JANUARY/FEBRUARY 2002
Volume 13, Number 1

© Copyright 2002 by the American Chemical Society

Bioconjugate Chemistry

EDITORIAL: What's New

We welcome the new members of the *Bioconjugate Chemistry* Editorial Advisory Board for 2002:

Dr. Sylvia Daunert, Department of Chemistry, University of Kentucky

Dr. Alexander V. Kabanov, Department of Pharmaceutical Sciences, University of Nebraska Medical Center

Thanks to Our Reviewers

It is a pleasure to acknowledge the contributions of the reviewers of manuscripts submitted in 2001 for publication in *Bioconjugate Chemistry*. Their unselfish service has been essential in the shaping of the twelfth volume of the journal. The scientific community is fortunate that its members are willing to share their time and specialized knowledge in this way. The reviewers are listed on the following page.

Claude F. Meares

Editor-in-Chief

10.1021/bc010189j CCC: $22.00 © 2002 American Chemical Society
Published on Web 01/16/2002

List of Reviewers

Maciej Adamczyk
Carolyn J. Anderson
Steven M. Ansell
Yasushi Arano
James R. Ballinger
J. A. Barrett
Jean-Paul Behr
Donald E. Bergstrom
Purshotam Bhan
Gary S. Bignami
Philip J. Blower
Alexei A. Bogdanov
Martin W. Brechbiel
Donald J. Buchsbaum
Herbert Cheung
Paul Chinn
Sylvia Daunert
Gary S. David
Mark E. Davis
Edith Dellacherie
Ruth Duncan
Ramon Eritja
Joan Estelrich
Raymond A. Firestone
Alan J. Fischman
Benoît Frisch
Michael J. Gait
Jean Gariépy
Kieran F. Geoghegan
David A. Goodwin
David W. Grainger
Marc M. Greenberg
Hermann J. Gruber
Elisha Haas
Bruce D. Hammock
M. Frederick Hawthorne
Claude Hélène
Jorge Heller
Donald J. Hnatowich
Leaf Huang
Ferenc Hudecz
Yuji Inada
David S. Jones
Rudy L. Juliano
Alexander V. Kabanov
Yoko Kanazawa
John Katzenellenbogen
John F. W. Keana
David E. Kerr
Hiromi Kitano
Hisataka Kobayashi
Jindrich Kopecek
Bennett C. Laguzza
David Lawrence
Stephen J. Lippard
Shuang Liu
Harri Lönnberg
Timo Lovgren
Atsushi Maruyama
Steve A. Matello
James A. McCloskey
Richard D. McCullough
Thomas J. Meade
Claude F. Meares
Damon L. Meyer
Patrick Midoux
Takeshi Miyata
Dennis Ng
Peter E. Nielsen
Makiya Nishikawa
Sean O'Malley
Leslie E. Orgel
David Oupicky
William M. Pardridge
David Piwnica-Worms
Tariq M. Rana
Jean-Serge Remy
Mark A. Reynolds
Kevin G. Rice
Annie C. Roche
Steven R. Roffler
Buck E. Rogers
Gregory J. Russell-Jones
Ahmad Safavy
Harri Salo
Michael Sánger
P. August Schubiger
Jody Schultz
Frank Seela
Nadrian Seeman
Peter D. Senter
Leonard W. Seymour
Jumi Shin
John E. Shively
Bradley D. Smith
Kevin M. Smith
Richard D. Smith
Caroline J. Springer
C. Y. Stein
Stanley Stein
Michael Sun
Håkan P. Svensson
Timothy M. Swager
Francis C. Szoka, Jr.
Donald A. Tomalia
Vladimir P. Torchilin
Vladimir S. Trubetskoy
Eishun Tsuchida
Ching-Hsuan Tung
Francesco M. Veronese
Wynn A. Volkert
Ernst Wagner
Alan Wahl
David S. Watt
Michael J. Welch
Eric Wickstrom
D. Scott Wilbur
Meir Wilchek
A. P. Wolffe
George Y. Wu
Samuel Zalipsky

BC010189J

COMMUNICATIONS

Gold Nanoparticle-Mediated Transfection of Mammalian Cells

Kulmeet K. Sandhu,[†] Catherine M. McIntosh,[†] Joseph M. Simard,[†] Sallie W. Smith,[‡] and Vincent M. Rotello*,[†]

Department of Chemistry and Department of Veterinary & Animal Science, University of Massachusetts, Amherst, Massachusetts 01003. Received August 16, 2001

Mixed monolayer protected gold clusters (MMPCs) functionalized with quaternary ammonium chains efficiently transfect mammalian cell cultures, as determined through β-galactosidase transfer and activity. The success of these transfection assemblies depended on several variables, including the ratio of DNA to nanoparticle during the incubation period, the number of charged substituents in the monolayer core, and the hydrophobic packing surrounding these amines. Complexes of MMPCs and plasmid DNA formed at w/w ratios of 30 were most effective in promoting transfection of 293T cells in the presence of 10% serum and 100 μM chloroquine. The most efficient nanoparticle studied (MMPC **7**) was ~8-fold more effective than 60 kDa polyethylenimine, a widely used transfection agent.

Gene transfer can be performed using either viral or synthetic gene delivery systems (*1*−*11*). While viral vectors are widely used, synthetic transfection systems provide several advantages including their ease of production *(7)* and the reduced risk of cytotoxicity (*7*, *12*) and immune responses (*3*, *4*, *7*, *12*, *13*). A variety of cationic systems have been studied for complexation and transport of negatively charged DNA, including peptides (*2*, *7*), liposomes containing cationic lipids (*14*), poly(lysine) (*6*), polyethylenimine (*3*), cationic polymers (*4*, *11*), PAMAM dendrimers (*1*, *5*, *10*), and more recently, silica nanoparticles (*8*, *9*).

Mixed monolayer protected gold clusters (MMPCs) represent a unique platform for transfection because of their ease of fabrication, especially in contrast to the complex synthesis required to produce the higher-generation dendrimer counterparts (*15*). In addition to simple hydrogen bonding or electrostatic moieties, biological tags capable of targeting the plasmid to a specific cell type are available (*7*) and can be introduced in postfabrication steps since subsequent modification of the monolayer is also facile. Cationic MMPCs bind very efficiently to DNA; in recent studies we have demonstrated that the interaction between cationic gold nanoparticles and DNA is efficient enough to totally inhibit in vitro DNA transcription by T7 RNA polymerase (*16*).

To explore the utility of MMPCs for transfection, MMPCs featuring a 2 nm gold core, with a total diameter of 6 nm, were fabricated. In comparison with other nanoparticle systems studied (*8*, *9*), we expect that the smaller size of the MMPCs should increase the efficiency of both the DNA−MMPC complex internalization and the subsequent release of the plasmid from the cationic MMPC surfaces. For our studies, we fabricated MMPCs modified with quaternary ammonium salts and tested their ability to transfect plasmid DNA (Figure 1).[1] The effect of varying cationic coverage was explored by comparing MMPCs **1**−**5**, constructed using differing

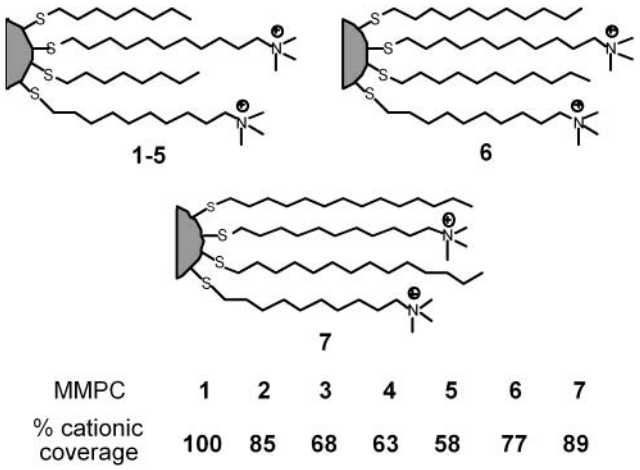


Figure 1. MMPCs used for transfection.

* Corresponding author: Vincent M. Rotello, Department of Chemistry LGRT 701, 710 N. Pleasant St., University of Massachusetts, Amherst, MA 01003. rotello@cisco.chem.umass.edu. Phone: (413) 545-2058. Fax: (413) 545-4490.

[†] Department of Chemistry.

[‡] Department of Veterinary & Animal Science.

[1] MMPCs were prepared as previously described in Simard, J., Briggs, C., Boal, A. K., and Rotello, V. M. (2000) *Chem. Commun.* 1943. Briefly, for **1**−**5**, 50 mg of octanethiol colloid was stirred for two days in THF with 10−100 mg of *N*,*N*,*N*-trimethyl(11-mercaptoundecyl)ammonium chloride. For **6** and **7**, 62 mg of undecanethiol colloid and 50 mg of tetradecanethiol colloid were stirred with 50 mg of ammonium thiol, respectively. After exchange, the MMPCs were purified by mulitple precipitations from dichloromethane. The colloids were characterized using UV, NMR, and TEM methods.

10.1021/bc015545c CCC: $22.00 © 2002 American Chemical Society
Published on Web 12/12/2001

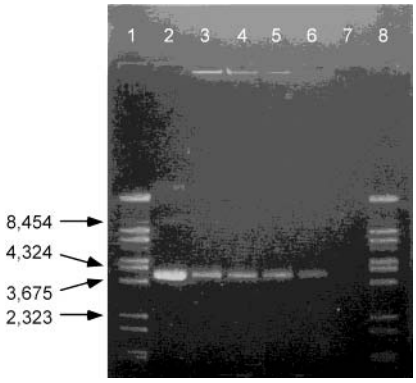


Figure 2. Agarose gel electrophoresis of the MMPCs and DNA. Exterior lanes contain molecular weight markers. The second lane is DNA alone at 9.5 nM; lanes 3−7 contain increasing amounts of MMPC **3** (2.4 μM, 3 μM, 4 μM, 6 μM, and 12 μM, respectively). As the nanoparticle concentration increases, more DNA is retained at the baseline, with complete complexation observed at 12 μM MMPC **3** or at a 790:1 MMPC **3** to DNA mole ratio. Decreasing fluorescence of the DNA fraction at the baseline may be due to absorption of the emitted light by the gold cores or the exclusion of ethidium bromide from the bound and condensed DNA (*17*).

ratios of octanethiol to ammonium thiol.[2] The effect of alkyl chain length on transfection was studied using MMPCs **6** and **7**, prepared with undecanethiol and tetradecanethiol, respectively.

Preliminary evidence for efficient MMPC−plasmid association was provided by the complete inhibition of electrophoretic mobility of the plasmids upon addition of cationic MMPCs. Gel electrophoresis of pET16B plasmids after incubation with MMPC **3** for 0−30 min showed the presence of only two bands of DNA: one at the baseline and one at the expected molecular weight for a single plasmid (Figure 2).[3] The ability of the nanoparticles to completely inhibit the DNA from progressing toward the positive electrode and the lack of any intermediate assemblies indicates either that the complexes formed were completely charge neutralized or that the resultant complexes were too large to enter the gel.[4]

Preliminary investigations focused on optimization of transfection conditions. Transfection was first compared in different environments: in the presence of both serum and chloroquine (chlq), transfection was improved in comparison to controls, as demonstrated using MMPC **3** (Figure 3a). For all further studies, a medium containing 100 μM chloroquine[5] and 10% serum was used.[6] To determine the optimal MMPC−plasmid ratio, increasing amounts of MMPC **3** were added to 250 μL of medium containing 5 μg of β-galactiosidase plasmid (Figure 3b).[7] Maximum transfection of β-galactosidase reporter gene

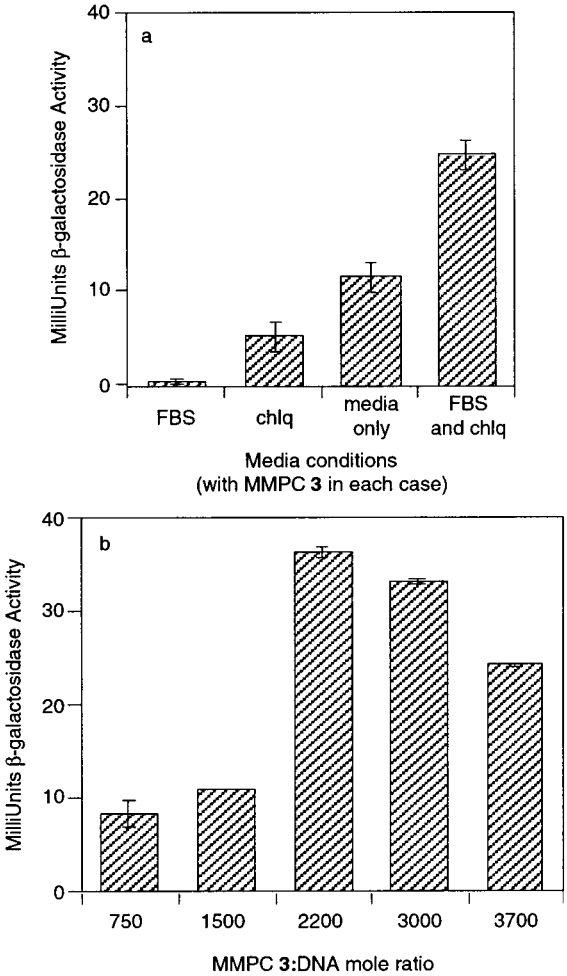


Figure 3. Efficiency of transfection as a function of (a) chloroquine (chlq) and serum (FBS) with a 2200:1 MMPC **3**:DNA ratio and (b) varying MMPC concentrations.[9] Levels of β-galactosidase were determined by comparison to a standard curve using known protein concentrations.

plasmid into 293T cells occurred at a MMPC:plasmid mole ratio of 2200:1. Further increases in MMPC concentration above this value resulted in a slow decrease in transfection efficiency.[8] Significantly, the optimal DNA−MMPC ratio for transfection was higher than that required for complete retardation of electrophoretic mobility (vide supra). This is consistent with previous studies that have shown overall net-positively charged assemblies to provide more efficient transfection (*9*, *18*, *19*).

[2] Cationic coverage of each MMPC was calculated by end-group analysis using NMR integration.

[3] Gels were prepared with 0.6% agarose, run for 60−90 minutes at 80 V, and visualized using ethidium bromide. pET16B plasmids encoding cellular retinoic acid binding protein consist of approximately 6200 base pairs. The molecular weights are composed of linear DNA, whereas the DNA of the pET vector (seen at approximately 4000 base pairs) corresponds to a circular strand. The small band evident in lane 2 at a higher MW is most likely due to incomplete purification of the DNA and is not expected to bias the results observed.

[4] Similar DNA:MMPC assemblies were prepared and characterized via methods in reference 16.

[5] Cholorquine is believed to disrupt the endosomal vesicle, resulting in increased passage of the transfection vector to the cytosol (*1*, *2*, *9*, *11*).

[6] β-Galactosidase plasmid DNA at 0.02 mg/mL was mixed with MMPC at 5 mg/mL. The complexes were then diluted with DMEM containing 10% FBS and 100 mM chloroquine. The human embryonic kidney cells (293T) were washed once with PBS and incubated with the MMPC/DNA complexes for 3 h at 37 °C in 5% CO_2. The cells were washed once with PBS and incubated for 48 h in DMEM + 10% FBS. The enzyme activities were then assayed using a β-galactosidase kit (Promega). The BCA assay (Pierce) was used to determine total protein content. Control experiments performed using naked DNA, nanoparticles alone, and neither DNA nor nanoparticles exhibited no measurable β-galactosidase activity (results not shown).

[7] The CMV-β-galactosidase plasmid is composed of approximately 7200 base pairs.

[8] Decreasing levels of β-galactosidase expression may be due to low level toxicity of the MMPCs (LD_{50} = 1.8 μM (a 2900:1 MMPC:DNA molar ratio) as determined for MMPC **3** using a WST-1 assay). This is ~165-fold higher than that of PEI (*9*).

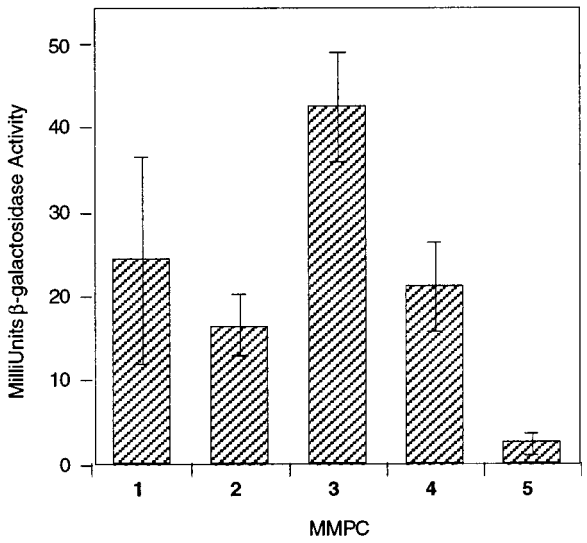


Figure 4. Transfection of β-galactosidase mediated by formation of various MMPC−DNA complexes at 2200:1 nanoparticle/DNA ratio.

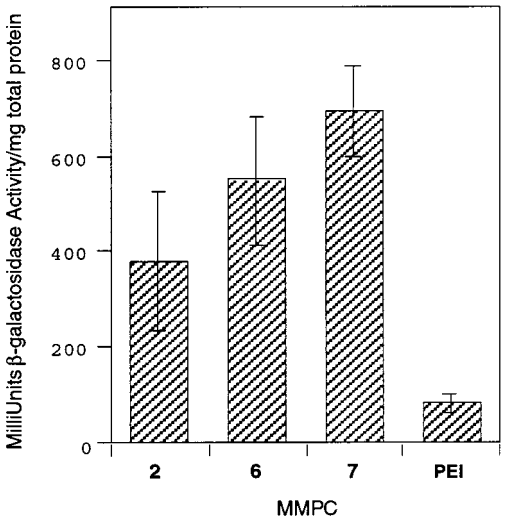


Figure 5. Transfection with MMPCs **2**, **6**, **7** (2200:1 nanoparticle/DNA ratio) and PEI (60 kDa).

We next explored the effect of the ratio of quaternary ammonium endgroups to hydrophobic chains (Figure 4). All of the gold nanoparticles were able to promote transfection in the presence of chloroquine and serum, with MMPC **3** proving to be the most effective of the octanethiol substituted particles. This suggests that either the charge/particle ratio or the hydrophobicity of the MMPCs is an important determinant of transfection efficiency.

The effect of the chain length of the monolayer was determined by testing the transfection efficiency of MMPCs **6** and **7** (Figure 5). In these studies, increasing transfection efficiency was observed with increasing chain length. All three nanoparticles were more efficient than polyethylenimine (PEI), with MMPC **7** being approximately eight times as effective as PEI.[10]

In summary, we have demonstrated the efficient transfection of plasmids encoding β-galactosidase into 293T cells, confirming the viability of MMPCs as transfection agents. The efficiency of the transfection process is determined by several parameters, including the ratio of MMPC:DNA used in initial complexation, the surface coverage of quaternary ammonium salts, and the length of the uncharged thiol chain. Further studies of the role of monolayer structure and functionality are currently underway and will be reported in due course.

[9] MMPC concentrations were determined by weight (based on an average molecular weight of 60000 for the nanoparticle, see ref 20) and DNA concentrations measured by UV-vis.

[10] PEI experiments performed as described in ref 9.

ACKNOWLEDGMENT

We thank Lila Gierasch and Jennifer Habink for the donation of cells containing the pET16B plasmid. We also thank Barbara A. Osborne for the use of her tissue culture facility. This research was supported by the National Science Foundation (DMR-9809365 for MRSEC instrumentation) and the National Institutes of Health (GM-59249 and GM-62998). V.M.R. acknowledges the Alfred P. Sloan Foundation, the Camille and Henry Dreyfus Foundation, and is a Cottrell scholar of Research Corporation. C.M.M. acknowledges support from the National Institutes of Health Chemistry-Biology Interface Training Grant GM-08515.

LITERATURE CITED

(1) Luo, D., and Saltzman, W. M. (2000) Enhancement of transfection by physical concentration of DNA at the cell surface. *Nat. Biotechnol. 18*, 893−895.

(2) Singh, D., Bisland, S. K., Kawamura, K., and Gariepy, J. (1999) Peptide-based intracellular shuttle able to facilitate gene transfer in mammalian cells. *Bioconjugate Chem. 10*, 745−754.

(3) Coll, J. L., Chollet, P., Brambilla, E., Desplanques, D., Behr, J. P., and Favrot, M. (1999) In vivo delivery to tumors of DNA complexed with linear polyethylenimine. *Hum. Gene Ther. 10*, 1659−1666.

(4) Lynn, D. M., and Langer, R. (2000) Degradable poly(beta-amino esters): Synthesis, characterization, and self-assembly with plasmid DNA. *J. Am. Chem. Soc. 122*, 10761−10768.

(5) Tang, M. X., Redemann, C. T., and Szoka, F. C. (1996) In vitro gene delivery by degraded polyamidoamine dendrimers. *Bioconjugate Chem. 7*, 703−714.

(6) Perales, J. C., Ferkol, T., Molas, M., and Hanson, R. W. (1994) An Evaluation of Receptor-Mediated Gene-Transfer Using Synthetic DNA-Ligand Complexes. *Eur. J. Biochem. 226*, 255−266.

(7) Morris, M. C., Chaloin, L., Heitz, F., and Divita, G. (2000) Translocating peptides and proteins and their use for gene delivery. *Curr. Opin. Biotechnol. 11*, 461−466.

(8) Kneuer, C., Sameti, M., Haltner, E. G., Schiestel, T., Schirra, H., Schmidt, H., and Lehr, C. M. (2000) Silica nanoparticles modified with aminosilanes as carriers for plasmid DNA. *Int. J. Pharm. 196*, 257−261.

(9) Kneuer, C., Sameti, M., Bakowsky, U., Schiestel, T., Schirra, H., Schmidt, H., and Lehr, C. M. (2000) A nonviral DNA delivery system based on surface modified silica-nanoparticles can efficiently transfect cells in vitro. *Bioconjugate Chem. 11*, 926−932.

(10) Bielinska, A. U., Chen, C. L., Johnson, J., and Baker, J. R. (1999) DNA complexing with polyamidoamine dendrimers: Implications for transfection. *Bioconjugate Chem. 10*, 843−850.

(11) Arigita, C., Zuidam, N. J., Crommelin, D. J. A., and Hennink, W. E. (1999) Association and dissociation characteristics of polymer/DNA complexes used for gene delivery. *Pharm. Res. 16*, 1534−1541.

(12) Luo, D., and Saltzman, W. M. (2000) Synthetic DNA delivery systems. *Nat. Biotechnol. 18*, 33−37.

(13) Tripathy, S. K., Black, H. B., Goldwasser, E., and Leiden, J. M. (1996) Immune responses to transgene-encoded proteins limit the stability of gene expression after injection of

replication-defective adenovirus vectors. *Nat. Med. 5*, 545−550.
(14) Colin, M., Harbottle, R. P., Knight, A., Kornprobst, M., Cooper, R. G., Miller, A. D., Trugnan, G., Capeau, J., Coutelle, C., and Brahimi-Horn, M. C. (1998) Liposomes enhance delivery and expression of an RGD-oligolysine gene transfer vector in human tracheal cells. *Gene Ther. 11*, 1488−1498.
(15) Tomalia, D. A., Naylor, A. N., and Goddard, W. A., III. (1990) Starburst dendrimers: Molecular level control of size, shape, surface, chemistry and topology. *Angew. Chem., Int. Ed. Engl. 29*, 138−175.
(16) McIntosh, C. M., Esposito, E. A., Boal, A. K., Simard, J. M., Martin, C. T., and Rotello, V. R. (2001) Inhibition of DNA Transcription Using Cationic Mixed Monolayer Protected Gold Clusters. *J. Am. Chem. Soc. 123*, 7626−7629.
(17) Gershon, H., Ghirlando, R., Guttman, S. B., Minsky, A. (1993) Mode of Formation and Structural Features of DNA Cationic Liposome Complexes Used for Transfection. *Biochemistry 32*, 7143−7151.
(18) Truong-Le, V. L., Walsh, S. M., Schweibert, E., Mao, H. Q., Guggino, W. B., August, J. T., and Leong, K. W. (1999) Gene transfer by DNA-gelatin nanospheres. *Arch. Biochem. Biophys. 361*, 47−56.
(19) Wolfert, M. A., Schacht, E. H., Toncheva, V., Ulbrich, K., Nazarova, O., and Seymour, L. W. (1996) Characterization of vectors for gene therapy formed by self-assembly of DNA with synthetic block copolymers. *Hum. Gene Ther. 7*, 2123-2133.
(20) Hostetler, M. J., Wingate, J. E., Zhong, C.-J., Harris, J. E., Vachet, R. W., Clark, M. R., Londono, J. D., Green, S. J., Stokes, J. J., Wignall, G. D., Glish, G. L., Porter, M. D., Evans, N. D., Murray, R. W. (1998) Alkanethiolate Gold Cluster Molecules with Core Diameters from 1.5 to 5.2 nm: Core and Monolayer Properties as a Function of Core Size. *Langmuir 14*, 17−30.

BC015545C

ARTICLES

In Vivo Tumor Delivery of a Recombinant Single-Chain Fv::Tumor Necrosis Factor: A Fusion Protein

Stephen P. Cooke,* R. Barbara Pedley, R. Boden, Richard H. J. Begent, and Kerry A. Chester

CRC Targeting and Imaging Group, Academic Department of Oncology, Royal Free and University College Medical School, University College, London, NW3 2PF, U.K. Received December 20, 2000

Locoregional and intratumoral administration of tumor necrosis factor α (TNFα) has been successful in obtaining inhibition or regression of tumor growth in the clinic. This potent antitumor activity of TNFα has not yet been exploited as a systemic agent in cancer therapy, mainly due to high levels of toxicity to normal tissues before a therapeutic dose of TNFα in the tumor has been achieved. To address this, we have targeted TNFα using antitumor antibodies. We have used a genetic fusion of human recombinant TNFα with MFE-23, a single-chain Fv antibody fragment directed against carcinoembryonic antigen. MFE-23::TNFα fusion protein is isolated in high yields (28 mg/L) from bacterial inclusion bodies and purified to homogeneity by affinity chromatography. It is a 144 kDa trimer in native form and possesses the antigen-binding activity of the sFv and the cytotoxicity to both WEHI 164 and a human adenocarcinoma cell line (LoVo) of rhTNFα. Radiolabeled MFE-23::TNFα binds both human and mouse TNF receptor 1 in vitro and is able to localize effectively in nude (nu/nu) mice bearing human LS174T xenografts; tumor/tissue ratios of 21:1 and 60:1 are achieved 24 and 48 h after intravenous injection. These studies indicate that MFE-23::TNFα will provide an effective means for systemically administered cancer therapy with TNFα.

INTRODUCTION

Tumor necrosis factor α (TNFα) is a pleiotropic cytokine produced by a variety of human cells particularly activated macrophages and monocytes. It has the ability to kill tumor cells by binding to two cell surface receptors, TNFR1 and TNFR2 (p55 and p75), thereby inducing apoptosis by activation of the death pathway (Laster et al., 1988; Itoh and Nagata, 1993). Studies involving regional (Lejeune, 1995; Moritz et al., 1989; Abbruzzese et al., 1989; Mavligit et al., 1992) or intratumoral (Watanabe et al., 1994) injection of TNFα in humans, where high tumor levels of the cytokine can be achieved, have demonstrated tumor regression, especially when administered in combination with interferon-γ. This has been particularly impressive in trials involving isolated limb perfusion (Lejeune, 1995; Abbruzzese et al., 1989) and raises the question of whether these results could be matched using TNFα administered to patients via a simple intravenous injection.

The use of TNFα as a systemic agent for cancer therapy is restricted by the short circulatory half-life of the molecule and its severe side effects ranging from headache, chills, and fever to systemic shock and sepsis (Asher et al., 1987; Rosenberg et al., 1988). Thus, normal tissue toxicity is limiting before a therapeutic dose to the tumor can be achieved, and therefore, the potent antitumor activity of TNFα remains unharnessed for systemic therapy. Various targeting strategies have been developed to address this with the aim of achieving higher doses of TNFα at the tumor site coupled with a low systemic concentration. Systemic delivery of TNFα by liposomes (Manusama et al., 1998) or dextran and metal coordination to improve tumor penetration and retention of TNFα (Tabata et al., 1999) have been explored, but more specific targeting can be achieved using tumor-selective antibodies. Indirect approaches using bispecific (antitumor/anti-TNFα) antibodies to capture TNFα at the tumor site (Robert et al., 1996) or avidin−antibody complexes to target biotinylated TNFα (Moro et al., 1997; Gasparri et al., 1999), have met with some success, but these systems are complex. More straightforward approaches using antibodies directly linked to TNFα are attractive and have shown efficacy in animal models using chemical conjugates of whole antibody coupled to TNFα (Gillies et al., 1993; Pietersz et al., 1998). However, chemical conjugates have demonstrated poor tumor penetration (possibly due in part to their large size), which results in low amounts of TNFα localizing in the tumor tissue. Attempts to optimize the direct antibody targeting approach by using recombinant fusion proteins of TNFα with single-chain Fv antibody fragments (sFvs) have shown encouraging results such as specific cytotoxicity in vitro (Hoogenboom et al., 1991; Yang et al., 1995) and reduction in tumor volume in mice bearing Le^{Y+} xenografts (Scherf et al., 1996). However, these promising therapies were hampered by poor yield of fusion protein, preventing further study and development of a clinically useful product. We describe the production, purification, characterization, and tumor targeting of MFE-23::TNFα fusion protein, which overcomes this obstacle.

* To whom correspondence should be addrssed. Tel: +44 020 7794 0500 ext 5495. Fax: +44 020 7794 3341. E-mail: s.cooke@ucl.ac.uk.

10.1021/bc000178a CCC: $22.00 © 2002 American Chemical Society
Published on Web 12/22/2001

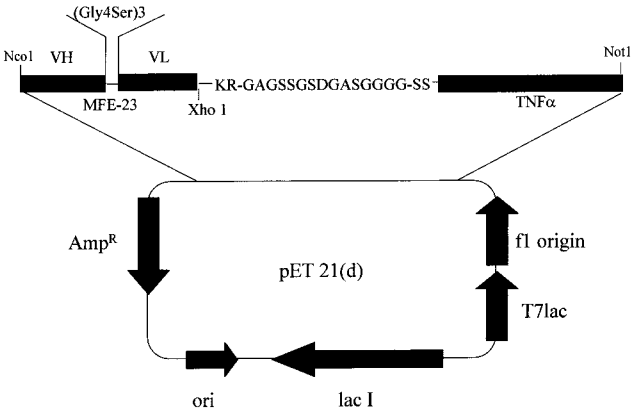


Figure 1. Schematic of MFE-23::TNFα/pET21(d). MFE-23::TNFα was inserted into pET21(d) via Nco1 and Not1 restriction sites. The flexible linker between the sFv and the TNFα is also shown.

MFE-23 is a filamentous bacteriophage-derived sFv (Chester et al., 1994) that has been shown to localize safely and effectively to carcinoembryonic antigen (CEA) expressing tumors in clinical trials (Begent et al., 1996; Mayer et al., 2000). CEA was chosen as a target because, with highly specific antibodies, it is only detectable on tumors and on the luminal surface of the gut, which is not accessible to IgG antibodies. CEA is expressed on most gastrointestinal carcinomas and on a proportion of breast, lung, and ovarian carcinomas. MFE-23 is readily expressed in bacteria and was selected to bind with high affinity ($K_D = 2 \times 10^{-9}$ M) for CEA (20). The MFE::TNFα fusion protein aims to reduce sequestration and increase tumor concentrations of systemically administered TNFα.

EXPERIMENTAL PROCEDURES

Subcloning of MFE-23::TNFα Plasmid. The expression vector pUC119SNpolymyc containing the MFE23::TNFα fusion protein (a kind gift from Philipp Holliger, LMB, Cambridge, UK) was purified from the *Escherichia coli* strain TG1 using standard methods. The MFE-23::TNFα gene was released from the plasmid by digestion with restriction endonucleases Nco1 and Not1 (5 units/μg DNA; 4 h; 37 °C) and ligated into the expression vector pET21(d) prior to electroporation into *E. coli* strain BL21(DE3)pLysS. A schematic of the resulting expression vector pET21(d) MFE-23::TNFα is shown in Figure 1.

Expression in Inclusion Bodies. Five individual colonies of BL21 (DE3 pLysS) containing the MFE-23::TNFα gene and controls containing the "empty" pET 21(d) vector alone were selected and grown in 50 mL culture broth (2TY + 0.1% glucose + 100 mg/mL ampicillin). When an OD_{600} of 0.9 was reached, the cultures were induced with 2 mM isopropylthiogalactoside (IPTG) for 16 h at 30 °C. Cultures were then centrifuged at 4000 rpm for 15 min, and the pellet was incubated in lysis buffer (0.1 M Tris, 20 mM EDTA pH8.0 containing 200 mg/mL lysozyme) for 1 h at room temperature followed by the addition of NaCl to 0.5 M and Triton-X 100 to a final concentration of 2%. After the pellet was incubated a further 3 h, tubes were centrifuged at 25000*g* for 1 h to isolate the inclusion body fraction. Inclusion bodies were washed three times in wash buffer (0.1 M Tris, 20 mM EDTA pH 8.0) before freezing at −70 °C overnight. The inclusion body pellet was resuspended in a second lysis buffer (0.1 M tris pH 8.0, 2 mM EDTA, 300 mM DTE, 8 M urea) and incubated overnight at room temperature. Tubes were centrifuged at 30000*g*, and the supernatant was recovered. Aliquots were analyzed for protein production by SDS−PAGE (stained with Coomassie Blue). The supernatants containing protein of the expected molecular weight were pooled and dialyzed extensively against 8 M urea to remove all DTE prior to refolding.

Refolding and Purification by Affinity Chromatography. The refolding protocol was based on that of Scherf et al. (1996). Single aliquots (5−10 mL) of supernatant were added every 30 min to 1 L of refolding buffer (0.1 M Tris pH 8.0, 2 mM EDTA, 1 mM reduced glutathione (GSSG), 1 mM oxidized glutathione (GSG), 0.5 M L-arginine) and allowed to refold at 4 °C for 96 h with constant agitation. The resulting protein solution (1200 mL) was filtered to remove aggregates before passage through an CNBr-activated Sepharose-CEA affinity column. The solution was circulated though the column via a peristaltic pump, and the column was washed with 50 mL of PBS before bound protein was eluted by the addition of 5 mL aliquots of 50 mM diethylamine. Optical density measurements were taken ($OD_{280\ nm}$), and fractions containing protein were pooled and dialyzed into PBS before being sterile filtered, aliquoted, and stored at −70 °C. This affinity chromatography procedure was repeated three times.

SDS−PAGE and Western Blot Analysis. For the initial analysis of the crude supernatants and controls obtained after inclusion body lysis, 20 μL samples were loaded into the wells of a 10% polyacrylamide gel under reducing conditions alongside molecular markers covering a range of molecular weights from 250 to 4 kDa. After electrophoresis, gels were stained with Coomassie Blue and destained in water/acetic acid/methanol until bands were visible.

After refolding of the fusion protein from the inclusion body supernatant and purification by affinity chromatography, 20 μL samples were loaded into the wells of a 10% polyacrylamide gel under reducing conditions. After electrophoresis, the gels were cut in half and proteins transferred to PVDF membranes. After being blocked in 5% Marvel, blots were incubated with either rabbit anti-MFE or rabbit anti-human TNFα polyclonal antibodies diluted 1:500 in 1% Marvel in PBS/0.1% Tween-20 for 1 h. After being washed with PBS/0.1% Tween-20, blots were incubated with goat anti-rabbit IgG conjugated to horseradish peroxidase (HRP) diluted 1:2000 for 1 h prior to visualization with diaminobenzidine/H_2O_2.

Assessment of CEA Binding Activity. ELISA plates were coated with CEA at 2 μg/mL and blocked for 1 h with 5% Marvel in PBS/0.1% Tween-20. Fusion protein was serially diluted in PBS/0.1% Tween-20 and 100 mL added to the wells in duplicate. Plates were washed, and 100 mL rabbit anti-MFE or rabbit anti-human TNFα polyclonal antibodies were added at 1:500 for 1 h followed by 100 μL of goat anti-rabbit IgG conjugated to HRP at 1:2000 for a further 1 h. Plates were developed by addition of 100 μL of *o*-phenylenediamine (OPD)/H_2O_2 in citrate buffer pH 5.0. The reaction was stopped by the addition of 50 μL of 4 M HCl and plates read at 490 nm on an ELISA plate reader.

Native Molecular Weight Determination. One hundred micrograms of purified fusion protein was loaded onto a Superose 12 size-exclusion column and analyzed by fast-performance liquid chromatography. One milliliter fractions were collected, and absorbance at $OD_{280\ nm}$ was used as the readout. The column was first calibrated by addition of 100 μg each of protein of known molecular weight (MFE-23; 28 kDa, IgG; 150 kDa, b-amylase; 205 kDa, apoferritin; 440 kDa and thyroglobu-

lin; 690 kDa) and a calibration curve of molecular weight versus elution volume constructed. The fraction number of the eluted peak was determined relative to these standards and the molecular weight estimated from the calibration curve.

Cytotoxicity Assay for TNFα Activity. The TNFα-sensitive cell line WEHI 164 was used in this assay. Cells were plated at 2×10^5 cells/well in 96-well plates and incubated overnight at 37 °C/5%CO_2. Cells were treated with actinomycin D at 10 μg/mL before addition of fusion protein or rhTNFα controls in tripling dilutions (adjusted to yield from 1000 pg/mL to 4 pg/mL w/v TNFα), in triplicate in 200 μL culture medium. sFv MFE-23 alone was used as control (also at 1000 pg/mL to 4 pg/mL). Culture medium alone was used as a negative control. Plates were incubated overnight before addition of 10 μL of a 5 mg/mL solution of MTT [3-(4,5-Dimethylthiazol-2-yl)-2,5-diphenyltetrazolium bromide]/well. After a further 4 h incubation at 37 °C, cells were lyzed by addition of 100 μL of 10% SDS in 0.01 N HCl. Color development was allowed to proceed overnight at 37 °C, and plates were read at 570 nm on an ELISA plate reader. The reduction in optical density is a measure of decreased cell viability. Results were expressed in terms of percentage cytotoxicity using the formula $[(OD_{max} - OD_{sample})/(OD_{max} - OD_{min})] \times 100$, where OD_{max} is the optical density of wells containing culture medium alone and OD_{min} is the optical density at which no viable cells were visible by phase-contrast microscopy. The differences between sets of triplicate wells were tested for significance using a nonpaired, single tail students t-test, and significance in the text refers to a p value of <0.05.

In Vivo Studies. *Xenograft.* The human colon adenocarcinoma cell line LS174T was used to develop a xenograft model in the flank of female (nu/nu) mice. Subsequent passaging was by s.c. implantation of small tumor pieces (~1 mm^3). The tumor is a moderately differentiated CEA-producing adenocarcinoma with small glandular ascini, which secretes no measurable CEA into the circulation (Pedley et al., 1993).

Radiolabeling and Biodistribution Studies. Fusion protein was labeled at 0.15 MBqmg^{-1} with $Na^{125}I$ by the chloramine T method (Fraker and Speck, 1978). Briefly, 18 MBq $Na^{125}I$ was added to the fusion protein (100 mg). After mixing, 100 mL of chloramine T (2 mg/mL) was added and reaction stopped after 30 s by the addition of 100 mL of L-tyrosine (2 mg/mL). Radiolabeled protein was separated from free ^{125}I by passage down a PD-10 desalting column. Incorporation of radiolabel was assessed by thin-layer chromatography and CEA binding activity by affinity chromatography. Four groups of nude mice bearing LS174T human tumor xenografts (4 mice per group) were injected with 1.1 MBq (6.2 μg) radiolabeled fusion protein and sacrificed 3, 6, 24, and 48 h postinjection. Selected normal tissues and tumors were then removed for comparative assessment using a gamma counter as previously described (Pedley et al., 1996). Results were expressed as percentage injected dose per gram of tissue and as tumor:tissue ratios.

Isolation of Intact Fusion Protein from Excised Tumors. Tumors were excised from host animals as described previously (Bhatia et al., 2000) 2 and 4 h postinjection of 28 μg of radiolabeled MFE-23::TNFα fusion protein, snap frozen, and stored at −70 °C before use. Blood samples were also taken, and the serum obtained was stored at −70 °C. Tumors were thawed, weighed, and homogenized in 20 mM HEPES buffer containing 2 mM EDTA and 100 μg/mL protease inhibitor cocktail (Sigma, Poole, UK). Samples of tumor homogenate and serum were loaded into the wells of 12% polyacrylamide gels and subjected to electrophoresis. A radiolabeled sFv was loaded as a control along with molecular weight markers. Gels were stained with Coomassie blue and destained in water/acetic acid/methanol until protein bands were visible. Gels were then exposed to phosphor image plates (Amersham Pharmacia Biotech UK, Little Chalfont, U.K.) for 120 h before analysis on a phosphor imager (Amersham Pharmacia Biotech UK, Little Chalfont, U.K.).

TNF Receptor Binding Studies. Fusion protein was radiolabeled with $Na^{125}I$ as described above. Labeled protein (~0.5 μg/0.05 MBq) was added to 200 μL of PBS and injected onto a Superose 12 size-exclusion column, and 2 mL fractions were collected. The fractions were then counted on a γ counter. For receptor binding studies, the fusion protein (~1 μg) was incubated with 3 μg of recombinant human TNF receptor 1/Fc chimera or recombinant mouse TNF receptor 1/Fc chimera (R&D Systems, Oxford, U.K.) for 15 min at room temperature prior to injection onto the column. Fractions were collected and counted as for fusion protein alone. The peak position was related to protein standards and molecular weight estimated by reference to the calibration curve constructed as above.

Cytotoxicity to Human Tumor Cells. The human colon adenocarcinoma cell line LoVo was used in this assay. Cells were plated at 1×10^5/well in culture medium and grown overnight. The cytotoxicity assay was carried out as outlined above for the WEHI cells. Fusion protein or rhTNFα controls were added in 10-fold dilutions (adjusted to yield from 1000ng/mL to 1pg/mL w/v TNFα), in triplicate in 200 μL culture medium. sFv MFE-23 alone was used as control (at the same proportion relative to TNFα as present in the fusion protein: 1530 ng/mL to 1.53 pg/mL). Percent cell death was calculated as outlined above for WEHI cells.

RESULTS

Expression and Purification of MFE-23::TNFα. MFE-23::TNFα was the major protein expressed in *E. coli* inclusion bodies after subcloning into the expression vector pET 21(d). The major protein band was seen in all five separate inclusion body extracts that were tested for fusion protein expression by SDS−PAGE prior to refolding. All five samples showed a major band of 48 kDa (Figure 2a), which is the estimated molecular weight of a MFE-23::TNFα monomer. This band was absent in the control cells. Approximately 10−14% of the extracted MFE-23::TNFα was subsequently refolded into the correct conformation for CEA binding as determined by the yields of CEA-binding material eluted from Sepharose-coupled CEA column. The CEA binding material eluted from this column was analyzed by SDS−PAGE, and the results are shown in Figure 2b. These indicate high-grade purity of MFE-23::TNFα since only a single band of 48 kDa remains. From the optical density measurements it was calculated that the yield of purified, refolded MFE-23::TNFα was 27.65 μg/mL bacterial culture.

Western Blot Analysis and CEA Binding ELISA. Both these methods of analysis demonstrated that the fusion protein comprised MFE-23 and TNFα. Western blot analysis showed that the protein was intact and antibodies to both MFE-23 and human TNFα reacted with the 48 kDa molecule. Antibody to MFE-23 also indicated some breakdown of the molecule, but the amount of smaller molecular weight proteins was low compared with the amount of intact fusion protein

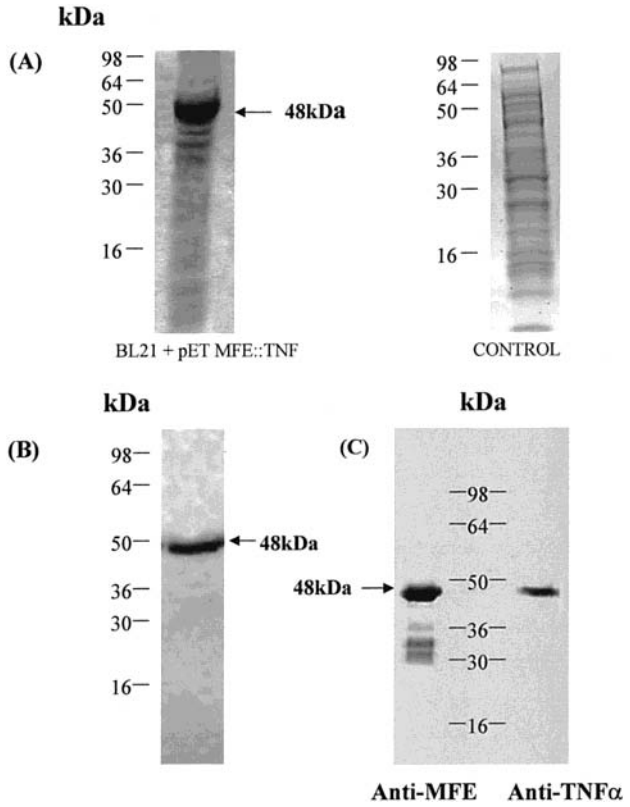


Figure 2. (A) Reducing SDS−PAGE gel showing expression of the 48 kDa MFE::TNFα fusion protein in inclusion body extracts. Twenty microliters of protein solution was loaded into each lane and stained with Coomassie blue. The 48 kDa protein comprises the majority of the total protein extracted from the bacterial inclusion body pellet; control cells do not show any major band at this molecular weight. (B) MFE-23::TNFα after refolding in redox buffer for 96 h and purification by affinity chromatography on a CEA column. (C) western blot analysis of MFE-23::TNFα showing reactivity of the 48kDa fusion protein with both anti-MFE-23 and anti-TNFα polyclonal antibodies. A small amount of breakdown product is also detected by the anti-MFE-23 antibody. Ten microliters of SeeBlue marker was loaded onto all gels to facilitate size estimation. M = molecular weight markers.

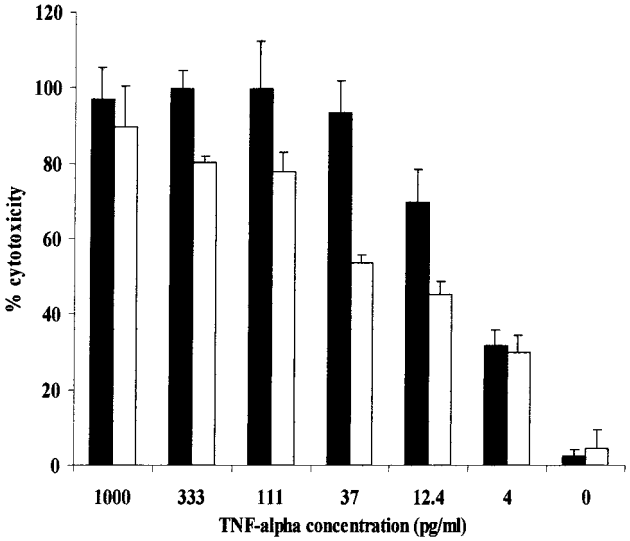


Figure 3. Cytotoxicity assay for TNFα bioactivity against actinomycin D-treated, TNFα-sensitive WEHI 164 cells. Recombinant human TNFα and MFE-23::TNFα were diluted from 1000 to 4 pg/mL (w/vTNFα) before addition to the assay plates. Medium alone represented no cytokine. Recombinant human TNFα yields maximum toxicity (no viable cells remaining) at a concentration of 100 pg/mL. MFE-23::TNFα is significantly less cytotoxic ($p < 0.05$) at all doses except 1000 and 4 pg/mL and on average 19% less toxic over the dose range tested. Control protein MFE-23 showed no toxicity to the WEHI 164 cells (data not shown). Results are expressed as mean ± SD of triplicate wells are representative of three separate experiments. TNFα, solid black; MFE-23::TNFα, white.

(Figure 2c). ELISA analysis of CEA-coated wells confirmed that the MFE-23::TNFα had specificity for CEA and reacted with antibodies to TNFα (data not shown).

Native Molecular Weight Determination. To determine the molecular weight of MFE-23::TNFα in its native form, 100 μg was passed down a Superose 12 size-exclusion column and the molecular weight estimated by comparison of the position of the eluted peak to those of molecular weight standards on a calibration curve for the column. A single peak was obtained centered around fraction 26 which corresponded to an estimated molecular weight of 144 kDa (91% of the injected protein) confirming that the fusion protein assumed a trimeric structure upon refolding. A smaller peak at around fraction 32−34 corresponded to the molecular weight of free MFE-23 (approximately 28 kDa) comprising 9% of the injected protein. No free TNFα was detected. Experiments performed after six weeks of storage at −70 °C gave identical results suggesting that the fusion protein is stable under these storage conditions (data not shown).

Cytotoxicity of MFE-23::TNFα. ***WIHI 164 Cells.*** We used the TNFα-sensitive cell line WEHI 164 to demonstrate that the fusion protein retained TNFα-mediated cytotoxicity in a standard MTT assay. The MFE-23::TNFα fusion protein exhibited a dose-dependent cytotoxic effect upon the WEHI cells that was significantly lower than that of recombinant human TNFα (rhTNFα) at 333, 111, 37, and 12 pg/mL but not so at 1000 and 4 pg/mL. However, MFE-23::TNFα was only on average 19% less cytotoxic over the dose range tested in the assay demonstrating that fusion to MFE-23 did not result in loss of cytotoxicity. Cell death was maximal (no intact cells visible by phase contrast microscopy) at a rhTNFα concentration of 100 pg/mL. There was no toxicity observed when cells were treated with MFE-23 alone (data not shown). Figure 3 shows the data for rhTNFα and MFE-23::TNFα expressed in terms of mean percent cytotoxicity.

Biodistribution Studies. Four groups of nude mice bearing LS174T human tumor xenografts (four mice per group) were injected with 1.1 MBq (6.2 μg) of radiolabeled MFE-23::TNFα fusion protein. Mice were sacrificed 3, 6, 24, and 48 h postinjection and tissues harvested and assessed using a γ counter. Figure 4a shows percent injected dose of fusion protein per gram tissue (% ID/g) at 3, 6, 24, and 48 h post intravenous administration of MFE-23::TNFα. Rapid clearance of the fusion protein was observed from all tissues tested within 24 h with selective retention of the molecule in the tumor. A maximum of 4.33% ID/g tumor was seen 6 h postinjection, falling to 1.99 and 1.58% ID/g tumor after 24 and 48 h, respectively. The same results are expressed as tumor/tissue ratios in Figure 4b to illustrate this tumor selectivity more clearly. Here, the retention of the fusion protein within the tumor is highlighted with tissue:blood ratios of 21:1 and 60:1 being achieved after 24 and 48 h, respectively. Liver and kidney were the only normal tissues to show retention of the fusion protein at these time points (liver = 0.14 and 0.087% ID/g; liver:blood ratio 2.12 and 4.4: kidney = 0.23 and 0.16% ID/g tissue; kidney/blood ratio 3.62 and 8.02) after 24 and 48 h,

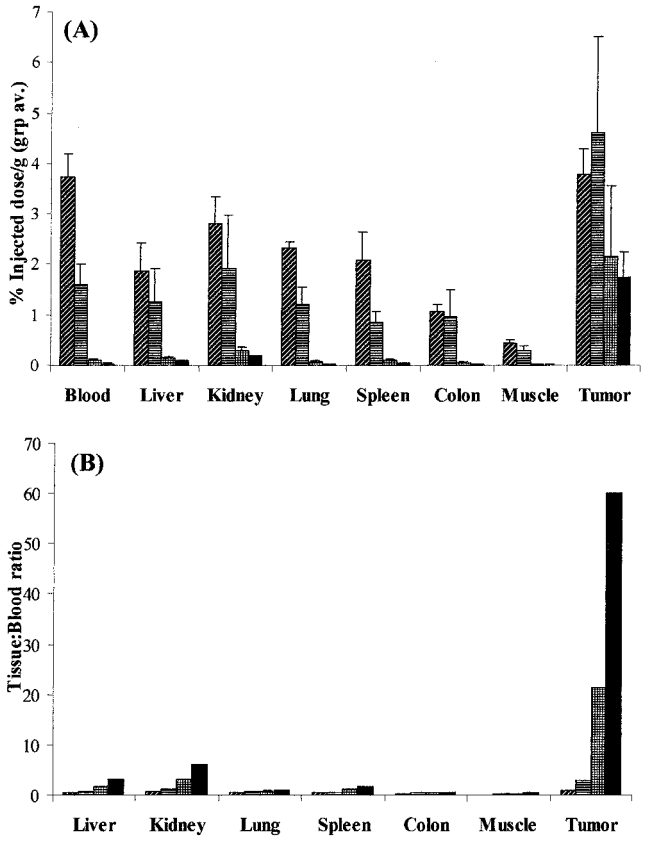


Figure 4. (A) Biodistribution of ^{125}I-MFE-23::TNFα in nude mice bearing the LS174T xenograft. Mice were injected with 1.1 Mbq (6.2 μg) ^{125}I-labeled MFE-23::TNFα and tissues excised 3, 6, 24, and 48 h post-fusion protein injection. After digestion in 7 M KOH, tissues were counted on a γ counter and radioactivity was assessed. Rapid clearance of the fusion protein was observed from all tissues tested within 24 h with selective retention of the molecule in the tumor. A maximum of 4.33% ID/g tumor was seen 6 h post-injection, falling to 1.99 and 1.58% ID/g tumor after 24 and 48 h, respectively. Columns, means of groups of four animals; bars, SD. (B) Tumor-to-tissue ratios obtained 3, 6, 24, and 48 h post-fusion protein injection. Tumor/blood ratios of 21:1 and 60:1 were achieved after 24 and 48 h, respectively. Columns, means of groups of four animals. Key: 3 h post-injection, diagonal cross-hatch; 6 h post-injection, horizontal cross-hatch; 24 h post-injection, black check; 48 h post-injection, solid black.

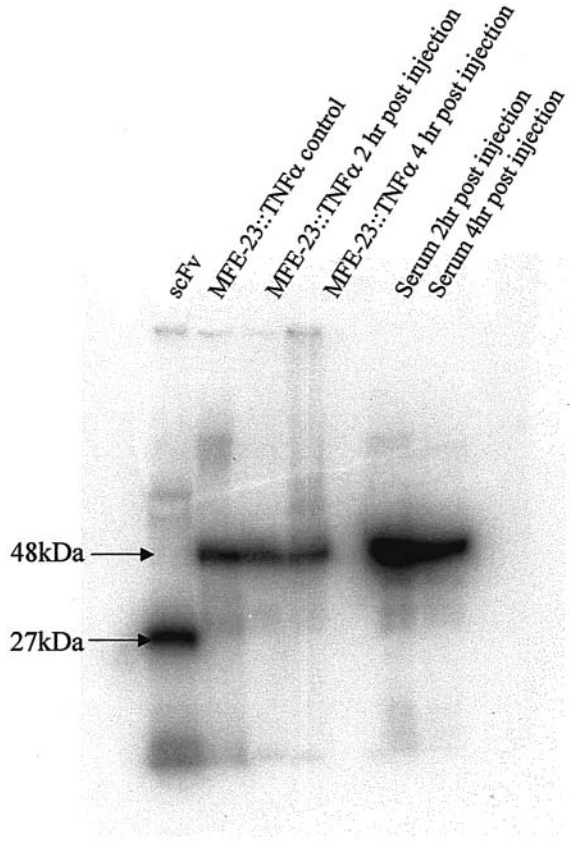


Figure 5. Extraction of intact MFE-23::TNFα from tumor homogenates and mouse serum. Mice were injected with 28 μg of ^{125}I MFE-23::TNFα and sacrificed 2 and 4 h post-injection. Blood and tumor were then taken. After homogenization and SDS−PAGE, a band of approximately 48 kDa can clearly be seen in the tumor extracts both 2 and 4 h post-injection of radiolabeled fusion protein. A band of the same molecular weight is seen in the serum. A ^{125}I-labeled sFv was loaded as a molecular weight control (27 kDa).

respectively. These data clearly demonstrate that MFE-23::TNFα shows high tumor specificity coupled with low uptake and retention by normal tissues or blood.

Isolation of MFE-23::TNFα from Tumors. Phosphor image analysis of the polyacrylamide gels showed a strong band of approximately 48 kDa in both tumor and blood samples (Figure 5). The intensity of the bands in the serum samples is greater at 2 h than at 4 h postinjection suggesting clearance of the fusion protein from the blood, supporting the evidence obtained from the biodistribution data. No free MFE or TNFα can be seen in any of the samples suggesting that the fusion protein is stable in vivo. This supports in vitro data obtained by incubating the fusion protein with human serum for 1 h or mouse serum for 2 and 4 h at 37 °C followed by analysis by FPLC. No degradation of the fusion protein was evident from these experiments (data not shown). Early time points were selected to give the best chance of detecting the fusion protein while still in the circulation to assess its resistance to degradation. The 48 kDa band present on the gels represents MFE-23::TNFα monomer, as the hydrophobic interactions which hold the TNFα trimer together are destroyed by SDS-sample buffers.

TNFα Receptor Binding Studies. To demonstrate that MFE-23::TNFα was able to bind TNF receptors after the radiolabeling procedure, ^{125}I-MFE-23::TNFα was preincubated with either recombinant human TNF receptor 1/Fc or mouse TNF receptor 1/Fc before loading onto a Superose 12 size-exclusion column for analysis by gel filtration chromatography. The results are shown in Figure 6. Radiolabeled, trimeric fusion protein was eluted from the column in fractions that corresponded to a molecular weight of approximately 144 kDa (Figure 6a) as read off the column calibration curve. After a 15 min incubation at room temperature with recombinant human TNF receptor 1/Fc chimera (which is a homodimer of approximately 120 kDa in native form), the peak was seen to shift from around fraction 26 to fractions 18−21 indicating an increase in the molecular weight of the radiolabeled species. This peak corresponded to a range of molecular weights consistent with the TNF trimer binding between one and three receptor molecules (Figure 6b). The peak was centered around fraction 19 suggesting the predominant species was a TNF trimer bound to two receptor molecules (estimated mw = 360 kDa, theoretical mw = 384 kDa). Similar results were obtained when ^{125}I-MFE-23::TNFα was preincubated with recombinant mouse TNF receptor 1/Fc chimera, indicating that the fusion protein effectively bound and complexed both human and murine TNF receptor mol-

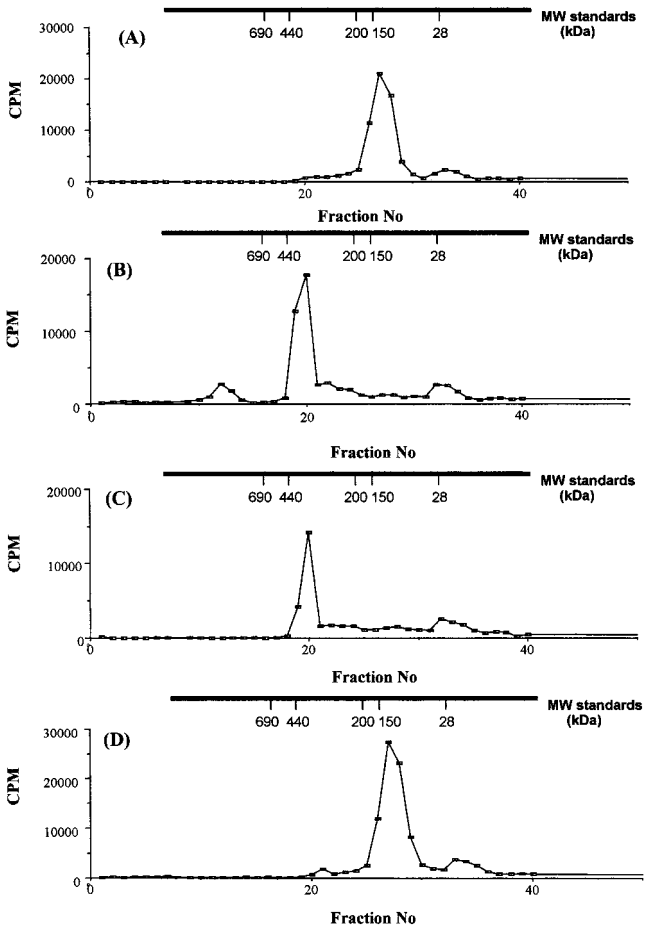


Figure 6. MFE-23::TNFα was preincubated for 15 min at room temperature with either human TNF R1/Fc or mouse TNF R1/Fc prior to loading onto a Superose 12 size-exclusion column calibrated with proteins of known molecular weight. After incubation with recombinant human (b) or recombinant mouse (c) TNF R1/Fc, an increase in molecular weight was seen (represented by the protein eluting at a lower fraction number; ~18−21 as opposed to ~26) indicating complex formation. Native fusion protein (a), or fusion protein incubated 0.1% BSA/0.1% HSA prior to loading (d) eluted with a molecular weight of ~144 kDa representing uncomplexed trimer. Molecular weight standards are indicated at the top of the figure.

ecules (Figure 6c). To control for the effects of the human serum albumin (HSA) and bovine serum albumin (BSA) included in the buffer solutions used to resuspend the recombinant receptor molecules, the fusion protein was incubated with PBS containing 0.1% BSA/0.1% HSA (concentrations identical to those in the buffers). The peak eluted in its original position around fraction 26 (Figure 6d). These data is consistent with the fusion protein retaining the ability to bind to TNFα receptors after radiolabeling.

Cytotoxicity to Human Tumor Cells (LoVo). LoVo cells were chosen for this assay because, unlike LS174T, they are susceptible to TNF-mediated cytotoxicity. Figure 7 shows that MFE-23::TNFα is as effective as TNFα alone at killing LoVo cells in vitro. Both the fusion protein and TNFα show identical LD_{50} values of 0.6 ng/mL. MFE-23 alone was used as a control and did not show any cytotoxic effects above background. Trypan blue exclusion showed 18% of cultured LoVo cells were not viable and this was taken as a measure of the background cell death in the cytotoxicity assays. These results confirm that MFE-23::TNFα is able to kill human tumor cells at the same concentrations as native TNFα.

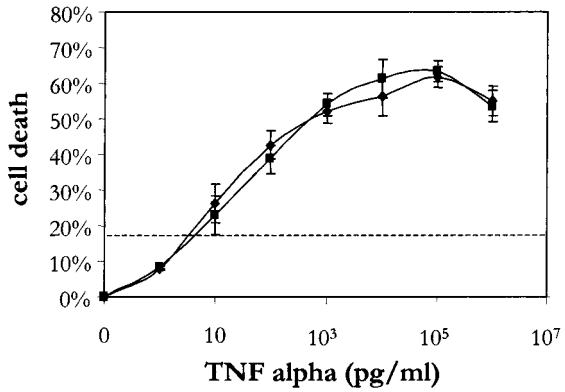


Figure 7. Cytotoxicity assay for TNFα cytotoxicity against actinomycin D-treated, LoVo tumor cells. Recombinant human TNFα and MFE-23::TNFα were diluted from 1000 to 1 pg/mL (w/vTNFα) before addition to the assay plates. Medium alone represented no cytokine. Both TNFα and the fusion protein show identical LD_{50} values of 0.6 ng/mL. Control protein MFE-23 showed no toxicity to the tumor cells above background (- - -) (data not shown). Results are expressed as mean + SD of triplicate wells and are representative of three separate experiments. TNFα, diamonds; MFE-23::TNFα, squares.

DISCUSSION

This study demonstrates that it is possible to localize TNFα to tumors in vivo by fusing it to a high-affinity antitumor antibody, despite the molecule retaining affinity for TNF receptors in normal tissues. MFE-23::TNFα was successfully refolded from bacterial inclusion bodies as a biologically active trimer with a yield of ~28 μg/mL. The molecule bound both human and murine TNF receptor 1, localized effectively to human tumor xenografts in a mouse model and killed tumor cells in in vitro assays.

Over the past decade, recombinant technology has been applied by a number of other groups to produce TNFα-linked antibodies. Some of the earliest used hybridoma cells engineered to produce an anti-transferrin receptor Fab linked to TNFα (Hoogenboom et al., 1991). The fusion protein had cytotoxic activity but it could not be isolated in sufficient amounts to enable tumor specificity studies to be undertaken. Another promising fusion protein incorporated TNFα fused to a sFv (B1) directed to the Le^{Y+} antigen (Scherf et al., 1996). This bacterially expressed fusion protein showed specificity for target cells and inhibited tumor growth in mice bearing MCF-7 (Le^{Y+}) tumors using a dose of 75 μg B1::TNFα injected on days 10, 12, and 14 after tumor implantation. However, the major problem was, again, that the fusion protein was only produced at a final concentration of 0.4 μg/mL. These reports highlighted a major problem facing workers attempting to produce TNFα-based fusion proteins for cancer therapy, namely low yields. This poses a significant problem as larger amounts are required for clinical use. Better yields (10 μg/mL) were obtained with an anti-TAG 72 sFv fused to TNFα (Yang et al., 1995). This fusion protein had anti-TAG 72 immunoreactivity and was cytotoxic in vitro but it was expressed as a mixture of monomer, dimer and trimer. TNFα is only fully biologically active in its trimeric form. In contrast to these reports, MFE-23::TNFα was expressed at high yields (~28 μg/mL) and exclusively as a trimer. This high expression may be due, in part, to the fact that the parent sFv can be expressed at high concentrations (~25 μg/mL) as a soluble protein and has been found to be particularly stable. This coupled with the slow refolding protocol in a "redox" environment may contribute significantly to the

yield of correctly folded MFE-23::TNFα recovered. This yield will be substantially improved by the use of fermenter technology and alternative expression systems such as *Pichia pastoris*.

An advantage conferred by the fact that MFE-23::TNFα is expressed as a trimer was that it retained its toxicity in standard WEHI 164 cell cytotoxicity assays. This will to be a major advantage if the molecule is successfully targeted to tumors without causing significant side effects due to "nontumor-specific" TNF receptor binding.

MFE-23::TNFα also proved cytotoxic to a human tumor cell line (LoVo) after treatment with actinomycin-D, showing LD_{50} values identical to that of recombinant human TNFα alone. Because LoVo cells express high levels of TNF receptors (data not shown), enhanced specificity due to the MFE-23 was not evident in the assays. The MFE-23 moiety did, however, rapidly localize the TNFα to the tumor and so did impart specificity in vivo although not in vitro.

The specific effects of TNFα on tumors include induction of necrosis (Abbruzzese et al., 1989), vascular hemorrhage (Watanabe et al., 1988), augmentation of the lethal effects of radiation against certain tumor cell lines (Chen et al., 1995; Mauceri et al., 1996), and an increase in vascular permeability (Rowlinson Busza et al., 1995). The effective harnessing of these properties while at the same time minimizing the less desirable effects to normal tissues is an important goal. MFE-23::TNFα represents a significant step in this direction. Reduction in cytotoxicity of the TNFα molecule is desirable if systemic side effects or sequestration of the protein by cellular and soluble receptors is to be avoided. It is the uptake of TNFα by TNF receptors by normal cells that results in poor tumor localization because of the reduction in the amount of injected TNFα able to reach the tumor. Indeed, natural mechanisms such as soluble TNF receptors in the blood, which are there primarily to protect against the nonspecific effects of endogenous TNFα, are a possible barrier to high tumor uptake of TNFα-based fusion proteins (Engelmann et al., 1989).

Reduction in cytotoxicity due to receptor sequestration can be countered by the rapid sFv-directed accumulation of the cytokine at the tumor site. Thus, high local doses may be achieved with lower, less toxic doses administered systemically. This argument is supported by the data presented here. We have shown that radiolabeled MFE-23::TNFα rapidly and efficiently localizes to tumors even though it is still able to bind both human and mouse TNF receptor type 1 (p55). In our in vitro experiments, all fusion protein was bound by receptor after a fifteen-minute incubation. These data, coupled with that shown by the biodistribution experiments, clearly demonstrate that ^{125}I-labeled MFE-23::TNFα is able to "bypass" blood-borne receptors and localize in LS174T human tumor xenografts with a positive (1.45) tumor/blood ratio observed as early as 3 h postinjection. This rises rapidly, culminating in a ratio of 60:1 after 48 h, corresponding to 1.58% injected dose/gram tumor (the maximum being 4.33% ID/g after 6 h). Most importantly, the phosphor image experiments on homogenized tumor extracts show unequivocally that the figures are due to localized, intact fusion protein and not free MFE-23 or TNFα. The high affinity of MFE-23 for CEA may play a large part in this, coupled with the overall size of the fusion protein (144 kDa) which gives good tumor retention. It is possible therefore, to target TNFα specifically to tumors without unacceptable "losses" en route.

It should be noted that TNFα binds with a higher affinity to human receptors than to murine receptors and also binds both human TNF R1 and TNF R2 (as opposed to TNF R1 only in the mouse model). This suggests that sequestration may be more of a problem in patients than in mice. The engineering of mutant TNFα molecules with reduced affinity for human TNF receptors will provide a way forward if this presents obstacles in the clinic (Cha et al., 1998). Another approach may be to use TNFα molecules specifically engineered to have sole affinity for human TNF R1, the receptor thought to be primarily responsible for inducing cytotoxic activity (Sato et al., 1998) rather than TNF R2, that is thought to be responsible for cellular activation (and thus unwanted side effects). Scherf et al. (1996) addressed the problem of nontumor specific toxicity by fusion the TNFα to the scFv via its C-terminus. This had the effect of reducing the cytotoxicity in in vitro assays 50-fold as the fusion protein was severely compromised in its ability to form active trimers. We have shown that this may not be necessary if the targeting scFv is of sufficiently high affinity to localize the fusion protein rapidly. MFE-23 has an affinity of 2×10^{-9} M, much higher than the anti-LeY antigen scFv used by Scherf et al. (of the order of 10^{-6} M). This higher affinity may mean that lower doses of a more active molecule may be given in a clinical situation with fewer side effects.

The fact that MFE-23::TNFα is a trimeric molecule also brings advantages in terms of avidity and consequent tumor retention. We have shown in other studies that higher avidity and a larger size will facilitate the retention of antibody-targeted therapeutics in viable areas of the tumor long after they have cleared from the blood and other tissues (Flynn et al.; in press). This is supported by the tumor:tissue ratios obtained with MFE-23::TNFα which increase up to 48 h postinjection.

Other workers have attempted to localize TNFα to tumors in animal models by a variety of different methods not involving fusion proteins. Robert et al. (1996) were successful in obtaining a high degree of localization of ^{125}I-labeled TNFα (^{125}I-TNFα) in tumor-bearing mice after prior injection of a bispecific mAb (BAb) directed against CEA and TNFα. Mice were treated with 3 μg of BAb followed by 1 μg of ^{125}I-TNFα 24 h later. At all time points, the Bab-injected mice showed specific tumor uptake of ^{125}I-TNFα.

The tumor/tissue ratios improved if a delay of 48 h before ^{125}I-TNFα injection was utilized. High doses of free ^{125}I-TNFα did diffuse rapidly into the tumors in control mice however, but this was followed by a rapid decrease in %ID/g tumor tissue and at no time was a significant, positive tumor/tissue ratio obtained. Although administration of the bispecific antibody followed by TNFα did result in tumor localization of the cytokine, the major advantage of our fusion protein-based approach is that no pre-injection of capture antibody is necessary and so this would be much more practical for clinical application. Similarly, a genetic fusion protein is likely to provide a simpler therapeutic option than other methods of targeting such as Cu2+-dextran (Tabata et al., 1999) or TNFα-biotin conjugates (Moro et al., 1997; Gasparri et al., 1999) which are all multistep approaches. MFE-23::TNFα is also a very "adaptable" molecule. The genetic "cassette" can be easily modified, both in terms of the sFv used to target or the cytokine used as effector, making this an agent that can be tailored to different tumors or cell types depending upon there susceptibility to certain agents.

In summary, we have produced a sFv::TNFα fusion protein in high yield that is biologically active in its

native form and retains affinity for both CEA and for both murine and human TNF receptors. Most importantly, despite its receptor binding capability, the fusion protein is still able to localize rapidly and effectively to tumors in vivo. This work indicates that MFE-23::TNFα has potential to deliver TNFα-meditated cancer therapy in the clinic.

ACKNOWLEDGMENT

This work was supported by the Cancer Research Campaign.

LITERATURE CITED

Abbruzzese, J., Levin, B., Ajani, J. A., Faintuch, J. S., Saks, S., Patt, Y. Z., Edwards, C., Ende, K., and Gutterman, J. U. (1989) Phase 1 trial of human γ-interferon and recombinant human tumor necrosis factor in patients with advanced gastrointestinal cancer. *Cancer Res. 49*, 4057−4061.

Asher, A. L., Mule, J. J., Riechert, C. M., Shiloni, E., and Rosenberg, S. A. (1987) Studies of the antitumor efficacy of systemically administered recombinant tumor necrosis factor against several murine tumors *in vivo. J. Immunol. 138*, 963−974.

Bhatia, J., Chester, K. A., Sharma, S. K., Pedley, R. B., Boxer, G., Robson, L., and Begent, R. H. J. Purification and characterization of a *Pichia pastoris* expressed MFE-23::CpG2 glycosylated fusion protein. (2000) *Brit. J. Cancer* (British Cancer Research Meeting abstracts), in press.

Cha, S.-S., Kim, J.-S., Cho, H.-S., Shin, N.-K., Jeong, W., Shin, H.-C., Kim, Y. J., Hahn, J. H., and Oh, B.-H. (1995) High-resolution crystal structure of a human tumor necrosis factor-a mutant with low systemic toxicity. (1998) *J. Biol. Chem. 273*, 2153−2160.

Chen, M., Quintans, J., Fuks, Z., Thompson, C., Kufe, D. W., and Weichselbaum, R. R. Suppression of Bcl-2 messenger RNA production may mediate apoptosis after ionising radiation, tumor necrosis factor α and ceramide. *Cancer Res. 55*, 991−994.

Chester, K. A., Begent, R. H., Robson, L., Keep, P., Pedley, R. B., Boden, J. A., Boxer, G., Green, A., Winter, G., Cochet, O., and Hawkins, R. E. (1994) Phage libraries for generation of clinically useful antibodies. *Lancet 343*, 455−456.

Begent, R. H., Verhaar, M. J., Chester, K. A., Casey, J. L., Green, A. J., Napier, M. P., Hope-Stone, L. D., Cushen, N., Keep, P. A., Johnson, C. J., Hawkins, R. E., Hilson, A. J., and Robson, L. (1996) Clinical evidence of efficient tumor targeting based on single-chain Fv antibody selected from a combinatorial library. *Nature Med. 2*, 979−984.

Engelmann, H., Aderka, D., Rubinstein, M., Rotman, D., and Wallach, D. A. (1989) Tumor necrosis factor-binding protein purified to homogeneity from human urine protects cells from tumor necrosis factor toxicity. *J. Exp. Med. 264*, 11974−11980.

Flynn, A. A., Pedley, R. B., Green, A. J., Boxer, G. M., Boden, R., Bhatia, J., Morris, R., and Begent, R. H. J. Antibody characteristics can influence the effectiveness of Radioimmunotherapy by selectively targeting radiosensitive areas of tumor. *Int. J. Radiat. Biol.* (in press).

Fraker, P. J., and Speck, J. C. (1978) Protein and cell membrane iodinations with a sparingly soluble chloroamide, 1,3,4,6-tetrachloro-3α,6α-diphenylglycoluril. *Biochem. Biophys. Res. Commun. 80*, 849−857.

Gasparri, A., Moro, M., Curnis, F., Sacchi, A., Pagano, S., Veglia, F., Casorati, G., Siccardi, A. G., Dellabona, P., and Corti, A. (1999) Tumor pretargeting with avidin improves the therapeutic index of biotinylated tumor necrosis factor α in mouse models. *Cancer Res. 59*, 2917−2923.

Gillies, S. D., Young, D., Lo, K.-M., and Roberts, S. (1993) Biological activity and in vivo clearance of antitumor antibody/cytokine fusion proteins. *Bioconjugate Chem. 4*, 230−235.

Hoogenboom, H. R., Volckaert, G., and Raus, J. C. M. (1991) Construction and expression of antibody-tumor necrosis factor fusion proteins. *Mol. Immunol. 32*, 1027−1037.

Itoh, N., and Nagata, S. (1993) A novel protein required for apoptosis-mutational analysis of human Fas antigen. *J. Biol. Chem. 268*, 10932−10937.

Laster, S. M., Wood, J. G., and Gooding, L. R. (1988) Tumor necrosis factor can induce both apoptotic and necrotic forms of cell lysis. *J. Immunol. 141*, 2629−2634.

Lejeune, F. J. (1995) High-dose recombinant tumor necrosis factor (rTNFα) administered by isolation perfusion for advanced tumors of the limbs: a model for biochemotherapy of cancer. *Eur. J. Cancer 31A*, 1009−1016.

Manusama, E. R., Nooijen, P. T. G. A., Tebhagen, T. L. M., Vanderveen, A. H., Devries, M. W. R., Dewilt, J. H. W., Vanijken, M. G., Marquet, M. G., and Eggermont, A. M. M. (1998) Tumor necrosis factor alpha in isolated perfusion systems in the treatment of cancer: The Rotterdam preclinical program. *Semin. Surg. Oncol. 14*, 232−237.

Mauceri, H. J., Hanna, N. H., Wayne, J. D., Hallahan, D. E., Hellman, S., and Weichselbaum, R. R. (1996) Tumor necrosis factor alpha (TNFα) gene therapy targeted by ionising radiation selectively damages tumor vasculature. *Cancer Res. 56*, 4311−4314.

Mavligit, G. M., Zukiwski, A. A., Charnsangavej, C., Humberto Carrasco, C., Wallace, S., and Gutterman, J. U. (1992) Regional biologic therapy: hepatic arterial infusion of recombinant human tumor necrosis factor in patients with liver metastases. *Cancer (Phila) 69*, 557−561.

Mayer, A., Tsiompanou, E., O'malley, D., Boxer, G. M., Bhatia, J., Flynn, A. A., Chester, K. A., Davidson, B. R., Lewis, A. A. M., Winslet, M. C., Dhillon, A. P., Hilson, A. J. W., and Begent, R. H. J. (2000) Radioimmunoguided surgery in colorectal cancer using a genetically engineered anti-CEA single chain Fv antibody. *Clin. Cancer Res.* (in press).

Moritz, T., Niederle, N., Baumann, J., May, D., Kurscel, E., Osieka, R., Kempini, J., Schlick, E., and Schmidt, C. (1989) Phase 1 study of recombinant human tumor necrosis factor-α in advanced malignant disease. *Cancer Immunol. Immunother. 29*, 144−150.

Moro, M., Pelagi, M., Fulci, G., Paganelli, G., Dellabona, P., Casorati, G., Siccardi, Ag., and Corti, A. (1997) Tumor cell targeting with antibody-avidin complexes and biotinylated tumor necrosis factor alpha. *Cancer Res. 57*, 1922−1928.

Pedley, R. B., Boden, J. A., Boden, R., Dale, R., and Begent, R. H. J. (1993) Comparative radioimmunotherapy using intact or $F(ab')_2$ fragments of ^{131}I anti-CEA antibody in a colonic xenograft model. *Brit. J. Cancer 68*, 69−73.

Pedley, R. B., Boden, J. A., Boden, R., Boxer, G. M., Flynn, A. A., Keep, P. A., and Begent, R. H. J. (1996) Ablation of colorectal xenografts with combined radioimmunotherapy and tumor blood flow modifying agents. *Cancer Res. 56*, 3293−3300.

Pietersz, G. A., Toohey, B., and Mckenzie, I. F. C. (1998) In vitro and in vivo evaluation of human tumor necrosis factor alpha (hTNF alpha) chemically conjugated to monoclonal antibody. *J. Drug Targeting 5*, 109−120.

Robert, B., Mach, J.-P., Mani, J.-C., Yehou, M., Folli, S., Artus, J.-C., and Pelegrin, A. (1996) Cytokine targeting in tumors using a bispecific antibody directed against carcinoembryonic antigen and tumor necrosis factor alpha. *Cancer Res. 56*, 4758−4765.

Rosenberg, S. A., Schwarz, S. L., and Spiess, P. J. (1988) Combination immunotherapy for cancer: synergistic antitumor interactions of interleukin-2,α-interferon, and tumor infiltrating lymphocytes. *J. Natl. Cancer Inst. 80*, 1393−1397.

Rowlinson Busza, G., Maraveyas, A., and Epenetos, A. A. (1995) Effect of tumor necrosis factor on the uptake of specific and control monoclonal antibodies in a human tumor xenograft model. *Brit. J. Cancer 71*, 660−665.

Sato, T., Yamauchi, N., Sasaki, H., Takahashi, M., Okamoto, T., Sakamaki, S., Watanabe, N., and Niitsu, Y. (1998) An apoptosis-inducing gene therapy for pancreatic cancer with a combination of 55-kDa tumor necrosis factor (TNF) receptor gene transfection and mutein TNF administration. *Cancer Res. 58*, 1677−1683.

Scherf, U., Benhar, I., Webber, K. O., Pastan, I., and Brinkmann, U. (1996) Cytotoxic and antitumor activity of recombinant tumor necrosis factor-B1(Fv) fusion protein on LeY antigen-expressing human cancer cells. *Clin. Cancer Res. 2*, 1523−1531.

Tabata, Y., Noda, Y., Matsui, Y, and Ikada, Y. (1999) Targeting of tumor necrosis factor to tumor by use of dextran and metal coordination. *J. Controlled Release 59*, 187−196.

Watanabe, N., Niitsy, Y., Umeno, H., Kuriyama, H., Neda, H., Yamauchi, N., Maeda, M., And Urushizaki, I. (1988) Toxic effect of tumor necrosis factor on tumor vasculature in mice. *Cancer Res. 48*, 2179−2183.

Watanabe, N., Yamauchi, N., Maeda, M., Neda, H., Tsuji, N., Okamoto, T., Tsuji, N., Akiyama, S., Sasaki, H., And Niitsu, Y. (1994) Recombinant human tumor necrosis factor causes regression in patients with advanced malignancies. *Oncology 51*, 360−365.

Yang, J., Moyana, T., and Xiang, J. (1995) A genetically engineered single-chain Fv/TNF molecule possesses the anti-tumor immunoreactivity of Fv as well as the cytotoxic activity of tumor necrosis factor. *Mol. Immunol. 32*, 873−881.

BC000178A

CORRECTIONS

Volume 13, Number 1, January/February, 2002.

Stephen P. Cooke,* R. Barbara Pedley, R. Boden, Richard H. J. Begent, and Kerry A. Chester

IN VIVO TUMOR DELIVERY OF A RECOMBINANT SINGLE CHAIN FV::TUMOR NECROSIS FACTOR-α FUSION PROTEIN

Page 7. An incorrect manuscript title appears in the published manuscript. The corrected title appears above.

BC020015H

10.1021/bc020015h
Published on Web 01/30/2002

Development of a Conjugate of ^{99m}Tc-EC with Aminomethylenediphosphonate in the Search for a Bone Tracer with Fast Clearance from Soft Tissue

Kristin Verbeke,[†,§] Jef Rozenski,[‡] Bernard Cleynhens,[†] Hubert Vanbilloen,[†] Tjibbe de Groot,[†] Nancy Weyns,[†] Guy Bormans,[†] and Alfons Verbruggen*[,†]

Laboratory of Radiopharmaceutical Chemistry, University Hospital Gasthuisberg, Herestraat 49, B-3000 Leuven, and Rega Institute for Medical Research, University of Leuven, Belgium. Received December 29, 2000; Revised Manuscript Received August 30, 2001

For the currently used ^{99m}Tc-labeled diphosphonates such as ^{99m}Tc-MDP and ^{99m}Tc-HDP, the required interval of 2.5 to 3 h between injection and the scintigraphic bone imaging is an inconvenience. The present study was set up in an attempt to develop a technetium-99m-labeled diphosphonate with efficient bone uptake and more rapid clearance from blood and soft tissue by renal extraction and excretion so that it would be possible to start imaging as early as 1 h after injection. A conjugate of the new renal tracer agent ^{99m}Tc-ethylene dicysteine (^{99m}Tc-L,L-EC), covalently bound via one of its carboxylates with aminomethylenediphosphonic acid (AMDP), was synthesized in seven steps. EC-AMDP could be labeled easily and efficiently with ^{99m}Tc at pH ≥12 and room temperature. Analysis using ion pair reversed phase high performance liquid chromatography showed the formation of a mixture of two main compounds with reproducible relative ratios, which were stable as a function of time. In a baboon, the scintigraphic images obtained with the new agent showed good quality bone scans, with clear visualization of the skeleton and low soft tissue activity at respectively 1 and 2 h after injection.

INTRODUCTION

Radionuclide bone imaging is the most common clinical investigation in nuclear medicine. Since the mid-1970s, the bone scan has replaced the X-ray skeletal survey because of its 95% sensitivity in detecting metastatic disease and because this radioisotopic technique allows detection of some lesions several months earlier than with X-ray examination. The reason for the latter lies in the fact that the bone scan demonstrates osseous remodeling, which must precede and is the cause of structural changes seen on the X-ray image (*1*).

For more than 20 years, ^{99m}Tc-labeled diphosphonates have been the radiopharmaceuticals of choice for radioisotopic bone scanning. The tracer agents most widely used at present are complexes of ^{99m}Tc with methylenediphosphonate (^{99m}Tc-MDP) and hydroxymethylenediphosphonate (^{99m}Tc-HMDP) (*2*−*4*).

Despite their wide clinical use, ^{99m}Tc-diphosphonates suffer from a number of suboptimal properties. First, they are fairly weak chelates and, therefore, tend to degrade with time and produce pertechnetate as an impurity. The use of a suitable antioxidant such as ascorbic acid, gentisic acid, or *p*-aminobenzoic acid helps to overcome this problem (*5*). Second, ^{99m}Tc-diphosphonates are not single, well-defined chemical species, but mixtures of short- and long-chain polymers in which one or more technetium atoms are bridged by two or several phosphate and hydroxyl ligands. Different polymers can have a different degree of ionization and biological behavior. Analysis by high-pressure liquid chromatography (HPLC) has also revealed that the relative amounts of the different species in a ^{99m}Tc-diphosphonate preparation vary as a function of time after reconstitution (*6*−*10*). In addition, the diphosphonate group is necessary both for the complexation of ^{99m}Tc and the uptake of the complex in the skeleton (*11*). This may have the disadvantage that a phosphonate group involved in the binding of ^{99m}Tc has a reduced ability of binding to the bone surface. Following intravenous administration, the uptake of ^{99m}Tc-diphosphonates in bone is almost complete 1 h after injection, but the clearance from soft tissue proceeds more slowly (*12*). For this reason, a time interval of 2 to 4 h is required between injection of the radiopharmaceutical and the bone scanning. This necessary delay is an important inconvenience for the nuclear medicine personnel and for the patients, especially for children.

Therefore, it would be a major improvement for nuclear medicine if the ^{99m}Tc-diphosphonates could be modified in such a way that:

(a) they still have a high and rapid uptake in the skeleton with the same lesion-to-normal bone activity ratio;

(b) the clearance from soft tissue by the kidneys followed by excretion into the urine would be much faster. In an ideal situation, it should be possible to obtain good quality scintigraphic images already 1 h after injection with the same clinical information as now after 3−4 h.

Therefore, the aim of the present study was the development of a "new generation" bone-seeking radiopharmaceutical with the above-described characteristics. For this purpose, a strategy was designed in which a diphosphonate is conjugated to a stable and easy to

* To whom correspondence should be addressed. Phone: 32-16-343732. Fax: 32-16-343891. e-mail: alfons.verbruggen@uz.kuleuven.ac.be.

[†] University Hospital Gasthuisberg.

[‡] Rega Institute for Medical Research.

[§] Postdoctoral fellow of the Fund for Scientific Research, Flanders.

10.1021/bc0001600 CCC: $22.00 © 2002 American Chemical Society
Published on Web 12/27/2001

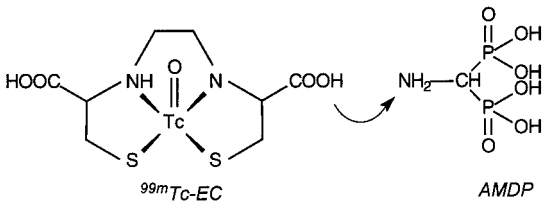


Figure 1. Structure of ^{99m}Tc-EC and aminomethylenediphosphonate (AMDP).

prepare ^{99m}Tc complex with known very rapid active renal excretion. In this conjugate, the diphosphonate would be "free" (i.e., not bound to Tc) and thus retain its full ability for binding to the bone surface. On the other hand, the ^{99m}Tc-labeled renal agent would ensure both a stable binding of the radionuclide (^{99m}Tc) and a rapid urinary elimination of the fraction of the tracer agent not bound to the skeleton.

For different reasons, we selected the complex of ^{99m}Tc with L,L-ethylene dicysteine (^{99m}Tc-L,L-EC, Figure 1) as the ^{99m}Tc-labeled renal agent to which the diphosphonate can be bound. It is a very stable and easy to prepare ^{99m}Tc complex with the highest plasma clearance by renal extraction ever reported for a ^{99m}Tc-compound (*13*). In humans the 1-h plasma clearance of ^{99m}Tc-L,L-EC is 75% of the Hippuran clearance as compared to about 60% for ^{99m}Tc-MAG3 (*14*, *15*). Moreover, it has in its structure two carboxylic groups of which one can be omitted without significantly affecting the renal excretion characteristics (*16*). This means that one of the carboxylates can be used for coupling to a diphosphonate bearing an amino group in its structure. Aminomethylenediphosphonate (AMDP, Figure 1) is such a diphosphonate and was selected as the diphosphonate part of our new compound. Preliminary experiments have demonstrated that during labeling of equimolar amounts of EC and a diphosphonate with ^{99m}TC, the radionuclide exclusively binds to the EC ligand and not to the diphosphonate (*17*), which in this way retains its full ability for binding to the bone surface.

MATERIALS AND METHODS

Materials. Thin-layer chromatography (TLC) was carried out using precoated TLC plates (Alugram SIL G/UV254, Macherey-Nagel, Düren, Germany). For purification by column chromatography, silica gel (MN Kieselgel 60, 70−230 mesh ASTM, Macherey-Nagel) was used. L,L-Ethylene dicysteine (***1***) and the tetraethyl ester of 1-aminomethylenediphosphonic acid (***5***) were prepared as described elsewhere (*18*−*20*).

^{1}H and ^{13}C NMR spectra were obtained on a Varian Gemini 200 spectrometer (Varian, Palo Alto, CA). Chemical shifts are reported in ppm relative to the standard reference tetramethylsilane. Liquid secondary ion mass spectra (LSIMS) were recorded on a Kratos Concept IH mass spectrometer (Kratos Analytical, Manchester, UK) controlled by a Masspec II data system (MSS, Manchester, UK) and obtained in a negative (-LSIMS) ion mode. Negative mode electrospray ionization (-ESI) mass spectra were acquired on an orthogonal acceleration time-of-flight mass spectrometer (qTof-2, Micromass, Manchester, UK).

^{99m}Tc-MDP was prepared by reconstitution of a conventional MDP labeling kit with sodium [^{99m}Tc]pertechnetate solution from a ^{99m}Tc generator (Ultratechnekow-FM, Mallinckrodt Medical, Petten, The Netherlands).

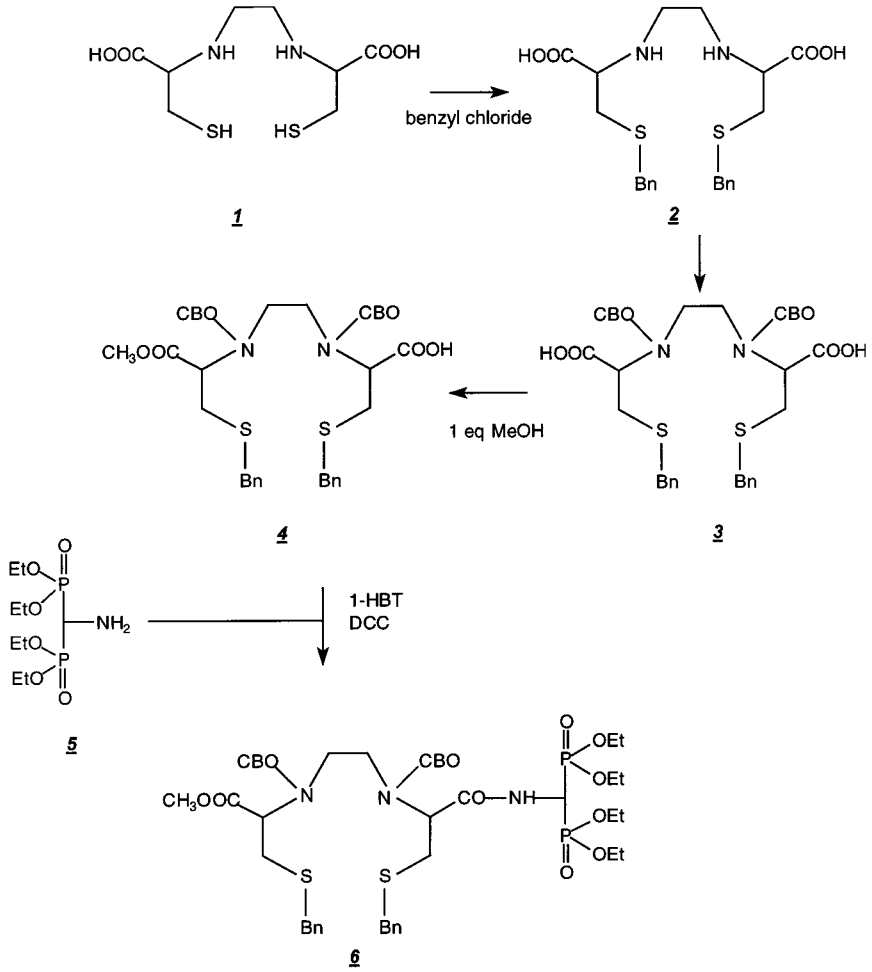
***S,S′*-Bis-benzyl-L,L-1,2-ethylene Dicysteine (2).** 1,2-L,L-Ethylene dicysteine (**1**, 41.37 g, 154 mmol) was dissolved in liquid ammonia (1000 mL) in a two-necked flask with a dewar cooler, and the mixture was stirred vigorously. Sodium (12.8 g, 555 mmol) was added until a blue color persisted for at least 15 min. Ammonium chloride was then added in portions till decoloration. After dilution with liquid ammonia (400 mL), benzyl chloride (40 mL, 320 mmol) was added dropwise. After stirring for 30 min, the liquid ammonia was removed by evaporation at room-temperature overnight. Water (600 mL) was then added, and the solution was washed with ether (3 × 200 mL). The water layer was acidified to pH 2 with 6 M HCl. The precipitate formed was filtered off and washed successively with water, ethanol, acetone, and finally with ether and dried under vacuum to yield 25.99 g (60%) of a white product (Scheme 1).

***N,N′*-Bis-carbobenzyloxy-*S,S′*-bis-benzyl-1,2-L,L-ethylene Dicysteine (3).** In a 2000-mL beaker *S,S′*-bis-benzyl-1,2-L,L-ethylene dicysteine **2** (27.2 g, 60 mmol) was suspended in water (1000 mL) and dissolved by addition of 1 M NaOH up to pH 11. After cooling to 0−5 °C, benzyl chloroformate (27 mL, 180 mmol) was added dropwise over a period of 30 min while the pH was maintained at 11 by addition of 4 M NaOH. After washing with ether (300 mL), the water layer was acidified to pH 2 with 6 M HCl and extracted with EtOAc (3 × 300 mL). The combined organic layers were dried over Na_2SO_4 and evaporated to yield a yellow oil which was purified by column chromatography using gradient mixtures of methanol in CH_2Cl_2/acetic acid (100:1, V/V). Evaporation of the fractions containing the pure main compound as shown by TLC (CH_2Cl_2−methanol−HOAc, 95:5:1, R_f = 0.7) yielded 26.8 g of a colorless oil. ^{1}H NMR: ($CDCl_3$): δ 2.6−3.1 (4H, m, 2 x CH−CH_2−S); 3.3−3.5 (4H, m, 2 x CH_2−N-); 3.7 (4H, 2 x s, 2 x S−CH_2−Ar); 4.3 (2H, m, 2 x N−C*H*−COO-); 5.5 (4H, m, 2 x Ar−CH_2−O−CO-); 7.3 (20H, m, 4 x CH_2−*Ar*); 9.0 (2H, br s, 2 x CH−COO*H*).

***N,N′*-Bis-carbobenzyloxy-*S,S′*-bis-benzyl-1,2-L,L-ethylene Dicysteine Monomethyl Ester (*4*).** To a solution of **3** (3.58 g, 5 mmol) and (dimethylamino)-pyridine (DMAP, 61 mg, 0.5 mmol) in a mixture of methanol (0.2 mL, 5 mmol) and CH_2Cl_2 (50 mL) at 5 °C was added dicyclohexylcarbodiimide (DCC, 1.031 g, 5 mmol), and the reaction mixture was stirred overnight at room temperature. After removal of the precipitate (dicyclohexylurea), the filtrate was evaporated and the residual oil purified by column chromatography using gradient mixtures of hexane and CH_2Cl_2 as the mobile phase. A colorless oil (1.56 g, 42%) was obtained. ^{1}H NMR: ($CDCl_3$): δ 2.5−3.1 (4H, m, 2 x CH−CH_2−S); 3.3−3.8 (4H, m, 2 x CH_2−N-; 3H, s, COOCH_3); 3.6 (4H, 2 x s, 2 x S−CH_2−Ar); 4.1−4.6 (2H, m, 2 x N−C*H*−COO-); 5.1 (4H, m, 2 x Ar−CH_2−O−CO-); 7.3 (20H, m, 4 x CH_2−*Ar*); 8.3 (H, br s, CH−COO*H*).

Ethylene-l-(*S*-benzyl-*N*-carbobenzyloxycysteine methyl ester)-2-*S*-benzyl-*N*-carbobenzyl-oxy-cysteinylmethylenediphosphonic Acid Tetraethyl Ester (6). To a solution of **4** (1.56 g, 2.14 mmol) and 1-hydroxybenzotriazole (HBT, 0.29 g, 2.14 mmol) in acetonitrile (20 mL) at 0−5 °C was added DCC (0.442 g, 2.14 mmol), and the mixture was stirred for 30 min. After addition of 1-aminomethylenediphosphonic acid tetraethyl ester (**5**) (0.648 g, 2.14 mmol) in one portion, stirring was continued overnight at room temperature. The precipitate was removed by filtration, the filtrate evaporated, and the residue purified by column chromatography using gradient mixtures of methanol in CH_2Cl_2 to yield **6** as a colorless oil (1.1 g). ^{1}H NMR ($CDCl_3$): δ 1.25 (12H, m, 4 x O−CH_2−CH_3); 2.5−2.9 (4H, m, CH−CH_2−S); 3.4 (1H, m, CO−NH−C*H*); 3.3−3.8 (11H, m, COOCH_3,

Scheme 1. Synthesis of the Fully Protected EC-AMDP Conjugate (6)



2 x CH_2−N, 2 x S-CH_2−Ar); 4.2 (8H, m, 4 x O−CH_2−CH_3); 4.4 (2H, m, N−C*H*−CO); 5.1 (4H, m, 2 x Ar−CH_2−O−CO); 7.3 (20H, m, 4 x CH_2−*Ar*). ^{13}C NMR ($CDCl_3$): δ 16.3 (O−CH_2−*C*H_3); 30.8, 30.9 (2 x CH−*C*H_2−S); 35.5 (CO−NH−*C*H); 36.1, 36.3 (2 x S−*C*H_2−Ar); 45.8, 46.4 (*2* x *C*H_2−N); *52*.3 (COO*C*H_3); 58.2,60.1 (2 x N−*C*H−CO); 63.6 (O−*C*H_2−CH_3); 67.6,68.0 (2 x Ar−*C*H_2−O−CO); 127.1, 128.5, 135.9, 137.4 (Ar); 156.8 (Ar−CH_2−O−*C*O); 170.4 (*C*O−NH−CH); 170.9 (*C*OOCH_3). MS LSIMS (nba): $[M - H]^-$ 1015.6.

Ethylene-l−L-cysteine-2-L-cysteinyl-aminomethylenediphosphonic Acid (7b). To a solution of **6** (1.016 g, 1 mmol) in CH_2Cl_2 (10 mL) at 0 °C was added trimethylsilyl bromide (TMSBr, 2 mL, 15 mmol). After stirring at room temperature for 72 h, the reaction mixture was evaporated, and to the residue was added methanol (10 mL). After stirring during 1.5 h, the methanol was removed by evaporation, and the residue was dried in a vacuum over P_2O_5. After addition of a mixture of methanol (10 mL) and 1 M NaOH (6 mL), the mixture was refluxed during 2 h. The solvent was evaporated, and the residual solid was stirred in methanol (20 mL). The white precipitate was filtered off, washed with methanol, and dried under a stream of nitrogen (intermediate **7a**, Scheme 2). MS-ESI: *m/z* calcd for $C_{39}H_{44}N_3O_{13}P_2S_2$ $[M - H]^-$ 888.1790; found 888.1780.

The precipitate (50 mg) was dissolved in liquid ammonia (20 mL), and pieces of sodium were added until a blue color persisted for 4 h. After decoloration with NH_4-Cl, the ammonia was removed under a stream of nitrogen, and the residual solid (**7b**, Scheme 2) was dried in a vacuum and used as such for labeling experiments.

Labeling with ^{99m}Tc and Analysis. Direct labeling of **7b** with ^{99m}Tc was performed by addition of 100 μg of $SnCl_2 \cdot 2H_2O$, dissolved in 25 μL of 0.05 M HCl, and 1 mL of eluate of a commercial generator containing 370−3700 MBq ^{99m}Tc in the form of sodium pertechnetate to a labeling vial containing 1 mg of **7b** (EC-AMDP) dissolved in 1 mL of 0.2 M NaOH.

After incubation for a few minutes at room temperature, the labeling reaction was analyzed by ion-pair reversed phase high-pressure liquid chromatography (IP-RP-HPLC). The system consisted of a Merck-Hitachi ternary gradient pump (model L-6200 intelligent pump, Merck, Darmstadt, Germany), a Valco N6 injector (Alltech, Deerfield, IL), and a 250 mm × 4.6 mm Hypersil ODS 5 μm column (Shandon Scientific, Maidstone, England). After application of the sample, the column was eluted with gradient mixtures of water, methanol, 0.008 M tetrabutylammonium hydroxide, and 0.0013 M MDP (pH 7.5) (see Table 1). The radioactivity in the column effluent was monitored with a 2-in. NaI(T1) scintillation detector and recorded on an IBM-compatible PC equipped with an integration program (Rachel, Lablogic, Sheffield, England).

Biodistribution in Rats. The ^{99m}Tc-EC-AMDP labeling mixture was used as such or its main components were isolated using the RP-HPLC described above. The labeling reaction mixture or the HPLC isolated peaks were diluted to a concentration of 0.37 MBq/mL with saline. Male rats (body mass 60−80 g) were sedated by im injection of 0.1 mL of a 1 to 4 diluted solution of Hypnorm (Duphar, Weesp, The Netherlands). Then, 0.2 mL of the diluted tracer solution was injected via a tail

Scheme 2. Deprotection of the Fully Protected Intermediate To Obtain the EC-AMDP Conjugate

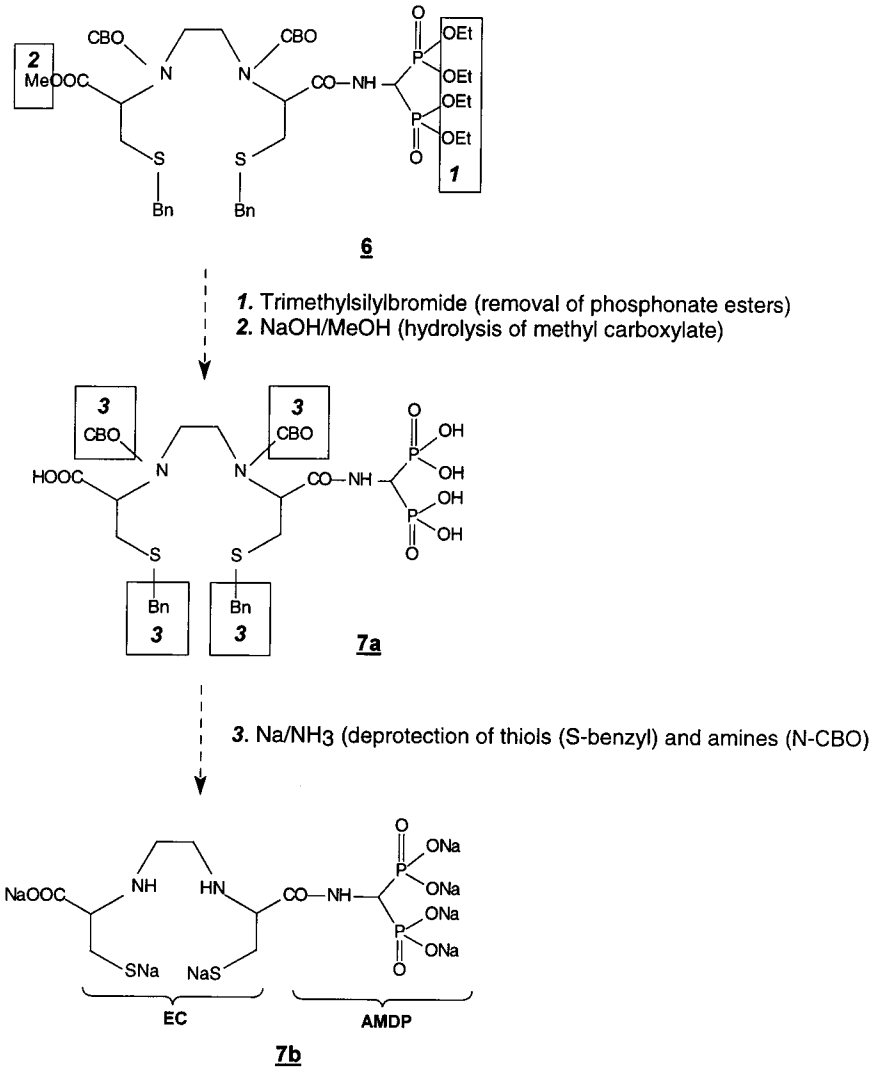


Table 1. Composition of the Mobile Phase Used in the HPLC Analysis as a Function of Time (linear gradient)[a]

time (min)	% A	% B
0	100	0
5	50	50
10	50	50
25	0	100
30	0	100
35	100	0

[a] A: water containing 10% MeOH, 0.008 M tetrabutylammonium hydroxide (TBAH) and 0.0013 M MDP (pH 7.5). B: water−methanol (40:60, V/V), containing 0.008 M TBAH and 0.0013 M MDP (pH 7.5). Flow rate: 1 mL/min.

vein into each of six rats. The rats were sacrificed by decapitation at fixed time intervals (two rats at 30, 60, and 120 min postinjection (p.i.), respectively) and the organs were dissected. The left and right femur were carefully cleaned and weighed. The activity in all organs and other body parts was counted in an automated sample counter (1480 Wizard3", Wallac, Turku, Finland) and corrected for background radiation and physical decay during counting. Results were expressed as percentage of injected activity, equal to the sum of the net activity in all organs. Blood was assumed to be 7% of the body mass.

Biodistribution in Rabbits. ^{99m}Tc-MDP or ^{99m}Tc-labeled EC-AMDP (without HPLC purification) were diluted with saline to a concentration of 37 MBq/mL. A male albino rabbit (body mass 3.0 kg) was sedated by im injection of 0.75 mL of Imalgène (Rhône Mérieux, Lyon, France), and 1 mL of the diluted tracer solution was injected via an ear vein. After 60 min, whole body images were acquired during 6 min using a gamma camera (BIAD XLT 24, Trionix, Twinsburg, OH), equipped with a low energy ultra resolution parallel collimator (LEUR-parallel) and connected to a data system SUN (Sparc station 10, Trionix).

Evaluation in a Baboon. A male baboon (body mass approximately 21 kg) was anaesthetized by intramuscular injection of 75 mg of ketamine (Imalgène). Anaesthesia was sustained with Fluothane. Then, 185 MBq of the radiolabeled preparation (^{99m}Tc-MDP or ^{99m}Tc-EC-AMDP, both without HPLC-purification), adjusted to pH 7 with 0.2 M phosphate buffer, was injected via a limb vein. Whole body images were taken at different time intervals postinjection using a dual head gamma camera as described above for the rabbit study. At fixed time intervals (2, 5, 7, 10, 15, 20, 30, 45, 60, 80, 100, 120 min p.i.) a 2-mL blood sample was taken in heparinized tubes (Monoject H100, Sherwood Medical, Balleymoney, Ireland). After centrifugation for 10 min at 1000 g plasma samples of approximately 0.5 g were pipetted in tubes, weighed, and counted as described above.

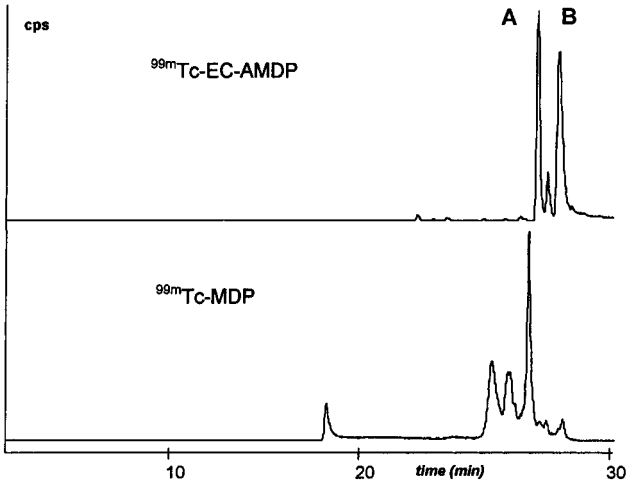


Figure 2. Ion pair RP-HPLC chromatograms of ^{99m}Tc-EC-AMDP and ^{99m}Tc-MDP. For conditions: see Materials and Methods.

RESULTS AND DISCUSSION

Synthesis of the EC-AMDP Conjugate. A multistep procedure has been designed to obtain the conjugate of ethylene dicysteine with aminomethylenediphosphonate in reasonable yields (Schemes 1 and 2). Since EC contains in its structure six functional groups (2 thiols, 2 amines, 2 carboxyl functions), a complex strategy of protection and deprotection of the respective functional groups had to be applied. The thiols were protected with a benzyl group, the amines with a carbobenzyloxy (CBO) group, and one of the carboxylates as a methyl ester (Scheme 1). The preparation of the monomethyl ester was performed by reaction of the diacid with 1 equiv of methanol in the presence of DMAP and DCC, followed by purification of the reaction product. In this way, a reasonable yield (42%) of the monoester was obtained. In addition, the four phosphonate groups of AMDP had to be protected as their ethyl ester to allow purification and confirmation of the identity of the precursors, the intermediates, and the fully protected EC-AMDP conjugate. Removal of the different protective groups was performed successfully in three steps using trimethylsilyl bromide for the phosphonate esters, alkaline hydrolysis of the methyl ester of the EC-moiety, and finally treatment with sodium in liquid ammonia to remove the *S*-benzyl and N-CBO groups (Scheme 2). Characterization of the intermediates by either NMR or mass spectrometry was possible up to intermediate **7a**, but was unsuccessful for the final fully deprotected conjugate **7b** because of high salt concentrations in the reaction product. In fact, the compound obtained after deprotection of the *S*-benzyl and N-CBO groups by treatment of **7a** with sodium in liquid ammonia was not further purified due to the small amounts available and the difficulty of chromatographic desalting of the highly polar conjugate **7b** and it was used as such for labeling with technetium-99m.

Table 3. Femur to Blood Activity Ratios for ^{99m}Tc-MDP and ^{99m}Tc-EC-AMDP (total preparation and HPLC-isolated peaks) in Rats (n = 2)

		30 min	60 min	120 min
^{99m}Tc-MDP		12.4	35.8	48.4
^{99m}Tc-EC-AMDP	total	19.9	55.1	98.0
	peak A	23.9	106.3	363.5
	peak B	26.9	50.2	745.9

Labeling of EC-AMDP with ^{99m}Tc and Analysis. Labeling of the conjugate with ^{99m}Tc was performed in the same conditions as described for EC, i.e., by a direct labeling procedure at alkaline pH and room temperature. As mentioned higher, previous experiments had indicated that the complexation strength of the N_2S_2-ligand EC is much higher than that of the diphosphonate. Therefore, there is no doubt that technetium is bound only by the N_2S_2-ligand and not by the diphosphonate moiety. Analysis of the labeling reaction product by ITLC showed that the solution did not contain measurable amounts of pertechnetate or ^{99m}Tc in colloidal form. Further analysis by IP-RP-HPLC showed the formation of a mixture of three compounds, of which the relative amounts were reproducible and constant as a function of time after preparation (Figure 2). The different peaks could easily be separated by HPLC and were stable after isolation. The HPLC-chromatogram of ^{99m}Tc-MDP clearly shows different complexes of which the relative amounts varied as a function of time after reconstitution and which were not reproducible. When one of the components of ^{99m}Tc-MDP was isolated by HPLC, it gradually converted to the other components as a function of time. In the biodistribution studies, ^{99m}Tc-MDP was always used as the complete preparation.

Biological Evaluation in Rats. The results of the biodistribution studies in rats of ^{99m}Tc-MDP and ^{99m}Tc-EC-AMDP (total preparation) at 30, 60, and 120 min p.i. are shown in Table 2. The activity in the femur is almost identical for ^{99m}Tc-MDP and ^{99m}Tc-EC-AMDP at 30 and 60 min p.i., whereas at 120 min p.i. ^{99m}Tc-EC-AMDP has a clearly higher uptake in bone than ^{99m}Tc-MDP. At each time point, the residual activity in the blood is lower for the new ^{99m}Tc-labeled conjugate, and as a result, the femur to blood activity ratios found with the total preparation are significantly higher for ^{99m}Tc-EC-AMDP than for ^{99m}Tc-MDP (Table 3). The femur to blood activity ratio of the ^{99m}Tc labeled EC-diphosphonate conjugate at 1 h p.i. is higher than the same ratio for ^{99m}Tc-MDP at 2 h p.i. In biodistribution studies with the isolated peaks A and B, the femur to blood activity ratios are significantly higher than for the total preparation. This indicates that the total preparation contains some constituents, possibly not eluted from HPLC, with lower affinity for the bone. In the muscles and the hepatobiliary system, the activity is low at all tested time points for each of the preparations tested. The activity not taken up in the bone is excreted rapidly via the kidneys to the urine, and its percentage is almost similar for the two preparations.

Table 2. Biodistribution in Rats of ^{99m}Tc-MDP (n = 2) and ^{99m}Tc-EC-AMDP (n = 6) at 30, 60, 120 min p.i.

		% of injected dose				
	time p.i. (min)	kidneys+urine	liver+intestines	blood	%/g muscle	%/g femur
^{99m}Tc-MDP	30	22.0	1.8	4.5	0.2	12.9
	60	24.4	1.2	1.9	0.4	15.1
	120	24.2	1.2	1.3	0.1	15.4
^{99m}Tc-EC-AMDP	30	26.7	1.7	2.7	0.2	12.7
	60	22.4	1.3	1.2	0.1	14.8
	120	26.4	0.8	0.5	0.0	29.4

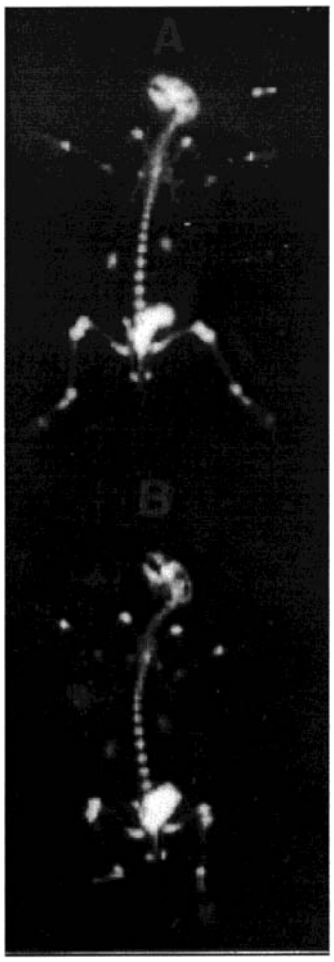


Figure 3. Whole body images of a rabbit 1 h after injection of ^{99m}Tc-EC-AMDP (A) and ^{99m}Tc-MDP (B) (*total preparation*).

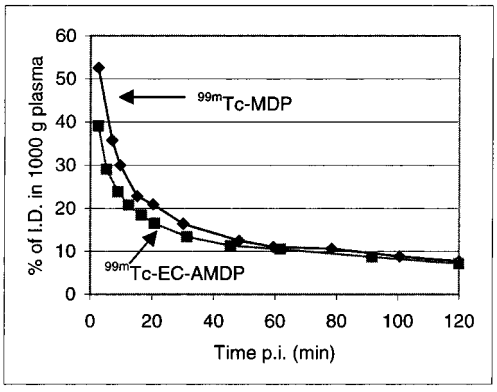


Figure 4. Plasma disappearance curves in a baboon for ^{99m}Tc-MDP and ^{99m}Tc-EC-AMDP.

Evaluation in a Rabbit. The scintigraphic images obtained in a rabbit at 1 h p.i. are shown in Figure 3. Both tracer agents allow a clear visualization of the skeleton and a net distinction between the respective vertebrae and ribs. Uptake in soft tissue is low, and it is clear that the activity not bound to the skeleton is excreted through the kidneys. The image quality is quite similar for both compounds.

Biological Evaluation in a Baboon. Figure 4 shows the plasma disappearance curve in a baboon for ^{99m}Tc-MDP and ^{99m}Tc-EC-AMDP (total preparation) during 2 h after injection. Both tracer agents behave in nearly the same way, although the clearance of ^{99m}Tc-EC-AMDP from plasma is somewhat faster. This may be related to a slightly faster renal extraction or to a faster distribution to the extravascular space. Whole body scintigraphic images obtained 2 h after injection of both agents are shown in Figure 5. As in the rabbit study, nearly identical images are obtained with the two radiopharmaceuticals. This means that the newly developed ^{99m}Tc-diphosphonate conjugate has the characteristics of a suitable bone scanning agent, with almost the same contrast between soft tissue and bone as obtained with ^{99m}Tc-MDP.

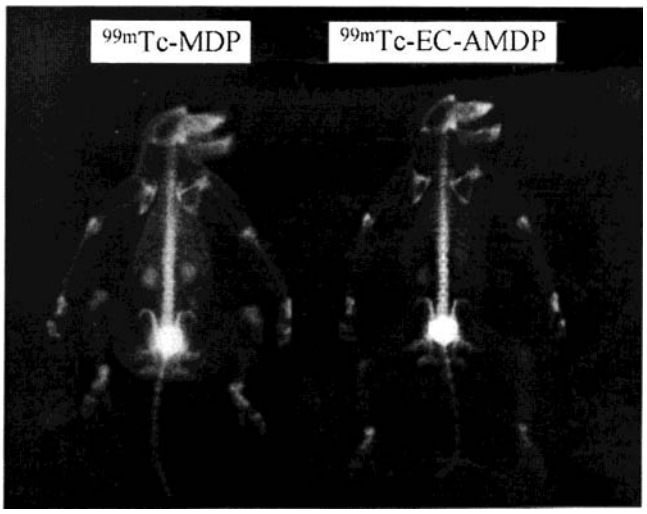


Figure 5. Whole body images 2 h after injection of ^{99m}Tc-MDP and ^{99m}Tc-EC-AMDP in a baboon.

CONCLUSION

The results shown in this paper are part of a research project with the aim to develop a "new generation" bone scanning agent with improved characteristics as compared to the currently used ^{99m}Tc-diphosphonates. The intended improvements concern the stability of the tracer agent, its clearance rate from soft tissue, and its uptake in the bone. For this purpose, a ^{99m}Tc-labeled renal tracer agent with known rapid active renal excretion (^{99m}Tc-ethylene dicysteine) was conjugated to a diphosphonate. In this concept, the EC moiety of the new tracer agent is assumed to be responsible for both the stable binding of the ^{99m}Tc radionuclide and the rapid urinary excretion of the fraction not bound to the bone. The diphosphonate moiety in this compound is not involved in the binding of ^{99m}Tc and thus fully available for binding to the skeleton.

Up to now, the most favorable results have been obtained with the ^{99m}Tc-complex of the conjugate between ethylene dicysteine and aminomethylenediphosphonate, coupled by amide formation between a carboxylate of EC and the amine of AMDP. We have synthesized several other conjugates and evaluated them as their ^{99m}Tc-complexes (*21*) (to be submitted for publication).

In rats, ^{99m}Tc-EC-AMDP showed very promising characteristics with clearly higher femur to blood and femur to muscle activity ratios than ^{99m}Tc-MDP. Especially when the HPLC-isolated peaks A and B were used, these ratios were favorably high. This suggested that an optimized preparation containing only peak A and peak B of ^{99m}Tc-EC-AMDP would constitute a bone-seeking radiopharmaceutical with more rapid clearance from soft tissue and higher uptake in the skeleton than the currently used ^{99m}Tc-diphosphonates.

In the rabbit and the baboon, the scintigraphic images obtained with the new agent (total preparation) showed good quality bone scans with clear visualization of the

skeleton and low soft tissue activity at respectively 1 and 2 h after injection. The fact that the plasma activity disappearance in the baboon was only slightly faster for ^{99m}Tc-EC-AMDP than for ^{99m}Tc-MDP indicates that the new tracer is a good bone-scanning agent, but in this species not a significant improvement as compared to the currently available ^{99m}Tc-diphosphonates. On the other hand, the new ^{99m}Tc-labeled EC-AMDP conjugate has the clear advantage over the common ^{99m}Tc diphosphonates of a high stability and a constant composition as a function of time.

The development and evaluation of further derivatives on the basis of the new concept may eventually result in a ^{99m}Tc-labeled tracer agent with the intended biological characteristics.

LITERATURE CITED

(1) Subramamian, G., McAfee, J. G., O'Mara, R. E., et al. (1971) Tc-99m polyphosphate PP46: A new radiopharmaceutical for skeletal imaging. *J. Nucl. Med. 12*, 399.

(2) Yano, Y., McRae, J., Van Dyke, D. C., and Angor, H. 0. (1973) Technetium-99m labeled stannous ethane-l-hydroxyl-1,1-diphosphonate: a new bone scanning agent. *J. Nucl. Med. 14*, 73−78.

(3) Castronovo, F. P., and Callahan, R. J. (1972) New bone scanning agent: Tc-99m labeled 1-hydroxyethylidene-1,1-disodium diphosphonate. *J. NucI. Med. 13*, 823−827.

(4) Subramanian, G., McAfee, J. G., Blair, R. J., Mehler, A., and Connort, T. (1972) Tc-99mEHDP: a potential radiopharmaceutial for skeletal imaging. *J. Nucl. Med. 13*, 947−950.

(5) Cleynhens, B., Bormans, G., Van Nerom, C., De Roo, M., and Verbruggen, A. (1991) Evaluation of the efficacy of different antioxidants in Tc-99m MDP preparations, in *Nuclear Medicine. The state of the art of Nuclear Medicine in Europe* (H. A. E. Schmidt, and J. B. van der Schoot, Eds.) pp 133−135, Schattauer, Stuttgart-New York.

(6) Baldas, J., and Bonnyman, J. (1985) Substitution reactions of $^{99m}TcNCl_4^-$ − A route to a new class of ^{99m}Tc-radiopharmaceuticals. *Int. J. Appl. Radiat. Isot. 36*, 133−139.

(7) Pinkerton, T., Heineman, W., and Deutch, E. (1980) Separation of technetium hydroxyethylidene diphosphonate complexes by anion-exchange high performance liquid chromatography. *Anal. Chem. 52*, 1106−1110.

(8) Srivastava, S., Bandyopadhyay, D., Meinken, G. et al. (1981) Characterization of ^{99m}Tc-bone agents (MDP, EHDP) by reversed phase and ion exchange high performance liquid chromatography. *J Nucl. Med. 22*, P69.

(9) Tanabe, S., Zodda, J., Deutsch, E., and Heineman, W. (1983) Effect of pH on the formation of Tc($NaBH_4$)-MDP radiopharmaceutical analogues. *Int. J. Appl. Radiat. Isot. 34*, 1577−1584.

(10) Hoch, D., and Pinkerton, T. (1986) Reversed-phase HPLC of ^{99m}Tc methylenediphosphonate bone imaging kits with quantification of pertechnetate. *Appl. Radiat. Isot. 37*, 593−598.

(11) Subrahamian, G., McAfee, J. G., Blair, R. J, Kollfelz, F. A., and Thomas, F. P. (1975) Technetium-99m methylene diphosphonate − a superior agent for skeletal imaging: comparison with other technetium complexes. *J. NucI. Med. 16*, 744−755.

(12) Fogelman, I. (1982) Diphosphonate bone scanning agents − current concepts. *Eur. J. Nucl. Med 7*, 506−509.

(13) Verbruggen, A. M., Nosco, D. L., Van Nerom, C. G., Bormans, G. M., Adriaens, P. J.; DeRoo, M. J. (1991) Technetium-99m−L,L-ethylene dicysteine: a renal imaging agent 1. Labeling and evaluation in animals. *J. NucI. Med. 33*, 551−557.

(14) Van Nerom, C., Bormans, G., De Roo, M., and Verbruggen, M. (1993) First experience in healthy volunteers with technetium-99m L,L-ethylene dicysteine, a new renal imaging agent. *Eur. J. Nucl. Med. 20*, 738−746.

(15) Van Nerom, C., Bormans, G., Bauwens, J., Vandecruys, A., De Roo, M., and Verbruggen, A. (1991) Comparative evaluation of ^{99m}Tc-L,L-ethylene dicysteine and ^{99m}Tc-MAG3 in volunteers, in *Nuclear Medicine. The state of the art of Nuclear Medicine in Europe* (H. A. E. Schmidt, and J. B. van der Schoot, Eds.) pp 290−292, Schattauer, Stuttgart-New York.

(16) Cleynhens, B., Vanbilloen, H., Seuntjens, E. et al. (1994) Comparison of labeling characteristics of ^{99m}Tc-ethylene dicysteine and its mono-acid derivative ^{99m}Tc-ethylene cysteamine cysteine. *J. Labeled Compd. Radiopharm. 36*, 19−22.

(17) Crombez, D., Cleynhens, B., Bormans, G., De Roo, M., and Verbruggen, A. (1991) Comparison of the chelating strength of different tetraligand systems. *Eur. J. Nucl. Med. 18*, 605.

(18) Blondeau, P., Berse, C., and Gracel, D. (1967) Dimerisation of an intermediate during the sodium in liquid ammonia reduction of L-thiazolidine-4-carboxylic acid. *Can. J. Chem. 45*, 49.

(19) Hormi, O., Pajunen, E., Avall, A., and Pannaren, P. (1990) A cheap approach to tetraethyl-methylenediphosphonates. *Synth. Commun. 20*, 1865−1667.

(20) Sturz, G., and Guervenau, J. (1991) Synthesis of novel gem-biphosphonates. *Synthesis 8*, 661−662.

(21) Cleynhens, B., Vanbilloen, H., Delvaux, C., and Verbruggen, A. (1999) Synthesis and evaluation in rats of a bisconjugate of Tc-99m-EC with aminomethylene-diphosphonic acid. *Eur. J. Nucl. Med. 26*, 1193.

BC0001600

Novel Functional Biodegradable Polymer: Synthesis and Anticoagulant Activity of Poly(γ-Glutamic Acid)sulfonate (γ-PGA-sulfonate)

Michiya Matsusaki,[†] Takeshi Serizawa,[†] Akio Kishida,[‡] Takeshi Endo,[§] and Mitsuru Akashi*[,†]

Department of Applied Chemistry and Chemical Engineering, Faculty of Engineering, Kagoshima University, I-21-40 Korimoto, Kagoshima 890-0065, Japan, Department of Biomedical Engineering, National Cardiovascular Center Research Institute, 5-7-1 Fujishiro-dai, Suita, Osaka 565-8565, Japan, and Faculty of Engineering, Yamagata University, 4-13-16 Johnan, Yonezawa 992-8510, Japan. Received January 29, 2001; Revised Manuscript Received August 15, 2001

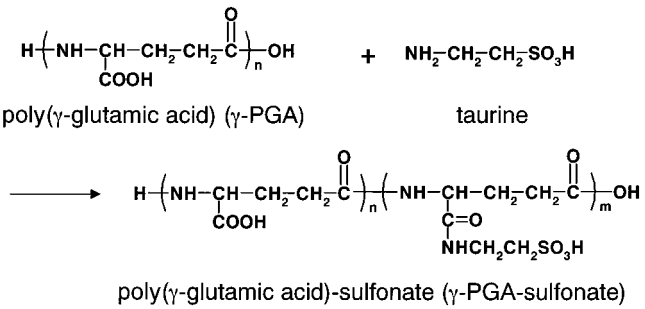
γ-Poly(glutamic acid) (γ-PGA), which is produced by *Bacillus subtilis*, was sulfonated using 2-aminoethane-1-sufonic acid (taurine) in the presence of 1-ethyl-3-(3-dimethylaminopropyl)carbodiimide (WSC) to give sulfonated γ-PGA (γ-PGA-sulfonate). From ^{1}H NMR spectroscopy and IR spectroscopy, it was confirmed that taurine was introduced to the side chain of γ-PGA via an amide linkage. By altering the synthetic conditions, it was possible to control the content of sulfonate in γ-PGA-sulfonate. Anticoagulant activity was investigated in order to evaluate the biological activity of γ-PGA-sulfonate by the Lee−White test. The clotting time was prolonged when the concentration of γ-PGA-sulfonate on the degree of sulfonation was increased. It becomes clear that γ-PGA-sulfonate is potentially useful for various medical applications, such as drug delivery, tissue engineering, and medical materials.

INTRODUCTION

Biodegradable polymers are used in a wide variety of applications, such as suture materials, bone fixation materials, environmental materials, and in drug delivery systems. Recently, further application of biodegradable polymers has been desired in many situations, such as a simuli−responsible drug delivery system and tissue engineering. However, it is difficult to prepare such functional biodegradable polymers because most biodegradable polymers have a simple chemical structure and lack reactive main or side chains. Some researchers have tried to prepare the functional biodegradable polymers. Ohya and co-workers have studied polydepsipeptides, which are copolymers of α-amino acids and α-hydroxy acids having a reactive side chain (*1*, *2*). Mikos and co-workers have synthesized poly(propylene fumarate) (PPF), which is a reactive unsaturated functional biodegradable polymer (*3*, *4*). These polymers have unique properties and are further improved in performances as compared with the conventional ones; however, there are so many aspects of the demands to biodegradable polymers.

For tissue engineering applications, there are some special demands to biodegradable polymers (in many cases, to scaffolds). A typical one is the ability of incorporating growth factors. Others are the fabrication of a complex shape, degradation rate control, and stimuli responsibility. On the other hand, when biodegradable polymers are used in biomedical fields, the polymers should be metabolized in biological systems at a final stage. So, α-hydroxy acids, amino acids, and lipids are currently used. When one would synthesize novel functional biodegradable polymers, one should use the same resources, which have functional groups or double bonds in their chemical structure.

Scheme 1. Synthesis of Poly(γ-glutamic acid Sulfonate) (γ-PGA-Sulfonate)



Poly(γ-glutamic acid) (γ-PGA) is bioproduct which is secreted by a *Bacillus subtilis* strain, *B. subtilis F-2-01* (*5*), and is mass produced by fermentation. The molecular weight of γ-PGA is very high (100 000−1 000 000), and this is a unique character of γ-PGA. Some researchers have tried to use γ-PGA as a novel biodegradable polymer by modifying the γ-PGA side chain. Kubota et al. have reported alkaline hydrolysis of γ-PGA (*6*) and esterification of the carboxyl group for the purpose of providing better solubility in organic solvents (*7*) or for the preparation of fiber (*8*). Kunioka et al. have studied the cross-linking reaction of γ-PGA by γ irradiation (*9*, *10*). Hara has reported the preparation of γ-PGA hydrogel for applications as an environmental material (*11*). We have also reported the polyion complex formation between γ-PGA and chitosan (*12*) and polymer drug (*13*). For further applications, we tried to prepare the sulfonated γ-PGA (γ-PGA-sulfonate).

Generally, it is well-known that heparin has many biological activities, such as anticoagulant activity, stabilizing activity of growth factors, antiviral activity, and

* To whom correspondence should be addressed. Phone: +81-99-285-8320. Fax: +81-99-255-1229. E-mail: akashi@apc.kagoshima-u.ac.jp.
† Kagoshima University.
‡ National Cardiovascular Center Research Institute.
§ Yamagata University.

10.1021/bc010008d CCC: $22.00 © 2002 American Chemical Society
Published on Web 12/20/2001

plasma clearing activity. Various heparinoids were synthesized, and their biological activities were studied. Sulfated naturally occurring polysaccharides have been studied, such as dextran, chitin, and chitosan (*14*−*17*). Synthetic polymers, such as poly(vinyl sulfonate) and polysaccharide derivatives having sulfamide and *O*-sulfonic acid groups (*18*, *19*), are the examples. The heparinoid, having antiviral activity or cell growth stimulation activity, are also the examples (*20*−*23*).

In this study, the sulfonic group was introduced into γ-PGA by using 2-aminoethane-1-sulfonic acid (taurine) in order to obtain sulfonated γ-PGA (γ-PGA-sulfonate). γ-PGA-sulfonate was inspired from the chemical structure of heparin, which is well-known to have anticoagulant activity and biodegradability. Biodegradable γ-PGA-sulfonate could be termed "a bioinspired material" and is expected to have heparin-like biological activities.

Taurine is one of the most abundant amino acids in animal tissues and is described as an essential amino acid for human and other mammalian species. Taurine has been reported to have several putative roles, functioning as a neurotransmitter, a neuromodulator, and a neurogrowth factor and functioning in membrane stabilization. Studies of sulfonation by conjugation with taurine have been reported in amino acids and oligopeptides (*24*, *25*). Sulfonation of γ-PGA using taurine is a new trial in the meaning of the modification of γ-PGA in aqueous media. Because of the high molecular weight and poor solubility to aqueous media, the chemical modification of γ-PGA was done in organic media. In this study, the preparation of γ-PGA aqueous solutions and esterification reactions were studied (in detail). The anticoagulant activity of γ-PGA-sufonated was also investigated.

MATERIALS AND METHODS

Materials. γ-PGA (MW 1 230 000, MW/M_n 1.20) was kindly donated by Meiji Seika Kaisya, Ltd. (Tokyo, Japan) and was used without further purification. Sodium hydrogen carbonate, 1-ethyl-3-(3-dimethylaminopropyl)carbodiimide (WSC), taurine, and sodium dextran sulfate (DS) were purchased from Wako Pure Chemical Industries (Osaka, Japan). Heparin sodium salt, polyvinyl sulfuric acid potassium salt (PVS), and calcium chloride were purchased from Nacalai Tesque (Kyoto, Japan). Poly(*p*-styrenesulfonic acid sodium salt) (PSS) was purchased from Tokyo Kasei (Tokyo, Japan).

Synthesis of γ-PGA-Sulfonate. Adequate amounts of sodium hydrogen carbonate, γ-PGA, WSC, and taurine were dissolved in 30 mL of pure water under magnetic stirring for 30 min at 0 ∼ 4 °C. The reaction solution was maintained for 24 h at ambient temperature. The reaction solution was dialyzed using a Spectra/Pore membrane (wt off molecular weight of 50 000) for 3 days. γ-PGA-sulfonate was obtained by freeze-drying for 3 days. The reaction conditions are shown in Table 1.

Anticoagulant Activity Test (Lee−White Test). The Lee−White test was carried out as follows. One milliliter of human whole blood, which was collected with a 21-gauge needle, was added to tubes each containing 1 mg/mL of each sample solution (sample tubes) and to an empty tube (reference tube). These tubes were allowed to stand for 3 min at 37 °C. After 3 min, the reference tube was tilted, and if the reference tube was not clotted, the tube was tilted every 30 s until clotting occurred. When the reference tube had clotted, the sample tubes were tiled every 30 s until the contents of these tubes were clotted. In vitro clotting time was evaluated using the following equations:

Lee−White clotting time =
time which sample tube was clotted −
time which reference tube was clotted

Table 1. Preparation of γ-PGA-sulfonate[a]

runs	γ-PGA (mmol)	taurine (mmol)	WSC (mmol)	yield (%)	sulfonate content[b] (%)
1	5	5	2.5	58	25
2	5	5	5	61	51
3	5	5	10	64	81
4	5	0.5	5	53	13
5	5	2.5	5	61	37
6	5	5	5	61	51
7	5	10	5	56	54
8	5	50	5	63	48

[a] Reaction time was 24 h at room temperature. [b] The sulfate content against total carboxyl groups was estimated by a ^{1}H NMR spectrum.

Hydrolysis Testing of γ-PGA and γ-PGA-Sulfonate. γ-PGA (MW = 350 000) and γ-PGA-sulfonate (10% and 90%, MW = 150 000) were dissolved in a 0.2 M phosphate buffer (pH = 7.4), and the concentration of samples was prepared at 0.1 wt %. Samples were stored at 80 °C until several hydrolysis times, molecular weights, and molecular weight distributions were measured by gel permeation chromatography (GPC) (TSK-GEL G5000PW and G4000PW$_{xL}$ column; flow rate was 1.0 mL/min), calibrated with pullulan (Shodex STANDARD P-82) standards.

RESULTS AND DISCUSSION

Synthesis of γ-PGA-Sulfonate. Figure 1 shows the ^{1}H NMR spectra of γ-PGA, taurine, and γ-PGA-sulfonate (the synthetic condition is no. 2 in Table 1). All of the peaks corresponding to γ-PGA and the CH_2 of taurine were observed after the reaction. The peak of a CH_2 next to a nitrogen atom was shifted from 3.4 ppm in taurine to 3.6 ppm in γ-PGA-sulfonate, indicating that taurine was introduced into γ-PGA by an amide linkage.

Figure 2 shows the FT-IR spectra of γ-PGA and γ-PGA-sulfonate. The peaks at 1100−1200 and 1350 cm^{-1} for γ-PGA-sulfonate show the asymmetric and symmetric stretching vibration modes of S (=O_2), respectively. These peaks were not observed for γ-PGA. The peaks at 1600 cm^{-1} of amide I and 1650 cm^{-1} of amide II were similarly observed for γ-PGA and γ-PGA-sulfonate. It was also confirmed that a carboxyl group of the side chain of γ-PGA was converted to an amide group, because a peak at 1750 cm^{-1} which corresponds to carbonyl vibration mode of carboxyl groups in γ-PGA was reduced in γ-PGA-sulfonate. These results indicated that γ-PGA-sulfonate was prepared by the conjugation of taurine with γ-PGA.

Sawa et al. has reported the molecular structure analysis of γ-PGA by IR spectra and by optical rotatory dispersion curves (*26*). Their report indicated that H-α-PGA (COOH type) was an α-helix structure, H-γ-PGA (COOH type) was a parallel β structure, and Na-γ-PGA (COONa type) was a random structure. In this study, Na-γ-PGA (COONa type) was used, so γ-PGA-sulfonate was thought to be a random structure. In Figure 2, when the FT-IR spectrum of γ-PGA is compared with that of γ-PGA-sulfonate, the reduction of a carboxyl group peak and the increase of sulfone group peaks were observed. Other changes of spectra were not observed. Accordingly,

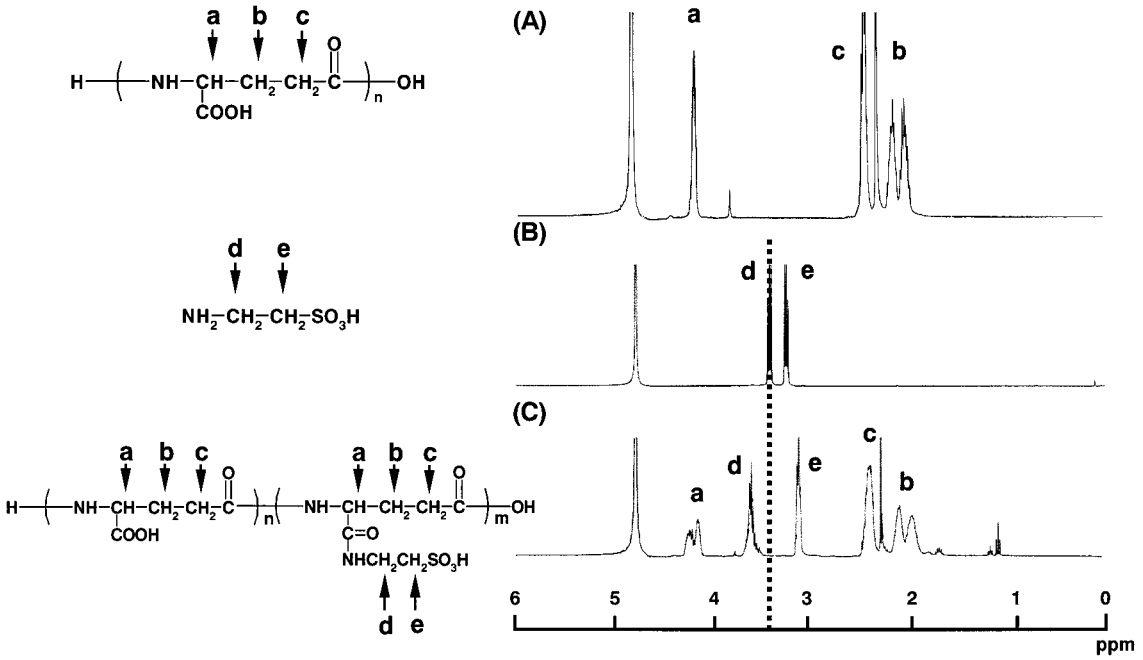


Figure 1. ^{1}H NMR spectra of (A) γ-PGA, (B) taurine, and (C) γ-PGA-sulfonate in D_2O.

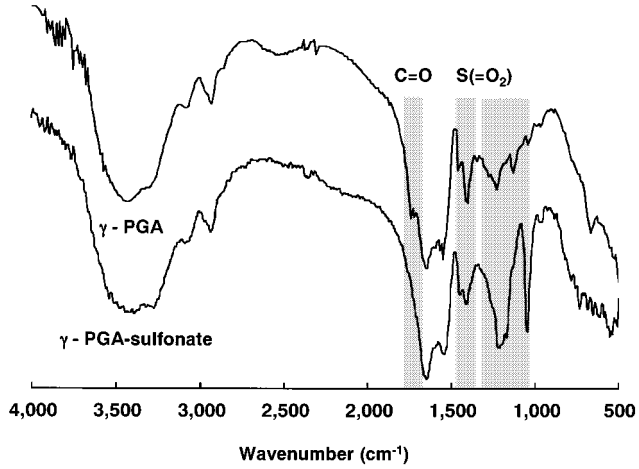


Figure 2. FT-IR spectra of γ-PGA and γ-PGA-sulfonate.

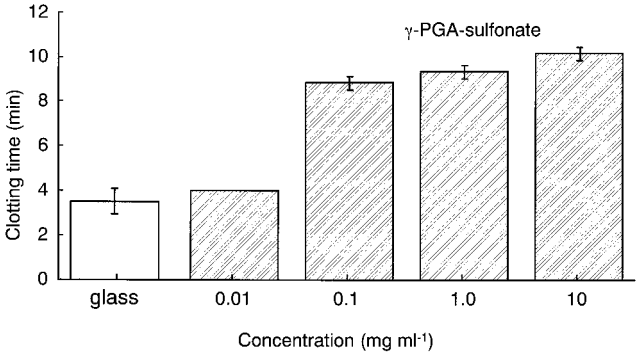


Figure 3. Effect of concentration on anticoagulant activity ($n = 3$).

the molecular structure of γ-PGA-sulfonate is confirmed to be a random structure. γ-PGA-sulfonate is thought to have an extended structure, because of ion repulsion by a sulfonic group.

It is expected that the solubility of γ-PGA-sulfonate is different from that of γ-PGA by sulfonic group. The solubility of γ-PGA was compared with that of γ-PGA-sulfonate. γ-PGA was dissolved in a pH > 7.4 aqueous solution. However, it was only dissolved in DMF, NMP, and DMSO and was not dissolved in other organic solvents. The solubility of γ-PGA-sulfonate was better than that of γ-PGA. For example, γ-PGA-sulfonate was dissolved in all pH's for aqueous solutions, and it had a good solubility in organic solvents (DMF, NMP, and so forth). This result confirmed that the properties of γ-PGA-sulfonate were different from those of γ-PGA.

Control of Sulfonate Content. The amount of taurine and WSC in feed was varied in order to control the sulfonate content. The yield and sulfonate content in the γ-PGA-sulfonate are shown in Table 1. The sulfonate content increased with increasing WSC in feed, resulting in a maximum content of 81%. On the other hand, when the amount of taurine in feed was also increased in the presence of a constant concentration at WSC (5 mmol), the sulfonate content was not increased to more than approximately 50%. Yields were around 60% under all preparing conditions. These results indicated that, in order to control sulfonate content, changing the WSC amount is most valuable.

Anticoagulant Activity Test (Lee−White Test). It is expected that γ-PGA-sulfonate has various biological activities. In this study, anticoagulant activity was investigated as a typical bioactive evaluation of γ-PGA-sulfonate. Anticoagulant activity was evaluated by the Lee−White test. Figure 3 shows the dependence of the clotting time on the γ-PGA-sulfonate concentration. The clotting time increased with an increase in the γ-PGA-sulfonate concentration. This result indicates that the anticoagulant activity of γ-PGA-sulfonate was concentration-dependent. Figure 4 shows the dependence of the anticoagulant activity on the degree of sulfonation. The clotting time of all γ-PGA-sulfonate samples were prolonged when they were compared to those of γ-PGA. This result indicates that γ-PGA-sulfonate obtained anticoagulant activity as a result of introducing taurine. Moreover, the clotting time increased with an increase in the degree of sulfonation.

Figure 5 compares the anticoagulant activity of γ-PGA-sulfonate, heparin, dextran sulfate (DS), poly(vinyl sul-

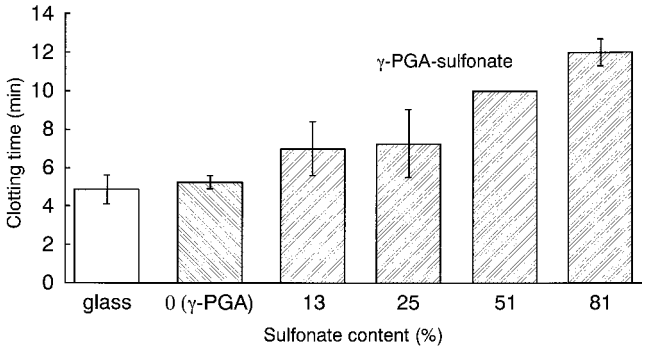


Figure 4. Effect of sulfonate content on anticoagulant activity ($n = 3$). Solution concentration was 1 mg mL^{-1}.

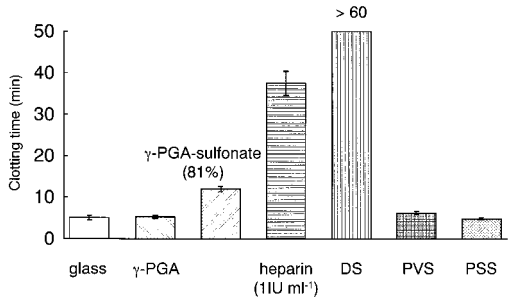


Figure 5. Comparison of anticoagulant activity between γ-PGA-sulfonate, heparin, dextran sulfate (DS), poly(vinyl sulfuric acid) (PVS), and poly(styrene sulfonic acid) (PSS) ($n = 3$). Solution concentration was 1 mg mL^{-1}.

furic acid) (PVS) and poly(styrene sulfonic acid) (PSS). The concentration of each solution was 1 mg mL^{-1}, and heparin was used at a concentration of 1 IU mL^{-1} (approximately 6 μg/mL). The anticoagulant activity of γ-PGA-sulfonate was not high as compared with heparin or DS. However, it was possible to realize the anticoagulant activity on γ-PGA by the introduction of taurine. γ-PGA-sulfonate can be prepared on a large scale, suggesting that the sulfonation of γ-PGA has significant implications.

In this study, the anticoagulant activity of γ-PGA-sulfonate was evaluated by the Lee−White test using human whole blood. It was indicated that γ-PGA-sulfonate has higher anticoagulant activity than synthetic sulfated polymers, such as PSS and PVS. However, it is difficult to clarify the mechanism of anticoagulant activity by the Lee−White method. We have reported that not only the interaction with antithrombin III but also activated partial thromboplastin time (aPTT), prothrombin time (PT), thrombin time (TT) tests recognize the mechanism of anticoagulant activity of poly(glucosyloxyethyl methacrylate)sulfate [poly(GEMA)-sulfate] (*27*, *28*). The results described that the antioagulant activity mechanism of poly(GEMA) sulfate was different from heparin. The mechanism of anticoagulant activity of γ-PGA-sulfonate will be evaluated in the future.

Hydrolysis Testing of γ-PGA and γ-PGA-Sulfonate. The hydrolysis of γ-PGA has been reported in detail. Kubota et al. have investigated the alkaline hydrolysis of γ-PGA for the purpose of obtaining various molecular weights of γ-PGA (*6*). It was possible to obtain the expected molecular weight of γ-PGA by controling the NaOH concentration. Kunioka et al. have also reported the effect of temperature on the hydrolysis of γ-PGA hydrogel prepared by γ irradiation. The rate of hydrolysis increased with an increase in hydrolysis temperature. On

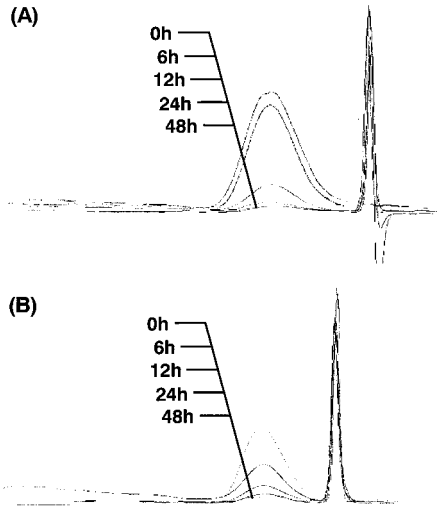


Figure 6. Degradation behavior of (A) γ-PGA and (B) 10% γ-PGA-sulfonate.

the basis of these observations, it is expected that γ-PGA-sulfonate is biodegradable polymer. In this study, the hydrolysis of γ-PGA and γ-PGA-sulfonate (10 and 90%) was evaluated in a phosphate buffer (pH = 7.4) at 80 °C.

After 6, 12, 24, 48 h, the hydrolysis reaction was stopped by cooling at 4 °C, and the molecular weight of each sample was measured by GPC. Figure 6 shows the GPC profiles of the hydrolysis of γ-PGA and γ-PGA-sulfonate (10%). High molecular weight polymers and oligomers coexisted without any intermediate molecular weight polymers. The ratio of high molecular weight polymers against its oligomer (molecular weight of about 2000) increased with an increase in time, indicating the hydrolysis of the polymers. Ninety percent of the γ-PGA-sulfonate showed a similar tendency (data not shown). Figure 7 indicated the existence ratio of high molecular weight polymer and oligomer estimated by GPC. The change of existence ratio of oligomer γ-PGA and γ-PGA-sulfonate has a similar tendency; however, the existence ratio of oligomer γ-PGA-sulfonate was more rapidly changed as compared to that of γ-PGA. It was confirmed that the hydrolysis ratio of γ-PGA-sulfonate was more rapid than that of γ-PGA. Further, the hydrolysis ratio of 90% γ-PGA-sulfonate was faster than that of 10% γ-PGA-sulfonate, indicating that the introduction of sulfonic groups to γ-PGA accelerate the polymer hydrolysis.

The hydrolysis mechanisms of γ-PGA and γ-PGA-sulfonate were suggested as follows. γ-PGA-sulfonate was thought to be more extended than γ-PGA, because of electrostatic repulsion of sulfonic groups. Accordingly, it was presumed that water molecules can readily attach the polymers, resulting that the hydrolysis of γ-PGA-sulfonate was easier and faster than that of γ-PGA. The hydrolysis ratio of 90% γ-PGA-sulfonate was faster than that of 10% γ-PGA-sulfonate, because 90% γ-PGA-sulfonate has many sulfonic groups. In addition, the pH of the neighborhood of the polymer seemed to be lowered by the introduction of a sulfonic group, resulting that the acid hydrolysis of the polymers was accelerated. For these reasons, the hydrolysis rate of γ-PGA-sulfonate was dependent on the degree of sulfonation.

The hydrolysis of γ-PGA and γ-PGA-sulfonate had high molecular weight polymers and oligomers without any intermediate molecular weight polymers. It was thought that when hydrolysis was started, hydrolysis of γ-PGA

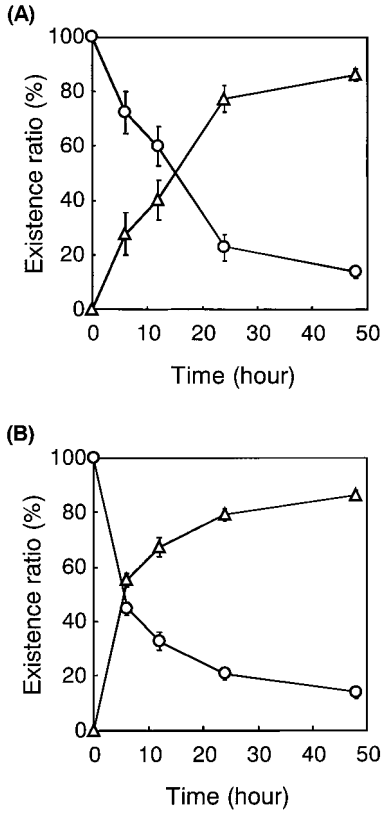


Figure 7. Existence ratio of (○) high molecular weight polymers and (△) oligomers was estimated by GPC: (A) γ-PGA and (B) 10% γ-PGA-sulfonate.

and γ-PGA-sulfonate seemed to rapidly proceed to the oligomer level. So, it was presumed that Figure 6 was only confirming the high molecular weight polymer and low molecular weight polymer (oligomer) peaks. This result was not clear in this study. Accordingly, further study of the hydrolysis mechanism of γ-PGA and γ-PGA-sulfonate will be done in the future.

It was confirmed that γ-PGA and γ-PGA-sulfonate had degradability. In this study, a hydrolysis test was carried out at 80 °C as an acceleration test. It is expected that γ-PGA-sulfonate will be hydrolyzed in vivo.

γ-PGA is a component of Japanese traditional food *Natto*; in other words, γ-PGA is edible natural product. In the meaning of toxicity, γ-PGA is very safe; however, the biocompatibility of γ-PGA is now investigated. Taurine exists in animal tissues, and is an essential amino acid for mammalian species. So, the toxicity of taurine is thought to be very low. It is expected that γ-PGA-sulfonate is a nontoxic material. The toxicity test of γ-PGA-sulfonate will be done in the future.

CONCLUSION

γ-PGA-sulfonate was prepared by the reaction of taurine with γ-PGA. Results indicated that the sulfonate content could be controlled by changing the WSC amount. γ-PGA-sulfonate was found to have anticoagulant activity. Anticoagulant activity was dependent on the concentration and sulfonate content of γ-PGA-sulfonate. γ-PGA-sulfonate has the potential to combine with cytokines, such as basic fibroblast growth factor, and to form polyion complexes with cationic biodegradable polymers. γ-PGA-sulfonate is expected to have applications in a wide variety of areas, such as drug delivery systems, environmental materials, tissue engineering, and medical materials.

ACKNOWLEDGMENT

This study was partially supported by a Grant-in-Aid for Scientific Research (B) from the Japan Society for the Promotion of Science.

LITERATURE CITED

(1) Ouchi, T., Nozaki, T., Ishikawa, A., Fujimoto, I., and Ohya, Y. (1997) Synthesis and enzymatic hydrolysis of lactic acid−depsipeptide copolymers with functionalized pendant groups. *J. Polym. Sci., Part A*: *Polym. Chem. 35*, 377−383.

(2) Ouchi, T., Seike, H., Nozaki, T., and Ohya, Y. (1998) Synthesis and characteristics of polydepsipeptide with pendant thiol group. *J. Polym. Sci., Part A*: *Polym. Chem. 36*, 1283−1290.

(3) Suggs, L. J., Payne, R. G., and Mikos, A. G. (1997) Synthesis and Characterization of a block copolymer consisting of poly(propylene fumarate) and poly(ethylene glycol). *Macromolecules 30*, 4318−4323.

(4) Suggs, L. J., Kao, E. Y., Palombo, L. L., Krishnan, R. S., Widmer, M. S., and Mikos, A. G. (1998) Preparation and characterization of poly(propylene fumarate-*co*-ethylene glycol)hydrogels. *J. Biomater. Sci., Polymer Ed. 9*, 653−666.

(5) Kubota, H., Matsunobu, T., Uotani, K., Takebe, H., Satoh, A., Tanaka, T., and Taniguchi, M. (1993) Production of poly(γ-glutamic acid) by *Bacillus subtilis* F-2-01. *Biosci. Biotechnol. Biochem. 57*, 1212−1217.

(6) Kubota, H., Nambu, Y., and Endo, T. (1992) Alkaline hydrolysis of poly(γ-glutamic acid) produced by microorganism. *Polym. Prepr., Japan 41*, 1074−1076.

(7) Kubota, H., Nambu, Y., and Endo, T. (1995) Convenient esterification of poly(γ-glutamic acid) produced by microorganism with alkyl halides and their thermal properties. *J. Polym. Sci., Part A*: *Polym. Chem. 33*, 85−88.

(8) Yahata, K., Sadanobu, J., and Endo, T. (1992) Preparation of poly-α-bynzyl-γ-glutamate fiber. *Polym. Prepr., Japan 41*, 1077−1079.

(9) Kunioka, M. (1993) Production and reaction by γ irradiation of poly(γ-glutamic acid) from *Bacillus subtilis* IFO3335. *Polym. Prepr., Japan 42*, 3751−3753.

(10) Kunioka, M. (1994) Biosynthesis of poly(γ-glutamic acid) in *Bacillus subtilis* IFO3325 and cross-linking reaction by γ irradiation of poly(γ-glutamic acid). *Stud. Polym. Sci. 12*, 425−432.

(11) Hara, T. (1999) Synthesis and Application of *Natto* resin produced by γ irradiation. *Hoshasen to Sangyo 81*, 37−41.

(12) Tachaboonyakiat, W., Serizawa, T., Endo, T., and Akashi, M. (2000) The influence of molecular weight over the ultrathin films of biodegradable polyion complexes between chitosan and poly(γ-glutamic acid). *Polym. J. 32*, 481−485.

(13) Serizawa, T., Goto, H., Kishida, A., Endo, T., and Akashi, M. (1999) Improved alternate deposition of biodegradable naturally occurring polymers onto a quartz crystal microbalance. *J. Polym. Sci., Part A*: *Polym. Chem. 36*, 801−804.

(14) Mauzac, M., and Jozefonvictz, J. (1984) Anticoagulant activity of dextran derivatives. Part I: Synthesis and characterization. *Biomaterials 5*, 301−304.

(15) Nishimura, S., and Tokura, S. (1987) Preparation and antithrombogenic activities of heparinoid from 6-*O*-(carboxymethyl)chitin. *Int. J. Biol. Macromol. 9*, 225−232.

(16) Muzzarelli, R. A. A., Tanfani, F., and Emanuelli, M. (1984) Sulfated *N*-(carboxymethyl)chitosans: Novel blood anticoagulants. *Carbohydr. Res. 126*, 225−231.

(17) Doctor, V. M., Lewis, D., Coleman, M., Kemp, M. T., Marbely, E., and Sauls, V. (1991) Anticoagulant properties of semisynthetic polysaccharide sulfates. *Thromb. Res. 64*, 413−425.

(18) Ito, Y., Iguchi, Y., Kashiwagi, T., and Imanishi, Y. (1991) Synthesis and nonthrombogenicity of polyethrurethaneurea film grafted with poly(sodium vinyl sulfonate). *J. Biomed. Mater. Res. 25*, 1347−1361.

(19) Hatanaka, K., Yoshida, T., Miyahara, S., Sato, T., Ono, F., Uryu, T., and Kuzuhara, H. (1987) Synthesis of new heparinoids with high anticoagulant activity. *J. Med. Chem. 30*, 810−814.

(20) Choi, Y. S., Yoshida, T., Mimura, T., Kaneko, Y. Nakashima, H., Yamamoto, N., and Uryu, T. (1996) Synthesis of sulfated octadecyl *ribo*-origosaccharides with potent anti-AIDS virus activity by ring-opening polymerization of a 1,4-anhydroribose derivative. *Carbohydr. Res. 282*, 113−123.

(21) Hattori, K., Yoshida, T., Nakashima, H., Premanathan, M., Aragaki, R., Mimura, T., Kaneko, Y., Yamamoto, N., and Uryu, T. (1998) Synthesis of sulfonated amino-polysaccharides having anti-HIV and blood anticoagulant activities. *Carbohydr. Res. 312*, 1−8.

(22) Nishimura, S., Kai, H., Shinada, K., Yoshida, T., Tokura, S., Kurita, K., Nakashima, H., Yamamoto, N., and Uryu, T. (1998) Regioselective syntheses of sulfated polysaccharides: specific anti-HIV-1 activity of novel chitin sulfates. *Carbohydr. Res. 306*, 427−433.

(23) Yano, K., Tsuda, E., Ueda, M., and Higashi, K. (1998) Natural hepatocyte growth factor (HGF) from human serum and a bound form of recombinant HGF with heparan sulfate are indistinguishable in their physicochemical properties. *Int. J. Biol. Macromol. 23*, 227−235.

(24) Gerhard, B., and Albert, H. (1993) Preparation of amino-sulfonic acid amino acid and peptide derivatives as immunostimulants. *Eur. Pat. Appl.* 18.

(25) Vaclav, C., and Dieter, J. H. (1994) Enzymic approach to the synthesis of taurine-containing peptides. *Int. J. Pept. Protein Res. 44*, 466−471.

(26) Sawa, S., Murakawa T., Watanabe T., Murao S., and Omata S. (1973) Studies on the physicochemical properties of polyglutamic acid produced by *Basillus subtilis* No. 5E. *Nippon Nogei Kagaku Kaishi. 47*, 167−175.

(27) Akashi, M., Sakamoto, N., Suzuki, K., and Kishida, A. (1996) Synthesis and anticoagulant activity of sulfated glucoside-bearing polymers. *Bioconjugate Chem. 7*, 393−395.

(28) Sakamoto, N., Shioya, T., Kishida, A., and Akashi, M. (1997) Preparation and anticoagulant surface properties of glucoside- or sulfated glucoside- bearing polymer-grafted poly(ethylene) films. *Macromol. Symp. 120*, 159−167.

BC010008D

Synthesis of Cyclopentadienyltricarbonyl Rhenium Phenyltropanes by Double Ligand Transfer: Organometallic Ligands for the Dopamine Transporter

Richard R. Cesati III,[†] Gilles Tamagnan,*[,‡] Ronald M. Baldwin,[‡,§] Sami S. Zoghbi,[‡] Robert B. Innis,[‡] Nora S. Kula,[∥] Ross J. Baldessarini,[∥] and John A. Katzenellenbogen*[,†]

Department of Chemistry, University of Illinois, 600 South Mathews Avenue, Urbana, Illinois 61801, Yale University School of Medicine/VA Connecticut HCS, West Haven, Connecticut 06516, RadioTracer Inc., New Haven, Connecticut 06521, and Mailman Research Center, McLean Division of Massachusetts General Hospital, Belmont, Massachusetts 02478 . Received January 31, 2001; Revised Manuscript Received August 15, 2001

Cyclopentadienyltricarbonyl rhenium ($CpRe(CO)_3$) systems can be prepared from ferrocenes and perrhenate by a double ligand transfer (DLT) reaction that gives reasonable yields and shows excellent functional group tolerance. We used this reaction for the direct preparation of $CpRe(CO)_3$−phenyltropane conjugates. Such agents, when labeled with technetium-99m, might function as imaging agents for the dopamine transporter (DAT) system that would be useful for assessing the onset and severity of Parkinson's disease. Of the $CpRe(CO)_3$−tropane conjugates prepared by the DLT reaction (as well as other analogues prepared by related methods), those substituted at the *N*-8 position seem most promising; their affinity for the DAT in all cases was high, and their ferrocene precursors for the DLT reaction can be prepared in a convenient manner. By contrast, the 3*β*-conjugates were poor DAT binders. The modular nature of these systems offers considerable flexibility that could be used to improve the binding characteristics of these compounds further.

INTRODUCTION

The dopamine transporter (DAT) serves a critical modulatory role in dopamine (DA) neurotransmission, removing released transmitter from the synapse by transporting it back into the presynaptic terminal (*1*). Because of its crucial function, DAT is a target for drug therapy (e.g., Ritalin for attention deficit and hyperactivity disorder) and for drugs of abuse (e.g., cocaine) and has been extensively studied both by in vitro methods and through in vivo imaging. Because DAT serves as a marker of DA terminal innervation of the striatum, DAT-based images have been proposed as an early diagnostic test for Parkinson's disease (PD) (*2*). The development of DAT imaging as an objective biological marker for PD would be extremely useful for assessing potential agents for neuroprotection and approaches to neuronal restoration (*3*, *4*). In addition, it might also provide a secondary marker in individuals with varying clinical symptoms that would allow for the mapping of disease subsets (*5*).

To date, radionuclide imaging of the DAT has been dominated by compounds such as the iodophenyltropane *β*-CIT (**I**, Figure 1), labeled with iodine-123 (*6*). However, production of the I-123 radionuclide requires daily delivery from cyclotrons, limiting its availability and increasing its cost. Because of this limitation, several research groups have developed DAT-binding radiotracers that use technetium-99m as a practical and widely available, low-cost alternative radionuclide, together with single photon emission computed tomography (SPECT) DAT imaging.

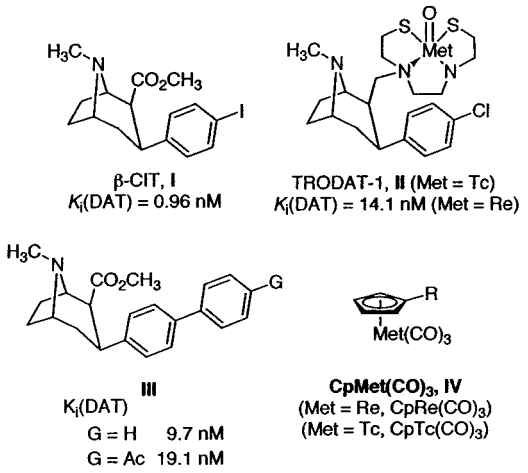


Figure 1. Synthetic ligands for the DAT.

Kung and co-workers reported successful SPECT DAT imaging using a technetium-99m complex of an N_2S_2 chelate conjugated at the 2*β*-position of 3*β*-(4-chlorophenyl)-8-methyl-8-azabicyclo[3.2.1]octane (TRODAT-1 (**II**), Figure 1) (*7*−*9*). The in vivo pharmacological specificity of this agent was shown in animal experiments by selective blocking with the DAT binding agent, *β*-CIT (**I**). The corresponding rhenium analogue displayed an inhibition constant (K_i) of 14.1 nM toward DAT. Madras and co-workers have reported a similar result with one of a series of N_2S_2 chelate analogues of the fluorophenyltropane CFT conjugated at the *N*-8 position (*10*). Together,

* To whom correspondence should be addressed. J.A.K., Tel: (217)333-6310. Fax: (217)333-7325. E-mail: jkatzene@uiuc.edu. G.T., Tel: (203)932-5711 × 3590. Fax: (203)937-2897. E-mail: gilles.tamagnan@yale.edu.

[†] University of Illinois.

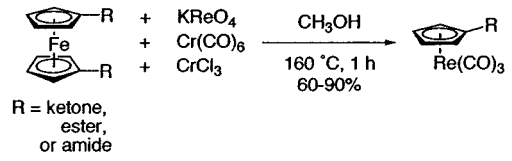
[‡] Yale University School of Medicine/VA Connecticut HCS.

[§] RadioTracer Inc..

[∥] Mailman Research Center.

10.1021/bc010011x CCC: $22.00 © 2002 American Chemical Society
Published on Web 12/27/2001

Scheme 1



these studies demonstrate that technetium-99m can be incorporated into a radiotracer that has a high affinity for the target site, crosses the blood−brain barrier, and concentrates in the appropriate target regions in the brain. However, both tracers showed relatively high nonspecific uptake, which may be a consequence of the high molecular weight of these agents and their large lipophilic metal complexes.

In a related effort, we have investigated the use of the stable substituted η^5-cyclopentadienyltricarbonyl rhenium and technetium organometallic complexes for radiolabeling biologically interesting molecules; these complexes are abbreviated collectively as $CpMet(CO)_3$ complexes (Met = metal) or individually as cyclopentadienyltricarbonyl rhenium ($CpRe(CO)_3$) for the rhenium and $CpTc(CO)_3$ for the technetium analogues (**IV**, Figure 1). As compared to the more widely used high oxidation state metal−oxo complexes (e.g., **II**, Figure l), $CpMet(CO)_3$ complexes exhibit high chemical and metabolic stability, are lipophilic and relatively small, and, unlike many inorganic chelates, do not possess additional stereocenters (Figure 1) (*11*−*13*). Thus, they appear to be promising for the development of novel metal-labeled DAT imaging agents. However, until recently, the synthesis of these organometallic species has required harsh conditions and multistep procedures. Recent reports describing the preparation and use of low valent (i.e., $Met(CO)_3^+$) technetium and rhenium are encouraging (*14*−*18*).

The suitability of tropane $CpMet(CO)_3$ conjugates as DAT ligands was shown by a series of $CpRe(CO)_3$ and manganese conjugates with nanomolar affinity (*19*). One of these, the ester of 2β-hydroxymethyl-3β-(4-[^{123}I]-iodophenyl)tropane with carboxycyclopentadienyltricarbonyl rhenium radiolabeled with iodine-123 ([^{123}I]YP116), was shown to bind specifically to striatal DAT in rats and baboons and showed SPECT regional uptake curves similar to those of [^{123}I]FPCIT (*20, 21*).

The first practical radiochemical preparation of substituted $CpMet(CO)_3$ complexes was the double ligand transfer (DLT) reaction, originally reported by Martin Wenzel in 1992 (*22*). We recently reported an improved version of the DLT reaction that minimized formation of unwanted byproducts (Scheme 1) (*23*). This remarkable transformation involves the in situ reduction/carbonylation of the permetalate species, followed by selective ring transfer from an appropriately substituted ferrocene precursor. The reaction occurs in a single pot and in most cases is limited to ferrocenes substituted with electron-withdrawing groups. However, the major drawback in the initial uses of the DLT reaction for labeling biomolecules is in the additional steps needed to conjugate the substituted $CpMet(CO)_3$ to the biological molecule of interest (*24*). Recent developments in our laboratory, which provide alternative routes to $CpRe(CO)_3$ complexes without a requirement for substitution with an electron-withdrawing group, include the "three-component condensation" reaction (*25*−*27*) and the stannane approach (*28*).

To extend the DLT methodology further and to expand structure−activity relationships for organometallic DAT imaging agents, we designed a direct version of the DLT reaction, applied it to a series of ferrocenyl phenyltropane conjugates, and measured the binding affinity of these new compounds to monoamine transporters. Although the rhenium compounds could be made more efficiently without going through the ferrocene intermediate, the purpose was to develop methods that could be applied to short-lived γ-emitting radiotracers. Additional ligands were made by the three-component condensation. Besides the innate interest in the rhenium compounds as organometallic DAT ligands, they serve as analogues of radioactive rhenium and technetium agents that could serve for SPECT imaging. Clearly, the conditions for metal incorporation (high temperature and pressure in organic solvent, chromatographic purification) are far from the characteristics of commercial ^{99m}Tc radiopharmaceutical kits, namely, mild reduction and complexation in aqueous solution. Stepwise investigation of the approach involved first determining the feasibility with respect to making the metal compounds and suitable biological properties. In a preliminary report (*29*), the technetium-99m analogue of one candidate, *N*-(4-$CpRe(CO)_3$-4-oxobutyl)norCCT (**5a**), was prepared and found to bind specifically to mouse striatum in vivo.

EXPERIMENTAL SECTION

General Comments. In general, the product was isolated by quenching of the reaction in an aqueous solution, exhaustive extraction with an organic solvent, drying over an anhydrous salt, filtration, evaporation on a rotary evaporator, and purification by flash chromatography (*30*) on Woelm silica gel (0.040−0.063 mm). Workup is indicated by the phrase "product isolation" followed, in parentheses, by a listing of quenching agent, extraction solvent, and drying agent if not $MgSO_4$, which is not listed and "purification" followed, in parentheses, by the elution solvent used in the flash chromatography.

All reactions were performed under a dry (Drierite) argon atmosphere. Unless otherwise specified, reagents and solvents used in this study were obtained from commercial sources (Aldrich, Strem, or Fluka) and were used without further purification. Temperatures refer to that of the reaction bath. Acetonitrile, triethylamine, methylene chloride, and toluene were distilled from calcium hydride under a nitrogen atmosphere. Oxalyl chloride was distilled from and stored over calcium hydride before use. Tetrahydrofuran (THF) was distilled from sodium/benzophenone ketal under a nitrogen atmosphere. Dimethylformamide (DMF) was dried with barium oxide and distilled from and stored over 4 Å molecular sieves. Methanol was distilled from magnesium activated with iodine and stored over 3 Å molecular sieves. Hexanes (mixed isomers) were distilled from $CaSO_4$ before use in flash chromatography. Butyllithium (Aldrich) was titrated using *N*-pivaloyl-*o*-toluidine according to a literature method (*31*).

Reaction progress was monitored by analytical thin-layer chromatography (TLC) on 0.25 mm Merck F-254 silica gel glass plates, visualizing with potassium permanganate or Dragendorff's reagent or quenching of UV illumination at 254 nm.

Melting points were determined using a Thomas−Hoover melting point apparatus and are uncorrected. ^{1}H and ^{13}C nuclear magnetic resoance (NMR) spectra were recorded on a U400, U500, or KECK750 Varian FT-NMR spectrometer. Chemical shifts (δ) are reported in parts per million (ppm) downfield from internal tetramethylsilane or by reference to proton resonances resulting from

incomplete deuteration of the NMR solvent. Low resolution electron impact (EI) mass spectra were obtained on a Finnigan MAT CH5 or VG Instruments 70-VSE spectrometer. High-resolution EI mass spectra were obtained on a Finnigan MAT 731 spectrometer. Both low-resolution and high-resolution chemical ionization (CI) mass spectra were obtained on a VG Instruments 70-VSE spectrometer. All fast atom bombardment (FAB) mass spectra were obtained on a VG Instruments ZAB-SE mass spectrometer. Elemental and DSC analyses were performed by the Microanalytical Service Laboratory of the University of Illinois.

Ferrocenecarbonyl chloride (*32*) and cyclopentadienyltricarbonyl rhenium carbonyl chloride (*33*) have been previously prepared. Ferrocenecarboxylic acid is available commercially, whereas cyclopentadienyltricarbonyl rhenium carboxylic acid was prepared by DLT reaction of 1,1′-methoxycarbonylferrocene followed by saponification. Iodocyclopentadienyltricarbonyl rhenium was prepared by an existing method (*34*). 8-Methyl-3β-[4-(trimethylstannanyl)phenyl]-8-azabicyclo[3.2.1]octane-2-carboxylic acid methyl ester (*35*), 3β-[4-chlorophenyl]-8-azabicyclo-[3.2.1]octane-2-carboxylic acid methyl ester (nor-CCT, **1**) (*36*), and 1-(*tert*-butyldimethylsiloxy)-4-iodobutane (**17**) (*37*) were prepared as previously described. Reactions performed using palladium catalysts were degassed using a standard freeze−pump−thaw method.

Cautionary Note for the DLT Reactions (*23*). Pressure tubes were placed within a specially made solid aluminum block containing holes drilled deep enough to admit the tubes to about three-fourths of their height and wide enough to allow room for some added mineral oil. The tubes and aluminum base were covered with a matching hollow aluminum screw cap, equipped with a small hole aligned with one drilled in the base (to the same depth as those for the pressure tubes) to hold a metal thermometer. This containment device minimized the potential danger of explosions during heating, allowed for the efficient stirring of the reactions, and enabled the reaction temperature to be monitored readily. All manipulations of sealed reaction tubes during and after the reactions were done in a fume hood with suitable protective equipment: blast shield, full face visor, and heavy gloves.

(4-Bromobutanoyl)ferrocene (4) (*38*). To a suspension of aluminum chloride (1.40 g, 10.5 mmol) in CH_2Cl_2 (4 mL) was added 4-bromobutanoyl chloride (1.16 mL, 10.0 mmol) as a solution in CH_2Cl_2 (4 mL) dropwise via a cannulus at room temperature. After 2 h, the now homogeneous solution was cooled to −10 °C and added via a cannulus to a solution of ferrocene (1.86 g, 10.0 mmol) in CH_2Cl_2 (24 mL) cooled to 0 °C. The now purple solution was allowed to warm to room temperature and stirred for 16 h. This solution was then diluted with CH_2Cl_2 and poured over ice-H_2O. Product isolation (saturated $NaHCO_3$, CH_2Cl_2), filtration through Celite, and purification (R_f 0.45 in CH_2Cl_2) afforded an orange solid (2.78 g, 83%); mp 58.0−61.1 °C. This solid should be stored in the freezer to prevent decomposition. ^{1}H NMR ($CDCl_3$, 500 MHz): δ 4.81 (t, 2H, J = 1.80 Hz), 4.52 (t, 2H, J = 1.86 Hz), 4.22 (s, 5H), 3.57 (t, 2H, J = 6.23 Hz), 2.94 (t, 2H, J = 6.83 Hz), 2.27 (quin, 2H, J = 6.54 Hz). ^{13}C NMR ($CDCl_3$, 125 MHz): δ 203.0, 78.8, 72.3, 69.8, 69.2, 37.2, 34.0, 26.9. MS (CI, CH_4): m/z (relative intensity) 337 (M + 3, 29), 336 (M + 2, 27), 335 (M + 1, 29), 334 (M^+, 25), 255 (100). High-resolution mass spectroscopy (HRMS) calcd for $C_{14}H_{15}Br^{56}FeO$, 333.9656; found, 333.9656. Anal. Calcd for $C_{14}H_{15}BrFeO$: C, 50.19; H, 4.51; Br, 23.85. Found: C, 50.02; H, 4.19; Br, 24.20.

3β-(4-Chlorophenyl)-8-(4-ferrocenyl-4-oxobutyl)-8-azabicyclo[3.2.1]octane-2β-carboxylic Acid Methyl Ester (5). To a solution of **1** (246.4 mg, 0.881 mmol) and **4** (885.2 mg, 2.64 mmol) in toluene (12.3 mL) were added triethylamine (12.3 mL, 88.1 mmol) and KI (27.7 mg, 0.220 mmol) successively. The mixture was then heated to reflux and stirred overnight. After the solution was cooled to room temperature, all volatile material was removed in vacuo. Purification (R_f 0.14 in 2% Et_3N/18% Et_2O/80% hexanes) afforded an orange solid (318 mg, 68%). ^{1}H NMR ($CDCl_3$, 500 MHz): δ 7.23 (AA′ of AA′XX′, 2H, J_{AX} = 8.78 Hz, J_{AA} = 2.14 Hz), 7.19 (XX′ of AA′XX′, 2H, J_{AX} = 8.55 Hz, J_{XX} = 2.3 Hz), 4.80 (m, 2H), 4.48 (m, 2H), 4.22 (s, 5H), 3.73 (dd, 1H, J = 6.84, 2.67 Hz), 3.52 (s, 3H), 3.40 (dt, 1H, J = 6.62, 2.61 Hz), 2.95 (m, 3H), 2.65 (ddd, 1H, J = 16.77, 7.63, 5.97 Hz), 2.59 (td, 1H, J = 12.60, 3.4 Hz), 2.33 (m, 2H), 2.11 (m, 1H), 2.01 (m, 1H), 1.85 (tt, 1H, J = 13.83, 6.71 Hz), 1.66 (m, 4H). ^{13}C NMR ($CDCl_3$, 125 MHz): δ 204.8, 171.8, 141.8, 131.4, 128.6, 128.0, 79.1, 72.1, 72.0, 69.8, 69.4, 69.2, 62.6, 61.5, 52.7, 52.6, 51.0, 36.7, 34.0, 33.8, 26.0, 25.9, 23.4. MS (CI, CH_4): m/z (relative intensity) 534 (M + 1, 100), 292 (40), 255 (15), 228 (69). HRMS calcd for $C_{29}H_{33}Cl^{56}FeNO_3$, 534.1498; found, 534.1493.

[3β-(4-Chlorophenyl)-8-(4-ferrocenyl-4-oxobutyl)-8-azabicyclo[3.2.1]oct-2β-yl]methanol (6). To a solution of [3β-(4-chlorophenyl)-8-azabicyclo[3.2.1]oct-2-yl]-methanol (**2**, 36.3 mg, 0.144 mmol) and **4** (145 mg, 0.433 mmol) in toluene (1.7 mL) were added triethylamine (1.71 mL, 12.3 mmol) and KI (5.3 mg, 0.032 mmol) successively. The mixture was then heated to reflux and stirred overnight. After the mixture was cooled to room temperature, all volatile material was removed in vacuo. Purification (R_f 0.15 in 2% Et_3N/48% Et_2O/50% hexanes) afforded an orange solid (68.2 mg, 94%). ^{1}H NMR ($CDCl_3$, 500 MHz): δ 7.29 (m, 4H), 4.82 (m, 2H), 4.50 (t, 2H, J = 1.99 Hz), 4.21 (s, 5H), 3.77 (dd, 1H, J = 11.12, 2.06 Hz), 3.62 (dd, 1H, J = 6.65, 1.37 Hz), 3.49 (dt, 1H, J = 6.48, 3.24 Hz), 3.37 (dd, 1H, J = 11.14, 2.53 Hz), 3.10 (dt, 1H, J = 12.58, 5.95 Hz), 2.84 (td, 2H, J = 7.15, 2.03 Hz), 2.51 (td, 1H, J = 13.18, 3.10 Hz), 2.43 (t, 2H, J = 7.07 Hz), 2.10 (m, 2H), 1.95 (quin, 2H, J = 7.16 Hz), 1.75 (m, 2H), 1.66 (ddd, 1H, J = 12.80, 5.40, 3.00 Hz), 1.52 (dq, 1H, J = 5.83, 2.61 Hz). ^{13}C NMR ($CDCl_3$, 189 MHz): δ 204.0, 141.1, 131.8, 129.7, 128.3, 78.8, 72.2, 72.1, 69.8, 69.3, 69.2, 66.9, 65.1, 60.1, 52.9, 45.3, 37.0(2), 36.8, 26.6, 25.4, 23.0. MS (FAB): m/z (relative intensity) 506 (M + 1, 2), 460 (4), 424 (2), 366 (3), 307 (35), 289 (17), 154 (100), 136 (56). HRMS calcd for $C_{28}H_{33}Cl^{56}FeNO_2$, 506.1549; found, 506.1548.

3β-(4-Iodophenyl)-8-(4-ferrocenyl-4-oxobutyl)-8-azabicyclo[3.2.1]octane-2β-carboxylic Acid Methyl Ester (7). To a solution of 3β-(4-iodophenyl)-8-azabicyclo-[3.2.1]octane-2β-carboxylic acid methyl ester (norCIT (**3**), 180 mg, 0.485 mmol) and **4** (812 mg, 2.42 mmol) in toluene (20 mL) were added triethylamine (11.5 mL, 82.6 mmol) and KI (13.6 mg, 0.108 mmol) successively. The mixture was then heated to reflux and stirred overnight. After the mixture was cooled to room temperature, all volatile material was removed in vacuo. Purification (R_f 0.24 in 2% Et_3N/28% Et_2O/70% hexanes) afforded an orange solid (210 mg, 69%). ^{1}H NMR ($CDCl_3$, 500 MHz): δ 7.29 (AB, 4H, J_{AB} = 8.45 Hz), 4.80 (m, 2H), 4.48 (m, 2H), 4.22 (m, 5H), 3.73 (dd, 1H, J = 6.00, 3.10 Hz), 3.52 (s, 3H), 3.39 (dt, 1H, J = 5.80, 2.08 Hz), 2.94 (m, 3H), 2.64 (ddd, 1H, J = 16.54, 7.38, 6.00 Hz), 2.57 (td, 1H, J = 12.57, 2.43 Hz), 2.33 (m, 2H), 2.11 (m 1H), 2.00 (m, 1H), 1.84 (tt, 1H, J = 13.57, 6.79 Hz), 1.66 (m, 4H). ^{13}C NMR ($CDCl_3$, 125 MHz): δ 204.7, 171.8, 143.1, 136.9,

129.5, 127.9, 79.3, 72.2, 72.1, 69.8, 69.4, 69.3, 62.8, 61.4, 52.7, 52.6, 51.0, 36.8, 34.0, 33.9, 26.1, 26.0, 23.5. MS (CI, CH_4): *m*/*z* (relative intensity) 626 (M + 1, 100), 384 (61), 22 (74). HRMS calcd for $C_{29}H_{33}I^{56}FeNO_3$, 626.0855; found, 626.0846.

8-(3-Benzyloxycarbonyl-propyl)-3*β*-(4-Chlorophenyl)-8-azabicyclo[3.2.1]octane-2*β*-carboxylic Acid Methyl Ester (8). To a solution of **1** (1.20 g, 4.30 mmol) and 4-bromobutyric acid benzyl ester (1.32 g, 5.10 mmol) in toluene (40 mL) were added triethylamine (5 mL) and KI (50.0 mg, 0.397 mmol) successively. The mixture was then heated to reflux and stirred overnight. After the mixture was cooled to room temperature, all volatile material was removed in vacuo. Purification (5% Et_3N/30% Et_2O/65% hexanes) afforded a colorless oil (1.4 g, 75%). ^{1}H NMR ($CDCl_3$, 300 MHz): δ 7.35 (m 5H), 7.21 (dd, 4H, J = 8.7 Hz), 5.12 (s, 2H), 3.65 (m, 1H), 3.42 (s, 3H), 3.39 (m, 1H), 2.90 (m, 2H), 2.60−2.40 (m, 4H), 2.27 (m, 2H), 2.00 (m, 2H), 1.85−1.60 (m, 4H).

8-(3-Carboxypropyl)-3*β*-(4-Chlorophenyl)-8-azabicyclo[3.2.1]octane-2*β*-carboxylic Acid Methyl Ester (9). A solution of **8** (1.00 g, 2.20 mmol) and 100 mg of 3% Pd/C in methanol (20 mL) was stirred under an atmosphere of hydrogen (35 psi) for 2 h. Filtration over Celite and removal of the solvent gave **9** as a colorless oil (740 mg, 95%), which was used without further purification. ^{1}H NMR (CD_3COCD_3, 300 MHz): δ 7.29 (dd, 4H, J = 8.4 Hz), 4.3 (m, 1H), 3.75−3.55 (m, 2H), 3.40 (s, 3H), 3.35 (m, 1H), 3.20−3.05 (m, 2H), 2.74 (dt, 1H, J = 12.8, 5.0 Hz), 2.48−2.10 (m, 6H), 1.98−1.85 (m, 3H).

3*β*-(4-Chlorophenyl)-8-(4-cyclopentadienyltricarbonyl rhenium butanoyl)-8-azabicyclo[3.2.1]octane-2*β*-carboxylic Acid Methyl Ester (10). $(Et_4N)_2[ReBr_3(CO)_3]$ (50 mg, 0.065 mmol) was dissolved in acetonitrile (2 mL) and treated with silver trifluoromethanesulfonate (53.4 mg, 0.208 mmol) in one portion. The mixture was stirred for 5 min, and the yellow silver bromide precipitate was removed by filtration using a Pasteur pipet fitted with a cotton plug. The resulting colorless solution was added directly to a previously prepared solution containing **9** (40.4 mg, 0.110 mmol) and triethylamine (36 μL, 0.260 mmol) in acetonitrile (1 mL). The mixing of the two solutions resulted in the formation of a white precipitate. To this suspension was added (102.5 mg, 0.195 mmol, 1.90 mmol CpN_2/g polymer) in one portion. The mixture was then fitted with a reflux condenser and heated to 80 °C for 45 min. After the mixture was cooled to room temperature, the mixture was concentrated under a stream of nitrogen. Purification (R_f 0.11 in 2% Et_3N/13% EtOAc/85% hexanes) afforded a pale yellow oil (38 mg, 70%). ^{1}H NMR ($CDCl_3$, 500 MHz): δ 7.28 (dd, 4H, J = 8.4 Hz), 5.55 (t, 2H, J = 2.3 Hz), 5.15 (t, 2H, J = 2.4 Hz), 3.67 (dd, 1H, J = 7.3, 3.3 Hz), 3.45 (s, 3H), 3.37 (dt, 1H, J = 6.6, 2.5 Hz), 2.94 (dt, 1H, J = 12.8, 5.0 Hz), 2.89 (t, 1H, J = 4.3 Hz), 2.58−2.40 (m, 4H), 2.28 (m, 2H), 2.07 (m, 1H), 1.98 (m, 1H), 1.81−1.56 (m, 4H). MS (FAB): *m*/*z* (relative intensity) 700 (M + 1, 4), 460 (4), 307 (36), 289 (17), 154 (100), 136 (59). HRMS calcd for $C_{27}H_{28}ClNO_7{}^{187}Re$, 700.1112; found, 700.1112.

Ferrocenecarbonyl Chloride (12). Ferrocenecarboxylic acid (200 mg, 0.869 mmol) was suspended in dry CH_2Cl_2 (5 mL) at 0 °C. Oxalyl chloride (100 μL, 1.13 mmol) was then added dropwise, followed by several drops of DMF. Vigorous gas evolution ensued, and the mixture became a dark red homogeneous solution. After 1 h, the solution was warmed to room temperature, and all of the volatile material was removed under a stream of nitrogen. The residue was dissolved in hot petroleum ether and filtered through paper. The petroleum ether was then removed in vacuo to afford a dark red solid (200 mg, 93%). This compound was used without purification directly in the preparation of compound **14**.

Cyclopentadienyltricarbonyl Rhenium Carbonyl Chloride (13). Cyclopentadienyltricarbonyl rhenium carboxylic acid (200 mg, 0.527 mmol) was suspended in dry CH_2Cl_2 (5 mL) at 0 °C. Oxalyl chloride (60 μL, 0.685 mmol) was then added dropwise, followed by several drops of DMF. Vigorous gas evolution ensued. After 1 h, the solution was warmed to room temperature, and all of the volatile material was removed under a stream of nitrogen. The residue was dissolved in hot hexanes and filtered through paper. The hexanes were then removed in vacuo to afford a white solid (120 mg, 62%). This compound was used without purification directly in the preparation of compound **14a**.

8-Methyl-3*β*-(4-ferrocenylphenyl)-8-azabicyclo-[3.2.1]octane-2*β*-carboxylic Acid Methyl Ester (14). To a solution of **12** (143 mg, 0.575 mmol) and benzyl bis-(triphenylphosphino) palladium chloride (2.2 mg, 2.9 μmol) in chloroform (1 mL) was added 8-methyl-3*β*-[4-(trimethylstannanyl)-phenyl]-8-azabicyclo[3.2.1]octane-2*β*-carboxylic acid methyl ester (*35*) (**11**, 255.1 mg, 0.604 mmol) as a solution in chloroform (1 mL). The flask was fitted with a reflux condenser, and the solution was heated to reflux for 1 h or until palladium black precipitated from the solution. After the solution was cooled to room temperature, the now red solution was placed directly on a silica column. Purification (R_f 0.26 in 2% Et_3N/58% Et_2O/40% hexanes) afforded a red solid (100 mg, 37%). ^{1}H NMR ($CDCl_3$, 500 MHz): δ 7.84 (AA′ of AA′XX′, 2H, J_{AX} = 8.47 Hz, J_{AA} = 1.95 Hz), 7.35 (XX′ of AA′XX′, 2H, J_{AX} = 8.10 Hz, J_{XX} = 2.28 Hz), 4.90 (m, 2H), 4.56 (m, 2H), 4.20 (s, 5H), 3.60 (dd, 1H, J = 7.47, 3.35 Hz), 3.52 (s, 3H), 3.40 (dt, 1H, J = 6.62, 3.31 Hz), 3.06 (dt, 1H, J = 12.76, 5.06 Hz), 2.98 (ddd, 1H, J = 5.01, 3.47, 1.11 Hz), 2.64 (td, 1H, J = 12.61, 2.93 Hz), 2.24 (m, 1H), 2.24 (s, 3H), 2.13 (m, 1H), 1.75 (m, 2H), 1.64 (ddd, 1H, J = 13.20, 9.43, 4.12 Hz). ^{13}C NMR ($CDCl_3$, 189 MHz): δ 198.7, 172.0, 147.3, 137.3, 128.1, 127.2, 78.5, 72.3, 72.2, 71.6, 71.5, 70.2, 65.3, 62.2, 52.6, 51.2, 42.0, 33.9, 33.8, 25.9, 25.2. MS (EI, 70 eV): *m*/*z* (relative intensity) 471 (M^+, 84), 97 (64), 83 (100). HRMS calcd for $C_{27}H_{29}{}^{56}FeNO_3$, 471.1497; found, 471.1493.

8-Methyl-3*β*-[4-(carbonyl cyclopentadienyltricarbonyl rhenium)phenyl]-8-azabicyclo[3.2.1]octane-2*β*-carboxylic Acid Methyl Ester (14a). To a solution of cyclopentadienyltricarbonyl rhenium carbonyl chloride (**13**, 38.5 mg, 96.8 μmol) and benzyl chloro-bis-(triphenylphosphino) palladium (0.37 mg, 0.48 μmol) in chloroform (1 mL) was added **11** (42.9 mg, 0.102 mmol) as a solution in chloroform (1 mL). The flask was fitted with a reflux condenser, and the solution was heated to reflux for 1 h or until palladium black precipitated from the solution. After the solution was cooled to room temperature, the yellow solution was placed directly on a silica column. Purification (R_f 0.24 in 2% Et_3N/68% Et_2O/30% hexanes) afforded a white solid (55 mg, 92%). ^{1}H NMR ($CDCl_3$, 500 MHz): δ 7.72 (AA′ of AA′XX′, 2H, J_{AX} = 8.32 Hz, J_{AA} = 1.95 Hz), 7.35 (XX′ of AA′XX′, 2H, J_{AX} = 8.35 Hz, J_{XX} = 2.15 Hz), 6.06 (t, 2H, J = 2.26 Hz), 5.44 (t, 2H, J = 2.30 Hz), 3.60 (dd, 1H, J = 6.56, 2.92 Hz), 3.51 (s, 3H), 3.39 (m, 2H), 3.04 (dt, 1H, J = 12.69, 5.20 Hz), 2.96 (m, 1H), 2.61 (td, 1H, J = 12.52, 2.78 Hz), 2.24 (m, 1H), 2.24 (s, 3H), 2.13 (m, 1H), 1.73 (m, 2H), 1.62 (ddd, 1H, J = 13.29, 9.51, 4.14 Hz). ^{13}C NMR ($CDCl_3$, 125 MHz): δ 192.0, 189.3, 171.9, 148.9, 134.8, 128.3, 127.6, 96.1, 89.7, 89.6, 85.2, 65.2, 62.1, 52.5, 51.2, 41.9, 33.9, 33.7, 25.8, 25.1. MS (EI, 70 eV): *m*/*z* (relative intensity) 621 (M^+,

24), 97 (53), 83 (100). HRMS calcd for $C_{25}H_{24}NO_6{}^{187}Re$, 621.1161; found, 621.1155.

(7*R*,5*S*)-7-(4-Chlorophenyl)-5-pyrrolidin-1-yl-cyclohept-1-enecarboxylic Acid Methyl Ester (15). To a solution of **1** (44.4 mg, 0.159 mmol) and 1-bromo-4-chlorobutane (91 μL, 0.794 mmol) in toluene (10 mL) were added triethylamine (250 μL, 1.79 mmol) and KI (6.6 mg, 0.040 mmol) successively. The mixture was then heated to reflux and stirred overnight. After the mixture was cooled to room temperature, all volatile material was removed. Purification (R_f 0.21 in 2% Et_3N/68% Et_2O/30% hexanes) afforded a colorless oil (34 mg, 58%). ^{1}H NMR ($CDCl_3$, 500 MHz): δ 7.24 (AA′ of AA′XX′, 2H, $J_{AX} = 8.49$ Hz, $J_{AA} = 2.30$ Hz), 7.19 (d, 1H, $J = 9.20, 5.95$ Hz), 7.15 (XX′ of AA′XX′, 2H, $J_{AX} = 8.39$ Hz, $J_{XX} = 2.41$ Hz), 4.02 (ddd, 1H, $J = 11.72, 6.77, 1.55$ Hz), 3.57 (s, 3H), 2.78 (ddtd, 1H, $J = 14.57, 12.35, 6.20, 1.94$ Hz), 2.57 (m, 6H), 2.28 (dddd, 1H, $J = 14.60, 9.06, 5.37, 3.01$ Hz), 2.09 (m, 2H), 1.95 (ddd, 1H, $J = 14.29, 12.06, 9.88$ Hz), 1.77 (m, 5H). ^{13}C NMR ($CDCl_3$, 125 MHz): δ 167.9, 143.4, 140.8, 134.7, 131.9, 128.6, 128.6, 59.8, 51.7, 50.7, 45.6, 36.6, 30.0, 23.3, 22.6. MS (EI, 70 eV): *m*/*z* (relative intensity) 333 (M^+, 11), 318 (4), 304 (10), 274 (6), 208 (48), 97 (100). HRMS calcd for $C_{19}H_{24}ClNO_2$, 333.1496; found, 333.1491.

Benzoylferrocene (16). To a suspension of aluminum chloride (376.3 mg, 2.82 mmol) in CH_2Cl_2 (1 mL) was added benzoyl chloride (312 μL, 2.69 mmol) as a solution in CH_2Cl_2 (1 mL) dropwise via a cannulus at room temperature. After 2 h, the homogeneous solution was cooled to −10 °C and added via a cannulus to a solution of ferrocene (500 mg, 2.69 mmol) in CH_2Cl_2 (5 mL) cooled to 0 °C. The now purple solution was allowed to warm to room temperature and stirred for 16 h. This solution was then diluted with CH_2Cl_2 and poured over ice-H_2O. Product isolation (saturated $NaHCO_3$, CH_2Cl_2), filtration through Celite, and purification (R_f 0.21 in CH_2Cl_2) afforded red crystals (631 mg, 81%); mp 107.3−108.9 °C. ^{1}H NMR ($CDCl_3$, 500 MHz): δ 7.90 (m, 2H), 7.55 (m, 1H), 7.47 (m, 2H), 4.91 (t, 2H, $J = 1.88$ Hz), 4.59 (t, 2H, $J = 2.00$ Hz), 4.21 (s, 5H). ^{13}C NMR ($CDCl_3$, 125 MHz): δ 199.2, 139.8, 131.5, 128.2, 128.1, 78.1, 72.5, 71.5, 70.2. MS (EI, 70 eV): *m*/*z* (relative intensity) 290 (M^+, 100), 197 (10), 141 (10), 133 (14), 56 (12). HRMS calcd for $C_{17}H_{14}{}^{56}FeO$, 290.0394; found, 290.0395.

4-*tert*-Butyldimethylsilyloxy-1-(cyclopentadienyltricarbonyl rhenium)butane (18). To a solution of cyclopentadienyltricarbonyl rhenium (335.3 mg, 1.00 mmol) in THF (10 mL) at −78 °C was added BuLi (617 μL, 1.00 mmol). After 3 h at −78 °C, **17** (628.6 mg, 2.00 mmol) was added and the temperature was maintained for an additional 2 h. The solution was then allowed to warm to room temperature and stirred overnight. Product isolation (H_2O, EtOAc) and purification (R_f 0.23 in 5% EtOAc/hexanes) afforded a colorless oil (250 mg, 48%). ^{1}H NMR ($CDCl_3$, 500 MHz): δ 5.24 (s, 4H), 3.62 (m, 2H), 2.43 (m, 2H), 1.58−1.54 (m, 4H), 0.89 (s, 9H), 0.05 (s, 6H). ^{13}C NMR ($CDCl_3$, 125 MHz): δ 194.6, 111.6, 83.5, 82.9, 62.7, 32.3, 28.2, 27.9, 25.9, 18.3,−5.3. MS (EI, 70 eV): *m*/*z* (relative intensity) 523 (M + 1, 18), 507 (16), 465 (41), 409 (15), 391 (100). HRMS calcd for $C_{18}H_{27}O_4{}^{187}ReSi$, 522.1236; found, 524.1399.

4-Hydroxy(cyclopentadienyltricarbonyl rhenium)-butane (19). To a solution of silyl ether **18** (240 mg, 0.460 mmol) in THF (5 mL) was added a 1 M solution of Bu_4NF in THF (920 μL, 0.920 mmol) dropwise at 0 °C. After 1 h at 0 °C, TLC indicated complete conversion of the starting material to a more polar compound. Product isolation (H_2O, Et_2O) and purification (R_f 0.26 in 50% EtOAc/hexanes) afforded a colorless oil (180 mg, 96%). ^{1}H NMR ($CDCl_3$, 500 MHz): δ 5.25 (s, 4H), 3.68 (m, 2H), 2.46 (m, 2H), 1.67−1.57 (m, 4H). ^{13}C NMR ($CDCl_3$, 125 MHz): δ 194.5, 111.3, 83.6, 82.8, 62.4, 32.2, 27.9 (2). MS (EI, 70 eV): *m*/*z* (relative intensity) 408 (M^+, 45), 380 (23), 348 (31), 322 (100), 304 (23), 263 (34), 85 (35), 71 (48), 57 (67). HRMS calcd for $C_{12}H_{13}O_4{}^{187}Re$, 408.0371; found, 408.0372.

4-*p*-Toluenesulfonyloxy-1-(cyclopentadienyltricarbonyl rhenium)butane (20). Alcohol **19** (90 mg, 0.221 mmol) was dissolved in pyridine (5 mL) and cooled to 0 °C. *p*-Toluenesulfonyl chloride (63.2 mg, 0.331 mmol) was added in one portion, and the solution was placed in the freezer overnight. Product isolation (saturated $CuSO_4$, Et_2O) and purification (R_f 0.33 in 30% EtOAc/Hexanes) afforded a yellow oil (100 mg, 81%). ^{1}H NMR ($CDCl_3$, 500 MHz): δ 7.79 (AA′ of AA′XX′, 2H, $J_{AX} = 8.36$ Hz, $J_{AA} = 2.05$ Hz), 7.36 (m, 2H), 5.24 (t, 2H, $J = 2.16$ Hz), 5.19 (t, 2H, $J = 2.26$ Hz), 4.04 (t, 2H, $J = 6.33$ Hz), 2.46 (s, 3H), 2.37 (m, 2H), 1.71 (m, 2H), 1.53 (m, 2H). ^{13}C NMR ($CDCl_3$, 125 MHz): δ 194.3, 144.9, 132.9, 129.9, 127.9, 110.4, 83.7, 82.9, 69.8, 28.4, 27.6, 27.4, 21.6. MS (EI, 70 eV): *m*/*z* (relative intensity) 562 (M^+, 68), 534 (63), 478 (51), 332 (100), 91 (52). HRMS calcd for $C_{19}H_{19}O_6S^{187}Re$, 562.0460; found, 562.0458.

3β-(4-Chlorophenyl)-8-(4-cyclopentadienyltricarbonyl rhenium-butyl)-8-azabicyclo[3.2.1]octane-2β-carboxylic Acid Methyl Ester (21). To a solution of **1** (49.8 mg, 0.178 mmol) and tosylate **20** (100 mg, 0.178 mmol) in toluene (10 mL) were added triethylamine (250 μL, 1.79 mmol) and KI (5.6 mg, 0.045 mmol) successively. The mixture was then heated to reflux and stirred overnight. After the solution had cooled to room temperature, all volatile material was removed in vacuo. Purification (R_f 0.24 in 2% Et_3N/28% Et_2O/70% hexanes) afforded a yellow oil (61 mg, 51%). ^{1}H NMR ($CDCl_3$, 500 MHz): δ 7.23 (AA′ of AA′XX′, 2H, $J_{AX} = 8.59$ Hz, $J_{AA} = 2.29$ Hz), 7.18 (XX′ of AA′XX′, 2H, $J_{AX} = 8.54$ Hz, $J_{XX} = 2.59$ Hz), 5.24 (m, 4H), 3.66 (dd, 1H, $J = 7.12, 3.29$ Hz), 3.48 (s, 3H), 3.38 (dt, 1H, $J = 6.63, 3.32$ Hz), 2.97 (dt, 1H, $J = 12.80, 5.06$ Hz), 2.89 (m, 1H), 2.54 (td, 1H, $J = 12.37, 2.99$ Hz), 2.39 (m, 2H), 2.25 (ABt, 2H, $J_{AB} = 12.19$ Hz, $J_t = 6.68$ Hz), 2.09 (tdd, 1H, $J = 12.70, 7.10, 4.09$ Hz), 1.99 (tdd, 1H, $J = 12.76, 6.57, 4.66$ Hz), 1.71 (ddd, 1H, $J = 13.35, 9.45, 4.28$ Hz), 1.65 (dddd, 1H, $J = 12.45, 4.74, 3.40, 1.18$ Hz), 1.61 (ddd, 1H, $J = 13.39, 9.43, 4.28$ Hz), 1.52 (m, 2H), 1.43 (m, 2H). ^{13}C NMR ($CDCl_3$, 125 MHz): δ 194.6, 171.9, 141.8, 131.4, 128.7, 128.0, 111.8, 83.6, 82.9, 82.8, 62.9, 61.3, 52.9, 52.8, 51.0, 34.0, 33.8, 29.2, 28.5, 27.9, 26.0. MS (EI, 70 eV): *m*/*z* (relative intensity) 669 (M^+, 62), 638 (9), 610 (14), 458 (51), 429 (38), 292 (100), 97 (56). HRMS calcd for $C_{27}H_{29}ClNO_5{}^{187}Re$, 669.1292; found, 669.1297.

8-Methyl-3β-[4-(Cyclopentadienyltricarbonyl rhenium)phenyl]-8-azabicyclo[3.2.1]octane-2β-carboxylic Acid Methyl Ester (22). Compound **11** (70 mg, 0.166 mmol) and iodocyclopentadienyltricarbonyl rhenium (33.4 mg, 0.166 mmol) were dissolved in DMF (5 mL) at room temperature. Bis(triphenylphosphino)-dichloro palladium (2.3 mg, 3.3 μmol) was added to the solution, which was subsequently degassed and stirred overnight. Product isolation (saturated LiCl, Et_2O) and purification (R_f 0.22 in 2% Et_3N/68% Et_2O/30% hexanes) afforded a white powder (63 mg, 64%). ^{1}H NMR ($CDCl_3$, 400 MHz): δ 7.22 (AA′ of AA′XX′, 2H, $J_{AX} = 8.40$ Hz, $J_{AA} = 2.20$ Hz), 7.14 (m, 2H), 5.64 (m, 2H), 5.29 (m, 2H), 3.49 (dd, 1H, $J = 6.80, 2.80$ Hz), 3.40 (s, 3H), 3.29 (tt, 1H, $J = 6.40, 3.20$ Hz), 2.93 (dt, 1H, $J = 12.40, 5.20$ Hz), 2.83 (m, 1H), 2.50 (td, 1H, $J = 12.40, 2.80$ Hz), 2.15 (s, 3H), 2.12 (m, 1H), 2.03 (m, 1H), 1.64 (m, 2H), 1.54 (ddd,

1H, J = 13.20, 9.60, 4.40 Hz). ^{13}C NMR ($CDCl_3$, 100 MHz): δ 194.6, 172.5, 144.2, 129.5, 128.1, 126.4, 109.4, 84.6, 84.5, 82.0, 81.9, 65.7, 62.6, 53.1, 51.6, 42.3, 34.3, 33.9, 26.3, 25.5. MS (EI, 70 eV): *m/z* (relative intensity) 593 (M^+, 73), 565 (15), 534 (19), 97 (68), 83 (100). HRMS calcd for $C_{24}H_{24}NO_5{}^{187}Re$, 593.1212; found, 593.1212.

Typical Experimental Procedure for DLT Reactions (See Cautionary Note at the Start of the Experimental Section). Reactions were performed in 4 mL threaded pressure tubes sealed with Teflon screw caps with O-rings (all purchased from Ace Glass). An egg-shaped (1 cm) stir bar was used to stir each reaction. Potassium perrhenate (1 molar equiv), chromium hexacarbonyl (5.61 equiv), chromium chloride (2.01 equiv), and the appropriate ferrocene (3.13 equiv) were combined in an oven-dried 4 mL pressure tube containing a magnetic stir bar. Dry methanol (500 μL) was added, and the tube was flushed with argon and then rapidly sealed. The heterogeneous mixture was placed in the reaction vessel described above and heated to 160 °C for 30 min. The tube was then carefully removed and placed directly into a water bath at room temperature: the solution was homogeneous when it came out of the reaction vessel. After 10 min, ice was added to the bath. Following an additional 10 min, the tube was transferred to a −78 °C bath before it could safely be opened. The reaction mixture was then diluted with CH_2Cl_2 and transferred to a 20 mL scintillation vial. The volatile components were removed under a stream of nitrogen, and the residue was purified on silica.

3β-(4-Chlorophenyl)-8-(4-cyclopentadienyltricarbonyl rhenium-4-oxobutyl)-8-azabicyclo[3.2.1]octane-2β-carboxylic Acid Methyl Ester (5a). The typical procedure for the DLT reaction, given above, was used with potassium perrhenate (8.7 mg, 0.030 mmol), chromium hexacarbonyl (36.9 mg, 0.168 mmol), chromium chloride (9.5 mg, 0.060 mmol), and ferrocene **5** (50 mg, 0.094 mmol). Purification (2% Et_3N/48% Et_2O/50% hexanes) afforded a dark brown oil (9.7 mg, 47%). ^{1}H NMR data for this compound were identical to that previously reported in the literature (*33*).

[3β-(4-Chlorophenyl)-8-(4-cyclopentadienyltricarbonyl rhenium-4-oxobutyl)-8-azabicyclo[3.2.1]oct-2β-yl]methanol (6a). The typical procedure for the DLT reaction, given above, was used with potassium perrhenate (11.0 mg, 0.038 mmol), chromium hexacarbonyl (46.8 mg, 0.213 mmol), chromium chloride (12.1 mg, 0.076 mmol), and ferrocene 6, 60 mg, 0.119 mmol). Purification (R_f 0.16 in 2% Et_3N/68% Et_2O/30% hexanes) afforded a dark brown oil (6.6 mg, 27%). ^{1}H NMR ($CDCl_3$, 500 MHz): δ 7.28 (m, 4H), 6.05 (ddt, 2H, J = 9.06, 3.14, 1.67 Hz), 5.40 (m, 2H), 3.75 (dd, 1H, J = 11.27, 2.23 Hz), 3.57 (dd, 1H, J = 6.94, 2.08 Hz), 3.45 (dt, 1H, J = 6.48, 2.86 Hz), 3.33 (dd, 1H, J = 11.12, 2.58 Hz), 3.09 (dt, 1H, J = 12.57, 5.95 Hz), 2.72 (ABt, 2H, J_{AB} = 16.88 Hz, J_t = 7.20 Hz), 2.47 (td, 1H, J = 13.13, 3.24 Hz), 2.36 (t, 2H, J = 6.93 Hz), 2.08 (m, 2H), 1.91 (quin, 2H, J = 7.25 Hz), 1.73 (m, 2H), 1.64 (ddd, 1H, J = 12.84, 5.59, 2.90 Hz), 1.50 (dq, 1H, J = 6.12, 2.37 Hz). ^{13}C NMR ($CDCl_3$, 125 MHz): δ 194.9, 191.9, 141.1, 131.9, 129.7, 128.4, 96.0, 88.0, 87.9, 85.5, 85.3, 66.9, 65.1, 60.2, 52.5, 45.3, 36.9, 36.7, 36.3, 26.5, 25.4, 23.0. MS (FAB): *m/z* (relative intensity) 656 (M + 1, 11), 307 (31), 289 (16), 154 (100), 136 (72). HRMS calcd for $C_{26}H_{28}ClNO_5{}^{187}Re$, 656.1214; found, 656.1223.

3β-(4-Iodophenyl)-8-(4-cyclopentadienyltricarbonyl rhenium-4-oxobutyl)-8-azabicyclo[3.2.1]octane-2β-carboxylic Acid Methyl Ester (7a). The typical procedure for the DLT reaction, given above, was used with potassium perrhenate (4.6 mg, 0.016 mmol), chromium hexacarbonyl (21.1 mg, 0.096 mmol), chromium chloride (5.1 mg, 0.032 mmol), and ferrocene **7** (10 mg, 0.016 mmol). Purification (R_f 0.26 in 2% Et_3N/28% Et_2O/70% hexanes) afforded a dark brown oil (6.5 mg, 52%). ^{1}H NMR ($CDCl_3$, 500 MHz): δ 7.58 (AA′ of AA′XX′, 2H, J_{AX} = 8.46 Hz, J_{AA} = 2.15 Hz), 7.00 (m, 2H), 6.06 (ABt, 2H, J_{AB} = 3.08 Hz, J_t = 1.62 Hz), 5.39 (dtd, 2H, J = 10.95, 2.76, 1.72 Hz), 3.66 (m, 1H), 3.48 (s, 3H), 3.36 (m, 1H), 3.10 (ABd, 2H, J_{AB} = 7.29 Hz, J_d = 4.76 Hz), 2.92 (m, 2H), 2.83 (dt, 1H, J = 16.89, 7.38 Hz), 2.55 (m, 2H), 2.27 (t, 2H, J = 6.10 Hz), 2.07 (m, 1H), 1.98 (m, 1H), 1.70 (m, 4H). ^{13}C NMR ($CDCl_3$, 125 MHz): δ 195.9, 192.0, 171.9, 143.0, 136.9, 129.4 (2), 96.4, 88.1, 88.0, 85.5, 85.0, 62.9, 61.2, 58.4, 52.5, 52.2, 51.0, 35.9, 33.9, 26.0, 25.9, 23.5. MS (CI, CH_4): *m/z* (relative intensity) 776 (M + 1, 95), 650 (18), 397 (100), 271 (19). HRMS calcd for $C_{27}H_{28}INO_6{}^{187}Re$, 776.0519; found, 776.0523.

8-Methyl-3β-[4-(carbonyloxycyclopentadienyltricarbonyl rhenium)phenyl]-8-azabicyclo[3.2.1]octane-2β-carboxylic Acid Methyl Ester (14a). The typical procedure for the DLT reaction, given above, was used with potassium perrhenate (3.3 mg, 0.011 mmol), chromium hexacarbonyl (14 mg, 0.064 mmol), chromium chloride (3.6 mg, 0.023 mmol), and ferrocene **14** (5.6 mg, 0.012 mmol). Purification (R_f 0.24 in 2% Et_3N/68% Et_2O/30% hexanes) afforded a dark brown oil (3.1 mg, 42%). ^{1}H NMR data for this compound were identical to those for the compound synthesized by palladium coupling described above.

Benzoylcyclopentadienyltricarbonyl Rhenium (16a). The typical procedure for the DLT reaction, given above, was used with potassium perrhenate (31.9 mg, 0.110 mmol), chromium hexacarbonyl (135.9 mg, 0.618 mmol), chromium chloride (35 mg, 0.221 mmol), and ferrocene **16** (100 mg, 0.345 mmol). Purification (R_f 0.06 in 10% EtOAc/hexanes) afforded an orange solid (25 mg, 50%), which could be recrystallized from ethanol/water to afford white crystals. Spectroscopic data for this compound matched that previously reported (*39*). ^{1}H NMR ($CDCl_3$, 500 MHz): δ 7.78 (m, 2H), 7.59 (m, 1H), 7.48 (m, 2H), 6.06 (t, 2H, J = 2.46 Hz), 5.46 (t, 2H, J = 2.33 Hz). MS (EI, 70 eV): *m/z* (relative intensity) 440 (M^+, 50), 412 (28), 356 (100), 328 (51), 302 (38). HRMS calcd for $C_{15}H_9O_4{}^{187}Re$, 440.0058; found, 440.0051.

Monoamine Transporter Binding Affinity Assays. Competitive binding assays were used to measure affinity of the new ligands to the DA, serotonin (5-HT), and norepinephrine (NE) transporters, using previously published methods (*40*−*42*). Briefly, brain tissue was obtained from adult male Sprague−Dawley rats, dissecting out striatum (caudate−putamen) for DAT and frontoparietal cortex for 5-HTT (serotonin transporter) and norepinephrine transporter (NET). Tissue was homogenized and washed in ice-cold assay buffer (see below); tissue pellets were stored at −70 °C until use and then suspended in assay buffer.

Radioligands for the competitive binding assay were [*propylene*-2,3-^{3}H]GBR-12935 (13 Ci/mmol; Kd = 1.0 nM) for DAT, [*phenyl*-6′-^{3}H]paroxetine (20 Ci/mmol, Kd = 150 pM) for 5-HTT, and [*N*-methyl-^{3}H]nisoxetine (85 Ci/mmol; Kd = 800 pM) for NET, all obtained from NEN/Dupont (Boston, MA).

Binding assays were carried out in triplicate at 100, 1000, and 10 000 nM with the following assay buffer, radioligands, and ligands for defining nonspecific binding: for DAT, Tris citrate buffer (50 mM, pH 7.4, containing 120 mM NaCl and 4 mM $MgCl_2$) with radioligand [^{3}H]GBR-12935 at a test concentration (*C*) of 400 pM, for 45 min on ice, using excess (2.5 μM) unlabeled

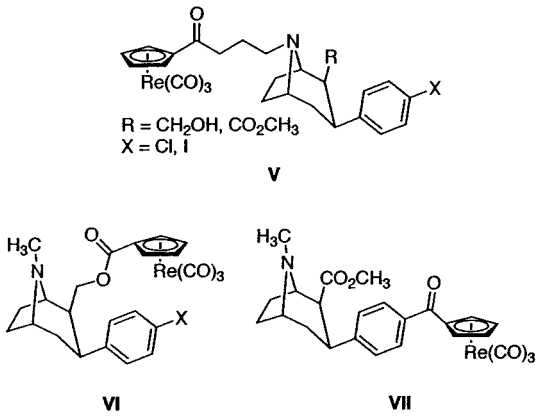


Figure 2. New $CpRe(CO)_3$ phenyltropane conjugates.

GBR-12909 (RBI, Natick, MA); for 5-HTT, Tris HCl buffer (50 mM, pH 7.4, with 120 mM NaCl and 5 mM KCl), radioligand [^{3}H]paroxetine ($C = 200$ pM) for 60 min at 20 °C, using excess (2 μM) fluoxetine HCl (Lilly Labs) as blank; for NET, Tris HCl buffer (50 mM, pH 7.4, with 300 mM NaCl and 5mM KCl), radioligand [^{3}H]nisoxetine ($C = 270$ pM) for 180 min at 4 °C, using excess (2 μM) desipramine HCl (RBI) as blank.

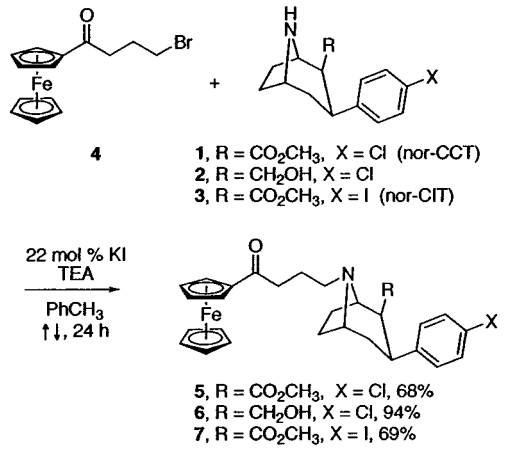
Concentration−inhibition curves were analyzed by the Allfit program (*43*) adapted to the Macintosh (*42*) to determine $IC_{50} \pm$ SE, and converted to $K_i \pm$ SE (nM) by the Cheng−Prusoff equation $K_i = IC_{50}/(1 + C/K_d)$ (*44*).

RESULTS AND DISCUSSION

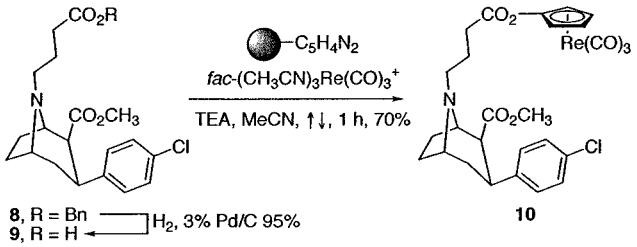
Compound Design. Structure−activity relationships in the phenyltropane series (*45*) show tolerance at the 2β-, 3β-, and 8-(*N*-) position with respect to DAT binding affinity; results of substitution on the 4′-(para) position of the 3β-phenyl group depend on the specific structures (*46*, *47*). For *N*-substitution, a chain length of four is in the effective range for obtaining high affinity ligands for DAT (*48*). Coupling this information with the requirement for an electron-withdrawing group on the cyclopentadienyltricarbonylmetal substituent for the DLT reaction to proceed efficiently (*23*) suggested the structures in Figure 2 (V−VII) as the primary targets. Compounds **10**, **21**, and **22** were selected as representative structures that could be made by techniques other than the DLT reaction. These three compounds were prepared to explore further structure−affinity relationships of $CpRe(CO)_3$-substituted tropanes as ligands for the monoamine transporters. Preliminary experiments to make $CpRe(CO)_3$ or $CpTc(CO)_3$ ester VI (Figure 2) by the DLT were largely unsuccessful (*49*), probably because of transesterification with the methanol solvent during the DLT reaction (*23*); thus, the preparation of compounds in this series was not explored further. Methanolysis of the C-2β methoxycarbonyl group in V and VII, on the other hand, regenerates the same compound and is of no consequence.

***N*-Alkylation of Nortropanes.** *N*-Alkylation of the nortropanes is readily accomplished with alkyl halides and sulfonates, using the weak base triethylamine; stronger bases, such as carbonates, result in significant epimerization of the C-2β methoxycarbonyl group to the thermodynamically more stable C-2α isomer (*50*). Systems with a four-atom linker between the nitrogen and the metallocene (**5**−**7**) were prepared using (4-halobutanoyl)ferrocenes (Scheme 2). These alkylating agents can be prepared by Friedel−Crafts monoacylation of ferrocene with the (4-halobutanoyl)chlorides, under carefully controlled conditions (*38*). Although (4-chlorobutanoyl)ferrocene was unreactive in tropane *N*-alkylations, the corresponding bromo compound **4** afforded the desired ferrocenyl phenyltropanes (**5**−**7**) in moderate yields.

Scheme 2



Scheme 3



Ester **10** was made by the three-component condensation (Scheme 3), through which carboxylic acids can be attached directly as acyloxy links to the cyclopentadienyl ring of $CpMet(CO)_3$ systems (*25*). The required carboxylic acid precursor **9** was prepared by alkylation of **1** with benzyl 4-bromobutanoate to afford the benzyl ester **8**. Removal of the benzyl ester protecting group by hydrogenolysis was initially accompanied by aromatic ring dechlorination. However, reducing the catalyst loading to 3% Pd/C resulted in selective removal of the benzyl ester. The acid **9** was converted to the desired $CpRe(CO)_3$ phenyltropane complex **10** in good yield by the three-component condensation, using *fac*-$(CH_3CN)_3Re(CO)_3^+$ and polymer-supported diazocyclopentadiene (*26*).

Substitution at the Para Position of the 3β-Phenyl Group. We initially intended to prepare the differentially substituted diaryl ketones **14** and **14a** (Scheme 4) from β-CIT (**I**) using a Suzuki carbonylative cross-coupling reaction (*51*, *52*). We tested a model Suzuki reaction of ferroceneboronic acid with 4-iodotoluene in the presence of bis(triphenylphosphine)dichloro palladium and potassium carbonate under one atmosphere of carbon monoxide, obtaining 20% yield of coupling product. The low yield might be explained by steric hindrance in the ferroceneboronic acid (*27*). Nevertheless, we attempted this reaction on the hydroxymethyl analogue of CIT (rather than on β-CIT itself, to avoid the risk of epimerization at C-2 by potassium carbonate), but we did not obtain any cross-coupled product.

We were able to prepare the desired ketones using the Stille reaction, however (*53*). Compound **11**, which has been used for the preparation of iodine-123-labeled β-CIT (**I**), can be synthesized directly from β-CIT by treatment with hexamethyldistannane in the presence of a palladium catalyst (*35*). Ferrocenecarbonyl chloride (**12**) and

Scheme 4

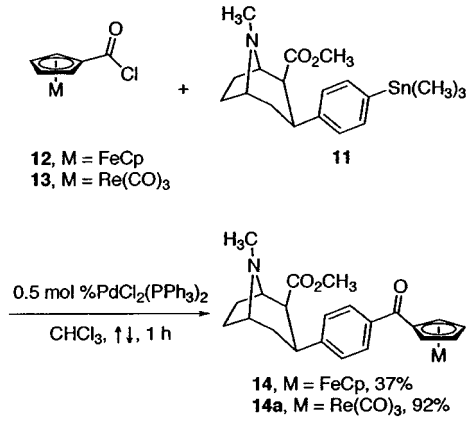
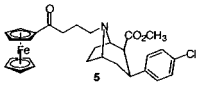
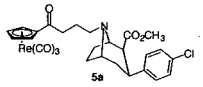
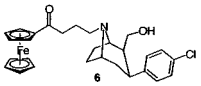
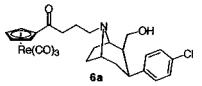
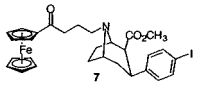
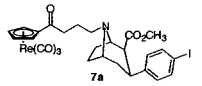
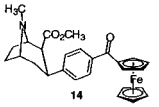
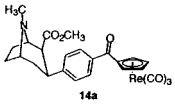


Table 1. Structures and Isolated Yields in the Direct DLT Reaction

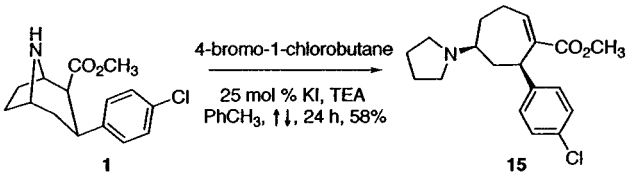
entry	reactant	Yield [a]	product
1		47%	
2		27%	
3		52%	
4		42%	
5		50%	

[a] Isolated yield following silica chromatography.

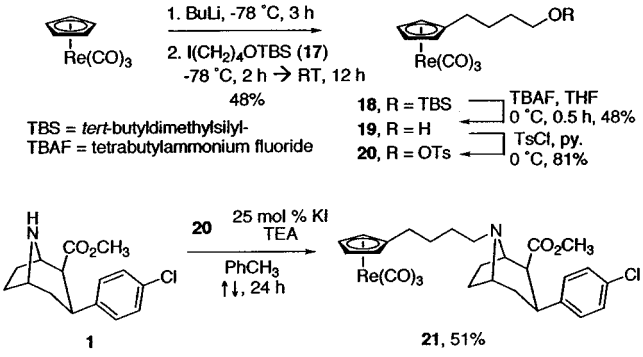
cyclopentadienyltricarbonyl rhenium carbonyl chloride (**13**) were prepared by treatment of the corresponding carboxylic acids with oxalyl chloride. They reacted with the tin precursor **11** and bis(triphenylphosphino)dichloro palladium to afford the desired biaryl ketones **14** and **14a** (Scheme 4). These reactions were performed on recrystallized acid chlorides; reaction yields were significantly lower with unpurified material.

DLT Reactions of Ferrocenyl Phenyltropanes. DLT reactions of ferrocenes with rhenium (Table 1; cf. Scheme 1) gave yields of 27−52%, in keeping with previously reported results on simpler molecules. The DLT reaction continues to display an impressive tolerance for functional groups. Previous reports had shown that ferrocene amides and monoketones were unaffected by this reaction, whereas aldehydes and alkynes underwent methanol addition (*25*). Esters underwent transesterification with the methanol solvent but successfully underwent the DLT (*25*). The present results show that alcohols, tertiary amines, and aryl halides also survive the high temperature and reducing conditions of this reaction. We considered that the extended conjugation in the biaryl ketone linkage of structure **VII** (Figure 2) might provide additional activation for the DLT reaction. As it turned out, ferrocene **14** underwent DLT with yields (42%) in the high range of examples tested, similar to the alkyl ketones (e.g., **5** and **7**). To determine whether the tropane part of the structure might be responsible

Scheme 5



Scheme 6



for lowering yields, the simpler benzophenone analogue **16** was synthesized. However, the DLT reaction reaction yield with this precursor was similar to that of **14**.

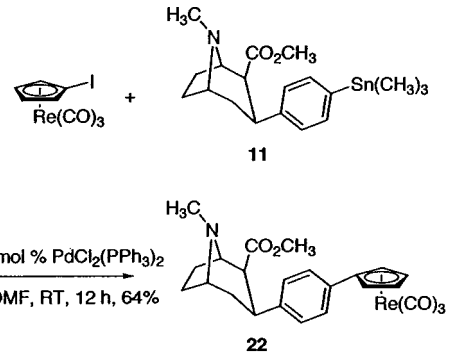
Directly Linked CpRe(CO)$_3$ Phenyltropanes. Although it would be difficult to prepare systems such as the alkyl CpRe(CO)$_3$ derivatives **21** and **22** by the DLT reaction because they lack the activating carbonyl link, our recently described approach using cyclopentadienyl tin precursors could ultimately be used to prepare the technetium-99m compounds (*28*). Initially, the planned synthetic route to these complexes was by alkylation of a suitable haloalkyl tropane precursor with the lithium anions generated from CpRe(CO)$_3$. However, when we attempted to prepare a potential 4-chlorobutyl-tropane alkylating precursor by the reaction of **1** with 1-bromo-4-chlorobutane, we obtained the ring-opened material **15** as the exclusive product (Scheme 5), presumably the result of double alkylation to form a spiro quaternary ammonium salt that then underwent β-elimination.

To avoid this difficulty, we reversed the sequence of alkylation steps, preparing first a 4-halobutyl CpRe(CO)$_3$ system (Scheme 6) and then coupling it to the *N*-8 position of the nortropane. The anion of CpRe(CO)$_3$, generated by treatment with butyllithium, underwent reaction with **17** to give 4-(*tert*-butyldimethylsilyloxy)-1-(cyclopentadienyltricarbonyl rhenium)-butane (**18**) (Scheme 6), which underwent smooth deprotection upon treatment with tetrabutylammonium fluoride. Reaction of the *p*-toluenesulfonate ester (**20**) of alcohol **19** with nortropane **1** afforded the desired CpRe(CO)$_3$ phenyltropane conjugate (Scheme 6).

The biarene **22**, an analogue of conjugate **14a**, was synthesized in a manner analogous to the method described previously (cf. Scheme 4). Iodocyclopentadienyltricarbonyl rhenium was coupled with aryl stannane **11** in the presence of a palladium catalyst to afford the desired biarene **22** (Scheme 7). The three-component condensation or our more recent approach using cyclopentadienyl tin precursors might provide an efficient route for preparing the analogous technetium-99m compound (*27*, *28*).

DAT Binding Affinities of CpRe(CO)$_3$ Phenyltropane Conjugates. The three monoamine transmitters—DA, 5-HT, and NE—have distinct functions in the brain,

Scheme 7



with corresponding significance for ligands that bind to them. For instance, disturbances in DA are associated with psychosis and motion disorders, and disturbances in 5-HT and NE are associated with mood disorders (*54*, *59*, *60*). Cocaine binds with similar affinity to DAT and 5-HTT (*55*), leading to its spectrum of pharmacological effects, and phenyltropanes display a range of selectivities, mostly for DAT and 5-HTT. A selective ligand for NET would be of interest because none is yet known that would be suitable for in vivo imaging. Selectivity is not so critical for quantitating DAT in the striatum, where the transporter is highly concentrated (>90%). Thus [^{123}I]β-CIT, which has comparable affinity to DAT and 5-HTT (*56*), is effective in measuring DAT in striatum but less so for detecting DAT in low-density extrastriatal areas.

A competitive in vitro radioligand binding assay was used to determine the affinity of the new tropane derivatives for the three monoamine transporters in rat brain tissue (Table 2, listed in order of decreasing DAT affinity). Overall, the DAT binding affinity pattern of the nine compounds reported in Table 2 is reflected in their affinities to the other two transporters, 5-HTT and NET: For comparison, β-CIT (**I**) has an affinity $K_i = 0.96$ nM for DAT in the same assay (*56*). The *N*-8-substituted tropanes (compounds **5**, **5a**, **6**, **6a**, **10**, and **21**) had high or at least moderate affinities, whereas the 3β-substituted systems (compounds **14**, **14a**, and **22**) had negligible affinities. Within the former, high-affinity group, however, there were some differences. The rank order for the six highest affinity compounds for the 5-HTT was nearly the same as that for the DAT, with the exception of compound **5**, which had a much higher affinity for 5-HTT, and compound **21**, which was fifth ranked on DAT but third ranked on 5-HTT. By contrast, the affinity for NET was uniformly low, with only ferrocene **6** having affinity in the low nanomolar range. (*56*, *25*, *27*, *28*).

The low affinity of the 3β-phenyl conjugates **14** and **14a** was unexpected in the light of the affinity (K_i 10−19 nM) of the biphenyl derivatives **III** (*47*). To see if this difference was a result of the overall bulk or to the different steric and electronic configuration of a biphenyl vs benzoyl type linkage, we synthesized and tested the biphenyl analogue **22**. The binding affinity was in the same range as the benzoyl analogues, showing that the ketone was not the deciding factor. These results agree with observed trends that the effect of substituents at the para position of the 3β-phenyl substituent cannot be predicted reliably with our current knowledge. Notably, the ferrocene precursors **5**, **6**, and **14** had binding profiles similar to the rhenium compounds, suggesting that the second cyclopentadienyl ligand on divalent iron in the sandwich compound has an effect similar to that of the tricarbonyl−rhenium(I) moiety. These properties make minimization of the ferrocene precursor in the final radiopharmaceutical necessary, either by purification or by clever choice of reaction conditions to selectively inactivate the iron compound.

As compared to other rhenium and technetium complexes targeting DAT, the *N*-substituted CpRe(CO)$_3$ analogues showed more favorable binding characteristics. The affinity of the rhenium analogue of TRODAT-1 is on the order of 14.1 nM for DAT and 360 nM for 5-HTT (*57*), and these are reflected in the modest in vivo target-to-background ratio (striatum/cerebellum = 3−3.5) as compared to a value of 4−7 for [^{123}I]β-CIT (*35*). The rhenium analogue of technepine was reported to have a K_i of 6.0 nM to DAT and 124 nM to 5-HTT (*58*), but quantitative in vivo data have not appeared. An imaging study in baboons with a tropane-CpRe(CO)$_3$ radiotracer labeled with ^{123}I showed an in vivo uptake and distribution similar to that of [^{99m}Tc]TRODAT-1 (*20*).

CONCLUSIONS

In this work, we present the first application of the DLT reaction for the direct preparation of CpRe(CO)$_3$−phenyltropane conjugates. In the new examples, we show that the DLT gives reasonable yields and continues to show broad functional group tolerance. In principle, the synthetic utility of this direct synthesis is greater for preparing radioactive rhenium and technetium compounds, where metal incorporation must be close to the final step in the synthesis. Technetium may be predicted to be more reactive chemically, although this is offset with technetium-99m because of the very low concentration of metal under practical conditions of labeling. Initial attempts to synthesize the technetium-99m analogue of **5a** have in fact shown that high levels of incorporation could be achieved, albeit at high temperature and pressure (*47*). Additional work will be needed to make the labeling conditions practical for routine radiopharmaceutical preparation. Of the CpRe(CO)$_3$−tropane conjugates we have investigated, those substituted at the *N*-8 position seem most promising; their affinity for the DAT in all cases was high, and their ferrocene precursors can be prepared in a convenient manner. By contrast, the 3β-conjugates showed low DAT binding. The modular nature

Table 2. Affinities (K_i, nM; Mean ± SEM) of Phenyltropane Conjugates

compd	metal	position	linkage	2β-	DAT	5-HTT	NET
5[a]	Fe	*N*-	ketone	ester	2.31 ± 0.16	0.22 ± 0.03	20.3 ± 4.7
5a[a]	Re	*N*-	ketone	ester	2.81 ± 0.50	0.63 ± 0.01	161 ± 32
6	Fe	*N*-	ketone	alcohol	3.66 ± 0.20	5.03 ± 0.35	2.30 ± 0.20
10	Re	*N*-	carboxylate	ester	4.18 ± 0.33	5.28 ± 0.21	74.0 ± 8.2
21	Re	*N*-	alkyl	ester	5.45 ± 0.64	1.14 ± 0.16	199 ± 30
6a	Re	*N*-	ketone	alcohol	13.0 ± 1.8	13.3 ± 1.0	39.2 ± 6.5
22	Re	3β-*para*	(direct)	ester	>10 000	~10 000	>10 000
14	Re	3β-*para*	ketone	ester	>30 000	>10 000	>30 000
14a	Re	3β-*para*	ketone	ester	>10 000	>10 000	>30 000

[a] Reported in ref *19*.

of these systems, however, allows considerable synthetic flexibility, which might be used to further improve the behavior of these compounds.

ACKNOWLEDGMENT

We are grateful for support of this research through a fellowship from the U.S. Army Breast Cancer Research Program (DAMD17-97-1-7292 to R.R.C.), a National Cancer Institute traineeship (PHS 5 T32 CA09067 to R.R.C.), and research grants from the Department of Energy (DE FG02 86ER60401 to J.A.K. and DE FG02 84ER60218 to R.M.B.) and Department of Veterans Affairs (Merit Review to R.B.I.). NMR spectra were obtained in the Varian Oxford Instrument Center for Excellence in NMR Laboratory. Funding for this instrumentation was provided in part from the W. M. Keck Foundation, the National Institutes of Health (PHS 1 S10 RR104444-01), and the National Science Foundation (NSF CHE 96-10502). Mass spectra were obtained on instruments supported by grants from the National Institute of General Medical Sciences (GM 27029), the National Institutes of Health (RR 01575), and the National Science Foundation (PCM 8121494).

LITERATURE CITED

(1) Kuhar, M. J., Sanchez-Roa, P. M., Wong, D. F., Dannals, R. F., Grigoriadis, D. E., Lew, R., and Milerger, M. (1990) Dopamine transporter: Biochemistry, pharmacology, and imaging. *Eur. J. Neurol. Suppl. Jpn. 30*, 15−20.

(2) Seibyl, J. P., Marek, K., Sheff, K., Zoghbi, S. S., Baldwin, R. M., Charney, D. S., van Dyck, C. H., and Innis, R. B. (1998) [^{123}I]β-CIT and [^{123}I]FPCIT SPECT measurement of dopamine transporters in healthy subjects and Parkinson's patients. *J. Nucl. Med. 39*, 1500−1508.

(3) Sawle, G., and Myers, R. (1993) Role of positron emission tomography in the assessment of human transplantation. *Trends Neurosci. 16*, 260−264.

(4) Tomac, A., Linqvist, E., Lin, L. F., Ogren, S., Young, D., Hoffer, B., and Olson, L. (1995) Protection and repair of the nigrostriatal dopaminergic system by GDNF in vivo. *Nature 373*, 335−339.

(5) Jankovic, J., McDermott, M., Carter, J., Gauthier, S., Goetz, C., Golbe, L., Huber, S., Koller, W., Olano, C., Shoulson, I., Stern, M., Tanner, C., Weiner, W., and Parkinson Study, G. (1990) Variable expression of Parkinson's disease: a baseline analysis of the DATATOP cohort. *Neurology 40*, 1529−1534.

(6) Carroll, F. I., Scheffel, U., Dannals, R. F., Boja, J. W., and Kuhar, M. J. (1995) Development of imaging agents for the dopamine transporter. *Med. Res. Rev. 15*, 419−444.

(7) Kung, H. F. (1996) Development of radiopharmaceuticals for imaging CNS receptors. *Current Directions in Radiopharmaceutical R&D*, Kluwer, London, pp 99−113.

(8) Kushner, S. A., McElgin, W. T., Kung, M. P., Mozley, P. D., Plossl, K., Meegalla, S. K., Mu, M., Dresel, S., Vessotskie, J. M., Lexow, N., and Kung, H. F. (1999) Kinetic modeling of ^{99m}Tc TRODAT-1: A dopamine transporter imaging agent. *J. Nucl. Med. 40*, 150−158.

(9) Mozley, P. D., Stubbs, J. B., Plossl, K., Dresel, S. H., Barraclough, E. D., Alavi, A., Araujo, L. I., and Kung, H. F. (1998) Biodistribution and dosimetry of TRODAT-1, a technetium-99m tropane for imaging dopamine transporers. *J. Nucl. Med. 39*, 2069−2076.

(10) Madras, B. K., Jones, A. G., Mahmood, A., Zimmerman, R. E., Garada, B., Holman, B. L., Davison, A., Blundell, P., and Meltzer, P. C. (1996) Technepine: a high-affinity ^{99m}Tc probe to label the dopamine transporter in brain by SPECT imaging. *Synapse 22*, 239−246.

(11) Chi, D. Y., O'Neil, J. P., Anderson, C. J., Welch, M. J., and Katzenellenbogen, J. A. (1994) Homodimeric and heterodimeric bis(amino thiol) oxometal complexes with rhenium(V) and technetium(V). Control of heterodimeric complex formation and an approach to metal complexes that mimic steroid hormones. *J. Med. Chem. 37*, 928−937.

(12) Hom, R. K., Chi, D. Y., and Katzenellenbogen, J. A. (1996) Heterodimeric bis(amino thiol) complexes of oxorhenium(V) and oxotechnetium(V) that mimic the structure of steroid hormones. Synthesis and stereochemical issues. *J. Org. Chem. 61*, 2624−2631.

(13) Hom, R. K., and Katzenellenbogen, J. A. (1997) Synthesis of a tetradentate oxorhenium(V) complex mimic of a steroidal estrogen. *J. Org. Chem. 62*, 6290−6297.

(14) Alberto, R., Egli, A., Abram, U., Hegetschweiler, K., and Gramlich (1994) Synthesis and reactivity of $[NEt_4]_2[ReBr_3(CO)_3]$—formation and structural characterization of the clusters $[NEt_4][Re_3(\mu 3\text{-}OH)(\mu\text{-}OH)_3(CO)_9]$ and $[NEt_4][Re_2(\mu\text{-}OH)_3(CO)_6]$ by alkaline titration. *J. Chem. Soc., Dalton Trans.* 2815−2820.

(15) Alberto, R., Schibli, R., Egli, A., Schubiger, A. P., and Abram, U. (1998) A novel organometallic aqua complex of technetium for the labeling of biomolecules—Synthesis of $[Tc\text{-}99m(OH_2)_3(CO)_3]^+$ from $[Tc\text{-}99m(TcO_4)]^-$ in aqueous solution and its reaction with a bifunctional ligand. *J. Am. Chem. Soc. 120*, 7987−7988.

(16) Alberto, R., Schibli, R., Schubiger, P. A., Abram, U., and Hubener, R. (1996) A simple single-step synthesis of $[Tc\text{-}99(Tc_3H_3)(CO)_{12}]$ From $[(TcO_4)\text{-}Tc\text{-}99]^-$ and its X-ray crystal structure—application to the production of no-carrier added $[(Re_3H_3)\text{-}Re\text{-}188(Co)_{12}]$. *Chem. Commun.* 1291−1292.

(17) Le Bideau, F., Kaloum, E. B., Haquette, P., Kernbach, U., Marrot, J., and Stephan, E. (2000) New and efficient routes to $CpRe(CO)_3$ substituted steroids. *Chem. Commun.* 211−212.

(18) Top, S., Morel, P., Pankowski, H., and Jaouen, G. (1996) Rapid and mild synthesis of $[Re_2(CO)_{10}]$ by reduction of $[NH_4][ReO_4]$ at atmospheric CO pressure. *J. Chem. Soc., Dalton Trans.* 3611−3612.

(19) Tamagnan, G., Gao, Y., Xu, L., Kula, N. S., Baldessarini, R. J., and Neumeyer, J. L. (1999) Nonisotopic surrogates for technetium as ligands for monoamine transporters. *Adv. Neurol. 80*, 99−103.

(20) Baldwin, R. M., Tamagnan, G., Zoghbi, S. S., Al-Tikriti, M. S., and Innis, R. B. (1999) Brain uptake and dopamine transporter binding of an I-123 labeled cyclopentadienyltricarbonylrhenium tropane conjugate. *J. Nucl. Med. 40*, 38P.

(21) Baldwin, R. M., Zea-Ponce, Y., Al-Tikriti, M. S., Zoghbi, S. S., Seibyl, J. P., Charney, D. S., Hoffer, P. B., Wang, S., Milius, R. A., Neumeyer, J. L., and Innis, R. B. (1995) Regional brain uptake and pharmacokinetics of [^{123}I]*N*-ω-fluoroalkyl-2β-carboxy-3β-(4-iodophenyl)nortropane esters in baboons. *Nucl. Med. Biol. 22*, 211−219.

(22) Wenzel, M. (1992) Tc-99m-Labeling of cymantrene-analogues with different substituents. A new approach to Tc-99m radiopharmaceuticals. *J. Labelled Compd. Radiopharm. 31*, 641−650.

(23) Spradau, T. W., and Katzenellenbogen, J. A. (1998) Preparation of cyclopentadienyltricarbonylrhenium complexes using a double ligand transfer reaction. *Organometallics 17*, 2009−2017.

(24) Spradau, T. W., and Katzenellenbogen, J. A. (1998) Protein and peptide labeling with (cyclopentadienyl)tricarbonyl rhenium and technetium. *Bioconjugate Chem. 9*, 765−772.

(25) Minutolo, F., and Katzenellenbogen, J. A. (1998) A convenient three-component synthesis of substituted cyclopentadienyl tricarbnyl rhenium complexes. *J. Am. Chem. Soc. 120*, 4514−4515.

(26) Minutolo, F., and Katzenellenbogen, J. A. (1999) A polymer-supported phosphazine as a stable and practical reagent in the three-component synthesis of cyclopentadienyl tricarbonyl rhenium Complexes. *Angew. Chem., Int. Ed. 38*, 1617−1620.

(27) Minutolo, F., and Ktzenellenbogen, J. A. (1998) Boronic acids in the three-component synthesis of carbon-substituted cyclopentadienyl tricarbonyl rhenium complexes. *J. Am. Chem. Soc. 120*, 13264−13265.

(28) Cesati, R. R., III, and Katzenellenbogen, J. A. (2001) One-pot formation of substituted cyclopentadienyl and indenyltricarbonyl rhenium complexes through in situ generation of cyclopentadienyl- and indenyltributylstannanes. *J. Am. Chem. Soc. 123*, 4093−4094.

(29) Tamagnan, G., Cesati, R. R., III, Zoghbi, S. S., Varrone, A., Al-Tikriti, M. S., Seibyl, J. P., Kula, N., Baldessarini, R.

J., Katzenellenbogen, J. A., Innis, R. B., and Baldwin, R. M. (2000) Labeling, dopamine transporter affinity, and brain uptake of the first cyclopentadienyltricarbonyl [^{99m}Tc]technetium tropane conjugate. *J. Nucl. Med. 41*, P38.

(30) Still, W. C., Kahn, M., and Mitra, A. (1978) Rapid chromatographic technique for preparative separations with moderate resolution. *J. Org. Chem. 43*, 2923−2926.

(31) Suffert, J. (1989) Simple Direct Titration of Organolithium Reagents Using *N*-Pivaloyl-*o*-toluidine and/or *N*-Pivaloyl-*o*-benzylaniline. *J. Am. Chem. Soc. 54*, 509−510.

(32) Wenzel, M., and Saidi, M. (1993) Brain affinity of ^{99m}Tc labeled esters of cytectrene carbonic acid. *J. Labelled Compd. Radiopharm. 33*, 77−80.

(33) Neumeyer, J. L., Tamagnan, G., and Gao, Y. (1997) Synthesis of ferrocenyl phenyltropane analogues and their radio-transformation to technetium neuroprobes for mapping monoamine reuptake sites. US Patent 5,700,446.

(34) Spradau, T. W., and Katzenellenbogen, J. A. (1998) Ligands for the estrogen receptor, containing cyclopentadienyltricarbonylrhenium units. *Bioorg. Med. Chem. Lett. 8*, 3235−3240.

(35) Baldwin, R. M., Zea-Ponce, Y., Zoghbi, S. S., Laruelle, M., Al-Tikriti, M. S., Sybirska, E. H., Neumeyer, J. L., Milius, R. A., Wang, S., Stabin, M., Smith, E. O., Charney, D. S., Hoffer, P. B., and Innis, R. B. (1993) Evaluation of the monoamine uptake site ligand [^{123}I]methyl 3β-(4-iodophenyl)tropane-2β-carboxylate ([^{123}I]β-CIT) in nonhuman primates: pharmacokinetics, biodistribution, and SPECT brain imaging coregistered with MRI. *Nucl. Med. Biol. 20*, 597−606.

(36) Boja, J. W., Kuhar, M. J., Kopajtic, M., Yang, E., Abraham, P., Lewin, A. H., and Carroll, F. I. (1994) Secondary amine analogues of 3β-(1′-substituted phenyl)tropane-2β-carboxylic acid esters and *N*-norcocaine exhibit enhanced affinity for serotonin and norepinephrine transporters. *J. Med. Chem. 37*, 1220−1223.

(37) Harusawa, S., Tomii, S., Takehisa, C., Ohishi, H., Yoneda, R., and Kurihara, T. (1992) [3,3]Sigmatropic ring expansion of cyclic thionocarbonates. VII. On the formation of eight-membered thionocarbonates as the intermediates. *Chem. Pharm. Bull. 40*, 2279−2282.

(38) Fort, Y., Caubère, P., Gautier, J. C., and Mondet, J. C. (1993) Synthesis in the ferrocenyl series I. Preparation of ω-haloalkanoylferrocenes. *J. Organomet. Chem. 452*, 111−113.

(39) Jones, S. S., Rausch, M. D., and Bitterwolf, T. E. (1993) A facile syntheic route to (η^5-benzoylcyclopentadienyl)metal complexes. *J. Organomet. Chem. 450*, 27−32.

(40) Kula, N. S., Baldessarini, R. J., Tarazi, F. I., Fisser, R., Wang, S., Trometer, J., and Neumeyer, J. L. (1999) [^{3}H]β-CIT: a radioligand for dopamine transporters in rat brain tissue. *Neuropharmacology 385*, 291−294.

(41) Tejani-Butt, S. M. (1992) [^{3}H]Nisoxetine: A radioligand for quantitation of norepinephrine uptake sites by autoradiography or by homogenate binding. *J. Pharmacol. Exp. Ther. 260*, 427−436.

(42) Baldessarini, R., Kula, N., Campbell, A., Bakthavachalam, V., Yuan, J., and Neumeyer, J. (1992) Prolonged D2 antidopaminergic activity of alkylating and nonalkylating derivatives of piperone in rat brain. *Mol. Pharmacol. 42*, 856−863.

(43) Munson, P., and Rodbard, D. (1980) LIGAND: A versatile computerized approach for characterization of ligand bindin systems. *Anal. Biochem. 107*, 220−239.

(44) Cheng, Y., and Prusoff, W. (1973) Relationship between the inhibition constant (Ki) and the concentration of inhibitor which causes 50% inhibition (IC_{50}) of an enzymatic reaction. *Biochem. Pharmacol. 22*, 3099−3108.

(45) Singh, S. (2000) Chemistry, design, and structure−activity relationship of cocaine antagonists. *Chem. Rev. 100*, 925−1024.

(46) Davies, H. M. L., Kuhn, L. A., Thornley, C., Matasi, J. J., Sexton, T., and Childers, S. R. (1996) Synthesis of 3β-aryl-8-azabicyclo[3.2.1]octanes with high binding affinity and selectivity for the serotonin transporter. *J. Med. Chem. 39*, 2554−2558.

(47) Tamagnan, G., Baldwin, R. M., Kula, N. S., Baldessarini, R. J., and Innis, R. B. (2000) Synthesis and monoamine transporter affinity of 2β-carbomethoxy-3β-(2″-, 3″-, and 4″-substituted) biphenyltropanes. *Bioorg. Med. Chem. Lett. 10*, 1783−1785.

(48) Tamagnan, G., Gao, Y., Wang, S., Kula, N. S., Baldessarini, R. J., and Neumeyer, J. L. (1997) Monoamine transporter affinity for *N*-substituted analogues of 2β-carbomethoxy-3β-(4′-iodophenyl)tropane (β-CIT). *Bioorg. Med. Chem. Lett. 7*, 337−340.

(49) Zoghbi, S. S., Tamagnan, G., Baldwin, R. M., Gao, Y., Neumeyer, J. L., Baldessarini, R., Charney, D. S., Seibyl, J. S., and Innis, R. B. (1997) Synthesis of a dopamine transporter binding cyclopentadiene phenyltropane conjugate complexed with Re and Tc-99m. *J. Nucl. Med. 38*, 100P.

(50) Clarke, R. L., Daum, S. J., Gambino, A. J., Aceto, M. D., Pearl, J., Levitt, M., Cumiskey, W. R., and Bogado, E. F. (1973) Compounds affecting the central nervous system. 4. β-Phenyltropane-2-carboxylic esters and analogues. *J. Med. Chem. 16*, 1260−1267.

(51) Ishiyama, T., Kizaki, H., Hayashi, T., Suzuki, A., and Miyaura, N. (1998) Palladium-catalyzed carbonylative cross-coupling reaction of aryl bromides with aryl electrophiles: Synthesis of biaryl ketones. *J. Org. Chem. 63*, 4726−4731.

(52) Ishiyama, T., Kizaki, H., Miyaura, N., and Suzuki, A. (1993) Synthesis of unsymmetrical biaryl ketones via palladium-catalyzed carbonylative cross-coupling reaction of arylboronic acids with iodoarenes. *Tetrahedron Lett. 34*, 7595−7598.

(53) Farina, V., Krishnamurthy, V., and Scott, W. J. (1998) *The Stille Reaction*, Wiley-Interscience, New York.

(54) Cooper, J. R., Bloom, F. E., and Roth, R. H. (1991) *The Biochemical Basis of Neuropharmacology*, 6th ed., Oxford University Press, New York.

(55) Boja, J. W., and Kuhar, M. J. (1989) [^{3}H]Cocaine binding and inhibition of [^{3}H]dopamine uptake is similar in both the rat striatum and nucleus accumbens. *Eur. J. Pharmacol. 173*, 215−217.

(56) Neumeyer, J. L., Baldessarini, R. J., Kula, N. S., and Tamagnan, G. (1998) Novel phenyltropanes: affinity to monoamine transporters in rat forebrain. *Progress in Alzheimer's and Parkinson's Disease*, Plenum Press, New York, pp 739−745.

(57) Kung, M.-P., Stevenson, D. A., Plossl, K., Meegalla, S. K., Beckwith, A., Essman, W. D., Mu, M., Lucki, I., and Kung, H. F. (1997) [^{99m}Tc]TRODAT-1: a novel Tc-99m complex as a dopamine transporter imaging agent. *Eur. J. Nucl. Med. 24*, 372−380.

(58) Meltzer, P. C., Blundell, P., and Madras, B. K. (1998) Structure activity relationships of inhibition of the dopamine transporter by 3-arylbicyclo[3.2.1]octanes. *Med. Chem. Res. 8*, 12−34.

(59) Baldessarini, R. J. (2001) Drugs and the treatment of psychiatric disorders: Antidepressant and antianxiety agents. In *Goodman and Gilman's The Pharmacological Basis of Therapeutics* (Hardman, J. G., Limbird, L. E., Gilman, A. G., Eds.) McGraw-Hill Press, New York, 10th ed. Chapter 19, pp 447−483.

(60) Baldessarini, R. J., and Tarazi, F. I. (2001) Drugs and the treatment of psychiatric disorders: Antipsychotic and antimanic agents. In *Goodman and Gilman's The Pharmacological Basis of Therapeutics* (Hardman, J. E., Limbird, L. E., Gilman, A. G., Eds.) McGraw-Hill Press, New York, 10th ed., Chapter 20, pp 485−520.

BC010011X

An Anti-CD33 Antibody–Calicheamicin Conjugate for Treatment of Acute Myeloid Leukemia. Choice of Linker

Philip R. Hamann,*,† Lois M. Hinman,† Carl F. Beyer,† Delores Lindh,† Janis Upeslacis,† David A. Flowers,‡ and Irwin Bernstein‡

Wyeth-Ayerst Research, 401 North Middletown Road, Pearl River, New York 10965 and Fred Hutchinson Cancer Research Center, 1124 Columbia Street, Seattle, Washington 98109. Received February 19, 2001; Revised Manuscript Received October 15, 2001

The anti-CD33 antibody, P67.6, has been chosen to target the potently cytotoxic calicheamicin antitumor antibiotics to acute myeloid leukemia (AML) due to the presence of CD33 on >80% of patient samples and its lack of expression outside the myeloid cell lineages, especially its lack of expression on pluripotent stem cells. Previous calicheamicin conjugates relied on the attachment of a hydrazide derivative to the oxidized carbohydrates that occur naturally on antibodies. This results in a "carbohydrate conjugate" capable of releasing active drug by hydrolysis of a hydrazone bond in the lysozomes where the pH is low. Conjugates have now been made that are formed by reacting a calicheamicin derivative containing an activated ester with the lysines of antibodies. This results in an "amide conjugate" that is stable to hydrolysis, leaving the disulfide that is present in all calicheamicin conjugates as the likely site of drug release from the conjugate. In this article, these two classes of calicheamicin–antibody conjugates are compared for potential use in AML with the anti-CD33 antibody P67.6. Conjugates of P67.6 are shown to require the site of hydrolytic release afforded by the carbohydrate conjugates in order to retain good potency and selectivity in vitro, in vivo, and ex vivo. The P67.6 carbohydrate conjugate of calicheamicin is selectively cytotoxic at <0.006 ng/mL of calicheamicin equivalents (cal equiv) toward HL-60 promyelocytic leukemia cells in tissue culture. Long-term, tumor-free survivors are seen in xenograft models when mice bearing HL-60 subcutaneous tumors are treated with the P67.6 carbohydrate conjugate at a dose of 300 μg/kg cal equiv given three times. This conjugate also selectively inhibits the formation of colonies from AML marrow samples at 2 ng/mL cal equiv. The P67.6 carbohydrate conjugate of calicheamicin therefore appears to have promise as an antibody-targeted chemotherapeutic agent for CD33-positive diseases such as AML.

INTRODUCTION

The calicheamicins are highly potent antitumor antibiotics of the enediyne family. Originally isolated from a broth extract of the soil microorganism *M. echinospora* ssp. *calichensis*, the calicheamicins were detected in a screen for potent DNA damaging agents (*1*). The parent of this family of xenobiotics, calicheamicin γ_1^I (**1**, Figure 1), has been shown to associate with the minor groove of DNA and, following reduction with glutathione (*2*), to cause sequence-specific, double-stranded DNA cleavage (*3*, *4*). Due to their unique mode of action and potency, several analogues of the calicheamicins have been tested in preclinical models as potential antitumor agents. Their development as single agent therapies has not been pursued because of delayed toxicities that limit the therapeutic dose range for treatment. However, their potency makes them ideal for antibody-targeted chemotherapy, where limits in antigen expression make the potency of the cytotoxic agent crucial (*5*, *6*).

A series of conjugates of the calicheamicins and the CTM01 anti-MUC1 antibody has previously been reported (*7*, *8*). Initial examination of the structural requirement for the calicheamicin portion of the conjugate led to the selection of the "carbohydrate conjugate" (**4**) which contains NAc-gamma calicheamicin[1] as the calicheamicin core, a disulfide stabilized by two adjacent methyl groups, and a hydrazone linkage to the oxidized carbohydrates of the antibody as a site of hydrolytic release. It is unknown why the N-acylated calicheamicin derivatives make better conjugates, but the stabilized disulfide is likely to prevent the premature release of calicheamicin from a conjugate by circulating reduced thiols, such as glutathione. Further work showed that the inclusion of the hydrazone was not necessary for this anti-MUC1 antibody, and that the "amide conjugate" (**7**) that lacks this site of hydrolysis was equivalent or superior in all preclinical models examined, especially against resistant cell lines.[2] This article describes an extension of this work to an anti-CD33 antibody.

* To whom correspondence should be addressed. Phone: (845) 732-3423. Fax: (845) 732-5561. E-mail: hamannp@war.wyeth.com.

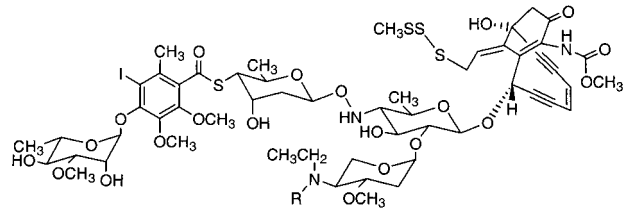
† Wyeth-Ayerst Research.

‡ Fred Hutchinson Cancer Research Center.

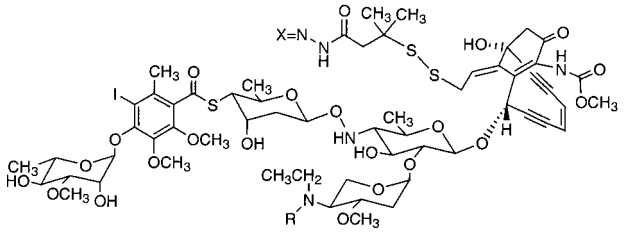
[1] Abbreviations: AML, acute myeloid leukemia; cal equiv, calicheamicin equivalents; DM, dimethyl; DMA, dimethyl acid; DMH, dimethyl hydrazide; FBS, fetal bovine serum; gamma, calicheamicin γ_1^I, MTD, maximum tolerated dose; NAc, *N*-acetyl; OSu, N-hydroxysuccinimide; PBS, phosphate-buffered saline; PSCs, pleuripotent stem cells.

[2] Hamann, P. R., Hinman, L. M., Beyer, C. F., Greenberger, L., Lin, C., Lindh, D., Menendez, A. T., Upeslacis, J., and Wallace, R. An anti-MUC1 antibody-calicheamicin conjugate for treatment of solid tumors, choice of linker and overcoming drug resistance. To be submitted for publication.

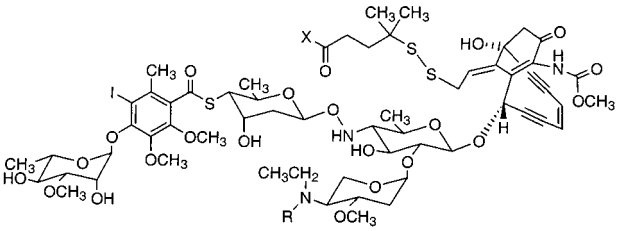
10.1021/bc0100206 CCC: $22.00 © 2002 American Chemical Society
Published on Web 12/19/2001



1, Calicheamicin γ_1^I (gamma), R = H
2, NAc-gamma calicheamicin, R = acetyl



3, NAc-gamma calicheamicin DMH, X = H_2
4, Carbohydrate conjugate, X = Antibody-CH=
(hydrazone with oxidized antibody)



5, NAc-gamma calicheamicin DMA, X = OH
6, NAc-gamma calicheamicin DMA, OSu ester,
X = N-succinimidyloxy
7, Amide conjugate, X = Antibody-NH
(amide bond to lysine groups)

Figure 1. Structures of calicheamicin derivatives and conjugates.

P67.6 is a murine IgG_1 antibody that targets CD33-positive cells of the myeloid lineage. In the hematopoietic cascade, expression of cell surface markers changes as a function of differentiation. The earliest cells which are capable of self-renewal and differentiation are the PSCs. PSCs are CD33-negative and, as they mature, they undergo extensive changes (*9*). Through one branch of hematopoiesis, PSCs differentiate into CD33-positive myeloid stem cells. AML is a disorder that is believed to result predominantly from a malignant transformation of CD33-positive myeloid stem cells, but not from PSCs. Greater than 80% of AML patients show expression of the CD33 antigen (a 67 kD cell surface glycoprotein) on the leukemic cell population (*10*).

Clinical studies with ^{125}I-labeled P67.6 demonstrate that this antibody has high selectivity for tumor targets, and that it is rapidly and efficiently internalized into antigen positive cells (*11, 12*). Internalization is widely held to be important for good activity for antibody-targeted chemotherapy. On the basis of our previous experience with the targeted delivery of the calicheamicins, P67.6 should be an excellent candidate for targeted chemotherapy for the treatment of AML by rapidly and effectively delivering the calicheamicin into CD33-positive cells. Any nonleukemic CD33-positive myeloid cells, which might also be destroyed during the course of therapy, can be regenerated by differentiation of the nonmalignant, CD33-negative PSCs (*13*).

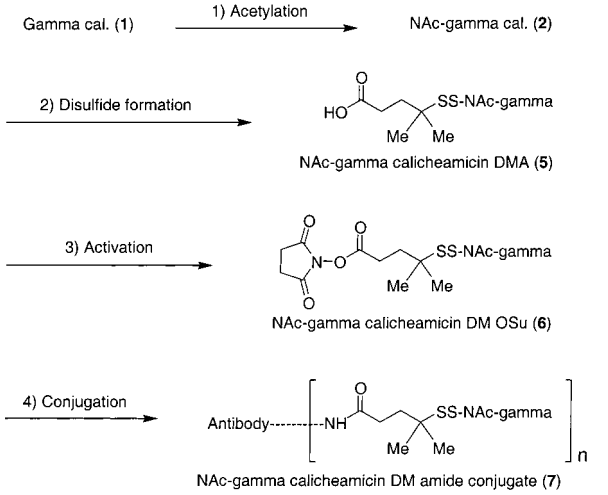


Figure 2. Synthetic scheme for preparation of amide conjugates.

This article summarizes the biological activities of two classes of calicheamicin conjugates made with the P67.6 antibody, a carbohydrate conjugate that contains a site of hydrolytic release and an amide conjugate that does not. It is clear from the results, which contrast with that of the CTM01 antibody, that the disulfide present in all calicheamicin conjugates is insufficient for efficient release of the calicheamicin from P67.6 and that the site of hydrolytic release offered by the hydrazone is essential for activity. With such a site of release, the carbohydrate conjugate is an exciting potential treatment for AML.

EXPERIMENTAL PROCEDURES

Monoclonal Antibodies. Antibodies were prepared by Celltech Therapeutics, Ltd., Slough, UK (now Celltech Chiroscience, plc). P67.6 was purified from tissue culture supernatants. MOPC-21, a murine plasmacytoma antibody (*14*) that does not bind to human tumor cells, was used as a negative control. P67.6 was radiolabeled with [^{125}I]diiodinated Bolton-Hunter reagent purchased from New England Nuclear as previously published (*7*).

Calicheamicin Derivatives. The synthesis of NAc-gamma calicheamicin DMH (**3**, Figure 1) has been previously reported (*7*). The synthesis of NAc-gamma calicheamicin DMA, *N*-hydroxysuccinimide ester (**6**) is as follows. (See Figure 2.)

The required linker, 4-mercapto-4-methylpentanoic acid (**8**), was made by routine synthetic procedures as follows. Reaction of epoxymethylpropane with potassium thiocyanate was followed by distillation of the organic layer to give 2,2-dimethylthiirane. Reaction of the thiirane with the sodium anion of ethyl cyanoacetate in ethanol was followed by filtration, concentration, precipitation with water, and drying in vacuo to give 2-imino-5,5-dimethyl-tetrahydro-thiophene-3-carboxylic acid ethyl ester. This compound was hydrolyzed under reflux with sodium hydroxide followed by acidification with HCl, extraction with methylene chloride, and evaporation to an oil which was heated at 165 °C followed by distillation to give 5,5-dimethyl-dihydro-thiophen-2-one. Hydrolysis of this compound followed by carefully acidifying with HCl, extracting with methylene chloride, and concentrating gave 4-mercapto-4-methylpentanoic acid (**8**) as an oil. This compound was characterized by mass spectroscopy, ^{1}H NMR, ^{13}C NMR, and elemental analysis.

To NAc-gamma calicheamicin (**2**) at a concentration of 2 mg/mL in acetonitrile at −15 °C was added 5 mol equiv

of 4-mercapto-4-methylpentanoic acid (**8**) and 6 mol equiv of triethylamine. After 24 h at −15 °C, the volatile organic solvents were evaporated at reduced pressure, and the crude product was chromatographed on Bio-Sil A using a gradient of 0 to 5% methanol in chloroform. Pure fractions, as assessed by TLC, were pooled, evaporated to a glass, dissolved in chloroform, and added to rapidly stirring hexane to produce a flocculent solid. Filtration and drying in vacuo gave the 4-mercapto-4-methylpentanoic acid disulfide derivative of *N*-acetyl γ_1^I calicheamicin (NAc-gamma calicheamicin DMA, **5**) as an amorphous, white powder.

To NAc-gamma calicheamicin DMA (**5**) at a concentration of 5 mg/mL in acetonitrile at ambient temperature was added 3 mol equiv of N-hydroxysuccinimide and 5 mol equiv of 1-(3-(dimethylamino)propyl)-3-ethylcarbodiimide hydrochloride (EDCI). After 3 h the volatile organic solvents were evaporated at reduced pressure and the crude product was chromatographed on Bio-Sil A using a gradient of 0 to 5% methanol in chloroform. Pure fractions, as assessed by TLC, were pooled, evaporated to a glass, dissolved in chloroform, and added to rapidly stirring hexane to produce a flocculent solid. Filtration and drying in vacuo gave NAc-gamma calicheamicin DMA, *N*-hydroxysuccinimide ester (**6**) as an amorphous, white powder.

These calicheamicin derivatives were well characterized by mass spectroscopy, ^{1}H NMR, ^{13}C NMR, elemental analysis, and IR and UV spectroscopy.

Antibody Conjugates. The synthesis of the carbohydrate conjugates (**4**) of NAc-gamma calicheamicin DMH have been reported previously (*7*). Drug loadings of 2 to 3 mol of calicheamicin per mole of antibody were seen, and free calicheamicin (structure **3**) was normally 1−3%.

Conjugates of NAc-gamma calicheamicin DMA, *N*-hydroxysuccinimide ester (amide conjugates, **7**) were prepared as follows. Four to six molar equivalents of NAc-gamma calicheamicin DMA, *N*-hydroxysuccinimide ester (**6**) in DMF (final concentration of DMF, 15%) were added to the antibody of interest at a concentration of 2 to 5 mg/mL in 50 mM phosphate buffer, pH 7.4, with 100 mM NaCl. After gently shaking the reaction overnight, the solvent was exchanged on a Sephadex G-25 column to remove the small organic species, and the product was purified by size exclusion on S-200 gel using the above buffer system to remove aggregates. Pooled monomer was concentrated by ultrafiltration, and the resultant amide conjugate (**7**) showed 1−3% aggregate by size exclusion HPLC (Zorbax GF-250, 0.2 M phosphate, pH 7.0) and no significant free drug (<0.5%) by reversed-phase HPLC. Drug and protein concentrations were determined spectroscopically using the extinction coefficients of the calicheamicin at 333 nm and the antibody at 280 nm as well as a correction factor for the absorbance of calicheamicin at 280 nm (mg/mL cal equiv = A_{333}/2.85, mg/mL protein = ($A_{280} - 3 \times A_{333}$)/1.43) cal equiv (calicheamicin equivalents) are in terms of either NAc-gamma calicheamicin DMA or DMH, which have the same molecular weight. Typically, recovery of antibody in the final product was 80%, drug loadings were 2 to 3 mol of calicheamicin per mole of antibody, and free calicheamicin (Structure **5**) was 0.5−1%.

Relative Immunoaffinity Assay. Relative immunoaffinities of P67.6 conjugates were determined in a competitive binding assay in which varying concentrations of test conjugate were allowed to compete with a fixed amount of [^{125}I]-P67.6 for binding to a fixed number of viable cells. The concentration of test conjugate required to obtain 50% inhibition of binding of the labeled antibody was compared with the concentration of a reference preparation of native hP67.6 required for 50% inhibition.

HEL 92.1.7 cells were collected by centrifugation, counted, resuspended in fresh medium at 10^7 cells per mL, and chilled on ice. Samples for assay were adjusted to 200 mg protein/mL in medium, and six serial 4-fold dilutions of each were prepared, for a total of seven concentrations of each sample. The reference hP67.6 was diluted in the same way: 0.05 mL of each dilution was transferred to a 12 × 75 mm plastic tube, and 0.05 mL of [^{125}I]-P67.6 was added. The tubes were mixed and incubated at 4 °C. Then 0.1 mL of chilled cell suspension was added to each tube, and all tubes were mixed again and incubated for 1 h at 4 °C. The final concentration of [^{125}I]-P67.6 was 1 μg/mL.

Controls to determine maximal binding and nonspecific binding were included in each assay. Maximal binding was determined by mixing 0.05 mL of medium, 0.05 mL of [^{125}I]-P67.6, and 0.1 mL of cells; nonspecific binding was determined by mixing 0.05 mL of 500 μg/mL of P67.6, 0.05 mL of [^{125}I]-P67.6, and 0.1 mL of cells.

At the end of the incubation, cells were washed twice with 3 mL of cold PBS by centrifugation and resuspension. The cells were resuspended in 0.5 mL of PBS and transferred to clean tubes, and radioactivity was determined in a γ-counter. The percent inhibition of binding was calculated, and the concentration required to inhibit 50% of binding was determined from a plot of inhibition versus binding.

Cells and Culture Methods. HL-60 human promyelocytic leukemia (CCL 240), Raji human Burkitt lymphoma (CCL 86), and HEL 92.1.7 human erythroleukemia (TIB 180) were obtained from the American Type Culture Collection. The standard methods used for cell culture have been described previously (*1*), except that 10% fetal calf serum was used for HL-60 cells.

In Vitro Testing. Concentrations of the test substances were all normalized to equivalents of calicheamicin (NAc-gamma DMH or NAc-gamma DMA, which have the same molecular weight), and a medium control was included. Triplicate 0.1 mL aliquots of cell suspension were added to microtiter wells already containing 0.1 mL aliquots of sample. The cells were incubated for 3 days, at which time 0.1 mL of supernatant was removed and replaced with 0.2 uCi of [^{3}H]thymidine in 0.1 mL of fresh medium. Incubation was resumed for an additional 24 h at which point the cells were harvested and counted. Growth inhibition curves of each drug or conjugate were plotted and the IC_{50} value (concentration of drug equivalents needed for 50% [^{3}H] thymidine uptake inhibition) of each sample was determined.

In Vivo Testing. The HL-60 human xenograft tumor was developed from the line received from the American Tissue Culture Collection and was passaged as an ascites in athymic mice. The ascites were harvested from donor mice, and 8×10^6 cells were routinely implanted subcutaneously into other athymic mice. Tumors were staged to a size of about 150 mg prior to drug treatment, and test samples were injected intraperitoneally, usually as three doses, 4 days apart (QD 4 × 3). Treatment started the day after tumor staging, which was usually 6 days after implantation. Control animals were injected with saline. There were usually 10 animals in a control group and five in each test group. Tumor mass was determined by measuring the tumor diameter once weekly for at least 28 days after the start of treatment.

Ex Vivo Testing. Samples of marrow from pediatric patients enrolled on CCSG protocol 213 were collected

in preservative-free heparin and sent to Seattle at initial diagnosis. These specimens were separated by Ficoll-Hypaque density centrifugation (specific gravity 1.077 g/mL) (Pharmacia, Inc., Piscataway, NJ). The mononuclear cells were pelleted and suspended in 10% dimethyl sulfoxide (Sigma, St. Louis, MO) and 90% newborn calf serum (Hyclone Laboratories, Loan, UT), at a concentration of 10^7 cells/mL and aliquoted in 1 mL volumes in cryovials (Nalge Co., Rochester, NY). Cells were then allowed to freeze overnight in a −80 °C mechanical freezer after which they were transferred to either a liquid nitrogen freezer or a −135 °C mechanical freezer. Samples previously found to grow colonies in the colony-forming assay were used for testing.

Cells were thawed in a 37 °C water bath and transferred to 10 mL of RPMI containing 10% fetal bovine serum and 100 U/mL deoxyribonuclease 1 Type II (Sigma). Cells were then washed twice in RPMI/10% FBS, counted, and suspended to a concentration of 10^6 viable cells/mL in RPMI containing 2% FBS. Cells were then incubated at 37 °C in the dark for 2 h in the presence of a CD33-antibody conjugate or, as a nonbinding control, a MOPC-21 antibody conjugate. After incubation, cells were washed three times in RPMI/2% FBS and suspended in 300 μL of human placental conditioned medium. Cells were then placed in triplicate 35-mm culture dishes (Nunc, Naperville, IL) containing 900 μL of Iscove's Modified Dulbecco's Medium, 0.9% methylcellulose (Stem Cell Technologies Inc., Vancouver, BC, Canada), supplemented with 20% FBS, 1% bovine serum albumin (Intergen Co., Purchase, NY), 1×10^{-4} mol/mL 2-mercaptoethanol (Sigma, St. Louis, MO), and 10% human placental conditioned medium, IL-3 (100 ng/mL) and erythropoietin (epo, 2 U/mL, Amgen, Thousand Oaks, CA). Cells were cultured at a concentration of 50000 cells per dish at 37 °C in a 5% CO_2 in air-humidified atmosphere. Colonies were counted after 10−12 days of incubation.

RESULTS

Carbohydrate and Amide Conjugates of P67.6. P67.6 was conjugated to calicheamicin by two methods. One method involved oxidizing the naturally occurring carbohydrates of the antibody (*15*) and reacting the resultant aldehydes with a calicheamicin derivative referred to as NAc-gamma calicheamicin DMH (**3**) (see Figure 1 for structures). This method produces a "carbohydrate conjugate" that has a hydrazone bond that is hydrolytically labile, especially at the low pH found in lysosomes (*16*, *17*). The second method (Figure 2) involves reacting the ϵ-amino groups of lysines on the antibody with a calicheamicin derivative referred to as NAc-gamma calicheamicin DMA, OSu ester (**6**). This method produces an "amide conjugate" which does not have a bond that is hydrolytically labile under physiological conditions. Both of these conjugates contain a disulfide bond that can react with glutathione to release an active calicheamicin derivative from the antibody and must be fully reduced by glutathione in the course of the cytotoxic mechanism of the calicheamicins (*2*). Both of these conjugates also contain a disulfide stabilized by two methyl groups and an aminosugar that is acetylated, as was shown to be optimum for calicheamicin conjugates (*7*).

Comparative in Vitro Activity. The in vitro cytotoxic activities of these conjugates are shown in Table 1. Both conjugates and various reference samples were incubated with CD33-positive HL-60 cells and CD33-negative Raji cells, and the IC_{50} values are given in cal equiv. The P67.6 carbohydrate conjugate was more than 7000-fold more potent than the P67.6 amide conjugate toward the antigen-positive cells. The specificity index of the P67.6 carbohydrate conjugate was greater that 100-fold, while the P67.6 amide conjugate showed modest specificity for antigen-positive cells. Both types of conjugates retained good immunoaffinities. Also presented in Table 1 are results for several controls, which showed that P67.6 alone was not toxic to either cell type, that the admixture of P67.6 and NAc-gamma calicheamicin DMH was not different than NAc-gamma calicheamicin DMH (**3**) alone, and that the calicheamicin derivatives were less potent than the carbohydrate conjugate toward the HL-60 target cells.

Table 1. Comparison of the in Vitro Cytotoxicity of Carbohydrate and Amide Conjugates of P67.6

sample	rel affinity[a]	IC_{50} (ng/mL)[b] HL-60	Raji	Raji/ HL-60[c]
P67.6 carbohydrate conjugate (**4**)	0.87	<0.006	0.79	>132
P67.6 amide conjugate (**7**)	0.79	44.1	353	8
NAc-γ DMH (**3**) + P67.6	0.88	0.74	1.07	1.4
NAc-γ DMH (**3**)	–	0.56	1.36	2.43
NAc-γ (**2**)	–	0.41	0.70	1.71
native P67.6	1.00	>100[d]	>100[d]	–

[a] Relative affinity in a competitive assay versus radioiodinated P67.6. [b] Doses are given in cal equiv. The corresponding amount of antibody is on average 40-fold greater. [c] Ratio of the two IC50's. [d] Concentration of antibody alone equivalent to that of either conjugate at the dose of cal equiv given in table. Actual concentration of antibody 4 μg/mL.

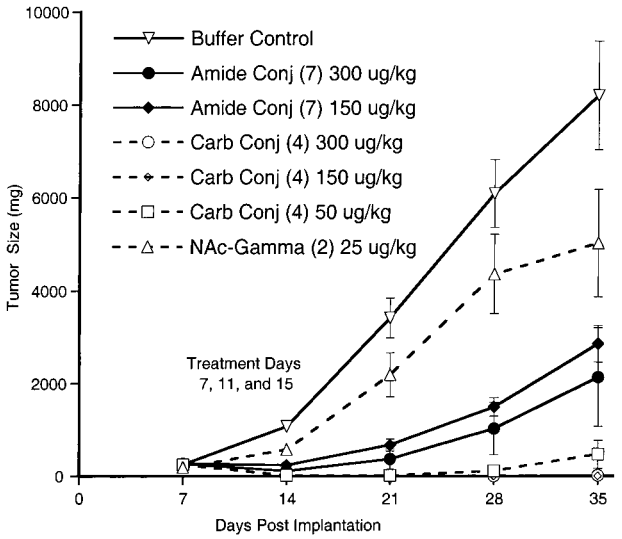


Figure 3. Time-course of the response of HL-60 xenograft tumors to amide and carbohydrate conjugates of P67.6. The doses are given in cal equiv. The corresponding amount of antibody is 40-fold greater. This experiment is representative of the general results seen with these conjugates.

Comparative in Vivo Activity. Carbohydrate and amide conjugates of P67.6 were further compared in vivo for antitumor effects against HL-60 tumor xenografts implanted subcutaneously in nude mice. The results of one such test are presented in Figure 3. The two conjugates and NAc-gamma calicheamicin (**2**) were administered three times at the doses indicated spaced by 4 days starting on day seven post tumor implantation. In this test, no deaths were noted in the conjugate-treated groups during the 42-day duration of the study, while in the group treated with NAc-gamma calicheamicin (**2**), one

Table 2. Comparison of the Ex Vivo Inhibition of Colony Formation. Single Experiment

	amide conjugate (**7**)	carbohydrate conjugate (**4**)
media	14.5 ± 2.0	14.5 ± 2.0
drug control (**5** and **3**, respectively)	10.3 ± 3.2	15.3 ± 3.6
CTM01 conjugate (control)	10.5 ± 2.5	14.5 ± 1.9
P67.6 conjugate	10.0 ± 4.4	3.7[a] ± 1.4

[a] Significantly different from the P67.6 amide conjugate as well as from all other samples in the carbohydrate conjugate column at $p < 0.02$.

Table 3. Comparison of the Ex Vivo Inhibition of Colony Formation. Composite Results

sample	no. of patients	no. with specific inhibition 25−59%	60−89%	≥90%
P67.6 amide conjugate (**7**)	12	4	2	0
P67.6 carbohydrate conjugate (**4**)	12	1	4	4

of five animals had died at the 75 μg/kg dose and all were dead at the 150 μg/kg dose (data not shown). This experiment showed that the P67.6 carbohydrate conjugate was significantly more active than the P67.6 amide conjugate at all three doses tested. The P67.6 carbohydrate conjugate produced nine tumor-free survivors out of 10 treated animals in the 300 and 150 μg/kg × 3 treatment groups, whereas no tumor-free animals were seen with the P67.6 amide conjugate at any dose.

Comparative ex Vivo Activity. Testing of the P67.6 amide and carbohydrate conjugates was carried out on pediatric AML patient samples. In one experiment, eight pediatric AML samples were tested with these two conjugates as well as control conjugates made with the nonbinding antibody CTM01 and also appropriate unconjugated drug controls. The data, shown in Table 2, indicate that at 2 ng/mL cal equiv only the targeting antibody conjugate made with a hydrolyzable linker is capable of inhibiting colony formation in the majority of samples, as indicated by the averages. Although there were individual patient samples that were inhibited by the amide conjugate, the average of all eight patients showed no statistical difference from media alone. In a total of three experiments, run with various combinations of the available samples, 12 different pediatric AML samples were tested with both the P67.6 amide and carbohydrate conjugates. The results, summarized in Table 3, show that at 2 ng/mL cal equiv there was some growth inhibition of AML colony-forming cells using the amide conjugate, while substantially more growth inhibition was seen using the carbohydrate conjugate.

DISCUSSION

Antibody-targeted chemotherapy has been studied for many years by numerous academic and pharmaceutical research groups. Aside from the requirement for an antibody that targets a pertinent, internalizing antigen, there appears to be two major criteria that need to be satisfied for activity. The first of these is that the antigen must be capable of carrying enough of the drug into the cell to deliver a toxic dose. Three factors come into play here: the antigenic density and turnover rate, the molar loading of drug on the antibody, and the inherent potency of the drug. The antigenic density and turnover rate is difficult to alter in patients, while the drug loading is difficult to increase significantly beyond a certain level. The potency of the drug, however, can vary by many orders of magnitude, depending on the choice an investigator makes (*5*, *18*). The calicheamicins are one of the most potent classes of natural products, and this allows calicheamicin conjugates to target a relatively broad range of antigens, including those with relatively low expression, such as CD33 (*19*).

The second requirement for antibody-targeted chemotherapy is that a mechanism must be incorporated into the conjugate design to allow for drug release after internalization into the target cells. Two of the most common sites of drug release are disulfide linkages and hydrazones. The former allows for reductive release of the drug, presumably through interaction with glutathione, while the latter allows for hydrolytic release in the acidic lysozomes where many antibody/antigen complexes end up after internalization.

Conjugates of calicheamicin, by the nature of their structure and mechanism of DNA damage, always have a disulfide present that can serve as a site of release of the calicheamicin from the antibody. Indeed, increasing the stability of this disulfide leads to a marked improvement in the therapeutic index of the conjugates (*8*). However, the desire to have site-selective conjugation led to the initial use of the procedure developed by Cytogen that involves the oxidation of the naturally occurring carbohydrates in the hinge region of the antibody and reacting the resultant aldehydes with nucleophiles, usually hydrazides. The carbohydrate conjugates that are formed are capable of releasing active drug by hydrolysis in the lysozomes where the pH is low (*16*, *17*).

A new class of calicheamicin conjugate has now been made that is based on the reaction of an activated ester derivative with the lysines on the antibody. The resultant amide conjugate does not contain a hydrazone bond and is therefore stable to hydrolysis under physiological conditions, but still contains a disulfide bond. These conjugates can therefore be used to answer a basic question about the requirements for efficient release of a cytotoxic agent such as the calicheamicins from various antibodies. The results in this article show that for the anti-CD33 antibody P67.6, the amide conjugates do not exhibit potent, selective cytotoxicity while the carbohydrate conjugates do. Thus, the disulfide bond does not appear to be an efficient site of release with this antibody.

Although carbohydrate conjugates were initially made with calicheamicin because the use of the carbohydrates precludes reactions near the antigen-binding site, the amide conjugate of P67.6 retains virtually all of its binding affinity when an amide conjugate is produced. Indeed, only one out of almost two dozen antibodies has lost any significant immunoaffinity when a calicheamicin amide conjugate was made (data not shown).

In vitro, the P67.6 amide conjugate is about 100-fold less potent than the calicheamicin reference drugs. This is indicative of unproductive metabolism due to insufficient release of an active calicheamicin derivative intracellularly. On the other hand, the P67.6 carbohydrate conjugate is at least 100-fold more cytotoxic than the calicheamicin reference compounds. This perhaps surprising result may be due to the efficient internalization, release, and utilization of the calicheamicin once carried into the cell by the antibody. The significant cytotoxicity of the P67.6 carbohydrate conjugate against the CD33-negative Raji cells during long-term exposure is presumed to be due to the result of the slow extracellular release and subsequent uptake of the NAc-gamma calicheamicin DMH (**6**) from the conjugate.

In vivo, the P67.6 amide conjugate does show significant inhibition of tumor growth of the HL-60 tumor in nude mice but was incapable of producing any long-term, tumor-free survivors, even at the highest doses tested.

In contrast, the P67.6 carbohydrate conjugate was capable of eradicating the tumors routinely at the two highest doses tested. Similar conjugates of other antibodies which do not bind to HL-60 cells show no significant effects on HL-60 xenografts, and conjugates of P67.6 do not show significant effect on xenograft tumors that do not express the CD33 antigen (data not shown). The unconjugated calicheamicin derivatives that have been tested as controls in this and similar experiments show at best modest antitumor effects at the MTD.

Ex vivo experiments were done to examine the response of a number of AML biopsies, thereby giving reassurance that the results with the HL-60 cells were not dependent on some unusual property of that cell line. A comparison of the activity of the two P67.6 conjugates in the ex vivo experiments clearly shows that the carbohydrate conjugate is superior and is capable of inhibiting colony formation in a significant percentage of patient samples. It should be noted that 100% inhibition is not necessarily desirable in this assay, as the formation of normal colonies from CD33-negative precursors is possible. The absolute predictive value of this assay is questionable, because only about 25% of AML patient samples grow colonies under these conditions. However, the results clearly show a difference for the two classes of conjugate and also indicate the possibility of selective cytotoxicity toward leukemic cells in at least a subset of patients.

The consistent results from these three test systems, in vitro, in vivo, and ex vivo, clearly show the need for a site of hydrolytic release in the linker between the calicheamicin and the P67.6 antibody even though a disulfide is present. Preliminary experiments indicated that reduction of the hydrazone bond in the carbohydrate conjugate of P67.6 with cyanoborohydride led to a conjugate that resembled the amide conjugate in its properties (data not shown). This would tend to preclude any special effect of attaching the calicheamicin to a carbohydrate reside being responsible for the observed activity.

It is unclear at this point why a site of hydrolytic release is necessary. HL-60 cells are relatively small and rich in lysozomes. Processed fragments of antibody appear in the cell supernatant quickly after treatment with radiolabeled antibody (*20*). Perhaps the calicheamicin is externalized with such fragments when only the disulfide bond is available for calicheamicin release, but when a hydrazone bond is present, the calicheamicin is released from the antibody before these fragments leave the cell. This is consistent with the known internalization of P67.6 into lysozomes (*20*) and the acid nature of this subcellular compartment (*16*, *17*). Initial experiments with tritium-labeled calicheamicin derivatives to explore this issue have been unsuccessful because of the unavailability of tritiated reagents with high enough specific activity to follow the low levels of the very potent calicheamicin derivatives in cells. It should be noted that although both disulfides and hydrazones are viewed as acceptable sites for cleaving chemoimmunoconjugates to release an active drug, there is no prior publication that examines the comparison of a drug conjugate made with a disulfide with that made with a hydrazone.

For calicheamicin conjugates the results with P67.6 have been shown not to be general. Indeed, for the anti-MUC1 antibody, CTM01 (*21*), a hydrolyzable bond had no benefit, and the amide conjugate was equivalent or superior in all preclinical models that were examined, especially against resistant cell lines.[2,3] The combined results for these two antibodies indicate that one optimal design of conjugate does not exist for all antibodies. Each antibody must be examined separately, and a variety of different types of conjugates must be tried in order to individually optimize a specific delivery system. The contrasting results obtained with the anti-P67.6 and anti-MUC1 antibody conjugates probably depend more on the physiology of the target cells and the antigen that is targeted than on any specific properties of the antibodies or cytotoxic agent.

In conclusion, a calicheamicin conjugate of the anti-CD33 antibody is a potent and selective agent targeted toward CD33-positive cells in cell culture, in xenograft experiments, and in ex vivo models of AML, as long as a site of hydrolytic release is present. Thus, the P67.6 carbohydrate conjugate of calicheamicin was envisioned to be an effective new agent for the treatment of AML and other CD33-positive diseases. The P67.6 antibody has been humanized and, as the result of an unexpected problem, the carbohydrate conjugate has been abandoned and replaced by a conjugate containing a bifunctional linker that attaches to lysines on the antibody, but that allows for formation of the hydrazone that is needed for activity (*22*). This improved conjugate, referred to as CMA-676 and assigned the generic name of gemtuzumab ozogamicin, has successfully completed initial clinical trials (*23*, *24*) and has been approved under the name Mylotarg by the FDA as the first antibody-targeted chemotherapeutic agent.

ACKNOWLEDGMENT

We would like to thank Irwin Hollander for helpful discussion, technical help, and editorial assistance, George Ellestad for helpful scientific discussions, and Martha Godwin and J. Philip James for technical support.

LITERATURE CITED

(1) Lee, M. D., Dunne, T. M., Chang, C. C., Morton, G. O., and Borders, D. B. (1987) Calicheamicins, a novel family of antitumor antibiotics, 1: Chemistry and partial characterization of γ_1^I. *J. Am. Chem. Soc. 109*, 3464−3466.

(2) Myers, A. G., Cohen, S. B., and Kwon, B. M. (1994) A study of the reaction of Calicheamicin γ_1^I with glutathione in the presence of double-stranded DNA. *J. Am. Chem. Soc. 116*, 1255−1271.

(3) Ellestad, G. A., Ding, W.-D., Zein, N., and Townsend, C. A. (1995) DNA-cleaving properties of calicheamicin γ_1^I. *Enediyne Antibiotics as Antitumor Agents* (D. B. Borders, and T. W. Doyle, Eds.) pp 137−160, Marcel Dekker, New York.

(4) Lee, M. D., Ellestad, G. A., and Borders, D. B. (1991) Calicheamicins: discovery, structure, chemistry, and interaction with DNA. *Acc. Chem. Res. 24*, 235−43.

(5) Liu, C., and Chri, R. V. J. (1997) The development of antibody delivery systems to target cancer with highly potent maytansinoids. *Exp. Opin. Invest. Drugs 6*, 169−172.

(6) Chari, R. V. J., Jackel, K. A., Bourret, L. A., Derr, S. M., Tadayoni, B. M., Mattocks, K. M., Shah, S. A., Liu, C., Blaettler, W. A., and Goldmacher, V. S. (1995) Enhancement of the selectivity and antitumor activity of a CC-1065 analogue through immunoconjugate formation. *Cancer Res. 55*, 4079−4084.

(7) Hinman, L. M., Hamann, P. R., Wallace, R., Menendez, A. T., Durr, F. E., and Upeslacis, J. (1993) Preparation and characterization of monoclonal antibody conjugates of the calicheamicins: a novel and potent family of antitumor antibiotics. *Cancer Res. 53*, 3336−3342.

[3] Hamann, P. R., Hinman, L. M., Beyer, C. F., Lindh, D., and Mountain, A. A calicheamicin conjugate with a fully humanized anti-MUC1 antibody shows potent antitumor effects in breast and ovarian tumor xenografts. To be submitted for publication.

(8) Hinman, L. M., Hamann, P. R., and Upeslacis, J. (1995) Preparation of conjugates to monoclonal antibodies. *Enediyne Antibiotics as Antitumor Agents* (D. B. Borders, and T. W. Doyle, Eds.) pp 87−106, Marcel Dekker, New York.

(9) Andrews, R. G., Singer, J. W., and Bernstein, I. D. (1989) Precursors of colony-forming cells in humans can be distinguished from colony-forming cells by expression of the CD33 and CD34 antigens and light scatter properties. *J. Exp. Medicine 169*, 1721−31.

(10) Keating, M. J., Estey E., and Kantarjian H. (1993) *Acute leukemia. Cancer, Principles and Practice of Oncology* (V. T. DeVita, Jr., S. Hellman, and S. A. Rosenberg, Eds.) pp 1938−64, JB Lippincott Company, Philadelphia.

(11) Appelbaum, F. R., Matthews, D. C., Eary, J. F., Badger, C. C., Kellogg, M., Press, O. W., Martin, P. J., Fisher, D. R., Nelp, W. B., Thomas, E. D., and Bernstein, I. D. (1992) The use of radiolabeled anti-CD33 antibody to augment marrow irradiation prior to marrow transplantation for acute myelogenous leukemia. *Transplantation 54*, 829−833.

(12) van der Jagt, R. H. C., Badger, C. C., Appelbaum, F. R., Press, O. W., Matthews, D. C., Eary, J. F., Krohn, K. A., and Bernstein, I. D. (1992) Localization of radiolabeled antimyeloid antibodies in a human acute leukemia xenograft tumor model. *Cancer Res. 52*, 89−94.

(13) Bernstein, I. D., Singer, J. W., Andrews, R. G., Keating, A., Powell, J. S., Bjornson, B. H., Cuttner, J., Najfeld, V., Reaman, G., Raskind, W., Sutton, D. M., and Fialkow, P. J. (1987) Treatment of acute myeloid leukemia cells in vitro with a monoclonal antibody recognizing a myeloid differentiation antigen allows normal progenitor cells to be expressed. *J. Clin. Invest. 79*, 1153−59.

(14) Melchers, F. (1970) Biosynthesis of the carbohydrate portion of immunoglobulins. *Biochem. J. 119*, 765−772.

(15) Rodwell, J. D., Alvarez, V. L., Lee, C., Lopes, A. D., Goers, J. W. F., King, H. D., Powsner, H. J., and McKearn, T. J. (1986) Site-specific covalent modification of monoclonal antibodies: in vitro and in vivo evaluations. *Proc. Natl. Acad. Sci. U.S.A. 83*, 2632−6.

(16) Van Dyke, R. W., Root, K. V., Schreiber, J. H., and Wilson, J. M. (1992) Role of CFTR in lysosomal acidification. *Biochem. Biophys. Res. Commun. 184*, 300−5.

(17) Ohkuma, S., and Poole, B. (1978) Fluorescence probe measurement of the intralysosomal pH in living cells and the perturbation of pH by various agents. *Proc. Natl. Acad. Sci. U.S.A. 75*, 3327−31.

(18) Trail, P. A., Willner, D., Lasch, S. J., Henderson, A. J., Hofstead, S., Casazza, A. M., Firestone, R. A., Hellström, I., and Hellström, K. E. (1993) Cure of xenografted human carcinoma by Br96-doxorubicin immunoconjugates. *Science 261*, 212−215.

(19) Xu, Y., and Scheinberg, D. A. (1995) Elimination of human leukemia by monoclonal antibodies in an athymic nude mouse leukemia model. *Clin. Cancer Res. 1*, 1179−87.

(20) Press, O. W., Shan, D., Howell-Clark, J., Eary, J., Appelbaum, F. R., Matthews, D., King, D. K., Haines, A. M. R., Hamann, P., Hinman, L., Shochat, D., and Bernstein, I. D. (1996) Comparative metabolism and retention of iodine-125, yttrium-90, and indium-111 radioimmunoconjugates by cancer cells. *Cancer Res. 56*, 2123−9.

(21) Aboud-Pirak, E., Sergent, T., Otte-Slachmuylder, C., Abarca, J., Trouet, A., and Schneider, Y.-J. (1988) Binding and endocytosis of a monoclonal antibody to a high molecular weight human milk fat globule membrane-associated antigen by cultured MCF-7 breast cancer cells. *Cancer Res. 48*, 3188−3196.

(22) Hamann, P. R., Hinman, L. M., Hollander, I., Beyer, C. F., Lindh, D., Holcomb, R., Hallett, W., Upeslacis, J., Shochat, D., Mountain, A., Flowers, D. A., and Bernstein, I. (2002) Gemtuzumab ozogamicin, a potent and selective anti-CD33 antibody-calicheamicin conjugate for treatment of acute myeloid leukemia. *Bioconjugate Chem. 13*, 47−58.

(23) Sievers, E. L., Appelbaum, F. R., Spielberger, R. T., Forman, S. J., Flowers, D., Smith, F. O., Shannon-Dorcy, K., Merger, M. S., and Bernstein, I. D. (1999) Selective ablation of acute myeloid leukemia using antibody-targeted chemotherapy: A phase I study of an anti-CD33 calicheamicin immunoconjugate. *Blood 93*, 3678−84.

(24) Sievers, E. L., Larson, R. A., Estey, E., Stadtmauer, E. A, Roy, D.-C. C., Spielberger, R., Tarantolo, S., Berger, M. S., Eten, C., Manley, L., Bernstein, and Appelbaum, I. F. (1999) Preliminary results of the efficacy and safety of CMA-676 in Patients with AML in first relapse. *Proceedings of The American Society of Clinical Oncology (ASCO) 18*, 7a, abstr. 21, Lippencott, Williams, and Wilkins, Baltimore, MD.

BC0100206

Gemtuzumab Ozogamicin, A Potent and Selective Anti-CD33 Antibody−Calicheamicin Conjugate for Treatment of Acute Myeloid Leukemia

Philip R. Hamann,*,† Lois M. Hinman,† Irwin Hollander,† Carl F. Beyer,† Delores Lindh,† Ryan Holcomb,† William Hallett,† Hwei-Ru Tsou,† Janis Upeslacis,† Dan Shochat,† Andrew Mountain,‡ David A. Flowers,§ and Irwin Bernstein§

Wyeth-Ayerst Research, 401 North Middletown Road, Pearl River, New York 10965, Celltech Chiroscience, plc., 216 Bath Rd, Slough, England, SL1-4EN Berkshire, and Fred Hutchinson Cancer Research Center, 1124 Columbia Street, Seattle, Washington 98109. Received February 19, 2001; Revised Manuscript Received October 15, 2001

CD33 is expressed by acute myeloid leukemia (AML) cells in >80% of patients but not by normal hematopoietic stem cells, suggesting that elimination of $CD33^+$ cells may be therapeutically beneficial. A conjugate of a calicheamicin hydrazide derivative attached via hydrazone formation to the oxidized carbohydrates of the anti-CD33 murine antibody P67.6 had been chosen for use in AML prior to humanization of this antibody. However, the CDR-grafted humanized P67.6 could not be used to make the carbohydrate conjugate because of the unexpected sensitivity of this antibody to periodate oxidation. Exploration of a series of bifunctional linkers resulted in a new class of calicheamicin conjugates, termed the hybrid conjugates, that allows for the attachment of the calicheamicin to lysines but incorporates the site of hydrolytic release, a hydrazone, previously shown to be required for activity. The optimized conjugate chosen for clinical trials, gemtuzumab ozogamicin ("gem-ozo", Mylotarg, formerly designated CMA-676), was significantly more potent and selective than the carbohydrate conjugate it replaced. It was selectively cytotoxic to HL-60 leukemia cells in tissue culture with an IC_{50} in the low to sub-pg cal/mL range (cal = calicheamicin equivalents). Doses of gem-ozo as low as 50 μg cal/kg given three times to mice bearing HL-60 xenografts routinely resulted in long-term, tumor-free survivors, while a nonbinding control conjugate was relatively inactive. Gem-ozo at a concentration of 2 to 10 ng cal/mL selectively inhibited leukemia colony formation by marrow cells from a significant proportion of AML patients. Gem-ozo has also shown significant activity against AML in Phase II trials and is the first antibody-targeted chemotherapeutic agent approved by the FDA.

INTRODUCTION

In the 25 years since the development of methods for preparing monoclonal antibodies, there have been numerous attempts to use these proteins as effective vehicles for targeting cytotoxic agents to human cancers. Although there are now several antibodies approved for treatment and various radioimmunoconjugates appear to be progressing toward eventual approval, conjugates of cytotoxic agents such as phytotoxins and traditional chemotherapeutic agents have met with little or no general success due to a variety of problems (*1*). What may be required are agents that are less immunogenic than toxins, such as ricin, yet more potently cytotoxic than traditional anticancer drugs. Potential agents would include antitumor antibiotics such as the potently cytotoxic calicheamicins. These potently cytotoxic natural products are members of the enediyne family of antitumor antibiotics that, even at sub-picomolar concentrations, produce double-stranded DNA cleavage (*2*, *3*). They may offer significant advantages over previous antibody-targeted agents, because they are roughly 1000-fold more cytotoxic than clinically used anticancer agents but have much lower immunogenicity than ricin. Conjugates of other potent cytotoxic agents have been published (*4*, *5*), but no direct comparison with calicheamicin conjugates is possible due to differences in the antibodies and testing systems.

AML[1] is a malignancy that affects 2.4/100000 people each year in the US and, although the majority of patients show a response to initial chemotherapy, less than 30% of patients survive for 3 years. The targeted CD33 antigen of this report is a 67 kD cell surface glycoprotein that is expressed by leukemia cells from >80% of AML patients (*6*). Although CD33 is expressed on normal progenitor and mature myeloid cells, it is not expressed on immature pluripotent stem cells that account for in vivo transplantation of hematopoietic function (*7*−*10*). CD33 was also selected because it is internalized (*11*), a property widely accepted to be crucial for successful antibody-target chemotherapy.

Evidence suggests that in some leukemias, $CD33^-$ precursors are essentially normal in origin since they establish nonclonal hematopoiesis in long-term marrow

* To whom correspondence should be addressed. Phone: (845) 602-3423. Fax: (845) 602-5561. E-mail: hamannp@war.wyeth.com.
† Wyeth-Ayerst Research.
‡ Celltech Chiroscience.
§ Fred Hutchinson Cancer Research Center.

[1] Abbreviations: AML, acute myeloid leukemia; cal, equivalents of calicheamicin (NAc gamma DMH, molecular weight 1478; CDR, complimentarity-determining region; DMH, dimethyl hydrazide; FBS, fetal bovine serum; gem-ozo, gemtuzumab ozogamicin; HAMA, human-antimurine antibody; hP67.6, humanized P67.6; NAc-gamma, *N*-acetyl gamma calicheamicin.

10.1021/bc010021y CCC: $22.00 © 2002 American Chemical Society
Published on Web 12/19/2001

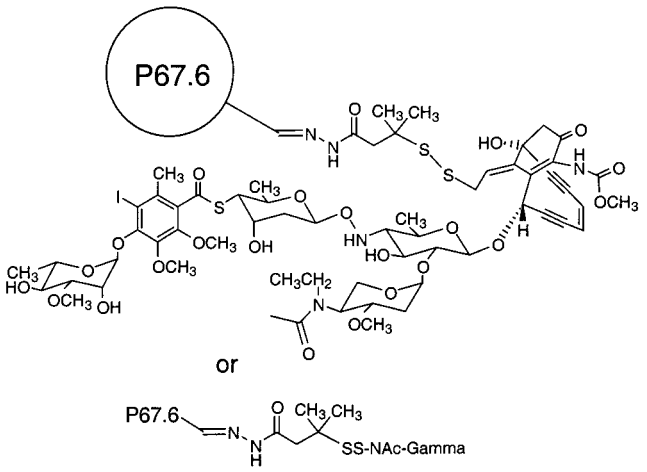


Figure 1. P67.6 carbohydrate conjugate of NAc-gamma calicheamicin DMH made by oxidizing the naturally occurring carbohydrate residues and reacting the resultant aldehydes with the calicheamicin hydrazide derivative.

cultures (*12, 13*). Thus, any nonleukemic $CD33^+$ myeloid cells killed during therapy would be regenerated from differentiating nonmalignant $CD33^-$ stem cells. However, one study appeared to show that primitive hematopoietic precursors isolated from AML specimens engrafted leukemic hematopoiesis in immunodeficient mice (*14*). This observation has been taken to suggest that the predominant cells of malignant origin in this case were $CD33^-$. This discrepancy might ultimately be clarified by clinical trials of an anti-CD33 immunoconjugate.

Studies of a radiolabeled anti-CD33 antibody have demonstrated rapid binding and efficient internalization by $CD33^+$ cells in spleen, marrow, and blood, suggesting that a toxic agent could be efficiently delivered to target cells (*15, 16*). However, the level of CD33 expressed on leukemia cells appears to be relatively low, which limits the amount of a cytotoxic agent that can be delivered by a conjugate. For example, in HL-60 promyelocytic leukemia cells, CD33 expression was estimated at 10^4 copies per cell (*17, 18*). It is therefore crucial that a potent cytotoxic agent, such as the calicheamicins, be used for conjugates that target this antigen (*19*).

The calicheamicins are highly potent antitumor antibiotics of the enediyne family. Originally isolated from a broth extract of the soil microorganism *Micromonospora echinospora*, ssp. *calichensis,* the calicheamicins were detected in a screen for potent DNA damaging agents (*20*). The parent of this family of xenobiotics, calicheamicin γ_1^I, has been shown to associate with the minor groove of DNA and, following reduction with glutathione (*21*), to cause sequence-specific DNA cleavage (*2, 3*). Due to their mode of action and potency, several analogues of the calicheamicins have been tested in preclinical models for their usefulness as antitumor agents. They have not been pursued as single agent therapies because of delayed toxicities in animal models that limit the therapeutic dose range for treatment and because of the ideal properties of the calicheamicins for targeted delivery.

Earlier work with calicheamicin conjugates of the murine, anti-CD33 antibody P67.6 showed that a site of hydrolytic release, as supplied by a hydrazone, was necessary for potent and selective cytotoxicity in tissue culture and for maximum efficacy in xenograft models of AML in athymic mice (*22*). A carbohydrate-based conjugate (Figure 1) was chosen that was made by oxidizing the naturally occurring carbohydrate-residues in P67.6 with periodate and reacting the resultant aldehydes with a hydrazide derivative of calicheamicin, NAc-gamma calicheamicin DMH (*23*). This conjugate showed potent, specific antitumor activity in models of AML. To minimize the potential for immune responses in human trials, the P67.6 antibody has been humanized by CDR-grafting with the intent of doing clinical trials with the hP67.6-NAc-gamma calicheamicin DMH conjugate. In this article is described the unexpected problem that arose in making this conjugate and the redesign of the conjugate that not only solved the problem but resulted in a more potent and selective agent. This conjugate, gemtuzumab ozogamicin (Mylotarg, formerly known as CMA-676), has now shown activity in clinical trials for AML (*24, 25*) and has been approved by the FDA for the treatment of relapsed AML.

EXPERIMENTAL PROCEDURES

Syntheses of the Bifunctional Hybrid Linkers. The following linkers were purchased: 4-formylbenzoic acid (Linker **b)** (Aldrich), 4′-formylphenoxyacetic acid (Linker **f)** (Fluka), and 4-(4′-acetylphenyl)butanoic acid (Linker **i)** (Salor). All other starting materials, solvents, and reagents were purchased from Aldrich and were used as received.

4-[4′-(4″-Fluorobenzoyl)phenoxy]butanoic Acid (Linker a). A solution of 3.98 g (18.4 mmol) of 4-fluoro-4′-hydroxybenzophenone and 5.37 g (27.6 mmol) of ethyl 4-bromobutyrate in 1 mL of anhydrous DMF was stirred for 48 h under an atmosphere of dry nitrogen with 7.64 g (55.2 mmol) of potassium carbonate and 0.31 g (1.84 mmol) of potassium iodide. The reaction mixture was then evaporated under vacuum, and the residue was partitioned between ether and water. The organic phase was separated, washed three times with water, dried with magnesium sulfate, filtered, and evaporated under vacuum. The crude yellow solid product was recrystallized from ether providing 2.97 g (49%) of 4-[4′-(4″-fluorobenzoyl)phenoxy]butanoic acid, ethyl ester as white crystals. Mp 57−59 °C; IR (KBr): 1735, 1645 cm^{-1}; FAB-MS: 311 ($M + H^+$). Anal. Calcd for $C_{19}H_{19}O_4F$: C, 69.08; H, 5.80; F, 5.75; O, 19.37. Found: C, 69.09; H, 5.62; F, 5.95; O, 19.34.

To a stirred solution of 0.48 g (1.45 mmol) of 4-[4′-(4″-fluorobenzoyl)phenoxy]butanoic acid, ethyl ester in 25 mL of methanol/water (3:2) was added 0.32 g (2.25 mmol) of potassium carbonate, and the reaction was stirred for 18 h under an argon atmosphere. Next, the reaction mixture was evaporated under vacuum and the residue dissolved in 20 mL of a 0.1 N solution of sodium hydroxide. This basic solution was washed with ether, the aqueous phase acidified by addition of sodium bisulfate, and the resulting mixture extracted with ethyl acetate. This solution was then dried with magnesium sulfate, filtered, and evaporated. The crude white solid was recrystallized from an ether−hexane mixture leaving 0.16 g (36%) of 4-[4′-(4″-fluorobenzoyl)phenoxy]butanoic acid as white crystals. Mp 109−111 °C; IR (KBr): 1735, 1700 1640 cm^{-1}; ^1H NMR ($CDCl_3$, 400 MHz): 10.5−9.65 (br s, 1H, COOH), 7.79 (m, 4H, C2″, C6″, C3′, and C5′), 7.15 (t, 2H, $J = 8.6$ Hz, C3″ and C4″), 6.95 (d, $J = 8.8$ Hz, 2H, C2′ and C6′), 4.12 (t, $J = 6.0$ Hz, 2H, C4), 2.62 (t, $J = 7.2$ Hz, 2H, C2), 2.17 (m, 2H, C3); FTMS: 301.08799 ($M - H^+$, theoretical 301.08816), Anal. Calcd for $C_{17}H_{15}O_4$ F: C, 67.54; H, 5.00; F, 6.28; O, 21.18. Found: C, 67.28; H, 4.89; F, 6.41; O, 21.42.

4-(4′-Formyl-2′-methoxyphenoxy)butanoic Acid (Linker c). 4-Hydroxy-3-methoxybenzyl alcohol (1 g, 6.49 mmol) was treated under dry nitrogen with 1.73 g (7.13

mmol) of ethyl 4-bromobutyrate, 2.69 g (19.5 mmol) of potassium carbonate, and a catalytic amount (97.2 mg, 0.65 mmol) of sodium iodide in 2 mL of anhydrous DMF for 48 h. The reaction mixture was then evaporated under vacuum, and the residue was partitioned between ether and water. The organic phase was separated, washed three times with water, dried with magnesium sulfate, filtered, and evaporated under vacuum to give 821 mg of 4-[4′-(hydroxymethyl)-2′-methoxyphenoxy]butanoic acid, ethyl ester as a light brown oil (47%). IR (neat): 3500, 1730, 1620, 1600 cm^{-1}; CI-MS: 269 ($M + H^+$), 251, 223, 195. This material was taken on to the following step without additional purification or further characterization.

4-[4′-(Hydroxymethyl)-2′-methoxyphenoxy]butanoic acid, ethyl ester (431 mg, 1.61 mmol) was dissolved in 100 mL of methylene chloride and stirred with 1.0 g (4.8 mmol) of pyridinium chlorochromate for 4 h before filtering through a Celite pad. The reaction mixture was then diluted with an equal volume of ether, precipitating out salts. This mixture was then filtered through a silica gel pad using ether, and the filtrate evaporated, giving 280 mg (65%) of 4-(4′-formyl-2′-methoxyphenoxy)butanoic, ethyl ester as a colorless oil. IR (neat): 1730, 1690, 1600, 1580 cm^{-1}. This material was taken on to the following step without additional purification or further characterization.

4-(4′-Formyl-2′-methoxyphenoxy)butanoic acid, ethyl ester (240 mg, 0.90 mmol) was dissolved in 3 mL of methanol/water (3:2) and treated with 435 mg (3.15 mmol) of potassium carbonate. The reaction was stirred for 18 h under an argon atmosphere. Next, the reaction mixture was evaporated under vacuum and the residue dissolved in 200 mL of a 0.1 N solution of sodium hydroxide. This basic solution was washed with ether, the aqueous phase acidified by addition of sodium bisulfate, and the resulting mixture was extracted with ethyl acetate. This solution was then dried with magnesium sulfate, filtered, and evaporated to give 125 mg (58%) of 4-(4′-formyl-2′-methoxyphenoxy)butanoic acid as a white powder. Mp 143−148 °C; ^1H NMR ($CDCl_3$, 400 MHz): 9.85 (s, 1H, CHO), 7.45−7.40 (m, 2H, C3′ and C4′), 6.98 (d, $J = 8.4$ Hz, 1H, C5′), 4.17 (t, $J = 6.2$ Hz, 2H, C4), 3.92 (s, 3H, OCH_3), 2.64 (t. $J = 7.1$ Hz, 2H, C2), 2.22 (m, 2H, C3); IR (KBr): 3575, 3500, 1720, 1700, 1680, 1600, 1585 cm^{-1}; FTMS: 239.09131 ($M + H^+$, theoretical 239.09140).

4-(2′-Oxoethoxy)benzenepropanoic Acid (Linker d). A mixture of 4′-hydroxybenzenepropanoic acid (500 mg, 3.01 mmol), 892 mg (7.52 mmol) of allyl bromide, and 1.28 g (10.8 mmol) of potassium carbonate in 4 mL of anhydrous DMF was stirred at room temperature for 12 h. This mixture was diluted with 20 mL of ether and washed five times with 20 mL of water. The organic layer was then washed successively with 20 mL of saturated sodium bicarbonate solution and 20 mL of saturated sodium chloride solution. The organic layer was separated, dried over magnesium sulfate, filtered, and concentrated under vacuum to give 610 mg (82%) of 2-propenyl-4-(2′-propenyloxy)benzenepropanoic ester as a colorless oil. IR (neat): 3450, 1740, 1650, 1610, 1510 cm^{-1}; CI-MS: 247 ($M + H^+$), 229, 215, 187, 175. This material was taken on to the following step without additional purification or further characterization.

A solution of 2-propenyl-4-(2′-propenyloxy)benzenepropanoic ester (271 mg, 1.1 mmol) in 9 mL of methanol/water (3:2) at room temperature was treated with 0.14 mL (1.4 mmol) of 10 M aqueous sodium hydroxide. The solution was allowed to stir for 1 h then acidified with 5 mL of 10% sodium bisulfate solution and extracted with 25 mL of ethyl acetate. The organic layer was washed with saturated sodium chloride solution, dried over magnesium sulfate, and concentrated under vacuum to give 196 mg (86%) of 4-(2′-propenyloxy)benzenepropanoic acid as a white powder. Mp 88−89 °C; IR (KBr): 3200, 1720, 1700, 1610 cm^{-1}; CI-MS: 207 ($M + H^+$), 189, 175, 147; Analysis calc′d for $C_{12}H_{14}O_3$: C, 69.89; H, 6.84; found: C, 69.87; H, 6.68. This material was taken on to the following step without additional purification or further characterization.

A solution of 4-(2′-propenyloxy)benzenepropanoic acid (120 mg, 0.58 mmol) in 5 mL of methylene chloride was cooled to −78 °C. Ozone was introduced by bubbling the gas into the solution through a glass tube until a blue color persisted. The solution was then purged with a stream of argon, and 1 mL of methyl sulfide was added. The solution was diluted with 20 mL of ether and washed with water. The organic layer was separated and allowed to stand over magnesium sulfate and then concentrated under vacuum to give 100 mg (82%) of 4-(2′-oxoethoxy)-benzenepropanoic acid as a white powder. Mp 95−100 °C; ^1H NMR ($CDCl_3$, 300 MHz): 9.86 (s, 1H, CHO), 7.15 (d, $J = 8.6$ Hz, 2H, C2′ and C6′), 6.83 (d, $J = 8.6$ Hz, 2H, C3′ and C5′), 4.55 (s, C1′), 2.91 (t, $J = 7.4$ Hz, 2H, C2), 2.65 (t, $J = 7.4$ Hz, C1); IR (KBr): 3400, 1740, 1720, 1610 cm^{-1}; FTMS: 207.06638 ($M - H^+$, theoretical 207.06628).

4-(4′-Formylphenoxy)butanoic Acid (Linker e). 4-Hydroxybenzyl alcohol (1 g, 8.06 mmol) was stirred with 1.73 g (8.86 mmol) of ethyl 4-bromobutyrate, 3.34 g (24.2 mmol) of potassium carbonate, and a catalytic amount (120 mg 0.81 mmol) of sodium iodide in 1.80 mL of anhydrous DMF for 48 h under an atmosphere of dry nitrogen. The reaction mixture was then evaporated under vacuum, and the residue was partitioned between ether and water. The organic phase was separated, washed three times with water, dried with magnesium sulfate, filtered, and evaporated under vacuum to give 1.73 g of 4-[4′-(hydroxymethyl)phenoxy]butanoic acid, ethyl ester as a light brown oil (90%). IR (neat): 3400, 1730, 1610, 1580, 1510 cm^{-1}; CI-MS: 238 (M^+), 221, 115. This material was taken on to the following step without additional purification or further characterization.

A mixture of 230 mg (0.97 mmol) of 4-[4′-(hydroxymethyl)phenoxy]butanoic acid, ethyl ester, 624.2 mg (2.9 mmol) of pyridinium chlorochromate, and 3 g of powdered 4 Å molecular sieve was stirred in 2 mL of methylene chloride at room temperature for 3 h. The mixture was diluted with 20 mL of ether, filtered, and concentrated under vacuum to give 175 mg (76%) of a light yellow oil. The oil (150 mg, 0.63 mmol) was dissolved in 2.3 mL of methanol/water (3:2) and treated with 307 mg (2.22 mmol) of potassium carbonate and stirred in 6 mL of methanol/water (3:2) at room temperature for 8 h. The solution was then concentrated under vacuum. The residue was dissolved in 10 mL of 0.1 N sodium hydroxide solution and washed with 20 mL of ether. The aqueous layer was separated and acidified with sodium bisulfate and extracted with ethyl acetate. The resulting organic layer was washed with saturated sodium chloride solution and then dried over magnesium sulfate. The mixture was then filtered and concentrated under vacuum to give 100 mg (75%) of 4-(4′-formylphenoxy)butanoic acid as a white powder. ^1H NMR ($CDCl_3$, 400 MHz): 9.89 (s, 1H, CHO), 7.83 (d, $J = 8.4$ Hz, 2H, C3′ and C5′), 7.00 (d, $J = 8.4$ Hz, 2H, C2′ and C6′), 4.13 (t, $J = 6.1$ Hz, 2H, C4), 2.61 (t, $J = 7.2$ Hz, 2H, C2), 2.17 (m, 2H, C3); IR (KBr): 3000, 1740, 1660 cm^{-1}; FTMS: 209.08080 ($M + H^+$, theoretical 209.08084).

4-[(2′-Acetyl-1′-naphthalenyl)oxy]butanoic Acid (Linker g). A 3.42 g (18.37 mmol) sample of 1-hydroxy-2-acetonaphthone and 5.0 g (50 mmol) of ethyl 4-bromobutyrate in 10 mL of anhydrous DMF was stirred for 48 h under an atmosphere of dry nitrogen with 13.7 g (100 mmol) of potassium carbonate and 0.5 g (3.3 mmol) of potassium iodide. The reaction mixture was then evaporated under vacuum, and the residue was partitioned between ether and water. The organic phase was separated, washed three times with water, dried with magnesium sulfate, filtered, and evaporated under vacuum. The crude product was dried under high vacuum at 60 °C to give 5.21 g (94%) of 4-[(2′-acetyl-1-naphthalenyl)oxy]butanoic acid, ethyl ester as a golden liquid. IR (neat): 1730, 1665 cm^{-1}; FAB-MS: 301($M + H^+$). Anal. Calcd for $C_{18}H_{20}O_4$: C, 71.98; H, 6.71. Found: C, 72.11; H, 6.58.

A sample of 2.84 g (9.46 mmol) of 4-[(2′-acetyl-1′-naphthalenyl)oxy]butanoic acid, ethyl ester was dissolved in 150 mL of methanol/water (3:2), with stirring. Then 2.1 g (15 mmol) of potassium carbonate was added, and the reaction was stirred for 18 h under an argon atmosphere. Next, the reaction mixture was evaporated under vacuum and the residue dissolved in 200 mL of a 0.1 N solution of sodium hydroxide. This basic solution was washed with ether, the aqueous phase acidified by addition of sodium bisulfate, and the resulting mixture extracted with ethyl acetate. This solution was then dried with magnesium sulfate, filtered, and evaporated. The crude product was recrystallized from ethyl acetate/ether to give 1.15 g (45%) of 4-[(2′-acetyl-1′-naphthalenyl)oxy]-butanoic acid as golden crystals. Mp 104−06 °C; IR (KBr): 1720, 1640 cm^{-1}; ^1H NMR ($CDCl_3$, 400 MHz): 8.18 (m, 1H, C8′), 7.85 (m, 1H, C5′), 7.69 (d, $J = 8.6$ Hz, 1H, C3′), 7.63 (d, $J = 8.6$ Hz, 1H, C4′), 7.60−7.54 (m, 2H, C6′ and C7′), 4.08 (t, $J = 6.4$ Hz, 2H, C4), 2.75 (s, 3H, $COCH_3$), 2.73 (t, $J = 7.3$ Hz, 2H, C2), 2.29 (m, 2H, C3); FTMS: 295.09396 ($M + Na^+$, theoretical 295.09408). Anal. Calcd for $C_{16}H_{16}O_4$: C, 70.58; H, 5.92. Found: C, 70.40; H, 5.89.

4-(4′-Acetylphenoxy)butanoic Acid (Linker h). A solution of 0.90 g (6.61 mmol) of 4-hydroxyacetophenone and 1.93 g (9.92 mmol) of ethyl 4-bromobutyrate in 1.80 mL of anhydrous DMF was stirred for 48 h under an atmosphere of dry nitrogen with 2.74 g (19.8 mmol) of potassium carbonate and 0.110 g (0.66 mmol) of potassium iodide. The reaction mixture was then evaporated under vacuum and the residue partitioned between ether and water. The organic phase was separated, washed three times with water, dried with magnesium sulfate, filtered, and evaporated under vacuum to give a brown solid. This was recrystallized from ether/hexane. The beige crystals were air-dried, leaving 0.84 g (51%) of 4-(4′-acetylphenoxy)butanoic acid, ethyl ester. Mp 59−61 °C; IR (KBr): 1740, 1670 cm^{-1}; FAB-MS: 251.1283 ($M + H^+$, theoretical 251.1285). Anal. Calcd for $C_{14}H_{18}O_4$: C, 67.18; H, 7.25;. Found: C, 67.16; H, 7.16. This material was taken on to the following step without additional purification or further characterization.

A sample of 0.25 g (1.00 mmol) of 4-(4′-acetylphenoxy)-butanoic acid, ethyl ester was dissolved in 15 mL of methanol/water (3:2). Then, 0.21 g (1.50 mmol) of potassium carbonate was added, and the reaction was stirred for 18 h under an argon atmosphere. Next, the reaction mixture was evaporated under vacuum and the residue dissolved in 20 mL of a 0.1 N solution of sodium hydroxide. This basic solution was washed with ether, the aqueous phase acidified by addition of sodium bisulfate, and the resulting mixture extracted with ethyl acetate. This solution was then dried with magnesium sulfate, filtered, and evaporated, leaving an off-white solid, which was recrystallized from ethyl acetate by the addition of an equal volume of ether. This provided 0.18 g (80%) of 4-(4′-acetylphenoxy)butanoic acid as light beige crystals. Mp 148−50 °C; IR (KBr): 3063, 2918, 2666, 2593, 2575, 2515, 1729, 1644, 1597, 1514, 1366, 1314, 1264, 1017, 881, 848 cm^{-1}; UV (CH_3OH): 273 nm (a = 76.2 $Lg^{-1}cm^{-1}$), 218 nm (a = 49.4 Lg^{-1} cm^{-1}); ^1H NMR (DMSO-d_6, 400 MHz): 12.18 (br s, 1H, COOH), 7.92 (d, $J = 8.9$, 2H, C3′ and C5′), 7.03 (d, $J = 8.9$ Hz, 2H, C2′ and C6′), 4.08 (t, $J = 6.4$ Hz, C4′), 2.52 (s, 3H, CH_3), 2.40 (t, $J = 7.3$ Hz, C2′), 1.97 (m, 2H, C3′); ^{13}C NMR (DMSO-d_6, 400 MHz): 196.2 (C═O), 174.0 (COOH), 162.4 (C1), 130.5 (C3 and C5), 129.9 (C4), 114.2 (C2 and C6), 67.0 (C4′), 30 (C2′), 26.4 (CH_3), 24.1 (C3′); FTMS: 223.09649 ($M + H^+$, theoretical 223.09649). Anal. Calcd for $C_{12}H_{14}O_4$: C, 64.85; H, 6.35. Found: C, 64.82; H, 6.28.

Synthesis of Calicheamicin Derivatives. HPLC retention times refers to a C_{18} Vydac analytical column (250 × 4.6 mm) run at 1 mL/min with a linear gradient of 35−65% acetonitrile/50 mM $NH_4H_2PO_4$. UV spectra were run in acetonitrile at approximately 5 μg/mL.

Synthesis of Hydrazone 2h. *N*-Acetyl gamma calicheamicin DMH (**1**) (5 mg) was dissolved in 250 μL of anhydrous ethyl alcohol containing 3.8 mg (5 equivalents) of hybrid Linker **h** and 15 μL of acetic acid. The reaction was allowed to stir for 18 h at 37 °C. The solvents were then removed under vacuum, and the crude product was purified on BioSil-A using a gradient of 0 to 20% methanol in chloroform. Removal of the solvents gave 4.6 mg (80%) of hydrazone **2h** as a glassy solid. Precipitation of this material from chloroform containing 5% methanol into a 1:1 mixture of ether and hexanes gave hydrazone **2h** as a slightly off white, amorphous powder. HPLC retention time: 6.4 min, FAB-MS: 1682.7 ($M + H^+$), required for $C_{73}H_{96}IN_5O_{25}S_3 + H^+$, 1682.5; ^1H NMR ($CDCl_3$ + 5% CD_3OD, 300 MHz): 9.2 (s, 1H, COOH), 9.1 (br s, 1H, 18C−NH−N═), 7.72 (d, $J = 8.7$ Hz, 2H, 22), 6.92 (d, $J = 8.7$ Hz, 2H, 23), 6.42 (br t, $J = 7$ Hz, 1H, 14), 6.25 (d, $J = 1.5$ Hz, 1H, 8), 5.92 (d, $J = 9.5$ Hz, 1H, 4), 5.81 (dd, $J = 9.5$, 1.5 Hz, 1H, 5), 5.66 (d, $J = 1.5$ Hz, 1H, 1D), 5.61 (br d, $J = 2.2$ Hz, 1H, 1E), 5.05 (dd, $J = 11.5$, 1.6 Hz, 1H, 1B), 4.72 (m, 1H, 5E), 4.62 (d, $J = 7.8$ Hz, 1H, 1A), 4.56 (m, 1H, 3E), 4.47 (m, 1H, 2D), 4.26 (m, 1H, 3B), 4.19 (m, 1H, 5D), 4.10 (m, 2H, 25), 4.08 (m, 1H, 5B), 4.06 (m, 1H, 3A), 4.02 (m, 1H, 15), 3.89 (s, 3H, 2C-OCH_3), 3.84 (s, 3H, 3C−OCH_3), 3.82 (m, 1H, 3D), 3.74 (m, 1H, 15), 3.67 (m, 1H, 4B), 3.65 (m, 1H, 5A), 3.63 (bs, 3H, 10-$NHCOOCH_3$), 3.62 (m, 1H, 2A), 3.6 (m, 1H, 4D), 3.57 (s, 3H, 3D-OCH_3), 3.4 (m, 1H, 5E), 3.37 (s, 3H, 3E-OCH_3), 3.30 (m, 2H, 4E-NCH_2CH_3), 3.12 (d, $J = 17.6$ Hz, 1H, 12), 3.0 (m, 1H, 4E), 2.85 (d, $J = 17.6$ Hz, 1H, 12), 2.54 (m, 2H, 27), 2.52 (m, 2H, 17), 2.4 (m, 1H, 2E), 2.33 (m, 1H, 4A), 2.20 (s, 3H, 19), 2.10 (m, 2H, 26), 2.08 (s, 3H, 4E-$NCOCH_3$), 1.99 (m, 1H, 2B), 1.76 (m, 1H, 2B), 1.48 (s, 3H, 16a), 1.454 (s, 3H, 16b), 1.42 (d, $J = 6.2$ Hz, 3H, 6B), 1.34 (m, 1H, 2E), 1.30 (d, $J = 6.1$ Hz, 3H, 6A), 1.28 (d, $J = 6.1$ Hz, 3H, 6D), 1.19 (t, $J = 7.2$ Hz, 3H, 4E−N−CH2CH_3); ^{13}C NMR ($CDCl_3$ + 5% CD_3OD, 300 MHz): 192.4 (C1C-CO), 192.4 (C11), 175.5 (C28), 173.0 ($NCOCH_3$), 172.8 (C20), 172.3 (C18), 166.5 (C21), 159.9 (C24), 155.0 ($NHCOOCH_3$), 151.5 (C4C), 150.4 (C2C), 146.7 (C3C), 142.9 (C13), 135.9 (C10), 133.4 (C9), 133.2 (C6C), 130.2 (C1C), 128.1 (C14), 127.5 (C22), 125.0 (C4), 122.4 (C5), 114.4 (C23), 102.8 (C1D), 101.3 (C1A), 101.1 (C2), 99.8 (C1B), 97.5 (C1E), 97.2 (C7), 93.5 (C5C), 87.2 (C3), 82.4 (C6), 80.7 (C3D), 77.6 (C2A), 72.5 (C3E), 71.9 (C4D), 71.7 (C5D), 71.2 (C1), 70.9 (C8), 70.6 (C3A), 69.4 (C5A), 69.2

(C5B), 68.0 (C4A), 67.9 (C3B), 67.6 (C25), 66.8 (C2D), 64.2 (C4E), 61.6 ($C2C-OCH_3$), 60.8 ($C3C-OCH_3$), 58.9 (C5E), 57.2 ($C3D-OCH_3$), 56.8 ($C3E-OCH_3$), 53.3 (C12), 52.4 ($NHCOOCH_3$), 51.3 (C4B), 49.7 (C16), 47.6 (NCH_2CH_3), 42.9 (C17), 41.2 (C15), 37.2 (C2B), 36.5 (C2E), 30.3 (C27), 28.0 (C16b), 27.8 (C16a), 25.2 ($C6C-CH_3$), 24.4 (C26), 22.6 ($NCOCH_3$), 22.2 (C19), 18.8 (C6B), 17.9 (C6A), 17.4 (C6D), 14.0 (NCH_2CH_3); IR ($CHCl_3$): 3400−2800, 1727, 1679, 1512, 1460, 1378, 1322, 1249, 1178, 1140, 1111, 1077, 990, 667 cm^{-1}; CD (CH_3OH): $\Delta\epsilon_{312} = -44$, $\Delta\epsilon_{272} = 51$; UV ($CH_3OH$): 286 nm ($\epsilon = 31600$); HR−FAB-MS: 1682.46323 ($M + H^+$), required for $C_{73}H_{96}IN_5O_{26}S_3 + H^+$, 1682.46231. Anal. Calcd for $C_{73}H_{96}IN_5O_{26}S_3$: C, 52.11; H, 5.75; N, 4.16; I, 7.54; S, 5.72. Found: C, 51.98; H, 5.68; N, 3.95; I, 7.56; S, 5.54.

The rest of the hydrazones were made by the same procedure. The ^1H NMR spectra were analogous to that of hydrazone **2a**. The resonances due to the calicheamicin portion were virtually identical to those found in either *N*-acetyl gamma calicheamicin DMH (**1**) or hydrazone **2h**, with the variation in shifts being less than 0.1 ppm. The resonances from the hybrid linker portion of the hydrazones were also very close to those of the starting material, with the obvious exception of the hydrogens very close to the hydrazone itself. The methyl group from the acetophenones appeared at around 2.2 ppm, the hydrogen from aldehydes was shifted upfield by about 2.0 ppm, and aromatic protons adjacent to the hydrazones were shifted upfield by around 0.2 ppm.

Additional data for these compounds is as follows.

Hydrazone 2a: HPLC retention time: 8.4 min, FAB-MS: 1762.6 ($M + H^+$), 1779.5 ($M + NH_4^+$); required for $C_{78}H_{97}FIN_5O_{26}S_3 + H^+$, 1762.5, for $+ NH_4^+$, 1779.5; UV_{max} at 284 nm.

Hydrazone 2b: HPLC retention time: 5.2 min, FAB-MS: 1610.2 ($M + H^+$), 1627.0 ($M + NH_4^+$); required for $C_{69}H_{88}IN_5O_{25}S_3 + H^+$, 1610.4, for $+ NH_4^+$, 1627.4; UV_{max} at 292 and 302 nm.

Hydrazone 2c: HPLC retention time: 5.5 min, FAB-MS: 1699.2 ($M + H^+$); required for $C_{73}H_{96}IN_5O_{27}S_3 + H^+$, 1698.5; UV_{max} at 284, 300, and 316 nm.

Hydrazone 2d: HPLC retention time: 6.0 min, FAB-MS: 1669 ($M + H^+$), 1686 ($M + NH_4^+$); required for $C_{72}H_{94}IN_5O_{26}S_3 + H^+$, 1668.4, for $+ NH_4^+$, 1685.4.

Hydrazone 2e: HPLC retention time: 6.1 min, FAB-MS: 1668.4 ($M + H^+$), required for $C_{72}H_{94}IN_5O_{26}S_3 + H^+$, 1668.4; UV_{max} at 291 nm.

Hydrazone 2f: HPLC retention time: 4.4 min, FAB-MS: 1641.0 ($M + H^+$), required for $C_{70}H_{90}IN_5O_{26}S_3 + H^+$, 1640.5; UV_{max} at 291 and 305 nm.

Hydrazone 2g: HPLC retention time: 7.8 min, FAB-MS: 1732.1 ($M + H^+$), 1749.6 ($M + NH_4^+$); required for $C_{77}H_{98}IN_5O_{26}S_3 + H^+$, 1731.5, for $+ NH_4^+$, 1748.5.

Hydrazone 2i: HPLC retention time: 6.4 min, FAB-MS: 1666.5 ($M + H^+$), 1683.3 ($M + NH_4^+$); required for $C_{73}H_{96}IN_5O_{25}S_3 + H^+$, 1666.5, for $+ NH_4^+$, 1683.5; UV_{max} at 281 nm.

Synthesis of *N*-Hydroxysuccinimide Ester 3h. Hydrazone **2h** (3.5 mg) was reacted with *N*-hydroxysuccinimide (5 equiv) and EDCI (10 equiv) in 1 mL of 5% DMF/acetonitrile at room temperature for 5 h. The reaction was stripped to dryness under reduced pressure. The product was purified on BioSil-A with a step gradient of 0 to 20% methanol in chloroform. Removal of the solvents gave 3.0 mg (80%) of *N*-hydroxysuccinimide ester **3h** as a glassy solid. Precipitation of this material from chloroform containing 5% methanol into a 1:1 mixture of ether and hexanes gave *N*-hydroxysuccinimide ester **3h** as a slightly off white, amorphous powder. HPLC retention time: 7.5 min. $[\alpha]^{25} = -156.5$ °C; ^1H NMR ($CDCl_3 + 5\%$ CD_3OD, 400 MHz): 8.69 (s, 1H, 18C−NH−N═), 7.75 (d, $J = 8.7$ Hz, 2H, 22), 6.95 (d, $J = 8.7$ Hz, 2H, 23), 6.38 (br t, $J = 7$ Hz, 1H, 14), 6.23 (d, $J = 1.5$ Hz, 1H, 8), 5.90 (d, $J = 9.5$ Hz, 1H, 4), 5.80 (dd, $J = 9.5$, 1.5 Hz, 1H, 5), 5.72 (d, $J = 1.5$ Hz, 1H, 1D), 5.63 (br d, $J = 2.2$ Hz, 1H, 1E), 5.03 (dd, $J = 11.5$, 1.6 Hz, 1H, 1B), 4.70 (m, 1H, 5E), 4.61 (d, $J = 7.8$ Hz, 1H, 1A), 4.6 (m, 1H, 3E), 4.49 (m, 1H, 2D), 4.31 (m, 1H, 3B), 4.20 (m, 1H, 5D), 4.10 (m, 2H, 25), 4.07 (m, 1H, 5B), 4.03 (m, 1H, 3A), 3.91 (m, 1H, 15), 3.89 (s, 3H, $2C-OCH_3$), 3.84 (s, 3H, $3C-OCH_3$), 3.8 (m, 1H, 3D), 3.76 (m, 1H, 15), 3.75 (m, 1H, 4B), 3.65 (m, 1H, 5A), 3.63 (bs, 3H, 10-$NHCOOCH_3$), 3.62 (m, 1H, 2A), 3.6 (m, 1H, 4D), 3.57 (s, 3H, $3D-OCH_3$), 3.4 (m, 1H, 5E), 3.37 (s, 3H, $3E-OCH_3$), 3.30 (m, 2H, $4E-N-CH_2CH_3$), 3.12 (d, $J = 17.6$ Hz, 1H, 12), 3.0 (m, 1H, 4E), 2.85 (m, 2H, 27), 2.85 (bs, 4, 30), 2.72 (d, $J = 17.6$ Hz, 1H, 12), 2.5 (m, 2H, 17), 2.4 (m, 1H, 2E equatorial), 2.33 (m, 1H, 4A), 2.25 (m, 2H, 26), 2.18 (s, 3H, 19), 2.08 (s, 3H, $4E-N-COCH_3$), 2.0 (m, 1H, 2B), 1.8 (m, 1H, 2B), 1.50 (s, 3H, 16a), 1.44 (s, 3H, 16b), 1.42 (d, $J = 6.2$ Hz, 3H, 6B), 1.4 (m, 1H, 2E axial), 1.31 (d, $J = 6.1$ Hz, 3H, 6A), 1.31 (d, $J = 6.1$ Hz, 3H, 6D), 1.19 (t, $J = 7.2$ Hz, 3H, $4E-N-CH_2CH_3$); ^{13}C NMR ($CDCl_3$, 400 MHz): 192.1 ($C1C-CO$), 191.9 (C11), 172.6 ($NCOCH_3$), 172.2 (C20), 169.1 (C29), 169.0 (C18), 168.2 (C28), 165.9 (C21), 165.9 (C24), 155.0 ($NHCOOCH_3$), 151.5 (C4C), 150.6 (C2C), 143.2 (C3C), 143.0 (C13), 136.6 (C10), 133.4 (C9), 133.2 (C6C), 130.2 (C1C), 127.6 (C14), 127.6 (C22), 124.6 (C4), 123.1 (C5), 114.6 (C23), 102.6 (C1D), 101.3 (C1A), 101.1 (C2), 99.7 (C1B), 98.2 (C7), 97.8 (C1E), 93.5 (C5C), 87.0 (C3), 83.0 (C6), 80.8 (C3D), 77.6 (C2A), 72.5 (C3E), 71.8 (C4D), 71.6 (C5D), 71.1 (C1), 71.1 (C8), 70.5 (C3A), 69.1 (C5A), 69.1 (C5B), 68.4 (C4A), 68.4 (C3B), 67.0 (C2D), 66.0 (C25), 64.4 (C4E), 61.7 ($C2C-OCH_3$), 60.9 ($C3C-OCH_3$), 58.9 (C5E), 57.2 ($C3D-OCH_3$), 57.0 ($C3E-OCH_3$), 53.1 (C12), 52.4 ($NHCOOCH_3$), 51.7 (C4B), 49.7 (C16), 47.6 (NCH_2CH_3), 42.9 (C27), 41.4 (C15), 36.9 (C2B), 36.7 (C2E), 28.4 (C17), 27.9 (C16b), 27.8 (C16a), 25.6 (C30), 25.3 ($C6C-CH_3$), 24.4 (C26), 22.6 (C19), 22.4 ($NCOCH_3$), 19.0 (C6B), 17.8 (C6A), 17.6 (C6D), 13.9 (NCH_2CH_3); IR (KBr): 3420 (br), 2700, 1815, 1785, 1739, 1675, 1635 (sh), 1617, 1521, 1420, 1150, 1140, 1110, 1070, 800−600, 570, 480 cm^{-1}; UV (CH_3CH_2OH): 285 nm ($a = 18.60$ Lg^{-1} cm^{-1}); FAB-MS: 1779.5 ($M + H^+$), required for $C_{81}H_{101}IN_6O_{28}S_3 + H^+$, 1779.5; HR−FAB-MS: 1801.458 ($M + Na^+$) (requires 1801.461). Anal. Calcd for $C_{81}H_{101}IN_6O_{28}S_3$: C, 51.96; H, 5.61; N, 4.72; S, 5.41; I 7.13. Found: C, 51.63; H, 5.71; N, 4.39; S, 5.25; I, 7.43.

The rest of the *N*-hydroxysuccinimide esters were made by the same procedure. The ^1H NMR spectra were virtually identical to those of the corresponding hydrazone made with the same hybrid linker, with the variation in shifts being less than 0.1 ppm, except for the appearance of the succinimide protons as a broad singlet at around 2.8 ppm and a slight downfield shift of the protons alpha to the *N*-hydroxysuccinimide ester.

Additional data for these compounds is as follows.

***N*-Hydroxysuccinimide ester 3a:** HPLC retention time: 9.3 min, FAB-MS: 1860 ($M + H^+$), 1877 ($M + NH_4^+$); required for $C_{82}H_{100}IN_6O_{28}S_3 + H^+$, 1859.5, $+ NH_4^+$, 1876.5; UV_{max} at 284 nm.

***N*-Hydroxysuccinimide ester 3b:** HPLC retention time: 6.6 min, FAB-MS: 1708 ($M + H^+$), 1725 ($M + NH_4^+$); required for $C_{73}H_{91}IN_6O_{27}S_3 + H^+$, 1707.4, for $+ NH_4^+$, 1724.4; UV_{max} at 310 nm.

***N*-Hydroxysuccinimide ester 3c:** HPLC retention time: 6.6 min, FAB-MS: 1795.8 ($M + H^+$), required for $C_{77}H_{99}IN_6O_{29}S_3 + H^+$, 1795.5.

***N*-Hydroxysuccinimide ester 3d:** HPLC retention time: 7.1 min, FAB-MS: 1765.2 ($M + H^+$), 1783 ($M + NH_4^+$); required for $C_{76}H_{97}IN_6O_{28}S_3 + H^+$, 1765.4, for $+ NH_4^+$, 1782.4.

***N*-Hydroxysuccinimide ester 3e:** HPLC retention time: 7.0 min, FAB-MS: 1765.3 ($M + H^+$), required for $C_{76}H_{97}IN_6O_{28}S_3 + H^+$, 1765.5, UV_{max} at 289 nm.

***N*-Hydroxysuccinimide ester 3f:** HPLC retention time: 6.5 min, FAB-MS: 1737.4 ($M + H^+$), required for $C_{74}H_{93}IN_6O_{28}S_3 + H^+$, 1737.4.

***N*-Hydroxysuccinimide ester 3g:** HPLC retention time: 9.4 min, FAB-MS: 1829 ($M + H^+$), 1846 ($M + NH_4^+$); required for $C_{81}H_{101}IN_6O_{28}S_3 + H^+$, 1828.5, for $+ NH_4^+$, 1845.5.

***N*-Hydroxysuccinimide ester 3i:** HPLC retention time: 7.7 min, FAB-MS: 1763.7 ($M + H^+$), required for $C_{77}H_{99}IN_6O_{27}S_3 + H^+$, 1763.5.

Conjugates. The synthesis of the carbohydrate conjugates of NAc-gamma calicheamicin DMH (Figure 1) have been reported previously (*26*). Drug loadings of 2 to 3 mol of calicheamicin per mole of antibody were seen and free calicheamicin (hydrazide **1**) was normally 1−3%.

The general procedure for the synthesis of hybrid conjugates of calicheamicin is exemplified by the synthesis of conjugate **4h**.

To hP67.6 at pH 7.8 in phosphate buffer (50 mM sodium phosphate, 100 mM NaCl) containing 60 mM sodium caprylate was added 6 equiv of NAc-gamma calicheamicin DMH AcBut, *N*-hydroxysuccinimide ester (**3h**) in sufficient propylene glycol to give a final concentration of 30% propylene glycol. After 3 h at 25 °C, the product was filtered through a Millex HV filter and purified by gel filtration on Sephacryl S-200 using 50 mM phosphate, 100mM NaCl at pH 7.4. The final monomeric product represented a 60% yield of protein and had a loading of 2.5 mol/mol of the calicheamicin derivative as assessed by UV (protein at 280 nm and drug at 333 nm).

Antibody and Cell Lines. MOPC-21, hP67.6, and hCTM01 were prepared at Celltech, Ltd., Slough, England (now Celltech Chiroscience, plc.). The HL-60 promyelocytic leukemia cells are ATCC CCL 240 and Raji human Burkitt lymphoma cells are ATCC CCL 86. HEL 92.1.7 human erythroleukemia (TIB 180) were obtained from the American Type Culture Collection.

Relative immunoaffinity of the antibodies and conjugates was measured by a competitive radioimmunoassay (RIA) in which several dilutions of the test sample competed with radioiodinated mP67.6 for binding to live cells. For each assay, 10^6 HEL 92.1.7 cells in 0.1 mL were incubated with 0.05 mL of 4 μg/mL ^{125}I-mP67.6 (Bolton-Hunter labeling, specific activity about 0.3−0.5 μCi/μg) and serial 4-fold dilutions of the test samples, the highest concentration being 200 μg/mL. After a 1 h incubation at 0−4 °C, the cells were washed three times with cold Dulbecco's phosphate-buffered saline (PBS) and transferred to fresh tubes and counted. Binding inhibition curves were plotted and IC_{50} values for each conjugate were compared with that of the unmodified control antibody as a relative measure of retention of immunoaffinity.

In Vitro Testing. Test samples were adjusted to 1 or 0.1 μg cal/mL (cal = calicheamicin equivalents) in medium (RPMI-1640 containing 5% heat-inactivated fetal bovine serum, 5 μg/mL insulin, 5 μg/mL transferrin, 5 ng/mL sodium selenite, 100 U/mL penicillin, and 0.1 μg/mL streptomycin) and six serial 10-fold dilutions were made. CD33-positive HL-60 cells or CD33-negative Raji cells were mixed with the sample dilutions in 12 × 75 mm plastic tubes (final cell concentrations 50,000/mL) and incubated at 37 °C in 5% CO_2/air for 1 h. Cells were washed twice by centrifugation, resuspended in fresh medium at 10,000/mL, and plated in triplicate in 96-well flat-bottom tissue culture plates at 200 μL/well. Cells were labeled with [^{3}H]thymidine during the final 24 h of a 3-day culture period. The percent inhibition of [^{3}H]-thymidine incorporation was plotted versus sample concentration, and the concentration that gave 50% inhibition was interpolated. Maximal inhibition was determined from the highest concentration of NAc gamma that killed all cells, and no inhibition was determined from medium controls.

In Vivo Testing. The HL-60 human xenograft tumor was developed from the ATCC line and was passaged as ascites in athymic mice. The ascites were harvested from donor mice, and 8×10^6 cells were implanted subcutaneously into athymic mice. Tumors were staged to a size of 200 mg prior to intraperitoneal treatment with three doses spaced 4 days apart (days 1, 5, and 9). Control animals were injected with the same phosphate-buffered saline used for the conjugates and conjugates were dosed at 25 (except for the MOPC-21 conjugate), 50, 150, and 300 μg cal/kg. There were 10 animals in the control group and five in each test group. Tumor mass was determined by measuring the tumor diameter once weekly for a minimum of 35 days after the start of treatment.

Ex Vivo Testing. Leukemia samples giving rise to colonies in semisolid medium were used. Cells were thawed in a 37 °C water bath and transferred to 10 mL of RPMI containing 10% calf bovine serum and 100 U/mL deoxyribonuclease 1 Type II (Sigma). Cells were then washed twice in RPMI/10% FBS, counted, and suspended to a concentration of 10^6 viable cells/mL in RPMI containing 2% FBS. Cells were then incubated at 37 °C in the dark for 2 h in the presence of gem-ozo or, as a nonbinding control, the equivalent CTM01 conjugate (for adult samples) or MOPC-21 conjugate (for pediatric samples). After incubation, cells were washed three times in RPMI/2% FBS and suspended in 300 μL of human placental conditioned medium. Cells were then placed in triplicate 35-mm culture dishes (Nunc, Naperville, IL) containing 900 μL of Iscove's Modified Dulbecco's Medium, 0.9% methylcellulose (Stem Cell Technologies Inc., Vancouver, BC, Canada), supplemented with 20% FBS, 1% bovine serum albumin (Intergen Co., Purchase, NY), 1×10^{-4} mol/mL 2-mercaptoethanol (Sigma, St. Louis, MO), and 10% human placental conditioned medium, IL-3 (100 ng/mL) and erythropoietin (epo, 2 U/mL, Amgen, Thousand Oaks, CA). Cells were cultured at a concentration of 50000 cells per dish at 37 °C in a 5% CO_2 in air-humidified atmosphere. Colonies were counted after 10−12 days of incubation. Previously frozen samples from pediatric patients were obtained from the Children's Cancer Group AML reference laboratory, and adult samples were obtained from patients enrolled in SWOG protocol 8600 were graciously provided by Dr. Cheryl Willman, University of NM.

RESULTS

Humanization. A conjugate consisting of a calicheamicin hydrazide derivative attached to the oxidized carbohydrates on the anti-CD33 antibody P67.6 had been selected for further development. To avoid HAMA responses to conjugates of murine P67.6 in AML patients, a humanized version of the antibody, hP67.6, was constructed which contains the complimentarity-determining regions of the murine version but human IgG_4 kappa sequences in the remainder (*27*). Competitive

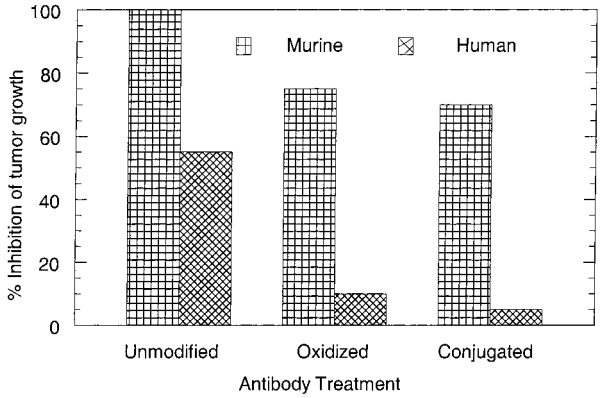


Figure 2. Relative affinity of murine and human P67.6 in the native, oxidized, and conjugated state as determined in a competitive radioimmunoassay.

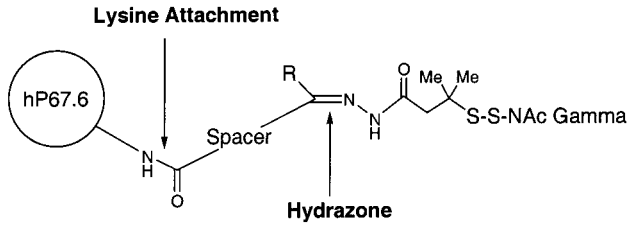


Figure 3. Strategy for hybrid conjugates.

binding assays with radiolabeled antibodies indicated roughly 50% less immunoreactivity with hP67.6 versus the murine antibody (see Figure 2). However, the periodate oxidation required in preparing a hP67.6 calicheamicin carbohydrate conjugate resulted in a virtually total loss of immunoreactivity, and alternative oxidation techniques or the use of potentially protective additives were unsuccessful. Milder oxidation with periodate reduced drug loading by about 50%, but resulted in a conjugate that still retained around 50% of its original immunoreactivity (i.e., 25% that of the murine antibody). These detrimental changes were reflected in a 4-fold loss of potency of the conjugate against HL-60 cells in vitro, while in HL-60 bearing athymic mice, only 6 of 33 survivors were rendered tumor-free with this conjugate as compared with 13 of 14 in the corresponding groups treated with the mP67.6 conjugate ($p < 0.001$).

Conjugate Redesign. One solution to the inability to make suitably active hydrazone conjugates via oxidation of the carbohydrates was to design a conjugate that utilizes lysine attachment, but which incorporates a hydrazone bond. This can be achieved as shown in Figure 3. Lysine attachment via amide bonds avoids the use of the carbohydrate oxidation technology. The spacer allows for separation of the two reactive functionalities in the bifunctional linker and, along with the R group, allows the hydrolytic stability of the hydrazone bond to be varied. The synthesis of such "hybrid" conjugates is shown in Figure 4, where an aryl group (Ar) was chosen as the spacer. The same calicheamicin derivative, NAc-gamma calicheamicin DMH (**1**), that was released from the earlier carbohydrate conjugate of P67.6 is condensed with a carbonyl compound. This calicheamicin hydrazone **2** then has the appended carboxylic acid activated to form derivative **3** before reaction with an antibody to form a hybrid conjugate **4**.

A broad variety of carbonyl-containing carboxylic acids were examined as linkers. This included both aliphatic as well as aromatic aldehydes and ketones and one benzophenone. The carboxylic acid included both ali-

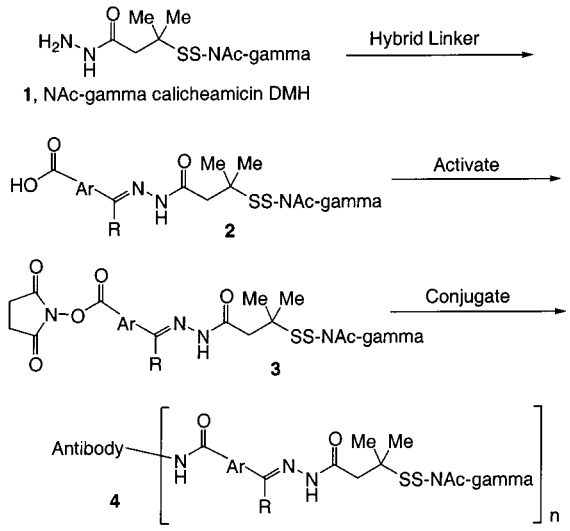


Figure 4. Synthesis of hybrid conjugates.

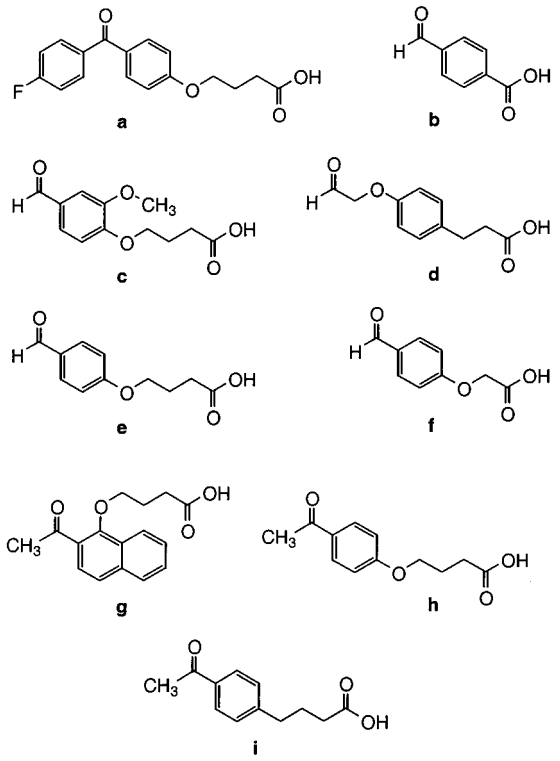


Figure 5. Selected hybrid linkers.

phatic and aromatic acids. One common factor in all these structures was the inclusion of an aromatic spacer, in part to preclude interaction of the two reactive ends. Of the 36 hybrid linkers examined (*28*), the structures of nine representative compounds are shown in Figure 5.

Selection of a Hybrid Linker. All of the linkers reacted smoothly to form hydrazones **2** (Figure 4), although benzophenones such as Linker **a** required more forcing conditions than the other types of carbonyls. Reaction of the carboxylic acid to form activated esters **3** and conjugation to hP67.6 was possible for all of the linkers, but with some notable differences. α-Phenoxy acids such as **2f** gave more impurities and lower yields on activation and conjugation. Activated aromatic acids such as **3b** reacted more sluggishly and required longer reaction times. Numerous aromatic substituents were examined (those illustrated plus halo, nitro, amino, and

Table 1. Properties of Calicheamicin Hybrid Derivatives and Conjugates

	% hydrolysis[a]		hP67.6	in vitro cytotoxicity[b]		xenograft[d]	ex vivo
derivative	pH 7.4	pH 4.5	conjugate	IC_{50} (ng cal/mL)	selectivity[c]	inhib, T/C	inhib[e]
2a	1	25	**4a**	99	3	ND	ND
2b	0	56	**4b**	4.0	>125	ND	63%
2c	7	48	**4c**	3.8	575	ND	ND
2d	90	100	**4d**	2.2	125	ND	71%
2e	5	60	**4e**	0.52	2900	12%	98%
2f	0	84	**4f**	0.22	1600	29%	95%
2g	0	16	**4g**	0.061	5000	36%	76%
2h[f]	6	97	**4h**[f]	0.040	6400	0%	96%
2i	8	100	**4i**	0.012	25000	10%	99%

[a] In 24 h at 37 °C. [b] Doses are given in equivalents of NAc-gamma calicheamicin DMH. The corresponding amount of antibody is on average 40-fold greater. [c] Ratio of the IC_{50} of the hCTM01 control conjugate and the hP67.6 hybrid conjugate, each made with the hybrid linker indicated, versus HL-60 target cells. [d] Percent inhibition of treated animal with respect to control animals for HL-60 xenograft at day 28 with a dose of 50 μg cal/kg × 3, 0% T/C = no detectable tumor. [e] Percent inhibition of colony formation at 1 μg cal/mL with AML patient marrow samples versus nonbinding control conjugate. [f] Made with AcBut linker.

ester), but none had any beneficial effect on activity of the conjugates of hP67.6.

To provide an estimate of the relative stability of the new hydrazones (**2**, Figure 4) as an estimate of the hydrolytic stability of their conjugates, they were examined by incubating a dilute aqueous solution at 37 °C in pH 4.5, 5.5, 6.5, and 7.4 buffers for 3 h and 24 h and monitoring the disappearance of hydrazone and the appearance of NAc-gamma calicheamicin DMH (**1**) by reversed-phase HPLC. The degree of hydrolysis varied greatly, and representative data from samples at pH 7.4 and 4.5 are included in Table 1, columns 1−3. These two pH's were considered most important because they approximate the pH in circulation and in lysosomes, respectively.

Reasonable loadings of these calicheamicin hydrazone derivatives on antibody (>1.5 mol/mol) were obtained only at the expense of protein recovery due to significant aggregate formation. This was particularly the case for the murine antibody, but even hP67.6 gave more aggregate than seen in the past with the earlier two classes of calicheamicin conjugates (*22*). Modification of the conjugation conditions was required to circumvent this problem and make monomeric conjugates in a manner appropriate for clinical trials (*29*).

Initial biological testing of these conjugates relied on in vitro cytotoxicity and selectivity, as given in Table 1, columns 4−6. In vivo and/or ex vivo testing was done on selected conjugates to further characterize some of the more promising conjugates, as included in Table 1, columns 7 and 8. Of all the conjugates tested, the ones made with Linker **h** (nicknamed the AcBut linker) gave the most consistent activity in all the tests. This linker was therefore chosen as the basis for the hP67.6 conjugate taken on to clinical trials. The hP67.6-NAc-gamma calicheamicin DMH AcBut conjugate (Figure 6) was given the trivial designation of CMA-676 and has been assigned the generic name gemtuzumab ozogamicin (gem-ozo) and the trade name of Mylotarg.

Characterization of Gem-Ozo. The in vitro assay comparing the cytotoxicity of gem-ozo with the mP67.6-NAc-gamma calicheamicin DMH conjugate (the previously characterized carbohydrate conjugate) shown in Table 2 indicates that gem-ozo was 45-fold more potent against HL-60 cells and 70-fold more specific than the carbohydrate conjugate relative to control cells. Gem-ozo was also 100,000-fold more cytotoxic than the corresponding AcBut-linked conjugate of MOPC-21, an antibody which does not bind to either cell line. Gem-ozo, as well as the P67.6 carbohydrate conjugate, was more cytotoxic toward $CD33^+$ cells than the calicheamicin derivative from which they were made.

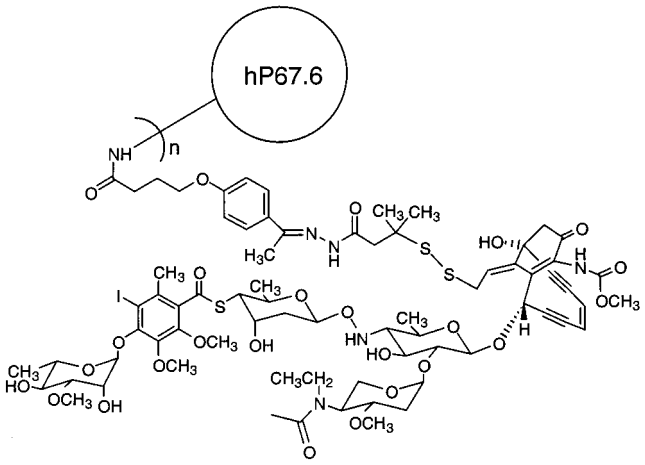


Figure 6. Gemtuzumab ozogamicin (gem-ozo) or Mylotarg. The drug loading, *n*, is 2 to 3 mol/mol.

Table 2. In Vitro Cytotoxicity and Selectivity of Gem-Ozo

	IC_{50} (ng cal/mL)[a]		
sample	HL-60 Cells	Raji Cells	IC_{50} (Raji) ÷ IC_{50} (HL-60)
gem-ozo	0.00046	35.7	78000
mP67.6-carbohydrate conjugate	0.0205	23	1100
MOPC-21 AcBut conjugate	42	52	1.2
NAc-gamma calicheamicin DMH (**1**)	9.2	4.7	0.5

[a] Doses are given in equivalents of NAc-gamma calicheamicin DMH. The corresponding amount of antibody is on average 40-fold greater.

In athymic mice implanted with HL-60 xenografts, both gem-ozo and the earlier carbohydrate conjugate induced complete tumor regression by day 28 with no tumor regrowth at day 100 in 5 out of 5 mice in each of the top two doses examined (300 and 150 μg cal/kg times 3 doses) (cal = calicheamicin equivalents) (Figure 7). However, gem-ozo was more efficacious than the carbohydrate conjugate at the lowest dose given (25 μg cal/kg times three doses). A chemically equivalent AcBut conjugate of the MOPC-21 antibody showed no significant effects at lower doses. At the highest dose used (300 μg cal/kg times three doses), there were no tumor free survivors compared to 5/5 in the gem-ozo treated group. Figure 8 shows the time course of this response for the three gem-ozo treatment groups. The maximum tolerated

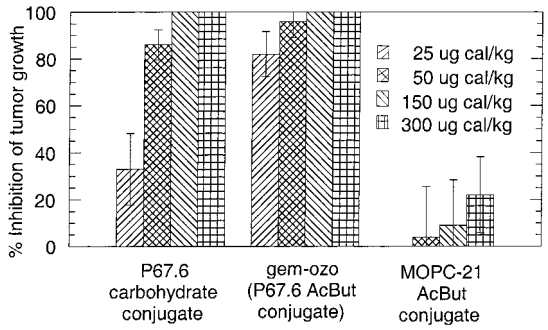


Figure 7. Response of HL-60 xenograft tumors to gem-ozo. The loading of calicheamicin on antibody is 2.5 mol/mol. Doses in protein equivalents are therefore 40-fold higher. Error bars represent the standard error of the mean.

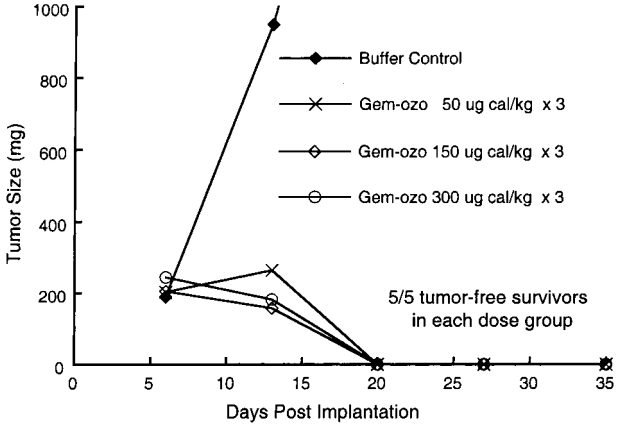


Figure 8. Time-course of the response of HL-60 xenograft tumors to gem-ozo. The loading of calicheamicin on antibody is 2.5 mol/mol. Doses in protein equivalents are therefore 40-fold higher.

Table 3. Gem-Ozo Induced Selective Inhibition of Colony Formation by Leukemic Marrow Cells

	concentrated (ng cal/mL)[a]	total no. samples	0−25% inhib	25−60% inhib	60−90% inhib	>90% inhib
adult	2	27	17	6	3	1
samples	10	27	12	3	6	6
pediatric	2	15	2	5	3	5
samples	10	5	0	1	1	3

[a] Equivalents of NAc-gamma calicheamicin DMH. The corresponding amount of antibody is 40-fold greater.

dose for gem-ozo in these experiments varied from 300 to 400 μg cal/kg given three times.

Analysis of the ability of gem-ozo to inhibit leukemia colony formation in diagnostic marrow specimens from 27 adult and 15 pediatric AML patients indicated effective inhibition of colony formation at doses of either 2 or 10 ng cal/mL (Table 3). The percent inhibition given in the table is with respect to that of an assay done with a calicheamicin control conjugate made from a nonbinding antibody. This control conjugate was prepared with the same linker and calicheamicin derivative and a nonbinding antibody, either MOPC-21 or the humanized anti-PEM antibody hCTM01 (*30*). Growth inhibition was less marked in the adult samples due presumably to differences between the leukemias occurring in the two age groups, although, at a dose of 10 ng cal/mL, 6 out of 27 adult samples showed >90% inhibition with respect to a nonspecific control conjugate. Although significant cytotoxic effects against AML cells were not observed in all patient samples tested, the factors predictive of response or lack thereof to gem-ozo by the colony-forming cells in a given leukemia sample were not obvious. Some of the colonies that did form following treatment with the conjugate could have been derived from normal $CD33^-$ precursors; however, some appeared to have abnormal morphology consistent with leukemic colonies.

DISCUSSION

Background. A series of conjugates of the calicheamicins and the anti-MUC1 antibody CTM01 has previously been reported (*26, 31*). Initial examination of the structural requirements for the calicheamicin portion of these conjugates was made using carbohydrate conjugates, which contain a hydrolytically labile hydrazone linkage between a calicheamicin hydrazide derivative and the oxidized carbohydrates of the antibody. The optimal conjugates contained NAc-gamma calicheamicin as the calicheamicin core and a disulfide stabilized by two adjacent methyl groups. Further work showed that the inclusion of the hydrazone was not necessary for the CTM01 antibody and that an "amide" conjugate that was lacking this site of hydrolysis was equivalent or superior in all preclinical models examined, especially against resistant cell lines (*32, 33*). This work with CTM01 is in dramatic contrast to that with P67.6. For this antibody, the carbohydrate conjugate was shown to be superior to the amide conjugate (*22*), presumably due to the need for hydrolytic release of the calicheamicin from the antibody in the acidic lysosomes.

The reason calicheamicin conjugates of P67.6 are significantly more potent and selective when the linker contains a site for intracellular hydrolytic release is unclear, but it is consistent with the fact that P67.6 is internalized into lysosomes (*34*), an acidic compartment (*35, 36*) that would provide an environment for greatly enhanced hydrolysis over that seen at the pH found in circulation. HL-60 cells are metabolically very active and thus may require the rapid release of an active calicheamicin derivative by hydrolysis, which would be faster in the endosomes/lysosomes than disulfide exchange would likely be. Overall, the data summarized above for P67.6 and CTM01 indicate the importance of designing linkers specific for the individual target cell type.

Although the murine P67.6 carbohydrate conjugate is a potent, selective agent in models of AML, the humanized antibody could not be oxidized to make the desired conjugate without significant losses in immunoaffinity and/or drug loading. Preliminary experiments indicated that an oxidatively sensitive methionine residue near the CDR's that originated with the human sequences might be the reason for this sensitivity to oxidation. This necessitated the design of a new class of calicheamicin conjugates.

Design and Chemistry of Hybrid Conjugates. The hybrid conjugates (Figure 3), which were envisioned as the replacement for the P67.6 carbohydrate conjugate, contain both lysine attachment to the antibody through amide formation, which obviates the need for oxidation of the carbohydrates, and a hydrazone linkage, which allows for the necessary hydrolytic release. The choice of the spacer and the R group affects the stability of the hydrazone and allows for variation in the degree of hydrolyzability. Not only can the chemical properties of the linker be varied to optimize the efficacy of the conjugate, but only a single species of hydrazone is produced. With the carbohydrates as the source of aldehydes, multiple species are present which all hydrolyze at different rates, some slower and others faster than

what is optimum for best activity. These new hybrid conjugates therefore have the potential to be even more active and more selective than the carbohydrate conjugates.

Selection of a Hybrid Linker. Numerous linkers were examined (Figure 5) to ascertain the structural properties necessary for optimal activity. Past experience indicates a reasonable correlation between in vitro, in vivo, and ex vivo activity for conjugates of P67.6. Therefore, initial screening of the hybrid conjugates of hP67.6 relied on in vitro data. The results with 36 hybrid linkers showed a good correlation between the ability to hydrolyze the hydrazone bond in the calicheamicin-linker adducts, **2**, and the in vitro potency and selectivity, with certain exceptions noted below. Table 1 shows representatives of the broad variety of the linker structural types that were examined. Various benzaldehyde and acetophenone derivatives made conjugates with good activity. No substituents on the aromatic ring were found that appeared to improve activity, consistent with the functional nature of the linkers. Benzophenones such as Linker **a** made poor conjugates, consistent with the greater stability of the hydrazone to hydrolysis.

One exception to the correlation between ease of hydrolysis and activity is the group of conjugates made with aliphatic aldehydes and ketones, exemplified by Linker **d**. The hydrazone bond in this conjugate is too unstable. Even freshly prepared batches of conjugate contained significant amounts of unconjugated calicheamicin, and conjugates examined after the biological testing contained almost all of the calicheamicin in unconjugated form. Conjugates made with other linkers contained significantly lower amount of unconjugated calicheamicin (1−3%).

One other exception to the correlation between hydrolyzability and cytotoxicity is the group of conjugates made with linkers containing naphthylene spacers, exemplified by Linker **g**. Conjugates made with such linkers were more active, especially in vitro, than would be expected based on their relatively slow hydrolysis. Although the reasons for this unexpected activity are unclear, conjugates containing such linkers did not prove to be the best overall in terms of in vivo, in vitro, and ex vivo activity.

The best conjugates were made with unsubstituted acetophenones, and the "AcBut" linker (Linker **h**, 4-(4-acetylphenoxy)butanoic acid), which appeared to afford the most favorable balance between hydrolytic stability in physiological buffers (pH 7.4) and efficient drug release at the pH of lysosomes (∼4), was chosen for its good overall activity. The resultant conjugate with hP67.6 was designated CMA-676 and given the generic name of gemtuzumab ozogamicin (gem-ozo).

Characterization of Gem-Ozo. Gem-ozo has a drug loading of 2−3 mol of calicheamicin per mole of antibody, comparable to that seen with calicheamicin carbohydrate or amide conjugates. The hybrid calicheamicin conjugate gem-ozo showed higher potency and selectivity than the earlier carbohydrate conjugate in cell culture, perhaps because the calicheamicin derivative is released at close to maximum efficiency from gem-ozo. Indeed, the 2000-fold increase in potency of gem-ozo over that of the parent drug is unusual for antibody-targeted chemotherapy, which often lose 100-fold potency upon derivatization and conjugation.

In addition to the remarkably high potency and selectivity in cell culture, gem-ozo is curative of the HL-60 xenograft in nude mice over a roughly 6-fold dose range. A comparable conjugate of a nontargeting antibody is virtually inactive in this model, while the previous carbohydrate conjugate shows somewhat less activity at the lowest dose tested. In ex vivo colony-forming assays, a significant percent of marrow samples are inhibited by gem-ozo. Attempts to elucidate the factors responsible for a response or lack thereof by looking at such factors as MDR and antigen expression have so far met with failure. However, it is clear that gem-ozo has significant activity in a subpopulation of patient samples in this assay. It is impossible to quantify the fraction of the total population that might be treated successfully from these data, as only about 25% of patient bone marrow samples form colonies in this assay. Taken together, the preclinical data presented in this article indicate that the hybrid conjugates as exemplified by this AcBut conjugate constitute a new, improved class of calicheamicin conjugates.

The effectiveness of gem-ozo in preclinical models as well as in clinical trials (vida infra) is attributed to the use of a potent cytotoxic agent, an internalizing target antigen with restricted expression and easy accessibility, and a custom-made, well-controlled, hydrolyzable bond with the AcBut linker. The hydrolytic release of the drug from the conjugate that results from the use of this novel, bifunctional linker (presumably in the acidic endosomes/lysosomes of the target cells) appears to be very important for the intracellular trafficking of the calicheamicins when targeting $CD33^+$ myeloid leukemia cells (*22*).

Aside from these considerations of design and mechanism of action, gem-ozo has demonstrated an acceptable safety profile in clinical trials as a single agent while achieving remissions in 38% of patients with AML in first relapse (*24*, *25*). In addition, as indication of the significantly decreased tendency for immune responses in patients in comparison to ricin conjugates, where virtually every patient shows an anti-ricin response, there were only two immune responses reported to gem-ozo in the Phase I trial (*24*) and none reported in the Phase II trial (*25*).

The clinical efficacy of the immunoconjugate described in these studies has recently been demonstrated in clinical trials using gem-ozo as single-agent therapy. In a Phase I dose escalation trial (*24*), 40 patients with advanced $CD33^+$ AML were treated to determine the toxicity and maximally tolerated dose of gem-ozo. In contrast to the significant toxicity observed with most therapies for AML, treatment with gem-ozo was remarkably well tolerated, with fever and chills as the most common clinical side effect. Furthermore, a relatively long half-life of approximately 2 days was observed. Clinical responses were observed in this group of patients with advanced disease, with leukemia cells eliminated from blood and marrow in eight patients, three of whom also showed complete recovery of normal hematopoietic function with a duration of response of from 140 to >623 days.

In a Phase II single-agent trial (*25*) to establish efficacy in patients with AML who relapsed after an initial remission in response to conventional chemotherapy, analysis of the 142 patients enrolled in three separate trials revealed 30% remissions as defined by disappearance of morphologically detectable leukemia from the blood and marrow, recovery of the peripheral granulocyte count to greater than 1,500/mm^3, and independence from platelet transfusion. Median relapse-free and landmark survival for these patients was 6.8 months and 12 months, respectively. The probability of survival at one year for all patients that underwent treatment was 31%. The toxicity profile of Mylotarg appears to be different

from that of traditional chemotherapy for AML, with lower incidences of mucositis and infections being noteworthy.

These results overall support the notion that the pluripotent stem cells may be predominately, if not completely, normal in some patients with AML, enabling reestablishment of normal hematopoiesis by remaining $CD33^-$ cells. Based on the preclinical and clinical data presented here, gem-ozo appears promising as an effective and, in some respects, less toxic new therapy for AML. On the basis of phase II data, Mylotarg, a representative of the new, improved hybrid class of calicheamicin conjugates, has become the first antibody-targeted chemotherapeutic agent approved by the FDA.

LITERATURE CITED

(1) Cf. Kreitman, R. J., Wilson, W. H., White, J. D., Stetler-Stevenson, M., Jaffe, E. S., Giardina, S., Waldmann, T. A., and Pastan, I. (2000) Phase I trial of recombinant immunotoxin anti-Tac(Fv)-PE38 (LMB-2) in patients with hematologic malignancies. *J. Clin. Oncol. 18*, 1622−1636.

(2) Ellestad, G. A., Ding, W.-D., Zein, N., and Townsend, C. A. (1995) DNA-cleaving properties of calicheamicin γ_1^I. *Enediyne Antibiotics as Antitumor Agents* (D. B. Borders, and T. W. Doyle, Eds.) pp 137−160, Marcel Dekker, New York.

(3) Lee, M. D., Ellestad, G. A., and Borders, D. B. (1991) Calicheamicins: Discovery, structure, chemistry, and interaction with DNA. *Acc. Chem. Res. 24*, 235−243.

(4) Liu, C., and Chari, R. V. J. (1997) The development of antibody delivery systems to target cancer with highly potent maytansinoids. *Expert Opin. Invest. Drugs 6*, 169−172.

(5) Chari, R. V. J., Jackel, K. A., Bourret, L. A., Derr, S. M., Tadayoni, B. M., Mattocks, K. M., Shah, S. A., Liu, C., Blättler, W. A., and Goldmacher, V. S. (1995) Enhancement of the selectivity and antitumor activity of a CC-1065 analogue through immunoconjugate formation. *Cancer Res. 55*, 4079−4084.

(6) Keating, M. J., Estey, E., and Kantarjian, H. (1993) Acute leukemia. *Cancer, Principles and Practice of Oncology* (V. T. DeVita, Jr., S. Hellman, and S. A. Rosenberg, Eds.) pp 1938−1964, JB Lippincott Company, Philadelphia.

(7) Andrews, R. G., Torok-Strob, B., and Bernstein, I. D. (1983) Myeloid-associated differentiation antigens on stem cells and their progeny identified by monoclonal antibodies. *Blood 62*, 124−132.

(8) Griffin, J. D., Linch, D., Sabbath, K., Larcom, P., and Schlossman, S. F. (1984) A monoclonal antibody reactive with normal and leukemic human myeloid progenitor cells. *Leuk. Res. 8*, 521−534.

(9) Dinndorf, P. A., Andrews, R. G., Benjamin, D., Ridgway, D., Wolff, L., and Bernstein, I. D. (1986) Expression of normal myeloid-associate antigens by acute leukemia cells. *Blood 67*, 1048−1053.

(10) Andrews, R. G., Singer, J. W., and Bernstein, I. D. (1989) Precursors of colony-forming cells in humans can be distinguished from colony-forming cells by expression of the CD33 and CD34 antigens and light scatter properties. *J. Exp. Medicine 169*, 1721−1731.

(11) van der Jagt, R. H. C., Badger, C. C., Appelbaum, F. R., Press, O. W., Matthews, D. C., Eary, J. F., Krohn, K. A., and Bernstein, I. D. (1992) Localization of radiolabeled antimyeloid antibodies in a human acute leukemia xenograft tumor model. *Cancer Res. 52*, 89−94.

(12) Bernstein, I. D., Singer, J. W., Smith, F. O., Andrews, R. G., Flowers, D. A., Petersens, J., Steinmann, L., Najfeld, V., Savage, D., Fruchtman, S., Arlin, Z., and Fialkow, P. J. (1992) Differences in the frequency of normal and clonal precursors of colony-forming cells in chronic myelogenous leukemia and acute myelogenous leukemia. *Blood 79*, 1811−1816.

(13) Bernstein, I. D., Singer, J. W., Andrews, R. G., Keating, A., Powell, J. S., Bjornson, B. H., Cuttner, J., Najfeld, V., Reaman, G., Raskind, W., Sutton, D. M. C., and Fialkow, P. J. (1987) Treatment of acute myeloid leukemia cells in vitro with a monoclonal antibody recognizing a myeloid differentiation antigen allows normal progenitor cells to be expressed. *J. Clin. Invest. 79*, 1153−1159.

(14) Bonnet, D., and Dick, J. E. (1997) Human acute myeloid leukemia is organized as a hierarchy that originates from a primitive hematopoietic cell. *Nature Medicine 3*, 730−737.

(15) Appelbaum, F. R., Matthews, D. C., Eary, J. F., Badger, C. C., Kellogg, M., Press, O. W., Martin, P. J., Fisher, D. R., Nelp, W. B., Thomas, E. D., and Bernstein, I. D. (1992) The use of radiolabeled anti-CD33 antibody to augment marrow irradiation prior to marrow transplantation for acute myelogenous leukemia. *Transplantation 54*, 829−833.

(16) Caron, P. C., Dumont, L., and Scheinberg, D. A. (1998) Supersaturating infusional humanized anti-CD33 monoclonal antibody HuM195 in myelogenous leukemia. *Clinical Cancer Res. 4*, 1421−1428.

(17) Tanimoto, M., Scheinberg, D. A., Cordon-Cardo, C., Huie, D., Clarkson, B. D., and Old, L. J. (1989) Restricted expression of an early myeloid and monocytic cell surface antigen defined by monoclonal antibody M195. *Leukemia 3*, 339−348.

(18) Xu, Y., and Scheinberg, D. A. (1995) Elimination of human leukemia by monoclonal antibodies in an athymic nude mouse leukemia model. *Clinical Cancer Res. 1*, 1179−1187.

(19) Cf. Trail, P. A., Willner, D., Lasch, S. J., Henderson, A. J., Hofstead, S., Casazza, A. M., Firestone, R. A., Hellström, I., and Hellström, K. E. (1993) Cure of xenografted human carcinomas by Br96-doxorubicin immunoconjugates. *Science 261*, 212−215.

(20) Lee, M. D., Dunne, T. M., Siegel, M. M., Chang, C. C., Morton, G. O., and Borders, D. B. (1987) Calicheamicins, a novel family of antitumor antibiotics, 1. Chemistry and partial structure of calicheamicin γ_1^I. *J. Am. Chem. Soc. 109*, 3464−3466.

(21) Myers, A. G., Cohen, S. B., and Kwon, B. M. (1994) A study of the reaction of Calicheamicin γ_1 with glutathione in the presence of double-stranded DNA. *J. Am. Chem. Soc. 116*, 1255−1271.

(22) Hamann, P. R., Hinman, L. M., Beyer, C. F., Lindh, D., Upeslacis, J., Flowers, D. A., and Bernstein, I., An anti-CD33 antibody-calicheamicin conjugate for treatment of acute myeloid leukemia; Choice of linker. *Bioconjugate Chem. 13*, 40−46.

(23) Rodwell, J. D., Alvarez, V. L., Lee, C., Lopes, A. D., Goers, J. W. F., King, H. D., Powsner, H. J., and McKearn, T. J. (1986) Site-specific covalent modification of monoclonal antibodies: In vitro and in vivo evaluations. *Proc. Natl. Acad. Sci. U.S.A. 83*, 2632−2636.

(24) Sievers, E. L., Appelbaum, F. R., Spielberger, R. T., Forman, S. J., Flowers, D., Smith, F. O., Shannon-Dorcy, K., Merger, M. S., and Bernstein, I. D. (1999) Selective ablation of acute myeloid leukemia using antibody-targeted chemotherapy: A phase I study of an anti-CD33 calicheamicin immunoconjugate. *Blood 93*, 3678−84.

(25) Sievers, E. L., Larson, R. A., Stadtmauer, E. A., Estey, E., Löwenberg, B., Dombret, H., Karanes, C., Theobald, M., Bennett, J. M., Sherman, M. L., Berger, M. S., Eten, C. B., Loken, M. R., van Dongen, J. J. M., Bernstein, I. D., Appelbaum, F. R. (2001) Efficacy and safety of gemtuzumab ozogamicin in patients with CD33-positive acute myeloid leukemia in first relapse. *J. Clin. Oncol. 19*, 3244−3254.

(26) Hinman, L. M., Hamann, P. R., Wallace, R., Menendez, A. T., Durr, F. E., and Upeslacis, J. (1993) Preparation and characterization of monoclonal antibody conjugates of the calicheamicins: a novel and potent family of antitumor antibiotics. *Cancer Res. 53*, 3336−3342.

(27) Baker, T. S., Bose, C. C., Caskey-Finney, H. M., King, D. J., Lawson, A. D., Lyons, A., Mountain, A., Owens, R. J., Rolfe, M. R., Sehdev, M., Yarranton, G. T., and Adair, J. R. (1994) Humanization of an anti-mucin antibody for breast and ovarian cancer therapy. *Adv. in Exp. Med. Biol. 1994*, 35361−35382.

(28) Hamann, P. R., Hinman, L., Hollander, I., Holcomb, R., Hallett, W., Tsou, H.-R., and Weiss, M. J. (1998) Calicheamicin conjugates with hybrid linkers. US patent no. 5,773,001.

(29) Hamann, P. R., Hollander, I., Kunz, A., and Kunstman, M., Unpublished results.

(30) Aboud-Pirak, E., Sergent, T., Otte-Slachmuylder, C., Abarca, J., Trouet, A., and Schneider, Y.-J. (1988) Binding and endocytosis of a monoclonal antibody to a high molecular weight human milk fat globule membrane-associated antigen by cultured MCF-7 breast cancer cells. *Cancer Res. 48*, 3188−3196.

(31) Hinman, L. M., Hamann, P. R., and Upeslacis, J. (1995) Preparation of conjugates to monoclonal antibodies. *Enediyne Antibiotics as Antitumor Agents* (D. B. Borders, and T. W. Doyle, Eds.) pp 87−105, Marcel Dekker, New York.

(32) Hamann, P. R., Hinman, L. M., Beyer, C. F., Greenberger, L., Lin, C., Lindh, D., Menendez, A. T., Upeslacis, J., and Wallace, R., An anti-MUC1 antibody-calicheamicin conjugate for treatment of solid tumors, choice of linker and overcoming drug resistance. Unpublished results.

(33) Hamann, P. R., Hinman, L. M., Beyer, C. F., Lindh, D., and Mountain, A., A calicheamicin conjugate with a fully humanized anti-MUC1 antibody shows potent antitumor effects in breast and ovarian tumor xenografts. Unpublished results.

(34) Press, O. W., Shan, D., Howell-Clark, J., Eary, J., Appelbaum, F. R., Matthews, D., King, D. J., Haines, A. M. R., Hamann, P., Hinman, L., Shochat, D., and Bernstein, I. D. (1996) Comparative metabolism and retention of iodine-125, yttrium-90, and indium-111 radioimmunoconjugates by cancer cells. *Cancer Res. 56*, 2123-2129.

(35) Van Dyke, R. W., Root, K. V., Schreiber, J. H., and Wilson, J. M. (1992) Role of CFTR in lysosome acidification. *Biochem. Biophys. Res. Commun. 184*, 300−305.

(36) Ohkuma, S., Poole, B. (1978) Fluorescence probe measurement of the intralysosomal pH in living cells and the perturbation of pH by various agents. *Proc. Natl. Acad. Sci. U.S.A. 75*, 3327−3331.

BC010021Y

Polycationic Telomers and Cotelomers for Gene Transfer: Synthesis and Evaluation of Their an Vitro Transfection Efficiency

Nathalie Van Craynest,[†] Catherine Santaella,[†,‡] Otmane Boussif,[§,||] and Pierre Vierling*[,†]

Laboratoire de Chimie Bio-Organique, UMR 6001 CNRS, Université de Nice Sophia-Antipolis, Faculté des Sciences, 06108 Nice Cédex 2, France, and Transgène SA, 11 rue de Molsheim, 67082 Strasbourg Cédex, France. Received March 2, 2001; Revised Manuscript Received May 15, 2001

We report on the synthesis of a series of lipopolyamine telomers, [I(Asp)-14,n_A(NH), I(His)-18,n_A(NH), I-18,n_B(NMe), Gal-n_A(NH)], and random cotelomers, [I-18,n_A(NH)-n_B(NMe) and I-18,n_A(NH)-n_C(OH)], and on their in vitro gene transfer capability. They were obtained by a telomerization process of various amino-acrylamide taxogens with various lipophilic thiol telogens which might also contain an aspartic or a histidine residue or with a thiogalactosyle derivative. For *N*/*P* ratios (*N* = number of (co)telomer amine equivalents, *P* = number of DNA phosphates) from 0.8 to 10, these polyamine (co)telomers condensed DNA, with or without the use of DOPE, forming (co)teloplexes of mean sizes less than 200 nm, except for *N*/*P* 1.25 for which precipitates were observed. Some trends, structure−transfection efficiency relationships, were established. Thus, aspartic-containing telomers were found to lead to efficient formulations for plasmid delivery to A549 cells and for *N*/*P* ratios from 1.25 to 5.

INTRODUCTION

Transgene expression mediated by (poly)cationic lipid- or polymer-plasmid DNA complexes (lipoplexes or polyplexes, respectively) represents an attractive alternative to the use of viral vectors in gene therapy. Synthetic nonviral gene transfer vectors, which are free from the risks associated with viral vectors, may represent more suitable gene delivery systems for repetitive use and will be of considerable potential to the gene therapy field. Although viral vectors are very efficient for gene delivery, their use suffers indeed from a number of disadvantages, including safety (possible presence of replication-competent virions, insertional mutagenesis, and specific immune response) and practical issues relating to quality control and high-cost and problematic large-scale production (*1*).

Over the past decade, a large variety of (poly)cationic lipids, liposomes (including highly fluorinated ones (*2*)), lipopolymers, and (co)polymers (*3*−*11* and references therein), have been used extensively to deliver genes to a large variety of cell lines and tissues. Several studies have shown that in vitro and in vivo transfection with complexed DNA can vary in function of, among others, the cationic components (lipid, polymer), the lipid composition of the lipoplexes (presence of helper lipids), and the size of the complexes. Currently, little is known concerning the intracellular traffic after endocytosis of the DNA complexes, and the ongoing research remains empirical. Consequently, there is a need to develop new compounds, especially cationic ones, with characteristics and properties different from those already described. Recently, as a contribution into this field, some of us have reported on teloplexes (e.g., DNA complexes formulated with lipopolyamine telomers) as alternative efficient gene transfer agents (*12*). These lipopolyamine telomers were obtained from telomerizing one polymerizable acrylamide M monomer, comprising a (poly)amine precursor, in the presence of a hydrophobic long-chain thiol (L-SH). The lipopolyamine telomers thus obtained, of formula L-S-(M)*n*-H, show lower degrees of polymerization ($1 \leq n < 200$) (*10*, *12*) and, hence, rather lower molecular weights than (M)*n* compounds obtainable with classic polymerization processes ($n \gg 200$) (*8*−*10*, *12*).

We report herein on the synthesis of new (lipo)polyamine telomers and random cotelomers (Figure 1), on their capabilities of compacting and transferring DNA into a cell, and on their effect on cell viability. This second generation of cationic (lipo)polyamine telomers and cotelomers shows a modular structure aimed at modulating the physicochemical and biological properties (e.g., chemical stability, biodegradability, toxicity, biodisponibility, and transfection efficacy) of the teloplexes and cotelolexes they form with DNA. This modular structure design was partly deduced from the SAR analysis performed with the first generation of telomers (*12*). The telomer's or cotelomer's polar moiety includes a variable number (from 15 to 90) of primary or tertiary amine functions or a random combination of primary and tertiary amine or polyol (tris(hydroxymethyl)methyl THM) functions, respectively. This polar moiety is connected to a hydrophilic galactosyl or a hydrophobic residue which might also contain an aspartic or a histidine amino acid. The galactosyl residue was selected in order to show the importance, with respect to transfection, of the hydrophilic or hydrophobic character of the moiety connected to the polyamine polar head. The neutral, hydrophilic THM and also the galactosyl residue were selected for improving the cell viability of the DNA complexes (*7*, *9*). The two amino acids were selected for the pK_a of their acid (pK_a 3.9) or imidazole (pK_a 6.1) functions, respectively, which could increase the buffering capacity of the DNA complexes inside the endosomes or lysosomes,

* Corresponding author. E-mail: vierling@unice.fr. Phone: 33 4 92 07 61 43. Fax: 33 4 92 07 61 51.

[†] Laboratoire de Chimie Bio-Organique.

[‡] Present address: Laboratoire d'Ecologie Microbienne de la Rhizosphère, UMR CNRS-CEA 163, DSV/DEVM.

[§] Transgène SA.

[||] Present address: Aventis Pharma.

10.1021/bc010047p CCC: $22.00 © 2002 American Chemical Society
Published on Web 12/13/2001

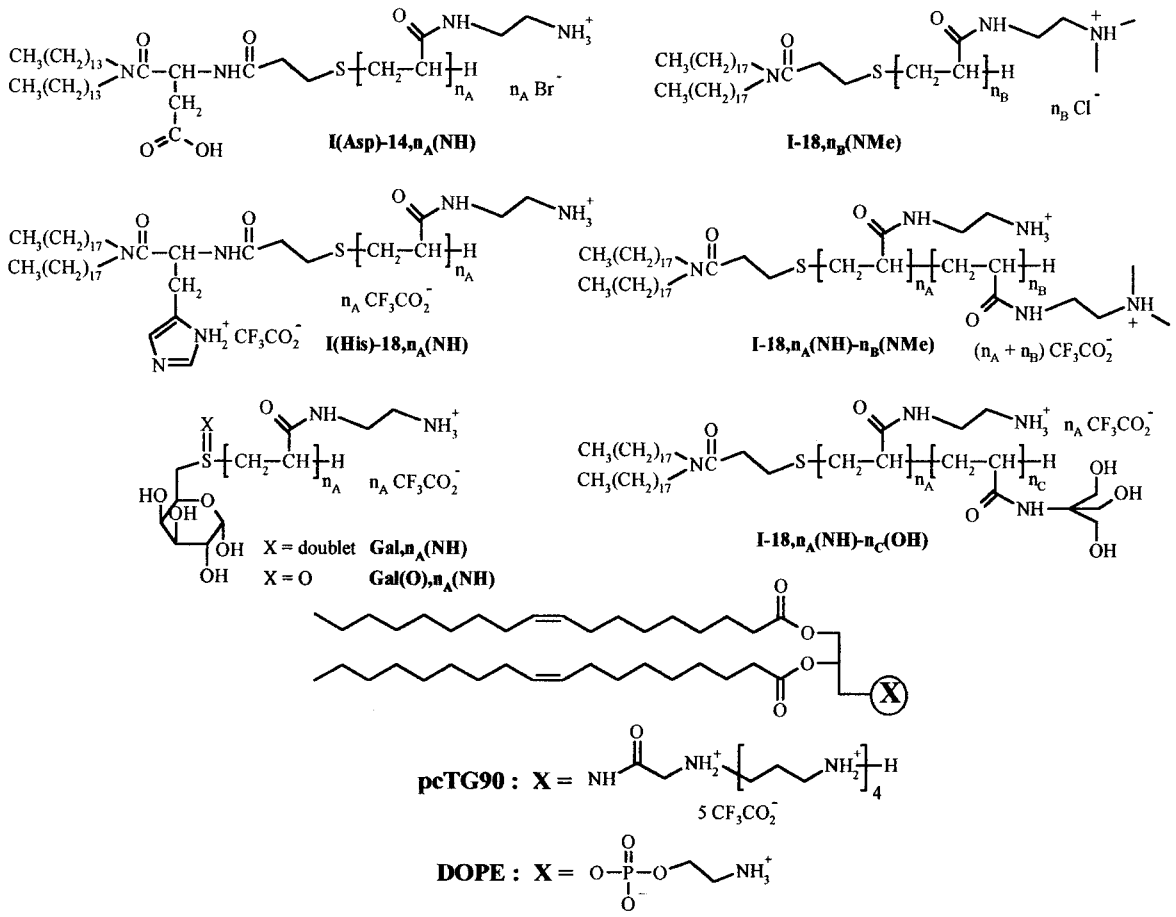


Figure 1. Molecular structure of the lipopolycationic telomers and cotelomers and of the pcTG90/DOPE reference gene transfer lipids used in this study.

causing their disruption and, thus, enhancing DNA cytoplasmic delivery (*4*, *13*); for example, the transfection efficiency of polylysines was improved when these polymers were partially substituted with histidyl residues (*11*). As the use of colipids such as DOPE (*14*, *15*) (which, when used alone, do not enhance gene transfer) was found in several cases to enhance transfection, we report also on the transfection efficacy of the lipotelomers used in conjunction with DOPE.

EXPERIMENTAL SECTION

General Experimental and Analytical Conditions. Most of the reactions were performed in anhydrous solvents under dry and oxygen-free nitrogen. The purifications by column chromatography were carried out using silica gel 60 (Merck, Whitehouse Station, NJ; 70−230 mesh) and chloroform ($CHCl_3$), dichloromethane (CH_2Cl_2), methanol (MeOH), diethyl ether (Et_2O), or mixtures thereof as indicated. The advance of the polymerization reaction was followed by thin-layer chromatography (TLC) on silica plates F_{254} (Merck). The following developing systems were used: UV light, $KMnO_4$, H_2SO_4/MeOH, DTNB (5,5′-dithiobis(2-nitrobenzoic acid)), and ninhydrin reagent (Sigma, St. Louis, MO). The syntheses of telogen I-SH and of taxogen **A** (*N*-[2-[(BOC)-aminoethyl]]acrylamide) have been performed as described in ref *12*. Taxogen **C** (*N*-tris(hydroxymethyl)-methylacrylamide) was purchased from Aldrich.

^1H and ^{13}C NMR spectra were recorded at 200 and 50.3 MHz, respectively, on a Bruker AC-200. Chemical shifts were measured relative to $CHCl_3$ (δ 7.27) or CH_3OD (δ 3.35) for ^1H, relative to $CDCl_3$ (δ 76.9) for ^{13}C, and expressed indirectly in relation to TMS. The following abbreviations are used to describe the signal multiplicities: s (singlet), d (doublet), t (triplet), q (quadruplet), and m (multiplet). Chemical shifts are expressed in ppm and listed as follows: shift in ppm (multiplicity, integration, coupling, and attribution). Mass spectra (MS) were recorded on a Finningan MAT TSQ 7000 equipped with an atmospheric pressure ionization (API) source. Electrospray ionization mass spectrometry (ESI-MS) was used depending on the polar moiety of the molecules to be studied. This method used in positive mode can give either a $M + H^+$ or a $M + Na^+$ signal.

Synthesis of Telogen I(Asp(OBzl))-SH. *H-Asp(OBzl)-N,N-ditetradecanamide TFA,* ***(1)***. A total of 126 mg (0.31 mmol) of ditetradecylamine (*12*), 0.12 mL (0.92 mmol) of NEt_3, and 144 mg (0.31 mmol) of PyBrop (Novabiochem) were added to a solution of 100 mg (0.31 mmol) of BOC-Asp(OBzl)-OH (Bachem) in 2 mL of CH_2Cl_2. After 24 h of reflux, $CHCl_3$ was added, and the organic phase was washed successively with $KHSO_4$ 5%, $NaHCO_3$ 8%, and H_2O and then dried over Na_2SO_4. The residue obtained after evaporation was chromatographed on a silica gel column ($CHCl_3$ to $CHCl_3/CH_3OH$, 99/1, v/v), giving 156 mg (0.22 mmol, 71%) of BOC-Asp(OBzl)-*N*,*N*-ditetradecanamide as a colorless oil. [TLC ($CHCl_3/CH_3OH$, 85/15, ninhydrin): $R_f = 0.8$. ^1H NMR ($CDCl_3$): 0.80 (t, 6H, J = 6.0 Hz, CH_3), 1.05−1.35 (m, 44H, $(CH_2)_{11}$), 1.35−1.60 (m, 13H, Me(BOC)), CH_2CH_2N), 2.55 and 2.76 (AB part of an ABX system, 2H, $^2J_{AB}$ = 15.6 Hz, $^3J_{AX}$ = 7.0 Hz, $^3J_{BX}$ = 6.0 Hz, CH_2CH), 3.00−3.40 (m, 4H, CH_2N), 4.80−4.95 (m, 1H, CH), 5.02 (s, 2H, CH_2Ph), 5.32 (d, 1H, J = 9.4 Hz, NH), 7.25 (s, 5H, Ph). ^{13}C NMR ($CDCl_3$): 14.2

(CH_3); 22.7 (CH_2CH_3); 28.3 (Me(BOC)); 26.9, 27.0, 27.5, 29.3, 29.4, 29.6, 29.7 ((CH_2)$_{11}$); 32.0 ($CH_2CH_2CH_3$); 38.4 (CH_2CO); 46.4, 47.4, 48.0 (CH_2N, CH_2Ph); 66.6 (CH); 79.9 (C(BOC)); 128.2, 128.3, 128.5 (CH=CH(Ph)); 135.8 (C=CH(Ph)); 154.9 (CO(BOC)); 170.3 (CO_2); 170.5 (CON).] This compound was then placed into 4.2 mL (54.5 mmol) of trifluoroacetic acid (TFA; Aldrich) for 1 h at room temperature (RT). Excess TFA was eliminated by evaporation with cyclohexane, giving 126 mg (0.22 mmol, 100%) of **1** as a colorless oil. [TLC ($CHCl_3$/CH_3OH, 95/5, ninhydrin): $R_f = 0.6$. ^{1}H NMR ($CDCl_3$): 0.83 (t, 6H, J = 6.0 Hz, CH_3), 1.05−1.75 (m, 48H, (CH_2)$_{12}$), 2.70−3.60 (m, 6H, CH_2N, CH_2CH), 4.55−4.75 (m, 1H, CH), 5.08 (m, 2H, CH_2Ph), 7.28 (s, 5H, Ph). ^{13}C NMR ($CDCl_3$): 14.2 (CH_3); 22.8 (CH_2CH_3); 26.9, 27.1, 27.3, 28.8, 29.3, 29.5, 29.6, 29.8 ((CH_2)$_{11}$); 32.0 ($CH_2CH_2CH_3$); 35.4 (CH_2CO); 46.7, 47.3, 48.0 (CH_2N,CH_2Ph); 67.7 (CH); 128.7 (CH=CH(Ph)); 135.1 (C=CH(Ph)); 161.9 (q, $^2J_{CF}$ = 35 Hz, CF_3CO_2); 167.1 (CO_2); 169.7 (CON).]

3-Mercaptopropanamide-Asp(OBzl)-N,N-ditetradecanamide, [I(Asp(OBzl))-SH]. To 154 mg (0.21 mmol) of **1** were added 0.1 mL (0.72 mmol) of NEt_3 and 2 mL (0.30 mmol) of a 0.15 M 3-mercaptopropionic acid (Aldrich) in CH_2Cl_2. After being cooled to 0 °C, 45 mg (0.33 mmol) of HOBt (Sigma), then 64 mg (0.33 mmol) of EDC (Aldrich), and 1 mL of CH_2Cl_2 were added. After 17 h at RT, $CHCl_3$ was added, and the organic phase was washed successively with $NaHCO_3$ 8%, $KHSO_4$ 5%, and then H_2O. After being dried over Na_2SO_4, evaporation, and chromatography (CH_2Cl_2/hexane, 8/2, v/v to CH_2Cl_2), one obtained 65 mg (0.09 mmol, 43%) of I(Asp(OBzl))-SH as a colorless oil. [TLC ($CHCl_3$, ninhydrin, DTNB): $R_f = 0.2$. ^{1}H NMR ($CDCl_3$): 0.80 (t, 6H, J = 6.0 Hz, CH_3), 1.05−1.75 (m, 48H, (CH_2)$_{12}$), 1.49 (t, 1H, J = 8.2 Hz, SH), 2.39 (t, 2H, J = 6.5 Hz, CH_2CONH), 2.50−2.90 (m, 4H, CH_2SH, CH_2CH), 3.00−3.45 (m, 4H, CH_2N), 5.02 (s, 2H, CH_2Ph), 5.22 (td, 1H, J = 7.5 Hz and J = 6.5 Hz, CH), 6.94 (t, 1H, J = 6.5 Hz, NH), 7.26 (s, 5H, Ph). ^{13}C NMR ($CDCl_3$): 14.2 (CH_3); 20.4 (CH_2SH); 22.8 (CH_2CH_3); 26.9, 27.1, 29.3, 29.5, 29.8 ((CH_2)$_{11}$); 32.0 ($CH_2CH_2CH_3$); 38.2 (CH_2CO_2); 40.2 (CH_2-CONH); 46.0, 46.6, 48.2 (CH_2N, CH_2Ph); 66.8 (CH); 128.4, 128.5, 128.6 (CH=CH(Ph)); 135.7 (C=CH(Ph)); 170.1, 170.3 (CO).]

Synthesis of Telogen I(His(BOC))-SH. *H-His(BOC)-N,N-dioctadecanamide, (**2**).* To a solution of 500 mg (1.04 mmol) of Fmoc-His(BOC)-OH (Bachem) in 2 mL of $CHCl_3$ were added 0.15 mL (1.04 mmol) of NEt_3 and 488 mg (1.04 mmol) of PyBrop and then 1.09 g (2.09 mmol) of dioctadecylamine (Fluka) in 15 mL $CHCl_3$. The resulting mixture was stirred for 4 h at RT. The organic phase was washed with H_2O, dried over Na_2SO_4, concentrated, and then chromatographed ($CHCl_3$), yielding 550 mg (0.56 mmol, 53%) of Fmoc-His(BOC)-*N,N*-dioctadecanamide as a colorless oil. [TLC ($CHCl_3$/CH_3OH, 99/1, $KMnO_4$): R_f = 0.7. ^{1}H NMR ($CDCl_3$): 0.84 (t, 6H, J = 6.0 Hz, CH_3), 1.05−1.50 (m, 64H, (CH_2)$_{16}$), 1.50−1.80 (m, 9H, Me-(BOC)), 2.75−3.70 (m, 6H, CH_2N, CH_2im), 4.10−4.45 (m, 3H, CH_2CH(Fmoc)), 4.94 (td, 1H, J = 8.0 Hz, J = 8.7 Hz, $CHCH_2$im), 5.90 (d, 1H, J = 8.7 Hz, NH), 7.15 (s, 1H, CH=C(im)), 7.05−7.45 (m, 4H, Fmoc), 7.55 (d, 2H, J = 8.0 Hz, Fmoc), 7.70 (d, 2H, J = 8.0 Hz, Fmoc), 7.96 (s, 1H, CH=N(im)). ^{13}C NMR ($CDCl_3$): 14.2 (CH_3); 22.7 (CH_2CH_3); 27.9 (Me(BOC)); 27.0, 27.1, 27.7, 29.5, 29.8 ((CH_2)$_{14}$); 32.0 ($CH_2CH_2CH_3$); 33.0 (CH_2im); 46.4, 47.3 (CH_2NCO); 48.0 (CH_2CH(Fmoc)); 51.1 ($CHCH_2$im); 67.2 (CH_2CH(Fmoc)); 85.4 (C(BOC)); 114.8 (CH=C(im)); 136.8 (CH=C(im)); 139.0 (CH=N(im)); 120.0, 125.3, 127.1, 127.7 (CH=CH(Fmoc)); 141.3, 144.1 (C=C(Fmoc)); 147.0 (CO(BOC)); 155.8 (CO(Fmoc)); 171.2 (CO).] Fmoc deprotection of 390 mg (0.39 mmol) of this compound was performed in 10 mL of a $^1/_2$ morpholine/DMF mixture at RT for 2 h, affording, after evaporation and chromatography of the residue ($CHCl_3$ to $CHCl_3$/CH_3OH, 99/1, v/v), 187 mg (0.24 mmol, 62%) of **2** as a colorless oil. [TLC ($CHCl_3$/CH_3OH, 9/1, UV, ninhydrin): $R_f = 0.5$. ^{1}H NMR ($CDCl_3$): 0.80 (t, 6H, J = 6.0 Hz, CH_3), 1.05−1.30 (m, 60H, (CH_2)$_{15}$), 1.30−1.45 (m, 4H, CH_2CH_2NCO), 1.45−1.60 (m, 9H, Me(BOC)), 2.50 and 2.85 (AB part of an ABX system, 2H, $^2J_{AB}$ = 14.0 Hz, $^3J_{AX}$ = 8.0 Hz, $^3J_{BX}$ = 5.5 Hz, CH_2im), 2.90−3.55 (m, 4H, CH_2NCO), 3.90 (X part, 1H,$^3J_{XB}$ = 8.0 Hz, $^3J_{XA}$ = 5.5 Hz, $CHCH_2$im), 7.10 (s, 1H, CH=C(im)), 7.98 (s, 1H, CH=N(im)).]

3-Mercaptopropanamide-His(BOC)-N,N-dioctadecanamide, (I(His(BOC))-SH). To a solution of 120 mg (0.16 mmol) of **2** in 1.5 mL of CH_2Cl_2 at 0 °C, were added 14 μL (0.15 mmol) of 3-mercaptopropionic acid, 23 mg (0.17 mmol) of HOBt, and 33 mg (0.17 mmol) of EDC. After 12 h at RT, $CHCl_3$ was added, and the organic phase was washed with 8% $NaHCO_3$ and H_2O and then dried over Na_2SO_4. After evaporation and chromatography (CH_2Cl_2 to CH_2Cl_2/Et_2O, 9/1, v/v), 31 mg (0.03 mmol, 23%) of I(His(BOC))-SH as a colorless oil was obtained. [TLC ($CHCl_3$/CH_3OH, 98/2, UV, DTNB, $KMnO_4$): $R_f = 0.4$. ^{1}H NMR ($CDCl_3$): 0.80 (t, 6H, J = 6.0 Hz, CH_3), 1.05−1.45 (m, 64H, (CH_2)$_{16}$), 1.45−1.75 (m, 9H, Me(BOC)), 2.35−2.55 (m, 2H, CH_2CO), 2.55−3.50 (m, 8H, CH_2im, CH_2SH, CH_2N), 5.00−5.30 (m, 1H, $CHCH_2$im), 6.70−6.85 (m, 1H, NH), 7.10 (s, CH=C(im)), 7.95 (s, CH=N(im)). ^{13}C NMR ($CDCl_3$): 14.2 (CH_3); 20.4 (CH_2SH); 22.8 (CH_2CH_3); 27.9 (Me(BOC)); 26.9, 27.1, 27.6, 29.4, 29.8 ((CH_2)$_{14}$); 32.0 ($CH_2CH_2CH_3$); 32.1 (CH_2im); 40.4 (CH_2CO); 46.4, 48.0 (CH_2N); 48.8 ($CHCH_2$im); 85.5 (C(BOC)); 114.7 (CH=C(im)); 136.8 (C=CH(im)); 138.8 (C=N(im)); 147.5 (CO(BOC)); 170.0, 170.8 (CO).]

Synthesis of Telogen. *6-Deoxy-6-thio-1,2:3,4-di-O-isopropylidene-D-galactopyranose, (PGal-SH).* To a solution of 1.2 g (4.7 mmol) of 1,2:3,4-di-*O*-isopropylidene-D-galactopyranose (Aldrich) in 120 mL of toluene were added 3.7 g (14.0 mmol) of PPh_3 (Aldrich), 1.0 g (14.0 mmol) of imidazole (Aldrich), and 2.4 g (9.4 mmol) of iodine (Aldrich). After 4 h of reflux, the reaction mixture was stirred with saturated $NaHCO_3$ for 5 min. Iodine was then added until the organic phase became yellow. After 15 min, the organic phase was extracted with $Na_2S_2O_3$ until decoloration, washed with H_2O, and then dried over Na_2SO_4. After evaporation, the residue was extracted with Et_2O, concentrated, and chromatographed (petroleum ether to petroleum ether/Et_2O, 7/3, v/v), yielding 1.6 g (4.2 mmol, 89%) of 6-deoxy-6-iodo-1,2:3,4-di-*O*-isopropylidene-D-galactopyranose as a pale-yellow powder. [TLC (petroleum ether/Et_2O, 1/1, H_2SO_4): $R_f = 0.9$. ^{1}H NMR ($CDCl_3$): 1.25, 1.27, 1.36, 1.46 (s, 12H, CH_3); 3.12 and 3.24 (AB part of an ABX system, 2H, $^2J_{AB}$ = 9.9 Hz, $^3J_{AX}$ = 6.9 Hz, $^3J_{BX}$ = 6.9 Hz, $GalH_6$); 3.85 (dt, 1H, $^3J_{AX}$ = 6.9 Hz, $^3J_{BX}$ = 6.9 Hz, $^3J_{5-4}$ = 1.8 Hz, $GalH_5$); 4.22 (dd, 1H, $^3J_{2-1}$ = 5.0 Hz, $^3J_{2-3}$ = 2.5 Hz, $GalH_2$); 4.32 (dd, 1H, $^3J_{4-3}$ = 7.8 Hz, $^3J_{4-5}$ = 1.8 Hz, $GalH_4$); 4.53 (dd, 1H, $^3J_{3-4}$ = 7.8 Hz, $^3J_{3-2}$ = 2.5 Hz, $GalH_3$); 5.46 (d, 1H, $^3J_{1-2}$ = 5.0 Hz, $GalH_1$). ^{13}C NMR ($CDCl_3$): 2.3 (CH_2I); 24.4, 24.8, 25.9, 26.0 (CH_3); 68.9 ($GalC_4$); 70.5 ($GalC_3$); 71.1 ($GalC_2$); 71.5 ($GalC_5$); 96.6 ($GalC_1$); 108.8, 109.5 ($C(CH_3)_2$).] A solution of this iodo derivative (200 mg, 0.54 mmol) and 123 mg of thiourea in 1 mL of CH_3CN and 1 mL of DMF was heated at 110 °C for 36 h until complete comsumption (TLC monitoring). Then, a solution of 50 mg (1.25 mmol) of NaOH in 0.5 mL of H_2O was added, and the resulting mixture was heated at 100 °C for 3 h. After evaporation, the residue was extracted with $CHCl_3$, and the organic

phase was washed with $KHSO_4$ (pH 5) and H_2O and then dried over Na_2SO_4. Chromatography of the residue (hexane/Et_2O, 95/5 to Et_2O, v/v) yielded 128 mg (0.23 mmol, 86%) of disulfide 6-6′-dithiobis(6-deoxy-1,2:3,4-di-*O*-isopropylidene-D-galactopyranose) as a white powder. Reduction of this disulfide was performed by stirring this powder with 107 mg (0.69 mmol) of DTT (Aldrich) and 0.1 mL (0.69 mmol) of NEt_3 in 1 mL of $CHCl_3$ for 3 h. Workup, as described for the disulfide, and chromatography (petroleum ether to petroleum ether/Et_2O, 95/5, v/v) yielded 107 mg (0.38 mmol, 72% with respect to the iodo derivative) of PGal-SH as a colorless oil. [TLC (petroleum ether/Et_2O, 7/3, DTNB, H_2SO_4): $R_f = 0.6$. ^{1}H NMR ($CDCl_3$): 1.22, 1.24, 1.33, 1.43 (s, 12H, CH_3); 1.48−1.56 (m, 1H, SH); 2.48−2.73 (m, 2H, $GalH_6$); 3.67 (td, 1H, $^3J_{5-6} = 6.9$ Hz, $^3J_{5-4} = 1.8$ Hz, $GalH_5$); 4.19−4.26 (m, 2H, $GalH_2$, $GalH_4$); 4.52 (dd, 1H, $^3J_{3-4} = 7.8$ Hz, $^3J_{3-2} = 2.5$ Hz, $GalH_3$); 5.42 (d, 1H, $^3J_{1-2} = 5.0$ Hz, $GalH_1$). ^{13}C NMR ($CDCl_3$): 24.2, 24.3 (CH_3); 24.8 ($GalC_6$); 25.8, 25.9 (CH_3); 69.7 ($GalC_4$); 70.4 ($GalC_3$); 70.7 ($GalC_2$); 71.1 ($GalC_5$); 96.4 ($GalC_1$); 108.5, 109.1 ($C(CH_3)_2$).]

Synthesis of Taxogen *N*-[2-(Dimethylaminoethyl)]-acrylamide (As Its HCl Salt), (B). A solution of 2 mL (18.3 mmol) of *N*,*N*-dimethylethylenediamine (Fluka) in 25 mL of CH_2Cl_2 was added dropwise, at 0 °C and over a 3 h period, to a solution of 2.2 mL (27.4 mmol) of acryloyl chloride in 18 mL of CH_2Cl_2. After 2 h at 0 °C and 2 h at RT, the mixture was evaporated to dryness, yielding taxogen **B** as a white powder which was used without further purification. [TLC ($CHCl_3$/CH_3OH, 6/4, UV, $KMnO_4$): $R_f = 0.4$. ^{1}H NMR (CD_3OD): 3.00 (s, 6H, CH_3); 3.40, 3.72 (t, t, 2H, 2H, $^3J = 6.0$ Hz, $NHCH_2CH_2N$); 5.77 (dd, 1H, $^2J = 3.8$, $^3J = 8.1$ Hz, CH_2=CH); 6.28 (dd, 1H, $^2J = 3.8$, $^3J = 17.0$ Hz, CH_2=CH); 6.38 (dd, 1H, $^3J = 8.1$, $^3J = 17.0$ Hz, CH_2=CH). ^{13}C NMR (CD_3OD): 34.2 (CH_2NH), 42.3 (CH_3), 56.7 (CH_2N), 126.0 (CH_2=CH), 130.1 (CH=CH_2), 167.5 (CO).]

Synthesis of Telomers I(Asp)-14,n_A(NH), I(His)-18,n_A(NH), Gal,n_A(NH), Gal(O),n_A(NH), and I-18,n_B(NMe). *General Procedure for the (Co)telomerization Reactions.* An acetonitrile (or methanol) solution of telogen I(Asp(OBzl))-SH, I(His(BOC))-SH, PGal-SH, or I-SH, and of taxogen **A** or **B** or of a mixture of **A** and **B** or **A** and **C**, at a fixed taxogen(s)/telogen molar ratio, was heated to 50 °C before the addition of AIBN ($^1/_4$ to $^1/_2$ equiv with respect to telogen). The reaction medium was stirred under reflux until the telogen had disappeared (followed by TLC/DTNB) (∼24 h). The solution was then concentrated and chromatographed on a silica column (eluent was $CHCl_3$ to $CHCl_3$/MeOH, 8/2, v/v; excluding telomers and cotelomers deriving from taxogen **B**) and fractionated by gel permeation chromatography on a Sephadex LH 20 column (Sigma) with $CHCl_3$ or MeOH as eluent. The structures were determined by ^{1}H and ^{13}C NMR and by mass spectrometry. The aDP*n* (=*n*) values were determined by ^{1}H NMR on each collected fraction.

General Procedure for the TFA Deprotection of the BOC-(Co)telomers. The deprotection of telomers I(His(BOC))-18,n_A(NHBOC), PGal,n_A(NHBOC), and PGal(O),n_A-(NHBOC) and of cotelomers I-18,n_A(NHBOC),n_B(NMe) and I-18,n_A(NHBOC),n_C(OH) was quantitatively achieved by dissolving and keeping these telomers in a large excess of TFA at RT for 1 h. The excess of TFA was removed by evaporation in the presence of cyclohexane and by gel permeation on a Sephadex LH20 column. The respective telomers I(His)-18,n_A(NH), Gal,n_A(NH), and Gal(O),n_A(NH) and cotelomers I-18,n(NH),n_B(NMe) and I-18,n(NH),n_C(OH) as their TFA salts were obtained in the form of white solids.

Synthesis of Telomers I(Asp(OBzl))-14,n_A(NHBOC) and I(Asp)-14,n_A(NH). The telomerization protocol applied to telogen I(Asp(OBzl))-SH (32 mg, 0.04 mmol) and taxogen **A** (195 mg, 0.91 mmol) at a taxogen/telogen molar ratio of 20, led, after chromatography and fractionation, to telomers I(Asp(OBzl))-14,20(NHBOC) (138 mg) and I(Asp(OBzl))-14,70(NHBOC) (64 mg) of aDP*n* = 20 and 70, respectively. The aDP*n*, determined by ^{1}H NMR, is equal to 3Hx/2Hz or to 2Hy/3Hz, with Hx and Hy being the integration of the signal corresponding to the taxogen ethyldiamido methylenes and BOC methyl groups, respectively, and Hz the integration of the signal corresponding to the telogen terminal methyl groups. Telomers I(Asp)-14,n_A(NH) were obtained quantitatively by simultaneous Bzl and BOC deprotection of telomers I(Asp(OBzl))-14,n_A(NHBOC), which was achieved by dissolving and keeping these telomers in a large excess of 30% HBr/AcOH (Aldrich) at 0 °C for 2 h.

I(Asp(OBzl))-14,20(NHBOC). ^{1}H NMR ($CDCl_3$): 0.80 (t, 6H, $J = 6.0$ Hz, CH_3), 1.05−1.20 (m, 44H, $(CH_2)_{11}$), 1.20−1.60 (m, (9*n* + 4)H, CH_2CH_2N, Me(BOC)), 1.60−2.90 (m, (3*n* + 7)H, CH_2CO, CH_2S, CH_2CHCO), 2.90−4.00 (m, (4*n* + 4)H, CH_2N, CH_2NHCO), 5.05 (s, 2H, CH_2Ph), 5.10−5.40 (m, 1H, CH), 5.40−6.50 (m, *n*H, NH), 7.30 (s, 5H, Ph). ^{13}C NMR ($CDCl_3$): 14.2 (CH_3); 22.7 (CH_2CH_3); 28.5 (Me(BOC)); 26.9, 27.0, 27.5, 29.3, 29.6 ($(CH_2)_{10}$); 31.9 ($CH_2CH_2CH_3$); 46.1, 46.7, 48.1 (CH_2N, CH_2Ph); 66.7 (CH); 79.5 (C(BOC)); 128.3, 128.5 (CH(Ph)); 135.6 (C(Ph)); 156.6 (CO(BOC)); 170.2 (CO); 175.9 (CHCONH). The resonances corresponding to the CH_2CH carbons appear as a large signal between 32 and 38 ppm and those corresponding to the CH_2CH and $NHCH_2CH_2NH$ carbons between 38 and 45 ppm. The CH_2S and CH_2CO signals are not detected.

I(Asp(OBzl))-14,70(NHBOC). ^{1}H NMR ($CDCl_3$) was identical to that of I(Asp(OBzl))-14,20(NHBOC) but with $n = 70$.

I(Asp)-14,20(NH). ^{1}H NMR (CD_3OD): 0.90 (t, 6H, $^3J = 6.0$ Hz, CH_3), 1.05−1.30 (m, 44H, $(CH_2)_{11}$), 1.40−2.15 (m, (2*n* + 2)H, CH_2CH_2N, CH_2CHCO), 2.15−3.00 (m, (*n* + 9)H, CH_2CO, CH_2S, CH_2CHCO), 3.00−3.40 (m, (2*n* + 4)H, CH_2N, CH_2NHCO), 3.40−3.90 (m, 2*n*H, $CH_2NH_3^+$), 5.00−5.20 (m, 1H, CH). ^{13}C NMR (CD_3OD): 14.4 (CH_3); 23.6 (CH_2CH_3); 30.4, 30.7 ($(CH_2)_{10}$); 33.0 ($CH_2CH_2CH_3$); 38.4 (CH_2NHCO); 40.8 ($CH_2NH_3^+$); 178.3 (CHCONH). The resonances corresponding to the CH_2CH carbons appear as large signals between 32 and 38 ppm and between 40 and 45 ppm, respectively. The $COCH_2CH_2$-SCH_2 and $COCHCH_2CO$ signals are not detected.

I(Asp)-14,70(NH). ^{1}H NMR (D_2O): identical to that of I(Asp)-14,20(NH) but with $n = 70$. ^{13}C NMR (D_2O): 37.0 (CH_2NHCO), 38.9 ($CH_2NH_3^+$), 42.6 (CH_2CHCO), 177.2 (CONH). The resonances corresponding to the CH_2CH carbons appear as large signals between 32 and 38 ppm. The $COCH_2CH_2SCH_2$, $CH_3(CH_2)_{13}N$, and $COCHCH_2CO$ signals are not detected.

Synthesis of Telomers I(His(BOC))-18,n_A(NHBOC) and I(His)-18,n_A(NH). When applied to telogen I(His(BOC))-SH (20 mg, 0.02 mmol) and taxogen **A** (202 mg, 0.94 mmol) at a taxogen/telogen molar ratio of 40, the telomerization procedure yielded telomers I(His(BOC))-18,20(NHBOC) (26 mg), I(His(BOC))-18,30(NHBOC) (40 mg), and I(His(BOC))-18,90(NHBOC) (156 mg) of aDP*n* = 20, 30, and 90, respectively. The determination of aDP*n*, by ^{1}H NMR, was performed as those for telomers I(Asp(OBzl))-14,n_A(NHBOC). Deprotection of telomers I(His(BOC))-18,n_A(NHBOC) with TFA afforded telomers I(His)-18,n_A(NH).

I(His(BOC))-18,n_A(NHBOC), n_A = 20, 30, and 90. ^{1}H NMR ($CDCl_3$): 0.81 (t, 6H, J = 6.0 Hz, CH_3), 1.10−1.75 (m, 60H, $(CH_2)_{15}$), 1.40−1.80 (m, (9n + 13)H, CH_2CH_2N, Me(BOC)), 1.80−3.50 (m, (7n + 11)H, CH_2CO, CH_2S, CH_2im, CH_2N, CH_2CHCO, CH_2NHCO), 4.90−6.50 (m, (n + 1)H, CH, NH(BOC)), 6.5−8.0 (m, (n + 2)H, NH, im).

I(His)-18,n_A(NH) with n_A = 20, 30, and 90. ^{1}H NMR (CD_3OD): 0.87 (t, 6H, J = 6.0 Hz, CH_3), 1.10−1.40 (m, 60H, $(CH_2)_{15}$), 1.40−1.80 (m, 4H, CH_2CH_2N), 1.80−3.50 (m, (7n + 11)H, CH_2CO, CH_2S, CH_2im, CH_2N, CH_2CHCO, CH_2NHCO, C$H_2NH_3^+$), 4.90−5.20 (m, 1H, CH).

n_A = 20. ^{13}C NMR (CD_3OD): 14.1 (CH_3); 22.7 (CH_2CH_3); 26.9, 27.1, 27.7, 29.4, 29.7 ($(CH_2)_{14}$); 32.0 (CH_2CH_2CH_3); 37.5 (CH_2NHCO); 39.9 ($CH_2NH_3^+$); 47.0, 48.5 (CH_2N, CH); 118.0 (CH=C(im)); 118.3 (q, $^1J_{CF}$ = 292 Hz, CF_3); 134.0 (CH=C(im), CH=N(im)); 163.0 (q, $^2J_{CF}$ = 35 Hz, $CF_3CO_2^-$); 170.3, 171.1 (CO); 177.5 (CHCONH). The resonances corresponding to the CH_2CH carbons appear as large signals between 32 and 38 ppm, and between 40 and 45 ppm, respectively. The CH_2CO, CH_2S, and CH_2im signals are not detected.

n_A = 30 and 90. ^{13}C NMR (CD_3OD): 37.1 (CH_2NHCO), 39.7 ($CH_2NH_3^+$), 118.3 (q, $^1J_{CF}$ = 292 Hz, CF_3), 163.0 (q, $^2J_{CF}$ = 35 Hz, $CF_3CO_2^-$), 177.6 (CHCONH). The resonances corresponding to the CH_2CH carbons appear as large signals between 32 and 38 ppm and between 40 and 45 ppm, respectively. The $COCH_2CH_2SCH_2$, CH_3-$(CH_2)_{13}N$, and $COCHCH_2im$ signals are not detected.

Synthesis of Telomers PGal,n_A(NHBOC), PGal(O),n_A(NHBOC), Gal,n_A(NH), and Gal(O),n_A(NH), with n_A = 15 and 30. When applied to telogen PGal-SH (16 mg, 0.06 mmol) and taxogen **A** (250 mg; 0.12 mmol) at a taxogen/telogen molar ratio of 20, the telomerization protocol afforded telomers PGal,15(NHBOC) (205 mg) and PGal,30(NHBOC) (46 mg) of aDPn = 15 and 30, respectively. The aDPn, as determined by ^{1}H NMR, is equal to 5Hx/2Hz or to 5Hy/9Hz, with Hx and Hy being the integration of the signal corresponding to the taxogen ethyldiamido methylenes and BOC methyl groups, respectively, and Hz the integration of the signal corresponding to the galactosyle CH protons groups.

Oxidation of telomers PGal,n_A(NHBOC) in commercial diethyl ether under oxygen afforded quantitatively telomers PGal(O),n_A(NHBOC). Their oxidation was attested by ESI-MS.

Deprotection of PGal,n_A(NHBOC) and PGal(O),n_A-(NHBOC) with TFA afforded Gal,n_A(NH) and Gal(O),n_A-(NH), respectively.

PGal,n_A(NHBOC) and PGal(O),n_A(NHBOC), with n_A = 15 and 30. ^{1}H NMR ($CDCl_3$): 1.00−1.60 (m, (9n + 12)H, CH_3), 1.60−2.60 (m, (3n − 1)H, CH_2CHCO), 2.60−4.00 (m, (4n + 4)H, CH_2S, CH_2NHCO), 4.05−4.15 (m, 1H, $GalH_5$), 4.15−4.35 (m, 2H, $GalH_2$, $GalH_4$), 4.55−4.65 (m, 1H, $GalH_3$), 5.40−5.50 (m, 1H, $GalH_1$), 5.50−6.50 (m, nH, NH). ^{13}C NMR ($CDCl_3$): 24.4, 25.1, 26.0 ($(CH_3)_2$C); 28.5 (Me(BOC)); 70.5, 70.9, 71.8, 71.9 ($GalC_2$, $GalC_3$, $GalC_4$, $GalC_5$); 96.4 ($GalC_1$); 79.5 (C(BOC)); 108.6, 109.3 (C$(CH_3)_2$); 156.7 (CO(BOC)); 176.1 (CHCONH). The resonances corresponding to the CH_2CH carbons appear as large signals between 32 and 38 ppm and those corresponding to the CH_2CH and CH_2NHCO between 40 and 45 ppm. The CH_2S signals are not detected. ESI-MS of PGal,15(NHBOC) shows the presence of compounds with n = 2 to 21 [m/z = (276.3 + 214.2n + 23) with n = 2 to 10 in agreement with the masses calculated for $[C_{12}H_{20}O_5S + n(C_{10}H_{18}N_2O_3) + Na^+]$ and n = 2 to 10; m/2z = (138.1 + 107.1n + 23) with n = 7 to 21 in agreement with the masses calculated for $[C_{12}H_{20}O_5S + n(C_{10}H_{18}N_2O_3) + 2Na^+]/2$ and n = 7 to 21]. ESI-MS of PGal(O),15(NHBOC) shows the presence of compounds with n = 2 to 21 [m/z = (292.3 + 214.2n + 23) with n = 2 to 10 in agreement with the masses calculated for $[C_{12}H_{20}O_6S + n(C_{10}H_{18}N_2O_3) + Na^+]$ and n = 2 to 10; m/2z = (146.1 + 107.1n + 23) with n = 7 to 21 in agreement with the masses calculated for $[C_{12}H_{20}O_6S + n(C_{10}H_{18}N_2O_3) + 2Na^+]/2$ and n = 7 to 21].

Gal,n_A(NH) and Gal(O),n_A(NH), with n_A = 15 and 30. ^{1}H NMR (CD_3OD): 1.25−2.05 (m, (2n − 2)H, CH_2CHCO), 2.05−2.95 (m, (n + 5)H, CH_2S, CH_2CHCO), 2.95−3.90 (m, 4nH, NHCH_2C$H_2NH_3^+$). The $GalH_X$ resonances are not detected. ^{13}C NMR (CD_3OD): 38.3 (CH_2NHCO); 40.4 ($CH_2NH_3^+$), 118.3 (q, $^1J_{CF}$ = 292 Hz, CF_3), 163.0 (q, $^2J_{CF}$ = 35 Hz, $CF_3CO_2^-$), 178.0 (CHCONH). The resonances corresponding to the CH_2CH carbons appear as large signals between 32 and 38 ppm and between 40 and 45 ppm, respectively. The $GalC_X$ and CH_2S signals are not detected.

Synthesis of Telomers I-18,35(NMe) and I-18,80(NMe). When applied to telogen I-SH (112 mg, 0.18 mmol) and taxogen **B** (164 mg, 0.92 mmol) at a taxogen/telogen molar ratio of 5, the telomerization protocol afforded, after purification and fractionation on a Sephadex LH20 column (MeOH), telomers I-18,35(NMe) (37 mg) and I-18,80(NMe) (114 mg) of aDPn = 35 and 80, respectively. The aDPn, as determined by ^{1}H NMR, is equal to 3Hx/2Hz or to Hy/Hz, with Hx and Hy being the integration of the signal corresponding to the taxogen NCH_2CH_2N methylenes and N-methyl groups, respectively, and Hz the integration of the signal corresponding to the telogen terminal methyl protons. These telomers were isolated as their Cl^- salts.

I-18,n_B(NMe), with n_B = 35 and 80. ^{1}H NMR ($CDCl_3$ + CD_3OD): 0.80 (t, 6H, J = 6.0 Hz, CH_3), 1.10−1.30 (m, 60H, $(CH_2)_{15}$), 1.30−1.90 (m, (2n + 2)H, CH_2CH_2N, CH_2CHCO), 1.90−2.80 (m, (n + 7)H, CH_2S, CH_2CO, CH_2CHCO), 2.80−3.10 (m, 6nH, NMe), 3.10−4.00 (m, (4n + 4)H, CH_2N, CH_2NHCO). ^{13}C NMR ($CDCl_3$ + CD_3OD): 14.6 (CH_3); 23.7 (CH_2CH_3); 27.1, 28.1, 28.8, 30.4, 30.7 ($(CH_2)_{14}$); 33.0 (CH_2CH_2CH_3); 36.0 (CH_2NHCO); 44.2 (NMe); 58.1 (CH_2NMe); 177.8 (CHCONH). The resonances corresponding to the CH_2CH carbons appear as large signals between 32 and 38 ppm and between 40 and 45 ppm, respectively. The CH_2S, CH_2N, and CH_2CO signals are not detected.

Synthesis of Cotelomers I-18,n_A(NHBOC)-n_B(NMe) and I-18,n_A(NH)-n_B(NMe). *Cotelomer I-18,8(NHBOC)-17(NMe).* The general telomerization protocol, when applied to telogen I-SH (40 mg, 0.06 mmol) and taxogens **A** (140 mg, 0.65 mmol in 2 mL of CH_3CN) and **B** (117 mg, 0.65 mmol, 1 mL of CH_3OH) (i.e., at a taxogen **A** (or **B**)/telogen molar ratio of 10) afforded, after purification on a Sephadex LH20 column ($CHCl_3$), cotelomer I-18,8(NHBOC)-17(NMe) (282 mg) as a white powder.

Cotelomer I-18,10(NHBOC)-1(NMe). (555 mg) was obtained, using the telomerization protocol from telogen I-SH (129 mg, 0.21 mmol), taxogens **A** (455 mg, 2.12 mmol) and **B** (38 mg, 0.21 mmol) (i.e., taxogen **A**/telogen and taxogen **B**/telogen of 10 and 1, respectively).

The aDPn_A and aDPn_B values, as determined by ^{1}H NMR, are equal to 2Hx/3Hz and to Hy/Hz, respectively, with Hx and Hy being the integration of the signal corresponding to the taxogen Me(BOC) and N-methyl groups, respectively, and Hz the integration of the signal corresponding to the telogen terminal methyl protons.

Cotelomers I-18,n_A(NH)-n_B(NMe) were obtained by deprotection of the BOC cotelomers in TFA using the general deprotection protocol. After an anion exchange

on a resin (TFA form), they were further purified on a Sephadex LH20 column and isolated as their TFA salts.

I-18,n_A(NHBOC)-n_B(NMe), with (n_A = 8, n_B = 17) and (n_A = 10, n_B = 1). ^{1}H NMR ($CDCl_3$): 0.88, (t, 6H, J = 6.0 Hz, CH_3), 1.05−1.30 (m, 60H, $(CH_2)_{15}$), 1.30−1.60 (m, ($9n_A$ + 4)H, CH_2CH_2N, Me(BOC)), 1.60−2.00 (m, ($2n_A$ + $2n_B$ − 2)H, CH_2CHCO), 2.00−2.85 (m, (n_A + n_B + 7)H, CH_2S, CH_2CO, CH_2CHCO), 2.85−3.05 (m, $6n_B$H, NMe), 3.05−3.90 (m, ($4n_A$ + $4n_B$ + 4)H, CH_2N, CH_2NHCO), 5.40−6.50 (m, n_AH, N*H*(BOC)). ^{13}C NMR ($CDCl_3$): 14.1 (CH_3); 22.7 (CH_2CH_3); 28.5 (Me(BOC)); 27.0, 27.1, 27.8, 29.4, 29.7 ($(CH_2)_{14}$); 31.9 ($CH_2CH_2CH_3$); 43.9 (NMe); 46.3, 48.2 (CH_2N); 58.1 (CH_2NMe); 79.4 (C(BOC)); 156.6 (CO(BOC)); 175.9 (CHCONH). The resonances corresponding to the CH_2CH carbons appear as a large signal between 32 and 38 ppm and those corresponding to the CH_2CH and $NHCH_2CH_2NHBOC$ between 38 and 45 ppm. The CH_2S and CH_2CO signals are not detected.

I-18,n_A(NH)-n_B(NMe), with (n_A = 8, n_B = 17) and (n_A = 10, n_B = 1). ^{1}H NMR (CD_3OD): 0.95 (t, 6H, J = 6.0 Hz, CH_3), 1.15−1.45 (m, 60H, $(CH_2)_{15}$), 1.45−2.00 (m, ($2n_A$ + $2n_B$ + 2)H, CH_2CH_2N, CH_2CHCO), 2.00−2.90 (m, (n_A + n_B + 7)H, CH_2S, CH_2CO, CH_2CHCO), 2.90−3.05 (m, $6n_B$H, NMe), 3.05−3.90 (m, ($4n_A$ + $4n_B$ + 4)H, CH_2N, CH_2NHCO). ^{13}C NMR (CD_3OD): 14.4 (CH_3); 23.6 (CH_2-CH_3); 27.7, 27.9, 30.3, 30.4, 30.7 ($(CH_2)_{14}$); 33.0 (CH_2CH_2-CH_3); 35.7, 38.2 (CH_2NHCO); 40.4 ($CH_2NH_3^+$); 43.8 (NMe); 58.0 (CH_2NMe); 118.0 (q, $^1J_{CF}$ = 292 Hz, CF_3); 162.8 (q, $^2J_{CF}$ = 35 Hz, $CF_3CO_2^-$); 177.9 (CHCONH). The resonances corresponding to the CH_2CH carbons appear as a large signal between 32 and 38 ppm and between 38 and 45 ppm, respectively. The CH_2S, CH_2N, and CH_2CO signals are not detected.

Synthesis of Cotelomers I-18,10(NHBOC)-10(OH) and I-18,10(NH)-10(OH). The general telomerization protocol when applied to telogen I-SH (57 mg, 0.09 mmol) and taxogens **A** (200 mg, 0.93 mmol) and **C** (163 mg, 0.93 mmol) (i.e., at a taxogen **A** (or **C**)/telogen molar ratio of 10) afforded, after purification on a Sephadex LH20 column (CH_3OH), cotelomer I-18,10(NHBOC)-10(OH) (369 mg) as a white powder. The aDPn_A and aDPn_C values, as determined by ^{1}H NMR, are equal to 2Hx/3Hz and to Hy/Hz, respectively, with Hx and Hy being the integration of the signal corresponding to the taxogen **A** BOC methyl group and taxogen **C** methylene CH_2OH groups, respectively, and Hz the integration of the signal corresponding to the telogen terminal methyl protons.

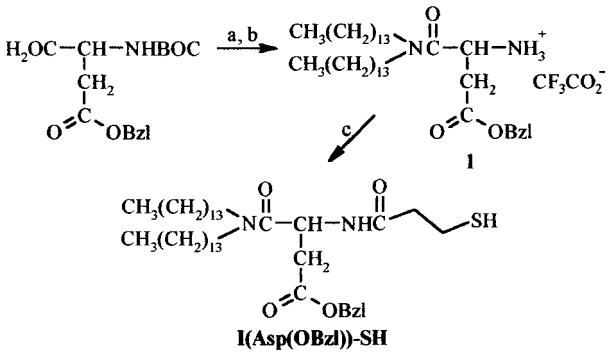
Cotelomer I-18,10(NH)-10(OH) was obtained by deprotection of the BOC cotelomer in TFA using the general TFA deprotection protocol.

I-18,10(NHBOC)-10(OH). ^{1}H NMR (CD_3OD): 0.88, (t, 6H, J = 6.0 Hz, CH_3), 1.15−1.35 (m, 60H, $(CH_2)_{15}$), 1.35−2.00 (m, ($11n_A$ + $2n_C$ + 2)H, CH_2CH_2N, CH_2CHCO, Me(BOC)), 2.00−3.00 (m, (n_A + n_C + 7)H, CH_2S, CH_2CO, CH_2CHCO), 3.00−3.50 (m, ($4n_A$ + 4)H, CH_2N, CH_2NHCO), 3.60−4.10 (m, $6n_C$H, CH_2OH) with n_A = 10 and n_C = 10. ^{13}C NMR (CD_3OD): 14.4 (CH_3); 23.7 (CH_2CH_3); 28.9 (Me(BOC)); 28.0, 30.4, 30.7 ($(CH_2)_{14}$); 33.0 ($CH_2CH_2CH_3$); 40.6, 41.0 (CH_2NHCO); 62.4, 63.9 ($C-CH_2OH$); 80.3 (C(BOC)); 158.4 (CO(BOC)); 177.5 (CHCONH). The resonances corresponding to the CH_2CH carbons appear as a large signal between 32 and 38 ppm and between 42 and 45 ppm, respectively. The CH_2S, CH_2CO, and CH_2N signals are not detected.

I-18,10(NH)-10(OH). ^{1}H NMR (CD_3OD): 0.90 (t, 6H, J = 6.0 Hz, CH_3); 1.15−1.40 (m, 60H, $(CH_2)_{15}$), 1.45−2.05 (m, ($2n_A$ + $2n_C$ + 2)H, CH_2CH_2N, CH_2CHCO), 2.05−3.00 (m, (n_A + n_C + 7)H, CH_2S, CH_2CO, CH_2CHCO), 3.00−3.25 (m, $2n_A$H, CH_2NHCO), 3.25−4.00 (m, ($2n_A$ + $6n_C$ + 4)H, CH_2N, $CH_2NH_3^+$, CH_2OH) with n_A = 10 and n_C = 10. ^{13}C NMR (CD_3OD): 15.8 (CH_3); 25.1 (CH_2CH_3); 29.2, 29.4, 31.8, 32.1, 32.2 ($(CH_2)_{14}$); 34.5 ($CH_2CH_2CH_3$); 39.7 (CH_2NHCO); 41.8 ($CH_2NH_3^+$); 62.8, 64.0, 65.2 ($C-CH_2OH$); 119.5 (q, $^1J_{CF}$ = 292 Hz, CF_3); 164.3 (q, $^2J_{CF}$ = 35 Hz, $CF_3CO_2^-$); 179.8 (CHCONH). The resonances corresponding to the CH_2CH carbons appear as a large signal between 35 and 39 ppm and between 43 and 46 ppm, respectively. The CH_2S, CH_2N, and CH_2CO signals are not detected.

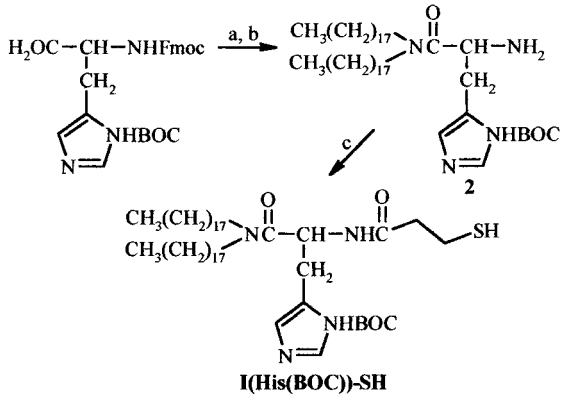
Preparation of Complexes Composed of the Polyamine Telomer Compounds and Plasmid pTG11033. The plasmid pTG11033 was produced by Transgène SA (Strasbourg, France). The endotoxin content of the plasmid preparation was checked using a Limulus Amebocyte Lysat kit (Biogenic, France). This value was below 1 endotoxin unit (e.u.)/mg of plasmid, hence below the 5 e.u./mg of DNA recommended for in vivo protocols. The

Scheme 1. Synthesis of Taxogen I(Asp(OBzl))-SH



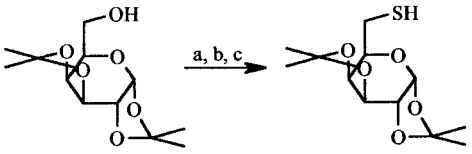
a: $(CH_3(CH_2)_{13})_2N$ / PyBrop / NEt_3 / CH_2Cl_2
b: TFA
c: H_2OC-CH_2-CH_2-SH / HOBt / EDC / NEt_3 / CH_2Cl_2

Scheme 2. Synthesis of Taxogen I(His(BOC))-SH



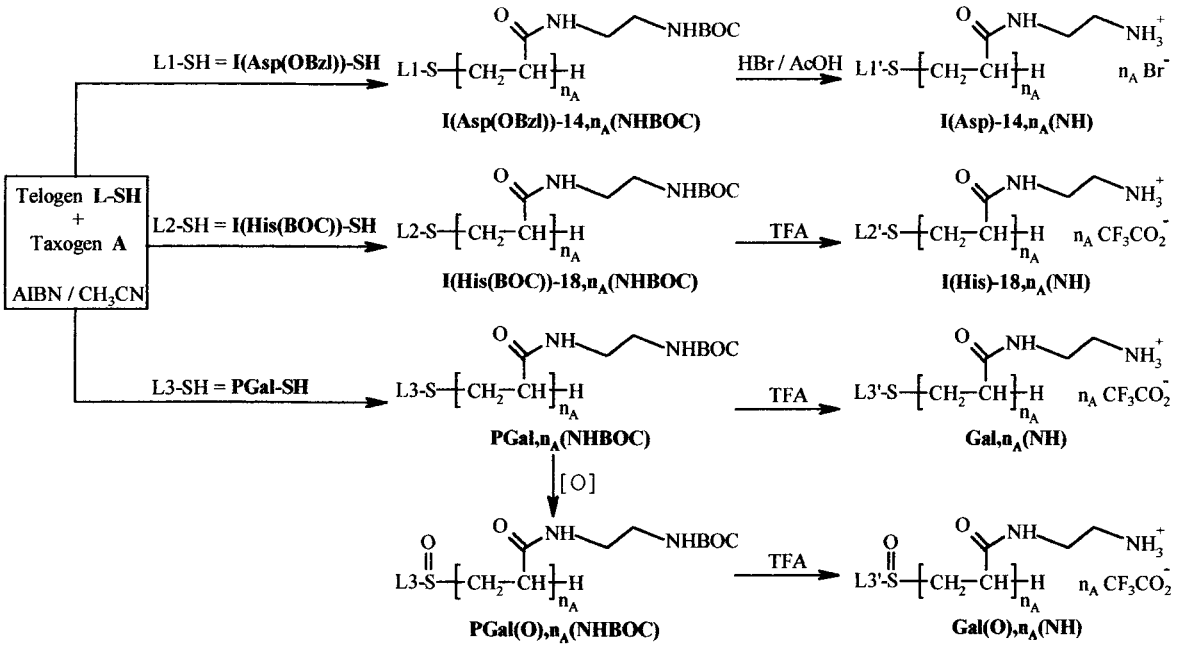
a: $(CH_3(CH_2)_{17})_2N$ / PyBrop / NEt_3 / $CHCl_3$
b: morpholine / DMF
c: H_2OC-CH_2-CH_2-SH / HOBt / EDC / CH_2Cl_2

Scheme 3. Synthesis of Taxogen PGal-SH



a: Ph_3P / imidazole / I_2/ toluene
b: thiourea / CH_3CN, DMF / H_2O, NaOH
c: DTT / NEt_3 / $CHCl_3$

Scheme 4. Synthesis of Telomers I(Asp)-14,*n*(NH), I(His)-18,*n*(NH), Gal,*n*(NH), and Gal(O),*n*(NH)



Scheme 5. Synthesis of Telomers I-18,*n*(NMe) and Cotelomers I-18,n_A(NH)-n_B(NMe) and I-18,n_A(NH)-n_C(OH)

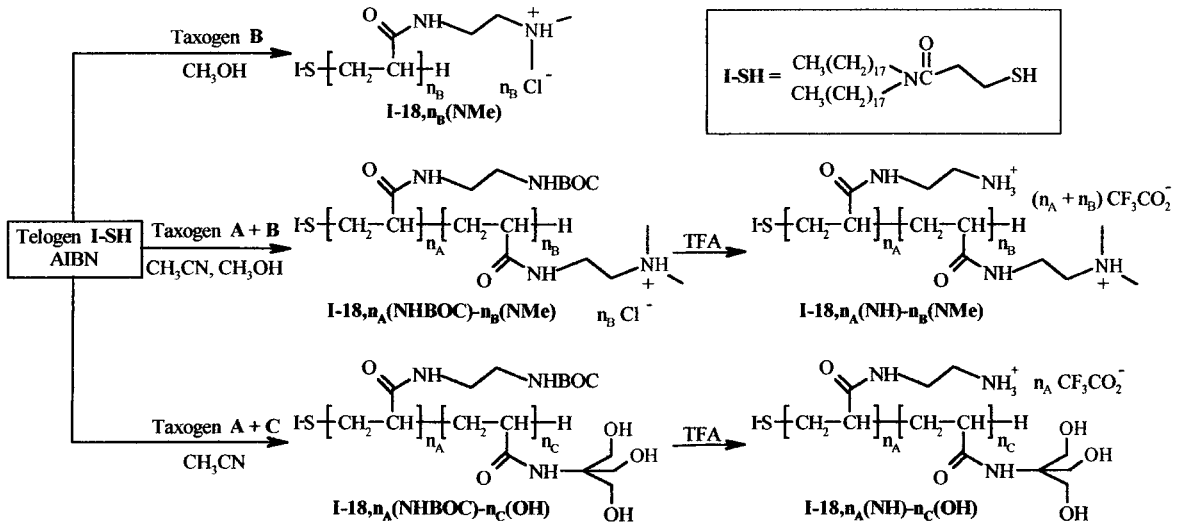


Table 1. Telomerization of Telogens I(Asp(OBzl))-SH, I(His(BOC))-SH, PGal-SH or I-SH with Taxogen A or B, Cotelomerization of Telogen I-SH with a Mixture of Taxogens A and B or A and C, and Code Name of the Isolated (co)Telomers (after Deprotection)

telogen	taxogen(s)	aDP*n*[a] (n_A, n_B, n_A/n_B, or n_A/n_C)	(co)telomercode name
I(Asp(OBzl))-SH	**A**	20	I(Asp)-14,20(NH)
		70	I(Asp)-14,70(NH)
I(His(BOC))-SH	**A**	20	I(His)-18,20(NH)
		30	I(His)-18,30(NH)
		90	I(His)-18,90(NH)
PGal-SH	**A**	15	Gal,15(NH)
		30	Gal,30(NH)
I-SH	**B**	30	I-18,30(NMe)
		80	I-18,80(NMe)
I-SH	**A** + **B**	8/17	I-18,8(NH)-17(NMe)
	A + **B**	10/1	I-18,10(NH)-1(NMe)
I-SH	**A** + **C**	10/10	I-18,10(NH)-10(OH)

[a] aDP*n* = average degree of polymerization as determined by ^{1}H NMR. In the case of the (co)telomers deriving from taxogen **A**, the aDP*n* values were determined on the corresponding BOC-protected (co)telomers.

quantities of compound used were calculated according to the desired DNA concentration of 0.1 mg/mL, the charge ratio, the molar weight, and the number of potential positive charges in the selected compound. The polyamine (co)telomer/DNA complex is formulated by adding a desired volume of (co)telomer preparation at a concentration of 10 mg/mL (in a 20 mM HEPES buffer (pH 7.5), containing 10% DMSO and 10% EtOH) to the

Table 2. Mean Sizes Determined by Light Scattering Spectroscopy of the (Co)teloplexes Formed between Plasmid PTG11033 and I(Asp)-14,n_A(NH), I(His)-18,n_A(NH), or Gal,n_A(NH) Telomers or I-18,n_A(NH)-n_B(NMe) and I-18,n_A(NH)-n_C(OH) Cotelomers

	(co)teloplexes			
			mean diameter in nm (SD)	
(co)telomers[a]	n_A, n_B, n_A/n_B, or n_A/n_C	*N*/*P* ratio[b]	alone	with DOPE
I(Asp)-14,n_A(NH)	20	10	120 (20)	120 (40)
	70	10	130 (40)	120 (40)
I(His)-18,n_A(NH)	30	10	140 (50)	100 (15) 80%[c]
				340 (80) 20%[c]
	90	10	150 (35)	170 (60)
I-18,n_B(NMe)	35	10	235 (75)	230 (80)
	80	10	220 (70)	225 (80)
I-18,n_A(NH)-n_B(NMe)	8/17	10	200 (70)	210 (75)
	10/1	10	230 (70)	215 (80)
I-18,n_A(NH)-n_C(OH)	10/10	10	205 (60)	245 (90)
Gal,n_A(NH)	15	10	460 (150) 20%[c]	nt[e]
			3150 (460) 80%[c]	
	30	10	100 (40)	nt[e]
I(Asp)-14,n_A(NH)	20	5	100 (15) 83%[c]	210 (80)
			320 (50) 17%[c]	
	70	5	160 (60)	155 (55)
I(His)-18,n_A(NH)	30	5	170 (60)	200 (70)
	90	5	170 (55)	150 (30)
I-18,n_B(NMe)	35	5	260 (80)	240 (80)
	80	5	230 (75)	240 (85)
I-18,n_A(NH)-n_B(NMe)	8/17	5	245 (85)	245 (70)
	10/1	5	335 (120)	360 (130)
I-18,n_A(NH)-n_C(OH)	10/10	5	215 (75)	260 (100)
Gal,n_A(NH)	15	5	p[d]	nt[e]
	30	5	200 (50)	nt[e]
I(Asp)-14,n_A(NH)	20	2.5	290 (100)	330 (100)
	70	2.5	170 (65)	165 (50)
I(His)-18,n_A(NH)	30	2.5	p[d]	p[d]
	90	2.5	230 (80)	175 (55)
I-18,n_A(NMe)	35	2.5	p[d]	p[d]
	80	2.5	p[d]	p[d]
I-18,n_A(NH)-n_B(NMe)	8/17	2.5	345 (110)	p[d]
	10/1	2.5	p[d]	p[d]
I-18,n_A(NH)-n_C(OH)	10/10	2.5	235 (75)	275 (95)
Gal,n_A(NH)	15	2.5	p[d]	p[d]
	30	2.5	p[d]	p[d]
I(Asp)-14,n_A(NH)	20	0.8	310 (50) 55%[c]	300 (110)
			1000 (150) 45%[c]	
	70	0.8	210 (70)	200 (70)
I(His)-18,n_A(NH)	30	0.8	250 (90)	220 (75)
	90	0.8	265 (90)	225 (70)
I-18,n_B(NMe)	35	0.8	770 (80)	530 (200)
	80	0.8	585 (200)	370 (130)
I-18,n_A(NH)-n_B(NMe)	8/17	0.8	5320 (990)	540 (200)
	10/1	0.8	465 (170)	500 (180)
I-18,n_A(NH)-n_C(OH)	10/10	0.8	p[d]	p[d]
Gal,n_A(NH)	15	0.8	300 (100)	nt[e]
	30	0.8	200 (60)	nt[e]

[b] *N* = amine equivalents, *P* = plasmid phosphate equivalents. [c] Percent (%) of the overall population. [d] p = precipitate. [e] nt = not tested. [a] All of the (co)telomers listed in this table led with plasmid pTG11033 to precipitates for *N*/*P* 1.25, whether used alone or with DOPE.

desired volume of DNA solution to reach desired DNA concentration (for example, 0.1 mg/mL), as described in ref *12*. When the composition further comprises DOPE, the desired volume of a DOPE solution (10 mg/mL) in chloroform (to get mol/mol cationic telomer/DOPE) was added to the volume of polyamine (co)telomer solution (10 mg/mL in $CHCl_3$). The mixture was then transferred to a borosilicate glass tube and evaporated. The film thus obtained was dissolved in DMSO/EtOH and diluted in a 20 mM HEPES buffer to obtain a preparation at a (co)telomer concentration of 10 mg/mL, containing 10% DMSO and 10% EtOH.

Measurement of the Size of the (Co)teloplexes. The average sizes were measured by photon correlation spectroscopy using a Coulter N4Plus particle size analyzer. The analyses were performed at 25 °C, after equilibrating the sample at 25 °C for 20 min. The sample was diluted with a 20 mM HEPES in the measurement tube and homogenized. These analysis were carried out on complexes having a 20 μg/mL concentration of DNA. The formulations and analyses were reproduced twice.

Agarose Gel Electrophoresis. Each sample (0.5 μg of plasmid) was analyzed by electrophoresis for about 90 min under 75 V/cm through a 0.8% agarose gel in TAE 1x (Tris−acetate−EDTA) buffer. The DNA was visualized in 400 mL of a TAE buffer containing 40 μL of ethidium bromide (Sigma; 10 mg/mL). The plasmid integrity in each sample (0.25 μg) was confirmed by electrophoresis after decomplexing the lipoplex (10 μL of a plasmid 0.05 mg/mL) with sodium dodecyl sulfate, SDS (10 μL, 80 g/L).

In Vitro Transfection of A549 cells. Twenty-four hours before transfection, A549 cells (epithelial cells derived from human pulmonary carcinoma) were grown in Dulbeco-modified Eagle culture medium (DMEM),

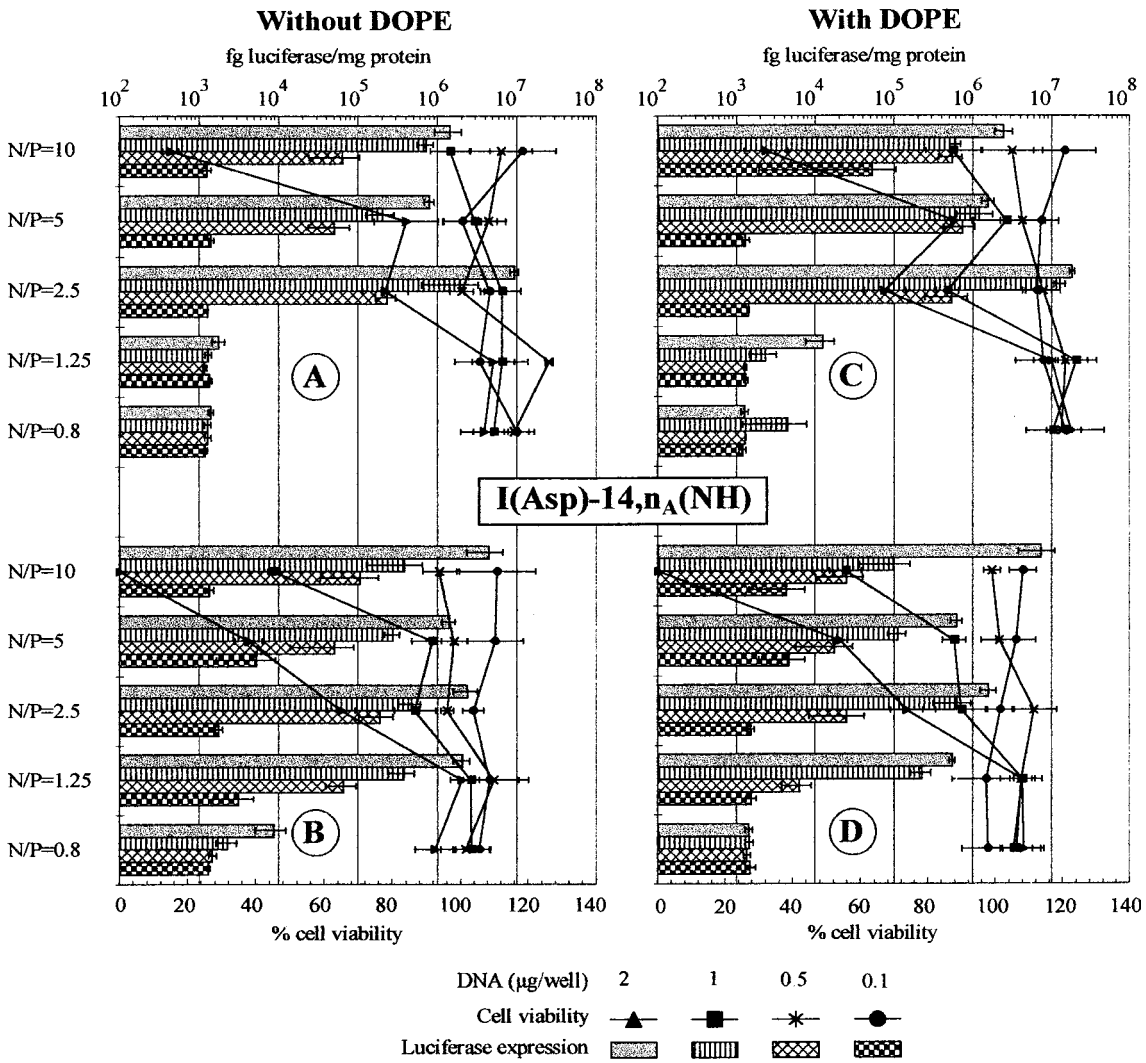


Figure 2. Luciferase expression (bars) and cell viability (points) of the pTG11033 teloplexes made with I(Asp)-14,n_A(NH) telomers or with I(Asp)-14,n_A(NH)/DOPE (1/1 mol) lipids (A and C, $n_A = 20$; B and D, $n_A = 70$) in A549 cells. Means ± SEM are given.

containing 1% glutamine (200 mM; Sigma), 0.4% gentamicine (10 μg/mL; Sigma), and 10% fetal calf serum, FCS (Gibco BRL) in 96-well plates (2×10^4 cells per well), in a wet (37 °C), and 5% CO_2/95% air atmosphere. The volume of the DNA/polyamine telomer complex (20, 10, 5, and 1 μL, respectively) was diluted to 100 μL in DMEM supplemented with 10% FCS in order to obtain various amounts of DNA (2, 1, 0.5, and 0.1 μg, respectively) in the preparation. The culture medium was removed and replaced by 100 μL of DMEM supplemented with 10% FCS and containing the desired amount of DNA. After 4 and 24 h, 50 and 100 μL of DMEM supplemented with 30% and 10% FCS, respectively, were added.

Forty-eight hours after transfection, the culture medium was discarded, and the cells were washed with 100 μL of PBS and then lysed with 50 μL of a lysis buffer (Promega). The lysates were frozen at −32 °C, awaiting the analysis of luciferase activity. This measurement was done for 10 s on 10 μL of the lysis mixture in a Berthold LB96P luminometer in dynamic mode, using the "Luciferase" determination system (Promega) in 96-well plates. The total protein concentration per well was determined using conventional techniques (BCA test; Pierce). For cells grown in the absence of DNA complexes, a well contains around 30−50 μg of proteins. Each (co)telomer/DNA complex was formulated twice, and each formulation was tested twice.

Statistical Analyses. Statistical analyses were performed using a Student *t* test. The difference between two means was considered as significant when the probability *p* is ≤ 0.05.

RESULTS AND DISCUSSION

Telogen Synthesis. Telomerization and cotelomerization reactions were performed with telogen I(Asp(OBzl))-SH, I(His(BOC))-SH, or PGal-SH (the syntheses of which are outlined in Schemes 1−3 respectively) or with I-SH whose synthesis has already been described (*12*).

I(Asp(OBzl))-SH (Scheme 1) was obtained in three steps by (i) condensing BOC-Asp(OBzl)-OH (activated by action of PyBrop) with ditetracylamine, then BOC-deprotection with TFA, followed by coupling to mercaptopropionic acid using HOBt/EDC as coupling reagents (30% overall yields). I(His(BOC))-SH (Scheme 2) was obtained from Fmoc-His(BOC)-OH using a similar strategy except the Fmoc deprotection step which was performed by action of morpholine (10% overall yields). The synthesis of PGal-SH (Scheme 3) was achieved starting from the isopropylidene-protected galactopyranose synthon, using a procedure described in the literature with some modifications (*16*). The free hydroxyl was first replaced by a iodo group by action of PPh_3/imidazole/I_2.

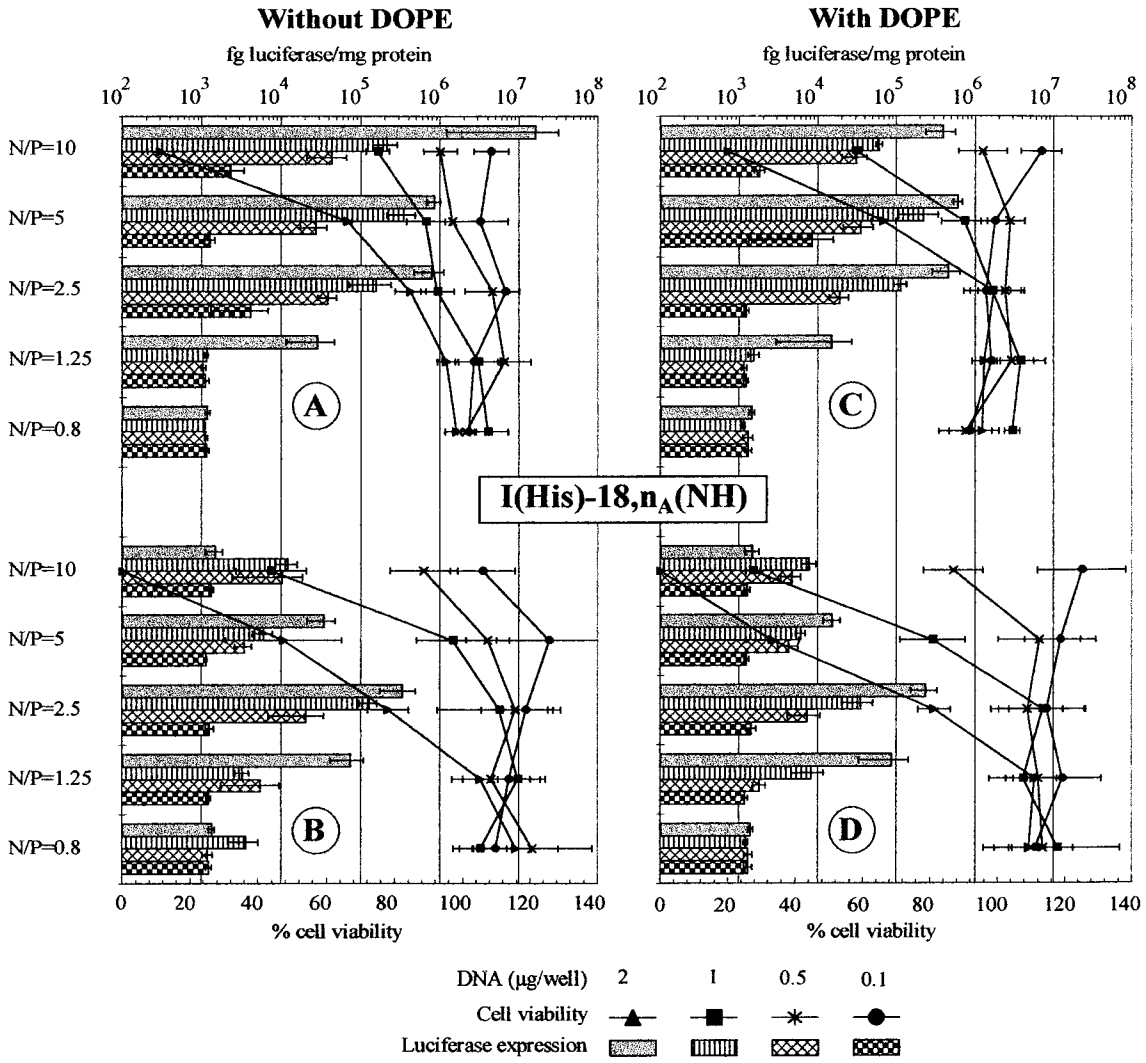


Figure 3. Luciferase expression (bars) and cell viability (points) of the pTG11033 teloplexes made with I(His)-18,n_A(NH) telomers or with I(His)-18,n_A(NH)/DOPE (1/1 mol) lipids (A and C, $n_A = 30$; B and D, $n_A = 90$) in A549 cells. Means ± SEM are given.

The iodo derivative was then converted into the corresponding disulfide by action of thiourea and oxidation and then into the PGal-SH thiol afterward by DTT reduction of disulfide.

Telomer and Cotelomer Synthesis. All telomerization and cotelomerization reactions (Schemes 4 and 5) were performed under nitrogen by refluxing in acetonitrile or in MeOH (i) taxogen **A** or **B** or a mixture of taxogens **A** and **B** or **A** and **C**, (ii) the thiols I(Asp(OBzl))-SH, I(His(BOC))-SH, PGal-SH, or I-SH in fixed taxogen/telogen concentration and ratio, and (iii) AIBN. At the end of the reaction, the solvent was evaporated under reduced pressure and the residue purified and fractionated by gel permeation chromatography on a Sephadex LH20 column and, when appropriate, chromatography on a silica column. This allows to separate the (co)telomers from AIBN and residual disulfide which has formed during telomerization. The *N*-BOC-telomers and cotelomers obtained from taxogen **A** and from telogen I(His(BOC))-SH, PGal-SH, or I-SH were deprotected in excess TFA at RT, and those obtained from telogen I(Asp(OBzl))-SH were deprotected in excess of HBr/AcOH. These (poly)cationic telomers and random cotelomers were isolated as TFA or Br salts by evaporation of excess reagent in the presence of cyclohexane followed by lyophilisation. Quantitative deprotection was confirmed by ^{1}H NMR (absence of the signal corresponding to the BOC and, when appropriate, Bzl protons of the starting material). For each telogen and taxogen(s), the different telomers isolated and their code name are reported in Table 1. Oxygen- and peroxide-free solvents were used throughout these experimental procedures in order to avoid oxidation of sulfur into sulfoxide in the (co)telomers. Oxidation of Gal,n_A(NHBOC) was indeed observed when these derivatives were placed in commercial diethyl ether, yielding Gal(O),n_A(NHBOC) (Scheme 4).

For each fraction collected, the average polymerization degrees (aDPn_A) of telomers resulting from taxogen **A** and the average copolymerization degrees (aDPn_A,n_B and aDPn_A,n_C) of cotelomers resulting from a mixture of taxogens **A** and **B** or **A** and **C**, respectively, were determined by ^{1}H NMR on the BOC-protected (co)telomers. The n_A, n_B, and n_C values were calculated by comparing the integration of the NCH_2CH_2NHBOC signals with that of (i) the terminal methyl chain protons, for the I(His)- and I(Asp)-based telomers, or the isopropylidene methyl and sugar CH protons, for the Gal-based telomers, (ii) the terminal methyl chain and NMe_2 protons for the cotelomers obtained from taxogen **A** and **B**, and (iii) the terminal methyl chain and methylene CH_2OH protons, for the cotelomers obtained from taxogen **A** and **C.** The aDPn_B values of telomers I-18,n_B(NMe) were also determined by ^{1}H NMR by comparing the integration of the NMe_2 protons with that of the terminal methyl chain

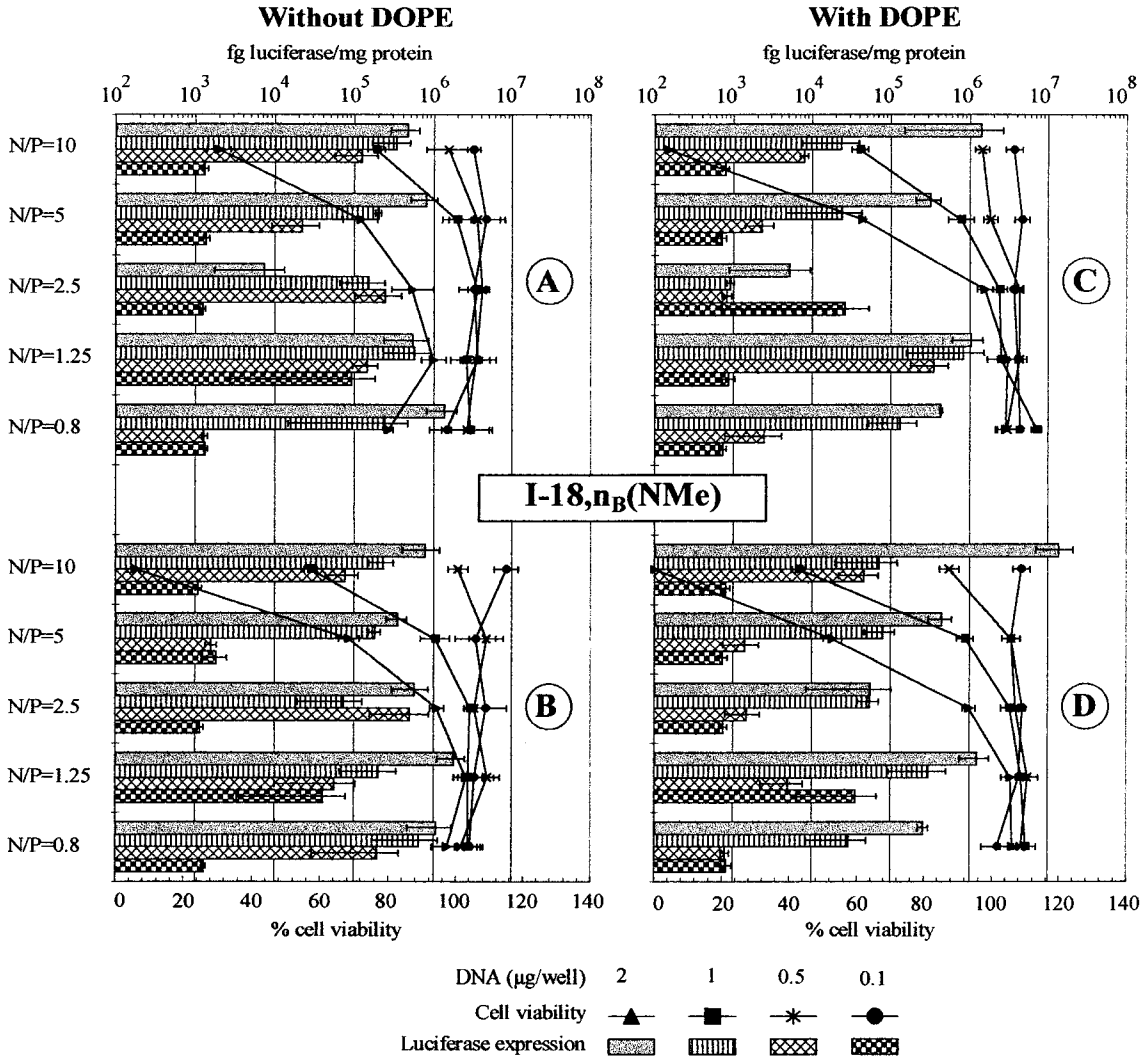


Figure 4. Luciferase expression (bars) and cell viability (points) of the pTG11033 teloplexes made with I-18,n_B(NMe) telomers or with I-18,n_B/(NMe)/DOPE (1/1 mol) lipids (A and C, $n_B = 35$; B and D, $n_B = 80$) in A549 cells. Means ± SEM are given.

protons. ESI-MS was further used to confirm the structure and polydispersity of the Gal-telomers and oxidation of sulfur into sulfoxide.

(Lipo)polyplex Formation and Characterization. The capability of the polyamine (co)telomers to condense DNA and to form (co)teloplexes was analyzed with or without an equimolar amount of the helper phospholipid DOPE except the Gal telomers which were used as unique component. The size of the DNA complexes (which is an important parameter to control when in vivo uses are contemplated or when their in vitro transfection efficiency is evaluated (*17*, *18*)) was analyzed by light scattering spectroscopy. These studies were performed with a pTG11033 plasmid, also used for the in vitro transfection assays described in the following paragraphs. The preparation of the (co)teloplexes relies on the dilution from a DMSO/EtOH lipo(co)telomer (and eventually DOPE) solution in a HEPES buffer (20 mM; pH 7.5) using *N*/*P* ratios of 10, 5, 2.5, 1.25, and 0.8 (*N* = number of amine functions of the (co)telomer, *P* = number of DNA phosphates). Table 2 collects the mean particle diameters measured for the different (co)teloplexes.

These formulations were also analyzed by gel electrophoresis, which showed the presence of fully complexed plasmid (not accessible to ethidium bromide) for all *N*/*P* 10 to 1.25 formulations and for the I-18,10(NH)-10(OH) *N*/*P* 0.8 one. Complexed DNA, but accessible to ethidium bromide, was detected, however, for the I-18,8(NH)-17(NMe) and I-18,n_B(NMe) *N*/*P* 0.8 formulations, while the presence of "free" DNA was also seen for the I(Asp)-14,n_A(NH), I(His)-18,n_A(NH), I-18,10(NH)-1(NMe), Gal,n_A(NH), and Gal(O),n_A(NH) *N*/*P* 0.8 formulations (data not shown). When gel electrophoresis of the (co)-teloplexes was performed in the presence of detergent SDS, dissociation of the complexes was observed in most cases except for teloplexes formulated with I(Asp)-14,70(NH), I(His)-18,90(NH), Gal,30(NH), and Gal(O),30(NH) whatever the *N*/*P* ratio and for teloplexes Gal,15(NH) and Gal(O),15(NH) for *N*/*P* ratios higher than 1.25. DOPE, when used as co-lipid with the lipo(co)-telomers for the formulation of the (co)teloplexes, had no effect neither on DNA complexation nor on complex dissociation by SDS.

Several conclusions concerning the influence of the (co)telomer molecular structure on the stability of the teloplexes with respect to dissociation initiated by SDS can be drawn from these experiments. As expected from the stronger phosphate/NH_3^+ interactions as compared with the phosphate/$NHMe_2^+$ ones, a greater stability was observed for the teloplexes formulated with the "NH_3^+" telomers than for those made from the "$NHMe_2^+$" telomers, whatever the polymerization degree of the telomer. However, the higher this polymerization degree, the higher the stability of the teloplexes. Indeed, teloplexes

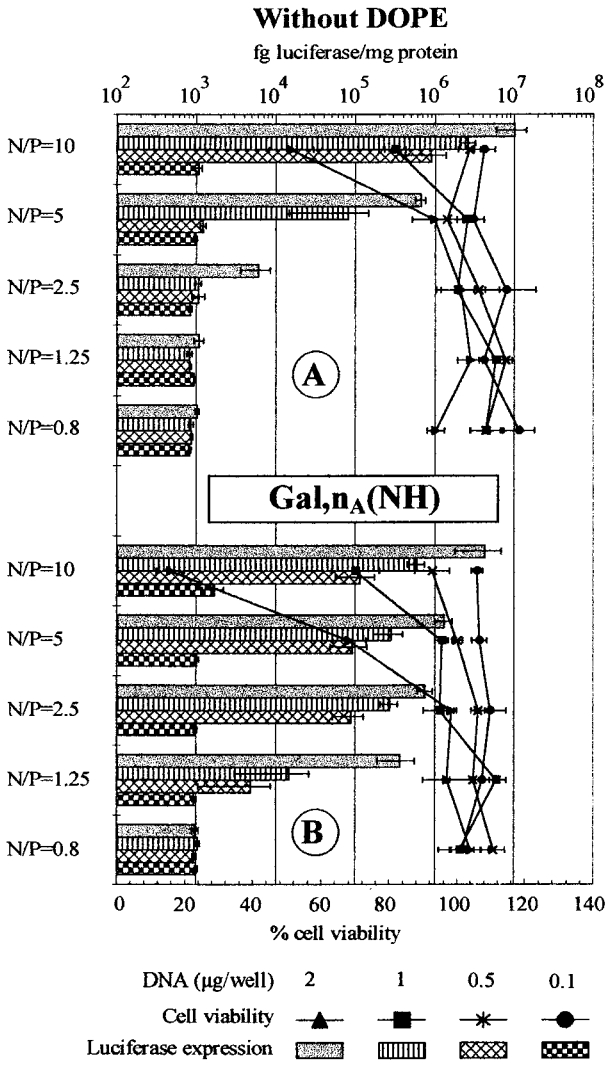


Figure 5. Luciferase expression (bars) and cell viability (points) of the pTG11033 teloplexes made with Gal,n_A(NH) telomers (A, $n_A = 15$; B, $n_A = 30$) in A549 cells. Means ± SEM are given.

formulated with telomers of aDP$n \geq 30$ were not dissociated in the presence of SDS. The stability of the teloplexes with respect to dissociation was further found to be unaffected by replacing part of the amino groups by the THM polyol residue and was increased by replacing the hydrophobic chains for the hydrophilic galactosyl residue.

Our particle size measurements showed a strong dependence of size and aggregation with the formulation's *N*/*P* ratio, as is generally found in the literature (*12*, *19*). For *N*/*P* ratios ≥ 2.5, most of the polyamine (co)telomer compounds were able, with or without the addition of an equimolar amount of DOPE, to condense DNA into (co)teloplexes of a mean size in the 100−450 nm range. In most cases, these preparations consisted further in a single population of particles. While precipitates were obtained for *N*/*P* 1.25 and frequently for *N*/*P* 2.5, larger-sized complexes (200−770 nm) were detected for *N*/*P* 0.8.

In terms of telomer chemical structure impact on teloplex size and stability (with respect to aggregation), the behavior of Gal,15(NH) telomers as compared to that of lipotelomers of similar polymerization degree is worth noting. Indeed, one often observed with Gal,15(NH) a polydisperse population of large-sized teloplexes that further tend to precipitate, while stable formulations were observed with the lipotelomers.

In Vitro Transfection. The transfection potency of the (co)telomers, with and without DOPE, was assayed in vitro on lung epithelial A549 cells, from human pulmonary carcinoma. Although transfection efficiencies with DNA complexes, including the first generation of teloplexes (*12*), are generally impaired in the presence of serum in the culture medium, these experiments were, nevertheless, run in the presence of 10% fetal calf serum. These assays were performed using the luciferase reporter plasmid pTG11033 (pCMV-intronHMG-luciferase-SV40pA; 9572 bp). All teloplex formulations, even those who precipitated, were tested. The transfection efficiency of the teloplexes (expressed in femtogram (fg) of luciferase (luc)/mg of protein) was evaluated for various amounts of DNA (2, 1, 0.5, and 0.1 μg/well) as compared to naked DNA and to the reference lipoplexes based on pcTG90/DOPE N/P 5 (1:1 molar ratio). For higher DNA amounts (e.g., 4 μg/well), the transfection, even if higher, was in most cases accompanied by a poor cell survival. The cationic pcTG90 amphiphile (see structure in Figure 1) is among the most efficient lipid for the transfection of A549 cells, with the highest level of luciferase expression being observed for the pcTG90/DOPE N/P 5 lipoplexes (these levels are further higher than those measured under the same conditions with Transfectam alone or Transfectam/DOPE (*2*), which is a highly efficient synthetic gene transfer agent widely documented in literature; see refs *4* and *8*). Cells treated with naked DNA under equivalent conditions showed expression levels of about 10^{2-3} fg of luc/mg of protein. The effect on cell viability of the (co)teloplexes was also checked by determining the total protein amount per well of the transfected cells relative to that measured for untreated cells (for which the total protein amount per well is in a 30−50 μg/well range).

The transfection and cell viability results are illustrated in Figures 2−7 for the (co)teloplexes formulated with (co)telomers I(Asp)-14,n_A(NH), I(His)-18,n_A(NH), I-18,n_B(NMe), Gal-n_A(NH), I-18,n_A(NH)-n_B(NMe), and I-18,10(NH)-10(OH), respectively. These results indicate that the polyamine (co)telomers do enable transfection of the plasmid into the cells. All of the (co)teloplexes tested so far showed indeed a higher efficiency to transfect A549 cells than naked DNA. For the lowest amount of plasmid used (i.e., 0.1 μg/well), the luciferase expression levels stood between 10^2 and 10^4 fg of luc/mg of protein.

The transfection efficiency and the cell tolerance of the (co)teloplexes depends further on the amount of DNA, on the *N*/*P* ratio as well as on the (co)teloplex formulation (DOPE added or not), and on the chemical structure of the (co)telomers. It usually increased on increasing the DNA amount from 0.1 to 2 μg/well, for which a plateau of luciferase expression (from 10^6−10^7 fg of luc/mg of protein) seemed to be reached. This plateau was often attained for a DNA amount of 0.5−1 μg/well. Irrespective of the amount of plasmid used, luciferase expression levels usually grew when the *N*/*P* ratio increased from 0.8 to 2.5−5 and then stood at a plateau. Simultaneously, cell tolerance decreased with the DNA amount or *N*/*P* ratio increase (see Figures 2−7). However, it remained very high (i) for DNA ≤ 1 μg/well, even for an *N*/*P* ratio of 10, and (ii) for DNA ≤ 2 μg/well, providing *N*/*P* ≤ 5.

This transfection efficiency and toxicity increase when raising the cationic charge of the (co)teloplexes is in line with the behavior of most lipoplexes and polyplexes reported in the literature. This is probably related to an

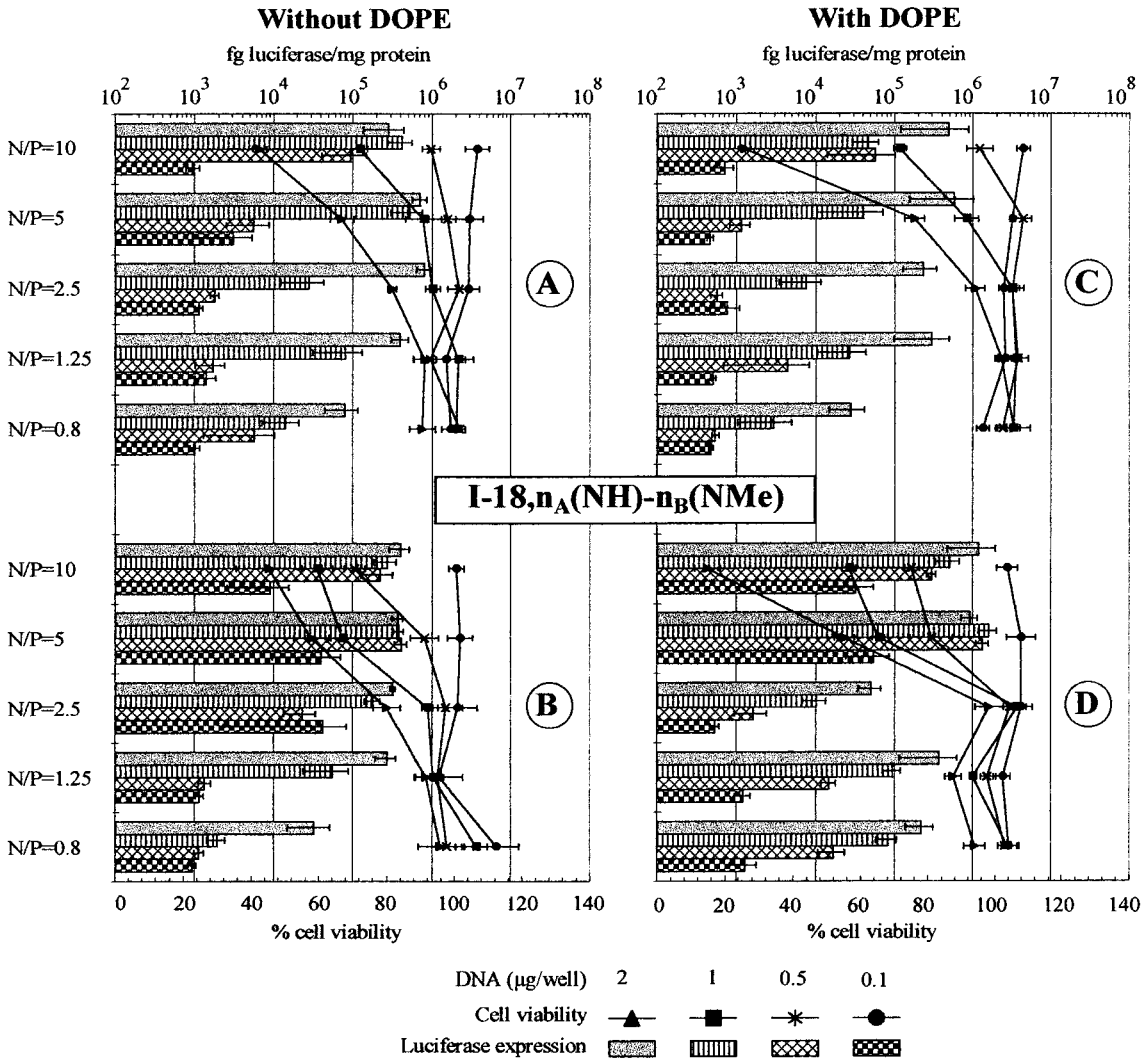


Figure 6. Luciferase expression (bars) and cell viability (points) of the pTG11033 coteloplexes made with I-18,n_A(NH)-n_B(NMe) cotelomers or with I-18,n_A(NH)-n_B(NMe)/DOPE (1/1 mol) lipids (A and C, $n_A = 8$, $n_B = 17$; B and D, $n_A = 10$, $n_B = 1$) in A549 cells. Means ± SEM are given.

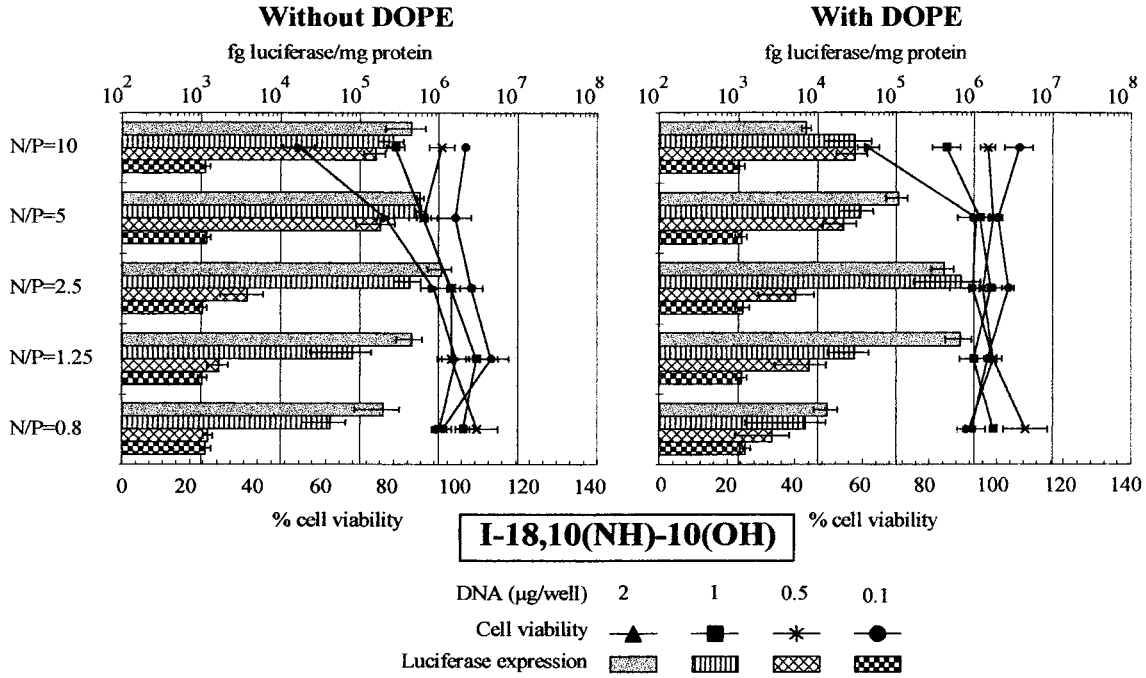


Figure 7. Luciferase expression (bars) and cell viability (points) of the pTG11033 coteloplexes made with I-18,10(NH)-10(OH) cotelomers or I-18,10(NH)-10(OH)/DOPE (1/1 mol) lipids in A549 cells. Means ± SEM are given.

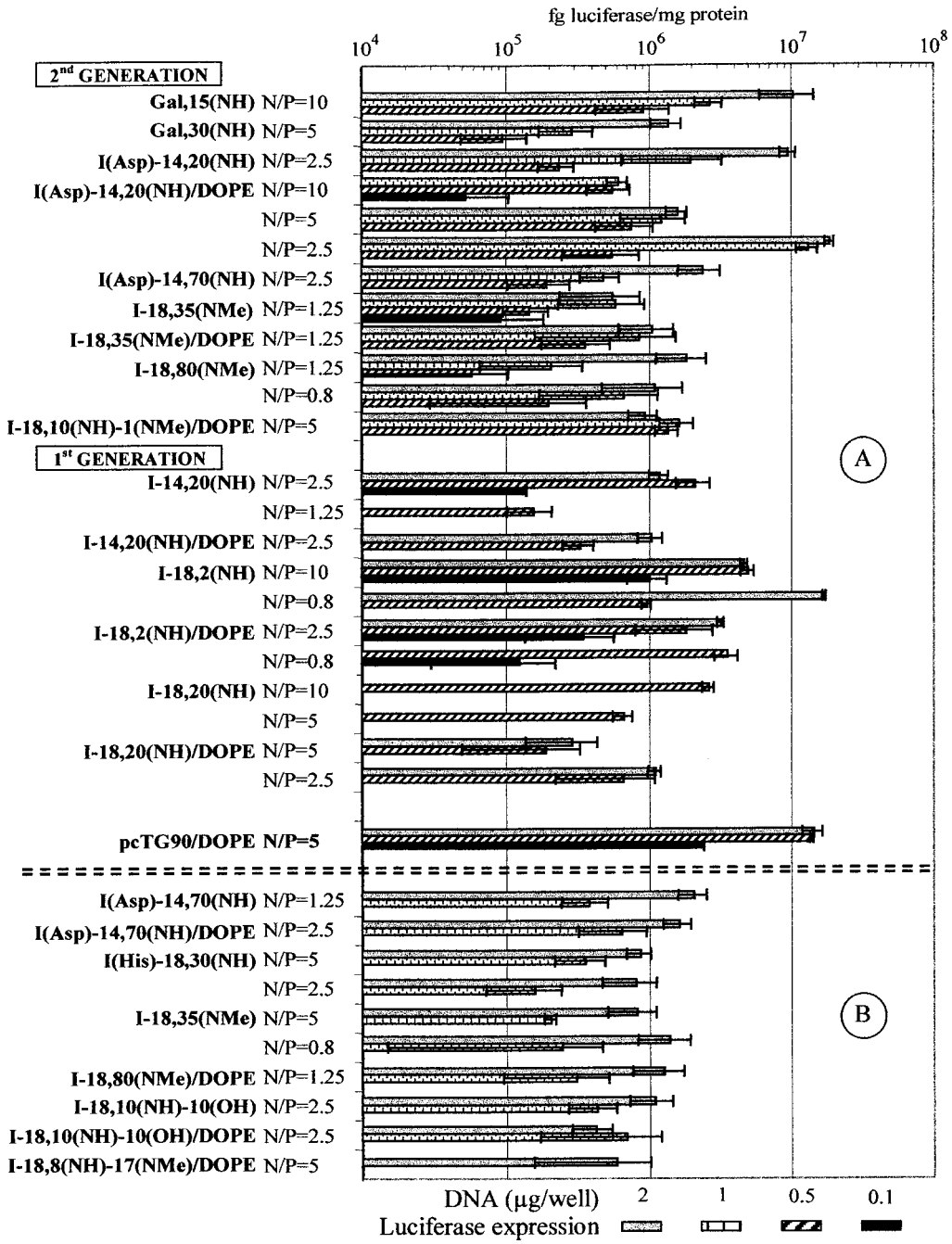


Figure 8. Most efficient second generation (co)teloplexes (selection criteria for A: transfection efficiency ≥ 10^5 fg of luc/mg of protein and cell viability > 50% for a DNA amount ≤ 0.5 μg/well; selection criteria for B: transfection efficiency ≥ 10^5 fg of luc/mg of protein and cell viability > 50% for a DNA amount ≤ 2 μg/well) described in this study as compared with the most efficient first second generation teloplexes and with the reference pcTG90/DOPE (1/1 mol; *N/P* 5) in A549 cells (data from ref *12*). Means ± SEM are given.

increase of the complex's cell uptake, which remains at a level compatible with cell growth providing that the *N/P* ratio is not higher than 5. For *N/P* 10, the (co)teloplexes became more toxic for the cells, likely as a result of a higher level of uptake, of cell membrane disruption, or as a result of the presence of a high amount of free uncomplexed (co)telomer.

When compared to the reference pcTG90/DOPE N/P 5 lipoplexes and to some teloplexes of the first generation which display a high transfection efficiency (10^6−10^7 fg of luc/mg of protein) already for DNA amounts ≤ 0.5 μg/well, several of the formulations investigated here, which are listed in panels A and B of Figure 8, were found to be as efficient in mediating DNA transfer and expression. However, such high luciferase levels were most often attained for a DNA amount ≥ 1 μg/well. When considering more severe selection criteria (DNA amounts of 0.5 and 0.1 μg/well), only a few of these (co)teloplexes (panel A of Figure 8) led to substantial transgene expression levels that are, however, in a 10^5−10^6 fg of luc/mg of protein range, hence below those measured for the reference and for the first generation of teloplexes (*12*). Overall, the transfection efficiency of the first generation of teloplexes was not found to be improved with these new (co)teloplexes (see also next section).

Concerning the effects on A549 cell transfection resulting from the formulation of the (co)teloplexes with DOPE, no helper effect of DOPE could be detected, the transfection efficiency upon DOPE addition to 180 formulations being statistically unaffected, in line with our

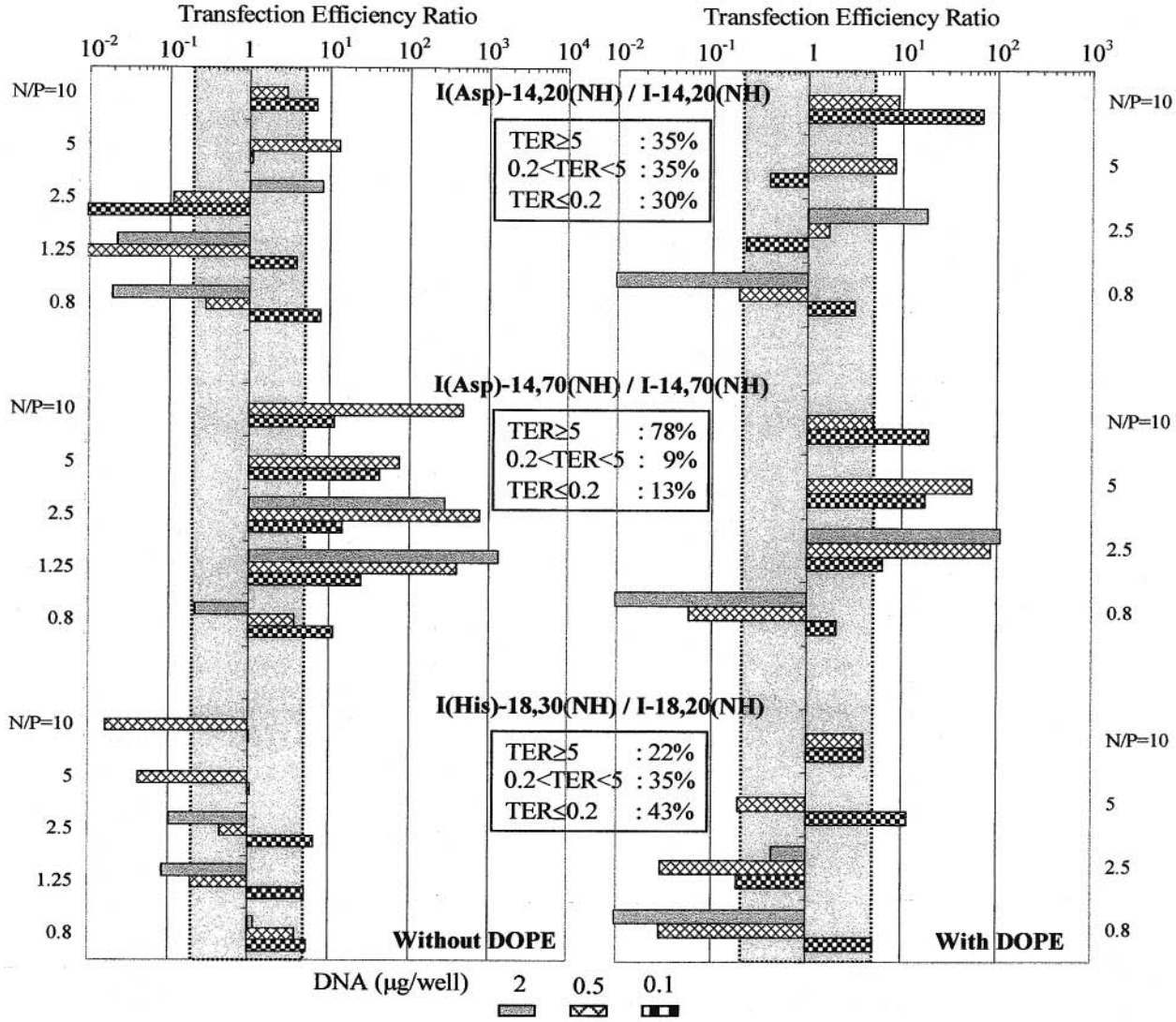


Figure 9. Impact on transfection efficiency of the aspartic or histine residue. TER is the ratio of luciferase amount measured for the formulations with telomer I(Asp)-14,n_A(NH) or I(His)-18,n_A(NH) versus that measured for the corresponding ones with the I-14,n_A(NH) or I-18,n_A(NH) homologues, respectively. The impact is significant if TER is not within the 0.2−5 range ($p < 0.05$ in a pairwise comparison). The percentages given in the boxes for each couple of telomers correspond to the percentages of formulations (with and without DOPE) for which TER were higher than 5, within the 0.2−5 range or below 0.2, respectively.

previous report on the first generation of telomers (*12*). Indeed, as compared to their respective teloplexes formed without DOPE, the luciferase expression remained unchanged for at least 73% of the formulations tested, a decrease or an increase of transfection being observed for nearly 20% or 7% of the formulations, respectively (data not shown).[1] Further, most of the 20% of formulations for which a transfection decrease was observed concerned the cotelomer- and the $NHMe_2^+$ telomer-based complexes.

Structure/Transfection Efficiency Relationships. One of the objectives of this study was also aimed at determining structural elements of the (co)telomers that favor or increase their transfection potential. The structural modifications that were investigated here concern (i) the number of amine functions, (ii) the nature of the polyamine polar head (primary vs tertiary amine, a combination of primary amines with tertiary amines, or with polyol (e.g., THM) residues), (iii) the presence of a low pK_a functional group (e.g., an aspartic or a histidine amino acid) between the lipophilic chains and the polar head, (iv) the replacement of a hydrophilic (galactosyl) moiety for lipophilic chains, or (v) the oxidation state of sulfur (thioether or sulfoxide linkage).

In the previous study concerning telomers I-m,n_A(NH) (with $m = 14$ or 18), it was shown that an optimum of transfection was attained for a number of amine functions, n_A, in the 2−20 range which decreased slightly for higher n_A values (*12*). We found here with the new series of telomers that their degree of polymerization (within the 20−90 range investigated) had almost no impact on their transfection efficiency. Indeed, when increasing the number of amine functions from 20 to 70 in the I(Asp)-14,n_A(NH) series, from 30 to 90 in the I(His)-18,n_A(NH) series, or from 35 to 80 in the I-18,n_B(NMe) series, the luciferase expression levels were statistically not affected for at least 80%, 78%, or 84% of the formulations, respectively (data not shown; see also note 1).

Where the impact on transfection of replacing part or all NH_3^+ functions by $NHMe_2^+$ ones in the polyamine

[1] The difference in transfection efficiency of two formulations is considered as significant if the ratio of luciferase amount (Transfection Efficiency Ratio (TER)) measured for the two formulations is out of the 0.2−5 range and associated with a $p < 0.05$ in a pairwise comparison. Only the formulations with cell viability > 50% were considered for TER calculations.

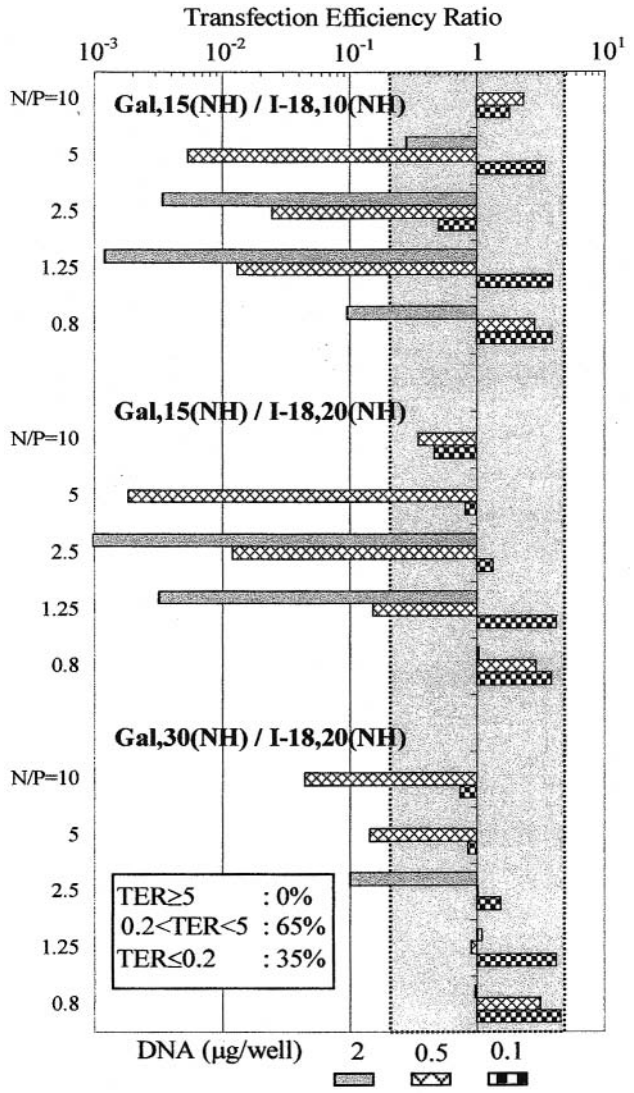


Figure 10. Impact on transfection efficiency of the hydrophilic (Gal) residue versus the hydrophobic moiety. TER is the ratio of luciferase amount measured for the formulations with telomer Gal,n_A(NH) versus that measured for the corresponding ones with I-18,n_A(NH) homologues. The impact is significant if TER is not within the 0.2−5 range ($p < 0.05$ in a pairwise comparison). The percentages given in the box correspond to the mean percentages of formulations, irrespectively of n_A, for which TER were higher than 5, within the 0.2−5 range or below 0.2, respectively.

telomers is concerned, transgene expression was statistically not modified by a partial [e.g., I-18,10(NH) vs I-18,10(NH)-1(NMe) and I-18,20(NH) vs I-18,8(NH)-17(NMe)] or a full [e.g., I-18,20(NH) or I-18,50(NH) vs I-18,35(NMe) and I-18,60(NH) vs I-18,80(NMe)] replacement for almost 50% of the formulations, the effects (increase or decrease of transfection) being rather at random for the remaining 50% of formulations (data available as Supporting Information; see also note 1). One should, however, underscore that cell viability was generally improved by the replacement of the primary amines by the tertiary ones.

Concerning the impact on transfection of replacing part of the primary amine functions by polyol THM residues, transgene expression was not modified for at least 70% of the formulations (I-18,10(NH) teloplexes versus I-18,10(NH)-10(OH) coteloplexes), while cell viability was to some extend improved (data available as Supporting Information; see also note 1). Similar results were also noticed for polylysines and polyallylamines after partial glycolylation (*7*) and for copolymers deriving from 2-(dimethylamino)ethyl methacrylate and ethoxytriethylene glycol methacrylate (*9*).

Importantly, as illustrated in Figure 9, it appeared that introducing an aspartic acid into the telomer structure of I-14,70(NH) improved its transfection efficiency (in some cases by more than 2 orders of magnitude). Seventy-eight percent of the teloplexes based on I(Asp)-14,70(NH) (some of which are as efficient as the pcTG90/DOPE N/P 5 reference; see Figure 8) gave rise to at least a 10-fold higher luciferase expression level than those formulated with I-14,70(NH). This tendency is, however, not confirmed for the I(Asp)-14,20(NH)-based teloplexes as compared to the I-14,20(NH) ones; if transfection was indeed improved for 35% of these formulations, it remained at the same level and decreased for another 35% and 30%, respectively. By contrast, insertion of histidine into the telomer backbone was statistically found to reduce transgene expression; 43% of the I(His)-18,30(NH) formulations were less efficient than their corresponding I-18,20(NH) teloplexes, while the opposite result was found for only 22% of the I(His)-18,30(NH) versus I-18,20(NH) formulations. These results contrast to some extent with the higher transfection potential found for histidylated polylysine polymers (which contained around 70 histidine residues) as compared with that of polylysines (*11*).

Replacing the hydrophobic chains for a hydrophilic galactose residue was found most frequently not to affect transfection. Indeed, 65% of the I-18,10(NH) and I-18,20(NH) lipoteloplexes displayed transgene expression levels comparable to those measured for their corresponding Gal,15(NH) and Gal,30(NH) teloplexes (Figure 10). However, this replacement led for the remaining 35% of formulations to a substantial transfection decrease (1 to 3 orders of magnitude). Concomitantly, cell viability was most often found to be improved for the galactosyl-based teloplexes. The higher transfection potential of the lipophilic telomers is in line with several reports in the literature which showed a substantial increase of the transfection efficiency for polylysines (*20*) and other polycationic polymers (*10*) upon conjugation to lipophilic residues.

Concerning the impact of the oxidation state of sulfur (thioether or sulfoxide linkage) on transfection, no significant effect could be evidenced, with Gal,n_A(NH) formulations and their Gal(O),n_A(NH) homologues giving rise to comparable luciferase expression levels (data not shown).

CONCLUSION

The present work suggests that some of the second generation of (co)telomers display a promising potential as synthetic vectors for gene delivery. The variation of structure parameters allowed the establishment of structure−activity relationships and the optimization of the (co)teloplex formulation, where both high transfection levels and cell viability were achieved. Thus, aspartic-containing telomers were found to lead to efficient formulations for plasmid delivery to A549 cells and for *N*/*P* ratios from 1.25 to 5. Some of these telomers are currently investigated for in vivo studies.

ACKNOWLEDGMENT

We wish to thank Transgène, SA (Strasbourg, France) for financial support and Dr. B. Cavallini (Transgène) for supplying with plasmid. We also thank Drs. D.

Heissler and A. Nazih (ULP Strasbourg) for the synthesis of pcTG90. Thanks to Dr. H.V.J. Kolbe for his interest into this project and for helpful discussions.

Supporting Information Available: Two figures showing the effect of DOPE and the effect of the NH_3/$NHMe_2$ or NH_3/OH (THM) replacement on the transfection efficiency of the (co)teloplexes, respectively. This material is available free of charge via the Internet at http://pubs.acs.org.

LITERATURE CITED

(1) Wivel, N. A., and Wilson J. M. (1998) Methods of gene delivery. *Hematol. Oncol. Clin. North Am. 12*, 483−501.

(2) Gaucheron, J., Santaella, C., and Vierling, P. (2001) Highly fluorinated lipospermines for gene transfer: synthesis and evaluation of their in vitro transfection efficiency. *Bioconjugate Chem. 12*, 114−128.

(3) Felgner, P. L., Gadek, T. R., Holm, M., Roman, R., Chan, H. W., Wenz, M., Northrop, J. P., Ringold, G. M., and Danielsen, M. (1987) Lipofection: a highly efficient, lipid-mediated DNA-transfection procedure. *Proc. Natl. Acad. Sci. U.S.A. 84*, 7413−7417.

(4) Remy, J. S., Abdallah, B., Zanta, M. A., Boussif, O., Behr, J. P., and Demeinex, B. (1998) Gene transfer with lipospermines and polyethylenimines. *Adv. Drug Delivery Rev. 30*, 85−95.

(5) Byk, G., Dubertret, C., Escriou, V., Frederic, M., Jaslin, G., Rangara, R., Pitard, B., Crouzet, J., Wils, P., Schwartz, B., and Scherman D. (1998) Synthesis, activity, and structure−activity relationship studies of novel cationic lipids for DNA transfer. *J. Med. Chem. 41*, 224−235.

(6) Miller, A. D. (1998) Cationic liposomes for gene therapy. *Angew. Chem., Int. Ed. 37*, 1768−1785.

(7) Boussif, O., Delair, T., Brua, C., Veron, L., Pavirani, A., and Kolbe, H. V. J. (1999) Synthesis of polyallylamine derivatives and their use as gene transfer vectors in vitro. *Bioconjugate Chem. 10*, 877−883.

(8) Van de Wetering, P., Moret, E. E., Schuurmans-Nieuwenbroek, N. M. E., Van Steenbergen, M. J., and Hennink, W. E. (1999) Structure/activity relationships of water-soluble cationic methacrylate/methacrylamide polymers for nonviral gene delivery. *Bioconjugate Chem. 10*, 589−597.

(9) Van de Wetering, P., Moret, E. E., Schuurmans-Nieuwenbroek, N. M. E., Van Steenbergen, M. J., Crommelin, D. J. A., and Hennink, W. E. (2000) Copolymers of 2-(dimethylamino)ethyl methacrylate with ethoxytriethylene glycol methacrylate or *N*-vinyl-pyrrolidone as gene transfer agents. *J. Controlled Release 64*, 193−203.

(10) Oupicky, D., Konak, C., Ulbrich, K., Wolfert, M. A., and Seymour, L. W. (2000) DNA delivey systems based on complexes of DNA with synthetic polycations and their copolymers. *J. Controlled Release 65*, 149−171.

(11) Midoux, P., and Monsigny, M. (1999) Efficient gene transfer by histidylated polylysine/pDNA complexes. *Bioconjugate Chem. 10*, 406−411.

(12) Verderone, G., Van Craynest, N., Boussif, O., Santaella, C., Bischoff, R., Kolbe, H. V. J., and Vierling, P. (2000) Lipopolycationic telomers for gene transfer: synthesis and evaluation of their in vitro transfection efficiency. *J. Med. Chem. 43*, 1367−1379.

(13) Haensler, J., and Szoka, F. C. (1993) Polyamidoamine cascade polymers mediate efficient transfection of cells in culture. *Bioconjugate Chem. 4*, 372−379.

(14) Felgner, P. L., Holm, M., and Chan, H. (1989) Cationic liposome mediated transfection. *Proc. West. Pharmacol. Soc. 32*, 115−121.

(15) Gao, X., and Huang., L. (1993) Cationic liposomes and polymers for gene transfer. *J. Liposome Res. 3*, 17−30

(16) Garegg, P. J., and Samuelsson, B. (1980) Novel reagent system. *J. Chem. Soc., Perkin Trans. 1* 2866−2869.

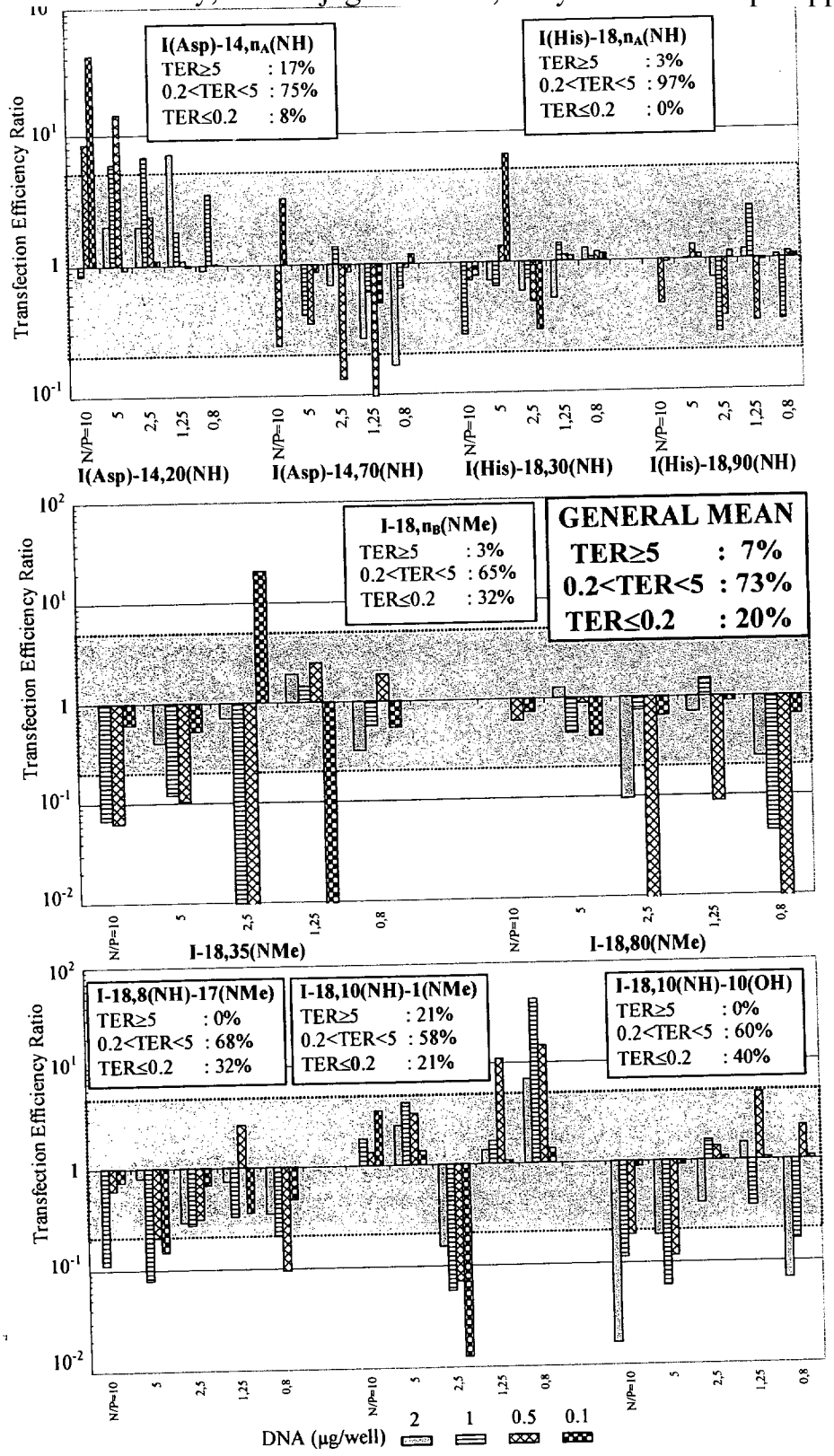
(17) Boussif, O., Zanta, M. A., and Behr, J. P. (1996) Optimized galenics improve in vitro gene transfer with cationic molecules up to 1000-fold. *Gene Ther. 3*, 1074−1080.

(18) Thierry, A. R., Rabinovich, P., Peng, L. C., Mahan, L. C., Bryant, J. L., and Gallo, R. C. (1997) Characterization of liposome-mediated gene delivery: expression, stability and pharmacokinetics of plasmid DNA. *Gene Ther. 4*, 226−237.

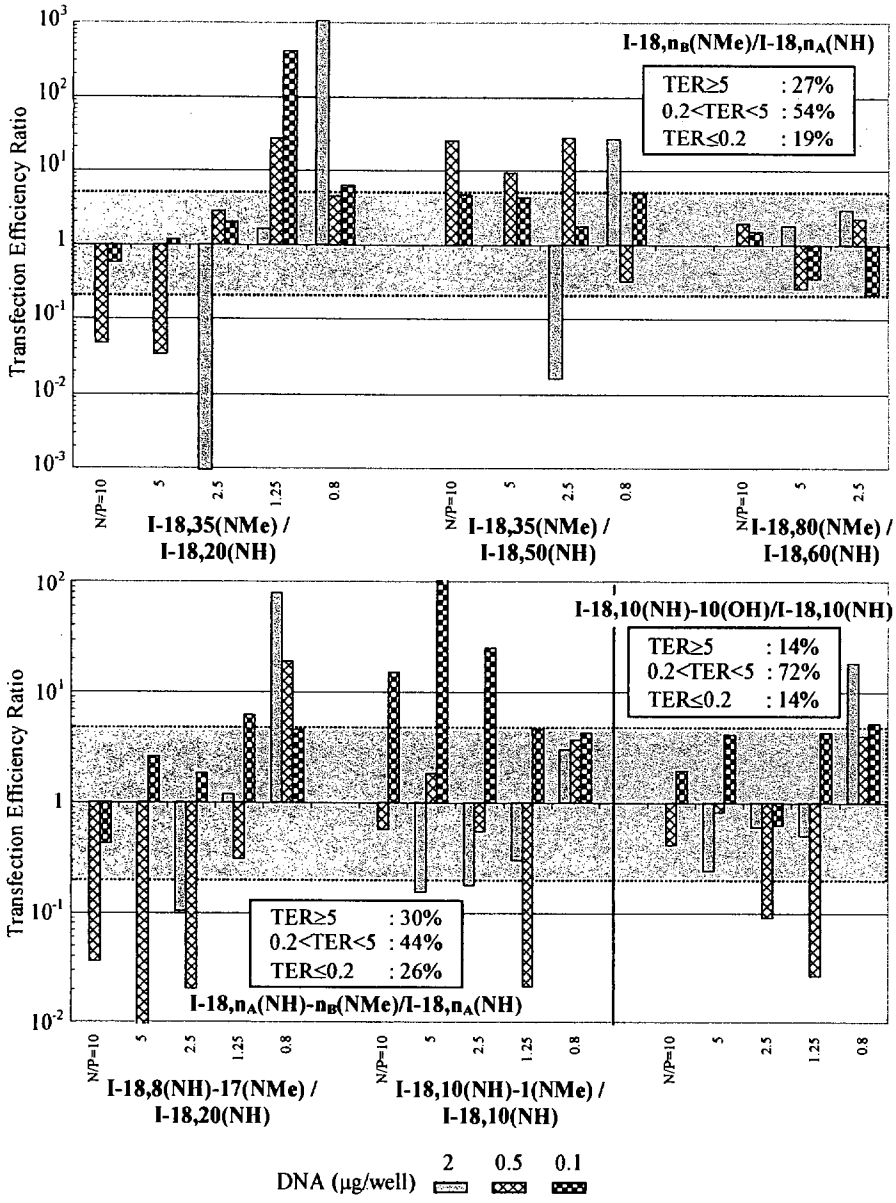
(19) Pitard, B., Aguerre, O., Airiau, M., Lachagès, A.-M., Boukhnikachvili, T., Byk, G., Dubertret, C., Herviou, C., Scherman, D., Mayaux, J.-F., and Crouzet, J. (1997) Virus-sized self-assembling lamellar complexes between plasmid DNA and cationic micelles promote gene transfer. *Proc. Natl. Acad. Sci. U.S.A. 94*, 14412−14417.

(20) Zhou, X. H., Klibanov, A. L., and Huang, L. (1991) Lipophilic polylysines mediate efficient DNA transfection in mammalian cells. *Biochim. Biophys. Acta 1065*, 8−14.

BC010047P



Supplementary material 1 : Effect of DOPE on the transfection efficiency of the (co)teloplexes. The transfection efficiency ratio, TER, is the ratio of luciferase amount measured for the formulation with DOPE vs that measured for the corresponding one without DOPE. The impact is significant if TER is not within the 0.2 – 5 range ($p < 0.05$ in a pair-wise comparison). The percentages given in the boxes correspond to the mean percentages of formulations, irrespectively of n_A or of n_B, for which TER is higher than 5, within the 0.2 – 5 range or below 0.2, respectively. The general mean percentages correspond to the percentages of formulations, irrespectively of the nature of the (co)teloplexes, for which TER were higher than 5, within the 0.2 – 5 range or below 0.2, respectively.



Supplementary material 2 : Effect of the $NH_3/NHMe_2$ or NH_3/OH (THAM) residue replacement on the transfection efficiency of the (co)teloplexes . The transfection efficiency ratio, TER, is the ratio of luciferase amount measured for the formulations with **I-18,n_B(NMe)**, **I-18,n_A(NH)-n_B(NMe)** or **I-18,10(NH)-10(OH)** vs that measured for the corresponding ones with **I-18,n_A(NH)**. The impact is significant if TER is not within the 0.2 – 5 range ($p < 0.05$ in a pair-wise comparison). The percentages given in the boxes correspond to the mean percentages of formulations, irrespectively of n_A and of n_B, for which TER were higher than 5, within the 0.2 – 5 range or below 0.2, respectively.

Poly[Lys-(AEDTP)]: A Cationic Polymer That Allows Dissociation of pDNA/Cationic Polymer Complexes in a Reductive Medium and Enhances Polyfection

Chantal Pichon,[†] Eric LeCam,[‡] Brigitte Guérin,[†] Dominique Coulaud,[‡] Etienne Delain,[‡] and Patrick Midoux*,[†]

Centre de Biophysique Moléculaire, CNRS UPR 4301, rue Charles Sadron, F-45071 Orléans Cedex 02, France, and Laboratoire de Microscopie Moléculaire et Cellulaire, CNRS UMR 8532, Institut Gustave Roussy, rue Camille Desmoulins, F-94805 Villejuif Cedex, France. Received March 13, 2001; Revised Manuscript Received October 8, 2001

Polyplexes of high stability resulting from the condensation of a plasmid DNA by a cationic polymer are widely used to develop polymer-based gene delivery systems. However, the plasmid must be released from its vector once inside the cells for an efficient expression of the exogenous gene in the cell nucleus. We have designed a disulfide-containing cationic polymer termed poly[Lys-(AEDTP)] which allowed for the formation of polyplexes and the release of the plasmid in a reductive medium. The amino groups of polylysine were substituted with 3-(2-aminoethyldithio)propionyl residues in order to have each amino group of poly[Lys-(AEDTP)] interacting with a phosphate DNA linked to the polymer backbone via a disulfide bond. As evidenced by agarose gel electrophoresis and ethidium bromide/pDNA fluorescence restoration, poly[Lys-(AEDTP)] polyplexes were decondensed and the plasmid released upon treatment with either dithiothreitol, glutathione in the presence of glutathione reductase, or the thioredoxin reductase. Electron microscopy showed that polyplexes exhibiting spherical particles of a mean size at about 100 nm were decondensed in the presence of glutathione and exhibited filamentous aggregates. Finally, we found that the transfection of 293T7 and HepG2 cells was 10- and 50-fold more efficient with poly[Lys-(AEDTP)] polyplexes, respectively, than with poly[Lys] polyplexes. These results indicate that disulfide-containing cationic polymers must be borne in mind for developping polymer-base gene delivery systems.

INTRODUCTION

The self-assembly of plasmid DNA (pDNA) in an aqueous solution via cooperative electrostatic interactions with cationic polymers such as polylysine is the basis of the development of synthetic vectors for gene therapy (*1*−*4*). This assembly induces the condensation of pDNA allowing for the formation of cationic polyplexes (DNA/cationic polymer complexes) and an increase of its cellular uptake. Once internalized, the intracellular trafficking of polyplexes and the mechanism allowing pDNA to reach the cell nucleus is still unclear. It is supposed that polyplexes route via endocytic vesicles, polyplexes, or pDNA are delivered in the cytosol and then imported in the cell nucleus. pDNA/polylysine complexes are highly stable, and pDNA is protected from nuclease digestion in serum and in cell extracts (*5*, *6*). However, the polyplexes stability could be a limiting factor for the transfection efficiency by preventing the pDNA release and the accessibility of gene expression machinery. The release of pDNA from polyplexes could be, indeed, required for either its delivery in the cytosol, its import in the cell nucleus, or the gene expression. Several lines of evidence suggest that a decrease of the strength of the electrostatic interactions between pDNA and polylysine favors the dissociation of polyplexes inside the cells and enhances the transfection efficiency. Indeed, the reduction of the number of positive charges on polylysine after a partial substitution of the ϵ-amino groups with uncharged residues, such as carbohydrate moieties (*7*) or polyhydroxyalcanoyl (gluconoyl) residues (*8*), was found to facilitate in vitro dissociation of polyplexes and to increase the transfection efficiency. In the same way, complexes between pDNA and an EGF−polylysine conjugate gave a better transfection when the size of polylysine was shortened because the stability of polyplexes was reduced (*9*).

Here, we describe the synthesis of a 3-(2-aminoethyldithio)propionyl-substituted polylysine conjugate, termed poly[Lys-(AEDTP)],[1] in which the lysyl ϵ-amino groups of polylysine are substituted with 3-(2-aminoethyldithio)-propionyl residues. Therefore, the amino groups of poly-[Lys-(AEDTP)] interacting with the pDNA phosphates are linked to the polymer backbone via a disulfide bond. This cationic polymer enables the formation of polyplexes with pDNA, which is expected to be released upon the cleavage of the disulfide bonds in a reductive medium, such as the cytosol and the cell nucleus. We show that these polyplexes are dissociated in the presence of reducing substances, including dithiothreitol (DTT), glu-

* Corresponding author. Phone: +33(0)2 38 25 55 95. Fax: +33 (0)2 38 25 78 07. E-mail: midoux@cnrs-orleans.fr.

[†] Centre de Biophysique Moléculaire, CNRS UPR 4301.

[‡] Laboratoire de Microscopie Moléculaire et Cellulaire, CNRS UMR 8532.

[1] Abbreviations: AEDTP, 3-(2-aminoethyldithio)propionyl residues; dp, degree of polymerization; DTT, dithiothreitol; EDTA, ethylenediamine tetraacetic acid; HB, 10 mM Hepes buffer (pH 7.4); PB, 0.1 M potassium phosphate buffer (pH 7.5) containing 2 mM EDTA; PDP, 3-(2-pyridyldithio)propionyl residues; poly-[Lys], poly-L-lysine.

10.1021/bc015503o CCC: $22.00 © 2002 American Chemical Society
Published on Web 12/13/2001

tathione, and thioredoxin. In addition, the transfection efficiency of poly[Lys-(AEDTP)] polyplexes is increased up to 50-fold as compared to polylysine polyplexes.

MATERIAL AND METHODS

Preparation of 3-(2-Pyridyldithio)propionyl-Substituted Polylysine (Poly[Lys-(PDP)]). Poly-L-lysine, HBr 30 000−50 000 (poly[Lys], dp = 190) (Bachem Feinchemikalien, Bubendorf, Switzerland) was changed to polylysine *p*-toluenesulfonate salt as described previously (*10*). Poly[Lys]-*p*-toluenesulfonate salt (100 mg, 1.75 μmol) in 5 mL dimethyl sulfoxide (Sigma-Aldrich, L'Isle d'Abeau Chesnes, France) in the presence of diisopropylethylamine (51 μL, 350 μmol; Aldrich) was reacted for 24 h at 20 °C with *N*-succinimidyl-3-(2-pyridyldithio)-propionate (SPDP) (110 mg, 352 μmol; Sigma). Polylysine substitution with 3-(2-pyridyldithio)propionyl residues (PDP) was monitored by thin-layer chromatography (TLC) on silica gel plates (Kieselgel 60 F_{254}, Merck, Darmstadt, Germany) in a chloroform/methanol/water (6:6:1 v/v/v) mixture under a UV lamp (polymer, R_f = 0; SPDP, R_f = 0.7) and upon ninhydin reaction. The reaction was stopped when the total substitution of the amino groups of polylysine with PDP residues was evidenced by the absence of staining after ninhydrin reaction. The polymer was precipitated by adding 10 vol of distilled water, and the precipitate was collected by centrifugation (1800*g* for 15 min) and dried under vacuum.

Preparation of 3-(2-Aminoethyldithio)propionyl-Substituted Polylysine (Poly[Lys-(AEDTP)]. Poly-[Lys-(PDP)] (45 mg, 0.95 μmol) was dissolved by warming in 4 mL of dimethyl sulfoxide and was reacted at 20 °C with mercapthoethylamine-*p*-toluenesulfonate salt. The reaction was monitored by the release of pyridine-2-thione. Briefly, 30 μL of reaction mixture was added to 200 μL of dimethyl sulfoxide; pyridine-2-thione was then extracted with 2 mL of ethyl acetate, and upon centrifugation, the absorbance of the supernatant was recorded at 377 nm. The absorbance was compared to that obtained with a sample after addition of an excess of mercapthoethylamine-*p*-toluenesulfonate salt (30 μL of 50 mg/mL). The reaction was complete after the addition of 62 mg (250 μmol) of mercapthoethylamine-*p*-toluenesulfonate salt. The polymer was purified by adding 10 vol of 2-propanol, and the precipitate was collected by centrifugation (1800*g* for 15 min). The pellet was washed with 2-propanol, collected by centrifugation (1800*g* for 15 min), dissolved in distilled water, and freezed-dried. ^{1}H NMR spectroscopy at 300 MHz in D_2O showed that the eight methylene protons ($1HC_8$, $2HC_9$, $2HC_{10}$, and $2HC_{11}$; Figure 1) corresponding to AEDTP residues exibited two equal peaks at 2.7 and 2.9 ppm. The value of one proton determined from the integration value of those peaks was equal to that from the six methylene protons ($1HC_3$, $1HC_4$, and $1HC_5$) of lysine residues, indicating that polylysine was practically completely substituted with AEDTP residues.

Plasmids. pSV2Luc was a 5 kb plasmid DNA encoding the firefly luciferase gene under the control of the SV40 large T antigen promoter (*11*). pUT650 plasmid (5.15 kb plasmid; CAYLA, Toulouse, France) was an expression vector encoding the firefly luciferase gene under the control of the human cytomegalovirus promoter. pUT650 was used to transfect the cells because the strength of the CMV promoter was higher than that of the SV40.

Release of pDNA from Poly[Lys-(AEDTP)]. *Agarose Gel Electrophoresis. Effect of DTT.* Twenty micrograms of pSV2Luc in 280 μL of 10 mM Hepes buffer (pH 7.4) (HB) was mixed with either poly[Lys-(AEDTP)] (80 μg) or polylysine (40 μg) in 120 μL of HB. After 30 min at 20 °C, 50 μL of polyplexes solution was incubated at 37 °C in the absence or in the presence of 0.1 M DTT (5 μL of a 1 M aqueous solution). Samples (20 μL) were then analyzed by agarose gel electrophoresis. Electrophoresis was performed for 2 h under 80 V/cm, through a 0.8% agarose gel containing ethidium bromide (1 μg/mL of gel) in a Tris−borate−EDTA buffer (95 mM Tris, 89 mM boric acid, 2.5 mM EDTA, and 10 mM DTT (pH 8.6)).

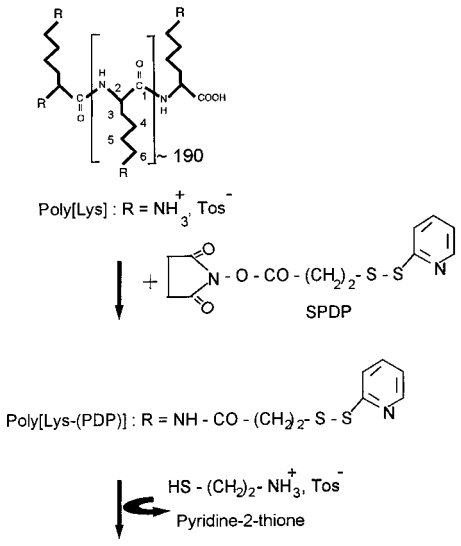


Figure 1. Schematic synthesis of poly[Lys-(AEDTP)].

Effect of Glutathione and Thioredoxin Reductase. A 0.4 M gluthatione reduced-form (Sigma) stock solution was prepared in 0.1 M potassium phosphate buffer (pH 7.5), containing 2 mM EDTA (PB) and adjusted to pH 7.5 with a 10 N NaOH solution. Complexes prepared as described previously were incubated for 2 h at 37 °C in PB in the presence of either (a) 20 mM glutathione, 2 units/mL glutathione reductase (from yeast; Roche Diagnostics, Grenoble, France), and 0.5 mM NADH (Sigma) or (b) 2 units/mL thioredoxin reductase (from *Escherichia coli*; Sigma) and 0.5 mM NADPH (Sigma). Samples (20 μL) were then analyzed by agarose gel electrophoresis as described previously.

Ethidium Bromide/pDNA Fluorescence Restoration. pSV2Luc plasmid (20 μg in 0.5 mL of HB) was mixed with either polylysine (40 μg) or poly[Lys-(AEDTP)] (100 μg) in 0.5 mL of HB. After 30 min at 20 °C, ethidium bromide (40 μL of a 0.1 mg/mL solution in HB) was then added, and polyplexes were incubated at 37 °C in the absence or the presence of either 0.1 M DTT (5 μL of a 1 M aqueous solution) or 10 mM glutathione reduced form. The fluorescence intensity of the solution was measured at 585 nm upon excitation at 540 nm.

ζ Potential and Size Measurements. Poly[Lys-(AEDTP)] (100 μg in 120 μL of HB) and polylysine (40 μg in 120 μL of HB) were complexed with pSV2Luc by mixing the polymers to 20 μg of plasmid in 280 μL of HB. The mixed solution was allowed to stand for 30 min at 20 °C before being diluted with 2 mL of HB. The ζ potential was measured by using a ZetaSizer 3000 (Malvern Instruments, Orsay, France) with the following parameters: viscosity, 0.891 cP; dielectric constant, 79; temperature, 25 °C; F (Ka), 1.50 (Smoluchowsky); maxi-

mum voltage of the current, 15 V. Measurements were performed five times with zero field correction. The ζ potential was calculated by using the Smoluchowsky approximation. The size was determined by quasi-elastic laser light scattering using the ZetaSizer 3000 with a sample refractive index of 1.59 and a viscosity of 0.89. Measurements were performed 10 times and the size was calculated by using the automatic mode. The system was calibrated by using a -50 ± 5 mV and 200 ± 5 nm standard dts 5050 from Malvern.

Cells and Cell Culture. 293T7 (human embryonic kidney-producing T7 RNA polymerase) (*12*) and HepG2 (human hepatoma cells, ATCC HB 8065) were cultured in DMEM (Gibco, Life Technologies, Renfrewshire, U.K.) and MEM, respectively. Culture media were supplemented with 10% heat-inactivated fetal bovine serum (FBS; Gibco), 2 mM L-glutamine (Gibco), and antibiotics (100 units/mL of penicillin and 100 mg/mL of streptomycin; Gibco). Cells were grown at 37 °C in a humidified atmosphere containing 5% CO_2 and 95% air. Cells were mycoplasma free, as evidenced by the bisbenzimidazole negative test (Hoechst 33258) (*13*).

Polyfection. Poly[Lys-(AEDTP)] (20 μg in 30 μL of HB) or polylysine (15 μg in 30 μL of HB) were complexed by mixing the polymers to 5 μg pUT650 in 70 μL of HB. The solution was allowed to stand for 30 min at 20 °C before diluted with 1 mL of culture medium supplemented with 10% FCS and made 100 μM chloroquine (phosphate salt; Sigma). Adherent cells ($(2-4) \times 10^5$ cells) were plated (day 0) in 4 cm^2 culture dishes (12-well culture plates). On day 1, the medium was removed, and 1 mL of polyplexes-containing medium was added into each well. After a 4 h incubation at 37 °C, the medium was removed, and cells were further incubated at 37 °C in 2 mL of the complete culture medium.

Luciferase Assay. Luciferase gene expression was measured by monitoring the luminescence activity according to De Wet et al. (*14*). The medium was discarded, and cells were washed three times with PBS. The homogenization buffer (200 μL of 8 mM $MgCl_2$, 1 mM DTT, 1 mM EDTA, 1% Triton $\times$ 100, 15% glycerol, 25 mM Tris−phosphate buffer (pH 7.8)) was poured into each well, and tissue culture plates were kept for 15 min at 20 °C. The solution was recovered and spun down (5 min at 800*g*). Ninety-five microliters of a 2 mM ATP solution in the homogenization buffer without Triton $\times$ 100 was added to 60 μL of supernatant, and the solution was shaken with a vortex. The luminescence was recorded for 4 s in a Lumat LB 9501 luminometer (Berthold, Wildbach, Germany) upon addition of 150 μL of a 167 mM luciferin solution in water. Measurements were done in duplicate. The data shown correspond to the number of relative light units (RLU) from 10^6 cells. The number of RLU of 1 pg/mL of luciferase was 2000 under these assay conditions.

Transmission Electron Microscopy (TEM). Ten micrograms of pUT650 in 70 μL of HB were complexed with 40 μg of poly[Lys-(AEDTP)] in 30 μL of HB. After 30 min at 20 °C, polyplexes were diluted with either 1 mL of HB or 1 mL of HB containing 10 mM glutathione reduced form. Samples were observed by TEM as already described (*15*). Five microliters of mixture were deposited on a carbon-coated copper grid, which was activated by a slow discharge in the presence of pentylamine. The sample was washed out with 2% uranyl acetate in water, blotted, and dried on a filter. Observation was made in the dark-field mode with a LEO-Zeiss 902 microscope, with filtering out inelastic electrons for contrast improvement.

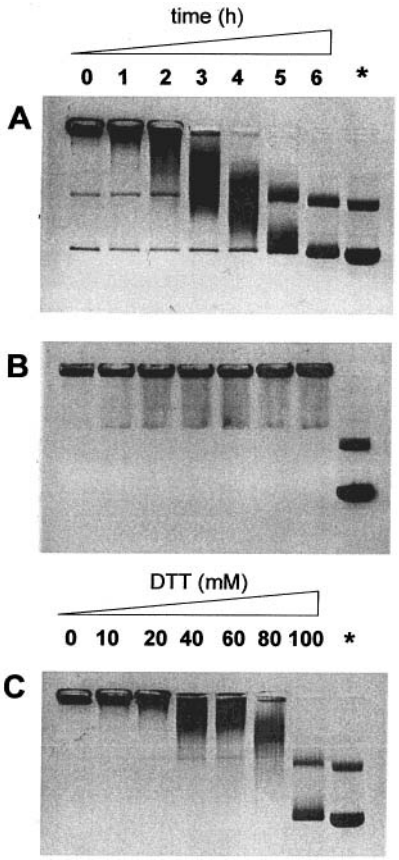


Figure 2. DTT releases pDNA from poly[Lys-(AEDTP)]. pSV2luc (20 μg in 280 μL of 10 mM HB) was mixed with either (A) poly[Lys-(AEDTP)] (80 μg) or (B) polylysine (40 μg) in 120 μL of HB. After 30 min at 20 °C, polyplexes (50 μL, 2.5 μg of plasmid) were incubated at 37 °C for various times in the presence of 0.1 M DTT. (C) Polyplexes (50 μL, 2.5 μg of plasmid) were incubated for 6 h at 37 °C in the presence of various DTT concentrations. Samples (20 μL) were analyzed by 0.8% agarose gel electrophoresis and DNA visualized with ethidium bromide.

RESULTS

Poly[Lys-(AEDTP)] was synthesized from poly-L-lysine with a degree of polymerization of 190 (Figure 1). First, poly-L-lysine was totally substituted with 3-(2-pyridyldithio)propionyl residues. The reaction was easily monitored on TLC after the reaction of the free amino groups with ninhydrin. The substitution was complete as evidenced by the absence of coloration when polylysine was reacted in the presence of 1.1 equiv of SPDP/polylysine amino group. Then, activated thiol groups were reacted with mercaptoethylamine to give 3-(2-aminoethyldithio)propionyl residues. The reaction was monitored by measuring the absorbance at 377 nm of released pyridine-2-thione. The absorbance was maximal when 1.4 equiv of mercaptoethylamine/PDP group were added; the absorbance corresponded to that obtained upon the reduction of the PDP groups in the presence of 5 equiv of mercaptoethylamine/PDP group.

Poly[Lys-(AEDTP)] was able to form complexes with pDNA via electrostatic interactions between pDNA phosphates and the amino groups of the cationic polymer. As shown by agarose gel electrophoresis, the migration of 2.5 μg of pDNA was indeed completely retarded in the presence of 10 μg of poly[Lys-(AEDTP)] (polymer/DNA molar ratio of 150, amine/phosphate ratio of 2.8; Figure 2A, line 0). Similar results were obtained with a DNA/polymer ratio of 10/50 (μg/μg). The polyplexes solution contained homogeneous particles of 110 nm in diameter

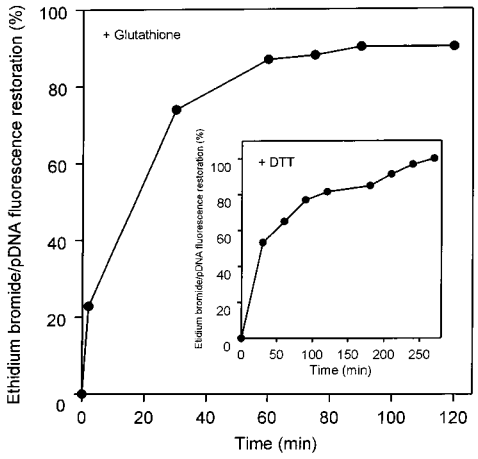


Figure 3. Glutathione-induced pDNA decondensation. Ethidium bromide/pDNA fluorescence restoration. pSV2luc (20 μg in 0.5 mL of HB) was mixed with poly[Lys-(AEDTP)] (100 μg) in 0.5 mL of HB. After 30 min at 20 °C, polyplexes were incubated for various times at 37 °C in the presence of either 10 mM glutathione or (inset) 0.1 M DTT. Ethidium bromide (40 μL of a 0.1 mg/mL solution in HB) was then added, and the fluorescence intensity of the solution was measured at 585 nm upon excitation at 540 nm.

and exhibited a ζ potential of $+15 \pm 4$ mV. Comparatively, 2.5 μg of pDNA completely condensed in the presence of 5 μg of polylysine (polymer/DNA molar ratio of 120, amine/phosphate ratio of 2.2; Figure 2B, line 0), formed polyplexes particles of 100 nm in diameter, and exhibited a ζ potential of $+17 \pm 2$ mV.

pDNA Release from Poly[Lys-(AEDTP)]. The cleavage of the disulfide bonds of poly[Lys-(AEDTP)] was expected to induce the dissociation of polyplexes and the release of pDNA. First, DTT was used in order to reduce disulfide bonds, and the release of pDNA was monitored by an agarose gel electrophoresis. After incubation of pDNA/poly[Lys-(AEDTP)] in the presence of 0.1 M DTT for 6 h at 37 °C, pDNA migrated as free pDNA, showing the total release of pDNA from poly[Lys-(AEDTP)] after cleavage of the disulfide bonds (Figure 2A). In contrast, no release of pDNA was found for pDNA/polylysine complexes in the presence of DTT (Figure 2B). The release was dependent on the DTT concentration; it was efficient with at least 40 mM DTT (Figure 2C). A cleavage of the disulfide bonds with DTT before mixing poly[Lys-(AEDTP)] with pDNA did not allow for the formation of polyplexes (data not shown). Second, the release of pDNA was also monitored by following the ethidium bromide/DNA fluorescence restoration. In the absence of poly[Lys-(AEDTP)], ethidium bromide mixed with pDNA exhibited a fluorescence emission centered at 585 nm. In polyplexes, the binding of ethidium bromide cannot intercalate between the base pairs of the DNA double helix and does not fluoresce. Conversely, when pDNA is decondensed or released from polyplexes, an intense fluorescence signal is emitted. In the presence of either poly[Lys-(AEDTP)] or polylysine with a DNA/polymer molar ratio leading to a complete condensation of the pDNA, the fluorescence intensity measured after adding ethidium bromide was 25% of that obtained with free pDNA. Thus, pDNA decondensation allowing the binding of ethidium bromide to pDNA will restore the fluorescence intensity. As shown in Figure 3 (inset), pDNA/poly[Lys-(AEDTP)] complexes incubated at 37 °C in the presence of 0.1 M DTT led to pDNA decondensation. No effect was observed with pDNA/polylysine complexes (data not shown). Although 80% of the fluorescence intensity was restored

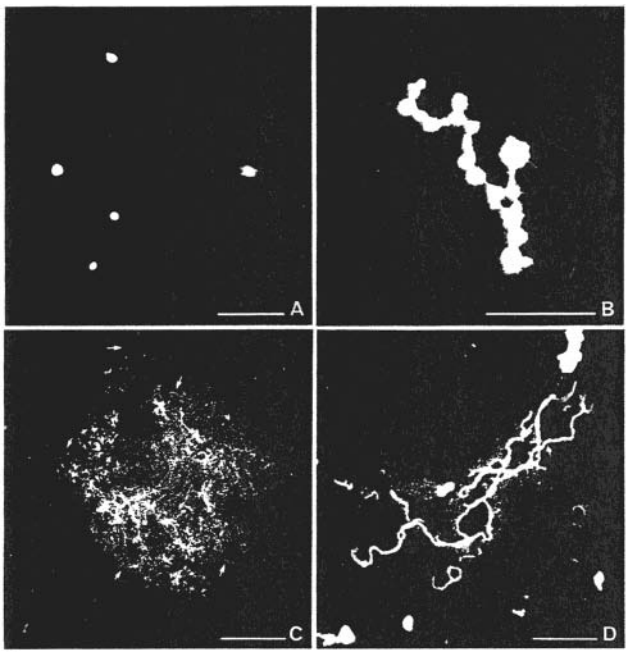


Figure 4. Electron microscopy observation of polyplexes made with poly[Lys-(AEDTP)]. Observations were performed by annular dark-field EM after adsorption of the molecules on activated carbon films and uranyl acetate staining, as described in Material and Methods. (A) After 30 min, the polyplexes were condensed in spherical particles of about 100 nm. (B) In the presence of glutathione (15 min), we observed decondensation of the complexes and fusion events. (C) Decondensation increased with time (1 or 2 h in the presence of glutathione). Arrows indicate fibrillate structures corresponding to DNA. (D) Formation of filamentous aggregates were frequently observed (same conditions). (Scale: the bars correspond to 500 nm.)

after a 2 h incubation, pDNA did not migrate under electrophoresis (Figure 2A). This indicated that pDNA was not still released. Ethidium bromide/DNA fluorescence restoration is a more sensitive method to check polyplexes modification than the mobility shift assay in agarose gel electrophoresis. The binding of ethidium bromide to pDNA does not require a complete dissociation of the polyplexes; a decondensation of pDNA after cleavage of a few disulfide bonds of poly[Lys-(AEDTP)] is enough to allow for the binding of ethidium bromide. In contrast, the migration of pDNA in an agarose gel electrophoresis requires the release of pDNA.

Attempts were also performed to check the release of pDNA under physiological conditions. The effect of glutathione on polyplexes stability, the main reductive substance contained in the cytosol, was monitored by electrophoresis and ethidium bromide/DNA fluorescence restoration. As with DTT, the incubation of poly[Lys-(AEDTP)] with 10 mM glutathione prior its mixing with pDNA did not allow for the formation of polyplexes (data not shown). As shown in Figure 3, 50% and 90% of the fluorescence intensity was restored after 20 min and 1 h incubation at 37 °C in the presence of 10 mM glutathione, respectively, suggesting that, as with DTT, glutathione induced a rapid decondensation of pDNA upon disulfide bond cleavage. However, glutathione was not as efficient as DTT to release pDNA. Indeed, when pDNA/poly[Lys-(AEDTP)] complexes were treated with glutathione for 6 h at 37 °C, only a low amount of pDNA migrated in agarose gel electrophoresis. This was sustained by electron microscopy. TEM showed the high level of condensation of polyplexes, with spherical particles of a mean size at about 100 nm (Figure 4A). In the presence of glutathione, numerous events of particles fusions appears

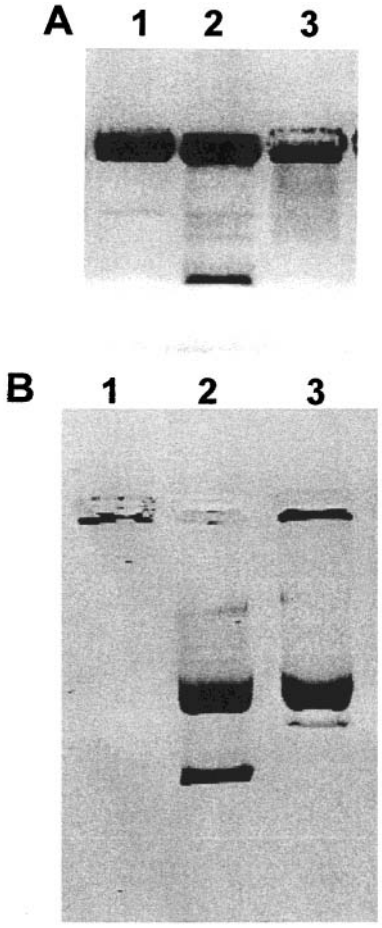


Figure 5. Release of pDNA from polyplexes made with poly-[Lys-(AEDTP)]. pSV2Luc (10 μg) was complexed with poly[Lys-(AEDTP)] (40 μg). Complexes were reduced for 2 h at 37 °C under indicated conditions, analyzed by 0.8% agarose gel electrophoresis, and DNA visualized with ethidium bromide: (A) lane 1, polyplexes before reduction; lane 2, polyplexes incubated in the presence of 20 mM glutathione, 2 units/mL glutathione reductase, and 0.5 mM NADH; lane 3, as in lane 2 but without glutathione; (B) lane 1, polyplexes before reduction; pDNA (lane 2) and polyplexes (lane 3) incubated in the presence of 2 units/mL thioredoxin reductase and 0.5 mM NADPH.

after 15 min (Figure 4B), resulting of some decondensation of the polyplexes; free pDNA molecules became visible at the periphery of the complexes. Decondensation increased with time, as illustrated in Figure 4C, after 1 or 2 h of incubation. Very frequently, complexes reorganization could occur through the formation of filamentous aggregates (Figure 4D with a granular background-containing released polymer from the complexes (parts C and D of Figure 4). However, the release of pDNA by glutathione was facilitated in the presence of glutathione reductase and NADH (Figure 5A). It was successfully induced by thioredoxin reductase itself in the presence of NADPH (Figure 5B). Despite the fact that the release of pDNA from polyplexes was not complete, these results still demonstrate that pDNA release can occur under reductive conditions inside the cells.

Enhancement of the Transfection Efficiency. HepG2 and 293T7 cells were transfected for 4 h with pCMVLuc complexed with either poly[Lys-(AEDTP)] or polylysine in the presence of 100 μM chloroquine. An enhancement of the transfection efficiency was obtained with the plasmid complexed with poly[Lys-(AEDTP)] as compared to that of the plasmid complexed with poly-

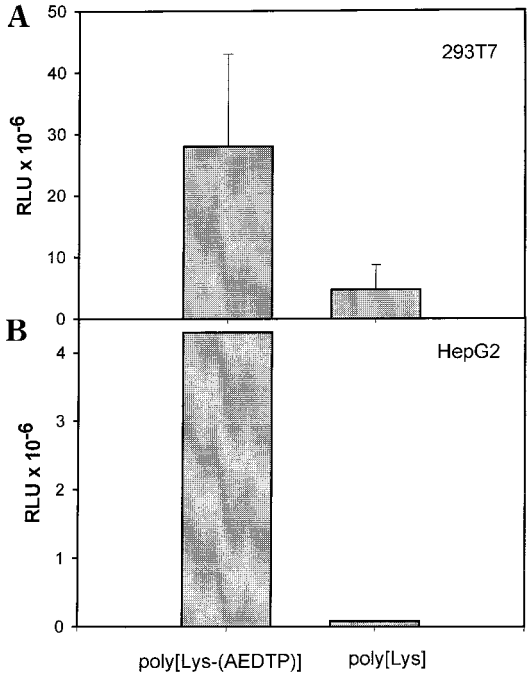


Figure 6. Poly[Lys-(AEDTP)]-mediated polyfection. (A) 293T7 cells and (B) HepG2 cells were incubated for 4 h at 37 °C with 5 μg of pUT650 complexed with either poly[Lys-(AEDTP)] (20 μg) or poly[Lys] (15 μg) in the presence of 10% FCS and 100 μM chloroquine. The luciferase activity was measured after a 48 h culture and expressed as RLU/10^6 cells.

lysine. The luciferase activity into HepG2 and 293T7 cells was 50- and 10-fold higher, respectively (Figure 6).

DISCUSSION

A disulfide-containing cationic polymer was designed to favor polyplexes dissociation and the release of the plasmid in a reductive medium. The substitution of each lysyl ϵ-amino group of polylysine with a 3-(2-aminoethyldithio)propionyl residue gave poly[Lys-(AEDTP)] in which all of the 190 amino groups were linked to the polylysine backbone via a disulfide bond. After mixing with pDNA, this cationic polymer induces DNA condensation and the formation of homogeneous particles with a diameter and a ζ potential similar to that of polyplexes made with polylysine. The main interesting feature of poly[Lys-(AEDTP)] is that pDNA can be released under reductive conditions found inside the cells either in the cytosol or the nucleus. We found that the luciferase activity was higher in cells transfected with poly[Lys-(AEDTP)] polyplexes than in cells transfected with polylysine polyplexes. Assuming a similar (i) uptake by the cells of polyplexes made with poly[Lys-(AEDTP)] or polylysine which exhibited similar size and charge and (ii) delivery of pDNA in the cytosol in the presence of chloroquine, the enhanced transfection with poly[Lys-(AEDTP)] polyplexes could be attributed to a better polyplexes dissociation upon the cleavage of the disulfide bonds of the polymer. This statement is supported by in vitro data showing that, in vitro under physiological conditions, glutathione induces a clear decondensation of pDNA with a significant release of the plasmid in the presence of glutathione reductase found in the cytosol of mammalian cells which has a broad substrate specificity.

Poly[Lys-(AEDTP)] was the first disulfide-containing cationic polymer reported for cell transfection. Conversely, it has been shown that cationic lipids such as 1′, 2′ dioleoyl-*sn*-glycero-3′-succinyl-2-hydroxyethyl dis-

ulfide ornithine conjugate (DOGSDSO) (*16*), the cholesteryl hemidithiodiglycolyl tris(aminoethyl)amine (CHD-TAEA) (*17*), spermine-derived amino acid linked via a disulfide bond to various hydrophobic entities (*18*), and lipoic acid-derived amphiphiles (*19*) were more efficient than their nondisulfide analogues in transfecting cells. The reduction of the disulfide bond in the cytosol, which released the pDNA as well as a reduced toxicity of these lipids by an increase of their degradation, were claimed to be involved in the efficiency of the transfection. In complexes with lipoic acid-derived amphiphiles, it was shown that pDNA was rapidly and largely released in the presence of thioredoxin (*19*). However, the release in the presence of glutathione alone was at the level we found for pDNA/poly[Lys-(AEDTP)] complexes. In the case of cationic polymers, it has been reported that the cross-linking of polyplexes via disulfide bonds, termed "caged DNA", allowing for a better stability in the extracellular medium of polyplexes, increased also the transfection efficiency (*20*, *21*). In this case, the elevation of the transfection efficiency was supposed to come from the reduction in the cytosol of the disulfide bonds leading to a decrease of the stability of polyplexes.

It is still ill-known whether the unpackaging of pDNA inside the cells could improved the transfection efficiency. Recent data have shown that an increase of the transfection efficiency of EGF−polylysine/DNA complexes was correlated to the unpackaging of pDNA and the decrease of the polyplexes stability according to the length of polylysine (*9*). Indeed, polyplexes made with polylysine of dp = 190 were more stable than polyplexes made with polylysine of dp = 36 but less efficient in transfecting cells. A fluorescence microscopy analysis showed that both pDNA and polymer were present inside the nucleus of few cells when EGF−polylysine polyplexes were made with polylysine of dp = 190, indicating that polyplexes were not dissociated. Conversely, only the pDNA was detected inside the cell nucleus when polyplexes were made with polylysine of dp = 36, indicating that polyplexes were dissociated. These data indicate that a better dissociation of polyplexes leads to a better accessibility of the plasmid to the nuclear machinery for the gene expression. Up to now, it is not clear in the case of nondividing cells whether a nuclear import of 100 nm polyplexes can occur through the nuclear pores, even when polyplexes carry nuclear localization signals. Thus, an unpackaging of the pDNA complexed with disulfide-containing cationic polymers such as poly[Lys-(AEDTP)] in the cytosol would favor its passage through the nuclear pores. At least, a decondensation of the plasmid without a complete release might protect it against degradation by cytosolic nucleases (*20*). Conversely, after the cell division, a disulfide-containing cationic polymer could favor the release of pDNA and facilitate the gene expression.

Disulfide-containing cationic polymers reducible in the cytosol could be also useful for the delivery of RNA and oligonucleotides. Indeed, cationic polymers have been used to deliver antisense or triple helix-forming oligonucleotides after the formation of complexes (*22*−*27*). Because, once in the cytosol, oligonucleotides penetrate rapidly by simple diffusion in the cell nucleus (*28*−*31*); a facilitated dissociation in the cytosol of oligonucleotide polyplexes could be achieved by using poly[Lys-(AEDTP)]. The self-assembly of RNA with a cationic polymer could also be a promising strategy to introduce RNA suitable to inhibit protein synthesis with a therapeutic effect or to express antigenic proteins (*32*−*34*). With this aim, we propose the use of poly[Lys-(AEDTP)]-like cationic polymers to complex mRNA in order to increase both its protection from nuclease degradation in the extracellular medium, its cellular uptake, its an unpackaging in the cytosol, and its transcription by the cytosolic machinery.

In conclusion, disulfide-containing cationic polymers could be good carriers for the delivery of plasmids, RNAs, and oligonucleotides. Further works are in progress to improve their efficiency. They include (i) the study of the influence of the number of disulfide bonds per polymer on the kinetic of the nucleic acids release under cytosolic conditions and (ii) the linkage of devices exhibiting fusogenic features such as histidyl residues to increase the escape of polyplexes from endocytic vesicles (*35*, *36*).

ACKNOWLEDGMENT

We thank Céline Zuber for her skillful technical assistance. We thank Drs. M. Brisson and L. Huang (University of Pittsburgh, Pittsburgh) for 293T7 cells. This work was partly supported by grants from Agence Nationale de Recherche sur le Sida (ANRS, n^0 97003). P.M. is Research Director at INSERM, C.P. an Assistant Professor at the University of Orléans, EL Chargé de Recherche at CNRS, and E.D. Research Director at CNRS.

LITERATURE CITED

(1) Zauner, W., Ogris, M., and Wagner, E. (1998) Polylysine-based transfection systems utilizing receptor-mediated delivery. *Adv. Drug Delivery Rev. 30*, 97−113.

(2) Mahato, R. I., Smith, L. C., and Rolland, A. (1999) Pharmaceutical perspectives of nonviral gene therapy. *Adv. Genet. 41*, 95−156.

(3) Garnett, M. C. (1999) Gene-delivery systems using cationic polymers. *Crit. Rev. Ther. Drug Carrier Syst. 16*, 147−207.

(4) Kabanov, V. A., and Kabanov, A. V. (1998) Interpolyelectrolyte and block ionomer complexes for gene delivery: physicochemical aspects. *Adv. Drug Deliv. Rev. 30*, 49−60.

(5) Chiou, H. C., Tangco, M. V., Levine, S. M., Robertson, D., Kormis, K., Wu, C. H., and Wu, G. Y. (1994) Enhanced resistance to nuclease degradation of nucleic acids complexed to asialoglycoprotein-polylysine carriers. *Nucleic Acids Res. 22*, 5439−46.

(6) Dash, P. R., Toncheva, V., Schacht, E., and Seymour, L. W. (1997) Synthetic polymers for vectorial delivery of DNA: characterization of polymer-DNA complexes by photon correlation spectroscopy and stability to nuclease degradation and disruption by polyanions in vitro. *J. Controlled Release 48*, 269−276.

(7) Erbacher, P., Roche, A. C., Monsigny, M., and Midoux, P. (1995) Glycosylated polylysine/DNA complexes: gene transfer efficiency in relation with the size and the sugar substitution level of glycosylated polylysines and with the plasmid size. *Bioconjugate Chem. 6*, 401−410.

(8) Erbacher, P., Roche, A. C., Monsigny, M., and Midoux, P. (1997) The reduction of the positive charges of polylysine by partial gluconoylation increases the transfection efficiency of polylysine/DNA complexes. *Biochim. Biophys. Acta 1324*, 27−36.

(9) Schaffer, D. V., Fidelman, N. A., Dan, N., and Lauffenburger, D. A. (2000) Vector unpacking as a potential barrier for receptor-mediated polyplex gene delivery. *Biotechnol. Bioeng. 67*, 598−606.

(10) Derrien, D., Midoux, P., Petit, C., Negre, E., Mayer, R., Monsigny, M., and Roche, A. C. (1989) Muramyl dipeptide bound to poly-L-lysine substituted with mannose and gluconoyl residues as macrophage activators. *Glycoconjugate J. 6*, 241−255.

(11) Brasier, A. R., Tate, J. E., and Habener, J. F. (1989) Optimized use of the firefly luciferase assay as a reporter gene in mammalian cell lines. *BioTechniques 7*, 1116−1123.

(12) Brisson, M., He, Y., Li, S., Yang, J. P., and Huang, L. (1999) A novel T7 RNA polymerase autogene for efficient cytoplasmic expression of target genes. *Gene Ther. 6*, 263−270.

(13) Chen, T. R. (1977) In situ detection of mycoplasma contamination in cell cultures by fluorescent Hoeschst 33258 stain. *Exp. Cell Res. 104*, 255−262.

(14) De Wet, J. R., Wood, K. V., De Luca, M., Helinsky, D. R., and Subramani, S. (1987) Firefly luciferase gene: structure and expression in mammalian cells. *Mol. Cell. Biol. 7*, 725−737.

(15) Delain, E., and Le Cam, E. (1995) The spreading of nucleic acids, in *Visualization of nucleic acids* (G. Morel, Ed.), pp 35−56, CRC Press, Boca Raton, FL.

(16) Tang, F., and Hughes, J. A. (1998) Introduction of a disulfide bond into a cationic lipid enhances transgene expression of plasmid DNA. *Biochem. Biophys. Res. Commun. 242*, 141−145.

(17) Tang, F., and Hughes, J. A. (1999) Use of dithiodiglycolic acid as a tether for cationic lipids decreases the cytotoxicity and increases transgene expression of plasmid DNA in vitro. *Bioconjugate Chem. 10*, 791−796.

(18) Wetzer, B., Byk, G., Frederic, M., Airiau, M., Blanche, F., Pitards, B., and Scherman, D. (2001) Reducible cationic lipids for gene transfer. *Biochem. J. 356*, 747−756.

(19) Balakirev, M., Schoehn, G., and Chroboczek, J. (2000) Lipoic acid-derived amphiphiles for redox-controlled DNA delivery. *Chem. Biol. 7*, 813−819.

(20) Trubetskoy, V. S., Budker, V. G., Hanson, L. J., Slattum, P. M., Wolff, J. A., and Hagstrom, J. E. (1998) Self-assembly of DNA-polymer complexes using template polymerization. *Nucleic Acids Res. 26*, 4178−4185.

(21) Lechardeur, D., Sohn, K. J., Haardt, M., Joshi, P. B., Monck, M., Graham, R. W., Beatty, B., Squire, J., O'Brodovich, H., and Lukacs, G. L. (1999) Metabolic instability of plasmid DNA in the cytosol: a potential barrier to gene transfer. *Gene Ther. 6*, 482−497.

(22) McKenzie, D. L., Kwok, K. Y., and Rice, K. G. (2000) A potent new class of reductively activated peptide gene delivery agents. *J. Biol. Chem. 275*, 9970−9977.

(23) Wu, G. H., and Wu, C. H. (1992) Specific inhibition of hepatitis B viral gene expression in vitro by targeted antisense oligonucleotides. *J. Biol. Chem. 267*, 12436−12439.

(24) Citro, G., Perrotti, D., Cucco, C., D'Agnano, I., Sacchi, A., Zupi, G., and Calabretta, B. (1992) Inhibition of leukemia cell proliferation by receptor-mediated uptake of c-myc antisense oligodeoxynucleotides. *Proc. Natl. Acad. Sci. U.S.A. 89*, 7031−7035.

(25) Citro, G., Szczylik, C., Ginobbi, P., Zupi, G., and Calabretta, B. (1994) Inhibition of leukemia cell proliferation by folic acid−polylysine-mediated introduction of c-myb antisense oligodeoxynucleotides into HL60 cells. *Br. J. Cancer 69*, 463−467.

(26) Stewart, A. J., Pichon, C., Meunier, L., Midoux, P., Monsigny, M., and Roche, A. C. (1996) Enhanced biological activity of antisense oligonucleotides complexed with glycosylated poly-L-lysine. *Mol. Pharmacol. 50*, 1487−1494.

(27) Pichon, C., Bello-Roufai, M., Monsigny, M., and Midoux, P. (2000) Histidylated oligolysines increase the transmembrane passage and the biological activity of antisense oligonucleotides. *Nucleic Acids Res. 28*, 504−512.

(28) Leonetti, J. P., Mechti, N., Degols, G., Gagnor, C., and Lebleu, B. (1991) Intracellular distribution of microinjected antisense oligonucleotides. *Proc. Natl. Acad. Sci. U.S.A. 88*, 2702−2706.

(29) Chin, D. J., Green, G. A., Zon, G., Szoka, F. C., and Straubinger, R. M. (1990) Rapid nuclear accumulation of injected oligodeoxyribonucleotides. *New Biol. 2*, 1091−1100.

(30) Fisher, T. L., Terhorst, T., Cao, X., and Wagner, R. W. (1993) Intracellular disposition and metabolism of fluorescently labeled unmodified and modified oligonucleotides microinjected into mammalian cells. *Nucleic Acids Res. 21*, 3857−3865.

(31) Lukacs, G. L., Haggie, P., Seksek, O., Lechardeur, D., Freedman, N., and Verkman, A. S. (2000) Size-dependent DNA mobility in cytoplasm and nucleus. *J. Biol. Chem. 275*, 1625−1629.

(32) Boczkowski, D., Nair, S. K., Nam, J. H., Lyerly, H. K., and Gilboa, E. (2000) Induction of tumor immunity and cytotoxic T lymphocyte responses using dendritic cells transfected with messenger RNA amplified from tumor cells. *Cancer Res. 60*, 1028−1034.

(33) Heiser, A., Dahm, P., Yancey, D. R., Maurice, M. A., Boczkowski, D., Nair, S. K., Gilboa, E., and Vieweg, J. (2000) Human dendritic cells transfected with RNA encoding prostate-specific antigen stimulate prostate-specific CTL responses in vitro. *J. Immunol. 164*, 5508−5514.

(34) Elbashir, S. M., Harborth, J., Lendeckel, W., Yalcin, A., Weber, K., and Tuschl, T. (2001) Duplexes of 21-nucleotide RNAs mediate RNA interference in cultured mammalian cells. *Nature 411*, 494−498.

(35) Midoux, P., and Monsigny, M. (1999) Efficient gene transfer by histidylated polylysine/pDNA complexes. *Bioconjugate Chem. 10*, 406−411.

(36) Pichon, C., Bello Roufaï, M., Monsigny, M., and Midoux, P. (2000) Histidylated oligolysines increase the transmembrane passage and the biological activity of antisense oligonucleotides. *Nucleic Acids Res. 28*, 504−512.

BC015503O

Synthesis and Characterization of Phenothiazine Labeled Oligodeoxynucleotides: Novel 2′-Deoxyadenosine and Thymidine Probes for Labeling DNA

Xi Hu, Mark T. Tierney, and Mark W. Grinstaff*

Department of Chemistry, Paul M. Gross Chemical Laboratory, Duke University, Durham, North Carolina 27708. Received April 15, 2001; Revised Manuscript Received August 15, 2001

A facile procedure for the incorporation of phenothiazine at the terminus of oligodeoxynucleotides is reported. Phenothiazine is covalently linked to the 5′-position of 2′-deoxyadenosine and thymidine. Next, the corresponding phosphoramidites are prepared, and then the labeled nucleosides are incorporated in DNA using an automated DNA solid-phase synthesizer. Phenothiazine labeled oligodeoxynucleotides form stable B-form duplexes with similar melting temperatures, CD spectra, and DSC traces compared to unlabeled DNA duplexes. The favorable photophysical properties of phenothiazine are also retained after covalent attachment to the oligodeoxynucleotide.

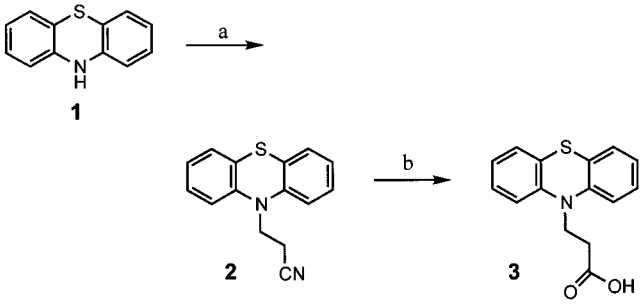
INTRODUCTION

Organic and inorganic chromophores possessing well-defined spectroscopic and redox properties are of interest for mechanistic studies of DNA mediated charge transfer (*1*−*15*) and for optimizing DNA diagnostic devices (*16*−*21*). Both of these interests require synthetic control over the site-specific location of the probe on the duplex. Current automated DNA synthesis technology offers a convenient and high-yielding procedure for synthesizing such duplexes. By selecting the appropriate derivatized phosphoramidite probe, this approach enables labeling at specific sites (phosphate, ribose, nucleobase) and sequence locations on the oligodeoxynucleotide. Intercalating probes such as anthraquinone and $Ru(phen)_2(dppz)^{2+}$ when covalently attached to DNA are typically tethered to the 5′- or 3′-terminal phosphate of the oligodeoxynucleotide (*1*, *2*). Yet intercalating probes alter the DNA duplex structure as evident by an increase in melting temperature and by crystallographic examination of the DNA π-stack (*22*). Nonintercalating tethered probes are less explored and provide an opportunity to assess the role of location site and the mode of attachment on duplex hybridization and on charge transfer chemistry. To expand the current repertoire of probes available for study (*23*), we are synthesizing oligodeoxynucleotides labeled at the 5-position of uridine (*24*−*27*), C8 position of 2′-deoxyadenosine (*28*), 5′-terminal phosphate (*29*, *30*), and the 5′-position of thymidine (*31*) with spectroscopic and/or redox-active chromophores. Herein, we describe the synthesis of two novel phenothiazine-2′-deoxyadenosine and -thymidine nucleosides and the incorporation of these labeled pyrimidine and purine nucleosides in oligodeoxynucleotides.

EXPERIMENTAL PROCEDURES

Reagents were purchased from Aldrich or Acros as highest purity grades and used without further purification. All solvents were freshly distilled under inert atmosphere prior to use unless otherwise noted. Dichloromethane (CH_2Cl_2) and acetonitrile (CH_3CN) were distilled from CaH_2. Ethyl ether and THF were distilled from sodium/benzophenone. Anhydrous DMF was obtained from Aldrich. All reactions were performed under inert atmosphere unless otherwise noted. Absorption spectra and melting curves were measured on a diode array spectrometer. CD spectra were recorded on a spectropolarimeter. Calorimetric data were obtained using a VP-DSC from MicroCal Inc. MALDI-TOF mass spectra of oligodeoxynucleotides were obtained using a PerSeptive Biosystems Voyager-DE Biospectrometry Workstation operating in the negative ion mode using a hydroxypicolinic acid matrix. NMR spectra were recorded on a spectrometer operating at 400 MHz. Fast atom bombardment mass spectra (FABMS) were obtained on a JEOL JMS-SX102A spectrometer using a 3-nitrobenzyl alcohol matrix.

Scheme 1. Synthesis of PTZ-Acid[a]



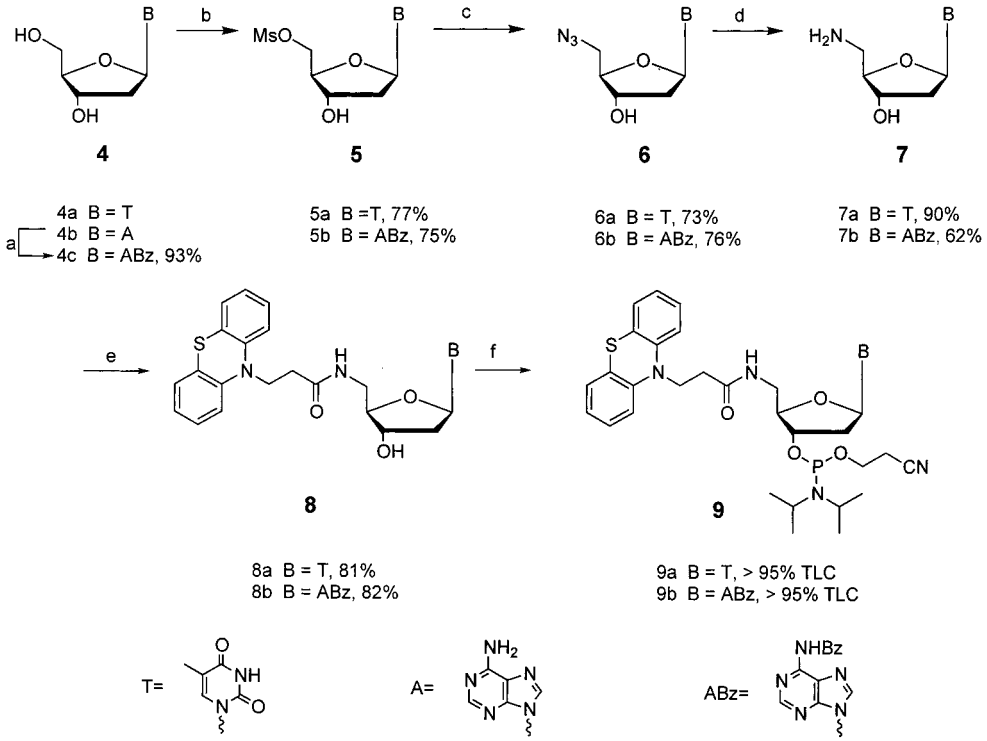
[a] Key: (a) acrylonitrile, $NBu_4^+OH^-$, 87% yield; (b) NaOH, aqueous MeOH, 56% yield.

Syntheses. *3-Phenothiazin-10-ylpropionitrile* ***2***. In a modification of a previous report by Godefroi and Wittle (*32*), phenothiazine (2.0 g; 1.0 mmol) was suspended in acrylonitrile (15 mL) and cooled to 0 °C. Tetrabutylammonium hydroxide (50% in water; 0.1 mL) was added and the mixture allowed to slowly warm to room temperature (Scheme 1). An exothermic reaction occurred immediately. Once the reaction subsided, dioxane (25 mL) was added and the mixture was heated to reflux for 1 h. The mixture was poured in water with vigorous stirring, and the resulting tan solid was filtered. Recrystallization from

* Corresponding author: mwg@chem.duke.edu; http://www.chem.duke.edu/~mwg/labgroup.

10.1021/bc0100509 CCC: $22.00 © 2002 American Chemical Society
Published on Web 12/27/2001

Scheme 2. Synthesis of PTZ-Phosphoramidites[a]



[a] Key: (a) TMSCl, BzCl/pyridine, 25 °C, 2.5 h, H_2O, NH_4OH, 0 °C, 10 min; (b) MsCl/pyridine, 0 °C, 12 h; (c) LiN_3/DMF, 90 °C, 3 h; (d) H_2, Pd/C, 50 psi, 25 °C 5 h; (e) **3**, CDI/DMF, LH-20/THF, 25 °C, 18 h; (f) 2-cyanoethyl *N*,*N*′-diisopropylchlorophosphoramidite, DIPEA, CH_3CN, 25 °C, 2 h.

acetone gave **2** as a white solid (2.2 g; 87% yield). This material was used directly in the next step.

3-Phenothiazin-10-ylpropionic Acid ***3***. This compound was prepared from **2** using the hydrolysis method described by Godefroi and Wittle (56% yield) (*32*). FAB-HRMS calcd (found) for $C_{15}H_{13}NO_2S$ (M^+) 271.0667 (271.0666).

6-N-Benzoyl-2′-deoxyadenosine ***4c.*** The reaction was performed following the literature procedure by Jones (*33*) to afford **4c** in 93% yield. This procedure also required transient protection of the 5′- and 3′-hydroxyls by TMS-Cl in pyridine, followed by addition of benzoyl chloride to protect the free amine and subsequent deprotection of the hydroxyls by ammonium hydroxide (*33*). ^{1}H NMR (DMSO-d_6): δ 2.32−2.40 (m, 1H, C2′), 2.77−2.83 (m, 1H, C2′), 3.51−3.67 (m, 2H, C5′), 3.90 (q, J = 2.8 Hz, 1H, C4′), 4.45−4.46 (m, 1H, C3′), 5.05 (s, 1H, 5′-OH), 5.39 (s, 1H, 3′-OH), 6.48 (t, J = 6.8 Hz, 1H, C1′), 7.55−8.06 (m, 5H, benzoyl), 8.69 (s, 1H, C2), 8.75 (s, 1H, C8), 11.20 (s, 1H, amide). FAB-MS calcd (found) for M^+ + H: 356.13 (356.09).

5′-O-Methanesulfonylthymidine ***5a.*** The reaction was based on a literature procedure (*34*). Thymidine **4a** (2.90 g, 12.0 mmol) was dissolved in 10 mL of dry pyridine and cooled to −10 °C. Next, mesyl chloride (14 mmol) was added dropwise over a period of 20 min (Scheme 2). The reaction mixture was then held at 0 °C for 12 h. The next day, 10 mL of methanol was added to quench the reaction, and the solvents were evaporated via high vacuum. The resulting crude product was checked by TLC and purified by column chromatography (silica gel, CH_3OH:$CHCl_3$ = 1:9). A white solid **5a** was obtained (2.95 g, 77% yield). ^{1}H NMR (DMSO-d_6): δ 1.78 (s, 3H, 5-methyl), 2.08−2.22 (m, 2H, C2′), 3.22 (s, 3H, mesyl), 3.98 (q, 1H, C4′), 4.23−4.28 (m, 1H, C3′), 4.36−4.39 (m, 2H, C5′), 5.49 (d, J = 4.4 Hz, 1H, 3′-OH), 6.22 (t, J = 7.2 Hz, 1H, C1′), 7.48 (s, 1H, C6), 11.25 (s, 1H, N3). FAB-MS calcd (found) for M^+ + H: 321.07 (321.06).

5′-O-Methanesulfonyl-6-N-benzoyl-2′-deoxyadenosine ***5b.*** Synthesized from **4c** in a similar manner as **5a**, 75% yield. ^{1}H NMR (DMSO-d_6): δ 2.40−2.47 (m, 1H, C2′), 2.88−2.96 (m, 1H, C2′), 3.16 (s, 1H, mesyl), 4.11−4.15 (m, 1H, C4′), 4.38−4.49 (m, 2H, C5′), 4.54−4.56 (m, 1H, C3′), 5.64 (d, J = 4.0 Hz, 1H, 3′-OH), 6.54 (t, J = 6.8 Hz, 1H, C1′), 7.55−8.06 (m, 5H, benzoyl), 8.65 (s, 1H, C2), 8.76 (s, 1H, C8), 11.20 (s, 1H, amide). FAB-MS calcd (found) for M^+ + H: 434.11 (434.10).

5′-Azido-5′-deoxythymidine ***6a***. A solution of **5a** (1.84 g, 5.75 mmol) in 15 mL of DMF containing lithium azide (1.60 g, 32.6 mmol) was refluxed at 90 °C under nitrogen. After 3 h, the reaction was stopped and the solvent was removed under vacuum. The resulting crude product was purified by column chromatography (silica gel, CH_3OH:$CHCl_3$ = 1:9) to afford **6a** (1.12 g, 73% yield). ^{1}H NMR (DMSO-d_6): δ 1.78 (s, 3H, 5-methyl), 2.16−2.34 (m, 2H, C2′), 3.38−3.56 (m, 2H, C5′), 3.92 (q, J = 4.8 Hz, 1H, C4′), 4.31−4.33 (m, 1H, C3′), 5.50 (s, 1H, 3′-OH), 6.13 (t, J = 7.2 Hz, 1H, C1′), 7.48 (s, 1H, C6), 11.25 (s, 1H, N3). FAB-MS calcd (found) for M^+ + H: 268.10 (268.12).

5′-Azido-6-N-benzoyl-2′,5′-dideoxyadenosine ***6b.*** Synthesized from **5b** in a similar manner as **6a**, 76% yield. ^{1}H NMR (DMSO-d_6): δ 2.45 (m, 1H, C2′), 2.97 (m, 1H, C2′), 3.51−3.67 (m, 2H, C5′), 3.99−4.03 (m, 1H, C4′), 4.47−4.49 (m, 1H, C3′), 5.52 (d, J = 4.0 Hz, 1H, 3′-OH), 6.52 (t, J = 6.8 Hz, 1H, C1′), 7.52−8.04 (m, 5H, benzoyl), 8.68 (s, 1H, C2), 8.76 (s, 1H, C8), 11.20 (s, 1H, amide). FAB-MS calcd (found) for M^+ + H: 381.13 (381.14).

5′-Amino-5′-deoxythymidine ***7a.*** A solution of 5′-azido-2′-deoxythymidine **6a** (1.12 g, 4.2 mmol) in 30 mL of methanol containing 10% Pd/C was shaken under 50 psi of hydrogen for 5 h. The catalyst was removed by filtration, and the filtrate was then concentrated to

dryness via evaporation. The resulting crude product was purified by column chromatography (silica gel, CH_3OH:$CHCl_3$ = 1:7) to yield **7a** (0.91 g, 90% yield). ^{1}H NMR DMSO, δ 1.78 (s, 3H, 5-methyl), 2.08−2.18 (m, 2H, C2′), 2.75 (s, 2H, amine), 3.50−3.60 (m, 2H, C5′), 3.64 (q, J = 3.2 Hz, 1H, C4′), 4.18−4.20 (m, 1H, C3′), 5.20 (s, 1H, 3′-OH), 6.14 (t, J = 7.2 Hz, 1H, C1′), 7.68 (s, 1H, C6). FAB-HRMS calcd (found) for $C_{10}H_{16}N_3O_4$ (MH^+): 242.1143 (242.1141).

5′-Amino-6-N-benzoyl-2′,5′-dideoxyadenosine ***7b.*** Synthesized from **6b** in a similar manner as **7a**, 62% yield.^{1}H NMR (DMSO-d_6): δ 2.31−2.36 (m, 1H, C2′), 2.71−2.89 (m, 3H, C5′+C2′), 3.16 (s, 2H, amine), 3.81 (q, J = 4.4 Hz, 1H, C4′), 4.43−4.45 (m, 1H, C3′), 5.31 (s, 1H, OH), 6.45 (t, J = 6.8 Hz, 1H, C1′), 7.52−8.05 (m, 5H, benzoyl), 8.70 (s, 1H, C2), 8.74 (s, 1H, C8). FAB-HRMS calcd (found) for $C_{17}H_{19}N_6O_3$ (MH^+): 355.1520 (355.1518).

N-(5′-Amino-5′-deoxythymidine)-3-phenothiazin-10-ylpropionamide ***8a.*** A solution of 3-phenothiazin-10-ylpropionic acid **3** (0.28 g, 1.0 mmol) and carbonyldiimidazole (CDI[1]) (0.24 g, 1.5 mmol) in 8 mL of dry DMF was stirred under nitrogen for 1 h at 25 °C. The mixture was then diluted with 17 mL of dry THF, followed by addition of the LH-20 resin (0.43 g, excess) to quench the excess CDI. An hour later, LH-20 was removed, and **7a** (0.24 g, 1.0 mmol) was added to the reaction mixture. After stirring for 12 h, the reaction was stopped, and the solvents were removed. Column chromatagraphy (silica gel, CH_3OH:$CHCl_3$ = 1:9) yielded a white solid (0.40 g, 81% yield). ^{1}H NMR (DMSO-d_6): δ 1.72 (s, 3H, 5-methyl), 1.98−2.08 (m, 2H, C2′), 2.55 (t, J = 7.2 Hz, 2H, PTZ N-CH_2), 3.20−3.38 (m, 2H, C5′), 3.68−3.69 (m, 1H, C4′), 4.07−4.12 (m, 3H, carbonyl-CH_2 and C3′), 5.24 (d, J = 4.4 Hz, 1H, 3′-OH), 6.08 (t, J = 7.2 Hz, 2H, C1′), 6.87−7.16 (m, 8H, aromatic H of PTZ), 7.42 (s, 1H, C6), 8.08 (t, J = 6.0 Hz, 1H, amide NH), 11.25 (s, 1H, C3). ^{13}C NMR: δ 13.0, 34.1, 39.4, 41.9, 43.9, 72.1, 84.6, 85.8, 110.6, 116.3, 123.5, 124.1, 128.0, 128.6, 137.1, 145.3, 151.4, 164.6, 171.3. FAB-HRMS calcd (found) for $C_{25}H_{26}N_4O_5S$ (M^+): 494.1618 (494.1621).

N-(5′-Amino-6-N-benzoyl-2′,5′-dideoxyadenosine)-3-phenothiazin-10-ylpropionamide ***8b.*** Synthesized from **7b** in a similar manner as **8a**, 82% yield. ^{1}H NMR (DMSO-d^6): δ 2.25−2.31 (m, 1H, C2′), 2.55−2.60 (m, 2H, PTZ-N-CH_2), 2.75−2.78 (m, 1H, C2′), 3.27−3.43 (m, 2H, C5′), 3.86−3.90 (m, 1H, C4′), 4.03−4.08 (m, 2H, carbonyl-CH_2), 4.37 (m, 1H, C3′), 5.37 (d, J = 4.0 Hz, 1H, 3′-OH), 6.41 (t, J = 6.8 Hz, 1H, C1′), 6.84−7.14 (m, 8H, PTZ), 7.48−8.01 (m, 5H, benzoyl), 8.12 (t, J = 6.0 Hz, 1H, PTZ amide), 8.62 (s, 1H, C2), 8.68 (s, 1H, C8), 11.14 (s, 1H, benzoyl amide). ^{13}C NMR: δ 34.1, 39.5, 42.1, 43.9, 72.5, 84.8, 86.8, 116.4, 123.4, 124.1, 127.1, 128.0, 128.6, 129.4, 133.4, 134.3, 144.4, 145.3, 151.4, 152.4, 152.8, 166.6, 171.2. FAB-HRMS calcd (found) for $C_{32}H_{29}N_7O_4S$ (M^+): 607.2002 (607.1996).

N-(5′Amino-3′-cyanoethoxydiisopropylaminophosphine-5′-deoxythymidine)-3-phenothiazin-10-ylpropionamide ***9a.*** 2-Cyanoethyl *N,N′*-diisopropylcholophosphoramidite (140 μL, 0.62 mmol) was added to a solution of **8a** (0.191 g, 0.39 mmol) in 20 mL of dry CH_3CN containing diisopropylethylamine (0.31 mL). The reaction mixture was stirred under nitrogen for 2 h. The solvent was then removed and the product checked by ^{31}P NMR($CDCl_3$): δ 149.5 and 149.9 observed. TLC: >95% yield.

N-(5′-Amino-3′-cyanoethoxydiisopropylaminophosphine-6-N-benzoyl-2′,5′-dideoxyadenosine)-3-phenothiazin-10-ylpropionamine ***9b.*** Synthesized in a similar manner as **9a**. ^{31}P NMR($CDCl_3$): δ 149.6 and 150.0 observed. TLC: >95% yield.

Oligodeoxynucleotide Syntheses. Oligodeoxynucleotide syntheses were performed on an ABI 395 DNA synthesizer from the 3′ to 5′ end using standard automated DNA synthesis protocols as shown in Scheme 3 (1.0 μmol scale). A 0.1 M solution of **9a** (or **9b**) in dry acetonitrile was prepared and installed on the DNA synthesizer in a standard reagent bottle. Normal solid-phase oligodeoxynucleotide synthesis was performed. In the last step, the PTZ-modified phosphoramidite was introduced and allowed to react with the oligodeoxynucleotide for 15 min. The PTZ-labeled oligodeoxynucleotides were cleaved from the column and deprotected in 30% NH_4OH at 55 °C for 16 h. MALDI mass spectrometry of the PTZ-oligodeoxynucleotides confirmed their formation.

	10	**11**	**12**	**13**	**14**
calcd	5436.8	5129.9	4205.7	5445.6	5141.4
found	5437.8	5128.5	4207.1	5448.4	5144.7

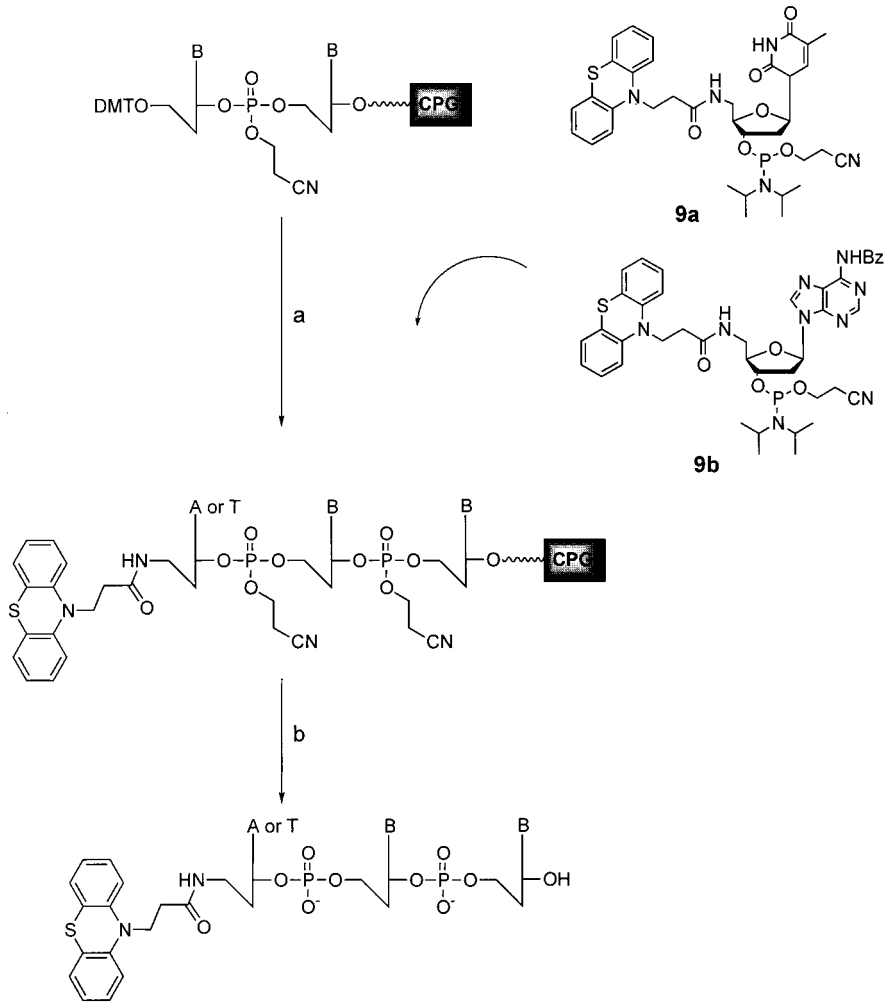
HPLC Purification of the Oligodeoxynucleotides. HPLC purification of the PTZ-labeled oligodeoxynucleotides was accomplished on a Rainin HPLC instrument. Reverse phase chromatography was performed on a C18 column (25 cm × 4.6 mm) with acetonitrile (ACN) and 0.1 M triethylamine acetate (TEAA) as eluting solvents. A flow rate of 3 mL/min was used, and the concentration of ACN was increased from 5% to 50% over 40 min. The retention times of the labeled oligodeoxynucleotides were well separated from those of the unlabeled oligodeoxynucleotide products (12−13 min).

Melting Curves. The stability of the duplex formed between two complementary oligodeoxynucleotides was determined from the melting curve profiles as a function of temperature. The T_m value was determined from the first derivative. The concentrations of stock solutions of oligodeoxynucleotide single strands were determined from the UV−vis absorbance spectra. Enzyme digestion of the oligdeoxynucleotides to yield the individual nucleotides with Nuclease P1 *Penicillium citrinum* was performed by the addition of 1 μL of a 1 mg/mL solution of enzyme to 5.0 μL of oligodeoxynucleotide single strand solution and 44.0 μL of 20 mM sodium acetate buffer at pH 5.5. The solutions were incubated at 55 °C for 30 min. A sample of 20.0 μL of digest solution was diluted to 2.00 mL with water, and the absorption spectrum was measured. The total molar absorptivity was determined from the sum of all the individual contributions of each nucleoside and PTZ. The concentrations of the stock solutions were then calculated. Equimolar amounts of each single strand were measured out of the stock solutions, combined, and diluted with phosphate buffer (5 mM NaH_2PO_4, 50 mM NaCl, pH = 7) to the appropriate concentration for UV−vis measurements. The solution was heated to 90 °C for 3 min and allowed to slowly cool to room temperature. After cooling, the thermal denaturation experiment was performed using the following parameters on a HP UV−vis: (a) monitoring wavelength, 260 nm, (b) temperature range, 25−70 °C, (c) temperature step, 1.0 °C, (d) averaging time constant, 15 s, (e) 0.5 °C rate of change.

Calorimetry. A VP-DSC from MicroCal Inc. with a cell volume of 0.5136 mL was used to determine the calorimetric profiles of labeled and unlabeled DNA

[1] [1]Abbreviations: DIPEA = *N,N*-diisopropylethylamine; CDI = carbonyldiimidazole; DMT = dimethoxytrityl; PTZ = phenothiazine.

Scheme 3. Synthesis of PTZ-Labeled Oligodeoxynucleotides[a]



[a] Key: (a) normal synthesis; (b) 30% NH_3, 55 °C, 16 h. B = A, C, G, or T.

duplexes. Samples were scanned from 10 °C to 80 °C using a constant rate of 30 °C/h. Prior to each experiment, the buffer was scanned to produce a stable baseline, and then the DNA sample (37.5 μM) was scanned repeatedly until a reproducible calorimetric transition curve was obtained. Subtraction of buffer baseline and normalization of sample concentration yielded the desired heat capacity versus temperature curve. The enthalpy of transition during the melting process was determined from the area under this heat capacity peak.

RESULTS AND DISCUSSION

To capitalize on solid-phase DNA synthesis technology and the flexibility that this automated and modular approach brings to the synthesis of site-specifically labeled oligodeoxynucleotides (*35*), we require redox probes that are (1) sufficiently soluble as the labeled nucleoside phosphoramidite in acetonitrile for solid-phase reactions, (2) stable to the standard oligodeoxynucleotide syntheses and deprotection reactions so as to prevent undesired side reactions leading to loss of Watson−Crick base pairing selectivity (*36*) or decomposition, and (3) amenable to covalent attachment to both purine and pyrimidine nucleosides. The chromophore, phenothiazine (PTZ), satisfies these requirements and is known to be a low potential reductant ($PTZ^{+\bullet}$/PTZ; 0.59 V vs SCE) (*37*). The one-electron oxidized product, $PTZ^{+\bullet}$, is also spectroscopically characterized (λ_{max} = 510 nm) (*38*, *39*). Moreover, previous reports have successfully described the use of PTZ with photoexcited inorganic chromophores such as $*Ru(bpy)_3^{2+}$ to study reductive electron-transfer reactions in peptide (*37*, *39*) and DNA (*40*) assemblies.

The PTZ-derivatized 5′-deoxythymidine and *N*-benzoyl-2′,5′-dideoxyadenosine phosphoramidites, **9a** and **9b**, respectively, for automated DNA synthesis were synthesized as shown in Schemes 1−3. The 3-phenothiazin-10-ylpropionic acid, **3**, was prepared by first reacting PTZ with acrylonitrile in the presence of tetrabutylammonium hydroxide (87% yield), followed by hydrolysis with sodium hydroxide in aqueous methanol to afford the product in 56% yield (*32*). As shown in Scheme 2, the 5′-position of thymidine was converted from a hydroxyl to an amine in three consecutive steps. First, thymidine was treated with an equal amount of methanesulfonyl chloride in dry pyridine to afford **5a** (*34*). Next, the 5′-mesyl group was substituted with lithium azide to yield **6a**. Finally, **6a** was reduced with H_2 and Pd/C to give the 5′-amino-5′-deoxythymidine, **7a** in 90% yield. This reduction method was preferred to that of using triphenylphosphine and ammonium hydroxide (72% yield). The primary hydroxyl of 2′-deoxyadenosine was converted to an amine in a similar manner, except that the primary amine was first protected with a benzoyl group (Scheme 2). This step required transient protection of the 5′- and 3′-hydroxyls by TMS-Cl in pyridine, followed by addition of benzoyl chloride and subsequent deprotection of the hydroxyls by ammonium hydroxide (*33*). Unlike the thymidine synthesis, the reduction of **6b** to **7b** was best achieved using

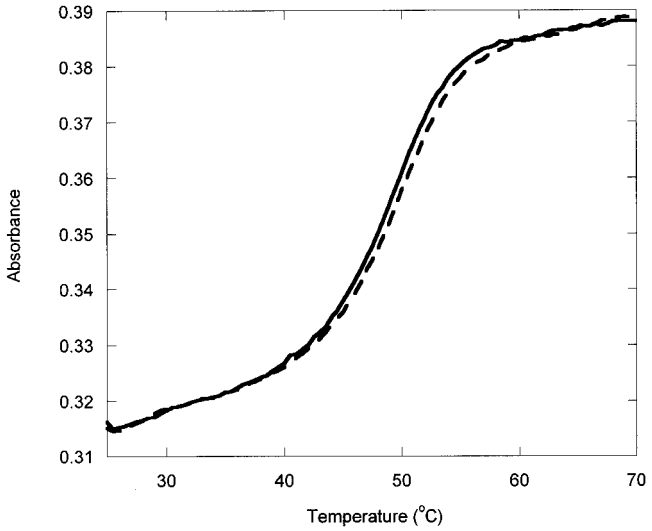


Figure 1. Melting curve for PTZ-dT labeled (**11·21**; dashed line) and unlabeled (**16·21**; solid line) oligodeoxynucleotide duplexes.

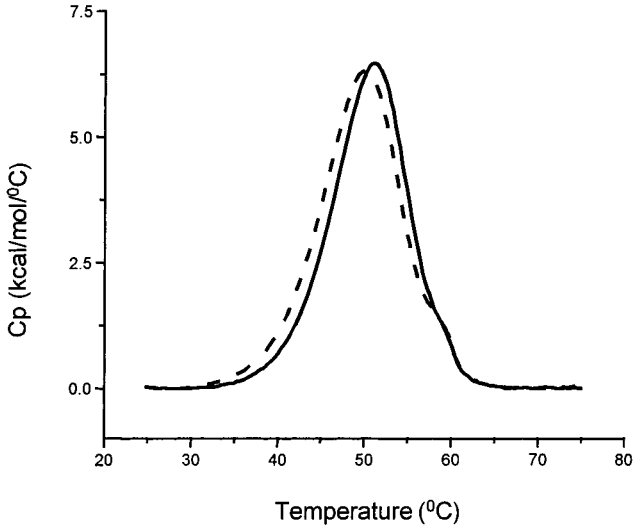


Figure 2. A heat capacity vs temperature transition curve for PTZ-dT labeled (**11·21**; dashed line) and unlabeled (**16·21**; solid line) oligodeoxynucleotide duplexes.

Table 1. PTZ-Labeled Oligodeoxynucleotides

10	5′-^{PTZ}TTGCTACAAACTGTTG A-3′
11	5′-^{PTZ}TGCTACAAACTGTTG A-3′
12	5′-^{PTZ}TTCAACAGTTTGT-3′
13	5′-^{PTZ}ATGCTACAAACTGTTGA-3′
14	5′-^{PTZ}AGCTACAAACTGTTGA-3′
15	5′-TTGCTACAAACTGTTG A-3′
16	5′-TGCTACAAACTGTTG A-3′
17	5′-TTCAACAGTTTGT-3′
18	5′-ATGCTACAAACTGTTG A-3′
19	5′-AGCTACAAACTGTTG A-3′
20	5′-TCAACAGTTTGTAGCAA-3′
21	5′-TCAACAGTTTGTAGCA-3′
22	5′-ACAAACTGTTGAA-3′
23	5′-TCAACAGTTTGTAGCAT-3′
24	5′-TCAACAGTTTGTAGCT-3′

Pd/C hydrogenation. The carboxylic acid derivatized PTZ, **3**, was then coupled to 5′-amino-5′-deoxythymidine (**7a**) or *N*-benzoyl 5′-amino 2′,5′-dideoxyadenosine (**7b**) in DMF using CDI (Scheme 2). Other amide forming strategies using DCC or the NHS activated ester were explored, but yielded less product. Finally, **8a** and **8b** were reacted with 2-cyanoethyl-*N*,*N*′-diisopropylchlorophosphoramidite in dry CH_3CN to afford the PTZ-phosphoramidite, **9a** and **9b**. The PTZ-thymidine and PTZ-2′-deoxyadenosine phosphoramidites were now ready for use in an oligodeoxynucleotide synthesizer (ABI 392).

Standard solid-phase oligodeoxynucleotide syntheses were performed (*35*, *41*), except that in the last coupling step the PTZ-modified thymidine or 2′-deoxyadenosine phosphoramidite was introduced as shown in Scheme 3. All syntheses were performed at the 1.0 μmol scale using the standard coupling protocol except that the final step proceeded for 15 min to ensure sufficient reaction time for **9a** and **9b**. Collection and analysis of the DMT-fractions during automated synthesis showed efficient phosphoramidite couplings throughout the procedure, with both the standard pyrimidine and purine nucleosides (>98%) and **9a** and **9b** coupled in ≈80%. Once synthesized, the PTZ-labeled oligodeoxynucleotides were cleaved from the column, and the nitrogenous bases and phosphate groups were deprotected in 30% ammonium at 55 °C. The oligodeoxynucleotides (see Table 1) were subsequently purified by RP-HPLC and analyzed by MALDI mass spectrometry.

A temperature change of approximately 1 °C is observed in the melting temperature between the unlabeled and PTZ-dA or PTZ-dT labeled oligodeoxynucleotides as determined by temperature-dependent optical measurements (see Figure 1 and Table 2). This difference in melting temperature is small indicating that labeling the 5′-terminal nucleotide of the oligodeoxynucleotide does not dramatically alter the DNA duplex structure. Differential scanning calorimetry (DSC) data provide additional insight into the thermodynamic consequences of PTZ labeling at the ribose (*42*, *43*). As shown in Table 2, the transition enthalpies ($\Delta H°$) of the PTZ-T and PTZ-A labeled and unlabeled 16-mer duplexes are 71.0, 70.6, 66.8, and 68.0 kcal/mol, respectively. The differences in transition enthalpy change ($\Delta\Delta H°$) for the unlabeled and labeled dT and dA duplexes are 0.4 and 1.2 kcal/mol, respectively. These $\Delta H°$ values are deduced from the heat capacity/temperature relationship, such as the one shown in Figure 2 for the PTZ-dT (**11•21**) labeled and unlabeled (**16•21**) duplex. The free energies ($\Delta G°$) at 25 °C for the PTZ-dT and -dA labeled and unlabeled 16-mer duplexes are 5.4, 5.6, 4.9, and 5.0 kcal/mol, respectively. There is only a modest decrease in free energy ($\Delta\Delta G°$) of 0.2 kcal/mol or less for the labeled duplex relative to the unlabeled duplex. The heat capacity traces shown in Figure 2 for the PTZ-T-labeled duplex can also be fit to a two-state model, and the calculated van't Hoff enthalpy (ΔH_v) is 70.4 kcal/mol. This value is similar to the measured enthalpy. These data suggest that a two-state (all-or-none) helix to coil transition occurs in the labeled and

Table 2. Optical and DSC Thermodynamic Data for the PTZ-dT Labeled and Unlabeled Duplexes

	optical data	DSC data				
duplex	T_m °C ± 0.5	T_m °C ± 0.5	ΔH (kcal/mol) ± 1.0	ΔH_v (kcal/mol) ± 1.0	ΔS (cal/mol) ± 3.0	ΔG at 25 °C (kcal/mol) ± 0.1
11·21	49.7	49.6	71.0	70.4	220.1	5.4
16·21	49.6	50.7	70.6	74.6	218.1	5.6
14·24	51.0	48.4	66.8	69.5	207.8	4.9
19·24	49.7	48.6	68.0	70.9	211.4	5.0

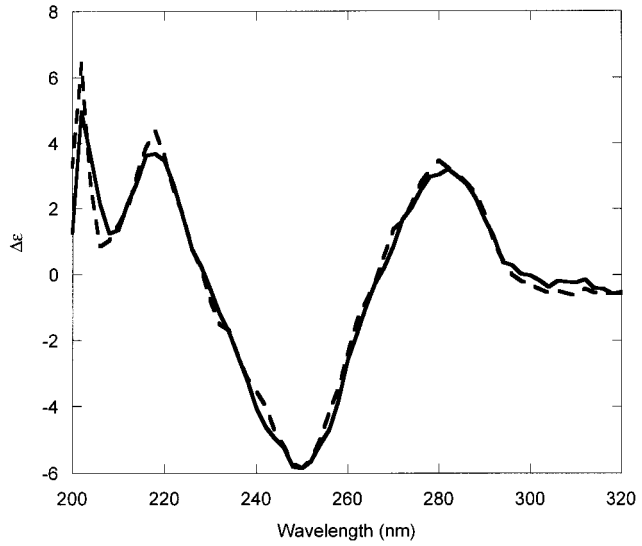


Figure 3. CD spectra of PTZ-dT labeled (**11·21**; solid line) and unlabeled (**16·21**; dashed line) oligodeoxynucleotide duplexes.

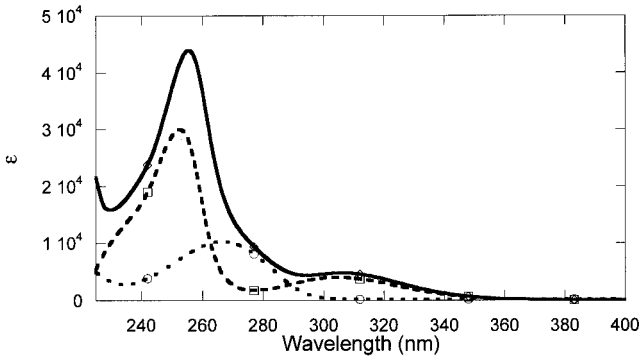


Figure 4. UV-vis spectra of PTZ-acid (**3**, dashed line), thymidine (**4a**, dotted line), and PTZ-thymidine (**8**, solid line).

unlabeled duplexes, and that introduction of PTZ does not generate intermediate states. The formation of a well-defined DNA duplex structure is also supported by circular dichroism (CD) spectroscopy. Figure 3 shows the CD spectra for the unlabeled (**16•21**) and PTZ-thymidine labeled (**11•21**) duplexes. Circular dichroism spectra (*44*) of the unlabeled, PTZ-thymidine labeled, and PTZ-adenosine labeled are similar, and the spectral features for B-DNA are present.

Covalent attachment of PTZ to the 2′-deoxynucleoside or oligodeoxynucleotide does not alter its spectroscopic properties. The UV−vis spectra of PTZ-labeled thymidine (**8a**), phenothiazine (**3**), and thymidine (**4a**) are shown in Figure 4 (1:1 CH_3CN:H_2O). The electronic spectrum of **8a** is a summation of PTZ and thymidine. Specifically the PTZ π-to-π and weak π-to-n absorption are observed at 250 and 306 nm, respectively. The thymidine π-to-n absorption is at 267 nm (Figure 4) (*45*). The PTZ-labeled oligodeoxynucleotide possess an absorption at 260 nm, but the absorption of PTZ at lower energy is masked by the DNA. Excitation of **8a** or **8b** at 315 nm produces an emission centered at 450 nm in 1:1 CH_3CN:H_2O in agreement with the reported literature value (*45*). Likewise, the excitation spectra of ss **14**, and ds **14•24** in phosphate buffer (50 mM NaCl, 5 mM NaH_2PO_4, pH = 7) possess a maximum at 315 nm, and the corresponding emission spectra possess a broad emission centered at 450 nm.

CONCLUSION

The site-specific labeling of oligodeoxynucleotides at a 5′-terminal thymidine or 2′-deoxyadenosine with phenothiazine is reported. The PTZ-labeled oligodeoxynucleotides form stable B-form duplexes with melting temperatures comparable to the unlabeled analogues. Similar results are also observed with oligodeoxynucleotides labeled with PTZ at the nucleobase (*28*) and 5′-terminal phosphate (*30*) indicating that PTZ is amenable to covalent attachment to DNA at different locations. Calorimetric data on the unlabeled and PTZ labeled duplexes reveal only a slight decrease in stability upon labeling with PTZ. The spectroscopic properties of PTZ are retained when the complex is covalently attached to DNA at the 5′-terminal thymidine or 2′-deoxyadenosine position. In summary, these two novel PTZ-modified thymidine and 2′-deoxyadenosine increase the number of well-characterized probes available for study, and the corresponding PTZ-labeled oligodeoxynucleotides are of use for DNA-mediated charge-transfer studies. Photophysical studies are currently underway to monitor the electron-transfer intermediate ($PTZ^{+\bullet}$) in a site-specifically labeled duplex containing PTZ and the inorganic chromophore, $Ru(bpy)_3^{2+}$.

ACKNOWLEDGMENT

This work was supported in part by the Army Office of Research. We thank Dr. T. Christensen for help with the calorimetry experiments. M.W.G. also thanks the Pew Foundation for a Pew Scholar in the Biomedical Sciences, the Alfred P. Sloan Foundation for a Research Fellowship, and the Dreyfus Foundation for a Camille Dreyfus Teacher Scholar.

Supporting Information Available: Proton NMR spectra and HPLC of **8a** and **8b**, and MALDI spectra of **10**, **11**, **12**, **13**, and **14**. This material is available free of charge via the Internet at http://pubs.acs.org.

LITERATURE CITED

(1) Holmlin, R. E., Dandliker, P. J., and Barton, J. K. (1997) Charge Transfer through the DNA Base Stack. *Angew. Chem., Int. Ed. Engl. 36*, 2714−2730.

(2) Schuster, G. B. (2000) Long-Range Charge Transfer in DNA: Transient Structural Distorations Control the Distance Dependence. *Acc. Chem. Res. 33*, 253−260.

(3) Kelley, S. O., and Barton, J. K. (1999) in *Metal Ions in Biological Systems* (A. Sigel, and H. Sigel, Eds.) Vol. 36, pp 211−249, Marcel Dekker, New York.

(4) Netzel, T. L. (1998) in *Organic and Inorganic Photochemistry* (V. Ramamurthy, and K. S. Schanze, Eds.) pp 1−54, Marcel Dekker, New York.

(5) Ratner, M. (1999) Electronic Motion in DNA. *Nature 397*, 480−481.

(6) Diederichsen, U. (1997) Charge Transfer in DNA: A Controversy. *Angew. Chem., Int. Ed. Engl. 36*, 2317−2319.

(7) Netzel, T. L. (1998) Present Status and Future Directions of Research in Electron-Transfer Mediated by DNA. *J. Biol. Inorg. Chem. 3*, 210−214.

(8) Grinstaff, M. W. (1999) How Do Charges Travel Through DNA-An Update on a Current Debate. *Angew. Chem., Int. Ed. 38*, 3629−3635.

(9) Murphy, C. J., Arkin, M. R., Jenkins, Y., Ghatlia, N. D., Bossmann, S. H., Turro, N. J., and Barton, J. K. (1993) Long-Range Photoinduced Electron Transfer Through a DNA Helix. *Science 262*, 1025−1029.

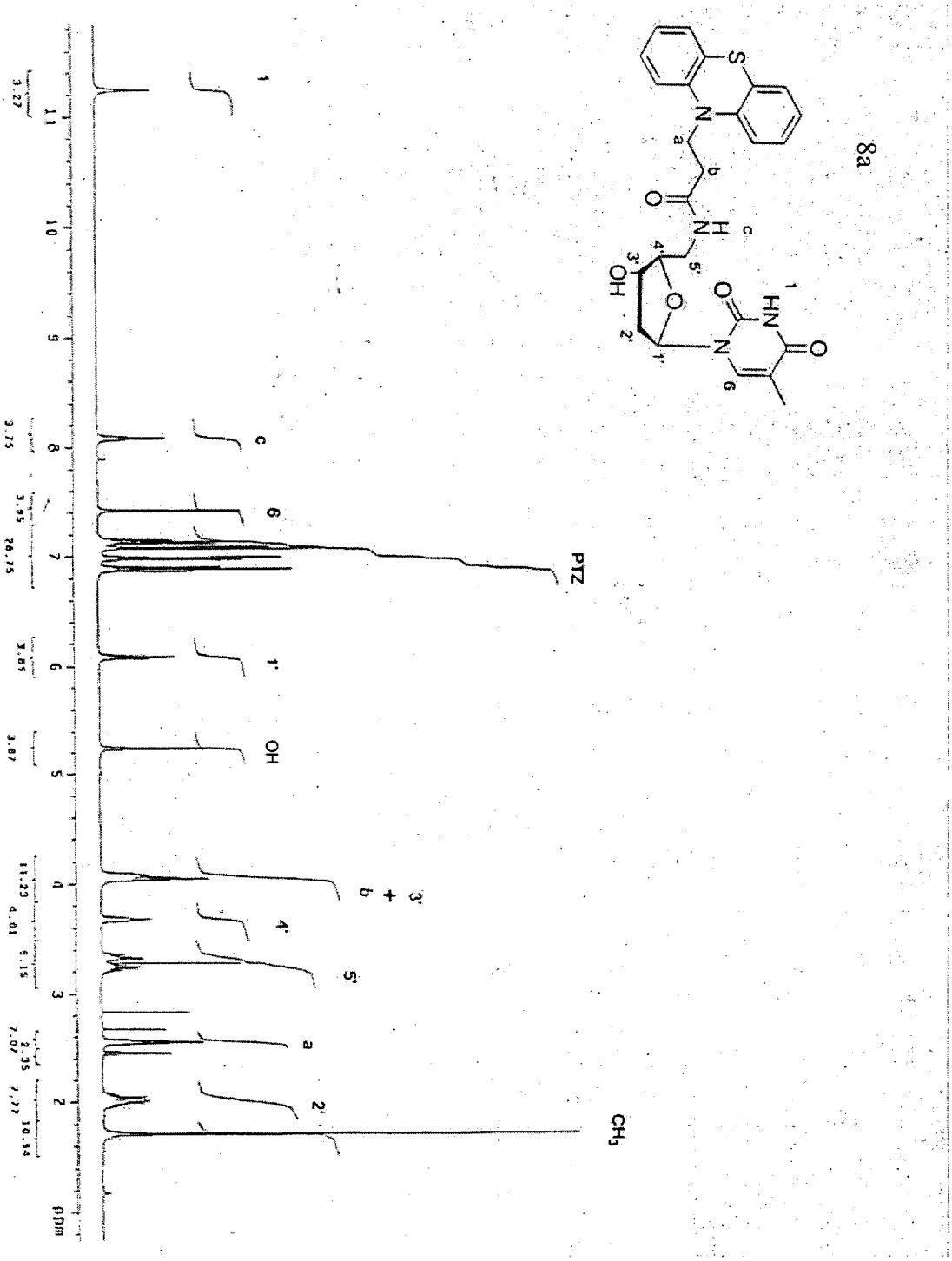
(10) Hall, D. B., Holmlin, R. E., and Barton, J. K. (1996) Oxidative DNA Damage through Long-Range Electron Transfer. *Nature 382*, 731−735.

(11) Lewis, F. D., Wu, R., Zhang, Y., Letsinger, R. L., Greenfield, S. R., and Wasielewski, M. R. (1997) Distance-Dependent Electron Transfer in DNA Hairpins. *Science 277*, 673−676.
(12) Meggers, E., Michel-Beyerle, M. E., and Giese, B. (1998) Sequence Dependent Long-Range Hole Transport in DNA *J. Am. Chem. Soc., 120*, 12950−12955.
(13) Meggers, E., Kusch, D., Spichty, M., Wille, U., and Giese, B. (1998) Electron Transfer through DNA in the Course of Radical-Induced Strand Cleavage. *Angew. Chem., Int. Ed. 37*, 460−462.
(14) Henderson, P. T., Jones, D., Hampikian, G., Kan, Y., and Schuster, G. B. (1999) Long-Distance Charge Transport in Duplex DNA: The Phonon-Assisted Polaron-Like Hopping Mechanism. *Proc. Natl. Acad. Sci. 96*, 8353−8358.
(15) Ly, D., Sanii, L., and Schuster, G. B. (1999) Mechanism of Charge Transport in DNA: Internally-Linked Anthraquinone Conjugates Support Phonon-Assisted Polaron Hopping. *J. Am. Chem. Soc. 121*, 9400−9410.
(16) Thorp, H. H. (1998) Cutting Out the Middleman: DNA Sensors Based on Electrochemical Oxidation. *Trends Biotechnol. 16*, 117−121.
(17) Ontko, A. C., Armistead, P. M., Kirrcus, S. R., and Thorp, H. H. (1999) Electrochemical Detection of Single-Stranded DNA Using Polymer-Modified Electrodes. *Inorg. Chem. 38*, 1842−1846.
(18) Welch, T. W., Corbett, A. H., and Thorp, H. H. (1995) Electrochemical Determination of Nucleic Acid Diffusion Coefficients through Noncovalent Association of Redox-Active Probes. *J. Phys. Chem. 99*, 11757−11763.
(19) Xu, X.-H., and Bard, A. J. (1995) Immobilization and Hybridization of DNA on an Aluminum(III) Alkanebisphosphonate Thin Film with Electrogenerated Chemiluminescent Detection. *J. Am. Chem. Soc. 117*, 2627−2631.
(20) Hasshimoto, K., Ito, K., and Ishimori, Y. (1994) Sequence-specific Gene Detection with a Gold Electrode modified with DNA Probes and an Electrochemically Active Dye. *Anal. Chem. 66*, 3830−3833.
(21) Kelley, S. O., Jackson, N. M., Hill, M. G., and Barton, J. K. (1999) Long-Range Electron Transfer through DNA Films. *Angew. Chem., Int. Ed. 38*, 941−944.
(22) Sarma, R. H., and Sarma, M. H. (1992) *Structure and Function, Volume I: Nucleic Acids*, Adenine Press, Albany.
(23) Beilstein, A. E., Tierney, M. T., and Grinstaff, M. W. (2000) Site-Specifically Labeled Metallo-Oligodeoxynucleotides. *Comments Inorg. Chem. 22*, 105−127.
(24) Khan, S. I., Beilstein, A. E., and Grinstaff, M. W. (1999) Automated Solid-Phase Synthesis of Site-Specifically Labeled Ruthenium-Oligonucleotides. *Inorg. Chem. 38*, 418−419.
(25) Khan, S. I., and Grinstaff, M. W. (1999) Palladium(0)-Catalyzed Modification of Oligonucleotides during Automated Solid-Phase Synthesis. *J. Am. Chem. Soc. 121*, 4704−4705.
(26) Khan, S. I., Beilstein, A. E., Tierney, M. T., Sykora, M., and Grinstaff, M. W. (1999) Solid-Phase Synthesis and Photophysical Properties of DNA Labeled at the Nucleobase with $Ru(bpy)_2(4\text{-m-pa-bpy})^{2+}$. *Inorg. Chem. 38*, 5999−6002.
(27) Beilstein, A. E., and Grinstaff, M. W. (2000) On-Column Derivatization of Oligodeoxynucleotides with Ferrocene. *Chem. Commun.* 509−510.
(28) Tierney, M. T., and Grinstaff, M. W. (2000) Synthesis and Stability of Oligodeoxynucleotides Containing C8-Labeled 2-Deoxyadenosine: Novel Redox Nucleobase Probes for DNA Mediated Charge-Transfer Studies. *Org. Lett. 2*, 3413−3416.
(29) Khan, S. I., Beilstein, A. E., Sykora, M., Smith, G. D., Hu, X., and Grinstaff, M. W. (1999) Automated Solid-Phase DNA Synthesis and Photophysical Properties of Oligonucleotides Labeled at the 5′-Terminus with $Ru(bpy)_3^{2+}$. *Inorg. Chem. 38*, 3922−3925.
(30) Tierney, M. T., and Grinstaff, M. W. (2000) Synthesis and Characterization of Fluorenone, Anthraquinone, and Phenothiazine Labeled Oligodeoxynucleotides: 5′-Probes for DNA Redox Chemistry. *J. Org. Chem. 65*, 5355−5359.
(31) Hu, X., Smith, G. D., Sykora, M., Lee, S. J., and Grinstaff, M. W. (2000) Automated Solid-Phase Synthesis and Photophysical Properties of Oligodeoxynucleotides Labeled at 5′-Amino-Thymidine with $Ru(bpy)_3^{2+}$. *Inorg. Chem. 39*, 2500−2504.
(32) Godefroi, E. F., and Wittle, E. L. (1956) The Preparation of Some Derivitives of β-(10-Phenothizinyl)propionic Acid and β-(2-Chloro-10-Phenothizinyl)propionic Acid. *J. Org. Chem. 21*, 1163−1168.
(33) Ti, G. S., Gattney, B. L., and Jones, R. A. (1982) Transient Protection: Efficient One-flask Synthesis of Protected Deoxynucleosides. *J. Am. Chem. Soc. 104*, 1316−1319.
(34) Horwitz, J. R., Chua, J., and Noel, M. (1964) Nucleosides V. The Monomesylates. *J. Org. Chem. 29*, 2076−2078.
(35) Caruthers, M. H. (1991) Chemical Synthesis of DNA and DNA Analogues. *Acc. Chem. Res. 24*, 278−284.
(36) Watson, J. D., and Crick, F. H. (1953) *Nature 171*, 737−738.
(37) Mecklenburg, S. L., Peek, B. M., Schoonover, J. R., McCafferty, D. G., Wall, C. G., Erickson, B. W., and Meyer, T. J. (1993) Photoinduced Electron Transfer in Amino Acid Assemblies. *J. Am. Chem. Soc. 115*, 5479−5495.
(38) Mecklenburg, S. L., McCafferty, D. G., Schoonover, J. R., Peek, B. M., Erickson, B. W., and Meyer, T. J. (1994) Spectroscopic Study of Electron Transfer in a Trifunctional Lysine with Anthraquinone as the Electron Acceptor. *Inorg. Chem. 33*, 2974−2983.
(39) McCafferty, D. G., Friesen, D. A., Danielson, E., Wall, C. G., Saderholm, M. J., Erickson, B. W., and Meyer, T. J. (1996) Photochemical Energy Conversion in a Helical Oligoproline Assembly. *Proc. Natl. Acad. Sci. 93*, 8200−8204.
(40) Tierney, M. T., Khan, S. I., Sykora, M., and Grinstaff, M. W. (2000) Electron Transfer in an Oligodeoxynucleotide Duplex: Direct Observation of an Electron-Transfer Product. *J. Phys. Chem. B. 104*, 7574−7576.
(41) Gait, M. J. *Oligonucleotide Synthesis: A Practical Approach*; IRL Press, Washington, DC, 1984.
(42) Marky, L. A., and Breslauer, K. J. (1987) Calculating Thermodynamic Data for Transitions of any Molecularity from Equilibrium Melting Curves. *Biopolymers 26*, 1601−1620.
(43) Breslauer, K. J. (1986) in *Thermodynamic Data for Biochemistry and Biotechnology* (H. J. Hinz, Ed.) pp 403−427, Springer-Verlag: Berlin.
(44) Johnson, W. C. (1994) *CD of Nucleic Acids*, VCH, New York.
(45) Kawanishi, Y., and Tazuke, S. (1986) Coulombic Effect of Photoinduced Electron-Transfer Reactions between Phenothiazine and Violgens. *J. Phys. Chem. 90*, 2469−2475.

BC0100509

© 2001 American Chemical Society, Bioconjugate Chem., Hu bc0100509 Supporting Info Page 1

NMR of PTZ-T



© 2001 American Chemical Society, Bioconjugate Chem., Hu bc0100509 Supporting Info Page 2

HPLC of PTZ-T

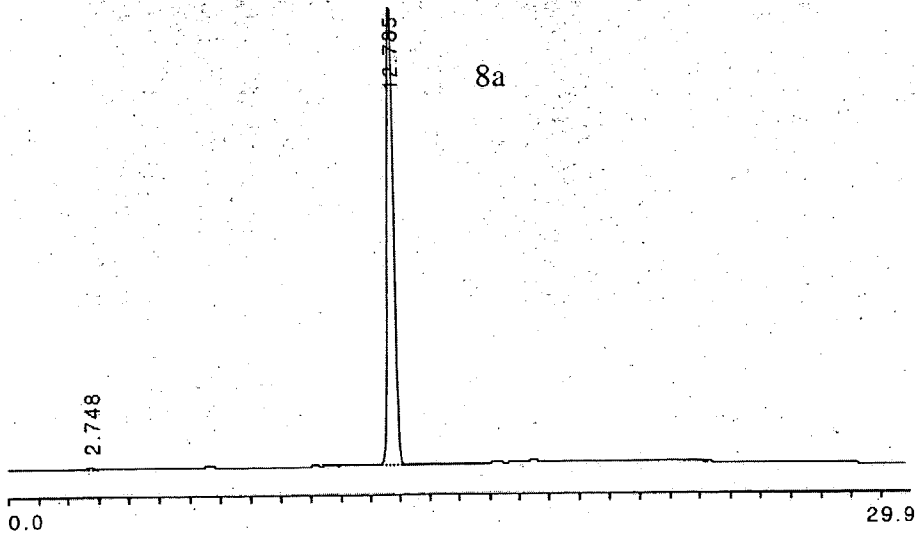
Date: Sun, Nov 18, 2001 7:39 PM
Data: xinucleoside5-18NOV101-003

PTZ-T

Sample: 89A Os w/ dG

Method: xinucleoside5
Inject Vol: 25
Sampling Int: 0.1 Seconds

Data:

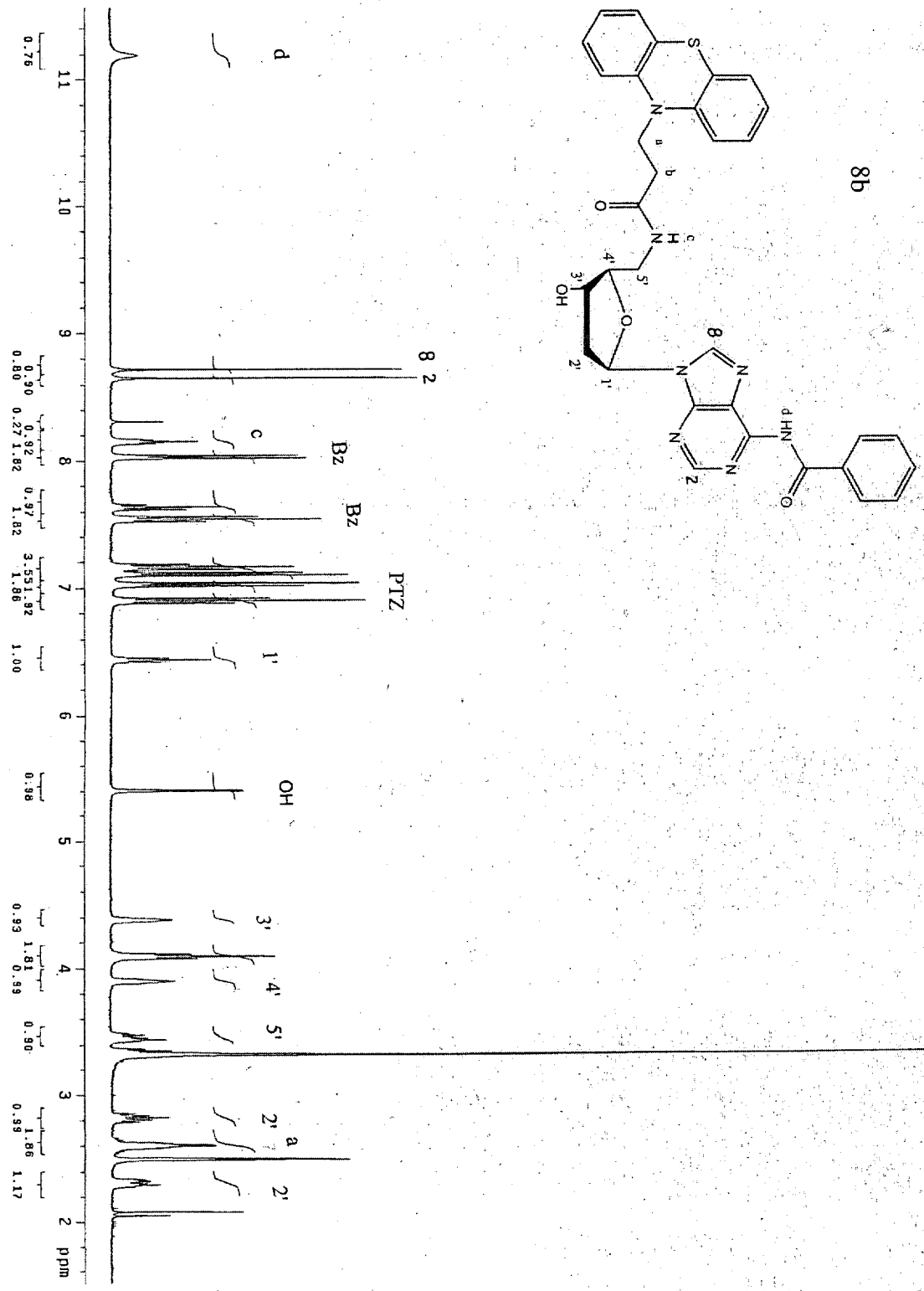


Analysis: Channel A

Peak No.	Time	Type	Height(μV)	Area(μV-sec)	Area%
1	2.748	N	1346	13680	0.343
2	12.785	N	346605	3967933	99.656
Total Area				3981613	99.999

© 2001 American Chemical Society, Bioconjugate Chem., Hu bc0100509 Supporting Info Page 3

NMR of PTZ-A



© 2001 American Chemical Society, Bioconjugate Chem., Hu bc0100509 Supporting Info Page 4

HPLC of PTZ-A

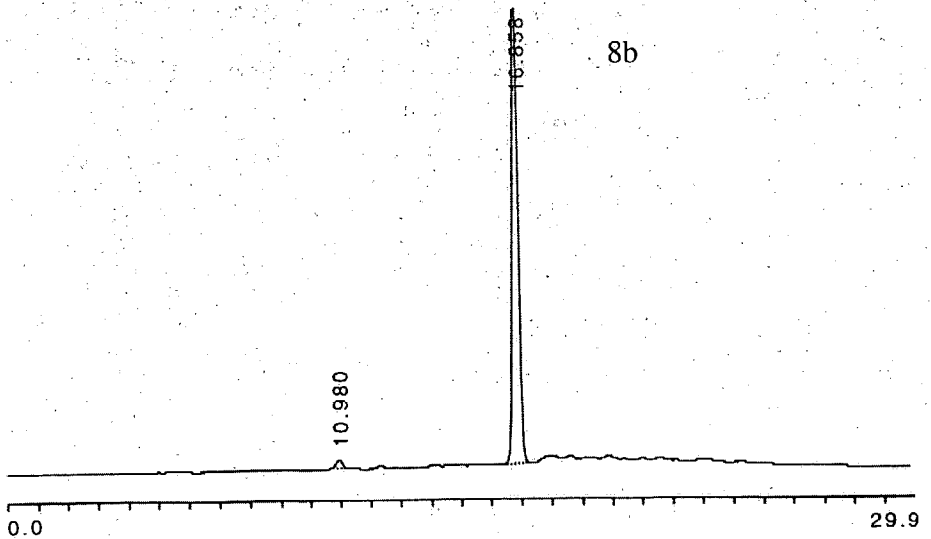
PTZ-A

Date: Sun, Nov 18, 2001 6:22 PM
Data: xinucleoside5-18NOV101-001

Sample: 89A Os w/ dG

Method: xinucleoside5
Inject Vol: 25
Sampling Int: 0.1 Seconds

Data:



Analysis: Channel A

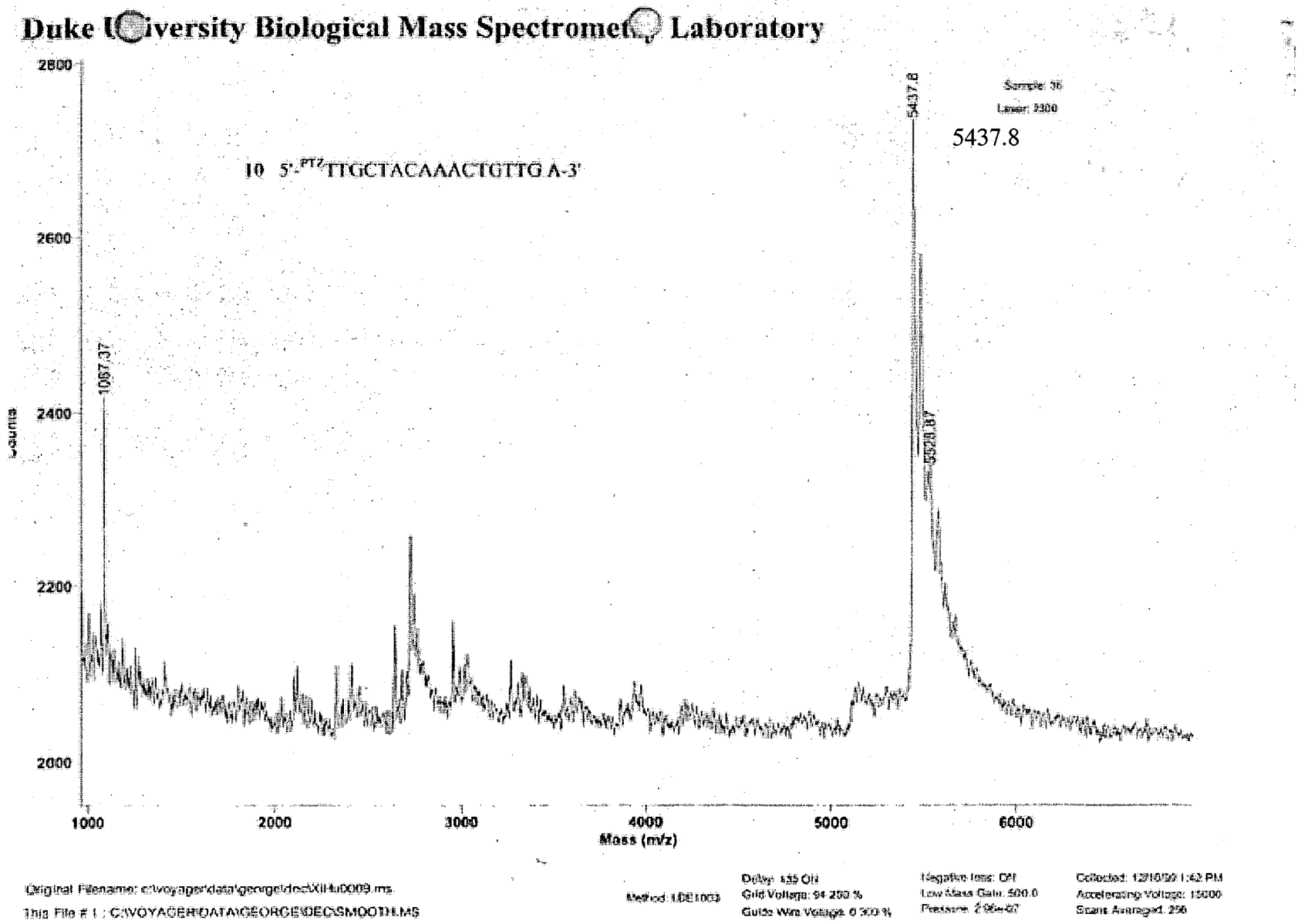
Peak No.	Time	Type	Height(μV)	Area(μV-sec)	Area%
1	10.980	N	2868	30977	1.959
2	16.858	N	148224	1549685	98.040
Total Area				1580662	99.999

© 2001 American Chemical Society, Bioconjugate Chem., Hu bc0100509 Supporting Info Page 5

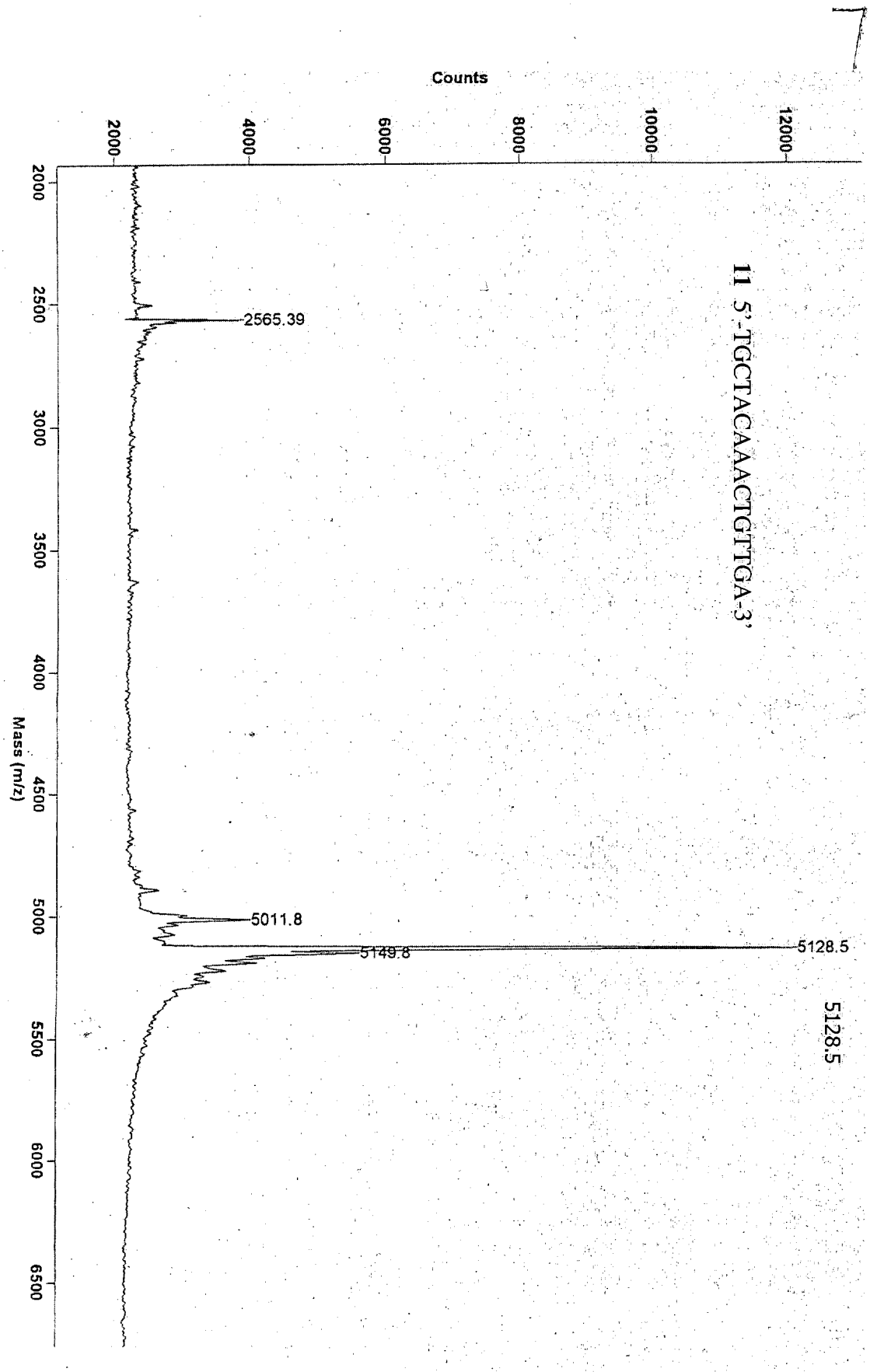
Purity determination by HPLC

The purity of the compounds was determined on a Rainin HPLC instrument system with Adsorbosphere Nucleoside-Nucleotide column (from Alltech, 250 mm × 4.6 mm). Aqueous solution containing 5 mM $N(Bu)_4(H_2PO_4)$ and 60 mM NH_6PO_4 (solvent A), and 5 mM $N(Bu)_4(H_2PO_4)$ in methanol (solvent B) were used as eluting solvents. A flow rate of 1.5 mL/min was used and the concentration of B was increased from 50% to 80% over 30 minutes.

© 2001 American Chemical Society, Bioconjugate Chem., Hu bc0100509 Supporting Info Page 6



© 2001 American Chemical Society, Bioconjugate Chem., Hu bc0100509 Supporting Info Page 7



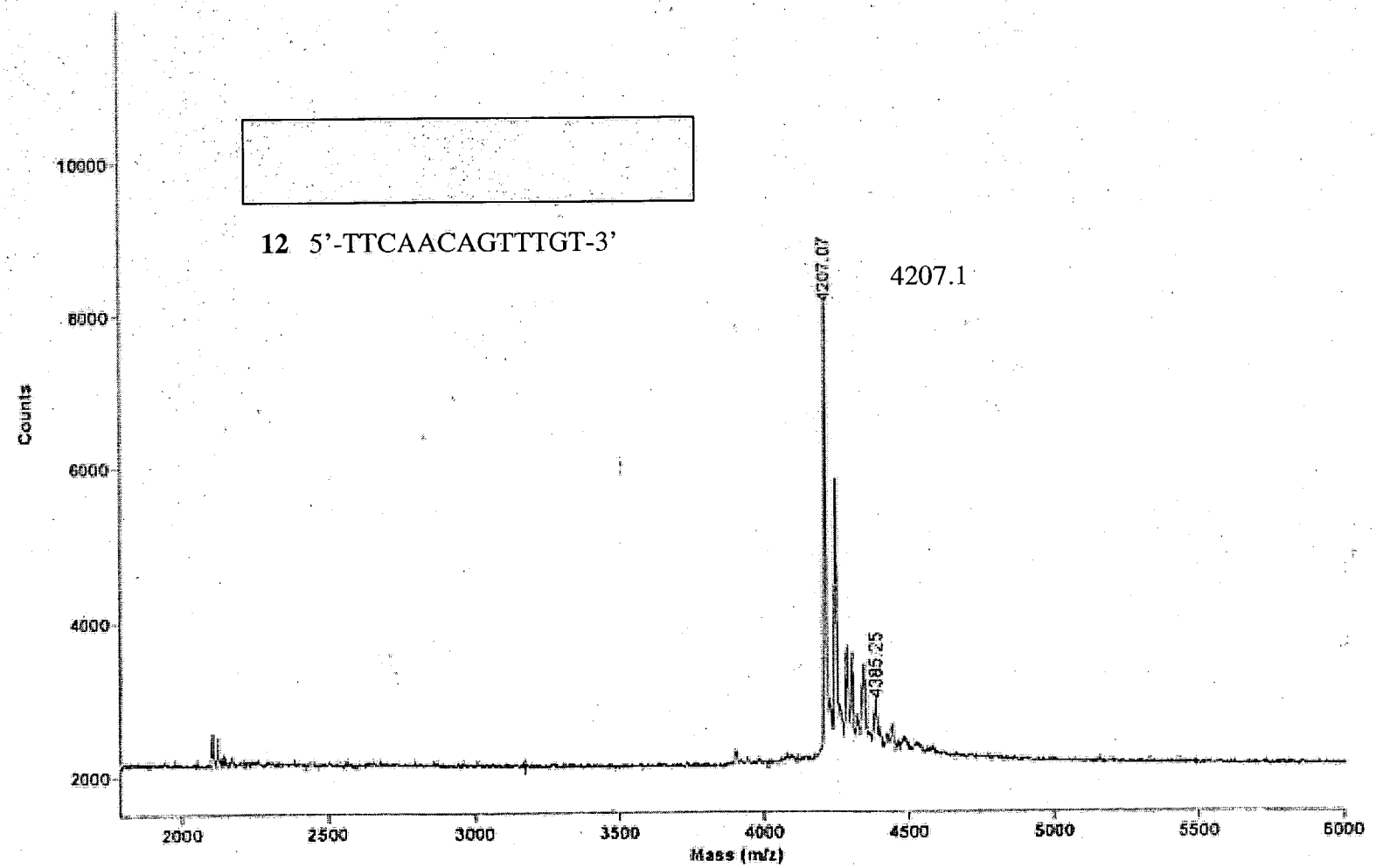
© 2001 American Chemical Society, Bioconjugate Chem., Hu bc0100509 Supporting Info Page 8

PerSeptive Biosystems

Original Filename: c:\voyager\data\guest\georgeJuly00\XHu_J603.ms
This File # 4 : C:\VOYAGER\DATA\GUEST\GEORGEJULY00\XHU_J603.MS
Comment:

Method: LDE1003
Accelerating Voltage: 25000
Grid Voltage: 94.250 %
Guide Wire Voltage: 0.200 %
Delay: 225 ON
Sample: 13

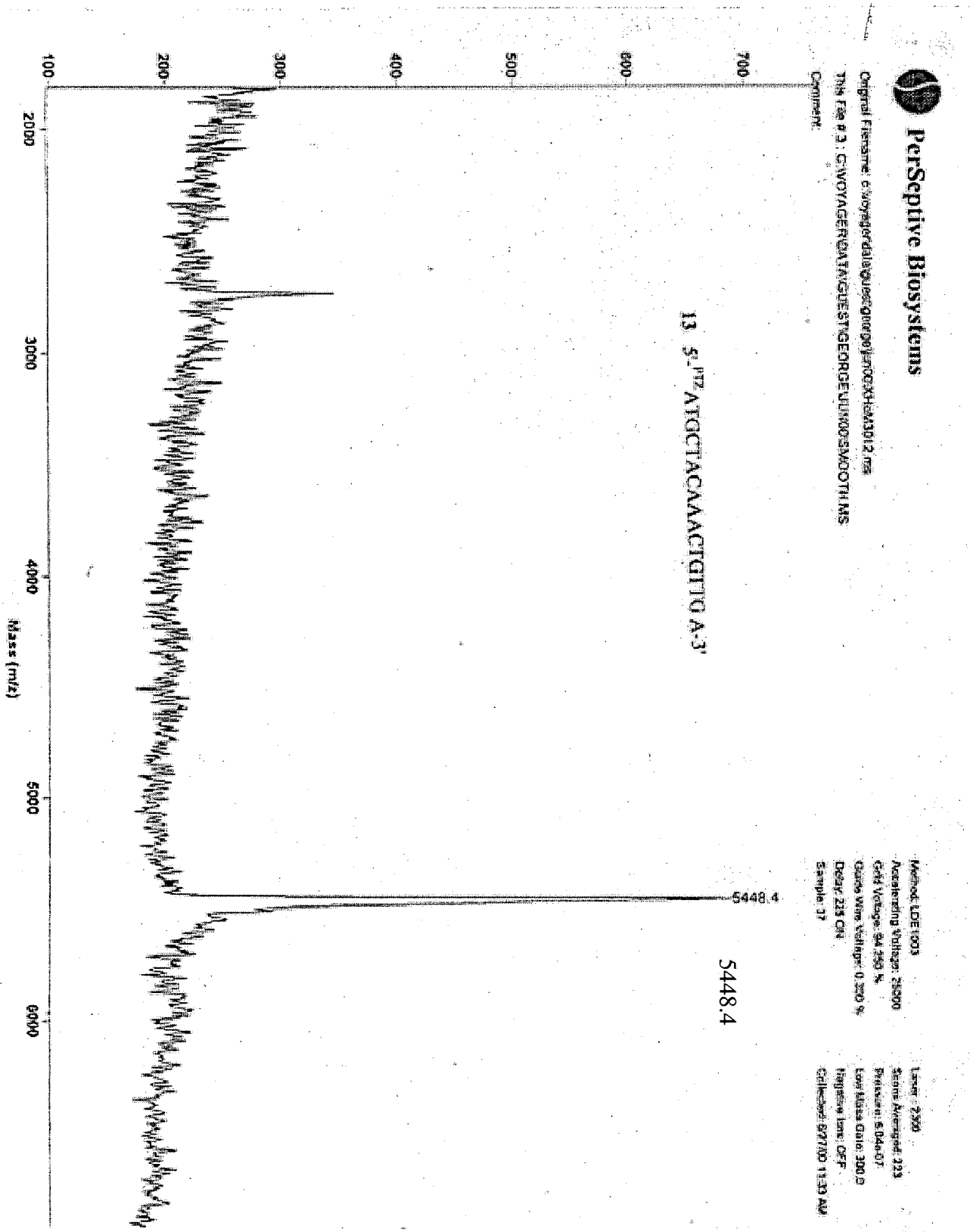
Laser: 2400
Scans Averaged: 256
Pressure: 4.84e-07
Low Mass Gate: 200.0
Negative Ions: OFF
Collected: 7/11/00 4:55 PM



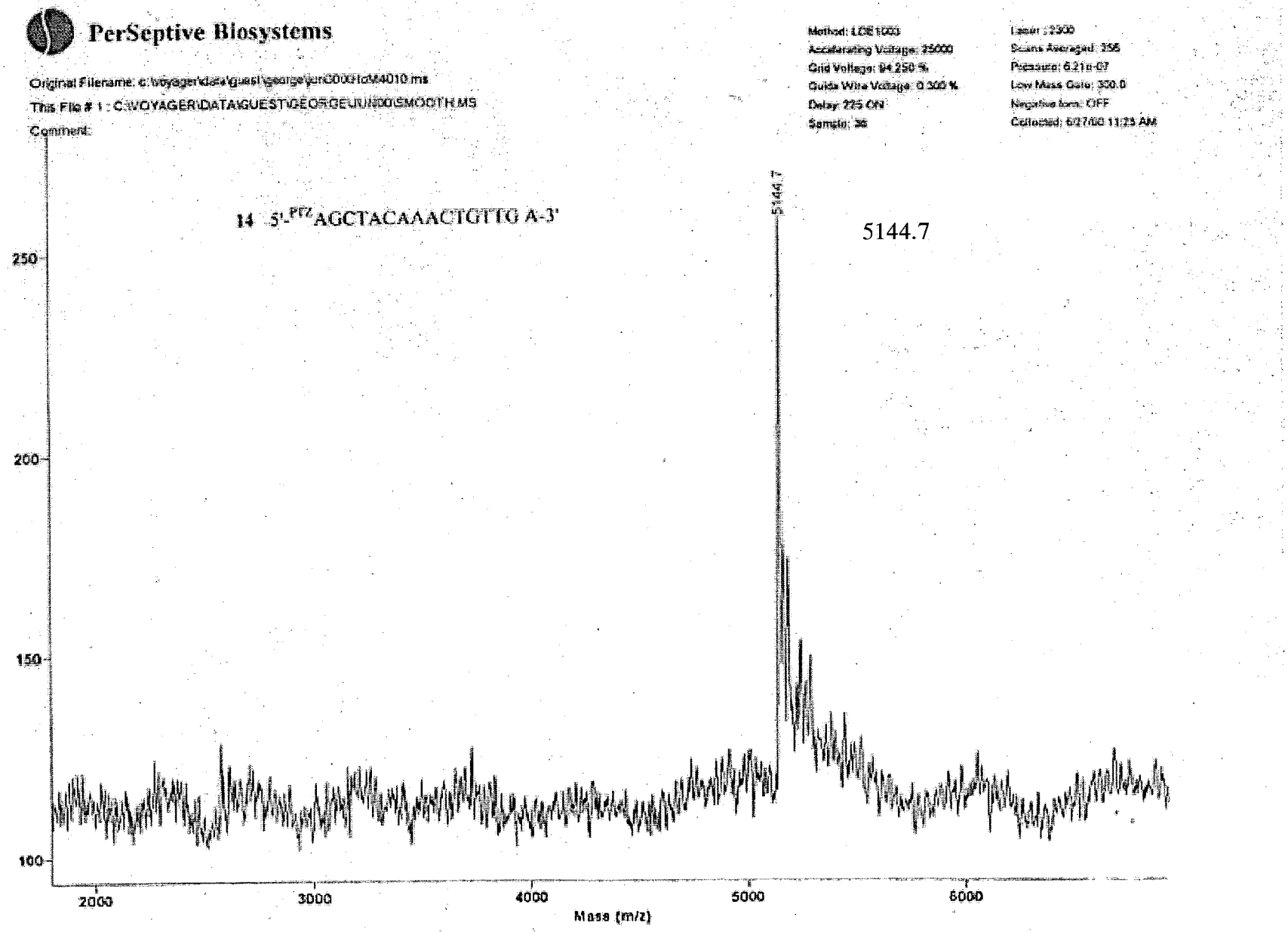
12 5’-TTCAACAGTTTGT-3’

4207.1

© 2001 American Chemical Society, Bioconjugate Chem., Hu bc0100509 Supporting Info Page 9



© 2001 American Chemical Society, Bioconjugate Chem., Hu bc0100509 Supporting Info Page 10



Immobilization of Biomolecules on Polyurethane Membrane Surfaces

Patrick Reichmuth,[†] Hans Sigrist,[‡] Martin Badertscher,[§] Werner E. Morf,[†] Nicolaas F. de Rooij,[†] and Ernö Pretsch*[,§]

Institute of Microtechnology (IMT), University of Neuchâtel, Rue Jaquet-Droz 1, CH-2007 Neuchâtel, Switzerland, Centre Suisse d'Electronique et de Microtechnique SA (CSEM), Rue Jaquet-Droz 1, CH-2007 Neuchâtel, Switzerland, and Swiss Federal Institute of Technology (ETH), Laboratorium für Organische Chemie, Universitätstrasse 16, CH-8092 Zürich, Switzerland. Received May 21, 2001

Lipophilic polymer membranes incorporating binding sites are widely used in various potentiometric, amperometric, and optical sensors. Here, we report on the biofunctional modification of the surface of a Ca^{2+}-selective membrane. A photoactivatable biotin derivative was synthesized and covalently immobilized on a soft polyurethane membrane. The modified polymer was characterized by X-ray photoelectron spectroscopy (XPS) as well as by potentiometric measurements. The selective binding of streptavidin by the photo-cross-linked biotin derivative was demonstrated. The surface coverage obtained with different experimental protocols was analyzed by autoradiography using [^{35}S]-streptavidin. The new approach may significantly extend the scope of applicability of potentiometric sensors.

INTRODUCTION

Lipophilic polymeric membranes incorporating ion-selective ligands (ionophores) and ion exchangers are widely applied in potentiometric sensors (*1*, *2*). The emf response is in most cases governed by the phase boundary potential that is defined by the bulk properties of the membrane and the sample (*1*, *3*). Plasticized poly(vinyl chloride) is the most widely used membrane matrix, but polymers with low glass transition temperatures such as polyurethanes (*4*), silicon rubber (*5*−*8*), and polyacrylates (*9*, *10*) have also been used without plasticizer. Owing to their relatively good biocompatibility, polyurethanes, especially the commercially available Tecoflex, are the best investigated alternatives to PVC (*4*, *11*−*13*). Usually, the ion exchanger and the ionophore are simply dissolved in the polymer matrix, but in other cases they have also been covalently bound to the polymer backbone (*6*, *9*, *10*, *14*−*16*). To improve the biocompatibility, the surface of potentiometric sensor membranes has been modified by covalent attachment of poly(ethylene oxide) (*17*), heparin (*18*), or theophylline (*19*). So far, however, a surface modification of ion-selective electrode membranes with specific, biofunctional binding sites has not yet been reported.

On the other hand, a number of techniques have been used to create selective reaction layers by covalently binding organic compounds to various substrates. One of the most versatile methods is photo-cross-linking using agents that form nitrenes, carbenes, or ketyl radicals upon irradiation (*20*). For example, Yan et al. used functionalized perfluorophenyl azides to pattern the surface of polystyrene (*21*, *22*). Similarly, Hengsakul et al. used an azidobenzene derivative of biotin for protein patterning of polystyrene or nitrocellulose surfaces (*23*). Several biotin derivatives with photosensitive groups have been described in the literature (*24*−*30*). More recently, carbene-generating photobiotins were used for the segregation of micrometer-sized domains of glassy-carbon, quartz, and polymer surfaces (*31*), for the preparation of bioprobes such as a photoaffinity taxoid probe (*32*), or for a photoaffinity labeling system for a glycosyltransferase (*33*).

Here we report on the synthesis of a novel photoactive biotin derivative **5** (Figure 1), its immobilization on the surface of an ion-selective polyurethane membrane (Tecoflex, **6** in Figure 1), and its interaction with streptavidin. The long-term goal of these studies is the development of new sensors to monitor guest molecules that are selectively complexed by host molecules immobilized on the sensor surface. The basic idea is to realize systems that yield a response signal due to the alteration of ion fluxes, similar to the principle used in channel-mimetic sensors (*34*). Instead of using an external current, the response would depend on zero-current transmembrane ion fluxes. The relevance of such fluxes has been demonstrated recently (*35*−*37*). At submicromolar sample activities, flux modulation may have a dramatic effect on the emf response of polymer membrane electrodes (*38*−*41*).

EXPERIMENTAL PROCEDURES

General Methods. Reagents and solvents were reagent-grade and used without further purification, except for THF, which was distilled. Tecoflex SG-80A was purchased from Thermedics Inc. (Woburn, MA). *N*,*N*-Dicyclohexyl-*N*,*N*-dioctadecyl-3-oxapentanediamide (ETH 5234), sodium tetrakis[3,5-bis(trifluoromethyl)phenyl]-borate (NaTFPB), and streptavidin from *Streptomyces avidinii* were obtained from Fluka AG (CH-9471 Buchs, Switzerland). *N*-[3-[3-(trifluoromethyl)diazirine-3-yl]phenyl]-4-maleimidobutyramide (**1**, MAD) was synthesized by

* To whom correspondence should be addressed. Phone: +41 1 632 29 26. Fax: +41 1 632 11 64. E-mail: pretsch@org.chem.ethz.ch.
[†] IMT, University of Neuchâtel.
[‡] CSEM, University of Neuchâtel.
[§] ETH Zürich.

10.1021/bc015515+ CCC: $22.00 © 2002 American Chemical Society
Published on Web 12/19/2001

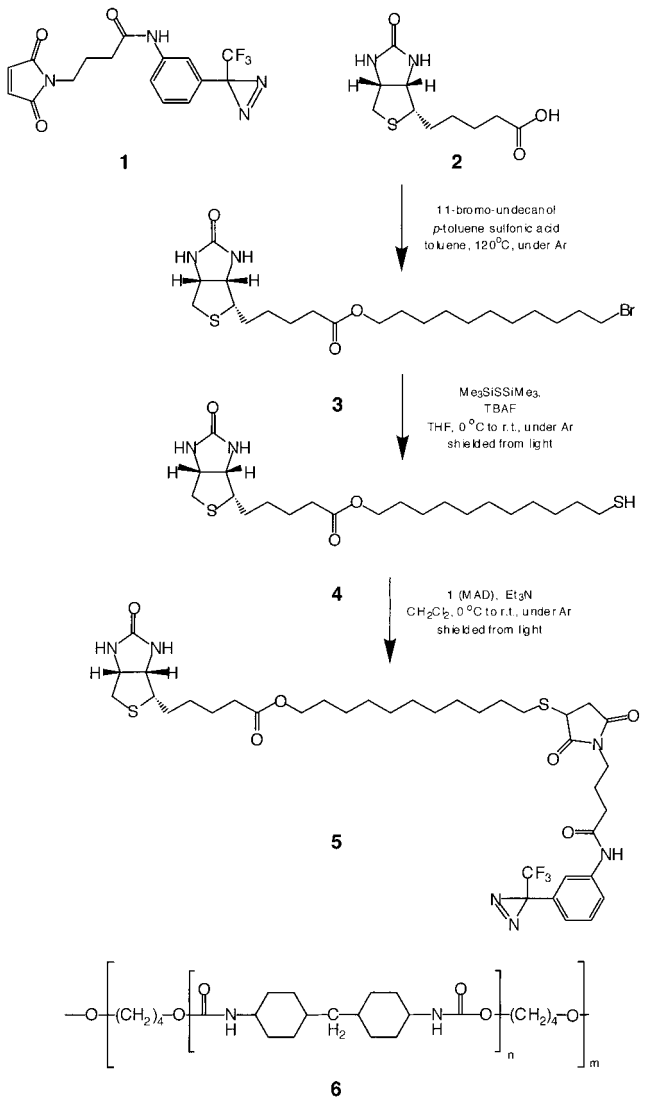


Figure 1. Synthetic pathway to biotin derivative **5**.

Collioud et al. (*42*). [^{35}S]-Streptavidin from Amersham (CH-8600 Dübendorf, Switzerland) had a specific activity of 7.4−74 TBq mmol^{-1}. Gold (99.99%) was obtained from Balzers AG (FL-9496 Balzers, Liechtenstein). Aqueous solutions were prepared with freshly deionized water (18.0 MΩ cm specific resistance) obtained with a NANOpure reagent-grade water system (Barnstead, CH-4009 Basel, Switzerland).

All reactions were performed in standard glassware. Evaporation and concentration in vacuo were done at water aspirator pressure, and compounds were dried at 10^{-2} mbar. Flash column chromatography was made with SiO_2 60 (220−440 mesh, 0.035−0.070 mm) from Fluka, TLC aluminum plates coated with SiO_2 60 F_{254} were from E. Merck, and the substances were visualized by UV light at 254 or 366 nm. TLC glass plates coated with SiO_2 (Silgur-25 UV_{254}) were from Macherey-Nagel (CH-4702 Oensingen, Switzerland). The following instruments were used: melting points, Büchi melting point apparatus (CH-9239 Flawil, Switzerland); IR spectra, 883 infrared spectrophotometer from Perkin-Elmer; UV/vis spectra, Uvikon 940 from Kontron Instruments; EI-MS, VG Tribid instrument, 70 eV; ESI-MS, Finnigan TSQ 7000 instrument; NMR spectra, Varian Gemini 200 (200 MHz) or Bruker AMX-2−500 (500 MHz) spectrometer at 300 K, with solvent peaks as reference.

Syntheses. *Synthesis of (3aS,4S,6aR)-11-Bromoundecyl 5-(Hexahydro-2-oxo-1H-thieno[3,4-d]imidazol-4t-yl)-pentanoate (**3** in Figure 1).* A mixture of biotin (**2**, 1.350 g, 5.5 mmol), 11-bromo-1-undecanol (6.940 g, 27.6 mmol), *p*-toluenesulfonic acid (0.105 g, 0.55 mmol), and toluene (34 mL) was stirred and refluxed at 120 °C for 48 h under argon (*43*). The reaction mixture was cooled to room temperature. Precipitated unreacted biotin was separated by filtration, the solvent was removed in vacuo, and the residue was purified by flash chromatography (MeOH/CH_2Cl_2 5:95) to give **3** as a white solid (1.970 g, 70%). Anal. ($C_{21}H_{37}N_2O_3SBr$) C, H, N, O, S, Br. Mp: 103.5−104.0 °C. IR ν_{max} (cm^{-1}): 3462, 2929, 2853, 1705, 1597. ^{1}H NMR (500 MHz, CD_2Cl_2, δ): 1.28−1.47 (m, 16H), 1.57−1.74 (m, 6H), 1.85 (m, −CH_2CH$_2$Br, 2H), 2.31 (t, J = 7.4 Hz, −CH_2C(O)OCH$_2$−, 2H), 2.71 (d, J = 12.6 Hz, −CHCH_2S−, 1H), 2.90 (dd, J = 12.6 Hz, J = 5.0 Hz, −CHCH_2S−, 1H), 3.17 (m, −SCH−, 1H), 3.42 (t, J = 6.9 Hz, −CH_2Br, 2H), 4.03 (t, J = 6.9 Hz, −OCH_2−, 2H), 4.30 (m, −NHCHCH$_2$−, 1H), 4.48 (m, −NHCH(CH−)$_2$, 1H), 5.43 (s, −NHCH(CH−)$_2$, 1H), 5.73 (s, −NH-CHCH$_2$−, 1H). ^{13}C NMR (125 MHz, CD_2Cl_2, δ): 25.28, 26.33, 28.57, 28.70, 28.78, 29.07, 29.15, 29.65, 29.81, 29.86, 29.88, 33.31 (−CH$_2$CH$_2$Br), 34.31, 34.68, 41.04 (−CH$_2$S−), 55.90 (−SCH−), 60.54 (−NCHCH$_2$), 62.28 (−NCH(CH−)$_2$), 64.82 (−C(O)OCH$_2$−), 163.94 (−NC(O)N−), 173.95 (−C(O)O−). EI-MS *m*/*z* (relative intensity): M$^+$ 476.1 (1), 418.1 (3), 227.1 (10), 166.1 (19).

*Synthesis of (3aS,4S,6aR)-11-Sulfanylundecyl 5-(Hexahydro-2-oxo-1H-thieno[3,4-d]imidazol-4t-yl)pentanoate (**4** in Figure 1).* A stirred solution of **3** (1.000 g, 2.09 mmol) in THF was cooled to −10 °C, and hexamethyldisilathiane (2.20 mL, 10.45 mmol) and TBAF (10.5 mL, 1.0 M solution in THF with 5% water, 10.45 mmol) were added (*44*). The resulting reaction mixture was allowed to warm to room temperature while it was stirred. The reaction was carried out under argon and under shielding from ambient light in order to avoid photoinduced side reactions. After 20 min, the reaction mixture was washed with 20 mL of aqueous ammonium chloride (saturated) and 10 mL of CH_2Cl_2. Recrystallization from CH_2Cl_2 and hexane gave **4** as white solid (0.673 g, 75% yield). Anal. ($C_{21}H_{38}N_2O_3S_2$) H, N; C: calcd, 58.57; found, 57.94; S: calcd 14.89; found, 14.31 (the ^{1}H NMR spectrum indicated that some disulfides occurred as impurities in the product). Mp: 99.5−101.0 °C. IR ν_{max} (cm^{-1}): 3462, 2929, 2853, 1705, 1597. UV (CH_2Cl_2) λ_{max} (log ϵ): 219 (0.48). ^{1}H NMR (500 MHz, CD_2Cl_2, δ): 1.28−1.47 (m, 17H), 1.57−1.74 (m, 6H), 1.87 (m, −CH_2CH$_2$SH, 2H), 2.31 (t, J = 7.4 Hz, −CH_2C(O)OCH$_2$−, 2H), 2.50 (q, J = 7.4, −CH_2-SH, 2H), 2.71 (d, J = 12.7 Hz, −CHCH_2S−, 1H), 2.91 (dd, J = 12.7, 5.0 Hz, −CHCH_2S−, 1H), 3.16 (m, −SCH−, 1H), 4.03 (t, J = 6.8 Hz, −OCH_2−, 2H), 4.30 (m, −NHCHCH$_2$−, 1H), 4.48 (m, −NHCH(CH−)$_2$, 1H), 5.44 (s, −NHCH(CH−)$_2$, 1H), 5.71 (s, −NHCHCH$_2$−, 1H). ^{13}C NMR (125 MHz, CD_2Cl_2, δ): 24.96 (−CH$_2$SH), 25.28, 26.33 28.71, 28.78 (2C), 29.08, 29.47, 29.66, 29.90 (3C), 34.32, 34.53, 41.04 (−CH$_2$S−), 55.90 (−SCH−), 60.54 (−NCCH$_2$), 62.27 (−NC(CH−)$_2$), 64.82 (−C(O)OCH$_2$−), 163.91 (−NC(O)N−), 173.95 (−C(O)O−). EI-MS *m*/*z* (relative intensity): (M + 1)$^+$ 431.2 (49), M$^+$ 430.2 (13), 397.3 (26), 227.1 (76), 166.0 (83).

*Synthesis of (3aS,4S,6aR)-11-[[3-(3-Trifluoromethyl-3H-diaziren-3-yl)phenylamino][1-(4-oxobutyl)pyrrolidine-2,5-dioxo-3-yl]thio]undecyl 5-(Hexahydro-2-oxo-1H-thieno-[3,4-d]imidazol-4t-yl)pentanoate (**5** in Figure 1).* To a solution of **4** (7.32 mg, 17 μmol) in CH_2Cl_2 (3 mL) at 0 °C was added a solution of **1** (6.23 mg, 17 μmol) in 0.2 mL CH_2Cl_2, followed by 5 drops of triethylamine. The mixture

was allowed to reach room temperature and then was stirred for 7 h. The reaction was shielded from light in order to avoid photoinduced side reactions and was carried out under argon. The resulting mixture was concentrated under reduced pressure, and the residue was purified by chromatography on a silica glass plate (hexane/1,2-dichloroethane/acetonitrile/ethanol 40:30:24:6) to give **5** as a diastereoisometric mixture in form of a white solid (11.1 mg, 82% yield). ^{1}H NMR (200 MHz, $CDCl_3$, δ): 1.28−1.49 (m, 16H), 1.57−1.74 (m, 8H), 2.04 (m, $-NCH_2CH_2CH_2CO-$, 2H), 2.33 (m, $-CH_2COOCH_2-$, $-NCH_2CH_2CH_2CO-$, 4H), 2.50 (dd, J = 18.7, 3.3 Hz, $-CH_2CH_2S-$, 2H), 2.69−3.00 (m, $-CHCHS-$, $-SCHCH_2-$CO−, 4H), 3.07−3.24 (m, $-SCHCHNH$, 1H), 3.58−3.76 (m, $-NCH_2-$, $-SCHCO$, 3H), 4.07 (t, J = 6.6 Hz, $-OCH_2-$, 2H), 4.35 (m, $-NHCHCH_2-$, 1H), 4.53 (m, $-NHCH(CH-)_2$, 1H), 4.88 (s, $-NHCH(CH-)_2$, 1H), 5.06 (s, $-NHCHCH_2-$, 1H), 6.94 (d, J = 7.1 Hz, Ar H, 1H), 7.34 (t, J = 7.9 Hz, Ar H, 1H), 7.48 (s, Ar H, 1H), 7.67 (d, J = 7.5 Hz, Ar H, 1H), 8.55 (d, J = 5.4 Hz, −NH-Ar, 1H). ESI-MS m/z: $(M + 1)^+$ 797, $(M + Na)^+$ 819, $(M + K)^+$ 835.

Atomic Force Microscopy (AFM). Glass microscope slides covered with an Au layer were prepared according to a standard procedure for self-assembled monolayers (*45*). Solution aliquots of pure Tecoflex were cast onto the gold substrate (1.0 × 1.0 cm^2) resulting in a membrane of 200 μm thickness. An Autoprobe CP from Park Scientific Instruments was used to image the pure Tecoflex membrane. The images were collected in intermittent-contact mode, in room atmosphere, and at ambient temperature. Commercially available silicon cantilevers with high aspect ratio tips were used.

X-ray Photoelectron Spectroscopy (XPS). The gold substrates covered with pure Tecoflex were washed in ethanol and dried for 1 h at room temperature under high vacuum (10^{-2} mbar). Then 25 μL of a solution of **1** (2.7 mM in ethanol) was deposited. The samples were dried under a vacuum of 20 mbar for 1 h at room temperature. For XPS-studies after photobinding, the samples were irradiated for 20 min using a Stragene UV Stratalinker 350 nm light source with a radiance of 0.95 mW cm^{-2} and washed in hexane and in ethanol (*42*, *46*). Photolyses were done at ambient temperature (20−25 °C). The surface of dry membrane films was analyzed via XPS under an ultrahigh vacuum of 10^{-9} mbar. Spectra were collected with a Perkin-Elmer 5700 spectrometer (Perkin-Elmer, Norwalk, CT) using an Al Kα X-ray source ($h\nu$ = 1486.7 eV) with an emission power of 350 W to stimulate photoelectron emission. A spherical analyzer with an investigation area of 0.80 mm^2 was used, and the hydrocarbon C1s peak was referenced at 285 eV. Samples were analyzed at 45° takeoff angle (the angle between the surface normal and the analyzer lens axes). An average of three measurements was obtained. Data were collected and stored on a Perkin-Elmer computer, which also controlled the spectrometer. Software provided with the instrument was used to interpret the data.

Potentiometry. The ion-selective membranes contained 2.0 wt % (25.0 mmol kg^{-1}), ETH 5234, 1.0 wt % (11.0 mmol kg^{-1}) NaTFPB, and Tecoflex. A membrane of 100 μm thickness was obtained by casting a solution of 316.80 mg of the membrane components, dissolved in 2.5 mL THF, into a glass ring (60 mm i.d.) fixed on a glass plate covered with a Teflon foil. For each ISE, a disk of 7 mm diameter was punched from the membrane and glued to plasticized PVC tubing with THF. The inner filling solution was 0.05 M Na_2EDTA, 10^{-3} M $CaCl_2$, and 0.06 M NaOH (pH 8.9, calculated ion activity $a_{Ca^{2+}}$ = 2.3 × 10^{-12} M). A diaphragm separated the internal filling solutions from the reference half cell (Ag/AgCl in 0.1 M KCl. The ISEs were conditioned for 2 d in a solution of 5 × 10^{-5} M 2-morpholinoethanesulfonic acid (MES) and 5 × 10^{-5} M NaOH (pH 6.5). Measuring solutions were prepared by successive automatic dilution of stock solutions with a Liquino 711 and two Dosino 700 instruments (Metrohm AG, CH-9010 Herisau). Potentials were measured with a 16-channel electrode monitor EMF16 (Lawson Labs Inc., Malvern, PA 19355) at room temperature (20−21 °C) in solutions stirred with a rod stirrer. An Ag/AgCl reference electrode (Metrohm, type 6.0729.100) with a 1 M KCl bridge electrolyte was used. All EMF values were corrected for the liquid-junction potential at the sample/bridge electrolyte interface using the Henderson equation (*3*).

For the preparation of ISEs with immobilized **5**, ISE membranes were washed in deionized water and dried under vacuum (20 mbar) for 1 h at room temperature. Then 40 μL of an acetonitrile (MeCN) solution of **5** (0.28 mM) were deposited on each membrane. The samples were dried for 1 h under a vacuum of 20 mbar at room temperature. For photobinding, the ISEs were irradiated for 20 min using a Stragene UV Stratalinker 350 nm light source with a light intensity of 0.95 mW cm^{-2} and washed in MeCN. Photolyses were done at ambient temperature (20−25 °C). The conditioned ISEs were set, before the streptavidin incubation, into a solution of 0.02% polyoxyethylenesorbitan monolaurate (Tween 20) for 20 min. A 0.1 M MES buffer of pH 6.1 (with NaOH) was used for the streptavidin binding experiments. The concentration of streptavidin in the MES buffer was 42 μg mL^{-1} (0.7 μM), and the reaction of this solution with the surface was allowed to proceed for 1 h. The membranes were rinsed with water in order to remove unbound streptavidin and set back into the conditioning solution for 1 h before the potentiometric measurements.

Radiochemistry. Glass slides (0.8 × 0.8 cm^2) were covered with a membrane which had the same composition as the one used in the potentiometric experiments. All samples were washed in acetonitrile (MeCN) and dried under vacuum (10^{-2} mbar) for 1 h at room temperature. Samples of series A and B: deposition of 25 μL of a solution of **5** (2.3 mM in MeCN), drying for 10 min under high vacuum of 0.05 mbar at room temperature, UV irradiation, washing in MeCN. Samples of series C: deposition of 25 μL of **5** (2.3 mM in MeCN), drying for 20 min under 0.05 mbar at r.t., UV-irradiation, washing in MeCN. Samples of series D, E, and F: deposition of 25 μL **5** (2.3 mM in MeCN), drying for 80 min under 0.05 mbar at rt, UV irradiation, washing in MeCN. Samples of series G: deposition of a pure MeCN drop, drying for 80 min under 0.05 mbar at rt, UV irradiation, washing in MeCN. Samples of series H and I: only washing in MeCN. All photobinding experiments were carried out employing a high-pressure mercury lamp (Osram HBO 350 W) mounted in a SUSS LH 1000 lamp house equipped with a shutter to control exposure times. The samples were irradiated for 200 s with a light intensity of 1.14 W cm^{-2} at 365 nm at ambient temperature (20−25 °C).

After the photoimmobilization, the glass slides with the membrane were conditioned in water for 2 d. A 0.1 M MES buffer of pH 6.1 (with NaOH) was used for the streptavidin binding. The protein concentrations in the MES buffer were 21 μg mL^{-1} (0.35 μM) streptavidin (not radiolabeled) and 3.1 ng mL^{-1} (52 pM) [^{35}S]-streptavidin with an activity of 15.4 × 10^3 Bq mL^{-1}. After being rinsed with water in order to remove unbound streptavidin,

Table 1. Elemental Analysis of Tecoflex Membranes with and without MAD

analytical method	C (%)	O (%)	N (%)	F (%)
combustion analysis[a]	78.57	19.05	2.38	
XPS[a]	78.08	20.98	0.95	
XPS[b]	77.97	19.52	1.80	0.35

[a] MAD was not photoimmobilized on the membrane surface. [b] MAD was photoimmobilized on the membrane surface.

Table 2. Surface Densities of [^{35}S]-Streptavidin on Tecoflex Membranes

series[a]	vacuum time (min)	cross-linking of **5**	treatment with Tween	density of streptavidin (ng cm^{-2})[b]
A	10	yes	no treatment	311 ± 43
B	10	yes	before streptavidin	45 ± 9
C	20	yes	before streptavidin	42 ± 19
D	80	yes	no treatment	134 ± 33
E	80	yes	after streptavidin	152 ± 81
F	80	yes	before streptavidin	30 ± 9
G	80	no	no treatment	17 ± 3
H	0	no	no treatment	26 ± 17
I	0	no	before streptavidin	22 ± 14

[a] The capital letters correspond to the series described in the Experimental Procedures and Figure 3. [b] The radiolabel densities were quantified by autoradiography. Error bounds correspond to standard deviations obtained from five measurements (four in series F).

the samples were set back into the conditioning solution for 1 h, and dried at room temperature for 15 h. As shown in Table 2, some sample series were set into a solution of 0.02% Tween 20 for 20 min before or after the streptavidin incubation. Autoradiography of the dried glass slides with the membranes was done with storage screens from Molecular Dynamics (Sunnyvale, CA), which were exposed for 12 h. For quantification, a PhosphorImager from Molecular Dynamics and an external one-point calibration ($n = 5$) with [^{35}S]-streptavidin was used. All work with radioactivity was performed in a certified laboratory.

RESULTS AND DISCUSSION

In this work, the surface of an ion-selective polyurethane membrane was modified by photocross-linking of biotin. First, the morphology of a pure Tecoflex membrane without **1** was mapped out using atomic force microscopy (AFM). The surface structure of the Tecoflex membrane was featureless with a root-mean-square roughness of about 0.7 nm. The height differences between the lower and higher spots were around 3 nm. Nurdin et al. (*47*) found for a similar polyurethane surface, after drying it in the vacuum, a peak-to-valley distance of about 15 nm. The plain and homogeneous surface morphology of the investigated polyurethane is well suited for the planned application. In the next step, X-ray photoelectron spectroscopy (XPS) was used to obtain evidence for the cross-linking of **1** to the polyurethane membrane surface. Tecoflex membranes with and without **1** were examined by XPS for providing a qualitative and quantitative analysis of their surface. No fluorine was detected in the case of membranes without **1** (Table 1). There are small differences between the surface concentrations determined from the XPS analysis (Table 1, second row) and the bulk membrane composition found from the elemental analysis (Table 1, first row). This may be the consequence of a phase separation that takes place at the few outermost molecular layers of the polyurethane, where little or no hard segments were found in earlier studies (*48*, *49*). For the membrane with **1**, the detection of fluorine is a clear evidence for the successful photoimmobilization on the membrane surface (*46*).

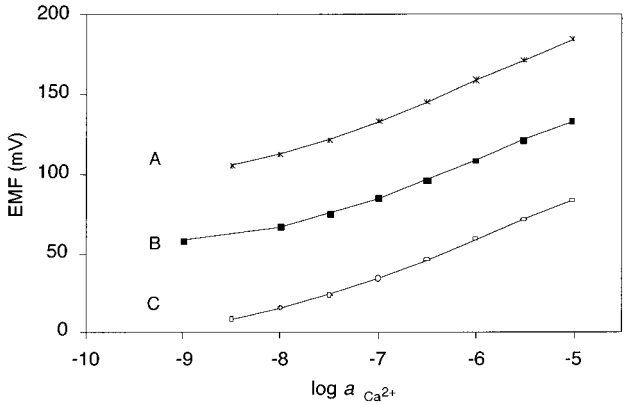


Figure 2. Response of ISEs based on the calcium-selective ionophore ETH 5234, NaTFPB and Tecoflex: A, without B and C with surface modification with **5**; C, after incubation with a streptavidin solution. Inner filling solution: 0.05 M Na_2EDTA, 10^{-3} M $CaCl_2$, and 0.06 M NaOH (pH 8.9). Sample solution: $CaCl_2$ in a buffer of 5×10^{-5} M 2-morpholinoethanesulfonic acid (MES) and 5×10^{-5} M NaOH (pH 6.5). Electrode slopes (mV dec^{-1} in the range 10^{-5} M bis 10^{-7} M): A, 25.8; B, 24.3; C, 25.0.

On the basis of the positive results of the above-described preliminary experiments, a biotin derivative with a covalently attached photo-cross-linking unit was designed and synthesized. The synthetic pathway to the novel photobiotin **5** with the carbene-generating trifluoromethylaryldiazirine group is shown in Figure 1. Brooks et al. demonstrated recently that photo-cross-linking of a related photobiotin (*31*) was more efficient than for the nitrene derivative used in their earlier studies (*31*). The photo-cross-linking unit is a derivative of *N*-[3-[3-(trifluoromethyl)diazirine-3-yl]phenyl]-4-maleimidobutyramide (**1**, MAD), which has been shown to have excellent properties in several earlier studies (*20*). To obtain optimal binding characteristics of streptavidin, a spacer with a carbon chain of 11 CH_2 groups is interposed between the biotin moiety and the photocross-linker (*24*, *25*). The intermediate product **4**, a thiol-bearing biotin derivative was prepared by a simpler procedure and in a higher yield than for similar compounds described previously (*26*−*30*).

The influence of the surface modification on the potentiometric response behavior of membrane-based sensors was investigated for Ca^{2+}-selective electrodes. A complete coverage of the membrane with a dense layer of proteins may be expected to result in a different response signal of the respective ISE. The experiments were performed using calcium-selective electrodes based on Tecoflex membranes. The biotin derivative **5** was photoimmobilized onto the surface of the membranes containing the Ca^{2+}-selective ionophore ETH 5243 and the ion exchanger NaTFPB (see the Experimental Procedures). To achieve detection limits in the nanomolar range (*39*, *50*), the inner filling solution of these ISEs contained a high sodium activity and a low calcium activity established with EDTA as ion-buffering system. The calibration curves of an untreated membrane (A) and one with immobilized biotin (B) were found to be virtually identical (Figure 2). This is even true for membrane B after incubation in a streptavidin solution (curve C). In all cases, it is possible to measure calcium activities down to the nanomolar range. It appears that the surface-immobilized biotin−streptavidin conjugate does not influence the potentiometric response of these sensors.

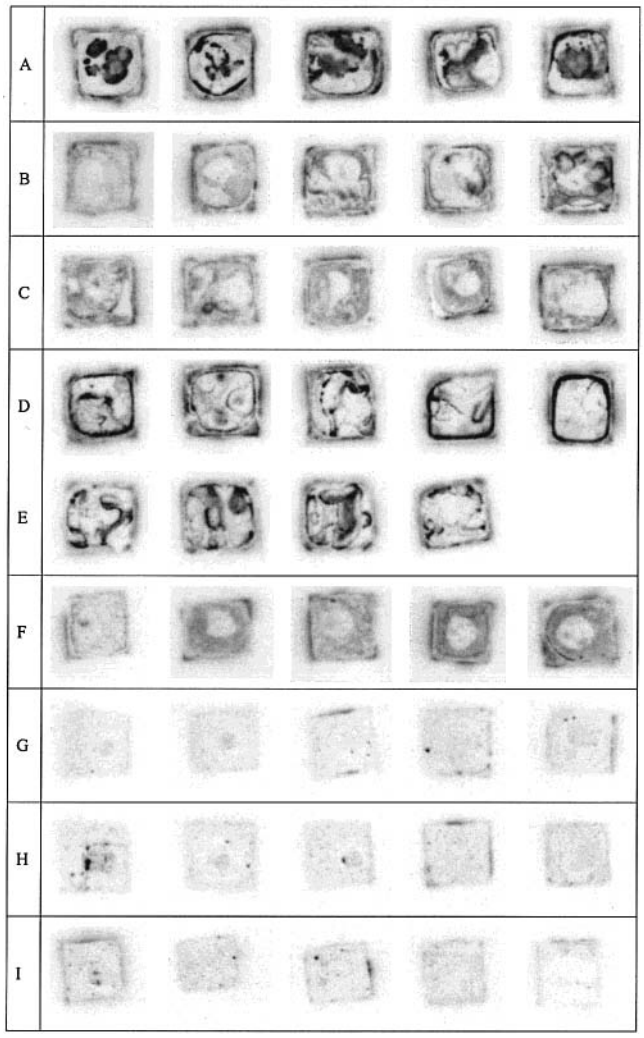


Figure 3. Autoradiographic measurements on Tecoflex films-coated (8 × 8 mm) glass slides, after incubation into a solution of [^{35}S]-streptavidin. The darkness is proportional to the density of bound or adsorbed [^{35}S]-streptavidin. Contact times before photo-cross-linking (in min): A, B, 10; C, 20; D−F, 80; blank samples: GI. Tween 20 was applied before streptavidin for samples B, C, and F and after streptavidin for membranes E. The density values shown in the five columns were determined from repeated experiments under identical conditions.

Evidently, the exchange of calcium ions at the interface between membrane and sample solution is not blocked by the binding of streptavidin. This implies that the streptavidin layer on the membrane surface cannot be very dense. To confirm this hypothesis, the surface coverage is analyzed experimentally in the following section.

The distribution of covalently bound biotin accessible for conjugation with streptavidin was monitored by autoradiography using the soft β-emitter [^{35}S]-streptavidin as radiolabel. The experiments were performed on Tecoflex membranes that had the same composition as the ones used for the ISE measurements. From the data shown in Figure 3 and Table 2, it is evident that the membranes with photoimmobilized biotin (A − F) bind a significantly larger amount of [^{35}S]-streptavidin than the ones without biotin (G and H). Consequently, the cross-linked biotin derivative is able to bind [^{35}S]-streptavidin on the polyurethane surface, and its biological activity is apparently not affected by the photochemical immobilization process. Although some adsorption of streptavidin occurs even for membranes without biotin, the effect is in all cases smaller than for membranes with biotin. While the surface distribution of the labeled streptavidin strongly varies from experiment to experiment (rows in Figure 3), the variation of the total amount within a given series of experiments is much smaller (Table 2, last column). The nonuniform distribution of the labeled streptavidin on membranes A−F must be caused by irregular photoimmobilization of **5**, since the [^{35}S]-streptavidin coverage on membranes G−I without immobilized biotin is found to be much more homogeneous, as shown in Figure 3. The heterogeneity of the coverage by **5** after deposition and vacuum treatment can even be observed with a magnifying glass. Previously, nonuniform immobilization of photobiotin was also reported for the case of solid substrates (*51*). AFM images also indicated that the distribution of streptavidin on biotinylated surfaces is nonuniform, and that the proteins tend to cluster (*52*). More than 80% of the adsorbed proteins were found in clusters of three or more molecules (*28*). Similarly, it was found that only a part of biotin is able to bind avidin if it is immobilized on a surface (*51*).

One of the reasons for the heterogeneous photoimmobilization may be the low photocoupling efficiency. For example, it was found in previous studies that the photocoupling efficiency of MAD-[^{35}S]Cys to polystyrene is only 7% (*42*). In the present system, the diffusion of the biotin derivative **5** into the polyurethane membrane before cross-linking may also have an effect. The diffusion coefficient of organic compounds in such membranes is on the order of 10^{-8} cm^2 s^{-1} (*1*). Assuming that compound **5** is sufficiently soluble in Tecoflex, one would expect a mean diffusion distance of 35 and 49 μm after 10 and 20 min, respectively. The amount of biotin available for the surface reaction would decrease accordingly. The measured dependence of the streptavidin density on the contact time before photo-cross-linking suggests such an influence. Figures 3 A vs D, as well as Figure 3 B and C vs F, indicate that an effect is well observable after contact times of 80 min, but the differences are small between 10 and 20 min.

To reduce nonspecific adsorption of proteins, the corresponding substrates are occasionally treated with a surfactant (*53*). Experiments were done in these lines with the nonionic surfactant Tween 20. If the surfactant is applied before the contact of the biotinylated membrane with [^{35}S]-streptavidin, the surface concentration of bound proteins is heavily reduced (see A vs B and D vs F in Figure 3 and Table 2). However, as demonstrated by the experiments H and I, this decrease is not due to a reduction of the nonspecific adsorption. It might rather be a consequence of an accumulation of Tween 20 at the membrane surface (*54*, *55*) and its competitive binding to the protein (*56*). In striking contrast, a treatment of the membranes after conjugation with [^{35}S]-streptavidin does not affect the surface concentration at all (see D and E in Figure 3 and Table 2).

Before performing the radiochemistry experiments, the membranes were kept 2 d in distilled water. As indicated by control experiments without conditioning (not shown) this did not significantly influence the measured [^{35}S] activity. Thus, once the biotin derivative is bound to the surface, it forms a rather stable layer despite the presence of a soft polymer substrate. Using the density of a two-dimensional crystalline streptavidin (C2,2,2) monolayer (262 ng cm^{-2}) (*30*, *57*) the percentage of the protein bound relative to the amount required for a compact monolayer can be calculated. It is 120% for membrane A and 50−60% for membranes D and E with long contact times before photoimmobilization.

CONCLUSIONS

We demonstrated that biotin can be covalently immobilized on the surface of a soft polyurethane and that the immobilized biotin is capable of binding streptavidin. Films made from Tecoflex, the applied polyurethane, seem to be ideally suited as substrate because of their very plain surface. While the total amount of streptavidin bound to the biotinylated polyurethane is rather close to that required for a compact monolayer, the uniformity varied significantly. Such a variation was also observed earlier with hard substrates (*51*).

ACKNOWLEDGMENT

This work was financially supported by the Swiss National Science Foundation, the National Institutes of Health (Grant No. R01-GM59716), and Orion Research, Inc. (Beverly, MA). We gratefully acknowledge the help of Martin Püntener and André Müller concerning the syntheses, Andrea Rainelli for some preliminary measurements, Prof. Roel Prins for permission to use his AFM instrument, and Prof. Nicholas Spencer for performing the XPS measurements.

LITERATURE CITED

(1) Bakker, E., Bühlmann, P., and Pretsch, E. (1997) Carrier-based ion-selective electrodes and bulk optodes. 1. General characteristics. *Chem. Rev. 97*, 3083−3132.

(2) Bühlmann, P., Pretsch, E., and Bakker, E. (1998) Carrier-based ion-selective electrodes and bulk optodes. 2. Ionophores for potentiometric and optical sensors. *Chem. Rev. 98*, 1593−1687.

(3) Morf, W. E. *The Principles of Ion-Selective Electrodes and of Membrane Transport*; Elsevier: New York, 1981.

(4) Cha, G. S., Liu, D., Meyerhoff, M. E., Cantor, H. C., Midgley, A. R., Goldberg, H. D., and Brown, R. B. (1991) Electrochemical performance, biocompatibility, and adhesion properties of new polymer matrices for solid-state ion sensors. *Anal. Chem. 63*, 1666−1672.

(5) Pick, J., Toth, K., Pungor, E., Vasak, M., and Simon, W. (1973) A potassium-selective silicone-rubber membrane electrode based on a neutral carrier. *Anal. Chim. Acta 64*, 477−480.

(6) Reinhoudt, D. N., Engbersen, J. F. J., Brzózka, Z., van den Vlekkert, H. H., Honig, G. W. N., Holterman, H. A. J., and Verkerk, U. H. (1994) Development of K^+-selective chemically modified field effect transistors with functionalized polysiloxane membranes. *Anal. Chem. 66*, 3618−3623.

(7) Oh, B. K., Kim, C. Y., Lee, H. J., Rho, K. L., Cha, G. S., and Nam, H. (1996) One-component room-temperature vulcanizing-type silicone rubber-based calcium-selective electrodes. *Anal. Chem. 68*, 503−508.

(8) Malinowska, E., Oklejas, V., Hower, R. W., Brown, R. B., and Meyerhoff, M. E. (1996) Enhanced electrochemical performance of solid-state ion sensors based on silicon rubber membranes. *Sens. Actuators B33*, 161−167.

(9) Heng, L. Y., and Hall, E. A. H. (2000) Producing "self-plasticizing" ion-selective membranes. *Anal. Chem. 72*, 42−51.

(10) Malinowska, E., Gawart, L., Parzuchowski, P., Rokicki, G., and Brzózka, Z. (2000) Novel approach of immobilization of calix[4]arene type ionophore in "self-plasticized" polymeric membrane. *Anal. Chim. Acta 421*, 93−101.

(11) Wang E., and Meyerhoff, M. E. (1993) Evaluation of polyurethane-based membrane matrixes for optical ion-selecitve sensors. *Anal. Lett. 26*, 1519−1533.

(12) Lindner, E., Cosofret, V. V., Ufer, S., Buck, R. P., Kao, W. J., Neuman, M. R., and Anderson, J. M. (1994) Ion-selective membranes with low plasticizer content: Electroanalytical characterization and biocompatibility studies. *J. Biomed. Mater. Res. 28*, 591−601.

(13) Yun, S. Y., Hong, Y. K., Oh, B. K., Cha, G. S., Nam, H., Lee, S. B., and Jin, J.-I. (1997) Potentiometric properties of ion-selective electrode membranes based on segmented polyether urethane matrices. *Anal. Chem. 69*, 868−873.

(14) Daunert, S., and Bachas, L. G. (1990) Ion-selective electrodes using an ionophore covalently attached to carboxylated poly(vinyl chloride). *Anal. Chem. 62*, 1428−1431.

(15) Kusy, R. P., Whitley, J. Q., Buck, R. P., Cosofret, V. V., and Lindner, E. (1994) Syntheses and kinetics of piperazine-modified poly(vinyl chloride)s for use as fixed-site proton carrier membranes. *Polymer 35*, 2141−2147.

(16) Kimura, K., Matsuba, T., Tsujimura, Y., and Yokoyama, M. (1992) Unsymmetrical Calix[4]arene Ionophore/Silicone Rubber Composite Membranes for High-Performance Sodium Ion-Sensitive Field-Effect Transistors. *Anal. Chem. 64*, 2508−2511.

(17) Espadas-Torre, C., and Meyerhoff, M. E. (1995) Thrombogenic properties of untreated and poly(ethylene oxide) modified polymeric matrixes useful for preparing intraarterial ion-selective electrodes. *Anal. Chem. 67*, 3108−3114.

(18) Brooks, K. A., Allen, J. R., Feldhoff, P. W., and Bachas, L. G. (1996) Effect of surface-attached heparin on the response of potassium-selective electrodes. *Anal. Chem. 68*, 1439−1443.

(19) Kuijpens, J. M. H., Kardaun, G. A., Blezer, R., Pijpers, A. P., and Koole, L. H. (1995) Immobilization of theophilline on medical-grade polyurethane inhibits surface-induced activation of blood platelets. *J. Am. Chem. Soc. 117*, 8691−8697.

(20) Sigrist, H., Collioud, A., Clemence, J., Gao, H., Sanger, M., and Sundarababu, G. (1995) Surface immobilization of biomolecules by light. *Opt. Eng. 35*, 2339−2348.

(21) Yan, M., Cai, S. X., Wybourne, M. N., and Keana, J. F. W. (1993) Photochemical functionalization of polymer surfaces and the production of biomolecule-carrying micrometer-scale structures by deep-UV litography using 4-substituted perfluoropheny azides. *J. Am. Chem. Soc. 115*, 814−816.

(22) Yan, M., Cai, S. X., Wybourne, M. N., and Keana, J. F. W. (1994) N-hydroxysuccinimide ester functionalized perfluoropheny azides as novel photoactive heterobifunctional crosslinking agents. The covalent immobilization of biomolecules to polymer surfaces. *Bioconjugate Chem. 5*, 151−157.

(23) Hengsakul, M., and Cass, A. E. G. (1996) Protein patterning with a photoactivable derivative of biotin. *Bioconjugate Chem. 7*, 249−254.

(24) Torres-Rodriguez, L. M., Roget, A., Billon, M., and Bidan, G. (1998) Synthesis of a Biotin Functionalized Pyrrole and Its Electropolymerization: Toward a Versatile Avidin Biosensor. *Chem. Commun. 21*, 1993−1994.

(25) Wang, Y. L., and Bobbitt, D. R. (1994) Binding Characteristics of Avidin and Surface Immobilized Octylbiotin − Implications for the Development of Dynamically Modified Optical-Fiber Sensors. *Anal. Chim. Acta 298*, 105−112.

(26) Dubrovsky, T. B. (2000) *Protein Architecture*, pp 25−54, Marcel Dekker: New York.

(27) Busse, S., Kashammer, J., Kramer, S., and Mittler, S. (1999) Gold and Thiol Surface Functionalized Integrated Optical Mach−Zender Interferometer for Sensing Purposes. *Sens. Actuators B 60*, 148−154.

(28) Perez Luna, V. H., O Brien, M. J., Opperman, K. A., Hampton, P. D., Lopez, G. P., Klumb, L. A., and Stayton, P. S. (1999) Molecular Recognition Between Genetically Engineered Streptavidin and Surface-Bound Biotin. *J. Am. Chem. Soc. 121*, 6469−6478.

(29) Knoll, W., Zizlsperger, M., Liebermann, T., Arnold, S., Badia, A., Liley, M., Piscevic, D., Schmitt, F. J., and Spinke, J. (2000) Streptavidin Arrays as Supramolecular Architectures in Surface-Plasmon Optical Sensor Formats. *Colloids Surf. A 161*, 115−137.

(30) Jung, L. S., Nelson, K. E., Campbell, C. T., Stayton, P. S., Yee, S. S., Perez-Luna, V., and Lopez, G. P. (1999) Surface Plasmon Resonance Measurement of Binding and Dissociation of Wild-Type and Mutant Streptavidin on Mixed Biotin-Containing Alkylthiolate Monolayers. *Sens. Actuators B 54*, 137−144.

(31) Brooks, S. A., Dontha, N., Davis, C. B., Stuart, J. K., O'Neill, G., and Kuhr, W. G. (2000) Segregation of micrometer-dimension biosensor elements on a variety of substrate surfaces. *Anal. Chem. 72*, 3253−3259.

(32) Lin, S., Fang, K., Hashimoto, M., Nakanishi, K., and Ojima, I. (2000) Design and synthesis of a novel photoaffinity taxoid as a potential probe for the study of paclitaxel-microtubules interactions. *Tetrahedron Lett. 41*, 4287−4290.

(33) Hatanaka, Y., Hashimoto, M., Nishihara, S., Narimatsu, H., and Kanaoka, Y. (1996) Synthesis and characterization of a carbene-generating biotinylated *N*-acetylglucosamine for photoaffinity labeling of β-(1→4)-galactosyltransferase. *Carbohydr. Res. 294*, 95−108.

(34) Bühlmann, P., Aoki, H., Xiao, K. P., Amemiya, S., Tohda, K., and Umezawa, Y. (1998) Chemical sensing with chemically modified electrodes that mimic gating at biomembranes incorporating ion-channel receptors. *Electroanalysis 10*, 1149−1158.

(35) Sokalski, T., Ceresa, A., Zwickl, T., and Pretsch, E. (1997) Large improvement of the lower detection limit of ion-selective polymer membrane electrodes. *J. Am. Chem. Soc. 119*, 11347−11348.

(36) Morf, W. E., Badertscher, M., Zwickl, T., de Rooij, N. F., and Pretsch, E. (1999) Effects of ion transport on the potential response of ionophore-based membrane electrodes: A theoretical approach. *J. Phys. Chem. B 103*, 11346−11356.

(37) Bakker, E., and Pretsch, E. (2001) Potentiometry at trace levels. *Trends Anal. Chem. 20*, 11−19.

(38) Sokalski, T., Zwickl, T., Bakker, E., and Pretsch, E. (1999) Lowering the detection limit of solvent polymeric ion-selective electrodes. 1. Modeling the influence of steady-state ion fluxes. *Anal. Chem. 71*, 1204−1209.

(39) Sokalski, T., Ceresa, A., Fibbioli, M., Zwickl, T., Bakker, E., and Pretsch, E. (1999) Lowering the detection limit of solvent polymeric ion-selective membrane electrodes. 2. Influence of composition of sample and internal electrolyte solution. *Anal. Chem. 71*, 1210−1214.

(40) Ye, Q., and Meyerhoff, M. E. (2001) Rotating electrode potentiometry: Lowering the detection limits of nonequilibrium polyion-sensitive membrane electrodes. *Anal. Chem. 73*, 332−336.

(41) Vigassy, T., Morf, W. E., Badertscher, M., Ceresa, A., de Rooij, N. F., and Pretsch, E. (2001) Making use of ion fluxes through potentiometric sensor membranes: ISEs with step responses at critical ion activities. *Sens. Actuators B 76*, 476−481.

(42) Collioud, A., Clémence, J. F., Sänger, M., and Sigrist, H. (1993) Oriented and Covalent Immobilization of Target Molecules to Solid Supports: Synthesis and Application of a Light-Activatable and Thiol-Reactive Cross-Linking Reagent. *Bioconjugate Chem. 4*, 528−536.

(43) Crisp, G. T., and Gore, J. (1997) Biotin Derivates as Gelators of Organic Solvents. *Synth. Commun. 27*, 2203−2216.

(44) Hu, J., and Fox, M. A. (1999) A Convenient Trimethylsilylthioxy-Dehalogenation Reaction for the Preparation of Functionalized Thiols. *J. Org. Chem. 64*, 4959−4961.

(45) Fibbioli, M., Bandyopadhyay, K., Liu, S.-G., Echegoyen, L., Enger, O., Diederich, F., Bühlmann, P., and Pretsch, E. (2000) Redox-active self-assembled monolayers as novel solid contacts for ion-selective electrodes. *Chem. Commun.* 339−340.

(46) Leonard, D., Chevolot, Y., Bucher, O., Sigrist, H., and Mathieu, H. J. (1998) ToF-SIMS and XPS Study of Photoactivatable Reagents Designed for Surface Glycoengineering − Part I. N-(m-(3-(trifluoromethyl)diazirine-3-yl)phenyl)-4-maleimido-butyramide (MAD) on Silicon, Silicon Nitride and Diamond. *Surf. Interface Anal. 26*, 783−792.

(47) Nurdin, N., and Descouts, P. (1995) Effect of Toluene Extraction on Biomer TM Surface: II. An Atomic Force Microscopy Study. *J. Biomater. Sci. Polymer. 7*, 425−438.

(48) Chen, Z., Ward, R., Tian, Y., Eppler, A. S., Shen, Y. R., and Somorjai, G. A. (1999) Surface Composition of Biopolymer Blend Biospan-SP/Phenoxy and Biospan-F/Phenoxy Observed with SFG, XPS, and Contact Angle Goniometry. *J. Phys. Chem. B 103*, 2935−2942.

(49) Hearn, M. J., Briggs, D., Yoon, S. C., and Ratner, B. D. (1987) SIMS and XPS Studies of Polyurethane Surfaces 2. Polyurethanes with Fluorinated Chain Extenders. *Surf. Interface Anal. 10*, 384−391.

(50) Ceresa, A., Sokalski, T., and Pretsch, E. (2001) Influence of Key Parameters on the Lower Detection Limit and Response Function of Solvent Polymeric Membrane Ion-Selective Electrodes. *J. Electroanal. Chem. 501*, 70−76.

(51) Brooks, S. A., Ambrose, W. P., and Kuhr, W. G. (1999) Micrometer Dimension Derivatization of Biosensor Surfaces Using Confocal Dynamic Patterning. *Anal. Chem. 71*, 2558−2563.

(52) Dontha, N., Nowall, W. B., and Kuhr, W. G. (1997) Generation of Biotin/Avidin/Enzyme Nanostructures with Maskless Photolithography. *Anal. Chem. 69*, 2619−2625.

(53) Wahlgren, M., Welin-Klintström, S., and Karlsson, C. A.-C., Eds. *Interactions Between Proteins and Surfactants at Solid Interfaces*; Marcel Dekker, 1998.

(54) Ye, Q., Vincze, A., Horvai, G., and Leermakers, F. A. M. (1998) Partial blocking of ion transport at the interface of an ion-selective liquid membrane electrode by neutral surfactants. Experiments and computer simulation. *Electrochim. Acta 44*, 125−132.

(55) Malinowska, E., and Meyerhoff, M. E. (1998) Influence of nonionic surfactants on the potentiometric response of ion-selective polymeric membrane electrodes designed for blood electrolyte measurements. *Anal. Chem. 70*, 1477−1488.

(56) Duhamel, R. C., and Whitehead, J. S. (1990) In *Avidin−Biotin Technology* (Wilchek, M., Bayer, E. A., Eds.) Vol. 184, pp 210−207, Academic Press, San Diego.

(57) Darst, S. A., Ahlers, M., Meller, P. H., Kubalek, E. W., Blankenburg, R., Ribi, H. O., Ringsdorf, H., and Kornberg, R. D. (1991) Two-Dimensional Crystals of Streptavidin on Biotinylated Lipid Layers and Their Interactions with Biotinylated Macromolecules. *Biophys. J. 59*, 387−396.

BC015515+

An Efficient Binding Chemistry for Glass Polynucleotide Microarrays

Paul H. Lee,[†] Samuel P. Sawan,[‡] Zora Modrusan,[†] Lyle J. Arnold, Jr.,[†] and Mark A. Reynolds*[,†]

Incyte Genomics, Microarray Research and Development, 6519 Dumbarton Circle, Fremont, California 94555 and University of Massachusetts, Department of Chemistry, One University Avenue, Lowell, Massachusetts 01854. Received June 29, 2001; Revised Manuscript Received September 10, 2001

A variety of methods have been described for making synthetic polynucleotide microarrays. These include in situ synthesis directly on the array surface, for example, by photolithography or ink-jet printing technologies, and the application of presynthesized polynucleotides that are derivatized with various nucleophiles or electrophiles. In the latter case, a variety of surface chemistries have been developed, and several are available commercially. These chemistries must be compatible with nanoliter-scale volumes of polynucleotide reagents, which contact the array over a small portion of their surface. We reasoned that a three-dimensional polymer coating could potentially offer greater surface contact and higher binding efficiency. Here we describe a polyethylenimine-based coating chemistry that provides exceptional binding and hybridization characteristics. In our preferred process, size-fractionated polyethylenimine polymers are cross-linked onto an aminopropylsilanated glass surface in the presence of cyanuric chloride. The resulting three-dimensional coating binds polynucleotides through a mixture of covalent and noncovalent interactions as evidenced by comparisons between 5′-aminoalkyl modified and unmodified polynucleotides. Binding and hybridization comparisons are presented including analogous two-dimensional electrophilic and electrostatic chemistries.

INTRODUCTION

Microarray platform development has accelerated in recent years for a variety of biological applications. These include gene and protein expression profiling, where hundreds to thousands of biomolecules are analyzed simultaneously (*1*, *2*). Recent improvements have been driven by an increasing need for sensitivity and precision (*3*), as multivariate analyses and database approaches become more commonly employed (*4*). In the case of microarrays that are prepared by deposition (spotted arrays), a robust binding chemistry is essential for optimal performance. Such chemistry must be capable of binding the deposited target molecules with high efficiency without compromising their ability to bind their intended query molecules. Moreover, reproducible performance between batches is essential for generating data of sufficient quality to be incorporated into a relational database.

Over the past several years we have developed and optimized a commercial cDNA-based microarray platform (LifeArray) for gene expression profiling. This platform utilizes PCR-amplified cDNA clones that are representative of publicly available and proprietary expressed gene sequences. Our standard production process has been described previously (*5*). Briefly, the PCR-amplified products are spotted onto an aminopropylsilanated glass surface (up to 10000 spots over a 12 × 12 mm area). In our standard dual channel format, mRNA samples from two different tissues (for example a reference pool and a diseased or drug-challenged tissue) are labeled with two different fluorescent dyes (cyanine-3 and cyanine-5) by reverse transcription. The resulting cDNA probes are pooled, copurified, and hybridized together on the array. The arrays are then detected with a dual laser scanner and analyzed using GEMTools image analysis software. This process generally yields greater than 2.5 logs dynamic range, has a sensitivity of 1:100000 (about 1 copy per cell), and can detect greater than 1.7-fold differential gene expression at ≥99.5% confidence (*6*).

Recently, our laboratory developed a synthetic polynucleotide microarray platform (Z. Modrusan et al., manuscript in preparation). This platform offers several potential advantages compared to our standard cDNA microarrays, including the ability to generate arrays from sequences for which no cDNA clones are yet available and the possibility of higher gene discrimination by avoiding repetitive and homologous sequences. The development of synthetic polynucleotide microarrays with sensitivity and precision rivaling our commercial cDNA platform proved to be a considerable challenge. For example, a survey of commonly reported and commercially available glass chemistries resulted in sensitivities that were at best about 10-fold lower than cDNA microarrays (M. A. Reynolds and P. H. Lee, data not shown). On the basis of these results, we decided to examine cross-linked polymer chemistries, assuming that this approach might enable a higher density of bound polynucleotide per unit surface area.

Several cross-linked polymer chemistries have already been described for microarray applications. These include polyacrylamide gel pads (*7*, *8*) and mixed dendrimers that are synthesized in situ (*9*). Polyethylenimine has been used successfully for the chromatographic separation of nucleic acids (*10*) and also as a transfection agent for plasmids and antisense oligonucleotides (*11*). It is relatively inexpensive and can be size fractionated and characterized prior to conjugation. We reasoned that this

* To whom correspondence should be addressed. Telephone (510) 739-2134; Fax (510) 739-2200; E-mail markr@Incyte.com.
[†] Incyte Genomics.
[‡] University of Massachusetts.

10.1021/bc015523q CCC: $22.00 © 2002 American Chemical Society
Published on Web 12/14/2001

Table 1. Synthetic Polynucleotides Used in Binding and Hybridization Experiments

name	sequence
YCF115	5′- CTGCAACAACTGAGAGGGCAAGGATATAC-ATAAAAATAGCCTACAAATTCTGAACTCTG-3′
Cy3-YCF115	5′- Cy3- CTGCAACAACTGAGAGGGCAAGGATATAC-ATAAAAATAGCCTACAAATTCTGAACTCTG −3′
YCF115−NH_2	5′-NH_2-(C6)- CTGCAACAACTGAGAGGGCAAGGATATAC-ATAAAAATAGCCTACAAATTCTGAACTCTG −3′
Cy3-YCF115−NH_2	5′-NH_2-(C6)- CTGCAACAACTGAGAGGGCAAGGATATAC-ATAAAAATAGCCTACAAATTCTGAACTCTG −Cy3−3′
YCF3−NH_2	5′-NH_2-(C6)- GCTGCATTTTCCAATTTCAGGATAAGT-TCTTCGTCTAATATAACTGTAGTGGTTCTGAA-3′
Cy3-YCF3−NH_2	5′-NH_2-(C6)- GCTGCATTTTCCAATTTCAGGATAAGT-TCTTCGTCTAATATAACTGTAGTGGTTCTGAA-Cy3−3′

polymer might also enhance the binding and hybridization of polynucleotides on microarrays, due to its electrostatic character and three-dimensional structure. Here we describe a method of conjugating polyethylenimine onto glass microarray surfaces. The method involves cyanuric chloride, a multifunctional cross-linking agent that provides residual electrophilic activity for reaction with deposited polynucleotides.

MATERIALS AND METHODS

Unless noted otherwise, all glass chemistry was conducted in a particle-free fume hood configured for HEPA filtration (Clean Air Products, Minneapolis, MN). Coated slides were stored desiccated at room temperature until used. Commercial poly-L-lysine coated glass slides were purchased from Sigma (Poly-Prep Slides, St. Louis, MO).

Preparation of Aminopropylsilanated Glass Slides (APS slides). Glass microscope slides (Corning, purchased from VWR Scientific, Part No. 48312-036) were cleaned in an ultrasonic bath (Branson Ultrasonics Corp., Danbury, CT) with 1% SDS followed by 4% aqueous hydrofluoric acid. The slides were then dried in an oven at 110 °C. After cooling to room temperature in the hood, the slides were immersed in a solution of 3-aminopropyltrimethoxysilane (0.05% w/v in 95% ethanol, Aldrich, Milwaukee, WI), rinsed several times with 95% ethanol, and then cured in an oven at 110 °C.

Preparation of Cyanuric Chloride-Activated Slides (CC-slides). Aminopropylsilanated slides were immersed in a stirred slurry of cyanuric chloride (12.7 g, Aldrich, Milwaukee, WI) and sodium carbonate (25 g) in *n*-hexane (1 L) at 4 °C for 1 h. The slides were then rinsed with *n*-hexane in an ultrasonic bath and air-dried.

Reaction of Cyanuric Chloride-Activated Slides with Polyethylenimine (PEI-slides). CC-slides were immersed in a stirred 0.1% aqueous solution of polyethylenimine (Aldrich Lot No. 40.872-7, average M_n ca. 10000 (GPC), average Mw ca. 25000 (LS), branched polymer) at 4 °C for 1 h with ultrasonication. The slides were then rinsed several times in deionized water with ultrasonication and air-dried.

Second Reaction of Polyethylenimine-Coated Slides with Cyanuric Chloride (P-slides). PEI-slides were reacted a second time with cyanuric chloride as described above (CC-slides) to cross-link the polyethylene polymers on the surface and to provide residual electrophiles for reaction with spotted analytes. After rinsing with *n*-hexane, these slides were further rinsed with acetone before air-drying.

FTIR-ATR Spectroscopy. The chemically modified slides were analyzed on a Nexus Model 470 instrument to confirm coating compositions (Nicolet Instrument Corp.).

Dynamic Contact Angle Measurements. Surface wetability and surface roughness were measured using a Model DCA315 dynamic contact angle analyzer (Cahn Instruments, Inc., CA). Each value reported represents the average of six independent measurements over a 2.5-cm × 3.5-cm area with an advancing speed of 80 μm/s. Distilled water and methylene iodide were used as test liquids with a two-parameter surface energy model[12] to isolate the London dispersion (d) and Keesom polar (p) contributions to the solid vapor surface tension, γ_s.

$$\gamma_s = \gamma_s^{\,d} + \gamma_s^{\,p}$$

The method of analyzing contact angle data according to the above surface energy model has been described by Kaelble (*13*).

$$(1 + \cos\theta_1)\gamma_1 = 2\,[(\gamma_1^{\,d}\,\gamma_s^{\,d})^{1/2} + (\gamma_1^{\,p}\,\gamma_s^{\,p})^{1/2}]$$

$$(1 + \cos\theta_2)\gamma_2 = 2[(\gamma_2^{\,d}\,\gamma_s^{\,d})^{1/2} + (\gamma_2^{\,p}\,\gamma_s^{\,p})^{1/2}]$$

In the case of water and methylene iodide, the solid vapor surface tension parameters have already been described: $\gamma_{water}{}^{d} = 22.1$, $\gamma_{water}{}^{p} = 50.7$ erg/cm^2; for methylene iodide $\gamma_{CH_2I_2}{}^{d} = 44.1$, $\gamma_{CH_2I_2}{}^{p} = 6.7$ erg/cm^2 (*14*). The slides were first assayed in distilled water, dried overnight in a dust-free fume hood, and then analyzed in methylene iodide.

Fluorescent Probe for Reactive Cyanuric Chloride Residues. An amino-reactive fluorescent dye was prepared to probe the various glass coatings containing reactive cyanuric chloride residues. FluoroLink Cy3 monofunctional dye (Amersham-Pharmacia Biotech) was reacted with a 5-fold molar excess of 1,7-diaminoheptane (Aldrich Chemical Co., Milwaukee, WI) to generate an amino-reactive fluorescent probe for surface characterization. Slides were reacted with an aqueous solution of the resulting dye mixture (1 μM final concentration of Cy3 dye) for 30 min at room temperature, washed sequentially with 0.1 N NaOH, 0.2% SDS, and deionized water, and then spun dry. Samples of "capped" surfaces containing cyanuric chloride residues were pretreated with 1,7-diaminohexane (1 mM in distilled water overnight at room temperature) before reaction with the fluorescent dye reagent.

Polynucleotide Reagents. Synthetic 59-mer polynucleotides modified with primary alkylamino moieties and/or cyanine dyes were purchased from Operon Technologies (Alameda, CA, YCF115 sequences, see Table 1) and TriLink Biotechnologies (San Diego, CA, YCF3 sequences, see Table 1). Each polynucleotide targets an inter-ORF region of *S. cerevisiae*. The regions selected are approximately 1000 bp in length and contain minimal sequence homology against any known expressed human gene sequence. Polynucleotide concentrations were determined by absorbance spectroscopy using a molar

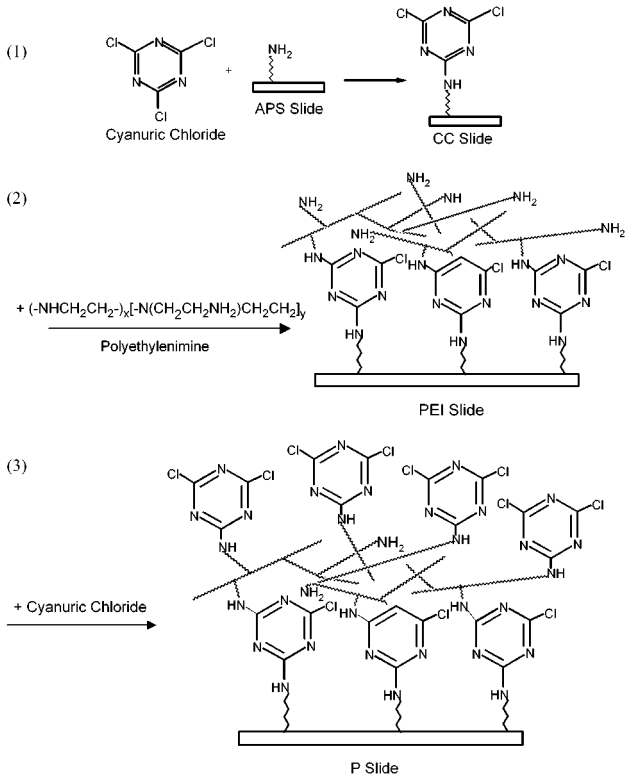


Figure 1. Schemes for the synthesis of APS, CC, PEI, and P glass surface coatings.

extinction coefficient (260 nm) of 5.7×10^5 $M^{-1}cm^{-1}$. Stock solutions were prepared in 2X SSC buffer (300 mM NaCl, 30 mM sodium citrate, pH 7.0).

Microarray Fabrication and Polynucleotide Binding. A dilution series of each polynucleotide (containing 10-mol % of the corresponding Cy3-labeled polynucleotide as an internal standard) was prepared in 4-fold replication in microtiter plates. All dilutions were made in 2X SSC buffer (2.5−20 μM final concentrations). Microarraying was performed in the Incyte Genomics microarray facility (80−100 μm spots at 180-μm spacing, center to center). For postprocessing, the slides were rinsed in 0.2% SDS for 2 min followed by three 1 min rinses in deionized water. Next, they were treated with 0.2% I-Block reagent (Tropix, Bedford, MA) in 1X Dulbecco's phosphate-buffered saline (Life Technologies, Gaithersburg, MD) at 60 °C for 30 min. Finally, they were washed again in 0.2% SDS and water as described above. These microarrays were analyzed for Cy3-dye fluorescence (see below) to determine percent bound polynucleotide = (avg. Cy3 fluorescent counts after washing)/(avg. Cy3 fluorescent counts post-arraying) × 100.

Table 2. Dynamic Contact Angle Measurements for Chemically Modified Glass Slides[a]

surface	θ_{H_2O}	$\theta_{CH_2I_2}$	γ^d(erg/cm^2)	γ^p(erg/cm^2)	γ(erg/cm^2)
APS slides	72.5	40.2	33.7	7.5	41.2
CC slides	87.2	37.7	38.5	1.4	39.9
PEI slides	62.8	32.0	35.7	11.6	47.4
P slides	72.0	37.0	35.2	7.3	42.5

[a] The standard deviations for θ_{H_2O} and $\theta_{CH_2I_2}$ were less than 2° and 1°, respectively.

Preparation of Inter-ORF *S. cerevisiae* RNA Transcripts for Probe Generation. T7 RNA transcripts were generated from PCR-amplified yeast templates by incorporating a T7 promoter sequence in the upstream PCR primer and a polyA sequence in the downstream PCR primer. The resulting in vitro RNA transcripts were then purified, quantified, and included in every probe labeling reaction at specified inputs (see below).

Probe Labeling and Hybridization. Synthetic yeast RNA transcripts corresponding to target polynucleotides (1 ng) were added to complex human placenta mRNA (200 ng, Biochain Institute, Hayward, CA) and then fluorescently labeled by reverse-transcription with cyanine-5 (Cy5) fluorescent dye (GEMbright labeling kit, Incyte Genomics) as previously described (*6*). The resulting Cy5-labeled cDNA probes were purified by size exclusion chromatography (TE-30 column, Clontech, Palo Alto, CA), ethanol-precipitated, and then resuspended in 24 μL of hybridization buffer (5X SSC, 0.2% SDS, 1 mM DTT).

The resuspended fluorescent cDNA probes were applied to the microarrays under 22 × 22 mm glass cover slips, placed in sealed chambers to prevent evaporation, and then incubated at 60 °C for 6 h. After hybridization, the microarrays were washed in 0.1X SSC/1 mM DTT at 45 °C for 10 min.

Scanning and Data Analysis. The microarrays were scanned at 532 nm (cyanine-3) and 635 nm (cyanine-5) using a dual-laser confocal fluorescence scanner (Axon Instruments, Foster City, CA) at 10 μm resolution. These signals were collected with 16-bits-per-pixel resolution. In the case of nonarrayed slides treated with amino-reactive Cy3-dye reagent, the images were analyzed with

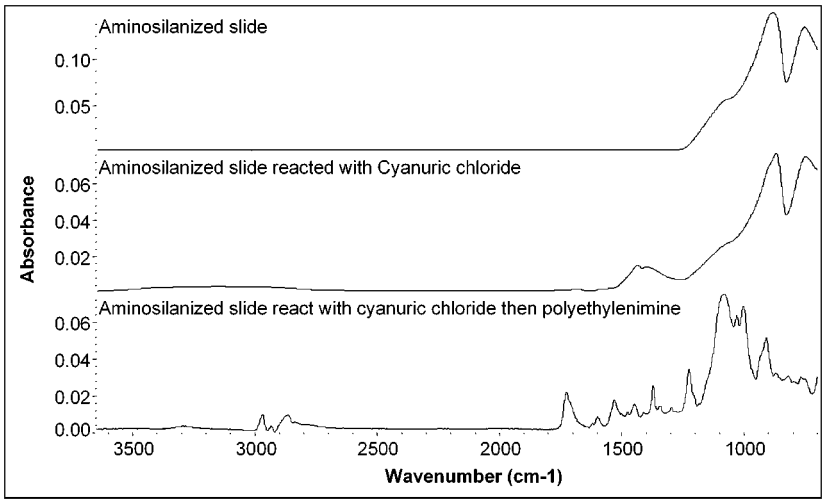


Figure 2. FTIR spectra for APS, CC, and PEI surface coatings.

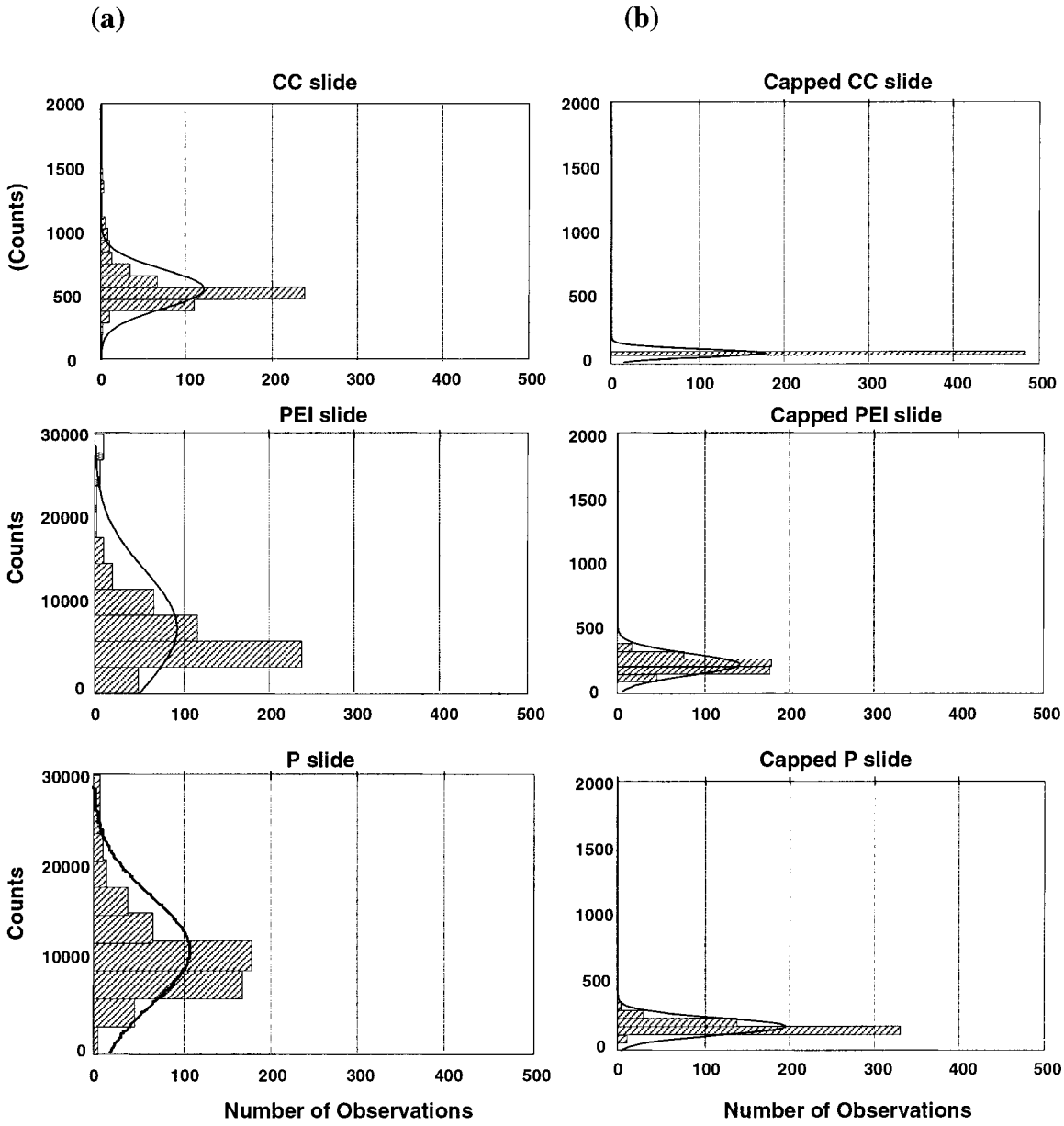


Figure 3. Histograms of scanned surface fluorescence intensities for chemically modified glass slides after treatment with an aminoreactive fluorescent dye, Cyanine-3. (a) Uncapped slides. (b) Capped slides.

GenePix software provided by the manufacturer. To monitor polynucleotide binding (Cy3 channel) and hybridization (Cy5 channel), the images were analyzed with GEMTools image analysis software (Incyte Genomics) to provide corrected signal intensities including local background subtraction. Tab-delineated text files were exported from GEMTools for graphical analysis using Microsoft Excel software. Reported signals are the average of 160 data points (80 spots per slide × 2 slides per assay). Error bars are one standard deviation from the mean.

RESULTS

Synthesis and Characterization of Glass Coatings. Figure 1 summarizes the steps used to prepare the two- and three-dimensional surface coatings described in this study. Each step was monitored by FTIR spectroscopy to confirm chemical modification (Figure 2). FTIR spectra were unchanged before and after treatment of the glass slides with aminopropyltrimethoxysilane, indicating that the thickness of this layer was below the detection limit of the instrument (i.e., less than about 1 μm). However, resonance in the range of ~1260 to 1540 cm^{-1} could be detected after treatment with cyanuric chloride (CC slides), indicative of 1,3,5-triazine ring stretching. Further reaction with polyethylenimine (PEI slides) resulted in a number of new resonances detected, including peaks at 2864 and 2975 cm^{-1} that are indicative of $-CH_2-$ stretching.

Surface wetability, commonly defined as the contact angle resulting when a liquid spot contacts a surface, was measured after each of the treatment steps using dynamic contact angle analysis (see Materials and Methods). The application of two different solvents of widely different known polarities (water and methylene iodide) enabled determinations of surface energy for each surface (Table 2). The observed increase in γ^d and decrease in γ^p after treatment with cyanuric chloride (CC slides) is consistent with a decrease in the polar nature of the surface. After reaction with polyethylenimine (PEI slides), γ^d decreased slightly and γ^p increased dramatically, consistent with an increase in surface polarity. Further

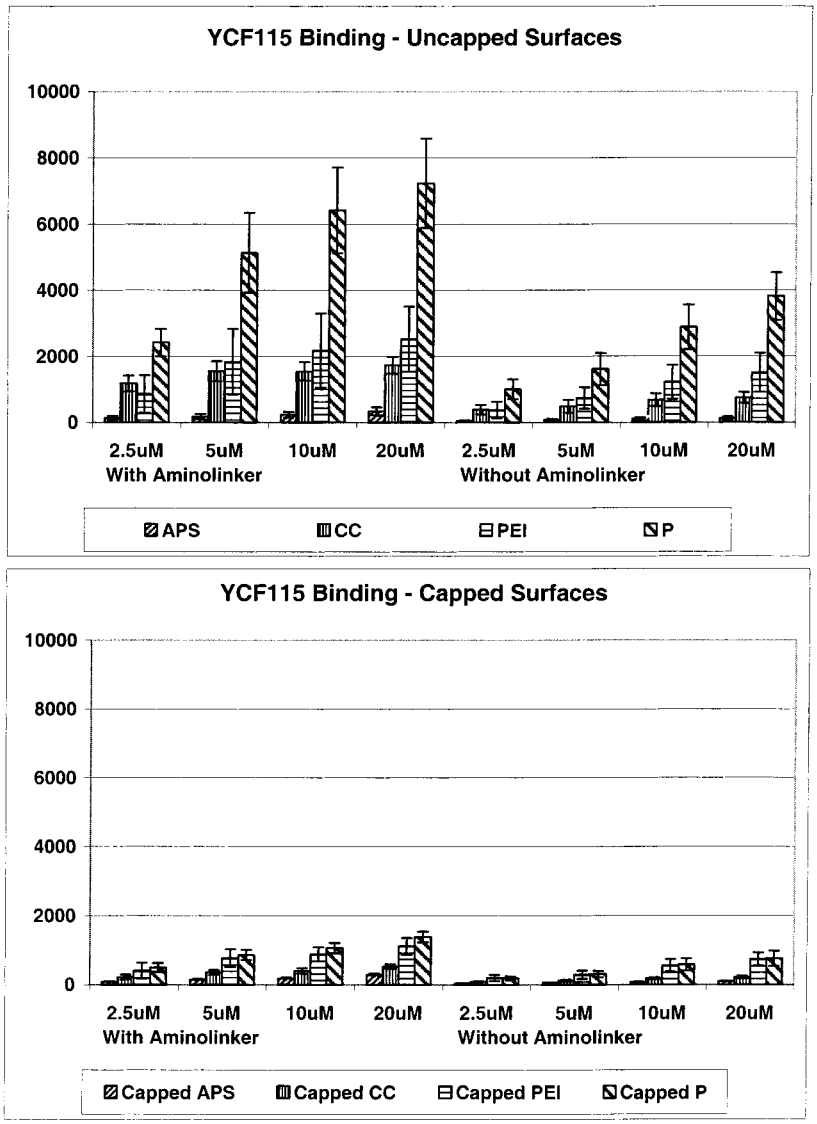


Figure 4. Averaged fluorescent binding signals (Cy3) for spotted polynucleotides after washing. Polynucleotides used in this experiment had the sequence designation "YCF115" (see Table 1). (a) Uncapped slides. (b) Capped slides.

reaction with cyanuric chloride (P slides) decreases γ^p and leaves γ^d essentially unchanged, indicating that a majority of amino moieties exposed to solvent are unreacted with cyanuric chloride.

The availability of reactive electrophiles on each glass coating was probed with an amino-reactive Cy3 fluorescent dye. Capped slides that had been pretreated with 1,7-diaminoheptane were included in this experiment for comparison (see Materials and Methods). Histograms of the resulting fluorescent signals before and after capping are shown in Figures 3a and 3b, respectively. In each case, the fluorescent signals from capped slides were significantly reduced, demonstrating that the capping reaction was greater than 97% efficient. In the absence of capping, CC slides showed considerably less fluorescence than P slides, consistent with their respective two- and three-dimensional surface characteristics. P slides were more fluorescent than PEI slides as expected based on their additional treatment with cyanuric chloride. However, the data indicates that PEI slides retain considerable electrophilic activity (presumably due to residual mono- and bis-functional cyanuric chloride residues at the interface between APS and polyethylenimine layers).

Covalent Contribution to Surface Binding. To assess the contribution of reactive cyanuric chloride residues to polynucleotide binding, samples of CC, PEI, and P slides were pretreated with 1,7-diaminoheptane ("capped") prior to arraying, as described in the previous section. The contribution of covalent reaction chemistry to polynucleotide binding can be inferred by comparing data from uncapped and capped slides, respectively. Polynucleotides with and without alkylamino modification were included in this assessment (see Table 1). The averaged polynucleotide binding signals (Cy3-channel) are summarized in Figure 4. As predicted, the covalent binding contribution was higher for the three-dimensional surfaces (PEI and P) compared to the two-dimensional CC surface. P slides showed the highest covalent contribution, indicating that reactive cyanuric chloride residues are readily accessible to spotted polynucleotides. PEI slides showed a lower covalent contribution, suggesting that cyanuric chloride residues are less accessible on this coating. It is interesting to note that some covalent contribution can also be attributed to the unmodified polynucleotide (i.e., no alkylamino linker). This indicates that other nucleophilic groups of the polynucleotide are also able to react with cyanuric

Table 3. Relative Percentages of Deposited Polynucleotide[a]

	APS, %	CC, %	PEI, %	P, %
2.5 μM	4.1	20	30	35
5.0 μM	2.7	17	26	29
10 μM	2.1	12	18	21
20 μM	2.0	9	13	16

[a] Based on averaged Cy3 signals pre- and postwashing.

chloride residues. The data from unmodified polynucleotide bound to the capped surfaces provides a relative measure of noncovalent binding (Figure 4b). In this case, the P and PEI slides performed similarly, and both showed increased binding relative to the CC and APS surfaces. These data indicates that P and PEI slides bind spotted polynucleotides through a combination of covalent and noncovalent interactions. Overall, the relative ranking for polynucleotide binding was P > PEI > CC > APS.

Relationship between Polynucleotide Binding and Hybridization. A two-color format was employed to monitor polynucleotide binding and probe hybridization in Cy3 and Cy5 channels, respectively. In this case, the slides were scanned pre- and postwashing. The percentages of deposited polynucleotide retained on each surface are summarized in Table 3. As in the previous experiment, the relative ranking was P > PEI > CC > APS. In each case, the amounts of bound polynucleotide increased with their prearrayed concentrations. However, the percentages of retained polynucleotide decreased at higher concentrations (Table 3). As observed in the previous experiment, the two-dimensional surfaces (APS and CC) showed lower binding efficiencies over the concentration range investigated, whereas the three-dimensional surfaces (PEI and P) showed higher binding efficiencies (up to 35% in the case of P slides).

The microarrayed slides were then hybridized to a complementary RNA transcript in the presence of a complex RNA background (human placenta mRNA) to provide a relative measure of their binding and hybridization efficiencies. For comparison purposes, commercial poly-L-lysine-coated glass slides were included in this experiment. The averaged binding (Cy3) and hybridization (Cy5) signals are summarized in Figure 5. In general, the hybridization signals showed a good correlation with the binding signals, although they appeared to plateau above 10 μM arrayed polynucleotide in the case of the P surface (Figure 5b).

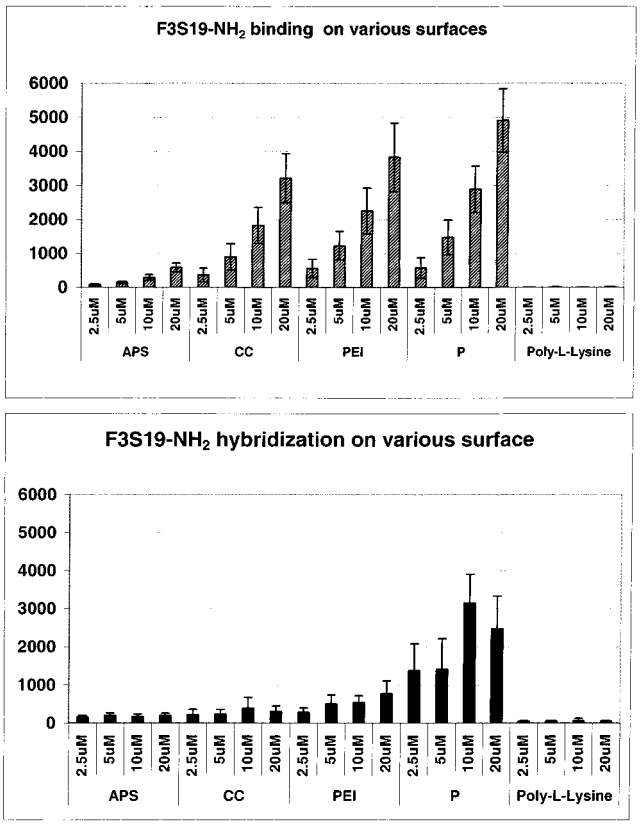


Figure 5. Comparison of averaged binding (Cy3) and hybridization (Cy5) signals for various chemically modified glass slides. Only polynucleotides modified with alkylamino linkers were used in this experiment. These polynucleotides had the sequence designation "YCF3" (see Table 1). (a) Binding signals (Cy3). (b) Hybridization signals (Cy5).

CONCLUSIONS

The results presented in this study demonstrate that glass coatings containing polyethylenimine provide enhanced binding of spotted polynucleotides. In particular, the P coating provided the best overall binding and hybridization performance. A number of other binding chemistries have been investigated in our laboratory, both on two-dimensional APS coatings and three-dimensional polyethylenimine coatings (data now shown). These include surface derivatization with reactive alkyl and aryl esters, aldehydes, and isothiocyanates, as have been described elsewhere (*15*−*17*). In practice, cyanuric chloride has provided the best and most consistent binding results.

The commercial polylysine surface showed low binding and hybridization efficiency according to our experimental conditions. It is possible that alternative conditions could improve the binding performance of this surface (i.e., different array buffers, wash conditions, etc.), but this possibility was not explored in detail.

In summary, a glass coating comprising polyethylenimine and reactive cyanuric chloride residues has been developed for the production of spotted polynucleotide microarrays. This surface binds polynucleotides through a combination of covalent and noncovalent interactions. The application of this surface to the production of polynucleotide microarrays is currently being investigated in our laboratory. Polynucleotide microarrays generated with this coating have discriminated gene transcripts sharing up to about 80% sequence identity (human cytochrome P-450 family, M. A. Reynolds, unpublished results). Preliminary studies with microarrays targeting human gene transcripts demonstrate comparable specificity and sensitivity to our commercial cDNA platform for gene expression profiling (Z. Modrusan, manuscript in preparation).

ACKNOWLEDGMENT

We thank Scott Braxton and Tod Bedilion for early contributions to this work. We also thank Rick Johnston, Scott Winder, and Sang Park for guidance and assistance with surface analyses.

LITERATURE CITED

(1) Ramsay, G. (1998) DNA chips: state-of-the art. *Nature Biotechnol. 16*, 40−44.

(2) MacBeath, G., and Schreiber, S. L. (2000) Printing proteins as microarrays for high-throughput function determination. *Science 289*, 1760−1763.

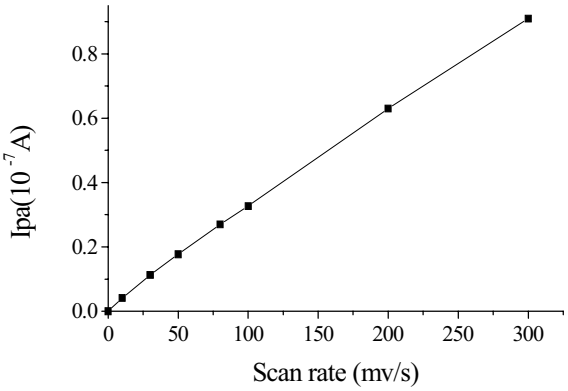
(3) Manduchi, E., Grant, G. R., McKenzie, S. E., Overton, G. C., Surrey, S., and Stoeckert, C. J., Jr. (2000) Generation of

patterns from gene expression data by assigning confidence to differentially expressed genes. *Bioinformatics 16*, 685−698.
(4) Hughes, T. R., Marton, M. J., Jones, A. R., Roberts, C. J., Stoughton, R., Armour, C. D., Bennett, H. A., Coffey, E., Dai, H., He, Y. D., Kidd, M. J., King, A. M., Meyer, M. R., Slade, D., Lum, P. Y., Stepaniants, S. B., Shoemaker, D. D., Gachotte, D., Chakraburtty, K., Simon, J., Bard, M., and Friend, S. H. (2000) Functional discovery via a compendium of expression profiles. *Cell 102*, 109−126.
(5) Evertsz, E., Starink, P., Gupta, R., and Watson, D. (2000) Technology and Applications of Gene Expression Microarrays. *Microarray Biochip Technology* (M. Schena, Ed.) pp 149−166, BioTechniques Books Division, Natick, MA.
(6) Yue, H., Eastman, P. S., Wang, B. B., Minor, J., Doctolero, M. H., Nuttall, R. L., Stack, R., Becker, J. W., Montgomery, J. R., Vainer, M. and Johnston, R. (2001) An evaluation of the performance of cDNA microarrays for detecting changes in global mRNA expression. *Nucleic Acids Res. 29*, E41.
(7) Guschin, D., Yershov, G., Zaslavsky, A., Gemmell, A., Shick, V., Proudnikov, D., Arenkov, P. and Mirzabekov, A. (1997) Manual manufacturing of oligonucleotide, DNA, and protein microchips. *Anal.,Biochem. 250*, 203−211.
(8) Vasiliskov, A. V., Timofeev, E. N., Surzhikov, S. A., Drobyshev, A. L., Shick, V. V., and Mirzabekov, A. D. (1999) Fabrication of microarray of gel-immobilized compounds on a chip by copolymerization. *Biotechniques 27*, 592.
(9) Beier, M., and Hoheisel, J. D. (1999) Versatile derivatisation of solid support media for covalent bonding on DNA-microchips. *Nucleic Acids Res. 27*, 1970−1977.
(10) Lawson, T. G., Regnier, F. E., and Weith, H. L. (1983) Separation of synthetic oligonucleotides on columns of microparticulate silica coated with cross-linked polyethylene imine. *Anal. Biochem. 133*, 85−93.
(11) Boussif, O., Lezoualc'h, F., Zanta, M. A., Mergny, M. D., Scherman, D., Demeniex, B., and Behr, J.-P. (1995) A versatile vector for gene and oligonucleotide transfer into cells in culture and in vivo: polyethyenimine. *Proc. Natl. Acad. Sci. U.S.A. 92*, 7297−7301.
(12) Cirlin, E. H., and Kaelble, D. H. (1973) Roughness and anisotropy effects on wettability of poly(tetrafluoroethylene) and sodium-treated poly(tetrafluoroethylene). *J. Polym. Sci., Polym. Phys. Ed. 11*, 785−799.
(13) Kaelble, D. H. (1971) *Physical Chemistry of Adhesion*, John Wiley & Sons, Inc., New York.
(14) Owens, D. K. (1969) Estimation of the surface energy of polymers. *J. Appl. Polym. Sci. 13*, 1741−1747.
(15) Guo, Z., Guilfoyle, R. A., Thiel, A. J., Wang, R., and Smith, L. M. (1994) Direct fluorescence analysis of genetic polymorphisms by hybridization with oligonucleotide arrays on glass supports. *Nucleic Acids Res. 22*, 5456−5465.
(16) Zammatteo, N., Jeanmart, L., Hamels, S., Courtois, S., Louette, P., Hevesi, L., and Remacle, J. (2000) Comparison between different strategies of covalent attachment of DNA to glass surfaces to build DNA microarrays. *Anal. Biochem. 280*, 143−150.
(17) Chrisey, L. A., Lee, G. U., and O'Ferrall, C. E. (1996) Covalent attachment of synthetic DNA to self-assembled monolayer films. *Nucleic Acids Res. 24*, 3031−3039.

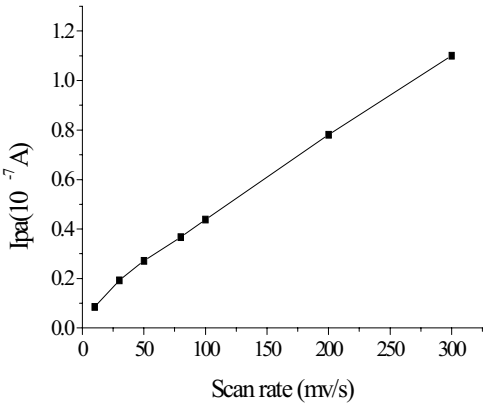
BC015523Q

Supporting information

1 Plots of Ip~V for HS-ODN modified electrodes. The peak current is directly proportional to the scan rate, which is a characteristic of a surface process

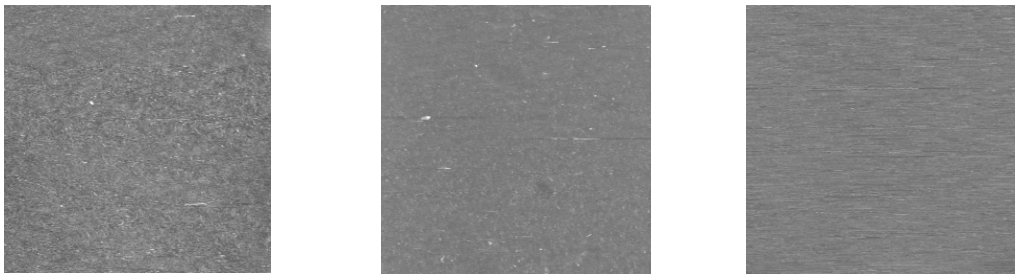


Plot of Ipa~V for HS-dsODN/Au in 20μM $Co(phen)_3^{3+/2+}$ 5mM KNO_3



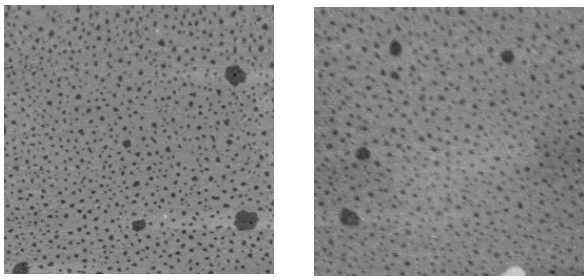
Plot of Ipa~V for HS-ssODN/Au in 20μM $Co(phen)_3^{3+/2+}$ 5mM KNO_3

2 EC-STM images of the bare gold surface and MCH on Au (111) surface. The images kept unchanged as the potential shifting from –300mV to 600mV. These control data could suggest that the changes of the HS-dsODN EC-STM images don't result from some type of potential dependent artifact.



A 200mV B -300mV C 600mV

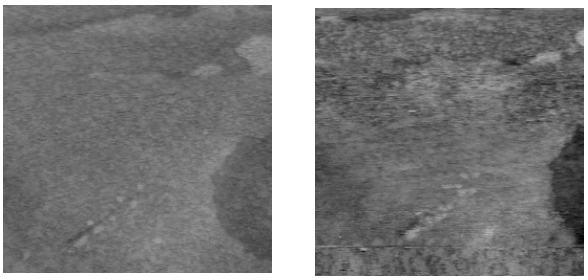
EC-STM images (150nm×150nm) of bare Au (111) at potentials of 200mV (A), -300mV (B) and 600mV (C) recorded in the solution of 10mMTE buffer containing 10 mMNaCl pH 7.4.



A –300mV B 600mV

EC-STM images (150nm×150nm) of MCH at potentials of -300mV(A) and 600mV(B) recorded in the solution of 10mMTE buffer containing 10 mMNaCl pH 7.4.

3 EC-STM images of HS-ssODN on Au (111) surface. No distinct changes in the surface structure of HS-ssODN were observed with the variation of applied potential.



A –300mV B 600mV

EC-STM images (100nm×100nm) of HS-ssODN on Au (111) surface at potentials of -300mV (A) and 600mV (B) recorded in the solution of 10mMTE buffer containing 10 mMNaCl pH 7.4.

Investigation of DNA Orientation on Gold by EC-STM

Zhi-Ling Zhang, Dai-Wen Pang,* and Rong-Ying Zhang

Department of Chemistry, Wuhan University, Wuhan 430072, P. R. China

Jia-Wei Yan and Bing-Wei Mao

State Key Laboratory for Physical Chemistry of Solid Surfaces, Xiamen University, Xiamen 361005

Yi-Peng Qi

Department of Virology, Wuhan University, Wuhan 430072, P. R. China . Received July 8, 2001; Revised Manuscript Received October 18, 2001

The immobilization of thiol-derivatized DNA on a Au (111) single crystal surface by self-assembly has been investigated by electrochemical scanning tunneling microscopy (EC-STM). Continuous potential-dependent orientation changes of double-stranded oligodeoxynucleotides (ODN) have been observed in a certain potential range from 200 to 600 mV (versus SCE). It is suggested that the DNA duplexes stand straight on the gold surface at potentials negative of the potential of zero charge (pzc) and then lay down on the surface when the potential shifts positively. These results are in agreement with the expectation based on the Coulombic interaction consideration between negatively charged DNA helices and gold surface. As the applied potential shifts positively, the surface charge changes from negative to positive, that is, the Coulombic force between negatively charged DNA helices and gold surfaces changes from repulsion to attraction. However, for the single-stranded oligodeoxynucleotides, no distinct changes in the surface structure were observed with the applied potential.

INTRODUCTION

The immobilization of DNA is of great importance for the investigation of interaction between DNA and other molecules by surface-based methods, as well as for DNA biosensors (including genochips) with potential use in disease diagnosis and genome sequencing. Many researchers have highlighted the immobilization and characterization of DNA on surfaces. Numerous methods, including X-ray photoelectron spectroscopy (XPS) (*1*, *2*), ellipsometry (*1*), electrochemical method (*3*−*5*), neutron reflectivity (*6*), surface plasmon resonance (SPR) (*5*, *7*), Raman spectroscopy (*8*), and STM (*8*) have been used to study this highlighted topic. However various fundamental and underlying problems, such as the relationship between structure and orientation of surface-anchored DNA and their biological affinity, the relation between the microenvironment on the electrode surface, and the behavior of DNA-modified electrodes, still remain as open questions. The imaging of DNA immobilized on the surface, which could provide detailed and direct recognition of the structure and orientation of the immobilized DNA, has explored very little. By using scanning probe microscopy (SPM), this goal can be achieved. Scanning tunneling microscopy (STM) (*9*−*16*) and atom force microscopy (AFM) (*17*−*21*) have been used for investigation of the DNA structure. These techniques can, in principle, reach atomic resolution and can be operated under the natural conditions, for instance, in aqueous solution and at ambient temperature and pressure, under which conditions the biomolecules behave naturally.

Barton and co-workers investigated the applied potential effect on the orientation of self-assembled DNA helices on gold by electrochemical in-situ atom force microscopy (EC-AFM) (*21*). They found that the monolayer height varied with the applied potential, but no clear and detailed image of the DNA monolayer was acquired.

We report herein the immobilization of thiol-derivatized oligodeoxynucleotides (HS-ODN) containing 15 base pairs on gold via self-assembly and the direct EC-STM observation of ODN monolayer on Au (111) surface. It was found that the STM images of double-stranded oligodeoxynucleotides changed with the applied potential, and the results seemed to agree with electrostatic interaction between negatively charged ODN helices and gold surface. However, perhaps due to their poor rigidity, the images of single-stranded oligodeoxynucleotides were not very clear and seemed not to change with applied potential.

EXPERIMENTAL PROCEDURES

Materials. All solutions were prepared with deionized water (≥18MΩ·cm) from a Millipore MilliQ system. Oligodeoxynucleotides were purchased from Shanghai Sangon Biotechnical Co. Ltd. and used without further purification. A sequence of 5′-TGT ACA GTC ATC GGG-3′ had a 6-mercaptohexyl linker at the 5′-terminus, the control sample had the same sequence but no 6-mercaptohexyl linker contained, and the complementary strand was 5′-CCC GAT GAC TGT ACA-3′. All oligodeoxynucleotides were dissolved in 10 mM pH 7.4 Tris-HCl buffer containing 1 mM EDTA (TE buffer). Double-stranded oligodeoxynucleotides were prepared through hybridization before immobilized on gold surfaces. Hybridization

* Corresponding author Tel: +86-027-87686380; Fax: +86-027-87882661; e-mail: dwpang@whu.edu.cn.

10.1021/bc0155263 CCC: $22.00 © 2002 American Chemical Society
Published on Web 12/13/2001

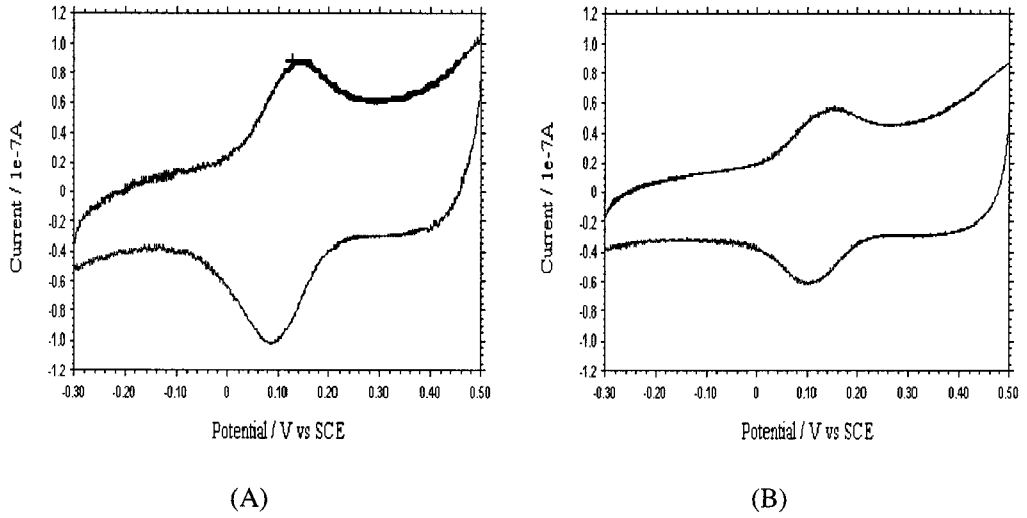


Figure 1. Cyclic voltammograms of 20 μM $Co(phen)_3^{3+/2+}$ on (A) HS-dsODN/Au and (B) HS-ssODN/Au electrodes in 5mM KNO_3; scan rate, 100 mV/s.

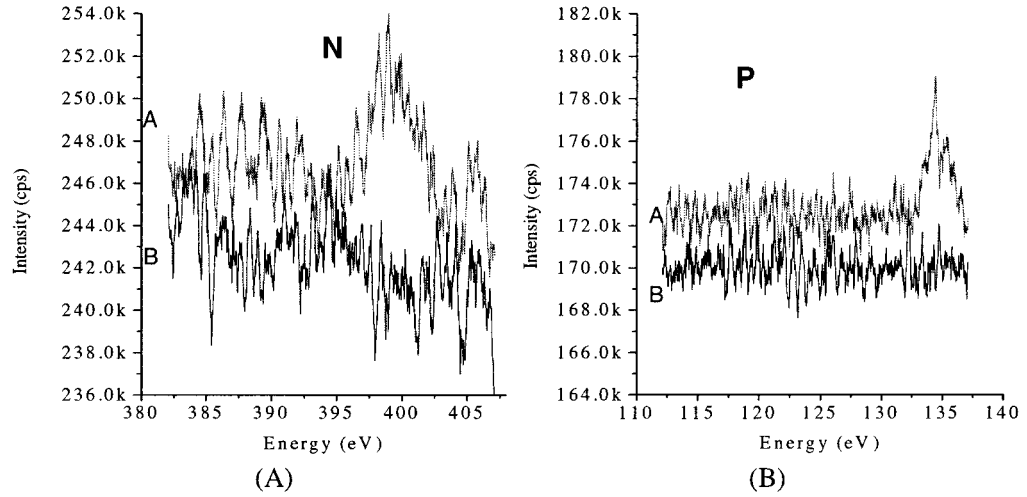


Figure 2. XPS N1s and P2p spectra of (A) thiol-derivatized (HS-dsODN) and (B) non-thiol-derivatized (dsODN) dsODN.

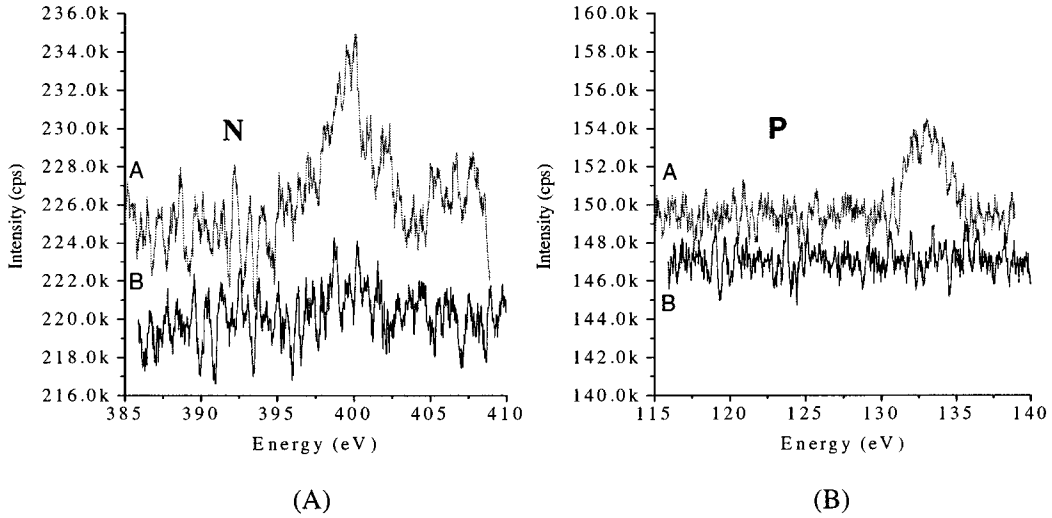


Figure 3. XPS N1s and P2p spectra of (A) thiol-derivatized (HS-ssODN) and (B) non-thiol-derivatized (ssODN) ssODN.

was performed at 37 °C for 120 min in TE buffer (pH 7.4) containing 0.5 M NaCl.

Preparation of the DNA-Modified Gold Electrodes. A flame-annealed Au (111) surface for EC-STM measurements prepared as reported previously (*8*) or a pretreated gold electrode for cyclic voltammetry (CV) had been immersed in 8.1 μM thiol-derivatized oligodeoxynucleotide (pH 7.4 TE buffer, 0.5 M NaCl) (HS-ODN) for 12 h at 4 °C, followed by a thorough rinse with deionized water to remove unbound ODN; thus, an electrode modified with a self-assembled monolayer of ODN obtained. The concentration of oligodeoxynucleotides in XPS

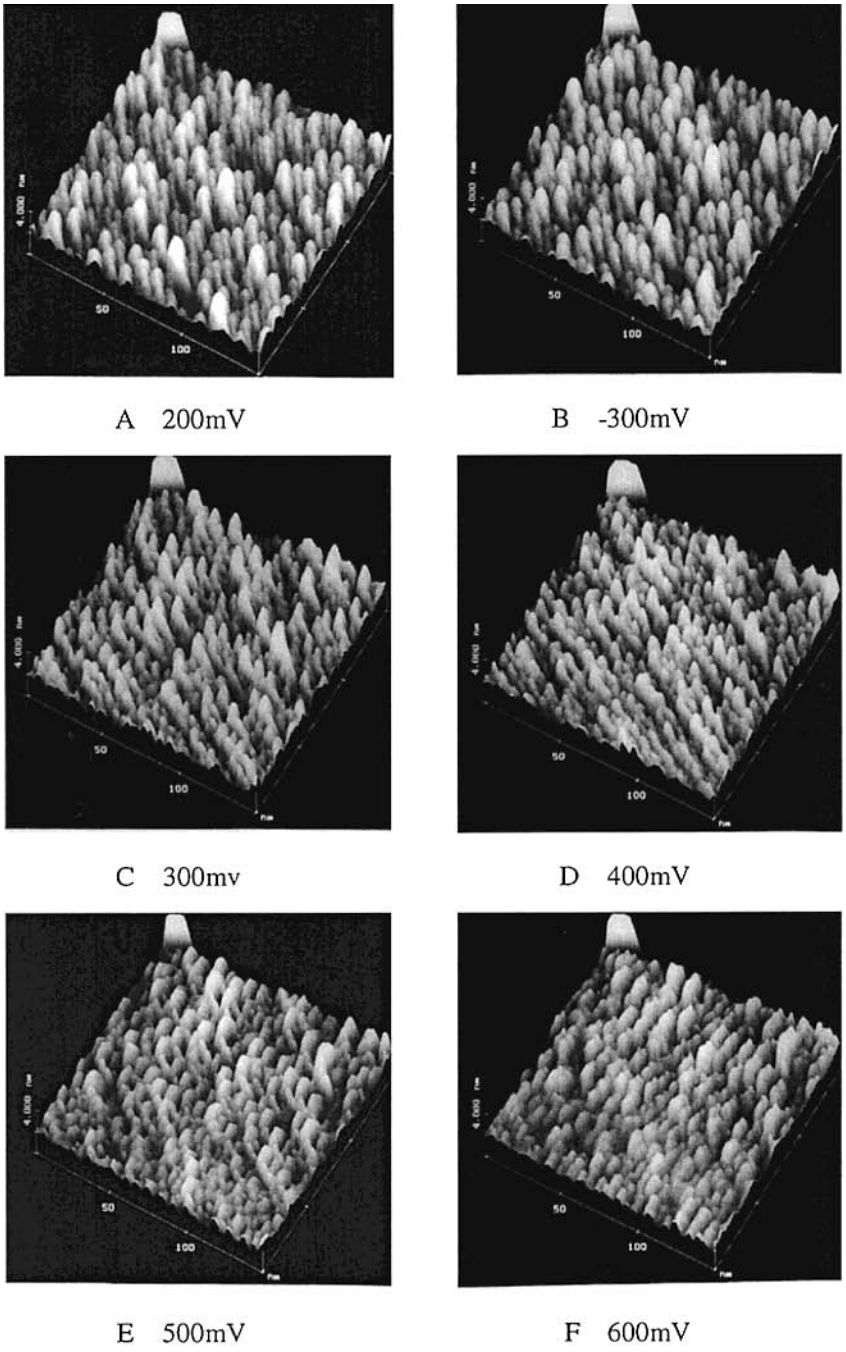


Figure 4. EC-STM 3D images (150 nm × 150 nm) of HS-dsODN on Au (111) recorded in the solution of 10 mM TE buffer containing 10 mM NaCl pH 7.4 at various potentials, (A) 200 mV, (B) −300 mV, (C) 300 mV, (D) 400 mV, (E) 500 mV, (F) 600 mV.

measurements was 2 μM. The preparation of the control electrode followed the same procedure described above except for the control sample of ODN used instead.

Instrumentation. All STM images were acquired on a Naonscope IIIa (Digital Instruments) operated under the constant current mode with an electrochemically etched tungsten tip coated with polymethylstyrene. Monatomic height steps of bare gold surfaces in air were observed clearly under the conditions used. EC-STM images were recorded in the solution of TE buffer containing 10 mM NaCl with a tunneling current of 3 nA over the potential range of −300 to +600 mV (versus SCE). The potential was first decreased with an interval of 100 from 200 to −300 mV and then gradually back to 600 mV.

XPS experiments were conducted on a VG ESCA-LAB MKII spectrometer with Mg radiation. The data were processed with an XPS-AES sampling/processing program (Version 5.0, Tsinghua University). The radiation gun was operated at 11 KV and 20 mA; 25 scans were used, and the PE mode was used for the analyzer with 100 eV pass energy. The sensitivity factors of N and P are 0.42 and 0.39, respectively; all the XPS data discussed below are corrected with these sensitivity factors.

Cyclic voltammograms (CV) were recorded on a CHI 660A electrochemical workstation using a Pt wire and a SCE as the counter and the reference electrode, respectively. $Co(phen)_3^{3+/2+}$ (20 μM) was used as an electrochemical probe for ODN detection on gold. All solutions were deaerated with high purity nitrogen and kept under a nitrogen atmosphere throughout the electrohemical measurements. All reported potentials were against the SCE.

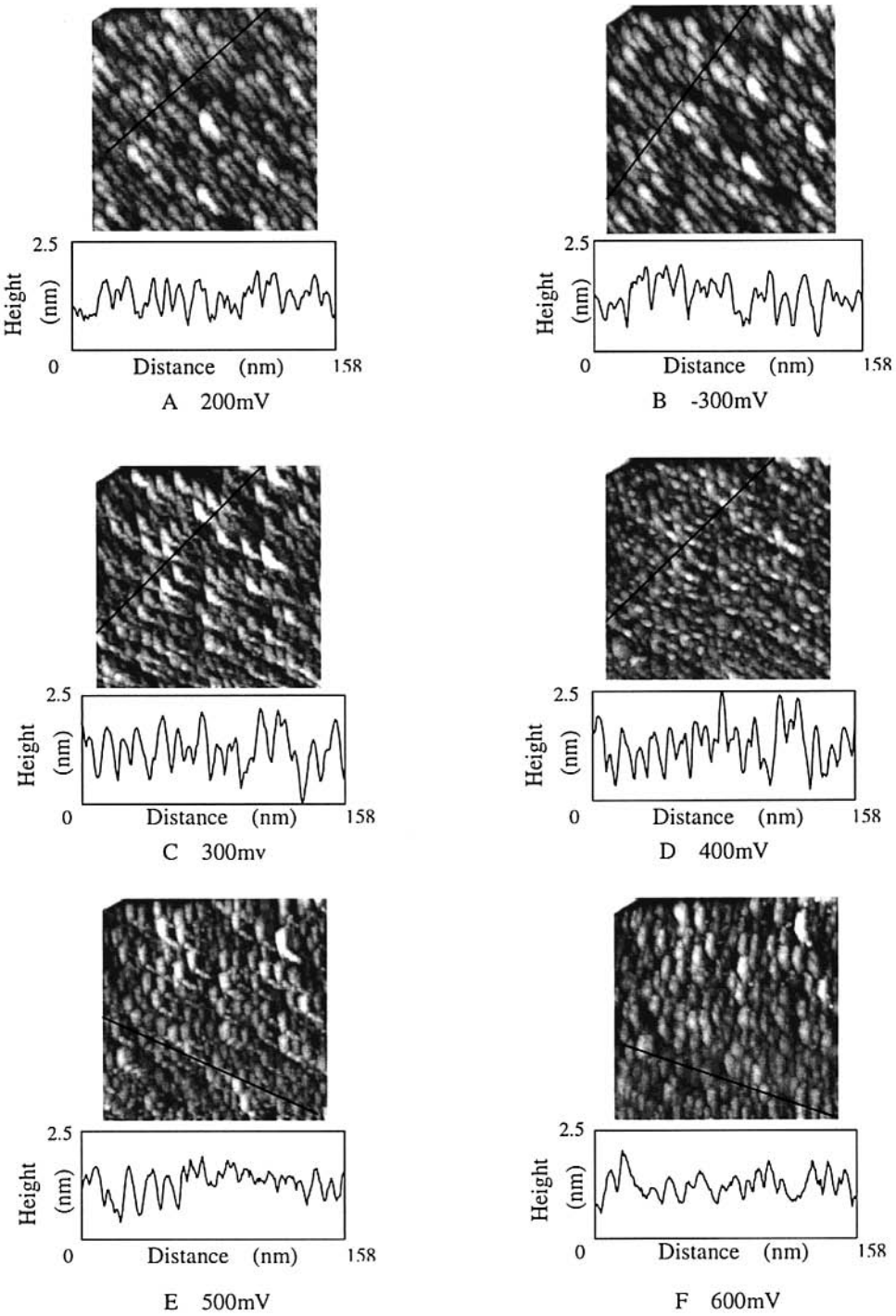


Figure 5. Cross-sectional profiles of dsODN EC-STM images at various potentials (A) 200 mV, (B) −300 mV, (C) 300 mV, (D) 400 mV, (E) 500 mV, (F) 600 mV.

RESULTS AND DISCUSSION

As demonstrated in our previous work (*4*), at the concentration used in the experiments, $Co(phen)_3^{3+/2+}$ had little electrochemical response at the bare gold electrode, but a pair of redox peaks was generated at an ODN-modified gold electrode, which resulted from the enrichment of $Co(phen)_3^{3+/2+}$ at the modified electrode because of the strong interaction between $Co(phen)_3^{3+/2+}$ and ODN (*22*, *23*). Therefore, the redox process can be used to verify whether the oligodeoxynucleotides were anchored on the gold surface or not. The cyclic voltammograms for $Co(phen)_3^{3+/2+}$ at HS-dsODN and HS-ssODN modified electrodes (denoted as HS-dsODN/Au and HS-ssODN/Au, respectively) are given in Figure 1. Evident peaks with a formal potential ($E^{0'}$) of 126 mV at HS-dsODN/Au or 116 mV at HS-ssODN/Au, as shown in Figure 1, suggest that ODNs have been immobilized on the electrode surfaces. The peak current is directly proportional to the scan rate, which is a characteristic of the surface process. The value of peak potential separation, ΔE_p, of 46 mV at HS-dsODN/Au or 53 mV at HS-ssODN at a scan rate of 100 mV/s also characterizes the surface process.

The N 1s (*1*) and P 2p (*8*) peaks in the XPS spectra can provide further reliable evidence for the immobilization of ODNs. The buffer solutions contained no phosphorus element, and there was no XPS-detectable nitrogen from bare gold surfaces exposed to buffer solutions. So we may conclude that any observed N 1s and P 2p

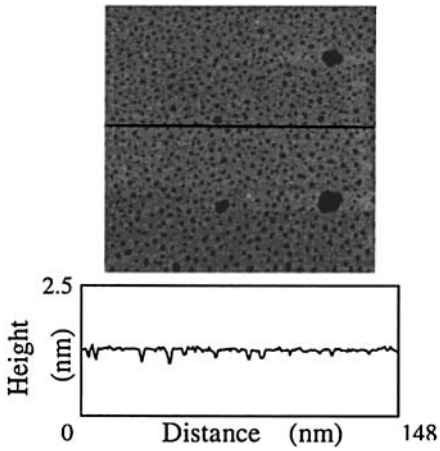


Figure 6. EC-STM image (150 nm × 150 nm) of MCH at potential of 200 mV recorded in the solution of 10 mM TE buffer containing 10 mM NaCl pH 7.4, and the cross-sectional profile. The images at other potential just keep unchanged (see Supporting Information).

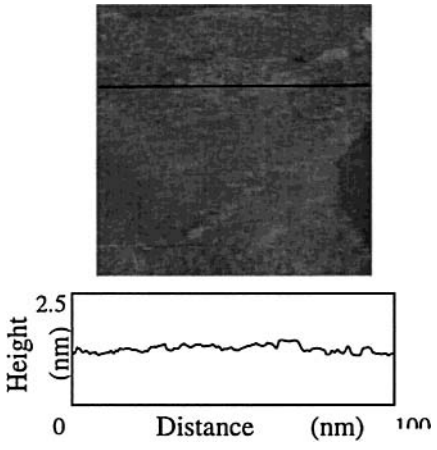


Figure 7. EC-STM image (100 nm × 100 nm) of HS-ssODN at potential of 200 mV recorded in the solution of 10 mMTE buffer containing 10 mMNaCl pH 7.4, and the cross-sectional profile.

signals originate exclusively from the nitrogen-containing bases and phosphate groups of ODN, respectively. In this case, the peak area ratio of N 1s to P 2p should be equal to the molar ratio of nitrogen to phosphorus in DNA. Figure 2 shows the XPS N1s and P2p data of the HS-dsODN/Au and the non-thiol-derivatized dsODN, which support that the HS-dsODN has been attached to the gold surface through the thiol−gold bond by self-assembly. There are very little XPS signals of the control samples, which indicates that nonspecific adsorption of ODN on gold surfaces can be ignored. The peak area ratio of N 1s to P 2p is 3.1, which is close to the value of 3.5 of molar nitrogen-to-phosphorus ratio of HS-dsODN. The XPS N1s and P2p spectra of the HS-ssODN and the non-thiol-derivatized ssODN are shown in Figure 3. The peak area ratio for HS-ssODN is 3.0, which is also close to its molar ratio of nitrogen to phosphorus.

The effect of the applied potential on the surface orientation of ODN was investigated by EC-STM. The image of uniformly and ordered structure of HS-dsODN on Au (111) at 200 mV (Figure 4a) indicates that the HS-dsODN stands straight up on the gold side by side with the thiol-end tethered on the gold and the other end floating in the buffer solution. This ordering may be a result of the electrostatic repulsion between the negatively charged deoxyribose-phosphate backbones of neighboring DNA helices. The cross-sectional profile indicated by a line on this image is shown in Figure 5a. The dsODN rods are measured to be 3 ± 1 nm in diameter, which is similar to that of B-form DNA helix reported by Watson and Crick (*24*). However, the height of dsODN rod measured is smaller than the expected height of 5.1 nm deduced from the 15 base-pair DNA helix structure. The apparent height difference between the measured and the expected is mainly due to the compact character of the dsODN monolayer. The HS-dsODN is perpendicular to the surface, which restricts both the precise measurement of the height of 15-base-pair dsODN and clear imaging of the dsODN helix structure. Moreover, the ends of dsODN helices tethering the surface seem to be interconnected as shown in the cross-sectional profile.

This orientation maintained when potential was decreased from 200 mV to −300 mV as shown in Figures 4a and 4b. To avoid hydrogen evolution, which would destroy the DNA monolayer, further decrease of potential was not attempted. Distinct change of the DNA helix orientation was observed, when potential was reversed to above 200 mV. The DNA helices start to tilt at 300 mV, and the tilted degree increases upon increasing the potential as shown in Figures 4c and 4d. As the applied potential was further increased to 500−600 mV, significant orientation changes were observed as can be seen in Figures 4e and 4f. The DNA helices no longer stand straight on but lie flat on the gold surface in this potential region. The cross-sectional profiles at different potentials are shown in Figure 5. The surface modified with the mercaptohexanol (MCH) exhibits the typical pinhole structure of thioalcohol self-assembly monolayer, instead of the ordered dsODN rod array on HS-dsODN modified gold surface. Moreover the image remained unchanged with varying potential as shown in Figure 6.

This potential dependent orientation change is attributed to the requirement of minimum electrostatic repulsion between the DNA and the gold surface. Both the density and polarity of electric charges on the gold electrode surface will change with the potential if the electrode is driven away from the potential of zero charge (pzc). According to the reference (*25*), the value of pzc on Au (111) is 0.258 V versus SCE. Since the gold surface is negatively charged at the potentials negative of the pzc, as mentioned by Barton (*20*), the negatively charged DNA helices orient themselves vertically to minimize the electrostatic repulsion with the gold surface. Nevertheless, the electrostatic repulsion becomes weaker as the potential shifts positively. It is expected that as the potential is increased across the pzc, the Coulombic interaction between DNA helices and gold surfaces changes from repulsive to attractive, which is favorable for the DNA duplexes leaning toward gold surface. Eventually, the DNA helices tend to lie flat on the surface in virtue of Coulombic attractive forces.

Figure 7 shows EC-STM images of HS-ssODN modified Au (111) at 200 mV. The gold surface exhibits an irregular configuration with the ssODN strands standing on the gold surface in a disorderly fashion. We believe that the difference in rigidity between dsODN and ssODN is mainly responsible for the distinctly different behaviors of the two DNA molecules on the surface. Both the rigidity of double-stranded ODN arising from Watson and Crick helix structure and the electrostatic repulsion between the DNA helices make the contribution in forming the regular arrangement. Since the single-stranded DNA cannot form stable and rigid helix structure, it is not surprising that ssODN does not form the ordered arrangement on the surface. Moreover, for its

poor rigidity, immobilized ssODN might dangle left and right along with the scrape of the tungsten tip. So the image of ssODN was blurred to some extent due to its irregular arrangement on gold surfaces, and no ssODN rod image as clear as dsODN could be obtained. No distinct changes in the surface structure of HS-ssODN were observed with the variation of applied potential, as shown in Supporting Information.

CONCLUSIONS

In summary, EC-STM has been applied to study the behaviors of dsODN and ssODN containing 15 base pairs tethered on Au (111) surface through self-assembly. It is found that dsODN changes its orientation on gold with the applied potential while ssODN does not. The electrostatic interaction between HS-dsODN and gold surface plays an important role for the orientation change of dsODN on gold. The results presented in this paper show that a uniform and compact dsODN monolayer can be formed readily on gold surfaces through self-assembly. The orientation of dsDNA on metal substrates can be controlled by the applied potential. Thus, an appropriate method to acquire desired DNA surface orientation has been developed.

ACKNOWLEDGMENT

This work was supported by the National Natural Science Foundation of China (Grant Nos. 29773034; 39770220), National Outstanding Young Investigator Fund (No. 20025311), and the State Key Laboratory for Physical Chemistry of Solid Surfaces (Xiamen University, Grant No. 9916). The authors also wish to thank Professor Zhong-Qun Tian, Professor Zhong-Hua Lin, Dr. Bin Ren, Professor Shui-Jiu Wang, Ms. Jing Tang, and Mr. Yi-An Chen for their kind help.

Supporting Information Available: Plots of Ip-V for HS-ODN modified electrodes. EC-STM images of the bare gold surface and MCH on Au (111) surface. EC-STM images of HS-ssODN on Au (111) surface. This material is available free of charge via the Internet at http://pubs.acs.org.

LITERATURE CITED

(1) Herne, T. M., and Tarlov, M. J. (1997) Characterization of DNA probes immobilized on gold surface. *J. Am. Chem. Soc. 119*, 8916−8920.

(2) Strother, T., Cai, W., Zhao, X. S, Hamers, R. J., and Smith, L. M. (2000) Synthesis and characterization of DNA-modified cilicon (111) surface. *J. Am. Chem. Soc. 122*, 1205−1209.

(3) Steel, A. B., Herne, T. M., and Tarlov, M. J. (1998) Electrochemical quantitation of DNA immobilized on gold. *Anal. Chem. 70*, 4670−4677.

(4) Pang, D. W., and Abruña, H. D. (1998) Micromethod for the investigation of the interactions between DNA and redox-active molecules. *Anal. Chem. 70*, 3160−3169.

(5) Yang, M. S., Yau, H. C. M., and Chan, H. L. (1998) Adsorption kinetics and ligand-binding properties of thiol-modified double-stranded DNA on a gold surface. *Langmuir 14*, 6121−6129.

(6) Levicky, R., Herne, T. M., Tarlov, M. J., and Satija, S. K. (1998) Using self-assembly to control the structure of DNA monolayers on gold: a neutron reflectivity study. *J. Am. Chem. Soc. 120*, 9787−9792.

(7) Peterlinz, K. A., Georgiadis, R. M., Herne, T. M., and Tarlov, M. J. (1997) Observation of hybridization and dehybridization of thiol-tethered DNA using two-color surface plasmon resonance spectroscopy. *J. Am. Chem. Soc. 119*, 3401−3402.

(8) Zhao, Y. D., Pang, D. W., Hu, S., Wang, Z. L., Cheng, J. K., Qi, Y. P., Dai, H. P., Mao, B. W., Tian, Z. Q., Luo, J., and Lin, Z. H. (1999) DNA-modified electrodes Part 3.: spectroscopic characterization of DNA modified gold electrodes. *Anal. Chim. Acta 388*, 93−101.

(9) Beebe, J. P., Wilson, T. E., Ogletree, D. F., Katz, J. E., Balhorn, R., Salmeron, M. B., and Siekhaus, W. J. (1989) Direct observation of native DNA structures with the scanning tunneling microscope. *Science 243*, 370−372.

(10) Lee, G., Arscott, P. G., Bloomfield, V. A., and Evans, D. F. (1989) Scanning tunneling microscopy of nucleic acids. *Science 244*, 475−477.

(11) Lindsay, S. M., Thundat, T., Nagahara, L., Knipping, U., and Rill, R. L. (1989) Images of the DNA double helix in water. *Science 244*, 1063−1064.

(12) Cricenti, A., Selci, S., Felici, A. C., Generosi, R., Gori, E., Djaczenko, W., and Chiarotti, G. (1989) Molecular structure of DNA by scanning tunneling microscopy. *Science 245*, 1226−1227.

(13) Arscott, P. G., Lee, G., Bloomfield, V. A., and Evans, D. F. (1989) Scanning tunneling microscopy of Z-DNA. *Nature 339*, 484−486.

(14) Driscoll, R. J., Youngquist, M. G., and Baldeschwieler, J. D. (1990) Atomic-scale imaging of DNA using scaning tunneling microscopy. *Nature 346*, 294−296.

(15) Amrein, M., Dürr, R., Staslak, A., Gross, H., and Travaglini, G. (1989) Scanning tunneling microscopy of uncoated recA-DNA complexes. *Science 243*, 1708−1711.

(16) Kim, Y., Long, E. C., Barton, J. K., and Lieber, C. M. (1992) Imaging of oligonucleotide-metal complexes by scanning tunneling microscopy. *Langmuir 8*, 496−500.

(17) Yokota, H., Sunwoo, J., Sarikaya, M., Ger van den Engh, and Adbersold R. (1999) Spin-stretching of DNA and protein molecules for detection by fluorescence and atomic force microscopy. *Anal. Chem. 71*, 4418−4422.

(18) O'Brien, J. C., Stickney, J. T., and Porter, M. D. (2000) Self-assembled double-stranded DNA (dsDNA) microarrays for protein: dsDNA screening using atomic force microscopy. *J. Am. Chem. Soc. 122*, 5004−5005.

(19) Yokota, H., Fung, K., Trask, B. J., Ger van den Engh, Sarikaya, M., and Adbersold, R. (1999) Sharp DNA bends as landmarks of protein-binding sites on straightened DNA. *Anal. Chem. 71*, 1663−1667.

(20) Sun, H. B., and Yokota, H. (2000) MutS-mediated detection of DNA mismatches using atomic force microscopy. *Anal. Chem. 72*, 3138−3141.

(21) Kelly, S. O., Barton, J. K., Jackson, N. M., McPherson, L. D., Potter, A. B., Spain, E. M., Allen, M. J., and Hill, M. G. (1998) Orienting DNA helices on gold using applied electric fields. *Langmuir 14*, 6781−6785.

(22) Millan, K. M., Spurmanis, A. J., and Mikkelsen, S. R. (1992) Covalent immobilization of DNA onto glassy carbon electrodes. *Electroanalysis 4*, 929−932.

(23) Carter, M. T., Rodriguez, M., and Bard, A. J. (1989) Voltammetric studies of the interaction of metal chelats with DNA. 2. tris-chelated complexes of Cobalt(III) and Iron(II) with 1,10-phenanthriline and 2,2′-bipyridine. *J. Am. Chem. Soc. 111*, 8901−8911.

(24) Watson, J. D., and Crick, F. H. C. (1953) Molecular structure of nucleic acids. a structure for deoxyribose nucleic acid. *Nature 171*, 737−738.

(25) Hamelin, A., and Lecoeur, J. (1971) Behavior of single-crystal gold electrode in diluted solutions of sodium fluride. *Collect. Czech. Chem. Commun. 36*, 714−721.

BC0155263

Vinyl Sulfone Bifunctional Derivatives of DOTA Allow Sulfhydryl- or Amino-Directed Coupling to Antibodies. Conjugates Retain Immunoreactivity and Have Similar Biodistributions

Lin Li,[†] Shih-Wa Tsai,[†] Anne-Line Anderson,[‡] David A. Keire,[§] Andrew A. Raubitschek,[‡] and John E. Shively*[,†]

Division of Immunology, Beckman Research Institute of the City of Hope, Duarte, California 91010, Department of Radioimmunotherapy, City of Hope Medical Center, Duarte, California 91010, and CURE Digestive Diseases Research Center, UCLA School of Medicine, Los Angeles, California 90095.
Received July 24, 2001; Revised Manuscript Received October 25, 2001

We have synthesized a bifunctional vinyl sulfone−cysteineamido derivative of DOTA (1,4,7,10-tetraazacyclododecane-1,4,7,10-tetraacetic acid) that can be conjugated to the sulfhydryls of mildly reduced recombinant antibody (chimeric anti-CEA antibody cT84.66) at pH 7 or to the amino groups of lysine residues at pH 9. The conjugation is sulfhydryl specific at pH 7 (case 1), and amino specific at pH 9 (case 2) as long as the antibody has no free sulhydryl groups. At a molar ratio of 50 BCA (bifunctional chelating agent) to mAb, the number of chelates conjugated is 0.8 for case 1, and 4.6 for case 2. The resulting conjugates can be radiolabeled with ^{111}In to high specific activity (5 mCi/mg) with high efficiency (>95%) at 43 °C in 60 min. The radiolabeled conjugates retained >95% immunoreactivity and are stable in serum containing 1mM DTPA over 3 d. When the radiolabeled conjugates were injected into nude mice bearing LS174T human colon tumor xenografts, over 40% ID/g accumulated in tumors during the period 24−72h. Tumor-to-blood ratios were 4.5, 3.5, and 2.5 for the sulfhydryl coupled conjugate at 24, 48, and 72 h, respectively, and 2.7, 2.5, and 2.3 for the amino-coupled conjugate at the same time points. For other organs the biodistributions were nearly identical whether the conjugates were attached via sulfhydryl or amino groups. These novel BCAs are easy to synthesize, offer versatile conjugation options, and give equivalent biodistributions that result in high tumor uptake and good tumor-to-blood ratios.

INTRODUCTION

Bifunctional chelating agents (BCAs[1]) are routinely conjugated to recombinant antibodies for radiolabeling with radiometals such as ^{111}In for radioimmunoimaging and ^{90}Y for radioimmunotherapy (*1*−*4*). The main advantages of this approach is the ability to radiolabel the conjugate just prior to use and the exceptional stability of the chelated metal, preventing the release of the radionuclide from the conjugate. Starting with BCAs derived from EDTA (*5*, *6*), and then DTPA (*7*−*11*), and more recently DOTA (*12*−*16*), increasingly more stable radiometal−chelate−antibody conjugates have been crafted. Nonetheless, the approach has certain drawbacks inherent in the biodistribution of the antibody which in the case of intact antibody can be deposited in the liver (*17*−*21*), and in the case of antibody fragments, in the kidney (*22*−*25*). High uptake in normal tissues is due to the deposition of free antibody or antibody antigen conjugates in the liver for intact antibody (*21*) and to renal filtering and reabsorption for antibody fragments (*26*). In both cases, the exceptional stability of the radiometal−chelate and the lack of metabolizing enzymes prevents the excretion of these end-products from the lysosomal compartment. While it is assumed that the antibodies are completely degraded in the lysosome, releasing radiometal−chelate, it has only been proven in a few cases (*27*−*31*). In addition, the site of BCA conjugation to the antibody may play a key role in the fate of the radiolabel in both the tumor and normal organs. Furthermore, it is essential that the BCA be conjugated to the antibody without impairment of immunoreactivity. Since a major goal of the field is to reduce normal tissue uptake without decreasing the tumor uptake, we have investigated new BCA derivatives of DOTA that include the possibility of site-specific conjugation and linker specific cleavage. In previous work we showed that a maleimidocysteineamido derivative of DOTA coupled to sulfhydryl groups of mildly reduced intact antibody underwent pH dependent cleavage at the resulting succinimido groups (*32*), lowering blood levels while preserving high tumor uptake (*33*). However, the results were only a marginal improvement over our use of DOTA-active ester conjugated antibody (*34*, *35*). Oxidation of the thioether linker to a sulfone linker further increased the rate of linker bond cleavage, but the rate of blood clearance was too high, preventing good tumor uptake (*33*). Similar approaches utilizing ester linkers for reducing blood levels have been reported, but also suffer from lower blood levels to the point of reducing

* To whom correspondence should be addressed. e-mail: jshively@coh.org.
[†] Beckman Research Institute of the City of Hope.
[‡] City of Hope Medical Center.
[§] UCLA School of Medicine.

[1] Abbreviations: BCA, bifunctional chelating agent; CEA, carcinoembryonic antigen; DOTA, 1,4,7,10-tetraazacyclododecane-1,4,7,10-tetraacetic acid; EDC, 1-ethyl-3-[3-(dimethylamino)propyl]carbodiimide; DTPA, diethylenetriaminepentaacetic acid; HSA, human serum albumin; sulfo-NHS, *N*-hydroxysulfosuccinimide; TCEP, tris(carboxyethyl)phosphine; VSC-DOTA, vinyl sulfone-cysteineamido-DOTA.

10.1021/bc015535b CCC: $22.00 © 2002 American Chemical Society
Published on Web 12/14/2001

tumor uptake (*21*, *36*−*38*). A similar problem is found in using antibody fragments, which clear the blood rapidly, but also give low tumor uptake (*25*). Thus, it is clear that the price of lowering blood levels is the concomitant lowering of tumor uptake, an unacceptable consequence in either radioimmunoimaging or radioimmunotherapy. A possible solution to the problem is the synthesis of BCAs with organ-specific cleavable linkers. Arano and co-workers (*26*, *39*−*41*) have synthesized C-terminal Lys linkers for a radioiodinated hippuric acid−Fab conjugatethat lowered kidney uptake by 50%. Meares and coworkers (*42*−*44*) have synthesized DOTA with cathepsin cleavable linkers for use in lowering liver levels. In the work reported here, we have made new derivatives of DOTA that incorporate a vinyl sulfone-based linker that shows versatility in terms of conjugation to either sulfhydryl or amino groups of antibodies. The BCA is easy to synthesize from readily available chemicals and gives high radiolabeling yields when conjugated to either sulfhydryl or amino groups. The biodistributions in tumor-bearing animals is nearly equivalent, suggesting that the site of conjugation has not affected either the tumor or normal organ uptake. The new BCA may be useful in preventing the impairment of immunoreactivity in cases where coupling through amino groups is problematic.

EXPERIMENTAL PROCEDURES

General. DOTA trisodium salt and the free acid were purchased from Parish Chemical Co. (Orem, UT) and Macrocyclics, Inc. (Richardson, TX), respectively. DTPA was obtained from Fluka (Milwaukee, WI), vinyl sulfone from Aldrich (Milwaukee, WI), Chelex 100 from BioRad (Hercules, CA), and L-cysteine from Sigma (St. Louis, MO). Ultrapure water (18 MΩ-cm) was used to make all buffers that were passed over Chelex 100 and pH adjusted if necessary. $^{111}InCl_3$ was obtained from NEN Life Science products, Inc. (Boston, MA). The anti-CEA chT84.66 has been previously described (*35*, *45*). HPLC and TLC were performed as previously described (*32*). Mass spectra were recorded on a Finnigan LCQ ion trap mass spectrometer using a custom nanospray interface. NMR spectra were recorded on a Varian Unity Plus 500 MHz spectrometer. Proton chemical shifts are reported relative to HOD (4.80 ppm). Antibody concentrations were calculated at 280 nm (A_{280}, 1 mg/mL = 1.42). UV spectrophometry was performed on a Shimadzu UV160 instrument using a 1 cm cell. Melting points were recorded on a Thomas-Hoover uni-melt apparatus and are uncorrected. SDS and IEF gel electrophoresis was performed on a Pharmacia PhastGel apparatus according to the manufacturer's instructions.

Vinyl Sulfone−Cysteineamido−DOTA (VSC-DOTA; 2). Cysteineamido-DOTA (**1**) was synthesized as previously reported (*46*). To a solution of 3.24 mg (6.1 μmol) of **1** in 0.6 mL of 50 mM, pH 7.5 potassium phosphate was added 0.06 mL of 0.1 M DTT (6 mmol) and stirred for 0.5 h at RT under Ar. Vinyl sulfone (6.6 μL (64 μmol) in 0.6 mL of DMF was added with continuous stirring for 5 h at RT. A second aliquot was added and the reaction continued for another 22 h (final vol = 1.2 mL, 5.3 mM **1**, 107 mM vinyl sulfone). The excess vinyl sulfone was extracted with ethyl acetate (2 mL, ×3). The aqueous layer was adjusted to pH 8.4, applied to a BioRad Ag1-X4 column (HCO_2^- form, 1 × 10 cm), washed with 30 mL of water, and eluted stepwise with 0.05−2 M HCO_2H (5 mL per step). The product (**2**) was found in fractions 8−13 by ESI/MS. The product was repeatedly lyophilyzed from water to remove excess HCO_2H (yield 3.4 mg). The product had the expected protonated mass by ESI/MS (626.71, expected; 626.73, observed), gave a single spot on TLC, and had a melting point of 140−142 °C. Proton NMR (H_2O): δ 2.92 (m, 2H, $SCH_2CH_2SO_2$), δ 3.10 (m, 2H, $SCH_2CH_2SO_2$), δ 3.10−3.45 [br, 16H, (CH_2-NCH_2) × 4], δ 3.53 (dd, 2H, CH_2SO_2), δ 3.45, 3.70, 3.84 (s, 6H, NCH_2CO_2H), δ 4.39 (m, 1H, $NHCHCO_2H$), δ 6.42 (dd, 2H, SO_2CHCH_2), δ 6.88 (dd, 1H, SO_2CHCH_2), δ 8.20 (d, 1H, CONH−CH).

Preparation of Amino-Conjnugated BCA Antibody (VSC-DOTA-NH-chT84.66). chT84.66 (FW= 150000, 1.0 mg, 6 nmol, at 10 mg/mL, 60 μM) was dialyzed vs 20 mM, pH 7.0 sodium phosphate buffer (three changes, × 1 L, 4 °C) and adjusted to pH 9.0 with 200 mM, pH 10 sodium phosphate (final volume, 0.1 mL). VSC-DOTA (0.1 mL of **2**, FW= 625, 0.7 mg, 1.12 μmol at 1.88 mg/mL, 3.1 mM in 50 mM, pH 9.0 sodium phosphate) was added and the solution rotated at 10 rpm for 4 h at 25 °C. The conjugate was dialyzed vs 250 mM NH_4 acetate (three changes, × 1 L, 4 °C).

Preparation of Sulfhydryl-Conjnugated BCA Antibody (VSC-DOTA-SH-chT84.66). chT84.66 was dialyzed as above and reduced with TCEP (20 μL of 10 mM in 50 mM sodium phosphate, pH 7.0) under argon for 2.5 h at 25 °C. TCEP was removed on a spin column (1 mL of Sephadex G25−50, 1200 rpm, 2 min) under argon. To 1.0 mg (60 nmol) of reduced chT84.66 in 0.1 mL of 50 mM sodium phosphate, pH 7, was added 0.1 mL of 3 mM (300 nmol) of VSC-DOTA (**2**) in the same buffer. The solution was rotated under argon overnight at 25 °C and dialyzed vs NH_4 acetate as described above. In parallel, 1 mg of TCEP reduced chT84.66 in 0.15 mL was reacted with 0.1 mL of 3 mM MC-DOTA and run as a control.

Radiolabeling of VSC-DOTA-chT84.66. The conjugates were radiolabeled with $^{111}InCl_3$ as previously described (*47*). For the animal studies, the conjugates (0.3 mL of 1 mg/mL in 250 mM NH_4 acetate, pH 5.7) were incubated with 0.3 mCi of ^{111}In (0.15 mL of 0.04 M HCl plus 0.03 mL of 250 mM NH_4 acetate, pH 5.7) for 60 min at 43 °C. Excess ^{111}In was chelated with 1 mM DTPA and the radiolabeled product purified on a TosoHaas TSK−Gel G2000SW column (0.75 × 30 cm in saline, 0.5 mL/min, 0.5 mL fractions). The protein peak was mixed with 1 drop of 25% (w/v) of HSA. In other test labelings, 1.0 mCi of ^{111}In was added to 0.2 mg of conjugate and the specific activity determined by ITLC (kit 151−770, Biodex, Medical, New York). Determination of the number of chelates per conjugate and the immunoreactivity was performed as previously described (*5*).

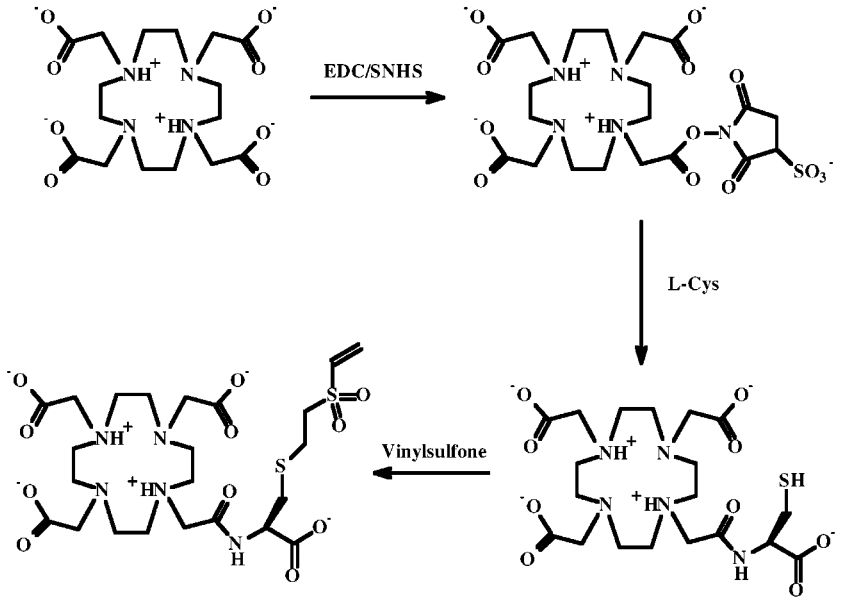
Stability Studies. Aliquots (0.5 mL) of the radiolabeled conjugates in 1% HSA were mixed with 0.05 mL of 10 mM DTPA, stored at 37 °C and injected at various time points onto a Pharmacia Superose 12HR column (as above) to determine the amount of radiolabel in the conjugate and DTPA.

Animal Biodistributions. Groups of five nude mice (Charles River) bearing LS174T human colon tumor xenografts (ave size = 1.5 mg ± 0.5 at t = 0 h) were injected with 2 μCi (2 μg) of radiolabeled conjugate via tail vein. Animals were sacrificed at 0, 12, 24, 48, 72, and 96 h after injection. Major organs, tumor, and blood were weighed, radioactivity was measured, and the results were expressed as mean %ID/g ± SD.

RESULTS

Synthesis and Antibody Conjugation. The synthesis of VSC-DOTA (**2**) is shown in Scheme 1. The product gave the expected proton NMR spectrum and protonated

Scheme 1



mass by ESI/MS and was free of DOTA and the bis-derivative. The reactivity of **2** to free L-cysteine was confirmed by ESI/MS (data not shown). At pH 7, only the mono-derivative was formed, suggesting that the thiol and not the α-amino group of L-cysteine was reactive under these conditions. When VSC-DOTA was incubated for 1−7 d in pH 7 PBS and analyzed by RP-HPLC, there was no evidence of chemical instability (data not shown).

Since VSC-DOTA was expected to react with the ϵ-amino group on the lysines of proteins at pH 9−10, we investigated the reaction of VSC-DOTA with antibody over the pH range of 7−9. The degree of conjugation was determined by IEF gel electrophoresis, wherein conjugation of the acidic BCA to antibody results in a dramatic shift of the antibody to a more acidic pI. The results of the conjugation reaction at pH 7, 8, and 9 shown in Figure 1A, lanes 3−5, demonstrate that little or no reaction occurs at pH 7, while substantial amounts of conjugate are formed at pH 9. The results at pH 8 are intermediate, with <20% product formed. The results at 37 °C, pH 9 demonstrate the expected effect of temperature on the extent of reaction (Figure 1A, lane 6). The products show no change in mobility when run on SDS gel electrophoresis under nonreducing conditions (data not shown). On the basis of these results, we reasoned that sulfhydryl specific conjugation could be performed at pH 7 with little or no conjugation at amino groups, while amino group specific conjugation could be performed at pH 9, as long as no free sulfhydryl groups are present. Since the cysteine residues in most antibodies are engaged in disulfide bonds, this criterion is easily met. In addition, under mild reducing conditions (no denaturing agents), only the hinge disulfides of antibodies are reduced, allowing site-specific conjugation at just these sulfhydryl groups (*48*, *49*). The conjugation of VSC-DOTA to mildly reduced chT84.66 at pH 7 shown in Figure 1B, lane 4, demonstrates that >90% of the antibody is conjugated under these conditions. It should be noted that either DTT or TCEP were successfully used as reducing agents. We prefer TCEP because a lower molar excess is required and since removal of the reducing agent by spin columns is not quantitative, better conjugation yields are routinely obtained.

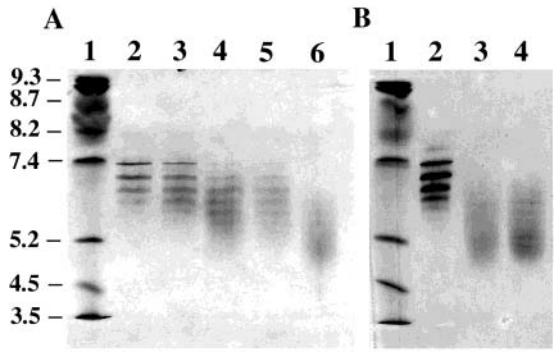


Figure 1. Analysis of VSC-DOTA-mAb conjugates by IEF gel electrophoresis. A: Lane 1: IEF standards; Lane 2: chT84.66 control; Lane 3: 30 μM chT84.66, 1.5 mM VSC-DOTA, pH 7.0, RT, 4h; Lane 4: 30 μM chT84.66, 1.5 mM VSC-DOTA, pH 8.0, RT, 4 h; Lane 5: 30 μM chT84.66, 1.5 mM VSC-DOTA, pH 9.0, RT, 4 h; Lane 6: 30 μM chT84.66, 1.5 mM VSC-DOTA, pH 9.0, 37 °C, 4 h. B: Lane 1: IEF standards; Lane 2: chT84.66 control; Lane 3: 30 μM chT84.66 reduced with 0.5 mM TCEP, the TCEP removed by spin column, and reacted with 1.5 mM MC-DOTA, pH 7.0, RT, 4 h; Lane 4: 30 μM chT84.66, reduced with 0.5 mM TCEP, the TCEP removed by spin column, and reacted with 1.5 mM VSC-DOTA, pH 7.0, RT, 4 h.

The number of chelates per antibody as determined by trace labeling with ^{111}In in a standard solution of $InCl_3$ is shown in Table 1. At pH 7 and with a 50:1 molar ratio of VSC-DOTA to mAb, mildly reduced antibody gave 0.8 chelates/mAb out of a theoretical of 8 for a human IgG1 hinge. At pH 9 with the same molar ratio of VSC-DOTA to mAb, unreduced mAb gave 4.6 chelates/mAb. Radiolabeling of these two conjugates with $^{111}InCl_3$ gave similar percent radiolabeling efficiencies, specific activities, and

Table 1. Radiometal Labeling and Immunoreactivity of VSC-DOTA-mAb[a]

sample	chelates/ mAb	labeling ratio (mCi/mg)	% efficiency	% immuno-reactivity
SH-mAb	0.8	1.0−5.0	>98	>98
NH-mAb	4.5	1.0−5.0	>98	>98

[a] VSC-DOTA was coupled to either SH or NH groups in the mAb as described in the text. The number of chelates per mAb was determined by trace labeling with ^{111}In in a standard solution of $InCl_3$. The labeling ratio was performed with 0.3 mCi of ^{111}In and 0.3 mg of conjugate in 0.3 mL of 0.25 mM ammonium acetate (pH 5.7), or 1.0 mCi of ^{111}In and 0.2 mg of conjugate in 0.2 mL of ammonium actetate (pH 5.7). Immunoreactivity was performed as described in Methods.

Table 2. Biodistribution of ^{111}In-Labeled VSC-DOTA-SH mAb in Nude Mice Bearing LS174T Xenografts[a]

	0 h	12 h	24 h	48 h	72 h	96 h
blood	47.97	23.83	15.00	7.33	3.98	2.49
	(2.58)	(2.43)	(2.07)	(3.78)	(2.51)	(3.02)
liver	7.30	6.65	10.15	14.91	19.60	18.83
	(0.25)	(1.94)	(1.90)	(6.27)	(7.19)	(3.32)
spleen	5.41	5.18	5.93	7.76	6.41	7.69
	(1.22)	(0.57)	(0.95)	(2.54)	(2.25)	(2.27)
kidney	6.36	5.62	4.36	3.46	2.82	2.63
	(1.43)	(0.46)	(0.56)	(1.08)	(0.46)	(0.43)
lung	14.01	8.59	5.50	2.99	1.87	0.90
	(3.27)	(1.26)	(0.72)	(1.36)	(0.88)	(0.59)
tumor	1.59	37.08	43.61	42.01	40.43	39.57
	(0.47)	(4.09)	(4.91)	(12.73)	(6.96)	(18.97)
carcass	1.57	2.58	2.15	1.47	1.05	0.96
	(0.15)	(0.10)	(0.29)	(0.48)	(0.26)	90.51)

[a] Five animals per group were injected with 4 μCi (4 μg) of VSC-DOTA coupled to chT84.66 via the hinge SH groups and radiolabeled with ^{111}In. The results are reported as mean %ID/g (±SD).

Table 3. Biodistribution of ^{111}In-Labeled VSC-DOTA-NH mAb in Nude Mice Bearing LS174T Xenografts[a]

	0 h	12 h	24 h	48 h	73 h	96 h
blood	47.61	17.98	17.50	8.98	5.84	3.08
	(2.97)	(6.29)	(6.74)	(3.18)	(4.14)	(4.50)
liver	9.16	12.38	13.93	16.27	19.64	18.42
	(0.97)	(3.77)	(5.75)	(4.25)	(5.36)	(4.79)
spleen	7.25	6.35	8.09	7.77	10.07	9.06
	(0.68)	(0.73)	(2.34)	(2.00)	(2.08)	(2.09)
kidney	7.29	4.24	5.03	3.44	2.60	2.15
	(1.36)	(1.14)	(1.77)	(0.87)	(0.79)	(0.76)
lung	13.07	5.63	6.58	3.44	2.58	1.45
	(1.18)	(1.79)	(2.58)	(1.30)	(1.57)	(1.63)
tumor	1.26	21.66	38.54	39.27	45.76	33.85
	(0.40)	(5.02)	(13.60)	(10.19)	(18.25)	(14.52)
carcass	1.76	2.20	2.64	1.72	1.43	0.89

[a] Five animals per group were injected with 4 μCi (3.4 μg) of VSC-DOTA coupled to chT84.66 via NH groups and radiolabeled with ^{111}In. The results are reported as mean %ID/g (± SD).

immunoreactivities (Table 1). When the radiolabeled conjugates were incubated in 1% HSA and 1 mM DTPA for 1−7d, negligible loss of radioactivity was seen to DTPA (Table 1). In addition, their immunoreactivities were >95% when radiolabeled, bound to excess CEA, and analyzed by gel filtration chromatography. Since their immunoreactivities were similar, we used these conjugates for a direct comparison in animal biodistribution studies.

Comparative Animal Biodistributions of [^{111}In]-VSC-DOTA-SH-chT84.66 and [^{111}In]VSC-DOTA-NH-chT84.66. The two ^{111}In-radiolabeled conjugates were injected into nude mice bearing human colon tumor xenografts and their biodistributions compared (Tables 2 and 3). The overall biodistributions are quite similar, resulting in maximal and sustained tumor uptake of 35−45% ID/g from 24 to 96 h. During the same time period the blood activity drops from about 45% ID/g to 2−3% ID/g. A comparison of tumor to blood curves over the time course suggests that the SH conjugate may be superior to the NH conjugate. Paradoxically, this difference may be due to a slightly slower blood clearance curve for the SH conjugate, resulting in higher uptake. A close analysis of the normal organs reveals nearly identical uptake levels and time courses for the spleen, kidney, and lung, but there are some interesting differences in the liver. The SH conjugate shows lower liver uptake at the earlier time points, suggesting that the NH conjugate accumulates more rapidly in the liver. This result would also account for their observed differences in blood clearance curves.

DISCUSSION

In a search for site-specific BCA derivatives of DOTA we first synthesized a bis-maleimidohexane derivative of cysteineamido-DOTA (*32*). Maleimide is a commonly used reagent that undergoes sulfhydryl specific Michael additions that are thought to be chemically stable (*50*). Although this BCA allowed site-specific conjugation to the sulfhydryl groups of mildly reduced mAb, it proved to be chemically labile, undergoing pH-dependent hydrolysis at its resulting succinimidyl bonds (*32*). Surprisingly, this phenomenon did not prevent good tumor uptake in animal biodistribution studies (*33*). As a result, we proposed that further increasing the chemical lability of the linker may be beneficial, since this would result in lower blood levels. Indeed, oxidation of the thioether bond in the linker to a sulfone increased the chemical lability of the BCA (*32*), but the BCA decomposed too rapidly to allow good tumor uptake. On the basis of these studies, we decided to investigate other Michael addition linkers as candidates for site-specific conjugation to mAbs. We chose vinyl sulfone for its well-documented reaction with sufhydryl groups (*51*). However, we realized from the outset that vinyl sulfone can also react with amino groups (*52*, *53*), and thus we were interested in seeing if this reaction could be controlled by manipulation of the reaction pH.

Vinyl sulfone is a viscous liquid with poor solubility in water, but when dissolved in DMF or acetonitrile reacts well with Michael acceptors in aqueous medium. In the synthesis of the title compound (**2**), we demonstrated a facile reaction between vinyl sulfone and cysteineamido-DOTA. Unlike the maleimido derivatives, the vinyl sulfone derivative of cysteineamido-DOTA is stable in PBS at pH 7. When **2** was reacted with chT84.66 at pH 7, no conjugate was formed unless the mAb was mildly reduced prior to reaction. In addition, we showed that the mAb conjugated with **2** at pH 9 to a greater extent (no. chelates/mAb) as it did to reduced mAb at pH 7 using the same molar ratio of **2** to mAb. Thus, we demonstrated that this BCA can be conjugated to the same mAb via different chemical linkages using pH and reducing agents to convey linkage specificity.

Since the biodistributions of radiolabeled mAbs is highly dependent on the mode of attachment of the radiolabel, it is always interesting to compare BCAs conjugated to the same mAb via different chemical linkages. In most cases, it is difficult to perform this type of comparative study. However, in this study, we have an almost ideal model. In one case, the same BCA is conjugated to sulfhydryl groups, and in the other case, amino groups, but the resulting BCA/mAb ratios are different. Even so, the resulting biodistributions are quite similar. When we compare these results to our previous studies in which DOTA was conjugated to chT84.66 by an active ester derivative of DOTA (*34*, *35*), we find that the uptake curves are similar for both tumor and normal tissues. This suggests that linkage of DOTA based BCAs to mAbs via amides, amine, or sulfhydryl bonds results in similar tissue, including tumor, uptakes, and metabolism. Thus, if one wants to manipulate normal or tumor uptake and metabolism of DOTA-based BCAs, it is necessary to explore other modes of chemical linkage or to insert linkers which have built-in chemical or biological lability. Examples of such linkers have been described by Meares (*21*), Arano (*54*), and ourselves (*32*).

When we examined the comparative biodistributions of the SH and NH BCA-chT84.66 conjugates in more detail, we noticed some intriguing trends. They include

the higher blood levels, higher tumor levels, and lower liver levels for the BCA chT84.66 SH conjugate at early time points 0−24 h. These three "organs" are interdependent in their biodistributions as follows: high tumor uptake is dependent on maintaining high blood levels, especially early in a biodistribution. If the blood is cleared by any mechanism, including rapid liver uptake, then blood and tumor levels will fall together. Thus, the lower liver uptake seen at early time points for the SH conjugate leads to higher blood levels and ultimately to higher tumor uptake which is sustained at later time points. While the biological reasons for these differences are unknown at this time, we can speculate that this mode of conjugation will lead to incremental improvements in the human, where most biodistributions are predicted from the animal model.

In summary, we have prepared a new BCA that allows site-specific conjugation to most mAbs either via sulfhydryl or amino groups by manipulating pH and use of reducing agents. The ^{111}In-radiolabeled versions of these conjugates give more or less equivalent animal biodistributions to previously described ^{111}In-radiolabeled BCA-mAbs, including are own version using the active ester of DOTA (*34*, *35*). This approach should have utility, allowing the investigator to chose one type of chemistry over the other depending on the restrictions implied by a given antibody. Finally, the improvement in tumor to blood and tumor-to-liver ratios seen for the SH-specific conjugate may translate into improved performance in the clinic.

ACKNOWLEDGMENT

The authors thank Stefanie Wright for the animal studies. This research was funded by NCI grant CA43904 (A.A.R. and J.E.S.) and the Department of the Army Grant DAMD 17-98-1-8031 (J.E.S.).

LITERATURE CITED

(1) Anderson, C. J., and Welch, M. J. (1999) Radiometal-labeled agents (non-technetium) for diagnostic imaging. *Chem. Rev. 99*, 2219−2234.

(2) Gansow, O. A. (1991) Newer Approaches to the Radiolabeling of Monoclonal Antibodies by Use of Metal Chelates. *Int. J. Radiat. Appl. Instrum. Part B Nucl. Med. Biol. 18*, 369−381.

(3) Meares, C. F. (1986) Chelating Agents for the Binding of Metal Ions to Antibodies. *Int. J. Radiat. Appl. Instrum. Part B Nucl. Med. Biol. 13*, 311−318.

(4) Liu, S., and Edwards, D. S. (2001) Bifunctional chelators for therapeutic lanthanide radiopharmaceuticals. *Bioconjugate Chem. 12*, 7−34.

(5) Meares, C. F., McCall, M. J., Reardan, D. T., Goodwin, D. A., Diamanti, C. I., and McTigue, M. (1984) Conjugation of Antibodies with Bifunctional Chelating Agents: Isothiocyanate and Bromoacetamide Reagents, Methods of Analysis, and Subsequent Addition of Metal Ions. *Anal. Biochem. 142*, 68−78.

(6) Brechbiel, M. W., Gansow, O. A., Atcher, R. W., Schlom, J., Esteban, J., Simpson, D. E., and Colcher, D. (1986) Synthesis of 1-(*p*-Isothiocyanatobenzyl) Derivatives of DTPA and EDTA. Antibody Labeling and Tumor-Imaging Studies. *Inorg. Chem. 25*, 2772−2781.

(7) Brechbiel, M. W., and Gransow, O. A. (1991) Backbone-substituted DTPA ligands for ^{90}Y radioimmunotherapy. *Bioconjugate Chem. 2*, 187−194.

(8) Cummins, C. H., Rutter, E. W., and Fordyce, W. A. (1991) A convenient synthesis of bifunctional chelating agents based on diethylenetriaminepentaacetic acid and their coordination chemistry with yttrium (III). *Bioconjugate Chem. 2*, 180−186.

(9) Hnatowich, D. J., Virzi, F., and Doherty, P. W. (1985) DTPA-Coupled Antibodies Labeled with Yttrium-90. *J. Nucl. Med. 26*, 503−509.

(10) Westerberg, D. A., Carney, P. L., Rogers, P. E., Kline, S. J., and Johnson, D. K. (1989) Synthesis of Novel Bifunctional Chelators and Their Use in Preparing Monoclonal Antibody Conjugates for Tumor Targeting. *J. Med. Chem. 32*, 236−243.

(11) Corson, D. T., and Meares, C. F. (2000) Efficient multigram synthesis of the bifunctional chelating agent (S)-1-p-isothiocyanatobenzyl-diethylenetetraaminepentaacetic acid. *Bioconjugate Chem. 11*, 292−299.

(12) Cox, J. P. L., Jankowski, K. J., Kataky, R., Parker, D., Beeley, N. R. A., Boyce, B. A., Eaton, M. A. W., Millar, K., Millican, A. T., Harrison, A., and Walker, C. (1989) Synthesis of a Kinetically Stable Yttrium-90 Labeled Macrocycle-Antibody Conjugate. *J. Chem. Soc., Chem. Commun.* 797−798.

(13) Deshpande, S. V., DeNardo, S. J., Kukis, D. L., Moi, M. K., McCall, M. J., DeNardo, G. L., and Meares, C. F. (1990) Yttrium-90-labeled monoclonal antibody for therapy: labeling by a new macrocyclic bifunctional chelating agent. *J. Nucl. Med. 31*, 473−479.

(14) Meares, C. F., Moi, M. K., Diril, H., Kukis, D. L., McCall, M. J., Deshpande, S. V., DeNardo, S. J., Snook, D., and Epenetos, A. A. (1990) Macrocyclic chelates of radiometals for diagnosis and therapy. *Br. J. Cancer 62*, Suppl. X, 21−26.

(15) Smith-Jones, P. M., Fridrich, R., Kaden, T. A., Novak-Hofer, I., Siebold, K., Tschudin, D., and Maecke, H. R. (1991) Antibody Labeling with Copper-67 Using the Bifunctional Macrocycle 4-[(1,4,8,11-Tetraazacyclotetradec-1-yl)methyl]-benzoic Acid. *Bioconjugate Chem. 2*, 415−421.

(16) Kline, S. J., Betebenner, D. A., and Johnson, D. K. (1991) Carboxymethyl-Substituted Bifunctional Chelators: Preparation of Aryl Isothiocyanate Derivatives of 3-(Carboxymethyl)-3-azapentanedioic Acid, 3,12-Bis(carboxymethyl)-6,9-dioxa-3,12-diazatetradecanedioic Acid, and 1,4,7,10-Tetraazacyclododecane-*N*,*N*′,*N*″,*N*‴-tetraacetic Acid for Use as Protein Labels. *Bioconjugate Chem. 2*, 26−31.

(17) Halpern, S. E., Hagan, P. L., Garver, P. R., Koziol, J. A., Chen, A. W. N., Frincke, J. M., Bartholomew, R. M., David, G. S., and Adams, T. H. (1983) Stability, Characterization, and Kinetics of ^{111}In-labeled Monoclonal Antitumor Antibodies in Normal Animals and Nude Mouse-Human Tumor Models. *Cancer Res. 43*, 5347−5355.

(18) Jakowatz, J. G., Beatty, B. G., Vlahos, W. G., Porudominsky, D., Philben, V. J., Williams, L. E., Paxton, R. J., Shively, J. E., and Beatty, J. D. (1985) High-Specific-Activity ^{111}In-labeled Anticarcinoembryonic Antigen Monoclonal Antibody: Biodistribution and Imaging in Nude Mice Bearing Human Colon Cancer Xenografts. *Cancer Res. 45*, 5700−5706.

(19) Larson, S. M., and Carrasquillo, J. A. (1988) Advatages of radioiodine over radioindium labeled monoclonal antibodies for imaging solid tumors. *Nucl. Med. Biol. 15*, 231−233.

(20) Wong, J. Y. C., Thomas, G. E., Yamauchi, D. M., Williams, L. E., Odom-Maryon, T. L., E. J. M., Neumaier, M., Wu, A. M., Primus, F. J., Shively, J. E., and Raubitschek, A. A. (1997) Clinical evaluation of an ^{111}In labeled anti-CEA chimeric monoclonal antibody in patients with metastatic CEA producing malignancies. *J. Nucl. Med. 38*, 1951−1959.

(21) Meares, C. F., McCall, M. J., Deshpande, S. V., DeNardo, S. J., and Goodwin, D. A. (1988) Chelate radiochemistry: cleavable linkers lead to altered levels of radioactivity in the liver. *Int. J. Cancer (suppl.) 2*, 99−102.

(22) Bujis, W. C. A. M., Massuger, L. F. A. G., Claessens, R. A. M. J., Kenemans, P., and Corstens, F. H. M. (1992) Dosimetric evaluation of immunoscintigraphy using indium-11-labeled monoclonal antibody fragments in patients with ovarian cancer. *J. Nucl. Med. 33*, 1113−1120.

(23) Govindan, S. V., Shih, L. B., Goldenberg, D. M., Sharkey, R. M., Karacay, H., Donnelly, J. E., Losman, M. J., Hansen, H. J., and Griffiths, G. L. (1998) 90-Yttrium-labeled complementarity-determining-region grafted monoclonal antibodies for radioimmunotherpay: radiolabeling and animal biodistribution studies. *Bioconjugate Chem. 9*, 773−782.

(24) Yemul, S., Leon, J. A., Pozniakoff, T., Esser, P. D., and Estabrook, A. (1993) Radioimmunoimaging of human breast carcinoma xenografts in nude mouse model with ^{111}In labeled new monoclonal antibody EBA-1 and F(ab′)2 fragments. *Nucl. Med. Biol. 20*, 325−335.

(25) Yokota, T., Milenic, D. E., Whitlow, M., and Schlom, J. (1992) Rapid tumor penetration of a single-chain Fv and comparison with other immunoglobulin forms. *Cancer Res. 52*, 3402−3408.

(26) Arano, Y. (1998) Strategies to reduce renal radioactivity levels of antibody fragments. *Quart. J. Nucl. Med. 42*, 262−270.

(27) Duncan, J. R., and Welch, M. J. (1993) Intracellular metabolism of indium-111 DTPA labeled receptor targeted proteins. *J. Nucl. Med. 34*, 1728−1738.

(28) Duncan, J. R., Stephenson, M. T., Wu, H. P., and Anderson, C. J. (1997) Indium-111-diethylenetriamine pentaacetic acid octreotide is delivered in vivo to pancreatic, tumor cell, renal, and hepatocyte lysosomes. *Cancer Res. 57*, 659−671.

(29) Franano, F. N., Edwards, W. B., Welch, M. J., and Duncan, J. R. (1994) Metabolism of receptor targeted ^{111}In-DTPA-glycoporteins: identification of ^{111}In-DTPA-epsilon-lysine as the primary metabolic and excretory product. *Nucl. Med. Biol. 21*, 1023−1034.

(30) Novak-Hofer, I., Amstutz, H. P., Macke, H. R., Schwartzbach, R., Zimmermann, K., Morgenthaler, J.-J., and Schubiger, P. A. (1995) Cellular processing of copper-67 labeled monoclonal antibody chCE7 by human neuroblastoma cells. *Cancer Res. 55*, 46−50.

(31) Tsai, S. W., Li, L., Williams, L. E., Anderson, A.-L., Raubitschek, A. A., and Shively, J. E. (2001) Metabolism and renal clearance of ^{111}In-labeled DOTA conjugated antibody fragments. *Bioconjugate Chem. 12*, 264−270.

(32) Lewis, M. R., and Shively, J. E. (1998) Maleimidocysteineamido-DOTA derivatives. New reagents for radiometal chelate conjugation to antibody sulfhydryl groups undergo pH-dependent clevage reactions. *Bioconjugate Chem. 9*, 72−86.

(33) Williams, L. E., Lewis, M. R., Bebb, G. G., Clarke, K. G., Odom-Maryon, T. L., Shively, J. E., and Raubitschek, A. A. (1998) Biodistribution of ^{111}In and ^{90}Y labeled DOTA and maleimidocysteineamido-DOTA conjugated to chimeric anti-carcinoembryonic antigen antibody in xenograft bearing nude mice: comparison of stable and chemically labile linker systems. *Bioconjugate Chem. 9*, 87−93.

(34) Lewis, M. R., Raubitschek, A. A., and Shively, J. E. (1994) A facile, water-soluble method for modification of proteins with DOTA. Use of elevated temperature and optimized pH to achieve high specific activity and high chelate stability in radiolabeled immunoconjugates. *Bioconjugate Chem. 5*, 565−576.

(35) Williams, L. E., Primus, F. J., Wong, J. Y. C., Wu, A. M., Odom-Maryon, T. L., Johnson, D. K., Hefta, L. J. F., Shively, J. E., and Raubitschek, A. A. (1996) Biodistribution of an ^{111}In or ^{90}Y labeled chimeric anti-CEA monoclonal antibody (cT84.66) following its large scale production in a bioreactor. *Tumor Targeting 2*, 116−124.

(36) Haseman, M. K., Goodwin, D. A., Meares, C. F., Kaminski, M. S., Wensel, T. G., McCall, M. J., and Levy, R. (1986) Metabolizable 111-In-chelate conjugated anti-iodiotype monoclonal antibody for radioimmunodetection of lymphoma in mice. *Eur. J. Nucl. Med. 12*, 455−460.

(37) Paik, C. H., Yokoyama, K., Reynolds, J. C., Quadri, S. M., Min, C. Y., Shin, Y., Maloney, P. J., Larson, S. M., and Reba, R. C. (1989) Reduction of background activities by introduction of a diester linkage between antibody and a chelate in radioimmunodetection of tumor. *J. Nucl. Med. 30*, 1693−1701.

(38) Deshpande, S. V., DeNardo, S. J., Meares, C. F., McCall, M. J., Adams, G. P., and DeNardo, G. L. (1989) Effect of different linkage between chelates and monoclonal antibodies on levels of radioactivity in the liver. *Nucl. Med. Biol. 16*, 587−597.

(39) Arano, Y., Mukai, T., Uezono, T., Wakisaka, K., Motonari, H., Akizawa, H., Taoka, Y., and Yokoyama, A. (1994) A biological method to evaluate bifunctional chelating agents to label antibodies with metallic radionuclides. *J. Nucl. Med. 35*, 890−898.

(40) Arano, Y., Wakisaka, K., Ohmono, Y., Uezono, T., Akizawa, H., Nakayama, M., Sakahara, H., Tanaka, C., Konishi, J., and Yokoyama, A. (1996) Assessment of radiochemical design of antibodies using an ester bond as the metabolizable linkage: evaluation of maleimidoethyl 3-(tri-*n*-butylstannyl)-hippurate as a radioiodination reagent of antibodies for diagnostic and therapeutic applications. *Bioconjugate Chem. 7*, 628−637.

(41) Fujioka, Y., Arano, Y., Ono, M., Uehara, T., Ogawa, K., Namba, S., Saga, T., Nakamoto, Y., Mukai, T., Konishi, J., and Saji, H. (2001) Renal metabolism of 3′-iodohippuryl Nϵ-maleoyl-L-lysine (HML)-conjugated Fab fragments. *Bioconjugate Chem. 12*, 178−185.

(42) Li, M., and Meares, C. F. (1993) Synthesis, metal chelate stability studies, and enzyme digestion of a peptide-linked DOTA derivative and its corresponding radiolabeled immunoconjugates. *Bioconjugate Chem. 4*, 275−283.

(43) Peterson, J. J., Pak, R. H., and Meares, C. F. (1999) Total solid-phase synthesis of 1,4,7,10-tetraazacyclododecane-N,N′,N″,N″-tertraacetic acid functionalized peptides for radioimmunotherpay. *Bioconjugate Chem. 10*, 316−320.

(44) Peterson, J. J., and Meares, C. F. (1999) Enzymatic cleavage of peptide linked radiolabels from immunoconjugates. *Bioconjugate Chem. 10*, 553−557.

(45) Neumaier, M., Shively, L., Chen, F.-S., Gaida, F.-J., Ilgen, C., Paxton, R. J., Shively, J. E., and Riggs, A. D. (1990) Cloning of the Genes for T84.66, an Antibody That Has a High Specificity and Affinity for Carcinoembryonic Antigen, and Expression of Chimeric Human/Mouse T84.66 Genes in Myeloma and Chinese Hamster Ovary Cells. *Cancer Res. 50*, 2128−2134.

(46) Lewis, M. R., and Shively, J. E. (1998) Maleimidocysteineamido-DOTA Derivatives: New Reagents for Radiometal Chelate Conjugation to Antibody Hinge Region Sulfhydryl Groups Undergo pH-Dependent Cleavage Reactions. *Bioconjugate Chem. 9*, 72−86.

(47) Williams, L. E., Lewis, M. R., Bebb, G. G., Clarke, K. G., Odom-Maryon, T. L., Shively, J. E., and Raubitschek, A. A. (1998) Biodistribution of ^{111}In- and ^{90}Y-Labeled DOTA and Maleimidocysteineamido-DOTA Conjugated to Chimeric Anti-Carcinoembryonic Antigen Antibody in Xenograft-Bearing Nude Mice: Comparison of Stable and Chemically Labile Linker Systems. *Bioconjugate Chem. 9*.

(48) Gunewardena, P., and Cook, K. B. (1966) 1,4-Dithiothreitol as a Reagent for Reductive Degradation of Human γG Globulin. *Biochem. J. 99*, 8P.

(49) Willner, D., Trail, P. A., Hofstead, S. J., King, H. D., Lasch, S. J., Braslawsky, G. R., Greenfield, R. S., Kaneko, T., and Firestone, R. A. (1993) (6-Maleimidocaproyl)hydrazone of Doxorubicin- -A New Derivative for the Preparation of Immunoconjugates of Doxorubicin. *Bioconjugate Chem. 4*, 521−527.

(50) Gregory, J. D. (1955) The Stability of *N*-Ethylmaleimide and its Reaction with Sulfhydryl Groups. *J. Am. Chem. Soc. 77*, 3922−3923.

(51) Houen, G., and Jensen, O. M. (1995) Conjugation to preactivated proteins using divinyl sulfone and iodoacetic acid. *J. Immunol. Methods 181*, 187−200.

(52) Friedman, M., and Finley, J. W. (1975) Reactions of proteins with ethyl vinyl sulfone. *Int. J. Pept. Protein Res. 7*, 481−486.

(53) Masri, M. S., and Friedman, M. (1988) Protein reactions with methyl and ethyl vinyl sulfones. *J. Protein Res. 7*, 49−54.

(54) Arano, Y., Fujioka, Y., Akizawa, H., Ono, M., Uehara, T., Wakisaka, K., Nakayama, M., Sakahara, H. K. J., and Saji, H. (1999) Chemical design of radiolabeled antibody fragments for low renal radioactivity levels. *Cancer Res. 59*, 128−134.

BC015535B

High Throughput Magnetic Resonance Imaging for Evaluating Targeted Nanoparticle Probes

Dagmar Högemann, Vasilis Ntziachristos,[§] Lee Josephson,[§] and Ralph Weissleder*

Center for Molecular Imaging Research, Massachusetts General Hospital, Charlestown, Massachusetts 02129.
Received August 21, 2001; Revised Manuscript Received October 26, 2001

The ability to image specific molecular targets in vivo would have significant impact in allowing earlier disease detection and in tailoring molecular therapies. One of the rate-limiting steps in the development of novel compounds as reporter probes has been the lack of cell-based, biologically relevant, high throughput screening methods. Here we describe the development and validation of magnetic resonance imaging (MRI) as a technique to rapidly screen compounds that are potential MR reporter agents for their interaction with specific cellular targets. We show that MR imaging can (1) evaluate thousands of samples simultaneously and rapidly, (2) provide exceedingly accurate measurements, and (3) provide receptor binding/internalization data as validated by radioactive assays. The technique allows the screening of libraries of peptide−nanoparticle conjugates against target cells and the identification of conjugates that may be subsequently used as reporter agents in vivo. The technology should greatly accelerate the development of target-specific or cell-specific MR contrast agents.

INTRODUCTION

The sequencing of the human genome has led to a large number of potential targets for drug development and necessitated ever more efficient strategies for compound synthesis and compound evaluation. Current therapeutic drugs address roughly 500 different molecular targets (45% receptors, 30% enzymes, 25% other targets). Estimates of potential future drug targets are in excess of 5000 to 10000. The large number of potential targets can be contrasted with the handful of specific imaging agents available clinically. One of the clearly identified bottlenecks in drug development generally, and targeted imaging agents in particular, has been the development of efficacy testing methodologies that are both highly relevant to the intended use of the drug and amenable to high throughput screening.

The goal of this study was to develop and validate magnetic resonance imaging (MRI) as a high throughput screening (HTS) modality for examining the interactions between superparamagnetic nanoparticles and cells in the wells of microtiter plates. To accomplish this we used a recently developed technology that allows the attachment of a variety of biological molecules to iron oxide nanoparticles with the retention of biological activity. Proteins such as transferrin (*1*), peptides such as the membrane translocating tat peptide of the HIV tat protein (*2*, *3*), and oligonucleotides of various sequences (*4*) have been attached to an aminated, cross-linked iron oxide nanoparticle (amino-CLIO) and used in a variety of applications.

We first evaluated MR imaging as an analytical method by examining the reproducibility and detectability of nanoparticles in microtiter plates using a clinical MR imaging system. Afterward we used a transferrin−nanoparticle conjugate to validate the method for determining nanoparticle binding and uptake by cells expressing differing levels of the transferrin receptor. Finally, we synthesized a limited library of peptide−nanoparticle conjugates and screened the library using the MR imaging method.

Use of the MR imager permitted up to 1920 samples to be imaged in about 50 min acquiring more than 38000 individual data points in multiecho trains. Using this approach it appears feasible to analyze upward of 20000 experimental samples per day, a number that is currently only limited by the design and availability of better magnetic coils and stronger gradients to achieve higher spatial resolutions. Imaging of large numbers of biological samples in HTS fashion with a clinical MR imager may accelerate the discovery of new targeted MR contrast agents.

MATERIALS AND METHODS

Synthesis of Amino-CLIO Nanoparticles. Monocrystalline iron oxide nanoparticles were prepared through the reaction of iron salts with ammonium hydroxide in the presence of T10 dextrans. The dextrans were then modified in the presence of epichlorohydrin according to previous reports to yield cross-linked iron oxide nanoparticles (CLIO-10). CLIO was finally treated with ammonia to yield amino-CLIO, to obtain reactive groups for the covalent binding of bifunctional linking reagents (*2*, *4*).

Peptide Synthesis. Peptides were synthesized for attachment to the aminated nanoparticle, amino-CLIO. The peptides included the tat peptide of HIV, a well-established membrane translocation signal (GRKKRRQRRRGYK(FITC)C-NH_2), short poly-arginyl peptides which might act as membrane translocating signals (*5*, *6*), and control peptides. Peptides were synthesized on an automatic synthesizer (PS3, Rainin, Woburn, MA) by Fmoc chemistry and underwent reaction with fluorescein isothiocyanate (FITC) to facilitate the determination of the

* Corresponding author: Ralph Weissleder, MD, Ph.D.,Center for Molecular Imaging Research, Massachusetts General Hospital, Bldg. 149 13th Street, #5406, Charlestown, MA 02129. Tel.: (617) 726 5788. Fax: (617) 726 5708. E-mail: weissleder@helix.mgh.harvard.edu.

§ Contributed equally.

10.1021/bc015549h CCC: $22.00 © 2002 American Chemical Society
Published on Web 01/16/2002

number of peptides attached per nanoparticle (*2*). Peptides were purified by C18 reversed-phase HPLC and characterized by MALDI-MS. The sequences of the peptides used and values of their molecular weights, as M + 1 (calculated/found), were RRK(FITC)C-NH_2 (951.08/951.47), GRRK(FITC)C-NH_2 (1008.13/1007.97), GRRRRK(FITC)C-NH_2 (1320.51/1321.77), GRRGRRK-(FITC)C-NH_2 (1377.54/1377.55), GRRRRGGGGK(FITC)C-NH_2 (1547.69/1548.66), GRKKRRQRRRGYK(FITC)C-NH_2 (2237.54/2238.54), CGGGPQRYGNQWAVGHLM-NH_2 (1931.13/1391.95), CGVYGWGMGLHGPQRNQA-NH_2 (1931.13/1932.15), and TMG-RRRRRGYK(FITC)-GCG-NH_2 (1689.77/1690.81). TMG stands for tetramethylguanidium and is a capping group on the N-terminal residue of the peptide.

Synthesis of a Limited Library of Peptide−Nanoparticle Conjugates. Peptides were conjugated to amino-CLIO either with long chain *N*-succinimidyl 3-(2-pyridyldithio)propionate (lc-SPDP, Molecular Biosciences, Boulder, CO) or with succinimidyl iodoacetate (SIA, Molecular Biosciences). For the former, 1 mL of amino-CLIO (9.25 mg iron in 5 mM citrate buffer, pH 8), 0.67 mL of PBS (pH 8), and 1.3 mL of 3.4×10^{-2} M (in DMSO) lc-SPDP were incubated for 2 h at room temperature to yield activated CLIO particles. Low molecular weight impurities were removed by filtration through Sephadex G-25 columns equilibrated with PBS, pH 8. Peptides and activated CLIO were mixed at equal molar ratios of peptides and 2-pyridyl disulfide groups in PBS, pH 8, and allowed to react for 18 h at room temperature. Nonreacted peptides were separated from peptide−nanoparticles using magnetic columns (Macs separation columns, Miltenyi Biotec, CA). For the latter, 1.5 mL of amino-CLIO (39 mg iron in 5 mM citrate buffer, pH 8) were reacted with 3 mL of 4.9×10^{-2} M (in DMSO) SIA for 2 h at room temperature. The mixture was separated over Sephadex G25, and the void volume with iron oxide particles was collected. The CLIO particles were mixed with 13 mg of GRKKRRQRRRGYK(FITC)C-NH_2 dissolved in 3 mL of 0.02 M citrate, pH 6.5, and allowed to stand for 3 h at room temperature. The mixture was then applied to the column above to remove nonreacted peptide. Peptide attachment was quantified from absorption of the conjugate (extinction coefficient of 73000 M^{-1} cm^{-1} at 494 nm in 0.1 M phosphate buffer). For non-FITC labeled peptide conjugates, peptide was released by DTT and attachment was determined by HPLC. Standards of the coupled peptide were used whose mass was determined by amino acid analysis. Conjugates had between 2 and 12 mol of peptide per mole of nanoparticles based on 2064 iron atoms per crystal (*7*). Conjugates are denoted as $(\text{peptide sequence})_n$-SS-CLIO or $(\text{peptide sequence})_n$-SC-CLIO where the letters SS or SC indicate disulfide or thioether linking groups, respectively, and n is the number of peptides coupled per particle.

Synthesis of Transferrin−Nanoparticle Conjugate. Transferrin (Tf) was attached to CLIO-NH_2 according to a protocol optimized in an earlier study (*1*). The linker in the current study was SIA (Molecular Biosciences). In brief, 1 mL of amino-CLIO (9.25 mg iron in 5 mM citrate buffer, pH 8), 0.67 mL of PBS (pH 8), and 1.3 mL of 3.4×10^{-2} M (in DMSO) SIA were incubated for 2 h at room temperature to yield activated CLIO particles. Human diferric transferrin was activated through thiolation of primary amine groups (*1*). Tf-SH and iodoacetylated CLIO were mixed at equal molar ratios of transferrin and iodoacetate groups in PBS, pH 8. The mixture was incubated for 18 h at room temperature. Nonreacted Tf-SH was separated from Tf-nanoparticles using Macs separation columns (Miltenyi Biotec). On average each superparamagnetic particle contained one transferrin molecule covalently attached. The transferrin−nanoparticle conjugate is denoted as Tf-SC-CLIO.

Magnetic Resonance Imaging. A 1.5 T superconducting magnet (Signa 5.0; GE Medical Systems, Milwaukee, WI) was used. A standard quadrature extremity coil was chosen to obtain a homogeneous field of view over the well plates. The imaging protocol consisted of a T2-weighted spin−echo sequence (TR 3000 ms, variable TE 15−1200 ms; total of 20−24 echo times). The 1.5 mm imaging slices were carefully placed to avoid partial volume effects. At a field of view (FOV) of 12 × 9 cm and a 256 × 192 imaging matrix, each voxel had a volume of 0.33 mm^3, and image acquisition time was 10.12 min per number of excitation (NEX).

Data Analysis. The MR images obtained at various echo times (TE's) were processed to obtain T2 maps. To automate the calculations a script was written in Matlab (Matlab 6.0; The MathWorks, Natick, MA). In this routine, signal intensities of each voxel were fitted for exponential decay according to the following equation: $SI = A \times e^{(-TE/T2)} + B$; with SI = signal intensity, TE = echo time, A = amplitude, B = offset. Following this calculation, the T2 maps underwent semiautomatic segmentation of the areas of the different wells (IPLab 3.5.2; Scanalytics, Fairfax, VA). The first step was to employ a median filter to change each pixel value to the median value within a neighborhood of 3 × 3 pixels. This filter reduced the noise from isolated pixels without affecting the average T2 values. All regions of interest were simultaneously defined through a one step thresholding function with the threshold set to a value just above the background of the plastic material of the plate. Applying an erode function that computes the minimum value of the pixels within the neighborhood and assigns it to the target pixel made sure that indeed no voxels outside the wells were included into the measurements. The average values of the T2 relaxation times were measured automatically, and the data was exported to a spreadsheet.

Evaluation of Levels of Transferrin Receptor Expression in Different Cell Lines by MR Imaging. 9L gliosarcoma clones, differing in expression of the transferrin receptor (8), were cultivated in Dulbecco's modified Eagle's medium (DMEM, Cellgro, Mediatech, Washington, DC) containing 10% fetal bovine serum (FBS, Cellgro) and were used to validate MR measurements of receptor binding and internalization of transferrin-CLIO. One hundred thousand cells/well of the different clones were grown in 24 well plates (Falcon, Becton Dickinson, Lincoln Park, NJ). The following day the binding and uptake of radioactive labeled transferrin and of Tf-SC-CLIO conjugate were determined. In the radioactive assay different concentrations of unlabeled diferric transferrin (1 nM to 10 μM in DMEM, 10% FBS) were added immediately prior to the addition of ^{125}I-transferrin (0.25 nM in DMEM, 10% FBS) (*1*). After incubation for 2 h at 37 °C, the cells were washed three times with Hanks's Balanced Salt Solution (HBSS, BioWhittaker, Walkersville, MD) and detached with trypsin (0.05% trypsin, 0.53 mM ethylenediaminetetraacetic acid). Cell-associated radioactivity was counted in a gamma-counter (1282 Compugamma CS, LKB Wallac, Sweden). In the MRI assay cells were incubated in the presence of different concentrations of Tf-SC-CLIO (0.018−1.8 mM iron). To control for receptor specificity, cells were also incubated with nonconjugated CLIO (7.2 mM iron)

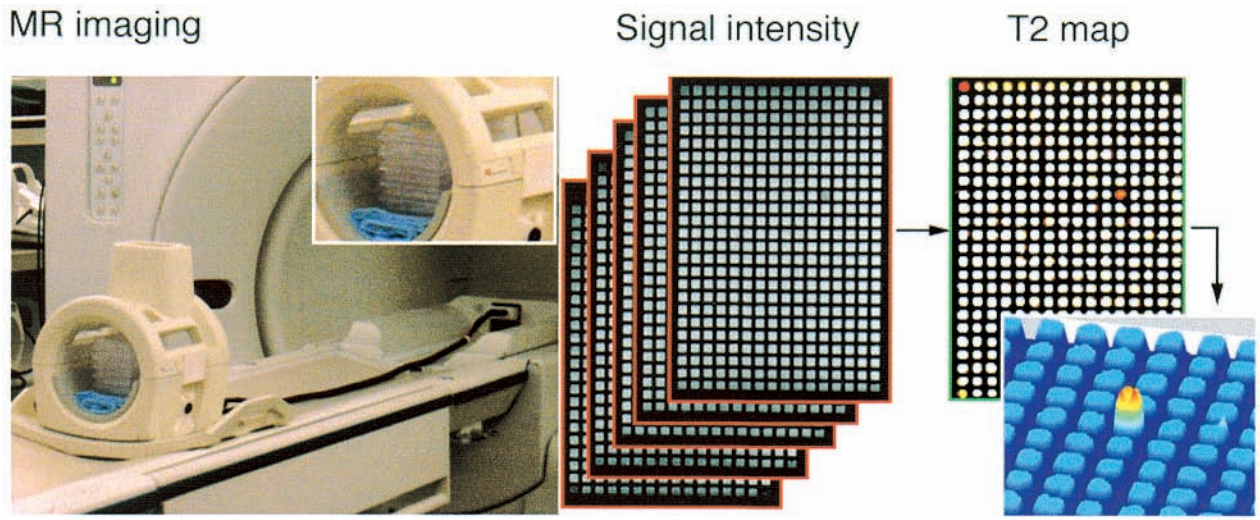


Figure 1. Use of a MR imager for high throughput screening. Microtiter plates were imaged in a quadrature coil with different pulse sequences (variable TE) to yield a series of images for each plate. Signal intensity data were processed to yield a T2 map indicating wells with "hits".

as well as with Tf-SC-CLIO (7.2 mM iron) in the presence of a 100-fold excess of nonconjugated transferrin. Nonspecific binding to the wells was ruled out through the incubation of the culture plates with Tf-SC-CLIO (7.2 mM iron) in the absence of cells. After incubation at 37 °C for 2 h, cells were washed three times with Hanks's Balanced Salt Solution (HBSS, Bio-Whittaker, Walkersville, MD). Cells were lysed in 60 μL of PBS, pH 8, containing 1% Triton X-100 and an aliquot of 5 μL was used to determine the number of cells per well by protein analysis (BCA, Pierce, Rockford, IL). Lysates were transferred to the wells of 384 well plates and centrifuged at 700 rpm for 2 min (Sorvall 7 RT, Kendro Laboratory Products, Newtown, CT) to remove air bubbles. MR imaging and the determination of the T2 values were carried out as described above. The quantification of cell-associated iron concentration was determined from T2 values of nanoparticle standards (1.46 to 29.2 μM iron).

Evaluation of a Limited Library of Peptide−Nanoparticles Conjugates for Cell Uptake by MR Imaging. Peptide−nanoparticle conjugates were evaluated for their cell-association and ability to serve as reagents for cell labeling and tracking (*3*). 9L gliosarcoma cells were cultivated as described above. One hundred thousand cells/well were grown in 24 well plates. The following day 9L gliosarcoma cells were incubated with the various peptide−CLIO conjugates at iron concentrations ranging from 0.0018 to 1.8 mM. After the 1 h incubation at 37 °C, the cells were washed three times with HBSS and lysed in 60 μL of PBS, pH 8, containing 1% Triton X-100. Lysates were transferred to the wells of 384 well plates and centrifuged at 700 rpm for 2 min. MR imaging and the determination of the T2 values were carried out as described above.

RESULTS

We performed three types of experiments to evaluate MR imaging as a HTS method for samples in microtiter plates. They were (a) analysis of signal intensity variation, (b) analysis of T2 variation, and (c) validation of ligand/receptor interaction in a cell based system expressing different levels of receptor. Finally, with the principles of the method established, we used the method to analyze the components of a limited superparamagnetic particle library for uptake into cells. We evaluated two different types of microtiter plates: 384 (60 μL volume per well) and 1536 (10 μL) well plates. All data were obtained with the 384 well configuration except where noted. The general procedure for the MR imaging of iron oxide nanoparticles in microtiter plates is shown in Figure 1.

Table 1. Reproducibility of Signal Intensity Determination at Different Nanoparticle Concentrations (384 well microtiter plate, 16 × 20 Wells, TR/TE = 3000/100)

well no.	0.009 mM	0.018 mM	0.09 mM	0.18 mM
1	1125.03	921.20	322.47	163.56
2	1094.76	922.88	314.25	162.21
3	1116.99	946.24	284.98	159.03
4	1087.80	945.53	264.03	143.14
5	1082.16	1007.67	254.20	137.18
.	.	.	.	.
320	1375.01	1078.91	399.06	130.82
mean	1106.16	952.42	391.41	154.11
SD	79.00	91.46	40.13	10.03
SEM	4.42	5.11	2.24	0.56
99%	11.38	13.17	5.78	1.44
95%	8.66	10.02	4.40	1.10

Analysis of Signal Intensity and T2 Variation. Before utilizing the microtiter plates to screen for nanoparticle interactions with cells by MR imaging, we tested the reproducibility of the measurements of signal intensities and T2 values. Signal intensities were determined for wells over the entire plate at four nanoparticle concentrations. At an echo time of 100 ms an area of 16 × 20 wells provided a 99% confidence interval with individual wells being within 1−2% of the mean signal intensity at all nanoparticle concentrations (Table 1). The reproducibility of the technique was unaffected by stacking plates up to six high during signal acquisition. This enabled data to be obtained simultaneously on 1920 samples of six 384 well plates.

To quantify the changes in signal intensities depending on the different concentrations of nanoparticles, we calculated the changes of the transverse relaxation times (T2). The reproducibility with which T2 could be determined was analyzed for wells over the entire plate (Figure 2A), and the chi-square of the exponential decay curve fit of signal intensities against echo times is shown in Figure 2B. The reproducibility of T2 values determined for 320 wells is shown in Table 2. Again the 99%

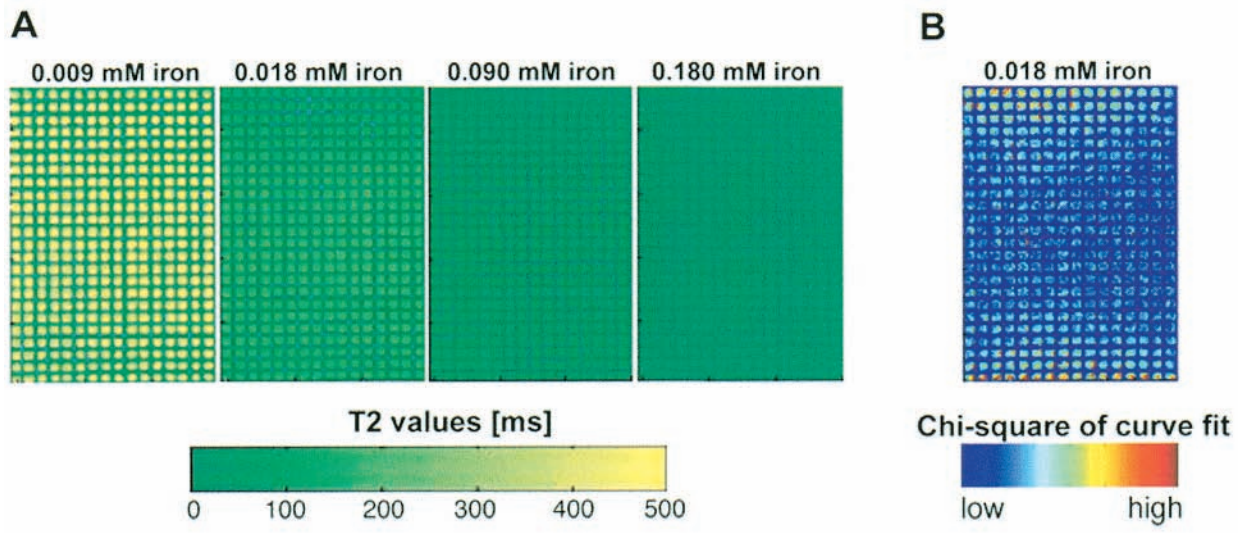


Figure 2. Uniformity of T2 values determined by imaging 384 well microtiter plates. A. Images of plates contained four nanoparticle concentrations. T2 is displayed as a color map from yellow (low nanoparticle concentration, high T2) to green (high nanoparticle concentration, low T2). B. The accuracy of the fitting procedure as a function of plate geometry. Signal intensities were plotted against echo times and T2 values were calculated by curve fitting for exponential decay. The chi-square of each respective curve fit is displayed as a color map from blue (low value of chi-square) to red (high value of chi-square).

Table 2. Reproducibility of T2 Determination at Different Nanoparticle Concentrations (384 well microtiter plate, 16 × 20 Wells, TR/TE = 3000/15−1200)

well no.	0.009 mM	0.018 mM	0.09 mM	0.18 mM
1	485.39	208.59	54.09	30.41
2	494.61	209.93	53.91	29.26
3	457.06	207.42	56.85	29.67
4	459.51	206.16	56.68	29.80
5	434.51	205.29	56.78	30.20
.	.	.	.	.
320	478.63	208.43	57.17	30.70
mean	459.0322	201.46	55.50	30.04
SD	38.4995	12.59	2.94	0.67
SEM	2.15	0.70	0.16	.038
99%	5.54	1.81	0.42	0.10
95%	4.22	1.38	0.32	0.07

confidence interval for individual T2 measurements was within 1−2% of the mean.

The reproducibility of T2 determinations was further evaluated over successively smaller areas (fields of view, FOV) for a 384 well plate as shown in Table 3. This experiment, performed to determine the "sweet spot" over which variations would be smallest, evaluated FOV's ranging from 8066 mm^2 (384 wells) to 672 mm^2 (32 wells). The standard deviation ranged from a high of 13.56 ms (mean 233.71 ms), when 384 wells were imaged, to 9.95 ms (mean 235.88 ms), when only the central 32 wells were imaged. Reproducibility of T2 determination is a function of FOV, though values from the entire plate should be sufficiently accurate for most compound or cell line screening experiments.

The data acquisition of 1536 well plates led to similar results as the 384 well format, but required a higher spatial resolution (matrix: 512 × 512) and therefore a two times longer imaging time.

The ability of the imaging method to detect nanoparticles is shown in Figure 3. Figure 3A shows the progressive decrease in T2 values as a colorized map for duplicate samples as the nanoparticle concentration was increased from 0 to 29.2 μM iron. Values of T2 were plotted against iron concentrations as shown in Figure 3B. The relaxivity, R2 was 188.5 $[mM \times s]^{-1}$ with a high coefficient of correlation, $r^2 = 0.999$. Nanoparticle concentrations in the low micromolar range of iron could be distinguished from zero with visual or graphical analyses. Since there are 2064 iron atoms per particle (*7*), iron oxide particle concentrations can be readily detected in the low nanomolar concentration range.

Determining Transferrin Receptor Expression Using a Transferrin−Nanoparticle Conjugate. The expression of the transferrin receptor has been used as a marker gene for imaging transgene expression (*1*, *8*). Five 9L gliosarcoma cell lines differing in transferrin receptor expression were incubated either with the nanoparticle conjugate Tf-SC-CLIO or with ^{125}I labeled Tf under identical conditions. As shown in Figure 4A, which summarizes the imaging results as a colorized T2 map, cell lines were evaluated in duplicate wells after incubation with Tf-SC-CLIO at concentrations ranging from 0.018 mM to 1.8 mM iron. Figure 4B compares the T2 values for duplicate samples of the five cell lines. Three data sets from separate experiments underwent t-test analysis and representative p values are shown. There was no statistically significant difference in T2 between the duplicates of each sample, however, significant differences in transferrin receptor expression were identified among different clones as indicated. ANOVA analysis confirmed the differentiation of five clones by MRI ($p < 0.001$).

The correlation between nanoparticle uptake determined by MR imaging and the cell-associated radioactivity determined with ^{125}I-Tf was examined as shown in Figure 4C. Cell-associated iron was determined from T2 (Figure 4B) using a standard curve of nanoparticles (Figure 3B). The binding and uptake of Tf-SC-CLIO paralleled the binding and uptake of ^{125}I-Tf with a high coefficient of correlation, $r^2 = 0.996$.

Screening a Limited Library of Peptide−Nanoparticle Conjugates for Cell Binding/Uptake. We then employed the HTS MR imaging technique to evaluate a series of peptide−CLIO conjugates for their binding and/or uptake by 9L gliosarcoma cells as shown in Figure 5. Conjugates were evaluated for their ability to become cell-associated and thereby serve as reagents for labeling cells for tracking by MR. Magnetic cell labeling has become an essential tool for tracking stem and progenitor cells in vivo and for isolating homed cells from tissues

Table 3. Reproducibility of T2 Determination as a Function of Area (field of view, FOV) at 0.018 mM Iron

FOV (mm^2)	8066	7394	6722	6050	5377	4705	4033	3361	2689	2017	1344	672
384 plate	384	352	320	288	256	224	192	160	128	96	64	32
mean	233.7	234.8	234.1	235.2	235.7	236.6	236.5	236.5	236.7	236.4	235.9	235.9
SD	13.56	12.85	12.79	11.51	10.96	10.46	10.33	10.24	10.1	9.2	9.64	9.95
SEM	0.69	0.68	0.71	0.68	0.68	0.70	0.75	0.81	0.89	0.94	1.21	1.76
99%	1.78	1.76	1.84	1.75	1.76	1.80	1.92	1.41	2.30	2.42	3.10	4.53
95%	1.36	1.34	1.40	1.33	1.34	1.37	1.46	1.07	1.75	1.84	2.36	3.45
1536 plate[a]	1536	1408	1280	1152	1024	896	768	640	512	384	256	128

[a] Number of wells of 1536 plate in the FOV used for imaging a 384 well plate.

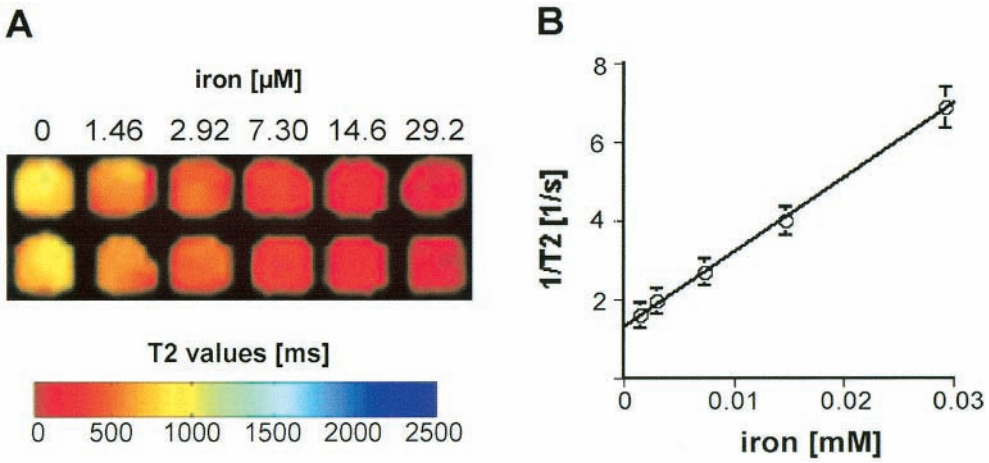


Figure 3. Detection of nanoparticles by MR imaging. A. Duplicate wells with increasing concentrations of nanoparticles were imaged by MR imaging, and the T2 maps were calculated. B. 1/T2 values were plotted versus the iron concentrations to determine the relaxivity R2.

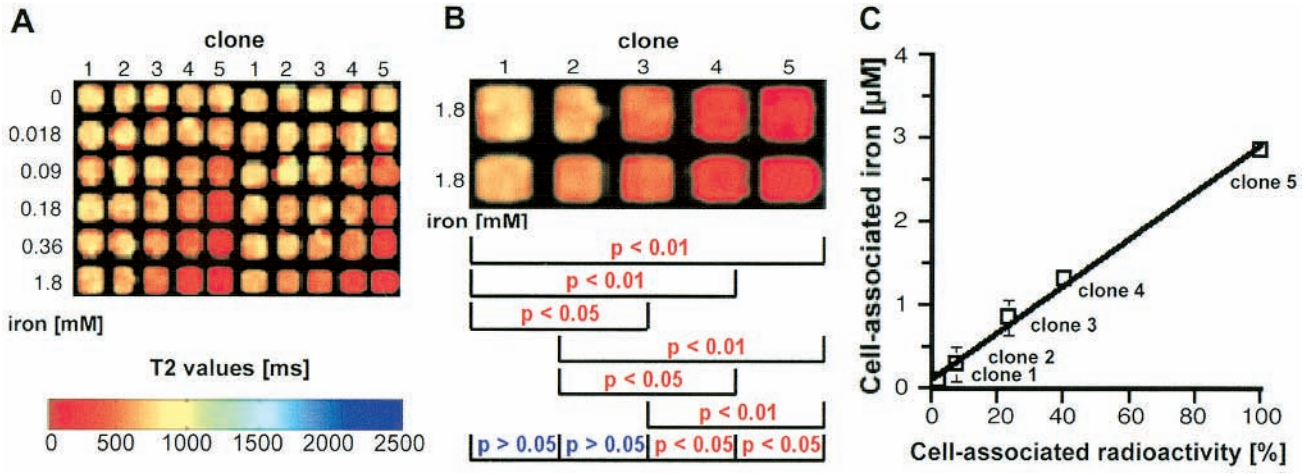


Figure 4. Imaging of transferrin receptor expression. A. Uptake of the nanoparticle conjugate Tf-SC-CLIO by clones 1−5 expressing different levels of the transferrin receptor. Cells were incubated with 0.018 to 1.8 mM iron in Tf-SC-CLIO. Data are expressed as a T2 color map. B. Comparison of T2 values of duplicate wells of clones 1−5 at 1.8 mM Tf-SC-CLIO from Figure 4A. T2's of pairs of clones were evaluated for significance of differences. C. Correlation of receptor expression determined by cell-associated Tf-SC-CLIO (T2 values Figure 4B) or cell-associated ^{125}I-Tf.

(*3*). The highest cellular uptake was observed for the conjugate $(GRKKRRQRRRGYKC\text{-}N)_{11}$-SC-CLIO which led to the lowest T2 values after incubation with 1.8 mM iron (G10) and 0.18 mM iron (B9), with T2 changes still detectable at 0.018 mM iron (D7) (Figure 5). $(GRKKRRQRRRGYKC\text{-}N)_5$-SS-CLIO (1.8 mM iron, D13 and 0.18 mM iron, D5) was the second best conjugate in terms of cell labeling. Finally, $(TMG\text{-}RRRRRGYKGCG\text{-}N)_5$-SS-CLIO also showed some minor efficacy (1.8 mM iron, D12 and 0.18 mM iron, F5) (Figure 5).

DISCUSSION

We used a clinical MR imaging system (1.5 T, 64 MHz) widely available in medical institutions and a conventional send-and-receive quadrature extremity coil to image superparamagnetic nanoparticles in microtiter plates. A major question regarding the use of MR imaging in this fashion is the reproducibility of the data obtained. An imaging protocol where the FOV was <7000 mm^2, corresponding to 320 samples for a 384 well plate, was found to give satisfactory reproducibility. As is apparent from Tables 1 and 2, the reproducibility with which nanoparticle concentrations could be determined was high, with in 99% of the cases the true measurement being within 1−2% of the measured mean. This accuracy is similar to other detection technologies and one of the best for magnetic measurements of small samples (<100 μL).

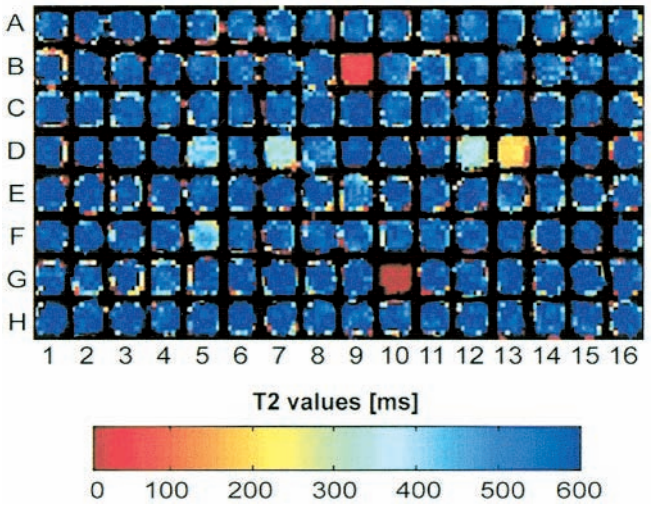


Figure 5. Use of MR imaging to evaluate a limited library of peptide−nanoparticle conjugates. Data are displayed as a T2 color map. The lead candidate was GRKKRRQRRRGYK(FITC)C-$NH_2)_{11}$-SC-CLIO at 1.8 mM iron (G10) and 0.18 mM iron (B9).

To determine how accurate the MR measurements were, we tested a single model compound against a panel of cell lines varying in transferrin receptor expression, which mimics the variable receptor expression seen in different tumors. As shown in Figure 4, based on the comparison of radioactive and superparamagnetic nanoparticle uptake data, measurements by MR imaging were exceedingly accurate.

We then incubated one model cell line with a limited peptide−nanoparticle library of conjugates, to compare their ability to be associated and internalized by cancer cells. Peptide−nanoparticle libraries can be generated by using the linker-chemistry that was developed earlier for the attachment of peptides and proteins to nanoparticles (*1*, *2*). Testing even a limited library of nanoparticle conjugates for cell uptake using conventional, single point relaxometry would have taken days and required sample volumes of 0.5 mL per data point. In contrast, the current assay took less than 4 h for imaging and data analysis and used sample volumes of 60 μL per well. Of the different peptide−nanoparticle conjugates tested a tat-derived peptide with a high valency had the highest uptake. Further studies will employ the HTS MRI technique to systematically screen libraries where peptide sequence, spacer arm chemistry, and valency (number of peptides per particle) will be varied.

The development of high throughput screening methods toward reading equipment capable of ever higher throughputs, lower costs, and higher sensitivities of detection is an ongoing feature of modern drug development. Use of imaging technology (e.g., MR imaging, nuclear imaging, optical imaging) as detection devices for HTS has a number of significant advantages. Imaging modalities have the ability to rapidly obtain signal intensity data of small samples in a field of view comparable to microtiter plates. The capabilities demonstrated here offer a new approach to the discovery of MR imaging reporter agents. The concentrations of labels in individual wells can be determined from signal intensity measurements, and the imaging modality can be used for a variety of tasks such as library deconvolution, determining the pharmacokinetics of internalization, or screening cell lines for the ability to internalize a given ligand. With the approach outlined here, the same imaging modality can be used for compound screening (cell uptake), animal models, and final clinical use. The current approach is well suited to the design of high affinity, targeted ligands for MR imaging and may have a significant impact on the development of new agents that are at the heart of molecular imaging research.

ACKNOWLEDGMENT

The authors thank Dr. Ching H. Tung and Dr. Mark D. Savellano for providing some of the peptides as well as Dr. Ming Zhao and Dr. Nikolay Sergeyev for the preparation and characterization of some of the peptide−CLIO conjugates. We also would like to thank Dr. James P. Basilion and Dr. J. Manuel Perez for the very helpful discussions regarding cell clones and 1536 well plates, respectively. The work was supported by NIH grants RO1 CA 85240, RO1 CA86782, and P50 CA86355. Dr. Dagmar Högemann is a recipient of a fellowship from the Deutsche Forschungsgemeinschaft, Germany.

LITERATURE CITED

(1) Högemann, D., Josephson, L., Weissleder, R., and Basilion, J. P. (2000) Improvement of MRI probes to allow efficient detection of gene expression. *Bioconjugate Chem. 11*, 941−946.

(2) Josephson, L., Tung, C. H., Moore, A., and Weissleder, R. (1999) High-efficiency intracellular magnetic labeling with novel superparamagnetic-Tat peptide conjugates. *Bioconjugate Chem. 10*, 186−191.

(3) Lewin, M., Carlesso, N., Tung, C. H., Tang, X. W., Cory, D., Scadden, D. T., and Weissleder, R. (2000) Tat peptide-derivatized magnetic nanoparticles allow in vivo tracking and recovery of progenitor cells. *Nat. Biotechnol. 18*, 410−414.

(4) Josephson, L., Perez, J. M., and Weissleder, R. (2001) Magnetic nanosensors for the detection of oligonucleotide sequences. *Angew. Chem., Int. Ed. 40*, 3204−3206.

(5) Rothbard, J. B., Garlington, S., Lin, Q., Kirschberg, T., Kreider, E., McGrane, P. L., Wender, P. A., and Khavari, P. A. (2000) Conjugation of arginine oligomers to cyclosporin A facilitates topical delivery and inhibition of inflammation. *Nat. Med. 6*, 1253−1257.

(6) Wender, P. A., Mitchell, D. J., Pattabiraman, K., Pelkey, E. T., Steinman, L., and Rothbard, J. B. (2000) The design, synthesis, and evaluation of molecules that enable or enhance cellular uptake: peptoid molecular transporters. *Proc. Natl. Acad. Sci. U.S.A. 97*, 13003−13008.

(7) Shen, T., Weissleder, R., Papisov, M., Bogdanov, A., Jr., and Brady, T. J. (1993) Monocrystalline iron oxide nanocompounds (MION): physicochemical properties. *Magn. Reson. Med. 29*, 599−604.

(8) Weissleder, R., Moore, A., Mahmood, U., Bhorade, R., Benveniste, H., Chiocca, E. A., and Basilion, J. P. (2000) In vivo magnetic resonance imaging of transgene expression. *Nat. Med. 6*, 351−355.

BC015549H

Magnetic Resonance Imaging of Inducible E-Selectin Expression in Human Endothelial Cell Culture

Hye Won Kang, Lee Josephson, Alexander Petrovsky, Ralph Weissleder, and Alexei Bogdanov, Jr.*

Center for Molecular Imaging Research, Department of Radiology, Massachusetts General Hospital, Harvard Medical School, Building 149, 13th Street, Charlestown, Massachusetts 02129. Received August 28, 2001; Revised Manuscript Received December 3, 2001

Covalent conjugates of the cross-linked iron oxide nanoparticles (CLIO) and high-affinity ($K_d^{app} = 8.5$ nM) anti-human E-selectin (CD62E) F(ab′)$_2$ fragments were prepared and tested in vitro to establish feasibility of endothelial proinflammatory marker magnetic resonance (MR) imaging. The conjugates were obtained by using thiol−disulfide exchange reaction between 3-(2-pyridyl)propionyl-CLIO and *S*-acetylthioacetate-modified F(ab′)$_2$ fragments. The purified CLIO−F(ab′)$_2$ conjugates (average hydrodynamic diameter 40.6 nm) were used in experiments with the live human endothelial umbilical vein cells (HUVEC). Cells treated with IL-1β expressed E-selectin and showed a 100−200 times higher binding of CLIO particles (83−104 ng iron/million cells) than control cells. The binding resulted in a high superparamagnetism of HUVEC with the transverse water proton relaxation time (T2) decrease to 30−40 ms in cell precipitates. Cells did not bind/internalize CLIO−F(ab′)$_2$ conjugates prepared using a control fragment or nonconjugated iron oxide particles before or after treatment with IL-1β. MR imaging of cells showed a highly specific T2-weighted signal darkening associated with cells treated with IL-1β and incubated with anti-E selectin. Demonstration of MR imaging of E-selectin expression justifies further development of MR-targeted agents for monitoring tumor vascular endothelial proliferation, angiogenesis, and atherosclerosis.

INTRODUCTION

Noninvasive imaging of endothelial cell surface marker expression in vivo represents an avenue for identifying early signs of tumor angiogenesis (reviewed in ref 1; *2*) and arthritis and inflammation (*3*, *4*, *5*) as well as atherosclerosis (*6*, *7*). For example, recent research demonstrated feasibility of targeted ^{18}F-labeled peptides (*8*) as well as paramagnetic agents (*2*, *9*) in detecting $\alpha v\beta 3$ integrin expression in endothelial cells lining tumor vessels. Alternatively, several other endothelial cell surface markers or adhesion-promoting molecules including endoglin (*10*) and fibronectin isoform B−FN (*11*) were investigated for imaging endothelial proliferation. There is a significant wealth of evidence suggesting that the expression of E-selectin (CD62E) (*12*), a proinflammatory marker of endothelial cells, is upregulated in proliferating endothelial cells (*13*). E-selectin overexpression was colocalized with dividing microvascular endothelial cells in tissues with active angiogenesis (*14*). In tumors, E-selectin-positive vessels are preferentially found in vascular-rich areas (*15*). In contrast to cell-surface associated E-selectin, levels of cell-shedded soluble E-selectin (sE-selectin) do not usually correlate with primary tumor angiogenesis but are frequently elevated in patients with active metastasis (*16*, *17*). Apart from E-selectin-specific diagnostic probes for angiogenesis, another potentially important application of E-selectin targeted imaging is in detection of early changes in endothelial phenotype linked to atherosclerotic plaque formation (*18*).

The goal of the current study was to develop a MR-detectable reporter with high affinity to E-selectin with an ultimate goal to image E-selectin expression in vivo with high resolution. Since superparamagnetic particles are detectable in tissues at relatively low concentrations of iron oxide (*19*), we chose to couple well-characterized high-affinity anti-human E-selectin antibody fragment (H18/7 (*12*)) to novel cross-linked iron oxide nanoparticles, CLIO[1] (*20*). Here we demonstrate that (1) the antibody−CLIO conjugate retains its specificity for E-selectin; (2) E-selectin expression can be detected by MR imaging in human endothelial cell culture.

MATERIALS AND METHODS

Cross-Linked Iron Oxide (CLIO). Dextran-coated iron oxide cross-linked with epichlorohydrin (cross-linked iron oxide, CLIO) was functionalized as described in (*20*, *21*) and reacted with *N*-succinimidyl-3-(2-pyridyl)dithiopropionate (SPDP) to yield CLIO bearing 3-(2-pyridyl)-propionyl residues (CLIO-SS-2Py). Analysis of CLIO-bound 2-pyridyl disulfide groups was performed by using dithiotrietol (DTT) reduction. Briefly, 50 μL of the CLIO-SS-2Py solution was added to 75 μL of DTT (20 mM) in PBS, pH 7.4 for 30 min. Pyridine-2-thione was separated from CLIO using Microcon 30 concentrators (Amicon, Beverly, MA) and absorbance at 343 nm (ϵ= 8100 M^{-1} cm^{-1}) was measured in the flow-through fraction.

F(ab′)$_2$ fragment of monoclonal anti-human E selectin antibody (H18/7, Vascular Research Division, Department of Pathology, Brigham and Women's Hospital) (90 nmol) was radioiodinated with ^{125}I using IodoGen (Pierce Chemical Co) as described by the manufacturer. Labeled antibody fragment was purified using P-6 gel Minicolumn (Bio-Rad, Hercules CA) equilibrated with PBS pH 7.2. Final specific radioactivity was 1.3−1.5 × 10^6 cpm/μg.

* To whom correspondence should be addressed: abogdanov@helix.mgh.harvard.edu.

[1] Abbreviations: CLIO, cross-linked iron oxide; SS-2Py, 2-pyridyl disulfide; SATA, succinimidyl *S*-acetylthioacetate.

10.1021/bc0155521 CCC: $22.00 © 2002 American Chemical Society
Published on Web 12/22/2001

Modification of F(ab′)$_2$ Fragment with *N*-Succinimidyl *S*-Acetylthioacetate. Conjugation of *N*-succinimidyl *S*-acetylthioacetate (*22*) (SATA, Molecular Biosciences, Boulder, CO) to the antibody fragment was accomplished by adding 27 nmol SATA from 0.5 mg/mL stock solution in DMF to 200 μg F(ab′)$_2$ solution (3.5 mg/mL in 0.05 M sodium bicarbonate pH 8.5, containing ^{125}I-F(ab′)$_2$ final specific activity 1·10^5 cpm/μg) and incubating with agitation for 2 h. The 15:1 mol:mol ratio of SATA to mAb was optimal as established in preliminary experiments. The SATA-modified F(ab′)$_2$ fragment was deacetylated by adding an equal volume of 25 mM hydroxylamine, 10 mM EDTA in PBS (pH 7.4) to F(ab′)$_2$−SATA. The excess of free thioacetic acid was removed by passing modified F(ab′)$_2$ through a P-6 gel centrifugation Minicolumn equilibrated with bicarbonate buffer (pH 8.4). Purified thioacetyl-F(ab′)$_2$ was then immediately used for conjugation to CLIO-SS-2Py.

Conjugation of Thioacetyl-F(ab′)$_2$ to CLIO-SS-2Py. An aliquot of CLIO-SS-2Py containing 340 μg Fe was added to 200 μg of thioacetyl-F(ab′)$_2$ in 0.05 M sodium bicarbonate, pH 8.5. The mixture was incubated overnight with mixing at 4 °C. A magnetic separation column (Macs, Miltenyi Biotec, CA) was used to separate the unbound mAb from iron oxide particles. The column was prewashed with 5 mL of degassed buffer (0.05 M sodium bicarbonate, pH 8.5). The reaction mixture was loaded on a column in the presence of external magnetic field. The column was washed twice with 5 mL of degassed buffer to remove nonbound antibody fragment. CLIO−F(ab′)$_2$ conjugate was eluted from the column in the absence of external magnetic field by washing the column with 0.05 M sodium bicarbonate, pH 8.5. The final concentration of iron in purified CLIO−F(ab′)$_2$ was 0.3−0.6 mg/mL. Purified CLIO−F(ab′)$_2$ was kept at 4 °C before use. In control experiments, anti-human IgG mouse monoclonal antibody fragment (control F(ab′)$_2$, Pierce Chemical Co) was conjugated to CLIO-SS-2Py and resultant conjugate was purified using the procedure described above.

Characterization of CLIO−F(ab′)$_2$. Iron concentration was determined as in (*23*). F(ab′)$_2$ concentration was measured by using gamma counting (Compugamma, Wallac, Turku Finland) or determined using BCA kit (Pierce Chemical Co). The size of initial CLIO and conjugates was determined using laser light scattering corrected for scattering properties of particles with different hydrodynamic radii (Zetasizer 3000HS/IHPL; Malvern Instruments Inc.).

Cell Culture Experiments. Human umbilical vein endothelial cells (HUVEC) were provided by Vascular Research Division, Department of Pathology, Brigham and Women's Hospital. HUVEC cells were plated in a gelatin-coated plastic flask containing endothelial cell growth basal medium (EBM) with endothelial growth supplements (Clonetics, BioWhittaker Inc.). Homogeneity of HUVEC culture was checked using flow-cytometry (FACScalibur, Becton-Dickinson) by using rat anti-human CD31 antibody (BD PharmIngen, San Diego CA) followed by anti-rat fluorescein-labeled antibody. To determine apparent dissociation constant (K_D^{app}) for H18/7 F(ab′)$_2$ HUVE cells were plated in 96-well plate and grown to confluency. Cells were treated with human recombinant interleukin-1β (hrIL-1β), freshly prepared by diluting 5μg/mL stock solution 100-fold in sterile HBSS, 10% FBS, 25mM Hepes pH 7.2. Human rIL-1β solution was added to EBM (final concentration −250 pg/mL). Control cells were left untreated. Cells were incubated for 4 h at 37 °C, washed twice with EBM and incubated with ^{125}I-F(ab′)$_2$ that was serially diluted in the medium (1000−1 ng/well) at 4 °C for 30 min. After the extensive washings, cells were solubilized in 1% Igepal/0.1% SDS and radioactivity in lysates was determined using gamma-counting.

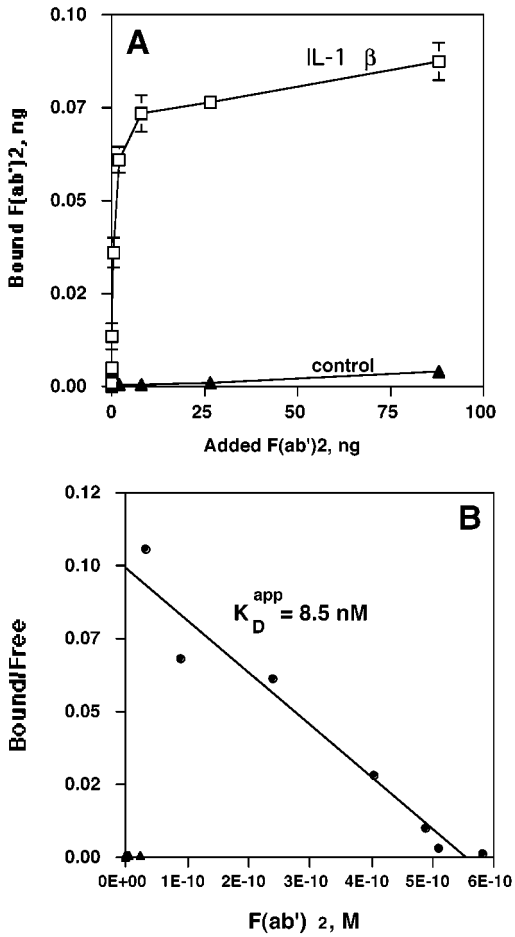


Figure 1. (A) Binding of ^{125}I-labeled H18/7 F(ab′)$_2$ to HUVEC stimulated by IL-1b treatment (squares) and to control HUVEC (triangles). (B) Scatchard plot of binding results presented in A. Circles, IL-1β treated cells; triangles, control cells.

To test the binding of CLIO−F(ab′)$_2$ conjugate to activated or nontreated cells, HUVEC were cultured in 6-well plates until confluence. Expression of E-selectin was induced as described above. Inducible expression of E-selectin on HUVECs after treating cells with IL-1β was verified by FACS after incubating treated and control cells with H18/7 antibody fragment followed by phycoerythrin-labeled goat anti-mouse F(ab′)$_2$ antibody (BD PharmIngen). The medium was replaced with the IL-1β containing EBM, and cells were incubated at 37 °C in 6% CO_2 atmosphere for 2 h. The medium was then replaced with fresh EBM (2 mL/well) containing 20 μL of CLIO−F(ab′)$_2$ conjugate (6.3 μg iron/mL; 400 ng F(ab′)$_2$/mL). Alternatively, an equivalent amount of control, antibody-free CLIO preparation or nonspecific CLIO−F(ab′)$_2$ conjugate were added to each well. The plates were agitated using a rotary incubator for 1 h. The cells were washed three times with HBSS, 10% FBS, 25 mM Hepes pH 7.2, and detached by scraping. Approximately 6.5 ± 0.5 × 10^6 cells were used to prepare samples for MR imaging. Cells were sedimented in 0.25 mL PCR tubes. The total volume of cells and medium was adjusted to 70 μL. The cell layer in the tubes was usually 2.9 ± 0.4 mm high (pellet volume 25 ± 6 μL). Tubes were filled with HBSS, 10% FBS, 25mM Hepes pH 7.2 solution and

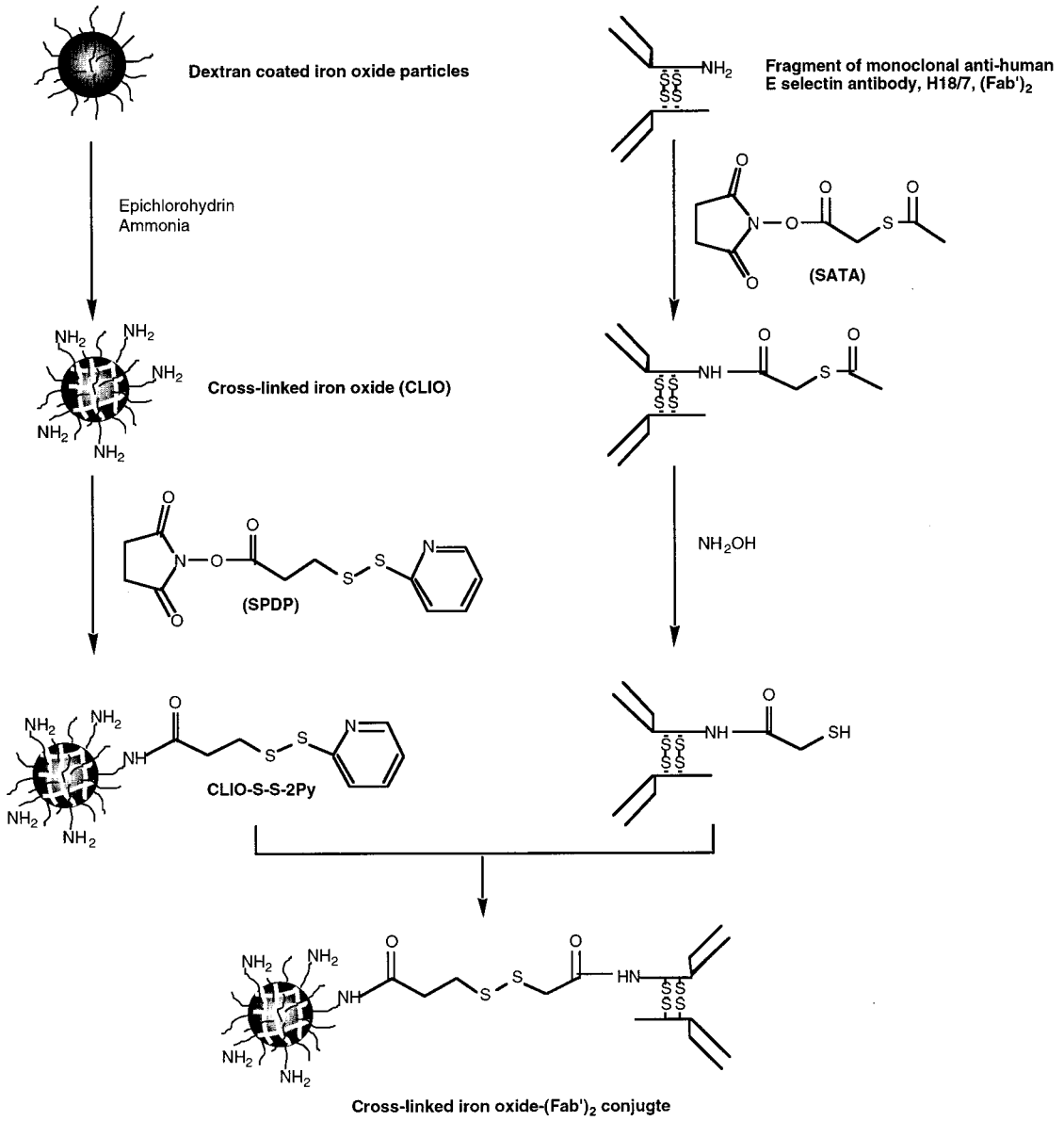


Figure 2. Schema of CLIO−F(ab′)$_2$ synthesis.

subjected to MR imaging. The amount of F(ab′)$_2$ and iron bound to cells was estimated using ^{125}I radioactivity counting (Compugamma, LKB, Gaithersburg, MD) using a previously determined F(ab′)$_2$/Fe ratio in CLIO−F(ab′)$_2$ preparations.

MR Imaging. MRI was performed using a clinical 1.5 T superconducting magnet (Signa 5.0, GE Medical Systems, Milwaukee, WI) and a 3.5 in. surface coil. A T2 weighted spin−echo sequences (TR 3000 ms, variable TE 16−100 ms and 1.0 mm imaging slice) were used for imaging and T2 relaxation time measurements. All sample tubes were placed in water to avoid artifacts during MR imaging. Signal intensity values were measured using IP Lab software (Signal Analytics, Vienna, VA). Relaxation time (T2) values were estimated using monoexponential decay fit as described (*20*) using Prism 2 software (GraphPad Software Inc.).

RESULTS AND DISCUSSION

Previous research suggested that in vivo detection of E-selectin expression by endothelial cells can be of prime importance for tumor angiogenesis imaging and potentially in imaging events preceding the atherosclerotic plaque formation. The expression of E-selectin is transcriptionally upregulated as a result of endothelial cell exposure to several cytokines (e.g., IL-1β and TNFα) and lipopolysaccharide (*24*, *25*, *26*). As demonstrated previously, several monoclonal antibodies to human E-selectin detects inducible E-selectin expression on human endothelial cells with high specificity (*12*, *27*). E-selectin targeted immunoliposomes and anti-E-selectin−hirudin conjugates prepared using H18/7 antibody (*12*) were previously shown to bind to activated human endothelial cells in vitro at the levels exceeding 200-fold those of control cells (*28*, *29*). These findings suggest that the H18/7 antibody or its fragments can potentially serve as excellent targeting ligand for designing imaging probes. In the current research we set forth to chemically link an F(ab′)$_2$ fragment isolated from H18/7 to the surface of cross-linked iron oxide particles (CLIO) and to investigate the utility of resultant CLIO−F(ab′)$_2$ conjugate for MR imaging of inducible E-selectin expression.

Initially, we tested the specificity of H18/7 F(ab′)$_2$ binding to IL-1β-treated cells and determined the apparent K_d. Even at very high antibody/cell ratio (100 ng Fab/10^4 cells) specific binding of antibody fragment was 100-

Table 1. Differential Binding of CLIO−F(ab′)$_2$ to HUVEC Cells in the Presence or Absence of IL-1β Treatment

preparation/batch	CLIO−F(ab′)$_2$ #1[a]		CLIO−F(ab′)$_2$ #2	
HUVEC, IL-1β treatment	+	−	+	−
Iron binding, ng/mLn cells**	104 ± 12	2.1	83 ± 10	0.4
F(ab′)$_2$ binding ng/mLn cells[b]	5.5 ± 0.8	0.1	12 ± 1.4	.05
T2, ms	29 ± 2	>1500	40 ± 17	1465

[a] CLIO−F(ab′)$_2$ batch #1: 0.6 mg Fe/mL; 40.8 μg F(ab′)$_2$/mL (molar ratio Fe/F(ab′)$_2$ = 15); batch #2: 0.31 mg Fe/mL; 44.1 μg F(ab′)$_2$/mL (molar ratio Fe/F(ab′)$_2$ = 7). [b] Data presented as: mean ± SD (n = 2).

times higher than the nonspecific uptake (Figure 1A). The apparent dissociation constant of H18/7 F(ab′)$_2$ was estimated as 8.5 nM for IL-1β-treated cells (Figure 1B) suggesting high affinity interaction and potential utility of H18/7 F(ab′)$_2$ for further in vitro and in vivo experiments. To prepare a conjugate of F(ab′)$_2$ with MR imaging probe, cross-linked iron oxide (CLIO) was chosen because of high stability of these particles and controllable chemistry of surface modification. To conjugate antibody fragment to CLIO, the latter was first modified with SPDP to attach pyridyl-disulfide groups to the surface of nanoparticles (*20*) (Figure 2). The resultant preparation contained approximately 27 2-pyridyldithio groups per iron oxide nanoparticle. We then covalently modified F(ab′)$_2$ amino groups with *N*-succinimidyl thioacetate (SATA) to attach protected sulfhydryl groups to F(ab′)$_2$ (*22*) (Figure 2). This conjugation was carried out at the ratio of 1:15 (F(ab′)$_2$:SATA mol/mol). As determined using an IL-1β activation test, modification with SATA resulted in a negligible loss of specificity and was thus used in further experiments as the standard coupling procedure. Our results are in agreement with previous work (*22*) showing that F(ab′)$_2$:SATA ratios 1:10−1:15 are optimal for antibody modification. The next coupling step included deacetylation with hydroxylamine in PBS followed by reacting thioacetyl-F(ab′)$_2$ with CLIO-SS-2Py. The conjugates purified on magnetic columns from the unbound antibody contained 453 ± 145 μg iron and 42.5 ± 1.6 μg F(ab′)$_2$ per mL (4.7 10^{-5} mol F(ab′)$_2$/mol iron). This ratio corresponds to an approximately 10−15% binding yield, assuming that each iron oxide crystal contains approximately 2064 atoms of iron (*23*). One to two molecules F(ab′)$_2$ were conjugated for each 10 nanoparticles. This ratio can be potentially increased by using alternative conjugation strategies or higher initial antibody/iron ratios. However, our results demonstrate that a decrease of Fe/F(ab′)$_2$ ratio does not necessarily result in a dramatic contrast enhancement of E-selectin-positive cells (see Table 1 and Figure 4). Using LALLS we determined that at the chosen ratio of the reactants the hydrodynamic diameter increased 1.6 times from 27.7 nm (nonreacted CLIO) to 40.6 nm (CLIO−F(ab′)$_2$ (polydispersity 0.22−0.28, Figure 3). This was apparently a consequence of F(ab′)$_2$ covalent attachment as the size of conjugates remained constant for almost two months, suggesting a very limited aggregation and sufficient stability of the conjugate. We determined that the further aggregation of CLIO−F(ab′)$_2$ particles was limited to approximately 1% of the total particle number (the size of the aggregates ranged between 150 and 274 nm).

In experiments involving binding of CLIO−F(ab′)$_2$ to HUVEC, either IL-1β activated, or control, we observed a very highly specific binding to activated endothelial cells (Table 1). By using a ^{125}I -labeled CLIO−F(ab′)$_2$ preparation, we determined that on the average, 0.14 ± 0.05% of initially added iron oxide was bound to IL-1β-treated HUVEC if CLIO−F(ab′)$_2$ was added to cells at the concentration of 1.2−2.4 μg iron/mL. In the absence of IL-1β pretreatment only 0.02−0.06% of iron was taken up by the endothelial cells under similar conditions. Thus, our results indicate that CLIO-bound antibody preserved its specificity (approximately 50-fold higher binding to activated than to control cells) and that the HUVECs bind CLIO−F(ab′)$_2$ with the high efficiency (approximately 0.1 pg iron/cell). The shortening of T2 relaxation times of water was clearly dependent on the amount of iron associated with the cells (Table 1). Cells incubated with CLIO−F(ab′)$_2$ conjugate were further subjected to MR imaging to determine whether differential binding of CLIO−F(ab′)$_2$ to nontreated vs IL-1β-treated cells could be verified by MR imaging and MR signal intensity measurements. As shown in Figure 4, T2-weighted MR spin−echo images revealed remarkable differences in signal intensities of IL-1β treated and control cells. Interleukin-treated endothelial cells showed a stronger contrast enhancement in two independent experiments performed using different batches of the conjugate (Table 1). There was no detectable MR signal intensity change observed in pellets of cells incubated with CLIO−F(ab′)$_2$ without pretreatment with IL-1β.

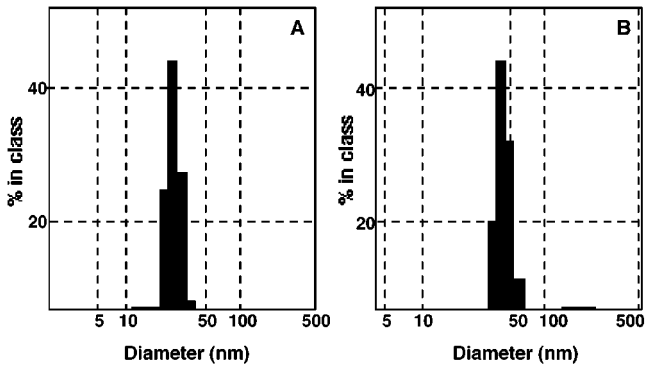


Figure 3. Size distribution of CLIO modified with SPDP (A) and CLIO−F(ab′)$_2$ (B) particles measured using laser light scattering (Zetasizer 3000, Malvern Instruments Inc.).

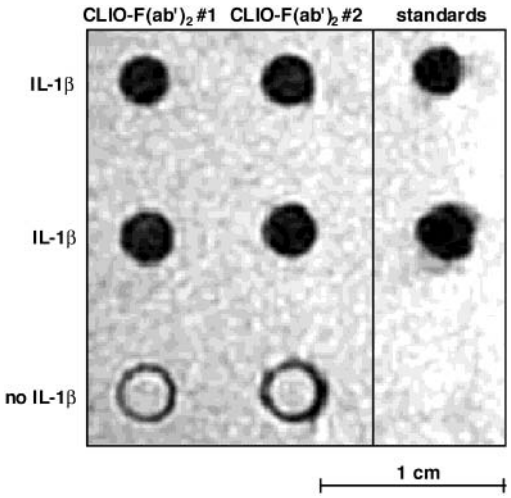


Figure 4. MR imaging of HUVEC precipitates in PCR tubes. Cells were incubated with CLIO−F(ab′)$_2$ #1 (samples 1−3) or CLIO−F(ab′)$_2$ #2 (samples 4−6). Samples 1, 2, 4, 5, HUVEC IL-1β treated cells; samples 3, 6, control, nontreated cells. Sample 7: CLIO−F(ab′)$_2$ solution at 0.05 mg iron/mL. Sample 8: CLIO−F(ab′)$_2$ solution at 0.1 mg iron/mL. MR imaging was performed using T2 weighted spin−echo sequence (TE 100/TR 3000), 1.5 mm imaging slice (1.5 T). Field of view , 3 in.

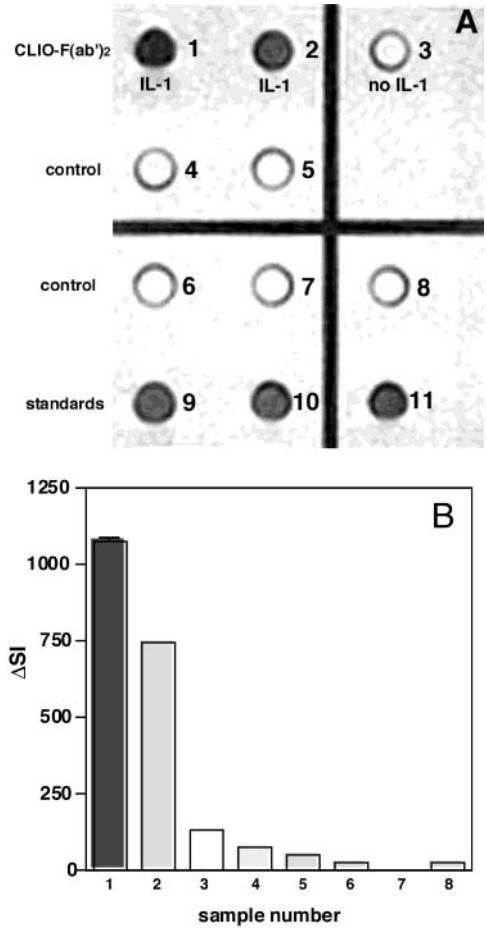


Figure 5. (A**)** MR imaging of HUVEC precipitates **1**, IL-1β-pretreated cells incubated with CLIO−F(ab′)$_2$ #1; **2**, IL-1β-pretreated cells incubated with CLIO−F(ab′)$_2$ #1 in the presence of 10-fold excess of free H18/7 F(ab′)$_2$; **3**, control cells incubated with CLIO−F(ab′)$_2$ #1; **4**, IL-1β-pretreated cells incubated with CLIO-SS-Py; **5**, IL-1β-pretreated cells incubated with MION; **6** and **7,** IL-1β-pretreated cells incubated with CLIO−nsF(ab′)$_2$ (control nonspecific F(ab′)$_2$); **8**, control cells incubated with CLIO-nsF(ab′)$_2$ were incubated for 30 min with 0.5 μg iron/mln cells and washed); **9**−**11**, CLIO−F(ab′) $_2$ standard solutions (0.18 ± 0.01 mg/mL). MR imaging was performed using T2 weighted spin−echo sequence (TE 100/TR 3000), 1.0 mm imaging slice (1.5 T). Field of view, 3 in. (B) Region-of-interest T2-weighted MR signal intensity analysis in samples **1**−**8** (see Figure 4A). The MR signal of water was subtracted from MR signal intensity measurements. Data presented as mean ± SD.

Thus, this result is in agreement with quantitative analysis of CLIO−F(ab′)$_2$ binding to HUVECs (Table 1). However, since an increase of CLIO−F(ab′)$_2$ uptake after IL-1β treatment could be a result of additional cytokine-mediated activation of adsorptive endocytosis or pinocytosis of particles (*30*), we set forth to test this using several control preparations. We compared binding of H18/7 F(ab′)$_2$ conjugated to CLIO with a nonspecific CLIO−F(ab′)$_2$ conjugate as well as unconjugated CLIO or MION (non-cross-linked) iron oxide (*30*). The results of MR imaging (Figure 5 A and B) clearly demonstrate that the profound signal intensity changes detected in IL-1β-activated HUVECs incubated with CLIO−F(ab′)$_2$ do not stem from the augmentation of nonspecific uptake mechanisms since cells incubated in the presence of control nanoparticles did not show any measurable uptake either before or after the IL-1β treatment (Figure 5A, samples 4−8). Interestingly, a 10-fold molar excess of free H18/7 F(ab′)$_2$ over the CLIO-conjugated F(ab′) inhibited binding and uptake by IL-1β treated cells only by 20% on the average. The further increase of free H18/7 F(ab′)$_2$ concentration to the level of 25-fold molar excess in the incubation medium resulted in a 76% of inhibition of the binding and uptake by HUVEC. One of the potential explanations for the observed effect is in that the antibody-conjugated particle has a higher valency, i.e., a higher avidity to the cell surface than F(ab′)$_2$ as a result of multipoint interaction with receptors expressed on the cell surface, the effect well studied in cell-targeted liposome experiments (*28, 31*). In addition, E-selectin is rapidly and constitutively internalized by IL-1β treated HUVEC (*32*) which may result in efficient endocytosis of many E-selectin bound particles by activated endothelial cells.

In conclusion, we demonstrated that H18/7 or control F(ab′)$_2$ fragments can be covalently modified with SATA and attached to superparamagnetic nanoparticles using thiol−disulfide exchange reaction. Anti-E selectin nanoparticles bound with high specificity to IL-1β stimulated HUVECs. We further demonstrated that specific interaction between CLIO−F(ab′)$_2$ and HUVEC can be directly imaged using MRI. This suggests potential in vivo utility of anti-E-selectin targeting for imaging endothelial activation and potentially, angiogenesis. In designing E-selectin-targeted agent we utilized CLIO particles that have a relatively long blood half-life (655 ± 37 min in mice at a dose of 10 mg Fe/kg, P. Wunderbaldinger, personal communication) and the antibody fragment lacking the Fc fragment. Both of these factors can potentially decrease the uptake of anti-E-selectin−CLIO in the liver, the major site of iron oxide elimination from the bloodstream (*30*). Overall, our experiments provide preliminary evidence of the feasibility of E-selectin imaging and justify further development of MR-targeted agents for monitoring proinflammatory markers associated with tumor vascular endothelial proliferation, angiogenesis, and atherosclerosis.

ACKNOWLEDGMENT

The authors acknowledge the help of Jeanne-Marie Kiely for providing H18/7 antibody fragment, Kay Case for assistance with endothelial cell culture, and Dr. Michael Gimbrone, Jr. for useful comments (Vascular Research Division, Department of Pathology, Brigham and Women's Hospital Boston MA). This work has been supported in part by 1P50CA86355-01 (R.W.) and 5RO1 CA74424-01 (AB). A.P. was supported in part by the Russian Department of Education Presidential Award.

LITERATURE CITED

(1) Brasch, R., Pham, C., Shames, D., Roberts, T., van Dijke, K., van Bruggen, N., Mann, J., Ostrowitzki, S., and Melnyk, O. (1997) Assessing tumor angiogenesis using macromolecular MR imaging contrast media. *J. Magn. Reson. Imag. 7*, 68−74.

(2) Sipkins, D. A., Cheresh, D. A., Kazemi, M. R., Nevin, L. M., Bednarski, M. D., and Li, K. C. (1998) Detection of tumor angiogenesis in vivo by alphaVbeta3-targeted magnetic resonance imaging. *Nat. Med. 4*, 623−626.

(3) Keelan, E. T., Harrison, A. A., Chapman, P. T., Binns, R. M., Peters, A. M., and Haskard, D. O. (1994) Imaging vascular endothelial activation: an approach using radiolabeled monoclonal antibodies against the endothelial cell adhesion molecule E-selectin. *J. Nucl. Med. 35*, 276−281.

(4) Chapman, P. T., Jamar, F., Keelan, E. T., Peters, A. M., and Haskard, D. O. (1996) Use of a radiolabeled monoclonal antibody against E-selectin for imaging of endothelial activation in rheumatoid arthritis. *Arthritis Rheum. 39*, 1371−1375.

(5) Zinn, K. R., Chaudhuri, T. R., Smyth, C. A., Wu, Q., Liu, H. G., Fleck, M., Mountz, J. D., and Mountz, J. M. (1999) Specific

targeting of activated endothelium in rat adjuvant arthritis with a 99mTc-radiolabeled E-selectin-binding peptide. *Arthritis Rheum. 42*, 641−649.
(6) Houston, P., Goodman, J., Lewis, A., Campbell, C. J., and Braddock, M. (2001) Homing markers for atherosclerosis: applications for drug delivery, gene delivery and vascular imaging. *FEBS Lett. 492*, 73−77.
(7) Schmitz, S. A., Coupland, S. E., Gust, R., Winterhalter, S., Wagner, S., Kresse, M., Semmler, W., and Wolf, K. J. (2000) Superparamagnetic iron oxide-enhanced MRI of atherosclerotic plaques in Watanabe hereditable hyperlipidemic rabbits. *Invest. Radiol. 35*, 460−771.
(8) Haubner, R., Wester, H. J., Weber, W. A., Mang, C., Ziegler, S. I., Goodman, S. L., Senekowitsch-Schmidtke, R., Kessler, H., and Schwaiger, M. (2001) Noninvasive imaging of alpha(v)beta3 integrin expression using 18F-labeled RGD-containing glycopeptide and positron emission tomography. *Cancer Res. 61*, 1781−1785.
(9) Anderson, S. A., Rader, R. K., Westlin, W. F., Null, C., Jackson, D., Lanza, G. M., Wickline, S. A., and Kotyk, J. J. (2000) Magnetic resonance contrast enhancement of neovasculature with alpha(v)beta(3)-targeted nanoparticles. *Magn. Reson. Med. 44*, 433−9.
(10) Bredow, S., Lewin, M., Hofmann, B., Marecos, E., and Weissleder, R. (2000) Imaging of tumour neovasculature by targeting the TGF-b binding receptor endoglin. *Eur. J. Cancer 36*, 675−681.
(11) Neri, D., Carnemolla, B., Nissim, A., Leprini, A., Querze, G., Balza, E., Pini, A., Tarli, L., Halin, C., Neri, P., Zardi, L., and Winter, G. (1997) Targeting by affinity-matured recombinant antibody fragments of an angiogenesis associated fibronectin isoform. *Nat. Biotechnol. 15*, 1271−1275.
(12) Bevilacqua, M. P., Pober, J. S., Mendrick, D. L., Cotran, R. S., and Gimbrone, M. A., Jr. (1987) Identification of an inducible endothelial-leukocyte adhesion molecule. *Proc. Natl Acad. Sci. U.S.A. 84*, 9238−9242.
(13) Bischoff, J., Brasel, C., Kraling, B., and Vranovska, K. (1997) E-selectin is upregulated in proliferating endothelial cells in vitro. *Microcirculation 4*, 279−287.
(14) Kraling, B. M., Razon, M. J., Boon, L. M., Zurakowski, D., Seachord, C., Darveau, R. P., Mulliken, J. B., Corless, C. L., and Bischoff, J. (1996) E-selectin is present in proliferating endothelial cells in human hemangiomas. *Am. J. Pathol. 148*, 1181−1191.
(15) Mayer, B., Spatz, H., Funke, I., Johnson, J. P., and Schildberg, F. W. (1998) De novo expression of the cell adhesion molecule E-selectin on gastric cancer endothelium. *Langenbecks Arch. Surg. 383*, 81−86.
(16) Hebbar, M., Revillion, F., Louchez, M. M., Vilain, M. O., Fournier, C., Bonneterre, J., and Peyrat, J. P. (1998) The relationship between concentrations of circulating soluble E-selectin and clinical, pathological, and biological features in patients with breast cancer. *Clin. Cancer Res. 4*, 373−380.
(17) Wittig, B. M., Kaulen, H., Thees, R., Schmitt, C., Knolle, P., Stock, J., Meyer zum Buschenfelde, K. H., and Dippold, W. (1996) Elevated serum E-selectin in patients with liver metastases of colorectal cancer. *Eur. J. Cancer 32A*, 1215−1218.
(18) Gimbrone, M. A., Jr., Topper, J. N., Nagel, T., Anderson, K. R., and Garcia-Cardena, G. (2000) Endothelial dysfunction, hemodynamic forces, and atherogenesis. *Ann. N.Y. Acad. Sci. 902*, 230−239.
(19) Zimmer, C., Weissleder, R., O'Connor, D., LaPointe, L., Brady, T., and Enochs, W. (1995) Cerebral iron oxide distribution: in vivo mapping with MR imaging. *Radiology 196*, 521−527.
(20) Hoegmann, D., Josephson, L., Weissleder, R., and Basilion, J. P. (2000) Improvement of MRI probes to allow efficient detection of gene expression. *Bioconjugate Chem. 11*, 941−946.
(21) Josephson, L., Tung, C. H., Moore, A., and Weissleder, R. (1999) High-efficiency intracellular magnetic labeling with novel superparamagnetic-Tat peptide conjugates. *Bioconjugate Chem. 10*, 186−191.
(22) Duncan, R. J. C., Weston, P., and Wrigglesworth, R. (1983) A new reagent which may be used to introduce sulfhydryl group into proteins, and its use in the preparation of counjugate for immunoasay. *Anal. Biochem. 132*, 68−73.
(23) Shen, T., Weissleder, R., Papisov, M., Bogdanov, A., Jr., and Brady, T. J. (1993) Monocrystalline iron oxide nanocompounds (MION): physicochemical properties. *Magn. Reson. Med. 29*, 599−604.
(24) Bagby, G. C. (1989) Interleukin-1 and hematopoiesis. *Blood Rev. 3*, 152−161.
(25) Luscinskas, F. W., Brock, A. F., Arnaout, M. A., and Gimbrone, M. A. (1989) Endothelial-leukocyte adhesion molecule-1-dependent and leukocyte (CD11/CD18)-dependent mechanisms contribute to polymorphonuclear leukocyte adhesion to cytokine-activated human vascular endothelium. *J. Immunol. 142*, 2257−2263.
(26) Montgomery, K. F., Osborn, L., Hession, C., Tizard, R., Goff, D., Vassallo, C., Tarr, P. I., Bomsztyk, K., Lobb, R., and Harlan, J. M. (1991) Activation of endothelial-leukocyte adhesion molecule 1 (ELAM-1) gene transcription. *Proc. Natl. Acad. Sci. U.S.A. 88*, 6523−6527.
(27) Peters, A. M. (1998) The use of nuclear medicine in infection. *Brit. J. Radiol. 71*, 252−261.
(28) Spragg, D. D., Alford, D. R., Greferath, R., Larsen, C. E., Lee, K. D., Gurtner, G. C., Cybulsky, M. I., Tosi, P. F., Nicolau, C., and Gimbrone, M. A., Jr. (1997) Immunotargeting of liposomes to activated vascular endothelial cells: a strategy for site-selective delivery in the cardiovascular system. *Proc. Natl. Acad. Sci. U.S.A. 94*, 8795−8800.
(29) Kiely, J. M., Cybulsky, M. I., Luscinskas, F. W., and Gimbrone, M. A., Jr. (1995) Immunoselective targeting of an anti-thrombin agent to the surface of cytokine-activated vascular endothelial cells. *Arteriosclerosis, Thromb. Vasc. Biol. 15*, 1211−1218.
(30) Moore, A., Weissleder, R., and Bogdanov, A., Jr. (1997) Uptake of dextran-coated monocrystalline iron oxides in tumor cells and macrophages. *J. Magn. Reson. Imag. 7*, 1140−1145.
(31) Papahadjopoulos, D., Heath, T., Bragman, K., and Matthay, K. (1986) New methodology for liposome targeting to specific cells. *Ann. N.Y. Acad. Sci.* 446, 341−348.
(32) von Asmuth, E. J., Smeets, E. F., Ginsel, L. A., Onderwater, J. J., Leeuwenberg, J. F., and Buurman, W. A. (1992) Evidence for endocytosis of E-selectin in human endothelial cells. *Eur. J. Immunol. 22*, 2519−2526.

BC0155521

Preparation and Functional Evaluation of RGD-Modified Proteins as $\alpha_v\beta_3$ Integrin Directed Therapeutics

Robbert J. Kok,*,§ Astrid J. Schraa,‡,§ Erwin J. Bos, Henk E. Moorlag,‡ Sigridur A. Ásgeirsdóttir,§ Maaike Everts,§ Dirk K. F. Meijer, and Grietje Molema†

Groningen University Institute for Drug Exploration (GUIDE), Department of Pharmacokinetics and Drug Delivery, University Centre for Pharmacy, A. Deusinglaan 1, 9713 AV Groningen, The Netherlands. Received October 3, 2001; Revised Manuscript Received November 16, 2001

Tumor blood vessels can be selectively targeted by RGD-peptides that bind to $\alpha_v\beta_3$ integrin on angiogenic endothelial cells. By inhibiting the binding of these integrins to its natural ligands, RGD-peptides can serve as antiangiogenic therapeutics. We have prepared multivalent derivatives of the cyclic RGD-peptide c(RGDfK) by covalent attachment of the peptide to side chain amino groups of a protein. These RGDpep−protein conjugates inhibited $\alpha_v\beta_3$-mediated endothelial cell adhesion in vitro, while conjugates prepared with a control RAD-peptide showed no activity. Radiobinding and displacement studies with endothelial cells demonstrated an increased affinity of the RGDpep−protein conjugates compared to the free peptide, with IC_{50} values ranging from 23 to 0.6 nM, depending on the amount of coupled RGDpep per protein. Compared to the parental RGD-peptide and the related RGD-peptide ligand c(RGDfV), the RGDpep−protein conjugates showed a considerable increase in affinity (IC_{50} parent RGDpep: 818 nM; IC_{50} c(RGDfV): 158 nM). We conclude that the conjugation of RGD-peptides to a protein, resulting in products that can bind multivalently, is a powerful approach to increase the affinity of peptide ligands for $\alpha_v\beta_3/\alpha_v\beta_5$ integrins.

INTRODUCTION

The formation of new blood vessels is essential for the supply of oxygen and nutrients to proliferating tumor cells. Antitumor therapies that aim at the endothelium of these newly formed tumor blood vessels seem attractive for several reasons. First, the disruption of one blood vessel will result in the killing of a multitude of tumor cells, as shown by inhibiting angiogenesis or by inducing tumor vasculature selective blood coagulation (*1*). Second, endothelial cells of tumor blood vessels are normal, nontransformed cells and therefore less likely to become resistant to antitumor therapy than tumor cells. Last, the endothelium lining the blood vessels is easily accessible for systemically applied therapeutics.

Newly formed blood vessels are characterized by the expression of surface molecules that are not present on resting endothelium (*2*). One of these so-called angiogenic markers is the $\alpha_v\beta_3$ integrin. Cyclic peptides containing a conformationally restrained Arg-Gly-Asp (RGD) sequence have been developed as ligands for $\alpha_v\beta_3$ and the closely related $\alpha_v\beta_5$ integrin (*3*). For instance, the dicyclic peptide CDCRGDCFC (RGD-4C)[1] has been used as a targeting moiety to selectively deliver doxorubicin to angiogenic blood vessels (*4*). A drawback of the RGD-4C peptide is the instability of the two disulfide bridges that maintain the specific three-dimensional structure of the peptide (*5*). A chemically more stable peptide with high affinity for $\alpha_v\beta_3$ integrin and moderate affinity for $\alpha_v\beta_5$ integrin is the cyclic pentapeptide c(RGDfV) (*6, 7*). This peptide consists of a head-to-tail cyclic ring containing one D-amino acid and is currently under investigation for tumor imaging and antitumor radiotherapy (*8*).

The present study describes the development of conjugates of the RGD-peptide c(RGDfK) coupled to the side chain amino groups of a protein backbone (Figure 1). Such conjugates have some favorable characteristics that are not present in the parental peptide. For instance, multiple peptide ligands can be attached covalently to the protein. Theoretically, the resulting multivalency of such a conjugate should result in increased avidity for $\alpha_v\beta_3/\alpha_v\beta_5$ integrins. Furthermore, the larger molecular size of such conjugates often results in longer circulation times in the body (*9*). Finally, our goal is to apply RGDpep−protein conjugates as carrier molecules in drug targeting strategies aiming at angiogenic endothelial cells. The larger size of the RGDpep−protein conjugates allows the attachment of multiple drug molecules, instead of the 1:1 coupling ratio of the RGD-4C-doxorubicin construct mentioned above.

In the current study, a series of conjugates were prepared consisting of different amounts of the RGD-peptide c(RGDfK) and a nonrelevant IgG protein backbone. The binding characteristics of such preparations

* To whom correspondence should be addressed. Phone: +31-50-3637627. Fax: +31-50-3633247. E-mail: r.j.kok@farm.rug.nl.

§ Members of UNYPHAR, a network collaboration between the universities of Groningen, Leiden, Utrecht, and the pharmaceutical company Yamanouchi.

‡ Department of Pathology and Laboratory Medicine, Medical Biology section, Tumor Immunology Laboratory.

† Department of Pharmacokinetics and Drug Delivery and Department of Pathology and Laboratory Medicine.

[1] Abbreviations used: RGD-4C, CDCRGDCFC; RGDpep, c(RGDf(ϵ-*S*-acetylthioacetyl)K); RADpep, c(RADf(ϵ-*S*-acetylthioacetyl)K); HuMab, human-anti-mouse antibody; SIA, *N*-succinimidyl iodoacetate; AEC, 3-amino-9-ethylcarbazole; OPD, *o*-phenylenediamine dihydrochloride; GARPO, goat-anti-rabbit-immunoglobulin horseradish peroxidase conjugate; DTDP, 2,2′-dithiodipyridine; mcKLH, mariculture keyhole limpet hemocyanin; PVDF, poly(vinylidene difluoride); HUVEC, human umbilical vein endothelial cells; tTF, truncated Tissue Factor; TNFα, tumor necrosis factor α; IL-2, interleukin-2.

10.1021/bc015561+ CCC: $22.00 © 2002 American Chemical Society
Published on Web 12/01/2001

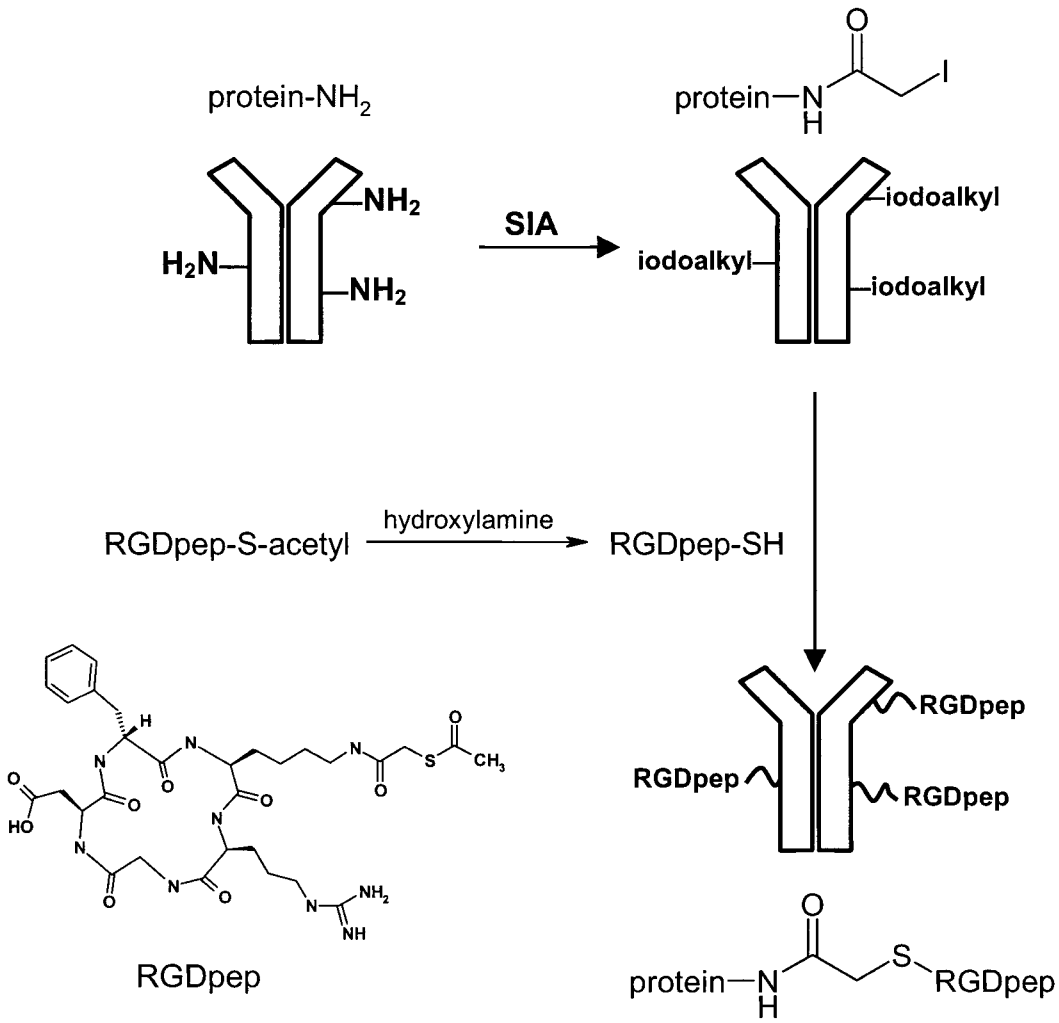


Figure 1. Synthesis of RGDpep−protein conjugates. The iodoacetyl linker (SIA) is coupled to primary amino groups of the protein. After purification by gel filtration, this product is allowed to react in the following reaction. After in situ removal of the protecting thioacetyl group of the peptide with hydroxylamine, RGDpep is coupled via its thiol group with the iodoacetyl group on the protein, resulting in a thioether linkage between RGDpep and protein.

to endothelial cells were studied and compared with those of single monovalent RGD-peptide ligands.

EXPERIMENTAL PROCEDURES

Chemicals and Proteins. All chemicals were used as supplied without further purification. The cyclic RGD-peptide c(RGDf(ϵ-*S*-acetylthioacetyl)K) and the RAD analogue c(RADf(ϵ-*S*-acetylthioacetyl)K), hereafter referred to as RGDpep and RADpep, respectively, were prepared by Ansynth (Roosendaal, The Netherlands). RGD-4C was kindly provided by F. M. H. de Groot (Nijmegen, The Netherlands). c(RGDfV) was obtained from Biomol (Omnilabo International BV, Breda, The Netherlands). HuMab was obtained from the University Hospital Groningen as leftovers from clinical application and consisted of a humanized antibody recognizing an irrelevant human nonendothelial antigen not of interest for our studies. *N*-Succinimidyl iodoacetate (SIA), 3-amino-9-ethyl-carbazole (AEC), *o*-phenylenediamine dihydrochloride tablets (OPD), vitronectin, and crystal violet were obtained from Sigma (St. Louis, MO). 2,2′-Dithiodipyridine (DTDP) was obtained from Fluka (Buchs, Switzerland). L-Cysteine hydrochloride was obtained from Merck (Darmstadt, Germany). Imject Mariculture Keyhole Limpet Hemocyanin (mcKLH), Freund's complete adjuvant, and Freund's incomplete adjuvant were obtained from Pierce (Rockford, IL). Goat-anti-rabbit-peroxidase (GARPO) was obtained from Dako A/S (Glostrup, Denmark). Fibronectin was obtained from Chemicon (Temecula, CA).

Preparation of anti-RGDpep Antiserum. A polyclonal rabbit antiserum was raised against an RGDpep-KLH conjugate in which RGDpep was linked to preactivated mcKLH according to the suppliers protocol. Approximately 600 μg RGDpep-KLH (600 μL) was mixed with an equal volume of Freund's complete adjuvant and injected subcutaneously into a Chinchilla rabbit (Harlan, Zeist, The Netherlands). At 14-day intervals, the immune response was boosted with the injection of RGDpep-KLH emulgated in Freund's incomplete adjuvant (two separate injections of 0.3 mL of emulgate). Blood was collected before immunization and 7 days after immunization. A total of three boosts was needed to obtain adequate anti-RGDpep titers.

Preparation and Characterization of RGDpep−Protein and RADpep−Protein Conjugates. RGDpep or RADpep were coupled in a two-step reaction to the lysine residues in the protein as described below. The iodoacetyl linker molecule SIA was coupled to the primary amino groups of the protein. After purification by size-exclusion chromatography, the SIA-activated proteins were mixed with the peptide and allowed to react after in situ deprotection of the thioacetyl group with hydroxylamine (Figure 1). The peptide:protein ratio of

the conjugate was controlled by varying the amounts of SIA and protein. The peptide was always added in a 2-fold molar excess over the amount of iodoacetyl reagent. To deactivate iodoacetyl groups that had not reacted with the peptide, a final conjugation step was performed with cysteine.

Synthesis of RGDpep−HuMab(I). HuMab (2 mg, 13 nmol) was diluted in PBS to a concentration of 4 mg mL^{-1}. A freshly prepared solution of SIA (19 μg, 67 nmol, 10 mg mL^{-1} in dimethylformamide) was added slowly while the reaction vial was protected from light. The mixture was allowed to react for 1 h at room temperature under gentle mixing. The crude product was purified by sephadex gel filtration (2 serial Hitrap 5 mL desalting columns, Pharmacia Biotech, Roosendaal, The Netherlands) using PBS as eluent at a flow rate of 0.5 mL min^{-1}. The protein-containing fraction was used directly in the following coupling reaction with the peptide. RGDpep (96 μg, 133 nmol), dissolved in an acetonitrile−water mixture (1:4) at a concentration of 10 mg mL^{-1}, was added dropwise to the activated protein. After addition of 100 μL of a freshly prepared hydroxylamine solution (1 M in water), the mixture was allowed to react overnight at room temperature. Remaining iodoacetyl groups were quenched with cysteine (24 μg of hydrochloride salt, 133 nmol, freshly dissolved in water at a concentration of 10 mg mL^{-1}) after which the mixture was reacted for another 1 h. Unreacted reagents were removed by dialysis against PBS at 4 °C. The final product was filtered through a 0.2 μm filter and stored at 4 °C or at −20 °C until further use.

*Synthesis of RGD*pep−Hu*Mab(II)−(IV) and RADpep−HuMab Conjugates.* RGDpep−HuMab and RADpep−HuMab conjugates differing in peptide:protein ratios were prepared according to the same protocol as described above for RGDpep−HuMab(I), using the following amounts of reagents (HuMab/SIA/peptide/cysteine): RGDpep−HuMab(II): 13/133/267/267 nmol; RGDpep−HuMab(III): 13/267/533/533 nmol; RGDpep−HuMab(IV): 13/667/1333/1333; RADpep−HuMab(II): 13/133/267/267 nmol; RADpep−HuMab(IV): 13/667/1333/1333. The amount of hydroxylamine solution (100 μL) was not changed in the various synthesis procedures.

SDS PAGE Analysis and Western Blotting. The covalent coupling of RGDpep or RADpep to the IgG protein in the conjugates was demonstrated by western blotting, followed by immunodetection of coupled peptides in the blotted proteins. For this, the conjugates were subjected to SDS−PAGE analysis performed on a mini-PROTEAN II system (Bio-rad, Veenendaal, The Netherlands) using 7.5% polyacrylamide Tris HCl gels. Samples were prepared for analysis in sample buffer without β-mercaptoethanol (nonreducing conditions) or with β-mercaptoethanol (reducing conditions) to disrupt disulfide bonds between the HuMab IgG subunits. Runned gels were either stained for protein (Coomassie Brilliant Blue staining) or blotted on poly(vinylidene difluoride) membranes (PVDF western blotting membranes, Roche Molecular Biochemicals, Almere, The Netherlands), followed by immunostaining for RGDpep or RADpep using anti-RGDpep polyclonal rabbit antiserum/GARPO/AEC detection. Prestained protein markers (precision prestained molecular weight markers, Bio-rad) were run together with the samples in a separate lane.

Size-Exclusion Chromatography. Molecular size of the prepared conjugates was also analyzed by size-exclusion chromatography under normal conditions, to demonstrate the absence of polymerized IgG or other aggregated proteins due to the conjugation procedures. Separations were performed on a FPLC system equipped with a Superdex 200 HR10/30 column (Pharmacia) and UV detection (214 nm), using PBS at a flow rate of 0.4 mL min^{-1} as mobile phase. HuMab, RGDpep−HuMab(IV), and RADpep−HuMab(IV) conjugates were diluted to a concentration of 100 μg mL^{-1} in PBS, of which 200 μL was injected into the system.

Determination of RGDpep-to-Protein Ratio. The protein content of the conjugates was determined by Lowry (*10*). The number of coupled RGDpep molecules was determined by ELISA using the anti-RGDpep antiserum. Wells were coated with serial dilutions of the RGDpep−protein conjugates for 2 h at 37 °C, washed with 25 mM Tris HCl buffer pH 8 containing 150 mM NaCl and 0.05% Tween 20 and incubated for 1 h with anti-RGDpep antiserum (1:1000 in PBS) at 37 °C, followed by standard detection with GARPO/OPD. The absorbance at 490 nm was measured on a ThermoMax microplate reader (Molecular Devices, Sunnyvale, CA). For each RGDpep−HuMab conjugate, the protein concentration at which 50% of the maximum absorbance was measured (EC_{50}) was calculated by nonlinear regression (Graphpad Prism). The relative RGDpep:protein ratio in each conjugate was calculated by normalization of the EC_{50} to the value of the RGDpep−HuMab(I) conjugate.

An estimate of the absolute RGDpep:protein ratio was obtained by determination of the amount of introduced iodoacetyl groups in the RGDpep−HuMab(IV) conjugate. This number was calculated by reacting the intermediate product SIA−HuMab(IV) with excess cysteine and titration of the remaining amount of free thiol groups with DTDP. In brief, HuMab (13 nmol, 4 mg mL^{-1} in PBS) was reacted with SIA (667 nmol) and purified by gel filtration as described above. To a 1 mL aliquot of the protein-containing fraction were added cysteine (1333 nmol, dissolved in water at a concentration of 10 mg mL^{-1}) and hydroxylamine (100 μL of a freshly prepared 1 M solution in water), and the mixture was stirred for 4 h at room temperature. A 100 μL aliquot was analyzed for thiol content by addition of 900 μL of PBS and 10 μL of DTDP solution (10 mg mL^{-1} in acetone), followed by immediate mixing and measurement of the absorbance at 343 nm. Calibration curves were prepared from a freshly prepared cysteine stock solution. To correct for oxidation of cysteine or consumption of the free thiol other than by reaction with the coupled iodoacetyl groups, a control experiment was performed in which HuMab (13 nmol, 4 mg mL^{-1} in PBS) was *not* reacted with SIA, but otherwise treated similarly as described above. The absolute iodoacetyl:protein ratio of the SIA−HuMab(IV) conjugate was calculated from the decrease in the molar amount of cysteine, corrected for oxidation, and from the protein content of the purified protein.

Cells. Human umbilical vein endothelial cells (HUVEC) were isolated by the method previously described by Mulder (*11*) and cultured on 1% gelatin-precoated plastic tissue culture plates or flasks (Costar Europe, Badhoevedorp, The Netherlands) at 37 °C under 5% CO_2/95% air. The culture medium consisted of RPMI 1640 (BioWittaker, Verviers, Belgium) supplemented with 20% heat-inactivated fetal calf serum (Integro BV, Zaandam, The Netherlands), 2 mM L-glutamine (GIBCO−BRL, Paisley, Scotland), 5 U mL^{-1} heparin (Leo Pharmaceutical Products BV, Weesp, The Netherlands), 100 U mL^{-1} penicillin (Yamanouchi Pharma BV, Leiderdorp, The Netherlands), 100 μg mL^{-1} streptomycin (Radiumfarma-Fisiopharma, Milan, Italy), and 50 μg mL^{-1} endothelial cell growth factor supplement extracted from bovine brain. After attaining confluence, cells were detached

from the surface by trypsin/EDTA (0.5/0.2 mg mL^{-1} in PBS) and split at a 1:3 ratio. HUVEC were used up to passage three.

The H5V mouse endothelioma cell line was kindly provided by Dr. A. Vecchi (Milan, Italy). H5V cells were grown in plastic tissue culture flasks or plates at 37 °C under 5% CO_2/95% air. The culture medium consisted of DMEM supplemented with 10% heat-inactivated FCS, 2 mM L-glutamine, and 300 μg mL^{-1} gentamicin. After attaining confluence, cells were detached from the surface by trypsin/EDTA (0.5/0.2 mg mL^{-1} in PBS) and split at a 1:3 ratio.

Endothelial Cell Adhesion Assay. The functional integrity of the coupled RGDpep was studied in an $\alpha_v\beta_3$-dependent adhesion assay as previously described with minor modifications (*12*). Briefly, flat bottom 96-wells culture plates were coated overnight with vitronectin (500 ng/well in PBS) at 4 °C. Wells were blocked with 1% BSA for 2 h at 37 °C and washed two times with PBS. Trypsinized HUVEC were resuspended in serum-free medium, incubated for 15 min on ice with RGDpep−HuMab or RADpep−HuMab conjugates, and subsequently plated at 2×10^4 cells/well. After incubation at 37 °C for 24 h, unattached cells were removed by rinsing the wells with PBS. Attached cells were fixed in 2% paraformaldehyde, stained with 0.5% crystal violet, and quantified by measuring the absorbance at 575 nm on an Emax microplate reader (Molecular Devices, Sunnyvale, CA). Control experiments included incubations with free RGDpep or RADpep, and adhesion experiments in wells coated with fibronectin, in which case the endothelial cell adhesion is independent of the availability of $\alpha_v\beta_3/\alpha_v\beta_5$ integrins due to adherence via $\alpha_5\beta_1$ integrin. Nonspecific binding of H5V cells was determined by adhesion onto BSA-coated wells.

Radiobinding Assays. The affinity of RGDpep−HuMab conjugates for $\alpha_v\beta_3/\alpha_v\beta_5$ integrin was studied using cells expressing these integrins rather than isolated receptors, to allow cross-linking and possible integrin multimerization in intact cell membranes. RGDpep−HuMab(IV) was radiolabeled with ^{125}I to a specific activity of 0.4 MBq μg^{-1} by a chloramine-T method (*13*). Confluent H5V cell layers in 24-well plates were preincubated for 15 min on ice with binding buffer (50 mM Tris-HCl buffer pH 7.4 supplemented with 150 mM NaCl, 1 mM $CaCl_2$, 1 mM $MgCl_2$, 1mM $MnCl_2$ and 1% BSA). After preincubation, the buffer was replaced by binding buffer containing 70000 cpm of ^{125}I-RGDpep−HuMab(IV) and appropriate dilutions of nonlabeled RGDpep−HuMab conjugates, followed by incubation of the cells for 4 h at 4 °C. After sampling of the supernatant, the cells were washed three times with binding buffer and lysed with 1 M NaOH (30 min at 37 °C). Radioactivity was counted in a LKB multichannel counter (LKB, Bromma, Sweden). Control experiments included competition experiments with RADpep−HuMab conjugates, free RGDpep and RADpep, as well as with c(RGDfV) and RGD-4C.

The K_d of ^{125}I-RGDpep−HuMab(IV) was calculated by nonlinear regression to the Michaelis−Menten equation[2] using the Multifit program (Department of Pharmacokinetics and Drug Delivery, University Centre for Pharmacy, Groningen, The Netherlands). IC_{50} values of RGDpep−HuMab conjugates and RGD-peptides were calculated by nonlinear regression (Graphpad Prism) using a one-site competition model[2].

Statistics. Statistical significance of differences was tested using the two-sided Student's t-test, assuming equal variances.

RESULTS

Preparation and Characterization of Peptide−Protein Conjugates. The peptide RGDpep and its nonbinding counterpart RADpep were coupled covalently to primary amino groups of the HuMab protein after initial derivatization with a iodoacetyl linker (Figure 1). To obtain conjugates with different numbers of coupled peptide, we used ratios of iodoacetyl reagent (SIA) and HuMab of 5:1, 10:1, 20:1, and 50:1 for RGDpep−HuMab-(I) to (IV), respectively. We demonstrated the covalent attachment of RGDpep to HuMab by SDS−PAGE analysis and immunoblotting with a polyclonal anti-RGDpep antiserum (Figure 2). Analysis of samples that were treated with β-mercaptoethanol revealed that the peptide was coupled in both IgG heavy and light chain subunits of the protein. Anti-RGDpep antiserum cross-reacted with RADpep−protein conjugates, but not with conjugates prepared with the iodoacetyl linker and unrelated peptides (data not shown). Therefore, this analysis method could also be applied for the analysis of RADpep−HuMab conjugates.

The covalent conjugation of RGDpep to the HuMab protein was also studied by anti-RGDpep ELISA. This method showed a clear correlation between the RGDpep incorporation and the added equivalents of coupling reagent during the synthesis (Figure 3). From these data, we conclude that we prepared a series of RGDpep−protein conjugates with increasing amounts of coupled RGDpep. In addition, we performed an indirect determination of the number of coupled RGDpep groups for the SIA−HuMab(IV) by reacting the introduced iodoacetyl groups with excess cysteine followed by titration of the remaining free thiol groups with DTDP. This analysis yielded an average of 23 coupled iodoacetyl groups per protein.

Size-exclusion chromatography of the peptide−protein conjugates demonstrated the absence of polymerized protein or other aggregates (Figure 4). A small-increase in molecular size of the conjugates was observed compared to the native IgG protein, both after coupling of RGDpep and RADpep ligands to HuMab.

Endothelial Cell Adhesion Assay. To test the functional integrity of the covalently attached RGDpep, we studied the effect of the RGDpep−HuMab conjugates on the adhesion of endothelial cells on vitronectin-coated surfaces. Figure 5 shows that RGDpep−HuMab conjugates strongly inhibited attachment of HUVEC on vitronectin-coated wells. Similar results were obtained when the adhesion of HUVEC was inhibited by incubation with free RGDpep or with other $\alpha_v\beta_3$ and $\alpha_v\beta_5$ binding peptides such as c(RGDfV) and RGD-4C. In contrast, RADpep−HuMab conjugates had no effect on vitronectin-mediated adhesion. From this, we concluded that the RGDpep−HuMab conjugates functionally interacted with $\alpha_v\beta_3/\alpha_v\beta_5$ in a similar fashion as other RGD-peptide ligands for these integrins. As expected, no inhibition of adhesion by RGDpep−HuMab conjugates was observed in fibronectin-coated wells, which allows HUVEC attachment via both $\alpha_5\beta_1$ and $\alpha_v\beta_3$ integrin (data not shown).

Radiobinding Assays. We studied the binding specificity and affinity of the RGDpep−HuMab conjugates for $\alpha_v\beta_3/\alpha_v\beta_5$-expressing H5V cells with the radioiodinated

[2] One-site binding model: (pmol bound) = $(B_{max})([pM])/(K_d + [pM])$; two-site binding model: (pmol bound) = $(B_{max_1})([pM])/(K_{d_1} + [pM]) + (B_{max_2})([pM])/(K_{d_2} + [pM])$; one-site competition model: % binding = $(100\%)/(1 + 10^{(\log(M) - \log EC_{50})})$.

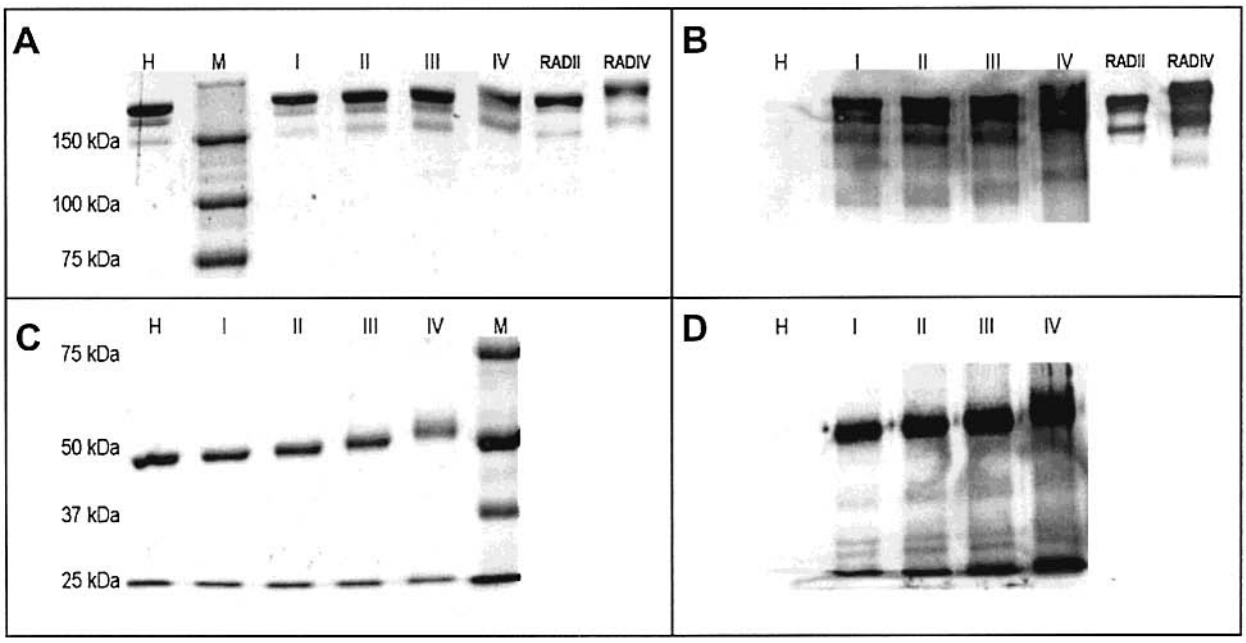


Figure 2. SDS PAGE (A, C) and western blot (B, D) analysis of RGDpep−HuMab conjugates. Panel A: nonreducing conditions, protein staining (Coomassie Brilliant Blue); Panel B: nonreducing conditions, anti-RGDpep immunostaining; Panel C: reducing conditions, protein staining; Panel D: reducing conditions, anti-RGDpep immunostaining. Lanes: (H) HuMab; (M) molecular weight markers; (I to IV) RGDpep−HuMab(I)−(IV); (RADII and -IV) RADpep−HuMab(II) and -(IV).

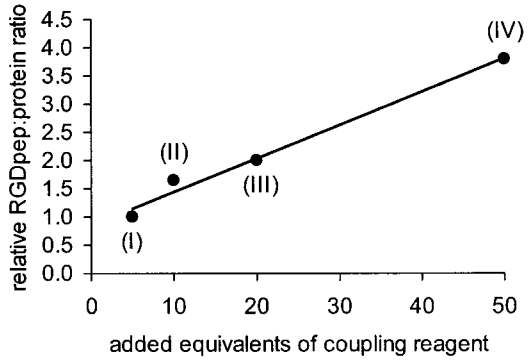


Figure 3. Determination of covalently incorporated RGDpep in RGDpep−HuMab conjugates. Values between parentheses denote the corresponding RGDpep−HuMab conjugate. RGDpep was determined by ELISA using a specific anti-RGDpep antiserum. The relative RGDpep:protein ratio was calculated from the EC_{50} of each conjugate, as determined from the half-maximal OD_{490} absorbance of serial dilutions in the ELISA, and normalized to the value of the RGDpep−HuMab(I) conjugate. See Experimental Procedures for a detailed description of the determination of the relative RGDpep:protein ratio.

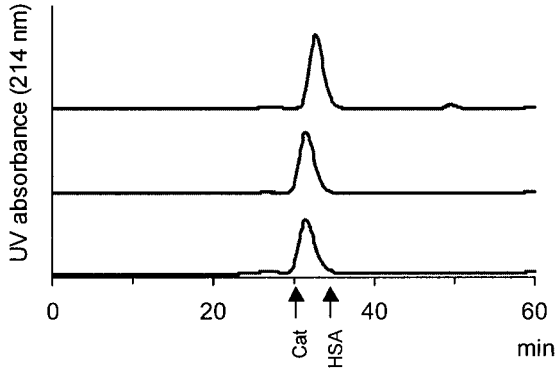


Figure 4. Size-exclusion chromatography of HuMab (upper), RGDpep−HuMab(IV) (middle), and RADpep−HuMab(IV) (bottom). Separations were performed under normal conditions on a Superdex 200 HR10/30 column. Arrows denote the peak elution time of catalase (Cat, 232 kDa) and human serum albumin (HSA, 67 kDa).

RGDpep−HuMab(IV) conjugate. By using whole cells, multivalent binding and clustering of receptors is studied in the natural context of the integrins. The radiobinding experiments were carried out in a Tris binding buffer pH 7.4 supplemented with 1 mM Ca^{2+}, 1mM Mg^{2+}, and 1 mM Mn^{2+}, since these divalent cations are important for the interaction of $\alpha_v\beta_3$ integrin with its ligands (*14*). Experiments in buffers lacking one or more of these cations showed lower absolute binding of ^{125}I-RGDpep−HuMab(IV) (Schraa, A. J., unpublished results).

^{125}I-labeled RGDpep−HuMab(IV) binding could be blocked almost completely by micromolar concentrations of either c(RGDfV) or RGD-4C (Figure 6), indicating that the radiolabeled conjugate bound specifically via its coupled RGDpep groups to the cells. Besides the 50 μM concentration shown in Figure 6, c(RGDfV) at a concentration of 1 M inhibited the binding of ^{125}I-RGDpep−HuMab(IV) to 2.0 ± 0.2% (data not shown).

The specific binding of ^{125}I-RGDpep−HuMab(IV) to the cells was saturable, although maximal binding was not reached at the highest concentration tested (Figure 7). The K_d of RGDpep−HuMab(IV) binding was calculated by nonlinear regression analysis. Assuming two binding sites, which resulted in a better fit of the data than a monovalent model ($p < 0.01$), the analysis yielded binding constants of 0.38 and 22 nM for K1 and K2, respectively (95% confidence intervals: $0.28 < K1 < 0.49$ nM, $0 < K2 < 92$ nM).

We compared the affinities of the RGDpep−HuMab conjugates to the affinity of the parental RGD-peptide by performing competitive displacement studies with the ^{125}I-RGDpep−HuMab(IV) conjugate (Figure 8). All four RGDpep−HuMab conjugates showed a considerable increase in affinity compared to the monovalently binding parental RGD-peptide. Fitting the data with nonlinear regression yielded IC_{50} values presented in Table 1. To compare these data with affinity data of other RGD-peptide ligands, we also determined the IC_{50} of the previously reported c(RGDfV) in our experimental setup

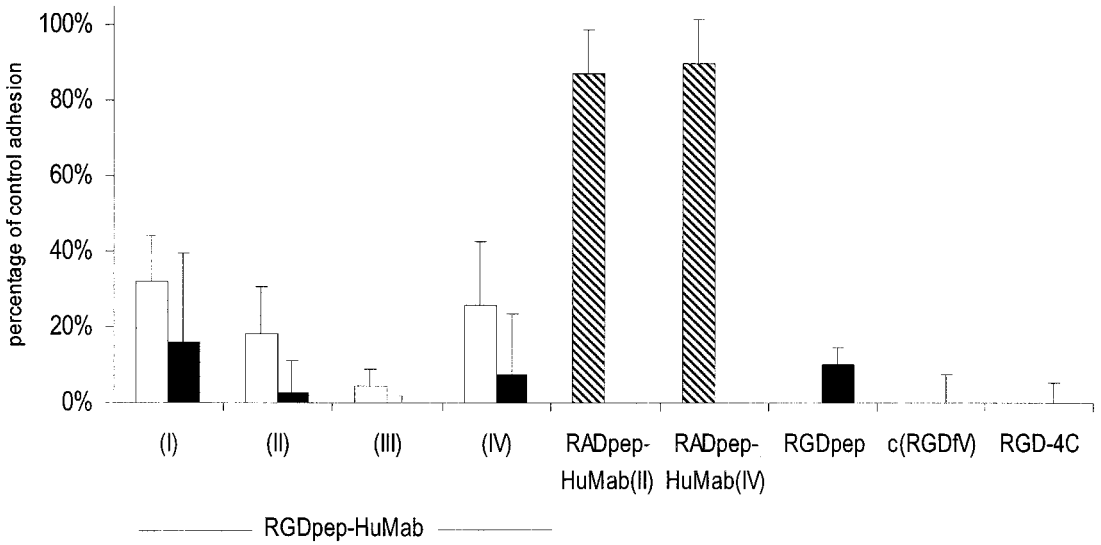


Figure 5. Inhibition of $\alpha_v\beta_3/\alpha_v\beta_5$ mediated adhesion of HUVEC to vitronectin by RGDpep−HuMab conjugates. Adhesion of HUVEC on vitronectin in the absence of inhibitor was set at 100%. Concentration of inhibitors: 500 nM (open bars), 700 nM (hatched bars), 1 μM (closed bars). Values are mean of triplicate assays ± SD. For all RGDpep−HuMab conjugates and RGD-peptides, adhesion of HUVEC significantly differed from control ($p < 0.05$).

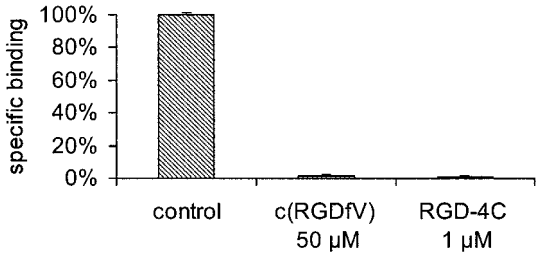


Figure 6. Binding of ^{125}I-RGDpep−HuMab(IV) to H5V endothelial cells. Specific binding of a tracer dose (70000 cpm) of ^{125}I-RGDpep−HuMab(IV) could be inhibited by excess of reported RGD-peptide ligands for $\alpha_v\beta_3/\alpha_v\beta_5$ integrin, c(RGDfV), and RGD-4C. Values are mean of triplicate assays ± SD.

(158 nM). The RGDpep used for preparation of our constructs, c(RGDf(ϵ-*S*-acetylthioacetyl)K), competed at a 5-fold higher IC_{50} than c(RGDfV), likely resulting from the attachment of the acetylthioacetyl linker group.

Competition experiments with RADpep and RADpep−HuMab conjugates showed no inhibition of ^{125}I-RGDpep−HuMab(IV) binding, even at the highest concentration tested. Again, this demonstrates that the binding of ^{125}I-RGDpep−HuMab(IV) is specifically mediated via the coupled RGDpep groups.

DISCUSSION

The present study describes the preparation and characterization of multivalent derivatives of a peptide that binds to $\alpha_v\beta_3$ and $\alpha_v\beta_5$ integrins via an Arg-Gly-Asp sequence. We coupled this RGDpep chemically to a protein and demonstrated that such RGDpep−protein conjugates bind to endothelial cells with dramatically increased affinity. Since the binding of the RGDpep−protein conjugates can be inhibited by the free RGDpep and other RGD-peptides, but not by similarly prepared RADpep−protein conjugates, we concluded that RGDpep−protein conjugates bind to the cells via the coupled RGDpep groups.

The type of RGD-peptide that was used in the present study binds specifically and with high affinity to $\alpha_v\beta_3$ integrin due to the special constrained conformation of the RGD sequence (*6*). This special RGD conformation is induced by both the unnatural D-amino acid and the head-to-tail cyclization of the pentapeptide. Since such peptide structures cannot be encoded by a recombinant DNA sequence, we have chosen for classical chemical coupling techniques to prepare RGDpep−protein derivatives. In these conjugates, the peptide was coupled via a relatively short linker to amino groups of the HuMab

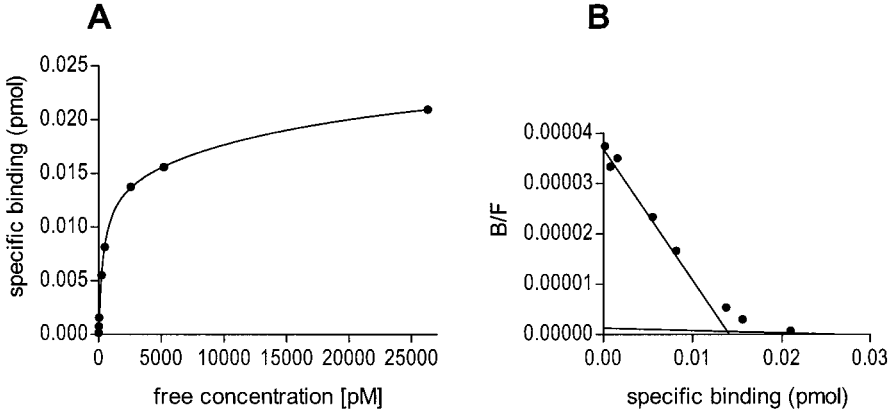


Figure 7. Specific binding of ^{125}I-RGDpep−HuMab(IV) to H5V endothelial cells after incubation for 4 h at 4 °C. Panel A: Specific binding of ^{125}I-RGDpep−HuMab(IV) (pmol/well) plotted against the free concentration of the compound [pM]. Panel B: Scatchard plot of ^{125}I-RGDpep−HuMab(IV) binding. B/F: ratio of specific binding and free concentration (pmol/pM). Fitted lines in both panels were drawn using the K_d and B_{max} values calculated by nonlinear regression analysis.

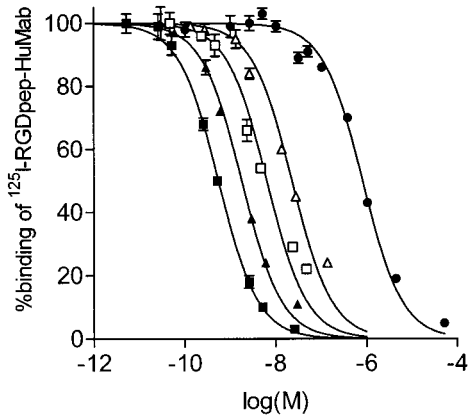


Figure 8. Competitive displacement of ^{125}I-RGDpep−HuMab-(IV) binding by RGDpep−HuMab conjugates and parental RGDpep. H5V cells were incubated with ^{125}I-RGDpep−HuMab-(IV) (tracer dose, 70000 cpm) and appropriate dilutions of nonlabeled compounds. Cell-associated radioactivity in the absence of competitor was set at 100%. Closed circles: RGDpep; open triangles: RGDpep−HuMab(I); open squares: RGDpep−HuMab(II); closed triangles: RGDpep−HuMab(III); closed squares: RGDpep−HuMab(IV). Values are mean of triplicate assays ± SD.

Table 1. Affinity Data of RGDpep−HuMab Conjugates and RGD-Peptides. Competitive Binding Experiments Were Performed on $\alpha_v\beta_3$ Integrin Expressing H5V Cells with Radiolabeled RGDpep−HuMab(IV) Conjugate and the Peptide−Protein Conjugates or Peptides Products Listed below. IC_{50} Values Were Calculated from the Data Presented in Figure 8

product	IC_{50} (nM)	increase in affinity[a]
RADpep	>5000[b]	
RGDpep	818	1
c(RGDfV)	158	5
RGDpep−HuMab(I)	23.2	35
RGDpep−HuMab(II)	6.5	125
RGDpep−HuMab(III)	2.0	410
RGDpep−HuMab(IV)	0.6	1297
RADpep−HuMab(II)	>667[b]	
RADpep−HuMab(IV)	>667[b]	

[a] The increase in affinity was calculated by dividing the IC_{50} of RGDpep by the IC_{50} of the tested product. [b] Highest tested concentration. No inhibition of ^{125}I−RGDpep−HuMab(IV) binding was observed at this concentration.

protein. Since the RGD-binding site of integrins is located in a cleft between the two subunits of the integrin, the pharmacological activity of RGD-peptide could be lost due to steric hindrance of the protein backbone. The spacer in our conjugates accounts for 10 atoms, counted from protein backbone to the ϵ-amino group of the lysine in the c(RGDfK) ring structure. This value fits in the spacer requirements found by Kantlehner and colleagues, who demonstrated that c(RGDfK) coupled via an 8-atom spacer lost its activity, while a 15-atom spacer allowed the peptide to interact freely with its receptor (*15*). Clearly, the binding of our conjugates to endothelial cells and the inhibition of adhesion of HUVEC onto vitronectin-coated wells demonstrate the functional activity of our constructs with $\alpha_v\beta_3$ integrin.

We determined the amount of coupled RGDpep ligands in our conjugates by an anti-RGDpep ELISA, which enabled us to calculate relative RGDpep:protein ratios ranging from 1 to 3.8. In addition, we determined the amount of introduced iodoacetyl groups of the SIA−HuMab(IV) conjugate. From this experiment an absolute RGDpep:protein ratio for the RGDpep−HuMab(IV) conjugate of 23 was established. Since the RGDpep−HuMab-(I) conjugate was prepared using 5 equiv of SIA reagent, the maximal amount of coupled RGDpep molecules in the RGDpep−HuMab(IV) conjugate based on the ELISA would be 19, which is lower than the absolute ratio of 23. Likely, the observed discrepancy results from an underestimation of the relative RGDpep:protein ratio, due to steric hindrance of anti-RGDpep antibody binding in the higher loaded conjugates.

Commonly, the degree of protein modification is calculated indirectly, for instance by TNBS derivatization of remaining primary amino groups (*16*). This approach proved to be inaccurate for our conjugates, due to the low protein concentration of the products. Alternatively, the number of coupled peptides can be derived from the change in apparent molecular weight demonstrated by gel electrophoresis or chromatography (*17*). However, our products showed only small differences compared to the parent protein, probably due to the constrained structure of the RGDpep ligand, although immunostaining clearly demonstrated the presence of the peptide in all conjugates. The large molecular weight of HuMab and the expected heterogeneity of the conjugates would furthermore not allow proper mass spectrometry analysis of the conjugates.

We studied the affinity of our conjugates for cells expressing $\alpha_v\beta_3/\alpha_v\beta_5$ integrins using the radiolabeled RGDpep−HuMab(IV) conjugate, which contained the highest number of coupled RGDpep ligands. ^{125}I-RGDpep−HuMab(IV) bound in a saturable manner to these endothelial cells, although complete saturation of binding was not observed at highest concentration tested. Assuming two binding sites in the fitting model gave better results than a one-binding site model. Whether the conjugate actually binds via two RGDpep-integrin interactions cannot be concluded from our data. More likely, the found binding constants are apparent K_d values.

To compare the binding affinities of the RGDpep−HuMab conjugates with those of free RGDpep and references from the literature, we determined the IC_{50} values of the various RGD-containing compounds (Table 1). The increase in IC_{50} correlated with the number of coupled RGDpep groups for the series of RGDpep−HuMab conjugates. Since the affinity increased to a larger extent than can be accounted for by the number of coupled RGDpep ligands, only cooperative binding due to multivalency can explain these data. Compared to the single RGDpep ligand, an increase in IC_{50} was found of over 3 orders of magnitude for the most potent RGDpep−HuMab conjugate, while about 23 RGDpep ligands have been incorporated in this product. Compared to the reference c(RGDfV), an increase in affinity of up to 250-times was calculated for the RGD-HuMab(IV) product. In comparison, the most potent structure derived from c(RGDfV), c(RGDf(N-Me)V) (EMD121974), binds to $\alpha_v\beta_3$ with an affinity 4.3 times higher than c(RGDfV) (*18*).

To summarize, the coupling of the peptide RGDpep to a protein yielded multivalent conjugates with a strongly increased affinity for $\alpha_v\beta_3$ integrin and/or $\alpha_v\beta_5$ integrin compared the parental peptide. These conjugates were capable of inhibiting the interaction between $\alpha_v\beta_3/\alpha_v\beta_5$ integrins and vitronectin and therefore may display antiangiogenic effects when administered in vivo. In addition, RGDpep-conjugation might be of use for targeting of therapeutic proteins to tumor blood vessels. Candidate proteins for such an approach currently under investigation in our laboratory include truncated Tissue Factor (tTF), that selectively induces blood coagulation in tumor blood vessels when properly bound to receptors on the tumor endothelium (*19*). Initial experiments with RGDpep-tTF conjugates demonstrated that RGDpep-tTF

was still capable of inducing blood coagulation in vitro (Schraa, A. J., unpublished results). Alternatively, RGDpep−protein conjugates can be prepared that induce tumor endothelial cell killing. Examples of proteins that can be used in the latter approach are TNFα and IL-2, both activating the immune system, or glucose oxidase, which generates toxic reactive oxygen species (*20*−*22*). Finally, endothelial delivery of small drug molecules or toxic molecules can be achieved using RGDpep as a targeting device. The validity of such an approach has already been demonstrated with the RGD-4C−doxorubicin prodrug, which displayed a strong antitumor effect (*4*). Preparations based on this approach can either consist of soluble macromolecules, such as proteins or polymeric backbones, or liposomal formulations as recently proposed by Kessler et al. (*23*, *24*).

ACKNOWLEDGMENT

A.D. Berendsen is kindly acknowledged for assisting in the radiobinding experiments, and J.H. Pol from the Department of Nuclear Medicine for radiolabeling of the conjugates. HUVEC and H5V cells were kindly provided by the RuG/AZG Endothelial Cell Facility.

LITERATURE CITED

(1) Griffioen, A. W., and Molema, G. (2000) Angiogenesis: potentials for pharmacologic intervention in the treatment of cancer, cardiovascular diseases, and chronic inflammation. *Pharmacol. Rev. 52* (*2*), 237−268.

(2) Ruoslahti, E., and Rajotte, D. (2000) An address system in the vasculature of normal tissues and tumors. *Annu. Rev. Immunol. 18*, 813−827.

(3) Koivunen, E., Wang, B., and Ruoslahti, E. (1995) Phage libraries displaying cyclic peptides with different ring sizes: ligand specificities of the RGD-directed integrins. *Biotechnology (N. Y.) 13* (*3*), 265−270.

(4) Arap, W., Pasqualini, R., and Ruoslahti, E. (1998) Cancer treatment by targeted drug delivery to tumor vasculature in a mouse model. *Science 279* (*5349*), 377−380.

(5) Assa-Munt, N., Jia, X., Laakkonen, P., and Ruoslahti, E. (2001) Solution structures and integrin binding activities of an RGD peptide with two isomers. *Biochemistry 40* (*8*), 2373−2378.

(6) Haubner, R., Gratias, R., Diefenbach, B., Goodman, S. L., Jonczyk, A., and Kessler, H. (1996) Structural and functional aspects of RGD-containing cyclic pentapeptides as highly potent and selective integrin alpha-v-beta-3 antagonists. *J. Am. Chem. Soc. 118*, 7461−7472.

(7) Lohof, E., Planker, E., Mang, C., Burkhart, F., Dechantsreiter, M. A., Haubner, R., Wester, H. J., Schwaiger, M., Holzemann, G., Goodman, S. L., and Kessler, H. (2000) Carbohydrate Derivatives for Use in Drug Design: Cyclic alpha(v)-Selective RGD Peptides. *Angew. Chem., Int. Ed. 39* (*15*), 2761−2764.

(8) Haubner, R., Wester, H. J., Reuning, U., Senekowitsch-Schmidtke, R., Diefenbach, B., Kessler, H., Stocklin, G., and Schwaiger, M. (1999) Radiolabeled alpha(v)beta3 integrin antagonists: a new class of tracers for tumor targeting. *J. Nucl. Med. 40* (*6*), 1061−1071.

(9) Meijer, D. K. F., and Ziegler, K. (1993) Mechanisms for the hepatic clearance of oligopeptides and proteins. Implications for rate of elimination, bioavailability and cell-specific drug delivery to the liver. *Biological Barriers to Protein Delivery* (K. L. Audus, T. J. Raub, Eds.) pp 339−408, Plenum Press, New York.

(10) Lowry, O. H., Rosebrough, N. J., Farr, A. L., and Randall, R. J. (1951) Protein measurement with the Folin Phenol reagent. *J. Biol. Chem. 193*, 265−275.

(11) Mulder, A. B., Blom, N. R., Smit, J. W., Ruiters, M. H., van der, M. J., Halie, M. R., and Bom, V. J. (1995) Basal tissue factor expression in endothelial cell cultures is caused by contaminating smooth muscle cells. Reduction by using chymotrypsin instead of collagenase. *Thromb. Res. 80* (*5*), 399−411.

(12) Ruegg, C., Yilmaz, A., Bieler, G., Bamat, J., Chaubert, P., and Lejeune, F. J. (1998) Evidence for the involvement of endothelial cell integrin alphaVbeta3 in the disruption of the tumor vasculature induced by TNF and IFN-gamma. *Nat. Med. 4* (*4*), 408−414.

(13) Hunter, W. M., and Greenwood, F. C. (1962) Preparation of iodine-131 labeled human growth hormone of high specific activity. *Nature 194* (*4827*), 495−496.

(14) Legler, D. F., Wiedle, G., Ross, F. P., and Imhof, B. A. (2001) Superactivation of integrin alphavbeta3 by low antagonist concentrations. *J. Cell Sci. 114* (*Pt 8*), 1545−1553.

(15) Kantlehner, M., Finsinger, D., Meyer, J., Schaffner, P., Jonczyk, A., Diefenbach, B., Nies, B. and Kessler, H. (1999) Selective RGD-mediated adhesion of osteoblasts at surfaces of implants. *Angew. Chem., Int. Ed. 38* (*4*), 560−562.

(16) Habeeb, A. F. S. A. (1966) Determination of free amino groups in proteins by trinitrobenzenesulfonic acid. *Anal. Biochem. 14*, 328−336.

(17) Beljaars, L., Molema, G., Schuppan, D., Geerts, A., De Bleser, P. J., Weert, B., Meijer, D. K. F., and Poelstra, K. (2000) Successful targeting of albumin to rat hepatic stellate cells using albumin modified with cyclic peptides that recognize the collagen type VI receptor. *J. Biol Chem. 275* (*17*), 12743−12751.

(18) Dechantsreiter, M. A., Planker, E., Matha, B., Lohof, E., Holzemann, G., Jonczyk, A., Goodman, S. L., and Kessler, H. (1999) *N*-Methylated cyclic RGD peptides as highly active and selective alpha(V)beta(3) integrin antagonists. *J. Med. Chem. 42* (*16*), 3033−3040.

(19) Huang, X., Molema, G., King, S., Watkins, L., Edgington, T. S., and Thorpe, P. E. (1997) Tumor infarction in mice by antibody-directed targeting of tissue factor to tumor vasculature. *Science 275* (*5299*), 547−550.

(20) Curnis, F., Sacchi, A., Borgna, L., Magni, F., Gasparri, A., and Corti, A. (2000) Enhancement of tumor necrosis factor alpha antitumor immunotherapeutic properties by targeted delivery to aminopeptidase N (CD13). *Nat. Biotechnol. 18* (*11*), 1185−1190.

(21) Lode, H. N., Moehler, T., Xiang, R., Jonczyk, A., Gillies, S. D., Cheresh, D. A., and Reisfeld, R. A. (1999) Synergy between an antiangiogenic integrin alphav antagonist and an antibody-cytokine fusion protein eradicates spontaneous tumor metastases. *Proc. Natl. Acad. Sci. U.S.A. 96* (*4*), 1591−1596.

(22) Christofidou-Solomidou, M., Pietra, G. G., Solomides, C. C., Arguiris, E., Harshaw, D., FitzGerald, G. A., Albelda, S. M., and Muzykantov, V. R. (2000) Immunotargeting of glucose oxidase to endothelium in vivo causes oxidative vascular injury in the lungs. *Am. J. Physiol. Lung Cell. Mol. Physiol. 278* (*4*), L794-L805.

(23) Kok, R. J., Asgeirsdottir, S. A., and Verweij, W. R. (2001) Development of proteinaceous drug targeting constructs using chemical and recombinant DNA approaches. *Drug targeting: organ-specific strategies* (G. Molema, D. K. F. Meijer, Eds.) pp 275−308, Wiley-VCH, Weinheim, Germany.

(24) Marchi-Artzner, V., Lorz, B., Hellerer, U., Kantlehner, M., Kessler, H. and Sackmann, E. (2001) Selective adhesion of endothelial cells to artificial membranes with a synthetic RGD-lipopeptide. *Chemistry 7* (*5*), 1095−1101.

Neoglycoconjugates of Mannan with Bovine Serum Albumin and Their Interaction with Lectin Concanavalin A

D. Mislovičová,*,† J. Masárová,† J. Švitel,‡ R. Mendichi,# L. Šoltés,§ P. Gemeiner,† and B. Danielsson‡

Institute of Chemistry, Slovak Academy of Sciences, SK-842 38 Bratislava, Slovakia, Pure and Applied Biochemistry, Lund University, S-22100 Lund, Sweden, Institute of Macromolecular Chemistry, National Research Council, I-20133 Milan, Italy, and Institute of Experimental Pharmacology, Slovak Academy of Sciences, SK-842 16 Bratislava, Slovakia. Received June 1, 2001; Revised Manuscript Received October 8, 2001

Neoglycoconjugates were prepared from mannan isolated from yeast *Saccharomyces cerevisiae* and activated by periodate oxidation to create aldehyde groups. Various degrees of oxidation introduced 11−28 aldehyde groups per mannan molecule and simultaneously resulted in a molar mass decrease from 46 to 44.5−31 kDa. The activated mannans were subsequently conjugated with bovine serum albumin forming neoglycoconjugates. Some parameters of these mannan−bovine serum albumin conjugates were characterized: saccharide content 25−30% w/w, molar mass within the range 169−246 kDa, and polydispersion (M_w/M_n) from 2.8 to 3.6. The interaction of these conjugates with lectin concanavalin A was studied using three different methods: (i) quantitative precipitation in solution; (ii) sorption to concanavalin A immobilized on bead cellulose; and (iii) kinetic measurement of the interaction by surface plasmon resonance. Quantitative precipitation assay showed only negligible differences in the precipitation course of original mannan and the corresponding mannan−bovine serum albumin conjugates. Both the sorption method (equilibrium method) and the surface plasmon resonance measurement (kinetic method) demonstrates that the values of dissociation constant K_D of all synthetic neoglycoconjugates were within the range 10^{-7}−10^{-8} mol·L^{-1} (close to $K_D = 10^{-8}$ mol·L^{-1} determined by the sorption method for the original mannan). In conclusion, characterization of synthetic neoglycoconjugates confirmed that the method used for their preparation retained the ability of mannan moiety to interact with concanavalin A.

INTRODUCTION

Carbohydrate moiety in glycoproteins modifies the physicochemical and biological properties of the proteins to which they are attached. By their conjugation with carbohydrate derivatives, the synthetic glycoproteins (neoglycoproteins) can be obtained. Neoglycoconjugates are compounds that in useful ways emulate the behavior of the natural glycoconjugates. Neoglycoproteins can be also prepared from bioactive proteins such as enzymes, immunoglobulins, or growth factors. A variety of strategies have been employed in preparing neoglycoproteins (neoglycoenzymes) using mono-, oligo-, or polysaccharides (Magnusson et al., 1994; Lee and Lee, 1997).

Neoglycoproteins containing mannosylated serum albumin were prepared and used as carriers for selective delivery of drugs to cell membranes. These neoglycoproteins are specifically recognized by membrane lectins of liver (Beljaars et al., 1999; Franssen et al., 1993). Mannosylated bovine serum albumin conjugates were utilized as carriers for receptor-mediated drug delivery to treat macrophage-associated diseases (Chakraborty et al., 1990) and for increase of oligonucleotide internalization in cells (expressing mannose-6-phosphate specific membrane lectins) at inhibition of gene expression (Bonfils et al., 1992). Polysaccharides from certain microorganisms were effectively converted into vaccines by partial hydrolysis and by reductive amination with appropriate protein carriers (Jennings and Sood, 1994).

The biospecific affinity of glycoconjugate to lectins originates from the specific saccharide contained in the protein/enzyme molecule. The immobilization procedures based on binding of glycoenzyme to lectin−matrix (in the case of having a strong affinity to this lectin) are gaining increasing acceptance (Saleemuddin, 1999) in the last years. The synthesis of neoglycoenzymes may therefore serve for preparation of modified enzymes with biospecific affinity to lectins, which could be utilized in such immobilization techniques.

Mannan is a polysaccharide with strong affinity (Jennings and Sood, 1994) to lectin concanavalin A (Con A)[1] and therefore is important for glycoprotein synthesis for their prospective use in lectinology. It was found out that

* To whom correspondence should be sent. Institute of Chemistry SAS, Dúbravská cesta 9, SK-842 38 Bratislava, Slovakia; fax: +421 2 59410222; e-mail: chemmisl@savba.sk.

† Institute of Chemistry, Slovak Academy of Sciences.

‡ Lund University.

National Research Council.

§ Institute of Experimental Pharmacology, Slovak Academy of Sciences.

[1] Abbreviations: BSA, bovine serum albumin; *SC* mannan, mannan from *Saccharomyces cerevisiae*; Con A, concanavalin A; BC, bead cellulose; CHTBC, chloro-1,3,5-triazine bead cellulose; Con A-TBC, Con A-triazine bead cellulose; α-MMP, methyl α-D-mannopyranoside; HEPES, *N*-(2-hydroxyethyl)piperazine-*N*′-(2-ethanesulfonic acid); M1−M5, samples of mannan dialdehydes; RM1−RM5, samples of reduced mannan dialdehydes; CM1−CM3, samples of mannan-BSA conjugates; SEC, size exclusion chromatography; HPLC, high performance liquid chromatography; HPSEC, high performance size exclusion chromatography; MALC, multiangle light scattering; SCV, single capillary viscometer; SPR, surface plasmon resonance; M_w, weight-average molecular mass; M_p, molecular mass of the apex of the peak.

10.1021/bc015517u CCC: $22.00 © 2002 American Chemical Society
Published on Web 12/19/2001

the polymer carrying multiple specific mannosyl residues exhibited a several times higher affinity toward Con A than methyl α-D-mannopyranoside (α-MMP) considered to be the most interacting monosaccharide (Mortell et al., 1996). This was proved by synthetic multivalent mannosylated clusters (glycodendrimers) which were shown to be high-affinity ligands for mannose specific lectins (Roy et al., 1998). Yeast mannans are extensively branched polymers (Goldstein and Poretz, 1986) where the presence of extended sequences of α-D-(1 → 2)-linked mannose residues in their macromolecules provides sites for interaction with Con A. The interaction of yeast mannan (as a natural multivalent ligand) with Con A is comparable with affinity of 16-mer mannosyl-dendrimer (Pagé et al., 1996). The mannan from *Saccharomyces cerevisiae* (*SC*) was previously used for determination of binding properties of natural and synthetic α-D-mannosyl ligands, e.g., inhibition effect of these ligands on yeast mannan precipitation with Con A was investigated (Goldstein and Hayes, 1978; Pagé et al. 1996). The idea of mannan conjugation with protein, to incorporate the polysaccharide properties into protein molecule, was applied in the last years to preparation of synthetic antigens. The high-molar-mass mannans exhibit immunogenic activity (Young et al., 1998); therefore, the synthetic mannan−protein conjugates (antigens) induce the protective antibody response (Han et al., 1999; Apostolopoulos et al., 2000), but the mannan−protein conjugates have not yet been investigated from the point of view of their interaction with lectins.

The aim of this study was to develop a method to prepare conjugates of *SC* mannan with bovine serum albumin (BSA) with retained lectin-binding affinity of mannan moiety. Three principally different methods to exhaustively investigate mannan−BSA conjugates interaction with Con A were used.

EXPERIMENTAL PROCEDURES

Materials. The mannan isolated from *Saccharomyces cerevisiae* (average molar mass ≈ 46 kDa) was kindly provided by Dr. Šandula (Institute of Chemistry, SAS, Slovak Republic) (Šandula and Vojtková-Lepšíková, 1974). BSA was purchased from IMUNA, Šarišské Michaľany, Slovak Republic, sodium cyanoborohydride ($NaCNBH_3$) was obtained from Fluka Chemie AG, Buchs, Switzerland, and sodium borohydride ($NaBH_4$) and sodium periodate ($NaIO_4$) were the products of Lachema, Brno, Czech Republic. Lectin Con A for precipitation and sorption experiments was obtained from Lectinola, Prague, Czech Republic. α-MMP was purchased from Fluka Chemie AG, Buchs, Germany. Bead cellulose Perlose MT-50 (BC) was supplied by Lovochemie, Lovosice, Czech Republic. Chloro-1,3,5-triazine bead cellulose (CHTBC) was prepared according to the procedure described in our previous work (Mislovičová et al. 1995). The content of 3% w/w of nitrogen and 1.5% w/w of chlorine were determined (10% w/w of chlorotriazine group/dry sorbent).

Con A and *N*-(2-hydroxyethyl)piperazine-*N′*-(2-ethanesulfonic acid) (HEPES) used in the SPR method were purchased from Sigma, St. Louis, USA. The SPR chips CM-5, covered with carboxymethylated dextran and an amine coupling kit, were purchased from BIACORE (Uppsala, Sweden). Other reagents were of the analytical grade.

Preparation of Mannan Conjugates with BSA. 100 mg of *SC* mannan was dissolved in a subsequent volumes of 0.05 mol·L^{-1} aqueous solution of sodium periodate:

1 mL − molar ratio $NaIO_4$/mannosyl unit = 0.054 (sample M1)

2 mL − molar ratio $NaIO_4$/mannosyl unit = 0.135 (sample M2)

3.5 mL − molar ratio $NaIO_4$/mannosyl unit = 0.270 (sample M3)

7 mL − molar ratio $NaIO_4$/mannosyl unit = 0.540 (sample M4)

10 mL − molar ratio $NaIO_4$/mannosyl unit = 0.710 (sample M5).

Reaction mixtures were stirred in the dark at 4 °C during 1 h. Then the reactions were stopped by addition of ethylene glycol (1 mL) and stirred 1 h. Low molecular weight compounds were removed from the mixture by dialysis (Spectra Por dialysis tubing MWCO 6000−8000) against water at 4 °C in the dark. Obtained aqueous solutions of oxidized polysaccharides were lyophilized. The amount of aldehyde groups was determined in lyophilizates by the Park-Johnson method (Park and Johnson, 1949). Mannan dialdehydes M1, M2, and M3 were used for conjugation with bovine serum albumin. The mixtures of each three mannan dialdehydes (M1−M3) in 0.05 mol·L^{-1} phosphate buffer of pH 7 (4 mL, c = 10 mg·mL^{-1}) with a solution of BSA (4 mL, c = 10 mg·mL^{-1} of the same buffer) and a solution of $NaCNBH_3$ (2.5 mL, c = 10 mg·mL^{-1} of the same buffer) were stirred at room temperature. The reaction was stopped after 24 h by addition of $NaBH_4$ in 0.05 mol·L^{-1} borate buffer of pH 9.5 (ca. 50 mol of $NaBH_4$ were added to the determined aldehyde groups, c = 5 mg·mL^{-1}) to reduce the remaining aldehyde groups. The reduction was proceeded by stirring at room temperature for 6 h. The products were adjusted with 4 mol·L^{-1} HCl to pH 6−7 and dialyzed against H_2O. Unreacted mannans and BSA were removed by ultrafiltration (YM 100, Amicon Inc., Beverly, USA), and the resulting water solutions of conjugates were lyophilized. The contents of saccharides (Saha and Brewer, 1994) and proteins (Lowry et al., 1951) in lyophilizates were determined. The content of nitrogen was determined by elemental analysis of conjugates (EA 1108 CHN-O analyzer, Milan, Italy).

Determination of the Molar Mass of the Mannans. M_w of the original as well as of the oxidized mannan samples (after their reduction with $NaBH_4$) (Masárová et al., 2001) were determined by the HPSEC method. HPLC system (Shimadzu, Wien, Austria) was composed of a high-pressure pump LC-10AD, a membrane degasser GT-104, an injector Rheodyne 77251, and a differential refractometer RID-6A. The system was calibrated with a set of pullulans with M_w = 5−100 kDa (Macherey-Nagel, Düren, Germany). The solutions of calibrating pullulans as well as of tested mannans (c = 1 mg·mL^{-1} of water) were applied onto a HEMA BIO 100 column (8 × 250 mm, 10-μm particle size) obtained from Tessek, Prague, Czech Republic, and eluted with 0.02 mol·L^{-1} phosphate buffer at flow rate 0.4 mL·min^{-1} at ambient temperature. The volume of injected sample was 0.02 mL. The chromatographic data were processed by Class-VP-chromatography software (Shimadzu, Wien, Austria).

Determination of the Molar Mass of the Mannan−BSA Conjugates. The molecular characterization of the starting (nonconjugated) mannan and BSA and of the mannan−BSA conjugates was performed by a multidetector size exclusion chromatography (SEC) system. The system consisted of an Alliance 2690 separation module, a 410 differential refractometer from Waters (Milford, MA), a homemade single capillary viscometer (SCV), and an additional multiangle laser light scattering

Table 1. Characteristics of Modified Mannans and Their Interaction with Con A Determined by SPR

sample	content of aldeh. groups before reduc. n(aldeh.)/n(polysach.)	M_p[a] [kDa]	polydispersion index M_w/M_n	k_a [M^{-1} s^{-1}]	k_d [s^{-1}]	K_D [M]
mannan	1	46.0	1.3	3.64×10^2	3.93×10^{-4}	1.08×10^{-6}
RM1	11	44.5	1.4	5.25×10^2	2.58×10^{-4}	4.91×10^{-7}
RM2	20	42.0	1.4	2.56×10^2	3.77×10^{-4}	1.47×10^{-6}
RM3	28	40.0	1.7	1.69×10^2	3.86×10^{-4}	2.28×10^{-6}
RM4	22[b]	37.0	1.8	1.08×10^2	3.06×10^{-4}	2.83×10^{-6}
RM5	13[b]	31.0	2.0	0.42×10^2	1.15×10^{-3}	2.74×10^{-5}

[a] Determined by HPSEC (HEMA BIO 100 column) and RI detection. [b] Determined in a soluble part.

(MALS) Dawn DSP-F photometer from Wyatt (Santa Barbara, CA). The SEC-MALS-SCV system was described in detail elsewhere (Wyatt, 1993; Mendichi et al., 1995; Mendichi and Giacometti Schieroni, 1999). The experimental SEC conditions were the following: 0.5 mol·L^{-1} NaCl at 35 °C as mobile phase, 0.8 mL·min^{-1} of flow rate, and 200 μL of injection volume. The column set was composed of two OHpak Shodex columns (KB-806 and KB-805) (8 × 300 mm, 13-μm particle size) from Showa Denko (Tokyo, Japan).

The differential refractive index increment, dn/dc, of the mannan−BSA conjugates with respect to the mobile phase was measured by a KMX-16 differential refractometer from LDC Milton Roy (Riviera Beach, FL).

Quantitative Precipitation Assay. Precipitation of *SC* mannan as well as mannan−BSA conjugates (CM1−CM3) with Con A was assayed in phosphate buffer of pH 7 containing 0.05 mol·L^{-1} sodium phosphate, 0.1 mol·L^{-1} NaCl, 0.1 mmol·L^{-1} $CaCl_2$, and 0.1 mmol·L^{-1} $MnCl_2 \times 4$ H_2O. The total volume of precipitation tests was 1 mL containing 230 μg·mL^{-1} of Con A and various concentrations of mannan (within the range from 20 to 190 μg·mL^{-1}) or conjugate (within the range from 10 to 120 μg·mL^{-1} of the conjugate saccharide). The samples were shaken at 25 °C for 2 h. The precipitates were separated in a microcentrifuge MPW-310 (Mechanika Precyzyjna, Warszawa, Poland) at 10 000 min^{-1} (8400*g*) during 10 min, washed twice with 1 mol·L^{-1} NaCl, centrifuged, and subsequently dissolved in 0.05 mol·L^{-1} phosphate buffer adjusted to pH 10.5 with 1 mol·L^{-1} NaOH. These solutions were analyzed for saccharides (Saha and Brewer, 1994) and proteins (Lowry et al., 1951). In each experiment (at the peak of maximum precipitation), the test was done in parallel in the presence of 0.05 mol·L^{-1} of methyl α-D-mannopyranoside (α-MMP) to confirm the specific interaction.

Sorption Experiments. Con A was bound to the chloro-1,3,5-triazine bead cellulose (CHTBC) matrix by the method described earlier (Mislovičová et al., 1995). The sorption of mannan−BSA (CM1−CM3) conjugates on Con A-TBC matrix (containing 3.61 mg of Con A/g of wet sorbent) was performed in 0.05 mol·L^{-1} phosphate buffer (pH 7) with 0.1 mol·L^{-1} NaCl containing 0.1 mmol·L^{-1} $CaCl_2$ and 0.1 mmol·L^{-1} $MnCl_2 \times 2$ H_2O. Suspensions of Con A-TBC prepared from 0.1 g of sorbent and 1 mL of individual mannan−BSA conjugate solutions (40−200 μg of conjugate or 10−70 μg expressed as the saccharide in the above-mentioned buffer) were shaken slowly at 25 °C for 2 h. At the same time, the blank experiment was performed, where the nonderivatized bead cellulose and maximum amount of pertinent conjugate in suspension was used. Then the supernatants were separated by twice centrifugation at 10 000 min^{-1} (8400*g*). Saccharides and proteins in the obtained supernatants were determined. The amounts of the adsorbed conjugate were calculated as the difference between the contents of saccharides and proteins in supernatants obtained in sorption on BC and on Con-A TBC. The same adsorption experiment was performed with *SC* mannan to compare the behavior of original mannan with mannan−BSA conjugates. Dissociation constants and binding capacities were calculated by rearrangement of the adsorption isotherm equation to the Scatchard plot $Q^* = Q_m - K_D Q^*/C^*$ (Chern et al., 1999), where C^* is the concentration of sorbate in solution in equilibrium, Q^* is the amount of sorbate adsorbed on the sorbent at equilibrium, Q_m is the maximum adsorption capacity of the adsorbent, and K_D is the dissociation constant of sorbate.

Surface Plasmon Resonance Measurement. The SPR measurements were performed with a BIACORE 2000 (Biacore AB, Sweden) operated with a BIAcore Control Software 1.2. All measurements were performed at 25 °C, at a flow rate of 5 μL·min^{-1}. The buffer of pH 7.4 consisted of 0.01 mol·L^{-1} *N′*-(2-hydroxyethyl)piperazine-*N′*-(2-ethanesulfonic acid) (HEPES), 0.15 mol·L^{-1} NaCl, 1 mmol·L^{-1} Ca^{2+}, and 1 mmol·L^{-1} Mn^{2+}. The chip surface was modified by covalently bound Con A using the amine coupling kit. The interaction with Con A was investigated by the injection of 50 μL of sample containing 1 mg·mL^{-1} mannan (RM1−RM5) or mannan−BSA conjugate (CM1−CM3). The chip surface was regenerated by the injection of 20 μL of 5 mg·mL^{-1} *p*-aminophenyl-α-D-mannopyranoside after each measurement. The association (k_a) and dissociation (k_d) rate constants as well as dissociation equilibrium contants (K_D) were calculated (Shinohara et al., 1994).

RESULTS AND DISSCUSION

Oxidized Mannans and their Interaction with Con A. The first step at the conjugation of mannan with BSA was the oxidation of *SC* mannan with periodate to obtain its reactive form. Mannan structure is changed after oxidation, and mannose rings and side chains can be cleaved, which results in a molecular mass decrease. A set of five mannans (M1−M5) oxidized to a different degree (from 11 to 28 of the aldehyde groups per mannan molecule; Table 1, second column) having partially degraded chains (M_p decreases from 46 to 31 kDa; Table 1, third column) and values of polydispersion index within the range from 1.4 to 2.0 (Table 1, fourth column) were prepared. HPSEC chromatograms of these samples are shown in Figure 1.

The oxidation of *SC* mannan was described in more detail in our previous work (Masárová et al., 2001). Quantity of produced aldehyde groups (degree of oxidation) and decrease of M_p of prepared mannan dialdehydes (degree of degradation) were observed. Practically no degradation of polysaccharide chain was observed at the lowest periodate concentration. Degree of degradation was increased with increasing amount of periodate. Samples M4 and M5 were partly insoluble, probably in consequence of the formation of intramolecular hemiac-

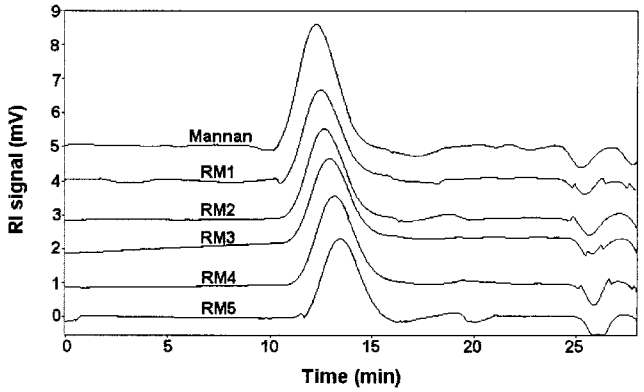


Figure 1. Chromatograms of mannan and oxidized mannan (after reduction) samples obtained by HPSEC chromatography on column HEMA BIO 100. The solutions of calibrating pullulans as well as of tested mannans (c = 1 mg·mL^{-1} of water) were applied onto a HEMA BIO 100 column (8 × 250 mm, 10-μm sorbent of particle size) and eluted with 0.02 mol·L^{-1} phosphate buffer at a flow rate of 0.4 mL·min^{-1} and at ambient temperature. The volume of injected sample was 0.02 mL. The chromatographic data were processed by Class-VP-chromatography software.

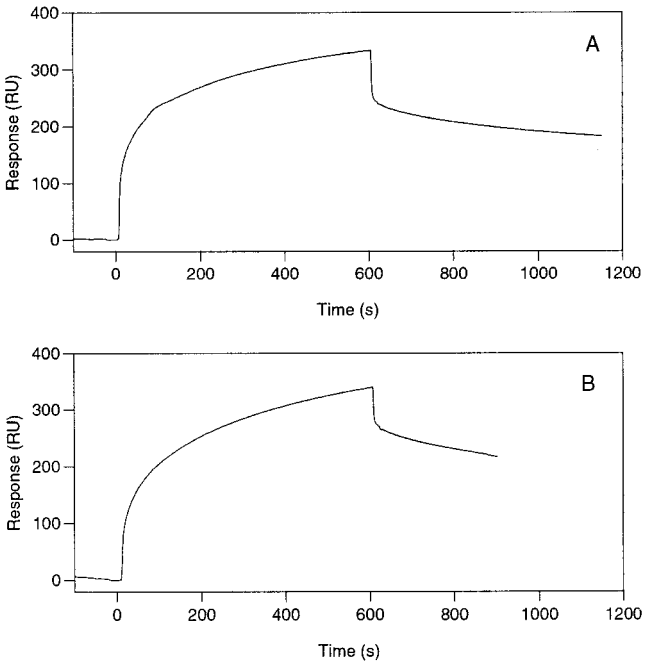


Figure 2. Surface plasmon resonance measurement of the interaction of Con A with mannan. SPR measurements were performed with BIACORE 2000 using the chip with modified surface with covalently bound Con A at a flow rate of 5 μL·min^{-1} with buffer of pH 7.4 consisting of 0.01 mol·L^{-1} HEPES, 0.15 mol·L^{-1} NaCl, 1 mmol·L^{-1} Ca^{2+}, and 1 mmol·L^{-1} Mn^{2+}. The interaction of samples with Con A was investigated by the injection of 50 μL of samples containing 1 mg/mL mannan or mannan-conjugate. Panel A − original mannan; panel B − oxidized mannan M2 after reduction (RM2).

etal bonds. Degree of oxidation and molar mass of these samples therefore could be determined only in the soluble part. By using of higher amount of periodate, higher degradation of polysaccharide chains was going on to the detriment of oxidation.

As it was mentioned above, the activation of mannan has an effect on its structure. The changes of mannan structure has an influence on affinity of mannan samples to lectin Con A. This effect was investigated with mannans that were activated, and subsequently the active groups were reduced. The oxidized mannans were reduced (RM samples) to eliminate chemical reaction of polysaccharide active groups (aldehyde) with amino groups of Con A. The results from precipitation experiments of modified mannans with Con A were presented in a previous paper (Masárová, et al., 2001). Intensive precipitation of mannan and RM1−RM3 samples with Con A was observed. On the other hand, the samples RM4 and RM5 precipitated with Con A weakly. In the present work, the interaction of these modified mannans with Con A was investigated by the SPR method. Figure 2 shows SPR sensorgrams of mannan and the sample RM2 using a chip with surface modified by immobilized Con A. Table 1 shows the calculated kinetic parameters of interactions of original mannan and all the five RM samples with Con A. Gradually reduced mannan affinity to Con A after its modification was observed. There is obvious a correlation of the degree of degradation, and supposed change of mannan structure, with the values of obtained association constants. Surprisingly, the value of k_a of original mannan was not determined to be the highest. We concluded that the oxidized *SC* mannans prepared by mild periodate oxidation (M1−M3) are suitable for the preparation of glycoproteins conjugates. The character (size and valency) of modified mannan in these samples did not change significantly, and therefore they maintained the affinity to Con A.

Preparation and Characterization of Mannan−BSA Conjugates. The three oxidized mannans with the best affinity to Con A (M1, M2, and M3) were used to prepare three BSA conjugates (CM1, CM2, and CM3). The method of reductive amination (described in Experimental Procedures) was used, where the weight ratio mannan/BSA = 1:1 was applied. The content of mannan, M_w, and the polydispersion M_w/M_n in conjugates were determined. The determined characteristics of obtained neoglycoconjugates as well as original mannan and BSA are shown in Table 2.

Table 2. Molecular Characteristics of Mannan, BSA, and Three Mannan−BSA Conjugates

conjugate	content of sacch. [%]	content of prot. [%]	content of N [%]	M_w[a] [kDa]	polydispers. index M_w/M_n
BSA	0	100	14.00	66.7	1.0
mannan	100	0		53.0	1.3
CM1	25	75	10.96	176.2	2.8
CM2	28	72	10.49	246.3	3.2
CM3	30	70	10.33	169.1	3.6

[a] Determined by HPSEC (two Shodex columns) and LS detection.

The conjugation method used produces a mixture of neoglycoconjugates of variable M_w, due to the polydispersion of oxidized mannan, and various stoichiometric mannan to BSA ratios. The polydispersion and modality of the prepared conjugates were estimated by HPSEC experiments on the tandem columns HEMA BIO 1000 + HEMA BIO 100 using UV detection (chromatograms are shown in Figure 3) as well as on the Shodex OH Pak column using LS detector. The high polydispersion of all three samples (≈3) was found. The problems with association of these conjugates caused the difficulties with the determination of their M_w. (It is seen in Figure 3—the first high-molar mass peak shows conjugates in associated form). The conformation of the conjugates was very compact because the gyration radius was low, considering the molecular mass, and the signal of the online viscometer was practically absent. The samples were quite polydisperse, and we can only estimate approximate mannan/BSA ratios (from the determined weight ratio

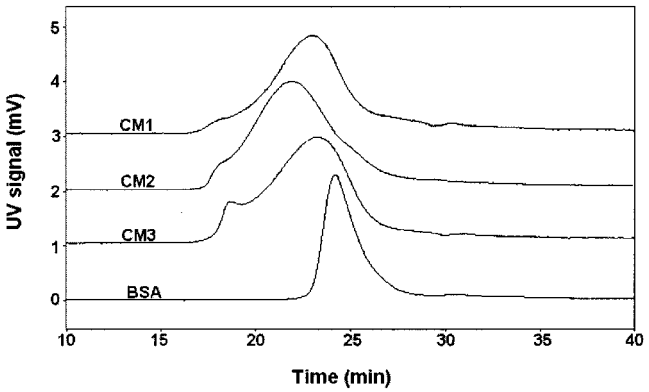


Figure 3. Chromatograms of mannan−BSA conjugates obtained by HPSEC chromatography on two columns HEMA BIO 100 and HEMA BIO 1000. The solutions of tested mannan−BSA conjugates and BSA ($c = 1$ mg·mL^{-1} of water) were applied onto a set of HEMA BIO 100 and HEMA BIO 1000 columns (size of both was 8 × 250 mm with 10-μm particle size of sorbent) and eluted with 0.02 mol·L^{-1} phosphate buffer at a flow rate of 0.5 mL·min^{-1} and at ambient temperature. The volume of injected sample was 0.02 mL. The chromatographic data were processed by Class-VP-chromatography software.

of mannan to BSA in conjugates and M_w of conjugates). We suppose that CM1 contains mainly conjugates with approximately one mannan molecule per two molecules of BSA. The samples CM2 and CM3 are mixtures of 1:1 and 1:2 stoichiometric ratios.

Interaction of Mannan−BSA Conjugates with Con A. The interaction of mannan−BSA conjugates with concanavalin A was studied using three different methods: (i) quantitative precipitation; (ii) sorption method; and (iii) kinetic measurement of the interaction by surface plasmon resonance (SPR).

In the quantitative precipitation method both interacting molecules, neoglycoprotein and Con A, are present in the solution. The measured parameter here is the amount of precipitate obtained at equilibrium. The precipitation profiles of mannan−BSA conjugates with Con A are presented in Figure 4, panel A. The values in precipitation dependence are obtained as the average of two experiments. The similar aggregation course of original mannan and of its conjugates with BSA was determined. Figure 4, panel B, shows dependences of the calculated molar ratios of *SC* mannan and conjugated mannans to Con A in precipitates on the initial concentration of mannan (original or conjugated) in the test. It can be seen that the molar ratio of mannan/Con A in precipitate was achieved to be only 0.5 in the case of original mannan, but the ratios near to 1 were determined for all three conjugates. During precipitation of mannan−BSA conjugates with Con A aggregates with higher content of mannan are formed than in the case of original mannan, what is caused probably by partial association of mannan−BSA conjugates (observed at HPSEC analysis).

The sorption experiments were performed on Con A-TBC MT-50 sorbent with small diameter of pores, to eliminate the sorption of conjugates into pores. Therefore, only the sorption of conjugates on the surface of cellulose beads could be expected. The sorbent with 3.61 mg of Con A/1 g of wet BC was used. The Langmuir isotherm curves (panel A) and the Scatchard plots (panel B) for mannan as well as mannan−BSA samples adsorbed on Con A-bead cellulose are shown in Figure 5. The obtained results are as average of two experiments. Equilibrium concentration of mannan conjugates in solution as well as of their amount adsorbed on Con A-TBC was expressed

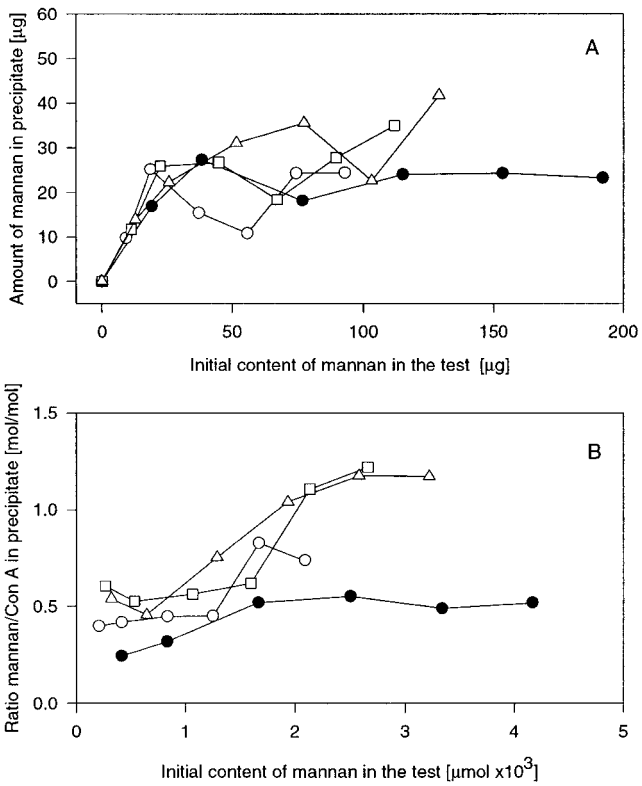


Figure 4. Precipitation of mannan and mannan−BSA conjugates with concanavalin A. Precipitation was performed in 0.05 mol·L^{-1} phosphate buffer of pH 7 containing 0.1 mol·L^{-1} NaCl, 0.1 mmol·L^{-1} Ca^{2+}, and 0.1 mmol·L^{-1} Mn^{2+}. The total volume of precipitation tests was 1 mL containing 230 μg·mL^{-1} Con A and various concentrations of mannan (from 20 to 190 μg·mL^{-1}) or conjugate (from 10 to 120 μg·mL^{-1} of the conjugate saccharide). The samples were shaken at 25 °C for 2 h. The precipitates were centrifugated, washed twice with 1 mol·L^{-1} NaCl, centrifugated, and dissolved in 0.05 mol·L^{-1} phosphate buffer adjusted to pH 10.5. These solutions were analyzed for saccharides and proteins. Panel A, dependences of mannan content (original or in conjugate) in precipitate on the initial content of mannan (original or in conjugate) in the test. Panel B, dependences of the molar ratio mannan (original or in conjugate)/Con A in precipitate on the initial content of mannan (original or in conjugate) in the test. -●- original mannan, -○- CM1, -□- CM2, -△- CM3.

as the mannan concentration. The values of K_D and Q_m estimated from the Scatchard plot and expressed as mannan−BSA conjugates are listed in Table 3. The results obtained by sorption experiments also confirmed that affinity of mannan molecules in conjugates with BSA to Con A was retained. CM2 conjugate showed the highest affinity to immobilized Con A among the three tested conjugates.

Kinetic measurement of the interaction between the neoglycoconjugates and Con A was performed using a biosensor based on surface plasmon resonance. This technique has been previously used for lectin−lipopolysaccharide interaction characterization (Shinohara et al., 1994; Mann et al., 1998; Haselye et al., 1999). SPR uses continuous flow technology and enables one to monitor the interaction in real time in comparison to the sorption method which provides data at equilibrium. In our study, Con A was immobilized on the SPR chip surface, and the interaction of neoglycoconjugates present in solution was monitored. The courses of measurements were similar to that presented in Figure 1; therefore, we present here only the calculated constants summarized in Table 4. The values of dissociation constant K_D are similar to those determined by isothermal adsorption. This demonstrates

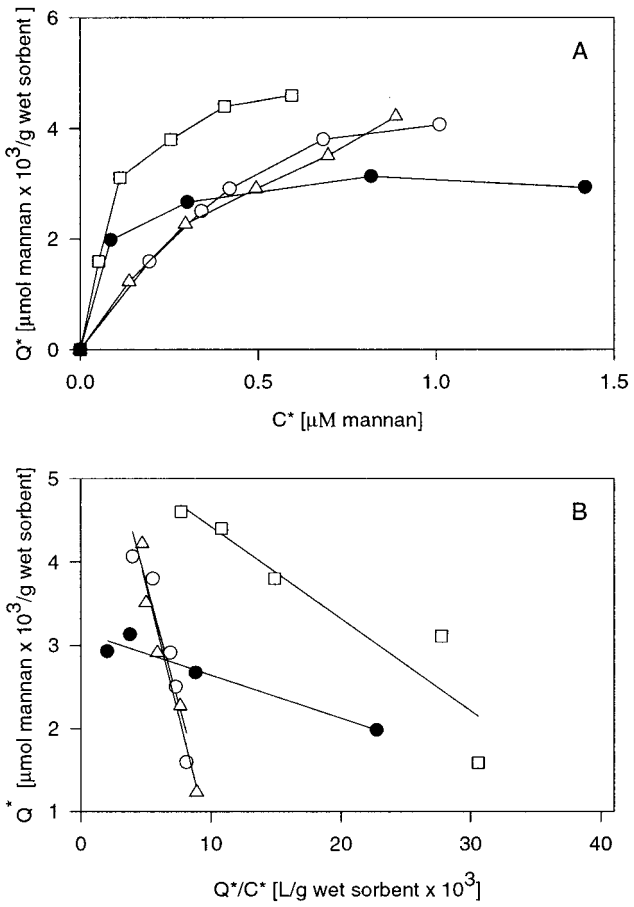


Figure 5. Sorption of mannan−BSA conjugates on Con A-TBC MT-50. The sorption of mannan and mannan−BSA was done in 0.05 mol·L^{-1} phosphate buffer (pH 7) with 0.1 mol·L^{-1} NaCl containing 0.1 mmol·L^{-1} Ca^{2+} and 0.1 mmol·L^{-1} Mn^{2+}. Suspension of Con A-TBC MT-50 (containing 3.61 mg of Con A/g of wet sorbent) prepared from 0.1 g of wet sorbent and 1 mL of individual mannan or mannan−BSA conjugate solutions (from 10 to 70 μg expressed as the saccharide in the above-mentioned buffer) were shaken slowly at 25° C for 2 h. The sorbents were centrifugated, and the saccharide and proteins in supernatants were determined. The amounts of the adsorbed conjugate were calculated as the difference between the contents of saccharides and proteins in supernatants obtained in sorption on blank BC and on Con-A TBC (sorbate is expressed as the content of mannan). Panel A, Langmuir isotherm. Panel B, Scatchard plot; -●- original mannan, -○- CM1, -□- CM2, -△- CM3.

Table 3. Langmuir Parameters for Adsorption of Mannan and Its Conjugates with BSA Determined on Con A Bead Cellulose Sorbent

sorbate	Q_m [μmol of sorbate/ g of wet sorbent]	K_D [mol sorbate·L^{-1}]	R^a
mannan SC	3.16×10^{-3}	5.2×10^{-8}	0.941
CM1	8.68×10^{-3}	5.67×10^{-7}	0.962
CM2	3.44×10^{-3}	8.98×10^{-8}	0.945
CM3	5.71×10^{-3}	2.81×10^{-7}	0.721

[a]Correlation coefficient.

a very good agreement of methods based on measurement at equilibrium (sorption method) and the method based on kinetic measurement (SPR method). We suppose the kinetic behavior of neoglycoconjugates is mainly affected by the two main influences: percentual content of saccharide (Table 2) and modification of mannan which changes kinetic properties of mannan itself (Table 1). The best interaction with Con A was experimentally observed for CM2. CM2 showed the highest kinetic association constant k_a determined by SPR and the lowest equilibrium dissociation constant K_D confirmed by both sorption and SPR method. Another parameter that may influence the interaction of neoglycoproteins are molecular weight and polydispersion. It is interesting that the highest molar mass using HPSEC method was determined for the conjugate CM2.

Table 4. Constants of Mannan−BSA Conjugates Interaction with Con A Determined by SPR

sample	k_a [M^{-1} s^{-1}]	k_d [s^{-1}]	K_D [M][a]
CM1	6.62×10^{2}	3.52×10^{-4}	5.32×10^{-7}
CM2	1.06×10^{3}	3.43×10^{-4}	3.25×10^{-7}
CM3	6.45×10^{2}	3.24×10^{-4}	5.02×10^{-7}

[a]Mol of mannan−BSA conjugate/L.

CONCLUSIONS

Oxidative modification of mannan results in changes in its interaction with Con A and consequently also influences properties of mannan−BSA neoglycoconjugates. Measurement of the interaction of neoglycoconjugates with Con A confirmed that the method used for their preparation retained the ability of the mannan moiety to interact with the lectin concanavalin A. It was observed by both the sorption and the SPR method that binding of mannan moiety of neoglycoprotein is similar as compared to the original mannan; it can be documented by the values of K_D (within the range 10^{-7} and 10^{-8} mol·L^{-1}). The measurements of molar mass and polydispersion suggest that in this conjugation method it is difficult to control structure of prepared conjugates. We suppose that conjugates of various BSA/mannan ratios may be present and also association of conjugates, which influences M_W determination, may occur. Nevertheless, the mannan−BSA conjugates with very similar M_w, polydispersion, composition, and affinity to Con A were obtained at the same condition of their conjugation and separation. This method and obtained experiences may find application in glycosylation of proteins/enzymes, for preparation of biologically active glycoconjugates (e.g., vaccines, markers) or generally as an immobilization technique for glycoproteins.

ACKNOWLEDGMENT

This work was supported by the Slovak Agency for Science VEGA via Grants No. 2/1047/21 and 1/7347/20. J.S. acknowledges support from EC (contract QLK1-CT-1999-51347). We thank D. Žišková for the technical assistance at the interaction experiments.

LITERATURE CITED

(1) Apostolopoulos, V., Pietersz, G. A., Gordon, S., Martinez-Pomarez, L., and McKenzie, I. F. C. (2000) Aldehyde-mannan antigen complexes target the MHC class I antigen-presentation pathway. *Eur. J. Immunol. 30*, 1714−1723.

(2) Beljaars, L., Molema, G., Weert, B., Bonnema, H., Olinga, P., Groothuis, G. M. M., Meijer, D. K. E., and Pelstra, K. (1999) Albumin modified with mannose 6-phosphate: a potential carrier for selective delivery of antifibrotic drugs to rat and human hepatic stellate cells. *Hepatology 29*, 1486−1493.

(3) Bonfils, E., Depierreux, C., Midoux, P., Thuong, N. T., Monsigny, M., and Roche, A. C. (1992) Drug targeting: synthesis and endocytosis of oligonucleotide−neoglycoprotein conjugates. *Nucleic Acids Res. 20*, 4621−4629.

(4) Chakraborty, P., Bhaduri, A. N., and Das, P. K. (1990) Sugar receptor mediated drug delivery to macrophages in the therapy of experimental visceral Leishmaniasis. *Biochem. Biophys. Res. Commun. 166*, 404−410.

(5) Chern, C. S., Lee, C. K., and Tsai, Y. J. (1999) Isothermal equilibrium adsorption of concanavalin A on dextran-modified poly(methyl methacrylate) latex particles. *Colloid Polym. Sci. 277*, 528−534.

(6) Franssen, E. J. F., Jansen, R. W., Vaalburg, M., and Meijer, D. K. F. (1993) Hepatic and intrahepatic targeting of an antiinflammatory agent with human serum albumin and neoglycoproteins as carrier molecules. *Biochem. Pharmacol. 45*, 1215−1226.

(7) Goldstein, I. J., and Poretz, R. D. (1986) Interaction of Concanavalin A with polysaccharides and glycoconjugates. *The Lectins, Proterties, Functions and Applications in Biology and Medicine* (I. E. Liener, N. Sharon, I. J. Goldstein, Eds.) pp 62−67, Academic Press, Orlando.

(8) Goldstein, I. J., and Hayes, C. E. (1978) The lectins: Carbohydrate-binding proteins of plants and animals. *Adv. Carbohydr. Chem. Biochem.* (P. S. Tipson, D. Horton, Eds.) Vol. 35, pp 128−206, Academic Press, New York.

(9) Han, Y., Ulrich, M. A., and Cutler, J. E. (1999) *Candida albicans* mannan extract-protein conjugates induce a protective immune response against experimental Candidiasis. *J. Infect. Dis. 179*, 1477−1484.

(10) Haselye, S. R., Talaga, P., Kamerling, J. P., and Vliegenthart, J. F. G. (1999) Characterization of the carbohydrate binding specificity and kinetic parameters of lectins by using surface plasmon resonance. *Anal. Biochem. 274*, 203−210.

(11) Jennings, H. J., and Sood, R. K. (1994) Synthetic glycoconjugates as human vaccines. *Neoglycoconjugates: Preparation and Application* (Y. C. Lee, R. T. Lee, Eds.) pp 325−371, Academic Press, San Diego.

(12) Lee, R. T., and Lee, Y. C. (1997) Neoglycoconjugates. *Glycosciences. Status and Pespectives* (H. J. Gabius, S. Gabius, Eds.) pp 55−73, Chapmann and Hall, Weinheim.

(13) Lowry, O. H., Rosenbrough, N. J., Farr, A. L., and Smith, F. (1951) Protein measurement with the Folin phenol reagent. *J. Biol. Chem. 193*, 265−275.

(14) Magnusson, G., Chernyak, A. Y., Kihlberg, J., and Konorov, L. O. (1994) Synthesis of neoglycoconjugates. *Neoglycoconjugates: Preparation and Application* (Y. C. Lee, R. T. Lee, Eds.) pp 90−143, Academic Press, San Diego.

(15) Mann, D. A., Kana, M., Maly, D. J., and Kiessling, L. L. (1998) Probing low affinity and multivalent interactions with surface plasmon resonance: Ligands for Concanavalin A. *J. Am. Chem. Soc. 120*, 10575−10582.

(16) Masárová, J., Mislovičová, D., and Gemeiner, P. (2001) Optimization of dextran and mannan dialdehydes preparation. Examination of their biospecific interaction with Concanavalin A. *Chem. Papers. 55*, 130−155.

(17) Mendichi, R., and Giacometti Schieroni, A. (1999) Use of the single-capillary viscometer detector, on-line to a size exclusion chromatography system, with a new pulse-free pump. *ACS Symposium Series* (T. Provder, Ed.) Vol. 731, pp 66−83, American Chemical Society, Washington, DC.

(18) Mendichi, R., Audisio, G., Maffei Facino, R., Carini, M., Giacometti Schieroni, A., and Saibene, L. (1995) Use of size exclusion chromatography to study the protective effect of radical scavengers on the oxygen free-radical induced degradation of hyaluronic acid. *Int. J. Polym. Anal. Character. 1*, 365−371.

(19) Mislovičová, D., Chudinová, M., Gemeiner, P., and Dočolomanský, P. (1995) Affinity chromatography of invertase on Concanavalin A-bead cellulose matrix: the case of an extraordinary strong binding glycoenzyme. *J. Chromatogr. B 664*, 145−153.

(20) Mortell, K. H., Weatherman, R. V., and Kiessling, L. L. (1996) Recognition specificity of neoglycopolymers prepared by ring-opening metathesis polymerization. *J. Am. Chem. Soc. 118*, 2297−2298.

(21) Pagé, D., Zanini, D., and Roy, R. (1996) Macromolecular recognition: Effect of multivalency in the inhibition of binding of yeast mannan to Concanavalin A and Pea lectins by mannosylated dendrimers. *Bioorgan. Med. Chem. 4*, 1949−1961.

(22) Park, J. T., and Johnson, M. J. (1949) A submicrodetermination of glucose. *J. Biol. Chem. 181*, 149−151.

(23) Roy, R., Pagé, D., Perez, S. F., and Bencomo, V. V. (1998) Effect of shape, size, and valency of multivalent mannosides on their binding properties to phytohemagglutinins. *Glycoconjugate J. 15*, 251−263.

(24) Saha, S. K., and Brewer, C. F. (1994) Determination of the concentration of oligosaccharides, complex type carbohydrates, and glycoproteins using the phenol/sulfuric acid method. *Carbohyd. Res. 254*, 157−167.

(25) Saleemuddin, M. (1999) Bioaffinity based immobilization of enzymes. *Adv. Biochem. Eng./Biotechnol. 64*, 204−226.

(26) Shinohara, Y., Kim, F., Shimizu, M., Goto, M., Tosu, M., and Hasegawa, Y. (1994) Kinetic measurement of the interaction between an oligosaccharide and lectins by a biosensor based on surface plasmon resonance. *Eur. J. Biochem. 223*, 189−194.

(27) Šandula, J., and Vojtková-Lepšíková, A. (1974) Immunochemical studies on mannans of the genus *Saccharomyces*. *Folia Microbiol. 19*, 94−101.

(28) Wyatt, P. J. (1993) Light scattering and the absolute characterization of macromolecules. *Anal. Chim. Acta 272*, 1−40.

(29) Young, M., Davies, M. J., Bailey, D., Gradwell, M. J., Smestad-Paulsen, B., Wold, J. K., Barnes, R. M. R., and Hounsell, E. F. (1998) Characterization of oligosaccharides from an antigenic mannan of *Saccharomyces cerevisiae*. *Glycoconjugate J. 15*, 815−822.

BC015517U

TECHNICAL NOTES

Synthesis of Novel Glycolipids That Bind HIV-1 Gp120

Rachel Y. LaBell, Neil E. Jacobsen, Jacquelyn Gervay-Hague, and David F. O'Brien*

The University of Arizona, Department of Chemistry, Tucson. Arizona 85721 . Received July 24, 2001

As part of a research effort to design and prepare high affinity ligands for the galactosyl ceramide (GalCer) binding site on the HIV cell surface glycoprotein, gp120, several GalCer analogues have been prepared and characterized. The molecular design of analogues permits independent variations of the carbohydrate, the length of a hydrophilic spacer between the ligand and the lipid, and the composition of the hydrophobic lipid chains. Five different galactosyl analogues were synthesized having hydrophilic spacers of tri-, tetra-, and penta-ethylene glycol separating the carbohydrate from the lipid region which has either oleoyl or stearoyl lipid chains. The synthetic design allows for a convergent synthesis of the three components of the glycolipid conjugate. The structural characterization includes the proton and carbon chemical shifts, which were assigned after analysis of 1D and 2D NMR spectra.

INTRODUCTION

HIV-1 can gain entry into human T-cells by the initial binding of an associated surface glycoprotein (gp120) to the critical domain receptor (CD4) on the T-cell membrane surface. Subsequently, a cascade of events occur leading to HIV-1 replication which ultimately causes impairment of the immune system as HIV infection progresses to AIDS. However, an alternative receptor has been discovered that mediates the infection of CD4 negative cells (*1*−*3*). This galactosyl ceramide (GalCer) receptor is present on the surface of many types of cells including colorectal cells and vaginal epithelial cells (*4*).

GalCer (Figure 1) is a relatively simple glycosphingolipid consisting of a single galactose unit bound via a β-linkage to ceramide. In biological membranes, the galactose portion is displayed very close to the membrane surface. Several laboratories have shown that the length of the spacer group between an antigen and its anchoring lipid can affect the efficiency of binding to antibodies. For example, Ringsdorf et al. found that extending fluorescein away from the membrane surface with a tetraethylene glycol spacer increased the binding of fluorescein to its antibody (*5*). The use of a hydrophilic linker as a spacer group in glycolipids has been reported to enhance the specific interaction of carbohydrates with receptor proteins (*6, 7*). Therefore, we elected to design GalCer analogues with variable length hydrophilic linkers to investigate the effect of spacer group length on the binding of galactosyl lipids with gp120.

The β configuration of galactose is believed to be necessary for effective binding of GalCer to gp120 (*8*). One problem with GalCer is the susceptibility of the anomeric linkage to cleavage by glycosidases. The replacement of the anomeric oxygen with carbon stabilizes the anomeric linkage and is reported to have little effect on the binding of galactose to gp120 (*9, 10*).

The third variable considered in the glycolipid is the nature of the lipid chains. There seems to be conflicting evidence in the literature about whether variation in the lipid chains can influence the binding of GalCer analogues to gp120. Silberger and Bhat provided evidence that variation of the GalCer fatty acid chain length from 16 to 24 carbons showed little effect on binding efficiency when ^{125}I-labeled gp120 was incubated with GalCer doped liposomes (*8*). Other authors reported that varying the GalCer fatty acid chain length from 1 to 14 has a distinct effect on the binding of GalCer analogues to rgp120 in an ELISA-type assay (*9*). Rico-Lattes has reported that a seven-carbon fatty acid chain showed no activity while a ten-carbon chain showed weak activity in binding to SPC3 peptide which mimics the V3 loop of gp120 (*11*). This literature provides evidence that a sufficiently long hydrophobic lipid chain is necessary to effectively anchor the lipid into the membrane, and there is little additional effect on binding efficiency.

The second issue concerning the lipid chains is the presence of unsaturation. GalCer fatty acid is saturated to the extent that it exists in microdomains in biological membranes (*12*). Lipids with an unsaturation in the chains tend to not form domains in biological membranes because they do not pack together well and are more fluidlike. Lipids with saturated chains tend to form domains because the lipid chains pack efficiently and are more solidlike. Whether GalCer analogues that do not form domains will bind to gp120 has not been systematically investigated. Therefore, the design allows for the synthesis of both saturated and unsaturated analogues that will allow evaluation of this variable.

In an effort to design GalCer analogues that could compete with the binding of gp120 to GalCer, a versatile synthetic scheme was developed. The analogue design permits the independent variation of three components that could increase binding: carbohydrate head group, hydrophilic spacer group, and lipid tails. The synthesis of these GalCer analogues is convergent with respect to each component. The hydrophilic spacer is derived from commercially available oligo-ethylene glycols by dif-

10.1021/bc015533r CCC: $22.00 © 2002 American Chemical Society
Published on Web 12/08/2001

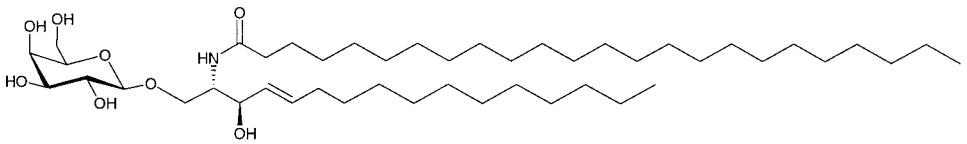
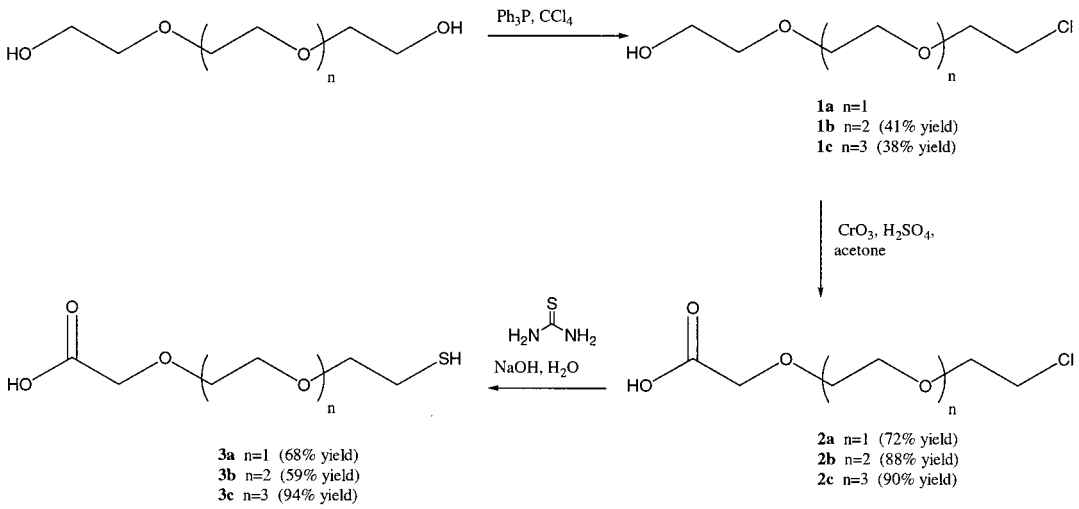
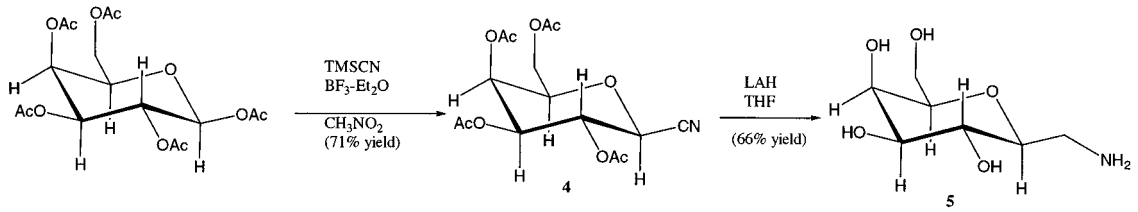


Figure 1. Structure of galactosyl ceramide.

Scheme 1



Scheme 2



ferentiation of the end groups. The carbohydrate head group is derived from β-D-galactose pentaacetate by conversion into the *C*-glycoside using trimethylsilyl cyanide (TMSCN). The lipid chains can be easily obtained by reaction of any long chain alcohol with maleic anhydride to form the maleic diester. Variation of one or more of these components has the potential to affect the binding affinity of the analogue to gp120.

RESULTS

The synthesis started with a commercially available spacer, 2-(2-chloroethoxy)ethoxyethanol (**1a**). The corresponding longer spacers were derived from tetraethylene glycol and pentaethylene glycol by monochlorination with triphenylphosphine and carbon tetrachloride (Scheme 1) (*16*). The statistical mixture of dichloride, monochloride, and diol were separated by silica gel chromatography. In each spacer the remaining alcohol underwent Jones oxidation to give the corresponding monochlorocarboxylic acids **2a**,**b**,**c** (*15*). The synthesis of each spacer is completed by conversion of the ω-chloro carboxylic acid to the ω-thiol by reaction with thiourea, sodium hydroxide, and water **3a**,**b**,**c** (*15*). The literature procedure was modified by addition of 1 equiv of sodium iodide to form the iodide in-situ and improve yields up to 96%. The galactose portion was synthesized from β-D-galactose pentaacetate by displacing the anomeric acetate using TMSCN in the presence of $BF_3 \cdot OEt_2$ **4** (Scheme 2) (*17*). Only the β anomer is formed because of participation of the C-2 acetate (*17*). The peracetylated *C*-galactose was reduced with lithium aluminum hydride in THF to remove all the acetates and convert the cyano group to methylene amine **5** (*18*). There was some acyl migration from the C-2 to the primary amine during the reaction followed by reduction of the amide to give 18% ethylamine as a byproduct.

Two different lipid chains were used to synthesize the five Gal-Cer analogues. The unsaturated series of glycolipids were made using oleoyl alcohol. These analogues were synthesized in order to investigate the effect of non-domain-forming glycolipids on binding affinity. The saturated series was made using stearoyl alcohol. Saturated glycolipids have the propensity to form domains when mixed with dioleoyl phosphatidylcholine (DOPC).

The unsaturated lipid was prepared (Scheme 3) from maleic anhydride and oleoyl alcohol with a catalytic amount of *p*-toluenesulfonic acid in chloroform to give the desired unsaturated diester. The conjugated double bond of the maleic ester provides a site for nucleophilic addition of the ω-thiol carboxylic acid **3a**,**b**,**c**. The product is a lipid-spacer conjugate with a carboxylic acid end group **7a**,**b**,**c** (*19*).

The last step of the synthesis is the formation of an amide bond between the carboxylic acid of the lipid **7a**,**b**,**c** and the *C*-galactoside **6**. The acid was combined with pentafluorophenyl trifluoroacetate to form the activated pentafluoro ester followed by addition of **6** (*20*). Low yields are a result of minimal solubility of the deprotected carbohydrate in DMF. The unsaturated series of glycolipid molecules are named according to the carbohy-

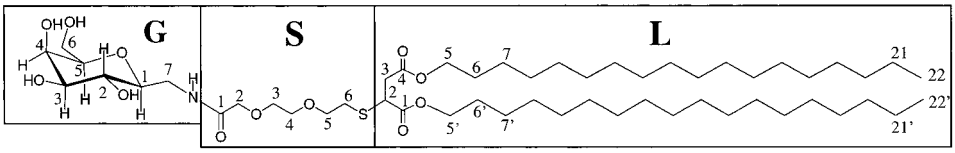
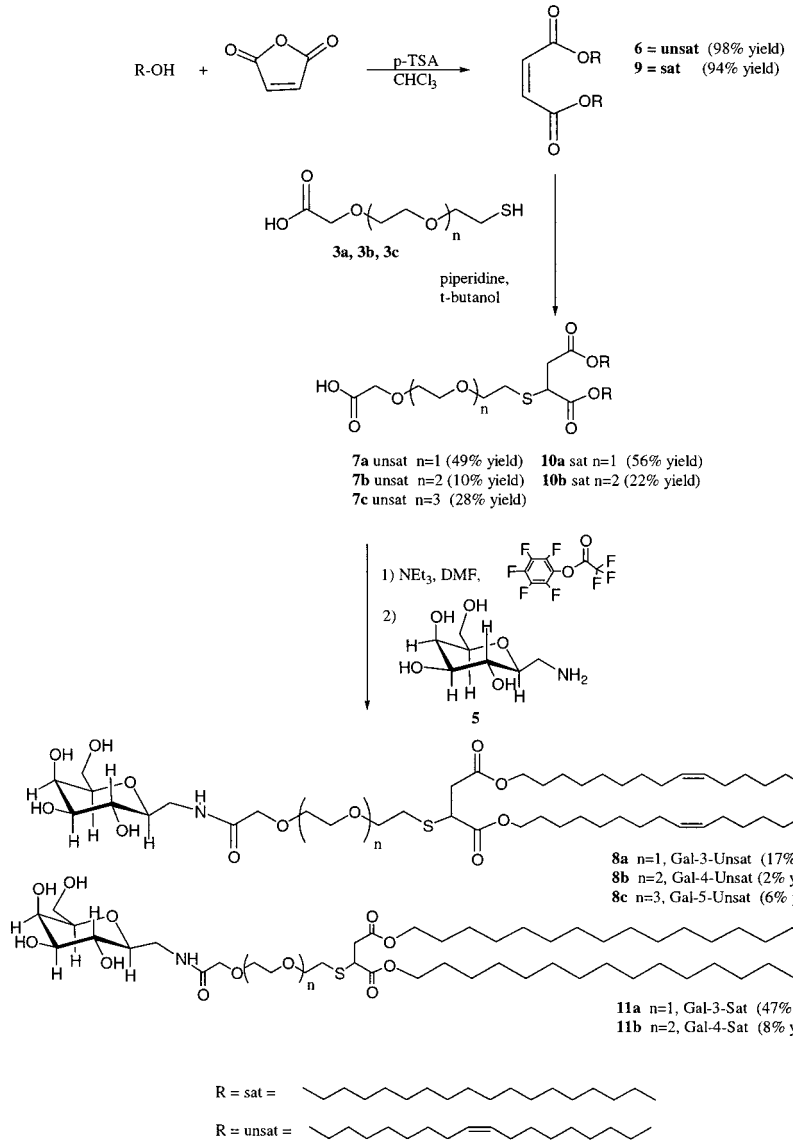


Figure 2. Numbering scheme for NMR assignments.

Scheme 3



drate, Gal; the length of the ethylene glycol spacer: 3, 4, or 5; and the nature of the lipid chain: oleoyl (unsat) or stearoyl (sat). Hence the unsaturated series is referred to as Gal-3-Unsat, Gal-4-Unsat, and Gal-5-Unsat.

The saturated series (Scheme 3) was prepared by the same reaction sequence except that the starting alcohol was stearoyl alcohol and the resulting maleic ester has saturated lipid chains **9**. The spacer−lipid conjugate **10a**,**b** and the final glycolipids **11a**,**b** were formed in the same manner as the unsaturated series to give Gal-3-Sat and Gal-4-Sat.

NMR chemical shift assignments were made for Gal-3-Sat, a representative glycolipid analogue (Figure 2). 2D-NMR data (HMQC, HMBC, and COSY) was acquired and analyzed to assign all protons and carbons. NMR chemical shift assignments (Table 1) were obtained by analysis of the HMBC data (Figure 4). The G4 (equatorial) proton signal has small coupling constants and thus can be located in the HSQC spectrum (Figure 3) as a sharp, positive cross-peak. G7 and G6 diastereotopic pairs can also be identified in the HSQC, with the G7 carbon 20 ppm upfield of the G6 carbon since it is bonded to amide nitrogen instead of oxygen. Clear HMBC connectivities allow assignment of the entire *C*-glycoside, with confirmation from the DQF−COSY (data not shown). An HMBC cross-peak from one of the G7 protons to the S1 (carbonyl) carbon verifies the spacer attachment through the amide linkage, and HMBC and COSY connections lead to assignment of the entire spacer. One of the S6 protons shows an HMBC connection through the thioether linkage to the L2 carbon, connecting the spacer to the lipid moiety. The more downfield of the lipid carbonyl

Table 1. Chemical Shift Assignments for Gal-3-Sat in $CDCl_3/CD_3OD$ (1:1)

position[a]	$\delta(^1H)$	mult[b]	J(Hz)	$\delta(^{13}C)$	HMBC carbons
G1	3.15	ddd	9.4,6.4,2.9	79.70	G2,G3
G2	3.39	m		69.85	G1,G3
G3	3.40	m		75.49	
G4	3.80	dd	2.7,1.0	70.47	G3,G5
G5	3.41	m		79.78	G1,G4,G6
G6a	3.69	dd	11.6,6.9	62.75	G5
G6b	3.60	d	11.7	62.75	G4,G5
G7a	3.63	d	13.9	41.14	G1,G2
G7b	3.40	m		41.14	G1,G2,S1
S1				172.56	
S2	3.94	s	J_{AB} 15.7	71.07	S1,S3
S3	3.61	m		71.67	S4
S4	3.59	m		70.95	S3
S5	3.62	m		71.26	S4
S6a	2.87	dt[c]	13.6(J_{AB}),6.4	31.96	S5
S6b	2.79	dt	13.7(J_{AB}),6.4	31.96	S5,L2
L1				173.09	
L2	3.65	dd	10.5,5.2	42.91	L1,L3,S6
L3a	2.87	dd	16.9,10.4	37.49	L1,L2
L3b	2.6	dd	16.9,5.3	37.49	L1,L2,L4
L4				171.92	
L5a	4.06	dt	10.7(J_{AB}),6.6	66.12	L4,L6,L7/7′
L5b	4.05	dt	10.7(J_{AB}),6.6	66.12	L4,L6,L7/7′
L5a′	3.998	dt	10.9(J_{AB}),6.7	66.54	L1,L6′,L7/7′
L5b′	3.992	dt	10.9(J_{AB}),6.7	66.54	L1,L6′,L7/7′
L6	1.54	m		29.41	L5,L7
L6′	1.58	m		29.38	L5′,L7′
L7	1.24	m		26.70	
L7′	1.28	m		26.70	L5′
				30.07(2)[d]	
				30.16(2)	
				30.35(1)	
L8-L19/	1.20	m		30.37(1)	
L8′-L19′				30.40(2)	
				30.46(2)	
				30.49(14)	
L20/L20′	1.19	m		32.75	
L21/L21′	1.22	m		23.45	L20/L20′
L22/L22′	0.77	t	7.0	14.51	L20/L20′,L21/L21′

[a] See Figure 2 for numbering system. Lower-case a and b refer to diastereotopic protons in methylene groups which are not stereospecifically assigned. [b] d = doublet, t = triplet, dd = doublet of doublets, dt = doublet of triplets, ddd = double double doublet, m = multiplet. [c] Doublet coupling listed first for all dt. [d] Estimated number of carbons shown in parentheses.

carbons was assigned to L1 due to its proximity to the thioether. HMBC connectivities across the ester linkages in the lipid portion allow unambiguous assignment of the L5 and L5′ (differing in both ^1H and ^{13}C shifts) and the L6 and L6′ (differing in ^1H shifts) positions. Approximately eight carbons from the L8-L19/L8′-L19′ portion of the lipid chains were resolved in the 1D ^{13}C spectrum but could not be assigned (Table 1).

DISCUSSION

Binding of the unsaturated GalCer analogues to gp120 has already been assessed by total internal reflection fluorescence spectroscopy (TIRF) (*21*). Fluorescently tagged recombinant gp120 was allowed to bind to the monolayer surface containing GalCer analogues and an equilibrium measurement of protein bound to the monolayer was accomplished using TIRF. The binding studies investigated the effect of varying the spacer length on binding affinity of GalCer analogues to gp120. The analogues bind cooperatively to gp120 when doped at 5 mol % in a monolayer of DOPC. The binding curves were extrapolated to obtain binding affinity constants (K_a) of 2×10^6. The protein coverage was determined and highest protein coverage was achieved with a spacer group of triethylene glycol. Therefore, a critical spacer arm length has been determined for these GalCer analogues (*21*). A comparative study of the saturated and unsaturated GalCer analogues will be reported elsewhere.

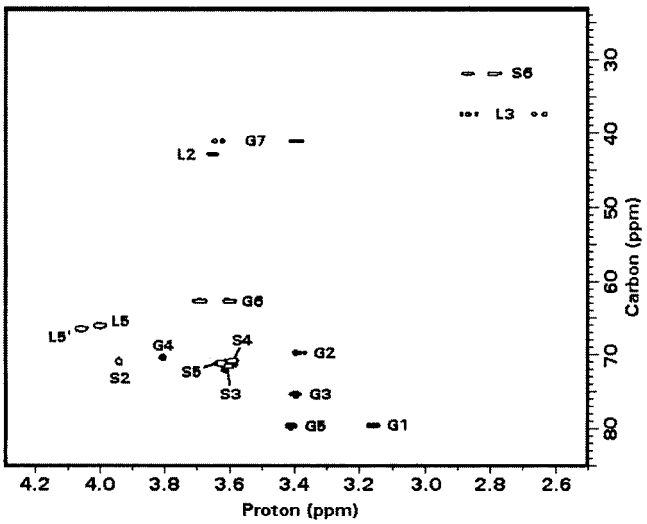


Figure 3. Portion of the edited 2D Gradient-Selected HSQC spectrum of Gal-3-Sat in $CD_3OD/CHCl_3$ (1:1). Data were acquired in TPPI mode with 512 complex pairs in t_2, 750 increments of t_1, and 8 scans per t_1 increment. A skewed, 45°-shifted sinebell was applied in both dimensions with zero-filling to a final real matrix of 2048 (F_2) × 1024 (F_1) data points. Single contours (open) are shown for negative (CH_2) cross-peaks with many contours (filled) for positive (CH_3, CH) cross-peaks.

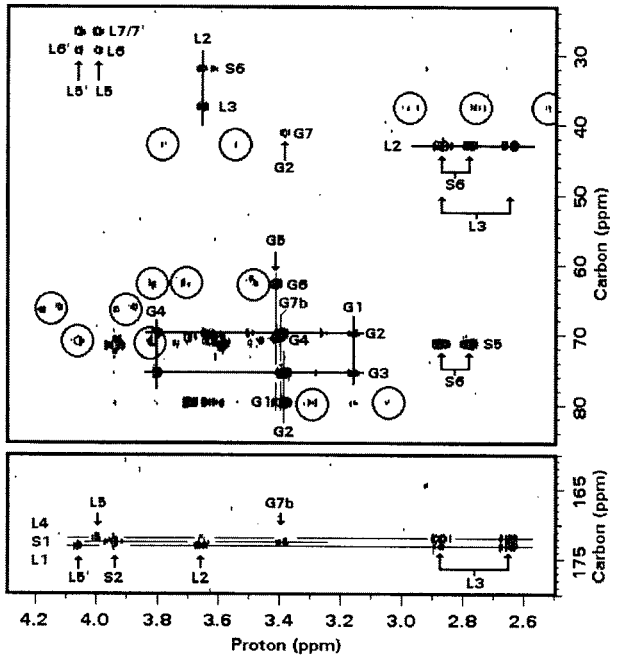


Figure 4. Two portions of the phase-sensitive 2D Gradient-Selective HMBC spectrum of Gal-3-Sat in $CD_3OD/CHCl_3$ (1:1). Data were acquired in echo-antiecho mode with 2048 complex pairs in t_2, 356 increments of t_1, and 16 scans per t_1 increment using a TANGO sequence and a gradient to dephase ^{13}C-bound proton signals before the start of the HMBC (Kover, K. E., personal communication). A 90°-shifted sinebell was applied in both dimensions with zero-filling to a final real matrix of 2048 (F_2) × 1024 (F_1) data points. Single contours (open) are shown for negative cross-peaks with many contours (filled) for positive cross-peaks. Circles indicated one-bond correlations.

This research has led to the development of a versatile synthesis of glycolipids that conjugate a carbohydrate, spacer group, and a lipid. These analogues should improve attempts to design and synthesize new HIV-1 therapies using membrane-tethered receptors for gp120.

EXPERIMENTAL SECTION

General Procedures. All materials were obtained from commercial sources and used without additional purification, unless otherwise noted. 1D ^{1}H and ^{13}C NMR spectra were recorded on Varian Gemini-200, Varian Unity-300 MHz, Bruker DRX-500 or Bruker DRX-600 spectrometers. 1D ^{1}H spectra were referenced to internal tetramethylsilane (0 ppm) and 1D ^{13}C spectra are referenced to the solvent ^{13}C signal, ($CDCl_3$ at 77.0 ppm and CD_3OD at 49.0 ppm). NMR spectra for Gal-3-Sat (^{1}H, ^{13}C, HSQC (*13*), HMBC (*13*), and DQF−COSY (*14*) were acquired on a Bruker DRX-600 spectrometer with a 5 mm Bruker TXI triple-resonance three-axis gradient probe at 25 °C. The sample (30 mg) was dissolved in 0.6 mL of $CDCl_3/CD_3OD$ (1:1). The spectral widths were 4.6 ppm (^{1}H) and 200 ppm (^{13}C) for the 2D spectra. Data were processed and plotted using Felix2000 (Molecular Simulations, San Diego, CA). All 2D spectra were referenced using specific signals in the 1D spectra, which were referenced to internal tetramethylsilane (0 ppm) for ^{1}H and CD_3OD (49.15 ppm) for ^{13}C.

(2-{2-[2-Chloroethoxy]ethoxy}ethoxy)acetic Acid (2b). A mixture of (2-{2-[2-chloroethoxy]ethoxy}ethoxy)-ethanol (3.00 g, 14.2 mmol) in acetone (60 mL) was stirred at room temperature as 6 mL of a 2.67 M Jones reagent (*15*) was added dropwise over 15 min. The reaction was stirred for an additional 30 min followed by addition of 3 drops of 2-propanol. Water (40 mL) was added to the mixture followed by removal of the acetone in vacuo. Saturated NaCl solution (20 mL) was added, and the aqueous mixture was extracted with $CHCl_3$ (7 × 30 mL). The organic layers were combined and dried with anhydrous $MgSO_4$. The product was visualized with bromocresol green on a silica gel TLC plate after elution with 30:5:3 $CHCl_3$/EtOH/HOAc, with an R_f value of 0.5. The solvent was removed in vacuo, and the product was purified by silica gel column chromatography in 30:5:3 $CHCl_3$/EtOH/HOAc to yield 2.63 g of product in 82% yield. ^{1}H NMR (300 MHz, $CDCl_3$) δ 3.50−3.65 (m, 12H), 4.15 (s, 2H), 10.63 (bs, 1H). ^{13}C NMR (75 MHz, $CDCl_3$) δ 42.5, 68.0, 70.1, 70.2, 70.7, 71.0, 173.8. High-resolution mass spectrum (FAB^+) calcd for $C_8H_{15}O_5Cl$ $(MH)^+$: 227.0686. Found: 227.0680.

(2-{2-[2-(2-Mercaptoethoxy)ethoxy]ethoxy}ethoxy)-acetic Acid (3c). (2-{2-[2-(2-Chloroethoxy)ethoxy]ethoxy}-ethoxy)acetic acid (2.60 g, 9.63 mmol) was combined with thiourea (2.93 g, 38.5 mmol) and sodium iodide (1.45 g, 9.63 mmol) in 40 mL of water, and the reaction mixture was heated at refluxed for 4 h. After addition of 52 mL of 2.5 M, heating was continued for another 4 h. The reaction was cooled to room temperature, and the pH was adjusted to 1 with concentrated HCl. The aqueous mixture was extracted with $CHCl_3$ (7 × 40 mL), and the organic layers were combined and dried with anhydrous $MgSO_4$. The product was visualized with bromocresol green on a silica gel TLC plate after elution with 3:2 $CHCl_3$/EtOH, with an R_f value of 0.30. The solvent was removed in vacuo, and the resulting oil was purified on neutral alumina column chromatograpy using a gradient starting with 6:1 $CHCl_3$/EtOH and ending with 60:40:5 $CHCl_3$/EtOH/HOAc to yield 2.43 g of a colorless oil with a 94% yield. ^{1}H NMR (300 MHz, $CDCl_3$) δ 1.55 (t, J = 8.6 Hz, 1H), 2.64 (q, J = 7.3 Hz, 2H), 3.53−3.73 (m, 14H), 4.14 (s, 2H). ^{13}C NMR (75 MHz, $CDCl_3$) δ 24.0, 68.3, 70.0, 70.3, 70.4, 70.9, 72.7, 174.2. High-resolution mass spectrum (FAB^+) calcd for $C_{10}H_{21}O_6S$ $(MH)^+$: 269.1059. Found: 269.1067.

2-[2-(2-Carboxymethyoxyethoxy)ethylsulfanyl]-succinic Acid dioctadec-9-enyl Ester (7a). Butenedioic acid dioctadec-9-enyl ester (cis) (0.660 g, 1.07 mmol) was dissolved in 40 mL of 2-propanol at 80 °C under an Ar atmosphere. In a separate vial, [2-(2-mercaptoethoxy)-ethoxy]acetic acid (**3a**) (0.193 g, 1.07 mmol) was titrated to pH of 8 with 15% NaOH. The basic solution was added to the reaction mixture followed by a catalytic amount of piperidine (2 drops). The reaction was heated at reflux for 1 h. Solvent was removed in vacuo, and the residue was taken up in water (20 mL). The pH was adjusted to 4 with 10% HCl, and the resulting solution was extracted with ethyl acetate (4 × 80 mL). The organic layers were combined and dried with anhydrous $MgSO_4$, and the solvent was removed in vacuo. The product was visualized by phosphomolybdic acid on a silica gel TLC plate after elution with 9:1 $CHCl_3$/MeOH, giving an R_f of 0.25. The product was purified by silica gel column chromatography using pure $CHCl_3$ to elute the starting ester, followed by 9:1 $CHCl_3$/MeOH to elute the product. A colorless oil (0.50 g) was obtained in 59% yield. ^{1}H NMR (200 MHz, $CDCl_3$) δ 0.85 (t, J = 6.8 Hz, 6H), 1.25 (m, 44H), 1.58 (t, J = 7.6 Hz, 4H), 1.98 (q, J = 5.8 Hz, 8H), 2.57−3.03 (m, 4H), 3.59−3.76 (m, 6H), 4.04 (t, J = 7.0 Hz, 2H), 4.10−4.13 (m, 2H), 5.46 (t, J = 5.2 Hz, 4H). ^{13}C NMR (50 MHz, $CDCl_3$) δ 14.1, 22.6, 25.8, 27.2, 28.5, 29.2, 29.3, 29.4, 29.5, 29.7, 30.8, 31.9, 36.5, 41.7, 65.2, 65.6, 70.0, 70.4, 127.9, 129.9, 170.6, 171.7. Electrospray mass spectrum calcd. for $C_{46}H_{84}O_8S$ $(M)^-$: 796.4. Found: 795.5.

2-{2-[2-(2-Carboxymethoxyethoxy)ethoxy]-ethylsulfanyl}succinic Acid dioctadec-9-enyl Ester (7b). Prepared in a silimar manner to (**7a**). ^{1}H NMR (300 MHz, $CDCl_3$) δ 0.85 (t, J = 7.48 Hz, 6H), 1.17−1.35 (m, 44H), 1.53−1.67 (m, 4H), 1.94−2.02 (m, 8H), 2.55−2.69 (m, 1H), 2.74−2.95 (m, 2H), 3.58−3.71 (m, 12H), 3.99−4.13 (m, 6H), 5.31 (t, J = 5.28 Hz, 4H). ^{13}C NMR (75 MHz, $CDCl_3$) δ 14.0, 21.6, 21.7, 22.6, 25.7, 27.1, 28.4, 29.1, 29.3, 29.4, 29.6, 30.7, 31.8, 36.4, 36.7, 41.7, 65.0, 65.5, 68.4, 68.9, 70.0, 70.2, 129.6, 129.8, 170.6, 171.0, 171.6. Electrospray mass spectrum cald for $C_{48}H_{88}O_9S$ $(M)^-$: 840.0. Found: 839.3.

2-(2-{2-[2-(2-Carboxymethoxyethoxy)ethoxy]-ethoxy}ethylsulfanyl)succinic Acid Dioctadec-9-enyl Ester (7c). Prepared in a silimar manner to (**7a**). ^{1}H NMR (300 MHz, $CDCl_3$) δ 0.86 (t, J = 7.0 Hz, 6H), 1.23−1.30 (m, 44H), 1.51−1.65 (m, 6H), 1.86−2.03 (m, 8H), 2.65 (dd, J = 16.8, 4.4 Hz, 1H), 2.73−3.35 (m, 6H), 3.58−3.70 (m, 10H), 3.96−4.14 (m, 6H), 5.32 (t, J = 5.3 Hz, 4H). ^{13}C NMR (75 MHz, $CDCl_3$) δ 14.1, 22.6, 25.7, 25.8, 27.1, 28.5, 29.2, 29.3, 29.4, 29.5, 29.7, 30.9, 31.8, 36.5, 41.6, 65.1, 65.5, 70.0, 70.2, 129.7, 129.9, 170.6, 171.6. Electrospray mass spectrum calcd. for $C_{50}H_{92}O_{10}S$ $(M)^-$: 884.0. Found: 883.1.

2-[2-(2-Carboxymethoxyethoxy)ethylsulfanyl]-succinic Acid Dioctadecyl Ester (10a). Prepared in a silimar manner to (**7a**). ^{1}H NMR (300 MHz, $CDCl_3$) δ 0.84 (t, J = 6.4 Hz, 6H), 1.21 (m, 60H), 1.58 (p, J = 11.8, 5.9 Hz, 4H), 2.64 (dd, J = 17.0, 11.0 Hz, 1H), 2.74−2.98 (m, 4H), 3.61−3.73 (m, 6H), 4.01−4.13 (m, 6H). ^{13}C NMR (75 MHz, $CDCl_3$) δ 14.1, 22.7, 25.7, 25.8, 28.5, 29.2, 29.3, 29.5, 29.6, 29.7, 30.8, 31.9, 36.5, 41.7, 62.3, 65.2, 65.6, 68.6, 70.1, 70.4, 71.0, 76.6, 78.9, 170.7, 171.7. High-resolution mass spectrum (FAB^+) calcd for $C_{46}H_{89}O_8S$ $(MH)^+$: 801.6278. Found: 801.6289.

2-{2-[2-(2-Carboxymethoxyethoxy)ethoxy]-ethylsulfanyl}succinic Acid Dioctadecyl Ester (10b). Prepared in a silimar manner to (**7a**). ^{1}H NMR (300 MHz, $CDCl_3$) δ 0.88 (t, J = 7.6 Hz, 6H), 1.25 (m, 60H), 1.62 (p, J = 12.7, 6.8 Hz, 4H), 2.68 (dd, J = 17.1, 11.7 Hz, 1H), 2.77−3.01 (m, 4H), 3.61−3.78 (m, 10H), 4.06 (t, J = 7.3 Hz, 2H), 4.10−4.17 (m, 4H). ^{13}C NMR (75 MHz, $CDCl_3$)

δ 14.1, 22.7, 25.8, 28.5, 29.2, 29.4, 29.5, 29.6, 29.7, 31.0, 31.9, 36.6, 41.7, 65.2, 65.6, 70.1, 70.5, 70.6, 170.7, 171.7. Electrospray mass spectrum cald for $C_{48}H_{92}O_9S$ $(M)^-$: 845.3. Found: 845.0.

Gal-3-Unsat (8a). 2-[2-(2-Carboxymethyoxyethoxy)-ethylsulfanyl]succinic acid dioctadec-9-enyl ester (**7a**) (165 mg, 0.21 mmol) was dissolved in 1.0 mL of DMF followed by addition of triethylamine (117 μL, 0.84 mmol) and pentafluorophenyltrifluoroacetate (55 μL, 0.32 mmol) via a Hamilton syringe. The reaction mixture was stirred at room temperature for 2 h to allow formation of the activated pentafluorophenyl ester. The *C*-glycoside amine (**5**) (40 mg, 0.21 mmol) was added, and the reaction was allowed to stir overnight. A solution of 10% $NaHCO_3$ (10 mL) was added directly to the reaction mixture, and then the aqueous layer was extracted with $CHCl_3$ (4 × 10 mL). The organic extracts were combined and dried with anhydrous $MgSO_4$, and the product was visualized with phosphomolybdic acid on a silica gel TLC plate. The R_f was 0.3 when eluted with 9:1 $CHCl_3$/MeOH. The product was purified by silica gel chromatography using a gradient solvent system starting with pure $CHCl_3$ followed by 99:1, 95:1, and 9:1 $CHCl_3$/MeOH. The product (32 mg) was obtained as a colorless, viscous liquid in 17% yield. ^{1}H NMR (600 MHz, CD_3OD) δ 0.80 (t, J = 6.9 Hz, 6H), 1.19 (m, 44H), 1.51−1.57 (m, 4H), 1.94 (m, 8H), 2.65 (d, J = 16.9 Hz, 1H), 2.74−2.88 (m, 3H), 3.21 (m, 8H), 3.30 (q, J = 6.9 Hz, 1H), 3.36 (d, J = 5.9 Hz, 2H), 3.39 (t, J = 6.0 Hz, 1H), 3.55−3.68 (m, 10 H), 3.76 (bs, 1H), 3.92 (s, 2H), 3.98 (q, J = 6.9 Hz, 2H), 4.04 (dt, J = 2.6, 6.5 Hz, 2H), 5.25 (t, J = 4.6 Hz, 4H). ^{13}C NMR (150 MHz, CD_3-OD) δ 14.1, 22.6, 25.8, 27.2, 28.5, 29.2, 29.3, 29.4, 29.5, 29.7, 31.0, 31.9, 36.5, 39.7, 41.7, 50.8, 63.2, 65.3, 69.9, 70.0, 70.1, 70.2, 70.7, 76.4, 76.6, 76.8, 77.8, 78.8, 129.7, 129.9, 170.7, 171.6, 172.4. High-resolution mass spectrum (FAB^+) calcd for $C_{53}H_{97}NO_{12}S$ $(MH)^+$: 972.6810. Found: 972.6815.

Gal-4-Unsat (8b). Prepared in a silimar manner to (**8a**). ^{1}H NMR (600 MHz, $CD_3OD/CDCl_3$) δ 0.86 (t, J = 6.7 Hz, 6H), 1.19−1.34 (m, 44H), 1.50−1.65 (m, 4H), 1.99 (q, J = 12.6, 5.9 Hz, 8H), 2.66 (dd, J = 17.0, 5.5 Hz, 1H), 2.82 (q, J = 6.9 Hz, 1H), 2.88−2.98 (m, 3H), 3.27 (q, J = 8.8 Hz, 1H), 3.37−3.43 (m, 4H), 3.45−3.52 (m, 6H), 3.58−3.70 (m, 10H), 3.73−3.76 (m, 1H), 3.78−3.84 (m, 1H), 3.86−3.91 (m, 1H), 4.02−4.07 (m, 4H), 4.11 (t, J = 6.9 Hz, 2H), 5.33 (p, J = 3.3, 6.9 Hz, 4H. Electrospray ionization mass spectrum (ESI^+) calcd for $C_{55}H_{101}NO_{13}S$ $(MH)^+$: 1016.34. Found: 1016.3.

Gal-5-Unsat (8c). Prepared in a silimar manner to (**8a**). ^{1}H NMR (600 MHz, $CD_3OD/CDCl_3$) δ 0.86 (t, J = 7.1 Hz, 6H), 1.19−1.34 (m, 44H), 1.52−1.65 (m, 4H), 1.99 (q, J = 12.4, 5.9 Hz, 8H), 2.66 (dd, J = 17.0, 5.4 Hz, 1H), 2.82 (q, J = 6.7 Hz, 1H), 2.88−2.98 (m, 3H), 3.23−3.31 (m, 3H), 3.47−3.52 (m, 3H), 3.59−3.70 (m, 14H), 3.78−3.84 (m, 2H), 3.85−3.90 (m, 2H), 3.95−4.06 (m, 7H), 4.11 (*t*, J = 7.1 Hz, 2H), 5.33 (*p*, J = 3.1, 6.3 Hz, 4H). Mass spectrum (FAB^+) calcd for $C_{57}H_{105}NO_{14}S$ $(MH)^+$: 1060.7. Found: 1061.2.

Gal-3-Sat (11a). Prepared in a silimar manner to (**8a**). ^{1}H and ^{13}C assignments: see Table 1. High-resolution mass spectrum (FAB^+) calcd for $C_{53}H_{101}NO_{12}S$ $(MH)^+$: 976.7123. Found: 976.7156.

Gal-4-Sat (11b). Prepared in a silimar manner to (**8a**). ^{1}H NMR (300 MHz, $CDCl_3$) δ 0.87 (t, J = 7.0 Hz, 6H), 1.25 (m, 60H), 1.61 (p, J = 12.0, 5.0 Hz, 4H), 2.67 (dd, J = 16.4, 6.1 Hz, 1H), 2.77−3.01 (m, 4H), 3.25−3.37 (m, 2H), 3.48−3.55 (m, 2H), 3.62−3.72 (m, 14H), 3.85 (t, J = 6.5 Hz, 2H), 4.03−4.15 (m, 10H). ^{13}C NMR (75 MHz, $CDCl_3$) δ 14.1, 22.7, 25.7, 25.8, 28.5, 29.2, 29.3, 29.5, 29.7, 30.8, 31.9, 36.5, 39.7, 41.7, 65.2, 65.7, 67.5, 70.1, 70.2, 70.5, 70.9, 77.4, 170.7, 171.6. Low resolution mass spectrum (FAB^+) calcd for $C_{55}H_{105}NO_{13}S$ $(MH)^+$: 1020.7. Found: 1021.3.

ACKNOWLEDGMENT

This research was supported by NIH (AI 40359). Scientific discussions with Dr. A. Somogyi and Dr. A. S. Bhat are gratefully acknowledged.

LITERATURE CITED

(1) Fantini, J., Cook, D. G., Nathanson, N., Spitalnik, S. L., and Gonzalez-Scarano, F. (1993) Infection of colonic epithelial cell lines by type 1 human immunodeficiency virus is associated with cell surface expression of galactosylceramide, a potential alternative gp120 receptor. *Proc. Natl. Acad. Sci. U.S.A. 90*, 2700−2704.

(2) Blanzat, M., Perez, E., Rico-Lattes, I., Prome, D., Prome, J. C., and Lattes, A. (1999) New catanionic glycolipids. 1. Synthesis, characterization, and biological activity of double-chain and gemini catanionic analogues of galactosylceramide (gal.beta.1cer). *Langmuir 15*, 6163−6169.

(3) Cook, D. G., Fantini, J., Spitalnik, S. L., and Gonzalez-Scarano, F. (1994) Application of high-performance thin-layer chromatography to investigate interactions between human immunodeficiency virus type 1 glycoprotein gp 120 and galactosylceramide. *Methods Mol. Genet. 4*, 86−92.

(4) Delezay, O., Yahi, N., and Fantini, J. (1996) Detection of functional galactosylceramide (GalCer) receptors on CD4-negative HIV-1 target cells. *Perspect. Drug Discovery Des. 5*, 192−202.

(5) Ahlers, M., Muller, W., Reichert, A., Ringsdorf, H., and Venzmer, J. (1990) Specific Interactions of Proteins with Functional Lipid Monolayers − Ways of Simulating Biomembrane Processes. *Angew. Chem., Int. Ed. Engl. 29*, 1269−1285.

(6) Adachi, K., Yamada, Y., Wada, H., Kameyama, A., Ishida, H., and Kiso, M. (1998) Synthesis of sialyl Lewis X ganglioside analogues containing a variable length spacer between the sugar and lipophilic moieties. *J. Carbohydr. Chem. 17*, 595−607.

(7) Sasaki, A., Murahashi, N., Yamada, H., and Morikawa, A. (1994) Syntheses of novel galactosyl ligands for liposomes and their accumulation in the rat liver. *Biol. Pharm. Bull. 17*, 680−685.

(8) Bhat, S., Spitalnik, S. L., Gonzalez-Scarano, F., and Silberberg, D. H. (1991) Galactosyl ceramide or a derivative is an essential component of the neural receptor for human immunodeficiency virus type 1 envelope glycoprotein gp120. *Proc. Natl. Acad. Sci. U.S.A. 88*, 7131−7134.

(9) Bertozzi, C. R., Cook, D. G., Kobertz, W. R., Gonzalez-Scarano, F., and Bednarski, M. D. (1992) Carbon-linked galactosphingolipid analogues bind specifically to HIV-1 gp120. *J. Am. Chem. Soc. 114*, 10639−41.

(10) Bertozzi, C., and Bednarski, M. (1996) Synthesis of C-glycosides; stable mimics of O-glycosidic linkages. *Front. Nat. Prod. Res. 1*, 316−351.

(11) Rico-Lattes, I., Gouzy, M.-F., Andre-Barres, C., Guidetti, B., and Lattes, A. (1998) Synthetic bolaamphiphilic analogues of galactosylceramide (GalCer) potentially binding to the V3 domain of HIV-1 gp 120: key role of their hydrophobicity. *New J. Chem. 22*, 451−457.

(12) Brown, D. A., and London, E. (2000) Structure and Function of Sphingolipid and Cholesterol-rich Memebrane Rafts. *J. Biol. Chem. 275*, 17221−17224.

(13) Willker, W., Leibfritz, D., Kerssebaum, R., and Bermel, W. (1993) *Magn. Reson. Chem. 31*, 287−292.

(14) Piantini, U., Sorensen, O. W., and Ernst, R. R. (1982) *J. Am. Chem, Soc. 104*, 6800−6801.

(15) Frisch, B., Boeckler, C., and Schuber, F. (1996) Synthesis of short polyoxyethylene-based heterobifunctional cross-linking reagents. Application to the coupling of peptides to liposomes. *Bioconjugate Chem. 7*, 180−186.

(16) Lee, J. B., and Downie, I. M. (1967) Sugar esters. IV. The preparation of chloro esters under essentially neutral conditions. *Tetrahedron 23*, 359−363.

(17) De las Heras, F. G., and Fernandez-Resa, P. (1982) Synthesis of ribosyl and arabinosyl cyanides by reaction of 1-O-acyl sugars with trimethylsilyl cyanide. *J. Chem. Soc., Perkin Trans. 1* 903−907.

(18) BeMiller, J. N., Yadav, M. P., Kalabokis, V. N., and Myers, R. W. (1990) N-substituted (.beta.-D-galactopyranosylmethyl)-amines, C-.beta.-D-galactopyranosylformamides, and related compounds. *Carbohydr. Res. 200*, 111−126.

(19) Neumann, R., and Ringsdorf, H. (1986) Peptide liposomes from amphiphilic amino acids. *J. Am. Chem. Soc. 108*, 487−490.

(20) Wilbur, D. S., Hamlin, D. K., Vessella, R. L., Stray, J. E., Buhler, K. R., Stayton, P. S., Klumb, L. A., Pathare, P. M., and Weerawarna, S. A. (1996) Antibody fragments in tumor pretargeting. Evaluation of biotinylated Fab' colocalization with recombinant streptavidin and avidin. *Bioconjugate Chem. 7*, 689−702.

(21) Gu, Y., LaBell, R., O'Brien, D. F., and Saavedra, S. S. (2001) Quantitative studies of binding between synthetic galactosyl ceramide analogues and HIV-1 Gp120 at planar membrane surfaces. *Angew. Chem., Int. Ed. 40*, 2320−2322.

BC015533R

Site-Specific Modification of de Novo Designed Coiled-Coil Polypeptides with Inorganic Redox Complexes

Anna Fedorova and Michael Y. Ogawa*

Department of Chemistry and Center for Photochemical Sciences, Bowling Green State University, Bowling Green, Ohio 43403. Received August 9, 2001; Revised Manuscript Received October 26, 2001

A stepwise procedure for preparing of site-specific binuclear metallopeptides is described. The modification procedure involves the alkylation of a cysteine side chain by reaction with $[Ru(bpy)_2(phen\text{-}ClA)]^{2+}$, where bpy = 2,2′-bipyridine and phen-ClA = 5-chloroacetamido-1,10-phenanthroline, followed by the coordination of a ruthenium pentammine complex to a histidine residue located elsewhere along the sequence. The apo and metalated versions of the peptides C10H21(30-mer) and H10C21(30-mer) display circular dichroism spectra having minima at 208 and 222 nm, with $\theta_{222}/\theta_{208} = 1.04$ to indicate that these peptides exist as α-helical coiled-coils in aqueous solution. When the ruthenium polypyridyl complex is attached to C10H21(30-mer), the Δ-*l* and Λ-*l* diastereomers of the resulting metallopeptide can be readily separated from each other by reversed-phase HPLC. However, in the case of the related H10C21(30-mer) metallopeptide, the two diastereomers cannot be chromatographically resolved. These results indicate how the subtle interplay between peptide conformation/sequence and metal complex geometry may alter some of the physical characteristics of metallopeptides.

INTRODUCTION

The incorporation of extrinsic metal centers into proteins and polypeptides has facilitated the study of biological electron-transfer mechanisms (*1, 2*) and, more recently, the de novo design of minimalistic metalloprotein structures (*3*−*9*). Such procedures commonly involve either metal coordination to natural amino acid side chains such as histidine (*4, 8, 10, 11*) or cysteine (*6, 12*−*14*) or the use of non-natural amino acids that contain metal binding sites (*15, 16*). Our group has used previously developed histidine coordination methods to prepare a new series of synthetic metalloproteins (*3, 5*) in which the self-assembled α-helical coiled-coil motif (*17*) is employed as a well-defined protein scaffold upon which metal-based electron donors and acceptors can be attached. Our studies have demonstrated that such systems can undergo either long-range, intraprotein electron-transfer across a well-defined, yet noncovalent, peptide-peptide interface (*5*) or inter-protein electron transfers whose rates can be modulated by electrostatic protein−protein interactions (*3*). In both these cases, the electron-transfer event involved inorganic cofactors that were placed on separate peptide strands of the α-helical coiled-coil. In other situations, it may be desirable to place such cofactors at different positions along the backbone of a single peptide chain. However, the preparation of such peptides presents a special synthetic challenge as coordinatively unsaturated metal complexes can react promiscuously with a variety of potential ligands. Thus, the reaction of inorganic reagents with polypeptides often yields a mixture of difficult-to-separate substitutional isomers. The situation becomes even more complicated when two different metal complexes are to be bound to specific positions along the sequence of a given protein or polypeptide (*18*). In this paper, we present a straightforward solution to this problem in which a thiol-specific metalation reaction is used to attach a coordinatively saturated ruthenium polypyridyl group to a cysteine residue, followed by the coordination of a ruthenium pentammine site to a histidine residue located elsewhere along the sequence. Details of the synthesis, purification, and characterization of these peptides are described here, and their electron-transfer properties will be discussed elsewhere (*19*). It is also reported that the specific placement of a chiral ruthenium polypyridyl complex within the peptide can significantly alter the way the peptide interacts with solid chromatographic supports: one substitutional isomer of the ruthenium polypyridyl-containing metallopeptides, [(Ru-phen)-C10]H21-(30-mer), can be resolved into its two diastereomers by reversed-phase HPLC, whereas the other, H10[(Ru-(phen)-C21](30-mer), cannot. These results indicate that the derivatization of polypeptides with inorganic complexes can subtly alter the physical properties of the macromolecule.

* To whom correspondence should be addressed. Phone: (419) 372-2809. Fax: (419) 372-9809. E-mail: mogawa@bgnet.bgsu.edu.

EXPERIMENTAL SECTION

General Methods. UV−vis, electrochemical, and MALDI-TOF mass spectral measurements were performed as previously described (*5*). Electrospray ionization mass spectra (ESI-MS) were obtained on a Bruker Daltonics Esquire LC-MS at the Department of Chemistry of the University of Toledo, Toledo, OH.

All peptide metalation reactions were monitored by HPLC on a semipreparative reversed-phase C_{18} column (Zorbax 300SB-C_{18}, 9.4 × 250 mm, 5 μm particle size, 300 Å pore size) with an AB gradient of 1% B/min for 20 min followed by a gradient of 0.5% B/min. For both gradients, the flow rate was 2 mL/min and solvent A was 0.1% (v/v) HTFA in water and solvent B was 0.1% (v/v) HTFA in acetonitrile. Purification of bulk quantities of the peptides was achieved using a preparative C_{18} column

10.1021/bc015544k CCC: $22.00 © 2002 American Chemical Society
Published on Web 12/19/2001

(Zorbax 300SB-C_{18}, 21.1 mm × 25 cm, 7 μm particle size, 300 Å pore size) using the same gradient as described above but at a flow rate of 5 mL/min.

Peptide Synthesis. Solid-phase techniques were used to prepare the 30-residue polypeptides, C10H21(30-mer): Ac-K-(IEALEGK)(ICALEGK)(IEALEHK)(IEALEGK)-G-amide, and H10C21(30-mer): Ac-K-(IEALEGK)-(IHALEGK)-(IEALECK)(IEALEGK)-G-amide, on an Applied Biosystems model 433A peptide as previously described (*5*). ESI-MS *m/z* (ion): found for C10H21(30-mer) 1088.2 ($[M + 3H^+]^{3+}$), 816.4 ($[M + 4H^+]^{4+}$) 653.4 ($[M + 5H^+]^{5+}$), 544.6 ($[M + 6H^+]^{6+}$; for H10C21(30-mer**)** 1088.1 ($[M + 3H^+]^{3+}$), 816.5 ($[M + 4H^+]^{4+}$), 653.3 ($[M + 5H^+]^{5+}$), 544.6 ($[M + 6H^+]^{6+}$.

Synthesis of $[Ru(bpy)_2(phen\text{-}ClA)](PF_6)_2$. *N,N′*-Dicyclohexylcarbodiimide (DCC) (2.5 g, 1.2 mmol) was added to a solution of chloroacetic acid (2.55 g, 2.7 mmol) dissolved in anhydrous ethyl acetate (75 mL). A white precipitate was seen to form immediately, and the mixture was stirred at ambient temperature for 2 h. The reaction mixture was then filtered, and the volume of the filtrate was reduced by rotary evaporation to yield chloroacetic anhydride as a viscous yellow oil. The oil was dissolved in acetonitrile (30 mL) and added to a solution of $[Ru(bpy)_2(phen\text{-}NH_2)](PF_6)_2$ (2 g, 2 mmol) in acetonitrile (100 mL), where bpy = 2,2′-bipyridine and phen-NH_2 = 5-amino-1,10-phenanthroline. The mixture was stirred overnight, and the acetonitrile was then removed by rotary evaporation. The resulting solid was redissolved in a minimal amount of methanol and precipitated with the addition of saturated NH_4PF_6 (aq). The $Ru(bpy)_2(phen\text{-}ClA)](PF_6)_2$, where phen-ClA = 5-chloroacetamido-1,10-phenanthroline, was collected by vacuum filtration as an orange solid, washed with water followed by diethyl ether, and stored at room temperature in the dark. ESI-MS *m/z* (ion): 830.3 ($[M - PF_6^-]^+$), 684.3 ($[M - 2PF_6^- + e^-]^+$).

Synthesis of $[Ru(bpy)_2(phen\text{-}IA)](PF_6)_2$. This synthesis was performed as outlined above for $[Ru(bpy)_2(phen\text{-}ClA)](PF_6)_2$ except iodoacetic acid was used in place of chloroacetic acid. ESI-MS *m/z* (ion): 922.1 ($[M\text{-}PF_6\text{-}]^+$), 776.2 ($[M\text{-}2PF_6\text{-}+e^-]^+$).

Peptide Labeling with $[Ru(bpy)_2(phen\text{-}ClA)](PF_6)_2$. In a typical procedure, a sample of either C10H21(30-mer) or H10C21(30-mer) (5 mg, 1.28 μmol) was dissolved in 100 mM phosphate buffer (1 mL, pH 7.0), and the resulting solution was purged with argon gas for 15−20 min. To this was added solid tris(2-carboxyethyl)phosphine (ca. 5 mg, 0.017 mmol). After being stirred under an argon atmosphere for ca. 20 min, the solution was neutralized by the dropwise addition of 1 N NaOH (aq). A solution of $[Ru(bpy)_2(phen\text{-}ClA)](PF_6)_2$ (10 mg, 0.01 mmol) dissolved in *N,N*-dimethylformamide (ca. 0.5 mL) was then added to the reaction mixture. After the mixture was stirrred for 4−5 h at room temperature, it was applied directly onto a size-exclusion column (Biogel P-2) that was previously equilibrated with 0.1 N trifluoroacetic acid (HTFA). Elution with the HTFA solution yielded the peptide fraction first followed by the hydrolyzed metal complex. The collected peptide fraction was then analyzed by HPLC and in cases where unreacted apo-peptide was detected, the metalation procedure was repeated using a fresh sample of $[Ru(bpy)_2(phen\text{-}ClA)](PF_6)_2$. ESI-MS *m/z* (ion): found for [(Λ-*l*)(Ru-phen)-C10]H21(30-mer*)* 978. 2 ($[M + 4H^+]^{4+}$), 782.6 ($[M + 5H^+]^{5+}$), 652.4 ($[M + 6H^+]^{6+}$), 559.3 ($[M + 7H^+]^{7+}$; for [(Δ-*l*)(Ru-phen)-C10]H21(30-mer*)* 978. 1 ($[M + 4H^+]^{4+}$), 782.7 ($[M + 5H^+]^{5+}$), 652.5 ($[M + 6H^+]^{6+}$), 559.6 ($[M + 7H^+]^{7+}$; for H10[(Δ-*l* + Λ-*l*)(Ru(phen)-C21](30-mer) 978.

(a)

a b c d e f g

Ac-K-(IEALEGK)-(I-**C/H**-ALEGK)-(IEALE-**H/C**-K)-(IEALEGK)-G-amide

1 10 21 30

(b)

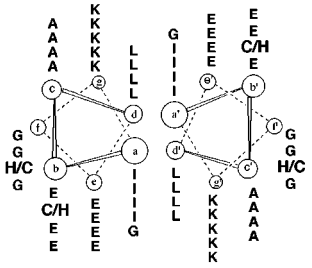


Figure 1. (a) Differences in the primary sequence of the C10H21(30-mer) and H10C21(30-mer) peptides. (b) Helical wheel diagram of the peptides.

3 ($[M + 4H^+]^{4+}$), 782.8 ($[M + 5H^+]^{5+}$), 652.4 ($[M + 6H^+]^{6+}$), 559.4 ($[M + 7H^+]^{7+}$).

Peptide Labeling with $[Ru(NH_3)_5Cl](TFA)$. The $Ru(bpy)_2(phen)$-labeled peptides [(Λ-*l*)(Ru-phen)-C10]-H21(30-mer*)* and the diastereomeric mixture H10[(Δ-*l* + Λ-*l*)(Ru(phen)-C21](30-mer) were metalated at their histidine side chains by treatment with aquopentammineruthenium(II) as described previously for the metalation of related coiled-coil peptides (*3*, *5*). However, in the present study, the reaction mixtures were treated with 0.1 N HTFA for 2−3 h prior to purification by reversed-phase HPLC. ESI-MS *m/z* (ion): found for [(Δ-*l*)(Ru-phen)-C10][$Ru(NH_3)_5$H21](30-mer*)* 1366.5 ($[M + 3H^+]^{3+}$), 1024.4 ($[M + 4H^+]^{4+}$), 819.9 ($[M + 5H^+]^{5+}$); for [$Ru(NH_3)_5$-H10][(Δ-*l* + Λ-*l*)(Ru(phen)-C21](30-mer) 1366.1 ($[M + 3H^+]^{3+}$), 1024.1 ($[M + 4H^+]^{4+}$), 819.8 ($[M + 5H^+]^{5+}$).

RESULTS AND DISCUSSION

Synthesis of the C10H21(30-mer) and H10C21(30-mer) Apopeptides. Solid-phase techniques were used to prepare the 30-residue polypeptides, C10H21(30-mer): Ac-K-(IEALEGK)(ICALEGK)(IEALEHK)(IEALEGK)-G-amide, and H10C21(30-mer): Ac-K-(IEALEGK)-(IHALEGK)-(IEALECK)(IEALEGK)-G-amide. These sequences are based on a seven residue heptad repeat, $(abcdefg)_n$, in which positions *a* and *d* are occupied by hydrophobic amino acids, positions *b*, *c*, and *f* are occupied by hydrophilic residues, and positions *e* and *g* are occupied by oppositely charged residues. Such sequences have been designed by Hodges and co-workers (*17*) to spontaneously form two-stranded α-helical coiled-coils, which can be described as being an intertwining of 2 α-helices to from a left-handed supercoil. The amino acid sequences of C10H21(30-mer) and H10C21(30-mer) differ from one another only in their placement of the cysteine and histidine residues along the peptide chain (Figure 1). Specifically, cysteine residues were located at either position 10 or 21 of the sequence to allow coupling to a ruthenium tris(bipyridyl) complex. Histidine residues were also placed at either positions 21 or 10 of the sequence to afford the coordination of a pentammineruthenium(II) center along the same peptide chain.

Synthesis of H10[(Ru(phen)-C21] (30-mer). The cysteine side chain of H10C21(30-mer) was alkylated by treatment with $[Ru(bpy)_2(phen\text{-}ClA)](PF_6)_2$, where phen-ClA = 5-chloroacetamido-1,10-phenanthroline and the cysteine residue occupies the most solvent-exposed position *(f)* of the third heptad of the peptide sequence. In this procedure, the ruthenium starting material was

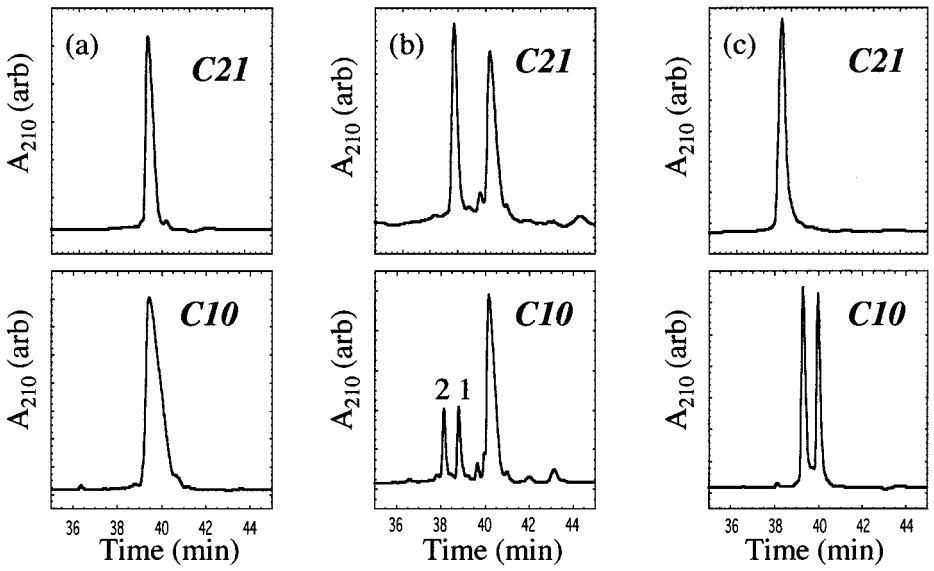


Figure 2. HPLC profiles monitoring the reaction between the H10C21(30-mer) peptide and $Ru(bpy)_2(phen\text{-}ACl)(PF_6)_2$ (top) and between the C10H21(30-mer) peptide and $Ru(bpy)_2(phen\text{-}ACl)(PF_6)_2$ (bottom): (a) apo-peptide before reaction, (b) intermediate stage of the reaction, (c) purified final product. Note that for C10H21(30-mer) two product peaks (**1** and **2**) are seen in the HPLC profile.

prepared by a carbodiimide coupling reaction involving chloroacetic acid and $[Ru(bpy)_2(phen\text{-}NH_2)]$. The alkylation reaction was monitored by reversed-phase HPLC (Figure 2 (top)), which showed that the peak corresponding to the apo-peptide diminished in intensity as a new product peak appeared at a somewhat shorter retention time. Electrospray ionization mass spectrometry showed that the product had a charge-to-mass ratio consistent with that expected for H10[(Ru(bpy)$_2$(phen)-C21](30-mer). The UV−vis spectrum of the product is very similar to that of $[Ru(bpy)_2(phen\text{-}ClA)]^{2+}$, having maxima at 286 and 450 nm, but has a significantly larger absorbance at 210−220 nm due to the presence of the peptide backbone. Additional HPLC experiments showed that metalation of the H10C21(30-mer) occurs in competition with hydrolysis of the $[Ru(bpy)_2(phen\text{-}ClA)]^{2+}$ starting material, as evidenced by the appearance of a new HPLC peak at shorter retention times than that of the ruthenium starting material.

The alkylation of sulfhydryl groups with 5-iodoacetamido-1,10-phenanthroline (phen-IA) has previously been used as a convenient method for attaching metal-binding sites onto the surfaces of proteins, where subsequent treatment of the modified protein with transition metal reagents has led to the creation of specific DNA cleaving agents (*13*, *14*). In related work, luminescent probes (*12*) were attached to the cysteine-containing proteins human serum albumin and human immunoglobulin G, by first reacting $[Ru(bpy)_2Cl_2]$ with phen-IA and then treating the protein with the resulting metal complex. However, in our hands this preparation of the ruthenium reactant gave a mixture of two products as observed by reversed-phase HPLC. The ESI-MS of these products indicated that they were $[Ru(bpy)_2(phen\text{-}IA)]^{2+}$ and $[Ru(bpy)_2(phen\text{-}ClA)]^{2+}$, of which the latter species was likely due to a halogen-exchange involving propitious chloride in solution. HPLC experiments also showed that when the mixture of $[Ru(bpy)_2(phen\text{-}IA)]^{2+}$ and $[Ru(bpy)_2(phen\text{-}ClA)]^{2+}$reactants was treated with H10C21(30-mer), the iodo species hydrolyzed very rapidly and the metalation of the peptide appeared to proceed only from the $[Ru(bpy)_2(phen\text{-}ClA)]^{2+}$ precursor. Indeed, when authentic samples of $[Ru(bpy)_2(phen\text{-}IA)]^{2+}$ and $[Ru(bpy)_2(phen\text{-}ClA)]^{2+}$ were reacted separately with the peptide, it was found that metalation occurred only from the chloro starting material and not the iodo species. This behavior is in contrast to that reported for the metalation of human serum albumin and human immunoglobulin G in which the $[Ru(bpy)_2(phen\text{-}ClA)]^{2+}$ species was observed to be nonreactive (*12*).

Synthesis of [Ru(phen)-C10]H21(30-mer). The cysteine side chain of C10H21(30-mer) was alkylated by treatment with $[Ru(bpy)_2(phen\text{-}ClA)]^{2+}$ as described above. It is noted that the sequence of this peptide places the cysteine residue at position (*b*) of the second heptad repeat. In contrast to the behavior previously described for the metalation of H10C21(30-mer), it was observed that the alkylation of C10H21(30-mer) produced two distinct product peaks (Figure 2 (bottom)). The UV−vis spectra of both species were identical to that of H10[(Ru-(phen)-C21](30-mer), and ESI-MS showed that they both had the charge-to-mass ratio expected for the desired metallopeptide. The circular dichroism spectrum (not shown) of the faster eluting product consists of negative bands appearing at 208 and 222 nm with $[\theta]_{222}/[\theta]_{208} = 1.04$ which indicates that the peptide exists as an α-helical coiled-coil (*17*). These features are also observed in the CD spectrum of the H10C21(30-mer) apopeptide (data not shown). However, the spectrum of the first ruthenated product displays an additional set of features that consists of a strong negative peak at 270 nm, a strong positive peak at 290 nm, a broad negative peak at ca. 420 nm, and a weak positive peak at 470 nm. By analogy to the CD properties of related systems, this latter set of transitions are assigned to the Λ configuration of the octahedral ruthenium polypyridyl complex (*20*, *21*). Thus, the faster eluting product is identified as being the Λ-*l* diastereomer which results from coupling the chiral metal complex to the *l*-polypeptide. The CD spectrum of the slower eluting product is nearly identical to the one described above except that it displays transitions arising from the metal complex corresponding to the Δ configuration. Thus, reaction of C10H21(30-mer) with $[Ru(bpy)_2(phen\text{-}ClA)]^{2+}$ produces the two diastereomers (Λ-*l* and Δ-*l*) of the [(Ru(phen)-C10]H21(30-mer) metallopeptide, which are resolvable by reversed-phase HPLC. It is noted, however, that the two diastereomers of the related H10[(Ru(phen)-C21](30-mer) metallopep-

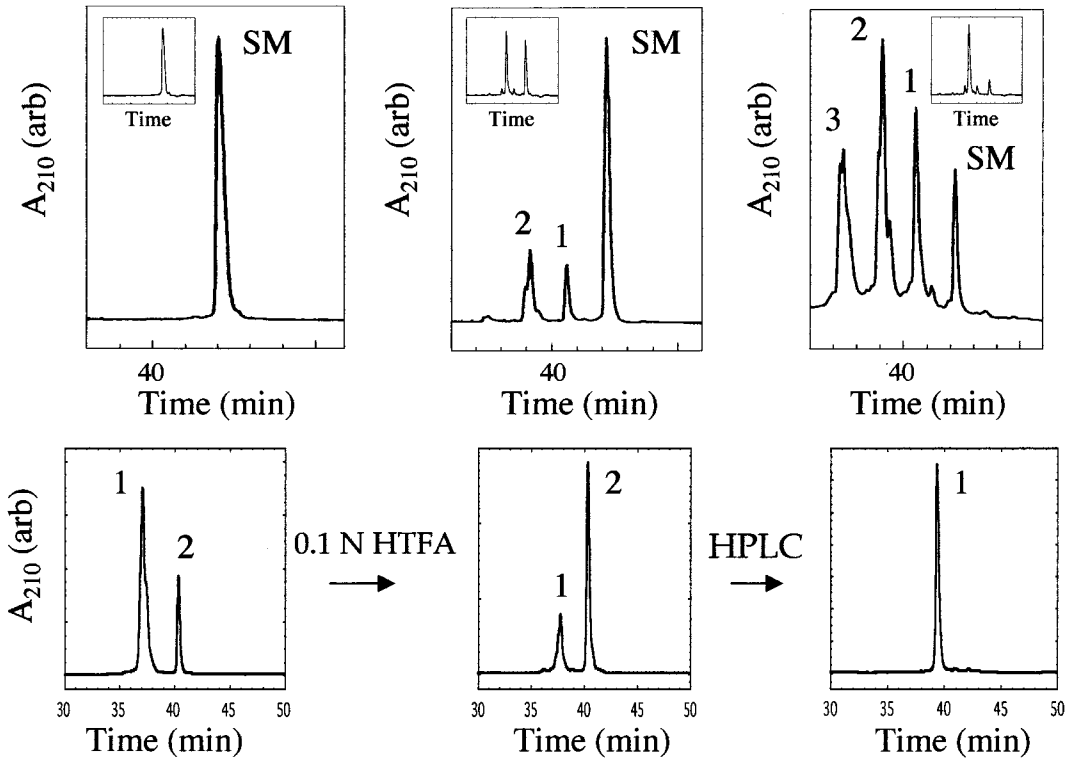


Figure 3. (Top) HPLC profiles showing the progress of the reaction between the H10[(Ru(bpy)$_2$(phen)-C21](30-mer) peptide and $RuA_5(H_2O)^{2+}$ after (a) 0, (b) 1, and (c) 6 h. At longer reaction times, three product peaks are observed (1−3) along with that of the unreacted starting material (SM). The insets show the progress of the corresponding metalation reaction using the related peptide H21(30-mer) (*5*), which undergoes conversion to a single metalated product. (Bottom) HPLC profiles showing that the treatment of product **2** with 0.1 N HTFA results in its conversion to product **1**, which can be separated by HPLC.

tide could not be separated under identical HPLC conditions. Thus, the specific placement of the ruthenium polypyridyl complex within the peptide sequence (i.e., a "b" position on C10H21(30-mer) vs a "f" position on H10C21(30-mer)) sufficiently alters the physical properties of the metallopeptide to yield significantly different HPLC properties of the two sets of metallopeptides.

Synthesis of [Ru(NH$_3$)$_5$-H10][(Δ-l + Λ-l)(Ru(phen)-C21](30-mer). The histidine side chains of the H10[(Ru(phen)-C21](30-mer) metallopeptide were coordinated to a ruthenium pentammine center by treating a diastereomeric mixture (Δ-*l* + Λ-*l*) of the metallopeptide with aquopentammineruthenium(II) made in situ by reducing chloropentammineruthenium(III) chloride with zinc amalgam. Similar procedures have been used to metalate the histidine residues of a variety of native heme proteins (*11*) and synthetic polypeptides (*3*, *5*, *7*). As monitored by reversed-phase HPLC (Figure 3), the reaction of [Ru(NH$_3$)$_5$(H$_2$O)]$^{2+}$ with H10[(Ru(phen)-C21](30-mer), whose two diastereomers appear as a single HPLC peak, results in the appearance of at least three new product peaks, labeled **1**−**3**. This behavior is in contrast to that previously observed for metalation of the related H21(30-mer) polypeptide (*5*) where only a single product peak appeared in the HPLC profile (insets, Figure 3).

The differential pulse polarogram of peak **1** (not shown) consists of a single reduction wave at −0.18 V vs Ag/Ag$^+$ that appears at a similar potential to those of [Ru(NH$_3$)$_5$-H21](30-mer) (*5*), and Ru(NH$_3$)$_5$ bound to His33 of cytochrome *c* (*11*). This peak is therefore assigned to the desired product, [Ru(NH$_3$)$_5$-H10][(Ru(phen)-C21](30-mer). ESI-MS data support this assignment and it is noted that changes in the spectrometer voltage can yield mass spectra that are either consistent with the formulation, [Ru(NH$_3$)$_5$-H10][(Ru(phen)-C21](30-mer), or with the complete loss of the ammonia ligands, as was previously seen in the case of ruthenium ammine labeled cytochrome *c* (*22*).

The polarograms from peaks **2** and **3** each show two reduction waves that appear at −0.18 and −0.32 V vs Ag/Ag$^+$, to suggest the presence of two types of peptide-bound ruthenium pentammine species in these samples. Based on model studies (*23*), the more anodic peak is assigned to the existence of pentamminecarboxylatoruthenium species bound to one or more of the glutamic acid residues in the peptide. However, the ESI-MS of **2** and **3** are identical to that of **1** and it is possible that the carboxylato bound ruthenium complexes dissociate under the MS conditions employed. Thus, to test for the existence of acid-bound ruthenium complexes, products **2** and **3** were isolated by HPLC and dissolved in 0.1 N HTFA for several hours. HPLC analysis (Figure 3) of the resulting solutions showed that this treatment produced the clean conversion of products **2** and **3** into product **1** which suggests the dissociation of carboxylato bound species at low pH.

Synthesis of [(Ru(phen)-C10][(Λ-l)Ru(NH$_3$)$_5$-H21]-(30-mer). The [(Ru(phen)-C10]H21(30-mer) was reacted with aquopentammine ruthenium (II) as described above. However, since the HPLC profile of the starting metallopeptide was complicated by the resolution of its two diastereomers, only the Λ-*l* diastereomer was used in the reaction. The HPLC results again show the presence of multiple product peaks which can be converted to a single peak by treatment with dilute acid.

SUMMARY

A stepwise procedure for the preparation of site-specific, binuclear metallopeptides has been described. The peptide modification proceeds first through the

alkylation of a cysteine side-chain with $[Ru(bpy)_2(phen\text{-}ClA)]^{2+}$, followed by the coordination of a ruthenium pentammine complex to a histidine residue located elsewhere along the sequence. Circular dichroism spectroscopy shows that both the apo and metalated peptides adopt the conformation of an α-helical coiled-coil in aqueous solution. When the ruthenium polypyridyl complex is attached to C10H21(30-mer), the Δ-*l* and Λ-*l* diastereomers of the resulting metallopeptide are readily separated from each another by reversed-phase HPLC. However, when the reaction occurs with H10C21(30-mer), the two peptide diastereomers cannot be chromatograpically resolved. These results demonstrate that the metalation of different positions of the coiled-coil sequence significantly affects the way the resulting peptide interacts with solid supports. An examination of the wheel diagram depicted in Figure 1 shows that the cysteine residue of C10H21(30-mer) is placed at a "b" position of the heptad which is located somewhat close to the peptide-peptide interface. It is speculated that the peptide-bound ruthenium polypyridyl complex may experience a restricted conformational environment that may facilitate its diastereomeric resolution by reversed-phase HPLC. In contrast, the cysteine residue in H10C21-(30-mer) is located at the most highly solvent-exposed position "f" of the heptad repeat, and presumably experiences a significant degree of conformational freedom. These results indicate that the subtle interplay between peptide conformation/sequence and metal complex geometry may be used to control some of the physical characteristics of metallopeptides.

ACKNOWLEDGMENT

We thank Mr. Jedrzej Romanowicz for obtaining the ESI-MS data. This work was supported by the National Institutes of Health through Grant Nos. GM 61171 and GM60258 and the Petroleum Research Fund through Grant No. 34901-AC. A.F. acknowledges predoctoral support from the Harold and Helen McMaster Foundation.

LITERATURE CITED

(1) Winkler, J. R., Di Bilio, A. J., Farrow, N. A., Richards, J. H., and Gray, H. B. (1999) Electron-tunneling in biological molecules. *Pure Appl. Chem. 71*, 1753−1764.

(2) Ogawa, M. Y. (1999) in *Molecular and Supramolecular Photochemistry* (Ramamurthy, V., and Schanze, K. S., Eds.) pp 113−150, Marcel Dekker, Inc., New York.

(3) Kornilova, A. Y., Wishart, J. F., and Ogawa, M. Y. (2001) The effect of surface charges on the rates of intermolecular electron-transfer between de novo designed metalloproteins. *Biochemistry* **2001**, *40*, 12186−12192.

(4) Schnepf, R., Horth, P., Bill, E., Wieghardt, K., P., H., and Haehnel, W. (2001) De novo design and characterization of copper centers in synthetic four-helix-bundle proteins. *J. Am. Chem. Soc. 123*, 2186−2195.

(5) Kornilova, A. Y., Wishart, J. F., Xiao, W., Lasey, R. C., Fedorova, A., Shin, Y. K., and Ogawa, M. Y. (2000) Design and characterization of a synthetic electron-transfer protein. *J. Am. Chem. Soc. 122*, 7999−8006.

(6) Farrer, B. T., McClure, C. P., Penner-Hahn, J. E., and Pecoraro, V. L. (2000) Arsenic(III)−cysteine interactions stabilize three-helix bundles in aqueous solution. *Inorg. Chem. 39*, 5422−5423.

(7) Mutz, M. W., Case, M. A., Wishart, J. F., Ghadiri, M. R., and McLendon, G. L. (1999) De Novo Design of Protein Function: Predictable Structure-Function Relationships in Synthetic Redox Proteins. *J. Am. Chem. Soc. 121*, 858−859.

(8) Gibney, B. R., and Dutton, P. L. (1999) Histidine placement in de novo heme proteins. *Protein Sci. 8*, 1888−1898.

(9) Rau, H. K., DeJonge, N., and Haehnel, W. (1998) Modular synthesis of de novo designed metalloproteins for light-induced electron transfer. *Proc. Natl. Acad. Sci. U.S.A. 95*, 11526−11531.

(10) Di Bilio, A. J., Dennison, C., Gray, H. B., Ramirez, B. E., Sykes, A. G., and Winkler, J. R. (1998) Electron transfer in ruthenium-modified plastocyanin. *J. Am. Chem. Soc. 120*, 7551−7556.

(11) Isied, S. S., Kuehn, C., and Worosila, G. (1984) Ruthenium-modified cytochrome *c*: temperature dependence of the rate of intramolecular electron-transfer. *J. Am. Chem. Soc. 106*, 1722−1726.

(12) Castellano, F. N., Dattelbaum, J. D., and Lakowicz, J. R. (1998) Long-lifetime Ru(II) complexes as labeling reagents for sulfhydryl groups. *Anal. Biochem. 255*, 165−170.

(13) Ebright, R. H., Ebright, Y. W., Pendergrast, P. S., and Gunasekera, A. (1990) Conversion of a helix-turn-helix motif sequence-specific DNA binding protein into a site-specific DNA cleaving agent. *Proc. Natl. Acad. Sci, U.S.A. 87*, 2882−2886.

(14) Chen, C. B., and Sigman, D. S. (1987) Chemical conversion of a DNA-binding protein into a site-specific nuclease. *Science 237*, 1197−1201.

(15) Hurley, D. J., Roppe, J. R., and Tor, Y. (1999) Coordination compounds as building blocks: simple synthesis of Ru(II)-containing amino acids and peptides. *Chem. Commun.* 993−994.

(16) Kise Jr., K. J., and Bowler, B. E. (1998) Enantioselective synthesis of an unnatural bipyridyl amino acid and its incorporation into a peptide. *Tetahedron*: *Asymmetry 9*, 3319−3324.

(17) Hodges, R. S. (1996) De novo design of α-helical proteins: basic research to medical applications. *Biochem. Cell Biol. 74*, 133−154.

(18) Dahiyat, B. I., Meade, T. J., and Mayo, S. L. (1996) Site-specific modification of alpha-helical peptides with electron donors and acceptors. *Inorg. Chim. Acta 243*, 207−212.

(19) Fedorova, A., and Ogawa, M. Y. (Manuscript in preparation).

(20) Dmochowski, I. J., Winkler, J. R., and Gray, H. B. (2000) Enantiomeric discrimination of Ru-substrates by cytochrome P450-cam. *J. Inorg. Biochem. 81*, 221−228.

(21) Luo, J., Wishart, J. F., and Isied, S. S. (1998) Site-dependent stereoselective binding of ruthenium aquobipyridine complexes to histidine side-chains in horse heart cytochrome *c*. *J. Am. Chem. Soc. 120*, 12970−12971.

(22) Fenwick, C. W., English, A. M., and Wishart, J. F. (1997) pH and driving force dependence of intramolecular oxyferryl heme reduction in myoglobin. *J. Am. Chem. Soc. 119*, 4758−4764.

(23) Ohyoshi, A., and Yoshikuni, K. (1979) The polarographic reduction and UV spectral properties of pentamminecarboxylatoruthenium(III) complexes. *Bull. Chem. Soc. Jpn. 52*, 3105−3106.

BC015544K

2′-Modified Nucleosides for Site-Specific Labeling of Oligonucleotides

Elizabeth S. Krider, Jeremiah E. Miller, and Thomas J. Meade*

Division of Biology and the Beckman Institute, California Institute of Technology, Pasadena, California 91125.
Received August 16, 2001

We report the synthesis of 2′-modified nucleosides designed specifically for incorporating labels into oligonucleotides. Conversion of these nucleosides to phosphoramidite and solid support-bound derivatives proceeds in good yield. Large-scale synthesis of 11-mer oligonucleotides possessing the 2′-modified nucleosides is achieved using these derivatives. Thermal denaturation studies indicate that the presence of 2′-modified nucleosides in 11-mer duplexes has minimal destabilizing effects on the duplex structure when the nucleosides are placed at the duplex termini. The powerful combination of phosphoramidite and support-bound derivatives of 2′-modified nucleosides affords the large-scale preparation of an entirely new class of oligonucleotides. The ability to synthesize oligonucleotides containing label attachment sites at 3′, intervening, and 5′ locations of a duplex is a significant advance in the development of oligonucleotide conjugates.

INTRODUCTION

Substituents at the 2′-ribose position of nucleosides are important structural and mechanistic probes of nuclease resistance and ribozyme catalysis (*1*). These nucleosides are used in the development of antisense therapeutics (*1b*) and the rapid screening of oligonucleotide sequences displaying high affinity toward protein targets (*2*). Nucleosides containing a primary amine at the 2′ position facilitate the incorporation of several reporter molecules or labels into oligonucleotides (*3*). This is accomplished by (a) introducing the amine-containing nucleoside into an oligonucleotide using standard automated DNA synthesis, (b) purifying the resulting oligonucleotide, (c) reacting the reporter group with the amine-containing oligonucleotide, and (d) isolating the conjugate. Labels such as fluorescent dyes (*3a,c*), aromatic and aliphatic isocyanates (*3b,d*), and transition metal complexes (*3e*) have been successfully incorporated into oligonucleotides using this method.

Our objective is to develop new methods of incorporating labels, namely transition metal complexes, into DNA site-specifically (*4*). To this end we have designed nucleosides containing bidentate amine groups at the 2′-ribose position to which transition metal complexes are chelated (Figure 1). This site on the ribose ring is selected so that both solid support-bound and phosphoramidite forms of the nucleosides can be prepared. The solid support-bound nucleoside is used as the starting material in oligonucleotide synthesis, whereas the phosphoramidite monomer can be introduced at any later position in the oligonucleotide sequence. As a result, labels can be incorporated at the 3′, intervening, or 5′ locations of an oligonucleotide. We report the synthesis of 2′-modified nucleosides as both solid support-bound and phosphoramidite derivatives and their incorporation into oligonucleotides via solid-phase methods. Thermal denaturation studies of the resulting oligonucleotides indicate that the presence of the 2′-modified nucleosides has only a slight destabilizing effect on the duplex structure.

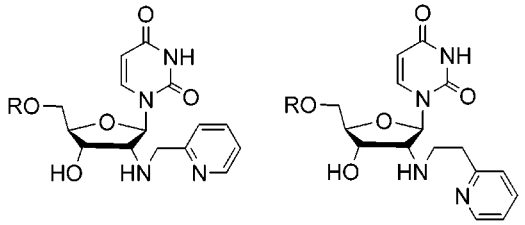


Figure 1. Structure of nucleosides with bidentate ligands at the 2′ ribose position (R = 4,4′-dimethoxytrityl).

EXPERIMENTAL PROCEDURES

General. ^{1}H and ^{31}P spectra were acquired on either Varian 300 or 500 spectrometers. Chemical shifts are reported in parts per million and referenced to the proton chemical shifts of deuterated solvent, trimethylsilane, or 85% H_3PO_4 in H_2O. Reagents and starting materials were used as received from Aldrich. Flash chromatography was performed on EM Science/Merck silica gel 60 (230−400 mesh). Thin-layer chromatography (TLC) was performed on 0.25 mm Merck precoated silica plates (60 F_{254}). Enzymes were purchased from Pharmacia. Mass spectrometry was performed at the Caltech Peptide/Protein Microanalytical Laboratory.

5′-*O*-(4,4′-Dimethoxytrityl)-2,2′-*O*-anhydro-1-(β-D-arabinofuranosyl)uracil, **1.** This compound was prepared from the reaction of 2,2′-*O*-anhydro-1-(β-D-arabinofuranosyl)uracil and 4,4′-dimethoxytrityl chloride as previously described (*5*).

5′-*O*-(4,4′-Dimethoxytrityl)-2′-*N*,3′-*O*-(2-oxooxazolidinyl)-2′-aminomethylpyridyl-2′-deoxyuridine, **2a.** To a solution of **1** (2.2 g, 4.2 mmol) in pyridine (40 mL) was added 1,1′-carbonyldiimidazole (1.01 g, 6.2 mmol). After 30 h of stirring at ambient temperature, the solvent was removed and the residue was resuspended in dichloromethane (40 mL); DIEA (1.1 mL, 6.3 mmol) and AMPy (649 μL, 6.3 mmol) were delivered to the solution. After 60 h of stirring at ambient temperature, the reaction was quenched with 5% citric acid, extracted with fresh dichloromethane, dried over Na_2SO_4, and concentrated

10.1021/bc0155465 CCC: $22.00 © 2002 American Chemical Society
Published on Web 12/08/2001

to an oil. The residue was dissolved in tetrahydrofuran (25 mL), DBU (628 μL, 4.2 mmol) was added to the flask, and the solution was refluxed for 46 h. The solvent was removed, and the residue was purified on silica (using 22% EtOAc in dichloromethane containing 1% TEA and 3% methanol) to afford **2a** in 20% yield (548 mg, 828 μmol). ^{1}H NMR ($CDCl_3$, 500 MHz) δ 3.48−3.58 (m, 2H), 3.78 (s, 6H), 4.35−4.40 (m, 1H), 4.54 (d, 1H), 4.75 (dd, 2H), 5.14−5.17 (m, 1H), 5.41 (d, 1H), 6.06 (d, 1H), 6.82 (d, 4H), 7.21−7.30 (m, 9H), 7.33−7.37 (m, 2H), 7.53 (d, 1H), 7.69 (t, 1H), 8.51 (d, 1H), 8.84 (s, 1H). ESI-MS mass calcd for $C_{37}H_{35}N_4O_8$ $(M + H)^+$: 663.24. Found: 663.2.

5′-*O*-(4,4′-Dimethoxytrityl)-2′-*N*,3′-*O*-(2-oxooxazolidinyl)-2′-aminoethylpyridyl-2′-deoxyuridine, **2b.** To a solution of **1** (1.0 g, 1.9 mmol) in pyridine (30 mL) was added 1,1′-carbonyldiimidazole (0.460 g, 2.8 mmol). After 30 h of stirring at ambient temperature, the solvent was removed by rotary evaporation and the residue was resuspended in dichloromethane (30 mL); DIEA (500 μL, 2.85 mmol) and AEPy (340 μL, 2.85 mmol) were delivered to the solution. After 60 h of stirring at ambient temperature, the reaction was worked up as described for **2a**. The residue was dissolved in THF (11 mL), DBU (284 μL, 1.9 mmol) was added to the flask, and the solution was refluxed for 46 h. The solvent was removed by rotary evaporation, and the residue was purified on silica (eluting with 5−15% methanol in EtOAc) to afford **2b** in 10% yield (127 mg, 188 μmol). ^{1}H NMR ($CDCl_3$, 300 MHz) δ 3.07−3.39 (m, 2H), 3.43−3.60 (m, 2H), 3.74−3.77 (m, 6H), 3.93−4.04 (m, 1H), 4.26−4.31 (m, 1H), 4.64 (dd, 2H), 5.09−5.14 (m, 1H), 5.35 (d, 1H), 6.09 (d, 1H), 6.84 (d, 4H), 7.15−7.39 (m, 11H), 7.59−7.69 (m, 2H), 8.57 (d, 1H). ESI-MS mass calcd for $C_{38}H_{37}N_4O_8$ $(M + H)^+$: 677.25. Found: 677.2.

5′-*O*-(4,4′-Dimethoxytrityl)-2′-aminomethylpyridyl-2′-deoxyuridine, **3a.** Compound **2a** (242 mg, 0.36 mmol) was suspended in dioxane (6 mL), 4 M NaOH (4.7 mL), and methanol (4.7 mL), and the mixture was stirred at 50 °C for 36 h. The solvents were removed by rotary evaporation, and the residue was dissolved in dichloromethane (55 mL). The solution was extracted with brine, dried over sodium sulfate, and evaporated to dryness to give **3a** in 92% yield (216 mg, 0.34 mmol). ^{1}H NMR ($CDCl_3$, 300 MHz) δ 3.3 (s(br), 4H), 3.73−3.78 (m, 6H), 3.94−4.02 (m, 1H), 4.1 (d, 1H), 4.2 (s, 1H), 5.3 (d, 1H), 6.1 (d, 1H), 6.7 (dd, 4H), 7.1−7.3 (m, 11H), 7.5−7.6 (m, 2H), 8.4 (s, 1H). ESI-MS mass calcd for $C_{36}H_{37}N_4O_7$ $(M + H)^+$: 637.26. Found: 637.2.

5′-*O*-(4,4′-Dimethoxytrityl)-2′-aminomethylpyridyl-2′-deoxyuridine, **3b.** Compound **2b** (1.7 g, 2.51 mmol) was suspended in dioxane (43 mL), 4 M NaOH (26 mL), and methanol (26 mL), and the mixture was stirred at room temperature for 20 h. The reaction was heated at 60 °C for an additional 2 h, after which the solvents were removed by rotary evaporation. The residue dissolved in dichloromethane, extracted with brine, dried over sodium sulfate, and evaporated to dryness. The material was purified on silica (eluting with 23% ethyl acetate in dichloromethane containing 1% each of methanol and triethylamine) to give **3b** in 88% yield (1.44 g, 2.21 mmol). ^{1}H NMR ($CDCl_3$, 500 MHz) δ 3.03 (t, 2H), 3.12−3.25 (m, 2H), 3.43−3.53 (m, 3H), 3.80 (s, 6H), 4.29 (s, 1H), 4.49 (d, 1H), 5.37 (d, 1H), 5.94 (d, 1H), 6.14 (s(br), 1H), 6.85 (d, 4H), 7.18−7.33 (m, 10H), 7.40 (d, 1H), 7.67 (t, 1H), 7.74 (d, 1H), 8.49 (d, 1H). ESI-MS mass calcd for $C_{37}H_{39}N_4O_7$ $(M + H)^+$: 651.27. Found: 651.2.

5′-*O*-(4,4′-Dimethoxytrityl)-*N*$^{2′}$-trifluoroacetamido-2′-deoxyuridine, **4.** This compound was prepared either from reaction of 2′-amino-5′-*O*-(4,4′-dimethoxytrityl)-2′-deoxyuridine and ethyl trifluoroacetate (*5*) or from reaction *N*$^{2′}$-trifluoroacetyl-2′-amino-2′-deoxyuridine and 4,4′-dimethoxytrityl chloride as previously described (*3a*).

5′-*O*-(4,4′-Dimethoxytrityl)-2′-aminomethylpyridyl −2′-deoxyuridine-3′-*O*-succinate, 5. Compound **3a** (100 mg, 0.157 mmol), DMAP (9.4 mg, 0.5 equiv), and succinic anhydride (17.3 mg, 1.1 equiv) were suspended in dry pyridine (1 mL) and allowed to stir under argon for 2 h, at which time an additional 0.2 equiv of succinic anhydride was added. The reaction proceeded overnight at room temperature, after which the solvent was removed. The residue was dissolved in dichloromethane (20 mL) and stirred with an equal volume of 5% $NaHCO_3$ solution for 2 h. The mixture was partitioned, and the organic phase was extracted with brine. Each phase was back-extracted once. The combined organic phases were washed with cold 5% citric acid and concentrated to a small volume (3−5 mL). The sample was precipitated in stirring hexanes, and the white solid **5** was collected by filtration in 60% yield (69 mg, 0.094 mmol). ^{13}C NMR (75 MHz, CD_3CN) δ 178.82, 174.10, 165.67, 160.11, 158.27, 156.03, 146.0, 145.95, 136.96, 136.76, 136.6, 133.06, 131.32, 129.47, 128.77, 127.74, 122.9, 114.45, 114.0, 102.0, 88.12, 85.33, 73.0, 72.88, 65.04, 56.03, 30.98. ESI-MS mass calcd for $C_{40}H_{39}N_4O_{10}$ $(M - H)^-$: 735.27. Found: 735.2.

5′-*O*-(4,4′-Dimethoxytrityl)-*N*$^{2′}$-trifluoroacetamido-2′-deoxyuridine-3′-*O*-succinate, 6. Compound **4** (100 mg, 0.156 mmol), DMAP (9.4 mg, 0.5 equiv), and succinic anhydride (17.2 mg, 1.1 equiv) were suspended in dry pyridine (2 mL) and stirred under argon for 2 h. An additional 0.2−0.5 equiv of succinic anhydride was added, and the reaction proceeded at room-temperature overnight. The reaction was worked according to the procedure given for **5**. A white powder **7** was isolated in 74% yield (85 mg, 0.115 mmol). ^{13}C NMR (75 MHz, CD_3CN) δ 175.04, 172.80, 163.85, 160.13, 140.71, 131.42, 130.35, 129.32, 128.96, 128.43, 114.60, 114.23, 103.97, 86.30, 84.29, 74.18, 64.77, 56.42, 55.77, 30.49. ESI-MS mass calcd for $C_{36}H_{33}N_3O_{11}$ $(M - H)^-$: 740.21. Found: 740.2.

5′-*O*-(4,4′-Dimethoxytrityl)-2′-aminomethylpyridyl-2′-deoxyuridine-3′-*O*-succinated Support, 7. Compound **7** was prepared by suspending the solid support (controlled pore glass derivatized with long-chain alkylamine, 500 Å pore size, 350 mg) in dry dichloromethane (5 mL) and adding TEA (250 μL) and **5** (180 mg, 245 μmol); HOBT (33 mg, 245 μmol) and BOP (119 mg, 270 μmol) were added to the suspension. The mixture was agitated for 16 h at room temperature, filtered, and washed with dichloromethane (2 × 10 mL). The solid was transferred to a separate flask and suspended in pyridine (7.5 mL). Acetic anhydride (1−2 mL) and *N*-methylimidazole (100 μL) were added to the flask, and the mixture was agitated overnight. The solid was filtered and washed with pyridine (3 × 10 mL), methanol (3 × 10 mL), dichloromethane (3 × 10 mL), and diethyl ether (3 × 10 mL). The white solid **7** was dried in vacuo. The nucleoside loading was determined spectrophotometrically to be 60 μmol/g (*6*).

5′-*O*-(4,4′-Dimethoxytrityl)-*N*$^{2′}$-trifluoroacetamido-2′-deoxyuridine-3′-*O*-succinated Support, 8. Compound **8** was prepared using the same method described for **7**. The nucleoside loading for **8** was 52 μmol/g.

5′-*O*-(4,4′-Dimethoxytrityl)-2′-aminomethylpyridyl-2′-deoxyuridine-3′-*O*-(2-cyanoethyl *N*,*N*-Diisopropylaminophosphoramidite), 9. While under argon **3a** (200 mg, 0.314 mmol) was dissolved in dry dichloromethane (2 mL) containing DIEA (220 μL, 4 equiv). The reaction vessel was degassed several times prior to

the addition of 2-chlorocyanoethyl *N*,*N*-diisopropylaminophosphoramidite (105 μL, 1.5 equiv) dropwise over 5 min. A positive ninhydrin test indicated formation of the desired product. After 50 min the reaction was diluted with 200 μL of methanol and evaporated to dryness. The residue was applied to silica (eluting with 0−80% dichloromethane in hexane containing 1% TEA) to give an off-white powder **9** in 57% yield (151 mg, 0.180 mmol). ESI-MS mass calcd for $C_{45}H_{52}N_6O_8P$ $(M - H)^-$: 835.37. Found: 835.4.

5′-*O*-(4,4′-Dimethoxytrityl)-*N*$^{2'}$-trifluoroacetamido-2′-deoxyuridine-3′-*O*-(2-cyanoethyl *N*,*N*-diisopropylaminophosphoramidite), **10.** While under argon **4** (100 mg, 0.163 mmol) was dissolved in dry dichloromethane (2 mL) containing DIEA (110 μL, 4 equiv). The reaction vessel was degassed several times prior to the addition of 2-chlorocyanoethyl *N*,*N*-diisopropylaminophosphoramidite (53 μL, 1.5 equiv) dropwise over 5 min. A positive ninhydrin test indicated formation of the desired product. After 90 min the reaction was diluted with ethyl acetate which had been previously washed with cold 10% sodium carbonate. The organic layer was extracted twice with cold 10% sodium carbonate and once with brine. The organic fraction was dried over sodium sulfate and evaporated to an oil. The residue was purified on silica (eluting with 20% hexane in dichloromethane containing 2% methanol and 1% TEA) to yield an off-white powder **10** in 77% yield (105 mg, 0.125 mmol). ^{1}H NMR (CD_3CN, 300 MHz) δ 1.26 (d, 12H), 3.4 (m, 2H), 3.5 (m, 2H), 3.6−3.8 (m, 3H), 3.79 (s, 6H), 4.1 (m, 2H), 4.3 (m, 1H), 4.4 (m, 1H), 4.5 (m, 1H), 4.7 (m, 1H), 4.8 (m, 1H), 5.4 (d, 1H), 5.8 (s, 1H), 6.1 (d, 1H), 6.9 (m, 4H), 7.3 (m, 9H), 7.5 (m, 2H), 7.6 (t, 1H), 7.9 (s, 1H). ^{31}P NMR (CD_3CN, 300 MHz) δ 153.13 and 154.06 ppm observed for the diastereomers. ESI-MS mass calcd for $C_{41}H_{46}F_3N_5O_9P$ $(M - H)^-$: 840.31. Found: 840.2.

Oligonucleotide Synthesis. Protected deoxyribonucleoside phosphoramidites and other reagents required for solid-phase DNA synthesis were purchased from Applied Biosystems, Incorporated (ABI). All oligonucleotides were synthesized on a 1.0 μmole scale. Solid supports (**7**, **8**) were packed in column assemblies purchased from ABI and contained approximately 23 mg of derivatized resin, depending on the nucleoside loading. The initial coupling steps in each synthesis were increased from 30 s to 2 min. The concentration of phosphoramidites (**9**, **10**) typically ranged from 0.1 to 0.18 M in dry acetonitrile. The coupling time for **9** and **10** was 15 min.

Oligonucleotides **11**, **13**, and **14** were synthesized with the terminal dimethoxytrityl (DMT) group retained. Oligonucleotide **12** was prepared with the 5′-DMT group removed prior to cleavage and deprotection. Oligonucleotides **11**−**13** were cleaved from the solid support with concentrated ammonia during the automated synthesis routine and deprotected for either 16 h at 55 °C or 4 h at 65 °C. Oligonucleotide **14** was cleaved manually in 5 mL of concentrated ammonia for 16 h at 55 °C. Oligonucleotides **15**−**18** were prepared by standard trityl-off procedures.

Oligonucleotide Purification. Deprotected oligonucleotides containing a 5′-DMT group were suspended in 20% triethylammonium bicarbonate buffer (1.0 M, pH 8.5) in water and injected onto a reverse phase VYDAC 201HS1022 C18 column. Preparative HPLC was performed with a Waters 600E Controller and 994 Diode Array Detecter, using the following gradient: 0−100% B over 50 min, where A = 0.1 M triethylamine acetate, 2% acetonitrile; B = 0.05 M triethylamine acetate, 50% acetonitrile. The collected peaks were dried in vacuo and further purified using Waters C18 Classic SepPak cartridges. The amount of purified oligonucleotide was determined spectrophotometrically, with ϵ_{260} values given in parentheses: **11** (119800 M^{-1} cm^{-1}), **12** (115150 M^{-1} cm^{-1}), **13** (95900 M^{-1} cm^{-1}), **14** (97250 M^{-1} cm^{-1}).

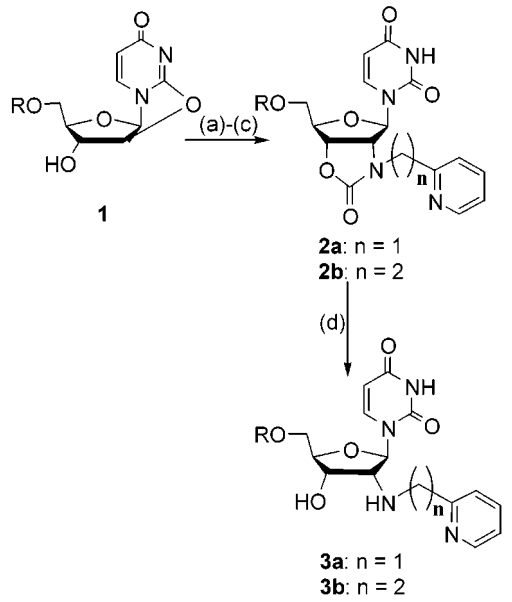
Oligonucleotides **11**, **13**, and **14** were detritylated according to the procedure outlined by ABI manual and desalted using SepPak cartridges (*7*). The detritylated oligonucleotides were further purified using a weak anion exchange column purchased from SynChroPak (AX-100, analytical, semiprep), using the following gradient: 0−90% B over 35 min, where A = 50 mM sodium phosphate (pH 5.9), 30% methanol; B = 50 mM sodium phosphate (pH 5.9), 30% methanol, 1 M ammonium sulfate. The collected peaks were desalted using SepPak cartridges and assayed as described above.

Oligonucleotide Yield. The overall yield of each modified oligonucleotide, following HPLC purification and workup, ranged from 30 to 40%, based on a 12-μmol synthesis. The detritylated, purified oligonucleotides **11**−**14** were characterized by MALDI-TOF mass spectrometry: **11**, calculated, 3355 [M], found, 3356.24 $[M - H]^-$; **12**, calculated, 3408 [M], found, 3407.17 $[M-H]^-$; **13**, calculated, 3230 [M], found, 3228.38 $[M - H]^-$; **14**, calculated, 3320 [M], found, 3319.43 $[M - H]^-$.

Enzymatic Digestion of Oligonucleotides and HPLC Analysis. Approximately 10−30 nmol of purified oligonucleotide was subjected to enzymatic digestion analysis. The digest cocktail (55 μL/sample) contained bacterial alkaline phosphatase (4 μL, 10 μL/unit) and snake venom phosphodiesterase (2.4 μL, 1 mL/mg), in 1 M $MgCl_2$ (0.8 μL), 0.5 M Tris buffer, pH 7.5 (3.5 μL). The reaction mixture was incubated at 37 °C for 8−16 h. The reaction was stopped by adding 3 M sodium acetate (7 μL) and ethanol (155 μL) to the samples, which were then frozen on dry ice (10 min) and centrifuged (10 min) at 4 °C. The supernatants were removed and transferred to new tubes, each containing 452 μL of ethanol. The samples were frozen and centrifuged; the resulting supernatants were removed and dried in vacuo. The samples were dissolved in water (200 μL) and injected onto a reverse phase Vydac (201HS54 4.6 mm × 25 cm, 5 μm, 90 Å) or Prism (Keystone Scientific, 4.6 × 250 mm, 5 μm, 100 Å) C18 column. The product nucleosides were eluted within 20 min, according to either of the following gradients: (Vydac) 0−30% B over 20 min then 30−100% B over 10 min, where A = 0.1 M triethylamine acetate, 2% acetonitrile, B = 0.05 M triethylamine acetate, 50% acetonitrile; (Prism) 0−17% B over 15 min then 17−75% B over 18 min, where A = 0.1 M triethylamine acetate, pH 7.0, 2% acetonitrile, B = 100% acetonitrile. The resulting peaks were compared against the appropriate set of nucleoside standards for a given oligonucleotide sequence.

Thermal Denaturation Measurements. Individual oligonucleotides were hybridized to their complementary strands in 50 mM NaP_i buffer (pH 7.0), 0.5 M NaCl, to give solutions that were 2.7 μM in each strand. The samples were heated for 20 min at 70 °C and cooled to 4 °C overnight. Thermal denaturation profiles were measured at 260 nm with an Hewlett-Packard diode array UV−vis spectrophotometer equipped with a Peltier temperature controller and interfaced with a personal computer. Samples were equilibrated at 20 °C for 10−20 min prior to data collection. Absorbance values were taken over a temperature range of 20−70 °C, with measurements made every 0.5 °C with an equilibration time of 60 s for each point. Each hybrid went through 2−4

Scheme 1[a]



[a] Reagents: (a) $(imid)_2CO$, pyridine, rt, 30 h; (b) NH_2R (R = CH_2pyr, CH_2CH_2pyr), DIEA, CH_2Cl_2, rt, 60 h; (c) DBU, THF, reflux, 46 h; (d) 6 N NaOH, dioxane, CH_3OH, 50 °C, 36 h. Abbreviation: R = 4,4′-dimethoxytrityl.

separate heat-cool cycles, and the T_m values obtained from these heating and cooling traces were averaged to give the final T_m value. Standard deviations were calculated for each duplex.

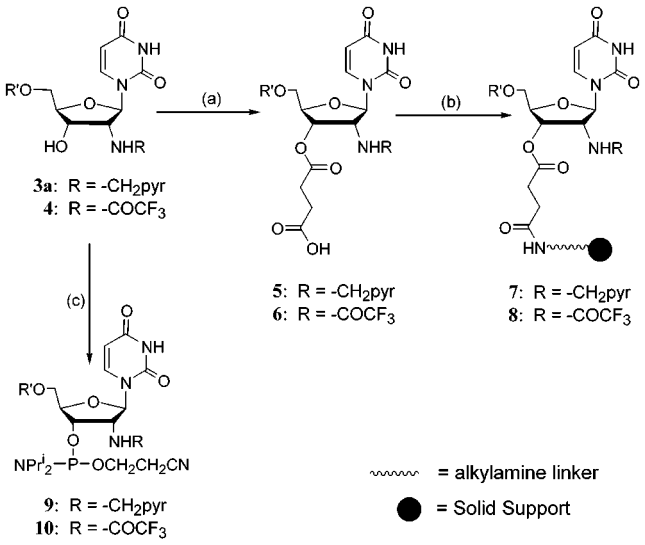
RESULTS

Synthesis of 2′-Modified Nucleosides. Nucleosides with bidentate amine groups such as aminomethylpyridine (AMPy) (*8*) and aminoethylpyridine (AEPy) at the 2′ ribose position were prepared as shown in Scheme 1. This approach was based on methods developed recently for incorporating 2′-*N*-alkylamino substituents into nucleosides (*9*). Nucleoside **1** was converted to the 3′-*N*-alkyl carbamate upon prolonged treatment with carbonyl diimidazole in pyridine; this was followed by the addition of AMPy or AEPy in the presence of DIEA and dichloromethane. Subsequent cyclization in THF using the cyclization agent DBU produced either **2a** or **2b** in yields of 20% and 10%, respectively. Prolonged heating of **2a** and **2b** in a basic dioxane−methanol solution caused deprotection at the 2′,3′-positions, giving **3a** and **3b** in high yield (92% and 88%, respectively).

Derivatization of solid supports with 2′-modified nucleosides was achieved according to Scheme 2. Nucleoside **4** was prepared according to previously published procedures (*3a, 5, 10*). Both **3a** and **4** were treated with succinic anhydride to give the corresponding hemisuccinates **5** and **6** in yields of 60% and 74%, respectively (*6, 11*). Solid supports such as controlled pore glass (CPG) containing long-chain alkylamine groups were derivatized with **6** using *p*-nitrophenol and DCC. This method resulted in solid supports with low nucleoside loading. Subsequent attempts to prepare the nucleoside-modified solid supports employed the coupling agent BOP in the presence of HOBT and TEA (*12*). The unreacted amine groups were treated with acetic anhydride, and the nucleoside loadings of the solid supports **7** and **8** were determined by spectrophotometric assay (60 and 52 μmol/g, respectively) (*6*).

The preparation of phosphoramidite derivatives of nucleosides **3a** and **4** relied on standard methods (*3a, 6, 10*). Nucleosides **3a** and **4** were treated with 2-chlorocyanoethyl *N*,*N*-diisopropylaminophosphoramidite in the presence of DIEA to give **9** and **10** in 57% and 77% yield, respectively (Scheme 2).

Scheme 2[a]



[a] Reagents: (a) succinic anhydride, pyridine, DMAP, rt, 16 h; (b) solid support, TEA, HOBT, BOP, CH_2Cl_2, rt, 16 h; acetic anhydride, *N*-methylimidazole, pyridine, rt, 12 h; (c) amidite, DIEA, CH_2Cl_2, rt, 50 min. Abbreviation: R′ = 4,4′-dimethoxytrityl.

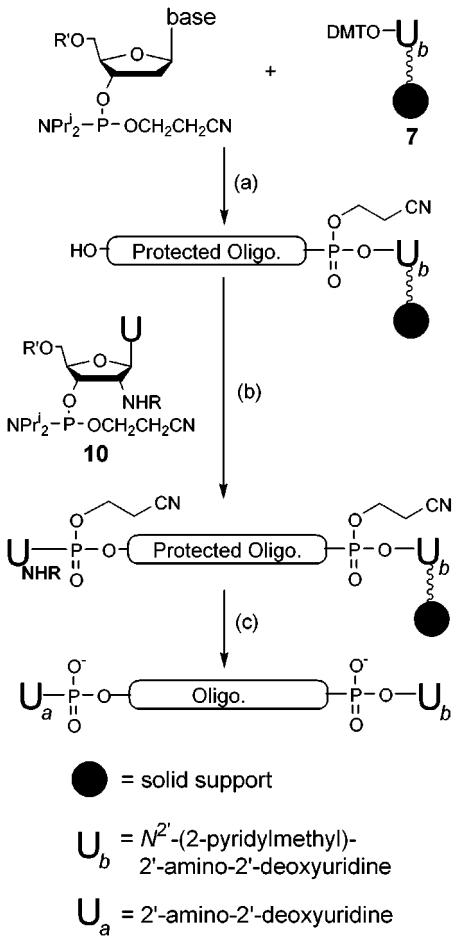
Oligonucleotide Synthesis. A series of oligonucleotides were prepared from the support-bound and phosphoramidite nucleoside derivatives as outlined in Scheme 3 (see Table 1 for sequences). To maximize coupling, the reaction time for the first step was increased from 30 s to 2 min (yield > 95%). The reaction times for **9** and **10** were 15 min in length, leading to coupling yields > 90%.

All oligonucleotides were cleaved from the solid support with concentrated ammonia as a part of the automated synthesis routine, except in the case of **14**, which was manually cleaved. The yield of purified oligonucleotide for **11**−**14** ranged from 30 to 40%, which was comparable to those values observed for **15**−**18**. Results from MALDI-TOF mass spectrometry on **11**−**14** were in excellent agreement with the calculated values. Further characterization of these oligonucleotides was achieved by enzymatic digestion with alkaline phosphatase and phosphodiesterase (Figure 2) (*7*). Analysis of the digestion products showed the expected distribution of nucleosides determined for each oligonucleotide sequence (*13*).

Thermal Denaturation Studies. We investigated the thermal stability of duplexes containing 2′-modified nucleosides. Table 2 shows the transition melting temperatures (T_m) for each duplex prepared in 50 mM sodium phosphate buffer (pH 7.0) containing 0.5 M sodium chloride. The T_m of the 11-mer duplex formed by the unmodified oligonucleotides **15** and **16** was 48 °C. When one 5′-terminal nucleoside from this duplex was substituted with either 2′-amino-2′-deoxyuridine ($\mathbf{U_a}$) or $N^{2'}$-(2-pyridylmethyl)-2′-amino-2′-deoxyuridine ($\mathbf{U_b}$), the T_m value remained unchanged (T_m = 47 °C for duplexes **11**:**15** and **12:16**). When both $\mathbf{U_a}$ and $\mathbf{U_b}$ were incorporated at the 5′ ends of the same duplex (**11:12**), the T_m value decreased to 45 °C.

The small change in the melting profile was similar to the results obtained with duplexes of identical length, GC content, and type of nucleoside modification, but of different sequence. This second set of duplexes contained

Scheme 3[a]



[a] Steps in the synthesis of oligonucleotide **14**: (a) detritylation of **7**; monomer coupling; normal synthesis cycle; (b) coupling of **10**; (c) cleavage and deprotection. R = $COCF_3$, R′ = 4,4′-dimethoxytrityl.

Table 1. Oligonucleotide Sequences[a]

sequence	abbreviation
5′-**U$_a$**CAGCTGTAGA	**11**
5′-**U$_b$**CTACAGCTGA	**12**
5′-**U$_a$**CTCCTACAC**U$_a$**	**13**
5′-**U$_a$**CTCCTACAC**U$_b$**	**14**
5′- TCTACAGCTGA	**15**
5′- TCAGCTGTAGA	**16**
5′- TCTCCTACACT	**17**
5′- AGTGTAGGAGA	**18**

[a] The symbol **U$_a$** denotes 2′-amino-2′-deoxyuridine; **U$_b$** denotes $N^{2'}$-(2-pyridylmethyl)-2′-amino-2′-deoxyuridine.

2′-modified nucleosides at both the 3′ and 5′ ends of the same strand. Duplex **13:18** contained **U$_a$** nucleosides at the 5′ and 3′ termini, whereas duplex **14:18** contained **U$_a$** at the 5′ end and **U$_b$** at the 3′ end. The T_m values (46 °C) for duplexes **13:18** and **14:18** decreased slightly in comparison to the value of the unmodified duplex **17:18** (T_m = 48 °C; Figure 3).

DISCUSSION

Synthetic Strategy. Two general methods exist for preparing oligonucleotides containing transition metal complexes. One method involves the synthesis of nucleosides that possess metal-binding ligands, followed by incorporation of these modified nucleosides into oligonucleotides and subsequent metal complexation at the specific attachment sites (*3e, 14*). The second method

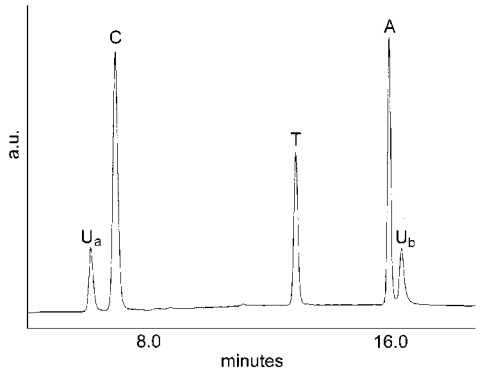


Figure 2. Products of enzymatic digestion of **14** as analyzed by reverse-phase HPLC.

Table 2. Thermal Denaturation Temperatures for Oligonucleotides Containing 2′-Substituted Nucleosides

duplex	T_m[a] (°C)	modification[b]
15:16	48.2 ± 0.5	none
11:15	46.6 ± 0.4	5′ **U$_a$**
12:16	46.7 ± 0.4	5′ **U$_b$**
11:12	45.0 ± 0.5	5′ **U$_a$**, 5′ **U$_b$**
17:18	47.6 ± 0.2	none
13:18	45.8 ± 0.5	5′ **U$_a$**, 3′ **U$_a$**
14:18	46.2 ± 0.5	5′ **U$_a$**, 3′ **U$_b$**

[a] Values determined in 50 mM NaP_i buffer (pH 7.0) containing 0.5 M NaCl. The concentration of each oligomer was 2.7 μM. [b] The symbol **U$_a$** denotes 2′-amino-2′-deoxyuridine; **U$_b$** denotes $N^{2'}$-(2-pyridylmethyl)-2′-amino-2′-deoxyuridine.

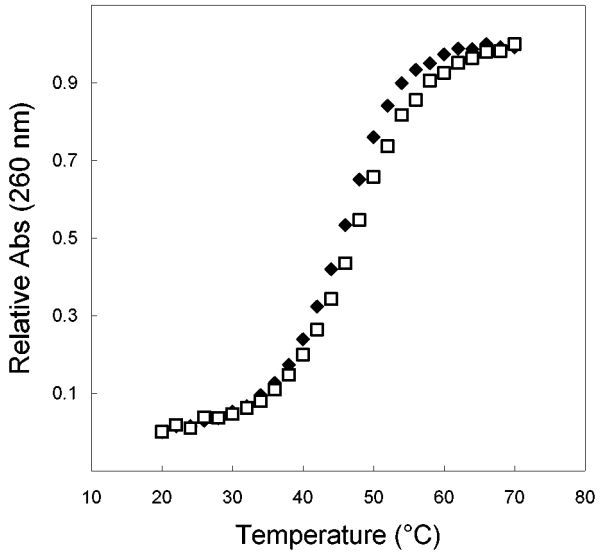


Figure 3. Thermal denaturation curves for the unmodified duplex **17:18** (□) and modified duplex **14:18** (◆).

entails the synthesis of metal-containing nucleosides that are incorporated during solid-phase oligonucleotide synthesis (*4ab, 15*). The 2′-modified nucleosides described in this work can be used in either method, resulting in oligonucleotides site-specifically labeled with metal complexes (*3e, 4*).

The choice of 2′-substituents described here are based on ligands that avidly bind transition metal complexes, such as AMPy and AEPy (*16*). The site-specific labeling of oligonucleotides with metal reagents is of considerable interest for several reasons. Recent experiments involving ruthenium-modified duplexes have shown that DNA can mediate energy and electron transfer reactions (*3e, 15f, 17*). Additionally, metal-modified primers have been used in dideoxy DNA sequencing techniques and elec-

trochemistry-based DNA assays (*18*). Therefore, nucleosides containing metal-binding ligands such as those in Figure 1 can facilitate the use of metal complexes as probes of nucleic acid structure and function (*3e, 4*).

Synthesis of 2′-Modified Nucleosides. The synthesis of nucleosides containing 2′-*N*-alkylamino substituents is an extension of methods developed by Sebesta, McGee, and co-workers (*9*). The yields of isolation determined for **2a** and **2b** are lower than those observed for nucleosides containing similarly bulky substituents and may be attributed to the purification conditions required for DMT-protected vs silyl-protected intermediates (*9a*). The products **3a** and **3b** are isolated in yields comparable to the yields reported by Sebesta for similar 2′-modified nucleosides.

The preparation of solid supports derivatized with 2′-modified nucleosides is complicated by the poor steric accessibility of the 3′ ribose site (*19*). The steric bulk at the 2′ position hinders the reaction of the 3′ hydroxyl with succinic anhydride. Succination of **3a** and **4** proceeds in reasonable yields and demonstrates that both small and large functional groups at the 2′ position can be tolerated in the succination step. High nucleoside loadings for **7** and **8** are achieved using the coupling agent BOP and an excess of nucleoside hemisuccinate in the derivatization step. While the solid support employed here is glass-based, the method is applicable to other supports containing long-chain alkylamine linkers.

Successful derivatization of supports with nucleosides such as **3a** and **4** affords the synthesis of 3′ oligonucleotide conjugates in which the label is incorporated *directly* on the ribose ring. This is a significant advance since the current preparation of 3′ oligonucleotide conjugates is achieved with supports containing either nucleosides with *base-tethered* primary amine groups (*20*) or *nonnucleosidic* amine derivatives (*21*). The ribose is an attractive attachment site since the labels introduced here cause fewer perturbations to the secondary duplex structure than labels attached to the nucleoside base (*4*). Additionally, the absence of a long linker between the attachment site and the incorporated label minimizes disruptions to the hydrogen bonding capacity of the oligonucleotide conjugate.

Oligonucleotide Synthesis with 2′-Modified Nucleosides. The successful large-scale synthesis of several 11-mer oligonucleotides validates the utility of 2′-modified nucleosides as support-bound and phosphoramidite derivatives (Table 1). Oligonucleotide synthesis beginning with **7** or **8** proceeds with minor modification to the automated protocol. The coupling yields of phosphoramidites **9** and **10** are acceptable for routine oligonucleotide preparation, and the purification of the several 11-mer modified oligonucleotides is straightforward. The isolation yields for **11**−**14** are comparable to values determined for oligonucleotides **15**−**18** under identical synthetic and purification conditions, implying that the use of 2′-modified nucleosides does not compromise the overall yield.

Effect of 2′-Modified Nucleosides on Duplex Stability. The presence of nucleosides containing ribose substituents at the 2′ position causes slight destabilization to the modified duplexes, as assessed by thermal denaturation studies. Interestingly, analysis of the transition melting (T_m) temperatures listed in Table 2 suggests that the T_m values are influenced by the number of 2′-modified nucleosides present in a duplex, not the size of the 2′ substituent. For example, thermal denaturation of duplexes **11:15** and **12:16** produces identical T_m values, despite the difference in the size of the 2′ substituent (−NH_2 vs AMPy). The T_m of **11:12** shows the effect of placing two 2′-modified nucleosides at the 5′ ends of the duplex. Similar results are obtained with a second set of duplexes identical in length, GC content, and type of nucleoside modification. The placement of two 2′-modified nucleosides at the 5′ and 3′ ends of the same strand results in duplexes destabilized by 1−2 °C (**13:18** and **14:18** vs **17:18**). We conclude that the extent of duplex destabilization is the same when two 2′-modified nucleosides are introduced at either (1) the 5′ and 3′ ends of a one strand hybridized to its complement, or (2) the 5′ ends of complementary strands.

Compared to 2′-*deoxy*nucleosides, 2′-*amino*nucleosides favor the 2′-endo sugar conformation to a higher degree (*22*). This observation suggests that 2′-aminonucleosides should stabilize DNA/DNA duplexes. However, T_m data for a series of 9-mer duplexes containing a 2′-aminonucleoside in the middle of the sequence indicate that the presence of these modified nucleosides has a destabilizing effect (*3a*). Our work shows that placement of the 2′-amino-modified nucleosides at the ends of the duplexes minimizes the destabilization imposed by the altered sugar conformation.

CONCLUSION

We report the synthesis of 2′-modified nucleosides designed specifically for incorporating reporter molecules into oligonucleotides. Because these nucleosides contain modifications to the ribose ring (as opposed to the nucleobase), they are important contributions to current library of modified nucleosides. The introduction of metal-binding ligands at the 2′ position is achieved after two steps. Conversion of these nucleosides to solid support-bound and phosphoramidite derivatives proceeds in good yield. The powerful combination of these derivatives affords the preparation of an entirely new class of oligonucleotide conjugates—those which contain label attachment sites at 3′, intervening, and 5′ sites of a duplex.

Thermal denaturation studies indicate that the presence of 2′-modified nucleosides in 11-mer duplexes has a slight destabilizing effect on the duplex structure. This effect is limited by the selective placement of these nucleosides at the ends of the duplexes. Interestingly, the size of the metal-binding substituent does not influence the magnitude of the destabilization. This characteristic makes these 2′-modified nucleosides even more attractive for use in the site-specific incorporation of reporter molecules into oligonucleotides.

The methodologies employed here can be extended to other modified nucleosides. Succination yields for nucleosides containing metal-binding ligands at locations other than the 2′ position are expected to be much higher due to the absence of steric constraints. While the solid support is glass-based, the method is applicable to other solid supports containing any long-chain alkylamine linker. The library of solid supports containing modified nucleosides can be significantly expanded with the coupling conditions described here. These nucleoside reagents will enable the incorporation of labels known to be useful probes of nucleic acid structure and function.

ACKNOWLEDGMENT

The authors wish to thank Thomas W. Welch, C. J. Yu, Jeffrey J. Rack, and Natia L. Frank for helpful discussions. This work was supported by NIST (ATP) Award 70NANB5H1031, Jet Propulsion Laboratory (JPL 67192), and the Beckman Institute Biological Imaging Center.

Supporting Information Available: MALDI-TOF mass spectra for **11**−**13**. HPLC of digestion products of **11**−**13**. This material is available free of charge via the Internet at http://pubs.acs.org.

LITERATURE CITED

(1) (a) Verma, S., and Eckstein, F. (1998) Modified Oligonucleotides: Synthesis and Strategy for Users. *Annu. Rev. Biochem. 67*, 99−134. (b) Eaton, B. E., and Pieken, W. A. (1995) Ribonucleotides and RNA. *Annu. Rev. Biochem. 64*, 837−863. (c) Aurup, H., Williams, D. M., and Eckstein, F. (1992) 2′-Fluoro-2′-deoxynucleoside and 2′-Amino-2′-deoxynucleoside 5′-Triphosphates As Substrates For T7 RNA-Polymerase. *Biochemistry 31*, 9636−9641.

(2) (a) Tuerk, C., and Gold, L. (1990) Systematic Evolution of Ligands By Exponential Enrichment − RNA Ligands to Bacteriophage-T4 Dna-Polymerase. *Science 249*, 505−510. (b) Lin, Y., Qiu, Q., Gill, S. C., and Jayasena, S. D. (1994) Modified Rna Sequence Pools For in-Vitro Selection. *Nucleic Acids Res. 22*, 5229−5234.

(3) (a) Aurup, H., Tuschi, T., Benseler, F., Ludwig, J., and Eckstein, F. (1994) Oligonucleotide duplexes containing 2′-amino-2′-deoxycytidines: thermal stability and chemical reactivity. *Nucleic Acids Res. 22*, 20−24. (b) Sigurdsson, S. T., and Eckstein, F. (1996) Site specific labeling of sugar residues in oligoribonucleotides: Reactions of aliphatic isocyanates with 2′ amino groups. *Nucleic Acids Res. 24*, 3129−3133. (c) Kuznetsova, K. G., Romanova, E. A., Volkov, E. M., Tashlitsky, V. N., Oretskaya, T. S., Krynetskaya, N. F., and Shabarova, Z. A. (1993) *J. Bioorg. Chem. (Moscow) 19*, 455−466. (d) Sigurdsson, S. T., Tuschl, T., and Eckstein, F. (1995) Probing RNA Tertiary Structure − Interhelical Cross-Linking of the Hammerhead Ribozyme. *RNA-Publ. RNA Soc. 1*, 575−583. (e) Meade, T. J., and Kayyem, J. F. (1995) Electron Transfer through DNA: Site-Specific Modification of Duplex DNA with Ruthenium Donors and Acceptors. *Angew. Chem., Int. Ed. Engl. 34*, 352−353.

(4) (a) Krider, E. S., Rack, J. J., Frank, N. L., and Meade, T. J. (2001) Automated Synthesis of 3′-Metalated Oligonucleotides. *Inorg. Chem. 40*, 4002−4009. (b) Rack, J. J., Krider, E. S., and Meade, T. J. (2000) Spectroscopy and Electrochemistry of Ruthenium-Modified Nucleic Acids: Design of a Novel Metal-Binding Nucleoside. *J. Am. Chem. Soc. 122*, 6287−6288.

(5) McGee, D., Vaughn-Settle, A., Vargeese, C., and Zhai, Y. (1996) 2′-Amino-2′-deoxyuridine via an intramolecular cyclization of a trichloroacetimidate. *J. Org. Chem. 61*, 781−785.

(6) Gait, M., Ed. (1984) *Oligonucleotide Synthesis: A Practical Approach*, Oxford University Press, Oxford.

(7) (1992) *Evaluating and Isolating Synthetic Oligonucleotides: The Complete Guide*, Perkin-Elmer/Applied Biosystems Division, Publication no. 239902, Foster City, CA.

(8) Abbreviations: AMPy, aminomethylpyridine; AEPy, aminoethylpyridine; BOP, benzotriazol-1-yloxytris(dimethylamino)phosphonium hexafluorophosphate; DBU, 1,8-diazabicyclo-[5.4.0]undec-7-ene; DCC, dicyclohexylcarbodiimide; DIEA, diisopropylethanolamine; DMAP, (dimethylamino)pyridine; DMT, 4,4′-dimethoxytrityl; EtOAC, ethyl acetate; HOBT, hydroxybenzotriazole; MALDI-TOF, matrix-assisted laser desorption-time-of-flight; TEA, triethylamine; THF, tetrahydrofuran.

(9) (a) Sebesta, D. P., O'Rourke, S. S., Martinez, R. L., Pieken, W. A., and McGee, D. P. C. (1996) 2′-Deoxy-2′-alkoxylaminouridines: Novel 2′-substituted uridines prepared by intramolecular nucleophilic ring opening of 2, 2′−O-anhydrouridines. *Tetrahedron 52*, 14385−14402. (b) McGee, D. P. C., Sebesta, D. P., O'Rourke, S. S., Martinez, R. L., Jung, M. E., and Pieken, W. A. (1996) Novel nucleoside va intramolecular functionalization of 2,2′-anhydrouridine derivatives. *Tetrahedron Lett. 37*, 1995−1998.

(10) Pieken, W. A., Olsen, D. B., Benseler, F., Aurup, H., and Eckstein, F. (1991) Kinetic characterization of ribonuclease-resistant 2′-modified hammerhead ribozymes. *Science 253*, 314−317.

(11) Caruthers, M. H., Barone, A. D., Beaucage, S. L., Dodds, D. R., Fisher, E. F., McBride, L. J., Matteucci, M., Stabinsky, Z., and Tang, J.-Y. (1987) In *Methods in Enzymology: Recombinant DNA* (R. W. a. L. Grossman, Ed.) vol. 154, pp 287−313, Academic Press, Inc., New York

(12) Knorr, R., Trzeciak, A., Bannwarth, W., and Gillessen, D. (1989) New coupling reagents in peptide chemistry. *Tetrahedron Lett. 30*, 1927−1930.

(13) Supporting data can be found in the Supporting Information.

(14) (a) Ledoan, T., Perrouault, L., Chassignol, M., Thuong, N. T., and Helene, C. (1987) Sequence-Targeted Chemical Modifications of Nucleic-Acids By Complementary Oligonucleotides Covalently Linked to Porphyrins. *Nucleic Acids Res. 15*, 8643−8659. (b) Bannwarth, W., Schmidt, D., Stallard, R. L., Hornung, C., Knorr, R., and Muller, F. (1988) Bathophenanthroline-Ruthenium(Ii) Complexes As Non-Radioactive Labels For Oligonucleotides Which Can Be Measured By Time-Resolved Fluorescence Techniques. *Helv. Chim. Acta 71*, 2085−2099. (c) Chen, C. H. B., and Sigman, D. S. (1988) Sequence-Specific Scission of Rna By 1,10-Phenanthroline Copper Linked to Deoxyoligonucleotides. *J. Am. Chem. Soc. 110*, 6570−6572. (d) Telser, J., Cruickshank, K. A., Schanze, K. S., and Netzel, T. L. (1989) DNA oligomers and duplexes containing a covalently attached derivative of tris(2,2′-bipyridine)ruthenium(II) − Synthesis and characterization by thermodynamic and optical spectroscopic measurements. *J. Am. Chem. Soc. 111*, 7221−7226. (e) Modak, A. S., Gard, J. K., Merriman, M. C., Winkeler, K. A., Bashkin, J. K., and Stern, M. K. (1991) Toward chemical ribonucleases II. Synthesis and characterization of nucleoside-bipyridine conjugates − hydrolytic cleavage of RNA by their copper(II) complexes. *J. Am. Chem. Soc. 113*, 283−291. (f) Jenkins, Y., and Barton, J. K. (1992) A sequence-specific molecular light switch − tethering of an oligonucleotide to a dipyridophenazine complex of ruthenium(II). *J. Am. Chem. Soc. 114*, 8736−8738. (g) Bashkin, J. K., Frolova, E. I., and Sampath, U. S. (1994) Sequence-specific cleavage of HIV messenger-RNA by a ribozyme mimic. *J. Am. Chem. Soc. 116*, 5981−5982. (h) Arkin, M. R., Stemp, E. D. A., Pulver, S. C., and Barton, J. K. (1997) Long-range oxidation of guanine by Ru(III) in duplex DNA. *Chem., Biol. 4*, 389−400. (i) Inoue, H., Furukawa, T., Shimizu, R., Tamura, T., Matsui, M. N., and Ohtsuka, E. (1999) Efficient site specific cleavage of RNA using a terpyridine−copper(II) complex joined to a 2′-O-methyloligonucleotide by a nonflexible linker. *Chem. Commun.*, 45−46. (j) Wiederholt, K., and McLaughlin, L. W. (1999) A 2,2′-bipyridine ligand for incorporation into oligodeoxynucleotides: synthesis, stability and fluorescence properties of ruthenium-DNA complexes. *Nucleic Acids Res. 27*, 2487−2493. (k) Ortmans, I., Content, S., Boutonnet, N., Kirsch-De Mesmaeker, A., Bannwarth, W., Constant, J. F., Defrancq, E., and Lhomme, J. (1999) Ru-labeled oligonucleotides for photoinduced reactions on targeted DNA guanines. *Chem. Eur. J. 5*, 2712−2721. (l) Holmlin, R. E., Dandliker, P. J., and Barton, J. K. (1999) Synthesis of metallointercalator-DNA conjugates on a solid support. *Bioconjugate Chem. 10*, 1122−1130. (m) Khan, S. I., and Grinstaff, M. W. (1999) Palladium(0)-catalyzed modification of oligonucleotides during automated solid-phase synthesis. *J. Am. Chem. Soc. 121*, 4704−4705.

(15) (a) Bannwarth, W., and Schmidt, D. (1989) A simple specific labeling for oligonucleotides by bathophenanthroline-Ru(II) complexes as nonradioactive label molecules. *Tetrahedron Lett. 30*, 1513−1516. (b) Manchanda, R., Dunham, S. U., and Lippard, S. J. (1996) Automated solid-phase synthesis of site-specifically platinated oligodeoxyribonucleotides. *J. Am. Chem. Soc. 118*, 5144−5145. (c) Schliepe, J., Berghoff, U., Lippert, B., and Cech, D. (1996) Automated solid-phase synthesis of platinated oligonucleotides via nucleoside phosphonates. *Angew. Chem., Int. Ed. 35*, 646−648. (d) Magda, D., Crofts, S., Lin, A., Miles, D., Wright, M., and Sessler, J. L. (1997) Synthesis and kinetic properties of ribozyme analogues prepared using phosphoramidite derivatives of dysprosium(III) texaphyrin. *J. Am. Chem. Soc. 119*, 2293−2294. (e) Meggers, E., Kusch, D., and Giese, B. (1997) An

efficient synthesis of enantiomerically pure Delta- and Lambda-ruthenium(II)-labeled oligonucleotides. *Helv. Chim. Acta 80*, 640−652. (f) Hurley, D. J., and Tor, Y. (1998) Metal-containing oligonucleotides: Solid-phase synthesis and luminescence properties. *J. Am. Chem. Soc. 120*, 2194−2195. (g) Khan, S. I., Beilstein, A. E., Smith, G. D., Sykora, M., and Grinstaff, M. W. (1999) Synthesis and excited-state properties of a novel ruthenium nucleoside: 5-[Ru(bpy)(2)(4-m-4′-pa-bpy)](2+)-2′-deoxyuridine. *Inorg. Chem. 38*, 2411−2415. (h) Khan, S. I., Beilstein, A. E., Sykora, M., Smith, G. D., Hu, X., and Grinstaff, M. W. (1999) Automated solid-phase DNA synthesis and photophysical properties of oligonucleotides labeled at the 5′-terminus with Ru(bpy)(3)(2+). *Inorg. Chem. 38*, 3922−3925. (i) Lewis, F. D., Helvoigt, S. A., and Letsinger, R. L. (1999) Synthesis and spectroscopy of Ru(II)-bridged DNA hairpins. *Chem. Commun.*, 327−328. (j) Hu, X., Smith, G. D., Sykora, M., Lee, S. J., and Grinstaff, M. W. (2000) Automated solid-phase synthesis and photophysical properties of oligodeoxynucleotides labeled at 5′-aminothymidine with Ru(bpy)-(2)(4-m-4′-cam-bpy)(2+). *Inorg. Chem. 39*, 2500−2504.

(16) (a) Brown, G. M., Weaver, T. R., Keene, F. R., and Meyer, T. J. (1976) Oxidation of Coordinated Diamines in Bis(2,2′-bipyridine) Complexes of Ruthenium. *Inorg. Chem. 15*, 190−196. (b) Juris, A., Balzani, V., Barigelletti, F., Campagna, S., Belser, P., and Vonzelewsky, A. (1988) Ru(II) polypyridine complexes − photophysics, photochemistry, electrochemistry, and chemiluminescence. *Coord. Chem. Rev. 84*, 85−277.

(17) (a) Fu, P. K. L., and Turro, C. (1999) Energy transfer from nucleic acids to Tb(III): Selective emission enhancement by single DNA mismatches. *J. Am. Chem. Soc. 121*, 1−7. (b) Bannwarth, W., Pfleiderer, W., and Muller, F. (1991) Energy-transfer within oligonucleotides from a lumazine (= pteridine-2,4(1H,3H)-dione) chromophore to bathophenanthroline-ruthenium(II) complexes. *Helv. Chim. Acta 74*, 1991−1999. (c) Bannwarth, W., and Muller, F. (1991) Energy-transfer from a lumazine (= pteridine-2,4(1H,3H)-dione) chromophore to bathophenanthroline-ruthenium(II) complexes during hybridization processes of DNA. *Helv. Chim. Acta 74*, 2000−2008. (d) Holmlin, R. E., Dandliker, P. J., and Barton, J. K. (1997) Charge transfer through the DNA base stack. *Angew. Chem., Int. Ed. 36*, 2715−2730. (e) Fukui, K., and Tanaka, K. (1998) Distance dependence of photoinduced electron transfer in DNA. *Angew. Chem., Int. Ed. 37*, 158−161. (f) Okahata, Y., Kobayashi, T., Tanaka, K., and Shimomura, M. (1998) Anisotropic electric conductivity in an aligned DNA cast film. *J. Am. Chem. Soc. 120*, 6165−6166. (g) Harriman, A. (1999) Electron tunneling in DNA. *Angew. Chem., Int. Ed. 38*, 945−949. (h) Kelley, S. O., and Barton, J. K. (1999) Electron transfer between bases in double helical DNA. *Science 283*, 375−381. (i) Tierney, M. T., Sykora, M., Khan, S. I., and Grinstaff, M. W. (2000) Photoinduced electron transfer in an oligonucleotide duplex: observation of the electron-transfer intermediate. *J. Phys. Chem. B 104*, 7574−7576. (j) Lewis, F. D., Wu, T. F., Liu, X. Y., Letsinger, R. L., Greenfield, S. R., Miller, S. E., and Wasielewski, M. R. (2000) Dynamics of photoinduced charge separation and charge recombination in synthetic DNA hairpins with stilbenedicarboxamide linkers. *J. Am. Chem. Soc. 122*, 2889−2902.

(18) (a) Bannwarth, W. (1989) Bathophenanthroline Ru(II) complexes as nonradioactive labels for dideoxy DNA sequencing. *Analytical Biochemistry 181*, 216−219. (b) Yu, C. J., Yowanto, H., Wan, Y. J., Meade, T. J., Chong, Y., Strong, M., Donilon, L. H., Kayyem, J. F., Gozin, M., and Blackburn, G. F. (2000) Uridine-conjugated ferrocene DNA oligonucleotides: Unexpected cyclization reaction of the uridine base. *J. Am. Chem. Soc. 122*, 6767−6768.

(19) Goodchild, J. (1990) Conguates of oligonucleotides and modified oligonucleotides: A review of their synthesis and properties. *Bioconjugate Chem. 1*, 165−191.

(20) Ueno, Y., Mikawa, M., and Matsuda, A. (1998) Nucleosides and nucleotides. 170. Synthesis and properties of oligodeoxynucleotides containing 5-[*N*-[2-[*N*,*N*-bis(2-aminoethyl)amino]-ethyl]carbamoyl]-2′-deoxyuridine and 5-[*N*-[3-[*N*,*N*-bis(3-aminopropyl)amino]propyl]carbamoyl]-2′-deoxyuridine. *Bioconjugate Chem. 9*, 33−39.

(21) (a) Haralambidis, J., Duncan, L., Angus, K., and Tregear, G. W. (1990) The synthesis of polyamide oligonucleotide conjugate molecules. *Nucleic Acids Res. 18*, 493−499. (b) Asseline, U., and Thuong, N. T. (1990) New solid-phase for automated synthesis of oligonucleotides containing an aminoalkyl linker at their 3′ end. *Tetrahedron Lett. 31*, 81−84. (c) Reed, M. W., Adams, A. D., Nelson, J. S., and Meyer, R. B. (1991) Acridine-derivatized and cholesterol-derivatized solid supports for improved synthesis of 3′-modified oligonucleotides. *Bioconjugate Chem. 2*, 217−225. (d) Petrie, C. R., Reed, M. W., Adams, A. D., and Meyer, R. B. (1992) An Improved Cpg Support For the Synthesis of 3′-Amine-Tailed Oligonucleotides. *Bioconjugate Chem. 3*, 85−87. (e) Thaden, J., and Miller, P. S. (1993) Automated Synthesis of Oligodeoxyribonucleoside Methylphosphonates Having [*N*-(3-Aminoprop-1-yl)-*N*-(2-hydroxyethyl)-2-aminoethyl] Phosphate or Methylphosphonic Acid At the 3′ End Using a Modified Controlled-Pore Glass Support. *Bioconjugate Chem. 4*, 395−401. (f) Nelson, P. S., Frye, R. A., and Liu, E. (1989) Bifunctional oligonucleotide probes synthesized using a novel CPG support are able to detect single base pair mutations. *Nucleic Acids Res. 17*, 7187−7194. (g) Nelson, P. S., Kent, M., and Muthini, S. (1992) Oligonucleotide labeling methods III: direct labeling of oligonucleotides Employing a novel, nonnucleosidic, 2-aminobutyl-1,3-propanediol backbone. *Nucleic Acids Res. 20*, 6253−6259. (h) Hovinen, J., Guzaev, A., Azhayeva, E., Azhayev, A., and Lonnberg, H. (1995) Imidazole tethered oligodeoxyribonucleotides: Synthesis and RNA cleaving activity. *J. Org. Chem. 60*, 2205−2209. (i) Mullah, B., and Andrus, A. (1997) Automated synthesis of double dye-labeled oligonucleotides using tetramethylrhodamine (TAMRA) solid supports. *Tetrahedron Lett. 38*, 5751−5754. (j) Mullah, B., Livak, K., Andrus, A., and Kenney, P. (1998) Efficient synthesis of double dye-labeled oligodeoxyribonucleotide probes and their application in a real time PCR assay. *Nucleic Acids Res. 26*, 1026−1031. (k) McMinn, D. L., Matray, T. J., and Greenberg, M. M. (1997) Efficient solution phase synthesis of oligonucleotide conjugates using protected biopolymers containing 3′-terminal alkylamines. *J. Org. Chem. 62*, 7074−7075. (l) McMinn, D. L., and Greenberg, M. M. (1998) Postsynthetic conjugation of protected oligonucleotides containing 3′-alkylamines. *J. Am. Chem. Soc. 120*, 3289−3294. (m) Kahl, J. D., and Greenberg, M. M. (1999) Solution-phase bioconjugate synthesis using protected oligonucleotides containing 3′-alkyl carboxylic acids. *J. Org. Chem. 64*, 507−510.

(22) Benseler, F., Williams, D., and Eckstein, F. (1992) Synthesis of suitably protected phosphoramidites of 2′-fluoro-2′-deoxyguanosine and 2′-Amino-2′-deoxyguanosine for incorporation into oligoribonucleotides. *Nucleosides Nucleotides 11*, 1333−1351.

BC0155465

MARCH/APRIL 2002
Volume 13, Number 2

© *Copyright 2002 by the American Chemical Society*

Bioconjugate Chemistry

COMMUNICATIONS

Total Analysis and Purification of Cellular Proteins Binding to Cisplatin-Damaged DNA Using Submicron Beads

Takenori Tomohiro,*,† Jun-ichi Sawada,‡ Chika Sawa,‡ Hironori Nakura,‡ Shuhei Yoshida,† Masato Kodaka,† Mamoru Hatakeyama,§ Haruma Kawaguchi,§ Hiroshi Handa,‡ and Hiroaki Okuno†

Institute of Molecular and Cell Biology, National Institute of Advanced Industrial Science and Technology (AIST), Tsukuba, Ibaraki 305-8566, Japan, Faculty of Bioscience and Biotechnology, Tokyo Institute of Technology, Yokohama 226-8501, Japan, and Faculty of Science and Technology, Keio University, Yokohama 223-8522, Japan. Received September 27, 2001

A high-performance affinity purification technique has been developed for cisplatin (CDDP)-damaged DNA binding proteins directly from crude nuclear extracts of HeLaS3 cell using novel submicron beads synthesized by copolymerization of styrene and glycidyl methacrylate (GMA). The beads dramatically decreased both nonspecific protein adsorption on solid surfaces and elution volume and simplified the handling procedure. Preparation of the beads for purification was carried out by immobilization of telomeric repeats, $(TTAGGG)_n$, on the surface after the reaction with CDDP. At least nine proteins clearly showed higher affinity to CDDP−DNA and were identified by amino acid sequence analysis including HMGB (high mobility group), hUBF (human upstream binding factor), and Ku autoantigen, which were previously reported to be components of CDDP-damaged DNA binding proteins.

INTRODUCTION

Cisplatin (*cis*-diamminedichloroplatinum(II), CDDP) has been widely used as a chemotherapeutic agent in several types of cancer including ovarian, testicular, bladder, small-cell lung, cervical, and head and neck carcinomas. One key step in its mechanism is the binding to DNA, which induces transcriptional interruption (*1*, *2*), cell cycle arrest (*3*), DNA repair (*4*), programmed cell death (apoptosis) via phosphorylation of tumor suppressor protein p53 (*5*), etc. The coordination binding of CDDP unwinds and bends the double helical DNA, especially in the case of intrastrand cross-links to G-rich sequences such as GG and AG (*6*). Various anticancer phenomena based on DNA-damage are attributable to the interactions between CDDP−DNA and some cellular proteins such as HMG-domain proteins acting as triggers (*7*, *8*). Though the purification of proteins binding to CDDP−DNA complexes was performed using affinity chromatography on cellulose (*9*), the efficiency was not

* To whom correspondence should be addressed. Phone: +81-298-61-6124. Fax: +81-298-61-6123. E-mail: t.tomohiro@aist.go.jp.
† National Institute of Advanced Industrial Science and Technology (AIST).
‡ Tokyo Institute of Technology.
§ Keio University.

10.1021/bc015560h CCC: $22.00 © 2002 American Chemical Society
Published on Web 03/03/2002

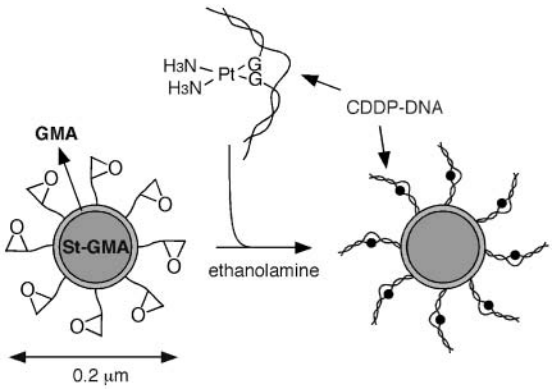


Figure 1. Preparation scheme of CDDP−DNA fixed beads.

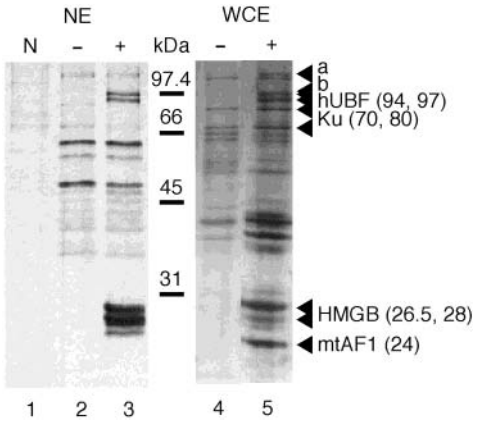


Figure 2. Affinity purification of CDDP−DNA binding proteins by salt elution. +, CDDP−DNA fixed beads; −, DNA fixed beads; N, DNA free beads; lane 1−5, proteins in the first elution from the beads with the buffer containing 1.0 M KCl; lane 1, DNA-free beads using NE; lane 2, DNA-fixed beads using NE; lane 3, CDDP−DNA-fixed beads using NE; lane 4, DNA-fixed beads using WCE; lane 5, CDDP−DNA-fixed beads using WCE. Arrows indicate the proteins that were identified this time.

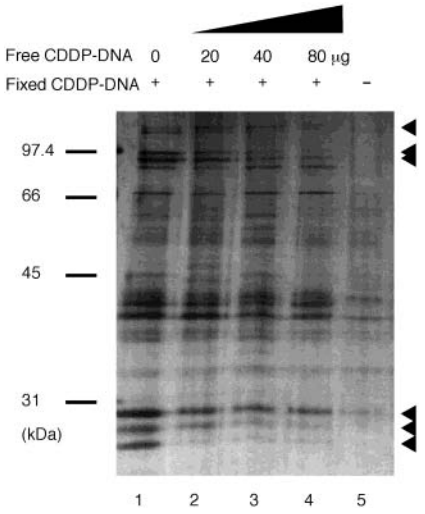


Figure 3. Competition analysis of CDDP−DNA binding proteins. +, CDDP−DNA fixed beads; −, DNA fixed beads; lane 1−5, proteins eluted from CDDP−DNA fixed beads using WCE; lane 1, without competitor (free CDDP−DNA); lane 2−4, including certain amount of competitor; lane 5, using DNA-fixed beads as a control. Arrows indicate the proteins whose amount was changed by addition of free CDDP−DNA as a competitor.

satisfactory because of the low binding ability. To solve this problem, we have developed novel submicron latex beads synthesized by copolymerization of styrene and GMA in a soap-free aqueous solution (*10*), with which drug receptors (*11*) and transcription factors (*12*) were successfully purified with high efficiency. In the present paper, we show for the first time that affinity proteins of CDDP−DNA can be totally analyzed in a very simple way by using whole protein extracts.

The human telomere, a G-rich region as tandem repeats of TTAGGG located at the ends of chromosomes, is important for stabilization of chromosomes, cell aging, and cancer growth (*13*). As the telomere length is known to be shortened by the treatment of CDDP in HeLa cells (*14*, *15*), there is a high possibility that the complex formation of CDDP and telomere is closely related to anticancer activity. Our attention was, therefore, focused on the interaction between the CDDP-telomere and cellular affinity proteins.

RESULTS AND DISCUSSION

Two complementary oligonucleotides, 5′- GGTTAGGGTTAG-3′ and 5′-CCCTAACCCTAA-3′, were chemically synthesized, annealed, 5′-phosphorylated, and ligated to give, on the average, several hundred base pairs of telomeric repeats, followed by gel filtration on Sephadex G-50. The telomeric repeats were reacted with CDDP in 10 mM phosphate buffer in the dark at 37 °C for 1 day according to the ref 15. The platinated DNA showed a gel mobility shift, and the platination reaction was pursued by gel electrophoresis using RI-labeled DNA. The platinum contents were determined by atomic absorption spectroscopy (AA) on a Varian spectrAA-400 spectrophotometer to get the bound drug-to-nucleotide $(D/N)_b$ of 0.079−0.083. A 100 mg amount of the resultant CDDP−DNA complex was reacted with the latex beads through the reaction between the surface epoxy groups and the amino groups of nucleic bases at the extruding ends of the double-strand DNA at 50 °C for 1 day, followed by masking the unreacted epoxy groups with ethanolamine (Figure 1). The yield of CDDP−DNA fixed on the beads (2−3 μg per mg of beads) was calculated from the amount of the unreacted DNA, and those beads showed a minimum amount of nonspecific protein absorption compared with the case of beads with a large amount of DNA on the surface. The DNA-fixed beads without CDDP and the ethanolamine-treated beads without DNA were also prepared as control samples.

Nuclear extracts (NE) and whole cell extracts (WCE) of HeLaS3 cells were prepared according to the methods of Dignam (*16*) and Manley (*17*), respectively. The DNA-fixed beads (2 mg) were suspended in 0.5 mL of NE or WCE including 20 μg of single-strand DNA and 2 μg of poly dI-dC in a 1.5 mL centrifuge tube. After incubation at 0 °C for 1 h, proteins were purified by the salt elution method as follows. The beads were spun down by brief centrifugation and washed three times with 0.1 mL of HEPES buffer containing 20 mM HEPES (pH 7.9), 10% glycerol, 5 mM $MgCl_2$, 0.2 mM EDTA, 0.5 mM dithiothreitol (DTT), and 0.1 M KCl and then washed five times with 0.1 mL of the buffer solution containing 0.4 M KCl. The proteins adsorbed on the beads were eluted three times with 0.1 mL of the buffer solution containing 1.0 M KCl. The proteins in each buffer solution were subjected to electrophoresis by SDS−PAGE, whose separated bands were detected by staining with silver (Figure 2). The affinity of eluted proteins to CDDP−DNA was confirmed by competition experiments in which certain amounts of free CDDP−DNA were added to the protein solution before incubation at 0 °C (Figure 3).

Figure 2 clearly shows the high-performance purification of CDDP−DNA affinity proteins. Compared with CDDP-free DNA beads (lane 2 or lane 4), some bands (especially 26.5, 28, 94, and 97 kDa) were recognized in the eluants from CDDP−DNA beads (lane 3 or lane 5) by silver staining. By using beads without DNA, adsorption of proteins was little observed under these conditions (lane 1). At least nine proteins had higher affinity to CDDP−DNA than to DNA without CDDP. Most of these proteins were identified by amino acid sequence analysis to be HMGB proteins (26.5 and 28 kDa), hUBF (human upstream binding factor, heterodimer of 94 and 97 kDa) proteins, and Ku autoantigen (heterodimer of 70 and 80 kDa), which were reported to interact with both telomeric repeat and CDDP−DNA as a part of DNA-dependent protein kinase (*18*, *19*). We further found mtTF1 (mitochondrial transcription factor 1, 24 kDa) as a new affinity protein and two other proteins whose biological functions are under investigation. Recent papers reported some relationship between telomere and DNA damage by CDDP in telomerase activity (*20*) and p53 dependent apoptosis (*21*), while the telomere is well-known as a transcriptional silent part of the genome.

It should be emphasized that the present technique is exceedingly simple (one-pot purification) and efficient despite using crude whole protein extracts in comparison with the ordinary affinity chromatography on cellulose or agarose that are more laborious procedures. Recently, affinity purification by Sepharose column chromatography was reported for CDDP−DNA (*22*). The new latex beads have the following characteristics superior to the conventional materials. Since the beads can be essentially treated as hard spheres with fairly monodisperse diameter (200 nm on average), chemical and physical reactions are not affected by diffusion-controlled processes inside the beads, which provide a homogeneous environment for binding between DNA and proteins. Subsequent polymerization of GMA after the styrene−GMA copolymerization makes the surface of the beads rather hydrophilic, which significantly reduces nonspecific adsorption of proteins on the beads. Easy removal of proteins from the beads through washing without requiring stringent conditions (e.g., high salt concentration) made it possible to isolate CDDP−DNA affinity proteins with binding constants relatively lower than those of sequence-specific DNA binding proteins. In addition, large surface area per weight (20 m^2 per 1 g) provides sufficient capacity to purify proteins in a milligram scale. Degree of the dilution of eluted proteins depends on the volume of the solution used for elution from the beads. Usually, only 50−100 μL of buffer is used for 1−10 mg of beads. Therefore, a precipitation procedure of the eluted proteins was not necessary to detect them by ordinary staining.

CONCLUSIONS

In the present method, an extensive analysis of binding proteins is generally possible under various conditions even when crude whole protein solutions are used. In addition, this simplified technique for affinity purification may be useful for screening chemical libraries to create new drugs and their receptor library in a short time directly from crude cell extracts.

ACKNOWLEDGMENT

Financial support from the New Energy and Industrial Technology Development Organization (NEDO) is gratefully acknowledged.

LITERATURE CITED

(1) Vichi, P., Coin, F., Renaud, J. P., Vermeulen, W., Hoeijmakers, J. H., Moras, D., and Egly, J. M. (1997) Cisplatin- and UV-damaged DNA lure the basal transcription factor TFIID/TBP. *EMBO J. 16*, 7444−7456.

(2) Zhai, X., Beckmann, H., Jantzen, H. M., and Essigmann, J. M. (1998) Cisplatin-DNA adducts inhibit ribosomal RNA synthesis by hijacking the transcription factor human upstream binding factor. *Biochemistry 37*, 16307−16315.

(3) Agami, R., and Bernards, R. (2000) Distinct initiation and maintenance mechanisms cooperate to induce G1 cell cycle arrest in response to DNA damage. *Cell 102*, 55−66.

(4) Tanaka, H., Arakawa, H., Yamaguchi, T., Shiraishi, K., Fukuda, S., Matsui, K., Takei, Y., and Nakamura, Y. (2000) A ribonucleotide reductase gene involved in a p53-dependent cell-cycle checkpoint for DNA damage. *Nature 404*, 42−49.

(5) Oda, K., Arakawa, H., Tanaka, T., Matsuda, K., Tanikawa, C., Mori, T., Nishimori, H., Tamai, K., Tokino, T., Nakamura, Y., and Taya, Y. (2000) p53AIP1, a Potential mediator of p53-Dependent apoptosis, and its regulation by Ser-46-phosphorylated p53. *Cell 102*, 849−862.

(6) Burstyn, J. N., Heiger-Bernays, W. J., Cohen, S. M., and Lippard, S. J. (2000) Formation of *cis*-diamminedichloroplatinum(II) 1,2-intrastrand cross-links on DNA is flanking-sequence independent. *Nucleic Acids Res. 28*, 4237−4243.

(7) Lippart, B., Ed. (1999) *Cisplatin, Chemistry and Biochemistry of a Leading Anticancer Drug*, Wiley-VCH, New York.

(8) Jamieson, E. R., and Lippard, S. J. (1999) Structure, recognition, and processing of cisplatin−DNA adducts. *Chem. Rev. 99*, 2467−2498.

(9) Hughes, E. N., Engelsberg, B. N., and Billings, P. C. (1992) Purification of nuclear proteins that bind to cisplatin-damaged DNA: identity with high mobility group proteins 1 and 2. *J. Biol. Chem. 267*, 13520−13527.

(10) Wada, T., Watanabe, H., Kawaguchi, H., and Handa, H. (1995) DNA Affinity Chromatography. *Methods Enzymol. 254*, 595−604.

(11) Shimizu, N., Sugimoto, K., Tang, J., Nishi, T., Sato, I., Hiramoto, M., Aizawa, S., Hatakeyama, M., Ohba, R., Hatori, H., Yoshikawa, T., Suzuki, F., Oomori, A., Tanaka, H., Kawaguchi, H., Watanabe, H., and Handa, H. (2000) High-performance affinity beads for identifying drug receptors. *Nature Biotech. 18*, 877−881.

(12) Inomata, Y., Kawaguchi, H., Hiramoto, M., Wada, T., and Handa, H. (1992) Direct purification of multiple ATF/E4TF3 polypeptides from HeLa cell crude nuclear extracts using DNA affinity latex particles. *Anal. Biochem*. 206, 109−114.

(13) Rudolph, K. L., Chang, S., Lee, H. W., Blasco, M., Gottlieb, G. J., Greider, C., and DePinho, R. A. (1999) Longevity, stress response, and cancer in aging telomerase-deficient mice. *Cell 96*, 701−712.

(14) Bodnar, A. G., Ouellette, M., Frolkis, M., Holt, S. E., Chiu, C.-P., Morin, G. B., Harley, C. B., Shay, J. W., Lichtsteiner, S., and Wright, W. E. (1998) Extension of life-span by introduction of telomerase into normal human cells. *Science 279*, 349−352.

(15) Ishibashi, T., and Lippard, S. J. (1998) Telomere loss in cells treated with cisplatin. *Proc. Natl. Acad. Sci. U.S.A. 95*, 4219−4223.

(16) Dignam, J. D., Lebovitz, R. M., and Roeder, R. G. (1983) Accurate transcription initiation by RNA polymerase II in a soluble extract from isolated mammalian nuclei. *Nucleic Acids Res. 11*, 1475−1489.

(17) Manley, J. L., Fire, A., Cano, A., Sharp, P. A., and Gefter, M. L. (1980) DNA-dependent transcription of adenovirus genes in a soluble whole-cell extract. *Proc. Natl. Acad. Sci. U.S.A. 77*, 3855−3859.

(18) Samper, E., Goytisolo, F. A., Slijepcevic, P., van Buul, P. P. W., and Blasco, M. A. (2000) Mammalian Ku86 protein prevents telomeric fusions independently of the length of TTAGGG repeats and the G-strand overhang. *EMBO Rep. 11*, 244−252.

(19) Turchi, J. J., Patrick, S. M., and Henkels, K. M. (1997)

Mechanism of DNA-dependent protein kinase inhibition by *cis*-diamminedichloroplatinum(II)-damaged DNA. *Biochemistry 36*, 7586−7593.
(20) Kiyozuka, Y., Yamamoto, D., Yang, J., Uemura, Y., Senzaki, H., Adachi, S., and Tsubura, A. (2000) Correlation of chemosensitivity to anticancer drugs and telomere length, telomerase activity and telomerase RNA expression in human ovarian cancer cells. *Anticancer Res. 20*, 203-212.
(21) Akeshima, R., Kigawa, J., Takahashi, M., Oishi, T., Kanamori, Y., Itamochi, H., Shimada, M., Kamazawa, S., Sato, S., and Terakawa, N. (2001) Telomerase activity and p53-dependent apoptosis in ovarian cancer cells. *Br. J. Cancer 84*, 1551−1555.
(22) Turchi, J. J., Henkels, K. M., Hermanson, I. L., and Patrick, S. M. (1999) Interactions of mammalian proteins with cisplatin-damaged DNA. *J. Inorg. Biochem. 77*, 83−87.

BC015560H

ARTICLES

Formation of a Bioconjugate Composed of Hemin, Smectite, and Quaternary Ammonium Chloride That Is Soluble and Active in Hydrophobic Media

Masaru Kurosawa, Tetsuji Itoh, Yoh Kodera, Ayako Matsushima, Misao Hiroto, Hiroyuki Nishimura, and Yuji Inada*

Toin Human Science and Technology Center, Department of Biomedical Engineering, Toin University of Yokohama, Kurogane-cho, Aoba-ku, Yokohama 225−8502. Received November 2, 2000; Revised Manuscript Received August 27, 2001

Hemin (Fe^{3+}) was adsorbed onto synthetic smectite (clay mineral) intercalated with a quaternary alkenylammonium compound, dioleyldimethylammonium chloride (DOA), to form a hemin−smectite−DOA conjugate. The hemin−smectite−DOA conjugate was soluble in organic solvents such as benzene and toluene to form a transparent colloidal solution with a light yellow color. Its absorption spectrum in benzene showed two bands, 600 and 568 nm, in the visible region and a sharp Soret band at 400 nm with the molar extinction coefficient of 7.5×10^4 M^{-1} cm^{-1}. The formation of the conjugate of smectite and DOA was confirmed by X-ray diffraction analysis: the basal spacing, *d*(001), of hemin−smectite−DOA conjugate was 19 Å which is an expansion of the interlayer space by 5 Å based upon the basal spacing of smectite of 14 Å. Hemin−smectite−DOA conjugate catalyzed the peroxidase-like reaction in organic solvents using benzoyl peroxide as the hydrogen acceptor and leucocrystal violet as the hydrogen donor. The temperature-dependent peroxidase-like activity of the conjugate was compared with peroxidase activity of horseradish peroxidase. The hemin−smectite−DOA conjugate exhibited higher activity as the temperature was increased from 30 to 70 °C, while horseradish peroxidase activity was reduced as the temperature was increased.

INTRODUCTION

Hemin (Fe^{3+}), a prosthetic group of heme-proteins and enzymes, plays an important role by itself in oxido-reductions such as oxidation of a compound with peroxide. Hemin (Fe^{3+}) liberated from holoenzyme is not soluble in neutral aqueous solution and in organic solvents such as benzene and chloroform. However, hemin (Fe^{3+}) itself has a catalytic potential, and several studies have been performed concerning the peroxidase activity (*1*) and catalase activity (*2*) in aqueous solution. It should be noted that hemin molecules tend to aggregate and dimerize in aqueous solutions (*3*), and its catalytic activity is often decreased through dimerization and polymerization (*4*). There are several ways of avoiding the aggregation and dimer formation of hemin (Fe^{3+}) (*5*), and the utilization of detergents was found to be one of the simple but useful techniques (*6*). On the other hand, hemin (Fe^{3+}) has been seldom used as a catalyst in organic media because it is not soluble in organic media.

Chemical modification of proteins with poly(ethylene glycol) (PEG),[1] a nontoxic, nonimmunogenic, and amphipathic polymer, has been extensively studied for the purpose of applying proteins to biomedical and biotechnological processes (*7*, *8*). In the biotechnology field, PEG-modified hydrolases, which are soluble and active in hydrophobic media, catalyze the reverse reactions of hydrolysis, ester synthesis, and ester exchange reactions (*9*, *10*). Along this line of investigations, Takahashi et al. (*11*) prepared PEG-modified hemin (Fe^{3+}) with peroxidase activity in hydrophobic media.

Recently, we have found a clay mineral, smectite, having a catalytic function as seen in a living body, by binding it with bioactive substances. The heme (Fe^{2+})−smectite conjugate, formed by combining smectite with heme (Fe^{2+}), has similar properties to those of hemoglobin or myoglobin in terms of adsorption and desorption of oxygen and carbon monoxide (*12*). Furthermore, chlorophyll *a*−smectite conjugate, smectite conjugated with chlorophyll *a* in place of heme (Fe^{2+}), has proved to be stable in sunlight and to produce hydrogen gas (*13*).

The present study deals with a conjugate of hemin (Fe^{3+}), smectite, and quaternary ammonium compound, dioleoyldimethylammonium chloride (DOA). The layer of smectite was expanded by conjugating with DOA, and consequently the hemin−smectite−DOA conjugate became soluble in organic solvents such as benzene and toluene to form a transparent colloidal solution. Furthermore, the conjugate had a peroxidase-like activity in hydrophobic media.

EXPERIMENTAL PROCEDURES

General. Hemin (crystalline) and horseradish peroxidase (116 purpurogallin units/mg solid) was purchased

* To whom correspondence should be addressed. Phone: +81-45-974-5060. Fax: +81-45-972-5972.

[1] Abbreviations: DOA, dioleyldimethylammonium chloride; PEG, poly(ethylene glycol).

10.1021/bc000133+ CCC: $22.00 © 2002 American Chemical Society
Published on Web 02/21/2002

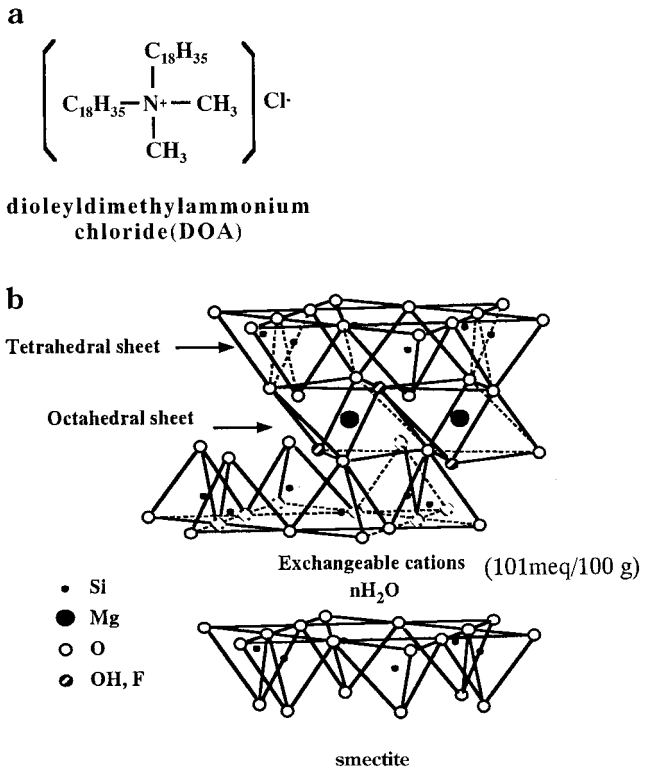


Figure 1. (a) Structure of dioleyldimethylammonium chloride (DOA). (b) The chemical structure of smectite in a crystal state consists of two sheets of linked SiO_4 tetrahedra sandwiching an octahedral cation (Mg) between them, and the interlayer. Elemental composition Si 8.00, Mg 5.65, Li 0.70, Na 1.05; transmittance 95% in 1% aqueous solution at 500 nm; and methylene blue absorption 101 milliequiv per 100 g.

from Sigma Chemical Co. (St. Louis, MO). Dioleoyldimethylammonium chloride (DOA) was kindly provided by Nippon Oil and Fats Co., Ltd. (Tokyo, Japan). Smectite powder (hectorite), which was hydrothermally synthesized by Torii et al. (*14*), was obtained from Co-op Chemical Co., Ltd. (Tokyo, Japan). The chemical structure and property of DOA and smectite were shown in Figure 1. Leucocrystal violet was obtained from Tokyo Kasei Kogyo Co., Ltd. (Tokyo, Japan). Other reagents used were of analytical grade.

Preparation of Hemin−Smectite−DOA Conjugate. The hemin (Fe^{3+})−smectite conjugate was prepared from hemin and smectite by the method of Itoh et al. (*12*). To 36 mL of acetone solution containing hemin (0.9 mg) was added 300 mg of smectite powder. The suspension was shaken for 1 h at 25 °C to establish the adsorption equilibrium between hemin (Fe^{3+}) and smectite. The hemin (Fe^{3+})−smectite conjugate thus formed was collected by centrifugation and was dried under reduced pressure. The amount of hemin (Fe^{3+}) adsorbed onto smectite was spectrophotometrically determined by measuring the absorbance of the supernatant liquid obtained by centrifugation of the sample suspension.

Since smectite[2] has cation-exchange properties of 101 mequiv/100 g of smectite, hemin−smectite conjugate must be bound with quaternary alkenylammonium compound, dioleyldimethylammonium chloride (DOA) (Figure 1a), with ion-exchange reaction. To 20 mL of hemin−smectite conjugate dissolved in water (15 mg/mL) was added 0.68 mL of DOA colloidal solution (70%), and the suspension was then stirred for 7 h at 25 °C to form hemin−smectite−DOA conjugate. The conjugate was collected by centrifugation and was dried under reduced pressure. The absorption spectra of hemin−smectite in water and hemin−smectite−DOA conjugates in organic solvents were measured with a Shimadzu MPS-2000 multipurpose spectrophotometer (Kyoto, Japan). One gram of hemin−smectite−DOA conjugate consists of 2 mg of hemin, 633 mg of smectite, and 365 mg of DOA. X-ray powder diffraction (XRD) analyses were carried out with a Rigaku diffractometer (RTP-300) using monochromatized Cu Kα radiation.

Measurement of Peroxidase Activity of Hemin−Smectite−DOA Conjugate in Organic Solvents. The peroxidase activity of hemin−smectite−DOA conjugate was tested by the modified method of Ajima et al. (*16*). The first series of experiments was conducted by measuring the peroxidase activity of hemin−smectite−DOA conjugate (0−0.32 μM) in an organic solvent, benzene. The reaction system consists of benzoyl peroxide (0−0.66 mM) as a hydrogen acceptor and leucocrystal violet (16.7 mM) as a hydrogen donor. The reaction was carried out for 5 min at 25 °C in the dark. The peroxidase activity of hemin−smectite−DOA conjugate in benzene was spectrophotometrically determined by measuring the amount of oxidized crystal violet using the molar extinction coefficient of $\epsilon_{604\ nm} = 1.2 \times 10^5\ M^{-1}\ cm^{-1}$ (*17*). The second series of experiments was conducted by measuring temperature-dependent peroxidase activity of hemin−smectite−DOA conjugate using benzoyl peroxide and leucocrystal violet as well as horseradish peroxidase using hydrogen peroxide and guaiacol. The peroxidase activity of the conjugate in toluene was spectrophotometrically determined by measuring the absorbance change of oxidized crystal violet at 604 nm/min at temperatures from 30 to 70 °C. As a control experiment, the peroxidase activity of the horseradish peroxidase, instead of hemin−smectite−DOA conjugate, in 0.1 M phosphate buffer (pH 7.4) was determined as follows: the reaction system consisted of horseradish peroxidase in 0.1 M phosphate buffer (pH 7.4), hydrogen peroxide (0.13 mM), and guaiacol (0.28 mM), and its activity was spectrophotometrically determined by measuring the absorbance change of oxidized guaiacol at 460 nm/min at temperatures from 30 to 70 °C.

RESULTS AND DISCUSSION

Absorption Spectra of Hemin−Smectite Conjugate in Water and Hemin−Smectite−DOA Conjugate in Benzene. Hemin, or ferriprotoporphyrin, is practically insoluble in water and in organic solvents except for strong organic bases such as trimethylamine and dimethylaniline. Hemin conjugated with smectite, hemin−smectite conjugate, was soluble in water to form a brownish, transparent colloidal solution. Addition of DOA, quaternary alkenylammonium compound, to hemin−smectite conjugate in water caused the precipitation of hemin−smectite−DOA in which DOA was bound to smectite by a cation-exchange reaction in the interlayer space of hemin−smectite. Then hemin−smectite−DOA conjugate was dissolved in hydrophobic media such as benzene and toluene.

[2] The smectite (hectorite), which was hydrothermally synthesized, had unique physical and chemical properties such as high transparency in water, cation exchange, and the ability to form organic and inorganic interlayer complex (*14*). Expandable phyllosilicates have a structure composed of alternating 2:1 layer, which consists of two sheets of linked SiO_4 tetrahedra sandwiching octahedral cations, Mg, between them (Figure 1 b). The 2:1 layers, which have a net negative charge (layer charge), are loosely tied together by interlayer cations. Water also is present between the layers.

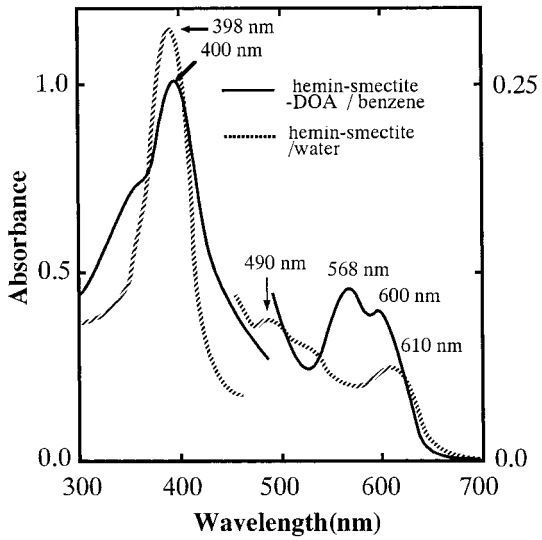


Figure 2. Absorption spectra of hemin–smectite–DOA conjugate and hemin–smectite conjugate. The spectrum of hemin (Fe^{3+})–smectite–DOA conjugate (13 μM) in benzene is shown by a solid line with a sharp Soret band at 400 nm. The spectrum of hemin (Fe^{3+})–smectite conjugate (10 μM) in water is shown by a dotted line with a sharp Soret band at 398 nm.

Figure 2 presents the absorption spectra of hemin–smectite–DOA conjugate in benzene (solid line) and hemin–smectite conjugate in water (dotted line). The absorption spectrum of hemin–smectite–DOA conjugate in benzene has the absorption maxima at 568 nm with a shoulder at 600 nm and Soret band at 400 nm in visible region. The molar extinction coefficient at the Soret band was calculated to be $\epsilon_{400\ nm} = 7.5 \times 10^4\ M^{-1}cm^{-1}$ in benzene (Table 1). On the other hand, the spectrum of hemin–smectite conjugate in water shows two peaks at 610 and 490 nm and the sharp Soret band at 398 nm with $\epsilon_{398\ nm} = 11.6 \times 10^4\ M^{-1}\ cm^{-1}$ in water which is closely in agreement with the molar extinction coefficient of monomeric hematin in water, $12.2 \times 10^4\ M^{-1}\ cm^{-1}$ (*15*). Table 1 summarizes the physicochemical and spectrophotometric properties of hemin–smectite–DOA conjugate together with its compositions. As is clear from the table, the basal spacing of smectite was determined to be 14 Å and that of smectite conjugated with DOA was determined to be 19 Å, indicating an expansion of the interlayer space by 5 Å. Furthermore, the layer of smectite conjugated with hemin was hardly expanded as described above. Therefore, it can be reasonably assumed that hemin is adsorbed onto surface of smectite, and DOA is intercalated in the basal spacing of smectite. Although hemin–smectite conjugate became easily soluble in water to form a transparent colloidal solution with a dark brown color, the conjugate is never soluble in benzene. However, hemin–smectite–DOA conjugate was freely soluble in organic solvents such as benzene and toluene to form a transparent colloidal solution with light yellow color (Figure 2). The solubility of hemin–smectite–DOA conjugate together with its components are shown in Table 1.

Table 1. Physicochemical and Spectrophotometric Properties of Hemin–Smectite–DOA Conjugate Together with Its Compositions

conjugate	*d* (001), Å	Soret band, nm (ϵ_{mM})	solubility[a] water	solubility[a] benzene
DOA[b]	-	-	±	+
hematin	-	398 (122)[c]	±	−
smectite	14	−	+	−
hemin–smectite	14	398 (116)	+	−
hemin–smectite–DOA	19	400 (75)	−	+

[a] +, −, ±: transparent colloidal solution, insoluble, and sparingly soluble, respectively. [b] Dioleyldimethylammonium chloride. [c] Monomeric hematin (*15*).

Peroxidase Activity of Hemin–Smectite–DOA Conjugate in Hydrophobic Media. The finding shown above leads to the study on the peroxidase activity induced by hemin–smectite–DOA conjugate in organic solvents. The first series of experiments was conducted with oxidation of leucocrystal violet (AH) by benzoyl peroxide in the presence of hemin–smectite–DOA conjugate in benzene as shown below (Scheme 1).

Scheme 1

$$\text{Peroxide} + 2\text{AH} \xrightarrow[\text{hemin-smectite-DOA conjugate}]{\text{in benzene}} \text{Reduced peroxide} + 2\text{A}$$

Figure 3a shows the oxidation of leucocrystal violet (AH) with benzoyl peroxide by the catalytic action of hemin–smectite–DOA conjugate with various concentrations (0–0.32 μM) in benzene. The oxidation of leuco-

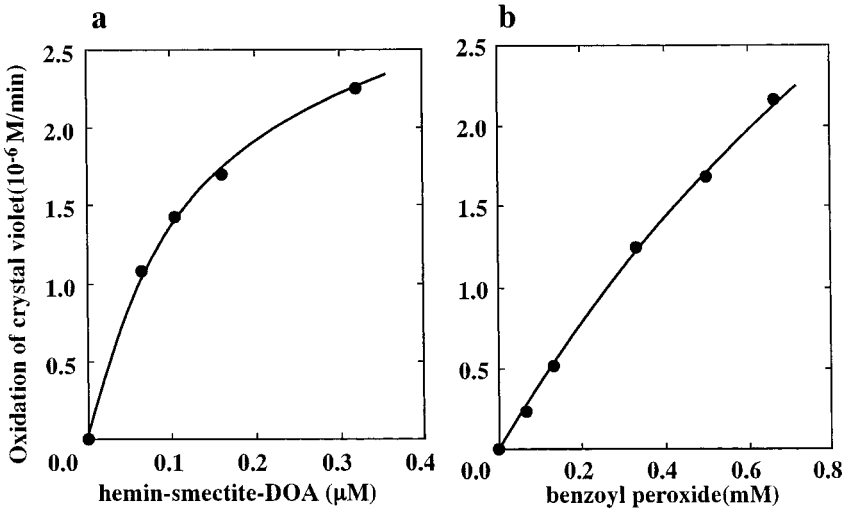


Figure 3. (a) Oxidation of leucocrystal violet (16.7 mM) with benzoyl peroxide (0.66 mM) in benzene by the catalytic action of hemin–smectite–DOA conjugate with various concentrations (0–0.32 μM). (b) Oxidation of leucocrystal violet (16.7 mM) with benzoyl peroxide (0–0.66 mM) in benzene by the catalytic action of hemin–smectite–DOA conjugate (0.32 μM) at 25 °C.

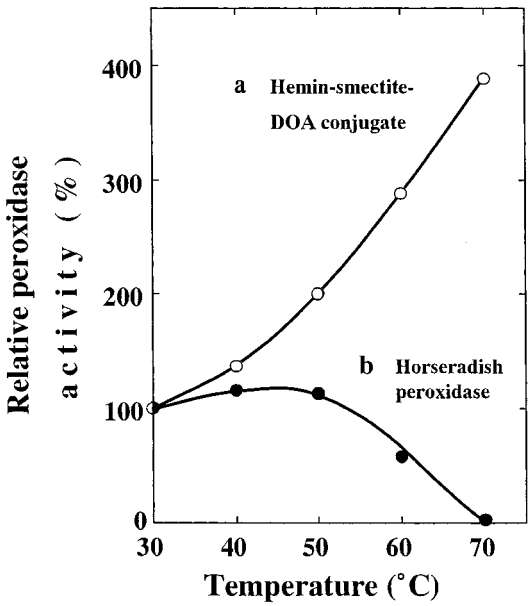


Figure 4. Temperature-dependent peroxidase activity of hemin−smectite−DOA conjugate in hydrophobic media (toluene) and of horseradish peroxidase in hydrophilic media [0.1 M phosphate buffer (pH 7.4)]. Curve a: Oxidation of leucocrystal violet (16.7 mM) with benzoyl peroxide (0.66 mM) by hemin−smectite−DOA conjugate (0.32 μM). Curve b: Oxidation of guaiacol (0.28 mM) with hydrogen peroxide (0.13 mM) by horseradish peroxidase (0.26 purpurogallin units).

crystal violet was linearly enhanced by increasing the amount of the conjugate in the reaction system. No reaction took place in the absence of the conjugate. The similar line of study was conducted by changing the benzoyl peroxide concentration. Figure 3b shows the oxidation of leucocrystal violet by the catalytic action of hemin−smectite−DOA conjugate (0.32 μM) in the presence of benzoyl peroxide (0−0.66 mM) in benzene. Crystal violet in the reduced form was linearly oxidized by the enhancement of benzoyl peroxide concentration in benzene. From the results obtained above, it can be concluded that hemin−smectite−DOA conjugate has peroxidase activity in an organic solvent.

Heat stability of peroxidase activity was tested for hemin−smectite−DOA conjugate and horseradish peroxidase at the temperature range from 30 to 70 °C. Although the absolute activity of horseradish peroxidase is much higher than that of the conjugate at 30 °C, these activities at 30 °C are regarded as 100%. Figure 4 shows the temperature-dependent activity curves of the conjugate and horseradish peroxidase. The peroxidase-like activity of the conjugate is enhanced by increasing the temperature (curve a). On the other hand, the enzymic activity of horseradish peroxidase is lowered by increasing temperature and is completely lost at 70 °C, due to the protein denaturation (curve b). From the result obtained above, the hemin−smectite−DOA conjugate may be available to be catalyst in hydrophobic media at high temperature.

A similar line of studies has been successfully carried out with the conjugate of chlorophyll adsorbed onto clay minerals such as bentonite and smectite which are closely associated with the development of the photochemical function of chlorophylls (*13, 18−20*). Chlorophyll−smectite conjugate becomes soluble in aqueous solution, although chlorophylls are never soluble in water. chlorophyll−poly(vinylpyrrolidone)−smectite conjugate with the absorption maximum at 677 nm was extensively photostable and catalyzed hydrogen gas evolution by the illumination of visible light in aqueous solution.

Along this line of investigations, the organic insolubility of hemin becomes soluble by conjugating with smectite and DOA, and the conjugate exerts peroxidase-like activity in organic media as well.

ACKNOWLEDGMENT

The authors are grateful to Dr. Toshi Tsuzuki and Dr. Hiroaki Kaji, and to Showa Denko K.K. for his basic and technical advice in the X-ray powder diffraction (XRD) analyses.

LITERATURE CITED

(1) Tohjo, M., Nakamura, Y., Kurihara, K., Samejima, T., Hachimori, Y., and Shibata, K. (1962) Peroxidase activity of hemoproteins. IV. Hematin complexes as model enzymes of peroxidase. *Arch. Biochem. Biophys. 99*, 222−240.

(2) Brown, S. B., Dean, T. C., and Jones, P. (1970) Catalytic activity of iron(III)-centred catalysts. Role of dimerization in the catalytic action of ferrihaems. *Biochem. J. 117*, 741−744.

(3) Brown, S. B., Dean, T. C., and Jones, P. (1970) Aggregation of ferrihaems. Dimerization and protolytic equilibria of protoferrihaem and deuterioferrihaem in aqueous solution. *Biochem. J. 117*, 733−739.

(4) Jones, P., Robson, T., and Brown, S. B. (1973) The catalase activity of ferrihaems. *Biochem. J. 135*, 353−359.

(5) Dunford, H. B., and Stillman, J. S. (1976) On the function and mechanism of action of peroxidases. *Coord. Chem. Rev. 19*, 187−251.

(6) Simplicio, J. (1972) Hemin monomers in micellar sodium lauryl sulfate. A spectral and equilibrium study with cyanide. *Biochemistry 11*, 2525−2528.

(7) Kodera, Y., Matsushima, A., Hiroto, M., Nishimura, H., Ishii, A., Ueno, T., and Inada, Y. (1998) Pegylation of proteins and bioactive substances for medical and technical applications. *Prog. Polym. Sci. 23*, 1233−1271.

(8) Inada, Y., Yoshimoto, T., Matsushima, A., and Saito, Y. (1986) Engineering physicochemical and biological properties of proteins by chemical modification. *Trends Biotechnol. 4*, 68−73.

(9) Inada, Y., Nishimura, H., Takahashi, K., Yoshimoto, T., Saha, A. R., and Saito, Y. (1984) Ester synthesis catalyzed by poly(ethylene glycol)-modified lipase in benzene. *Biochem. Biophys. Res. Commun. 122*, 845−850.

(10) Matsushima, A., Kodera, Y., Hiroto, M., Nishimura, H., and Inada, Y. (1996) Bioconjugates of proteins and poly(ethylene glycol): potent tools in biotechnological processes. *J. Mol. Catal. B: Enzym. 2*, 1−17.

(11) Takahashi, K., Matsushima, A., Saito, Y., and Inada, Y. (1986) Poly(ethylene glycol)-modified hemin having peroxidase activity in organic solvents. *Biochem. Biophys. Res. Commun. 138*, 283−288.

(12) Itoh, T., Yamada, T., Kodera, Y., Matsushima, A., Hiroto, M., Sakurai, K., Nishimura, H., and Inada, Y. (2001) Hemin (Fe^{3+})- and heme (Fe^{2+})-smectite conjugates as a model of hemoprotein based on spectrophotometry. *Bioconjugate Chem. 12*, 3−6.

(13) Itoh, T., Ishii, A., Kodera, Y., Matsushima, A., Hiroto, M., Nishimura, H., Tsuzuki, T., Kamachi, T., Okura, I., and Inada, Y. (1998) Photostable chlorophyll *a* conjugated with poly(vinylpyrrolidone)−smectite catalyzes photoreduction and hydrogen gas evolution by visible light. *Bioconjugate Chem. 9*, 409−412.

(14) Torii, K., and Iwasaki, T. (1987) Synthesis of hectorite. *Clay Sci. 6*, 1−16.

(15) Inada, Y., and Shibata, K. (1962) The Soret band of monomeric hematin and its changes on polymerization. *Biochem. Biophys. Res. Commun. 9*, 323−327.

(16) Ajima, A., Cao, S. G., Takahashi, K., Matsushima, A., Saito, Y., and Inada Y. (1987) An attempt to determine lipid

peroxides with poly(ethylene glycol)-modified hemin. *Biotech. Appl. Biochem. 9*, 53−57.
(17) Herz, M. L., Feldman, D., and Healy E. M. (1976) Reaction of substituted malachite green cations with cyanide ion. *J. Org. Chem. 41*, 221−225.
(18) Ishii, A., Itoh, T., Kageyama, H., Mizoguchi, T., Kodera, Y., Matsushima, A., Torii, K., and Inada, Y. (1995) Photostabilization of chlorophyll *a* adsorbed onto smectite. *Dyes Pigments 28*, 77−82.
(19) Kodera, Y., Kageyama, H., Sekine, H., and Inada, Y. (1992) Photostable chlorophylls conjugated with montmorillonite. *Biotechnol. Lett. 14*, 119−122.
(20) Ishii, A., Itoh, T., Kodera, Y., Matsushima, A., Hiroto, M., Nishimura, H., and Inada, Y. (1997) Photostable chlorophyll *a*-bentonite conjugate exhibits high photosensitive activity. *Res. Chem. Intermed. 23*, 683−689.

BC000133+

Electrochemical Detection of Gene Expression in Tumor Samples: Overexpression of Rak Nuclear Tyrosine Kinase

Paul M. Armistead and H. Holden Thorp*

Department of Chemistry and Lineberger Comprehensive Cancer Center, University of North Carolina at Chapel Hill, Chapel Hill, North Carolina 27599-3290. Received December 13, 2000; Revised Manuscript Received March 2, 2001

Absolute quantification of Rak nuclear tyrosine kinase mRNA in breast tissue samples was determined by competitive RT-PCR. The total RNA from the same samples was also chemically amplified through conventional RT-PCR, and the relative amounts of these amplified RT-PCR products were determined by adsorption onto an indium tin oxide (ITO) electrode followed by electrochemical detection. The electrochemical detection was performed using the inorganic metal complex $Ru(bpy)_3^{2+}$ (bpy = 2,2′ bipyridine) to catalyze the oxidation of the guanine residues of the immobilized RT-PCR products. Using the competitive RT-PCR values as standards, it was found that an optimized conventional RT-PCR coupled with electrochemical detection provides a simple method for measuring relative gene expression among a series of mRNA samples from breast tumors. The use of electrochemical detection potentially eliminates the need for gel electrophoresis and fluorescent or radioactive labels in detecting the target genes.

Abnormalities in the expression of specific genes have been linked to a large and increasing number of diseases (*1*−*7*). The identification of overexpressed genes provides a promising framework for identifying diagnostics as well as protein or small molecule drugs; this approach has been particularly successful in studies of HER2-neu in breast cancer (*8*−*10*). Several methods are currently available to quantify mRNA expression in biological samples; these methods typically provide semiquantitative information in some whole genome expression assays and absolute quantification in some single gene assays (*11*−*16*). Easily automated methods for detecting relative gene expression would allow for routine use of gene expression in diagnostics and drug discovery (*17*, *18*).

Our laboratory has developed a method for detecting trace nucleic acids based on electrocatalysis with cyclic voltammetric detection (*19*−*21*). In these experiments, DNA molecules are adsorbed onto indium tin oxide (ITO) electrodes with a surface area of 12.6 mm^2, placed in an electrochemical cell containing 10 μM of the electron-transfer mediator $Ru(bpy)_3^{2+}$ (bpy = 2,2′-bipyridine), and detected via catalytic oxidation of the guanine base according to the following reactions (*22*):

$$Ru(bpy)_3^{2+} \rightarrow Ru(bpy)_3^{3+} + e^- \quad (1)$$

$$Ru(bpy)_3^{3+} + \text{guanine} \rightarrow Ru(bpy)_3^{2+} + \text{guanine}^+ \quad (2)$$

The resulting cyclic voltammmogram shows a dramatic enhancement in the $Ru(bpy)_3^{2+}$ oxidation wave as the generated $Ru(bpy)_3^{3+}$ is recycled to $Ru(bpy)_3^{2+}$ by electrons from the guanine bases. Experiments with model PCR products showed that the sensitivity of this system was 44 amol/mm^2 of electrode area, which translates to a detection limit for the 12.6 mm^2 electrodes of roughly 550 amol (*23*). A number of other electrochemical techniques are under development, and the advantages of electrochemical approaches have been discussed in detail (*24*−*29*). In this application, the electrochemical technique can be used to replace gel electrophoresis performed following the RT-PCR protocol. The electrochemical technique could ultimately be performed in a miniaturized electrode array for analysis in high throughput without fluorescent or radioactive labels.

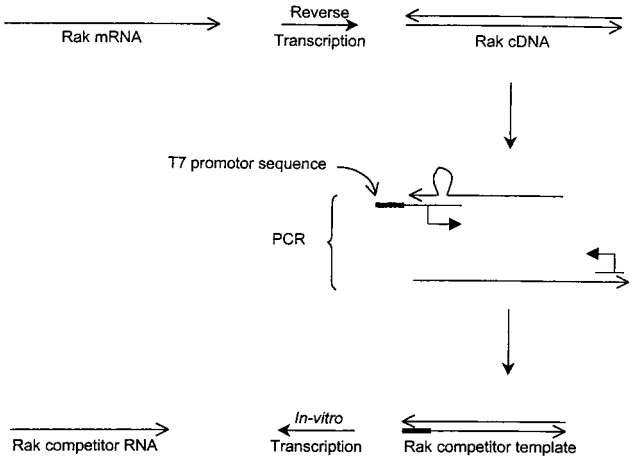
We report here that our electrochemical technique can be used to determine the mRNA expression level of Rak nuclear tyrosine kinase in a series of breast tissue samples. Rak (also called Frk) is a distant relative in the Src family of tyrosine kinases and is overexpressed in roughly 30% of human epithelial (breast and colon) cancers (*30*). The absolute quantity of Rak mRNA measured by competitive RT-PCR (*14*) ranged from 440 to 2300 zmol/μg of total RNA in breast tissues, which are typical values for the mRNA of signaling molecules (*16*). The same samples were analyzed by conventional RT-PCR with electrochemical detection (*23*), and a strong correlation was observed between the electrochemical current and the absolute quantity of mRNA determined by competitive RT-PCR.

EXPERIMENTAL SECTION

Materials and Reagents. All oligonucleotides were synthesized at the Lineberger Comprehensive Cancer Center Nucleic Acid Core Facility at the University of North Carolina at Chapel Hill. Tissue Samples were from the Tissue Procurement Facility at UNC-CH. Of the seven tissue samples studied, sample 35A was normal tissue, sample 54B was a primary tumor with no signs of invasion through the basal lamina, and the others were invasive breast tumors. Sample 35B was an invasive breast tumor from the same patient as sample 35A. BT-474 cells were a gift from the lab of Dr. Bill Cance. All water used was in-house distilled water that was further purified on a Milli-Q water purification system. Water for use in RNA manipulations was further treated with diethyl pyrocarbonate, DEPC, (Sigma, St. Louis, MO). *N*,*N*-Dimethyl formamide, sodium phosphate, sodium acetate, and sodium chloride were from Mallinckrodt

10.1021/bc000129y CCC: $22.00 © 2002 American Chemical Society
Published on Web 02/06/2002

Scheme 1



(Paris, KY). $Ru(bpy)_3Cl_2$ was purchased from Aldrich (Milwaukee, WI) and purified by recrystallization from acetonitrile. ITO electrodes were purchased from Delta Technologies (Stillwater, MN). Total RNA from both cell culture and tissue samples was purified on Qiagen RNeasy columns according to the manufacturer's directions. All electrochemical measurements were performed in a one-compartment cell on an Princeton Applied Research (Princeton, NJ) model 273A potentiostat that was controlled by a Pentium computer. An Ag/AgCl reference electrode was used (Cypress Systems, Lawrence, KS), and a platinum wire was used as the auxiliary electrode. Fluorescent staining of DNA in agarose was performed using SYBR-green (Molecular Probes, Eugene, OR). Fluorescently stained gels were scanned on a Molecular Dynamics (San Jose, CA) Storm 860 phosphorimager using the blue fluorescence mode. Scanned gels were analyzed using ImageQuaNT software.

Competitive RT-PCR. Synthesis of an appropriate Rak mRNA competitor followed the strategy outlined in Scheme 1 (*15*). A Rak RT-PCR product was produced that contained the T7 promoter sequence as well as a "loop-out" region. The reverse transcription was carried out as follows. A 14-μL reaction mix consisting of 1 μg of total BT-474 RNA, 714 μM dNTPs (Amersham), and 0.4 μg/μL random hexamers (Life Technologies) was prepared. The mix was heated to 75 °C for 3 min and immediately cooled on ice. To the mix was added 4 μL of 5× buffer (Life Technologies), 1 μL of RNasin (Promega), and 1 μL (200 U) of M-MLV reverse transcriptase (Life Technologies). The reaction was allowed to proceed for 1 h at 42 °C and then stopped by heating the mix to 90 °C for 10 min.

A 50-μL PCR was made that contained 5 μL of the reverse transcription mix in 1× buffer, 2.5 mM $MgCl_2$, 125 μM dNTPs, 250 nM forward primer (TAA TAC GAC TCA CTC TAG GGC CTA TCT GGA GTC TCG GAA GCA GAT TTT GGA CTT GCC AGA), 250 nM reverse primer (GGG CAC CTG TCA TAC CAC TGT), and 1 U Taq polymerase (Life Technologies). The reaction was performed with 1 cycle of 95 °C for 5 min followed by 30 cycles of 94 °C for 20 s, 62 °C for 30 s, 72 °C for 40 s, and 1 cycle 72 °C for 5 min. The purity of the product was determined by agarose gel electrophoresis. The gel revealed a single band at the appropriate size (250 bp). The PCR product was purified on Qiagen Qiaquick PCR purification columns.

In vitro transcription was performed by assembling a 20-μL reaction mix that contained 40 mM Tris (pH = 7.5), 10 mM $MgCl_2$, 10 mM DTT, 8 mM NTPs, 50 μg/mL BSA, 170 nM PCR template, and 1× T7 polymerase that was a gift from the lab of Dr. Kevin Weeks. The reaction was allowed to proceed for 7 h at 37 °C. Following the reaction, 1 μL of DNase (Ambion) was added to the reaction and allowed to incubate for 30 min. To the reaction, were added 15 μL of 5 M ammonium acetate, 15 μL of 100 mM sodium EDTA, and 100 μL of DEPC water. The reaction was extracted with acid phenol/chloroform/isoamyl alcohol. The organic phase was back-extracted with 50 μL of DEPC water. The 200 μL of aqueous mix was precipitated with ice cold 2-propanol overnight. The RNA pellet was resuspended in TE buffer and run on a 4% denaturing polyacrylamide gel. The transcription products were visualized by UV shadowing, and the single visible product was cut from the gel using a clean razor blade. The gel fragment was placed into 300 μL of eluting solution containing 500 mM ammonium acetate, 1 mM EDTA, and 0.2% SDS (Ambion). The gel slice was kept in the solution overnight at 4 °C. The eluting solution was transferred from the gel slice, and the eluted RNA was ethanol precipitated overnight revealing a glassy pellet. The pellet was resuspended in TE buffer. The amount of product, 1.8 μg (23 pmol), was determined by UV−vis spectroscopy at 260 nm.

Competitive RT-PCR was performed by preparing 6 reverse transcription mixes for each tissue sample. A 15-μL reaction mix was prepared that contained 0.5 μg of total RNA, a known quantity of the competitor (either 31.3, 62.5, 125, 250, 500, or 1000 zmol), 667 μM dNTPs, and 667 nM reverse primer. The mixes were heated and cooled on ice as described above. To each mix was added 4 μL of 5× buffer and 1 μL (200 U) of M-MLV reverse transcriptase. The reverse transcription and PCR were performed as described above except a different forward primer (GGC CTA TCT GGA GTC TCG GAA) was used. Each reaction mix was run on a 2% agarose gel and stained with SYBR-Green for 20 min. Staining with SYBR-Green was performed after the electrophoresis to minimize measurement errors due to dye migration in the gel. The stained gel was scanned with a Molecular Dynamics Storm 860 phosphorimager in the blue fluorescence mode. The band intensities resulting from both the native Rak mRNA amplification (296 bp) and the competitor RNA amplification (232 bp) were measured, and background fluorescence was subtracted. For each tissue sample, the logarithm of the competitor signal/native signal in each mix was plotted vs the logarithm of the amount of competitor added for each mix. The best linear fit was calculated, and the antilogarithm of x at $y = 0$ was calculated. This value yielded the absolute quantity of Rak mRNA in the tissue sample.

Conventional RT-PCR Amplification of Rak. RT-PCR of Rak was performed on all tissue samples in parallel, except sample 55B, which did not yield enough RNA. Six reverse transcription reactions were assembled (1 for each sample). Each 15-μL reaction contained 0.5 μg of total RNA, 0.4 μg/μL random hexamers, and 667 μM dNTPs. The random hexamers and dNTPs were originally pooled into a master mix and then pipetted into each individual reverse transcription mix. The mixes were heated and cooled as described above. Four microliters of 5× buffer and 1 μL (200 U) of M-MLV were added. These reagents were premixed to ensure that equivalent amounts of enzyme were added to each reverse transcription reaction. The reactions were again performed at 42 °C for 1 h and were stopped by heating to 90 °C for 10 min.

PCR was assembled for each tissue sample as a 100-μL solution that contained 10 μL of reverse transcription

mix, 1× buffer, 2.5 mM $MgCl_2$, 125 μM dNTPs, 250 nM forward primer (GGC CTA TCT GGA GTC TCG GAA), 250 nM reverse primer (GGG CAC CTG TCA TAC CAC TGT), and 2 U Taq polymerase. The reagents were premixed except the reverse transcription mix. Ninety microliters of the master mix was added to 10 μL of the reverse transcription mix. This step again ensured that equivalent amounts of Taq were added to each reaction. The reaction proceeded as follows: 1 cycle of 95 °C for 5 min followed by 28 cycles of 94 °C for 20 s, 62 °C for 30s, 72 °C for 40 s, and 1 cycle 72 °C for 5 min. Five microliters of each product were analyzed by agarose gel electrophoresis.

Purification of Rak RT-PCR Products. After RT-PCR, 90 μL of each PCR were purified on Qiagen Qiaquick PCR purification columns. The purification was performed according to the manufacturer's instructions, except for the final elution step. At this step, each column was treated with 30 μL of 10 mM sodium acetate pH = 8.0 (pH raised by addition of sodium hydroxide). The columns were allowed to sit for one minute and were then centrifuged at 14 000 rpm for 2 min. Again, 5 μL of each product was analyzed by agarose gel electrophoresis. The pre- and post-purification gels were used to confirm that the relative amounts of RT-PCR among samples did not change significantly after purification.

Electrochemical Detection of Rak RT-PCR Products. ITO electrodes were cleaned using the protocol of Willit and Bowden (*31*). The electrodes were cleaned by sonication in 2-propanol for 15 min, and twice in Milli-Q water each time for 15 min. The electrodes were air-dried. For each electrode, 5 μL of purified PCR product were added to 45 μL of DMF. The DMF mixtures were pipetted onto the electrodes, which were placed in a constant humidity chamber for 30 min (*23*). The electrodes were then washed in Milli-Q water for 3 min on a rotary mixer and allowed to air-dry.

The DNA modified electrodes were placed in a one-compartment electrochemical cell. The cell contained 150 μL of 10 μM $Ru(bpy)_3^{2+}$ in 50 mM sodium phosphate buffer at pH = 7.0. Electrochemical detection was performed using cyclic voltammetry at a scan rate of 10 V s^{-1}. The potential range was 0−1300 mV. All measurements were made relative to an Ag/AgCl reference electrode. Because of the large charging currents generated at this fast scan rate, background subtraction was performed. The background scans were taken with no $Ru(bpy)_3^{2+}$ at ITO electrodes that had been treated with a 9:1 DMF/sodium acetate solution (without DNA) and washed as above. The background electrodes were placed in the same electrochemical cell, and cyclic voltammetry was performed only in the presence of 50 mM sodium phosphate. Immobilized DNA was quantitated by comparison of catalytic currents for DNA-modified electrodes scanned with $Ru(bpy)_3^{2+}$ compared to the currents obtained for $Ru(bpy)_3^{2+}$ only on electrodes not modified with DNA.

RESULTS AND DISCUSSION

Absolute Quantification of Rak mRNA in Breast Tissue Samples. Competitive RT-PCR was performed on the seven breast tissue samples and BT-474 cells following a procedure adapted from published protocols (*14*). A typical agarose gel of a competitive RT-PCR is shown in Figure 1 (top). Quantities of amplified material and internal standard were determined by fluorescence and plotted as in Figure 1 (bottom). The linear fits from all of the analyses had an average R-value of 0.99 ± 0.01

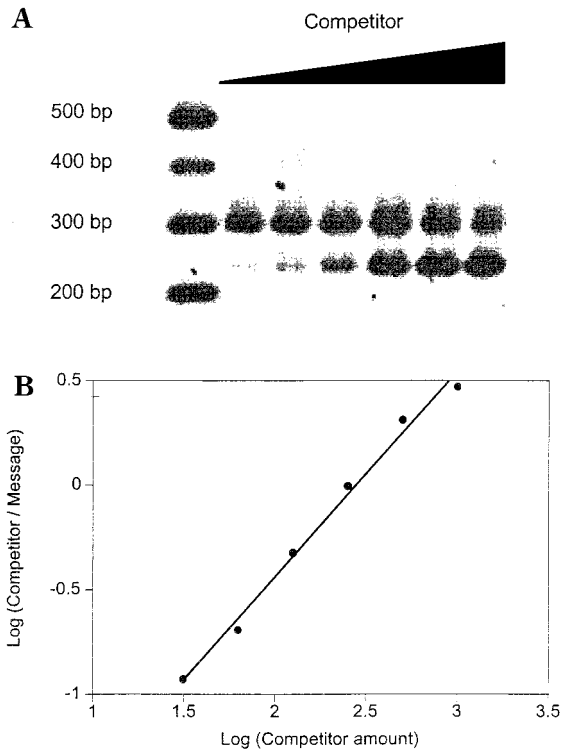


Figure 1. Results of competitive RT-PCR for sample 35B. (A) Agarose gel showing that as the amount of competitor added to each reaction is increased, the ratio of the amount of native RT-PCR product (296 bp) decreases relative to the amount of competitor RT-PCR product (232 bp). (B) The logarithm of the band intensity ratio versus the logarithm of the quantity of competitor.

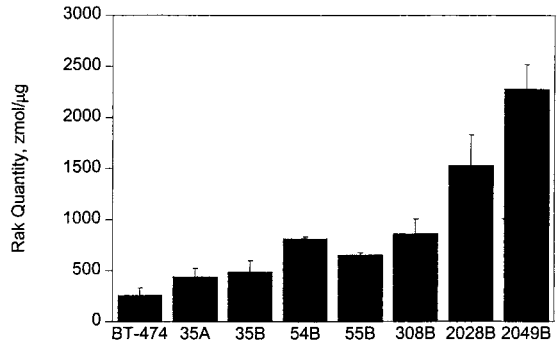


Figure 2. Quantity of Rak mRNA from competitive RT-PCR given as zmol of Rak mRNA per μg of total RNA for the specified sample. Quantities determined for each sample as in Figure 1.

and an average slope of 0.98 ± 0.14. Observation of slopes near unity indicates that the standard RNA is behaving as a proper competitor (*32*).

The competitive RT-PCR results for the seven breast tissues and BT-474 cells are shown in Figure 2. Rak mRNA expression ranged from 440 zmol/μg of total RNA in normal breast tissue (sample 35A) to 2300 zmol/μg of total RNA in sample 2049B. A greater than 2-fold increase in expression (compared to normal sample 35A) was observed in two of the six breast cancer samples, which is consistent with the finding of Cance et al. that Rak is overexpressed in roughly 30% of breast tumors (*30*). The six samples examined here were for the purposes of demonstrating the electrochemical method and not meant to reflect a statistically relevant population; nevertheless, the determined quantities and trends are entirely consistent with the biological expectations. While Rak overexpression is clearly evident, it should be

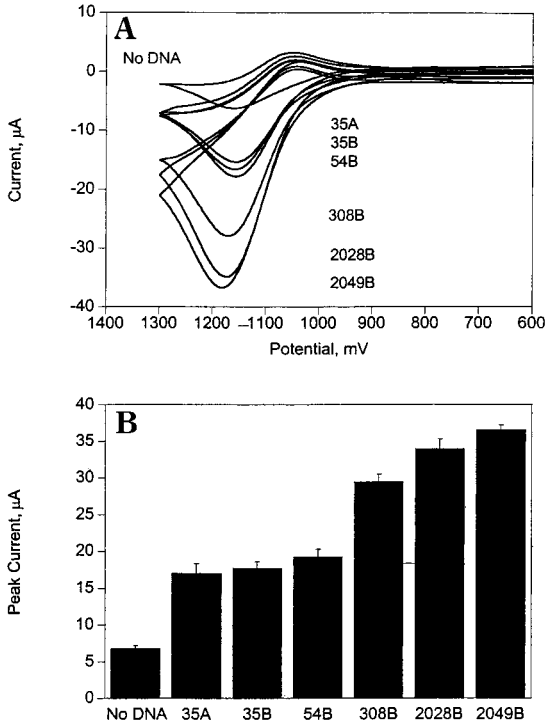


Figure 3. (A) Cyclic voltammograms for ITO electrodes with no DNA or modified with the RT-PCR products from six breast tissue samples at a scan rate of 10 V/s with 10 μM $Ru(bpy)_3^{2+}$ in 50 mM phosphate buffer (pH 7). (B) Peak current for each sample.

noted that the magnitude of overexpression is relatively mild, expecially when compared to other oncogenes such as HER-2, which can vary in expression over 3 orders of magnitude (*16*, *33*).

Electrochemical Quantification of Rak RT-PCR Products. For electrochemical analysis, conventional RT-PCR was performed on each tissue sample, and the resulting PCR reactions were purified to remove the unreacted nucleotides and pyrophosphate, which inhibit adsorption of the DNA onto the electrode (*23*). Agarose gel electrophoresis was performed on all of the samples both before and after the purification step to ensure that purification did not affect the relative quantities of the Rak PCR products. After purification, the PCR products were adsorbed to the electrodes using a procedure similar to that we have published previously (*23*).

Electrochemical detection of the Rak RT-PCR products was performed by cyclic voltammetry in the presence of $Ru(bpy)_3^{2+}$. We have shown previously that the peak currents obtained by this method increase with increasing amounts of adsorbed PCR product (*23*). We have also determined previously that a scan rate of 10 V/s and a 10 μM concentration of $Ru(bpy)_3^{2+}$ provide the optimal sensitivity (*23*). Here we apply this method to clinical samples for the first time. Representative cyclic voltammograms of $Ru(bpy)_3^{2+}$ at unmodified electrodes (no DNA) and at ITO electrodes modified with the Rak RT-PCR products from the breast tissue samples are shown in Figure 3 along with a bar graph giving the peak currents and associated errors.

Figure 4 shows the correlation between the peak currents determined by cyclic voltammetry and the absolute quantity of mRNA applied to the electrode determined by competitive RT-PCR. A good correlation is observed between the expression level and the electrochemical signal. The signal appears to maximize somewhat for the higher expression levels. We have

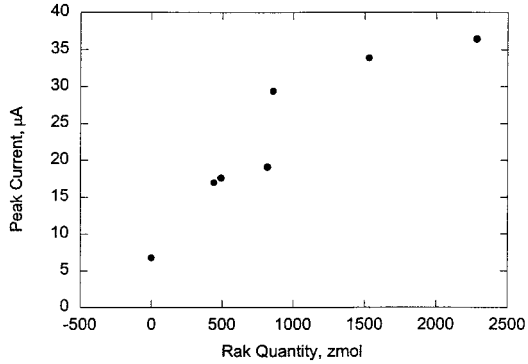


Figure 4. Plot of the absolute quantity of Rak mRNA in the series of breast tumor samples (Figure 2) versus the peak current from the corresponding cyclic voltammograms (Figure 3). Note that the error bars for each axis are given in Figures 2 and 3.

shown previously that the electrochemical method exhibits a high dynamic range for PCR amplicons applied to electrodes and directly quantitated by radiolabeling (*23*); quantities of immobilized PCR products spanning 2 orders of magnitude give distinct electrochemical signals. Thus, the saturation in Figure 4 at high copy numbers is likely due to the reduced dynamic range of the conventional RT-PCR compared to that of competitive RT-PCR (*14*) and not to a lower dynamic range of the electrochemical method as compared to fluorescence detection. The accuracy of the electrochemical method is therefore more than sufficient to distinguish changes in the quantities of conventional RT-PCR products. In particular, the two samples indicating overexpression (2028B and 2049B) were identified using both methods.

CONCLUSIONS

Rak mRNA is expressed in the range of 100−2300 zmol/μg of total RNA in seven breast tissue samples and BT-474 cells as determined by competitive RT-PCR. In this group, 2 of 6 breast tumors expressed Rak at a level more than twice that of normal breast tissue (sample 35A). This result supports the findings of Cance and Liu that Rak is overexpressed in roughly 30% of all invasive breast tumors (*30*). A semiquantitative conventional RT-PCR approach coupled with electrochemical detection led to similar Rak expression data. The two breast tumors with the highest absolute Rak mRNA quantity also gave the largest electrochemical signals (which were also 2× greater than the electrochemical signal from sample 35A). The magnitude of the differences in expression from sample to sample was diminished in the conventional RT-PCR versus the competitive RT-PCR measurements, probably as a result of the reduced dynamic range of the conventional method. Catalytic electrochemical detection of RT-PCR products offers a rapid method for determining the relative amount of a specific mRNA in a series of biological samples. The adsorption of DNA to the ITO electrodes is complete in 30 min, and performing the cyclic voltammogram takes less than 1 s.

LITERATURE CITED

(1) Andreelli, F., Laville, M., Ducluzeau, P. H., Vega, N., Vallier, P., Khalfallah, Y., Riou, J. P., and Vidal, H. (1999) Defective regulation of phosphatidylinositol-3-kinase gene expression in skeletal muscle and adipose tissue of noninsulin-dependent diabetes mellitus patients. *Diabetologia 42*, 358−364.

(2) Callahan, L. M., Vaules, W. A., and Coleman, P. D. (1999) Quantitative decrease in syaptophysin message expression and increase in cathepsin D message expression in Alzheimer

disease neurons containing neurofibrillary tangles. *J. Neuropath. Exp. Neurol. 58*, 275−287.
(3) Chan, H. S., Gallie, B. L., DeBoer, G., Haddad, G., Ikegaki, N., Dimitroulakos, J., Yeger, J., and Ling, V. (1997) MYCN protein expression as a predictor of neuroblastoma prognosis. *Clin. Cancer Res. 3*, 1699−1706.
(4) Condorelli, G., Vigliotta, G., Iavarone, C., Caruso, M., Tocchetti, C. G., Andreozzi, F., Cafieri, A., Tecce, M. F., Formisano, P., Beguinot, L., and Beguinot, F. (1998) PED/PEA-15 gene controls glucose transport and is overexpressed in type 2 diabetes mellitus. *EMBO J. 17*, 3858−3866.
(5) Heffernan, J. M., Eastwood, S. L., Nagy, Z., Sanders, M. W., McDonald, B., and Harrison, P. J. (1998) Temporal cortex synaptophysin mRNA is reduced in Alzheimer's disease and is negatively correlated with the severity of dementia. *Exp. Neurol. 150*, 235−239.
(6) Howard, E. F., Chen, Q., Cheng, C., Carroll, J. E., and Hess, D. (1998) NF-kappa B is activated and ICAM-1 gene expression is upregulated during reoxygenation of human brain endothelial cells. *Neurosci. Lett. 243*, 199−203.
(7) Iadecola, C., Salkowski, C. A., Zhang, F., Aber, T., Nagayama, M., Vogel, S. N., and Ross, M. E. (1999) The transcription factor interferon regulatory factor 1 is expressed after cerebral ischemia and contributes to ischemic brain injury. *J. Exp. Med. 189*, 719−727.
(8) Lopez, A. M., Pegram, M. D., Slamon, D. J., and Landaw, E. M. (1999) A Model-Based Approach for Assessing in vivo Combination Therapy Interactions. *Proc. Natl. Acad. Sci. U.S.A. 96*, 13023−13028.
(9) Slamon, D. J., Godolphin, W., and Jones, L. A. (1989) Studies of the HER-2/neu Proto-oncogene in Human Breast and Ovarian Cancer. *Science 244*, 707−712.
(10) Slamon, D. J., Clark, G. M., Wong, S. G., Levin, W. J., Ullrich, A., and McGuire, W. L. (1987) Human Breast Cancer: Correlation of relpase and Survival with Amplificaiton of the HER-2/*neu* Oncogene. *Science 235*, 177−182.
(11) Bourcigaux, N., Gaston, V., Logie, A., Bertagna, X., Le Bouc, Y., and Gicquel, C. (2000) High expression of cyclin E and G1 CDK and loss of function of p57KIP are involved in proliferation of malignant sporadic adrencortical tumors. *J. Clin. Endocrinol. Metab. 85*, 322−330.
(12) Strehlow, D., Jelasta, A., Strehlow, K., and Korn, J. H. (1999) A potential role for protease nexin 1 in the pathogenesis of scleroderma. *J. Clin. Invest. 103*, 1179−1190.
(13) Chan, S. D. H., Dill, K., Blomdahl, J., and Wada, H. G. (1996) Nonisotopic Quantitation of mRNA Using a Novel RNase Protection Assay: Measurement of erbB-2 mRNA in Tumor Cell Lines. *Anal. Biochem. 242*, 214−220.
(14) Wang, A. M., Doyle, M. V., and Mark, D. F. (1989) Quantitation of mRNA by the polymerase chain reaction. *Proc. Natl. Acad. Sci. U.S.A. 86*, 9717−9721.
(15) Totze, G., Sachinidis, A., Vettre, H., and Ko, Y. (1996) Competitive reverse transcription/polymerase chain reaction for the quantification of p53 and mdm2 mRNA expression. *Mol. Cell. Probes 10*, 427−433.
(16) Revillion, F., Hornez, L., and Peyrat, J.-P. (1997) Quantification of c-erbB-2 expression in breast cancer by competitive RT-PCR. *Clin. Chem. 43*, 2114−2120.
(17) DeRisi, J. L., Iyer, V. R., and Brown, P. O. (1997) Exploring the Metabolic and Genetic Control of Gene Expression on a Genomic Scale. *Science 278*, 680−686.
(18) Schena, M., Shalon, D., Davis, R. W., and Brown, P. O. (1995) Quantitative Monitoring of Gene Expression Patterns with a Complementary DNA Microarray. *Science 270*, 467−470.
(19) Thorp, H. H. (1998) Cutting Out the Middleman: DNA Biosensors Based on Electrochemical Oxidation. *Trends Biotechnol. 16*, 117−121.
(20) Napier, M. E., and Thorp, H. H. (1997) Modification of Electrodes with Dicarboxylate Self-Assembled Monolayers for Attachment and Detection of Nucleic Acids. *Langmuir 13*, 6342−6344.
(21) Napier, M. E., Loomis, C. R., Sistare, M. F., Kim, J., Eckhardt, A. E., and Thorp, H. H. (1997) Probing Biomolecule Recognition with Electron Transfer: Electrochemical Sensors for DNA Hybridization. *Bioconjugate Chem. 8*, 906−913.
(22) Johnston, D. H., Glasgow, K. C., and Thorp, H. H. (1995) Electrochemical Measurement of the Solvent Accesibility of Nucleobases Using Electron Transfer between DNA and Metal Complexes. *J. Am. Chem. Soc. 117*, 8933−8938.
(23) Armistead, P. M., and Thorp, H. H. (2000) *Anal. Chem. 72*, 3764−3770.
(24) Wang, J., Cai, X., Rivas, G., Shiraishi, H., Farias, P. A. M., and Dontha, N. (1996) DNA Electrochemical Biosensor for the Detection of Short DNA Sequences Related to the Human Immunodeficiency Virus. *Anal. Chem. 68*, 2629−2634.
(25) Millan, K. M., Saraullo, A., and Mikkelsen, S. R. (1994) Voltammetric DNA Biosensor for Cystic Fibrosis Based on a Modified Carbon Paste Electrode. *Anal. Chem. 66*, 2943−2948.
(26) Hashimoto, K., Ito, K., and Ishimori, Y. (1994) Sequence-Specific Gene Detection with a Gold Electrode Modified with DNA Probes and an Electrochemically Active Dye. *Anal. Chem. 66*, 3830−3833.
(27) Kelley, S. O., Boon, E. M., Barton, J. K., Jackson, N. M., and Hill, M. G. (1999) Single-Base Mismatch Detection Based on Charge Transduction Through DNA. *Nucl. Acids Res. 27*, 4830−4837.
(28) Johnston, D. H., Glasgow, K. C., and Thorp, H. H. (1995) Electrochemical Measurement of the Solvent Accessibility of Nucleobases Using Electron-Transfer Between DNA and Metal Complexes. *J. Am. Chem. Soc. 117*, 8933−8938.
(29) Kayyem, J. F. (1999) DNA Diagnostics Using Electronic Detection. *Clin. Chem. 45*, S12−S12.
(30) Cance, W. G., Craven, R. J., Bergman, M., Xu, L., Alitalo, K., and Liu, E. T. (1994) Rak, a Novel Nuclear Tyrosine Kinase Expressed in Epithelial Cells. *Cell Growth Dif. 5*, 1347−1355.
(31) Willit, J. L., and Bowden, E. F. (1990) Adsorption and Redox Thermodynamics of Strongly Adsorbed Cytochrome *c* on Tin Oxide Electrodes. *J. Phys. Chem. 94*, 8241−8246.
(32) Raeymaekers, L. (1995) A commentary on the practical applications of competitive PCR. *Genome Res. 5*, 91−94.
(33) Schneenberger, C., Eder, S., Speiser, P., and Zeillinger, R. (1996) Competitive Reverse Transcriptase-PCR: an Improved Method for Determination of *c-erb*B-2 Gene Expression. *Anticancer Res. 16*, 849−852.

BC000129Y

Protamine-Fragment Peptides Fused to an SV40 Nuclear Localization Signal Deliver Oligonucleotides That Produce Antisense Effects in Prostate and Bladder Carcinoma Cells

Luba Benimetskaya,[†] Nancy Guzzo-Pernell,[‡] Su-Ting Liu,[‡] Johnathan C. H. Lai,[†] Paul Miller,[§] and C. A. Stein*[,†,||]

Howard Florey Institute of Experimental Physiology and Medicine, University of Melbourne, Parkville, Victoria, 3052, Australia, Departments of Medicine and Pharmacology, Columbia University, College of Physicians and Surgeons, 630 W. 168 Street, New York, New York 10032, and Department of Biochemistry and Molecular Biology, Bloomberg School of Public Health, Johns Hopkins University School of Medicine, 615 N. Wolfe Street, Baltimore, Maryland 21287. Received July 20, 2001

The development of antisense technology has focused on improving methods for oligonucleotide delivery into cells. In the present work, we describe a novel strategy for oligonucleotide delivery based on a bifunctional peptide composed of a C-terminal protamine-fragment that contains a DNA-binding domain and an N-terminal nuclear localization signal sequence derived from the SV40 large-T antigen (The sequences of two of the peptides are R6WGR6−PKKKRKV [s-protamine-NLS] and R4SR6FGR-6VWR4−PKKKRKV [l-protamine-NLS]). We demonstrated, by intrinsic fluorescence quenching, that peptides of this class form complexes with oligodeoxynucleotides. To evaluate delivery, we used a 20-mer phosphorothioate oligomer (Isis 3521) targeted to the 3′-untranslated region of the PKC-α mRNA and G3139, an 18-mer phosphorothioate targeted to the first six codons of the human bcl-2 open reading frame, and complexed them with either of two peptides (s- or l-protamine-NLS). These peptides bind to and deliver antisense oligonucleotides to the nucleus of T24 bladder and PC3 prostate cancer cells, as demonstrated by confocal microscopy. Furthermore, as shown by Western and Northern blotting, the peptide−oligonucleotide complexes produced excellent downregulation of the expression of the complementary mRNAs, which in turn resulted in downregulation of protein expression. However, under certain circumstances (predominately in PC3 cells), incubation of the cells with chloroquine was required to produce antisense activity. Using this strategy, PKC-α protein and mRNA expression in T24 and PC3 cells and bcl-2 expression in PC3 cells was reduced by approximately 75 ± 10% at a minimum concentration of oligomer of 0.25 μM, in combination with 12−15 μM peptide. On the basis of our results, we conclude that arginine-rich peptides of this class may be potentially useful delivery vehicles for the cellular delivery of antisense oligonucleotides. This new strategy may have several advantages over other methods of oligonucleotide delivery and may complement already existing lipid-based technologies.

INTRODUCTION

Antisense oligonucleotides, especially those containing the phosphorothioate backbone, are currently in clinical trials as potential therapeutic agents and also may be valuable reagents for the validation of gene function. However, at least in tissue culture, antisense oligonucleotides almost invariably must be condensed with a delivery reagent to ensure adequate cellular uptake and release from sequestered sites in the endosomes/lysosomes. The most commonly employed delivery reagents are cationic lipids (e.g., Lipofectin, Lipofectamine), but these reagents may contribute their own cytotoxic effects, which would thus affect the phenotype produced after treatment of the cells with the antisense effector molecule.

Accordingly, a large number of peptide delivery vehicles for antisense oligonucleotides have been devised. Tung and Stein (*1*), in their recent review of covalent peptide−oligonucleotide conjugates, have listed approximately 20 peptides that increase the delivery of oligonucleotides to cells. These include pH sensitive fusogenic peptides (*2*−*5*), Antennapedia-type peptides (*6*, *7*), and the HIV tat C-terminus peptide (*8*, *9*). Other peptides that have been covalently conjugated to oligonucleotides include the ER-retaining peptide YKDEL (*10*) and various nuclear localization signal peptides (including the PKKKRKV sequence derived from the SV40 large-T antigen (*11*−*14*).

Noncovalent peptide oligonucleotide complexes have also been employed to increase cellular delivery (reviewed by (*15*)). Morris et al. (*16*) used a 27-mer peptide, called MPG, which was composed of the N-terminal domain of the HIV gp41 fusion sequence fused to the C-terminal domain derived from the nuclear localization signal derived from the SV40 large-T antigen. Nuclear localization of oligonucleotide in fibroblasts was observed. Pichon et al. (*3*) employed a permeabilizing peptide derived ultimately from an analogue of the N-terminal sequence of the HA2 subunit of the influenza virus hemagglutinin. Permeabilization was successful as judged by the nuclear localization of a fluoresceinated oligonucleotide. This

* Corresponding author: Phone: 212-305-3606; Fax: 212-305-7348; E-mail: stein@cuccfa.ccc.columbia.edu.
[†] Department of Medicine, Columbia University.
[‡] University of Melbourne.
[§] Johns Hopkins University School of Medicine.
[||] Department of Pharmacology, Columbia University.

10.1021/bc010068j CCC: $22.00 © 2002 American Chemical Society
Published on Web 02/14/2002

same group (*17*) subsequently employed histidylated oligolysines to deliver antisense oligonucleotides targeted to ICAM-1, which demonstrated excellent antisense activity.

However, with this exception, in almost all the examples of peptide-mediated delivery given above, it is unclear if any sequence specific downregulation of the expression of a target mRNA was observed. In this work we have produced a bifunctional peptide comprising a C-terminal DNA-binding domain which is a protamine fragment, and an N-terminal nuclear localization signal derived from the SV40 large-T antigen. We demonstrate that peptides of this class both bind to and deliver antisense oligonucleotides to cells, and in addition, permit antisense activity by the oligonucleotide. However, in some cases, nuclear delivery, as well as antisense competency, only occur if the cells are pretreated with the lysosomotropic agent chloroquine, thus highlighting the difficulties that oligonucleotide/peptide complexes have in penetrating the endosomal barrier unassisted.

The antisense oligonucleotides we have employed are the 20-mer phosphorothioate antisense PKC-α, first developed by Dean and colleagues (*18*), which we have recently used to evaluate a novel type of porphyrin carrier (*19*). This oligomer, and G3139, the 18-mer antisense bcl-2 oligonucleotide (*20*) we have also employed in this study, are widely considered to be sequence-specific inhibitors of gene expression. Because of this property, they are both well suited for the evaluation of a novel delivery strategy.

MATERIALS AND METHODS

Peptide Synthesis. The preparation of these peptide sequences required the difficult coupling of multiple positively charged amino acid monomers adjacent to each other. To prepare them in reasonable yields, we used the following monomers, reagents and conditions: Fmoc-Arg-(Pbf)-OH (pentamethyldihydrobenzofuransulfonyl), Fmoc-Ser(tBu)-Opfp (*tert*-butyl), Fmoc-Trp(tBoc)-Opfp (*tert*-butyloxycarbonyl), Fmoc-Lys(tBoc)-Opfp (*tert*-butyloxycarbonyl), Fmoc-Lys(Mtt)-OH (methoxytrityl), Fmoc-Phe-Opfp, Fmoc-Gly-Opfp, Fmoc-Val-Opfp and Fmoc-Val-OH. The resin used was PAC−PEG-PS, (PerSeptive Biosystems, UK). Amino acids, *N*,*N*-dimethylformamide (DMF), 2-(1*H*-benzotriazole-l-yl)-1,1,3,3-tetramethyluronium hexafluorophosphate, DIPEA (diisopropylethylamine), and TFA (triethylsiliane) were purchased from Auspep Australia. HOBt (1-Hydroxybenzotriazole) was purchased from Fluka, TIS (triethylsilane) from Aldrich, and piperidine from Merck.

A 0.05 mmol scale peptide synthesis, using PAC−PEG-PS resin with a loading of 0.19 mmol/g, was carried out on a Rainin PS3 Automated Solid-Phase Peptide Synthesizer. Fmoc-amino acids were used in 5 mol equiv and activated with 5 mol equiv of HOBt or HBTU in 1 M DIPEA (in DMF) for 5 min, followed by a 35 min coupling. HBTU was used for the free alcohols and HOBt for the Opfp esters. Fmoc deprotection was carried out in 20% piperidine in DMF. Cleavage and side chain deprotection involved treating the peptide with a mixture containing 95% TFA, 2.5% TIS, and 2.5% H_2O, for 2 h at room temperature with constant stirring. The peptide was then isolated by ether extraction.

Purification and Characterization of the Peptides. Reverse phase HPLC was carried out using a Vydac 218TP C18 protein and peptide RP 5 μM column (4.6 × 250 mm) on a Waters 996 Photodiode Array Detector. Samples were monitored at 254 nm.

A mobile gradient buffer of 0.1% TFA and HPLC grade acetonitrile (0−60% in 30 min) were employed. The retention times for the peptides (not all of which were employed as delivery agents) are R6WGR6 (18 min), R6WGR6−PKKKRKV (19 min), R6WGR6−PKGKRKV (21min), R6WGR6−KPKRKVK (19 min), R4SR6FGRVWR4 (21.5 min), R4SR6FGR6VWR4−PKKKRKV (25.5 min), R4SR6FGR6VWR4−PKGKRKV (20 min), and R2FGR2VWR2 (19 min).

Matrix assisted laser desorption ionization-time-of-flight mass spectrometry (MALDI-TOF) was carried out on a Bruker Biflex spectrometer, and all data was collected and analyzed using Solaris software. Peptides were analyzed in positive linear mode as 50 ρM in 3:7 acetonitrile/water and 0.1% trifluoroacetic acid.

Cell Culture. Cells were obtained from American Type Culture Collection (12301 Parklawn Drive, Rockville, MD 20852). T24 cells were grown in McCoy's 5A medium (Gibco BRL, Grand Island, NY), containing 10% (v/v) heat-inactivated (56 °C) fetal bovine serum (FBS) (Gibco BRL, Grand Island, NY), supplemented with 25 mM Hepes, 100 units/mL penicillin G sodium, and 100 μg/mL streptomycin sulfate. PC3 cells were grown in RPMI 1640 medium (Gibco BRL), containing 10% (v/v) FBS, to which were added 2 mM glutamine, 1 mM sodium pyruvate, and 0.1 mM nonessential amino acids. Stock cultures were maintained at 37 °C in a humidified 5% CO_2 incubator.

Reagents. The anti-PKC-α mouse monoclonal antibody was purchased from Transduction Laboratories (Lexington, KY). The anti-bcl-2 mouse monoclonal antibody was purchased from Dako (Carpinteria,CA). The anti-mouse horseradish peroxidase conjugated secondary antibody was from Amersham (Arlington Heights, IL).

Synthesis of Oligonucleotides. Phosphorothioate oligonucleotides were synthesized on an Applied Biosystems (Foster City, CA) model 380B DNA. Following cleavage from controlled pore glass support, oligodeoxynucleotides were base-deblocked in ammonium hydroxide at 60 °C for 8 h and purified by reversed phase HPLC [0.1 M triethylammonium bicarbonate (TEAB)/acetonitrile, PRP-1 support]. Oligomers were detritylated in 3% acetic acid and precipitated with 2% lithium perchlorate/acetone, dissolved in sterile water, and reprecipitated as the sodium salt from 1 M NaCl/ethanol. Concentrations were determined by UV spectroscopy.

The sequences of the oligonucleotides used were Isis 3521 (targeted to the 3′ region of the PKC-α mRNA), 5′-GTTCTCGCTGGTGAGTTTCA-3′ (*18*); G3139 (targeted to the first six codons of the human bcl-2 open reading frame), 5′-TCTCCCAGCGTGCGCCAT-3′ (*20*). The sequence of the control, scrambled oligonucleotide (Isis 4559) is 5′-GGTTTTACCATCGGTTCTGG-3′ (*18*).

Treatment of Cells with Oligonucleotide−Peptide Complexes. Cells were grown in six-well plates until 65−75% confluent. The peptides, at the stated peptide/oligonucleotide molar ratios, were diluted in 200 μL of distilled water, and oligonucleotide was then added to the required concentration. The solution was mixed gently and incubated at room temperature for 30 min to allow oligonucleotide−peptide complexes to form. Then, 300 μL of Opti-MEM media was added, and the solution was mixed and overlaid onto the cells, which had been rinsed with Opti-MEM medium and pretreated with 500 μL 50 μM chloroquine for 15 min (the chloroquine with final concentration 25 μM was allowed to remain in solution during incubation with the complexes). The cells were then incubated at 37 °C for 5 h or refed with complete media containing 10% FBS and allowed to

incubate for an additional 19 h (for PKC-α) or 68 h (for bcl-2) before cell lysis and extract preparation.

Fluorescence Titrations. Fluorescence experiments were performed on an Aminco Bowman series 2 luminescence spectrometer (SLM Aminco, Urbana, IL). The intrinsic tryptophan fluorescence of peptide was excited at 290 nm, and the emission spectrum was recorded between 310 and 410 nm with a spectral band-pass of 4 nm. A fixed concentration of protein (0.5 μM) was titrated by increasing the concentration of Isis 3521 (from 0 to 0.35 μM) at room temperature in PBS buffer. Curve fitting was performed with the Grafit program (Excel Software).

Confocal Microscopy. T24 cells were seeded in glass bottom microwells (MatTec Corp., Ashland, MA) and treated with 5′-fluorescein-Isis 3521 (2 μM) complexed with 15 μM s-protamine-NLS in the presence of 25 μM chloroquine at 37 °C for 5 h. Cellular internalization was examined using an LSM 410 laser scanning confocal microscope (Zeiss, Thornwood, NY) equipped with a krypton/argon laser and attached to a Zeiss Axiovert 100 TV microscope. The 515−540 nm band-pass for fluorescein was used. Z-series were taken of a 1 to 2 micron optical section at 2 μm intervals. For measurements, a maximum projection of all sections was employed. Images were printed using Adobe Photoshop.

Western Blotting. Cells were treated with oligodeoxynucleotide−peptide complexes, scraped, washed with cold PBS, and then extracted in 40−50 μL of lysis buffer [50 mM Tris-HCl, pH 7.5; 1% NP-40; 0.25% sodium deoxycholate; 150 mM NaCl; 1 mM EGTA; 50 μg/mL Pefablock SC; 15 μg/mL aprotinin, leupeptin, chymostatin, and pepstatin A; 1 mM Na_3VO_4; 1 mM NaF] at 4 °C for 1 h. Cell debris was removed by centrifugation at 14000*g* for 20 min at 4 °C. Protein concentrations were determined using the Bio-Rad protein assay system (Bio-Rad Laboratories, Richmond, CA).

Aliquots of cell extracts containing 20−30 μg of protein were resolved by 10% or 12% SDS−polyacrylamide gel electrophoresis and transferred to Hybond ECL filter paper (Amersham, Arlington Heights, IL). Filters were incubated at room temperature for 1−2 h in Blotto A [5% nonfat milk powder in TBS-T: 10 mM Tris-HCl, pH 8.0, 150 mM NaCl, 0.05% Tween 20 (for PKC-α) and 5% BSA in PBS, 0.5% Tween (for Bcl-2)] and then probed overnight at 4 °C with 1:1000 dilution of anti-PKC-α or 1:500 dilution of anti-Bcl-2 in Blotto A. After washing in TBS-T or PBS-T buffer (3 × 7 min, room temperature), filters were incubated for 1 h at room temperature in 5% milk/TBS-T or 5% milk/PBS-T buffer containing a 1:3000 dilution of peroxidase-conjugated anti-mouse secondary antibody. The filters were then washed (3 × 10 min, room temperature), and ECL was performed according to the manufacturer's instructions.

Northern Blot Analysis. Total cellular RNA was isolated using TRIZOL Reagent (Gibco BRL). 30−40 μg was resolved on 1.2% agarose gel containing 1.1% formaldehyde and transferred to Hybond-N nylon membranes (Amersham). Human PKC-α and bcl-2 cDNA probes were ^{32}P-radiolabeled with [α-^{32}P]dCTP by random primer labeling using a commercially available kit (Promega) according to the manufacturer's instructions. The blots were then hybridized with the cDNA probes in 50% formamide, 5X SSC, 5X Denhardt's solution, 0.5% SDS and 0.1 mg/mL of salmon sperm DNA overnight at 42 °C. The filters were washed at room temperature, twice for 15 min in 2X SSC and 0.1% SDS, once for 20 min in 1X SSC and 0.1% SDS, and finally twice for 15 min in 0.1X SSC and 0.1% SDS at 65 °C. The filters were exposed to Kodak X-ray film for 12−24 h with intensifying screens at −70 °C and then developed.

Cellular Viability Assay. Cells were seeded in 96-well tissue culture plates and treated the next day with oligonucleotide−peptide complexes in the presence of 25 μM chloroquine for 5 h at 37 °C. At the end of this time, the Opti-MEM media was then replaced with complete media containing various concentrations of paclitaxel. After 3 days treatment with paclitaxel (at the indicated concentrations as described in the Results), cellular viability was determined by MTT (3-(4,5-dimethylthiazol-2-yl)-2,5-diphenyltetrazolium bromide) assay. Briefly, the cells were incubated for 4 h at 37 °C, 5% CO_2 with 0.5 mg/mL MTT in complete media. An equal volume of solubilization solution (10% SDS in 0.01 M HCl) was then added and allowed to incubate overnight at 37 °C. After the formazan crystals were dissolved, the plates were read on a Dynatech MR600 Microplate Reader at 540 nm.

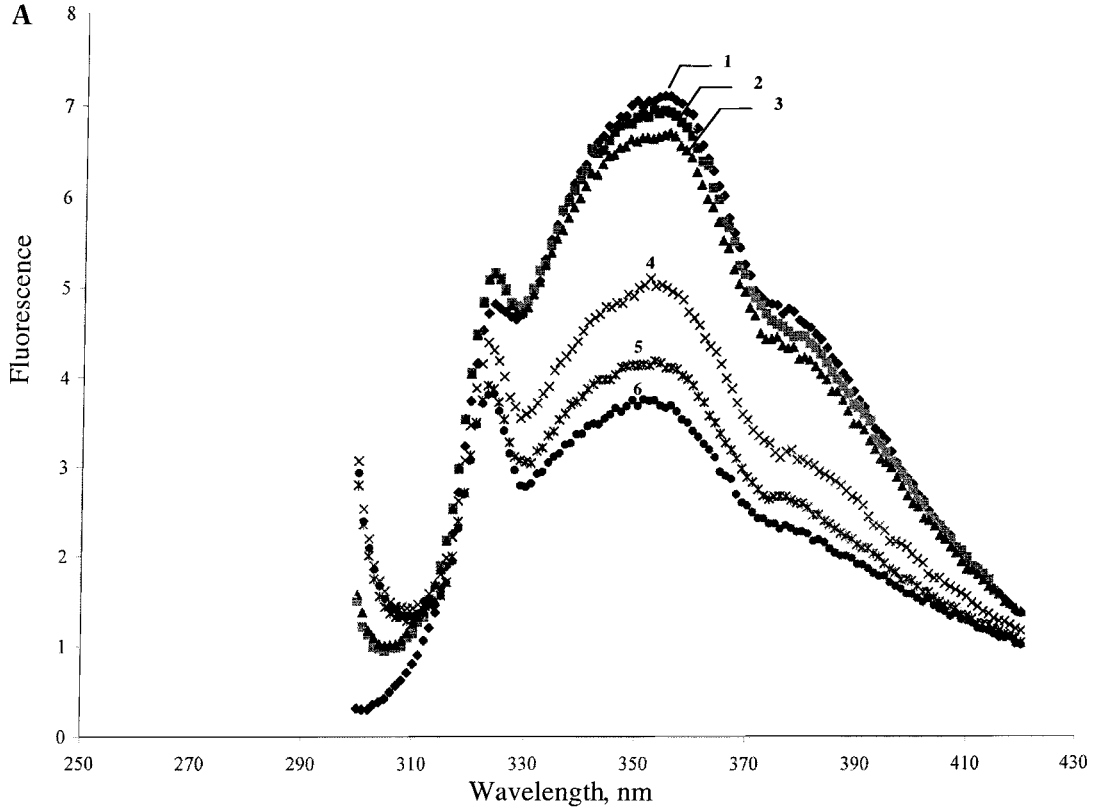
Experiments were performed in quadruplicate and data are expressed as the mean absorbance ± the SD. Statistical analysis of the results was performed using the Analysis ToolPack provided by Microsoft Excel. A Student's two-sample t-test, assuming unequal variances, was used to determine the equality of the means of two samples (* = $p < 0.05$).

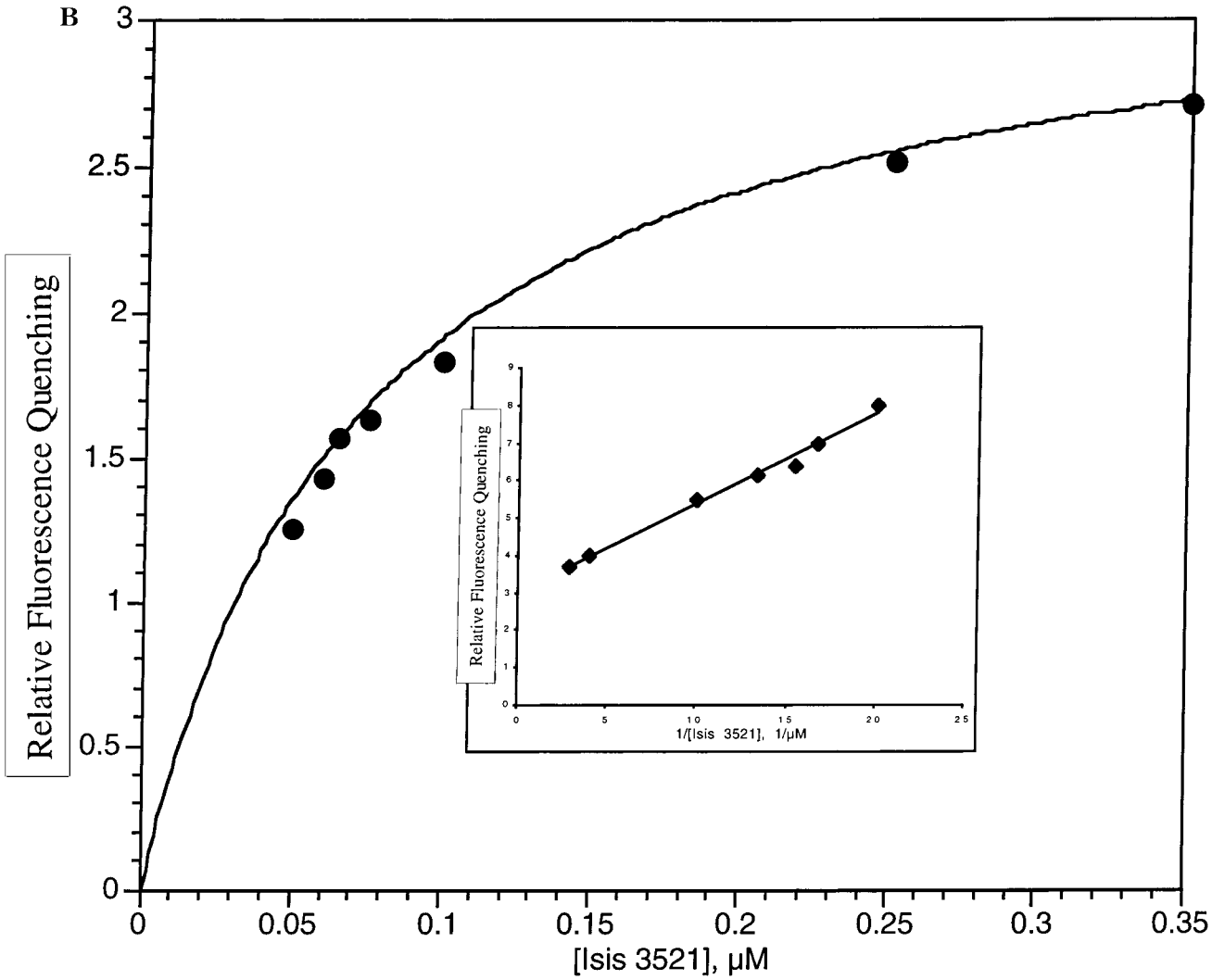
RESULTS

Peptides Form Complexes with Oligodeoxynucleotides. The interaction of Isis 3521, a 20-mer phosphorothioate antisense oligonucleotide, with protamine-NLS peptides was evaluated by fluorescence spectroscopy. The peptide contains a single Trp residue, which can be excited at 290 nm and emits fluorescent light at 330 nm. The ability of a bound oligonucleotide to quench this fluorescent emission constitutes a relatively sensitive probe for the monitoring of molecular interactions.

As shown in Figure 1A, the titration of a 0.5 μM solution of l-protamine-NLS with increasing concentrations of Isis 3521, both in PBS and in Opti-MEM (without serum, to mimic our transfection conditions), led to dramatic fluorescence quenching. At low oligonucleotide concentration (relative to l-protamine-NLS peptide) a plot of the decrease in fluorescence (due to quenching) vs oligonucleotide concentration fits an equation of the Michaelis−Menton type (Figure 1B). A Lineweaver−Burke (double reciprocal) plot gives K_d = 80 nM (R^2 = 0.99). However, as oligonucleotide concentration is increased, Trp fluorescence continues to decline, but a similar plot no longer fits a Michaelis−Menton-type equation, and the binding becomes increasingly complex (not shown). Similarly, for the s-peptide-NLS, the binding at relatively low oligonucleotide concentration also fits a single-site model of the Michaelis−Menton type (Figure 1C). A Lineweaver−Burke plot of the data gives K_d = 2 μM. At higher oligonucleotide concentration, the single site binding model also breaks down. For both peptides, these data are somewhat approximate because we could not obtain measurements at lower oligonucleotide concentrations than those indicated.

Protamine-NLS Peptides Deliver Oligonucleotides to the Cell Nucleus. We evaluated the ability of the protamine-NLS peptides to deliver the oligonucleotides into the cell nucleus by confocal microscopy. 5′-Fluorescein-labeled ISIS 3521 (2 μM) was complexed with s-protamine-NLS-peptide (15 μM) and incubated with T24 cells in the presence of chloroquine (25 μM). As shown in Figure 2, the peptide effectively delivered fluoresceinated oligonucleotide to the cell nucleus after


A
Fluorescence
Wavelength, nm
1
2
3
4
5
6


B
Relative Fluorescence Quenching
[Isis 3521], μM
Relative Fluorescence Quenching
1/[Isis 3521], 1/μM

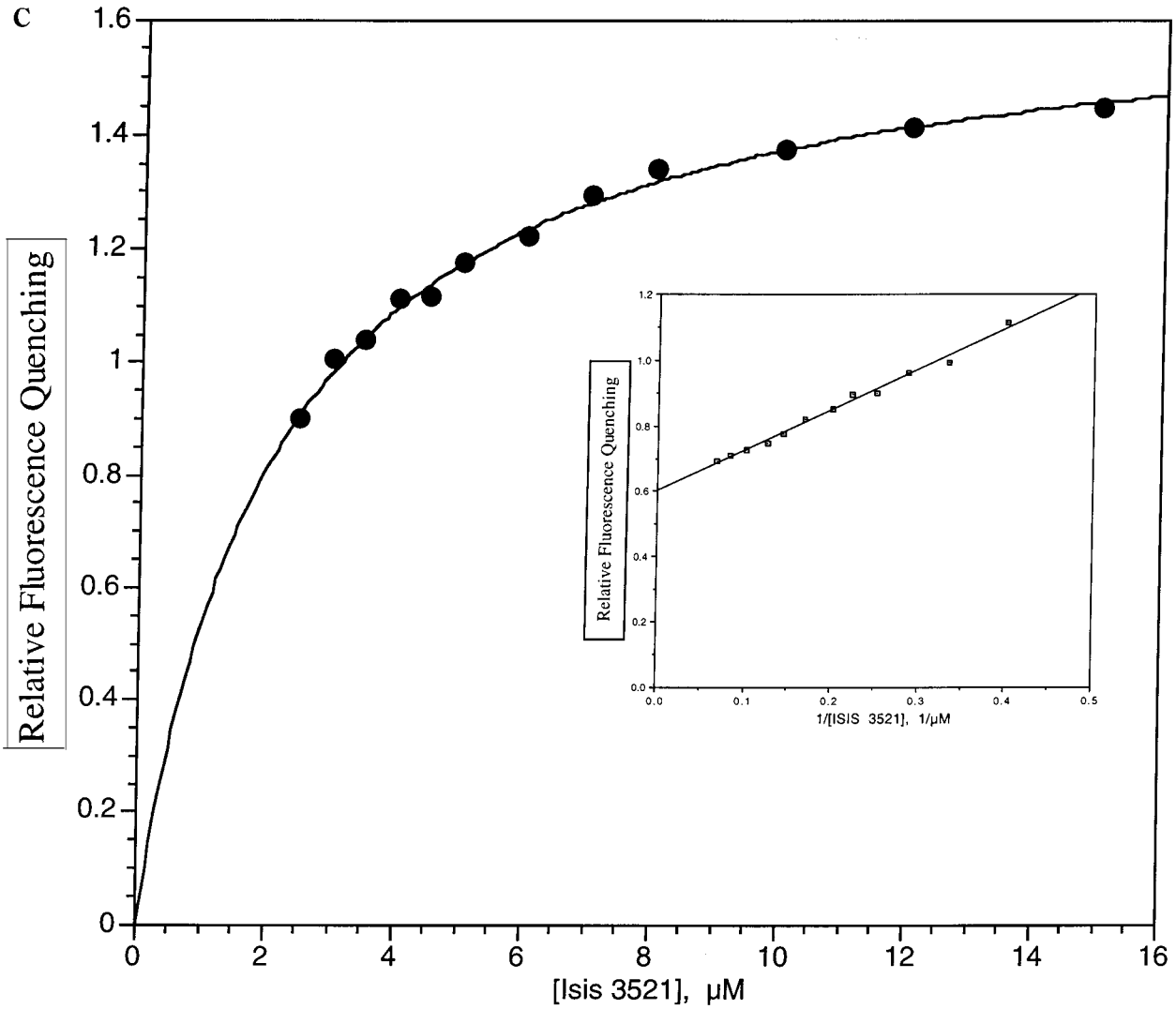


Figure 1. (A) Binding of l-protamine-NLS (0.5 μM) to increasing concentrations of Isis 3521 as monitored by intrinsic fluorescence quenching. The concentrations of Isis 3521 are (traces 1−6, respectively) 0, 0.06, 0.075, 0.1, 0.25, and 0.35 μM. The fluorescence of l-protamine-NLS was excited at 290 nm, and the emission spectrum was recorded between 310 and 410 nm. (B) Relative fluorescence of l-protamine-NLS at 350 nm plotted as a function of the concentration of Isis 3521, with extrapolation to zero concentration. The solid line represents the data plotted as per the Michaelis−Menton equation. The insert depicts a Lineweaver−Burke (double reciprocal) plot of these data. (C) Relative fluorescence of s-protamine-NLS at 350 nm plotted as a function of the concentration of Isis 3521, with extrapolation to zero concentration. The solid line represents the data plotted as per the Michaelis−Menton equation. The insert depicts the Lineweaver−Burke (double reciprocal) plot of these data.

an incubation time of 5 h. In the absence of peptide, oligonucleotides were internalized poorly by the cells, with most of the internalized material accumulating in a punctate pattern, signifying localization in vesicular structures (endosomes/lysosomes; not shown).

Surprisingly, under the same conditions and reagent concentrations, the s-protamine-(scrambled)NLS also promotes the delivery of the oligonucleotide to the nucleus (not shown). However, as described below, when delivered in this fashion, the oligonucleotide does not downregulate the expression of PKC-α protein as determined by Western blotting.

Peptide−Oligodeoxynucleotide Complexes Demonstrate Antisense Activity. *1. s-Protamine-NLS Complexes with Oligonucleotides.* Experiments using the protamine-NLS peptides to deliver antisense oligonucleotides were performed in T24 bladder carcinoma and PC3 prostate carcinoma cells. In addition to the 20-mer ISIS 3521, we also employed the 18-mer phosphorothioate oligonucleotide G3139, which is targeted to the first six codons of the human bcl-2 open reading frame. The

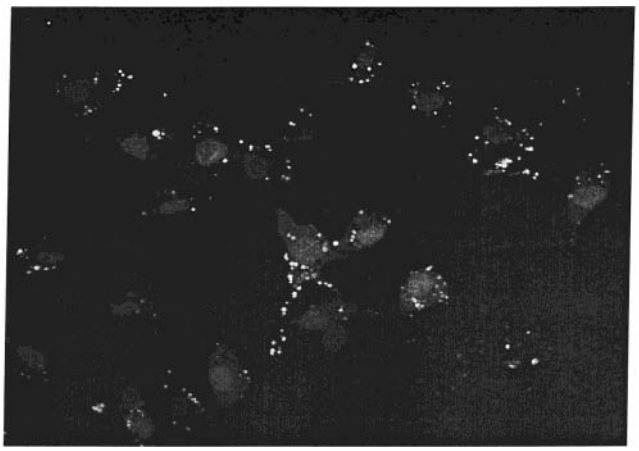


Figure 2. s-Protamine-NLS-mediated delivery of Isis 3521 in T24 bladder carcinoma cells. Cells were treated for 5 h at 37 °C with 5′-fluorescein-labeled Isis 3521 (2 μM) complexed to s-protamine-NLS (15 μM) in the presence of 25 μM chloroquine. Cellular localization was monitored by confocal microscopy, as described in the text.

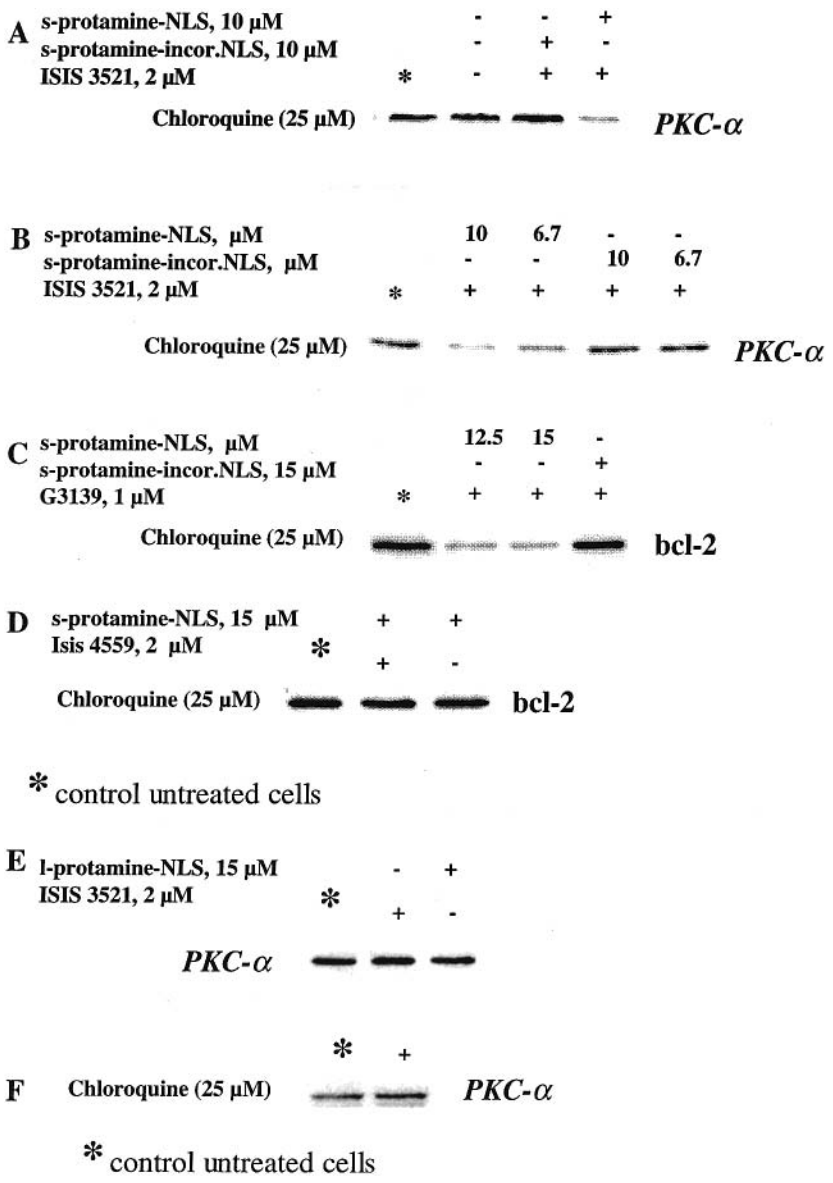


Figure 3. Inhibition of PKC-α protein expression by Isis 3521 (2 μM) (A, B) complexed with s-protamine-NLS (at the stated concentrations) in T24 (A) and PC3 (B) cells. (C) Inhibition of bcl-2 protein expression by G3139 (2 μM) complexed with s-protamine-NLS (15 μM) in PC3 cells. (D) Control oligonucleotide Isis 4559 complexed with s-protamine-NLS has no effect on bcl-2 expression in PC3 cells. (E) Uncomplexed l-protamine-NLS (15 μM) and Isis 3521 oligonucleotide in the presence of 25 μM chloroquine have no effect on PKC-α protein expression in PC3 cells. (F) Chloroquine (25 μM) alone has no effect on PKC-α protein expression in T24 cells. Cells were treated with complexes of Isis 3521 or G3139 oligonucleotides/s-protamine-NLS or control s-protamine-(incorrect)-NLS in the presence of 25 μM chloroquine for 5 h at 37 °C. 19 h (for PKC-α) or 67 h (for bcl-2) later, total protein was harvested, and Western blot analysis (25−30 μg of protein/lane) performed with anti-PKC-α and anti-bcl-2 antibodies as described in the Materials and Methods.

optimum incubation time of the cells with the peptide/oligonucleotide complexes was 5 h for Isis 3521 and G3139, followed by incubation periods of 24 h and 3 days, respectively.

To generate antisense effects, cells treated with s-protamine-NLS complexes with oligonucleotides were also pretreated with 50 μM chloroquine for 15 min. The chloroquine (final concentration = 25 μM) was allowed to remain in solution during incubation with the complexes (i.e., for 5 h). s-Protamine-NLS, when complexed to ISIS 3521 (2 μM), yielded significant antisense activity in both T24 (Figure 3A) and PC-3 cells (Figure 3B). By Western blotting and scanning densitometry, the expression of the PKC-α (T24 and PC3 cells) and Bcl-2 (Figure 3C; PC3 cells only) proteins were all reduced by approximately 70−80%. Naked oligomer (i.e., not complexed with peptide), at the identical concentration (2 μM) + 50 μM chloroquine preincubation and then 25 μM during the incubation period, was completely ineffective (Figure 3E), most likely because of the sequestration of the oligonucleotides in endosomes/lysosomes, as demonstated by confocal microscopy. A control, scrambled phosphorothioate oligonucleotide (Isis 4559; 2 μM)) complexed with the s-protamine-NLS-peptide, and ISIS 3521 complexed with s-protamine-(incorrect)-NLS-peptide under identical conditions (+ 50 μM chloroquine preincubation and then 25 μM during the incubation period), did not produce any reduction in target PKC-α protein levels in either T24 or PC3 cells (Figure 3A and 3B). Furthermore, 25 μM chloroquine alone did not downregulate PKC-α expression (Figure 3F), and neither the l-protamine-NLS alone (15 μM) nor Isis 3521 alone (Figure 3E) were active.

In addition, G3139 when complexed to s-protamine-NLS-peptide was "antisense" active in PC3 cells (Figure

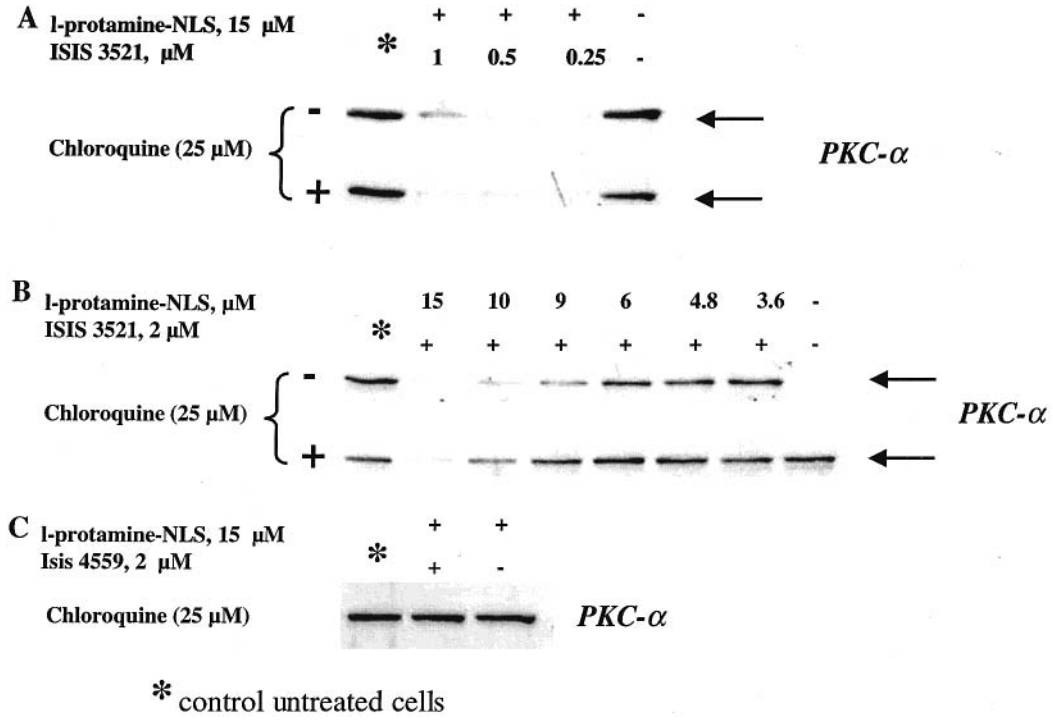


Figure 4. Inhibition of PKC-α protein expression in T24 cells by Isis 3521 (at the stated concentrations) complexed with l-protamine-NLS (15 μM) (A) and Isis 3521 (2 μM)/l-protamine-NLS (at the stated concentrations) (B) in the presence or absence of chloroquine. (C) Control oligonucleotide Isis 4559 (2 μM) complexed with l-protamine-NLS (15 μM), and uncomplexed l-protamine-NLS (15 μM), in the presence of 25 μM chloroquine, have no effect on PKC-α protein expression in T24 cells. Cells were treated with complexes of Isis 3521 or Isis 4559/l-protamine-NLS in the presence or absence of chloroquine for 5 h at 37 °C. 19 h later, total protein was harvested, and Western blot analysis (25−30 μg of protein/lane) was performed as described in the text.

3C). Similar controls as employed above (scrambled oligonucleotide Isis 4559, incorrect NLS sequence (15 μM), chloroquine alone (50 μM pretreatment then 25 μM during incubation; Figure 5C) were all totally inactive. However, we were not able to inhibit the expression of bcl-2 protein expression in T24 cells at any concentration of peptide/oligonucleotide complex.

2. l-Protamine-NLS Complexes with Oligonucleotides. We also evaluated the ability of a longer protamine peptide to diminish PKC-α and Bcl-2 protein expression in T24 and PC3 cells. Complexes of this peptide with the ISIS 3521 or the G3139 oligonucleotides were active over approximately the same concentration range in both cell lines. In T24 cells, as shown in the Western blots in Figure 4A and 4B, pretreatment by 50 μM chloroquine, and then treatment with 25 μM chloroquine during the incubation time was not necessary for the induction of an antisense effect. Instead, at a constant 2 μM concentration of Isis 3521 (Figure 4B), the concentration of peptide required for equivalent downregulation of PKC-α protein expression was slightly, but not dramatically, increased in the absence of chloroquine. At constant l-protamine-NLS concentration (15 μM; Figure 4A), the oligonucleotide concentrations required for maximal downregulation of PKC-α activity were also virtually identical in the presence and absence of chloroquine. However, the l-protamine-NLS (15 μM) complex with a control oligomer, Isis 4559 (2 μM; Figure 4C), did not produce any downregulation of PKC-α expression under the same experimental conditions. Congruent with these observations, the 8.5 kb and 4.0 kb PKC-α mRNA transcripts, as demonstrated by Northern blotting, were downregulated in the absence of chloroquine (Figure 6A).

In contrast, in PC3 prostate cancer cells, chloroquine (50 μM pretreatment + 25 μM during the incubation time) was still required for antisense activity. As shown in Figure 5A, a molar ratio of l-protamine-NLS/Isis 3521 of 7.5 provided maximal downregulation of PKC-α protein expression until a concentration of 1.9/0.25 μM was achieved. However, at a constant concentration of l-protamine-NLS (15 μM), Isis 3521 concentrations as low as 0.25 μM were still active (Figure 5B). Nevertheless, a decrease in peptide concentration to 10 μM virtually eliminated the antisense effect of Isis 3521. Similar to what was observed in the T24 cells, the control oligomer Isis 4559 (2 μM) complexed with 15 μM l-protamine-NLS was equally ineffective in the PC3 cells (Figure 5D). Furthermore, an l-protamine-NLS peptide in which the NLS sequence was mutated from PKKKRKV to PKGK-RKV did downregulate PKC-α protein expression (Figure 5D), but not quite to the same extent as the NLS peptide with the correct sequence.

G3139 (2 μM-0.25 μM) in complex with l-protamine-NLS (15−10 μM; Figure 5C) could effectively downregulate the expression of both bcl-2 protein (after 3 days) and mRNA (after 1 day; Figure 6B), but again only after pretreatment of the PC3 cells with 50 μM chloroquine and then treatment with 25 μM chloroquine during the incubation time. However, at lower peptide concentrations, antisense inhibition was lost (Figure 5C).

Downregulation of PKC-α Increases Sensitivity of T24 Bladder Carcinoma Cells to Paclitaxel. Reductions in cell proliferation was determined by MTT assay. Data are shown in Figure 7A and 7B, as determined after 3 days of drug treatment. This followed 24 h treatment of the T24 cells by complexes of s-protamine-NLS (15 μM)/Isis 3521 (2 μM) complexes and pretreatment of the cells with 50 μM chloroquine and then treatment with 25 μM during the incubation period. Isis 3521, s-protamine-NLS peptide, and 50 μM and then 25 μM chloroquine alone had no effect on cell viability, as assessed by MTT assay. Complexes of s-protamine-NLS

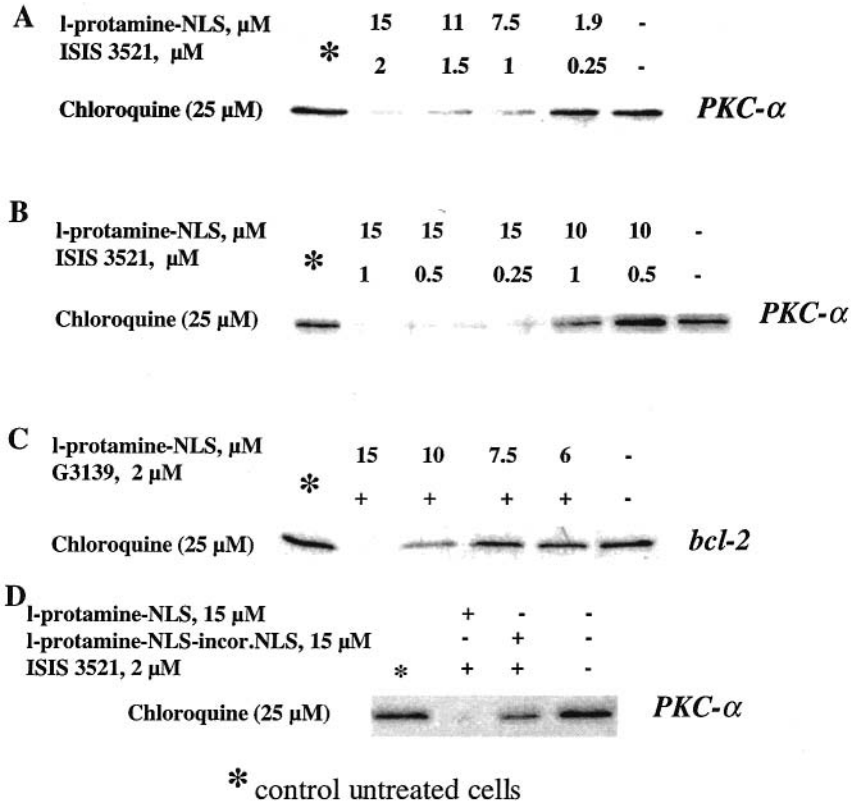


Figure 5. Inhibition of PKC-α protein expression by Isis 3521 (at the stated concentrations) complexed with l-protamine-NLS (at the stated concentrations) in PC3 cells (A, B). (C) Inhibition of bcl-2 protein expression by G3139 (2 μM) complexed with l-protamine-NLS (at the stated concentrations) in PC3 cells. (D) Complexes of Isis 3521/l-protamine-(incorrect)-NLS in the presence of 25 μM chloroquine have a diminished effect on PKC-α protein expression in PC3 cells, while chloroquine alone (25 μM) has no effect. Cells were treated with complexes of Isis 3521 or Isis 4559/l-protamine-NLS or complexes of Isis 3521/l-protamine-(incorrect)-NLS in the presence of 25 μM chloroquine for 5 h at 37 °C. 19 h later, total protein was harvested, and Western blot analysis (25−30 μg of protein/lane) was performed, as described in the text.

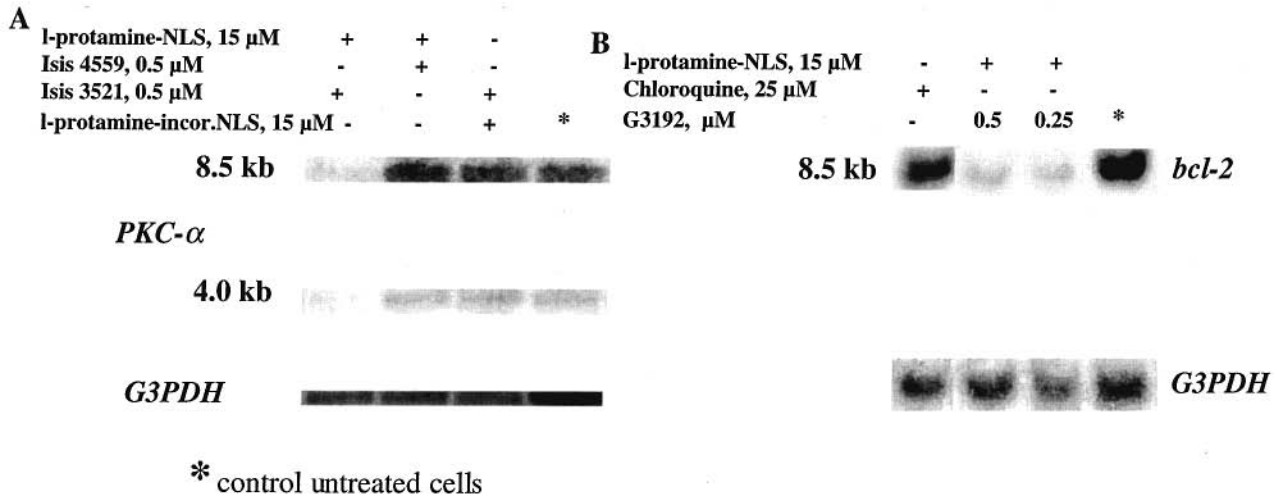


Figure 6. Inhibition of PKC-α mRNA expression by Isis 3521 (0.5 μM) complexed with l-protamine-NLS (15 μM) in T24 cells (A) and bcl-2 mRNA expression by G3139 (0.25 and 0.5 μM) complexed with l-protamine-NLS (15 μM) in PC3 cells (B). Cells were treated with complexes of Isis 3521, G3139 or control oligonucleotide Isis 4559/l-protamine-NLS in the presence of 25 μM chloroquine for 5 h at 37 °C. 19 h later, total mRNA was isolated, and Northern blot analysis was performed as described in the Materials and Methods. 30−40 μg of mRNA was loaded in each lane of the 1.2% denaturing agarose gel, transferred to Hybond-N nylon membranes, and probed with either a PKC-α, bcl-2, or control G3PDH cDNA probe.

(scrambled)-peptide/Isis 3521 reduced cellular viability to a much lesser extent. Only treatment of the cells with s-protamine-NLS/Isis 3521 was able to reduce cellular viability.

DISCUSSION

The peptides in this study were designed in an attempt to satisfy the major requirements for efficient oligonucleotide delivery to the cell nucleus, and, what is of course the ultimate goal, the retention of antisense activity. We believe that these requirements for peptide sequence include (1) the ability to bind to oligodeoxynucleotides, (2) the ability of the peptide−oligonucleotide complexes to penetrate the endosomal/lysosomal membrane, and (3) the ability of the peptide to promote nuclear localization.

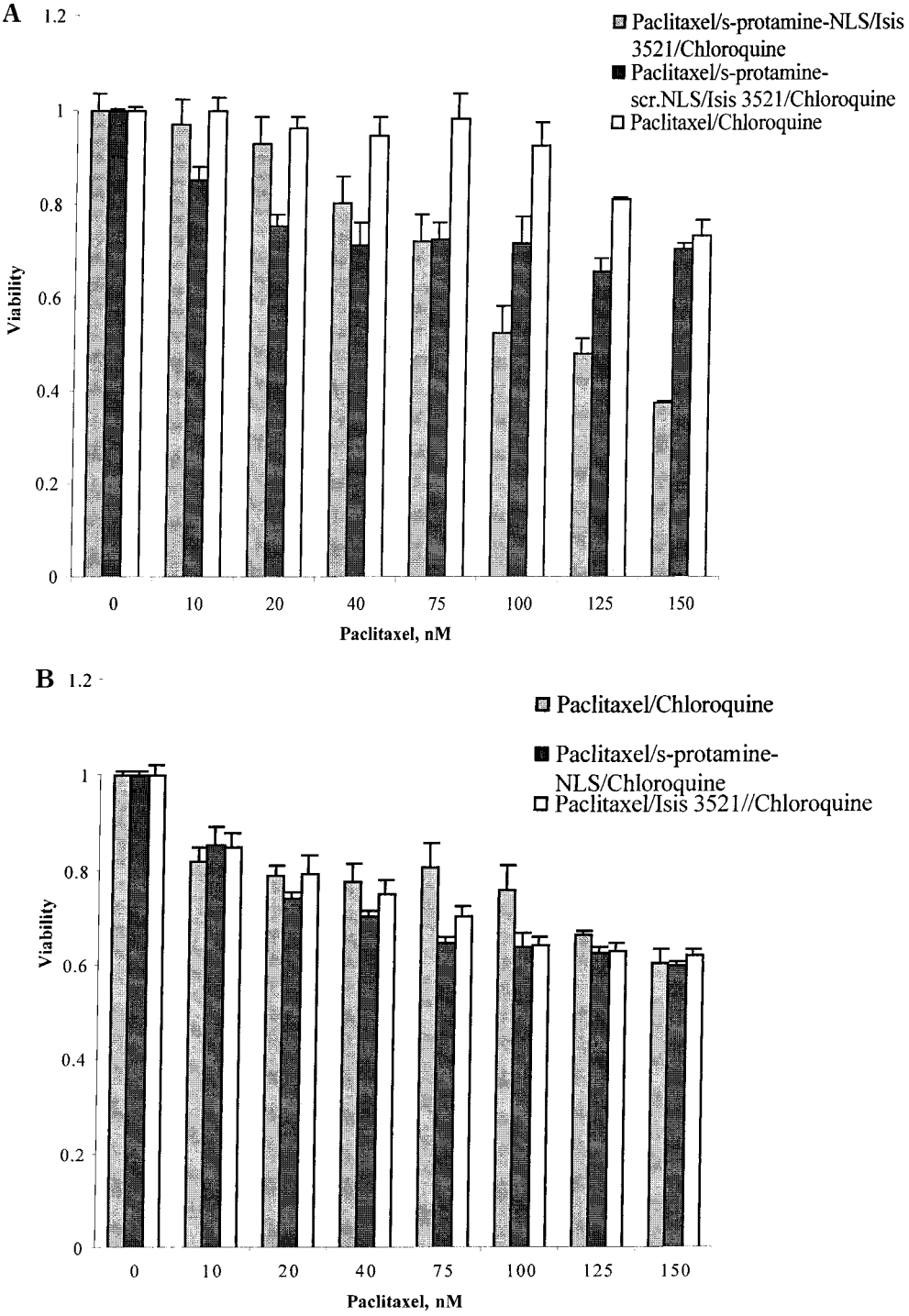


Figure 7. (A) Diminution in T24 cellular viability induced by the Isis 3521/s-protamine-NLS complex in response to increasing concentrations of paclitaxel. Neither control s-protamine-(scrambled)-NLS complexed to Isis 3521 (A), nor s-protamine-NLS or Isis 3521 alone (B) have any significant effect on T24 cellular viability in response to increasing concentrations of paclitaxel. Cells were treated with Isis 3521 complexed to s-protamine-NLS or s-protamine-(scrambled)-NLS or either s-protamine-NLS or Isis 3521 alone in the presence of 25 μM chloroquine for 5 h at 37 °C. The Opti-MEM media was then replaced with complete media containing various concentrations of paclitaxel. After 3 days of incubation, the MTT assay was performed. The absorbance at 540 nm was normalized to the controls to determine cellular viability. Experiments were performed in quaduplicate, and data are expressed as the mean absorbance ± the SD. A Student's two-sample t-test assuming unequal variances was used to determine the equality of the means of two samples (* = p <0.05).

The peptides described in this work satisfy criteria 1 and 3, and with the addition of chloroquine, all of them.

Bull protamine is a 50 amino acid peptide with an arginine rich central domain (ARYRCCLTHSGSRCR-RRRRRRC **RRRRRRFGRRRRRR** VCCRRYTVI.RC-TRQ). The short (s) sequence that we have tested is the central region highlighted in bold, with the exception that we have replaced the phe (F) with a trp (W) amino acid in order to provide an intrinsic fluorescent probe. This region was chosen because it provides the required arginine-rich sequence for oligonucleotide binding, but lacks cysteines which could promote dimerization. The long (l) protamine sequence contains the region in bold above, but the F is retained. Instead, the l-protamine sequence deletes the C and extends the R residues on both the N-and C-termini, as shown in Table 1.

Table 1. Peptides Used in This Work

peptide	sequence	mw	m/z^{+1}
s-protamine	R6WGR6	2134.88	2136.88
s-protamine-NLS	R6WGR6−PKKKRKV	2998.97	3000
s-protamine-(incorrect)-NLS	R6WGR6−PK**G**KRKV	2927.97	2931
s-protamine-(scrambled)-NLS	R6WGR6−KPKRKVK	2998.97	2999.14
l-protamine	R4SR6FGR6VWR4	3716.30	3717.03
l-protamine-NLS	R4SR6FGR6VWR4−PKKKRKV	4580.90	4580.9
l-protamine-(incorrect)NLS	R4SR6FGR6VWR4−PK**G**KRKV	4509.93	4509.9

It is known that the positively charged guanidinium functional groups (pK_a = 12.5) electrostatically interact with the negatively charged phosphate backbone of DNA. These charge based interactions result in an overall charge neutralization leading to condensation of DNA.

In general, studies of protamine interactions have been carried out for double-stranded DNA. These have involved X-ray diffraction, Raman spectra, chemical reaction, and optical detection of magnetic resonance (*21*−*24*). Some of the reports are conflicting, but regardless it is now thought that the interaction of protamine and double-stranded DNA involves binding to the major groove with a β-form DNA and β-conformation for the protamine (*21*, *23*). Unfortunately, the interaction of protamine with single-stranded DNA remains poorly understood. Nevertheless, protamine is known to be an efficient condensing peptide and has been shown to enhance transfection (*25*) and lipid-mediated gene transfer (*26*). In these experiments, the binding of increasing concentrations of oligonucleotide to a much larger concentration of s-protamine-NLS fits a single-site binding model of the Michaelis−Menton type, with K_d as derived from the Lineweaver−Burke analysis equaling 75 nM. The binding of additional molecules of s-protamine-NLS to oligonucleotide is mathematically complex, but on the basis of the spectroscopic measurements, Trp fluorescence is 100% quenched at a peptide/oligomer molar ratio of 4:1 (charge ratio of approximately 3.15:1).

Arginine-rich peptides (e.g., Tat-(48−60) appear to be able to be internalized even at 4 °C by an endocytosis-independent pathway (*27*). Despite this, it seems unlikely that an arginine-rich peptide, when complexed with negatively charged oligonucleotides, will undergo endocytosis-dependent internalization. Experiments with the lysosomotropic agent chloroquine support this idea.

Chloroquine is a weak base (pK_a 10.2 and 8.1) that accumulates in endosomes/lysosomes in a time and concentration-dependent manner. It has been used extensively to improve nuclear delivery of plasmids, but to the best of our knowledge only rarely, if at all, for similar purposes for oligonucleotides (*28*). Intralysosomal concentrations of chloroquine may reach 9 mM, and the compound acts as a buffer to prevent the continuous endosomal acidification process (*29*). This causes a rise in intraendosomal osmolarity and its eventual lysis, releasing peptide/oligonucleotide complexes into the cytoplasm (the "proton sponge" hypothesis (*30*)). It is also possible that, in addition to this mechanism, chloroquine causes some degree of intraendosomal dissociation of the peptide/oligonucleotide complex (*29*). This dissociation may to some extent contribute to the retention of antisense activity (see below), but is probably overshowed in extent by peptide-mediated nuclear delivery.

A large family of nuclear localization signals exists, but the simian virus 40 (SV40 T) large T antigen nuclear localization sequence was chosen because it has resulted in efficient DNA transfer into the nucleus of various cell types, and has enhanced transgene expression (*31*−*34*). The peptide we employed (^{126}PKKKRKV^{132}) consists of a basic stretch of amino acids containing five consecutive positively charged residues, which are necessary for binding to the nuclear import protein karyopherin α (also known as importin α) (*35*). This complex then binds to importin β and, with the assistance of the GTPase Ran, is carried through the nuclear pore by mechanisms that are still poorly defined. Nevertheless, particles as large as 25 nm have been shown to be transported into the nucleus in this fashion (*35*). Since in preliminary experiments the particle size of the complexes is nearly 300 nm, significant intracellular decomposition must be occurring.

Lys-128 appears to be crucial for nuclear import (*36*). In this work, we have mutated Lys-128 to Gly and were unable to detect antisense downregulation of PKC-α protein expression. While these data strongly argue for the importance of the NLS in the generation of an antisense effect, other data suggest its role may be complex. For example, an s-protamine-NLS, in which the NLS has been scrambled, also promoted delivery of oligonucleotides to the nucleus, but did not downregulate the expression of PKC-α protein. This observation may suggest that the binding of the NLS to nuclear elements promotes dissociation of the oligonucleotide/peptide complex that results from particle degradation, thereby increasing the level of free nuclear oligonucleotide. However, this is speculative and other explanations may also be possible.

In summary, we have found a novel, efficient, arginine-peptide (and frequently, chloroquine) dependent way to transfer oligonucleotides into the nucleus of T24 and PC3 cells, where they produce downregulation of protein expression that is consistent with antisense effects. Provided that these substances can be manufactured at reasonable cost, they may be important complements to traditional cationic lipids as transfection vehicles.

ACKNOWLEDGMENT

C.A.S. and P.M. were funded by NIH R01 GM58791. N.G.P. and S.T.L. were supported by a National Health and Medical Research Council of Australia, Block Grant (#983001), to the Howard Florey Institute.

LITERATURE CITED

(1) Tung, C. H., and Stein, S. (2000) Preparation and applications of peptide−oligonucleotide conjugates. *Bioconjugate Chem. 11*, 605−618.

(2) Ha, H. C., Sirisoma, N. S., Kuppusamy, P., Zweier, J. L., Woster, P. M., and Casero, R. A., Jr. (1998) The natural polyamine spermine functions directly as a free radical scavenger. *Proc. Natl. Acad. Sci. U.S.A. 95*, 11140−11145.

(3) Pichon, C., Freulon, I., Midoux, P., Mayer, R., Monsigny, M., and Roche, A. C. (1997) Cytosolic and nuclear delivery of oligonucleotides mediated by an amphiphilic anionic peptide. *Antisense Nucleic Acid Drug Dev. 7*, 335−343.

(4) Parente, R. A., Nadasdi, L., Subbarao, N. K., and Szoka, F. C., Jr. (1990) Association of a pH-sensitive peptide with membrane vesicles: role of amino acid sequence. *Biochemistry 29*, 8713−8719.

(5) Wyman, T. B., Nicol, F., Zelphati, O., Scaria, P. V., Plank, C., and Szoka, F. C., Jr. (1997) Design, synthesis, and characterization of a cationic peptide that binds to nucleic acids and permeabilizes bilayers. *Biochemistry 36*, 3008−3017.

(6) Derossi, D., Joliot, A. H., Chassaing, G., and Prochiantz, A. (1994) The third helix of the Antennapedia homeodomain translocates through biological membranes. *J. Biol. Chem. 269*, 10444−10450.

(7) Derossi, D., Chassaing, G., and Prochiantz, A. (1998) Trojan peptides: the penetratin system for intracellular delivery. *Trends Cell Biol. 8*, 84−87.

(8) Fawell, S., Seery, J., Daikh, Y., Moore, C., Chen, L. L., Pepinsky, B., and Barsoum, J. (1994) Tat-mediated delivery of heterologous proteins into cells. *Proc. Natl. Acad. Sci. U.S.A. 91*, 664−668.

(9) Chen, L. L., Frankel, A. D., Harder, J. L., Fawell, S., Barsoum, J., and Pepinsky, B. (1995) Increased cellular uptake of the human immunodeficiency virus-1 Tat protein after modification with biotin. *Anal. Biochem. 227*, 168−175.

(10) Arar, K., Monsigny, M., and Mayer, R. (1993) Synsesis of defined oligonucleotide−peptide conjugates containing a KDELt signal sequence. *Tetrahedron Lett. 34*, 3087−3090.

(11) de La Torre, B. G., Albericio, F., Saison-Behmoaras, E., Bachi, A., and Eritja, R. (1999) Synthesis and binding properties of oligonucleotides carrying nuclear localization sequences. *Bioconjugate Chem. 10*, 1005−1012.

(12) Eritja, R., Pons, A., Escarceller, M., Giralt, E., and Albericio, F. (1991) Synthesis of defined peptide−oligonucleotide hybrids containing a nuclear transport signal sequence. *Tetrahedron 47*, 4113−4120.

(13) Reed, M. W., Fraga, D., Schwartz, D. E., Scholler, J., and Hinrichsen, R. D. (1995) Synthesis and evaluation of nuclear targeting peptide-antisense oligodeoxynucleotide conjugates. *Bioconjugate Chem. 6*, 101−108.

(14) Neves, C., Byk, G., Scherman, D., and Wils, P. (1999) Coupling of a targeting peptide to plasmid DNA by covalent triple helix formation. *FEBS Lett. 453*, 41−45.

(15) Lebedeva, I., Benimetskaya, L., Stein, C. A., and Vilenchik, M. (2000) Cellular delivery of antisense oligonucleotides. *Eur. J. Pharm. Biopharm. 50*, 101−119.

(16) Morris, M. C., Vidal, P., Chaloin, L., Heitz, F., and Divita, G. (1997) A new peptide vector for efficient delivery of oligonucleotides into mammalian cells. *Nucleic Acids Res. 25*, 2730−2736.

(17) Pichon, C., Roufai, M. B., Monsigny, M., and Midoux, P. (2000) Histidylated oligolysines increase the transmembrane passage and the biological activity of antisense oligonucleotides. *Nucleic Acids Res. 28*, 504−512.

(18) Dean, N. M., and McKay, R. (1994) Inhibition of protein kinase C-alpha expression in mice after systemic administration of phosphorothioate antisense oligodeoxynucleotides. *Proc. Natl. Acad. Sci. U.S.A. 91*, 11762−11766.

(19) Benimetskaya, L., Takle, G. B., Vilenchik, M., Lebedeva, I., Miller, P., and Stein, C. A. (1998) Cationic porphyrins: novel delivery vehicles for antisense oligodeoxynucleotides. *Nucleic Acids Res. 26*, 5310−5317.

(20) Jansen, B., Schlagbauer-Wadl, H., Brown, B. D., Bryan, R. N., van Elsas, A., Muller, M., Wolff, K., Eichler, H. G., and Pehamberger, H. (1998) bcl-2 antisense therapy chemosensitizes human melanoma in SCID mice. *Nat. Med. 4*, 232−234.

(21) Puigjaner, L. C., Fita, I., Arnott, S., Chandrasekaran, R., and Subirana, J. A. (1986) Modelling and refinement of the crystal structure of nucleoprotamine from Gibbula divaricata. *J. Biomol. Struct. Dyn. 3*, 1067−1078.

(22) Campos, J. L., and Subirana, J. A. (1987) The complex of poly (dG). poly (dC) with arginine: stabilization of the B form and transition to multistranded structures. *J. Biomol. Struct. Dyn. 5*, 15−19.

(23) Hud, N. V., Milanovich, F. P., and Balhorn, R. (1994) Evidence of novel secondary structure in DNA-bound protamine is revealed by Raman spectroscopy. *Biochemistry 33*, 7528−7535.

(24) Prieto, M. C., Maki, A. H., and Balhorn, R. (1997) Analysis of DNA-protamine interactions by optical detection of magnetic resonance. *Biochemistry 36*, 11944−11951.

(25) Boulikas, T. (1997) Nuclear localization signal peptides for the import od plasmid DNA in gene therapy. *Int. J. Oncol. 10*, 301−309.

(26) Sorgi, F. L., Bhattacharya, S., and Huang, L. (1997) Protamine sulfate enhances lipid-mediated gene transfer. *Gene Ther. 4*, 961−968.

(27) Futaki, S., Suzuki, T., Ohashi, W., Yagami, T., Tanaka, S., Ueda, K., and Sugiura, Y. (2001) Arginine-rich peptides. An abundant source of membrane-permeable peptides having potential as carriers for intracellular protein delivery. *J Biol. Chem. 276*, 5836−5840.

(28) Erbacher, P., Roche, A. C., Monsigny, M., and Midoux, P. (1996) Putative role of chloroquine in gene transfer into a human hepatoma cell line by DNA/lactosylated polylysine complexes. *Exp. Cell Res. 225*, 186−194.

(29) Wolfert, M. A., and Seymour, L. W. (1998) Chloroquine and amphipathic peptide helices show synergistic transfection in vitro. *Gene Ther. 5*, 409−414.

(30) Behr, J. P. (1997) The proton sponge: a trick to enter cells the viruses did not exploit. *Chimica 51*, 34.

(31) Collas, P., Husebye, H., and Alestrom, P. (1996) The nuclear localization sequence of the SV40 T antigen promotes transgene uptake and expression in zebrafish embryo nuclei. *Transgen. Res. 5*, 451−458.

(32) Collas, P., and Alestrom, P. (1997) Rapid targeting of plasmid DNA to zebrafish embryo nuclei by the nuclear localization signal of SV40 T antigen. *Mol. Mar. Biol. Biotechnol. 6*, 48−58.

(33) Wienhues, U., Hosokawa, K., Hoveler, A., Siegmann, B., and Doerfler, W. (1987) A novel method for transfection and expression of reconstituted DNA- protein complexes in eukaryotic cells. *DNA 6*, 81−89.

(34) Kaneda, Y., Iwai, K., and Uchida, T. (1989) Increased expression of DNA cointroduced with nuclear protein in adult liver. *Science 243*, 375−378.

(35) Zanta, M. A., Belguise-Valladier, P., and Behr, J. P. (1999) Gene delivery: a single nuclear localization signal peptide is sufficient to carry DNA to the cell nucleus. *Proc. Natl. Acad. Sci. U.S.A. 96*, 91−96.

(36) Colledge, W. H., Richardson, W. D., Edge, M. D., and Smith, A. E. (1986) Extensive mutagenesis of the nuclear location signal of simian virus 40 large-T antigen. *Mol. Cell Biol. 6*, 4136−4139.

BC010068J

Reversible Surface Thiol Immobilization of Carboxyl Group Containing Haptens to a BIAcore Biosensor Chip Enabling Repeated Usage of a Single Sensor Surface

Ulrich Schlecht,† Yoko Nomura, Till Bachmann,† and Isao Karube*

Research Center for Advanced Science and Technology, University of Tokyo, 4-6-1 Komaba, Meguro-ku, Tokyo 153-8904, Japan. Received February 1, 2001

We describe a reversible immobilization method for carboxyl group containing haptens that makes the repeated usage of a BIAcore biosensor chip possible. Haptens which are immobilized according to the surface thiol method can be removed completely from the sensor surface again by a reducing step. In the first part of our study, analogues of the herbicides 2,4-dichlorophenoxyacetic acid and 2,4,5-trichlorophenoxyacetic acid were immobilized in succession to a biosensor surface of a BIAcore surface plasmon resonance instrument according to the thiol coupling method. Direct kinetic analysis of these ligands to a polyclonal *anti*-2,4-dichlorophenoxyacetic acid antibody were performed using these biosensor surfaces. In the second part of the study, different amounts of 2,4-dichlorophenoxyacetic acid were sequentially immobilized onto the same biosensor surface in order to generate a calibration plot for 2,4-dichlorophenoxyacetic acid. Using this plot, the quantitative detection of the herbicide down to a concentration of 0.1 μg/mL, the maximum admissible concentration of pesticides in drinking water, is possible.

INTRODUCTION

2,4-Dichlorophenoxyacetic acid (2,4-D) and 2,4,5-trichlorophenoxyacetic acid (2,4,5-T) are common herbicides used for the control of weeds that can potentially contaminate groundwater and drinking water supplies. It has been reported that exposure of humans to 2,4-D produces acute congestion of all organs and degenerative changes in ganglionic cells of the central nervous system (*1*). 2,4-D is also a carcinogen, causing soft-tissue sarcoma in humans (*2*) and malignant lymphoma in dogs (*3*). Toxicity of 2,4,5-T is mainly based on its contamination by dioxins, such as TCDD and PCDD, during its production (*4*). In the European Community (EC) countries, the maximum admissible concentration for pesticides in drinking water is 0.1 μg/mL for any substance and 0.5 μg/mL for the combined total of pesticides (*5*). Rapid, easy, and economical methods for the detection of these pesticides, most of which are low molecular weight ligands (haptens), are of great importance.

In the past few years, different approaches to the detection of pesticides have been described, for example, capillary gas chromatography with ion trap detection (*6*), piezoelectric biosensors (*7*), fiber-optic immunosensors (*8*), and amperometric cholinesterase biosensors (*9*). Beyond these techniques, the development of the surface plasmon resonance (SPR) technology has opened up a new and elegant way to detect haptens quantitatively. For instance, assays for the detection of the herbicides atrazine (*10*) and simazine (*11*) on the basis of the competition principle have been established. In the present study, we have detected 2,4-D for the first time using the BIAcore SPR technology and, in addition, we describe a new method of detection.

* To whom correspondence should be sent. Tel: +81-3-54525220. Fax: +81-3-5452-5227. E-mail: karube@bio.rcast.u-tokyo.ac.jp.

† Institute for Technical Biochemistry, University of Stuttgart.

The specific chemistry of 2-(2-pyridinyldithio)ethaneamine hydrochloride (PDEA) that is normally used to perform site-controlled coupling of proteins to biosensor surfaces in the BIAcore system (*12*, *13*) inspired us to develop a reusable biosensor. With the described PDEA-dependent thiol coupling method (*14*), haptens containing a carboxyl group (i.e., 2,4-D) can be immobilized to a biosensor surface and removed again by a reducing step with a dithiothreitol solution. Using one biosensor chip, a calibration plot for the model compound 2,4-D has been generated that makes the quantitative detection of this herbicide down to a concentration of 0.1 μg/mL, the maximum admissible concentration of this pesticide in drinking water, possible.

The BIAcore SPR technology is also a powerful tool for binding affinity studies of haptens to related antibodies. The most common approach involves a competitive study in which an immobilized ligand and a soluble ligand free in solution compete for binding sites on a single analyte (solution competition) (*15*, *16*). The advantage of the solution competition experiment is that a single biosensor surface can be utilized for the determination of equilibrium association and dissociation constants (K_A and K_D, respectively) for a series of related analogues. Unfortunately, the method does not provide apparent association and dissociation rate constants (k_a and k_d, respectively). These constants characterize the association and the dissociation phases of antibodies binding to ligands in particular. They are often more reliable than the equilibrium constants. One way to determine these parameters is by direct kinetic analysis. The analogues are immobilized to the sensor surface, normally according to the amino-coupling method, and the antibody is injected over the surface at different concentrations (*17*). The disadvantage of this method is the necessity of a different sensor surface for each analogue tested (*18*), as the amino-coupling method is irreversible. Sensor chips from BIAcore are of high-quality in terms of a well-defined

10.1021/bc0100399 CCC: $22.00 © 2002 American Chemical Society
Published on Web 01/25/2002

surface chemistry, but they are, at the same time, expensive. It is, therefore, of great interest to establish a fully reversible immobilization method which makes the repeated usage of a biosensor surface possible.

Our novel approach allows for the economical direct kinetic binding studies of several ligands to related antibodies. Different ligands can be reversibly immobilized to the surface. We have carried out direct kinetic analysis of binding parameters of a polyclonal *anti*-2,4-D antibody to 2,4-D and 2,4,5-T analogues using one sensor chip.

MATERIALS

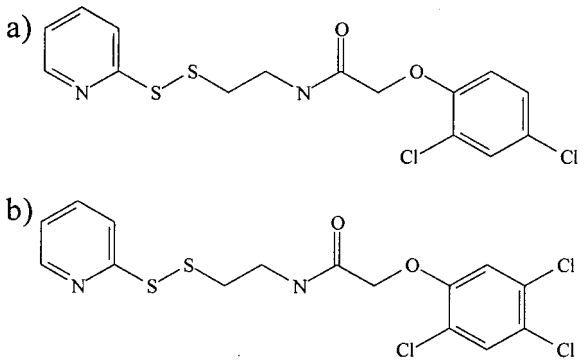
2,4-D, 2,4,5-T, and all other reagents were obtained from Wako Pure Chemical Industries, Ltd. (Tokyo, Japan) unless otherwise noted. Sodium formate and formic acid were obtained from Kanto Chemicals Co., Inc. (Tokyo, Japan). Cystamine hydrochloride was purchased from Tokyo Kasei (Tokyo, Japan). Surface plasmon resonance measurements were carried out on a BIAcore 3000 (BIAcore AB, Uppsala, Sweden) automated system using C1 four-channel sensor chips (BIAcore AB, Uppsala, Sweden). Reagents for the BIAcore instrument consisted of a HBS-EP buffer [10 mM HEPES (pH 7.4), 150 mM NaCl, 3 mM EDTA, and 0.005% polysorbate 20 (v/v)], BIAnormalizing solution [70% (w/w) glycerol], a coupling kit (containing *N*-hydroxysuccinimide (NHS), *N*-ethyl-*N*-[3-(diethylamino)propyl] carbodiimide (EDC) and 1 M ethanolamine hydrochloride (pH 8.5)), and the thiol-coupling reagent 2-(2-pyridinyldithio)ethaneamine hydrochloride (PDEA), all from BIAcore. The polyclonal *anti*-2,4-D antibody was obtained from Guildhay, Ltd. (Guildford, Surrey, U.K.).

METHODS

Immobilization of 2,4-D Analogues to a C1-Sensor Chip. All of the experiments were carried out at 25 °C and with a flow rate of 5 μL/min. Immobilization of 2,4-D to a C1-sensor chip, which has a flat carboxymethylated surface without dextran matrix, was performed according to the surface thiol method described in the BIAapplications Handbook (*14*). Briefly, the biosensor surface was normalized with BIAnormalizing solution and primed with a HBS-EP buffer. It was then activated by a 2 min injection of a solution of 0.2 M EDC and 0.05 M NHS. Cystamine dihydrochloride (40 mM, solved in 100 mM boric acid (pH 8.5)) was then injected (3 min), followed by a 3 min injection of 100 mM dithiothreitol (DTT) reducing solution (solved in 100 mM boric acid (pH 8.5)) to reduce the dithio bridges of the immobilized cystamine. Two flow cells of the biosensor chip were prepared in the described way. In the following experiments, except for the linked reactions control experiment, one was used as the measuring cell and the other as the reference cell.

A mixture consisting of 50 μL of 45 mM PDEA (solved in an MES buffer (pH 5.0)), 50 μL of NHS (0.1 M), 50 μL of EDC (0.4 M), and 50 μL of 1.81 mM 2,4-D (solved in a 10 mM PBS buffer (pH 7.4)) was incubated on ice for 1 h to obtain PDEA/2,4-D conjugates (Scheme 1a). The mixture was then injected over the modified biosensor surface of the measuring cell (7 min) in order to immobilize 2,4-D analogues; the thiopyridone leaving group from the PDEA/2,4-D conjugate was set free, and a new dithio bridge between the surface thiol and the thiol of the 2,4-D analogue was formed. A 4 min injection of PDEA/NaCl solution (20 mM PDEA and 1 M NaCl in a 100 mM formate buffer (pH 4.3)) followed to block remaining unreacted active thiol groups in both flow cells.

Scheme 1. PDEA/2,4-D and PDEA/2,4,5-T Conjugates[a]



[a] (a) PDEA/2,4-D conjugate and (b) PDEA/2,4,5-T conjugate, which consist of a thiopyridone ring (leaving group) and the 2,4-D analogue or the 2,4,5-T analogue, respectively. The analogs are bound to the biosensor surface during the immobilization step.

Linked Reactions Control Experiments. For the linked reactions control experiment, 100 nM *anti*-2,4-D antibody solution was injected for 1, 3, and 20 min over the measuring cell of the prepared biosensor surface at a flow rate of 5 μL/min. The biosensor surface was regenerated after each run with a 100 mM hydrochloric acid wash (1 min).

Direct Kinetic Binding Analysis. To determine binding affinity parameters of *anti*-2,4-D antibodies to immobilized 2,4-D analogues, we injected five concentrations of *anti*-2,4-D antibody solution (37.5, 75, 150, 300, and 600 nM) over the biosensor surface. The biosensor surface was regenerated after each run with a 100 mM hydrochloric acid wash (1 min). Sensorgrams for each solution were obtained in duplicate. The fitting of the curves to the bivalent analyte model (*19*) was carried out by the BIAevaluation software (version 3.1).

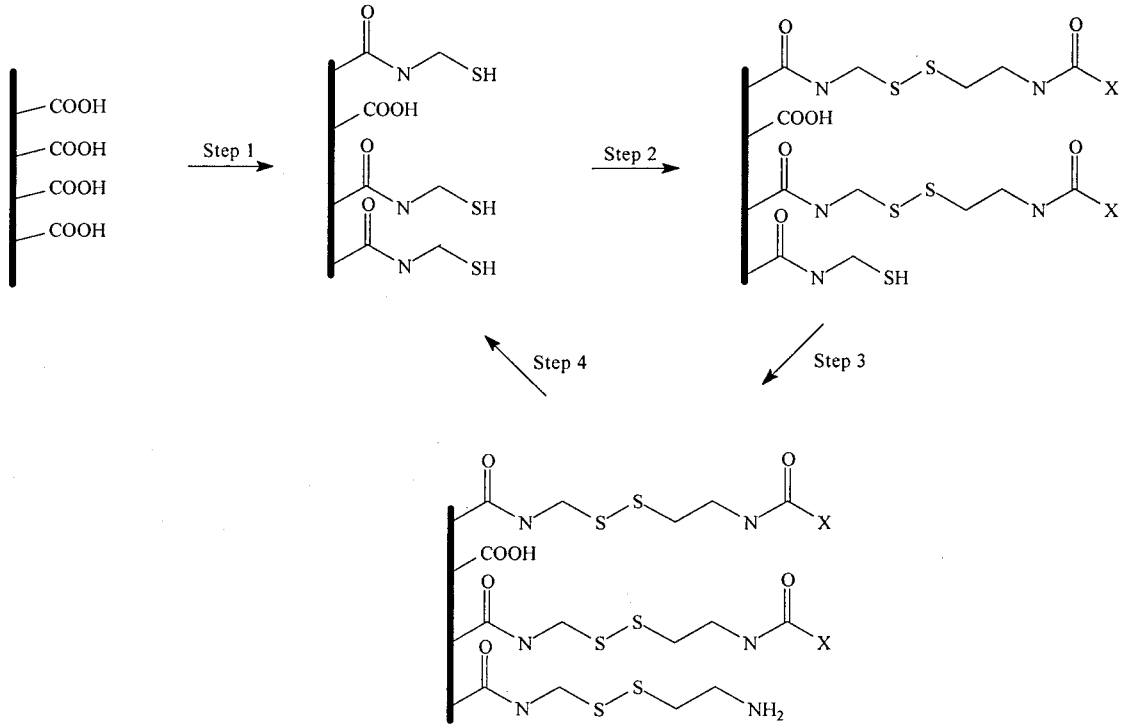
Removal of 2,4-D Analogues from the C1-Sensor Chip. 2,4-D Analogues were removed from the biosensor surface by injection of a 100 mM DTT reducing solution for 4 min. To ensure that all analogues had been removed, a 600 nM *anti*-2,4-D antibody solution was injected for 2 min.

Scheme 2 shows in an overview the preparation of the C1-sensor chip, the immobilization of carboxyl group containing hapten analogues, the blocking of unreacted thiol groups, and the removal of the analogues from the surface.

Cross-Reactivity Study. A mixture consisting of 50 μL of PDEA (45 mM in an MES buffer (pH 5.0)), 50 μL of NHS (0.1 M), 50 μL of EDC (0.4 M), and 50 μL of 1.57 mM 2,4,5-T (solved in a 10 mM PBS buffer (pH 7.4)) was incubated on ice for 1 h to obtain PDEA/2,4,5-T conjugates (Scheme 1b). The mixture was then injected for 7 min over the biosensor surface of the measuring cell, from which the 2,4-D analogues had been removed before, to immobilize the 2,4,5-T analogues. To determine binding affinity parameters of *anti*-2,4-D antibodies to immobilized 2,4-D analogues, we injected five concentrations of *anti*-2,4-D antibody solution (37.5, 75, 150, 300, and 600 nM) over the biosensor surface. The biosensor surface was regenerated after each run with a 100 mM hydrochloric acid wash (1 min). Sensorgrams for each solution were obtained in duplicate. The fitting of the curves was carried out as described previously.

Creation of a Calibration Plot for 2,4-D Using a C1-Sensor Surface. A second C1-sensor chip was prepared according to the surface thiol method as described previously. Eight mixtures consisting of 50 μL of 45 mM

Scheme 2. Overview of the Preparation of a C1-sensor Chip, the Immobilization of Analogs of Carboxyl Group Containing Haptens, the Blocking of Unreacted Thiol Groups, and the Removal of the Analogs from the Surface[a]



[a] (Step 1) Carboxyl groups on the biosensor surface are activated by the injection of a mixture of 0.2 M EDC and 0.05 M NHS (1:1) for 2 min. A 40 mM cystamine dihydrochloride solution is injected for 3 min. The dithio bridges of the immobilized cystamine are reduced by injection of a 100 mM DTT solution for 3 min. (Step 2) PDEA/*x* conjugates (*x* stands for carboxyl group containing haptens, like 2,4-D or 2,4,5-T) are injected over the sensor surface. The dithio bridges between thiopyridone, the *x* analogue is cleaved, and a new bridge between a thiol group on the sensor surface and the analogue is formed. (Step 3) Unreacted thiol groups on the sensor surface are blocked by injection of a PDEA/NaCl solution. (Step 4) Dithio bridges between the analogues and the thiol groups on the sensor surface are cleaved by a reducing step. After the reducing step, a 600 nM *anti*-2,4-D antibody solution is injected for 2 min in order to ensure that all 2,4-D analogues have been removed.

PDEA (solved in an MES buffer (pH 5.0)), 50 μL of NHS (0.1 M), 50 μL of EDC (0.4 M), and 50 μL of 2,4-D (0, 1.8, 4.5, 13.5, 27, 54, 180, and 450 μM solved in a 10 mM PBS buffer (pH 7.4)) were incubated for 1 h on ice. These mixtures were sequentially injected over the biosensor surface (7 min) of the measuring cell in order to immobilize 2,4-D analogues. A 4 min injection of PDEA/NaCl solution (20 mM PDEA and 1 M NaCl in a 100 mM formate buffer (pH 4.3)) followed to block remaining unreacted active thiol groups in both flow cells.

Immobilized levels of 2,4-D analogues were detected by injecting a 600 nM *anti*-2,4-D antibody solution (2 min) and measuring the shift of the relative response 2 min postinjection in the measuring and the reference cell. The antibody solution was injected 5 to 10 times, depending on how fast a stable relative response level was reached.

The biosensor surfaces were regenerated after each run by washing three times with 100 mM hydrochloric acid (1 min). To remove all 2,4-D analogues from the biosensor surface before the injection of a new 2,4-D/PDEA/NHS/EDC mixture, a DTT reducing solution was injected over the biosensor surface for 4 min. To ensure that all 2,4-D analogues were removed by this reducing step, *anti*-2,4-D antibodies (600 nM) were injected over the biosensor surface (2 min).

RESULTS

Immobilization of 2,4-D Analogues on a C1-Sensor Chip and Linked Reactions Control Experiment. After conjugation of 2,4-D analogues to a C1-sensor chip by the thiol coupling method, an immobilization level of 10 RU was found. Sensorgrams obtained from the linked reactions control experiment are shown in Figure 1. The three sensorgrams show differently shaped association and dissociation profiles for increasing reaction times. This indicates a multistep reaction between the ligands on the biosensor surface and the soluble analyte. Because the analyte is a bivalent antibody, we have assumed that these results reflect its binding to one or two ligands on the surface. Dissociation of the antibody from the surface also occurs in two steps.

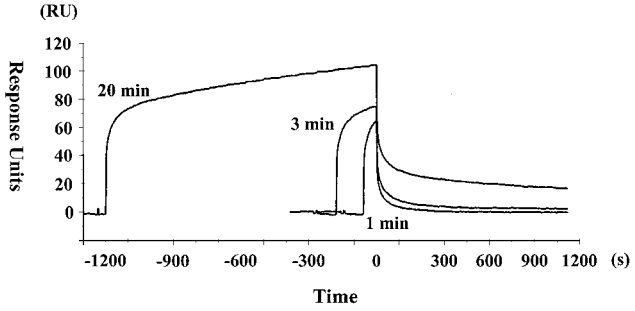


Figure 1. Linked reactions control experiment performed with *anti*-2,4-D antibodies injected over C1-sensor chip with immobilized 2,4-D analogues. A 100 nM *anti*-2,4-D antibody solution was injected for 1, 3, and 20 min over the prepared biosensor surface at a flow rate of 5 μL/min.

Determination of Binding Affinities of *Anti*-2,4-D Antibodies to 2,4-D Analogues. Sensorgrams which were obtained during the binding studies and which were fitted according to the bivalent analyte model are depicted in Figure 2. Binding parameters are shown in Table 1. Binding of the first ligand molecule is described

Table 1. Overview of the Binding Parameters Obtained from Direct Kinetic Analysis

hapten	k_a1 (1/Ms)[a]	k_d1 (1/s)[b]	K_D (1/M)	k_a2 (1/RUs)[c]	k_d2 (1/s)[d]	K_D2 (1/RU)
2,4-D	7.52×10^3	0.024	3.19×10^{-6}	8.09×10^{-5}	2.00×10^{-2}	2.47×10^2
2,4,5-T	6.42×10^3	0.215	3.35×10^{-5}	0.215	0.149	0.693

[a] Association rate constant for A + B = AB. [b] Dissociation rate constant for AB = A + B. [c] Association rate constant for AB + B = AB2. Note that the association rate constants for the second binding are 1/RUs, not 1/Ms. This is because the reaction involves complex (in RU) binding to ligand (in RU). [d] Dissociation rate constant for AB2 = AB + B. (A stands for antibody. B stands for immobilized ligand.)

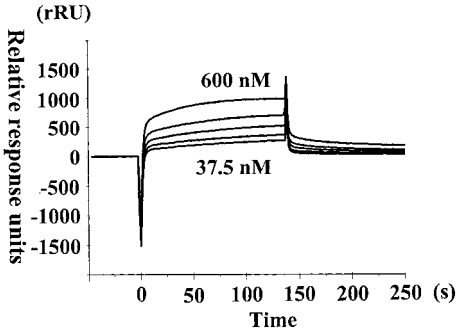


Figure 2. Direct kinetic analysis of binding of *anti*-2,4-D antibodies to 2,4-D analogues immobilized to a C1-sensor chip. Five concentrations of *anti*-2,4-D antibody solution (37.5, 75, 150, 300, and 600 nM) were injected over the biosensor surface for 2 min at a flow rate of 5 μL/min. The biosensor was regenerated after each run with a 100 mM hydrochloric acid wash (1 min).

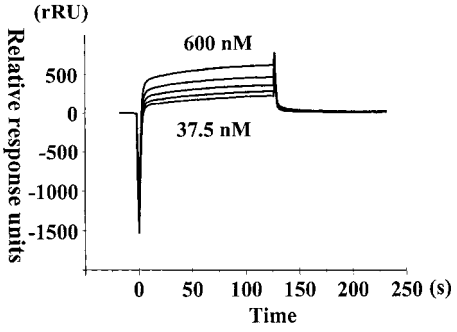


Figure 3. Direct kinetic analysis of binding of *anti*-2,4-D antibodies to 2,4,5-T analogues immobilized to a C1-sensor chip. Five concentrations of *anti*-2,4-D antibody solution (37.5, 75, 150, 300, and 600 nM) were injected over the biosensor surface for 2 min at a flow rate of 5 μL/min. The biosensor was regenerated after each run with a 100 mM hydrochloric acid wash (1 min).

by a single set of rate constants so that the two sites on the analyte are equivalent in the first binding step. Binding of the second ligand molecule is described by a second set of rate constants. The first and the second equilibrium dissociation constant calculated for *anti*-2,4-D antibodies binding to 2,4-D analogues is 3.19×10^{-6} M^{-1} and $2.47 \times 10^{+2}$ RU^{-1}, respectively.

Removal of 2,4-D Analogues from the C1-Sensor Chip. All 2,4-D analogues could be removed from the biosensor surface after reduction with a 100 mM DTT solution. No remaining 2,4-D analogues conjugated to the biosensor surface could be detected by injecting a 600 nM *anti*-2,4-D antibody solution; the relative responses (signal in the measuring cell minus the signal in the reference cell) were always decreased to nearly 0 RU.

Immobilization of 2,4,5-T Analogues on the C1-Sensor Chip and Cross-Reactivity Study. After conjugation of 2,4,5-T analogues to the C1-sensor chip, an immobilization of 8 RU was found. Sensorgrams which were obtained during the binding studies and which were fitted according to the bivalent analyte model are shown in Figure 3. Binding parameters are shown in Table 1. The first and the second equilibrium dissociation constant for *anti*-2,4-D antibodies binding to 2,4,5-T analogues is 3.35×10^{-5} M^{-1} and 6.93×10^{-1} RU^{-1}, respectively. The cross-reactivity of the *anti*-2,4-D antibody to 2,4,5-T is, therefore, 10%.

Creation of a Calibration Curve for 2,4-D. As expected, the relative response level increased with the concentration of 2,4-D in the mixtures and, therefore, with the amount of immobilized 2,4-D analogues. To obtain a calibration curve, the antibody solution was injected 5 to 10 times, depending on how fast a stable relative response level was reached. We have found that the relative response decreases during the first few cycles of detection, as shown in Figure 4, and we think this is due to a removal of only loosely bound 2,4-D analogues from the biosensor surface during the washes with 100 mM hydrochloric acid. Therefore, we have repeated the detection steps until the average of five relative responses had a standard deviation of 10%. The calibration plot of

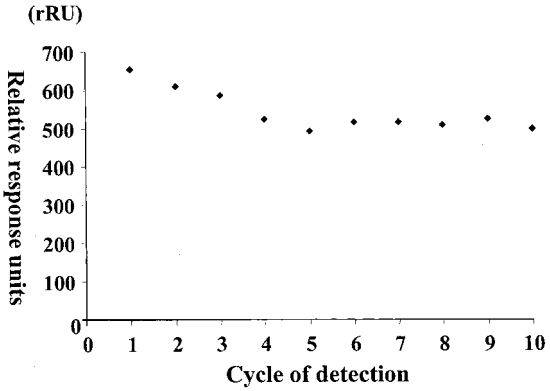


Figure 4. Stability of the relative response levels during detection of 2,4-D analogues. A mixture of PDEA, NHS, EDC, and 450 μM 2,4-D was injected over a C1-sensor chip, which was prepared according to the surface thiol method. Immobilized levels of 2,4-D analogues were detected by injection of a 600 nM *anti*-2,4-D antibody solution. After each detection cycle, the antibodies were washed from the surface by injection of a 100 mM hydrochloride solution (3 times). During the first few cycles, the relative response levels decreased because of the removal of only loosely bound 2,4-D analogues until it became stable.

the average relative responses versus the concentration of 2,4-D in the immobilized mixtures is depicted in Figure 5.

The relative responses after reduction with DTT reducing solution were always decreased to nearly 0 RU. A detection of 2,4-D analogues down to a concentration of 0.1 μg/mL was possible. In this case, the average relative response and standard deviation were 34.6 and 2.4 RU (7%), respectively.

DISCUSSION

The analytical system, BIAcore (*20*), is based on a biosensor that uses surface plasmon resonance to monitor the adsorption of biomolecules on a sensor chip. The SPR phenomenon measures changes in the refractive index in the vicinity of the surface. Such changes are correlated to the change in adsorbed mass (*21*), which makes it

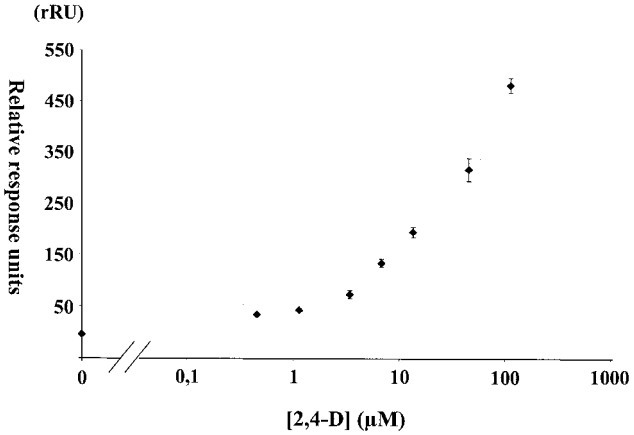


Figure 5. Logarithmic calibration plot for 2,4-D. Mixtures consisting of PDEA, NHS, EDC, and eight different concentrations of 2,4-D (0, 1.8, 4.5, 13.5, 27, 54, 180, and 450 μM) were sequentially injected over a C1-sensor chip, which was prepared according to the surface thiol method. Immobilized 2,4-D analogues were detected by a 600 nM *anti*-2,4-D antibody solution. After each run, the biosensor surface was regenerated with a 100 mM hydrochloric acid wash (1 min). The antibody solution was injected until the average of five relative responses had an SD of 10%. 2,4-D analogues were removed from the biosensor surface by reduction with a 100 mM DTT solution.

suitable for the detection of biomolecules. The larger the mass of the analyte used, the larger the instrumental response; low molecular weight analytes, like herbicides and peptides, only generate a minimal instrument response. An experiment in which the low molecular weight species is conjugated to the biosensor surface is, therefore, advantageous with regard to the generation of an instrument response upon binding of the macromolecular analyte. In this case, the low molecular weight ligand normally is immobilized to the biosensor surface by the amino-coupling method (*18*, *22*, *23*). A big disadvantage of this approach is that it necessitates the production of a different biosensor for each analogue studied, as the amino-coupling method is irreversible. We have, therefore, developed a method by which a hapten can be immobilized to and removed from one single biosensor surface of a BIAcore sensor chip for at least seven times. Considering that a BIAcore biosensor allows for 50−100 analytical cycles, depending on regeneration conditions (*20*), our method makes an even higher frequency of analytical cycles possible to be carried out.

We report, for the first time, a PDEA-dependent conjugation of haptens to a biosensor surface. Every hapten which contains a carboxyl group and which can, therefore, be conjugated to PDEA is suitable for this immobilization method. Because small molecules generally have fewer functional groups available for coupling to biosensor surfaces, in many cases they have to be modified for incorporation of a linker functionality (*18*, *23*), like a carboxyl group, for example. Also, such modified haptens are suitable for the immobilization method described here.

To obtain a calibration curve for the herbicide 2,4-D, seven different amounts of 2,4-D analogues were immobilized to the biosensor surface of a C1-sensor chip. Detection of 2,4-D analogues down to a concentration of 0.1 μg/mL, which is the maximum admissible concentration of pesticides in drinking water, was possible. A drawback with our method is that other haptens bearing carboxyl groups, such as amino acids or carboxyl acids that are present in environmental samples, might interfere with the amount of immobilized 2,4-D analogues.

In comparison to environmental samples, solutions for binding affinitiy studies are well-defined and, therefore, more suitable for our method. In this study, 2,4-D analogues were immobilized on a C1-sensor chip, and direct kinetic analysis was performed. The sensorgrams obtained were fitted according to the bivalent analyte model, which delivered detailed information about the first and the second binding steps of the bivalent analytes to the immobilized haptens. We have used the same biosensor surface to immobilize 2,4,5-T analogues for direct kinetic analysis. This shows that our method allows for easy and economical direct kinetic analysis of binding of several ligands to related antibodies. Cross-reactivity studies can be performed as shown in this paper.

The equilibrium dissociation constants (K_D) calculated for the first (and the second) site binding were 3×10^{-6} M^{-1} ($2.5 \times 10^{+2}$ RU^{-1}) and 3×10^{-5} M^{-1} (7×10^{-1} RU^{-1}) for 2,4-D and 2,4,5-T analogues, respectively, showing a reasonable selectivity of the antibody. The previously published equilibrium dissociation constants for the binding of *anti*-2,4-D antibodies to 2,4-D were 7×10^{-8} M^{-1} and 4×10^{-8} M^{-1} (*6*, *24*). These values showed a tighter binding than those we obtained. This might be due to the fact that we used polyclonal antibodies which were not purified and not due to the immobilization method itself.

CONCLUSION

We describe a reversible immobilization method for low molecular weight ligands containing carboxyl groups to biosensor surfaces of a BIAcore surface plasmon resonance instrument. Our method allowed us to obtain a calibration curve for the detection of the commonly used herbicide 2,4-D and to perform direct kinetic analysis of the binding affinity of a polyclonal *anti*-2,4-D antibody to the analogues of the haptens 2,4-D and 2,4,5-T using only one biosensor surface of a BIAcore sensor chip. There may be drawbacks in the described method of detection, namely, that other substances present in the environmental sample which also carry a carboxyl group might interfere with the level of immobilized 2,4-D. We have proved, however, that our method of immobilization, quantitative detection, and removal of the haptens works in principle. Regarding the kinetic analysis, we have obtained very detailed information. Apparent association and dissociation constants for the first and the second binding step of the bivalent analyte to the immobilized ligands were determined. Calculated equilibrium dissociation constants were smaller as compared to those shown in other publications, but purified monoclonal antibodies or F_{ab} fragments should deliver much better results.

ACKNOWLEDGMENT

This research was supported by the German Academic Exchange Service (DAAD).

LITERATURE CITED

(1) Matsumura, F. (1994) Differential toxicities of insecticides and halogenated aromatics. *International Encyclopedia of Pharmacology and Therapeutics, Section 113*, p 453, Pergamon Press, New York.

(2) Ibrahim, M. A., Bond, G. G., Burke, T. A., Cole, P., Dost, F. N., Enterline, P. E., Gough, M., Greenberg, R. S., Halperin, W. E., McConnel, E., Munro, I. C., Swenberg, J. A., Zahm, S. H., and Graham, J. D. (1991) Weight of the evidence on the human carcinogenicity of 2,4-D. *Environ. Health Perspect. 96*, 213

(3) Carlo, G. L., Cole, P., Miller, A. B., Munro, A. I. C., Solomon, K. R., and Squire, R. A. (1992) Review of study reporting an association between 2,4-dichlorophenoxyacetic acid and canine malignant lymphoma. *Regul. Toxicol. Pharmacol. 16*, 245.

(4) Neuberger, M., Rappe, C., Begek, S. Cai, H., Hansson, M., Jaeger, R., Kundi, M., Lim, C. K., Wingfors, H., and Smith, A. G. (1999) Persistent health effect of dioxin contamination in herbicide production. *Environ. Res., Sect. A 81*, 206−214.

(5) Wittmann. C., and Hock, B. (1991) Development of an ELISA for the analysis of atrazine metabolites deethylatrazine and deisopropylatrazine. *J. Agric. Food Chem. 39*, 1194−1200.

(6) Pena, A. L. S., and Silveira, I. N. (1997) Determination of chlorophenoxy herbicides in waters by capillary gas chromatography with ion trap detection. *J. Chromatogr., A 758*, 324−331.

(7) Horacek, J., and Skládal, P., (1997) Improved direct piezoelectric biosensors operating in liquid solution for the competitive label-free immunoassay of 2,4-dichlorophenoxyacetic acid. *Anal. Chim. Acta 347*, 43−50.

(8) Mosiello, L., Nencini, L., Serge, L., and Spano, M. (1997) A fibre-optic immunosensor for 2,4-dichlorophenoxyacetic acid detection. *Sens. Actuators, B 38−39*, 353−359.

(9) Medyantseva, E. P., Vertlib, M. G., Kutyreva, M. P., Khaldeeva, E. I., Budnikov, G. K., and Eremin, S. A. (1997) The specific immunochemical detection of 2,4-dichlorophenoxyacetic acid and 2,4,5-trichlorophenoxyacetic acid pesticides by amperometric cholinesterase biosensors. *Anal. Chim. Acta 347*, 71−78.

(10) Minunni, M., and Mascini, M. (1993) Detection of pesticide in drinking water using real-time biospecific interaction analysis (BIA). *Anal. Lett. 26*, 1441−1460.

(11) Harris, R. D., Luff, B. J., Wilkinson, J. S., Piehler, J., Brecht, A., Gauglitz, G., and Abuknesha, R. A. (1999) Integrated optical surface plasmon resonance immunoprobe for simazine detection. *Biosens. Bioelectron. 14*, 377−386.

(12) Catimel, B., Nerrie, M., Lee, F. T., Scott, A. M., Ritter, G., Welt, S., Old, L. J., Burgess, A. W., and Nice, E. C. (1997) Kinetic analysis of the interaction between the monoclonal antibody A33 and its colonic epithelial antigen by the use of an optical biosensor. A comparison of immobilization strategies. *J. Chromatogr., A 776*, 15−30.

(13) Löfas, S., Johnsson, B., Edström, A., Hansson, A., Lindquist, G., Müller Hillgren, R., and Stigh, L. (1995) Methods for site controlled coupling to carboxymethyldextran surfaces in surface plasmon resonance sensors. *Biosens. Bioelectron. 10*, 813−822.

(14) (1998) *BIAapplications Handbook,* pp 4/6−4/15, BIAcore AB, Uppsala, Sweden.

(15) Karlsson, R. (1994) Real-time competitive kinetic analysis of interactions between low-molecular-weight ligands in solution and surface-immobilized receptors. *Anal. Biochem. 221*, 142−151.

(16) Sternesjo, A., Mellgren, C., and Bjorck, L. (1995) Determination of sulfamethazine residues in milk by surface plasmon resonance-based biosensor assay. *Anal. Biochem. 226*, 175−181.

(17) Alfthan, K. (1998) Surface plasmon resonance biosensors as a tool in antibody engineering. *Biosens. Bioelectron. 13*, 653−663.

(18) Adamczyk, M., Gebler, J. C., Gunasekera, A. H., Mattingly, P. G., and Pan, Y. (1997) Immunoassay reagents for thyroid testing. 2. Binding properties and energetic parameters of a T4 monoclonal antibody and its Fab fragment with a library of thyroxine analogue biosensors using surface plasmon resonance. *Bioconjugate Chem. 8*, 133−145.

(19) (1997) *BIAevaluation Software Handbook (version 3.0),* pp C9−C12, BIAcore AB, Uppsala Sweden.

(20) Malmquist, M. (1993) Biospecific interaction analysis using biosensor technology. *Nature 361*, 186−187.

(21) Karlsson, R. Mo, J. A., and Holmdahl, R. (1995) Binding of autoreactive mouse *anti* type II collagen antibodies derived from the primary and the secondary immune response investigated with the biosensor technique. *J. Immunol. Methods 188*, 63−71.

(22) Weller, M. G., Schuetz, A. J., Winklmair, M., and Niesser, R., (1999) Highly parallel affinity sensor for the detection of environmental contaminants in water. *Anal. Chim. Acta 393*, 29−41.

(23) Adamczyk, M., Johnson, D. D., Mattingly, P. G., Moore, J. A., and Pan, Y. (1998) Immunoassay Reagents for thyroid testing. 3. Determination of the solution binding affinities of a T4 monoclonal antibody Fab fragment for a library of thyroxine analogues using surface plasmon resonance. *Bioconjugate Chem. 9*, 23−32.

(24) Skládal, P., Minunni, M., Mascini, M., Koláø, V., and Fránek, M. (1994) Characterization of monoclonal antibodies to 2,4-dichlorophenoxyacetic acid using a piezoelectric quartz crystal microbalance in solution. *J. Immunol. Methods 176*, 117−125.

BC0100399

Enzyme-Assisted Synthesis and Structure Characterization of Glucuronide Conjugates of Methyltestosterone (17α-methylandrost-4-en-17*β*-ol-3-one) and Nandrolone (estr-4-en-17*β*-ol-3-one) Metabolites

Tiia Kuuranne,[†,‡] Olli Aitio,[‡] Mikko Vahermo,[†] Eivor Elovaara,[§] and Risto Kostiainen*[,†,‡]

Viikki Drug Discovery Technology Center, FIN-00014 University of Helsinki, Finland, Division of Pharmaceutical Chemistry, Department of Pharmacy, P.O. Box 56, Viikinkaari 5E, FIN-00014 University of Helsinki, Finland, and Laboratory of Toxicokinetics and Metabolism, Department of Industrial Hygiene and Toxicology, Finnish Institute of Occupational Health, FIN-00250 Helsinki, Finland . Received March 15, 2001; Revised Manuscript Received October 5, 2001

A new and useful method based on enzyme-assisted synthesis was developed for producing 3α-*O*-*β*-D-glucuronide conjugates from synthetic phase I metabolites of methyltestosterone and nandrolone. The formed glucuronide conjugates of 17α-methyl-5α-androstane-3α,17*β*-diol (I), 17α-methyl-5*β*-androstane-3α,17*β*-diol (II), 5α-estran-3α-ol-17-one (III), and 5*β*-estran-3α-ol-17-one (IV) are urinary metabolites, indicating the human misuse of the above-mentioned anabolic androgenic steroids (AAS). The common lack of reference material precludes the use and validation of these biomarkers in human doping control. Liver microsomes from Aroclor 1254-induced rats were used as a highly active source of mammalian UDP-glucuronosyltransferases (UGT, EC 2.4.1.17). After purification by protein precipitation, liquid−liquid extraction (dichloromethane), C-18 solid-phase extraction, and lyophilization, the steroid glucuronide structures were characterized by ^{1}H and ^{13}C NMR spectroscopy and tandem mass spectrometry. The enzymatic method was highly stereoselective, producing a single major conjugate from the parent steroids I−IV. The stereochemically pure steroid glucuronide conjugates were recovered in milligram amounts (1.0−2.8 mg, yield 12−29%), which is sufficient for veterinary and human doping control analyses; for pharmaco-, toxico-, and enzyme kinetic studies in the pharmaceutical industry; for clinical laboratories; and for forensic medicine. A new sensitive LC-MS method was developed for controlling the product purity in syntheses, as well as for enzyme kinetic characterization of AAS-metabolizing UGT activities in rat liver toward the aglycones I−IV. In this study, the UGT enzymes responsible for the formation of 3α-O-linked glucuronides from the substrates I, II, III, and IV exhibited the specific enzyme activity values: 25, 124, 48, and 212 nmol/mg microsomal protein in a 2-h incubation, respectively.

INTRODUCTION

Methyltestosterone (17α-methylandrost-4-en-17*β*-ol-3-one) and nandrolone (estr-4-en-17*β*-ol-3-one) are exogenous anabolic androgenic steroids (AAS) and widely misused in human sports. Because of their nonpolar character, AAS are extensively metabolized by routes involving functionalization (phase I) and conjugation (phase II) reactions prior to excretion in urine. AAS molecules with a 3-keto-4-ene structure undergo enzymatic reduction of the C4−C5 double bond in the A-ring as a rate-limiting step, which is catalyzed by 5α- and 5*β*-reductases (Figure 1). As soon as the double bond is reduced, the 3-keto-group is transformed mainly to a 3α-hydroxy structure (*1*, *2*). Phase I reactions thus provide attachment sites for subsequent conjugation reactions mediated by phase II metabolism. For AAS, the main conjugation pathway is glucuronidation (*3*), an S_N2 reaction between the donating coenzyme uridine-5′-

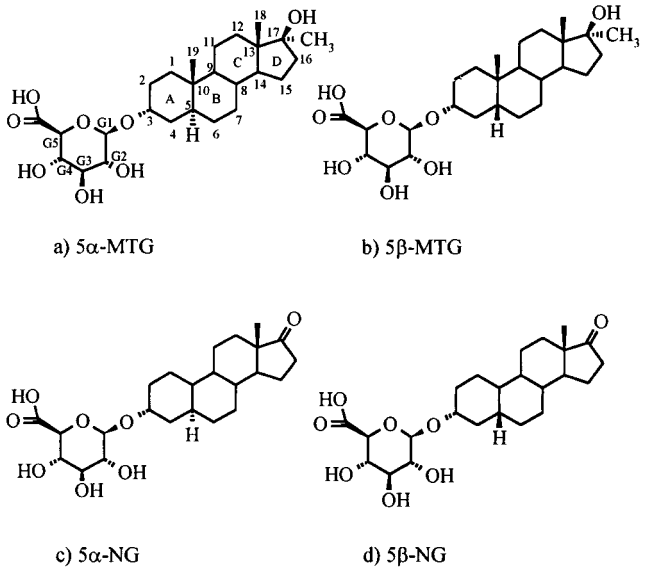


Figure 1. Structures and nomenclature of AAS glucuronides. (a) 17α-methyl-5α-androstane-17*β*-ol-3α-*O*-(*β*)-glucuronide, (b) 17α-methyl-5*β*-androstane-17*β*-ol-3α-*O*-(*β*)-glucuronide, (c) 5α-estran-17-one-3α-*O*-(*β*)-glucuronide, and (d) 5*β*-estran-17-one-3α-*O*-(*β*)-glucuronide.

* Corresponding author, Tel.: +358-(0)9-191 59 134, Fax: +358-(0)9-59 556, e-mail: risto.kostiainen@helsinki.fi.

† Viikki Drug Discovery Technology Center, University of Helsinki.

‡ Division of Pharmaceutical Chemistry, University of Helsinki.

§ Finnish Institute of Occupational Health.

10.1021/bc010038g CCC: $22.00 © 2002 American Chemical Society
Published on Web 02/06/2002

Table 1. Yields of the Syntheses and Kinetic Data of Steroid Glucuronides

		bulk synthesis[b]		reaction velocity:[c] enzymic glucuronidation activity (nmol/mg protein per 2 h) at different substrate concentrations (μM)						
substrate[a]	product (glucuronide)	yield (mg)	yield (%)	1	10	50	100	250	1000	exogenous source [ref]
I	5α-MTG 17α-methyl-5α-androstan-17β-ol-3α-*O*-glucuronide	1.0	12	0.6	4.9	18	21	20	25	mestanolone, methyltestosterone, oxymetholone [*1, 2, 39*]
II	5β-MTG 17α-methyl-5β-androstan-17β-ol-3α-*O*-glucuronide	2.8	29	0.9	8.3	40	79	124	124	methandriol, methyltestosterone, metandienone [*1, 2, 39*]
III	5α-NG 5α-estran-17-one-3α-*O*-glucuronide	1.3	16	0.7	3.7	18	30	45	48	nandrolone [*1, 2, 39*]
IV	5β-NG 5β-estran-17-one-3α-*O*-glucuronide	1.1	13	1.0	10.1	44	83	178	212	nandrolone [*1, 2, 39*]

[a] (I) 17α-methyl-5α-androstane-3α,17β-diol; (II) 17α-methyl-5β-androstane-3α,17β-diol; (III) 5α-estran-3α-ol-17-one; (IV)5β-estran-3α-ol-17-one. [b] 1 mM substrate and 5 mM UDPGA concentrations used for the biosyntheses (duration 24 h). [c] Assayed with liver microsomes from Aroclor 1254 treated rats under conditions essentially the same as in bulk syntheses.

diphospho-α-D-glucuronic acid (UDPGA) and a nucleophilic steroid aglycone, yielding β-D-glucuronides through a configurational inversion of the α-glycosidic bond (*4*). Steroids possessing either a 3α- or 17β-hydroxyl group are predominantly metabolized by the UGT-mediated pathway (*5*), whereas steroids with the 3β-hydroxyl structure are mostly excreted as sulfates (*6, 7*). Studies with isoenzyme preparations of animal and human UGTs, obtained by protein purification or by cDNA-expression techniques, have revealed that members of both the UGT1 and UGT2 families carry out C18 and C19 steroid glucuronidation (*3, 8*−*16*).

The development of a synthesis method for the production of AAS glucuronides is of great interest due to the current lack of commercial reference compounds, especially in the case of exogenous AAS. In addition to veterinary and human doping control analyses, synthetic steroid glucuronides are applicable as reference material for analyses in the pharmaceutical industry, clinical laboratories, and forensic medicine. Regarding recent advances in method development, the adoption of liquid chromatography−mass spectrometry (LC-MS) techniques provides an alternative pathway for direct and straightforward analysis of nonvolatile steroid conjugates, offering a rapid analysis system under the growing pressure of sample input.

Reports of chemical syntheses of steroid glucuronide conjugates have been widely published (*17*−*22*). The problem with the classical synthesis is the possible formation of a racemic mixture of α/β-anomer and additional byproducts (*18*). Enzyme-assisted synthesis may offer an elegant way to produce stereochemically pure steroid glucuronides by virtue of the stereoselectivity encountered in nature for biochemical catalysts, i.e., UGT enzymes (*3*). Methods using rat liver preparations as a source of conjugating enzymes have been described for a structurally diverse group of substrates, e.g., *p*-nitrophenol (*23*); a series of nitrogen-containing antidepressants (*24*); nitrocatechols (*25, 26*); androsterone, androstanediol, dihydrotestosterone (*27*); epitestosterone (*28*); and testosterone (*29*−*31*).

The purpose of the present study was to develop and optimize a synthesis method for enzyme-assisted production of *O*-glucuronide conjugates derived from four AAS metabolites relevant to human metabolism and the abuse of exogenous steroids. The steroid aglycones 17α-methyl-5α-androstane-3α,17β-diol (I), 17α-methyl-5β-androstane-3α,17β-diol (II), 5α-estran-3α-ol-17-one (III), and 5β-estran-3α-ol-17-one (IV) each yielded a major product corresponding to the 3α-*O*-glucuronides referred to as 5α-MTG, 5β-MTG, 5α-NG, and 5β-NG (Figure 1). The synthesized products were characterized by NMR and tandem mass spectrometry and used as reference material for the development of a sensitive LC-MS method suitable for our present and future UGT enzyme kinetic studies.

EXPERIMENTAL SECTION

Chemicals. Steroid aglycones I, III, and IV (see Table 1) were purchased from Steraloids (Wilton, NH). Compound II was synthesized in our laboratory by the synthesis route of Shinohara (*32*), and the structure of the product was confirmed with the GC-EI/MS method against a standard reference of 17α-methyl-5β-androstane-3α,17β-diol. UDPGA was from Boehringer-Mannheim, and D-saccharic acid 1,4-lactone and androsterone glucuronide (internal standard) from Sigma Chemicals (St. Louis, MO). Aroclor 1254 (RCS-088/Analabs, Lot No K040) was from the Foxboro Company (North Haven, CT 06473). Solvents were of HPLC-grade. All other reagents were of analytical grade.

Preparation of Liver Microsomes. Adult female Wistar rats from Helsinki University Breeding Centre (n = 8, weight 224 ± 18 g) were killed on day 8 after administration of Aroclor 1254 (500 mg/4 mL olive oil/kg body weight on day 1, and 125 mg/1 mL/kg on day 6, intraperitoneally). The livers were perfused in situ with saline before being removed and stored at −70 °C. Liver microsomes were prepared by differential centrifugation (*33*), and the protein concentration (37.6 mg/mL) was determined according to the method of Lowry et al. (*34*). The treatment of the animals was approved by the local Ethical Committee for Animal Studies.

Bulk Synthesis. The reaction mixtures for enzyme-assisted synthesis of steroid glucuronides consisted of 1 mM of the lipophilic steroid substrates I, II, III, or IV (dissolved in 2 mL of methanol); 5 mM $MgCl_2$; 5 mM D-saccharic acid 1,4-lactone (a β-glucuronidase inhibitor); and 5 mM UDPGA in 50 mM K−Na-phosphate buffer (pH 7.4) and contained 20 mg of rat liver microsomal protein in a final volume of 20 mL. The concentration of methanol was limited to 10% to avoid protein denaturation. The enzyme reactions (started by UDPGA addition) were carried out at 37 °C (in a water bath) for 24 h in a glass vial with magnet stirring. The synthesis reaction was terminated with 2 mL of water-saturated dichloromethane (*29*), which was added for protein precipitation (15 min in an ice bath) and extraction of the residual steroid aglycone and nonpolar impurities from the synthesis mixture. A clear aqueous phase was separated by

centrifugation (14000 rpm, 10 min). The supernatant obtained was acidified with 4 N perchloric acid to ensure the neutral form of steroid glucuronides for their retention and cleanup by solid-phase extraction (SPE) with a C-18 cartridge (100 mg, International Sorbet Technology). The column was conditioned with 2.5 mL of methanol and then acidified with 2.5 mL of 1 N HCl. After loading of the sample (5 mL per a cartridge), polar impurities were removed with 2.5 mL of water and the final elution was performed with 2.5 mL of methanol. Methanol was evaporated to dryness (N_2, 60 °C), and the dry residue, which was reconstituted to 3 mL with water, was frozen and lyophilized. This step enabled the formation of white crystals of steroid glucuronides.

Mass Spectrometric Characterization. The mass spectra were recorded by Perkin-Elmer Sciex API 300 (Sciex, Concord, Canada) triple quadrupole instrument equipped with electrospray ion source (ESI). Samples were introduced by loop injection, and both positive and negative ion MS and MS/MS spectra were measured. Operation parameters, as well as the MS and MS/MS behavior of the glucuronides studied, have been presented in detail earlier (*35*).

LC-MS Procedure. The LC-MS method was developed for the detection of synthesis impurities and for the enzyme kinetic studies. Liquid chromatography consisted of Perkin-Elmer LC 200 Series micro pump and Series 200 autosampler, and Phenomenex Luna C-18 (150 × 1.0 mm, particle size 5 μm) micro column. The total eluent flow of 100 μL/min was split after the column by a ratio of 1:10 (ICP-04−20, LC-Packings). HPLC eluent A was 15 mM ammonium acetate/formic acid buffer (pH 4.2) in water:acetonitrile (9:1, v/v), and eluent B included the same buffer and acetonitrile but in a reversed ratio (1:9, v/v). The gradient was set as a linear increase of the eluent B content from 10% to 50% in 15 min, corresponding to an actual acetonitrile gradient from 18% to 50%. The column was equilibrated for 11 min after each analysis. The injection volume was 5 μL.

NMR Spectroscopy. Steroid glucuronides were dissolved in 40 μL of acetone-d_6. The NMR experiments were carried out on a Varian Unity 500 spectrometer at 23 °C using a gHX nano-NMR probe. For the DQFCOSY (*36*) experiment (16 scans per t_1 value), a matrix of $2k \times 256$ points was collected and zero-filled to $2k \times 512$. A cosine-bell weighting function was used in both dimensions. For the HMQC (*37*) and HMBC (*38*) spectra (32 and 64 scans per t_1 value, respectively), matrixes of $2k \times 256$ and $2k \times 128$ points were recorded and zero-filled to $2k \times 512$ and $2k \times 256$ points, respectively. A cosine-bell weighing function was used. The average $^1H-^{13}C$ coupling constant was estimated to be 150 Hz and Δ_2 was 60 ms. The ^1H and ^{13}C chemical shifts were referenced to residual acetone, 2.05 and 29.92 ppm, respectively.

Enzyme Activity Studies. The kinetic data obtained for microsomal UGT activity toward the parent steroid aglycones I, II, III, and IV represent mean values of duplicate incubations performed and analyzed all on the same day. In enzyme activity assays the final incubation volume was 100 μL, the microsomal protein content 100 μg, and the test concentration of each substrate 1, 2.5, 5, 10, 25, 50, 100, 250, 500, and 1000 μM. Otherwise, the composition of the reaction mixture was the same as in bulk synthesis. The glucuronidation reaction (preincubated for 11min) was started with the addition of UDPGA, incubated for 2 h at 37 °C before being stopped with 10 μL of 4 N perchloric acid and by chilling the sample tubes for 15 min in an ice bath (protein precipitation). An internal standard, androsterone glucuronide (10 μM), was added prior to centrifugation (14000 rpm, 10 min). The supernatant was cleaned up by the same C-18 SPE procedure as in bulk synthesis, with the exception that the final elution was in 500 μL acetonitrile. The sample was evaporated to dryness (N_2, 60 °C) and diluted in 100 μL of eluent A for LC-MS analysis. The four most concentrated samples of each series (substrate concentration 100−1000 μM) were additionally diluted 10-fold with eluent A to ensure that the measurement was within the dynamic range of ESI-MS. The steroid glucuronide formation was calculated by using the ratio of the peak area of ammonium adduct $[M + NH_4]^+$ of analyte (A_A) and that of the internal standard (A_{ISTD}), i.e., $v = A_A/A_{ISTD}$.

RESULTS AND DISCUSSION

Bulk Synthesis. Figure 1 shows the steroidal 3α-*O*-β-D-glucuronides (5α- and 5β-MTG, 5α- and 5β-NG) formed from 17α-methyl-5α-androstane-3α,17β-diol (I), 17α-methyl-5β-androstane-3α,17β-diol (II), 5α-estran-3α-ol-17-one (III), and 5β-estran-3α-ol-17-one (IV) by means of enzyme-driven syntheses. The compounds I and 5α-MTG can be detected in human urine after dosing with mestanolone, methyltestosterone, or oxymetholone, and the compounds II and 5β-MTG after methandriol, methyltestosterone, or metandione intake (*39*). The compounds III, IV, 5α-NG, and 5β-NG originate from nandrolone metabolism (*39*). Notably, we used liver microsomes from female rats pretreated with a mixture of polychlorinated biphenyls (Aroclor 1254) as the enzyme source. According to human excretion studies, the metabolites synthesized here (Figure 1 and Table 1) are, evidently, also formed in man (*1*, *2*, *39*). The method described in this work is suitable for producing milligram quantities of stereochemically pure steroid glucuronides at reasonable costs. This amount is enough for metabolic in vitro studies as well as for doping control analysis. The concentrations in these analyses are typically below 1 μg/mL, and therefore standard material of 1 mg of steroid glucuronide is enough for more than 1000 analyses.

The data in Table 1 summarize the results for bulk syntheses of the four steroid glucuronides illustrated in Figure 1. We also show the results from the short-term kinetic studies describing the reaction velocities of the present enzyme-driven syntheses. The UGT activities in rat liver microsomes were tested toward the parent steroids I − IV at 10 different substrate concentrations (1−1000 μM) using a reaction time of 2 h and a 5 mM UDPGA concentration. These findings suggested that at a 250−1000 μM substrate concentration the reaction velocity is maintained nearly at maximum for each substrate (I−IV). The efficiency of the rat enzyme source to glucuronidate different steroids exhibited an 8-fold difference. This was revealed by the specific enzyme activities varying from 25 to 212 nmol/mg protein per 2 h (Table 1). Moreover, the 5α-MTG and 5α-NG products were clearly formed at lower specific rates than the 5β-MTG and 5β-NG anomers. Despite careful optimization of the initial reaction conditions (substrate, UDPGA, and microsomal protein), the yields of single syntheses remained lower than expected by the reaction velocities measured for the biosyntheses of 2 h (Table 1). A plausible explanation may lie in the uncertainty of maintaining the optimal reaction conditions throughout an incubation time extended over up to 24 h. Another obvious reason for low yields is the poor solubility of the substrates in aqueous incubation media. This problem could be only partly resolved by addition of methanol,

Table 2. Mass Spectrometric Data of Steroid Glucuronides; *m/z* (rel abundance)[a]

ion	5α-MTG	5β-MTG	5α-NG	5β-NG
	Positive Ion MS			
$[M + Na]^+$	505 (36)	505 (38)	n.d.[b]	475 (43)
$[M + NH_4]^+$	500 (100)	500 (100)	470 (100)	470 (100)
	Negative Ion MS			
$[M - H]^-$	481 (100)	481 (100)	451 (100)	451 (100)
Positive Ion MS/MS, Precursor $[M + NH_4]^+$, Collision Offset, 25 V				
$[M + NH_4]^+$	500 (3)	500 (1)	470 (7)	470 (4)
$[M + H]^+$	n.d.	n.d.	453 (7)	453 (2)
$[M + H - 2H_2O]^+$	447 (1)	447 (1)	417 (5)	417 (20)
$[M + H - Glu]^+$	n.d.	n.d.	277 (19)	277 (72)
$[M + H - Glu - H_2O]^+$	289 (16)	289 (22)	259 (100)	259 (100)
$[M + H - Glu - 2H_2O]^+$	271 (100)	271 (100)	241 (54)	241 (68)
$[Glu + H]^+$	177 (6)	177 (2)	177 (25)	177 (7)
$[Glu + H - H_2O]^+$	159 (10)	159 (3)	159 (37)	159 (15)
$[Glu + H - 2H_2O]^+$	141 (12)	141 (6)	141 (56)	141 (25)
Negative Ion MS/MS, Precursor $[M - H]^-$, Collision Offset, 40 V				
$[M - H]^-$	481 (89)	481 (100)	451 (52)	451 (57)
$[M - H - H_2O]^-$	463 (6)	463 (6)	433 (5)	433 (3)
$[M - H - CH_3COOH]^-$	421 (2)	421 (3)	391 (5)	391 (5)
$[M - H - 118]^-$	363 (5)	363 (4)	n.d.	333 (4)
$[M - H - 134]^-$	347 (1)	347 (2)	317 (4)	317 (2)
$[M - H - Glu - 2H]^-$	303 (1)	303 (4)	273 (12)	273 (3)
$[Glu - H]^-$	175 (28)	175 (15)	175 (2)	n.d.
$[Glu - H - H_2O]^-$	157 (36)	157 (18)	157 (11)	157 (9)
$[Glu - H - H_2O - CO]^-$	129 (16)	129 (9)	n.d.	129 (6)
$m/z = 113$	(90)	(59)	(75)	(55)
$m/z = 95$	(10)	(6)	(12)	(7)
$m/z = 85$	(100)	(41)	(100)	(100)
$m/z = 75$	(89)	(49)	(82)	(82)
$m/z = 59$	(12)	(3)	(6)	(5)

[a] See nomenclature in Figure 1. [b] n.d. = not detected.

because the amount of organic solvent must be less than 10% to avoid denaturation of enzyme catalysts.

The purity of the synthesis products was characterized with LC-MS. The total ion chromatograms showed only one intense peak corresponding to the steroid glucuronide, and no impurities were detected. Despite a complex incubation matrix containing biological material, a simple procedure based on protein precipitation and liquid−liquid extraction with dichloromethane followed by C-18 SPE was adequate for efficient and rapid cleanup of the syntheses. The chemical stability of aryl and alkyl glucuronides has earlier been reported to be good (*18*). However, during our LC-MS studies it was evident that acid-catalyzed methylation of the glucuronide moiety occurred in standard samples, which were stored in a freezer for more than two weeks in the presence of methanol and at pH 4.2. Stock solutions were therefore prepared in acetonitrile and stored in a freezer for several months without any detectable changes in the steroid glucuronide structure.

Mass Spectrometry. The abundant ammonium adduct ions $[M + NH_4]^+$ and deprotonated molecules $[M - H]^-$ recorded in positive and negative ESI-MS, respectively, indicate the correct molecular weights of the synthesized steroid glucuronides. The product ion spectra of $[M + NH_4]^+$ and $[M - H]^-$ show diagnostic product ions $[M + H - Glu]^+$, $[M + H - Glu - H_2O]^+$, $[M + H - Glu - 2H_2O]^+$ and $[M - H - Glu - 2H]^-$, indicating clearly the presence of the glucuronide moiety (Table 2). These ions also provide strong evidence for the expected *O*-glucuronidation. The product ions $[Glu + H]^+$, $[Glu + H - H_2O]^+$, $[Glu - H]^-$, and $[Glu - H - H_2O]^-$ provide further evidence for the presence of the glucuronide moiety. The isomers 5α-NG and 5β-NG can be distinguished according to the ratio of relative abundances of product ions $[M + H - Glu]^+/[M + H - Glu - H_2O]^+$, which is significantly higher for 5β-NG than for 5α-NG. However, the product ion spectra of 5α-MTG and 5β-MTG pair were strongly analogous and thus without a distinction of isomers. A more detailed discussion about MS and MS/MS behavior of the compounds is presented in our earlier paper (*35*).

NMR Spectroscopy. For structural analysis, the ^1H and ^{13}C spectra of each steroid glucuronide were assigned. The ^1H signals were assigned from DQFCOSY,

Table 3. ^1H and ^{13}C NMR Chemical Shifts [ppm][a]

^1H	5α-MTG	5β-MTG	5α-NG	5β-NG	^{13}C	5α-MTG	5β-MTG	5α-NG	5β-NG
GH1	4.443	4.511	4.451	4.512	GC1	102.35	102.16	102.37	102.26
GH2	3.254	3.204	3.249	3.191	GC2	74.32	74.48	74.44	74.42
GH3	3.463	3.445	3.455	3.436	GC3	77.14	77.14	77.15	77.16
GH4	3.621	3.609	3.619	3.604	GC4	72.56	72.59	72.56	72.62
GH5	3.838	3.842	3.842	3.838	GC5	75.78	75.86	75.82	75.87
H1	1.395	0.961	1.264	1.538	C1	33.08	35.86	24.50	31.99
H1′	1.395	1.826	1.643	1.691	C2	25.83	27.33	29.86	26.54
H2	1.528	1.307	1.321	1.197	C3	74.07	78.94	73.68	78.95
H2′	1.823	1.791	2.014	1.787	C4	34.99	34.93	39.90	34.97
H3	3.957	3.680	4.006	3.686	C5	39.91	42.91	36.87	36.52
H4	1.454	1.547	1.183	1.615	C6	29.03	27.77	34.00[b]	26.43
H4′	1.454	1.820	1.795	1.678	C7	32.05	26.91	30.46[b]	25.68
H5	1.644	1.396	1.507	1.800	C8	36.99	37.55	41.41	42.06
H6	0.117	1.247	1.019[b]	1.256	C9	55.00	41.30	48.98	39.39
H6′	1.173	1.877	1.572[b]	1.941	C10	n.d.	n.d.	47.45	40.86
H7	0.890	1.110	1.019[b]	1.192	C11	21.03	21.11	25.46	25.55
H7′	1.668	1.437	1.776[b]	1.553	C12	32.38	32.60	32.47	32.51
H8	1.435	1.492	1.284	1.282	C14	51.56	51.45	51.32	51.08
H9	0.720	1.43[c]	0.717	1.320	C15	23.81	23.91	21.99	22.13
H10	n.d.[d]	n.d.	0.808	1.416	C16	39.28	39.44	35.86	35.93
H11	1.277	1.29[c]	1.138	1.106	C17(CH_3)	26.24	26.31	-	-
H11′	1.576	1.48[c]	1.839	1.763	C18(CH_3)	14.35	14.36	13.85	13.89
H12	1.240	1.314	1.185	1.264	C19(CH_3)	11.59	23.65	-	-
H12′	1.487	1.507	1.693	1.712					
H14	1.213	1.326	1.326	1.415					
H15	1.222	1.227	1.532	1.526					
H15′	1.55[c]	1.548	1.921	1.930					
H16	1.590	1.617	1.990	1.996					
H16′	1.825	1.833	2.378	2.376					
H17(CH_3)	1.169	1.192	-	-					
H18(CH_3)	0.842	0.839	0.849	0.848					
H19(CH_3)	0.831	0.958	-	-					

[a] See nomenclature in Figure 1. [b] C6−H6,H6′ and C7−H7,H7′ may have to be interchanged. [c] From HMQC. [d] n.d., not determined.

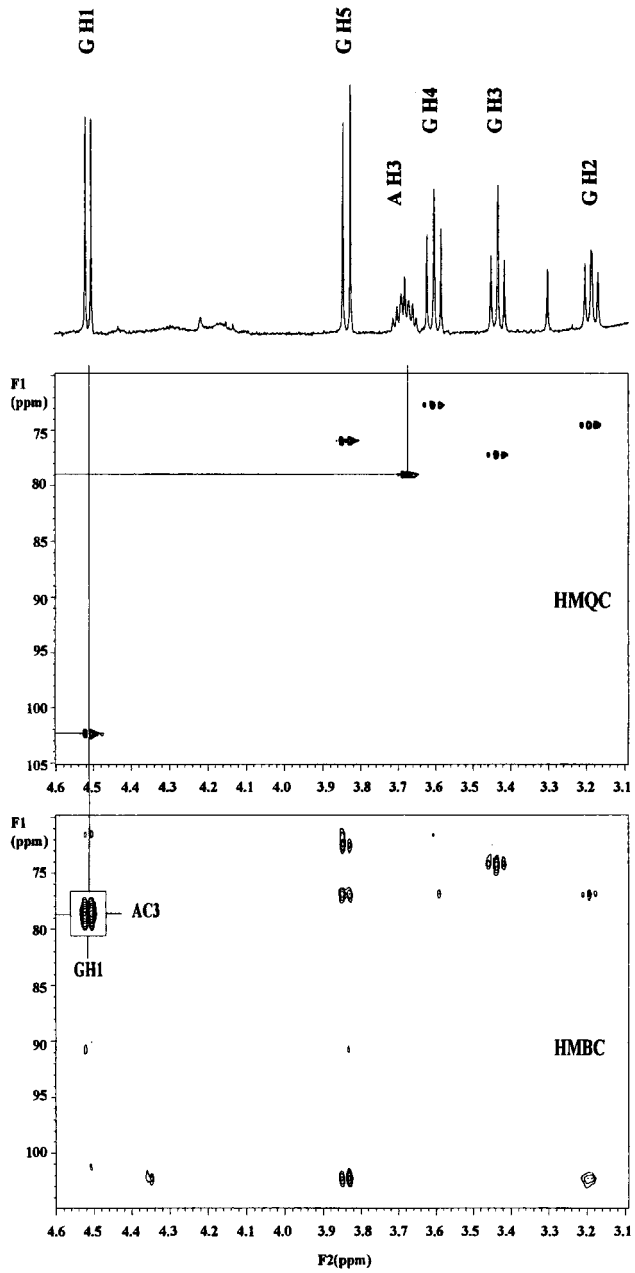


Figure 2. Expansion of 1D, HMQC and HMBC spectra of 5β-NG. In the 1D spectrum, a typical aglycone H3 resonance (AH3) of a H3β−H5β configuration is seen. The solid lines in HMQC and HMBC spectra with $J_{GH1,GH2}$ = 7.7 Hz establish the glycosidic linkage to be β(1→3).

and the corresponding ^{13}C resonances were located from the HMQC spectrum (Table 3). The anomericity of the glucuronide moieties was determined from the vicinal coupling constant $^3J_{GH1,GH2}$. As the measured coupling constants of 7.7−7.8 Hz are typical values between two axial protons (*40*), the β-configuration was confirmed. The aglycone H3 resonance in the ^1H spectra of 5α-MTG and 5α-NG appears as a quintet with a coupling constant of ∼2.5 Hz as expected for the H3β-H5α steroids (*41*). On the other hand, the corresponding H3 resonance in ^1H spectra of 5β-MTG and 5β-NG is a multiplet of seven peaks (Figure 2), which is the typical pattern for the H3β-H5β-configuration (*41*). These results confirm the expected anomericity at H5 for each steroid. Finally, the positions of the glycosidic linkages of each steroid glucuronide were identified from the interglycosidic correlation in the HMBC spectra. In each HMBC spectra the resonance correlating H1 of the glucuronide to C3 of the aglycone was observed (Figure 2).

Liquid Chromatography−Mass Spectrometry. A sensitive LC-MS method was developed for the determination of steroid-glucuronidation activities. Steroid glucuronide structures possess neither chromophores nor fluorophores, and therefore conventional LC methods based on UV or fluorescence detection are not applicable. The method showed a good linearity as indicated by the calibration curves, which were linear over a wide concentration range of 10 to 5000 ng/mL and exhibited correlation coefficients (r^2) between 0.9989 and 0.9993. The quantitation limit of the present method was sufficient for the determination of steroid metabolizing UGT activity in small-volume enzyme assays (100 μL) with a very low aglycone (I, II, III, IV) concentration, starting from 1 μM and upward (Table 1). It is of the utmost importance to work with diluted samples due to the limited dynamic range of ESI-MS. The signal saturation at higher concentrations than 10−50 μM is due to droplet surface saturation in the ESI process (*42*).

Enzyme Kinetics. The velocity of the pathway forming glucuronides linked to the 3α-OH moiety of the parent AAS substrates I−IV was measured in hepatic microsomes from Aroclor-induced rats and with the LC-MS method described above. This UGT activity was readily quantitated even at a substrate concentration as low as 1 μM. The actual reaction rates and their dependence on the aglycone concentrations were measured at a 2 h time point and under the same conditions as used in the bulk syntheses. Because the glucuronidation activities obtained (Table 1) were not fully consistent with the assay conditions required for the determination of enzyme kinetic parameters, no K_m or V_{max} values are given. Our results on enzyme kinetics are in line with reports suggesting that the glucuronidation of hydroxyandrogens shows a high degree of stereo- and regioselectivity (*5*). The 5α-structured steroids, both C18 and C19 steroids, were glucuronidated in all test concentrations (1−1000 μM) at a clearly lower velocity than the corresponding 5β-anomers. It is also noteworthy, that our NMR data supports the assumption that 17α-CH_3 substitution hinders 17β-OH glucuronidation, and the glucuronides detected in the present biosyntheses were linked only to the 3α-hydroxy positions. Yields of the steroid glucuronides 5α-MTG, 5α-NG, and 5β-MTG were reflected by the specific activities assayed at 0.1 to 1 mM substrate concentrations. In this context, 5β-NG was a clear exception.

ACKNOWLEDGMENT

Ms. Leena Luukkanen is gratefully acknowledged for her excellent guidance with enzyme-assisted syntheses, Mr. Antti Leinonen and Dr. Kimmo Kuoppasalmi for scientific support, and the National Technology Agency (TEKES) together with the University Pharmacy (YA) for financial support.

LITERATURE CITED

(1) Schänzer, W. (1996) Metabolism of anabolic androgenic steroids: 5α- and 5β-reduction of 3-keto-4-ene steroids, Recent advances in doping analysis (4), in *Proceedings of the Manfred Donike Workshop on Dope Analysis,* March 17−22, 1996, pp 185−201.

(2) Schänzer, W. (1996) Metabolism of anabolic androgenic steroids. *Clin. Chem. 42,* 1001−1020.

(3) Mackenzie, P. I., Rodbourne, L., and Stranks, S. (1992) Steroid UDP glucuronosyltransferases. *J. Steroid Biochem. Mol. Biol. 43,* 1099−1105.

(4) Mulder, G. J., Coughtrie, M. W. H., and Burchell, B. (1990) Glucuronidation. *Conjugation reactions in drug metabolism* (G. J. Mulder, Ed.) p 51, Taylor & Francis, Great Britain.
(5) Jin, C.-J., Mackenzie, P. I., and Miners, J. O. (1997) The regio- and stereoselectivity of C19 and C21 hydroxysteroid glucuronidation by UGT2B7 and UGT2B11. *Arch. Biochem. Biophys. 341, 2*, 207−211.
(6) Makin, H. L. J., and Trafford, D. J. H. (1972) The chemistry of the steroids. *Clinics Endocrin. Metab. 1*, 333−360.
(7) Shackleton, C. H. L. (1986) Profiling steroid hormones and urinary steroids. *J. Chromatogr. Biomed. Appl. 379*, 91−156.
(8) Mackenzie, P. I., and Owens, I. S. (1983) Purification of a form of mouse liver UDP glucuronosyltransferase which glucuronidates androgens. *J. Steroid Biochem. 19*, 1097−1102.
(9) Beaulieu, M., Lévesque, E., Barbier, O., Turgeon, D., Bélanger, G., Hum, D. W., and Bélanger, A. (1998) Isolation and characterization of a simian UDP-glucuronosyltransferase UGT2B18 active on 3-hydroxyandrogens. *J. Mol. Biol. 275*, 785−794.
(10) Bélanger, G., Barbier, O., Hum, D. W., and Bélanger, A. (1999) Molecular cloning, expression and characterization of a monkey steroid UDP-glucuronosyltransferase, UGT2B19, that conjugates testosterone. *Eur. J. Biochem. 260*, 701−708.
(11) Guillemette, C., Hum, D. W., and Bélanger, A. (1995) Specificity of glucuronosyltransferase activity in the human cancer cell line LNCaP, evidence for the presence of at least two glucuronosyltransferase enzymes. *J. Steroid Biochem. Mol. Biol. 55*, 355−362.
(12) Coffman, B. L., King, C. D., Rios, G. R., and Tephly, T. R. (1998) The glucuronidation of opioids, other xenobiotics, and androgens by human UGT2B7Y(268) and UGT2B7H(268). *Drug Metab. Dispos. 26*, 73−77.
(13) Falany, C. N., Green, M. D., and Tephly, T. R. (1987) The enzymatic mechanism of glucuronidation catalyzed by two purified rat liver steroid UDP-glucuronosyltransferases. *J. Biol. Chem. 262*, 1218−1222.
(14) Falany, C. N., Green, M. D., Swain, E., and Tephly, T. R. (1986) Substrate specificity and characterization of rat liver *p*-nitrophenol, 3α-hydroxysteroid and 17*β*-hydroxysteroid UDP-glucuronosyltransferases. *Biochem. J. 238*, 65−73.
(15) Oguri, K., Kurogi, A., Yamabe, K., Tanaka, M., Yoshisue, K., Ishii, Y., and Yoshimura, H. (1996) Purification of a phenobarbital-inducible UDP-glucuronosyltransferase isoform from dog liver which catalyzes morphine and testosterone glucuronidation. *Arch. Biochem. Biophys. 325*, 159−166.
(16) Hum, D. W., Bélanger, A., Lévesque, É., Barbier, O., Beaulieu, M., Albert, C., Vallée, M., Guillemette, C., Tchernof, A., Turgeon, D., and Dubois, S. (1999) Characterization of UDP-glucuronosyltransferases active on steroid hormones. *J. Steroid Biochem. Mol. Biol. 69*, 413−423.
(17) Kaspersen, F. M., and Van Boeckel, C. A. (1987) A review of the methods of chemical synthesis of sulphate and glucuronide conjugates. *Xenobiotica 17*, 1451−1471.
(18) Stachulski, A. V., and Jenkins, G. N. (1998) The synthesis of O-glucuronides. *Nat. Prod. Rep. 15*, 173−186.
(19) Conrow, R. B., and Bernstein, S. (1971) Steroid conjugates. VI. An improved Koenings-Knorr synthesis of aryl glucuronides using cadmium carbonate, a new effective catalyst. *J. Org. Chem. 36*, 863−870.
(20) Sanaullah, and Bowers, L. D. (1996) Facile synthesis of [16, 16, 17-$^2H_3$]-testosterone, -epitestosterone and their glucuronides and sulfates. *J. Steroid Biochem. Mol. Biol. 58*, 225−234.
(21) Chung, B. C., Mallamo, J. P., Juniewicz, P. E., and Shackleton, C. H. L. (1992) Synthesis of deuterium-labeled 5α-androstane-3α, 17*β*-diol and its 17*β*-glucuronide. *Steroids 57*, 530−536.
(22) Rao, P. N., Rodriguez, A. M., and Miller, D. W. (1986) Synthesis of 5α-androstane-3α, 17*β*-diol 3- and 17-glucuronides. *J. Steroid Biochem. 25*, 417−421.
(23) Lehman, J. P., Ferrin, L., Fenselau, C., and Yost, G. (1981) Simultaneous immobilization of cytochrome P-450 and glucuronyltransferase for synthesis of drug metabolites. *Drug Metab. Dispos. 9*, 15−18.
(24) Lehman, J. P., Fenselau, C., and Depaulo, J. R. (1983) Quaternary ammonium-linked glucuronides of amitriptyline, imipramine, and chlorpromazine. *Drug Metab. Dispos. 11*, 221−225.
(25) Luukkanen, L., Kilpeläinen, I., Kangas, H., Ottoila, P., Elovaara, E., and Taskinen, J. (1999) Enzyme-assisted synthesis and structural characterization of nitrocatechol glucuronides. *Bioconjugate Chem. 10*, 150−154.
(26) Lautala, P., Kivimaa, M., Salomies, H., Elovaara, E., and Taskinen, J. (1997) Glucuronidation of entacapone, nitecapone, tolcapone, and some other nitrocatechols by rat liver microsomes. *Pharm. Res. 14*, 1444−1448.
(27) Rittmaster, R. S., Leopold, C. A., and Thompson, D. L. (1989) Androgen glucuronyl transferase activity in rat liver, evidence for the importance of hepatic tissue in 5α-reduced androgen metabolism. *J. Steroid Biochem. 33*, 1207−1212.
(28) Falany, C. N., and Tephly, T. R. (1983) Separation, purification and characterization of three isoenzymes of UDP-glucuronosyltransferase from rat liver microsomes. *Arch. Biochem. Biophys. 227*, 248−258.
(29) Rao, G. S., Haueter, G., Rao, M. L., and Breuer, H. (1976) An improved assay for steroid glucuronosyl transferase in rat liver microsomes. *Anal. Biochem. 74, 1*, 35−40.
(30) Numazawa, M., Suzuki, K., and Nambara, T. (1977) Glucuronidation of testosterone by rat liver microsomes. *Chem. Pharm. Bull. 25*, 420−426.
(31) Pacifici, G. M., Gucci, A., and Giuliani, L. (1997) Testosterone sulphatation and glucuronidation in the human liver: interindividual variability. *Eur. J. Drug Metab. Pharmacokinet. 22*, 253−258.
(32) Shinohara, Y., Baba, S., and Kasuya, Y. (1984) Synthesis of deuterium labeled 17-methyl-testosterone. *Steroids 44*, 253−260.
(33) Luukkanen, L., Elovaara, E., Lautala, P., Taskinen, J., and Vainio, H. (1997) Characterization of 1-hydroxypyrene as a novel marker substrate of 3-methylcholantrene-inducible phenol UDP-glucuronosyltransferase(s). *Pharmacol. Toxicol. 80*, 152−158.
(34) Lowry, O. H., Rosebrough, N. J., Farr, A. L., and Randall, R. J. (1951) Protein measurement with the Folin phenol reagent. *J. Biol. Chem. 193*, 265−275.
(35) Kuuranne, T., Vahermo, M., Leinonen, A., and Kostiainen, R. (2000) Electrospray and atmospheric pressure chemical ionization tandem mass spectrometric behavior of eight anabolic steroid glucuronides. *J. Am. Soc. Mass Spectrom. 11*, 722−730.
(36) Marion, D., and Wüthrich, K. (1985) Application of phase sensitive two-dimensional correlated spectroscopy (COSY) for measurements of 1H-1H spin−spin coupling constants in proteins, *Biochem. Biophys. Res. Commun. 117*, 967−974.
(37) Summers, M. F., Marzili, L. G., and Bax, A. (1986) Complete proton and carbon-13 assignments of coenzyme B12 through the use of new two-dimensional NMR experiments. *J. Am. Chem. Soc. 108*, 4285−4294.
(38) Bax, A., and Summers, M. F. (1986) ^1H and ^{13}C assignments from sensitivity-enhanced detection of heteronuclear multiple-bond connectivity by 2D multiple quantum NMR. *J. Am. Chem. Soc. 108*, 2093−2094.
(39) Schänzer, W. and Donike, M. (1993) Metabolism of anabolic steroids in man: synthesis and use of reference substances for identification of anabolic steroid metabolites. *Anal. Chim. Acta 275*, 23−48.
(40) Van Halbeek, H. NMR spectroscopy of carbohydrates. A tutorial, American Chemical Society 205th National Meeting, Denver, CO, 1993.
(41) Kirk, D. N., Gaskell, S. J., and Marples, B. A. (1995) Spectroscopic methods of steroid analysis, in *Steroid analysis* (H. L. J. Makin, D. B. Gower, and D. N. Kirk, Eds.) p 72, Chapman & Hall, Great Britain.
(42) Kostiainen, R., and Bruins, A. (1994) Effect of multiple sprayers on dynamic range and flow rate limitations in electrospray and ionspray mass spectrometry. *Rapid Commun. Mass Spectrom. 8*, 549−558.

BC010038G

A Homogeneous DNA Hybridization System by Using A New Luminescence Terbium Chelate

Shinji Sueda,[†] Jingli Yuan,[‡] and Kazuko Matsumoto*,[†]

Department of Chemistry, Waseda University, 3-4-1 Okubo, Shinjuku-ku, Tokyo 169-8555, Japan, and Department of Analytical Chemistry, Dalian Institute of Chemical Physics, Chinese Academy of Sciences, Dalian, China. Received April 16, 2001; Revised Manuscript Received December 7, 2001

Homogeneous DNA hybridization assay based on the luminescence resonance energy transfer (LRET) from a new luminescence terbium chelate, *N*,*N*,*N*^{1},*N*^{1}-[2,6-bis(3′-aminomethyl-1′-pyrazolyl)-4-phenylpyridine]tetrakis(acetic acid) (BPTA)-Tb^{3+} (λ_{ex} = 325 nm and λ_{em} = 545 nm) to an organic dye, Cy3 (λ_{ex} = 548 nm and λ_{em} = 565 nm), has been developed. In the system, two DNA probes whose sequences are complementary to the two different consecutive sequences of a target DNA are used; one of the probes is labeled with the Tb^{3+} chelate at the 3′-end, and the other is with Cy3 at the 5′-end. Labeling of the Tb^{3+} chelate is accomplished via the linkage of a biotin-labeled DNA probe with the Tb^{3+} chelate-labeled streptavidin. Strong sensitized emission of Cy3 was observed upon excitation of the Tb^{3+} chelate at 325 nm, when the two probe DNAs were hybridized with the target DNA. The sensitivity of the assay was very high compared with those of the previous homogeneous-format assays using the conventional organic dyes; the detection limit of the present assay is about 30 pM of the target DNA strand.

INTRODUCTION

Several homogeneous DNA hybridization assay systems have been reported (*1*−*4*), in which fluorescence resonance energy transfer (FRET) is used, and the target DNAs can be detected in a homogeneous solution without time-consuming and tedious immobilization of the DNAs or separation of the reaction solution (*5*). In the FRET assay, two DNA probes, each being complementary to the two different consecutive regions of a target DNA, are used. One probe has a donor dye while the other an acceptor dye. The target DNA is detected in a homogeneous manner by monitoring the sensitized emission of the acceptor resulting from the hybridization reaction. In most of the systems developed so far, organic dyes are employed as the donor−acceptor pair. However, the sensitivities of such systems are insufficient for practical use. Such low sensitivity is mostly due to the existence of the substantial background caused by the donor emission and the directly excited acceptor emission.

To circumvent this problem, we have directed our attention to the lanthanide chelates as the energy donor and have already developed a homogeneous DNA hybridization system using the BHHCT-Eu^{3+} chelate as the donor and Cy5 as the acceptor (*6*−*8*). Some of the lanthanide chelates exhibit marked distinct luminescence properties (*9*−*14*): the luminescence emission profiles of the lanthanide chelates are very sharp, usually with the fwhm of ca. 10 nm; the Stokes shift is large, usually in the range of several hundreds of nanometers; the excitation is 300−350 nm and the emission is 615 nm for the Eu^{3+} chelate and 545 nm for the Tb^{3+} chelate. Therefore, the sensitized emission band of the organic dye acceptor can easily be distinguished from the excitation light and the emission of the lanthanide chelate donor. Also, the directly excited acceptor emission is effectively suppressed to almost zero, because the absorption spectra of the acceptor organic dyes hardly overlap on those of the donor lanthanide chelates and therefore the excitation wavelength, owing to the large Stokes shift of the lanthanide chelates. Moreover, the lifetimes of the lanthanide chelates are very long (∼1 ms), and as a result, the sensitized emission of the acceptor also becomes long-lived. Thus, by employing time-resolved luminescence measurement, luminescence of the short-lived species including the directly excited acceptor emission can be eliminated (*11*−*14*).

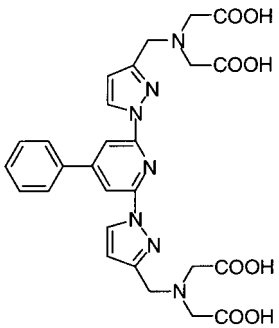


Figure 1. Structure of the BPTA ligand.

Recently, we have developed a new luminescent terbium chelate, *N*,*N*,*N*^{1},*N*^{1}-[2,6-bis(3′-aminomethyl-1′-pyrazolyl)-4-phenylpyridine]tetrakis(acetic acid), (BPTA)-Tb^{3+} (Figure 1). The synthesis and the fluorescence properties of the chelate were detailed in the previous paper (*15*). The Tb^{3+} chelate exhibits strong luminescence characteristic of Tb^{3+} ion at 545 nm by the excitation of the ligand (325 nm), whose lifetime is over 2 ms. In the present manuscript, a homogeneous DNA hybridization assay system based on the luminescence resonance

* To whom correspondence should be addressed. Phone: +81-3-5286-3108. Fax: +81-3-5273-3489. E-mail: kmatsu@mn.waseda.ac.jp.
[†] Waseda University.
[‡] Chinese Academy of Sciences.

10.1021/bc010049+ CCC: $22.00 © 2002 American Chemical Society
Published on Web 02/22/2002

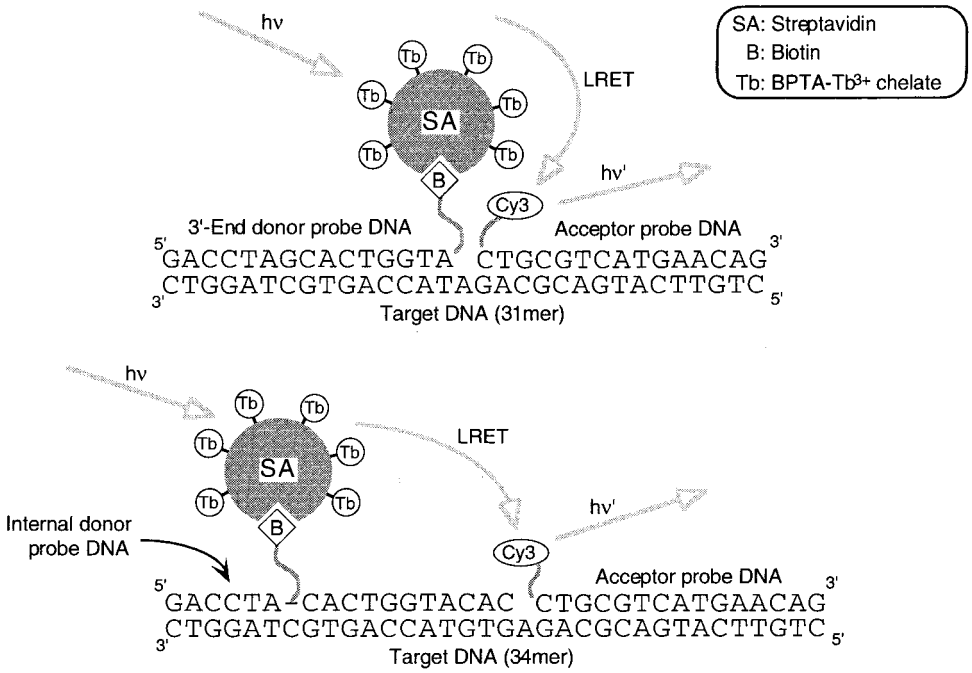


Figure 2. Principle of the homogeneous DNA hybridization assay in the present work.

energy transfer (LRET) from the BPTA−Tb^{3+} chelate to an organic dye, Cy3, is reported.

The principle of our method is illustrated in Figure 2. The acceptor Cy3 was directly introduced into the 5′-end of the probe DNA. On the other hand, the donor Tb^{3+} chelate was indirectly introduced into the probe DNA via the biotin−streptavidin bridge: the donor probe DNA was prepared by addition of the Tb^{3+} chelate-labeled streptavidin to the biotin-labeled probe DNA. In the system, the sensitized emission of Cy3 is observed via LRET in the presence of the target DNA, but not in the absence of the target DNA. Therefore, the target DNA can be detected by monitoring the sensitized emission of Cy3, in a homogeneous solution without the conventional immobilization and separation steps. In the present work, two kinds of donor probe DNAs were used, which differ in the biotin labeling position: one has a biotin label at the 3′-end (3′-end donor probe), and the other has in the internal position (internal donor probe). These two donor probe DNAs serve to examine the effect of the distance between the donor and acceptor on the energy transfer efficiency.

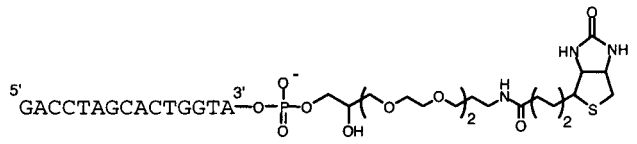
EXPERIMENTAL PROCEDURES

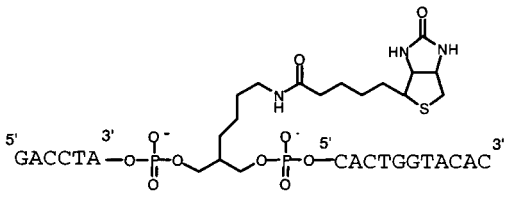
The Labeling of Streptavidin with the BPTA−Tb^{3+} Chelate. The synthesis of BPTA was reported in the previous paper (*15*). Streptavidin (SA) was labeled with BPTA by using the succinimidyl monoester of BPTA (NHS−BPTA) according to the procedure slightly modified from that of our previous report (*15*) as follows. Ten milligrams (1.5×10^{-2} mmol) of NHS−BPTA and 5 mg (8.3×10^{-5} mmol) of SA were dissolved in 0.1 M carbonate buffer (pH 9.1) (10 mL). After the solution was stirred for 4 h at room temperature, the solution was dialyzed three times against 3 L of 0.1 M $NaHCO_3$ containing 0.25 g of NaN_3, each time for 24 h at 4 °C. The labeling ratio of BPTA to SA was determined as SA-$(BPTA)_{26}$ by using the absorbance of the labeled SA solution and the molar extinction coefficient of BPTA. The complexation with Tb^{3+} was achieved by dilution of the labeled SA solution (1 mL) with 50 mM Tris-HCl buffer (pH 7.8) (24 mL) containing equimolar amount of $TbCl_3$ and incubation for a few minutes at room temperature. The luminescence of the Tb complex appeared immediately. Dilution of a nonlabeled SA solution with the same $TbCl_3$ buffer solution did not give luminescence, which confirmed that Tb^{3+} binds to BPTA and gives the luminescence. The high stability of the BPTA−Tb^{3+} complex was confirmed by the two experiments: First, the competitive binding assay with EDTA showed that the binding constant of the free BPTA with Tb^{3+} is higher than that of EDTA ($K_a > 10^{18}$). Second, the Tb^{3+} titration with BPTA labeled to SA by monitoring the Tb^{3+} luminescence showed that the chelate formation is stoichiometric in the concentration range less than that of the presence work.

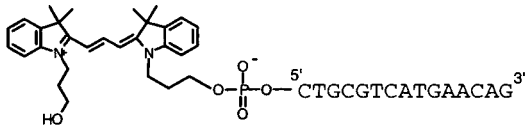
Preparation of the Probe DNAs and the Target DNAs. Figure 3 shows the probe DNAs and the target DNAs used in the present work. The 31mer and 34mer were used as the target DNAs in the 3′-end biotin probe system and the internal biotin probe system, respectively. All DNAs (oligonucleotides) were prepared on a fully automated DNA synthesizer according to the standard phosphoramide coupling method. Biotin was introduced into the 3′-end and the internal position of the oligonucleotides by using biotin TEG CPG and biotin TEG phosphoramidite (Glen Research), respectively, whereas Cy3 was introduced with Cy3 phosphoramidite (Glen Research). The purification of the oligonucleotides was carried out with reversed-phase HPLC.

Hybridization Condition. The target oligonucleotides and probe oligonucleotides were mixed at a desired ratio in the buffer containing 10 mM Tris-HCl (pH 7.8) and 0.5 M NaCl. Oligonucleotides were annealed by heating at 50 °C for 15 min and cooling to room temperature.

Luminescence Energy Transfer Measurement. To a solution of the hybridized oligonucleotides was added the solution of BPTA−Tb^{3+}-labeled SA at an 1:1 molar ratio of SA to the biotinylated DNA. The final concentrations of the probe DNAs and labeled SA were 50 nM or 10 nM. After the solution was incubated for 1 h at room temperature, the luminescence was measured with the excitation at 325 nm. The luminescence was measured







31mer 5'CTGTTCATGACGCAGATACCAGTGCTAGGTC3'

34mer 5'CTGTTCATGACGCAGAGTGTACCAGTGCTAGGTC3'

Figure 3. Sequences of the target DNAs and the probe DNAs used in the present study. The hybridization sites on the target DNAs are underlined.

on a LS-50B (Perkin-Elmer) fluorometer equipped with a Xenon flash lamp (10 μs-pulse width and repetition rate of 50 Hz). A 420 nm cut off filter was employed to eliminate the second-order scattering light. The spectra of LRET were measured in two modes. One is a normal luminescence mode, in which all the luminescence was recorded over a gate period of 80 μs after pulse excitation without delay time. The other is the time-resolved luminescence mode, in which luminescence is recorded over a gate period of 500 μs with 40 μs of delay time after pulse excitation. In this time-resolved mode, the luminescence of only the long-lived species can be detected; the fluorescence of the short-lived species are eliminated. Luminescence decay curves were obtained by measuring the luminescence intensity at 565 nm with the gate period of 10 μs gate period after the appropriate delay time. By varying the delay time, the luminescence decay curves were constructed.

RESULTS

Spectral Characteristics of the Donor and Acceptor. The emission spectrum of the BPTA−Tb^{3+} chelate bound to SA, and the emission and absorption spectra of Cy3 bound to the oligonucleotide are shown in Figure 4. The emission peak of the Tb^{3+} chelate overlaps on the absorption spectrum of Cy3, satisfying the requirement for luminescence resonance energy transfer. It should also be noted that the emission intensity of the Tb^{3+} chelate at the Cy3 emission maximum of 565 nm is very weak; the emission intensity of the Tb^{3+} chelate at 565 nm is 250 times lower than that at the Tb^{3+} chelate maximum of 545 nm. Therefore, high signal/background ratio is obtained when the sensitized emission of the acceptor is monitored at 565 nm, resulting in the highly sensitive detection of the target DNA.

Measurement of the Emission Spectra in the Normal Luminescence Mode. Figure 5 shows the

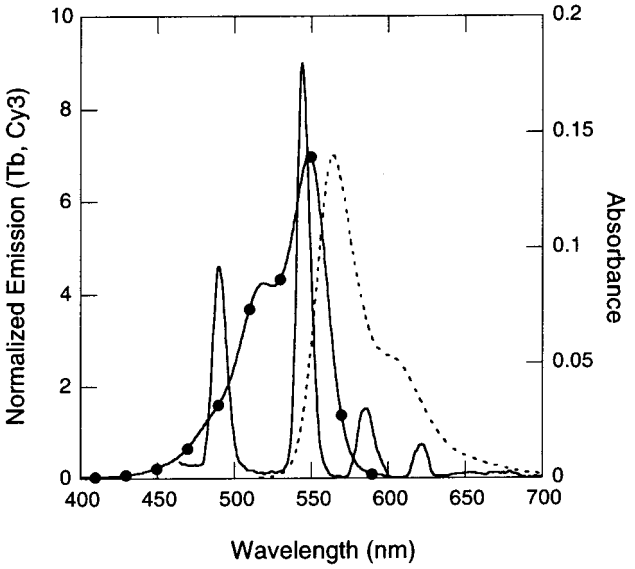


Figure 4. Spectra of the BPTA−Tb^{3+} chelate bound to SA, and Cy3 bound to the oligonucleotide. The solid line is the emission spectrum (λ_{ex} = 325 nm) of the BPTA−Tb^{3+} chelate, and the dashed line and the solid line with dots are the emission spectrum (λ_{ex} = 545 nm) and absorption spectrum of Cy3, respectively.

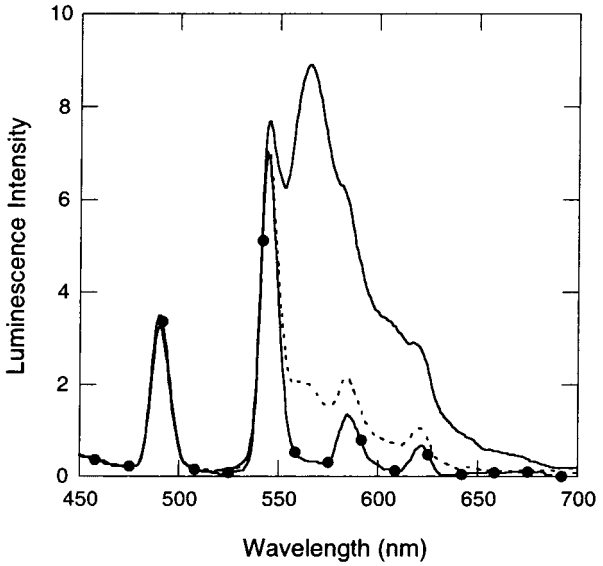


Figure 5. Comparison of the emission spectra obtained in the normal luminescence detection mode. Solid line represents the emission spectrum obtained for the 3′-end donor probe DNAs in the presence of its target DNA (31mer). Dashed line represents the emission spectrum obtained for the internal donor probe DNAs in the presence of its target DNA (34mer). Solid line with dots represents the emission spectrum observed in the absence of the target DNAs. Both of the 3′-end donor system and the internal donor system gave the identical spectrum in the absence of the target DNAs. The concentrations of the probe DNAs, the target DNAs, and SA were 50 nM.

emission spectra obtained in the normal luminescence mode, i.e., the spectra measured without delay time. The comparison of the emission spectra in the presence and absence of the target DNAs shows that the sensitized emission of Cy3 is observed only in the presence of the target DNAs. The sensitized emission is stronger in the 3′-end donor probe system than the internal donor probe system, and this is due to the well-known relation that the energy transfer efficiency decreases with R^{-6}, where R is the distance between the donor and the acceptor (*16*). The biotin is separated from Cy3 by 11 base pairs (ca.

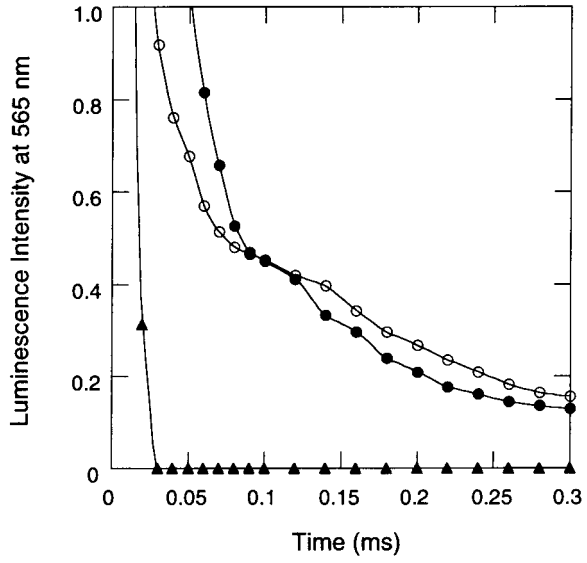


Figure 6. The luminescence decay curves of Cy3 observed at 565 nm. Closed circles are for the 3′-end donor probe DNA, and open circles are for the internal donor probe DNA. Both of the two curves were obtained in the presence of the target DNAs. The curve with triangles was obtained in the absence of the donor probe. The concentrations of the probe DNAs, the target DNAs, and SA were 50 nM.

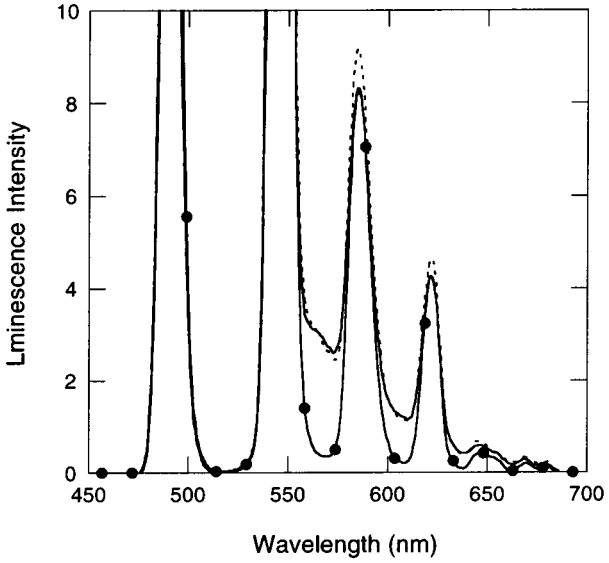


Figure 7. Comparison of the emission spectra observed in the time-resolved luminescence mode. The spectra were obtained with 40 μs delay time and 500 μs gate time. Solid line represents the emission spectrum obtained for the 3′-end donor probe DNA in the presence of its target DNA (31mer). Dashed line represents the emission spectrum obtained for the internal donor probe DNA in the presence of its target DNA (34mer). Solid line with dots represents the emission spectrum observed in the absence of the target DNAs (an identical spectrum was obtained for the both donor probe DNAs systems). The concentrations of the probe DNAs, the target DNAs, and SA were 50 nM.

35 Å) in the internal donor probe system, whereas the separation is only a single base in the 3′-end donor probe system. It is notable that the intensity of the sensitized emission obtained in the 3′-end donor probe system is significantly strong; the signal/background ratio at 565 nm is approximately 30:1 (the signal/background ratio represents the ratio of the emission intensities at 565 nm in the presence and absence of the target DNA).

Measurement of the Luminescence Decay Curves. Since the lifetime of the BPTA−Tb^{3+} chelate is very long (>2 ms), it is expected that the sensitized emission of the acceptor, Cy3, also becomes long-lived. The luminescence decay curves were measured for the sensitized emission by monitoring the intensity at 565 nm (Figure 6). Clearly, the lifetimes of the sensitized emission in both of the donor probe systems are longer-lived than that obtained in the absence of the donor probe DNAs. While exact quantitative determination of the lifetime is not possible in the present LRET, where multiple donor molecules with various distances to the acceptor molecule transfer the energy, the lifetimes were roughly estimated in the range of a few tens to a few hundreds microseconds. This long-lived property clearly demonstrates that the observed emission of Cy3 in the presence of the target DNAs is due to LRET. In Figure 6, while the luminescence intensity is stronger during the initial 0.1 ms for the 3′-end biotin probe system than for the internal biotin probe system, this relation is reversed after 0.1 ms. This means that the lifetime of the sensitized emission of Cy3 becomes longer as the distance between the donor and the acceptor increases. This behavior is explained by the mechanism of LRET as follows: when the distance is short, the efficiency of the energy transfer increases, and the lifetime of the Tb^{3+} chelate becomes short. At the same time, the lifetime of the acceptor, Cy3 decreases, since the donor Tb^{3+} chelate becomes short-lived. Therefore, the lifetime of the sensitized emission is shorter in the 3′-end biotin probe system, in which energy transfer occurs more effectively.

Measurement of the Emission Spectra in the Time-Resolved Luminescence Mode. It was found in the above decay curves that the sensitized emission of Cy3 is moderately long-lived (microsecond order) and therefore can be monitored in the time-resolved luminescence mode. Figure 7 shows the observed time-resolved luminescence spectra in the presence and absence of the target DNAs. In this detection mode, the intensity of the sensitized emission at 565 nm is almost the same in both of the two donor probe DNA systems. As shown in the decay curve experiment, the intensity of the sensitized emission is stronger during the initial 0.1 ms for the 3′-end biotin probe system than for the internal biotin probe system; however, this relation is reversed after 0.1 ms. In this work, the time-resolved spectra were obtained with the gate period of 0.5 ms after 0.04 ms of the delay time. It seems that the intensities of the sensitized emission of the Cy3 happened to be the same in both of the two probe DNA systems under the present condition.

Contrary to our expectation, the signal/background ratio at 565 nm in the time-resolved mode is lower (approximately 10:1) than that in the normal luminescence mode (approximately 30:1). In the present LRET assay, multiple Tb^{3+} chelates labeled to a large streptavidin molecule act as the donor, and the energy transfer occurs between these multiple Tb^{3+} donors and a single Cy3 molecule. The distances of the Tb^{3+} chelates to the Cy3 molecule span a substantial range, since the Tb^{3+} chelates are bound to a large streptavidin molecule. Some of the chelates efficiently transfer the absorbed energy to Cy3, whereas others do not, depending on the distance. Under such circumstances, the lifetime of the Tb^{3+} chelate is still longer than that of Cy3. At 565 nm, the Tb^{3+} chelate has weak emission. This weak emission is really weak compared to the sensitized emission of Cy3 in the normal luminescence measurement, however becomes moderately strong and constitutes the background in the time-resolved measurement, since both of the intensities are collected after 0.04 ms of delay time.

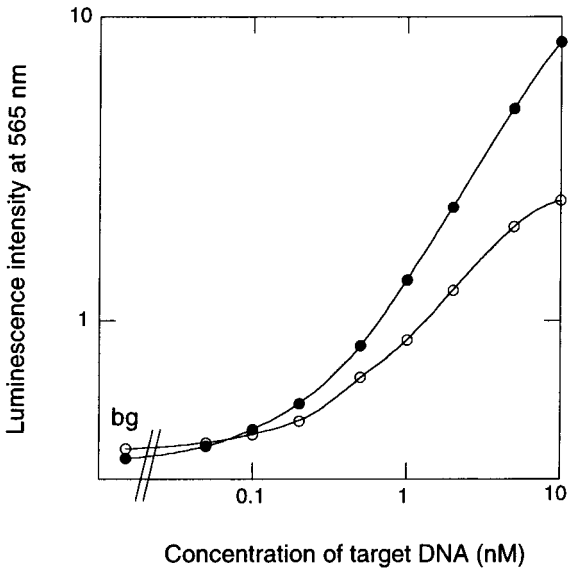


Figure 8. The plot of the Cy3 emission intensity at 565 nm against the concentration of the target DNA (31mer). The plot was obtained for the 3′-end donor probe DNA system. Closed circles are for the normal luminescence mode, and the open circles are for the time-resolved luminescence mode. The concentrations of the probe DNAs and SA were 10 nM.

This is the reason for the low signal/background ratio at 565 nm in Figure 7 than in Figure 5.

The Sensitivities for DNA Detection in the Two Detection Methods. The sensitivity of the present method was examined by using the 3′-end biotin probe system. Figure 8 shows the plot of the Cy3 emission intensity at 565 nm against the concentration of the target DNA. Figure 8 shows both of the normal mode and the time-resolved mode. The detection limit was determined as the concentration corresponding to the twice amount of the background standard deviation. Detection limits in the normal mode and the time-resolved mode are about 30 pM and 50 pM, respectively, when 10 nM of the probe DNA was used. These detection limits are 2 orders of magnitude superior to that obtained with the previous homogeneous hybridization assay (*17*).

DISCUSSION

In the present work, a homogeneous DNA hybridization assay has been developed based on the luminescence resonance energy transfer from the BPTA−Tb^{3+} chelate to Cy3. Two systems differing in the distance between the donor and the acceptor were constructed by using two donor probe DNAs, one having the biotin label at the 3′-end and the other at the internal position. As expected, the emission was more effectively sensitized in the system of the 3′-end biotin probe. By using the 3′-end biotin system, the high signal/background ratio (30:1) was obtained at 565 nm in the normal luminescence mode. Such a high signal/background ratio cannot be achieved in the systems using organic dyes as the donor−acceptor pairs. The emission and absorption peak profiles of the organic dye pairs are broad and overlap to each other to some extent; as a result, the emission of the donor and the directly excited emission of the acceptor cause substantial background to the sensitized emission. However, in our system using the Tb^{3+} chelate as the donor, the emission of the donor hardly interferes with the sensitized emission, because the emission profile of the Tb^{3+} chelate is very sharp and the emission intensity is very weak at the maximum emission wavelength of Cy3. The directly excited emission of the acceptor is also very effectively suppressed, since Cy3 is scarcely excited at the excitation wavelength for the Tb^{3+} chelate, 325 nm (the molar extinction coefficient of Cy3 at 325 nm is about one-eightieth of that at its maximum absorption wavelength, 548 nm).

The detection limit of the present method is excellent, due to the high signal/background ratio and the very effective energy transfer. The Tb^{3+} chelate is multiply labeled onto the probe DNA by using the streptavidin−biotin interaction, and causes strong sensitized emission of Cy3. Such multiple labeling strategy was not effective for enhancing the fluorescence of the acceptor in the conventional donor organic dye system, due to π-stacking and reabsorption of the emitted fluorescence of the donor (*18*). The Tb^{3+} chelate molecules do not stack to each other and do not quench their emission since they have a large Stokes shift.

Under the time-resolved luminescence measurement condition (delay time 40 μs, gate time 500 μs), the intensity of the sensitized emission of the acceptor was almost the same between the 3′-end donor probe system and the internal donor probe system. This behavior is explained by the LRET property that as the distance between the donor and the acceptor increases, the efficiency of the energy transfer is decreased, whereas the lifetime of the sensitized emission is increased. In the time-resolved mode, the signal/background ratio at 565 nm is markedly low, as compared with that in the normal luminescence mode, though the emission in the latter mode contains a considerable contribution from the direct excitation of the Cy3 acceptor. Consequently, the detection limit is better in the normal luminescence mode than in the time-resolved mode. However, the time-resolved detection mode is still attractive, especially for the samples containing many impurities or coexisting materials, since the background emission caused by the short-lived species can be eliminated by the time-resolved mode. Considering these LRET characteristics, the optimal distance between the donor and the acceptor and the optimal measurement conditions must be found, and such parameters are expected to depend on the nature of the samples.

ACKNOWLEDGMENT

This work has been supported by CREST (Core Research for Evolutional Science and Technology) of Japan Science and Technology Corporation (JST) and the Grant-in-Aid for COE Research, Ministry of Education, Culture, Sports, Science and Technology (MEXT).

LITERATURE CITED

(1) Heller, M. J., and Morrison, L. E. (1985) Chemiluminescent and Fluorescent Probes for DNA Hybridization Systems. *Rapid Detection and Identification of Infectious Agents* (Kingsbury, D. T., and Falkow, S., Eds.) pp 245−256, Academic Press, New York.

(2) Matthews, J. A., and Kricka, L. J. (1988) Analytical Strategies for the Use of DNA Probes. *Anal. Biochem. 169*, 1−25.

(3) Cardullo, R. A., Agrawal, S., Flores, C., Zamecnik, P. C., and Wolf, D. E. (1988) Detection of Nucleic Acid Hybridization by Nonradiative Fluorescence Resonance Energy Transfer. *Proc. Natl. Acad. Sci. U.S.A. 85*, 8790−8794.

(4) Mergny, J.-L., Boutorine A. S., Garestier, T., Belloc, F., Rougée, M., Bulychev, N. V., Koshikin, A. A., Bourson, J., Lebedev, A. V., Valeur, B., Thuong, N. T., and Hélène, C. (1994) Fluorescence Energy Transfer as a Probe for Nucleic Acid Structures and Sequences. *Nucleic Acids Res. 22*, 920−928.

(5) Sambrook, J., Fritsch, E. F., and Maniatis, T. (1994) In situ Hybridization of Bacteriophage λ Plaques. *Molecular Cloning* (Nolan, C., Ed.) p 2.108−2.117, Cold Spring Harbor Laboratory Press, New York.
(6) Sueda, S., Yuan, J., and Matsumoto, K. (2000) Homogeneous DNA Hybridization Assay by Using Europium Luminescence Energy Transfer. *Bioconjugate Chem. 11*, 827−831.
(7) Yuan, J., and Matsumoto, K. (1998) A New Tetradentate β-Diketonate-Europium Chelate That Can Be Covalently Bound to Proteins for Time-Resolved Fluoroimmunoassay. *Anal. Chem. 70*, 596−601.
(8) Yoshikawa, K., Yuan, J., Matsumoto, K., and Kimura, H. (1999) Time-Resolved Fluorometric Detection of DNA Using a Tetradentate β-Diketonate Europium Chelate as a Label. *Anal. Sci. 15*, 121−124
(9) Horrocks, W. D., and Albin, J. M. (1984) Lanthanide Ion Luminescence in Coordination Chemistry and Biochemistry. *Prog. Inorg. Chem. 31*, 1−104.
(10) Sabbatini, N., Guardigli, M., and Lehn, J.-M. (1993) Luminescence Lanthanide Complexes as Photochemical Supramolecular Devices. *Coord. Chem. Rev. 123*, 201−228.
(11) Prat, O., Lopez, E., and Mathis, G. (1991) Europium (III) Cryptate: A Fluorescent Label for the Detection of DNA Hybrids on Solid Support. *Anal. Biochem. 195*, 283−289.
(12) Seveus, L., Väisälä, M., Syrjanen, S., Sandberg, M., Kuusisto, A., Harju, R., Salo, J., Hemmilä, I., Kojola, H., and Soini, E. (1992) Time-Resolved Fluorescence Imaging of Europium Chelate Label in Immunohistochemistry and In Situ Hybridization. *Cytometry 13*, 329−338.
(13) Mathis, G. (1993) Rare Earth Cryptate and Homogeneous Fluoroimmunoassays with Human Sera. *Clin. Chem. 39*, 1953−1959.
(14) Selvin, P. R., and Hearst, J. E. (1994) Luminescence Energy Transfer Using a Terbium Chelate: Improvements on Fluorescence Energy Transfer. *Proc. Natl. Acad. Sci. U.S.A. 91*, 10024−10028.
(15) Yuan, J., Wang, G., Majima, K. and Matsumoto, K. (2001) Synthesis of a Terbium Fluorescence Chelate and Its Application to Time-Resolved Fluoroimmunoassay. *Anal. Chem. 73*, 1869−1876.
(16) Selvin, P. R. (1995) Fluorescence Resonance Energy Transfer. *Methods Enzymol. 246*, 300−334.
(17) Oser, A., and Valet, G. (1993) Nonradioactive Assay of DNA Hybridization by DNA-Template-Mediated Formation of a Ternary Tb(III) Complex in Pure Liquid Phase. *Angew. Chem., Int. Ed. Engl. 29*, 1167−1169.
(18) Haralambidis, J., Angus, K., Pownall, S., Duncan, L., Chai, M., and Treager, G. W. (1990). The preparation of polyamide-oligonucleotide probes containing multiple nonradioactive labels. *Nucleic Acids Res. 18*, 501−505.

BC010049+

Star Structure of Antibody-Targeted HPMA Copolymer-Bound Doxorubicin: A Novel Type of Polymeric Conjugate for Targeted Drug Delivery with Potent Antitumor Effect

Marek Kovář,[†] Jiří Strohalm,[‡] Tomáš Etrych,[‡] Karel Ulbrich,[‡] and Blanka Říhová*[,†]

Institute of Microbiology, Academy of Sciences of the Czech Republic, Vídeňská 1083, 142 20 Prague 4, Czech Republic, and Institute of Macromolecular Chemistry, Academy of Sciences of the Czech Republic, Heyrovsky Square 2, 162 06 Prague 6, Czech Republic. Received June 29, 2001; Revised Manuscript Received December 14, 2001

The aim of this study was to compare the properties and antitumor potential of a novel type of antibody-targeted *N*-(2-hydroxypropyl)methacrylamide (HPMA) copolymer-bound doxorubicin conjugates with star structure with those of previously described classic antibody-targeted or lectin-targeted HPMA copolymer-bound doxorubicin conjugates. Classic antibody-targeted conjugates were prepared by aminolytic reaction of the multivalent HPMA copolymer containing side-chains ending in 4-nitrophenyl ester (ONp) reactive groups with primary NH_2 groups of the antibodies. The star structure of antibody-targeted conjugates was prepared using semitelechelic HPMA copolymer chains containing only one reactive *N*-hydroxysuccinimide group at the end of the backbone chain. In both types of conjugates, B1 monoclonal antibody (mAb) was used as a targeting moiety. B1 mAb recognizes the idiotype of surface IgM on BCL1 cells. The star structure of the targeted conjugate had a narrower molecular mass distribution than the classic structure. The peak in the star structure was around 300−350 kDa, while the classic structure conjugate had a peak around 1300 kDa. Doxorubicin was bound to the HPMA copolymer via Gly-Phe(D,L)-Leu-Gly spacer to ensure the controlled intracellular delivery. The release of doxorubicin from polymer conjugates incubated in the presence of cathepsin B was almost twice faster from the star structure of targeted conjugate than from the classic one. The star structure of the targeted conjugate showed a lower binding activity to BCL1 cells in vitro, but the cytostatic activity measured by [^{3}H]thymidine incorporation was three times higher than that seen with the classic conjugate. Cytostatic activity of nontargeted and anti-Thy 1.2 mAb (irrelevant mAb) modified HPMA copolymer-bound doxorubicin was more than hundred times lower as compared to the star structure of B1 mAb targeted conjugate. In vivo, both types of conjugates targeted with B1 mAb bound to BCL1 cells in the spleen with approximately the same intensity. The classic structure of the targeted conjugate bound to BCL1 cells in the blood with a slightly higher intensity than the star structure. Both types of targeted conjugates had a much stronger antitumor effect than nontargeted HPMA copolymer-bound doxorubicin and free doxorubicin. The star structure of targeted conjugate had a remarkably higher antitumor effect than the classic structure: a single intravenous dose of 100 μg of doxorubicin given on day 11 completely cured five out of nine experimental animals whereas the classic structure of targeted conjugate given in the same schedule only prolonged the survival of experimental mice to 138% of control mice. These results show that the star structure of antibody-targeted HPMA copolymer-bound doxorubicin is a suitable conjugate for targeted drug delivery with better characterization, higher cytostatic activity in vitro, and stronger antitumor potential in vivo than classic conjugates.

INTRODUCTION

Cytostatic drugs that are used for conventional chemotherapy of cancer do not show any specific accumulation within the tumor but, due to the higher sensitivity of rapidly dividing cancer cells to these drugs, some preferential killing is achieved. Unfortunately, also tissues containing highly proliferating cells such as bone marrow and epithelia are very often seriously damaged by conventional chemotheraphy, and these toxic side-effects are limiting factors for the chemotherapy dosage. It has been reported that conjugation of the free drug to a polymeric carrier reduces its nonspecific toxicity (*1*, *2*) and markedly prolongs its blood half-life (*3*). A conjugate of a synthetic, water-soluble and biocompatible copolymer based on *N*-(2-hydroxypropyl)methacrylamide (HPMA) and containing doxorubicin bound via the Gly-Phe(D,L)-Leu-Gly spacer, called PK1, is undergoing phase I/II clinical study in UK (*4*), and a conjugate containing doxorubicin and IgG was successfully used in the Czech Republic with a human patient with generalized breast carcinoma (*5*).

The idea of increasing the therapeutic effect and minimizing the side-toxicity of common anticancer drugs is very attractive. This could be achieved by site-specific drug delivery using a targeting moiety specifically recognizing tumor cells. Targeted HPMA copolymer-bound drugs have previously been shown to have antitumor effect in vitro and in vivo (*6*). These conjugates consist

* To whom the correspondence should be addressed. Phone: +420 2 475 23 43. Fax: +420 2 472 11 43. E-mail: rihova@biomed.cas.cz.

[†] Institute of Microbiology.

[‡] Institute of Macromolecular Chemistry.

10.1021/bc010063m CCC: $22.00 © 2002 American Chemical Society
Published on Web 02/12/2002

of a HPMA copolymer backbone to which the drug and the targeting moiety are conjugated via a biodegradable spacer Gly-Phe(D,L)-Leu-Gly. This spacer ensures a controlled intracellular release of the bound drug. The targeting moieties to be used can be monoclonal or polyclonal antibodies (*7*), saccharides (*8*), lectins (*9*), and hormones (*10*). The risk of arising of antibodies directed against the targeting moiety after repeated administration, as commonly seen with immunotoxins, is lowered thanks to the decreased immunogenicity of proteins bound to HPMA copolymer (*11*).

Decisive in antibody-targeted drug delivery is the selection of appropriate surface receptor for targeting. In many experimental and preclinical studies, receptors such as carcinoembryonic antigen (*12*), α-fetoprotein (*13*), CD5 (*14*), CD22 (*15*), and many others have been explored. In this study, we have used as a tumor model system murine BCL1 leukemia. It is B-cell derived malignancy and BCL1 cells thus possess surface IgM. We have used the B1 monoclonal antibody (mAb) recognizing the idiotype of surface IgM on BCL1 cells as targeting moiety. Since the idiotype of each clone of B-cells is a unique structure, we have used a strictly tumor-specific marker for drug targeting. Moreover, the surface IgM on B-cells has been shown as a receptor with a high level of expression and rapid internalization after ligand binding (*16, 17*).

Antibody-targeted or lectin-targeted HPMA copolymer-bound doxorubicin conjugates were shown to exhibit binding to target cells, cytostatic activity in vitro, and antitumor effect in vivo (*18*). These conjugates were prepared by an aminolytic reaction of the multivalent HPMA copolymer containing ONp reactive groups with antibody molecules (the IgG molecule contains more than 70 amino groups of lysine residues). Since there are many reactive groups distributed along the both HPMA copolymer and antibody molecule, two or more molecules of the antibody can be joined together to form a high-molecular weight branched structure (classic structure, Figure 1A). Recently, we have introduced a novel type of antibody-targeted HPMA copolymer-bound doxorubicin of a star structure. In this type of conjugate, HPMA copolymer chains containing only one reactive *N*-hydroxysuccinimide group at the end of the molecule react with the amino groups of the only one molecule of antibody (Figure 1B). This means that the star structure of HPMA copolymer-bound doxorubicin targeted with antibody is a more homogeneous and better characterized conjugate than the classic structure.

The purpose of this study was (a) to synthesize and characterize a star conjugate and a classic conjugate of HPMA copolymer-bound doxorubicin targeted with B1 mAb, (b) to compare the binding activity of free B1 mAb, B1mAb in the star conjugate and in classic conjugate, (c) in vitro evaluate cytostatic activity of both types of HPMA copolymer-bound doxorubicin targeted with B1 mAb and compare it to the cytostatic activity of nontargeted and anti-Thy 1.2 mAb containing (irrelevant antibody) conjugate using tumor cell line BCL1, and (d) to determine the binding capacity to target cells and antitumor potential of star and classic structure of HPMA copolymer-bound doxorubicin targeted with B1 mAb in vivo.

MATERIAL AND METHODS

Chemicals. 1-Aminopropan-2-ol, glutathione (GSH), ethylenediaminetetraacetic acid (EDTA), 3-sulfanylpropionic acid (MPA), methacryloyl chloride, glycyl-D,L-phenylalanine, L-leucyl-glycine, 4-nitrophenol, *N*-hydroxysuccinimide, 1-hydroxybenzotriazole, triethylamine (TEA), *N,N′*-dicyclohexylcarbodiimide (DCCI), 2,2′-azobisisobutyronitrile (AIBN), phthalaldehyde (OPA), 5-thio-D-glucose, dimethyl sulfoxide (DMSO), dimethyl formamide (DMF), and doxorubicin hydrochloride (Dox·HCl) were from Fluka AG (Buchs, Switzerland). All other chemicals and solvents were of analytical grade. The solvents were dried and purified by conventional procedures and distilled before use.

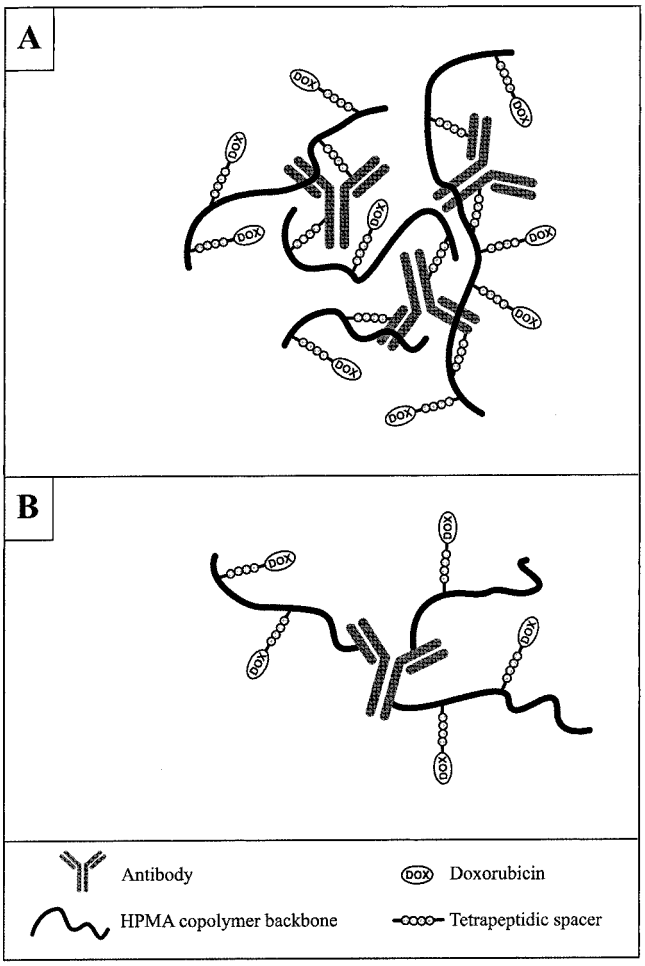


Figure 1. Schematic drawing of the classic structure of antibody-targeted HPMA copolymer-bound doxorubicin conjugate (A) and the star structure of antibody-targeted HPMA copolymer-bound doxorubicin conjugate (B).

Synthesis of Monomers. All monomers were prepared as previously described. Briefly, *N*-(2-hydroxypropyl)methacrylamide (HPMA) was prepared by methacryloylation of 1-aminopropan-2-ol in methylene chloride (*19*), methacryloylglycyl-D,L-phenylalanyl-L-leucylglycine 4-nitrophenyl ester (Ma-Gly-Phe(D,L)-Leu-Gly-ONp) by methacryloylation of Gly-Phe-Leu-Gly tetrapeptide following its synthesis from Boc-GlyPheOH and H-LeuGly-OMe (*20*) (chromatographically pure product, mp = 134−136 °C, amino acid analysis: Gly:L-Phe:D-Phe:L-Leu = 2.04:0.54:0.46:1.00), and methacryloylglycyl-DL-phenylalanyl-L-leucylglycyl doxorubicin amide (Ma-Gly-Phe(D,L)-Leu-Gly-Dox) by the reaction of Ma-Gly-Phe(D,L)-Leu-Gly-ONp with Dox·HCl in DMF in the presence of TEA (*19*) (TLC in chloroform:methanol 8:1 mixture showed two spots at $R_f = 0.46$ and $R_f = 0.4$ corresponding to the D-Phe and L-Phe isomers; HPLC showed a single peak at 18.22 min (UV detection at 230 and 484 nm); amino

acid analysis Gly:L-Phe:D-Phe:L-Leu = 2.04:0.54:0.46:1.00).

Synthesis of Polymer Precursors and Polymer−Doxorubicin Conjugates. Polymer-bound doxorubicin (conjugate 1), classic and star polymer conjugates of doxorubicin with B1mAb antibody (conjugate 2 and conjugate 3), and the classic polymer conjugate of doxorubicin with anti-Thy1,2 antibody (conjugate 4) were prepared from polymer precursors as described (*19*). Briefly, polymer−Dox conjugate 1 was prepared from the polymer precursor I by its reaction with Dox·HCl carried out in the presence of TEA in DMSO. Classic polymer conjugates 2 and 4 were prepared by the reaction of the polymer precursor II with Dox·HCl in the presence of TEA in DMSO, followed by the reaction of such intermediate with the respective antibody in saline solution at controlled pH (7.6 and 8) using pH stat Radiometer Copenhagen. Star conjugate 3 was prepared from the semitelechelic, succinimide group-containing polymer precursor III, by its reaction with the anti-Thy1,2 antibody in phosphate buffer at pH 7.3−7.8. Polymer precursors I and II were prepared by radical precipitation copolymerization of HPMA with Ma-Gly-Phe(D,L)-Leu-Gly-ONp in acetone (initiator AIBN, 0.6 wt %; concentration of monomers 12.5 wt %; molar ratio HPMA: Ma-Gly-Phe(D,L)-Leu-Gly-ONp 5:1 (precursor I) or 10:1 (precursor II); 60 °C; 24 h) as described (*20, 21*). Semitelechelic polymer precursor III was prepared by radical precipitation copolymerization of HPMA with Ma-Gly-DL-Phe-L-Leu-Gly-Dox carried out in acetone and initiated with AIBN in the presence of 3-sulfanylpropionic acid as a chain-transfer agent. Copolymerization was followed by the reaction of the terminal COOH group-containing copolymer with *N*-hydroxysuccinimide in DMF using DCCI method (*19*).

Characterization of Polymer Precursors and Polymer Conjugates. Polymer precursors I and II were characterized by UV spectrophotometry (the content of oligopeptide side chains terminated in 4-nitrophenoxy groups (ONp)) (*20*), by amino acid analysis (LDC Analytical, Riviera Beach, FL, precolumn OPA derivatization) and by liquid chromatography (weight- and number-average molecular weights, M_w and M_n) after aminolysis of reactive groups with 1-aminopropan-2-ol. Polymer−Dox conjugates were characterized and tested for the content of free polymer, free drug, or protein by GPC (Sepharose 4B/6B) or FPLC Pharmacia equipped with Superose 6 column (RI and UV detectors) and by electrophoresis (Pharmacia-LKB Phast System, SDS PAGE, gels with gradient 4−15). Molecular weights of all final conjugates and polymer precursors were determined using liquid chromatograph ÄKTA-Pharmacia equipped with Superose 6 or TSK 5000 PW columns and RI (refractive index) and multiangle light scattering DAWN-DSP−F (Wyatt Technology Corp.) detectors. The protein content in the conjugates was estimated by amino acid analysis (LDC Analytical, Riviera Beach, FL, precolumn OPA derivatization) and Dox content by UV spectrophotometry (*22*). Neither GPC nor electrophoresis showed significant amounts of free protein in the conjugates and the content of free Dox in the conjugate was less than 0.05% of the total Dox content.

Release of Dox from the Conjugates. Release of Dox from polymer conjugates was tested in phosphate buffer pH 6 after their incubation in cathepsin B solution at 37 °C. Incubation medium was 0.1 M sodium phosphate, 0.05 M NaCl, 1 mM EDTA, 5 mM reduced glutathione, and 0.5 μM cathepsin B. The activity of the cysteine proteinase cathepsin B was determined using Bz-Arg-NAp as a substrate (*20*). In all cases, final Dox concentration was 0.5 mM. At predetermined time intervals the samples were tested for the content of free Dox. The amount of Dox released from the polymer conjugate was determined after its extraction from the incubation media into chloroform. A mixture of 0.1 mL of sample solution and 0.3 mL of buffer (0.2 M Na_2CO_3/$NaHCO_3$, pH 9.8) was extracted with 0.6 mL of chloroform. HPLC (Tessek gel C18 column, methanol−water gradient 10−90% methanol, fluorescent detector with excitation at 488 nm and emission at 560 nm) was used to determine the amount of free Dox. The calibration (yield of extraction) was carried out using Dox·HCl. All drug-release data are expressed as the amount of free Dox relative to the total Dox content in the conjugate.

Monoclonal Antibody (mAb). Monoclonal antibody directed against the idiotype of surface IgM of BCL1 cells, clone B1, is of the IgG1 isotype (*23*). For these studies, B1 mAb was purified from Balb/c mouse ascitic fluid by a combination of 45% saturated ammonium sulfate precipitation and protein A affinity chromatography. The concentration was determined by spectrophotometry (λ = 280 nm) and the purity was checked by SDS−PAGE.

Tumor Lines and Tissue Culture Condition. The murine B cell leukemia BCL1 was purchased from the American Type Culture Collection (ATCC, Rockville, MD). It is a well-described cell line that grows rapidly and consistently in immunocompetent Balb/c mice. Routine culture and all in vitro experiments with BCL1 cell line were conducted in RPMI 1640 medium with extra L-glutamine (300 μg/mL), sodium pyruvate (110 μg/mL), 2-mercaptoethanol (5×10^{-5}M), HEPES (10mM), penicillin (100 units/mL), streptomycin (100 μg/mL), and 10% v/v 0.1 μm filtered fetal bovine serum. Cells in exponential growth with viability greater than 95% were used for all experiments. Cultures were maintained at 37 °C in 5% CO_2. The murine B cell lymphoma 38C13 is a cell line with characteristics similar to the BCL1 cell line, and both lines express membrane IgM but do not secrete it. For this reason we decided to use the 38C13 cell line as control cells for in vitro binding studies. Routine culture and all experiments with 38C13 cell line were conducted in the same medium and under the same conditions as with BCL1 cell line.

Mice. Mice of inbred strain Balb/c were obtained from the breeding colony of the Institute of Physiology (Academy of Sciences of the Czech Republic) and kept in standard housing. Animals 9−15 weeks of age and in the 19−22 g weight range were used in in vivo experiments. All experiments were approved by the Animal Welfare Committee of the Institute of Microbiology Academy of Sciences of the Czech Republic.

Biotinylation of Free mAb and Targeted Conjugates Containing mAb. B1 mAb was biotinylated using EZ-Link Sulfo-NHS-LC−Biotin (Pierce). Briefly, 2 mg of B1 mAb in 1 mL of PBS (pH 8.0) was mixed with 100 μL of 1.5 mg/mL Sulfo-NHS-LC−Biotin solution. After a 45-min incubation at room temperature, unreacted biotin was removed by dialysis. The degree of biotinylation was determined using HABA (Pierce), and about 4 biotins per molecule of IgG were found. Conjugates containing B1 mAb as a targeting moiety were biotinylated under the same conditions as free B1 mAb, but the degree of biotinylation was not determined because of the presence of doxorubicin.

Fluorescence-Activated Cell Sorter Analysis (FACS). For in vitro binding studies, BCL1 cells were collected from an exponential growth phase culture. They were centrifuged for 5 min at 300 g, washed twice with PBS

with 1% of calf albumin and 0.1% of sodium azide (FACS solution), resuspended in FACS solution, and counted in trypan blue. Cell density was adjusted to 1×10^7 cells/mL and 0.1 mL of this cell suspension was added to each test tube. From this moment on, all test tubes with cells were maintained on ice (0 °C), and all solutions added were adjusted to this temperature. Cells were again centrifuged for 5 min at 300 g and 100 μL of tested samples in different concentrations was then added. The cells were incubated for 45 min and then washed three times with FACS solution. Streptavidine−FITC conjugate at appropriate dilution was added for 30 min. Finally, the cells were washed three times and then resuspended in 0.5 mL of FACS solution. For in vivo binding studies, Balb/c mice 30 days after intraperitoneal administration of 5×10^5 BCL1 cells were intravenously injected with tested samples (250 μg of B1 mAb). At 45 min after the administration the mice were sacrificed, and spleen and 100 μL of blood from each mouse were placed in precooled test tubes containing 5 IU of heparine. Spleen was homogenized, and both the homogenate and blood were transferred to lysis solution to eliminate erythrocytes. After lysis, splenocytes and peripheral blood leucocytes were washed twice with FACS solution, centrifuged for 5 min at 300 g and streptavidin−FITC conjugate at appropriate dilution was added for 30 min. Finally, the cells were washed three times and resuspended in 0.5 mL of FACS solution. At least 7500 live cells were analyzed for each measurement.

Proliferation Assay in Vitro. BCL1 cells were collected from an exponential growth phase culture. They were centrifuged for 5 min at 300 g, washed, resuspended in fresh culture medium, and counted in trypan blue. Cell density was adjusted to 5×10^4 cells/mL, and 0.2 mL of this cell suspension was loaded by multichannel pipet into each well of Nunc 96-well flat-bottomed plates. The tested samples were then added to the wells to achieve the desired concentrations; the final well volume was 0.25 mL and cell density 1×10^4 cells/well, with five wells for each test condition. The plates were cultured in 5% CO_2 for 72 h at 37 °C, after which 18.5 kBq of [^{3}H]thymidine in 50 μL was added per well, followed by another 6 h incubation. The cells were then collected using a cell harvester (Tomtec, Orange, CT) onto glass fiber filters (filtermat, Wallac, Finland). When the mixture was dried, a sheet of solid scintillator-Meltilex (Wallac) was placed together with a filtermat containing 96 samples in a sample bag and run together through a heat sealer (Microsealer, Wallac). Counting was performed in 1450 MicroBeta TriLux (Wallac).

Treatment of Established BCL1 Leukemia in Vivo. BCL1 cells were collected from an exponential growth phase culture. They were centrifuged for 5 min at 300 g, washed, resuspended in fresh culture medium, and counted in trypan blue. An amount of 5×10^5 BCL1 cells in 0.5 mL culture medium were inoculated intraperitoneally on day 0 to Balb/c mice. Treatment with targeted HPMA copolymer-bound doxorubicin was given intravenously either as a single or as three injections and always began on the 11th day. The second injection was given on the 14th day and the third injection on the 17th day. One dose contained either 50 μg of free doxorubicin or 100 μg of HPMA copolymer-bound doxorubicin. Control mice were injected with only physiological solution. Nine or 10 mice were used for each experimental group.

Statistical Analysis. The Wilcoxon's statistics (multiple comparison method) and Student's *t*-test were used to evaluate the differences among experimental groups. *P* values <0.01 were taken as statistically significant.

Table 1. Characteristics of Polymer Precursors and Antibody-Targeted HPMA Copolymer-Bound Doxorubicin Conjugates

				Content of:		
		M_w		ONp	Dox	mAb
Sample	Structure	(kDa)	M_w/M_n	(mol%)	(wt%)	(wt%)
Conjugate 1	P-GFLG-Dox	26	1.7		6.8	
Conjugate 2	P (GFLG-Dox; GFLG-B1 mAb) (star structure)	320	2.4		3.35	51
Conjugate 3	P (GFLG-Dox; GFLG-B1 mAb) (classic structure)	1300	~5		4.0	25
Conjugate 4	P (GFLG-Dox; GFLG-a-Thy 1.2) (classic structure)	1250	~5		4.54	25
Precursor I	P-GFLG-ONp	23	1.35	5.1		
Precursor II	P-GFLG-ONp	19	1.30	9.0		
Precursor III	P-(GFLG-Dox)-OSu	13	1.40		6.0	

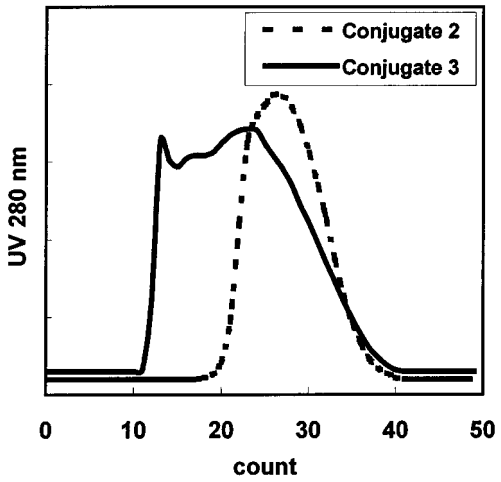


Figure 2. GPC analysis of the classic structure of HPMA copolymer-bound doxorubicin targeted with B1 mAb (Conjugate 3) and the star structure of HPMA copolymer-bound doxorubicin targeted with B1 mAb (Conjugate 2).

RESULTS

Characterization of Synthesized HPMA Copolymer-Bound Doxorubicin Conjugates and Rate of Doxorubicin Release. Conjugates of two structures (Figure 1) consisting of HPMA copolymer, the anticancer drug doxorubicin, and targeting antibody have been synthesized. For characteristics of polymer precursors and polymer conjugates see Table 1. All doxorubicin-bearing conjugates contained <0.1 wt % free doxorubicin (referred to the total doxorubicin content). The molecular mass of the classic structure of antibody-targeted HPMA copolymer-bound doxorubicin was approximately 1300 kDa and polydispersity was broad (Figure 2). The star structure of targeted conjugate exhibited properties of a well-defined and more uniformly characterized conjugate, with molecular mass of 300−350 kDa and low polydispersity. Release profiles of doxorubicin from the HPMA copolymer-bound doxorubicin conjugates after their incubation with cathepsin B are shown in Figure 3. Nontargeted HPMA copolymer-bound doxorubicin conjugate released 49.8% of doxorubicin after 49 h of incubation. The star structure of targeted conjugate showed a lower release rate (38%) and the classic structure of targeted conjugate released only 21.5% of the bound doxorubicin.

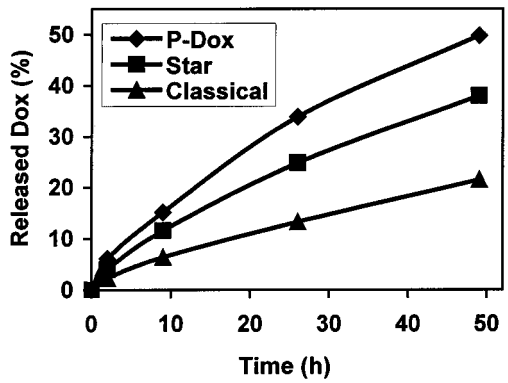


Figure 3. Release profiles of doxorubicin from nontargeted HPMA copolymer-bound doxorubicin (P-Dox), the star structure of HPMA copolymer-bound doxorubicin targeted with B1 mAb (star) and the classical structure of HPMA copolymer-bound doxorubicin targeted with B1 mAb (classical). Release of doxorubicin from polymer conjugates was tested at 37 °C in phosphate buffer pH 6 and in the presence of 0.5 μM cathepsin B.

In Vitro Binding of Free B1 mAb, Classic Structure, and Star Structure of HPMA Copolymer-Bound Doxorubicin Targeted with B1 mAb to Target BCL1 Cells and to 38C13 Cells Used as a Negative Control. Fluorescence activated cell sorter analysis (FACS) was used to evaluate the intensity and specificity of binding of HPMA copolymers containing doxorubicin and targeted with B1 mAb. Free B1 mAb and both types of targeted conjugates were biotinylated to enable the use of FITC-labeled streptavidin for secondary labeling. We tested the intensity of binding at concentrations of 100, 10, and 1 μg/mL of B1 mAb; the corresponding mean fluorescence intensities for free B1 mAb were 2340, 1230, and 220. The classic structure of HPMA copolymer-bound doxorubicin targeted with B1 mAb showed a slightly lower level of binding if compared to the free B1 mAb and the corresponding mean fuorescence intensities were 1700, 708, and 95.4, respectively. The level of binding of the star structure of HPMA copolymer-bound doxorubicin targeted with B1 mAb was considerably lower than that seen with free B1 mAb, with corresponding mean fluorescence intensities of 621, 145, and 25.5, respectively. BCL1 cells treated only with FITC-labeled streptavidin at a concentration equal to that used for secondary labeling showed mean fluorescence intensity of 4.44. Since the conjugate of antibody and synthetic copolymer containing doxorubicin could show nonspecific binding activity, we decided to evaluate the binding of both types of targeted conjugates to control cells. 38C13 cell line was used as appropriate control cells because their characteristics are similar to those of BCL1 cells (see Materials and Methods). Even at a concentration of 100 μg/mL of B1 mAb neither the classic nor the star structure of HPMA copolymer-bound doxorubicin targeted with B1 mAb bound to 38C13 cells (Figure 4).

Cytostatic Activity of Classic and Star Structure of HPMA Copolymer-Bound Doxorubicin Targeted with B1 mAb in Vitro. In Vitro inhibition of cell proliferation of the BCL1 cell line was determined by [^{3}H]-thymidine incorporation. Concentrations of doxorubicin required for 50% inhibiton of cell proliferation (IC_{50}) of the BCL1 cancer cell line are summarized in Table 2. The star structure of HPMA copolymer-bound doxorubicin targeted with B1 mAb showed three times higher cytostatic activity than the classic structure. Both targeted conjugates exhibited a much higher cytostatic activity than nontargeted HPMA copolymer-bound doxorubicin. To prove that higher cytostatic activity of HPMA copolymer-bound doxorubicin targeted with B1 mAb is due to the specific binding of the targeting moiety to the target BCL1 cells, we used HPMA copolymer-bound doxorubicin conjugated with irrelevant anti-Thy 1.2 mAb as control. This conjugate had the same cytostatic activity as nontargeted HPMA copolymer-bound doxorubicin. Furthermore, the cytostatic activity of both classic and star structure of HPMA copolymer-bound doxorubicin targeted with B1 mAb can be strongly reduced (15 and 12 times, respectively) by free B1 mAb. This mAb does not have any effect on the proliferation of BCL1 cells alone (not shown).

In Vivo Binding of Free B1 mAb, Classic and Star Structure of HPMA Copolymer-Bound Doxorubicin Targeted with B1 mAb to Peripheral Blood Leukocytes (PBL) and to Spleen Cells of Balb/c Mouse Bearing BCL1 Leukemia. Fluorescent activated cell sorter analysis (FACS) was used to evaluate the binding capacity of HPMA copolymers containing doxorubicin and targeted with B1 mAb. Biotinylated free B1 mAb and both types of targeted conjugates were intravenously administered (250 μg B1 mAb/dose) to Balb/c mice bearing BCL1 leukemia. Figure 5 demonstrates that 45 min after the application of free B1 mAb and classic structure of HPMA copolymer-bound doxorubicin targeted with B1 mAb these structures bound to the target cells and noticeably separated BCL1 cells in blood from other nonmalignant PBL. The star structure of HPMA copolymer-bound doxorubicin targeted with B1 mAb also bound to BCL1 cells but separation from other PBL was not as significant as that seen with free B1 mAb and the classic structure of targeted conjugate. Binding of free B1 mAb and both types of targeted conjugates to spleen cells of Balb/c mice bearing BCL1 leukemia is shown in Figure 6. In this case, 45 min after intravenous application the classic and the star structure of HPMA copolymer-bound doxorubicin targeted with B1 mAb bound to the target BCL1 cells with comparable binding capacity. Corresponding mean fluorescence intensities were 8.65 and 7.13, respectively. Free B1 mAb showed a higher binding capacity and the corresponding mean fluorescence intensity was 15.3. Mean fluorescence intensities of control spleen cells (no secondary labeling) for free B1 mAb and both types of targeted conjugates were within the range 2.26−2.59.

Treatment of Balb/c Mice with Established BCL1 Leukemia by Classic and Star Structure of HPMA Copolymer-Bound Doxorubicin Targeted with B1 mAb. For the in vivo experiments, 5×10^5 BCL1 tumor cells were administered intraperitoneally to Balb/c mice and the treatment (50 μg of free doxorubicin or 100 μg of HPMA copolymer-bound doxorubicin) was always begun on the 11th day. In the first experiment we tested the effect of three intravenous doses given on the 11th, 14th, and 17th day. As shown in Figure 7, free doxorubicin significantly prolonged the survival of the experimental mice to 143% relative to the control. However, nontargeted HPMA copolymer-bound doxorubicin prolonged the survival of experimental mice to only 112% relative to control mice (not statistically significant). Both the classic and the star structure of HPMA copolymer-bound doxorubicin targeted with B1 mAb strongly prolonged the survival of experimental mice. The result of this experiment would be probably much better than shown in Figure 7 if the experimental mice did not contract systemic staphylococcus infection, which was most probably the reason of their death. We did not find any mice to have splenomegalia, which is the major symptom of

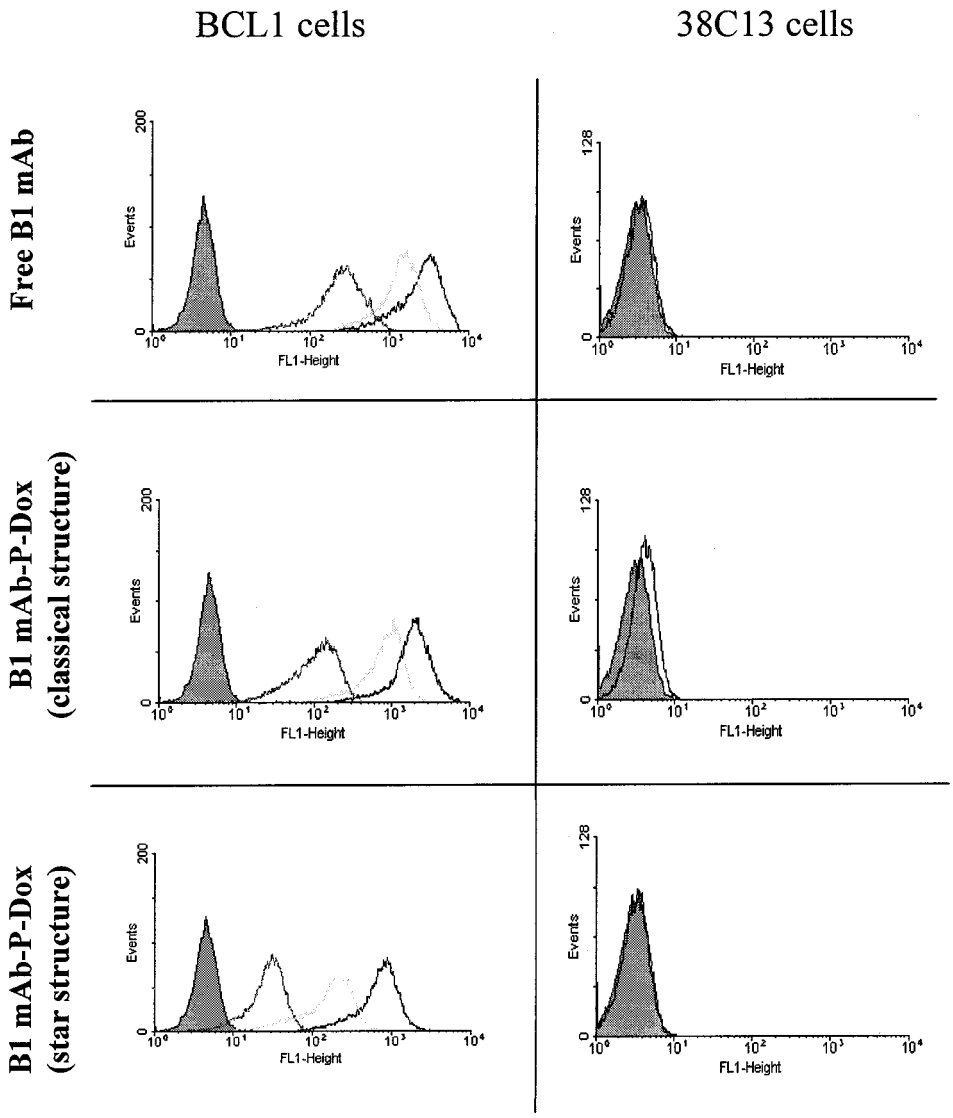


Figure 4. Flow cytometry analysis of biotinylated free B1 mAb, the classical structure and the star structure of HPMA copolymer-bound doxorubicin targeted with B1 mAb (B1 mAb-P-Dox). B1 mAb is anti-idiotype antibody which specifically recognizes the idiotype of surface IgM of BCL1 cells. 38C13 cells also express surface IgM but with a different idiotype. Grey peaks represent the background staining with the secondary FITC-labeled streptavidin alone. BCL1 cells were treated with 100 μg/mL (solid line), 10μg/mL (gray line), and 1 μg/mL (dotted line) of biotinylated B1 mAb.

progression of BCL1 leukemia. In further experiment we decided to use only one dose given on the 11th day. The results of this experiment is shown in Figure 8. As in the previous experiment, treatment with free doxorubicin significantly prolonged the survival of experimental mice (114% relative to control mice) while nontargeted HPMA copolymer-bound doxorubicin prolonged the survival of experimental mice to only 106% relative to control mice (not statistically significant). The classic structure of HPMA copolymer-bound doxorubicin targeted with B1 mAb prolonged the survival of experimental mice to 138% relative to control mice (statistically significant) but did not bring about any total recovery. The star structure of HPMA copolymer-bound doxorubicin targeted with B1 mAb showed an extraordinary effect. It completely cured five out of nine experimental mice and extended the average lifespan of the remaining mice to 258% of that found in the controls. In the last in vivo experiment we tested whether free B1 mAb can block or reduce the strong antitumor effect of the star structure of HPMA copolymer-bound doxorubicin targeted with B1 mAb as it can be seen in vitro. The targeted conjugate was given intravenously on the 11th day in an amount of 75 μg doxorubicin/dose which corresponds to 1.13 mg of B1 mAb. Free B1 mAb was given in two injections (0.4 mg intraperitoneally and 0.8 mg intravenously) separated by 1 h. Figure 9 demonstrates that free B1 mAb did not block the effect of the star structure of HPMA copolymer-bound doxorubicin on the survival of experimental mice. The star structure of targeted conjugate given alone again demonstrated a powerful therapeutic effect, curing completely 7 out of 9 experimental mice. Free B1 mAb did not have any effect on the survival of experimental mice. Moreover, free B1 mAb caused an immediate death of two experimental mice when intravenously injected.

DISCUSSION

Antibody-targeted HPMA copolymer-bound doxorubicin conjugates have been reported in many studies (*24*−*26*) as perspective anticancer drugs. These conjugates were prepared by aminolysis of ONp groups of the HPMA copolymer with the amino group of daunosamine in doxorubicin molecule. It was followed by the reaction of the rest of ONp groups of the HPMA copolymer with

Table 2. IC_{50} Values Determined in Cell Line BCL1 for Different Samples of HPMA Copolymer-Bound Doxorubicin[a]

Sample	IC_{50} concentration (nM Dox) ± SD
P-GFLG-Dox	1450 ± 167
P(GFLG-Dox)(GFLG-a-Thy 1.2 mAb) (classic structure)	1470 ± 179
P(GFLG-Dox)(GFLG-B1 mAb) (classic structure)	32.6 ± 9.2
P(GFLG-Dox)(GFLG-B1 mAb) (star structure)	10.5 ± 3.1
P(GFLG-Dox)(GFLG-B1 mAb) (classic structure) + 20 μg/ml B1 mAb[b]	502 ± 183
P(GFLF-Dox)(GFLG-B1 mAb) (star structure) + 20 μg/ml B1 mAb[b]	121 ± 38
Dox	1.6 ± 0.39

[a] IC_{50} values were evaluated as concentration of doxorubicin which inhibits after 72 h of cultivation (see Material and Methods) the incorporation of [^{3}H]thymidine by BCL1 cells to 50% of the control cell level. The activity of control cells was always higher than 30 000 cpm/well. Experiments were repeated twice with similar results. P-GFLG-Dox: HPMA copolymer-bound doxorubicin, a-Thy 1.2 mAb-GFLG-P-GFLG-Dox: HPMA copolymer-bound doxorubicin targeted with anti-Thy 1.2 mAb, B1 mAb-GFLG-P-Dox: HPMA copolymer-bound doxorubicin targeted with B1 mAb, Dox: free doxorubicin. [b] Free B1 mAb was added to the cells just prior to targeted conjugate.

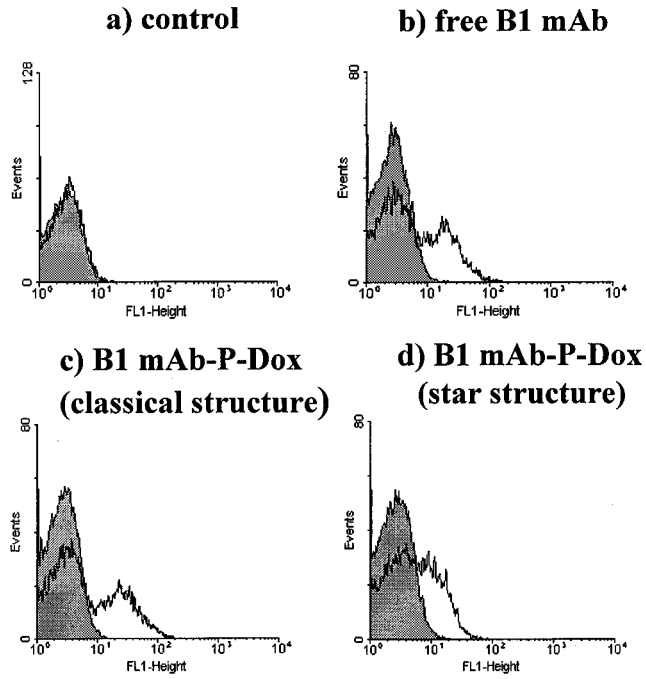


Figure 5. Binding of biotinylated free B1 mAb, the classical structure, and the star structure of HPMA copolymer-bound doxorubicin targeted with B1 mAb (B1 mAb-P-Dox) to peripheral blood leukocytes (PBL) of Balb/c mice bearing BCL1 leukemia after intravenous application of 250 μg of B1 mAb. PBL were isolated 45 min after sample application and secondary labeled by streptavidin-FITC conjugate as described in Material and Methods. Grey peaks represent control (no secondary labeling). Control mouse was injected with physiological solution only.

amino groups of lysine residues in the antibody molecule. Unfortunately, in the reaction of the multivalent polymer precursor with the multivalent antibody, branching reaction cannot be avoided. The effect of branching can be minimized by careful performance and control of pH, ionic strength and temperature of the reaction. Nevertheless, the reaction product is still a mixture of molecules consisting of a single antibody modified with polymer chains, and molecules containing two or more antibody molecules connected by many polymer chains into a branched structure (Figure 1A). Consequently, the molecular weight of such conjugate is high and its polydispersity is fairly broad. This means that the proper characterization of its molecular structure is rather difficult. On the other hand, an advantage of this aminolytic conjugation is the relative ease of performance on a large scale.

With the aim of preparing an antibody-targeted HPMA copolymer-bound doxorubicin conjugate with a better-defined structure, we synthesized a new type of conjugate with a star structure. In this conjugate some of the amino groups (usually 40−45%) of the antibody molecule are modified with HPMA copolymer chains, each of them being attached to the antibody via the polymer end-chain carbonyl group. Analogous to the classic-structure conjugate, the polymers are bearing doxorubicin molecules attached via biodegradable oligopeptide spacers. Similarly, the paper of Wang et al. (*27*) describes the synthesis of starlike *N*-(2-hydroxypropyl)methacrylamide copolymers. The authors of this paper also used semitelechelic HPMA copolymers with terminal COOH, which was activated with *N*-hydroxysuccinimide. In contrast to our paper, Wang et al. conjugated the above-described semitelechelic HPMA copolymers to PAMAM dendrimers. Such conjugate does not possess any targeting moiety and thus cannot be classified as a tumor-specific drug delivery system.

We have used in this study the tetrapeptidic spacer Gly-Phe(D,L)-Leu-Gly which is commonly used as optimal linker between the drug and the HPMA copolymer backbone. In the past we tested the efficacy of conjugates with spacers containing only D-phenylalanine or only L-phenylalanine. In the presence of cathepsin B and after 24 h of incubation, the Gly-Phe(L)-Leu-Gly spacer releases 35% of bound doxorubicin, Gly-Phe(D)-Leu-Gly spacer releases 12% and Gly-Phe(D,L)-Leu-Gly spacer releases 22% of bound doxorubicin.

Surprisingly, using a spacer containing both isomers of phenylalanine gives the best cytostatic activity in vitro and antitumor effect in vivo. No explanation why conjugates with Gly-Phe(D,L)-Leu-Gly spacer show the highest cytostatic activity is available at the moment. Recently, we have also introduced HPMA copolymer-bound doxorubicin conjugates with pH sensitive bond between the drug and the spacer. In this type of conjugates doxorubicin is attached to the spacer through a hydrazone bond. Hydrazone bond is relatively stable at physiological pH 7.4 but it is quickly hydrolyzed at pH 5. So, unlike aminolytically bound doxorubicin, the drug can be released in endosomes since lysosomal proteases are not required and the pH in this cell compartment is favorable. HPMA copolymer conjugates with doxorubicin conjugated through a hydrazone bond exhibit very high cytostatic activity in vitro against a variety of different tumor cell lines including those with a limited content of lysosomes (*28*).

Different release profiles of doxorubicin from HPMA copolymer conjugates after their incubation with cathe-

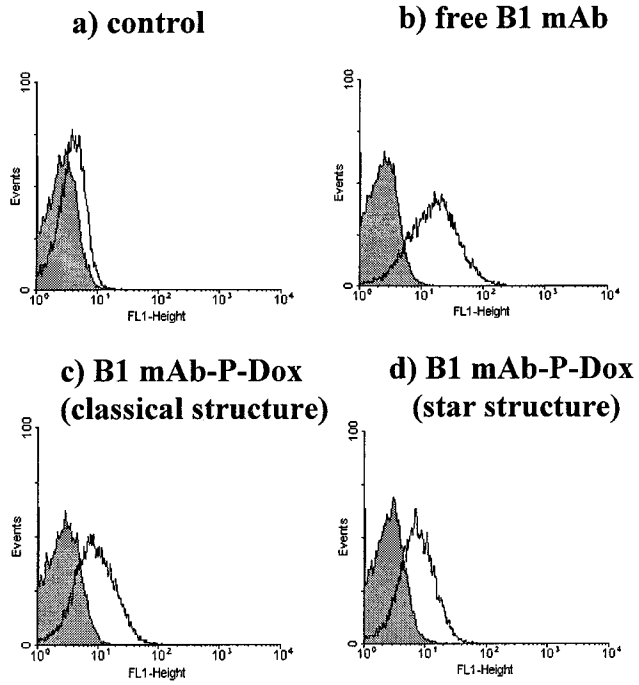


Figure 6. Binding of biotinylated free B1 mAb, the classical structure, and the star structure of HPMA copolymer-bound doxorubicin targeted with B1 mAb (B1 mAb-P-Dox) to spleen cells of Balb/c mice bearing BCL1 leukemia after intravenous application of 250 μg of B1 mAb. Spleen cells were isolated 45 min after sample application and secondary labeled by streptavidin−FITC conjugate as described in Material and Methods. Grey peaks represent control (no secondary labeling). Control mouse was injected with physiological solution only.

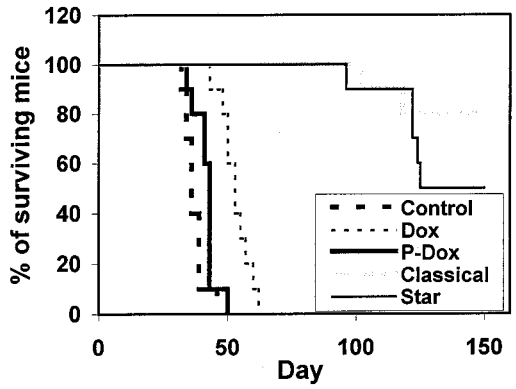


Figure 7. Effect of free doxorubicin (Dox), HPMA copolymer-bound doxorubicin (P-Dox), the classical structure of HPMA copolymer-bound doxorubicin targeted with B1 mAb (Classical), and the star structure of HPMA copolymer-bound doxorubicin targeted with B1 mAb (Star) on the survival of Balb/c mice bearing BCL1 leukemia. The treatment consisted of three intravenous doses given on the 11th, 14th, and 17th day. Each dose contained 50 μg of free doxorubicin or 100 μg of HPMA copolymer-bound doxorubicin. Control mice were injected with the same volume (250 μL) of physiological solution.

psin B are probably due to the different molecular structure of the conjugate and accessibility of the doxorubicin bound to the tetrapeptide spacer. Steric hindrances to the access of the enzyme to the macromolecular substrate could explain the decrease in the rate of doxorubicin release. The steric hindrances are the highest in the branched high molecular-weight conjugate with classic structure. This type of conjugate thus shows the slowest doxorubicin release rate. Steric hindrances are lower in the case of the star structure. The star structure is a conjugate with central antibody molecule surrounded

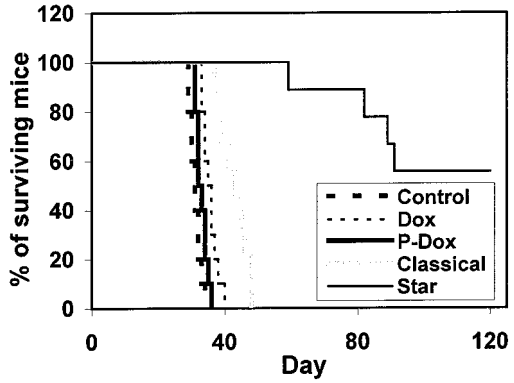


Figure 8. Effect of free doxorubicin (Dox), HPMA copolymer-bound doxorubicin (P-Dox), the classical structure of HPMA copolymer-bound doxorubicin targeted with B1 mAb (Classical), and the star structure of HPMA copolymer-bound doxorubicin targeted with B1 mAb (Star) on the survival of Balb/c mice bearing BCL1 leukemia. The treatment consisted of one intravenous dose given on the 11th day. The dose contained 50 μg of free doxorubicin or 100 μg of HPMA copolymer-bound doxorubicin. Control mice were injected with the same volume (250 μL) of physiological solution.

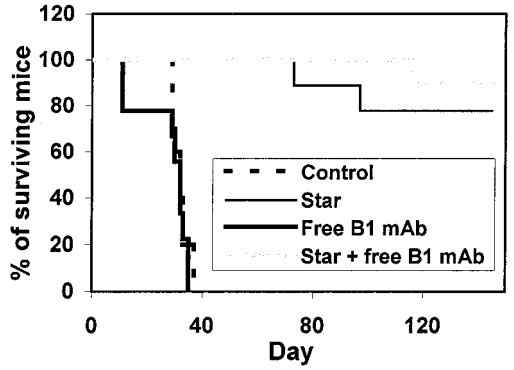


Figure 9. Effect of star structure of HPMA copolymer-bound doxorubicin targeted with B1 mAb (Star), free B1 mAb and a combination of free B1 mAb and the star structure of HPMA copolymer-bound doxorubicin targeted with B1 mAb on the survival of Balb/c mice bearing BCL1 leukemia. Free B1 mAb was given in two injections (125 μL) separated by 1 h (0.4 mg intraperitoneally followed by 0.8 mg intravenously). Targeted conjugate was given in one intravenous injection containing 75 μg of doxorubicin. Combination of free B1 mAb and targeted conjugate was given in two injections (125 μL and 187.5 μL) separated by 1 h (0.4 mg of free B1 mAb intraperitoneally followed by a mixture of 0.8 mg of free B1mAb and targeted conjugate containing 75 μg of doxorubicin intravenously). All treatments were given on the 11th day and control mice were injected intravenously with 187.5 μL of physiological solution.

by the HPMA copolymer chains exposing doxorubicin on the surface. This probably provides faster doxorubicin release. Finally, nontargeted HPMA copolymer-bound doxorubicin is a simple conjugate without antibody showing the fastest doxorubicin release. Differences in the molecular structure of the two antibody-targeted conjugates could also explain the different binding activity to BCL1 cells in vitro. In the star structure where the single antibody molecule is surrounded by the HPMA copolymer chains, the binding site of the antibody could be partially masked and blocked in its binding to its epitope. Moreover, the accessibility of biotins for streptavidine−FITC conjugate on the antibody molecule in the star structure could be lower than the accessibility of biotins in a branched high-molecular-weight antibody-targeted conjugate (classic conjugate).

Our results demonstrate that both antibody-targeted HPMA copolymer-bound doxorubicin conjugates have strong cytostatic activity in vitro. The low cytostatic activity of nontargeted HPMA copolymer-bound doxorubicin reflects the fact that this conjugate has no specific receptor on target cells. It is taken up only by fluid-phase pinocytosis (*29*), which is a slow process and requires a high concentration of the conjugate to produce cytostatic activity. The presence of irrelevant (anti-Thy 1.2) antibody in the conjugate does not enhance its cytostatic activity. This provides an evidence that BCL1 cells take up also this conjugate only by fluid-phase pinocytosis and that other mechanisms such as endocytosis via Fc receptors are not involved. By contrast, HPMA copolymer-bound doxorubicin conjugates targeted with anti-idiotype B1 mAb bind specifically to target BCL1 cells and produce strong cytostatic activity. Anti-idiotype antibodies have been previously used for constructing different immunotoxins (*30, 31*). Here we demonstrate that also a water-soluble polymer-bound drug system based on HPMA copolymer is efficient in anti-idiotype targeting. Direct correlation was reported between the intensity of binding of targeted cytostatic drugs or immunotoxins to target cells and their respective cytotoxicities. Despite this fact, we found that the star structure of HPMA copolymer-bound doxorubicin binds to BCL1 cells with lower activity than the classic structure of targeted conjugate, but it shows a higher cytostatic activity. The discrepancies between the intensity of binding and cytostatic activities may reflect different processing and intracellular release of the targeted drug (*32*). Intracellular release of the bound drug is probably faster within the star structure of the targeted conjugate as documented in vitro (Figure 3). As described for immunotoxins, the cellular internalization rate and intracellular destination are more critical factors in targeted drug efficacy than the number and binding of cell surface receptors (*33*). Nevertheless, our other experimental data shows that the star structure of HPMA copolymer-bound doxorubicin targeted with monoclonal antibody is more effective than the classic structure also in the case of anti-CD71 targeting using B cell lymphoma 38C13 cell line (Kovář, preliminary results) and anti-Thy 1.2 targeting using T cell lymphoma EL4 cell line (*34*).

We have used in our in vivo experiments different doses of free doxorubicin and HPMA copolymer-bound doxorubicin. It was repeatedly shown that conjugation of doxorubicin to HPMA copolymer reduces the cellular toxicity of the drug. For example, the recommended Phase II dose of PK1 is 280 mg/m^2 every 3 weeks in contrast to the free doxorubicin which is given at 60−80 mg/m^2. This means that HPMA copolymer-bound doxorubicin is given at a 3.5−4.6 higher dose than the free drug. We have used only twice higher doses of HPMA copolymer-bound doxorubicin than free doxorubicin. Twice higher doses for HPMA copolymer-bound doxorubicin have already been used in the model of murine T-cell lymphoma EL4 by targeting HPMA copolymer-bound doxorubicin to Thy 1.2 antigen (*35*). The much stronger antitumor effect of the star structure as compared with the classic structure of targeted conjugate against established BCL1 leukemia demonstrates that the molecular design of conjugates for targeted drug delivery is essential for their biological properties. Among the most important factors that influence the activity of such conjugates are the rate of release of the bound drug (*28*), rate of internalization and intracelular pathway, biodistribution and pharmacokinetics. Our preliminary data shows that the star structure of HPMA copolymer-bound doxorubicin targeted with mAb has a prolonged blood-elimination profile if compared to the classic structure. Both types of antibody-targeted conjugates were injected to mice and the blood of these mice was analyzed for the content of the conjugate 24 h after administration. We found less than 5% of administered dose of the conjugate with a classic structure but more than 25% of administered dose of the conjugate with a star structure (*34*). This slower elimination of the star structure of antibody-targeted conjugate is probably a very important feature responsible for its higher antitumor effect.

ACKNOWLEDGMENT

The authors thank Dr. Wyatt for the kind loan of the multiangle light scattering detector DAWN-DSP-F (Wyatt Technology Corp., Santa Barbara, CA). This research was supported by the Institutional Research Concept No. AVOZ5020903, by the grant AS CR No. S5020101, and by the grant GA AS CR No. A4050201.

LITERATURE CITED

(1) Rossmann, P., Říhová, B., Strohalm, J., and Ulbrich, K. (1997) Morphology of rat kidney and thymus after native and antibody-coupled cyclosporin A application (reduced toxicity of targeted drug). *Folia Microbiol. Praha 42*, 277−87.

(2) Šťastný, M., Ulbrich, K., Strohalm, J., Rossmann, P., and Říhová, B. (1997) Abnormal differentiation of thymocytes induced by free cyclosporine is avoided when cyclosporine bound to *N*-(2-hydroxypropyl)methacrylamide copolymer carrier is used. *Transplantation 63*, 1818−1827.

(3) Říhová, B., Vereš, K., Fornůsek, L., Ulbrich, K., Strohalm, J., Větvička, V., Bilej, M., and Kopeček, J. (1989) Action of the polymeric prodrugs based on *N*-(2-hydroxypropyl)methacrylamide. 2. Body distribution and T cell accumulation of ^{125}DNM. *J. Controlled Release 10*, 37−49.

(4) Vasey, P. A., Kaye, S. B., Morrison, R., Twelves, C., Wilson, P., Duncan, R., Thomson, A. H., Murray, L. S., Hilditch, T. E., Murray, T., Burtles, S., Fraier, D., Frigerio, E., and Cassidy, J. (1999) Phase I clinical and pharmacokinetic study of PK1 [*N*-(2-hydroxypropyl)methacrylamide copolymer doxorubicin]: first member of a new class of chemotherapeutic agents-drug-polymer conjugates. Cancer Research Campaign Phase I/II Committee [see comments]. *Clin. Cancer Res. 5*, 83−94.

(5) Říhová, B., Strohalm, J., Kubáčková, K., Jelínková, M., Hovorka, O., Kovář, M., Plocová, D., Šírová, M., Šťastný, M., Rozprimová, L., and Ulbrich, K. (2002) Acquired and specific immunological mechanisms co-responsible for efficacy of polymer-bound drugs. *J. Controlled Release 78*, 97−114.

(6) Jelínková, M., Strohalm, J., Plocová, D., Šubr, V., Šťastný, M., Ulbrich, K., and Říhová, B. (1998) Targeting of human and mouse T-lymphocytes by monoclonal antibody-HPMA copolymer-doxorubicin conjugates directed against different T-cell surface antigens. *J. Controlled Release 52*, 253−70.

(7) Říhová, B. (1995) Antibody-targeted polymer-bound drugs. *Folia Microbiol. Praha 40*, 367−84.

(8) Pimm, M. V., Perkins, A. C., Duncan, R., and Ulbrich, K. (1993) Targeting of *N*-(2-hydroxypropyl)methacrylamide copolymer-doxorubicin conjugate to the hepatocyte galactose-receptor in mice: visualisation and quantification by gamma scintigraphy as a basis for clinical targeting studies. *J. Drug Target. 1*, 125−31.

(9) Wirth, M., Hamilton, G., and Gabor, F. (1998) Lectin-mediated drug targeting: quantification of binding and internalization of Wheat germ agglutinin and *Solanum tuberosum* lectin using Caco-2 and HT-29 cells. *J. Drug Target. 6*, 95−104.

(10) O'Hare, K. B., Duncan, R., Strohalm, J., Ulbrich, K., and Kopečková, P. (1993) Polymeric drug-carriers containing doxorubicin and melanocyte-stimulating hormone: in vitro and in vivo evaluation against murine melanoma. *J. Drug Target. 1*, 217−29.

(11) Flanagan, P. A., Duncan, R., Říhová, B., Šubr, V., and Kopeček, J. (1990) Immunogenicity of protein-*N*-(2-hydroxypropyl)methacrylamide conjugates in A/J and B10 mice. *J. Bioact. Compat. Polym. 5*, 151−166.

(12) Corvalan, J. R., Smith, W., Gore, V. A., and Brandon, D. R. (1987) Specific in vitro and in vivo drug localisation to tumour cells using a hybrid-hybrid monoclonal antibody recognising both carcinoembryonic antigen (CEA) and vinca alkaloids. *Cancer Immunol. Immunother. 24*, 133−7.

(13) Tsukada, Y., Ohkawa, K., and Hibi, N. (1987) Therapeutic effect of treatment with polyclonal or monoclonal antibodies to alpha-fetoprotein that have been conjugated to daunomycin via a dextran bridge: studies with an alpha-fetoprotein-producing rat hepatoma tumor model. *Cancer Res. 47*, 4293−5.

(14) Manske, J. M., Buchsbaum, D. J., Hanna, D. E., and Vallera, D. A. (1988) Cytotoxic effects of anti-CD5 radioimmunotoxins on human tumors in vitro and in a nude mouse model. *Cancer Res. 48*, 7107−14.

(15) Vervoordeldonk, S. F., Merle, P. A., van Leeuwen, E. F., von dem Borne, A. E., and Slaper Cortenbach, I. C. (1994) Preclinical studies with radiolabeled monoclonal antibodies for treatment of patients with B-cell malignancies. *Cancer 73*, 1006−11.

(16) Denis, O., Macedo Soares, F., Latinne, D., Nisol, F., and Bazin, H. (1994) In vivo study of mIgM and mIgD cross-linking on murine B cells. *Scand. J. Immunol. 39*, 625−32.

(17) Mitchell, R. N., Shaw, A. C., Weaver, Y. K., Leder, P., and Abbas, A. K. (1991) Cytoplasmic tail deletion converts membrane immunoglobulin to a phosphatidylinositol-linked form lacking signaling and efficient antigen internalization functions. *J. Biol. Chem. 266*, 8856−60.

(18) Říhová, B., Jelínková, M., Strohalm, J., Šťastný, M., Hovorka, O., Plocová, D., Kovář, M., Dráberová, L., and Ulbrich, K. (2000) Antiproliferative Effect of a Lectin- and Anti-Thy-1.2 Antibody Targeted HPMA Copolymer-Bound Doxorubicin on Primary and Metastatic Human Colorectal Carcinoma and on Human Colorectal Carcinoma Transfected with the Mouse Thy-1.2 Gene. *Bioconjug. Chem. 11*, 664−673.

(19) Ulbrich, K., Šubr, V., Strohalm, J., Plocová, D., Jelínková, M., and Říhová, B. (2000) Polymeric drugs based on conjugates of synthetic and natural macromolecules. I. Synthesis and physicochemical characterisation. *J. Controlled Release 64*, 63−79.

(20) Rejmanová, P., Pohl, J., Baudyš, M., Kostka, V., and Kopeček, J. (1983) Polymers containing enzymatically degradable bonds. 8. Degradation of oligopeptide sequences in *N*-(2-hydroxypropyl)methacrylamide) copolymers by bovine spleen cathepsin B. *Makromol. Chem. 184*, 2009−2020.

(21) Kopeček, J., Rejmanová, P., and Chytrý, V. (1981) Polymers containing enzymatically degradable bonds. 1. Chymotrypsin catalyzed hydrolysis of *p*-nitroanilides of phenylalanine and tyrosine attached to side-chains of copolymers of *N*-(2-hydroxypropyl)methacrylamide. *Makromol. Chem. 182*, 799−809.

(22) Šubr, V., Strohalm, J., Ulbrich, K., Duncan, R., and Hume, I. C. (1992) Polymers containing enzymatically degradable bonds, XII. Effect of spacer structure on the rate of release of daunomycin and adriamycin from poly[*N*-(2-hydroxypropyl)methacrylamide] copolymer drug carriers in vitro and antitumor activity measured in vivo. *J. Controlled Release 18*, 123−132.

(23) Brissinck, J., Demanet, C., Moser, M., Leo, O., and Thielemans, K. (1991) Treatment of Mice Bearing BCL1 Lymphoma with Bispecific Antibodies. *J. Immunol. 147*, 4019−4026.

(24) Říhová, B. and Kopeček, J. (1985) Biological properties of targetable poly *N*-(2-hydroxypropyl)methacrylamide-antibody conjugates. *J. Controlled Release 2*, 289−310.

(25) Říhová, B., Kopeček, J., Kopečková Rejmanova, P., Strohalm, J., Plocová, D., and Semorádová, H. (1986) Bioaffinity therapy with antibodies and drugs bound to soluble synthetic polymers. *J. Chromatogr. 376*, 221−33.

(26) Šťastný, M., Strohalm, J., Plocová, D., Ulbrich, K., and Říhová, B. (1999) A possibility to overcome P-glycoprotein (PGP)-mediated multidrug resistance by antibody-targeted drugs conjugated to *N*-(2-hydroxypropyl)methacrylamide (HPMA) copolymer carrier. *Eur. J. Cancer 35*, 459−66.

(27) Wang, D., Kopečková, P., Minko, T., Nanayakkara, V., and Kopeček J. (2000) Synthesis of starlike *N*-(2-hydroxypropyl)-methacrylamide copolymers: potential drug carriers. *Biomacromolecules 1*, 313−19.

(28) Říhová, B., Etrych, T., Pechar, M., Jelínková, M., Šťastný, M., Hovorka, O., Kovář, M., and Ulbrich, K. (2001) Doxorubicin bound to a HPMA copolymer carrier through hydrazone bond is effective also in a cancer cell line with a limited content of lysosomes. *J. Controlled Release 74*, 225−232.

(29) Duncan, R., Kopečková Rejmanová, P., Strohalm, J., Hume, I., Cable, H. C., Pohl, J., Lloyd, J. B., and Kopeček, J. (1987) Anticancer agents coupled to *N*-(2-hydroxypropyl)methacrylamide copolymers. I. Evaluation of daunomycin and puromycin conjugates in vitro. *Br. J. Cancer 55*, 165−74.

(30) Walbridge, S. and Rybak, S. M. (1994) Immunotoxin therapy of leptomeningeal neoplasia. *J. Neurooncol. 20*, 59−65.

(31) DeShambo, R. M. and Krolick, K. A. (1986) Selective in vitro inhibition of an antibody response to purified acetylcholine receptor by using anti-idiotypic antibodies coupled to the A chain of ricin. *J. Immunol. 137*, 3135−9.

(32) Marks, A., Ettenson, D., Bjorn, M. J., Lei, M., and Baumal, R. (1990) Inhibition of human tumor growth by intraperitoneal immunotoxins in nude mice. *Cancer Res. 50*, 288−92.

(33) Recht, L. D., Raso, V., Davis, R., and Salmonsen, R. (1996) Immunotoxin sensitivity of Chinese hamster ovary cells expressing human transferrin receptors with differing internalization rates. *Cancer Immunol. Immunother. 42*, 357−61.

(34) Jelínková, M., Ulbrich, K., Strohalm, J., Etrych, T., Šírová, M., and Říhová, B. (2000) Use of "star-like" macromolecular prodrugs in cancer therapy. *Proceed. Int'l. Symp. Control. Relat. Bioact. Mater. 27*, 84−85.

(35) Říhová, B., Jelínková, M., Strohalm, J., Šubr, V., Plocová, D., Hovorka, O., Novák, M., Plundrová, D., Germano, Y., and Ulbrich, K. (2000) Polymeric drugs based on conjugates of synthetic and natural macromolecules. II. Anti-cancer activity of antibody or (Fab′)(2)-targeted conjugates and combined therapy with immunomodulators. *J. Controlled Release 64*, 241−61.

BC010063M

Conjugates Bearing Multiple Formyl-Methionyl Peptides Display Enhanced Binding to but Not Activation of Phagocytic Cells

Shahriar Pooyan,[†,‡] Bo Qiu,[†] Marion M. Chan,[§] Dunne Fong,[†] Patrick J. Sinko,[∥] Michael J. Leibowitz,[⊥,⊗] and Stanley Stein*[,†,‡,⊥]

Department of Molecular Genetics and Microbiology, UMDNJ-Robert Wood Johnson Medical School, Piscataway, New Jersey 08854; Center for Advanced Biotechnology and Medicine, Piscataway, New Jersey 08854; Departments of Chemistry and Cell Biology and Neurosciences, Rutgers University,Rutgers, Piscataway, New Jersey 08854; Cancer Institute of New Jersey, New Brunswick, New Jersey 08903; Department of Microbiology and Immunology, Temple University School of Medicine, Philadelphia, Pennsylvania 19140; and Department of Pharmaceutics, School of Pharmacy, Rutgers University, Piscataway, New Jersey 08854. Received July 3, 2001; Revised Manuscript Received November 12, 2001

N-Formyl-methionyl peptides can specifically bind to surface receptors on phagocytic cells. A single copy of *N*-formyl-methionine-leucine-phenylalanine (fMLF) covalently linked to a poly(ethylene glycol)-based polymer displayed reduced binding avidity (K_d = 190 nM) for differentiated HL-60 cells relative to free fMLF (K_d = 28 nM). Increasing the number of fMLF residues (up to eight) attached to a single polymer results in enhanced avidity for these cells (K_d = 0.18 nM), which appears to be independent of whether the polymer backbone is linear or branched. However, no conjugate showed enhanced ability to activate phagocytic cells, relative to the free peptide (EC_{50} = 5 nM), as measured by transient stimulation of release of calcium ions from intracellular stores into the cytoplasm. A polymer bearing four fMLF and four digoxigenin residues showed specific enhancement in binding to differentiated HL-60 cells and mouse peritoneal macrophages in situ relative to a polymer lacking fMLF; no such enhancement was seen in binding to receptor-negative lymphocytic Jurkat cells. These results suggest that multiple fMLF residues linked to a drug-delivery polymer can be used to target appended drugs to phagocytic cells with relatively little toxicity due to cellular activation.

INTRODUCTION

Therapeutic drugs are generally administered via oral or parenteral routes, so that they are widely distributed throughout the body, although only one organ or tissue might be affected by the disease being treated. By targeting a drug to the site of the disease, it should be possible to achieve a higher and more effective dose where needed and a lower and less toxic dose in unaffected tissues. The present study focuses on targeting drugs to macrophages and related phagocytic cells of the reticuloendothelial system, such as monocytes and dendritic cells. Macrophage targeting could be especially useful for therapy of AIDS and tuberculosis, since these cells represent a major reservoir for propagation of the causative virus and bacterium, respectively, as well as for the AIDS-associated opportunistic infection, leishmaniasis, caused by a tropical protozoan. Macrophage targeting has been studied before, examples being the use of nanoparticles for antileishmanial drugs (Venier-Julienne et al., 1995), glycoside-liposomes for antituberculosis drugs (Medda et al., 1995), and mannosylated replacement enzyme for Gaucher's disease (Mistry et al., 1996). To achieve macrophage targeting for AIDS, reverse transcriptase inhibitors have been covalently attached to lipoproteins (Mankertz et al., 1996), noncovalently adsorbed into colloidal nanoparticles (Lobenberg and Kreuter, 1996), and incorporated into erythrocytes (Rossi et al., 1998). In this report, macrophage targeting is based on the chemotactic peptide, *N*-formyl-methionine-leucine-phenylalanine (fMLF),[1] which is indicative of a bacterial infection since all bacterial (but not eukaryotic) proteins are synthesized with *N*-formyl-methionine as their N-terminal amino acid. Monocyte-derived dendritic cells (Randolph et al., 1998), which migrate to lymph nodes and which can be infected by both M-tropic and T-tropic strains of HIV-1, also bind and respond to fMLF (Benelli et al., 1998). The high affinity receptor for fMLF is found on phagocytes and some other cells, while sequence-related low affinity and orphan receptors are more widely distributed (reviewed by Prossnitz and Ye, 1997; Le et al., 2001). Expression of the fMLF receptor has been shown to be sufficient to enable normally receptor nega-

* Address correspondence to this author at the Center for Advanced Biotechnology and Medicine, 679 Hoes Lane, Piscataway, NJ 08854. Phone: 732-235-5319. Fax: 732-235-4850. E-mail: stein@cabm.rutgers.edu.

† Departments of Chemistry and Cell Biology and Neurosciences, Rutgers University.

‡ Center for Advanced Biotechnology and Medicine.

§ Temple University School of Medicine.

∥ Department of Pharmaceutics, Rutgers University.

⊥ UMDNJ−Robert Wood Johnson Medical School.

⊗ Cancer Institute of New Jersey.

[1] Abbreviations: DCM, dichloromethane; DIG, digoxigenin; DIPC, diisopropylcarbodiimide; 4-DMAP, 4-(dimethylamino)-pyridine; DMF, *N*,*N*-dimethylformamide; fMLF, formyl-methionine-leucine-phenylalanine; HBSS, Hanks's Balanced Salt Solution; NHS, *N*-hydroxysuccinimide; PBS, phosphate-buffered saline; PEG, poly(ethylene glycol); PEG/A, linear PEG-aspartate copolymer; PTSA, *p*-toluenethiosulfonic acid; tBoc, *tert*-butyloxycarbonyl; TFA, trifluoroacetic acid.

10.1021/bc0100657 CCC: $22.00 © 2002 American Chemical Society
Published on Web 03/03/2002

tive cells to specifically bind to fMLF (Prossnitz et al., 1993).

We have developed a novel method of targeting drug delivery to phagocytic cells based on a poly(ethylene glycol) (PEG) carrier possessing multiple sites for covalent attachment of targeting groups and drug moieties (Huang et al., 1998). Whereas the bioreversible disulfide bond had been proposed for reversibly appending the therapeutic agent to the carrier and delivering it to cellular targets (Huang et al., 1998), the present studies used the more stable amide bond for appending the reporter group, digoxigenin, as a surrogate drug substance. To achieve high affinity binding to fMLF receptors, we explored the concept of using multiple copies of this ligand on the carrier polymer. In addition to achieving strong and specific binding to the fMLF receptor, a clinically acceptable targeted drug−carrier conjugate should not activate macrophages, thereby avoiding undesired side effects. A previously proposed solution was to use a receptor antagonist as the targeting group. This could be accomplished by replacing the formyl group on the targeting peptide ligand with a branched carbamate structure, such as the *tert*-butyloxycarbonyl group (tBoc) commonly used as a blocking group in peptide synthesis (Derian et al., 1996). However, this substitution was found to weaken receptor binding 100-fold (K_d increased from 0.033 to 4.5 μM) (Derian et al., 1996). Based on studies using carrier polymers bearing different numbers of fMLF ligands, we now report that we have found a method by which macrophages can be targeted but not activated, by attaching multiple fMLF moieties to a single drug-carrying polymer.

EXPERIMENTAL PROCEDURES

Materials. *N*-Formyl-methionine-leucine-phenylalanine (fMLF) peptide was purchased from Sigma (St. Louis, MO). Radioactive [^{45}Ca]calcium chloride (specific activity 16 mCi/mg) and fML[^{3}H]F (40 Ci/mmol) were from DuPont-NEN Research Products (Boston, MA). The human cells used in this study (HL-60 and Jurkat T-cells) were purchased from the American Type Culture Collection (Manassas, VA). Branched amino-PEGs with three (10 kDa), four (10 kDa), or eight arms (20 kDa) and α,ω-diamino-PEG (3.4 kDa) were purchased from Shearwater Polymers (Huntsville, AL). Dichloromethane (DCM) and *N*,*N*-dimethylformamide (DMF) were purchased from Fisher Scientific (Pittsburgh, PA). Trifluouroacetic acid (TFA), diiosopropylcarbodiimide (DIPC), and *p*-toluenethiosulfonic acid (PTSA) were obtained from Aldrich Chemical (Milwaukee, WI). *N*-Hydroxysuccinimide-digoxigenin (NHS-DIG) was obtained from Boehringer-Mannheim (Indianapolis, IN). Fluorescamine was a gift from S. Udenfriend. Hanks's balanced salt solution (HBSS) and RPMI 1640 tissue culture medium were purchased from GIBCO (Grand Island, NY).

Quantitation of Primary Amino Groups. Fluorescamine (Udenfriend et al., 1972) was used to monitor conversion of primary amines to amides. A fluorescence signal is obtained only by reaction with primary amines and not with amides or with secondary or aromatic amines. To each well of the 96-well plates, 0.1 mL of sample was added. Then 0.05 mL of 0.2 M borate buffer (pH 9.3) was added to each well, and 0.05 mL of fluorescamine (0.5 mg/mL in acetonitrile) was added and mixed immediately. The fluorescence intensity was measured at an excitation wavelength of 390 nm and emission wavelength of 475 nm.

Synthesis of Linear PEG−Aspartate Copolymer. This carrier copolymer was prepared by copolymerization of tBoc-aspartic acid and α,ω-diamino-PEG (3400 Da), using a modification of previous methods (Nathan et al., 1993; Poiani et al., 1994). The tBoc group was removed by treatment with TFA, thereby providing primary amino groups (NH_2) for attachment of fMLF. Copolymer size was determined by size exclusion chromatography using PEG−tyrosine molecular weight standards prepared by us. The molecular weight was estimated to be 29 kDa. The structure of the resulting copolymer ($m \sim 8$, $n \sim 75$) is

$$\text{H-[NHCH}_2\text{CH}_2(\text{OCH}_2\text{CH}_2)_n\text{NHCOCH}_2\text{-CH(NH}_2\text{)CO]}_m\text{-OH}$$

Conjugation of PEG−Aspartate Copolymer with fMLF and DIG. Linear PEG−aspartate (PEG/A) copolymer (about 10 mg) was reacted with 7-fold excess (relative to amino groups) of fMLF peptide, 3.5 molar excess of DIPC, and 0.5 equiv of PTSA and 4-(dimethylamino)-pyridine (4-DMAP) in DMF:DCM (1:1 v/v). The total volume of the reaction was adjusted to 1 mL. The reaction mixture was incubated at room temperature for 24 h with gentle stirring. Then the polymer was precipitated with 10 volumes of ice-cold ethyl ether and dissolved in 90% phosphate-buffered saline (PBS) pH = 7.4, 10% acetonitrile. The unreacted peptide was separated from polymer by ultrafiltration with Microcon 10 (molecular weight cutoff = 10 kDa Amicon/Millipore, Inc., Bedford, MA). The retentate was dried and dissolved in PBS. The extent of peptide conjugated to the polymer was estimated using the fluorescamine assay. Separately, 4 mg of PEG/A or 4 mg of PEG/A−fMLF was reacted with 1 mg of NHS-DIG, dissolved in DMSO, in 0.5 mL of PBS, adjusted with NaOH to pH 8.0, with stirring overnight. The products were precipitated with ether, dissolved in PBS, and separated from the unreacted reagent by ultrafiltration with Microcon 10. The products were PEG/A−$fMLF_4$ and PEG/A−$fMLF_4$−DIG_4, and PEG/A−DIG_8.

Conjugation of fMLF with Branched (B) PEG. Addition of fMLF to the eight-arm branched amino-PEGs was accomplished in a similar manner as above. To achieve a range of molar ratio of fMLF conjugated to the copolymer, three sets of reactions with 14-, 8-, and 2-fold excess fMLF were set up. Fluorescamine assay was used to determine the average extent of conjugation of fMLF on the polymer, which was 8 (100%), 5.5 (68%), and 1.1 (14%) fMLF residues per polymer, respectively, for each reaction. These products are denoted B8-PEG−$fMLF_8$, B8-PEG−$fMLF_{5.5}$, and B8-PEG−$fMLF_{1.1}$, respectively. Similarly, a 14-fold molar excess of fMLF was used for reactions with three-arm and four-arm branched amino-PEGs to achieve100% coupling, yielding B3-PEG−$fMLF_3$ and B4-PEG−$fMLF_4$.

Competitive Receptor Binding Assay. HL-60 cells were propagated in RPMI 1640 supplemented with 2 mM L-glutamine and 10% (v/v) heat-inactivated fetal bovine serum and were subcultured every 3 days at a ratio of 1:4. Cells were grown at 37 °C in an atmosphere of 5% CO_2. Dimethyl sulfoxide (DMSO, 1.3%) was added to the culture (3×10^5 cells/mL) 48 h before the binding assay to initiate cellular differentiation. Differentiated HL-60 cells (2×10^5) were washed with PBS, pH 7.4, and resuspended in 1.77 mM KH_2PO_4, 8.0 mM Na_2HPO_4, 0.117 M NaCl, 0.15 mM $CaCl_2$, 0.5 mM MgCl, and 1% bovine serum albumin (binding buffer) with fML[^{3}H]F (30,000 cpm) and unlabeled fMLF (0.1 nM-200 nM) or conjugate. The cells were incubated for 15 min at 37 °C with gentle shaking. They were collected by centrifuga-

tion at 3000*g* for 5 min at room temperature. The supernatant was removed, and cells were resuspended in 0.1 mL of binding buffer and carefully added to the very top of tubes (Denville Scientific, South Plainfield, NJ, catalog #C19002) that contained 0.3 mL of 10% sucrose. They were centrifuged for 5 min at 12000*g*. The cells settled to the bottom, and any unbound ligand remained in the middle of the tube. The tubes were placed in dry ice for 5 min, and then their bottoms were cut off to collect the cells. Cell-bound and free radioactivity were determined by liquid scintillation counting. The value of K_d for each curve was determined graphically using the Cricket Graph program.

Intracellular Calcium Assay. HL-60 cells (2×10^5 cells/mL) were grown in the presence of 1.3% DMSO for 5 days. For each time course experiment, 2×10^6 cells were resuspended in 5 mL of HBSS containing 2 mCi/mL of $^{45}CaCl_2$ as the sole source of calcium. After 90 min incubation at 37 °C, cells were washed twice as above with cold HBSS. Vesicle-associated and cytoplasmic ^{45}Ca were measured prior to and at 1, 2, 3, 4, 5, and 10 min after the addition of the fMLF or conjugated compounds. The EC_{50} for cellular activation is the concentration of each compound tested resulting in 50% maximal stimulation of calcium efflux by this assay. Cell pellets were treated with 0.5% Triton X-100/0.1 M NaOH and centrifuged in tubes containing 0.3 mL of 10% sucrose, and radioactivity associated with the pellets was measured; this represents vesicle-associated ^{45}Ca. The top portion of the tube, which contained the cytoplasmic ^{45}Ca was also measured. The peak level of transient increase in cytoplasmic calcium and decrease in vesicle-associated calcium represents efflux of calcium from intracellular storage compartments that is stimulated by fMLF interaction with membrane receptors (Montero et al., 1994; Klinker et al., 1996; Azuma et al., 1996; Anderson and Mohamed Goolam, 1997).

Uptake by HL-60, Jurkat and Peritoneal Cells. Human Jurkat T-cell growth conditions were the same as for HL-60 cells, except that the subcultivation ratio was 1:3. Jurkat cells (2×10^5) or fully differentiated HL-60 cells were washed twice with PBS and incubated in binding buffer (see above) with conjugate for 30 min at 37 °C. Each conjugate (1 μg, dissolved at a concentration of 33 nM) was used in these experiments. Cells were lysed, the membranes and cell debris were removed by centrifugation (5 min at 14000*g*), and the enzyme-linked immunosorbant assay (ELISA) for DIG was performed on the supernatant as described below. To study primary peritoneal cells, BALB/c mice were injected in the peritoneal cavity with 5 μg of PEG/A−DIG_4-$fMLF_4$ ($n = 3$ mice), or PEG/A−DIG_8 ($n = 4$ mice). After 1 h, the cavity was flushed with medium, and cells were collected and washed twice with cold PBS, as described above.

Cells were resuspended in 100 μL of PBS, containing 0.6% Tween 20, vortexed briefly, and kept on ice for 30 min. Microscopic examination confirmed complete cell lysis. Uptake of DIG was determined by ELISA of the supernatant. Anti-DIG-Fab fragment and anti-DIG-horseradish peroxidase (POD) were purchased from Boehringer Mannheim. Anti-DIG-Fab (1 mg/mL) was diluted 1:100 and anti-DIG−POD (150 U/mL) was diluted 1:10000. ELISA was performed according to the manufacturer's procedure. DIG content was proportional to the difference in absorbance at 495 and 450 nm. A standard curve for PEG/A−DIG_8 and PEG/A−$fMLF_4$−DIG_4 was included in each assay. To account for the potential different amounts of peritoneal cells from each mouse, the results were normalized to the amount of protein, as measured with the Bradford assay (BioRad, Hercules, CA).

For all cell uptake experiments, statistical significance of the differences between experimental groups was evaluated using the two-sample t-test for independent samples with unequal variance.

RESULTS

Competitive Binding of fMLF Conjugates to Differentiated HL-60 Cells. To determine the effect of different numbers of targeting groups on polymer avidity for differentiated HL-60 cells, conjugates were tested for their binding activity, measured by their ability to compete with fML[H^3]F for cell binding. The HL-60 cells used for these experiments were differentiated for 48 h with DMSO. HL-60 cells treated with DMSO for 5 days yielded similar results (data not shown). However, HL-60 cells that were not subjected to a differentiation-inducing regimen did not bind to fMLF (data not shown). HL-60 cells, which are derived from human promyelocytic leukemia cells, have the capacity to respond to many stimuli to differentiate into many cell types of the monocytic−granulocytic class. The categorization of the differentiated states by the nomenclature for normal cell types is somewhat arbitrary, since the cells tend to have properties that overlap these categories. Although DMSO is considered to induce cells to differentiate along the granulocytic pathway, the final phenotype of these cells is not identical to normal granulocytes (reviewed by Collins, 1987). The functional properties of HL-60 differentiated cells are similar (although not identical) to neutrophils (Dahlgren et al., 1987). They are able to undergo azurophilic granule release and to generate O_2^- (Seifert et al., 1992). Expression of the receptor for fMLF is one of the early events of differentiation of HL-60 cells and its presence is the only requirement for binding of fMLF to these cells (Prossnitz et al.,. 1993). In this work these differentiated HL-60 cells are used as a model cell system; these cells have some properties of both macrophages and neutrophils, but are not identical with either cell type.

Figures 1 and 2 show the result of competitive binding studies. The conjugates tested included PEG/A−$fMLF_4$, PEG/A−$fMLF_4$−DIG_4, PEG/A−DIG_8, B8-PEG−$fMLF_{1.1,5.5,8}$, B4-PEG−$fMLF_4$, and B3-PEG−$fMLF_3$. The amount of fML[H^3]F was kept constant while the concentration of each conjugate was varied. The binding curves (Figures 1 and 2) show that the specific binding is about 75% of the total binding, since about 25% of maximum ligand binding was nonspecific in that it was not subject to competition at any concentration of any competitor. The binding constant (K_d) estimated here for fMLF is 28 nM, which is close to that (33 nM) determined by Derian et al. (1996). As can be seen in Figure 1 and Table 1, the increased K_d of B8-PEG−$fMLF_{1.1}$ (190 nM) relative to the free fMLF peptide (28 nM) indicates that attachment to the polymer reduces the avidity of the peptide for binding to cellular receptors. However, polymers with multiple fMLF moieties attached showed increased avidity for differentiated HL-60 cells, with B8-PEG−$fMLF_8$ showing the lowest K_d (0.18 nM) and the greatest avidity relative to the number of fMLF peptides [$K_d \times$ (no. of fMLF) = 0.18 nM $\times$ 8 = 1.44 nM].

The size or shape of the polymer does not seem to play a major role in avidity of binding, since the linear polymer with four copies of fMLF showed properties similar to its branched counterpart, both displaying a K_d of about

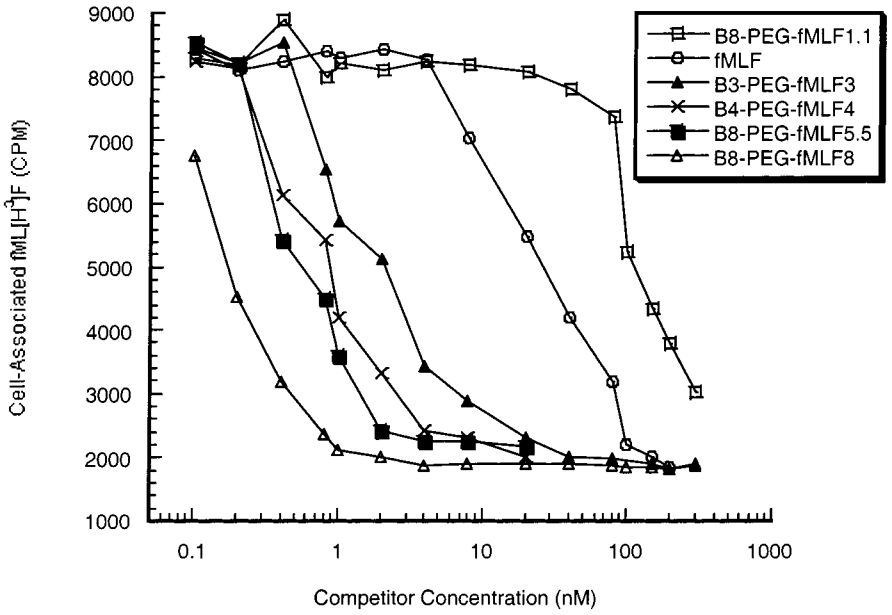


Figure 1. Competition of free and branched polymer-conjugated fMLF for binding to differentiated HL-60 cells. Varying concentrations of the indicated compounds were tested for their ability to compete with fML[^{3}H]F for binding to DMSO-differentiated HL-60 cells, as described in Experimental Procedures. These results are the means of three independent assays; for each data point, the maximal deviation from the mean among these assays was 3%.

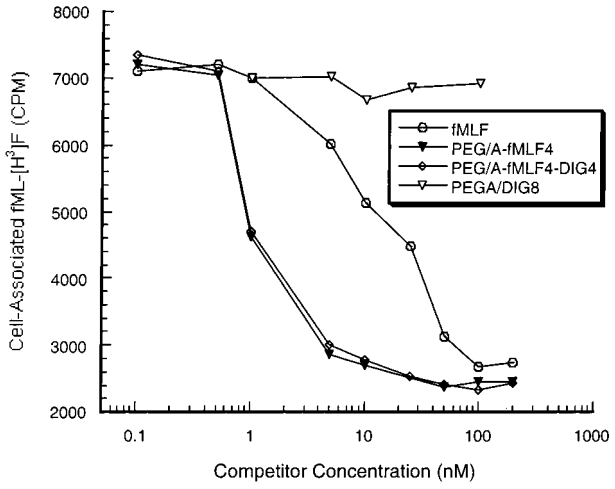


Figure 2. Competition of free and linear polymer-conjugated fMLF for binding to differentiated HL-60 cells. The experiment was performed as in Figure 1. The results shown are the means of three independent assays; the maximal deviation from the mean among these assays was 8%.

1 nM (Table 1). Furthermore, whether the other four potential attachment sites on the linear PEG/A were either unoccupied or were occupied with DIG made little difference in the K_d (Figure 2, Table 1). Thus, additional moieties such as therapeutic drugs could be added to the targeting polymer without compromising the binding avidity.

Cellular Activation of HL-60 Cells. Upon binding of the chemotactic peptide to the G-protein coupled receptor, one of the early events related to cellular activation is the release of Ca^{2+} from membrane-bound intracellular compartments into the cytoplasm (Azuma et al., 1996; Anderson and Mahomed Goolam, 1997; Prossnitz et al., 1999). This assay for cellular activation was used because it is the earliest measurable event after fMLF binding along the complex activation pathway. The release of calcium is rapid, reaching its maximum value in 2−3 min followed by slow recovery to near basal level (Figure 3). Similar kinetics of calcium release were observed in the response of differentiated HL-60 cells to free fMLF and to polymers bearing multiple fMLF moieties (Figure 3 and data not shown). As was the case for binding to these cells, B8-PEG−fMLF$_{1.1}$ showed reduced ability relative to free fMLF to activate differentiated HL-60 cells, with virtually no flux of calcium even at 100 nM polymer. Activation also resembled binding in being enhanced by the presence of multiple fMLF moieties on a polymer, so that three fMLF residues on a polymer yielded readily detectable activation and four fMLF residues on a polymer were about as potent as free fMLF by this assay (Figure 4 and Table 1). However, unlike the binding assay, the Ca^{2+} efflux into the cytoplasm did not further increase as the copy number of fMLF per polymer increased beyond 4 (Figure 4 and Table 1). All of the conjugates with the copy number of fMLF ≥ 4 showed similar half-maximal release of intracellular calcium (EC_{50}, as determined graphically using the Cricket Graph program) of about 5 nM of conjugate, which is approximately the same as the EC_{50} value (4.7 nM) for the free peptide (Table 1). Thus, the presence of multiple ligands (>3) on PEG does not increase the activation potency as much as it increases binding avidity for differentiated HL-60 cells.

Comparison of cellular binding and activation by various conjugates (Table 1) reveals that while no conjugate is more potent in activating differentiated HL-60 cells than is free fMLF, the avidity of conjugate for these cells increases with increasing number of fMLF moieties. This increase is most remarkable when expressed as K_d for the conjugate, but is still evident when a relative avidity is calculated per peptide, by multiplying the K_d of the polymer by the average number of fMLF moieties that it carries. The ratio of avidity ($1/K_d$) to cellular activation ("toxicity") activity ($1/EC_{50}$), measured by EC_{50}/K_d, is 0.168 for free fMLF and increases from 5.05 to 27.8 for conjugates as number of fMLF moieties increases from 3 tof 8. Although the effect of molecular shape was not systematically studied, note that both avidity and cellular activation activity were nearly the same for branched and linear polymers harboring four copies of fMLF.

Table 1. Binding and Cell Activation by Conjugates

competitor	avidity: K_d (nM)	cell activation: EC_{50} (nM)	relative avidity: $K_d \times$ no. of fMLF	avidity/activation: EC_{50}/K_d
fMLF	28	4.7	28	0.168
B8-PEG−$fMLF_{1.1}$	190	–	209	–
B3-PEG−$fMLF_3$	1.9	9.6	5.7	5.05
B4-PEG−$fMLF_4$	0.8	5.0	3.2	6.25
B8-PEG−$fMLF_{5.5}$	0.5	5.3	2.75	10.6
B8-PEG−$fMLF_8$	0.18	5.0	1.44	27.8
PEG/A−$fMLF_4$	1.1	ND	4.4	–
PEG/A−$fMLF_4$−DIG_4	1.2	5.9	4.8	4.92

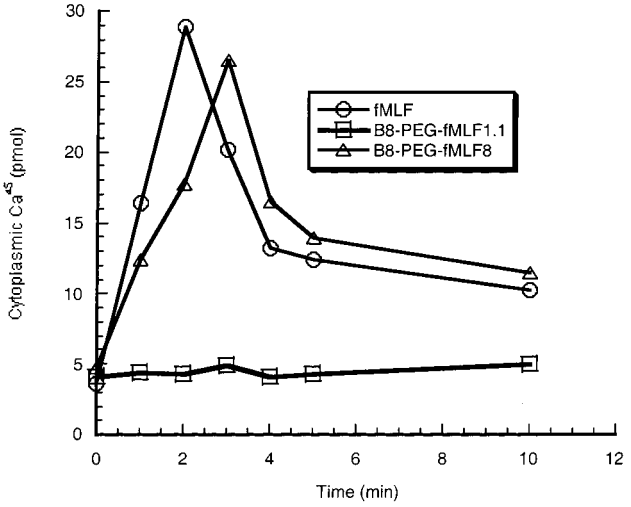


Figure 3. Time course of calcium release from intracellular stores in differentiated HL-60 cells. Release of ^{45}Ca into the cytoplasmic compartment of differentiated HL-60 cells was measured at various times after addition of fMLF or the conjugated polymers. Similar time courses were observed when the added compounds were at concentrations between 1 and 100 nM.

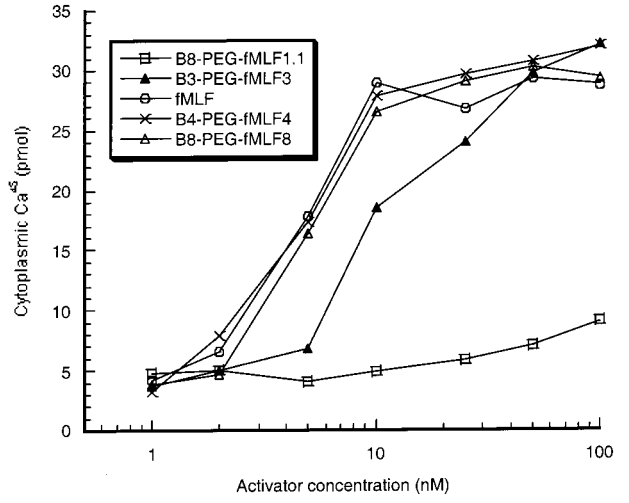


Figure 4. Calcium mobilization in differentiated HL-60 cells by fMLF and polymer-conjugated fMLF. The peak value of calcium release after addition of the indicated fMLF derivatives at various concentrations was measured as shown in Figure 3. Each data point is the mean of at least two independent experiments; for all data points the variation between repeat measurements was less than 8.2%.

Targeting Drugs to Cells. To directly show the accumulation of PEG/A−drug−ligand conjugates, PEG/A−$fMLF_4$−DIG_4 (333 nM) was incubated with differentiated HL-60 cells. The DIG ELISA demonstrated that 18% of this conjugate had been internalized by these cells (Figure 5). When the negative control conjugate, PEG/A−DIG_8, was incubated with HL-60 cells, 4.7% uptake

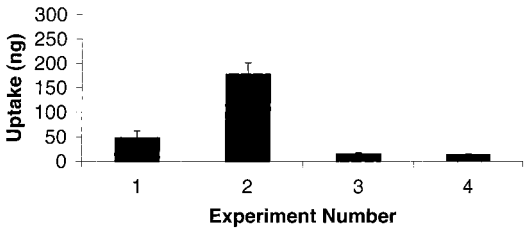


Figure 5. Uptake of PEG/A−$fMLF_4$−DIG_4 and PEG/A−DIG_8 by phagocytic cells. Uptake of the indicated conjugate by cells was measured by ELISA for DIG, as described in Experimental Procedures. Uptake of PEG/A−$fMLF_4$−DIG_4 (experiments 2 and 4) and PEG/A−DIG_8 (experiments 1 and 3) to DMSO-differentiated HL-60 cells (experiments 1 and 2) and Jurkat T-cells (experiments 3 and 4) were measured (n = 3). The total conjugate added to each culture was 1 μg.

was observed. This much lower accumulation ($P < 0.006$) in the absence of fMLF confirmed the importance of this ligand in the interaction of conjugates with differentiated HL-60 cells. Lymphocytic Jurkat cells, which do not express the fMLF receptor, accumulated both PEG/A−DIG_8 (1.5%) and PEG/A−$fMLF_4$−DIG_4 (1.3%) to a much lesser extent than did differentiated HL-60 cells (Figure 5). The difference between uptake of the nontargeted conjugate by differentiated HL-60 cells and Jurkat cells was significant ($P < 0.003$), as was the difference between these two cell types for uptake of the targeted conjugate ($P < 0.004$). Note that for the Jurkat cells, there was no significant difference between the uptake of the two conjugates ($P = 0.80$). These values represent nonspecific cellular binding of polymers. These results indicate the specificity of binding of PEG/A−$fMLF_4$−DIG_4 to differentiated HL-60 cells. The 4.7% accumulation of PEG/A−DIG_8 by differentiated HL-60 cells might reflect the tendency of these cells to bind and phagocytose polymeric PEG/A molecules nonspecifically.

Injection of PEG/A−$fMLF_4$−DIG_4 into the peritoneal cavity of BALB/c mice was used to determine the in vivo properties of this conjugate, in contrast to using the differentiated HL-60 cell line. The mice in this study were not injected with thioglycol, and, therefore, the macrophages in the peritoneal cavity were not activated. These nonactivated peritoneal cells accumulated DIG to about a 5-fold greater extent ($P < 0.0003$) from the targeted conjugate, PEG/A−$fMLF_4$−DIG_4, than from the nontargeted conjugate, PEG/A−DIG_8 (Figure 6). In fact, 17% of the administered PEG/A−$fMLF_4$−DIG_4 was taken up by peritoneal cells, whereas they accumulated only 3.3% of the nontargeted PEG/A−DIG_8. This low level of accumulation of nontargeted DIG is not surprising, since we have shown that in culture there is some nonspecific binding of PEG/A to promyelocytic HL-60 cells (Figure 5). Peritoneal incubation for less than 1 h (15 or 30 min) gave similar results (data not shown). It should be noted that the DIG that was accumulated in cells is expected to remain conjugated to its PEG/A carrier, but this was not confirmed.

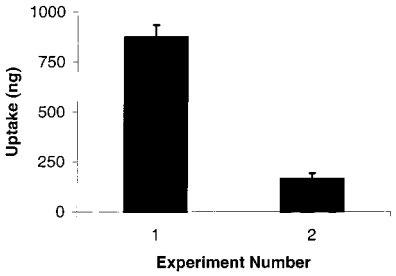


Figure 6. Specific targeting of peritoneal macrophages by fMLF. Each BALB/C mouse was injected intraperitoneally with 5 μg of PEG/A−fMLF$_4$−DIG$_4$ (experiment 1, $n = 3$) or PEG/A−DIG$_8$ (experiment 2, $n = 4$). After 1 h, the peritoneal cavity was flushed, and cells were collected and lysed as described in Experimental Procedures. ELISA was performed to determine intracellular digoxigenin; a standard curve for digoxigenin was included on every assay plate. The results are normalized to the amount of protein in each lysate, to correct for variations in cell number and efficiency of lysis.

DISCUSSION

In this study, we have demonstrated the ability of multiple fMLF moieties to target a polymeric drug delivery molecule (Huang et al., 1998) to phagocytic cells. Such phagocytic cells populate the reticuloendothelial system and play a key role in host defense against bacteria (Seifert and Schultz, 1991). Macrophages recognize bacteria through a specific receptor for peptides containing *N*-formyl-methionine, which is the initiating amino acid in prokaryote protein synthesis. The high affinity formyl methionine receptor (referred to here as the fMLF receptor) is a member of the G-protein coupled receptor family (Gierschik et al., 1991; Prossnitz and Ye, 1997; Le et al., 2001). The binding of fMLF to this receptor initiates a series of cascades, resulting in chemotaxis (Martinet et al., 1994) and cellular activation (Montero et al., 1994). Since this receptor is present on phagocytic cells, such as macrophages and neutrophils (Niedel et al., 1980), it could serve as a targeting ligand for delivering drugs to these cells. Although binding of fMLF initiates the activation process, activation is not required for cellular uptake of fMLF (Prossnitz et al., 1999).

Our approach to drug delivery is based on the use a PEG-based carrier with multiple attachment sites to which drugs or targeting moieties can be linked. By appending drugs via the bioreversible disulfide bond, which can be designed to varying degrees of susceptibility to cleavage by reducing agents (Huang et al., 1998), the circulating time of the carrier can be adjusted, allowing it to reach the targeted cells, before releasing its drug cargo. The multiple attachment sites on the PEG-based carrier can not only provide a high payload of drug, but also can be used for appending one or more moieties for targeting specific cellular receptors or promoting cell uptake of the conjugate. In this study, the enhancement in avidity for the targeted receptor on phagocytic cells by multivalent binding of the fMLF ligand is demonstrated. Thus, a concentration of only 0.18 nM B8-PEG−fMLF$_8$ is needed to get 50% occupancy of the differentiated HL-60 cell surface fMLF receptors, as opposed to 190 nM for B8-PEG−fMLF$_{1.1}$, with only one appended ligand, an increase in avidity of more than 1000-fold (Table 1).

The molecular basis of enhanced avidity by multivalency of ligand attachment to a single polymeric carrier molecule is not obvious. It is possible that such multimeric ligands show their enhanced binding by interacting with multiple cellular receptors. Since a single fMLF moiety bound to a branched PEG polymer shows less avidity for differentiated HL-60 cells than does the free peptide, it seems likely that the bulky carrier group sterically interferes with ligand interaction with its cellular receptor, but this interference is overcome by peptide multivalency on the polymer. This behavior of fMLF conjugated to PEG-based polymers resembles that described for α-sialoside groups, the ligands for the hemagglutinin protein of influenza virus. When a single α-sialoside is linked to a polyacrylamide polymer, the conjugate binds less avidly to the hemagglutinin receptor on the virus than does a low molecular weight form of the ligand (Lees et al., 1994). However polyacrylamides bearing many copies of the ligand show vastly greater binding avidity than the free ligand (Lees et al., 1994; Sigal et al., 1996).

After binding of the free fMLF chemotactic peptide to a phagocytic cell, a rapid receptor-mediated internalization takes place (Niedel et al., 1979). Our results suggest that polymers with multiple fMLF moieties are capable of binding to and/or entering cells in culture and in vivo. In the present study we have not fully defined the possible mechanism of internalization and have only used the model indicator compound digoxigenin stably linked by an amide bond to the carrier polymer rather than an actual therapeutic agent. We are currently studying the subcellular localization of delivered compounds and determining the kinetics of release of a disulfide-linked model drug from the targeted conjugate upon its uptake by phagocytic cells.

A potential cause of adverse effects of targeting fMLF receptors on phagocytes is cellular activation caused by this interaction. Cellular activation is mediated by a complex chain of signal transduction events (reviewed by Prossnitz and Ye, 1997) and can be monitored by the mobilization of calcium from intracellular stores (Camps et al., 1992). This transient increase in intracellular free calcium correlates with acidification and stimulation of superoxide (O^{2-}) release. The level of free fMLF required for half-maximal effect on Ca^{2+} release has been reported to be 2−4 nM (Wenzel-Seifert and Seifert, 1990), in approximate agreement with our determination of 5 nM, while the EC_{50} for superoxide production has been reported to be 15−30 nM fMLF (Klinker et al., 1996). In this study all conjugates with four or more copies of fMLF and free fMLF displayed an EC_{50} value of about 5 nM for calcium release (Table 1 and Figure 4). Therefore, the cooperative effect that was observed in binding is less pronounced for cellular activation. This difference indicates that polymers targeted to phagocytic cells with multiple fMLF moieties should be much more potent as targeting agents than as cellular activators. At a concentration of 1 nM of B8-PEG−fMLF$_8$, nearly 100% of the fMLF receptors were occupied by the targeted drug carrier, whereas little or no cellular activation occurred.

PEG-based copolymers have been found to be biocompatible and are currently being developed for multiple in vivo applications (Poiani et al., 1994). These include the use of biotin targeting moieties to promote sodium-dependent multivitamin transporter (SMVT) mediated transport of molecules across the intestinal epithelium (Ramanathan et al., 2001). In the present study, the high molecular weight (>20 KDa) and inertness of PEG-based conjugate would be expected to confer on appended drugs an extended in vivo half-life and protection from degradative processes and immune system surveillance (Davis et al., 1981). Therefore, we propose that a PEG-based carrier containing multiple copies of fMLF can be used to target drugs to macrophages and other phagocytic cells

without the adverse effects of activation of these cells. Furthermore, the lack of enhancement of cellular activation by polymers carrying multiple targeting fMLF groups might indicate that drugs appended to such polymers would be less likely to be inactivated by the many degradative mechanisms induced by phagocyte activation.

ACKNOWLEDGMENT

This study was funded by grants from the Campbell Foundation (M.J.L.) and Award R01 AI45555-01 from the NIH (M.M.C.). S.P. was supported by IMSD Award R25 GM55145-05 from the NIH (M.J.L.). We thank L. Covey and J.A. Langer for critical comments on this manuscript.

LITERATURE CITED

(1) Anderson, R., and Mahomed Goolam, A. (1997) Calcium efflux and influx in f-met-leu-phe (fMLP)-activated human neutrophils are chronologically distinct events. *Clin. Exp. Immunol. 110*, 132−138.

(2) Azuma, E. K., Yuo, A, Matsushima, K., Kasahara, T., Mizoguchi, H., Saito, M., Takaku, F., and Kitagawa, S. (1996) Activation and priming of human monocytes by monocyte chemotactic and activating factor: Cooperation with other inflammatory cytokines and close association between an increase in cytoplasmic free Ca^{2+} and intracellular acidification. *Exp. Hematol. 24*, 169−175.

(3) Benelli, R., Mortarini, R., Anichini, A., Giunciuglio D., Noonan D. M., Monatalti, S., Tacchetti, C., and Albini, A. (1998) Monocyte-derived dendritic cells and monocytes migrate to HIV−Tat RGD and basic peptides. *AIDS 12*, 261−268.

(4) Camps, M., Carozzi, A., Schnabel, P., Scheer, A., Parker, P. J., and Gierschik, P. (1992) Lysosome-selective stimulation of phospholipaseC-b_2 by G-protein-bg-subunits. *Nature 369*, 684−686.

(5) Collins, S. J. (1987) The HL-60 promyelocytic leukemia cell line: Proliferation, differentiation, and cellular oncogene expression. *Blood 70*, 1233−1244.

(6) Dahlgren, C., Anderson, T., and Stendahl, O. (1987) Chemotactic factor binding and functional capacity: A comparison between human granulocytes and differentiated HL-60 cells. *J. Leukocyte Biol. 42*, 245−252.

(7) Davis, S., Abuchowiski, A., Park, Y. K., and Davis, F. E. (1981) Alteration of the circulating half-life and antigenic properties of bovine adenosine deaminase in mice by attachment of poly(ethylene glycol). *Clin. Exp. Immunol. 46*, 649−652.

(8) Derian, C. K., Solomon, H. F., Higgins, J. D., III, Beblavy M. J., Santulli, R. J., Bridger, G. J., Pike, M. C., Kroon, D. J., and Fischman, A. J. (1996) Selective inhibition of *N*-formylpeptide-induced neutrophil activation by carbamate-modified peptide analogues. *Biochemistry 35*, 1265−1269.

(9) Gierschik, P., Moghtader, R., Straub, C., Dietrich, K., and Jacobs, K. H. (1991) Signal amplification in HL-60 granulocytes. Evidence that the chemotactic peptide receptor catalytically activates guanine-nucleotide-binding regulatory proteins in native plasma membranes. *Eur. J. Biochem. 197*, 725−732.

(10) Huang, S.-Y., Pooyan, S., Wang, J., Choudhury, I., Leibowitz, M. J., and Stein, S. (1998) A poly(ethylene glycol) copolymer for carrying and releasing multiple copies of cysteine-containing peptides. *Bioconjug. Chem. 9*, 612−617.

(11) Klinker, J. F., Wenzel-Seifert, K., and Seifert, R. (1996) G-Protein-coupled receptors in HL-60 human leukemia cells. *Gen. Pharmacol. 27*, 33−54.

(12) Le, Y., Oppenheim, J. J., and Wang, J. M. (2001) Pleiotropic roles of formyl peptide receptors. *Cytokine Growth Factor Rev. 12*, 91−105.

(13) Lees, W. J., Spaltenstein, A., Kingery-Wood, J. E., and Whitesides, G. M. (1994) Polyacrylamides bearing pendant alpha-sialoside groups strongly inhibit agglutination of erythrocytes by influenza A virus: Multivalency and steric stabilization of particulate biological systems. *J. Med. Chem. 37*, 3419−3433.

(14) Lobenberg, R., and Kreuter, J. (1996) Macrophage targeting of azidothymidine: a promising strategy for AIDS therapy. *AIDS Res. Human Retrovirol. 12*, 1709−1715.

(15) Mankertz, J. Matthes, E. Rokos, K. von Baeyer, H, Pauli, G., and Riedel, E. (1996) Selective endocytosis of fluorothymidine and azidothymidine coupled to LDL into HIV infected mononuclear cells. *Biochim. Biophys. Acta 1317*, 233−237.

(16) Martinet, Y., Martinet, N., Vignaud, J. D., and Plenat, F. (1994) Blood monocytes chemotaxis. *J. Immunol. Methods 174*, 209−214.

(17) Medda, S. Das, N. Mahato, S. B., Mahadaven, P. R., and Basu, M. K. (1995) Glycoside-bearing liposome delivery systems against macrophage-associated disorders involving *Mycobacterium leprea* and *Mycobacterium tuberculosis*. *Indian J. Biochem. Biophys. 32*, 147−151

(18) Mistry, P. K., Wraight, E. P., and Cox, T. M. (1996) Therapeutic delivery of proteins to macrophages: implications for treatment of Gaucher's disease. *Lancet 348*, 1555−1559.

(19) Montero, M., Garcia-Sancho, J., and Alvarez, J. (1994) Activation by chemotactic peptide of a receptor-operated Ca^{2+} entry pathway in differentiated HL60 cells. *J. Biol. Chem. 269*, 29451−29456.

(20) Nathan, A., Zalipsky, S., Ertel, S. I., Agathos, S. N., Yarmush, M. L., and Kohn J. (1993) Copolymers of lysine and poly(ethylene glycol): a new family of functionalized drug carriers. *Bioconjug. Chem. 4*:54−62, 410.

(21) Niedel, J. E., Kahane, I., and Cuatrecasas, P. (1979) Receptor-mediated internalization of fluorescent chemotactic peptide by human neutrophils. *Science 205*, 1412−1414.

(22) Niedel, J., Kahane, I., Lachman, L., and Cuatrecasas, P. (1980) A subpopulation of cultured human promyelocytic leukemia cells (HL-60) displays the formyl peptide chemotactic receptor. *Proc. Natl. Acad. Sci. U.S.A.* 77, 1000−1004.

(23) Poiani, G. J. Riley, D. J., Fox, J. D., Kemnitzer, J. E., Gean, K. F., and Kohn, J. (1994) Conjugation of *cis*-4-hydroxy-L-proline and poly(PEG-Lys), a water soluble poly(ether urethane): Synthesis and evaluation of antifibrotic effect in vitro and in vivo. *Bioconjugate Chem. 5*, 621−630.

(24) Prossnitz, E. R., Gilbert, T. L., Chiang, S., Campbell, J. J., Qin, S., Newman, W., Sklar, L. A., and Ye, R. D. (1999) Multiple activation steps of the *N*-formyl peptide receptor. *Biochemistry 38*, 2240−2247.

(25) Prossnitz, E. R., Quechenberger, O., Cochrane, C. G., and Ye, R. D. (1993) Signal transducing properties of the N-formyl peptide receptor expressed in undifferentiated HL60 cells. *J. Immunol. 151*, 5704−5715.

(26) Prossnitz, E. R., and Ye, R. D. (1997) The N-formyl peptide receptor: A model for the study of chemoattractant receptor structure and function. *Pharmacol. Ther. 74*, 73−102.

(27) Randolph, G. J., Beaulieu, S., Lebecque, S., Steinman, R. M., and Muller, W. A. (1998) Differentiation of monocytes into dendritic cells in a model of transendothelial trafficking. *Science 282*, 480−483.

(28) Ramanathan, S., Pooyan, S., Stein, S., Prasad, P. D., Wang, J., Leibowitz, M. J., Ganapathy, V., and Sinko, P. J. (2001) Targeting the sodium-dependent multivitamin transporter (SMVT) for improving the oral absorption properties of a retro-inverso Tat nonapeptide. *Pharm. Res. 18*, 950−956.

(29) Rossi, L. Brandi G., Schiavano G. F., Balestra, E., Millo, E., Scarfi, S., Damonte, G., Gasparini, A., Magnani, M. Perno, C. F., Benatti, U., and De Flora, A. (1998) Macrophage protection against human immunodeficiency virus or herpes simplex virus by red blood cell-mediated delivery of a heterodinucleotide of aziothymidine and acyclovir. *AIDS Res. Human Retrovirol. 14*, 435−444.

(30) Seifert R., and Schultz, G. (1991) The superoxide-forming NADPH oxidase of phagocytes: an enzyme regulated by multiple mechanisms. *Rev. Physiol. Biochem. Pharmacol. 117*, 1−338.

(31) Seifert, R., Serke, S., Huhn, D., Bessler, W. G., Hauschildt S., Metzegae, J., Wiesmuller, K.-H., and Jung, G. (1992) Incomplete functional differentiation of HL-60 leukemic cells by synthetic lipopropeptides. Partial inhibition by pertussis toxin of enhanced superoxide formation. *Eur. J. Biochem. 203*, 143−151.

(32) Sigal, G. B., Mammen, M., Dahmann, G., and Whitesides, G. M. (1996) Polyacrylamides bearing pendant α-sialoside groups strongly inhibit agglutination of erythrocytes by influenza virus: The strong inhibition reflects enhanced binding through cooperative polyvalent interactions. *J. Am. Chem. Soc. 116*, 3789−3800.

(33) Udenfriend, S., Stein, S., Bohlen, P., and Dairman, W. (1972) Fluorescamine, a new reagent for assay of amino acids, peptides, proteins and other primary amines in the picomole range. *Science 178*, 871.

(34) Venier-Julienne, M. C., Vouldoukis, I., Monjour, L., and Benoit, J. P. (1995) In vitro study of the anti-leishmanial activity of biodegradable nanoparticles. *J. Drug Targeting 3*, 23−29.

(35) Wenzel-Seifert, K., and Seifert, R. (1990) Nucleotide-, chemotactic peptide- and phorbal ester induced exocytosis in HL-60 leukemic cells. *Immunobiol. 181*, 298−316.

BC0100657

Chemical Synthesis of *Escherichia Coli* ST_h Analogues by Regioselective Disulfide Bond Formation: Biological Evaluation of an ^{111}In-DOTA−Phe^{19}-ST_h Analogue for Specific Targeting of Human Colon Cancers

Hariprasad Gali,[†] Gary L. Sieckman,[§] Timothy J. Hoffman,[†,‡,§] Nellie K. Owen,[†] Dana G. Mazuru,[†] Leonard R. Forte,[§,⊥] and Wynn A. Volkert*[,†,§]

Research Service, Harry S. Truman Memorial Veterans' Administration Hospital, Columbia, Missouri 65201 and Departments of Radiology, Pharmacology and Internal Medicine, University of Missouri−Columbia, Columbia, Missouri 65211. Received July 6, 2001; Revised Manuscript Received October 18, 2001

New human *Escherichia coli* heat-stable peptide (ST_h) analogues containing a DOTA chelating group were synthesized by sequential and selective formation of disulfides bonds in the peptide. This synthetic approach utilizes three orthogonal thiol-protecting groups, Trt, Acm, and t-Bu, to form three disulfide bonds by successive reactions using 2-PDS, iodine, and silyl chloride−sulfoxide systems. The DOTA−ST_h conjugates exhibiting high guanylin/guanylate cyclase-C (GC-C) receptor binding affinities were obtained with >98% purity. In vitro competitive binding assays, employing T-84 human colon cancer cells, demonstrated the IC_{50} values of <2 nM for GC-C receptor binding suggesting that the new synthetic ST_h analogues are biologically active. In vitro stability studies of the ^{111}In-DOTA−Phe^{19}-ST_h conjugate incubated in human serum at 37 °C under 5% CO_2 atmosphere revealed that this conjugate is extremely stable with no observable decomposition at 24 h postincubation. HPLC analysis of mouse urine at 1 h pi of the ^{111}In-DOTA−Phe^{19}-ST_h conjugate showed only about 15% decomposition suggesting that the ^{111}In-DOTA−Phe^{19}-ST_h conjugate is highly stable, even under in vivo conditions. In vivo pharmacokinetic studies of the ^{111}In-DOTA−Phe^{19}-ST_h conjugate in T-84 human colon cancer derived xenografts in SCID mice conducted at 1 h pi showed an initial tumor uptake of 2.04 ± 0.30% ID/g at 1 h pi with efficient clearance from the blood pool (0.23 ± 0.14% ID/g, 1 h pi) by excretion mainly through the renal/urinary pathway (95.8 ± 0.2% ID, 1 h pi). High tumor/blood, tumor/muscle, and tumor/liver ratios of approximately 9:1, 68:1, and 26:1, respectively, were achieved at 1 h pi The specific in vitro and in vivo uptake of the radioactivity by human colonic cancer cells highlights the potential of radiometalated-DOTA−ST_h conjugates as diagnostic/therapeutic radiopharmaceuticals.

INTRODUCTION

Heat-stable (ST) peptides are secreted by several enteric bacteria such as *Escherichia coli*, *Yersinia enterocolitica*, and *Vibrio cholerae non-01* (*1*−*3*). ST peptides bind to guanylin/guanylate cyclase-C (GC-C) receptors that are selectively expressed in apical membranes of intestinal mucosal cells (*4*−*6*). It is reported that functional GC-C receptors are also expressed on human colon cancer cells (*7*−*9*). Considerable efforts have been and are being made to investigate the relationship between structural characteristics of ST peptides and receptor-mediated cellular and physiological response (*5*, *10*−*15*). It has been shown that the GC-C receptor binding domain consists of a sequence of 13 amino acid residues with six cysteines forming three disulfide bonds that are critical for the construction of the three-dimensional tertiary structure (*5*, *11*, *12*). The six cysteines can adopt 15 possible different disulfide arrangements, and only one of them exhibits high GC-C receptor binding affinity and full biological activity (*15*). Thus, in the synthesis of biologically active ST analogues, correct formation of the three disulfide bonds is critical.

The widely used method for the synthesis of ST peptides and their analogues involves simultaneous folding and disulfide bond formation of the fully deprotected peptide by air-oxidation in aqueous solutions (*10*−*12*, *15*−*19*). Reproducible production of the correct conformer is challenging, particularly if there is a large chemical moiety attached to the native peptide sequence that may substantially alter the thermodynamic and steric properties of the system during the folding. To achieve improved synthetic reproducibility, we followed a new synthetic strategy, similar to that described by Akaji et al. (*20*) for synthesizing human insulin, utilizing three well-known orthogonal thiol-protecting groups, Trt, Acm, and t-Bu, to form three disulfide bonds by successive reactions using 2-PDS, iodine, and silyl chloride−sulfoxide system (*20*−*25*). Herein, we report two novel ST_h analogues containing a DOTA chelating agent, synthesized by sequential and selective formation of disulfide bonds. The ST_h analogues synthesized for these studies have the identical structure as the ST peptide

* To whom correspondence should be sent: Prof. Wynn A. Volkert, Radiopharmaceutical Sciences Institute, 143 Major Hall, DC200.0 HSC, University of Missouri−Columbia, Columbia, MO 65212. E-mail: VolkertW@health.missouri.edu, Phone: 573-882-6759, Fax: 573-882-6129.

[†] Department of Radiology, University of Missouri−Columbia.

[§] Harry S. Truman Memorial Veterans' Administration Hospital.

[‡] Department of Internal Medicine, University of Missouri−Columbia.

[⊥] Department of Pharmacology, University of Missouri−Columbia.

10.1021/bc010062u CCC: $22.00 © 2002 American Chemical Society
Published on Web 02/19/2002

originated from *E. coli* that colonize the human gut (*5*), except that the C-terminal Tyr^{19} residue was replaced by the Phe^{19} residue. This substitution does not alter the biological activity or receptor affinity of the corresponding ST analogue. Utilization of the selective deprotection approach makes it possible to synthesize the entire linear DOTA−ST$_h$ conjugates on the resin prior to S−S bond formation, in contrast to forming the S−S bonds on the binding sequence prior to conjugation with a DOTA moiety (*26*). The in vitro binding of these two ST peptides to GC-C receptors expressed on human colon cancer T-84 cells was measured, and the in vivo stability and pharmacokinetics were assessed in tumor-bearing SCID mice.

EXPERIMENTAL SECTION

All solvents were either ACS certified or HPLC grade. Solvents were obtained from Fisher Scientific and used as received. The fmoc-Phe-Wang resin, Rink Amide MBHA resin, and fmoc-protected amino acids were purchased from Calbiochem-Novabiochem Corp (San Diego, CA) and the other peptide reagents from Applied Biosystems, Inc (Foster City, CA). DOTA-tris(*tert*-butyl ester) was purchased from Macrocyclics (Dallas, TX) and fmoc-6-aminohexanoic acid from Advanced ChemTech (Louisville, KY). All other reagents were purchased from Aldrich Chemical Co. $^{111}InCl_3$ was obtained from Mallinckrodt Medical, Inc (St. Louis, MO) as a 0.05 N HCl solution. ^{125}I-Tyr^5-6-Ahx-Phe^{19}-ST$_h$ and ^{125}I-Tyr^5-Phe^{19}-ST$_h$ were synthesized according to the previously published procedure.[19] Human colon carcinoma T-84 cells were obtained from American Type Culture Collection (ATCC) and maintained and grown for use in these studies in the University of Missouri Cell and Immunology Core facilities. Electrospray mass spectral analyses were performed by Synpep Corporation (Dublin, CA).

High Performance Liquid Chromatography (HPLC). High performance liquid chromatography (HPLC) analyses were performed on a Waters 600E system equipped with Varian 2550 variable absorption detector, Packard Radiometic 150TR flow scintillation analyzer, sodium iodide crystal radiometric detector, Eppendorf TC-50 column temperature controller, and Hewlett-Packard HP3395 integrators. HPLC solvents consisted of H_2O containing 0.1% trifluoroacetic acid (Solvent A) and acetonitrile containing 0.1% trifluoroacetic acid (Solvent B). Conditions: A Phenomenex Jupiter C-18 (5 μm, 300 Å, 4.6 × 250 mm) column was used with a flow rate of 1.5 mL/min. The column temperature was maintained at 35 °C. Gradient I begins with a solvent composition of 95% A and 5% B followed by a linear gradient to 30% A and 70% B in 25 min, after which the column is reequilibrated. Gradient II begins with a solvent composition of 80% A and 20% B followed by a linear gradient to 70% A and 30% B in 30 min, after which the column is reequilibrated.

DOTA−[Cys^{6,11}, Cys(Acm)^{7,15}, Cys(tBu)^{10,18}]-Phe^{19}-ST$_h$ (1). Linear peptide **1** synthesis was carried out on a Perkin-Elmer Applied Biosystems Model 432 automated peptide synthesizer employing traditional fmoc chemistry with HBTU activation of carboxyl groups on the reactant with the N-terminal amino group on the growing peptide anchored via the C-terminus to the resin. Fmoc-Phe-Wang resin (25 μmol), fmoc-protected amino acid with appropriate side-chain protections (75 μmol), and DOTA-tris(*tert*-butyl ester) (75 μmol) were used for the synthesis. The final product was cleaved by a standard procedure using a cocktail containing thioanisol, water, ethanedithiol, and trifluoroacetic acid in a ratio of 2:1:1:36 and precipitated into methyl *tert*-butyl ether and dried. Yield of the crude peptide was 90% (60 mg).

DOTA−6-Ahx-NSSNY-NH$_2$. The same solid-phase peptide synthetic procedure described to produce linear peptide **1** was used to prepare the DOTA−6-Ahx-NSSNY-NH$_2$ conjugate (this ^{111}In-DOTA−6-Ahx-NSSNY-NH$_2$ conjugate was used as a non-GC-C receptor binding control in in vivo studies) except that Rink Amide MBHA resin replaced the fmoc-Phe-Wang resin, and fmoc-6-aminohexanoic acid added, in the reaction sequence. Electrospray MS calcd *m/z* for $C_{45}H_{71}N_{13}O_{18}$ [M + H]$^+$: 1082.5; found: 1082.7.

DOTA−[Cys(Acm)^{7,15}, Cys(tBu)^{10,18}]-Phe^{19}-ST$_h$ (2). DOTA−[Cys^{6,11}, Cys(Acm)^{7,15}, Cys(tBu)^{10,18}]-Phe^{19}-ST$_h$ **1** (63 mg, 22.6 μmol) was dissolved in water (110 mL), and the pH of the solution was adjusted to 8.6 using 0.1 M NH_4OH (3.5 mL). To this solution was added dropwise 2,2′-dithiodipyridine (2-PDS) (10 mg, 45.5 μmol) in methanol (15 mL) while stirring at room temperature. The stirring was continued for 1 h, and the reaction mixture was concentrated and filtered. The filtrate was purified on the HPLC (t_R = 17.6 min, Gradient I) and lyophilized to give pure DOTA−[Cys(Acm)^{7,15}, Cys(tBu)^{10,18}]-Phe^{19}-ST$_h$ **2** as a white powder in a yield of 29% (18.3 mg). Electrospray MS calcd *m/z* for $C_{109}H_{168}N_{28}O_{38}S_6$ [M + H]$^+$: 2670.0; found: 2670.0.

DOTA−[Cys(tBu)^{10,18}]-Phe^{19}-ST$_h$ (3). DOTA−[Cys(Acm)^{7,15}, Cys(tBu)^{10,18}]-Phe^{19}-ST$_h$ **2** (18 mg, 6.5 μmol) was dissolved in 80% aqueous methanol (7 mL), and 1 M HCl (40 μL, 2.0 equiv) was added. To this solution was added dropwise iodine (40 mg, 157 μmol) dissolved in methanol (0.5 mL) while stirring at room temperature. The stirring was continued for 30 min, and then 1 M ascorbic acid (0.5 mL) was added to reduce the excess iodine. The reaction mixture was concentrated, purified on the HPLC (t_R = 18.6 min, Gradient I) and lyophilized to give pure DOTA−[Cys(tBu)^{10,18}]-Phe^{19}-ST$_h$ **3** as a white powder in a yield of 62% (10.2 mg). Electrospray MS calcd *m/z* for $C_{103}H_{156}N_{26}O_{36}S_6$ [M + H]$^+$: 2526.0; found: 2526.0.

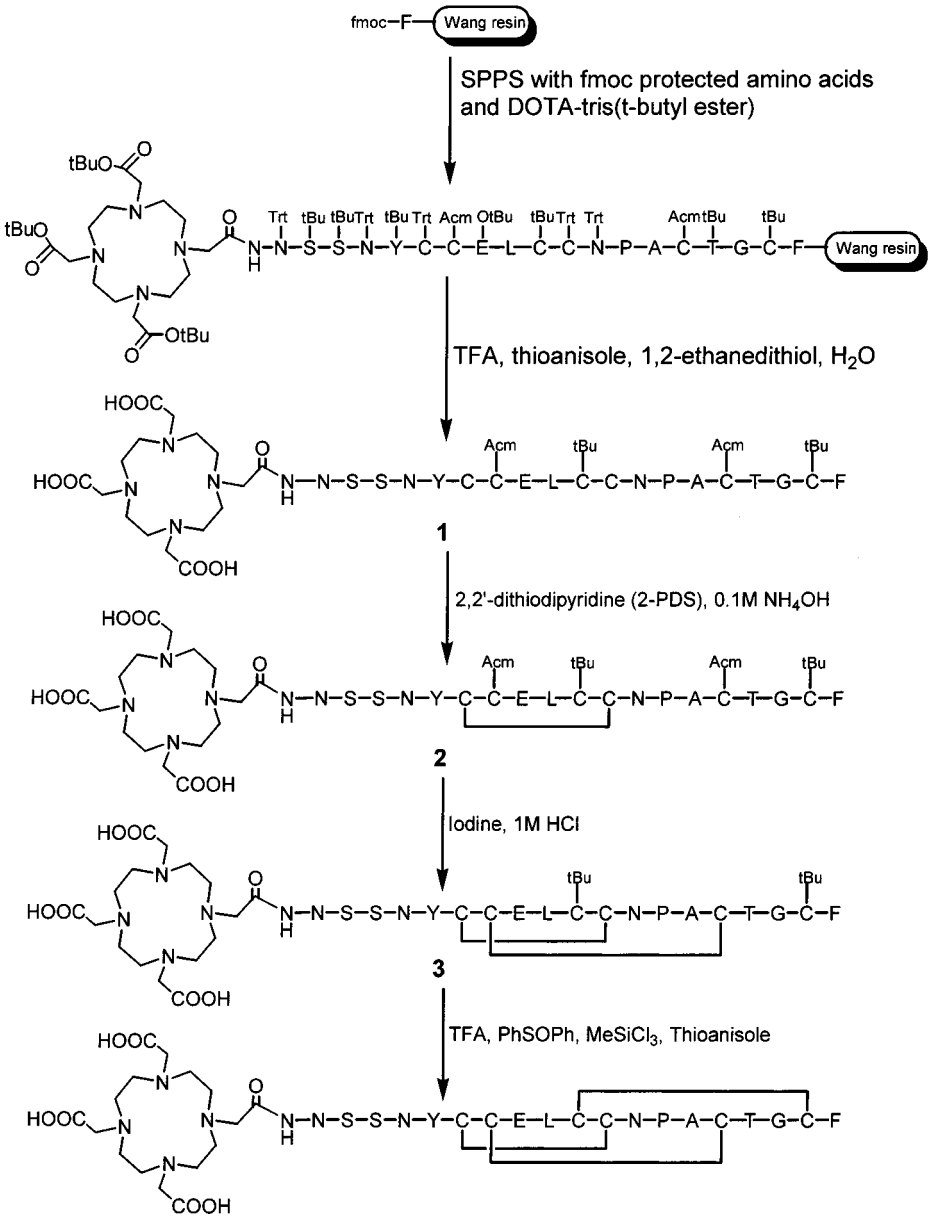
DOTA−Phe^{19}-ST$_h$ (4). To a solution of DOTA−[Cys(tBu)^{10,18}]-Phe^{19}-ST$_h$ **3** (10 mg, 4.0 μmol) in TFA (5 mL) were added PhS(O)Ph (12 mg, 15 equiv) and thioanisole (80 μL, 160 equiv). To this solution was added CH_3SiCl_3 (110 μL, 22 equiv) while stirring at room temperature. The stirring was continued for 45 min, and then the reaction mixture was added to methyl-*tert*-butyl ether (40 mL) and extracted with water (2 × 10 mL). The aqueous solution was neutralized with 10% NH_4OH, concentrated, purified on the HPLC (t_R = 20.0 min, Gradient II), and lyophilized to give pure DOTA−Phe^{19}-ST$_h$ **4** as a white powder in a yield of 6% (0.6 mg). Electrospray MS calcd *m/z* for $C_{95}H_{138}N_{26}O_{36}S_6$ [M + H]$^+$: 2411.8; found: 2412.0.

DOTA−6-Ahx-Phe^{19}-ST$_h$. The same synthetic procedure described to produce DOTA−Phe^{19}-ST$_h$ **4** was used to prepare the DOTA−6-Ahx-Phe^{19}-ST$_h$ analogue except that the fmoc-6-aminohexanoic acid was added in the reaction sequence. Overall yield (starting from resin): 1.5%; electrospray MS calcd *m/z* for $C_{101}H_{149}N_{27}O_{37}S_6$ [M + H]$^+$: 2524.9; found: 2525.0.

Phe^{19}-ST$_h$. The same synthetic procedure described to produce DOTA−Phe^{19}-ST$_h$ **4** was used to prepare the Phe^{19}-ST$_h$ analogue except that the DOTA-tris(*tert*-butyl ester) was deleted from the reaction sequence. Overall yield (starting from resin): 1.6%; electrospray MS calcd *m/z* for $C_{79}H_{112}N_{22}O_{29}S_6$ [M + H]$^+$: 2025.6; found: 2025.6.

In-DOTA−Phe^{19}-ST$_h$. A solution of DOTA−Phe^{19}-ST$_h$ **4** (0.5 mg) in 0.2 M tetramethylammonium acetate (0.5 mL) was added to indium chloride (1.0 mg). The pH of

Scheme 1. Synthesis of DOTA−ST_h Conjugate



the reaction mixture was adjusted to 5.8 (Scheme 2). The reaction mixture was incubated for 1 h at 80 °C. The resultant In-DOTA−Phe^{19}-ST_h conjugate was purified by reversed-phase HPLC (t_R = 17.7 min, Gradient II). Electrospray MS calcd *m*/*z* for $C_{95}H_{135}N_{26}O_{36}S_6In$ $[M + H]^+$: 2523.7; found: 2524.0.

^{111}In Labeling. An aliquot of $^{111}InCl_3$ (0.5−2.5 mCi, 1.85−9.25 MBq, 50 μL) was added to a solution of DOTA−Phe^{19}-ST_h **4** (50 μg) or DOTA−6-Ahx-NSSNY-NH_2 (50 μg) in 0.2 M tetramethylammonium acetate (400 μL). The pH of the reaction mixture was adjusted to 5.8. The reaction mixture was incubated for 1 h at 80 °C. An aliquot of 0.002 M EDTA (50 μL) was added to the reaction mixture to complex the unreacted $^{111}In^{3+}$. The resultant ^{111}In-DOTA−Phe^{19}-ST_h and ^{111}In-DOTA−6-Ahx-NSSNY-NH_2 conjugates were obtained as single products and purified by HPLC. The ^{111}In-DOTA−Phe^{19}-ST_h (t_R = 17.7 min, Gradient II) eluted approximately 2.3 min before the nonmetalated DOTA−Phe^{19}-ST_h conjugate (t_R = 20.0 min, Gradient II) enabling collection of the high-specific activity, NCA ^{111}In-DOTA−Phe^{19}-ST_h conjugate. An isocratic HPLC solvent program of 95% A and 5% B was used to separate ^{111}In-DOTA−6-Ahx-NSSNY-NH_2 (t_R = 5.5 min) from the excess unlabeled DOTA−6-Ahx-NSSNY-NH_2 (t_R = 9.7 min). Both purified ^{111}In-DOTA−Phe^{19}-ST_h and ^{111}In-DOTA−6-Ahx-NSSNY-NH_2 conjugates were concentrated by passing through a 3M Empore C-18 HD high performance extraction disk (7 mm/3 mL) cartridge and eluting with 33% ethanol in 0.1 M NaH_2PO_4 buffer (400 μL). The concentrated fraction was diluted with 0.1 M NaH_2PO_4 buffer (2 0.3 mL, pH 7) to make the final concentration of ethanol in the solution <5%.

In Vitro Competitive Cell Binding Assay. The IC_{50} values of In-DOTA−Phe^{19}-ST_h, DOTA−Phe^{19}-ST_h, DOTA−6-Ahx-Phe^{19}-ST_h, and Phe^{19}-ST_h conjugates were determined in human colon cancer T-84 cells by a competitive displacement cell binding assay using ^{125}I-Tyr^5-6-Ahx-Phe^{19}-ST_h. Briefly, 3×10^6 cells suspended in DMEM/F-12 media containing 14.4 mM MES and 2% BSA, pH-5.5, were incubated at 37 °C for 1 h in the presence of approximately 20000 cpm ^{125}I-Tyr^5-6-Ahx-Phe^{19}-ST_h and

Scheme 2. Indium-111 Labeling of DOTA−ST$_h$ Conjugate

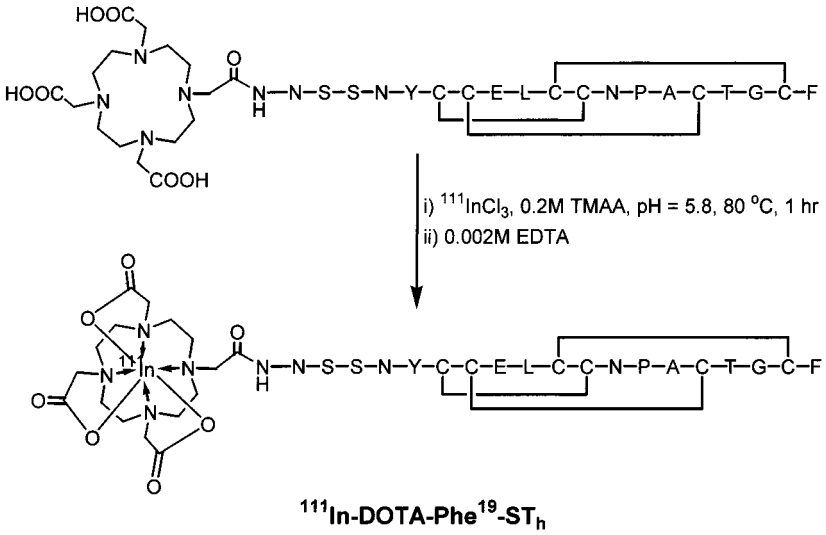


Table 1. In Vitro IC$_{50}$ Values (n = 3 or 4 separate experiments performed in duplicate) Measured from a Competitive Binding Assay with ST$_h$ Analogs vs ^{125}I-Tyr^5-6-Ahx-Phe^{19}-ST$_h$ with Human Colon Cancer T-84 Cells

ST$_h$ analog	IC$_{50}$ (nM)
In-DOTA−Phe^{19}-ST$_h$	3.3 ± 2.0
DOTA−Phe^{19}-ST$_h$	0.6 ± 0.1
DOTA−6-Ahx-Phe^{19}-ST$_h$	1.6 ± 1.2
Phe^{19}-ST$_h$	0.5 ± 0.1

an increasing concentration of ST$_h$ conjugates. After the incubation, the reaction medium was aspirated, and cells were washed three times with media. The radioactivity bound to the cells was counted in a Packard Riastar gamma counting system. The %^{125}I-Tyr^5-6-Ahx-Phe^{19}-ST$_h$ bound to cells was plotted vs increasing concentrations of ST$_h$ conjugate to determine the respective IC$_{50}$ values (Table 1, Figure 1). In-DOTA−6-Ahx-NSSNY-NH$_2$, evaluated using this same system, does not exhibit measurable binding to GC-C receptors (i.e., IC$_{50}$ > 10^5 M). For statistical considerations, three separate in vitro cell binding experiments with each conjugate were performed in duplicate.

Scatchard Analysis. Scatchard analysis was performed in human colon cancer T-84 cells by a receptor-binding assay using ^{125}I-Tyr^5-Phe^{19}-ST$_h$ and Phe^{19}-ST$_h$. Briefly 2.2 × 10^6 cells suspended in DMEM/F-12 media containing 14.4 mM MES and 2% BSA, pH-5.5, were incubated at 37 °C for 1 h in the presence of approximately 27000 cpm ^{125}I-Tyr^5-Phe^{19}-ST$_h$ and an increasing concentration of Phe^{19}-ST$_h$. After the incubation, the reaction medium was aspirated, and cells were washed three times with media. The radioactivity bound to the cells was counted in a Packard Riastar gamma counting system. The experiment was performed in duplicate, and average values were used for the calculations. The total bound peptide (B, both radioactive and nonradioactive) was obtained by multiplying the fraction of bound labeled peptide with the total concentration of peptide (both radioactive and nonradioactive). The total free peptide (F, both radioactive and nonradioactive) was obtained by subtracting the total bound peptide from the total concentration of peptide. The nonspecific binding was neglected in the calculations as it was <3%. The ratio of concentration of total bound and total free peptide (B/F) was plotted vs total bound peptide (B) to determine

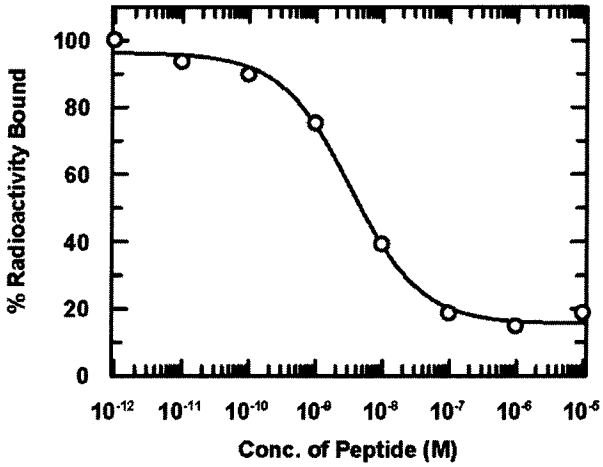


Figure 1. Competitive binding curve of In-DOTA−Phe^{19}-ST$_h$ vs ^{125}I-Tyr^5-6-Ahx-Phe^{19}-ST$_h$ in T-84 cells. IC$_{50}$ of In-DOTA−Phe^{19}-ST$_h$ is 3.3 ± 2.0 nM.

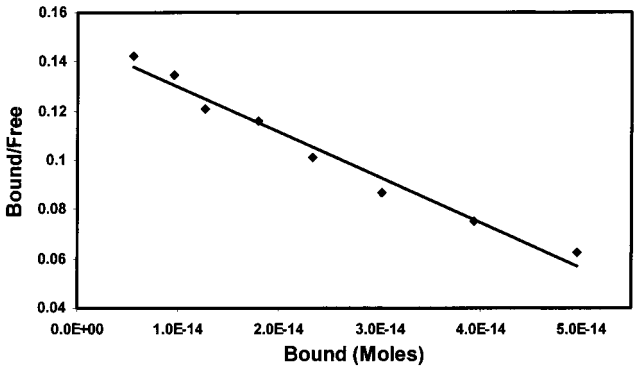


Figure 2. Scatchard plot of ^{125}I-Tyr^5-Phe^{19}-ST$_h$ in T-84 cells. K_d = 1.8 nM and number of receptors per cell at equilibrium (calculated using B_{max} value) = 21715.

the K_d (−1/slope) and B_{max} (X-intercept) values. The number of receptors per cell was calculated from the B_{max} (Figure 2).

In Vitro Stability Studies of ^{111}In-DOTA−Phe^{19}-ST$_h$ in Human Serum. A sample of HPLC purified ^{111}In-DOTA−Phe^{19}-ST$_h$ (100−500 μCi, 3.7−18.5 MBq, 100 μL) was added to 1 mL of human serum in a culture tube and incubated at 37 °C at pH 7.4−7.8 under 5% CO_2 atmosphere. An aliquot of the serum sample (1 μCi, 37

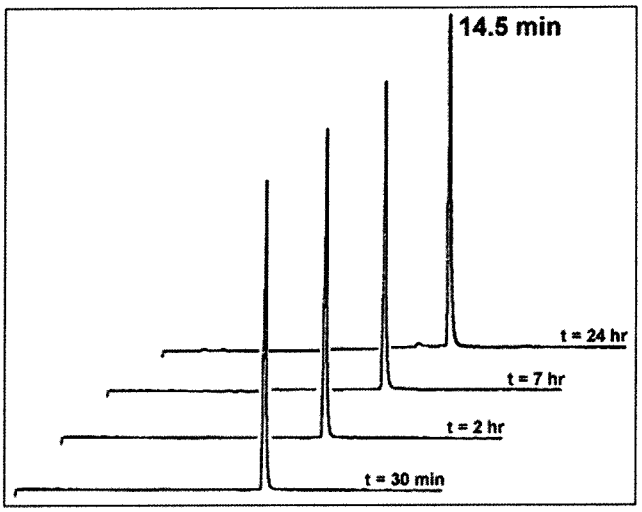


Figure 3. HPLC chromatogram (Gradient I, radiometric detector) of the ^{111}In-DOTA−Phe^{19}-ST$_h$ conjugate incubated in human serum at 37 °C, pH 7.4−7.8, under 5%CO_2 atmosphere. The peaks are normalized to full scale.

KBq, 2−15 μL) was injected into HPLC (Gradient I, radiometric detector) at 30 min, 2, 4, 7 and 24 h to analyze the stability of the ^{111}In-DOTA−ST in human serum (Figure 3). The experiment was performed in duplicate.

In Vivo Pharmacokinetic Studies of ^{111}In-DOTA−Phe^{19}-ST$_h$ in SCID Mice. Four- to five-week old female ICR SCID (severely compromised immunodeficient) outbred mice were obtained from Taconic (Germantown, NY). The mice were housed five animals per cage in sterile microisolator cages in a temperature- and humidity-controlled room with a 12-h light/12-h dark schedule. The animals were fed autoclaved rodent chow (Ralston Purina Company, St. Louis, MO) and water ad libitum. Animals were housed one week prior to inoculation of tumor cells and anesthetized for injections with isoflurane (Baxter Healthcare Corp., Deerfield, IL) at a rate of 2.5% with 0.4 L oxygen through a nonrebreathing anesthesia vaporizer.

Human colon cancer T-84 cells were injected on the bilateral subcutaneous (sc) flank with ~5 × 10^6 cells in a suspension of 100 μL of normal sterile saline per injection site. T-84 cells were allowed to grow in vivo two to three weeks postinoculation, developing tumors ranging in sizes from 0.02 to 1.30 g. The biodistribution and uptake of ^{111}In-DOTA−Phe^{19}-ST$_h$ in tumor-bearing SCID mice was studied. The mice (average weight, 25 g) were injected with aliquots (50−100 μL) of the radiolabeled peptide solution (55−75 kBq) in each animal via the tail vein. Tissues, organs, and tumors were excised from the animals sacrificed at 1 h postinjection (pi). For blocking studies, an access of nonradioactive 6-Ahx-Phe^{19}-ST$_h$ (100 μg) was also injected along with the radiolabeled peptide solution. The radioactivity was measured in a NaI counter and the percent-injected dose per organ and the percent-injected dose per gram tissue were calculated (Table 2). Animal studies were conducted in accordance with the highest standards of care as outlined in the NIH guide for Care and Use of Laboratory Animals and the Policy and Procedures for Animal Research at the Harry S. Truman Memorial Veterans' Hospital and according to approved protocols.

In Vivo Stability Studies of ^{111}In-DOTA−Phe^{19}-ST$_h$ in CF1 Normal Mice. HPLC purified ^{111}In-DOTA−Phe^{19}-ST$_h$ (30−40 μCi, 1.11−1.48 MBq, 100 μL) was injected into normal CF1 mice via the tail vein. The analysis of ^{111}In

Table 2. Biodistribution (% ID/g of tissue) of ^{111}In-DOTA−Phe^{19}-ST$_h$ in T-84 Tumor Bearing SCID Mice at 1 h pi[a]

tissue	^{111}In-Phe^{19}-DOTA−ST$_h$	blocking[b]	^{111}In-DOTA−NSSNY-NH_2
blood	0.23 ± 0.14	0.69 ± 0.23	0.36 ± 0.26
heart	0.00 ± 0.00	0.30 ± 0.06	0.16 ± 0.10
lung	0.20 ± 0.07	0.61 ± 0.17	0.33 ± 0.18
liver	0.08 ± 0.01	0.31 ± 0.10	0.19 ± 0.05
spleen	0.08 ± 0.09	0.76 ± 0.77	0.25 ± 0.34
stomach	0.08 ± 0.04	0.20 ± 0.05	0.11 ± 0.07
large intestine	0.27 ± 0.06	0.25 ± 0.08	0.16 ± 0.03
small intestine	0.76 ± 0.14	0.23 ± 0.06	0.36 ± 0.15
kidney	2.16 ± 0.31	16.37 ± 11.67	7.02 ± 0.91
muscle	0.03 ± 0.02	0.14 ± 0.07	0.08 ± 0.13
pancreas	0.02 ± 0.03	0.26 ± 0.08	0.10 ± 0.05
tumor	2.04 ± 0.30	0.81 ± 0.25	0.36 ± 0.19
urine (% ID)	95.8 ± 0.2	88.8 ± 6.1	94.7 ± 2.5
tumor/blood	8.9 ± 5.6	1.2 ± 0.5	1.0 ± 0.9
tumor/muscle	68.0 ± 46.4	5.8 ± 3.4	4.5 ± 7.7
tumor/liver	25.5 ± 4.9	2.6 ± 1.2	1.9 ± 1.1

[a] Values are expressed as the mean ± SD; $N = 3$. [b] To determine the nonspecific uptake of radioactivity a GC−C-receptor-blocking dose of 6-Ahx-Phe^{19}-ST$_h$ (100 μg) was co-injected intravenously along with the ^{111}In-DOTA−Phe^{19}-ST$_h$.

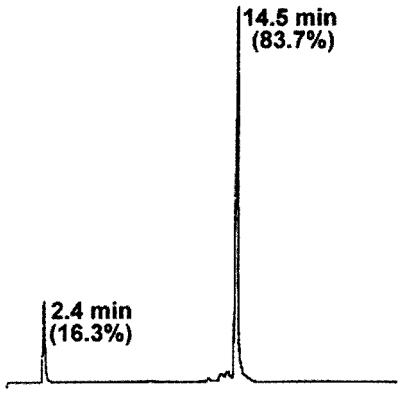


Figure 4. HPLC chromatogram (Gradient I, radiometric detector) of the mouse urine at 1 h pi of the ^{111}In-DOTA−Phe^{19}-ST$_h$.

products excreted into the urine was performed by HPLC using 25 μL aliquots of urine collected from CF1 mice 1 h after iv injection of ^{111}In-DOTA−Phe^{19}-ST$_h$ (Figure 4). At 1 h pi approximately 95% of the injected dose had been excreted into the urine (Table 2).

RESULTS AND DISCUSSION

We recently reported results of studies with an indium-111 labeled DOTA−NCS-6-Ahx-Phe^{19}-ST$_h$ analogue that demonstrated a specific binding affinity for human colon cancer cells both in vitro and in vivo (*26*, *27*). Also we have reported results of studies with another ST$_h$ analogue (DOTA−6-Ahx-Phe^{19}-ST$_h$), in which the chelating framework DOTA−NCS was replaced by DOTA. These data showed that ^{111}In-DOTA−6-Ahx-Phe^{19}-ST$_h$ analogue exhibited increased tumor uptake and reduced kidney retention of the radioactivity producing improved tumor-to-background ratios in T-84 tumor bearing SCID mice when compared to the corresponding DOTA−NCS conjugate (*28*). The DOTA−6-Ahx-Phe^{19}-ST$_h$ analogue was synthesized by random air-oxidation of fully deprotected (reduced) DOTA−6-Ahx-[Cys^{6,7,10,11,15,18}]-Phe^{19}-ST$_h$ in 0.1M NH_4OH (*28*). Although we obtained biologically active DOTA−6-Ahx-Phe^{19}-ST$_h$ analogue with this method, the reproducibility of the generating pure biologically active peptide in consistent yields was poor. Furthermore, when

we tried to synthesize an analogue containing no alkyl chain spacer (DOTA−Phe^{19}-ST$_h$), for studying the effect of alkyl chain spacer on the in vivo biodistribution and pharmacokinetics properties of radiometalated DOTA−ST$_h$ conjugates, using the above method we did not get any product. These results suggested that the attachment of a bulky and polar DOTA group at the amino terminus of the native ST$_h$ peptide impeded proper folding of the peptide. To overcome this problem, we followed a new synthetic strategy, similar to that described by Akaji et al. (*20*) for synthesizing human insulin, using three well-known orthogonal thiol protecting groups to form three regioselective disulfide bonds as required to retain full biological activiy (Scheme 1). The amino acid sequence, of all the ST conjugates reported herein, is identical to the heat-stable enterotoxin ST$_h$ excreted by the human strain of *Escherichia coli* except the C-terminal tyrosine in the 19th position is replaced by phenylalanine (i.e., Phe^{19}).

The first step in the synthesis of DOTA−Phe^{19}-ST$_h$ **4** involves the synthesis of fully protected DOTA−[Cys(Trt)^{6,11}, Cys(Acm)^{7,15}, Cys(tBu)^{10,18}]-Phe^{19}-ST$_h$ on the Wang resin on an automated peptide synthesizer system using traditional fmoc chemistry. Upon cleavage of the fully protected ST$_h$ analogue from the resin using standard TFA cocktail, the crude DOTA−[Cys^{6,11}, Cys(Acm)^{7,15}, Cys(tBu)^{10,18}]-Phe^{19}-ST$_h$ **1** was obtained in a yield of about 90%. The formation of the first disulfide bond was carried out by treating an aqueous solution of **1** with 2,2′-dithiodipyridine (2-PDS) at pH 8.6 (Scheme 1). The 2-PDS reagent selectively reacts only with free thiol group present on the cysteine-containing peptide, forming the S−S-pyridyl derivative of the peptide and 2-thiopyridone. The S−S-pyridyl side chain of cysteine was then attacked by another free thiol group present in the same peptide to form an intramolecular S−S bond (*23*). Thus, the two reduced cysteine residues present on the linear peptide **1** were converted to the oxidized form upon treatment with 2-PDS (*23*). The first folded peptide, DOTA−[Cys(Acm)^{7,15}, Cys(tBu)^{10,18}]-Phe^{19}-ST$_h$ **2**, was obtained in a yield of about 30−40% after HPLC purification using gradient I elution program. The second disulfide bond formation was carried out using a widely employed iodine oxidation method (*20*, *24*, *25*). The two Acm-protected cysteines present in the cyclic peptide **2** were oxidized to form a second S−S bond and the other two tBu protected cysteines remained stable to iodine oxidation. The second folded peptide, DOTA−[Cys-(tBu)^{10,18}]-Phe^{19}-ST$_h$ **3**, was obtained in a yield of about 50−60% after purification on HPLC (Gradient I) (Scheme 1). DOTA−[Cys(tBu)^{10,18}]-Phe^{19}-ST$_h$ **3** exhibited slightly more hydrophobic character than DOTA−[Cys(Acm)^{7,15}, Cys(tBu)^{10,18}]-Phe^{19}-ST$_h$ **2** and eluted about 1 min later during HPLC (Gradient I). The final specific disulfide bond formation was achieved by the treatment of **3** in TFA with methyltrichlorosilane in the presence of diphenyl sulfoxide (Scheme 1). Methyltrichlorosilane in the presence of diphenyl sulfoxide in TFA cleaves the tBu protecting group of the cysteines to form the S−S bond directly by a reduction−oxidation reaction mechanism.[20−22] Pure DOTA−Phe^{19}-ST$_h$ **4** was obtained in yields of about 20−30% after purification on HPLC (Gradient II). The overall yield was about 0.6−1.6% starting from resin with purity >98% as confirmed by HPLC. DOTA−Phe^{19}-ST$_h$ **4** exhibited more hydrophilic character than DOTA−[Cys(tBu)^{10,18}]-Phe^{19}-ST$_h$ **3** and eluted about 4 min earlier on the HPLC (Gradient I). For the purification at the last step of the synthesis, Gradient II was used since the resolution of HPLC peaks (byproducts and other impurities) was optimal. The characterization of product formation at each step was carried out by electrospray mass spectrometry.

Indium-111 labeling as well as the nonradioactive indium metalation of the DOTA−Phe^{19}-ST$_h$ **4** was carried out using $^{111}InCl_3$ (or $InCl_3$) at pH 5.8 and heating at 80 °C for 1 h. The ^{111}In-DOTA−Phe^{19}-ST$_h$ (t_R = 17.7 min, Gradient II) eluted approximately 2.3 min before the nonmetalated DOTA−Phe^{19}-ST$_h$ conjugate (t_R = 20.0 min, Gradient II) enabling collection of the high-specific activity, NCA ^{111}In-DOTA−Phe^{19}-ST$_h$ conjugate. The nonradioactive In-DOTA−Phe^{19}-ST$_h$ conjugate (t_R = 17.7 min, Gradient II) was purified on HPLC and characterized by electrospray mass-spectrometry. The identical HPLC retention times of both radioactive and nonradioactive indium complexes of DOTA−Phe^{19}-ST$_h$ conjugate confirms that the structure at both the micro- and macroscopic level is the same.

The binding affinity of the ST$_h$ analogues, synthesized herein, to GC-C receptors was determined by performing in vitro competitive cell binding assay in human colon cancer T-84 cells. Results from these cell binding assay studies with In-DOTA−Phe^{19}-ST$_h$, DOTA−Phe^{19}-ST$_h$, DOTA−6-Ahx-Phe^{19}-ST$_h$, and Phe^{19}-ST$_h$ analogues vs ^{125}I-Tyr^5-6-Ahx-Phe^{19}-ST$_h$ performed in human colonic cancer T-84 cells demonstrated that all ST$_h$ analogues bind to the GC-C receptors present on these cells with high specificity and affinity (i.e., IC$_{50}$ values measured for the In-DOTA−Phe^{19}-ST$_h$ and DOTA−Phe^{19}-ST$_h$ are 3.3 ± 2.0 and 0.6 ± 0.1 nM, respectively) (Table 1, Figure 1). IC$_{50}$ values measured for metalated and nonmetalated DOTA−6-Ahx-Phe^{19}-ST$_h$ analogues, synthesized by regioselective disulfide bond formation strategy, were found to be identical to those previously synthesized by a random air-oxidation method and similar to those reported earlier for ST peptides (*28*). Interestingly, these values are lower than those reported recently for binding of indium-metalated and nonmetalated DOTA−NCS−ST$_h$ analogues to human colonic cancer cell lines (i.e., T-84, LS-180, and CaCO-2 cells) (*26*, *27*). These in vitro cell binding studies demonstrates that the conformation produced by regioselective disulfide bond formation strategy in the ST$_h$ conjugates, reported herein, is biologically active and binds to GC-C receptors with high affinity. Scatchard analysis of the data obtained from the receptor-binding studies performed in T-84 cells yielded a linear plot with K_d value of 1.8 nM (Figure 2). The number of active receptors per cell at equilibrium (calculated using B_{max} value) was found to be about 21715. These values are in agreement with the results previously reported by Carrithers et al. for low affinity ST receptor binding sites expressed on T-84 cells (*7*).

The in vitro stability studies in human serum shows that no measurable decomposition of the ^{111}In-DOTA−Phe^{19}-ST$_h$ conjugate occurs ≥24 h postincubation at 37 °C (Figure 3). The HPLC (Gradient I) analysis of CF1 normal mice urine at 1 h pi of the ^{111}In-DOTA−Phe^{19}-ST$_h$ shows only about 15% decomposition (Figure 4). These stability studies demonstrate that the three-dimensional structure of the ST provides protection from enzymatic degradation under both in vitro and in vivo conditions and are consistent with previous reports demonstrating that ST-peptides have exceptionally high in vitro and in vivo metabolic stability (*4*, *10*).

In vivo biodistribution studies of the ^{111}In-DOTA−Phe^{19}-ST$_h$ were performed in healthy SCID mice xenografted with human colonic tumors derived from T-84 cells. Table 2 summarizes results of the biodistribution pattern of the ^{111}In-DOTA−Phe^{19}-ST$_h$ in tumor-bearing

SCID mice at 1 h pi. High tumor uptake of 2.04 ± 0.30% ID/g was observed with only 0.23 ± 0.14% ID/g in blood stream at 1 h pi. The radioactivity cleared rapidly from the blood stream with 95.8 ± 0.2% ID found in the urine at 1 h pi. The primary route of clearance of the ^{111}In-DOTA−Phe^{19}-ST$_h$ is via the kidneys into the urine (Table 2). There is only 0.09 ± 0.01% ID, 0.18 ± 0.01% ID, and 1.09 ± 0.04% ID found in the liver, large intestine, and small intestine at 1 h pi, respectively. Thus, a maximum of approximately 1.4% ID that had cleared from circulation and was excreted into the intestines by the hepatobiliary route by 1 h. It is also important to note that there is minimal uptake of the ^{111}In-DOTA−Phe^{19}-ST$_h$ in other organs, other than the kidneys, indicating that these normal tissues and organs exhibit no or minimal GC-C receptor expression, which is consistent with previous reports (*4*−*9*, *27*, *28*). The retention of the radioactivity in the kidneys (Table 2) is reduced substantially when compared to previously reported ^{111}In-DOTA−NCS−ST$_h$ analogue (*27*). The reason for this is not understood but may relate to the lower lipophilicity of the ^{111}In-DOTA−Phe^{19}-ST$_h$ conjugate. The fact that there is minimal accumulation of ^{111}In-DOTA−Phe^{19}-ST$_h$ in the intestines demonstrates that, when this ST-analogue is administered intravenously, it does not have access to the GC-C receptors expressed only on the luminal side of the normal intestinal enterocytes (*7*, *29*−*31*). In contrast, GC-C receptors expressed on colorectal tumor cells are accessible to iv-injected radiolabeled ST analogues (*7*, *29*−*31*). The high tumor to blood, tumor to muscle, and tumor to liver ratios in T-84 tumor-bearing mice of about 9, 68, and 25.5, respectively, at 1 h pi (Table 2) demonstrate the potential of using the ^{111}In-DOTA−Phe^{19}-ST$_h$ as a radiopharmaceutical for imaging colorectal tumors in humans.

To demonstrate that the ^{111}In-DOTA−Phe^{19}-ST$_h$ uptake in T-84 tumors is specific and receptor-mediated, biodistribution studies were performed using a nonspecific peptide, ^{111}In-DOTA−6-Ahx-NSSNY-NH$_2$ (which has similar pharmacokinetic properties to that of ^{111}In-DOTA−Phe^{19}-ST$_h$), in T-84 tumor-bearing SCID mice. An uptake value of 0.36 ± 0.19% ID/g in the tumors was observed at 1 h pi which is representative of nonspecific localization by the normal blood supply in tumors (Table 2). Further verification of tumor specificity is demonstrated by coinjection of an excess (100 μg) of nonradioactive 6-Ahx-Phe^{19}-ST$_h$ along with the ^{111}In-DOTA−Phe^{19}-ST$_h$ in T-84 tumor-bearing SCID mice. In these studies an uptake of 0.81 ± 0.25% ID/g was observed in the tumor at 1 h pi (Table 2), which is about 60% lower uptake than the tumor uptake of ^{111}In-DOTA−Phe^{19}-ST$_h$ when no blocking agent was coinjected (Table 2). The cause of the marked increased degree of ^{111}In-localization in the kidneys (Table 2) with coinjection of excess nonradioactive 6-Ahx-Phe^{19}-ST$_h$ is unknown. Results from these two experiments clearly demonstrates that the ^{111}In-DOTA−Phe^{19}-ST$_h$ binds selectively to the GC-C receptors present on the T-84 tumor cells under in vivo conditions.

CONCLUSION

The synthetic strategy described successfully demonstrates that ST$_h$ analogues containing a DOTA chelating framework that bind with high affinity to GC-C receptors on human colon cancer cells can be produced by regioselective formation of disulfide bonds following SPPS of the linear DOTA-conjugated sequence. The in vitro studies performed in human colon cancer T-84 cells showed that both the metalated and nonmetalated DOTA−ST$_h$ analogues bind to GC-C receptors for guanylin/ST peptides with high specificity and affinity. The in vivo biodistribution of the ^{111}In-DOTA−Phe^{19}-ST$_h$ peptide in SCID mice xenografted with T-84 human colonic tumors showed high uptake of ^{111}In-conjugate in tumors coupled with rapid clearance from the blood stream almost entirely via the renal/urinary pathway. The results from these studies demonstrate that the radiometalated DOTA−ST$_h$ analogues are promising candidates for further development as diagnostic and/or therapeutic radiopharmaceuticals for use in patients with colorectal cancers (*32*−*35*).

ACKNOWLEDGMENT

This work was supported by funding from DOE Grant No. DEFG0289ER8075 and by the Department of Radiology at the University of Missouri-Columbia. The material is the result of work supported with resources and the use of facilities at the Harry S. Truman Memorial Veterans' Administration Hospital.

LITERATURE CITED

(1) Smith H. W., and Gyles C. L. (1970) The relationship between two apparently different enterotoxins produced by enteropathogenic strains of *Escherichia coli* of porcine origin. *J. Med Microbiol. 3*, 387−401.

(2) Pai C. H., and Mors V. (1978) Production of enterotoxin by Yersinia enterocolitica. *Infect. Immun. 19*, 908−911.

(3) Takao T., Shimonishi Y., Kobayashi M., Nishimura O., Arita M., Takeda T., Honda T., and Miwatani T. (1985) Amino acid sequence of heat-stable enterotoxin produced by *Vibrio cholerae* non-01. *FEBS Lett. 193*, 250−254.

(4) Giannella R. A. (1995) *Escherichia coli* heat-stable enterotoxins, guanylins, and their receptors: What are they and what do they do? *J. Lab. Clin. Med. 125*, 173−181.

(5) Forte L. R. (1999) Guanylin regulatory peptides: Structure, biological activity mediated by cyclic GMP and pathobiology. Regulatory. *Peptides 81*, 25−39.

(6) Drewett J. G., and Garbers D. L. (1994) The family of guanylyl cyclase receptors and their ligands. *Endocr. Rev. 15*, 135−162.

(7) Carrithers S. L., Parkinson S. J., Goldstein S. D., Park P. K., Robertson D. C., and Waldman S. A. (1994) *Escherichia coli* heat-stable toxin receptors in human colonic tumors. *Gastroenterology 107*, 1653−1661.

(8) Carrithers S. L., Parkinson S. J., Goldstein S. D., Park P. K., Urbanski R. W., and Waldman S. A. (1996) *Escherichia coli* heat-stable enterotoxin receptors − A novel marker for colorectal tumors. *Dis. Colon Rectum 39*, 171−181.

(9) Carrithers S. L., Barber M. T., Biswas S., Parkinson S. J., Park P. K., Goldstein S. D., and Waldman S. A. (1996) Guanyly cyclase C is a selective marker for metastatic colorectal tumors in human extraintestinal tissue. *Proc. Natl. Acad.. Sci. U.S.A. 93*, 14827−14832.

(10) Ozaki H., Sato T., Kubota H., Hata Y., Katsube Y., and Shimonishi Y. (1991) Molecular structure of the toxin domain of heat-stable enterotoxin produced by a pathogenic strain of *Escherichia coli*. A putative binding site for a binding protein on rat intestinal epithelial cell membranes. *J. Biol. Chem. 266*, 5934−5941.

(11) Sato T., Ozaki H., Hata Y., Kitagawa Y., Katsube Y., and Shimonishi Y. (1994) Structural characteristics for biological activity of heat-stable enterotoxin produced by enterotoxigenic *Escherichia coli*: X-ray crystallography of weakly toxic and nontoxic analogues. *Biochemistry 33*, 8641−8650.

(12) Carpick B. W., and Gariepy J. (1991) Structural characterization of functionally important regions of the *Escherichia coli* heat-stable enterotoxin STIb. *Biochemistry 30*, 4803−4809.

(13) Staples S. J., Asher S. E., and Giannella R. A. (1980) Purification and characterization of heat-stable enterotoxin produced by a strain of *E. coli* pathogenic for man. *J. Biol. Chem. 255*, 4716−4721.

(14) Greenberg R. N., Dunn J. A., and Guerrant R. L. (1983) Reduction of the secretory response to *Escherichia coli* heat-stable enterotoxin by thiol and disulfide compounds. *Infect. Immun. 41*, 174−180.

(15) Gariepy J., Judd A. K., and Schoolnik G. K. (1987) Importance of disulfide bridges in the structure and activity of *Escherichia coli* enterotoxin ST1b. *Proc. Natl. Acad Sci. U.S.A. 84*, 8907−8911.

(16) Kubota H., Hidaka Y., Ozaki H., Ito H., Hirayama T., Takeda Y., and Shimonishi Y. (1989) A long-acting heat-stable enterotoxin analogue of enterotoxigenic *Escherichia coli* with a single D-amino acid. *Biochem. Biophys. Res. Commun. 161*, 229−235.

(17) Aimoto S., Watanabe H., Ikemura H., Shimonishi Y., Takeda T., Takeda Y., and Miwatani T. (1983) Chemical synthesis of a highly potent and heat-stable analogue of an enterotoxin produced by a human strain of enterotoxigenic *Escherichia coli*. *Biochem. Biophys. Res. Commun. 112*, 320−326.

(18) Houghten R. A, Ostresh J. M., and Klipstein F. A. (1984) Chemical synthesis of an octadecapeptide with the biological and immunological properties of human heat-stable *Escherichia coli* enterotoxin. *Eur. J. Biochem. 145*, 157−162.

(19) Hamra F. K., Forte L. R., Eber S. L., Pidhorodeckyj N. V., Krause W. J., Freeman R. H., Chin D. T., Tompkins J. A., Fok K. F., Smith C. E., Duffra K. L., Siegel N. R., and Currie M. G. (1993) Uroguanylin: structure and activity of a second endogenous peptide that stimulates intestinal guanylate cyclase. *Proc. Natl. Acad. Sci. U.S.A. 90*, 10464−10468.

(20) Akaji K., Fujino K., Tatsumi T., and Kiso Y. (1993) Total synthesis of human insulin by regioselective disulfide formation using the silyl chloride-sulfoxide method. *J. Am. Chem. Soc. 115*, 11384−11392.

(21) Koide T., Otaka A., Suzuki H., and Fujii N. (1991) Selective conversion of S-protected cysteine derivatives to cystine by various sulphoxide-silyl compounds/trifluoroacetic acid system. *Synlett* 345−346.

(22) Akaji K., Tatsumi T., Yoshida M., Kimuru t., Fujiwara Y., and Kiso Y. (1991) Synthesis of cystine-peptide by a new disulphide bond-forming reaction using the silyl chloride-sulphoxide system. *J. Chem. Soc. Chem. Commun.* 167−168.

(23) Maruyama K., Nagasawa H., and Suzuki A. (1999) 2,2′-Bipyridyl disulfide rapidly induces intramolecular disulfide bonds in peptides. *Peptides 20*, 881−884.

(24) Kudryavtseva E. V., Sidorova M. V., and Evstigneeva R. P. (1998) Some peculiarities of synthesis of cysteine-containing peptides. *Russ. Chem. Rev. 67*, 545−562.

(25) Kamber B. Hartmann A. Eisler K., Riniker B., Rink H., Sieber P., and Rittel W. (1980) 96. The synthesis of cystine peptides by iodine oxidation of S-trityl-cysteine and S-acetamidomethyl-cysteine peptides. *Helv. Chim. Acta 63*, 899−915.

(26) Gali H., Sieckman G. L., Hoffman T. J., Kiefer G. E., Chin D. T. Forte L. R., and Volkert W. A. (2001) Synthesis and In Vitro Evaluation of a ^{111}In-Labeled ST-peptide Analogue for Specific Targeting of Guanylin Receptors on Human Colonic Cancers. *Anticancer Res. 21*, 2785−2792.

(27) Gali H., Sieckman G. L., Hoffman T. J., Owen N. K., Chin D. T., Forte L. R., and Volkert W. A. (2001) In Vivo Evaluation of an ^{111}In-Labeled ST-Peptide Analogue for Specific-Targeting of Human Colon Cancers. *Nucl. Med. Biol. 28*, 903−909.

(28) Gali H., Sieckman G. L., Hoffman T. J., Owen T. J., Chin D. T., Forte L. R., and Volkert W. A. (2001) In vitro and in vivo characterization of a new receptor specific indium-111 labeled DOTA-ST conjugate for targeting guanylin receptors in human colon cancer cells. *J. Labelled Cpd. Radiopharm. 44*, Suppl. 1, S682−S84.

(29) Almenoff J. S., Willims S. I., Scheving L. A., Judd A. K., and Schoolnik G. K. (1993) Ligand-based histochemical localization and capture of cells expressing heat-stable enterotoxin receptors. *Mol. Microbiol. 8*, 865−873.

(30) Crissinger K. D., Kvietys P. R., and Granger D. N. (1990) Pathophysiology of gastrointestinal mucosal permeability. *J. Intern. Med. 732*, 145−154.

(31) Forte L. R., and Currie M. G. (1995) Guanylin: a peptide regulator of epithelial transport. *FASEB J. 9*, 643−650.

(32) Liu, S., and Edwards, S. D. (1999) ^{99m}Tc-Labeled small peptides as diagnostic radiopharmaceuticals. *Chem. Rev. 99*, 2235−2268.

(33) Okarvi, S. M. (1999) ^{99m}Tc-Labeled small peptide-based radiopharmaceuticals: An overview. *Nucl. Med. Commun. 20*, 1093−1112.

(34) Hoffman T. J., Quinn T. P., and Volkert W. A. (2001) Radiometalated receptor-avid peptide conjugates for specific in vivo targeting of cancer cells. *Nucl. Med. Biol. 28*, 527−539.

(35) Volkert, W. A., and Hoffman, T. J. (1999) Therapeutic radiopharmaceuticals. *Chem. Rev. 99*, 2269−2292.

BC010062U

Synthesis of Sulfhydryl Cross-Linking Poly(Ethylene Glycol)-Peptides and Glycopeptides as Carriers for Gene Delivery†

Youmie Park, Kai Y. Kwok, Chawki Boukarim, and Kevin G. Rice*

College of Pharmacy, 428 Church Street, University of Michigan, Ann Arbor, Michigan 48109-1065. Received July 16, 2001; Revised Manuscript Received January 7, 2002

Sulfhydryl cross-linking poly(ethylene glycol) (PEG)-peptides and glycopeptides were prepared and tested for spontaneous polymerization by disulfide bond formation when bound to plasmid DNA, resulting in stable PEG-peptide and glycopeptide DNA condensates. A 20 amino acid synthetic peptide possessing a single sulfhydryl group on the N-terminal cysteine, with two or five internal acetamidomethyl (Acm)-protected cysteine residues, was reacted with either PEG vinyl sulfone or iodoacetamide tyrosinamide triantennary *N*-glycan. Following RP-HPLC purification, Acm groups were removed by silver tetrafluoroborate to generate sulfhydryl cross-linking PEG-peptides and glycopeptide that were characterized by either ^{1}H NMR or LC−MS. Sulfhydryl cross-linking PEG-peptides and glycopeptides were found to bind to plasmid DNA and undergo disulfide cross-linking resulting in stable DNA condensates with potential utility for in vivo gene delivery.

INTRODUCTION

Nonviral gene delivery relies upon carrier molecules to bind to plasmid DNA, resulting in the formation of DNA condensates that target to the desired cell-type and mediate transient expression of the encoded gene (*1*). To be therapeutically useful, it is essential to develop sophisticated nonviral gene delivery polymers that can be systematically optimized to mediate high levels of gene expression in vivo (*2*, *3*).

Low molecular weight (LMW)[1] peptide carriers have been substituted for high molecular weight (HMW) polylysine and shown to mediate efficient in vitro gene transfer (*4*, *5*). Even though LMW peptides are potentially less toxic than HMW peptides when used in vivo, LMW peptide DNA condensates are not sufficiently stable in the circulation and target tissue (*6*). Cross-linking strategies have been developed to stabilize LMW peptide DNA condensates during transit in the blood and once inside the target cell (*7*, *8*). Glutaraldehyde is one such cross-linking agent that has been shown to retard LMW peptide DNA condensate metabolism in the liver, thereby affording in vivo gene expression (*6*).

To ensure proper targeting to the desired cell type, poly(ethylene glycol) (PEG) has been attached to LMW peptides and used to form DNA condensates possessing a steric layer that blocks nonspecific binding of serum proteins (*9*, *10*). Likewise, LMW glycopeptides possessing either terminal galactose or mannose residues have been incorporated onto the surface of DNA condensates for the purpose of targeting either the asialoglycoprotein receptor or mannose receptor (*6*, *11*).

More recently, peptides containing multiple cysteine residues that undergo sulfhydryl cross-linking when bound to plasmid DNA have been used to form stable peptide DNA condensates that mediate in vitro gene expression (*12*, *13*). This cross-linking strategy is attractive because, in principle, the degree of stability can be controlled by the number and type of sulfhydryl groups in a peptide and the release of DNA is triggered by the reducing environment of the endosome or cytosol (*14*). This same strategy has been applied to prepare detergents containing sulfhydryl groups that dimerize when bound to DNA to form cationic lipids (*15*−*17*). These lipoplexes are reportedly more homogeneous in particle size and exhibit higher in vitro gene transfer activity because of a triggered release of DNA in the cytosol. Despite progress in the development of sulfhydryl cross-linked gene delivery systems, to date, none of these agents have been tested for in vivo gene delivery. To do this would require derivatization to install a targeting ligand as well as a steric stabilizing agent to form blood-compatible DNA condensates.

In the present study, we have extended the concept of LMW sulfhydryl cross-linking peptides by preparing PEG-peptides and glycopeptides that are able to bind DNA and undergo disulfide bond formation to create stable condensates. The synthesis of these DNA binding molecules represents a significant advance in the design of LMW carriers properly derivatized to test whether sulfhydryl cross-linking peptides will function to mediate in vivo gene expression.

MATERIALS AND METHODS

PEG-vinyl sulfone (PEG-VS, 5 kDa) was purchased from Fluka (Ronkonkoma, NY). Tris(2-carboxyethyl)-phosphine hydrochloride (TCEP) was purchased from Pierce (Rockford, IL). N-terminal Fmoc-protected Boc-Lys, Boc-Trp, and Trt-Cys and 9-hydroxybenzotriazole (HOBt), diisopropylcarbodiimide (DIC), and diisopropyl-

† The authors acknowledge financial support provided by NIH Grant GM48049 and Selective Genetics.

* To whom correspondence should be addressed. Phone: 734-763-2032. Fax: 734-763-2022. E-mail: krice@umich.edu.

[1] Abbreviations: Acm, acetamidomethyl; DTT, dithiothreitol; EDT, 1,2-ethane dithiol; ESI-MS, electrospray ionization mass spectrometry; Fmoc, N$^{\alpha}$-9-fluorenylmethyloxycarbonyl; ^{1}H NMR, proton nuclear magnetic resonance spectroscopy; LC−MS, liquid chromatography−mass spectrometry; LMW, low molecular weight; PEG-VS, poly(ethylene glycol) vinyl sulfone; QELS, quasi-elastic light scattering; RP-HPLC, reversed-phase high performance chromatography; TCEP, tris(2-carboxyethyl)phosphine hydrochloride; TFA, trifluoroacetic acid.

10.1021/bc010070a CCC: $22.00 © 2002 American Chemical Society
Published on Web 02/13/2002

Table 1. ^{1}H NMR Chemical Shifts[a] and MS for PEG-peptides and Glycopeptides

structure[b]	3	4	5	6	8	9
PEG CH_2	3.630	3.704	3.629	3.764		
OCH_3	3.382	3.382	3.380	3.382		
Lys α	4.223	4.332	4.222	4.250	4.298	4.223
β	1.705	1.806	1.708	1.712	1.785	1.816
γ	1.363	1.445	1.366	1.352	1.433	1.443
δ	1.616	1.695	1.616	1.618	1.695	1.701
ϵ	2.925	3.000	2.924	2.926	3.004	3.006
Trp b	7.211	7.251	7.217	7.223	7.296	7.290
d	7.430	7.448	7.427	7.431	7.505	7.506
e	7.164	7.163	7.175	7.177	7.247	7.248
f	7.090	7.013	7.086	7.095	7.158	7.165
g	7.566	7.581	7.551	7.549	7.629	7.626
Tyr a					7.120	7.128
b					6.811	6.819
Acm (CH_3)	2.019, 2.034	2.031			2.035, 2.049	2.024, 2.035
GlcNAc (H1)						
1					5.032	5.039
2					4.608	4.618
5					4.556	4.585
5′					4.583	4.585
7					4.538	4.585
Gal (H1)						
6					4.468	4.468
6′					4.468	4.468
8					4.468	4.468
Man (H1)						
4					5.121	5.123
4′					4.926	4.927
NAc						
1					2.035	2.034
2					2.077	2.076
5					2.049	2.047
5′					2.049	2.047
7					2.067	2.076
mass (obs/calc)					(4914.9/4915.5) (4772.9/4773.4)[c]	(5053.0/5052.5) (4697.5/4697.1)[c]

[a] Chemical shifts are reported relative to acetone (2.225 ppm) internal standard at 23 °C. [b] See Figures 1, 3, and 5 for nomenclature. [c] Represents the mass following removal of Acm from glycopeptides **8** and **9**.

ethylamine (DIPEA) were obtained from Advanced ChemTech (Lexington, KY). Substituted Wang resin for peptide synthesis was obtained from ChemImpex (Wood Dale, IL). N-terminal Fmoc-protected acetamidomethyl (Acm)-protected cysteine was purchased from Novabiochem (La Jolla, CA). *N*,*N*-Dimethylformamide (DMF), trifluoroacetic acid (TFA), acetic anhydride, acetonitrile, acetic acid, ether, and piperidine were purchased from Fisher Scientific (Pittsburgh, PA). CM Sephadex cation-exchange resin and anisole were from Sigma (St. Louis, MO). Silver tetrafluoroborate was from Aldrich (Milwaukee, WI). SYBR-Gold was purchased from Molecular Probes, Inc. (Eugene, OR). Thiazole orange was a gift from Beckton Immunocytometry Systems (San Jose, CA). The 5.6 kb plasmid pCMVL encoding the reporter gene luciferase under the control of the cytomegalovirus promoter was a gift from Dr. M. A. Hickman at the University of California, Davis, CA (*18*). Peptide synthesis was performed on a computer interfaced model 90 Advanced ChemTech solid-phase peptide synthesizer (Lexington, KY). Preparative and analytical HPLC columns were purchased from Vydac (Hesperia, CA). HPLC was performed using a computer-interfaced HPLC and fraction collector from ISCO (Lincoln, NE). Electrospray ionization mass spectrometry (ESI-MS) was performed using a Finnigan LCQ mass spectrometer (San Jose, CA) interfaced with an analytical HPLC from Hitachi (San Jose, CA). ^{1}H NMR was generated on a Bruker 500 MHz spectrometer operated at 23 °C.

Peptide Synthesis and Characterization. CWC(Acm)K_{15}C(Acm)K (**1**) and CW(C(Acm)K_3)$_4$C(Acm)K (**2**) were synthesized using standard Fmoc procedures with HOBt and DIC double couplings followed by N-capping with acetic anhydride after each coupling to avoid deletion sequences. The peptide was cleaved from the resin and side-chain-protecting groups were removed (except for Acm protecting groups on internal cysteines) by reaction with TFA/EDT/water (95/2.5/2.5, v/v/v) for 1 h.

Peptides **1** and **2** were purified to homogeneity by injecting 1 *μ*mol onto a semipreparative RP-HPLC column (2 × 25 cm) eluted at 10 mL/min with 0.1% (v/v) TFA and a gradient of acetonitrile (5−25% over 30 min) while monitoring tryptophan absorbance at 280 nm. The major peak eluting at 15 min for **1** or 22 min for **2** was collected and pooled from multiple injections, concentrated by rotary evaporation, lyophilized, and stored dry at −20 °C. The purified peptides were reconstituted in 0.1% TFA and quantified by tryptophan absorbance ($\epsilon_{280\ nm} = 5600\ M^{-1}\ cm^{-1}$).

Synthesis of PEG-VS-CWCK_{15}CK (5) and PEG-VS-CW(CK_3)$_4$CK (6). PEG-peptides **5** and **6** (Table 1) were synthesized by reacting 1.25 *μ*mol of peptide **1** or **2** with 25 *μ*mol of TCEP and 37 *μ*mol of PEG-VS at room temperature (RT) for 24 h in 4 mL of a 0.1 M sodium phosphate buffer (pH 7.0) (*9*). The reaction was monitored by injecting 5 nmol onto analytical RP-HPLC eluted at 1 mL/min with 0.1% TFA and an acetonitrile gradient of 5−65% over 30 min while detecting by $Abs_{280\ nm}$.

PEG-peptides were purified from unreacted PEG-VS by chromatography on a CM Sephadex cation exchange column (1.5 × 35 cm) eluted with 180 mL of water to remove unreacted PEG-VS and then 180 mL of 2 M sodium chloride while detecting by $Abs_{280\ nm}$. The PEG-peptide peak eluting between 240 and 264 mL was

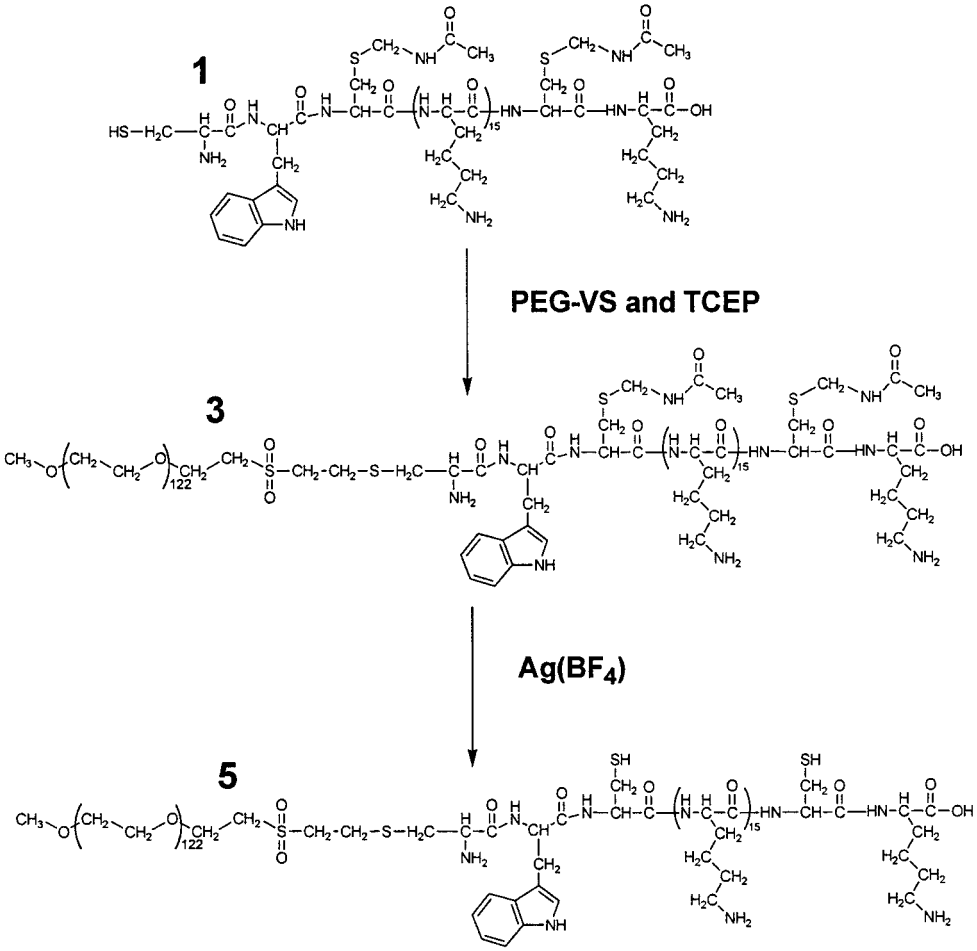


Figure 1. Synthesis of PEG-VS-CWCK$_{15}$CK (**5**). Peptide **1** was reacted with PEG-VS to form PEG-peptide **3** in the presence of TCEP. Acm protecting groups on internal cysteine residues were removed by silver tetrafluoroborate to generate PEG-peptide **5**.

pooled, dialyzed in 1000 MWCO tubing for 12 h against water, and lyophilized. PEG-peptides **3** or **4** were purified by applying 1 μmol onto semipreparative RP-HPLC (2 × 25 cm) eluted at 10 mL/min with 0.1% TFA and a gradient of acetonitrile (5−65% over 30 min) while detecting Abs$_{280\ nm}$.

Final deprotection of PEG-peptides **3** or **4** was accomplished by dissolving 5 μmol in 1 mL of cold TFA followed by the addition of silver tetrafluoroborate (20 equiv/Acm group) and anisol (10 equiv/Acm group) and reaction at 4 °C for 1 h with stirring (*19*). PEG-peptides were recovered as the silver salt by centrifugation of the precipitate formed in 60% (v/v) diethyl ether, then redissolved in 0.1 M acetic acid containing DTT (40 equiv/Acm group), and reacted at RT for 3 h. Following centrifugation to remove insolubles, deprotected PEG-peptides **5** or **6** were purified on semipreparative RP-HPLC eluted as described previously. The isolated product was freeze-dried and reconstituted in 0.1% TFA and reanalyzed by analytical HPLC to determine purity. PEG-peptides **3**−**6** were prepared for ^{1}H NMR by repeated freeze-drying in D_2O followed by dissolving the sample in 0.5 mL of D_2O (99.96%), containing 0.1% acetone as an internal standard, and analyzed on a Bruker 500 MHz NMR spectrometer operating at 23 °C.

Synthesis of Triantennary-CWCK$_{15}$CK (10) and Triantennary-CW(CK$_3$)$_4$CK (11) Glycopeptide. A triantennary *N*-glycan was purified as a Boc tyrosinamide derivative from bovine fetuin (*20*) and converted into the iodoacetamide triantennary *N*-glycan following the removal of Boc as previously reported (*21*). Iodoacetamide

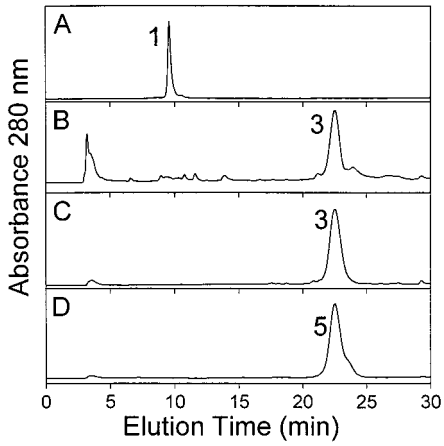


Figure 2. RP-HPLC analysis of PEG-VS-CWCK$_{15}$CK (**5**) synthesis. RP-HPLC analysis of the reaction of peptide **1** and PEG-VS verified the complete consumption of **1** (panel A versus B) with the formation of PEG-peptide **3** (panel B). Purification of **3** via ion-exchange chromatography and RP-HPLC to remove residual PEG-VS resulted in its rechromatograph as single peak (panel C). Following removal of the Acm protecting groups, PEG-peptide **5** chromatographed coincidently with PEG-peptide **3** (panel D). The peaks are numbered according to the nomenclature in Figure 1.

triantennary *N*-glycan **7** (100 nmol) was conjugated to either peptide **1** (125 nmol) or **2** by reaction for 12 h at RT in 400 μL of a 0.2 M Tris buffer (pH 8.0). The resulting glycopeptide was purified by injecting 100 nmol onto a semipreparative RP-HPLC column (2 × 25 cm) eluted at

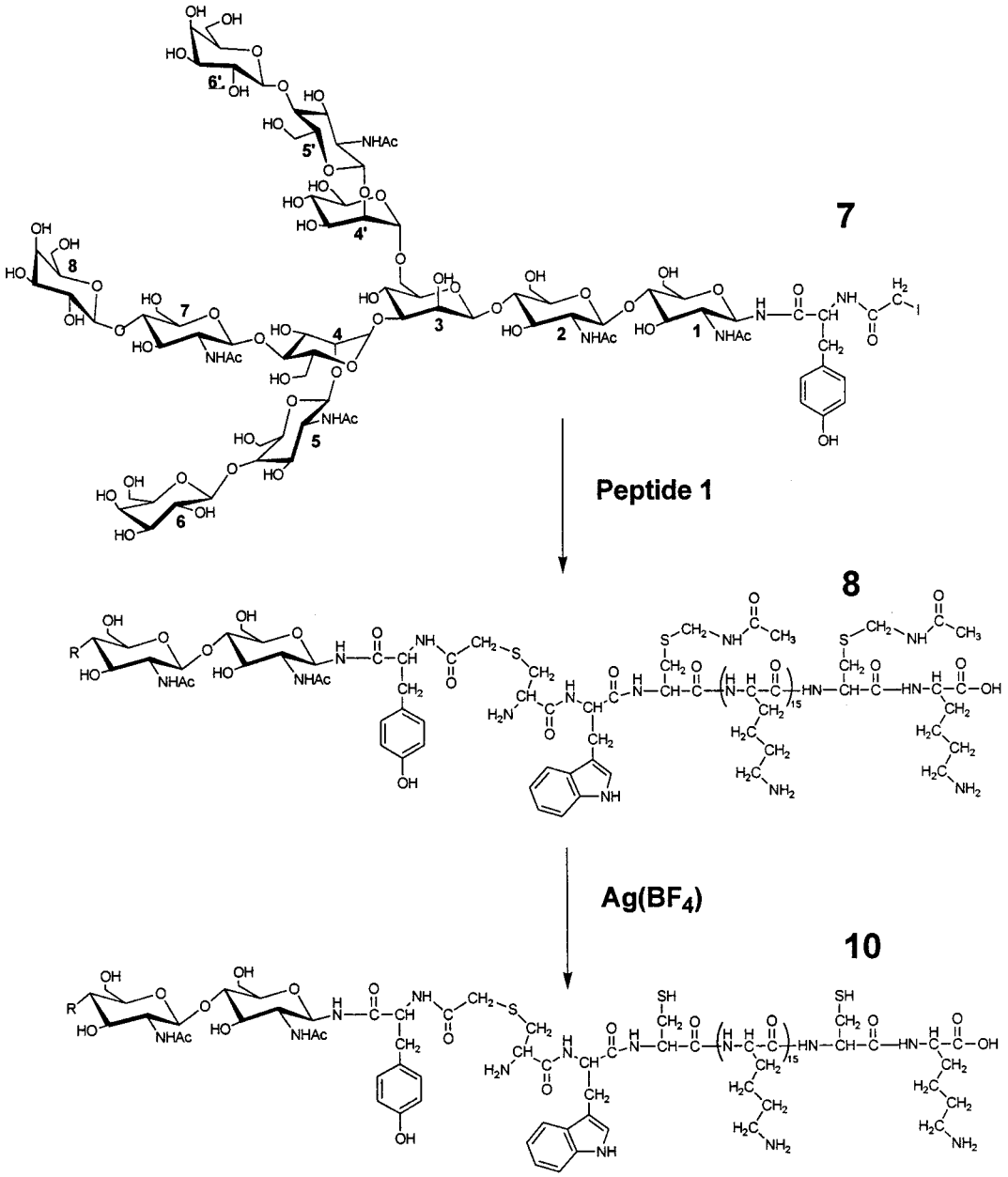


Figure 3. Synthesis of triantennary-CWCK$_{15}$CK (**10**). *N*-iodoacetylated *N*-glycan **7** reacted with peptide **1** to form glycopeptide **8**. Subsequent removal of the Acm protecting groups on internal cysteine residues by silver tetrafluoroborate led to the formation of glycopeptide **10**. R represents the remainder of the triantennary *N*-glycan.

10 mL/min with 0.1% TFA and a gradient of 5−20% acetonitrile over 30 min. The peaks eluting at either 18 or 22 min, representing glycopeptide **8** or **9**, were pooled and lyophilized. Glycopeptides were characterized by ^{1}H NMR, as described previously, and also by LC−MS by injecting 2.5 nmol onto an analytical RP-HPLC column (0.47 × 25 cm) eluted at 1 mL/min with 0.1% acetic acid containing 0.02% (v/v) TFA and an acetonitrile gradient of 1−25% over 30 min. The RP-HPLC eluent was directly infused into the electrospray ionization source of a Finnigan LCQ mass spectrometer, and mass spectral data was obtained in the positive mode. Glycopeptides **8** and **9** were deprotected as described previously, resulting in the generation of final products **10** and **11** that were purified on semipreparative RP-HPLC, reconstituted in 0.1% TFA, quantified by Abs$_{280\ nm}$ ($\epsilon_{280\ nm}$ = 6930 M^{-1} cm^{-1}), and then characterized by LC−MS.

Formulation of Peptide DNA Condensates. PEG-peptide **5** or glycopeptide **10** DNA condensates were prepared by combining 7.5−60 nmol in 750 μL of 5 mM Hepes (pH 7.4) with 75 μg of DNA (pCMVL in 750 μL of Hepes) while vortexing, followed by equilibration at RT for 4 h. Peptide binding to DNA was monitored by a fluorescent dye displacement assay. A 1 μg aliquot of the peptide DNA condensate was diluted to 1 mL in Hepes containing 0.1 μM thiazole orange. The fluorescence of the intercalated dye was measured on an LS50B fluorometer (Perkin-Elmer, U.K.) in a microcuvette by exciting at 500 nm while monitoring emission at 530 nm. Fluorescence blanks were subtracted from all values before data analysis.

The particle size of peptide DNA condensates was analyzed at a DNA concentration of 50 μg/mL in 5 mM Hepes (pH 7.0) at a peptide/DNA charge ratio of 2:1 by quasi-elastic light scattering (QELS). The mean diameter and population distribution were computed from the diffusion coefficient using a multimodal cumulate analysis supplied by the manufacturer. The particle surface

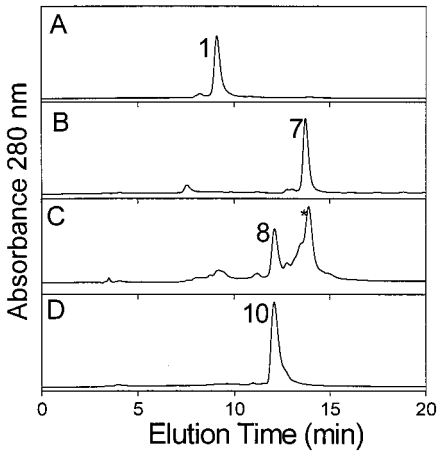


Figure 4. RP-HPLC analysis of triantennary-CWCK$_{15}$CK (**10**)-synthesis. RP-HPLC analysis of the reaction of peptide **1** (panel A) with *N*-glycan **7** (panel B) established the consumption of both starting materials and the formation of glycopeptide **8** and a byproduct (*) determined to be dimeric peptide **1** (panel C). Purification of **8**, followed by the removal of the Acm protecting groups and repurification, yielded glycopeptide **10**, which re-chromatographed as a single peak. The peaks are numbered according to the nomenclature in Figure 3.

charge was determined by ζ potential analysis using a Brookhaven ZetaPlus from Brookhaven Instruments (Worestershire, U.K.).

The kinetics of inter-peptide sulfhydryl cross-linking within peptide DNA condensates was studied indirectly by monitoring the displacement of a SYBR-Gold intercalator dye from DNA condensates as a function of time (*12, 13*). SYBR-Gold was combined with 1 mL of 20 μg/mL peptide DNA condensates prepared at a peptide stoichiometry of 0.4 nmol of peptide/μg of DNA. Immediately after mixing PEG-peptide or glycopeptide and DNA, the fluorescence intensity (E_x, 495 nm; E_m, 537 nm) was continuously monitored for 3 h.

RESULTS

Synthesis and Characterization of Sulfhydryl Cross-Linking Carriers. The synthetic scheme for generating PEG-peptides is illustrated in Figure 1. The individual steps of the reaction were monitored by analytical RP-HPLC (Figure 2). PEG-VS (5 kDa) was reacted with either peptide **1** (Figure 2A) or **2** in the presence of TCEP to generate PEG-peptide **3** (Figure 2B) or **4**. RP-HPLC analysis demonstrated complete consumption of peptide **1** in 12 h to produce PEG-peptide **3** or **4**. Excess PEG-VS was needed to drive the reaction to completion and then removed as a void peak during chromatography on a cation-exchange column. Without this step, PEG-VS and the PEG-peptide coeluted during preparative RP-HPLC. Removal of the Acm protecting groups followed by semipreparative RP-HPLC resulted in a 38% isolated yield of PEG-peptide **5** or **6** that rechromatographed to 96% purity on analytical RP-HPLC (Figure 2D).

Sulfhydryl cross-linking glycopeptides were prepared as illustrated schematically in Figure 3. Monomeric peptide **1** or **2** reacted with iodoacetamide triantennary *N*-glycan **7** (Figure 4B) to generate glycopeptide **8** or **9** and dimeric-peptide as a byproduct. Comparison of the RP-HPLC retention time of peptide **1** (Figure 4A) with that of iodoacetamide triantennary *N*-glycan (Figure 4B) and the crude reaction product (Figure 4C) established the formation of glycopeptide **8** which elutes at 12 min and dimeric peptide **1** as a byproduct eluting at 14 min.

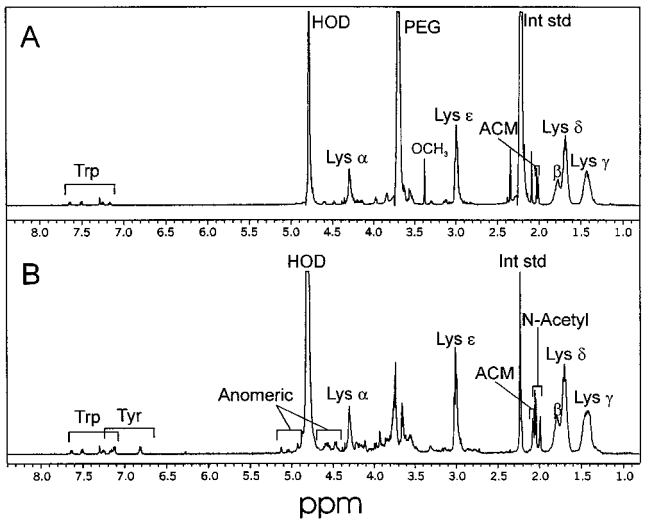


Figure 5. ^{1}H NMR analysis of PEG-peptide **3** and glycopeptide **8**. The ^{1}H NMR spectra of Acm-protected PEG-peptide **3** (panel A) and glycopeptide **8** (panel B) are illustrated. Each spectrum shows characteristic resonances for the peptide lysine side chain α, β, γ, δ, and ϵ protons as well as tryptophan anomeric protons. The PEG methylene resonances at 3.7 ppm (panel A) were integrated relative to lysine ϵ to establish a 1:1 conjugate. Panel B illustrates tyrosine aromatic resonances in addition to Gal (6,6′,8), GlcNAc (1,2,5,5′,7), and Man (4,4′) anomeric resonances as well as GlcNAc *N*-acetyl resonances. Both conjugates possess resonances at 2.019−2.049 ppm arising from the Acm methyl groups.

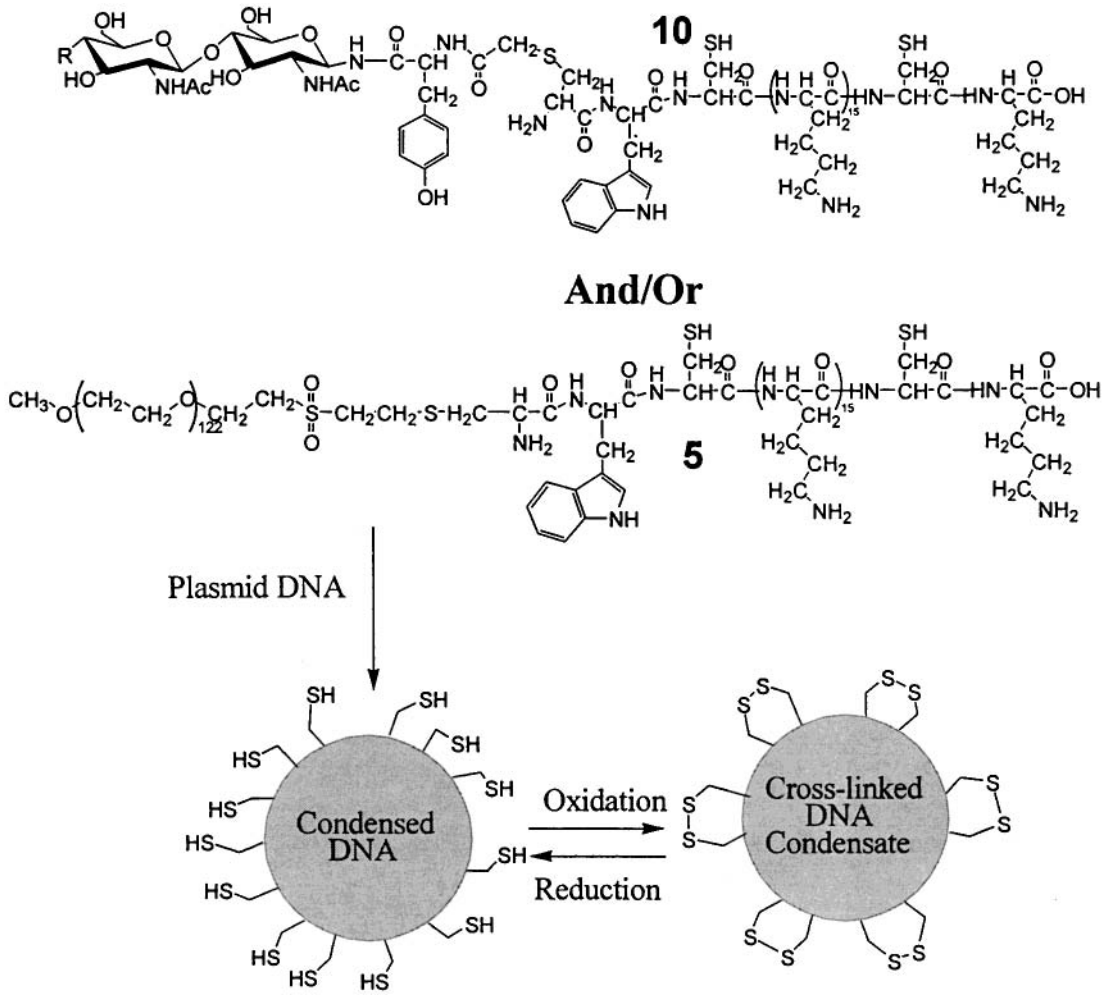
TCEP was omitted from the reaction because it was incompatible with the iodoacetamide *N*-glycan. Excess peptide **1** was used to drive the formation of glycopeptide to completion but also led to the formation of dimeric-peptide **1**. Following RP-HPLC purification of **8**, deprotection afforded glycopeptide **10**, which was isolated in 26% yield at >95%, purity as determined by analytical RP-HPLC (Figure 4D).

^{1}H NMR of PEG-peptide **3** verified the presence of signals arising from both the peptide and PEG (Figure 5A; Table 1) including resonances assigned to lysine as well as the tryptophan aromatic resonances in each spectrum (Figure 5A; Table 1). The integration intensity of the PEG methylene signal at 3.630 ppm relative to the lysine ϵ signal at 2.925 ppm established a 1:1 conjugate of PEG-peptide. Complete deprotection of PEG-peptide **3** to form **5** established the disappearance of methyl resonances of the Acm protecting groups at 1.959 and 1.944, respectively. PEG-peptides were not amendable to LC−MS because of their heterogeneity in PEG.

^{1}H NMR was also used to characterize the structure of glycopeptides **8** and **9** (Figure 5B; Table 1). Each glycopeptide possessed characteristic resonances assigned to the lysine α, β, δ, γ, and ϵ protons, tryptophan and tyrosine protons, anomeric resonances of GlcNAc, Man, and Gal and the GlcNAc *N*-acetyl signals. In contrast to PEG-peptides, LC−MS was successfully applied to characterize the Acm deprotection of glycopeptides **8** and **9**. The observed mass for glycopeptide **8** was *m*/*z*: 4914.9 prior to deprotection which converted to *m*/*z*: 4772.9 for glycopeptide **10** following a loss of two Acm groups. Similarly, glycopeptide **9**, possessing five Acm-protected cysteine residues, had a mass of *m*/*z*: 5053.0, which, upon treatment with silver tetrafluoroborate, converted quantitatively to glycopeptide **11** possessing a mass of *m*/*z*: 4697.5.

Formulation of Sulfhydryl Cross-Linked DNA Condensates. The ability of PEG-peptide **5** or glycopep-

Scheme 1. Formation of Cross-Linked Glycdopeptide and PEG-peptide DNA Condensates[a]



[a] PEG-peptide or glycopeptide DNA condensates are formed instantly through ionic binding of the peptide to the DNA backbone followed by inter-peptide oxidation to form disulfide bonds that reversibly stabilize the DNA condensates.

tide **10** to cross-link upon binding to plasmid DNA, as depicted in Scheme 1, was compared to that of alkylated-CWK_{18} ($AlkCWK_{18}$), which cannot undergo sulfhydryl cross-linking when bound to DNA. The stoichiometry of peptide needed to completely condense DNA was evaluated by monitoring a decrease in fluorescence intensity of thiazole orange while titrating increasing amounts of peptide (Figure 6). The results established that PEG-peptide **5** required a charge ratio of 1.7 to maximally displace fluorophore, whereas glycopeptide **10** and $AlkCWK_{18}$ were nearly equivalent in forming condensates at a charge ratio slightly above 1.

The particle size and ζ potential of DNA condensates formed at a 2:1 charge ratio were compared when using $AlkCWK_{18}$, PEG-peptide **5**, and glycopeptide **10** (Table 2). Each formed DNA condensates that had a major population (90 vol %) of particles that were approximately 60−90 nm in diameter and a minor population of approximately 200−280 nm in diameter. PEG-peptide **5** formed condensates possessing a ζ potential of +6 mV, because of the formation of a steric layer, relative to +32−34 mV determined for glycopeptide **10** or $AlkCWK_{18}$ DNA condensates.

The kinetics of sulfhydryl cross-linking was examined using a fluorescent displacement assay (*12, 13*). In a control experiment, the binding of $AlkCWK_{18}$ to DNA in the presence of SYBR-Gold led to an immediate quench followed by constant fluorescence intensity over time,

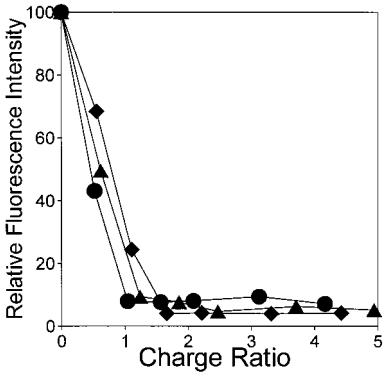


Figure 6. Relative binding affinity of peptides to DNA. The intensity of thiazole orange fluorescence was measured following titration of 7.5−60 pmols of either $AlkCWK_{18}$ (σ), PEG-peptide **5** (υ), or glycopeptide **10** (λ), with 75 ng of a 5.6 kb plasmid in 1 mL of 5 mM Hepes (pH 7.4). The decrease in the fluorescence intensity at a calculated peptide ($R-NH_3^+$) to DNA (PO_4^-) charge ratio of 0−1 results from peptide displacement of the fluororphore from DNA. At a charge ratio of 1 or higher, the asmyptote predicts the stoichiometry at which peptide binding to DNA is saturated.

because this peptide is incapable of forming cross-links (Figure 7). Because of its higher affinity for DNA, HMW polylysine (dp, 1007) displaced fluorophore more efficiently than $AlkCWK_{18}$, resulting in a lower fluorescence intensity that also remains constant with time (not

Table 2. Particle Size and ζ Potential Analysis of DNA Condensates

formulation[a]	particle size[b] (nm)	ζ potential[c] (mV)
$AlkCWK_{18}$ DNA	59 ± 6	34 ± 2
PEG-peptide **5** DNA	91 ± 7	6 ± 1
Glycopeptide **10** DNA	102 ± 18	32 ± 2

[a] DNA condensates prepared at a DNA concentration of 20 μg/mL and peptide to DNA stoichiometry of 0.4 nmol/μg of DNA corresponding to a 2:1 charge ratio in 5 mM Hepes (pH 7.4). [b] Mean and standard deviation of five analyses. [c] Mean and standard deviation of 10 determinations.

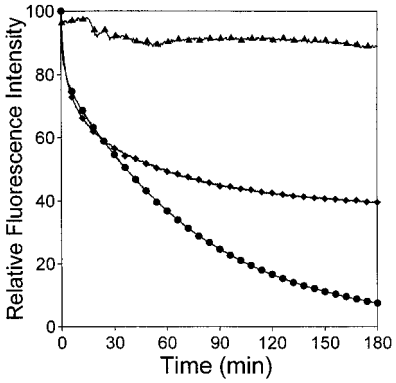


Figure 7. Kinetics of cross-linking. The fluorescence intensity of SYBR-Gold was monitored at (E_x, 495 nm; E_m, 537 nm) over time following formation of peptide DNA condensates prepared by combining 8 nmol of either $AlkCWK_{18}$ (σ), PEG-peptide **5** (υ), or glycopeptide **10** (λ), with 20 μg of DNA in 1 mL of buffer. The decrease in fluorescence intensity over 3 h represents the time course of carrier cross-linking on DNA.

shown) (*12*, *13*). Alternatively, PEG-peptide **5** initially binds to DNA and displaces SYBR-Gold, resulting in comparable fluorescence intensity to that of $AlkCWK_{18}$. However, upon polymerization, the binding affinity increases, leading to a progressive decrease in the fluorescence intensity over time. Comparison of the kinetics of fluorescence decrease determined for PEG-peptide **5** and glycopeptide **10** binding to DNA revealed that the reaction is nearly complete after 3 h but that glycopeptide **10** was more efficient at displacing fluorophore (Figure 7).

DISCUSSION

The ability to synthesize homogeneous LMW carriers provides an important opportunity to systematically change their structure and to determine how single or multiple changes influence the properties of the resulting DNA formulation and gene transfer properties either in vitro or in vivo. This distinct advantage of LMW carriers over HMW carriers provides sufficient justification for their development as gene transfer agents for treating human diseases.

A major challenge when developing LMW nonviral gene delivery carriers is the need for transient stabilization in the circulation, target tissue, and cytosol. One strategy to achieve this is to reversibly cross-link carrier molecules bound to DNA (Scheme 1). This requires the synthesis of homogeneous monomers with precise structures designed to trigger the release of DNA at a strategic location in the cell.

Among the cross-linking strategies under investigation, sulfhydryl cross-linked peptides or cationic lipids have emerged as promising carriers for DNA because the trigger is the reducing environment in the endosome or cytosol (*22*). Consequently, sulfhydryl cross-linked peptide DNA condensates and cationic lipids demonstrate higher levels of transfection in vitro when compared to un-cross-linked DNA condensates (*12*, *13*).

To take the next step toward advancing this concept, a test of their in vivo efficacy is necessary. To do this requires functionalization of a cross-linking peptide with a targeting ligand and PEG chain. Add-mixtures of glycopeptide and PEG-peptide can then be used to create DNA cocondensates that incorporate both carrier molecules in a ratio reflected by the add-mixture ratio (*9*). In previous studies, an add-mixture of carriers was used to systematically optimize DNA targeting to hepatocytes mediated by a triantennary *N*-glycan or to Kupffer cells by a high-mannose *N*-glycan (*11*, *23*).

The difficulty in preparing sulfhydryl cross-linking PEG-peptides and glycopeptides is in accomplishing a site specific coupling to the peptide. We have previously described the synthesis of PEG-Cys-Trp-Lys_{18} and *N*-glycan-Cys-Trp-Lys_{18} based on coupling to a single thiol in the peptide. The methodology described in the present paper extends upon this concept by installing internally masked Acm-protected cysteine residues that are only unmasked following conjugation of PEG or *N*-glycan to an exposed sulfhydryl on cysteine. Silver tetrafluoroborate treatment (*19*) was sufficiently mild to allow for the unmasking of the internal cysteine residues without causing a side reaction with PEG or *N*-glycan, as demonstrated by characterization of the fully deprotected product. ESI-MS was the most convenient method of verifying the complete removal of Acm groups; however, this approach was only amendable to glycopeptides analysis because PEG-peptides (with or without Acm) did not produce ion clusters corresponding to a discrete mass.

The synthesis proved versatile enough to allow for the preparation of glycopeptides and PEG-peptides that contained either two or five cross-linking sulfhydryl groups capable of producing DNA condensates of different reductive stability. In addition, it should be possible to position the trityl protected cysteine at different locations throughout the peptide to determine if the location of a PEG chain or *N*-glycan will influence the physical or biological properties of the resulting cross-linked DNA condensates.

Sulfhydryl cross-linking PEG-peptides and glycopeptides formed small electropositive DNA condensates (102 nm or less in mean diameter) with reduced surface charge when PEG was present as a steric layer. The relative DNA binding affinities of PEG-peptides and glycopeptides were comparable to an underivatized peptide of similar length. Likewise, the kinetics of sulfhydryl cross-linking appears to be complete in approximately 3 h, in close agreement with the rate of cross-linking underivatized sulfhydryl cross-linking peptides (*12*, *13*).

In conclusion, the synthetic methods described have led to the preparation of PEG-peptides and glycopeptides that form cross-linked DNA condensates. A detailed examination of the in vivo properties of these DNA condensates will be reported as part of an ongoing investigation aimed at developing LMW DNA carrier molecules that function in vivo.

LITERATURE CITED

(1) Felgner, P. L. (1997) Nonviral strategies for gene therapy. *Sci. Am. 276*, 102−106.

(2) Mahato, R. I. (1999) Nonviral peptide-based approaches to gene delivery. J. *Drug Targeting 7*, 249−268.

(3) Pouton, C. W., and Seymour, L. W. (1998) Key issues in nonviral gene delivery. *Adv. Drug Delivery Rev. 34*, 3−19.

(4) Wadhwa, M. S., Collard, W. T., Adami, R. C., McKenzie, D. L., and Rice, K. G. (1997) Peptide-Mediated Gene Delivery: Influence of Peptide Structure on Gene Expression. *Bioconjugate Chem. 8*, 81−88.

(5) Plank, C., Tang, M. X., Wolfe, A. R., and Szoka, F. C., Jr. (1999) Branched cationic peptides for gene delivery: role of type and number of cationic residues in formation and in vitro activity of DNA polyplexes. *Hum. Gene Ther. 10*, 319−332.

(6) Collard, W. T., Yang, Y., Kwok, K. Y., and Rice, K. G. (2000) Biodistribution, metabolism, and in vitro gene expression of glycopeptide poly(ethylene glycol) DNA co-condensates. *J. Pharm. Sci. 89*, 499−512.

(7) Trubetskoy, V. S., Budker, V. G., Hanson, L. J., Slattum, P. M., Wolff, J. A., and Hagstrom, J. E. (1998) Self-assembly of DNA-polymer complexes using template polymerization. *Nucleic Acids Res. 26*, 4178−4185.

(8) Adami, R. C., and Rice, K. G. (1999) Metabolic stability of glutaraldehyde cross-linked peptide DNA condensates. *J. Pharm. Sci. 88*, 739−746.

(9) Kwok, K. Y., McKenzie, D. L., Evers, D. L., and Rice, K. G. (1999) Formulation of highly soluble poly(ethylene glycol)-peptide DNA condensates. *J. Pharm. Sci. 88*, 996−1003.

(10) Kwoh, D. Y., Coffin, C. C., Lollo, C. P., Jovenal, J., Banaszczyk, M. G., Mullen, P., Phillips, A., Amini, A., Fabrycki, J., Bartholomew, R. M., Brostoff, S. W., and Carlo, D. J. (1999) Stabilization of poly-L-lysine/DNA polyplexes for in vivo gene delivery to the liver. *Biochim. Biophys. Acta 1444*, 171−190.

(11) Yang, Y., Park, Y., Man, S., Liu, Y., and Rice, K. G. (2001) Cross-linked low molecular weight glycopeptide mediated gene delivery: relationship between DNA metabolic stability and the level of transient gene expression in vivo. *J. Pharm. Sci. 90*, 2010−2022.

(12) McKenzie, D. L., Kwok, K. Y., and Rice, K. G. (2000) A potent new class of reductively activated peptide gene delivery agents. *J. Biol. Chem. 275*, 9970−9977.

(13) McKenzie, D., Smiley, B., Kwok, K. Y., and Rice, K. G. (2000) Low molecular weight disulfide cross-linking peptides as nonviral gene delivery carriers. *Bioconjugate Chem. 11*, 901−911.

(14) Schaffer, D. V., Fidelman, N. A., Dan, N., and Lauffenburger, D. A. (2000) Vector unpacking as a potential barrier for receptor-mediated polyplex gene delivery. *Biotechnol. Bioeng. 67*, 598−606.

(15) Balakirev, M., Schoehn, G., and Chroboczek, J. (2000) Lipoic acid-derived amphiphiles for redox-controlled DNA delivery. *Chem. Biol. 7*, 813−819.

(16) Tang, F., and Hughes, J. (1999) Use of dithiodiglycolic acid as a tether for cationic lipids decreases the cytoxicity and increases transgene expression of plasmid DNA in vitro. *Bioconjugate Chem. 10*, 791−796.

(17) Ouyang, M., Remy, J. S., and Szoka, F. C., Jr. (2000) Controlled template-assisted assembly of plasmid DNA into nanometric particles with high DNA concentration. *Bioconjugate Chem. 11*, 104−112.

(18) Hickman, M. A., Malone, R. W., Lehmann-Bruinsma, K., Sih, T. R., Knoell, D., Szoka, F. C., Walzem, R., Carlson, D. M., and Powell, J. S. (1994) Gene expression following direct injection of DNA into liver. *Hum. Gene Ther. 5*, 1477−1483.

(19) Yoshida, M., Akaji, K., Tatsumi, T., Iinuma, S., Fujiwara, Y., Kimura, T., and Kiso, Y. (1990) Synthesis of porcine brain natriuretic peptide-32 using silver tetrafluoroborate as a new deprotecting reagent of the S-trimethylacetamidomethyl group. *Chem. Pharm. Bull. 38*, 273−275.

(20) Tamura, T., Wadhwa, M. S., and Rice, K. G. (1994) Reducing-end modification of N-linked oligosaccharides with tyrosine. *Anal. Biochem. 216*, 335−344.

(21) Collard, W. T., Evers, D. L., and McKenzie, D. L. (2000) Synthesis of homogeneous glycopeptides as DNA targeting agents. *Carbohydr. Res. 323*, 176−184.

(22) Kwok, K. Y., Yang, Y., and Rice, K. G. (2001) Evolution of cross-linked nonviral gene delivery systems. *Curr. Opin. Mol. Ther. 3*, 142−146.

(23) Collard, W. T., Yang, Y., Kwok, K. Y., and Rice, K. G. (2000) Biodistribution, metabolism, and in vivo gene expression of glycopeptide poly(ethylene glycol) DNA co-condensates. *J. Pharm. Sci. 89*, 499−512.

BC010070A

Solid-State NMR Investigation of Indomethacin−Cyclodextrin Complexes in PEG 6000 Carrier

Marie Wulff,[†] Maggie Aldén,*[,†] and Jörgen Tegenfeldt[‡]

Department of Physical and Inorganic Pharmaceutical Chemistry, Box 580, Biomedical Center, Uppsala University, SE-751 23 Uppsala, Sweden, and Department of Materials Chemistry, Ångström Laboratory, Box 538, Uppsala University, SE-751 21 Uppsala, Sweden. Received December 13, 2000; Revised Manuscript Received June 18, 2001

Various solid dispersions of α-, *β*- and *γ*-cyclodextrin (CD) in PEG 6000 with and without the addition of 5% w/w indomethacin were prepared by the melting method using the original components. The samples were investigated by solid-state ^{13}C NMR, and the interactions between the drug and the cyclodextrins were evaluated. The indomethacin−*γ*-CD phase with tetragonal symmetry found in a previous X-ray study gave chemical shifts which suggested that this phase is a complex between indomethacin and *γ*-CD. Evidence of an indomethacin−*β*-CD complex were found. A distribution of the chemical shifts for *β*-CD was attributed to the possible formation of different types of complexes between indomethacin and *β*-CD. No complex formation was found in the α-CD system. The degree of relative crystallinity of the samples in the *γ*-CD system was measured by ^{1}H NMR, X-ray powder diffraction (XRD), differential scanning calorimetry (DSC), and modulated-temperature DSC (MTDSC). The results obtained by the NMR, XRD, and DSC techniques showed that the dispersions were less crystalline than the pure polymer carrier, and the dispersion containing the indomethacin−*γ*-CD complex had the lowest degree of crystallinity. By the MTDSC method a deviation was found for the PEG 6000/indomethacin dispersion. This emphasizes that the different techniques give specific information on the crystallinity.

INTRODUCTION

Cyclodextrins (CDs) are cyclic oligosaccharides consisting of six (α-CD), seven (*β*-CD), or eight (*γ*-CD) α-1,4-linked glucose units. These toroidal molecules enclose cavities of approximately 5−8 Å in diameter (*1*) and have, due to their particular conformation, the ability to form inclusion complexes with a variety of guest molecules. Through the inclusion complexation various physicochemical properties of the guest molecules are modified. These complexes can increase the stability and improve the solubility and bioavailability of molecules of pharmaceutical interest (*2*). Inclusion of the nonsteroidal antiinflammatory agent indomethacin in *β*-cyclodextrin has been described to improve the oral administration and limit the gastric irritation and the ulcerative side effects of the drug (*3*).

In aqueous solutions, addition of water-soluble polymers can both enhance and reduce cyclodextrin complexation of a guest molecule (*4*). It has been found (*5*) that α-CD forms complexes with poly(ethylene glycol) (PEG) of various molecular weights to give crystalline complexes in high yields, although *β*-CD did not. On the other hand *β*-CD and *γ*-CD form complexes with other polymers such as polypropylene glycol (PPG) and polyisobutylene (PIB), while α-CD does not form a complex with either of these polymers (*6*).

In a recent study (*7*) the melting method was investigated as a possible method for producing drug/cyclodextrin inclusion compounds dispersed in a polymer, forming a solid dispersion. This type of solid dispersion has tremendous potential in the area of controlled release dosage forms. Moreover, in recent years, the melting method has enjoyed a renaissance in the form of hot melt extrusion (*8*), which should make it possible to overcome problems in scale-up. In the study (*7*), evidence of a complex between indomethacin and *β*-CD and *γ*-CD, respectively, dispersed in PEG 6000 were found, while no complexation of indomethacin with α-CD could be detected. Dissolution tests performed (*7*) showed that the CDs have a delaying effect on the release of indomethacin from PEG 6000 in the order α-CD < *γ*-CD ≤ *β*-CD. In the present work studies on these ternary systems were performed, by solid-state NMR, to elaborate bonding conditions between the components. For investigations of the short-range order in the solid state, ^{13}C NMR was used as a sensitive tool giving information concerning specific interactions in the powder samples.

An essential property of solid dispersions at dissolution and technical handling is the crystallinity of the sample. To determine the degree of crystallinity of polymer-based systems can be a very complex task. In this study the degree of crystallinity of some samples was investigated by three different techniques: ^{1}H NMR, X-ray diffraction, and modulated-temperature DSC (MTDSC). A tentative discussion of the various results that were obtained is presented.

EXPERIMENTAL SECTION

Materials. Indomethacin (IM) (Sigma, St. Louis, MO), a drug with low aqueous solubility, has the formula $C_{19}H_{16}ClNO_4$, M_w = 357.8 g/mol, and mp 162 °C. Poly(ethylene glycol) (PEG) 6000 (Janssen, Geel, Belgium and

* To whom correspondence should be addressed, Telephone: +46 18 471 43 69, Telefax: +46 18 471 43 77, E-mail: maggie.alden@farmaci.uu.se.

[†] Department of Physical and Inorganic Pharmaceutical Chemistry, Uppsala University.

[‡] Department of Materials Chemistry, Uppsala University.

10.1021/bc000156o CCC: $22.00 © 2002 American Chemical Society
Published on Web 02/27/2002

Table 1. Phase Analysis of Solid Dispersions by X-ray Powder Diffraction, Modified from Reference 7

sample	phases
PEG 6000 + 5% w/w indomethacin	PEG 6000, indomethacin
PEG 6000 + 10% w/w α-CD	PEG 6000, α-CD
PEG 6000 + 5% w/w indomethacin + 13% w/w α-CD	PEG 6000, α-CD, indomethacin
PEG 6000 + 10% w/w *β*-CD	PEG 6000, *β*-CD
PEG 6000 + 5% w/w indomethacin + 14% w/w *β*-CD	PEG 6000, *β*-CD, IM/*β*-CD complex
PEG 6000 + 20% w/w *γ*-CD	PEG 6000/*γ*-CD
PEG 6000 + 5% w/w indomethacin + 19% w/w *γ*-CD	PEG 6000/*γ*-CD, IM/*γ*-CD complex

Fluka, Buchs, Switzerland) has the formula $HO(C_2H_4O)_nH$, where $n \approx 140$, and the average $M_w = 5600-7000$. Cyclodextrins (CDs): α-CD (Sigma), formula $C_{36}H_{60}O_{30}$, $M_w = 972.9$ g/mol; *β*-CD (Sigma), formula $C_{42}H_{70}O_{35}$, $M_w = 1135$ g/mol; *γ*-CD (Fluka, Switzerland), formula $C_{48}H_{80}O_{40}$, $M_w = 1297$ g/mol.

Methods. *Preparation of Samples.* Various solid dispersions of α-CD, *β*-CD, and *γ*-CD in PEG 6000 with and without the addition of 5% w/w indomethacin were prepared by the melting method in a Carbolite furnace HRF 7/22 with an Eurotherm 818P Programmer at a temperature of 120 °C.

For several reasons the concentration of CD was kept as low as possible and did not exceed 20% w/w in any sample; the viscosity of the melt increases with increased CD concentration and complicates the handling of the samples. It is also desirable that pharmaceutical formulations contain as small an amount of CD as possible since excess cyclodextrin can reduce, for example, drug bioavailability and preservative efficacy (*4*).

The samples were brought to room temperature by fast cooling (50−100 °C/s), and after at least 24 h the dispersions were pulverized in a mortar and sieved to obtain the 300−500 *μ*m fraction. Since a small amount of water may be absorbed by these samples, measures were taken to minimize the water absorption.

Solid-State NMR. The NMR measurements were performed using a Bruker MSL 300 spectrometer equipped with a 7 T magnet. Carbon-13 CPMAS NMR spectra were recorded at room temperature at 75 MHz using 4 mm o.d. zirconium oxide rotors and spinning at about 3−7 kHz. For the spectra presented in this paper, the spinning rate was 7 kHz. The proton and carbon radiofrequency fields used during cross-polarization and decoupling correspond to 4 *μ*s 90° pulses. The cross-polarization contact time was 1 ms. Proton NMR spectra were recorded at 300 MHz and at 25.0 °C. The length of the 90° pulse was 1.5 *μ*s.

X-ray Diffraction (XRD). Phase analysis was made by X-ray powder diffraction using a STOE position sensitive detector (PSD) system (Germany) with Ge monochromatized Cu $K\alpha_1$ radiation. A linear detector covering 7° at 155 mm distance was operated in a scanning mode. Room-temperature runs were performed by rotating the powder attached to a cellulose membrane about the normal to the membrane plane. All phases present could be identified by means of characteristic nonoverlapping peaks (*9*).

Modulated-Temperature Differential Scanning Calorimetry (MTDSC). The samples were analyzed in the temperature range of 10−120 °C using an oscillating Seiko DSC 220 differential scanning calorimeter SSC/5200H (Japan). The samples (4.4−5.4 mg) were kept in aluminum pans in an atmosphere of nitrogen. An amplitude of 2, 4, or 6 °C and a frequency of 0.02 Hz were selected in the oscillating mode together with a heating rate of 2.5 or 5 °C/min. The selected values give both heating and cooling in the temperature cycle and a degree of oscillation (*10*) of 0.96−1.9. The calorimeter was temperature- and heat-calibrated with indium, tin, gallium, and mercury as standards. The three heat of fusion values determined are the reversible c_p-component, ΔH_c, the irreversible kinetic component, ΔH_k, and the conventional component, ΔH. The results are presented as mean values with the standard deviations based on three to five determinations.

RESULTS AND DISCUSSION

The phase analysis of the samples, by X-ray powder diffraction, was performed in a previous work (*7*). Some of the results are presented in Table 1. In the dispersion of 5% indomethacin in PEG 6000 both indomethacin and PEG were present as pure phases. The dispersions of 10% α-CD and *β*-CD, respectively, in PEG 6000 formed two-phase systems. It should be noted that a small amount of the CDs may be dissolved in the PEG structure, forming a solid solution. This phase can, however, not be distinguished from the pure PEG phase due to the detection limit of the XRD equipment. The notation PEG 6000 in Table 1 thus represents the pure PEG phase or a mixture of the pure phase and the solid solution $(PEG)_{1-y}CD_y$. In the case of *γ*-CD, however, solid solutions were formed in all samples with ≤20% *γ*-CD. In the PEG/α-CD/IM dispersion the three components were all observed as pure phases. Upon addition of 14% *β*-CD to the PEG/IM only two phases were *observed* in the diffraction pattern, one of them PEG and the other *β*-CD. No diffraction lines from pure indomethacin were observed. This fact shows that indomethacin was incorporated in the structure, not as a pure phase though, but possibly as a complex with *β*-CD. In the sample where 19% *γ*-CD was added to the PEG/IM dispersion several new diffraction lines appeared beside the PEG lines. This new well-defined phase was supposed to be an indomethacin−*γ*-CD complex with tetragonal structure that was dispersed in the PEG structure.

Investigation of Inclusion Complexes by Solid-State ^{13}C NMR. In Figure 1 the ^{13}C NMR spectrum of pure indomethacin is shown. The spectra of the dispersions PEG/IM and PEG/CD/IM are presented in Figure 2a−d. The chemical shift data for the carbons in CDs in pure and dispersed states are presented in Table 2.

Indomethacin. The structural formulas of indomethacin is depicted in Figure 1 with the different carbon atoms denoted by appropriate numbers together with the ^{13}C NMR spectrum. The different peaks could be identified by the spectrum presented for indomethacin in liquid solution (*11*). The carbon peaks that are resolved in the spectra of the dispersions are marked. Peaks marked with + are sidebands resulting from the sample spinning.

PEG/Indomethacin. The PEG 6000/IM spectrum is essentially a superposition of the spectra from the two components (Figure 2a). The peak at approximately 72 ppm is the PEG peak while the others arise from indomethacin. This indicates that there is no interaction between the polymer and indomethacin that is changing the short-range order.

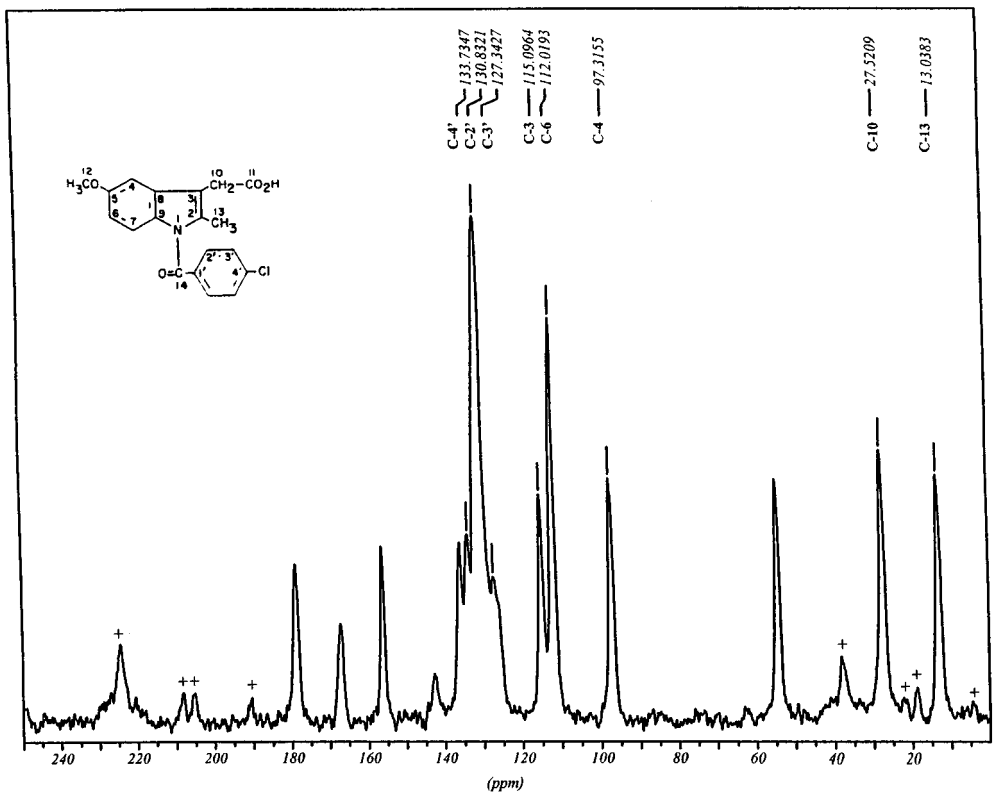
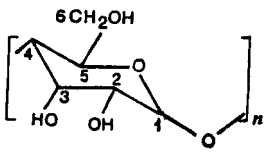


Figure 1. ^{13}C NMR spectrum of pure indomethacin. Peaks marked with + are sidebands resulting from the sample spinning.

Table 2. Chemical Shifts (ppm) of the Carbons in Cyclodextrin[g] in Pure and Dispersed States

carbon	δ_0[a]	δ_1[b]	$\Delta\delta_1$[c]	δ_2[d]	$\Delta\delta_2$[a]	$\Delta\delta_3$[f]
			α-CD, $n = 6$			
C-1	101.93	102.74	0.81	101.76	−0.18	−0.98
C-4	80.92	81.44	0.52	81.00	0.08	−0.44
C-2,3,5	73.17	72.29	-0.88	71.94	−1.23	−0.35
C-6	60.70	61.25	0.55	60.49	−0.21	−0.76
			β-CD, $n = 7$			
C-1	102.64	102.67	0.03	102.09	−0.55	−0.58
C-4	81.60	80.91	-0.69	80.76	−0.84	−0.15
C-2,3,5	72.17	72.98	0.81	71.98	−0.19	−1.00
C-6	60.77	60.10	-0.67	60.14	−0.63	0.04
			γ-CD, $n = 8$			
C-1	102.32	103.35	1.03	103.27	0.95	−0.08
C-1	96.61	100.96	4.35	100.48	3.87	−0.48
C-1				97.70	1.09	−3.26
C-4	79.70	80.80	1.10	81.58	1.88	0.78
C-4				78.79	−0.91	−2.01
C-2,3,5	73.63	72.90	-0.73	72.55	−1.08	−0.35
C-6	61.72	60.60	-1.12	62.28	0.56	1.68
C-6				59.64	−2.08	−0.96

[a] Pure CD. [b] PEG 6000/CD. [c] $\Delta\delta_1 = \delta_1 - \delta_0$. [d] PEG 6000/CD/IM. [e] $\Delta\delta_2 = \delta_2 - \delta_0$. [f] $\Delta\delta_3 = \delta_2 - \delta_1$. [g] Structural formula of cyclodextrin.



Cyclodextrins (CDs). The chemical shift data for the carbons in pure cyclodextrins, presented in Table 2, and the spectra obtained are in agreement with the ^{13}C NMR chemical shifts measured by Furó et al. (*12*) on hydrated and anhydrous cyclodextrins. The C-1 and C-6 peaks were resolved, while the C-4 lines were close to the range of the C-2,3,5 resonances that could not be separated clearly. The structural formulas of the cyclodextrins are also given in Table 2.

PEG/Cyclodextrin. The observed chemical shifts of the carbons of α-, β-, and γ-CD in the PEG/CD and PEG/CD/IM dispersions, respectively, are presented in Table 2. The broad peak at approximately 72 ppm arises from both PEG 6000 and the C-2,3,5 carbons in the cyclodextrins that give chemical shifts at almost the same location due to the similarity in chemical composition. The PEG/α-CD and PEG/β-CD dispersions give spectra which are essentially superpositions of the spectra from the pure phases. All changes in chemical shifts are less than 1 ppm.

In the PEG/γ-CD dispersion, however, the C-1 and C-4 peaks have moved 1−4 ppm downfield, while the C-2,3,5 and C-6 peaks have moved approximately 1 ppm upfield. The large shift seen for C-1 can depend on differences in water content between the treated γ-CD and the dispersions, since the hydrated and anhydrous form of γ-CD have different chemical shifts (*12*). The spectral resolution was somewhat better for the dispersions, and therefore several chemical shift data for C-1, C-4 and C-6 were obtained. Nevertheless, the shifts for these carbons were significant. A structure might be formed where the PEG molecules or their hydroxyl end groups interact with the cyclodextrin, changing the chemical shift in a way similar to that obtained when water is present (*12*).

It has been shown in a recent study (*7*) that up to 20 w/w % γ-CD can dissolve in PEG 6000, forming a solid solution. The single-stranded PEG helix has an average width of 7.6 Å (*13*), and the γ-CD has a cavity diameter of 7.5−8.3 Å (*4*). There is thus a possibility that the PEG helices penetrate the γ-CD cavities forming a solid solution of γ-CD in PEG 6000 where part of the PEG molecules are forming inclusion complexes with γ-CD. A structure similar to this has been found for the complex formed between γ-CD and the water-soluble polymer polyisobutylene (PIB) (*6*).

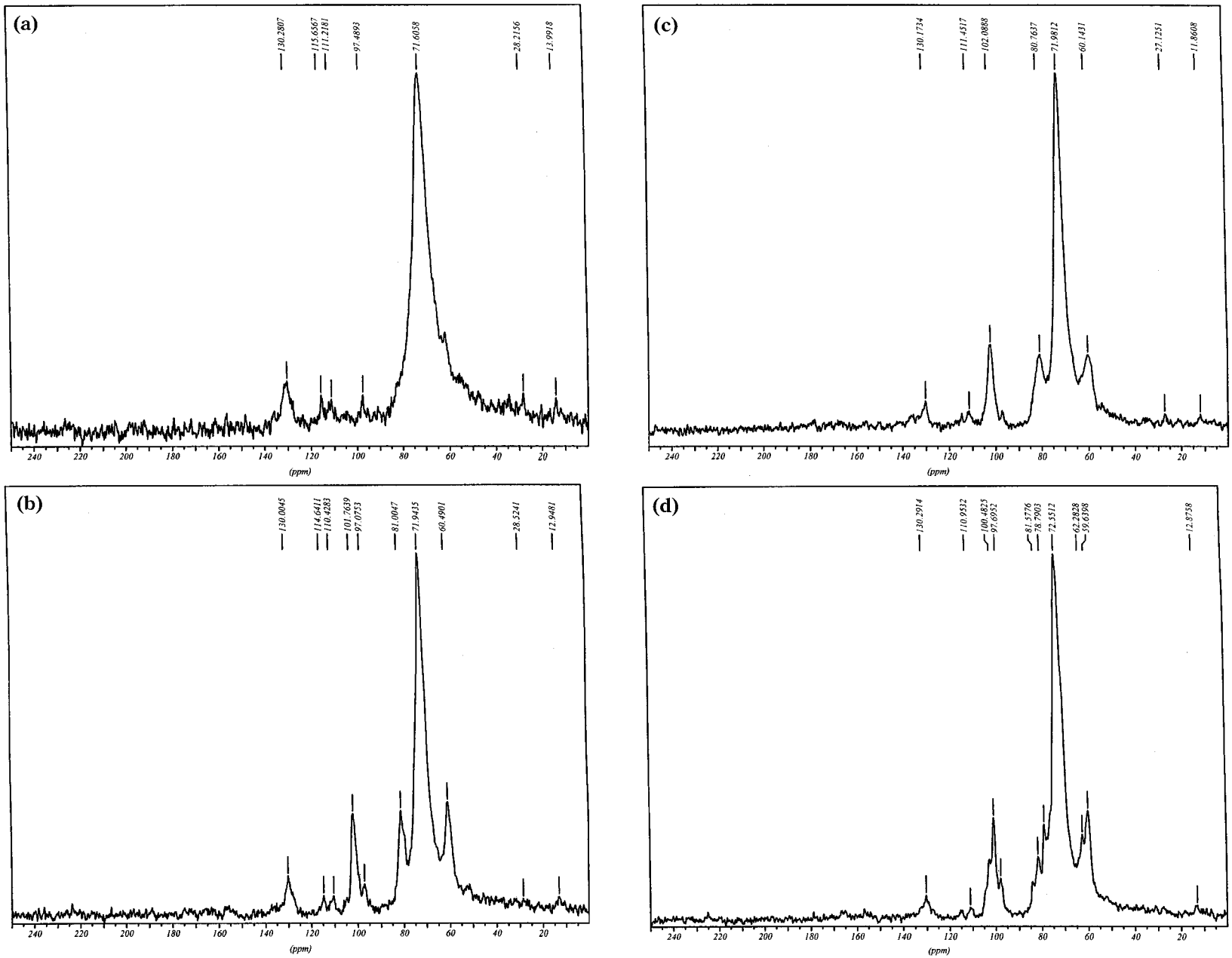


Figure 2. (a) ^{13}C NMR spectrum of PEG 6000 + 5% indomethacin, (b) ^{13}C NMR spectrum of PEG 6000 + 13% α-CD + 5% indomethacin, (c) ^{13}C NMR spectrum of PEG 6000 + 14% β-CD + 5% indomethacin, (d) ^{13}C NMR spectrum of PEG 6000 + 19% γ-CD + 5% indomethacin.

PEG/CD/Indomethacin. In the PEG/IM and PEG/α-CD/IM dispersions (Figure 2a and 2b) the C-2′, C-3, and C-6 peaks of IM at 131, 115, and 111 ppm, respectively, are fully resolved, and the intensity distributions of these are similar. The magnitude of the C-3 and C-6 peaks are almost equal, while the C-2′ peak has twice the intensity of the former. In the PEG/β-CD/IM and PEG/γ-CD/IM samples (Figure 2c and 2d), however, these peaks are much weaker, and a somewhat different intensity distribution was observed. The C-2′, C-3, and C-6 carbons might thus be influenced by the addition of β- or γ-CD.

Indomethacin possesses two different lipophilic parts, namely the phenyl ring and the indole ring, that are able to interact with the nonpolar cavity of CD.

It has been reported (*14*) that the six-membered ring of the indole unit of the indomethacin molecule (carbons C-4 and C-6 in Figure 1) is strongly affected by the formation of the β-CD-indomethacin inclusion complex in aqueous solution. The C-4 peak at 97 ppm is unfortunately not resolved in the CD dispersions in this study due to overlapping with the chemical shift of C-1 in anhydrous cyclodextrins. The results from (*14*) are, however, at variance with the data reported by others (*15*, *16*, *17*) who claim that the *p*-chlorobenzoic part of the indomethacin molecule (carbons C-1′, C-2′, C-3′, and C-4′ in Figure 1) is included in the β-CD channel in aqueous solution. Fronza et al. combined experimental data from 1D NOE and 2D ROESY experiments with theoretical energy calculations, taking into account the existence of two diastereometric forms of indomethacin (*E* and *Z*). The *Z* form is the most thermodynamically stable form and consequently the dominant isomer in solution. However, they found that the complexation selectively stabilizes the *E* isomer with respect to *Z*. One should, however, bear in mind that these results concern the complex in aqueous solution. In the solid state, with a polymer matrix as solvent, the conditions for complex formation may be different, and possibly here both isomers form complex with CD. In the present study the C-1′ peak (130 ppm), which lies very close to the C-2′ peak, is not fully resolved, while the C-3′ and C-4′ peaks at 127 and 134 ppm, respectively, do not appear distinctly in the spectra of the dispersions.

The relation between the C-13 and C-10 peaks at 13 and 28 ppm, respectively, seems also to be affected in the CD dispersions. In the PEG/IM, PEG/α-CD/IM, and PEG/β-CD/IM samples as in pure indomethacin, these two peaks are of the same magnitude, while the C-10 peak has almost disappeared in the γ-CD dispersion. The observations indicate that at least part of the indomethacin molecule experiences a somewhat different surrounding depending on the character of the CD that is added.

Carbon-13 signals from guest molecules are known to be, in many instances, lost or obscured because the amount of the guest molecules is usually low compared with that of the glucose residues. Therefore, the effect of a possible inclusion of indomethacin on the ^{13}C chemical shifts of the CDs were studied, and the results are presented in Table 2. The distinct spectral change on complex formation especially in the C-1, C-4, and C-6 region might arise from a macrocyclic conformational change associated with the inclusion of the guest molecule.

For γ-CD, C-1 and C-4 signals showed a shift 1−4 ppm downfield, while C-2,3,5 signals showed a shift 1 ppm in the opposite direction compared to pure γ-CD. The C-6 carbon located at the exterior of the torus also showed a shift of 2 ppm upfield. These results indicate that indomethacin may interact with γ-CD not only at the interior of the cavity but could also effect, directly or indirectly, the hydrogen bonds at the top of the torus where C-6 is located. In Table 2 the effect of the addition of indomethacin to the PEG/CD dispersion is also calculated. Shifts larger than 1 ppm were only obtained in the γ-CD system, again for the C-1, C-4, and C-6 carbons. A prostaglandin $F_{2\alpha}$−γ-cyclodextrin complex has been reported (*18*) to form a structure similar to the *n*-propyl alcohol−γ-cyclodextrin complex (*19*). These compounds were proposed to have a channel structure with a tetragonal or a hexagonal close packing of the cylinders of γ-CD molecules corresponding to the hydrated and anhydrous form of γ-CD, respectively. In the study by Uekama et al. (*18*) the ^{13}C chemical shifts from the individual carbons of the γ-CD in the prostaglandin $F_{2\alpha}$−γ-cyclodextrin complex were found to be 103.5 ppm (C-1), 81.7 ppm (C-4), 72.6 ppm (C-3,2,5), and 60.0 ppm (C-6), respectively. The shifts observed for the carbons in γ-CD in the indomethacin−γ-CD complex (Table 2) are in good agreement with these values. It is thus probable that the indomethacin−γ-CD complex has a similar bonding between the indomethacin and CD molecules as in the prostaglandin−γ-CD complex. The indomethacin−γ-CD phase found in a previous X-ray experiment (*7*) and appointed a tetragonal symmetry might thus be a complex between indomethacin and γ-CD where the inclusion complex forms a tetragonal packing of cylinders.

For the β-CD system a broadening of the CD peaks compared to the spectrum of the pure CD was observed. This might arise from a distribution of the chemical shift of the carbons or an increased disorder in the surroundings of the β-CD molecules. A recent molecular modeling study of β- and γ-cyclodextrin complexes (20) demonstrates the high capability of deformation of β-CD, which could accommodate several types of ligands. Indomethacin exists in two diastereometric forms (*E* and *Z*) and different parts of the indomethacin molecule has been reported (*14*, *15*, *16*, *17*) to form complex with β-CD, which could explain the distribution of the chemical shift of the β-CD carbons.

For α-CD, the peak at 73 ppm showed a shift approximately 1 ppm upfield both with and without indomethacin. This peak arise from the C-2,3,5 carbons in the cyclodextrin and from the PEG carbons. In the case of α-CD this shift may depend on an interaction with the polymer, α-CD has been reported to form complexes with poly(ethylene glycol) of various molecular weight to give crystalline complexes (*5*). Since C-3-H and C-5-H groups are oriented at the center of the cavity, these carbons may be particularly affected by the shielding due to hydrophobic interactions.

Investigation of Crystallinity. The degree of relative crystallinity of some of the solid dispersions and the solid solutions was investigated using different techniques: ^1H NMR, XRD, and two different DSC methods. We chose to investigate the samples where γ-CD was added to the PEG or the PEG/IM system. In the former a solid solution was formed while in the latter case a new phase could be identified that probably is an inclusion complex (Table 1).

Solid State ^1H NMR. The line-width of a ^1H NMR spectrum is a probe of the strength of interactions between atoms or molecules in a polymer sample, or the molecular flexibility. At room temperature the relaxation rate is faster for protons in crystalline PEG than for those in the amorphous phase (*21*). The two components appear at the same resonance frequency but exhibit different line widths, arising from PEG chain segments with different dynamic properties. In PEG, the rigid, crystalline mate-

Table 3. Crystallinity Determined by ^{1}H NMR and Crystallite Sizes Determined by XRD in the 2θ Range 14.14−15.60

sample	peak area gaussian	peak area lorentzian	^{1}H NMR crystallinity (%)	crystallite size (Å) $d = 6.06$ *hkl* (0.21)	crystallite size (Å) $d = 5.87$ *hkl* (110)	*R* value[a] (%)
PEG 6000 (treated)	9.95	4.87	67	579.4	893.3	2.35
PEG 6000 + IM	2.83	3.75	43	430.0	629.6	2.31
PEG 6000 + γ-CD	6.66	7.68	46	450.3	624.5	1.91
PEG 6000 + IM + γ-CD	2.43	5.23	32	404.8	525.5	2.14

[a] $R = \sqrt{\Sigma w(I_o - I_c)^2 / \Sigma w I_o^2}$.

rial gives rise to a broad component with a Gaussian shape, while the signal from the flexible polymer chains in the amorphous phase is a Lorentzian (*21*). The relative area of the broad peak is directly related to the fraction of PEG forming crystalline material in a one-component system. The crystallinity is thus compared with the amorphous part within the same sample. The crystallinity measured as the ratio between the relative area of the broad peak and the total area of the peak is presented in Table 3. When samples contain several components in varying amounts and in different phases, the interpretation is, however, not as straightforward as for a pure polymer sample. The effect of a macroscopic inhomogeneity can influence the response of the sample. Furthermore, the number of protons and relaxation times may differ for indomethacin and the CDs compared to PEG. It is also possible that crystalline regions apart from PEG give rise to narrow peaks with Lorentzian shape.

It can be seen from Table 3 that the ratio for treated PEG 6000 (67%) was decreased to the same extent by addition of indomethacin (43%) and γ-CD (46%), indicating that the PEG structure is somewhat disordered by the distribution of indomethacin and γ-CD, respectively, leading to a decrease in crystallinity. The value obtained for the PEG/γ-CD/IM dispersion (32%) was even lower, indicating a structure of still more amorphous character.

X-ray Diffraction. Most of the X-ray methods for estimating the crystallinity fall into three general categories: separation of the crystalline and amorphous scattering, differential intensity measurements where data are compared with crystalline and amorphous standards, and absolute methods where X-ray scattering equations are used directly (*22*). Crystalline and amorphous scattering are usually separated using some sort of profile-fitting technique. In such analyses the XRD peaks are resolved in Gaussians or Lorentzians or a combination of the two. The curves have three parameters to define the position (x_0), the height (I_0), and the half-width (H) of the peak in the diffractogram.

The shape of the peaks was in this work determined by a profile-fitting program from Siemens (PROFILE, 1996), and the profile function used was the Gaussian split function. When the size of the individual crystals is less than about 0.1 μm (1000 Å), the term "particle size" or crystallite size is usually used. Crystallite sizes can be calculated from the Scherrer formula, eq 1:

$$t = \frac{0.9\lambda}{B \cos \theta} \tag{1}$$

where B = broadening of diffraction line measured at half-maximum intensity and t = diameter of crystal particle (*9*).

Perfect crystallites with long-range order give narrow diffraction lines and thus large particle sizes. Small crystallites giving broad diffraction lines indicate higher short-range order derived from a more amorphous structure. The maximum size measurement by line broadening is close to 2000 Å using a diffractometer (*9*). In a perfect homogeneous material the crystallite sizes that are obtained should be the same, regardless of which reflection that is used for the calculation. This is not the case for the distribution of crystalline and amorphous parts in a polymer. In the crystalline state, PEG, the matrix used here, form lamellae, which can be organized into spherulites. The lamellae built by PEG chains grow in the *z*-direction leaving amorphous areas between them. The spherulites consists of a lamellae layers in the radial direction separated by amorphous parts (*23*). It should thus be emphasized that the same value of the crystallite sizes can hardly be expected from different reflections in a PEG sample. It is, however, possible to compare the values obtained for the same reflection in different PEG samples.

Two different PEG 6000 reflections, with Miller indices *hkl* (011) and *hkl* (210), respectively, were selected, representing a 2θ range with no overlapping from the adjacent, very broad high-intensity peak at 19°. In Table 3 the crystallite sizes calculated from ref 1 are presented together with the *R*-values, and the diffractogram of PEG 6000 together with the peak profile-fitting is shown in Figure 3. In the profile fitting of the peak the measure of agreement between the observed intensity I_o and the calculated intensity I_c is given by the reliability *R*, in this case the weighted *R*-value, defined by eq 2:

$$R = \sqrt{\frac{\sum w(I_o - I_c)^2}{\sum w I_o^2}} \tag{2}$$

where w is a weighing factor that considers the accuracy of the measurement of each peak. A perfect fit gives an *R*-value of 0. A good fit ranges from 1% to 5% depending on the number of data points in the region to fit.

It can be seen from Table 3 that the crystallite sizes are lower in the dispersions than in pure PEG 6000. The particle size in the dispersions PEG/IM and PEG/γ-CD are similar, whereas the ternary dispersion have even smaller crystallite sizes. Our analysis of degree of crystallinity has been made using results from an experiment aimed for phase analysis where a rather short exposure time was used.

Differential Scanning Calorimetry (DSC) and Modulated-Temperature Differential Scanning Calorimetry (MTDSC). The two-phase model (a perfect crystalline and a perfect amorphous phase), although the simplest, is still the most widely used model for defining the degree of crystallinity (*24*). The degree of crystallinity is determined by comparing the heat of fusion value obtained for a sample with a standard defined as 100% crystalline material. In the method the ΔH of the sample is thus compared with the ΔH for an external standard. The difficulty in this method is to find and characterize a 100% crystalline reference. Since PEG 6000 is a semicrystalline polymer and far from 100% crystalline, a comparison between the samples and pure PEG 6000

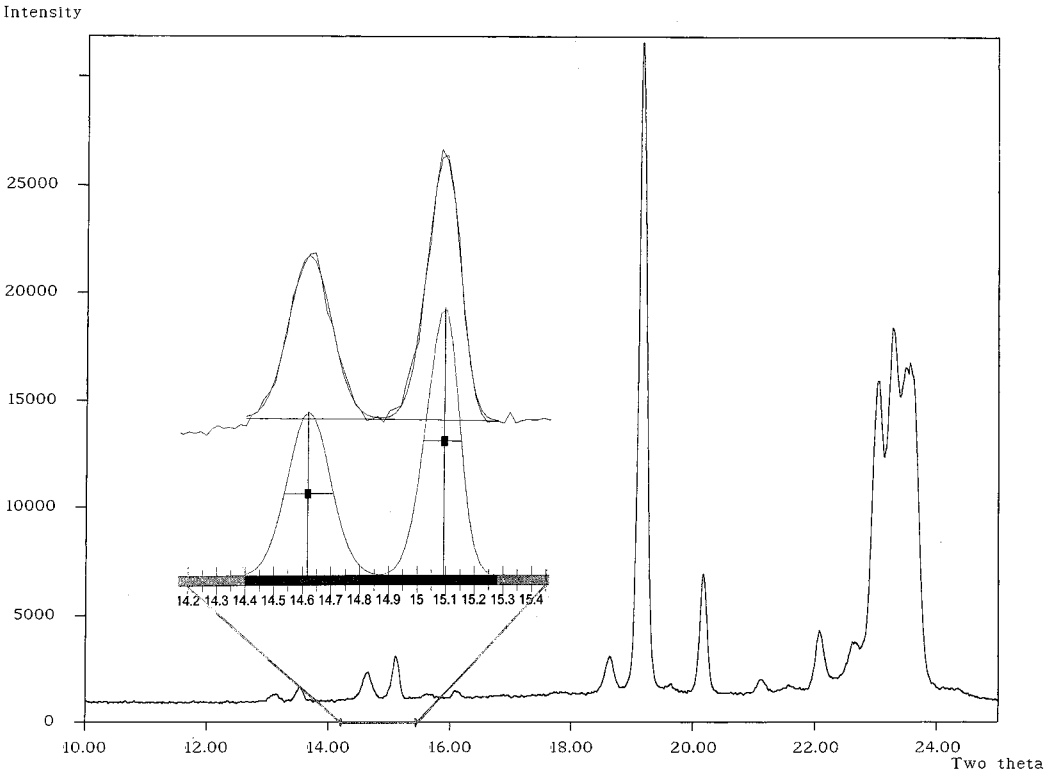


Figure 3. X-ray diffractogram of PEG 6000 (treated) and Gaussian profile-fitted peaks of PEG at $2\theta = 14.62$ and $2\theta = 15.09$, respectively.

only gives a rough estimation if the crystallinity increases or decreases.

The crystallinity values presented in Figure 4a are calculated as the ratio $\Delta H_{\text{sample}}/\Delta H_{\text{PEG 6000}}$ and show lower crystallinity for the dispersions than for pure PEG 6000.

A much more informative method might be offered by the MTDSC method. Three heat of fusion values are obtained with this method: the reversing c_p-component, ΔH_c, the nonreversing kinetic component, ΔH_k, and the conventional component, ΔH. In a previous study it was found that the ratio $\Delta H_c/\Delta H$ might be a possible measure of the degree of crystallinity in a system at certain operational settings defined as degrees of oscillation (*10*). The term degree of oscillation, DO, is a dimension-less quantity defined by a combination of amplitude, frequency, and heating rate giving a certain weight to the c_p component of the total energy. If the DO is selected in such a way that both heating and cooling is obtained in each period, theoretically, both melting and crystallization can occur in each of the modulations. With this technique the transformation energy of the crystalline parts of a sample is compared with the total transformation energy in the same sample. To ensure good reproducibility, there should be at least five modulations under the melting transition, and the sample temperature must follow the modulation during the whole course of the thermal event (*25*). Three DO combinations were selected from a previous study (*10*) that give both heating and cooling in the temperature cycle. A DO ~1−2 was recommended for this particular polymer system for a frequency of 0.02 Hz. A higher DO usually gives better standard deviations but at the cost of less differentiation between the samples. It should be emphasized that only results obtained with the same DO can be compared. The ratio $\Delta H_c/\Delta H$ with standard deviation for the samples obtained with three different degree of oscillation, DO, is presented in Figure 4b. The value 0.96 is the lower limit of DO for this particular system (*10*) which can explain the larger standard deviations obtained for this combination.

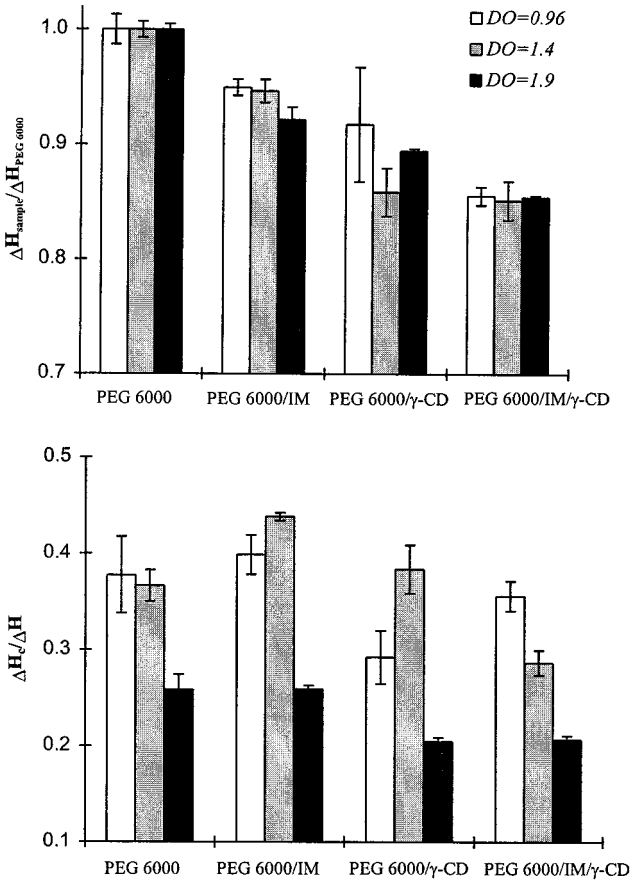


Figure 4. $\Delta H_{\text{sample}}/\Delta H_{\text{PEG 6000}}$ for PEG 6000 dispersions, $\Delta H_c/\Delta H$ for PEG 6000 dispersions.

The ratio $\Delta H_c/\Delta H$ for treated PEG 6000 was not changed or slightly increased by the addition of 5% indomethacin. With an addition of 20% γ-CD to PEG 6000, the ratio was lowered or almost equal for all combinations considering the standard deviations. The dispersion with 5% indomethacin and 19% γ-CD in PEG 6000 had a lower ratio than pure PEG 6000 for all DO, implying a less crystalline structure.

DISCUSSION

On comparison between the methods that were used, it is important to be conscious of what information that is obtained by each technique. In the ^{1}H NMR method the response of all the protons in the samples was measured. These protons are primarily PEG protons, since the polymer is the main component of the dispersions (76−95% w/w), and the carrier also has the highest content of protons per molecule. In the XRD method the crystallite sizes were calculated from two PEG reflections, and the information obtained thus concerned the crystallinity of the PEG matrix. The ΔH method, based on the two-phase model, considered the transformation energy of *all* phases in the sample and compared it with an external reference, namely pure PEG 6000. In the MTDSC method the transformation energy of *all* the crystalline parts of a sample that respond to a cyclic temperature modulation was measured and related to the total transformation energy of the same sample.

The relative crystallinity of the samples predicted by the NMR and the XRD methods are in good accordance with each other. The addition of IM or γ-CD to PEG 6000 decreases the crystallinity of the system. Particles of indomethacin dispersed in the carrier can be expected to distort the PEG structure, and the model proposed above for the solid solution of γ-CD in PEG 6000, where the γ-CD molecules may be thread on the PEG chains or helices, would also lead to a disturbance in the crystalline lamellae structure. However, the DSC and MTDSC methods indicate a difference in crystallinity between the two dispersions PEG 6000/IM and PEG 6000/γ-CD whereas the NMR and XRD methods did not. The results obtained are not necessarily contradictory. The presence of indomethacin particles or γ-cyclodextrin molecules may disturb the PEG matrix to the same extent, but the additives might not respond equally to the cyclic temperature modulation or have the same effect on the total energy of the sample. The ternary dispersion PEG/IM/γ-CD exhibited the lowest degree of crystallinity of the samples as predicted by all methods used. A possible explanation is that the indomethacin−γ-CD complex forms larger particles than pure indomethacin and that the tetragonal packing of the complexes disturbs the host PEG structure to a greater extent than does pure γ-CD.

CONCLUSIONS

The addition of different cyclodextrins to the dispersion of 5% indomethacin in PEG 6000 changed the short-range order in the samples to a varying extent. The NMR spectra of the PEG 6000/IM and PEG 6000/α-CD/IM dispersions were essentially superpositions of the pure components. In the PEG 6000/β-CD/IM dispersion a broadening of the peaks was obtained which was attributed to a distribution of the chemical shifts. Different parts of the indomethacin molecule can bind to β-CD and thereby give several types of complexes. The change in the chemicals shifts of the CD carbons in the PEG 6000/γ-CD/IM dispersion indicated a bond between γ-CD and indomethacin.

The degree of relative crystallinity of the samples in the γ-CD system, obtained by the different methods (^{1}H NMR, XRD, DSC, and MTDSC) showed that the dispersions were less crystalline than the pure polymer and that the dispersion containing the indomethacin−γ-CD complex had the lowest degree of relative crystallinity. Only the MTDSC method deviated, giving differentiation between the PEG 6000/IM and PEG 6000/γ-CD dispersions. Furthermore, equal or higher relative crystallinity for the PEG 6000/IM dispersion than for pure PEG 6000 was obtained, depending on operational parameters. When using different techniques for the determination of relative crystallinity, it is important to be aware of the kind of information that is obtained by the respective experiment.

ACKNOWLEDGMENT

The authors are grateful to MSc Marie Herstedt for assistance in the NMR laboratory, and to Dr Nils-Olov Ersson for skillful help with the XRD profile-fitting procedure. Financial support from The Royal Swedish Academy of Sciences and The Swedish Research Council for Engineering Sciences is gratefully acknowledged.

LITERATURE CITED

(1) Saenger, W. (1980) Cyclodextrin inclusion compounds in research and industry. *Angew. Chem., Int. Ed. Engl. 19*, 344−362.

(2) Duchêne, D., and Wouessidjewe, D. (1990) Pharmaceutical uses of cyclodextrins and derivates. *Drug Dev. Ind. Pharm. 16*, 2487−2499.

(3) Szejtli, J., and Szente, L. (1981) Interactions between indomethacin and β-cyclodextrin. *Pharmazie 36*, 694−698.

(4) Loftsson, T., and Brewster, M. E. (1996) Pharmaceutical applications of cyclodextrin. 1. Drug solubilization and stabilization. *J. Pharm. Sci. 85*, 1017−1025.

(5) Harada, A., and Kamachi, M. (1990) Complex formation between poly (ethyleneglycol) and α-cyclodextrin. *Macromolecules 23*, 2821−2823.

(6) Harada, A., Li, J., Suzuki, S., and Kamachi, M. (1993) Complex formation between polyisobutylene and cyclodextrins: Inversion of chain-length selectivity between β-cyclodextrin and γ-cyclodextrin. *Macromolecules 26*, 5267−5268.

(7) Wulff, M., and Aldén, M. (1999) Solid-state studies of drug-cyclodextrin inclusion complexes in PEG 6000 prepared by a new method. *Eur. J. Pharm. Sci. 8*, 269−281.

(8) Leuner, C., and Dressman, J. (2000) Improving drug solubility for oral delivery using solid dispersions. *Eur. J. Pharm. Biopharm. 50*, 47−60.

(9) Cullity, B. D. (1978) *Elements of X-ray diffraction*, 2nd ed., Addison-Wesley, Reading, MA.

(10) Aldén, M., Wulff, M., and Herdinius, S. (1995) Influence of selected variables on heat of fusion determinations by oscillating DSC. *Thermochim. Acta 265*, 89−102.

(11) Singh, S. P., Parmar, S. S., Stenberg, V. I., and Farnum, S. A. (1978) Carbon-13 nuclear magnetic resonance spectra of antiinflammatory drugs: Phenylbutazone, Oxyphenbutazone and Indomethacin. *J. Heterocycl. Chem. 15*, 13−16.

(12) Furó, I., Pócsik, I., Tompa, K., Teeäär, R., and Lippmaa, E. (1987) C.P.-D.D.-M.A.S. ^{13}C−N.M.R. Investigations of anhydrous and hydrated cyclomalto-oligosaccharides: The role of water of hydration. *Carbohydr. Res. 166*, 27−33.

(13) Yang, R., Yang, X. R., Evans, D. F., Hendrickson, W. A., and Baker, J. (1990) Scanning Tunneling Microscopy Images of Poly(ethylene oxide) Polymers: Evidence for Helical and Superhelical Structures. *J. Phys. Chem. 94*, 6123−6125.

(14) Djedaïni, F., Lin, S. Z., Perly, B., and Wouessidjewe, D. (1990) High-field nuclear magnetic resonance techniques for the investigation of a β-cyclodextrin: indomethacin inclusion complex. *J. Pharm. Sci. 79*, 643−646.

(15) Fronza, G., Mele, A., Redenti, E., and Ventura, P. (1996) ^{1}H NMR and molecular modeling study on the inclusion complex β-cyclodextrin−indomethacin. *J. Org. Chem. 61*, 909−914.
(16) Backensfeld, T., Müller, B. W., Wiese, M., and Seydel, J. K. (1990) Effect of cyclodextrin derivatives on the indomethacin stability in aqueous solution. *Pharm. Res. 7*, 484−490.
(17) Hoshino, T, Tagawa, T., Hirayama, F., Otagiri, M., and Uekama, K. (1982) *Yakugaru Zasshi 102*, 1184−1190.
(18) Uekama, K., Hirayama, F., Fujise, A., Otagiri, M., Inaba, K., and Saitô, H. (1984) Inclusion complexation of prostaglandin $F_{2\alpha}$ with γ-cyclodextrin in solution and solid phases. *J. Pharm. Sci. 73*, 382−384.
(19) Takeo, K., and Kuge, T. (1970) Complexes of starchy materials with organic compounds. Part IV. X-ray diffraction of γ-cyclodextrin complexes. *Agr. Biol. Chem. 34*, 568−574.
(20) Piel, G., Dive, G., Evrard, B., Van Hees, T., Henry de Hassonville, S., and Delattre, L. (2001) Molecular modeling study of β- and γ-cyclodextrin complexes with miconazole. *Eur. J. Pharm. Sci. 13*, 271−279.
(21) Johansson, A., and Tegenfeldt, J. (1992) NMR study of crystalline and amorphous poly(ethylene oxide). *Macromol. 25*, 4712−4715.
(22) Murthy, N. S. (1982) Analysis of X-ray diffraction data from polymers by profile fitting. *Am. Lab. 14*, 70−75.
(23) Prud'homme, R. E. (1982) Fractionation in mixtures of poly(ethylene oxide) fractions during crystallization. *J. Polym. Sci. 20*, 307−317.
(24) Chen, H.-L., and Hwang, J. C. (1995) Some comments on the degree of crystallinity defined by the enthalpy of melting. *Polymer 36*, 4355−4357.
(25) Reading, M., Luget, A., and Wilson, R. (1994) Modulated differential scanning calorimetry. *Thermochim. Acta 238*, 295−307.

BC000156O

Porphyrin, Chlorin, and Bacteriochlorin Isothiocyanates: Useful Reagents for the Synthesis of Photoactive Bioconjugates†

J. M. Sutton,‡ O. J. Clarke,§ N. Fernandez,‡ and R. W. Boyle*,§

Department of Biological Sciences, University of Essex, Colchester CO4 3SQ, U.K., and Department of Chemistry, University of Hull, Hull HU6 7RX, U.K. Received August 20, 2001; Revised Manuscript Received January 4, 2002

A novel method for conjugating porphyrins and related molecules to proteins has been developed. The method, which involves synthesizing porphyrins, chlorins, and bacteriochlorins bearing a single amine-reactive isothiocyanate group represents a facile system for protein labeling with these photoactive species. Problems associated with the noncovalent binding of porphyrins to proteins are highlighted, and a method for purifying conjugates to yield exclusively covalently bound porphyrin protein species is demonstrated. Biological activity of porphyrin−bovine serum albumin conjugates formed and purified by these methods is demonstrated using laser scanning confocal microscopy.

INTRODUCTION

Porphyrins and their derivatives are of wide general interest because of the range of potential applications associated with these molecules; included among these are photodynamic therapy (PDT) (*1*−*4*) and fluorescence imaging (*5*). Addition reactions at the "exocyclic" double bonds of the porphyrins, which include OsO_4-mediated dihydroxylation reactions (*6*−*10*), leads to the generation of chlorins and bacteriochlorins, which absorb light more efficiently in the red and near-infrared regions of the spectrum. PDT applications, where light penetration through tissue is a limiting factor, are most effective using light in the 600−800 nm range, thus making chlorins and bacteriochlorins particularly suitable on purely photophysical grounds. Furthermore, as porphyrins, chlorins, and bacteriochlorins fluoresce at different wavelengths (*11*) and also have unusually large Stokes shifts (>200 nm), their use in multicolor fluorescence analysis could be envisaged. In both cases, however, the accurate targeting of the chromophore against tissue to be photosensitized or imaged is important.

Porphyrins and their derivatives have been conjugated with several proteins of biological importance, such as human and bovine serum albumins (*12*−*15*), monoclonal antibodies (*16*−*20*), and lipoproteins (*21*, *22*); this has allowed for their use as photosensitizers and imaging agents to be exploited in a more selective and controlled manner than was previously possible. The majority of bioconjugations involving porphyrin derivatives have relied on natural products such as haematoporphyrin (*13*, *16*, *17*) or chlorin e_6 (*15*, *20*, *22*) and have made use of carbodiimide or *N*-hydroxysuccinimide ester (NHS)-based bioconjugation protocols. These porphyin derivatives, however, contain multiple reactive functionalities, which can lead to cross-linking problems. Many bioconjugates of porphyrin and protein formed as previously described also incorporate significant amounts of noncovalently bound (NCB) porphyrin (*13*, *16*, *17*). Some attempts have been made to remove NCB porphyrin derivatives from bioconjugates, but these have usually involved gel permeation chromatography, which is not effective in removing large amounts of strongly NCB material. Hamblin et al. (*15*) successfully removed NCB material using acetone precipitation, which allowed the NCB chlorin e_6, retained in the supernatant, to be removed by successive washes. In PDT applications, the presence of some NCB porphyrin may not negate photosensitization entirely, as a number of NCB complexes or conjugates containing NCB porphyrin derivatives have been used successfully (*13*, *16*, *17*); however, it will decrease the desired selectivity for target tissue. In fluorescence-activated flow cytometry, the fluorophore is usually conjugated directly to a monoclonal antibody (Mab) or indirectly using an avidin−biotin interaction (i.e., biotinylated Mab/avidin−fluorophore conjugate) (*23*). In such applications, NCB porphyrin derivatives can present a major problem, as lipophilic porphyrin molecules can transfer to cell membranes and lead to large errors during flow cytometric analysis.

Recently, bioconjugates of porphyrins with bovine serum albumin (BSA) and a maleylated derivative (mal-BSA) have been successfully used to target particular cell types. BSA and mal-BSA bind selectively to ligands of the macrophage scavenger receptor; then, following cellular internalization by receptor-mediated endocytosis, the porphyrin-derived bioconjugates have been successfully used to image and photosensitize these cells (*13*−*15*, *22*, *23*).

In the study described herein, we have attempted to develop an improved bioconjugation technique for porphyrin derivatives and also to identify structural features which can minimize noncovalent binding (NCB) of porphyrins to protein.

EXPERIMENTAL PROCEDURES

Instrumentation and Materials. Melting points are uncorrected and were recorded on a Kolfer hot-plate microscope. ^1H and ^{13}C NMR spectra were recorded on a JEOL EX270 FT-NMR spectrometer and are referenced

† The authors thank the Wellcome trust for financial support (052724).

* Corresponding author. Phone: (01482) 466353. Fax: (01482) 466410. E-mail: r.w.boyle@hull.ac.uk.

‡ University of Essex.

§ University of Hull.

10.1021/bc015547x CCC: $22.00 © 2002 American Chemical Society
Published on Web 02/21/2002

downfield to tetramethylsilane. IR spectra were obtained using a Nicolet series 1600 FTIR spectrophotometer. Nominal mass spectra were obtained using a Kratos Kompact MALDI II spectrometer, EI biotech instrument, or a FAB autospec machine using NOBA matrix. Accurate masses were obtained from EPSRC Mass Spectrometry Service, Swansea, Wales. UV−visible spectra were obtained using Unicam UV-2 or UV-4 spectrometers and were taken in dichloromethane (DCM), unless otherwise stated. Fluorescent measurements were taken using a Perkin-Elmer LS50 spectrophotometer. All commercial chemicals and solvents were of reagent grade or higher and were used as received, unless otherwise specified. TLC analyses were performed on Merck silica-gel 60 plates (F254, 500 μm thickness). Merck silica-gel 60 (230−400 mesh) was used for flash chromatographic purification with all of the crude reaction mixtures being preadsorbed onto silica gel prior to separation, unless otherwise stated. All purified compounds were found to contain only one component by TLC analysis. HeLa cells were obtained in-house.

Chemistry: 5-(4-Methoxyphenyl)dipyrromethane (1). Dipyrromethane **1** was synthesized according to the method of Boyle et al. (*25*). The crude reaction mixture was purified by chromatography, eluting with *n*-hexane/DCM (3:7), to afford the pure product as an off-white solid (4.3 g, 50%); $R_f = 0.33$ (DCM); IR (Nujol, cm^{-1}) ν_{max}: 3382 (br s, NH), 1598 (C═C), 1300, 1050; UV−vis (MeOH) λ_{max} (relative intensity), nm: 224 (1.0); ^{1}H NMR (270 MHz, $CDCl_3$, δ): 7.87 (br s, 2H, *NH*), 7.10 (m, 2H, $J = 8.8$ Hz, *5-m-Ar*), 6.83 (m, 2H, $J = 8.8$ Hz, *5-o-Ar*), 6.66 (m, 2H, *1-H*), 6.14 (m, 2H, *2-H*), 5.89 (m, 2H, *3-H*), 5.40 (s, 1H, *5-H*); MALDI-MS *m/z*: 252.4 (M^+, 100%).

5-(3,4,5-Trismethoxyphenyl)dipyrromethane (2). Dipyrromethane **2** was synthesized according to the method of Boyle et al. (*25*). The reaction mixture was recrystallized from hot ethyl acetate/*n*-hexane and gave the required dipyrromethane as a white solid (5.41 g, 68%); $R_f = 0.44$ (DCM/ethyl acetate, 20:1); IR (Nujol, cm^{-1}) ν_{max}: 3378 (br s, NH), 1594 (C═C), 1233, 1040; UV−vis (MeOH) λ_{max} (relative intensity), nm: 222 (1.0), 280 (0.75); ^{1}H NMR (270 MHz; $CDCl_3$, δ): 8.07 (br s, 2H, *NH*), 7.53 (m, 2H, *1-H*), 6.68 (s, 2H, *5-o-Ar*), 6.37 (m, 2H, *2-H*), 5.93 (m, 2H, *3-H*), 5.38 (s, 1H, *5-H*), 3.80 (s, 3H, *p-OCH$_3$*), 3.73 (s, 6H, *m-OCH$_3$*); ^{13}C (68 MHz; $CDCl_3$, δ): 152.7, 137.3, 136.1, 131.8, 116.7, 107.9, 106.6, 104.9, 60.3, 55.5, 43.7; MALDI-MS *m/z*: 311.2 ($[M - 1]^+$, 100%).

5-(4-Acetamidophenyl)dipyrromethane (3). Dipyrromethane **3** was synthesized according to the method of Boyle et al. (*25*). The crude product was recrystallized from hot ethyl acetate/*n*-hexane and afforded the required dipyrromethane as a white solid (8.0 g, 68%); $R_f = 0.35$ ($CHCl_3$/ethyl acetate, 1:1); IR (Nujol, cm^{-1}) ν_{max}: 3409 (NH, *amide*), 3248 (br s, *NH*), 1650 (*C═O*), 1593 (*C═C*), 1320, 1009; UV−vis (MeOH) λ_{max} (relative intensity), nm: 224 (1.0); ^{1}H NMR (270 MHz, $CDCl_3$, δ): 8.00 (br s, 2H, *NH*), 7.40 (m, 2H, $J = 8.5$ Hz, *5-o-Ar*), 7.30 (br s, 1H, *NH-acetamide*), 7.13 (m, 2H, $J = 8.5$ Hz, *5-m-Ar*), 6.68 (m, 2H, *1-H*), 6.16 (m, 2H, *2-H*), 5.90 (m, 2H, *3-H*), 5.42 (s, 1H, *5-H*), 2.14 (s, 3H, *CH$_3$*); ^{13}C NMR (68 MHz, $CDCl_3$, δ): 168.4, 138.2, 136, 132.4, 128.9, 120.3, 117.2, 108.4, 107.1, 43.4, 24.5; MALDI-MS *m/z*: 279.4 (M^+, 100%).

5-(4-Acetamidophenyl)-15-(4-methoxyphenyl)porphyrin (4). The DPP was synthesized according to the method of Boyle et al. (*25*). The resulting mixture of three porphyrins was chromatographed, eluting initially with DCM to allow for the removal of 5,15-(4-methoxy)-DPP, and then continuing with ethyl acetate/DCM (1:4) to elute the required product as purple crystals (150 mg, 12%); $R_f = 0.40$ (DCM/MeOH, 19:1); mp 305−307 °C (dec); UV−vis (DCM) λ_{max} (relative intensity), nm: 410 (1.0), 502 (0.04), 538 (0.02), 578 (0.015), 630 (0.01); ^{1}H NMR (270 MHz, $CDCl_3$, δ): 10.35 (s, 2H, *10+20-H*), 9.43 (d, 4H, $J = 4.8$ Hz, *β-H*), 9.14 (d, 4H, $J = 4.8$ Hz, *β-H*), 8.65 (m, 2H, $J = 7.2$ Hz, *5-m-Ar*), 8.22−8.12 (m, 4H, (overlapping), $J = 8.1$ Hz, *5+15-o-Ar*), 7.56 (m, 2H, $J = 8.1$ Hz, *15-m-Ar*), 4.14 (s, 3H, *CH$_3$*), −3.00 (br s, 2H, *NH*); MALDI-MS *m/z*: 550.3 (M^+, 100%).

5-(4-Aminophenyl)-15-(4-methoxyphenyl)porphyrin (6) (General Procedure A). 5-(4-Acetamido phenyl)-15-(4-methoxyphenyl)porphyrin **4** (1 equiv, 100 mg, 0.182 mmol) was dissolved in 5 M aqueous HCl (100 mL) and the solution heated for 3 h under reflux. The hot reaction mixture was concentrated in vacuo to yield a crude green solid. The solid was redissolved in a mixture of DCM/triethylamine (9:1) (200 mL) and stirred for 10 min at room temperature. The solution was then washed with water (3 × 200 mL) and saturated brine (200 mL), and the organic layer separated, dried (Na_2SO_4), and then concentrated in vacuo. The crude purple solid was chromatographed, eluting with DCM, and gave the desired porphyrin as a purple crystalline solid (51 mg, 54%), $R_f = 0.30$ (DCM); mp 300 °C (dec); UV−vis (DCM) λ_{max} (relative intensity), nm: 410 (1.0), 503 (0.045), 538-(0.02), 578 (0.015), 630 (0.005); fluorescence (DCM): λ_{max} 634 nm (λ excitation = 410 nm); ^{1}H NMR (270 MHz, $CDCl_3$, δ): 10.30 (s, 2H, *10+20-H*), 9.39 (d, 4H, $J = 4.9$ Hz, *β-H*), 9.17 (d, 2H, $J = 4.9$ Hz, *β-H*), 9.10 (d, 2H, $J = 4.9$ Hz, *β-H*), 8.19 (m, 2H, $J = 8.8$ Hz, *15-o-Ar*), 8.07 (m, 2H, $J = 8.1$ Hz, *5-o-Ar*), 7.35 (m, 2H, $J = 8.8$ Hz, *15-m-Ar*), 7.14 (m, 2H, $J = 8.1$ Hz, *5-m-Ar*), 4.13 (s, 3H, *CH$_3$*), 4.08 (br s, 2H, *NH*), −3.06 (br s, 2H *NH*); MALDI-MS *m/z*: 508.3 ($[M + 1]^+$, 100%). ES-HRMS Anal. Calcd. for $C_{33}H_{26}N_5O$ ($[M + 1]^+$), 508.2137; found, 508.2144.

5-(4-Isothiocyanatophenyl)-15-(4-methoxyphenyl)-porphyrin (8) (General Procedure B). To a stirred solution of **6** (1 equiv, 50 mg, 0.099 mmol) in freshly distilled DCM (20 mL) was added 1,1′-thiocarbonyldi-2(1*H*)-pyridone (2 equiv, 46 mg, 0.198 mmol). The reaction was allowed to stir under argon for 2 h at room temperature, after which the reaction mixture was concentrated in vacuo. The crude residue was chromatographed, eluting with DCM, and afforded the title compound as a purple crystalline solid (45.7 mg, 92%); $R_f = 0.86$ (DCM); mp >350 °C (dec); UV−vis (DCM) λ_{max}, nm: 411, 505, 541, 576, 630; ^{1}H NMR (270 MHz, $CDCl_3$, δ): 10.32 (s, 2H, *10+20-H*), 9.13−9.43 (m, 4H, *β-H*), 9.11 (d, 2H, $J = 5$ Hz, *β-H*), 9.02 (d, 2H, $J = 5$ Hz, *β-H*), 8.27 (m, 2H, $J = 8$ Hz, *5-o-Ar*), 8.19 (m, 2H, $J = 8$ Hz, *15-o-Ar*), 7.69 (m, 2H, $J = 8$ Hz, *5-m-Ar*), 7.36 (m, 2H, $J = 8$ Hz, *15-m-Ar*), 4.13 (s, 3H, *OCH$_3$*), −3.12 (br s, 2H, *NH*). FAB-HRMS Anal. Calcd. for $C_{34}H_{23}N_5OS$ (M^+), 549.1623; found, 549.1604.

5-(4-Acetamidophenyl)-15-(3,4,5-trimethoxyphenyl)porphyrin (5). DPP was synthesized according to the method of Boyle et al. (*25*). The crude porphyrin mixture was chromatographed, eluting with DCM/ethyl acetate (4:1), and afforded the required product as a purple crystalline solid (198 mg, 7.2%); $R_f = 0.37$ (DCM/ethyl acetate, 4:1); mp >350 °C (dec); UV−vis (DCM) λ_{max}, nm: 407, 504, 539, 576, 632; ^{1}H NMR (270 MHz, $CDCl_3$/DMSO-d_6, 1:1, δ): 10.42 (s, 2H, *10+20-H*), 10.27 (br s, 1H, *NH*), 9.50 (d, 4H, $J = 5$ Hz, *β-H*), 9.20 (d, 2H, $J = 5$ Hz, *β-H*), 9.13 (d, 2H, $J = 5$ Hz, *β-H*), 8.18 (m, 2H, $J = 8$

Hz, *5-o-Ar*), 8.12 (d, 2H, $J = 8$ Hz, *5-m-Ar*), 7.54 (s, 2H, *15-o-Ar*), 4.14 (s, 3H, *15-p-OCH$_3$*), 4.02 (s, 6H, *15-m-OCH$_3$*), 2.32 (s, 3H, *CH$_3$*); MALDI-MS *m/z*: 609 (M^+, 100%).

5-(4-Aminophenyl)-15-(3,4,5-trimethoxyphenyl)-porphyrin (7). Porphyrin **5** was converted into the aminoporphyrin **7** following general procedure A. The crude purple solid was chromatographed, eluting with DCM to afford the title compound as a purple crystalline solid (168 mg, 94.8%); $R_f = 0.49$ (DCM/ethyl acetate, 5:1); mp >350 °C (dec); UV−vis (DCM) λ_{max}, nm: 410, 505, 542, 578, 634; ^{1}H NMR (270 MHz, $CDCl_3$, δ): 10.19 (s, 2H, *10+20-H*), 9.28 (d, 4H, $J = 5$ Hz, *β-H*), 9.08 (d, 4H, $J = 5$ Hz, *β-H*), 7.96 (m, 2H, $J = 8$ Hz, *5-o-Ar*), 7.37 (s, 2H, *15-o-Ar*), 7.01 (d, 2H, $J = 8.1$ Hz, *5-m-Ar*), 6.85 (br s, 2H, *NH$_2$*), 3.90 (s, 9H, *15-o/p-OCH$_3$*), −3.18 (br s, 2H, *NH*); ^{13}C NMR (68 MHz, $CDCl_3$, δ): 159.1, 147.6, 147, 146.1, 145.1, 143.3, 136, 131.6, 131.4, 131.3, 131.2, 130.8, 119.9, 118.2, 113.9, 113.8, 105.1, 100, 55.7; MALDI-MS *m/z*: 568 (M^+, 100%).

5-(4-Isothiocyanatophenyl)-15-(3,4,5-trimethoxyphenyl)porphyrin (9). Porphyrin **9** was synthesized from **7** using general procedure B. The crude residue was chromatographed, eluting with DCM to afford the required product as a purple crystalline solid (102 mg, 95.5%); $R_f = 0.72$ (DCM); mp >350 °C (dec); UV−vis (DCM) λ_{max}, nm: 410, 504, 539, 576, 631; ^{1}H NMR (270 MHz, $CDCl_3$, δ): 10.28 (s, 2H, *10+20-H*), 9.35−9.38 (m, 4H, *β-H*), 9.17 (d, 2H, $J = 5$ Hz, *β-H*), 8.98 (d, 2H, $J = 5$ Hz, *β-H*), 8.20 (m, 2H, $J = 8$ Hz, *5-o-Ar*), 7.63 (m, 2H, $J = 8$ Hz, *5-m-Ar*), 7.50 (s, 2H, *15-o-Ar*), 4.20 (s, 3H, *15-p-OCH$_3$*), 3.98 (s, 6H, *15-m-OCH$_3$*), −3.15 (br s, 2H, *NH*); ^{13}C NMR (68 MHz, $CDCl_3$, δ): 151.6, 147.2, 146.7, 145.3, 145.2, 140.6, 137.8, 136.8, 136.4, 135.7, 131.2, 131.9, 131.8, 131.1, 130.4, 124.3, 119.2, 117.2, 112.9, 105.5, 61.3, 56.4. FAB-HRMS Anal. Calcd for $C_{36}H_{27}N_5O_3S$ ([M + H]$^+$), 610.1913; found, 610.1914.

5-(4-Hydroxyphenyl)dipyrromethane (11). The dipyrromethane was synthesized according to the method of Boyle et al. (*25*). The crude dipyrromethame was chromatographed, eluting initially with $CHCl_3$, and then gradient eluting to $CHCl_3$/ethyl acetate (1:1). The required product was obtained as a pale pink crystalline solid (6.36 g, 65%); $R_f = 0.18$ ($CHCl_3$); mp 158−160 °C; IR (Nujol, cm^{-1}) υ_{max}: 3409 (NH), 2968 (OH); ^{1}H NMR (270 MHz, DMSO-d_6, δ): 10.48 (br s, 2H, *NH*); 9.19 (br s, 1H, *OH*), 7.07 (m, 2H, $J = 8.1$ Hz, *5-m-Ar*), 6.90 (m, 2H, $J = 8.1$ Hz, *5-o-Ar*), 6.59 (m, 2H, *1-H*), 5.89 (m, 2H, *2-H*), 5.63 (m, 2H, *3-H*), 5.23 (s, 1H, *5-H*); ^{13}C NMR (68 MHz, DMSO-d_6, δ): 155.6, 134.2, 133.8, 129, 117.4, 116.7, 114.8, 107.2, 106.9, 105.9; MALDI-MS *m/z*: 237 (M^+, 100%).

5-(4-*tert*-Butyldiphenylsilyloxyphenyl)dipyrromethane (12). Imidazole (712 mg, 10 mmol) and *tert*-butylchlorodiphenylsilane (1.3 mL, 5 mmol) were dissolved in anhydrous DMF (2.0 mL, distilled from CaH_2, 0.1 Torr), and the reaction mixture was stirred under argon for 5 min at room temperature. Dipyrromethane **11** (1.0 g, 4.2 mmol) was added, and stirring was continued for a further 17 h under the same conditions. The crude reaction mixture was diluted with ethyl acetate (100 mL) and washed with water (3 × 100 mL) and saturated brine (100 mL). The organic layer was separated and dried (Na_2SO_4) before concentration in vacuo to yield a crude brown oil. The crude product was chromatographed, eluting with DCM, and afforded the title compound as viscous tan oil (1.57 g, 78.8%); $R_f = 0.42$ (DCM); IR (Nujol, cm^{-1}) υ_{max}: 3315 (NH); ^{1}H NMR (270 MHz, $CDCl_3$, δ): 7.52−7.62 (m (overlapping), 4H, *NH* and *Si-o-Ar*); 7.21−7.27 (m, 6H, *Si-m/p-Ar*), 6.75 (m, 2H, $J = 8.6$ Hz, *5-o-Ar*), 6.59 (m, 2H, $J = 8.6$ Hz, *5-m-Ar*), 6.39 (m, 2H, *1-H*), 5.96 (m, 2H, *2-H*), 5.67 (m, 2H, *3-H*), 5.10 (s, 1H, *5-H*), 1.00 (s, 9H, *^{t}Bu*); ^{13}C NMR (68 MHz, $CDCl_3$, δ): 154.9, 135.9, 135.2, 134.9, 133.3, 133.2, 130.3, 130.1, 129.5, 128.2, 120.1, 117.5, 108.6, 107.4, 43.4, 27, 19.9; FAB-MS *m/z*: 474 ([M + H]$^+$, 55%), 410 ([M − C_4H_4N]$^+$, 90%).

5-(4-Acetamidophenyl)-15-(4-*tert*-butyldiphenylsilyloxyphenyl)porphyrin (13). Porphyrin **13** was synthesized according to the method of Boyle et al. (*25*). The porphyrin mixture was chromatographed, eluting with DCM/ethyl acetate (1:1) to give the required product as a purple crystalline solid (317 mg, 42%); $R_f = 0.44$ (DCM/ethyl acetate, 1:1); mp >350 °C (dec); UV−vis (DCM) λ_{max}, nm: 410, 504, 539, 599, 656; ^{1}H NMR (270 MHz, $CDCl_3$, δ): 10.10 (s, 2H, *10+20-H*), 9.26 (d, 2H, $J = 5$ Hz, *β-H*), 9.18 (d, 2H, $J = 5$ Hz, *β-H*), 8.99 (d, 4H, $J = 5$ Hz, *β-H*), 8.61−8.70 (m, 4H, *Si-o-Ar*), 8.21 (br s, 1H, *NH*), 8.10 (m, 2H, $J = 8$ Hz, *5-o-Ar*), 7.93−7.99 (m, 6H, *Si-m/p-Ar*), 7.84 (m, 2H, $J = 8$ Hz, *15-o-Ar*), 7.36 (m, 2H, $J = 8$ Hz, *5-m-Ar*), 7.21 (m, 2H, $J = 8$ Hz, *15-m-Ar*), 2.24 (s, 3H, *CH$_3$*), 1.31 (s, 9H, *^{t}Bu*), −3.11 (br s, 2H, *NH*); FAB-MS *m/z*: 774 ([M + H]$^+$, 100%).

5-(4-Aminophenyl)-15-(4-*tert*-butyldiphenylsilyloxyphenyl)porphyrin (14). Porphyrin **13** was hydrolyzed following general procedure A. The residual crude purple solid was chromatographed, eluting with DCM/ethyl acetate (4:1) to afford the title compound as a purple crystalline solid (90 mg, 97%); $R_f = 0.8$ (DCM/ethyl acetate, 1:1); mp >350 °C (dec); UV−vis (DCM) λ_{max}, nm: 411, 505, 543, 579, 636; ^{1}H NMR (270 MHz, $CDCl_3$, δ): 10.23 (s, 2H, *10+20-H*), 9.24 (m, 4H, *β-H*), 6H, *Si-o-Ar* and *15-o-Ar*), 9.14 (d, 2H, $J = 5$ Hz, *β-H*), 9.00 (d, 2H, $J = 5$ Hz, *β-H*), 7.98 (m, 2H, $J = 8$ Hz, *5-o-Ar*), 7.96 (m (overlapping)), 7.54 m, (6H, *Si-m/p-Ar*), 7.14 (m, 2H, $J = 8$ Hz, *15-m-Ar*), 7.08 (m, 2H, $J = 8$ Hz, *5-m-Ar*), 4.0 (br s, 2H, *NH$_2$*), 1.30 (s, 9H, *^{t}Bu*), −3.11 (br s, 2H, *NH*); ^{13}C NMR (68 MHz, $CDCl_3$, δ): 155.6, 150.5, 147.9, 147.6, 147.3, 146.1, 144.9, 135.9, 135.7, 135.6, 134.1, 133, 131.4, 131.3, 131.1, 130.9, 130.1, 127.9, 120.4, 119.6, 119.3, 118.7, 118.5, 113.7, 105, 26.7, 19.6; FAB-MS *m/z*: 732 (M^+, 50%), 716 ([M − NH_2]$^+$, 9%), 674 ([M − $C(CH_3)_3$]$^+$, 3%).

5-(4-Isothiocyanatophenyl)-15-(4-*tert*-butyldiphenylsilyloxyphenyl)porphyrin (15). Porphyrin **14** was converted into the isothiocyanate using general procedure B. The crude reaction mixture was chromatographed, eluting with DCM which gave the required compound as a purple crystalline solid (133 mg, 97%); $R_f = 0.6$ (DCM/hexane, 1:1); mp >350 °C (dec); UV−vis (DCM) λ_{max}, nm: 410, 504, 539, 576, 631; ^{1}H NMR (270 MHz, $CDCl_3$, δ): 10.27 (s, 2H, *10+20-H*), 9.36 (m, 4H, *β-H*), 9.01 (d, 2H, $J = 5$ Hz, *β-H*), 8.97 (d, 2H, $J = 5$ Hz, *β-H*), 8.21 (m, 2H, $J = 8$ Hz, *5-o-Ar*), 7.95−7.98 (m (overlapping)), 6H, *15-o-Ar* and *Si-o-Ar*), 7.64 (m, 2H, $J = 8$ Hz, *5-m-Ar*), 7.53−7.55 (m, 6H, *Si-m/p-Ar*), 7.20 (m, 2H, $J = 8$ Hz, *15-m-Ar*), 1.30 (s, 9H, *^{t}Bu*), −3.18 (br s, 2H, *NH*); ^{13}C NMR (68 MHz, $CDCl_3$, δ): 155.7, 147.4, 146.6, 145.2, 145, 140.7, 135.8, 135.7, 135.6, 133.9, 133, 131.9, 131.5, 131.2, 131, 130.3, 130.1, 127.9, 124.3, 119.5, 118.5, 116.8, 105.4, 26.7, 19.7; FAB-MS *m/z*: 536 ([M + H]$^+$, 100%).

5-(4-Isothiocyanatophenyl)-15-(4-hydroxyphenyl)-porphyrin (10). To a stirred solution of porphyrin **15** (100 mg, 0.13 mmol) in freshly distilled DCM (20 mL) was added tetrabutylammonium fluoride (40.5 mg, 0.16

mmol). The reaction was allowed to proceed under argon for 1 h at room temperature. The solvent was removed in vacuo to yield a crude purple solid. The crude product was purified by chromatography, eluting with DCM and afforded the title compound as a purple crystalline solid (63.5 mg, 92%); $R_f = 0.67$ (DCM); mp >350 °C (dec); UV−vis (MeOH) λ_{max}, nm: 408, 505, 540, 576, 630; ^{1}H NMR (270 MHz, $CDCl_3$/DMSO-d_6, 1:1, δ): 10.34 (s, 2H, *10+20-H*), 9.43 (m, 4H, *β-H*), 9.16 (m, 2H, *β-H*), 9.02 (m, 2H, *β-H*), 8.25 (m, 2H, *15-o-Ar*), 8.05 (m, 2H, *5-o-Ar*), 7.71 (m, 2H, *15-m-Ar*), 7.30 (m, 2H, *5-m-Ar*), −3.16 (br s, 2H, *NH*); ^{13}C NMR (68 MHz, $CDCl_3$/DMSO-d_6, 1:1, δ): 156.9, 146.9, 146, 144.5, 144.3, 139.9, 135.6, 135.3, 135.1, 131.5, 131.1, 130.8, 130.4, 129.8, 123.8, 119.5, 116.1, 113.7, 104.8. FAB-HRMS (FAB) Anal. Calcd. for $C_{33}H_{21}N_5OS$ ([M + H]$^+$), 536.1545; found, 536.1548.

5-(4-Acetamidophenyl)-10,15,20-tri-(4-methoxyphenyl)porphyrin (18). Porphyrin **18** was synthesized according to the method of Adler et al. (*29*). The crude mixture of porphyrin isomers was purified by chromatography, eluting with DCM/ethyl acetate (4:1) to afford the required product as a purple crystalline solid (1.77 g, 7.5%); $R_f = 0.5$ (DCM/ethyl acetate, 4:1); mp >350 °C (dec); UV−vis (DCM) λ_{max}, nm: 423, 520, 554, 594, 651; ^{1}H NMR (270 MHz, $CDCl_3$, δ): 8.87 (s, 8H, *β-H*), 8.17−8.09 (m, 8H, *5+10+15+20-o-Ar*), 7.91 (m, 2H, $J = 8$ Hz, *5-m-Ar*), 7.78 (br s, 1H, *NH*), 7.29−7.26 (m, 6H, *10+15+20-m-Ar*), 4.09 (s, 9H, CH_3), 2.36 (s, 3H, CH_3), −2.77 (br s, 2H, *NH*); MALDI-MS *m/z*: 762 (M$^+$, 100%).

5-(4-Aminophenyl)-10,15,20-tri-(4-methoxyphenyl)-porphyrin (20). Porphyrin **18** was converted into **20** following general procedure A. The crude purple solid was chromatographed, eluting with DCM/ethyl acetate (4:1), and gave the title compound as a purple crystalline solid (437 mg, 93%); $R_f = 0.84$ (DCM/ethyl acetate, 4:1); mp >350 °C (dec); UV−vis (DCM) λ_{max}, nm: 421, 516, 553, 591, 652; ^{1}H NMR (270 MHz, $CDCl_3$, δ): 8.93−8.86 (m, 8H, *β-H*), 8.13 (m, 6H, $J = 8$ Hz, *10+15+20-o-Ar*), 7.99 (m, 2H, $J = 8$ Hz, *5-o-Ar*), 7.29 (m, 6H, $J = 8$ Hz, *10+15+20-m-Ar*), 7.07 (m, 2H, $J = 8$ Hz, *5-m-Ar*), 4.10 (s, 9H, CH_3), 4.03 (br s, 2H, NH_2), −2.74 (br s, 2H, *NH*); ^{13}C NMR (68 MHz, $CDCl_3$, δ): 159.4, 135.7, 135.6, 134.7, 120.5, 113.5, 112.2, 55.6; MALDI-MS *m/z*: 720 (M$^+$, 100%).

5-(4-Aminophenyl)-10,15,20-tri-(4-hydroxyphenyl)-porphyrin (22) (General Procedure C). To a stirred solution of **20** (1 equiv, 100 mg, 0.139 mmol) in freshly distilled DCM (50 mL) was added boron tribromide (15 equiv, 197 μL, 2.08 mmol). The reaction was allowed to proceed under argon for 17 h at room temperature. The reaction mixture was cooled to 0 °C then treated with water (2.0 mL) and allowed to warm to room temperature for a further 1 h. The reaction was then concentrated in vacuo and redissolved in a (9:1) mixture of DCM/triethylamine (100 mL). The solution was washed with water (3 × 100 mL) and saturated brine (100 mL), the organic layer separated, dried (Na_2SO_4), and then concentrated in vacuo. The crude purple solid was then chromatographed, eluting with DCM/MeOH (5:1) to afford the title compound as a purple crystalline solid (72 mg, 77%); $R_f = 0.48$ (DCM/MeOH, 9:1); mp >350 °C (dec); UV−vis (MeOH) λ_{max}, nm: 423, 517, 554, 592, 651; ^{1}H NMR (270 MHz, DMSO-d_6, δ): 10.00 (br s, 3H, *OH*), 8.91−8.84 (m, 8H *β-H*), 7.99 (m, 6H, $J = 8$ Hz, *10+15+20-o-Ar*), 7.85 (m, 2H, $J = 8$ Hz, *5-o-Ar*), 7.21 (m, 6H, $J = 8$ Hz, *10+15+20-m-Ar*), 7.00 (m, 2H, $J = 8$ Hz, *5-m-Ar*), 5.60 (br s, 2H, *NH*), −2.85 (br s, 2H, *NH*); ^{13}C NMR (67.5 MHz, DMSO-d_6, δ): 157.4, 148.6, 135.4, 131.9, 131.8, 131.6, 131.5, 131.2, 131.1, 131, 130.9, 128.4, 121.2, 119.8, 119.6, 114.9, 113.9, 112.5; MALDI-MS *m/z*: 677 (M$^+$, 100%).

5-(4-Isothiocyanatophenyl)-10,15,20-tri-(4-hydroxyphenyl)porphyrin (16). Porphyrin **22** was converted into isothiocyanate **16** following general procedure B. The solid was chromatographed, eluting with DCM/MeOH (9:1) and gave the required product as a purple crystalline solid (48 mg, 91%); $R_f = 0.4$ (DCM/MeOH, 9:1); mp >350 °C (dec); UV−vis (MeOH) λ_{max}, nm: 422, 519, 556, 590, 651; ^{1}H NMR (270 MHz, DMSO-d_6, δ): 9.99 (br s, 3H, *OH*), 8.89−8.78 (m, 8H, *β-H*), 8.27 (m, 2H, $J = 8$ Hz, *5-o-Ar*), 7.99 (m, 6H, $J = 8$ Hz, *10+15+20-o-Ar*), 7.86 (m, 2H, $J = 8$ Hz, *5-m-Ar*), 7.20 (m, 6H, $J = 8$ Hz, *10+15+20-m-Ar*), −2.91 (br s, 2H, *NH*); ^{13}C NMR (68 MHz, DMSO-d_6, δ): 162.3, 161.2, 158.4, 141.5, 140.9, 137.4, 137.3, 135.8, 135.5, 135.4, 134.4, 131.8, 131.7, 131.3, 129.9, 124.5, 120.6, 120.3, 120, 119.6, 117.6, 114.1, 113.9, 105.7, 104.8. FAB-HRMS Anal. Calcd. for $C_{45}H_{29}N_5O_3S$ ([M + H]$^+$), 720.2069; found, 720.2095.

5-(4-Acetamidophenyl)-10,15,20-tri-(3,5-dimethoxyphenyl)porphyrin (19). Porphyrin **19** was synthesized according to the procedure of Adler et al. (*29*). The crude reaction mixture was purified by chromatography, eluting with DCM/ethyl acetate (4:1) and afforded the title compound as a purple crystalline solid (1.55 g, 9%); $R_f = 0.50$ (DCM/ethyl acetate, 4:1); mp >350 °C (dec); UV−vis (DCM) λ_{max}, nm: 421, 515, 551, 590, 650; ^{1}H NMR (270 MHz, $CDCl_3$, δ): 10.42 (br s, 1H, *NH*), 8.93−8.86 (m, 8H, *β-H*), 7.44 (m, 2H, $J = 8$ Hz, *5-o-Ar*), 7.38 (s, 6H, *10+15+20-o-Ar*), 7.07 (m, 2H, $J = 8$ Hz, *5-m-Ar*), 6.99 (s, 3H, *10+15+20-p-Ar*), 3.93 (s, 18H, *10+15+20-m-OCH_3*), 2.23 (s, 3H, CH_3), −2.96 (br s, 2H, *NH*); ^{13}C NMR (68 MHz, $CDCl_3$, δ): 168.7, 167.9, 160.3, 158.6, 143.1, 139.3, 135.6, 134.5, 131.8, 131.4, 131.3, 131.1, 129, 120, 119.6, 119.4, 119, 117.3, 113.5, 103.9, 23.9, 20.4; MALDI-MS *m/z*: 852 (M$^+$, 100%).

5-(4-Aminophenyl)-10,15,20-tri-(3,5-dimethoxyphenyl)porphyrin (21). Porphyrin **21** was synthesized by hydrolysis of **19** following general procedure A. The crude purple solid was purified by chromatography, eluting with DCM/ethyl acetate (4:1) and gave the desired product as a purple crystalline solid (426 mg, 89.7%); $R_f = 0.89$ (DCM/ethyl acetate, 4:1); mp >350 °C (dec); UV−vis (DCM) λ_{max}, nm: 422, 517, 553, 593, 651; ^{1}H NMR (270 MHz, $CDCl_3$, δ): 8.93 (m, 8H, *β-H*), 7.98 (m, 2H, $J = 8$ Hz, *5-o-Ar*), 7.40 (s, 6H, *10+15+20-o-Ar*), 7.06 (m, 2H, $J = 8$ Hz, *5-m-Ar*), 6.90 (s, 3H, *10+15+20-p-Ar*), 3.96 (s, 18H, *10+15+20-m-OCH_3*), −2.80 (br s, 2H, *NH*); ^{13}C NMR (68 MHz, $CDCl_3$, δ): 159.3; 146.5, 144.6, 144.5, 136.1, 132.7, 131.4, 130.2, 121.4, 120.1, 119.8, 115.7, 114.3, 113.9, 100.6, 20.13; MALDI-MS *m/z*: 809 (M$^+$, 100%).

5-(4-Aminophenyl)-10,15,20-tri-(3,5-dihydroxyphenyl)porphyrin (23). Porphyrin **21** was converted into **23** following general procedure C. The solid residue was chromatographed, eluting with $CHCl_3$/MeOH (9:1) to afford the title compound as a purple crystalline solid (667 mg, 75%); $R_f = 0.19$ ($CHCl_3$/MeOH, 9:1); mp >350 °C (dec); UV−vis (DCM) λ_{max}, nm: 422, 517, 553, 592, 649; ^{1}H NMR (270 MHz, DMSO-d_6, δ): 9.75 (br s, 6H, *10+15+20-m-OH*); 8.94 (s, 8H, *β-H*), 7.87 (m, 2H, $J = 8$ Hz, *5-o-Ar*), 7.06 (s, 6H, *10+15+20-o-Ar*), 7.02 (m, 2H, $J = 8$ Hz, *5-m-Ar*), 6.69 (s, 3H, *10+15+20-p-Ar*), 5.56 (br s, 2H, NH_2), −2.95 (br s, 2H, *NH*); ^{13}C NMR (68 MHz, DMSO-d_6, δ): 156.5, 156.4, 148.6, 142.9, 142.8, 135.5, 130.7−131.3, 128.3, 127.5, 121.5, 119.7, 119.2, 114.1, 113.9, 112.5, 102.3; MALDI-MS *m/z*: 726 (M$^+$, 100%).

5-(4-Isothiocyanatophenyl)-10,15,20-tri-(3,5-dihydroxyphenyl)porphyrin (17). Porphyrin **17** was syn-

thesized from **23** using general procedure B. The solid was purified by chromatography, eluting with $CHCl_3$/MeOH (9:1) which afforded the required product as a purple crystalline solid (67.5 mg, 64%); $R_f = 0.29$ ($CHCl_3$/MeOH, 9:1); mp >350 °C (dec); UV−vis (MeOH) λ_{max}, nm: 422, 516, 552, 592, 648; ^{1}H NMR (270 MHz, 25% CD_3OD in $CDCl_3$, δ): 9.0−8.76 (m, 8H, *β-H*), 8.19 (m, 2H, $J = 8$ Hz, *5-o-Ar*), 7.64 (m, 2H, $J = 8$ Hz, *5-m-Ar*), 7.12 (s, 6H, *10+15+20-o-Ar*), 6.77 (s, 3H, *10+15+20-p-Ar*); ^{13}C NMR (68 MHz, 25% CD_3OD in $CDCl_3$, δ): 155.8, 143.6, 142, 141.2, 136.1, 135.2, 134, 130.9, 123.9, 120.1, 120, 119.9, 117.6, 114.7, 107.1, 101. ES-HRMS Anal. Calcd. for $C_{45}H_{29}N_5O_6S$ ([M + H]$^+$), 768.1914; found, 768.1908.

5-(4-Acetamidophenyl)-10,15,20-tri-(4-pyridyl)porphyrin (25). Porphyrin **25** was synthesized by Adler condensation (*29*). The crude product was chromatographed, eluting with $CHCl_3$/MeOH (19:1), giving the required product as a purple crystalline solid (526 mg, 4%); $R_f = 0.22$ ($CHCl_3$/MeOH, 19:1); mp >350 °C (dec); UV−vis (DCM) λ_{max}, nm: 418, 514, 548, 587, 644; ^{1}H NMR (270 MHz, $CDCl_3$, δ): 10.35 (br s, 1H, *NH*), 9.10−9.15 (m, 6H, *10+15+20-m-Pyr*), 9.06−8.84 (m, 8H, *β-H*), 8.28−8.21 (m, 8H, *5-o-Ar* and *10+15+20-o-Pyr*), 8.07 (m, 2H, $J = 8$ Hz, *5-m-Ar*), 2.49 (s, 3H, CH_3), −2.79 (br s, 2H, *NH*); ^{13}C NMR (68 MHz, $CDCl_3$, δ): 175.2, 150.1, 149.6, 149.4, 149.3, 149, 148.2, 145.1, 142.5, 140.1, 134.7, 123.9, 123.8,123.3, 122.2, 122.1, 121.5, 121.1, 117.9, 110.2, 110.1, 106.9, 26.8; MALDI-MS *m/z*: 675 (M$^+$, 100%).

5-(4-Aminophenyl)-10,15,20-tri-(4-pyridyl)porphyrin (26). Porphyrin **25** was converted into the required product following general procedure A. The crude purple solid was purified by chromatography, eluting with $CHCl_3$/MeOH (20:1), and gave the product as a purple crystalline solid (422 mg, 90%); $R_f = 0.31$ ($CHCl_3$/MeOH, 20:1); mp >350 °C (dec); UV−vis (DCM) λ_{max}, nm: 418, 515, 552, 592, 653; ^{1}H NMR (270 MHz, $CDCl_3$, δ): 9.04 (m, 6H, $J = 5$ Hz, *10+15+20-m-Pyr*), 9.01−8.80 (m, 8H, *β-H*), 8.16 (m, 6H, $J = 5$ Hz, *10+15+20-o-Pyr*), 7.98 (m, 2H, $J = 8$ Hz, *5-o-Ar*), 7.08 (m, 2H, $J = 8$ Hz, *5-m-Ar*), 4.09 (br s, 2H, NH_2), −2.86 (br s, 2H, *NH*); ^{13}C NMR (68 MHz, $CDCl_3$, δ): 150, 149.8, 148.5, 148.4, 2, 146.5, 135.9, 131.7, 129.5, 122.7, 117.9, 117.4, 116.7, 113.6; FAB-MS *m/z*: 633 (M$^+$, 100%).

5-(4-Isothiocyanatophenyl)-10,15,20-tri-(4-pyridyl)-porphyrin (27). Porphyrin **26** was converted to **27** utilizing general procedure B. The crude product was dissolved in a minimum amount of chloroform and chromatographed, eluting with $CHCl_3$/MeOH (49:1) which yielded the title compound as a purple crystalline solid (104 mg, 98%); $R_f = 0.57$ ($CHCl_3$/MeOH, 49:1); mp >350 °C (dec); UV−vis (DCM) λ_{max}, nm: 417, 514, 548, 587, 643; ^{1}H NMR (270 MHz, $CDCl_3$, δ): 9.06 (m, 6H, $J = 5$ Hz, *10+15+20-m-Pyr*), 8.67 (br s, 8H, *β-H*), 8.21−8.15 (m, 8H, *10+15+20-o-Pyr* and *5-o-Ar*), 7.65 (m, 2H, $J = 8$ Hz, *5-m-Ar*), −2.91 (br s, 2H, *NH*); ^{13}C NMR (68 MHz, $CDCl_3$, δ): 149.8, 148.4, 140.6, 136.9, 135.4, 131.6, 129.3, 124.7, 119.7, 117.6, 117.4; FAB-MS *m/z*: 675.7 (M$^+$, 100%). ES-HRMS Anal. Calcd. for $C_{42}H_{26}N_8S$ ([M + H]$^+$), 675.2079; found, 675.2078.

5-(4-Isothiocyanatophenyl)-10,15,20-tri-(4-*N*-methylpyridiniumyl)porphyrin triiodide (24). To a solution of **27** (50 mg, 74 μmol) in anhydrous DMF (10 mL, distilled from CaH_2, 0.1 Torr) was added iodomethane (1 mL, 16 mmol). The reaction was stirred under argon for 3 h at room temperature. Upon completion of the reaction, excess DMF was removed in vacuo (0.1 Torr) at 30−40 °C to yield the title compound as a lustrous purple solid (77 mg, 95%); $R_f = 0.32$ (5 M KNO_3-(aq)/MeCN, 1:4); mp >350 °C (dec); UV−vis (H_2O) λ_{max}, nm: 423, 520, 585; ^{1}H NMR (270 MHz, DMSO-d_6, δ): 9.50 (m, 6H, $J = 6$ Hz, *10+15+20-m-Pyr*), 9.16 (m, 8H, *β-H*), 9.03 (m, 6H, $J = 6$ Hz, *10+15+20-o-Pyr*), 8.32 (m, 2H, $J = 8$ Hz, *5-o-Ar*), 7.96 (m, 2H, $J = 8$ Hz, *5-m-Ar*), 4.74 (br s, 9H, *CH$_3$-pyr*), −3.03 (br s, 2H, *NH*); ^{13}C NMR (67.5 MHz, DMSO-d_6, δ): 156.4, 156.3, 144.1, 139.7, 135.4, 134.7, 132, 130.6, 124.8, 121.1, 115.3, 114.7, 47.9; FAB-MS *m/z*: 719 ([M + H$^+$], 100%), 704 (M − *CH$_3$*, 26%), 689 (M − *2xCH$_3$*, 20%), 674 (M − *3xCH$_3$*, 5%). ES-HRMS Anal. Calcd. for $C_{45}H_{35}N_8S$ ([M + H]$^+$), 719.2705; found, 719.2686.

5-(4-Isothiocyanatophenyl)-10,15,20-tris(4-*N*-methylpyridiniumyl)porphyrin trichloride (28). To a solution of **24** (30 mg, 27 μmol) in anhydrous MeOH (30 mL) was added Amberlite IRA 400 (1.0 g), and the mixture was stirred for 1 h at room temperature. Amberlite IRA 400 resin was filtered under vacuum, and the porphyrin filtrate was recovered, dried (Na_2SO_4), and concentrated in vacuo to yield the required product as a purple crystalline solid (22 mg, 96%). Porphyrins **24** and **28** were distinguished only by their respective solubilities in water.

5-(4-Fluorenylmethylaminophenyl)-15-(4-methoxyphenyl)porphyrin (35). To a stirred solution of porphyrin **6** (28 mg, 55 μmol) in anhydrous 1,4-dioxane (2.5 mL) was added solid sodium hydrogen carbonate (6 equiv, 28 mg, 0.33 mmol). To this mixture was then added a solution of 9-fluorenylmethyl chloroformate (2 equiv, 0.11 mmol, 28.5 mg) in 1,4-dioxane (0.5 mL) under N_2. The reaction flask was covered with aluminum foil to exclude light and stirred at room temperature for a period of 3 h. At this time, the reaction was complete (as monitored by TLC). The 1,4-dioxane was removed in vacuo and the residue partitioned between water (25 mL) and DCM (2 × 25 mL). The combined organic extracts were washed with saturated brine (25 mL), then dried (Na_2SO_4), filtered, and concentrated in vacuo. The required porphyrin was obtained by chromatography, eluting with DCM. The desired porphyrin was obtained as purple crystals (38 mg, 95%); $R_f = 0.39$ (DCM); mp 292−295 °C (dec); UV−vis (DCM) λ_{max} (relative intensity), nm: 410 (1.0), 505 (0.042), 541 (0.02), 578 (0.015), 633 (0.01); fluorescence (DCM): λ_{max} 635 nm (λ excitation = 410 nm); ^{1}H NMR (270 MHz, $CDCl_3$, δ): 10.35 (s, 2H, *10+20-H*), 9.69 (br s, 1H, *NH*), 9.44 (d, 4H, $J = 4.8$ Hz, *β-H*), 9.12 (d, 4H, $J = 4.8$ Hz, *β-H*), 8.20−8.17 (m (overlapping), 4H, $J = 8.1$ Hz, *5+15-o-Ar*), 7.85 (m, 4H, *5+15-m-Ar*), 7.76−7.66 (m, 2H, *fluoreno-Ar*), 7.51−7.30 (m, 6H, *fluoreno-Ar*), 4.69 (d, 2H, $J = 7.2$ Hz, CH_2), 4.30 (t, 1H, $J = 7.2$ Hz, *CH*), 4.13 (s, 3H, CH_3), −3.15 (br. s, 2H, *NH*); MALD-MS *m/z*: 731.5 ([M + H]$^+$, 100%), 508.3 ([M − FMOC + 2]$^+$, 50%). ES-HRMS Anal. Calcd. for $C_{48}H_{36}N_5O_3$ ([M + H]$^+$), 730.2818; found, 730.2809.

17,18-Dihydroxy-5-(4-aminophenyl)-15-(4-methoxyphenyl)chlorin and 7,8-Dihydroxy-5-(4-aminophenyl)-15-(4-methoxyphenyl)chlorin Regioisomers (31/32). Porphyrin **6** (28 mg, 55.2 μmol) was converted into the required mixture of chlorin regioisomers following the procedure of Sutton et al. (*26*). The crude reaction mixture was then chromatographed, eluting with 1% MeOH in DCM. First, some unreacted starting material was eluted, then the higher R_f chlorin isomer **31** eluted as a brown-purple crystalline solid; $R_f = 0.28$ (DCM/MeOH, 19:1). The lower R_f isomer **32** was obtained by further elution with 2.5% MeOH in DCM and gave also a brown-purple crystalline solid; $R_f = 0.17$ (DCM/MeOH, 19:1).

High R_f Chlorin Regioisomer. 17,18-Dihydroxy-15-(4-methoxy phenyl)-5-(4-aminophenyl)chlorin was assigned previously (*26*) (7.0 mg, 24%); mp 165−167 °C (dec); UV−vis (DCM) λ_{max} (relative intensity), nm: 401 (0.99), 414 (1.0), 503 (0.08), 535 (0.07), 582 (0.035), 636 (0.22); fluorescence (DCM): λ_{max} 639 nm (λ excitation = 412 nm); ^{1}H NMR (270 MHz, 10% CD_3OD in $CDCl_3$, δ): 9.95 (s, 1H, *10-H*), 9.42 (s, 1H, *20-H*), 9.17 (d, 1H, J = 4.8 Hz, *β-H*), 9.03 (d, 1H, J = 4.0 Hz, *β-H*), 8.97 (s, 2H, *β-H*) 8.78 (d, 1H, J = 4.8 Hz, *β-H*), 8.51 (d, 1H, J = 4.8 Hz, *β-H*), 8.05 (m, 2H, J = 8.9 Hz, *o-Ar*), 7.94 (m, 2H, J = 8.1 Hz, *o′-Ar*), 7.25 (m, 2H, J = 8.9 Hz, *m-Ar*), 7.12 (m, 2H, J = 8.1 Hz, *m′-Ar*), 6.42 (d, 1H, J = 6.5 Hz, *17-H*), 6.03 (d, 1H, J = 6.5 Hz, *18-H*), 4.08 (s, 3H, CH_3), (*NH*'s exchanged and *OH*'*s* not observed); MALDI-MS *m*/*z*: 542.2 ([M + H]$^+$, 100%). ES-HRMS Anal. Calcd. for $C_{33}H_{28}N_5O_3$ ([M + H]$^+$), 542.2192; found, 542.2187.

Low R_f Chlorin Regioisomer. 7,8-Dihydroxy-5-(4-aminophenyl)-15-(4-methoxyphenyl)chlorin (8.5 mg, 30%); mp 168−171 °C (dec); UV−vis (DCM) λ_{max} (relative intensity), nm: 401(0.99), 413 (1.0), 507 (0.08), 536 (0.06), 586 (0.025), 637 (0.20); fluorescence (DCM): λ_{max} 639 nm (λ excitation = 412 nm); ^{1}H NMR (270 MHz, 10% CD_3-OD in $CDCl_3$, δ): 9.96 (s, 1H, *20-H*), 9.40 (s, 1H, *10-H*), 9.18 (d, 1H, J = 4.8 Hz, *β-H*), 9.05 (d, 1H, J = 4.8 Hz, *β-H*), 8.98 (d, 1H, J = 4.0 Hz, *β-H*) 8.92 (d, 1H, J = 4.0 Hz, *β-H*), 8.74 (d, 1H, J = 4.0 Hz, *β-H*), 8.58 (d, 1H, J = 4.0 Hz, *β-H*), 8.13 (m, 1H, J = 8.9 Hz, *o-Ar*), 8.08 (m, 1H, J = 8.9 Hz, *o-Ar*), 7.95 (m, 1H, J = 8.1 Hz, *o′-Ar*), 7.79 (m, 1H, J = 8.1 Hz, *o′-Ar*), 7.36 (m, 1H, J = 8.9 Hz, *m-Ar*), 7.30 (m, 1H, J = 8.9 Hz, *m-Ar*), 7.11 (m, 1H, J = 8.1 Hz, *m′-Ar*), 7.05 (m, 1H, J = 8.1 Hz, *m′-Ar*), 6.42 (d, 1H, J = 6.5 Hz, *7-H*), 6.09 (d, 1H, J = 6.5 Hz, *8-H*), 4.11 (s, 3H, CH_3), (*NH*'s exchanged and *OH*'s not observed); MALDI-MS *m*/*z*: 542.2 ([M + H]$^+$, 100%). ES-HRMS Anal. Calcd. for $C_{33}H_{28}N_5O_3$ ([M + H]$^+$), 542.2192; found, 542.2185.

17,18-Dihydroxy-5-(4-isothiocyanatophenyl)-15-(4-methoxyphenyl)chlorin (29). The higher R_f regioisomeric chlorin **31** (17.5 mg, 23.2 μmol) was converted into the corresponding isothiocyanate following general procedure B. The resulting organic extract was filtered, concentrated, and then chromatographed, eluting with 1% MeOH in DCM to afford **29**. The title compound was isolated as a brown-purple crystalline solid (17 mg, 90%); R_f = 0.36 (DCM/MeOH, 19:1); mp 155−158 °C (dec); UV−vis (DCM) λ_{max} (relative intensity), nm: 410 (1.0) 505 (0.09), 534 (0.06), 586 (0.04), 637 (0.18); fluorescence (DCM): λ_{max} 639 nm (λ excitation = 412 nm); ^{1}H NMR (270 MHz, 10% CD_3OD in $CDCl_3$, δ): 10.0 (s, 1H, *10-H*), 9.45 (s, 1H, *20-H*), 9.20 (d, 1H, J = 4.8 Hz, *β-H*), 9.06 (d, 1H, J = 4.0 Hz, *β-H*), 9.02 (d, 1H, J = 4.8 Hz, *β-H*) 8.84 (d, 1H, J = 4.8 Hz, *β-H*), 8.64 (d, 1H, J = 4.0 Hz, *β-H*), 8.55 (d, 1H, J = 4.8 Hz, *β-H*), 8.21 (m, 1H, J = 8.1 Hz, *5-o-Ar*), 8.15 (m, 1H, J = 8.1 Hz, *5-o-Ar*), 8.05 (m, 1H, J = 8.9 Hz, *15-o-Ar*) 7.93 (m, 1H, J = 8.9 Hz, *15-o-Ar*), 7.65 (m, 2H, *5-m-Ar*), 7.24 (m, 2H, *15-m-Ar*), 6.43 (d, 1H, J = 6.5 Hz, *17-H*), 6.04 (d, 1H, J = 6.5 Hz, *18-H*), 4.08 (s, 3H, CH_3), (*NH*'s exchanged and *OH*'s not observed); MALDI-MS *m*/*z*: 583.7 ([M + H]$^+$, 100%). ES-HRMS Anal. Calcd. for $C_{34}H_{26}N_5O_3S$ ([M + H]$^+$), 584.1757; found, 584.1756.

***cis/trans*-7,8,17,18-Tetrahydroxy-5-(4-fluorenylmethylaminophenyl)-15-(4-methoxyphenyl)bacteriochlorins (36/37).** Porphyrin **35** (35 mg, 48.0 μmol) was converted into the required mixture of bacteriochlorin stereoisomers by minor modification of the procedure of Sutton et al. (*26*) (reaction carried out using 1,4-dioxane (5 mL) to allow for the dissolution of **35**). The crude reaction mixture was chromatographed, eluting initially with 1% MeOH in DCM to remove chlorin byproducts. Further elution with 2% MeOH/DCM allowed for the isolation of both stereoisomeric bacteriochlorin tetrols. The higher R_f *trans*-bacteriochlorin isomer **36** was isolated as a pink-green crystalline solid (6 mg, 15%); R_f = 0.25 (DCM/MeOH, 19:1); mp 142−145 °C (dec); UV−vis (DCM) λ_{max} (relative intensity), nm: 374 (1.0) 512 (0.23), 702 (0.52); fluorescence (DCM): λ_{max} 708 nm (λ excitation = 512 nm); ^{1}H NMR (270 MHz, 10% CD_3-OD in $CDCl_3$, δ): δ 9.20 (s, 2H, *10+20-H*), 8.78 (d, 2H, J = 4.0 Hz, *β-H*), 8.36 (d, 2H, J = 4.0 Hz, *β-H*), 7.95 (m, 2H, *o-Ar*), 7.85 (m, 2H, J = 7.3 Hz, *fluoreno-Ar*), 7.79 (m, 2H *o′-Ar*), 7.65 (m, 2H, *m′-Ar*), 7.47−7.38 (m, 6H, *fluoreno-Ar*), 7.24 (m, 2H, *m-Ar*), 6.27−6.24 (m, 2H, *7+17-H*), 5.85 (m, 2H, *8+18-H*), 4.65 (d, 2H, J = 7.2 Hz, CH_2), 4.39 (t, 1H, J = 7.2 Hz, *CH*), 4.06 (s, 3H, CH_3), −1.94 (br s (partly exchanged), 2H, *NH*), (*OH*'s not observed); MALDI-MS *m*/*z*: 800.4 ([M + H]$^+$, 100%). ES-HRMS Anal. Calcd. for $C_{48}H_{40}N_5O_7$ ([M + H]$^+$), 798.2927; found, 798.2921.

The lower R_f *cis*-bacteriochlorin isomer **37** was isolated as a pink-green crystalline solid (8.5 mg, 21%); R_f = 0.2 (DCM/MeOH, 19:1); mp 148−150 °C (dec); UV−vis (DCM) λ_{max} (relative intensity), nm: 374 (1.0) 512 (0.24), 703 (0.54); fluorescence (DCM): λ_{max} 708 nm (λ excitation = 512 nm); ^{1}H NMR (270 MHz, 10% CD_3OD in $CDCl_3$, δ): 9.12 (s, 2H, *10+20-H*), 8.76 (d, 2H, J = 4.8 Hz, *β-H*), 8.34 (d (overlapping), 2H, J = 4.8 Hz, *β-H*), 8.02 (m, 2H, *o-Ar*), 7.85 (m (obscured), 2H, J = 8.0 Hz, *o′-Ar*), 7.83 (m, 2H, J = 7.3 Hz, *fluoreno-Ar*), 7.76 (m, 2H, J = 8.0 Hz, *m′-Ar*), 7.50−7.38 (m, 6H, *fluoreno-Ar*), 7.24 (m, 2H, *m-Ar*), 6.27−6.23 (m, 2H, *7+17-H*), 5.85−5.82 (m, 2H, *8+18-H*), 4.65 (d, 2H, J = 7.2 Hz, CH_2), 4.39 (t, 1H, J = 7.2 Hz, *CH*), 4.05 (s, 3H, CH_3), −1.88 (br s (partly exchanged), 2H, *NH*), (*OH*'s not observed); MALDI-MS *m*/*z*: 800.4 ([M + H]$^+$, 100%). ES-HRMS Anal. Calcd. for $C_{48}H_{40}N_5O_7$ ([M + H]$^+$), 798.2927; found, 798.2921.

***cis*-7,8,17,18-Tetrahydroxy-5-(4-isothiocyanatophenyl)-15-(4-methoxyphenyl)bacteriochlorin (30) (General Procedure E).** The *cis*-bacteriochlorin **37** (8.5 mg, 10.7 μmol) in 25% MeOH in DCM (1.25 mL) was treated with piperidine (50 equiv, 53 μL, 0.53 mmol) and left to stir for a period of 3 h at room temperature under N_2 with light excluded. The reaction mixture was concentrated in vacuo (0.1 Torr) to remove all traces of piperidine. The crude amine **34** was then converted into the required isothiocyanate following general procedure B. The *cis*-bacteriochlorin isothiocyanate was isolated as a pink-green crystalline solid (5.0 mg, 76%); R_f = 0.40 (DCM/MeOH, 19:1); mp 132−135 °C (dec); UV−vis (DCM) λ_{max} (relative intensity), nm: 375 (1.0) 516 (0.22), 702 (0.48); fluorescence: λ_{max} 709 nm (λ excitation = 516 nm); ^{1}H NMR (270 MHz, 10% CD_3OD in $CDCl_3$, δ): 9.20 (s, 1H, *meso-H*), 9.18 (s, 1H, *meso-H*), 8.77 (d, 2H, J = 4.8 Hz, *β-H*), 8.40 (d, 1H, J = 4.8 Hz, *β-H*), 8.34 (d, 1H, J = 4.8 Hz, *β-H*), 8.14 (m, 2H, *o-Ar*), 8.05 (m, 2H, *o′-Ar*), 7.42−7.08 (m, 4H, *5+15-m-Ar*), 6.20 (m, 2H, *7+17-H*), 5.98 (m, 1H, *8-H*), 5.93 (m, 1H, *18-H*), 4.04 (s, 3H, CH_3), −1.80 (br s, 2H, partly exchanged-*NH*), (*OH*'s not observed); MALDI-MS *m*/*z*: 618.9 ([M + H]$^+$, 100%). ES-HRMS Anal. Calcd. for $C_{34}H_{28}N_5O_5S$ ([M + H]$^+$), 618.1815; found, 618.1810.

17,18-Dihydroxy-5-(4-acetamidophenyl)-15-(4-methoxyphenyl)chlorin/7,8-dihydroxy-5-(4-acetamidophenyl)-15-(4-methoxyphenyl)chlorin Regioisomers (38/39) and *cis/trans*-7,8,17,18-Tetrahydroxy-5-(4-acetamidophenyl)-15-(4-methoxyphenyl)-bacteriochlorin Stereoisomers (40/41). Porphyrin **4** (100 mg, 0.18 mmol) was converted, in a single reaction,

to a mixture of chlorin diols/bacteriochlorin tetrols following the procedure of Sutton et al. (*26*). After 38 h, the reaction was stopped. The crude reaction mixture was then chromatographed, eluting with 2% MeOH in DCM to give, first, some unreacted starting material and then the higher R_f chlorin isomer **38** as a brown-purple crystalline solid (5 mg, 5%). The lower R_f isomer **39** was obtained by further elution with 3.5% MeOH in DCM and gave also a brown-purple crystalline solid (7.0 mg, 7%). Further elution with 5% MeOH in DCM afforded the required *trans*/*cis*-bacteriochlorin tetrols **40** and **41** as pink/green solids ((5.0 mg, 5%) and (7.0 mg, 7%), respectively).

*High R_f Chlorin Regioisomer **38***. 17,18-Dihydroxy-15-(4-methoxyphenyl)-5-(4-acetamidophenyl)chlorin was assigned on the basis of past data (*26*); R_f = 0.40 (DCM/MeOH, 37:3); mp 186−188 °C (dec); UV−vis (DCM) λ_{max} (relative intensity), nm: 410(1.0), 505.5 (0.12), 535 (0.08), 585.5 (0.05), 637 (0.18); fluorescence (DCM): λ_{max} 639 nm (λ excitation = 410 nm); ^{1}H NMR (270 MHz, $CDCl_3$, δ): 9.97 (s, 1H, *10-H*), 9.42 (s, 1H, *20-H*), 9.19 (d, 1H, J = 4.0 Hz, *β-H*), 9.03 (d, 1H, J = 4.0 Hz, *β-H*), 8.98 (d, 1H, J = 4.8 Hz, *β-H*) 8.89 (d, 1H, J = 4.0 Hz, *β-H*), 8.70 (d, 1H, J = 4.8 Hz, *β-H*), 8.52 (d, 1H, J = 4.8 Hz, *β-H*), 8.14−8.10 (m, 3H, *5-o*/*m-Ar*), 7.96−7.82 (m, 3H, *5+15-o*/*m-Ar*), 7.50 (s, 1H, *NH*), 7.34 (m, 2H, *15-m-Ar*), 6.48 (m, 1H, *17-H*), 6.20 (m, 1H, *18-H*), 4.08 (s, 3H, *CH*$_3$), 2.38 (s, 3H, *CH*$_3$), −1.89, −2.20 (s, 2H, *NH*); MALDI-MS *m*/*z*: 582.6 ([M + H]$^+$, 100%). ES-HRMS Anal. Calcd. for $C_{35}H_{28}N_5O_4$ ([M + H]$^+$), 582.2141; found, 582.2137.

*Low R_f Chlorin Regioisomer **39***. 7,8-Dihydroxy-5-(4-acetamidophenyl)-15-(4-methoxyphenyl)chlorin; R_f = 0.35 (DCM/MeOH, 37:3); mp 182−185 °C (dec); UV−vis (DCM) λ_{max} (relative intensity), nm: 410(1.0), 505.5 (0.1), 535 (0.07), 585 (0.04), 636 (0.19); fluorescence (DCM): λ_{max} 639 nm (λ excitation = 410 nm); ^{1}H NMR (270 MHz, 10% DMSO-d_6 in $CDCl_3$, δ): 9.96 (s, 1H, *10-H*), 9.92 (s, 1H, *NH*), 9.42 (s, 1H, *20-H*), 9.22 (m, 1H, *β-H*), 9.02 (d, 1H, J = 4.8 Hz, *β-H*), 9.00 (m, 1H, *β-H*) 8.92 (m, 1H, *β-H*), 8.70 (d, 1H, J = 4.8 Hz, *β-H*), 8.53 (m, 1H, *β-H*), 8.18−7.91 (m, 6H, *5+15-o*/*m-Ar*), 7.33−7.28 (m, 2H, *15-m-Ar*), 6.36 (m, 1H, *7-H*), 5.96 (m, 1H, *8-H*), 4.10 (s, 3H, *CH*$_3$), 2.30 (s, 3H, *CH*$_3$), −1.74, −2.17 (s, 2H, *NH*); MALDI-MS *m*/*z*: 582.6 ([M + H]$^+$, 100%). ES-HRMS Anal. Calcd. for $C_{35}H_{28}N_5O_4$ ([M + H]$^+$), 582.2141; found, 582.2135.

*High R_f trans-Bacteriochlorin **40***. R_f = 0.29 (DCM/MeOH, 37:3:1); mp 152−155 °C (dec); UV−vis (DCM) λ_{max} (relative intensity), nm: 373.5 (1.0) 514 (0.25), 702 (0.49); fluorescence (DCM): λ_{max} 708 nm (λ excitation = 514 nm); ^{1}H NMR (270 MHz, DMSO-d_6, δ): 10.27 (s, 1H, *NH*), 9.16 (s, 2H, *10+20-H*), 8.96 (d, 2H, J = 4.0 Hz, *β-H*), 8.24 (d, 2H, J = 4.0 Hz, *β-H*), 7.99−7.89 (m, 6H, *5+15-o*/*m-Ar*), 7.25 (m, 2H, *15-m-Ar*), 6.30 (m, 2H, *7+17-H*), 6.15 (m, 2H, *8+18-H*), 5.63 (m, 2H, *OH*), 5.32 (m, 2H, *OH*), 3.99 (s, 3H, *CH*$_3$), 2.20 (s, 3H, *CH*$_3$), −1.87 (br s, 2H, *NH*); MALDI-MS *m*/*z*: 616.3 ([M + H]$^+$,100%). ES-HRMS Anal Calcd. for $C_{35}H_{30}N_5O_6$ ([M + H]$^+$), 616.2196; found, 616.2192.

*Low R_f cis-Bacteriochlorin **41***. R_f = 0.24 (DCM/MeOH, 19:1); mp 148−151 °C (dec); UV−vis (DCM) λ_{max} (relative intensity), nm: 373.5 (1.0) 514.5 (0.24), 703 (0.50); fluorescence (DCM): λ_{max} 708 nm (λ excitation = 514 nm); ^{1}H NMR (270 MHz, 20% CD_3OD in $CDCl_3$, δ): 9.20 (s, 2H, *10+20-H*), 8.78 (m, 2H, *β-H*), 8.35 (m, 2H, *β-H*), 8.05 (m, 2H, *5-o-Ar*), 7.89−7.86 (m, 3H, *5+15-o*/*m-Ar*), 7.75 (m, 1H, *15-o-Ar*), 7.20−7.17 (m, 2H, *15-m-Ar*), 6.25 (m, 2H, *7+17-H*), 5.86 (m, 2H, *8+18-H*), 4.06 (s, 3H, *CH*$_3$), 2.31 (s, 3H, *CH*$_3$) (*NH*'s exchanged); MALDI-MS *m*/*z*: 616.4 ([M + H]$^+$, 100%). ES-HRMS Anal. Calcd. for $C_{35}H_{30}N_5O_6$ ([M + H]$^+$), 616.2196; found, 616.2192.

Preparation of Bioconjugates: 2,3-Dihydroxy-5-(4-methoxyphenyl)-15-(4-isothiouridophenyl)chlorin-BSA Bioconjugate (General Procedure D). In a typical bioconjugation procedure, a stock solution of the 2,3-dihydroxy-5-(4-methoxyphenyl)-15-(4-isothiocyanatophenyl)chlorin 29 (higher R_f regioisomer) in anhydrous DMSO (10 mg mL^{-1}) was prepared. To a stirred solution of BSA (1 equiv, 10 mg, 0.15 μmol) in a sodium bicarbonate/sodium carbonate buffer (1 mL, pH 9.2) was added a solution of the isothiocyanate (10 mg mL^{-1} stock solution; 10 equiv, 88 μL, 1.52 μmol). The reaction vessel was protected from light and agitated for a period of 16 h at room temperature. The bioconjugate was purified by gel-filtration using a sodium phosphate buffer (0.5 M, pH 7.0) pre-equilibrated PD-10 gel filtration column, eluting with the same buffer.

BSA-Haematoporphyrin Bioconjugate. Haematoporphyrin (18.0 mg, 30 μmol), *N*-hydroxysuccinimide (6.9 mg, 60 μmol), and DCC (12.5 mg, 60 μmol) in anhydrous DMSO (1.0 mL) were stirred overnight at room temperature to facilitate the formation of the activated NHS-ester(s) of haematoporphyrin. To a solution of BSA (10 mg, 0.15 μmol) in sodium bicarbonate/sodium carbonate buffer (1 mL, pH 9.2) was added, from the stock solution, haemotoporphyrin-NHS (10 equiv, 50 μL, 1.52 μmol). The reaction vessel was protected from light and agitated, at room temperature, for a period of 16 h. The bioconjugate was purified by gel-filtration using a sodium phosphate buffer (0.5 M, pH 7.0) pre-equilibrated PD-10 gel filtration column, eluting with the same buffer.

Characterization of Bioconjugates: Gel Electrophoresis. Bioconjugates were characterized by sodium dodecyl sulfate−polyacrylamide gel electrophoresis (SDS−PAGE), which were performed for 45 min at 200 V and 400 mA. Stacking gels of 4% were used, and 12% or 15% separating gels were used for BSA and avidin, respectively. The running buffer used was 0.1% (w/v) SDS in a 125 mM Tris-gylcine buffer (pH 8.9). Electrophoresis was performed under nonreducing conditions with samples containing 25% Tris-HCl (125 mM, pH 6.8), 20% (w/v) glycerol 4% (w/v) and 0.03% bromophenol blue. For SDS−PAGE analysis of avidin bioconjugates, the protein solution, in loading buffer, was heated to 95 °C for 1 min. This was undertaken to ensure that all avidin entered the gel (without this, little avidin bioconjugate entered the gel because of the high isoelectric point of avidin, which resulted in extensive aggregation in the loading gel). After electrophoresis, gels were first photographed under 360 nm UV illumination using a Kodak instamatic camera fitted with a 570 nm long pass filter and then silver-stained using the method of Heukenshoven and Dernick (*27*).

Noncovalent-Binding Studies: Utilizing Chemically Unreactive Fluorescent Probe/Protein Mixtures. To investigate the levels of NCB typical for these potential fluorescent probes, we undertook the synthesis of chlorin **39** and bacteriochlorin **41** examples. The chlorin **39** and bacteriochlorin **41** were then mixed with BSA independently using general procedure D. The colored bands obtained from all PD-10 gel permeation columns were analyzed by UV−vis spectroscopy. Similar mixtures containing unreactive fluorescein and haemotoporphyrin derivative were also analyzed using the same procedure, to establish a comparison of their possible NCB interactions with proteins. SDS−PAGE analysis was used to show that the removal of noncovalently bound fluorescent probes from proteins was possible.

Hela Cell Transfer Experiment Utilizing Crude Bioconjugates and NCB Fluorescent Probe/Protein Mixtures. Further investigation of the potential problems associated with the use of impure bioconjugates, that contain a NCB fluorescent probe, was undertaken with the use of epithelial human carcinoma cell line (HeLa). Products, obtained by mixing capped chlorin **39** and bacteriochlorin **41** with BSA, were purified by gel permeation chromatography (PD-10) and adjusted to varying concentrations (2.5−25 mg mL^{-1}) made up to 3 mL, and their fluorescence intensity was measured. Similar mixtures were then made up to the same final concentration, but to each was added 500 000 HeLa cells. The mixtures were then agitated for 5 min to allow any probe transfer to occur. Each sample was centrifuged at 1000*g* for 3 min, and the fluorescence of the supernatant was remeasured. Finally, the pellets of HeLa cells were resuspended by agitation, and a final fluorescence measurement was taken.

Purification of Bioconjugates: Using SDS−PAGE Electroelution. Following gel permeation chromatography, the BSA bioconjugates were further purified by SDS−PAGE to remove a NCB fluorescent probe. The purified bioconjugates were then recovered using a Millipore centrilutor microelectroeluter (Fisher Life Sciences, U.K.), this device incorporates removable Centricon filter units so as to allow electroeluted proteins to be washed successively with PBS prior to concentration by centrifugation. YM-30 Centricon concentrators were used for BSA bioconjugates. Electroelution was achieved using 200 V (50 mA) and took between 2 and 3 h. The concentrated, purified bioconjugates were then collected in the retentate vials of the filter units by inversion and centrifugation. Sodium azide (2 M, 20 mL) was added, and the bioconjugates were stored at 4 °C.

Using the Acetone Precipitation Method. Initial attempts at the removal of the NCB fluorescent probe were undertaken using the procedure of Hamblin et al. (*15*). Briefly, this involved the slow addition of ACS grade acetone (10*x*) to the crude bioconjugate preparations at 4 °C (approximate concentration of 2.5 mg mL^{-1}). After 6 h, the suspension was centrifuged at 4000*g*, and the supernatant was removed. The pellet was resuspended in the same volume of acetone, and the centrifugation was repeated. After a further three washes, the bioconjugates were redissolved in 1 mL of PBS and exhaustively dialyzed against 2 L of PBS for 2 days to remove all traces of acetone. The semipurified bioconjugates were then analyzed by SDS−PAGE and TLC (1:1 mixture of 10% aqueous ammonium chloride and MeOH).

Confocal Laser Scanning Microscope Analysis of BSA Bioconjugates. A preliminary examination of the intracellular localization of BSA bioconjugates was undertaken using fluorescence microscopy. The HeLa cell line was chosen for the microscope studies, and a number of 5 cm culture dishes, with 22 × 22 mm^2 microscope cover slips inside, were seeded with 5×10^5 HeLa and allowed to grow in 5.0 mL media for 2 days until the monolayer of cells generated was about 75% confluent. Further incubation with a range of concentrations of BSA bioconjugates were then undertaken for 30 min prior to cell fixing with 4% formaldehyde and further washings. The cover slips were then placed on histological slides with PBS and fixed along their edges with grease. A Biorad Radiance-2000 confocal laser scanning microscope was then used with argon-ion laser excitation at 514 nm, fluorescent images being collected after passage through a 570 or 640 nm long pass filter.

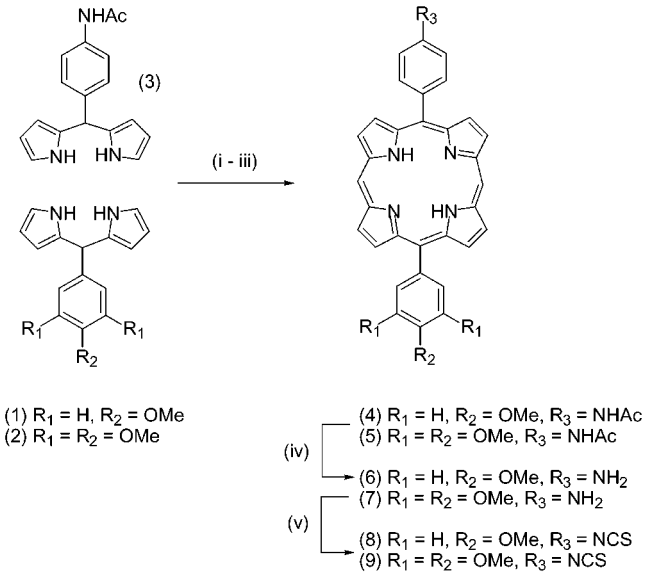
RESULTS AND DISCUSSION

The majority of attempts at covalently conjugating porphyrin type molecules with biological targeting agents, such as serum albumins (*12*−*15*), monoclonal antibodies (*16*−*20*), and lipoproteins (*21*, *22*), have generally involved the use of carbodiimide or NHS ester-based coupling methodologies. These coupling methods, however, have their drawbacks; carbodiimide-mediated conjugations are slow and invariably lead to extensive loss of porphyrin as the stable *N*-acyl urea derivative; also, both methods can lead to cross-linking when using naturally occurring porphyrins containing multiple carboxyl groups. To overcome these drawbacks, we have become interested in the synthesis and elaboration of a range of synthetic porphyrin derivatives for use in bioconjugation. These derivatives, while still containing the important porphine core, have allowed us to produce fluorescent probes and PDT agents containing a single reactive isothiocyanato (ITC) functionality (*26*, *28*). Although this eliminates the problems associated with cross-linking, another problem has become apparent during our studies. Bioconjugate preparation using tetrapyrrole derivatives invariably result in the formation of noncovalent complexes (*13*, *16*, *17*). For lipophilic derivatives, the level of NCB can significantly exceed that of covalent binding. The NCB complexes formed between lipophilic or amphiphilic porphyrins and proteins are stable and cannot be separated using conventional gel permeation (size exclusion) chromatography. Clearly, the use of such NCB complexes can lead to loss of specificity because of chromophore transfer to serum proteins or cellular membranes. We therefore set out to study, and address, the problem of NCB in the synthesis of photoactive bioconjugates.

Initial Synthetic Studies on Diphenylporphyrin (DPP)-Based Molecular Probes. We have recently been developing DPP's as core structures for the synthesis of imaging agents and PDT photosensitizers. Using methodologies developed within our laboratories (*26*, *28*), we initially synthesized diphenylporphyrin isothiocyanates **8** and **9** bearing different methoxy substitution patterns. This was undertaken in an attempt to induce solubility of the reactive porphyrin isothiocyanate (PITC) in DMSO or DMF "stock" solutions commonly used in protein bioconjugations (most lipophilic porphyrins are almost completely insoluble in DMSO or DMF and completely insoluble in aqueous bioconjugation buffers). Separate acid-catalyzed condensations of the dipyrromethanes **1** and **2** with the *N*-acetyl derivative **3** and trimethyl orthoformate gave the corresponding monoacetamidoporphyrins **4** and **5** (Scheme 1). Hydrolysis of **4** and **5** followed by treatment of the resulting amines **6** and **7** with 1,1′-thiocarbonyldi-2(1*H*)-pyridone (TDP) (*4*, *5*) afforded PITCs **8** and **9**. PITC **8** was found to be completely insoluble in DMSO, DMF, MeOH, and EtOH alike, although PITC **9** was soluble in DMSO. DMSO cosolvent stock solution of **9** was therefore prepared at a standard concentration of 10 mg mL^{-1}, and a 100 μL aliquot of this solution was slowly added to 1 mL of a bicarbonate buffer at pH 9.2, to simulate a typical bioconjugation procedure. Unfortunately, the addition of the cosolvent stock solution to the aqueous buffer resulted in the immediate precipitation of porphyrin. Although PITC **9** was soluble in DMSO and DMF, the inclusion of two extra methoxy groups apparently did not represent a large enough increase in polarity to allow bioconjugation in aqueous media.

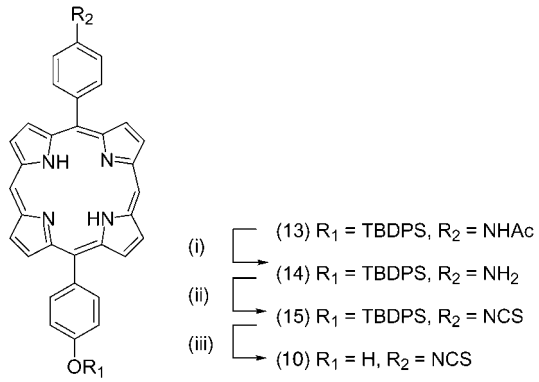
As bioconjugations involving the isothiocyanate group are often carried out in carbonate/bicarbonate buffers

Scheme 1[a]



[a] Conditions: (i) trichloroacetic acid, trimethylorthoformate, DCM, RT, 3.5 h; (ii) pyridine, RT, 16 h; (iii) air, RT, 3 h; (iv) 5 M HCl(aq), 80 °C, 3 h; (v) TDP, DCM, RT, 2 h.

Scheme 2[a]



[a] Conditions: (i) 5 M HCl(aq), 80 °C, 3 h; (ii) TDP, DCM, RT, 5 h; (iii) TBAF, DCM, RT, 1 h.

(typical pH = 9.2), we rationalized that the synthesis of the monophenoxy PITC derivative **10** might give rise to enhanced solubility in basic buffer systems, because of its partial ionization at this pH (pK_a phenol = 10). The condensation of the phenolic dipyrromethane **11** with **3** was carried out in a manner analogous to that in Scheme 1. Yields of unsymmetrically substituted porphyrin from this reaction were low (<1%), and the high polarity of the required acetamidohydroxy-DPP made it difficult to separate chromatographically. We therefore sought an alternative method for the synthesis of this potentially useful DPP (Scheme 2).

The hydroxy group of dipyrromethane **11** was protected with the *tert*-butyldiphenylsilyl (TBDPS) group using standard methodology (TBDPSCl/imidazole in DMF) to afford TBDPSO-dipyrromethane **12**, which was then condensed as previously with dipyrromethane **3**. The resulting unsymmetrically substituted acetamidoporphyrin **13** was formed in unusually high yield (42%), possibly because of the presence of the bulky TBDPS group greatly reducing self-condensation. Regioselective hydrolysis of DPP **13** gave the corresponding amine **14**, with no significant hydrolysis of the TBDPS group, and treatment of **14** with TDP gave the corresponding PITC derivative **15**. Deprotection of **15** was carried out in DCM with tetrabutylammonium fluoride (TBAF) and gave PITC **10** without any degradation of the isothiocyanato functionality. Unfortunately, PITC **10** was found to be insoluble in basic buffer solutions. However, **10** was found to be readily soluble in DMSO and, to a lesser extent, soluble in DMF. When a DMSO cosolvent stock solution of **10** (100 μL, 25.7 mM) was added to a bicarbonate buffer solution, as described for **9**, the porphyrin remained in solution for 2−3 min before visible precipitation commenced. The use of increased quantities of DMSO cosolvent (up to a final concentration of 30% DMSO in buffer) produced no noteworthy increase in the solubility of **10**. Much to our disappointment, the use of 3,4- and 3,5-dihydroxy derivatives of **10** (data not given) also showed no significant improvement upon the solubility observed for **10.** Despite its sparing solubility under aqueous conditions, the bioconjugation of **10** with BSA was investigated and is discussed later.

Synthetic Studies Toward Water-Soluble TPP Isothiocyanates. The synthesis of TPP derivatives has been developed over many years and now allows for routine access to multigram quantities of functionalized porphyrins. In our initial studies toward TPP based PITCs, we synthesized a number of hydroxy analogues, which included **16** and **17**, to allow for a direct comparison with hydroxy DPP counterparts under bioconjugation conditions (Scheme 3). PITC **16** was found to be readily soluble in DMSO and DMF but did not retain solubility when added to aqueous buffer, with precipitation detected after only 10 min. Fortunately, hexahydroxy PITC **17** remained completely soluble when dissolved in a typical bioconjugation solution (10% DMSO/pH 9.2 buffer) for 16 h at 4 °C.

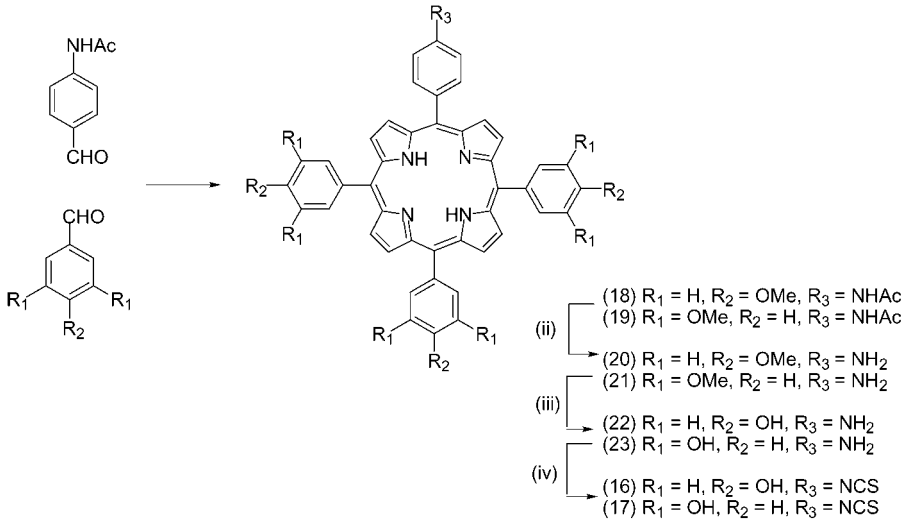
Synthesis of Water-Soluble TPP Isothiocyanate. As a logical extension of our search for highly hydrophilic PITCs, we envisaged that combining three water-solubilizing *N*-methylpyridinium cations and a reactive isothiocyanate group, as in PITC **24**, would give full water solubility and allow facile bioconjugation, with a minimum loss of label and reduce, if not eliminate, NCB. The synthetic route to the tri-(*N*-methylpyridiniumyl)-PITCs **24** and **28** is shown in Scheme 4.

Synthetic Studies into the Generation of Wavelength-Shifted Porphyrin Derivatives Suitable for Bioconjugation: Formation of Chlorins and Bacteriochlorins by OsO_4-Mediated Dihydroxylation of Porphyrins. The synthesis of porphyrin derivatives such as chlorins and bacteriochlorins offers easy access to molecules which exhibit favorable optical properties and may be beneficial in PDT and fluorescence imaging applications. Investigations into the use of porphyrin derivatives for conversion to wavelength-shifted dihydroxychlorins and tetrahydroxybacteriochlorins by osmium tetroxide-mediated oxidation were therefore undertaken. Unfortunately, because of the relative inactivity of the TPP β-positions toward OsO_4, presumably because of steric effects, reactions were found to take many weeks using standard conditions (*9*, *10*) and gave very low yields. To overcome these problems, and as a result of recent work within our laboratories (*25*, *26*, *28*), we turned our attention back to DPP derivatives. DPPs were found to undergo facile dihydroxylation (*26*), giving total yields of diphenylchlorin diols (DPCH) and diphenylbacteriochlorin tetrols (DPBC), in many cases above 80%.

Scheme 5 shows the synthetic pathway employed for the preparation of the reactive chlorin- and bacteriochlorin-isothiocyanato derivatives **29** and **30**.

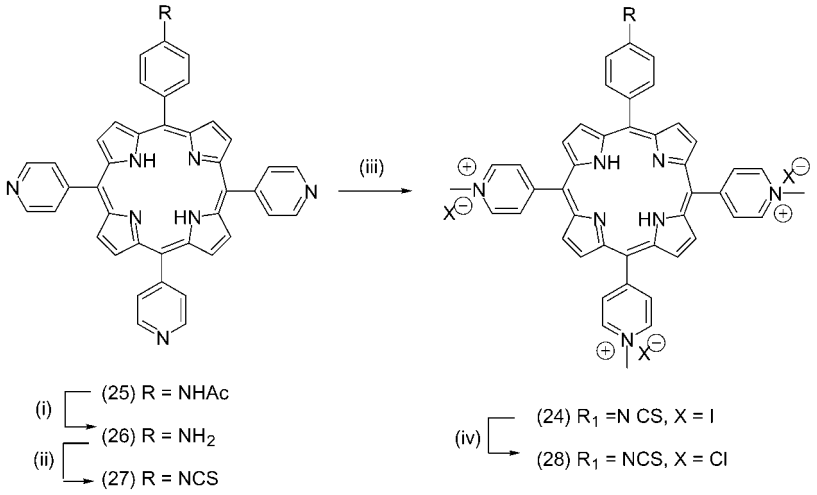
Generation of BSA Bioconjugates Using PITC Derivatives. A comparative bioconjugation study of all

Scheme 3[a]



[a] Conditions: (i) propionic acid, 90 °C, 0.5 h; (ii) 5 M HCl(aq), 80 °C, 3 h; (iii) BBr_3, DCM, 17 h; (iv) TDP, DCM, RT, 2 h.

Scheme 4[a]



[a] Conditions: 5 M HCl(aq), 80 °C, 3 h; (ii) TDP, DCM, RT, 2 h; (iii) MeI, DCM, 3 h; (iv) Amberlite IRA 400, MeOH, RT, 1 h.

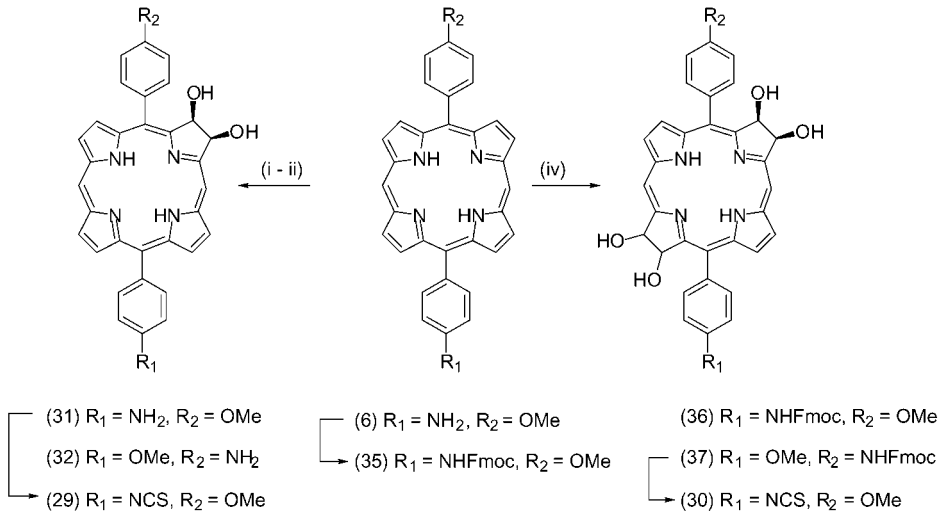
PITC derivatives with BSA, as a model protein, was now undertaken. Aliquots, containing 10 equiv of PITCs were taken from 10 mg mL^{-1} stock solutions in DMSO and added dropwise to 10 mg samples of BSA that were predissolved and equilibrated in a carbonate/bicarbonate buffer (pH = 9.2). Final concentrations of DMSO in buffer were approximately 10%. Examination of solubility clearly indicated an encouraging trend, with the PITCs increasing solubility in DMSO and DMF cosolvent (seen from **9**, **10**, **16**, and **17**). The tri-(*N*-methylpyridiniumyl)-Cl-PITC **28** was found to be completely soluble under the bioconjugation conditions used for isothiocyanates. An examination of the solubility characteristics of the chlorin and bacteriochlorin PITCs **29** and **30** during typical bioconjugations has shown that they lie somewhere between that of the tri- and hexa-hydroxy substituted TPPs **16** and **17**. On these occasions, precipitation of the reactive PITC derivatives did not visibly occur for up to 30 min. Therefore, the use of OsO_4-mediated oxidation of DPPs has the double advantage of producing products that contain both favorable solubility and also improved spectroscopic characteristics.

Initial purification of bioconjugates by gel permeation chromatography (PD-10) also indicated that as the polarity, and therefore the hydrophilicity, of the reactive PITC increased, so did the amount of nonbioconjugated material retained at the top of the gel column. This has implications for the use of lipophilic porphyrins in bioconjugation and indicates that resulting bioconjugates will contain significant proportions of NCB porphyrins. For PDT applications, the presence of some NCB porphyrin "complex" does not necessarily negate activity (*13*, *16*, *17*); however, to maximize specificity of the photosensitizer conjugate, it is clearly desirable to minimize this parameter. The preceding argument applies to an even greater extent for fluorescence imaging applications.

Characterization of BSA Bioconjugates. SDS−PAGE analysis of a range of BSA biconjugates, obtained after gel permeation chromatography, has shown that bioconjugations using all but the most water-soluble PITC **28** result in the formation of substantial amounts of PITC/protein NCB complex. Figure 1 shows a typical SDS−PAGE analysis of a conjugate formed from BSA and PITC **17**. Qualitative analysis of image A (lanes 1 and 2) clearly shows the presence of NCB free porphyrin that has not been removed by gel permeation chromatography. A similar scenario was also evident from SDS−PAGE analysis of all other BSA bioconjugation mixtures, in varying degrees, after initial gel permeation.

Investigations of NCB Associated with the Use of Lipophilic PITC in Protein Bioconjugations. To investigate, in more detail, the problems that proteins

Scheme 5[a]



[a] Conditions: (i) 2.5 equiv of OsO_4, 10% pyridine/$CHCl_3$, RT, 72 h; (ii) H_2S(g), RT, 5 min; (iii) TDP, DCM, RT, 2 h; (iv) FmocCl, $NaHCO_3$, 1,4-dioxane, RT, 3 h; (v) 5.0 equiv of OsO_4, 1% pyridine/1,4-dioxane, RT, 72 h; (vi) piperidine, 25% MeOH/DCM, RT, 3 h; (vii) TDP, DCM, RT, 2 h.

with associated lipophilic NCB porphyrin can cause, DPP **4**, DPCH **39**, and DPBC **41** were prepared. These unreactive probes were then mixed with BSA separately under standard bioconjugating conditions and passed through gel permeation columns in order to simulate typical bioconjugation protocols. The colored bands eluted were analyzed by UV−vis spectroscopy and indicated the presence of a NCB probe (DPP 412 nm; DPCH 411 nm; DPBC 376 nm) and protein (282 nm). BSA mixtures contained approximately 2, 1, and 0.6 mol of NCB−DPP, DPCH, and DPBC per mole of protein, respectively. With typical bioconjugations giving degrees of labeling (DOL) of between 2.5 and 5 mol of porphyrin per mole protein in total; this level of NCB represents a significant problem to be overcome. For comparison, haematoporphyrin-NHS ester and fluorescein isothiocyanate (FITC) gave levels of NCB of 0.75 and 0.1 mol of chromophore per mole protein, respectively. It therefore appears that NCB is a much less significant problem for FITC bioconjugates (SDS−PAGE analysis of crude FITC bioconjugates showed almost negligible NCB probe at the gel front). Further investigations of the BSA complexes formed with capped DPP, DPCH, and DPBC indicated that NCB probe actively transfers to cell membranes nonspecifically and rapidly. This was demonstrated by measuring the fluorescence prior to and after mixing of NCB complexes with HeLa cells. Cells were agitated with each complex for 5 min, then the resulting mixtures were centrifuged, and the fluorescence of the supernatant remeasured. BSA mixtures showed marked reductions in fluorescence for the chlorin **39**, with lesser reductions for the bacteriochlorin **41**. More interestingly, the fluorescence of resuspended HeLa cells now showed intense fluorescence corresponding to chlorin and bacteriochlorin, with respective values of 3 and 1, relative to the initial values for these conjugates in solution. Comparison of fluorescence arising from supernatant and cells surprisingly showed greater relative intensity from cells than from the original solution of conjugate prior to mixing with cells. It seems likely that this reflects a lowering of fluorescence quenching in the membrane, as compared to the protein. Experiments repeated with crude bioconjugate mixtures containing NCB and covalently bound porphyrin, chlorin, and bacteriochlorin also showed transfer of fluorophore to the cell membrane but at reduced levels, reflecting the inability of covalently bound fluorophore to transfer to the cell membrane. Reanalysis of supernatants from these experiments by SDS−PAGE, and comparison to gels run before mixing with cells, indicated significant reductions in NCB porphyrin, chlorin, and bacteriochlorin but no reduction in covalently bound material.

To address the problems associated with PITC bioconjugates which contain appreciable amounts of NCB material, we have investigated a number of methods for their removal.

Purification of Porphyrin Chlorin- and Bacteriochlorin-Derived Bioconjugates: Removal of NCB PITC Impurities. To facilitate the removal of the NCB porphyrin, chlorin, and bacteriochlorin from covalent bioconjugates, a number of methods were investigated. We noted from many SDS−PAGE analyses the presence of front running NCB fluorescent probe in bioconjugates purified by gel permeation chromatography (except with water soluble PITC **28**). We therefore decided to recover pure bioconjugates from preparative SDS−PAGE. The procedure involved excising the gel area corresponding to fluorescent labeled protein, followed by electroelution using the same conditions as for the initial SDS−PAGE.

Photographs of the SDS−PAGE gels for a typical bioconjugate (BSA−porphyrin **17**) are shown in Figure 1. Gel A clearly indicates the presence of NCB porphyrin, which can be seen running at the electrophoresis front (bottom of the gel) as a purple stain along with the blue marker dye. Gel B represents the conjugate after purification by electroelution, except for lane 7 which is a control lane of unpurified conjugate for comparison. Gels C and D are the same gels as A and B but have been visualized under UV light, as opposed to white light, to visualize the fluorescent porphyrin. Again, lanes 1−6 in gel D represent conjugate purified by electroelution. Finally, gels E and F are the same gels as A and B and C and D, respectively; however, the gels have now been stained with silver nitrate to visualize protein. Lane 8 shows the visualized molecular weight markers, indicating that the major protein band in gel F corresponds to BSA.

To quantify the levels of NCB material, a number of PITC derivatives were bioconjugated to BSA, using probes of varying lipophilicity (trihydroxy-TPP **16**, DPCH **29**, DPBC **30** and tri-(*N*-methylpyridiumyl)-TPP **28**). An

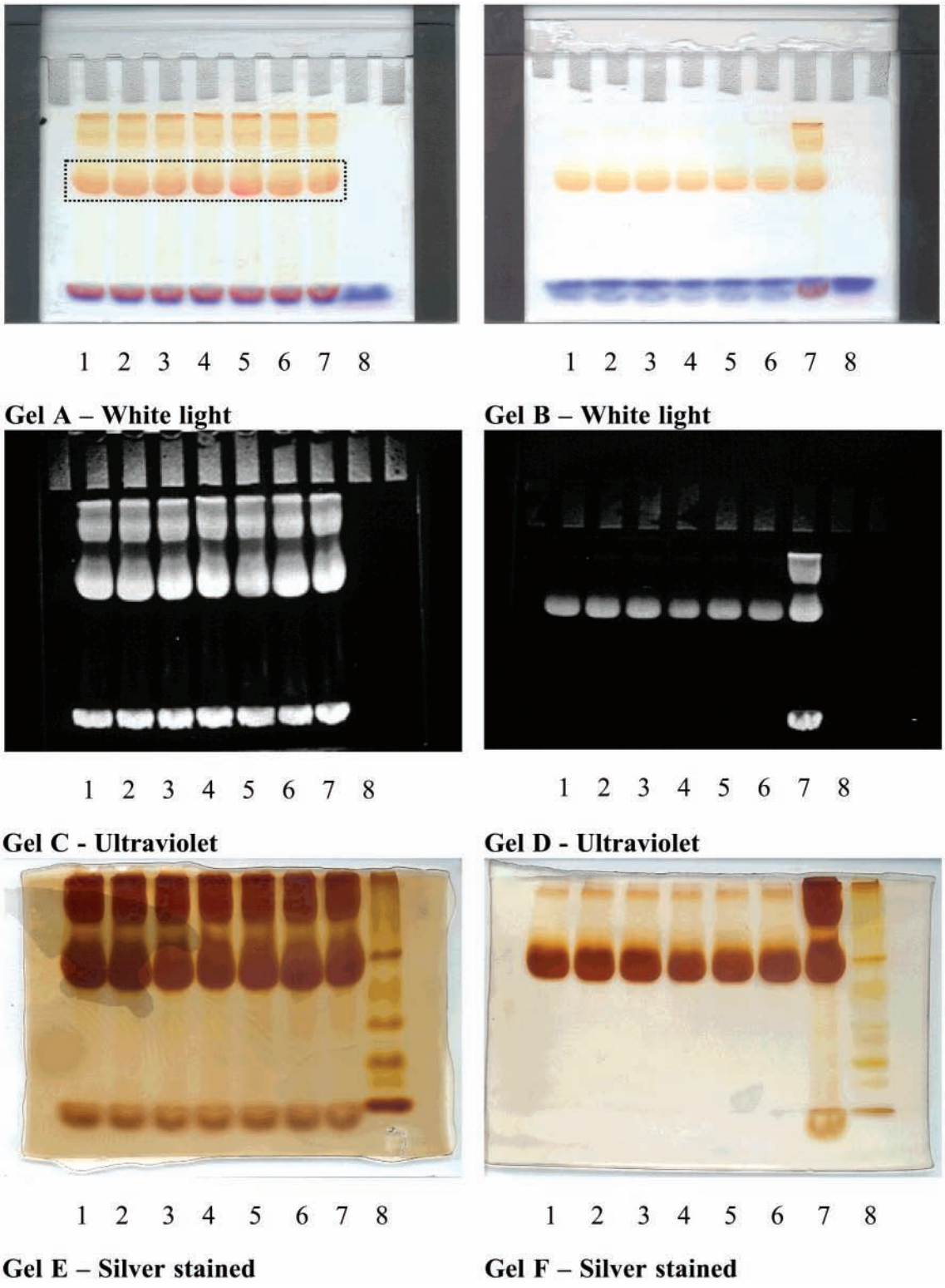


Figure 1. SDS−PAGE gels for BSA−porphyrin (**17**) conjugate before (A, C, E) and after (B, D, F) purification by electroelution.

examination of the proportions of NCB material pre- and post-SDS−PAGE electroelution is given in Table 1. The data clearly indicate that as the PITC derivative increases in polarity, so the level of NCB material drops, with the bioconjugate formed from tri-(*N*-methylpyridium)-PITC **28** having very low levels of NCB, similar to that found for conjugates prepared using commercial FITC. Analysis of DOL data from conjugates pre- and postelectrophoretic purification show interesting trends. Pre-electrophoretic purification, but post-gel permeation chromatography, which has been the usual method for purification of porphyrin conjugates to date, DOL values are inversely proportional to hydrophilicity for the analogous TPP derivatives **16**, **17**, and **28** and also for analogous DPP chlorin and bacteriochlorin **29** and **30**. The same data postelectrophoretic purification, however, reveals a much greater contribution to DOL value for NCB material for the less hydrophilic porphyrin derivatives. Interestingly, we repeated a previously reported NHS ester-mediated conjugation for haematoporphyrin

Table 1. Degree of Labelling for PITC-BSA Conjugates Pre- and Postelectroelution with Percentages of Noncovalent Binding[a]

PITC	degree of labeling electroelution		% NCB
	pre	post	
$TPP(OH)_3$ (**16**)	7:1	2:1	71
$TPP(OH)_6$ (**17**)	6:1	4:1	33
$chlorin(OH)_2$ (**29**)	3:1	2:1	33
$bacteriochlorin(OH)_4$ (**30**)	0.5:1	0.35:1	30
TPP-(methylpyridiniumyl) (**28**)	2:1	1.9:1	5

non-PITC	pre	post	% NCB
haematoporphyrin	4:1	3.4:1	15
fluorescein	3.3:1	3.2:1	3

[a] Haematoporphyrin and fluorescein BSA conjugates are included for comparison.

with BSA (*13*) and analyzed the product for percentage NCB. The result indicated a 15% contribution from NCB haematoporphyrin. It would seem, then, that SDS−PAGE offers the ability to quantify levels of NCB in the conjugation of porphyrins to proteins and can also be used to obtain 100% covalently bound conjugates for study. Although the method used here is obviously suited to small-scale preparations, commercial large-scale preparative electrophoresis apparatus is available, which could be used to produce larger amounts of purified conjugates.

Scanning Confocal Laser Microscopy Studies of BSA PITC Derivatives. The use of protein-photosensitizer (PS) conjugates to obtain specific targeting of a particular cell type may constitute an improvement in PDT. One method, which is becoming increasingly popular, is the generation PS−protein conjugates (usually of BSA, mal-BSA, or LDL) that bind to specific cell surface receptors. Following cellular internalization by receptor-mediated endocytosis, the PS−protein bioconjugate has

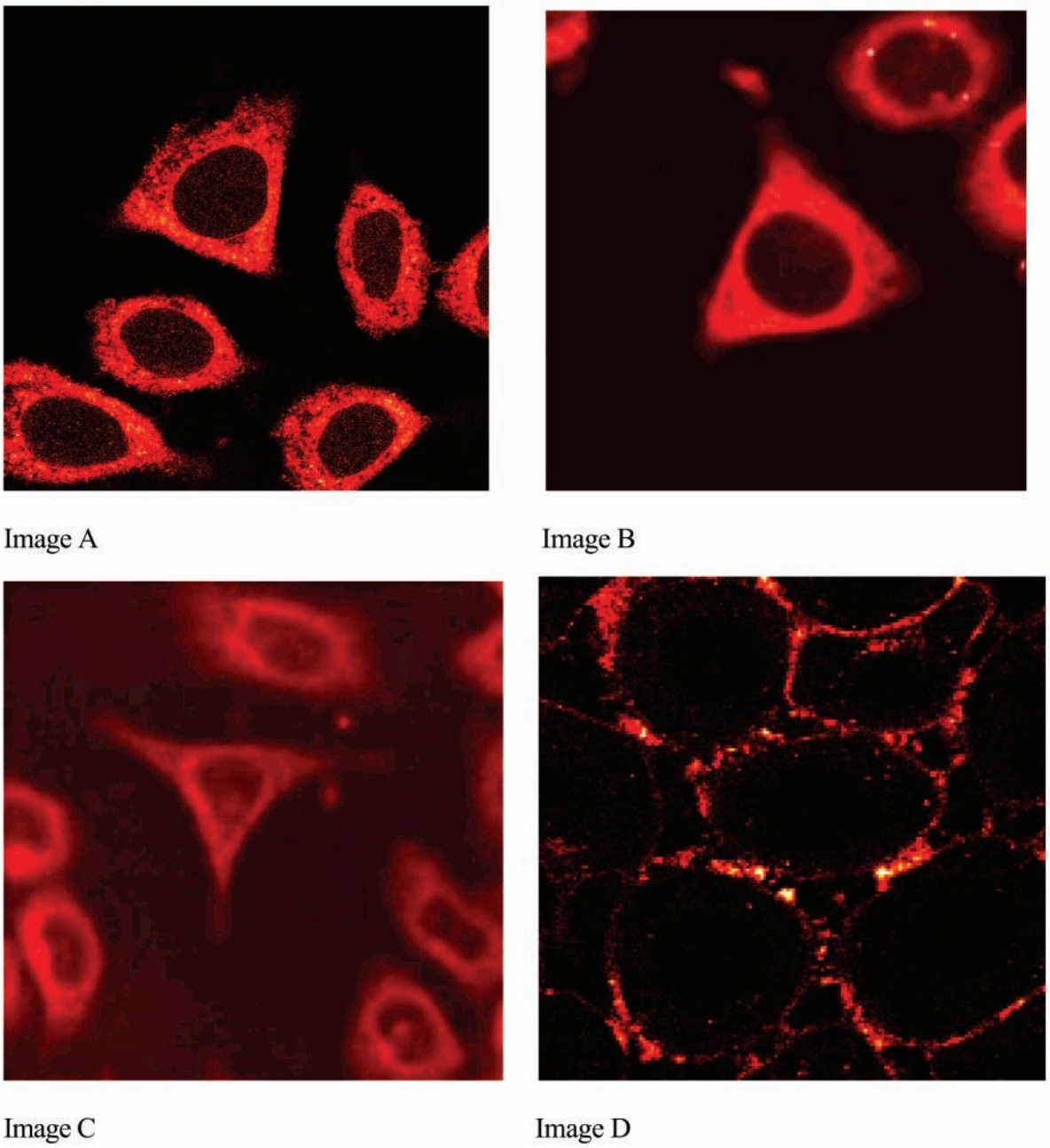


Figure 2. CLSM images of HeLa cells incubated with (A) BSA−porphyrin (**17**) conjugate, (B) BSA−chlorin (**29**) conjugate, (C) BSA−bacteriochlorin (**30**), and (D) Unconjugated porphyrin (**23**).

been successfully used to target destruction of specific cells (*13*−*15*, *22*, *23*).

We therefore undertook a preliminary examination of the intracellular localization of bioconjugates of BSA with a representative porphyrin (**17**), chlorin (**29**), and bacteriochlorin (**30**) using human cultured carcinoma cells (HeLa). HeLa cells overexpress receptors for human serum albumin relative to similar noncarcinoma cells, and as there is a 87% homology between BSA and HSA, it was hoped BSA conjugates would be processed by the HSA receptors. The bioconjugates were first purified vigorously by SDS−PAGE electroelution and then incubated with HeLa cells prior to fixing and imaging by confocal laser scanning microscopy (CLSM). Figure 2 (images A−C) shows CLSM images taken through the center of the cells. Clearly, all BSA conjugates penetrate the cell but are excluded from the nucleus or are subjected to efficient quenching of fluorescence in this cellular region. Images of BSA or PBS controls showed insignificant autofluorescence at the same detector collecting level. However, the control images taken after identical incubation conditions with unconjugated porphyrin (**23**) showed that fluorescence was localized exclusively in the extracellular space (Figure 2, image D), demonstrating that conjugation to the BSA is required in order for probe internalization to occur. Further investigations into the exact mode of cellular entry and intracellular distribution are currently underway within our laboratory.

In conclusion, we have developed methods for the synthesis and bioconjugation of water soluble tri-(*N*-methlpyridiniumyl)porphyrin derivatives typified by PITC **28** with proteins and shown that their increased hydrophilicity minimizes the amount of NCB porphyrin. We have also developed a range of wavelength-shifted chlorin and bacteriochlorin isothiocyanate derivatives **29**/**30** from the OsO_4-mediated oxidation of DPPs, which have been used to generate bioconjugates with BSA. We have highlighted the problem of NCB associated with the use of lipophilic and amphiphilic porphyrin derivatives in bioconjugation and have successfully overcome them by using SDS−PAGE electroelution to obtain bioconjugates of superior quality which retain no NCB material. Furthermore, we have highlighted a potential source of error in using molecular probes containing NCB porphyrins because of the active transfer of NCB porphyrins from protein to cell membranes. This would severely limit the use of these probes in applications such as flow cytometry. Work is currently underway within our laboratory to utilize this technology to generate specific immunoconjugates for use in multicolor FACS analysis and as PDT sensitizers. Finally, we have used the CLSM technique to demonstrate the potential use of purified BSA conjugates as a delivery vehicle for porphyrins, chlorins, and bacteriochlorins.

ACKNOWLEDGMENT

The authors thank EPSRC Mass Spectrometry Service, Swansea, for analysis. The authors also thank Drs. Peter O'Toole and Ian Morrison for their assistance with CLSM and flow cytometric analysis and Huguette Savoie for cell culture support.

LITERATURE CITED

(1) Sternberg, E. D., and Dolphin, D. (1996) Pyrrolic photosensitizers. *Curr. Med. Chem. 3*, 239−272.

(2) Jasat, A., and Dolphin, D. (1997) Expanded porphyrins and their heterologs. *Chem. Rev. 97*, 2267−2340.

(3) Dolphin, D., and Brückner, C. (1998) Porphyrin-based photosensitizers for use in photodynamic therapy. *Tetrahedron 54*, 4151−4202.

(4) Ali, H., and van Lier, J. E. (1999) Metal complexes as photo- and radiosensitizers. *Chem. Rev. 99*, 2379−2450.

(5) Boyle, R. W., and Dolphin, D. (1996) Structure and biodistribution relationships of photodynamic sensitizers. *Photochem. Photobiol. 63*, 469−485.

(6) Chang, C. K., and Sotiriou, C. (1985) C-hydroxychlorins and C-methylchlorins−A convenient route to heme-D and Bonellin model compounds. *J. Org. Chem. 50*, 4989−4991.

(7) Bonnett, R. Nizhmick, A. N., and Berenbaum, M. C. (1989) Second generation tumor photosensitizers−The synthesis of octaalkyl chlorins and bacteriochlorins with graded amphiphilic character. *J. Chem. Soc., Chem. Commun.* 1822−1823.

(8) Adams, K. R., Berenbaum, M. C., Bonnett, R., Nizhmick, A. N., and Salgado, A. (1992) 2nd generation tumor photosensitizers−The synthesis and biological activity of octaalkyl chlorins and bacteriochlorins with graded amphiphilic character. *J. Chem. Soc., Perkin Trans. 1* 1465−1470.

(9) Brückner, C., and Dolphin, D. (1995) 2,3-*vic*-Dihydroxy-*meso*-tetraphenylchorins from the osmium tetroxide oxidation of *meso*-tetraphenylporphyrin. *Tetrahedron Lett. 36*, 3295−3298.

(10) Brückner, C., and Dolphin, D. (1995) β,β'-Hydroxylation of *meso*-Tetraphenylchlorins and Metallochlorins. *Tetrahedron Lett. 36*, 9425−9428.

(11) Gouterman, M. (1978) Optical spectra and electronic structure of porphyrins and related rings. *The Porphyrins* (D. Dolphin, Ed.), Vol. III, pp 1−165, Academic Press, New York.

(12) Parr, G. R., and Pasternack, R. F. (1977) The interactions of some water-soluble porphyrins and metalloporphyrins with human serum albumin. *Bioinorg. Chem. 7*, 277−282.

(13) Hamblin, M. R., and Newman, J. (1994) Photosensitizer targeting in photodynamic therapy. I. Bioconjugates of haematoporphyrin with albumin and transferrin. *J. Photochem. Photobiol., B 26*, 45−56.

(14) Brasseur, N. R., Langlois, C., La Madeleine, R., van Lier, J. E., and Oullet (1999) Receptor-mediated targeting of phthalocyanines to macrophages via covalent coupling to native or maleylated bovine serum albumin. *Photochem. Photobiol. 69*, 345−352.

(15) Hamblin, M. R., Miller, J. L, and Ortel B. (2000) Scavenger receptor targeted photodynamic therapy. *Photochem. Photobiol. 72*, 533−540.

(16) Mew, D., Wat, C−K., Towers, G. H. N., and Levy, J. G. (1983) Photoimmunotherapy: Treatment of animal tumors with tumor-specific monoclonal antibody-hematoporphyrin conjugates. *J. Immunol. 130*, 1473−1477.

(17) Donald, P. J., Cardiff, R. D., and Kendall, K. (1991) Monoclonal antibody-porphyrin conjugates for head and neck cancer: The possible magic bullet. *Otolaryngol.-Head Neck Surg. 6*, 781−787.

(18) Milgrom, L. R., and O'neill, F. (1995) Towards synthetic-porphyrin/monoclonal antibody bioconjugates. *Tetrahedron 51*, 2137−2144.

(19) Vrouenraets, M. B., Visser, G. W. M., Stewart, F. A., Stigter, M., Oppelaar, H., Postmus, P. E., Snow, G., and van Dongen, G. A. M. S. (1999) Development of *meta*-tetrahydroxyphenylchlorin-monoclonal antibody conjugates for photoimmunotherapy. *Cancer Res. 59*, 1505−1513.

(20) Del Governatore, M, Hamblin, M. R., Piccinini, E. E., Ugolini, G., and Hasan, T. (2000) Targeted photodestruction of human colon cancer cells using charged 17.1A chlorin e_6 immunoconjugates. *Br. J. Cancer 82*, 56−64.

(21) Hamblin, M. R., and Newman, J. (1994) Photosensitizer targeting in photodynamic therapy. II. Bioconjugates of haematoporphyrin with serum lipoproteins. *J. Photochem. Photobiol., B 26*, 147−157.

(22) Schmidt, U., Diddens, H., Birngruber, R., and Hasan, T. (1997) Photodynamic targeting of human retinoblastoma cells using covalent low-density lipoprotein conjugates. *Br. J. Cancer 75*, 54−61.

(23) Nagae, T., Louie, A. Y., Aizawa, K., Ishimaru, S., and Wilson, S. E. (1998) Selective targeting and photodynamic destruction of intimal hyperplasia by scavenger-receptor mediated protein−chlorin e_6 conjugates. *J. Cardiovasc. Surg. (Torino) 39*, 709−715.

(24) Drouet, M., and Lees, O. (1993) Clinical applications of flow cytometry in hematology and immunology. *Biol. Cell 78*, 73−78.

(25) Boyle, R. W., Brckner, C., Posakony, J., James, B. R., and Dolphin, D. (1998) 5-Phenyldipyrromethane and 5,15-diphenylporphyrin. *Org. Synth. 76*, 287−293.

(26) Sutton, J. M., Fernandez, N., and Boyle, R. W. (2000) Functionalised diphenylchlorins and bacteriochlorins—Their synthesis and bioconjugation for targeted photodynamic therapy and tumour cell imaging. *J. Porphyrin Phthalocyanines 4*, 655−658.

(27) Heukenshoven, J., and Dernick, R. (1985) Simplified method for silver staining of proteins in polyacryalamide gels and the mechanism of silver staining. *Electrophoresis 6*, 103−106.

(28) Clarke, O. J., and Boyle, R. W. (1999) Isothiocyanatoporphyrins, useful intermediates for the conjugation of porphyrins with biomolecules and solid supports. *J. Chem. Soc., Chem. Commun.* 2231−2232.

(29) Adler, A. D., Longo, F. R., Finarelli, J. D., Goldmacher, J., Assour, J., and Korsakoff, L. (1967) A simplified synthesis for *meso*-tetraphenyl porphyrins. *J. Org. Chem. 32*, 476.

(30) McOmie, J. F. W., Wattis, M. L., and West, D. E. (1968) Demethylation of aryl ethers by boron tribromide. *Tetrahedron 24*, 2289−2292.

(31) Pasternack, R. F., Huber, P. R., Boyd, P., Engasser, G., Francesconi, L., Gibbs, E., Fasella, P., Cerio-Venturo, G., and deC. Hinds, L. (1972) Water soluble porphyrins. *J. Am. Chem. Soc. 94*, 4511−4517.

(32) Bedner, E., Halicka, H. D., Cheng, W., Salomon, T., Deptala, A., Gorczyca, W., Melamed, M. R., and Darzynkiewicz, Z. (1999) High affinity binding of fluorescein isothiocyanate to eosinophils detected by laser scanning cytometry: A potential source of error in analysis of blood samples utilizing fluorescein-conjugated reagents in flow cytometry. *Cytometry 36*, 77−82.

BC015547X

Tat Peptide Directs Enhanced Clearance and Hepatic Permeability of Magnetic Nanoparticles

Patrick Wunderbaldinger,[†] Lee Josephson,*[,†] and Ralph Weissleder

From the Center of Molecular Imaging Research, Massachusetts General Hospital, Harvard Medical School, Boston, Massachussets. Received October 5, 2001

Superparamagnetic nanoparticles have a number of important biomedical applications, serving as MR contrast agents for imaging specific molecular targets, as reagents for cell labeling and cell tracking, and for the isolation of specific classes of cells. We have determined the physical and biological properties of MION-47 and amino-CLIO, nanoparticles which serve as precursors for the synthesis of targeted MR contrast agents, and Tat-CLIO, a nanoparticle used as a cell labeling reagent. Blood half-lives for MION-47 and amino-CLIO were 682 ± 34 and 655 ± 37 min, respectively. The attachment of 9.7 tat peptides per crystal to amino-CLIO resulted in a reduction in blood half-life to 47 ± 6 min. MION-47, amino-CLIO, and Tat-CLIO were present in highest concentrations in liver and spleen and lymph nodes, where concentrations for all three nanoparticles ranged from 8.80 to 6.11% of injected dose per gram. Twenty-four hours after the intravenous injection of amino-CLIO, the nanoparticle was concentrated in cells surrounding hepatic blood vessels (endothelial and Kupffer cells), in a fashion similar to that obtained with other nanoparticle preparations. In contrast, Tat-CLIO was present as numerous discrete foci of intense fluorescence throughout the parenchyma. Using the peptide as a component of future nanoparticles, it might be possible to design sensors for the detection of macromolecules present in intracellular compartments.

INTRODUCTION

The ability to induce the internalization of therapeutic agents by attachment to positively charged peptides has suggested a variety of new approaches to drug design including new forms of cyclosporin A (*1*), improved radiotherapy based on the nuclear localization of toxic radioisotopes (*2*), and the enhanced delivery of therapeutic proteins or DNA (*3*−*5*). Peptides with membrane translocating properties include the tat peptide from the HIV tat protein, polyarginyl peptides, and penetrin (the third helix homeodoman of antenapedia) (*1, 6, 7*).

We have shown that the attachment of tat peptides to a superparamagnetic iron oxide known as Tat-CLIO (Tat-cross-linked iron oxide) induces the intracellular accumulation of iron oxide and makes cells highly detectable by magnetic resonance imaging (*8*). Uses of Tat-CLIO include labeling stem cells homing to bone marrow (*9*), labeling T cells homing to the spleen (*10*), labeling neuroprogenitor cells migrating in the developing mouse brain (*11*), and labeling T cells invading diabetic insulitic lesions (*12*) (Table 1). Tat-CLIO uptake is not associated with toxicity (*8*−*10*).

A key question concerning the usefulness of the tat peptide for the delivery of diagnostic and sensing agents involves the fate of tat peptide conjugates after clearance from the vascular compartment. If tat-conjugates move beyond cells bordering the vascular compartment, a new capability to deliver cell impermeable drugs to a wide range of different cell types throughout an organ can be imagined. We therefore chose to examine the in vivo behavior of Tat-CLIO, a nanoparticle developed for cell labeling applications. We examined the physical and biological properties of Tat-CLIO by comparison with two nanoparticles, MION-47 and amino-CLIO, which have served as precursors for the synthesis of Tat-CLIO and targeted nanoparticles generally. Here we report that the attachment of the tat peptide enhances nanoparticle clearance from the vascular compartment and that nanoparticles were found throughout the liver, rather than in cells adjacent to the vascular compartment (endothelial cells/Kupffer cells). This observation opens exciting opportunities for the delivery of intracellular sensing molecules that will allow in vivo molecular imaging.

EXPERIMENTAL PROCEDURES

Synthesis of Magnetic Nanoparticles. The synthesis of nanoparticles used here, MION-47, amino-CLIO, and Tat-CLIO, follows the scheme shown in Figure 1. Amino-CLIO was synthesized by cross-linking MION-47 in strong base with epichlorohydrin followed by reaction with ammonia to provide primary amino groups (*8, 13, 14*). The original synthesis of Tat-CLIO (*8*) was modified to ensure that FITC, used to tract the nanoparticle in fluorescent microscopy studies, could not be cleaved from the nanoparticle in vivo. We used succinimidyl iodoacetate (SIA) as a bifunctional conjugating reagent because it forms a stable thioether linkage between peptide and amino-CLIO. Our earlier synthesis used *N*-succinimidyl 3-(-pyridyldithio)propionate (SPDP), which results in a reducing-environment-sensitive, disulfide linkage between peptide and nanoparticle. Second, our earlier synthesis used GGC*GRKKRRQRRR*K(FITC)-NH_2 as the tat peptide, which features a cysteine residue near the N terminus and a C-terminal lysine modified by FITC. The current study used the peptide *GRKKRRQRRR*GYK-

* Corresponding author: Lee Josephson, Ph.D. MGH-CMIR; Building 149, 13th Street, Room 5406, Charlestown, MA 02129. Office: 617-726-5788. Fax: 617-726-5708. E-mail: josephso@helix.mgh.harvard.edu.

[†] P.W. and L.J. contributed equally.

10.1021/bc015563u CCC: $22.00 © 2002 American Chemical Society
Published on Web 02/12/2002

Table 1. Summary of Magnetic Nanoparticles Used in Current and Previous Studies

compound	primary use	ref
MION-47	monocrystalline iron oxide nanoparticles (MION) used as a blood pool agent and as a lymphotrophic conrast agent	15, 23
Amino-CLIO	an aminated, cross-linked iron oxide (CLIO) used as a precursor in the synthesis of other nanoparticles	8, 13, 14
Tat-CLIO	a cell labeling and cell tracking reagent synthesized from amino-CLIO	9

(FITC)C-NH_2. The C-terminal cysteine side chain is modified by the attachment to the CLIO nanoparticle, while the penultimate lysine is modified by attachment of FITC (Figure 1). Unlike our original Tat-Clio nanoparticle, cleavage of the naturally occurring amino acids providing the membrane translocation sequence will result not result in a separation of FITC from the nanoparticle. To verify the stability of the current Tat-CLIO, the nanoparticle was incubated with 10 μg/mL trypsin, 10 μg/mL chymotrypsin, or 10 mM DTT at 37 °C for 4 h. All treatments failed to separate FITC from the nanoparticle, based on its inability to pass through an ultrafiltration membrane.

*GRKKRRQRRR*GYK(FITC)C$-NH_2$ was synthesized with Fmoc chemistry and labeled with FITC, MALDI-MS $(M+1)^+$: 2237.54 (calc.), 2237.2 (found) as described (*8*). Italicized residues are the membrane translocation sequence of the tat peptide. One and a half milliliters of amino-CLIO (39 mg Fe, 0.70 mmol) in 5 mM sodium citrate, pH 8 was reacted with succinimidyl-iodoacetate or SIA (42 mg, 0.12 mmol) (Molecular Biosciences, Boulder CO) dissolved in DMSO (3 mL). Reaction was for 2 h at room temperature. The mixture was separated on a Sephadex G-25 column (30 × 1.5 cm) and the void volume with iron oxide was collected. To the iron oxide was added 13 mg of peptide dissolved in 3 mL of 0.02 M citrate, pH 6.5 and the mixture was allowed to stand for 3 h at room temperature. The mixture was then applied to the column above to remove unreacted peptide.

Isotopic Labeling of Magnetic Nanoparticles. To prepare indium-labeled MION-47 or indium-labeled amino-CLIO, nanoparticles were dialyzed against 0.01M sodium carbonate, pH 11−11.5. To 0.5 mL of nanoparticle (10 mg Fe, 0.178 mmol) was added diethylenetriaminpentaacetic acid dianhydride (DPTA anhydride, Aldrich, Milwaukee, WI), in 100 μL of DMSO (0.5 mg, 1.4 μmol of DTPA anhydride). The mixture was allowed to stand for 90 min, and the addition of DTPA anhydride was repeated. To remove unreacted DTPA, the mixture was applied to Sephadex G-25 column PD-10 columns equilibrated with 0.02 M citrate, pH 6.5, and the dark void volume was collected. One millicurie of $^{111}InCl_3$ (NEN, Boston MA) was then added and the mixture allowed to stand at room temperature for 4 h. The mixture was added to a Sephadex G-25 PD-10 column equilibrated with the above buffer and which had been spun (4 min × 2000 g) to remove entrapped fluid. The sample was added and the column spun again and the flow through taken.

For indium labeled Tat-CLIO, to 0.6 mL Tat-CLIO (2.1 mg Fe, 0.038 mmol) was added to 0.1 mL of 0.1 M Borate, pH 8.5, and 0.07 mL of 2.8 mM DTPA anhydride (0.20

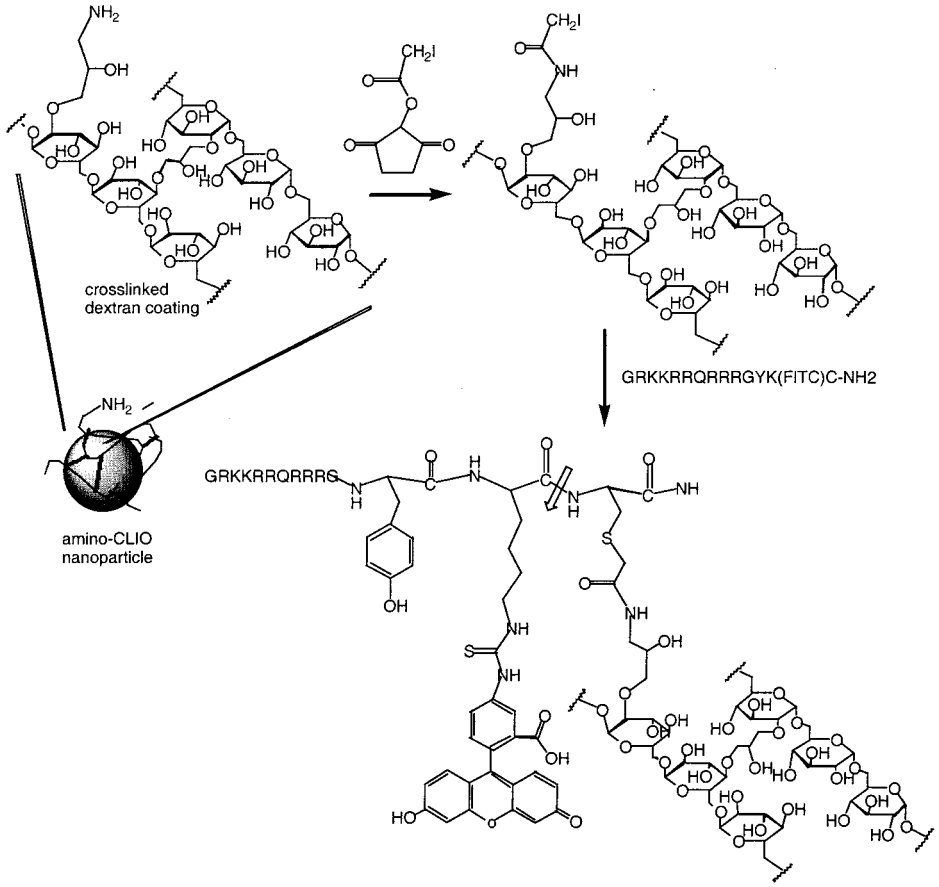


Figure 1. Scheme for the synthesis of Tat-CLIO.

Table 2. Physical and Biological Properties of Magnetic Nanoparticles

agent	size (nm)	R1 ($mM^{-1}\,s^{-1}$)	R2 ($mM^{-1}\,s^{-1}$)	peptides per crystal	blood $T_{1/2}$ (min)
MION-47	27.5 ± 6.8	21.9 ± 3.6	44.6 ± 7.1	NA	682 ± 34
Amino-CLIO	29.8 ± 5.0	23.2 ± 1.9	54.9 ± 15	NA	655 ± 37
Tat-CLIO	65.2 ± 7.3	22.9 ± 1.3	73.4 ± 17.8	11.6 ± 1.7	47 ± 6

μmol) in DMSO. The mixture was allowed to stand 4 h at room temperature and separated on a PD-10 column equilibrated as above. One millicurie of $^{111}InCl_3$ was added and the mixture allowed to stand overnight. Removal of unreacted indium was by centrifugation as above.

To prepare fluorescein isothiocyanate (FITC)-labeled CLIO, 1 mL of amino-CLIO (26 mg Fe, 0.464 mmol) was dialyzed against sodium carbonate as above and 1 mL of 0.01 M FITC (10 μmol) in sodium carbonate was added. The mixture was allowed to stand for 1 h at room temperature and FITC removed with a PD-10 G-25 column in citrate as above.

Characterization of Nanoparticles. Size was determined by laser light scattering using a Coulter N4 particle size analyzer. Relaxivity (R1 and R2) were measured at 0.47 T as described. Iron was measured spectrophotometrically. Details are provided elsewhere (*8, 13*). The number of tat peptides attached was determined from the OD_{493} of a solution of Tat-CLIO of known iron concentration. The OD_{493} of a similar iron concentration of amino-CLIO was subtracted and the peptide concentration calculated from the difference using an extinction coefficient for fluorescein of 73000 $M^{-1}\,cm^{-1}$. Results are expressed as the number of peptides per crystal assuming 2064 iron atoms per crystal (*15*).

Animal Studies. For biodistribution studies, female Balb C mice (six animals per agent) (Charles River Breeding Laboratories, NC) (weight 20−30 g, retired breeders) were used. Mice were anesthetized by an intraperitoneal (IP) injection of ketamine (80 mg(kg) and xylazine (12 mg/kg; Parker-Davis, Morris Plains, NJ/Miles, Shawnee Mission, KS). They were then injected intravenously (iv) through the tail vein with ^{111} In-labeled contrast agents at a dose of 10 mg Fe/kg. Twenty-four hours later animals were sacrificed by an ip injection of pentobarbital (Anpro Pharmaceutical, Arcadia, CA). Brain, heart, intestine, liver, spleen, kidney, muscle, bone, lung, paraaortic and inguinal lymph nodes, and body fluids (blood and urine) were excised, weighed, sealed in test tubes, and counted in a well counter (Wallace, Turku, Finland). Tissue concentration was expressed as percentage of injected dose per gram of tissue (%ID/g).

Blood half-life was calculated from blood radioactivity at various time points after animals were injected. Blood (120 μL) was withdrawn at various known time points between 1 and 24 h postinjection for five animals per agent (MION-47 and amino-CLIO: 1, 5, 8, 12, 18, and 24 h; Tat-CLIO: 1, 2, 4, 8, 12, 18, and 24 h). Half-life was obtained by fitting blood radioactivity to a single-exponential equation use for a one-compartment open pharmacokinetic model:

$$C(t) = C(0)e^{-kt}$$

$C(t)$ is blood radioactivity at time t after injection, $C(0)$ is the concentration of the colloid in the blood at the moment of injection time, k is the decay constant, and t is time after injection. Animal protocols were approved by the Institutional Review Committee on Animal Care and were conducted in accordance with National Animal Welfare guidelines.

All statistical calculations were made using SAS software (SAS Institute, Cary, NC). Results are expressed as mean (±SD).

Fluorescence Microscopy. To visualize the intrahepatic distribution of iron oxides, fluorescence microscopy in the green channel was used (excitation at 485 nm, emission at 530 nm). Mice were injected with FITC labeled amino-CLIO or Tat-CLIO, which has an FITC residue on the tat peptide, at 10 mg/kg and sacrificed 24 h later. Immediately after sacrifice animals were perfused with heparinized 5% glucose to reduce background fluorescence from blood. The liver was then removed, placed in freezing mounting liquid, and frozen in liquid nitrogen. The frozen tissue was cut into 5 μm thick sections for microscopic examination. Fluorescence microscopy on liver tissue was performed on air-dried, unembedded, and unfixed sections. This was done to prevent leaching of Tat-CLIO from the tissue during fixation, bleaching artifacts, and other distortions. HeLa cell images are from ref 8 and were obtained under similar conditions (unfixed, unembedded). Images were collected using a cooled, charge-coupled device (Photometrics, Tucson, AZ) with appropriate filters for excitation and emission (Omega Optics, Brattleboro, VT).

RESULTS AND DISCUSSION

The sizes, magnetic properties and numbers of tat peptides for MION-47 and amino-CLIO and Tat-CLIO are shown in Table 2. Values are the means plus/minus one standard deviation for four lots of MION-47 or amino-CLIO and for three lots of Tat-CLIO. Values are consistent with earlier studies of the physical properties of these materials (*8, 16−18*). Biological data were obtained with one of the three lots of Tat-CLIO that had 9.7 tat peptides attached per crystal.

The blood half-lives of MION-47, amino-CLIO, and Tat-CLIO were determined by sampling blood radioactivity at various time points after injection with results summarized Table 2. Data fit the one compartment model well, with correlation coefficients (r^2 values) of 0.959 for MION-47, 0.997 for amino-CLIO, and 0.98 for Tat-CLIO. Half-lives for MION-47 and amino-CLIO were similar, 682 ± 34 min and 655 ± 37 min, respectively. Thus the cross-linking and amination of the dextran surface of MION-47, to yield amino-CLIO (Figure 1), did not alter the physical properties (size and relaxivity) or the blood half-life. MION has a long blood half-life in rats and humans, i.e., 252 min in rats (*18*) and greater than 24 h in humans (*19*). The attachment of tat peptides resulted in a reduction of blood half-life from 655 ± 37 for amino-CLIO to 47 ± 6 min for Tat-CLIO.

MION-47, amino-CLIO, and Tat-CLIO had similar biodistributions; see Table 3. Each had the highest concentrations in the liver, spleen and lymph nodes, ranging from 8.80 to 6.11% ID/g, which suggests that all three nanoparticles were removed by phagocytes of the reticuloendothelial system. The enhanced clearance of Tat-CLIO is likely due to the enhanced interaction of Tat-CLIO with phagocytes mediated by the tat peptide itself or by enhanced opsonin-mediated phagocytosis.

To compare the distributions of Tat-CLIO and amino-CLIO after clearance, fluorescence microscopy of the liver

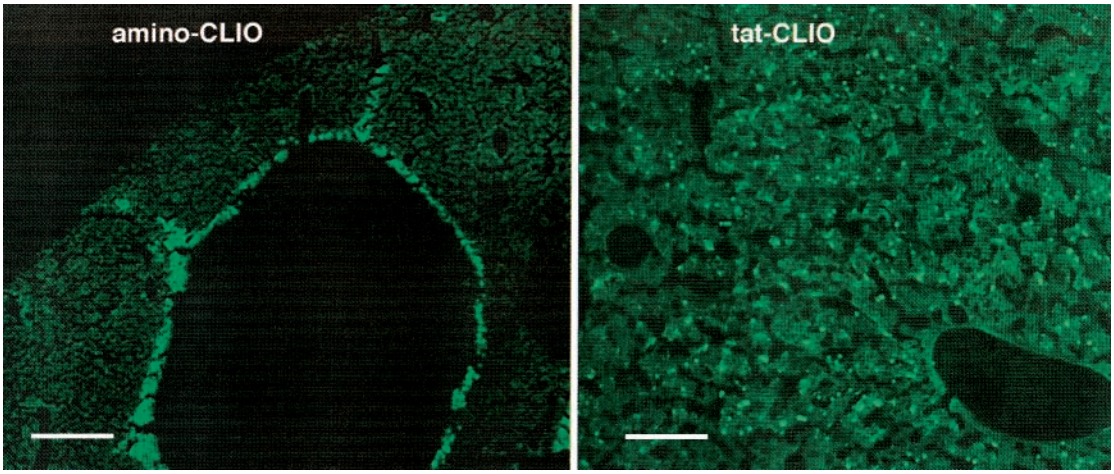


Figure 2. Fluorescence microscopy of livers of mice injected with amino-CLIO or Tat CLIO. Line is a scale marker indicating 50 microns.

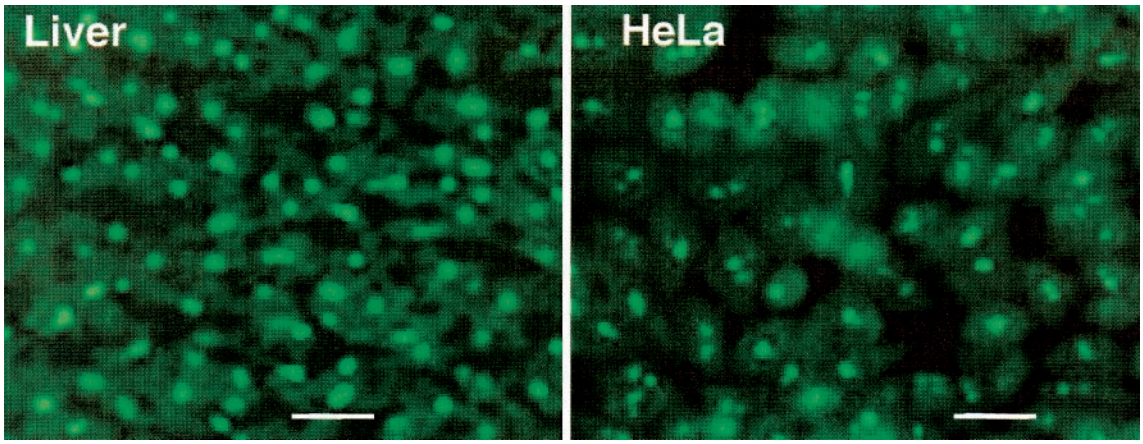


Figure 3. Fluorescence microscopy of livers of mice injected with amino-CLIO and HeLa cells in culture incubated with tat-CLIO. White line indicates 10 microns.

Table 3. Biodistribution of Nanoparticles[a]

organ	MION-47 (%ID/g)	Amino-CLIO (%ID/g)	Tat-CLIO (%ID/g)
liver	8.8 ± 0.27	8.28 ± 0.45	8.53 ± 0.3
lymph node	8.79 ± 0.21	8.75 ± 0.26	6.4 ± 0.1
spleen	6.13 ± 0.21	6.11 ± 0.35	6.27 ± 0.18
kidney	2.94 ± 0.78	2.9 ± 0.51	1.87 ± 0.38
lung	1.82 ± 0.21	1.92 ± 0.27	1.92 ± 0.39
bone	1.69 ± 0.49	1.79 ± 0.25	1.0 ± 0.21
fat	1.84 ± 0.17	1.81 ± 0.41	0.72 ± 0.13
muscle	1.97 ± 0.31	1.91 ± 0.25	0.92 ± 0.19
brain	0.38 ± 0.09	0.17 ± 0.03	0.09 ± 0.02
blood	2.23 ± 0.45	2.2 ± 0.3	0.49 ± 0.19

[a] %ID/g = percent injected dose per gram.

was performed because it achieved high concentrations of Tat-CLIO and because of its well-defined vasculature and large vessel-free regions. Amino-CLIO was concentrated along the hepatic vessels in endothelial cells and/or Kupffer cells as shown in Figure 2, a pattern similar to that seen when MION accumulates in rat liver. MION shows reticuloendothelial uptake, with an absence of iron in hepatocytes (*20*). However, the pattern of hepatic fluorescence obtained after Tat-CLIO administration was quite different, with numerous discrete foci of intense fluorescence throughout the parenchyma and a notable absence of fluorescence surrounding blood vessels. This indicates that Tat-CLIO passes from the vascular compartment, and through cells surrounding blood vessels, to obtain a parenchymal distribution. The distribution of Tat-CLIO fluorescence was analyzed at higher magnification as shown in Figure 3. The distribution of fluorescence appears to be similar to that seen when HeLa cells are incubated with Tat-CLIO, where Tat-CLIO shows a pronounced nuclear accumulation. It appears that attachment of the tat peptide to magnetic nanoparticles reduces blood half-life and leads to a broad parenchymal intrahepatic distribution in the liver, while the organ biodistribution is determined by the nanoparticlate rather than the presence of the tat peptide.

Our results can be compared with studies using protein transduction domains such as the tat peptide to induce enzymes to penetrate tissues after injection. Fusion proteins of the tat protein with β-galactosidase or of the tat peptide with β-glucuronidase have been synthesized and exhibit enhanced tissue penetration after injection (*21, 22*). On the other hand a tat-β-galactosidase, prepared by the conjugation of between one and two peptides per mole of enzyme, concentrated perivascularly after injection (*6*). Schwarze et al. have proposed that protein denaturation plays a role in the cellular uptake of their conjugates.

The label to which the tat peptide is attached here, amino-CLIO, is extremely robust and cannot undergo temperature dependent changes in physical state similar to denaturation. Cross-linked dextran-coated iron oxide (amino-CLIO) can withstand abusive treatments, such as incubation at 121 °C for 30 min, without a change in size, blood half-life, or loss of its dextran coat (Josephson, unpublished observations). Second, the use of Tat-CLIO for cell tracking by MR requires the highly magnetic form

the iron oxide (superparamagnetic iron oxide), which requires preservation of the iron oxide crystals in their original form (greater than 3 nm in diameter with an inverse spinel crystal structure). The magnetic integrity of the iron oxide must be maintained after internalization because of the profound effect that Tat-CLIO loaded cells have on MR images (*9*, *10*). Finally, as explained above, the FITC label of the Tat-CLIO nanoparticle used here cannot be separated from the nanoparticle with the chemistry employed.

Our finding that the tat peptide can affect the delivery of magnetic nanoparticles might provide the basis for the design of new types of magnetic nanoparticle based diagnostic agents. We have recently demonstrated that magnetic nanoparticles can serve as sensitive biosensors for the sequence specific detection of nucleic acids by NMR (*14*). The addition of the tat peptide to such biosensors may provide a signal for their membrane translocation or nuclear localization in vivo. Alternatively, it may be possible to add the tat peptide sequence to direct the intracellular disposition of nanoparticles targeted to cells by antibodies or receptor binding ligands.

ACKNOWLEDGMENT

P. Wunderbaldinger was supported by the Austrian Science Fund (FWF), Vienna, Austria.

LITERATURE CITED

(1) Rothbard, J. B., Garlington, S., Lin, Q., Kirschberg, T., Kreider, E., McGrane, P. L., et al. (2000) Conjugation of arginine oligomers to cyclosporin A facilitates topical delivery and inhibition of inflammation. *Nat. Med. 6*, 1253−7.

(2) Polyakov, V., Sharma, V., Dahlheimer, J. L., Pica, C. M., Luker, G. D., and Piwnica-Worms, D. (2000) Novel Tat-peptide chelates for direct transduction of technetium-99m and rhenium into human cells for imaging and radiotherapy. *Bioconjugate Chem. 11*, 762−71.

(3) Ford, K. G., Souberbielle, B. E., Darling, D., and Farzaneh, F. (2001) Protein transduction: an alternative to genetic intervention? *Gene Ther. 8*, 1−4.

(4) Eguchi, A., Akuta, T., Okuyama, H., Senda, T., Yokoi, H., Inokuchi, H., et al. (2001) Protein transduction domain of HIV-1 Tat protein promotes efficient delivery of DNA into mammalian cells. *J. Biol. Chem. 9*, 9.

(5) Snyder, E. L., and Dowdy, S. F. (2001) Protein/peptide transduction domains: potential to deliver large DNA molecules into cells. *Curr. Opin. Mol. Ther. 3*, 147−52.

(6) Fawell, S., Seery, J., Daikh, Y., Moore, C., Chen, L. L., Pepinsky, B., et al. (1994) Tat-mediated delivery of heterologous proteins into cells. *Proc. Natl. Acad. Sci. U.S.A. 91*, 664−8.

(7) Derossi, D., Chassaing, G., and Prochiantz, A. (1998) Trojan peptides: the penetratin system for intracellular delivery. *Trends. Cell Biol. 8*, 84−7.

(8) Josephson, L., Tung, C. H., Moore, A., and Weissleder, R. (1999) High-efficiency intracellular magnetic labeling with novel superparamagnetic-Tat peptide conjugates. *Bioconjugate Chem. 10*, 186−91.

(9) Lewin, M., Carlesso, N., Tung, C. H., Tang, X. W., Cory, D., Scadden, D. T., et al. (2000) Tat peptide-derivatized magnetic nanoparticles allow in vivo tracking and recovery of progenitor cells. *Nat. Biotechnol. 18*, 410−4.

(10) Dodd, C. H., Hsu, H., Chu, W., Yang, P., Zhang, H., Mountz, J. D., et al. (2001) Normal T-cell response and in vivo magnetic resonance imaging of T cells loaded with HIV transactivator-peptide-derived superparamagnetic nanoparticles. *J. Immunol. Methods 256*, 89−105.

(11) Turnbull, D. H., Wadghiri, Y. Z., Josephson, L., and Wichterje, H. (2001) In vivo MR microspectroscopy of neural migration in the mouse brain. *Int. Soc. Magn. Reson. Med., Meeting Abstr.*

(12) Moore, A., Sun, Z., Cory, D., Lipes, M., and Weissleder, R. (2001) Detection of the immune cells labeled with superparamagnetic nanoparticles in Type 1 Diabetes, in *Advances in assays, molecular labels, signaling and detection*, Proceedings of Cambridge Healthtech Institute's 5th Annual Meeting, Washington, DC.

(13) Hogemann, D., Josephson, L., Weissleder, R., and Basilion, J. P. (2000) Improvement of MRI probes to allow efficient detection of gene expression. *Bioconjugate Chem. 11*, 941−6.

(14) Josephson, L., Perez, J. M., and Weissleder, R. (2001) Magnetic nanosensors for the detection of oligonucleotide sequences. *Angew. Chem. Int. Ed. 40*, 3204−3206.

(15) Shen, T., Weissleder, R., Papisov, M., Bogdanov, A., Jr., and Brady, T. J. (1993) Monocrystalline iron oxide nanocompounds (MION): physicochemical properties. *Magn. Reson. Med. 29*, 599−604.

(16) Jung, C. W. (1995) Surface properties of superparamagnetic iron oxide MR contrast agents: ferumoxides, ferumoxtran, ferumoxsil. *Magn. Reson. Imaging 13*, 675−91.

(17) Jung, C. W., and Jacobs, P. (1995) Physical and chemical properties of superparamagnetic iron oxide MR contrast agents: ferumoxides, ferumoxtran, ferumoxsil. *Magn. Reson. Imaging 13*, 661−74.

(18) Jung, C. W., Weissleder, R., Josephson, L., Bengele, H., and Brady, T. J. (1996) Physical properties of MION-46 and AMI-227, in the Proceedings of the International Society of Magnetic Resonance and Medicine, New York.

(19) McLachlan, S. J., Morris, M. R., Lucas, M. A., Fisco, R. A., Eakins, M. N., Fowler, D. R., et al. (1994) Phase I clinical evaluation of a new iron oxide MR contrast agent. *J. Magn. Reson. Imaging 4*, 301−7.

(20) Van Beers, B. E., Sempoux, C., Materne, R., Delos, M., and Smith, A. M. (2001) Biodistribution of ultrasmall iron oxide particles in the rat liver. *J. Magn. Reson. Imaging 13*, 594−9.

(21) Schwarze, S. R., Ho, A., Vocero-Akbani, A., and Dowdy, S. F. (1999) In vivo protein transduction: delivery of a biologically active protein into the mouse. *Science 285*, 1569−72.

(22) Xia, H. M. Q., and Davidson, B. L. (2001) The HIV tat protein transduction domain improves the biodistribution of beta-glucuronidase expressed from recombinant viral vectors. *Nature Biotechnol. 19*, 640−644.

(23) Weissleder, R., Heautot, J. F., Schaffer, B. K., Nossiff, N., Papisov, M. I., Bogdanov, A., Jr., et al. (1994) MR lymphography: study of a high-efficiency lymphotrophic agent. *Radiology 191*, 225−30.

BC015563U

Cysteine-Free Mutant of Aequorin as a Photolabel in Immunoassay Development

Suresh Shrestha,[†] Insook R. Paeng,[‡] Sapna K. Deo,[†] and Sylvia Daunert*,[†]

Departments of Chemistry and Pharmaceutical Sciences, University of Kentucky, Lexington, Kentucky 40506-0055 and Department of Chemistry, Seoul Women's University, Seoul, Korea.
Received April 5, 2001; Revised Manuscript Received September 27, 2001

The bioluminescent protein aequorin is a sensitive label that has been employed in a number of analytical applications. A mutant of aequorin with enhanced stability produced recombinantly in our laboratory has been employed as a label in the development of an immunoassay for digoxin. Digoxin is a cardiac glycoside used in the treatment of congestive heart failure. This drug has a very narrow therapeutic range of 0.8−2.0 ng/mL (1.0−2.5 nmol/L), thus requiring therapeutic drug monitoring. In this study, a derivative of digoxigenin was chemically conjugated to the mutant aequorin, and the resulting protein−digoxigenin derivative conjugates were characterized in terms of their luminescence properties. A solid-phase immunoassay for digoxin was then developed. The detection limit of the assay for digoxin was 1×10^{-12} M. To demonstrate the use of this mutant aequorin as a label in biological sample analysis without any need for pretreatment of the samples, the assay was tested in serum spiked with digoxin. Interference from digoxin analogues was also evaluated to determine the specificity of the assay.

INTRODUCTION

Aequorin, a calcium-binding photoprotein, was originally isolated from the jellyfish *Aequorea victoria* in Friday Harbor, Washington (*1*). The holoprotein consists of apoaequorin (189 amino acid residues), a chromophore (coelenterazine), and molecular oxygen (*2*). The photoprotein is activated by calcium, which binds to the three EF-hand structures present within the protein molecule (*3*). These EF-hand structures are characteristic of the calcium-binding protein family. Upon addition of calcium, aequorin undergoes a conformational change leading to oxidation of bound coelenterazine to coelenteramide with the subsequent release of CO_2 and a flash of light ($\lambda_{max} = 469$ nm) (*4*).

Aequorin has been employed in a variety of analytical and biological applications. It has been used in the measurement of calcium in various intracellular compartments (*5*). Highly sensitive binding assays and immunoassays have been developed for peptidic and nonpeptidic analytes using aequorin as a label (*6, 7*). A proteolytic bond cleavage assay has also been developed using an aequorin fusion protein (*8*). Since aequorin can be detected down to attomole levels, it has been employed in the determination of biotin in single cells and in picoliter-volume vials (*9*−*11*). In addition, aequorin-labeled probes have been used as an alternative to radiolabels in nucleic acid hybridization assays (*12, 13*).

Several mutational studies have been performed on aequorin to elucidate the effects of various amino acids on the activity of the protein (*14*−*16*). Among them, cysteine-free mutants have shown to increase the protein's luminescence activity. The luminescence activity of the mutant was found to be higher (124%) when compared to that of native protein (100%) (*17, 18*). Although the specific cause for the higher activity is not yet clear, it has been suggested that the cysteines present in the native protein are not essential in the generation of the luminescence activity (*19*). We have postulated that presence of disulfide bonds in the native protein may introduce conformational constraints in the protein structure leading to a reduction in the bioluminescence activity (*19*). In addition to an increased activity, the cysteine-free mutant does not need the addition of a reducing agent to prevent dimerization of the protein, thus increasing the stability of the protein.

The goal of this study was to investigate the performance of this cysteine-free mutant of aequorin constructed previously in our laboratory as a label in immunoassay development. Bioluminescence is a relatively rare phenomenon in nature; thus, when aequorin is used as a label in biological sample analysis it offers the advantage of producing a low background signal (*3*). Therefore, we decided to investigate the detection ability of this mutant of aequorin in the analysis of biological samples and without performing any pretreatment steps.

Digoxin was selected as a model analyte for the study. Digoxin is a cardiac glycoside used in the treatment of congestive heart failure and supraventricular arrhythmias (*20, 21*). It has a narrow therapeutic window of 0.8−2.0 ng/mL with a potential of fatal toxicity. Hence, it frequently needs therapeutic drug monitoring (TDM) (*22*).

For the purpose of this study, a derivative of digoxigenin was employed for its chemical conjugation to the lysine residues of the mutant aequorin. Several mutant aequorin−digoxigenin derivative conjugates with various mole ratios of digoxin to aequorin were prepared and were characterized in terms of their luminescence properties and binding ability to an anti-digoxin antibody. Dose−response curves were generated for digoxin in a sequential binding format. The optimized assay was used

* Corresponding author: Sylvia Daunert; Phone: (859) 257-7060; Fax: (859) 323-1069; E-mail: daunert@pop.uky.edu.
[†] University of Kentucky.
[‡] Seoul Women's University.

10.1021/bc010044c CCC: $22.00 © 2002 American Chemical Society
Published on Web 02/21/2002

to perform serum analysis with spiked digoxin without any pretreatment of the samples. To determine the specificity of the immunoassay, the assay was also employed to determine the effect of structurally similar compounds to digoxin.

MATERIALS AND METHODS

Reagents. Tris(hydroxymethyl)aminomethane (Tris) free base, ethylenediaminetetraacetic acid (EDTA) sodium salt, glucose, digoxin, monoclonal biotinylated anti-digoxin antibody, digitoxin, bufalin, oleandrin, and human sera were purchased from Sigma (St. Louis, MO). Digoxigenin-3-*O*-methycarbonyl-ϵ-aminocaproic acid *N*-hydroxysuccinimide ester (derivative of digoxigenin) was obtained from Roche Molecular Biochemicals (Indianapolis, IN). Reactibind 96-well neutravidin-coated white polystyrene microtiter plates and biotin-free bovine serum albumin (BSA) were from Pierce (Rockford, IL). Microlite 2 polystyrene microtiter plates were purchased from Dynex (Chantilly, VA). The Bradford protein assay kit was obtained from Bio-Rad Laboratories (Hercules, CA). Coelenterazine was obtained from Biosynth International (Naperville, IL). Luria Bertani (LB) broth was from Gibco-BRL (Gaitherburg, MD). All solutions were prepared using deionized (Milli-Q Water Purification System, Millipore, Bedford, MA) distilled water. All chemicals were reagent grade or better and were used as received.

Apparatus. Ion-exchange chromatography was performed using a BioCAD-SPRINT perfusion chromatography system by Perseptive Biosystems (Cambridge, MA). Fractions containing the mutant aequorin protein were lyophilized using a VirTis Bench Top 3 freeze-dryer (Gardiner, NY). The purity of the aequorin protein was verified by sodium dodecyl sulfate−polyacrylamide gel electrophoresis (SDS−PAGE) on a Phast System by Pharmacia Biotech (Uppsala, Sweden). Absorbance measurements were performed using a HP 8453 UV−Vis spectrophotometer from Hewlett-Packard (Waldbronn, Germany). Bioluminescence measurements were taken on a MLX microtiter plate luminometer from Dynex (Chantilly, VA) using a 100 μL-fixed volume injector. All luminescence intensities reported are the average of a minimum of three replicates and have been corrected for the contribution of the blank.

Expression and Isolation of Mutant Aequorin. *Bacillus subtilis* (*B. subtilis*) cells containing plasmid pSD110 consisting of the gene for mutant apoaequorin were grown in 250 mL of LB broth containing kanamycin (30 μg/mL) for 16 to 18 h. The plasmid pSD110 consists of sequence for signal peptide fused to the gene for mutant apoaequorin. Thus, the expressed protein was secreted out in the culture media. The culture was centrifuged at 13800 × g for 30 min at 4 °C, and the supernatant was collected. The supernatant containing the mutant protein was filtered through 0.2 μm membrane filter to remove any cell debris. The pH of the protein solution was then adjusted to 4.2 by adding glacial acetic acid in order to precipitate the protein. The precipitated protein was collected by centrifugation at 13800 × g for 30 min at 4 °C.

Purification of the Mutant Protein. The precipitate containing the mutant protein was resuspended in 30 mM Tris-HCl, pH 7.0 containing 2 mM EDTA, and it was filtered using 0.2 μm filter. The filtered protein was purified by perfusion anion exchange chromatography using a column consisting of a quarternized polyethyleneimine (HQ) as a stationary phase. A salt gradient from 0.0 to 0.5 M NaCl was employed to elute the protein. Fractions containing the photoprotein were pooled together and lyophilized after adding glucose at a final concentration of 30 mM for protein stability. The lyophilized protein was resuspended in distilled deionized water and immediately dialyzed against 50 mM sodium bicarbonate buffer of pH 8.3 containing 4 mM EDTA to remove excess salt from the protein solution. The purity of the mutant protein was verified by SDS−PAGE using 12.5% polyacrylamide gels, which were developed by silver staining. The protein concentration was determined using the Bradford protein assay, with BSA as the standard.

Preparation of Mutant Apoaequorin−Digoxigenin Derivative Conjugates. To prepare apoaequorin−digoxigenin derivative conjugates, various amounts of derivative of digoxigenin were reacted with a fixed amount of mutant apoaequorin. Five different mole ratios of digoxigenin derivative to mutant apoaequorin, namely, 25/1, 50/1, 100/1, 250/1, and 500/1 were prepared. The digoxgenin derivative in anhydrous dimethyl sulfoxide was added to a solution of mutant apoaequorin in 50 mM sodium bicarbonate, pH 8.3, containing 4 mM EDTA. The reaction was allowed to proceed for 4 h at 4 °C while stirring. After that, a 5-fold molar excess of coelenterazine was added to the reaction mixture, and the solution was incubated for 15 h at 4 °C. After the conjugation reaction was completed, an excess of unconjugated analyte and an excess of coelenterazine were removed by passing the mixture through a Sephadex G-25 size-exclusion column. The concentration of each conjugate was determined using a standard Bradford assay.

Bioluminescence Emission Study. A volume of 100 μL of various conjugates at a concentration of 1.0×10^{-7} M were added to a Microlite 2 polystyrene microtiter plate, and the bioluminescence was measured by injecting 100 μL of luminescence triggering buffer (100 mM Tris-HCl, 100 mM $CaCl_2$, pH 7.5). The bioluminescence signal was collected at 0.1-s interval over a 3-s time period.

Calibration Plot of Mutant Aequorin−Digoxigenin Derivative Conjugates. A stock solution of conjugates (8.0×10^{-7} M) were serially diluted in assay buffer (30 mM Tris-HCl, 4 mM EDTA, 150 mM NaCl, pH 7.5, containing 0.1% (w/v) biotin-free BSA) and the bioluminescence intensity of 100 μL of each dilution was measured after injecting 100 μL of luminescence-triggering buffer.

Binder−Dilution Study. A biotinylated anti-digoxin antibody of differing concentrations were prepared in the dilution buffer (100 mM sodium phosphate, pH 7.4, containing 150 mM NaCl and 0.1% (w/v) biotin-free BSA) and 100 μL of each dilution was immobilized on a neutravidin coated plate with constant shaking for 2 h at room temperature. The plate was then washed three times with wash buffer (30 mM Tris-HCl, 4 mM EDTA, 150 mM NaCl, pH 7.5 containing 0.1% (w/v) biotin-free BSA). Digoxigenin derivative−aequorin conjugate, 50/1 (100 μL, 1×10^{-9} M), in assay buffer was then added to the plate containing immobilized antibody. The plate was incubated for an additional 2 h with shaking at room temperature. The plate was then washed three times with the wash buffer, and the bioluminescence intensity was measured by injecting 100 μL of the luminescence-triggering buffer.

Association−Time Study. For this study, a biotinylated anti-digoxin antibody (100 μL, 2.0 μg/mL) was immobilized on the neutravidin-coated wells of the microtiter plate, as described previously. Next, a volume of

100 μL of the conjugate, 50/1, of concentration 1×10^{-9} M was added to the plate, and the plate was incubated for various time periods with shaking. The plate was then washed three times with the wash buffer, and the luminescence intensity was measured in the presence of 100 μL of luminescence-triggering buffer.

Dose−Response Curves for Digoxin. A stock solution of digoxin of a concentration 1×10^{-3} M was serially diluted in dilution buffer. For the assay, 100 μL of digoxin ranging in concentration from 1×10^{-5} M to 1×10^{-13} M were incubated with immobilized biotinylated anti-digoxin antibody (2 μg/mL) for 2 h at room temperature with shaking. Following this incubation period, the plate was washed three times with wash buffer. A volume of 100 μL of conjugate, 50/1, of concentration 1×10^{-9} M was then added and allowed to incubate with shaking for an additional 2 h at room temperature. After a washing step, the luminescence intensity was measured as described previously. Dose−response curves were also generated in a similar manner for the 25/1 digoxigenin derivative−aequorin conjugate with differing anti-digoxin antibody concentrations. For this, a volume of a 100 μL of a protein conjugate of 5×10^{-11} M concentration was employed, along with 0.5 and 2.0 μg/mL of anti-digoxin antibody, respectively.

Determination of Degree of Conjugation. The degree of conjugation for each conjugate was determined by a simultaneous spectrophotometric assay for two component system by following a previously reported protocol (*23*). For that, absorbance measurement was done at two different wavelengths (λ_1 = 265 nm and λ_2 = 278 nm). Following equations were used to calculate the concentration of the digoxin

$$A_{\lambda 1} = a_{x\lambda 1} b c_x + a_{y\lambda 1} b c_y$$

$$A_{\lambda 2} = a_{x\lambda 2} b c_x + a_{y\lambda 2} b c_y$$

where, $A_{\lambda 1}$ = absorbance at λ_1, b = path length = 1, x = component 1, y = component 2, $a_{x\lambda 1}$ = molar absorptivity of compound 1 at λ_1, c_x = concentration of compound 1.

Recovery Study of Digoxin in Serum. A volume of 100 μL of serum samples were spiked with standard amounts of digoxin. Next, 100 μL of these samples was incubated with immobilized biotinylated anti-digoxin antibody, for 2 h at room temperature followed by a washing step. A volume of 100 μL of the conjugate (25/1) of 5×10^{-10} M concentration was then added to the plate and incubated for 2 h. After a washing step, the luminescence intensity was measured as described previously. Percent recoveries of digoxin in serum samples were determined from the dose−response curve.

Cross-Reactivity Study. A cross-reactivity study was performed in the same way as the studies conducted for digoxin in serum. Various concentrations of compounds structurally similar to digoxin such as bufalin, oleandrin, and digitoxin were spiked in the serum, and the percent cross-reactivity was determined from the dose−response curve generated for digoxin.

RESULTS AND DISCUSSION

Luminescent proteins have become popular reporters due to their ease of handling and inherent sensitivity. Aequorin is one such luminescent protein that has been used as a highly sensitive label in analytical assay systems. Native aequorin contains three cysteine residues in its primary structure, which necessitates the presence of disulfide reducing agents at all times to prevent dimerization of the protein leading to loss in its activity (*14*). Furthermore, the presence of reducing agents can also have a negative effect on the binding capacity of antibodies as they consist of disulfide bonds linking their heavy chains with light chains that together form the binding site for antigens. We have demonstrated that a cysteine-free mutant of aequorin constructed using genetic engineering tools can overcome these problems associated with the native protein. Moreover, this cysteine-free mutant protein has been found to be more active than the wild-type protein (*17*).

Table 1. Characteristics of Aequorin−Digoxin Conjugates.

initial ratio (aequorin:digoxigenin derivative)	degree of conjugation	detection limit (M)	half-life (s)
cysteine-free aequorin	N/A	7.0×10^{-12}	1.22
25/1	1.1	8.0×10^{-12}	1.30
50/1	2.0	5.0×10^{-11}	1.17
100/1	4.0	2.0×10^{-10}	1.27
250/1	4.0	4.0×10^{-10}	1.22
500/1	4.1	1.0×10^{-9}	1.22

In this study, the performance of this mutant aequorin as a label in the development of an immunoassay for the determination of digoxin in biological samples was investigated. As mentioned earlier, patients taking digoxin need to be monitored frequently because of the narrow therapeutic range of this drug. Thus, assays for digoxin that are highly sensitive, rapid, and selective are required. Several immunoassays have been developed for analyzing digoxin and are commercially available. For example, Vitros digoxin immunoassay by Johnson & Johnson Clinical Diagnostics is based on competition between the digoxin and digoxin-peroxidase conjugate for binding to anti-digoxin antibody (*22*). AxSYM Digoxin II is an automated immunoassay for digoxin developed by Abbott Laboratories which uses an alkaline phosphotase conjugate of digoxin in an heterogeneous format (*22*).

The mutant aequorin can be produced using recombinant DNA technique in a highly reproducible manner and in unlimited amounts, thus reducing the reagent cost (*1*). For that, the cysteine-free mutant aequorin was expressed in *B. subtilis* using plasmid pSD110 constructed in our laboratory (*6*). The expressed protein was collected from the culture media by acid precipitation. The crude protein was purified using perfusion anion-exchange chromatography, and the concentration of the protein was determined by Bradford assay. The yield of the protein was found to be 8.38 mg of protein per liter of culture.

Several aequorin−digoxigenin derivative conjugates were prepared by reacting an excess of an *N*-hydroxysuccinimide ester derivative of digoxigenin at various mole ratios with the lysine residues of mutant aequorin as described in the Experimental Section. All the conjugates were characterized in terms of their luminescence properties, detection limits, and half-lives, as shown in Table 1. The detection limit for each conjugate was determined using calibration curves generated by employing varying amounts of conjugates. As it can be seen in Table 1, the detection limit increased with the increasing molar ratios of digoxigenin derivative to aequorin. This can be explained by the fact that an increased molar ratio of digoxigenin derivative to aequorin in the conjugation reaction results in the conjugates with a higher number of digoxigenin derivative bound to the protein. Some of these digoxigenin derivative can bind to the active site of the protein affecting the protein activity, and consequently providing a poor detection limit. However, con-

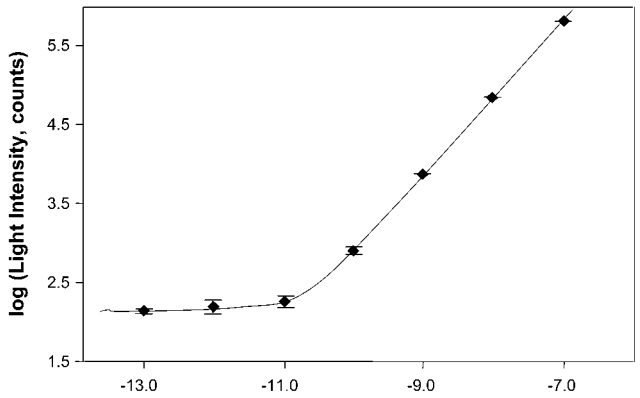


Figure 1. Calibration curve study of the 50/1 aequorin−digoxigenin derivative conjugate. Data are the average plus ± one standard deviation ($n = 3$).

jugates containing approximately one digoxigenin derivative per aequorin molecule were as active as unmodified aequorin. The bioluminescence half-lives of all the conjugates were found to be comparable to the half-life of nonconjugated mutant aequorin. Performance of the conjugates was also evaluated in terms of change in the luminescence activity of aequorin−digoxigenin derivative conjugate in a solution phase in the presence of anti-digoxin antibody. None of the conjugates exhibited any homogeneous change in bioluminescence signal, indicating that the binding event between aequorin-labeled analyte and antibody does not have any effect on the activity of the protein. On the basis of the results obtained above, we decided to use an digoxigenin derivative−aequorin conjugate, 50/1, for further studies. The conjugate 50/1 showed good bioluminescence activity with a low detection limit. The conjugate 25/1 provided a better detection limit than the conjugate 50/1; however, the probability of attachment of digoxigenin derivative to aequorin in a conjugation reaction is higher for the molar ratio of 50/1 of aequorin to digoxin.

A concentration of 1×10^{-9} M of the conjugate 50/1 was selected from the calibration study for further studies as this is a relatively low concentration of protein capable of generating a signal that is well above the background. A typical calibration curve for 50/1 conjugate is presented in Figure 1.

The next step in the study was to determine the amount of antibody to be used in subsequent experiments. For that purpose, a binder−dilution curve was generated (see Figure 2). The biotinylated anti-digoxin antibody was immobilized on a neutravidin-coated plate by taking advantage of the strong binding affinity of neutravidin for biotin. A concentration of antibody of 2 μg/mL was selected from the linear portion of the binder−dilution curve for further studies. This concentration of antibody was chosen in order to achieve a low detection limit while keeping a high signal.

To reduce the total assay time, the optimum time required for binding of the aequorin−digoxigenin derivative conjugate to the antibody was determined by generating an association curve. The association study shown in Figure 3 was performed in the same manner as the binder−dilution study, except that the incubation time for binding the mutant aequorin−digoxigenin derivative conjugate to the antibody was varied. An association time of 2 h was selected since there is no substantial increase in binding after 2 h of incubation.

After evaluating various parameters, such as optimum amount of conjugate, antibody, and time, a dose−

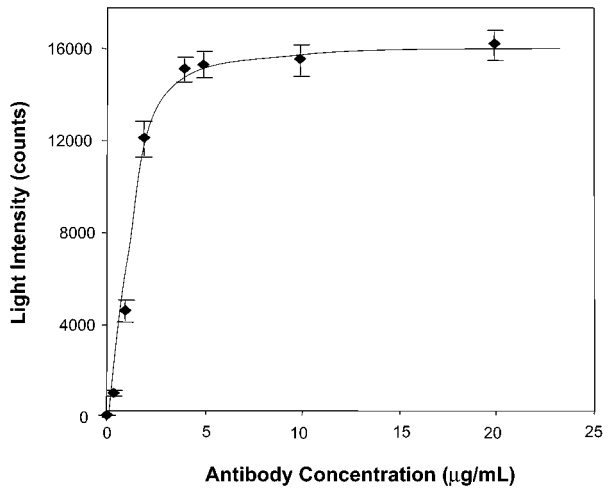


Figure 2. Binder−dilution study conducted using a 100 μL of 1×10^{-9} M 50/1 conjugate with 100 μL of the varying anti-digoxin antibody concentrations. Data are the average plus ± one standard deviation ($n = 3$).

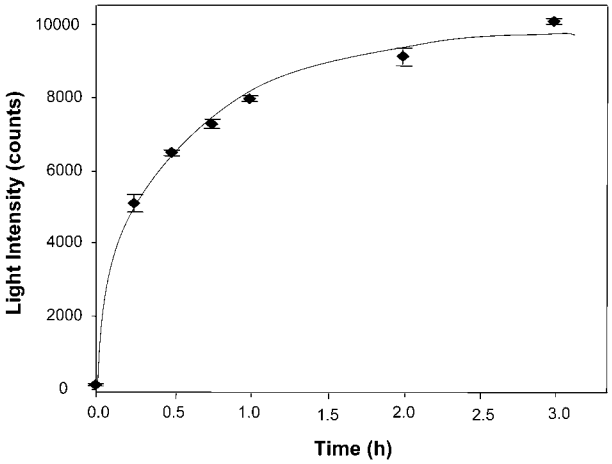


Figure 3. Association time study performed using 100 μL of 1×10^{-9} M 50/1 conjugate, and 100 μL of 2 μg/mL anti-digoxin antibody varying the incubation time period. Data are the average plus ± one standard deviation ($n = 3$).

response curve was generated for digoxin using the conjugate 50/1 in a sequential binding mode. The sequential binding mode has the advantage of producing a lower detection limit compared to the competitive binding mode. When the dose−response curve was generated using the competitive binding mode, a detection limit of 1×10^{-9} M was obtained (data not shown). To generate a dose−response curve in sequential binding format, various concentrations of free digoxin were incubated with the immobilized antibody followed by a washing step. Next, the conjugate was added and the luminescence intensity was measured. The dose−response curve obtained is shown in Figure 4. The study indicated that as expected the luminescence intensity was lower at higher concentrations of free digoxin and that the intensity of the signal increased with decreasing amounts of the digoxin. From this curve, a working range of 4 orders of magnitude was obtained and the detection limit was determined to be 3×10^{-10} M (S/N = 3).

The degree of conjugation was determined for all the conjugates prepared using a spectrophotometric method reported previously (Table 1) (*23*). The results showed that the conjugate 25/1 has 1.1 digoxigenin derivatives per aequorin molecule. Conjugate 50/1 resulted in 2.0 digoxigenin derivatives per aequorin. The other conju-

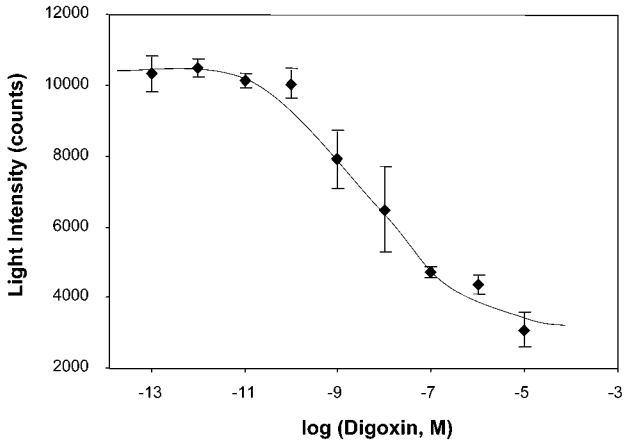


Figure 4. Dose−response curve generated in a sequential binding mode using 100 μL of 1×10^{-9} M 50/1 conjugate and 100 μL of 2 μg/mL anti-digoxin antibody. A stock solution of digoxin was serially diluted and used in the concentration range from 1×10^{-5} to 1×10^{-13} M. Data are the average plus ± one standard deviation ($n = 3$).

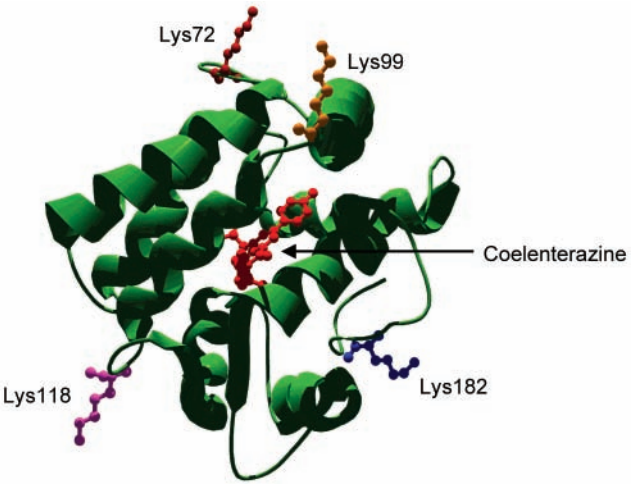


Figure 5. The three-dimensional X-ray crystal structure of aequorin showing the lysine residues 72, 99, 118, and 182. The figure was prepared using Swiss-PdbViewer (*24*) and rendered using POVRAY (*32*).

gates, 100/1, 250/1, and 500/1 had a degree of conjugation of 4.0, 4.0, and 4.1 digoxigenin derivatives per aequorin, respectively. Given these results, it appears that a maximum of four lysine molecules are being conjugated with the digoxigenin derivative employed. An examination of the X-ray crystal structure of aequorin using Swiss-PdbViewer (*24*) revealed that out of the fourteen lysines in the protein, Lys118 and Lys99 are the most accessible to the solvent with ≥62% and 52% accessible surface, respectively (Figure 5). The residues Lys72, Lys182, and Lys88 are also exposed to the solvent but to a lesser degree. The residue Lys72 has ≥43% accessible surface and residues Lys182 and Lys88 have ≥41% accessible surface. Among other lysines, Lys17 and Lys56 have 35% and 31% accessible surface, respectively. The remaining lysine residues, Lys59, 30, 39, 87, 96, 130, and 134 have less than 25% accessible surfaces. We also examined the crystal structure using Swiss-PdbViewer for the possibility of lysine residues forming ionic bonds with nearby aspartate or glutamate residues. We found that Lys30, 56, and 88 are within 3 Å from Glu76, Asp60, and Asp92, respectively. These lysine residues may form ionic bonds and thus may not be available for conjugation. Therefore, on the basis of our conjugation results

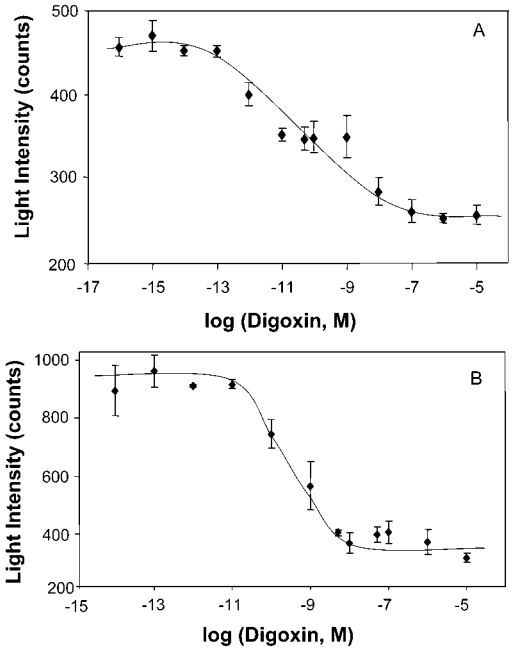


Figure 6. Dose−response curves for digoxin generated using 100 μL of 5×10^{-11} M 25/1 aequorin−digoxigenin derivative conjugate with 100 μL of (A) 0.5 μg/mL and (B) 2 μg/mL anti-digoxin antibody. Data are the average plus ± one standard deviation ($n = 3$).

as well as on the X-ray crystal structure analysis, we postulate that Lys118 and Lys99 are the ones that are most likely conjugated with digoxigenin derivative followed by Lys72 and Lys182.

Since better detection limits will be achieved from the system with only one analyte conjugated per label, digoxigenin derivative−aequorin conjugate 25/1 would provide better detection limit than the conjugate 50/1 (*25*). Thus, dose−response curves were also generated using conjugate 25/1. Two different concentrations of anti-digoxin antibody, 0.5 μg/mL and 2 μg/mL, were employed in the study (Figure 6). When the concentration of anti-digoxin antibody was increased from 0.5 μg/mL to 2 μg/mL, the curve became steeper, and as expected the detection limit for digoxin worsened. This is because as the amount of binder is increased, more free-analyte is required to compete with the labeled analyte. A detection limit of 1.0×10^{-12} M was obtained for digoxin using 0.5 μg/mL of antibody (Figure 6A). The dose−response curve generated using 2 μg/mL of anti-digoxin antibody has a dynamic range of 3 orders of magnitude and a detection limit for digoxin of 1.0×10^{-11} M (Figure 6B). The detection limits were calculated by measuring the signal at three times the standard deviation of the blank. The sensitivity of the assay when calculated in terms of standard deviation at zero dose (σ) (*26*) showed that a lower value of σ was obtained using 2 μg/mL antibody as compared to 0.5 μg/mL of the antibody. Thus, the system is more sensitive when 2 μg/mL of antibody is employed in the study. In general, a better detection limit for digoxin was obtained employing the conjugate 25/1 than when the conjugate 50/1 was used.

The assay developed was employed in the analysis of digoxin spiked in serum samples to determine the effect of the serum matrix on the detection of aequorin. Although this study is not equivalent to real patients sample analysis, it can serve as a good model. It has been found that myocardial digoxin concentration reaches steady state with serum digoxin concentration after several hours of the oral dose (*20*). Thus, digoxin is

Table 2. Percent Recovery of Digoxin in Serum.

spiked concentrations (ng/mL)	percent recovery[a]
0.5	116.7 ± 0.4
0.8	101.5 ± 2.4
1.5	108.2 ± 0.5
2.2	105.1 ± 1.8

[a] Percent recovery is calculated as follows: (concentration obtained from immunoassay)/(spiked concentration) × 100%.

routinely monitored in the serum of the patients. The advantage of using aequorin as a label in serum analysis is that the samples do not need any pretreatment due to the absence of background signal. Before performing the serum sample analysis, we investigated the effect of serum on aequorin activity by incubating the aequorin−digoxigenin derivative conjugates in both buffer and in serum. No effect of the serum matrix was observed on the activity of conjugates (data not shown). To mimic digoxin in the real sample, standard amounts of digoxin corresponding to the therapeutic range were spiked into the serum aliquots and employed in the study. Serum sample analyses were performed using the conjugate 25/1. The percent recoveries of digoxin in serum samples were determined from the dose−response curve generated for digoxin standards (Table 2). The results indicated that the matrix in the serum has very little effect on the assay.

In the development of an immunoassay, the specificity of the assay is very important, especially in assays for drugs with narrow therapeutic range. The presence of compounds similar in structure to the target analyte in the sample can provide with erroneous results if the assay is not selective. Since the therapeutic range of digoxin is narrow, its accurate determination in the presence of interferents is essential (*27*). There are several other drugs used in this cardiac treatment that have the structures similar to digoxin. For example, digitoxin, a structurally related cardiac glycoside to digoxin, has been found to decrease the apparent digoxin concentration in the sample (*28*, *29*). Oleandrin, another cardiac glycoside, present in the oleander plant and used in low doses to treat heart diseases competes with digoxin for the binding to the antibody (*28*, *30*). Bufalin is a cardioactive compound found in the venom of the Chinese toad, and it is also known to interfere in the assessment of digoxin concentration (*28*, *31*). These three compounds were tested for their cross-reactivity in our immunoassay. Aliquots of serum were spiked with various concentrations of these compounds in the absence of digoxin. Serum samples were spiked with the therapeutic amount of digitoxin and bufalin. Oleandrin was used in higher concentration than the other two as the micromolar concentration of oleandrin in serum has been found to provide apparent digoxin concentration in nanomolar range. The assay was conducted using aequorin−digoxin conjugate 1:25, and the percent cross-reactivities were determined from the dose−response curve generated for digoxin. None of the three compounds showed any significant cross-reactivity with the digoxin antibody (Table 3).

Stability studies were also performed for the conjugates in terms of retention of the luminescence activity of aequorin over time. All the conjugates were found to be stable for at least four months when stored in liquid form in Tris buffer (30 mM Tris-HCl pH 7.5 containing 2 mM EDTA) at 4 °C.

Table 3. Cross-Reactivity Study.

compounds added in serum	spiked concentrations (ng/mL)	percent cross-reactivity[a]
digitoxin	10.0	3.2 ± 1.3
	50.1	0.7 ± 0.1
	100.2	0.2 ± 0.1
bufalin	10.0	1.1 ± 1.4
	50.3	0.2 ± 0.1
	100.1	0.1 ± 0.1
oleandrin	9976.9	$2.5 \times 10^{-3} \pm 1.9 \times 10^{-3}$
	49884.6	$6.4 \times 10^{-4} \pm 1.0 \times 10^{-4}$
	99769.1	$3.3 \times 10^{-4} \pm 2.0 \times 10^{-4}$

[a] Percent cross-reactivity is calculated as follows: (Concentration obtained from immunoassay)/(Spiked concentration) × 100%.

In conclusion, a highly sensitive assay for digoxin was developed using a cysteine-free mutant of aequorin. We have demonstrated that a cysteine-free mutant of aequorin offers an excellent alternative to native aequorin to use as a label in the development of immunoassays where cysteines in the native protein are undesirable. This mutant of aequorin was found to be as sensitive as the native aequorin. Its performance in the development of immunoassay for digoxin has shown that this mutant can be used as a label in any immunoassays that require sensitive detection and therapeutic drug monitoring. The conjugates prepared retained their bioluminescence activity and had a long shelf life. This study also showed that the mutant aequorin can be effectively used in the assays requiring real sample analysis, and more importantly, no pretreatment of the samples is required, indicating minimal matrix effect. A detection limit for digoxin of 1×10^{-12} M (femtomoles of drug in the sample) was achieved using this cysteine-free mutant of aequorin. Furthermore, no significant cross-reactivity was observed from structurally similar compounds to digoxin.

ACKNOWLEDGMENT

This work was supported by grant from the National Institutes of Health (GM47915). S.D. is a Cottrell Scholar and a Lilly Faculty Awardee. S.S. thanks the Kentucky Research Challenge Trust Fund (RCTF) for a Predoctoral Fellowship.

LITERATURE CITED

(1) Lewis, J. C., and Daunert, S (2000) Photoproteins as luminescent labels in binding assays. *Fresenius J. Anal. Chem. 346*, 1.

(2) Kendall, J. M., and Badminton, M. N. (1998) *Aequorea victoria* bioluminescence moves into an exciting new era. *Trends Biotechnol. 16*, 216.

(3) Ohmiya, Y., and Hirano, T. (1998) Shining the light: mechanism of the bioluminescence reaction of calcium binding photoproteins. *Chem. Biol. 3*, 337.

(4) Jones, K., Keenan, M., and Keenan, M. (1999) Glowing jellyfish, luminescence and a molecule called coelenterazine. *Trends Biotechnol. 17*, 477.

(5) Brini, M., Pinton, P., Pozzan, T., and Rizzuto, R. (1999) Targeted recombinant aequorins: tools for monitoring [Ca^{2+}] in the various compartments of a living cell. *Microsc. Res. Technol. 46*, 380.

(6) Lewis, J. C., Cullen, L. C., and Daunert, S. (2000) Site-specifically labeled photoprotein-thyroxine conjugates using aequorin mutants containing unique cysteine residues: applications for binding assays (Part II). *Bioconjugate Chem. 11*, 65.

(7) Ramanathan, S., Lewis, J. C., Kindy, M. S., and Daunert, S. (1998) Heterogeneous Bioluminescence Binding Assay for an Octapeptide using Recombinant Aequorin. *Anal. Chim. Acta 369*, 181.

(8) Deo, S., Lewis, J. C., and Daunert S. (2000) Detection of proteolytic bond cleavage using recombinant aequorin. *Anal. Biochem. 281*, 87.

(9) Feltus, A., Grosvenor, A. L., Conover, R. C., Anderson, K. W., and Daunert, S. (2001) Detection of biotin in individual sea urchin oocytes using a bioluminescence binding assay. *Anal. Chem. 73* (7), 1403.

(10) Crofcheck, C. L., Grosvenor, A. L., Anderson, K., Lumpp, J. K., Scott, D., and Daunert, S. (1997) Detecting Biomolecules in Picoliter Vials using Aequorin Bioluminescence. *Anal. Chem. 69*, 4768.

(11) Grosvenor, A. L., Feltus, A., Conover, R. C., Daunert, S., and Anderson, K. W. (2000) Development of binding assays in microfabricated picoliter vials: an assay for biotin. *Anal. Chem. 72* (11), 2590.

(12) Galvan, B., and Christopoulos, T. K. (1996) Bioluminescence Hybridization Assays using Recombinant Aequorin: Application to the Detection of Prostate-Specific Antigen mRNA. *Anal. Chem. 20*, 3545.

(13) Actor, J. K., Kuffner, T., Hunter, C. S., and McNicholl, J. M. (1998) A flash-type bioluminescent immunoassay that is more sensitive than radioimaging: quantitative detection of cytokine cDNA inactivated and resting human cells. *J. Immunol. Methods 211*, 65.

(14) Tsuji, F. I., Inouye, S., Goto, T., and Sakaki, Y. (1986) Site-specific mutagenesis of the calcium-binding photoprotein aequorin. *Proc. Natl. Acad. Sci U.S.A. 83*, 8107.

(15) Ohmiya, Y., Ohashi, M., and Tsuji, F. I. (1992) Two excited states in aequorin bioluminescence induced by tryptophan modification. *FEBS Lett. 301*, 197.

(16) Ohmiya, Y., and Tsuji, F. I. (1993) Bioluminescence of the Ca^{2+}-binding photoprotein, aequorin, after histidine modification. *FEBS Lett. 320*, 267.

(17) Lewis, J. C., Lopez-Moya, J. J., and Daunert, S. (2000) Bioluminescence and secondary structure properties of aequorin mutants produced for site-specific conjugation and immobilization. *Bioconjugate Chem. 11*, 65.

(18) Deo, S. K., Lewis, J. C., and Daunert, S. (2001) C-terminal and N-terminal fusions of aequorin with small peptides in immunoassay development. *Bioconjugate Chem.* 12, 378.

(19) Kurose, K., Inouye, S., Sakaki, Y., and Tsuji, F. I. (1989) Bioluminescence of the Ca^{2+}-binding photoprotein aequorin after cysteine modification. *Proc. Natl. Acad. Sci. U.S.A. 86*, 80.

(20) Tzou, M. C., Reuning, R. H., and Sams, R. A. (1997) Quantitation of interference in digoxin immunoassay in renal, hepatic, and diabetic disease. *Clin. Pharmacol. Ther. 61*, 429.

(21) Datta, P., Hinz, V., and Klee, G. (1996) Comparison of four digoxin immunoassays with respect to interference from digoxin-like immunoreactive factors. *Clin. Biochem. 29*, 541.

(22) De, B. K., Booth, D. D., Magee, P. J., Moore, M. L., Preuss, T. M., Rose, T. A., and Roberts, W. L. (1999) Analytic performance of two automated nonpretreatment digoxin immunoassays. *Ther. Drug Monit. 21*, 123.

(23) Bachas, L. G., and Meyerhoff, M. E. (1986) Homogeneous enzyme-linked competitive binding assay for the rapid determination of folate in vitamin tablets. *Anal. Chem. 58*, 956.

(24) Guex, N., and Peitsch, M. C. (1997) SWISS-MODEL and the Swiss-PdbViewer: An environment for comparative protein modeling. *Electrophoresis 18*, 2714.

(25) Diamandis, E. P., and Christopoulos, T. K., Eds. (1996) *Immunoassay*, Academic Press, San Diego, CA.

(26) Ekins, R., and Edwards, P. (1997) Point on the meaning of sensitivity *Clin. Chem. 43*, 1824.

(27) Datta, P., Xu, L., Malik, S., Landicho, D., Ferreri, L., Halverson, K., Roby, P. V., Zebelman, A. M., and Kenny, M. A. (1996) Effect of antibody specificity on results of selected digoxin immunoassays among various clinical groups. *Clin. Chem. 42*, 373.

(28) Dasgupta, A., and Scott, J. (1998) Unexpected suppression of total digoxin concentrations by cross-reactants in the microparticle enzyme immunoassaay. *Am. J. Clin. Pathol. 110*, 78.

(29) Dasgupta, A., Wells, A., and Datta, P. (1999) Effect of digoxin Fab antibody on the measurement of total and free digitoxin by fluorescence polarization and a new chemiluminescent immunoassay. *Ther. Drug Monit. 21*, 251.

(30) Osterloh, J., Harold, S., and Pond, S. (1982) Oleander interference in the digoxin immunoassay in a fatal ingestion. *JAMA 247*, 1596.

(31) Chern, M. S., Ray, C. Y., and Wu, D. (1991) Biological intoxication to digitalis like substances after ingestion of cooked toad soup. *Am. J. Cardiol. 67*, 443.

(32) POVRAY. Persistence of Vision Raytracer version 3.1 (http://www.povray.org).

BC010044C

Noninvasive Imaging of Peripherally Injected Alzheimer's Disease Type Synthetic Aβ Amyloid In Vivo

Jeffrey R. Marshall,[†] Evelyn R. Stimson,[†] Joseph R. Ghilardi,[‡] Harry V. Vinters,[§] Patrick W. Mantyh,[‡] and John E. Maggio*[,†]

Department of Pharmacology and Cell Biophysics, University of Cincinnati, College of Medicine, 231 Albert B. Sabin Way, Cincinnati, Ohio 45267, University of Minnesota, Department of Preventive Sciences−Neurosystems, 515 Delaware Street SE, Minneapolis, Minnesota 55455, and Department of Pathology and Laboratory Medicine and Brain Research Institute, 10833 Le Conte Avenue, University of California Los Angeles Medical Center, Los Angeles, California 90095. Received June 9, 2001; Revised Manuscript Received August 15, 2001

The pathological hallmark of Alzheimer's disease (AD) is accumulation in the brain of amyloid composed of the 40-mer peptide Aβ. Many fundamental questions about the biology of (AD) remain unanswered because there is currently no method of quantifying Aβ amyloid in vivo. A noninvasive method of detecting and quantifying Aβ amyloid in vivo would have wide application for the premortem diagnosis of AD and the efficient evaluation of candidate therapeutics aimed at inhibiting the formation and growth of Aβ amyloid. Taking advantage of the extraordinarily high affinity of Aβ for itself, we have synthesized an N′-terminal diethylenetriaminepentaacetic acid (DTPA) derivative of Aβ possessing the kinetic activity and specificity for Aβ amyloid desired of a probe to be used for noninvasive imaging. DTPA-Aβ(3−40) is readily labeled with $^{111}InOAc_3$ to yield a stable probe with exquisite specificity for naturally occurring and synthetic Aβ amyloid in vitro. Moreover, ^{111}In-DTPA-Aβ(3−40), administered intravascularly can specifically deposit onto and label previously injected synthetic Aβ amyloid and be imaged in vivo with a γ camera. The present results demonstrate the design, synthesis, and use of an Aβ amyloid-specific probe and methods for its use as a noninvasive imaging agent. In vivo imaging of Aβ amyloid represents an important step toward the development of biochemically based objective tools for the assessment of progression of AD and efficacy of potential therapeutics.

INTRODUCTION

Approximately 20 human diseases known as amyloidoses have as a common feature the ordered assembly of naturally occurring nonpathogenic peptides and proteins into insoluble fibrillar polymers ("amyloid"), which accumulate and are associated with damage to surrounding tissue (*1*, *2*). The ordered self-assembly of the amyloid forming proteins into β-sheet structures continues to be the focus of research aimed at understanding the pathogenesis of these diseases (*3*) as well as the development of therapeutic interventions (*4*, *5*).

The most common amyloidosis and most common neurodegenerative disease is Alzheimer's disease (AD). Almost a century after its first description (*6*), AD is a major cause of morbidity and mortality among the elderly, affects 40−60% of the population over 85 years of age, and ranks as the third leading cause of death in the elderly population of the developed world behind cardiovascular disease and cancer (*3*). The pathological hallmark of AD is the presence of cerebrovascular and parenchymal amyloid in the brain, concentrated in the hippocampus, amygdala, and cerebral cortex (*3*, *7*−*13*). The major constituent of these amyloid plaques is the human β-amyloid peptide (Aβ), a 39−43 residue peptide (*14*−*16*) of unknown function produced by the proteolytic cleavage of the much larger amyloid precursor protein by two enzymes, β and γ secretase (*17*−*19*). Aβ is expressed constitutively in most tissues as a natural product; its production is not pathogenic, as it is found in similar total concentrations (nM) in both AD positive and negative individuals (*20*−*22*).

Aβ amyloid also exerts a pathological influence peripherally in human skeletal muscle. Inclusion body myositis (IBM) is the most common skeletal muscle disorder in adults, with a typical onset at age 50 or older (*23*, *24*). Both AD and IBM occur as age-dependent, sporadic, or genetically complex familial diseases and share multiple pathologic traits resulting in progressive tissue degeneration. Among a number of features common to AD and IBM, the pathology resulting from the accumulation of Congo red (an amyloid-specific dye) positive fibrillar Aβ deposits continues to be central to investigations aimed at elucidating these diseases (*25*). It is likely that AD and IBM also share pathogenic steps of disease progression given their mutual Aβ amyloid accumulations, and an increased understanding of one of these diseases may provide further details about the other. At present, many questions about the biology of these Aβ amyloidoses remain unanswered because there is currently no method of detecting and quantifying Aβ amyloid in vivo.

Historically, administration of Congo red (sodium diphenyldiazo-bis-α-naphthylamine sulfonate), introduced in 1923 (*26*), had been used to diagnose the presence of systemic amyloidosis by the measurement of the optical density of serum before and after administration and the amount of Congo red excreted in the

* Corresponding author. Phone: (513) 558-2302. Fax: (513) 558-1169. E-mail: John.Maggio@uc.edu.
[†] University of Cincinnati.
[‡] University of Minnesota.
[§] University of California.

10.1021/bc010066z CCC: $22.00 © 2002 American Chemical Society
Published on Web 01/05/2002

patients' urine (*27*). This method proved unreliable because it lacked the sensitivity (high proportion of false negatives), utility, and safety to be used as a diagnostic or research tool. More recently, noninvasive imaging of peripheral amyloid using radiolabeled purified human serum amyloid P (SAP) has been demonstrated and advanced toward clinical use (*28*, *29*).

Attempts at noninvasive detection of Aβ amyloid in vivo have been made using antibodies (*30*), Congo red derivatives (*31*, *32*), and other amyloid-specific dyes (*33*−*35*). Radiolabeled derivatives of Aβ show exquisite sensitivity at detecting Aβ amyloid in brain sections (*36*−*39*) and have been shown to label brain amyloid in vivo in both rodents (*36*) and primates (*38*). Despite these advances, the goal of noninvasive in vivo Aβ amyloid detection has remained elusive because of one or more shortcomings in sensitivity, specificity, kinetics, or accessibility.

Here, we report the design and synthesis of an Aβ derivative in which the two N-terminal amino acid residues have been replaced with the high affinity (K_d = 10^{-29} M) (*40*) ^{111}In chelating moiety diethylenetriaminepentaacetic acid (DTPA). We show that the resulting Aβ derivative, DTPA-Aβ(3−40), can be rapidly and easily labeled with ^{111}In, yielding a radiotracer that closely tracks the kinetic activity and specificity of the previously characterized (*39*, *41*−*43*) ^{125}I-Aβ in vitro. Further, we illustrate that ^{111}In-DTPA-Aβ(3−40), administered intravascularly, can deposit onto peripheral synthetic Aβ amyloid in the biceps femoris muscle of a rat and be imaged noninvasively with a γ camera in vivo. This is, to our knowledge, the first time that Aβ amyloid has been detected and imaged noninvasively in a living animal. This demonstration is a significant step toward the development of an imaging agent with the requisite properties for detection and measurement of Alzheimer's disease Aβ amyloid in vivo.

EXPERIMENTAL PROCEDURES

Synthetic Peptides and Radiolabeling. Aβ(1−40), the major form of Aβ found in human CSF (*14*, *21*), and DTPA-Aβ(3−40), synthesized by fluorenylmethoxycarbonyl (Fmoc) chemistry and purified by HPLC (>98%), were purchased (Quality Controlled Biochemicals, Hopkington, MA) and stored lyophilized at −20 °C. DTPA was added as the dianhydride (Aldrich Chemical Co., Inc., Milwaukee, WI) to the amino terminus of Aβ(3−40) during solid-phase synthesis (Figure 1). The purified peptides were characterized by analytical RP-HPLC (to 98%), amino acid analysis, and matrix-assisted time-of-flight mass spectrometry (Aβ(1−40) = 4329.86; DTPA-Aβ(3−40) = 4520.82).

Aβ(1−40) was radioiodinated (^{125}I at tyrosine-10, methionine-35 as native thioether) with Na^{125}I (Amersham, Arlington Heights, IL) as previously described (*39*) and was purified to a specific activity of 2000 Ci/mmol (10^9 dpm/μg; 1 ^{125}I molecule/Aβ peptide). The labeled peptide was stored at −20 °C in the eluting HPLC mobile phase with 2-mercaptoethanol (0.5%) added to prevent oxidation during storage.

$^{111}InCl_3$ in 40 mM HCl (Nycomed Amersham, Cincinnati, OH) was converted to $^{111}InOAc_3$ by the addition of 0.5 M NaOAc (pH 6) to yield final concentrations of 33 mM HCl and 83 mM NaOAc (*44*). One hundred microliters (1.2 mCi, 26 pmol ^{111}In) of this $^{111}InOAc_3$ stock solution was added to 10 nmol of DTPA-Aβ(3−40) dissolved in 900 μL of ammonium succinate buffer to achieve a final buffer concentration of 50 mM (pH 3). After 60 s

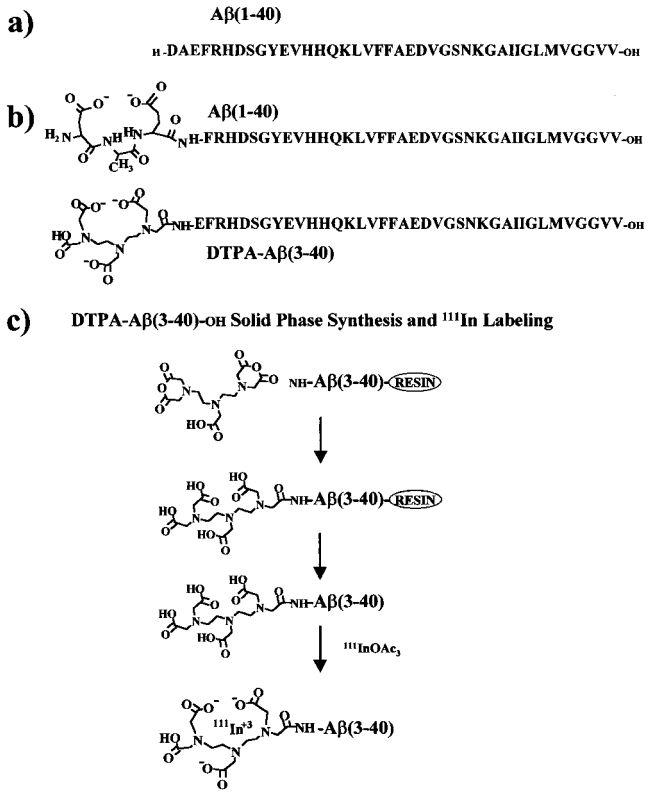


Figure 1. (a) Amino acid sequence of Aβ(1−40) and (b) N′-terminal chemical structure of Aβ(1−40) and DTPA-Aβ(3−40). (c) Solid-phase synthesis of DTPA-Aβ(3−40) using DTPA dianhydride and ^{111}In labeling with $^{111}InOAc_3$.

at room temperature with gentle manual mixing, the reaction was stopped by the addition of 2 mL of 1 mM DTPA free acid in 10 mM aqueous trifluoroacetic acid (TFA) (pH 2). The labeled peptide was purified from the ^{111}In-DTPA using a Sep-Pak Light (Waters Corp., Milford, MA) reversed-phase chromatography cartridge and a stepwise gradient of 0%, 10%, 20%, 40%, 60%, 80%, 90%, 95%, and 100% MeOH/EtOH (50:50) in 10 mM TFA (pH 2) (Figure 2a). Elution fractions 7−9 (200 μL each) were pooled and stored in the eluting mobile phase (approximately 85% MeOH/EtOH in 10 mM aqueous TFA) at room temperature (4 °C for size exclusion stability testing) until used for experiments. Using the 385:1 ratio of DTPA-Aβ(3−40):^{111}In with the conditions described above, ^{111}In labeling of DTPA-Aβ(3−40) is scalable to yield low μCi to high mCi amounts of ^{111}In-DTPA-Aβ(3−40). For in vitro experiments, stock solutions of ^{111}In-DTPA-Aβ(3−40) were diluted to the desired concentrations directly into the assay buffers.

Size exclusion chromatography (SEC) (FPLC; Amersham Pharmacia, Piscataway, NJ) was performed as described (*45*) to characterize the assembly state and stability of the radiotracers. Briefly, ^{125}I-Aβ(1−40) (calculated MW = 4455) or ^{111}In-DTPA-Aβ(3−40) (calculated MW = 4631) were diluted to about 2×10^5 cpm/mL in a 100 mM Tris buffer (0.01% BSA; pH 7.5), centrifuged for 10 min at 14 000*g*, loaded onto a Superdex 75 (10 mm i.d., 30 cm length) column, and eluted with a 100 mM Tris buffer (pH 7.5) at 30 mL/h. Thirty second elution fractions were collected and quantified with a γ counter. The SEC characterization was performed daily for 9 consecutive days using freshly prepared radiotracer (day 1) stored at 4 °C and 20 °C. Standard radiation safety handling precautions and shielding were used to minimize exposure during all experiments which employed the use of ^{111}In or ^{125}I.

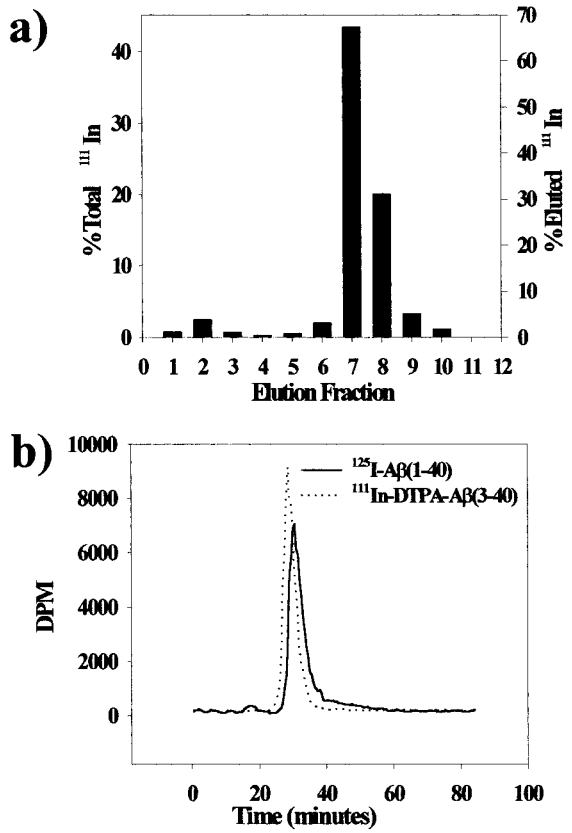


Figure 2. DTPA-Aβ(3−40) efficiently labels with ^{111}In. (a) Approximately 65% of total ^{111}In added to the labeling reaction and greater than 95% of ^{111}In eluted from the labeling reaction are eluted in the peptide fractions. (b) SEC of ^{111}In-DTPA-Aβ-(3−40) and ^{125}I-Aβ(1−40) indicate they are soluble monomers.

Deposition onto AD and Synthetic Aβ Amyloid In Vitro. Synthetic amyloid was prepared as previously described (*46*). Briefly, fibrillar aggregates were prepared from solutions of 10^{-4} Aβ in phosphate-buffered saline (PBS) (pH 7.5). Aβ(1−40) was dissolved in PBS, resulting in a clear solution with no evidence of flocculation or incomplete dissolution. Immediately following dissolution, peptide solutions were incubated under vigorous agitation (Teflon-coated magnetic stir bar at 800 rpm) at room temperature for up to 24 h until visible turbidity no longer increased. After aggregation, the suspensions were frozen on dry ice and stored at −20 °C until used. Synthetic amyloid plates (*46*) were prepared by diluting the aggregated Aβ(1−40) in 0.1% gelatin (60 °C) to yield 10 μg of peptide/mL of final concentration. The resulting suspension was aliquotted onto glass microscope slides for autoradiography or into flexible 96-well assay plates at 1.0 μg of Aβ peptide/well, dried overnight at 60 °C, and stored at room temperature. For deposition assays, the synthetic amyloid plates were preincubated with PBS, (0.1% BSA; pH 7.5) for 30 min. The preincubation buffer was removed, and 100 pM ^{125}I-Aβ(1−40) or 12.5 pM ^{111}In-DTPA-Aβ(3−40) in the PBS buffer was added to each well. After the incubation period (5−240 min), the radiotracer solution was removed, and wells were washed three times with an automated 96-well plate washer (Bio-Tek Instruments, Inc., Winooski, VT), separated, and quantified with a γ counter.

For a test of biological stability, 6.25 pM ^{111}In-DTPA-Aβ(3−40) was used to compare deposition kinetics onto synthetic amyloid in heparinized (250 IU/mL) fresh whole rat blood (collected using cardiac puncture immediately before the experiment) and PBS buffer in parellel. Deposition times of 15, 45, 120, and 1380 min in either buffer or blood were used, and workup was as described previously.

Deposition of ^{125}I-Aβ(1−40) and ^{111}In-DTPA-Aβ(3−40) radiotracers onto immobilized synthetic amyloid and slide-mounted tissue sections for autoradiography was performed as described (*39*, *41*, *46*, *47*). Tissue sections were preincubated at room temperature for 30 min with a PBS deposition buffer (0.1% BSA, 0.004% bacitracin, 0.0002% chymostatin, and 0.0002% leupeptin (pH 7.5)). After preincubation, the buffer was drained from the tissue, and fresh buffer containing the desired concentration of ^{125}I-Aβ(1−40) or ^{111}In-DTPA-Aβ(3−40) was added. After incubation, radiotracer was drained and aspirated from the slides, and the slides were washed three times for 3 min each in PBS (0.1% BSA; pH 7.5) followed by two 5 s rinses in distilled water. Dried slides were placed on film, stored at room temperature for desired exposure, and developed with a Kodak XOMAT film processor.

Immunohistochemical confirmation of Aβ was performed as described (*48*). Sections were washed in Tris-buffered saline (TBS; 140mM NaCl, 2.7 mM KCl, and 24.8 mM Tris, (pH 7.4)) for 20 min followed by 10 min in ethanol/distilled water (1:1). Sections were then washed three times for 10 min each in TBS, washed in blocking solution containing TBS and 10% normal goat serum (NGS) for 30 min, and incubated overnight at 23 °C in TBS containing 1% NGS and polyclonal anti-Aβ (R1282; 1:1500) raised against unaggregated synthetic Aβ(1−40). Three 10 min washes in TBS preceded a 1 h incubation at 23 °C in TBS containing 1% NGS and biotinylated donkey antirabbit IgG (1:500; Jackson ImmunoResearch, West Grove, PA). Sections were washed three times for 10 min each in TBS followed by incubation for 45 min at 23 °C in TBS containing 1% NGS and fluorescein (FITC)-conjugated avidin (1:200; Jackson ImmunoResearch). Sections were again washed three times for 10 min each with TBS and coverslipped using PBS/glycerol (1:1). Immunofluorescence was examined using a MRC-1024 Confocal Imaging System equipped with a krypton/argon ion laser in conjunction with an Olympus BX-75 microscope. Thioflavine S detection of Aβ amyloid was performed by fixing the tissue sections with a 4% paraformaldehyde solution for 30 min followed by a 5 min rinse in each 50% and 80% ethanol. Sections were then incubated in a 1% solution of Thioflavin S for 15 min followed by three 5 min washes in 80% ethanol. Thioflavin S fluorescence was examined using a Zeiss Axioplan microsope imaging system. Labeled sections were imaged using filters appropriate for the specific visualization of either fluorescein or Thioflavin S.

Imaging Synthetic Amyloid In Vivo. All animal experiments were performed under a University of Cincinnati IACUC-approved animal protocol in an AALAC-accredited facility. Five Sprague Dawley rats (100−300 g; Harlan, Indianapolis, IN) were anesthetized with a ketamine (60 mg/mL)/xylazine (12 mg/mL) cocktail. The posterior legs of each animal were clipped and scrubbed, and either synthetic Aβ amyloid (1 μg/μL, 0.9% NaCl) or vehicle was injected into the rat biceps femoris muscle. Animals recovered from anesthesia and were housed individually for one week with food and water ad libitum prior to injection of ^{111}In-DTPA-Aβ(3−40) and in vivo imaging. Pooled elution fractions collected from ^{111}In-DTPA-Aβ(3−40) synthesis were concentrated by evaporation and reconstituted in PBS (pH 6.0; 0.05% Tween 80) prior to injection. Animals were briefly anesthetized using isoflurane, and ^{111}In-DTPA-Aβ(3−40) was injected

(100 μL/min, 2 μCi/μL ^{111}In-DTPA-Aβ(3−40)) into a tail vein. At time intervals from 5 min to 7 days postinjection, animals were anesthetized with isoflurane for in vivo planar γ camera imaging. A Siemens LEM portable γ camera, equipped with both parallel hole and pinhole collimators, was used to image the labeled synthetic amyloid in vivo. After the appropriate survival time, the animals were anesthetized for a final time with a ketamine (60 mg/mL)/xylazine (12 mg/mL) cocktail and then rapidly perfused through the left ventricle with ice cold heparinized (250 IU/mL) saline (0.9% NaCl). After perfusion, the animals were dissected, and the muscle tissue was frozen, blocked, and sectioned with a cryostat microtome onto glass slides for autoradiography and Thioflavin S staining.

RESULTS

Synthesis and ^{111}In Labeling of DTPA-Aβ(3−40). After solid-phase peptide synthesis, DTPA-Aβ(3−40) (Figure 1) was deprotected, cleaved from the resin, and purified. DTPA-Aβ(3−40) has a molecular weight of only 176 Da greater than the naturally occurring Aβ(1−40) and, when labeled with ^{111}In at neutral pH, has an N′-terminal charge difference of only +1. The peptide is efficiently and stably labeled with ^{111}In (Figure 2a). DTPA-Aβ(3−40) can be labeled in high yield in 60 s, and longer incubation under these conditions did not improve the labeling efficiency or total yield of labeled peptide (data not shown). The conditions employed yield ^{111}In-DTPA-Aβ(3−40) with a specific activity of approximately 122 Ci/mmol with 65% ^{111}In incorporation, and scale-up is straightforward. SEC (*45*) (Figure 2b) confirmed that the ^{111}In-DTPA-Aβ(3−40) and ^{125}I-Aβ(1−40) used in these experiments were nonaggregated monomeric solutions. As expected, freshly prepared ^{111}In-DTPA-Aβ(3−40) elutes slightly earlier than monomeric ^{125}I-Aβ(1−40) (Figure 2b). Further, SEC confirmed the stability of ^{111}In-DTPA-Aβ-(3−40) as it remains in monomeric form with no detectable dissociation of ^{111}In for at least three ^{111}In half-lives when stored at either 20 or 4 °C (data not shown).

In Vitro Deposition Activity of ^{111}In-DTPA-Aβ(3−40). Successful in vivo amyloid detection and quantification using a radiolabeled Aβ derivative such as ^{111}In-DTPA-Aβ(3−40) depends on the ability of this derivative to specifically bind to and deposit onto endogenous amyloid plaques. Figures 3 and 4 show that ^{111}In-DTPA-Aβ(3−40) does specifically deposit onto both cerebrovascular and parenchymal Aβ amyloid in human AD brain tissue in vivo. Serial sections (Figure 3a,b) show that the same amyloid deposits labeled by ^{125}I-Aβ(1−40) are labeled by ^{111}In-DTPA-Aβ(3−40). High signal-to-noise exhibited on the human AD tissue sections and negligible signal on age-matched non-AD control serial sections (Figure 3d,e) further demonstrate that these radiolabeled Aβ derivatives are specific for the Aβ amyloid. Moreover, ^{111}In-DTPA-Aβ(3−40) shows significantly improved sensitivity over ^{125}I-Aβ(1−40) (Figure 3a,b), although the ^{125}I-Aβ(1−40) label has a much higher specific activity.

To confirm that ^{111}In-DTPA-Aβ(3−40) is depositing onto and labeling Aβ in the human tissue sections, a human AD tissue section was doubly labeled with ^{111}In-DTPA-Aβ(3−40) and Aβ-specific polyclonal antibody (R1282). ^{111}In-DTPA-Aβ(3−40) exhibits intense and specific labeling of cerebrovascular (CVA) and parenchymal senile plaque (SP) Aβ amyloid (Figure 4). The same CVA and SP (indicated with arrows in Figure 4) that labeled with ^{111}In-DTPA-Aβ(3−40) also labeled with the anti-Aβ antibody. Thioflavin S staining (Figure 4d,e) similarly validates the specificity of ^{111}In-DTPA-Aβ(3−40). ^{111}In-DTPA-Aβ(3−40) labels Aβ amyloid with great sensitivity, and the physical properties (specific activity, half-life, and decay energy) of ^{111}In enable excellent autoradiography resolution, as demonstrated by the ability to resolve the microvasculature lumen containing Aβ amyloid (indicated by arrow in Figure 4b).

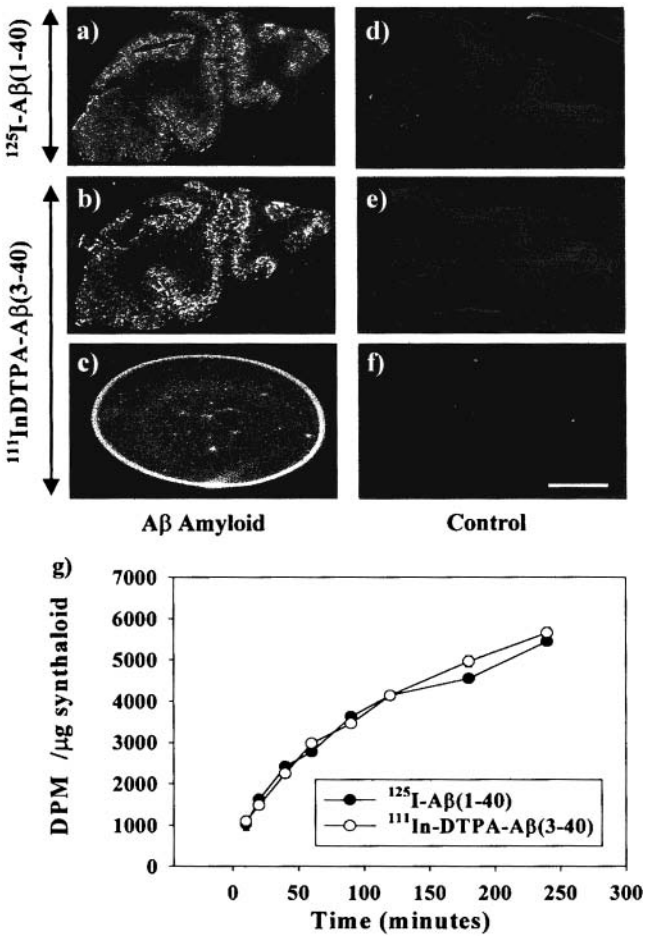


Figure 3. In vitro deposition and Aβ amyloid labeling with ^{111}In-DTPA-Aβ(3−40). Darkfield film autoradiograms of (a, b) 15.5 pM ^{111}In-DTPA-Aβ(3−40) or 125 pM ^{125}I-Aβ(1−40) incubated for 3 h on unfixed human AD cortex tissue sections, (c) immobilized synthetic Aβ amyloid, (d, e) age matched human control tissue sections, and (f) immobilizing polymer control with exposure times of 50 h for ^{111}In-DTPA-Aβ(3−40) (specific activity = 122 Ci/mmol) (for b, e, c, f) and 120 h for ^{125}I-Aβ(1−40) (specific activity = 2000 Ci/mmol) (for a, d) (scalebar = 1 cm). (g) Deposition kinetics of 12.5 pM ^{111}In-DTPA-Aβ(3−40) and 100 pM ^{125}I-Aβ(1−40) deposited onto synthetic Aβ amyloid. Error bars (mostly within symbols) represent mean ± SEM of six replicates.

The ability of ^{111}In-DTPA-Aβ(3−40) to deposit onto and label synthetic amyloid (*46*) was examined. Autoradiography of ^{111}In-DTPA-Aβ(3−40) incubated with synthetic Aβ amyloid immobilized onto a microscope slide versus control (Figure 3c,f) shows that ^{111}In-DTPA-Aβ(3−40) labels synthetic amyloid with high specificity. Comparison of deposition kinetics revealed a similar time course for ^{111}In-DTPA-Aβ(1−40) and ^{125}I-Aβ(1−40) (Figure 3g). Deposition kinetics onto synthetic amyloid in fresh heparinized whole rat blood revealed remarkable stability of ^{111}In-DTPA-Aβ(3−40). After a 23 h incubation, the amount of ^{111}In-DTPA-Aβ(3−40) deposited in the rat blood was 58% of that deposited in the buffer control (Table 1).

Table 1. In-DTPA-Aβ(3−40)Deposition onto Synthetic Amyloid in Fresh Heparinized Whole Rat Blood

time (min)	buffer control (DPM/μg of synthetic amyloid ± SEM)	fresh rat blood (DPM/μg of synthetic amyloid ± SEM)	fresh rat blood (% of buffer control)
15	347 ± 20	385 ± 30	111
45	582 ± 43	730 ± 37	125
120	981 ± 19	1262 ± 75	129
1380	3329 ± 127	1946 ± 115	58

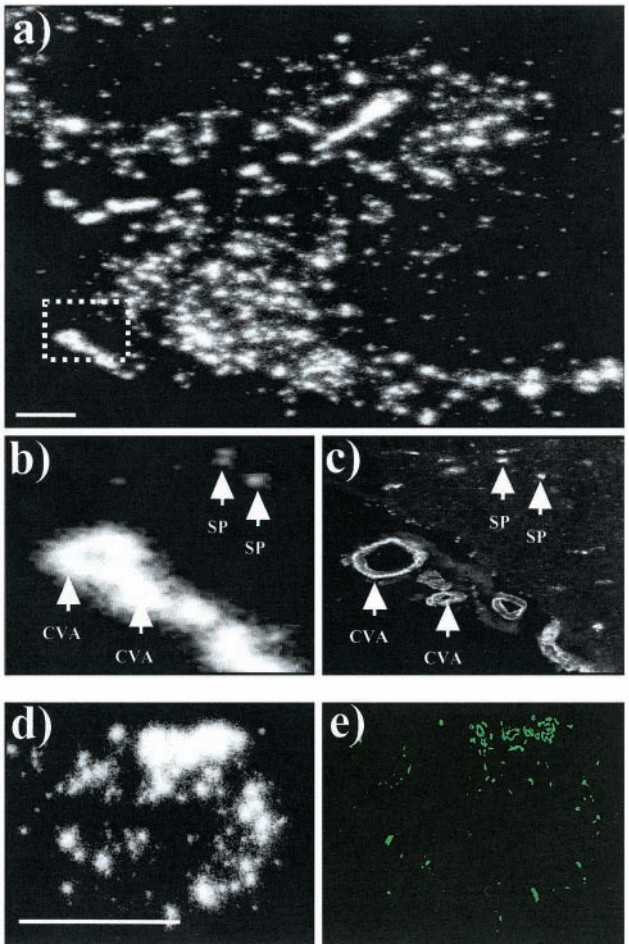


Figure 4. (a) ^{111}In-DTPA-Aβ(3−40) in vitro deposition onto and labeling of Aβ amyloid in unfixed human cortex tissue. Expansion of area indicated by dotted box in (a) is shown in (b) and (c). (b) ^{111}In-DTPA-Aβ(3−40) and (c) polyclonal anti-Aβ antibody R1282 labels showing that ^{111}In-DTPA-Aβ(3−40) deposits onto and labels both cerebrovascular amyloid (CVA) and parenchymal senile plaques (SP) (indicated by arrows). Another human AD cortex section doubly labeled with (d) ^{111}In-DTPA-Aβ(3−40) and (e) Thioflavin S confirms amyloid specificity of ^{111}In-DTPA-Aβ(3−40) (scalebars = 1 mm).

Noninvasive Imaging of Synthetic Amyloid In Vivo with ^{111}In-DTPA-Aβ(3−40). The specificity and sensitivity of ^{111}In-DTPA-Aβ(3−40) at deposition and labeling of naturally occurring and synthetic Aβ amyloid in vitro encouraged us to determine the ability of ^{111}In-DTPA-Aβ(3−40) to deposit onto and label synthetic Aβ amyloid in vivo. ^{111}In-DTPA-Aβ(3−40) injected intravenously (tail vein) deposits onto and labels synthetic Aβ amyloid previously implanted in rat muscle tissue, allowing the Aβ amyloid to be imaged in vivo as shown in Figure 5. The specific labeling of the synthetic Aβ amyloid was imaged with a planar γ camera using high-energy parallel and pinhole collimators and could be detected from 5 min up to 7 days following the injection of ^{111}In-DTPA-Aβ(3−40). Pinhole γ-camera images of rat leg muscle injected with either synthetic Aβ amyloid (Figure 5a) or vehicle (Figure 5b) 1 week earlier demonstrate the

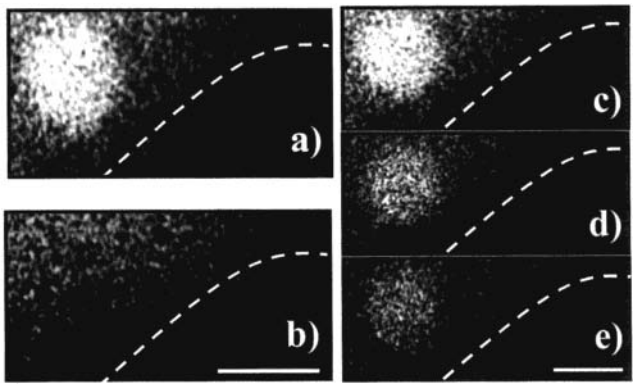


Figure 5. Planar γ-camera images of rat leg in vivo, with biceps femoris muscle containing 150 μg of (a) synthetic Aβ amyloid or (b) an equivalent volume of vehicle (10 min image acquisition time). Images were acquired using a Siemens LEM γ camera with a high-resolution pinhole collimator 97 h postinjection of ^{111}In-DTPA-Aβ(3−40). Signal decay exhibited by images acquired at (c) 97 h, (d) 121 h, and (e) 165 h postinjection of ^{111}In-DTPA-Aβ(3−40). Dashed lines represent the outline of the rat leg (scalebars = 10 mm).

specificity of ^{111}In-DTPA-Aβ(3−40) as an imaging agent for the synthetic Aβ amyloid in vivo. The optimal signal-to-noise ratio for specifically labeled synthetic Aβ amyloid above background radioactivity was attained at approximately 48 h postinjection of ^{111}In-DTPA-Aβ(3−40). Total signal decreased over time with clearance and radioactive decay of the ^{111}In label (Figure 5c−e) and could be compensated for by increasing the image acquisition time (data not shown).

After in vivo imaging, animals were sacrificed and perfused through the left ventricle. Additional γ-camera images acquired postmortem verified the position of the synthetic Aβ amyloid and specificity of the ^{111}In-DTPA-Aβ(3−40) radiotracer. Film autoradiography on tissue sections cut transverse to the synthetic Aβ amyloid injection track confirm that ^{111}In-DTPA-Aβ(3−40) did specifically deposit onto and label the synthetic Aβ amyloid (Figure 6a). Thioflavin S stained the tissue sections in the same region shown to be positive by autoradiography and confirmed that ^{111}In-DTPA-Aβ(3−40) specifically deposited onto and labeled individual synthetic Aβ amyloid aggregates (Figure 6b).

DISCUSSION

The need for a tool to detect and measure Aβ amyloid noninvasively in a living animal or human is well-established. Neuropathological observations in humans (*49*) and animal models (*9*, *33*, *35*, *36*, *38*, *48*, *50*) of AD indicating a direct correlation between disease symptoms and amyloid burden are fundamental to the amyloid hypothesis (*7*, *12*). The characterization of two transgenic animal models of inclusion body myositis, a skeletal muscle Aβ amyloidosis, also imply this relationship (*51*, *52*). To date, a thorough evaluation of this hypothesis has been elusive because there is currently no method of detecting and measuring the salient pathological feature, Aβ amyloid, in vivo.

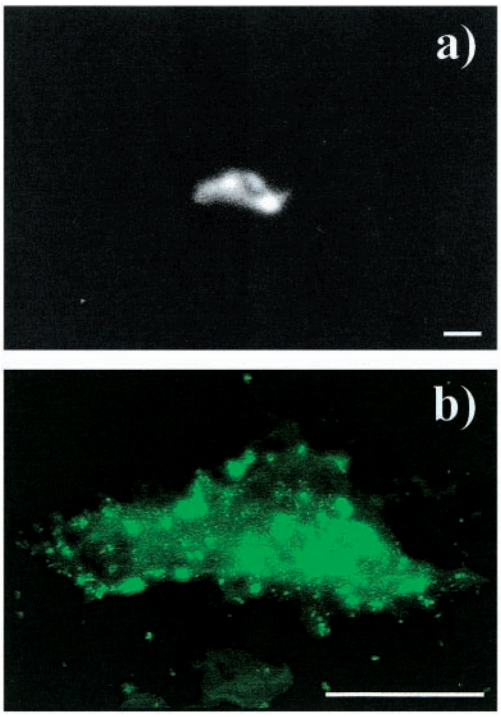


Figure 6. (a) Rat biceps femoris muscle tissue section darkfield film autoradiogram (20 h exposure, scalebar = 2 mm) showing synthetic Aβ amyloid labeled in vivo with ^{111}In-DTPA-Aβ(3−40). (b) Thioflavin S image of the same section confirming the presence of individual synthetic Aβ amyloid aggregates within the tissue area labeled with ^{111}In-DTPA-Aβ(3−40) (scalebars = 250 μm).

The most sensitive and specific method described to date for labeling Aβ amyloid in vitro has been the use of ^{125}I-radiolabeled Aβ peptide (*39*). The specificity results from the extraordinary affinity of Aβ for itself and the sensitivity from the high specific activity of the radiolabeled Aβ (2000 Ci/mmol; 1 ^{125}I molecule/peptide) (*39*, *41*). ^{125}I-Aβ has been shown to accurately track the intrinsic deposition and aggregation activity of unlabeled Aβ in a wide range of experiments in vitro (*39*, *41*, *45*, *46*).

The first significant advance toward the development of a noninvasive in vivo Aβ amyloid imaging agent was the demonstration that ^{125}I-Aβ(1−40), administered intravascularly, crosses the BBB and labels Aβ amyloid in aged primate brain in vivo (*38*). Later studies in transgenic mice using an ^{125}I-Aβ derivative (*36*) or a small fluorescent molecule able to cross the BBB (*35*) are the only known reports of molecules which label brain amyloid in vivo. Antibodies used to label amyloid have the necessary sensitivity and specificity but cannot cross the blood brain barrier (BBB) and, thus, lack accessibility to the lesions of AD (*30*). Several Congo red derivatives (*31*, *32*) or other dye molecules (*35*) have been investigated, and some have successfully overcome the accessibility issue (*35*); but these reagents lack the specificity to label only amyloid and exclude the neurofibrillar pathology found in several other human neurodegerative diseases and the ability to distinguish among amyloidoses derived from different protein precursors. Magnetic resonance imaging techniques have been applied to image Aβ amyloid in tissue samples but have not been advanced to in vivo use (*50*, *53*). Fluorescent microscopy imaging techniques requiring tissue/bone removal for signal detection have had some success at detecting amyloid plaques in the outermost 100 μm of cortex in live transgenic mice (*54*, *55*). However, all of these invasive methods do not facilitate the repetition required to evaluate the amyloid hypothesis or therapeutic efficacy in a single animal.

^{125}I-Aβ crosses the BBB intact in several animals including mice (*56*), rats (*57*), guinea-pigs (*58*), and primates (*59*) and is believed to be carried by a specific transport mechanism (*36*, *58*, *59*). Evidence that BBB permeability can be improved by chemical modification of Aβ (*36*) provides additional support for using radiolabeled Aβ derivatives toward the development of an in vivo Aβ amyloid imaging agent.

Success in detecting and quantifying amyloid by radiochemical imaging in vivo requires an isotope of appropriate energy for nuclear medicine imaging techniques such as planar γ scintigraphy, single photon emission computed tomography (SPECT), or positron emission tomography (PET). The half-life must be long enough to allow sufficient time for radiolabeling, purification to high specific activity, administration, and specific deposition onto the existing endogenous Aβ amyloid. The isotope half-life must also allow background (nonspecifically bound radiotracer) clearance without significantly compromising the intensity of the signal. The intrinsic kinetics (*39*, *43*) of Aβ amyloid deposition fundamental to the use of Aβ derivatives as in vivo imaging agents (Figure 3g) preclude the use of the very short-lived positron-emitting isotopes. A great deal of the signal and specific activity would be lost in the process of labeling and purifying the probes, and multiple half-lives would pass during the deposition process prior to achieving the optimal signal-to-noise ratio for in vivo imaging. The optimal γ decay energy range for SPECT or planar γ scintigraphy is 140−300 keV. Thus, imaging with ^{125}I, a low energy (30 keV) and relatively long half-life isotope, is practical only in tissue sections postmortem. In contrast, ^{123}I has a decay energy (159 keV) suitable for imaging in vivo; however, its relatively short half-life (13.3 h) would prevent its use in Aβ-derivative amyloid imaging agents. A preferable isotope, widely available and used extensively for diagnostic imaging in research and in the clinic, is ^{111}In (γ = 173 and 247 keV, $t_{1/2}$ = 2.8 days) (*40*).

The high affinity trivalent metal chelating moeity diethylenetriaminepentaacetic acid (DTPA) is established (*40*) as a tool for labeling proteins with ^{111}In and has previously been used (*37*) to label Aβ with ^{111}In. In the present study, the two N-teminal residues of Aβ have been replaced with a single DTPA moeity (Figure 1). The conjugation of DTPA to the N terminus of Aβ(3−40) avoids altering the chemical structure of Aβ at Lys16 or Lys28 (*37*) within the Aβ(10−35) sequence shown to be fundamental to the deposition competence of Aβ (*47*). Altering the chemical structure within this key central sequence risks compromising the deposition activity or specificity of the radiotracer. The rapid (60 s) and efficient (Figure 2a) labeling of DTPA-Aβ(3−40) with ^{111}In and purification of ^{111}In-DTPA-Aβ(3−40) produce a radiotracer possessing the specificity and sensitivity desired of an Aβ derivative for use as a noninvasive in vivo Aβ amyloid imaging agent.

As discussed previously, the extraordinary high specific affinity of Aβ for itself confers the specificity of ^{125}I-Aβ(1−40) for Aβ amyloid. Experiments comparing ^{125}I-Aβ(1−40) and ^{111}In-DTPA-Aβ(3−40) demonstrate equally high specificity of ^{111}In-DTPA-Aβ(3−40) for naturally occurring and synthetic Aβ amyloid in vitro (Figure 3). This specificity has been confirmed using two supplemental labels: an Aβ-specific antibody and the amyloid-specific dye Thioflavin S (Figures 3 and 4). As Aβ amyloid peptide probes retain specificity in vivo (*38*), the improved

sensitivity afforded by the physical properties of ^{111}In supported the advancement of ^{111}In-DTPA-Aβ(3−40) to in vivo imaging assays.

As an extension of previous work which showed the ability of ^{125}I-Aβ(1−40) to deposit onto naturally occurring Aβ amyloid plaques in vivo in a primate model of AD (*36*, *38*), we used an in vivo model consisting of peripherally injected synthetic Aβ amyloid to determine whether ^{111}In-DTPA-Aβ(3−40) could be used for noninvasive detection of Aβ amyloid by imaging in a living animal. ^{111}In-DTPA-Aβ(3−40) is able to deposit onto and label synthetic Aβ amyloid in vivo (Figure 5a,b) with specificity comparable to that observed in vitro. The sensitivity evident in vitro is also apparent in vivo and demonstrated by the ability of the γ camera to easily detect, resolve, and image the specifically labeled Aβ amyloid in 10 min (Figure 5). The amount of Aβ amyloid imaged in vivo in Figure 5 is 150 μg, significantly less than that found experimentally (*60*) or theoretically (*61*) in an AD brain. The amount of radiotracer (1.2 mCi) is significantly less than the amount of ^{111}In used in clinical procedures. To the best of our knowledge, the present study is the first report of noninvasive imaging of Aβ amyloid in vivo.

The principle that Aβ amyloid can be imaged noninvasively is established for the first time in the present study. The imaging methods present an example of how these procedures could be adapted to repeated image acquisitions throughout the life of a single animal to monitor the progression of Aβ amyloid burden or the efficacy of potential therapeutics. Furthermore, the sensitivity of γ scintigraphy for detecting the ^{111}In label would allow for efficient screening in multiple animals with little additional time invested relative to the current postmortem methods of detecting and quantifying Aβ amyloid.

The present results describe the development of an Aβ amyloid-specific probe with appropriate kinetics for noninvasive in vivo imaging. We demonstrate the specificity for Aβ amyloid and the sensitivity of imaging with ^{111}In-DTPA-Aβ(3−40) in vitro and in vivo. A desirable property of an AD Aβ amyloid probe, to avoid intrathecal application, is accessibility, the ability of the probe to cross the BBB, and enter the central nervous system. The most desirable method of administration of ^{111}In-DTPA-Aβ(3−40) is intravenous; however, other techniques for delivery to the CNS including injection directly across the BBB into the cerebrospinal fluid, and the use of hyperosmotic mannitol are available and have been effective in animals and humans. The imaging procedures described in the present study would not change following the administration of ^{111}In-DTPA-Aβ(3−40) with either of these methods. The minimal trauma resulting from these administration methods would be transient.

A method for specific in vivo detection and quantification of Aβ amyloid would provide a tool for efficient diagnosis and the capacity to monitor the progression of AD or IBM in an objective, symptom-independent manner. The present study demonstrates a significant step toward the development of such a tool. The ability to evaluate the progression of the disease and the relationship of amyloid burden to symptoms using a single subject over time and the evaluation of candidate therapeutic agents aimed at inhibiting the formation and growth of Aβ amyloid plaques would be a material advance in basic and clinical research related to Alzheimer's Disease.

ACKNOWLEDGMENT

We thank Dr. Dennis Selkoe for his generous gift of antiserum R1282, The University of Cincinnati Hospital Department of Nuclear Medicine for use of the γ camera, Dr. L. C. Washburn for providing $^{111}InCl_3$ and valuable technical advice, and Drs. Randall Sakai and Li Yun Ma for access to their cryostat microtome. This work was supported by NIH (Grant AG12853) and the Alzheimer's Association (Grant ZEN-1842).

LITERATURE CITED

(1) Kelly, J. W. (1997) Amyloid fibril formation and protein misassembly: a structural quest for insights into amyloid and prion diseases. *Structure 5*, 595−600.

(2) Kelly, J. W. (1998) The environmental dependency of protein folding best explains prion and amyloid diseases. *Proc. Natl. Acad. Sci. U.S.A. 95*, 930−2.

(3) Teplow, D. B. (1998) Structural and kinetic features of amyloid β-protein fibrillogenesis. *Amyloid 5*, 121−42.

(4) Lansbury, P. T., Jr. (1997) Inhibition of amyloid formation: a strategy to delay the onset of Alzheimer's disease. *Curr. Opin. Chem. Biol. 1*, 260−7.

(5) Lansbury, P. T., Jr. (1999) Evolution of amyloid: what normal protein folding may tell us about fibrillogenesis and disease. *Proc. Natl. Acad. Sci. U.S.A. 96*, 3342−4.

(6) Alzheimer, A. (1907) Uber eine eigenartige Erkrankung der Hirnrinde. *Allg. Z. Psychiatr. Psych.-Gerichtl. Med. 64*, 146−148.

(7) Selkoe, D. J. (1999) Translating cell biology into therapeutic advances in Alzheimer's disease. *Nature 399*, A23−31.

(8) Braak, H., de Vos, R. A., Jansen, E. N., Bratzke, H., and Braak, E. (1998) Neuropathological hallmarks of Alzheimer's and Parkinson's diseases. *Prog. Brain Res. 117*, 267−85.

(9) Mattson, M. P., Barger, S. W., Furukawa, K., Bruce, A. J., Wyss-Coray, T., Mark, R. J., and Mucke, L. (1997) Cellular signaling roles of TGF β, TNF α, and β APP in brain injury responses and Alzheimer's disease. *Brain Res. Rev. 23*, 47−61.

(10) Miller, D. L., Papayannopoulos, I. A., Styles, J., Bobin, S. A., Lin, Y. Y., Biemann, K., and Iqbal, K. (1993) Peptide compositions of the cerebrovascular and senile plaque core amyloid deposits of Alzheimer's disease. *Arch. Biochem. Biophys. 301*, 41−52.

(11) Price, J. L., and Morris, J. C. (1999) Tangles and plaques in nondemented aging and "preclinical" Alzheimer's disease. *Ann. Neurol. 45*, 358−68.

(12) Selkoe, D. J. (1991) The molecular pathology of Alzheimer's disease. *Neuron 6*, 487−98.

(13) Selkoe, D. J. (1994) Alzheimer's disease: a central role for amyloid. *J. Neuropathol. Exp. Neurol. 53*, 438−47.

(14) Seubert, P., Vigo-Pelfrey, C., Esch, F., Lee, M., Dovey, H., Davis, D., Sinha, S., Schlossmacher, M., Whaley, J., Swindlehurst, C., and et al. (1992) Isolation and quantification of soluble Alzheimer's β-peptide from biological fluids. *Nature 359*, 325−7.

(15) Kang, J., Lemaire, H. G., Unterbeck, A., Salbaum, J. M., Masters, C. L., Grzeschik, K. H., Multhaup, G., Beyreuther, K., and Muller-Hill, B. (1987) The precursor of Alzheimer's disease amyloid A4 protein resembles a cell-surface receptor. *Nature 325*, 733−6.

(16) Goldgaber, D., Lerman, M. I., McBride, O. W., Saffiotti, U., and Gajdusek, D. C. (1987) Characterization and chromosomal localization of a cDNA encoding brain amyloid of Alzheimer's disease. *Science 235*, 877−80.

(17) Esler, W. P., Kimberly, W. T., Ostaszewski, B. L., Diehl, T. S., Moore, C. L., Tsai, J. Y., Rahmati, T., Xia, W., Selkoe, D. J., and Wolfe, M. S. (2000) Transition-state analogue inhibitors of γ secretase bind directly to presenilin-1. *Nat. Cell Biol. 2*, 428−34.

(18) Vassar, R., Bennett, B. D., Babu-Khan, S., Kahn, S., Mendiaz, E. A., Denis, P., Teplow, D. B., Ross, S., Amarante, P., Loeloff, R., Luo, Y., Fisher, S., Fuller, J., Edenson, S., Lile,

J., Jarosinski, M. A., Biere, A. L., Curran, E., Burgess, T., Louis, J. C., Collins, F., Treanor, J., Rogers, G., and Citron, M. (1999) β-secretase cleavage of Alzheimer's amyloid precursor protein by the transmembrane aspartic protease BACE. *Science 286*, 735−41.

(19) Zhang, Z., Nadeau, P., Song, W., Donoviel, D., Yuan, M., Bernstein, A., and Yankner, B. A. (2000) Presenilins are required for γ-secretase cleavage of β-APP and transmembrane cleavage of Notch-1. *Nat. Cell Biol. 2*, 463−5.

(20) Mattson, M. P. (1997) Cellular actions of β-amyloid precursor protein and its soluble and fibrillogenic derivatives. *Physiol. Rev. 77*, 1081−132.

(21) Scheuner, D., Eckman, C., Jensen, M., Song, X., Citron, M., Suzuki, N., Bird, T. D., Hardy, J., Hutton, M., Kukull, W., Larson, E., Levy-Lahad, E., Viitanen, M., Peskind, E., Poorkaj, P., Schellenberg, G., Tanzi, R., Wasco, W., Lannfelt, L., Selkoe, D., and Younkin, S. (1996) Secreted amyloid β-protein similar to that in the senile plaques of Alzheimer's disease is increased in vivo by the presenilin 1 and 2 and APP mutations linked to familial Alzheimer's disease. *Nat. Med. 2*, 864−70.

(22) Shoji, M., Golde, T. E., Ghiso, J., Cheung, T. T., Estus, S., Shaffer, L. M., Cai, X. D., McKay, D. M., Tintner, R., Frangione, B., and et al. (1992) Production of the Alzheimer amyloid β protein by normal proteolytic processing. *Science 258*, 126−9.

(23) Askanas, V., Engel, W. K., Yang, C. C., Alvarez, R. B., Lee, V. M., and Wisniewski, T. (1998) Light and electron microscopic immunolocalization of presenilin 1 in abnormal muscle fibers of patients with sporadic inclusion-body myositis and autosomal-recessive inclusion-body myopathy. *Am. J. Pathol. 152*, 889−95.

(24) Querfurth, H. W., Suhara, T., Rosen, K. M., McPhie, D. L., Fujio, Y., Tejada, G., Neve, R. L., Adelman, L. S., and Walsh, K. (2001) β-Amyloid peptide expression is sufficient for myotube death: implications for human inclusion body myopathy. *Mol. Cell. Neurosci. 17*, 793−810.

(25) Askanas, V., and Engel, W. K. (1998) Sporadic inclusion-body myositis and its similarities to Alzheimer disease brain. Recent approaches to diagnosis and pathogenesis, and relation to aging. *Scand. J. Rheumatol. 27*, 389−405.

(26) Bennhold, H. (1923) *Deutsch Arch. Klin. Med. 142*, 32.

(27) Blum, A., and Sohar, E. (1962) The Diagnosis of Amyloidosis: Ancillary Procedures. *Lancet* 721.

(28) Hawkins, P. N., Lavender, J. P., and Pepys, M. B. (1990) Evaluation of systemic amyloidosis by scintigraphy with ^{123}I-labeled serum amyloid P component. *N. Engl. J. Med. 323*, 508−13.

(29) Gillmore, J. D., Madhoo, S., Pepys, M. B., and Hawkins, P. N. (2000) Renal transplantation for amyloid end-stage renal failure-insights from serial serum amyloid P component scintigraphy. *Nucl. Med. Commun. 21*, 735−40.

(30) Friedland, R. P., Shi, J., Lamanna, J. C., Smith, M. A., and Perry, G. (2000) Prospects for noninvasive imaging of brain amyloid β in Alzheimer's disease. *Ann. N. Y. Acad. Sci. 903*, 123−8.

(31) Klunk, W. E., Debnath, M. L., and Pettegrew, J. W. (1994) Development of small molecule probes for the β-amyloid protein of Alzheimer's disease. *Neurobiol. Aging 15*, 691−8.

(32) Klunk, W. E., Jacob, R. F., and Mason, R. P. (1999) Quantifying amyloid β-peptide (Aβ) aggregation using the Congo red-Aβ (CR-aβ) spectrophotometric assay. *Anal. Biochem 266*, 66−76.

(33) Dezutter, N. A., Dom, R. J., de Groot, T. J., Bormans, G. M., and Verbruggen, A. M. (1999) 99mTc-MAMA-chrysamine G, a probe for β-amyloid protein of Alzheimer's disease. *Eur. J. Nucl. Med. 26*, 1392−9.

(34) Zhen, W., Han, H., Anguiano, M., Lemere, C. A., Cho, C. G., and Lansbury, P. T., Jr. (1999) Synthesis and amyloid binding properties of rhenium complexes: preliminary progress toward a reagent for SPECT imaging of Alzheimer's disease brain. *J. Med. Chem. 42*, 2805−15.

(35) Skovronsky, D. M., Zhang, B., Kung, M. P., Kung, H. F., Trojanowski, J. Q., and Lee, V. M. (2000) In vivo detection of amyloid plaques in a mouse model of Alzheimer's disease. *Proc. Natl. Acad. Sci. U.S.A. 97*, 7609−14.

(36) Wengenack, T. M., Curran, G. L., and Poduslo, J. F. (2000) Targeting Alzheimer amyloid plaques in vivo. *Nat. Biotechnol. 18*, 868−872.

(37) Kurihara, A., and Pardridge, W. M. (2000) Aβ(1−40) peptide radiopharmaceuticals for brain amyloid imaging: ^{111}In chelation, conjugation to poly(ethylene glycol)-biotin linkers, and autoradiography with Alzheimer's disease brain sections. *Bioconjugate Chem. 11*, 380−6.

(38) Ghilardi, J. R., Catton, M., Stimson, E. R., Rogers, S., Walker, L. C., Maggio, J. E., and Mantyh, P. W. (1996) Intra-arterial infusion of [^{125}I]Aβ(1−40) labels amyloid deposits in the aged primate brain in vivo. *NeuroReport 7*, 2607−11.

(39) Maggio, J. E., Stimson, E. R., Ghilardi, J. R., Allen, C. J., Dahl, C. E., Whitcomb, D. C., Vigna, S. R., Vinters, H. V., Labenski, M. E., and Mantyh, P. W. (1992) Reversible in vitro growth of Alzheimer disease β-amyloid plaques by deposition of labeled amyloid peptide. *Proc. Natl. Acad. Sci. U.S.A. 89*, 5462−6.

(40) Jasanada, F. (1996) Indium-111 Labeling Low-Density Lipoproteins with the DTPA-Bis(stearylamide): Evaluation as a Potential Radiopharmaceutical for Tumor Localization. *Bioconjugate Chem. 7*, 72−81.

(41) Esler, W. P., Stimson, E. R., Ghilardi, J. R., Vinters, H. V., Lee, J. P., Mantyh, P. W., and Maggio, J. E. (1996) In vitro growth of Alzheimer's disease β-amyloid plaques displays first-order kinetics. *Biochemistry 35*, 749−57.

(42) Esler, W. P., Felix, A. M., Stimson, E. R., Lachenmann, M. J., Ghilardi, J. R., Lu, Y. A., Vinters, H. V., Mantyh, P. W., Lee, J. P., and Maggio, J. E. (2000) Activation barriers to structural transition determine deposition rates of Alzheimer's disease aβ amyloid. *J. Struct. Biol. 130*, 174−83.

(43) Esler, W. P., Stimson, E. R., Jennings, J. M., Vinters, H. V., Ghilardi, J. R., Lee, J. P., Mantyh, P. W., and Maggio, J. E. (2000) Alzheimer's disease amyloid propagation by a template-dependent dock-lock mechanism. *Biochemistry 39*, 6288−95.

(44) Hnatowich, D. J., and McGann, J. (1987) DTPA-coupled proteins—procedures and precautions. *Int. J. Rad. Appl. Instrum., Part B 14*, 563−8.

(45) Walsh, D. M., Lomakin, A., Benedek, G. B., Condron, M. M., and Teplow, D. B. (1997) Amyloid β-protein fibrillogenesis. Detection of a protofibrillar intermediate. *J. Biol. Chem. 272*, 22364−72.

(46) Esler, W. P., Stimson, E. R., Ghilardi, J. R., Felix, A. M., Lu, Y. A., Vinters, H. V., Mantyh, P. W., and Maggio, J. E. (1997) A β deposition inhibitor screen using synthetic amyloid. *Nat. Biotechnol. 15*, 258−63.

(47) Esler, W. P., Stimson, E. R., Ghilardi, J. R., Lu, Y. A., Felix, A. M., Vinters, H. V., Mantyh, P. W., Lee, J. P., and Maggio, J. E. (1996) Point substitution in the central hydrophobic cluster of a human β-amyloid congener disrupts peptide folding and abolishes plaque competence. *Biochemistry 35*, 13914−21.

(48) Weldon, D. T., Rogers, S. D., Ghilardi, J. R., Finke, M. P., Cleary, J. P., O'Hare, E., Esler, W. P., Maggio, J. E., and Mantyh, P. W. (1998) Fibrillar β-amyloid induces microglial phagocytosis, expression of inducible nitric oxide synthase, and loss of a select population of neurons in the rat CNS in vivo. *J. Neurosci. 18*, 2161−73.

(49) Cummings, B. J., Pike, C. J., Shankle, R., and Cotman, C. W. (1996) β-amyloid deposition and other measures of neuropathology predict cognitive status in Alzheimer's disease. *Neurobiol. Aging 17*, 921−33.

(50) Benveniste, H., Einstein, G., Kim, K. R., Hulette, C., and Johnson, G. A. (1999) Detection of neuritic plaques in Alzheimer's disease by magnetic resonance microscopy. *Proc. Natl. Acad. Sci. U.S.A. 96*, 14079−84.

(51) Fukuchi, K., Pham, D., Hart, M., Li, L., and Lindsey, J. R. (1998) Amyloid-β deposition in skeletal muscle of transgenic mice: possible model of inclusion body myopathy. *Am. J. Pathol. 153*, 1687−93.

(52) Jin, L. W., Hearn, M. G., Ogburn, C. E., Dang, N., Nochlin, D., Ladiges, W. C., and Martin, G. M. (1998) Transgenic mice overexpressing the C-99 fragment of βPP with an α-secretase site mutation develop a myopathy similar to human inclusion body myositis. *Am. J. Pathol. 153*, 1679−86.

(53) Benveniste, H., Kim, K., Zhang, L., and Johnson, G. A. (2000) Magnetic resonance microscopy of the C57BL mouse brain. *Neuroimage 11*, 601−11.

(54) Hyman, B. T. (2001) Molecular and anatomical studies in Alzheimer's disease. *Neurologia 16*, 100−4.

(55) Bacskai, B. J., Kajdasz, S. T., Christie, R. H., Carter, C., Games, D., Seubert, P., Schenk, D., and Hyman, B. T. (2001) Imaging of amyloid-β deposits in brains of living mice permits direct observation of clearance of plaques with immunotherapy. *Nat. Med. 7*, 369−372.

(56) Maness, L. M., Banks, W. A., Podlisny, M. B., Selkoe, D. J., and Kastin, A. J. (1994) Passage of human amyloid β-protein 1−40 across the murine blood-brain barrier. *Life Sci. 55*, 1643−50.

(57) Ghersi-Egea, J. F., Gorevic, P. D., Ghiso, J., Frangione, B., Patlak, C. S., and Fenstermacher, J. D. (1996) Fate of cerebrospinal fluid-borne amyloid β-peptide: rapid clearance into blood and appreciable accumulation by cerebral arteries. *J. Neurochem. 67*, 880−3.

(58) Martel, C. L., Mackic, J. B., McComb, J. G., Ghiso, J., and Zlokovic, B. V. (1996) Blood-brain barrier uptake of the 40 and 42 amino acid sequences of circulating Alzheimer's amyloid β in guinea pigs. *Neurosci. Lett. 206*, 157−60.

(59) Mackic, J. B., Stins, M., McComb, J. G., Calero, M., Ghiso, J., Kim, K. S., Yan, S. D., Stern, D., Schmidt, A. M., Frangione, B., and Zlokovic, B. V. (1998) Human blood-brain barrier receptors for Alzheimer's amyloid-β 1−40. Asymmetrical binding, endocytosis, and transcytosis at the apical side of brain microvascular endothelial cell monolayer. *J. Clin. Invest. 102*, 734−43.

(60) Wang, J., Dickson, D. W., Trojanowski, J. Q., and Lee, V. M. (1999) The levels of soluble versus insoluble brain Aβ distinguish Alzheimer's disease from normal and pathologic aging. *Exp. Neurol. 158*, 328−37.

(61) Selkoe, D. J., Abraham, C. R., Podlisny, M. B., and Duffy, L. K. (1986) Isolation of low-molecular-weight proteins from amyloid plaque fibers in Alzheimer's disease. *J. Neurochem. 46*, 1820−34.

BC010066Z

Immobilization of Pectin Fragments on Solid Supports: Novel Coupling by Thiazolidine Formation

Fanny Guillaumie,[†,‡] Owen R. T. Thomas,[‡] and Knud J. Jensen*[,†]

Center for Process Biotechnology, Biocentrum-DTU, Building 223, Søltofts Plads, and Department of Chemistry, Building 201, Kemitorvet, Technical University of Denmark, DK-2800 Kgs. Lyngby, Denmark. Received July 26, 2001; Revised Manuscript Received October 18, 2001

As a prerequisite to solid-phase and sequence analyses and for the study of the fine structure of pectin, we have developed oriented and chemoselective methodologies to couple model pectin fragments onto a solid support. Polyethylene glycol polyacrylamide (PEGA) resins were selected due to their excellent swelling properties in a wide range of solvents, including water, and their easy accessibility to enzymes. Following appropriate derivatization of amino-terminated PEGA resins, oligomers of α-D-galacturonic acid (GalA), up to the trimer, were anchored to the support through their reducing end. In addition to reductive amination, the strategies included the formation of an oxime bond, a glycosyl hydrazide, and a pyroglutamyl ring. Further, we developed a new immobilization approach based on the formation of a thiazolidine ring. All methods proved efficient and did not require modification of the GalA oligomers prior to coupling. In addition, very mild conditions and few steps for derivatization of the support were required. Immobilization by thiazolidine ring and oxime bond formation were the preferred methods, given the stability of the linkages formed, their compatibility with aqueous solvents, the few number of steps required, and their potential for application to larger pectin fragments. Thiazolidine and pyroglutamyl anchoring were developed further by the insertion of a disulfide bond which allowed release of the saccharides under mild, selective conditions.

INTRODUCTION

Pectin is a complex polysaccharide that occurs in the primary cell walls and the middle lamella of higher plants (*1*). The main feature of pectin is a linear chain of α-(1→4)-linked D-galacturonic acid units (the so-called 'smooth region') in which varying proportions of the carboxylic acid groups have been converted to methyl esters. The smooth region is interrupted by α-(1→2)-linked L-rhamnose units (the so-called 'hairy region'), carrying further neutral carbohydrate side chains, typically consisting of D-galactose and D-arabinose (*1*). The remarkable gelling properties of pectin have been widely exploited in the food industry for the production of jams, marmalades, and other fruit based products. Pectin has also been used as a stabilizer in dairy products (*2*) and for medical preparations as an antidiarrheal, detoxicant, or in the regulation and the protection of gastrointestinal tract (*1*).

Pectin has been the subject of numerous studies, many of which focused on structure elucidation in pectin (*3*−*9*), binding of pectin with metal ions (*10*−*13*), synthesis of pectin fragments (*14*−*17*), and the development of new analytical methods for pectin structure elucidation (*18*−*20*). However, despite all of these efforts, much still remains to be learned about structure−function relationships in pectin.

Immobilization of pectin fragments on a solid support may prove to be an important technique in the study of fine structure−function relationships in pectin. For example, immobilization would allow solid-phase analysis of the pectin molecule to be carried out and would serve as a prerequisite to sequencing. Moreover, an immobilization strategy could be a useful tool for the determination of the factors influencing the formation of 'egg-box' cavities in pectin. The 'egg-box' model has been proposed for the gelation of low methyl esterified pectin (*21*). It involves the intermolecular binding of two non-esterified segments or two whole pectin chains with interstices in which calcium ions may pack and coordinate.

A number of coupling methods have been developed for the synthesis of glycoconjugates and for the immobilization of oligosaccharides. Reductive amination was one of the first methods to be implemented in the preparation of glycoconjugates (*22*−*24*) and in the coupling of carbohydrates onto solid supports (*25*−*27*). The reactivity toward the reducing end of carbohydrates can be enhanced by substituting amino groups with hydrazide functions. This technique has recently proved to be efficient for the immobilization of simple oligosaccharides on an ELISA plate (*28*). The oxime linkage has also been used to prepare glycoconjugates (*29*) and to immobilize short oligosaccharides on ELISA plates (*28*). Furthermore, small oligosaccharides have been coupled to solid supports (*30*) and glycoconjugates have been prepared (*31*, *32*) by formation of a glycosyl amide linkage. However, none of the above coupling chemistries have so far been applied to the immobilization of polyuronic acids such as pectin or heparin. The formation of a thiazolidine ring has found application in the synthesis of peptide dendrimers (*33*), but has not been applied to the preparation of glycoconjugates nor to the immobilization of oligosaccharides. All of the aforementioned strategies will introduce a stable linkage between the saccha-

* To whom correspondence should be addressed at the present address: Department of Chemistry, Royal Veterinary and Agricultural University, Thorvaldsensvej 40, DK-1871 Frederiksberg C (Copenhagen), Denmark, Phone: + 45 3528 2430, Fax: + 45 3528 2398, E-mail: kjj@kvl.dk.

† Chemistry Department.

‡ Center for Process Biotechnology, Biocentrum-DTU.

10.1021/bc0155364 CCC: $22.00 © 2002 American Chemical Society
Published on Web 03/03/2002

ride and the support. Accordingly, in this paper we report on the use of these methodologies for anchoring GalA[1] oligomers onto solid supports. Further, to allow for release of immobilized structures, we have modified the thiazolidine and pyroglutamyl immobilization strategies by including a cleavable disulfide bond. Polyethylene glycol polyacrylamide (PEGA) resin was selected as the solid phase in these studies due to its compatibility with a wide range of solvents, including water, and its accessibility to enzymes with a molecular weight of up to 70 kDa.

MATERIALS AND METHODS

The amino-functionalized PEGA resins (0.4 mmol/g, 150−300 μm, 11.19 wt % in MeOH or 0.2 mmol/g, 300−500 μm, 9.41 wt % in MeOH) used in this study were kindly supplied by Dr. Andrew Coffey of Polymer Laboratories, UK. The PEGA resins were weighed wet, unless stated otherwise. All chemical reagents and solvents were purchased from Sigma-Aldrich Denmark A/S (Vallensbaek Strand, Denmark). All amino acids were of the L-configuration.

General. Melting points were uncorrected. ^{1}H NMR and ^{13}C NMR spectra were recorded on a Varian Mercury 300 instrument equipped with a four-nuclei probe operating at 300.06 and 75.45 MHz, respectively, or on a Varian Unity Inova 500 equipped with a H−C−P probe operating at 499.87 and 125.69 MHz, respectively. FAB-MS analyses were performed on a VG TRIO-2 quadrupole mass spectrometer equipped with a combined electron impact/chemical ionization ion source. The samples were analyzed in the chemical ionization mode with ammonia as reagent gas. ES-MS analyses were conducted on a Micromass LCT mass spectrometer or on a ion trap Esquire-Bruker instrument at Danisco Cultor A/S (Copenhagen, Denmark). Elemental analyses were conducted at the Department of Chemistry, University of Copenhagen. Analytical HPLC was performed with a Waters chromatography system (600E pump, 996 photodiode array (PDA) detector, 717 Plus autosampler, Millenium32 control software) on a 3.0 × 50 mm Waters X-Terra RP_{18} column (3.5 μm particle size), using H_2O (A) and CH_3CN (B) as eluents. The following program was applied: after 0.1 min at 100% A, 0% B, a linear gradient (0−95% B) was applied over the next 5.9 min; the eluent composition was then maintained at 5% A, 95% B for a further 1 min before applying a step change to 100% A, 0% B over 0.1 min to regenerate the column; a flow rate of 1.20 mL/min was employed at all stages. Individual peaks were analyzed by their UV-spectra. All solid-phase reactions were performed in plastic syringes equipped with a polypropylene filter. Before saccharide coupling, all the resins were washed with an increasing concentration of Et_2O in CH_2Cl_2 (0%, 1 × 5 min; 25%, 1 × 5 min; 50%, 1 × 5 min; 75%, 1 × 5 min; 100%, 2 × 5 min) and dried in vacuo for 18 h to give dry PEGA resins suitable for weighing.

Loading Determination by Trityl (Trt) Group Quantitation. The '*indirect method*' was applied to the resins **A**, **B**, **G**, and **H**. Each coupling took place at room temperature and for 1 h. Derivatized resin was washed with CH_2Cl_2−DMF (9:1, 3 × 1 min, 1 × 5 min) and treated with TrtCl (5 equiv) with DIEA (10 equiv) in CH_2Cl_2-DMF (9:1) (*34*). Excess reagents and solvents were removed by filtration, the resin was washed with CH_2Cl_2 (5 × 1 min) and treated with TrtCl (5 equiv) and diisopropylethylamine (DIEA, 10 equiv) in CH_2Cl_2. This coupling step was repeated once. Solvents and unreacted materials were removed by filtration. The resin was then washed with CH_2Cl_2 (3 × 1 min) and treated with TFA−CH_2Cl_2 (1:1) in the presence of Et_3SiH (6 equiv) (*35*). The filtrate was collected, and the resin was washed with two extra portions CH_2Cl_2. The filtrate was evaporated to dryness, redissolved into CH_3CN (1 mL), analyzed by HPLC, and the absorbance of TrtH was read at 226 nm. The amount *n* (mmol) of Trt groups was calculated using a standard curve. The resin was washed with an increasing concentration of Et_2O in CH_2Cl_2 (0%, 1 × 5 min; 25%, 1 × 5 min; 50%, 1 × 5 min; 75%, 1 × 5 min; 100%, 2 × 5 min), dried in vacuo for 18 h, and weighed (*m*). The ratio between *n* and *m* gave the loading of the resin in mmol/g. '*Direct method*': Trt-protected resins **E** and **F** were washed with CH_2Cl_2 (3 × 1 min) and treated with TFA−CH_2Cl_2 (1:1) in the presence of Et_3SiH (6 equiv) (*35*). In each case, the filtrate was collected, and the resin was washed with two extra portions CH_2Cl_2. The filtrate was evaporated to dryness, redissolved into CH_3CN (1 mL), and analyzed by HPLC. The absorbance of TrtH was read at 226 nm and the amount *n* (mmol) of Trt groups was calculated using a standard curve. The resin was washed with an increasing concentration of Et_2O in CH_2Cl_2 (0%, 1 × 5 min; 25%, 1 × 5 min; 50%, 1 × 5 min; 75%, 1 × 5 min; 100%, 2 × 5 min), dried in vacuo for 18 h, and weighed (*m*). The ratio between *n* and *m* gave the loading of the resin in mmol/g.

Determination of Immobilization Efficiency by Anthrone Assay. Resins **A**, **C**, **G**, and **H** prior to immobilization and after immobilization were treated as follows. The resin was washed with an increasing concentration of Et_2O in CH_2Cl_2 (0%, 1 × 5 min; 25%, 1 × 5 min; 50%, 1 × 5 min; 75%, 1 × 5 min; 100%, 2 × 5 min), and dried in vacuo for 18 h. A small portion of the resin (1−5 mg) was weighed in a 1.5 mL safelock plastic vial. Water (0.5 mL) was added, followed by anthrone solution (0.2% in concentrated H_2SO_4, 1 mL) (*36*). The samples were shaken vigorously for 3 min, incubated at 100 °C for 5 min, and cooled in an ice bath for 3 min. A 300 μL amount was transferred to an ELISA plate, and the optical density was read at 570 nm in a microtiter plate reader (Anthos reader 2001, Anthos Labtech Instruments, Salzburg, Austria). The difference in optical density between the pre- and the postimmobilization resins was used as a measure of the amount of GalA units immobilized.

Determination of Immobilization Efficiency by the Ellman Test. Pre- and postimmobilization resins (resins **E** and **F**) were treated as follows. The resin was washed with an increasing concentration of Et_2O in CH_2Cl_2 (0%, 1 × 5 min; 25%, 1 × 5 min; 50%, 1 × 5 min; 75%, 1 × 5 min; 100%, 2 × 5 min), dried in vacuo for 18 h. A small portion of resin (1−4 mg) was treated with a 0.01 M solution of 5,5′-dithiobis(2-nitrobenzoic acid) (DTNB) in aq Na_2HPO_4 buffer (0.1 M, pH 8.5, 400 μL) (*37, 38*). Water (600 μL) was added, and the sample was shaken for 20 min at room temperature and analyzed by reversed-phase HPLC in an isocratic mode using H_2O

[1] Abbrevations: H-Aoa-OH, aminooxy acetic acid; Boc, *tert*-butoxycarbonyl; Cys, cysteine; DIEA, diisopropylethylamine; DMF, dimethylformamide; DTNB, 5,5′-dithiobis(2-nitrobenzoic acid); DTT, dithiothreitol; GalA, α-D-galacturonic acid; $(GalA)_2$, α-D-GalA-(1→4)-D-GalA; $(GalA)_3$, α-D-GalA-(1→4)-α-D-GalA-(1→4)-D-GalA; Glu, glutamic acid; HL, high loading; LL, low loading; PyBOP, (benzotriazol-1-yloxy)tripyrrolidinophosphonium hexafluorophosphate; HBTU, *N*-[(1*H*-benzotriazol-1-yl)-(dimethylamino)methylene]-*N*-methylmethanaminium hexafluorophosphate *N*-oxide; HOBt, 1-hydroxybenzotriazole; PEGA, polyethylene glycol polyacrylamide; Pyr, pyridine; rt, room temperature; Trt, trityl.

as the eluent. The absorbance of the released thiol anion was read at 412 nm, and the amount of resin-bound free thiol groups was determined using a calibration curve with H-Cys-OMe·HCl as a standard.

Preparation of Aminooxy-Terminated Resins (A). Reactions were carried out in a 20 mL syringe, and the washing volumes were 8 mL. Amino PEGA resin (3.8 g, 0.4 mmol/g) was washed with DMF (3 × 1 min), swollen in DMF (1 × 10 min), and washed with 10% DIEA in DMF (3 × 1 min) and DMF (3 × 1 min), respectively. N^{β}-Boc-aminooxy acetic acid (N^{β}-Boc-Aoa-OH, 100 mg, 0.52 mmol), (benzotriazol-1-yloxy)tripyrrolidinophosphonium hexafluorophosphate (PyBOP, 271 mg, 0.52 mmol), and 1-hydroxybenzotriazole (HOBt, 70 mg, 0.52 mmol) were dissolved in DMF (7 mL). DIEA (157 μL, 0.92 mmol) was then added, and the solution was added to the resin. The syringe was shaken at room temperature for 1.2 h, after which a qualitative ninhydrin test was negative. Solvents and unreacted materials were filtered off, and the resin was washed with DMF (4 × 1 min) and CH_2Cl_2 (2 × 1 min, 1 × 5 min and 2 × 1 min). Removal of Boc groups was accomplished by treatment with TFA−CH_2Cl_2 (1:1, 8 mL) for 1 h at room temperature.

Preparation of Carboxylic Acid-Terminated Resins (B). Reactions were performed in a 50 mL syringe, and the washing volumes were 15 mL. Amino PEGA resin (8.94 g, 0.4 mmol/g) was washed and swollen with the same solvents as for **A**. Succinic anhydride (160 mg, 1.6 mmol) and HOBt (162 mg, 1.2 mmol) were dissolved in DMF (13 mL), DIEA (308 μL, 1.8 mmol) was added, and the solution was added to the resin. The syringe was shaken at room temperature for 1.5 h. Excess reagents and solvents were filtered off, and the resin was washed with DMF (4 × 1 min) and MeOH (4 × 1 min). At this point, a ninhydrin test was negative. The resin was stored wet in MeOH at 5 °C until further use.

Preparation of Hydrazide-Terminated Resins (C). A portion of resin **B** (1.98 g, 0.11 mmol) was transferred to a 10 mL syringe. The washing volumes were 4 mL. The resin was washed with DMF (1 × 1 min, 1 × 10 min, and 1 × 1 min). *N*-[(1*H*-Benzotriazol-1-yl)(dimethylamino)methylene]-*N*-methylmethanaminium hexafluorophosphate *N*-oxide (HBTU, 173 mg, 0.46 mmol) and HOBt (62 mg, 0.46 mmol) were dissolved in DMF (3 mL). DIEA (88 μL, 0.51 mmol) was then added, followed by hydrazine monohydrate (28 μL, 0.57 mmol), and the mixture was added to the resin. After 2 h coupling at room temperature, solvents and unreacted compounds were removed by filtration, and the resin was washed with DMF (4 × 1 min) and MeOH (4 × 1 min).

Preparation of Thiol-Terminated Resins (D). Resin **B** (3.30 g, 0.19 mmol) was transferred into a 20 mL syringe. Washing volumes were 6 mL. The resin was washed with DMF (1 × 1 min, 1 × 10 min, and 1 × 1 min). *S*-(2-Pyridylthio)cysteamine hydrochloride (*39*) (212 mg, 0.95 mmol), HBTU (288 mg, 0.76 mmol), and HOBt (103 mg, 0.76 mmol) were dissolved in DMF (6 mL). After addition of DIEA (146 μL, 0.86 mmol), the solution was added to the resin. After shaking for 2 h at room temperature, the resin was washed with DMF (4 × 1 min), H_2O (4 × 1 min), and aq NaOAc buffer (0.1 M, pH 4.8, 2 × 1 min). Pyridine-2-thione was removed from the support by treatment with a solution of dithiothreitol (DTT) (147 mg, 0.95 mmol) in aq NaOAc buffer (7 mL). After 2 h at room temperature, solvents and excess reagents were filtered off, and the resin was washed with H_2O (4 × 1 min) and then with MeOH (3 × 1 min).

Preparation of Cysteine (Cys)-Terminated Resins (E). *Synthesis of Boc-Cys(Trt)-NH-$(CH_2)_2$-S-S-Pyr.* Boc-Cys(Trt)-OH (566 mg, 1.22 mmol) was dissolved in CH_3CN (10 mL). HBTU (512 mg, 1.35 mmol) and NEt_3 (340 μL, 2.44 mmol) were then added, followed by *S*-(2-pyridylthio)cysteamine hydrochloride (*39*) (771 mg, 1.22 mmol). Complete dissolution was accomplished by addition of water (1 mL). After overnight stirring at room temperature, a white precipitate formed. It was isolated by filtration and dried under reduced pressure (1st crop). The filtrate was diluted with EtOAc (40 mL), washed with 1 M aq HCl (3 × 15 mL), saturated aqueous $NaHCO_3$ (3 × 15 mL), and brine (3 × 15 mL), dried over $MgSO_4$, and concentrated to afford white crystals (2nd crop). Fractions 1 and 2 were identified as the title compound (753 mg, 98%), mp 131−134 °C. ^{1}H NMR ($CDCl_3$) δ 1.41 (s, 9 H, CH_3), 2.56 (dd, 1 H, H-β^a (Cys), *J* 5.2 Hz, *J* 12.5 Hz), 2.71 (dd, 1 H, H-β^b (Cys), *J* 7 Hz, *J* 12.5 Hz), 2.86 (m, 2 H, CH_2-S, *J* 1.8 Hz, *J* 5.8 Hz), 3.50 (m, 1 H, CH_2-NH), 4.01 (dd, 1 H, H-α (Cys), *J* 0.8 Hz, *J* 5.4 Hz), 7.06−7.61 (m, 18 H, H arom.), 8.47 (d, 1 H, H-3′ (Pyr), *J* 4.9 Hz). ^{13}C NMR ($CDCl_3$) δ 28.58 (*C*H$_3$, ^{t}Bu), 34.59 (C-β, Cys), 37.62 (*C*H$_2$-S), 38.87 (*C*H$_2$-N), 52.17 (S-*C*Ph$_3$), 67.34 (C-α, Cys), 121.19 (C-6′, Pyr), 121.38 (C-4′, Pyr), 127.07 (Trt), 128.45 (Trt), 129.79 (Trt), 137.15 (C-3′, Pyr), 144.66 (Trt), 150.24 (C-3′, Pyr), 159.22 (*C*O, Boc), 170.64 (*C*O, Cys). ES-MS, calcd. for $C_{34}H_{37}N_3O_3S_3$: 631.20. Found: *m*/*z* 670.11 $[M + K]^+$, 654.13 $[M + Na]^+$, 632.18 $[M + H]^+$, 243.42 $[Trt]^+$. Anal. Calcd for $C_{34}H_{37}N_3O_3S_3$: C, 64.63; H, 5.90; N, 6.65; S,15.22. Found: C, 64.29; H, 5.82; N, 6.65; S, 14.91. Thiol-terminated resin **D** (376 mg, 29 μmol) was weighed in a 10 mL syringe. Washing volumes were 4 mL. Boc-Cys(Trt)-NH-$(CH_2)_2$-S-S-Pyr (72 mg, 0.114 mmol) was dissolved in MeOH (4 mL) and added to the resin. The resin was shaken at room temperature for 2 h and washed with MeOH (4 × 1 min) and CH_2Cl_2 (2 × 1 min, 1 × 5 min, 2 × 1 min). The resin was stored wet at 5 °C and Boc and Trt groups were cleaved with TFA−CH_2Cl_2 (1:1) in the presence of Et_3SiH (15 equiv) prior to coupling.

Preparation of Cys-Terminated Resins (F). '**F** high loading' (**F**-HL): the reactions were performed in a 10 mL syringe, and the washing volumes were 4 mL. Amino-terminated PEGA resin (1.79 g, 0.4 mmol/g) was washed with DMF (3 × 1 min), swollen in DMF (1 × 10 min), and washed with DIEA−DMF (1:9, 3 × 1 min) and DMF (3 × 1 min), respectively. Boc-Cys(Trt)-OH (148 mg, 0.32 mmol) was coupled in the presence of PyBOP (125 mg, 0.24 mmol), HOBt (32 mg, 0.24 mmol), and DIEA (62 μL, 0.36 mmol) in DMF (4 mL) at room temperature. After 1 h, a qualitative ninhydrin test showed complete incorporation of the Cys derivative. The resin was then washed with DMF (3 × 1 min) and CH_2Cl_2 (2 × 1 min, 1 × 5 min, 2 × 1 min) and stored wet at 5 °C. Deprotection of Boc and Trt groups was accomplished with TFA−CH_2Cl_2 (1:1) in the presence of Et_3SiH (15 equiv) immediately prior to sugar immobilization.

'**F** low loading' (**F**-LL): a parallel experiment was conducted using a low loading amino PEGA resin (2.13 g, 0.2 mmol/g) in a 10 mL syringe. Boc-Cys(Trt)-OH (74 mg, 0.16 mmol) was reacted with PyBOP (63 mg, 0.12 mmol), HOBt (16 mg, 0.12 mmol) and DIEA (31 μL, 0.18 mmol) in DMF (4 mL). The coupling was performed at room temperature and was complete within 1 h, according to a qualitative ninhydrin test. Washing conditions were similar to the ones described above. Boc and Trt groups were removed by TFA−CH_2Cl_2 (1:1) in the presence of Et_3SiH (15 equiv) prior to immobilization (see below).

Preparation of Glutamic Acid (Glu)-Terminated Resins (G). *Synthesis of Boc-Glu(O^{t}Bu)-NH-(CH$_2$)$_2$-S-S-Pyr.* A solution of Boc-Glu(O^{t}Bu)-OH (249 mg, 0.82 mmol), HBTU (341 mg, 0.9 mmol), NEt_3 (286 μL, 2.05 mmol), and *S*-(2-pyridylthio)cysteamine hydrochloride (*39*) (200 mg, 0.90 mmol) in CH_3CN (8 mL) was stirred at room temperature. After 15 h, the mixture was diluted with EtOAc (35 mL), washed sequentially with 1 M aq HCl (3 × 12 mL), saturated aqueous $NaHCO_3$ (3 × 12 mL), and brine (3 × 12 mL), dried over $MgSO_4$, and concentrated to a foam identified as the title compound (352 mg, 91%). ^{1}H NMR ($CDCl_3$) δ 1.35 (s, 9 H, CH_3), 1.37 (s, 9 H, CH_3), 1.80 (m, 1 H, H-β^a), 1.97 (m, 1 H, H-β^b), 2.26 (m, 2 H, H-γ), 2.84 (t, 2 H, CH_2-S, *J* 6.1 Hz), 3.46 (m, 2 H, CH_2-NH), 4.03 (dd, 1 H, H-α, *J* 7.1 Hz), 7.08 (m, 1 H, H-4′ Pyr), 7.57 (m, 2 H, H-5′ Pyr, H-6′ Pyr), 7.82 (s, 1 H, N*H*), 8.44 (m, 1H, H-3′ Pyr). ^{13}C NMR (CD_3OD) δ 27.23 (*C*H$_3$, Boc), 27.40 (C-β), 27.57 (*C*H$_3$, ^{t}Bu), 27.69 (C-γ), 31.57 (*C*H$_2$-S), 37.91 (*C*H$_2$-NH), 54.42 (C-α), 79.62 ((CH$_3$)$_3$-*C*, Boc), 80.63 ((CH$_3$)$_3$-*C*, ^{t}Bu), 120.39 (C-6′, Pyr), 121.30 (C-4′, Pyr), 137.85 (C-5′, Pyr), 149.47 (C-3′, Pyr), 159.74 (*C*O, Boc), 172.74 (*C*O, Glu, side chain), 173.55 (*C*O, Glu). ES-MS, calcd. for $C_{21}H_{33}N_3O_5S_2$: 471.19. Found: *m*/*z* 494.29 [M + Na]$^+$, 472.31 [M + H]$^+$, 416.33 [M − ^{t}Bu + 2H]$^+$, 372.37 [M − Boc + 2H]$^+$, 316.35 [M − Boc − ^{t}Bu + 3H]$^+$. Resin **D** (275 mg, 29 μmol) was weighed in a 10 mL syringe. Washing volumes were 4 mL. Boc-Glu(O^{t}Bu)-NH−(CH$_2$)$_2$-S-S-Pyr (54 mg, 0.114 mmol) was dissolved in MeOH (0.7 mL), the volume was adjusted to 4 mL with MeOH, and the solution was added to the resin. During coupling for 2 h at room temperature, a yellow coloration was observed, indicative of the release of pyridine-2-thione. The resin was then washed with MeOH (4 × 1 min) and stored wet at 4 °C until further use.

Preparation of Glu-Terminated Resins (H). Reactions were carried out in a 10 mL syringe. The washing volumes were 4 mL. The initial washing and coupling procedures were identical to the ones described above for the preparation of Cys terminated resins using Boc-Cys-(Trt)-OH. In this case, Boc-Glu(O^{t}Bu)-OH (97 mg, 0.32 mmol) was anchored to amino PEGA resin (1.79 g, 0.4 mmol/g) in the presence of PyBOP (125 mg, 0.24 mmol), HOBt (32 mg, 0.24 mmol), and DIEA (62 μL, 0.36 mmol). According to a qualitative ninhydrin test, coupling was completed within 1 h at room temperature. The resin was then washed with DMF (3 × 1 min) and CH_2Cl_2 (2 × 1 min, 1 × 5 min, 2 × 1 min) and stored wet at 5 °C until deprotection and further derivatization.

Model Reactions in Solution. *Preparation of a Model Glycosyl Hydrazide.* GalA (1.3 g, 6.14 mmol) was dissolved in MeOH (dried over 3 Å molecular sieves, 12 mL), and acetic acid hydrazide (500 mg, 6.75 mmol) (*40*) was added. The mixture was stirred at 65 °C for 7 h. Formation of a precipitate was observed. It was collected by centrifugation and dried under reduced pressure (1st crop). The filtrate was concentrated to a pale yellow solid in vacuo (2nd crop). Fractions 1 and 2 gave 1.53 g (99%) of the acyclic glycosyl hydrazide (*E*/*Z* = 2:1, based on the assumption that δ_Z(H-1) > δ_E(H-1)). ^{1}H NMR (DMSO-d_6) δ 1.85 (s, 1 H, CH_3, *Z*), 2.05 (s, 2 H, CH_3, *E*), 3.45 (d, 1 H, H-3, *J* 9.4 Hz), 3.80 (d, 1 H, H-4, *J* 9.4 Hz), 4.24 (m, 2 H, H-2, H-5), 7.35 (d, 0.66 H, H-1, *E*, *J* 5.7 Hz), 7.46 (d, 0.33 H, H-1, *Z*, *J* 5.9 Hz), 10.84 (s, 0.66 H, N*H*, *E*), 10.99 (s, 0.33 H, N*H*, *Z*). ^{13}C NMR (DMSO-d_6) δ 20.96 (*C*H$_3$, *E*), 21.74 (*C*H$_3$, *Z*), 70.33 (C-2), 70.62 (C-4), 71.98 and 72.06 (C-3), 72.66 and 72.77 (C-5), 149.35 (C-1, *E*), 152.03 (C-1, *Z*), 166.0 (*C*(O), Ac, *Z*), 172.27 (*C*(O), Ac, *E*), 176.04 (C-6). FAB-MS, calcd for $C_8H_{14}N_2O_7$: 250.08. Found: *m*/*z* 170 [M + 3H$_2$O + 2NH$_4$]$^{2+}$, 153 [M + 3H$_2$O + 2H]$^{2+}$.

Preparation of a Model Thiazolidine. H-Cys-OMe.HCl (1 g, 5.8 mmol) (*41*) was dissolved in H_2O (10 mL). K_2CO_3 was added until neutral pH. The solution was extracted with Et_2O (5 × 5 mL), and the combined extracts were dried over $MgSO_4$ and concentrated in vacuo. Residual H-Cys-OMe (100 mg, 0.74 mmol) was dissolved in MeOH (5 mL), and a solution of GalA (157 mg, 0.74 mmol) in MeOH (5 mL) was added. The clear mixture (pH 4) was stirred at room temperature. After 24 h, TLC (eluent CH_2Cl_2−MeOH, 1:1) showed complete disappearance of the starting material. The solvent was then evaporated in vacuo. Purification on a short silica column using MeOH as eluent gave the thiazolidine derivative in 50% yield and as two diastereomers (*R* and *S* configurations at C-1, GalA). ^{13}C NMR (D_2O) δ 35.87 and 36.47 (C-β, Cys), 52.23 and 52.36 (*C*H$_3$, Cys), 64.58 and 65.00 (C-α, Cys), 68.76 and 69.98 (C-1, GalA), 70.97−72.30 (C-2, C-3, C-4, GalA), 76.07 and 76.23 (C-5, GalA), 169.93 (*C*(O), Cys). FAB-MS, calcd for $C_{10}H_{17}NO_8S$: 311.07. Found: *m*/*z* 294 [M + H − H$_2$O]$^+$, 276 [M + H − 2H$_2$O]$^+$.

Immobilization Techniques. *Immobilization via Reductive Amination.* The reaction was performed in a 5 mL syringe, and the washing and reaction volumes were 2 mL. Hydrazide-terminated resin **C** (100 mg dry, 38 μmol) was washed with DMF (2 × 1 min, 1 × 5 min, 2 × 1 min). GalA (40 mg, 0.19 mmol) was dissolved in DMF−AcOH (99:1). The solution was then added to the resin, and following addition of $NaBH_3CN$ (24 mg, 0.38 mmol), the syringe was shaken at room temperature. After 24 h, the solvent and excess reagents were filtered off, and the resin was washed with DMF (4 × 1 min) and stored at 5 °C until quantitation. A similar procedure was applied to immobilize α-D-GalA-(1→4)-D-GalA ((GalA)$_2$, 10 mg, 27 μmol) on resin **C** (14 mg dry, 5 μmol) in the presence of $NaBH_3CN$ (4 mg, 54 μmol). α-D-GalA-(1→4)-α-D-GalA-(1→4)-D-GalA ((GalA)$_3$, 5.9 mg, 11 μmol) was also coupled to resin **C** (6 mg dry, 2 μmol) using $NaBH_3CN$ (7 mg, 11 μmol). In these two cases, 2 mL syringes were used, and the washing and reaction volumes were 1 mL. The anthrone assay was used to determine the coupling efficiencies.

Immobilization via Oxime Formation. The immobilization reaction was performed in a 5 mL syringe, and the washing and reaction volumes were 2 mL. Aminooxy-terminated resin (128 mg dry, 44 μmol) was first washed with DMF−H_2O (1:1, 1 × 1 min, 1 × 5 min, 2 × 1 min) and DMF−0.1 M aq NaOAc, pH 4.76 (1:1, 3 × 1 min). GalA (42 mg, 0.2 mmol) was dissolved in DMF−0.1 M aq NaOAc, pH 4.8 (1:1), and the solution was added to the resin. The syringe was placed in a sand bath at 40 °C for 24 h. The solvents and unreacted compounds were removed by filtration, and the resin was washed with H_2O (4 × 1 min) and stored at 5 °C until quantitation. The same procedure was applied to immobilize (GalA)$_2$ (9.5 mg, 26 μmol) on aminooxy-terminated resins **A** (14 mg dry, 5 μmol) and (GalA)$_3$ (4.4 mg, 8 μmol) on resin **A** (5.6 mg dry, 2 μmol). In these latter cases, 2 mL syringes were used, and the washing and reaction volumes were reduced to 1 mL. Coupling efficiencies were determined by anthrone assay.

Immobilization via Glycosyl Hydrazide Formation. Resin **C** (100 mg dry, 38 μmol) was weighed in a 5 mL syringe. Washing volumes were 2 mL. The resin was washed with MeOH (2 × 1 min, 1 × 5 min, 2 × 1 min). GalA (40 mg, 0.19 mmol) was dissolved in MeOH (2 mL), and the solution was added to the resin. The syringe was placed in a sand bath at 65 °C. After 20 h, the solvents

and excess reagents were removed by filtration. The resin was washed with MeOH (4 × 1 min), and stored at 5 °C until quantitation. Similar experiments were conducted in 2 mL syringes (the washing and reaction volumes were 1 mL) to immobilize $(GalA)_2$ (10 mg, 27 μmol) and $(GalA)_3$ (6.2 mg, 11 μmol) on resin **C** (14 mg dry, 5 μmol or 6 mg dry, 2 μmol, respectively). In the latter case, the reaction time was extended to 46 h. The reactions were quantified by the anthrone assay.

Immobilization via Thiazolidine Formation. The coupling reactions were performed in 2 mL syringes, and the washing volumes were 1.5 mL. Resins **E** (20 mg dry, 0.6 μmol) was treated with TFA−CH_2Cl_2 (1:1, 1.5 mL) in the presence of Et_3SiH (2 μL, 12 μmol) for 1 h at room temperature. It was then washed with CH_2Cl_2 (4 × 1 min) and with CH_3CN-H_2O−0.1 M aq NaH_2PO_4 buffer, pH 8.5 (1:1:1, 2 × 1 min). GalA (0.2 mg, 1 μmol) was dissolved into CH_3CN-H_2O−0.1 M aq NaH_2PO_4 buffer, pH 8.5 (1:1:1, 1.5 mL), and the solution (pH 4) was added to the resin. After 48 h at room temperature, the resins were washed with CH_3CN (4 × 1 min) and stored at 5 °C until quantitation. The same procedure was repeated with resin **F**-HL (20 mg dry, 2 μmol) and resin **F**-LL (20 mg dry, 0.8 μmol) with Et_3SiH (5 μL, 31 μmol and 2 μL, 12 μmol, respectively) and GalA (0.6 mg, 3 μmol and 0.2 mg, 1 μmol, respectively). A similar procedure was applied using the same amount of resins **E**, **F**-HL, and **F**-LL and $(GalA)_2$ (0.4 mg, 1 μmol; 1 g, 3 μmol and 0.4 mg, 1 μmol, respectively) as a substrate. Similarly, $(GalA)_3$ (1.4 mg, 3 μmol and 0.5 mg, 1 μmol, respectively) was coupled to Cys-terminated resins **F**-HL (20 mg dry, 2 μmol) and **F**-LL (20 mg dry, 0.8 μmol), respectively. The Ellman test was used to determine the coupling efficiencies.

Immobilization via Pyroglutamyl Formation. Reactions were carried out in 2 mL syringes, and the washing volumes were 1.5 mL. Resin **G** (20 mg dry, 2 μmol) and resin **H** (20 mg dry, 6 μmol) were washed with CH_2Cl_2 (3 × 1 min, 1 × 3 min) and deprotected with TFA−CH_2Cl_2 (1:1, 1.5 mL) and Et_3SiH (5 μL, 30 μmol; 11 μL, 70 μmol, respectively) at room temperature. After 1 h, the solvents and excess reagents were filtered off, and the resin was washed with CH_2Cl_2 (3 × 1 min) and DMF (3 × 1 min, 1 × 3 min). GalA (2 mg, 96 μmol and 5 mg, 23 μmol, respectively) and imidazole (1 mg, 14 μmol and 2.4 mg, 35 μmol, respectively) were dissolved in DMF (1 mL), and the solutions were added to the resins. The syringes were placed in a sand bath at 60 °C for 24 h. After filtration, the resins were washed with DMF (2 × 1 min). Solutions of PyBOP (7 mg, 14 μmol and 18 mg, 35 μmol, respectively) and imidazole (1 mg, 14 μmol and 2.4 mg, 35 μmol, respectively) in DMF (1 mL) were added to the resins. Coupling took place at room temperature for 4 h. Solvents and excess reagents were removed by filtration, and the resins were finally washed with DMF (3 × 1 min), H_2O (2 × 5 min), and DMF (2 × 1 min) and stored at 5 °C until quantitation. In a parallel fashion, $(GalA)_2$ (2 mg, 5 μmol and 4.4 mg, 12 μmol) was coupled to resin **G** (10 mg dry, 1 μmol) and resin **H** (10 mg dry, 3 μmol), respectively, using 2 mL syringes and washing with 1 mL solvent. Quantitation by anthrone assay provided data on the coupling efficiencies.

Cleavage of Immobilized Pectin Fragment from the Support. The cleavage reactions were performed in 2 mL syringes, and the washing volumes were 1 mL. Resins **E** (4.3 mg) and **G** (7 mg), both derivatized with GalA, were washed with H_2O (3 × 1 min) and 50 mM tris(hydroxymethyl)aminomethane buffer (pH 8, 3 × 1 min) and then treated with DTT (1 mg, 6 μmol) in the same buffer (pH 8, 0.8 mL) at room temperature. After 22 h, the filtrates from the cleavage reactions were collected and combined with H_2O washes (2 × 1 min). H_2O (5 mL) was then added to each filtrate, and the samples were freeze-dried. For resin **E**, ES-MS, calcd for $C_{11}H_{20}N_2O_7S_2$: 356.07. Found: *m/z* 395.07 $[M + K]^+$, 379.09 $[M + Na]^+$, 281.20 $[M - C_2H_6NS + H]^+$. For resin **G**, ES-MS, calcd for $C_{13}H_{20}N_2O_8S$: 364.09. Found: *m/z* 363.06 $[M - H]^-$.

RESULTS AND DISCUSSION

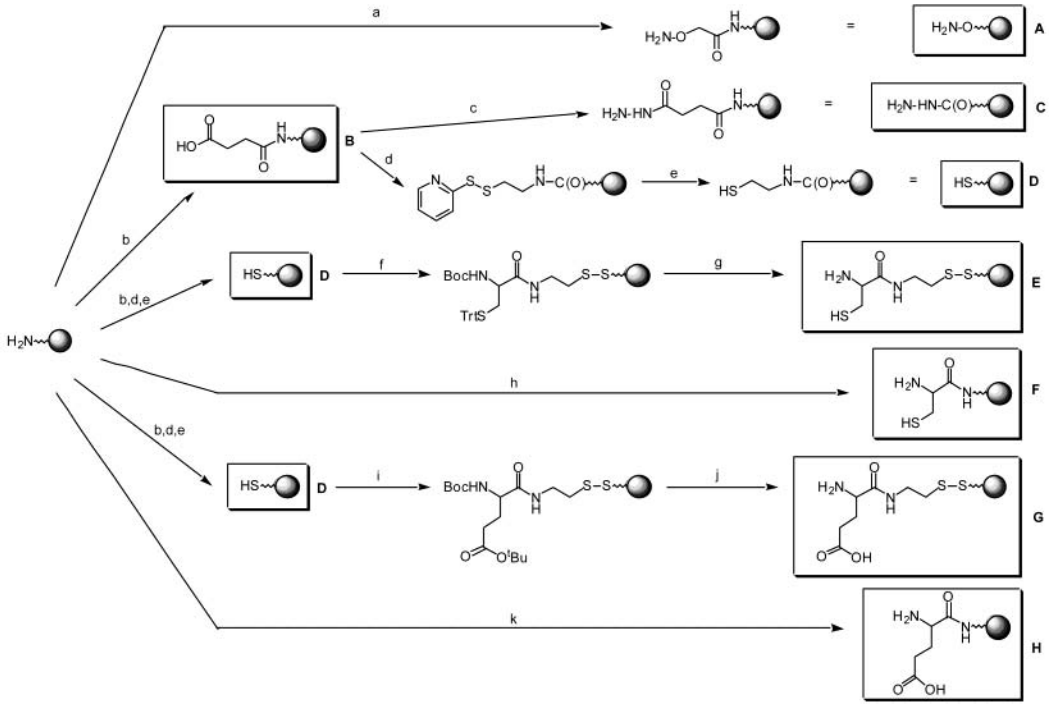
In this comprehensive study, we present the development of efficient methodologies for the stable, covalent, and chemoselective anchoring of oligomers of GalA onto a solid support. To ensure that the methods developed could also be used for longer pectin fragments, the oligogalacturonides were *not* derivatized and were immobilized through their reducing end, which provides a unique functionality in the molecule. Several functional groups were installed on amino-terminated PEGA resins by classical solid-phase manipulations prior to immobilization of small GalA oligomers (see Scheme 1). These functionalities included amino, hydrazide, Cys, and Glu moieties. For two of the supports, we also synthesized variants containing a disulfide bridge which, under mild reducing conditions, allows cleavage and release of the immobilized material into solution.

Preparation of Activated Solid Supports. Resin **A** was prepared by coupling N^{β}-Boc-Aoa-OH to amino PEGA resin (0.4 mmol/g). Free aminooxy groups were obtained upon treatment with TFA in CH_2Cl_2. The corresponding loading was determined via an 'indirect method', in which trityl groups were coupled to the aminooxy-terminated groups on the support and subsequently released into solution for quantitation (*34*). Cleavage of the Trt groups with TFA−CH_2Cl_2 (1:1) was optimized by trapping of the released trityl cation with Et_3SiH to form TrtH (*35*). For the loading determination, it was essential to efficiently dry and accurately weigh functionalized PEGA resins. For this purpose, we developed a procedure in which the resin was allowed to collapse gradually using an increasing concentration of Et_2O in CH_2Cl_2 followed by drying in vacuo (*42*). This 'indirect method' was applied to resin **A** and gave a loading of 0.34 mmol/g (Table 1).

The first step in the preparation of a hydrazide support was coupling of succinic anhydride to amino-terminated PEGA resins (0.4 mmol/g, HL and 0.2 mmol/g, LL) using HOBt and DIEA in DMF. The obtained resin **B** (HL) was further derivatized to resin **C** by treatment with hydrazine monohydrate in the presence of standard coupling reagents. The loading of hydrazide resin **C** was 0.38 mmol/g, according to an 'indirect' trityl quantitation as described above (see Table 1).

For the preparation of a thiol-functionalized support, *S*-(2-pyridylthio)cysteamine hydrochloride was synthesized following a literature procedure (*39*) and coupled to **B** (LL) under standard coupling conditions. Subsequent treatment with DTT at pH 4.8 cleaved the disulfide bridge to give free thiol groups of resin **D** (see Scheme 1). A yellow coloration was observed, indicating release of pyridine-2-thione into solution. Resin **D** was then reacted with synthesized Boc-Cys(Trt)-NH-$(CH_2)_2$-S-S-Pyr via a disulfide exchange reaction in MeOH. Final deprotection of the Boc and Trt groups in the presence of Et_3SiH (*35*) afforded Cys-functionalized resin **E**. The release of Trt groups in the last deprotection step was also used to determine the loading of resin **E** ('direct method'). It was found to be 0.03 mmol/g (Table 1). The low value of the loading may be attributed to the large

Scheme 1. Preparation of Various Activated Solid Supports from Amino-Terminated PEGA Resins (0.2 mmol/g or 0.4 mmol/g)[a]



[a] (a) (*i*) N^{β}-Boc-Aoa-OH, PyBOP, HOBt, DIEA, DMF, rt, 1.2 h, (*ii*) TFA−CH_2Cl_2 (1:1), rt, 1 h; (b) succinic anhydride, HOBt, DIEA, DMF, rt, 1.5 h; (c) hydrazine monohydrate, HBTU, HOBt, DIEA, DMF, rt, 2 h; (d) *S*-(2-Pyridylthio)cysteamine hydrochloride, HBTU, HOBt, DIEA, DMF, rt, 2 h; (e) DTT, H_2O, pH 4.8, rt, 2 h; (f) Boc-Cys(Trt)-NH−$(CH_2)_2$−S−S−Pyr, MeOH, rt, 2 h; (g) TFA−CH_2Cl_2 (1:1), Et_3SiH, rt, 1 h; (h) (*i*) Boc-Cys(Trt)-OH, PyBOP, HOBt, DIEA, DMF, rt, 1 h, (*ii*) TFA−CH_2Cl_2 (1:1), Et_3SiH, rt, 1 h; (i) Boc-Glu(O^tBu)-NH-$(CH_2)_2$-S-S-Pyr, MeOH, rt, 2 h; (j) TFA−CH_2Cl_2 (1:1), rt, 1 h; (k) (*i*) Boc-Glu(O^tBu)-OH, PyBOP, HOBt, DIEA, DMF, rt, 1 h, (*ii*) TFA−CH_2Cl_2 (1:1), rt, 1 h.

Table 1. Efficiencies for the Immobilization of Oligomers of GalA

			% coupling efficiency[b] (uncertainty)		
coupling technique	initial resin[a]	loading (mmol/g)	GalA	$(GalA)_2$	$(GalA)_3$
reductive amination	**C**	0.38[c]	93 (± 13)[e]	81 (± 15)[e]	n.d.
glycosyl hydrazide	**C**	0.38[c]	117 (± 21)[e]	89 (± 21)[e]	75 (± 23)[e]
oxime	**A**	0.34[c]	117 (± 23)[e]	120 (± 31)[e]	62 (± 15)[e]
thiazolidine 1	**F**	0.10[d]	quant.[g]	quant.[g]	quant.[g]
thiazolidine 2	**E**	0.03[d]	quant.[g]	quant.[g]	n.d.
glycosyl amide 1	**H**	0.29[c]	97 (± 18)[e]	71 (± 14)[e]	n.d.
glycosyl amide 2	**G**	0.12[c]	90 (± 7)[f]	75 (± 12)[f]	n.d.

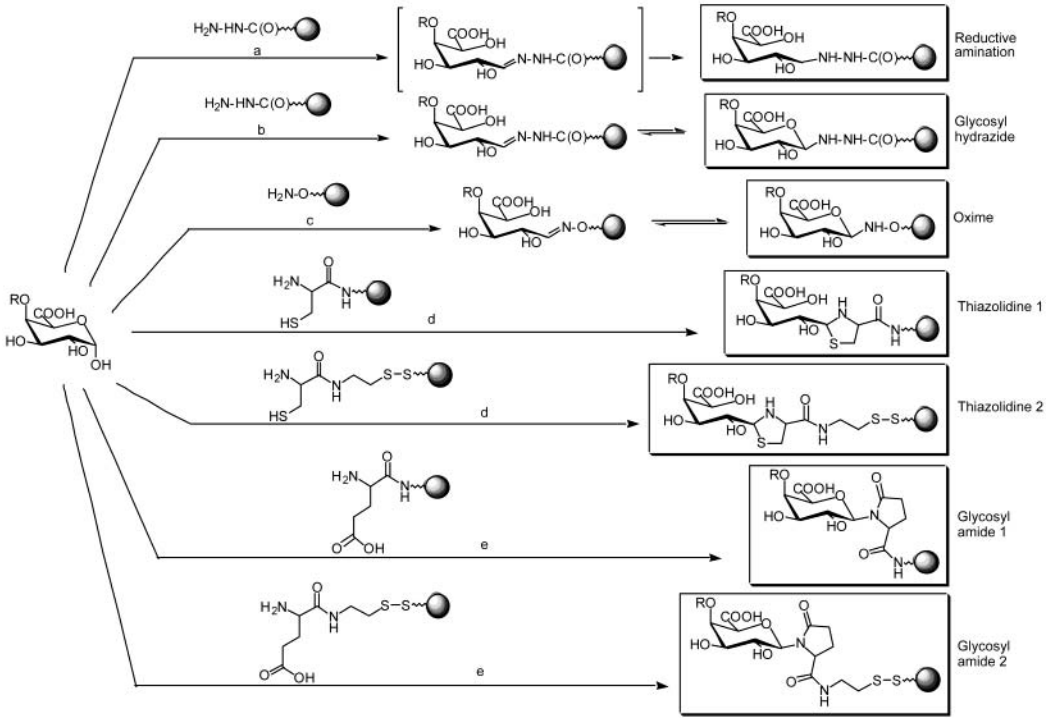
[a] See Scheme 1. [b] Based on the initial resin loading. [c] By 'indirect' trityl quantitation. [d] By 'direct' trityl quantitation. [e] Anthrone assay; assumptions: 0.05 mmol/g uncertainty on the loading, 0.2 mg uncertainty on the mass. [f] Anthrone assay; assumptions: 0.02 mmol/g uncertainty on the loading, 0.2 mg uncertainty on the mass. [g] Quantitative based on negative Ellman test. n.d. = not determined.

number of steps from the starting material amino PEGA resins and/or to an incomplete coupling of Boc-Cys(Trt)-NH-$(CH_2)_2$-S-S-Pyr on thiol-functionalized support. Cys-terminated support **F**, with a permanent linkage, was directly obtained from amino PEGA resins (0.4 mmol/g) by standard coupling of Boc-Cys(Trt)-OH followed by acidic treatment under similar conditions as described for **E**. Direct quantitation of the amount of Trt groups released in the last step gave a loading of 0.10 mmol/g (Table 1). Access to resin **F** was faster and easier than to resin **E**, but in the latter case, a cleavable linker was installed through the disulfide bond.

A similar strategy to that used for **E** and **F** was applied to install Glu moieties on solid support. Resin **D** was functionalized with synthesized Boc-Glu(O^tBu)-NH-$(CH_2)_2$-S-S-Pyr and the protecting groups were further removed under acidic conditions to give **G**. The loading was 0.12 mmol/g, according to an 'indirect' trityl quantitation (Table 1). As in **E**, the disulfide bridge introduced a potentially cleavable linkage. Alternatively, Boc-Glu(^{t}Bu)-OH was coupled to amino-terminated PEGA resin (0.4 mmol/g). Subsequent deprotection allowed access to Glu-terminated resin, **H** (loading 0.29 mmol/g, after 'indirect' trityl quantitation; Table 1). Resins **A**, **C**, **E**, **F**, **G**, and **H** were then available for immobilization of pectin fragments.

Methods for the Immobilization of GalA Oligomers. Seppälä and Mäkelä (*22*) reported on the use of hydrazide groups as an alternative to amino groups to enhance, via the α-effect, the reactivity during coupling with various neutral oligosaccharides. In case of solid-supported reductive aminations, coupling conditions were also optimized by careful choice of the solvent and the reagents (*43*). These observations were combined and applied to immobilize model pectin fragments, GalA and $(GalA)_2$, on a hydrazide-terminated resin (see Scheme 2). Typically, the solid-phase reactions were performed in DMF−AcOH (99:1) using 5 equiv of oligogalacturonide and 10 equiv of $NaBH_3CN$ at room temperature for 24 h. For larger pectin fragments, an excess of resin should be used. The immobilization efficiency was determined by the anthrone assay, based on the initial loading of

Scheme 2. Methods for the Solid-Phase Immobilization of Model Pectin Fragments[a]



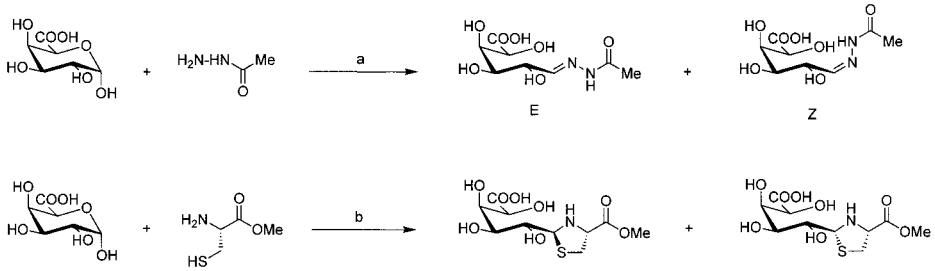
[a] (a) $NaBH_3CN$, DMF−AcOH (99:1), rt, 24 h; (b) MeOH, 65 °C, 20 h; (c) DMF−H_2O (1:1), pH 4.8, 40 °C, 24 h; (d) H_2O−CH_3CN (2:1), pH 4, rt, 24 h; (e) (*i*) imidazole, DMF, 60 °C, 24 h, (*ii*) PyBOP, imidazole, DMF, rt, 4 h.

resin **C**. This colorimetric method was chosen for several reasons. First, it is a general and well-established method for the quantitation of carbohydrates, including uronic acids (*36*). Second, it takes place at very low pH, using concentrated H_2SO_4, and high temperatures are required for the color development of the reagent. Such acidic conditions would cleave the glycosidic linkages along the oligogalacturonide chains, liberating single galacturonic acid units. These could then be quantified by comparison with standards. Furthermore, the harsh conditions were believed to dissolve the PEGA resin, allowing direct analysis of a solution containing oligogalacturonides. Contributions from the support were accounted for by comparing resin samples prior to and after immobilization. Analysis of GalA immobilized resin gave a 93 (±13)% coupling efficiency, which shows that one saccharide unit reacted with anthrone (Table 1). The uncertainty on the coupling efficiency, which takes into account intermediate uncertainties, was calculated using standard methods (Table 1). In case of $(GalA)_2$, the coupling efficiency was 81 (±15)%, when two saccharide units were cleaved and reacted with anthrone. These results prove that reductive amination with hydrazide is an effective method for the immobilization of unprotected GalA oligomers to solid supports. And, whereas conventional methods rely on affinity studies to estimate the degree of coupling (*28, 30*), the quantitation method developed hereby directly estimates the amount of pectin immobilized on the support. However, the data obtained are in contradiction with the literature (*36, 44, 45*). The mechanism for the reaction of anthrone with carbohydrates is complex and not fully elucidated: it involves the formation of strongly colored furfural derivatives when anthrone reacts with the aldehyde group at the reducing end of the carbohydrate. Since solid-phase anchoring of oligogalacturonides onto hydrazide-terminated resin under reducing conditions gives a modified saccharide, the reducing sugar is transformed into an open ring hydrazide. Thus, the anthrone assay was not expected to give a positive response when analyzing GalA-immobilized resin and to show two saccharide units when analyzing $(GalA)_2$ immobilized support.

A second approach which we have implemented for the immobilization of underivatized GalA oligomers was based on the formation of an oxime bond. This type of linkage has recently become a popular method for preparing bioconjugates (*46, 47*), peptide dendrimers (*48*), glycopeptides (*29*), carbopeptides (*49*), and carboproteins (*50*). The efficiency of the method relies on the ease of formation and on the good stability of the oxime linkage up to pH 9. This well-established methodology appears not to have been used for the immobilization of polyuronic acids. Oligogalacturonides, ranging from the monomer to the trimer, were coupled to resin **A** through the aldehyde group at their reducing end. Oxime formation took place under mild conditions, in DMF−H_2O (1:1), at 40 °C and pH 4.8 for 24 h (*33*). Incorporation of GalA oligomers was quantified by the anthrone assay. The coupling efficiencies, based on the initial loading of resin **A**, were 117 (±23)%, 120 (±31)% and 62 (±15)% for immobilized GalA, $(GalA)_2$, and $(GalA)_3$, respectively (Table 1). In each case, the contribution of the pre-immobilization resin was subtracted. In contrast to reductive amination, the sugar structure was preserved after coupling; an equilibrium between the closed ring and open ring forms might occur at the surface of the support. This efficient technique requires few derivatization steps on solid-phase and its compatibility with aqueous solvents makes it very attractive when using larger pectin fragments with limited solubilities.

The direct coupling between the reducing end of various neutral oligosaccharides with hydrazide groups has recently been investigated in carbohydrate recognition studies (*51*) and in the synthesis of surfactants (*52*), demonstrating the stability of the glycosyl hydrazide linkage under neutral to basic conditions. We decided to include this technique in our study, as an alternative to other linkage types. Prior to solid-phase immobilization,

Scheme 3. Solution Synthesis of Glycosylhydrazide and Thiazolidine Derivatives of GalA[a]



[a] (a) MeOH, 65 °C, 7 h; (b) MeOH, rt, 24 h.

a model study was conducted in solution (see Scheme 3). Following the conditions described by Augé and Lubin-Germain (*52*), GalA was coupled to acetic acid hydrazide (*40*) in MeOH at 65 °C for 7 h to give the corresponding glycosyl hydrazide in 99% yield. NMR analysis revealed the presence of two acyclic glycosyl hydrazides, most likely the *E* and *Z* isomers (2:1). These optimized conditions were then applied to the coupling of GalA, as well as its dimer and trimer to hydrazide functionalized resin **C** (Scheme 2). The reaction time was extended to 20 h to compensate for the slower reaction rates generally encountered with solid supports. Quantitation by the anthrone assay showed 117 (±21)%, 89 (±21)% and 75 (±23)% immobilization efficiencies for GalA, $(GalA)_2$, and $(GalA)_3$, respectively (Table 1). The coupling yield decreased with increasing size of the oligogalacturonides. Although an unsaturated hydrazone compound was isolated after solution synthesis, an equilibrium between this form and the closed ring glycosyl hydrazide might occur at the surface of the support. Despite its high coupling efficiency and its ease of preparation, this third approach suffers from poor stability of the linkage at low pH. Acid present in the media could indeed protonate the glycosidic nitrogen at the reducing end and cleave the glycosidic bond.

A well-documented methodology for the covalent linkage of oligosaccharides to other molecules or matrixes is based on the formation of a glycosylamine derivative. The reaction is reversible, and a further acylation step is required to stabilize the glycosylamine (*53*). This latter step can proceed by treatment with acetic anhydride (*30*). Alternatively, a method for the preparation of glycoconjugates has recently been developed by Quétard et al. (*31, 32*) in which various neutral oligosaccharides were reacted with glutamic acid derivatives to form the corresponding glycosylamines. In each case, stabilization of the linkage proceeded via an intramolecular acylation by the activated carboxyl group on the side chain of the glutamyl moiety. The potential of this elegant technique has not been exploited to a large extent, and we wish to report here its application to solid-phase immobilization of model pectin fragments. The designed solid-phase strategy included the introduction of two different spacers with a terminal Glu residue on the resin. Glu-functionalized resin **H** would allow for permanent immobilization, whereas resin **G** contained a linker cleavable in the form of a disulfide bridge. The attachment of GalA and $(GalA)_2$ proceeded according to the conditions described by Quétard et al. (*31, 32*). Typically, the reducing end of the oligomer of GalA was reacted with the amino group of the glutamyl acid in DMF in the presence of imidazole for 24 h to form a glycosylamine (Scheme 2). The reactivity was improved by increasing the temperature to 60 °C. After removal of the excess reagents, the coupling agent PyBOP was added, and the intramolecular acylation of the secondary amine and concomitant pyroglutamyl ring formation was allowed to proceed at room temperature for 4 h. Quantitation of the reaction was performed using the anthrone assay. Immobilization of GalA and $(GalA)_2$ on a short spacer resin (**H**-LL) proceeded with an efficiency of 97 (±18)% and 71 (±14)%, respectively (Table 1). Moreover, GalA and $(GalA)_2$ were immobilized on long spacer resin (**G**-HL) with equally high efficiency: 90 (±7)% and 75 (±12)% respectively (Table 1). In this latter case, an uncertainty of 0.02 mmol/g on the resin loading was assumed. Resin **H**-LL functionalized with GalA was treated with DTT. Subsequent cleavage of the disulfide bond released a pyroglutamyl derivative of GalA as the major compound upon MS analysis.

Finally, both early (*54*) and recent (*55*) studies reported on the formation of a thiazolidine ring when reacting a Cys derivative with an aldehyde. Various thiazolidine compounds have so far been prepared from carbohydrates (*56*−*60*), and the stability of the linkage over a large range of pH (3−9) has recently been illustrated in the synthesis of peptide dendrimers (*33*). However, this very efficient methodology has apparently not been extended to the preparation of larger glycoconjugates nor to immobilization on solid supports. We therefore decided to include the formation of a thiazolidine ring in our general strategy for the solid-phase immobilization of pectin fragments. First, optimization of the available conditions was required, and model reactions were conducted using GalA and Cys methyl ester (H-Cys-OMe, Scheme 3). According to earlier studies, the reaction between an 1,2-aminothiol and an aldehyde proceeds very rapidly at pH 4−5 (*54, 55*). Such acidic conditions were also preferred in order to avoid disulfide formation of the Cys residue. Reaction of GalA with H−Cys-OMe in MeOH gave the expected thiazolidine in 50% yield. These conditions were then modified for immobilization on a solid support. GalA, $(GalA)_2$, or $(GalA)_3$ dissolved in H_2O−CH_3CN (2:1) at pH 4 and were coupled to resins **E** or **F** at room temperature for 24 h (Scheme 2). The anthrone assay was not suitable for on-resin quantitation due to a very high absorbance of the preimmobilization resin. Support bound thiol nucleophiles could theoretically react with the carbonyl group of anthrone. The Ellman test is, however, a well-established assay for the quantitation of free thiol groups (*37, 38, 61*). It was used in our study as an alternative to the anthrone assay for this particular reaction. Conditions for the application of the Ellman test to our system were optimized in terms of sample preparation and analytical technique. Postimmobilization resins were analyzed for their content of free thiol groups, by treatment with the Ellman reagent, DTNB. In all cases, a negative test was obtained, corresponding to a quantitative coupling of the GalA oligomers (see Table 1). Disulfide formation between Cys moieties could in principle also account for a negative test, but this was ruled out by a control experiment on the preimmobiliza-

tion resins, which showed excellent response to the Ellman test. This last strategy therefore proved very efficient for the anchoring of pectin fragments on solid support. In addition, a very stable linkage was installed in a few steps. Finally, this coupling method was validated by conducting a cleavage test on resin **E** functionalized with GalA; reduction of the disulfide linkage with DTT released the corresponding thiazolidine derivative. Extension of this new coupling chemistry to immobilization of other oligosaccharides and the synthesis of glycoconjugates can easily be envisaged.

CONCLUSION

We have prepared new hydrazide, aminooxy, and glutamyl-functionalized PEGA supports designed for chemoselective immobilization of oligomers of GalA by hydrazide, oxime, and pyroglutamyl formation, respectively. As an alternative to these well-established immobilization chemistries, we also prepared Cys-functionalized PEGA resins to immobilize GalA oligomers by *novel* thiazolidine formation. In addition to supports which allow permanent and covalent anchoring of saccharides, we also developed Glu- and Cys-functionalized supports in which a cleavable disulfide linkage was inserted. This strategy allows release of the saccharide derivatives under mild selective conditions. The loading of each functionalized support was determined either by an 'indirect' trityl quantitation, based on a coupling-cleavage strategy, or by a 'direct' trityl quantitation, when trityl groups were part of the synthetic pathway.

All supports allowed for efficient immobilization of oligomers of GalA, i.e., unprotected uronic acids, under mild conditions and without modification of the oligosaccharide prior to immobilization. Most of the coupling chemistries were first validated in solution. The two preferred immobilization methods in this study were oxime formation and formation of a thiazolidine. We anticipate that the novel thiazolidine coupling chemistry may also be applied to the immobilization of other saccharides. These methods are currently being used in our laboratories in the solid-phase analysis and the sequencing of pectin fragments.

ACKNOWLEDGMENT

We wish to thank the following: Dr. Andrew Coffey (Polymer Laboratories, UK) for the gift of PEGA resins; Dr. Tove Christensen (Danisco Cultor, Denmark) for supplying GalA oligomers; Mr. Clive Phipps Walter of Danisco Cultor, Denmark, and Associate Professor Jørgen Øgaard Madsen and Mrs. Anne Hector from the Department of Chemistry, Technical University of Denmark, for performing various MS analyses. Finally, we are grateful to: Dr. Gerrit Limberg for initiating this project, the Danish Technical Science Research Council for financial support through a 'Centerkontrakt' grant, and the Alfred Benzon Foundation for a Bøje Benzon fellowship to K.J.J.

LITERATURE CITED

(1) Voragen, A. G. J., Pilnik, W., Thibault, J.-F., Axelos, M. A. V., and Renard, C. M. G. C. (1995) Pectins. *Food polysaccharides and their applications* (A. M. Stephen, Ed.) pp 287−339, Marcel Dekker Inc., New York.

(2) May, C. D. (1990) Industrial pectins: sources, production and applications. *Carbohydr. Polym. 12*, 79−99.

(3) Rombouts, F. M., and Thibault, J.-F. (1986) Enzymic and chemical degradation and the fine structure of pectins from sugar-beet pulp. *Carbohydr. Res. 154*, 189−203.

(4) Thibault, J.-F., Renard, C. M. G. C., Axelos, M. A. V., Roger, P., and Crépeau M.-J. (1993) Studies of the length of homogalacturonic regions in pectins by acid hydrolysis. *Carbohydr. Res. 238*, 271−286.

(5) Renard, C. M. G. C., Crépeau, M.-J., and Thibault, J.-F. (1999) Glucuronic acid directly linked to galacturonic acid in the rhamnogalacturonan backbone of beet pectins. *Eur. J. Biochem. 266*, 566−574.

(6) Limberg, G., Körner, R., Buchholt, H. C., Christensen, T. M. I. E., Roepstorff, P., and Mikkelsen, J. D. (2000) Quantification of the amount of galacturonic acid residues in blocksequences in pectin homogalacturonan by enzymatic fingerprinting with exo- and endo-polygalacturonase II from *Aspergillus niger*. *Carbohydr. Res. 327*, 321−332.

(7) Oosterveld, A., Beldman, G., Schols, H. A., and Voragen, A. G. J. (2000) Characterization of arabinose and ferulic acid rich pectic polysaccharides and hemicelluloses from sugar beet pulp. *Carbohydr. Res. 328*, 185−197.

(8) Marry, M., McCann, M. C., Kolpak, F., White, A. R., Stacey, N. J., and Keith, R. (2000) Extraction of pectic polysaccharides from sugar-beet cell walls. *J. Sci. Food. Agric. 80*, 17−28.

(9) Strasser, G. R., and Amadò, R. (2001) Pectic substances from red beet (*Beta vulgaris conditiva*). Part I. Structural analysis of rhamnogalacturonan I using enzymic degradation and methylation analysis. *Carbohydr. Polym. 44*, 63−70.

(10) Kawabata, A., Sawayama, S., Nakahara, H., and Kamata, T. (1981) Mechanism of association of various demethylated pectins by calcium ions. *Agric. Biol. Chem. 45*, 965−973.

(11) Thom, D., Grant, G. T., Morris, E. R., and Rees, D. A. (1982) Characterisation of cation binding and gelation of polyuronates by circular dichroism. *Carbohydr. Res. 100*, 29−42.

(12) Kohn, R. (1987) Binding of divalent cations to oligomeric fragments of pectin. *Carbohydr. Res. 160*, 343−353.

(13) Tibbits, C. W., MacDougall, A. J., and Ring, S. G. (1998) Calcium binding and swelling behaviour of a high methoxyl pectin gel. *Carbohydr. Res. 310*, 101−107.

(14) Nakahara, Y., and Ogawa, T. (1990) Synthesis of (1→4)-linked galacturonic acid trisaccharides, a proposed plant wound-hormone and a stereoisomer. *Carbohydr. Res. 200*, 363−375.

(15) Nolting, B., Boye, H., and Vogel, C. (2000) Synthesis of rhamnogalacturonan I fragments. *J. Carbohydr. Chem. 19*, 923−938.

(16) Kramer, S., Nolting, B., Ott, A.-J., and Vogel, C. (2000) Synthesis of homogalacturonan fragments. *J. Carbohydr. Chem. 19*, 891−921.

(17) Clausen, M. H., Jørgensen, M. R., Thorsen, J., and Madsen, R. (2001) A strategy for chemical synthesis of selectively methyl-esterified oligomers of galacturonic acid. *J. Chem. Soc., Perkin Trans. 1* 543−551.

(18) Zhong, H.-J., Williams, M. A. K., Goodall, D. M., and Hansen, M. E. (1998) Capillary electrophoresis studies of pectins. *Carbohydr. Res. 308*, 1−8.

(19) van Alebeek, G.-J. W. M., Zabotina, O., Schols, H. A., and Voragen, A. G. J. (2000) Esterification and glycosidation of oligogalacturonides: examination of the reaction products using MALDI-TOF MS and HPAEC. *Carbohydr. Polym. 43*, 39−46.

(20) Sinitsya, A., Copíková, J., and Pavlíková, H. (1998) ^{13}C CP/MAS NMR spectroscopy in the analysis of pectin. *J. Carbohydr. Chem. 17*, 279−292.

(21) Grant, G. T., Morris, E. R., Rees, D. A., Smith, P. J. C., and Thom, D. (1973) Biological interactions between polysaccharides and divalent cations: the egg-box model. *FEBS Lett. 32*, 195−198.

(22) Seppälä, I., and Mäkelä, O. (1989) Antigenicity of dextran-protein conjugates in mice. Effect of molecular weight of the carbohydrate and comparison of two modes of coupling. *J. Immunol. 143*, 1259−1264.

(23) Arndt, B., and Porro, M. (1991) Strategies for type-specific glycoconjugate vaccines of *Streptococcus pneumoniae*. *Adv. Exp. Med. Biol. 303*, 129−148.

(24) Schneller, M., and Geiger, R. E. (1992) An effective method for the synthesis of neoglycoproteins and neogangliosideproteins by use of reductively aminated sulfhydryl-containing carbohydrate conjugates. *Biol. Chem. 373*, 1095−1104.

(25) Baues, R. J., and Gray, G. R. (1977) Lectin purification on affinity columns containing reductively aminated disaccharides. *J. Biol. Chem. 252*, 57−60.
(26) Matsumoto, I., Kitagaki, H., Akai, Y., Ito, Y., and Seno, N. (1981) Derivatization of epoxy-activated agarose with various carbohydrates for the preparation of stable and high-capacity affinity adsorbents: their use for affinity chromatography of carbohydrate-binding proteins. *Anal. Biochem. 116*, 103−110.
(27) Matsumoto, I., Ito, Y., and Seno, N. (1982) Preparation of affinity adsorbents with Toyopearl gels. *J. Chromatogr. 239*, 747−754.
(28) Satoh, A., Fukui, E., Yoshino, S., Shinoda, M., Kojima, K., and Matsumoto I. (1999) Comparison of methods of immobilization to Enzyme-Linked Immunosorbent Assay plates for the detection of sugar chains. *Anal. Biochem. 275*, 231−235.
(29) Zhao, Y., Kent, S. B. H., and Chait, B. T. (1997) Rapid, sensitive structure analysis of oligosaccharides. *Proc. Natl. Acad. Sci. U.S.A. 94*, 1629−1633.
(30) Blomberg, L., Wieslander, J., and Norberg, T. (1993) Immobilization of reducing oligosaccharides to matrixes by a glycosylamide linkage. *J. Carbohydr. Chem. 12*, 265−276.
(31) Quétard, C., Normand-Sdiqui, N., Mayer, R., Strecker, G., Roche, A.-C., and Monsigny, M. (1997) Simple synthesis of novel glycosynthons: oligosylpyroglutamyl derivatives. *Carbohydr. Lett. 2*, 415−422.
(32) Quétard, C., Bourgerie, S., Normand-Sdiqui, N., Mayer, R., Strecker, G., Midoux, P., Roche, A.-C., and Monsigny, M. (1998) Novel glycosynthons for glycoconjugate preparation: oligosaccharylpyroglutamylanilide derivatives. *Bioconjugate Chem. 9*, 268−276.
(33) Shao, J., and Tam, J. P. (1995) Unprotected peptides as building blocks for the synthesis of peptide dendrimers with oxime, hydrazone and thiazolidine linkages. *J. Am. Chem. Soc. 117*, 3893−3899.
(34) Bunin, B. A. (1998) Successive amide alkylations: libraries from libraries, in *The Combinatorial Index*, pp 117−118, Academic Press, San Diego.
(35) Pearson, D. A., Blanchette, M., Baker, M. L., and Guindon C. A. (1989) Trialkylsilanes as scavengers for the trifluoroacetic acid deblocking of protecting groups in peptide synthesis. *Tetrahedron Lett. 30*, 2739−2742.
(36) Scherz, H., and Bonn, G. (1998) Reaction with anthrone, in *Analytical chemistry of carbohydrates* (G. T. Verlag, Ed.) pp 52−53, Thieme Medical Publishers, Inc., Stuggart, New York.
(37) Ellman, G. L. (1958) A colorimetric method for determining low concentrations of mercaptans. *Arch. Biochem. Biophys. 74*, 443−450.
(38) Ellman, G. L. (1959) Tissue sulfhydryl groups. *Arch. Biochem. Biophys. 82*, 70−77.
(39) Ebright, Y. W., Chen, Y., Pendergrast, P. S., and Ebright, R. H. (1992) Incorporation of an EDTA-metal complex at a rationally selected site within a protein: application to EDTA-iron DNA affinity cleaving with Catabolite gene Activator Protein (CAP) and Cro. *Biochemistry 31*, 10664−10670.
(40) Palla, G., Predieri, G., Domiano, P., Vignali, C., and Turner, W. (1986) Conformational behaviour and *E*/*Z* isomerization of *N*-acyl and *N*-aroylhydrazones. *Tetrahedron 42*, 3649−3654.
(41) Webb, R. G., Haskell, M. W., and Stammer, C. H. (1969) A Nuclear Magnetic Resonance method for distinguishing α-amino acids from β and γ isomers. *J. Org. Chem. 34*, 576−580.
(42) Tolborg, J. F., Petersen, L., Jensen, K. J., Mayer, C., Jakeman, D. L., Warren, R. A. J., and Withers, S. G. (2002) Solid-phase oligosaccharide and glycopeptide synthesis using glycosynthases, submitted.
(43) Sazaki, Y., and Coy, D. H. (1987) *Peptides 8*, 119−121.
(44) Momose, T., Ueda, Y., Sawada, K., and Sugi, A. (1957) Organic analysis. VIII. Reaction mechanism of anthrone with sugars. (1). *Chem. Pharm. Bull. 5*, 31−36.
(45) Momose, T., Ohkura, Y., and Hirauchi, K. (1963) Color reaction mechanism of anthrone with sugars. (2). Some reaction products of furfural with anthrone (Organic analysis. XLVII). *Chem. Pharm. Bull. 11*, 1364−1368.
(46) Webb, R. R., and Kaneko, T. (1990) Synthesis of 1-(aminooxy)-4-[(3-nitro-2-pyridyl)dithio]butane and 1-(aminooxy)-4-[(3-nitro-2-pyridyl)dithio]but-2-ene, novel heterobifunctional cross-linking reagents. *Bioconjugate Chem. 1*, 96−99.
(47) Mikola, H., and Hänninen, E. (1992) Introduction of aliphatic amino and hydroxy groups to keto steroids using O-substituted hydroxylamines. *Bioconjugate Chem. 3*, 182−186.
(48) Rose, K. (1994) Facile synthesis of homogeneous artificial proteins. *J. Am. Chem. Soc. 116*, 30−33.
(49) Brask, J., and Jensen, K. J. (2000) Carbopeptides: chemoselective ligation of peptide aldehydes to aminooxy-functionalized D-galactose template. *J. Pept. Sci. 6*, 290−299.
(50) Brask, J., and Jensen, K. J. (2001) Carboproteins: a 4-α-helix bundle protein model assembled on a D-galactopyranoside template. *Bioorg. Med. Chem. Lett. 11*, 697−700.
(51) Leteux, C., Childs, R. A., Chai, W., Stoll, M. S., Kogelberg, H., and Feizi, T. (1998) Biotinyl-L-3-(2-naphthyl)-alanine hydrazide derivatives of *N*-glycans: versatile solid-phase probes for carbohydrate-recognition studies. *Glycobiology 8*, 227−236.
(52) Augé, J., and Lubin-Germain, N. (2000) Glycosylhydrazides, a new class of sugar surfactant. Preparation and amphiphilic properties of 1-glycosyl-2-acylhydrazines. *J. Carbohydr. Chem. 19*, 379−392.
(53) Onodera, K., and Kitaoka, S. (1960) *N*-Acylation of unsubstituted glycosylamines. *J. Org. Chem. 25*, 1322−1325.
(54) Ratner, S., and Clarke, H. T. (1936) The action of formaldehyde upon cysteine. *J. Biol. Chem. 59*, 200−206.
(55) Liu, C.-F., and Tam, J. P. (1994) Chemical ligation approach to form a peptide bond between unprotected peptide segments. Concept and model study. *J. Am. Chem. Soc. 116*, 4149−4153.
(56) Bognár, R., Somogyi, L., and Györgydeák, Z. (1970) Substituierte Thiazolidine durch Reaktion von L-Cystein mit Monosacchariden. *Liebigs Ann. Chem. 738*, 68−78.
(57) Radomski, J., and Temeriusz, A. (1989) Thiazolidine-4(*R*)-carboxylic acids derived from sugars: part I, C-2-epimerisation in aqueous solutions. *Carbohydr. Res. 187*, 223−237.
(58) Siriwardena, A. H., Chiaroni, A., Riche, C., and Grierson, D. S. (1992) Synthesis of (6*R*,7*R*,8*S*,8a*R*)-6,7,8-trihydroxyperhydro[1,3]thiazolo[3,2-*a*]pyridine and its 8a*S*-epimer. Novel, biologically active analogues of castanospermine. *J. Org. Chem. 57*, 5661−5666.
(59) Marek, D., Wadouachi, A., Uzan, R., and Beaupère, D. (1996) A facile route to diastereomerically pure analogues of castanospermine and australine. *Tetrahedron Lett. 37*, 49−52.
(60) Marek, D., Wadouachi, A., and Beaupère, D. (1997) Synthesis of diastereomerically pure indolizidine and pyrrolizidine analogues from D-pentoses. *Tetrahedron: Asymmetry 8*, 3223−3230.
(61) Virgilio, A. A., and Ellman, J. A. (1994) Simultaneous solid-phase synthesis of β-turn mimetics incorporating side-chain functionality. *J. Am. Chem. Soc. 116*, 11580−11581.

BC0155364

Design of a Targeted Peptide Nucleic Acid Prodrug To Inhibit Hepatic Human Microsomal Triglyceride Transfer Protein Expression in Hepatocytes†

Erik A. L. Biessen,*,‡ Karen Sliedregt-Bol,§ Peter A. Chr. 'T Hoen,‡ Perry Prince,‡ Erica Van der Bilt,‡ A. Rob P. M. Valentijn,§ Nico J. Meeuwenoord,§ Hans Princen,|| Martin K. Bijsterbosch,‡ Gijs A. Van der Marel,§ Jacques H. Van Boom,§ and Theo J. C. Van Berkel‡

Division of Biopharmaceutics, Leiden/Amsterdam Center for Drug Research, Leiden University, P.O. Box 9503, 2300 RA Leiden, The Netherlands, Department of Organic Chemistry, Leiden University, P.O. Box 9502, 2300 RA Leiden, The Netherlands, and TNO-PG, Gaubius Laboratory, Leiden, The Netherlands.
Received August 22, 2001; Revised Manuscript Received November 23, 2001

In this study, we present the design and synthesis of an antisense peptide nucleic acid (asPNA) prodrug, which displays an improved biodistribution profile and an equally improved capacity to reduce the levels of target mRNA. The prodrug, $K(GalNAc)_2$-asPNA, comprised of a 14-mer sequence complementary to the human microsomal triglyceride transfer protein (huMTP) gene, conjugated to a high-affinity tag for the hepatic asialoglycoprotein receptor ($K(GalNAc)_2$). The prodrug was avidly bound and rapidly internalized by HepG2s. After iv injection into mice, $K(GalNAc)_2$-asPNA accumulated in the parenchymal liver cells to a much greater extent than nonconjugated PNA (46% ± 1% vs 3.1% ± 0.5% of the injected dose, respectively). The prodrug was able to reduce MTP mRNA levels in HepG2 cells by 35−40% ($P < 0.02$) at 100 nM in an asialoglycoprotein receptor- and sequence-dependent fashion. In conclusion, hepatocyte-targeted PNA prodrugs combine a greatly improved tropism with an enhanced local intracellular availability and activity, making them attractive therapeutics to lower the expression level of hepatic target genes such as MTP.

INTRODUCTION

Peptide nucleic acids (PNAs)[1] are oligonucleotide analogues in which the entire deoxyribose phosphate has been replaced with an *N*-(2-aminoethyl)glycine pseudopeptide backbone. Unlike conventional phosphorothioate antisense drugs that act by inducing RNase-H-mediated degradation of the target mRNA, PNAs inhibit gene expression by steric hindrance of enzyme/proteins responsible for DNA transcription, RNA splicing, and translation (*1*, *2*). Because of their electrical neutrality, chemo-enzymatic stability (*3*), and avidity of target-strand hybridization (*4*), PNAs hold great promise as antisense or antigene drugs (*1*, *2*). In addition, PNA hybridization is less tolerant toward mismatches, which makes PNAs more specific than conventional antisense drugs (*5*).

Widespread use of PNA-based therapy is, however, still hampered by the fact that PNAs display an even lower tendency to enter cells than phosphodiester or phosphorothioate oligodeoxynucleotides (ODNs) (*6*, *7*). Accordingly, therapeutic PNA activity has been demonstrated in cell free translation/transcription systems (*8*, *9*), in permeable *Escherichia coli* (*9*), and after microinjection into individual cells (*7*, *10*). In a recent study, Faruqui et al. (*11*) described that PNA uptake into fibroblasts could be considerably enhanced by streptolysin-O-mediated permeabilization. Improved delivery to Bowes cells was also observed after the coupling of PNA to intracellular translocation peptides (*12*). In vivo, however, the latter strategy requires the use of invasive local administration protocols. A strategy that exploits the potential of receptor-mediated endocytosis to improve cellular uptake of PNAs will probably be more feasible (*13*−*15*). Illustratively, Basu and Wickstrom demonstrated that the uptake of IGF1 receptor ligand-conjugated PNA by Jurkat cells is 5-fold higher, despite the moderate affinity of the tag (*13*). Successful in vivo delivery of PNAs to the brain could be realized by conjugation to transferrin receptor or OX26-specific antibodies (*14*, *15*). However, the extent of intracerebral penetration of PNA was still modest, and it remains to be established whether the recycling transferrin receptor leans itself for cellular accumulation of PNA drugs.

This study is aimed at devising a PNA-based therapy to down-regulate the expression of the human microso-

† This study was supported by grants from The Dutch Heart Foundation (M93.001) and from The Society of Technological Sciences (349-477).

* Corresponding author. Phone: (31)-71-527-6040. Fax: (31)-71−527−6032. E-mail: biessen@LACDR.LeidenUniv.nl.

‡ Division of Biopharmaceutics, Leiden/Amsterdam Center for Drug Research, Leiden University.

§ Department of Organic Chemistry, Leiden University.

|| Gaubius Laboratory, Leiden, The Netherlands.

[1] Abbreviations: (as)PNA, (antisense) peptide nucleic acid; ODN, oligodeoxynucleotide; (hu)MTP, (human) microsomal triglyceride transfer protein; GalNAc, *N*-acetyl-*β*-D-deoxygalactosamine; huGAPDH, human glyceraldehyde-3-phosphate dehydrogenase; BSA, bovine serum albumin; ASOR, asialoorosomucoid; DCC, *N*,*N*′-dicyclohexylcarbodiimide; DiPEA, *N*,*N*-diisopropylethylamine; BOP, benzotriazol-1-yl-oxy-tris(dimethylamino)phosphoniumhexafluorophosphate; DCM, dichloromethane; TFA, trifluoroacetic acid; DMAP, 4-(dimethylamino)pyridine; HOBT, *N*-hydroxybenzotriazole; DMF, *N*,*N*-dimethylformamide; HMBA, 4-hydroxymethylbenzoic acid; HATU, (1*H*-9-azabenzotriazole-1-yl)-1,1,3,3-tetramethyluroniumhexafluorophosphate; SDS−PAGE, sodium dodecyl sulfate−polyacrylamide gel electrophoresis; DMEM, Dulbeco's modified essential medium.

10.1021/bc015550g CCC: $22.00 © 2002 American Chemical Society
Published on Web 03/05/2002

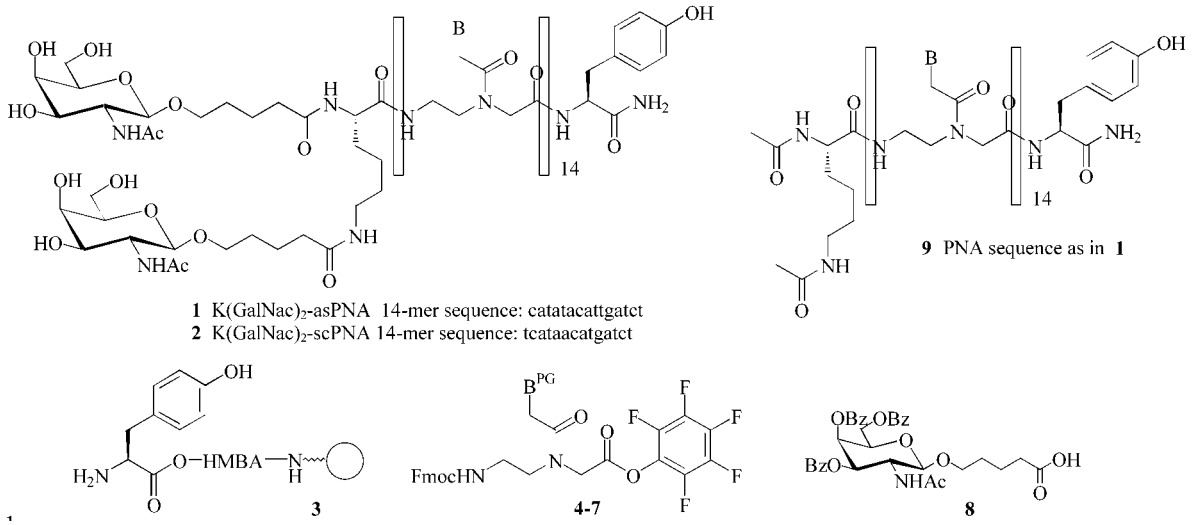


Figure 1. Chemical structures of building blocks **3**−**8** and lead compounds **1**, **2**, and **9**.

mal triglyceride transfer protein (huMTP) (*16*). HuMTP is a rate-limiting key enzyme in the assembly of atherogenic apolipoprotein B100-containing lipoproteins by parenchymal liver cells (*17*, *18*). This makes huMTP an excellent target for therapeutic intervention in patients that suffer from elevated plasma apoB100 levels. We now show in vitro and in vivo that parenchymal liver cell uptake of antisense PNAs can be considerably improved through targeting to the asialoglycoprotein receptor using a high-affinity tag for this receptor. In addition, the efficient target tissue uptake of antisense PNAs was found to be accompanied by a significantly enhanced ability of the PNA to inhibit MTP mRNA levels.

EXPERIMENTAL PROCEDURES

Materials. Tris-saturated biophenol (pH 8) was purchased from Biosolve Ltd., Valkenswaard, The Netherlands. Ribogreen was from Molecular Probes, Eugene, OR. Superscript II reverse transcriptase and RNaseH were obtained from Life Technologies, Frederick, MD. Oligonucleotides and Goldstar DNA polymerase were from Eurogentec, Seraing, Belgium. All other chemicals were of analytical grade. Human orosomucoid was isolated, subsequently desialylated enzymatically, and radioiodinated to yield [^{125}I]-asialoorosomucoid (ASOR), as previously described (*19*). All solvents were of analytical grade. Dry solvents were stored over molecular sieves 4 Å. Merck Kieselgel 60 F_{254} plates were used for TLC analysis. Compounds were visualized by charring with sulfuric acid/ethanol (1/4, v/v) or by dipping in a potassium hydroxide/ethanol/H_2O (v/v/v) solution followed by charring with a 0.3% solution of ninhydrine in acetic acid/*n*-butanol (3/100, v/v). Column chromatography was performed with Kieselgel 60, 230−400 mesh (Merck, Whitehouse Station, NJ). ^{1}H NMR spectra (300 MHz) were recorded with a Bruker WM-300 spectrometer. PEG-PS resin was purchased from Perkin-Elmer (Shelton, CT). Solid-phase synthesis was performed on an ABI 433 synthesizer. Products were analyzed with a Jasco HPLC system using a LiChrospher 100 RP-18 column (Merck; 5 μm, 4.6 × 250 mm). Electrospray mass-spectra were recorded with a Perkin-Elmer SCIEX API 165 single quadrupole LC/MS instrument. Matrix-assisted laser desorption ionization time-of-flight (MALDI-TOF) mass spectrometry was performed on a Perkin-Elmer/PerSeptive Biosystems Voyager-DE-RP MALDI-TOF mass spectrometer.

Synthesis. *Resin 3.* Resin **3** was prepared manually by shaking amino-PEG-PS resin (2.5 g, 38.4 μmol/g) overnight with a solution of 4-hydroxymethylbenzoic acid (HMBA; 150 mg, 10 eq), *N*,*N*′-dicyclohexylcarbodiimide (DCC), and 4-(dimethylamino)pyridine (DMAP) in *N*,*N*-dimethylformamide (DMF)/dichloromethane (1/1, v/v). The resin was washed three times with DMF, three times with methanol, and finally with ether before drying over P_2O_5. Subsequently, FmocTyr(O*t*Bu)-OH (129 mg, 10 eq) and benzotriazol-1-yl-oxy-tris(dimethylamino)phosphoniumhexafluorophosphate (BOP; 520 mg, 10 eq) were added to a suspension of the resin in DMF/dichloroethane (1/1, v/v). The mixture was shaken for 3 h. Capping was performed with benzoic anhydride (200 mg), after which a small resin sample (15 mg) was taken to determine the loading (33 μmol/g). Finally, the resin was treated with piperidine (10 mL, 20% in DMF) and trifluoroacetic acid (TFA) (10 mL, 95% in H_2O) to deprotect the tyrosine residue. A 14-mer PNA sequence was assembled on resin **3** (30 mg, 1 μmol) using the previously prepared (*20*, *21*) building blocks **4**−**7** in the presence of *N*,*N*-diisopropyl ethylamine (DiPEA) in *N*-methylpyrrolidone. The coupling procedure took approximately 1 h per building block.

*Target Compound (**1**, **2**, and **9**).* For the subsequent preparation of the PNA glycoconjugates (*1*, *2*) and acetylated control PNA (**9**), galactosamine derivative **8** was synthesized starting from galactosamine (Senn chemicals, Dielsdorf, Switzerland), as previously described (*22*). Resin **10** was treated with 25 eq of FmocLys(Fmoc)-OH (15 mg) and 2-(1*H*-9-azabenzotriazole-1-yl)-1,1,3,3-tetramethyluroniumhexafluorophosphate (HATU; 10 mg) using standard solid-phase coupling procedures (30 min), followed by deprotection with piperidine and manual addition of 60 mg of **8** (2 × 25 μmol per free amine), BOP (44 mg, 100 μmol), and DiPEA (100 μmol). The thus obtained resin **12** was washed and suspended in a saturated solution of ammonia in methanol at 55 °C, which resulted in liberation of compound **1** from the resin as well as deprotection of the sugar and PNA residues. The product was purified by reversed-phase HPLC using a 0.1% TFA/H_2O/acetonitrile gradient (5−50%) and eluted at 22% acetonitrile, as was established by LC/MS. After purification, compound **1** was characterized by MALDI-TOF. The scrambled PNA-conjugate **2** (for chemical structure see Figure 1) was prepared analogously, and for acetylated PNA (*9*), resin **11** was treated with piperi-

dine and capped with acetic acid anhydride after the coupling of **10** with 25 eq of FmocLys(Fmoc)-OH (15 mg) and HATU (10 mg). Both compounds were purified by reversed-phase HPLC as described for compound **1** and characterized. (Analysis for (**1** and **2**): LC/MS, found 1557 $(M + 3H)^{3+}$; MALDI-TOF, found 4668 $(M + H)^{+}$. Analysis for (**9**): LC/MS, found 1338 $(M + 3H)^{3+}$; MALDI-TOF, found 2073 $(M + 2H)^{2+}$.)

Animals. All animal work was approved by the regulatory authority of Leiden University and carried out in compliance with the guidelines issued by the Dutch government. C57Bl/6 mice were acquired from Charles Rivers (Someren, The Netherlands). The mice were male and 10−12 weeks old at the time of the study. Regular chow diet (Hope Farms, Woerden, The Netherlands) and water were provided ad libitum.

Radioiodination of PNA (Glycoconjugates). $K(GalNAc)_2$-asPNA and asPNA were radiolabeled at the C-terminal tyrosinamide, as previously described (*14*). In short, PNA (1.5 μg, 0.37 nmol), sodium [^{125}I]iodide (0.1 mCi, in 0.1 M NaOH) and chloramine T (2.8 μg) were mixed at a total volume of 40 μL of a phosphate buffer (pH = 7.4). After incubation for 1 min at ambient temperature, the reaction was quenched by adding sodium metabisulfite (11.7 μg), sodium iodide (10 μmol), and TFA (1%, v/v), and the solution was passed over a C18 Sep-Pak extraction cartridge (Waters Corp., Milford, MA). After the column was washed with 0.1% TFA/H_2O (4 mL) and 10% acetonitrile/0.1% TFA/H_2O (4 mL), the radioiodinated product was eluted by washing with 40% acetonitrile/0.1% TFA/H_2O (4 mL). The solvent was removed by lyophilization. The product was checked for purity on 20% SDS−PAGE. PNA associated radioactivity was more than 95%. The specific activity ranged from 1000 to 1200 dpm/ng.

In Vitro Binding and Uptake of K(GalNAc)$_2$-[^{125}I]-asPNA to HepG2 Cells. For uptake studies of $K(GalNAc)_2$-[^{125}I]asPNA, HepG2 cells (grown to confluency in 12-well tissue culture plates) were incubated for 15 min at 37 °C in Dulbecco's modified essential medium (DMEM) + 2% BSA with $K(GalNAc)_2$-[^{125}I]asPNA (0−100 nM), put on ice, washed twice with ice-cold DMEM + 2% (w/v) BSA, and incubated for 10 min at 4 °C with DMEM + 2% (w/v) BSA + EGTA (5 mM) to remove membrane-associated $K(GalNAc)_2$-[^{125}I]asPNA. Subsequently, cells were washed 3 times with Tris-buffered saline (50 mM Tris, 120 mM NaCl (pH 7.4); TBS) + 0.2% (w/v) BSA and once with TBS, and the cell-associated radioactivity was counted and corrected for protein content. Nonspecific uptake was determined in the presence of 100 mM of *N*-acetylgalactosamine. The viability of the cells was not significantly affected by the incubation protocol.

In Vivo Serum Clearance and Liver Association. C57Bl/6 mice were anaesthetised by subcutaneous injection of a cocktail containing ketamine·HCl, fentanyl citrate, droperidol, and fluanisone (75, 0.04, 1.1, and 0.75 mg/kg, respectively). [^{125}I]asPNA or $K(GalNAc)_2$-[^{125}I]asPNA (0.2 μg in 200 μL PBS) was injected into the inferior vena cava, and at the indicated times, the radioactivities in serum and liver were determined as described before (*23*). To assess the involvement of asialoglycoprotein receptors in liver uptake, we have monitored the liver uptake of $K(GalNAc)_2$-[^{125}I]asPNA injected into the vena cava at 1 min after intravenous injection of asialofetuin (15 mg/kg body weight).

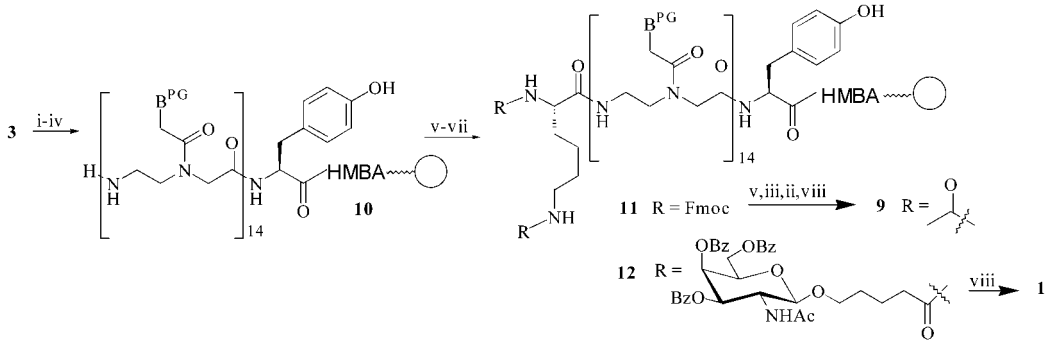
Contribution of Liver Cell Types to Hepatic Uptake. C57Bl/6 mice were anaesthetised by subcutaneous injection of a cocktail containing ketamine·HCl, fentanyl citrate, droperidol, and fluanisone (75, 0.04, 1.1, and 0.75 mg/kg, respectively) and subsequently injected with [^{125}I]asPNA or $K(GalNAc)_2$-[^{125}I]asPNA (0.2 μg in 200 μL PBS) as previously described. Ten minutes after injection, the portal vein was cannulated, and the liver was perfused at 4 °C with collagenase (0.01%, w/v) and parenchymal; Kupffer and endothelial liver cells were isolated by differential centrifugation and centrifugal elutriation, as previously described (*23*).

Quantitative Radioactive RT-PCR of Human MTP. The relative abundance of human MTP mRNA was monitored through quantitative RT-PCR with human glyceraldehyde-3-phosphate dehydrogenase (huGAPDH) as an internal standard. Total RNA was isolated from HepG2 cells by lysis in GTC buffer (4 M guanidinium isothiocyanate; 25 mM sodium citrate buffer (pH 7.0); 0.5% *N*-lauroyl sarcosine; and 0.1 M β-mercaptoethanol) according to Chomczynski and Sacchi (*24*). After phenol-chloroform extraction, the total RNA was precipitated by adding 2.5 volumes of ice-cold ethanol, and the pellet was washed twice with 70% ethanol and dissolved in 20 μL of a Tris/EDTA buffer (10 mM Tris-HCl, 1 mM EDTA (pH 8.0)). The RNA concentration in the samples was determined with the RNA-specific fluorescent dye Ribogreen according to the procedure of Jones et al. and using yeast tRNA as calibration standard (yield: 6−18 μg/6 × 10^5 HepG2 cells) (*25*). Total RNA (2 μg) was reverse-transcribed using 100 units of superscript II reverse transcriptase (Life Technologies, Gaithersburg, MD). To minimize reverse transcription reaction variability, all RNA samples were reverse-transcribed simultaneously with a reverse transcription "master mix". cDNAs were amplified for 22 cycles at 54 °C in the presence of [^{32}P]-α-dCTP (0.8 μCi) and Taq polymerase (0.4 units; Eurogentec, Brussels, Belgium) using huMTP primers (forward, 5′-GAA·TCC·TGA·TGG·TGA·TGA·TG; reversed, 5′-GTC·TTG·ATG·AGC·CTG·GTA·GG; 100 ng). Unless otherwise stated, huGAPDH primers (forward, 5′-GGT·GAA·GGT·CGG·AGT·CAA; reversed, 5′-GAG·GGA·TCT·CGC·TCC·TGG; 100 ng) were added after cycle 4. Amplicon formation was monitored through autoradiography using the phosphor-imager as described before (*33*). Formation of huMTP amplicons in the presence or absence of huGAPDH primers was identical. Intra-experimental variation in the huMTP-to-huGAPDH amplicon ratio amounted to 13% and 18%, starting from a single batch of cDNA and mRNA, respectively ($n = 5$).

Effect of (Glycoconjugated) PNA on the huMTP mRNA Level. The PNA effect studies were carried out as follows. Cell cultures of HepG2s were grown to 60−70% confluency in DMEM/Eagles minimal essential medium (1/4, v/v) supplemented with fetal calf serum (10%, v/v), glucose (3.5 mg/mL), nonessential amino acids (20 μM), and biotin (0.2 μg/mL) in a 12-well tissue culture plate. Two days before the experiment, sodium butyrate (2 mM) was added to the medium. Cells were incubated for 6 h at 37 °C in the absence or the presence of asPNA, $K(GalNAc)_2$-asPNA, or $K(GalNAc)_2$-scPNA (100 nM). To establish the involvement of the asialoglycoprotein receptor in PNA uptake, HepG2 cells were also incubated with the PNA (glycoconjugates) in the presence of 10 mM *N*-acetylgalactosamine. After incubation, medium was removed, 0.5 mL medium was added, and the cultures were incubated for 24 h at 37 °C. Cells were lysed in 0.5 mL GTC, after which the total RNAs were isolated and the huMTP-to-huGAPDH amplicon ratio was determined by quantitative radioactive RT-PCR as previously described.

Data Processing. Saturation binding data and substrate curves of initial uptake were analyzed according to a single-site binding model using nonlinear regression

Scheme 1. Assembly of Compound 1 on Solid Support



Reagents: (i) PNA building blocks **4**−**7**, DiPEA; (ii) capping (Ac_2O/HOBt/DiPEA); (iii) piperidine; (iv) repeat (i)−(iii); (v) FmocLys(Fmoc)-OH/HATU/DiPEA; (vi) piperidine; (vii) **8**, BOP/HOBt/DiPEA; (viii) NH_3, MeOH.

(Prism, GraphPAD Software, Inc., San Diego, CA). Displacement studies were analyzed according to a single-site competitive displacement model using nonlinear regression (*19*). Values are expressed as means ± SE. Data variance was analyzed statistically by means of one-way ANOVA with Dunnet's post-testing.

RESULTS

The synthesis on solid support of PNA-glycoconjugate **1** by a Fmoc/benzoyl strategy starts with the preparation of tyrosine-functionalized resin **3**, PNA monomers **4**−**7**, and readily accessible building block **8** (Figure 1). First, commercially available polystyrene resin was equipped with FmocTyr(O*t*Bu)-OH via a hydroxymethylbenzoic acid linker, followed by piperidine and TFA deprotection to give **3** (loading: 33 μmol/g). Then, the active esters of the respective PNA monomers **4**−**7** were prepared from the previously described Fmoc-protected backbone (*20*) and known Bz/*i*Bu-protected base acetic acids (*21*) in 72−80% yield. Finally, galactosamine was extended with a carboxylic acid spacer, as previously described, to afford compound **8** (*22*).

With all of the building blocks in hand, the antisense PNA sequence (asPNA; 5′-CAT·ATA·CAT·TGA·TCT-3′) was assembled on resin **3** (33 mg, 1 μmol) by repetitive coupling cycles using the building blocks **4**−**7** in the presence of DiPEA to give **10** (Scheme 1). Next, immobilized PNA fragment **10** was treated with FmocLys-(Fmoc)-OH in the presence of HATU/DiPEA. Subsequent deprotection of the lysine residue with piperidine allowed for the simultaneous introduction of both galactosamine moieties **8** mediated by BOP, *N*-hydroxybenzotriazole (HOBt), and DiPEA. Treatment of the obtained resin **12** with a saturated solution of ammonia in methanol resulted in cleavage of compound **1** (K(GalNAc)$_2$-asPNA) from the resin and concomitant removal of the nucleobase and sugar protecting groups. The conjugate was then purified by reversed-phase HPLC and characterized by LCMS and MALDI-TOF analysis. Analogously, the 14-mer *scrambled* PNA was conjugated to the divalent galactosamine cluster (**2**, K(GalNAc)$_2$-scPNA; Figure 1). For the synthesis of nonconjugated asPNA (9), resin **11** was treated with piperidine, capped, and subsequently cleaved from the resin, as previously described.

Target-Strand Hybridization. To verify whether the presence of the bulky K(GalNAc)$_2$ group interferes with the hybridization of PNA to the complementary target strand, thermal denaturation studies were performed for duplexes of asPNA or K(GalNAc)$_2$-asPNA and complementary DNA. The two melting curves largely concurred, yielding T_m values of 57.5 and 62.6 °C, respectively.

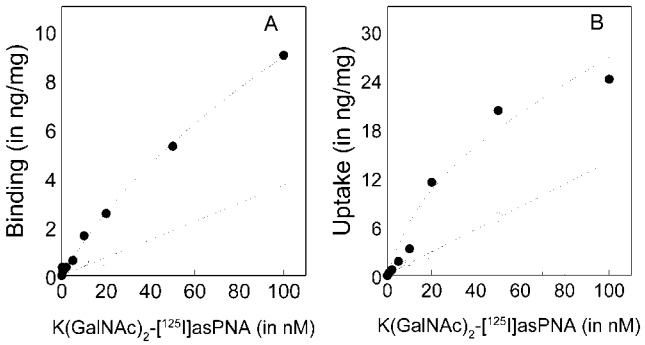


Figure 2. In vitro studies of K(GalNAc)$_2$-[^{125}I]asPNA binding and uptake by HepG2 cells. (A) HepG2s (1−2 × 10^6 cells) were incubated for 2 h at 4 °C in DMEM + 2% (w/v) BSA with 0−100 nM of K(GalNAc)$_2$-[^{125}I]asPNA in the absence (●) or presence (○) of 100 mM *N*-acetylgalactosamine. After incubation, cells were washed thoroughly, and cell binding was determined and corrected for cellular protein content. Total and nonspecific binding is given as mean of a duplicate experiment. (B) HepG2s (1−2 × 10^6 cells) were incubated for 1 h at 37 °C in DMEM + 2% (w/v) BSA with 0−100 nM of K(GalNAc)$_2$-[^{125}I]asPNA in the absence (●) or presence (○) of 100 mM *N*-acetylgalactosamine. After incubation, cells were put on ice and washed thoroughly, and membrane-bound radioactivity was removed by incubation for 5 min with 5 mM EGTA at 4 °C. Cell-associated radioactivity was counted and corrected for cellular protein content.

Apparently, the presence of the K(GalNAc)$_2$ group only slightly impairs PNA hybridization to the target strand.

In Vitro Studies. In vitro binding studies were performed to establish the effect of glycoconjugation on cellular uptake of PNA by HepG2s (Figure 2A). K(GalNAc)$_2$-[^{125}I]asPNA bound to HepG2s in a saturable fashion (B_{max} = 8.5 ng/mg) and with high affinity (K_d = 77 nM). The affinity of the glycoconjugate was only slightly lower than that of the K(GalNAc)$_2$ tag and that of PMEA-K(GalNAc)$_2$ (24 and 46 nM, respectively; *22*, *26*). Equilibrium binding of K(GalNAc)$_2$-[^{125}I]asPNA at 37 °C was rapidly achieved (within 10 min of incubation) (data not shown). Once bound, K(GalNAc)$_2$-[^{125}I]asPNA was efficiently internalized by HepG2 cells at a K_m of 25 nM (Figure 2B). The turn-over-rate of K(GalNAc)$_2$-[^{125}I]asPNA internalization by HepG2 cells as estimated from the B_{max} and V_{max} was approximately 20 min, suggesting that uptake of the glycoconjugate is an efficient process.

In Vivo Fate. Evidently, glycoconjugation has a stimulatory effect on the PNA uptake by HepG2 cells in vitro. A major issue to be addressed is whether the targeting capacity of the K(GalNAc)$_2$ tag is sufficiently high to overcome premature elimination of the PNA by renal clearance or competing uptake routes. Thus, we have compared the tissue distribution profile of the control, [^{125}I]asPNA, after intravenous injection into mice with

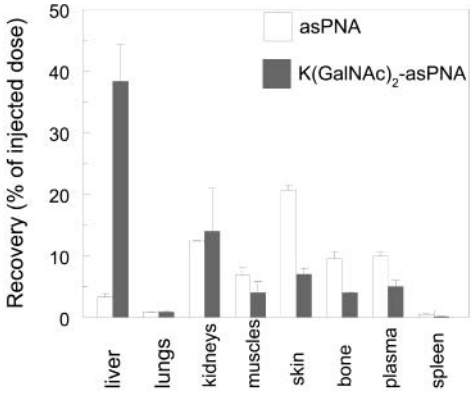


Figure 3. Tissue distribution of PNA (glycoconjugate). [^{125}I]-asPNA (open bars) or K(GalNAc)$_2$-[^{125}I]asPNA (closed bars) (1 μg dissolved in 100 μL PBS) were intravenously injected into mice. After 30 min, mice were sacrificed, and the indicated tissues were analyzed for radioactivity. Tissue recovery was corrected for the radioactivity from entrapped plasma. The recovery of radioactivity in the organs was >80%. Values are means (±SD) of a determination of three experiments.

that of K(GalNAc)$_2$-[^{125}I]asPNA. Preliminary experiments showed that the PNA (glycoconjugates) tended to form aggregates, which accumulated in lung tissue rather than liver (only 20% ± 4% of the injected dose). To avoid aggregate formation, radiolabeled PNA (glycoconjugates) were routinely incubated for 5 min at 96 °C in 50% formamide and subsequently lyophilised before use in further experiments. [^{125}I]asPNA and K(GalNAc)$_2$-[^{125}I]asPNA were equally rapidly cleared from the bloodstream, with a plasma half-life of 0.49 ± 0.08 min and 0.38 ± 0.04 min, respectively. By contrast, the tissue distribution profiles of [^{125}I]asPNA and K(GalNAc)$_2$-[^{125}I]asPNA differed considerably (Figure 3). [^{125}I]asPNA was recovered mainly in skin (20.7% ± 0.7%), kidney (12.4% ± 0.1%), bone (9.5% ± 1.2%), and plasma (10.0% ± 0.6%), whereas the liver appeared to be the major recovery site of K(GalNAc)$_2$-[^{125}I]asPNA (38% ± 6% at 30 min after injection). The accumulation of K(GalNAc)$_2$-[^{125}I]asPNA in skin, plasma, and bone was 2−3-fold lower than that of [^{125}I]asPNA. Hepatic uptake of K(GalNAc)$_2$-[^{125}I]asPNA peaked at 10 min after administration (49% ± 3% as compared to only 4.1% ± 0.3% for control PNA; $P < 0.001$) (Figure 4A). After preinjection of asialofetuin (15 mg/kg) to prevent asialoglycoprotein receptor-mediated uptake, the liver uptake of K(GalNAc)$_2$-[^{125}I]asPNA was significantly reduced to 18.6% ± 4.1% of the injected dose ($P < 0.001$). Of relevance, 97% ± 2% of the liver uptake of K(GalNAc)$_2$-[^{125}I]asPNA could be recovered in the parenchymal liver cells. This implies that 45.8% ± 0.9% of the total injected K(GalNAc)$_2$-[^{125}I]-asPNA reaches the aimed target, as compared to only 3.1% for non-conjugated [^{125}I]-asPNA (Figure 4B). Taken together, the aforementioned data indicate that the 15-fold stimulated hepatic uptake of the glycoconjugated PNA can be attributed almost exclusively to the asialoglycoprotein receptor.

Antisense Effect of Targeted PNAs. From the aforesaid studies, it is apparent that glycoconjugation stimulates the uptake of PNA by the aimed target both in vitro and in vivo. The next issue to be addressed is whether the stimulated cellular uptake is accompanied by an enhanced inhibitory activity of the asPNA. A quantitative radioactive RT-PCR-based assay was set up to measure huMTP mRNA levels. cDNA was amplified for various cycle numbers in the presence of [^{32}P]-α-dCTP and using huMTP and huGAPDH specific primer sets to determine

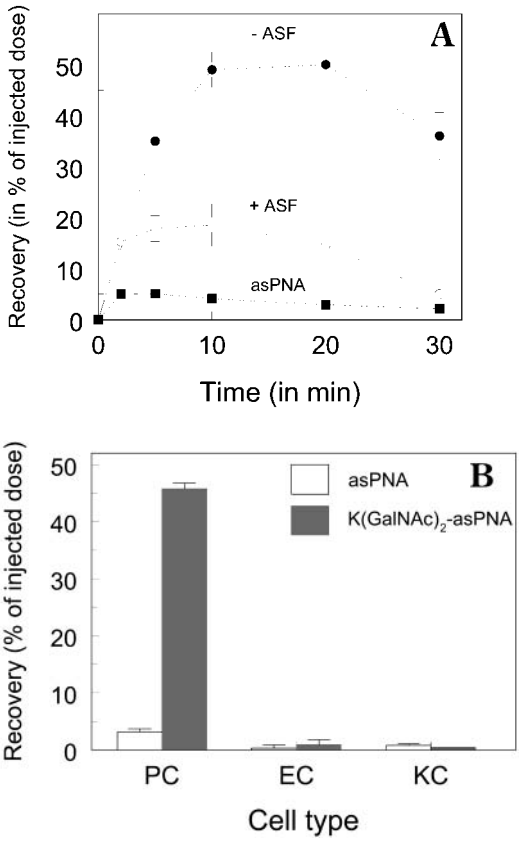


Figure 4. (A) Effect of asialofetuin treatment on the kinetics of liver uptake of PNA (glycoconjugate). [^{125}I]asPNA (1 μg, in 100 μl PBS) (■) or K(GalNAc)$_2$-[^{125}I]asPNA (1 μg in 100 μL PBS) (●, ○) was injected into mice that were injected at 1 min prior to administration of the radiolabel with PBS (100 μl; ●, ■) or PBS containing asialofetuin (15 mg/kg; 100 μl; ○). At the indicated times, radioactivities in the liver were determined. Values are means ± SD of three experiments. (B) Contribution of the various liver cell types to hepatic uptake of PNA (glycoconjugates). [^{125}I]asPNA (open bars) or K(GalNAc)$_2$-[^{125}I]-asPNA (closed bars) was intravenously injected into mice. At 10 min after injection, the liver was excised, and the various liver cell types were isolated by differential centrifugation and centrifugal elutriation. The recovery of radioactivity in the purified cell fractions was determined and corrected for protein content. From the specific recovery, the total contribution of the liver cell types could be calculated assuming the PC, EC, and KC to contribute 92.5%, 2.5%, and 3.1% to the total hepatic cell protein, respectively. Values are means ± SD of three experiments.

the optimal number of cycles (cycle titration). Under optimal conditions (annealing temperature and primer concentration), the logarithmic phase of the PCR amplification ranged from 12 to 21 cycles for huGAPDH and from 15 to 24 cycles for huMTP (Figure 5). For both genes, amplification efficiencies were >90%, both in the absence and presence of a second primer set (correlation coefficients >0.996). Starting from a single batch of cDNA and mRNA, assay variability amounted to 13% and 18% ($n = 5$), respectively, which is sufficiently low to allow for the detection of minor changes in the huMTP-to-huGAPDH mRNA ratio.

Next, we have assessed the effect of the PNA drugs on huMTP mRNA levels in vitro in HepG2 cells. HepG2 cells were incubated for 6 h at 37 °C with 100 nM of asPNA, K(GalNAc)$_2$-asPNA, or scrambled K(GalNAc)$_2$-scPNA and at 24 h after incubation assayed for huMTP and huGAPDH mRNA content. From Figure 6 it can be appreciated that the huMTP-to-huGAPDH amplicon

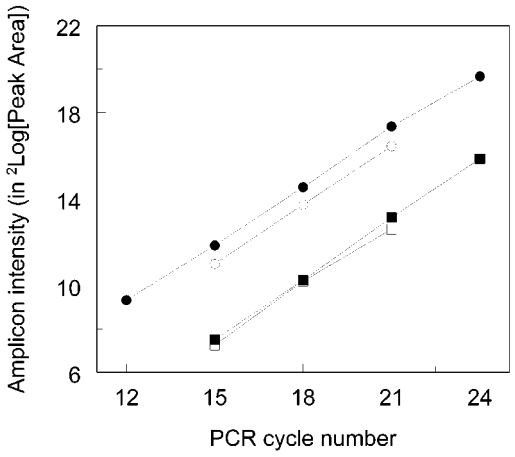


Figure 5. Optimization of the quantitative RT-PCR assay. Total RNA was isolated from HepG2 cells, after which mRNA (2 μg) was reverse-transcribed, and the huMTP cDNA and huGADPH cDNA were amplified for 12−24 cycles in the presence of [^{32}P]-″CTP, as described in the Experimental Procedures section. The PCR products were subjected to gel electrophoresis on 10% polyacrylamide, and the intensity of the [^{32}P]-huMTP and [^{32}P]huGAPDH bands were determined by autoradiography using the Phosphor-Imager. The intensities of the huMTP (■, □) and huGAPDH bands (●, ○) are plotted versus the number of PCR cycles. The PCR reaction was performed in the presence of a single (○, □) or both primer sets for huMTP and huGAPDH (■, ●).

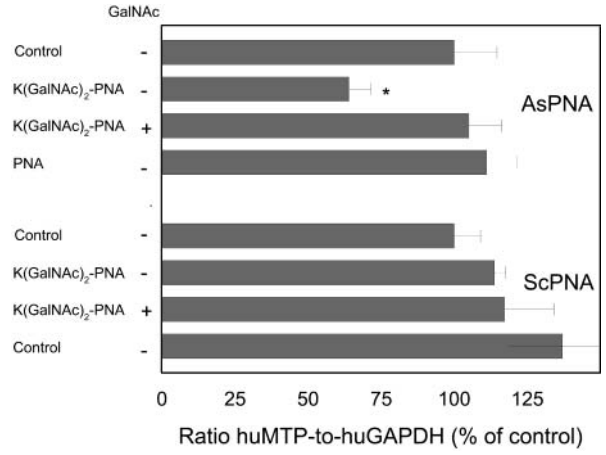


Figure 6. Effect of PNA (glycoconjugates) on MTP mRNA level by HepG2s. HepG2s, grown to 60−70% confluency, were incubated for 6 h at 37 °C without (control) or with PNA (glycoconjugates) (100 nM), washed, and incubated again for 24 h. After incubation, cells were lysed in GTC buffer, after which the total RNA was isolated. The huMTP to huGAPDH mRNA ratios were determined by quantitative radioactive RT-PCR using the Phosphor-Imager. To establish the involvement of the asialoglycoprotein receptor in the antisense effect, the above experiment was also performed in the presence of 10 mM *N*-acetylgalactosamine (GalNAc). Data are means ± SD of an experiment in hexaplo.

ratios were significantly reduced only after incubation with K(GalNAc)$_2$-asPNA (−36%, $P < 0.02$). Essentially similar results were obtained in an initial experiment (39% reduction in the huMTP-to-huGAPDH mRNA ratio after K(GalNAc)$_2$-asPNA treatment; not shown here). Ratios were unaffected after incubation of the HepG2s with nonconjugated asPNA or K(GalNAc)$_2$-scPNA. Importantly, the effect of K(GalNAc)$_2$-asPNA on huMTP-to-huGAPDH ratios was critically dependent on asialoglycoprotein receptor-mediated transport, as ratios were found to be unaffected after co-incubation with *N*-acetylgalactosamine.

DISCUSSION

Because of their electrical neutrality, chemo-enzymatic stability (*3*), and avidity of target-strand hybridization (*4*), PNAs hold great promise as antisense or antigene drugs (*1*, *2*). Nevertheless, they still have not redeemed their initial promise. Partly, this might be attributed to the unfavorable pharmacokinetics of PNAs in vivo (*14*, *15*, *27*) and the inability to enter cells in vitro (*6*, *7*). We (*26*, *29*) and others (*29*−*31*) have recently shown that the therapeutic profile of (oligo)nucleotides can be considerably improved by direct conjugation to a ligand for a receptor that is characteristic for the target tissue or by incorporation into tissue-specific drug carriers. In this study, we show that PNAs may equally benefit from hepatic delivery, as do conventional (oligo)nucleotide drugs. To this end, antisense PNA targeting the human MTP gene was conjugated to K(GalNAc)$_2$, a bivalent *N*-acetylgalactosamine-terminated scaffold with nanomolar affinity for the asialoglycoprotein receptor (*22*). From the thermal denaturation studies, we may conclude that conjugation of the asPNA sequence to K(GalNAc)$_2$ did not significantly affect target-strand hybridization, which is an absolute requisite for antisense drug activity.

The glycoconjugated asPNA was avidly bound to parenchymal liver cells and HepG2 cells at a similar affinity as reported earlier for K(GalNAc)$_2$ conjugated to an antiviral nucleoside (i.e., 46 nM (*26*)). The K(GalNAc)$_2$ tag conferred efficient uptake of PNA by human parenchymal liver as well as by hepatoma cells. A similar increase in PNA uptake by Jurkat cells was recently observed after conjugation to a D-peptide ligand for the IGF1 receptor (*13*).

In agreement with previous studies on the pharmacokinetics of PNAs (*14*, *15*, *27*), PNA displayed a fairly unspecific tissue distribution profile, with kidney, skin muscle, and bone being the major sites of accumulation. The PNA glycoconjugate, however, strongly accumulates in the liver at the dispense of skin, bone, serum, and muscle uptake. The hepatic uptake of the K(GalNAc)$_2$-asPNA could be prevented by prior injection of asialofetuin, indicating that the asialoglycoprotein receptor is responsible for the increased liver uptake. Given the stability of the PNA drug against proteases and nucleotidases (*3*), the observed decrease in liver associated K(GalNAc)$_2$-[^{125}I]asPNA after 20 min probably reflects proteolytic cleavage and subsequent deiodination of the C-terminal [^{125}I]tyrosinamide group rather than degradation of the antisense drug itself. In agreement, PAGE analysis of the liver extract for intact K(GalNAc)$_2$-[^{125}I]asPNA showed a half-life of 16 ± 4 min (data not shown). Intermediate PNA degradation products were not observed, which also points to proteolysis of the radiolabeled tyrosine moiety. Further study of the liver cell distribution profile showed that the parenchymal liver cell uptake increased almost 20-fold after glycoconjugation, which compares well with the targeting efficiencies that were obtained for ODN glycoconjugates (*28*) and for the K(GalNAc)$_2$ conjugate of an antiviral nucleoside (*26*). To date, successful PNA delivery to specific organs has only been reported by Pardridge et al. (*14*) and by Penichet et al. (*15*), showing a 15-fold enhanced brain accumulation of biotinylated anti-HIV asPNA after conjugation to an antibody against the transferrin receptor or Ox-26. However, it is not known whether the improved bioavailability of the PNA drug in the target cells resulted in a similarly enhanced therapeutic activity.

In this study, we demonstrate inhibition of huMTP expression in HepG2 cells after tagging of the asPNA

drug with a high-affinity ligand for the asialoglycoprotein receptor. The antisense PNA used in this study targeted the gene encoding huMTP (*16*), which catalyses a rate-limiting step in the assembly of proatherogenic apolipoprotein-B100-containing lipoproteins (*17*, *18*). Although, recently, a number of potent MTP inhibitors have been devised, these inhibitors also reduce intestinal MTP activity, which may be harmful. The antisense prodrugs, described in this study, may display a more favorable therapeutic profile, as their activity is more liver-specific and possibly, to a lesser extent, dictated by interindividual variations in pharmacodynamics. From secondary RNA structure analysis of the huMTP mRNA using the Zuker algorithm (Mfold, version 3.0), we have selected the nucleotide sequence 3133−3146 as a potential antisense prone site that is probably not involved in hairpin or pseudo-knot formation (*32*).

To enable the detection of minor changes in the relative huMTP level, a sensitive assay for quantification of huMTP mRNA levels in HepG2 cells was set up. Incubation of HepG2 cells with $K(GalNAc)_2$-asPNA led in two independent experiments to a significant reduction of huMTP mRNA levels of 35−40%. This reduction was not observed for scrambled PNA glycoconjugate, establishing the sequence-dependency of PNA induced inhibition of huMTP expression. The antisense effect was neither observed after blockage of the asialoglycoprotein receptor nor observed for the parental asPNA, implying that asialoglycoprotein receptor-mediated uptake is a sine-qua-non requisite for antisense activity of the tagged asPNA. It can be calculated that, under the assay conditions, approximately 15 ng $K(GalNAc)_2$-asPNA/mg cell protein will be taken up by HepG2 cells, corresponding with intracellular concentrations of 700 nM, which apparently is sufficient for antisense activity. Although the asPNA was targeting a sequence on the human MTP gene 3.1 kb downstream from the initiation codon, it was able to interdict transcription or post-transcriptional splicing in HepG2 cells. Homopyrimidine PNAs were reported to be capable of DNA double-strand invasion (*1*, *10*), but the mixed composition of the antisense PNA makes it rather unlikely that its inhibitory activity can be traced down either to duplex formation via Hoogsteen base-pairing or to triplex formation.

In conclusion, PNA glycoconjugates have been synthesized that avidly bind to, and are taken up by, HepG2 cells. The pharmacokinetics of the PNA glycoconjugates are superior to that of PNAs in that parenchymal liver cell uptake is increased by 20-fold, while PNA accumulation in skin, spleen, muscle, bone, and plasma was found to be 2−3-fold lower. The glycoconjugated antisense PNA interfered with the huMTP mRNA levels in HepG2 cells at concentrations as low as 100 nM in a sequence-dependent and receptor-mediated fashion. The aforesaid prodrug strategy for improved and cell-specific PNA delivery thus results in a considerably increased therapeutic activity of the antisense PNA drugs and may be valid also for PNAs directed against other target genes.

LITERATURE CITED

(1) Good, L., and Nielsen, P. E. (1997) Progress in developing PNA as a gene-targeted drug. *Antisense Nucleic Acid Drug Dev. 7*, 431−437.

(2) Ray, A., and Norden, B. (2000) Peptide nucleic acid (PNA): its medical and biotechnical applications and promise for the future. *FASEB J. 14*, 1041−1060.

(3) Demidov, V. V., Potaman, V. N., Frank-Kamenetskii, M. D., Egholm, M., Buchard, O., Sonnichsen, S. H., and Nielsen, P. E. (1994) Stability of peptide nucleic acids in human serum and cellular extracts. *Biochem. Pharmacol. 48*, 1310−1313.

(4) Egholm, M., Buchardt, O., Christensen, L., Behrens, C., Freier, S. M., Driver, D. A., Berg, R. H., Kim, S. K., Norden, B., and Nielsen, P. E. (1993) PNA hybridizes to complementary oligonucleotides obeying the Watson−Crick hydrogen-bonding rules. *Nature 365*, 566−568.

(5) Haaima, G., Lohse, A., Buchardt, O., and Nielsen, P. E. (1996) Peptide nucleic acids (PNAs) containing thymine monomers derived from chiral amino acids: hybridisation and solubility properties of D-lysine PNA. *Angew. Chem., Int. Ed. Engl. 35*, 1939−1942.

(6) Gray, G. D., Basu, S., and Wickstrom, E. (1997) Transformed and immortalized cellular uptake of oligodeoxynucleoside phosphorothioates, 3′-alkylamino oligodeoxynucleotides, 2′-*O*-methyloligoribonucleotides, oligodeoxynucleoside methylphosphonates, and peptide nucleic acids. *Biochem. Pharmacol. 53*, 1465−1476.

(7) Bonham, M. A., Brown, S., Boyd, A. L., Brown, P., II., Bruckenstein, D. A., Hanvey, J. C., Thomson, S. A., Pipe, A., Hassman, F., and Bisi, J. E. (1995) An assessment of the antisense properties of RNase H-competent and steric-blocking oligomers. *Nucleic Acid Res. 23*, 1197−1203.

(8) Nielsen, P. E., Egholm, M., and Buchardt, O. (1994) Sequence-specific transcription arrest by peptide nucleic acid bound to the DNA template strand. *Gene 149*, 139−145.

(9) Good, L., and Nielsen, P. E. (1998) Inhibition of translation and bacterial growth by peptide nucleic acid targeted to ribosomal RNA. *Proc. Natl. Acad. Sci. U.S.A. 95*, 2073−2076.

(10) Hanvey, J. C., Peffer, N. J., Bisi, J. E., Thomson, S. A., Cadilla, R., Josey, J. A., Ricca, D. J., Hassman, C. F., Bonham, M. A., Au, K. G., Carter, S. G., Bruckenstein, D. A., Boyd, A. L., Noble, S. A., and Babiss, L. E. (1992) Antisense and antigene properties of peptide nucleic acids. *Science 258*, 1481−1485.

(11) Faruqi, A. F., Egholm, M., and Glazer, P. M. (1998) Peptide nucleic acid-targeted mutagenesis of a chromosomal gene in mouse cells. *Proc. Natl. Acad. Sci. U.S.A. 95*, 1398−1403.

(12) Pooga, M., Soomets, U., Hallbrink, M., Valkna, A., Saar, K., Rezaei, K., Kahl, U., Hao, J. X., Xu, X. J., Wiesenfeld-Hallin, Z., Hokfelt, T., Bartfai, T., and Langel, U. (1998) Cell penetrating PNA constructs regulate galanin receptor levels and modify pain transmission in vivo. *Nat. Biotechnol. 16*, 857−861.

(13) Basu, S., and Wickstrom, E. (1997) Synthesis and characterization of a peptide nucleic acid conjugated to a D-peptide analogue of insulin-like growth factor 1 for increased cellular uptake *Bioconjugate Chem. 8*, 481−488.

(14) Pardridge, W. M., Boado, R. J., and Kang, Y. S. (1995) Vector-mediated delivery of a polyamide ("peptide") nucleic acid analogue through the blood-brain barrier in vivo. *Proc. Natl. Acad. Sci. U.S.A. 92*, 5592−5596.

(15) Penichet, M. L., Kang, Y. S., Pardridge, W. M., Morrison, S. L., and Shin, S. U. (1999) An antibody-avidin fusion protein specific for the transferrin receptor serves as a delivery vehicle for effective brain targeting: initial applications in anti-HIV antisense drug delivery to the brain. *J. Immunol. 163*, 4421−4426.

(16) Nakamuta, M., Chang, B. H., Hoogeveen, R., Li, W. H., and Chan, L. (1996) Mouse microsomal triglyceride transfer protein large subunit: cDNA cloning, tissue-specific expression, and chromosomal localization. *Genomics 33*, 313−316.

(17) Raabe, M., Veniant, M. M., Sullivan, M. A., Zlot, C. H., Bjorkegren, J., Nielsen, L. B., Wong, J. S., Hamilton, R. L., and Young, S. G. (1999) Analysis of the role of microsomal triglyceride transfer protein in the liver of tissue-specific knockout mice. *J. Clin. Invest. 103*, 1287−1298.

(18) Jamil, H., Chu, C. H., Dickson, J. K., Jr, Chen, Y., Yan, M., Biller, S. A., Gregg, R. E., Wetterau, J. R., and Gordon, D. A. (1998) Evidence that microsomal triglyceride transfer protein is limiting in the production of apolipoprotein B-containing lipoproteins in hepatic cells. *J. Lipid Res. 39*, 1448−1454.

(19) Biessen, E. A. L., Beuting, D. M., Vietsch, H., Bijsterbosch, M. K., and Van Berkel, T. J. C. (1994) Specific targeting of the antiviral drug 5-iodo-2′-deoxyuridine to the parenchymal liver cell using lactosylated poly-L-lysine. *J. Hepatol. 21*, 806−815.

(20) Thomson, S. A., Jossy, J. A., Cadilla, R., Gaul, M. D., Hassman, F., Luzzio, M. J., Pipe, A. J., Reed, K. L., Ricca, D. J., Wiethe, R. W., and Noble, S. A. (1995) *Tetrahedron 51*, 6179−6194.

(21) van der Laan, S. (1998) Design and Synthesis of Potential Antisense Probes, Thesis, Leiden University, Leiden, The Netherlands.

(22) Valentijn, A. R. P. M., Van der Marel, G. A., Sliedregt, L. A. J. M., Van Berkel, T. J. C., Biessen, E. A. L., and Van Boom, J. H. (1997) Solid-phase synthesis of lysine-based cluster galactosides with high affinity for the asialoglycoprotein receptor. *Tetrahedron 53*, 759−770.

(23) Nagelkerke, J. F., Barto, K. P., and Van Berkel, Th. J. C. (1983) In vivo and in vitro uptake and degradation of acetylated low-density lipoproteins by rat liver endothelial, Kupffer, and parenchymal cells. *J. Biol. Chem. 263*, 12221−12227.

(24) Chomczynski, P., and Sacchi, N. (1987) Single-step method of RNA isolation by acid guanidinium thiocyanate-phenol-chloroform extraction. *Anal. Biochem. 162*, 156−159.

(25) Jones, L. J., Yue, S. T., Cheung, C. Y., and Singer, V. L. (1998) RNA quantitation by fluorescence-based solution assay: RiboGreen reagent characterization. *Anal. Biochem. 265*, 368−374.

(26) Biessen, E. A. L., Valentijn, A. R. P. M., de Vrueh, R. L. A., Van de Bilt, E., Sliedregt, L. A. J. M., Prince, P., Bijsterbosch, M. K., Van Boom, J. H., Van de Marel, G. A., Abrahams, P. G., and Van Berkel, Th. J. C. (2000) New Hepatotrophic Prodrugs of the Antiviral Nucleoside 9-(2-Phosphonylmethoxyethyl)adenine with Improved Pharmacokinetics and Antiviral Activity. *FASEB J. 14*, 1784−1792.

(27) Hnatowich, D. J. (1997) Pharmacokinetics of 99mTc-labeled oligonucleotides. *Q. J. Nucl. Med. 41*, 91−100.

(28) Biessen, E. A. L., Vietsch, H., Rump, E. T., Fluiter, K., Kuiper, J., Bijsterbosch, M. K., and van Berkel, T. J. C. (1999) Targeted delivery of oligodeoxynucleotides to parenchymal liver cells in vivo. *Biochem. J. 340*, 783−792.

(29) Hangeland, J. J., Flesher, J. E., Deamond, S. F., Lee, Y. C., Ts'o, P. O. P., and Frost, J. J. (1997) Tissue distribution and metabolism of the [^{32}P]-labeled oligodeoxynucleoside methylphosphonate-neoglycopeptide conjugate, [YEE(ahGalNAc)$_3$]-SMCC-AET-pUmpT7, in the mouse. *Antisense Nucleic Acid Drug Dev. 7*, 141−149.

(30) Sugano, M., Makino, N., Sawada, S., Otsuka, S., Watanabe, M., Okamoto, H., Kamada, M., and Mizushima, A. (1998) Effect of antisense oligonucleotides against cholesteryl ester transfer protein on the development of atherosclerosis in cholesterol-fed rabbits. *J. Biol. Chem. 273*, 5033−5036.

(31) Lu, X. M., Fischman, A. J., Jyawook, S. L., Hendricks, K., Tompkins, R. G., and Yarmusch, M. L. (1994) Antisense DNA delivery in vivo: liver targeting by receptor-mediated uptake *J. Nucl. Med. 35*, 269−275.

(32) Mathews, D. H., Sabina, J., Zuker, M., and Turner, D. H. (1999) Expanded sequence dependence of thermodynamic parameters provides robust prediction of RNA secondary structure. *J. Mol. Biol. 288*, 911−940.

(33) 'T Hoen, P. A. Chr., Commandeur, J. N. M., Vermeulen, N. P. E., Van Berkel, Th. J. C., and Bijsterbosch, M. K. (2000) Selective induction of cytochrome P450 3A1 by dexamethasone in cultured rat hepatocytes *Biochem. Pharmacol. 60*, 1509−1518.

BC015550G

Preparation of a Conjugate of 2′,5′-Triadenylate 5′-Triphosphate and Biotinylated Firefly Luciferase and Its Use for Sensitive Bioluminescent Enzyme Immunoassay

Yoshiaki Seto,*[,†,‡] Katsushi Abe,[‡] Masao Itoh,[‡] and Hiroaki Sawai[†]

Department of Chemistry, Faculty of Engineering, Gunma University, 1-5-1 Tenjin-cho, Kiryu, Gunma, 376-8515, Japan and Biochemical Research Laboratory, Eiken Chemical Co., Ltd., 1381−3 Ohtawara, Tochigi, 324-0036, Japan. Received September 6, 2001; Revised Manuscript Received December 11, 2001

A bioluminescent enzyme immunoassay (BLEIA) for 2′,5′-oligoadenylate 5′-triphosphate (pppA2′-p5′A2′Ap5′A, 2-5A) was developed using a conjugate of 2-5A and firefly luciferase as a probe. The conjugate was prepared from a 2-5A derivative bearing a thiol group at the 2′(or 3′) end, and streptavidin (SA) bearing maleimide via a linker-arm and biotinylated luciferase. The thiol group of the 2-5A derivative was relatively stable under aerobic conditions and remained 100% and 56% intact at 25 °C after 1 and 96 h, respectively, without dimerization by aerobic oxidation. The thiol-modified 2-5A was coupled with the SA−maleimide conjugate, followed by complex formation with biotinylated firefly luciferase. BLEIA using this conjugate allowed for the direct analysis of 2-5A in a range of 5−500 fmol (0.1−10 nM in a 50 μL sample) and in a reaction time of 15 min. The measurement of microquantities of 2-5 A from various sources is easy to perform by this BLEIA, because no radioisotope labeled 2-5A was required as a probe.

INTRODUCTION

2′,5′-Oligoadenylate 5′-triphosphate (pppA2′p5′A2′p5′A), referred to as 2-5A, is synthesized from ATP by 2-5A synthetase, which is induced by interferon. The 2-5A binds and activates 2-5A−dependent RNase (RNase L), which degrades messenger and ribosomal RNA at a nanomolar concentration (*1*, *2*). This 2-5A system is implicated not only in interferon's antiviral action but also in cell growth regulation. Therefore, the measurement of nanomolar concentrations of 2-5A is useful for the study of the 2-5A system and for management of interferon therapy and diagnosis for viral diseases. Silvernan et al. and Hersh et al. reported radiobinding and radioimmuno assays for 2-5A using a ^{32}P-labeled 2-5A derivative which was synthesized enzymatically (*3*, *4*). Sawai et al. synthesized the 2-5A conjugate with β-alanyltyrosine and labeled the conjugate with ^{125}I for radioimmunoassay (RIA) (*5*). These methods require a radiolabeled 2-5A derivative as a probe. Recently, RIA methods have been replaced with nonradioisotope immunoassays using enzyme, fluorescence, or chemiluminescence. Nicolas et al. reported enzyme immunoassay for 2-5A using monoclonal antibody and peroxidase-2-5A conjugate, but this method required long reaction time for using a microtiter plate as the solid phase (*16*). Thus, we have explored nonradioisotope, sensitive, and rapid immunoassay to measure subnanomolar concentrations of 2-5A.

The bioluminescent enzyme, firefly luciferase, catalyses the oxidation of D-luciferin in the presence of adenosine 5′-triphosphate(ATP), Mg^{2+}, and molecular oxygen. The exited state oxyluciferin that is produced in the oxidation process generates light, forming a steady state oxyluciferin. This luminescence quantum yield is 0.88 and higher than any other bio- or chemiluminescence (*6*). For this high quantum yield, the firefly luciferase bioluminescent system has been applied to a genetic reporter in molecular biology and in ATP detection in microbiology (*7*, *8*). Tatsumi et al. developed a modified thermostable luciferase genetically and introduced D-biotin (*9*). The biotinylated luciferase can be used as a labeling enzyme for an antibody in an enzyme immunoassay (EIA). Ohkuma and Maeda et al. reported BLEIA for pepsinogen I and II using conjugates constructed from biotinylated luciferase, streptavidin (SA), and a biotinylated antibody (*10*). Recently we developed a BLEIA for thyroid stimulating hormone, in which the antibody was coupled with SA by a cross-linking agent and bound with biotinylated luciferase by a avidin−biotin complex (*11*). These BLEIA give highly sensitive analyses of the target molecules. Thus, we have studied the conjugation of 2-5A and luciferase for use in a BLEIA of 2-5A. For covalently linking 2-5A with SA, we derivatized 2-5A with cysteamine according to the method reported by Torrence et al. (*12*). Contrary to their report that the 2-5A−cysteamine conjugate was unstable because its free thiol group formed a disulfide linkage immediately by aerobic oxidation, we found that thiol-derivatized 2-5A is relatively stable and permitted the conjugation with SA by a bifunctional cross-linking agent bearing maleimide. The resulting 2-5A−SA conjugate was bound with biotinylated luciferase. This report describes the preparation and properties of the conjugates of 2-5A, and a BLEIA for 2-5A using the conjugate and a biotinylated luciferase as a probe.

MATERIALS AND METHODS

Materials. The 2′,5′-oligoadenylate-5′-triphosphate (2-5A) was prepared as described in a previous report (*13*).

* Corresponding author: Yoshiaki SetoAddress: Biochemical Research Laboratory, Eiken Chemical Co., Ltd., 1381-3 Ohtawara, Tochigi, 324-0036, Japan. Phone: 81-287-29-2003. Fax: 81-287-29-3456. E-mail: yoshiakiseto@eiken.co.jp.

† Department of Chemistry, Gunma University.

‡ Biochemical Research Laboratory, Eiken Chemical Co., Ltd.

10.1021/bc015554l CCC: $22.00 © 2002 American Chemical Society
Published on Web 02/21/2002

ATP and SA were purchased from Sigma (St. Louis, MO). *N*-(11-maleimidoundecanoyloxy)sulfosuccimide, sodium salt (Sulfo-KMUS), *N*-(2-acetamido)iminodiacetic acid (ADA), 2-[4-(2-hydroxyethyl)-1-piperazinyl]ethanesulfonic acid (HEPES), bis(2-hydroxyethyl)iminotris(hydroxymethyl)methane (Bis-Tris), and 1-ethyl-3-(3-dimethylaminopropyl)carbodiimide, hydrochloride (EDC or WSC) were obtained from Dojin (Kumamoto, Japan). Anti 2-5A polyclonal antibody was prepared as described previously (*14*). Anti rabbit IgG polyclonal antibody was from Shibayagi (Gunma, Japan). Block Ace was purchased from Dainippon Pharmaceutical (Osaka, Japan). Biotinylated thermostable recombinant firefly luciferase (bL248) was supplied by Kikkoman Corp. (Tokyo, Japan). D-Luciferin was purchased from Biosynth (Staad, Switzerland). Magnetic particle (Immtex MAG1803) was obtained from JSR (Tokyo, Japan).

HPLC. Analytical and fractional HPLC were carried out on a Wakosil DNA column (4.5 mm × 150 mm) using a linear gradient elution of 3−31% of solvent B. Solvent A was 50 mM triethylammonium acetate (TEAA) at pH 7.0 and solvent B was 70% acetonitrile in 50 mM TEAA (pH 7.0).

Preparation of Cystamine Derivative of pppA2′-p5′A2′p5′A (2−5A). To a 50 μL aqueous solution of 2-5A (9.0 ODU at 260 nm, 0.27 μmol) was added 3.8 μL of 0.1 M sodium metaperiodate in distilled water, and the solution was incubated for 25 min on an ice bath. To the reaction mixture, 2.5 μL of 0.1 M cystamine dihydrochloride in water was added and the pH immediately adjusted to 8.5 using 0.1 M NaOH and 1 M NaOH solution. After incubation for 15 min on an ice bath, 5.0 μL of 0.5 M sodium cyanoborohydride in water was added to the reaction mixture, and the pH was adjusted to 6.5 using 0.1 M HCl and 1 M HCl solution immediately. After incubation for 60 min on an ice bath, the product was checked and purified by reverse phase HPLC. Fractions containing 2-5A−cystamine were pooled and lyophilized. The yield was 37% (3.3 ODU at 260 nm, 0.1 μmol). ESI-MS: calculated $[M - H]^-$ *m/z* 1282.1 and $[M - 2H]^{2-}$ *m/z* 640.6, found 1282.2 and 640.6, respectively.

Reduction of 2-5A-Cystamine. To 100 μL of 2-5A−cystamine in distilled water (3.3 ODU at 260 nm, 0.1 μmol) was added 20 μL of 1.0 M dithiothreitol (DTT) in distilled water (DW), and the reaction mixture was incubated at 25 °C for 30 min. The product was checked and purified by reverse phase HPLC. Fractions containing 2-5A−cysteamine were pooled, lyophilized, and stored at −20 °C. The yield was 79% (2.6 ODU at 260 nm, 79 nmol). ESI-MS: calculated $[M - H]^-$ *m/z* 1207.1 and $[M - 2H]^{2-}$ *m/z* 603.1, found 1207.2 and 602.8, respectively.

Conjugation of 2-5A−Cysteamine with Streptavidin (SA). To 100 μL of 40 μM SA in phosphate buffer saline (PBS) was added 6.8 μL of 14.2 mM Sulfo-KMUS in dimethylformamide (DMF), and the solution was incubated at 30 °C for 60 min. The reaction mixture was passed through a PD-10 column using 0.1 M PB containing 5 mM EDTA (pH 7.2) as an elution buffer. The fractions containing SA-KMUS were collected and concentrated by a Centricon-30 centrifuge concentrator (Millipore, MA). The yield of SA-KMUS was 63% based on SA. To 280 μL of 9.0 μM SA-KMUS solution in PBS was added 4.8 μL of 790 μM 2-5A−cysteamine in 0.1 M PB containing 5 mM EDTA (pH 7.2), and the reaction mixture then incubated at 30 °C for 60 min. The product was passed through a PD-10 column using 0.1 M PB containing 5 mM EDTA (pH 7.2) as an elution buffer. Fractions containing 2-5A−cysteamine-SA (2-5A−SA) were collected and pooled. The yield was 20% based on SA-KMUS (0.192 OD at 280 nm, 0.5 nmol). The conjugate showed UV absorption at 280 and 260 nm in a 1 to 0.76 ratio. The numbers of the 2-5A molecule introduced to one molecule of SA was estimated as 1.2 from the ratio of the UV absorption of the conjugate at 260 nm and 280 nm, ascribed to 2-5A and SA, respectively.

Conjugate Formation between Biotinylated Luciferase (bL248) and 2-5A−SA. To 0.5 nmol of the 2-5A−SA solution, 50 nmol 2-mercaptoethanol was added to block the excess maleimide groups in the conjugate, and the mixture incubated at 25 °C for 30 min. Four hundred and seventy microliters of bL248 solution (2.4 mg mL^{-1}) in the storage buffer (0.1 M PB, 2 mM 2-mercaptoethanol, 1 mM EDTA, 10% glycerol) was added to 0.5 nmol 2-5A−SA solution and the mixture incubated at 25 °C for 60 min. The product was purified by Superdex 200HR 10/30 (Pharmacia) column chromatography using 0.1 M PB containing 0.15 M NaCl (pH 7.2) as an elution buffer. Fractions showing high immunological reactivity and enzyme activity were collected. This conjugate solution was diluted to 80 pM (based on enzyme concentration) with conjugate buffer (0.1 M PB containing 2.5 mM EDTA, 0.2% bovine serum albumin, 0.02% casein, and 0.05% NaN_3) and stored at 4 °C.

Immobilization of Anti-Rabbit IgG Polyclonal Antibody to Magnetic Particles. One milliliter of magnetic particle suspension (5 mg mL^{-1}) was washed 3 times with 1 mL of distilled water. The magnetic particles were resuspended with 500 μL of 0.2 M Bis-Tris buffer (pH 5.5), and then 500 μL of 10 mg mL^{-1} EDC in distilled water was added and the mixture stirred at 25 °C for 30 min. The suspension was washed three times with 1 mL of distilled water and with 500 μL of 0.1 M PB(pH 7.2) containing 0.4 M ammonium sulfate. The activated magnetic particles were resuspended with 500 μL of 0.1 M PB(pH 7.2) containing 0.4 M ammonium sulfate and 0.4 mg mL^{-1} anti-rabbit IgG antibody, and the mixture was stirred at 25 °C for 18 h. To the magnetic particles was added 1 mL of blocking buffer (0.05 M PB containing 20% Block Ace, pH 7.2), and the suspension was stirred at 25 °C for 3 h. After blocking buffer was removed from the suspension, 10 mL of stock buffer (0.05 M PB containing 5% Dextran T40, 0.2% bovine serum albumin and 0.1% NaN_3, pH 7.4) was added and stored at 4 °C.

Bioluminescent Enzyme Immunoassay for 2-5A. Immunoassay was carried out by the one-step competitive method. After 50 μL of sample was transferred to a polystyrene test tube (12 × 75 mm), 50 μL of the reaction buffer (0.05 M PB containing 5% Dextran T40, 0.2% bovine serum albumin, and 0.1% NaN_3, pH 7.4), 100 μL of 80 pM 2-5A−Lucferase conjugate solution, a 20 μL suspension of 1 mg mL^{-1} anti-rabbit IgG antibody immobilized on magnetic particles, and 100 μL of anti 2-5A rabbit serum, which was diluted 20,000-fold with the reaction buffer, were added to the test tube and stirred. The mixture was incubated at 25 °C for 15 min and washed with 0.05% Tween 20 in PBS (750 μL × 3). To the magnetic particles was added 100 μL of suspension buffer (50 mM Tris-HCl, pH 8.5), and the mixture stirred for 2 s. The test tube containing the suspension was placed on a luminometer (Lumat LB 9507, EG&G Berthold) and 100 μL of a substrate solution (940 μM luciferin, 2 mM ATP, 40 mM ADA, 16 mM MgSO4, 0.26 mM EDTA, 2 mM potassium pyrophosphate, pH 6.5) added. Luminescence intensity was measured by integrating the emission for 5 s (delay time 0.5 s).

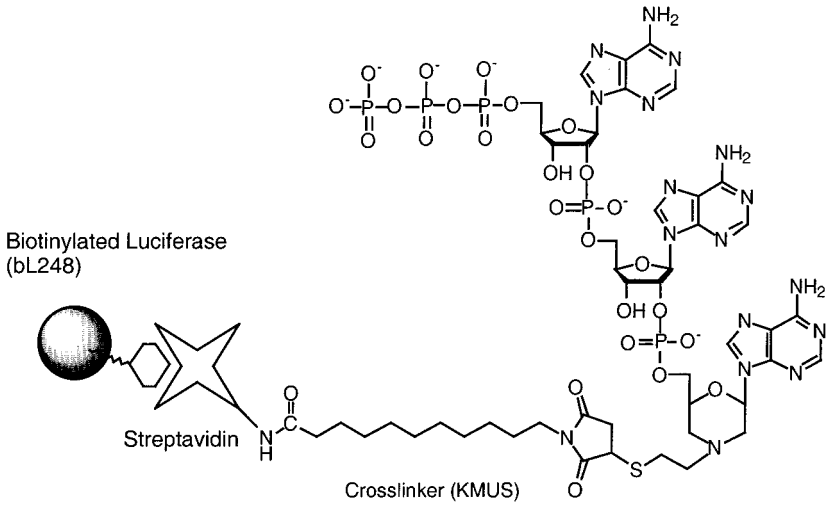
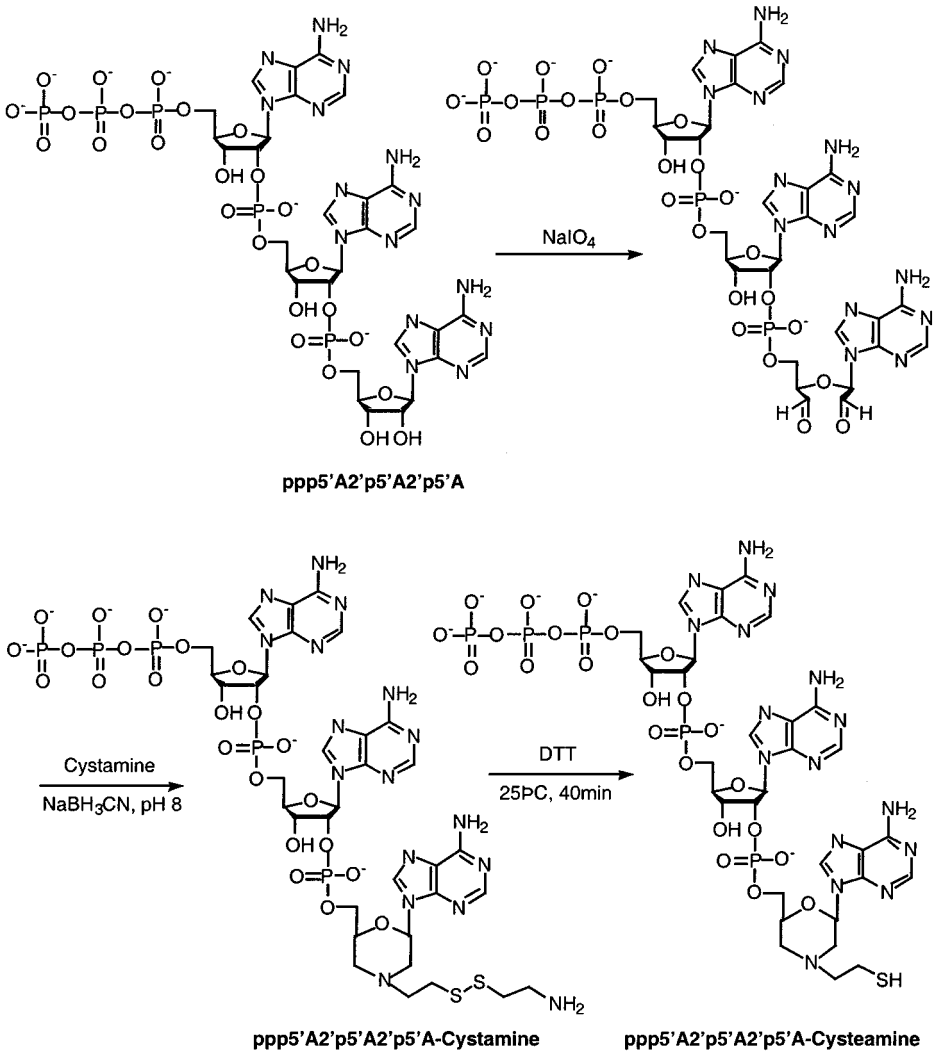


Figure 1. Structure ofbioluminescence enzyme conjugate with 2-5A.

Scheme 1. Preparation of 2−5A-cysteamine



RESULTS AND DISCUSSION

The conjugate of 2-5A used in this BLEIA was bound covalently to SA as shown in Figure 1. We initially prepared a 2-5A derivative bearing biotin and conducted complex formation between biotinylated 2-5A, SA, and biotinylated luciferase. However, simultaneous introduction of biotinylated luciferase and biotinylated 2-5A to SA was difficult to control, because binding of the high molecular weight biotinylated luciferase to SA is suppressed by the preferable binding of the low molecular weight biotinylated 2-5A to SA. Thus, we tried to prepare 2-5A conjugate linked to SA covalently. Several methods can be considered for the covalent conjugation of 2-5A with SA. A homobifunctional cross-linking reagent such as dialdehyde or disuccinmide, which is amine reactive, reacts with SA at both sites forming polymeric structures.

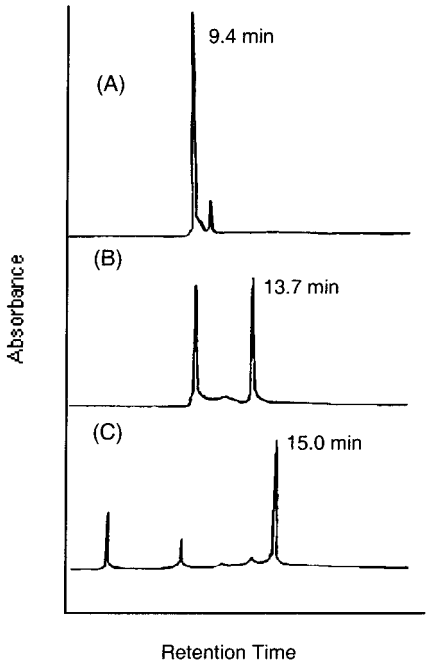


Figure 2. HPLC profiles of 2-5A−cysteamine preparation. (A) The peak at 9.4 min is 2-5A before derivatization. (B) Introduction of cystamine to 2-5A. The peak at 13.7 min is 2-5A−cystamine. (C) Reduction of 2-5A−cystamine with DTT. The peak at 15.0 min is 2-5A−cysteamine. The reaction conditions for the introduction of cystamine to 2-5A and for the reduction of 2-5A−cystamine are in Materials and Methods.

Therefore, we employed a heterobifunctional cross-linking reagent, Sulfo-KMUS, which has an amine reactive *N*-hydroxysuccinimide ester and a thiol reactive maleimide group. Reaction of SA with Sulfo-KMUS yielded SA-KMUS conjugate. No polymerization of SA took place with this cross-linking agent, as SA has no free thiol group. A thiol group has to be introduced into the 2′(or 3′) end of 2-5A for the binding of 2-5A with SA-KMUS, because the 5′-triphosphate moiety of 2-5A is very important in the activation of RNase L and in the binding of the polyclonal antibody to 2-5A used in the BLEIA. We chose cystamine to introduce a thiol group into 2-5A at the 2′(3′) end, as a cystamine moiety of the 2-5A derivative can be reduced easily with DTT to convert a thiol group. The coupling of 2-5A with cystamine was carried out by a modification of a published procedure (*5*, *12*, *14*) as shown in Scheme 1. A dialdehyde group was generated by oxidation of the 2′,3′ terminal diol group of 2-5A with sodium periodate. The dialdehyde group was then reacted with an amino group of cystamine and the resulting unstable Schiff base immediately reduced with sodium cyanoborohydride. The product, 2-5A−cystamine conjugate, was purified by reverse phase HPLC, the profile of which is shown in Figure 2. The peak at 13.7 min is due to 2-5A−cystamine and the other peak at 9.4 min to the unreacted 2-5A. The yield of 2-5A−cystamine after purification by HPLC was 37%. The cystamine moiety of the 2-5A derivative was reduced by 0.1M DTT to convert to 2-5A−cysteamine bearing an active thiol group. This reduction took place almost quantitatively, as shown in Figure 2(C). The purified 2-5A−cysteamine was isolated in 79% yield by HPLC.

Torrence et al. reported that the thiol group in the 2-5A−cysteamine conjugate was unstable and formed disulfide linkage immediately by aerobic oxidation, yielding the dimeric product $(2\text{-}5A\text{−}cysteamine)_2$ (*12*). We checked stability of the thiol group of 2-5A−cysteamine in water at 25 °C. The dimer formation by oxidation of

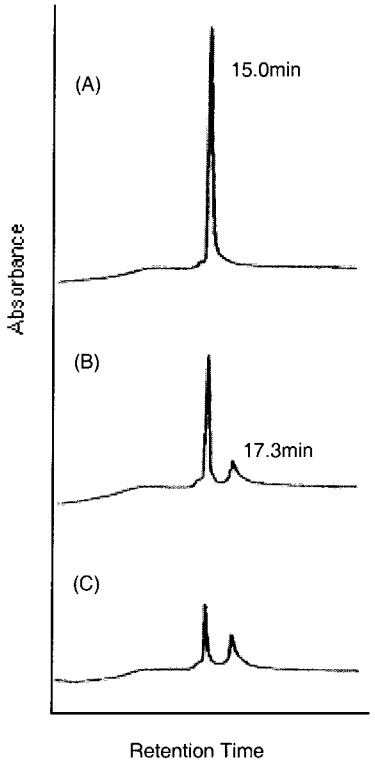


Figure 3. HPLC profiles of oxidation of 2-5A−cysteamine in aqueous solution. The profiles show a decrease of 2-5A−cysteamine (15.0 min) and an increase of its dimer (17.3 min) when 2-5A−cysteamine solution (0.5 mM) was kept at 25 °C for 1 h (A), 52 h (B), and 96 h (C).

2-5A−cysteamine was monitored by HPLC (Figure 3). The monomeric 2-5A−cysteamine remained at 100%, 72.5%, and 56% after 1, 52, and 96 h, respectively, at 25 °C. The identify of the resulting dimer was corroborated by ESI mass spectrometry (calculated $[M\text{-}2H]^{2-}$ *m*/*z* 1206.1 and $[M\text{-}3H]^{3-}$ *m*/*z* 803.7, found 1206.2 and 803.8, respectively). The dimer (peak at 17.3 min) was converted to 2-5A−cysteamine again by reduction with DTT as shown in Figure 4 (B). The thiol group of 2-5A−cysteamine is certainly unstable and was converted to the dimer by oxidation as Torrence et al. mentioned (*12*). However, reaction of 2-5A−cysteamine with the maleimide moiety of SA-KMUS proceeded more quickly than the dimerization. SA-KMUS was obtained from SA and sulfo-KMUS in 63% yield. Conjugate of 2-5A and SA-KMUS was isolated in 20% yield (based on SA-KMUS), as recovered in a small amount during purification by a PD-10 column. The average molar ratio of 2-5A to SA in the resulting 2-5A−SA conjugate was estimated to be 1.2 from the UV absorption at 260 and 280 nm, being the maximal absorption wavelengths of 2-5A and SA, respectively.

Thiol groups in the luciferase play an important role for enzyme activity (*15*). The excess unreacted maleimide groups in the 2-5A−SA conjugate will result in an inactivation of the enzyme by reacting with free thiol groups of the enzyme. Thus, 2-mercaptoethanol was added to the 2-5A−SA conjugate to block excess maleimide groups in the conjugate. The resulting 2-5A−SA conjugate was mixed with biotinylated luciferase to form the complex of 2-5A and luciferase as illustrated in Figure 1. BLEIA for 2-5A was carried out using the 2-5A−luciferase conjugate as a probe and was based on the one step competitive method. Very small amounts of anti-2-5A antibody and labeled 2-5A must be used for the highly sensitive immunoassay of 2-5A. However, the antibody was difficult to immobilize on a solid support in such a

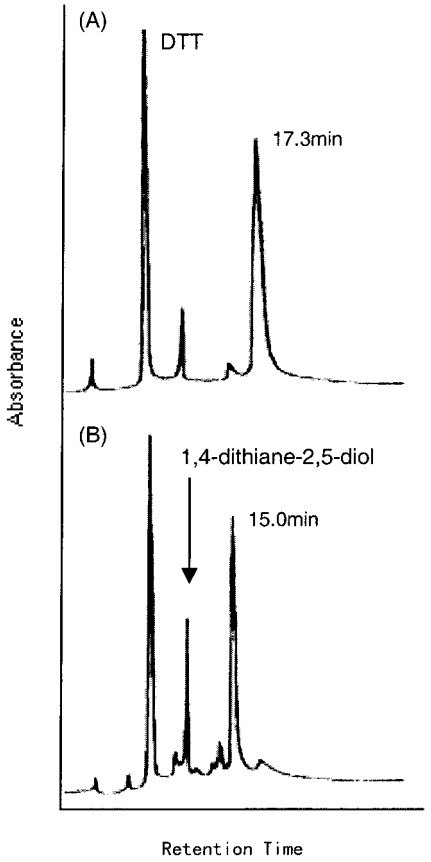


Figure 4. Reduction of the dimer to 2-5A−cysteamine(A) The dimer (0.1 mM) was treated with 0.1 M DTT for 1 min. The dimer was prepared by aerobic oxidation of 2-5A−cysteamine in water by passing O_2 gas at 25 °C for 5 days. The peak at 17.3 min is the dimer of 2-5A−cysteamine. (B) The dimer was treated with 0.1 M DTT for 40 min.

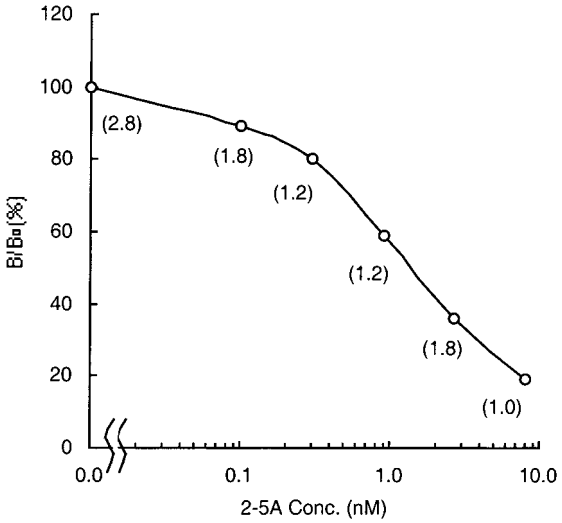


Figure 5. Standard BLEIA curve for 2-5A. Values in parentheses represent the coefficients of variation ($n = 6$). *B* is binding at the 2-5A concentration indicated, and B_0 is the maximum binding of labeled 2-5A in 0 nM 2-5A standard.

small amount. When the anti-2-5A antibody was not bound quantitatively on the solid support, the assay resulted in a low reproductivity. Therefore, we employed a second antibody method for the assay and the anti-rabbit IgG antibody was immobilized on magnetic particles. The second antibody on the magnetic particles bound with the anti-2-5A antibody, which captured the target 2-5A molecule or the probe labeled 2-5A in a

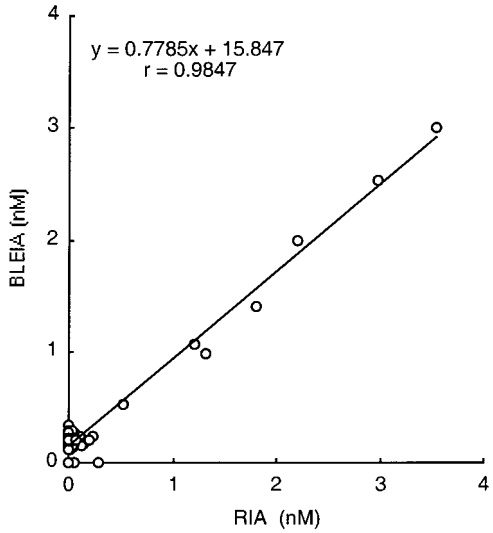


Figure 6. Correlation between this BLEIA and RIA. RIA was carried out by a previously described method (*5*).

sample solution. Magnetic particles could enhance the binding of the target molecule with their vast surface. The 2-5A and labeled 2-5A, captured by the antibody on the magnetic particles, could be separated easily from the unbound ones in the sample mixture by using a strong magnet. After the reaction mixture was removed from the test tube, the remaining magnetic particles were washed three times with a washing solution, and the substrate solution for luminescence was then added to the test tube containing the magnetic particle suspension in 50mM Tris-HCl (pH8.0), followed by luminescence measurement. A typical standard curve for 2-5A is shown in Figure 5. The measurable range of 2-5A was 0.1−10 nM. This range is sufficient in practical use for the assay of 2-5A from various sources, as 2-5A shows its biological activities at nanomolar concentrations. Reproduction of the assay for 2-5A was very good as shown in Figure 5. Variations of the assays at each concentration were 1.0−2.8%. The 2-5A concentrations measured by this BLEIA were compared with those measured by radioimmunoassay (RIA) (*5*) using 60 samples of human plasma. A good correlation between BLEIA and RIA was observed as shown in Figure 6.

CONCLUSIONS

A 2-5A derivative bearing cysteamine at 2′(or 3′) terminal was prepared for conjugation with biotinylated luciferase. The free thiol group of 2-5A−cysteamine was stable during the conjugation process with streptavidin. The 2-5A−SA conjugate formed a strong complex with biotinylated luciferase by biotin−streptavidin bonding. BLEIA for 2-5A using the conjugate of 2-5A and luciferase provides a highly sensitive measurement of 2-5A and is easy to perform compared with other methods, as no radioisotope is required for the assay. BLEIA for 2-5A in human plasma using this conjugate showed good correlation with the previously reported RIA method. Thus, this BLEIA would be useful for study of the 2-5A system and the diagnosis of infectious diseases, as well as for the management of patients undergoing interferon therapy, by measuring the 2-5A produced by 2-5A synthetase induced by interferon.

ACKNOWLEDGMENT

We thank Dr. Hiroki Tatsumi (Kikkoman Corp.) for providing the biotinylated thermostable recombinant

firefly luciferase (bL248) and Mr. Mikio Hikata (JSR Corp.) for providing the magnetic particles (Immtex-MAG1803) used in this study.

LITERATURE CITED

(1) Baglioni, C. (1979) Interferon-induced enzymatic activities and their role in the antiviral state. *Cell 17*, 255−64.

(2) Johnston, M. I., and Torrence, P. F. (1984) The role of interferon-induced proteins, double-stranded RNA, and 2′,5′-oligoadenylate on the interferon-mediated inhibition of viral translation, in *Interferon: Mechanism of Production and Action* (R. Friedman, Ed.) Vol. 3, pp 189−298.

(3) Silverman, R. H., Wreschner, D. H., Gilbert, C. S. and Kerr, I. M. (1981) Synthesis, characterization and properties of ppp-(A2′p)nApCp and related high-specific-activity ^{32}p-labeled derivatives of ppp(A2′p)nA. *Eur. J. Biochem. 115*, 79−85.

(4) Hersh, C. L., Reid, T. R., Friedman, R.; Stark G. R. (1984) Preparation, characterization, and use of an antiserum specific for 2′, 5′-oligoadenylates. *J. Biol. Chem. 259*, 1727−1730.

(5) Sawai, H., Ishibashi, K., Itoh, M. and Watanabe, S. (1985) Sensitive radioimmuno assay for 2′-5′-oligoadenylates using a novel ^{125}I-labeled derivative of 2′-5′-triadenylate 5′-triphosphate. *J. Biochem. 98*, 999−1005.

(6) DeLuca, M. and McElroy, W. D. (1981) Purification and properties of firefly luciferase. *Methods Enzymol. 57*, 3−15.

(7) Kricka, L. J. (1991) Chemiluminescence and bioluminescence techniques. *Clin. Chem. 37*, 1472−1481.

(8) Kricka, L. J. (1994) Selected strategies for improving sensitivity and reliability of immunoassays. *Clin. Chem. 40*, 347−357.

(9) Tatsumi, H., Fukuda, S., Kikuchi, M. and Koyama, Y. (1996) Construction of biotinylated luciferases using biotin acceptor peptides. *Anal. Biochem. 243*, 176−180.

(10) Ohkuma, H., Abe, K., Kosaka, Y. and Maeda, M. (1999) Simultaneous assay of pepsinogen I and pepsinogen II in serum by bioluminescent enzyme immunoassay using two kinds of *Luciola lateralis* luciferase. *Anal. Chim. Acta 395*, 265−272.

(11) Seto, Y., Ohkuma, H., Takayasu, S., Iba, T., Umeda, A. and Abe, K. (2001) Development of highly sensitive bioluminescent enzyme immunoassay with ultra-wide measurable range for thyroid-stimulating hormone using firefly luciferase. *Anal. Chim. Acta 429*, 19−26.

(12) Lesiak, K. and Torrence, P. F. (1997) Efficient functionalization of 2′-5′-oligoadenylates with sulfur. *Bioconjugate Chem. 8*, 199−203.

(13) Sawai, H., Shibata, T. and Ohno, M. (1981) Preparation of oligoadenylates with 2′,5′ linkage using Pb2+ ion catalyst. *Tetrahedron 37*, 4573−4576.

(14) Hansske, F. and Cramer, F. (1979) Modification of the 3′-terminus of tRNA by periodate oxidation and subsequent reaction with hydrazides. *Methods Enzymol. 59*, 172−181.

(15) Branchini, B. R., Magyar, R. A., Murtiashaw, M. H., Magnasco, N., Hinz, L. K. and Stroh, J. G. (1997) Inactivation of firefly luciferase with N−(iodoacetyl)-N′-(5-sulfo-1-naphthyl)ethylenediamine (I-AEDANS). *Arch. Biochem. Biophys. 340*, 52-58.

(16) Nicolas, M., Laurence, L., Luxembourg, A., Cailla, H and Marti, J. (1987) Enzyme immunoassay of 2′-5′-oligoadenylates at the femtomole level. *Ann. Inst. Pasteur Immunol. 138*, 83−96.

BC015554L

Synthesis of New Modified DNAs by Hyperthermophilic DNA Polymerase: Substrate and Template Specificity of Functionalized Thymidine Analogues Bearing an sp3-Hybridized Carbon at the C5 α-Position for Several DNA Polymerases

Hiroki Sawai,* Akiko Ozaki-Nakamura, Masayuki Mine, and Hiroaki Ozaki

Department of Applied Chemistry, Gunma University, Kiryu, Gunma 376-8515, Japan. Received September 12, 2001; Revised Manuscript Received December 31, 2001

Novel thymidine analogue triphosphates, which have an sp3-hybridized carbon at the C5 α-position with amino-linker arms, a methyl ester, or a carboxyl group at the C5 sidearm, were good substrates for primer-extension reactions by DNA polymerase from *Pyrococcus kodakaraensis* (KOD Dash DNA polymerase), yielding exclusively full-length products. The resulting modified DNA was further alllowed to react with a functional molecule such as fluorescein isothiocyanate. By contrast, only truncated products were formed from the thymidine analogue substrate bearing the amino-linker arm or the negatively charged carboxyl group using Taq, Tth DNA polymerase, or DNA polymerase I from *E. coli* (Klenow fragment). The results indicate either that the thymidine analogue was not accepted by the enzymes, or that the polymerases could not extend the products, once the analogue had been incorporated, depending on the type of the analogue. A conventional thymidine analogue bearing an aminopropenyl group at the C5-position was accepted by all enzymes, among which KOD Dash DNA polymerase showed the highest activity for the polymerization with this analogue. Templates bearing the thymidine analogues in place of one thymidine residue were read by KOD Dash, Taq, Tth DNA polymerases, and the Klenow fragment giving the full-length product. KOD Dash DNA polymerase could expand structural diversities of substrates that can be used to prepare modified DNAs.

INTRODUCTION

Modified oligonucleotides with a variety of functional groups are important tools for biological and biochemical studies (*1*−*3*). The C5-position of the pyrimidine ring is an ideal site for the modification, because it is located in the major groove of double-stranded DNA and does not inhibit A:T base pairing. Functional groups such as fluorophores (*3*, *4*), enzymes (*3*, *4*), biotin (*3*, *4*), metal chelators (*6*, *7*), polyamines (*8*), and intercalating agents (*9*, *10*) have been attached to C5 via amino-linker arms. Previously, we reported the synthesis of thymidine analogues, C5-substituted 2′-deoxyuridines bearing amino-linker arms at the C5-position, and their introduction into oligodeoxyribonucleotides (*11*, *12*). Usually, modified DNA is prepared chemically by using a DNA synthesizer.

However, if a DNA polymerase can accept modified nucleotides as substrates, modified DNA can be prepared enzymatically. The resulting modified DNA could be used as a DNA probe by attachment of a reporter group, or as a catalytic DNA by in vitro selection. Thus, nucleotide analogues that are substrates for DNA and RNA polymerases can be powerful tools for biochemical studies. Modified ribonucleoside 5′-triphosphates are substrates for several RNA polymerases, and are used to create various functionalized RNA molecules with catalytic activity or binding activity (*13*−*21*). However, there are a few examples of functionalized DNA molecules prepared using modified deoxynucleoside 5′-triphosphates, because DNA polymerases accept a limited range of molecular structures as a substrate. Some DNA polymerases can use 5′-triphosphates of modified 2′-deoxyuridines with a C5 side chain carrying an (*E*)-propenyl or propynyl group (*22*−*31*). Vent or Taq DNA polymerases can use 2′-deoxyuridine derivatives carrying a triple bond at the C5 α-position, yielding the corresponding modified DNAs (*24*, *26*, *29*). 2′-Deoxyuridine derivatives bearing a propenyl group at the C5 α-position are good substrates for Taq DNA polymerase, but poor substrates for Vent or Pfu DNA polymerase (*25*, *27*, *30*). The Klenow fragment incorporates 2′-deoxyuridine derivatives bearing a propenyl group at the C5-position, but with low efficiency (*22*, *23*). Reduction of the double or triple bond of the C5 propenyl- or alkynyl-substituted 2′-deoxyuridines significantly inhibits their function as a substrate (*30*). These results indicate that an sp- or sp2-hybridized carbon at the C5 α-position of the C5-substituted 2′-deoxyuridine is required as a substrate for some DNA polymerases (*22*−*31*). The differences in reactivity of C5-substituted 2′-deoxyuridines as a substrate may be due to the steric effect of a large side group, or to the ionic effect of a substituent group such as an amino group. The ability of the modified nucleotides as a substrate also depends on the kind of DNA polymerase.

We prepared several triphosphates of thymidine analogues, which have an sp3-hybridized carbon at the C5 α-position with either amino-linker arms or an ester or carboxylic group at the terminus, and have examined for their specificity as a substrate for several DNA polymerases in the primer-extension reaction. We have found that KOD Dash DNA polymerase readily uses the thymidine analogue nucleotides as a substrate and reads a template containing the modified thymidine, but no other DNA polymerase tested, including Taq DNA polymerase,

* Address correspondence to this author. E-mail: sawai@chem.gunma-u.ac.jp. Tel: 81-277-30-1220. Fax: 81-277-30-1224.

10.1021/bc010088l CCC: $22.00 © 2002 American Chemical Society
Published on Web 02/06/2002

can accept the thymidine analogues as a substrate. KOD Dash DNA polymerase is a hyperthermophilic DNA polymerase and now commercially available. The enzyme was originally isolated from the extremely thermophilic archaeum *Pyrococcus kodakaraensis*, found in a hot spring on Kodakara Island in southern Japan, and is reported to have high DNA polymerization activity with high fidelity (*32*). This is the first report that a thymidine analogue which has an sp3-hybridized carbon at the C5 α-position can function as a substrate. The enzyme also accepts the conventional thymidine analogues bearing an aminopropenyl group more readily than other enzymes. The finding that KOD Dash DNA polymerase has broader substrate specificity than other polymerases may expand the variety of nucleotide analogues that can be used for enzymatic modified DNA synthesis.

MATERIALS AND METHODS

Materials. 2′-Deoxynucleoside 5′-triphosphates (dATP, dGTP, dCTP, and TTP) were purchased from Seikagaku Kogyo. 2′-Deoxyuridine 5′-triphosphate (dUTP) was a gift from Mr. H. Kusakabe of Yamasa Co. Snake venom phosphodiesterase and alkaline phosphatase were from Worthington Biochemicals, and nuclease P1 was from Yamasa Co. Klenow fragment of *E. coli* DNA polymerase I and Taq DNA polymerase were purchased from Takara, and KOD Dash and Tth DNA polymerases were from Toyobo Co. [α-^{32}P]dGTP (800 Ci/mmol) and [α-^{33}P]ddNTP (A, G, C, and T) (1500 Ci/mmol, 450 μCi/mL) were from Amersham. C5-substituted 2′-deoxyuridine derivatives, 5-*N*-(6-trifluoroacetylaminohexyl)carbamoylmethyl-2′-deoxyuridine (**1**), 5-(methoxycarbonylmethyl)-2′-deoxyuridine (**2**), and 5-[*N*-2-[*N*,*N*-bis(2-trifluoroacetylaminoethyl)-amino]ethyl]carbamoylmethyl-2′-deoxyuridine (**3**), were prepared as described previously (*11*, *12*). A radiolabeled DNA marker was prepared from the template and primer DNA using a thermo sequenase radiolabeled terminator cycle sequence kit obtained from USB Co. according to the method of the manufacturer. All other chemicals were reagent grade and were used without further purification.

Oligonucleotides. Oligodeoxyribonulceotides were synthesized on an Applied Biosystems model 381 A DNA synthesizer using deoxyribonucleoside 2-cyanoethyl phosphoramidites. Normal nucleoside phosphoramidites were purchased from Applied Biosystems. Phosphoramidites of the thymidine analogues bearing ethylenediamine, hexamethylenediamine, and tris(2-aminoethyl)amine at the C5-position were prepared as described previously (*12*). Oligodeoxyribonucleotides (37mer) bearing a thymidine analogue in place of one thymidine residue were prepared along with the normal oligodeoxyribonucleotide, and used as the template for DNA polymerase reactions.

Analytical Methods and Gel Electrophoresis. ^{1}H and ^{31}P NMR spectra were obtained with a JEOL α-500. Triphosphates of 2′-deoxyuridine derivatives for NMR measurement were passed through a Dowex 50-WX-8 (Na^+ form) column to convert the triethylammonium salt to the sodium salt. Tetramethylsilane (TMS) and 85% phosphoric acid were used as the internal standards for ^{1}H and ^{31}P NMR, respectively. ESI mass spectra were recorded on a PE Sciex API-100. MALDI TOF mass spectra were taken with a Shimadzu AXIMA-CF. UV spectra were obtained with a Hitachi 3200 spectrometer. High-pressure liquid chromatography (HPLC) on an ODS-silica gel column (4 mm × 250 mm) was carried out with a linear gradient elution (2−40% acetonitrile in 50 mM triethylammonium acetate, pH 7.0) over 30−40 min at a flow rate of 1.0 mL/min. Gel electrophoresis was carried out using 0.5 mm thick denaturing15% polyacrylamide gels containing 7 M urea, and run at 2000 V for 2.5−3 h. The gels were autoradiographed with Kodak BioMax MS film at −70 °C.

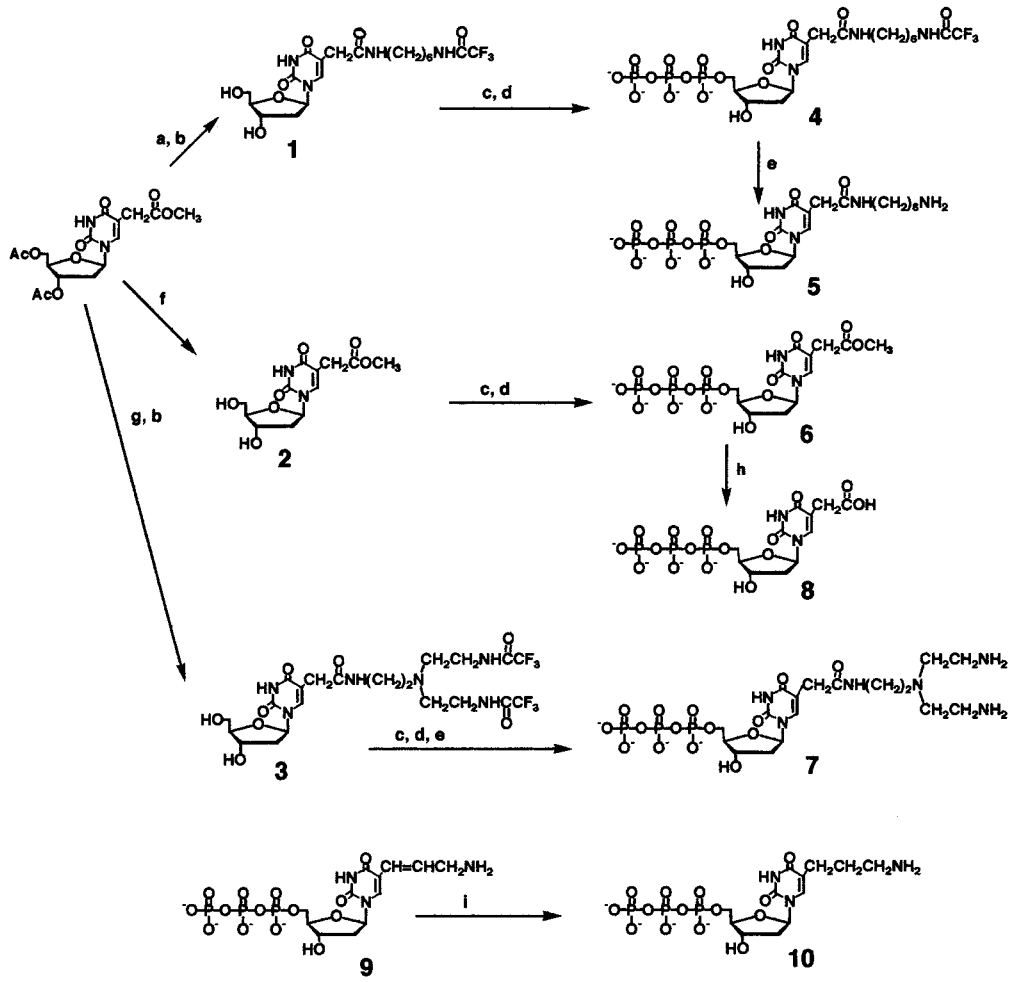
Synthesis of 5′-Triphosphates of 2′-Deoxyuridine Derivatives. *(A) 5-N-(6-Trifluoroacetylaminohexyl)carbamoylmethyl-2′-deoxyuridine 5′-Triphosphate (**4**).* 5′-Triphosphorylation of the modified nucleosides was carried out by the method described by Ludwig (*33*) as shown in Scheme 1. To a solution of **1** (143 mg, 0.30 mmol) in trimethyl phosphate (0.75 mL) was added phosphoryl chloride (60 μL, 0.64 mmol) with stirring on ice. After stirring for 2 h at 0 °C, the reaction mixture was added to a solution of 0.5 M tributylammonium pyrophosphate in dry DMF (3 mL) containing 0.3 mL of tributylamine, and the solution was stirred for 30 min at room temperature. The reaction mixture was poured into a 40 mL ether/acetone (1:1) solution containing $NaClO_4$-saturated acetone (2 mL) with stirring. The precipitates were collected, dried under vacuum, and redissolved in a small volume of water, and the products were separated on a column of DEAE-Sephadex A-25 using a linear gradient (0.1−1.0 M) of triethylammonium hydrogen carbonate (pH 7.5) as an eluent. The appropriate fractions containing (**4**) were collected and concentrated under vacuum to give white precipitates, which were further purified by column chromatography on an ODS-silica gel column (30 × 250 mm) with a linear gradient elution of acetonitrile (0−50%) in 50 mM triethylammonium acetate buffer (pH 7.0) to remove inorganic pyrophosphate and lyophilized. The yield of **4** was 13% (346 ODU at 260 nm). UV(H_2O): λ_{max}, 267 nm. ^{31}P NMR(D_2O): δ(ppm), −10.2(d, J = 20 Hz, P_γ), −10.9(d, J = 20 Hz, P_α), −22.6(t, J = 20 Hz, P_β). ^{1}H NMR(D_2O): δ-(ppm), 7.81(s, 1H, H-6), 6.27(t, 1H, H-1′), 4.58(q, 1H, H-3′), 4.15(m, 3H, H-4′+H-5′), 3.28(s, 2H, CH_2CO), 3.24−3.10(m, 4H, NCH_2+CH_2N), 2.34(m, 2H, H-2′), 1.51−1.25-(m, 8H, $(CH_2)_4$). ESI-Mass(negative mode): found 719.2; calcd for $[M-H^+]^-$, 719.1.

*(B) 5-N-(6-Aminohexyl)carbamoylmethyl-2′-deoxyuridine 5′-Triphosphate (**5**).* A portion of **4** (54 ODU at 260 nm) was dissolved in 1 M ammonium hydroxide solution (200 μL) and kept for 3 days at −20 °C to remove the protecting trifluoroacetyl group. The resulting triphosphate of 5-*N*-(6-aminohexyl)carbamoylmethyl-2′-deoxyuridine (**5**) was purified by ODS-silica gel column chromatography as described above and lyophilized. The yield was 24 ODU at 260 nm (44%). UV(H_2O): λ_{max}, 267 nm. ^{31}P NMR(D_2O): δ(ppm), −5.5(d, J = 20 Hz, P_γ), −10.2(d, J = 22 Hz, P_α), −20.9(t, J = 20, 22 Hz, P_β). ^{1}H NMR-(D_2O): δ(ppm), 7.93(s, 1H, H-6), 6.34(t, J = 7.0 Hz, 1H, H-1′), 4.77(m, 1H, H-3′), 4.24−4.17(m, 3H, H-47+H-5′), 3.38(s, 2H, CH_2CO), 3.21(t, J = 6.4 Hz, 2H, CH_2N), 2.96-(t, J = 7.5 Hz, 2H, NCH_2), 2.41(m, 2H, H-2′), 1.67−1.34-(m, 8H, $(CH_2)_4$). ESI-Mass(negative mode): found 623.2; calcd for $[M-H^+]^-$, 623.1.

*(C) 5-[N-2-[N,N-Bis(2-aminoethyl)amino]ethyl]carbamoylmethyl-2′-deoxyuridine 5′-Triphosphate (**7**).* Preparation of 5-[*N*-2-[*N*,*N*-bis(2-aminoethyl)amino]ethyl]carbamoylmethyl-2′-deoxyuridine 5′-triphosphate (**7**) was carried out by a similar procedure to that of **4** from the nucleoside **3** (182 mg, 0.30 mmol). The yield of **7** was 20% from **3** after removing the trifluoroacetyl group by treatment with ammonium hydroxide solution (457 ODU at 260 nm). UV(H_2O): λ_{max}, 267 nm. ^{31}P NMR(D_2O): δ(ppm), −9.6(br, P_γ), −10.9(br, P_α), −22.3(br, P_β). ESI-Mass-(negative mode): found 653.4; calcd for $[M-H^+]^-$, 653.5.

*(D) 5′-Triphosphates of 5-(Methoxycarbonylmethyl)-2′-deoxyuridine (**6**) and of 5-(Carboxymethyl)-2′-deoxyuri-*

Scheme 1. 5-Substituted 2′-Deoxyuridine Triphosphates, 4−10[a]



[a] (a) $H_2N(CH_2)_6NH_2$, MeOH; (b) CF_3COOEt, (dimethylamino)pyridine, MeOH; (c) $POCl_3$, $(MeO)_3PO$; (d) tributylammonium pyrophosphate, DMF; (e) 2 M NH_4OH; (f) triethylamine, MeOH; (g) $N(CH_2CH_2NH_2)_3$, MeOH; (h) 0.2 M NaOH; (i) 5% Pd-C, H_2.

*dine (**8**).* Triphosphorylation of compound **2** (90 mg, 0.3 mmol) was carried out by a similar procedure to that used for **1** as described above. Compound **6** was obtained in 7% yield from **2** (186 ODU at 260 nm). UV(H_2O): λ_{max}, 267 nm. ^{31}P NMR(D_2O): δ(ppm), −5.5(br, P_γ), −10.4(br, P_α), −22.6(br, P_β). ^{1}H NMR(D_2O): δ(ppm), 7.81(s, 1H, H-6), 6.21(dd, J = 6.7 Hz, J = 13.5 Hz, 1H, H-1′), 4.10−4.07(m, 2H, H-3′+H-4′), 4.03(m, 2H, H-5′), 3.60(s, 3H, CH_3), 3.40(s, 2H, CH_2CO), 2.28(m, 2H, H-2′). ESI-Mass(negative mode): found 539.0; calcd for $[M-H^+]^-$, 539.0.

To a solution of **6** (2.4 ODU at 260 nm, 0.27 mmol) in 15 μL of water was added 15 μL of 0.2 M NaOH solution, and the reaction mixture was kept overnight at 4 °C for hydrolysis of the methyl ester. The resulting triphosphate of 5-(carboxymethyl)-2′-deoxyuridine (**8**) was purified by HPLC on ODS-silica gel as described above. The yield was 2.0 ODU at 260 nm (0.23 μmol, 85%). UV(H_2O): λ_{max}, 267 nm. ESI-Mass(negative mode): found 526.2; calcd for $[M-H^+]^-$, 526.0.

*(E) 5′-Triphosphates of 5-(E)-(Aminopropenyl)-2′-deoxyuridine (**9**) and 5-(Aminopropyl)-2′-deoxyuridine (**10**).* Compound **9** was prepared from dUTP according to the published procedure (*22*). Hydrogenation of **9** (155 ODU at 260 nm) was carried out in the presence of 5% Pd-carbon (8 mg) in 2 mL of methanol/H_2O (9:1) containing 100 μL of 4 M acetic acid for 2 days under an atmospheric pressure of hydrogen. The reaction mixture was filtered through Celite, and the Celite was rinsed with 2 mL of methanol. The filtrate was evaporated under vacuum. The residue was separated by HPLC on ODS-silica gel as described above and lyophilized, giving **10** in 57% yield (88 ODU at 260 nm). UV(H_2O): λ_{max}, 268 nm. ^{31}P NMR(D_2O): δ(ppm), −4.6(br, P_γ), −10.2(br, P_α), −20.4(br, P_β). ^{1}H NMR(D_2O): δ(ppm), 7.86(s, 1H, H-6), 6.38(t, J = 1.1 Hz, 1H, H-1′), 4.69(m, 1H, H-3′), 4.27(br, 2H, H-4′+H-5′), 4.18(br, 1H, H-5′), 3.01(m, 1H, CH), 2.86(m, 1H, CH), 2.48(m, 1H, CH) 2.40(t, J = 5.8 Hz, 2H, H-2′), 2.2(m, 1H, CH), 1.93(m, 2H, CH_2). ESI-Mass(positive mode): found 523.8 and 546.0; calcd for $[M+H^+]^+$ and $[M+Na^+]^+$, 524.2 and 546.2, respectively.

Enzymatic Incorporation of Thymidine Analogues into DNA with KOD Dash, Taq, Tth DNA Polymerase, or DNA Polymerase I (Klenow Fragment). DNA polymerase reactions were performed using a 17mer oligodeoxyribonucleotide, 5′-TAATACGACTCACTATA-3′, as a primer and a 37mer oligodeoxyribonucleotide, 3′-ATTATGCTGAGTGATATCCTGTACTCCTAATGGGTAC-5′, as a template. The primer−template complex was prepared by heating a 1:1 mixture of the primer and the template strands in TE buffer (10 mM Tris-HCl and 0.1 mM EDTA, pH 8.0) to 90 °C for 2 min and then cooling.

KOD Dash DNA polymerase reaction was carried out in a mixture (10 μL) containing 0.5 unit of the enzyme, 0.2 μM primer−template complex, 20 μM substrates (dATP + dCTP + TTP or TTP analogue), 5 μM dGTP, and 1 μCi (800 Ci/mmol) of [α-^{32}P]dGTP in the buffer supplied by the maker or in 120 mM Tris-HCl (pH 8.0),

10 mM KCl, 6 mM $(NH_4)_2SO_4$, 0.1% Triton X-100, 0.01 mg/mL BSA, and 1.0 mM $MgCl_2$. Either unmodified TTP or a thymidine analogue triphosphate (**4**, **5**, **6**, **7**, **8**, **9**, or **10**) was used in each reaction. Control reactions without TTP were carried out under the same conditions. Reaction mixtures were incubated at 50 °C for 5 or 30 min, and quenched by addition of 6 μL of 90% formamide containing 0.1% xylenecyanol, 0.1% bromophenol blue, and 20 mM EDTA (pH 8.0). The solutions were heated for 3 min at 95 °C for denaturation, and then cooled. The reaction products were separated by electrophoresis in a 15% denaturing polyacrylamide gel containing 7 M urea. The gels were visualized by autoradiography.

Taq DNA polymerase reactions were conducted as described above in reaction mixture (10 μL) containing the primer−template complex, the substrates, 0.5 unit of enzyme in 10 mM Tris-HCl (pH 8.3), 50 mM KCl, and 1.5 mM $MgCl_2$ at 50 °C for 5 or 30 min.

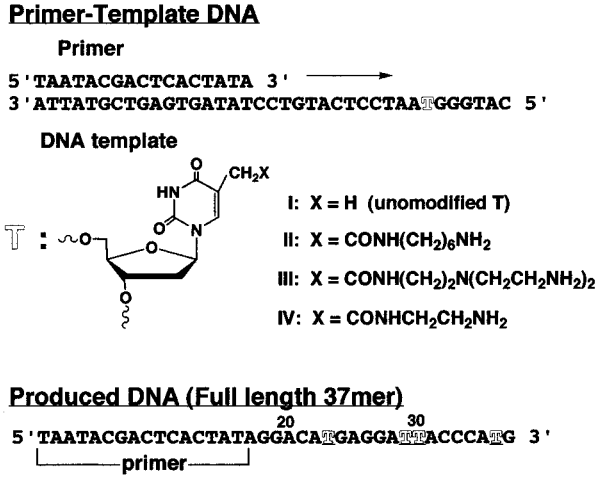
Tth DNA polymerase reactions were conducted as described above in reaction mixture (10 μL) containing the primer−template complex, the substrates, 0.5 unit of enzyme in 10 mM Tris-HCl (pH 8.0), 1.5 mM $MgCl_2$, 80 mM KCl, 500 μg/mL of bovine serum albumin, 0.1% sodium cholate, and 0.1% Triton X-100 at 50 °C for 5 or 30 min.

Reactions with the Klenow fragment were performed by a similar method as used for the KOD Dash DNA polymerase except for the reaction conditions. Each reaction mixture (10 μL) contained 0.5 unit of the enzyme, the primer−template complex, the substrates in 10 mM Tris-HCl (pH 8.0), and 5 mM $MgCl_2$. Reaction mixtures were incubated at 37 °C for 30 min.

Preparation of the Modified DNA in Large Quantity from the Thymidine Analogue 5, Its Characterization with a MALDI-TOF Mass Spectrometer, and Reaction with Fluorescein Isothiocyanate. A reaction mixture (1 mL) containing 5 units of KOD Dash DNA polymerase, a 0.1 μM sample of the 37mer DNA template, a 2 μM aliquot of the 17mer primer, 0.2 mM substrates (dATP + dCTP + dGTP + 5), and the buffer supplied by the maker was divided in 10 portions, and each 100 μL solution was transferred in a 0.5 mL tube. The polymerization reaction was carried out with a thermal cycler using the following program: 20 cycles of 20 s at 94 °C, 10 s at 40 °C, 30 s at 60 °C. The resulting 37mer DNA was extracted with PCI solution [phenol saturated with TE buffer/chloroform/isoamyl alcohol (25:24:1) twice, and then with CI solution (chloroform/isoamyl alcohol, 24:1)] and precipitated with ethanol. The product was further purified by HPLC on an ODS-silica gel column, giving 0.28 ODU at 260 nm of the DNA 37mer, whose mass spectrum was taken by a Shimazu AXIMA-CF MALDI-TOF mass spectrometer. Two peaks were present in the mass spectrum. One is due to the template DNA (found 11 370; calcd for $[M+H^+]^+$, 11 368), and the other is due to the modified DNA produced by the polymerization (found 11 937; calcd for $[M+H^+]^+$, 11 932). The DNA 37mer (0.1 ODU) was reacted with fluorescein isothiocyanate (5 mM) in the mixture (50 μL) containing 0.2 M sodium hydrogen carbonate buffer (pH 9.5) and 20% DMF at 37 °C for overnight. The reaction mixture was analyzed by HPLC monitoring by UV (260 nm) and fluorescence (excitation at 490 nm and emission at 520 nm).

Template Activity of Oligodeoxyribonucleotides Containing Thymidine Analogues. DNA polymerase reactions were carried out by the same method as described above using a 37mer modified oligodeoxyribonucleotide template and a 17mer oligodeoxyribonucleotide primer (Scheme 2). Templates contained, at position 31, either normal thymidine or a thymidine analogue bearing hexamethylenediamine, tris(2-aminoethyl)amine, or ethylenediamine at the C5 sidearm (X position). KOD Dash, Taq, and Tth polymerase reactions were performed at 50 °C for 1, 2, 5, or 20 min in reaction mixture (10 μL) containing 0.5 unit of DNA polymerase, 0.2 μM primer−template complex, 20 μM unmodified substrates (dATP, dCTP, and TTP), 5 μM dGTP, and 1 μCi (800 Ci/mmol) of [α-^{32}P]dGTP in the buffer for KOD Dash, Taq, and Tth DNA polymerases described above.

Scheme 2. Sequence of the Primer, the Template, and the Full-Length DNA Product[a]



[a]Templates were Prepared Chemically, and T represents either standard thymidine (I) or one of three modified thymidines (II−IV). In the product, T indicates the positions where the polymerase has to incorporate thymidine residues (modified or unmodified).

The reactions with the Klenow fragment were performed at 37 °C for 5, 10, 30, and 60 min in the reaction mixture (10 μL) containing 0.5 unit of enzyme, 0.2 μM primer−template complex, 20 μM unmodified substrates (dATP, dCTP, and TTP), 5 μM dGTP, and 1 μCi (800 Ci/mmol) of [α-^{32}P]dGTP in 10 mM Tris-HCl (pH 8.0) and 5 mM $MgCl_2$.

The polymerase reactions were stopped by addition of 3 μL of formamide dye, denatured, and analyzed by gel electrophoresis as described above.

RESULTS

A series of C5-substituted 2′-deoxyuridine derivatives were prepared from 3′,5′-di-*O*-acetyl-5-methoxycarbonylmethyl-2′-deoxyuridine, which was synthesized easily according to the method described previously (*11*). The 5′-triphosphorylation of the nucleosides was carried out by the one-pot method described by Ludwig (*32*) with a slight modification as shown in Scheme 1. The terminal amino-protecting trifluoroacetyl group of the triphosphate from **1** or **3** was removed by treatment with concentrated aqueous ammonia quantitatively at low temperature. The resulting terminal amino group can be further modified by reaction with a functional molecule such as fluorescein isothiocyanate. Conventional modified substrates, 5′-triphosphates of 5-(*E*)-(aminopropenyl)-2′-deoxyuridine (**9**) and 5-(aminopropyl)-2′-deoxyuridine (**10**), were also prepared to compare the substrate specificity for the DNA polymerases.

Enzymatic Incorporation of the Thymidine Analogues by DNA Polymerases. Compounds **4**, **5**, **6**, **7**, **8**, **9**, and **10** were tested as substrates for DNA poly-

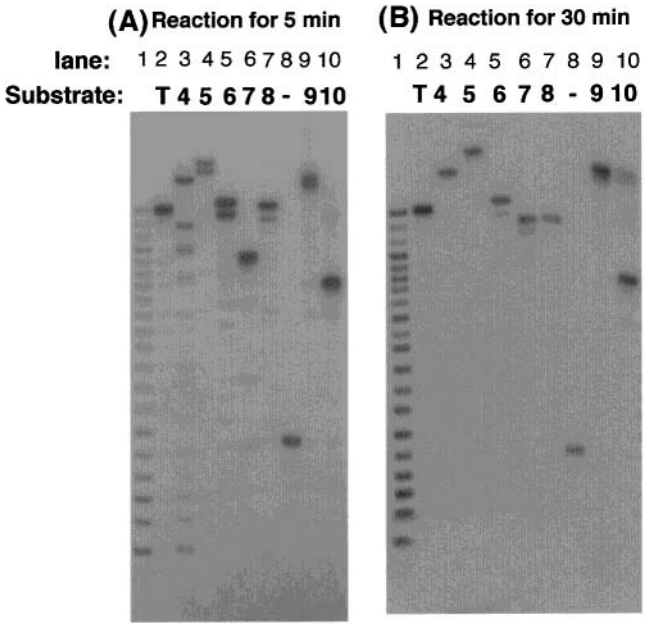


Figure 1. Autoradiogram of the products of primer extension reactions using KOD Dash DNA polymerase, and either normal TTP or modified as substrates. The reactions were done at 50 °C for 5 min (A) or 30 min (B) under the conditions described under Materials and Methods. Lane 1, marker DNA; lane 2, positive control (TTP+dATP+dCTP+dGTP); lane 3, **4**+dATP+dCTP+dGTP; lane 4, **5**+dATP+dCTP+dGTP; lane 5, **6**+dATP+dCTP+dGTP; lane 6, **7**+dATP+dCTP+dGTP; lane 7, **8**+dATP+dCTP+dGTP; lane 8, negative control (dATP+dCTP+dGTP); lane 9, **9**+dATP+dCTP+dGTP; lane 10, **10**+dATP+dCTP+dGTP.

merase I from *E. coli* (Klenow fragment), Taq, Tth, and KOD Dash DNA polymerases using the same amount of standard enzyme activity for comparison of activities against the modified substrate. The polymerization reactions with KOD Dash, Taq, and Tth DNA polymerases were carried out at 50 °C for 5 and 30 min, because the melting temperature of the primer−template complex was estimated to be a little lower than 50 °C under the reaction conditions (*34*). The polymerization reactions in the case of the Klenow fragment were done at 37 °C for 30 min. DNA polymerases extend the primer on the template (Scheme 2). Thus, when unmodified substrates and the same enzyme activities were used, all enzymes formed 37mer full-length DNA at the same rate. However, the ability of the modified thymidine triphosphates to function as a substrate depended on the type of modification, and on the polymerase.

KOD Dash DNA Polymerase Reactions. Figure 1A and Figure 1B show the KOD Dash DNA polymerase reactions for 5 and 30 min, respectively. The 37mer full-length DNA was the major product from the unmodified substrate (lane 2). The result of the control reaction with no TTP is shown in lane 8: the polymerization was completely stopped before the first T position, forming a 22mer DNA. In contrast to the other enzymes, KOD Dash DNA polymerase tolerated the modification, and readily accepted the modified substrates forming the full-length DNA. Thus 37mer DNAs were formed from compounds **4**, **5**, and **6** (lanes 3, 4, and 5) when the polymerization reaction was carried out for 30 min (B), although some short-chained DNAs were observed in the 5 min reaction (A). The 37mer DNA product containing trifluoroacetyl-protected hexamethylenediamine (compound **4**, lane 3) or hexamethylenediamine (compound **5**, lane 4) modified thymidine showed lower electrophoretic mobility than DNA containing unmodified thymidine (lane 2) or methoxycarbonyl-modified thymidine (compound **6**, lane 5). Attachment of a bulky substituent and a cationic protonated amino group presumably retarded the mobility of these modified DNAs. The structure of the modified 37mer obtained from compound **5** was confirmed by MALDI-TOF mass spectroscopy. The observed molecular weight of the modified 37mer, prepared in a large scale and isolated by HPLC, was 11 937, while the calculated mass number $([M+H])^+$ of the enzymatic product was 11 932. The modified DNA from **5** bearing a terminal amino group was further reacted with fluorescein isothiocyanate to furnish the fluorescence-labeled DNA. Treatment of the 37mer obtained from compound **4** with concentrated ammonium hydroxide removed the terminal trifluoroacetyl groups, giving the modified DNA with hexamethylenediamine, whose electrophoretic mobility was the same as the modified DNA obtained from compound **5**. KOD Dash DNA polymerase also accepted as a substrate the highly modified compound **7** (lane 6), which bears a bulky branched polyamine with two cationic protonated amino groups at the C5 sidearm. Incorporation of compound **7** and chain-elongation took place at the first T-23 position. However, the enzyme could not tolerate two successive incorporations of compound **7**, stopping at the T-30 position (lane 6). This enzyme could tolerate the substrate analogue **8** with an anionic carboxyl, yielding the full-length 37mer, although the 36mer was the main product in the case of the long reaction time (lane 7). The enzyme also accepted a conventional modified substrate, **9**, bearing an (*E*)-aminopropenyl group easily giving the corresponding 37mer DNA (lane 9). The analogue **10** bearing an aminopropyl group was partially accepted as a substrate. Small amounts of the full-length 37mer DNA were formed, although the main product was a truncated DNA 30mer in which the chain-elongation stopped at the two successive T positions (lane 10 of Figure 1B). The results indicate that, in contrast to the other DNA polymerases, the KOD Dash DNA polymerase can accept C5-substituted 2′-deoxyuridine with an sp3-hybridized carbon at the α-position as a substrate.

Taq and Tth DNA Polymerase Reactions. Polymerization reactions using Taq and Tth DNA polymerases are shown in Figure 2. Both enzymes showed similar behavior with the modified substrates. The full-length 37mer was exclusively formed after 5 min when the natural substrate TTP was used (Figure 2A, lane 2), while chain-elongation was completely stopped at the first T position, forming 22mer DNA in the control reaction without TTP (Figure 2A, lane 8). Small amounts of 38mer and 23mer DNAs were formed after 30 min due to the terminal transferase activity of the enzymes both with and without TTP, respectively (Figure 2B, lanes 2 and 8). Compounds **4** and **5** slowed elongation, forming mainly the 22mer DNA after 5 min (lanes 3 and 4). However, the enzymes accept compounds **4** and **5** slowly, and extend the polymerization reaction after the first single T position, and a substantial amount of 28mer DNA was formed after 30 min. The incorporation was completely inhibited at the two successive TT positions. The main polymerization product when using compound **6** was 28mer DNA after 5 min (Figure 2A, lane 5). Chain elongation took place after 30 min, forming 29mer and full-length 37mer DNAs (Figure 2B, lane 5). On the other hand, these enzymes could not use compounds **7** and **8**, giving only 22mer and 23mer DNA, although very small amounts of 28mer DNA were formed after 30 min (Figure 2B, lanes 6 and 7). The enzymes use compound **9**, giving full-length 37mer DNA after 30 min in accordance with

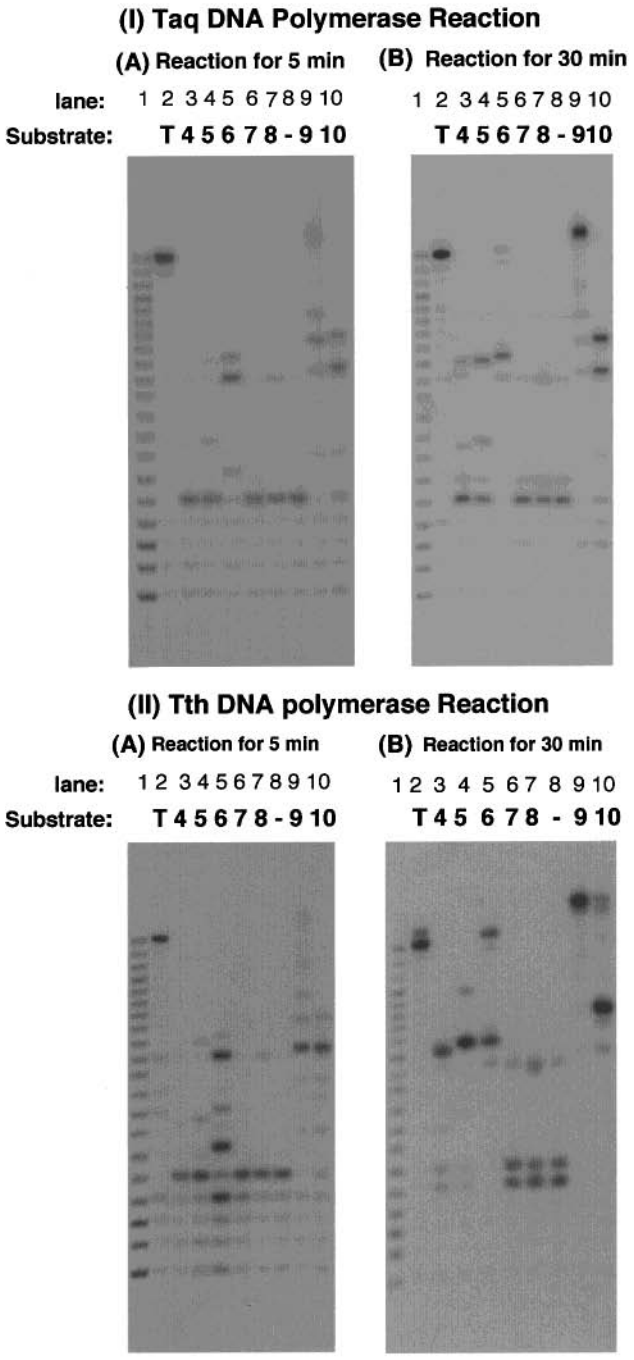


Figure 2. Autoradiogram of the products of primer extension reactions using Taq (I) and Tth (II) DNA polymerase, with various mixtures of nucleoside triphosphates (normal and/or modified). The reactions were done at 50 °C for 5 min (A) or 30 min (B) under the conditions described under Materials and Methods. Lane numbering is identical to that in Figure 1.

previous report (*25*, *30*), although 28mer and 29mer DNAs were the main products in the 5 min reaction (lane 9). Compound **10** was accepted by the enzyme at the first T-23 position, and chain-elongation continued beyond this point, but not at the two successive TT position giving the 28mer and 29mer DNAs (lane 10).

Polymerization Reactions with DNA Polymerase I from *E. coli* (Klenow Fragment). Figure 3 shows results of polymerization reactions with DNA polymerase I from *E. coli* (Klenow fragment). The 37mer full-length DNA was the major polymerization product when the unmodified substrate was used, although small amounts of 38mer and 36mer DNAs were also formed due to the

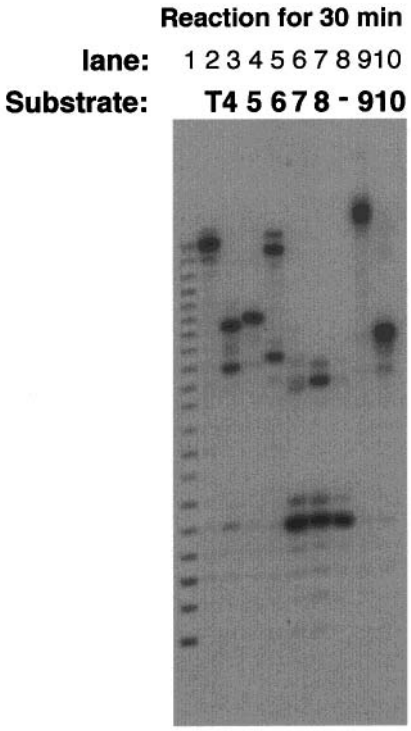


Figure 3. Autoradiogram of the products of primer extension reactions using DNA polymerase I from *E. coli* (Klenow fragment), with various mixtures of nucleoside triphosphates (normal and/or modified). The reactions were done at 37 °C for 30 min under the conditions described under Materials and Methods. Lane numbering is identical to that in Figure 1.

presence of terminal transferase and 3′-5′ exonuclease activities of the enzyme (lane 2). In the control reaction in which TTP was absent (lane 8), polymerization was completely stopped before the first T position, forming 22mer DNA, although small amounts of the 23mer were formed by the terminal transferase activity. Klenow fragment accepted compounds **4** and **5**, and extended the chain elongation at the first T-23 position. The enzyme could tolerate two successive incorporations of **4** or **5** at T-29 and T-30, but further chain-elongation was completely stopped, forming 30mer DNA (lanes 3 and 4). The enzyme also accepted compound **6** producing full-length 37mer DNA, along with substantial amounts of 36mer and 29mer, which were terminated at the T-36 and T-29 positions, respectively (lane 5). Compound **7** completely inhibited the enzyme. Thus, the main product was 22mer DNA which ended before the first T position, although very small amounts of 28mer DNA, in which chain-elongation was stopped before the double T position, were also formed (lane 6). Compound **8** was accepted to some extent by the enzyme, with formation of 28mer DNA, which passed through the T-23 but stopped before the two successive T (lane 7). With the conventional substrate analogue **9**, full-length 37mer DNA was formed as a sole product (lane 9). With compound **10**, only a truncated DNA 30mer was formed (lane 10). The results with compounds **9** and **10** are consistent with the previous report (*22*, *23*) in which the Klenow fragment accepts 2′-deoxyuridine derivatives bearing a propenyl group at the C5-position, but reduction of the double bond inhibits their function as a substrate. The formation of short DNAs with compounds **7** and **8** is due to inhibition of incorporation of the modified substrate. Inhibition of chain-elongation after incorporation results in the formation of the truncated DNA in the cases of compounds **4**, **5**, **6**, and **10**.

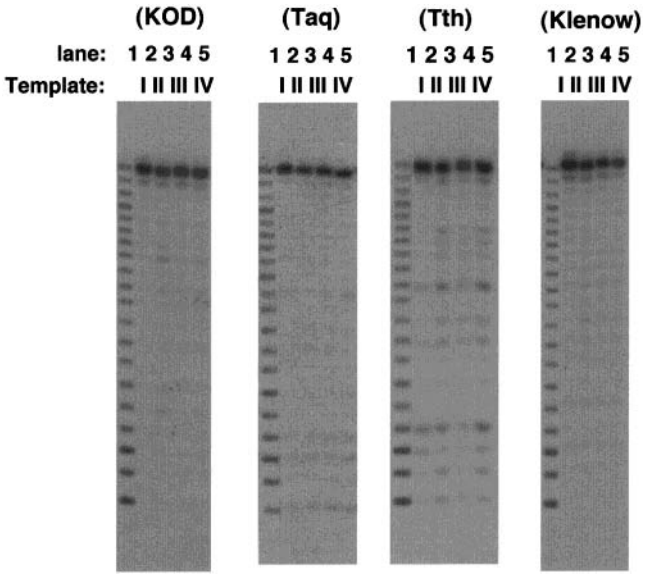


Figure 4. Autoradiogram of the products of primer extension on a DNA template bearing at position 31 either a normal thymidine residue or a C5-substituted 2′-deoxyuridine. The reactions were done at 50 °C for 5 min for Taq, Tth, and KOD Dash DNA polymerases, and at 37 °C for 30 min for Klenow fragment and under the conditions described under Materials and Methods, and unmodified 2′-deoxyribonucleoside triphosphates as substrates (TTP+dATP+dCTP+dGTP). Lane 1, marker DNA; lane 2, positive control (unmodified template I); lane 3, modified template II, bearing hexamethylenediamine at C5; lane 4, modified template III, bearing tris(2-aminoethyl)amine at C5; lane 5, modified template IV, bearing ethylenediamine at C5.

Template Activity of Oligodeoxyribonucleotides Containing Thymidine Analogues. Figure 4 illustrates the results of polymerization of unmodified substrates, dATP, dCTP, dGTP, and TTP, on modified DNA templates by KOD Dash, Taq, and Tth DNA polymerases and the Klenow fragment. The 37mer template DNA contains the thymidine analogue at the 31st position in place of a thymidine residue. All the DNA polymerases examined in this study read through the modified thymidine in the template, and accepted the complementary substrate and continued the chain-elongation until the end of the template, forming the full-length 37mer DNA.

DISCUSSION

We have examined the substrate activity of TTP analogues, **4**, **5**, **6**, **7**, and **8** along with the conventional **9** and **10**, for several DNA polymerases. Compounds **4**−**8** and **10** have an sp3-hybridized carbon at the C5 α-position with or without a bulky sidearm. Compounds **5** and **7** have one or two positively charged amino groups in the sidearm. Compound **8** bears a negatively charged carboxyl group. Compound **6** has a small noncharged substituent. Compound **9**, which has an (*E*)-aminopropenyl group at the C5-positon of 2′-deoxyuridine, is reported to be a good substrate for several DNA polymerases (*22*, *23*, *25*, *27*, *30*). On the other hand, the thymidine analogue **10**, the reduced product of **9**, is reported to be devoid of substrate activity for the enzymes (*27*, *30*). We found that KOD Dash DNA polymerase can accept various TTP analogues, **4**, **5**, **6**, **8**, and **9**, readily as substrates and the corresponding full-length 37mer DNA was formed. The enzyme also accepts compound **10**, although the full-length DNA was formed in modest yield. The enzyme, however, could not tolerate two successive incorporations of compound **7**. KOD Dash DNA polymerase is a hyperthermophilic DNA polymerase from thermophilic archaeum and is now commercially available. The enzyme is reported to have higher DNA polymerization activity with higher fidelity compared with other thermophilic DNA polymerases such as Taq DNA polymerase (*32*).

In contrast, compounds **4**, **5**, **6**, **7**, and **8** were poor substrates for Klenow fragment and Taq and Tth DNA polymerases. Compounds **4** and **5** gave only truncated DNA. A modest to substantial amount of the full-length 37mer DNA was obtained in addition to the truncated one when using compound **6** with these polymerases. The results of the DNA polymerization reaction by the Klenow fragment and Taq and Tth DNA polymerase confirm and extend the results reported previously (*22*−*30*). The 2′-deoxyuridine derivatives bearing a propenyl or propynyl linker at the C5 α-position are reported to function as substrates for several DNA polymerases, but the reduced product does not, indicating the possible requirement for an sp2- or sp-hybridized carbon at the C5 α-position (*22*−*30*). These results demonstrate that the ability of modified thymidine triphosphates to function as a substrate for DNA polymerases depends on the type of modification of the substrate and on the kind of polymerase.

KOD Dash DNA polymerase accepts the thymidine analogues which have an sp3-hybridized carbon at the C5 α-position, while other DNA polymerases cannot accept these analogues. The results are somewhat in contrast to the previous report on modified 2′-deoxyuridines, in which a propenyl or propynyl group at the C5 sidearm is required for the compound to be a substrate for DNA polymerase (*22*−*30*). Thus, this is the first example that C5-substituted 2′-deoxyuridine derivatives bearing an sp3-hybridized carbon at the C5 α-position are incorporated into DNA. All DNA polymerases examined in this study read through the thymidine modification in the template, giving the full-length DNA.

KOD Dash DNA polymerase may expand the range of structural modified substrates for enzymatic synthesis of modified DNAs. The resulting modified DNA can be further functionalized by reaction with a functional molecule such as fluorescein isothiocyanate. KOD Dash DNA polymerase and the thymidine analogues will be useful for preparing large quantities of modified DNA by PCR, and then in vitro selection of the functionalized DNA. The functionalized DNA synthesis by PCR using KOD Dash DNA polymerase and various thymidine analogues will be published elsewhere.

LITERATURE CITED

(1) Luyten, I., and Herdewijin, P. (1998) Hybridization properties of base-modified oligonucleotides within the double and triple helix motif. *Eur. J. Med. Chem. 33*, 515−576.
(2) Verma, S., and Eckstein, F. (1998) Modified oligonucleotides: Synthesis and strategy for users. *Annu. Rev. Biochem. 67*, 99−134.
(3) Ruth, J. L. (1991) Oligodeoxyribonucleotides with reporter groups attached to the base. In *Oligonucleotides and Analogues* (Eckstein, F., Ed.) pp 255−282, IRL Press, Oxford, U.K.
(4) Tesler, J. K., Cruickshank, A. L., Morrison, E., and Netzel, T. L. (1989) Synthesis and characterization of DNA oligomers and duplexes containing covalently attached molecular labels: Comparison of biotin, fluorescein, and pyrene labels by thermodynamic and optical spectroscopic measurements. *J. Am. Chem. Soc. 111*, 6966−6976.
(5) Jablonski, E. E., Moomaw, W., Tullis, R. H., and Ruth, L. L. (1986) Preparation of oligodeoxynucleotide-alkaline phosphatase conjugates and their use as hybridization probes. *Nucleic Acids Res. 14*, 6115−6128.
(6) Dreyer, G. B., and Dervan, P. B. (1985) Sequence-specific cleavage of single-stranded DNA: oligodeoxynucleotide-EDTA-Fe(II). *Proc. Natl. Acad. Sci. U.S.A. 82*, 968−972.

(7) Hurley, D. J., and Tot, Y. (1998) Metal containing oligonucleotides: sold-phase synthesis and luminescence properties. *J.. Am. Chem. Soc. 120*, 2194−2195.
(8) Ueno, Y., Mikawa, M., and Matsuda, A. (1998) Nucleosides and Nucleotides. 170. Synthesis and properties of oligodeoxyribonucleotides containing 5-[*N*-2-[[*N*,*N*-bis(2-aminoethyl)-amino]ethyl]carbamoyl]-2′-deoxyuridine and 5-[*N*-3-[[*N*,*N*-bis(3-aminopropyl)amino]propyl]carbamoyl]-2′-deoxyuridine. *Bioconjugate Chem. 9*, 33−39.
(9) Asseline, U., Bonfils, E., Dupret, D., and Thuong, N. T. (1996) Synthesis and binding properties of oligonucleotides covalently linked to an acridine derivative: new study of the influence of the dye attachment site. *Bioconjugate Chem. 7*, 369−379.
(10) Ozaki, H., Ogawa, Y., Mine, M., and Sawai, H. (1998) Effect of acridine with various linker arms attached to C5 position of 2′-deoxyuridine on the stability of DNA/DNA and DNA/RNA duplexes. *Nucleosides Nucleotides 8*, 911−923.
(11) Sawai, H., Nakamura, A., Sekiguchi, S., Yumoto, K., Endoh, M., and Ozaki, H. (1994) Efficient synthesis of new 5-substituted uracil nucleosides useful for linker arm incorporation. *J. Chem. Soc., Chem. Commun*., 1997−1998.
(12) Ozaki, H., Nakamura, A., Arai, M., Endoh, M., and Sawai, H. (1995) Novel C5-substituted 2′-deoxyuridine derivatives bearing amino-linker arms: Synthesis, incorporation into oligodeoxyribonucleotides, and their hybridization properties. *Bull. Chem. Soc. Jpn. 68*, 1981−1989.
(13) Aurup, H., Williams, D. M., and Eckstein, F. (1992) 2′-Fluoro- and 2′-amino-2′-deoxynucleoside 5′-triphosphates as substrates for T7 RNA polymerase. *Biochemistry 31*, 9636−9641.
(14) Dewey, T. M., Mundt, A. A., Crouch, G. J., Zyzniewski, M. C., and Eaton, B. E. (1995) New uridine derivatives for systematic evolution of RNA ligands by exponential enrichment. *J. Am. Chem. Soc. 117*, 8474−8475.
(15) Eaton, B. E., and Pieken, W. A. (1995) *Annu. Rev. Biochem. 64*, 837−863.
(16) Dewey, T. M., Zyzniewski, M. C., and Eaton, B. E. (1996) The RNA world: Functional diversity in a nucleoside by carboxyamidation of uridine. *Nucleosides Nucleotides 15*, 1611−1617.
(17) Tarasow, T. M., Tarasow, S. L., and Eaton, B. E. (1997) RNA-catalyzed carbon−carbon bond formation. *Nature 389*, 54−57.
(18) Wiegand, T. W., Janssen, R. C., and Eaton, B. E. (1997) Selection of RNA amide synthases. *Chem. Biol. 4*, 675−683.
(19) Tarasow, T. M., Tarasow. S. L., and Eaton, B. E. (2000) RNA diels-aldorases: relationships between unique sequences and catalytic function. *J. Am. Chem. Soc. 122*, 1015−1021.
(20) Vaish, N. K., Fraley, A. W., Szostak, J., and McLaughlin, L. W. (2000) Expanding the structural and functional diversity of RNA: analogue uridine triphosphates as candidates for in vitro selection of nucleic acids. *Nucleic Acids Res. 28*, 2316−2322.
(21) Trevisol, E., Defrange, E., Lhomme, J., Laayoun, A., and Cros, P. (2000) Synthesis of nucleoside triphosphates that contain an aminooxy function for post-amplification labeling. *Eur. J. Org. Chem. 2000*, 211−217.
(22) Langer, R. P., Waldrop, A. A., and Ward, D. C. (1981) Enzymatic synthesis of biotin-labeled polynucleotides: Novel nucleic acid affinity probes. *Proc. Natl. Acad. Sci. U.S.A. 78*, 6633−6637.
(23) Petrie, C. R., Adams, A. D., Stamn, M., Van Ness, J. S., Watanabe, M., and Meyer, R. B. (1991) A novel biotinylated adenylate analogue derived from pyrazolo[3,4-*d*]pyrimidine for labeling DNA probes. *Bioconjugate Chem. 2*, 441−446.
(24) Latham, J. A., Johnson, R., and Toole, J. J. (1994) The application of a modified nucleotide in aptamer selection: novel thrombin aptamers containing 5-(1-pentynyl)-2′deoxyuridine. *Nucleic Acids Res. 22*, 2817−2822.
(25) Sakthivel, K., and Barbas, C. F., III (1998) Expanding the potential of DNA for binding and catalysis: Highly functionalized dUTP derivatives that are substrate for thermostable DNA polymerases. *Angew. Chem., Int. Ed. Engl. 37*, 2872−2875.
(26) Battersby, T. R., Ang, D. N., Burgstaller, P., Jurczyk, S. C., Bowser, M. T., Buchanan, D. D., Kennedy, R. T., and Benner, S. A. (1999) Quantitative analysis of receptors for adenosine nucleotides obtained via in vitro selection from a library incorporating a cationic nucleotide analogue. *J. Am. Chem. Soc. 121*, 9781−9789.
(27) Godovikova, T. S., Kolpashchikov, D. M., Orlova, T. N., Richter, V. A., Ivanova, T. M., Grochovsky, S. L., Nasedkina, T. V., Victorova, L. S., and Poletaev, A. I. (1999) 5-[3-(*E*)-(4-azido-2,3,5,6-tetrafluorobenzamide)propenyl-1]-2′-deoxyuridine-5′-triphosphate substitutents for thymidine-5′-triphosphate in the polymerase chain reaction. *Bioconjugate Chem. 10*, 529−537.
(28) Perrin, D. M., Garestier, T., and Helene, C. (1999) Expanding the catalytic repertoire of nucleic acid catalyst: Simultaneous incorporation of two modified deoxyribonucleoside triphosphates bearing ammonium and imidazolyl functionalities. *Nucleosides Nucleotides 18*, 377−391.
(29) Santoro, S. W., Joyce, G. F., Sakthivel, K., Gramatikova, S., and Barabas, C. F., III (2000) RNA Cleavage by a DNA enzyme with extended chemical functionality. *J. Am. Chem. Soc. 122*, 2433−2439.
(30) Lee, S. E., Sidrov, A., Gourlain, T., Mignet, N., Thorpe, S. J., Brazier, J. A., Dickman, M. J., Hornby, D. P., Grasby, J. A., and Williams, D. M. (2001) Enhancing the catalytic repertoire of nucleic acids: a systematic study of linker length and rigidity. *Nucleic Acids Res. 29*, 1565−1573.
(31) Gourlain, T., Sidrov, A., Mignet, N., Thorpe, S. J., Lee, S. E., Grasby, J. A., and Williams, D. M. (2001) Enhancing the catalytic repertoire of nucleic acids. II. Simultaneous incorporation of amino and imidazoyl functionalities by two modified triphosphates during PCR. *Nucleic Acids Res. 29*, 1898−1905.
(32) Takagi, M., Nishioka, M., Kakihara, H., Kita, M., Inoue, H., Kawakami, B., Oka, M., and Imanaka, T. (1997) Characterization of DNA polymerase from *Pyrococcus* sp. strain of KOD1 and its application to PCR. *Appl. Environ. Microbiol. 63*, 4504−4510.
(33) Ludwig, J. (1981) A new route to nucleoside 5′-triphosphate. *Acta Biochem. Biophys. Acad. Sci. Hung. 16*, 131−133.
(34) Breslauer, J. K., Frank, R., Blöcker, H., and Markay, L. A. (1986) Predicting DNA duplex stability from the base sequence. *Proc. Natl. Acad. Sci. U.S.A. 83*, 3746−3750.

BC010088L

De Novo Synthesis of a New Diethylenetriaminepentaacetic Acid (DTPA) Bifunctional Chelating Agent

Ahmad Safavy,*[,§] Dale C. Smith, Jr.,[§] Alireza Bazooband,[†,‡] and Donald J. Buchsbaum[§]

Department of Radiation Oncology, University of Alabama at Birmingham, Birmingham, Alabama 35294, and Department of Pathology, University of Florida/Shands Jacksonville, Jacksonville, Florida 32209.
Received September 23, 2001; Revised Manuscript Received January 10, 2002

Diethylene triamine pentaacetic acid (DTPA) has been in extensive use as a metal chelator in the development of radiopharmaceuticals and contrast agents. The former application uses DTPA mostly as a bifunctional chelating agent (BCA) conjugated to tumor-targeting vehicles (TTVs) such as monoclonal antibodies (MAbs) and receptor-directed peptides. A new bifunctional DTPA derivative was synthesized by a fully organic scheme. This compound, N^4,N^{α},N^{α},N^{ϵ},N^{ϵ}-[pentakis(carboxymethyl)]-N^4-(carboxymethyl)-2,6-diamino-4-azahexanoic hydrazide (**20**) was prepared by a convergent synthesis strategy using N^{α}-benzyloxycarbonyl-2,3-diaminopropionic acid as the starting compound. This commercially available material was used to build a functionalized triamine which served as the molecular core template for assembling the target molecule. To evaluate the conjugation and radiolabeling capabilities of this new molecule, it was covalently attached to the *anti*-TAG-72 MAb, ΔCH2HuCC49, and the conjugate was radiolabeled in near-quantitative yields with yttrium-90 (^{90}Y) and lutetium-177 (^{177}Lu). Biodistribution of the ^{177}Lu-labeled DTPA−ΔCH2HuCC49 in tumor-bearing nude mice demonstrated preservation of the immunoreactivity of the MAb as indicated by high tumor uptake. In addition to the introduction of a new bifunctional DTPA, this work reports on a novel synthetic approach for preparation of this useful metal chelator and introduces a new conjugation protocol.

INTRODUCTION

Metallic nuclides have found increasingly important applications in diagnostic and therapeutic medicine (*1*−*3*). These, in the main part, include the use of transition metals as contrast agents in magnetic resonance imaging (*4*, *5*) and the development of radiopharmaceuticals, with the latter playing a major role in both diagnosis and therapy of neoplastic disease (*6*−*12*). Targeted delivery of radioactivity to malignant tissue through the application of monoclonal antibodies (MAbs)[1] (*13*) has progressed significantly by the development of MAb derivatives and fragments, and small-molecule peptides (*14*−*20*). In this regard, the design and development of synthetic BCAs for connecting these targeting vehicles to radioactive metals, and improvements in the related conjugation and chelation chemistries, have made significant contributions (*3*, *21*−*25*).

Several classes of BCAs have been reported in radioactive lanthanide and transition metal labeling procedures (*1*−*3*). An important series, the macrocyclic azacarboxylates (MACs), have demonstrated outstanding metal chelation and complex properties with members (DOTA and TETA) already in clinical trials. A large body of radioimmunoconjugate-related data, mainly based on the works of Meares et al., and Gansow and Brechbiel et al., is available for these compounds (*26*−*30*).

Acyclic analogues of MACs, represented by DTPA and EDTA, constitute another major class of BCAs. The iminocarboxylate compound DTPA has been used for the radiolabeling of MAb and peptide TTVs, particularly with the isotopes of yttrium (^{88}Y, ^{90}Y) (*31*−*33*), indium (^{111}In) (*34*−*37*), samarium (^{152}Sm, ^{153}Sm) (*38*, *39*), and lutetium (^{177}Lu) (*40*, *41*). These and other applications of DTPA, such as MRI (*4*, *5*, *42*) and luminescent lanthanide imaging (*43*), confer great importance to this compound. Two major protocols for conjugation of DTPA derivatives to MAbs, peptides, and nucleic acids have been reported, namely, the cyclic dianhydride (*44*, *45*) and isothiocyanate procedures (*46*). While most of the reported work on DTPA conjugation is based on these derivatives, difficulties may sometimes arise. The anhydride coupling may result in conjugation heterogeneity (i.e., mono- versus dicoupling) and is accompanied by the loss of one of the prospective metal chelating carboxyl groups. The latter feature may result in a less stable chelation product with the premature release of the activity in vivo (*47*). The isothiocyanate approach may also show some limited stability of the thiocyanate group and low aqueous solubility of these compounds. Nevertheless, routine

* To whom correspondence should be addressed at 1824 6th Avenue South, WTI 674 Birmingham, AL 35294-6832. E-mail: safavy@uab.edu.

§ University of Alabama at Birmingham.

† University of Florida/Shands Jacksonville.

‡ Present address: University of Florida/Shands Jacksonville, Department of Pathology, 655 W 8th Street Jacksonville, FL 32209.

[1] Abbreviations: BCA, bifunctional chelating agent; Boc, *tert*-butyloxycarbonyl; Cbz, benzyloxycarbonyl; DCC, dicyclohexylcarbodiimide; DIEA, diisopropylethylamine; DOTA, 1,4,7,10-tetraazacyclododecane-*N*,*N*′,*N*″,*N*‴-tetraacetic acid; DTPA, diethylenetriaminepentaacetic acid; ESMS, electrospray mass spectrometry; FWHM, full-width half-maximum; HOBT, 1-hydroxy benzotriazole; MAb, monoclonal antibody; MALDI MS, matrix-assisted laser desorption/ionization mass spectrometry; Phth, pthalyl; MRI, magnetic resonance imaging; TFA, trifluoracetic acid; TETA, 1,4,8,11-tetraazacyclotetradecane-*N*,*N*′,*N*″,*N*‴-tetraacetic acid; THF, tetrahydrofuran; TTV, tumor-targeting vehicle.

10.1021/bc0100861 CCC: $22.00 © 2002 American Chemical Society
Published on Web 02/16/2002

conjugation procedures are being conducted with these compounds.

In this paper, we report through a novel approach, the synthesis of a new bifunctional DTPA containing a hydrazide sidearm for TTV conjugation. The hydrazide function is placed on one of the methylene carbons of the skeletal core, thus leaving all five carboxyl groups available for metal chelation. This feature may lead to significantly better metal complex kinetics and stabilities, which are highly desirable features in diagnosis and therapy procedures. The hydrazide function allows for efficient and group-specific conjugation through a procedure developed in this laboratory for the covalent attachment of unprotected hydroxamate BCAs to Mabs (*22*). In contrast to the cyclic anhydride and isothiocyanate derivatives, the new DTPA hydrazide is stable, both in solid form and in solution, for extended periods of time. This stability is an important feature that may be particularly useful in the development of DTPA kits for clinical applications.

EXPERIMENTAL PROCEDURES

General Procedures. THF was ketyl distilled under argon. All other reagents and solvents were obtained from commercial suppliers and were used as received. ^{1}H NMR spectra were recorded on a Bruker ARX500 FT-NMR spectrometer. The chemical shifts were referenced to internal tetramethylsilane (TMS). ESMS spectra were recorded either on an API VI triple quadruple mass spectrometer (PE-Sciex, Toronto, Ontario) or Micromass Platform LCZ mass spectrometer (Beverly, MA). Thin layer chromatography (TLC) was performed with Whatman glass-backed silica gel plates (2.5 × 7.5 cm, coating thickness 250 μm, detected at 254 nm). Solvents for TLC were mixed on a v/v scale and are defined as follows: (A) chloroform/methanol, 90:10; (E) chloroform/methanol/acetic acid, 77:20:3. RP-HPLC was performed on a BioRad model 5000 Titanium system (BioRad, Richmond, CA) equipped with a model 1806 UV/Vis detector at 254 nm unless otherwise noted. HPLC solvents: H_2O containing 0.1% TFA; 60/40 CH_3CN/H_2O (v/v) containing 0.1% TFA, gradient elution. Analytical HPLC runs were performed on a C_{18} column (4.6 T 250 cm, Vydac, Hesperia, CA). Metal-free purified water (18.2 MΩ) was obtained from a Milli-QF system (Millipore, Bedford, MA). Retention times (t_R's) are reported in minutes at the specified wavelength (nm) with percent area under the peak in parentheses as a measure of compound purity. For analytical SEC−HPLC, a 7.5 mm × 25 cm G3000SW column (TosoHaas, Montgomeryville, PA) was used. A 10 mM PBS containing 10 mM Na_2SO_4 at pH 6.7 was used as solvent. Preparative SEC was carried out using Sephadex G-25 columns (PD-10, Pharmacia Biotech AB, Uppsala, Sweden) eluted with DPBS.

MALDI MS Analyses. Samples were analyzed in the positive mode on a Voyager Elite mass spectrometer with delayed extraction technology (PerSeptive Biosystems, Framingham, MA). The acceleration voltage was set at 25 kV, and 50−100 laser shots were summed. The matrix was Sinapinic acid, dissolved in a 50:50 (v/v) mixture of 0.1% TFA:acetonitrile. A 1 pmol/μL solution of bovine serum albumin was added as an internal standard. Equal volumes of sample and matrix were mixed on a smooth plate, and the average of three measurements were reported. For each reaction, the intact MAb was scanned as the control for evaluation of the following conjugation. The molecular weight increase of the OHA-MAb intermediate was calculated using the unconjugated MAb. The molecular weight of this intermediate then served as the control to measure the increase in the molecular weight of the final product conjugate. Each difference in molecular weight was divided by the molecular weight of the corresponding linker to measure the linker/MAb ratio.

High Resolution Mass Spectroscopy Procedure. The high-resolution liquid secondary ion mass spectra were acquired on a Micromass AutoSpec Magnetic Sector mass spectrometer (Beverly, MA) operated at a resolution of 10 000 (FWHM). All samples were run as approximately 1 μg/mL solutions in *m*-nitrobenzyl alcohol using matrix clusters or added peptides as reference peak.

Methyl N^{α}-(benzyloxy carbonyl)-2,3-diaminopropionate (2). A suspension of N^{α}-(benzyloxy carbonyl)-2,3-diaminopropionic acid (5.0 g, 21 mmol) in methanol (50 mL) was cooled to 0 °C while stirring under argon. A solution of 4 M HCl (40 mL) in dioxane was added dropwise, and the reaction was allowed to gradually warm to ambient temperature over 18 h. The solution was concentrated in vacuo to a white solid. This residue was triturated with diethyl ether (3 × 30 mL) to a fine powder that was dried in vacuo to yield **2** (6.0 g, 99%) as a white crystalline solid in high purity. mp 160−163 °C. R_f (A) 0.03, (E) 0.63. HPLC: t_R 12.97 min (>99%). ^{1}H NMR (500 MHz, DMSO-d_6) d 8.19 (br s, 4H,), 7.95 (br s, 1H), 7.35 (m, 5H), 5.07 (s, 2H), 4.43 (m, 1H), 3.63 (m, 2H), 2.50 (s, 3H). HRMS (FAB$^+$): 253.1195 ($C_{12}H_{16}N_2O_4$ + H requires 253.1188). MS(ES$^+$) 253. Anal. Calcd for $C_{12}H_{17}N_2ClO_4$: C, 49.9; H, 5.9; N, 9.7. Found: C, 50.0; H, 6.0; N, 9.8.

***N*-[1-(2,2-Diethoxy)ethyl]phthalimide (7).** A flask containing a solution of phthalic anhydride (22.2 g, 150 mmol), amino acetaldehyde diethyl acetal (20.0 g, 150 mmol), and DIEA (2.6 mL, 0.15 mmol) in toluene (100 mL) was fitted with a Dean−Stark trap and heated to 100 °C. TLC was used to follow the progress of the reaction. After 20 h, the reaction was complete, and the solution was concentrated in vacuo to a brown oil. The residue was taken up in ethyl acetate (100 mL) treated with charcoal, dried over $MgSO_4$, and filtered. The filtrate was concentrated in vacuo to a yellow-brown solid. The residue was eluted through a silica plug (4 × 6 cm) with chloroform and then recrystallized (2×) from ethyl acetate/hexanes (1:5, v/v) to afford **5** (27.1 g, 69%) as yellow plates in high purity. mp 72−73 °C. R_f (A) 0.89, (E) 0.94. HPLC: t_R 22.33 min (>99%). ^{1}H NMR (500 MHz, $CDCl_3$) d 7.85 (m, 2H), 7.55 (m, 2H), 4.88 (t, J = 5.7 Hz, 2H), 3.82 (d, J = 5.7 Hz, 1H), 3.74 (m, 2H), 3.54 (m, 2H), 1.16 (m, 6H). HRMS (FAB$^+$) 264.1232 ($C_{14}H_{17}NO_4$ + H requires 264.1235). MS(ES$^+$) 264. Anal. Calcd for $C_{14}H_{17}NO_4$: C, 63.9; H, 6.5; N, 5.3. Found: C, 64.1; H, 6.5; N, 5.4.

***N*-[(Formyl)methyl]phthalimide (8).** A solution of **7** (27.0 g, 0.10 mmol) in acetic acid/water (1:1, 200 mL) was stirred under an argon purge at 60 °C. TLC determined completion of the reaction after 48 h. The solution was concentrated, and $NaHCO_3$ was added to neutralize the mixture to pH 8. The solution was extracted with ethyl acetate (3 × 100 mL), and the combined extracts were washed with 10% citric acid solution (3 × 100 mL) and brine (1 × 100 mL), dried over $MgSO_4$, and filtered. The filtrate was concentrated in vacuo to give a yellow-orange solid. The latter was eluted through a silica plug (4 × 6 cm) with chloroform and then recrystallized (2×) from ethyl acetate/hexanes (2:5, v/v) to yield **8** (8.24 g, 43%) as white needles in high purity. mp 108−111 °C. R_f (A) 0.72, (E) 0.92. HPLC: t_R 11.61 min (>99%). ^{1}H NMR (500 MHz, $CDCl_3$) d 9.67 (s, 1H), 7.89 (m, 2H), 7.75 (m, 2H), 4.88 (s, 2H). HRMS (FAB$^+$) 190.0501 ($C_{10}H_7NO_3$

+ H requires 190.0504). MS (ES^+) 190. Anal. Calcd for $C_{10}H_7NO_3$: C, 63.5; H, 3.7; N, 7.4. Found: C, 63.1; H, 4.0; N, 7.3.

Methyl N^{α}-(Benzyloxycarbonyl)-6-(*N*-phthalimidyl)-2-amino-4-azahexanoate (9). A solution of **2** (6.1 g, 21.2 mmol), **8** (4.0 g, 21.2 mmol) in dry THF (175 mL) was stirred under argon, and sodium tri(acetoxy)borohydride (19.0 g, 186 mmol) was slowly added. The heterogeneous, reaction mixture was stirred under an argon atmosphere at ambient temperature for 18 h, after which time it was filtered through Celite (2×) and concentrated in vacuo to a yellow oil. The oil was dissolved in ethyl acetate (100 mL) and extracted with water (3 × 50 mL) and brine (1 × 50 mL). The organic phase was dried over $MgSO_4$ and filtered, and the filtrate was concentrated in vacuo to yield **7** (7.71 g, 86%) as a light yellow solid. mp 47−49 °C. R_f 0.08 (A), (E) 0.71. HPLC: t_R 17.53 min (>96%). ^{1}H NMR (500 MHz, $CDCl_3$) d 7.72 (m, 2H), 7.65 (m, 2H), 7.48 (m, 5H), 5.82 (br s, 1H), 4.45 (m, 1H), 3.5−3.9 (m, 6H), 2.15 (s, 3H). HRMS (FAB^+) 426.1676 ($C_{22}H_{23}N_3O_6$ + H requires 426.1665). MS (ES^+) 426. Anal. Calcd for $C_{22}H_{23}N_3O_6 \cdot {}^1/_4\ H_2O$: C, 61.6; H, 5.5; N, 9.7. Found: C, 61.5; H, 5.7; N, 9.7.

Methyl N^{α}, N^{ϵ}-Bis(benzyloxycarbonyl)-6-(*N*-phthalimidyl)-2-amino-4-azahexanoate (10). A solution of **9** (6.84 g, 16.1 mmol) and DIEA (3 mL, 17 mmol) in dioxane (100 mL) was cooled to 0 °C while stirring under argon. Benzyl chloroformate (BCF, 2.4 mL, 17 mmol) in dioxane (25 mL) was added dropwise through an addition funnel over 30 min, and the solution was allowed to warm to ambient temperature and stirred for 18 h. The solution was filtered to remove the solid precipitate, and the filtrate was in vacuo to a yellow oil. The oil was dissolved in ethyl acetate (75 mL), and the solution was extracted with 10% aqueous citric acid (3 × 50 mL), 10% aqueous $NaHCO_3$ (3 × 50 mL), and brine (1 × 50 mL), dried over $MgSO_4$, and filtered. The filtrate was concentrated in vacuo to a yellow oil. Flash chromatography on silica gel column (4 × 25 cm), eluted with 1.5% methanol in chloroform, afforded **10** (6.75 g, 75%) as a light yellow oil. R_f (A) 0.83, (E) 0.98. HPLC: t_R 30.62 min (>99%). ^{1}H NMR (500 MHz, $CDCl_3$) d 7.60−7.85 (m, 4H) 7.20−7.45 (m, 10H), 5.95 (br s, 1H), 5.12 (s, 2H), 4.63 (s, 2H), 4.45 (m, 1H), 3.4−3.9 (m, 6H), 1.62 (s, 3H). HRMS (FAB^+) 560.2047 ($C_{30}H_{29}N_3O_8$ + H requires 560.2032). MS (ES^+) 560. Anal. Calcd for $C_{30}H_{29}N_3O_8 \cdot {}^1/_2\ H_2O$: C, 63.4; H, 5.3; N, 7.4. Found: C, 63.7; H, 5.5; N, 7.1.

N^{α}, N^{ϵ}-Bis(benzyloxycarbonyl)-6-(*N*-phthalimidyl)-2-amino-4-azahexanoic Acid (14). A solution of **10** (6.8 g, 12.1 mmol) and 12 N HCl (30 mL) in dioxane (100 mL) was heated at 40 °C for 18 h. The solution was concentrated in vacuo to remove the dioxane. Water (20 mL) was added, and the mixture was extracted with ethyl acetate (3 × 50 mL). The combined ethyl acetate extracts were washed with brine (1 × 50 mL), dried over $MgSO_4$, and filtered. The filtrate was concentrated in vacuo to a yellow solid and triturated with diethyl ether (2 × 20 mL). Flash chromatography on a silica gel column (4 × 12 cm), eluted with a 2−15% methanol/chloroform gradient, afforded **14** (3.58 g, 54%) as a microcrystalline white solid. mp 53−55 °C. R_f (A) 0.19, (E) 0.89. HPLC: t_R 27.12 (>95%) min. ^{1}H NMR (500 MHz, $CDCl_3$) d 7.61−7.79 (m, 4H), 7.09−7.37 (m, 10H), 6.20 (br s, 1H), 5.10 (s, 2H), 4.94 (s, 2H), 4.47 (m, 1H), 3.49−3.82 (m, 6H). HRMS (FAB^+) 546.1902 ($C_{29}H_{27}N_3O_8$ + H requires 546.1876). MS (ES^+) 546. Anal. Calcd for $C_{29}H_{27}N_3O_8$: C, 63.8; H, 5.0; N, 7.7. Found: C, 63.5; H, 4.9; N, 7.7.

***N′*-(*tert*-Butyloxycarbonyl)-N^{α}, N^{ϵ}-bis(benzyloxycarbonyl)-6-(*N*-phthalimidyl)-2-amino-4-azahexanoic Hydrazide (15).** A solution of **14** (3.6 g, 6.5 mmol), HOBT, (1.0 g, 7.2 mmol), and *tert*-butylcarbazate (0.95 g, 7.2 mmol) in dry THF (30 mL) was cooled to 0 °C, and DIEA (1.2 mL, 7.2 mmol) was added under an argon atmosphere. A solution of DCC (1.48 g, 7.2 mmol) in THF (5 mL) was added dropwise to the solution over 5 min. The reaction gradually was warmed to ambient temperature and stirred for 18 h. The white precipitate was separated by filtration, and the filtrate was concentrated in vacuo to an oil. This was taken up in ethyl acetate (20 mL), extracted with 10% aqueous citric acid (3 × 10 mL), 10% aqueous $NaHCO_3$ (3 × 10 mL), and brine (1 × 10 mL), and dried over $MgSO_4$. Filtration and evaporation in vacuo yielded **15** (4.23 g, 98%) as an off-white solid. mp 83−85 °C. R_f (A) 0.53, (E) 0.96. HPLC: t_R 28.65 min (>96%). ^{1}H NMR (500 MHz, $CDCl_3$) d 8.23 (br s, 1H), 7.65−7.78 (m, 4H), 7.10−7.47 (m, 10H), 6.85 (br s, 1H), 6.72 (br s, 1H), 5.10 (s, 2H), 4.84 (s, 2H), 4.43 (m, 1H), 3.39−3.82 (m, 6H), 1.42 (9H, s). HRMS (FAB^+) 660.2663 ($C_{34}H_{37}N_5O_9$ + H requires 660.2669). MS (ES^+) 660. Anal. Calcd for $C_{34}H_{37}N_5O_9 \cdot H_2O$: C, 60.3; H, 5.8; N, 10.3. Found: C, 60.3; H, 5.4; N, 10.3.

***N′*-(*tert*-Butyloxycarbonyl)-N^{α}, N^{ϵ}-bis(benzyloxycarbonyl)-2,6-diamino-4-azahexanoic Hydrazide (16).** A solution of **15** (4.2 g, 6.7 mmol) and hydrazine (0.84 mL, 26.7 mmol) in absolute ethanol (120 mL) was heated to 50 °C for 18 h. The voluminous white precipitate was separated by filtration (2×), and the filtrate was concentrated in vacuo to an off-white solid. Flash chromatography on a silica gel column (2 × 18 cm), eluted with a 3−8% methanol/chloroform gradient, afforded **16** (2.1 g, 59%) as a glassy white solid. mp 56−58 °C. R_f (A) 0.31, (E) 0.72. HPLC: t_R 20.49 min (>99%). ^{1}H NMR (500 MHz, $CDCl_3$) d 7.10−7.47 (m, 10H), 6.65 (br s, 1H), 6.42 (br s, 1H), 5.10 (s, 4H), 4.39 (m, 1H), 3.39−3.92 (m, 6H), 1.39 (s, 9H). HRMS (FAB^+) 530.2657 ($C_{26}H_{35}N_5O_7$ + H requires 530.2614). MS (ES^+) 530. Anal. Calcd for $C_{26}H_{35}N_5O_7 \cdot {}^1/_2\ H_2O$: C, 58.0; H, 6.7; N, 13.0. Found: C, 57.8; H, 6.6; N, 12.6.

***N′*-(*tert*-Butyloxycarbonyl)-2,6-diamino-4-azahexanoic Hydrazide (17).** A solution of **16** (1.54 g, 2.91 mmol) in acetic acid/water (9:1, v/v, 30 mL) was hydrogenated with palladium on carbon (10%, 0.46 g) at 50 psi for 24 h. The solution was filtered through Celite, and the filtrate was concentrated in vacuo to a yellow oil. The residue was triturated with ethyl acetate (2 × 5 mL), dissolved in methanol (2 mL), and precipitated from diethyl ether (50 mL). The suspension was separated by centrifugation to afford a yellow residue that was dissolved in water (20 mL), and the solution was extracted with ethyl acetate (3 × 20 mL). Lyophilization and drying of the product in vacuo over P_2O_5 yielded **17** (1.23 g, 96%) as a hygroscopic, yellow glass. mp 62−66 °C. HPLC (214 nm) 8.74 min (>95%). ^{1}H NMR (500 MHz, D_2O) d 9.15 (br s, 1H); 8.69 (br s 1H); 3.29 (m, 1H), 4.1−6.2 (br 8H), 2.54−2.85 (m, 6H), 1.86 (s, 9H), 1.39 (s, 9H). HRMS (FAB^+) 262.1866 ($C_{10}H_{23}N_5O_3$ + H requires 262.1879). MS (ES^+) 262. Anal. Calcd for $C_{14}H_{31}N_5O_9 \cdot {}^3/_4\ H_2O$: C, 42.6; H, 8.3; N, 17.7. Found: C, 42.4; H, 8.0; N, 18.0.

***N′*-(*tert*-Butyloxycarbonyl)-2,6-diamino-4-azahexanoic N^4,N^{α},N^{α},N^{ϵ},N^{ϵ}-[pentakis(benzyloxycarbonyl)-methy]-2,6-diamino-4-azahexanoic Hydrazide (18).** A solution of the triflate of benzyl glycolate (1.0 mL, 1.95 mmol) in anhydrous CH_2Cl_2 (15 mL) was added to a suspension of **17** (0.13 g, 0.13 mmol) and DIEA (0.44 mL, 2.5 mmol) in CH_2C_{l2} (15 mL) at −78 °C under an argon atmosphere. The reaction was allowed to proceed for 18 h at −78 °C and then gradually allowed to warm to 0 °C temperature over 72 h. The solution was extracted with

10% aqueous $NaHCO_3$ (2 × 2 mL) and brine (1 × 2 mL) and concentrated in vacuo to a yellow-orange oil. The oil was extracted with diethyl ether (4 mL × 3), and the combined ether extracts were dried over $MgSO_4$, filtered and concentrated in vacuo. The residue was flash chromatographed on a silica gel column (2 × 15 cm), eluted with chloroform with 0−1% methanol and 0−1% triethylamine gradient to afford **18** (0.071 g, 25%) as a pale yellow oil. R_f (A) 0.72, (E) 0.89. HPLC: t_R 20.99 min (>99%). ^{1}H NMR (500 MHz, $CDCl_3$) d 7.26−7.41 (m, 25H), 5.08−5.12 (m, 10H), 3.51−3.82 (m, 17H), 1.46 (s, 9H). HRMS (FAB^+) 1002.4513 ($C_{55}H_{63}N_5O_{13}$ + H requires 1002.4501). MS (ES^+) 1002. Anal. Calcd for $C_{55}H_{63}N_5O_{13} \cdot H_2O$: C, 64.8; H, 6.4; N, 6.9. Found: C, 64.8; H, 6.3; N, 6.9.

***N′*-(*tert*-Butyloxycarbonyl)-N^4,N^α,N^α,N^ϵ,N^ϵ-[pentakis(carboxymethyl)]-2,6-diamino-4-azahexanoic Hydrazide (19).** A solution of **18** (0.07 g, 0.07 mmol) in methanol (8 mL) was hydrogenated over Pd/C (10%, 0.032 g) at ambient temperature and with hydrogen balloon for 24 h. The catalyst was separated by filtration through a 0.2 μm acrodisc syringe tip filter (Gelman Sciences, Ann Arbor, MI), and the filtrate was concentrated in vacuo to an off-white oil. The oil was dissolved in methanol (1 mL), and the product was precipitated from diethyl ether (35 mL) and separated by centrifugation. The product was dried in vacuo to yield **19** (0.038 g, 96%) as a hygroscopic white microcrystalline solid. HPLC (214 nm): t_R 10.02 min (>95%). mp: 152−155 °C. ^{1}H NMR (500 MHz, D_2O) d 1.42 (s, 9H), 3.10−3.54 (m, 17H). MS (ES^+) 552. Anal. Calcd for $C_{20}H_{35}N_5O_{13} \cdot H_2O$: CF_3COOH. Cold: C, 38.7; H, 5.3; N, 10.2. Found: C, 38.4; H, 5.4; N, 10.6.

N^4,N^α,N^α,N^ϵ,N^ϵ-[pentakis(carboxymethyl)]-N^4-(carboxymethyl)-2,6-diamino-4-azahexanoic Hydrazide (20). TFA was added to **19** (0.017 g, 0.03 mmol) and stirred for 35 min. The solution was concentrated in vacuo, the residue was dissolved in methanol (1 mL), and the product was precipitated (4×) from diethyl ether (35 mL). Centrifugation and drying of the collected product in vacuo yielded **20** (0.014 g, 81%) as hygroscopic white microcrystalline TFA salt. mp: 116−119 °C. HPLC (214 nm): t_R 3.0 min (>98%). ^{1}H NMR (500 MHz, D_2O) d 3.32−3.43 (m, 6H), 3.50−3.90 (m, 11H). ^{19}F NMR (564 MHz, D_2O) d −74.3 (s). MS (ES^+) 452.

MAb Conjugation. The DTPA hydrazide **20** was conjugated to the MAb ΔCH2HuCC49 through a ketone-hydrazide technique described previously (*22*). Briefly, 6-oxoheptanoic acid was first conjugated to the MAb at pH 8.1. After buffer exchange to 50 mM ammonium acetate (pH 5.5), the BCA was introduced at a molar ratio of 300 relative to the MAb. The solution was stirred at 4 °C for 16 h, and the product was purified by dialysis. Number of DTPAs per antibody (DTPA: MAB) was calculated by MALDI analyses as described before (*22*). This procedure resulted in a DTPA/MAb of 4.

^{90}Y- and ^{177}Lu-Labeling. The same labeling protocol was applied to both isotopes which were supplied (University of Missouri Research Reactor, St. Louis, MO, and NEN, Boston, MA, for ^{90}Y and ^{177}Lu, respectively) as trichloride salts. Briefly, the radiometal in HCl (3 μL) was incubated in 50 μL of acetate buffer (pH 5.5) at ambient temperature for 15 min and was added to the solution of the conjugate (120 μg) in the same buffer (63 μL). Near-quantitative radiolabeling yields (>96%) were obtained with both isotopes as indicated by size-exclusion HPLC, after 1 h incubation at ambient temperature. Under these conditions, a control unconjugated MAb showed about 0.3−4% nonspecific labeling depending on the type of the MAb.[2] Labeled conjugates were purified by gel filtration using PD-10 columns and phosphate-buffered saline as the eluent. One-milliliter fractions were collected with the conjugate eluting in fractions 3 and 4.

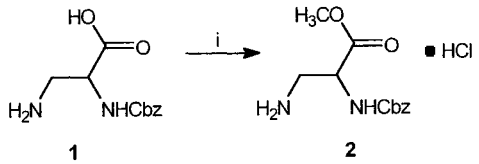
Animal Model. Athymic nude female *nu*/*nu* mice with a BALB/c background, were obtained from the National Cancer Institute Frederick Research Laboratory (Frederick, MD) and were kept under sterile conditions. Procedures to minimize discomfort, pain, and distress were in accord with the Animal Resource Program at the University of Alabama at Birmingham, accredited by the American Association for Accreditation of Laboratory Animal Care. The LS174T human colon cancer cells (American Type Culture Collection, Manassas, VA) were harvested and suspended in sterile PBS at a concentration of 7.5 × 10^8 viable cells/mL. Cell viability was determined by trypan blue dye exclusion. Two groups of animals (6 mice each) were injected i.p. with 10^8 viable cells in PBS. At a tumor diameter of 5−10 mm, 2 μCi of ^{177}Lu-DTPA−ΔCH2HuCC49 was injected i.p. into the mice and the animals were sacrificed 4 and 24 h after administration of the radiopharmaceutical. The radioactivity uptake of the tumor and normal tissues were measured in a gamma-counter, and the counts were used to calculate the percent injected dose per gram of tissue (%ID/g).

RESULTS AND DISCUSSION

Synthesis. In addition to the preparation of a bifunctional DTPA with a new conjugating functionality, a goal of this synthesis was to generate a DTPA precursor with full orthogonal protection of both the *metal-chelating* and the *conjugating* segments. Also, a fully organic phase synthetic strategy, without resorting to biphasic and/or aqueous and buffer-mediated steps, was of interest. All intermediate compounds, formed prior to the deprotected final products, were designed to be compatible with normal-phase silica gel chromatography to exclude any need for ion-exchange or reversed-phase procedures.

The convergent synthetic strategy is illustrated in Schemes 1−3. Commercially available Cbz-diamino propionic acid **1** (Scheme 1) was carboxy-protected, in near

Scheme 1[a]

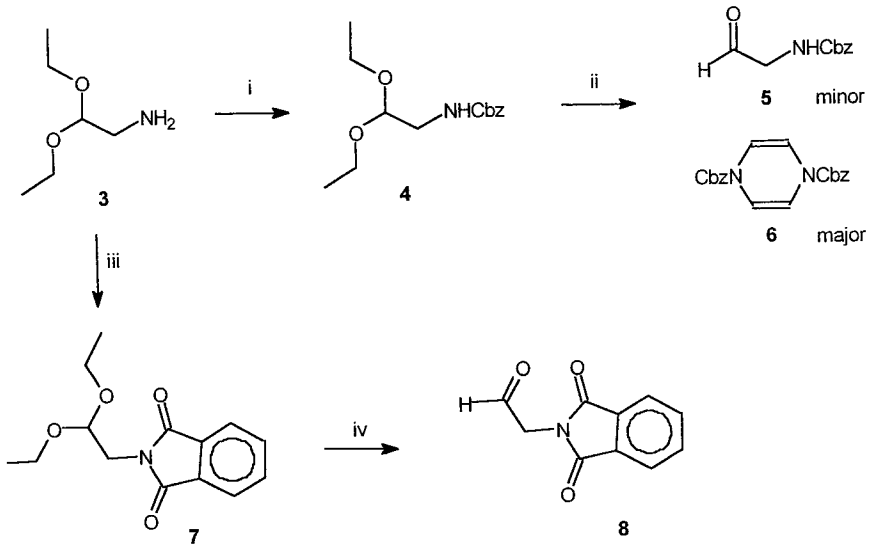


[a] (i) MeOH, HCl/dioxane, 0 °C → rt.

quantitative yields and in a dry methanol/HCl/dioxane solution (*48*), to the methyl ester **2** which served as part of the triamine backbone needed for assembling the molecular scaffold. Since at this stage, establishment of the synthetic protocol, and not the metal chelating features of the ligand, was of interest, the commercially available racemic mixture of diamino propionic acid was used as received. A logical approach to the formation of this triamine was coupling of **2** with a 2-amino ethanol derivative at its C2 position. A number of nucleophilic substitution reactions, between **2** and N-protected amino ethanol tosylates and triflates, were tried under different conditions and without satisfactory results. A second

[2] Radiolabeling of unconjugated mCC49 and HuCC49 resulted in 0.3 and 0.8% nonspecific labeling, respectively.

Scheme 2[a]



[a] (i) BCF, DIEA, dioxane; (ii) H^+; (iii) $(Phth)_2O$, DIEA, toluene; (iv) 50% HOAc, 60 °C.

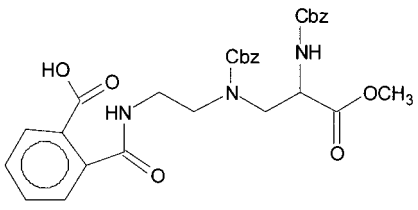
option, coupling of **2** with an N-protected amino acetaldehyde through Schiff base formation was therefore proposed. Of the two possibilities for protection of the amine **3**, i.e., Boc and Cbz, the former was eliminated due to incompatibility with a later step of the synthesis. Specifically, an acid removal of such a Boc group would also remove the *N′*-Boc protection of the hydrazide **16** (Scheme 3).

To test the Cbz option, amino acetaldehyde dimethyl acetal **3** was N-protected by benzyl chloroformate to form **4** (Scheme 2). Deblocking of the aldehyde group of **4** under different standard acidic conditions, and evaluation of the products by electrospray MS, indicated a minor formation of the desired aldehyde and a major product with a molecular weight of 350. Although this byproduct was not isolated, the MW points to the formation of an N^1,N^4-di(benzyloxycarbonyl)-1,4-dihydro pyrazine, **6**, resulting from a head-to-tail condensation of two molecules of the Cbz-aminoaldehyde. This competing reaction appears to have occurred shortly after the aldehyde formation, and due to the high thermodynamic stability of the dihydropyrazine structure. Formation of this compound drastically reduced the yield of the desired aldehyde and complicated the purification.

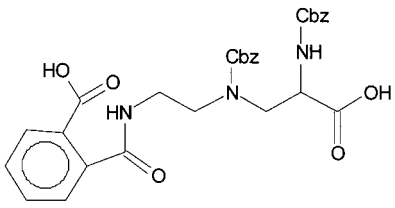
To circumvent this problem, we postulated that deprotonation of the amide nitrogen in the Cbz-protected amino aldehyde might prevent the formation of the unwanted pyrazine compound by blocking the head-to-tail aminoacetaldehyde condensations. Thus, compound **3** was N-protected by phthalic anhydride in toluene to afford compound **7** in 69% yield after purification (Scheme 2). Indeed, deprotection of compound **7** was a clean reaction affording the desired aldehyde **8** as the major product and with no significant formation of any byproducts. On the other hand, a series of standard acidic conditions to remove the acetal protection of **7** resulted either in low-yield and low-purity reactions or recovery of the starting material with no change. The deprotection, however, worked quite efficiently from both yield and purity standpoints, when aqueous acetic acid was used at elevated temperature. Both compounds **7** and **8** were readily purified by crystallization.

Condensation of the aldehyde **8** with the partially protected amine **2** was carried out, as shown in Scheme 3, in dry THF with in situ reduction of the resulting Schiff base intermediate by sodium acetoxy borohydride. The use of this reagent proved to be superior to $NaCNBH_3$ by affording high-purity products and better yields of recovery. Celite filtration and water/brine wash of the product solution afforded the amine **9** in 86% yield. This procedure provided **9** with sufficient purity for preparative purposes and required no further purification.

To prevent the interference of the secondary amine group of **9** with the coupling reaction used for the construction of the hydrazide conjugating function (see compound **15**), the former was blocked by a Cbz, which was the same as the protection used for the N^{α}-amine; both Cbz groups may now be removed as needed and in the same step. Masking of the secondary amine was carried out by a standard procedure, (*49*) using benzyl chloroformate in dioxane, which formed the fully protected compound **10** in over 88% yield and without needing chromatography.



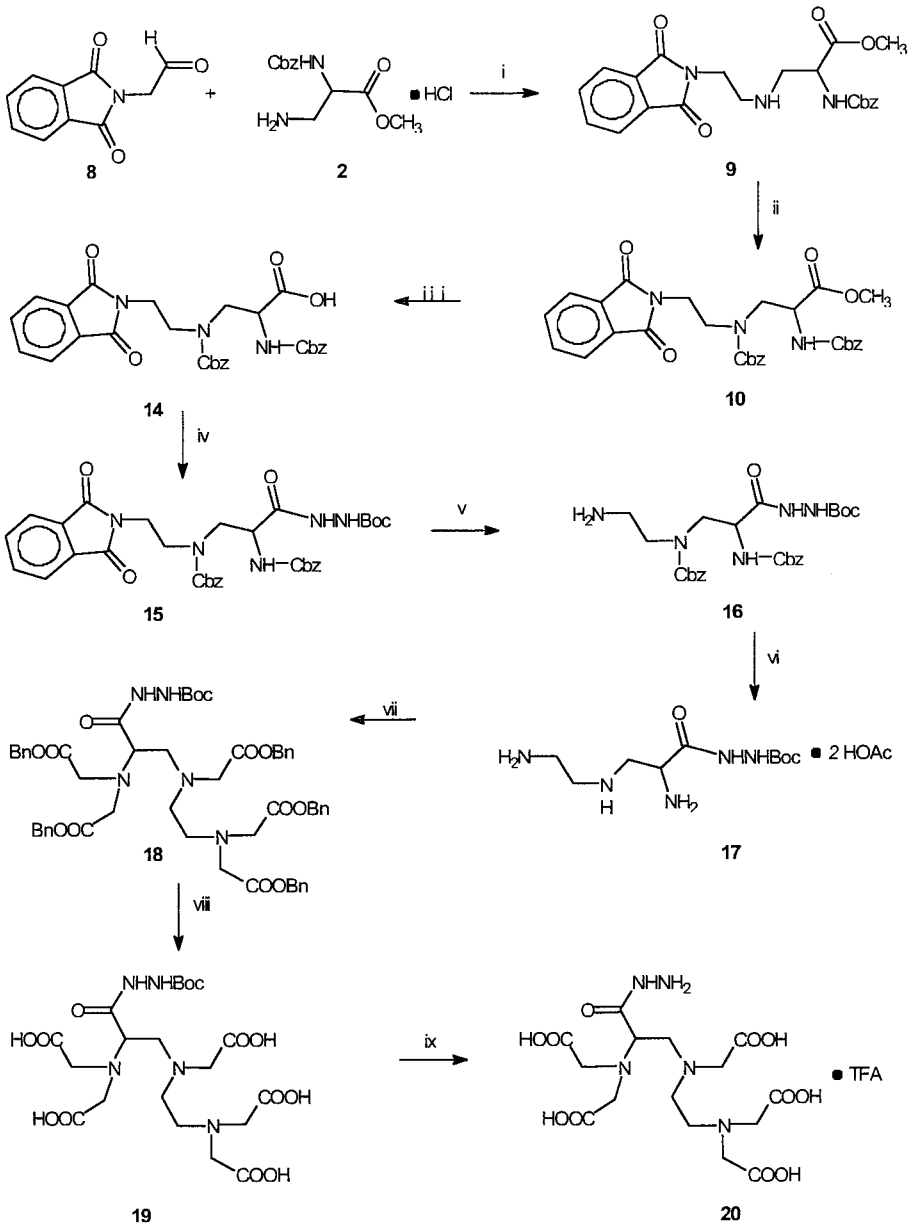
MW 577.206
11



MW 563.190
12

Despite the well-known ease of base hydrolysis of methyl esters, this method could not be applied to the deblocking of the ester **10**. Attempts to remove this ester group by equimolar concentrations of NaOH or KOH in methanol, methanol/water, and THF/water, and also with

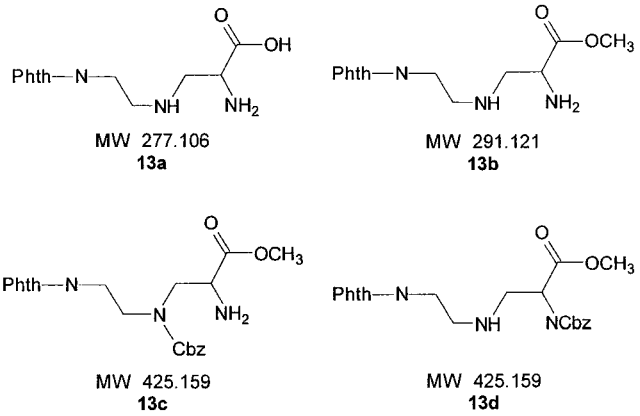
Scheme 3[a]



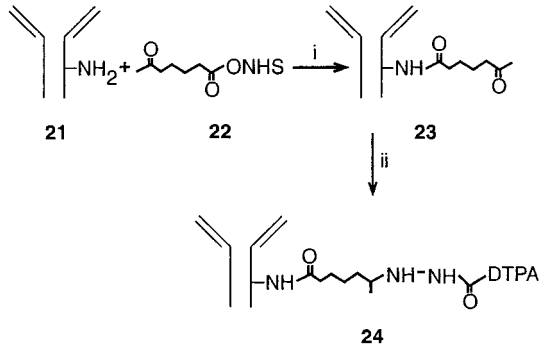
[a] (i) $Na(AcO)_3BH$, THF; (ii) BCF, DIEA, dioxane, 0 °C → rt; (iii) conc HCl, dioxane, 40 °C; (iv) Boc-$NHNH_2$, HOBT, DIEA, DCC, THF; (v) H_2NNH_2, EtOH, 50 °C; (vi) Pd/C (10%) H2, 90% HOAc; (vii) BnO_2CCH_2OTpf; CH_2Cl_2 −78 °C; (viii) Pd/C (10%), MeOH; (ix) TFA.

LiOH in wet methanol or THF/water, resulted mainly in the opening of the phthalimide ring and formation of the corresponding N-substituted phthalamic acid **11**, partially mixed with the demethylated compound, **12**. This was confirmed by the detection of these structures on ESMS as indicated by the *m*/*z* 577 and 563, for structures **11** and **12**, respectively. The same result was obtained when weaker bases such as $NaHCO_3$ and K_2CO_3 were used. A transesterification procedure using anhydrous TFA (*50*) was employed as an alternative route. Over 18 h at 40 °C, this reaction lead to a mixture of products as detected by ESMS. Possible structures based on the MS data are shown in structures **13a**−**d**.

On the basis of the esterification mechanism of the amino acid **1** to form this methyl ester, an acid hydrolysis with concentrated HCl, i.e., reversal of the esterification process was, therefore, proposed. Indeed, treatment of **10** with 25% of concentrated HCl in dioxane at 40 °C selectively removed the methyl ester, without disturbing other protecting groups, to afford the corresponding propionic acid **14** in 67% purified yield. The hydrazide conjugating function was then introduced into this



Scheme 4[a]



[a] (i) PBS, pH 8.1; (ii) **20**, acetate buffer, pH 5.5, 2-propanol, $NaCNBH_3$.

molecule by a HOBT-promoted carbodiimide reaction, resulting in the formation of **15** in 98% recovery.

To generate the triamine core, the three amine-protecting groups were to be removed in two separate reactions. From the results of the base hydrolysis of the methyl ester **10**, it was expected that the removal of the Cbz groups of **10**, prior to that of the phthalyl, would result in unwanted in situ ring opening reactions caused by the newly formed N^{α}- and N^{4}-amine groups. Therefore, compound **15** was first treated with excess hydrazine to afford the amine **16**, in 69% purified yield. The latter product was hydrogenated catalytically to the triamine **17**, in the form of a diacetate salt and at near quantitative yields.

Assembling the five metal-chelating arms on the amine backbone was carried out under completely organic conditions through a slight modification of the procedure reported by Pickersgill and Rapoport (*51*). Because of the mild conditions, this procedure has the advantage of minimizing the competing lactamization reactions, thereby resulting in an improvement in the yield of recovery of the target product. Thus, reaction of the triamine **17** with the triflate of benzyl glycolate, in dichloromethane and at low temperature, afforded the fully alkylated **18** as the major product.

Since the removal of all protecting groups in the last two steps of this synthesis generates highly polar products, obtaining a highly pure **18** was essential to avoid extensive purification of the polar products **19** and **20**. If performed carefully, both benzyl- and Boc-removal steps could be clean processes, resulting in a final-product BCA with acceptable purity for conjugation protocols.

Removal of the Boc and benzyl groups from compound **18** were carried out in two successive steps starting with catalytic hydrogenation in methanol. The hydrazide-protecting Boc group was then removed by acid treatment of **19** to afford the fully deblocked target molecule **20** in 81% yield. Our attempts to obtain a high-resolution MS on compounds **19** and **20** were not successful probably due to the excessively charged nature of these molecules (*52*). The ^{1}H NMR and ESMS, however, confirm the structure of **20** with a high (>98%) purity as indicated by reversed-phase HPLC. Furthermore, the MALDI-supported antibody conjugation of this compound, and subsequent high-yield radiolabeling reactions with both ^{90}Y and ^{177}Lu, provide indirect evidence for the formation of **20**.

Antibody Conjugation. To test the ability of this new DTPA molecule for conjugation to, e.g., proteins, a model experiment was performed (Scheme 4) using the MAbΔCH2HuCC49 (**21**), a domain-deleted humanized murine immunoglobulin, that binds to TAG-72, a pan-carcinoma antigen (*53*). The ΔCH2HuCC49 is reactive against adenocarcinomas including colorectal, ovarian, gastric, pancreatic, and non-small cell lung cancer.

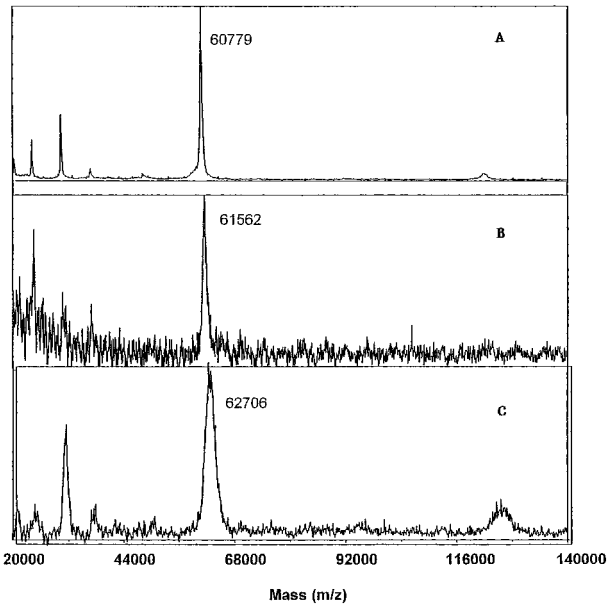


Figure 1. MALDI-TOF mass spectra of the starting MAb ΔCH2HuCC49 (A), the intermediate OHA−ΔCH2HuCC49 (B), and the final product conjugate DTPA−ΔCH2HuCC49 (C). Reaction progress is indicated by the corresponding increases in *m*/*z* values. MWs are shown at half-value from doubly charged species.

We have reported a conjugation procedure for the covalent attachment of unprotected hydroxamic acid BCAs, using a hydrazide conjugating function (*22*). In this procedure, a ketone-derived linker (**22**) is first implanted into the MAb molecule through an activated ester chemistry. With the ketone groups serving as "*hydrazide anchors*" (**23**), the BCA is then conjugated to the MAb, in a group-selective (ketone-directed) manner and with no conflict with the native amine groups of the protein. As compared to the isothiocyanate and cyclic anhydride protocols, this procedure uses a two-step protocol. The addition of an extra step, however, may be compensated by gains in the conjugation outcome as a result of the BCA stability.

Matrix-assisted laser desorption/ionization (MALDI) MS analyses of the conjugation products **23** and **24**, using MWs of the unconjugated starting MAb, the linker, and DTPA **20**, indicated a 4:1 DTPA-to-MAb ratio (Figure 1). Although this ratio is within an acceptable range of BCA-MAb substitution for radiolabeling and in vivo studies of the radiolabeled MAb conjugates, it could be varied by manipulating the conditions for the conjugation sequence of Scheme 4 (*22*).

Radiolabeling. Radiolabeling of the DTPA−ΔCH2-HuCC49 conjugate proceeded efficiently with two therapeutically important radiometals, ^{90}Y and ^{177}Lu. High yields of radiolabeling (>96%) confirmed the ability of the ligand to maintain its metal-chelating properties after conjugation to the MAb. The size-exclusion (SE) HPLC (Figure 2) and Sephadex-25 chromatography (PD-10, Figure 3 for ^{177}Lu only) showed the expected IgG elution patterns. The results of radiolabeling are shown in Table 1 which also demonstrate high specific activities for both ^{90}Y and ^{177}Lu conjugates.

Biodistribution. Tumor and normal tissue uptake of the ^{177}Lu-DTPA−ΔCH2HuCC49 was studied in LS174T-bearing athymic nude mice at two time points as shown

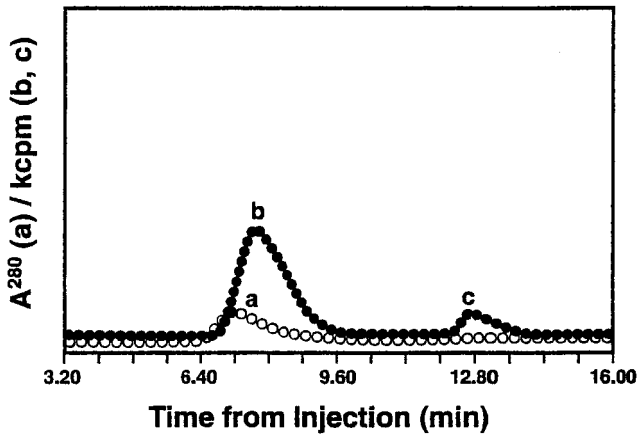


Figure 2. Analytical size-exclusion HPLC profile for ^{177}Lu-DTPA−ΔCH2HuCC49 as determined by UV (○) and radioactive (●) traces. Peaks a and b indicate conjugate elution, while c denotes unbound activity.

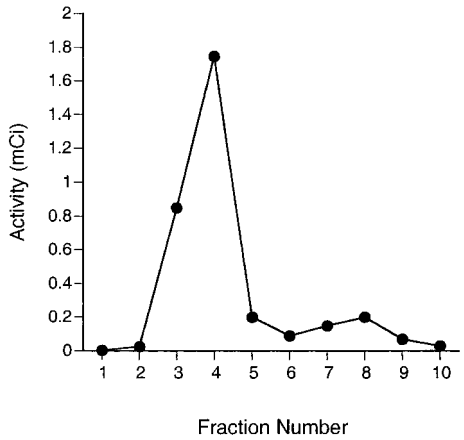


Figure 3. Preparative gel filtration profile for purification of ^{177}Lu-DTPA−ΔCH2HuCC49 on a Sephadex G25 column. Elution of the labeled antibody peaks in fractions 3 and 4 is followed by the later elution of the unbound activity in fractions 7−9.

Table 1. ^{90}Y and ^{177}Lu Labeling of DTPA−ΔCH2HuCC49 Conjugate

isotope	%RY[a]	SA[b]
^{90}Y	96	16
^{177}Lu	98	21

[a] Percent radiolabeling yield calculated from SE HPLC. [b] Specific activity in mCi/mg of conjugate.

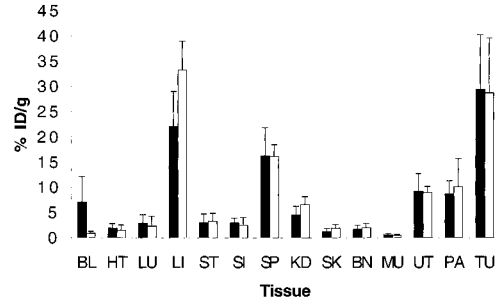


Figure 4. Biodistribution of ^{177}Lu-DTPA−ΔCH2HuCC49 in athymic nude mice bearing i.p. LS174T human colon carcinoma xenografts at 4 h (■) and 24 (□) postinjection as %ID/g for blood (BL), heart (HT), lungs (LU), liver (LI), stomach (ST), small intestine (SI), spleen (SP), kidneys (KD), skin (SK), bone (BN), muscle (MU), uterus (UT), pancreas (PA), and tumor (TU).

in Figure 4. The percent injected radioactivity uptake by unit weight of each tissue (%ID/g) for this conjugate showed a high tumor uptake, indicating that the immunoreactivity of the labeled conjugate was not affected by the conjugation and radiolabeling procedures. The conjugate also showed a blood clearance pattern characteristic of this antibody but had relatively high liver uptake. Work is in progress in this laboratory to evaluate the effect of different BCA-MAb linkers in reducing the liver activity (*54*−*58*). This biodistribution analysis, however, validates the conjugation and radiolabeling protocols used in this work for the production of therapeutically useful radiopharmaceuticals using the new DTPA hydrazide.

CONCLUSION

The metal-chelating agent DTPA has been extensively used for labeling of MAbs and peptides with such radioactive metals as ^{88}Y, ^{90}Y, ^{111}In, ^{152}Sm, ^{153}Sm, and ^{177}Lu, for diagnosis and therapy of malignancies, as well as a contrast agent in MRI and a metal-sequestering agent. Application of organic chelators in metal-tagging of biomolecules requires first the conjugation of the BCA to the latter, a procedure reported with a variety of mechanisms and functional groups. The DTPA-based BCAs used in the reported protocols are mainly either the cyclic dianhydride or isothiocyanate derivatives of this ligand. In this work, we report the synthesis of a novel derivative of this useful metal chelator, the hydrazide DTPA **20**, designed for a new and group-specific conjugation protocol. The synthetic strategy uses a novel approach in building the skeletal backbone of this molecule. This approach enjoys a totally organic route involving diagonally protected nonpolar intermediates, and resulted in the formation of the target DTPA product with a good overall yield and a final-product purity that was suitable for further conjugation procedures. Also, most steps of this synthesis produced, without a need for chromatography, intermediate compounds with purities suitable for preparative applications. The final-product BCA showed a high physical and chemical stability and remained intact over an extended period of time. Furthermore, the conjugation mechanism of this DTPA leaves all five carboxylate groups available for metal chelation, thus resulting in more stable metal complexes.

The ability of the new BCA **20** for covalent attachment to MAbs was tested by conjugation of this molecule to the MAbΔCH2HuCC49. Evaluation of the conjugation products by MALDI MS demonstrated the successful attachment of **20** to this antibody at a BCA/MAb ratio of 4. While the full deprotection of **20** generates a ready-to-conjugate heterobifunctional compound, removal of only the carboxyl group protection may afford a stable metal-chelating DTPA molecule for in vitro and in vivo studies of the corresponding metal complexes.

This new DTPA heterobifunctional chelating agent may serve to improve conjugation of this useful chelating agent to compounds of medical and biological applications, resulting in efficient and controllable protocols and producing reagents with high metal-chelating efficiencies.

ACKNOWLEDGMENT

The authors thank Dr. Michael G. Bartlett (University of Georgia College of Pharmacy) for providing the high resolution mass spectral data and helpful related discussions. Also, we thank Marion Kirk and Lori Coward (UAB Mass Spectroscopy Shared Facility), for running the ESMS and MALDI spectra, respectively, and Soneshia

McMillan for preparing the manuscript. This work was supported by NCI Grants CA62550 and CA78505.

LITERATURE CITED

(1) Volkert, W. A., and Hoffman, T. J. (1999) Therapeutic Radiopharmaceuticals. *Chem. Rev. 99*, 2269−2292.

(2) Jurisson, S., Berning, D., Jia, W., and Ma, D. (1993) Coordination compounds in nuclear medicine. *Chem. Rev. 93*, 1137−1156.

(3) Anderson, C., and Welch, M. J. (1999) Radiometal-labeled agents (non-technetium) for diagnostic imaging. *Chem. Rev. 99*, 2219−2234.

(4) Lauffer, R. B. (1987) Paramagnetic metal complexes as water proton relaxation agents for NMR imaging: theory and design. *Chem. Rev. 87*, 901−927.

(5) Caravan, P., Ellison, J. J., McMurry, T. J., and Lauffer, R. B. (1999) Gadolinium (III) chelates as MRI contrast agents: structure, dynamics, and applications. *Chem. Rev. 99*, 2293−2352.

(6) Goldenberg, D. M. (1997) Perspectives on oncologic imaging with radiolabeled antibodies. *Cancer 80*, 2431−2435.

(7) Buscombe, J. R., Cwikla, J. B., Thakrar, D. S., and Hilson, A. J. (1997) Scintigraphic imaging of breast cancer: a review. *Nucl. Med. Commun. 18*, 698−709.

(8) Mansi, L., Rambaldi, P. F., Cuccurullo, V., Pecori, B., Quarantelli, M., Fallanca, F., and Del Vecchio, E. (1997) Diagnostic and prognostic role of 99mTc−Tetrofosmin in breast cancer. *Q. J. Nucl. Med. 41*, 239−250.

(9) Hughes, O. D., Bishop, M. C., Perkins, A. C., Wastie, M. L., Denton, G., Price, M. R., Frier, M., Denley, H., Rutherford, R., and Schubiger, P. A. (2000) Targeting superficial bladder cancer by the intravesical administration of copper-67-labeled anti-MUCI mucin monoclonal antibody C595. *J. Clin. Oncol. 18*, 363−370.

(10) Lewis, J. S., Srinivasan, A., Schmidt, M. A., and Anderson, C. J. (1999) In vitro and in vivo evaluation of ^{64}Cu-TETA-Tyr^{3}-octreotate. A new somatostatin analog with improved target tissue uptake. *Nucl. Med. Biol. 26*, 267−273.

(11) Wahl, R. L. (1998) Overview of the current status of PET in breast cancer imaging. *Q. J. Nucl. Med. 42*, 1−7.

(12) Goldenberg, D. M. (1995) in *Cancer Therapy with Radiolabeled Antibodies* (D. M. Goldenberg, Ed.) CRC Press, Boca Raton, FL.

(13) Kohler, G. M., C. (1975) Continuous cultures of fused cells secreting antibody of predefined specificity. *Nature 256*, 495−497.

(14) Kousparou, C. A., Deonarain, M. P., and Epenetos, A. A. (2000) Advances in tumour targeting. *J. Int. Soc. Tumour Targeting 1*, 55−69.

(15) Cao, Y., and Suresh, M. R. (1998) Bispecific antibodies as novel bioconjugates. *Bioconjugate Chem. 9*, 635−644.

(16) Schmidt, S., Arndt, M., Braunagel, M., Moldernhauer, G., and Little, M. (2000) Construction and purification of a single-chain Fv antibody binding to the t-cell differentiation antigen CD28. *J. Int. Soc. Tumour Targeting 1*, 82−89.

(17) Khaw, B. A., Strauss, H. W., and Narula, J. (1993) "Magic bullets:" from muskets to smart bombs. *J. Nucl. Med. 34*, 2264−2268.

(18) Illidge, T. M., and Brock, S. (2000) Radioimmunotherapy of cancer: using monoclonal antibodies to target radiotherapy. *Curr. Pharm. Des. 6*, 1399−1418.

(19) Casey, J. L., King, D. J., Chaplin, L. C., Haines, A. M., Pedley, R. B., Mountain, A., Yarranton, G. T., and Begent, R. H. (1996) Preparation, characterisation and tumour targeting of cross-linked divalent and trivalent anti-tumour Fab' fragments. *Br. J. Cancer 74*, 1397−1405.

(20) Arap, W., Pasqualini, R., and Ruoslahti, E. (1998) Cancer treatment by targeted drug delivery to tumor vasculature in a mouse model. *Science 279*, 377−380.

(21) Safavy, A., Buchsbaum, D. J., and Khazaeli, M. B. (1993) Synthesis of N-[tris[2-[[N-(benzyloxy)amino]carbonyl]ethyl]-methyl]succinamic acid, trisuccin. Hydroxamic acid derivatives as a new class of bifunctional chelating agents. *Bioconjugate Chem. 4*, 194−198.

(22) Safavy, A., Khazaeli, M. B., Kirk, M., Coward, L., and Buchsbaum, D. J. (1999) Further studies on the protein conjugation of hydoxamic acid bifunctional chelating agents: Group-specific conjugation at two different loci. *Bioconjugate Chem. 10*, 18−23.

(23) Corson, D. T., and Meares, C. F. (2000) Efficient multigram synthesis of the bifunctional chelating agent (S)-1-p-isothiocyanatobenzyl-diethylenetriaminepentaacetic acid [correction of diethylenetetraminepentaacetic acid]. *Bioconjugate Chem. 11*, 292−299.

(24) Chappell, L. L., Dadachova, E., Milenic, D. E., Garmestani, K., Wu, C., and Brechbiel, M. W. (2000) Synthesis, characterization, and evaluation of a novel bifunctional chelating agent for the lead isotopes 203Pb and 212Pb. *Nucl. Med. Biol. 27*, 93−100.

(25) Chappell, L. L., Deal, K. A., Dadachova, E., and Brechbiel, M. W. (2000) Synthesis, conjugation, and radiolabeling of a novel bifunctional chelating agent for (225)Ac radioimmunotherapy applications. *Bioconjugate Chem. 11*, 510−519.

(26) Moi, M. K., Meares, C. F., McCall, M. J., Cole, W. C., and DeNardo, S. J. (1985) Copper chelates as probes of biological systems: stable copper complexes with a macrocyclic bifunctional chelating agent. *Anal. Biochem. 148*, 249−253.

(27) Moi, M. K., Meares, C. F., and DeNardo, S. J. (1988) The peptide way to macrocyclic bifunctional chelating agents: Synthesis of 2-(*p*-nitrobenzyl)-1,4,7,10-tetraazacyclododecane-*N*,*N*′,*N*″,*N*‴-tetraacetic acid and its study of its yttrium (III) complex. *J. Am. Chem. Soc. 110*, 6266−6267.

(28) Kumar, K., Magerstadt, M., and Gansow, O. (1989) Lead-(II) and bismuth (III) complexes of the polyazacycloalkane-*N*-acetic acids nota, dota, and teta. *J. Chem. Soc. Chem. Commun. 3*, 145.

(29) McMurry, T. J., Brechbiel, M., Kumar, K., and Gansow, O. A. (1992) Convenient synthesis of bifunctional tetraaza macrocycles. *Bioconjugate Chem. 3*, 108−117.

(30) Renn, O., and Meares, C. F. (1992) Large scale synthesis of bifunctional chelating agent 2-(*p*-nitrobenzyl)-1,4,7,10-tetraazacyclododecane-*N*,*N*′,*N*″,*N*‴,tetraacetic acid, and the determination of its enantiomeric purity by chiral chromatography. *Bioconjugate Chem. 3*, 563−569.

(31) Kobayashi, H., Wu, C., Yoo, T. M., Sun, B.-F., Drumm, D., Pastan, I., Paik, C. H., Gansow, O. A., Carrasquillo, J. A., and Brechbiel, M. W. (1998) Evaluation of the in vivo biodistribution of yttrium-labeled isomers of CHX-DTPA-conjugated monoclonal antibodies. *J. Nucl. Med. 39*, 829−936.

(32) Brechbiel, M. W., and Gansow, O. A. (1991) Backbone-substituted DTPA ligands for ^{90}Y. *Bioconjugate Chem 2*, 187−194.

(33) McMurry, T. J., Pippin, C. G., Wu, C., Deal, K. A., Brechbiel, M. W., Mirzadeh, S., and Gansow, O. A. (1998) Physical parameters and biological stability of yttrium (III) diethylenetriaminepentaacetic acid derivative conjugates. *J. Med. Chem. 41*, 3546−3549.

(34) Wong, J. Y., Thomas, G. E., Yamauchi, D., Williams, L. E., Odom-Maryon, T. L., Liu, A., Esteban, J. M., Neumaier, M., Dresse, S., Wu, A. M., Primus, F. J., Shively, J. E., and Raubitschek, A. A. (1997) Clinical evaluation of indium-111-labeled chimeric anti-CEA monoclonal antibody. *J. Nucl. Med. 38*, 1951−1959.

(35) Jasanada, F., Urizzi, P., Souchard, J. P., Le Gaillard, F., Favre, G., and Nepveu, F. (1996) Indium-111 labeling of low-density lipoproteins with the DTPA-bis(stearylamide): evaluation as a potential radiopharmaceutical for tumor localization. *Bioconjugate Chem. 7*, 72−81.

(36) Arano, Y., Uezono, T., Akizawa, H., Ono, M., Wakisaka, K., Nakayama, M., Sakahara, H., Konishi, J., and Yokoyama, A. (1996) Reassessment of diethylenetriaminepentaacetic acid (DTPA) as a chelating agent for indium-111 labeling of polypeptides using a newly synthesized monoreactive DTPA derivative. *J. Med. Chem. 39*, 3451−3460.

(37) Raderer, M., Kurtaran, A., Leimer, M., Angelberger, P., Niederle, B., Vierhapper, H., Vorbeck, F., Hejna, M. H., Scheithauer, W., Pidlich, J., and Virgolini, I. (2000) Value of peptide receptor scintigraphy using (123)I-vasoactive intes-

tinal peptide and (111)In-DTPA-D-Phel-octreotide in 194 carcinoid. *J. Clin. Oncol. 18*, 1331−1336.
(38) Ferro-Flores, G., Ramirez, F. D., Tendilla, J. I., Pimentel-Gonzalez, G., Murphy, C. A., Melendez-Alafort, L., Ascencio, J. A., and Croft, B. Y. (1999) Preparation and pharmacokinetics of samarium(III)-153-labeled DTPA-bis-biotin. Characterization and theoretical studies of the samarium(III)-152 conjugate. *Bioconjugate Chem. 10*, 726−734.
(39) Izard, M. E., Boniface, G. R., Hardiman, K. L., Brechbiel, M. W., Gansow, O. A., and Walkers, K. Z. (1992) An improved method for labeling monoclonal antibodies with samarium-153: use of the bifunctional chelate 2-(p-isothiocyanatobenzyl)-6- methyldiethylenetriaminepentaacetic acid. *Bioconjugate Chem. 3*, 346−350.
(40) Stimmel, J. B., and Kull, F. C., Jr. (1998) Samarium-153 and lutetium-177 chelation properties of selected macrocyclic and acyclic ligands. *Nucl. Med. Biol. 25*, 117−125.
(41) Safavy, A. (2000) Unpublished results.
(42) Rebizak, R., Schaefer, M., and Dellacherie, E. (1997) Polymeric conjugates of Gd^{3+}–diethylenetriaminepentaacetic acid and dextran. 1. Synthesis, characterization and paramagnetic properties. *Bioconjugate Chem 8*, 605−610.
(43) Li, M., and Selvin, P. R. (1997) Amine-reactive forms of a luminescent diethylenetriaminepentaacetic acid chelate of terbium and europium: attachment to DNA and energy transfer measurements. *Bioconjugate Chem. 8*, 127−132.
(44) Hnatowich, D. J., Layne, W. W., and Childs, R. L. (1982) The preparation and labeling of DTPA-coupled albumin. *Int. J. Appl. Radiat. Isot. 33*, 327−332.
(45) Hnatowich, D. J., Childs, R. L., Lanteigne, D., and Najafi, A. (1983) The preparation of DTPA-coupled antibodies radiolabeled with metallic radionuclides: an improved method. *J. Immunol. Methods 65*, 147−157.
(46) Brechbiel, M. W., Gansow, O. A., Atcher, R. W., Schlom, J., Esteban, J., Simpson, D. E., and Colcher, D. (1986) Synthesis of 1-(p-isothiocyanatobenzyl) derivatives of DTPA and EDTA: Antibody labeling and tumor-imaging studies. *Inorg. Chem. 25*, 2772−2781.
(47) Kozak, R. W., Raubitschek, A., Mirzadeh, S., Brechbiel, M. W., Junghaus, R., Gansow, O. A., Waldmann, T. A. (1989) Nature of the bifunctional chelating agent used for radioimmunotherapy with yttrium-90 monoclonal antibodies: Critical factors in determining *in vivo* survival and organ toxicity. *Cancer Res. 49*, 2639−2644.
(48) Xue, C. B., Wityak, J., Sielecki, T. M., Pinto, D. J., Batt, D. G., Cain, G. A., Sworin, M., Rockwell, A. L., Roderick, J. J., Wang, S., Orwat, M. J., Frietze, W. E., Bostrom, L. L., Liu, J., Higley, C. A., Rankin, F. W., Tobin, A. E., Emmett, G., Lalka, G. K., Sze, J. Y., Di Meo, S. V., Mousa, S. A., Thoolen, M. J., Racanelli, A. L., and Olson, R. E. (1997) Discovery of an orally active series of isoxazoline glycoprotein IIb/IIIa antagonists. *J. Med. Chem. 40*, 2064−2084.
(49) Bodanszky, M. (1993) *Principles of Peptide Synthesis*, 2nd ed., Springer-Verlag, Berlin.
(50) Tabor, D. C., and Evans Jr, S. A. (1982) Efficient demethylation of methyl esters with anhydrous trifluoroacetic acid. *Synth. Commun. 12*, 855−864.
(51) Pickersgill, I. F., and Rapoport, H. (2000) Preparation of functionalized, conformationally constrained DTPA analogues from L- or D-serine and *trans*-4-hydroxy-L-proline. Hydroxymethyl substituents on the central acetic acid and on the backbone. *J. Org. Chem. 65*, 4048−4057.
(52) Bartlett, M. G., personal communication.
(53) Johnson, V. G., Schlom, J., Paterson, A. J., Bennett, J., Magnani, J. L., and Colcher, D. (1986) Analysis of a human tumor-associated glycoprotein (TAG-72) identified by monoclonal antibody B72.3. *Cancer Res. 46*, 850−857.
(54) Pardridge, W. M., Kang, Y. S., Yang, J., and Buciak, J. L. (1995) Enhanced cellular uptake and in vivo biodistribution of a monoclonal antibody following cationization. *J. Pharm. Sci. 84*, 943−948.
(55) Haseman, M. K., Goodwin, D. A., Meares, C. F., Kaminski, M. S., Wensel, T. G., McCall, M. J., and Levy, R. (1986) Metabolizable 111In chelate conjugated anti-idiotype monoclonal antibody for radioimmunodetection of lymphoma in mice. *Eur. J. Nucl. Med. 12*, 455−460.
(56) Arano, Y., Wakisaka, K., Mukai, T., Uezono, T., Motonari, H., Akizawa, H., Kairiyama, C., Ohmomo, Y., Tanaka, C., Ishiyama, M., Sakahara, H., Konishi, J., and Yokoyama, A. (1996) Stability of a metabolizable ester bond in radioimmunoconjugates. *Nucl. Med. Biol. 23*, 129−136.
(57) Weber, R. W., Boutin, R. H., Nedelman, M. A., Lister-James, J., and Dean, R. T. (1990) Enhanced kidney clearance with an ester-linked ^{99m}Tc-radiolabeled antibody Fab′-chelator conjugate. *Bioconjugate Chem. 1*, 431−437.
(58) Arano, Y., Matsushima, H., Tagawa, M., Koizumi, M., Endo, K., Konishi, J., and Yokoyama, A. (1991) A novel bifunctional metabolizable linker for the conjugation of antibodies with radionuclides. *Bioconjugate Chem. 2*, 71−6.

BC0100861

Synthesis of the First Diethylenetriaminepentahydroxamic Acid (DTPH) Bifunctional Chelating Agent†,§

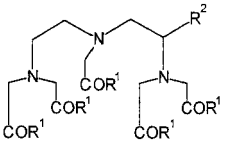
Ahmad Safavy,* Dale C. Smith Jr., Alireza Bazooband,‡ and Donald J. Buchsbaum

Department of Radiation Oncology, University of Alabama at Birmingham, Birmingham, Alabama 35294.
Received October 8, 2001; Revised Manuscript Received January 10, 2002

Synthesis of a new pentahydroxamic acid bifunctional chelating agent (BCA), constructed on the aminoazaalkyl core of diethylenetriaminepentaacetic acid (DTPA), is reported. Rational modifications in the structure of DTPA, which could result in an enhancement of its chelation properties, add to the collection of diagnostic and therapeutic metals bound by this chelator, and might implement significant improvements in the in vivo behavior of this compound, are described. Further improvements in the stability of the ligand−metal complexes of DTPA may improve both diagnostic and therapeutic outcomes such as tumor-to-normal tissue ratios and target-delivered radioactivity. A combination of hydroxamate functions with the azaalkyl backbone of DTPA might be a suitable approach to generate such higher stabilities. This rationale may be justified by the well-known affinity of hydroxamates against different transition metals and favorable properties of DTPA as a versatile chelator. Thus, the N^4,N^α,N^α,N^ϵ,N^ϵ-pentakis[[((*N*-hydroxy-*N*-methyl]carbonyl)methyl]-2, 6-diamino-4-azahexanoic hydrazide (**5**, DTPH) was designed and synthesized through a convergent synthesis and in 40.7% overall yield. Conjugation of this compound to the monoclonal antibody (MAb) ΔCh2HuCC49, used as a model protein, was carried out to evaluate the efficiency of this molecule as a BCA. Radiolabeling of the DTPH−ΔCH2HuCC49 conjugate with lutetium-177 (^{177}Lu) and biodistribution of the labeled conjugate in athymic nude mice, bearing LS174T human colon carcinoma xenografts, are reported.

INTRODUCTION

Diethylenetriaminepentaacetic acid (DTPA[1], **1**, Figure 1) has been widely used as a metal chelating agent in both diagnostic and therapeutic procedures. Although the use of this agent as a single-molecule metal chelator has been reported, its application as a conjugate to TVs, for the transfer of metallic nuclides to the site of the disease, has been more prominent. The latter application includes radiolabeling of MAbs and peptides with different metallic radionuclides such as yttrium (^{88}Y, ^{90}Y) (*1*−*3*), indium (^{111}In) (*4*−*7*), lead (^{203}Pb) (*8*), samarium (^{152}Sm, ^{153}Sm) (*9*, *10*), and lutetium (^{177}Lu) (*11*, *12*). Other applications of DTPA, such as in MRI (*13*−*15*) and luminescent lanthanide imaging (*16*), have also been demonstrated,



1: R^1 = OH; R^2 = H
2: R^1 = OH; R^2 = $CONHNH_2$
3: R^1 = OH; R^2 = CONHNHBoc
4: R^1 = NHOBn; R^2 = CONHNHBoc
5: R^1 = $N(CH_3)OH$; R^2 = $CONHNH_2$

Figure 1. Chemical structure of DTPH and other DTPA derivatives.

which, collectively, point to the importance of this compound in medicine. It may be, therefore, of interest to explore possibilities for the development of more improved derivatives of this molecule. These improvements may be accomplished through either or both of the following approaches: (i) developing a bifunctional DTPA with higher chemical stability, and (ii) designing derivatives that could generate metal complexes of better kinetic/thermodynamic properties. A new bifunctional DTPA hydrazide, using Schiff base formation for MAb conjugation, has been reported by Safavy et al. (*17*). This molecule (**2**) showed a high shelf stability and efficient antibody conjugation under mild conditions, which is expected to be compatible with the structural and immunoreactivity features of most peptides and proteins.

Improvement in the metal complex stability prevents the premature in vivo release of the complex metal, which could, in turn, result in high uptake in normal tissues as well as in low-efficiency treatment protocols. Furthermore, and in the case of immunoconjugates, this metal release is also a function of the BCA-TV bond stability. Readily cleavable covalent bonds, such as carboxylic

† This article is dedicated to Professor W. Franklin Gilmore on the occasion of his 67th birthday.

§ Presented in part at the 14th International Symposium on Radiopharmaceutical Chemistry, Interlaken, Switzerland, June 10−15, 2001.

* To whom correspondence should be addressed at 1824 6th Avenue South, WTI 674, Birmingham, AL 35294-6832. E-mail: safavy@uab.edu.

‡ Present address: University of Florida/Shands Jacksonville, Department of Pathology, 655 W 8th Street, Jacksonville, FL 32209.

[1] Abbreviations: BCA, bifunctional chelating agent; BOC, *tert*-butyloxycarbonyl; DIEA, diisopropylethylamine; DPBS, Dulbecco's phosphate-buffered saline; DTPA, diethylenetriaminepentaacetic acid; DTPH, diethylenetriaminepentahydroxamic acid; ESMS, electrospray mass spectrometry; HR, high-resolution; MAb, monoclonal antibody; MALDI, matrix-assisted laser desorption/ionization mass spectrometry; MRI, magnetic resonance imaging; OHA, 6-oxoheptanoic acid; Phth, pthalyl; SE, size-exclusion; TFA, trifluoroacetic acid; TLC, thin-layer chromatography; TV, targeting vehicle.

10.1021/bc010092x CCC: $22.00 © 2002 American Chemical Society
Published on Web 02/16/2002

esters, may be disrupted in vivo and in the presence of endogenous enzymes. The design of a potential BCA should, therefore, take into account both of these factors for an efficient site-directed delivery of the metal.

Hydroxamic acids have been noted for their favorable metal-chelating features (*18*). This has been the basis for their utilization in nature as iron-solubilizing agents (siderophores) produced by microorganisms (*19*−*23*). In drug development, hydroxamic acids have been the subject of much research in the development of enzyme inhibitors (*24*, *25*), as well as antithalassemic (*26*, *27*), antifungal (*28*), and antibacterial (*29*) agents, while hydroxamate-derived enkephalinase inhibitors have been proposed as nonopioid analgesic drug candidates (*30*−*32*). Furthermore, a trihydroxamate BCA, trisuccin, was reported by Safavy et al. as a radiometal-labeling bifunctional agent (*33*), and the use of this compound in radiolabeling of MAbs and peptides with rhenium-188 (^{188}Re) through a post-conjugation protocol has been reported (*34*). The post-conjugation route of indirect radiolabeling, as opposed to the "preformed chelate approach" (*35*, *36*), is a versatile techniques in preparation of rhenium and technetium radiopharmaceuticals that was not available as a routine procedure prior to the development of trisuccin. Thus, the potential of hydroxamic acids, along with the development of antibody conjugation and rhenium-labeling protocols using trisuccin, warranted studies on the design and synthesis of other hydroxamate BCAs.

In this paper, we report the synthesis of a novel heterobifunctional DTPA pentahydroxamate, DTPH, containing a hydrazide sidearm as the TV-conjugating moiety. In contrast to the cyclic anhydride DTPA, this hydrazide function forms the prospective linkages through one of the core ethylenediamine segments, leaving all five hydroxamate groups available for metal chelation. The hydrazide group is also compatible with free (unprotected) hydroxamate functions and allows for efficient and group-specific antibody conjugation as described before by Safavy et al. (*37*).

EXPERIMENTAL SECTION

General Procedures. Tetrahydrofuran (THF) was ketyl distilled under argon. All other reagents and solvents were obtained from commercial suppliers and were used as received. ^{1}H NMR spectra were recorded on a Bruker ARX500 FT-NMR spectrometer. The chemical shifts were referenced to tetramethylsilane as internal calibrator. Mass spectra in electrospray mode (ESMS) were recorded either on an API VI triple quadruple mass spectrometer (PE-Sciex, Toronto, Ontario) or Micromass Platform LCZ mass spectrometer (Beverly, MA). TLC was performed with Whatman glass-backed silica gel plates (2.5 cm × 7.5 cm, coating thickness 250 μ, 60 A, 254 nm). Solvents for TLC were mixed on a v/v scale and are defined as follows: (A) chloroform/methanol, 90:10; (E) chloroform/methanol/acetic acid, 77:20:3. Metal-free purified water (18.2 MΩ) was obtained from a Milli-QF system (Millipore, Bedford, MA). Melting points were performed in open capillary tubes and are uncorrected. For analytical SE HPLC, a 7.5 mm × 25 cm G3000SW column (TosoHaas, Montgomeryville, PA) was used. A 10 mM PBS containing 10 mM Na_2SO_4 at pH 6.7 was used as solvent. Preparative SE chromatography was carried out using Sephadex G-25 columns (PD-10, Pharmacia Biotech AB, Uppsala, Sweden) eluted with DPBS.

MALDI MS Procedure. Samples were analyzed in the positive mode on a Voyager Elite mass spectrometer with delayed extraction technology (PerSeptive Biosystems, Framingham, MA). The acceleration voltage was set at 25 kV, and 50−100 laser shots were summed. The matrix was sinapinic acid, dissolved in a 50:50 (v/v) mixture of 0.1% TFA/acetonitrile. A 1 pmol/μL solution of bovine serum albumin was added as an internal standard. Equal volumes of sample and matrix were mixed on a smooth plate, and the average of three measurements were reported. For each reaction, the intact MAb was scanned as the control for evaluation of the following conjugation. The molecular weight increase of the OHA-MAb intermediate was calculated using the unconjugated MAb. The molecular weight of this intermediate then served as the control to measure the increase in the molecular weight of the final product conjugate. Each difference in molecular weight was divided by the molecular weight of the corresponding linker to measure the linker/MAb ratio.

HR MS Procedure. The high-resolution liquid secondary ion mass spectra were acquired on a Micromass AutoSpec Magnetic Sector mass spectrometer (Beverly, MA) operated at a resolution of 10 000 (fwhm). All samples were run as approximately 1 μg/mL solutions in 3-nitrobenzyl alcohol using matrix clusters or added peptides as reference peak.

2-Bromo-*N*-benzyloxy-*N*-methylacetamide (19). A solution of *O*-benzylhydroxylamine·HCl (6.57 g, 41.2 mmol) and K_2CO_3 (17.04 g, 123.5 mmol) in dioxane/water (1:1, 125 mL) was cooled to 0 °C, and a solution of di-*tert*-butyl dicarbonate (9.02 g, 41.3 mmol) in dioxane was added dropwise over 20 min. The reaction was allowed to warm to ambient temperature and stirred vigorously for 20 h. The volatiles were removed in vacuo. The residue was taken up in ethyl acetate (100 mL) and extracted with water (3 × 50 mL), 10% aqueous citric acid (3 × 50 mL), and brine (1 × 20 mL), followed by drying over $MgSO_4$. The filtered solution was concentrated in vacuo to yield *O*-benzyl-*N*-Boc-hydroxylamine (8.93 g, 97.3%) as a colorless oil. R_f 0.86 (A), 0.54 ($CHCl_3$). ^{1}H NMR (500 MHz, $CDCl_3$) d 7.09−7.42 (m, 5H), 4.85 (s, 2H), 1.48 (s, 9H). A solution of *O*-benzyl-*N*-Boc-hydroxylamine (8.75 g, 39.2 mmol), iodomethane (14.5 mL. 235.25 mmol), and K_2CO_3 (5.82 g, 42.1 mmol) in acetone (75 mL) was heated at 50 °C with constant stirring. Reaction was complete after 8 days as monitored by TLC. The reaction mixture was filtered, and the volatiles were removed in vacuo. The oily residue was taken up in diethyl ether (100 mL) and extracted with $NaHCO_3$ (3 × 50 mL) and brine (1 × 50 mL) and dried over $MgSO_4$, and the solution was concentrated in vacuo to yield *O*-benzyl-*N*-Boc-*N*-methylhydroxylamine (9.13 g, 98.2%) as a colorless oil. R_f 0.90 (A), 0.68 ($CHCl_3$). ^{1}H NMR (500 MHz, $CDCl_3$) d 7.34−7.41 (m, 5H), 4.83 (s, 2H), 3.02 (s, 3H), 1.50 (s, 9H).

A flask was charged with the *O*-benzyl-*N*-Boc-*N*-methylhydroxylamine (8.38 g, 35.32 mmol), purged with argon, and cooled to 0 °C. Trifluoroacetic acid (65 mL) was slowly added over 10 min, and the solution was stirred for 1 h (**Caution: highly exothermic reaction**). All volatiles were removed in vacuo to give *O*-benzyl-*N*-methylhydroxylamine·TFA (8.79 g, 93.3%) as an off-white crystalline solid. mp 62−64 °C. R_f 0.65 (A), 0.18 ($CHCl_3$). ^{1}H NMR (500 MHz, $CDCl_3$) d 11.71 (s,1H); 7.32−7.37 (m, 5H), 5.06 (s, 2H), 2.96 (s, 3H). MS(ES+) 138.

A solution of bromoacetyl bromide (0.66 mL, 7.5 mmol) in THF (25 mL) was cooled to −78 °C under an argon purge, and dry K_2CO_3 (0.753 g, 5.52 mmol) was added. The reaction was vigorously stirred, and a solution of DIEA (0.95 mL, 5.1 mmol) and *O*-benzyl-*N*-methylhydroxylamine (1.26 g, 5.02 mmol) in THF (10 mL) was

added over 15 min. The reaction mixture was allowed to warm to 0 °C over 4 h. The reaction mixture was filtered, and the volatiles were removed in vacuo at ambient temperature. The oily residue was taken up in diethyl ether (20 mL), and the solution was extracted with 10% aqueous $NaHCO_3$ (3 × 5 mL) and brine (1 × 5 mL), dried over $MgSO_4$, and filtered. The filtrate was concentrated in vacuo to yield **19** (1.21 g, 93.5%) as a colorless oil. R_f 0.85 (A) 0.24. ^{1}H NMR (500 MHz, $CDCl_3$) d 7.39−7.41 (m, 5H), 4.94 (s, 2H) 3.91 (s, 2H), 3.27 (s, 3H). MS(ES+) 258.0, 260.0.

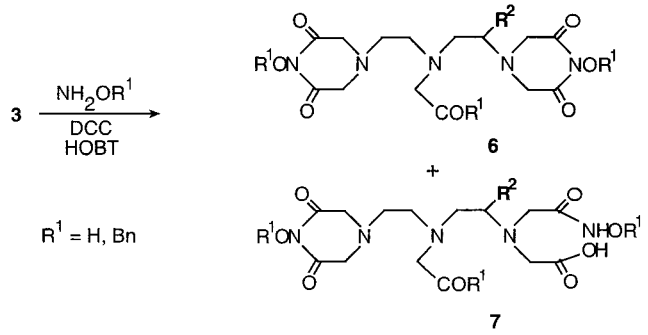
***N′*-BOC-N^4,N^a,N^a,N^e,N^e-pentakis[[((*N*-benzyloxy-*N*-methyl)amino)carbonyl]methyl]-2,6-diamino-4-azahexanoic Hydrazide (20).** A solution of *N′*-Boc-2-amino-3-[[2-(amino)ethyl]amino] propionic hydrazide **8** (0.137 g, 0.311 mmol) (*17*) and DIEA (0.84 mL, 4.67 mmol) was dissolved in DMF (2 mL). A solution of *O*-benzyl-2-bromo-*N*-methylacetohydroxamic acid **19** (1.21 g, 4.67 mmol) dissolved in CH_2Cl_2 was added to the reaction mixture at −50 °C, and the mixture was allowed to warm to ambient temperature over 48 h. The solution was concentrated in vacuo to a yellow-orange oil that was dissolved in ethyl acetate (4 mL). This solution was extracted with 10% aqueous citric acid, 10% aqueous $NaHCO_3$ (2 × 2 mL), and brine (1 × 2 mL) and was dried over $MgSO_4$. Removal of the solvent afforded an oily residue that was triturated with petroleum ether redissolved in ethyl acetate (0.5 mL). The product was then precipitated into a diethyl ether: petroleum ether solution (1:1, 35 mL). The yellow-orange solid was separated by centrifugation and dried in vacuo to yield **20** (0.230 g, 64.5%). mp 93−98 °C. R_f 0.52 (A), 0.86 (E). ^{1}H NMR (500 MHz, $CDCl_3$) d 7.26−7.36 (25H, m); 4.80−4.82 (10H, m); 3.61−3.82 (10H, b); 3.14−3.09 (15H, b); 2.61−2.87 (7H, m); 1.44 (9H, s); HRMS (FAB+) 1147.5748 ($C_{60}H_{79}N_{10}O_{13}$ requires 1147.5828). MS ES+ 1147.2.

***N′*-BOC-N^4,N^a,N^a,N^e,N^e-pentakis[[((*N*-hydroxy-*N*-methyl)amino)carbonyl]methyl]-2,6-diamino-4-azahexanoic Hydrazide (21).** A solution of **20** (0.228 g, 0.199 mmol) in methanol (8 mL) was hydrogenated at ambient temperature over palladium on carbon (10%, 0.046 g) under a hydrogen balloon for 24 h. The catalyst was separated by filtration through a 0.2 μm Acrodisc syringe tip filter (Gelman Sciences, Ann Arbor, MI), and the filtrate was concentrated in vacuo to an off-white oil. The oil was dissolved in methanol (1 mL) and precipitated from diethyl ether (35 mL). The solid was isolated by centrifugation and dried in vacuo to yield **21** (0.112 g, 80.7%) as a hygroscopic yellow-white microcrystalline solid. mp 136−139 °C. ^{1}H NMR (500 MHz, DMSO-d_6) d 3.76−3.82 (b, 15 H), 2.78−3.16 (m, 17 H), 1.48 (s, 9 H). HRMS (FAB+) 697.3489 ($C_{25}H_{49}N_{10}O_{13}$ requires 697.3481). MS ES+ 697.5.

***N^4,N^α,N^α,N^ϵ,N^ϵ*-pentakis[[((*N*-hydroxy-*N*-methyl]-carbonyl)methyl]-2,6-diamino-4-azahexanoic Hydrazide (5).** TFA (5 mL) was added to the Boc-protected **21** (0.154 g, 0.221 mmol), and the homogeneous solution was stirred for 65 min. The solution was concentrated in vacuo and dissolved in methanol (1 mL), and the product was precipitated (×2) from diethyl ether (35 mL). The solid product was separated by centrifugation and dried in vacuo to yield 0.123 g (78.3%) of **5** as a hygroscopic orange-yellow microcrystalline solid. mp 127−133 °C ^{1}H NMR (500 MHz, DMSO-d_6) d 3.76−3.82 (15 H, b); 2.85−3.21 (17 H, m). HRMS (FAB+) 597.2964 ($C_{20}H_{41}N_{10}O_{11}$ requires 597.2956). MS ES+: 597.2.

MAb Conjugation. The DTPA hydrazide **5** was conjugated to the MAb ΔCH2HuCC49 using ketone-hydrazide protocol described previously (*37*). Briefly, 6-oxoheptanoic acid was conjugated to the MAb in PBS, pH 8.1. The intermediate conjugate was purified by SE filtration in Centricon-50 against 50 mM ammonium acetate (pH 5.5). Compound **5** was added in the same buffer and at a molar ratio of 300:1 relative to the MAb. The homogeneous solution was stirred at 4 °C for 16 h, and the product conjugate was purified by dialysis. The number of DTPH molecules per antibody (DTPH:MAB) was calculated by MALDI MS as described previously (*37*). This procedure resulted in a DTPH/MAb of 2.2.

Scheme 1



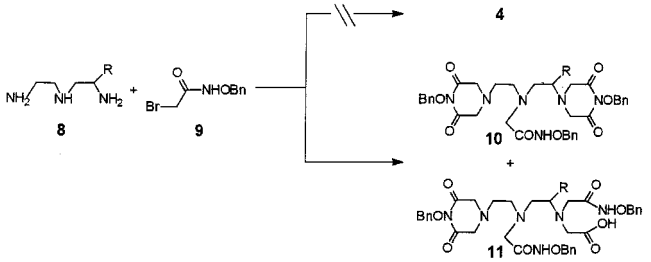
^{177}Lu-Labeling. The radioisotope was supplied (University of Missouri Research Reactor, St. Louis, MO) as lutetium chloride in 0.1 M HCl. The radiometal solution (3 μL) was incubated in 50 μL of acetate buffer (pH 5.5) at ambient temperature for 15 min and was added to the solution of the conjugate (120 μg) in the same buffer (63 μL). Radiolabeling yields (>96%) were assessed by SE HPLC, after 1 h incubation at ambient temperature. A control unconjugated MAb showed negligible nonspecific labeling under these conditions. The labeled conjugate was purified by gel filtration using a PD-10 column and phosphate-buffered saline as the eluant. One-milliliter fractions were collected with the conjugate eluting in fractions 3 and 4.

Animal Model. Athymic nude female *nu/nu* mice with a BALB/c background, obtained from the National Cancer Institute Frederick Research Laboratory (Frederick, MD), kept under sterile conditions, were used. Procedures to minimize discomfort, pain, and distress were in accord with the Animal Resource Program at the University of Alabama at Birmingham, accredited by the American Association for Accreditation of Laboratory Animal Care. The LS174T human colon cancer cells (American Type Culture Collection, Manassas, VA) were harvested and suspended in sterile PBS at 7.5 × 10^8 viable cells/mL. Two groups of animals (6 mice per group) were injected intraperitoneally (i.p.) with 10^8 viable cells in PBS. At a tumor diameter of 5−10 mm, 2 μCi of ^{177}Lu-DTPA-ΔCH2HuCC49 was injected i.p. into the mice, and the animals were dissected 4 and 48 h postinjection. The radioactivity uptake in the tumor, and normal tissues were measured in a gamma-counter and the counts were used to calculate the %ID/g values.

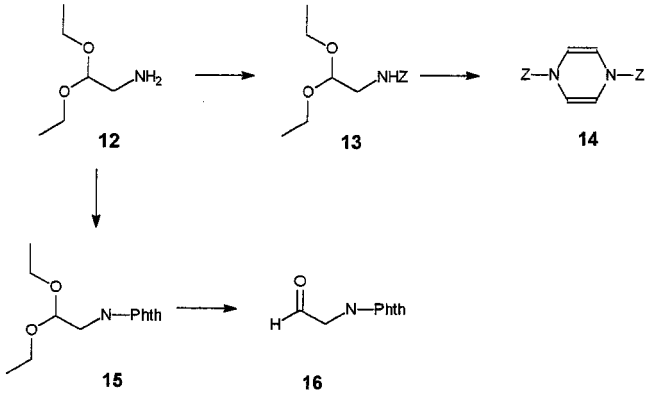
RESULTS AND DISCUSSION

A bifunctional DTPA molecule (**2**, Figure 1), containing a hydrazide function on the methylene backbone, has been recently prepared (*17*). The simplest approach to the synthesis of the target DTPH compound (**5**) seemed to be a direct reaction of the protected pentacarboxylate hydrazide **3**, with an excess of hydroxylamine and in the presence of a coupling reagent. This turned out to be not a simple task as shown in Scheme 1. Reaction of **3** with *O*-benzylhydroxylamine in DCC/HOBT reactions formed

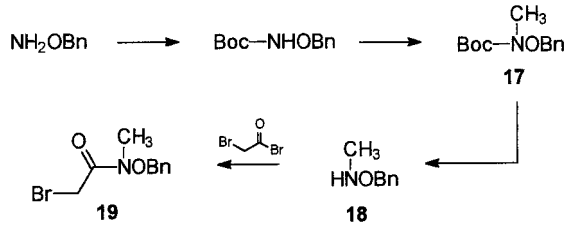
Scheme 2



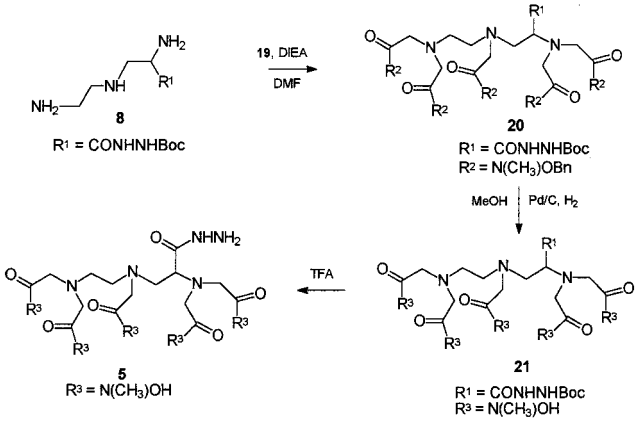
Scheme 3



Scheme 4



Scheme 5



the cyclized compounds **6** and **7** as the major products and with no or negligible quantities of **4**. Changing the reaction conditions, such as stoichiometry, solvent and temperature, did not improve the results, and longer reaction times converted **7** to **6**.

It was anticipated that a logical solution to this problem would be alkylation of the core diethylene triamine **8** by a reagent already equipped with a protected hydroxamic acid group as shown in Scheme 2. Thus, the functionalized triamine **8** (R = CONHNHBoc) (*17*) was reacted with 2-bromo *N*-benzyloxy acetamide **9** under basic conditions. Again, formation of cyclic products **10** and **11**, and not the desired product **4**, was observed. These results demonstrated the high stabilities of the cyclic structures to the extent of eliminating hydroxylamine and *O*-benzylhydroxylamine as two otherwise poor leaving groups.

In the course of the synthesis of the triamine **8**, formation of a 1,4-disubstituted dihydropyrazine **14**, and not the desired aldehyde, was noted as the major product of the amino aldehyde **13** deprotection as shown in Scheme 3 (17). This occurred only when the protected amine in **13** carried an amide proton. Removal of this proton, using phthalyl as the amine-protecting group (**15**), produced exclusively the target aldehyde **16** and through the same deblocking process.

N-Alkyl hydroxamates have been known to maintain their metal-chelating abilities (*19*, *21*, *27*). The bacterial siderophore, desferrioxamine, as well as some other natural-product siderophores, are potent *N*-alkylated hydroxamic acid chelators (*20*), both in the form of open-chain and cyclic compounds where the hydroxamic nitrogen is incorporated into the ring structure. We anticipated, therefore, that replacing the amide proton of the alkylating agent 2-bromo *N*-bezyloxyacetamide by a small alkyl group should prevent the unwanted cyclizations and still preserve the metal-chelating abilities of the molecule. Thus, 2-bromo-*O*-benzyloxy-*N*-methylacetamide (BNMA, **19**) was prepared by the procedure of Esteves et al. (*38*) with slight modification (Scheme 4). This modification afforded the *O*-benzyl-2-bromo-*N*-methylhydroxylamine in a significantly higher overall yield than reported previously. The improved method involves the N-protection of *O*-benzylhydroxylamine with Boc, instead of 2,2,2-trichloroacetylation, followed by methylation of *N*-Boc-*O*-benzylhydroxylamine with iodomethane at elevated temperature and for 8 days. Additionally, the reaction of *O*-benzyl-*N*-methylhydroxylamine with bromoacetyl bromide was improved by lowering the temperature to −78 °C and carrying out the reaction for 4 h to give the analytically pure product **19** at a higher yield than the one reported previously (93.5 versus 36% reported) (*37*).

Alkylation of the triamine **8** (*17*) with BNMA afforded the product **20** with only minor amounts of the cyclized compounds (Scheme 5). The orthogonally protected **20** was stable and withstood chromatographic purification procedures with no later cyclizations. Removal of the protecting groups by successive hydrogenation/acidolysis proceeded smoothly and with no effect on the structure of the molecule. This synthesis afforded the target product **5** in the form of its TFA salt and at 40.7% overall yield.

MAb Conjugation. A conjugation procedure has been reported for the covalent attachment of unprotected hydroxamic acids to antibodies, using a hydrazide conjugating function (*37*). In this procedure, a ketone-derived linker (6-oxoheptanoic acid) is first implanted into the MAb molecule by an activated ester coupling. With the ketone groups serving as hydrazide anchors, the BCA is then conjugated to the MAb, at a low pH and in a group-selective (ketone-directed) manner, and with no conflict with the native amine groups of the protein. This protocol was used here to conjugate the DTPH hydrazide **5** to the CH2 domain-deleted anti-TAG-72 antibody ΔCH2HuCC49.

MALDI MS analyses of the conjugation products and, using MWs of the unconjugated starting MAb, the linker, and **5**, indicated a DTPH-to-MAb ratio of 2.2 for this conjugation.

Radiolabeling. Radiolabeling of the DTPH-ΔCH2HuCC49 conjugate with ^{177}Lu proceeded at high yields of

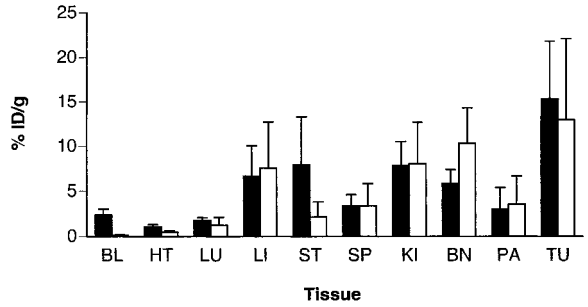


Figure 2. Biodistribution of ^{177}Lu-DTPH−ΔCh2HuCC49 in athymic nude mice bearing i.p. LS174T human colon cancer xenografts at 4 h (■) and 24 h (□) postinjection.

Table 1. Tumor-to-Normal Tissue Ratios for ^{177}Lu-DTPH−Δ*C*H2HuCC49 in LS174T-Bearing Athymic Nude Mice at 4 and 24 h Post-Injection

tissue	4 h	24 h
blood	6.4 ± 1.1	80.9 ± 18.9
heart	14.2 ± 2.7	27.0 ± 4.7
liver	8.5 ± 0.5	10.4 ± 0.3
lung	2.3 ± 1.3	1.7 ± 2.4
stomach	1.9 ± 0.3	5.9 ± 2.2
spleen	4.5 ± 0.6	3.8 ± 0.4
kidney	2.0 ± 0.3	1.6 ± 0.2
bone	2.6 ± 0.3	2.5 ± 0.2
pancreas	5.1 ± 1.1	3.6 ± 0.7

radiolabeling (>96%) confirming the ability of the ligand to maintain its metal-chelating properties after conjugation to the MAb. The SEC−HPLC and Sephadex-25 (PD-10) showed the expected IgG elution patterns.

Biodistribution. Tumor and normal tissue uptake of the ^{177}Lu-DTPH−ΔCH2HuCC49 were studied in athymic nude mice, implanted i.p. with LS174T human colon carcinoma cells, at two time points as shown in Figure 2. The %ID/g values for this conjugate showed tumor uptake of 15.3 ± 6.5 and 13.0 ± 9.1 at 4 and 24 h time-points, respectively. The respective blood %ID/g values were 2.4 ± 0.7 and 0.16 ± 0.05 at these time-points. The tumor-to-normal tissue ratios (Table 1) indicated positive values for all organs with the tumor-to-blood ratio increasing significantly from the 4-h to the 24-h time points. These results demonstrate that the immunoreactivity of the labeled conjugate was not affected by the conjugation and radiolabeling procedures and the conjugate had a rapid blood clearance pattern characteristic of this antibody. It is important to note, however, that the in vivo stability of the ^{177}Lu complex of DTPH may not be as high as that of its pentacarboxylate counterpart. This is based on the observation that the 24-h bone concentration of ^{177}Lu-DTPH-ΔCH2HuCC49 (Figure 2) is over three times that of a ^{177}Lu-labeled DTPA conjugate (*17*).

Conclusion. In an attempt to evaluate the possibilities of designing derivatives with improved properties, a heterobifunctional pentahydroxamate version of the routinely used chelating agent, DTPA, was synthesized. The rationale was the study of a combination of the azaalkyl backbone of DTPA with the metal-chelating hydroxamic acid functionality. The new DTPH molecule, carrying a hydrazide arm on the core chain, formed a covalent conjugate with the ΔCh2HuCC49 as a model antibody and at a DTPH/MAb ratio of 2.2. The ^{177}Lu-labeled conjugate showed tumor uptake in LS174T-bearing nude mice both at 4 and 24 h postinjection timepoints. This study demonstrates the feasibility of synthesis, antibody conjugation, and radiolabeling of this novel BCA and provides the information needed for moving into the next phase of this investigation, the evaluation of the molecule with other radioactive metals and its comparison with DTPA as a multimetal chelator.

ACKNOWLEDGMENT

The authors thank Dr. Michael G. Bartlett (University of Georgia College of Pharmacy) for high resolution mass spectral measurements and helpful discussions. Also, we thank Marion Kirk and Lori Coward (UAB Comprehensive Cancer Center Mass Spectroscopy Shared Facility) for running the ESMS and MALDI spectra, respectively, and Soneshia McMillan for preparing the manuscript. This work was supported by NCI Grants CA62550 and CA78505.

LITERATURE CITED

(1) Kobayashi, H., Wu, C., Yoo, T. M., Sun, B.-F., Drumm, D., Pastan, I., Paik, C. H., Gansow, O. A., Carrasquillo, J. A., and Brechbiel, M. W. (1998) Evaluation of the in vivo biodistribution of yttrium-labeled isomers of CHX-DTPA-conjugated monoclonal antibodies. *J. Nucl. Med. 39*, 829−936.

(2) Brechbiel, M. W., and Gansow, O. A. (1991) Backbone-substituted DTPA ligands for ^{90}Y. *Bioconjugate Chem. 2*, 187−194.

(3) McMurry, T. J., Pippin, C. G., Wu, C., Deal, K. A., Brechbiel, M. W., Mirzadeh, S., and Gansow, O. A. (1998) Physical parameters and biological stability of yttrium (III) diethylenetriaminepentaacetic acid derivative conjugates. *J. Med. Chem. 41*, 3546−3549.

(4) Wong, J. Y., Thomas, G. E., Yamauchi, D., Williams, L. E., Odom-Maryon, T. L., Liu, A., Esteban, J. M., Neumaier, M., Dresse, S., Wu, A. M., Primus, F. J., Shively, J. E., and Raubitschek, A. A. (1997) Clinical evaluation of indium-111-labeled chimeric anti-CEA monoclonal antibody. *J. Nucl. Med. 38*, 1951−1959.

(5) Jasanada, F., Urizzi, P., Souchard, J. P., Le Gaillard, F., Favre, G., and Nepveu, F. (1996) Indium-111 labeling of low-density lipoproteins with the DTPA-bis(stearylamide): evaluation as a potential radiopharmaceutical for tumor localization. *Bioconjugate Chem. 7*, 72−81.

(6) Arano, Y., Uezono, T., Akizawa, H., Ono, M., Wakisaka, K., Nakayama, M., Sakahara, H., Konishi, J., and Yokoyama, A. (1996) Reassessment of diethylenetriaminepentaacetic acid (DTPA) as a chelating agent for indium-111 labeling of polypeptides using a newly synthesized monoreactive DTPA derivative. *J. Med. Chem. 39*, 3451−3460.

(7) Raderer, M., Kurtaran, A., Leimer, M., Angelberger, P., Niederle, B., Vierhapper, H., Vorbeck, F., Hejna, M. H., Scheithauer, W., Pidlich, J., and Virgolini, I. (2000) Value of peptide receptor scintigraphy using (123)I-vasoactive intestinal peptide and (III)In-DTPA-D-Phel-octreotide in 194 carcinoid. *J. Clin. Oncol. 18*, 1331−1336.

(8) Srivastava, S. C., Mease, R. C., Meinken, G. E., Mausner, L. F., and Steplewski, Z. (1990) Development of a new radiolabel (203Pb) and new chelating agents for labeling monoclonal antibodies for imaging. *Acta Radiol. Suppl. 374*, 135−140.

(9) Ferro-Flores, G., Ramirez, F. D., Tendilla, J. I., Pimentel-Gonzalez, G., Murphy, C. A., Melendez-Alafort, L., Ascencio, J. A., and Croft, B. Y. (1999) Preparation and pharmacokinetics of samarium(III)-153-labeled DTPA-bis-biotin. Characterization and theoretical studies of the samarium(III)-152 conjugate. *Bioconjugate Chem. 10*, 726−734.

(10) Izard, M. E., Boniface, G. R., Hardiman, K. L., Brechbiel, M. W., Gansow, O. A., and Walkers, K. Z. (1992) An improved method for labeling monoclonal antibodies with samarium-153: use of the bifunctional chelate 2-(p-isothiocyanatobenzyl)-6- methyldiethylenetriaminepentaacetic acid. *Bioconjugate Chem. 3*, 346−350.

(11) Stimmel, J. B., and Kull, F. C., Jr. (1998) Samarium-153 and lutetium-177 chelation properties of selected macrocyclic and acyclic ligands. *Nucl. Med. Biol. 25*, 117−125.
(12) Safavy, A. (2000) Unpublished results.
(13) Lauffer, R. B. (1987) Paramagnetic metal complexes as water proton relaxation agents for NMR imaging: theory and design. *Chem. Rev. 87*, 901−927.
(14) Caravan, P., Ellison, J. J., McMurry, T. J., and Lauffer, R. B. (1999) Gadolinium (III) chelates as MRI contrast agents: structure, dynamics, and applications. *Chem. Rev. 99*, 2293−2352.
(15) Rebizak, R., Schaefer, M., and Dellacherie, E. (1997) Polymeric conjugates of Gd^{3+}-diethylenetriaminepentaacetic acid and dextran. 1 Synthesis, characterization and paramagnetic properties. *Bioconjugate Chem. 8*, 605−610.
(16) Li, M., and Selvin, P. R. (1997) Amine-reactive forms of a luminescent diethylenetriaminepentaacetic acid chelate of terbium and europium: attachment to DNA and energy transfer measurements. *Bioconjugate Chem. 8*, 127−132.
(17) Safavy, A., Smith, D. C., Bazooband, A., and Buchsbaum, D. J. (2002) De Novo Synthesis of a New Diethylenetriaminepentaacetic Acid (DTPA) Bifunctional Chelating Agent. *Bioconjugate Chem. 13*, 317−326.
(18) Munson, J. W. (1992) in *The Chemistry of Acid Derivatives* (S. Patai, Ed.) pp 849, J. Wiley and Sons, New York.
(19) Bergeron, R. J. (1984) Synthesis and solution structure of microbial siderophores. *Chem. Rev. 84*, 587−602.
(20) Miller, M. J. (1989) Synthesis and therapeutic potential of hydroxamic acid based siderophores and analogues. *Chem. Rev. 89*, 1563−1579.
(21) Bergeron, R. J., McManis, J. S., Phanstiel, O., IV, and Vinson, J. R. T. (1995) A versatile synthesis of deferrioxamine B. *J. Org. Chem. 60*, 109−114.
(22) Tufano, T. P., and Raymond, K. N. (1981) Coordination chemistry of microbial iron transport compounds. 21 Kinetics and mechanism of iron exchange in hydroxamate siderophore complexes. *J. Am. Chem. Soc. 103*, 6617−6624.
(23) Roosenberg, I., J. M., and Miller, M. J. (2000) Total synthesis of the siderophore danoxamine. *J. Org. Chem. 65*, 4833−4838.
(24) Natchus, M. G., Bookland, R. G., De, B., Almstead, N. G., Pikul, S., Janusz, M. J., Heitmeyer, S. A., Hookfin, E. B., Hsieh, L. C., Dowty, M. E., Dietsch, C. R., Patel, V. S., Garver, S. M., Gu, F., Pokross, M. E., Mieling, G. E., Baker, T. R., Foltz, D. J., Peng, S. X., Bornes, D. M., Strojnowski, M. J., and Taiwo, Y. O. (2000) Development of new hydroxamate matrix metalloproteinase inhibitors derived from functionalized 4-aminoprolines. *J. Med. Chem. 43*, 4948−4963.
(25) Barlaam, B., Bird, T. G., Lambert-Van Der Brempt, C., Campbell, D., Foster, S. J., and Maciewicz, R. (1999) New alpha-substituted succinate-based hydroxamic acids as TNFalpha convertase inhibitors. *J. Med. Chem. 42*, 4890−4908.
(26) Cohen, A. (1990) Current status of iron chelation therapy with deferoxamine. *Semin. Hematol. 27*, 86−90.
(27) Bergeron, R. J., Wiegand, J., McManis, J. S., and Perumal, P. T. (1991) Synthesis and biological evaluation of hydroxamate-based iron chelators. *J. Med. Chem. 34*, 3182−3187.
(28) Darwish, I. S., Patel, C., and Miller, M. J. (1993) Synthesis of the antifungal agent norneoenactin a. *J. Org. Chem. 58*, 6072−6075.
(29) Apfel, C., Banner, D. W., Bur, D., Dietz, M., Hirata, T., Hubschwerlen, C., Locher, H., Page, M. G., Pirson, W., Rosse, G., and Specklin, J. L. (2000) Hydroxamic acid derivatives as potent peptide deformylase inhibitors and antibacterial agents. *J. Med. Chem. 43*, 2324−2331.
(30) Fournie-Zaluski, M. C., Coric, P., Turcaud, S., Bruetschy, L., Lucas, E., Noble, F., and Roques, B. P. (1992) Potent and systemically active aminopeptidase N inhibitors designed from active-site investigation. *J. Med. Chem. 35*, 1259−1266.
(31) Fournie-Zaluski, M.-C., Coulaud, A., Bouboutou, R., Chaillet, P., Devin, J., Waksman, G., Costentin, J., and Roques, P. (1985) New bidentates as full inhibitors of enkephalin-degrading enzymes: Synthesis and analgesic properties. *J. Med. Chem. 28*, 1158−1169.
(32) Mimura, T., Nakamura, Y., Nishino, J., Sawayama, T., Komiya, T., Deguchi, T., Kita, A., Nakamura, H., and Matsumoto, J. (1992) A novel class of enkephalinase inhibitors containing a C-terminal sulfo group. *J. Med. Chem. 35*, 602−608.
(33) Safavy, A., Buchsbaum, D. J., and Khazaeli, M. B. (1993) Synthesis of N-[tris[2-[[N-(benzyloxy)amino]carbonyl]ethyl]-methyl]succinamic acid, trisuccin. Hydroxamic acid derivatives as a new class of bifunctional chelating agents. *Bioconjugate Chem. 4*, 194−198.
(34) Safavy, A., Khazaeli, M. B., Safavy, K., Mayo, M. S., and Buchsbaum, D. J. (1999) Biodistribution study of ^{188}Re-labeled trisuccin-HuCC49 and trisuccin-HuCC49ΔCH2 conjugates in athymic nude mice bearing intraperitoneal colon cancer xenografts. *Clin. Cancer Res. 5 (Suppl.)*, 2994s−3000s.
(35) Fritzberg, A. R., Abrams, P. G., Beaumier, P. L., Kasina, S., Morgan, A. C., Rao, T. N., Reno, J. M., Sanderson, J. A., Srinivasan, A., Wilbur, D. S., and Vanderheyden, J. L. (1988) Specific and stable labeling of antibodies with technetium-99m with a diamide dithiolate chelating agent. *Proc. Natl. Acad. Sci. U.S.A. 85*, 4025−4029.
(36) Gerretsen, M., Visser, G. W., van Walsum, M., Meijer, C. J., Snow, G. B., and van Dongen, G. A. (1993) ^{186}Re-labeled monoclonal antibody E48 immunoglobulin G-mediated therapy of human head and neck squamous cell carcinoma xenografts. *Cancer Res. 53*, 3524−3529.
(37) Safavy, A., Khazaeli, M. B., Kirk, M., Coward, L., and Buchsbaum, D. J. (1999) Further studies on the protein conjugation of hydoxamic acid bifunctional chelating agents: Group-specific conjugation at two different loci. *Bioconjugate Chem. 10*, 18−23.
(38) Esteves, M. A., Vaz, M. C. T., Goncalves, S., Farkas, E., and Santos, M. A. (1995) Siderophore analogues. Synthesis and chelating properties of a new macrocyclic trishydroxamate ligand. *J. Chem. Soc., Dalton Trans.*, 2564−2573.

BC010092X

Synthesis and Cleavage Experiments of Oligonucleotide Conjugates with a Diimidazole-Derived Catalytic Center

Birgit Verbeure, Carl Jeff Lacey, Mattheus Froeyen, Jef Rozenski, and Piet Herdewijn*

Laboratory of Medicinal Chemistry, Rega Institute for Medical Research, Katholieke Universiteit Leuven, Minderbroedersstraat 10, B-3000 Leuven, Belgium. Received October 5, 2001;
Revised Manuscript Received December 11, 2001

Ribonuclease mimics based on diimidazole derived constructs in combination with or without additional amino groups have been synthesized and conjugated to oligonucleotides. The imidazole moiety was used either unprotected, protected with a monomethoxytrityl group or a *tert*-butyloxy carbonyl group. Acylation reactions were carried out using the 3-acyl-1,3-thiazolidine-2-thione activation strategy. The peptides were coupled to the oligonucleotides with a mixture of PyBOP, DIEA an HOBt in DMF on solid support. The conjugates were purified by RP-HPLC and identified using negative ion mode mass spectrometry. Unfortunately, no cleavage of a linear RNA target under physiological conditions could be observed.

INTRODUCTION

The design and synthesis of a small synthetic molecule that mimics the active center of a naturally occurring ribonuclease and that is capable of cleaving RNA molecules is an interesting research subject (*1*). The conjugation of such an artificial ribonuclease to a nucleic acid, i.e., an antisense oligonucleotide, would potentially result in a ribonuclease capable of cleaving its target mRNA in a sequence-specific and RNA-selective manner. The study of these constructs could lead to more profound insights in the biochemical processes of hydrolysis in nature.

Nature has provided us with several examples of enzymes possessing phosphodiesterase activity. Studies to resolve the mechanism of pancreatic ribonuclease, RNase A, revealed the presence of two histidine groups around the catalytic center. The protonated imidazole group of His-119 and free imidazole moiety of His-12 have been shown to act as a general acid and general base catalyst, respectively, and hence promote the hydrolysis of phosphodiester bonds within RNA (*2*). Besides the imidazole moieties present in the enzyme's active center, the side chain amino group of Lys-41 would play an important role in the cleavage reaction as well by stabilization of the phosphorane intermediate. Several small organic molecules designed for cleaving RNA in a hydrolytic manner via an acid−base catalyzed mechanism have been reported in the past, including simple diamine or polyamine constructs, guanidine derivatives, or imidazole conjugates (*1*). Their potential as ribonuclease mimics might be elaborated by metal ion coordination due to the ability of imidazole rings to complex metal ions (*3*, *4*).

Our study on artificial ribonucleases has resulted in the synthesis of diimidazole derived constructs in combination with or without additional amino groups and their DNA conjugates. Monoimidazole conjugates of oligonucleotides have previously been reported to exhibit cleaving activity in the absence (*5*) and presence (*6*) of metal ions. However, the cleavage process of oligonucleotides bearing a histamine at the 3′-end in the presence of Zn^{2+} ions is not very efficient (*6*), i.e., 2−5% of RNA is cleaved in 19 h at room temperature. Since conjugation of an at random diimidazole construct to a strand of DNA does not promise the observance of hydrolytic activity, various backbones bearing juxtaposed functionalities have been used to link the catalytic unit to the oligonucleotide. The amino groups could provide additional charge stabilization on the transition-state or, in its protonated state, improve affinity for the phosphodiester backbone.

Different procedures for covalent derivatization of oligonucleotides have been reviewed recently by C. H. Tung (*7*). In the presented study, the RNase A mimics are to be conjugated to an amino-derivatized oligonucleotide via an amide linkage and are therefore provided by a free carboxy acid.

EXPERIMENTAL PROCEDURES

The ^{1}H NMR and ^{13}C NMR spectra were recorded with a Varian Gemini 200 spectrometer (Varian Inc., Palo Alto, CA). Trimethylsilane (TMS) was used as internal standard for the ^{1}H NMR spectra, $CDCl_3$ (δ = 77.0 ppm), DMSO-d_6 (δ = 39.7 ppm), or CD_3OD (δ = 49.0 ppm) for the ^{13}C NMR spectra (*s* = singlet, d = doublet, t = triplet, m = multiplet, br = broad, dAB = doublet in an AB system). Exact mass measurements were obtained performed on a quadrupole/orthogonal-acceleration time-of-flight (Q/oaTOF) tandem mass spectrometer (qTOF 2, Micromass, Manchester, UK) equipped with a standard electrospray ionization (ESI) interface. Samples were infused in a 2-propanol/water (1:1) mixture at 3 μL/min. Precoated SIL G/UV 254 plates (e.g., Silica gel/TLC-cards, Fluka Chemie, Steinheim, Switserland) were used for thin-layer chromatography (TLC), and products were visualized by UV-light, iodine staining, or ninhydrin and sulfuric acid/anisaldehyde spray. Column chromatography was performed on Acros silica gel (0.060−0.200 mm, Beerse, Belgium). Elemental analyses were performed at the University of Konstanz, Germany. Mixtures of solvents are given on a volume to volume basis (v/v) unless otherwise specified.

* To whom correspondence should be addressed: Tel: +32-16-337387; Fax: +32-16-337340; e-mail: Piet.Herdewijn@rega.kuleuven.ac.be.

10.1021/bc0155622 CCC: $22.00 © 2002 American Chemical Society
Published on Web 02/28/2002

For the 5′-amino derivatization of the oligo, the 5′-Amino Modifier 5 from Glen Research Corporation (Sterling, VA) was purchased. HPLC analysis and purification of the oligonucleotide conjugates was done with a Waters Nova-Pak C_{18} column (60 Å, 4 μm) on a Waters 600E instrument using Millenium software for data analysis (Waters Corp., Milford, MA), or with a Merck-Hitachi L-6200A intelligent pump and Pharmacia LKB−Uvicord SII spectrophotometer (Amersham-Pharmacia-Biotech, Freiburg, Germany). The ribooligonucleotides were assembled by Eurogentec (Gent, Belgium). All experiments were conducted in RNase-free water that was prepared by treatment of bi-distilled water with diethyl pyrocarbonate followed by sterilisation.

3-Acetyl-1,3-thiazolidine-2-thione (1). A round-bottom flask, fitted with an addition funnel and equipped with a magnetic stirring bar, was charged with 2-mercaptothiazoline (5.961 g, 50 mmol), 75 mL of dichloromethane (DCM), and triethylamine (Et_3N) (5.060 g, 6.93 mL, 50 mmol). The flask was immersed in an ice bath and stirred. A solution of acetyl chloride (3.925 g, 3.57 mL, 50 mmol) in DCM (65 mL) was placed in the addition funnel and added to the chilled solution dropwise over 45 min. The yellow mixture was stirred at ice bath temperature for an additional 1 h and then at room temperature overnight. The mixture was then extracted successively with 0.2 M citric acid solution and saturated NaCl solution. The organic layer was dried over Na_2SO_4, filtered, and concentrated. The crude material was purified by vacuum distillation: 88−90 °C, 1.0×10^{-1} mbar, 74%, $R_f = 0.60$ (CH_2Cl_2/EtOH 98:2), Upon chilling, the viscous yellow oil crystallized as clear yellow crystals. ^{1}H NMR ($CDCl_3$): δ 2.79 (s, 3H, COC*H*$_3$), 3.30 (t, 2H, ^3J = 7.6 Hz, thiazolidine-C5-*H*$_2$) and 4.589 (t, 2H, ^3J = 7.6 Hz, thiazolidine-C4-*H*$_2$); exact mass (ESI MS, $C_5H_7NOS_2$ + H): calculated 162.0047, found 162.0042.

***N*$^{\alpha}$-Acetyl-L-his-glyOH (3).** To a solution of **1** (161 mg, 1 mmol) in THF (3 mL) was added a solution of Et_3N (101 mg, 139 μL, 1 mmol) and L-his-glyOH (212 mg, 1 mmol) in 3 mL of H_2O. The solution was stirred at room temperature for 16 h, and the solvents were removed on the rotary evaporator. The residue was triturated with THF, the THF drawn off, and the process repeated. The solid was dissolved in 50 mL of boiling methanol. The solution was filtered hot and concentrated, and upon standing at room temperature, the product crystallized. The white product was collected by suction, washed with cold methanol, and dried in a vacuum. Yield: 143 mg, 56%, $R_f = 0.39$ ($CHCl_3$/MeOH/NH_4OH 5:4:1); ^{1}H NMR (DMSO-d_6): δ 1.80 (s, 3H, C*H*$_3$CO), 2.85 (m, 2H, Im-C*H*$_2$), 3.70 (m, 2H, NHC*H*$_2$CO$_2$H), 4.46 (m, 1H, C*H*CO), 6.82 (d, 1H, ^4J = 0.6 Hz, Im-C5-*H*), 7.635 (d, 1H, ^4J = 1 Hz, Im-C2-*H*), 8.01 (d, 1H, ^3J = 8 Hz, AcN*H*) and 8.23 (t, 1H, ^3J = 5.7 Hz, CON*H*CH$_2$); exact mass (ESI MS, $C_{10}H_{14}N_4O_4$, $[M + H]^+$): calculated: 255.1093; found: 255.1078. Elemental analysis: calculated: C 45.62, H 5.74, N 21.23, found: C 45.44, H 5.70, N 21.25.

3-(*O*$^{\gamma}$-Benzyl-*N*$^{\alpha}$-Fmoc-aspartyl)-1,3-thiazolidine-2-thione (5). A mixture of *N*$^{\alpha}$(Fmoc)-*O*^{4}(Bzl)-Asp(OH) (10 mmol, 4.45 g), 1 equiv of DCC (10 mmol, 2.06 g), and 1 equiv of 2-mercaptothiazoline (10 mmol, 1.2 g) in DCM (50 mL) was stirred and cooled on an ice bath. A catalytic amount of DMAP was added to start the reaction. The reaction mixture was stirred at 0 °C for 2 h. The precipitate was removed by filtration and the filtrate evaporated to dryness. The crude product was chromatographed on a silica gel column eluted with 30% ethyl acetate in hexane. Appropriate fractions were pooled and evaporated to dryness, which resulted in yellow foam. R_f = 0.77 (DCM/MeOH 98:2); yield = 90%; ^{1}H NMR ($CDCl_3$): δ 2.9−3.2 (m, 4H, thiazolidine-C$_4$-*H*$_2$, β-C*H*$_2$), 4.1−4.6 (m, 5H, thiazolidine-C$_4$-*H*$_2$, Fmoc-C*H*$_2$C*H*), 5.113 (s, 2H, C*H*$_2$C$_6$H$_5$), 5.964 (d, 1H, ^3J = 7.4 Hz, CON*H*), 6.249 (m, 1H, α-C*H*), 7.2−7.8 (m, 13H, aromatic H benzyl and Fmoc); ^{13}C NMR ($CDCl_3$): δ 28.804 (thiazolidine CH_2N), 36.634 (Asp β-CH_2), 46.953 (Fmoc 9′), 52.234 (Asp α-CH), 56.756 (thiazolidine CH_2S), 66.863 (Bn *C*H$_2$Ph), 67.227 (Fmoc CH_2O), 120.006 (Fmoc 4′/5′), 125.075 (Fmoc 1′/8′), 127.129, 127.746, 128.383, 128.504, 128.626 (Fmoc 2′/7′ and 3′/6′; Bn o and m and p), 135.394 (Bn i), 141.312 (Fmoc 11′/12′), 143.710 (Fmoc 10′/13′), 156.032 (Fmoc OCONH, 170.388 and 172.543 (Asp CONH, COO) 201.315 (thiazolidine N*C*SS); exact mass (ESI MS, $C_{29}H_{26}N_2O_5S_2$, $[M + H]^+$): calculated 547.1361, found 547.1354.

***N*^{1}-(TFA)-*N*^{im}-(Mmtr)-histamine (6a).** A suspension of histamine·2HCl (10 mmol, 1.84 g) in anhydrous pyridine (20 mL) was stirred at room temperature in the presence of a catalytic amount of DMAP. After the addition of 1.2 equiv of trifluoroacetic anhydride (12 mmol, 1.69 mL), the mixture was stirred for an additional 2 h. Subsequently, 1 equiv of monomethoxytrityl chloride (10 mmol, 3.08 g) was added and stirring continued overnight. The solution was concentrated, and 300 mL saturated sodium bicarbonate solution was added. The mixture was extracted three times with DCM (3 × 100 mL), and the combined organic layers were washed with water and brine. The organic layer was dried over Na_2SO_4. After filtration, the solution was evaporated to dryness in a vacuum. Chromatographic purification on a silicagel column (DCM/MeOH 98:2) yielded 4.6 g of a white solid. $R_f = 0.2$ (DCM/MeOH 98:2); yield = 96%; ^{1}H NMR ($CDCl_3$): δ 2.761 (t, 2H, ^3J = 6.2 Hz, Im-C*H*$_2$), 3.6241 (q, 2H, ^3J = 5.8 Hz, NHC*H*$_2$), 3.807 (s, 3H, OC*H*$_3$), 6.621 (s, 1H, Im-C$_5$-*H*), 6.8−7.5 (m, Mmtr, Im-C$_2$-*H*), 8.553 (br t, 1H, TFA-N*H*); ^{13}C NMR ($CDCl_3$): δ 26.194 (Im-*C*H$_2$CH$_2$NH), 39.608 (Im-CH$_2$*C*H$_2$NH), 55.208 (Mmtr, OCH$_3$), 74.967 (Mmtr, CPh$_3$), 113.329 (Mmtr, m′), 118.701 (Im C$_5$), 127.776 (Mmtr p), 128.080 (Mmtr o), 129.597 (Mmtr m), 131.115 (Mmtr o′), 134.301 (Im C$_4$), 138.368 (Im C$_2$), 138.672 (Mmtr i′), 142.557 (Mmtr i), 159.249 (Mmtr p′); exact mass (ESI MS, $C_{27}H_{24}N_3O_2F_3$, $[M + H]^+$): calculated 480.1898, found 480.1873.

***N*^{im}-(Mmtr)-Histamine *O*^{4}-Benzyl-*N*$^{\alpha}$-Fmoc-aspartamide (7).** A NaOH solution (30 mL of a 10% solution) was added to a solution of 9 mmol of (**6a**) in ethanol (30 mL), and the mixture was stirred at room temperature. After 30 min, analysis on TLC indicated complete deprotection of the aliphatic amine. DCM (300 mL) and water (300 mL) were added. The aqueous layer was extracted twice more with DCM. The combined organic layers were washed with brine and dried over anhydrous sodium sulfate. After evaporation of the filtrate to dryness in a vacuum, the residual crude amine (**6b**) was mixed with 9 mmol of **(5)** (9 g) in anhyd THF (50 mL) and stirred at room temperature for an additional 15 min after disappearance of the bright yellow color. After evaporation of the reaction mixture to dryness, the product was purified by silica gel column chromatography (DCM/MeOH 98:2). Appropriate fractions were pooled and evaporated to dryness to yield a white foam. $R_f = 0.88$ (DCM/MeOH 95:5); yield = 80%; ^{1}H NMR ($CDCl_3$): δ 2.678 (t, 2H, ^3J = 6.1 Hz, Im-C*H*$_2$), 2.938 (d AB, 2H, ^2J = 12.4 Hz, ^3J = 5.8 Hz and 4.4 Hz, β-C*H*$_2$), 3.512 (m, 2H, Im-CH$_2$C*H*$_2$), 3.750 (s, 3H, OC*H*$_3$), 4.127 (t, 1H, ^3J = 6.8 Hz, Fmoc-C*H*CH$_2$), 4.354 (d, 2H, ^3J = 7.4 Hz, Fmoc-CHC*H*$_2$), 4.550 (m, 1H, α-C*H*), 5.098 (d, 2H, C*H*$_2$C$_6$H$_5$), 6.050 (d, 1H, ^3J = 8.8 Hz, Fmoc-N*H*), 6.569 (d, 1H, Im-C$_5$-*H*), 6.75−7.8 (aromatic C), 7.720 (d, 1H, Im-C$_2$-*H*); ^{13}C NMR ($CDCl_3$):

δ 27.347 (Im-*C*H_2CH$_2$NH), 36.422 (Asp β-CH$_2$), 39.608 (Im-CH$_2$*C*H$_2$NH), 47.075 (Fmoc 9′), 51.202 (Asp α-CH), 55.148 (Mmtr, OCH$_3$), 66.711 (Fmoc-CH$_2$O), 67.136 (Bn *C*H$_2$Ph), 74.724 (Mmtr, CPh$_3$), 113.208 (Mmtr, m′), 118.519 (Im C$_5$), 119.946 (Fmoc 4′), 125.136 (Fmoc 1′), 127.108, 127.746, 127.989, 128.262, 128.596 (Fmoc 2′/7′ and 3′/6′; Mmtr o and p; Bn i and o and m), 129.627 (Mmtr m), 131.115 (Mmtr o′), 134.453 (Im C$_4$), 135.455 (Bn p), 138.550 (Mmtr i), 138.915 (Im C$_2$), 141.282 (Fmoc 11′/12′), 142.708 (Mmtr i), 143.710 (Fmoc 10′/13′), 156.032 (Fmoc OCONH, 159.098 (Mmtr p′), 169.963 (Asp COO), 171.572 (Asp CONH); exact mass (ESI MS, $C_{51}H_{46}N_2O_6$, $[M + H]^+$): calculated 810.3495, found 810.3519.

***N*^{Im}(Mmtr)-Urocanic Acid (9).** To a suspension of urocanic acid (0.69 g, 5 mmol) in anhydrous pyridine (20 mL) was added 1 equiv of monomethoxytrityl chloride (5 mmol, 1.54 g) and the reaction mixture was stirred overnight at room temperature. After concentration of the reaction mixture under vacuum, chloroform (200 mL) was added. The organic layer was washed twice with a citric acid solution (18% m/v) and once with brine, dried over anhydrous Na_2SO_4 and concentrated under vacuum. The reaction product was precipitated from diethyl ether and isolated as a white solid in 50% yield.

^{1}H NMR ($CDCl_3$): δ 3.816 (s, 3H, −O−C*H*$_3$), 6.5395 (d, 1H, ^3J = 15.4 Hz, HOOC−C*H*=CH-), 6.8−7.4 (m, 15H, aromatic H Mmtr and Im-C$_5$-*H*), 7.563 (d, 1H, ^3J = 15.6 Hz, Im-C*H*=CH-), 7.566 (s, 1H, Im-C$_2$-*H*); ^{13}C NMR ($CDCl_3$): δ 55.269 (Mmtr, −O−CH$_3$), 75.513 (Mmtr, CPh$_3$), 113.511 (Mmtr, m′), 116.334 (Im C$_5$), 124.225 (−CH=*C*H−COOH), 127.897 (Mmtr p), 128.262 (Mmtr o), 129.597 (Mmtr m), 131.145(Mmtr o′), 133.876 (Im C$_4$), 136.760 (Im-*C*H=CH-, 137.276 (Mmtr i′), 140.493 (Im C$_2$), 142.192 (Mmtr i), 159.371 (Mmtr p′), 171.693 (-*C*OOH); exact mass (ESI MS, $C_{26}H_{22}N_2O_3$ $[M-H]^-$): calculated 409.1552, found 409.1546.

***N*^{Im}(Mmtr)-imidazole acetic acid (10).** Imidazole acetic acid·HCl (1.62 g, 10 mmol) was suspended in DCM (40 mL). Subsequently, 3 equiv of triethylamine (30 mmol, 4.16 mL) and a catalytic amount of DMAP were added. After 15 min. stirring at 0 °C, 1 equiv of monomethoxytrityl chloride (3.08 g, 10 mmol) was added. After 1 h of reaction, an additional equiv of monomethoxytrityl chloride was added. After reaction, 50 mL of DCM was added. The solution was extracted with 5% (m/V) citric acid (100 mL), half saturated sodium chloride (100 mL) and two times with brine (75 mL). The organic layer was dried over anhydrous Na_2SO_4 and filtered, and the filtrate was evaporated to dryness in a vacuum. The residue was covered with 13.4 mL of 20% (m/V) potassium hydroxide in methanol and 3.4 mL of water. The mixture was boiled on a steam bath for 5 min and allowed to cool. After addition of 60 mL of water, the aqueous layer was extracted three times with diethyl ether (3 × 100 mL). The aqueous layer was chilled in an ice bath, and glacial acetic acid was added dropwise under stirring till pH 5. The mixture was extracted twice with DCM (200 mL). The combined organic layers were washed with brine, dried over anhydrous Na_2SO_4, and filtered. After evaporation of the solvent in a vacuum, the crude material was triturated in THF/diethyl ether (1:1) and placed in a refrigerator for several hours. The product was collected by filtration and washed with fresh chilled THF/diethyl ether, and the resulting white powder dried in a vacuum over P_2O_5. Yield = 77%; ^{1}H NMR (DMSO-d_6): δ 3.453 (s, 2H, Im-C*H*$_2$COOH), 3.768 (s, 3H, OC*H*$_3$), 6.769 (s, 1H, Im-C5-*H*), 6.95−7.12 and 7.35−7.46 (14H, aromatic H), 7.284 (d, 1H, Im-C2-*H*); ^{13}C NMR ($CDCl_3$): δ 34.289 (Im-*C*H$_2$CO), 55.322 (Mmtr, OCH$_3$), 74.322 (Mmtr, CPh$_3$), 113.687 (Mmtr, m′), 119.333 (Im C$_5$), 127.953, 128.408, 129.349, 130.897 (Mmtr p o m o′), 134.357, 134.812 (Im C$_4$ and Im C$_2$), 137.756 (Mmtr i′), 142.825 (Mmtr i), 158.911 (Mmtr p′), 172.448 (COOH); exact mass (ESI MS, $C_{25}H_{22}N_2O_3$, $[M + H]^+$): calculated: 399.1708; found: 399.1689.

***N*$^{\alpha}$(TFA)-*N*^{Im}(Mmtr)-histidine (11).** Histidine (10 mmol, 1.55 g) was suspended in a mixture of methanol (50 mL) and triethylamine (50 mmol, 7 mL). Five equivalents of ethyl trifluoroacetate (50 mmol, 6 mL) were added over a period of 30 min. After 2 h stirring at room temperature, the reaction mixture was evaporated till dryness in a vacuum. This crude reaction product was coevaporated twice with anhyd pyridine and finally suspended in anhyd pyridine (20 mL). One equivalent of monomethoxytrityl chloride (10 mmol, 3.08 g) was added and the reaction mixture stirred for 2 h at room temperature. EtOAc (300 mL) was added, and this solution was extracted twice with a citric acid solution (18% m/v), washed with brine, and dried over anhydrous sodium sulfate. During evaporation of the solvent under vacuum, the product precipitated as a white solid. Therefore, the mixture was placed in a refrigerator overnight and the product was collected by filtration, washed with freshly chilled EtOAc, and dried in a vacuum over P_2O_5. R_f = 0.25 (DCM/MeOH 95:5); yield = 92%; ^{1}H NMR ($CDCl_3$): δ 3.384 (dAB, 2H, ^2J = 14.6 Hz, ^3J = 3.3 Hz and 5.8 Hz, β-C*H*$_2$ (His)), 3.820 (s, 3H, OC*H*$_3$), 4.499 (m, 1H, α-C*H*), 6.584 (d, 1H, ^4J = 1.6 Hz, Im-C$_5$-*H*), 6.8−7.4 (aromatic H Mmtr), 7.424 (d, 1H, ^3J = 5.2 Hz, TFA-N*H*-), 7.881 (d, 1H, ^4J = 1.6 Hz, Im-C$_2$-*H*); ^{13}C NMR ($CDCl_3$): δ 27.195 (His, β-CH$_2$), 52.841 (His, α-CH$_2$), 55.269 (Mmtr, OCH$_3$), 76.682 (Mmtr, CPh$_3$), 113.724 (Mmtr, m′), 121.190 (Im C$_5$), 128.474 (Mmtr p), 128.656 (Mmtr o), 129.415 (Mmtr m), 131.054 (Mmtr o′), 131.651 (Im C$_4$), 132.845 (Im C$_2$), 137.124, 141.252 (Mmtr i), 159.614 (Mmtr p′), 172.452 (His −COOH); exact mass (ESI MS, $C_{28}H_{24}N_3O_4F_3$, $[M + H]^+$): calculated 524.1797, found 524.1792.

Coupling Procedure for Diimidazole Constructs 12, 13, and 14. The Fmoc-group was removed from compound **7** by treatment for 10 min with 20% piperidine in toluene. After evaporation to dryness in a vacuum, the residue was coevaporated with toluene two times more. The free amine was dissolved in DCM and added to a mixture of the acid **9**, **10**, or **11**, and DIEA in DMF. Consequently, 1 equiv of PyBOP was added to the reaction mixture. After stirring for 3 h at room temperature, the mixture was diluted with DCM and extracted twice with saturated $NaHCO_3$ solution. After washing with brine, the organic phase was dried over anhydrous Na_2SO_4, filtered, and evaporated to dryness in a vacuum. The product was further purified on silica gel column chromatography (DCM/MeOH 98:2).

Benzyl 3-[((2*E*)-3-{1-[(4-Methoxyphenyl)(diphenyl)methyl]-1*H*-imidazol-4-yl}-2-propenoyl)amino]-4-[(2-{1-[(4-methoxyphenyl)(diphenyl)methyl]-1*H*-imidazol-4-yl}ethyl)amino]-4-oxobutanoate (12). Additional extraction of a solution of the product in diethyl ether/ethyl acetate (4:1) with water (four times) was needed for complete purification. The product was isolated as a white foam in 78% yield. R_f = 0.52 (DCM/MeOH 95/5); ^{1}H NMR ($CDCl_3$): δ 2.671 (t, 2H, ^3J = 6.6 Hz, Im-C*H*$_2$CH$_2$), 2.878 (dAB, 2H, ^2J = 17.3 Hz, ^3J = 4.6 and 6.2 Hz, β-C*H*$_2$ (Asp)), 3.490 (m, 2H, Im-CH$_2$C*H*$_2$NH), 3.774 and 3.816 (2 × s, 2 × 3H, OC*H*$_3$), 4.896 (m, 1H, α-C*H* (Asp)), 5.087 (d, 2H, J = 1 Hz, C*H*$_2$C$_6$H$_5$), 6.573 (d, ^3J = 15 Hz, Im-CH=C*H*CO), 6.5−7.5 (aromatic H); ^{13}C NMR ($CDCl_3$): δ 27.620 (Im-*C*H$_2$CH$_2$), 35.845 (Asp

β-CH_2), 39.487 (Im-CH_2CH_2NH), 49.290 (Asp α-CH), 55.208 (Mmtr, OCH_3), 66.711 (Bn CH_2Ph), 74.815 and 75.270 (Mmtr, CPh_3), 113.269 (Mmtr, m′), 118.094 and 118.489 (Im C_5), 123.709 (Im-CH=*C*HCO), 127.928−131.145 (Mmtr p o m o′; Bn o m p), 134.059 and 134.544 (Im C_4), 135.546 (Bn p), 137.215 (Im-*C*H=CH), 138.520 and 138.611 (Mmtr i′), 140.068 (Im C_2), 142.344 and 142.799 (Mmtr i), 159.098 and 159.310 (Mmtr p′), 166.382 (=CH*C*ONH), 170.267, 171.846 (CONH; COO); exact mass (ESI MS, $C_{62}H_{56}N_6O_6$, $[M + H]^+$): calculated 981.4339, found 981.4312.

Benzyl 3-[({1-[(4-Methoxyphenyl)(diphenyl)methyl]-1*H*-imidazol-4-yl}acetyl)amino]-4-[(2-{1-[(4-methoxyphenyl)(diphenyl)methyl]-1*H*-imidazol-4-yl}ethyl)amino]-4-oxobutanoate (13). Complete purification was achieved by silica gel column chromatography using 2% methanol in ethyl acetate as the mobile phase. Appropriate fractions were pooled and evaporated to dryness in a vacuum to yield the product as a white foam. Yield 54%; $R_f = 0.28$ (DCM/MeOH 95/5); ^{1}H NMR ($CDCl_3$): 2.642 (t, 2H, $^3J = 6.7$ Hz, Im-CH_2CH$_2$), 2.876 (dAB, 2H, $^2J = 17$ Hz, $^3J = 5.2$ and 6.0 Hz, (Asp)), 3,431 (m, 2H, Im-CH_2CH_2NH), 3.477 (s, 2H, Im-CH_2CO), 3.783 and 3.794 (2 × s, 6H, 2 × OCH_3), 4.833 (m, 1H, α-C*H* (Asp)), 5.035 (d, 2H, CH_2Ph), 6.568 and 6.677 (2 × d, 2 × Im-C_5*H*), 6.778−7.377 (aromatic H), 7.650 (t, 1H, N*H*CH_2-CH_2-Im), 7.692 (d, 1H, OCN*H*CH (Asp)); ^{13}C NMR ($CDCl_3$): δ 27.863 (Im-*C*H_2CH_2NH), 35.845 (Asp β-CH_2), 36.057 (Im-*C*H_2CO), 39.578 (Im-CH_2*C*H_2NH), 49.260 (Asp α-CH), 55.208 (Mmtr, OCH_3), 66.499 (Bn CH_2Ph), 75.058-(d) (Mmtr, CPh_3), 113.238(d) (Mmtr, m′), 118.580 and 119.764 (2 × Im C_5), 128.019, 128.110, 128.201, 128.535, 129.718, 131.175 (Mmtr, p o m o′; Bn o m p), 134.423 (Im C_4), 135.606 (Bn p), 138.672 (Im C_2), 138.399 and 139.066 (Mmtr i′), 142.557 and 142.830 (Mmtr i), 159.219 (Mmtr p′), 170.267, 170.509, 171.602 (2 × CONH, COO); exact mass (ESI MS, $C_{61}H_{56}N_6O_6$, $[M + H]^+$): calculated 969.4329, found 969.4329.

Benzyl 3-({3-{1-[(4-Methoxyphenyl)(diphenyl)methyl]-1*H*-imidazol-4-yl}-2-[(trifluoroacetyl)amino]propanoyl}amino)-4-[(2-{1-[(4-methoxyphenyl)-(diphenyl)methyl]-1*H*-imidazol-4-yl}ethyl)amino]-4-oxobutanoate (14). After purification on silicagel column chromatography, appropriate fractions were pooled and evaporated to dryness in a vacuum to yield the product as a white foam. Yield 67%; $R_f = 0.55$ (DCM/MeOH 95/5); ^{1}H NMR ($CDCl_3$): δ 2.660 (t, 2H, $^3J = 6.60$ Hz, Im-CH_2CH$_2$), 2.822 (dAB, 2H, $^2J = 16.8$ Hz, $^3J = 5.3$ and 6.2 Hz, β-CH_2 (Asp)), 3.1−3.35 (m, 2H, β-CH_2 (His)), 3.651 (m, 2H, Im-CH_2CH_2NH), 3.825 and 3.816 (2 × s, 2 × 3H, OCH_3), 4.584 (m, 1H, α-C*H* (His)), 4.584 (m, 1H, α-C*H* (Asp)), 5.083 (d, 2H, $J = 4.4$ Hz, C$H_2C_6H_5$), 6.579 and 6.606 (2 × d, 2 × 1H, $J = 1.0$ and 1.2 Hz, 2 × Im-C_5-*H*), 6.8−7.4 (aromatic H), 7.453 and 7.495 (2 × d, 2 × 1H, $J = 1.4$ and 2.0 Hz, 2 × Im-C_2-*H*), 7.956 (d, 1H, $^3J = 5.76$ Hz, N*H* (His)), 8.462 (d, 1H, $^3J = 9.0$ Hz, N*H* (Asp)), 8.914 (t, 1H, $^3J = 5.58$ Hz, CON*H*CH_2CH_2-Im); ^{13}C NMR ($CDCl_3$): δ 28.106 (Im-*C*H_2CH_2NH), 29.411 (His β-CH_2), 35.693 (Asp β-CH_2), 39.942 (Im-CH_2*C*H_2NH), 49.563 (Asp α-CH), 53.357 (His α-CH_2), 55.178 (Mmtr, OCH_3), 66.529 (Bn CH_2Ph), 74.784 and 75.058 (Mmtr, 2 × CPh_3), 113.269 (Mmtr, m′), 118.519 and 120.340 (2 × Im C_5), 128.110, 128.262, 128.535, 129.567, 129.718, 131.084, 131.206 (Mmtr p o m o′; Bn o m p), 134.180 and 134.605 (Im C_4), 135.667 (Bn p), 138.368 and 138.733 (Mmtr i′), 138.884 (Im C_2), 142.435 and 142.799 (Mmtr i), 159.249 (Mmtr p′), 168.658, 169.902, 171.632 (2 × CONH, COO); exact mass (ESI MS, $C_{64}H_{58}N_7O_7F_3$, $[M + H]^+$): calculated 1094.4427, found 1094.4423.

Procedure for Ester Hydrolysis of Compounds 12 and 13. The compound **12** (or **13**) was dissolved in EtOH (5 mL) and a 10% NaOH (m/v) solution (1 mL) was added. After 30 min, DCM (200 mL) was added and the resulting solution was extracted with water and brine. The organic layer was dried over anhydrous sodium sulfate and evaporated in a vacuum. The products were further purified on silica gel column chromatography ($CHCl_3$/MeOH/Et_3N 95/5/0.5). The fractions containing the title compound were pooled and the solvent evaporated. Traces of Et_3N could be removed by extraction of a solution of the product in DCM with a 0.1 M citric acid solution.

3-[(3-{1-[(4-Methoxyphenyl)(diphenyl)methyl]-1*H*-imidazol-4-yl}acryloyl)amino]-4-[(2-{1-[(4-methoxyphenyl)(diphenyl)methyl]-1*H*-imidazol-4-yl}-ethyl)amino]-4-oxobutanoic Acid (15). The product was isolated as a hygroscopic, white solid. $R_f = 0.60$ ($CHCl_3$/MeOH/Et_3N 90/10/0.5); yield = 71%; ^{1}H NMR ($CDCl_3$): δ 2.62−2.84 (m, 4H, Im-CH_2CH$_2$ and β-CH_2 (Asp)), 3.418 (m, 2H, Im-CH_2CH_2NH), 3.787 and 3.809 (2 × s, 2 × 3H, OCH_3), 4.602 (m, 1H, α-C*H* (Asp)), 6.617 (d, $^3J = 15.8$ Hz, Im-CH=*C*HCO), 7.433 (d, $^3J = 15,4$ Hz, Im-CH=*C*HCO), 6.5−7.5 (aromatic H); ^{13}C NMR ($CDCl_3$): δ 26.588 (Im-*C*H_2CH_2), 38.182 (Asp β-CH_2), 39.396 (Im-CH_2*C*H_2NH), 50.504 (Asp α-CH), 55.239 (Mmtr, OCH_3), 75.300 and 75.847 (Mmtr, CPh_3), 113.451 (Mmtr, m′), 119.157 and 119.703 (Im C_5), 123.193 (Im-CH=*C*HCO), 126.987−131.115 (Mmtr p o m o′), 133.512 and 133.937 (Im C_4), 136.699 (Im-*C*H=CH), 137.245 (Mmtr i′), 139.825 (Im C_2), 141.859 and 142.253 (Mmtr i), 159.340 (Mmtr p′), 166.230 (=CH*C*ONH), 171.177, (CONH), 174.455 (COOH); exact mass (ESI MS, $C_{55}H_{50}N_6O_6$, $[M + H]^+$): calculated 891.3869, found 891.3863.

3-[({1-[(4-Methoxyphenyl)(diphenyl)methyl]-1*H*-imidazol-4-yl}acetyl)amino]-4-[(2-{1-[(4-methoxyphenyl)(diphenyl)methyl]-1*H*-imidazol-4-yl}ethyl)-amino]-4-oxobutanoic Acid (16). The product was isolated as a hygroscopic, white solid. $R_f = 0.42$ ($CHCl_3$/MeOH/Et_3N 90/10/0.5); yield = 55%; ^{1}H NMR ($CDCl_3$): δ 2.64−2.79 (m, 4H, Im-CH_2CH$_2$ and β-CH_2 (Asp)), 3.35−3.56 (4H: m, Im-CH_2CH_2; s (δ 3.502), Im-CH_2CO), 4.562 (m, 1H, α-C*H*), 6.589 and 6.728 (2 × s, 2 × 1H, 2 × Im-C_5-*H*), 7.667 (d, 1H, $^3J = 6.2$ Hz, α-C*H*); ^{13}CNMR ($CDCl_3$): δ 28.106 (Im-*C*H_2CH_2NH), 36.361 (Im-*C*H_2CO), 39.244 (Im-CH_2*C*H_2NH), 40.215 (Asp β-CH_2), 51.566 (Asp β-CH), 55.239 (Mmtr, OCH_3), 74.724 and 74.936 (Mmtr, CPh_3), 113.269 (Mmtr, m′), 118.519, 119.794, 128.019, 129.718, 131.175 (Mmtr p o m o′; Bn o m p), 134.575 and 134.969 (Im C_4), 138.368 (Mmtr i′), 138.793 (Im C_2), 142.678 and 142.799 (Mmtr i), 159.128 (Mmtr p′), 170.054, 171.116 (2 × CONH), 175.912 (COOH); exact mass (ESI MS, $C_{54}H_{50}N_6O_6$, $[M + H]^+$): calculated 879.3892, found 879.3869.

3-({3-{1-[(4-Methoxyphenyl)(diphenyl)methyl]-1*H*-imidazol-4-yl}-2-[(trifluoroacetyl)amino]-propanoyl}amino)-4-[(2-{1-[(4-methoxyphenyl)-(diphenyl)methyl]-1*H*-imidazol-4-yl}ethyl)amino]-4-oxobutanoic Acid (18). Compound **14** (500 mg, 0.45 mmol) was dissolved in 5 mL of EtOH and 1 mL of 10% NaOH solution was added. After 30 min, DCM (200 mL) was added and the solution was extracted with water and brine. The organic layer was dried over anhydrous Na_2SO_4 and evaporated in a vacuum. The residue was treated overnight with 5 equiv (calculated on the starting product, 2.25 mmol, 0.27 mL) of ethyl trifluoroacetate in a mixture of methanol (3 mL) and triethylamine (2.25 mmol, 0.3 mL). The product was isolated by extraction after the addition of 30 mL water with two times 30 mL chloroform. The combined organic layers were washed

twice with brine and dried over anhydrous Na_2SO_4 and filtered, and the filtrate was evaporated in a vacuum. The acid was further purified by silica gel column chromatography ($CHCl_3$/MeOH/Et_3N 95/5/0.5). The positive fractions were pooled, and the solvent was evaporated. The residue was dissolved in DCM and extracted with 0.2 M citric acid and washed with brine. The organic layer was dried over anhydrous Na_2SO_4, filtered, and evaporated in a vacuum to yield the title compound as a hygroscopic, white solid. R_f = 0.51 ($CHCl_3$/MeOH/Et_3N 90/10/0.5); yield = 60%; ^{1}H NMR ($CDCl_3$): δ 2.60−2.78 (m, 4H, Im-CH_2CH$_2$ and β-CH_2 (Asp)), 3.30−3.49 (m, 2H, Im-CH$_2$CH_2), 4.381 (q, 1H, J = 5.87 Hz, α-C*H* (Asp)), 4.664 (br m, 1H, α-C*H* (His)), 6.5−7.4 (aromatic H), 7,471 (t, 1H, OCN*H*CH$_2$), 7.846 (d, 1H, OCN*H*CH (Asp)), 8.795 (br s, 1H, OCN*H*CH (His)); ^{13}C NMR ($CDCl_3$): δ 27.863 (Im-*C*H$_2$CH$_2$NH), 29.654 (His β-CH$_2$), 39.305 (Im-CH$_2$*C*H$_2$-NH and Asp β-CH$_2$), 51.688 (Asp α-CH), 53.721 (His α-CH$_2$), 55.148 (Mmtr, OCH$_3$), 74.724, 113.178 (Mmtr, m′), 118.459 and 119.794 (2 × Im C$_5$), 127.958, 129.567, 131.054 (Mmtr p o m o′), 134.119 and 134.392 (Im C$_4$), 138.308 (Mmtr i′), 138.824 (Im C$_2$), 142.375 and 142.648 (Mmtr i), 159.098 (Mmtr p′), 168.506, 170.874 (2 × CONH), 175.123 (COOH); exact mass (ESI MS, $C_{57}H_{52}N_7O_7F_3$, $[M + H]^+$): calculated 1004.3958, found 1004.3967.

3-{[(9*H*-Fluoren-9-ylmethoxy)carbonyl]amino}-4-[(2-{1-[(4-methoxyphenyl)(diphenyl)methyl]-1*H*-imidazol-4-yl}ethyl)amino]-4-oxobutanoic Acid (20). Compound **7** was subjected to mild hydrolysis by the addition of 5 mL of 20% (m/v) potassium carbonate in water to a solution of 500 mg of the compound in 5 mL of ethanol. The reaction mixture was stirred at room temperature for 30 min. The reaction mixture was concentrated in a vacuum, diluted with 150 mL water, and extracted two times with DCM (2 × 75 mL). The pooled organic layers were washed 0.1 M citric acid and with brine, dried over anhydrous Na_2SO_4, and filtered, and the filtrate was evaporated to dryness in a vacuum. The product was purified by silica gel column chromatography (MeOH/DCM/Et_3N 10:90:0.5). The fractions containing the title compound were pooled and the solvent evaporated. Traces of Et_3N could be removed by extraction of a solution of the product in DCM with 0.1 M citric acid solution. The organic layer was dried over anhydrous Na_2SO_4, filtered, and evaporated in a vacuum to yield the title compound as a white solid. R_f = 0.13 (DCM/MeOH 95/5); yield = 63%; ^{1}H NMR ($CDCl_3$): δ 2.64−2.96 (m, 4H, Im-CH_2CH$_2$ and β-CH_2 (Asp)), 3.455 (m, 2H, Im-CH$_2$CH_2NH), 3.752 (s, 3H, OCH_3), 4.08−4.38 (m, 3H, Fmoc-C*H*CH$_2$ and Fmoc-CHCH_2) 4.470 (br q, 1H, α-C*H* (Asp)), 6.550 (d, 1H, J = 8.5 Hz, N*H* (Asp)), 6.593 (s, 1H, Im-C$_5$-*H*), 6.74−7.56 (aromatic H); ^{13}C NMR ($CDCl_3$): δ 26.710 (Im-*C*H$_2$CH$_2$NH), 38.668 (Asp β-CH$_2$), 39.426 (Im-CH$_2$*C*H$_2$NH), 47.075, 52.325 (Asp α-CH), 55.208 (Mmtr, OCH$_3$), 65.072, 66.833, 75.877 (Mmtr, CPh$_3$), 113.511 (Mmtr, m′), 119.794 ((Im C$_5$), 125.378, 126.987−131.115, 133.452 (Im C$_4$), 136.699, 137.245 (Im C$_2$), 141.221 and 141.798 (Mmtr i), 144.044, 144.196, 156.275, 159.371 (Mmtr p′), 171.086 (CONH), 175.365 (COOH); exact mass (ESI MS, $C_{44}H_{40}N_4O_6$, $[M + H]^+$): calculated 721.3025, found 721.3027.

3-(*N*$^\alpha$-TFA-*N*^{im}-*t*-Boc-L-histidyl)-thiazolidine-2-thione (21). Dicyclohexylcarbodiimide (DCC) (2.063 g, 10 mmol) was weighed into a round-bottom flask, equipped with a stirring bar, followed by thiazolidine-2-thione (MTA) (1.192 g, 10 mmol) and 20 mL (2 mL/mmol) of DCM. Once the DCC had dissolved, the flask was immersed in an ice bath. To the cold mixture was added N^α(TFA)-N^{im}(BOC)-L-histidine (3.513 g, 10 mmol) followed by DMAP (61 mg, 5 mol %). The well-stirred solution was kept at ice bath temperature for 135 min and then overnight at room temperature. The resulting yellow mixture was chilled in a refrigerator for several hours and filtered by suction, and the precipitated urea was washed with several small portions of fresh DCM. The solvent of the filtrate was stripped off, and the oil was taken up in diethyl ether and concentrated. Dissolution in ether and concentration were repeated until the product precipitated or crystallized. After chilling, the yellow crystals were collected by suction and washed with ether. R_f = 0.84 (DCM/MeOH 9:1); yield = 65%; ^{1}H NMR ($CDCl_3$): δ 1.62 (s, 9H, C[CH_3]$_3$), 3.25 (d, 2H, ^3J = 5.2 Hz, β-CH_2), 3.398 (m, 2H, thiazolidine-C$_5$-H_2), 4.581 (m, 2H, thiazolidine-C$_4$-H_2), 6.517 (br q, 1H, ^3J = 5.5 Hz, α-C*H*), 7.179 (d, 1H, ^4J = 0.8 Hz, Im-C4-*H*), 8.004 (d, 1H, ^4J = 1.4 Hz, Im-C2-*H*) and 8.458 (br d, ^3J = 5.2 Hz, TFA-N*H*); exact mass (ESI MS, $C_{16}H_{19}F_3N_4O_4S_2$, $[M + H]^+$): calculated: 453.0878; found: 453.0879. Elemental analysis: calculated: C42.48, H 4.25, N 12.35; found: C 42.56, H 4.38, N 12.41.

***N*$^\alpha$,*N*$^\delta$-bis(*N*$^\alpha$-TFA-*N*^{im}-*t*-Boc-L-histidyl)ornithine (22).** Ornithine·HCl (295 mg, 1.747 mmol) was dissolved in a mixture of MeOH (3.5 mL) and water (42 drops). To the resulting stirred solution was added Et_3N (354 mg, 484 μL, 3.494 mmol) and then a solution of **21** (1.72 g, 1.09 × 3.494 mmol) in 10.5 mL of THF. The mixture was stirred for 24 h. The solution was diluted with more MeOH and concentrated on a rotary evaporator. The residue was diluted with DCM (80 mL) and extracted with 0.2 M citric acid (80 mL). The organic layer was dried over anhydrous Na_2SO_4 and filtered, and the filtrate was concentrated. Purification was done by column chromatography (silica gel, DCM/MeOH 85:15). Appropriate fractions were pooled and evaporated to yield the title compound as clear glassy material. Yield: 34%; ^{13}C NMR (DMSO-d_6): δ 25.435 (γ-CH$_2$ (Orn)), 27.529 (CH$_3$), 27.863 (β-CH$_2$ (Orn)), 29.411 (β-CH$_2$ (His)), under DMSO (δ-CH$_2$ (Orn)), 53.176 (α-CH$_2$ (His)), 58.245 (α-CH$_2$ (Orn)), 85.470 (C[CH$_3$]$_3$), 107.474/113.211/118.978/124.714 (CF$_3$), 114.698 (Im-C5), 137.067 (Im-C4), 139.343 (Im-C2), 146.961 (NHCOO), 155.460/156.188/156.886/157.615 (*C*OCF$_3$), 169.057 and 169.512 (CONH), 174.520 (COOH); exact mass (ESI MS, $C_{31}H_{40}F_6N_8O_{10}$, $[M + H]^+$): calculated: 799.2850; found: 799.2842; elemental analysis: calculated: C 44.60, H 5.31, N 13.43; found C 44.77, H 5.07, N 13.68.

Benzyl *N*$^\alpha$,*N*$^\epsilon$-Bis(*N*$^\alpha$-TFA-*N*^{im}-*t*-Boc-L-histidyl)lysinate (23). Benzyl lysinate·2TsOH (1.161 g, 2 mmol) was covered with THF (10 mL). To the stirred mixture was added Et_3N (304 mg, 416 μL, 3 mmol), followed by dropwise addition of ethanol (approximately 0.5 mL) until a solution obtained. A solution of **21** (1.855 g, 4.1 mmol) in THF (10 mL) was added, followed by an additional 1 equiv of Et_3N. The solution was stirred at room temperature for 3 days. The reaction mixture was concentrated under reduced pressure, diluted with DCM (200 mL), and extracted with cold 0.2 M citric acid (200 mL), H_2O (200 mL), and brine (100 mL). The organic layer was dried over anhydrous Na_2SO_4 and filtered, and the filtrate was concentrated under reduced pressure. The crude material was purified by column chromatography (silica gel, CH_2Cl_2/MeOH 97.5:2.5). Appropriate fractions were pooled, and the solvent was evaporated to yield the title compound as clear glassy material. Yield = 84%, R_f = 0.09 (CH_2Cl_2/MeOH 97.5:2.5); ^{1}H NMR ($CDCl_3$): δ 1.36−1.54 (2 × m, 4H, γ and δ-CH_2 (Lys)), 1.603 (s, 18 H, 6 × CH$_3$), 1.786 (m, 2H, β-CH_2 (Lys)), 2.96−3.1 (m, 4H, 2 × β-CH_2

(His)), 3.182 (m, 2H, ϵ-CH_2 (Lys)), 4.45−4.65 (m, 3H, 2 × α-CH_2 (His) and α-CH_2 (Lys)), 5.138 (d, 2H, CH_2Ph), 7.205 (s, 2H, Im-C5-H), 7.339 (br s, 5H, Ph), 8.031 (m, 2H, Im-C2−H); exact mass (ESI MS, $C_{39}H_{48}F_6N_8O_{10}$, $[M + H]^+$): calculated: 903.3476; found: 903.3445; elemental analysis: C 51.62 H 5.39, N 12.35; found: C 51.34, H 5.33, N 12.38.

***N*$^{\alpha}$,*N*$^{\epsilon}$-Bis(*N*$^{\alpha}$-TFA-*N*^{im}-*t*-Boc-L-histidyl)lysine (24).** To a solution of **35** (1.00 g, 1.108 mmol) in 11 mL of ethanol under a positive N_2 pressure were added in succession Pd/C (10%) (1.0 g) and 1,4-cyclohexadiene (976 mg, 1.153 mL, 11.08 mmol). The mixture was stirred for 48 h, the catalyst removed by filtration, and the filtrate concentrated on a rotary evaporator. Column chromatography on silica gel eluted with DCM/MeOH (8:2) gave a pure product. Appropriate fractions were pooled and evaporated to yield the title compound as clear glassy material. R_f = 0.47 (DCM/MeOH 8:2); yield = 50%; ^{13}C NMR ($CDCl_3$): δ 22.218 (γ-CH_2 (Lys)), 27.650, 27.81 (δ-CH_2 (Lys)), 28.257 (β-CH_2 (Lys)), 30.443 (β-CH_2 (His)), 39.335 257 (ε-CH_2 (Lys)), 53.175 (257 (α-CH_2 (Lys and His)), 85.983 (*C*[CH_3]$_3$), 107.229/112.935/118.671/124.377 (CF_3), 115.090 (Im-C5), 136.972 (Im-C4), 138.126 (Im-C2), 146.715 (NCOO (BOC)), 156.852/157.610 (*C*OCF_3), 169.751 (CONH, COOH); exact mass (ESI MS, $C_{32}H_{42}F_6N_8O_{10}$, $[M + H]^+$): calculated: 813.3006; found: 813.3002; elemental analysis: calculated: C 46.77, H 5.27, N 13.64; found: C 46.07, H 5.41, N 13.38.

Bis{[2-(*N*$^{\alpha}$-TFA-*N*^{im}-*t*-Boc-L-histidyl)amino]ethyl}amine (25). *N*-(2-Aminoethyl)-1,2-diaminoethane (103 mg, 108 μL, 1 mmol) was dissolved in 2 mL of THF. To the stirred solution was added at room temperature a solution of **34** (905 mg, 2 mmol) in 6 mL of THF followed by Et_3N (101 mg, 139 μL, 1 mmol). After stirring for 1 h, the solvent was removed on a rotary evaporator. The crude mixture was purified by silica gel column chromatography eluting first with 9:1 DCM/MeOH and finally 8:2. Appropriate fractions were pooled and evaporated to yield the title compound as gummy material that upon chilling solidifies to a clear glass. R_f = 0.61 (DCM/MeOH 8:2); yield = 78%; ^{1}H NMR ($CDCl_3$): δ 1.607 (s, 18H, C[C*H*$_3$]$_3$), 2.752 (br m, 4H, C*H*$_2$NHC*H*$_2$), 3.095 (m, 4H, Im-C*H*$_2$), 3.325 (br m, 4H, CONHC*H*$_2$), 4.741 (br m, 2H, α-C*H*), 7.210 (s, 2H, Im-C$_4$-H), 7.474 (br m, 2H, his-CON*H*) and 8.52−8.78 (br d, 2H, TFA-N*H*); ^{13}C NMR ($CDCl_3$): δ 27.711 (CH_3), 29.593 and 29.805 (β-CH_2 (His)), 38.577 (CONH*C*H$_2$CH$_2$NH), 47.439 (CONHCH$_2$*C*H$_2$NH), 53.054 (α-CH_2 (His)), 86.044 (*C*[CH_3]$_3$), 115.241 (Im-C5), 107.168/112.904/118.641/124.346 (CF_3), 137.003 (Im-C4), 137.822 and 137.913 (Im-C2), 146.684 (NHCOO), 157.519/156.852 (*C*OCF_3), 169.902 and 170.084 (CONH); exact mass (ESI MS, $C_{30}H_{41}F_6N_9O_8$, $[M + H]^+$): calculated: 770.3060; found: 770.3061.

Bis{[2-(*N*$^{\alpha}$-TFA-*N*^{im}-*t*-Boc-L-histidyl)amino]propyl}amine (26). To a solution of *N*-(3-aminopropyl)-1,3-propanediamine (131 mg, 140 μL, 1 mmol) in THF (2 mL) was added a solution of **21** (905 mg, 2 mmol) in THF (6 mL). After stirring for 1 h at room temperature, the solution was concentrated to an oil on a rotary evaporator, and the crude material was purified by column chromatography (silica gel, DCM/MeOH first 9:1 then 8:2). Appropriate fractions were pooled and evaporated to yield the title compound as gummy material that upon chilling solidifies to a clear glass. R_f = 0.60 (DCM/MeOH 8:2); yield = 54%; ^{1}H NMR ($CDCl_3$): δ 1.42−1.75 (m, 22H, C(CH_3)$_3$ and $CH_2CH_2CH_2$), 2.44−2.70 (br m, 4H, C*H*$_2$-NC*H*$_2$), 2.94−3.28 (m, 4H, Im-C*H*$_2$), 3.28−3.50 (br m, 4H, his-NHC*H*$_2$), 4.74−4.88 (t, 1H, ^3J = 6.4 Hz, one α-C*H*), 4.88−5.02 (t, 1H, ^3J = 7.0 Hz, one α-C*H*), 7.20−7.28 (br s, Im-C4-*H*) and 7.86−8.80 (m, 4H, Im-C2-*H* and TFA-N*H*); ^{13}C NMR ($CDCl_3$): δ 27.741 (CH_3), 28.743 (β-CH_2 (His)), 29.927 and 30.352 (CONHCH$_2$C*H*$_2$CH$_2$NH), 36.938 and 37.787 (CONH*C*H$_2$CH$_2$CH$_2$NH), 45.830 and 46.741 (α-CH (His)), 53.205 and 53.357 (CONHCH$_2$CH$_2$*C*H$_2$NH), 85.832 (*C*[CH_3]$_3$), 112.995/118.762 (CF_3), 115.059 and 115.363 (Im-C5), 136.911 (Im-C4), 138.247 and 138.459 (Im-C2), 146.806 (NHCOO), 156.123/156.912/157.641/158.399 (*C*OCF_3), 169.599 and 170.084 (*C*ONH); exact mass (ESI MS, $C_{32}H_{45}F_6N_9O_8$, $[M + H]^+$): Calculated: 798.3373; Found: 798.3386.

Benzyl {Bis[(2-{*N*$^{\alpha}$-TFA-*N*^{im}-*t*-Boc-L-histidyl}amino)ethyl]amino}acetate (27). A round-bottom flask equipped with a stirring bar was charged with **24** (1.079 g, 1.402 × 10^{-3} mol), DCM (6 mL), benzyl bromoacetate (482 mg, 330 μL, 1.5 × 1.402 × 10^{-3} mol), and Et_3N (213 mg, 292 μL, 1.5 × 1.402 × 10^{-3} mol). The solution was stirred for 6 days. The mixture was concentrated to an oil on a rotary evaporator and purified by silica gel column chromatography eluting with DCM/MeOH (9:1). Appropriate fractions were pooled and evaporated to yield the title compound as gummy material that upon chilling solidifies to a clear glass. R_f = 0.73 (DCM/MeOH 9:1); yield = 87%; ^{1}H NMR ($CDCl_3$): δ 1.594 (s, 18H, C(C*H*$_3$)$_3$), 2.744 (q, 4H, ^3J = 5.4 Hz, C*H*$_2$NC*H*$_2$), 2.96−3.42 (m, 10H, Im-C*H*$_2$, BnO$_2$CC*H*$_2$, His-CONHC*H*$_2$), 4.748−4.948 (m, 2H, α-C*H*), 5.102 (s, 2H, PhC*H*$_2$), 7.199 (s, 2H, Im-C4-*H*), 7.30−7.40 (m, 5H, Ph), 8.007 (s, 2H, Im C2-*H*), 8.743 (br d, 1H, ^3J = 7 Hz, TFA-N*H*) and 8.930 (br d, 1H, ^3J = 7.4 Hz, TFA-N*H*); exact mass (ESI MS, $C_{39}H_{49}F_6N_9O_{10}$, $[M + H]^+$): calculated: 918.3584; found: 918.3586; elemental analysis: calculated: C 50.65, H 5.51, N 13.52; found: C 50.66, H 5.60, N 13.44.

Benzyl {bis[(2-{*N*$^{\alpha}$-TFA-*N*^{im}-*t*-Boc-L-histidyl}amino)propyl]amino}acetate (28). A mixture of **26** (427 mg, 5.35 × 10^{-4} mol), 1 mL of anhydrous DMF, benzyl bromoacetate (135 mg, 92 μL, 1.1 × 5.35 × 10^{-4} mol), and $NaHCO_3$ (49 mg, 1.1 × 5.35 × 10^{-4} mol) was stirred under a positive N_2 pressure at room temperature for 7 days. The mixture was concentrated on a rotary evaporator at 45 °C, and the crude material was purified by column chromatography (silica gel, CH_2Cl_2/MeOH 9:1). Appropriate fractions were pooled and evaporated to yield the title compound as gummy material that upon chilling solidifies to a clear glass. R_f = 0.75 (DCM/MeOH/H_2O 8:2:0.1); yield = 46%; exact mass (ESI MS, $C_{41}H_{53}F_6N_9O_{10}$, $[M + H]^+$): calculated: 946.3898; found: 946.3899.

{Bis[(2-{*N*$^{\alpha}$-TFA-*N*^{im}-*t*-Boc-L-histidyl}amino)ethyl]amino}acetic Acid (29). Compound **27** (586 mg, 6.38 × 10^{-4} mol) was dissolved in 6.4 mL (10 mL/mmol) of EtOH. The solution was stirred and placed under a positive N_2 pressure. Pd/C (10%) (586 mg, 1:1 catalyst/ester by weight) was added followed by 1,4-cyclohexadiene (512 mg, 604 μL, 10 × (6.38 × 10^{-4} mol)). The mixture was stirred for 2 days. The catalyst was filtered off, and the ethanol was removed on a rotary evaporator. Purification was carried out using silica gel column chromatography, eluting first with 9:1 DCM/MeOH and then 8:2. Appropriate fractions were pooled and evaporated to yield the title compound as gummy material that upon chilling solidifies to a clear glass. R_f = 0.20 (DCM/MeOH 8:2 (v/v)); yield = 69%; ^{1}H NMR ($CDCl_3$): δ 1.586 (s, 18H, C(C*H*$_3$)$_3$), 2.60−3.40 (br m, 14H, NHC*H*$_2$C*H*$_2$N, NC*H*$_2$-CO_2H and Im-C*H*$_2$), 4.74−4.98 (m, 2H, α-C*H*), 7.155 (s, 2H, Im-C4-*H*), 8.018 (s, 2H, Im-C2-*H*), and 8.16−8.62 (br m, 4H, TFA-N*H* and his-N*H*); ^{13}C NMR ($CDCl_3$): δ 27.803 (CH_3), 30.262 (β-CH_2 (Asp)), 37.455 (OCNH*C*H$_2$CH$_2$N), 53.421 (α-CH (Asp)), 54.392 (OCNHCH$_2$*C*H$_2$N), 57.8 (HOOC*C*H$_2$N), 85.989 (C[CH_3]$_3$), 113.094/115.340 (*C*OCF_3),

118.800 (Im-C5), 137.315 (Im-C4), 138.105 (Im-C2), 146.876 (NCOO), 157.136/157.864 (*C*OCF$_3$), 170.400 and, 170.643 (NCO and COOH); exact mass (ESI MS, $C_{32}H_{43}F_6N_9O_{10}$, $[M + H]^+$): calculated: 828.3115; found: 828.3103.

{Bis[(2-{*N*$^{\alpha}$-TFA-*N*^{im}-*t*-Boc-L-histidyl}amino)propyl]-amino}acetic Acid (30). Compound **28** was hydrogenolyzed as described for compound **29** during 45 h. After filtration and removal of ethanol from the filtrate, the crude material was purified by column chromatography (silica gel, DCM/MeOH/H_2O 8:2:0.1). Appropriate fractions were pooled and evaporated to yield the title compound as gummy material that upon chilling solidifies to a clear glass. R_f = 0.34 (CH_2Cl_2/MeOH/H_2O 8:2:0.1); yield = 60%; ^{13}C NMR ($CDCl_3$): δ 24.342 ($NHCH_2CH_2CH_2N$), 27.650 (CH_3), 29.987 (β-CH_2 (Asp)), 36.573 ($OCNHCH_2CH_2CH_2N$), 52.841 ($OCNHCH_2CH_2$-CH_2N), 53.539 (α-CH (Asp)), 85.832 (C[CH_3]$_3$), 112.935/118.671 (CF_3), 115.120 (Im-C5), 137.094 (Im-C4), 138.095 (Im-C2), 146.745 (NCOO), 157.034/157.762 (*C*OCF$_3$), 170.540 (N*C*OCH); exact mass (ESI MS, $C_{34}H_{47}F_6N_9O_{10}$, $[M + H]^+$): calculated: 856.3428; found: 856.3421. Elemental analysis: calculated: C 46.26, H 5.71, N 14.28; found C 45.67, H 5.79, N 14.16.

Bis(1-methyl-4-piperidinyl)methylamine·3HCl (33). A three-neck round-bottom flask containing a magnetic stirring bar, a reflux condenser, and an addition funnel were dried in an oven, assembled hot, and placed under a positive N_2 pressure. After cooling to room temperature, the flask was charged with Mg (2.072 g, 1.25 × 68.2 mmol). A solution of freshly distilled 4-chloro-1-methylpiperidine (10.937 g, 68.2 mmol) in dry THF (41 mL, 50 mL/0.1 mol of chloride) was transferred via a cannula into the addition funnel. The chloride solution was then added to the flask and the flask immersed in an oil bath preheated to 60 °C. A small crystal of I_2 and a drop of 1,2-dibromoethane were added, and the temperature was increased toward 80 °C. External heating was maintained from the onset of the Grignard reaction so that reflux continued for 6.5 h. A solution of 4-cyano-1-methylpiperidine (8.471 g, 68.2 mmol) in anhyd THF (34.1 mL, 50 mL/0.1 mol of nitrile) was transferred to the addition funnel via a cannula and added dropwise over 30 min to the refluxing Grignard mixture. Reflux was continued for 13.5 h after which time the flask was allowed to cool to room temperature and then immersed in an ice bath. Initial slow dropwise addition of 150 mL of methanol produced a solution which was then poured into 300 mL of chilled methanol, with an additional 50 mL added as a rinsing to the bulk solution. The flask was immersed in an ice bath, and, over a 13-min period, $NaBH_4$ (6.82 g, 1 g/10 mmol of nitrile) was added in portions to the well-stirred solution. The flask was removed from the ice bath and the solution stirred for 1.5 h, until gas evolution ceased. The solvents were stripped off, the residue was covered with a mixture of 150 mL of diethyl ether and 150 mL of THF, and the mixture was allowed to stand at room temperature so that the insoluble material separated. The solid was removed by suction filtration and washed well with Et_2O/THF (1:1). The combined filtrate was concentrated to a viscous oil, which, upon covering with DCM, deposited colorless needles which were removed by filtration and discarded. The filtrate was adjusted with DCM to a volume of 200 mL and extracted with 100 mL of 10% (m/v) NaOH. After the addition of saturated NaCl solution (100 mL), the aqueous layer was extracted with DCM (2 × 100 mL). The combined organic extracts were dried over anhydrous Na_2SO_4 and filtered, and the filtrate concentrated to an oil which was then heated to 55 °C under high vacuum for 2 h (crude yield: 11.25 g). The crude material (11.025 g) was dissolved at ice bath temperature in 50 mL of 6 N HCl. The acid was removed on a rotary evaporator. Dissolution in and removal of water followed by dissolution in and removal of ethanol left a clear gummy material which was crystallized by boiling in isopropyl alcohol and adding methanol in small portions until a solution was obtained. Upon standing at room temperature, fine powder-like crystals deposited from the solution. The flask was kept at 2 °C for 6 days. Due to the degree of hygroscopicity of the product, the supernatant was drawn off, the crystals washed with isopropyl alcohol, and the washing drawn off. The very hygroscopic, white crystals were dried in a vacuum in the presence of P_2O_5. The supernatant and the washing were combined and then concentrated until product appeared. Crystallization overnight at 2 °C produced a second crop, isolated as described above. R_f = 0.19 (DCM/MeOH/NH_4OH 8:2:0.2); yield = 61%; ^{1}H NMR (D_2O) δ 1.50−2.30 (m, 10H, piperidyl C3-*H*$_2$, C4-*H*, and C5−H_2), 2.888 (s, 6H, N−CH_3), 3.078 (br t, 4H, ^3J = 12.2 Hz, piperidyl C2- and C6-H_{ax}), 3.226 (br t, 1H, ^3J = 12.2 Hz, C*H*-NH_2) and 3.55−3.75(br m, 4H, piperidyl C2- and C6-H_{eq}). exact mass (ESI MS, $C_{13}H_{27}N_3$, $[M + H]^+$): calculated: 226.2283; found: 226.2260.

3-Ethoxycarbonyl-1,3-thiazolidine-2-thione (35). 2-Mercaptothiazoline (1,3-thiazolidine-2-thione, 2.38 g, 20 mmol) was placed in a round-bottom flask, equipped with a magnetic stirring bar and fitted with an addition funnel and $CaCl_2$ drying tube, and partially dissolved in anhydrous DCM (20 mL). After addition of Et_3N (2.024 g, 2.77 mL, 20 mmol) to the mixture, the flask was immersed in an ice bath. The addition funnel was charged with a solution of ethyl chloroformate (2.170 g, 1.91 mL, 20 mmol) in DCM (20 mL). The ethyl chloroformate solution was added dropwise to the cold and stirred reaction mixture over 15 min. The reaction mixture was stirred to room-temperature overnight. After being diluted with 100 mL of DCM, the reaction mixture was extracted with 0.2 M citric acid solution (100 mL), H_2O (100 mL), and brine (100 mL). The organic layer was dried over anhydrous Na_2SO_4 and filtered, and the filtrate was concentrated to a yellow oil. Purification was carried out using column chromatography (silica gel, DCM/EtOH 97.5:2.5). Appropriate fractions were pooled and evaporated to yield the title compound as a bright yellow oil. R_f = 0.71 (DCM/EtOH, 97.5:2.5); yield = 89%; ^{1}H NMR ($CDCl_3$): δ 1.372 (t, 3H, ^3J = 7.2 Hz, CH_3), 3.307 (t, 2H, ^3J = 7.5 Hz, thiazolidine-C5-*H*), 4.352 (q, 2H, ^3J = 7.1 Hz, OCH_2CH_3) and 4.528 (t, 2H, ^3J = 7.5 Hz, thiazolidiene-C4-*H*); ^{13}C NMR ($CDCl_3$): δ 13.953 (−CH_3), 28.097 (thiazolidine C5), 55.473 (thiazolidine C4), 63.637 (CH_2O), 151.167 (OCON), 199.728 (NCSS); exact mass (ESI MS, $C_6H_9NO_2S_2$, $[M + H]^+$): calculated: 192.0153; found: 192.0176.

Ethyl Bis(1-methyl-4-piperidinyl)methylcarbamate (36). Compound **33** (3.348 g, 10 mmol) was dissolved in ethanol (40 mL). To this solution were added Et_3N (3.036 g, 4.16 mL, 30 mmol) and a solution of **35** (1.913 g, 10 mmol) in THF (10 mL). The yellow solution was boiled at gentle reflux for 5 days. (Note: Initially, stirring at room temperature for several days produced little product, a result which indicates the steric hindrance associated with this primary amine.) The solvents were stripped off, and the crude residue was taken up in DCM and purified by column chromatography (silica gel, DCM/MeOH/NH_4OH 8:2:0.25). R_f = 0.51 (DCM/MeOH/NH_4OH, 8:2:0.2); yield = 68%; ^{1}H NMR ($CDCl_3$): δ 1.207 (t, 3H, ^3J = 7.1 Hz, CH_2CH_3), 1.28−1.71 (m, 10H, piperidinyl-

C3-H_2, C4-H_2 and C5-*H*), 1.74−1.96 (m, 4H, piperidinyl-C2-H_{ax} and piperidinyl-C6-H_{ax}), 2.871 (br d, 4H, ^2J = 11 Hz, piperidinyl-C2-H_{eq} and piperidinyl-C6-H_{eq}), 3.398 (br s, 1H, C*H*(NH)), 4.070 (q, 2H, ^3J = 7.2 Hz, COOCH_2) and 4.385 (br d, 1H, ^3J = 10.2 Hz, N*H*CO); exact mass (ESI MS, $C_{16}H_{31}N_3O_2$, $[M + H]^+$): calculated: 298.2494; found: 298.2498.

Ethyl Bis(1-ethoxycarbonyl-4-piperidinyl)methylcarbamate (34). Method A. The free base of **33** was prepared by dissolving the trihydrochloride (3.348 g, 10 mmol) in 5 mL of water and 10% (m/V) NaOH (16.1 mL, 1.5 × 30 mmol) and extracting with twice with 50 mL of DCM. The organic layers were pooled and extracted with of brine (40 mL), dried over anhydrous Na_2SO_4, and filtered. The filtrate was concentrated, and solid residue was dried under high vacuum, leaving 2.13 g (95%) of the free base. The triamine was then dissolved in anhydrous DCM in a two-neck 250 mL round-bottom flask equipped with a stirring bar, reflux condenser, addition funnel, and a $CaCl_2$ drying tube. To the solution were added $NaHCO_3$ (924 mg, 11 mmol) and ethyl chloroformate (1 mL, ∼10 mmol) dropwise. After stirring for 5 min, 8.37 mL of ethyl chlorofomate (total = 9.37 mL, 4.4 × 2 × 10 mmol) was added dropwise during 5 min. The mixture was then refluxed for 8 days with chloroformate and/or $NaHCO_3$ being added after 13.5 h (1.87 mL and 840 mg), 4 days (1.67 mL), 6 days (1 mL and 420 mg), and 7 days (1 mL and 420 mg). The mixture was diluted with DCM to a volume of 200 mL and poured onto crushed ice. After the ice had melted, the two layers were separated and the organic layer washed with 0.1 N HCl (200 mL), water (200 mL), and brine (100 mL). The organic layer was dried over anhydrous Na_2SO_4 and filtered, and the filtrate was concentrated to give 3.17 g of very viscous oil. This crude material was used as obtained for the subsequent hydrolysis.

Method B. A 250 mL round-bottom flask equipped with a magnetic stirring bar and reflux condenser was charged with **36** (2.023 g, 6.80 mmol), $NaHCO_3$ (571 mg, 6.80 mmol), and anhydrous DCM (80 mL) and placed under a positive N_2 pressure. To the stirred solution was added ethyl chloroformate (6.495 g, 5.72 mL, 60 mmol), and heating to reflux commenced. Chloroformate and/or $NaHCO_3$ were added after 67.5 h (1.14 mL and 571 mg), 79 h (1.14 mL and 571 mg), 91 h (1 mL and 571 mg), and 100 h (1 mL and 282 mg). Reflux was terminated after 115 h at which time the reaction mixture was diluted with DCM (150 mL) and poured into crushed ice (300 mL). After the ice melted the layers were separated, and the organic layer was washed with 0.1 N HCl (200 mL), water (200 mL), and brine (100 mL). The organic phase was dried over Na_2SO_4 and filtered. The filtrate was concentrated and dried well under vacuum. Upon standing for several days, the hard gum solidified to a white powdery material. Yield = 73%. As in Method A, the crude material can be used for subsequent hydrolysis. R_f = 0.88 (DCM/MeOH/NH_4OH, 8:2:0.2); exact mass (ESI MS, $C_{20}H_{35}N_3O_6$, $[M + H]^+$): calculated: 414.2604; found: 414.2635.

Di(4-piperidinyl)methylamine (37). To **34** was added slowly 26.4 mL of concentrated hydrochloric acid solution (0.88 mL/mmol of amine, based on starting triamine **33**). The mixture was heated at 60 °C. After 5.5 h, 5 mL of concentrated hydrochloric acid solution was added and the reaction mixture was refluxed for an additional 6 h. The cooled reaction mixture was poured into crushed ice, and the aqueous solution was extracted with DCM (2 × 40 mL). The water was stripped off, and the residue was taken up in ethanol and concentrated. This process was repeated several times until a dry glassy product remained. Mass spectral analysis revealed the presence of the desired product along with a monocarbamate species. Because of the difficulty to remove the third carbamate in acidic conditions, basic hydrolysis was carried out by dissolving the crude material in a mixture of 50 mL of ethanol and 30 mL of 50% (m/v) KOH (aq) and refluxing for 23 h. The alcohol was removed on a rotary evaporator, and the aqueous layer was extracted with diethyl ether. Saturated NaCl solution (10 mL) was added and extraction with DCM (4 × 50 mL) performed. The organic extracts were combined, dried over anhydrous Na_2SO_4, and filtered, and the filtrate was concentrated to an oil which crystallized. The proton NMR spectrum showed that the product was quite pure and, because of its tendency to absorb CO_2 readily, it was used immediately in the subsequent condensation step (vide infra). Yield = 1.02 g, R_f = 0.05 ($CHCl_3$/MeOH/NH_4OH 5:4:1). ^{1}H NMR ($CDCl_3/D_2O$): δ 1.10−1.80 (m, 10H, piperidinyl-C3-H_2, -C4-*H*, and -C5-H_2), 2.272 (t, 1H, ^3J = 5.1 Hz, C*H*(NH_2), 2.50−2.70 (m, 4H, piperidinyl-C2-H_{ax} and -C6-H_{ax}) and 3.04−3.20 (m, 4H, piperidinyl-C2-H_{eq} and -C6-H_{eq}). exact mass (ESI MS, $C_{11}H_{23}N_3$, $[M + H]^+$): calculated: 198.1970; found: 198.1979.

1-Triphenylmethyl-5-imidazoleacetic Acid (38). A 50 mL two-neck round-bottom flask equipped with a magnetic stirring bar, reflux condenser, and $CaCl_2$ drying tube was charged with imidazoleacetic acid·HCl (813 mg, 5 mmol), anhydrous DCM (15 mL), and Et_3N (506 mg, 693 μL, 5 mmol). Chlorotrimethylsilane (543 mg, 635 μL, 5 mmol) was added, and the suspension was refluxed for 2 h. The mixture was allowed to cool to room temperature, 5 mmol of Et_3N added, and reflux continued for 5 min. The reaction flask was again cooled to room temperature, a final 5 mmol portion of Et_3N was added followed by a solution of chlorotriphenylmethane (1.39 g, 5 mmol) in anhydrous DCM (15 mL), and the mixture was stirred for 3 h at room temperature. Methanol (500 μL) was added, the solution was stirred for several minutes, and the solvents were removed under reduced pressure. The residue was partitioned between $CHCl_3$ (100 mL) and cold 5% (m/V) citric acid (100 mL) and separated. The organic layer was then extracted once with brine, dried over Na_2SO_4, and filtered, and the filtrate was concentrated. The crude material was recrystallized from $CHCl_3$/hexane at room temperature and was isolated as a white solid by filtration. R_f = 0.27 (CH_2Cl_2/MeOH 9:1); yield = 90%; ^{1}H NMR ($CDCl_3$): δ 3.653 (s, 2H, −CH_2−CO_2H)-, 6.703 (d, 1H, ^4J = 1.6 Hz, Im-C4-*H*), 7.07−7.18 (m, 6H, phenyl-C2-*H* and -C6-*H*), 7.30−7.40 (m, 9H, phenyl-C3-*H*, -C4-*H* and -C5-*H*) and 7.510 (d, 1H, ^1J = 1.4 Hz); exact mass (ESI MS, $C_{24}H_{20}N_2O_2$, $[M + Na]^+$): calculated: 391.1423, found: 391.1443.

Bis(1-{[1-(triphenylmethyl)-1*H*-imidazol-5-yl]-acetyl}4-piperidinyl)methylamine (39). To a stirred suspension of **51** (3.904 g, 2.05x 0.169 mmol) in anhydrous DCM (21 mL, 2 mL/mmol) under N_2 pressure was added carbonyl diimidazole (1.802 g, 2.15 × 5.169 mmol) at once. The solution, resulting after vigorous gas evolution ceased, was stirred for 30 min, and then the reaction flask was immersed in an ice bath. A solution of **37** (1.02 g, 5.169 mmol) in DCM (10 mL) was added dropwise during 3 min. The reaction mixture was stirred at room-temperature overnight (13 h), diluted to 150 mL with DCM, extracted with water (2 × 150 mL) and brine (1 × 100 mL), dried over anhydrous Na_2SO_4, and filtered. The filtrate was concentrated under reduced pressure. Purification was performed using column chromatography (silica gel, DCM/MeOH, first 9:1, then 8:2). Appropriate

fractions were pooled and evaporated to yield the title compound as glassy material. A relatively large amount (1.26 g) of the triacylated material was obtained. R_f = 0.56 (DCM/MeOH 8:2); yield = 36%; exact mass (ESI MS, $C_{59}H_{59}N_7O_2$, $[M + H]^+$): calculated: 898.4808, found: 898.4789.

Bis{1-[2-(1*H*-imidazol-5-yl)ethyl]-4-piperidinyl}-methylamine (40). A two-neck round-bottom flask, reflux condenser and an addition funnel were dried in an oven and then assembled hot and placed under a positive N_2 pressure. Lithium aluminum hydride (254 mg, 3.75 × 1.781 mmol) was added and then covered with anhydrous THF (5 mL). The slurry was stirred and the flask immersed in an oil bath preheated at 65 °C. A sonicated suspension of diamide **39** (1.60 g, 1.781 mmol) in dry THF (15 mL) was transferred to the addition funnel via a cannula. Another 5 mL of anhydrous THF was used for rinsing, and the rinsing was added to the addition funnel in a like manner. The suspension was added dropwise to the slurry of $LiAlH_4$ during 1.33 h. A final 5 mL of anhydrous THF was used to rinse the system and was added to the reaction mixture. Throughout the addition, the temperature was maintained at 65−70 °C, resulting in gentle reflux. As diamide was added, the mixture would initially develop a greenish color, which changed to a reddish color as the reaction proceeded. When more diamide was added, the red color disappeared, giving way again to the green color. Once addition was complete, the temperature was increased to 80 °C and reflux continued for 130 min. during which time the mixture became fairly dark red. After being cooled to room temperature, the reaction was quenched by sequential addition of water (254 μL), 15% (m/v) NaOH (254 μL), and water (762 μL). The mixture was stirred for 1.5 h with intermittent triturating. The solid was removed by suction filtration through a sintered glass filter and washed several times with fresh THF. The filtrate was concentrated on a rotary evaporator, the residue covered with 13 mL of 50% HOAc, and the mixture heated on a boiling steam bath for 15 min. The walls of the flask were rinsed with 1 mL of 50% HOAc, and the mixture was cooled to room temperature, diluted with water (14.5 mL), and chilled in a refrigerator at 2 °C for 5 h. Insoluble trityl-containing byproducts were filtered off and washed several times with water while triturating. The filtrate was concentrated under reduced pressure, the residue redissolved in water, and the water stripped off. The crude material was purified by silica gel column chromatography. For the first column, elution was performed using $CHCl_3$/MeOH/NH_4OH_{concd} 5:4:1 (R_f = 0.75) and for the second MeOH/H_2O/NH_4OH_{concd} 9:0.5:0.5 (R_f = 0.28) was used. The product was dissolved in isopropyl alcohol, and the solution was filtered (0.45 μm filters) and concentrated. The residue was dried under high vacuum to yield the product as a dry, white foam. Yield = 38%; ^{1}H NMR (D_2O): δ 1.20−1.82 (m, 10H, piperidyl-C3-H_2, -C4-*H*, and -C5-H_2), 1.98−2.22 (m, 4H, piperidyl-C2-H_{ax} and -C6-H_{ax}), 2.34−2.44 (m,1H, C*H*(NH_2)), 2.54−2.88 (m, 8H, Im-CH_2CH_2), 2.94−3.14 (m, 4H, piperidinyl-C2-H_{eq} and -C6-H_{eq}), 6.909 (s, 2H, Im-C4-*H*) and 7.660 (d, 2H, ^4J = 1 Hz, Im-C2-*H*); ^{13}C NMR (CD_3OD): δ 25.023 (Im-CH_2), 27.633 and 30.213 (piperidyl-C3 and -C5), 39.288 (piperidyl-C4), 54.858 (piperidyl-C2 and -C6), 59.653 (Im-CH_2*C*H_2), 60.382 (C-[4-piperidyl]$_2$), 117.836 (Im-C5), 136.016 (Im-C4), 136.624 (Im-C2); exact mass (ESI MS, $C_{21}H_{35}N_7$, $[M + H]^+$): calculated: 386.3032, found: 386.3045.

4-[(Bis{1-[2-(1*H*-imidazol-5-yl)ethyl]-4-piperidinyl}-methyl)amino]-4-oxobutanoic acid (41) Primary amine **40** (152 mg, 3.89 × 10^{-4} mol) was placed in a round-bottom flask, equipped with a stirring bar and reflux condenser, and dissolved with heating at 80 °C in a mixture of anhydrous THF (6 mL) and anhydrous DMF (2 mL) while under positive N_2 pressure. After dissolution of the amine was complete, succinic anhydride (39 mg, 3.89 × 10^{-4} mol) was added in one portion and heating and stirring continued for 30 min. After the reaction mixture had cooled to room temperature, a small amount of water was added to dissolve the precipitated product, and the solvents were removed under reduced pressure. The residue was taken up in water and the solution concentrated, and this process was repeated twice with ethanol. The crude product was dissolved in a minimum amount of $CHCl_3$/MeOH/H_2O (5:4:1) and applied to a column of silica gel and eluted with $CHCl_3$/MeOH/NH_4OH_{concd} (5:4:1). The product was dissolved in water, filtered (0.45 μm filters), concentrated, and dried under high vacuum to yield the title compound as a white solid. R_f = 0.50 ($CHCl_3$/MeOH/NH_4OH 5:4:1); yield = 87%; ^{1}H NMR (D_2O): δ 1.22−1.94 (m, 10H, piperidyl-C3-H_2, -C4-*H*, and -C5-H_2), 2.42−2.54 (m, 4H, NHCH_2C$H_2$$CO_2$H), 2.54−2.76 (m, 4H, piperidyl-C2-H_{ax} and -C6-H_{ax}), 2.88−3.16 (m, 8H, Im-CH_2CH_2), 3.30−3.48 (m, 4H, piperidinyl-C2-H_{eq} and -C6-H_{eq}) and 3.653 (br t, 1H, ^3J = 5 Hz, C*H*(NH)); ^{13}C NMR (DMSO-d_6): δ 24.342 (Im-CH_2), 26.861 and 29.198 (piperidyl-C3 and -C5), 30.170 (NHCO*C*$H_2$$CH_2$COOH), 30.564 (NHCOC$H_2$*C*$H_2$COOH), 36.543 (piperidyl-C4), 53.358 (piperidyl-C2 and -C6), 55.574 (C-[4-piperidyl]$_2$), 58.214 (Im-CH_2*C*H_2), 117.490 (Im-C5), 134.700 (Im-C2 and Im-C4), 171.576 (CONH), 174.581 (COOH); exact mass (ESI MS, $C_{25}H_{39}N_7O_3$, $[M + H]^+$): calculated: 486.3192, found: 486.3198.

Oligodeoxynucleotide Synthesis. Assembly was done at a 2 μmol scale on an ABI 392A DNA synthesizer (Applied Biosystems, Perkin-Elmer, Foster City, CA) following standard procedures (*8*). For the 5′-amino modification, the 5′-amino-modifier was dissolved in anhydrous acetonitrile at a concentration of 0.11 M and allowed to react during 180 s. Detritylation was performed manually using 3% trichloroacetic acid (TCA) in DCM until no yellow color was formed upon addition of additional TCA in DCM solution. The internal amino-modifier (**67**) was dissolved in anhydrous acetonitrile (0.12 M) and incorporated in the oligonucleotide on the DNA synthesizer. The coupling procedure was slightly modified as well by increasing the reaction time. The detritylation procedure was extended to 3 × 20 s (from 3 × 12 s) because of the monomethoxytrityl protection of the 5′-OH instead of dimethoxytrityl protection used during standard oligonucleotide synthesis.

Procedure for 5′-Oligonucleotide Conjugation with the RNase A Mimics. After oligonucleotide synthesis at a 2 μM scale and deprotection of the 5′-amino linker, the solid support was transferred to a microtube with sintered glass filter. Twenty equivalents of the RNase A mimics (**3**, **15**, **16**, **18**, **20**, **22**, **24**, **29**, **30**, and **41**) relative to the theoretical amount of oligonucleotide (0.02 mmol) were weighed out in an eppendorf tube, and 100 μL of anhydrous DMF, 3 mg HOBt (0.022 mmol), and 3.5 μL DIEA (0.02 mmol) were added. In the case of **3** and **41** a suspension was formed. Upon addition of PyBOP (10.4 mg, 0.02 mmol) a clear solution was formed in all cases. The reaction mixture was added to the solid-phase-supported oligonucleotide and shaken overnight. Excess reagent was filtered off, and the solid was washed with anhydrous DMF (3 × 500 μL), acetonitrile (3 × 500 μL), and DCM (3 × 500 μL). For the preparation of **43**−**46**, the solid phase was treated with several quanti-

ties of a solution of 3% TCA in DCM until no yellow color formed anymore upon addition of an additional amount of TCA. The support was washed three times with 500 μL of DCM and was dried by passing nitrogen through the tube.

Cleavage and Deprotection with Ammonia/ Methylamine Mixture. The solid supported oligonucleotide conjugates **42**−**46** were transferred into a screw-capped vial, and 1 mL of a mixture of methylamine and 33% aqueous ammonia (1:1) (AMA) was added. The recipient was firmly closed and the mixture vortexed and allowed to react for 2 h at 25 °C. The mixture was vortexed again, and the oligonucleotide conjugates were isolated from the supernatant on a NAP-25 Sephadex column (Pharmacia, Amersham-Pharmacia-Biotech, Freiburg, Germany).

Cleavage and Deprotection with Aqueous Ammonia. The solid-supported oligonucleotide conjugates **47**−**51** were transferred into a screw-capped vial, and 1 mL of 33% aqueous ammonia was added. The recipient was firmly closed and the mixture vortexed and allowed to react for 16 h at 55 °C. The mixture was vortexed again, and the oligonucleotide conjugates were isolated from the supernatant on a NAP-25 Sephadex column.

Analysis and Purification of Conjugates by RP-HPLC. Analysis and purification of the conjugates by RP-HPLC employed buffers A (0.1 M triethylammonium acetate (TEAA), pH 7.0, freshly prepared from 1 M stock solution and filtered prior to use) and B (acetonitrile). For analytical purposes, a linear gradient of 0% to 20% B over 50 min was used. EDTA was added to the sample (final concentration 5 mM) and incubated for 10 min prior to injection. Monitoring was done at 260 nm.

Oligonucleotide Concentration Determination and Thermal Stability Studies. Oligonucleotide concentrations were determined by measuring the absorbance in pure RNase-free water at 260 nm at 80 °C, and the following extinction coefficients were used: adenine nucleotide $\epsilon = 15000$; thymine nucleotides $\epsilon = 8500$; guanine nucleotides $\epsilon = 12500$; cytosine nucleotides $\epsilon = 7500$; uridine nucleotides $\epsilon = 10000$. T_m values were determined in a buffer containing 0.1 M NaCl, 0.02 M potassium phosphate pH=7.5, 0.1 mM EDTA with a 4 μM concentration for each strand. Melting curves were obtained with a Cary 100 Bio spectrophotometer. Cuvettes were maintained at constant temperature by means of water circulation through the cuvette holder. The temperature of the solution was measured with a thermistor directly immersed in one of the cuvettes. Temperature control and data acquisition was done with an IBM-compatible computer using Cary WinUV thermal application software. The samples were heated at a rate of 0.2 °C·min^{-1} starting at 10 °C and heating to 80 °C. Melting temperatures were determined by plotting the first derivative of the absorbance versus temperature curve. Up and down curves showed identical T_m values. (no hysteresis effect observed).

Cleavage Experiments. The ribooligonucleotides were radiolabeled (^{32}P) at the 5′-end using T4 polynucleotide kinase (Gibco BRL) and [γ-^{32}P]adenosine 5′-triphosphate (ATP) (166500 GBq/mmol) by standard procedures (*9*) and purified on a NAP-5 column (Pharmacia). Stock solutions of the radiolabeled RNA target (0.5 μM) and of the oligonucleotide conjugates (2 μM) (**42**−**51**) were prepared. The oligonucleotide conjugate solution, 2.5 μL, was first mixed with 1 μL of EDTA solution (10 mM) and incubated for 10 min. Subsequently, the buffer solution (250 mM Tris·HCl pH 7.5 or 250 mM imidazole pH 7, 10 μL), the sodium and or potassium chloride solutions, and eventually the metal salts were added. The appropriate amount of RNase free water was added to a total volume of 45 μL. Finally, the radiolabeled ribooligonucleotides were added (5 μL, 0.5 μM), and the reaction mixtures were vortexed and centrifuged. The mixtures were incubated at 37 °C. After appropriate time intervals, samples (5 μL) were taken and mixed with an equal volume of stop mix (EDTA 50 mM, Xylene cyanol FF 0.1%, and bromophenol blue 0.1% in formamide). Alkaline hydrolysis ladders were obtained by incubation at 90 °C in 100 mM Na_2CO_3 solution. Samples were taken after 5, 7, 10, and 12 min. Samples were analyzed by denaturing PAGE (20% in the case of the 23-mer RNA substrate, 12% in the case of the 41-mer RNA substrate) containing urea (50%) with TBE buffer at 65 W for 1.5 h. Results were visualized by phosphorimaging (Packard Cyclone, Optiquant Software, Packard Instrument Company, Meriden, CT).

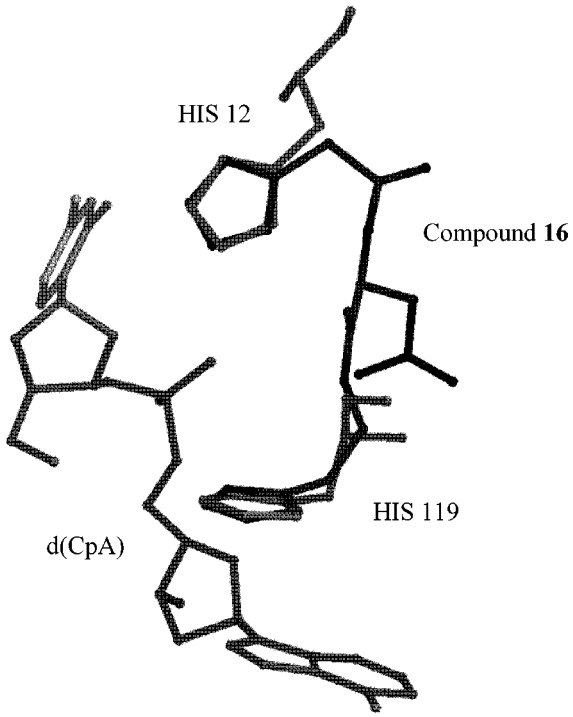


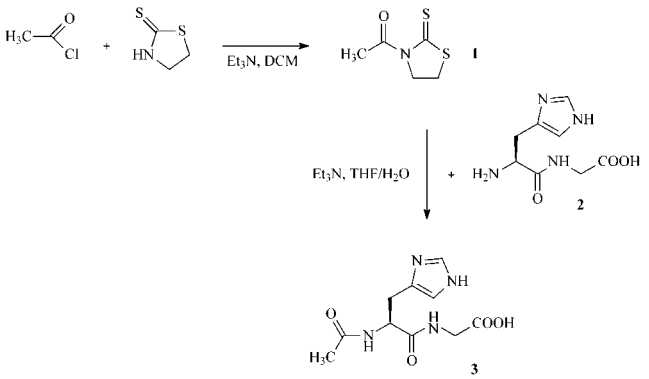
Figure 1. Flexible superposition of compound **16** on the active site histidines of ribonuclease A, shown together with a d(CpA) fragment.

Molecular Modeling Analysis. To preclude the synthesis of RNase A mimics unable to fit in the catalytic ribonuclease system, we did a preliminary check by molecular modeling. Models of structures **16**, **18**, and **24** have been created using Macromodel 5.0 (*10*), and their geometry (one conformation) was optimized in the Amber* force field (*11*) and written out as pdb files. Using a self-made flexible fit program, we investigated if it was possible to match the 2 imidazole functions in our molecules with the two histidines 12 and 119 in the Ribonuclease A enzyme. The X-ray structure of RNase A in complex with dinucleotide d(CpA) from Zegers et al. (*12*) was used as a template. The program varies all possible dihedral angles in the flexible molecule and uses the quaternion fit algorithm (*13*) together with an adaptive simulated annealing minimizer (asa) (*14*) to select the lowest root-mean-square deviation.

RESULTS AND DISCUSSION

The rationale for the synthesis of the proposed diimidazole conjugates is primarily based on some single

Scheme 1

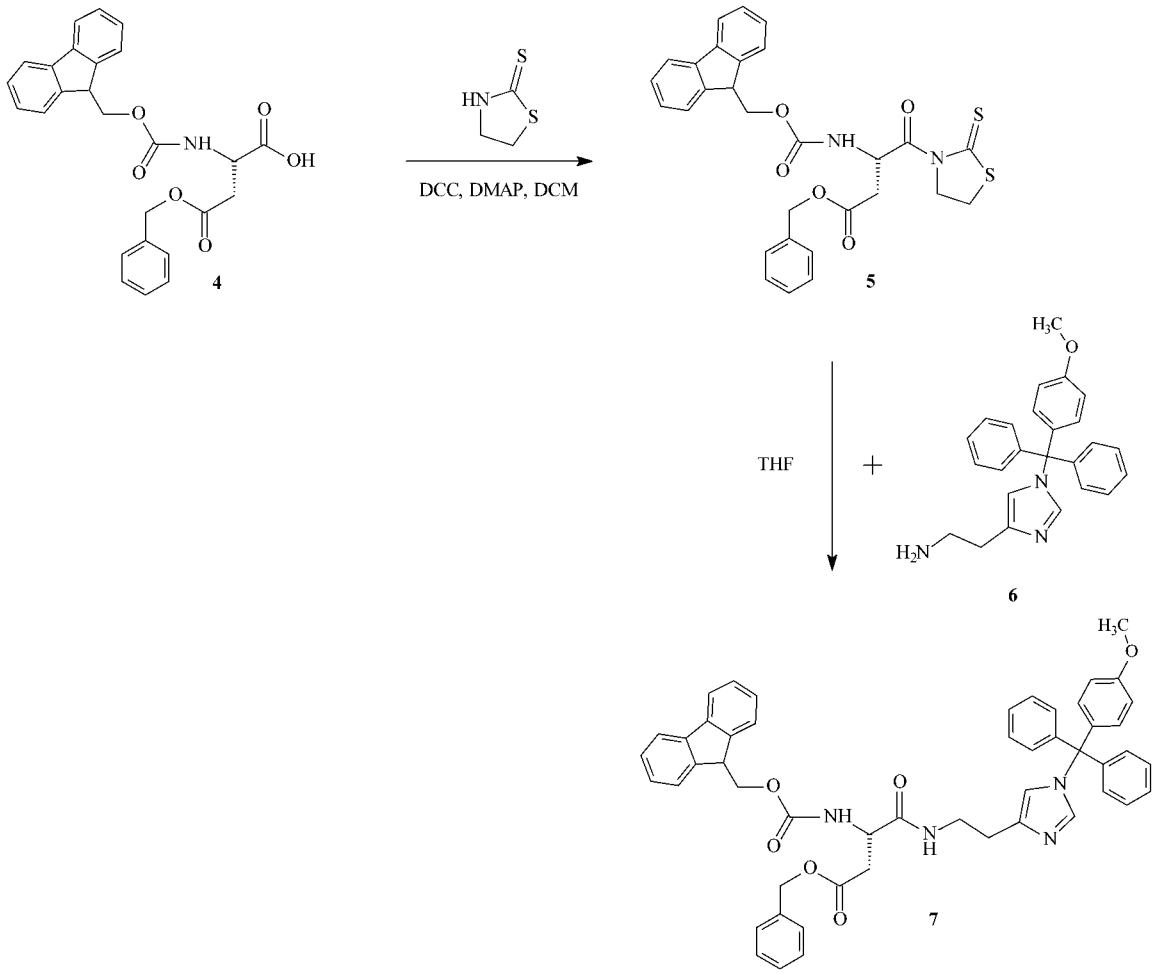


modeling experiments with compounds **16**, **18**, and **24**. The molecular modeling calculations show that there exists at least one conformation of compound **16** where the imidazole functions fit onto his-12 and his-119 of RNase A (Figure 1). The flexible backbone of compound **16** consisting of nine bonds does not hinder approaching the RNA fragment. The same calculations were performed on compounds **18** (10 bonds between the two imidazoles) and **24** (14 bonds) with similar results. These calculations can be extrapolated to the other compounds with similar backbones (**15**: 10 bonds with less flexibility than **18**, due to the presence of the double bond; **22**: 13 bonds; **29**: 14 bonds; **41**: 14 bonds with less flexibility than **24**, due to the presence of the piperidine rings) or longer backbones (**30**: 16 bonds). Moreover, several examples are described of peptide−acridine conjugates (*15*) and of diimidazole intercalator constructs (*16*) that are able to function as mimics of ribonucleases. In those examples, the imidazole groups are bond on a flexible (peptide) linker with 10 to 12 bonds between both imidazole residues.

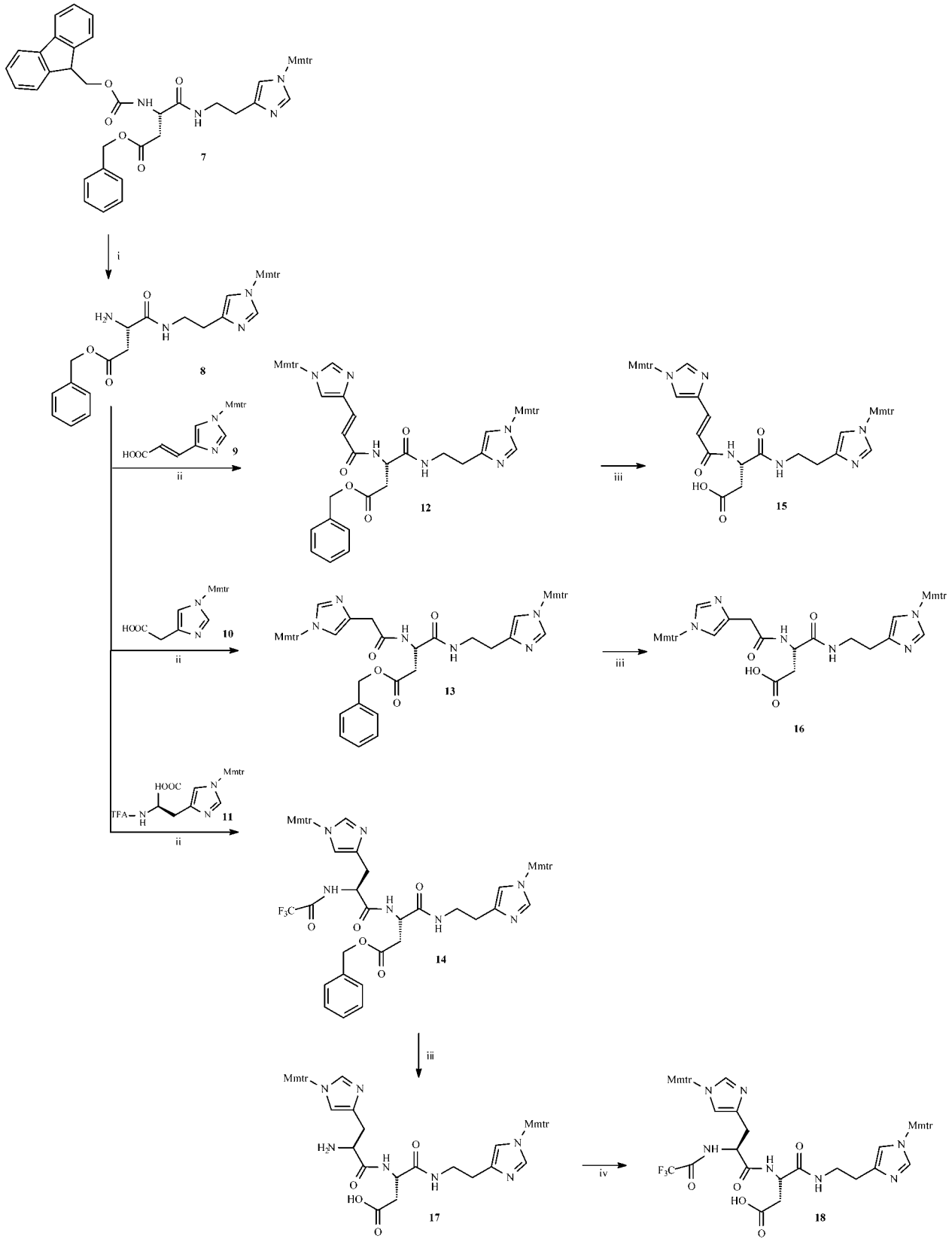
Synthesis of the RNase A Mimics. Although it has been shown that a free imidazole functionality does not interfere with the conjugation reaction on the oligonucleotide itself, the synthesis of these catalysts as fully protected molecules, with imidazole protection as well as protection of the free α-amino group of the amino acid, appeared very attractive as a useful intermediate from the point of view of solubility and stability. The monomethoxytrityl group (Mmtr) was the first protecting group of choice. The high acid lability of this group allowed its removal after conjugation with the oligonucleotide using the standard detritylation procedure of oligonucleotide chemistry, thereby allowing the evaluation of the coupling reaction. However, for the acylation procedures with an imidazole-containing molecule during the synthesis of the RNase A mimics, where the 3-acyl-1,3-thiazolidine-2-thione activation strategy was applied, the BOC group had to be used for the imidazole protection in order to obtain the desired activated compound. The amino groups were protected as trifluoro acetamides (TFA) or fluorenylmethoxycarbonyl amides (Fmoc).

For the synthesis of the monoimidazole compound, N^{α}-acetyl-L-histidylglycine (**3**), the dipeptide, L-histidylglycine (**2**), was modified by acetylation of the α-amino group

Scheme 2



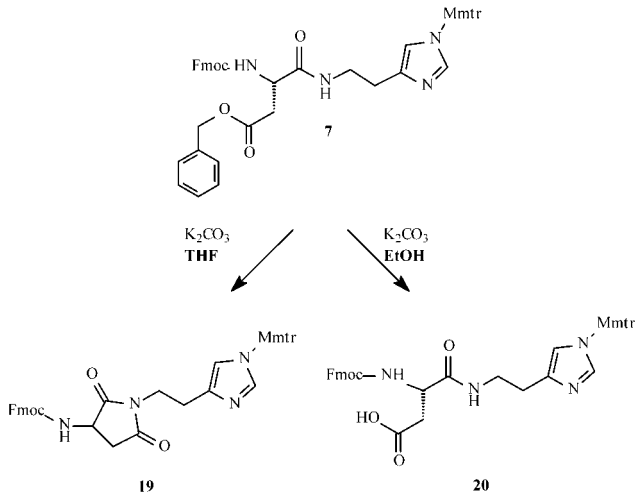
Scheme 3[a]



[a] i: Piperidine, toluene; ii: ByBOP, DIEA, DCM, DMF; iii: NaOH, EtOH, H_2O; iv: CF_3COOEt, Et_3N, MeOH.

of the histidyl residue (Scheme 1). The acetylation procedure was carried out based on the work of Nagao Y. et al., using a previously unreported reagent (*17*). Hereto, acetic acid was converted into its 3-acyl-1,3-thiazolidine-2-thione derivative (**1**) by the addition of acetyl chloride to a solution of 2-mercaptothiazoline and triethylamine. Of practical importance is the applicability of this strategy in aqueous solution in case the amino-substrate is not soluble in organic solvents (*18*), as it is the case for the acylation of L-histidylglycine.

Scheme 4

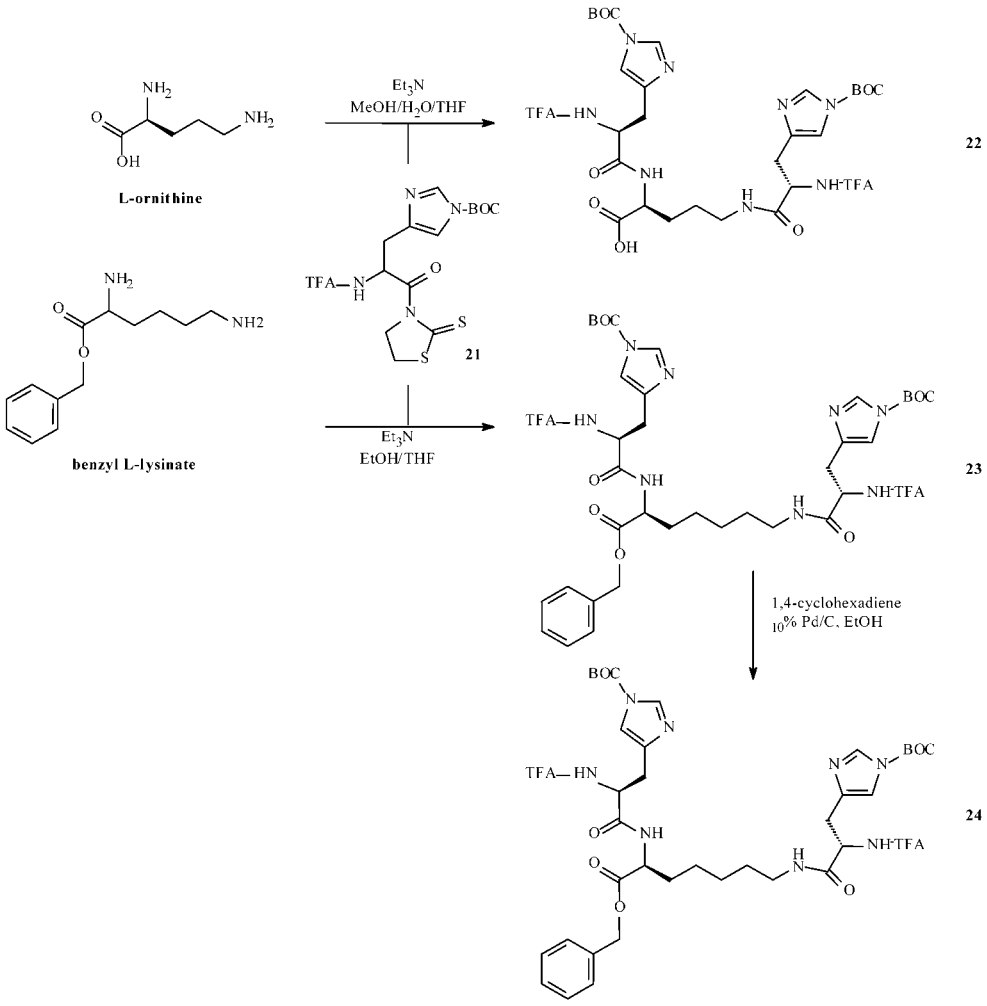


In a first series of multifunctional constructs, aspartic acid was used as the brace to attach imidazole groups on one side, providing on the other side a free carboxylic acid function for conjugation onto the oligonucleotide. Starting from O^{γ}-benzyl,N^{α}-[(9*H*-fluoren-9-ylmethoxy)-carbonyl]-L-aspartic acid (**4**) [N^{α}(Fmoc)-L-Asp(OBzl)-OH], the free α-carboxyl group was converted into a 3-acyl-1,3-thiazolidine-2-thione (**5**) (Scheme 2). This enabled the introduction of the first imidazole group by reaction with N^{im}-(Mmtr)-histamine (**6**). To allow introduction of the second imidazole moiety in the molecule (Scheme 3), the α-amino protecting group of protected aspartic acid (**7**) was removed, and the product was used in the following peptide coupling procedure without prior purification of the amine (*19*). The free amine of **8** was reacted with a carboxylic function on three slightly different imidazole containing molecules: N^{im}(Mmtr)-urocanic acid **9**, N^{im}-(Mmtr)-imidazole acetic acid **10**, and N^{α}(TFA)-N^{im}(Mmtr)-histidine **11** (Scheme 3).

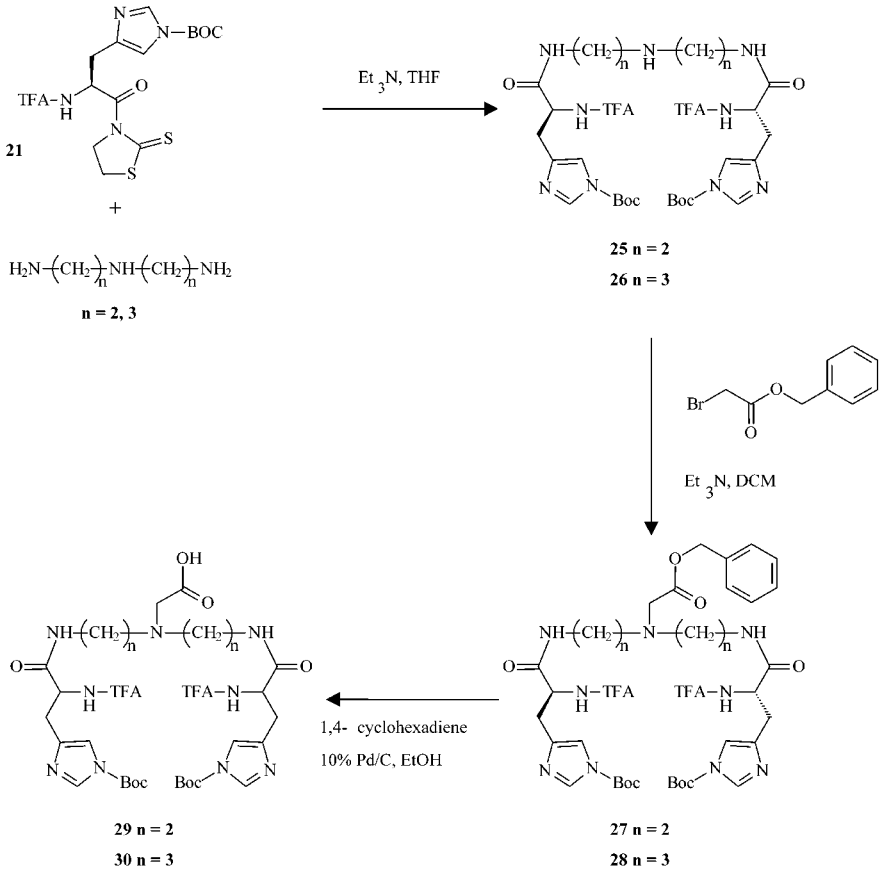
For the formation of the amide bond between the free amine of compound **8** and the free acids of **9**, **10**, and **11** respectively (Scheme 3), ByBOP was used as coupling reagent. It was observed that for the chromatographic purification of the reaction products, halogenated solvents are best to be excluded from the mobile phase in order to separate the desired product from tri(1-pyrrolidinyl)phosphine oxide, the product from PyBOP coupling (*20*). Finally, prior to conjugation with the oligonucleotide, the benzyl ester was cleaved by alkaline hydrolysis. Unfortunately, in the case of **14**, the trifluoroacetamide group was cleaved concomitantly. This could easily be restored by treatment of the product (**17**) with methyl trifluoroacetate in methanol.

A candidate molecule for coupling on the oligonucleotide was obtained by immediate benzyl ester hydrolysis of **7** by selective alkaline hydrolysis leaving the α-amino protecting group intact (Scheme 4). The use of an aqueous potassium carbonate solution in combination with THF as the organic solvent resulted in predominant aspartim-

Scheme 5



Scheme 6



ide formation (**19**) (*21, 22*). Substituting THF for ethanol resulted in the desired hydrolysis product (**20**).

A different scaffold for the synthesis of RNase A mimic's was found in the natural occurring amino acids lysine and ornithine. Because of the general applicability of the 3-acyl-1,3-thiazolidine-2-thione activation strategy for amide bond formation in polar solvents, acylation of both amines (α- and *δ*-amino (ornithine) and *ϵ*-amino (lysine), respectively) would preferentially be carried out following this procedure because of their solubility properties. The unactivated protected amino acid, N^{α}(TFA)-M^{im}(BOC)-His, was prepared as described by Smith T. H. et al. (*23*) and converted into the 3-acyl-1,3-thiazolidine-2-thione derivative.

For the coupling of **21** with ornithine, the amino acid was used in its free acid form. For the derivatization of lysine, the benzyl ester was used (Scheme 5). Although acylation of the side chain amine proceeds very rapidly, the α-amino group is somewhat less reactive toward 3-acyl-1,3-thiazolidine-2-thione compounds (*24*). The derivatization of ornithine under its free acid form resulted in only half the yield obtained with the benzyl ester of lysine. Subsequent removal of the benzyl group of **23** by catalytic transfer hydrogenation, lowered the total yield of the second approach, and compound **24** was obtained in the same overall yield as compound **22**.

Two other potential catalysts were synthesized by derivatization of dialkyl triamines, i.e., *N*-(2-aminoethyl)-1,2-ethanediamine and *N*-(3-aminopropyl)-1,3-propanediamine (Scheme 6). We observed that it was easily possible to selectively functionalize the primary amines of these triamines in the presence of the secondary amine. In comparison with acylation using thiazolidine-thione, CDI coupling exhibited slightly lower selectivity with these substrates. The diacylated products **25** and **26** appeared quite stable and could easily be alkylated with benzyl bromoacetate under standard conditions. Phase transfer hydrogenolysis of **27** and **28**, with 1,4-cyclohexadiene as the hydrogen source, easily cleaved the ester while leaving the protecting groups intact (*25*).

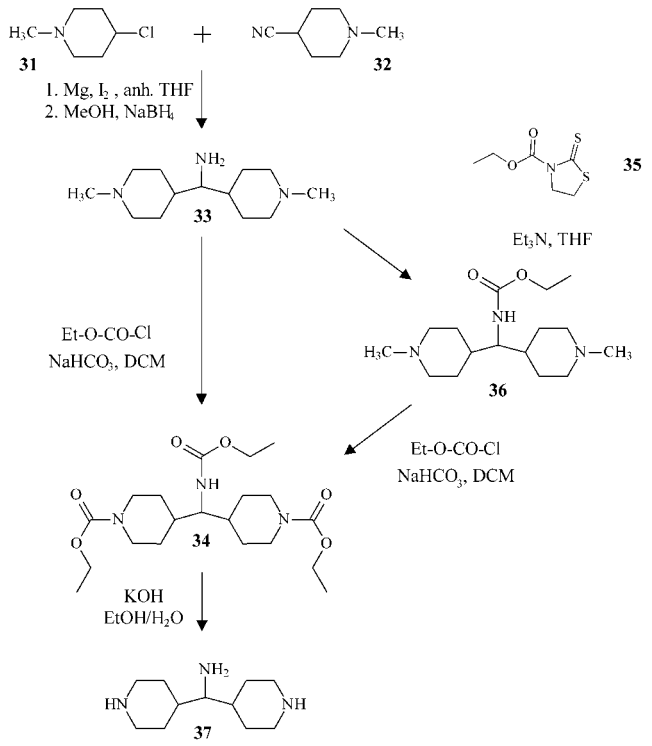
The final RNase A mimic synthesized was based on a bipiperidine moiety. A single amino-functionalized carbon atom was introduced between the two rings in order to be able to link the functionalized bipiperidine to an oligonucleotide.

For the synthesis of the bipiperidine scaffold (Scheme 7), bis(4-piperidinyl)methylamine (**37**), starting from 4-chloro-1-methylpiperidine (**31**) a Grignard reagent was prepared (*26*) that was reacted with 4-cyano-1-methylpiperidine (**32**) (*27*). The resulting imine was immediately reduced using sodium borohydride (*28*). To demethylate the piperidine amino groups, the product was treated with ethyl chloroformate to yield the triethyl carbamate (**34**), which was easily hydrolyzed (*29*). Though the treatment of **33** with ethyl chloroformate yielded the desired compound, a cleaner method was transformation of the primary amine of **33** into its ethyl carbamate (**36**) using 3-(ethyloxycarbonyl)-1,3-thiazolidine-2-thione (**35**)- prior to treatment of the tertiary amines with ethyl chloroformate.

For the introduction of the imidazole moieties (Scheme 8), the secondary amines were first acylated using N^{im}-(trityl)-imidazole acetic acid (**38**). To restore the basicity of the piperidine ring nitrogens, the resulting amide functions were reduced using lithium aluminum hydride. The bis-imidazole compound (**40**) possessing the central primary was succinylated to yield the final product (**41**) ready for conjugation.

Preparation of the Oligonucleotide Conjugates with the RNase A Mimics. For conjugation of the

Scheme 7

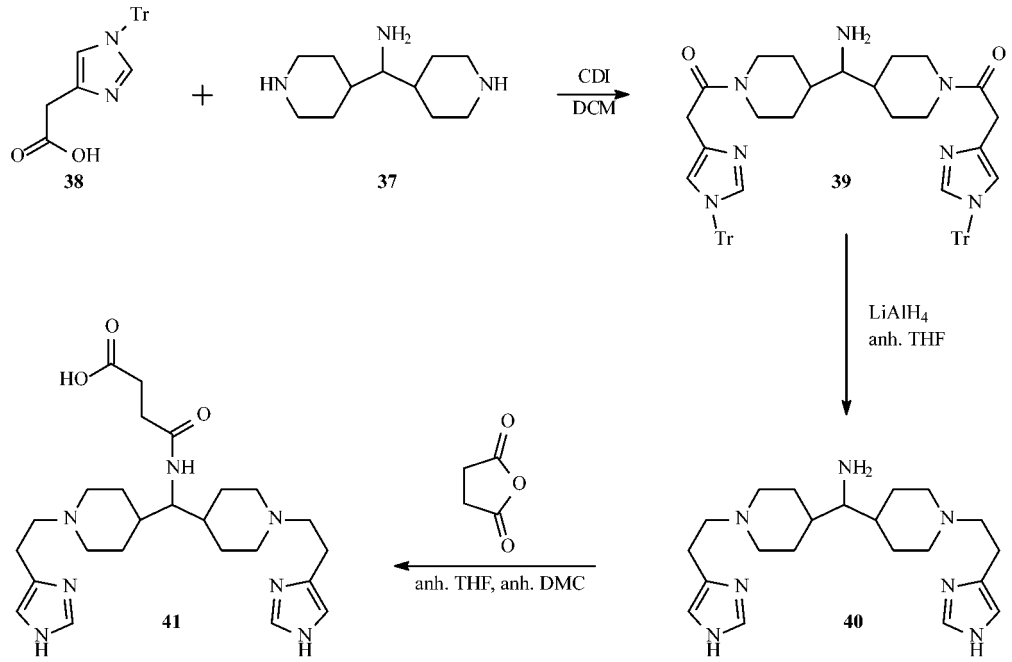


oligonucleotide at the 5′-position, the oligonucleotide was first functionalized with an amino group. The amino linker was introduced at the 5′-position by means of a phosphoramidite building block. The monomethoxytrityl group is easily removed using 3% TCA in dichloromethane. Conjugation of the synthesized constructs with the 5′-amino linker on the oligonucleotide was accomplished by activation of the carboxylic acid with PyBOP in the presence of 1 equiv of DIEA and HOBt in DMF. After 4 h of reaction, the beads were washed. In the case of **15**, **16**, **18**, and **20**, the imidazole protecting group, monomethoxytrityl, was removed by washing the solid support with 3% TCA in DCM, prior to the oligonucleotide cleavage and deprotection procedure using a 1/1 mixture of methylamine and ammonia at room temperature during 2 h. In the case of these aspartic acid based RNase A mimic conjugates, cleavage and deprotection using aqueous ammonia overnight at 55 °C lead to loss of the RNase A mimic from the oligonucleotide. The other conjugates with BOC imidazole protection had to be cleaved from solid support and deprotected under standard aqueous ammonia treatment (33%) overnight at 55 °C since no complete removal of the BOC protection was achieved following ammonia/methylamine treatment. The oligonucleotide conjugates were purified by C_{18} reversed phase HPLC. Confirmation of the identity of the oligonucleotide conjugates was obtained by negative ion mode mass spectrometry (Table 1). Direct infusion experiments show −5 to −7 charged molecules (Figure 2). Deconvolution of the spectra gives the molecular mass of the compound the charged species came from. A few spectra contained additional peaks due to sodium or potassium adducts. Capillary reversed phase liquid chromatography coupled experiments in some cases resulted in the appearances of additional peaks or complete shifts

Table 1. Overview of the Yield of the Coupling Reactions of the 5′-Amino-Modified Oligonucleotide with the RNase A Mimics and the Subsequent Result of Mass Spectral Analysis

compound	RNase A mimic	yield (%)	avg mass calcd (M)	avg mass found
42	3	94	4648.1	(M)4648.0
43	15	45	4740.2	(M) 4740.2
44	16	60	4728.2	(M) 4728.1
45	18	43	4757.2	(M) 4757.2
46	20	68	4620.1	(M) 4619.9
47	22	50	4799.3	(M) 4800.8
48	24	68	4814.3	(M) 4814.2, (M − H + Na) 4836.2; (M − H + K) 4852.1
49	29	57	4829.3	(M) 4829.6; (M − H + Na) 4841.2
50	30	40	4857.4	(M) 4857.4; (M − H + Na) 4879.2; (M − 2H + 2Na) 4911.0
51	41	40	4879.5	(M) 4878.7

Scheme 8



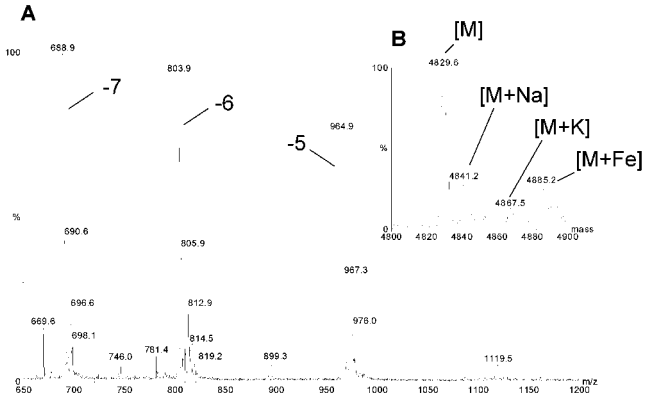


Figure 2. Mass spectrum of compound **49**: (A) the primary spectrum shows the −5 to −7 charged molecules; (B) deconvolution of the primary spectrum results in the average mass peak of the molecule together with the average mass peak of the sodium, potassium, and iron adduct.

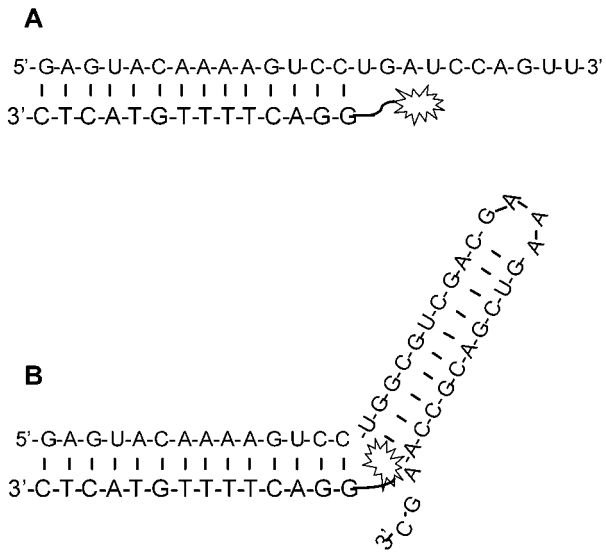


Figure 3. Structure of the RNA targets used for the evaluation of the oligonucleotide conjugates on their ribonuclease activity: the RNase A mimic is represented as a star. (A) Linear RNA target. (B) RNA target with hairpin structure.

in the spectra. Apparently, during the process of this capillary liquid chromatography, some of the oligonucleotide conjugates pick up metal ions by complexation from the material of the instruments. The same adducts were observed when comparing direct infusion mass experiments before and after C_{18} RP-HPLC purification. Addition of EDTA during the direct infusion mass experiments did reduce this phenomenon. This observation indicates the tendency of the compounds toward metal complexation and ensures there was no covalent modification of the oligonucleotide conjugates.

RNA Cleavage Experiments. To evaluate the synthesized conjugates on their potential as ribonuclease

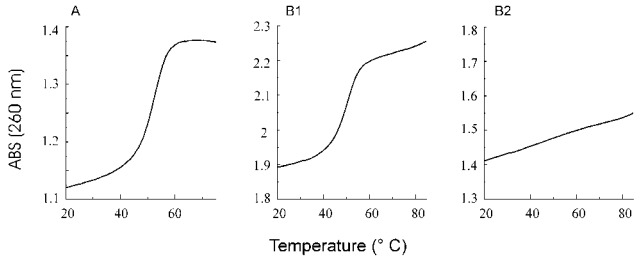


Figure 4. Determination of the melting temperature of duplexes formed between the oligodeoxynucleotide sequence used for the preparation of the oligonucleotide conjugates and (A) the linear RNA target, T_m = 52.3 °C, and (B) the hairpin RNA target. B2 is the curve of the hairpin without oligodeoxynucleotide (no T_m observed), and B1 shows a hyperchromic effect when oligodeoxynucleotide is present, T_m = 50.3 °C.

mimics, two RNA molecules were used as targets. First, a simple linear RNA 23-mer with single strand overhang of nine nucleotides at the 5′-end of the oligonucleotide conjugates (Figure 3A) was used, though the extensive dangling motion allowed in such a target could impede any interaction between the RNA molecule and the ribonuclease mimic. Therefore, a second RNA target was used where, next to the RNA/oligonucleotide−conjugate duplex, the RNA strand is believed to form a hairpin structure (Figure 3B). Some additional unpaired bases are present at the 3′-end, because unpaired (and bulged) regions are cleaved preferentially.

Prior to the cleavage experiments, the melting temperature (T_m value, Figure 4) of the duplex formed between the oligodeoxynucleotide and RNA strands was measured in order to ensure duplex formation at the temperature at which the cleavage experiments are performed. The T_m value for the association of the oligodeoxynucleotide with the linear RNA (Figure 3A) was observed to be 52.3 °C (Figure 4A). In the case of the hairpin RNA, T_m measurements were performed in the presence (Figure 4B1, T_m = 50.3 °C) as well as in the absence (Figure 4B2, no T_m value observed) of the oligodeoxynucleotide used in the oligonucleotide conjugates in order to ascertain the measured T_m value is correlated with the formation of a duplex between the oligodeoxynucleotide and RNA hairpin and that the T_m value is not correlated to the dissociation of the hairpin duplex structure itself. A T_m value for the hairpin structure itself could not be obtained, not even at very low salt concentration. However, the hairpin structure itself was chosen based on previously reported results which indicated the hairpin exhibits extraordinary stability (*30*). Since all exceeded 50 °C, it can be concluded that performing the cleavage tests at 37 °C will not impair association of the oligonucleotide conjugates with their target RNA sequence.

In a first experimental setup, the cleavage tests were performed under the conditions as suggested by Vlassov et al. (*31*) using Tris buffer or imidazole buffer, though

Table 2. Survey of the Conditions Used for Cleavage Experiments

	A	B	C	D	E	F	G	H	I
Tris buffer pH 7.5	50 mM		50 mM	50 mM	50 mM	50 mM	50 mM	50 mM	50 mM
imidazole buffer pH 7		50 mM							
NaCl	150 mM	150 mM	150 mM	75 mM		150 mM	150 mM	150 mM	150 mM
KCl				75 mM	150 mM				
EDTA	0.2 mM	0.2 mM	0.2 mM	0.2 mM	0.2 mM	0.2 mM	0.2 mM	0.2 mM	0.2 mM
$MgCl_2$	10 mM								
metal ion[a]						Zn^{2+}	Mn^{2+}	Cu^{2+}	Pb^{2+}

[a] Final concentration 2 mM.

no specific cuts could be observed. The inclusion of imidazole in the reaction buffer could serve as an exogeneous cleavage catalyst, which seems not to be the case here. Other experiments were performed where the amount of sodium chloride was changed, in combination with or replaced by potassium chloride, albeit without any success. A survey of the different conditions in which the oligonucleotide conjugates were tested is given in Table 2. Because of the tendency of some of the oligonucleotide conjugates to complex metal ions as observed during mass spectral analysis, the experimental setup was complemented with the addition of metal ions in order to cause target degradation. Addition of Mg^{2+}, Zn^{2+}, or Mn^{2+} did not result in any difference. The addition of Cu^{2+} and Pb^{2+} resulted in a complete and specific degradation of the target molecule.

Obviously, more tests can be envisioned in order to elicit hydrolytic RNA degradation. On the other hand, the aim of the project is to develop a method for sequence-specific RNA degradation, preferentially under near physiological conditions. Apparently, the tests performed do not indicate a tendency for successful cleavage under such conditions.

CONCLUSION

The development of organic hydrolytic cleavers occupies a special place in the category of artificial ribonucleases because of their RNA selectivity. Until now, the search for such cleavers was met with limited success because their cleavage capacity is less efficient than that of inorganic cleavers (*33*). The selection of organic functional groups used for this purpose is based on their presence in the active sites of some ribonucleases. We focused on the use of imidazole moieties as derived from RNase A (*32*) and the combination of imidazole and amino groups. The synthesis of the RNase A mimics was based on the proper derivatization with imidazole-containing moieties by amide bond formation of different molecules. These molecules served as linking arm between the imidazole and amino groups and between the cleaver and the oligonucleotide. Therefore, alternative strategies were explored for the selective acylation of polyamine compounds. It was found that thiazolide and imidazolide activation of the carboxy acid function leads to high discrimination for differences in nucleophilicity and sterical environment of the attacking amines. For the coupling of the RNase A mimics with the oligonucleotide, we used peptide bond chemistry. The peptide bond formation with a 5′-amino-functionalized oligonucleotide did work for all RNase A mimics albeit not always in the same extent.

Different conditions were used for the evaluation of the 5′-oligonucleotide conjugates, but no cleavage could be observed. More forcing reaction conditions could be envisioned for these cleavage tests, but the goal of the study was to develop ribonuclease mimics that can be used under physiological or near physiological conditions.

The reason for this failure could be due as well to the structure of the RNase A mimic as to an inappropriate target-selection. The flexibility of the linker between the RNase A mimic and the oligonucleotide as well as the flexibility of the backbone between the two imidazole functions is very high. In the case of the enzyme, RNase A, all participants in the enzymatic reactions are well anchored in the enzyme active site, which favors them entropically compared to the RNase A mimics. From this point of view, the synthesis of RNase mimics with a less flexible linker or the attachment of imidazole groups on a rigid scaffold may be envisaged. Vlassov et al. already emphasized the importance of target selection and structure. Our experiments were mainly carried out on linear nucleic acids while the experiments of Vlassov et al. (*34*) were conducted on $tRNA^{Phe}$. In conclusion, appropriate selection of cleavage agent, target, linker groups, and reaction conditions is needed to obtain a successful RNA-cleaver. It will be very difficult to mimic the in vivo situation by in vitro experiments to make this catalytic RNA-cleaving approach as successful as the natural systems (RNase's and ribozymes).

ACKNOWLEDGMENT

The authors thank K. U. Leuven (GOA 97/11) and F.W.O. for financial support. Dr. J. Lacey is grateful to the K. U. Leuven for a Research Fellowship. We are indebted to G. Schepers and Prof. A. Van Aerschot for the synthesis of the monomethoxytritylated aminoalkoxy derivitized oligonucleotides. We are indebted to C. Biernaux for editorial help. Authors thank the reviewers for helpful comments.

LITERATURE CITED

(1) Breslow, R., Dong, S. D., Webb, Y., and Xu, R. J. (1996) *J. Am. Chem. Soc. 118*, 6588.
(2) Ovinan, M., Kuusela, S., and Lönnberg, H. (1998) *Chem. Rev. 98*, 961−990.
(3) Reynolds, M. A., Beck, J. A., Say, P. B., Dweye, B. P., Daily, W. J., Vaghefi, M. M., Metzler, M. D., Klem, R. E., and Arnold, L. J., Jr. (1996) *Nucleic Acids Res. 24*, 760−765.
(4) Kuusela, S., Rantanen, M., and Lönnberg, H. (1995) *J. Chem. Soc. Perkin Trans. 2* 2269−2273.
(5) Zhdan, N. S., Kuznetsova, I. L., Vlasov, A. V., Sil'nikov, V. N., Zenkova, M. A., and Vlasov, V. V. (1999) *Bioorg Khim. 25*, 723−732.
(6) Hovinen, J., Guzaev, A., Azhayeva, E., Azhayev, A., and Lönnberg, H. (1995) *J. Org. Chem. 60*, 2205−2209.
(7) Tung, C. H., and Stein, S. (2000) *Bioconjugate Chem. 11* (5), 605−618.
(8) Gait, M. J. (1984) *Oligonucleotide Synthesis, a practical approach*, IRL Press, Oxford, Washington, DC.
(9) Maniatis, T., Fritsch, E., and Sambrook, J. (1989) *Molecular Cloning: A Laboratory Manual*, Cold Spring Harbor Laboratory, New York.
(10) Mohamadi, F., Richards, N. G. J., Guida, W. C., Liskamp, R., Lipton, M., Caufield, C., Chang, G., Hendrickson, T., and Still, W. C. (1990) *J. Comput. Chem. 11*, 440−467.
(11) Weiner, S. J., Kollman, P. A., Nguyen, D. T., and Case, D. A. (1986) *J. Comput. Chem. 7*, 230−252.
(12) Zegers, I., Maes, D., Dao-Thi, M. H., Poortmans, F., Palmer, R., and Wyns, L. (1994) *Protein Sci. 3*, 2322−2339.
(13) Heisterberg, D. Ohio Supercomputer Center, b. qfit, Computational Chemistry List, software archive, c. Kearsley S. K. (1990) *J. Comput. Chem. 11*, 1187−1192.
(14) Ingber, L. (1996) *Control Cybernetics 25*, 33−54.
(15) Tung, C.-H., Wei, Z., Leibowitz, M. J., and Stein, S. (1992) *Proc. Natl. Acad. Sci. U.S.A. 89*, 7114−7118.
(16) Nagao, Y., Miyasaka, T., Seno, K., and Fujita, E. (1984) *J. Chem. Soc., Perkin Trans. 1* 2439−2446. Nagao, Y., Miyasaka, T., Seno, K., Yagi, M., and Fujita, E. (1981) *Chem. Lett.* 463−466.
(17) Nagao, Y., Miyasaka, T., Seno, K., Yagi, M., and Fujita, E. (1981) *Chem. Lett.* 463−466.
(18) Smith, T. H., LaTour, J. V., Bochkariov, D., Chaga, G., and Nelson, P. S. (1999*) Bioconjugate Chem. 10*, 647−652. Furniss, B. S., Hannaford, A. J., Smith, P. W. G., and Tatchell, A. R. (1998) *Vogel's textbook of practical organic chemistry*, 5th ed., p 412.
(19) Huffman, W. F., Hall, R. F., Grant, J. A., and Holden, K. G. (1978) *J. Med. Chem. 21* (5), 413−415.
(20) Dölling, R., Beyermann, M., Haenel, J., Kernchen, F., Krause, E., Franke, P., Brudel, M., and Bienert, M. (1994) *J. Chem. Soc., Chem. Commun.* 853−854.

(21) Smith, T. H., LaTour, J. V., Bochkariov, D., Chaga, G., and Nelson, P. S. (1999) *Bioconjugate Chem. 10*, 647−652.
(22) Nagao, Y., Seno, K., Kawabata, K., Miyasaka, T., Takao, S., and Fujita, E. (1980) *Tetrahedron Lett. 21*, 841−844.
(23) Felix, A. M., Heimer, E. P., Lambros, T. J., Bougraki, C., and Meienhofer, J. (1978) *J. Org. Chem. 43*, 4194−4196.
(24) Šindelá•, K., Metyšová, J., Holubek, J., Svátek, E., Protiva, J., and Protiva, M. (1982) *Collect. Czech. Chem. Commun. 47*, 3077.
(25) Wagner, P. J., and Scheve, B. J. (1977) *J. Am. Chem. Soc. 99* (6), 3845−3847.
(26) Rinehart, K. L., Kobayashi, J., Harbour, G. C., Gilmore, J., Mascal, M., Holt, T. G., Shield, L. S., and Lafargue, F. (1987) *J. Am. Chem. Soc. 109*, 3378−3387.
(27) Abdel-Monem, M. M., and Portoghese, P. S. (1972) *J. Med. Chem. 15* (2), 208−210; Montzka, T. A., Matiskella, J. D., and Partyka, R. A. (1974) *Tetrahedron Lett. 14*, 1325−1327.
(28) Heus, H. A., and Pardi, A. (1991) *Science 253*, 191−194.
(29) Giegé, R., Felden, B., Zenkova, M. A., Sil'nikov, V. N., and Vlassov, V. V. (2000) *Methods Enzymol. 318*, 147−165.
(30) Häner, R., and Hall, J. (1997) *Antisense* and *Nucl. Ac. Drug Dev. 7*, 423−430. Trawick, B. N., Daniher, A. T., and Bashkin, J. K. *Chem. Rev. 98*, 939−960.
(31) Raines, R. T. (1998) *Chem. Rev. 98*, 1045−1065.
(32) Vlassov, V., Abramova, T., Godovikova, T., Giege, R., and Silnikov, V. (1997) *Antisense Nucl. Acid Drug Dev. 7*, 39−42.

BC0155622

Molecular Umbrella-Assisted Transport of Thiolated AMP and ATP Across Phospholipid Bilayers

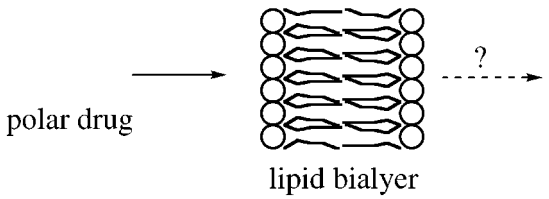
Vaclav Janout, Bingwen Jing, and Steven L. Regen*

Department of Chemistry, Lehigh University, Bethlehem, Pennsylvania 18015. Received October 9, 2001; Revised Manuscript Received December 4, 2001

Two molecular umbrella-nucleoside conjugates (**1a** and **1b**) have been synthesized via thiolate−disulfide displacement by adenosine 5′-*O*-(3-thiomonophosphate) and adenosine 5′-*O*-(3-thiotriphosphate) on an activated dimer derived from cholic acid, spermidine, and 5,5′-dithiobis-(2-nitrobenzoic acid). Both conjugates readily enter the aqueous compartment of liposomes made from 1-palmitoyl-2-oleyol-*sn*-glycero-3-phosphocholine (POPC) and release the free nucleoside upon reaction with entrapped glutathione. Approximately 50% of the thiolated form of AMP is released within 20 min at 23 °C; 120 min is required for a similar release of the thiolated form of ATP. The facile cleavage of these conjugates by glutathione, together with the fact that mammalian cells contain millimolar concentrations of this tripeptide in their cytoplasm, suggest that such chemistry may be extended to the practical development of prodrugs, e.g., antisense oligonucleotides that can be delivered into cells.

INTRODUCTION

Lipid bilayers play an essential role in cells by serving as barriers for transport (*1*). In particular, they permit the selective passage of those molecules and ions that are necessary for maintaining the living state. Due to their hydrophobic core, the ability of many classes of biologically active agents that have therapeutic potential (e.g., nucleosides, opioid pentapeptides, antisense oligonucleotides, and DNA) to enter cells has been limited (*2*−*15*). Finding ways to improve the bilayer transport of such molecules is a formidable challenge, and one that has important biomedical implications.



With this challenge in mind, we have introduced a unique class of amphiphilic molecules that interconvert between two different morphological states in response to changes in their microenvironment. These "amphomorphic" compounds, in a sense, mimic the structure and function of umbrellas by being able to cover an attached agent and shield it from an incompatible environment (*16*, *17*). Thus, when two or more facially amphiphilic units (i.e., rigid hydrocarbon units that maintain a hydrophobic and a hydrophilic face) are coupled to a suitable scaffold that contains a hydrophilic agent, immersion of such a molecule in an aqueous environment favors an exposed (or fully exposed) conformation, where hydrophobic interactions are maximized and where the hydrophilic faces are hydrated. When immersed in an hydrocarbon environment (e.g., the interior of a lipid bilayer), the umbrella then favors a shielded conformation such that intramolecular dipole−dipole and hydrogen bonding interactions are maximized, and the hydrophobic faces are solvated. A stylized illustration of a molecular umbrella in shielded, exposed, and fully exposed conformations is presented in Scheme 1. Here, each amphiphilic unit appears as a doubly shaded rectangle having a hydrophobic (darkened) and a hydrophilic (lightly shaded) face; the lightly shaded oval corresponds to a hydrophilic agent. Our working hypothesis has been that molecular umbrella conjugates can cross lipid bilayers through the following sequence of events: (i) diffusion to the membrane surface in an exposed or fully exposed state, (ii) insertion into the outer monolayer leaflet by flipping into a shielded state, (iii) diffusion to the inner monolayer leaflet, and (iv) entry into the adjoining aqueous phase via the reversal of steps ii and i (Scheme 2).

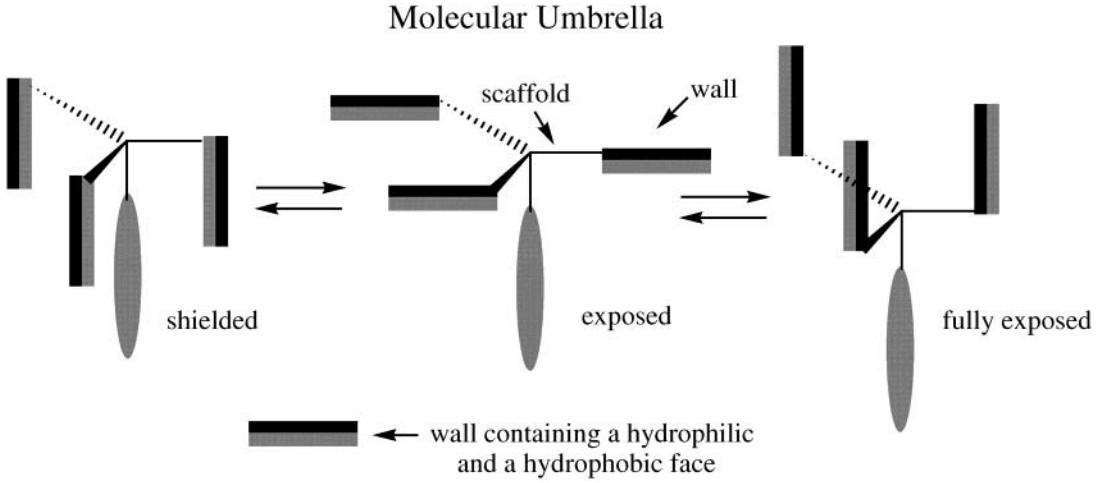
In recent studies, we have obtained compelling evidence for an "umbrella" mechanism of permeation for the transport of an umbrella conjugate of glutathione (γ-Glu-Cys-Gly, GSH) across phospholipid bilayers (*18*). Specifically, we found that the ability of this conjugate to cross these bilayers depended more on their facially amphiphilicity than on their hydrophobic/hydrophilic balance. Thus, the permeation of molecular umbrellas across lipid membranes takes place by a mechanism that is different from classic solution-diffusion pathways, where permeation rates are controlled by the permeant's solubility and diffusivity in the hydrocarbon region of the membrane (*3*).

In an effort to expand the scope of molecular umbrellas as membrane transporters, we have begun to turn our attention toward the bilayer transport of antisense oligonucleotides. As a first step in this direction, we sought to demonstrate the feasibility of transporting cleavable forms of adenosine 5′-monophosphate (AMP) and adenosine 5′-triphosphate (ATP) across phospholipid bilayers. Although several studies have been aimed at creating prodrugs of nucleoside 5′monophosphates, reports of membrane transporters of nucleoside 5′-triphosphates are rare. In one recent study, where it was

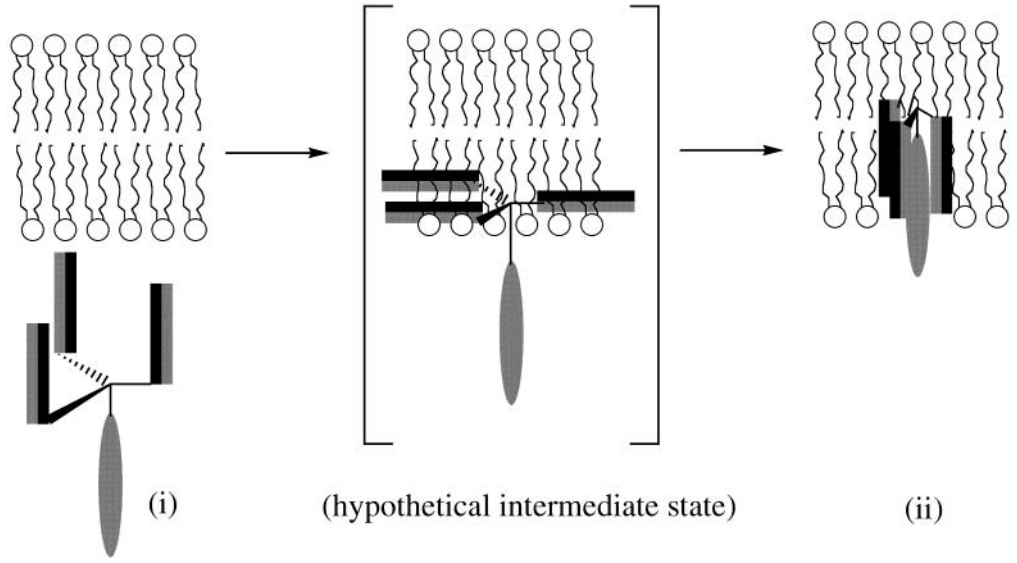
* To whom correspondence should be addressed. E-mail: slr0@lehigh.edu.

10.1021/bc015564m CCC: $22.00 © 2002 American Chemical Society
Published on Web 01/30/2002

Scheme 1



Scheme 2



claimed that a cholesteryloxycarbonyl−ATP conjugate releases of free ATP into the aqueous compartment of liposomes, the transport activity that was observed was only modest; ca. 10% after 9 days at an unspecified temperature (*19*). In this paper, we describe the synthesis of molecular umbrella conjugates of thiolated forms of AMP and ATP. We also show that these conjugates deliver the free nucleosides into liposomes, made from 1-palmitoyl-2-oleoyl-*sn*-glycero-phosphocholine (POPC), with half-lives that are less than 20 and 120 min at 23 °C for the monophosphate and triphosphate, respectively.

MATERIALS AND METHODS

General Methods. Unless stated otherwise, all reagents were obtained from commercial sources and used without further purification. 1-Palmitoyl-2-oleoyl-*sn*-glycero-phosphocholine was obtained from Avanti Polar Lipids (Alabaster, AL). Adenosine 5′-*O*-(3-thiotriphosphate) and adenosine 5′-*O*-(3-thiomonophosphate) were purchased from Fluka and used directly. 5,5′-Dithiobis-(2-nitrobenzoic acid) (Ellman's reagent) was purchased from Aldrich (Milwaukee, WI) and used as obtained. All dialysis experiments were made using a 1.5-mL equilibrium dialysis cell (Fischer Scientific) and SpectraPor #7 dialysis tubing (MWCO 50000). All ^{1}H NMR spectra were recorded on a Bruker 360 MHz instrument; chemical shifts are reported in ppm and are referenced to residual solvent. The buffer that was used in all experiments was composed of 0.1 M H_3BO_3 and 2 mM EDTA, where the pH was adjusted to 7.0 by use of 1 M NaOH. All UV spectra were recorded using a Cary 300 Bio UV/VIS spectrophotometer.

Molecular Umbrella−ATP Conjugate 1b. To a solution of 12.6 mg (5.7 μmol) of **6** in a mixture of 400 μL of CH_3OH and 150 μL of H_2O was added a solution that was made from 3.12 mg (5.7 μmol) of the tetralithium salt of adenosine 5′-*O*-(3-thiotriphosphate) and 150 μL of water. A homogeneous orange-colored solution was produced, and the solution was stirred for a total of 72 h at room temperature. Concentration under reduced pressure, followed by preparative thin-layer chromatography (silica gel, $CHCl_3/CH_3OH/H_2O$, 60/40/10, v/v/v), afforded 2.51 mg (24.9%) of the desired conjugate, **1b**, having R_f 0.45 and ^{1}H NMR (CD_3OD) δ 842 (d, 1 H), 8.19 (s, 1 H), 8.06 (m, 1 H), 7.70 (m, 2 H), 6.05 (m, 1 H), 4.67 (m, 1 H), 4.45 (m, 1 H), 4.25 (m, 3 H), 3.92 (m, 2 H), 3.78 (s, 2 H), 3.35 (m, 6 H), 3.00 (m, 4 H), 0.89−2.20 (m, 66 H), 0.68 (d, 6 H). HRMS for $C_{72}H_{110}N_9O_{24}P_3S_2Na_3$ (MNa^+) Calcd: 1710.6006. Found: 1710.6094.

Molecular Umbrella−AMP Conjugate (1a). Using procedures similar to those used for the synthesis of **1b**, the molecular umbrella−AMP conjugate (**1a**) was ob-

tained in a 53% isolated yield, having R_f 0.41 (silica gel, $CHCl_3/CH_3OH/H_2O$, 65/25/4, v/v/v) and ^1H NMR (CD_3OD) δ 841 (d, 1 H), 8.19 (s, 1 H), 8.03 (m, 1 H), 7.68 (m, 2 H), 6.06 (m, 1 H), 4.66 (m, 1 H), 4.30 (m, 1 H), 4.20 (m, 3 H), 3.92 (m, 2 H), 3.78 (s, 2 H), 3.35 (m, 6 H), 3.00 (m, 4 H), 0.90−2.25 (m, 66 H), 0.69 (d, 6 H). HRMS for $C_{72}H_{109}N_9O_{17}PS_2Na_2$ (MNa^+) Calcd: 1512.6910. Found: 1512.6959.

Vesicles for Transport Experiments. Typically, 2.0 mL of a 20 mg/mL solution of POPC in chloroform were transferred to a Pyrex test tube, and the solvent was evaporated by rotating the tube under a stream of nitrogen, resulting in a thin lipid film. The last traces of solvent were removed under reduced pressure (25 °C, 72 h, <0.2 Torr). To the dried film was added 2.20 mL of a 1.2 mM solution of glutathione that was prepared in borate buffer, which had been adjusted to pH 7.0 by addition of a few drops of 1 M NaOH. The mixture was vortexed for 40 s, incubated at room temperature for 5 min, vortexed for another 40 s, and incubated for 25 min at room temperature, while being maintained under an argon atmosphere. The dispersion was then subjected to six freeze/thaw cycles (−196 °C/30 °C), followed by extrusion through a 400 nm Nuclepore membrane (12 times) and a 200 nm Nuclepore membrane (15 times).

Gel Filtration Procedure. All gel filtrations were carried out via minicolumn centrifugation using prepacked Sephadex G-25, PD-10 (Pharmacia Biotech). Prior to use, the Sephadex G-25 was extensively rinsed with borate buffer. Typically, 1.0 mL of the dispersion was gel filtered (two times) using 5.0 g of Sephadex G-25 (fine), by expelling the void volume of the column via centrifugation (3 min). To confirm that all of external glutathione had been removed, an aliquot of the dispersion (400 μL) was dialyzed against 400 μL for 24 h at room temperature, using an equilibrium dialysis cell and SpectraPor #7 dialysis tubing (MWCO 50000). Analysis of the receiving side for thiol content (Ellman's reagent) showed a negligible concentration of glutathione, i.e., <0.1 μM.

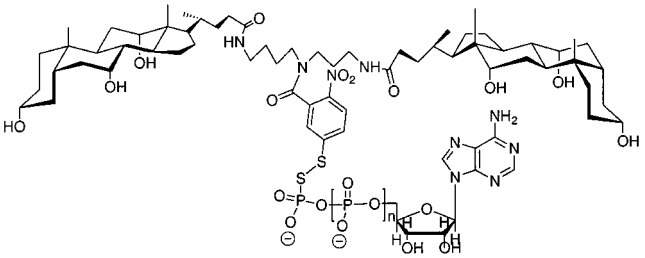
Reaction of Vesicle-Entrapped Glutathione with 1b. In a typical experiment, 600 μL of the vesicular dispersion was mixed with 600 μL of a 30 μM solution of **1b** in borate buffer, and half of the mixture was then added to a 0.7 mL UV cuvette. The rate of formation of **3** was then monitored as a function of time (λ_{max} 427 nm) up to 98% conversion. Careful subtraction of apparent absorbances due to light scattering was done in all cases.

In a separate experiment, 600 μL of the original vesicular dispersion was mixed with 600 μL of a 30 μM solution of **1b** in borate buffer, and half of this mixture was then dialyzed against 600 μM of borate buffer for 24 h. A portion of the receiving side (400 μL) was then mixed with 35 μL of 2 mM Ellman's reagent (pH 7.0), and the thiol content was then determined by measuring the absorption at 410 nm. Based on this analysis, the maximum concentration of glutathione that was present outside of the vesicles was determined to be <0.15 μM. Thus, the addition of **1b** does not induce significant leakage of glutathione from the vesicles.

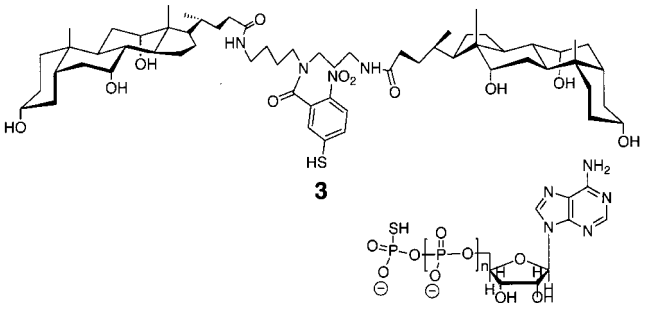
To confirm that the released nucleoside was captured within the vesicles, 400 μL of the disperson (taken from the source side of the dialysis cell after 24 h of reaction) was gel filtered using procedures described above. A 100 μL-aliquot of the void volume was then mixed with 300 μL of ethanol, followed by vortex mixing. The UV spectrum of the homogeneous solution (230−500 nm) was then recorded. After a background subtraction was made, using a similar solution that was devoid of **1b**, the nucleoside content (λ_{max} 260 nm) was determined.

RESULTS AND DISCUSSION

Design and Synthesis of Molecular Umbrella−Nucleoside Conjugates. The molecules that were chosen as synthetic targets for this study were conjugates **1a** and **1b**. Attack by glutathione on the disulfide moiety was expected to result in umbrella−nucleoside cleavage with the formation of **3**, **4a**, and **4b**. In one scenario (pathway A), attack on the disulfide linkage of the umbrella by the thiolate anion of glutathione results in the direct release of the free nucleoside and the formation of **5** (Scheme 3). Subsequent attack by a second glutathione molecule on **5** then liberates **3** plus the oxidized form of glutathione (GSSG). An alternative pathway (pathway B, not shown) is one in which glutathione initially attacks the sulfur atom of the nucleoside, thereby liberating **3**; subsequent attack by a second glutathione molecule on the resulting glutathione−nucleoside conjugate then affords **4a** or **4b** plus GSSG. Given the UV absorbances of **5** (λ_{max} 330 nm; ϵ 5.501 × 10^3 M^{-1} cm^{-1}, borate buffer, pH 7.0) and **3** (λ_{max} 427 nm; ϵ 7.007 × 10^3 M^{-1} cm^{-1}; borate buffer, pH 7.0), one might expect that insight into the preferred reaction pathway could be obtained by following the changes in the UV spectrum with time. An additional basis for the design of these conjugates stems from the fact that mammalian cells contain millimolar concentrations of glutathione. Thus, such conjugates have attractiveness from a prodrug standpoint.



1a, n=0
b, n=2



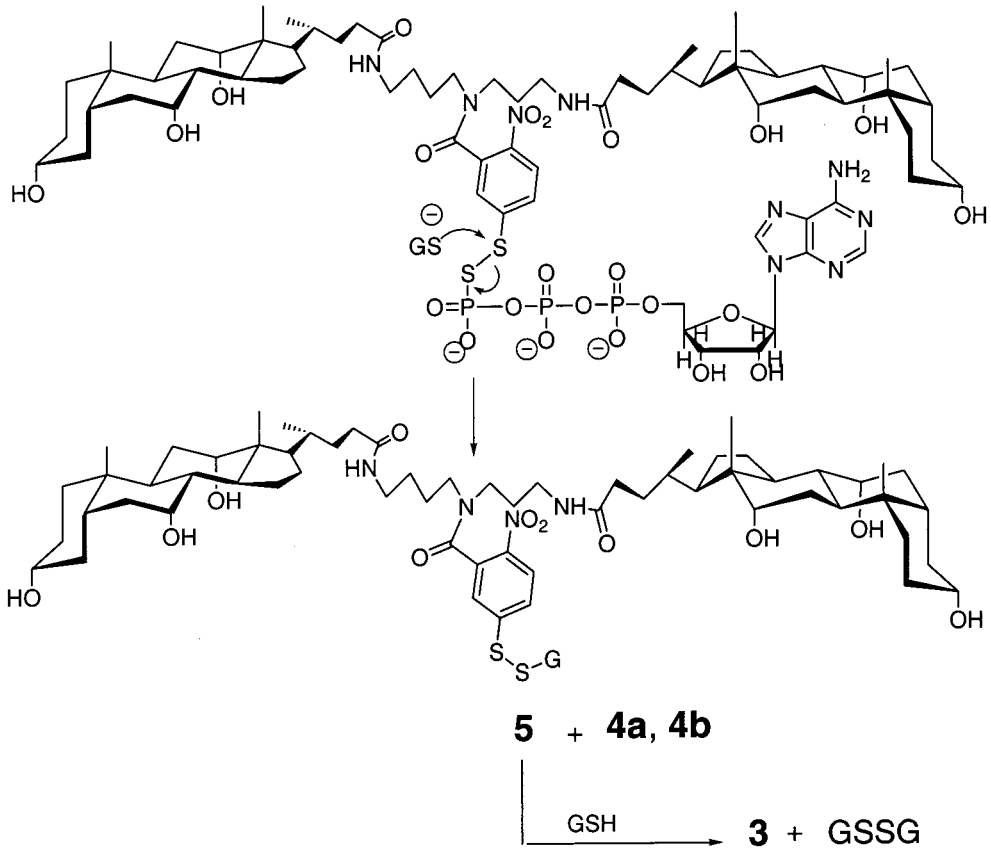
3

4a, n=0
b, n=2

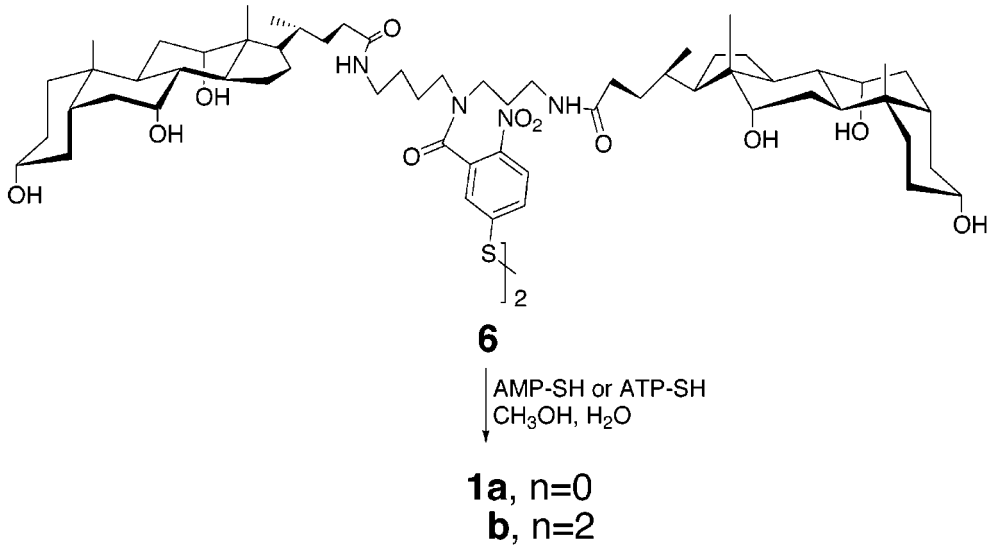
In Scheme 4 is shown the method by **1a** and **1b** were synthesized. In brief, molecular umbrella dimer, **6**, bearing a labile "Ellman's" moiety (previously described) was reacted with adenosine 5′-*O*-(3-thiotriphosphate) or adenosine 5′-*O*-(3-thiomonophosphate) in an aqueous methanolic solution (*18*, *20*). The desired conjugates were then isolated from the resulting equilibrium mixtures by preparative thin-layer chromatography.

Nature of Molecular Umbrella−Nucleoside Cleavage by Glutathione. To understand how these molecular umbrella−nucleosides are cleaved by glutathione, a solution of **1a** was treated with the peptide in borate

Scheme 3



Scheme 4



buffer. As is evident from Figure 1, the UV absorbance for **1a** (λ_{max} 349 nm; ϵ 7.007 × 10^3 M^{-1} cm^{-1}) disappears almost instantly and is replaced by the UV absorbance of **5** (λ_{max} 330 nm). The latter absorbance then decreases with time and is replaced with the absorbance of **3** (λ_{max} 427 nm). These results clearly indicate that pathway A (Scheme 3) is dominant, where initial attack by glutathione releases the free nucleoside and not **3** (λ_{max} 427 nm). On the basis of the spectral intensity that appeared at 427 nm, after **1a** had fully reacted (i.e., after 30 s of reaction), we estimate that ≥95% of the cleavage occurs via pathway A. Similar results were obtained with **1b**, except that the resolution of the UV absorbances was not as significant (not shown).

Umbrella-Assisted Bilayer Transport of Thiolated AMP and ATP. Large unilamellar vesicles (200 nm diameter) were prepared from 1-palmitoyl-2-oleoyl-*sn*-glycero-phosphocholine (POPC) via extrusion methods in the presence of 1.2 mM of glutathione (*20*). Nonentrapped GSH was then removed by gel filtration. In a typical bilayer transport experiment, a 30 mM POPC liposomal dispersion was mixed with an equal volume of a 28.6 μM solution of **1b** in borate buffer. Subsequent mixing was then carried out in the "source" side of a 1.5-mL equilibrium dialysis cell, which contained an equal volume of borate buffer in the "receiving" side. Agitation of the cell was made by use of a wrist-action shaker. Because of light scattering of the vesicles, the extent of molecular

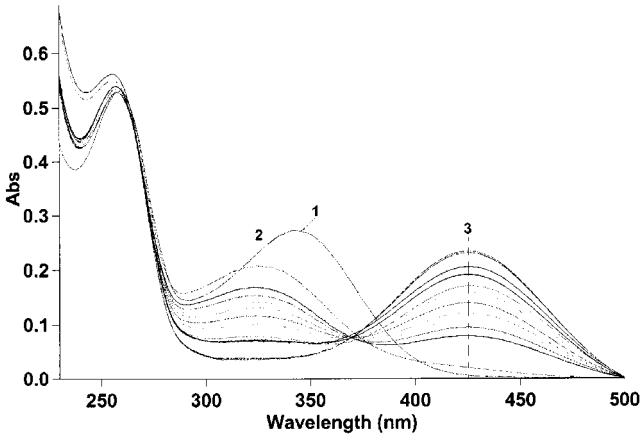


Figure 1. Spectral changes as a function of time for the reaction of 58 μM of **1a** with 220 μM glutathione in borate buffer (pH 7.0) at 25 °C. The λ_{max} for **1a** that appears at 349 nm (#1) was observed at the start of the reaction. After 30 s, a strong peak appeared with a λ_{max} at 330 nm (#2), which decreased in intensity; the lowest absorbance that is shown at this wavelength was observed after 65 min. A gradual "growing in" of the absorbance of **3** was observed at λ_{max} 427 nm (#3).

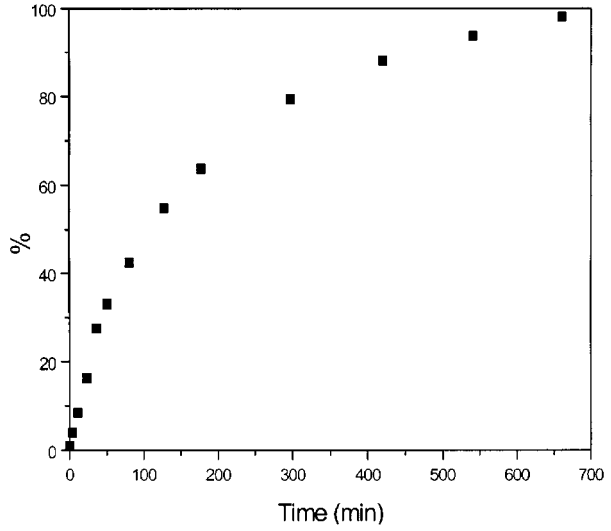


Figure 2. Plot of the percentage of **3** that is formed as a function of time, for the reaction of 15 μM **1a** with 14.3 mM POPC liposomes, containing 1.2 mM entrapped glutathione at 23 °C.

umbrella−nucleoside cleavage was monitored by following the appearance of **3** at 427 nm. A plot of the percent of **3** that is formed as a function of time is shown in Figure 2, which indicates that ca. 120 min is needed for generating ca. 50% of the reduced umbrella. Since the formation of **3** represents a slower second stage of the cleavage reaction (the initial stage being the direct release of the nucleoside), the time that is needed for releasing 50% of the free nucleoside into the aqueous interior of the vesicles must be <120 min. Analysis of the receiving side of the cell after 24 h for thiol content (Ellman's reagent) indicated a maximum glutathione concentration in the external bulk phase to be 0.31 μM. Thus, the extent of leakage that is induced by the presence of **1b** is exceedingly low, if at all.

To confirm that the released nucleoside (**4b**) was captured within the vesicles, a portion of a liposomal dispersion, which had been fully reacted, was mixed with ethanol to destroy the vesicles and then analyzed for **4b** (λ_{max} 260 nm). A second portion of the dispersion was subjected to gel filtration (to remove nonentrapped **4b**) and also analyzed for nucleoside content. Comparison of these two measurements indicate that >90% of **4b** was entrapped within the vesicles; that is <10% of the nucleoside was removed from the dispersion by gel filtration. A control experiment that was carried out, in which an aqueous solution of **4b** was mixed with an equal volume of POPC vesicles (loaded with 1.2 mM glutathione) showed the complete removal of the nucleoside via gel filtration. Analogous transport experiments that were carried out with **1a** gave similar results, except that the rate of appearance of **3** was faster; here, 50% of the conjugate was converted into **3** after 20 min.

CONCLUSIONS

The results reported herein demonstrate the feasibility of conjugating thiolated forms of AMP and ATP to molecular umbrellas and transporting these nucleosides across liposomal membranes. The facile cleavage of such conjugates by entrapped glutathione, together with the fact that mammalian cells contain millimolar concentrations of glutathione in their cytoplasm, suggests that this chemistry may be extended to the practical development of prodrugs, e.g., antisense oligonucleotides, which can be delivered into cells.

ACKNOWLEDGMENT

We are grateful to the National Institutes of Health (PHS Grant GM51814) for support of this research.

LITERATURE CITED

(1) Gennis, R. B. (1989) *Biomembranes: Molecular Structure and Function*, Springer-Verlag, New York.

(2) Juliano, R. L., Alahari, S., Yoo, H., Kole, R., and Cho, M. (1999) Antisense Pharmacodynamics. Critical Issues in the Transport and Delivery of Antisense Oligonucleotides. *Pharm. Res. 16*, 494.

(3) Ramaswami, V., Zhu, X., Romanowksi, M., Haaseth, R. C., Misicka, A., Lipkowski, A. W., Hruby, V. J., and O'Brien, D. F. (1996) Lipid Membrane Permeability of Modified c[D-Pen2, D.-Pen5]enkephalin Peptides. *Int. J. Pept. Protein Res. 48*, 87.

(4) Akhtar, S., Basu, S., Wickstrom, E., and Juliano, R. L. (1991) Interactions Of Antisense DNA Oligonucleotide Analogues With Phospholipid Membranes (Liposomes). *Nucleic Acids Res. 19*, 5551.

(5) Gerwitz, A. M., Stein, C. A., and Glazer, P. M. (1996) Facilitating Oligonucleotide Delivery: Helping Antisense Deliver On Its Promise. *Proc. Natl. Acad. Sci., U.S.A. 93*, 3161.

(6) Uhlmann, E., and Peyman, A. (1990) Antisense Oligonucleotides: A New Therapeutic Principle. *Chem. Rev. 90*, 544.

(7) Letsinger, R. L., Zhang, G., Sun, D. K., Ikeuchi, T., and Sarin, P. (1989) Cholesteryl-Conjugated Oligonucleotides: Synthesis, Properties, and Activity As Inhibitors Of Replication Of Human Immunodeficiency Virus In Cell Culture. *Proc. Natl. Acad. Sci., U.S.A. 86*, 6553.

(8) Kabanov, A. V., Vinogradov, S. V., Orchamenko, A. V., Krivonos A. V., Melik-Nubarov, N. S. Kiselev, V. I., and Severin, E. S. (1990) A New Class Of Antivirals: Antisense Oligonucleotides Combined With Hydrophobic Substituents Effectively Inhibit Influenza Virus Reproduction And Synthesis Of Virus-Specific Proteins In MDCK Cells. *FEBS Lett. 259*, 327.

(9) Lemaitre, M., Bayard, B., and LeBleu, B. (1987) Specific Antiviral Activity Of A Poly(L-lysine) conjugated Oligodeoxyribonucleotide Sequence Complementary To Vesicular Stomatitis Virus N Protein mRNA Initiation Stage. *Proc. Natl. Acad. Sci., U.S.A. 84*, 648.

(10) Leonetti, I. P.; Machy, P., Degols, G., LeBleu, B., and Leserman, L. (1990) Antibody-Targeted Liposomes Containing Oligodeoxyribonucleotides Complementary To Viral RNS

Selectively Inhibit Viral Replication. *Proc. Natl. Acad. Sci., U.S.A. 87*, 2448.
(11) Behr, J. P. (1993) Synthetic Gene-Transfer Vectors. *Acc. Chem. Res. 26*, 274.
(12) Behr, J. P. (1994) Gene Transfer With Synthetic Cationic Amphiphiles: Prospects For Gene Therapy. *Bioconjugate Chem. 5*, 382.
(13) Vigneron, J. P., Oudrhiri, N., Fauquent, M., Vergely, L., Bradley, J. C., Basseville, M., Lehn, P., and Lehn, J. M. (1996) Guanidinium-Cholesterol Cationic Lipids: Efficient Vectors For The Transfection of Eukaryotic Cells. *Proc. Natl. Acad. Sci., U.S.A. 93*, 9682.
(14) Walker, S., Sofia, M. J., Kakarla, R., Kogan, N. A., Wierichs, L., Longley, C. B., Bruker, K., Axelrod, H. R., Midha, S., Babu, S., and Kahne, D. (1996) Cationic Facial Amphiphiles: A Promising Class of Transfection Agents. *Proc. Natl. Acad. Sci., U.S.A. 93*, 1585.
(15) Lewis, J. G., Lin, K. Y., Kothavale, A., Flanagan, W. M., Mateucci, M. D., DePrince, R. B., Mook, R. A., Jr., Hendren, R. W., and Wagner, R. W. (1996) A Serum-Resistent Cytofectin For Cellular Delivery Of Antisense Oligodeoxynucleotides and Plasmid DNA. *Proc. Natl. Acad. Sci., U.S.A. 93*, 3176.
(16) Janout, V., Lanier, M., and Regen, S. L. (1996) Molecular Umbrellas. *J. Am. Chem. Soc. 118*, 1573.
(17) Janout, V., Lanier, M., Deng, G., and Regen, S. L. (1997) Evidence for Highly Cooperative Binding Between Molecular Umbrella-Spermine Conjugates and DNA. *Bioconjugate Chem. 8*, 891.
(18) Janout, V., Staina, I. V., Bandyopadhyay, P., and Regen, S. L. (2001) Evidence for an Umbrella Mechanism of Bilayer Transport. *J. Am. Chem. Soc. 123*, 9926.
(19) Kreimeyer, A., Andre, F., Gouyette, C., and Huynh-Dinh, T. (1998) Transmembrane Transport of Adenosine 5′-Triphosphate Using a Lipophilic Cholesteryl Derivative. *Angew. Chem., Int. Ed. 37*, 2853.
(20) Janout, V., Zhang, L., Staina, I. V., DiGiorgio, C., and Regen, S. L. (2001) Molecular Umbrella-Assisted Transport of Glutathione Across a Phospholipid Membrane. *J. Am. Chem. Soc. 123*, 5401.

BC015564M

Synthesis and Biologic Evaluation of a Radioiodinated Quinazolinone Derivative for Enzyme-Mediated Insolubilization Therapy

Nan-hui Ho, Ravi S. Harapanhalli, Bassam A. Dahman, Kai Chen, Ketai Wang, S. James Adelstein, and Amin I. Kassis*

Department of Radiology, Harvard Medical School, Goldenson Building B-242, 220 Longwood Avenue, Boston, Massachusetts 02115. Received October 15, 2001; Revised Manuscript Received January 25, 2002

We have developed a new strategy that aims to concentrate therapeutic radionuclides within solid tumors. This approach, which we have named EMIT (enzyme-mediated insolubilization therapy), is a method for enzyme-dependent, site-specific, in vivo precipitation of a radioactive molecule (from a water-soluble precursor) within the extracellular space of solid tumors. The prodrug, ammonium 2-(2′-phosphoryloxyphenyl)-6-iodo-4-(3*H*)-quinazolinone, labeled with iodine-125 (^{125}IPD) and its authentic compound labeled with iodine-127 (IPD) have been synthesized, purified, and characterized. The alkaline phosphatase (ALP)-mediated conversion of these water-soluble nonfluorescent prodrugs to the water-insoluble fluorescent species, iodine-125-labeled 2-(2′-hydroxyphenyl)-6-iodo-4-(3*H*)-quinazolinone (^{125}ID) and its iodine-127-labeled derivative (ID), has been demonstrated in vitro. Biodistribution studies in mice indicate that both ^{125}IPD and ^{125}ID are minimally retained by most tissues and organs. In addition, following its intravenous injection in mice, ^{125}IPD is localized in ALP-rich regions and converted to ^{125}ID, which remains indefinitely within the tissues where it is produced. We believe that EMIT is a strategy that will lead to the active and specific concentration and entrapment of therapeutic radionuclides within solid tumors, the consequent protracted irradiation of tumor cells within the range of the emitted particles, and the effective therapy of solid tumors.

INTRODUCTION

Monoclonal antibodies (mAb)[1] by virtue of their unique in vitro specificity and high affinity for their antigen have been considered particularly attractive as selective carriers of cancer radiotherapeutic atoms/molecules. While most published work on this subject has demonstrated their utility in the diagnosis and treatment of various tumors in *experimental animal models*, the use of radiolabeled mAb to target and treat solid tumors in cancer patients has been for the most part unsuccessful. This failure can be attributed to many causes, including (i) high activity in the whole body, which lowers the maximum tolerated dose (MTD), (ii) limited intratumoral diffusion of the radiolabeled protein molecules and heterogeneity of tumor-associated antigens, both of which lead to nonuniform distribution of the radionuclide within the tumor mass and the consequent sparing of many regions (because either they are outside the range of the emitted particles or they receive a sublethal dose), and (iii) low tumor uptake (∼0.01% injected dose per gram [% ID/g] of tumor in patients versus 5−50% ID/g of tumor in mice). It seems highly probable that the latter point, which is the most distinctive difference between the results obtained from studies in mice and in humans, is the principal factor that has generally led to the therapeutic ineffectiveness of radiolabeled antibodies in man.

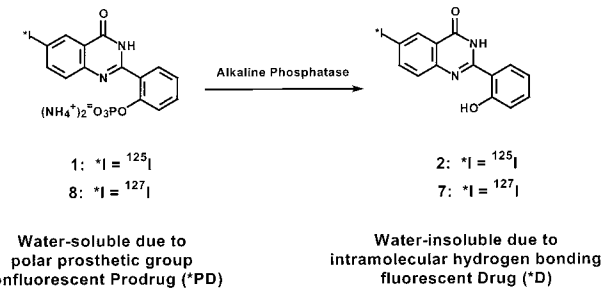
In an attempt to bypass some of these limitations, we have been developing a novel strategy that aims to concentrate radioactive molecules within solid tumors. The approach, which we have named EMIT (enzyme-mediated insolubilization therapy), is a method for enzyme-dependent, site-specific, in vivo precipitation of a water-soluble radioactive molecule within the extracellular space of solid tumors. In one of its embodiments, the radiolabeled prodrug is hydrolyzed to its water-insoluble form by a constitutive enzyme present in high concentrations within the tumor. In another embodiment, a mAb−enzyme conjugate is injected into tumor-bearing animals. Following its tumor targeting and partial clearance from normal tissues and organs (i.e., high tumor-to-normal-tissue ratios), a water-soluble radioactive substrate to the preadministered enzyme is injected. Owing to the negatively charged prosthetic group(s) present within the substrate, it is highly hydrophilic and consequently not internalized by mammalian cells. On enzymatic hydrolysis, this water-soluble molecule loses its prosthetic group, and the resulting compound is water insoluble and precipitates. The precipitated molecules are concentrated and trapped within the extracellular space of the targeted solid tumor. For EMIT, the substrate may be radiolabeled with an energetic α- (e.g., ^{211}At, ^{213}Bi) or β- (e.g., ^{131}I, ^{90}Y) particle-emitting radionuclide. Once precipitated and trapped within the tumor, the prolonged

* To whom correspondence should be addressed. Telephone: (617) 432-7777. FAX: (617) 432-2419. E-mail: amin_kassis@hms.harvard.edu.

[1] Abbreviations: mAb, monoclonal antibody; MTD, maximum tolerated dose; %ID/g, percentage injected dose per gram tissue or organ; EMIT, enzyme-mediated insolubilization therapy; ALP, alkaline phosphatase; HPLC, high performance liquid chromatography; THF, tetrahydrofuran; TLC, thin-layer chromatography; $T_{1/2}$, half-life; DMSO, dimethyl sulfoxide; ARG, autoradiography; IPD, iodinated prodrug, ammonium 2-(2′-phosphoryloxyphenyl)-6-iodo-4(3*H*)-quinazolinone; ID, iodinated drug, 2-(2′-hydroxyphenyl)-6-iodo-4(3*H*)-quinazolinone; ADRT, antibody-directed radioligand targeting; ADEPT, antibody-directed enzyme prodrug therapy; PD, prodrug; D, drug.

10.1021/bc010093p CCC: $22.00 © 2002 American Chemical Society
Published on Web 02/27/2002

Scheme 1. Conversion of Water-Soluble Prodrug to Water-Insoluble Drug



residence time should permit delivery of a high radiation dose to the tumor with a low dose to the rest of the body.

In 1994, Haugland et al. (*1*) described a class of novel substrates made from quinazolinones for the in vitro detection of cell-associated enzyme activity, particularly that of glycosidase, phosphatase, and sulfatase. When the enzyme acts on its weakly fluorescent water-soluble substrate, a highly fluorescent product insoluble in aqueous systems is formed. Using a similar approach, we have synthesized an iodinated (^{127}I/^{125}I) derivative of one of these substrates (Schemes 1−3), ammonium 2-(2′-phosphoryloxyphenyl)-6-iodo-4-(3*H*)-quinazolinone (**1** and **8**). In the presence of alkaline phosphatase (ALP), this water-soluble molecule is hydrolyzed to 2-(2′-hydroxyphenyl)-6-iodo-4-(3*H*)-quinazolinone (**2** and **7**), a water-insoluble alcohol that precipitates in aqueous solution. We plan to localize such molecules, when labeled with therapeutic radionuclides such as ^{131}I or ^{211}At, within solid tumors that are either innately rich in ALP or that have been pretargeted with an antitumor-antibody−ALP conjugate. We believe that the EMIT approach will lead to the active and specific concentration and entrapment of such therapeutic radionuclides in solid tumors, the consequent protracted irradiation of tumor cells within the range of the emitted particles, and effective therapies of solid tumors. To our knowledge, the use of prodrugs radiolabeled with therapeutic radionuclides has not been reported.

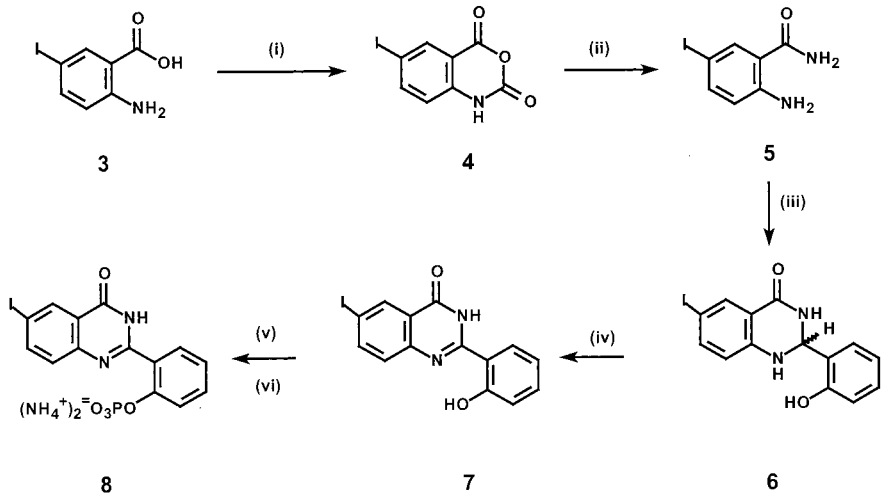
EXPERIMENTAL PROCEDURES

General Remarks. The reagents were obtained from Sigma Aldrich Chemical Company and used without further purification. Carrier-free sodium [^{125}I]iodide was obtained from Amersham Corporation. NMR spectroscopy was carried out on either a Varian XL-200 or a Varian XL-500 instrument. Electronspray mass spectra were recorded on a Micromass Platform LCZ mass analyzer. HPLC separations were performed on a reversed-phase Nova-Pak C_{18} column, 3.9 × 30 mm (Waters Corporation), at a flow rate of 1 mL/min. UV absorption (Waters 486 detector, 286 nm) and γ-ray detection were used to analyze the eluates. High-resolution mass spectrometry was performed on a Bruker Daltonics ApexII 3 T Fourier transform mass spectrometer. Elemental analyses were obtained from Oneida Research Services Incorporated, Oneida, NY.

Syntheses. *Iodoisotoic Anhydride (**4**).* 2-Amino-5-iodobenzoic acid (**3**, 2.0 g, 7.6 mmol, Aldrich) and triphosgene (2.26 g, 7.6 mmol) were dissolved in 20 mL of dry THF (freshly distilled from CaH_2) (Scheme 2). The reaction mixture was stirred at room temperature for 1 h. An off-white precipitate was formed, and TLC showed that **3** was consumed. The precipitate was filtered and washed with cold methanol. The crude product was redissolved in hot acetonitrile and crystallized (*2*). After drying in vacuo, **4** was obtained as a white solid (2.0 g, 90%); mp = 235 °C dec. ^{1}H NMR (DMSO-d_6) δ 6.94 (d, 1H, ar), 8.01 (d, 1H, ar), 8.11 (s, 1H, ar). ESI−HRMS calcd for $C_8H_4INO_3$−Na $[M + Na]^+$: 311.9128. Found: 311.9126. Anal. Calcd for $C_8H_4INO_3$: C, 33.25; H, 1.39; N, 4.85. Found: C, 33.44; H, 1.32; N, 4.90.

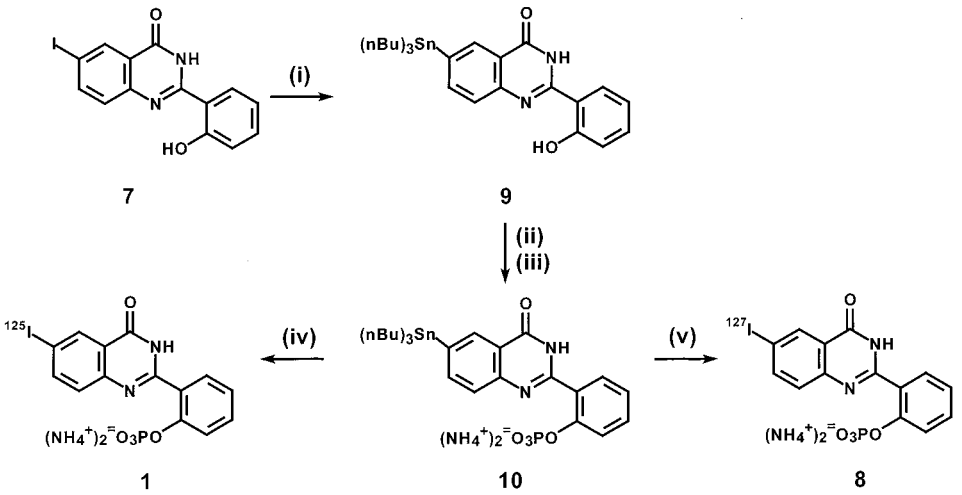
*Iodoanthranilamide (**5**).* A solution of **4** (2.0 g, 6.9 mmol) was suspended in 16 mL of THF. The reaction flask was cooled in an ice-bath. Then 1 mL of 28% aqueous ammonium hydroxide solution was added dropwise to the reaction mixture, accompanied by the evolution of gas. The solution became warm and started to boil. The reaction mixture was stirred for 15 min at 0 °C and 30 min at room temperature. At the end of the reaction, the solution became clear. The solvent was evaporated, and a white solid was obtained. The crude product was filtered to give **5** as a fluffy white solid (1.3 g, 72%). ^{1}H NMR (DMSO-d_6) δ 7.80 (s, 1H, ar), 7.37 (d, J = 8.5 Hz, 1H, ar), 7.13 (bs, 2H, NH_2), 6.69 (bs, 2H, *CO*NH_2), 6.54 (d, J = 8.5 Hz, 1H, ar). ESI−HRMS calcd for $C_7H_7IN_2O$ $[M + H]^+$: 262.9676. Found: 262.9674. Anal. Calcd for

Scheme 2. Pathway for the Synthesis of Ammonium 2-(2′-Phosphoryloxyphenyl)-6-iodo-4(3*H*)-quinazolinone (8) by Method A[a]



[a] Reagents and conditions: (i) triphosgene/THF; (ii) 28% aqueous ammonium hydroxide/THF; (iii) salicylaldehyde, *p*-toluenesulfonic acid; (iv) 2,3-dichloro-5,6-dicyano-1,4-benzoquinone; (v) phosphorus oxychloride/pyridine/0 °C; (vi) 28% aqueous ammonium hydroxide.

Scheme 3. Pathway for the Synthesis of Ammonium 2-(2′-Phosphoryloxyphenyl)-6-iodo-4(3*H*)-quinazolinone (1, 8) by Method B[a]



[a] Reagents and conditions: (i) dioxane/hexa-*n*-butylditin/palladium(0), reflux; (ii) phosphorus oxychloride/pyridine/0 °C; (iii) 28% aqueous ammonium hydroxide; (iv) $Na^{125}I$/iodobeads; (v) $Na^{127}I$/hydrogen peroxide/37 °C.

$C_7H_7IN_2O$: C, 32.08; H, 2.69; N, 10.69. Found: C, 32.30; H, 2.64; N, 10.78.

*2-(2′-Hydroxyphenyl)-6-iodo-2,3-dihydro-4(1H)-quinazolinone (**6**).* Iodoanthranilamide **5** (1.834 g, 7 mmol) and salicylaldehyde (0.9 mL, 8.4 mmol) were suspended in 25 mL of methanol and refluxed in the presence of catalytic amounts of *p*-toluenesulfonic acid (10%, 0.183 g) for 2 h. After being filtered and washed with cold methanol, **6** was obtained as a pale-yellow solid (2.42 g, 94%). ^{1}H NMR (DMSO-d_6) δ 9.87 (s, 1H), 8.40 (s, 1H), 8.13 (d, J = 8.0 Hz, 1H), 7.82 (s, 1H), 7.50 (t, J = 8.75 Hz, 1H), 7.20 (t, J = 8.5 Hz, 1H), 6.98 (d, J = 7.6 Hz, 1H), 6.82 (d, J = 7.6 Hz, 1H), 6.61 (d, J = 8.8 Hz, 1H), 5.99 (s, 1H). ESI−HRMS calcd for $C_{14}H_{11}IN_2O_2$ [M + H]$^+$: 366.9938. Found 366.9937. Anal. Calcd for $C_{14}H_{11}IN_2O_2$: C, 45.92; H, 3.03; N, 7.65. Found: C, 46.19; H, 2.74; N, 7.71.

*2-(2′-Hydroxyphenyl)-6-iodo-4(3H)-quinazolinone (**7**).* 2-(2′-Hydroxyphenyl)- 6-iodo-2,3-dihydro-4(1*H*)-quinazolinone **6** (1.831 g, 5 mmol) was oxidized by the addition of 2,3-dichloro-5,6-dicyano-1,4-benzoquinone (1.816 g, 8 mmol) in 20 mL of methanol. The suspension was refluxed for 2 h and turned a deep-orange color. After being filtered and washed with cold methanol, the light-yellow solid **7** was obtained (1.52 g, 83.5%). ^{1}H NMR (DMSO-d_6) δ 11.3 (s, N−H), 8.39 (s, H-7), 8.17 (d, J = 8.0 Hz), 8.12 (d, H-5, J = 8.75 Hz), 7.56 (d, H-4, J = 8.5 Hz), 7.44 (t, H-4′, J = 7.75 Hz), 6.99 (d, H-6′, J = 7.5 Hz), 6.95 (t, H-5′, J = 7.70 Hz). ESI−HRMS calcd for $C_{14}H_9IN_2O_2$ [M + H]$^+$: 364.9781. Found: 364.9772. Anal. Calcd for $C_{14}H_9IN_2O_2$: C, 46.18; H, 2.49; N, 7.69. Found: C, 45.96; H, 2.46; N, 7.73.

*2-(2′-Hydroxy)-6-tributylstannyl-4(3H)-quinazolinone (**9**).* To a stirred solution of **7** (0.50 g, 1.49 mmol) in 10 mL of dioxane was added hexa-*n*-butylditin (1.89 g, 3.12 mmol) followed by tetrakis(triphenylphosphine)palladium (17.0 mg, 0.015 mmol) as catalyst (Scheme 3). The solution was cloudy and yellow. The reaction mixture was refluxed for 1.5 h, and progress of the reaction was followed by silica gel TLC with methylene chloride:ethyl acetate (9:1) to test for the formation of a more nonpolar product. The solvent was evaporated, and the crude yellow solid was purified on a silica gel column eluted with a stepwise gradient, starting with hexane followed by hexane: dichloromethane (1:1). The solvent was removed to give a yellow fluorescent solid product **9** (0.4 g, 43%). ^{1}H NMR (DMSO-d_6) δ 8.24−8.6 (m, 2H, H-7, H-3′), 7.88 (d, H-5, ^3J = 7.80 Hz), 7.68 (d, H-4, ^3J = 8.10 Hz), 7.43 (t, H-5′, ^3J = 8.12 Hz), 6.98 (d, H-6′, ^3J = 9.0 Hz), 6.94 (t, H-4′, ^3J = 8.0 Hz), 1.51 (quintet, 6H′, CH_2CH$_2$Sn, ^3J = 7.70 Hz), 1.30 (sextet, 6H′, CH$_3$CH_2, ^3J = 7.30 Hz), 1.09 (dd, with Sn satellites, $^2J_{Sn-CH}$ = 52 Hz, 6H′, CH_2Sn, $^3J_{avg}$ = 8.0 Hz), 0.83 (t, 9H′, CH_3CH$_2$, ^3J = 7.30 Hz). Peak assignment was made using a combination of COSY (2D) and 1D proton NMR spectra. ESI−HRMS calcd for $C_{26}H_{36}N_2O_2$-Sn [M + H]$^+$: 529.1872. Found 529.1878. Anal. Calcd for $C_{26}H_{36}N_2O_2Sn$: C, 59.23; H, 6.88; N, 5.31. Found: C, 59.48; H, 6.75; N, 5.32.

*Ammonium 2-(2′-Phosphoryloxyphenyl)-6-tributylstannyl-4(3H)-quinazolinone (**10**).* To a stirred solution of **9** (54 mg, 0.108 mmol) in 1 mL of dry pyridine cooled to 0 °C was added dropwise phosphorus oxychloride (20 mg, 0.130 mmol) in 1 mL of dry pyridine. The solution turned yellow. The reaction mixture was stirred for 10 min at 0 °C and then quenched by adding 0.2 mL of 28% ammonium hydroxide solution. The solution was slightly basic (pH 9−10) on pH paper. The reaction mixture after quenching was orange-red. The solvent was evaporated, and a mixture of orange-red-yellow solid was obtained. The crude product was redissolved in methanol:acetate (1:1) and purified on a C_{18} column (Waters) using a stepwise gradient, starting with water followed by acetonitrile:water going from 30% to 50% acetonitrile. The solvent was evaporated under reduced pressure (rotary evaporator). An orange-red-yellow nonfluorescent solid (**10**) was obtained (57 mg, 80%). ^{31}P NMR (DMSO-d_6, H_3PO_4 as external reference) δ −17.2. ESI−HRMS calcd for $C_{26}H_{35}N_2O_5PSn$ [M − H]: 605.1228. Found: 605.1226.

*Ammonium 2-(2′-Phosphoryloxyphenyl)-6-iodo-4(3H)-quinazolinone (**8**). Method A.* 2-(2′-Hydroxy)-6-iodo-4-(3*H*)-quinazolinone (**7**, 0.1 g, 0.274 mmol) was added to 1 mL of dried pyridine at 0 °C, followed by phosphorus oxychloride (42 mg, 27 μL, 0.274 mmol) dissolved in 0.2 mL of dried pyridine under nitrogen gas (Scheme 2). The reaction was completed within 2 min as indicated by silica gel TLC (chloroform:ethyl acetate:methanol, 3:1:1). The reaction solution became less cloudy and was neutralized to pH 7.0 by adding 0.4 mL (10 mmol) of 28% ammonium hydroxide in 1.5 mL of water at 0 °C. During neutralization, the solution turned orange-red and then light-yellow. At the end of neutralization, the solution

stayed orange-red and some orange-red precipitate was formed. The solvent was evaporated, and a mixture of orange-red and yellow solid was obtained. The solid product was suspended in 2−3 mL of water. The orange-red solid was filtered. The yellow filtrate was purified by chromatography on a 12 cm^3 Sep-Pak Vac C_{18} cartridge (Waters) eluted with a stepwise gradient, starting with water (8 mL) followed by acetonitrile:water (2:1, 2 mL). A yellow solution containing UV−visible product was collected. The solvent was evaporated under reduced pressure (rotary evaporator). A yellow nonfluorescent solid (**8**) was obtained (80 mg, 62%). ^{1}H NMR (DMSO-d_6) δ 8.36 (d, H-7, ^4J = 3.5 Hz), 8.25 (dd, H-3′, ^3J = 13.5 Hz, ^4J = 2.5 Hz), 8.07 (dd, H-5, ^3J = 14.3 Hz, ^4J = 3.5 Hz), 7.53 (t, H-4′, ^3J = 13.5 Hz), 7.47 (d, H-4, ^3J = 14.5 Hz), 7.22 (t, H-5′, ^3J = 13.0 Hz), 7.08 (d, H-6′, ^3J = 13.5 Hz). ^{31}P NMR (DMSO-d_6, 85% H_3PO_4 as external reference) δ −14.5. ESI−HRMS calcd for $C_{14}H_8IN_2O_5P$ [M − H]: 440.9138. Found: 440.9146.

Method B. Ammonium 2-(2′-phosphoryloxyphenyl)-6-tributylstannyl-4(3*H*)-quinazolinone (**10**, 15 mg, 0.023 mmol) was dissolved in 0.4 mL of methanol (Scheme 3). Sodium iodide (30 mg, 0.2 mmol) in 0.2 mL of water was added, followed by 0.2 mL of diluted hydrogen peroxide (30% solution diluted 500-fold in water). A yellow precipitate formed immediately. The reaction vial was vortex-mixed and incubated for 15 min at 37 °C. Reversed-phase silica gel TLC (RPSF, Analtech) with acetonitrile:water (1:1) showed approximately 50% conversion. An additional 15-min incubation did not improve the conversion. The solvent was evaporated, and the product was purified by chromatography on a Sep-Pak Plus C_{18} cartridge (Waters) eluted with a stepwise gradient, starting with water followed by acetonitrile:water (2:1, 2 mL). A yellow solution containing a UV product was collected, and the solvent was evaporated to yield a yellow nonfluorescent solid. TLC (chloroform:methanol, 1:1) showed the same R_f value (0.6), and proton and ^{31}P NMR gave the same spectra as were obtained with the known compound **8** synthesized by the other route (Scheme 2). Product **8** was spotted on a TLC plate with alkaline phosphatase and Tris buffer. The TLC plate was incubated for 5 min at 37 °C. After developing the TLC with chloroform, a bright fluorescent spot was seen whose R_f value was the same as that of **7** (R_f = 0.33).

*Preparation of Radiolabeled (^{125}I) Ammonium 2-(2′-Phosphoryloxyphenyl)-6-iodo-4(3H)-quinazolinone (**1**).* Three iodobeads (Pierce) were placed in a reaction vial, followed by 20 μL of **10** (1 μg/μL solution) and 30 μL of 0.1 M borate buffer (pH = 8.3) (Scheme 3). The desired quantity of Na^{125}I (800 μCi, 100 μCi/μL in 0.1 M sodium hydroxide) was added. After 20 min at room temperature, an aliquot was removed for HPLC analysis (the reaction was not quenched with sodium bisulfite since we found that **1** was unstable in reducing reagents). The crude reaction mixture was then loaded on a Sep-Pak Plus C_{18} cartridge (Waters) for purification and separation from unreacted organotin precursor (**10**). The column was eluted with 1 mL of water, 2 mL of 10% acetonitrile in water to remove impurities, and finally with 20% acetonitrile in water. The purification was monitored by determining the radioactivity in each tube (Capintec) and analyzing the samples by autoradiography on reversed-phase TLC (acetonitrile:water, 1.5:2). Only the fractions containing a single radioactive spot that had the same R_f as authentic nonradioactive **8** were combined. Approximately 370 μCi of the product (**1**) eluted with the 20% acetonitrile (radiochemical yield, 46%; radiochemical purity, 98%). When **1** was cospotted with nonradioactive **8** on reversed-phase TLC (acetonitrile:water, 1.5:2), a single spot on autoradiograph was obtained that had the same R_f as **8**. Radiolabeled **1** coinjected with **8** into the HPLC showed a single radioactive peak (t_R = 14 min) that matched the t_R value of **8** (Figure 1).

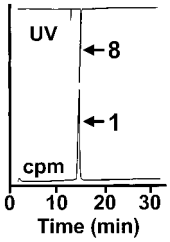


Figure 1. HPLC profile of **1** and **8**.

Biologic Studies. *Enzyme-Dependent Conversion of Prodrug (**8**) to Drug (**7**).* When the water-soluble ^{127}I-labeled **8** is incubated at 37 °C with alkaline phosphatase (ALP), a clearly visible precipitate is formed whose R_f on TLC corresponds to **7**. To assess the kinetics of this enzyme-based hydrolysis (i.e., conversion of **8** to **7**), **8** (60 μM) was mixed with 10 units of ALP in 0.1 M Tris (pH 7.2) containing 50 mM NaCl, 10 mM $MgCl_2$, and 0.1 mM $ZnCl_2$, and the reaction kinetics were followed over time using a Perkin-Elmer LS50B luminescence spectrometer with excitation at 340 nm and emission at 500 nm. The fluorescence intensity at 500 nm was then plotted as a function of time, the linear portions of the data points were fitted, and the slope was used to calculate the half-life ($T_{1/2\alpha}$ and $T_{1/2\beta}$) for the disappearance of **8**.

To assess further the kinetics of this enzyme-based hydrolysis, **8** (2.7 μM) was mixed with 40 units of ALP in buffer (pH 9.8), and the reaction kinetics were followed over time. A plot of reciprocal of the substrate (prodrug **8**) concentration (abscissa) versus reciprocal of reaction velocity (ordinate) furnished a straight Lineweaver−Burk line with a slope equal to K_m/V_{max}; K_m is Michaelis−Menten constant of ALP and V_{max} is maximum velocity.

*Enzyme-Dependent Conversion of Radioiodinated Prodrug (**1**) to Radioiodinated Drug (**2**).* To characterize the radioiodinated prodrug **1**, 5 units of ALP or heat-inactivated (70 °C, 2 h) ALP were incubated (37 °C) for 3 h with **1** (~10 μCi/100 μL of 0.1 M Tris buffer, pH 7.2). Samples were spotted on reversed-phase TLC plates that were then run in acetonitrile:water (1.5:2), and radioactivity was detected by autoradiography.

*Stability of Prodrug **1**.* To assess the chemical nature of the radioactivity in blood post intravenous injection (i.e., determine stability of **1** in blood), mice (n = 5) were injected with ~5 μCi of **1** and bled ~40 min later. The samples were pooled, and ethanol was added to precipitate the cells and proteins. Following centrifugation, the supernatant was spotted on TLC, and the plates were run in acetonitrile:water (1.5:2). Autoradiography was used to visualize the radioactivity on the plates.

*Biodistribution of ^{125}I-Labeled Prodrug (**1**) and Drug (**2**) in Normal Mice.* To determine normal-tissue localization of **1** and **2**, mice (n = 5/group) were injected iv or sc with one of the radioiodinated agents and, at 24 h, the animals were killed. The radioactivity associated with blood, heart, lungs, liver, spleen, kidneys, bladder, urine, stomach, small intestine, large intestine, muscles, skin, skeleton, and thyroid was determined in a gamma counter. Based on the injected activity and the weight of these fluids, tissues, and organs, the percentage injected dose per gram (% ID/g) was then calculated.

*Specific Localization of **1** in Alkaline Phosphatase-Rich Regions.* To demonstrate within an animal the conversion of the water-soluble radioiodinated **1** to the water-insoluble **2**, ALP was dissolved in saline (50, 100, 150, 200, 250, 300, 400 units/10 μL), and10 μL of the enzyme preparations was injected sc, with a 10-μL Hamilton syringe, in the forelimb of Swiss Alpine mice (n = 5/ALP concentration). Five minutes later, 20 μCi of **1** was injected iv (tail vein). The animals were killed 1 h later, and the radioactivity in the forelimbs was measured. As nonspecific controls, mice (n = 5) were injected sc (forelimb) with 200 units of heat-inactivated ALP (56 °C, 30 min) prior to the iv injection of **1**.

*Entrapment of **2** within Tissues.* To demonstrate that the water-insoluble ID is retained within the tissue where it is formed, 100 μCi of **7** and 2.5 mg of **2** were added to 100 μL of DMSO, and the sample was heated. Under these conditions, the water-insoluble iodinated (^{125}I/^{127}I) drug dissolves completely, forms a yellow solution, and remains in solution when the sample is cooled to room temperature. However, when 100 μL of water is added, a visible precipitate forms immediately. Five microliters of **7**−**2**-DMSO solution was injected sc into the right forelimb of Swiss Alpine mice (n = 15) and followed at once by 5 μL of saline (the immediate formation of turbidity was noted through the skin of the mice). For comparison, 5 μCi of **1** in 5 μL of saline was injected sc into the left forelimb of the same mice and followed immediately with 5 μL of DMSO. The animals were killed after 1, 24, and 48 h (n = 5/time point). The radioactivity associated with the forelimbs was measured, and the percentage of radioactivity remaining at the injection site was calculated.

RESULTS

Enzyme-Dependent Conversion of Prodrug (8) to Drug (7). When nonradiolabeled prodrug **8**, a nonfluorescent, water-soluble compound was incubated with alkaline phosphatase and the kinetics of the hydrolysis were followed with a luminescence spectrometer, a rapid increase in fluorescence intensity (excitation at 340 nm; emission at 500 nm) was observed, demonstrating the hydrolysis of **8** and the formation of **7** (Figure 2, top). Analysis of these data indicates the enzyme-dependent disappearance of **8** (or the appearance of **7**) is biphasic with a $T_{1/2\alpha}$ of 31 s and a $T_{1/2\beta}$ of 120 s (Figure 2, bottom). No fluorescence was detected when the enzyme was heat-inactivated prior to its incubation with **8**.

To assess the kinetics of this enzyme-based hydrolysis, the Michaelis−Menten constant of ALP (K_m) and maximum velocity (V_{max}) were determined by a straight Lineweaver−Burk line with a slope equal to K_m/V_{max}, where the y intercept of the line is $1/V_{max}$ and the x intercept is $-1/K_m$. The calculated K_m and V_{max} values, easily determined by extrapolating the straight line to its intercepts on the x and y axes, are 3.07×10^{-6} M and 2.11×10^{-8} M/min.

Enzyme-Dependent Conversion of Radioiodinated Prodrug (1) to Radioiodinated Drug (2). Reversed-phase TLC followed by autoradiography (ARG) was used to characterize the radiolabeled derivative **1** and confirm its ALP-dependent hydrolysis to **2**. When **1** was cospotted with nonradioactive **8**, a single spot was obtained (ARG) that has the same R_f as that of **8** (Figure 3). Furthermore, the incubation of **1** with ALP, but not heat-inactivated ALP, led to its complete conversion to **2** (Figure 3). The incubation of **1** with heat-inactivated ALP did not induce any hydrolysis.

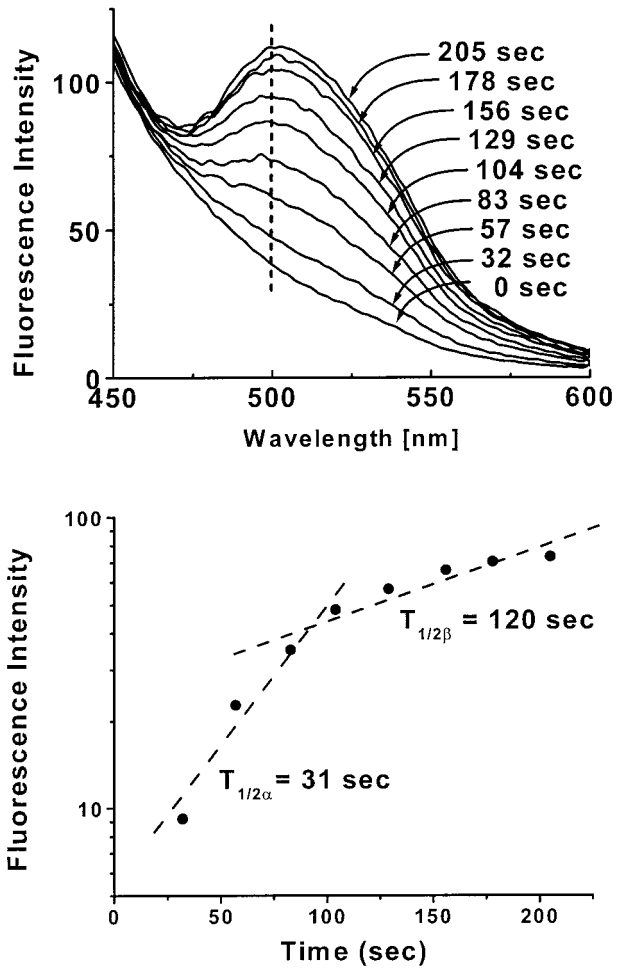


Figure 2. Kinetics of alkaline phosphatase-based hydrolysis of **8** to **7** at 37 °C. Top: change in fluorescence spectra of **8** as function of time. Bottom: change in fluorescence intensity of **8** at 500 nm as function of time. Linear fits were used to calculate the slopes (data points sets 1−4 and 4−9) and the corresponding $T_{1/2\alpha}$ and $T_{1/2\beta}$.

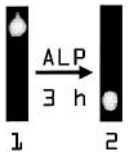


Figure 3. Autoradiograph demonstrating complete conversion of **1** to **2** after incubation in alkaline phosphatase at 37 °C for 3 h.

Stability of Prodrug 1. When the chemical nature of the radioactivity in blood post iv injection in mice was examined, autoradiography demonstrated (i) the presence of a single spot whose R_f is the same as that of **1**, and (ii) no evidence of free iodide.

Biodistribution of ^{125}I-Labeled Prodrug (1) and Drug (2) in Normal Mice. To assess whether ^{125}IPD (**1**) and ^{125}ID (**2**) are taken up and/or retained by normal tissues, the %ID/g was determined in blood and in various organs and tissues in mice injected iv or sc with ~5 μCi of each agent. For ^{125}IPD (Figure 4, top), the data indicate that (i) similar results were obtained regardless of the injection route, (ii) ~10% of the injected dose remained in the body of these animals, (iii) some radioactivity was present in the liver (6% ID/g), the kidneys (7% ID/g), and the thyroid (6−12% ID/g), and (iv) minimal amounts of radioactivity (<2% ID/g) were detected in blood and most organs and tissues. These results suggest

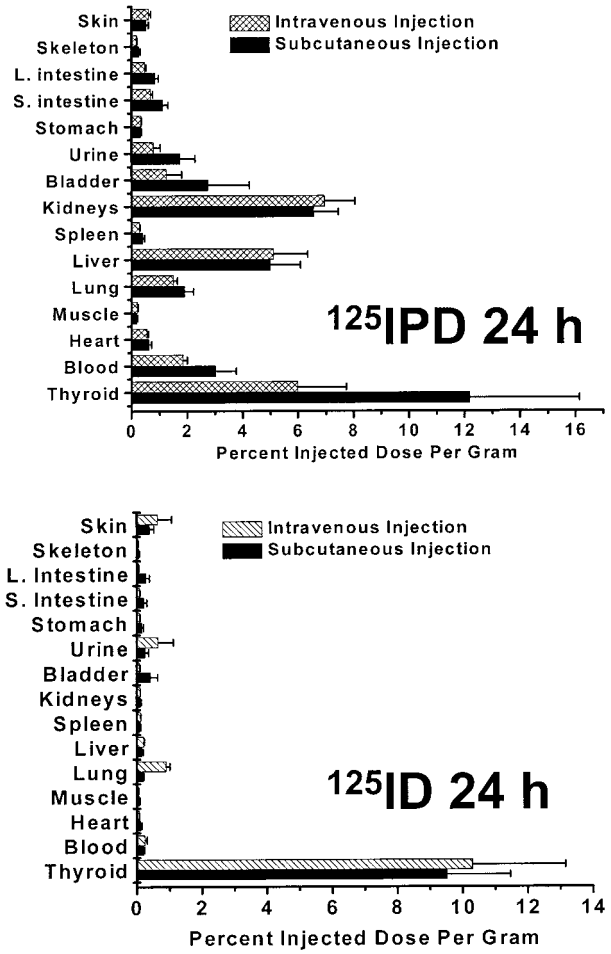


Figure 4. Percentage injected dose per gram of tissues, organs, and fluids 24 h post iv or sc injection of compound in normal mice. Top: **1**. Bottom: **2**.

that (i) **1** and/or its breakdown/hydrolysis product(s) are not taken up, hydrolyzed, or retained by most normal tissues and are rapidly excreted through the urinary system, (ii) some dehalogenation of the compound occurs, as exemplified by the presence of activity within the thyroid, and (iii) the accumulation of radioactivity within the liver and kidneys, which are rich in ALP, may be a result of the hydrolysis of **1** and the consequent formation of precipitated **2**. For ^{125}ID (Figure 4, bottom), minimal radioactivity was observed in all tissues except the thyroid.

Specific Localization of 1 in Alkaline Phosphatase-Rich Regions. To demonstrate the hydrolysis of water-soluble **1** to water-insoluble **2** in ALP-rich regions within an animal, mice were injected sc in the forelimb with ALP (or heat-inactivated ALP) and 5 min later iv (tail vein) with 20 μCi of **1**. The mice were killed 1 h later, and the radioactivity in the forelimb was measured. The data (Figure 5) demonstrate that the radioactive content of the forelimb of animals increased with enzyme dose and plateaued at the highest concentrations. That these increases were due to the enzymatic action of ALP was ascertained in studies that showed no increase in uptake in the forelimb of mice preinjected with heat-inactivated ALP (Figure 5). These results illustrate the specific dose-dependent accumulation of **1** (more accurately **2**) within ALP-containing sites in an animal.

Entrapment of 2 within Tissues. To assess the retention of water-insoluble **2** within the tissue where it is formed, ^{125}ID (**2**) was injected sc into the right forelimb

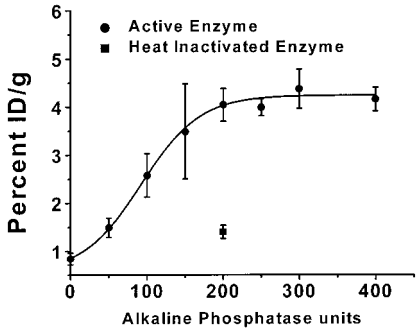


Figure 5. Accumulation of radioactivity in forelimbs of mice after sc injection of alkaline phosphatase followed 5 min later by iv injection of **1**.

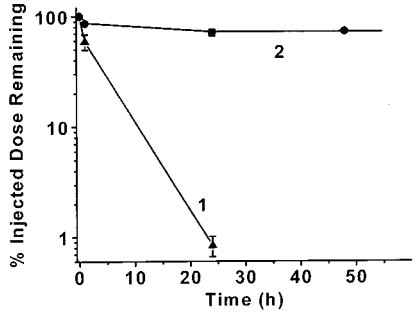


Figure 6. Retention of radioactivity in forelimbs of mice after sc injection of **1** and **2**.

of mice (for comparison, ^{125}IPD (**1**) was injected sc into the left forelimb). The animals were killed at various time periods, and the radioactivity associated with their forelimbs was determined. The data (Figure 6) demonstrate that while >99% of prodrug **1** had seeped from the sc pocket by 24 h, 71 ± 5% of the injected **2** activity remained at the injection site. As presented earlier (Figure 4, bottom), the radioactivity that escaped from sc injected **2** did not localize in any normal tissues within the animal. Finally, the results show no change in the radioactivity in the forelimbs of the animals (~72% injected dose) at 24 and 48 h (Figure 6), indicating that precipitated **2** is permanently and indefinitely trapped within tissues.

DISCUSSION

The treatment of solid tumors with current therapeutic agents continues to be a problem. Over the past two decades, some investigators have proposed two-step and three-step approaches in which a noninternalizing anti-tumor antibody is injected prior to the administration of a low-molecular-weight therapeutic molecule that has an affinity/reactivity with the preinjected antibody molecule. These systems can be categorized into two major classes: antibody-directed radioligand targeting (ADRT), and antibody-directed enzyme prodrug therapy (ADEPT).

The first strategy (ADRT) is based on the pretargeting of a monoclonal antibody (mAb) moiety that has the capacity to bind simultaneously to tumor cells and a radiotherapeutic molecule. For example, bispecific mAb, in which one valency is directed to a tumor-associated antigen while the other is directed to a radiolabeled molecule, have been preadministered into tumor-bearing animals, and after targeting and clearance of unbound material from the blood pool, the animals are injected with the radiolabeled molecule (*3*−*6*). Another system utilizes the high avidity of avidin or streptavidin for biotin ($k_d = \sim 10^{-15}$ M) to bind the radiolabeled molecule

to the pretargeted antibody (*7*−*10*). Both of these systems offer several potential advantages, most prominently (i) rapid blood clearance of the radiopharmaceutical, (ii) short residence of radioactivity in the body, (iii) low radiation doses to normal tissues, and (iv) cross-fire from the emitted long-range particles (α or *β*), negating the need for intracellular localization of the therapeutic agent. A recent report (*11*) that examined the therapeutic efficacy of a ^{90}Y-labeled biotin derivative post-pretargeting with an antitumor mAb−avidin conjugate in tumor-bearing mice showed that 100% of the treated animals were cured of their disease, clearly demonstrating the therapeutic potential of such two-step and three-step approaches.

In ADEPT, which was originally described by Philpott in 1973 (*12*) and later pursued by Bagshawe (*13*, *14*) and Senter (*15*, *16*), a noninternalizing antitumor-antibody−enzyme conjugate is injected into a tumor-bearing animal prior to the administration of a chemotherapeutic agent (prodrug, PD). The enzyme is chosen for its ability to convert the relatively noncytotoxic PD into a highly cytotoxic drug (D). The major advantages offered by ADEPT are (i) low normal tissue toxicity (PD is mildly toxic), (ii) specific conversion of PD in tumors, (iii) high PD-to-D turnover, and (iv) bystander effect (low-molecular-weight D can readily diffuse within the tumor mass and, hence, reach antigen-positive [antibody-targeted] as well as neighboring antigen-negative [antibody nontargeted] tumor cells). However, investigators have realized that, at a minimum, ADEPT has two major limitations: (i) to be therapeutically effective, the cytotoxic agent must be *internalized by each cell* within the tumor mass (*14*, *17*, *18*), and (ii) the toxic agents formed have relatively long biologic half-lives (*19*) and have been shown to escape from within the tumor mass, thereby increasing nonspecific normal tissue toxicity (*14*). Despite these shortcomings, various reports have demonstrated that the injection of prodrugs into tumor-bearing animals preinjected with mAb−enzyme conjugates will lead to tumor regression and delay in tumor growth (*16*, *20*). These findings, as well as those reported for ADRT, clearly demonstrate the credibility of such two- and three-step strategies for the treatment of solid tumors.

In this paper, we describe a novel approach, which we have named EMIT (enzyme-mediated insolubilization therapy), that we believe could fulfill many of the basic requirements for the effective therapy of solid tumors. The strategy combines the major advantages of the above-mentioned two approaches while negating their limitations. As mentioned earlier, EMIT is a method for the site-specific, in vivo conversion of a water-soluble radioactive molecule (**1**) to a water-insoluble radioactive molecule (**2**) by an enzyme present within a solid tumor. Since many tumors (e.g., prostate, osteosarcomas, teratocarcinomas) have been shown to innately express various phosphatases (*21*, *22*), we expect the hydrolysis of **1** (*IPD) within the extracellular spaces of such tumors and the indefinite entrapment of the precipitated radioiodinated **2**. Our current data, which demonstrate that ^{125}IPD concentrates at sites rich in ALP (Figure 5) and that, once formed, the ^{125}ID remains "indefinitely" within the tissue where it is produced (Figure 6), support these expectations. However, for those circumstances where the concentration of the enzyme within a tumor is too low to hydrolyze sufficient amounts of the IPD, the enzyme can be pretargeted to the tumor following its conjugation to a targeting moiety such as a noninternalizing ligand to a tumor-specific receptor or an antitumor antibody, i.e., utilizing the same approaches used in ADEPT. It is important to note that the EMIT approach bypasses the two main limitations reported for ADEPT since (i) the radiolabeled moiety does not need to be internalized (due to the cross-fire irradiation of cells within the range of the emitted α and *β* particles), and (ii) the precipitated molecules formed are trapped within the extracellular spaces of the tumor mass (the biologic half-time within the tumor will in effect equal the physical half-life of the isotope).

For our current studies, we have synthesized (Schemes 2 and 3) a phosporyloxyphenol derivative of a radioiodinated quinazolinone (**1**), a water-soluble molecule that is readily hydrolyzed to water-insoluble **2** when exposed to ALP (Scheme 1). While ALP may seem at first inappropriate for EMIT (it is present in most normal mammalian tissues and fluids), our data demonstrate that except for the liver (∼5% ID/g) and possibly the kidneys (∼6% ID/g), minimal radioactivity is detected and/or retained in all other normal tissues of mice following the injection of **1** (Figure 4, top). These results indicate that **1** is not taken up, concentrated, or hydrolyzed by most tissues. In addition, the choice of ALP is favored since (i) it is present in high concentration within various tumors (*21*, *22*), (ii) it has a very high second-order rate constant ($k_{cat}/K_M = 5 \times 10^7$ M^{-1} s^{-1}), (iii) the availability of its human form should eliminate/reduce its immunogenicity in humans, and (iv) ALP covalently bound to mAb has already been used to activate several chemotherapeutic prodrugs in vitro and to retard tumor growth in vivo (*15*, *16*, *23*−*28*).

We believe that the approach described in this paper should satisfy most of the requirements for an ideal radiotherapeutic agent, namely (i) rapid and efficient concentration by the tumor, (ii) retention by the tumor (i.e., very long effective clearance half-life), (iii) short residence time within normal tissues (i.e., short effective half-life in blood, bone marrow, and whole body), and (iv) high tumor-to-normal-tissue uptake ratios. Since the PD is labeled with an energetic particle emitter, the therapeutic potential of EMIT will depend on (i) attaining an intratumoral distribution that is sufficiently uniform to match the range of the emitted particles (all tumor cells are within the range of the emitted particles), and (ii) achieving an intratumoral concentration that is sufficiently high to deposit a tumoricidal dose in every cell that is within the range of the emitted particles. Experiments that address these issues are currently ongoing.

CONCLUSIONS

We have synthesized and characterized ^{125}I-labeled prodrug (**1**) and its nonradioactive analogue (**8**). The radiochemical yield for no-carrier-added **1** is 46% and the radiochemical purity over 98%. In vitro, water-soluble **8** is rapidly and completely converted to a water-insoluble fluorescent precipitate **7** in the presence of alkaline phosphatase. With the exception of the liver, and possibly the kidneys, the radioiodinated prodrug **1** is not taken up/hydrolyzed by normal tissues in mice. However, in ALP-rich regions in vivo, it is converted to **2**, which is indefinitely retained within the tissue where it is formed.

We believe EMIT to be a technology that will (i) lead to the active and specific concentration of therapeutic radionuclides within solid tumors, (ii) result in the indefinite entrapment of therapeutic radionuclides within solid tumors, (iii) lead to the protracted irradiation of tumor cells that are within the range of the emitted α (50−100 *μ*m) or *β* (0.1 mm−1 cm) particles, and (iv)

negate the limitations of current prodrug approaches and lead to more effective therapies of solid tumors.

ACKNOWLEDGMENT

The authors wish to thank Pulin Wang for his technical assistance.

LITERATURE CITED

(1) Haugland, R. P., Zhang, Y., Yue, S. T., Terpetschnig, E., Olson, N. A., Naleway, J. J., Larison, K. D., and Huang, Z. (1994) Enzymatic analysis using substrates that yield fluorescent precipitates. US Patent 5,316,906.

(2) Daly, W. H., and Poché, D. (1988) The preparation of N-carboxyanhydrides of α-amino acids using bis(trichloromethyl)carbonate. *Tetrahedron Lett. 29*, 5859−5862.

(3) Le Doussal, J.-M., Martin, M., Gautherot, E., Delaage, M., and Barbet, J. (1989) In vitro and in vivo targeting of radiolabeled monovalent and divalent haptens with dual specificity monoclonal antibody conjugates: enhanced divalent hapten affinity for cell-bound antibody conjugate. *J. Nucl. Med. 30*, 1358−1366.

(4) Le Doussal, J.-M., Gruaz-Guyon, A., Martin, M., Gautherot, E., Delaage, M., and Barbet, J. (1990) Targeting of indium 111-labeled bivalent hapten to human melanoma mediated by bispecific monoclonal antibody conjugates: imaging of tumors hosted in nude mice. *Cancer Res. 50*, 3445−3452.

(5) Peltier, P., Curtet, C., Chatal, J.-F., Le Doussal, J.-M., Daniel, G., Aillet, G., Gruaz-Guyon, A., Barbet, J., and Delaage, M. (1993) Radioimmunodetection of medullary thyroid cancer using a bispecific anti-CEA/anti-indium-DTPA antibody and an indium-111-labeled DTPA dimer. *J. Nucl. Med. 34*, 1267−1273.

(6) Bardiès, M., Bardet, S., Faivre-Chauvet, A., Peltier, P., Douillard, J.-Y., Mahé, M., Fiche, M., Lisbona, A., Giacalone, F., Meyer, P., Gautherot, E., Rouvier, E., Barbet, J., and Chatal, J.-F. (1996) Bispecific antibody and iodine-131-labeled bivalent hapten dosimetry in patients with medullary thyroid or small-cell lung cancer. *J. Nucl. Med. 37*, 1853−1859.

(7) Hnatowich, D. J., Virzi, F., and Rusckowski, M. (1987) Investigations of avidin and biotin for imaging applications. *J. Nucl. Med. 28*, 1294−1302.

(8) Paganelli, G., Riva, P., Deleide, G., Clivio, A., Chiolerio, F., Scassellati, G. A., Malcovati, M., and Siccardi, A. G. (1988) *In vivo* labelling of biotinylated monoclonal antibodies by radioactive avidin: a strategy to increase tumor radiolocalization. *Int. J. Cancer Suppl. 2*, 121−125.

(9) Pimm, M. V., Fells, H. F., Perkins, A. C., and Baldwin, R. W. (1988) Iodine-131 and indium-111 labelled avidin and streptavidin for pre-targetted immunoscintigraphy with biotinylated anti-tumour monoclonal antibody. *Nucl. Med. Commun. 9*, 931−941.

(10) Kassis, A. I., Jones, P. L., Matalka, K. Z., and Adelstein, S. J. (1996) Antibody-dependent signal amplification in tumor xenografts following pretreatment with biotinylated monoclonal antibody and avidin or streptavidin. *J. Nucl. Med. 37*, 343−352.

(11) Axworthy, D. B., Reno, J. M., Hylarides, M. D., Mallett, R. W., Theodore, L. J., Gustavson, L. M., Su, F.-M., Hobson, L. J., Beaumier, P. L., and Fritzberg, A. R. (2000) Cure of human carcinoma xenografts by a single dose of pretargeted yttrium-90 with negligible toxicity. *Proc. Natl. Acad. Sci. U.S.A. 97*, 1802−1807.

(12) Philpott, G. W., Shearer, W. T., Bower, R. J., and Parker, C. W. (1973) Selective cytotoxicity of hapten-substituted cells with an antibody-enzyme conjugate. *J. Immunol. 111*, 921−929.

(13) Bagshawe, K. D. (1987) Antibody directed enzymes revive anti-cancer prodrugs concept. *Br. J. Cancer 56*, 531−532.

(14) Bagshawe, K. D. (1994) Antibody-directed enzyme prodrug therapy. *Clin. Pharmacokinet. 27*, 368−376.

(15) Senter, P. D., Saulnier, M. G., Schreiber, G. J., Hirschberg, D. L., Brown, J. P., Hellström, I., and Hellström, K. E. (1988) Anti-tumor effects of antibody−alkaline phosphatase conjugates in combination with etoposide phosphate. *Proc. Natl. Acad. Sci. U.S.A. 85*, 4842−4846.

(16) Senter, P. D., Schreiber, G. J., Hirschberg, D. L., Ashe, S. A., Hellström, K. E., and Hellström, I. (1989) Enhancement of the *in vitro* and *in vivo* antitumor activities of phosphorylated mitomycin C and etoposide derivatives by monoclonal antibody−alkaline phosphatase conjugates. *Cancer Res. 49*, 5789−5792.

(17) Springer, C. J., Antoniw, P., Bagshawe, K. D., and Wilman, D. E. V. (1991) Comparison of half-lives and cytotoxicity of *N*-chloroethyl-4-amino and *N*-mesyloxyethyl-benzoyl compounds, products of prodrugs in antibody-directed enzyme prodrug therapy (ADEPT). *Anticancer Drug Des. 6*, 467−479.

(18) Melton, R. G., and Sherwood, R. F. (1996) Antibody−enzyme conjugates for cancer therapy. *J. Natl. Cancer Inst. 88*, 153−165.

(19) Antoniw, P., Springer, C. J., Bagshawe, K. D., Searle, F., Melton, R. G., Rogers, G. T., Burke, P. J., and Sherwood, R. F. (1990) Disposition of the prodrug 4-(bis(2-chloroethyl)-amino)benzoyl-L-glutamic acid and its active parent drug in mice. *Br. J. Cancer 62*, 909−914.

(20) Cheng, T.-L., Chen, B.-M., Chern, J.-W., Wu, M.-F., and Roffler, S. R. (2000) Efficient clearance of poly(ethylene glycol)-modified immunoenzyme with anti-PEG monoclonal antibody for prodrug cancer therapy. *Bioconjugate Chem. 11*, 258−266.

(21) Herz, F. (1985) Alkaline phosphatase isozymes in cultured human cancer cells. *Experientia 41*, 1357−1361.

(22) Harris, H. (1989) The human alkaline phosphatases: what we know and what we don't know. *Clin. Chim. Acta 186*, 133−150.

(23) Sahin, U., Hartmann, F., Senter, P., Pohl, C., Engert, A., Diehl, V., and Pfreundschuh, M. (1990) Specific activation of the prodrug mitomycin phosphate by a bispecific anti-CD30/anti-alkaline phosphatase monoclonal antibody. *Cancer Res. 50*, 6944−6948.

(24) Senter, P. D. (1990) Activation of prodrugs by antibody-enzyme conjugates: a new approach to cancer therapy. *FASEB J. 4*, 188−193.

(25) Wallace, P. M., and Senter, P. D. (1991) In vitro and in vivo activities of monoclonal antibody-alkaline phosphatase conjugates in combination with phenol mustard phosphate. *Bioconjugate Chem. 2*, 349−352.

(26) Haisma, H. J., Boven, E., van Muijen, M., De Vries, R., and Pinedo, H. M. (1992) Analysis of a conjugate between anti-carcinoembryonic antigen monoclonal antibody and alkaline phosphatase for specific activation of the prodrug etoposide phosphate. *Cancer Immunol. Immunother. 34*, 343−348.

(27) Senter, P. D., Wallace, P. M., Svensson, H. P., Vrudhula, V. M., Kerr, D. E., Hellström, I., and Hellström, K. E. (1993) Generation of cytotoxic agents by targeted enzymes. *Bioconjugate Chem. 4*, 3−9.

(28) Mamber, S. W., Mikkilineni, A. B., Pack, E. J., Rosser, M. P., Wong, H., Ueda, Y., and Forenza, S. (1995) Tubulin polymerization by paclitaxel (taxol) phosphate prodrugs after metabolic activation with alkaline phosphatase. *J. Pharmacol. Exp. Ther. 274*, 877−883.

BC010093P

Conjugation of Various Acridines to DNA for Site-Selective RNA Scission by Lanthanide Ion

Akinori Kuzuya, Kenzo Machida, Ryo Mizoguchi, and Makoto Komiyama*

Research Center for Advanced Science and Technology, The University of Tokyo, 4-6-1 Komaba, Meguro, Tokyo, 153-8904 Japan. Received October 30, 2001; Revised Manuscript Received December 10, 2001

Three types of DNA conjugates having 9-acridinecarboxamide, 9-aminoacridine, and 9-amino-6-chloro-2-methoxyacridine at the 5′-ends were synthesized and used for site-selective RNA scission together with another unmodified DNA and Lu(III) ion. The target phosphodiester linkages in the substrate RNA were selectively and efficiently activated and were hydrolyzed by free Lu(III) ion. The conjugate bearing 9-amino-6-chloro-2-methoxyacridine was the most active. However, its duplex with the substrate RNA was almost as stable as that of the 9-aminoacridine-bearing conjugate, which was much less active for the RNA activation. The 9-acridinecarboxamide-bearing conjugate was only marginally active. The substituents on the acridine groups in these conjugates positively participate in the present RNA activation, probably by fixing the orientation of the acridine rings.

INTRODUCTION

To date, various conjugates of oligonucleotides with intercalating agents have been prepared mainly because of their attractive potentials for biological applications (e.g., antisense technology and antigene technology) (*1*). Acridine is one of the most popularly studied intercalating agents (*2*−*4*).

Recently, we have found a unique function of the DNA conjugates, which bear 9-amino-6-chloro-2-methoxyacridine, in RNA scission (*5*, *6*). When these conjugates form heteroduplex with RNA, specific phosphodiester linkages in the RNA are efficiently activated and thus are selectively hydrolyzed by lanthanide ions (see Figure 1). It is noteworthy that these metal ions are never covalently bound anywhere and are freely moving around in the solutions. The intercalation of the acridine (as well as the resulting conformational change of RNA) is the key for this RNA activation, although the mechanistic details have not yet been sufficiently clarified.

In this study, we have synthesized three acridine−DNA conjugates to understand the roles of the substituents on the acridine groups for the RNA activation. The DNAs in these conjugates are complementary with the 5′-side portion of the substrate RNA and have different acridine moieties (i.e., 9-acridinecarboxamide, 9-aminoacridine, and 9-amino-6-chloro-2-methoxyacridine) at the 5′-ends (**2a**−**c** in Scheme 1). For site-selective RNA scission, they are combined with another unmodified DNA **3**, which is complementary with the remaining portion of the RNA, and Lu(III) ion. The melting temperatures of the corresponding DNA/RNA heteroduplexes are presented.

EXPERIMENTAL PROCEDURES

^{1}H NMR spectra were obtained on a JEOL JNM-A500 spectrometer. MALDI- and LI-TOF mass spectra were measured on a KRATOS Kompact MALDI 2 TOF-MS spectrometer. For sonic spray ionization (SSI) mass spectroscopy, a HITACHI M-8000 LC/3DQMS mass spectrometer was used.

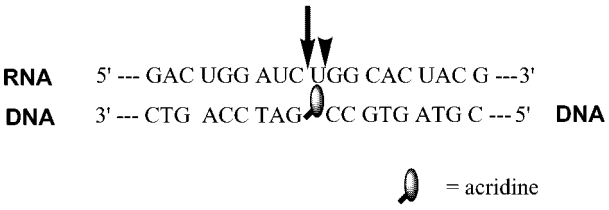
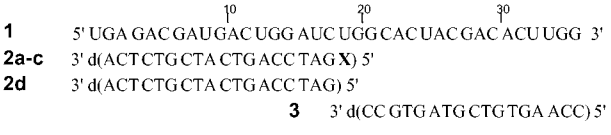
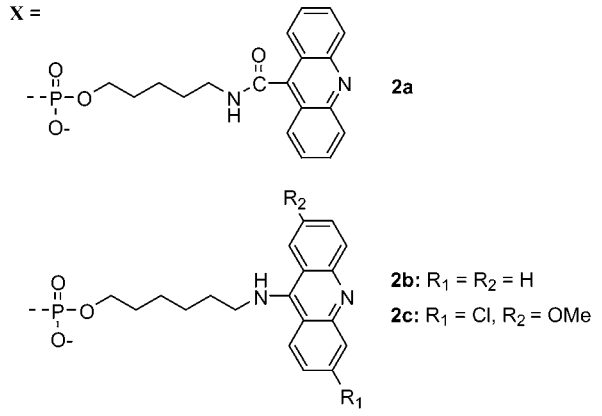


Figure 1. Schematic representation of the site-selective activation of RNA by acridine−DNA conjugates. The selective-scission sites are indicated by arrows.

Scheme 1



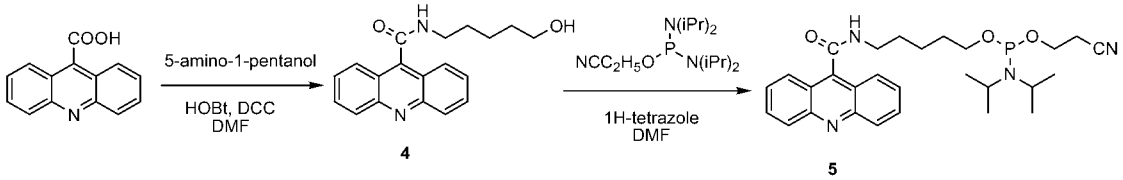


***N*-(5-Hydroxypentyl)-9-acridinecarboxamide (4).** To a solution of 9-acridinecarboxylic acid hydrate (1.0 g, 4.5 mmol), 5-amino-1-pentanol (0.49 mL, 4.5 mmol), and HOBt (0.67 g, 4.9 mmol) in DMF (25 mL) was added DCC (1.0 g, 4.9 mmol) by portions (Scheme 2). After overnight

* To whom correspondence should be addressed. Telephone: +81−3−5452−5200. Fax: +81−3−5452−5209. E-mail: komiyama@mkomi.rcast.u-tokyo.ac.jp.

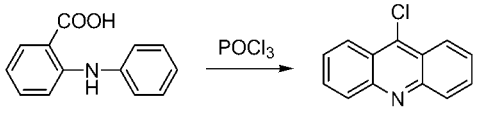
10.1021/bc015573v CCC: $22.00 © 2002 American Chemical Society
Published on Web 02/13/2002

Scheme 2



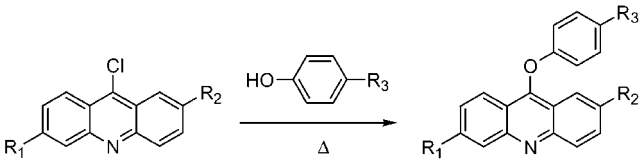
4 5

Scheme 3



6

Scheme 4



7: $R_1 = R_2 = R_3 = H$

8: $R_1 = R_3 = Cl$, $R_2 = OMe$

reaction, the solution was filtered and evaporated to dryness under reduced pressure. Washing with dilute HCl (50 mL) and ethyl acetate (50 mL) gave 0.92 g of **4** (67% yield) as white-yellow powder. TLC $R_f = 0.20$, 10:1 CH_2Cl_2/MeOH; ^{1}H NMR (DMSO-d_6) δ 9.00 (t, 1H, NH), 8.18 (d, 2H), 7.98 (d, 2H), 7.87 (t, 2H), 7.67 (t, 2H), 4.39 (t, 0.6H, OH), 3.49 (m, 0.5H), 3.44 (m, 1.5H), 3.33−3.25 (2H), 1.66 (m, 2H), 1.51−1.44 (m, 4H). MS (LI): *m*/*z* 309.1 (M + H).

Phosphoramidite Monomer 5. To a solution of **4** (0.30 g, 0.96 mmol) and 2-cyanoethyl *N*,*N*,*N*′,*N*′-tetraisopropylphosphorodiamidite (0.32 g, 1.1 mmol) in anhydrous DMF (6 mL) on ice was slowly added 1*H*-tetrazole (0.073 g, 1.1 mmol) in anhydrous DMF (6 mL) under nitrogen, and the mixture was stirred for 1 h at room temperature. After the solvent was removed, ethyl acetate (30 mL) was poured, and the organic layer was washed with saturated aqueous $NaHCO_3$ (10 mL × 2) and with brine (10 mL). This layer was dried over anhydrous Na_2SO_4 and concentrated under reduced pressure to afford 0.46 g of **5** (94% yield). This product was dissolved in anhydrous acetonitrile (0.5 M) and used for automated DNA synthesis without further purification. TLC $R_f = 0.71$, 10:1 CH_2Cl_2/MeOH. MS (SSI): *m*/*z* 509 (M + H), 531 (M + Na), 548 (M + K).

9-Phenoxyacridine (7). *N*-Phenylanthranilic acid (1.85 g, 8.7 mmol) and phosphoryl chloride (10 g, 65 mmol) were slowly heated to 90 °C (for 15 min) and then to 140 °C. After 2 h, excess phosphoryl chloride was evaporated, and chloroform (10 mL) was added to the residue. The mixture was poured into concentrated aqueous NH_3 (10 mL) containing crushed ice (25 g). When the solids disappeared, the aqueous layer was extracted twice with chloroform (20 mL), and the combined organic layer was dried over anhydrous Na_2SO_4, filtered, and evaporated to dryness. To the resultant 9-chloroacridine (**6** in Scheme 3), phenol (9.4 g) was added, and the mixture was stirred at 70 °C for 12 h (Scheme 4). Aqueous NaOH (2 N) was added dropwise to neutralize the solution, which was extracted with chloroform (50 mL × 3). The organic layer was dried with anhydrous Na_2SO_4 and concentrated under reduced pressure. The product was purified by silica gel column chromatography ($CHCl_3$) to afford 2.1 g of **7** (89% yield). TLC $R_f = 0.35$; ^{1}H NMR (DMSO-d_6) δ 8.23 (d, 2H), 8.04 (d, 2H), 7.88 (t, 2H), 7.59 (t, 2H), 7.32 (t, 2H), 7.08 (t, 1H), 6.88 (d, 2H). MS (LI): *m*/*z* 272.1 (M + H).

6-Chloro-9-(*p*-chlorophenoxy)-2-methoxyacridine (8). A mixture of 6,9-dichloro-2-methoxyacridine (1.39 g, 5.0 mmol) and *p*-chlorophenol (6.43 g, 50 mmol) was stirred at 100 °C for 12 h (Scheme 4). The solution was neutralized with aqueous NaOH (2 N). Resulting yellow precipitates were filtered, washed with large portions of water, and dried at 80 °C in vacuo (98% yield). ^{1}H NMR (DMSO-d_6) δ 8.31 (s, 1H), 8.19 (d, 1H), 8.03 (d, 1H), 7.66 (m, 2H), 7.43 (d, 2H), 7.22 (d, 2H), 7.21 (s, 1H), 7.01 (d, 2H), 6.82 (d, 2H), 3.86 (s, 3H, OMe). MS (LI): *m*/*z* 370.0 (M + H).

Preparation of Oligonucleotides. All the oligonucleotides were synthesized on an ABI 394 DNA synthesizer in 1 μmol scale. For the synthesis of **2b**, phenoxyacetyl (Pac)-protected dA, 4-isopropylphenoxyacetyl (^{i}Pr-Pac)-protected dG, and acetyl (Ac)-protected dC (from Glen Research Co.) were used. An extended coupling time of 10 min was adopted for the coupling of **5**. Unmodified DNA **2d** and **3** were synthesized with standard monomers.

Attachment of 9-Phenoxyacridine or 6-Chloro-9-(*p*-chlorophenoxy)-2-methoxyacridine to DNA. In the final coupling cycle for the synthesis of **2d**, an aminolinker C6, protected with a monomethoxytrityl (MMTr) group, was attached. The CPG column was removed from the synthesizer, and the MMTr group was taken off by passing 3% trichloroacetic acid in CH_2Cl_2 through the column with two glass syringes. The column was washed with CH_2Cl_2 (1 mL × 3) and filled with 1 M solution of **7** in DMF or **8** in THF (1 mL). After incubating the column at 60 °C for 4 h and at room-temperature overnight, it was washed with DMF (or THF: 1 mL × 3) and CH_2Cl_2 (1 mL × 3). The conjugates **2b** and **2c** were detached from the support and deprotected with 0.4 M methanolic NaOH (4:1 MeOH/H_2O) at room temperature for 16 h (*4*).

Purification and Characterization of the Acridine−DNA Conjugates. The oligonucleotides were purified by Poly-PaK II cartridges (Glen Research Co.) and then by a reversed-phase HPLC equipped with an RP−C18 column (Cica-Merck LiChroCART 125−4; a linear gradient of 5−25% acetonitrile in 50 mM ammonium formate over 20 min; flow rate 0.5 mL/min). They were characterized by mass spectroscopy in the negative ion mode (Table 1). Their base compositions were confirmed by the HPLC analyses on the digests with snake venom phosphodiesterase and alkaline phosphatase.

RNA Cleavage Assay. The substrate RNA **1** (5′-end ^{32}P-labeled with γ-^{32}P-ATP and T4 kinase, 1 μM), modified or unmodified DNA **2a**−**d** (10 μM), and another unmodified DNA **3** (10 μM) were dissolved in pH 8 Tris-HCl buffer (10 mM) containing 200 mM NaCl. The mixture was heated to 90 °C (for 1 min) and slowly cooled to room temperature. Then 1/10 volume of aqueous solution of $LuCl_3$ was added to the mixture (the final

Table 1. Mass Spectral Data and Base Compositions of 2a–c

	mass spectral data		base compositions		
	calcd (M − H)	found[a]	(A:T:G:C) theoretical value = 4:5:3:6	T_m (°C)	ΔT_m (°C)[b]
2a	5801.0	5801.2 ±0.3	4.2:5.0:3.0:6.0	66.0	2.9
2b	5787.0	5787.3 ±0.3	4.0:5.2:3.0:6.0	68.9	5.8
2c	5851.0	5851.7 ±0.3	3.9:5.2:2.8:6.0	69.1	6.0
2d				63.1	–

[a] Calibrated with two authentic DNA (calculated *m*/*z* 3642.6 and 7333.2) as internal standards. [b] The differences of T_m's from the value for the unmodified DNA **2d**.

concentration of Lu(III) was 100 μM). After 3 h at 37 °C, the reaction was quenched by 100 mM EDTA-2Na solution and analyzed on 20% denaturing PAGE. Imaging and quantification of RNA cleavage were carried out on a Fuji film FLA-3000G fluorescent imaging analyzer.

Measurement of Melting Temperature (T_m). The melting profiles of the duplexes were obtained on a JASCO V-530 spectrometer at 260 nm in a quartz cell of 1 cm path length. The specimens contained **2a**–**d** (1 μM), substrate RNA **1** (1 μM), and NaCl (200 mM) in pH 8 Tris-HCl buffer (10 mM). The heating rate was 1.0 °C/min.

RESULTS AND DISCUSSION

Syntheses of Acridine–DNA Conjugates (2a–c in Scheme 1). Three different types of DNA conjugates having an acridine at the 5′-end were synthesized in two strategies. The conjugate **2a** with 9-acridinecarboxamide was prepared using phosphoramidite chemistry, whereas 9-aminoacridine and 9-amino-6-chloro-2-methoxyacridine were directly attached to the end of DNA oligomer via an amino-linker (**2b** and **2c**).

The phosphoramidite monomer **5** bearing 9-acridinecarboxamide was synthesized as outlined in Scheme 2. 9-Acridinecarboxylic acid was condensed with 5-amino-1-pentanol, and the functionalized acridine **4** was then converted to **5** with 2-cyanoethyl *N*,*N*,*N*′,*N*′-tetraisopropylphosphorodiamidite. When this phosphoramidite monomer **5** was used for automated DNA synthesis together with the standard phosphoramidite monomers, however, the yield for the desired product **2a** was unexpectedly low. Probably the amide bond between the acridine and the linker arm was hydrolyzed under the deprotection conditions (concentrated aqueous NH_3, 55 °C, 6 h). In this study, this problem was successfully avoided by using Pac-dA, ^{i}Pr-Pac-dG, and Ac-dC, which can be deprotected under far milder conditions (room temperature, 2 h). Note that the linker length in **2a** is identical with that for other acridine–DNA conjugates **2b** and **2c**.

The HPLC chart of the purified product showed two peaks (**A** and **B** in Figure 2). The peak **A** was separated and analyzed by the HPLC. Interestingly, both the peaks **A** and **B** were observed again, and their relative intensities were the same as those in Figure 2. Similar results were obtained when the peak **B** was collected and analyzed. Furthermore, the mass spectroscopy on these two specimens gave the same molecular weights, which were in good agreement with the calculated mass of **2a** (*m*/*z* = 5801: Figure 3). Thus, we concluded that these peaks correspond to the two isomers of **2a**, which rapidly interconvert each other under ambient conditions. Probably, cis–trans isomerization of the amide bond is responsible for this isomerization.

The acridine–DNA conjugates bearing 9-aminoacridine or 9-amino-6-chloro-2-methoxyacridine (**2b** and **2c**) were prepared through 9-phenoxyacridine or 6-chloro-9-(*p*-chlorophenoxy)-2-methoxyacridine (**7** and **8**). *N*-Phenylanthranilic acid was reacted with phosphoryl chloride to afford 9-chloroacridine **6** (Scheme 3), which was converted to **7** with phenol (Scheme 4). From 6,9-dichloro-2-methoxyacridine as the starting material, **8** was synthesized in the same fashion. The DNA portion in **2b** and **2c** was prepared by using the synthesizer and an amino-linker was attached to its 5′-end. Then the CPG column was directly treated with **7** or **8**. With this simple method, the yield and purity of **2b** and **2c** were satisfactorily high. Both the observed molecular weights and the base compositions fairly agree with the calculated values (Table 1). Their structures have been concretely confirmed. The HPLC of the purified **2b** and **2c** showed a single peak (data not shown). In contrast with **2a**, these conjugates involve no amide linkages which can show cis–trans isomerization (vide ante).

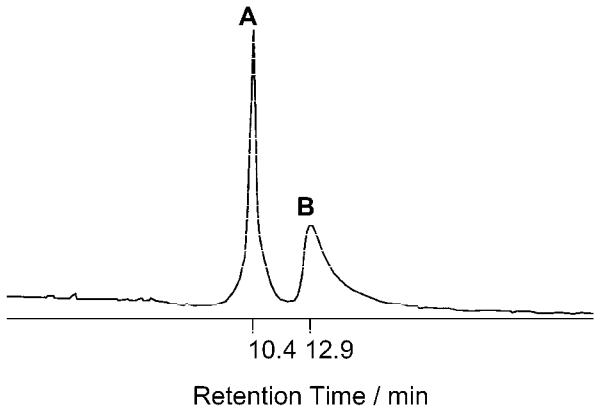


Figure 2. HPLC chart of purified **2a** monitored at λ = 260 nm.

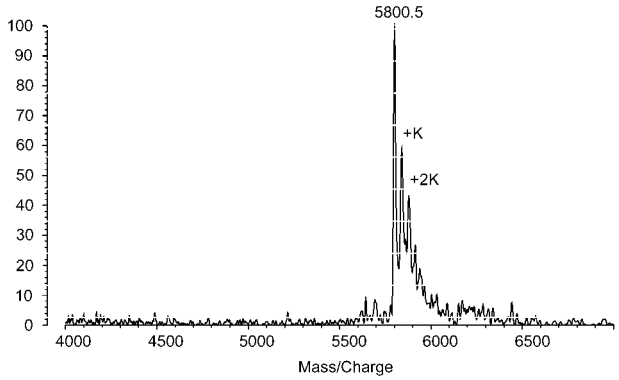


Figure 3. MALDI-TOF mass spectrum of the species for the peak A in Figure 1. Observed molecular weight of the species in the peak B was 5801.2.

Site-Selective RNA Scission Using the Acridine–DNA Conjugates. RNA cleavage assay was performed by combining **2a**–**d**, **3**, and the 36mer RNA **1** as the substrate in the presence of Lu(III) as cocatalyst (see Scheme 1). The results of PAGE analysis are presented in Figure 4. In the absence of the oligonucleotides (with only Lu(III)), RNA is cleaved randomly throughout the strand (lane 1). Lu(III) ion itself has no sequence-selectivity for RNA scission. When RNA is hybridized with the combination of the unmodified DNAs **2d** and **3**, RNA is cleaved at the 5′-sides of G-20, U-19, and C-18 (lane 2). However, the scission efficiencies are rather low. Here, all the nucleotides in the RNA, except for U-19, are forming base pairs with the DNAs.

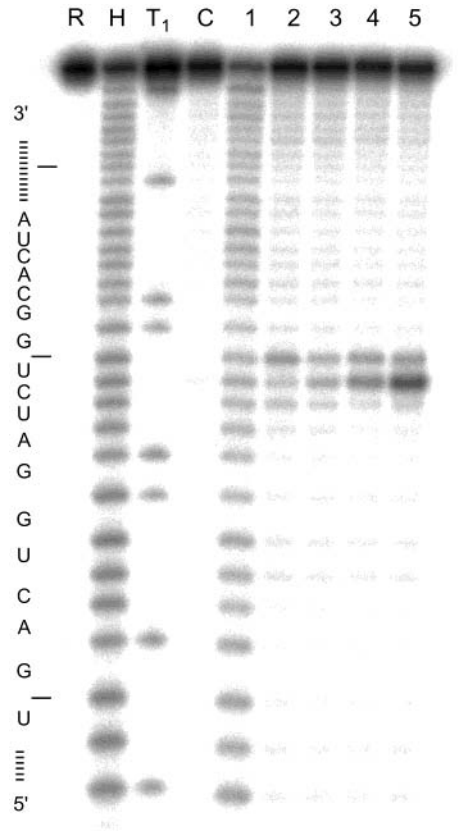


Figure 4. Site-selective scission of RNA **1** by the combinations of **2a**−**d**, **3**, and Lu(III) at 37 °C and pH 8 in 3 h. Lane 1, treatment with Lu(III) alone; lane 2, **2d** + **3** + Lu(III); lane 3, **2a** + **3** + Lu(III); lane 4, **2b** + **3** + Lu(III); lane 5, **2c** + **3** + Lu(III). In lane 1, the DNA, which has the same sequence as **1**, is added to make the phosphate concentration identical with that in lanes 2−5. R, no treatment of **1**; H, alkaline hydrolysis; T_1, RNase T_1 digestion; C, control (**1** was treated under the designated conditions, in the absence of Lu(III) and any DNA).

Quite significantly, the cleavage at U-19 is enormously accelerated when the acridine−DNA conjugate **2c** is used in place of **2d** (lane 5). Band intensity of the cleavage at U-19 in lane 5 (obtained with **2c)** is about 15 times as large as that in lane 2 (with **2d**), and 10 times as large as that of the random cleavage by Lu(III) in lane 1. The cleavage conversions for **2a**−**d** (together with **3** and Lu(III)), evaluated from Figure 4, are graphically presented in Figure 5. The target phosphodiester linkage in the RNA is greatly activated by the 9-amino-6-chloro-2-methoxyacridine in **2c** and is promptly hydrolyzed. Similarly, the 9-aminoacridine in **2b** also site-selectively activates the RNA (lane 4), although the effect is moderate. The scission rate by the **2b** + **3** + Lu(III) combination is about 40% of the value by the **2c** + **3** + Lu(III) combination. In contrast with the notable and site-specific RNA activation by these two conjugates, the DNA modified with 9-acridinecarboxamide (**2a**) scarcely activates the RNA (lane 3). The magnitude of the RNA activation is as follows: **2c** > **2b** ≫ **2d** ≈ **2a**.

When **1** is hybridized only with **2c** (in the absence of the second unmodified DNA **3**), the single-stranded portion of this RNA substrate is uniformly cleaved by Lu(III) ion (*5*). It is noteworthy that, without **3**, the scission at the target site is never accelerated by **2c**. Both **2c** and **3** are essential for the present RNA activation and its site-selective scission. In the ternary heteroduplex composed of **1**, **2c**, and **3**, the acridine is sandwiched between the neighboring two-base pairs (the CG and the GC pairs in this case). As the result, the RNA-base in front of the acridine (U-19) is partially pushed out, and the conformation of phosphate backbone is changed. The attacking 2′ OH is brought closer to the P-atom of scissile phosphate, and the intramolecular reaction is facilitated. The second DNA strand **3** is necessary for the acridine to interact efficiently with the RNA and to induce a sufficient conformational change. This argument is consistent with the finding that binding of two short DNAs to a long DNA is promoted by stacking interaction between the two base pairs which are located at the junction of these two short DNAs (*7*).

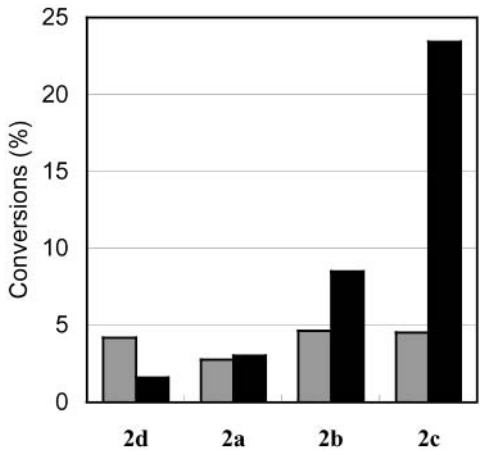


Figure 5. Conversions of the site-selective cleavages of **1** at G-20 and U-19 in 3 h. The hatched bars and the filled ones are for the cleavages at the 5′-sides of G-20 and U-19, respectively.

Thermodynamic Properties. To evaluate the strength of the interaction between the acridine and the RNA, T_m values of heteroduplexes of **1** with **2a**−**d** were measured (Table 1). All the acridines in the conjugates stabilize the duplex. The stabilizing effects of the 9-amino-6-chloro-2-methoxyacridine in **2c** and the 9-aminoacridine in **2b** are similar to each other ($\Delta T_m \approx 6$ °C). The 9-acridinecarboxamide in **2a** induces a smaller effect ($\Delta T_m = 2.9$ °C). In the reaction mixtures (pH 8), the major species of the 9-aminoacridine in **2b** and the 9-amino-6-chloro-2-methoxyacridine in **2c** are the corresponding cations (the pK_a value for 9-aminoacridine is 9.6 and that for 9-amino-6-chloro-2-methoxyacridine is 8.5 (*8*)). On the other hand, the 9-acridinecarboxamide in **2a** exists mostly as neutral species (the pK_a of methyl 9-acridinecarboxylate is 3.2 (*8*)). Relatively large duplex-stabilizing effects of the acridines in **2b** and **2c** are ascribed to their positive charges. Although the duplex-stabilizing effects of these acridines are similar, their RNA-activating capacities are significantly different from each other. Notable roles of both 6-chloro and 2-methoxy groups in **2c** are indicated. These bulky substituents orient the acridine on the intercalation, and probably this promotes the RNA activation. The positive charge on the acridine ring further assists this process. Interestingly, the order of the RNA activation (**2c** > **2b** ≫ **2d** ≈ **2a**) is the same as the order of antibacterial activities of these substituted acridines against some organisms (*8*). Importance of the acridine−RNA interaction for the present RNA activation is further supported.

In most of previously reported ribozyme-mimics, inorganic (*9*−*14*) or organic (*15*−*19*) catalysts were bound to oligonucleotides which are complementary with substrate RNA and localized near the target site. On the other hand, the present strategy utilizes site-selective RNA activation by noncovalent interactions with acridine−

DNA conjugates and has many advantages over these mimics. First, the fixation of catalysts to DNA oligomers, which often diminishes the catalytic abilities, is unnecessary. Second, various catalysts are easily applicable, since the systems are very simple.

ACKNOWLEDGMENT

This work was supported by Bio-oriented Technology Research Advancement Institution. The support by a Grant-in-Aid for Scientific Research from the Ministry of Education, Science, Sport, and Culture, Japan is also acknowledged.

LITERATURE CITED

(1) Asseline, U., Thuong, N. T., and Hélène, C. (1997) Synthesis and properties of oligonucleotides covalently linked to intercalating agents. *New J. Chem. 21*, 5−17.

(2) François, J. C., and Hélène, C. (1999) Recognition of hairpin-containing single-stranded DNA by oligonucleotides containing internal acridine derivatives. *Bioconjugate Chem. 10*, 439−446.

(3) Fukui, K., and Tanaka, K. (1996) The acridine ring selectively intercalated into a DNA helix at various types of abasic sites: double strand formation and photophysical properties. *Nucleic Acids Res. 24*, 3962−3967.

(4) Nelson, P. S., Kent, M., and Muthini, S. (1992) Oligonucleotide labeling methods 3. Direct labeling of oligonucleotides employing a novel, nonnucleosidic, 2-aminobutyl-1,3-propandiol backbone. *Nucleic Acids Res. 20*, 6253−6259.

(5) Kuzuya, A., and Komiyama, M. (2000) Noncovalent ternary systems (DNA-acridine hybrid/DNA/lanthanide(III)) for efficient and site-selective RNA scission. *Chem. Commun.* 2019−2020.

(6) Kuzuya, A., and Komiyama, M. (2000) Sequence-selective RNA scission by noncovalent combinations of acridine-tethered DNA and lanthanide(III) ion. *Chem. Lett.* 1378−1379.

(7) Koval, V. V., Lokteva, N. A., Karnaukhova, S. L., and Fedorova, O. S. (1999) Cooperative binding of oligonucleotides to adjacent sites of single-stranded DNA: sequence composition dependence at the junction. *J. Biomol. Struct. Dyn. 17*, 259−265.

(8) Albert, A. (1966) The connexion between antibacterial action and physicochemical properties in the acridine series. *The acridines*, 2nd ed., pp 434−467, Edward Arnold (Publishers) Ltd., London.

(9) Matsumura, K., Endo, M., and Komiyama, M. (1994) Lanthanide complex-oligo-DNA hybrid for sequence-selective hydrolysis of RNA. *J. Chem. Soc., Chem. Commun.* 2019−2020.

(10) Hall, J., Hüsken, D., and Häner, R. (1996) Towards artificial ribonucleases: the sequence-specific cleavage of RNA in a duplex. *Nucleic Acids Res. 24*, 3522−3526.

(11) Magda, D., Wright, M., Crofts, S., Lin, A., and Sessler, J. L. (1997) Metal complex conjugates of antisense DNA which display ribozyme-like activity. *J. Am. Chem. Soc. 119*, 6947−6948.

(12) Matsuda, S., Ishikubo, A., Kuzuya, A., Yashiro, M., and Komiyama, M. (1998) Conjugates of a dinuclear zinc(II) complex and DNA oligomers as novel sequence-selective artificial ribonucleases. *Angew. Chem., Int. Ed. 37*, 3284−3286.

(13) Inoue, H., Furukawa, T., Shimizu, M., Tamura, T., Matsui, M., and Ohtsuka, E. (1999) Efficient site-specific cleavage of RNA using a terpyridine-copper(II) complex joined to a 2′-*O*-methyloligonucleotide by a nonflexible linker. *Chem. Commun.*, 45−46.

(14) Putnam, W. C., Daniher, A. T., Trawick, B. N., and Bashkin, J. K. (2001) Efficient new ribozyme mimics: direct mapping of molecular design principles from small molecules to macromolecular, biomimetic catalysts. *Nucleic Acids Res. 29*, 2199−2204.

(15) Komiyama, M., Inokawa, T., and Yoshinari, K. (1995) Ethylenediamine-oligo DNA hybrid as sequence-selective artificial ribonuclease. *J. Chem. Soc., Chem. Commun.* 77−78.

(16) Hovinen, J., Guzaev, A., Azhayeva, E., Azhayev, A., and Lönnberg, H. (1995) Imidazole tethered oligodeoxyribonucleotides: synthesis and RNA cleaving activity. *J. Org. Chem. 60*, 2205−2209.

(17) Reynolds, M. A., Beck, T. A., Say, P. B., Schwartz, D. A., Dwyer, B. P., Daily, W. J., Vaghefi, M. M., Metzler, M. D., Klem, R. E., and Arnold, L. J., Jr. (1996) Antisense oligonucleotides containing an internal, nonnucleotide-based linker promote site-specific cleavage of RNA. *Nucleic Acids Res. 24*, 760−765.

(18) Endo, M., Azuma, Y., Saga, Y., Kuzuya, A., Kawai, G., and Komiyama, M. (1997) Molecular design for a pinpoint RNA scission. Interposition of oligoamines between two DNA oligomers. *J. Org. Chem. 62*, 846−852.

(19) Beloglazova, N. G., Sil′nikov, V. N., Zenkova, M. A., and Vlassov, V. V. (2000) Cleavage of yeast $tRNA^{Phe}$ with complementary oligonucleotide conjugated to a small ribonuclease mimic. *FEBS Lett. 481*, 277−280.

BC015573V

Effects of Coligand Variation on the In Vivo Characteristics of Tc-99m-Labeled Interleukin-8 in Detection of Infection

Huub J. J. M. Rennen,* Julliëtte E. van Eerd, Wim J. G. Oyen, Frans H. M. Corstens, D. Scott Edwards,† and Otto C. Boerman

Department of Nuclear Medicine, University Medical Center Nijmegen, Nijmegen, The Netherlands. Received November 22, 2001

In our previous studies, interleukin-8 (IL-8) was labeled with ^{99m}Tc using hydrazinonicotinamide (HYNIC) as bifunctional coupling agent and tricine as coligand. This preparation showed excellent characteristics for imaging of infection in a rabbit model of soft-tissue infection. In the present study, the propylaldehyde hydrazone formulation of HYNIC was introduced to stabilize HYNIC−IL-8. ^{99m}Tc−HYNIC−IL-8 was prepared using 5 different coligand formulations. The effect of these coligand formulations on the in vitro characteristics and in vivo behavior of ^{99m}Tc−HYNIC−IL-8 was investigated. HYNIC-conjugated IL-8 was labeled with ^{99m}Tc in the presence of either (A) tricine, (B) ethylenediaminediacetic acid (EDDA), (C) tricine and trisodium triphenylphosphinetrisulfonate (TPPTS), (D) tricine and nicotinic acid (NIC), or (E) tricine and isonicotinic acid (ISONIC). These preparations were characterized in vitro by RP-HPLC, determination of the octanol/water partition coefficient, stability studies, and receptor binding assays. The in vivo biodistribution of the radiolabel in rabbits with *E. coli*-induced soft-tissue infection was determined both by γ-camera imaging as well as by tissue counting at 6 h pi. Specific activity (MBq/μg) was highest for (ISO)NIC (up to 80) > TPPTS (40) > tricine (15) > EDDA (7). RP-HPLC and octanol/water partition coefficients showed a shift toward higher lipophilicity for the TPPTS preparation. The leukocyte receptor binding fractions were around 40−55% for all preparations except for TPPTS, which showed predominantly nonspecific binding. All preparations were stabilized in serum, but the stability in PBS was highest for NIC and TPPTS > EDDA > ISONIC > tricine. The in vivo biodistribution showed highest abscess/muscle for NIC and ISONIC (>200) > EDDA and tricine (∼100) > TPPTS (<40). Gamma camera imaging rapidly visualized the abscess from 2 h pi onward for all formulations. The abscess/background (A/B) at 6 h pi for ISONIC was significantly higher ($P < 0.05$) than that of tricine and the A/B of TPPTS was significantly lower ($P < 0.05$). IL-8 can be rapidly and easily labeled with ^{99m}Tc using HYNIC as a chelator in combination with various coligands. The most optimal infection imaging characteristics were found for formulations using nicotinic acid/tricine as coligand system combining a high specific activity and high in vitro stability with high abscess/muscle ratios (>200) and high abscess/background ratios (>20). Protein doses to be administered were as low as 70 ng/kg bodyweight. At these low protein doses, side effects are not to be expected in the human system. This paves the way for infection imaging studies in patients.

INTRODUCTION

Scintigraphic imaging of infectious and noninfectious inflammation is a powerful diagnostic tool in the management of patients with inflammatory disorders. Most inflammatory foci can be visualized accurately with ex vivo radiolabeled autologous leukocytes. However, preparation of this radiopharmaceutical is laborious and requires the handling of potentially contaminated blood with inherent risks for both personnel and patients.

There is an ongoing search for radiolabeling small molecules that bind to circulating leukocytes (in vivo labeling of leukocytes) after the relatively poor results obtained with large size monoclonal antibodies directed against leukocytes. These small molecules include chemotactic peptides (analogues of formyl-Met-Leu-Phe) and cytokines (e.g., the interleukins, platelet factor 4 derivatives) (for a review, see ref 1). We have actively pursued a research program to explore the potential of radiolabeled formyl-Met-Leu-Phe-Lys, interleukin-1, interleukin-8, and other cytokines for imaging inflammation.

Radiolabeled interleukin-8 (IL-8) proved to be the most promising candidate so far. IL-8 is a member of the CXC subfamily of chemokines, or chemotactic cytokines, in which the first two cysteine residues are separated by one amino acid residue. This cytokine binds the CXC type I (= IL-8 type A) and CXC type II (= IL-8 type B) receptors expressed on neutrophils and monocytes with high affinity (0.3−4 nM) (*2*, *3*). Hay and colleagues (*4*) studied the in vivo behavior of radioiodinated IL-8 in a rat model with carrageenan-induced sterile inflammations and found only modest target-to-background ratios of 2.5. In a pilot study in eight patients these investigators showed that a ^{123}I−IL-8 could visualize inflammatory foci (*5*).

We investigated the in vivo behavior of radiolabeled IL-8 in various models of infection and sterile inflammation in rabbits (*6*−*10*). Studies with ^{123}I-labeled IL-8

* Correspondence and reprint requests to Huub J. J. M. Rennen, Department of Nuclear Medicine, University Medical Center Nijmegen, P.O. Box 9101, 6500 HB Nijmegen, The Netherlands. Phone: +31-24-3615054. Fax: +31-24-3618942. e-mail: H.Rennen@nugen.azn.nl.

† DuPont Pharmaceuticals Company, North Billerica, MA.

10.1021/bc015579k CCC: $22.00 © 2002 American Chemical Society
Published on Web 02/21/2002

in rabbits with focal *E. coli* infection showed rapid accumulation of the radiopharmaceutical in the abscess (*6*, *7*). Abscess-to-contralateral muscle ratios exceeded 100 in this model within 8 h postinjection. A drawback of this preparation was its relatively low specific activity; the imaging dose of ^{123}I−IL-8 (25 μg/kg) caused a transient drop of peripheral leukocyte counts to 45%, followed by a leukocytosis (170% of preinjection level) during several hours. Moreover, ^{123}I is not a very suitable radionuclide for clinical imaging: it is expensive and the Bolton−Hunter labeling method used for preparing ^{123}I-labeled IL-8 is rather laborious.

For clinical application, a simple and rapid labeling procedure of IL-8, using the radionuclide ^{99m}Tc, is preferable. ^{99m}Tc combines highly favorable physical characteristics ($t_{1/2}$ = 6 h, E_{max} = 140 keV) with easy availability and low cost. In a subsequent study, IL-8 was labeled with ^{99m}Tc using hydrazinonicotinamide (HYNIC) as bifunctional coupling agent (*8*). HYNIC has been introduced by Abrams and co-workers (*11*) for labeling polyclonal IgG with ^{99m}Tc to image infections. Since the HYNIC group can only occupy one or two coordination sites in the technetium coordination sphere, an additional coligand is required. For labeling HYNIC conjugated IL-8 with ^{99m}Tc tricine was chosen as coligand, because specific activities obtained with this coligand are much higher than with, for example, glucoheptonate (*12*). The specific activity of the ^{99m}Tc-labeled IL-8 preparation was found to be 25× higher than the specific activity of the ^{123}I-labeled IL-8 preparation. In rabbits with *E. coli*-induced softtissue infection abscess to contralateral muscle ratios and abscess-to-blood ratios obtained with the ^{99m}Tc- and the ^{123}I-labeled preparation were similar. Preparing ^{99m}Tc-labeled IL-8 is easy and fast, offering a major advantage over the radioiodination procedure.

The aim of the present study was to improve the characteristics for imaging infection of a ^{99m}Tc-labeled IL-8 preparation together with a further increase in specific activity of the preparation, thus reducing the required IL-8 protein dose. Two aspects of the labeling procedure were further optimized.

First, a modified form of HYNIC was synthesized. To improve long-term stability Schwartz and co-workers introduced the use of a propylaldehyde hydrazone formulation to stabilize HYNIC-modified proteins (*13*, *14*). This protection of the hydrazine moiety of HYNIC ensures greater stability in aqueous solutions, and the hydrazone retains the capacity to produce enough free hydrazine for successful labeling with ^{99m}Tc.

Second, different coligand formulations were adopted in labeling HYNIC conjugated IL-8 with ^{99m}Tc. Babich and Fischman (*15*) were the first to show that the nature of the coligand has a distinctive influence on the biologic properties of the radioconjugate. Liu and Edwards et al. have performed systematic studies on labeling a HYNIC-conjugated platelet glycoprotein receptor antagonist with ^{99m}Tc using various coligand formulations: tricine; ethylenediaminediacetic acid (EDDA) (*16*); tricine in combination with water soluble phosphines (*17*); tricine in combination with imine-N-containing heterocycles (*18*).

In the present study HYNIC conjugated IL-8 was labeled with ^{99m}Tc using five different coligand systems: (i) tricine; (ii) EDDA; (iii) tricine in combination with trisodium triphenylphosphine-3,3′,3″-trisulfonate (TPPTS); (iv) tricine in combination with nicotinic acid; and (v) tricine in combination with isonicotinic acid (see Figure 1). The proposed structures (*16*−*18*) of the resulting binary technetium complexes [^{99m}Tc(IL-8−HYNIC)(tricine)$_2$] and [^{99m}Tc(IL-8−HYNIC)(EDDA)] and ternary

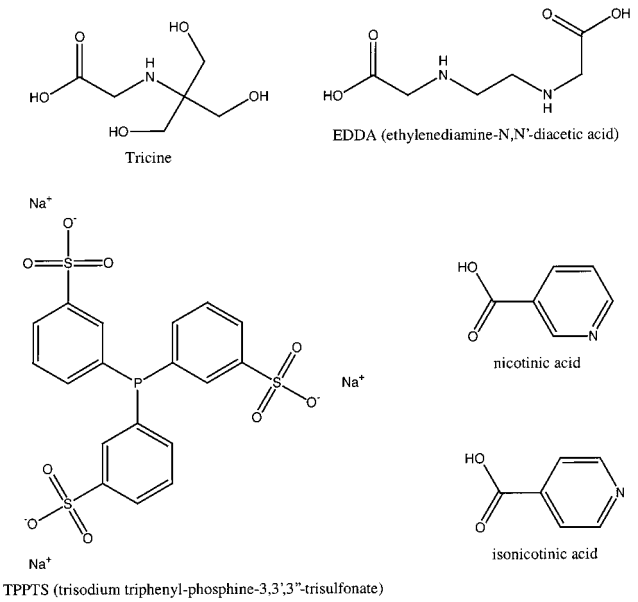


Figure 1. Structures of coligands used in this study.

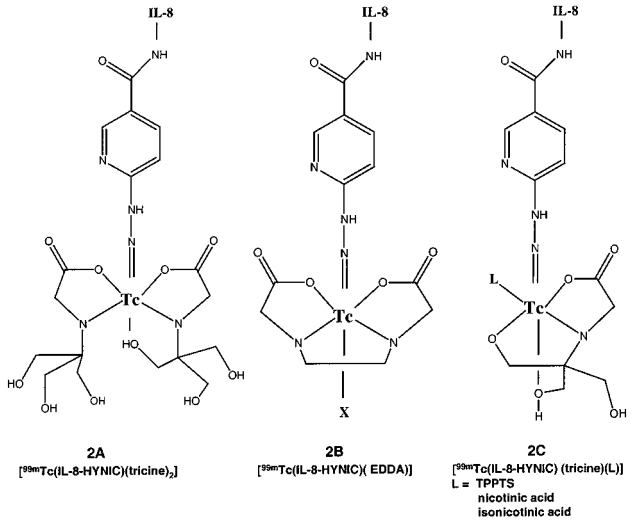


Figure 2. Binary technetium complexes (A) [^{99m}Tc(IL-8−HYNIC)(tricine)$_2$] and (B) [^{99m}Tc(IL-8−HYNIC)(EDDA)]. The exact nature of the bonding between the IL-8−HYNIC−^{99m}Tc core and EDDA is unclear. X is a supposed additional monodentate ligand, such as Cl^- (*16*). Ternary technetium complexes [^{99m}Tc(IL-8−HYNIC)(tricine)(L)] (L = TPPTS or nicotinic acid or isonicotinic acid) [Figure 2C].

technetium complexes [^{99m}Tc(IL-8−HYNIC)(tricine)(L)] (L = TPPTS or nicotinic acid or isonicotinic acid) are depicted in Figure 2. The effect of the coligand on the in vivo behavior of ^{99m}Tc-labeled IL-8 was investigated in a rabbit model of *E. coli*-induced soft tissue infection.

MATERIALS AND METHODS

Human recombinant IL-8 was kindly provided by Dr I. Lindley (Novartis, Vienna, Austria). Tricine (*N*-[tris-(hydroxymethyl)methyl]glycine) was purchased from Fluka, Buchs, Switzerland. EDDA (ethylenediaminediacetic acid), TPPTS (trisodium triphenylphosphine-3,3′,3″-trisulfonate), nicotinic acid, and isonicotinic acid were obtained from Sigma-Aldrich (St. Louis, MO).

Conjugation of HYNIC to IL-8. The propylaldehyde hydrazone of succinimidyl-hydrazinonicotinamide (HYNIC) was synthesized essentially as described by Abrams, Schwartz et al. (*11*, *13*). The IL-8−HYNIC conjugate was

prepared as described previously (*8*). Briefly, in a 1.5 mL vial, 4 μL of 1 M $NaHCO_3$, pH 8.2, was added to 35 μL of IL-8 (4.8 mg/mL). Subsequently, a 3-fold molar excess of HYNIC in 5 μL of dry DMSO was added dropwise to the mixture. After incubation for 5 min at room temperature, the reaction was stopped by adding an excess of 200 μL of 1 M glycine in phoshate-buffered saline (PBS). To remove excess unbound HYNIC, the mixture was extensively dialyzed against PBS (0.1−0.5 mL dialysis cell 3.5 MWCO, Pierce, Rockford, IL). Dialyzed samples of ca. 5 μg IL-8−HYNIC were stored at −20 °C.

Technetium-99m Labeling of HYNIC Conjugated IL-8. *(i) Tricine as Coligand.* Tricine−$SnSO_4$ kits (0.2 mL) were prepared containing 20 mg of tricine and 0.01 mg of $SnSO_4$ in 0.2 mL of PBS, pH 7.0. To prevent precipitation of tin colloid, $SnSO_4$ dissolved in 2 M HCl was added to a solution of tricine in PBS, and the pH was adjusted to 7.0 with 1.0 M NaOH. A 0.2 mL tricine−$SnSO_4$ kit and 100−350 MBq $^{99m}TcO_4^-$ in saline were added to 5 μg of thawed HYNIC−IL-8 and incubated at room temperature for 30 min.

(ii) EDDA as Coligand. A 10 μg amount of thawed HYNIC−IL-8 was incubated with 0.5 mL of solution of EDDA (10 mg/mL in PBS), 100−350 MBq $^{99m}TcO_4^-$ in saline, and 10 μL of tin(II) solution (1.0 mg/mL $SnSO_4$ in nitrogen-purged 0.1 N HCl) for 30 min at 70 °C.

(iii) TPPTS/Tricine as Coligands. A 5 μg amount of thawed HYNIC−IL-8 was incubated with 0.1 mL of solution of TPPTS (10 mg/mL in 25 mM benzoate buffer, pH 5.0), 0.3 mL of a tricine solution (100 mg/mL in 25 mM benzoate buffer, pH 5.0), 100−350 MBq $^{99m}TcO_4^-$ in saline, and 25 μL of tin(II) solution (1.0 mg/mL $SnSO_4$ in nitrogen-purged 0.1 N HCl) for 30 min at 70 °C.

(iv) Nicotinic Acid/Tricine as Coligands. A 5 μg amount of thawed HYNIC−IL-8 was incubated with 0.1 mL of solution of nicotinic acid (20 mg/mL in 25 mM benzoate buffer, pH 5.0), 0.4 mL of a tricine solution (100 mg/mL in 25 mM benzoate buffer, pH 5.0), 100−350 MBq $^{99m}TcO_4^-$ in saline, and 25 μL of tin(II)solution (1.0 mg/mL $SnSO_4$ in nitrogen purged 0.1 N HCl) for 30 min at 70 °C.

(v) Isonicotinic Acid/Tricine as Coligands. The labeling procedure was identical to the one above, using isonicotinic acid instead of nicotinic acid.

Chemical Characterization of ^{99m}Tc-Labeled IL-8 Preparations. *(i) Radiochemical Purity by ITLC.* The radiochemical purity was determined by instant thin-layer chromatography (ITLC) on ITLC−SG strips (Gelman Laboratories, Ann Arbor, MI) with 0.1 M citrate, pH 6.0, as the mobile phase.

(ii) Purification. Following the labeling reaction the reaction mixture was applied to a Sephadex G-25 column (PD-10; Pharmacia, Uppsala, Sweden) and eluted with PBS, 0.5% BSA, to purify the radiolabeled IL-8 conjugate.

(iii) Octanol/Water Partition Coefficient as a Measure of Lipophilicity. To determine the lipophilicity of the various ^{99m}Tc−HYNIC−IL-8 preparations, approximately 100 000 cpm of a purified preparation was diluted with PBS to a total volume of 3 mL. An equal volume of octanol was added, and the resulting biphasic system was mixed vigorously for 1 min and gently for another 10 min. The two phases were separated by centrifugation (10 min, 2000*g*), and 0.2 mL aliquots were taken from each layer. The partition coefficient was expressed as the ratio of cpm in the octanol phase to the cpm in the PBS phase.

(iv) Stability in PBS and in Serum. Following the labeling reactions, the five ^{99m}Tc-labeled IL-8 preparations were purified on a Sephadex G-25 column eluted with PBS without BSA. The stability of the purified preparations was monitored in PBS at room temperature and in human serum (1:5) at 37 °C for 6 h. At several time points postincubation (0, 2, 4, and 6 h), samples were analyzed for the amount of free radiolabel using ITLC. Samples of the serum incubated preparations were diluted 1:5 in PBS with 0.5% BSA before applying to the ITLC-strip in order to prevent protein overload of the strips by serum proteins.

(v) Analytical RP-HPLC. The radiochemical purity was determined by reversed phase high-performance liquid chromatography (RP-HPLC) (HP 1100 series, Hewlett-Packard, Palo Alto, CA) using an Agilent Zorbax Stable Bond Analytical 4.6 × 250 mm column (300SB−C8) at a flow rate of 1 mL/min. The radioactivity of the eluate was monitored using an in-line radiodetector (Flo-one Beta series A-100, Radiomatic, Meriden, CT).

Method 1. Solvents used: (A) 0.01% TFA in water; (B) 90% acetonitrile (ACN), 10% solution A. Gradient: from 70% A and 30% B to 45% A and 55% B in 30 min.

Method 2. Solvents used: (A) 10 mM phosphate buffer pH 6.0; (B) 100% ACN. Gradient: 0−3 min 0% B, 3−18 min 0%−30% B, 18−23 min 30% B, 23−33 min 30%−75% B, 33−34 min 70%−0% B.

Receptor Binding Assays. The receptor binding fraction (RBF) of the various ^{99m}Tc−HYNIC−IL-8 preparations was determined in receptor binding assays essentially as described by Lindmo et al. (*19*). The in vitro receptor binding assays were performed using Jurkat cells transfected with either IL-8 receptor 1 (CXCR1) or IL-8 receptor 2 (CXCR2), a kind gift of Drs. Loetscher and Baggiolini (Theodor Kocher Institute, University of Bern, Bern, Switzerland). The two cell lines were cultured at 37 °C in a humidified atmosphere of air/CO_2 (95:5) in RPMI 1640 medium (GIBCO, Gaithersburg, MD) containing 10% fetal calf serum and 1% glutamine, amino acids, and pyruvate. The medium also contained Pen/Strep, 5 × 10^{-5} M of β-mercaptoethanol, and 1.5 μg/mL puromycin for selection. Live Jurkat cells were centrifuged (5 min, 2000 g) and washed once with assay buffer (RPMI 1640, 0.5% BSA, 0.05% NaN_3). A series of serially diluted cell suspensions (0.125−2 × 10^8 cells/ml) of cells bearing CXCR1 and a second series bearing CXCR2 were incubated with 10000 cpm of a ^{99m}Tc-labeled IL-8 preparation in assay buffer. For each series, a duplicate of the lowest cell concentration was incubated in the presence of at least a 100-fold molar excess of unlabeled IL-8 to correct for nonspecific binding. After 30 min incubation at 37 °C, cells were centrifuged (5 min, 2000 g), and the radioactivity in the pellet (total bound radioactivity) was measured in a shielded well-type gamma counter (Wizard; Pharmacia, Uppsala, Sweden). The data were graphically analyzed in a modified Lineweaver−Burk plot: a double inverse plot of the conventional binding plot (specifically bound fraction versus cell concentration). The receptor-binding fraction at infinite cell excess was calculated by linear extrapolation to the ordinate.

Animal Studies. Abscesses were induced in the left thigh muscle of 25 female New Zealand rabbits (2.4−2.7 kg) with (1−2) × 10^{11} colony forming units (cfu) of *Escherichia coli* in 0.5 mL. During the procedure, rabbits were anaesthetized with a subcutaneous injection of a 0.6 mL mixture of fentanyl 0.315 mg/mL and fluanisone 10 mg/mL (Hypnorm, Janssens Pharmaceutical, Buckinghamshire, UK). The rabbits were divided into five groups of five animals (five animals per ^{99m}Tc−HYNIC−IL-8 coligand formulation). After 24 h, when swelling of the muscle was apparent, the rabbits were injected with 10−40 MBq ^{99m}Tc−HYNIC−IL-8 (protein dose 0.2−2 μg) via the ear vein. Three rabbits out of each group were

Table 1. In Vitro Characteristics of Five Different ^{99m}Tc-Labeled IL-8 Coligand Preparations[a]

coligand system	specific activity, MBq/μg	octanol/water partition	RBF: CXCR1, %	RBF: CXCR2, %	stability: PBS, %	stability: serum, %
tricine	15	0.017	50−55	40−45	15−20	>90
EDDA	7	0.0053	45−50	36−42	55−65	>90
TPPTS/tricine	40	0.033	n.s.[b]	n.s.	>90	>90
nicotinic acid/tricine	80	0.0046	46−50	42−45	>90	>90
isonicotinic acid/tricine	80	0.0049	50−54	40−45	40−45	>90

[a] Specific activities (MBq/μg), octanol/water partition coefficients, receptor binding fractions (RBF) (%) to Jurkat cells transfected with either IL-8 receptor 1 (CXCR1) or IL-8 receptor 2 (CXCR2) and stabilities in PBS and in serum (labeling efficiencies after 6 h of incubation). [b] n.s. = predominantly nonspecific cell binding.

used for gamma camera imaging. These rabbits were immobilized, placed prone on the gamma camera and images were recorded at 0, 2, 4, and 6 h pi with a single-head gamma camera (Orbiter, Siemens Medical Systems Inc., Hoffman Estates, IL) equipped with a parallel-hole low-energy all purpose collimator. Images were obtained with a 15% symmetrical window over the 140 keV energy peak of ^{99m}Tc. After acquisition of 100000−300000 counts, the images were digitally stored in a 256 × 256 matrix.

Scintigraphic images were analyzed quantitatively by drawing regions of interest (ROI) over the abscess and the uninfected contralateral thigh muscle (background). Abscess-to-background ratios were calculated.

After completion of the final imaging (6 h pi), all rabbits were killed with a lethal dose of sodium phenobarbital. Samples of blood, infected thigh muscle, uninfected contralateral thigh muscle, lung, spleen, liver, kidneys, and intestines were collected. The dissected tissues were weighed and counted in a gamma counter. To correct for radioactive decay, injection standards were counted simultaneously. The measured activity in samples was expressed as a percentage of injected dose per gram tissue (%ID/g). Additionally, total uptake of the radiopharmaceutical (%ID) was determined for kidneys and abscesses. Abscess-to-contralateral muscle ratios and abscess-to-blood ratios were calculated.

Statistical Analysis. All mean values are given as %ID/g, %ID or ratios ± 1 standard error of the mean (sem). The data were analyzed statistically using the one-way ANOVA with Dunnett's posttest (GraphPad Instat 3.00 Win 95, San Diego, CA) comparing data for the EDDA, the TPPTS, the nicotinic, and the isonicotinic preparation with data for the tricine preparation.

RESULTS

Radiolabeling and Characterization of ^{99m}Tc-Labeled IL-8 Preparations. Table 1 shows the specific activities (MBq/μg), the octanol/water partition coefficients, the receptor binding fractions RBF for CXCR1 and CXCR2 receptors, and the stability of the preparations in PBS and in serum. The five preparations will be denoted here by their main discriminating component: tricine, EDDA, TPPTS, nicotinic acid, and isonicotinic acid.

Radiolabeling of each of the five HYNIC−IL-8 coligand formulations was rapid and straightforward, resulting in high specific activities of four out of five formulations. With EDDA only a modest specific activity could be obtained (7 MBq/μg) as compared to tricine (15 MBq/μg), TPPTS (40 MBq/μg), and nicotinic acid and isonicotinic acid (up to 80 MBq/μg). In our experience, the protection of the hydrazine moiety with propylaldehyde resulted in a HYNIC-conjugated IL-8 product with increased stability (at −20 °C): it could be labeled with high labeling efficiency over longer time periods (several months). Using the same tricine coligand formulation, the specific activity of ^{99m}Tc-labeled hydrazine protected HYNIC−IL-8 was found to be 15 MBq/μg as compared to 3 MBq/μg for ^{99m}Tc-labeled free hydrazine HYNIC−IL-8 previously reported (*8*). Both products started at similar labeling efficiencies but the free hydrazine HYNIC−IL-8 product showed a gradual decrease in labeling efficiency over 3 months even when stored at −20 °C.

The lipophilicity as reflected in the octanol/water partition coefficient was highest for the TPPTS preparation. This is in line with the HPLC analyses (Figure 3) and a significantly higher liver uptake of the TPPTS preparation as found in the biodistribution (Table 2) (see below).

All the formulations with the exception of TPPTS showed similar RBF values for both receptors: between 45% and 55% for CXCR1 and between 36% and 45% for CXCR2. The TPPTS preparation showed predominantly nonspecific binding to the cells.

All radiolabeled IL-8 preparations were stable in human serum: after 6 h of incubation at 37 °C the amount of free radiolabel was less than 10% as determined by ITLC. However, the same preparations diluted in PBS showed a large variation in stability: after 6 h of incubation at room temperature the amount of free radiolabel was less than 10% for TPPTS and nicotinic acid only. For EDDA between 35 and 45% of the radiolabel was released, for isonicotinic acid between 55 and 60% and for tricine around 80%.

The radio-HPLC chromatograms (method 1) of tricine and of TPPTS are presented in Figure 3A and 3B. The tricine chromatogram shows a pertechnetate peak with retention time of 3.5 min (<1.5%) and a doublet peak of [^{99m}Tc(IL-8−HYNIC)(tricine)$_2$] with retention times of 10.3 and 10.9 min. The radiochromatograms of the EDDA, nicotinic acid, and isonicotinic acid preparations showed essentially the same profile. Retention times of the doublet peak were found at 10.3 and 10.9 min for EDDA, at 10.3 and 11.0 min for nicotinic, and at 10.4 and 11.1 min for isonicotic. The radiochromatogram of TPPTS turned out to be completely different: the major peak eluted much later (16.3 min) indicating the higher lipophilicity of the preparation. It might be the case that TPPTS interacts with the protein outside the protein−HYNIC-core. For instance, triarylphosphines such as TPPTS can reduce disulfide linkages, whereas maintenance of the disulfide structure is critical for IL-8 activity. The possibility of interaction of TPPTS with IL-8 outside the protein−HYNIC-core was investigated in an additional experiment. The radiochromatograms of a iodinated IL-8 preparation and the same preparation incubated at 70 °C for 30 min in the presence of an excess of TPPTS were compared (not shown). The ^{125}I-IL-8 radiochromatogram showed a profile similar to that of [^{99m}Tc-(IL-8−HYNIC)(tricine)$_2$] with a doublet at 11.2 and 11.9 min. The radiochromatogram of ^{125}I-IL-8 incubated with TPPTS was similar, indicating that (chemical) interaction

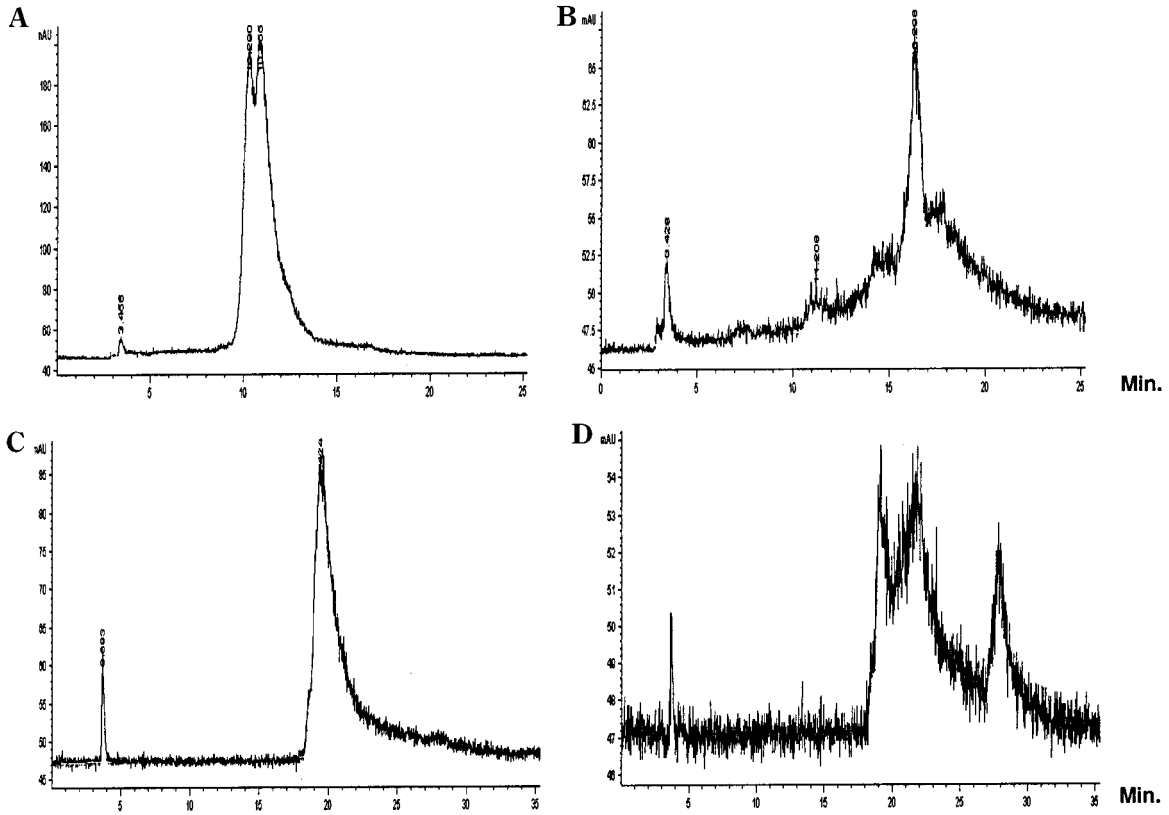


Figure 3. Radio-HPLC chromatograms of ^{99m}Tc-labeled IL-8 with (A) coligand tricine and (B) coligand TPPTS/tricine using HPLC method 1. Radio-HPLC chromatograms of ^{99m}Tc-labeled IL-8 with coligand nicotinic acid/tricine (Figure 3C) and coligand TPPTS/tricine (Figure 3D) using HPLC method 2.

Table 2. Biodistribution of Five Different ^{99m}Tc-Labeled IL-8 Coligand Preparations in Rabbits with *E. coli* Infections at 6 h pi (% ID/g, % ID or ratios, mean values ± SEM)

	%ID/g				
	tricine	EDDA	TPPTS/tricine	nicotinic/tricine	isonicotinic/tricine
blood	0.045 ± 0.005	0.024 ± 0.005	0.010 ± 0.001	0.030 ± 0.007	0.032 ± 0.003
muscle	0.0044 ± 0.0007	0.0037 ± 0.0001	0.0022 ± 0.0002	0.0024 ± 0.0003	0.0027 ± 0.0003
abscess	0.39 ± 0.02	0.42 ± 0.04	0.075 ± 0.004	0.55 ± 0.13	0.53 ± 0.07
lung	0.36 ± 0.03	0.39 ± 0.03	0.17 ± 0.04	0.31 ± 0.07	0.33 ± 0.02
spleen	0.86 ± 0.10	1.00 ± 0.15	1.01 ± 0.04	0.83 ± 0.20	0.98 ± 0.13
kidney	2.59 ± 0.14	2.86 ± 0.17	2.69 ± 0.11	1.75 ± 0.14	1.91 ± 0.13
liver	0.10 ± 0.01	0.12 ± 0.01	0.28 ± 0.01	0.10 ± 0.02	0.10 ± 0.02
intestine	0.030 ± 0.003	0.030 ± 0.001	0.019 ± 0.002	0.017 ± 0.002	0.019 ± 0.002
abscess/muscle	94 ± 12	116 ± 14	36 ± 5	248 ± 69	204 ± 24
abscess/blood	9.6 ± 2.0	22.3 ± 5.6	7.6 ± 0.8	18.6 ± 3.5	17.0 ± 2.3
%ID abscess	5.6 ± 0.2	6.0 ± 0.3	1.1 ± 0.1	6.5 ± 1.3	7.8 ± 0.5
%ID kidneys	43 ± 2	44 ± 1	48 ± 1	29 ± 2	34 ± 1

of TPPTS with IL-8 is not the principal determinant for the aberrant in vitro behavior of [^{99m}Tc(IL-8−HYNIC)-(tricine)(TPPTS)]. The characteristics of the mobile phase itself may explain the chromatographic behavior of TPPTS. The acidic sulfonate groups of TPPTS are partly protonated/deprotonated using the acidic TFA/ACN mobile phase of method 1. A mix of protonation states might be responsible for the broad and multispecies chromatogram of TPPTS. To investigate this, the acidic mobile phase of HPLC method 1 (diluted TFA/ACN) was replaced by a more pH neutral mobile phase in HPLC method 2 (phosphate buffer pH 6.0/ACN) in an additional experiment. The radio-HPLC chromatograms (method 2) of nicotinic acid (representative for tricine, EDDA, and isonicotinic acid) and of TPPTS are presented in Figure 3C and 3D. The nicotinic acid chromatogram showed a pertechnetate peak with a retention time of 3.7 min and a single peak of [^{99m}Tc(IL-8−HYNIC)(tricine)(nicotinic acid)] with a retention time of 19.4 min. The chromatogram of TPPTS showed a pertechnetate peak with a retention time of 3.7 min and, again, a multispecies pattern with peaks at 19.0, 21.8, and 27.8 min, indicating a higher lipophilicity of the TPPTS preparation.

Animal Studies. The coligand system clearly affected the biodistribution of ^{99m}Tc-labeled IL-8−HYNIC as showed in Table 2. Figure 4 summarizes the main in vivo characteristics: abscess/muscle and abscess/blood ratios and the principal routes of clearance (renally and/or hepatobiliary) of the five preparations. As compared to tricine, the EDDA preparation cleared faster from the blood, resulting in a significantly lower percentage of residual activity in the blood ($P < 0.05$) and (in combination with a similar muscle uptake) in a significantly higher abscess/blood ratio ($P < 0.05$) (Figure 4b). The biodistribution pattern of TPPTS was very different from the other ones. This preparation had a significantly reduced uptake in the abscess as well as in muscles, lungs, and intestines ($P < 0.05$). Blood clearance was much faster ($P < 0.001$), presumably due to a more than 2-fold higher uptake by the liver ($P < 0.001$). Lower lung

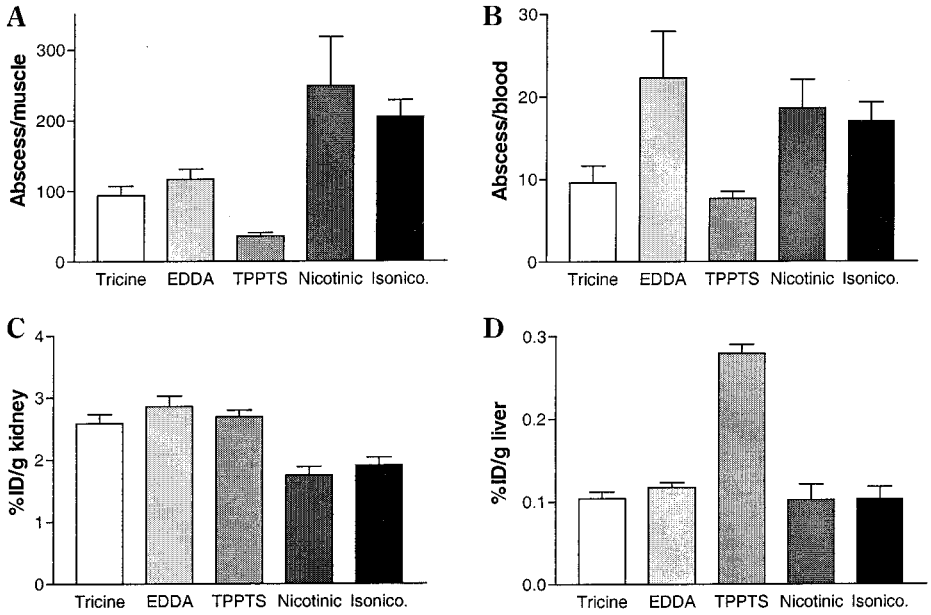


Figure 4. Biodistribution ratios: (A) abscess/muscle and (B) abscess/blood. Principal routes of clearance: (C) Renal and (D) hepatobiliar. The five different ^{99m}Tc-labeled IL-8 coligand preparations are named by their discriminating component (nicotinic = nicotinic acid; isonico. = isonicotinic acid). Data are taken from Table 2. The error bars indicate SEM.

uptake might suggest that there was less interaction of this preparation with leukocytes. The nicotinic acid and isonicotinic acid preparation had almost identical in vivo characteristics. In comparison to the tricine preparation, a significantly lower percentage residual activity in the muscles ($P < 0.001$ and $P < 0.05$, respectively) and intestines ($P < 0.001$) was found. Abscess/muscle ratio of the nicotinic acid preparation was significantly higher ($P < 0.05$) (Figure 4a). At 6 h pi, kidney uptake was significantly lower for nicotinic and isonicotinic acid ($P < 0.001$) (Figure 4c). All preparations were excreted renally except for the TPPTS preparation which partly cleared via the hepatobiliary route (Figure 4c and 4d).

The abscesses were clearly delineated on the images recorded from 2 h onward for all preparations with the exception of TPPTS (Figure 5). Quantitative analysis of the images indicated that the abscess/background ratios (A/B) improved with time for all preparations (Figure 6). The A/B at 6 h pi, of isonicotinic acid was significantly higher ($P < 0.05$) than that of tricine and the A/B of TPPTS was significantly lower ($P < 0.05$). Immediately after injection high kidney uptake was observed for all preparations, remaining prominent during the 6 h pi. In addition to this, high liver uptake was seen on all the TPPTS images.

DISCUSSION

In our previous study, IL-8 was conjugated with HYNIC and subsequently labeled with ^{99m}Tc using tricine as coligand (*8*). This preparation showed excellent characteristics as an infection imaging agent, approaching the characteristics of the ideal radiopharmaceutical for infection imaging: rapid and high accumulation in infectious foci together with rapid clearance from the blood and the nontarget tissues. The leukocyte receptor binding capacity was still largely preserved.

The primary concern in using IL-8 in vivo is that it is a highly potent activator of neutrophils. Administration doses of micrograms of IL-8 per kg of body-weight in healthy rabbits caused a serious but transient neutropenia followed by a leukocytosis lasting several hours (*6*). These side-effects are undesirable for a diagnostic utility in routine clinical practice. Our research program focused on increasing the specific activity of a radiolabeled IL-8 preparation in combination with preservation of the

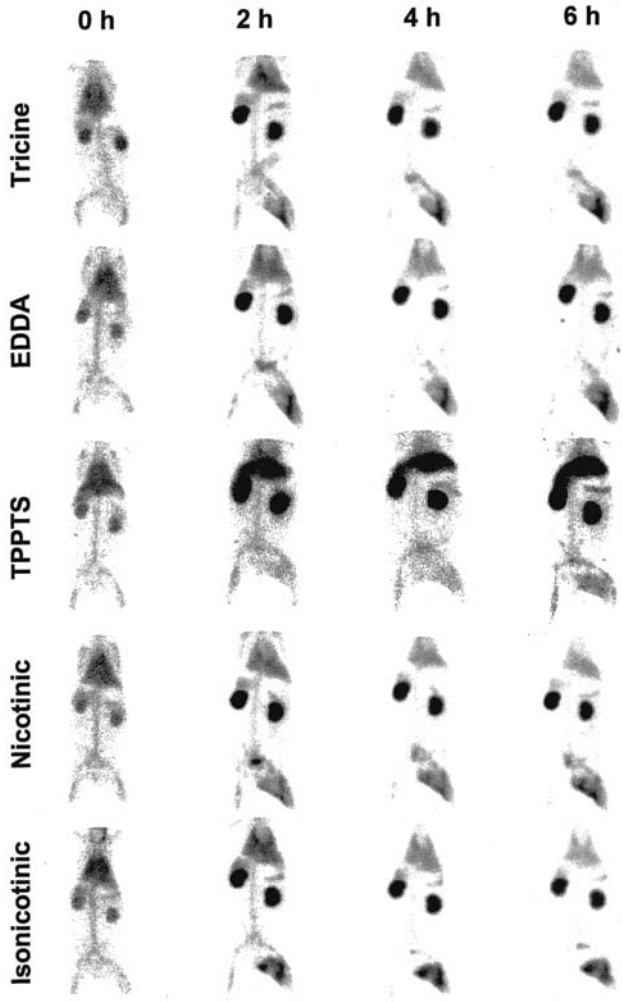


Figure 5. Images of rabbits with an *E. coli* abscess in the left thigh muscle at 1 min, 2, 4, and 6 h after injection of five different ^{99m}Tc−HYNIC−IL-8 coligand preparations.

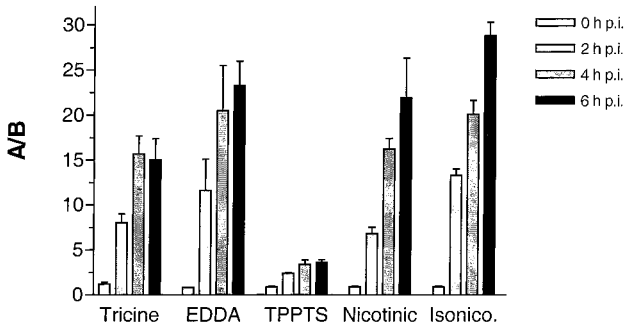


Figure 6. The abscess/background ratios as determined by quantitative analysis of the images of rabbits with *E. coli* infection injected with five different ^{99m}Tc−HYNIC−IL-8 coligand preparations. The coligand preparations are named by their discriminating component (nicotinic = nicotinic acid; isonico. = isonicotinic acid). The error bars indicate SEM.

leukocyte receptor binding capacity. A first and most important reduction of the amount of biologically active material to be injected was achieved with ^{99m}Tc−HYNIC−IL-8 (with coligand tricine) as compared to radioiodinated IL-8: 1 μg/kg ^{99m}Tc−HYNIC−IL-8 versus 25 μg/kg ^{123}I−IL-8 (*8*).

In the present study the bifunctional coupling agent HYNIC was adopted again for labeling IL-8 with technetium. A decisive improvement was obtained with a slightly modified HYNIC formulation: the propylaldehyde hydrazone formulation instead of the free hydrazine formulation (*13*). Protection of the hydrazine group of HYNIC in HYNIC-conjugated IL-8 resulted in a product with improved long-term stability resulting in an increased labeling efficiency using the same coligand tricine as in previous studies.

Further improvement was sought in the exploration of various coligands. Liu and Edwards et al. have performed systematic studies upon labeling a HYNIC-conjugated platelet glycoprotein receptor antagonist with ^{99m}Tc using various alternative coligand systems. The formulation with tricine was found to be unstable in solution, particularly under dilute conditions, and to exist in many isomeric forms (*16*). Increased stability of the complex and reduction of the number of isomers could be achieved by replacing tricine by other coligand systems such as EDDA (16), tricine/TPPTS (*17*), and tricine/(iso)-nicotinic acid (*18*). High specific activities were obtained with all these preparations, though the labeling efficiency using EDDA as coligand was not as high as that using the other coligand systems. Decristoforo and Mather described the preclinical evaluation of ^{99m}Tc-labeled HYNIC-conjugated somatostatin analogues using tricine, EDDA, and tricine in combination with nicotinic acid as coligands (*20*−*22*). These preparations showed preserved binding affinity for the somatostatin receptor. Again, reduced in vitro stability was found for the complex using tricine only as coligand, resulting in higher blood levels. The preparation using tricine/nicotinic acid produced significant levels of activity in the gastrointestinal tract. The preparation using EDDA showed the most promising overall biodistribution profile, though labeling efficiency was considerably lower. Consequently, a first clinical study was performed with this EDDA formulation (*23*).

Our findings concerning stability of the coligand complexes are in line with the above-reported results. The tricine formulation was found to be unstable in vitro under diluted conditions (PBS). Alternative coligand systems offered a solution toward more stable in vitro complexes, especially the TPPTS and the nicotinic acid preparations. In contrast, in serum all preparations proved to be equally stable. In a recent study Ono and co-workers have demonstrated that plasma proteins can stabilize ^{99m}Tc-labeled HYNIC-conjugated Fab fragments when tricine is used as coligand (*24*). The authors proposed that one of the tricine coligands is replaced by a plasma protein to generate higher molecular weight species that exhibit a slower blood clearance. This could explain not only the stability of the [^{99m}Tc(IL-8−HYNIC)-(tricine)$_2$] complex in serum, but also the relatively slow blood clearance of the [^{99m}Tc(IL-8−HYNIC)(tricine)$_2$] complex. In addition, Ono et al. found that replacement of one tricine molecule by a nicotinic acid molecule in the reported complexes resulted in a stabilized ternary ligand system which demonstrated a significantly faster blood clearance. We arrived at similar conclusions for [^{99m}Tc-(IL-8−HYNIC)(tricine)(nicotinic)].

It is rather surprising that the in vitro and in vivo properties of a 72 amino acid protein as IL-8 could be greatly affected by a coligand. Introduction of the bulky coligand TPPTS resulted in a severe reduction of in vitro receptor binding affinity, a shift in lipophilicity of the total complex, significant lower abscess uptake and lower blood levels, and a much higher liver uptake. Quality of the images was poor as compared to the other coligand systems. Several explanations can be given for the marked change in biodistribution pattern of TPPTS. First, TPPTS is considerably larger than the other coligands (Figure 1). TPPTS equals the size of approximately four amino acid residues, whereas the other coligands have the size of just one amino acid residue. Steric hindrance of the relatively bulky TPPTS group might, at least in part, explain the major impact on binding affinity toward the IL-8 receptors. Second, the charge of the complex is affected by the three TPPTS sulfonato groups. These sulfonato groups are expected to be deprotonated under physiologic conditions (*17*), which has a definite impact on the (local) electron distribution. We investigated the possibility of interaction of TPPTS with IL-8 outside the protein−HYNIC-core and compared the radiochromatograms of a iodinated IL-8 preparation with the same preparation incubated at 70 °C for 30 min in the presence of an excess of TPPTS. In this experiment the dramatic changes in RP-HPLC patterns were not seen as with the ^{99m}Tc-labeled IL-8 TPPTS preparation. Apparently, interaction of TPPTS with IL-8 outside the protein−HYNIC-core does not play a major role in explaining the aberrant in vitro and in vivo behavior of the TPPTS preparation.

The ^{99m}Tc−HYNIC−IL-8 EDDA preparation showed highly favorable characteristics for infection imaging. The preparation cleared relatively rapidly from the blood. EDDA is, however, not the coligand of choice for IL-8 for two reasons. First, the formulations using (iso)nicotinic acid generated higher abscess/muscle (and A/B) ratios. Second, the EDDA preparation had a relatively low specific activity. The specific activity of the tricine formulation was twice as high as that of EDDA, and with (iso)nicotinic acid, specific activities were up to 10 times higher (Table 1).

The most optimal characteristics for infection imaging were obtained with formulations using nicotinic acid or isonicotinic acid as coligands. With these coligands, specific activities 20-fold higher than those previously reported with the unprotected hydrazine and with tricine as coligand could be achieved, without compromising the receptor binding capacity. Administration of doses as low as 70 ng/kg ^{99m}Tc−HYNIC−IL-8 (versus 1 μg/kg previously reported) will suffice for imaging procedures.

Moreover, (iso)nicotinic acid showed the most favorable in vivo characteristics with abscess/muscle, abscess/blood, and ROI-derived abscess/background ratios being twice as high as those obtained with tricine. Its higher in vitro stability makes nicotinic acid the preferred coligand. Future experiments with ^{99m}Tc−HYNIC−IL-8 will exploit the advantages of the nicotinic acid/tricine coligand formulations. At low IL-8 protein doses of 70 ng/kg, side effects are not to be expected in the human system. This opens the way to infection imaging studies in patients.

CONCLUSION

IL-8 can be rapidly, easily, and efficiently labeled with ^{99m}Tc using (hydrazine protected) HYNIC as chelator and using various coligands. The most optimal infection imaging characteristics were found for formulations using nicotinic acid/tricine as coligands combining a high specific activity (up to 80 MBq/μg) and high in vitro stability with high abscess/muscle ratios (>200) and high abscess/background ratios (>20) in vivo. High quality images with clear delineation of infectious foci could be obtained within 2 h after injection of the radiopharmaceutical. The low administration doses of 70 ng/kg ^{99m}Tc−HYNIC−IL-8 paves the way for infection imaging studies in patients.

ACKNOWLEDGMENT

The authors thank G. Grutters (University of Nijmegen, Central Animal Laboratory) and C. Frielink (University Medical Center Nijmegen, Department of Nuclear Medicine) for their excellent technical assistance.

LITERATURE CITED

(1) Rennen, H. J., Boerman, O. C., Oyen, W. J., and Corstens, F. H. (2001) Imaging infection/inflammation in the new millennium. *Eur. J. Nucl. Med. 28*, 241−252.

(2) Lee, J., Horuk, R., Rice, G. C., Bennett, G. L., Camerato, T., and Wood, W. I. (1992) Characterization of two high affinity human interleukin-8 receptors. *J. Biol. Chem. 267*, 16283−16287.

(3) Cerretti, D. P., Kozlosky, C. J., VandenBos, T., Nelson, N., Gearing, D. P., and Beckmann, M. P. (1993) Molecular characterization of receptors for human interleukin-8, GRO/melanoma growth-stimulatory activity and neutrophil activating peptide-2. *Mol. Immunol. 30*, 359−367.

(4) Hay, R. V., Skinner, R. S., Newman, O. C., and et al. (1997) Scintigraphy of acute inflammatory lesions in rats with radiolabeled recombinant human interleukin-8. *Nucl. Med. Commun. 18*, 367−378.

(5) Gross, M. D., Shapiro, B., Skinner, R. S., Shreve, P., Fig, L. M., and Hay, R. V. (1996) Scintigraphy of osteomyelitis in man with human recombinant interleukin-8. *J. Nucl. Med. 37*, 25P.

(6) Van der Laken, C. J., Boerman, O. C., Oyen, W. J., Van de Ven, M. T., Ven der Meer, J. W., and Corstens, F. H. (1998) The kinetics of radiolabeled interleukin-8 in infection and sterile inflammation. *Nucl. Med. Commun. 19*, 271−281.

(7) Van der Laken, C. J., Boerman, O. C., Oyen, W. J., Van de Ven, M. T., Van der Meer, J. W., and Corstens, F. H. (2000) Radiolabeled interleukin-8: specific scintigraphic detection of infection within a few hours. *J. Nucl. Med. 41*, 463−469.

(8) Rennen, H. J., Boerman, O. C., Oyen, W. J., van der Meer, J. W., and Corstens, F. H. (2001) Specificand rapid scintigraphic detection of infection with ^{99m}Tc-labeled Interleukin-8. *J. Nucl. Med. 42*, 117−123.

(9) Gratz, S., Rennen, H. J., Boerman, O. C., Oyen, W. J., and Corstens, F. H. (2001) Rapid imaging of experimental colitis with ^{99m}Tc-Interleukin-8 in rabbits. *J. Nucl. Med. 42*, 917−923.

(10) Gratz, S., Rennen, H. J., Boerman, O. C., Oyen, W. J., Burma, P., and Corstens, F. H. (2001) ^{99m}Tc-Interleukin-8 for imaging acute osteomyelitis. *J. Nucl. Med. 42*, 1257−1264.

(11) Abrams, M. J., Juweid, M., tenKate, C. I, and et al. (1990) Technetium-99m-human polyclonal IgG radiolabeled via the hydrazino nicotinamide derivative for imaging focal sites of infection in rats. *J. Nucl. Med. 31*, 2022−2028.

(12) Larsen, S. K., Solomon, H. F., Caldwell, G., and Abrams, M. J. (1995) [99mTc]tricine: a useful precursor complex for the radiolabeling of hydrazinonicotinate protein conjugates. *Bioconjug. Chem. 6*, 635−638.

(13) Schwartz, D. A., Abrams, M. J., Gladomenico, C. M., and Zubieta, J. A. Certain pyridyl hydrazines and hydrazides useful for protein labeling. 1993; U.S. Patent 5,206,370.

(14) Edwards, D. S., Liu, S., Harris, A. R., Poirier, M. J., and Ewels, B. A. (1999) 99mTc-labeling of hydrazones of a hydrazinonicotinamide conjugated cyclic peptide. *Bioconjug. Chem. 10*, 803−807.

(15) Babich, J. W., and Fischman, A. J. (1995) Effect of "coligand" on the biodistribution of 99mTc-labeled hydrazinonicotinic acid derivatized chemotactic peptides. *Nucl. Med. Biol. 22*, 25−30.

(16) Liu, S., Edwards, D. S., Looby, R. J., Harris, A. R., Poirier, M. J., Barrett, J. A., Heminway, S. J., and Carroll, T. R. (1996) Labeling a hydrazino nicotinamide-modified cyclic IIb/IIIa receptor antagonist with 99mTc using aminocarboxylates as coligands. *Bioconjug Chem. 7*, 63−71.

(17) Edwards, D. S., Liu, S., Barrett, J. A., Harris, A. R., Looby, R. J., Ziegler, M. C., Heminway, S. J., and Carroll, T. R. (1997) New and versatile ternary ligand system for technetium radiopharmaceuticals: water soluble phosphines and tricine as coligands in labeling a hydrazinonicotinamide-modified cyclic glycoprotein IIb/IIIa receptor antagonist with 99mTc. *Bioconjug. Chem. 8*, 146−154.

(18) Liu, S., Edwards, D. S., and Harris, A. R. (1998) A novel ternary ligand system for 99mTc-labeling of hydrazino nicotinamide-modified biologically active molecules using imine-N-containing heterocycles as coligands. *Bioconjug. Chem. 9*, 583−595.

(19) Lindmo, T., Boven, E., Cuttitta, F., Fedorko, J., and Bunn, P. A. (1984) Determination of the immunoreactive fraction of radiolabeled monoclonal antibodies by linear extrapolation to binding at infinite antigen excess. *J. Immunol. Methods 72*, 77−89.

(20) Decristoforo, C., and Mather, S. J. (1999) Preparation, (99m)Tc-labeling, and in vitro characterization of hynic and N(3)S modified RC-160 and [Tyr3]-octreotide. *Bioconjug. Chem. 10*, 701−702.

(21) Decristoforo, C., and Mather, S. J. (1999) Technetium-99m somatostatin analogues: effect of labeling methods and peptide sequence. *Eur. J. Nucl. Med. 26*, 869−876.

(22) Decristoforo, C., Melendez-Alafort, L., Sosabowski, J. K., and Mather, S. J. (2000) 99mTc-HYNIC-[Tyr3]-octreotide for imaging somatostatin-receptor-positive tumors: preclinical evaluation and comparison with 111I*n*-octreotide. *J. Nucl. Med. 41*, 1114−1119.

(23) Decristoforo, C., Mather, S. J., Cholewinski, W., Donnemiller, E., Riccabona, G., and Moncayo, R. (2000) 99mTc-EDDA/HYNIC-TOC: a new 99mTc-labeled radiopharmaceutical for imaging somatostatin receptor-positive tumours; first clinical results and intra-patient comparison with 111In-labeled octreotide derivatives. *Eur. J. Nucl. Med. 27*, 1318−1325.

(24) Ono, M., Arano, Y., Mukai, T., Uehara, T., Fujioka, Y., Ogawa, K., Namba, S., Nakayama, M., Saga, T., Konishi, J., Horiuchi, K., Yokoyama, A., and Saji, H. (2001) Plasma protein binding of (99m)Tc-labeled hydrazino nicotinamide derivatized polypeptides and peptides. *Nucl. Med. Biol. 28*, 155−164.

BC015579K

TECHNICAL NOTES

Advantage of the Ether Linkage between the Positive Charge and the Cholesteryl Skeleton in Cholesterol-Based Amphiphiles as Vectors for Gene Delivery

Yamuna Krishnan Ghosh,[†] Sandhya S. Visweswariah,[‡] and Santanu Bhattacharya*[,†]

Department of Organic Chemistry, Indian Institute of Science, Bangalore 560 012, India. Received June 15, 2001

Twelve novel cationic cholesterol derivatives with different linkage types between the cationic headgroup and the cholesteryl backbone have been developed. These have been tested for their efficacies as gene transfer agents as mixtures with dioleoyl phosphatidylethanolamine (DOPE). A pronounced improvement in transfection efficiency was observed when the cationic center was linked to the steroid backbone using an *ether* type bond. Among these, cholest-5-en-3b-oxyethane-*N*,*N*,*N*-trimethylammonium bromide (**2a**) and cholest-5-en-3b-oxyethane-*N*,*N*-dimethyl-*N*-2-hydroxyethylammonium bromide (**3d**) showed transfection efficiencies considerably greater than commercially available reagents such as Lipofectin or Lipofectamine. To achieve transfection, **3d** did not require DOPE. Increasing hydration at the headgroup level for both ester- and ether-linked amphiphiles resulted in progressive loss of transfection efficiency. Transfection efficiency was also greatly reduced when a 'disorder'-inducing chain like an oleyl (*cis*-9-octadecenyl) segment was added to these cholesteryl amphiphiles. Importantly, the transfection ability of **2a** with DOPE in the presence of serum was significantly greater than for a commercially available reagent, Lipofectamine. This suggests that these novel cholesterol-based amphiphiles might prove promising in applications involving liposome-mediated gene transfection. This investigation demonstrates the importance of structural features at the molecular level for the design of cholesterol-based gene delivery reagents that would aid the development of newer, more efficient formulations based on this class of molecules.

INTRODUCTION

Aqueous suspensions of cationic cholesterol derivatives have been shown to bring about DNA transfection in cells with greater efficiency than for many commercially available formulations composed of cationic lipids based on the pseudoglyceryl skeleton (*1*, *2*). Such an alternative class of cytofectins (*3*) based on synthetic cationic cholesterol derivatives are currently receiving much attention for use in gene therapy (*4*−*8*). In addition, they are being utilized in the studies involving enzyme inhibition (*9*) for the design of membrane-spanning conductors (*10*) or in medicinal applications (*11*).

The surge in the utilization of cationic cholesterol derivatives as cytofectin over traditional cationic glycerol-based amphiphiles stems from one practical fact that the 3β-OH of cholesterol is easily amenable to functionalization, and this facilitates the generation of a range of new cationic cholesteryl derivatives. The emergence of this class of molecules as efficient cytofectins has prompted structural studies such as the headgroup variation and location of the positive charge on the cholesterol monomer (*12*). However, little is known on the effect of the *linkage* region, which connects the positive charge to the steroid backbone. Our preliminary studies (*2*) using COS-7 cells suggested that use of an ether linkage over the more frequently used hydrolytically scissile ester- or urethane-based linkage offers significant advantage in effecting gene transfer. In the present investigation we undertake a detailed study using several cationic cholesterol derivatives (Figure 1) for their utilization in transfection through various cell lines. To derive a relationship between headgroup hydration and transfection efficiency (TE) involving this class of cytofectins, we prepared cationic cholesterol derivatives bearing varying lengths of oligooxyethylene glycol units. Earlier investigations with cationic fatty acid derivatives of glycerol-based transfection reagents have already indicated a crucial relationship that exists between the TE and the headgroup solvation (*13*−*15*). Herein we present the results where the transfection abilities of various cationic cholesterol derivatives having different linker regions and altered levels of headgroup hydration yield a correlation between molecular structure and gene transfection efficiency.

2. MATERIALS AND METHODS

2.1. Materials. All reagents, solvents, and starting materials were obtained from the best known commercial sources and were distilled, recrystallized, or used without further purification, as appropriate (*16*). Thin layer

* To whom the correspondence should be addressed. Fax, +91-80-360-0529; e-mail: sb@orgchem.iisc.ernet.in; also at the Chemical Biology Unit of JNCASR, Bangalore 560 012, India.
[†] Department of Organic Chemistry.
[‡] Department of Molecular Reproduction Development and Genetics.

10.1021/bc010048h CCC: $22.00 © 2002 American Chemical Society
Published on Web 02/09/2002

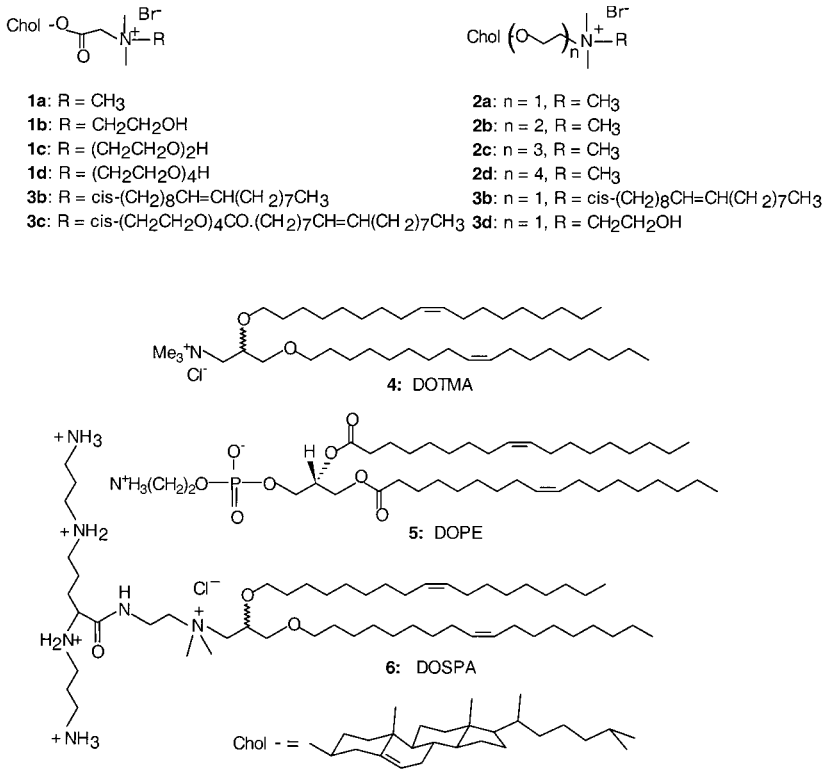


Figure 1. Molecular structures of the various Cytofectins and Helper Lipid (DOPE) employed in the present investigation.

chromatographic analyses were performed on silica gel-G (Merck) coated plates. Preparative chromatographic columns were packed with silica gel (60−120 mesh) obtained from Merck. 1,2-Dioleoyl-*sn*-glycero-3-phosphatidylethanolamine (DOPE) was purchased from Avanti Polar Lipids. Cholesterol was obtained Sigma (St. Louis, MO). *N,N*-Dimethylethanolamine was obtained from Aldrich and trimethylamine from Merck. Commercially available transfection reagents Lipofectin and Lipofectamine were obtained from GIBCO-BRL. Luciferase assay kit was obtained from Promega.

2.2 Synthesis. The syntheses of cationic cholesterol-based amphiphiles **1a**−**d** and **2a**−**d** have been reported elsewhere (*17*). Melting points were recorded in open capillaries and are uncorrected. ^{1}H NMR spectra were recorded on JEOL-JANL-LA-300 NMR spectrometers. Chemical shifts are reported in ppm downfield from the internal standard, tetramethylsilane. IR spectra were recorded on a Perkin-Elmer Model 781 spectrometer and are reported in wavenumbers (cm^{-1}). MALDI-TOF was recorded on a Kratos MALDI-TOF spectrometer.

General Procedure for the Synthesis of Cationic Cholesterol Derivatives. A solution of cholesteryl bromoacetate or 2-bromoethylcholesteryl ether (1 mmol) in dry acetone (20 mL) was refluxed for 12 h with the appropriate *N*-alkyl-*N,N*-dimethylamine. The white precipitate so formed was filtered off and washed with dry acetone. These were then recrystallized several times from dry acetone to give white solids, which were found to be pure by TLC, in yields of 88−95%. All compounds were found to be hygroscopic and existed as hydrates despite prolonged drying under vacuum and were characterized by IR, ^{1}H NMR, MALDI-TOF, and elemental analysis.

*Cholesteryl (2-N,N-dimethyl-N-oleylammonium bromide) acetate (**3a**).* Mp: 185−7 °C; IR ($CHCl_3$): 1735 cm^{-1}. ^{1}H NMR ($CDCl_3$, 300 MHz); δ: 0.65−2.45 (multiple peaks, 77 H), 3.48 (s, 8H), 4.623 (m, 3H), 5.34 (d, 1H). MALDI-TOF: 724 (M^+ − Br). Anal. Calcd for $C_{49}H_{88}O_2$-NBr·2.5H_2O: C, 69.39; H, 10.96; N, 1.65. Found: C, 69.4; H, 10.66; N, 1.79.

*Cholesteryl ((1-oleoyloxy-3,6,9-oxaundecano)-11-N,N,-dimethylammonium bromide) acetate (**3b**).* Mp: 88 °C; IR ($CHCl_3$): 1745 cm^{-1}. ^{1}H NMR ($CDCl_3$, 300 MHz); δ: 0.68−2.35 (multiple peaks, 77H), 3.62−3.7 (m, 18H), 3.98 (bs, 2H), 4.17−4.25 (m, 4H), 4.07 (t, 2H), 4.73−4.74 (m, 3H), 5.34−5.38 (m, 3H). MALDI-TOF: 913 (M^+ − Br). Anal. Calcd for $C_{57}H_{102}O_7$NBr·1.25H_2O: C, 67.39; H, 10.37; N, 1.38. Found: C, 67.76; H, 10.41; N, 1.02.

*Cholest-5-en-3β-oxyethane-N,N-dimethyl-N-(cis-9-octadecenyl)ammonium bromide (**3c**).* Isolated as white gum, 94 mg, 0.12 mmol, 59%. IR: 3240, 2930, 2865, 1465, 1350 cm^{-1}. ^{1}H NMR ($CDCl_3$, 300 MHz); δ: 0.67 (s, 3H), 0.85−2.35 (m, 72H), 3.20 (m, 1H), 3.40−3.60 (multiple peaks, 6H), 3.95 (s, 4H), 5.36 (d, J = 4.5 Hz, 1H). MALDI-TOF: 710 (M^+ − Br). Anal. Calcd for $C_{49}H_{90}$ONBr·1.5H_2O: C, 72.11; H, 11.49; N, 1.41. Found: C, 71.74; H, 11.59; N, 1.41.

*Cholest-5-en-3β-oxyethane-N,N-dimethyl-N-2-hydroxyethylammonium bromide (**3d**).* White solid, 98 mg, 0.17 mmol, 83%. IR: 3240, 2930, 2865, 1465, 1350 cm^{-1}. ^{1}H NMR ($CDCl_3$, 300 MHz); δ: 0.67 (s, 3H), 0.85−2.35 (m, 41H), 3.20 (m, 1H), 3.67 (s, 6H), 3.82−3.92 (m, 6H), 4.15 (s, 2H), 5.36 (d, J = 4.5 Hz, 1H). MALDI-TOF: 503 (M^+ − Br). Anal. Calcd for $C_{33}H_{60}O_2$ NBr· 0.5 H_2O: C, 66.98; H, 10.39; N, 2.37. Found: C, 67.28; H, 10.45; N, 2.06.

2.3. Liposome Preparation. A mixture of cationic amphiphile and DOPE in the desired molar ratio was dissolved in $CHCl_3$ in autoclaved Wheaton glass vials, and then solvent was evaporated under vacuum from the solutions to form respective thin films. These were resuspended in freshly autoclaved Milli-Q water. The final cationic cholesterol lipid/DOPE concentration was

0.2 mg/mL for all formulations. The mixture was left to hydrate at room temperature for ~6 h and then vortexed for 5 min followed by bath sonication for 15 min. The solutions were filtered under sterile conditions through a 0.22 mm filter (Sartorius) and stored at 4 °C. The diameters of the cationic liposomes prepared by this method ranged generally between 80 and 400 nm as checked by transmission electron microscopy of individual aliquots of sterile vesicular suspensions from respective cationic cholesterol derivatives with DOPE suspensions.

2.4. Plasmid DNA. Plasmid PRL-SV40 vector containing the luciferase reporter gene was amplified in *Escherichia coli* (DH5a) and purified using the QIAGEN Midi Prep Plasmid Purification protocol.

2.5. Transfection Procedure. A general procedure for a typical transfection was as follows. Cells were seeded in 24 well tissue culture plates (Nunc) the day before transfection in order to be approximately 40% confluent the next day. All cell lines (COS-7, NIH3T3, T84, and HEK293) were cultured in Dulbecco's Modified Eagle Medium (DMEM) supplemented with 10% fetal calf serum (FCS). Cells were routinely maintained on plastic 24 well tissue culture dishes (Nunc) at 37 °C in a humidified 5% CO_2/95% air-containing atmosphere. Plasmid DNA (0.3 μg) and the desired cationic cholesteryl amphiphile (4 μg) were each diluted in 100 μL of DMEM without FCS. After ≈5 min, the two solutions were combined and gently mixed, and the resulting solution was allowed to incubate for 15 min at room temperature to allow complex formation. The transfection mixture was then added (0.2 mL/well) to the cells that had been washed with serum free medium. After 8 h incubation at 37 °C, the transfection mixture was removed and 0.4 mL of 10% FCS was added to each well. The cells were harvested at 2 days post-transfection for monitoring of the transient expression of the luciferase gene. Control transfections were performed by using commercially available transfection reagents. The lipopolyamine Lipofectamine was used at a concentration of 4 μg/well. For transfection with the commercial grade Lipofectin−DNA complexes were obtained using the standard conditions specified by the manufacturer.

2.6. Transfections in the Presence of Serum. Transfections in the presence of serum were carried out in an identical manner with the transfection mixture being overlaid on wells containing an equal volume of 10% FCS such that the wells contained the lipid−DNA complex in 5% FCS. All experiments were performed in duplicate.

2.7. Luciferase Assay. Luciferase activities were assayed 48 h post-transfection using a modified procedure of De Wet ET al. (*18*). This is briefly presented herein. After removal of the culture medium, the cells were washed with cold phosphate buffer−saline and lysed by incubation with 60 μL of cell lysis buffer (25 mM Tris-phosphate buffer, pH = 7.8, 2 mM DTT, 2 mM CGTA, 10% glycerol, 1% Triton × 100). The lysate was clarified from insoluble material by centrifugation (for 5 s at 12000 × g). The supernatant was transferred to a new tube, and the pelleted cell debris was discarded. An aliquot (2 μL) of the cell extract at room temperature was mixed with 20 μL of Luciferin also at room temperature. Samples were placed in a photon counting luminometer (Turner Designs Model, TD 20/20 Luminometer), and the integration value of light emission was measured for 10 s. Protein concentrations were measured by using Bradford's method with BSA as a standard. Data for luciferase activity are expressed as relative light units (RLU)/mg of cell protein.

3. RESULTS AND DISCUSSION

3.1. Molecular Structures of Cytofectins. Figure 1 shows the molecular structures of the three families of cationic cholesterol-based amphiphiles (*cholamphiphiles*) **1**−**3**. We first synthesized two families of cationic cholamphiphiles, one where the charge is linked to the cholesteryl skeleton either via an *ester* or an *ether* bond. In cholesteryl derivatives **1a**−**d**, the cationic headgroup is linked to the 3b-cholesterol via an *ester* connection. In the derivatives **2a**-**d**, the cationic headgroup was linked to the hydrophobic cholesteryl backbone via an *ether* linkage. In view of the fact that there is a relation between headgroup hydration and transfection efficiency we chose oligooxyethylene residues as elements of hydration modulation at the headgroup. Hence in series **1a**−**d**, the positive charge is located at a fixed distance from the cholesteryl backbone, and the headgroup hydration is continually modified with the progressive increase in the number of oxyethylene units on the NMe_2^+ center. In addition, due to lack of information on the optimum location of the positive charge with respect to the hydrophobic backbone, **2a**−**d** were synthesized where cholesterol derivatives are connected to the cationic NMe_3^+ groups via varying lengths of an oligo-oxyethylene spacer units. The cationic NMe_3^+ group is therefore placed at incrementally greater distance from the cholesteryl backbone with the insertion of increasing number of oxyethylene units.

Membranes formed from the aqueous suspensions of these amphiphiles were found to be highly rigid. For instance, these aggregates were found to be thermally insensitive (*17*), as no solid-to-fluid transition was observed under either temperature-dependent fluorescence depolarization studies or differential scanning calorimetry. To examine the role of such thermally insensitive, rigid hydrophobic segments toward transfection, a flexible, fatty acyl chain namely the oleyl chain, was appended to **1a**, **1d**, and **2a**, to give **3a**−**c**. In addition, the ether analogue of **1b**, i.e., **3d** was also synthesized.

3.2. DNA Transfection Studies in COS-7 Cells. The potency of a given cytofectin toward DNA transfection was checked as follows. The cytofectin of interest was mixed with DOPE (**5**) in mole percentages of 20, 33, 50, 66, and 100 in separate vials, and the corresponding mixed liposomes were prepared as given in the Materials and Methods. Transfections were carried out with five different liposomal formulations, and the luciferase assay was used to quantitatively assess the corresponding transfection efficiencies. Two control transfections, with commercially available liposomal transfection reagents, i.e., Lipofectin (which is a 1:1 mixture of 1,2-dioleyloxypropyl-3-trimethylammonium bromide (DOTMA) **4**/DOPE) and Lipofectamine (a mixture of 1:1 DOSPA **6**/DOPE) were carried out every time. It was ensured that the variation of light units obtained for control transfections was not greater than 5%. Transfection efficiency (TE) of a given formulation is expressed as relative light units (RLU)/g protein content normalized with respect to Lipofectamine. Thus a plot of mol % cytofectin in DOPE versus the TE gave the transfection profile of the cytofectin so investigated. The transfection profile of the cytofectin shows the amount of DOPE required by the cytofectin for optimal transfection efficiency (OTE).

The transfection profiles so obtained for the ester-based series **1a**−**d** are presented in Figure 2. **1a** showed the highest activity in the series, with the most effective formulation being 1:2 **1a**/DOPE (Figure 2A). This formulation was at least three times more active than that

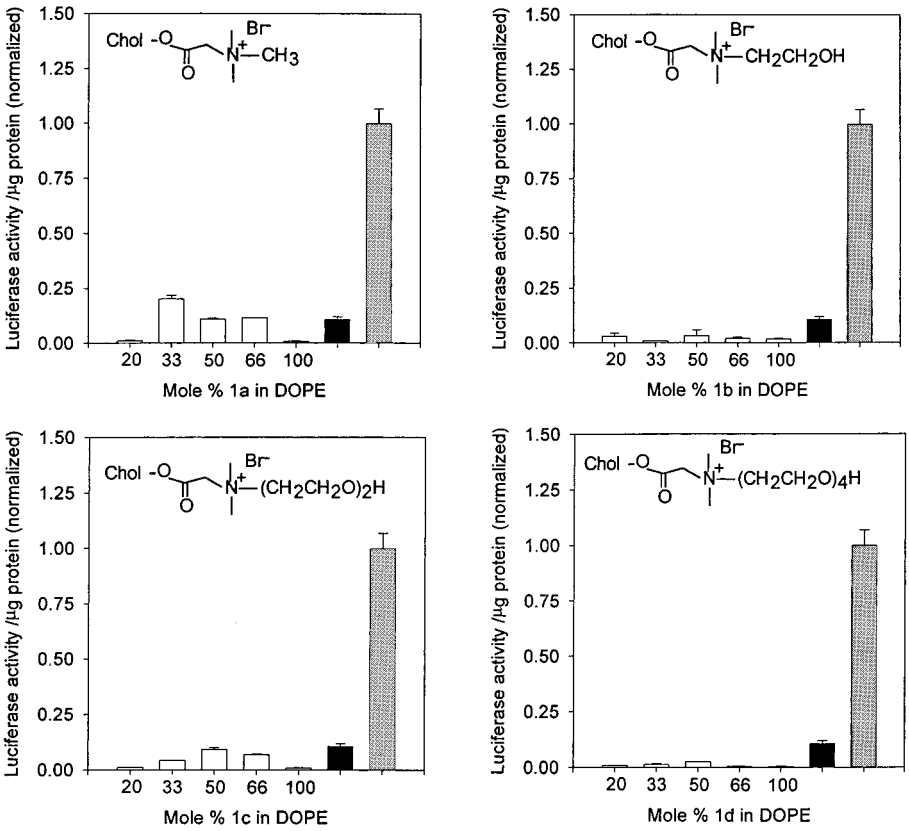


Figure 2. Comparison of transfection efficiencies of pGL3 control DNA using various compositions of **1a**−**d** in DOPE (open bar) with Lipfectamine (gray bar) and Lipofectin (black bar). DNA concentration was 0.3 μg/well and lipid concentration was 4.0 μg/well. Data are expressed as RLU/μg total protein content normalized to Lipofectamine.

of Lipofectin. The most active formulations for all the other compounds in this series were 1:1 formulations of cytofectin/DOPE (Figure 2B−D). OTE for a given cytofectin was found to decrease from **1a** to **1d**.

A similar study was carried out with the ether-based series of cytofectins **2a**−**d**. An appreciable improvement in transfection abilities was observed with the ether-linked cytofectins (Figure 3). **2a** was found to be the most active cytofectin in this series which showed an OTE as a 1:1 mixture with DOPE (Figure 3A). This mixture was found to transfect COS-7 cells at least 1.2 times as efficiently as Lipofectamine and over 1 order of magnitude as efficiently as Lipofectin. **2b** was most active as a 2:1 **2b**/DOPE mixture (Figure 3B) while 1:2 **2c**/DOPE and 1:2 **2d**/DOPE were the most active formulations for **2c** and **2d**, respectively (Figures 3C and 3D). OTE for a given cytofectin was again found to decrease from **2a** to **2d**. A close examination of the optimal transfection efficiencies of both the series revealed that without exception, all ether-based cytofectins in series **2a**−**d** showed TEs greater than 0.25, which is better than the OTE of the most efficient ester-based cytofectin formulation (1:2 **1a**/DOPE). This reflects the clear advantage the cytofectins with ether link possesses over their ester linked counterparts.

Appending **1a** and **2a** with oleyl chains to give **3a** and **3c** resulted in a decrease in transfection efficiencies for both compounds (not shown). This suggests that introduction of disorder-promoting elements reduce the activity of these cytofectins. Interestingly again in this series also, the ether-based analogue of **1b** i.e., **3d** was most active without DOPE and showed an OTE of 0.74 ± 0.03 at 100% of **3d**. Closer scrutiny of the molecular structures of **1a** and **2a**, **1b**, and **3d** as well as **3a** and **3b** reveal that these pairs are identical in all respects except for the fact that the ester link in the former is replaced by an ether link in the latter. A comparison of their OTEs normalized to Lipofectamine (Figure 4) shows that while **2d** transfects 600% as efficiently as **1d**, **3d** transfects ~15 times as efficiently as **1b** and **3b** transfects twice as well as **3a**. This reveals unambiguously that the ether-based lipids transfect DNA with much greater efficiency than their ester counterparts.

We then decided to study in detail two of the most efficient cytofectin formulations, i.e., 100% of **3d** and 1:1 **2a**/DOPE. Transfection efficiencies for the above formulations were optimized by varying DNA concentration from 0.76 mM to 30.3 mM while maintaining the lipid (liposomal formulation) concentration constant. Similarly the lipid concentration was varied from 3.85 mM to 77.04 mM (for 1:1 **2a**/DOPE) and up to 137 mM (for **3d**), keeping the DNA concentration constant. The 30 different assay conditions for each well for 1:1 **2a**/DOPE is shown in Figure 5. Figure 6 provides an overview of the reagent activity under all conditions elucidated in Figure 5. Transfection efficiencies for both cytofectin formulations increased with increasing concentrations of DNA till 1 μg/well. With a further increase in DNA concentration, transfection efficiencies decreased. This bell-shaped curve has been previously reported for other cationic lipid formulations and is most likely related to the oversaturation of the cationic charges by the excess DNA (*19*). The optimum DNA concentration of both 1:1 **2a**/DOPE and **3d** was 1.0 μg/well of DNA. However, the activity profiles of both formulations showed different characteristics. **2a** exhibited a bell-shaped dependence with lipid concentration (Figure 6A). For all DNA concentrations, the optimum [lipid]/[DNA] ratio was ~4. In contrast, **3d** showed a curve that saturated at an optimum [lipid]/[DNA] ratio of ~5 (Figure 6B).

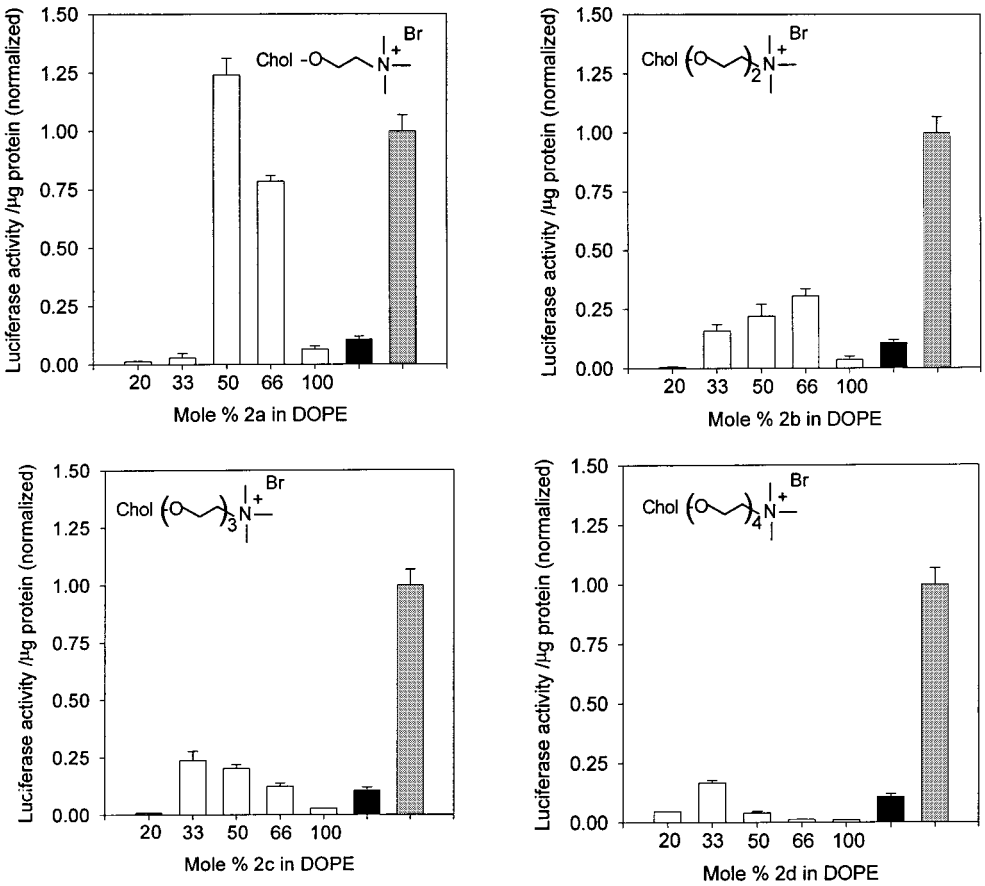


Figure 3. Comparison of transfection efficiencies of pGL3 control DNA using various compositions of **2a**−**d** in DOPE (open bar) with Lipfectamine (gray bar) and Lipofectin (black bar). DNA concentration was 0.3 μg/well and lipid concentration was 4.0 μg/well. Data are expressed as RLU/mg total protein content normalized to Lipofectamine.

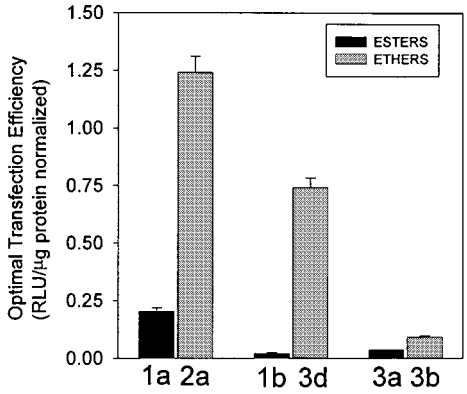


Figure 4. Comparison of transfection efficiencies of ether-based cationic cholesterol derivatives and the corresponding ester-based analogues.

3.3. Effect of Serum on Transfection Efficiency.

We then probed the efficiency of transfection of 1:1 **2a**/DOPE and **3d** in the presence of serum. Serum is known to inhibit the transfection due to the presence of negatively charged sulfate groups in certain constituents of serum which competes with the phosphodiester anions of the DNA backbone for the cationic liposome This presumably interferes with the formation of the cationic lipid−DNA complex and affects transfection efficiencies. To examine this aspect, transfections were carried out in the presence and absence of 10% fetal calf serum using the optimized conditions for the two formulations (Figure 7). A similar experiment was carried out with commercially available Lipofectamine as a comparison to evaluate the performance of these cationic cholesterol ether-based formulations. The conditions of Lipofectamine for transfection were maintained at those recommended

40,000 cells per well
0.2 mL volume
649 μg/μmole for 1:1 **2a**/DOPE
330 μg/μmole for DNA.

	1	2	3	4	5	6	
A	3.8	15.4	30.8	46.2	61.6	77.0	[Lipid](μM)
	0.8	0.8	0.8	0.8	0.8	0.8	[DNA](μM)
	5.1	20.0	40.7	61.0	81.4	101.7	[Lipid]/[DNA]
B	3.8	15.4	30.8	46.2	61.6	77.0	[Lipid](μM)
	3.8	3.8	3.8	3.8	3.8	3.8	[DNA](μM)
	1.0	4.1	8.1	12.2	16.2	20.3	[Lipid]/[DNA]
C	3.8	15.4	30.8	46.2	61.6	77.0	[Lipid](μM)
	7.6	7.6	7.6	7.6	7.6	7.6	[DNA](μM)
	0.5	2.0	4.1	6.1	8.1	10.2	[Lipid]/[DNA]
D	3.8	15.4	30.8	46.2	61.6	77.0	[Lipid](μM)
	15.1	15.1	15.1	15.1	15.1	15.1	[DNA](μM)
	0.3	1.0	2.0	3.1	4.1	5.1	[Lipid]/[DNA]
E	3.8	15.4	30.8	46.2	61.6	77.0	[Lipid](μM)
	30.3	30.3	30.3	30.3	30.3	30.3	[DNA](μM)
	0.1	0.5	1.0	1.5	2.0	2.5	[Lipid]/[DNA]

Figure 5. Concentration of cationic lipid **2a** and DNA in the transfection assay. Shown in the figure are the concentrations of cationic lipid and DNA that were present in the 30 wells of the transfection assay. Lipid concentration ranged from 3.8 to 77.0 μM (0.5 to 10 μg per well of the 1:1 **2a**/DOPE) and the DNA concentration from 0.8 to 30.3 μM (0.05−2 μg per well). DNA molarity was based on an average molecular weight of 330 per nucleotide monomer.

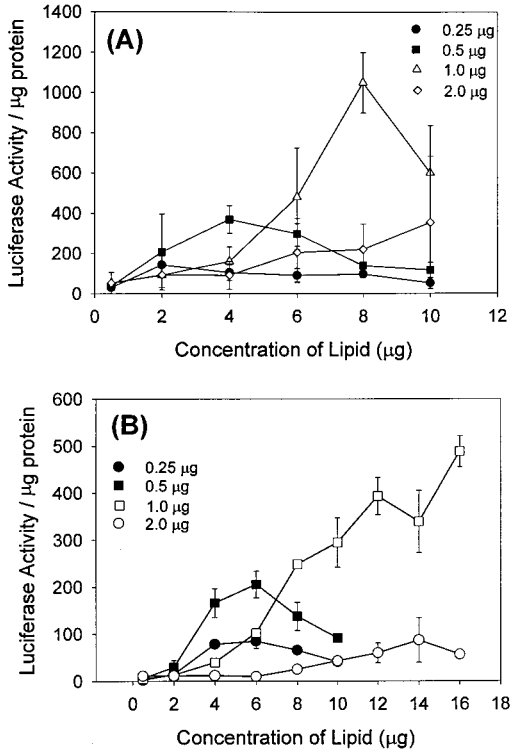


Figure 6. Optimization of Transfection Efficiency of 1:1 **2a**/DOPE (**A**) and **3d** (**B**) in DOPE. DNA concentrations were 0.05, 0.25, 1.0, and 2.0 μg/well. Data are expressed as RLU/μg of total cellular protein. Experiments were performed twice and in duplicate.

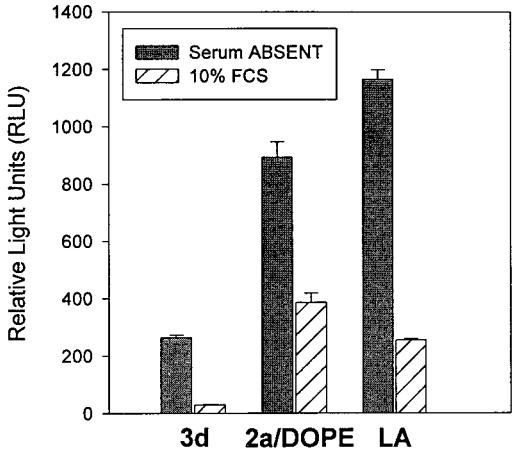


Figure 7. Transfection efficiencies in the presence of 10% FCS and absence of serum for **3d**, 1:1 **2a**/DOPE and LA (Lipofectamine). Concentration of DNA = 1.0 μg/well, concentration of **3** = 10 μg/well; LA = **2a**/DOPE = 4.0 μg/well. Data expressed as RLU for 10 μL of cell lysate.

by the manufacturers. In the presence of serum, the efficiency of **3d** was reduced to one-tenth of the activity in the absence of serum, showing that serum significantly hampers the ability of **3d** to transfect DNA. Lipofectamine activity in the presence of serum was suppressed to less than one-fourth of the transfection efficiency under serum-free conditions. In comparison, the efficiency of 1:1 **2a**/DOPE in the presence of serum was only reduced to ~50%. Thus, in the presence of serum, this formulation is about 1.4 times as efficient as Lipofectamine under these conditions.

These findings suggest that **2a** induces gene transfer by a mechanism that is probably different from the one mediated by Lipofectamine. Lipofectamine is composed of a lipid derivative of spermine (DOSPA) which at

Table 1. Optimal Transfection Efficiency of PGL3 DNA Using 1:1 2a/DOPE in Different Cell Lines

cell line	Luciferase activity (RLU/mg protein)	cell line	Luciferase activity (RLU/mg protein)
COS-7	1.1×10^6	NIH3T3	1.79×10^5
T84	3.36×10^4	HEK293	4.41×10^5

[a] Concentration of DNA = 1.0 μg/well; concentration of 1:1 **2a**/DOPE = 4.0 μg/well. Data expressed as RLU/mg of cellular protein content. Experiments were performed in duplicate.

physiological pH remains multiply protonated giving it a polycationic character. The large concentration of positive charges offered by this lipid on the membrane surface facilitates both DNA binding and fusion with the eukaryotic cell surface leading to efficient transfection. However, in the presence of serum the multicationic character of Lipofectamine makes it compete with serum against DNA, leading to significant suppression of transfection efficiency. On the other hand, **2a** possesses only one cationic center per molecule and is therefore not as drastically affected by serum.

The amount of extractable protein from treated cells was also determined (not shown) as an indication of the cytotoxicity of the treated cells. The total cellular protein for cells treated with 2 μg/well of DNA was about 80% of the untreated control. For DNA concentrations lower than 2 μg, the lowest protein content was observed for those conditions that showed the highest transfection efficiency, indicating that the lipid−DNA complex is slightly toxic. However, under optimized conditions, the toxicity of 1:1 **2a**/DOPE and **3d** were found to little lower than that of the Lipofectamine or Lipofectin−DNA complex.

Intrigued by the fact that **2a**/DOPE (1:1) induced excellent TE under various conditions in COS-7 cells, we proceeded to check its generality in conferring DNA transfection across other cell lines. Using the above determined optimized ratio of [lipid]/[DNA], 1:1 **2a**/DOPE was used to transfect cell lines such as HEK293, NIH3T3, and T84. Table 1 shows that the formulation 1:1 **2a**/DOPE is indeed able to transfect a number of cell lines. Even for a cell line such as T84, which is often not conducive to transfection, this formulation (1:1 **2a**/DOPE) shows reasonably high luciferase activity. Thus, as a liposomal transfection reagent, the cationic ether-based cholesterol derivative **2a** as a 1:1 formulation in DOPE is indeed quite versatile and efficient.

In summary, we have systematically investigated the transfection abilities of a number of new cytofectins based on cholesterol that vary in terms of linkage of the cationic charge to cholesterol. In addition, within a given series of identical linkages, the headgroup hydration was also progressively modified. In the ester-linked series **1a**−**d**, it was observed that the progressive introduction of oxyethylene units on a cationic center at a fixed location reduced the transfection efficiency. In addition, the introduction of oligooxyethylene units as a spacer in the linker region of the lipid monomer (Figure 4b) in the ether-linked series **2a**−**d** also resulted in a marked diminution of the transfection ability. Thus efficient transfection requires a rather "dry" positive charge located as close as possible to the steroid skeleton of the cytofectin. Introduction of a membrane 'disorder'-promoting element like an oleyl chain to **1a** and **2a** resulted in considerable loss of transfection efficiency. Thus, there seems to exist an optimum balance between rigidity and fluidity for this class of cytofectins. The effect of the nature of linkage was investigated in detail, and the

advantage of the ether linkage over the ester linkage was clearly evidenced.

ACKNOWLEDGMENT

This work was supported by a Swarnajayanti Fellowship grant of the Department of Science and Technology, Govt. of India, awarded to S.B..

NOTE ADDED AFTER ASAP POSTING

The version of this paper posted on February 9, 2002, had an incorrect structure of DOPE (**5**) in Figure 1. The corrected version was posted on March 20, 2002.

LITERATURE CITED

(1) Moradpour, D., Schauer, J. I., Zurawski, V. R., Jr., Wands, J. R., and Boutin, R. H. (1996) *Biochem. Biophys. Res. Commun. 221*, 82.
(2) Krishnan-Ghosh, Y., Visweswariah, S. S., and Bhattacharya, S. (2000) *FEBS Lett. 473*, 341.
(3) The active component of a liposomal transfection reagent, which is usually a cationic amphiphile is referred to as a cytofectin ('*cyto*' meaning 'cell' and '*fectin*' for 'transfection', that is, gene delivery and expression).
(4) For an excellent review, see: Miller A. D. (1998) *Angew. Chem., Int. Ed. 37*, 1768.
(5) Cooper, R. G., Etheridge, C. J., Stewart, L., Marshall, J., Rudginsky, S., Cheng, S. H., and Miller, A. D. **(**1998) *Chem. Eur. J. 4*, 137.
(6) Vigneron, J. P., Oudrhiri, N., Fauquet, M., Vergely, L., Bradley, J. C., Basseville, M., Lehn, P., and Lehn, J.-M. (1996) *Proc. Natl. Acad. Sci. U.S.A. 93*, 9682.
(7) Gao, X., and Huang, L. (1991) *Biochem. Biophys. Res. Commun. 179*, 280.
(8) Leventis, R., and Silvius, J. R. (1990) *Biochim. Biophys. Acta 1023*, 124.
(9) Bottega, R., and Epand, E. M. (1992) *Biochemistry 31*, 9025.
(10) Otto, S., Osifchin, M., and Regen, S. L. (1999) *J. Am. Chem. Soc. 121*, 7276.
(11) Kreimeyer, A., Andre, F., Guoyette, C., and Hyunh-Dinh, T. (1998) *Angew. Chem., Int. Ed. 37*, 2853.
(12) Fichert, T., Regelin, A., and Massing, U. (2000) *Bioorg. Med. Chem. Lett. 10*, 787.
(13) Webb, M. S., Hui, S. W., and Steponkus, P. L. (1993) *Biochim. Biophys. Acta. 1145*, 93.
(14) Bloomfield, V. A. (1996) *Curr. Opin. Struct. Biol. 6*, 334.
(15) Safinya, C. R., Koltover, I., and Raedler, J. (1998) *Curr. Opin. Coll. Interface Sci. 3*, 69.
(16) Perrin, D. A., Armarego, W. L., and Perrin, D. R. *Purification of laboratory chemicals*, 3rd ed., Pergamon: NY, 1990.
(17) Bhattacharya, S., and Krishnan-Ghosh, Y. (2001) *Langmuir 17*, 2067.
(18) De Wet, J. R., Wood, K. V., DeLuca M., Helsinki, D. R., Subramani, S. (1986) *Mol. Cell. Biol. 7*, 725.
(19) Rose, J. K., Buonocore, L., and Whitt, M. A. (1991) *BioTechniques 10*, 520.

BC010048H

CORRECTIONS

Volume 13, Number 1, January/February, 2002.

Stephen P. Cooke,* R. Barbara Pedley, R. Boden, Richard H. J. Begent, and Kerry A. Chester

IN VIVO TUMOR DELIVERY OF A RECOMBINANT SINGLE CHAIN FV::TUMOR NECROSIS FACTOR-α FUSION PROTEIN

Page 7. An incorrect manuscript title appears in the published manuscript. The corrected title appears above.

BC020015H

10.1021/bc020015h
Published on Web 01/30/2002

MAY/JUNE 2002
Volume 13, Number 3

© *Copyright 2002 by the American Chemical Society*

Bioconjugate Chemistry

COMMUNICATIONS

Facile Synthesis of Thiol-Reactive Cy3 and Cy5 Derivatives with Enhanced Water Solubility

Alexei Toutchkine, Perihan Nalbant, and Klaus M. Hahn*

Department of Cell Biology, Scripps Research Institute, 10550, N. Torrey Pines Road, BCC162, La Jolla, California 92037. Received September 25, 2001

The cyanine dyes Cy3 and Cy5 have proven valuable in numerous applications involving conjugation with proteins. Practical syntheses of lysine-selective, succinimidyl ester derivatives of these dyes have been published, and succinimidyl esters are commercially available. However, the published syntheses of cysteine-selective derivatives produce relatively low yields from expensive starting materials, or produce molecules with marginal water solubility for protein labeling. We report here facile syntheses (four steps, >50% overall yield) of iodoacetamide, sulfhydryl-reactive derivatives of the Cy3 and Cy5 fluorophores. These novel derivatives have good water solubility (>2.5 mM) and bear only one reactive side chain, reducing possible protein cross-linking encountered with previous derivatives.

INTRODUCTION

The cyanine dyes Cy3 and Cy5, originally described by Waggoner and co-workers (*1*, *2*), have proven their utility in a wide range of applications. These dyes are bright and photostable, and are well suited to microscopy of living cells. Lysine-reactive succinimidyl ester derivatives of Cy3 and Cy5 for protein labeling can be readily made using published syntheses (*2*, *3*) and are commercially available. Because lysine is relatively abundant in most proteins, lysine-reactive dyes are valuable for introducing several dyes on the same protein (i.e. in antibody labeling for immunofluorescence staining). Lysine-reactive dyes, however, cannot readily be used for precise site-specific dye attachment. Site-specific labeling is usually accomplished through conjugation to cysteine, which is less abundant and can be introduced at the desired site using molecular biology approaches. Site-specific labeling is important in many potentially valuable applications of the cyanine dyes, including fluorescence resonance energy transfer (FRET) microscopy, where dyes must be placed to respond to protein activity without perturbing normal biological behavior (*4*−*6*).

This paper addresses the current inaccessibility of water soluble, cysteine-reactive Cy3 and Cy5 derivatives. Ernst et al. have described cysteine-reactive analogues of these dyes which are substantially less water soluble than the lysine-reactive derivatives and are therefore difficult to use for protein labeling. More recently, Gruber et al. produced water-soluble cysteine-reactive derivatives by linking the succinimidyl ester of the lysine-reactive dyes to chains bearing different thiol-reactive groups (*7*). The dyes used as starting materials for this approach are available only in small quantities and are very expensive. Moreover, Gruber et al. did not prepare any iodoacet-

* To whom correspondence should be addressed. Phone (858) 784-8726, Fax (858) 784-8764, E-mail: khahn@scripps.edu.

10.1021/bc015558q CCC: $22.00 © 2002 American Chemical Society
Published on Web 03/27/2002

amido derivatives, which may be advantageous in certain applications.

Here we describe straightforward, high-yielding syntheses of Cy3 and Cy5 derivatives bearing cysteine-selective iodoacetamide reactive groups. The new syntheses place two water-solubilizing sulfonate groups on the dyes, producing reagents with good water solubility for practical protein labeling. Only a single reactive side chain is introduced, minimizing problems with protein cross-linking. The new dyes are referred to as neo-Cy3 and neo-Cy5.

EXPERIMENTAL PROCEDURES

Materials. Analytical grade reagents were purchased from major suppliers.

5-Chloroacetamido-1,3,3-trimethyl-2-methyleneindoline (IV) and 5-chloroacetamidomethyl-1,3,3-trimethyl-2-methyleneindoline (VII) were prepared by the method of Gale (*8*, *9*). The potassium salt of 2,3,3-trimethylindolenine-5-sulfonate was prepared by the method of Waggoner (*2*).

Methods. UV−vis spectra were measured using a Hewlett-Packard 8453 diode array spectrophotometer. Emission and excitation spectra were obtained using a Spex Fluorolog 2 spectrofluorometer at 23 °C. Quantum yields were measured using merocyanine 540 (*10*) or indotricarbocyanine (*11*) as internal standards (*12*). Mass spectra were obtained by MALDI−FT MS techniques on an IonSpec FT MS spectrometer. ^{1}H NMR spectra of 0.5% solutions in CD_3SOCD_3 were recorded on Bruker DRX-400 or DRX-500 spectrometers. The peaks corresponding to the residual protons of CD_3SOCD_3 (2.49 ppm) were used as internal reference. All operations with dyes were performed under dim light. Flasks containing dyes were wrapped with aluminum foil.

2,3,3-Trimethyl-1-(3-sulfonatopropyl)-3*H*-indolinium-5-sulfonate (I). The potassium salt of 2,3,3-trimethylindolenine-5-sulfonate (*2*) (1.49 g, 0.006 mol, vacuum-dried) and 1,3-propane sultone (0.80 g, 0.0066mol) were mixed in 10 mL of dichlorobenzene and heated at 120 °C for 12 h with stirring under nitrogen. The mixture was cooled, 1,2-dichlorobenzene was decanted, and the solid was washed with ether to give practically pure quaternary salt. The yield was 2.20 g (90%).

^{1}H NMR (500 MHz, DMSO-d_6): δ 1.52 (s, 6H, 2 × CH_3), 2.13 (p, $^3J_{H-H}$ = 7.5 Hz, 2H, $CH_2CH_2CH_2$), 2.65 (t, $^3J_{H-H}$ = 7.5 Hz, 2H, CH_2SO_3), 2.82 (s, 3H, CH_3), 4.61(t, $^3J_{H-H}$ = 7.5 Hz, 2H, CH_2N), 7.70−8.00 (m, 3H, aromatic ring).

2-{(*E*)-2-[Acetyl(phenyl)amino]ethenyl}-3,3-dimethyl-1-(3-sulfonatopropyl)-3*H*-indolinium-5-sulfonate (II). A mixture of the quaternary salt I (2.00 g) and *N*,*N*′-diphenylformamidine (2.00 g) in 10 mL of acetic acid−acetic anhydride (1:2) was heated to reflux for 2 h. The solvent was removed on a rotary evaporator, and the product was washed with acetone until free yellow powder was obtained. The yield was 2.64 g (97%).

^{1}H NMR (500 MHz, DMSO-d_6): δ 1.71 (s, 6H, 2 × CH_3), 1.84 (p, $^3J_{H-H}$ = 7.5 Hz, 2H, $CH_2CH_2CH_2$), 2.15 (s, 3H, CH_3CO), 2.65 (t, $^3J_{H-H}$ = 7.5 Hz, 2H, CH_2SO_3), 4.21(t, $^3J_{H-H}$ = 7.5 Hz, 2H, CH_2N), 5.40 (d, $^3J_{H-H}$ = 14 Hz, C=C−H), 7.50−8.00 (m, 3H, aromatic ring) 9.05 (d, $^3J_{H-H}$ = 14 Hz, C=C−H).

2-{(1*E*,3*Z*)-3-[5-(Iodoacetylamino)-1,3,3-trimethyl-1,3-dihydro-2*H*-indol-2-ylidene]prop-1-enyl}-1-(3-sulfonatopropyl)-3*H*-indolium-5-sulfonate (Neo-Cy3, VI). A mixture of 1.35 g of anyl II and 0.65 g of 5-chloroacetamido-1,3,3-trimethyl-2-methyleneindoline IV was heated in 20 mL of acetic anhydride at 130 °C with stirring under nitrogen for 45 min. The mixture was cooled to room temperature, and the dye was separated by filtration. The crude dye was chromatographed over silica gel, eluting with acetone−methanol (3:1), to yield 1.15 g (71%) of pure chloroacetamido cyanine V. This dye was refluxed for 3 h in methanol (30 mL) containing 2.0 g of sodium iodide. The solution was cooled, filtered and concentrated in a vacuum to 10 mL. The dye was precipitated by the addition of 100 mL of acetone to give 1.2 g of dye VI (92%). The analytical sample of the dye was purified by HPLC on a Vydac C-18 column (no. 218TP152022, 22 × 250 mm, 15−20 μm), 3 mL/min water−acetonitrile gradient.

^{1}H NMR (500 MHz, DMSO-d_6): δ 1.74 (s, 6H, 2 × CH_3), 1.76 (s, 6H, 2 × CH_3), 2.08 (p, $^3J_{H-H}$ = 7.0 Hz, 2H, $CH_2CH_2CH_2$), 2.70 (t, $^3J_{H-H}$ = 7.0 Hz, 2H, CH_2SO_3), 3.71 (s, 3H, CH_3, N−CH_3), 3.91 (s, 2H, CH_2, CH_2I), 4.30 (t, $^3J_{H-H}$ = 7.0 Hz, 2H, CH_2N), 6.48 (d, $^3J_{H-H}$ = 13.6 Hz, 1H, C=C−H), 6.62 (d, $^3J_{H-H}$ = 13.6 Hz, 1H, C=C−H), 7.48−7.90 (m, 6H, aromatics), 8.38 (t, $^3J_{H-H}$ = 13.6 Hz, C=C−H), 10.59 (s, 1H, NH−CO). MALDI−FTMS: MH^+ found: 750.0746, calculated: 750.0775.

2-[(1*E*,3*E*)-4-Acetyl(phenyl)aminobuta-1,3-dienyl]-3,3-dimethyl-1-(3-sulfonatopropyl)-3*H*-indolium-5-sulfonate (III). A mixture of the quaternary salt I (2.00 g) and malonaldehyde dianilide hydrochloride (0.65 g) in 10 mL of acetic acid−acetic anhydride (1:2) was heated at reflux for 2 h. The solution of anyl was cooled to room temperature and used without further purification in the next step.

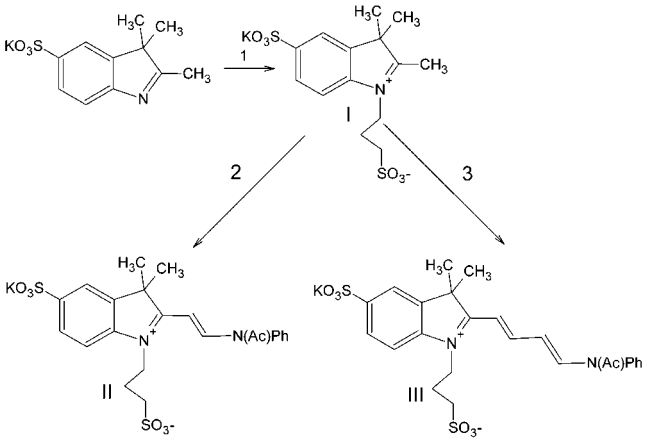
2-[(1*E*,3*E*,5*Z*)-5-(5-(Iodoacetylamino)-1,3,3-trimethyl-1,3-dihydro-2*H*-indol-2-ylidene)penta-1,3-dienyl]-1-(3-sulfonatopropyl)-3*H*-indolium-5-sulfonate (neo-Cy5, VIII). The solution of anyl III was mixed with 1.39 g of 5-chloroacetamidomethyl-1,3,3-trimethyl-2-methyleneindoline VII. The mixture was heated to 120 °C for 20 min and cooled to room temperature. The diethyl ether was added to the mixture to precipitate the dye. The crude dye was chromatographed over silica gel, eluting with acetone−methanol (3:1), to yield 2.14 g (61%) of pure chloroacetamido cyanine (VIII). This dye was refluxed in 30 mL of methanol containing 2.0 g of sodium iodide for 3 h. The solution was cooled, filtered, and concentrated in a vacuum to 10 mL. The dye was precipitated by the addition of 100 mL of acetone to give 2.30 g (95%) of dye IX. The analytical sample of the dye was purified by HPLC on a Vydac C-18 column (the same condition as for neo-Cy3 dye).

^{1}H NMR (400 MHz, DMSO-d_6): δ 1.67 (s, 12H, 4xCH_3), 1.98 (p, $^3J_{H-H}$ = 7.3 Hz, 2H, $CH_2CH_2CH_2$), 2.67 (t, $^3J_{H-H}$ = 7.3 Hz, 2H, CH_2SO_3), 3.60 (s, 3H, CH_3, N−CH_3), 3.71 (s, 2H, CH_2, CH_2I), 4.28 (t, $^3J_{H-H}$ = 7.3 Hz, 2H, CH_2N), 4.32 (d, $^3J_{H-H}$ = 5.6 Hz, 2H, CH_2−NH), 6.28 (d, $^3J_{H-H}$ = 14.1 Hz, 1H, C=C−H), 6.40−8.60 (m, 11H). MALDI−FTMS: MH^+found: 790.1078,calculated: 790.1088.

Preparation of Neo-Cy3−Cysteine Conjugate. A 30 mg amount of neo-Cy3 dye was added to 30 mg of cysteine in 2.0 mL of $NaHCO_3$−Na_2CO_3 buffer (pH = 8.0), and the mixture was stirred for 2 h at room temperature. Silica gel TLC (CH_3CN−H_2O: 90−10) showed complete consumption of starting dye. Several drops of hydrochloric acid were added to the mixture until pH = 5, and the conjugate was isolated by preparative HPLC on Vydac C18 column (same condition as for neo-Cy3 dye).

^{1}H NMR (500 MHz, DMSO-d_6): δ 1.74 (s, 6H, 2 × CH_3), 1.76 (s, 6H, 2 × CH_3), 2.08 (p, $^3J_{H-H}$ = 7.0 Hz, 2H, $CH_2CH_2CH_2$), 2.70 (t, $^3J_{H-H}$ = 7.0 Hz, 2H, CH_2SO_3), 3.71

Scheme 1. Synthesis of Acetanilidovinyl Salts[a]

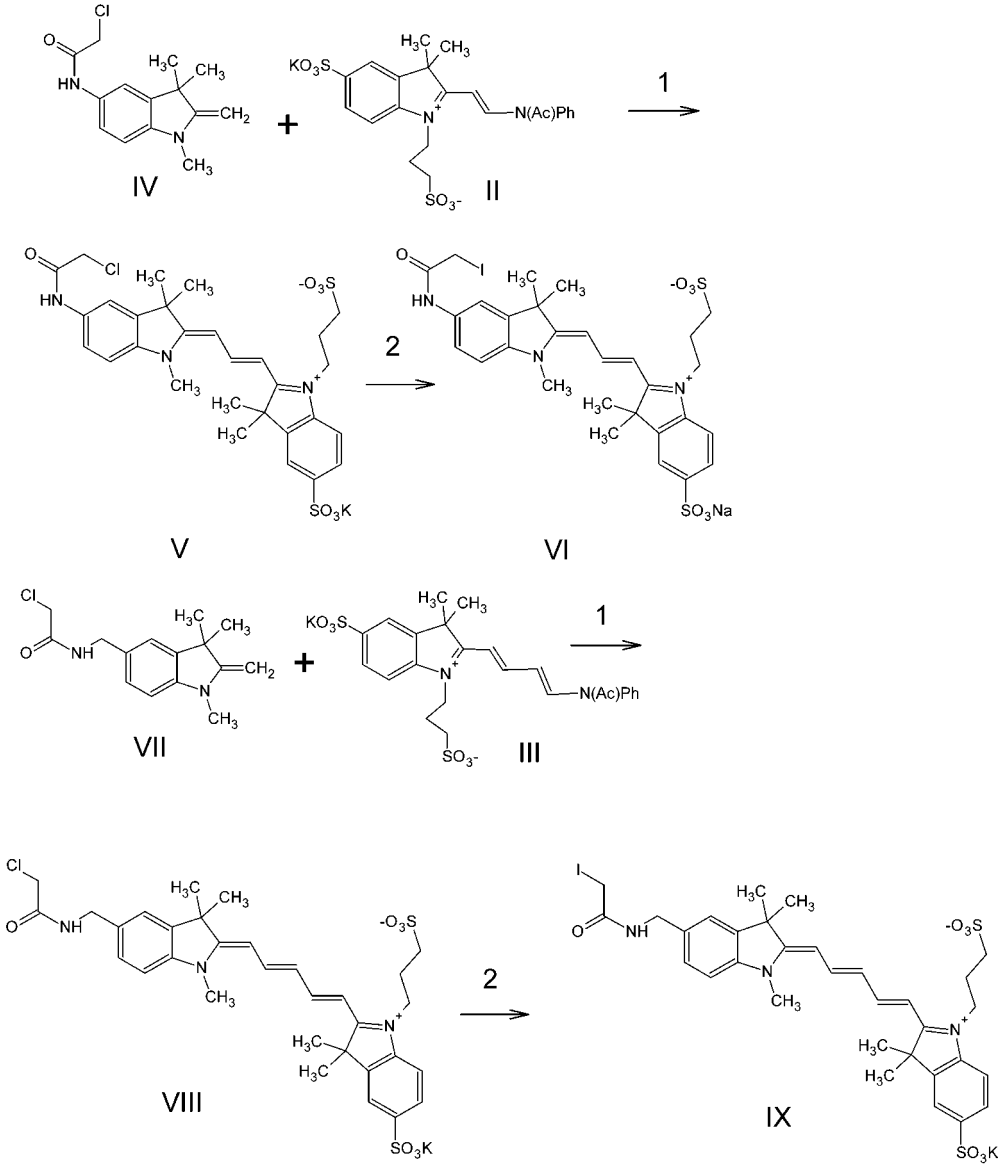


[a] Reagents and conditions: (1) propane sultone, 120 °C; (2) diphenylformamidine, Ac_2O; (3) malonaldehyde dianyl monochloride, $AcOH-Ac_2O$.

(s, 3H, CH_3, $N-CH_3$), 3.91 (s, 2H, CH_2, CH_2I), 4.30 (t, $^3J_{H-H}$ = 7.0 Hz, 2H, CH_2N), 6.48 (d, $^3J_{H-H}$ = 13.6 Hz, 1H, C=C−H), 6.62 (d, $^3J_{H-H}$ = 13.6 Hz, 1H, C=C−H), 7.48−7.90(m, 6H, aromatics), 8.38 (t, $^3J_{H-H}$ = 13.6 Hz, C=C−H), 10.59 (s, 1H, NH−CO). MALDI−FTMS: MH^+ found:743.1868, calculated: 743.185.

Protein Labeling. A fragment of Wiskott Aldrich Syndrome Protein (WASP, residues 201−320), mutated to contain a single cysteine (F271C), was labeled with Cy3 and separately with Cy5 dye. A stock solution of the dye in DMSO (10−20 mM) was added to 200 μL of protein solution (200 μM in sodium phosphate buffer, pH = 7.5), to produce a final dye concentration of 1−2 mM. The reaction mixture was incubated for 4 h at room temperature and then quenched by addition of 1 μL mercaptoethanol. The reaction mixture was spun at 12000 rpm for 2 min to remove any precipitates, which might have formed during the reaction, and the supernatant was purified using G25 sepharose gel filtration. The dye−protein adduct was clearly separated from free dye during gel-filtration. Purity of the conjugates was confirmed by SDS−PAGE electrophoresis. No free dye was seen in purified protein conjugates. Control samples of free dye were clearly visible on the gel at lower MW than protein. Conjugates formed single, highly colored fluorescent

Scheme 2. Synthesis of the Dyes[a]



[a] Reagents and conditions: (1) AcONa, Ac_2O, 120 °C; (2) NaI, MeOH, 65 °C.

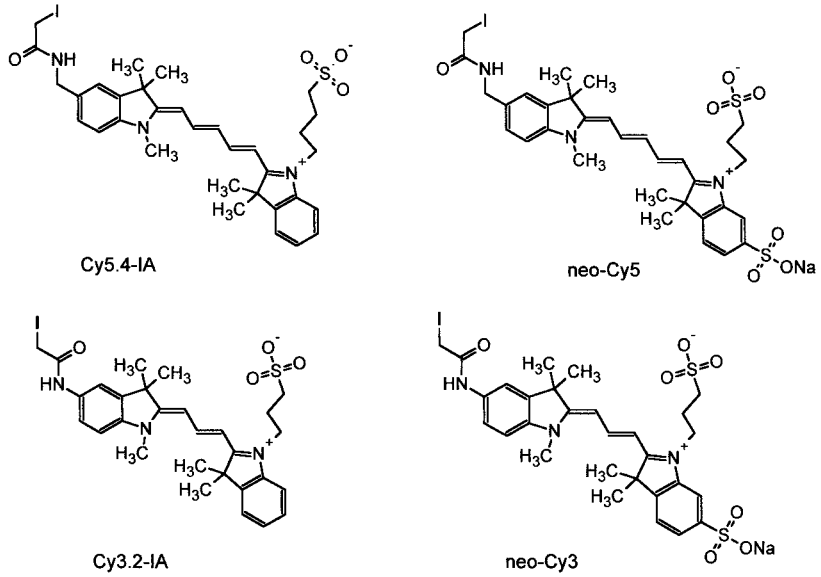


Figure 1. Structure of cysteine-reactive neo-Cy3 and neo-Cy5 dyes and previously described (*1*) Cy3.2-IA and Cy5.4-IA dye.

Table 1. Absorption and Fluorescence Data for Neo-Cy3, Neo-Cy5, and Labeled Substrates

dye	solvent	absorption, λ_{max}/nm (ϵ^a/M^{-1})	emission, λ_{max}/nm	ϕ^b
neo-Cy3, VI	PBS[c]	551 (98 000)	573	0.02
	MeOH	563 (95 000)	583	0.03
	DMSO	573 (97 000)	595	0.06
neo-Cy5, IX	PBS	643 (170 000)	660	0.10
	MeOH	648 (200 000)	665	0.22
	DMSO	656 (195 000)	675	0.25
neo-Cy3-cysteine	PBS	552 (107 000)	573	0.02
neo-Cy3-WASP fragment	PBS	551 (100 000)	572	0.02
neo-Cy5-WASP fragment	PBS	647 (180 000)	664	0.13
Cy3.2-IA[d]	EtOH	565 (116 000)	590	0.07
Cy5.4-IA[d]	EtOH	652 (128 000)	669	0.27

[a] Extinction coefficient, error is ±5%. [b] Quantum yield of fluorescence, error is ±10%. [c] Phosphate-buffered saline. [d] Reference 1.

protein bands with molecular weights corresponding to the WASP fragment. The dye-to-protein ratio was calculated by measuring protein and dye concentrations using absorbance spectroscopy as previously described (*13*). In each case this ratio was between 0.9 and 1.0.

RESULTS AND DISCUSSION

The most widely used thiol-reactive groups for protein modification are maleimide and iodoacetamide. Maleimide adducts have disadvantages in that they can hydrolyze, thereby causing significant changes in the fluorescence of protein conjugates, and they can undergo a nucleophilic ring-opening reaction with amines to yield cross-linked protein products (*13*). We therefore chose the iodoacetamide group as the reactive side chain for the new dyes. They contain one reactive side chain rather than the two found in some earlier derivatives. This abrogates problems of protein cross-linking and inhomogeneous conjugation sometimes seen during labeling.

The synthesis of both new cyanine dyes was accomplished using the same general method (*14*), in which Fischer's bases IV and VII were condensed with acetanilidovinyl salts II and III (Scheme 2). These straightforward syntheses produced the dyes in four steps with overall yields of 57% (neo-Cy3) and 50% (neo-Cy5). The reactivity of these iodoacetamido dyes was verified by facile formation of conjugates with cysteine and with purified protein (see Materials and Methods).

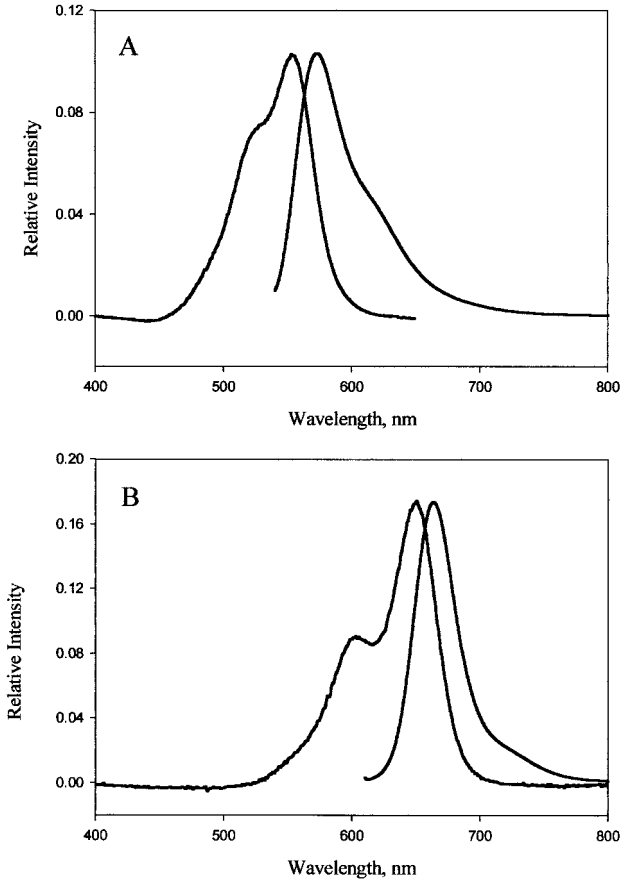


Figure 2. Normalized absorbance and fluorescence spectra of neo-Cy3-WASP (A) and neo-Cy5-WASP (B) conjugates in PBS (pH = 7.4), concentrations 1 μM.

Importantly, the neo-Cy dyes bear two sulfonate groups (Figure 1), and this leads to excellent water solubility (neo-Cy3, 3 mM; neo-Cy5, 2.5 mM), bringing accessible concentrations into the range typically used for protein labeling. The fluorescence properties of the neo-Cy dyes are given in Table 1. The quantum yields, extinction coefficients, and fluorescence maxima of the neo-Cy dyes deviate little from those reported for Cy3 and Cy5. As

with Cy3 and Cy5, the absorbance and emission maxima of the new dyes show little solvent sensitivity, while the quantum yields are greater in more hydrophobic (methanol) or more viscous (dimethyl sulfoxide) solvents (Table 1) as was previously reported for many polymethine dyes (*15*). The main nonfluorescent deactivation path for the exited state of cyanine dyes is photoisomerization around the central double bond, and the rate of this photoisomerization becomes smaller as hydrophobicity or viscosity of the solvent increases (*15*).

Attachment of the dyes to cysteine or to a protein (a fragment of WASP, see Materials and Methods) did not alter the dyes' favorable fluorescence properties (Table 1, Figure 2).

Both the absorbance and fluorescence spectra are similar to spectra of free dyes, indicating that there is no quenching of fluorescence after attachment of dyes to protein.

CONCLUSION

The many published applications of the original Cy3 and Cy5 dyes attest to their value. We hope that the straightforward syntheses presented here will make cysteine-reactive derivatives accessible to more researchers.

ACKNOWLEDGMENT

We are grateful to Velda Comstock for expert secretarial assistance. This work was supported by NIH grant GM57464 to K.M.H. and by a Leukemia & Lymphoma Society fellowship (3427-02) to A.T.

LITERATURE CITED

(1) Ernst, L. A., Gupta, R. K., Mujumdar, R. B., and Waggoner, A. S. (1989) Cyanine dye labeling reagents for sulfhydryl groups. *Cytometry 10*, 3−10.

(2) Mujumdar, R. B., Ernst, L. A., Mujumdar, S. R., Lewis, C. J., and Waggoner, A. S. (1993) Cyanine dye labeling reagents: sulfoindocyanines succinimidyl esters. *Bioconjugate Chem. 4*, 105−111.

(3) Reddington, M. V. (1998) New glycoconjugated cyanine dyes as fluorescent labeling reagents. *J. Chem. Soc., Perkin Trans. 1* 143−147.

(4) Kraynov, V. S., Chamberlain, C. E., Bokoch, G. M., Schwartz, M. A., Slabaugh, S., and Hahn, K. M. (2000) Localized Rac activation dynamics visualized in living cells. *Science 290*, 333−337.

(5) Kenworthy, A. K. (2001) Imaging protein−protein interactions using fluorescence resonance energy transfer microscopy. *Methods 24*, 289−296.

(6) Mi, Z., Mai, J., Lu, X., and Robbins, P. D. (2000) Characterization of a class of cationic peptides able to facilitate efficient protein transduction in vitro and in vivo. *Mol. Ther. 2*, 339−347.

(7) Gruber, H. J., Kada, G., Pragl, B., Riener, C., Hahn, C. D., Harms, G. S., Ahrer, W., Dax, T. G., Hohenthanner, K., and Knaus, H.-G. (2000) Preparation of Thiol-Reactive Cy5 Derivatives from Commercial Cy5 Succinimidyl Ester. *Bioconjugate Chem. 11*, 161−166.

(8) Gale, D. J., and Wilshire, J. F. K. (1974) Fibre-Reactive Basic Dyes. I−Polymethine Dyes Containing the N−Chloroacetyl Group. *J. Soc. Dyers Colour. 90*, 97−100.

(9) Gale, D. J., Lin, J., and Wilshire, J. F. K. (1977) The Amidomethylation and Bromination of Fisher's Base. The Preparation of Some New Polymethine Dyes. *Aust. J. Chem. 30*, 689−694.

(10) Onganer, Y., Yin, M., Bessire, D. R., Quitevis, E. L. (1993) Dynamic Solvatation Effects on the Cis−Trans Isomerization Reaction: Photoisomerization of Merocyanine 540 in Polar Solvents. *J. Phys. Chem. 97*, 2344−2354.

(11) Sims, P. J., Waggoner, A. S., Wang, C. H., and Hoffman, J. F. (1974) Studies on the mechanism by which cyanine dyes measure membrane potential in red blood cells and phosphatidylcholine vesicles. *Biochemistry 13*, 3315−3330.

(12) Demas, J. N., and Crosby, G. A. (1971) The Measurement of Photoluminescence Quantum Yields. A Review. *J. Phys. Chem. 75*, 991−1024.

(13) Haugland, R. P. (1996) *Handbook of Fluorescent Probes and Research Chemicals*; Molecular Probes Inc., Eugene, OR.

(14) Hamer, F. M. (1964) The Cyanine Dyes and Related Compounds, in *The Chemistry of Heterocyclic Compounds* (A. Wiessberger, Ed.) Interscience, New York.

(15) Mandal, D., Pal, S. K., Sukul, D., and Bhattacharyya, B. (1999) Photophysical Processes of Merocyanine 540 in Solutions and in Organized Media. *J. Phys. Chem. A 103*, 8156−8159.

BC015558Q

Low-Density Lipoprotein Reconstituted by Pyropheophorbide Cholesteryl Oleate as Target-Specific Photosensitizer

Gang Zheng,*,† Hui Li,† Min Zhang,†,§ Sissel Lund-Katz,‖ Britton Chance,‡ and Jerry D. Glickson†

Department of Radiology, Department of Biochemistry and Biophysics, University of Pennsylvania Medical School, Philadelphia, Pennsylvania 19104; and Department of Chemistry, Shanghai University, Shanghai 200436, China; and Department of Pediatric GI Nutrition, The Children's Hospital of Philadelphia, Philadelphia, PA 19104. Received December 14, 2001

To target tumors overexpressing low-density lipoprotein receptors (LDLr), a pyropheophorbide cholesterol oleate conjugate was synthesized and successfully reconstituted into the low-density lipoprotein (LDL) lipid core. Laser scanning confocal microscopy studies demonstrated that this photosensitizer-reconstituted LDL can be internalized via LDLr by human hepatoblastoma G_2 ($HepG_2$) tumor cells.

INTRODUCTION

Photodynamic therapy (PDT) is a promising cancer treatment that involves the combination of light and a photosensitizer, normally a porphyrin derivative. Each factor is harmless by itself, but when combined with oxygen they can produce lethal reactive oxygen species that kill tumor cells (*1*). Singlet oxygen ($^1O_2$) is a powerful, fairly indiscriminate oxidant that is generally recognized as the key agent of PDT-induced tumor necrosis. Because the diffusion range of $^1O_2$ is much smaller than the diameter of a single cell, the site of the primary generation of $^1O_2$ determines which subcellular structures may be attacked (*2*). Consequently, if a photosensitizer is preferentially localized in tumor cells, PDT-induced cellular damage will be highly tumor specific. Therefore, target-specific photosensitizers are desirable.

The LDL particle consists of a nonpolar core of neutral lipids (cholesterol esters, triglycerides) surrounded by a polar shell of phospholipid, unesterified cholesterol, and apolipoprotein B100 that is recognized by cell surface LDLr (*3*). A number of tumors overexpress LDLr to meet the high cholesterol demand for membrane synthesis. These include acute myelogenous leukemia (3- to 100-fold), colon cancer (6-fold), adrenal adenoma (8-fold), lung carcinoma, brain tumors, and metastatic prostate cancer (*4*−*6*). Therefore, numerous efforts have been made to use LDL as a vehicle for selective delivery of photosensitizers and other antitumor agents. Porphyrins are known for their ability to associate with LDL through direct incubation without inhibiting LDLr binding (*7*) or processing (*8*). Thus, many PDT agents were incorporated into LDL via this approach and showed improved activity (*9*). For example, a benzoporphyrin derivative (BPD) associated with LDL by simple mixing induced photodynamic cell killing 7-fold better than BPD alone (*10*). However, such a simple incubation method has a major drawback in that porphyrins can exchange between LDL, other phospholipids, and cell membranes, reducing the targeting specificity.

One of the most important methods for packaging and delivering LDL-targeting drugs is the LDL reconstitution approach. Kreiger et al. were the first to report that it is possible to reconstitute the core of LDL with exogenous neutral lipids or suitable hydrophobic compounds, and such reconstituted LDL (r-LDL) is essentially identical with native LDL in its ability to bind to LDLr, to be internalized by cells and to be hydrolyzed in lysosomes (*11*). Since r-LDL can be internalized exclusively by LDLr, many cytotoxic compounds were delivered to cancer cells using this method and showed good antitumor activity (*4*−*6*). However, competing with tumor for r-LDL are organs known to overexpress LDLr, particularly the liver and adrenals, leading to undesirable toxicity (*12*). In this regard, the PDT protocol utilizing photosensitizer based r-LDL will be more suitable because (1) organ selectivity of PDT will come from the ability to confine activation of the photosensitizer to the tumors by restricting the illumination to that specific region; (2) the photosensitizer itself should bear no dark toxicity; and (3) the photosensitizer phototoxicity can be postponed until after non-tumor-bound photosensitizer has been cleared from the body. Goldstein, Brown, and co-workers first introduced a pyrene-based r-LDL for targeted killing of cells by LDLr-mediated photosensitization (irradiation at 300−400 nm) (*13*). However, this pioneering approach has never been applied using porphyrins, the most useful PDT agents. We report here the design and synthesis of a novel chlorophyll-based photosensitizer containing anchors that render it compatible with LDL's phospholipid coat and lipophilic core. This new dye conjugate was successfully reconstituted into the LDL core, and such an r-LDL-based photosensitizer was internalized by tumor cells overexpressing LDLr and accumulated in intracellular compartments such as endosomes or lysosomes.

* Address correspondence to Dr. Gang Zheng, University of Pennsylvania, Chemistry Building, Box 66, 231 South 34th Street, Philadelphia, PA 19104. Tel: +1-215-898-3105. Fax: +1-215-573-2113. E-mail: zheng@rad.upenn.edu.

† Department of Radiology, University of Pennsylvania Medical School.

‡ Department of Biochemistry and Biophysics, University of Pennsylvania Medical School.

§ Shanghai University.

‖ Children's Hospital of Philadelphia.

10.1021/bc025516h CCC: $22.00 © 2002 American Chemical Society
Published on Web 04/18/2002

EXPERIMENTAL PROCEDURES

Materials and General Methods. Melting points (uncorrected) were measured with a Mel-Temp II apparatus. UV−vis spectra were recorded with a Beckman DU-600 spectrophotometer. ^{1}H NMR and ^{13}C NMR spectra were recorded with Bruker ASPECT 360 MHz instrument. Mass spectrometry analysis and elemental analysis were performed at the Mass Spectrometry Facility of the Department of Chemistry, University of Pennsylvania. 5-Androsten-17β-amino-3β-ol was purchased from Steraloid Inc., Newport, RI. Methyl pheophorbide *a* was obtained from *Spirulina pacifica* algae available from Cyanotech Corp., Hawaii. Other chemicals were purchased from Aldrich. Where necessary, solvents were dried before use. For TLC, EM Science TLC plates (silica gel 60 F_{254}) were used. Chlorophyll derivatives were visible without staining, and other compounds were stained with phosphomolybdic acid reagent. Reverse phase (RP) analytical HPLC was performed using a Zorbax RX-C8 (9.4 mm × 250 mm) column eluting at 1.0 mL/min with MeCN/phosphate buffer (25% to 95% MeCN gradient) with UV−vis detection at 414 nm.

5-Androsten-17β-Boc-amino-3β-ol (2). Di-*tert*-butyl dicarbonate (420 g, 1.90 mmol) was added to a solution containing 5-androsten-17β-amino-3β-ol (475 mg, 1.64 mmol) and triethylamine (0.27 mL, 1.94 mmol) in dichloromethane (50 mL). The reaction mixture was stirred at room temperature for 2 days. Evaporation of the solvent gave a white residue. This crude product was purified by silica gel column chromatography (30% ethyl acetate in hexanes) to give **2** as a white solid in 95% yield (610 mg, 1.57 mmol). Mp: 168−172 °C; exact mass calcd: 389.3; found by ESI-MS: 390.4 (MH^+). Anal. Calcd for $C_{24}H_{39}NO_3$: C, 73.99; H, 10.09; N, 3.60. Found: C, 73.52; H, 10.39; N, 3.19. ^{1}H NMR ($CDCl_3$): δ 5.34 (m, 1H, 6-H), 4.42 (brs, 1H, N−H), 3.53 (m, 2H, 3-H + 17-H), 2.27 (m, 2H), 2.17−1.92 (m, 2H), 1.90−1.70 (m, 3H), 1.69−1.49 (m, 6H), 1.48−1.32 (m, 3H), 1.44 (s, 9H for *tert*-butyl), 1.31−1.15 (m, 2H), 1.15−0.95 (m, 2H), 1.00 (s, 3H, 19-CH_3), 0.67 (s, 3H, 18-CH_3); ^{13}C NMR ($CDCl_3$): δ 156.2, 141.1, 121.5, 79.2, 71.9, 60.5, 53.0, 50.4, 42.8, 42.5, 37.5, 37.2, 36.8, 32.3, 31.8, 31.7, 29.0, 28.6, 28.6, 28.6, 23.7, 20.9, 19.6, 12.0.

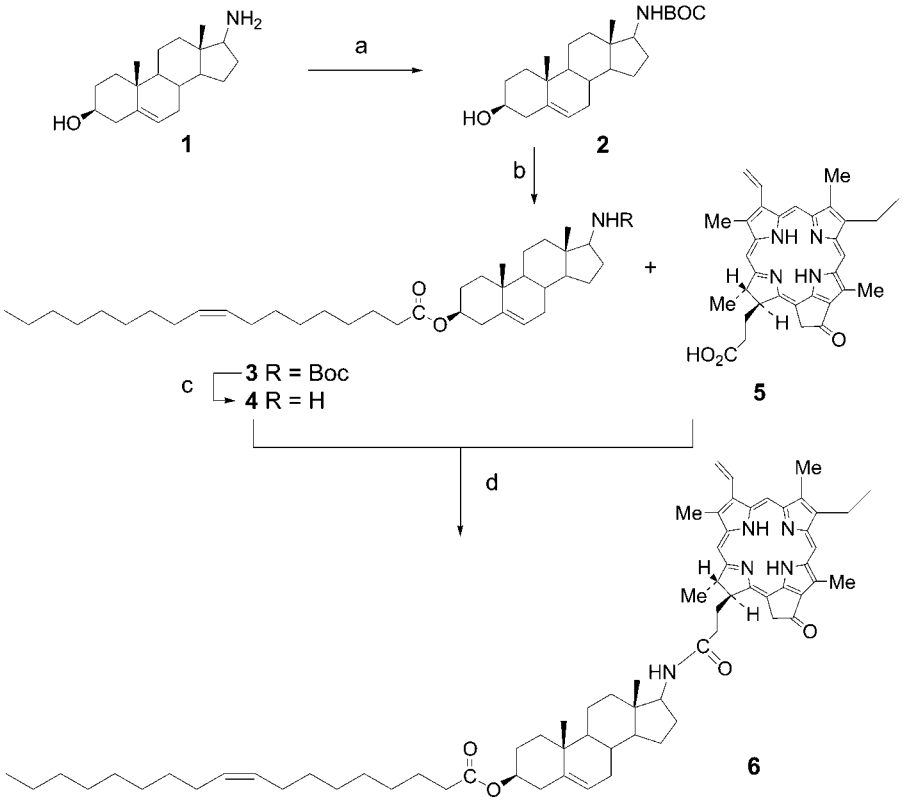
5-Androsten-17β-Boc-amino-3β-yl Oleate (3). Oleoyl chloride (710 mg, 2.35 mmol) was slowly added into a 20 mL pyridine solution of **2** (610 mg, 1.57 mmol). After 2 h, the reaction mixture was poured into 40 mL of ice−water. It was filtered and washed with water three times to give a crude residue. This crude product was then chromatographed on silica column with 10% ethyl acetate in hexanes to afford the title compound as sticky solid in 60% yield (615 mg, 0.94 mmol). Exact mass calcd: 653.5; found by ESI-MS: 654.6 (MH^+). Anal. Calcd for $C_{42}H_{71}NO_4$: C, 77.13; H, 10.94; N, 2.14. Found: C, 77.35; H, 11.41; N, 1.76. ^{1}H NMR ($CDCl_3$): δ 5.32 (m, 3H, 6-H + 2 × vinyl-H of oleate), 4.58 (m, 1H, 3-H), 4.41 (brs, 1H, N−H), 3.52 (m, 1H, 17-H), 2.28 (m, 4H), 2.17−1.70 (m, 10H), 1.61 (m, 8H), 1.50−1.38 (m, 2H), 1.43 (s, 9H for *tert*-butyl), 1.37−0.95 (m, 23H), 1.00 (s, 3H, 19-CH_3), 0.85 (t, 3H, terminal CH_3 of oleate), 0.65 (s, 3H, 18-CH_3); ^{13}C NMR ($CDCl_3$): δ 173.3, 139.4, 130.1, 129.9, 122.4, 78.1, 73.7, 60.5, 52.8, 50.2, 42.7, 38.3, 37.1, 37.0, 36.8, 34.8, 32.2, 32.1, 31.7, 29.9, 29.8, 29.7, 29.5, 29.5, 29.3, 29.3, 29.2, 29.2, 28.9, 28.6, 28.6, 28.6, 27.9, 27.4, 27.3, 25.2, 23.7, 22.8, 20.7, 19.5, 14.3, 11.9.

5-Androsten-17β-amino-3β-yl Oleate (4). Compound **3** (340 mg, 0.52 mmol) was dissolved in trifluoroacetic acid (5 mL), and the mixture was stirred at room temperature under argon atmosphere for 2.5 h. The acid was removed by rotavapor. Saturated aqueous Na_2CO_3 (5 mL) was added to the residue and then extracted with CH_2Cl_2 (3 × 10 mL), and the combined extracts were dried with Na_2SO_4. After the solvent was removed, the residue was dried under high vacuum and used for the conjugation step without further purification (260 mg, 0.47 mmol). Mass calcd for $C_{37}H_{63}NO_2$: 553.5; found by ESI-MS: 554.8 (MH^+).

Pyropheophorbide *a* (5). Methyl pheophorbide *a* (500 mg, 0.82 mmol) isolated from *Spirulina* algae was heated under refluxed temperature in collidine (100 mL) for 3 h under nitrogen atmosphere. The solution was evaporated under high vacuum, and the residue so obtained was chromatographed over an alumina column (Grade III) and eluted with CH_2Cl_2. Pyropheophorbide *a* methyl ester was crystallized from CH_2Cl_2/hexanes in 91% yield (411 mg, 0.75 mmol). This intermediate (250 mg, 0.46 mmol) was dissolved in THF (65 mL) and mixed with a solution containing LiOH (500 mg), methanol (7 mL), and water (3 mL). The mixture was stirred under argon atmosphere for 24 h. After workup, the crude product was chromatographed on a silica column with 10% methanol in CH_2Cl_2 to give the title compound in 82% yield (200 mg, 0.37 mmol). The spectral and physical data of compound **5** are consistent with the literature (*14*). Mp: 220−223 °C. UV−vis in CH_2Cl_2: 411 nm (ϵ 1.1 × 10^5), 509 (1.1 × 10^4), 537 (9.6 × 10^3), 611 (8.2 × 10^3), and 669 (4.5 × 10^4). Mass calcd for $C_{33}H_{34}N_4O_3$: 534.5; found by ESI-MS: 535.6 (MH^+) and 557.6 ($M + Na^+$). ^{1}H NMR ($CDCl_3$): 9.47, 9.35, and 8.53 (each s, 1H, 5-H, 10-H, and 20-H); 8.00 (dd, J = 17.7, 11.4 Hz, 1H, 3^1-CH=CH_2); 6.27 (d, J = 17.7 Hz, 1H, *trans*-3^2-CH=CH_2); 6.15 (d, J = 11.4 Hz, 1H, *cis*-3^2-CH=CH_2); 5.18 (ABX, 2H, 13^2-CH_2); 4.47 (q, J = 7.1, 1.9 Hz, 1H for 18-H); 4.29 (m, J = 7.8 Hz, 1H for 17-H); 3.68 (q, J = 7.4 Hz, 2H, 8-CH_2-CH_3); 3.64, 3.39, and 3.22 (each s, 3H, 12-CH_3, 2-CH_3 and 7-CH_3); 2.65 and 2.32 (each m, 2H, for 2 × 17^1-H and 2 × 17^2-H); 1.81 (d, J = 7.2 Hz, 3H, 18-CH_3); 1.70 (t, J = 8.3 Hz, 3H, 8-CH_2CH_3), 0.87 and −1.35 (each brs, 1H, 2 × N−H).

Pyropheophorbide Cholesterol Oleate (6). Compound **5** (45 mg, 0.084 mmol) was activated with DCC (20 mg, 0.097 mmol) and 1-hydroxybenzotriazole (14 mg, 0.103 mmol) in CH_2Cl_2 (2 mL) and added to a solution of the cholesterol oleate amine **4** (50 mg, 0.090) in CH_2Cl_2 (3 mL). After being stirred for 24 h, solvent was removed, and the crude product was purified by silica gel plate chromatography (3% methanol in CH_2Cl_2) to afford the desired conjugate in 20% yield (18 mg, 0.017 mmol). Analytical RP HPLC: t_R 35.81 min, 99%. UV−vis in CH_2Cl_2: 414 nm (ϵ 9.8 × 10^4), 510 (1.1 × 10^4), 541 (1.1 × 10^4), 610 (5.4 × 10^3), and 667 (4.5 × 10^4). Mass calcd for $C_{70}H_{95}N_5O_4$: 1070.7462 (MH^+); found by HRMS: 1070.7412 (MH^+); ^{1}H NMR ($CDCl_3$): 9.37, 9.33, and 8.55 (each s, 1H, 5-H, 10-H, and 20-H of pyro); 8.00 (dd, J = 17.7, 11.4 Hz, 1H, 3^1-CH=CH_2 of pyro); 6.28 (d, J = 17.7 Hz, 1H, *trans*-3^2-CH=CH_2 of pyro); 6.17 (d, J = 11.4 Hz, 1H, *cis*-3^2-CH=CH_2 of pyro); 5.31 (m, 3H, 2 × vinyl-H and 6-H of oleate), 5.23 (ABX, 2H, 13^2-CH_2 of pyro); 5.02 (m, 1H, N−H of cholesterol), 4.55 (m, 2H, 18-H of pyro, 3-H of cholesterol); 4.35 (m, J = 7.8 Hz, 1H for 17-H of pyro); 3.75 (m, 1H, 17-H of cholesterol), 3.63 (q, J = 7.4 Hz, 2H, 8-CH_2CH_3 of pyro); 3.47, 3.46 and 3.23 (each s, 3H, 12-CH_3, 2-CH_3 and 7-CH_3 of pyro); 2.71 and 2.46 (each m, 2H, for 2 × 17^1-H and 2 × 17^2-H of pyro); 2.22 (m, 6H of cholesterol oleate), 2.10−1.75 (m, 11H of cholesterol oleate), 1.70−0.95 (m, 39H of cholesterol oleate), 1.82 (d, J = 7.2 Hz, 3H, 18-CH_3 of pyro); 1.65 (t, J = 8.3 Hz, 3H, 8-CH_2CH_3 of pyro), 0.88 (m, 6H, 19-CH_3

Scheme 1. Synthesis of Cholesteryl Oleate Amine 4 and Its Corresponding Pyropheophorbide Conjugate 6



[a] Reagents (yields in parentheses): (a) $(BOC)_2O$, Et_3N, CH_2Cl_2, 24 h (95%); (b) oleoyl chloride, pyridine, 2 h (60%); (c) TFA, 2.5 h (90%); (d) DCC, 1-hydroxybenzotriazole, CH_2Cl_2, 24 h (20%).

of cholesterol and terminal CH_3 of oleate), 0.32 (s, 3H, 18-CH_3 of cholesterol).

LDL Reconstitution. LDL (1.9 mg) was lyophilized with 25 mg starch and then extracted three times with 5 mL of heptane at −5 °C. Following aspiration of the last heptane extract, 6 mg of pyropheophorbide cholesteryl oleate (**6**) was added in 200 μL of benzene. After 90 min at 4 °C, benzene and any residual heptane were removed under a stream of N_2 in an ice−salt bath for about 45 min. The r-(Pyro-CE)−LDL was solubilized in 10 mM Tricine, pH 8.2, at 4 °C for 24 h. Starch was removed from the solution by low-speed centrifugation (500*g*) and followed by a 20 min centrifugation (6000*g*). The reconstituted LDL was stored under an inert gas at 4 °C. The protein content of the specimen was determined by the Lowry method (*15*), and the fluorescence was measured using an LS-50B Fluorometer.

Cell Preparations. $HepG_2$ tumor cells, which were obtained from Dr. Theo van Berkel's laboratory from the University of Leiden in The Netherlands, were cultured in Dulbecco's modified Eagle's medium (DMEM) supplemented with 10% fetal bovine serum (FBS), 100 U/mL penicillin−streptomycin. Cells were grown at 37 °C in an atmosphere of 5% CO_2 in a humidified incubator.

Confocal Microscopic Studies. For confocal microscopic studies, $HepG_2$ cells were grown for 5 days in four-well Lab-Tek chamber slides (Naperville, IL). Before the cell experiments, the culture medium was replaced by preincubation medium (medium with 1% (w/v) BSA instead of FBS). The cells were washed three times with preincubation medium (for 15, 15, and 30 min) and cultured in this medium for a further 20 h. Experiments were started, after two quick washes with preincubation medium, by the addition of preincubation medium containing the indicated amounts of r-(Pyro-CE)-LDL and/or unlabeled LDL. After 3 h incubation at 37 °C, the cells were washed five times with ice-cold PBS containing 0.8% BSA, two times with PBS alone, and fixed for 20 min with 2% formaldehyde in PBS at room temperature. Then the chamber slides were mounted and sealed for confocal microscopic analysis.

RESULTS AND DISCUSSION

Our choice of the photosensitizer, pyropheophorbide *a*, is a stable analogue of natural chlorophyll *a*. It has excellent photophysical properties with long wavelength absorption of 667 nm. One of its derivatives, the hexyl ether analogue of pyropheophorbide *a* (Photochlor) is currently in phase I/II clinical trial at the Roswell Park Cancer Institute (Buffalo, NY) (*16*). As for the anchor, a cholesteryl oleate containing a primary amine linker was designed for conjugation with a variety of PDT agents. The oleate moiety contains one cis-double bond leading to a bent form of the long hydrocarbon chain that may facilitate the reconstitution process, whereas the cholesterol moiety will serve to anchor lipids in the core, thus eliminating nonspecific leakage.

To synthesize the desired cholesteryl oleate amine, we developed a very short and efficient pathway. As shown in Scheme 1, a commercially available cholesterol amine (**1**), 5-androsten-17β-amino-3β-ol (Steraloid Inc., Newport, RI), was first Boc-protected and esterified with oleoyl chloride. Deprotection of the amine at C-17 gave the corresponding cholesteryl oleate amine **4** in 60% overall yield. Coupling of amine **4** to pyropheophorbide *a* **5** (Scheme 1), obtained from *Spirulina* algae in short steps (*14*), yielded the desired conjugate **6** in sufficient quantities for LDL reconstitution studies. All new compounds were characterized by mass and NMR spectro-

scopic studies, and the purity of these compounds was confirmed by either elemental analysis or HPLC studies.

The pyropheophorbide cholesteryl oleate (**6**) so obtained was then used for reconstituting LDL. Following a modified Krieger's procedure as reported by Craig et al. (*17*), we were able to extract the native cholesteryl esters from the LDL lipid core and successfully replace them with our newly synthesized conjugate. The success of reconstitution was determined by a protein recovery assay following Lowry's method. Our pyropheophorbide cholesteryl oleate reconstituted LDL, r-(Pyro-CE)-LDL, yielded a 45% protein recovery comparable to the published data of 48% protein recovery (*17*) for other hydrophobic molecules. This LDL-based photosensitizer has long wavelength absorption of 667 nm and produces a fluorescence signal in the near-infrared (NIR) range (720 nm). Therefore, this photosensitizer can also be used for NIR detection of early cancers by optical imaging techniques.

To visualize LDLr-mediated internalization into the tumor cells, we performed laser scanning confocal microscopy studies on our newly synthesized r-(Pyro-CE)-LDL in $HepG_2$ tumor cells. Four sets of experiments were performed on a Leica TCS SPII laser scanning confocal microscope (Heidelberg, Germany). Figure 1 shows the confocal microscopic images of $HepG_2$ cells incubated with/without fluorescent probe (B, D, F, H) as well as corresponding bright field images (A, C, E, G). In a control experiment, $HepG_2$ cells were incubated with native LDL but without the photosensitizer at 37 °C for 3 h to determine any possible background fluorescence. As expected, no fluorescence signal could be detected without the photosensitizer (Figure 1B). After the incubation with 20 μg/mL of r-(Pyro-CE)-LDL, an intense fluorescence signal was observed distributing throughout the whole cell except for the nucleus, presumably in intracellular compartments such as endosomes or lysosomes (Figure 1D). To determine the specificity of this LDL-based photosensitizer toward LDL receptors, $HepG_2$ cells were incubated with either a 25-fold excess of unlabeled LDL in addition to the 20 μg/mL r-(Pyro-CE)-LDL or the same amount of Pyro-CE (compound **6**) without reconstitution into LDL. No fluorescence could be observed in both experiments (Figure 1F, 1H), which clearly indicates specific binding of the reconstituted LDL to the LDL receptors.

In summary, we have demonstrated that pyropheophorbide, a stable photosensitizer derived from chlorophyll *a*, can be covalently linked to the primary amine functional group of the cholesteryl oleate, which serves as a double anchor for the LDL lipid core and can be synthesized in short steps. We were able to successfully incorporate this dye conjugate into the LDL lipid core via the LDL reconstitution approach. By using laser scanning confocal microscopy, we have demonstrated that photosensitizer-reconstituted LDL can be internalized by $HepG_2$ tumor cells and, therefore, can be used as a PDT agent directed at LDLr-overexpressing tumors.

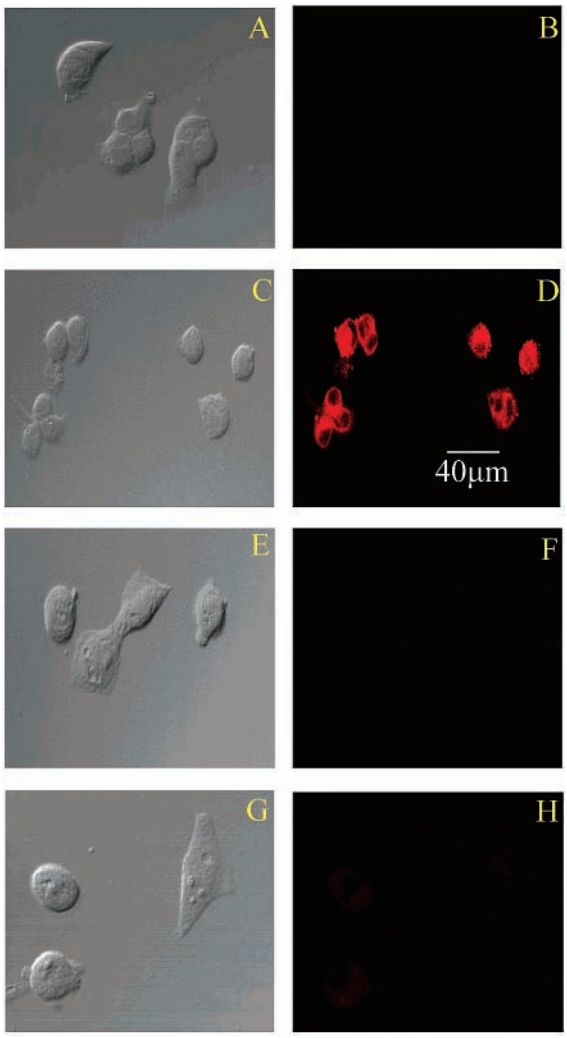


Figure 1. Fluorescence confocal microscopic images of $HepG_2$ tumor cells incubated with unlabeled LDL as control (B), 20 μg/mL of r-(Pyro-CE)-LDL for binding assay (D), 20 μg/mL of r-(Pyro-CE)-LDL with 25-fold excess of unlabeled LDL for competition assay (F), 20 μg/mL non-LDL-reconstituted Pyro-CE for comparison (H), as well as the corresponding bright field images (A, C, E, G).

ACKNOWLEDGMENT

We are grateful to Dr. Ponzy Lu of the Chemistry Department for accommodating our organic laboratory, to Ms. Jasmine X.-Y. Zhao of the Microscopy Core Facility of the Wistar Institute for taking confocal microscope images, to Mr. David Nelson and Mr. Dong Xin for technical assistance, and to Ms. Lida Gifford for critical reading of the manuscript. This research was supported by NIH contract BAA NO1-CM97065-02 and an Oncologic Foundation of Buffalo award. Partial support by NIH grants RO1 CA 83105-02, P20 CA86255-01, and HL 56083 are also acknowledged.

LITERATURE CITED

(1) (a) Dougherty, T. J., Gomer, C., Henderson, B. W., Jori, G., Kessel, D., Korbelik, M., Moan, J., and Peng, Q. (1998) Photodynamic therapy. *J. Natl. Cancer Inst. 90*, 889−905. (b) Sternberg, E. D., Dolphin, D., and Bruckner, C. (1998) Porphyrin-based photosensitizers for use in photodynamic therapy. *Tetrahedron 54*, 4151−4202. (c) Pandey, R. K., and Zheng, G. (2000) Porphyrins as Photosensitizers in Photodynamic Therapy. *Porphyrin Handbook* (Kadish, K., Smith, K. M., and Guilard, R., Eds.) pp 157−230, Vol. 6, Academic Press, New York.

(2) Moan, J. (1990) On the diffusion length of singlet oxygen in cells and tissues. *J. Photochem. Photobiol. B: Biol. 6*, 343−347.

(3) Brown, M. S., Kovanen, P. T., and Goldstein, J. L. (1980) Evolution of the LDL receptor concept − cultured cells to intact animals. *Ann. N.Y. Acad. Sci. 348*, 48−68.

(4) Lundberg, B. (1987) Preparation of drug-low-density lipoprotein complexes for delivery of antitumoral drugs via the low-density lipoprotein pathway. *Cancer Res. 47*, 4105−4108.

(5) Firestone, R. A. (1994) Low-density lipoprotein as a vehicle for targeting antitumor compounds to cancer cells. *Bioconjugate Chem. 5*, 105−113.
(6) Shaw, J. M., Shaw, K. V., Yanovich, S., Iwanik, M., Futch, W. S., Rosowsky, A., and Schook, L. B. (1987) Delivery of lipophilic drugs using lipoproteins. *Ann. N.Y. Acad. Sci. 507*, 252−271.
(7) Candide, C., Morliere, P., Maziere, J. C., Goldstein, S., Santus, R., Dubertret, S., Reyftmann, J. P., and Polonovski, J. (1986) In vitro interaction of the photoactive anticancer porphyrin derivative photofrin II with low-density lipoprotein, and its delivery to cultured human fibroblasts. *FEBS Lett. 207*, 133−138.
(8) de Smidt, P. C., Versluis, A. J., and van Berkel, T. J. C. (1993) Properties of incorporation, redistribution and integrity of porphyrin-low-density lipoprotein complexes. *Biochemistry 32*, 2916−2922.
(9) Reddi, E. (1997) Role of delivery vehicles for photosensitizers in the photodynamic therapy of tumors. *J. Photochem. Photobiol. B: Biol. 37*, 189−195.
(10) Allison, B. A., Waterfield, A. M., Richter, A. M., and Levy, J. G. (1991) The effects of plasma-lipoproteins on in vitro tumor cell killing and in vivo tumor photosensitization with benzoporphyrin derivative. *Photochem. Photobiol. 54*, 709−715.
(11) Krieger, M., McPhaul, M. J., Goldstein, J. L., and Brown, M. S. (1979) Replacement of neutral lipids of low-density lipoprotein with esters of long chain unsaturated fatty acids. *J. Biol. Chem. 254*, 3845−3853.
(12) Versluis, A. J., van Geel, P. J., Oppelaar, H., van Berkel, T. J. C., and Bijsterbosch, M. K. (1996) Receptor-mediated uptake of low-density lipoprotein by B16 melanoma cells in vitro and in vivo in mice. *Br. J. Cancer 74*, 525−532.
(13) Mosley, S. T., Goldstein, J. L., Brown, M. S., Falck, J. R., and Anderson, R. G. W. (1981) Targeted killing of cultured cells by receptor-mediated photosensitization. *Proc. Natl. Acad. Sci. U.S.A. 78*, 5717−5721.
(14) Pandey, R. K., Sumlin, A. B., Constantine, S., Aoudia, M., Potter, W. R., Bellnier, D. A., Henderson, B. W., Rodgers, M. A., Smith, K. M., and Dougherty, T. J. (1996) Alkyl ether analogues of chlorophyll-a derivatives 0.1. Synthesis, photophysical properties and photodynamic efficacy. *Photochem. Photobiol. 64*, 194−204.
(15) Lowry, O. H., Rosebrough, N. J., Farr, A. L., and Randall, R. J. (1951) Protein measurement with the Folin phenol reagent. *J. Biol. Chem. 193*, 265−275.
(16) Henderson, B. W., Bellnier, D. A., Greco, W. R., Sharma, A., Pandey, R. K., Vaughan, L., Weishaupt, K., and Dougherty, T. J. (1997) A quantitative structure−activity relationship for a congeneric series of pyropheophorbide derivatives as photosensitizers for photodynamic therapy. *Cancer Res. 57*, 4000−4007.
(17) Craig, I. F., Via, D. P., Mantulin, W. W., Pownall, H. J., Gotto, A. M., Jr., and Smith, L. C. (1981) Low-density lipoproteins reconstituted with steroids containing the nitrobenzoxadiazole. *J. Lipid Res. 22*, 687−696.

BC025516H

ARTICLES

Effect of Heme Structure on O_2-Binding Properties of Human Serum Albumin−Heme Hybrids: Intramolecular Histidine Coordination Provides a Stable O_2−Adduct Complex

Teruyuki Komatsu, Yasuko Matsukawa, and Eishun Tsuchida*,†

Department of Polymer Chemistry, Advanced Research Institute for Science and Engineering, Waseda University, Tokyo 169-8555, Japan. Received July 3, 2001; Revised Manuscript Received October 8, 2001

5,10,15,20-Tetrakis[(α,α,α,α-*o*-pivaloylamino)phenyl]porphinatoiron(II) and 5,10,15,20-tetrakis-{[α,α,α,α-*o*-(1-methylcyclohexanoylamino)]phenyl}porphinatoiron(II) complexes bearing a covalently bound 8-(2-methyl-1-imidazolyl)octanoyloxymethyl or 4-(methyl-L-histidinamido)butanoyloxymethyl side-chain [**FeRP(B)** series: R = piv or cyc, B = Im or His] have been synthesized. The histidine-bound derivatives [**FepivP(His)**, **FecycP(His)**] formed five N-coordinated high-spin iron(II) complexes in organic solvents under an N_2 atmosphere and showed large O_2-binding affinities in comparison to those of the 2-methylimidazole-bound analogues [**FepivP(Im)**, **FecycP(Im)**] due to the low O_2-dissociation rate constants. On the contrary, the difference in the fence groups around the O_2-coordination site (pivaloyl or 1-methylhexanoyl) did not significantly influence to the O_2-binding parameters. These four porphinatoiron(II)s were efficiently incorporated into recombinant human serum albumin (rHSA), thus providing the synthetic hemoprotein, the albumin−heme hybrid [rHSA−**FeRP(B)**]. An rHSA host absorbs a maximum of eight **FeRP(B)** molecules in each case. The obtained rHSA−**FeRP(B)** can reversibly bind and release O_2 under physiological conditions (in aqueous media, pH 7.3, 37 °C) like hemoglobin and myoglobin. As in organic solutions, the difference in the fence groups did not affect their O_2-binding parameters, but the axial histidine coordination significantly increased the O_2-binding affinity, which is again ascribed to the low O_2-dissociation rates. The most remarkable effect of the heme structure appeared in the half-life ($\tau_{1/2}$) of the O_2−adduct complex. The dioxygenated rHSA−**FecycP(His)** showed an unusually long lifetime ($\tau_{1/2}$: 25 h at 37 °C) which is ca. 13-fold longer than that of rHSA−**FepivP(Im)**.

INTRODUCTION

A recombinant human serum albumin (rHSA) incorporating 2-[8-(2-methyl-1-imidazolyl)octanoyloxymethyl]-5,10,15,20-tetrakis[(α,α,α,α-*o*-pivaloylamino)phenyl]porphinatoiron(II) [**FepivP(Im)**[1]] [albumin−heme; rHSA−**FepivP(Im)**] is an entirely synthetic hemoprotein which can reversibly bind and release O_2 under physiological conditions like that of hemoglobin (Hb) and myoglobin (Mb) (Tsuchida et al., 1999). The exchange transfusion with this rHSA−**FepivP(Im)** solution into anesthetized rats has shown that it becomes an O_2-carrying fluid as a red blood cell substitute (Tsuchida et al., 2000). The albumin−heme hybrid is now recognized to be one of the most promising materials not only as a blood replacement composition, but also as an O_2-carrying medicine which will be adopted for use in several clinical applications, such as myocardial infraction, anemia, and tracheal blockade, etc. Only one limitation of this material is the relatively short lifetime of the O_2−adduct complex; the half-life of the dioxygenated rHSA−**FepivP(Im)** at 37 °C (pH 7.3 under 100% O_2 atmosphere) was 2 h. We believe that it should be improved by the optimizing of the chemical structure of the incorporated heme. Actually, the relationship between the heme structure and the O_2-binding parameters has been elucidated, but its effect to the O_2−adduct stability is still controversial (Collman et al., 1983; Traylor et al., 1985). We have employed **FepivP(Im)** as an active site of the albumin−heme, in which the sterically hindered 2-methylimidazole coordination plays a crucial role to realize the similar O_2-binding affinity with red blood cells. On the other hand, the low-binding constant of the 2-methylimidazolyl N atom to the central iron(II) has also been postulated to lead the short lifetime of the dioxygenated species. Other factors that regulate the O_2-binding ability of the heme are the basicity of the imidazole ligand and the hydrophobicity of the cavity around the coordinated O_2. The pK_a of the histidine, which is found in nature, is 6.0. This

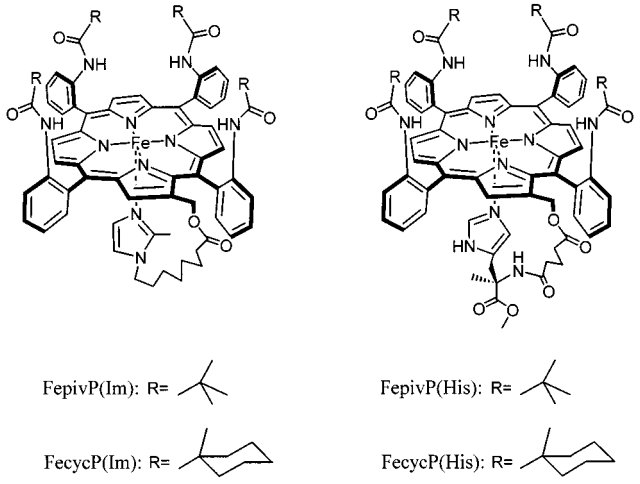
* To whom the correspondence should be addressed. Phone: +81 3−5286−3120; Fax: +81 3−3205−4740. e-mail: eishun@mn.waseda.ac.jp.

† CREST investigator, JST.

[1] Abbreviations: **FepivP(Im)**, 2-[8-(2-methyl-1-imidazolyl)-octanoyloxymethyl]-5,10,15,20-tetrakis[(α,α,α,α-*o*-pivaloylamino)phenyl]porphinatoiron; **FecycP(Im)**, 2-[8-(2-methyl-1-imidazolyl)octanoyloxymethyl]-5,10,15,20-tetrakis{[α,α,α,α-*o*-(1-methylcyclohexanoylamino)]phenyl}porphinatoiron; **FepivP(His)**, 2-(4-methyl-L-histidinamidobutanoyloxymethyl)-5,10,15,20-tetrakis-[(α,α,α,α-*o*-pivaloylamino)phenyl]porphinatoiron; **FecycP(His)**, 2-(4-methyl-L-histidinamidobutanoyloxymethyl)-5,10,15,20-tetrakis{[α,α,α,α-*o*-(1-methylcyclohexanoylamino)]phenyl}-porphinatoiron.

10.1021/bc010067r CCC: $22.00 © 2002 American Chemical Society
Published on Web 04/05/2002

value is significantly low compared to those of the *N*-alkylimidazole derivatives and may provide both a suitable O_2-binding affinity and a long lifetime. To increase the stability of the O_2−adduct complex of the albumin−heme hybrid, new porphinatoiron(II) derivatives with different substituents on the *distal* and *proximal* sides of the porphine planes [5,10,15,20-tetrakis[(α,α,α,α-*o*-pivaloylamino)phenyl]porphinatoiron(II) bearing a covalently bound 4-methyl-L-histidinamidobutanoyl-oxymethyl chains [**FepivP(His)**], and 5,10,15,20-tetrakis{[α,α,α,α-*o*-(1-methylcyclohexanoylamino)]-phenyl}porphinatoiron(II) with a 8-(2-methyl-1-imidazolyl)octanoyloxymethyl or the histidine side-chain [**FecycP(Im)** or **FecycP(His)**] have been synthesized. This paper describes the O_2-binding equilibria and kinetics of these newly synthesized **FeRP(B)** complexes in organic solvents and their rHSA hybrids in aqueous media. This is the first reported evaluation of the effect of the heme structure on the O_2-binding property of the albumin−heme hybrid.



EXPERIMENTAL PROCEDURES

Materials and Apparatus. Thin-layer chromatography was carried out on 0.2 mm precoated plates of silica gel 60 F_{254} (Merck). Purification was performed by silica gel 60 (Merck) column chromatography. Infrared spectra were measured with a JASCO FT/IR-410 spectrometer. ^{1}H NMR spectra were recorded using a JEOL Lambda 500 spectrometer. Chemical shifts were expressed in parts per million downfield from Me_4Si as an internal standard. FAB-MS spectra were obtained from a JEOL JMS−SX102A spectrometer. UV−vis absorption spectra were recorded on a JASCO V-570 spectrophotometer. 2-Hydroxymethyl-5,10,15,20-tetrakis[(α,α,α,α-*o*-pivaloylamino)phenyl]porphine (**3-piv**), 8-(2-methyl-1-imidazolyl)-octanoic acid, and 2-[8-(2-methyl-1-imidazolyl)octanoyloxymethyl]-5,10,15,20-tetrakis[(α,α,α,α-*o*-pivaloylamino)-phenyl]porphinatoiron(III) bromide [**FepivP(Im)Br**$^-$] were prepared according to our previously reported literature (Tsuchida et al., 1995). All solvents were purified by distillation before use. Other chemicals were commercial high-purity grades. The water used was deionized using a ADVANTEC GS-200 system. An rHSA (25 wt %) was provided from WelFide Corporation (Sumi et al., 1993).

Reduction of Ferric Complex to Ferrous Complex in Organic Solvent. Reduction to the porphinatoiron(II) complex was carried out using toluene (or benzene)−aq $Na_2S_2O_4$ in a heterogeneous two-phase system under aerobic conditions as previously reported (Tsuchida et a., 1995). After separation of the two phases, the organic layer containing the reduced compound was transferred into 1-cm quartz cuvette under an Ar atmosphre.

Resonance Raman Spectroscopy. RR spectra were obtained on a JASCO NRS-2000 laser Raman spectrometer equipped with a CCD multichannel detector. Excitation was carried out by the 457.9-nm line of an NEC GLG2162 Ar^+ ion laser at 25 °C. The details of the measurements were reported elsewhere (Komatsu et al., 1999; Wu et al., 1998).

Preparation of rHSA−FeRP(B) Hybrid. Aqueous ascorbic acid (15 mM, 20 μL) was added to an EtOH solution of **FeRP(B)** derivative (75 μM, 4 mL) under carbon monoxide (CO). After complete reduction of the central ferric ion, the UV−vis absorption spectrum showed a formation of the six-coordinated carbonyl complex. This EtOH solution was slowly injected into the phosphate buffer solution (33 mM, pH 7.3, 8 mL) of rHSA (4.69 μM) via the narrow tube under a CO atmosphere, and the mixture was dialyzed with cellulose membrane against phosphate buffer (pH 7.3) for 2 h and 15 h at 4 °C. We confirmed that the EtOH concentration in the solution reduced to less that 100 ppm. Finally, the total volume was adjusted to 15 mL, giving carbonyl rHSA−**FeRP(B)** solution (**FeRP(B)**/rHSA = 8 (mol/mol), [Fe] = 20 μM).

Binding Numbers of FeRP(B) into rHSA. Based on the absorbance intensity of the UV−vis absorption spectra of the rHSA−**FeRP(B)** hybrid with different **FeRP(B)**/rHSA mixing ratios, the binding numbers of **FeRP(B)** in the albumin host were assayed as previously reported (Komatsu et al., 1999). Furthermore, in the course of preparation of the hybrid, the remaining carbonyl **FeRP(B)** at the bottom of the round flask was extracted with $CHCl_3$ and its concentration was determined by the absorption spectra.

O_2-Coordination Equilibria and Kinetics. O_2-coordinations to **FeRP(B)** derivative are expressed by

$$\textbf{FeRP(B)} + O_2 \underset{k_{off}}{\overset{k_{on}}{\rightleftharpoons}} \textbf{FeRP(B)}{-}O_2 \qquad (1)$$

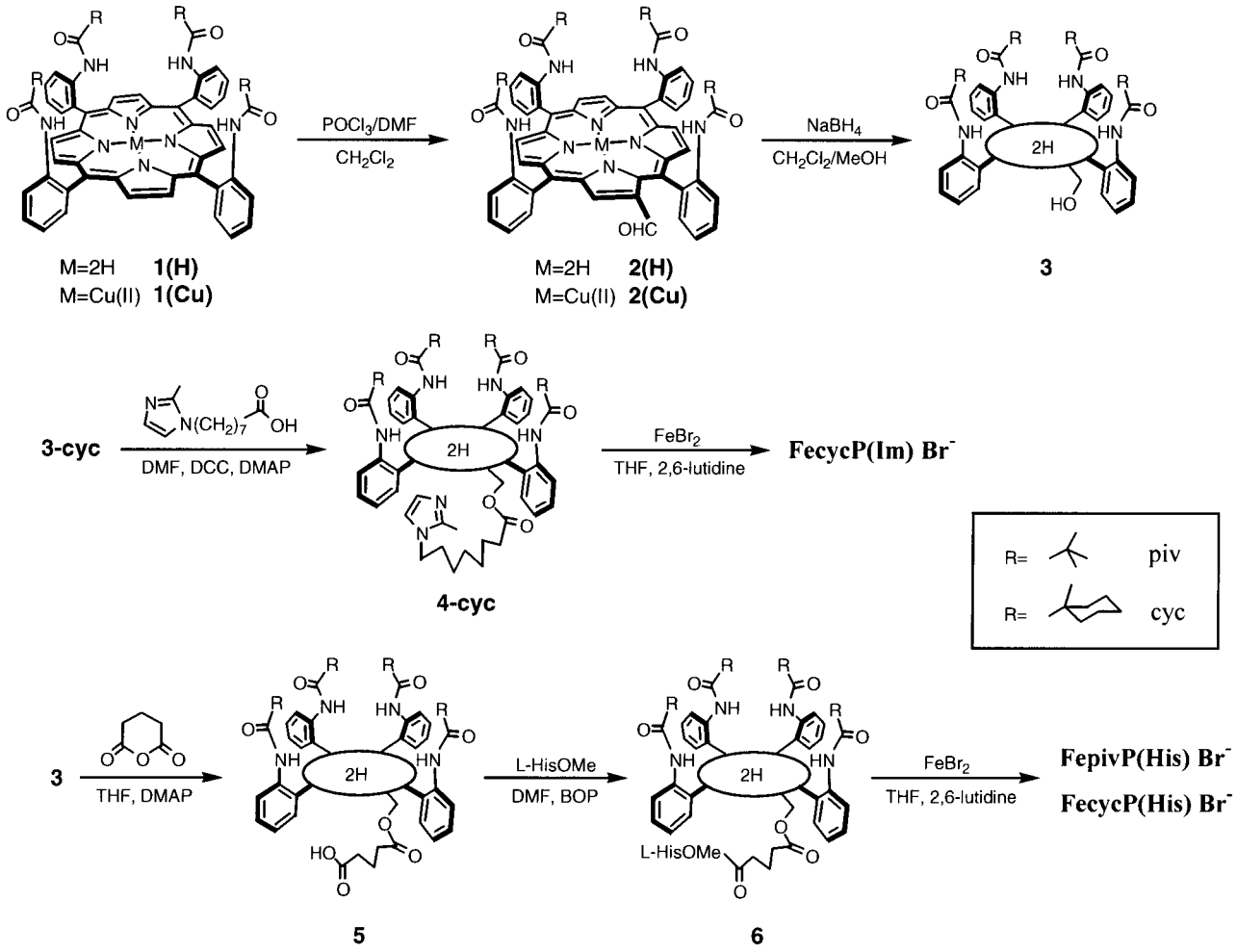
$$(K = k_{on}/k_{off})$$

The O_2-binding affinity ($P_{1/2} = 1/K$) of **FeRP(B)**s in organic solvents or their rHSA hybrids in aqueous media were determined by spectral changes at various partial pressure of O_2 as in previous literatures (Komatsu et al., 1999; Tsuchida et al., 1995). **FeRP(B)**s concentrations of 20 μM were normally used for UV−vis. absorption spectroscopy. The spectra were recorded within the range of 350−700 nm. The O_2-association and -dissociation rate constants (k_{on}, k_{off}) were measured by a competitive rebinding technique using a Unisoku TSP-600 laser flash photolysis apparatus (Collman et al., 1983; Tsuchida et al., 1995; Traylor et al., 1985). The absorption decays accompanied O_2-rebinding to **FeRP(B)**s in organic solvents obeyed single exponential, so that we applied a first-order kinetics to calculate the rates. On the other hand, rHSA−**FeRP(B)** in aqueous solution showed triphases. We used triple-exponential kinetics described elsewhere to analyze the absorption decays (Komatsu et al., 2000).

RESULTS AND DISCUSSION

Synthesis of FeRP(B) Complexes. We first report the synthesis of tetrakis[(α,α,α,α-*o*-amino)phenyl]porphinatoiron(II) derivatives with bulky fences around the

Scheme 1



O_2-coordination site (pivaloyl or 1-methylcyclohexanoyl) and a proximal base [2-methylimidazole or methyl-L-histidine (L-HisOMe)] at the β-pyrrolic position (Scheme 1, see Supporting Information). The parent porphines, namely 2-hydroxymethyl-5,10,15,20-tetrakis[(α,α,α,α-*o*-pivaloylamino)phenyl]porphine (**3-piv**) and 2-hydroxymethyl-5,10,15,20-tetrakis{[α,α,α,α-*o*-(1-methylcyclohexanoylamino)]phenyl}porphine (**3-cyc**) were prepared using the Vilsmeir reaction. The hydroxyl group was converted into a carboxylic acid chain by glutaric anhydride (**5**). Introduction of L-HisOMe into this carboxylic acid using DCC unfortunately failed. Several unknown products were detected. In contrast, the same coupling using benzotriazol-1-yloxytris(dimethylamine)phosphonium hexafluorophosphate (BOP) in a dry DMF solution yielded the target free-base compound (**6**) in high yield (~85%). Iron insertion was carried out using $FeBr_2$ in dry THF to afford the corresponding iron(III) complexes.

O_2-Binding Properties of FeRP(B)s in Organic Solvents. The UV−vis absorption spectrum of the toluene solution of **FecycP(Im)** with a 2-methyl-1-imidazolylalkyl arm under an N_2 atmosphere showed the formation of the five-N-coordinated complex (λ_{max}: 441, 539, 558 nm) as well as **FepivP(Im)** (not shown) (Tsuchida et al., 1995). The **FepivP(His)** and **FecycP(His)** with a proximal histidine also displayed the same spectral pattern (λ_{max}: 441, 544, 564 nm), which was constant in the range from 5 μM−1 mM at 10−70 °C. Resonance Raman (RR) spectroscopy of **Fepiv(His)** demonstrated a medium band at 219 cm^{-1}, which was assigned to the Fe(II)−N(imidazole) stretching mode,

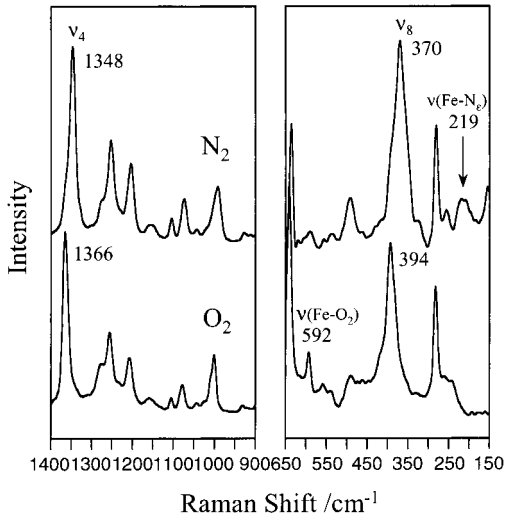


Figure 1. Resonance Raman spectra of **FepivP(His)** in benzene solution at 25 °C.

ν(Fe−N_ϵ) (Figure 1) (Hori et al., 1980; Wu et al., 1998). It can be concluded that the covalently linked histidine residue at the porphine periphery binds to the central iron(II) to give the five-coordinated high-spin iron(II) complex under an N_2 atmosphere in a fashion similar to the 2-methylimidazolated analogues [**FepivP(Im)** or **FecycP(Im)**].

Upon bubbling of O_2 or CO gas into the benzene solution of **FepivP(His)**, the UV−vis absorption spec-

Table 1. O_2-Binding Parameters of FeRP(B) in Organic Solvents at 25 °C

FeRP(B)	solvent	$P_{1/2}$ (Torr)	10^{-8} k_{on} (M^{-1} s^{-1})	10^{-3} k_{off} (s^{-1})
FepivP(Im)	toluene	38	1.6	79
FecycP(Im)	toluene	20	1.8	47
FepivP(His)	benzene	1.7	2.1	3.7
FecycP(His)	toluene	1.7	2.0	4.3

trum immediately changed to those of the O_2−adduct complex (λ_{max}: 429, 551 nm) or CO−adduct complex (λ_{max}: 428, 546 nm) (Komatsu et al., 2001). The dioxygenation was sufficiently stable and reversible at 25 °C depending on the O_2-partial pressure. In the RR spectrum, the ν(Fe−O_2) vibration of the dioxygenated **FepivP(His)** appeared at 592 cm^{-1} after O_2 bubbling. This peak suggests a typical end-on type O_2-coordination to the porphinatoiron(II). The skeletal modes of the porphine ring (ν_8 and ν_4) were also upshifted from 370 and 1348 cm^{-1} to 394 and 1366 cm^{-1}, respectively. These observations indicate the formation of the six-coordinated low-spin iron(II) complex of **FepivP(His)** (Burke et al., 1978; Hori et al., 1980; Wu et al., 1998). All the shifts were reversibly observed depending on the O_2 concentration. The RR spectra of **FecycP(His)** showed the same results as well.

The O_2-binding affinities ($P_{1/2}$), and O_2-association and -dissociation rate constants (k_{on}, k_{off}) of the **FeRP(B)**s in organic solvents are summarized in Table 1. The difference in the fence structure around the O_2-coordination site (pivaloyl or 1-methylhexanoyl) did not significantly influence their O_2-binding equilibria and kinetics. On the basis of the important earlier studies, the distal steric encumbrance only reduces the association rate for O_2 (Collman et al., 1983; Traylor et al., 1985). According to the hypothesis, the inner volume of the cavities, which are constructed using the four pivaloyl or 1-methylcyclohexanoyl groups on the porphine plane, should be of similar size. On the other hand, the axial histidine coordination significantly increased the O_2-binding affinity compared to those of the 2-methylimidazole bound analogues by a factor of 11−24, that is kinetically due to the low O_2-dissociation rate constants. It is generally recognized that the steric hindrance of the 2-methyl group of the axially coordinated imdazole decreases the O_2-binding affinity, giving the "Tense state" model of Hb (Collman et al., 1978). Our results on the large O_2-binding affinities of **FepivP(His)** and **FecycP(His)** correlate well with the theory of the former study.

To clarify the geometry of the bulky cyclohexanoyl fences and axial histidine coordination, the stereostructure of the dioxygenated low-spin complex of **FecycP(His)** was simulated by molecular dynamics (Figure 2). It was found that (i) the repulsions between the cyclohexanoyl fences do not induce a ruffling of the porphine plane, and (ii) the dihedral angle of the imidazole ring with respect to the porphine was 89.3°, suggesting that the imidazole N-coordination to the central iron(II) is not distorted by the rigid amide spacer between the porphine and HisOMe. It is also remarkable that (iii) the H atom of the imidazole cannot form a hydrogen bond with the neighboring carbonyl O atom, which is known to partially influence the dioxygenation of the heme.

We concluded that covalently attaching the histidine group directly to the porphine periphery provides the five-N-coordinated high-spin iron(II) complex and a large equilibrium constant for the O_2 binding in comparison to that of the 2-methylimidazolated analogue due to the small dissociation rate, even though its O_2-binding affinity was 6-fold lower than that of the *N*-alkylimidazole-coordinated one, 2-[8-(1-imidazolyl)octanoyloxymethyl]-5,10,15,20-tetrakis[(α,α,α,α-*o*-pivaloylamino)phenyl]-porphinatoiron(II) ($P_{1/2}$: 0.29 Torr) (Tsuchida et al., 1995). This is probably caused by the low σ-basicity of the histidine.

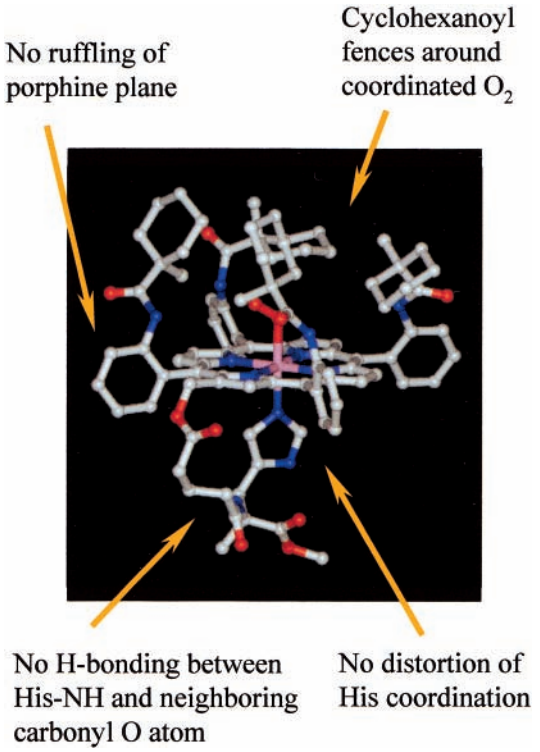


Figure 2. Simulated structure of the dioxygenated **FecycP(His)**. Molecular dynamics and minimization (force field: esff) were performed using an Insight II system (Molecular Simulations Inc.). The structure was generated by alternative minimizations and annealing dynamic calculations from 1000 to 100 K.

Anyway, these results are the first examples of the stable O_2−adduct complexes of the synthetic porphinatoiron(II)s with an intramolecularly coordinated proximal histidine and their O_2-binding equilibrium and kinetic parameters.

FeRP(B)s Incorporations into rHSA. A maximum of eight **FepivP(Im)** molecules were incorporated into certain domains of human serum albumin with binding constants from 10^6−10^4 M^{-1} (Komatsu et al., 1999). Other **FeRP(B)s** were also expected to bind to rHSA in a similar fashion, and the binding sites would also be identical. From the quantitative analyses of the absorption intensity for the Soret band of aqueous rHSA−**FecycP(His)**, the maximum binding numbers of **FecycP(His)** to an rHSA were determined to be eight by using molar extinction coefficient of the carbonyl heme complex. Actually, the unbound **FecycP(His)** remaining in the flask was less than 4% of the total amount of the heme in case of **FecycP(His)**/rHSA was eight (mol/mol). The other **FeRP(B)**s [**FepivP(His)**, **FecycP(Im)**] also showed the same results. The binding numbers are always eight and independent of the substituents and axial bases.

O_2-Coordination Properties of rHSA−FeRP(B). The UV−vis absorption spectrum of the aqueous rHSA hybrid including carbonyl **FepivP(His)** showed the formation of the typical CO-coordinated low-spin tetraphenylporphinatoiron(II) derivative (λ_{max}: 433, 548 nm) (Figure 3). Light irradiation using a 500-W halogen lamp

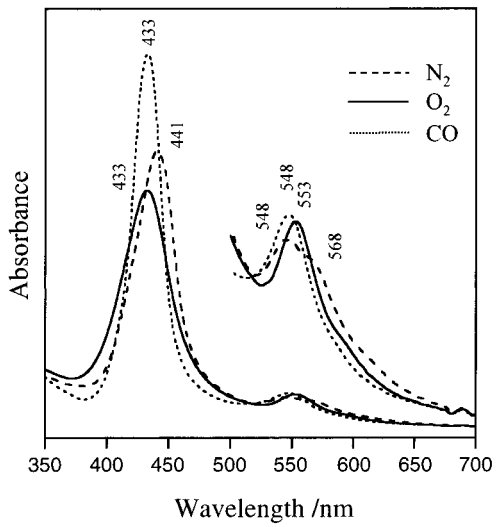


Figure 3. UV−vis absorption spectral changes of the rHSA−**FepivP(His)** in phosphate buffer solution (pH 7.3) at 25 °C.

Table 2. Absorption Maxima (λ_{max}) of rHSA−FeRP(B) Series in Phosphate Buffer Solution (pH 7.3) under N_2, O_2, and CO Atmosphere

rHSA−**FeRP(B)**	N_2	O_2	CO
rHSA−**FepivP(Im)**	443, 542, 567	426, 552	427, 539
rHSA−**FecycP(Im)**	445, 543, 567	428, 555	429, 545
rHSA−**FepivP(His)**	441, 548, 568	433, 553	433, 548
rHSA−**FecycP(His)**	442, 548, 568	429, 553	431, 548
Hb[a]	430, 555	415, 541, 576	419, 540, 569

[a] From Antonini et al. (1971).

of this solution under an O_2 atmosphere led to CO dissociation, affording the O_2−adduct complex (λ_{max}: 433, 553 nm). Upon exposure of the dioxygenated rHSA−**FepivP(His)** to N_2, the UV−vis absorption spectrum changed to that of the five-N-coordinated iron(II) complex with an intramolecularly coordinated axial histidine (λ_{max}: 441, 548, 568 nm). This O_2-binidng was reversibly observed and kinetically stable under physiological conditions (pH 7.3, 37 °C). Similar dioxygenations were also observed in the rHSA hybrids with **FecycP(Im)** and **FecycP(His)** (Table 2).

The laser flash photolysis experiments provided the k_{on} and k_{off} values of the O_2 binding to rHSA−**FeRP(B)**s, and a detailed kinetic analysis gave the following results. (i) The absorption decays accompanying the O_2 recombination were composed of three-phases of the first-order kinetics, therefore, the curves were fit by a triple-exponential equation, which is similar to the previously reported rHSA− **FepivP(Im)** (Komatsu et al., 2000). The minor, almost 10% component, which has the fastest rate constant, was independent of the O_2 concentrations. It should be correlated with a base elimination reaction (Geibel et al., 1978). (ii) From the careful inspections of the other two phases, the association rate constants for the fast and slow rebindings [k_{on}(fast) and k_{on}(slow)] of O_2 were calculated (Table 3). The k_{on}(fast) values are 4−6-times larger than k_{on}(slow). (iii) The concentration ratios of the fast and slow reactions were 2−3. Consequently, the O_2 association to the **FeRP(B)**s in the hydrophobic domains of the serum albumin is influenced by the molecular microenvironments around each O_2-coordination site, e.g., steric hindrance of the amino acid residue and difference in polarity. These observations coincided with our previous results on rHSA−**FepivP(Im)** (Komatsu et al., 2000).

Table 3. O_2-Binding Parameters of rHSA−FeRP(B) Series in Phosphate Buffer Solution (pH 7.3) at 25 °C

	10^{-6} k_{on} (M^{-1} s^{-1})		10^{-1} k_{off} (s^{-1})			
rHSA−**FeRP(B)**	fast	slow	fast	slow	$P_{1/2}$[a] (Torr)	$\tau_{1/2}$[b] (h)
rHSA−**FepivP(Im)**	34	9.5	75	20	13 (33)	2
rHSA−**FecycP(Im)**	46	7.3	98	16	13 (35)	9
rHSA−**FepivP(His)**	36	6.1	5.9	1.0	1 (3)	5
rHSA−**FecycP(His)**	54	8.8	8.9	1.4	1 (3)	25

[a] At 37 °C in parentheses. [b] At 37 °C.

The $P_{1/2}$ of the rHSA−**FeRP(B)**s were determined on the basis of the UV−vis. spectral changes during the O_2 titration (Table 3). According to the kinetic experiments, the $P_{1/2}$ values were divided into two components using our previously reported equation (Komatsu et al., 2000). Nevertheless, the calculated $P_{1/2}$ for the fast and slow phases were all identical in each case. The rHSA−**FepivP(Im)** and rHSA−**FecycP(Im)** showed the same O_2-binding affinities (13 Torr), indicating that the fence structures on the porphine plane cause only negligibly small changes in their O_2-equilibria and -kinetics even in albumin. In contrast, the axial histidine coordination provided a 13-fold larger O_2-binding affinity compared to those of the 2-methylimidazole-linked analogues, which is again ascribed to the low O_2-dissociation rate constants.

Accompanying the autoxidation of the central iron(II), the absorption band (λ_{max}: 552−555 nm) slowly disappeared at 37 °C, leading to the formation of the inactive iron(III) porphinate (Momenteau et al., 1994). The effect of the heme structure on the half-life ($\tau_{1/2}$) of the O_2−adduct complex was rather remarkable. (i) The cyclohexanoyl fences gave ca. 5-fold longer $\tau_{1/2}$ values compared to those of the pivaloyl derivatives, and (ii) the proximal histidine coordination increased $\tau_{1/2}$ by a factor of 3. As a result, (iii) the dioxygenated rHSA−**FecycP(His)** showed an unusually long lifetime ($\tau_{1/2}$: 25 h at 37 °C) which is ca. 13-fold longer than that of rHSA−**FepivP(Im)**.

In conclusion, recombinant human serum albumin incorporating **FeRP(His)**s having an intramolecularly coordinated histidine residue formed stable O_2−adduct complexes under physiological conditions. In particular, dioxygenated rHSA−**FecycP(His)** showed a high stability against the proton-driven oxidation, and its half-lifetime reached a value similar to that of the native Hb A ($\tau_{1/2}$: 36 h at 37 °C) (Mansouri et al., 1973). Although the O_2-binding affinity of rHSA−**FecycP(His)** is too high to use as a blood replacement composition, it can be utilized as an O_2-carrying medicine for oxygenation of the hypoxia region in cancer tissue, the preservation or circulation liquid for organs, and culture medium for the regeneration of tissues, etc. As a red blood cell substitute, rHSA−**FecycP(Im)**, which has a similar $P_{1/2}$ value to red blood cells, is full of promise. In the bloodstream, the apparent lifetime of the O_2-coordinated albumin−heme is prolonged by a factor of 4 (Tsuchida et al., 2000), so that the rHSA−**FecycP(Im)** is expected to transport O_2 in the circulatory system for more than 36 h. The preclinical test of the administration of rHSA−**FecycP(Im)** into anesthetized rats is currently underway.

ACKNOWLEDGMENT

This work was partially supported by the Core Research for Evolutional Science and Technology, JST, by Health Science Research Grants (Artificial Blood Project) of the Ministry of Health, Labor and Welfare, Japan, and

by a Grant-in-Aid for Scientific Research (No. 13650938) from the Ministry of Education, Culture, Sports, Science and Technology, Japan.

Supporting Information Available: Experimental details of the synthesis procedures (^{1}H NMR, IR, MS, UV−vis) of the all compounds in Scheme 1. This material is available free of charge via the Internet at http://pubs.acs.org.

LITERATURE CITED

(1) Antonini, E., and Brunori, M. (1971) in Hemoglobin and Myoglobin in Their Reactions with Ligands (A. Neuberger, E. L. Tatum, C. Rivat, Ed.), North-Holland Publ., Amsterdam.

(2) Burke, J. M., Kinchrad, J. R., Peters, S., Gagne, R. R., Collman, J. P., and Spiro, T. G. (1978) Structure-Sensitive Resonance Raman Bands of Tetraphenyl and "Picket Fence" Porphyrin-Iron Complexes, Including an Oxyhemoglobin Analogue. *J. Am. Chem. Soc. 100,* 6083−6088.

(3) Collman, J. P., Brauman, J. I., Doxsee, K. M. Halbert, T. R., and Suslick, K. S. (1978) Model Compounds for the T State of Hemoglobin. *Proc. Natl. Acad. Sci. U.S.A. 75,* 564−568.

(4) Collman, J. P., Brauman, J. I., Iverson, B. L., Sessler, J. L., Morris, R. M., and Gibson, Q. H. (1983) O_2 and CO Binding to Iron(II) Porphyrins: A Comparison of the "Picket Fence" and "Pocket" Porphyrins. *J. Am. Chem. Soc. 105,* 3052−3064.

(5) Geibel, J., Cannon, J., Campbell, D., and Traylor, T. G. (1978) Model Compounds for R-State and T-State Hemoglobins. *J. Am. Chem. Soc. 100,* 3575−3585.

(6) Hori, H. and Kitagawa, T. (1980) Iron-Ligand Stretching Band in the Resonance Raman Spectra of Ferrous Iron Porphyrin Derivatives. Importance as a Probe Band for Quaternary Structure of Hemoglobin. *J. Am. Chem. Soc. 102,* 3608−3613.

(7) Komatsu, T., Hamamatsu, K., Wu, J., and Tsuchida, E. (1999) Physicochemical Properties and O_2−Coordination Structure of Human Serum Albumin Incorporating Tetrakis-(*o*-pivalamido)phenylporphyrinatoiron(II) Derivatives. *Bioconjugate Chem. 10,* 82−86.

(8) Komatsu, T., Matsukawa, Y., and Tsuchida, E. (2000) Kinetics of CO and O_2 Binding to Human Serum Albumin-Heme Hybrid. *Bioconjugate Chem. 11,* 772−776.

(9) Komatsu, T., Matsukawa, Y., Miyatake, K., and Tsuchida, E. (2001) O_2-Adduct Complex of *meso*-Tetrakis(α,α,α,α-*o*-pivalamidophenyl)porphinatoiron(II) with an Intramolecularly Coordinated Proximal Histidine. *Chem. Lett. 2001,* 668−669.

(10) Momentau, M., and Reed, C. A. (1994) Synthetic Heme Oxygen Complexes. *Chem. Rev. 94,* 659−698.

(11) Monsouri, A., and Winterhalter, K. H. (1973) Nonequivalence of Chains in Hemoglobin Oxidation. *Biochemistry 12,* 4946−4949.

(12) Sumi, A., Ohtani, W., Kobayashi, K., Ohmura, T., Yokoyama, K., Nishida, M., and Suyama, T. (1993) Purification and Physicochemical Properties of Recombinant Human Serum Albumin, in *Biotechnology of Blood Proteins* (C. Rivat, J.-F. Stoltz, Eds.) Vol. 227, pp 293−298, John Libbey Eurotext, Montrouge.

(13) Traylor, T. G., Tsuchiya, S., Campbell, D., Mitchell, M., Stynes, D., and Koga, N. (1985) Anthracene Heme Cyclophanes. Steric Effects in CO, O_2, and RNC Binding. *J. Am. Chem. Soc. 107,* 604−614.

(14) Tsuchida, E., Komatsu, T., Kumamoto, S., Ando, K., and Nishide, H. (1995) Synthesis and O_2-Binding Properties of Tetraphenylporphyrinatoiron(II) Derivatives Bearing a Proximal Imidazole Covalently Bound at the β-Pyrrolic Position. *J. Chem. Soc., Perkin Trans. 2* 747−753.

(15) Tsuchida, E., Komatsu, T., Matsukawa, Y., Hamamatsu, K., and Wu, J. (1999) Human Serum Albumin Incorporating Tetrakis(*o*-pivalamido)phenylporphinatoiron(II) Derivative as a Totally Synthetic O_2-Carrying Hemoprotein. *Bioconjugate Chem. 10,* 797−802.

(16) Tsuchida, E., Komatsu, T., Hamamatsu, K., Matsukawa, Y., Tajima, M., Yoshizu, A., Izumi, Y., and Kobayashi, K. (2000) Exchange Transfusion with Albumin-Heme as an Artificial O_2-Infusion into Anesthetized Rats: Physiological Reponses, O_2-Delivery, and Reduction of the Oxidized Hemin Sites by Red Blood Cells. *Bioconjugate Chem. 10,* 797−802.

(17) Wu, J., Komatsu, T., and Tsuchida, E. (1998) Resonance Raman Studies of O_2-Binding to *ortho*-Substituted Tetraphenyl- and Tetranaphthyl-Porphyrinatoiron(II) Derivatives with a Covalently Linked Axial Imidazole. *J. Chem. Soc., Dalton Trans.* 2503−2506.

BC010067R

© 2002 American Chemical Society, Bioconjugate Chem., Komatsu bc010067r Supporting Info Page 1

5,10,15,20-Tetrakis{[α,α,α,α-*o*-(1-methylcyclohexanoylamino)]phenyl}porphine [1(H)-cyc]. Oxalyl chloride (19 mL, 132.3 mmol) was added to 1-methylcyclohexane carboxylic acid (2.11 g, 14.8 mmol) and stirred for 1 h at room temperature. After excess oxalyl chloride was removed *in vacuo*, dry THF (55 mL) solution of 5,10,15,20-tetrakis(α,α,α,α-*o*-amino)phenylporphine (0.4 g, 0.59 mmol) and pyridine (1.7 mL, 20.7 mmol) was added dropwise to the acid chloride at 5 °C under the darkness. The reaction mixture was stirred for 2 hr at room temperature, and brought to dryness on a rotary evaporator. $CHCl_3$ extracted the residue and washed with 5% aqueous NH_3 and water. The organic layer was then dried over anhydrous Na_2SO_4, and chromatographed on silica gel column using $CHCl_3$/Ethylacetate (10/1 v/v) as the eluent. The main band was collected and dried at room temperature for several hours *in vacuo* to give the compound **1(H)-cyc** as a purple solid (0.56g, 82 %). Rf = 0.50 ($CHCl_3$/Ethylacetate, 10/1 v/v). IR (NaCl) ν = 1691 (C=O(amide)), 3428 (NH(amide)) cm^{-1}. UV-Vis. ($CHCl_3$) λ_{max} = 423, 516, 549, 590, 647 nm. ^{1}H-NMR ($CDCl_3$) δ = -2.6 (2H, s, innerH), 0.1 (12H, s, 1-Me), 0.3 – 1.0 (40H, m, cyclohexyl), 7.5 (4H, t, phenyl-4), 7.6 (4H, s, amide-H), 7.8 (4H, t, phenyl-5), 7.9 (4H, d, phenyl-3), 8.8 (4H, d, phenyl-6), 8.9 (8H, s, pyrrole-β) ppm. FAB-MS: *m/z* 1172 [M^+].

5,10,15,20-Tetrakis{[α,α,α,α-*o*-(1-methylcyclohexanoylamino)]phenyl}porphinatocopper(II) [1(Cu)-cyc]. Methanol solution (2 mL) of $CuCl_2 \cdot 2H_2O$ (0.18 g, 1.15 mmol) was added to a $CHCl_3$ solution (10 mL) of **1(H)-cyc** (0.54 g, 0.46 mmol) in the presence of TEA (0.23 mL), and the mixture was stirred for 1 h at 65 °C. After confirming the reaction complete by measuring the vis. absorption spectrum, the solvents were removed by an evaporator. $CHCl_3$ extracted the residue and dried over anhydrous Na_2SO_4. The obtained mixture was chromatographed on a silica gel column using $CHCl_3$/Ethylacetate (5/1 v/v) as eluent. The major band was collected and dried at room temperature for several hours in *vacuo* to give the compound **1(Cu)-cyc** as a purple solid

© 2002 American Chemical Society, Bioconjugate Chem., Komatsu bc010067r Supporting Info Page 2

(0.45 mg, 79 %). Rf = 0.74 ($CHCl_3$/Ethylacetate, 5/1 v/v). IR (NaCl) ν = 1687 (C=O (amide)), 3434 (NH(amide)) cm^{-1}. UV-Vis. ($CHCl_3$) λ_{max} = 423, 541, 576 nm. FAB-MS: *m/z* 1233 [M^+].

2-Formyl-5,10,15,20-tetrakis{[α,α,α,α-*o*-(1-methylcyclohexanoylamino)] phenyl}porphinatocopper(II) [2(Cu)-cyc]. Phosphorus oxychloride (7.4 mL) was slowly dropped into DMF (6.3 mL) in an ice-water bath under an N_2 atmosphere and the mixture was stirred for 1 hr at room temperature, giving a pale orange Vilsmeir regent. A dry CH_2Cl_2 solution of **1(Cu)-cyc** (0.45 g, 0.36 mmol) was then added dropwise to this solution, and refluxed for 18 hr (the color of reactant changed to green). After cooling to the room temperature, saturated aqueous sodium acetate (300 mL) was carefully added to the mixture to neutralize the solution (the color of the organic layer was again turned to red). After additional stirring for 3 hr at 40°C, the mixture was extracted with $CHCl_3$. The organic phase was washed with water for several times, and dried over anhydrous Na_2SO_4. The evaporated residue was chromatographed on silica gel column using $CHCl_3$/Ethylacetate (6/1 v/v) as the eluent. The major band eluted was collected and dried at room temperature for several hours *in vacuo* to give the compound **2(Cu)-cyc** as a red-purple solid (0.22g, 50 %). Rf = 0.53 ($CHCl_3$/Ethylacetate, 5/1 v/v). IR (NaCl) ν = 1672 (C=O(formyl)), 1692 (C=O(amide)), 3428 (NH(amide)) cm^{-1}. UV-Vis. ($CHCl_3$) λ_{max} = 430, 552, 593 nm. FAB-MS: *m/z* 1262 [M^+ + H].

2-Formyl-5,10,15,20-tetrakis{[α,α,α,α-*o*-(1-methylcyclohexanoylamino)] phenyl}porphine [2(H)-cyc]. To a CH_2Cl_2 solution (8 mL) of **2(Cu)-cyc** (0.22 g, 0.174 mmol), conc. H_2SO_4 (2 mL) was added and vigously stirred for 10 min. The resulting green solution was added dropwise to CH_2Cl_2-ice-water (500 mL, 1:1 v/v) and slowly neutralized by $NaHCO_3$. The mixture was extracted by $CHCl_3$ and washed with water. After drying by Na_2SO_4, the organic layer was evaporated to dryness and the residue was chromatographed on silica gel column using $CHCl_3$/Ethylacetate (5/2 v/v) as

© 2002 American Chemical Society, Bioconjugate Chem., Komatsu bc010067r Supporting Info Page 3

the eluent. The main band was collected and dried at room temperature for several hours *in vacuo* to give compound **2(H)-cyc** as a purple solid (0.18 g, 84 %). Rf = 0.60 ($CHCl_3$/Ethylacetate 5/2 v/v). IR (NaCl) ν = 1672 (C=O(formyl)), 1691 (C=O(amide)), 3429 (NH(amide)) cm^{-1}. UV-Vis. ($CHCl_3$) λ_{max} = 432, 527, 555, 597, 662 nm. ^{1}H-NMR ($CDCl_3$) δ = -2.3 (2H, s, innerH), 0.1 – 0.2 (12H, d, 1-Me), 0.3 – 1.0 (40H, m, cyclohexyl), 7.4 – 7.6 (8H, m, amide-H, phenyl-4), 7.8 – 7.9 (8H, m, phenyl-3, 5), 8.7 – 8.9 (10H, m, pyrrole-βH, phenyl-6), 9.4 (1H, s, pyrrole-H), 9.6 (1H, s, formyl) ppm. FAB-MS: *m/z* 1200 [M^+].

2-Hydroxy-5,10,15,20-tetrakis{[α,α,α,α-*o*-(1-methylcyclohexanoylamino)] phenyl}porphine (3-cyc). $NaBH_4$ (53.6 mg, 1.47 mmol) was added to the CH_2Cl_2-MeOH solution (9.5 mL, 2.5/7 v/v) of **2(H)-cyc** (0.18 g, 0.15 mmol) under an Ar atmosphere under the ice-water bath, and stirred for 10 min. After adding water to stop the reaction, the mixture was extracted with $CHCl_3$. The organic phase was washed with water for several times, and dried over anhydrous Na_2SO_4. The evaporated residue was chromatographed on silica gel column using $CHCl_3$/MeOH (30/1 v/v) as the eluent. The major band eluted was collected and dried at room temperature for several hours *in vacuo* to give the compound **3-cyc** as a purple solid (144.2 mg, 80 %). Rf = 0.29 ($CHCl_3$/MeOH, 30/1 v/v). IR (NaCl) ν = 1690 (C=O(amide)), 3427 (NH(amide)) cm^{-1}. UV-Vis. ($CHCl_3$) λ_{max} = 423, 517, 548, 591, 645 nm. ^{1}H-NMR ($CDCl_3$) δ = -2.6 (2H, s, innerH), 0.1 (12H, m, 1-Me), 0.3 – 1.0 (40H, m, cyclohexyl), 4.9 (2H, q, -C<u>H</u>$_2$OH), 7.4 – 7.6 (8H, m, amide-H, phenyl-4), 7.7 – 7.8 (8H, m, phenyl-3, 5), 8.6 – 8.8 (10H, m, pyrrole-βH, phenyl-6), 9.0 (1H, s, pyrrole-H) ppm. FAB-MS: *m/z* 1202 [M^+].

2-[8-(2-Methyl-1-imidazolyl)octanoyloxymethyl]-5,10,15,20-tetrakis{[α,α,α,α -*o*-(1-methylcyclohexanoylamino)]phenyl}porphine (4-cyc). 8-(2-Methyl-1-imidazolyl)octanoic acid hydrochloride (74.0 mg, 0.287 mmol) and TEA (0.14 mL, 1.15 mmol) were dissolved in dry DMF (2 mL) and stirred for 10 min. After removing TEA

© 2002 American Chemical Society, Bioconjugate Chem., Komatsu bc010067r Supporting Info Page 4

under reduced pressure, **3-cyc** (35 mg, 29.1 μmol), DMAP (3.5 mg, 28.7 μmol), and DCC (100.7 mg, 0.488 mmol) were added to the solution and stirred for 96 hr at room temperature in the darkness. The deposited DCU was filtered off and the mother liquid was evaporated to dryness. After the residue was redisolved in benzene, insoluble DCU was further removed by filtration. Then the $CHCl_3$ solution of the material was slowly dropped into ice-cooled hexane. The red precipitate was collected and chromatographed on silica gel column using $CHCl_3$/MeOH (10/1 v/v) as the eluent. The major band was collected and dried at room temperature for several hours *in vacuo* to give the compound **4-cyc** as a purple solid (31.1 mg, 76 %). Rf = 0.60 ($CHCl_3$/MeOH, 10/1 v/v). IR (NaCl) ν = 1734 (C=O(ester)), 1685 (C=O(amide)) cm^{-1}. UV-Vis. ($CHCl_3$) λ_{max} = 423, 517, 547, 591, 645 nm. ^{1}H-NMR ($CDCl_3$) δ = -2.6 (2H, s, innerH), 0.1 (12H, d, 1-Me), 0.3 – 1.2 (40H, m, cyclohexyl), 1.3 – 1.4 (10H, m, $-(CH_2)_5-$), 1.6 (2H, m, $-O(C=O)CH_2-$), 2.4 (3H, s, 2MeIm), 3.8 (2H, t, $-CH_2$Im), 5.3 (2H, s, Por-$CH_2O(C=O)-$), 6.8, 6.9 (1H, 2s, Im), 7.4 – 7.5 (8H, m, amide-H, phenyl-4), 7.6 – 7.8 (8H, m, phenyl-3, 5), 8.7 – 8.8 (11H, m, pyrrole-βH, phenyl-6) ppm. FAB-MS: *m/z* 1408 [M^+].

FecycP(Im) Br$^-$. A dry THF solution (5 mL) of **4-cyc** (23.5 mg, 16.7 μmol) and 2,6-lutidine (21.3 μL, 0.193 mmol) was added dropwise to anhydrous $FeBr_2$ (200 mg) under dry N_2 atmosphere. The mixture was refluxed for 4 hr under N_2. The obtained solution was brought to dryness, and the residue was extracted with $CHCl_3$ and washed with water. After drying over anhydrous Na_2SO_4, the organic layer was evaporated and chromatographed on a silica gel column using $CHCl_3$/MeOH (10/1 v/v) as eluent. The major band was collected and dried at room temperature for several hours in *vacuo* to give the compound **FecycP(Im) Br$^-$** as a purple solid (17.6 mg, 74 %). Rf = 0.34 ($CHCl_3$/MeOH, 10/1 v/v). IR (NaCl) ν = 1740 (C=O(ester)), 1685 (C=O(amide)) cm^{-1}. UV-Vis. ($CHCl_3$) λ_{max} = 361, 420, 504, 580, 648, 682 nm. FAB-MS: *m/z* 1462 [M^+ – Br].

© 2002 American Chemical Society, Bioconjugate Chem., Komatsu bc010067r Supporting Info Page 5

2-(4-Carboxybutanoyloxymethyl)-5,10,15,20-tetrakis{[α,α,α,α-*o*-(1-methylcyclohexanoylamino)]phenyl}porphine (5-cyc). Gultaric acid anhydride (155 mg, 1.34 mmol) and DMAP (65.4 mg, 0.53 mmol) were added to a dry THF solution (15 mL) of **3-cyc** (0.54 g, 0.45 mmol), and the mixture was reacted for 18 hr at 60°C under an N_2 atmosphere. After evaporation of the solvent, the residue was extracted with $CHCl_3$ and washed with water. The organic layer was then dried with Na_2SO_4, and chromatographed on silica gel column using $CHCl_3$/MeOH (10/1 v/v) as the eluent. The major band was collected and reduced to a small volume on a rotary evaporator. The residue was dried at room temperature for several hours *in vacuo* to give the compound **5-cyc** as a purple solid (0.45g, 79 %). Rf = 0.49 ($CHCl_3$/MeOH, 5/1 v/v). IR (NaCl) ν = 1734 (C=O(ester)), 1688 (C=O(amide)) cm^{-1}. UV-Vis. ($CHCl_3$) λ_{max} = 423, 517, 547, 591, 645 nm. ^{1}H-NMR ($CDCl_3$) δ = -2.6 (2H, m, innerH), 0.1 (12H, s, 1-Me), 0.3 – 1.0 (40H, m, cyclohexyl), 2.0 (2H, t, -C$\underline{H_2}$COOH), 2.4 (4H, m, -O(C=O)C$\underline{H_2}$C$\underline{H_2}$-), 5.3 (2H, q, Por-CH_2O(C=O)-), 7.4 – 7.5 (8H, m, amide-H, phenyl-4), 7.7 – 7.8 (8H, m, phenyl-3, 5), 8.6 (1H, s, pyrrole-βH), 8.7 – 8.8 (10H, m, pyrrole-βH, phenyl-6) ppm. FAB-MS: *m/z* 1316 [M^+].

2-(4-Methyl-L-histidinamidobutanoyloxymethyl)-5,10,15,20-tetrakis{[α,α,α,α-*o*-(1-methylcyclohexanoylamino)]phenyl}porphine (6-cyc). **5-cyc** (46 mg, 35 μmol) and benzotriazol-1-yloxytris(dimethylamine)phosphonium hexafluorophosphate (BOP, 151 mg, 0.35 mmol) were mixed in a dry DMF including TEA (37.7 μL, 0.31 mmol) under an Ar atmosphere. After stirring for 10 min, the histidine methyl ester hydrochlolic acid (25.1 mg, 0.1 mmol) was added to the solution. The obtained mixture was reacted for 12 hr under an Ar atmosphere in the darkness. The reactant was slowly dropped into water, and the precipitation was collected by the glass filter. The obtained solid was dissolved in $CHCl_3$ and dried with Na_2SO_4. The organic layer was condensed and chromatographed on silica gel column using $CHCl_3$/MeOH (30/1 v/v) as the eluent.

© 2002 American Chemical Society, Bioconjugate Chem., Komatsu bc010067r Supporting Info Page 6

The main band was collected and reduced to a small volume on a rotary evaporator. The residue was dried at room temperature for several hours *in vacuo* to give the compound **6-cyc** as a purple solid (43.6 mg, 85 %). Rf = 0.16 ($CHCl_3$/MeOH, 20/1 v/v). IR (NaCl) ν = 1740 (C=O(ester)), 1684 (C=O(amide)) cm^{-1}. UV-Vis. ($CHCl_3$) λ_{max} = 423, 517, 549, 591, 646 nm. ^{1}H-NMR ($CDCl_3$) δ = -2.6 (2H, s, innerH), 0.0 – 0.1 (12H, m, 1-Me), 0.3 – 1.0 (40H, m, cyclohexyl), 1.9 (2H, t, -C$\underline{H_2}$CONH), 2.3 – 2.5 (4H, m, -O(C=O)C$\underline{H_2}$C$\underline{H_2}$-), 3.2 (2H, s, Im-C$\underline{H_2}$-), 3.7 (3H, m, His-O$\underline{Me}$), 4.9 (1H, m, His-CH_2C$\underline{H}$-), 5.2 – 5.4 (2H, q, Por-CH_2O(C=O)-), 7.1 (1H, s, Im), 7.4 – 7.5 (8H, m, amide-H, phenyl-4), 7.7 (1H, s, Im), 7.8 (8H, m, phenyl-3, 5), 8.7 – 8.8 (11H, m, pyrrole-βH, phenyl-6) ppm. FAB-MS: *m/z* 1466 [M^+ – H].

FecycP(His) Br^-. Iron insertion to the compound **6-cyc** was carried out using the same procedure for FecycP(Im) Br^- as described above. Rf = 0.44 ($CHCl_3$/MeOH = 10/1 (v/v)). IR (NaCl) ν = 1740 (C=O(ester)), 1693 (C=O(amide)) cm^{-1}. UV-Vis. ($CHCl_3$) λ_{max} = 354, 420, 505, 581, 648, 683 nm. FAB-MS: *m/z* 1521 [M^+–Br].

2-(4-Carboxybutanoyloxymethyl)-5,10,15,20-tetrakis[(α,α,α,α-*o*-pivaloyl-amino)phenyl]porphine (5-piv). The synthetic procedure for preparation of compound **5-piv** was similar to that used for **5-cyc**. Yield: 85%. Rf = 0.60 ($CHCl_3$/Ethylacetate, 5/1 v/v). IR (NaCl) ν = 1739 (C=O(ester)), 1691 (C=O(amide)) cm^{-1}. UV-Vis. ($CHCl_3$) λ_{max} = 421, 515, 547, 589, 650 nm. ^{1}H-NMR ($CDCl_3$) δ = -2.6 (2H, s, innerH), 0.0 – 0.1 (36H, m, t-Bu), 1.8 (2H, m, -CH_2C(=O)O-), 2.3 – 2.4 (4H, m, -O(C=O)C$\underline{H_2}$C$\underline{H_2}$-), 5.2 (2H, s, Por-CH_2O(C=O)-), 7.1 – 7.2 (4H, m, amide-H), 7.4 – 7.5 (4H, m, phenyl-4), 7.7 – 7.9 (8H, m, phenyl-3,5), 8.6 – 8.8 (11H, m, pyrrole-βH, phenyl-6) ppm. FAB-MS: *m/z* 1155 [M^+].

2-(4-Methyl-L-histidinamidobutanoyloxymethyl)-5,10,15,20-tetrakis[(α,α,α,α -*o*-pivaloylamino)phenyl]porphine (6-piv). The preparation of compound **6-piv** was similar to that used for **6-cyc**. Yield: 87%. Rf = 0.53 ($CHCl_3$/MeOH, 10/1 v/v).

© 2002 American Chemical Society, Bioconjugate Chem., Komatsu bc010067r Supporting Info Page 7

IR (NaCl) ν = 1740 (C=O(ester)), 1687 (C=O(amide)) cm^{-1}. UV-Vis. ($CHCl_3$) λ_{max} = 421, 516, 547, 590, 646 nm. ^{1}H-NMR ($CDCl_3$) δ = -2.6 (2H, s, innerH), 0.0 – 0.1 (36H, m, t-Bu), 1.9 (2H, t, -C$\underline{H_2}$(C=O)NH-), 2.3 – 2.4 (4H, m, -O(C=O)C$\underline{H_2}$C$\underline{H_2}$-), 3.2 (2H, s, Im-C$\underline{H_2}$-), 3.7 (3H, m, His-O$\underline{Me}$), 4.8 (1H, s, His-CH_2C$\underline{H}$-), 5.3 – 5.4 (2H, q, Por-CH_2O(C=O)-), 6.8 (1H, s, Im), 7.2 – 7.3 (4H, m, amide-H), 7.4 – 7.5 (4H, m, phenyl-4), 7.6 (1H, s, Im), 7.7 – 7.9 (8H, m, phenyl-3,5), 8.6 – 8.8 (11H, m, pyrrole-βH, phenyl-6) ppm. FAB-MS: *m/z* 1305 [M^+ – H].

FepivP(His) Br$^-$. Iron insertion to the compound **6-piv** was performed by the same procedure for FecycP(Im) Br$^-$ as described above. Rf = 0.39 ($CHCl_3$/MeOH = 10/1 (v/v)). IR (NaCl) ν = 1741 (C=O(ester)), 1682 (C=O(amide)) cm^{-1}. UV-Vis. ($CHCl_3$) λ_{max} = 353, 420, 507, 577, 645, 685 nm. FAB-MS: *m/z* 1361 [M^+–Br].

3-Methyladenine-DNA Glycosylase II: The Crystal Structure of an AlkA−Hypoxanthine Complex Suggests the Possibility of Product Inhibition

Michael Teale,*,‡ Jindrich Symersky,§ and Larry DeLucas§

Laboratory for Structural Biology, University of Alabama in Huntsville, Huntsville, Alabama 35899 and Center for Biophysical Sciences and Engineering, University of Alabama in Birmingham, Birmingham, Alabama 35294. Received July 12, 2001; Revised Manuscript Received October 31, 2001

Escherichia coli (*E. coli*) protein 3-methyladenine-DNA glycosylase II (AlkA) functions primarily by removing alkylation damage from duplex and single stranded DNA. A crystal structure of AlkA was refined to 2.0 Å resolution. This structure in turn was used to refine an AlkA−hypoxanthine (substrate) complex structure to 2.4 Å resolution. The complex structure shows hypoxanthine located in AlkA's active site stacked between residues W218 and Y239. The structural analysis of the AlkA and AlkA−hypoxanthine structures indicate that free hypoxanthine binding in the active site may inhibit glycosylase activity.

INTRODUCTION

AlkA[1] is one of two base excision repair (BER) enzymes produced by *E. coli* that remove the cytotoxic and mutagenic 3-methyladenine (3-mA); the other glycosylase is the Tag protein (Thomas et al., 1982). AlkA is produced constitutively in small amounts in *E. coli*. In the presence of an alkylating agent, the *adaptive response* is triggered (Evensen et al., 1982; Lindahl et al., 1988), and AlkA expression is increased 10 to 40-fold, resulting in cellular resistance to the alkylating agent (Karran et al., 1982; Nakabeppu et al., 1984). Alkylation of DNA from exposure to cellular (endogenous) alkylating agents or from those that are exogenous, results in a number of alkylation products targeted by AlkA for removal (Kaasen et al., 1986; Habarken et al., 1991; Saparbaev et al., 1994). Given the wide variety of AlkA substrates, it is reasonable to speculate that AlkA is present to remove alkylation damage that the Tag protein is unable to remove. It has been postulated that AlkA evolved to remove primarily 3-methylquanine (Bjelland et al., 1993). AlkA removes damaged bases from single-stranded DNA (Bjelland and Seeberg, 1996) and releases normal bases from duplex DNA (Berdal et al., 1998), indicating that AlkA on occasion orients undamaged bases in its active site such that they are susceptible to cleavage, which might be interpreted to mean that base movement into the active site is likely to result in cleavage.

As has been pointed out (Hollis et al., 2000), AlkA must search for substrate in a vast excess of DNA. It follows that cells would have developed an efficient mechanism to deal with the search for these substrates and thus the cytotoxic and mutagenic effects of alkylation damage. One search mechanism would require glycosylases to search indiscriminately by flipping every base encountered into its active site then cleaving (usually) only those bases that precisely fit the active site pocket (Hollis et al., 2000). Base flipping is believed to be the dominant mechanism for BER glycosylases (Mol et al., 1999). A more efficient search mechanism might be one in which the glycosylase searched the DNA by probing for substrate. Once the probe locates a target base, the base could be flipped out of the helix into the active site (occasionally flipping a normal base), and then the base could be cleaved. This supposition might be supported by the fact that AlkA's efficiency for removing normal bases is several orders of magnitude lower than that of 3-mA removal (Bjelland et al., 1996).

The cell must also deal efficiently with the resulting DNA base excision repair (BER) problem of toxicity resulting from apurinic and apyrimidinc sites (AP-sites). DNA glycosylases remove damaged DNA bases to protect cells from mutation and death. Yet, this relationship is vicarious at best, since removing damaged bases produces toxic AP-sites. The cell must balance its need to remove damaged bases with its need to repair the resulting AP-site. The cell may address this problem via the biochemical mechanism known as product inhibition. In product inhibition, one or more of the products of a given reaction may interact with the enzyme at the active site or a secondary site thereby inhibiting the enzyme's activity. The Tag DNA glycosylase from *E. coli* works in this manner (Bjelland et al., 1987). Tag has a much stricter substrate specificity than AlkA; Tag removes 3-mA and to a lesser extent 3-mG (Bjelland et al., 1987; Bjelland et al., 1993). Product inhibition could also be accomplished by rebinding to the AP-site (the other product of a base excision reaction), which would have the dual

* To whom correspondence should be addressed: Dr. Michael J. Teale, Laboratory for Structural Biology, John Wright Drive MSB room 339, University of Alabama at Huntsville, Telephone: (256) 824-6377, FAX: (256) 824-3204, E-mail: tealem@email.uah.edu.

‡ University of Alabama in Huntsville.

§ University of Alabama in Birmingham.

[1] Abbreviations and glossary: 3-methyladenine-DNA glycosylase II (AlkA); base excision repair (BER) is a noted mechanism for removing bases in DNA repair pathways; 3-methyladenine (3-mA) is a lethal alkylation product; uracil-DNA glycosylase UDG removes uracil from DNA; AP-sites are apurinic and apyrimidinic sites which are sites in DNA where the bases have been removed but the sugar and backbone atoms remain intact; TATA box binding proteins (TBP) are initiation factors.

10.1021/bc015527v CCC: $22.00 © 2002 American Chemical Society
Published on Web 04/03/2002

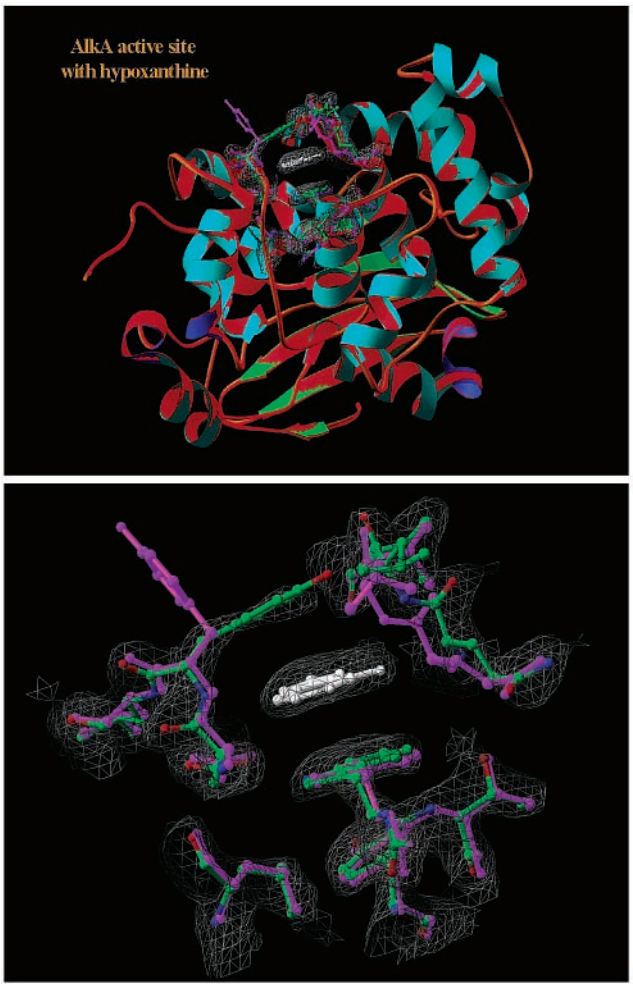


Figure 1. Upper panel: Ribbons diagram depicts two AlkA molecules superimposed red without hypoxanthine, cyan with hypoxanthine bound. White stick and ball model is hypoxanthine. Electron density outlines the hypoxanthine binding site and relevant residues (gray). Lower panel: Shows enlargement of hypoxanthine binding site. Purple stick and ball model shows side chain positions of residues with no hypoxanthine, green shows same residues with hypoxanthine.

purpose of removing AlkA from further activity and protecting the cell from the AP-site. Biochemical assays have shown that uracil-DNA glycosylase (UDG) actually binds to the AP-site more strongly than its target substrate (Bennet et al., 1993). In these reactions the AP-site acts as a competitive inhibitor at concentrations 2−3 orders of magnitude less than the noncompetitive product inhibitor, uracil. It was proposed that UDG cleaved its substrate, released the reaction products, and then rebound the AP-site (Parikh et al., 1998). This implies that some DNA glycosylases may have both reaction products (AP-sites and free damaged base) as inhibition substrates. Adenine in DNA molecules may under go oxidative deamination to form hypoxanthine, which is a substrate for AlkA albeit a weak substrate (Saparbaev, M. and Laval, J., 1994). Here we report the 2.4 Å resolution crystal structure of the E. coli AlkA protein complexed with reaction product free hypoxanthine. The hypoxanthine effectively blocks the active site by stacking between residues Y239 and W218 (Figure 1). The only other AlkA−ligand structure shows AlkA protein complexed to a duplex DNA molecule containing a ribose analogue, 1-azaribose (Hollis et al., 2000) in what might be called an AP-site analogue. Review of the AlkA−hypoxanthine complex structure shows that the hypoxanthine is not in the cleavage position as modeled by Hollis et al., but rather it is located in the general area of the 1-azaribose from the modified DNA. It is possible that the 1-azaribose bound an inhibition site similarly to that of the UDG AP-site inhibition model (Parikh et al., 1998). This putative orientation would probably be very similar to that of the base excision orientation.

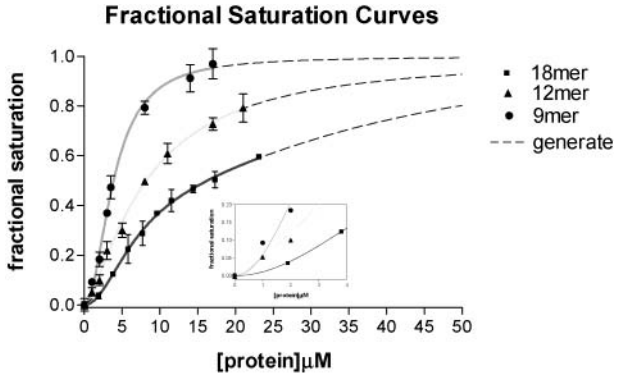


Figure 2. Binding isotherms of AlkA's interaction with normal DNA using 5 μM DNA were developed in an initial study using analytical ultra centrifugation techniques. The best-fit model was the Hill model when compared to a single noninteracting site model. Binding isotherms from 33mer DNA molecules were also obtained, using different DNA concentrations (data not shown), which also produced cooperative curves. The reduction in binding affinity with DNA length is due to nonspecific binding (McGhee et al., 1974). Experiments indicate that these binding isotherms are probably not due to end effects, and sedimentation equilibrium experiments gave binding stoichiometries of 2:1 for 9mers, 3:1 for 12mers, and 3:1 or 4:1 for 18mers.

A Hill analysis from an initial study of AlkA's interaction with undamaged DNA using analytical ultracentrifugation techniques (Figure 2) suggests that AlkA binds undamaged DNA as multiple monomers with a cooperative mechanism (Lebowitz et al., 1998; Teale, unpublished data). The positive cooperative nature of the binding curves suggests that the DNA and/or the protein change conformation upon binding. The structure reported by Hollis et al. shows the DNA separating at the point of AlkA binding. Yet, the DNA in the Hollis structure is not "normal" DNA. Given this, we point out that it is possible that AlkA binds this AP-site analogue as an inhibitor complex with K ∼ 100 pM (Hollis et al., 2000) with a putative AlkA function of protecting the cell from AP-site toxicity. A model where monomers combine on the DNA as the DNA strands and/or AlkA change conformation could explain the cooperative binding isotherms.

MATERIALS AND METHODS

AlkA Crystallization and X-ray Data Collection. AlkA was purified, concentrated, and stored with methods described (O'Connor et al 1993; Teale, unpublished results). The final storage concentration of AlkA was 158 mM (∼ 5 mg/mL) as measured by absorbance at 280 nm, extinction coefficient 2.16 (Pace et al., 1995). The storage buffer was 10 mM Tris-HCl pH 7.5 (KOH), 10 mM β-mercaptanoethanol, and 5% (w/v) glycerol, stored at −80 °C. The hanging drop vapor diffusion crystallization method was used with a 1:1 drop ratio (well/protein solution), and a well solution of 50 mM Hepes pH 6.9, 18% (w/v) poly(ethylene glycol) 8000, and 10 mM β-mercaptanoethanol at 22 °C. Crystals nucleated overnight and grew to a usable size in 4−6 days. The largest crystals were 0.3 × 0.3 × 0.15 mm; however, crystals that produced the best diffraction data were approximately 0.2 × 0.2 × 0.1 mm.

Table 1. Data Collection and Refinement Statistics

	AlkA-hypoxanthine	AlkA
unique reflections	19914	25541
completeness	96%	99%
resolution range (Å)	100−2.4	20−2.0
R_{merge} (%)[b]	3.8%	5.2%
R_{work}[c]	24.3%	18.8%
R_{free}[c]	25.7%	22.1%

[b] $R_{merge} = \sum|I_{obs} - <I>|/\sum I_{obs}$. [c] $R_{work} = ||F_o| - |F_c||/|F_o|$, R_{free} is the same parameter calculated with reserved reflections.

For data collection, crystals were transferred to droplets containing well buffer adjusted to 8%(w/v) glycerol as a cryoprotectant. Crystals were soaked for no more than 15 min. A single crystal was mounted from this droplet onto a Hampton 0.1 mm loop. The crystal was placed immediately into a nitrogen stream at approximately −180 °C. The loop size was selected to allow positioning of the crystal on the loop, minimizing the amount of trapped buffer around the crystal. X-ray diffraction data was collected using a Rigaku R-AXIS IV imaging-plate detector mounted on a Rigaku RU-200 rotating anode X-ray generator operated at 50 kV and 100 mA. A graphite monochromator yielded K radiation with the beam focused by Gobol mirrors. Data were indexed, integrated, and scaled using Denzo and ScalePack (Otwinowski et al., 1997). Completeness of data in the resolution range used for refinement was 96% (Table 1). The R_{sym} and average $I/\sigma(I)$ to 2.0 Å were 5.0 and 15, respectively. The space group was $P2_1$ with pseudo-C centering (seen as very weak reflections when $[h + k] = 2n + 1$), unit-cell parameters were $a = 58.17$, $b = 76.27$, $c = 61.69$, $\alpha = \gamma = 90°$, $\beta = 109.98°$. The Mathews (Mathews, 1968) coefficient was calculated to be 2.18 $Å^3$ Da^{-1}, which represents 44% solvent content for the unit cell with two AlkA monomers per asymmetric unit. The monomers are arranged head to tail in the asymmetric unit.

Cocrystallization of AlkA with hypoxanthine was carried out in hanging drops as described above in 7 mM hypoxanthine. A 0.32 M stock solution of hypoxanthine was made by dissolving hypoxanthine in concentrated well buffer (above), and then concentrated HCl was add until the solution cleared. The solution was then diluted to its final volume with distilled H_2O. The completed solution was filtered with a sterile 0.22 μm filter. A crystal was mounted and data collected as described above. The space group was $P2_1$ with unit cell parameters were $a = 58.17$, $b = 76.27$, $c = 61.87$, $\alpha = \gamma = 90°$, $\beta = 110.03°$.

Crystallographic Refinement and Model Building. The coordinates provided by Tom Ellenberger (see Acknowledgment) were used as the starting refinement model (water molecules not included) for AlkA. The initial R-factor was 30.7% and R-free 36.8% for the resolution range 20.0−2.0 with a 2-σ cutoff for the observed structure amplitudes (Table 1). Positional refinement of the model was performed using the programs X-PLOR (Brunger et al., 1992) and CNS. In alternating rounds of manual adjustments and positional refinement, the refined coordinates were compared with electron density maps with $2F_o - F_c$ and $F_o - F_c$ coefficients. Generally, no major adjustments were necessary other than for several side chain positions. After several rounds of positional refinement and manual adjustments the isotropic temperature factors (B-factors) of individual nonhydrogen atoms were refined. B-factor refinement produced a R-factor of 25.8% and R-free to 30.1%. At this stage of refinement, water molecules were added with regard to defined electron density, while maintaining acceptable intermolecular geometry. After several additional rounds of refinement, R-factors converged with final values: R-factor 18.8% and R-free 24.3%. The final model has 564 amino acid residues, and 379 water molecules with no significant residual electron density.

The coordinates refined above were used as the starting refinement model for the AlkA−hypoxanthine structure (water molecules not included). The initial R-factor was 28.65% and R-free 28.71% for the resolution range 100.0−2.4 with a 2.0 σ cutoff for the observed structure amplitudes. It was apparent in the initial $F_o - F_c$ maps that substantial electron density was present in the active site for hypoxanthine (Figure 1). The density was situated between residues W218 and Y239. Simulated annealing omit maps were generated using CNS scripts. The molecular structure of hypoxanthine was added to the electron density found in the active site. Positional refinement of the combined model was performed. After several rounds of refinement the R-factor values were: R-factor 25.77% and R-free 27.77%. At this point, automatic water selection from CNS was run, which chooses waters based on density maps and performs positional and B-factor refinement. Manual fitting of water positions was carried out using the computer program Chain (Sack, 1988). The final R-factor values were R-factor 22.1% and R-free 25.7%. The final model has 564 amino acid residues, 108 water molecules, and 2 hypoxanthine molecules.

RESULTS

The refined crystal structure of AlkA demonstrates that the monomer orientations in the unit cell are like those of the Labahn et al. (1996) structure. This orientation differs from the 2-fold noncrystallographic symmetry of an AlkA dimer observed in the AlkA structure determined by Yamagata et al. (1996).

A comparison between AlkA and AlkA-hypoxanthine structures shows residue Y239 positioned in the mouth of the active site with its side chain oriented away from the main body of the native AlkA structure (Figure 1, purple stick and ball model). In the AlkA−hypoxanthine structure, residue Y239 turned to block the active site (green stick and ball) with hypoxanthine situated at the opening to the active site (white stick and ball) stacked between residues Y239 and W218.

When residue Y239 rotates in toward the active site opening, its main chain atoms and those of the leucine loop directly across the active site opening are displaced laterally. The orientation of hypoxanthine at 2.4 Å resolution is based on the best fit to the electron density and the local chemistry.

DISCUSSION

AlkA exists as a three domain globular structure; domain 1 has strong structural homology to TATA box binding proteins (TBP), yet there is no sequence homology. There is probably a biological function of AlkA domain one, yet it remains unknown (Yagamata et al., 1996). Domains 2 and 3 define the glycosylase function and demonstrate that AlkA belongs to the helix−hairpin−helix (HhH) super family of DNA repair enzymes (Nash et al., 1996). This motif is found in domain 2 and consists of two α-helices connected by a four amino acid type II hairpin turn and plays a role in bending DNA (Hollis et al., 2000). The AlkA domain 3 helical-fold is similar to the domains containing iron−sulfur clusters in mismatch-adenine glycosylase (MutY)(Guan et al., 1998) and en-

donuclease III (EndoIII)(Kuo et al., 1994), which also have DNA glycosylase functions. AlkA has a leucine minor-groove-binding motif, possessed by DNA glycosylases in general (Mol et al., 1999), where a leucine (or glutamine) is positioned on a loop near the active site and probes the minor groove for substrate. Once a damaged base is located, this probe could take advantage of the possible base stack instabilities and altered minor groove structure due to alkylation (in AlkA's case) and cause the base to flip out of the helix. In this proposed flipping process the base must come in contact with residue Y239 (Figure 1).

Other glycosylase protein−DNA complex crystal structures show the glycosylase interacting with a base, and/or an AP site, or an AP-site analogue inhibitor (Lau et al., 1998; Barrett et al., 1998; Parikh et al., 1998; Hollis et al., 2000). The complex crystal structure of AlkA with an AP-site analogue inhibitor demonstrates inhibition ($K \sim 100$ pM) of AlkA's active site (Hollis et al., 2000). The inhibitor is in part a duplex DNA. The resulting structure is unusual in that it produces a pronounced bend (66°) in the DNA helix. This is unlike similar glycosylase structures as pointed out by Hollis et al. (Slupphaug et al., 1996; Vassylyev et al., 1995; Barrett et al., 1998; Lau et al., 1998). In an earlier study it was shown that a similarly modified DNA molecule designed to mimic a proposed reaction transition state also inhibited glycosylase activity (Schärer et al., 1995).

In the AlkA−hypoxanthine structure, the position of the hypoxanthine suggests a product inhibition mechanism, because the position of the hypoxanthine is similar to that of the 1-azaribose in the Hollis structure. If AlkA cleaved the hypoxanthine from DNA as modeled by Hollis et al., then the hypoxanthine bound as shown in Figure 1 is not in the cleavage position and thus it may have some other function. The AlkA−hypoxanthine complex crystallization conditions do not represent cellular reaction conditions; thus, the biological significance cannot be accessed from these results. However, the hypoxanthine binding at this position is unlikely to be merely a coincidence, given the positioning of the AP-site analogue inhibitor in the AlkA active site.

The complex structure reveals that the hypoxanthine locks up residues Y239 and W218. It's known that W218 is critical for binding substrate (Yamagata et al., 1996). This reaction product (free hypoxanthine) binding site might represent a product inhibitor site for reducing the enzyme activity of damaged base cleavage, thereby modulating the number of new AP-sites formed. By interacting with Y239 and W218, hypoxanthine effectively blocks the active site, which might give the cell time to repair existing AP-sites therefore preventing development of AP-site toxicity. This putative inhibition may very well be a weak interaction by design requiring large concentrations of product for inhibition. Product inhibition reactions could work in concert. Interaction between AlkA and the AP-site would inhibit development of toxicity, while the free damaged base, acting as an inhibitor, would limit new AP-site production.

Although it is still not completely understood, AlkA binding to undamaged DNA is an important aspect of DNA repair, and it has implications for glycosylase DNA interactions in general. The results described herein suggest the possibility of a mechanism for modulating AlkA−DNA interactions and perhaps this class of glycosylases in general.

ACKNOWLEDGMENT

We are very grateful to Tim O'Connor for an AlkA clone and purification protocol and to Tom Ellenberger of Harvard University for their AlkA coordinates. We are also grateful for the program Ribbons implemented by W. M. Carson carson@cmc.uab.edu, http://www.cmc.uab.edu/faculty_staff/carson/.

LITERATURE CITED

(1) Barrett, T. E., Savva, R., Panayotou, G., Barlow, T., Brown, T., Jiricny, J., and Pearl, H. L. (1998) Crystal Structure of a G: T/U Mismatch-Specific DNA Glycosylase: Mismatch Recognition by Complementary-Strand Interactions. *Cell 92*, 117−129.

(2) Bennett, S. E., Schimerlik, M. I., and Mosbaugh, D. W. (1993) Kinetics of the Uracil-DNA Glycosylase/Inhibitor Protein Association *J. Biol. Chem. 268*, No. 36, 26879−26885.

(3) Berdal, K. G., Johansen, R. F., and Seeberg, E. (1998) Release of normal bases from intact DNA by a native DNA repair enzyme. *EMBO J. 17*, No. 2, 363−367.

(4) Bjelland, S., and Seeberg, E. (1996) Different efficiencies of the Tag and AlkA DNA glycosylases from *Escherichia coli* in the removal of 3-methyladenine from single-stranded DNA. *FEBS Lett. 397*, 127−129.

(5) Bjelland, S., Bjoras, M., and Seeberg, E. (1993) Erling Excision of 3-methylquanine from alkylated DNA by 3-methyladenine DNA glycosylase I of *Escherichia coli. Nucleic Acids Research 21*, No. 9, 2045-2049.

(6) Brunger, A. T. (1992) X-PLOR, version 3.1. *A system for X-ray crystallography and NMR*, Yale University Press, New Haven, CT.

(7) Carson, M., and Bugg, C. E. (1986) Algorithm for Ribbon Models of Proteins. *J. Mol. Graphics 4*, 121−122.

(8) Evensen, G., and Seegerg, E. (1982) Adaptation to alkylation resistance involves the induction of a DNA glycosylase. *Nature 296*, 773−774.

(9) Guan, Y., Manuel, R. C., Arvai, A. S., Parikh, S. S., and Mol, C. D. (1998) MutY catalytic core, mutant and bound adenine structures define specificity for DNA repair enzyme super family. *Nat. Struct. Biol. 5*, 1058−64.

(10) Habarken, Y., Carter, C. A., Kirk, M. C., and Ludlum, D. B. (1991) Release of 7-alklyquanines from N-(2-Chloroethyl)-N′-cyclohexyl-*N*-nitrosourea modified DNA by 3-methyladenine DNA Glycosylase II. *Cancer Res. 51*, 499−503.

(11) Hollis, T., Ichikawa, Y., and Ellenberger, T. (2000) DNA bending and a flip-out mechanism for base excision by the helix-hairpin-helix DNA glycosylase, *Escherichia coli* AlkA. *EMBO J. 19*, 758−766, 2000.

(12) Jiang, F., and Kim, S.−H. (1991) "Soft docking": matching of molecular surface cubes. *J. Mol. Biol. 282*, 1061−1081.

(13) Kaasen, I., Evensen, G., and Seeberg, E. (1986) Amplified Expression of *tag*+ and *alkA*+ Genes in *Escherichia coli*: Identification of Gene Products and Effects on Alkylation Resistance. *J. Bacteriol. 186*, 642−647.

(14) Karran, P., Hjelmgren, T., and Lindahl, T. (1982) Induction of a DNA glycosylase for the *N*-methylated purines is part of the adaptive response to alkylating agents. *Nature* 770−773.

(15) Kuo, C. F., McRee, D. E., Fisher, C. L., O'Handley, S. F., Cunningham, R. P., Tainer, J. A. (1994) Atomic structure of the DNA repair [4Fe-4S] enzyme endonuclease III. *Science 258*, 434−40.

(16) Labahn, J., Scharer, O. D., Long, A., Ezaz-Nikpay, K., Verdine, G. L., and Ellenberger, T. E. (1996) Structural Basis for the Excision Repair of Alkylation-Damaged DNA. *Cell 86*, 311−319.

(17) Laskowski, R. A., MacArthur, M. W., Moss, D. S., and Thornton, J. M. (1993) PROCHECK: a program to check the stereochemical quality of protein structures. *J. Appl. Crystallog. 26*, 283−291.

(18) Lau, A. Y., Scharer, O. D., Samson, L., Verdine, G. L., and Ellenberger, T. (1998) Crystal Structure of a Human Alkybase-DNA Repair Enzyme Complexed to DNA: Mechanisms for Nucleotides Flipping and Base Excision. *Cell 95*, 249−258.

(19) Lebowitz, J., Teale, M. J., Schuck, P. W. (1998) Analytical Band Centrifugation of Proteins and Protein Complexes. *Biochem. Soc. Trans. 26*, 745−749.
(20) Lindahl, T., and Sedgwick, B. (1988) Regulation and expression of the adaptive response to alkylating agents. *Ann. Rev. Biochem. 57*, 133−157.
(21) Matthews, B. W. (1968) Solvent content of protein crystals. *J. Mol. Biol. 33*, 491−497.
(22) O′Connor, R. T. (1993) Purification and characterization of human 3-methyladenine-DNA glycosylase. *Nucl. Acids Res. 21*, 5561−5569.
(23) James, D., McGhee, and von Hippel, P. (1974) Theoretical Aspects of DNA-Protein Interactions: Cooperative and Non-cooperative Binding of Large Ligands to a One-dimensional Homogeneous Lattice. *J. Mol. Biol. 86*, 469−489.
(24) McGhee, J. D., and von Hippel, P. (1974) *J. Mol. Biol. 86*, 469−489.
(25) Mol, C. D., Arvai, A. S., Sanderson, R. J., Slupphaug, G., Kavli, B. (1995a) Crystal structure of human uracil-DNA glycosylase in complex with a protein inhibitor: protein mimicry of DNA. *Cell 82*, 701−8.
(26) Mol, C. D., Parikh, S. S., Putnam, C. D., Lo, T. P., and Tainer, J. A. (1999) DNA repair mechanisms for the recognition and removal of damaged DNA bases. *Annu. Rev. Biophys. Biomol. Struct. 28*, 101−28.
(27) Nakabeppu, Y., Miyata, T., Kondo, H., Iwanaga, S., and Sekiguchi, M. (1984) Structure and Expression of the *alkA* Gene of *Escherichia coli* Involved in Adaptive Response to Alkylating Agents. *J. Biol. Chem. 259*, 13730−13736.
(28) Nash, H. M., Bruner, S. D., Scharer, O. D., Kawate, T., and Addona, T. A. (1996) Cloning of a yeast 8-oxoguanine DNA glycosylase reveals the existence of a base-excision DNA-repair protein super-family. *Curr. Biol. 6*, 968−80.
(29) Otwinowski, O., and Minor, W. (1997) Processing of X-ray Diffraction Data in Collected in Oscillation Mode. *Methods Enzymol., Macromol. Crystallogr., A 276*, 307−326.
(30) Pace, C. N., Vajdos, F., Fee, L., Grimsley, G., and Gray, T. (1995) How to measure and predict the molar absorption coefficient of a protein. *Protein Sci. 4*, 2411−2423.
(31) Parikh, S. S., Mol, C. D., Slupphaug, G., Bharati, S., Krokan, H. E., and Tainer, J. A. (1998) Base excision repair initiation revealed by crystal structures and binding kinetics of human uracil-DNA glycosylase with DNA. *EMBO J. 17*, 17: 5214−5226.
(32) Saparbaev, M., and Laval, J. (1994) Excision of hypoxanthine from DNA containing dIMP residues by the *Escherichia coli*, yeast, rat, and human alkylpurine DNA glycosylases. *Proc. Natl. Acad. Sci. U.S.A. 91*, 5873−5877.
(33) Saparbaev, M., and Laval, J. (1994) Excision of hypoxanthine from DNA containing dIMP residues by the *Escherichia coli*, yeast, rat, and human alkylpurine DNA glycosylases. *Proc. Natl. Acad. Sci. U.S.A. 91*, 5873−5877.
(34) Schärer, Orlando D., Ortholand, Jean-Yves, Ganesan, A., Ezaz-Nikpay, Khosro, and Verdine, Gregory L. (1995) Specific Binding of the DNA Repair Enzyme AlkA to a Pyrrolidine-Based Inhibitor. *J. Am. Chem. Soc. 117*, 6623−6624.
(35) Slupphaug, G., Mol, C. D., Kavli, B., Arvai, A. S., Krokan, H. E., and Tainer, J. A. (1996) A nucleotide-flipping mechanism from the structure of human uracil-DNA glycosylase bound to DNA. *Nature 384*, 87−92.
(36) Teale, M. J., Bogart, T., and DeLucas, L. Binding Stoichiometries and Isotherms Indicate Cooperative Interactions Between AlkA and Normal Duplex DNA. Unpublished data.
(37) Thomas, L., Yang, C. H., and Goldthwait, D. A. (1982) Two DNA glycosylases in *Escherichia coli* which release primarily 3-methyladenine. *Biochemistry 21*, 1162−1169.
(38) Vassylyev, D. G., Kashiwagi, T., Mikami, Y., Ariyoshi, M., Iwai, S., Ohtsuka, E., and Morikawa, K. (1995) Atomic model of a pyrimidine dimer excision repair enzyme complexed with a DNA substrate: structural basis for damaged DNA recognition. *Cell 83*, 773−782.
(39) Yamagata, Y., Kato, M., Odawara, K., Tokuno, Y., Nakashima, Y., Matsushima, N., Yasumura, K., Tomito, K., Ihara, K., Fuji, Y., Nakabeppu, Y., Sekiguchi, M., and Fuji, S. (1996) Three-Dimensional Structure of a DNA Repair Enzyme, 3-methyladenine DNA Glycosylase II, from *Escherichia coli*. *Cell 86*, 311−319.

BC015527V

Monoclonal Antibodies That Recognize Minimal Differences in the Three-Dimensional Structures of Metal−Chelate Complexes

R. Mark Jones,[†] Haini Yu,[†] James B. Delehanty,[†] and Diane A. Blake*[,†,‡]

Department of Ophthalmology, Tulane University Health Sciences Center, New Orleans, Louisiana, 70112, and Tulane/Xavier Center for Bioenvironmental Research, New Orleans, Louisiana 70112. Received August 1, 2001; Revised Manuscript Received November 29, 2001

Immunization of BALB/c mice with a cadmium−chelate−protein conjugate resulted in the isolation of two hybridoma cell lines (A4 and E5) that synthesized antibodies with different variable regions, but similar metal−chelate affinity. The ability of these two monoclonal antibodies to interact with 12 different metal−chelate complexes was studied using the KinExA 3000 immunoassay instrument. The two antibodies showed the highest affinity for cadmium and mercury complexes of ethylenediamine *N*,*N*,*N*′,*N*′-tetraacetic acid (EDTA). The E5 antibody bound to EDTA complexes of cadmium and mercury with equilibrium dissociation constants (K_d) of 1.62×10^{-9} M and 3.64×10^{-9} M, respectively. The corresponding values for the A4 antibody were 14.7×10^{-9} M and 3.56×10^{-9} M. Addition of a cyclohexyl ring to the EDTA backbone increased the affinity of E5 for the metal−chelate haptens, while decreasing the binding of A4 to the same haptens. Based on available crystal structures, molecular models were constructed for five different divalent metal−chelate complexes. The models were compared to determine structural features of the haptens that may influence antibody recognition. Difference distance matrixes were used to identify areas of the metal−chelate haptens that differed in three-dimensional space. Antibody affinity correlated well with the extent of total structural difference for these metal−EDTA complexes.

INTRODUCTION

Half of the 20 amino acids have functional groups that can coordinate metal ions, and the resulting protein−metal complexes play a number of roles; they serve as electrophiles at active sites, redox centers, and foci for structural stabilization (*1*). Antibodies that bind metals and metal-containing antigens make up a special class of these metal-binding proteins. There are a number of reports of metal-binding antibodies. Myelomas producing Cu- and Ca-binding immunoglobulins were reported in the mid and late 1970s (*2*, *3*). More recently antibodies directed against glutathione− and chelate−metal complexes of Hg(II), In(III), Cd(II), and Pb(II) have been reported (*4*−*7*). These metal-specific monoclonal antibodies (mAbs)[1] have potential uses in both medicine and environmental analysis. Some metal-binding antibodies have had utility in tumor imaging and treatment (*8*). Immunoassays for specific metal ions have also been developed using metal-specific monoclonal antibodies as their primary reagent (*9*−*12*). These immunoassays, with sensitivities of sub-part per billion for some metal ions, will be useful adjuncts to more traditional analytical methods of metals analysis.

Metal-specific monoclonal antibodies also offer a unique opportunity to examine mechanisms of protein−metal interactions. The best studied metal-specific mAb is CHA255, which binds to In(III)−EDTA complexes (*13*). This antibody was studied in detail via X-ray crystallography and was shown to bind an In(III)−4-[*N*′-(2-hydroxyethyl)thioureido]-L-benzyl−EDTA (EOTUBE) complex through both direct metal coordination and ionic interactions with the chelate molecule. A histidine residue in the third complementarity determining region of the heavy chain (CDRH3) was shown to coordinate the In(III) ion. Contiguous to the histidine, an arginine appeared to ion-pair with one of the carboxylate arms of the In(III)−EOTUBE complex. When the In(III) was replaced with Fe(III), the affinity of CHA255 decreased 20-fold. The histidine in CDRH3 could no longer coordinate the Fe(III) due to changes in the conformation of the glycinate arms of the EDTA chelate. This study emphasized that the direct coordination of the metal by CHA255 was required for high affinity binding. The Cd(II)− and Hg(II)−EDTA specific antibody, 2A81G5, was homology modeled using CHA255 as a template (*6*). This model revealed a CDRH3 histidine residue in a similar metal-ion-coordinating orientation. Apart from this histidine, the two antibodies shared little CDR homology or binding similarities. The metal-ion selectivity of the CHA255 antibody could not be explained in terms of metal ion size or metal−chelate stability constants (*5*).

* To whom correspondence should be addressed: Department of Ophthalmology SL-69, Tulane University Health Sciences Center, 1430 Tulane Ave., New Orleans, LA 70112-2699: Tel.: 504-584-2478; Fax: 504-584-2684. E-mail: blake@tulane.edu.

[†] Tulane University Health Sciences Center.

[‡] Tulane/Xavier Center for Bioenvironmental Research.

[1] Abbreviations used: mAb, monoclonal antibody; EDTA, ethylenediamine-*N*,*N*,*N*′,*N*′-tetraacetic acid; EOTUBE, 4-[*N*′-(2-hydroxyethyl)thioureido]-L-benzyl−EDTA; CDR, complementarity determining regions; BSA, bovine serum albumin; KLH, keyhole limpet hemocyanin; ITCBE, 1-(4-isothiocyanobenzyl)-ethylenediamine-*N*,*N*,*N*′,*N*′-tetraacetic acid; CDTA, *trans*-1,2-cyclohexanediamino-*N*,*N*,*N*′,*N*′-tetraacetic acid; TMB, 3,3′,5,5′-tetramethylbenzidine; ELISA, enzyme-linked immunosorbent assay; PCR, polymerase chain reaction; HBS, HEPES buffered saline, (137 mM NaCl, 3 mM KCl, 10 mM Hepes); IgG, immunoglobulin G.; K_d, equilibrium dissociation constant; K_{on}, association rate constant; K_{off}, dissociation rate constant; DM, distance matrix; DDM, difference distance matrix; SDS−PAGE, sodium dodecyl sulfate polyacrylamide gel electrophoresis.

10.1021/bc0155418 CCC: $22.00 © 2002 American Chemical Society
Published on Web 03/30/2002

With the exception of Hg(II) and Mg(II), the metal-ion selectivity and affinity of the 2A81G5 antibody was found to correlate well with the atomic volume of the divalent metal ions (*6*). Both of these studies gave only cursory regard to the total metal−chelate structure, which is regulated by both ion size and coordination bond lability.

In the current study, we report the isolation and characterization of two monoclonal antibodies that showed similar metal−chelate affinities during initial screening studies. These two antibodies were subsequently found to have different N-terminal sequences in both their heavy and light chains. We have compared the ability of these two antibodies to bind to a variety of metal−chelate complexes and hypothesized about recognition mechanisms based on metal−chelate structure. The two antibodies were found to bind Cd(II)− and Hg(II)−chelate complexes with the highest affinity. Molecular modeling of five divalent metal−chelates with known crystal structures also allowed us to focus on differences in the metal−chelate hapten structures that may be important for antibody recognition.

EXPERIMENTAL PROCEDURES

Materials. Bovine serum albumin (BSA) (ultrapure) and an immunoglobulin G (IgG) isotyping kit were obtained from Boehringer Mannheim (Indianapolis, IN). Keyhole limpet hemocyanin (KLH) and 1-(4-isothiocyanobenzyl)ethylenediaminetetraacetic acid (ITCBE) were purchased from CalBiochem Corp. (La Jolla, CA). Centricon 30 microconcentrators were products of Amicon, Inc. (Beverly, MA). Metal ions were atomic absorption standards from Perkin-Elmer Corporation (Norwalk, CT). BALB/c AnNtacfBR inbred mice were purchased from Charles River Laboratories (Wilmington, MA). Ribi adjuvant was obtained from Ribi Immunochemicals (Hamilton, MT). HEPES, ethylenediamine-*N*,*N*,*N*′,*N*′-tetraacetic acid (EDTA), tissue culture medium, L-glutamine, HAT medium supplement, antibiotics, cyanogen bromide activated agarose, and goat anti-mouse IgG coupled to horseradish peroxidase were purchased from Sigma Chemical Co. (St. Louis, MO). Sodium dodecyl sulfate−polyacrylamide gel electrophesis (SDS−PAGE) reagents were obtained from Bio-Rad (Hercules, CA). Pyroglutmate amino peptidase was purchased from Panvera Corporation (Madison, WI). *trans*-1,2-Diaminocyclohexane-*N*,*N*,*N*′,*N*′-tetraacetic acid (CDTA) was purchased from Aldrich (Milwaukee, WI). 3,3′5,5′-Tetramethylbenzidine (TMB) microwell substrate was a product of Kirkegaard-Perry Laboratories (Gaithersburg, MD). Mini Problott membranes were obtained from Applied Biosystems (Foster City, CA). Immobilized protein G resin and BCA protein assay were purchased from Pierce Chemical Co. (Rockford, IL) and used according to the manufacturer's instructions.

Protein−Chelate Conjugates. Protein chelate conjugates were prepared as described in (*14*). A 20 mg/mL solution of protein (BSA or KLH) was prepared in phosphate-buffered saline (137 mM NaCl, 3 mM KCl, 10 mM sodium phosphate), pH 9.5. ITCBE and Cd(II) were added to the BSA solutions to achieve final concentrations of 1.36 mM and 1.4 mM, respectively. ITCBE and Cd(II) were added to KLH solutions in equimolar amounts to achieve a final concentration of 1.5 mM. The reactions were adjusted to pH 9.0 and stirred for 22 h at 25 °C. Unreacted low-molecular weight reagents were removed by buffer exchange using a Centricon 30 device that had been previously treated with EDTA and washed profusely with Hepes-buffered saline (HBS, 137 mM NaCl, 3 mM KCl, 10 mM Hepes), pH 7.4. The conjugates were washed five times with metal-free HEPES (0.1 M, pH 9.0) and twice with metal-free HEPES (0.1 M, pH 7.4). Protein conjugate concentration was determined using the Pierce BCA protein assay. The degree of conjugate substitution was quantified using the trinitrobenzenesulfonic acid method similar to that described in refs 15 and 16. The extent of substitution of free lysine residues was 15.8−17.0% for BSA conjugates and 15% for the KLH conjugate.

Mouse Immunization, Hybridoma Production, and Purification of Monoclonal Antibodies. Five 6-week old BALB/c AnNtacfBR mice were injected intraperitoneally with 50 μg of the Cd(II)−EDTA−KLH conjugate emulsified in Ribi adjuvant at days 0, 21, and then at 2-week intervals. Antibody response of each mouse was determined by indirect ELISA using both metal-free EDTA−BSA and cadmium-loaded conjugate (*6*). The mice showing highest antibody responses were given a final intraperitoneal boost of 50 μg of the KLH conjugate in phosphate-buffered saline (pH 7.4) 4 days prior to fusion. Mouse spleen cells were harvested, washed in RPMI 1640 medium, and fused with X63-Ag 8.653 myeloma cells. Supernatants from viable, replicating hybridoma clones were collected and screened for antibodies to a variety of metal−chelate complexes by competitive ELISA (described below). Hybridomas synthesizing and secreting metal-specific antibodies were subcloned twice by limiting dilution. Positive hybridoma clones were subcultured and frozen.

Ascites fluid was produced in BALB/c mice primed with Freund's incomplete adjuvant by intraperitoneal injection of 1.27×10^6 hybridoma cells. Ascites fluid was collected 10−15 days after the hybridoma injection. The clone E5 was difficult to grow as an ascites tumor, while clone A4 displayed no problems developing as ascites. The IgG fraction of ascites was isolated by affinity chromatography on immobilized protein G. A portion of the protein G purified antibody was further purified on a Cd(II)−EDTA−BSA affinity column. The Cd(II)−EDTA−BSA affinity-purified antibodies were separated under reducing conditions by SDS−PAGE and electroblotted to Mini Problott membranes. The heavy chain N-terminus of antibody E5 was blocked and required deblocking according to the method described in Mozdzanowski et. al prior to electrophoresis (*17*). The heavy and light chain proteins were excised, and N-terminal sequencing was performed at a commercial facility. The immunoglobulin subclass and light chain isotype of the antibodies were determined using an IsoStrip antibody isotyping kit according to the manufacture's instructions. Protein concentration was determined using the BCA protein assay kit.

Competitive ELISA. Competitive ELISAs were performed essentially as described in ref 11. Cd(II), Hg(II), Mn(II), Cu(II), Zn(II), Fe(III), Ni(II), In(III), Ag(I), Pb(II), Co(III), Mo(VI), and Ca(II) were tested for their ability to inhibit binding to the immobilized Cd(II)−EDTA−BSA conjugate in a HBS amended with 0.4 mM CDTA or 4.0 mM EDTA.

Determination of Equilibrium Dissociation Constants and Bimolecular Association Rate Constants. The KinExA 3000 (Sapidyne Instruments Inc., Boise, ID) is an automated flow fluorimeter used to determine the amount of antibody with unoccupied binding sites in a mixture of antibody and ligand (*18*). Binding experiments were performed by coating 200 mg of poly(methyl methacrylate) beads (63−103 μm) (Sapidyne Instruments, Inc.) with 1 mL Cd(II)−EDTA−BSA

conjugate (100 μg/mL). The conjugate and beads were rocked for 1 h at 37 °C. The beads were then pelleted and washed three times with 1 mL of HBS. The beads were blocked with 1 mL of 1% BSA in HBS at 37 °C for 1 h and stored in blocking buffer at 4 °C for up to six weeks. Detailed protocols for use of the KinExA instrument are available in ref 18.

Data acquisition and instrument control were accomplished using a PC interfaced with the KinExA and software distributed by Sapidyne, Inc. The resulting data was compiled using Microsoft Excel, and equilibrium dissociation constants were obtained from nonlinear regression analysis of the data using a one-site homogeneous binding model contained within SlideWrite Plus software (Version 5.0, Advanced Graphics, Inc, Encinitas, CA).

Modeling of Metal−Chelate Conjugates and Distance Matrixes. Crystal structures for Cd(II)−, Hg(II)−, Mn(II)−, In(III)−, Fe(III)−, Ni(II)−, and Zn(II)−EDTA complexes were obtained from the Cambridge Structural Database (*19*−*25*). Metal−EDTA structures were displayed on a Silicon Graphics Octane workstation with SYBYL 6.6 molecular modeling software (Tripos Associates, St. Louis, MO). The extended parameter set $TA_DEMOS/metals.tpd was used for metal recognition as provided by Tripos. The crystal structures were geometry-optimized using the standard Tripos molecular mechanics force field with 0.001 kcal/mol energy gradient convergence criterion. Interatomic distances were determined manually from the SYBYL menu using the ANALYSE>DISTANCE option. The atom numbering between the crystal structures varied, so the chelate−metal complexes were aligned and numbered according to ref 26. Distance Matrixes and Difference Distance Matrixes were built using the program Mathematica version 4.1 (Wolfram Research, Champaign, IL). The carbonyl oxygens (O2, O4, O6, and O8) (see Figure 3) were not included in the difference distance matrixes in order to reduce the size and complexity of Figure 4. Due to the planar nature of the carbonyl bond the distance information is mirrored by the metal-coordinating oxygens and thus would be repetitive.

RESULTS

Hybridoma Screen. Hybridoma cells were screened for antibodies that bound Cd(II)−EDTA−BSA and 49 positive clones were detected. The positive hybridomas were grouped based on the ability of their antibodies to be inhibited in competitive ELISA. Cells producing antibodies that showed little inhibition by soluble EDTA or Zn(II)−EDTA, but considerable inhibition by Cd(II)−EDTA, were selected for further analysis.

Cells in a single well showing activity were subcloned by limiting dilution and gave rise to two clones, A4 and E5. Supernatants from these two clones were again screened for their ability to be competitively inhibited by metal-free EDTA and Zn(II) or Cd(II) in a background of 5 mM EDTA. Both antibodies showed little inhibition by metal-free EDTA at concentrations as high as 5 mM (data not shown). As shown in Figure 1, addition of Zn(II) (765 μM)−EDTA inhibited A4 by 54% and E5 by 71%, while Cd(II) (445 μM)−EDTA inhibited 97% of the binding activities of the two antibodies. The initial interpretation of this screening data was that A4 and E5 were identical clones, and the differences in the competitive ELISA screen were due to variations of antibody concentration in the culture supernatants. Isotyping revealed that both mAbs were of the IgG1 subclass with κ light chains.

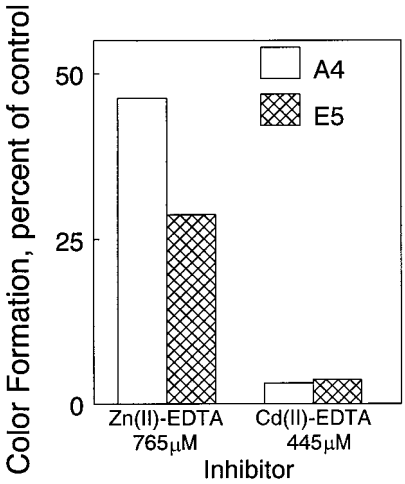


Figure 1. Hybridoma supernatant screen by competitive ELISA. The tissue culture supernatants from clones A4 and E5 were diluted in PBS containing 5 mM EDTA and tested by competitive ELISA for their ability to be inhibited by soluble Zn(II) (765 μM) or Cd(II) (445 μM) in a background of 5 mM EDTA.

Table 1. N-Terminal Amino Acid Sequence for A4 and E5 Variable Regions[a]

	heavy chain variable region sequence
A4	E V Q L Q Q S G A E L V K P G A S V K L S C S V T A
E5	Q V Q L K E S G P G L V A P S Q S L S I T

	light chain variable region sequence
A4	D I V M S Q F P S S L A V S T G E R V T M
E5	D V V M T Q T P L S L P V S L G X Q A X I

[a] An X indicates amino acid residues that could not be accurately determined from the data.

N-Terminal sequencing subsequently revealed that the two antibodies differed in amino acid sequence in the first framework region of both their light chain and heavy chain variable regions as shown in Table 1. Although these framework sequences do not define the antigen-binding domains of the antibodies, these data, taken with the differences observed in binding affinities (see below), indicate that A4 and E5 are two different antibodies.

Binding Specificity. Binding comparisons of A4 and E5 were initially performed using competitive ELISA (data not shown). The ELISA data identified trends that could be more rigorously studied using the KinExA 3000. The KinExA instrument allows the separation and quantification of unbound antibody in an equilibrium mixture of antibody, ligand, and antibody−ligand complexes. Unbound antibody is removed from the equilibrium mixture by a brief passage through a column of immobilized ligand. The equilibrium mixture is exposed to the column for approximately 240 ms, and thus the immobilized ligand acts merely as a trapping reagent to remove a portion of uncomplexed antibody from the mixture (*18*).

The KinExA instrument generates fluorescence curves as shown in Figure 2A. A portion of the curve (for this study between 300 and 399 s) was integrated, and the concentration of free, unbound antibody in each equilibrium mixture was determined from the integrated fluorescence. The fraction of occupied binding sites on the antibody molecule was taken as:

$$\frac{I_0 - I_{exp}}{I_0 - I_\infty} \quad (1)$$

Table 2. Binding (K_d, M) of Chelators and Chelated Metals to Antibodies A4 and E5

	A4		E5	
chelator	EDTA	CDTA	EDTA	CDTA
metal free	$>10^{-3}$	$(5.27 \pm 1.60) \times 10^{-4}$	$>10^{-3}$	$(2.27 \pm 0.34) \times 10^{-8}$
Cd(II)	$(1.47 \pm 0.24) \times 10^{-8}$	$(4.20 \pm 0.50) \times 10^{-8}$	$(1.62 \pm 0.14) \times 10^{-9}$	$(1.16 \pm 0.34) \times 10^{-9}$
Hg(II)	$(3.56 \pm 1.08) \times 10^{-9}$		$(3.64 \pm 1.33) \times 10^{-9}$	
In(III)	$(3.11 \pm 0.55) \times 10^{-7}$	$(6.90 \pm 2.00) \times 10^{-7}$	$(1.69 \pm 0.30) \times 10^{-7}$	$(3.23 \pm 0.83) \times 10^{-8}$
Mn(II)	$(4.71 \pm 0.88) \times 10^{-7}$	$(6.42 \pm 0.45) \times 10^{-6}$	$(1.45 \pm 0.09) \times 10^{-7}$	$(3.40 \pm 0.96) \times 10^{-9}$
Zn(II)	$(1.10 \pm 0.21) \times 10^{-6}$		$(1.18 \pm 0.13) \times 10^{-6}$	
Cu(II)	$(1.11 \pm 0.06) \times 10^{-6}$		$(1.80 \pm 0.23) \times 10^{-6}$	
Ni(II)	$(5.39 \pm 0.80) \times 10^{-6}$		$(1.10 \pm 0.50) \times 10^{-6}$	
Co(III)	$(3.04 \pm 0.17) \times 10^{-6}$		$(1.22 \pm 0.40) \times 10^{-6}$	
Fe(III)	$(6.03 \pm 1.08) \times 10^{-6}$		$(4.00 \pm 0.89) \times 10^{-6}$	
Ca(II)	$>1 \times 10^{-6}$		$>2 \times 10^{-6}$	
Pb(II)	$>1 \times 10^{-5}$		$>3 \times 10^{-5}$	

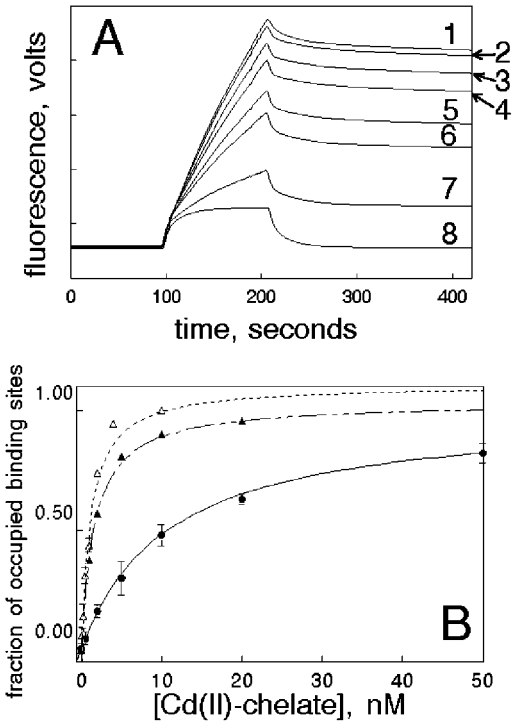


Figure 2. Determination of equilibrium dissociation constants for A4 and E5 to cadmium–chelate complexes. Panel A: Instrument response traces from the KinExA 3000. A4 inhibition by Cd(II) in a backgroud of 0.4 mM EDTA. Curve 1 corresponds to zero Cd(II) concentration, curve 8 corresponds to a saturating Cd(II) concentration (100 nM), and curves 2–7 correspond to Cd(II) concentrations of 0.5, 2,5, 10, 20, and 50 nM, respectively. Panel B: The fraction of occupied binding sites is determined by integrating a portion of the instrument response traces between 300 and 399 s, graphing against ligand concentration, and normalizing these integrated fluorescence curves. A4 binding to Cd(II)–EDTA is represented by closed circles (●). E5 binding to Cd(II)–EDTA is represented by closed triangles (▲), and E5 binding to Cd(II)-CDTA is represented by open triangles (△). Equilibrium dissociation constants are summarized in Table 1.

where I represents the integrated fluorescence and the subscripts 0, exp, and ∞ represent experimental traces corresponding to a ligand concentration of zero, an intermediate concentration, and a saturating ligand concentration, respectively. The fraction of occupied binding sites was plotted versus ligand concentration, and the equilibrium dissociation constant, K_d, was determined from a nonlinear regression fit of the data (example shown in Figure 2B) to the following rectangular hyperbola:

$$\text{fraction of occupied binding sites} = X/(X + K_d) \quad (2)$$

where X represents the free ligand concentration.

Both antibodies showed negligible affinity for metal-free EDTA as shown in Table 2. Antibody A4 bound most tightly to Hg(II)–EDTA complexes. Replacement of Hg(II) in the EDTA complex with Cd(II) decreased the affinity of A4 by 4-fold. Replacement with In(III) or Mn(II) lowered the K_d 2 orders of magnitude from that observed with the Hg(II)–EDTA complex. All other metal–EDTA complexes tested (Zn(II), Cu(II), Ni(II), Co(III), Fe(III), Ca(II), and Pb(II)) bound A4 more than 200-fold less tightly than Hg(II)–EDTA.

Of the EDTA complexes, E5 showed the highest affinity for Cd(II)–EDTA and only a 2-fold lower affinity for Hg(II)–EDTA (Table 2). Replacement of Cd(II) with In(III) or Mn(II) in the EDTA complex resulted in an approximate 100-fold decrease in affinity, while all other metals decreased the affinity of E5 for the metal–chelate complex by over 500-fold. The two antibodies bound EDTA complexes of Cd(II), Mn(II), and Ni(II) with differing affinities, but both antibodies bound the EDTA complexes of Hg(II), Zn(II), Co(III), Cu(II), Fe(III), and In(III) with very similar affinities.

When the structure of the chelator was changed by substituting CDTA for EDTA, antibody recognition of the metal-free CDTA was measurable (Table 2). A4 recognized metal-free CDTA with just under millimolar affinity, while E5 bound to metal-free CDTA with a surprisingly high affinity (22.7 nM). A4 bound less tightly to the metal–CDTA complexes than to the corresponding metal–EDTA complexes. Except for Mn(II)–CDTA, the average decrease in affinity of A4 for metal–CDTA complexes over metal–EDTA complexes was approximately 2-fold. The decrease for Mn(II)–CDTA versus Mn(II)–EDTA was just over 10-fold. In contrast, E5 bound more tightly to the metal–CDTA complexes than to the corresponding metal–EDTA complexes. E5 bound Cd(II)–CDTA slightly tighter than the Cd(II)–EDTA complex, but recognized Mn–CDTA with a 40-fold higher affinity than Mn(II)–EDTA. E5 also showed a 5-fold increase in affinity for In(III)–CDTA over the In(III)–EDTA complex.

Association and dissociation rate constant determinations were attempted for the Cd(II), Mn(II), In(III), and Hg(II) metal–chelate complexes and for the metal-free CDTA. The KinExA 3000 was used to determine bimolecular association rate constants in these procedures (*18*). The concentration of antigen was varied while maintaining a constant, but short reaction time. Antibody was injected into and mixed with a stream of antigen. This mixture was allowed to react for the 11 s it took the stream to flow from the injection point to the observation cell and interact with the bead column. The resulting fluorescent response curves were similar to those in Figure 2A, and a single-exponential function of

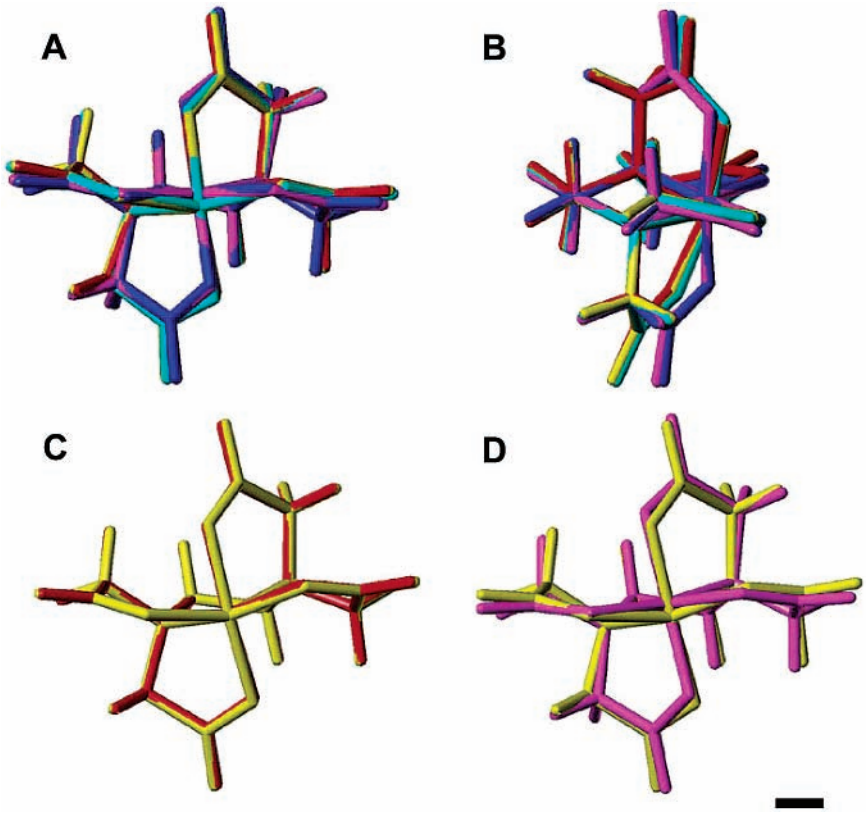


Figure 3. Energy-minimized crystal structures of metal−EDTA complexes. EDTA complexes of Cd(II), yellow; Hg(II), red; Mn(II), cyan; Ni(II), magenta; and Zn(II), blue. Panels A and B: Superimposed structures of all five complexes, shown from two different angles of view. Panel C: Superimposed structures of EDTA complexes of Cd(II) and Hg(II). Panel D: Superimposed structures of EDTA complexes of Cd(II) and Ni(II). Bar, 1 Å.

Table 3. Measurable Kinetic Constants for Antibodies A4 and E5[a]

ligand	association rate constant, $M^{-1}\ s^{-1}$	dissociation rate constant, s^{-1}
	Antibody A4	
Hg(II)−EDTA	$(3.96 \pm 0.9) \times 10^6$	0.014
Mn(II)−EDTA	$(6.64 \pm 1.7) \times 10^4$	0.031
	Antibody E5	
Hg(II)−EDTA	$(2.26 \pm 0.2) \times 10^6$	0.008
Cd(II)−EDTA	$(1.73 \pm 0.2) \times 10^7$	0.028

[a] Association rate constants were determined as described in the text. Values for dissociation rate constants were obtained by calculation from the association rate constant and the K_d.

time was fit to each data set (see ref 18 for details). Unfortunately, association rate constants for metal-free CDTA and the In(III)−chelate complexes with both antibodies, Cd(II)−EDTA with A4, and Mn(II)−EDTA with E5 were not measurable by this method. The antibody and metal−chelates had reached equilibrium in the 11 s allowed for the mixing reaction, indicating that the antibody had an on-rate for these ligands that was faster than the operational deadtime of the instrument.

The on-rate for Hg(II)−EDTA with A4 was 59-fold higher than that determined for Mn(II)−EDTA as shown in Table 3. The off rate was determined by the identity $K_d = K_{off}/K_{on}$. A4 dissociated from Mn(II)−EDTA at a rate 2× faster than that determined for Hg(II)−EDTA. The on-rate for E5 was 7.5-fold faster with Cd(II)−EDTA than with Hg(II)−EDTA, but it also dissociated 3.5-fold faster. The bimolecular association rate constants of both antibodies with Hg(II)−EDTA were similar.

Difference Distance Matrixes. The ability of the A4 and E5 antibodies to discern subtle differences in the structures of metal−chelate complexes was further investigated by analyzing the available crystal data for several of these complexes. Figure 3 shows the energy-minimized crystal structures for EDTA complexes of Cd(II), Hg(II), Mn(II), Ni(II), and Zn(II). As can be seen from the 1 Å bar at the bottom of the figure, these complexes are structurally very similar. In Panels A and B, all five structures were superimposed and displayed from two different angles of view. A superimposition of the two most structurally similar complexes under study, Cd(II)−EDTA and Hg(II)−EDTA, is shown in Panel C, while the superimposed structures of the two most dissimilar complexes, the Cd(II) and Ni(II) complexes, are displayed in Panel D. While comparisons of such three-dimensional projections provided an overall appreciation of the similarities and differences in these metal−EDTA complexes, they were not sufficient to quantify structural differences between the complexes. Distance matrixes (DMs) were therefore developed to compare the molecular structures of the metal−chelate complexes. The DM for one individual complex was subsequently subtracted from that of another complex to yield difference distance matrixes (DDMs), which identified areas in two metal−chelate structures under comparison where differences in the three-dimensional structures occurred. This analysis required that the atoms compared be numbered identically. Metal−EDTA crystal structures obtained from the Cambridge Structural Database all had different numbering schemes; these crystal structures were therefore renumbered according to the scheme used by Nesterova and Porai-Koshits (*26*), and the numbering scheme used in this analysis is shown in Panel C of Figure 4. The glycinate arms are labeled A−D to aid in their identification. Two examples of the DDMs are shown in Panels A

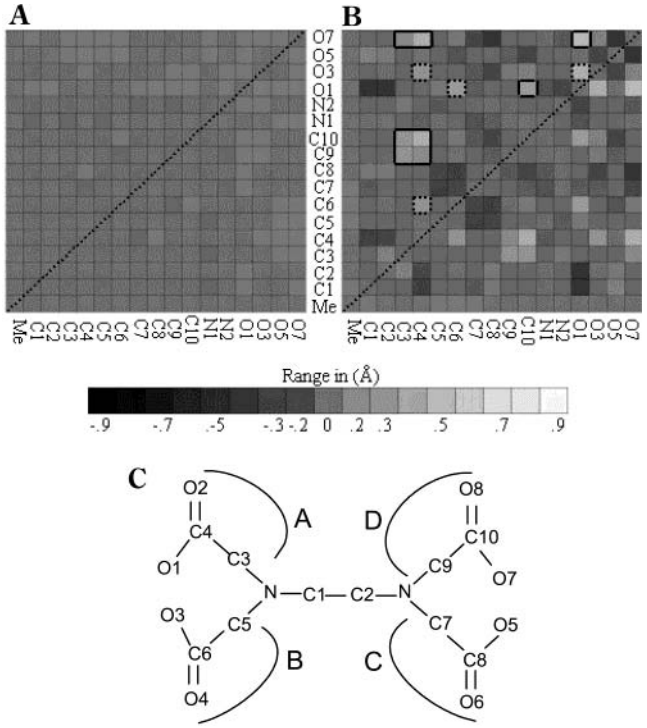


Figure 4. Difference distance matrixes. Panels A and B: The difference distance matrixes (DDM) were generated by subtracting the distance matrixes of two individual metal–chelate complexes (see Experimental Procedures), and the values were given a gray scale shade. Each square represents a value corresponding to the distance difference between the two atoms; therefore the lower right square represents the distance difference between the metal and oxygen 7. The entire bottom row of squares is distance differences from the metal atom. The dark dashed line separates the DDM into the two symmetric halves. This line runs through squares of zero value that can be used as a color reference with the range scale. Panel A: DDM for Cd(II)–EDTA minus Hg(II)–EDTA. The differences are all below 0.2 Å. Panel B: DDM for Cd(II)–EDTA minus Ni(II)–EDTA. The splotchy pattern reports atom distance differences up to 0.6 Å. Panel C: Distance matrixes require that the atoms compared be numbered identically. Metal–EDTA crystal structures obtained from the Cambridge Structural Database all had different numbering schemes; these crystal structures were renumbered according to the scheme used by Nesterova and Porai-Koshits (*26*). C1 was established by determining the ethylene carbon that was farthest from the metal ion. The glycinate arms are labeled A–D to aid in their identification.

and B of Figure 4 with the gray scale range (−0.9 Å to +0.9 Å) shown below. Figure 4A is the DDM for Cd(II)–EDTA minus Hg(II)–EDTA. The distance differences between atom positions in the Cd(II)–EDTA and Hg(II)–EDTA structures all fall below 0.2 Å, indicating that the three-dimensional structures of these two complexes are very similar (see also the superimposed structures in Figure 3C). In contrast, a number of differences are evident in the DDM for Cd(II)–EDTA minus Ni(II)–EDTA, shown in Figure 4B. Dark squares indicate distances in the Ni(II)–EDTA complex where the atoms are farther apart than corresponding atoms in the Cd(II)–EDTA structure; lighter squares indicate distances in the Ni(II)–EDTA complex where the atoms are closer together than atoms in the Cd(II)–EDTA structure. This analysis showed that the atoms of arm A (C3/C4/O1) (see Figure 4C) and the atoms of arm D (C9/C10/O7) were closer together in the Ni(II)–EDTA complex than in the Cd(II)–EDTA complex. When comparing the distance differences between the arms, compare the distance between the atoms C3 and C9, C4 and C10, and O1 and O7 (highlighted in Figure 4B by squares with bold edges). Lighter shading at the intersection of the atoms in arm A (C4/O1) with the atoms in arm B (C6/O3) (highlighted in Figure 4B by squares with dotted edges) indicates that these atoms are also closer together in the Ni(II)–EDTA complex than in the Cd(II)–EDTA complex. Worth noting is that O1 does not get closer to C5 or C9. This may indicate a rotation around the C–C bond in the glycinate arms. The dark shading at the intersection of C4 with C1/C2 and O1 with C1/C2 indicates that in the Ni(II)–EDTA complex these atoms were farther apart than in the Cd(II)–EDTA complex. This indicates arm A is further from the ethylene backbone in the Ni(II)–EDTA complex than the Cd(II) complex. This is counter-intuitive because Cd(II) has a larger ion size, but may be explained by crowding of the glycinate arms around the Ni(II) ion and forcing arm A to move away from the ion. The distances between the atoms in arm B (C5/C6/O3) with the atoms in arm C (C7/C8/O5) are farther apart from one another in the Ni(II)– compared to the Cd(II)–EDTA complex. These differences are mimicked by the Cd(II)–EDTA minus Zn(II)–EDTA difference matrix and similar differences are seen when either the Zn(II)– or Ni(II)–EDTA matrix is subtracted from the Mn(II)–EDTA matrix (data not shown).

In an effort to relate differences in the molecular shape of the metal–chelate complexes to their ability to be recognized by the A4 and E5 antibodies, the absolute values from one of the symmetric halves of the DDM were summed. This term is representative of the total differences between the two metal–chelate haptens being compared. The structures of five EDTA-chelated divalent metals (Cd, Hg, Ni, Mn, and Zn), available in the Cambridge Structural Database, were used in this comparison. As shown in Figure 5, when the total difference was related to the $-\log K_d$, an inverse relationship was observed. The metal–EDTA complex with the highest affinity for each antibody was used as the standard when the differences were calculated. The coefficient of determination (r^2) for the total difference related to the binding of A4 was very strong ($r^2 = 0.97$), while this relationship was only slightly weaker for E5 (r^2 of 0.84) (Figure 5).

DISCUSSION

Antigen specificity and antibody binding are believed to reside mainly in the CDRs found in the variable regions of the antibody molecule (*27*). The two antibodies examined in the present study differ in the N-terminal sequences of their light and heavy chain variable regions (Table 1). The differences in the N-terminal sequence data and the differences in affinity are compelling evidence that E5 and A4 are two different antibodies. Because of the differences in protein sequence and the similarities of activity in the initial screening, these two antibodies were chosen for a comparative binding study. Such a structure/function comparison requires the use of a number of structurally similar ligands to probe the antibody binding activity. The metal–chelate complexes offer a unique system whereby the hapten can be easily modified simply by changing the metal in the chelate complex. Larger hapten modifications can be made by replacing the chelate. For the metals examined in this study, the logarithms of the critical stability constants for EDTA range from 10.8 (Ca^{2+}) to 25.0 (Fe^{3+}), and those for CDTA from 17.5 (Mn^{2+}) to 28.7 (In^{3+}) (*28*). Under the conditions of our binding assays (400 μM chelator and 0.1 to 50 μM metal ion), it was reasonable to assume that all the metal ions in Table 2 existed as complexes with the chelator, and that the metal–chelate complex was the form that interacted with the antibody. The metal–

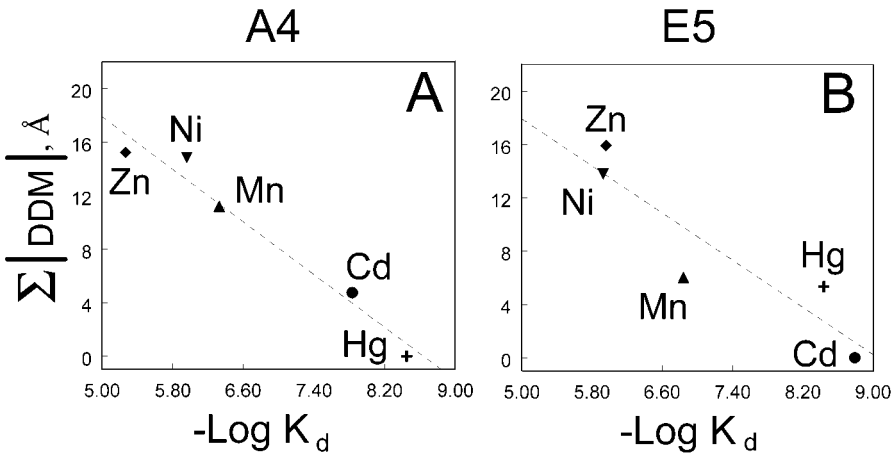


Figure 5. Changes in hapten shape correlate with antibody binding. One-half the sum of the absolute value of the DDM was plotted versus the negative logarithm of the equilibrium dissociation constant for the divalent metal ions modeled. Panel A: The relationship for A4 when the metal−EDTA DDMs are subtracted from the highest affinity ligand, Hg(II)−EDTA ($r^2 = 0.97$). Panel B: The relationship for E5 when the metal−EDTA DDMs are subtracted from the highest affinity ligand, Cd(II)−EDTA ($r^2 = 0.84$).

chelates used in this study exist in at least four distinct conformations. NMR studies have shown that these conformations arise primarily from the lability of the metal−ligand bonds and that the bond lability is dependent upon the identity of the metal ion (*29*, *30*). For example, the metal−oxygen bond of the Cd(II)−EDTA molecule is labile and rapidly rotates around the nitrogen−carbon bond, while the metal-nitrogen bond is longer lived and does not allow for complete dissociation between the chelate and metal (*29*). This may allow for rapid interconversion between different conformations of the Cd(II)−EDTA complex. In contrast, these NMR studies point out the longevity of both the metal−nitrogen and metal−oxygen coordination bonds in the Co(III)−EDTA complex, which may suppress rapid conformational conversion.

The crystal structures of Cd(II)−, Hg(II)−, In(III)−, and Mn(II)−EDTA were observed to be in the same stereoisomeric conformation as the In(III)−chelate complex in the CHA255 binding pocket (*13*, *20*−*22*, *24*). The crystal structures of Ni(II)−, Fe(III)−, and Zn(II)−EDTA, all recognized with lower affinity by both A4 and E5 antibodies, were in a second, different stereoisomeric conformation (*19*, *23*, *25*). Modeling and geometrical minimizing revealed that these original crystal structures were in the lowest energy conformation (data not shown). If the energy differences are indicative of conformer stability, then the metal−chelates' ability to exchange between conformations may play a role in how readily they adopt the proper conformation to fit into the antigen binding site of the antibodies.

The conformational changes of the chelate arms as they shift to accommodate various metal ions appear to be an important factor in antibody recognition. In our study, the DDM indicated that the major difference between the metal−EDTA haptens was the way in which the chelate arms encircled the metal ion. The strong correlation between the total difference in structure and binding activity for the divalent metal ions with A4 and E5 is striking, especially when the maximum, single distance difference between any of the atoms in the structures was 0.6 Å (Figure 4). The shifting of the chelate arms to accommodate metals was demonstrated when the separate crystal structures of the antibody CHA255 bound to In(III)− and Fe(III)−EDTA were solved (*13*); when Fe(III) replaced In(III) in the chelate complex, the conformation of the chelate arms around the metal changed and blocked the antibody coordination to the metal by the histidine, thus lowering the antibody's affinity. The crystallography data obtained with antibody CHA255 indicate that it is entirely plausible that the additive effects of these small differences can significantly alter antibody affinity.

Altering the chelate structure also played a major role in antibody affinity. The two antibodies showed opposite behavior when presented with CDTA-bound metals. In CDTA−metal complexes, the nitrogen becomes more basic due to the cyclohexyl ring; this serves to increase the strength of the nitrogen−metal bond and increase the metal−chelate stability. The stability constants for CDTA complexes are all higher than for their respective EDTA complexes (*28*). A4 bound less tightly to CDTA metal complexes than to the corresponding EDTA complexes, while E5 increased its affinity for the CDTA complexes. The increased affinity of E5 for the metal-free CDTA could be due to the positive hydrophobic interaction of the cyclohexyl ring with the antigen binding site. The same could be suggested for the affinity of A4 for the metal-free CDTA, but then we would expect an increase in affinity with metal-loaded CDTA. This is not what is observed. The increase in A4 affinity to metal-free CDTA may more likely be due to the preorganizing effect of the cyclohexyl group on the chelate; thus the normally nonstructured glycinate arms, as in EDTA, would now have a structured shape similar to the metal−chelated arms in metal-loaded EDTA (*31*). The decrease in A4's affinity for metal-loaded CDTA may be due to a negative hydrophobic interaction of the cyclohexyl portion of the chelate with the binding site.

The association rate constants may also yield information on how well the metal−chelates fit the binding site. Both antibodies have similar rate constants for Hg(II)−EDTA. The on-rate of A4 for Mn(II)−EDTA is almost 60-fold less than for Hg(II)−EDTA. The Mn(II) ion, like Co(III), Fe(III), and Ni(II), all have strong metal−oxygen bonds (*32*). If these smaller ions cannot convert rapidly to a conformation preferred by the antibody, it would most likely reduce the on-rate. Cd(II)−EDTA complexes were shown to have very labile metal−oxygen bonds (*29*). This fact, taken with the fast on-rate of Cd(II)−EDTA with E5, supports the idea of rapid interconversion assisting in binding to the protein.

Metal ion size has an effect on antibody affinity both through ionic radii and via the effect each metal has on the overall chelate complex conformation. This shape is directly related to the ion size and electronic properties

of the different metal ions. The information obtained from comparisons of the distance matrixes is superior to comparisons of ionic radii, because the DM compares the entire three-dimensional structure of the metal−chelate. We were able to demonstrate that Hg(II)− and Cd(II)−EDTA complexes appear very similar in three-dimensional shape, and these structural differences correlate well with antibody binding (Figure 5). Blake et al. used only the difference in ionic radii to correlate the affinity of mAb 2A81G5 to the metal ions, and the difference in ionic radii for Hg(II) from Cd(II) did not correlate well to antibody binding. Studies are in progress to further characterize the structure of the antibody binding sites of A4 and E5 and to develop models that may also correlate the effects of the electronic properties of the metal ions in antibody recognition.

ACKNOWLEDGMENT

The authors thank Drs. Thomas C. Bishop and Thomas E. Weise for advice and guidance on molecular modeling and for the use of the computing facilities in the Theoretical Molecular Biology Laboratory. Dr. Robert C. Blake II is acknowledged for his help in the binding studies and for his critical reading of this manuscript. This work was supported by a grant to D.A.B. from the Natural and Accelerated Bioremediation Research (NABIR) program, Biological and Environmental Research (BER), U.S. Department of Energy (grant #DE-FG02-98ER62704). The Theoretical Molecular Biology Laboratory at the Tulane/Xavier Center for Bioenvironmental Research was established under NSF Cooperative Agreement Number OSR-9550481/LEQSF (1996−1998)-SI-JFAP-04 and is also supported by the Office of Naval Research (NO-0014−99−1−0763).

LITERATURE CITED

(1) Glusker, J. P. (1991) *Adv. Protein Chem. 42*, 1−76.
(2) Baker, B. L., and Hultquist, D. E. (1978) *J. Biol. Chem. 253*, 8444−8451.
(3) Lindgarde, F., and Zettervall, O. (1974) *Scand. J. Immunol. 3*, 277−285.
(4) Wylie, D. E., Lu, D., Carlson, L. D., Carlson, R., Babacan, K. F., Schuster, S. M., and Wagner, F. W. (1992) *Proc. Natl Acad. Sci. U.S.A. 89*, 4104−4108.
(5) Reardan, D. T., Meares, C. F., Goodwin, D. A., McTigue, M., David, G. S., Stone, M. R., Leung, J. P., Bartholomew, R. M., and Frincke, J. M. (1985) *Nature 316*, 265−267.
(6) Blake, D. A., Chakrabarti, P., Khosraviani, M., Hatcher, F. M., Westhoff, C. M., Goebel, P., Wylie, D. E., and Blake, R. C., II. (1996) *J. Biol. Chem. 271*, 27677−27685.
(7) Khosraviani, M., Blake, R. C., II, Pavlov, A. R., Lorbach, S. C., Yu, H., Delehanty, J. B., Brechbiel, M. W., and Blake, D. A. (2000) *Bioconjugate Chem. 11*, 267−277.
(8) Doussal, J. M. L., Chetanneau, A., Gruaz-Guyon, A., Martin, M., Gautherot, E., Lehur, P. A., Chatal, J. F., Delaage, M., and Barbet, J. (1993) *J. Nuc. Med. 34*, 1662−1671.
(9) Wylie, D. E., Carlson, L. D., Carlson, R., Wagner, F. W., Schuster, S. M. (1991) *Anal. Biochem. 194*, 381−387.
(10) Blake, D. A., Pavlov, A. R., and Khosraviani, M. (1998) in *Current Protocols in Field Analytical Chemistry*, 3C.1.1−3C1.10, John Wiley and Sons, Inc., New York.
(11) Khosraviani, M., Pavlov, A. R., Flowers, G. C., and Blake D. A. (1998) *Environ. Sci. Technol. 32*, 137−142.
(12) Darwish, I. A., and Blake, D. A. (2001) *Anal. Chem. 73*, 1889−1895.
(13) Love, R. A., Villafranca, J. E., Aust, R. M., Nakamura, K. K., Jue, R. A., Major, J. G., Radakrishnan, R., and Butler, W. F. (1993) *Biochemistry 32*, 10950−10959.
(14) Chakrabarti, P., Hatcher, F. M., Blake, R. C., II., Ladd, P. A., Blake, D. A. (1994) *Anal. Biochem. 217*, 70−75.
(15) Cayot, P., and Tainturier, G. (1997) *Anal. Biochem. 249*, 184−200.
(16) Habeeb, A. F. (1966) *Anal. Biochem. 14*, 328−36.
(17) Mozdzanowski, J., Bongers, J., and Anumula, K. (1998) *Anal. Biochem. 260*, 183−187.
(18) Blake, R. C., II., Pavlov, A. R., and Blake, D. A. (1999) *Anal. Biochem. 272*, 123−134.
(19) Solans, X., Gali, S., Font-Altaba, M., Oliva, J., and Herrera, J. (1983) *Acta Crystallogr. C39*, 438−440.
(20) Albinati, A., Gramlich, V., Anderegg, G., Lianza, F., Petter, W., and Bommeli, H. (1998) *Inorg. Chem. Acta 274*, 219−223.
(21) Solans, X., Gali, S., Font-Altaba, M., Oliva, J., and Herrera, J. (1988) *Afinidad 45*, 243−248.
(22) Agre, V. M., Kozlova, N. P., Trunov, V. K., and Ershova, S. D. (1981) *Zh. Strukt. Khim. 22*, 138−146.
(23) Solans, X., Font-Altaba, M., and Garcia-Oricain, J. (1984) *Acta Crystallogr. C40*, 635−638.
(24) Agre, V. M., Sysoeva, T. F., Trunov, V. K., Efremov, V. A., Fridman, A., and Barkhanova, N. N. (1980) *Zh. Strukt. Khim. 21*, 110−117.
(25) Sysoeva, T. F., Starikova, Z. A., Leont′eva, M. V., and Dyatlov, N. M. (1990) *Zh. Strukt. Khim. 31*, 140−143.
(26) Nesterova, Y. M., and Porai-Koshits, M. A. (1982) *Koord. Khim. 8*, 994−1001.
(27) Paul, W. E., Ed. (1999) *Fundamental Immunology*, 4th ed., pp 58−60, Lippincontt-Raven Publishers, Philadelphia, PA.
(28) Martell, A. E., and Smith, R. M., Eds. (1998) *NIST Critically Selected Stability Constants of Metal Complexes* version 5.0, NIST Standard Reference Data, Gaithersburg, MD 20899.
(29) Kula, R. J., Sawyer, D. T., Chan, S. I., Finley, C. M. (1963) *J. Am. Chem. Soc. 85*, 2930−2936.
(30) Day, R. J., and Reilley, C. N. (1964) *Anal. Chem. 36*, 1073−1076.
(31) Brechbiel, M. W., Gansow, O. A., Pippin, C. G., Rogers, R. D., and Planalp, R. P. (1996) *Inorg. Chem. 35*, 6343−6348.
(32) Rettig, S. J., and Trotter, J. (1973) *Can. J. Chem 51*, 1303−1312.

BC0155418

Synthesis, Characterization, and Application of Cy-Dye- and Alexa-Dye-Labeled Hongotoxin$_1$ Analogues. The First High Affinity Fluorescence Probes for Voltage-Gated K^+ Channels

Bernt Pragl,[‡] Alexandra Koschak,[‡] Maria Trieb,[‡] Gerald Obermair,[‡] Walter A. Kaufmann,[‡] Uli Gerster,[‡] Eric Blanc,[§] Christoph Hahn,[#] Heino Prinz,[†] Gerhard Schütz,[#] Herve Darbon,[§] Hermann J. Gruber,[#] and Hans-Günther Knaus*[,‡]

Institut für Biochemische Pharmakologie, Universität Innsbruck, Peter Mayr-Strasse 1, A-6020 Innsbruck, Austria; Architecture et Fonction des Macromolecules Biologiques, UMR 6098-CNRS and Universities Aix-Marseille I and II.31, chemin Joseph-Aiguier, 13402 Marseille Cedex 20; Institut für Biophysik, Johannes-Kepler University, Altenberger Strasse 69, A-4040 Linz, Austria; and Max-Planck Institut für Ernährungsphysiologie, Rheinlanddamm 201, D-44139 Dortmund, Germany. Received August 9, 2001; Revised Manuscript Received November 7, 2001

Hongotoxin$_1$ (HgTX$_1$), a 39-residue peptide recently isolated from the venom of *Centruroides limbatus*, blocks the voltage-gated K^+ channels $K_v1.1$, $K_v1.2$, and $K_v1.3$ at picomolar toxin concentrations (Koschak, A., Bugianesi, R. M., Mitterdorfer, J., Kaczorowski, G. J., Garcia, M. L., and Knaus, H. G. (1998) *J. Biol. Chem. 273*, 2639−2644). In this report, we determine the three-dimensional structure of HgTX$_1$ using NMR spectroscopy (PDB-code: 1HLY). HgTX$_1$ was found to possess a structure similar to previously characterized K^+ channel toxins (e.g. margatoxin) consisting of a three-stranded antiparallel β-sheet (residues 2−4, 26−30, and 33−37) and a helical conformation (part 3_{10} helix and part α helix; residues 10−20). Due to the importance of residue Lys-28 for high-affinity interaction with the respective channels, lysine-reactive fluorescence dyes cannot be used to label wild-type HgTX$_1$. On the basis of previous studies (see above) and our NMR data, a HgTX$_1$ mutant (HgTX$_1$-A19C) was engineered, expressed, and purified. HgTX$_1$-A19C-SH was labeled using sulfhydryl-reactive Cy3-, Cy5-, and Alexa-dyes. Pharmacological characterization of fluorescently labeled HgTX$_1$-A19C in radioligand binding studies indicated that these hongotoxin$_1$ analogues retain high-affinity for voltage-gated K^+ channels and a respective pharmacological profile. Cy3- and Alexa-dye-labeled hongotoxin$_1$ analogues were used to investigate the localization of K^+ channels in brain sections. The distribution of toxin binding closely follows the distribution of $K_v1.2$ immunoreactivity with the highest expression levels in the cerebellar Purkinje cell layer. Taken together, these results demonstrate that fluorescently labeled HgTX$_1$ analogues comprise novel probes to characterize a subset of voltage-gated K^+ channels.

Current knowledge regarding the distribution and subunit composition of K^+ channels arises mainly from the use of antibodies directed against various ion channel subunits (Sheng et al., 1993; Knaus et al., 1996; Shamotienko et al., 1997; Koch et al., 1997; Knaus et al., 1996; Shamotienko et al., 1997; Koch et al., 1997). These antibodies are essential tools to enable high-resolution distribution studies clarifying the expression pattern of various K^+ channel subunits in various tissues or to establish their subunit composition (Shamotienko et al., 1997; Koch et al., 1997; Koschak et al., 1998; Koch et al., 1997; Koschak et al., 1998). However, production of selective antibodies is frequently hampered by a high degree of sequence conservation within several K^+ channel subfamilies (Chandy and Gutman, 1993). Moreover, these antibodies do not comprise a suitable tool to study native K^+ channels, as the tissues need to be fixed and permeabilized in order to allow antibody access to its intracellular binding site.

As an alternative, toxins have often been used to study native K^+ channels, mostly in functional assays (Miller, 1995; Tytgat et al., 1999; Tytgat et al., 1999). These K^+ channel toxins bind to the extracellular channel vestibule thereby physically occluding the ion conduction pathway (MacKinnon and Miller, 1988; MacKinnon and Miller, 1989; Gross and MacKinnon, 1996; Doyle et al., 1998; MacKinnon et al., 1998; MacKinnon and Miller, 1989; Gross and MacKinnon, 1996; Doyle et al., 1998; MacKinnon et al., 1998). Radioiodinated toxin analogues have extensively been used to map the distribution of toxin receptors through autoradiographic studies, to establish the pharmacological profile of various K^+ channels through radioligand binding studies, or to purify K^+ channels from native tissue thereby clarifying their subunit composition (Gehlert and Gackenheimer, 1993; Vazquez et al., 1990; Garcia-Calvo et al., 1994; Knaus et al., 1994; Vazquez et al., 1990; Garcia-Calvo et al., 1994; Knaus et al., 1994). However, use of these radioiodinated toxins for distribution studies is limited as the resolution of receptor autoradiography is notoriously low.

To overcome these limitations, several attempts were made to generate fluorescently labeled K^+ channel toxins. In most cases, direct fluorescence labeling procedures

* Corresponding author: Hans-Günther Knaus, Institut für Biochemische Pharmakologie, Peter-Mayr Strasse 1, A-6020 Innsbruck, Austria; Tel.: +43−512-507-3156; Fax: +43−512-507-2858; e-mail: hans.g.knaus@uibk.ac.at.

[§] Architecture et Fonction des Macromolecules Biologiques.

[‡] Universität Innsbruck.

[#] Johannes-Kepler University.

[†] Max-Planck Institut für Ernährungsphysiologie.

10.1021/bc015543s CCC: $22.00 © 2002 American Chemical Society
Published on Web 04/17/2002

were performed through incorporation via *N*-hydroxysuccinimidyl ester chemistry into ϵ-amino groups of lysine residues (Darbon and Angelides, 1984; Angelides, 1986; Angelides, 1989; Jones et al., 1989; Cohen et al., 1991; Angelides, 1986; Angelides, 1989; Jones et al., 1989; Cohen et al., 1991). However, lysine derivatization is often not desirable as they comprise crucial residues for high-affinity toxin interaction with the K^+ channel of interest (Park and Miller, 1992; Goldstein and Miller, 1993; Goldstein et al., 1994; Goldstein and Miller, 1993; Goldstein et al., 1994). Resulting toxin analogues often render a loss of affinity accompanied by an altered pharmacological profile.

In this paper, we report the three-dimensional structure of $HgTX_1$[1] determined through NMR experiments (PDB-code: 1HLY). On the basis of these NMR data and previous studies (Knaus et al., 1996; Koschak et al., 1998), we constructed, expressed, and purified a toxin analogue ($HgTX_1$-A19C) which carries a single free sulfhydryl group in the 'back' of the molecule, most opposite from the toxin's interaction surface with voltage-gated K^+ channels. This sulfhydryl group was used for derivatization with fluorescent dyes such as Cy3, Cy5, and the Alexa-dye-family. The resulting toxin analogues widely retain their pharmacological profile as shown in radioligand binding studies and fluorescence microscopy. Demonstrating one capability of these toxin analogues, $HgTX_1$-A19C−Cy3 was used to monitor the distribution of K_v1 channels in native brain tissue.

These toxin analogues will now allow 'real time' imaging of channels on living cells or heterogeneous tissues. In this respect they will overcome several limitations known to exist for radioligands or sequence specific antibodies. Additionally, they will enable quantification of ligand binding on the cellular level, even in heterologous tissues, or at the subcellular level.

EXPERIMENTAL PROCEDURES

Materials. *Escherichia coli* DH5a was used for plasmid propagation and strain BL21(DE3) for expression of the fusion protein. The plasmid pCI-neo was purchased from Promega (Mannheim, Germany), pcDNA3.1HisA from Invitrogen, and pUC from Boehringer-Mannheim (Mannheim, Germany). Restriction enzymes, Pfu-DNA-Polymerase, T4-DNA-Ligase, nucleotide triphosphates, and reagents for polymerase chain reaction were obtained from Boehringer Mannheim (Mannheim, Germany), tissue culture media and the LipofectAMINE reagent from GIBCO, Life Technology (Vienna, Austria), glass fiber filters (GF/C) from Whatman International (Maidstone, England), and polyethyleneimine and bovine serum albumin (BSA) from Sigma (Vienna, Austria). All other reagents were obtained from commercial sources and were of the highest purity grade commercially available. Cy3- and Cy5-NHS esters were purchased from Amersham-Pharmacia Biotech (Freiburg, Germany) while Cy5-PDP, Cy5-mal, and Cy3-mal were synthesized as described (Gruber et al., 2000). Alexa488-mal, Alexa546-mal, Alexa594-mal, Alexa660-mal, and Alexa680-mal were obtained from Molecular Probes Inc. (Eugene, OR; supplied as isomeric mixtures).

NMR Spectroscopy of Wild-Type $HgTX_1$. Recombinant wild-type $HgTX_1$ was produced as described previously (Koschak et al., 1998). Four milligrams of $HgTX_1$ was dissolved in a 0.5 mL mixture of H_2O and D_2O in a 9:1 ratio (v/v). The pH value of the $HgTX_1$ solution was 3.0 uncorrected for isotope effects. Amide proton exchange rate was determined after lyophilization and dissolution in 100% D_2O.

All 2D-^{1}H NMR measurements were obtained on a BRUKER DRX 500 spectrometer equipped with an HCN probe. Self-shielded triple axis gradients were used as previously described (Blanc et al., 1998). To solve assignment ambiguities, the experiments were performed at 283 and 300 K. All data were processed using the UXNMR Bruker's software running on a Silicon Graphics Indy R4400 workstation. Identification of amino acid spin systems and sequential assignment were done using the standard method described by Wuthrich (Wuthrich, 1986). Distance geometry calculations were performed with the variable target function program DIANA 2.8 (Guntert et al., 1991) following the well-established strategy for scorpion toxin structure determination (Blanc et al., 1998). The visual analysis of resulting structures was carried out with the TURBO−FRODO graphic software running on Silicon Graphics workstations. The quality of the structures was assessed using both PROCHECK 3.3 and PROCHECK−NMR software (Laskowski et al., 1993).

Plasmid Construction, Synthesis, and Purification of Recombinant $HgTX_1$-A19C. The plasmid pG9$HgTX_1$-A19C encodes a fusion protein of the T7 gene 9 product and $HgTX_1$, separated by six histidine residues and the factor Xa cleavage site. Polymerase chain reaction (PCR) was used to create cDNA mutations in the primary sequence of $HgTX_1$ described previously (Koschak et al., 1998). $HgTX_1$-A19C was generated by introducing cysteine at position 19 thereby replacing alanine. Mutations were introduced by the "gene SOEing" technique using mutagenic forward and reverse PCR primers (Horton et al., 1989). Desired mutations were verified by cDNA sequencing using the dideoxy chain termination method (Sanger et al., 1977). The fusion protein was expressed in *E. coli* and purified as described (Koschak et al., 1998). After purification of the fusion protein the toxin mutant was released by cleavage with trypsin. Purified fusion protein (20−40 mg) was incubated with 190 μL of trypsin solution (1 mg/100 μL H_2O) for 15 min at 22 °C. The cleavage mixture was applied to a cation-exchange column (MonoS HR5/5; Pharmacia) and $HgTX_1$-A19C was eluted with a linear gradient from 0 to 0.75 M NaCl in 20 mM borate pH 8.0 (over 40 min) at a flow rate of 0.6 mL/min. Cation exchange chromatography yielded two distinct peptide fractions (see Results). Each peptide fraction was applied separately to a C_{18} reversed-phase column (Vydac, 1 × 25 cm, 23 °C), and the respective toxin analogue was eluted with a linear gradient from 0 to 35% acetonitrile in 0.05% TFA (over 40 min) at a flow rate of 3 mL/min. Approximately equal amounts of two individual peptide isoforms, $HgTX_1$-A19C-βME and dimeric $HgTX_1$-A19C were obtained (see Results). Composition of the purified material was veri-

[1] Abbreviations: $AgTX_2$, agitoxin-2; βME, β-mercaptoethanol; BSA, bovine serum albumin; ChTX, charybdotoxin; Cy3, sodium 1-[5-(carboxyl)pent-1-yl]-2-[5-(3,3-dimethyl-1-ethyl-5-sulfonatoindolin-2-ylidene)-1-en-yl]-3,3-dimethyl-3*H*-indolium-5-sulfonate; Cy5, sodium 1-[5-(carboxyl)pent-1-yl]-2-[5-(3,3-dimethyl-1-ethyl-5-sulfonatoindolin-2-ylidene)-1,3-pentadien-1-yl]-3,3-dimethyl-3*H*-indolium-5-sulfonate; DTT, dithiothreitol; $HgTX_1$, hongotoxin-1; [^{125}I]$HgTX_1$-A19Y/Y37F, mono-[^{125}I]iodotyrosine-hongotoxin-1-A19Y/Y37F; IbTX, iberiotoxin; IC_{50}, concentration causing half-maximal inhibition; KTX, kaliotoxin; k_{+1}, association rate constant; k_{-1}, dissociation rate constant; K_d, dissociation constant; K_i, inhibition constant; mal, maleimide group; MgTX, margatoxin; n_H, pseudohill slope; NHS, *N*-hydroxysuccinimide; PDP, 3-(2-pyridyldithio)propionyl group; SDT, single dye tracing; TFA, trifluoroacetic acid.

fied by electrospray mass spectrometry. Aliquots were lyophilized and stored at −80 °C.

Reduction of Dimeric $HgTX_1$-A19C and $HgTX_1$-A19C-βME. For reduction of dimeric $HgTX_1$-A19C and $HgTX_1$-A19C-βME, aliquots of the respective peptides were dissolved in 0.1 M sodium phosphate buffer (pH 7.0) containing 10 mM DTT and incubated for 15 min at 22 °C. The reaction mixture was applied to a C_{18} reversed-phase column (Vydac, 0.45 × 25 cm, 23 °C). Reduced $HgTX_1$-A19C ($HgTX_1$-A19C-SH) was eluted with a linear gradient from 0 to 35% acetonitrile in 0.05% TFA (over 40 min) at a flow rate of 1 mL/min and stored as described above.

Synthesis of Fluorescently Labeled Hongotoxin$_1$ Analogues. *Conjugation of Cy5-PDP to $HgTX_1$-A19C−SH.* Cy5-PDP was synthesized as described for Cy5-mal (Gruber et al., 2000). Cy5-PDP was dissolved in 25% AcN and 0.05% TFA (in H_2O), an equimolar amount of $HgTX_1$-A19C-SH was added, and the reaction mixture was lyophilized. The reaction was started by addition of 100 μL aqueous buffer (100 mM NaCl, 50 mM NaH_2PO_4, pH 7.5 adjusted with NaOH, deoxygenated with N_2). The mixture was incubated under N_2 for 90 min at 37 °C (see Figure 3) and applied to a C_{18} reversed-phase column (Vydac, 0.45 × 25 cm, 23 °C). $HgTX_1$-A19C−Cy5 was eluted with a linear gradient from 0 to 35% acetonitrile in 0.05% TFA (over 40 min) at a flow rate of 1 mL/min.

Conjugation of Cy5-mal and Cy3-mal to $HgTX_1$-A19C−SH. Cy5-mal and Cy3-mal were synthesized as described for Cy5-mal (Gruber et al., 2000). A 3- or 5-fold molar excess of thiol-teactive Cy-dye was dissolved in 100 μL of aqueous buffer (150 mM NaCl, 50 mM NaH_2PO_4, pH 7.4 adjusted with NaOH) and applied to a vial containing lyophilized $HgTX_1$-A19C-SH. The reaction mixture was incubated for 90 min at 37 °C (see Figure 3) and applied to a C_{18} reversed-phase column (Vydac, 0.45 × 25 cm, 37 °C). $HgTX_1$-A19C−Cy5 and $HgTX_1$-A19C−Cy3 were eluted with a linear gradient from 0 to 35% acetonitrile in 0.05% TFA (over 40 min) at a flow rate of 1 mL/min. Due to the excess of dye no oxidation (dimerization) of the peptide could be detected.

Conjugation of Alexa488-mal, Alexa546-mal, Alexa594-mal, Alexa660-mal, and Alexa680-mal to $HgTX_1$-A19C−SH. A 25 μg or 50 μg amount of thiol-reactive Alexa-dye was dissolved in 200 μL of aqueous buffer (150 mM NaCl, 50 mM NaH_2PO_4, pH 7.4 adjusted with NaOH) and applied to a vial containing lyophilized $HgTX_1$-A19C-SH. The reaction mixture was incubated for 120 min at 37 °C (see Figure 3) and applied to a C_{18} reversed-phase column (Vydac, 0.45 × 25 cm, 23 °C). $HgTX_1$-A19C−Alexa488, $HgTX_1$-A19C−Alexa594, $HgTX_1$-A19C−Alexa660, and $HgTX_1$-A19C−Alexa680 were eluted with a linear gradient from 0 to 35% acetonitrile in 0.05% TFA (over 40 min) at a flow rate of 1 mL/min. $HgTX_1$-A19C−Alea546 was eluted with a linear gradient from 0 to 45% acetonitrile in 0.05% TFA (over 50 min) at a flow rate of 1 mL/min. Due to the excess of dye no oxidation (dimerization) of the peptide could be detected.

The structure of the compounds was verified by electrospray mass spectrometry. Aliquots of fluorescently labeled hongotoxin$_1$ analogues were lyophilized and stored at −80 °C.

Nano-Electrospray Mass Spectrometry. Nanoelectrospray mass spectrometry was performed with a Finnigan LCQ mass spectrometer equipped with a micromanipulator for the correct positioning of the nanospray needle. In short, capillaries (GC120F from Clark Instruments, Reading, United Kingdom) were pulled using the DMZ-universal puller (Zeitz-Instrumente GmbH, München, Germany). They were coated with gold using a Polaron SC7610 Sputter Coater (VG Microtech, Uckfield, United Kingdom) and a gold target. These needles were filled with 1−4 μL of aqueous solution and centrifuged for several seconds using a PicoFuge (Tomy Capsule, Tomy Tech Inc, Palo Alto, CA). The needles were mounted on the micromanipulator and were gently brought in contact with a surface near the inlet of the mass spectrometer. Air pressure was applied to the needle until a small droplet appeared on the tip. The needle was then adjusted 2.5 mm opposite the inlet of the heated cappillary. A potential of 900 V was applied to the needle. For measurements of aqueous solutions, the relative intensities of the corresponding peaks were maximized when the collision-induced decay at the inlet of the mass spectrometer was minimized. The tuning procedure of the mass spectrometer was applied for this purpose. The original data (i.e. abundance of the multiple charged peptide populations versus *m*/*z*) were deconvoluted into mass spectra (relative abundance versus mass) by means of the deconvolution software BioExplore. The error of the mass spectrometer was 100 ppm in the normal mass range (150−2000 *m*/*z*), which was used for all experiments.

Membrane Preparation and Binding Studies. Rat brain synaptic plasma membrane vesicles were prepared as previously described (Knaus et al., 1995). Membrane vesicles from HEK293 cells stably transfected with homotetrameric $K_v1.3$ channels were prepared as described (Helms et al., 1997). Binding experiments were carried out as previously described (Knaus et al., 1995). The incubation medium consisted of 20 mM Tris/HCl, pH 7.4, 0.1% BSA (rat brain membranes) or 20 mM TRIS/HCl, pH 7.4, 5 mM KCl, 0.1% BSA (HEK−$K_v1.3$ membranes). Nonspecific binding was defined in the presence of 1 nM recombinant $HgTX_1$ or MgTX, and incubation was carried out at 22−25 °C typically for 240 min.

Immunohistochemistry. Immunohistochemical distribution studies using an antibody directed against the voltage-gated K^+ channel $K_v1.2$ (anti-$K_v1.2_{(461-480)}$) were performed as previously published in detail (Koch et al., 1997).

Labeling of $K_v1.1$/$K_v1.2$ Channels with Fluorescent $HgTX_1$-A19C Analogues. Male Sprague−Dawley rats (250−300 g) were sacrificed by cervical dislocation, and their brains were rapidly removed and placed for 90 s in isopentane chilled to −40 °C. Thereafter, brains were transferred for 30 min at −30 °C and 10 μm horizontal sections were cut on a cryostat (Leitz, Germany) and thaw-mounted onto gelatin-coated glass slides. Sections were labeled in 20 mM Tris/HCl (pH 7.4), 10 mM NaCl, and 0.1% BSA for 12 h at 4 °C at a saturating concentration of $HgTX_1$-A19C−Alexa488, $HgTX_1$-A19C−Cy3, or $HgTX_1$-A19C−Alexa546 (2 nM). Nonspecific binding was determined in adjacent sections by inclusion of 100 nM $HgTX_1$. Sections were then rinsed four times 2 min each with in ice-cold 20 mM TRIS/HCl, pH 7.4, 10 mM NaCl. For fluorescence microscopy, the sections were embedded in pPD glycerol (30 mg of *p*-phenylendiamine dissolved in 10 mL of 10 mM Tris pH 8.0/90% glycerol (v/v), coverslipped, and sealed with nail polish.

Fluorescence images of the sections were obtained using a Zeiss Axiophot microscope (Carl Zeiss, Oberkochen, Germany) with a 40 × 1.3 NA oil immersion objective, a 20 × 0.5 NA objective, and a standard Rhodamine and FITC filter set. Images were captured by a Peltier cooled slow-scan CCD-camera system (Visitron Systems GmbH, Puchheim, Germany) at short exposure times (0.5−2 s)

and prepared for presentation with Metaview software (Metaview, Version 4.1, Universal Imaging Corp.).

Protein Determination. Protein concentration was determined as previously published (Bradford, 1976) using BSA as standard.

RESULTS

NMR Spectroscopy of Wild-Type $HgTX_1$. Approximately 10 mg of native $HgTX_1$ was purified from a 4 L of *E. coli* culture as described previously (Koschak et al., 1998) and a total of 4 mg of $HgTX_1$ subjected to NMR studies. Using this amount of toxin we were able to assign all spins unambiguously and to connect them in sequence. We collected a total of 380 NOEs which were then converted into distance constraints (144 intraresidue constraints, 109 sequential constraints, 41 medium range, and 59 long-range constraints). Study of the amide proton exchange rates led to the localization of 18 hydrogen bonds which were also converted into distance constraints. Finally, 27 measured coupling constants were converted into as many φ angle constraints.

The distance geometry calculations led to a single family of 25 structures. These structures, containing nonbonded bad contacts, were energy-minimized with the Powell algorithm of the XPLOR3.1 software (Brünger, 1992). The final set of 25 structures after energy minimization is of good quality as demonstrated by Procheck-NMR analysis. The negative van der Waals energy indicates the absence of nonbonded contacts. The correlation with the experimental restraints shows neither distance violation greater than 0.25 Å, nor angle violation greater than 5°. The low root-mean-square-deviation (RMSD) values of the bond lengths (0.012 Å) and the valence angles (2.9 Å) indicates that the covalent geometry is preserved for all 25 structures. The analysis of the Ramachandran plot shows (in PROCHECK software nomenclature) 80% of the residues in the most favored, 19% in the additional allowed regions, 1% in the generously allowed regions, and none in disallowed regions.

The final 25 calculated structures share the same fold and thus form a homologous family. The RMSD value of these 25 structures versus the calculated average structure is 0.57 Å for the backbone atoms and 1.10 Å for all heavy atoms. As shown in Figure 1, the backbone structure is well-defined all along the sequence. The results of structure analysis using TURBO−FRODO (Roussel and Cambillau, 1989) and PROCHECK−NMR (Laskowski et al., 1993) showed that residues G10 to C20 are in helical conformation with the first three residues in 3_{10} helix conformation and the seven following in pure α-helix. Further analysis of the distribution of φ/ψ angles and the location of hydrogen bonds indicated that three segments, 2 to 4, 26 to 30, and 33 to 37 form a three-stranded antiparallel β-sheet. This β-sheet is right-hand twisted and stabilized by standard hydrogen bonds. The two last strands of the β-sheet are connected by a well-defined type I′ β -turn centered between 31 and 32 (Margolskee et al., 1993). This β-sheet is connected to the α-helix through an $\alpha/\beta 5$ loop (Jones et al., 1989; Cohen et al., 1991; Park and Miller, 1992; Goldstein and Miller, 1993; Goldstein et al., 1994). On the basis of previous studies (Knaus et al., 1996; Koschak et al., 1998) and the NMR structure of $HgTX_1$, we were able to predict that mutations in position 19 will significantly alter neither the toxin's overall structure nor its interaction with the channel since this residue is located in the 'back' of the peptide, its side chain is oriented toward the solvent (see Figure 1) and it does not form part of the peptide's interaction surface with K^+ channels (Miller, 1995). Thus, we altered the synthetic $HgTX_1$ gene thereby substituting Ala19 for Cys19 (Koschak et al., 1998).

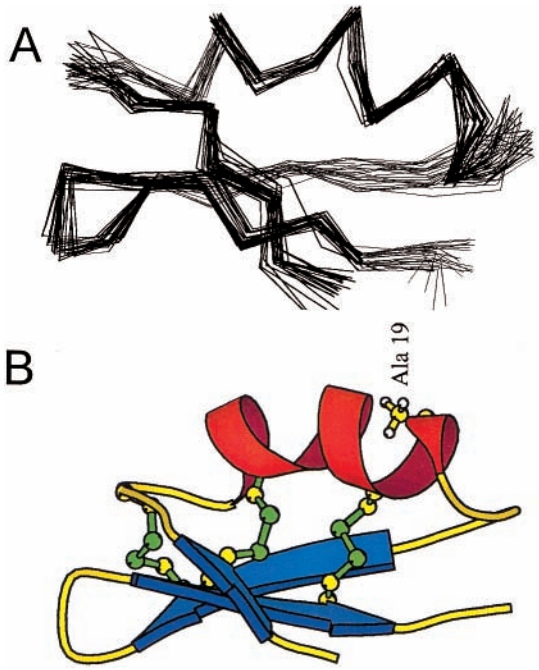


Figure 1. NMR spectroscopy of $HgTX_1$. Stereoview of the backbone (A) of the 25 best $HgTX_1$ structures superposed for best fit, and ribbon drawing of the averaged minimized $HgTX_1$ structure (B). The disulfide bridges are represented in balls and sticks, as well as A19 of $HgTX_1$.

Expression and Purification of $HgTX_1$-A19C. To obtain sufficient amounts of peptide for derivatization with fluorescence dyes, $HgTX_1$-A19C was recombinantly expressed in *E. coli* as part of a fusion protein (Figure 2A). Induction of the respective fusion protein was comparable to wild-type $HgTX_1$ (we determined an induction of 40−80 mg of protein/1500 mL of *E. coli* culture, data not shown). However, the final yield after cation exchange and reversed-phase chromatography was estimated to be only 11 ± 4% of the calculated theoretical yield (corresponding to 440−720 μg of $HgTX_1$-A19C/1500 mL of *E. coli* culture; $n = 4$). We currently favor the idea that the introduction of an additional Cys residue in position 19 impairs proper formation of the internal disulfide bonds of the toxins. Such an incompletely folded toxin analogue is expected to possess much lower resistance to trypsin and would therefore be degraded upon proteolytic release from the fusion protein (Koschak et al., 1998).

After partial purification of the fusion protein and cleavage with trypsin to release $HgTX_1$-A19C-SH, the peptide was purified to homogeneity by cation-exchange (Figure 2B) and C_{18} reversed-phase chromatography (Figure 2C). Cation-exchange chromatography yielded two distinct peptide fractions. Both peptides were subjected to electrospray mass spectrometry which yielded molecular weights of 4329.0 and 8506.0 Da, respectively (see Table 1). However, the calculated M_r for $HgTX_1$-A19C-SH is 4253 Da, a number which is significantly lower than that measured by mass spectrometry. The observed molecular weights are explainable by the formation of a disulfide bond between residue Cys19 (M_r 8506.0) or βME derivatization of this sulhydryl group of Cys19 (M_r 4329.0). Similar observations have been made for an IbTX mutant (which is preferentially isolated as a βME derivative (Knaus et al., 1996)) and for an $AgTX_2$

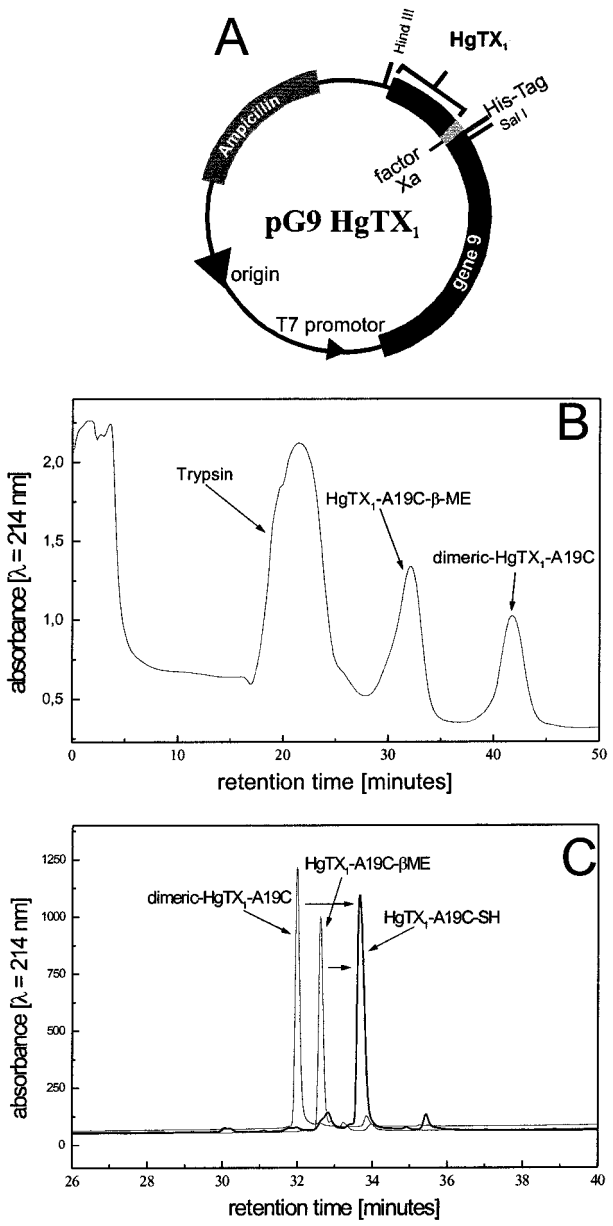


Figure 2. Design of the synthetic $HgTX_1$-A19C gene and purification of the recombinant toxin. (A) The plasmid map of pG9-$HgTX_1$-A19C shows the location of the $HgTX_1$-A19C gene, the factor Xa cleavage site and the T7 gene 9 fusion protein. (B) Cation exchange chromatography of ~ 1 mg trypsin-digested fusion protein loaded onto a MonoS HR5/5 column. Peaks 1, 2, and 3 correspond to trypsin, $HgTX_1$-A19C-βME, and dimeric $HgTX_1$-A19C. (C) Reversed-phase chromatography: Peak 2 and 3 were applied to a C_{18} reversed-phase HPLC. Aliquots of the $HgTX_1$-A19C dimer and $HgTX_1$-A19C-βME were incubated with 10 mM DTT to result in the free thiol form of $HgTX_1$-A19C. Elution of dimeric $HgTX_1$-A19C, $HgTX_1$-A19C-βME, and $HgTX_1$-A19C-SH is shown.

mutant (this toxin analogue quantitatively dimerizes during folding and isolation (Krezel et al., 1995)).

The individual fractions were tested for activity in [^{125}I]-$HgTX_1$-A19Y/Y37F binding to rat brain synaptosomal plasma membranes. Dimeric $HgTX_1$-A19C was a less potent inhibitor of [^{125}I]$HgTX_1$-A19Y/Y37F binding to rat brain synaptosomal plasma membranes compared to $HgTX_1$-A19C-βME and wild-type $HgTX_1$ (see Table 2).

Synthesis of Fluorescently Labeled Hongotoxin$_1$ Analogues. To selectively reduce the disulfide bond in the back of the toxin without disrupting the integrity of the internal disulfide bridges, both $HgTX_1$-A19C-βME and dimeric $HgTX_1$-A19C were incubated with DTT under carefully controlled conditions (see Methods). The peptide carrying a free sulfhydryl group ($HgTX_1$-A19C-SH) was easily identified by a change in retention time upon reversed-phase HPLC (Figure 2). The reduced toxin ($HgTX_1$-A19C-SH) was subjected to mass spectral analysis. A molecular weight of 4253 Da was determined which was identical to the calculated molecular weight. The reduction yield after reversed phase chromatography was estimated to be 90 ± 5% (n > 10). Equimolar amounts of $HgTX_1$-A19C-SH and the sulfhydryl-reactive Cy5-PDP were incubated in order to synthesize the respective fluorescently labeled toxin. For all other fluorescent dyes, a molar excess (see Experimental Procedures) over toxin was employed. The fluorescently labeled toxin mutants were isolated by reverse phase chromatography (see Figure 4) and the postulated structure (see Figure 3) was verified by electrospray mass spectrometry (see Table 1). The coupling yield after reversed-phase chromatography was estimated to be 95 ± 5% (n > 10). Noteworthy, coupling of $HgTX_1$-A19C-SH to maleimides will generate an asymmetric carbon and therefore lead to the formation of diastereomers (see Figure 3B).

Pharmacological Characterization of Fluorescently Labeled $HgTX_1$-A19C. To ascertain that wild-type $HgTX_1$ and the respective fluorescently labeled toxin analogue display similar affinities for native K_v1 channels, binding competition experiments using [^{125}I]$HgTX_1$-A19Y/Y37F were performed (Figure 7). As a tissue source, either rat brain synaptosomal membranes (which pre-

Table 1. Nano-Electrospray Mass Spectrometry[a]

$HgTX_1$-A19C-dye	mass (Da)
$HgTX_1$	4219
$HgTX_1$-A19C−βME	4329
$(HgTX_1\text{-A19C})_2$	8506
$HgTX_1$-A19C−Cy3	5144
$HgTX_1$-A19C-Cy5 (Cy5−PDP)	5037
$HgTX_1$-A19C-Cy5 (Cy5−mal)	5170
$HgTX_1$-A19C−Alexa488	4950
$HgTX_1$-A19C−Alexa546	5263
$HgTX_1$-A19C−Alexa594	5138
$HgTX_1$-A19C−Alexa660	5153
$HgTX_1$-A19C−Alexa680	5233

[a] Nano-electrospray mass spectrometry was performed with a Finnigan LCQ mass spectrometer. The original data (i.e. abundance of the multiple charged peptide populations versus m/z) were deconvoluted into mass spectra (relative abundance versus mass) by means of the deconvolution software BioExplore. Experiments were performed as described in Experimental Procedures.

Table 2. Pharmacological Characterization of Fluorescently Labeled $HgTX_1$-A19C Analogues[a]

$HgTX_1$-A19C−dye	IC_{50} (pM)
$HgTX_1$	0.5
$HgTX_1$-A19C−βME	0.6
$(HgTX_1\text{-A19C})_2$	6.4
$HgTX_1$-A19C−Cy3	2
$HgTX_1$-A19C-Cy5 (Cy5−PDP)	11.6
$HgTX_1$-A19C-Cy5 (Cy5−mal)	11.6
$HgTX_1$–A19C−Alexa488	2.8
$HgTX_1$-A19C−Alexa546	6.7
$HgTX_1$-A19C−Alexa594	4.2
$HgTX_1$-A19C−Alexa660	2
$HgTX_1$-A19C−Alexa680	5

[a] To ascertain whether $HgTX_1$, $HgTX_1$-A19C-βME, $(HgTX_1\text{-A19C})_2$, and a variety of fluorescently labeled $HgTX_1$-A19C analogues display a similar affinity for heterotetrameric native K_v1 channels, binding competition experiments using [^{125}I]$HgTX_1$-A19Y/Y37F were performed. As a tissue source, rat brain synaptosomal membranes were used. IC_{50}, concentration causing half-maximal inhibition.

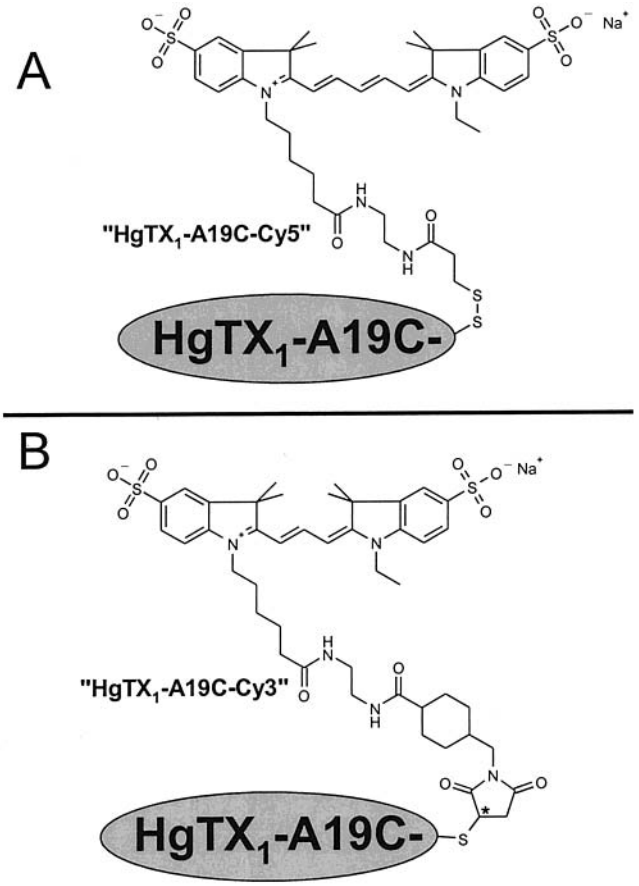


Figure 3. Coupling products of Cy5-PDP and Cy3-mal to the free thiol form of $HgTX_1$-A19C. Noteworthy, coupling of $HgTX_1$-A19C-SH to maleimides will generate an asymmetric carbon and therefore lead to the formation of diastereomers.

dominantly express heterotetrameric K_v1 channels formed by assembly of $K_v1.1$ and $K_v1.2$ (Koch et al., 1997)) or HEK-293 plasma membranes stably transfected with $K_v1.3$ were used (Figure 7). In both membrane preparations, [^{125}I]$HgTX_1$-A19Y/Y37F binds to a single class of sites that display a K_d of 0.15 pM (Koschak et al., 1998). The toxin analogue $HgTX_1$-A19C-βME retains this very high affinity for $K_v1.1/1.2$ channels as it displaces [^{125}I]-$HgTX_1$-A19Y/Y37F binding with an identical (compared to wild-type $HgTX_1$) IC_{50} value of 0.6 pM (see Table 2; $n = 6$). The respective dimeric toxin $(HgTX\text{-}A19C)_2$ suffers an approximately 10-fold loss in affinity (see Table 2; $n = 6$).

In good agreement with these data, $HgTX_1$-A19C−Cy5 displaces [^{125}I]$HgTX_1$A19Y/Y37F binding from native $K_v1.1/K_v1.2$ channels as well as from recombinant $K_v1.3$ channels with IC_{50} values of 11.6 pM ($n = 4$) and 1.3 pM ($n = 2$), respectively (Figure 7, open squares). By comparison, wild-type $HgTX_1$ inhibited [^{125}I]$HgTX_1$-A19Y/Y37F interactions with these membranes with IC_{50} values of 0.49 pM ($n = 3$) and 0.16 pM ($n = 2$), respectively (Figure 7, circles). These data indicate that $HgTX_1$-A19C−Cy5 binds to voltage-gated potassium channels with a slightly reduced binding potency (see Table 2).

To investigate the pharmacological profile of the other fluorescently labeled $HgTX_1$ analogues, they were screened in binding competition experiments using [^{125}I]$HgTX_1$-A19Y/Y37F and native $K_v1.1/1.2$ channels. All toxin analogues retain high affinity and a proper pharmacological profile (see Table 2; $n = 6$).

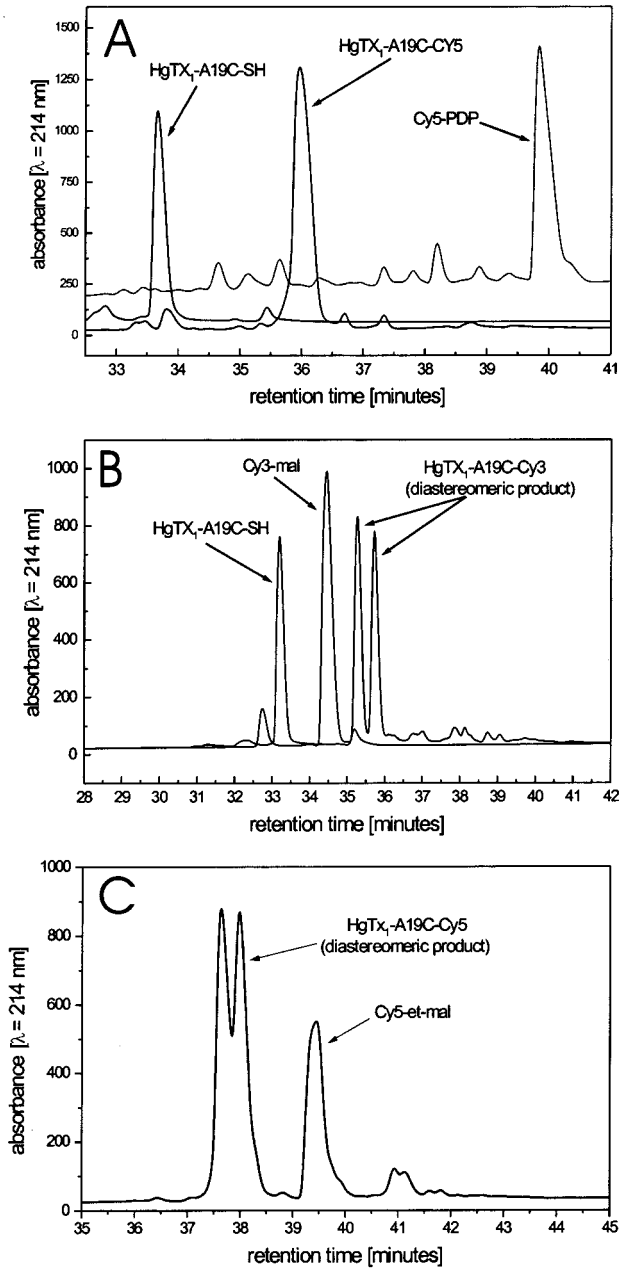


Figure 4. Coupling of thiol-reactive Cy5-PDP, Cy3-mal, and Cy5-mal to the free thiol form of $HgTX_1$-A19C. (A) $HgTX_1$-A19C-SH (peak 1) and Cy5-PDP (peak 3) were coupled, and the products were applied to a C_{18} reversed-phase HPLC. Elution of $HgTX_1$-A19C−Cy5 (Peak 2) is shown. (B) $HgTX_1$-A19C-SH (peak 1) and Cy3-mal (peak 2) were coupled as described in Experimental Procedures. Resulting products were applied to a C_{18} reversed-phase HPLC. Elution of the two diastereomers of $HgTX_1$-A19C−Cy3 (peaks 3 and 4) is shown. (C) The coupling mixture of $HgTX_1$-A19C-SH and Cy5-mal was applied to a C_{18} reversed-phase HPLC. Elution of the two diastereomers of $HgTX_1$-A19C−Cy5 (peaks 1 and 2) is shown.

We also monitored the effect of $HgTX_1$-A19C−Cy5 on recombinant $K_v1.3$ channels by means of electrophysiology. This toxin analogue completely supressed the K^+ current through these channels with a potency comparable to wild-type $HgTX_1$ (data not shown).

Localization of $HgTX_1$-Sensitive K^+ Channels in Native Rat Brain Sections. $HgTX_1$-A19C−Cy3, $HgTX_1$-A19C−Alexa488, and $HgTX_1$-A19C−Alexa546 were used to investigate the localization of native voltage-gated K_v1 channel in rat brain sections using fluorescence micros-

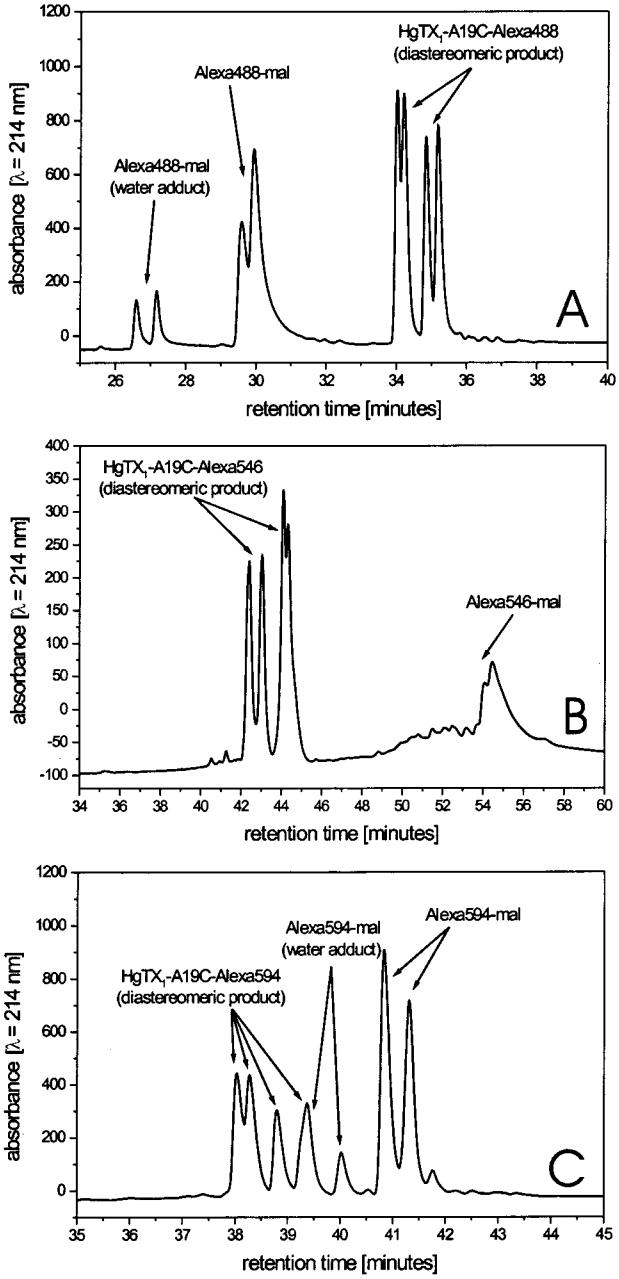


Figure 5. Coupling of thiol-reactive Alexa488-mal, Alexa546-mal, and Alexa594-mal to the free thiol form of $HgTX_1$-A19C. $HgTX_1$-A19C-SH and Alexa488-mal (A), Alexa 546-mal (B), or Alexa594-mal (C) were coupled as described in Experimental Procedures. Resulting products were applied to a C_{18} reversed-phase HPLC. Elution of the diastereomeric (one pair of diastereomers for each dye-isomer) coupling products is shown.

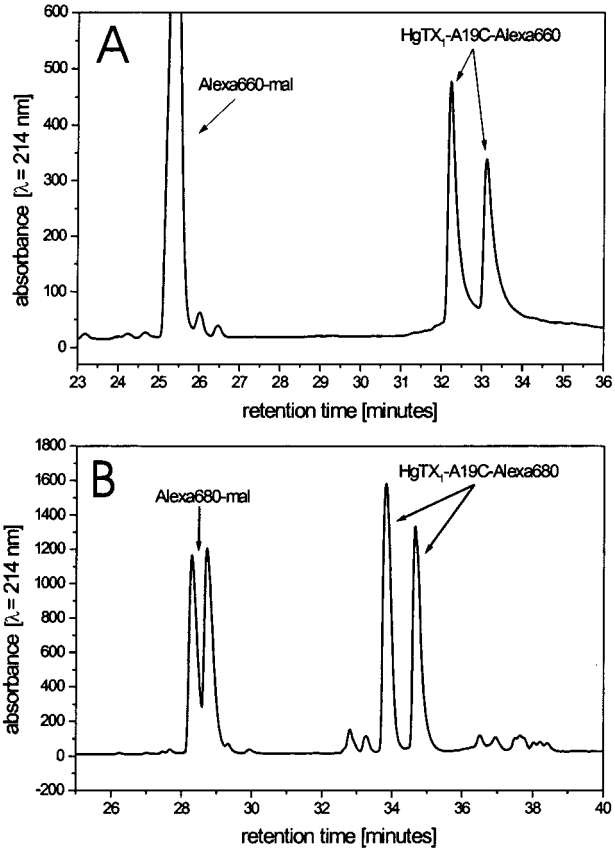


Figure 6. Coupling of thiol-reactive Alexa660-mal and Alexa680-mal to the free thiol form of $HgTX_1$-A19C. $HgTX_1$-A19C-SH and Alexa660-mal (A) or Alexa680-mal (B) were coupled as described in Experimental Procedures. Resulting products were applied to a C_{18} reversed-phase HPLC. Elution of the coupling products is shown.

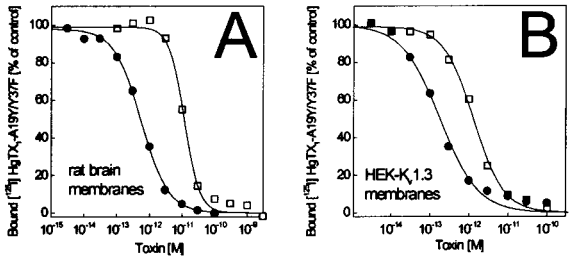


Figure 7. Functional characterization of $HgTX_1$-A19C−Cy5 − Radioligand Bindind Studies. (A) Rat brain membranes were incubated with 0.5 pM [^{125}I]$HgTX_1$-A19Y/Y37F in the absence or presence of increasing concentrations of $HgTX_1$ (circles, IC_{50} 0.5 pM; n_H 1.04) or $HgTX_1$-A19C−Cy5 (open squares, IC_{50} 11.6 pM; n_H 1.86) at room temperature for 2 h. (B) HEK−K_v1.3 membranes were incubated under the same conditions as described in (A). $HgTX_1$ (circles, IC_{50} 0.16 pM; n_H 0.89) and $HgTX_1$-A19C−Cy5 (squares, IC_{50} 1.3 pM; n_H 1.31). All displacement curves were computer fitted to the general dose−response curve as described in Experimental Procedures.

copy. Immunohistochemical studies using a sequence-directed antibody against K_v1.2 were performed.

High levels of $HgTX_1$-A19C−Cy3 binding were observed in the brainstem, cerebellum, and neocortex. The binding reaction was specific as no fluorescence signal was observed in the presence of 100 nM unlabeled $HgTX_1$ (data not shown). Under controlled conditions $HgTX_1$-A19C−Cy3 labeling resulted in specific staining of morphologically and anatomically well-defined neuronal structures which correspond to the immunohistochemical staining pattern using sequence-directed antibodies. The most prominent fluorescence signal was detected in the Purkinje cell layer of the rat cerebellum (Figure 8). This subregion of the cerebellum is known to harbor the highest density of K_v1.1/K_v1.2 channels of the entire rat CNS (Koch et al., 1997; Sheng et al., 1994; Wang et al., 1994; Wang et al., 1994; Koch et al., 1997). The channels are situated at pinceau terminals—giant basket cell synapses wrapping around the base of the Purkinje cell. Parallel experiments using a sequence-directed antibody against the voltage-gated K^+ channel K_v1.2 displayed a very similar distribution pattern (Figure 8B/D). Moreover, $HgTX_1$-A19C−Alexa488 and $HgTX_1$-A19C−Alexa546 show an identical distribution pattern compared to $HgTX_1$-A19C−Cy3 (Figure 9). In summary, the experiments confirm the suitability of this toxin for distribution

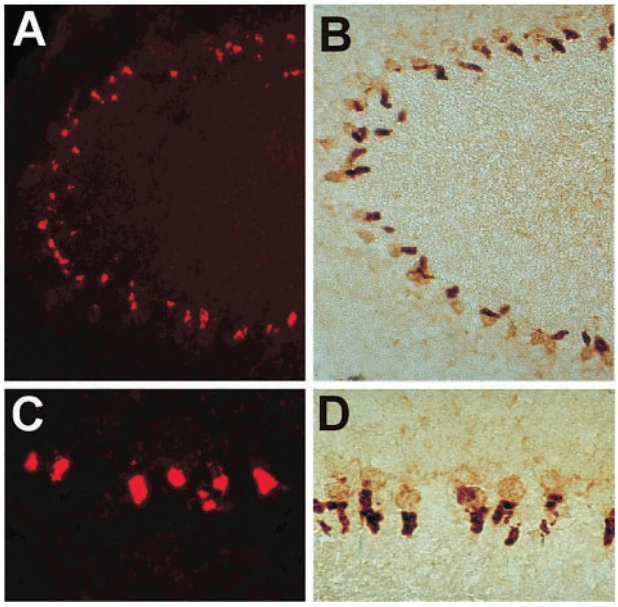


Figure 8. Application of HgTX1-A19C−Cy3 to fluorescence microscopy. Native 10 μm rat brain sections were incubated with 2 nM of $HgTX_1$-A19C−Cy3 overnight at 4 °C. Pinceau terminal staining in the cerebellum (A, B 20×, C, D 40×) is shown in comparison to K_v1.2 immunoreactivity.

studies of voltage-gated K^+ channel either in isolated cells (e.g. neurons in primary culture; recombinant channels in mammalian cell lines) or complex tissues (e.g. the brain).

DISCUSSION

Until now, fluorescently labeled K^+ channel toxins were synthesized by either covalent modification of lysine residues or toxin biotinylation (e.g. charybdotoxin (Robitaille et al., 1993) or apamin (Molecular Probes Inc., Eugene, OR)). However, in many instances, these procedures generate toxin analogues with reduced binding affinity and/or altered pharmacological profiles (H.G.K., unpublished observation). To circumvent these obstacles and to generate a fluorescently labeled $HgTX_1$ analogue which closely resembles wild-type $HgTX_1$ thereby preserving affinity and pharmacology, we adapted a recently developed strategy to radiolabel a structurally related toxin, namely IbTX, with [^{3}H] (Knaus et al., 1996). Our experiments were governed by studies in which ChTX (Goldstein et al., 1994), IbTX (Mullmann et al., 1999), KTX (Aiyar et al., 1996), and $AgTX_2$ (Gross and MacKinnon, 1996) were subjected to an extensive site-directed mutagenesis paradigm, coupled to functional screening of these mutant toxin analogues. These studies allowed the clear assignment of residues which are crucial for high affinity interaction with the respective channels. In addition, the NMR data presented in this paper enabled us to clearly assign residues which are known to be located opposite from the toxin's interaction surface with the voltage-gated K^+ channel K_v1.3 (Aiyar et al., 1995). As examplified for $HgTX_1$-A19C−Cy3, ion channel expression and distribution can be investigated in brain sections thereby complementing or even substituting antibody staining experiments. This approach offers the definite advantage that the respective tissue under investigation does not need to be fixed nor permeabilized before the staining reaction is performed. In contrast to all sequence-specific antibodies directed against individual ion channel subunits (which mostly recognize epitopes located on the intracellular side of the channel),

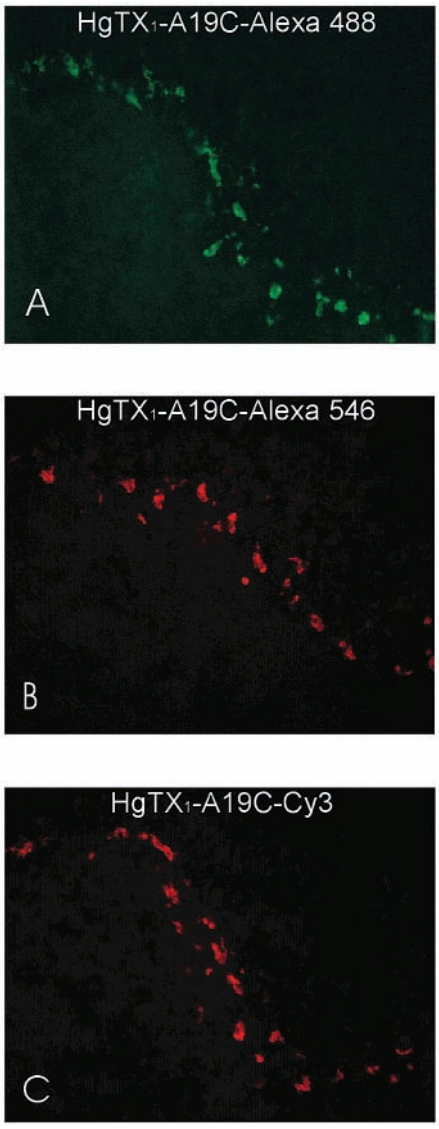


Figure 9. Comparison between $HgTX_1$-A19C−Alexa488, $HgTX_1$-A19C−Alexa546, and $HgTX_1$-A19C−Cy3 (fluorescence microscopy). Native 10 μm rat brain sections were incubated with 2 nM of $HgTX_1$-A19C−Alexa488 (A), $HgTX_1$-A19C−Alexa546 (B), and $HgTX_1$-A19C−Cy3 (C) overnight at 4 °C. Pinceau terminal staining in the cerebellum (A, B, C 20×) is shown.

most ion channel toxins bind to extracellular sites within the channel's vestibule (Gross and MacKinnon, 1996; Aiyar et al., 1995). In two very recent reports, we have shown that this toxin analogue can also be utilized to image individual ion channels in living cells by means of single dye tracing (SDT) experiments (Schütz et al., 2000a; Schütz et al., 2000b; Schütz et al., 2000a). For the first time, individual membrane proteins were visualized at a three-dimensional position of ~40 nm.

Besides studying individual ion channels at high spatial resolution through SDT experiments, a number of additional questions can now be addressed using fluorescently labeled K^+ channel toxins utilizing this general principle. Ion channel distribution studies could be extended to cultured neurons in order to address developmental changes in channel expression in distinct neuronal structures through fluorescence microscopy. An additional application is the monitoring of recombinant channel expression in, for example, mammalian cell lines. Individual cells could be screened based on the fluorescence signal, channel expression could be quantified, and

a single cell could be harvested and replated. Moreover, as only channels residing in the plasma membrane would be detected, precise information on the surface expression level could be obtained.

Soon this approach is going to be extended to produce and characterize additional ion channel-selective toxin analogues (e.g. iberiotoxin for BK channels or ω-conotoxin GVIA for a subset of voltage-gated Ca^{2+} channels). We aim to derivatize all these toxins by means of Förster donor−acceptor dye pairs (e.g. Cy3/Cy5 or Cy5/Cy5.5) and utilize them in fluorescence resonance energy transfer studies. Together with commercially available fluorescently labeled ion channel probes (e.g. dihydropyridines), these tools will help to address the issue of ion channel colocalization by means of two-photon laser miscroscopy and/or SDT experiments in native tissue.

ACKNOWLEDGMENT

We thank Drs. Hartmut Glossmann, Hans-Georg Schindler, and Bernhard Flucher for continuous support and discussion. This work is part of the Ph.D. diploma of B.P. This work was supported by research grants P12663-MED and P14594-PHA (Austrian Research Foundation) and European Community #BMH4-CT97-2118 and QLRT-1999-01356.

LITERATURE CITED

(1) Aiyar, J., Rizzi, J. P., Gutman, G. A., and Chandy, K. G. (1996) The signature sequence of voltage-gated potassium channels projects into the external vestibule. *J. Biol. Chem. 271*, 31013−31016.

(2) Aiyar, J., Withka, J. M., Rizzi, J. P., Singleton, D. H., Andrews, G. C., Lin, W., Boyd, J., Hanson, D. C., Simon, M., and Dethlefs, B. (1995) Topology of the pore-region of a K+ channel revealed by the NMR-derived structures of scorpion toxins. *Neuron 15*, 1169−1181.

(3) Angelides, K. J. (1986) Fluorescently labeled Na+ channels are localized and immobilized to synapses of innervated muscle fibres. *Nature 321*, 63−66.

(4) Angelides, K. J. (1989) Fluorescent analogues of toxins. *Methods Cell Biol. 29*, 29−58.

(5) Blanc, E., Romi-Lebrun, R., Bornet, O., Nakajima, T., and Darbon, H. (1998) Solution structure of two new toxins from the venom of the Chinese scorpion Buthus martensi Karsch blockers of potassium channels. *Biochemistry 37*, 12412−12418.

(6) Bradford, M. M. (1976) A rapid and sensitive method for the quantitation of microgram quantities of protein utilizing the principle of protein-dye binding. *Anal. Biochem. 72*, 248−254.

(7) Brünger, A. T. (1992) X-PLOR v3.1 Manual, Yale University, New Haven, CT.

(8) Chandy, K. G. and Gutman, G. A. (1993) Nomenclature for mammalian potassium channel genes. *Trends Pharmacol. Sci. 14*, 434.

(9) Cohen, M. W., Jones, O. T., and Angelides, K. J. (1991) Distribution of Ca2+ channels on frog motor nerve terminals revealed by fluorescent omega-conotoxin. *J. Neurosci. 11*, 1032−1039.

(10) Darbon, H. and Angelides, K. J. (1984) Structural mapping of the voltage-dependent sodium channel. Distance between the tetrodotoxin and Centruroides suffusus suffusus II beta-scorpion toxin receptors. *J. Biol. Chem. 259*, 6074−6084.

(11) Doyle, D. A., Morais, C. J., Pfuetzner, R. A., Kuo, A., Gulbis, J. M., Cohen, S. L., Chait, B. T., and MacKinnon, R. (1998) The structure of the potassium channel: molecular basis of K^+ conduction and selectivity. *Science 280*, 69−77.

(12) Garcia-Calvo, M., Knaus, H. G., McManus, O. B., Giangiacomo, K. M., Kaczorowski, G. J., and Garcia, M. L. (1994) Purification and reconstitution of the high-conductance, calcium-activated potassium channel from tracheal smooth muscle. *J. Biol. Chem. 269*, 676−682.

(13) Gehlert, D. R. and Gackenheimer, S. L. (1993) Comparison of the distribution of binding sites for the potassium channel ligands [125I]apamin, [125I]charybdotoxin and [125I]iodoglyburide in the rat brain. *Neuroscience 52*, 191−205.

(14) Goldstein, S. A. and Miller, C. (1993) Mechanism of charybdotoxin block of a voltage-gated K^+ channel. *Biophys. J. 65*, 1613−1619.

(15) Goldstein, S. A., Pheasant, D. J., and Miller, C. (1994) The charybdotoxin receptor of a Shaker K^+ channel: peptide and channel residues mediating molecular recognition. *Neuron 12*, 1377−1388.

(16) Gross, A. and MacKinnon, R. (1996) Agitoxin footprinting the shaker potassium channel pore. *Neuron 16*, 399−406.

(17) Gruber, H. J., Kada, G., Pragl, B., Riener, C., Hahn, C. D., Harms, G. S., Ahrer, W., Dax, T. G., Hohenthanner, K., and Knaus, H. G. (2000) Preparation of thiol-reactive Cy5 derivatives from commercial Cy5 succinimidyl ester. *Bioconjugate Chem. 11*, 161−166.

(18) Guntert, P., Braun, W., and Wuthrich, K. (1991) Efficient computation of three-dimensional protein structures in solution from nuclear magnetic resonance data using the program DIANA and the supporting programs CALIBA, HABAS and GLOMSA. *J. Mol. Biol. 217*, 517−530.

(19) Helms, L. M., Felix, J. P., Bugianesi, R. M., Garcia, M. L., Stevens, S., Leonard, R. J., Knaus, H. G., Koch, R., Wanner, S. G., Kaczorowski, G. J., and Slaughter, R. S. (1997) Margatoxin binds to a homomultimer of K(V)1.3 channels in Jurkat cells. Comparison with K(V)1.3 expressed in CHO cells. *Biochemistry 36*, 3737−3744.

(20) Horton, R. M., Hunt, H. D., Ho, S. N., Pullen, J. K., and Pease, L. R. (1989) Engineering hybrid genes without the use of restriction enzymes: gene splicing by overlap extension. *Gene 77*, 61−68.

(21) Jones, O. T., Kunze, D. L., and Angelides, K. J. (1989) Localization and mobility of omega-conotoxin-sensitive Ca^{2+} channels in hippocampal CA1 neurons. *Science 244*, 1189−1193.

(22) Knaus, H. G., Garcia-Calvo, M., Kaczorowski, G. J., and Garcia, M. L. (1994) Subunit composition of the high conductance calcium-activated potassium channel from smooth muscle, a representative of the mSlo and slowpoke family of potassium channels. *J. Biol. Chem. 269*, 3921−3924.

(23) Knaus, H. G., Koch, R. O., Eberhart, A., Kaczorowski, G. J., Garcia, M. L., and Slaughter, R. S. (1995) [125I]margatoxin, an extraordinarily high affinity ligand for voltage-gated potassium channels in mammalian brain. *Biochemistry 34*, 13627−13634.

(24) Knaus, H. G., Schwarzer, C., Koch, R. O., Eberhart, A., Kaczorowski, G. J., Glossmann, H., Wunder, F., Pongs, O., Garcia, M. L., and Sperk, G. (1996) Distribution of high-conductance $Ca^{(2+)}$-activated K^+ channels in rat brain: targeting to axons and nerve terminals. *J. Neurosci. 16*, 955−963.

(25) Koch, R. O., Wanner, S. G., Koschak, A., Hanner, M., Schwarzer, C., Kaczorowski, G. J., Slaughter, R. S., Garcia, M. L., and Knaus, H. G. (1997) Complex subunit assembly of neuronal voltage-gated K+ channels. Basis for high-affinity toxin interactions and pharmacology. *J. Biol. Chem. 272*, 27577−27581.

(26) Koschak, A., Bugianesi, R. M., Mitterdorfer, J., Kaczorowski, G. J., Garcia, M. L., and Knaus, H. G. (1998). Subunit composition of brain voltage-gated potassium channels determined by hongotoxin-1, a novel peptide derived from Centruroides limbatus venom. *J. Biol. Chem. 273*, 2639−2644.

(27) Krezel, A. M., Kasibhatla, C., Hidalgo, P., MacKinnon, R., and Wagner, G. (1995) Solution structure of the potassium channel inhibitor agitoxin 2: caliper for probing channel geometry. *Protein Sci. 4*, 1478−1489.

(28) Laskowski, R. A., MacArthur, M. W., Moss, D. M., and Thornton, J. M. (1993) A program to check the stereochemical quality of protein strutures. *J. Appl. Crystallogr. 26*, 283−291.

(29) MacKinnon, R., Cohen, S. L., Kuo, A., Lee, A., and Chait, B. T. (1998) Structural conservation in prokaryotic and eukaryotic potassium channels. *Science 280*, 106−109.

(30) MacKinnon, R. and Miller, C. (1988) Mechanism of charybdotoxin block of the high-conductance, Ca^{2+}-activated K^+ channel. *J. Gen. Physiol. 91*, 335−349.

(31) MacKinnon, R. and Miller, C. (1989) Mutant potassium channels with altered binding of charybdotoxin, a pore-blocking peptide inhibitor. *Science 245*, 1382−1385.

(32) Margolskee, R. F., McHendry-Rinde, B., and Horn, R. (1993) Panning transfected cells for electrophysiological studies. *Biotechniques 15*, 906−911.

(33) Miller, C. (1995) The charybdotoxin family of K+ channel-blocking peptides. *Neuron 15*, 5−10.

(34) Mullmann, T. J., Munujos, P., Garcia, M. L., and Giangiacomo, K. M. (1999) Electrostatic mutations in iberiotoxin as a unique tool for probing the electrostatic structure of the maxi-K channel outer vestibule. *Biochemistry 38*, 2395−2402.

(35) Park, C. S. and Miller, C. (1992) Mapping function to structure in a channel-blocking peptide: electrostatic mutants of charybdotoxin. *Biochemistry 31*, 7749−7755.

(36) Robitaille, R., Garcia, M. L., Kaczorowski, G. J., and Charlton, M. P. (1993) Functional colocalization of calcium and calcium-gated potassium channels in control of transmitter release. *Neuron 11*, 645−655.

(37) Roussel, A. and Cambillau, C. (1989) *Silicon Graphics Geometry Partner Directory* (Silicon Graphics, Mountain View, CA) pp 77−78.

(38) Sanger, F., Nicklen, S., and Coulson, A. R. (1977) DNA sequencing with chain-terminating inhibitors. *Proc. Natl. Acad. Sci. U.S.A 74*, 5463−5467.

(39) Schütz, G., Hesse, J., Freudenthaler, G., Pastushenko, V. P., Knaus, H. G., Pragl, B., and Schindler, H. (2000) 3D mapping of individual ion channels on living cells. *Single Mol. 1*, 153−157.

(40) Schütz, G., Pastushenko, V. P., Gruber, H. J., Knaus, H. G., Pragl, B., and Schindler, H. (2000) 3D Imaging of individual ion channels in live cells at 40 nm resolution. *Single Mol. 1*, 25−31.

(41) Shamotienko, O. G., Parcej, D. N., and Dolly, J. O. (1997) Subunit combinations defined for K+ channel Kv1 subtypes in synaptic membranes from bovine brain. *Biochemistry 36*, 8195−8201.

(42) Sheng, M., Liao, Y. J., Jan, Y. N., and Jan, L. Y. (1993) Presynaptic A-current based on heteromultimeric K+ channels detected in vivo. *Nature 365*, 72−75.

(43) Sheng, M., Tsaur, M. L., Jan, Y. N., and Jan, L. Y. (1994) Contrasting subcellular localization of the Kv1.2 K^+ channel subunit in different neurons of rat brain. *J. Neurosci. 14*, 2408−2417.

(44) Tytgat, J., Chandy, K. G., Garcia, M. L., Gutman, G. A., Martin-Eauclaire, M. F., van der Walt, J. J., and Possani, L. D. (1999) A unified nomenclature for short-chain peptides isolated from scorpion venoms: alpha-KTx molecular subfamilies. *Trends Pharmacol. Sci. 20*, 444−447.

(45) Vazquez, J., Feigenbaum, P., King, V. F., Kaczorowski, G. J., and Garcia, M. L. (1990) Characterization of high affinity binding sites for charybdotoxin in synaptic plasma membranes from rat brain. Evidence for a direct association with an inactivating, voltage-dependent, potassium channel. *J. Biol. Chem. 265*, 15564−15571.

(46) Wang, H., Kunkel, D. D., Schwartzkroin, P. A., and Tempel, B. L. (1994) Localization of Kv1.1 and Kv1.2, two K channel proteins, to synaptic terminals, somata, and dendrites in the mouse brain. *J. Neurosci. 14*, 4588−4599.

(47) Wuthrich, K. (1986) *NMR of protein and nucleic acids*, John Wiley and Sons, New York.

BC015543S

Solid-Phase Synthesis of Deglycobleomycins: A C-Terminal Tetraamine Linker That Permits Direct Evaluation of Resin-Bound Bleomycins

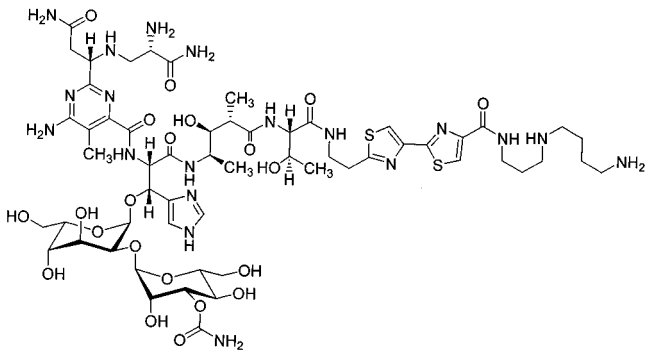
Zhi-Fu Tao, Christopher J. Leitheiser, Kenneth L. Smith, Shigeki Hashimoto, and Sidney M. Hecht*

Departments of Chemistry and Biology, University of Virginia, Charlottesville, Virginia 22901. Received September 8, 2001

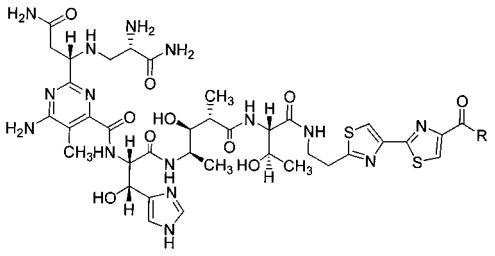
Deglycobleomycin analogues having different length polyamine side chains at the C-terminus were synthesized using a novel solid-phase synthesis strategy that produces fully deprotected deglycobleomycin congeners attached to the resin. Detailed studies of DNA cleavage by these compounds and their resin-bound counterparts using supercoiled plasmid DNAs and DNA restriction fragments as substrates revealed that (i) the length of the polyamine side chain of free deglycoBLM had limited effect on its DNA cleavage potency or sequence selectivity, and (ii) the nature of the linker moiety between the resin and attached deglycobleomycin had a more substantial effect on the potency of DNA cleavage, but no effect on sequence selectivity of resin-bound deglycoBLMs. Resin-bound **4** exhibited efficient DNA cleavage, indicating that its tetraamine linker moiety could be used for the elaboration and direct evaluation of bleomycin congeners attached to resins.

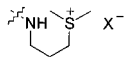
The bleomycins (BLMs),[1] exemplified by bleomycin A_5, are naturally occurring, peptide-derived antitumor agents (*1, 2*) that are used clinically for the treatment of several cancers, notably squamous cell carcinomas and malignant lymphomas (*3*). The antitumor activity of these BLMs is believed to depend on their ability to effect the selective cleavage of DNA (*1, 2, 4*−*9*) and possibly also RNA (*10*−*12*). Deglycobleomycin lacks the carbohydrate moiety but nonetheless exhibits DNA cleavage properties quite similar to those of bleomycin itself as regards potency, sequence selectivity, and actual chemistry of DNA degradation (*13*−*15*).

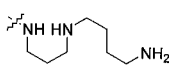
Numerous analogues of bleomycin and deglycobleomycin have been synthesized and characterized for their properties in DNA degradation (*16*−*35*). However, with the exception of our discovery that the carbohydrate moiety of bleomycin is not essential for DNA cleavage (*13*−*15*), none of the analogues reported to date can be argued to have improved properties, simplified structures, or to be more readily accessible by synthesis such that improved antitumor agents might be realized. We have developed two solid-phase strategies for synthesis of BLM analogues (*36, 37*), one goal of which is the elaboration of BLM-like species having specific improved properties. It should be possible to realize this goal through the synthesis and survey of large numbers of BLM analogues.



bleomycin A_5



deglycobleomycin A_2 R =  X^-

deglycobleomycin A_5 (**3**) R = 

Combinatorial chemistry has become a powerful tool for the organic and medicinal chemist. There are numerous ways in which libraries can be prepared and tested; solid-phase synthesis has been utilized widely for library construction (*38*−*43*). The assay of libraries on solid supports has been used successfully for the screening of medicinally important molecules and synthetic receptors (*44*−*50*).

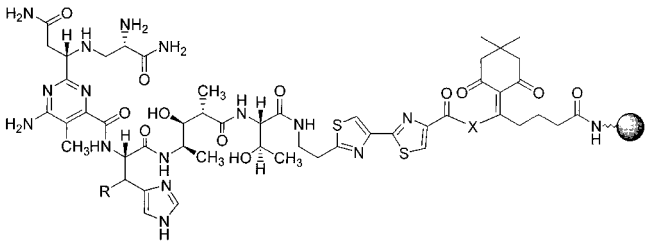
A key parameter that defines the potential utility of resin-bound ligands for assaying ligand−receptor inter-

* Address correspondence to Dr. Sidney M. Hecht, Department of Chemistry, University of Virginia, Charlottesville, VA 22901. Fax: (434) 924-7856. E-mail: sidhecht@virginia.edu.

[1] Abbreviations: BLM, bleomycin; Boc, *tert*-butoxycarbonyl; BOP, benzotriazol-1-yloxytris(dimethylamino)phosphonium hexafluorophosphate; Dde, 2-acetyldimedone; DIPEA, *N*,*N*′-diisopropylethylamine, Hünig's base; HATU, *O*-(7-azabenzotriazol-1-yl)- *N*,*N*,*N*′,*N*′-tetramethyluronium hexafluorophosphate; Fmoc, 9-fluorenylmethoxycarbonyl; HBTU, *O*-benzotriazolyl-*N*,*N*,*N*′,*N*′-tetramethyluronium hexafluorophosphate; HOBt, *N*-hydroxybenzotriazole; HOAt, 1-hydroxy-7-azabenzotriazole; TFA, trifluoroacetic acid; Tr, triphenylmethyl.

10.1021/bc010083o CCC: $22.00 © 2002 American Chemical Society
Published on Web 03/09/2002

action is the accessibility of resin-bound library members to the receptors. The recent finding (*51, 52*) that conjugation of BLM A_5 to a solid support via its C-terminus had little effect on its ability to mediate DNA cleavage encouraged us to identify a C-terminal linker applicable to direct evaluation of resin-bound DNA-cleaving bleomycin analogues. Reported herein are (i) the solid-phase syntheses of deglycoBLM analogues in which the C-terminal polyamine substituent is varied in a systematic fashion, and (ii) a characterization of DNA cleavage by these resin-free and resin-bound analogues, resulting in the identification of a C-substituent that facilitates the direct evaluation of resin-bound bleomycin analogues.



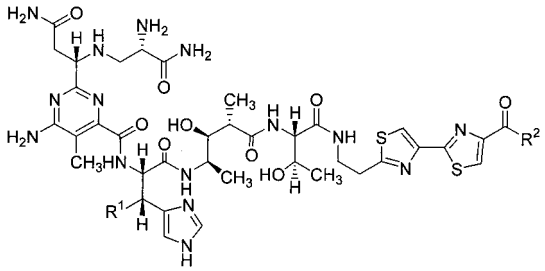
Resin-bound 1 R = H; X = $NH(CH_2)_4NH$
Resin-bound 2 R= H; X= $NH(CH_2)_3NH(CH_2)_4NH$
Resin-bound 3 R= OH; X = $NH(CH_2)_3NH(CH_2)_4NH$
Resin-bound 4 R = H; X = $NH(CH_2)_3NH(CH_2)_4NH(CH_2)_3NH$

EXPERIMENTAL PROCEDURES

Materials and General Techniques. Calf intestinal phosphatase (one unit is the amount of enzyme that hydrolyzes 1 μmol of *p*-nitrophenyl phosphate to *p*-nitrophenol in 1 min at 37 °C in a total reaction volume of 1 mL), *Eco*RV, *Hin*dIII (one unit is the amount of enzyme required to digest 1 μg of λ DNA in 1 h at 37 °C in a total reaction volume of 50 μL), T4 polynucleotide kinase (one unit is the amount of enzyme catalyzing the production of 1 nmol of acid-insoluble ^{32}P in 30 min at 37 °C under the following conditions: 70 mM Tris-HCl, pH 7.6, 10 mM $MgCl_2$, 5 mM DTT, 66 μM [γ-^{32}P]ATP (5×10^6 cpm/mmol), 0.26 mM 5′-OH terminating salmon sperm DNA). Plasmid pSP64 was cultured in *E. coli* and isolated using a Qiagen resin. Plasmid pB*R*322 DNA was purchased from New England Biolabs. [γ-^{32}P]ATP (7000 Ci/mmol) was obtained from ICN Radiochemicals, Inc. $Fe(NH_4)_2(SO_4)_2 \cdot 6H_2O$ (Aldrich) was used to prepare aqueous solutions for admixture with bleomycin; these were made immediately prior to use. Agarose gel electrophoresis was carried out in 90 mM Tris-borate buffer, pH 8.3, containing 5 mM EDTA. The agarose gel loading solution contained 30% glycerol and 0.05% (w/v) bromophenol blue. Polyacrylamide gel electrophoresis was carried out in 90 mM Tris-borate buffer, pH 8.3, containing 5 mM EDTA. The loading solution contained 80% formamide, 2 mM EDTA, 0.05% (w/v) xylene cyanol, and 0.05% (w/v) bromophenol blue. Chemical sequencing was carried out according to the method of Maxam and Gilbert (*53*). Distilled and deionized water from a Milli-Q system was autoclaved prior to use in all aqueous solutions in the DNA cleavage experiments. The 5′-^{32}P end labeled 158-bp DNA restriction fragment was prepared from pB*R*322 plasmid DNA according to reported procedures (*51, 52*).

Ultraviolet spectra were recorded on a Perkin-Elmer Lambda 20 UV−Vis spectrophotometer. ^1H NMR spectra were recorded on a General Electric QE-300 MHz NMR spectrophotometer using the residual HOD resonance at 4.80 ppm as an internal standard. HPLC purification was performed on a Varian 9012 HPLC gradient programmer system with a Perkin-Elmer LC-235 diode array detector. All synthetic reactions were carried out under nitrogen or argon. Anhydrous grade DMF, anhydrous grade piperidine, HATU, HOAt, trifluoroacetic acid, hydrazine monohydrate, and anhydrous grade Hunig's base were purchased from Aldrich chemicals. TentaGel resin, HBTU, HOBt, BOP, 9-fluorenylmethoxycarbonyl-β-alanine, and 9-fluorenylmethoxycarbamoylthreonine were purchased from NovaBiochem. Methylene chloride was distilled from calcium hydride. Fmoc cleavage was determined by UV measurement of the dibenzylfulvene−piperidine adduct formed upon treatment of the resin with piperidine (*54*). The optical density of 5540 M^{-1} at 290 nm and 7300 M^{-1} at 300 nm was used to calculate the loading from a known weight of dry resin.

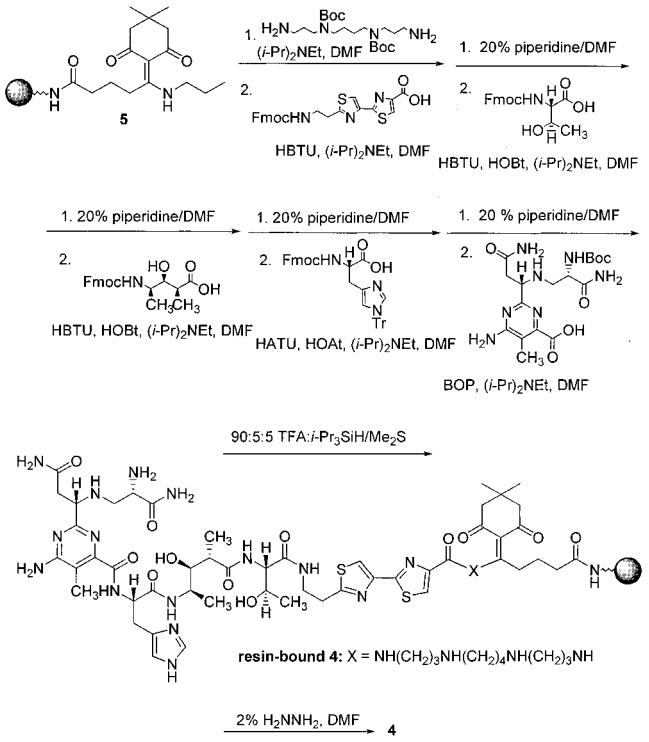
Molecular beacon DNA oligodeoxynucleotide, labeled with 5′ FAM and 3′ BHQ dyes, was custom-synthesized by Integrated DNA Technology, Inc. BHQ is a trademark of Biosearch Technologies, Inc.; the chemical structure has not been disclosed. Fluorescence image analysis was performed at the W. M. Keck Center for Cellular Imaging, University of Virginia, using an Olympus Infinity corrected inverted microscope.



1 R^1 = H; R^2 = $NH(CH_2)_4NH_2$
2 R^1 = H; R^2 = $NH(CH_2)_3NH(CH_2)_4NH_2$
3 R^1 = OH; R^2 = $NH(CH_2)_3NH(CH_2)_4NH_2$
4 R^1 = H; R^2 = $NH(CH_2)_3NH(CH_2)_4NH(CH_2)_3NH_2$

Synthesis of Resin-Bound DeglycoBLM 4. DeglycoBLM analogues **1**−**4** were prepared using closely related methods; these are exemplified by the synthesis of deglycoBLM **4**. To a suspension containing 200 mg (0.45 mmol/g) of TentaGel amino functionalized resin (**5**; Scheme 1) (*55*) was added a DMF solution containing 362 mg (0.90 mmol) of protected spermine and 313 μL (232 mg, 1.8 mmol) of Hunig's base. The reaction mixture was shaken for 24 h, and then the resin was filtered and washed successively for 30 s each with three 5-mL portions of DMF, three 5-mL portions of CH_2Cl_2, three 5-mL portions of methanol, and again with three 5-mL portions of DMF. A DMF solution containing 128 mg (0.27 mmol) of Fmoc-bithiazole, 102 mg (0.27 mmol) of HBTU, and 94 μL (70 mg, 0.54 mmol) of Hunig's base was added. After 30 min, the resin was filtered and washed successively for 30 s each with three 5-mL portions of DMF, three 5-mL portions of CH_2Cl_2, and again with three 5-mL portions of DMF. Quantitation of Fmoc cleavage indicated a loading of 0.17 mmol/g (57% yield for three steps). The resulting resin was treated for 5 min each with three 2-mL DMF solutions containing 20% piperidine in DMF. The resulting resin was washed for 30 s each with seven 5-mL portions of DMF, five 5-mL portions of CH_2Cl_2, and three 5-mL portions of DMF. A solution containing 35 mg (0.10 mmol) of Fmoc-threonine, 38 mg (0.10 mmol) of HBTU, 15 mg (0.10 mmol) of HOBt, and 36 μL (26 mg, 0.20 mmol) of Hunig's base in 0.5 mL of DMF was added. After 30 min the resin was filtered and washed with three 5-mL portions of DMF, three 5-mL portions of CH_2Cl_2, and again with three 5-mL

Scheme 1. Solid-Phase Synthesis of Resin-Bound and Free DeglycoBLM 4



portions of DMF. Quantitation of Fmoc cleavage indicated a loading of 0.17 mmol/g (>95%). The resin was treated for 5 min each with three 2-mL DMF solutions containing 20% piperidine in DMF. The resin was washed for 30 s each with seven 5-mL portions of DMF, five 5-mL portions of CH_2Cl_2, and three 5-mL portions of DMF. The resin was treated with a solution containing 37 mg (0.10 mmol) of Fmoc-methylvalerate, 38 mg (0.10 mmol) of HBTU, 15 mg (0.10 mmol) of HOBt, and 36 μL (26 mg, 0.20 mmol) of Hunig's base. After 30 min, the resin was filtered and washed for 30 s each with three 5-mL portions of DMF, three 5-mL portions of CH_2Cl_2, and again with three 5-mL portions of DMF. Quantitation of Fmoc cleavage indicated a loading of 0.15 mmol/g (94%). The resulting resin was treated for 5 min each with three 2-mL DMF solutions containing 20% piperidine in DMF and then washed for 30 s each with seven 5-mL portions of DMF, five 5-mL portions of CH_2Cl_2, and three 5-mL portions of DMF. The resin was treated with a solution containing 63 mg (0.10 mmol) of tritylated Fmoc histidine, 38 mg (0.10 mmol) of HATU, 16 mg (0.10 mmol) of HOAt, and 36 μL (26 mg, 0.20 mmol) of Hunig's base. After 30 min, the resin was filtered and washed for 30 s each with three 5-mL portions of DMF, three 5-mL portions of CH_2Cl_2, and with three 5-mL portions of methanol. The resulting resin was dried under diminished pressure over KOH pellets. A small sample (~20 mg) was treated for 5 min each with three 1-mL portions of 2% hydrazine in DMF (v/v). The resulting solution was concentrated under diminished pressure. The resulting oil was dissolved in 1 mL of an aq 0.1% TFA solution, frozen, and lyophilized to give an off-white solid: mass spectrum (electrospray) m/z 1249.4 $(M + H)^+$ and 1273.6 $(M + Na)^+$. A suspension containing 40 mg of the above resin swollen in 0.5 mL of DMF was treated for 5 min each with three 2-mL DMF solutions containing 20% piperidine in DMF. The resulting resin was washed for 30 s each with seven 5-mL portions of DMF, five 5-mL portions of CH_2Cl_2, and three 5-mL portions of DMF. The resin was treated with a cooled (0 °C) solution containing 5.0 mg (12 μmol) of Boc-pyrimidoblamic acid, 15 mg (35 μmol) of BOP, and 12 μL (9.0 mg, 70 μmol) of Hunig's base in 0.5 mL of DMF. After 16 h, the resin was filtered and washed for 30 s each with three 5-mL portions of DMF, three 5-mL portions of CH_2Cl_2, and three 5-mL portions of methanol. The resin was treated with a solution consisting of 100 μL of triisopropylsilane and 100 μL of dimethyl sulfide. The resin was shaken for 5 min and then 4 mL of trifluoroacetic acid was added to the suspension. After 4 h, the resin was filtered and washed with five 3-mL portions of CH_2Cl_2 and three 3-mL portions of methanol. The resulting resin was dried under diminished pressure over KOH pellets to give resin-bound deglycoBLM **4**.

Synthesis of DeglycoBLM 4. To a suspension containing 30 mg of resin-bound deglycoBLM **4** was added a 0.5 mL of DMF containing 2% hydrazine. The resin was filtered and then treated with three additional 0.5-mL portions of DMF containing 2% hydrazine. Each treatment was carried out for 5 min. The combined filtrate was concentrated under diminished pressure. The resulting oil was dissolved in 2 mL of CF_3COOH and added dropwise to cold (−20 °C) ether. The suspension was centrifuged and the ether decanted. The resulting solid was dissolved in water, frozen and lyophilized. HPLC of the crude material on an Alltech Alltima semipreparative C_{18} reversed-phase HPLC column (250 × 10 mm, 5 μm) was carried out using 0.1% aqueous CF_3COOH and CH_3CN as mobile phases. A linear gradient was employed starting from 88:12 0.1% aqueous $CF_3COOH-CH_3CN$ to 83:17 0.1% aqueous $CF_3COOH-CH_3CN$ over a period of 30 min at a flow rate of 4 mL/min. Fractions containing the desired product eluted after 12 min; these were collected and lyophilized. The yield was determined by ^1H NMR spectroscopy, by comparing the integration of the exocyclic methyl group on pyrimidoblamic acid vs the methyl signal resulting from a known concentration of *tert*-butyl alcohol, and then relating the calculated concentration to the amount of the di-*tert*-butoxycarbonyl spermine determined to have been attached to the resin initially. Yield 3.1 mg (66%); ^1H NMR (D_2O) δ 0.94 (d, 3H, J = 7.0 Hz), 0.99 (d, 3H, J = 7.0 Hz), 1.07 (d, 3 H, J = 7.0 Hz), 1.69 (m, 4H), 1.93 (s, 3H), 1.98 (m, 4H), 2.53 (t, 1H, J = 7.5 Hz), 2.63 (m, 2H), 3.03 (m, 12H), 3.21 (m, 4H), 3.44 (t, 2H, J = 7.0 Hz), 3.58 (t, 1H, J = 5.5 Hz), 3.64 (t, 1H, J = 5.0 Hz), 3.77 (t, 1H, J = 6.5 Hz), 3.97 (t, 2H, J = 6.0 Hz), 4.04 (t, 1H, J = 5.5 Hz), 4.12 (d, 1H, J = 5.5 Hz), 7.27 (s, 1H), 7.98 (s, 1H), 8.13 (s, 1H) and 8.59 (s, 1H); mass spectrum (electrospray), m/z 1114.6 $(M + H)^+$ (calculated 1114.4).

General Procedure for Relaxation of Plasmid DNA by DeglycoBLM Analogues. The reactions were performed in a 25 μL (total volume) reaction mixture containing 300 ng of pSP64 DNA, 10 mM sodium cacodylate, pH 7.0, and various concentrations of BLM (analogues) or Fe^{2+}. The concentrations of resin-bound deglycoBLM analogues are expressed as the concentration that would have been present in solution had the analogues not been attached to the resin. Each reaction mixture was incubated at 37 °C for 30 min, terminated by the addition of 5 μL of loading dye (30% glycerol containing 0.125% bromophenol blue) and applied to 1% agarose gel containing 0.5 μg/mL ethidium bromide. The gel was run in 90 mM Tris-borate buffer, pH 8.3, containing 5 mM EDTA at 138 V for 3−3.5 h; the DNA bands were visualized under UV light.

General Procedure for Degradation of 5′-^{32}P End Labeled DNA Duplexes by DeglycoBLM Analogues.

Reactions were carried out in 25 μL (total volume) of 10 mM sodium cacodylate, pH 7.0, containing ^{32}P-labeled DNA duplex (10^4 cpm) and the concentrations of reagents indicated in the figure legends. Each reaction mixture was incubated at 37 °C for 30 min, and then the reaction mixture was frozen in dry ice, lyophilized, and dissolved in gel loading solution (80% formamide, 2 mM EDTA, 0.05% (w/v) xylene cyanol, and 0.05% (w/v) bromophenol blue). The resulting solution was heated at 90 °C for 3 min, chilled on ice, and then applied to a 10% denaturing polyacrylamide gel. The gel was visualized by autoradiography or by use of a phosphorimager. The sites of cleavage mediated by (resin-bound) **1**−**4** were determined by comparison with Maxam−Gilbert DNA sequencing lanes (*53*).

Fluorescence Microscope Analysis of Beacon DNA Cleavage. A suspension of TentaGel-conjugated deglycoBLM **4** and agarose gel solution were prepared in 50 mM sodium cacodylate, pH 7.0, for the fluorescence microscopy studies. To a single well on a 96-well plate was added 35 μL of 2.4% agarose gel solution in 50 mM sodium cacodylate, pH 7.0; after solidification, this was followed by 20 μL of 500 μM TentaGel-conjugated deglycoBLM A_6 suspension in the same buffer, and an additional 35 μL of buffered 2.4% agarose gel solution. The resulting 55-μL suspension above the solidified gel was immediately mixed with a pipet tip. The plate was placed on ice for 20 min to facilitate solidification of the agarose mixture. A 30-μL solution of 1.5 μM beacon DNA solution was added to the agarose mixture containing the TentaGel beads. The plate was maintained on ice in the absence of light for 12 h to allow the beacon DNA to diffuse through the agarose gel. The final concentrations of deglycoBLM A_6 and beacon DNA were 0.11 mM and 0.37 μM, respectively. The supernatant on the agarose mixture was removed, and a gel piece containing the bleomycin bound resin was excised from the gel. The gel was sandwiched between two cover glass plates (22 × 22 mm), and the bleomycin was activated with 10 μL of 5 mM $Fe(NH_4)_2(SO_4)_2$ solution. Fluorescence images were taken every 5 min through an FITC filter (excitation at 480 ± 20 nm; fluorescence emission at 535 ± 25 nm).

RESULTS AND DISCUSSION

Solid-Phase Synthesis of DeglycoBLM Analogues. We have described a solid-phase synthesis of deglycoBLM A_5 (*36*), in which the final deprotection of acid-labile groups and detachment of the deglycoBLM from the solid support were accomplished simultaneously by treatment with CF_3COOH; therefore, fully deprotected resin-bound bleomycin analogues could not be obtained by this approach. Access to resin-bound, fully deprotected BLM analogues has been accomplished by the use of a solid-phase methodology (*37*) that employs a Dde-based linker (*54*). This linker has been shown to be stable to conditions used to remove both base and acid-labile protecting groups. As outlined in Scheme 1 starting from TentaGel-derived resin **5**, which was prepared according to reported procedures (*55*), Boc-protected spermine (*56*) was attached to the resin via a transamination procedure. The resulting primary amine was then condensed with the bithiazole moiety of bleomycin. For this purpose, Fmoc-protected bithiazole was activated with HBTU and Hunig's base in DMF; this solution was added to the resin containing a free primary amino group, and the mixture was shaken under N_2 at 25 °C for 30 min. The resin was then washed with DMF and CH_2Cl_2, and a small sample was utilized for qualitative verification of coupling by colorimetric assays using the Kaiser (*57*) and bromophenol blue (*58*) tests for amines. The extent of coupling was quantified by UV measurement following Fmoc cleavage with piperidine (*54*); this procedure indicated a loading of 0.17 mmol/g of resin, which represented a coupling efficiency of 57% for three steps. Successive treatments of the resin with 20% piperidine in DMF, followed by Fmoc threonine, resulted in successful synthesis of the tripeptide. The same procedure was used for attachment of Fmoc-methylvaleric acid, resulting in successive attachments of these two amino acids in yields of >95% (0.17 mmol/g) and 94% (0.15 mmol/g), respectively.

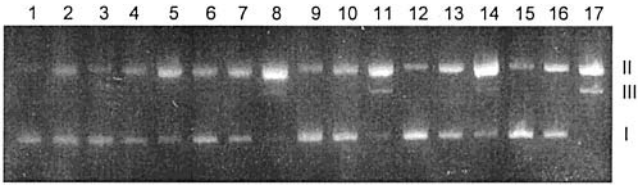


Figure 1. Relaxation of supercoiled pSP64 plasmid DNA by deglycoBLM analogues **1**−**4**. Lane 1: DNA alone; lane 2: 1.5 μM Fe^{2+}; lane 3: 3 μM **1**; lane 4: 1 μM **1** + 1.5 μM Fe^{2+}; lane 5: 3 μM **1** + 1.5 μM Fe^{2+}; lane 6: 3 μM **2**; lane 7: 1 μM **2** + 1.5 μM Fe^{2+}; lane 8: 3 μM **2** + 1.5 μM Fe^{2+}; lane 9: 3 μM **3**; lane 10: 1 μM **3** + 1.5 μM Fe^{2+}; lane 11: 3 μM **3** + 1.5 μM Fe^{2+}; lane 12: 3 μM **4**; lane 13: 1 μM **4** + 1.5 μM Fe^{2+}; lane 14: 3 μM **4** + 1.5 μM Fe^{2+}; lane 15: 3 μM deglycoBLM A_5; lane 16: 1 μM deglycoBLM A_5 + 1.5 μM Fe^{2+}; lane 17: 3 μM deglycoBLM A_5 + 1.5 μM Fe^{2+}.

The resin-bound oligopeptide was deblocked with piperidine in DMF and coupled with Fmoc histidine in the presence of the highly reactive coupling reagent HATU; the coupling efficiency was calculated as 95%, based on spectrophotometric assay of the dibenzylfulvene−piperidine adduct formed following treatment of a portion of the resin with piperidine (*54*). Boc pyrimidoblamic acid (*59*−*61*) was then coupled to the resin using BOP reagent and Hunig's base at 0 °C in the absence of light for 16 h. The resin was washed with DMF and methylene chloride, and the acid-sensitive trityl protecting group on histidine and Boc protecting group on pyrimidoblamic acid were removed simultaneously by treatment with 90:5:5 CF_3COOH−triisopropylsilane−Me_2S. This afforded fully deprotected resin-bound deglycoBLM **4**. A portion of resin-bound **4** was treated with 2% hydrazine in DMF to give deglycoBLM **4**; the structure was confirmed by ^{1}H NMR spectroscopy and electrospray ionization mass spectrometry. The yield of deglycoBLM **4** prepared by solid-phase synthesis was 66%. DeglycoBLMs **1**, **2**, and **3** were synthesized and characterized by following procedures analogous to those employed for analogue **4**.

DNA Cleavage Mediated by DeglycoBLM Analogues. The abilities of deglycoBLM analogues **1**−**4** to cleave DNA were investigated initially using supercoiled plasmid DNA as a substrate. As shown in Figure 1, deglycoBLM analogues **2**−**4** mediated DNA relaxation to roughly the same extent in the presence of Fe^{2+}; the cleavage mediated by Fe(II)·deglycoBLM A_5 was also determined for comparative purposes and shown to be quite similar. Thus the efficiency of DNA cleavage mediated by deglycoBLM analogue **4**, having three basic amino groups within the C-terminal substituent, was not significantly different in this assay than that of **2** or **3**, each of which contain two amino groups within the C-substituent. In comparison, analogue **1**, having a single amine within the C-substituent, was less efficient as a DNA cleaving agent. This finding was anticipated based on earlier studies of the effects of the number and spacing of positively charged groups in the C-substituent on the efficiency of DNA binding (*62*) and degradation (*63*).

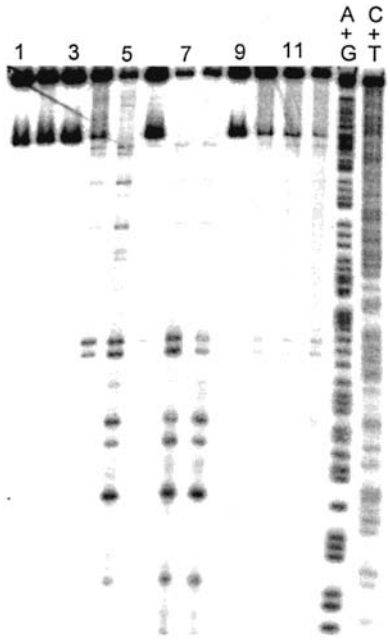


Figure 2. Cleavage of a 5′-^{32}P end-labeled 158-bp DNA restriction fragment by **1** and resin-bound **1**. Lane 1: DNA alone; lane 2: 15 μM Fe^{2+}; lane 3: 15 μM **1**; lane 4: 1.5 μM **1** + 15 μM Fe^{2+}; lane 5: 15 μM **1** + 15 μM Fe^{2+}; lane 6: 15 μM deglycoBLM A_2; lane 7: 1.5 μM deglycoBLM A_2 + 15 μM Fe^{2+}; lane 8: 15 μM deglycoBLM A_2 + 15 μM Fe^{2+}; lane 9: 200 μM resin-bound **1**; lane 10: 50 μM resin-bound **1** + 30 μM Fe^{2+}; lane 11: 100 μM resin-bound **1** + 30 μM Fe^{2+}; lane 12: 200 μM **1** + 30 μM Fe^{2+}.

DeglycoBLM analogues **2** and **3** have the same (spermidine) C-substituent, but differ in that analogue **2** contains a histidine moiety while **3** was synthesized using the amino acid analogue (*S*)-*erythro*-β-hydroxyhistidine; the OH group of the latter is the point of attachment of the disaccharide moiety in the BLMs (cf BLM A_5 and deglycoBLM A_5). The similar potencies of these two analogues in the experiment shown in Figure 1 argues that this OH group does not contribute to the efficiency of deglycoBLM-mediated DNA relaxation, a finding that is entirely consistent with a previous report from the Boger laboratory (*64*).

Also investigated was the sequence selectivity of DNA cleavage by these four deglycoBLMs. The substrate employed for this study was a 158-base pair DNA restriction fragment that has been employed previously as a substrate for Fe(II)·BLMs (*33,51,52*). As shown in Figures 2−4, and Figures 1 and 2 of the Supporting Information, each of the four analogues mediated sequence-selective cleavage of the DNA substrate in the same fashion as BLM itself. Thus the nature of the C-terminal substituent had little if any effect on sequence selectivity of DNA cleavage, as might have been anticipated based on earlier work (*28, 65*). The potency of DNA cleavage by **1**−**4** was investigated in direct comparison with a deglycoBLM congener obtained by HF-mediated cleavage of the sugar moiety (*66*). Thus deglycoBLM analogue **1** was compared directly with deglycoBLM A_2; both of these have a single positively charged group within the C-substituent, and the distance of these charged groups from the bleomycinic acid nucleus (*1*) is quite similar. As shown in Figure 2 and Supporting Information Figure 1, deglycoBLM analogue **1** and deglycoBLM A_2 were of comparable potency as DNA cleaving agents.

An analogous result was obtained for deglycoBLMs **2** and **3**, both of which contain spermidine C-substituents.

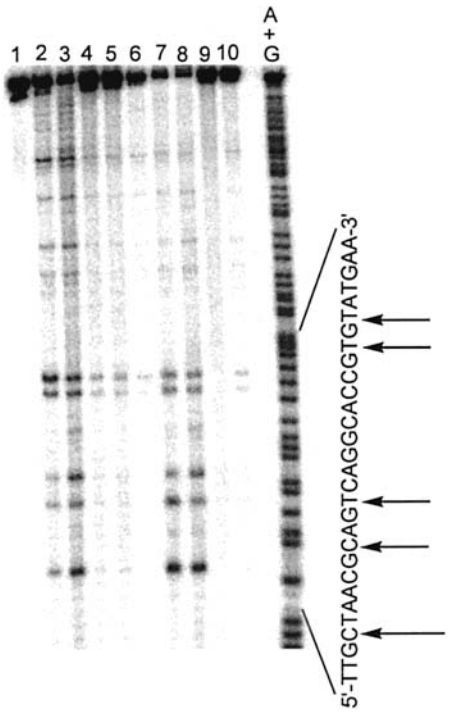


Figure 3. Cleavage of a 5′-^{32}P end-labeled 158-bp DNA fragment by **2**, **3**, resin-bound **2**, and resin-bound **3**. Lane 1: DNA alone; lane 2: 1 μM **2** + 10 μM Fe^{2+}; lane 3: 10 μM **2** + 10 μM Fe^{2+}; lane 4: 1 μM resin-bound **2** + 10 μM Fe^{2+}; lane 5: 10 μM resin-bound **2** + 10 μM Fe^{2+}; lane 6: 100 μM resin-bound **2** + 10 μM Fe^{2+}; lane 7: 1 μM **3** + 10 μM Fe^{2+}; lane 8: 10 μM **3** + 10 μM Fe^{2+}; lane 9: 1 μM resin-bound **3** + 10 μM Fe^{2+}; lane 10: 10 μM resin-bound **3** + 10 μM Fe^{2+}.

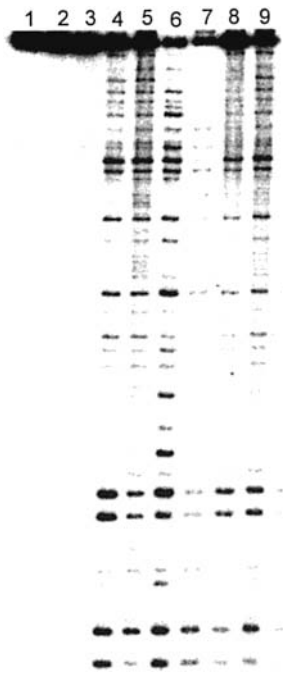


Figure 4. Cleavage of a 5′-^{32}P end-labeled 158-bp DNA fragment by **4** and resin-bound **4**. Lane 1: DNA alone; lane 2: 10 μM **4**; lane 3: 10 μM Fe^{2+}; lane 4: 1 μM **4** + 10 μM Fe^{2+}; lane 5: 10 μM **4** + 10 μM Fe^{2+}; lane 6: 0.1 μM BLM A_5 +10 μM Fe^{2+}; lane 7: 1 μM BLM A_5 +10 μM Fe^{2+}; lane 8: 10 μM resin-bound **4** + 10 μM Fe^{2+}; lane 9: 100 μM resin-bound **4** + 10 μM Fe^{2+}.

Their potencies of DNA cleavage assayed on a polyacrylamide gel (Figure 3) were the same, as had been noted in the supercoiled plasmid DNA relaxation assay (Figure 1). Further, assay of BLM **3** in direct comparison with

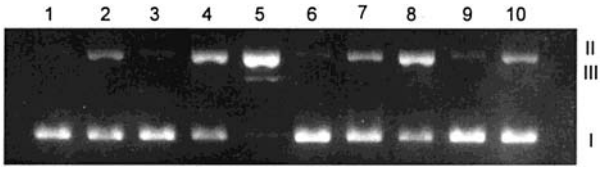


Figure 5. Relaxation of supercoiled pSP64 DNA by **1** and resin-bound **1**. Lane 1: DNA alone; lane 2: 1.5 μM Fe^{2+}; lane 3: 3 μM deglycoBLM A_2; lane 4: 1 μM deglycoBLM A_2 + 1.5 μM Fe^{2+}; lane 5: 3 μM deglycoBLM A_2 + 1.5 μM Fe^{2+}; lane 6: 3 μM **1**; lane 7: 1 μM **1** + 1.5 μM Fe^{2+}; lane 8: 3 μM **1** + 1.5 μM Fe^{2+}; lane 9: 10 μM resin-bound **1**; lane 10: 10 μM resin-bound **1** + 1.5 μM Fe^{2+}.

authentic deglycoBLM A_5, with which it was putatively identical, resulted in the same pattern and potency of cleavage of the 158-base pair DNA substrate when the BLMs were employed at each of two different concentrations (Supporting Information Figure 2).

Finally, comparison of deglycoBLM analogue **4** with BLM A_5 indicated good potency of cleavage by both (Figure 4), although the range of concentrations tested was not designed to permit a definitive assessment of the relative cleavage potencies of these two species.

DNA Cleavage Mediated by Resin-Bound DeglycoBLM Analogues. The successful synthesis of fully deprotected resin-bound deglycoBLM analogues has permitted an assessment of the ability to characterize these BLM analogue conjugates as DNA cleaving agents directly (*37*). It was anticipated that on-resin characterization might prove difficult for any of a few different reasons. These include simple lack of accessibility of the ligand to the target, as noted previously (*49*). Our earlier finding that BLMs tethered to each of two solid supports by linkers of three different lengths could all mediate DNA cleavage (*51, 52*) argued that the accessibility problem could be overcome by an appropriate choice of linkers. Potentially more serious was the observation that the attachment of BLM A_5 to a solid support resulted in a severalfold diminution in the potency of cleavage (*51, 52*). This effect was attributed to the attachment of BLMs to beads whose concentration in solution was (10^{12}−10^{13}-fold) lower than that usually employed for DNA cleavage by BLM, thus possibly diminishing the efficiency of encounter of BLMs by the DNA substrate. Since BLM A_5 was attached to the solid supports by utilizing a side chain amine to form an amide bond, it is also the case that the number of positively charged groups on the C-substituent would be reduced from 2 to 1; as illustrated in Figure 1, this could also potentially affect the efficiency of DNA binding and cleavage (*62, 63*). Accordingly, we sought to assess the DNA cleaving characteristics of deglycoBLM analogues having different numbers of positively charged functionalities within their C-substituents when the analogues were tested in resin-free or resin-bound form.

As shown in Figure 5, resin-bound deglycoBLM **1** gave only minimal cleavage of supercoiled plasmid DNA even when employed at high (i.e., 10 μM) concentration. An analogous effect was observed when resin-bound **1** was used in the presence of a ^{32}P-end labeled DNA duplex; no significant cleavage was observed in the presence of 200 μM resin-bound **1** + 30 μM Fe^{2+} (Figure 2). In comparison, the resin-free **1** gave detectable cleavage in the presence of 1.5 μM free **1** + 15 μM Fe^{2+}, and strong cleavage when 15 μM concentrations of free **1** and Fe^{2+} were present (Figure 2). Thus, attachment of this analogue to a solid support resulted in a much greater diminution in cleavage potency than had been observed previously for BLM A_5 (*51, 52*).

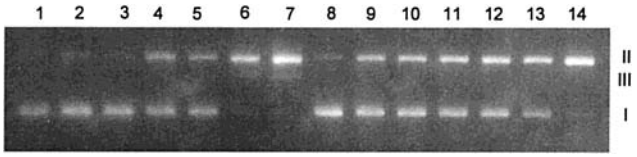


Figure 6. Relaxation of supercoiled pSP64 plasmid DNA by **4** and resin-bound **4**. Lane 1: DNA alone; lane 2: 1.5 μM Fe^{2+}; lane 3: 5 μM **4**; lane 4: 0.5 μM **4** + 1.5 μM Fe^{2+}; lane 5: 1 μM **4** + 1.5 μM Fe^{2+}; lane 6: 3 μM **4** + 1.5 μM Fe^{2+}; lane 7: 5 μM **4** + 1.5 μM Fe^{2+}; lane 8: 50 μM resin-bound **4**; lane 9: 0.5 μM resin-bound **4** + 1.5 μM Fe^{2+}; lane 10: 1 μM resin-bound **4** + 1.5 μM Fe^{2+}; lane 11: 3 μM resin-bound **4** + 1.5 μM Fe^{2+}; lane 12: 5 μM resin-bound **4** + 1.5 μM Fe^{2+}; lane 13: 10 μM resin-bound **4** + 1.5 μM Fe^{2+}; lane 14: 50 μM resin-bound **4** + 1.5 μM Fe^{2+}.

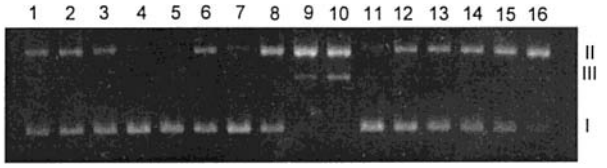


Figure 7. Relaxation of supercoiled pSP64 plasmid DNA cleavage by **3**, resin-bound **3** and resin-bound **4**. Lane 1: 100 μM resin-bound **3** + 1.5 μM Fe^{2+}; lane 2: 50 μM resin-bound **3** + 1.5 μM Fe^{2+}; lane 3: 10 μM resin-bound **3** + 1.5 μM Fe^{2+}; lane 4: 100 μM resin-bound **3**; lane 5: DNA alone; lane 6: 1.5 μM Fe^{2+}; lane 7: 5 μM **3**; lane 8: 1 μM **3** + 1.5 μM Fe^{2+}; lane 9: 3 μM **3** + 1.5 μM Fe^{2+}; lane 10: 5 μM **3** + 1.5 μM Fe^{2+}; lane 11: 50 μM resin-bound **4**; lane 12: 1 μM resin-bound **4** + 1.5 μM Fe^{2+}; lane 13: 5 μM resin-bound **4** + 1.5 μM Fe^{2+}; lane 14: 10 μM resin-bound **4** + 1.5 μM Fe^{2+}; lane 15: 25 μM resin-bound **4** + 1.5 μM Fe^{2+}; lane 16: 50 μM resin-bound **4** + 1.5 μM Fe^{2+}.

Although deglycoBLM analogues **2** and **3** exhibited greater potency than **1** in relaxing supercoiled plasmid DNA (Figure 1), these analogues also gave disappointing results when tested in their resin-bound forms. As shown in Figure 3, in the presence of 10 μM Fe^{2+}, analogues **2** and **3** gave readily detectable sequence selective DNA cleavage at 1 and 10 μM concentrations. In comparison, resin-bound **2** and **3** gave much weaker cleavage at all tested concentrations; the former species was utilized at concentrations up to 100 μM in the presence of 10 μM Fe^{2+}. Although **2** and **3** are formally analogues of BLM A_5, the conjugates of which do produce strong DNA cleavage in resin-bound form (*51, 52*), the (2−3-fold) diminution of DNA cleavage potency known to result from the absence of the BLM disaccharide moiety (*13*−*15*) was sufficient to compromise the ability of resin-bound **2** and **3** to produce a useful level of DNA damage.

In contrast, resin-bound **4** cleaved DNA very efficiently. A plasmid DNA relaxation assay (Figures 6 and 7) revealed that, in the presence of 1.5 μM Fe^{2+}, resin-bound **4** degraded the substrate significantly even at low micromolar concentrations (Figure 7, lanes 9−12) and completely degraded the DNA at 50 μM concentration. The potency of DNA cleavage by resin-bound **4** was further confirmed by high-resolution gel electrophoresis analysis of a 5′-^{32}P end labeled 158 base pair DNA fragment that had been treated with resin-bound **4**. As is clear from Figure 4, resin-bound **4** (lanes 8 and 9) cleaved the duplex with the same sequence selectivity and comparable potency as resin-free **4** (lanes 4 and 5) and natural BLM A_5 (lanes 6 and 7). The difference in potencies of DNA cleavage by resin-free and resin-bound analogue **4** was clearly less than 10-fold, demonstrating the ability of additional positively charged groups in the C-substituent to compensate for the absence of the BLM disaccharide moiety, as well as the attachment of the analogue to the TentaGel resin. It may be noted also that

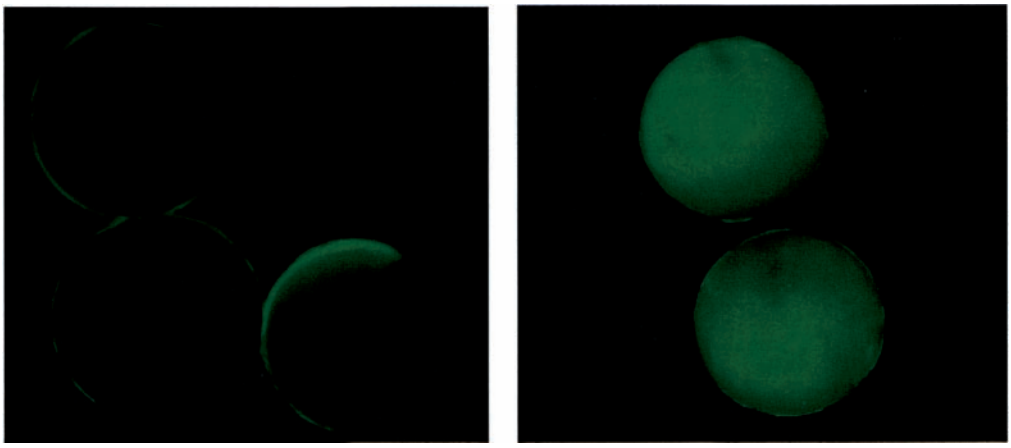


Figure 8. Fluorescence microscopy of TentaGel beads containing conjugated Fe(II)·deglycoBLM **4**. The images were recorded prior to Fe^{2+} addition (left) and 30 min after Fe^{2+} addition (right).

the sequence selectivity of DNA cleavage by resin-bound **4** was identical with that of resin-free **4** (Figure 4).

To evaluate the relative importance of the number of positive charges in the C-substituent vs conjugation to a resin on the efficiency of DNA cleavage, the ability of free **3** to effect plasmid DNA relaxation was compared to that of resin-bound **3** and resin-bound **4**. Resin-bound **3** has one fewer positively charged group than unbound **3** at physiological pH, while resin-bound **4** should have the same number as free **3**. As shown in Figure 7, neither resin-bound BLM analogue was nearly so potent as free **3** in effecting DNA relaxation, but resin-bound **4** was significantly more efficient than resin-bound **3**. Thus actual conjugation of a BLM to a solid support would seem to lower the efficiency of DNA cleavage primarily for reasons of localization of BLM to the (very small number of) resin beads, rather than by reducing the number of positively charged groups within the C-substituent. Nevertheless, it is clear from the foregoing results that the incorporation of additional positively charged groups can be effective in compensating for the loss of overall cleavage efficiency and can do so without altering the sequence selectivity of DNA cleavage. Resin-bound **4** exhibited strong DNA cleavage, indicating that the spermine-based linker in this analogue should be sufficient to permit the evaluation of many (deglyco)BLM analogues while they are still bound to the resin employed for their elaboration.

Molecular Beacon Assay Utilizing Fluorescence Microscopy. DNA cleavage by TentaGel-conjugated BLM **4** was also monitored by molecular beacon assay utilizing fluorescence microscopy (*37, 67*). A molecular beacon designed for bleomycin cleavage was shown to fluoresce following BLM-mediated DNA cleavage (*67*). The sequence of the molecular beacon used for the microscopy was 5′d($CGCT_3A_7GCG$); the beacon contained the fluorophore carboxyfluorescein (FAM) at the 5′-end and the "Black Hole Quencher" (BHQ) at the 3′-end. Though DABCYL has been used routinely as a quencher for commonly used fluorophores (*68*−*70*), the quenching efficiency is sometimes not high due to poor spectral overlap with the fluorescent dye (*71*). A new class of quencher, BHQ dye, has an absorption spectrum essentially superimposable with the emission maximum of FAM, and thus provided a significant increase in fluorescence resonance energy transfer (FRET). Therefore, a molecular beacon made with this quencher exhibited very low background fluorescence, enabling enhanced detection sensitivity. Beacon cleavage for visualization was carried out with the TentaGel embedded in an agarose gel medium to retard diffusion of the formed fluorescent cleavage products from the gel. Figure 8 shows the fluorescence images of beacon DNA cleavage by deglycoBLM A_6 without added Fe^{2+}, and 30 min after the addition of Fe^{2+}. As can be seen from the figure, fluorescence emission from each gel increased markedly after the addition of Fe^{2+}; the increase was also time dependent (not shown). The fluorescence intensity reached a maximum after about 40 min. No significant fluorescence increase was observed for beacon DNA treated with Fe^{2+} + TentaGel lacking a BLM A_6 moiety. These results demonstrate that beacon DNA cleavage by Fe(II)·BLM **4** can be monitored visually on individual beads, thus enabling the monitoring of BLM libraries elaborated on beads by split and mix synthesis.

ACKNOWLEDGMENT

We thank Michael Rishel for the β-hydroxyhistidine derivative employed in this study, and Dr. Ammasi Periasamy and Colten Noakes of the University of Virginia W. M. Keck Center for Cellular Imaging for technical assistance with the fluorescence microscopy. This work was supported by NIH Research Grants CA76297 and CA77284, awarded by the National Cancer Institute.

Supporting Information Available: Gel electrophoreses of the cleavage of a 5′-^{32}P end-labeled 158-bp DNA by **3** and synthetic deglycoBLM **1**. This material is available free of charge via the Internet at http://pubs.acs.org.

LITERATURE CITED

(1) Hecht, S. M. (1995) Bleomycin-group antitumor agents. *Cancer Chemotherapeutic Agents* (Foye, W. O., Ed.) pp 369−388, American Chemical Society, Washington, DC.
(2) Hecht, S. M. (2000) Bleomycin: new perspectives on the mechanism of action. *J. Nat. Prod. 63*, 158−168.
(3) Sikic, B. I., Rozencweig, M., and Carter, S. K., Eds. (1985) *Bleomycin Chemotherapy*, Academic Press, New York.
(4) Hecht, S. M. (1986) The chemistry of activated bleomycin. *Acc. Chem. Res. 19*, 383−391.
(5) Kozarich, J. W., and Stubbe, J. (1987) Mechanism of bleomycin-induced DNA degradation. *Chem. Rev. 87*, 1107−1136.
(6) Natrajan, A., and Hecht, S. M. (1993) Bleomycin: mechanism of polynucleotide recognition and oxidative degradation. *Molecular Aspects of Anticancer Drug−DNA Interactions* (Neidle, S., Waring, M. J., Eds.) pp 197−242, Macmillan, London.

(7) Kane, S. A., and Hecht, S. M. (1994) Polynucleotide recognition and degradation by bleomycin. *Prog. Nucl. Acid Res. Mol. Biol. 49*, 313−352.

(8) Burger, R. M. (1998) Cleavage of nucleic acids by bleomycin. *Chem. Rev. 98*, 1153−1169.

(9) Claussen, C. A., and Long, E. C. (1999) Nucleic Acid Recognition by Metal Complexes of Bleomycin. *Chem. Rev. 99*, 2797−2816.

(10) Hecht, S. M. (1994) RNA degradation by bleomycin, a naturally occurring bioconjugate. *Bioconjugate Chem. 5*, 513−526.

(11) Holmes, C. D., Duff, R. J., van der Marel, G. A., van Boom, J., and Hecht, S. M. (1997) On the chemistry of RNA degradation by Fe-bleomycin. *Bioorg. Med. Chem. 5*, 1235−1248.

(12) Hecht, S. M. (1998) RNA as a therapeutic target for bleomycin. *The Many Faces of RNA* (Eggleston, D. S., Prescott, C. D., Pearson, N. D., Eds.) pp 3−17, Academic Press, San Diego.

(13) Aoyagi, Y., Suguna, H., Murugesan, N., Ehrenfeld, G. M., Chang, L.-H., Ohgi, T., Shekhani, M. S., Kirkup, M. P., and Hecht, S. M. (1982) Deglycobleomycin: total synthesis and oxygen transfer properties of an active bleomycin analogue. *J. Am. Chem. Soc. 104*, 5237−5239.

(14) Oppenheimer, N. J., Chang, C., Chang, L.-H., Ehrenfeld, G., Rodriguez, L. O., and Hecht, S. M. (1982) Deglycobleomycin: degradation of DNA and formation of a structurally unique Fe(II)CO complex. *J. Biol. Chem. 257*, 1606−1609.

(15) Sugiyama, H., Ehrenfeld, G. M., Shipley, J. P., Kilkuskie, R. E., Chang, L.-H., and Hecht, S. M. (1985) DNA strand scission by bleomycin group antibiotics. *J. Nat. Prod. 48*, 869−877.

(16) Takita, T., Umezawa, Y., Saito, S., Morishima, H., Umezawa, H., Muraoka, Y., Suzuki, M., Otsuka, M., Kobayashi, S., and Ohno, M. (1981) Total synthesis of deglyco-bleomycin A_2. *Tetrahedron Lett. 22*, 671−674.

(17) Saito, S., Umezawa, Y., Morishima, H., Takita, T., Umezawa, H., Narita, M., Otsuka, M., Kobayashi, S., and Ohno, M. (1982) A new synthesis of deglyco-bleomycin A_2 aiming at the total synthesis of bleomycin. *Tetrahedron Lett. 23*, 529−532.

(18) Ohno, M. (1989) From natural bleomycins to man-made bleomycins. *Pure Appl. Chem. 61*, 581−584.

(19) Ohno, M., Otsuka, M. (1990) Synthetic study on man-made bleomycin based on the anticancer mechanism of natural bleomycin. *Recent Progress in the Chemical Synthesis of Antibiotics* (Lukacs, G., Ohno, M., Eds.) pp 387−414, Springer-Verlag: New York.

(20) Owa, T., Haupt, A., Otsuka, M., Kobayashi, S., Tomioka, N., Itai, A., Ohno, M., Shiraki, T., Uesugi, M., Sugiura, Y., and Maeda, K. (1992) Man-designed bleomycins: significance of the binding sites as enzyme models and of the stereochemistry of the linker moiety. *Tetrahedron 48*, 1193−1208.

(21) Boger, D. L., Teramoto, S., and Cai, H. (1997) *N*-Methyl threonine analogues of deglycobleomycin A_2: synthesis and evaluation. *Bioorg. Med. Chem. 5*, 1577−1589.

(22) Boger, D. L., Ramsey, T. M., Cai, H., Hoehn, S. T., Kozarich, J. W., and Stubbe, J. (1998) Assessment of the role of the bleomycin A_2 pyrimidoblamic acid C4 amino group. *J. Am. Chem. Soc. 120*, 53−65.

(23) Boger, D. L., Ramsey, T. M., Cai, H., Hoehn, S. T., and Stubbe, J. (1998) A systematic evaluation of the bleomycin A_2 L-threonine side chain: its role in preorganization of a compact conformation implicated in sequence-selective DNA cleavage. *J. Am. Chem. Soc. 120*, 9139−9148.

(24) Boger, D. L., and Cai, H. (1999) Bleomycin: synthetic and mechanistic studies. *Angew. Chem., Int. Ed. 38*, 448−476.

(25) Boger, D. L., Aquila, B. M., Tse, W. C., and Searcey, M. (2000) Synthesis and evaluation of a novel bleomycin A_2 analogue: continuing assessment of the linker domain. *Tetrahedron Lett. 41*, 9493−9498.

(26) Guajardo, R. J., Hudson, S. E., Brown, S. J., and Mascharak, P. K. (1993) $[Fe(PMA)]^{n+}$ ($n = 1,2$): good models of Fe-bleomycins and examples of mononuclear non-heme iron complexes with significant O_2-activation capabilities. *J. Am. Chem. Soc. 115*, 7971−7977.

(27) Kilkuskie, R. E., Suguna, H., Yellin, B., Murugesan, N., and Hecht, S. M. (1985) Oxygen transfer by bleomycin analogues dysfunctional in DNA cleavage. *J. Am. Chem. Soc. 107*, 260−261.

(28) Shipley, J. B., and Hecht, S. M. (1988) Bleomycin congeners exhibiting altered DNA cleavage specificity. *Chem. Res. Toxicol. 1*, 25−27.

(29) Hamamichi, N., Natrajan, A., and Hecht, S. M. (1992) On the role of individual bleomycin thiazoles in oxygen activation and DNA cleavage. *J. Am. Chem. Soc. 114*, 6278−6291.

(30) Kane, S. A., Natrajan, A., and Hecht, S. M. (1994) On the role of the bithiazole moiety in sequence-selective DNA cleavage by Fe·bleomycin. *J. Biol. Chem. 269*, 10899−10904.

(31) Zuber, G., Quada, J. C., Jr., and Hecht, S. M. (1998) Sequence selective cleavage of a DNA octanucleotide by chlorinated bithiazoles and bleomycins. *J. Am. Chem. Soc. 120*, 9368−9369.

(32) Katano, K., An, H., Aoyagi, Y., Overhand, M., Sucheck, S. J., Stevens, W. C., Jr., Hess, C. D., Zhou, X., and Hecht, S. (1998) Total synthesis of bleomycin group antibiotics. Total syntheses of bleomycin demethyl A_2, bleomycin A_2, and decarbamoyl bleomycin demethyl A_2. *J. Am. Chem. Soc. 120*, 11285−11296.

(33) Choudhury, A. K., Tao, Z.-F., and Hecht, S. M. (2001) Synthesis and DNA cleavage activity of a novel bleomycin A_5 glycoconjugate. *Org. Lett. 3*, 1291−1294.

(34) Grigg, G. W., Hall, R. M., Hart, N. K., Kavulak, D. R., Lamberton, J. A., and Lane, A. (1985) Amplification of the antibiotic effects of the bleomycins, phleomycins and tallysomycins: its dependence of the nature of the variable basic groups. *J. Antibiot. 38*, 99−110.

(35) Oakley, M. G., Turnbull, K. D., and Dervan, P. B. (1994) Synthesis of a hybrid protein containing the iron-binding ligand of bleomycin and the DNA-binding domain of hin. *Bioconjugate Chem. 5*, 242−247.

(36) Leitheiser, C. J., Rishel, M. J., Wu, X. H., and Hecht, S. M. (2000) Solid-phase synthesis of bleomycin group antibiotics. Elaboration of deglycobleomycin A_5. *Org. Lett. 2*, 3397−3399.

(37) Smith, K. L., Tao, Z.-F., Hashimoto, S., Leitheiser, C. J., Wu, X., and Hecht, S. M. (2002) Deglycobleomycin: Solid-phase synthesis and DNA cleavage by the resin-bound ligand. *Org. Lett.*, in press.

(38) Lam, K. S., Lebl, M., and Krchňák, V. (1997) The "one-bead-one-compound" combinatorial library method. *Chem. Rev. 97*, 411−448.

(39) Guillier, F., Orain, D., and Dradly, M. (2000) Linker and cleavage strategies in solid-phase organic synthesis and combinatorial chemistry. *Chem. Rev. 100*, 2091−2157.

(40) Wendeborn, S., De Mesmaeker, A., Brill, W. K.-D., and Berteina, S. (2000) Synthesis of diverse and complex molecules on the solid phase. *Acc. Chem. Res. 33*, 215−224.

(41) Toy, P. H., and Janda, K. D. (2000) Soluble polymer-supported organic synthesis. *Acc. Chem. Res. 33*, 546−554.

(42) Hall, D. G., Manku, S., and Wang, F. (2001) Solution- and solid-phase strategies for the design, synthesis, and screening of the libraries based on natural product templates: A comprehensive survey. *J. Comb. Chem. 3*, 125−150.

(43) Comely, A. C., and Gibson, S. E. (2001) Tracelessness unmasked: A general linker nomenclature. *Angew. Chem., Int. Ed. 40*, 1012−1032.

(44) Meldal, M., Svendsen, I., Breddam, K., and Auzanneau, F.-I. (1994) Portion-mixing peptide libraries of quenched fluorogenic substrates for complete subsite mapping of endoprotease specificity. *Proc. Natl. Acad. Sci. U.S.A. 91*, 3314−3318.

(45) Youngquist, R. S., Fuentes, G. R., Lacey, M. P., and Keough, T. (1995) Generation and screening of combinatorial peptide libraries designed for rapid sequencing by mass spectrometry. *J. Am. Chem. Soc. 117*, 3900−3906.

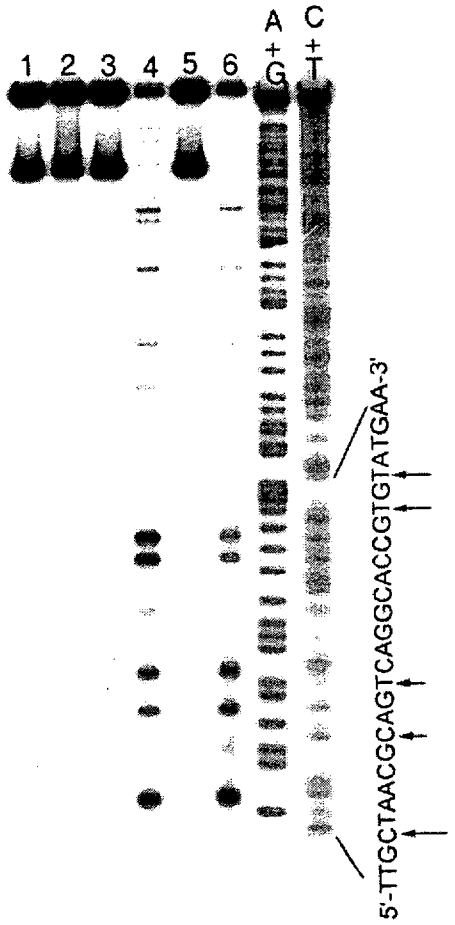
(46) Campbell, D. A., Bermak, J. C., Burkoth, T. S., and Patel, D. V. (1995) A transition state analogue inhibitor combinatorial library. *J. Am. Chem. Soc. 117*, 5381−5382.
(47) Bastos, M., Maeji, N. J., and Abeles, R. H. (1995) Inhibitors of human heart chymase based on a peptide library. *Proc. Natl. Acad. Sci. U.S.A. 92*, 6738−6742.
(48) Still, W. C. (1996) Discovery of sequence-selective peptide binding by synthetic receptors using encoded combinatorial libraries. *Acc. Chem. Res. 29*, 155−163.
(49) Smith, H. K., and Bradley, M. (1999) Comparison of resin and solution screening methodologies in combinatorial chemistry and the identification of a 100 nM inhibitor of trypanothione reductase. *J. Comb. Chem. 1*, 326−332.
(50) Papanikos, A., Rademann, J., and Medal, M. (2001) α-Ketocarbonyl peptides: A general approach to reactive resin-bound intermediates in the synthesis of peptide isosteres for protease inhibitor screening on solid support. *J. Am. Chem. Soc. 123*, 2176−2181.
(51) Abraham, A. T., Zhou, X., and Hecht, S. M. (1999) DNA cleavage by Fe(II)-bleomycin conjugated to a solid support. *J. Am. Chem. Soc. 121*, 1982−1983.
(52) Abraham, A. T., Zhou, X., and Hecht, S. M. (2001) Metallobleomycin-mediated cleavage of DNA not involving a threading intercalation mechanism. *J. Am. Chem. Soc. 123*, 5167−5175.
(53) Maxam, A. M., and Gilbert, W. (1980) Sequencing end-labeled DNA with base-specific chemical cleavages. *Methods Enzymol. 65*, 499−560.
(54) Bycroft, B. W., Chan, W. C., Hone, N. D., Millington, S., and Nash, I. A. (1994) Synthesis of the Spider Toxins Nephilatoxin-9 and -11 by a Novel Solid-Phase Strategy. *J. Am. Chem. Soc. 116*, 7415−7416.
(55) Chhababra, S. R., Khan, A. N., and Bycroft, B. W. (1998) Versatile Dde-based primary amine linkers for solid-phase synthesis. *Tetrahedron Lett. 39*, 3585−3588.
(56) Geall, A. J., and Blagbrough, I. S. (2000) Homologation of polyamines in the rapid synthesis of lipospermine conjugates and related lipoplexes, *Tetrahedron 56*, 2449−2460.
(57) Kaiser, E., Colescott, R. L., Bossinger, C. D., and Cook, P. I. (1970) Color test for detection of three terminal amino groups in the solid-phase synthesis of peptides. *Anal. Biochem. 34*, 595−598.
(58) Krchňák, V., Vagner, J., Safar, P., and Lebl, M. (1988) Amino acids and peptides 206. Noninvasive continuous monitoring of solid-phase peptide-synthesis by acid−base indicator. *Collect. Czech. Chem. Commun. 53*, 2542−2548.
(59) Aoyagi, Y., Chorghade, M. S., Padmapriya, A. A., Suguna, H., and Hecht, S. M. (1990) Synthesis of pyrimidoblamic acid and epipyrimidoblamic acid. *J. Org. Chem. 55*, 6291−6298.
(60) Umezawa, Y., Morishima, H., Saito, S., Takita, T., and Umezawa, H. (1980) Synthesis of the pyrimidine moiety of bleomycin. *J. Am. Chem. Soc. 102*, 6630−6631.
(61) Boger, D. L., Honda, T., and Dang, Q. (1994) Total synthesis of bleomycin A_2 and related agents. 2. Synthesis of (−)-pyrimidoblamic acid, *epi*-(+)-pyrimidoblamic acid, (+)-desacetamidopyrimidoblamic acid, and (−)-descarboxamidopyrimidoblamic acid. *J. Am. Chem. soc. 116*, 5619−5630.
(62) Kross, J., Henner, D. W., Hecht, S. M., Haseltine, W. A., Rodriguez, L., and Levin, M. D. (1982) Structural basis for the deoxyribonucleic acid affinity of the bleomycins. *Biochemistry 21*, 3711−3721.
(63) Berry, D. E., Chang, L.-H., and Hecht, S. M. (1985) DNA damage and growth inhibition in cultured human cells by bleomycin congeners. *Biochemistry 24*, 3207−3214.
(64) Boger, D. L., Teramoto, S, and Cai, H. (1996) Synthesis and evaluation of deglycobleomycin A_2 analogues containing a tertiary *N*-methyl amide and simple ester replacement for the L-histidine secondary amide: Direct functional characterization of the requirement for secondary amide metal complexation. *Bioorg. Med. Chem. 4*, 179−193.
(65) Kross, J., Henner, D. W., Hecht, S. M., and Haseltine, W. A. (1982) Specificity of deoxyribonucleic acid cleavage by bleomycin, phleomycin and tallysomycin. *Biochemistry 21*, 4310−4318.
(66) Kenani, A., Lamblin, G., and Hénichart, J. P. (1988) A convenient method for the cleavage of the D-mannosyl-L-glucose disaccharide from bleomycin A_2. *Carbohydr. Res. 177*, 81−89.
(67) Hashimoto, S., Wang, B., and Hecht, S. M. (2001) Kinetics of DNA cleavage by Fe(II)•bleomycins. *J. Am. Chem. Soc. 123*, 7437−7438.
(68) Tyagi, S., and Kramer, F. R. (1996) Molecular beacons: probes that fluoresce upon hybridization. *Nat. Biotechnol. 14*, 303−308.
(69) Tyagi, S., Bratu, D., and Kramer, F. R. (1998) Multicolor molecular beacons for allele discrimination. *Nat. Biotechnol 16*, 49−53.
(70) Biggins, J. B., Prudent, J. R., Marshall, D. J., Ruppen, M., and Thorson, J. S. (2000) A continuous assay for DNA cleavage: the application of "break lights" to enediynes, iron-dependent agents, and nucleases. *Proc. Natl. Acad. Sci. U.S.A. 97*, 13537−13542.
(71) Haugland, R. P. (1999) *Handbook of Fluorescent Probes and Research Chemicals*, 7th ed., Molecular Probes, Inc., Eugene, OR.

BC010083O

Figure 1S. Cleavage of a 5'-^{32}P end-labeled 158 base-pair DNA duplex by synthetic deglycoBLM **1** in the presence of Fe^{2+}. Lane 1, DNA alone; lane 2, 15 μM Fe^{2+}; lane 3, 15 μM deglycoBLM **1**; lane 4, 15 μM deglycoBLM **1** + 15 μM Fe^{2+}; lane 5, 15 μM deglycoBLM A_2; lane 6, 15 μM deglycoBLM A_2 + 15 μM Fe^{2+}.

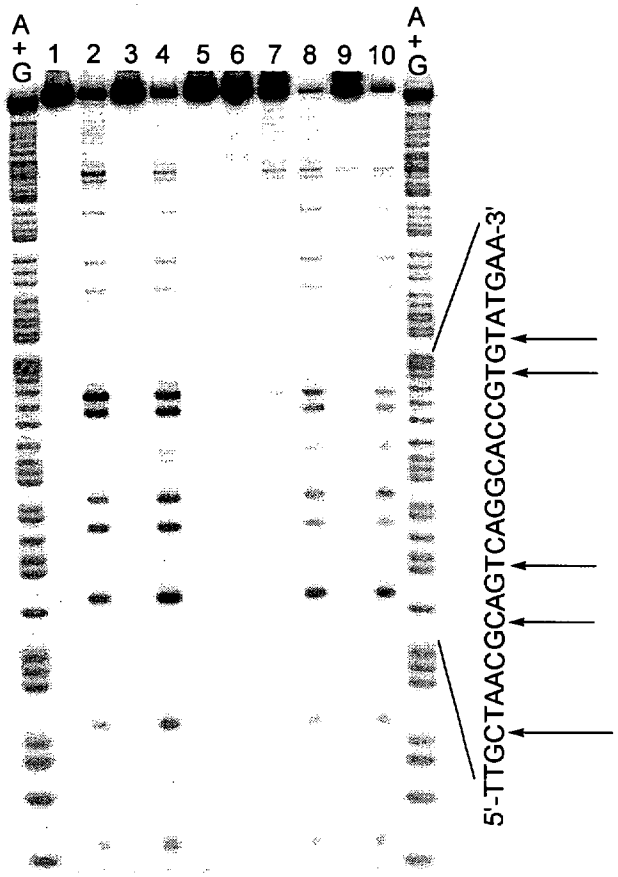
Figure 2S. Cleavage of a 5'-^{32}P end-labeled 158-bp DNA fragment cleavage by **3**. Lane 1: 1 μM **3**; lane 2: 1 μM **3** + 1 μM Fe^{2+}; lane 3: 1 μM deglycoBLM A_5; lane 4: 1 μM deglycoBLM A_5 + 1 μM Fe^{2+}; lane 5: DNA alone; lane 6: 10 μM Fe^{2+}; lane 7: 10 μM **3**; lane 8: 10 μM **3** + 10 μM Fe^{2+}; lane 9: 10 μM deglycoBLM A_5; lane 10: 10 μM deglycoBLM A_5 + 10 μM Fe^{2+}.

Figure 1S



3

Figure 2S



Boron-Containing Folate Receptor-Targeted Liposomes as Potential Delivery Agents for Neutron Capture Therapy

Xing Q. Pan,[#] Huaqing Wang,[#] Supriya Shukla,[#] Masaru Sekido,[#] Dianne M. Adams,[⊥] Werner Tjarks,[#] Rolf F. Barth,[⊥] and Robert J. Lee*[,#]

College of Pharmacy and Department of Pathology, The Ohio State University, Columbus, Ohio 43210. Received September 21, 2001; Revised Manuscript Received December 14, 2001

Boron neutron capture therapy (BNCT) depends on the selective delivery of a sufficient number of ^{10}B atoms to tumor cells to sustain a lethal $^{10}B(n,\alpha)^7Li$ reaction. Expression of FR frequently is amplified among human tumors. The goal of the present study was to investigate folate receptor (FR)-targeted liposomes as potential carriers for a series of boron-containing agents. Two highly ionized boron compounds, $Na_2[B_{12}H_{11}SH]$ and $Na_3(B_{20}H_{17}NH_3)$, were incorporated into liposomes by passive loading with encapsulation efficiencies of 6% and 15%, respectively. In addition, five weakly basic boronated polyamines were investigated. Two were the spermidine derivatives: N^5-(4-carboranylbutyl)spermidine·3HCl (SPD-5), N^5-[4-(2-aminoethyl-*o*-carboranyl)butyl]spermidine·4HCl (ASPD-5). Three were the spermine derivatives: N^5-(4-carboranylbutyl)spermine·4HCl (SPM-5), N^5-[4-(2-aminoethyl-*o*-carboranyl)-butyl]spermine·5HCl (ASPM-5), and N^5,N^{10}-bis(4-carboranylbutyl)spermine·4 HCl (SPM-5,10). These were incorporated into liposomes by a pH-gradient-driven remote-loading method with varying loading efficiencies, which were influenced by the specific trapping agent and the structure of the boron compound. Greater loading efficiencies were obtained with lower molecular weight boron derivatives, using ammonium sulfate as the trapping agent, compared to those obtained with sodium citrate. The in vitro uptake of folate-derivatized, boronated liposomes was investigated using human KB squamous epithelial cancer cells, which have amplified FR expression. Higher cellular boron uptake (up to 1584 μg per 10^9 cells) was observed with FR-targeted liposomes than with nontargeted control liposomes (up to 154 μg per 10^9 cells), irrespective of the chemical form of the boron and the method used for liposomal preparation. KB cell binding of the FR-targeted liposomes was saturable and could be blocked by 1 mM free folic acid. Our findings suggest that further evaluation of FR-targeted liposomes is warranted to assess their potential as boron carriers for neutron capture therapy.

INTRODUCTION

Boron neutron capture therapy (BNCT) currently is being evaluated as a modality for the treatment of primary and metastatic brain tumors and cutaneous and metastatic melanoma (Soloway et al., 1997; Barth et al., 1999; Hawthorne, 1998; Mishima et al., 2001). The effectiveness of BNCT depends on the selective accumulation of a sufficient concentration of the stable isotope, ^{10}B, in cancer cells, followed by neutron irradiation. The resulting nuclear reaction ($^{10}B[n,\alpha]^7Li$) yields tumoricidal high linear energy transfer (LET) α particles and recoiling ^7Li nuclei. Our efforts to improve the efficacy of BNCT have concentrated on (i) the development of novel boronated agents that have high boron content and exhibit selective uptake by tumor cells and favorable subcellular distribution (Soloway et al., 1997; Capala et al., 1996 and 1997) and (ii) methods to optimize the delivery of the two drugs that currently are being used clinically for BNCT: sodium borocaptate ($Na_2B_{12}H_{11}SH$ or BSH) and boronophenylalanine (BPA) (Barth et al., 1997 and 2000; Yang et al., 1997 and 2000). To maximize boron content, BNCT agents often consist of derivatives of one or more carborane cages, which contain 10 boron atoms. Boronated polyamines are potential delivery agents for BNCT due to their DNA-binding properties (Zhuo et al., 1999; Cai et al., 1997). The structures of a series of such derivatives, including two spermidine derivatives SPD-5 and ASPD-5, and three spermine derivatives SPM-5, ASPM-5, and SPM-5,10 (with two carborane cages), are shown in Figure 1. The polyamine moiety and, when present, the extra amino group provide hydrophilicity and aqueous solubility to these constructs. In contrast, the carboranyl moieties provide high molecular boron content, lipophilicity, and potential bilayer permeability upon deprotonation of the amino groups. Recently, a series of DNA-binding carborane-derivatized polyamines have been synthesized to facilitate the targeting of cellular DNA (Cai et al., 1997; Zhuo et al., 1999). Due to their superior boron-carrying capacity, Hawthrone and Shelly (1997) have carried out extensive studies on the incorporation of a variety of boronated agents into liposomes. The tumor-selective accumulation of boronated liposomes potentially can be further enhanced by introducing poly(ethylene glycol) (PEG)-derivatized lipids into the lipid bilayer to extend their systemic circulation time and a targeting ligand to increase selective tumor cell uptake (Yanagie et al., 2000).

FR, also known as the folate binding protein, is a glycosyl-phosphatidylinositol (GPI)-anchored membrane glycoprotein, which exhibits highly restricted normal

* Address correspondence to this author at College of Pharmacy, The Ohio State University, 542 Parks Hall, 500 W. 12th Ave., Columbus, OH 43210. Phone: (614) 292−4172; fax (614) 292−7766. e-mail: lee.1339@osu.edu.

[#] College of Pharmacy, The Ohio State University.

[⊥] Department of Pathology, The Ohio State University.

10.1021/bc015557y CCC: $22.00 © 2002 American Chemical Society
Published on Web 03/15/2002

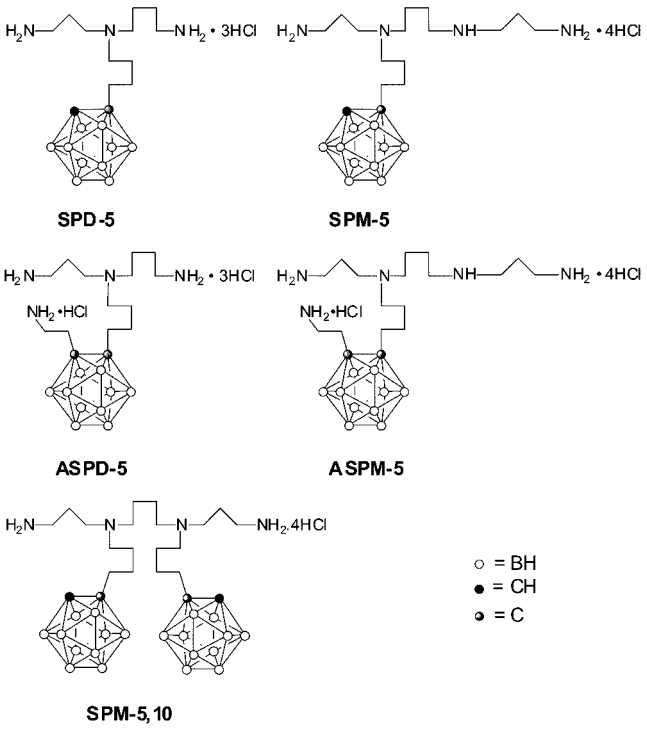


Figure 1. Structures of boronated polyamine derivatives that were studied.

tissue distribution, and is amplified in a variety of human cancers (Antony, 1996). Folic acid has been shown to retain its high affinity ($K_a \sim 10^{10}$ M^{-1}) for FR upon derivatization via its γ-carboxyl (Leamon and Low, 1991). Folate-derivatized bioconjugates, including liposomal drug carriers, have been successfully selectively targeted to FR-α in ovarian and other cancers, in which FR is overexpressed (Sudimack and Lee, 2000; Reddy and Low, 1998). Folate can be incorporated into liposomes via conjugation to either a phospholipid or a cholesterol anchor (Lee and Low, 1994; Gabizon et al., 1999, Guo et al., 2000). Passive and remote loading (Muggia, 2001) have been used to incorporate hydrophilic molecules into liposomes. The former is based on producing the liposomes in an aqueous solution of the molecule of interest, thereby encapsulating it in the entrapped volume. Typically, this method has limited encapsulation efficiency. In contrast, the remote loading method relies on the establishment of a transbilayer pH gradient in preformed liposomes, which contain a "trapping" agent consisting of a counterion (Nichols and Deamer, 1976; Johnsson et al., 1999) and often yields near-quantitative drug loading. Remote loading, however, is only applicable to weakly basic molecules that exhibit membrane permeability at a slightly basic pH, e.g., anthracyclines doxorubicin and daunorubicin (Muggia, 2001).

In the present study a series of boron containing polyamine derivatives have been incorporated into liposomes targeted to the tumor cells via the folate receptor (FR). Following this, we have evaluated the liposomal loading efficiency and in vitro tumor cell binding properties of a series of boronated compounds, including the anionic agents BSH and $Na_3(B_{20}H_{17}NH_3)$ (Feakes et al., 1994; Shelly et al., 1992) and cationic boronated polyamines. Two were the spermidine derivatives N^5-(4-carboranylbutyl)spermidine·3HCl (SPD-5) and N^5-[4-(2-aminoethyl-*o*-carboranyl)butyl]spermidine·4HCl (ASPD-5). Three were the spermine derivatives N^5-(4-carboranylbutyl)spermine·4HCl (SPM-5), N^5-[4-(2-aminoethyl-*o*-carboranyl)butyl]spermine·5HCl (ASPM-5), and N^5,N^{10}-bis(4-carboranylbutyl)spermine·4HCl (SPM-5,10) (Zhuo et al., 1999; Cai et al., 1997). The anionic agents and cationic boronated polyamines were incorporated into liposomes by passive entrapment and remote loading, respectively. Higher cellular uptake was observed with FR-targeted liposomes than with nontargeted liposomes irrespective of the chemical form of the boron and the method used in liposomal preparation. A detailed description of these findings is presented in the following report.

EXPERIMENTAL PROCEDURES

Reagents. BSH was purchased from Centronic Ltd. (Croydon,U.K). Na_3 ($B_{20}H_{17}NH_3$) was kindly provided by Drs. M. Frederick Hawthorne and Kenneth Shelly in the Department of Chemistry at the University of California at Los Angeles; boronated polyamines, including the two spermidine derivatives N^5-(4-carboranylbutyl)spermidine·3HCl (SPD-5) and N^5-[4-(2-aminoethyl-*o*-carboranyl)-butyl]spermidine·4HCl (ASPD-5), and the three spermine derivatives N^5-(4-carboranylbutyl)spermine·4HCl (SPM-5), N^5-[4-(2-aminoethyl-*o*-carboranyl)butyl]spermine·5HCl (ASPM-5), and N^5,N^{10}-bis(4-carboranylbutyl)spermine·4HCl (SPM-5,10) were synthesized in our laboratories as reported previously (Zhuo et al., 1999; Cai et al., 1997). Egg phosphatidylcholine was purchased from Avanti Polar Lipids (Alabaster, AL). PEG900-Cholesterol (PEG-Chol) was purchased from Fluka Chemical Co. (Milwaukee, WI). Folic acid and cholesterol (Chol) were purchased from Sigma Chemical Co. (St. Louis, MO). Folate-free RPMI 1640 medium and other tissue culture reagents were purchased from Gibco-BRL (Grand Island, NY). BCA Protein Assay Kit was purchased from Pierce Chemical Co. (Rockford, IL). Folate−poly(ethylene glycol) (MW $\sim$ 3350)−distearoyl phosphatidylethanolamine (folate−PEG−DSPE) was synthesized as described previously (Lee and Low, 1995). The final folate−PEG−DSPE product was purified on a silica gel (70−200 mesh) using a solvent gradient of 15 to 80% methanol in CH_2Cl_2. Product purity was confirmed by thin-layer chromatography analysis on silica gel GF (75:36:6 chloroform/methanol/water), as described previously (Gabizon et al., 1999) and showed a single spot ($R_f = 0.61$).

Cell Culture. KB human cancer cells (American Type Culture Collection # CCL 17), derived from an epidermal carcinoma of the oral cavity, were obtained as a gift from Dr. Philip S. Low at Purdue University (West Lafayette, IN). The cells were maintained in folate-free RPMI 1640 medium supplemented with 100 units/mL penicillin, 100 μg/mL streptomycin, and 5% fetal bovine serum, which provides the only source of folate. The cells were cultured as a monolayer in a humidified atmosphere containing 5% CO_2 at 37 °C.

Liposome Preparation. Small unilamellar vesicles (SUVs) were prepared by high-pressure polycarbonate membrane extrusion, as previously described (Lee and Low, 1995). Briefly, a lipid mixture of the desired composition (including folate−PEG−DSPE for the FR-targeted formulation), containing 30 mg of total phospholipids, was dissolved in chloroform, dried into a thin film under a stream of nitrogen, and then desiccated under vacuum for another 30 min. Boronated agents then were loaded into liposomes by either passive entrapment (during liposome formation) or remote loading (after liposome formation), as described in the following sections.

Passive Entrapment. The dried lipids were hydrated in a 0.5 mL of aqueous solution containing the boronated compound (5 mg/mL BSH or 16.5 mg/mL Na_3 ($B_{20}H_{17}$-

NH_3)). To facilitate lipid hydration, the mixture was subjected to vortex mixing followed by brief sonication in a bath sonicator and six cycles of freezing and thawing, which resulted in the formation of a heterogeneous population of lipidic vesicles. These were manually extruded six times through a 100-nm pore-size polycarbonate membrane using a handheld LiposoFast extruder (Avestin Inc., Ottawa, Canada) attached to two 0.5-mL gastight syringes. The resulting SUVs were purified from nonentrapped molecules by size exclusion chromatography on a 10 mL Sepharose CL-4B column (Sigma Chemical Co., St. Louis, MO) preequilibrated in a buffer consisting of 10 mM sodium phosphate buffer and 150 mM NaCl (phosphate-buffered saline, PBS, pH 7.4). The liposomes were eluted in the void volume fractions whereas the free boronated compounds were eluted in later fractions. Boron concentrations in each of the fractions were quantified by means of direct current plasma-atomic emission spectroscopy (DCP-AES) using a Spectraspan VB spectrometer (Applied Research Laboratories, La Brea, CA), as previously described (Barth et al., 1991). Encapsulation efficiencies were determined by calculating the total boron content in the liposomal fractions and the total boron eluted from the column, including both the liposomal and the free boron fractions, as indicated in the following equation:

$$\% \text{ encapsulation} = \text{liposomal boron}/(\text{liposomal boron} + \text{free boron}) \times 100\%$$

The mean diameter and size distribution of the liposomes were determined by photon correlation spectroscopy on a NICOMP 370 submicron particle analyzer. Phospholipid concentration was measured by an ammonium ferrothiocyanate partitioning colorimetic assay, as previously described (Stewart, 1980). The mean particle diameters were between 100 and 150 nm for all liposome preparations. Liposome samples were stored at 4 °C and used within 2 weeks of preparation, during which time no significant leakage (<1%) of the entrapped contents was detected by gel-filtration fractionation on a Sepharose CL-4B column.

Remote Loading. Boronated polyamine derivatives (SPD-5, ASPD-5, SPM-5, ASPM-5, and SPM-5,10) were incorporated into preformed liposomes via a transmembrane pH gradient. Briefly, SUVs were prepared using the above-described method by hydrating them in either 300 mM citric acid (pH 4.0) or 250 mM ammonium sulfate. Boron loading was accomplished by incubating the liposomes with the boronated polyamines, which each contained 1.1 mg (or ~0.1 mmol) of boron dissolved in HEPES buffered saline (HBS, 150 mM NaCl, 20 mM HEPES, pH 7.4), for 60 min at 60 °C. Liposomes then were separated from the free drug by gel-filtration on a Sepharose CL-4B column and characterized as described above.

Uptake of Boronated Liposomes by Cultured KB Cells. Monolayer cultures of KB cells in a logarithmic growth phase were disaggregrated by a short exposure to 0.5% trypsin. The cells then were sedimented by centrifugation at 500*g*, resuspended in folate-free RPMI 1640 media, divided into aliquots of 1×10^6 cells, and incubated with folate-derivatized or nontargeted control boronated liposomes for 2 h at 37 °C with gentle shaking. The number of cells was determined by counting using a hemocytometer. The cells then were sedimented at 500*g* and washed 2× with PBS, and the boron concentration in the supernatant and the cell pellet was measured by DCP-AES, as previously described (Barth et al., 1991).

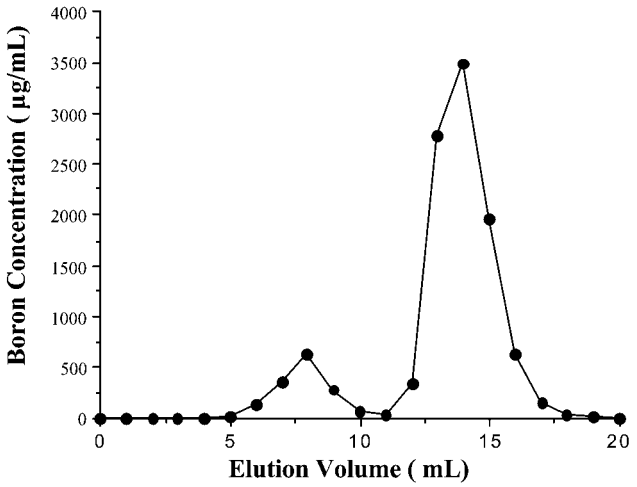


Figure 2. Size-exclusion chromatographic fractionation of L-[Na_3 ($B_{20}H_{17}NH_3$)] on a Sepharose CL-4B column. One milliliter of polycarbonate membrane extruded liposomes was loaded on to an 11-mL column, which had been prewashed with three volumes of PBS (pH7.4). Boron content in each elution fraction was determined by DCP-AES, as described in Experimental Procedures.

For FR blocking studies, the cells were incubated with boronated liposomes in the presence of 1 mM free folic acid. Cellular uptake was normalized to micrograms of boron per 10^9 cells by multiplying by the appropriate factor.

RESULTS

Liposomal Entrapment of BSH and $Na_3(B_{20}H_{17}NH_3)$. Boronated liposomes (SUVs), composed of egg PC/Chol/PEG-Chol (60:35:5, mole/mole), were prepared by lipid hydration in a solution of the anionic hydrophilic boron agent BSH or $Na_3(B_{20}H_{17}NH_3)$, followed by extrusion through a 100-nm pore-size polycarbonate membrane, as described in the Experimental Procedures. The 5 mol % PEG−Chol was incorporated in the liposome formulation to provide steric stabilization against plasma protein binding during systemic administration for future in vivo studies. Egg PC/Chol/PEG−Chol/folate−PEG−DSPE (60:35:4.5:0.5, mole/mole) was used in the preparation of FR-targeted liposomes. The liposome samples were fractionated on a Sepharose CL-4B column. As shown in a typical chromatogram (Figure 2), liposomal $Na_3(B_{20}H_{17}NH_3)$ (L-[$Na_3(B_{20}H_{17}NH_3)$]) could be efficiently separated from the unentrapped free drug using this method. The majority of the boron detected by DCP-AES was eluted in the low molecular weight fractions. Entrapment efficiencies, obtained for BSH and $Na_3(B_{20}H_{17}NH_3)$, were 6% and 15%, respectively. No significant differences were observed between the loading efficiency of FR-targeted and the nontargeted control liposomes (data not shown).

Liposomal Entrapment of Boronated Polyamines. Liposome loading was carried out by remote-loading methods based on the generation of a transmembrane pH gradient, as described in the Experimental Procedures. Either 300 mM sodium citrate (pH 4) or 250 mM ammonium sulfate was used as an intraliposomal trapping agent, which forms an insoluble complex with the boronated polyamines that have diffused across the lipid bilayer into the aqueous core of the liposomes. Identical lipid compositions, with or without the incorporation of folate−PEG−DSPE, were used, as described above for liposomes entrapping anionic boronated agents.

Table 1. The Entrapment Efficiency of Boronated Polyamines by Remote Loading (%)

boronated polyamine derivatives	trapping agent	
	sodium citrate	$(NH_4)_2SO_4$
SPD-5	30	93
ASPD-5	26	72
SPM-5	19	26
ASPM-5	13	45
SPM-5, 10	75	85

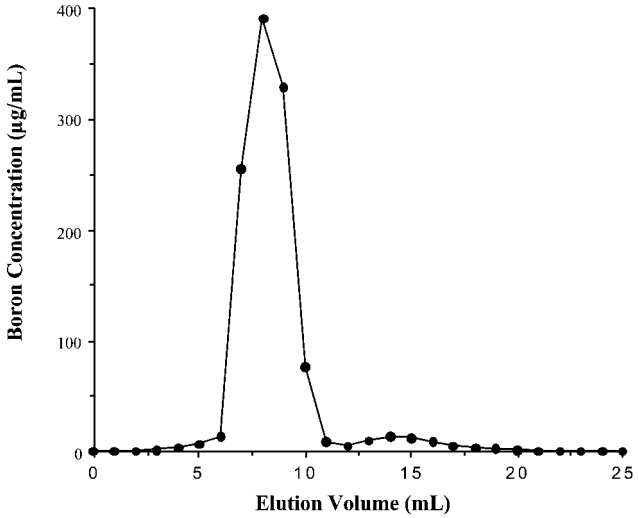


Figure 3. Size-exclusion chromatographic purification of L-[ASPD-5] on a Sepharose CL-4B column. One milliliter of polycarbonate membrane extruded liposomes was loaded on to an 11-mL column prewashed with three volumes of PBS (pH7.4). Boron content in each elution fraction was determined by DCP-AES, as described in Experimental Procedures.

The loading efficiencies were highly variable and ranged from 13% to 93%, as shown in Table 1. The boronated liposomes were easily separated from the free compound, as shown in a representative size-exclusion chromatogram of liposomes entrapping ASPD-5 (Figure 3). Comparing the various boronated polyamines with a single carborane moiety (SPD-5, ASPD-5, SPM-5, ASPM-5), the spermidine derivatives showed a higher entrapment efficiency compared to the spermine derivatives. Among the spermine derivatives, SPM-5,10, which has two attached carborane cages, showed a higher entrapment efficiency than SPM-5, which contains a single carborane moiety. Finally, liposome loading using ammonium sulfate as the trapping agent resulted in an overall higher efficiency of boron entrapment compared to procedures using sodium citrate as the trapping agent. Therefore, all liposomes containing the boronated polyamines used in subsequent tumor cell uptake studies were prepared using ammonium sulfate as the trapping agent. Incorporation of folate−PEG−DSPE did not significantly influence liposomal loading efficiency (data not shown).

Cellular Uptake of FR-Targeted Boronated Liposomes. To study the potential use of folate-derivatized liposomes as tumor cell selective delivery agents for BNCT, cellular binding of the liposomes was evaluated using cultured KB cells, which express amplified FR. A representative concentration dependent cellular uptake curve using liposome-entrapped BSH is shown in Figure 4. Greater cellular uptake of boron was obtained with folate-derivatized liposomal BSH (f-L-[BSH]) compared to the nontargeted control liposomes (L-[BSH]). Furthermore, the FR-targeted liposomes showed binding saturation at boron concentrations greater than 4 μM and this

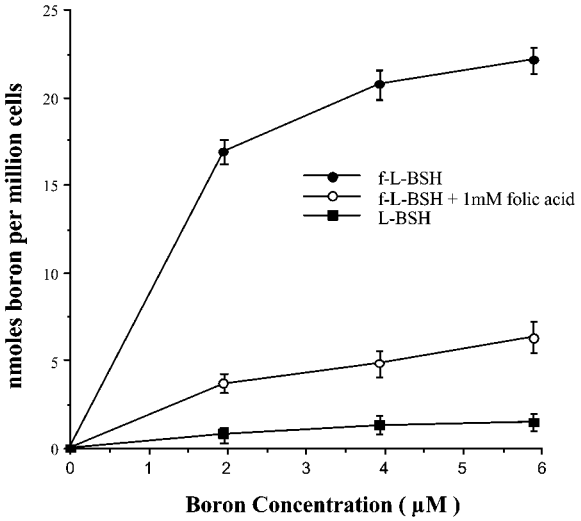


Figure 4. FR-mediated uptake of liposomal BSH in cultured KB cells. Tumor cells were suspended with trypsin and incubated with BSH-containing liposomes at the indicated boron concentrations for 2 h at 37 °C. Tumor cell associated boron was analyzed as described in Experimental Procedures.

was inhibited by 1 mM folic acid, suggesting that the uptake of f-L-BSH was dependent upon FR expression. The maximum boron uptake obtained with f-L-[BSH] was ~240 μg/10^9 cells.

Cellular uptake of boron, following a 2 h incubation at 37 °C with a variety of boronated agents, each containing 4 μM total boron, entrapped in either FR-targeted (f-L-[boron]) or nontargeted control liposomes (L-[boron]), are summarized in Table 2. There was a 2.3- to 49-fold higher boron uptake in cells treated with the f-L-[boron] compared to cells treated with L-[boron]. Furthermore, uptake of f-L-[boron] could be blocked by coincubation with 1 mM folic acid, indicating that cellular uptake was FR dependent. Boron delivery to KB cells generally was more efficient with f-L-[boron] containing the cationic polyamine derivatives compared to the liposomes containing the anionic boronated species. The maximum cellular uptake of f-L-[boron] was variable and was as high as 1584 μg per 10^9 cells with liposomes entrapping SPM-5,10.

DISCUSSION

In the present study, we have evaluated the incorporation of a series of carborane cage-containing derivatives into FR-targeted liposomes. Using either passive or remote loading techniques, the efficiency of loading and the cellular uptake of boron have been determined. Anionic carborane derivatives BSH and $Na_3(B_{20}H_{17}NH_3)$, which have very high boron content and are membrane impermeable due to their high degree of ionization (Hawthorne and Shelly, 1997), were loaded into SUVs by passive entrapment. In the absence of significant bilayer interactions, the liposomal entrapment efficiencies for water-soluble agents primarily will be determined by the percent entrapped volume, provided that solute concentrations reach equilibrium across the lipid bilayer during liposome preparation. Under these conditions, higher percentage entrapment can be achieved by (i) increasing the lipid concentration, (ii) adopting procedures to ensure equilibration of solute across the membrane, and (iii) increasing the mean vesicle diameter. A relatively small particle size is required for systemic liposomal drug delivery in order to enhance diffusion into the tumor. Therefore, we have selected a polycarbonate

Table 2. Uptake of Liposomal Boron Compounds by Cultured KB Cells

boron compounds	boron-to-lipid ratio × 10^3 (wt/wt)	f-L-[boron][a]	L-[boron][a]	f-L-[boron] + 1 mM folic acid
BSH	3.0	231 ± 40 [b]	14 ± 2	53 ± 10
$Na_3(B_{20}H_{17}NH_3)$	28	108 ± 26	2.2 ± 1.1	18 ± 12
SPD-5	34	671 ± 154	76 ± 8	297 ± 26
ASPD-5	26	770 ± 143	75 ± 30	352 ± 44
SPM-5	9.5	132 ± 21	17.6 ± 3	33 ± 3
ASPM-5	17	154 ± 29	67 ± 9	132 ± 18
SPM-5,10	31	1584 ± 56	154 ± 19	1331 ± 74

[a] f-L-[boron] designates the FR-targeted boron containing liposomes; L-[boron] designates the nontargeted control liposomes. [b] Boron concentrations were determined by means of DCP-AES. The values indicated were micrograms of boron per 10^9 cells ± standard deviation, based on three replicate samples for each compound.

membrane extrusion-based procedure to generate SUVs with mean diameters in the range of 100−150 nm. The entrapment efficiencies obtained for BSH and Na_3 ($B_{20}H_{17}NH_3$) (6% and 15%) were substantially higher than those reported previously (Mehta et al., 1996; Feakes et al., 1994). The lower entrapment efficiencies observed by Feakes et al. possibly could have been due to the small size of the liposomes (~60 nm), although differences in lipid compositions and the procedure used to prepare these liposome preparation also may have played a role. The difference in encapsulation efficiency of BSH and $Na_3(B_{20}H_{17}NH_3)$ may be due to differences in their binding affinity for the lipid bilayer. The incorporation of folate−PEG−DSPE, a targeting ligand for the FR, did not significantly affect liposomal loading efficiency. Further enhancement in entrapment efficiency might be achieved by increasing the lipid concentration during lipid hydration. Although much greater incorporation efficiencies can be achieved using lipophilic derivatives of carboranes, their high lipophilicity would reduce subcellular localization to the nucleus. A combination of encapsulation of hydrophilic boron agents with the incorporation of lipophilic carborane derivatives into the bilayer would maximize liposomal boron content and simultaneously allow the targeting of multiple intracellular targets. Further evaluation of this approach is warranted.

Boronated polyamines have been designed to target DNA following cellular uptake (Cai et al., 1997). The amphiphilicity and weakly basic properties of these agents make them suitable candidates for remote loading into liposomes. In contrast to passive entrapment, remote loading is achieved based on the bilayer permeability of boronated polyamines at basic pH and the formation of insoluble complexes between these agents and a trapping agent, which consist of either sodium citrate or ammonium sulfate. Remote loading procedures have been applied to anthracyclines, resulting in close to 100% entrapment (Muggia, 2001). In the present study, we compared the effectiveness of 300 mM sodium citrate and ammonium sulfate as trapping agents during remote loading. The latter was found to be more effective, possibly due to its greater capacity to form stable complexes with the boronated polyamines. Remote loading of weakly basic compounds into liposomes is presumably mediated by precipitation of the agent inside the liposome, either with citrate or sulfate as the counterion. Neither citrate nor sulfate ions are expected to cross the lipid bilayer, either alone or as a polyamine complex. Therefore, the observed differences in loading efficiency were possibly due to differences in intraliposomal pH values and the solubility product (K_{sp}) values for the polyamines with each type of counterions.

The liposomal loading efficiency also appeared to be influenced by the chemical structure of the boron derivatives. When only one carborane cage was present, higher percentages of boron encapsulation were observed when the ionic component was spermidine (SPD-5, ASPD-5) compared to those obtained with spermine (SPM-5, ASPM-5). It is possible that at a weakly basic pH the additional ionizable amine component and the corresponding increase in overall size of the molecule impeded diffusion of spermine derivatives across the phospholipid bilayer. In addition, the presence of two carborane cages (in SPM-5,10), which increased the lipophilicity of the molecule, appeared to facilitate liposome loading, suggesting that lipophilicity might be an additional determining factor for optimizing remote loading.

Based on the premise that cholesterol formed a stable lipophilic anchor for PEG, PEG900-Chol was incorporated into the liposomes to enhance their colloidal stability. A previous report (Beugin et al., 1998) has shown that PEG-Chol derivatives have lower critical micelle concentration (CMC) values than the corresponding PEG-PE derivatives and were stably incorporated into liposomes with similar efficiency and stability. In addition, Ishiwata et al. (1995) reported that PEG−Chol derivatives could prolong systemic circulation time of liposomes. Furthermore, our previous studies have shown that folate−PEG−Chol effectively targeted liposomes to tumor cells expressing amplified level of folate receptor (Guo and Lee, 2000).

Receptor-mediated targeting of boronated liposomes potentially may improve the delivery of boron to tumor cells. FR-targeted liposomes can be easily prepared through the incorporation of folate−PEG−DSPE, a lipophilic derivative of FR ligand folic acid. A proposed mechanism of FR-mediated intracellular boron delivery is shown in Figure 5. Compared to polypeptide-based targeting ligands, folate is small in size, readily available, easily amenable to liposomal incorporation, highly specific for FR positive tumor cells, nonimmunogenic, and selective for a cellular marker that has very limited normal tissue distribution and is widely overexpressed in a wide variety of tumors, including over 90% ovarian carcinomas (Garin-Chesa et al., 1993; Ross et al., 1994; Weitman et al., 1992). Boron uptake by FR-positive KB cells was much greater with FR-targeted f-L-[boron] liposomes compared to the nontargeted control liposomes. The variability in the boron delivery efficiencies of f-L-[boron] partly may be attributable to differences in boron loading efficiencies and boron-to-lipid ratios of the various liposomal preparations. Uptake of f-L-[boron] by KB cell was only partially blocked by 1 mM folic acid, which may have been due to increased binding affinity resulting from multivalent interactions between liposomes and cellular FRs.

The ultimate purpose of developing FR-targeted boronated liposomes is to selectively deliver sufficient quantities of boron to FR-expressing tumor cells. Comparison

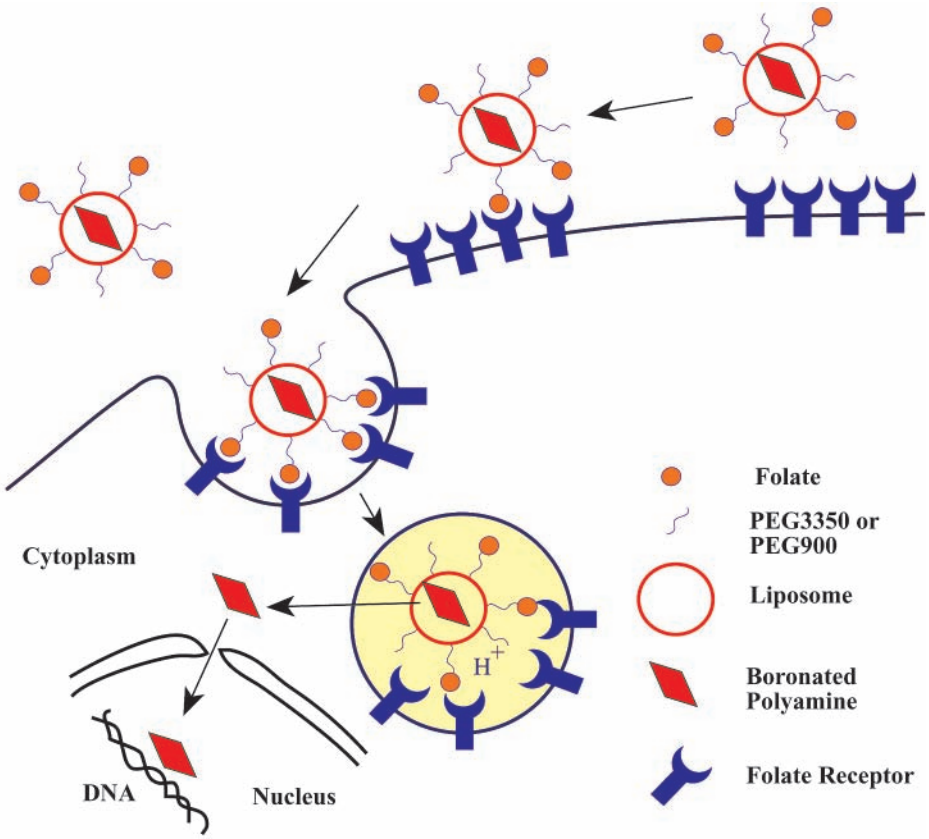


Figure 5. Proposed mechanism of intracellular boron delivery that involves both FR-mediated tumor cell targeting and intracellular DNA targeting. FR-targeted boronated polyamine containing liposomes are shown to be internalized by a cell via FR-mediated endocytosis. The encapsulated boron agent is then released into the cytosol via endosomal escape and bound to the DNA in the cellular nucleus.

of delivery efficiencies by different liposomal formulations, therefore, was based on exposing cells to the same concentrations of boron, rather than lipids. The FR targeting properties of folate-derivatized liposomes have been reported previously (Lee and Low, 1995) and, therefore, was not the main focus of the present study. The alternative would have been to keep the lipid concentration constant, which would result in variable amounts of boron. Results based on this strategy might be difficult to interpret since our data focused on measurements of cell-associated boron. The choice of 4 μM boron concentration in cellular binding studies was based on the finding that higher concentrations of boron and lipids resulted in significant nonspecific cellular uptake (data not shown).

The variability in cellular boron uptake and in FR-targeted-to-nontargeted enhancement ratios were influenced by a number of variables. These included (i) the lipid concentration used in the binding assay, (ii) the boron-to-lipid ratio of the liposomal formulation, and (iii) the ζ-potential of the liposomal surface, which was affected by binding of the cationic and lipophilic boronated polyamines. Data on cellular boron uptake indicated that boronated polyamine liposomal formulations with higher boron-to-lipid ratios generally had greater nonspecific cellular uptake. This suggests that uptake of FR-targeted liposomes may have been due to both receptor-mediated and nonspecific binding, which would increase with elevated ζ-potential due to greater liposome surface binding of the boronated polyamines.

In vivo tumor localization of boronated liposomes potentially can be affected by passive targeting due to increased endothelial permeability and limited lymphatic drainage frequently observed in solid tumors (Matsumura et al., 1986). Tumor-targeted immunoliposomes and FR-targeted liposomes have shown moderate enhancement in tumor accumulation compared to nontargeted liposomes, but the degree of enhancement was highly variable (Ishida et al., 2001; Park et al., 1997; Guo et al., 2000). For example, transferrin receptor-targeted immunoliposomes showed only a 2-fold increase in boron localization in a rat xenograft model (Maruyama et al., 1999; Ishida et al., 2001). Intratumoral and subcellular distribution of the boron are important determinants for the effectiveness of neutron capture therapy (Hartman et al., 1994). It is conceivable that FR-targeted liposomes may be more efficiently internalized by FR-bearing tumor cells following extravasation compared to nontargeted liposomes within the solid tumor.

In summary, we have shown that FR-targeted liposomes can deliver larger amounts of boron (up to 1584 μg/10^9 cells) to receptor positive tumor cells in vitro than any other delivery agent currently being investigated in our laboratories. This amount greatly exceeds the boron concentration (20−35 μg per gram of tumor) required to sustain a lethal $^{10}B(n,\alpha)^7Li$ capture reaction for BNCT. Boron delivery was selective to FR expressing cells since it can be blocked by excess free folate. Folate-derivatized liposomes containing boronated polyamines would be particularly attractive targeting agents since they also could deliver boron to cellular DNA. Further studies are warranted to evaluate the in vivo tumor localizing potential of these boron carriers in FR-positive tumor cells and their utility for BNCT.

ACKNOWLEDGMENT

This work has been supported by the National Institute of Health grant R01CA79758 and Department of Energy grant DE-FG02-98ERG295.

LITERATURE CITED

(1) Allen, T. M., Hansen, C., Martin, F., Redemann, C., and Yau-Young, A. (1991) Liposomes containing synthetic lipid derivatives of poly(ethylene glycol) show prolonged circulation half-lives in vivo. *Biochim. Biophys. Acta 1066*, 29−36.

(2) Antony, A. C. (1996) Folate receptors. *Annu. Rev. Nutr. 16*, 501−521.

(3) Barth, R. F., Adams, D. M., Soloway, A. H., Mechetner, E. B., Alam, F., and Anisuzzaman, A. K. (1991) Determination of boron in tissues and cells using direct-current plasma atomic emission spectroscopy. *Anal. Chem. 63*, 890−893.

(4) Barth, R. F., Soloway, A. H., Goodman, J. H., Gahbauer, R. A., Gupta, N., Blue, T. E., Yang, W., and Tjarks, W. (1999) Boron neutron capture therapy of brain tumors: an emerging therapeutic modality. *Neurosurgery 44*, 433−450.

(5) Barth, R. F., Yang, W., Rotaru, J. H., Moeschberger, M. L., Boesel, C. P., Soloway, A. H., Joel, D. D., Nawrocky, M. M., Ono, K., and Goodman, J. H. (2000) Boron neutron capture therapy of brain tumors: enhanced survival and cure following blood-brain barrier disruption and intracarotid injection of sodium borocaptate and boronophenylalanine. *Int. J. Radiat. Oncol. Biol. Phys. 47*, 209−218.

(6) Barth, R. F., Yang, W., Rotaru, J. H., Moeschberger, M. L., Joel, D. D., Nawrocky, M. M., Goodman, J. H., and Soloway, A. H. (1997) Boron neutron capture therapy of brain tumors: enhanced survival following intracarotid injection of either sodium borocaptate or boronophenylalanine with or without blood-brain barrier disruption. *Cancer Res. 57*, 1129−1136.

(7) Beugin, S., Edwards, K., Karlsson, G., Ollivon, M., and Lesieur, S. (1998) New sterically stabilized vesicles based on nonionic surfactant, cholesterol, and poly(ethylene glycol)-cholesterol conjugates. *Biophys. J. 74*, 3198−3210.

(8) Cai, J., Soloway, A. H., Barth, R. F., Adams, D. M., Hariharan, J. R., Wyzlic, I. M., and Radcliffe, K. (1997) Boron-containing polyamines as DNA targeting agents for neutron capture therapy of brain tumors: synthesis and biological evaluation. *J. Med. Chem. 40*, 3887−3896.

(9) Capala, J., Barth, R. F., Bailey, M. Q., Fenstermaker, R. A., Marek, M. J., and Rhodes, B. A. (1997) Radiolabeling of epidermal growth factor with ^{99m}Tc and in vivo localization following intracerebral injection into normal and glioma bearing mice. *Bioconjugate Chem. 8*, 289−295.

(10) Capala, J., Barth, R. F., Bendayan, M., Lauzon, M., Adams, D., Soloway, A. H., and Carlsson, J. (1996) Boronated epidermal growth factor as a potential targeting agent for boron neutron capture therapy of brain tumors. *Bioconjugate Chem. 7*, 7−15.

(11) Chonn, A., and Cullis, P. R. (1995) Recent advances in liposomal drug-delivery systems. *Curr. Opin. Biotechnol. 6*, 698−708.

(12) Feakes, D. A., Shelly, K., Knobler, C. B., and Hawthorne, M. F. (1994) $Na_3[B_{20}H_{17}NH_3]$: synthesis and liposomal delivery to murine tumors. *Proc. Natl. Acad. Sci. U.S.A. 91*, 3029−3033.

(13) Frisch, B., Muller, S., Briand, J. P., Van Regenmortel, M. H., and Schuber, F. (1991) Parameters affecting the immunogenicity of a liposome-associated synthetic hexapeptide antigen. *Eur. J. Immunol. 21*, 185−193.

(14) Gabizon, A., Horowitz, A. T., Goren, D., Tzemach, D., Mandelbaum-Shavit, F., Qazen, M. M., and Zalipsky, S. (1999) Targeting folate receptor with folate linked to extremities of poly(ethylene glycol)-grafted liposomes: in vitro studies. *Bioconjugate Chem. 10*, 289−298.

(15) Garin-Chesa, P., Campbell, I., Saigo, P. E., Lewis, J. L. Jr., Old, L. J., and Rettig, W. J. (1993) Trophoblast and ovarian cancer antigen LK26. Sensitivity and specificity in immunopathology and molecular identification as a folate-binding protein. *Am. J. Pathol. 142*, 557−567.

(16) Guo, W., Sudimack, J., and Lee, R. J. (2000) Receptor-specific delivery of liposomes via folate-PEG-chol. *J. Liposome Res. 10*, 179−195.

(17) Hartman, T., and Carlsson, J. (1994) Radiation dose heterogeneity in receptor and antigen mediated boron neutron capture therapy. *Radiother. Oncol. 31*, 61−75.

(18) Hawthorne, M. F. (1998) New horizon for therapy based on the boron neutron capture reaction. *Mol. Med. Today 4*, 174−181.

(19) Hawthorne, M. F., and Shelly, K. (1997) Liposomes as drug delivery vehicles for boron agents. *J. Neurooncol. 33*, 53−58.

(20) Ishida, O., Maruyama, K., Tanahashi, H., Iwatsuru, M., Sasaki, K., Eriguchi, M., and Yanagie, H. (2001) Liposomes bearing poly(ethylene glycol)-coupled transferrin with intracellular targeting property to the solid tumors in vivo. *Pharm. Res. 18*, 1042−1048.

(21) Ishiwata, H., Vertut-Doi, A., Hirose, T., and Miyajima, K. (1995) Physical-chemistry characteristics and biodistribution of poly(ethylene glycol)-coated liposomes using poly(oxyethylene) cholesteryl ether. *Chem. Pharm. Bull. 43*, 1005−1011.

(22) Johnsson, M., Bergstrand, N., and Edwards, K. (1999) Optimization of drug loading procedures and characterization of liposomal formulations of two novel agents intended for boron neutron capture therapy (BNCT). *J. Liposome Res. 9*, 53−79.

(23) Leamon, C. P., and Low, P. S. (1991) Delivery of macromolecules into living cells: a method that exploits folate receptor endocytosis. *Proc. Natl. Acad. Sci. U.S.A. 88*, 5572−5576.

(24) Lee, R. J., and Low, P. S. (1994) Delivery of liposomes to cultured KB cells via folate receptor-mediated endocytosis. *J. Biol. Chem. 269*, 3198−3204.

(25) Lee, R. J., and Low, P. S. (1995) Folate-mediated tumor cell targeting of liposome-entrapped doxorubicin in vitro. *Biochim. Biophys. Acta 1233*, 134−144.

(26) Lee, R. J., and Low, P. S. (1997) Folate-targeted liposomes for drug delivery. *J. Liposome Res. 7*, 455−466.

(27) Maruyama, K., Yanagie, H., ishida, O., Shinohara, A., Chiba, M., Eriguchi, M., Kobayashi, H., and Iwatsuru, M. (2000) Application of ^{10}BSH entrapped transferrin-PEG-liposome to boron neutron-capture therapy (BNCT) for solid tumor. *KURRI−KR*, 109−110.

(28) Matsumura, Y., and Maeda, H. (1986) A new concept for macromolecular therapeutics in cancer chemotherapy: mechanism of tumoritropic accumulation of proteins and the antitumor agent smancs. *Cancer Res 46*, 6387−6392.

(29) Mehta, S. C., Lai, J. C., and Lu, D. R. (1996) Liposomal formulations containing sodium mercaptoundecahydrododecaborate (BSH) for boron neutron capture therapy. *J. Microencapsul. 13*, 269−279.

(30) Mishima, Y., Kondoh, H., Yoshino, K., and Hiratsuka, J. (2001) Current clinical paradigms in melanoma BNCT, in *Frontiers in Neutron Capture Ther.* (M. F. Hawthorne, K. Shelly, and R. J. Wiersma, Eds.) pp 1365−1382, Plenum Publishers, New York.

(31) Muggia, F. M. (2001) Liposomes encapsulating anthracyclines: New therapeutic horizons. *Curr. Oncol. Rep. 3*, 156−162.

(32) Nichols, J. W., and Deamer, D. W. (1976) Catecholamine uptake and concentration by liposomes maintaining pH gradients. *Biochim. Biophys. Acta 455*, 269−271.

(33) Park, J. W., Hong, K., Kirpotin, D. B., Papahadjopoulos, D., Benz, C. C.(1997) Immunoliposomes for cancer treatment. *Adv. Pharmacol. 40*, 399−435.

(34) Reddy, J. A., Haneline, L. S., Srour, E. F., Antony, A. C., Clapp, D. W., and Low, P. S. (1999) Expression and functional characterization of the beta-isoform of the folate receptor on CD34(+) cells. *Blood 93*, 3940−3948.

(35) Reddy, J. A., and Low, P. S. (1998) Folate-mediated targeting of therapeutic and imaging agents to cancers. *Crit. Rev. Ther. Drug Carrier Syst. 15*, 587−627.

(36) Ross, J. F., Chaudhuri, P. K., and Ratnam, M. (1994) Differential regulation of folate receptor isoforms in normal and malignant tissues in vivo and in established cell lines. Physiologic and clinical implications. *Cancer 73*, 2432−2443.

(37) Shelly, K., Feakes, D. A., Hawthorne, M. F., Schmidt, P. G., Krisch, T. A., and Bauer, W. F. (1992) Model studies directed toward the boron neutron-capture therapy of cancer: boron delivery to murine tumors with liposomes. *Proc. Natl. Acad. Sci. U.S.A. 89*, 9039−9043.

(38) Soloway, A. H., Barth, R. F., Gahbauer, R. A., Blue, T. E., and Goodman, J. H. (1997) The rationale and requirements for the development of boron neutron capture therapy of brain tumors. *J. Neurooncol. 33*, 9−18.

(39) Stewart, J. C. (1980) Colorimetric determination of phospholipids with ammonium ferrothiocyanate. *Anal. Chem. 104*, 10−14.

(40) Sudimack, J., and Lee, R. J. (2000) Targeted drug delivery via the folate receptor. *Adv. Drug Deliv. Rev. 41*, 147−162.

(41) Tjarks, W., Barth, R. F., Rotaru, J. H., Adams, D. M., Yang, W., Kultyshev, R. G., Forrester, J., Barnum, B. A., Soloway, A. H., and Shore, S. G. (2001) *In vivo* evaluation of phosphorous-containing derivatives of dodecahydro- closo-dodecaborate for boron neutron capture therapy of gliomas and sarcomas. *Anticancer Res. 21*, 841−846.

(42) Weitman, S. D., Lark, R. H., Coney, L. R., Fort, D. W., Frasca, V., Zurawski, V. R. Jr., Kamen, B. A. (1992) Distribution of the folate receptor GP38 in normal and malignant cell lines and tissues. *Cancer Res. 52*, 3396−3401.

(43) Woodle, M. C., and Lasic, D. D. (1992) Sterically stabilized liposomes. *Biochim. Biophys. Acta 1113*, 171−199.

(44) Yanagie, H., Maruyama, K., Takizawa, T., Ogura, K., Matsumoto, T., Sakurai, Y., Kobayashi, T., Ono, K., Rant, J., Skvarc, J., Llic, R., Eriguchi, M., Shinohara, A., and Kobayashi, H. (2000) Tumor growth suppression by boron neutron capture therapy using PEG-liposomal boron delivery in vivo. *KURRI−KR* 101−102.

(45) Yanagie, H., Tomita, T., Kobayashi, H., Fujii, Y., Nonaka, Y., Saegusa, Y., Hasumi, K., Eriguchi, M., Kobayashi, T., and Ono, K. (1997) Inhibition of human pancreatic cancer growth in nude mice by boron neutron capture therapy. *Br. J. Cancer 75*, 660−665.

(46) Yang, W., Barth, R. F., and Adams, D. M. et al. (2000) Boron neutron capture therapy (BNCT) of brain tumors: Convection enhanced delivery of boronated epidermal growth factor to EGF receptor positive gliomas. *Neuro-Oncol. 2*, 304.

(47) Yang, W., Barth, R. F., Rotaru, J. H., Joel, D. D., Nawrocky, BA., and Goodman, J. H. (1997) Enhanced survival of glioma bearing rats following boron neutron capture therapy with blood-brain barrier disruption and intracarotid injection of boronophenylalanine. *J. Neuro. Oncol. 32*, 59−70.

(48) Yang, W., Barth, R. F., Rotaru, J. H., Moeschberger, M. L., Joel, D. D., Nawrocky, BA., Goodman, J. H., and Soloway, A. H. (1997) Boron neutron capture therapy of brain tumors: enhanced survival following intracarotid injection of sodium borocaptate with or without blood-brain barrier disruption. *Int. J. Rad. Oncol. Biol. Phys. 37*, 663−672.

(49) Zhuo, J.-C., Cai, J., Soloway, A. H., Barth, R. F., Adams, D. M., Ji, W., and Tjarks, W. (1999) Synthesis and biological evaluation of boron-containing polyamines as potential agents for neutron capture therapy of brain tumors. *J. Med. Chem. 42*, 1282−1292.

BC015557Y

Polyester Dendritic Systems for Drug Delivery Applications: Design, Synthesis, and Characterization

Henrik R. Ihre,[†] Omayra L. Padilla De Jesús,[†] Francis C. Szoka, Jr.,*[,‡] and Jean M. J. Fréchet*[,†]

Department of Chemistry, University of California, Berkeley, California 94720-1460 and School of Pharmacy, University of California, San Francisco, California 94143-0446. Received October 22, 2001

Attachment of drugs to high molecular weight polymers can significantly improve both tumor targeting and therapeutic efficacy due to the enhanced permeability and retention effect observed in tumor tissue. However, the commercial availability of well-defined water-soluble polymeric systems with narrow polydispersities that are biocompatible, nontoxic, and nonimmunogenic is rather limited. To address this need, we have investigated dendritic polymers as promising scaffolds for the preparation of new soluble polymeric drug carriers due to their well-defined molecular architecture and their multiplicity of surface sites. Herein we show the design and synthesis of dendritic polyester systems based on the monomer unit 2,2-bis(hydroxymethyl)propanoic acid as a possible versatile drug carrier. The potent anticancer drug doxorubicin was attached via a pH-sensitive linkage to one of the carriers presented, demonstrating the feasibility of using these polyester dendritic structures to prepare a viable polymer−drug conjugate.

INTRODUCTION

In the past few decades, there has been an increasing interest in the design and synthesis of polymeric systems with potential drug delivery applications, a concept initially introduced by Ringsdorf (*1*, *2*) and Kopeček (*3*−*5*). For certain medical treatments, such as chemotherapy, the use of high molecular weight (>20 000 Da) systems provide advantages compared to low molecular weight molecules (<1000 Da), that results in enhanced targeting of tumor tissue and efficiency of the treatment (*6*−*8*).

This effect is explained in part by the enhanced permeability and retention (EPR) phenomenon observed in tumor tissue (*9*−*11*). The EPR effect relies on the fact that the new blood capillaries formed by angiogenesis around tumor tissue, in contrast to normal tissue, are more loosely constructed with larger gaps between endothelial cells. This leaky character serves to supply oxygen and nutrients to the increasing number of neoplastic cells. However, this same physical characteristic also increases the possibilities of extravasation of larger molecules from the surrounding capillaries to the tumor tissue. Therefore, the less probable access of large molecules to normal healthy cells allows for the selectivity toward tumor tissue observed when using polymers as drug carriers. Furthermore, the access to lymphatic capillaries via the tumor is very limited, such that there is inadequate drainage of macromolecules from the tissue. Therefore, both the leaky capillaries that allow permeation of larger molecules and the absence of functional lymphatic drainage that causes accumulation provide an alternative means to passively target tumor tissue by using high molecular weight polymeric systems as drug carriers. The use of polymeric prodrugs also takes advantage of the endocytotic cell uptake mechanism, which contributes to bypass the multidrug resistance (MDR) effect observed in cancer cells (*12*, *13*). In addition, the coupling of an active drug to the appropriate polymeric backbone may overcome problems of water solubility, and lower the toxicity of the drug until it is delivered to the target tissue. The pharmacokinetics of the drug will also be affected, as the higher molecular weight of the conjugate increases its circulation time in the plasma. The combination of these factors makes the polymeric prodrug more accessible for accumulation in the target tissue, increasing the possibilities of improved delivery and efficacy (*7*, *8*).

Although there are many commercially available polymers, few of these polymeric systems possess properties that are suitable for drug delivery agents, such as water solubility, biocompatibility, nontoxicity, and nonimmunogenicity. One system that has been evaluated extensively in clinical trials is PK1, containing a polymeric backbone based on (2-hydroxypropyl)methacrylamide (HPMA) (*14*). Even though this system has shown very promising results in terms of its drug delivery capability, the reproducibility in the preparation of monodisperse poly(HPMA) remains a challenge (*15*, *16*). The broad polydispersity index (PDI) of most polymers may lead to irreproducible pharmacokinetic behavior due to the variation in the molecular weight distribution profile of the polymers from preparation to preparation. Therefore, the preparation of materials with low PDI (≤ 1.1) is essential for the development of systems with reproducible behavior.

Dendritic systems are excellent candidates for providing a well-defined molecular architecture, which is a result of a stepwise synthetic procedure consisting of coupling and activation steps (*17*−*19*). Dendrimers consist of branched, wedge-like structures called dendrons that are attached to a multivalent core, and emerge radially toward the periphery. The architecture and synthetic routes result in polymers with PDI near 1.00, as opposed to the much higher polydispersity of linear or hyperbranched structures (Figure 1). The flexibility to tailor both the core and surface of these systems make them very attractive, since different groups can be provided so as to optimize the properties of the drug carrier. For instance, the functional periphery can be

[†] University of California, Berkeley.
[‡] University of California, San Francisco.

10.1021/bc010102u CCC: $22.00 © 2002 American Chemical Society
Published on Web 04/24/2002

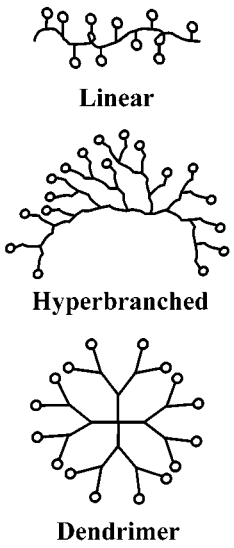


Figure 1. Schematic representation of the architectural differences between linear, hyperbranched, and dendritic polymers.

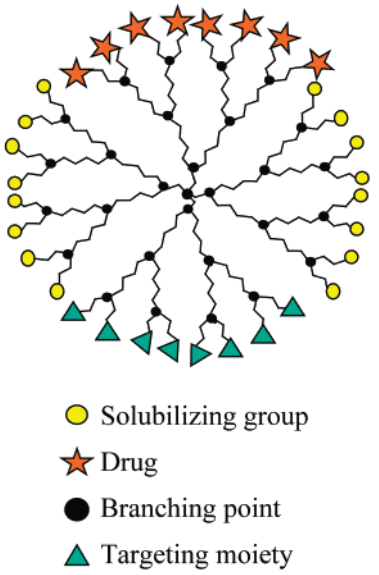


Figure 2. Schematic representation of a possible design for a dendritic drug carrier due to flexibility and versatility that dendritic systems provide.

altered for improving water solubility properties. Orthogonal terminal groups can also be incorporated for nonstatistical attachment of drugs and targeting moieties (Figure 2). The covalent character of dendrimers is also advantageous, providing a stable system that is not dependent on an appropriate dynamic equilibrium or thermodynamic factors that rule large systems, such as micelles and liposomes, formed by aggregation of smaller parts (*20*−*22*). These intrinsic properties of dendrimers make them interesting multivalent molecules that can serve as scaffolds for the preparation of new polymeric systems for drug delivery purposes (*23*−*29*). Nevertheless, the commercial availability of dendritic systems is limited. Currently, the only "commercially" available dendrimers are poly(amidoamine) (PAMAM) and poly(propyleneimine) (PPI) dendrimers. These systems are toxic in cells and animals due to their polycationic character (*30*−*32*). As a result, the search for new dendritic systems for drug delivery purposes is of considerable interest. Less toxic but rather small convergent "Fréchet-type" dendrons (*18*) and related building blocks are commercialized by TCI (Tokyo Kasei Kogyo Co.).

We report the design and synthesis of a polyester dendritic scaffold based on 2,2-bis(hydroxymethyl)propanoic acid. Three different model compounds were prepared as possible scaffolds for the preparation of actual drug carriers. The potent anticancer drug doxorubicin was attached to model compound **11**, showing the feasibility of preparing a polymer-drug conjugate with these polyester dendritic structures. The biological evaluation of these systems is reported elsewhere (*33*).

RESULTS AND DISCUSSION

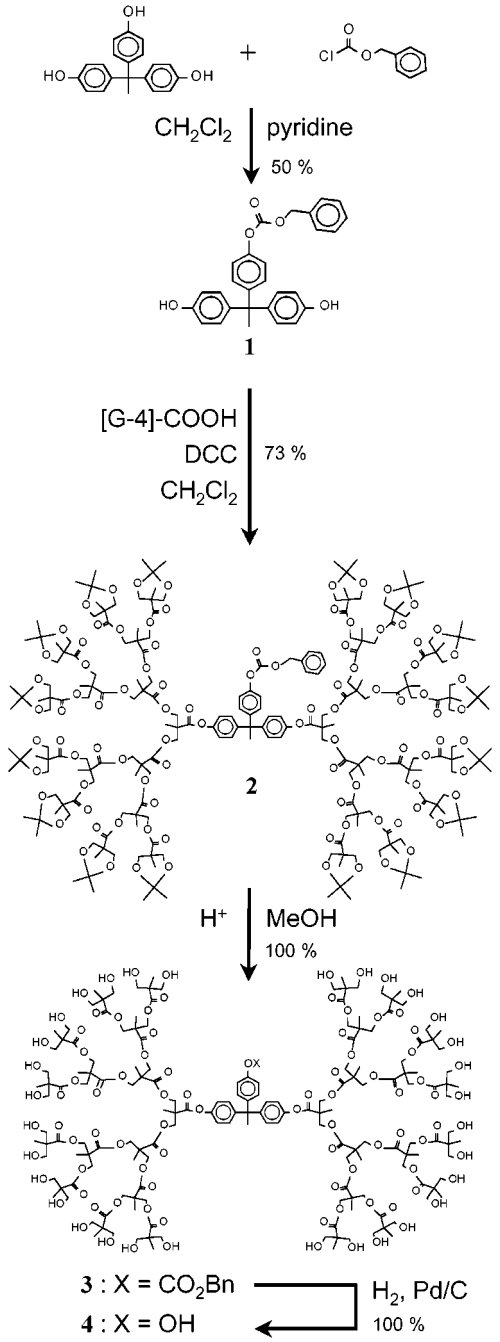
Design and Synthesis of Polymeric Carriers. The main advantages for the use of dendrimers as drug carriers reside in their multivalent design and their well-defined structure that results from the stepwise, iterative approach used in their preparation. This controlled synthesis allows the preparation of structures with specific, reproducible, and tunable characteristics. As previously stated, dendrimers would allow both control over the size of the drug−polymer conjugate, and over the functional groups used for drug and targeting moiety attachment. These groups may also be modified to improve the water solubility properties of the system. Furthermore, a well-defined system with low PDI also renders reproducible pharmacokinetic properties, which is important for the approval of new therapeutic agents by the FDA.

The monomer unit selected for the preparation of the dendritic scaffold, 2,2-bis(hydroxymethyl)propanoic acid, exhibits a set of unique advantages. This polyester system is water soluble in the uncharged state when the polyhydroxylated surface is exposed. This avoids the necessity of introducing functional groups that would contribute to water solubility by ionization, which can counteract the beneficial effect of the use of polymers. Generally, polycationic systems have shown to be toxic and quickly eliminated from circulation, while negatively charged systems often suffer from reduced uptake of molecules in cultured cells and rapid removal via the scavenger receptor in animals (*30*, *34*). In addition, even though polyester bonds are characterized by their susceptibility toward hydrolysis, an attractive feature for biodegradable systems (*35*, *36*), the sterically hindered ester bond of the monomer unit used makes this backbone more stable toward both nucleophilic attack and acid-catalyzed hydrolysis. However, if desired, the points of attachment of drugs to the dendrons and/or dendrons to the core can be designed for more rapid rates of hydrolysis. This feature is another advantage of the dendron architecture.

To perform preliminary biological evaluation of the dendritic scaffold proposed, three model compounds (**4**, **7**, **11**) of different molecular weights and architecture were prepared. The design and synthesis of the carriers are described below.

Model Compound ***4***. The monomer unit 2,2-bis(hydroxymethyl)propanoic acid was selected for the preparation of dendrimer **4**. The fourth generation dendrons [G-4] that compose **4** were synthesized using a double stage convergent approach as reported previously (*37*). In summary, two analogues of the monomer were prepared: the protected acid and the protected 1,3-diol. The protecting groups selected were a benzyl ester group and an isopropylidene ketal group, respectively, to provide access to an orthogonal selective deprotection. The carboxylic acid functionality of the focal point can be deprotected by hydrogenolysis, while the diol surface becomes exposed upon acid-catalyzed hydrolysis of the

Scheme 1



ketal groups. The peripheral hydroxyl groups were esterified by reacting one equivalent of the protected acid diol (HO_2-[G-1]-Bn) with two equivalents of the acid derivative of the monomer ([G-1]-COOH) in the presence of dicyclohexylcarbodiimide (DCC), forming the second generation dendron [G-2]. Following orthogonal deprotection of two samples of these [G-2] dendrons, the resulting [G-2]-OH_4 and [G-2]-COOH dendrons were coupled under DCC conditions to afford the [G-4] dendron in one step.

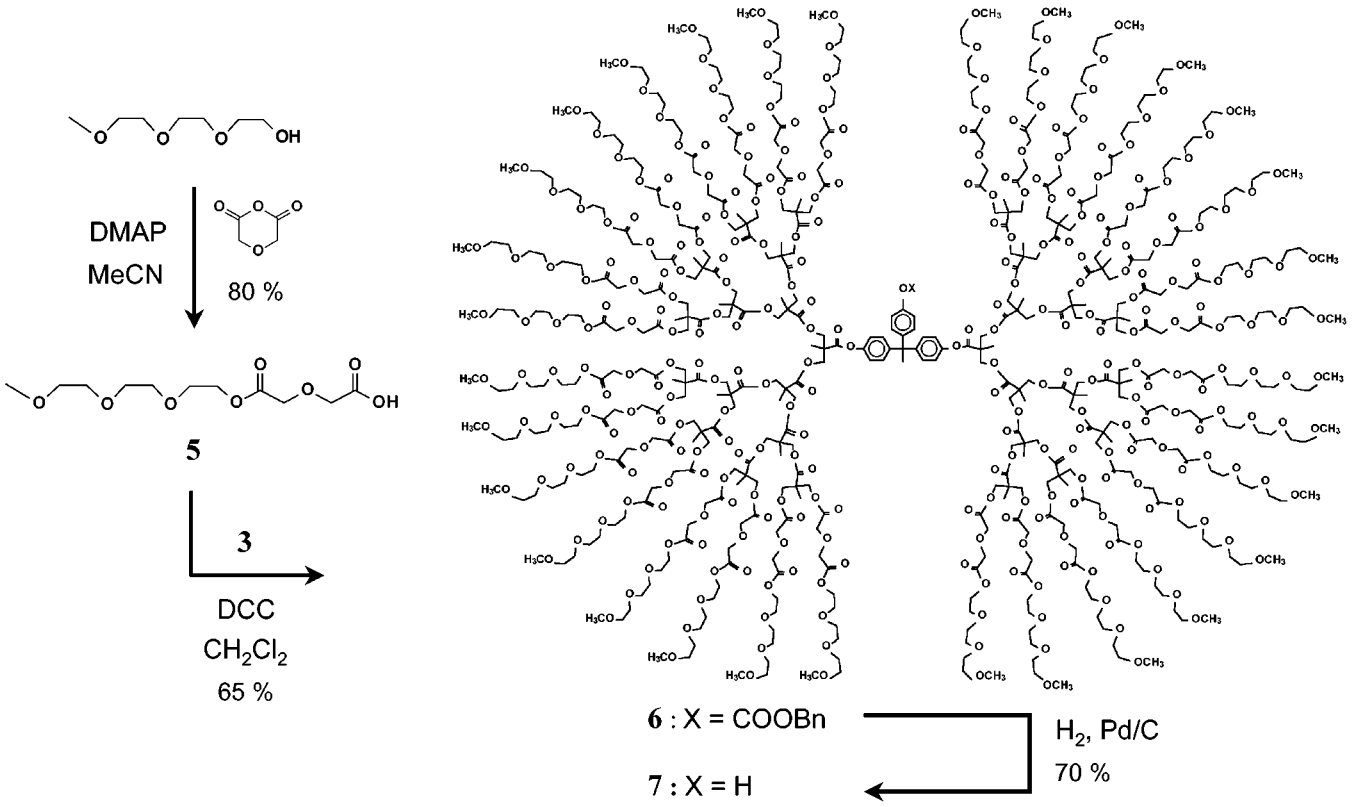
For the assembly of dendrimer **4** (Scheme 1), a monoprotected trisphenolic core was prepared (**1**) by reacting an excess of 1,1,1-tris(4-hydroxyphenyl)ethane with benzyl chloroformate, affording **1** in 50% yield after purification by column chromatography. Then, two equivalents of the [G-4]-COOH dendron were coupled to **1** in the presence of DCC. After coupling the dendrons to the bifunctional core, the isopropylidene ketal protecting groups were cleaved under mild acidic conditions, producing a highly water soluble system containing 32 free hydroxyl groups on the surface. Finally, the benzyl carbonate group was cleaved by hydrogenolysis to provide the free phenol for radiolabeling purposes in future biodistribution experiments, yielding dendrimer **4** with a molecular mass of 3790 Da (Scheme 1).

*Model Compound **7***. To evaluate the effect of increasing the mass of the dendritic system, a second dendritic model compound (**7**) was prepared. This system, consisting of dendrimer **4** with modified chain ends, has three times the molar mass of **4**. To increase the mass of dendrimer **4**, two different approaches were initially considered: (i) synthesizing higher generations of the dendrimer or (ii) simply coupling oligomeric groups to the chain ends of the preformed dendrimer. The former would require repetitive steps of activation, coupling, and purification for each generation as required by the protocols of dendrimer synthesis. Also, a potential difficulty would arise if steric hindrance at the focal point caused incomplete coupling for dendrimers of higher generations. The second approach, however, provides a significant increase in mass in a single step while still preserving the regular dendrimer structure. Thus, the second approach was followed.

For the preparation of **7** (Scheme 2) a capping agent consisting of monomethyl ether tri(ethylene glycol) was selected, since poly(ethylene glycol) and its derivatives are used extensively for biological applications due to their high water solubility and biocompatibility properties (*38*). To couple this moiety to the hydroxyl functionalized periphery of the dendrimer, an acid derivative of the monomethyl ether of tri(ethylene glycol) was prepared. Therefore, **5** was prepared by reaction of the monomethyl ether of tri(ethylene glycol) with diglycolic anhydride in the presence of (dimethylamino)pyridine (DMAP) as the catalyst. Compound **5** is more soluble in water than an analogous compound prepared from succinic anhydride we also prepared, and therefore was deemed to be better suited for our purposes. An excess of the capping agent **5** was reacted with the polyhydroxylated surface of **3** using DCC as the coupling agent to afford **6**. Although the surface of **6** with its methoxylated end groups is no longer reactive, our objective in preparing this dendritic molecule was to test the effect of increased mass and new building blocks on toxicity and biodistribution. If this system shows promising results after biological evaluation, an end-protected capping agent could be used instead of **5**. Finally, the phenolic protecting group located at the core of **6** was removed by hydrogenolysis to expose the free phenol for radio labeling purposes. The final product **7** has a theoretical mass of 12 182 Da; however, MALDI-TOF MS data suggest that coverage of the surface with **5** only occurred in a 90−95%, yielding a product with a mass of ca. 11 500 Da.

*Model Compound **11***. In contrast to the true dendrimer **4** and partly modified dendrimer **7**, model compound **11** is a hybrid macromolecule consisting of a commercially available 3-arm poly(ethylene oxide) (PEO) star and terminal dendritic polyester moieties (Scheme 3). The PEO star (MW = 22 550) used as a core for **11** contributes the majority of the molar mass of the hybrid. The linearity of the PEO arms also leads to a macromolecule with a larger hydrodynamic volume, which may contribute to an increase in plasma half-life without compromising either water solubility or biocompatibility (*38*). In addition, the star shape of the core provides a multivalency of three, as opposed to a valency of one for the more traditional monofunctionalized linear polymers.

Scheme 2



A divergent approach was followed for the synthesis of **11**. The same chemistry described above was used for the coupling steps and activation of the surface of the dendrons. To incorporate the dendritic moieties, the terminal hydroxyl groups of the PEO-star were coupled to the isopropylidene ketal derivative of the 2,2-bis-(hydroxymethyl)propanoic acid monomer unit in the presence of DCC. Activation of the chain ends of **8** was performed under mild acidic conditions to afford a star with six hydroxyl groups, each of which was further used for generation growth. Therefore, second generation dendrons were grown from the hexahydroxylated PEO core, eventually yielding product **11** with a total of 12 hydroxyl groups capable of further modifications (Scheme 3). Dendritic star **11** has a molar mass of ca. 23 500 Da and is highly water soluble (≥ 200 mg/mL). Unlike its dendrimer analogue **4**, the hybrid is not monodisperse but has a very low PDI reflecting that of its PEO core (PDI = 1.03). Due to their perfect structure, the incorporation of the dendritic moieties does not alter the polydispersity of the initial star affording a conjugate in which the periphery of the dendrons provides perfect multivalency with 12 hydroxyl groups available for both drug attachment and release. The PEO-star also contributes to the easy purification of **11** and its precursors by precipitation in diethyl ether affording a white solid, while the excess of reagents and byproducts remained in solution.

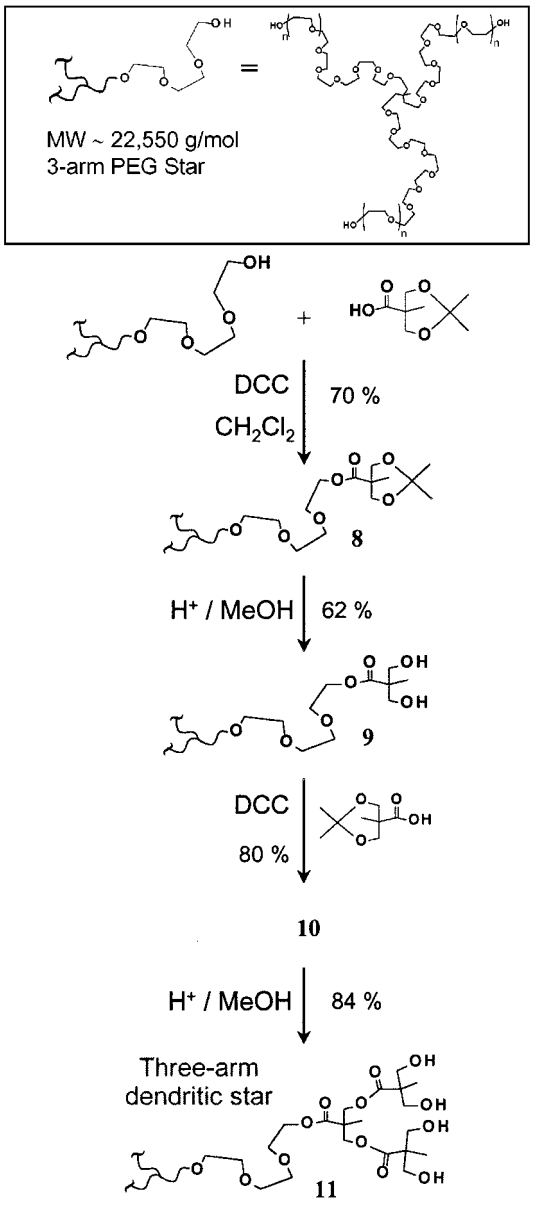
Model compound **11** does not contain a moiety that could be used as a handle for radiolabeling as was the case for **4** and **7**, each which contain a free phenolic group. Therefore, **11** was allowed to react with 2 equiv of 4-methoxyphenyl acetic acid per molecule of polymer under DCC coupling conditions, as shown in Scheme 4, to produce the statistically modified molecule **11a** that contains activated aromatic rings for radiolabeling and subsequent biodistribution studies.

Polymer−Drug Conjugate. Model compound **11** with its higher mass may exhibit the best properties of our three model compounds in terms of serum half-life (*7*). Therefore, a drug-conjugate was prepared from **11** to test the feasibility of the modification of the surface of these dendritic structures for attachment of a drug.

When preparing a polymer−drug conjugate, it is important to consider the mechanism of release and the location of the link used for drug attachment and release. A linkage that is stable under physiological conditions but sufficiently labile to be readily cleaved within the target tissue is the goal. The literature describes release mechanisms for covalently attached drugs that include acid-labile and enzyme-cleavable linkages (*39*−*43*). It has been difficult to specifically address enzyme cleavable linkages because enzymes levels vary at the target site and the rates of drug release from various systems can be appreciably influenced by the characteristics of the drug (*44*). On the other hand, the release rate of an acid labile linkage is often less affected by the type of drug after cellular uptake of the conjugate into the more acidic environment of the lysosomal cellular compartment. The environment around tumor tissue is also slightly more acidic than normal tissue. Therefore, an acid labile linkage might be suitable for drug release in the vicinity of a tumor even before the drug conjugate is internalized by the cancer cell.

The drug selected for the preparation of the drug−polymer conjugate was the anticancer drug doxorubicin (DOX). DOX contains several functional groups that could be utilized for polymer attachment. Typically, the sugar amino group has been used for the formation of hydrolyzable amide linkages. However, amide linkages may be too stable toward acid catalyzed hydrolysis. On the other hand, the keto group of DOX can be used to form an acid labile hydrazone linkage. An acid labile Schiff base could also be generated from this keto group,

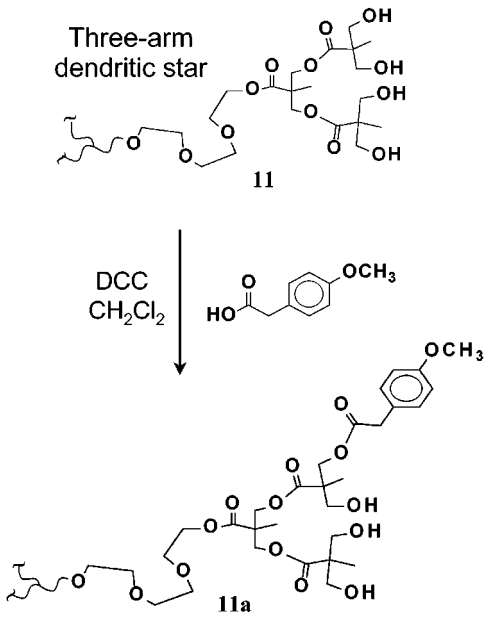
Scheme 3



but imines are thermodynamically less stable than hydrazones under physiological conditions (*45*). Therefore, the polyhydroxylated surface of the polyester dendrons on **11** was modified to produce hydrazides that could further be coupled to the ketone moiety of DOX, forming compound **15** that has the desired hydrazone linkage between the polymeric carrier and DOX.

For the surface modification of **11**, the hydroxyl groups were activated by reaction with an excess of 4-nitrochloroformate in the presence of pyridine, yielding **12** (Scheme 5). This activation step was followed by the displacement of 4-nitrophenol upon nucleophilic attack of *tert*-butyl carbazate in the presence of a catalytic amount of DMAP. It is noteworthy that this reaction could be driven to completion only when benzene was used as a solvent. The hydrazide groups of **13** were then deprotected using a (1:1) TFA/CH_2Cl_2 mixture to afford **14**. Finally, the polyhydrazide chain ends were coupled to an excess of DOX in acidic methanol, forming the hydrazone linkage between the polymeric carrier and the drug (Scheme 5). The product was isolated from the excess DOX by purification with Sephadex LH-20 resin. The coupling of DOX to the polyhydrazide surface proceeded to an extent

Scheme 4

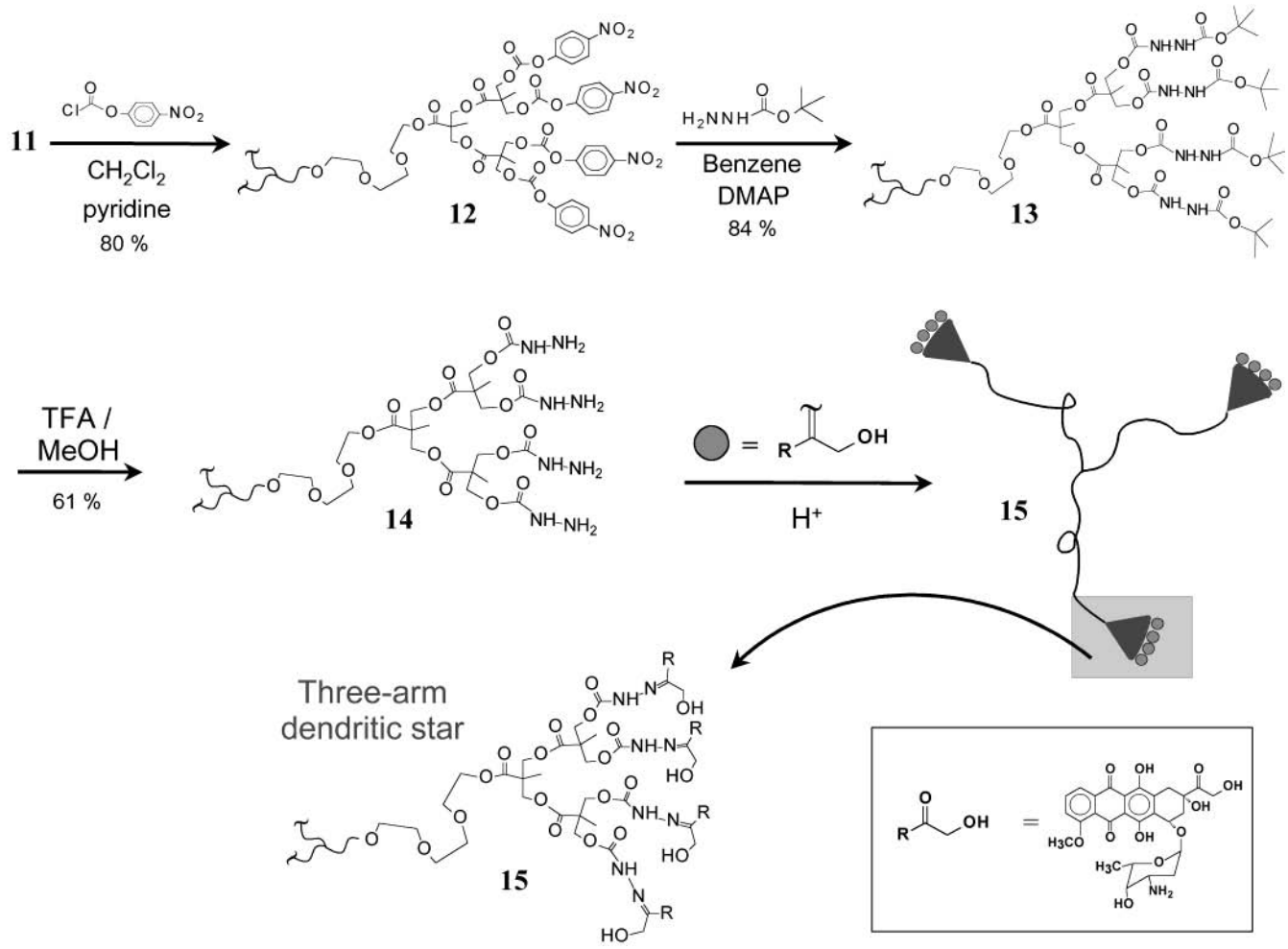


of only approximately 50% (6 out of 12 sites), based on MALDI-TOF MS and UV absorbance measurements, affording a conjugate with a mass of ca. 27 200 Da (**15**). The incomplete coupling observed in this reaction may be due to the reversible character of hydrazone formation under acid-catalyzed conditions (*46*). Conjugate **15**, obtained as a red solid, exhibited very different solubility properties when compared to its precursors. It was not soluble in common organic solvents such as tetrahydrofuran (THF) and CH_2Cl_2. However, it was soluble in MeOH and water, a finding that further supports the covalent character of **15** as opposed to a mixture of two separate compounds.

General Characterization. The techniques used for characterization of the dendrimers and 3-arm star PEO-dendrimer hybrids include ^{1}H NMR, ^{13}C NMR, size exclusion chromatography (SEC), electrospray MS, and MALDI-TOF MS. MALDI signals for model compound **4** and its precursors were not detected. However, the molecular ions and multiply charged species of the corresponding molecules were observed by electrospray MS. Peaks corresponding to incompletely deprotected chain ends were not observed. Even though SEC cannot detect small imperfections, it was a valuable technique for monitoring coupling of the dendrons to the trisphenolic core and to assess the purity after purification from any remaining [G-4]-COOH. MALDI-TOF MS was also the preferred technique for the characterization of **6** and model compound **7**, due to the small but inherent polydispersity of the short PEO moieties attached to the surface of the dendrimer. These PEO derivatives, although mainly consisting of three repeat units of ethylene glycol, also contained ca. 5% of the oligomers with two or four repeat units. Therefore, it imparted a wider range of molecular weights to the resulting molecule. However, SEC indicated a low polydispersity (PDI = 1.03) for this modified dendrimer. MALDI−TOF MS was also helpful in confirming the high degree of coupling (~ 95%) of **5** to the surface of **4**.

For the 3-arm star PEO-dendrimer hybrids the most valuable characterization technique was ^{1}H NMR. The signals corresponding to the quaternary methyl of the monomer unit (1.1−1.3 ppm), and the set of two singlets corresponding to the methyl groups of the isopropylidene

Scheme 5



ketal protecting group (~1.4 ppm) are very sharp and highly differentiated. These signals integrate well with the triplet (~ 4.3 ppm) of the terminal methylene alcohol of the PEO star formed after esterification. The methylene protons of the monomer unit are also well resolved. If the coupling reaction had been incomplete, these peaks would have been observed as several sets of signals, whereas just one sharp set was observed when the desired product was obtained. For the modification of **11**, ^{1}H NMR was also the most helpful technique because it was not possible to observe the individual signals corresponding to the dendritic units by ^{13}C NMR after introduction of the *t*-Boc groups on the surface and their cleavage (**13**, **14**). Only the individual signal of the PEO core (~ 70.4 ppm) was observed even with a variety of solvents and concentration conditions with overnight scanning at 125 MHz. In contrast, all of the signals were clearly present and correlated with the integration in the ^{1}H NMR analysis. MALDI-TOF MS also showed the general trend corresponding to an increase in the mass of these hybrids. A discrepancy in mass for **12** and **13** may be due to partial cleavage of the surface groups upon reaction with the acidic matrix. However, after cleavage of these groups (**14**), the mass correlates well with expected values. The characterization of **15** was made more difficult by the lack of detailed information available in the ^{1}H NMR spectrum with its very broad signals. In this case, MALDI-TOF MS and comparison of UV absorbance spectrum of **15** (λ = 490 nm) against a doxorubicin calibration curve were used to determine the degree of drug coupling on the surface of the carrier. SEC studies proved inconclusive due to solubility issues or the existence of strong interactions between the anthracene ring of DOX and the solid support leading to extreme peak broadening. However, Figure 3 shows the HPLC trace of the conjugate, which suggests a highly regular system.

Further evidence for the low polydispersity of the various carriers is demonstrated in Figure 4 in which precursors of **4** and **14** were evaluated since their highly hydrophilic surface leads to strong interactions with the solid support. These SEC measurements confirm the low polydispersities for **2**, **7**, and **13**, 1.01, 1.03, and 1.05, respectively, as well as the progressive decrease in retention time as a result of the increase in size for the three carriers.

CONCLUSIONS

The necessity for the development of low polydispersities and structurally well-defined polymeric systems with potential use as drug carriers has motivated the design and preparation of dendritic polymeric scaffolds based on an aliphatic polyester backbone derived from 2,2-bis(hydroxymethyl)propanoic acid as the building block. These systems were designed to meet the needs of their intended use as drug carriers, including water solubility, nontoxicity, and stability of the polymeric backbone. The low polydispersity of the model systems has been demonstrated. In addition, model compounds **4**, **7,** and **11** all showed excellent water solubility properties (≥ 200 mg/mL) making them excellent candidates

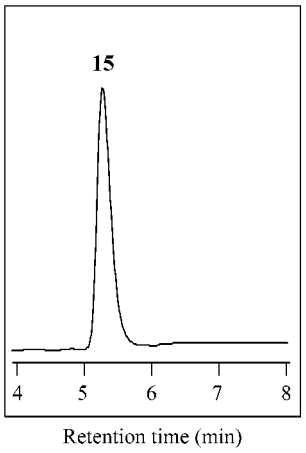


Figure 3. HPLC chromatogram of polymer−doxorubicin conjugate (**15**).

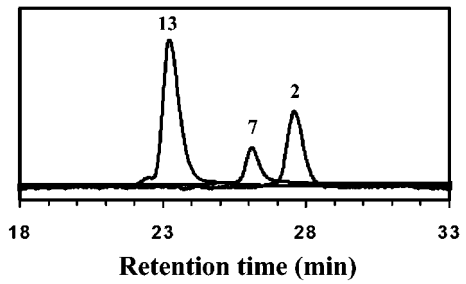


Figure 4. Size exclusion chromatography (SEC) traces of **2**, **7**, and **13** showing the low polydispersity of the systems prepared.

for further biological evaluation. In addition to the polymeric carriers, the feasibility for the modification of the surface of the polyester dendrimers and the preparation of a drug−polymer conjugate (**15**) have been demonstrated. The lack of quantitative coupling of DOX to the surface of the dendrons may be explained by thermodynamic factors due to the equilibrium conditions that prevail in the acid-catalyzed formation of the hydrazone linkage and perhaps some additional steric factors. These issues will be evaluated soon to optimize the coupling of the drug to the multifunctional carrier. Nevertheless, the carriers exemplified in this report show great promise due to their high degree of structure definition, polyvalency, and other desirable characteristics.

EXPERIMENTAL SECTION

General Procedures. All chemicals were purchased from Aldrich and used without any further purification. Solvents (Fischer) were reagent grade (99.9%). The 3-arm star poly(ethylene oxide) was purchased from Shearwater Polymers, Inc. (Huntsville, AL). ^{1}H and ^{13}C NMR spectra were recorded on Bruker AMX 300, AM 400 or DRX 500, as specified. The solvents used were $CDCl_3$ and DMSO-d_6. The solvent signals were used as internal standards for both ^{1}H NMR and ^{13}C NMR spectra. Size-exclusion chromatography (SEC) with double detection was performed at 45 °C on a chromatography line consisting of an M510 pump, a U6K universal injector, three 7-μm ultra-Styragel columns with pore sizes 100 Å, 500 Å, and a linear column, a differential refractive index (DRI) detector M410, and a photodiode array (PDA) detector M991 (Waters). THF was used as eluent at a nominal flow of 1 mL/min. The molecular weights and polydispersity were computed using a calibration curve constructed by polystyrene standards with narrow molecular weight distribution. Corrections for the flow rate fluctuation were made by using toluene as an internal standard. HPLC analysis was performed in a Model 2690 XE Alliance Separations module (Waters, USA) with built-in autoinjector and Photodiode Array detector (Waters 996). A Waters Symmetry C18 column (2.1 × 150 mm, 3.5 μm) was used with 40% phosphate buffer pH 7.0/60% methanol; 0.3 mL/min as mobile phase. MALDI-TOF MS data was collected on a PerSeptive Biosystems Voyager-DE instrument. The matrix used was α-cyano-4-hydroxycinnamic acid, and no silver trifluoroacetate was used. Electrospray and FAB mass spectrometry measurements were performed in the facilities of UC Berkeley. Elemental analyses were carried out by M-H-W Laboratories (Phoenix, AZ).

Preparation of Monoprotected Trisphenolic Core 1. The trisphenolic core (5.67 g, 18.51 mmol, 2 equiv) was dissolved in 150 mL of a 1:1 mixture of pyridine and CH_2Cl_2. The solution was placed in an ice bath and after stirring of the sample for 15 min, benzylchloroformate (1.58 g, 9.25 mmol, 1 equiv) was added dropwise. The reaction mixture was stirred for 1 h at 0 °C and warmed to room temperature. The solvent was evaporated and the residue was dissolved in CH_2Cl_2, followed by extraction with a 2 M HCl solution and H_2O. The organic layer was dried over $MgSO_4$, and the solvent was evaporated. The monoprotected product was separated from minor amounts of the diprotected product by column chromatography, using a gradient from CH_2Cl_2 to CH_2Cl_2/THF (1:1). A colorless solid product was obtained in a 50% yield (2.04 g, 4.63 mmol). IR (cm^{-1}, thin film from $CHCl_3$): 3359 (s), 1893, 1736. ^{1}H NMR ($CDCl_3$, 500 MHz): δ 2.10 (s, 3), 4.69 (s, 2), 5.26 (s, 2), 6.72 (d, 4, J = 8.5), 6.94 (d, 4, J = 8.5), 7.07 (m, 4), 7.40 (m, 3), 7.45 (m, 2). ^{13}C NMR ($CDCl_3$, 100 MHz): δ 30.80, 50.92, 70.37, 110.48, 114.65, 120.17, 128.56, 128.68, 128.77, 129.66, 129.81, 134.73, 141.30, 147.42, 149.08, 153.61. Calcd.: $[M]^+$ m/z = 440.162374. Found: LRFAB-MS: $[M]^+$ = 440, HRFAB-MS: $[M]^+$ = 440.16108. Anal. Calcd. for $C_{28}O_5H_{24}$: C 76.35%, H 5.49%. Found: C 73.05%, H 5.87%.

Preparation of the Isopropylidene Ketal Protected Dendrimer 2. The [G-4]-COOH polyester dendron (3.0 g, 1.4 mmol, 2.2 equiv), prepared as previously reported (*37*) and 0.17 g (0.66 mmol, 1.0 equiv) of the monoprotected tris phenolic core were dissolved in 3 mL of CH_2Cl_2. Following addition of 0.34 g of DCC (1.64 mmol, 2.5 equiv) and a catalytic amount of DPTS (0.08 g, 0.26 mmol, 0.40 equiv), the reaction mixture was stirred overnight at room temperature. The product was purified by column chromatography using a mixture of hexanes and ethyl acetate (20:80) as eluent to afford 1.23 g (73%) of a white solid. IR (cm^{-1}, thin film from $CHCl_3$): 2990, 1740 (br). ^{1}H NMR ($CDCl_3$, 300 MHz): δ 1.12 (s, 48), 1.26 (s, 24), 1.33 (s, 48), 1.39 (s, 48), 1.43 (s, 6), 2.16 (s, 3), 3.60 (d, 32, J = 11.7), 4.13 (d, 32, J = 11.7), 4.34 (m, 56), 5.25 (s, 2), 6.98 (d, 4, J = 8.7), 7.09 (bs,4), 7.11 (m, 8), 7.42 (m, 5). ^{13}C NMR ($CDCl_3$, 100 MHz): δ 17.51, 17.61, 18.42, 21.97, 25.13, 41.95, 46.67, 46.75, 46.99, 51.61, 64.74, 65.40, 65.83, 65.88, 70.28, 98.00, 120.44, 120.64, 128.47, 128.62, 128.71, 129.57, 129.74, 134.68, 146.02, 146.38, 148.49, 149.36, 153.51, 170.58, 171.38, 171.74, 173.39. Calcd: $[M]^+$ m/z = 4562.083502. Found: LRES-MS: $[MNa_2]^{+2}$ m/z = 2305.2, $[MNa_3]^{+3}$ m/z = 1544.7, $[MNa_4]^{+4}$ m/z = 1116.2. Anal. Calcd. for $C_{226}O_{95}H_{328}$: C 59.46%, H 7.24%. Found: C 59.60%, H 7.21%.

Preparation of Core-Monoprotected Dendrimer 3. For the deprotection of the hydroxyl groups of **2**, 1.12 g (0.22 mmol) of **2** was dissolved in 10 mL of methanol,

followed by the addition of 2 mL of 2 M H_2SO_4. The reaction mixture was stirred at room temperature for 2 days. The mixture was neutralized with a MeOH/NH_3 (1:1) solution. The ammonium sulfate salt was removed by filtration, and the solvent of the filtrate was evaporated to afford a quantitative yield (0.96 g) of a colorless solid product. IR (cm^{-1}, thin film from THF): 3369 (s), 2941, 1735 (s). ^{1}H NMR (DMSO-d_6, 500 MHz): δ 1.01 (s, 48), 1.14 (s, 24), 1.21 (s, 12), 1.36 (s, 6), 2.15 (s, 3), 3.45 (m, 64), 4.14 (bs, 32), 4.22 (bs, 16), 4.34 (d, 4, J = 9.5), 4.40 (d, 4, J = 9.5), 4.64 (bs, 32), 5.26 (s, 2), 7.12 (m, 12), 7.41 (m, 5). ^{13}C NMR (DMSO-d_6, 100 MHz): δ 16.73, 16.97, 17.17, 17.94, 30.45, 34.39, 46.30, 46.65, 50.27, 51.36, 63.72, 64.41, 65.37, 65.82, 69.83, 69.86, 120.75, 120.97, 124.94, 125.52, 128.41, 128.59, 129.46, 135.03, 146.18, 148.32, 148.97, 151.49, 152.96, 170.81, 171.49, 171.88, 174.07. Calcd: $[M]^+$ m/z = 3921.582700. Found: LRES-MS: $[MNa_2]^{+2}$ m/z = 1985.0, $[MNa_3]^{+3}$ m/z = 1330.9. Anal. Calcd for $C_{178}O_{95}H_{264}$: C 54.48%, H 6.78%. Found: C 54.23%, H 6.91%.

Preparation of Dendrimer 4. Dendrimer **3** (0.280 g, 0.071 mmol) was dissolved in 2 mL of ethyl acetate, and 0.04 g of Pd/C 10% was added. Following evacuation of the system, an atmosphere of H_2 under medium pressure was applied to the reaction mixture using a rubber balloon. After the sample was stirred vigorously for 6 h at room temperature, the catalyst was removed by filtration. A solid product was obtained in quantitative yield after evaporation of the solvent (0.27 g). IR (cm^{-1}, thin film from THF): 3367 (s), 2947, 1741 (s). ^{1}H NMR (DMSO-d_6, 500 MHz): δ 0.998 (s, 48), 1.136 (s, 24), 1.202 (s, 12), 1.348 (s, 6), 2.076 (s, 3), 3.363−3.505 (m, 64), 4.102 (bs, 32), 4.215 (bs, 16), 4.33 (d, 4, J = 9.5), 4.382 (d, 4, J = 9.5), 4.627 (bs, 32), 6.678 (d, 2, J = 8.0), 6.824 (d, 2, J = 8.0), 7.014 (m, 4), 7.102 (m, 4). ^{13}C NMR (DMSO-d_6, 125 MHz): δ 16.73, 16.95, 17.15, 17.94, 40.01, 46.28, 50.26, 63.69, 64.38, 65.03, 69.81, 120.72, 125.50, 128.08, 129.42, 137.64, 138.51, 147.01, 147.89, 170.83, 171.48, 171.86, 174.06. Calcd: $[M]^+$ m/z = 3789.86. Found: LRES-MS: $[MNa_2]^{+2}$ m/z = 1917.4, $[MNa_3]^{+3}$ m/z = 1286.0. Anal. Calcd for $C_{170}O_{93}H_{258}$: C 53.88%, H 6.86%. Found: C 51.96%, H 6.89%.

Preparation of 5. Tri(ethylene glycol) monomethyl ether (14.65 g, 89.20 mmol) was diluted with 60 mL of acetonitrile. DMAP (1.09 g, 8.92 mmol) used as a catalyst and diglycolic anhydride (10.87 g, 93.66 mmol) were added to the reaction mixture. After the reaction mixture was stirred for 24 h at room temperature, the solvent was evaporated and the crude product was diluted with 12 mL of acidified brine. The product was extracted with ethyl acetate. The combined organic layers were dried over $MgSO_4$. After removal of the drying agent by filtration, the solvent was evaporated to afford an 80% yield (20 g) of a colorless slightly viscous oil as a product. IR (cm^{-1}): 3400−2500 (br), 1753, 1140. ^{1}H NMR ($CDCl_3$, 400 MHz): δ 3.83 (s, 3), 3.56 (t, 2, J = 3.2), 3.66 (bs, 6), 3.72 (dt, 2, J = 3.2, 4.8), 4.25 (s, 2), 4.30 (s, 2), 4.35 (dt, 2, J = 3.2, 4.8). ^{13}C NMR (DMSO, 100 MHz): δ 58.72, 63.78, 63.98, 67.77, 68.13, 68.62, 70.19, 70.81, 71.62, 169.97, 171.88. Calcd: $[M]^+$ m/z = 280.115818. Found: LRES-MS $[M-H]^-$ m/z = 279.2. Anal. Calcd for $C_{11}O_8H_{20}$: C 47.14%, H 7.19%. Found: C 47.04%, H 6.96%.

Preparation of Surface Modified Dendrimer 6. The polyol **3** (0.94 g, 0.24 mmol, 1 equiv) was dissolved in 1 mL of pyridine and 15 mL of CH_2Cl_2. The acid derivative of tri(ethylene glycol) monomethyl ether (4.30 g, 15.36 mmol, 64 equiv) was added, followed by the addition of 3.17 g (15.36 mmol) of DCC and 1.02 g (3.48 mmol) of DPTS as a catalyst. The reaction mixture was stirred overnight at room temperature. The dicyclohexyl urea (DCU) formed as a byproduct was removed by filtration, and the solvent of the filtrate was evaporated. Trace amounts of DPTS present in the product were removed by filtration from a toluene solution and precipitation in diethyl ether. The colorless oily product was obtained in a 65% yield (1.91 g). IR (cm^{-1}, thin film from $CHCl_3$): 1737 (s), 1154 (s). ^{1}H NMR ($CDCl_3$, 400 MHz): δ 1.18 (bs, 72), 1.26 (s, 12), 1.41 (s, 6), 2.11 (s, 3), 3.32 (s, 96), 3.49 (m, 64), 3.59 (m, 224), 3.65 (m, 64), 4.19 (bs, 208), 4.24 (m, 64), 4.37 (m, 8), 5.21 (s, 2), 7.13 (m, 12), 7.30 (m, 5). ^{13}C NMR ($CDCl_3$, 125 MHz): δ 17.42, 17.63, 46.21, 46.49, 58.87, 63.81, 64.98, 67.61, 67.79, 68.73, 70.39, 70.42, 71.77, 120.45, 120.62, 128.40, 128.57, 129.69, 132.29, 169.21, 169.58, 171.35, 171.52. Calcd: $[M]^+$ m/z = 12,316.63. Found: MALDI-TOF MS: $[M]^+$ = 11,930, $[M]^{+2}$ = 23,505. Anal. Calcd for $C_{530}O_{319}H_{840}$: C 51.69%, H 6.87%. Found: C 51.60%, H 6.73%.

Preparation of Dendrimer 7. The precursor **6** (1.7 g, 0.138 mmol) was dissolved in 6 mL of ethyl acetate. After the addition of 0.16 g of Pd/C 10%, the system was evacuated and the reaction mixture was stirred overnight at room temperature under H_2 atmosphere at 700 psi. The catalyst was removed by filtration, and the solvent was evaporated, affording 1.17 g of the product as an oil (70%). IR (cm^{-1}, thin film from $CHCl_3$): 3485, 2887, 1737 (s), 1145 (s). ^{1}H NMR ($CDCl_3$, 400 MHz): δ 1.10 (s, 12), 1.17 (bs, 48), 1.24 (s, 24), 1.40 (s. 6), 2.04 (s, 3), 3.34 (s, 96), 3.51 (bs, 64), 3.61 (bs, 224), 3.67 (bs, 64), 4.21 (bs, 272), 6.69 (d, 2, J = 7), 6.85 (d, 2, J = 7), 6.94 (d, 4, J = 7), 7.07 (d, 4, J = 7). ^{13}C NMR ($CDCl_3$, 125 MHz): δ 17.02, 17.22, 17.48, 46.11, 46.41, 48.21, 51.04, 58.70, 61.30, 63.37, 63.72, 63.91, 64.99, 67.50, 67.70, 67.88, 68.04, 68.58, 69.99, 70.11, 70.17, 70.23, 70.28, 71.59, 72.16, 114.73, 120.33, 129.31, 129.56, 147.08, 148.10, 169.18, 169.56, 169.94, 171.18, 171.78, 172.89. Calcd: $[M]^+$ m/z = 12,182.17. Found: MALDI-TOF MS: $[M]^+$ = 11,458.

Preparation of 3-Arm Star PEO−Dendrimer Hybrid 8. The hydroxy terminated 3-arm PEO star of 22 550 Da (as measured by MALDI) (2.0 g, 0.1 mmol) and the propylidene ketal derivative of 2,2-bis(hydroxymethyl)propanoic acid were mixed and dissolved in 5 mL of CH_2Cl_2. DMAP was added as a catalyst (0.12 g, 1.0 mmol), followed by DCC (0.62 g, 3.0 mmol). The reaction mixture was stirred at room temperature under N_2 atmosphere for 3 h. After filtration of the DCU formed as a byproduct, the polymer was precipitated from CH_2Cl_2 solution into diethyl ether. The polymer was collected by filtration. Trace amounts of DMAP still present were removed by filtration after dissolving the polymer in benzene. The product was precipitated from the benzene solution directly into diethyl ether and filtered to yield 1.44 g (70%) of the product. IR (cm^{-1}, thin film from $CHCl_3$): 2874, 1730 (w), 1100 (s). ^{1}H NMR ($CDCl_3$, 400 MHz): δ 1.21 (s, 9), 1.38 (s, 9), 1.42 (s, 9), 3.46 (t, 16, J = 5.0), 3.64 (bs, 2140), 3.81 (t, 10, J = 5.0), 4.19 (d, 6, J = 10.8), 4.29 (t, 6, J = 4.8). ^{13}C NMR ($CDCl_3$, 125 MHz): δ 18.60, 22.98, 24.13, 41.69, 56.79, 63.63, 63.78, 65.84, 68.91, 70.46, 97.94, 174.04. Calcd: $[M]^+$ m/z = 23,018. Found: MALDI-TOF MS: $[M]^+$ = 23,000. Anal. for **8**: Found: C 54.56%, H 8.46%.

Preparation of Hybrid 9. A mixture of 1.24 g (0.06 mmol) of **8** in 6 mL of MeOH and 2 mL of a 2 M H_2SO_4 solution was stirred overnight at room temperature. The crude reaction mixture was neutralized with a 7 N solution of ammonia in methanol and the ammonium sulfate salt was filtered off. The product was then precipitated from the filtrate in diethyl ether. The white solid product was recovered in a 62% yield (0.77 g). IR

(cm^{-1}, thin film from $CHCl_3$): 3484, 2885, 1727 (w), 1102 (s). ^1H NMR ($CDCl_3$, 300 MHz): δ 1.11 (s, 9), 3.64 (bs, 2288), 4.33 (t, 6, $J = 4.8$). ^{13}C NMR ($CDCl_3$, 125 MHz): δ 17.06, 49.57, 56.75, 63.27, 63.59, 67.18, 68.70, 70.30, 84.09, 175.59. Calcd: $[M]^+$ $m/z = 22{,}895$. Found: MALDI-TOF MS: $[M]^+ = 22{,}890$. Anal. for **9**: Found: C 52.49%, H 8.40%.

Preparation of Hybrid 10. Polyol **9** (2.96 g, 0.15 mmol) was dissolved in 20 mL of CH_2Cl_2. DMAP (0.18 g, 1.45 mmol) and DCC (0.90 g, 4.34 mmol) were added and the reaction mixture was stirred overnight at room temperature under N_2 atmosphere. The DCU was filtered off and the product was precipitated from CH_2Cl_2 solution in diethyl ether affording a white powder in 80% yield. IR (cm^{-1}, thin film from $CHCl_3$): 2884, 1737, 1106 (s). ^1H NMR ($CDCl_3$, 300 MHz): δ 1.14 (s, 18), 1.20 (s, 9), 1.35 (s, 18), 1.40 (s, 18), 3.63 (bs, 2160), 4.14 (d, 12, $J =$ 11.7). ^{13}C NMR ($CDCl_3$, 125 MHz): δ 17.67, 18.50, 22.21, 24.94, 41.98, 46.68, 63.70, 64.21, 65.20, 65.88, 65.93, 68.79, 70.53, 98.05, 172.47, 173.47. Calcd: $[M]^+$ $m/z =$ 23,831. Found: TOF-MALDI MS: $[M]^+ = 23{,}801$. Anal. for **10**. Found: C 54.26%, H 9.01%.

Preparation of Hybrid 11. A solution of 2.71 g (0.13 mmol) of **10** in 12 mL of MeOH was mixed with 4 mL of 2 M H_2SO_4, and the mixture was stirred overnight at room temperature, then neutralized with 7 N ammonia solution in methanol. The ammonium salt was removed by filtration and the product was purified by precipitation in diethyl ether. The product was recovered in 84% (2.25 g). IR (cm^{-1}, thin film from $CHCl_3$): 3459, 1736, 1105. ^1H NMR ($CDCl_3$, 400 MHz): δ 1.07 (s, 18), 1.31 (s, 9), 3.64 (bs, 2437), 4.31 (m, 12), 4.40 (d, 6, $J = 11.2$). ^{13}C NMR ($CDCl_3$, 125 MHz): δ 17.11, 17.99, 46.44, 49.72, 63.68, 64.89, 67.56, 70.50, 173.01, 175.02. Calcd: $[M]^+$ $m/z = 23\,591$. Found: MALDI-TOF MS: $[M]^+ = 23\,583$. Anal. for **11**. Found: C 54.47%, H 9.04%.

Preparation of 11a. A solution of **11** (1.00 g, 0.042 mmol) in 5 mL of CH_2Cl_2 was treated with *p*-methoxyacetic acid (16 mg, 0.096 mmol), DMAP (58 mg, 0.474 mmol), and then DCC (20 mg, 0.097 mmol). The reaction mixture was stirred at room temperature for 5 h, and the product was precipitated from the reaction mixture into diethyl ether affording 0.86 g of product. IR (cm^{-1}, thin film from $CHCl_3$): 3449, 1731, 1135. ^1H NMR (DMSO-d_6, 300 MHz): δ 0.99 (s, 18), 1.16 (s, 9), 3.39 (bs, 3322), 4.09 (m, 20), 4.62 (t, 6, $J = 4.8$), 4.95 (t, 1, $J =$ 4.8), 6.85 (d, 6, $J = 9.0$), 7.11 (d, 6 $J = 9.0$). ^{13}C NMR ($CDCl_3$, 100 MHz): δ 17.10, 49.73, 70.49, 113.96, 130.22, 172.82, 176.10. Found: MALDI-TOF MS: $[M]^+ = 23\,897$. Anal. for **11a**. Found: C 54.89%, H 8.72%.

Preparation of Activated Hybrid 12. A solution of 1.07 g (0.05 mmol) of **11** in 4 mL of CH_2Cl_2 was treated with 0.25 mL of pyridine and 0.61 g (3.05 mmol) of 4-nitrophenyl chloroformate. The reaction mixture was stirred overnight at room temperature. The product was recovered in 80% yield after purification by precipitation from the reaction mixture into diethyl ether. IR (cm^{-1}, thin film from $CHCl_3$): 2883, 1774, 1737, 1626, 1593, 1527, 1107. ^1H NMR ($CDCl_3$, 400 MHz): δ 1.34 (s, 9), 1.36 (s, 18), 3.64 (bs, 2453), 4.27 (t, 6, $J = 4.8$ Hz), 4.39−4.53 (m, 36), 7.38 (d, 24, $J = 9.0$), 8.28 (d, 24, $J = 9.0$). ^{13}C NMR ($CDCl_3$, 125 MHz): δ 17.62, 46.56, 5.39, 63.68, 69.10, 70.50, 121.71, 125.28, 145.54, 152.04, 155.14, 170.98. Calcd: $[M]^+$ $m/z = 25\,571$. Found: MALDI-TOF MS: $[M]^+ = 25{,}100$. Anal. for **12**. Found: C 56.39%, H 8.96, N 0.70%.

Preparation of *t*-Boc Terminated Hybrid 13. The protected hydrazide was coupled to **12** by dissolving 0.84 g (0.04 mmol) of **12** in 5 mL of benzene, followed by the addition of DMAP (0.02 g, 0.15 mmol) and *tert*-butyl carbazate (0.29 g, 2.19 mmol). The reaction mixture was stirred at room temperature under N_2 atmosphere for 3 h. The product was purified by precipitation in diethyl ether. The white solid product was recovered by filtration in 84% yield (0.69 g). IR (cm^{-1}, thin film from $CHCl_3$): 3300, 2885, 1736, 1104. ^1H NMR ($CDCl_3$, 300 MHz): δ 1.18 (s, 18), 1.31 (s, 9), 1.46 (s, 108), 3.64 (bs, 2300), 4.30 (m, 36). Calcd: $[M]^+$ $m/z = 25{,}487$. Found: MALDI-TOF MS: $[M]^+ = 24\,501$. Anal. for **13**. Found: C 53.96%, H 8.37, N 1.34%.

Preparation of Hydrazide Terminated Hybrid 14. The *t*-Boc groups of **13** were cleaved by dissolving 0.62 g (0.03 mmol) of **13** in 4 mL of a (1:1) trifluoroacetic acid (TFA) and CH_2Cl_2 solution. The reaction mixture was stirred for 5 h and the product was precipitated in diethyl ether from the reaction mixture solution, yielding a white powdery product in 61% yield (0.36 g). IR (cm^{-1}, thin film from $CHCl_3$): 3282, 2884, 1737, 1105. ^1H NMR ($CDCl_3$, 300 MHz): δ 1.23 (s, 18), 1.29 (s, 9), 3.64 (bs, 2688), 4.26 (m, 36). Calcd: $[M]^+$ $m/z = 24{,}287$. Found: TOF-MALDI MS: $[M]^+ = 24{,}210$. Anal. for **14**. Found: C 53.33%, H 8.71, N 1.43%.

Preparation of Polymer−DOX Conjugate (15). The polyhydrazide **14** (0.22 g, 0.01 mmol) and an excess of the HCl salt of doxorubicin (95 mg, 0.16 mmol) were dissolved in 3 mL of MeOH. A drop of TFA was added as a catalyst. The reaction mixture was stirred overnight at room temperature. The polymer was precipitated in diethyl ether from the reaction mixture. The solid was recovered by filtration and washed with diethyl ether. The conjugate was purified from free doxorubicin by size exclusion chromatography using Sephadex LH-20 resin and MeOH as the mobile phase. The conjugate fractions were combined, and the solvent was evaporated. The conjugate was redissolved in distilled water and lyophilized, recovering 0.21 g of a spongy red solid as the product (78% based on half coupling). IR (cm^{-1}): 3100−1900 (br), 1739. ^1H NMR (DMSO-d_6, 300 MHz): δ 1.16 (bs, 42), 1.62−1.95 (m, 9), 2.10−2.31 (m, 7), 3.50 (bs, 2200), 3.92 (bs, 18), 4.15 (bs, 38), 4.43 (s, 8), 4.89−5.18 (m, 5), 5.28 (s, 3), 5.44 (d, 3), 5.84 (s, 3), 7.50−8.00 (m, 36). Calcd (full coupling): $[M]^+$ $m/z = 30\,395$. Found: MALDI-TOF MS: $[M]^+ = 27{,}242$. Anal. for **15**. Found: C 54.21%, H 8.57, N 1.43%.

ACKNOWLEDGMENT

We thank the National Science Foundation (DMR-9816166), the Department of Energy (Basic Energy Sciences, and MDI II), the National Institutes of Health, Grant GM65361, and the UC Breast Cancer Research and Development Program (6JB-0137) for support of this research.

LITERATURE CITED

(1) Ringsdorf, H. (1975) Structure and Properties of Pharmacologically Active Polymers. *J. Polym. Sci. Polym. Symp. 51*, 135−153.

(2) Bader, H., Ringsdorf, H., and Schmidt, B. (1984) Water-Soluble Polymers in Medicine. *Angew. Makromol. Chem. 123/124*, 457−485.

(3) Kopeček, J. (1977) Soluble biomedical polymers. *Polym. Med. 7*, 191−221.

(4) Kopeček, J. (1981) Soluble Polymers in Medicine, in *Systemic Aspects of Biocompatibility, II* (D. F. Williams, Ed.) pp 159−180, CRC Press, Boca Raton, FL.

(5) Kopeček, J., Kopečková, P., Minko, T., and Lu, Z. R. (2000) HPMA Copolymer-Anticancer Drug Conjugates: Design, Activity and Mechanism of Action. *Eur. J. Pharm. Biopharm. 50*, 61−81.

(6) Duncan, R. (1992) Drug-Polymer Conjugates: Potential for Improved Chemotherapy. *Cancer Res. 46*, 175−210.
(7) Maeda, H., Seymour, L. W., and Miyamoto, Y. (1992) Conjugates of Anticancer Agents and Polymers: Advantages of Macromolecular Therapeutics in Vivo. *Bioconjugate Chem. 3*, 351−362.
(8) Seymour, L. W., Miyamoto, Y., Maeda, H., Brereton, M., Strohalm, J., Ulbrich, K., and Duncan, R. (1995) Influence of Molecular Weight on Passive Tumour Accumulation of a Soluble Macromolecular Drug Carrier. *Eur. J. Cancer 31A*, 766−770.
(9) Matsumura, T., and Maeda, H. (1986) A New Concept for Macromolecular Therapeutics in Cancer Chemotherapy: Mechanism of Tumoritropic Accumulation of Proteins and the Antitumor Agent SMANCS. *Cancer Res. 46*, 6387−6392.
(10) Maeda, H., Wu, J., Sawa, T., Matsumura, Y., and Hori, K. (2000) Tumor Vascular Permeability and the EPR Effect in Macromolecular Therapeutics: A Review. *J. Control. Release 65*, 271−284.
(11) Seymour, L. W. (1992) Passive Tumor Targeting of Soluble Macromolecules and Drug Conjugates. *Crit. Rev. Ther. Drug 9*, 135−187.
(12) Cuvier, C., Roblot-Treupel, L., Milliot, J. M., Lizard, G., Chevillards, S., Manfait, M., Couvreur, P., and Poupon, M. F. (1992) Doxorubicin-loaded Nanospheres bypass Tumour Cell Multidrug Resistance. *Biochem. Pharmacol. 44*, 509−517.
(13) Omelyanenko, V., Kopečková, P., Gentry, C, and Kopeček, J. (1998) Targetable HPMA Copolymer-Adriamycin Conjugates: Recognition, Internalization, and Subcellular Fate. *J. Control. Release 53*, 25−37.
(14) Vasey, P. A., Kaye, S. B., Morrison, R., Twelves, C., Wilson, P., Duncan, R., Thomson, A. H., Murray, L. S., Hilditch, T. E., Murray, T., Burtles, S., Fraier, D., Frigerio, E., and Cassidy, J. (1999) Phase I Clinical and Pharmacokinetic Study of PK1 [N-(2-Hydroxypropyl)methacrylamide Copolymer Doxorubicin]: First member of a New Class of Chemotherapeutic Agents-Drug-Polymer Conjugates. *Clin. Cancer Res. 5*, 83−94.
(15) Ulbrich, K., Šubr, V., Strohalm, J., Plocavá, D., Jelínkova, M., and Říhová, B. (2000) Polymeric Drugs Based on Conjugates of Synthetic and Natural Macromolecules: I. Synthesis and Physicochemical Characterization. *J. Control. Release 64*, 63−79.
(16) Godwin, A., Hartenstein, M., Müller, A. H. E., and Brocchini, S. (2001) Narrow Molecular Weight Distribution Precursors for Polymer-Drug Conjugates. *Angew. Chem., Int. Ed. 40*, 594−597.
(17) Tomalia, D. A., and Durst, H. D. (1993) Genealogically Directed Synthesis − Starburst Cascade Dendrimers and Hyperbranched Structures. *Top. Curr. Chem. 165*, 193−313.
(18) Fréchet, J. M. J. (1994) Functional Polymers and Dendrimers − Reactivity, Molecular Architecture, and Interfacial Energy. *Science 263*, 1710−1715.
(19) Newkome, G. R., Moorefield, C. N., and Vögtle, F. (1996) Dendritic Macromolecules: Concepts, Synthesis, Perspectives, VCH: Weinheim, Germany.
(20) Kim, S. Y., Shin, I. L. G., Lee, Y. M., Cho, C. S., and Sung, Y. K. (1998) Methoxy poly(ethylene glycol) and e-caprolactone amphiphilic block copolymeric micelle containing indomethacin. II. Micelle formation and drug release behaviors. *J. Control. Release 51*, 13−22.
(21) Lasic, D. D. (1994) Sterically Stabilized Vesicles. *Angew. Chem., Int. Ed. Engl. 33*, 1685−1698.
(22) Evans, E., Klingenberg, D. J., Rawicz, W., and Szoka, F. (1996) Interactions between Polymer-Grafted Membranes in Concentrated Solutions of Free Polymer. *Langmuir 12*, 3031−3037.
(23) Liu, M., and Fréchet, J. M. J. (1999) Designing Dendrimers for Drug Delivery. *Pharm. Sci. Technol. Today 2*, 393−401.
(24) Liu, M., Kono, K., and Fréchet, J. M. J. (1999) Water-Soluble Dendrimer-Poly(ethylene glycol) Starlike Conjugates as Potential Drug Carriers. *J. Polym. Sci., Polym. Chem. 37*, 3492−3502.
(25) Kono, K., Liu, M., and Fréchet, J. M. J. (1999) Design of Dendritic Macromolecules Containing Folate or Methotrexate Residues. *Bioconjugate Chem. 10*, 1115−1121.
(26) Grayson, S. M., Jayaraman, M., and Fréchet, J. M. J. (1999) Convergent synthesis and 'surface' functionalization of a dendritic analogue of poly(ethylene glycol). *Chem. Commun. 14*, 1329−1330.
(27) Liu, M., Kono, K., and Fréchet, J. M. J. (2000) Water-soluble dendritic unimolecular micelles: Their potential as drug delivery agents. *J. Control. Release 65*, 12−131.
(28) Esfand, R., and Tomalia, D. A. (2001) Poly(Amidoamine) (PAMAM) Dendrimers: From Biomimicry to Drug Delivery and Biomedical Applications. *Drug Discovery Today 6*, 427−436.
(29) Haensler, J., and Szoka, F. C., Jr. (1993) Polyamidoamine Cascade Polymers Mediate Efficient Transfection of Cells in Culture. *Bioconjugate Chem. 4*, 372−379.
(30) Malik, N., Wiwattanapatapee, R., Klopsch, R., Lorenz, K., Frey, H., Weener, J. W., Meijer, E. W., Paulus, W., and Duncan, R. (2000) Dendrimers: Relationship Between Structure and Biocompatibility in Vitro, and Preliminary Studies on the Biodistribution of 125I-Labeled Polyamidoamine Dendrimers in Vivo. *J. Control. Release 65*, 133−148.
(31) Supattapone, S., Wille, H., Uyechi, L., Safar, J., Tremblay, P., Szoka, F. C. Jr., Cohen, F. E., Prusiner, S. B., and Scott, M. R. (2001) Branched Polyamines Cure Prion-Infected Neuroblastoma Cells. *J. Virol. 75*, 3453−3461.
(32) Duncan, R., and Malik, N. (1996) Dendrimers: Biocompatibility and Potential for Delivery of Anticancer Agents. *Proc. Int. Symp. Control. Release Bioact. Mater. 23*, 105−106.
(33) Padilla De Jesús, O. L., Ihre, H. R., Gagne, L., Fréchet, J. M. J., and Szoka, F. C., Jr. (2001) Polyester Dendritic Systems for Drug Delivery Applications: In Vitro and In Vivo Evaluation. *Bioconjugate Chem. 13*, 453−461.
(34) Meijer, D. K., and Molema, G. (1995) Targeting of drugs to the liver. *Semin. Liver Dis. 15*, 202−56.
(35) Lee, W. K., and Gardella, J. A. (2000) Hydrolytic kinetics of biodegradable polyester monolayers. *Langmuir 16*, 3401−3406.
(36) Breitenbach A., Li, Y. X., and Kissel, T. (2000) Branched biodegradable polyesters for parenteral drug delivery systems. *J. Control. Release 64*, 167−178.
(37) Ihre, H., Hult, A., Fréchet, J. M. J., and Gitsov, I. (1998) Double-Stage Convergent Approach for the Synthesis of Functionalized Dendritic Aliphatic Polyesters Based on 2,2-Bis(Hydroxymethyl)Propanoic Acid. *Macromolecules 31*, 4061−4068.
(38) Greenwald, R. B., Conover, C. D., and Choe, Y. H. (2000) Poly(Ethylene Glycol) Conjugated Drugs and Prodrugs: A Comprehensive Review. *Crit. Rev. Ther. Drug 17*, 101−161.
(39) Kaneko, T., Willner, D., Monkovíc, I., Knipe, J. O., Braslawsky, G. R., Greenfield, R. S., and Vyas, D. M. (1991) New Hydrazone Derivatives of Adriamycin and Their Immunoconjugates- a Correlation between Acid Stability and Cytotoxicity. *Bioconjugate Chem. 2*, 133−141.
(40) Guo, X., and Szoka, F. C., Jr. (2001) Steric Stabilization of Fusogenic Liposomes by a Low-pH Sensitive PEG-Diortho Ester-Lipid Conjugate. *Bioconjugate Chem. 12*, 291−300.
(41) Murthy, N., Stayton, P. S., and Hoffman, A. S. (2000) pH Sensitive Membrane Disruptive Pegylated Polycations. *Polym. Prepr., Am. Chem. Soc. Div. Polym. Chem. 41*, 1010−1011.
(42) Duncan, R., Cable, H. C., Lloyd, J. B., Rejmanova, P., and Kopeček, J. (1983) Degradation of Side-Chains of N-2-(Hydroxypropyl)Methacrylamide Copolymers by Lysosomal Thiol Proteinases. *Biosci. Rep. 2*, 1041−1046.
(43) Senter, P. D., Svensson, H. P., Schreiber, G. J., Rodriguez, J. L., and Vrudhula, V. M. (1995) Poly(Ethylene Glycol)-Doxorubicin Conjugates Containing B−Lactamase-Sensitive Linkers. *Bioconjugate Chem. 6*, 389−394.
(44) Melton, R. G., and Knox, R. J., Eds. (1999) *Enzyme Prodrug Strategies for Cancer Therapy*, Kluwer Academic/Plenum Publishers, New York.
(45) Lemieux, G. A., and Bertozzi, C. R. (1998) Chemoselective ligation reactions with proteins, oligosaccharides and cells. *Trends Biotechnol. 16*, 506−511.
(46) King, T. P., Zhao, S. W., and Lam, T. (1986) Preparation of Protein Conjugates via Intermolecular Hydrazone Linkage. *Biochemistry 25*, 5774−5779.

BC010102U

Polyester Dendritic Systems for Drug Delivery Applications: In Vitro and In Vivo Evaluation

Omayra L. Padilla De Jesús,[†] Henrik R. Ihre,[†] Lucie Gagne,[‡] Jean M. J. Fréchet,*[,†] and Francis C. Szoka, Jr.*[,‡]

Department of Chemistry, University of California, Berkeley, California 94720-1460 and School of Pharmacy, University of California, San Francisco, California 94143-0446. Received October 22, 2001

High molecular weight polymers (> 20 000 Da) have been widely used as soluble drug carriers to improve drug targeting and therapeutic efficacy. Dendritic polymers are exceptional candidates for the preparation of near monodisperse drug carriers due to their well-defined structure, multivalency, and flexibility for tailored functionalization. We evaluated various dendritic architectures composed of a polyester dendritic scaffold based on the monomer unit 2,2-bis(hydroxymethyl)propanoic acid for their suitability as drug carriers both in vitro and in vivo. These systems are both water soluble and nontoxic. In addition, the potent anticancer drug, doxorubicin, was covalently bound via a hydrazone linkage to a high molecular weight 3-arm poly(ethylene oxide)−dendrimer hybrid. Drug release was a function of pH, and the release rate was more rapid at pH < 6. The cytotoxicity of the DOX−polymer conjugate measured on multiple cancer lines in vitro was reduced but not eliminated, indicating that some active doxorubicin was released from the drug polymer conjugate under physiological conditions. Furthermore, biodistribution experiments show little accumulation of the DOX−polymer conjugate in vital organs, and the serum half-life of doxorubicin attached to an appropriate high molecular weight polymer has been significantly increased when compared to the free drug. Thus, this new macromolecular system exhibits promising characteristics for the development of new polymeric drug carriers.

INTRODUCTION

A variety of approaches have been implemented for the discovery of medicinal compounds, including the isolation of naturally occurring bioactive substances and the design and synthesis of new molecules with biological activity. Many compounds have been identified by these means, but the lack of selectivity of the majority of current highly toxic drugs used for chemotherapy has motivated the search for other means to improve their therapeutic efficacy and increase their selectivity (*1*).

In the past few decades, the use of polymers as carriers of both covalently bound (*2*−*5*) and physically entrapped drug molecules (*6*−*8*) has been widely explored. When a drug is linked to a polymer, it loses activity because it cannot interact with the drug target either due to steric constraints or the inability of the drug to reach the target site (*9*). Furthermore, the drug−polymer conjugate can no longer cross the cellular membrane by simple diffusion, but must do so by endocytosis. The resulting endosomal compartment containing the polymeric conjugate fuses with the more acidic lysosomal compartment (pH 4−5), whose hydrolytic enzymes then degrade the conjugate. This mechanism allows a more selective uptake of therapeutic agents, in contrast to small drugs that can easily diffuse into and out of the cell (*2, 10*). In certain cells, the endocytotic uptake enables drug−polymer conjugates to bypass multidrug resistance (MDR) mediated efflux mechanisms hence to overcome drug resistance in the cancer cells (*11, 12*). Furthermore, the anatomical differences between normal and tumor tissue allows for preferential accumulation of a polymeric drug in neoplastic tissue. High molecular weight polymers preferentially accumulate in solid tumor tissue due to a combination of the leaky character of tumor blood vessels formed during neo-angiogenesis and to limited lymphatic drainage. The combination of these two factors is responsible for the enhanced permeability and retention effect (EPR) observed with tumor tissue, which leads to a passive targeting of drugs to tumors (*13, 14*). In addition, the larger hydrodynamic volume of polymers contributes to the increased plasma half-life of the drug-polymer conjugates, increasing the probability of accumulation of the therapeutic agent in the tumor tissue by means of the EPR effect (*3, 15*). Drugs have also been conjugated to polymers to improve their water solubility properties, to decrease their toxicity due to local accumulation of the drug prior to reaching the target tissue, and to protect them from possible enzymatic degradation or hydrolysis.

Polymers previously evaluated for delivery of covalently attached drugs have primarily been random coil linear polymers such as poly(ethylene glycol) (PEG) (*16*), *N*-(2-hydroxypropyl)methacrylate (HPMA) (*17*), and styrene maleic anhydride (SMA) (*5*). However, the synthesis of some of these systems results in highly polydisperse materials with a wide range of molecular weights due to their mode of preparation (*18*). Molecules of different molecular weights found in a polydisperse sample will behave differently in the body. Therefore, either monodisperse or low-polydisperse (PDI < 1.1) polymers are required to achieve systems displaying homogeneous and reproducible pharmacokinetic properties. The intrinsic properties of dendrimers, with their well-defined structures and their flexibility for tailored functionalization, classify these molecules as good candidates for the assembly of multivalent drug carriers (*19*−*25*).

The well-designed step-by-step preparation of dendrimers results in a monodisperse system (*26*−*28*). Few dendritic systems have been evaluated previously, due to their lack of availability. At present, probably the best-known dendritic system is the polyamidoamine (PAMAM) Starburst family of dendrimers (*29*). These are

[†] University of California, Berkeley.
[‡] University of California, San Francisco.

10.1021/bc010103m CCC: $22.00 © 2002 American Chemical Society
Published on Web 04/24/2002

commercially available, but their polycationic character must be pacified to reduce their in vivo toxicity (*30*−*33*). In addition, their polyamidoamine linkage is resistant to degradation in the body. Another well-known dendritic system is based on the polyaryl ether convergent dendrimers (*34*). Although promising preliminary studies were performed with the latter by coupling the drug methotrexate (MTX) (*21*), these dendrimers also have a backbone that is inherently resistant to degradation and thus were thought to be less suitable for drug delivery purposes than other structures incorporating hydrolyzable linkages.

Thus, it is of interest to develop and evaluate novel water-soluble, biocompatible, dendritic systems. A polyester dendritic scaffold based on 2,2-bis(hydroxymethyl)-propanoic acid has been investigated as a possible drug carrier. Herein, the biological evaluation of various polyester dendritic model compounds is described. The biodistribution of a doxorubicin−polymer conjugate is also reported, as well as drug release studies. The synthesis and chemical characterization of the systems evaluated are reported elsewhere (*35*).

MATERIALS AND METHODS

Cell Culture. The murine melanoma cell line B16F10 was obtained from the UCSF Cell Culture Facility. The cells were cultured in prewarmed medium (MEM Eagle's with EBSS medium containing 10% fetal bovine serum, 1% MEM nonessential amino acids, 110 mg/L sodium pyruvate, and 1% penicillin−streptomycin) at 37 °C in a humidified atmosphere composed of 5% CO_2. MDA-MB-231 and MDA-MB-435 breast cancer cell lines were cultured in a medium consisting of Dulbecco's Modified Earl's medium (DME) H-16, containing 10% FBS and 1% MEM nonessential amino acids. The medium for culturing the monkey kidney fibroblast CV-1 cells consisted of DME H-21 (high glucose 4.5 g/L) containing 10% fetal bovine serum, 1% MEM nonessential amino acids, 1% HEPES buffer, and 1% penicillin−streptomycin. For all of our experiments, cells were harvested from subconfluent cultures using trypsin-versene (0.05 and 0.02% respectively) and were suspended in medium. Cell viability was determined using the trypan blue exclusion method.

Cell Cytotoxicity Assay. The cytotoxicity of the polymeric carriers, and of the free or conjugated doxorubicin, was determined using a target cell line and the sulforhodamine B assay (SRB) (*36*). The target cells used were murine B16F10 melanoma cells and the human breast cancer cell lines MDA-MD-231 and MDA-MD-435. Cells were seeded into a 96-well plate at a density of 3×10^4 cells/mL with 100 μL per well for 19 h (37 °C and 5% CO_2) before the assay. The medium of each well was then replaced by 100 μL of antibiotic-free medium containing various concentrations of the polymer with no drug, drug, or conjugated doxorubicin. The tests were conducted in replicates of four to eight for each drug dose. The cells were incubated at 37 °C/5% CO_2. Following the incubation period, the cells were fixed for 1 h at 4 °C by adding 25 μL of ice-cold 50% trichloroacetic acid (TCA) to the growth medium of each well. The wells were washed 5 times with cold water to remove the excess TCA and then air-dried at room temperature for several minutes. Once dry, each well received 100 μL of 0.4% SRB in 1% acetic acid followed with a 30-min incubation at room temperature. The SRB solution was then aspirated off the cells and the wells were quickly washed with 1% acetic acid. The wells were air-dried at room temperature for several minutes until moisture was no longer detected visually. The dye bound to the cells was solubilized by adding 100 μL of 10 mM Tris base, unbuffered, per well and agitated for 5 min at room temperature. The optical densities were obtained using an OPTIMAX microplate reader (Molecular Devices, Sunnyvale, CA) at a wavelength of 564 nm. OD measured on wells containing cells that did not receive the drug were considered to represent 100% growth, and OD measured on wells containing no cells but that received drug are considered to represent 0% growth. The IC50 is evaluated by comparing the OD of wells containing cells that were exposed to at least five doses.

Maximum Tolerated Polymer Intravenous Bolus Dose. The polymers were dissolved at 162 mg/mL in HBS. CD-1 female mice, 6−8 week-old, were injected with increasing volumes of polymer solution via the tail vein and observed for 24 h postinjection. All mice were then anesthetized with an intraperitoneal injection of ketamine cocktail (44 mg Ketamine; 2.5 mg Xylazine; 0.75 mg acepromazine in PBS per kg of body mass) and their liver dissected and observed under a dissecting microscope for signs of toxicity.

Radiolabeling Methods. Compound **I** and **II** were iodinated using carrier-free ^{125}I and the chloramine T reaction as previously described (*37*). The radiolabeled polymer was separated from noncovalently attached iodine on a Sephadex G-25 column. Compound **III** containing the methoxyphenol group was not readily radiolabeled when using the chloramines T reaction described in ref *37* but was readily radioiodinated using noncarrier iodine and an electrophilic protocol based upon Krummeich et al (*38*). In brief, 3 mg of **III** was dissolved in 0.25 mL of trifluoroacetic acid (TFA), and 0.01 mL of an aqueous solution of ^{125}I was added containing 1 mCi ^{125}I. Chloramine T (0.54 mg) dissolved in 0.05 mL of TFA was added to the mixture, and the reaction was heated at 60 °C for 5 min. The reaction was stopped by the addition of sodium metabisulfite, 1 mg in 0.01 mL of water, and the TFA was evaporated under a stream of nitrogen that was vented through a trap containing activated carbon (Dupont-New England Nuclear, MA). The residue was dissolved in 0.1 mL of 0.1 N NaOH containing 100 mM sodium metabisulfite and chromatographed on a column containing 1.8 mL bed volume of Dowex 2 anion-exchange resin. The radiolabeled polymer was eluted in the first 4 mL using water as the mobile phase. There was about a 20% incorporation of radioiodine into the polymer under these conditions. The mixture was rechromatographed two additional times, and greater than 99% of the radioactivity eluted with the polymer fraction. The radiolabeled material eluted in the void volume from a Sephadex 25 size exclusion column.

A suitable quantity of radiolabeled polymer was mixed with the nonradiolabeled polymer in sterile HBS to create a 10 mg/mL polymer concentration with a specific activity of 4 μCi/mL for use in the biodistribution studies.

Biodistribution Assays for Compounds I, II, and III. A known amount of radiolabeled polymer was added to a stock solution of nonradiolabeled polymer prepared at a concentration of 10 mg/mL in sterile HBS, and 100 μL was injected intravenously into 6−8 week-old CD-1 female mice. Each mouse was housed separately to collect the urine and feces. At different times postinjection, either three or four mice per group were anesthetized with an intraperitoneal injection of a ketamine cocktail and sacrificed. The feces and urine were collected. Each mouse was bled by heart puncture, and the volume of blood measured and transferred to a scintillation vial. The circulation system was perfused with PBS via the

right ventricle to reduce blood in the organs. All the organs were collected separately and transferred to preweighed scintillation vials. The carcass was sectioned into three portions and placed into preweighted vials. The radioactivity contained in each organ was counted on a Beckman Gamma 8000 Spectrometer (Irvine, CA) and expressed as counts per minute/gram of tissue. Using this procedure we were able to account for 95 ± 5% of the injected radioactivity.

Blood Clearance Assay for Compounds I, II, and III. Female mice of 6−8 week-old (Charles River) were injected with 1 mg of radiolabeled polymer in 100 μL of HBS via the tail vein. At time 3, 10, 30, 60, and 90 min postinjection, each mouse was anesthetized with isoflurane, and 50 μL of blood was collected from the orbital sinus using a heparinized capillary. The level of radioactivity (cpm) found in the blood was determined using a Beckman Gamma 8000 gamma spectrometer (Irvine, CA) and the elimination rate computed using a log−linear regression of CPM/mL blood versus time after injection.

Biodistribution Assay for Compound IV. A known amount of the doxorubicin conjugate was dissolved in a 5 mM HEPES and 5% glucose solution. CD-1 females mice at 6−8 weeks old were injected i. v. via tail with 200 μL of the conjugate solution. Four mice per group were anesthetized with a ketamine cocktail by i. p. injection. All mice were bled by heart puncture, and the volume of blood was measured and transferred to a scintillation vial. An injection of 1 mL of PBS to the right ventricle of the heart was used to flush the circulation system. The whole organs were dissected and their weight was recorded. The organs were put into 2 mL tubes containing 1 mL of acidified alcohol (90% 2-propanol/0.075 HCl) and zirconia beads, followed by homogenization (Bead Beater, Biospec, Bartlesville, OK) for 20 s at 5000 rpm. The blood was allowed to coagulate at 4 °C and then centrifuged for 10 min at 1000 rpm. The serum (upper phase) was collected, and its volume was recorded. An aliquot of 100 μL of serum was transferred to a 2-mL tube containing 1 mL of acidified alcohol. The homogenized organ samples and the sera were placed in the refrigerator for 24 h to extract the drug. The cell debris in the organ homogenates was removed by centrifugation at 14 000 rpm for 5 min at 4 °C. An aliquot (400 μL) of the supernatants were transferred to tubes containing 1.6 mL of acidified alcohol. For the quantification of doxorubicin present in the organs, drug-free homogenates of organs and sera from untreated mice were spiked with free doxorubicin. Various organs had different background fluorescence levels, which required separate calibration curves for each organ. Fluorescence emission from the drug was measured in fluorescence intensity units (Ex 490 nm: Em 590 nm) in a Quantech Turner fluorometer (Barnstead/Thermolyne, Dubuque, IO). Calibration curves were linear over two orders and drug levels to 10 ng/g organ could be reliably measured.

Confocal Microscopy. GFP transfected and nontransfected MDA-MB-435 cells were plated on sterilized 4-well slides by the addition of 1 mL of a 1×10^5 cells/mL solution. After incubation for 24 h, the media was gently removed and the cells were washed once with 1 mL of PBS, followed by the addition of 0.5 mL of media containing free doxorubicin and conjugated doxorubicin. The control cells contained only media. The concentration of free and conjugated doxorubicin equals the IC50 of free doxorubicin for this cell line, as determined previously in vitro experiments (0.62 mg/mL). Cells were incubated at 37 °C and 5% CO_2 for 1 and 24 h. After incubation the cells were fixed for 1 h at 4 °C in 1.0 mL of 4% paraformaldehyde in PBS. The cells were mounted in Vector Vectrashield (Burlingame, CA) for confocal microscopy. Confocal images were obtained using LaserSharpe software installed on a Bio-Rad (Hercules, CA) krypton−argon laser scanning confocal microscope (MRC-1024) outfitted with a Nikon Diaphot 200 microscope using an ×60 objective lens. 512 × 512 pixel sections were taken every 2 μm using all laser lines, 10% laser power, slow scan, and Kalman averaging of three scans. For both GFP transfected and untransfected MDA-MB-5 cells, doxorubicin was imaged by PMT1 using low signal amplification, an iris of 2.5, a gain of 1500, and a black level of −6. For the GFP transfected MDA-MB-5, GFP was imaged on PMT2 using an iris of 2.5, a gain of 1500, and a black level of −3. Images were analyzed using Confocal Assistant 4.02 software.

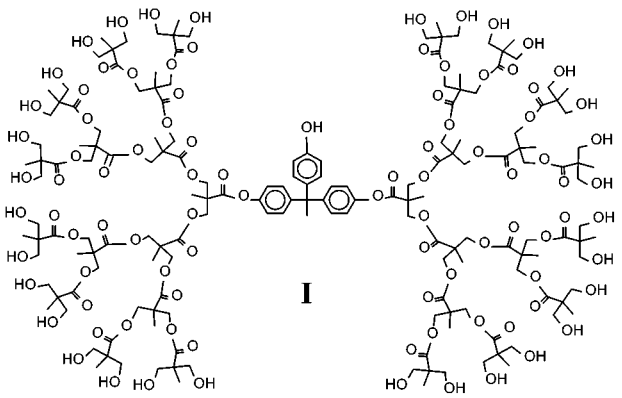


Figure 1. Dendritic polyester model compound **I** with molecular mass of 3790 Da.

Drug Release Studies as a Function of Buffer pH. A stock solution of conjugate was prepared using distilled water as a solvent. An aliquot of the stock solution was added to the respective prewarmed buffer solutions (37 °C), to initiate the reaction. The final concentration of the conjugate was of 3 mg/mL, 40 mM in buffer ion and 100 mM NaCl. Solutions at pH 2.4 (HCl), 4.5 (acetate), 5.5 (acetate), 6.5 (MES), and 7.0 (phosphate) were used to evaluate drug release as a function of pH. Quantification of drug released was performed by HPLC analysis on a model 2690 XE Alliance Separations module (Waters, USA) and a Photodiode Array detector (Waters 996). Aliquots of 10 μL were injected with built-in autoinjector at different times after the incubation started. The separation was carried out with a Waters Symmetry C18 column (2.1 × 150 mm, 3.5 μm) using a mobile phase consisting of 40% phosphate buffer pH 7.0 and 60% methanol at a flow rate of 0.3 mL/min. The data acquisition and processing were controlled by Millenium 32 software. In contrast to commonly used mobile phases for the separation of DOX conjugates from the free DOX, we used a neutral pH system, to minimize cleavage of DOX from the polymer during the analysis. A calibration curve was prepared with fresh doxorubicin and the extent of release was monitored by peak height based on the absorbance at 490 nm.

RESULTS AND DISCUSSION

Brief Description of Structure of Model Compounds Evaluated. Model compounds **I**, **II,** and **III** were evaluated as possible polymeric drug carriers (Figures 1−3). The common denominator of these systems is the polyester dendritic scaffold derived from the monomer unit 2,2-bis(hydroxymethyl)propanoic acid. These

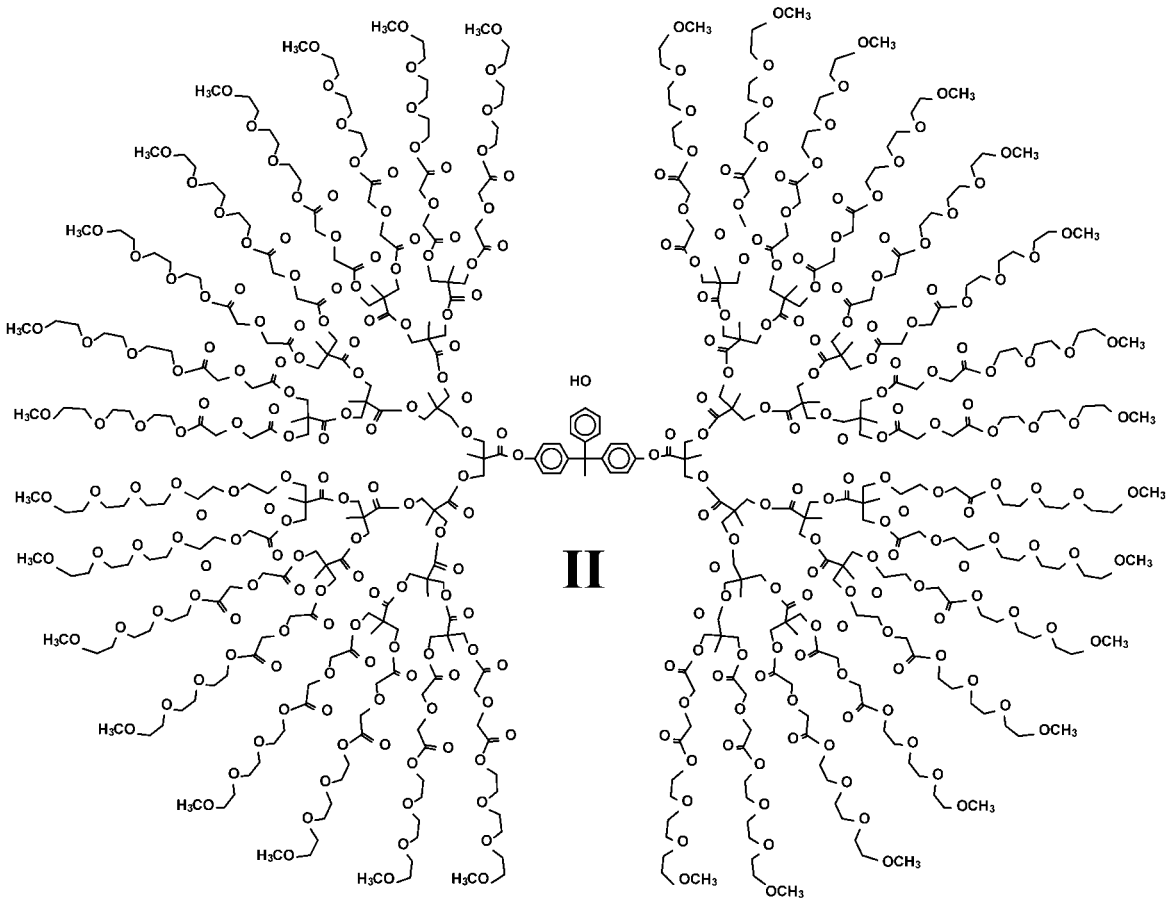


Figure 2. Modified dendritic polyester model compound **II** with molecular mass of 11 500 Da.

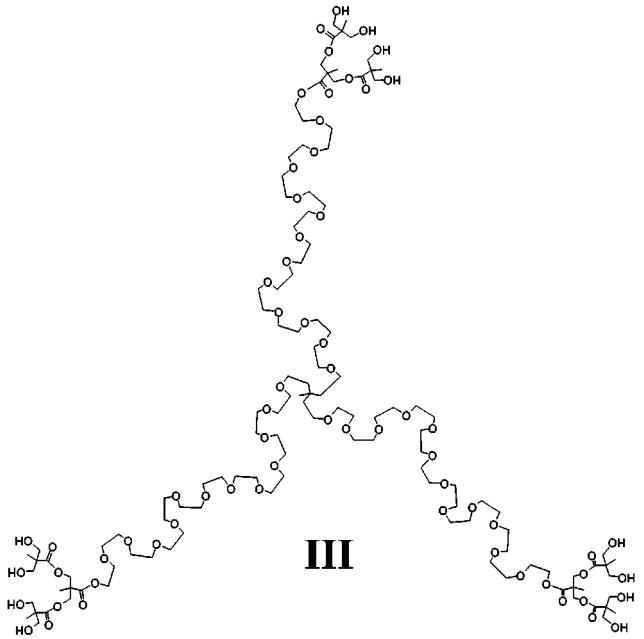


Figure 3. Model compound **III**, composed of 3-arm poly(ethylene oxide) star and [G-2] polyester dendrons (23 500 Da).

three polymers differ in molecular weight and architecture, so we could evaluate these factors on toxicity and biodistribution. Compounds **I** and **II** mainly consist of two fourth generation [G-4] polyester dendrons attached to a trisphenolic core. Carrier **I** has a molecular mass of 3790 Da and contains a fully activated surface with 32 hydroxyl groups, which can be further modified. The surface of **II** was modified with methoxy terminated tri(ethylene glycol) oligomeric units to increase the mass of the dendritic molecule by a factor of 3 in one single synthetic step, achieving a mass of 11 500 Da. An attractive feature of this polyester scaffold is that it is highly water soluble (at least 200 mg/mL) in an uncharged state, avoiding the necessity of introducing ionizable functional groups to achieve good solubility properties. This property decreases the possibilities for rapid elimination as is observed in the case for cationic systems, due to electrostatic interactions with the negatively charged cellular membranes and extracellular matrixes (*30*−*33*) or in the case of anionic systems due to their interaction with the scavenger receptor (*39*). Second, the sterically hindered ester bond of the monomer unit makes this backbone more stable toward both nucleophilic attack and acid-catalyzed hydrolysis avoiding its rapid and premature degradation.

In contrast to **I** and **II**, compound **III** consists of a hybrid between a 3-arm poly(ethylene oxide) (PEO) star and three [G-2] polyester dendritic units. This system has a molecular mass of ca. 23 500 Da, and its molecular architecture has a more linear character, as compared to the compact shape of the strictly dendritic systems **I** and **II**. In this instance, the trifunctional PEO core contributes most of the mass of the system. The advantages of using a star-PEO also include its contribution to biocompatibility and water solubility (*40*), without jeopardizing the polydispersity of the system, since star-PEO molecules with low polydispersity indices (PDI < 1.1) are commercially available. On the other hand, the [G-2] polyester dendrons of **III** provide the multivalency necessary for drug attachment. In contrast to linear polymers containing statistical amounts of reacting sites,

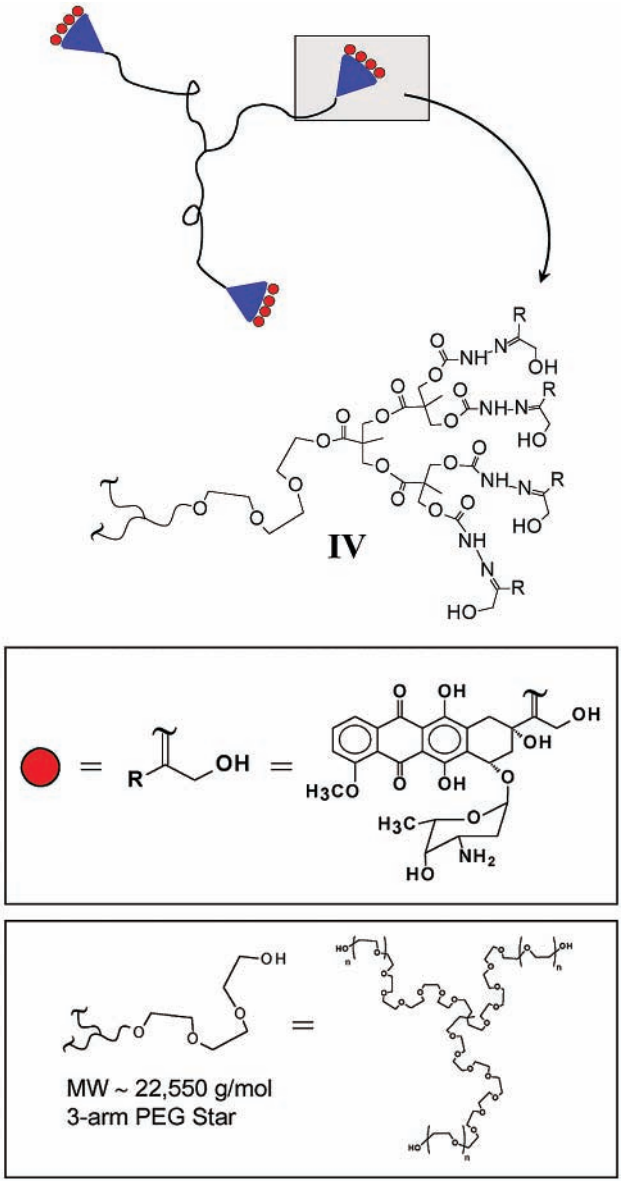


Figure 4. Model compound **IV**. Polymer drug conjugate consisting of modified **III** and doxorubicin using a hydrazone covalent bond as a linker.

this architecture provides a known and reproducible number of functional groups.

Finally, the drug−polymer conjugate **IV** (Figure 4) consists of the potent anticancer drug doxorubicin (DOX) and a derivative of the polymeric carrier **III**. DOX was covalently bound to the polymer by means of an acid-labile hydrazone linkage (*41*−*42*). An acid-labile linkage was selected because it can remain stable under physiological conditions, but once it is internalized in the cell by endocytosis, the more acidic environment of lysosomal compartments will trigger the release of the drug. An additional advantage of a pH-sensitive linker is that the release rate of the drug attached by an acid-labile linkage is often less affected by the type of drug than in the case of enzyme cleavable linkages, which have been difficult to address (*43*). Finally, the environment around tumor tissue is slightly more acidic than normal tissue; therefore, an acid labile linkage might be cleaved more rapidly in the vicinity of a tumor prior being internalized by the cancer cell.

Biological Evaluation of Model Compounds. *In Vitro Cytotoxicity of the Carriers.* In vitro studies were performed on the polymeric model compounds **I**, **II**, and **III** to evaluate the possible toxic effect of the polyester dendritic scaffold itself. The cell viability studies were performed on melanoma B16F10 cancer cells and cell proliferation was quantified by the sulforhodamine B assay (SRB), which measures the level of protein remaining on a cell culture dish. All of the polymers examined were well tolerated by cells in culture (Figure 5). For instance, after incubation for 48 h, cells exposed to **I** at a polymer concentration of 10 mg/mL retained 87% of the growth rate of the control cells. In the case of model compound **II**, cell proliferation was slightly suppressed to 81% of control at 5 mg/mL. Model compound **III**, the highest molecular weight carrier evaluated, also was very well tolerated with 87% of the growth rate of the control culture at 10 mg/mL of polymer (Figure 5).

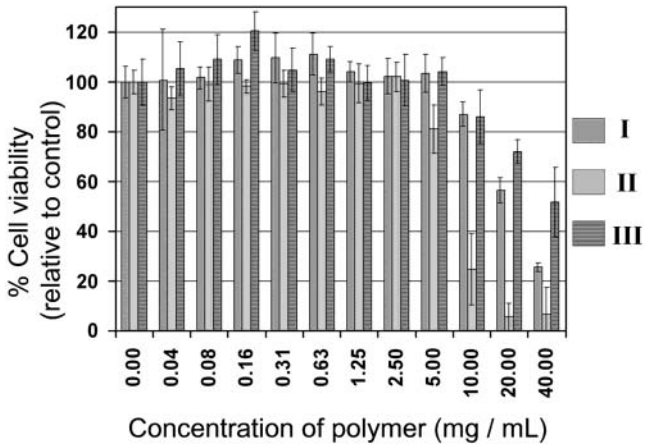


Figure 5. Cell viability results upon treatment of B16F10 cells with polymeric carriers **I**, **II**, and **III** after 48 h of incubation.

An interesting observation on this polymer is that even though there is an apparent growth inhibition at the highest concentrations, dead cells were not evident under microscopic observation even at 40 mg/mL, rather the cell density was decreased. This suggests a growth inhibition effect as a result of the very high polymer concentration. These results are very promising, considering that previously evaluated dendritic systems, such as PAMAM, polyethyleneimine and poly(ethylene oxide) grafted carbosilanes inhibit cell viability and induce hemolysis or cytolysis at concentrations much lower than 5 mg/mL (*31*).

In Vivo Tolerability of the Dendritic Polyesters. Nonionic polymers such as the poly(ethylene glycols) are very well tolerated upon injection into animals. Given the low toxicity of the polyester dendrimers in culture, we thought they would also be well tolerated upon injection into animals. However, we did not believe it warranted conducting a complete toxicity profile of the polymers at this stage of the investigation; rather, we undertook to learn if the polymers could be administered as an intravenous bolus at levels greater than 1 g/kg body weight in mice. If the polymers could be administered at this dose, a wide variety of drug delivery applications would be possible. Compound **I** was injected i.v. over a 10 s period into a number of animals at increasing doses. At the dose of 1.3 g/kg body weight, 1 of the 2 animals injected survived. In the animal that died, there was no evidence for blood hemolysis. The surviving animal was sacrificed at 24 h postinjection, the organs removed and visually examined. There was no gross evidence for toxicity in any organ examined.

Compound **III** was injected intravenous as a bolus into two mice at a dose of 1.3 g/kg body weight. Both mice

survived with no evidence for any adverse effect of the polymer. The animals were sacrificed at 24 h, the organs were removed and visually examined. There was no evidence for gross pathology in the liver, lungs, heart, kidney, or intestine.

These preliminary experiments confirmed that the polymers were very well tolerated in mice when administered by i.v. bolus. Upon the basis of this result, we decided to undertake biodistribution experiments at doses of 0.1 g/kg body weight. This is comparable to what has been used to study biodistribution of dextrans (*44*) and HPMA, polymers that have been used as drug carriers.

Biodistribution Studies. Dendrimer **I** was radiolabeled with ^{125}I, and the biodistribution of the radiolabeled polymer was monitored in CD-1 mice after intravenous administration. Polymer **I** was renally excreted and preferential accumulation in specific organs was not observed (Figure 6a). At 10 min postinjection, only 14% of the injected material remained in the serum, and the polymer was essentially completely excreted after 4 h. The low circulation time is most likely related to the compact shape of the branched dendritic structure and its modest molecular size.

Biodistribution of model compound **II** was evaluated and even though the mass of this system was 3 times larger than **I**, the polymer was also rapidly excreted in the urine. At 30 min postinjection, only 4% of the administered dose remained in serum, and after 5 h the material was essentially completely excreted from the body with no evidence for accumulation in any tissue (Figure 6b).

Model compound **III** was labeled with ^{125}I as well, but in contrast to **I** and **II** the radioactive label was attached to a *p*-methoxyphenyl acetic acid moiety that was statistically coupled to the surface of **III**. This compound exhibited a highly significant accumulation in the liver. At 10 min postinjection, 70% of injected dose is in the liver and 5% in serum. After 5 h, 53% of the injected dose was still found in the liver (Figure 6c).

This distribution behavior was not expected. One major difference between compound **III** and compounds **I** and **II** is that the labeled moiety was at the periphery of the PEO chains in **III**, as opposed to the well protected core in compounds **I** and **II**. This could possibly account for the liver uptake since it was previously observed that iodophenol containing PEGs would expose the methoxy iodophenol to the putative liver receptors whereas the iodophenol would be sterically hindered in compounds **I** and **II** (*37*). Another possibility is that the iodine-containing moiety was hydrolyzed from the polymer and incorporated into the liver rather than the model compound itself. Given the rapidity of uptake in the liver, this is unlikely. Moreover, iodinated polymer recovered from serum eluted in the high molecular weight fraction on a G-50 spin column. Thus, we attributed the biodistribution profile of compound **III** to the exposed iodinated phenol. Despite the uptake of **III** into the liver, we decided to prepare a polymer−doxorubicin conjugate with compound **III** for further biodistribution studies.

In addition to being a highly potent anticancer agent, doxorubicin is a fluorescent compound, providing a convenient analytical tool for monitoring distribution of the conjugate **IV**. In contrast to the radiolabeled **III**, the polymer−DOX conjugate **IV** showed no significant accumulation in any vital organ, including the liver, heart, and lungs (Figure 7). This is a significantly different distribution pattern than is observed for the free drug, which partitions into a variety of organs such as the liver

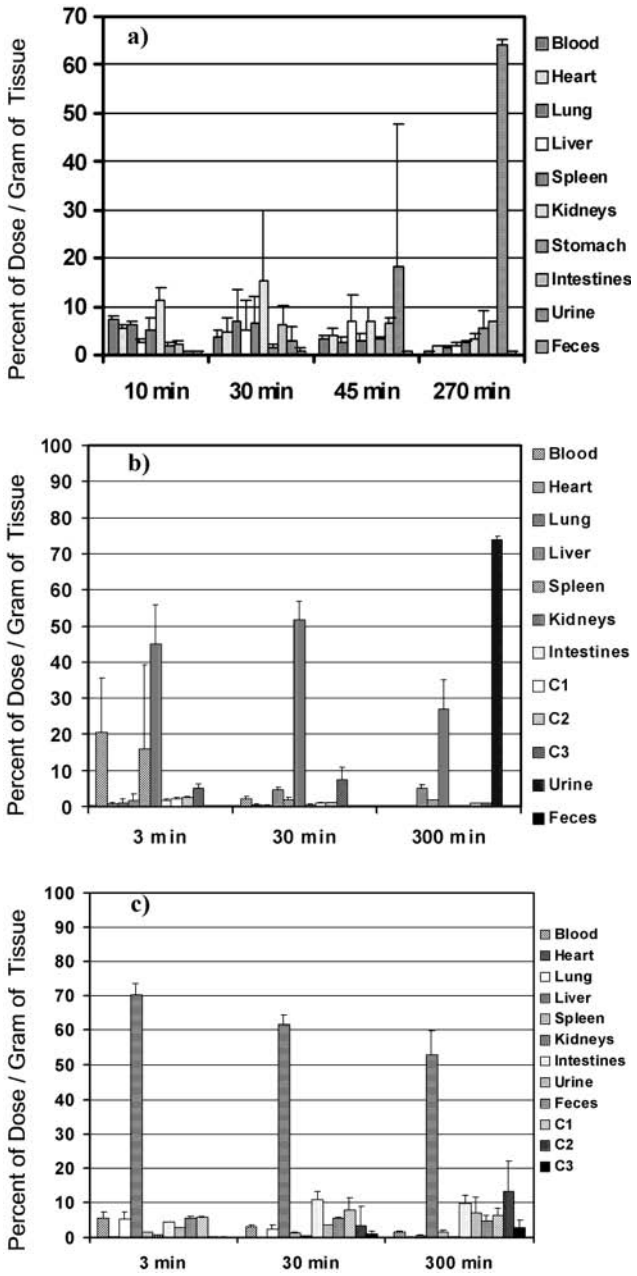


Figure 6. Biodistribution of model compounds (a) **I**, (b) **II**, and (c**) III**. The data are expressed in % of dose injected per gram of organ tissue. The blood is expressed in % of dose injected per mL, for ca. 2 mL of total blood volume in a CD-1 mouse.

and heart (*45*). Most importantly, conjugate **IV** had circulation half-life of 72 min, which is significantly longer than both the half-life of the free drug (ca. 8 min) and the carriers **I** and **II**. This demonstrates that the polymeric form of the carrier alters the pharmacokinetics and the distribution of the drug.

Drug Release Studies. One of the important features to take into consideration when designing polymeric carriers is the means of attachment of the molecule to be delivered. The nature of the attachment sites will determine whether selective release of the bioactive molecule can be attained. A hydrazone linkage was selected due to its known stability under neutral pH conditions and its ability to undergo hydrolysis under acidic conditions. The goal is to have a linkage that will be sufficiently labile at a pH range of 4−6 to provide a therapeutic level of the drug. This is the pH found in the endosomal and lysosomal environments, which are the

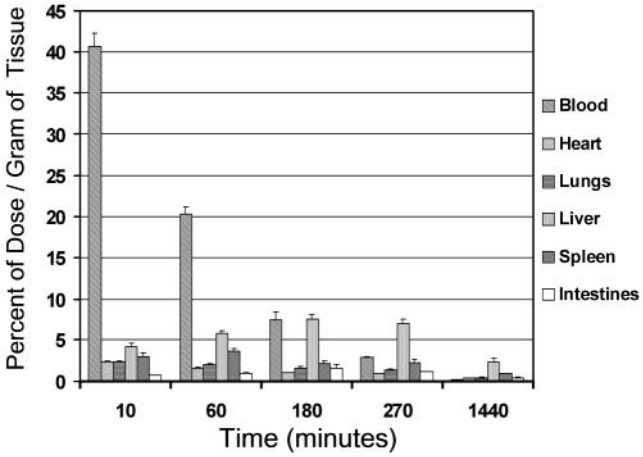


Figure 7. Biodistribution of **IV**.

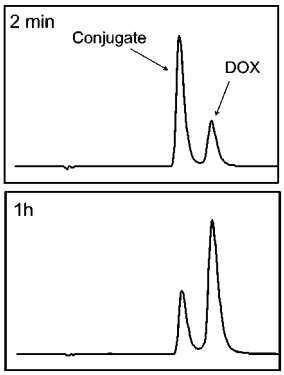


Figure 8. HPLC chromatogram showing increment in free drug concentration upon release from polymer conjugate **IV**. The detection was observed at 490 nm.

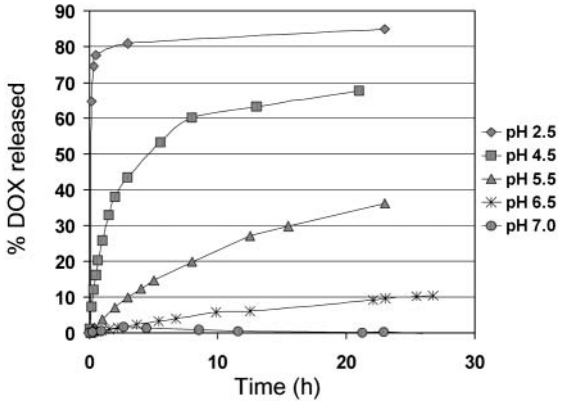


Figure 9. pH profile for release of doxorubicin from conjugate **IV**.

compartments where polymeric drugs are often internalized. The linkage we used and evaluated throughout this study is a hydrazone linkage.

Drug release was monitored by an HPLC method. Figure 8 shows the well-resolved peaks corresponding to the conjugate and free doxorubicin at retention times of 5.4 and 6.3 min, respectively. As shown in Figure 9, the hydrazone linkage is indeed very stable at neutral pH, while it is cleaved more rapidly under more acidic conditions. Due to the highly reversible character of the hydrolysis of hydrazone linkages, an apparent equilibrium is observed under the experimental nonsink conditions of the release assay. One can estimate the time for complete release of DOX from the conjugate based on the computed initial rates of release; a 100% release would

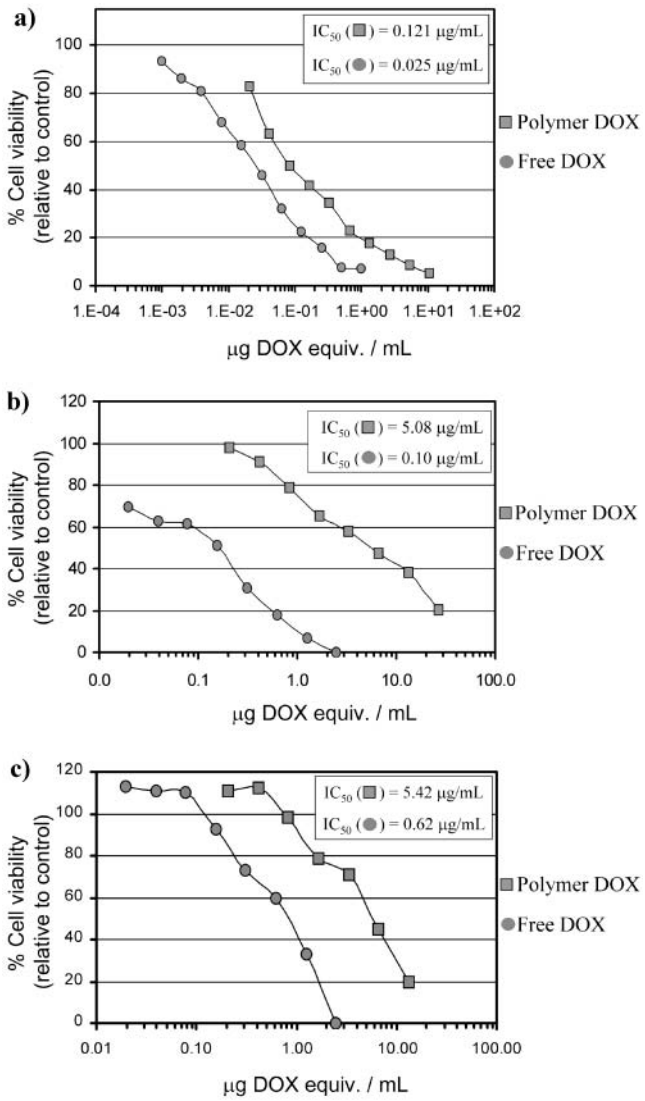


Figure 10. Comparative cell viability results upon treatment of (a) B16F10, (b) MDA-MB-231, and (c) MDA-MB-435 cell lines with bound DOX (**IV**) and free DOX. Results are compared in terms of DOX equivalents.

be achieved after 10 min, 3 h, 26.5 h, and 10 days for pH 2.5, 4.5, 5.5, and 6.5, respectively. Thus, the hydrazone linkage provides a suitable linker for a pH-dependent release that is compatible with conditions found in tumors.

Cytotoxicity of Drug−Polymer Conjugate in Vitro. The cell proliferation results suggest that these systems based on polyester dendrimers do not exhibit a significant toxic effect and the drug release rates from the hydrazone linker encouraged us to further evaluate model compound **IV** as a polymeric drug carrier. In vitro evaluation of the conjugate was performed in various cancer cell lines to compare the cytotoxic activity of the bound drug in relation to the free drug (Figure 10).

The three cell lines examined exhibited a range of sensitivity to the free doxorubicin, from 0.025 μg/mL for B16F10 to 0.62 μg/mL for the MDA-MB-435 cell lines. In all three cell lines examined, the free drug was considerably more potent than the drug−polymer conjugate (Figure 10); 6-fold in the B16F10 cells, 50-fold in the MDA-MB-231, and 9-fold in the MDA-MB-435 cells. In the experiments, the conjugated doxorubicin was chromatographed in a gel permeation column within 1 day of testing the material so that there was less than

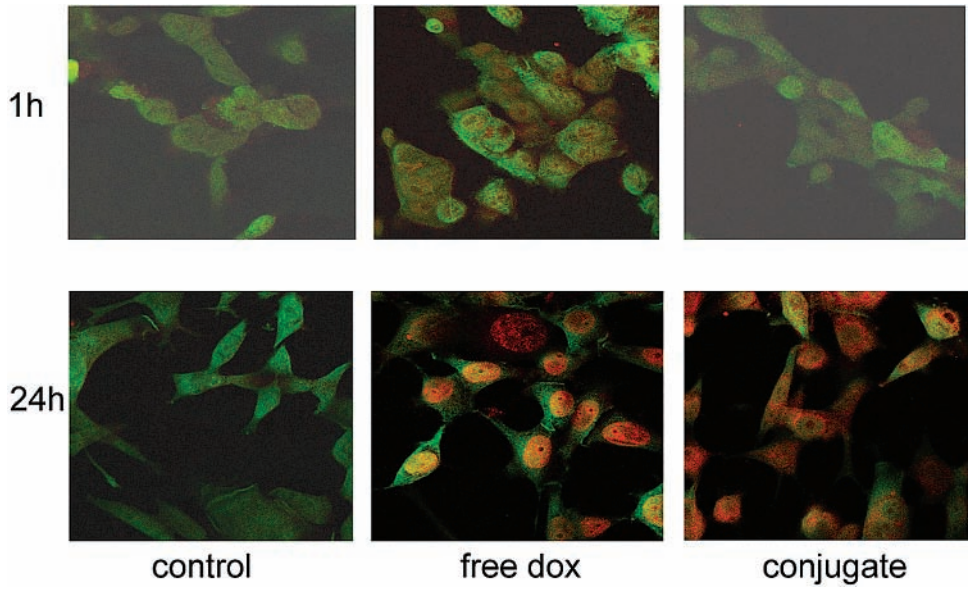


Figure 11. Fluorescence confocal microscopy images of localized DOX and DOX−polymer conjugate **IV** in MDA-MD-435 cells. MDA-MD-435 cells were grown to 40% confluence on sterilized coverslips and incubated for 1 and 24 h.

1% free doxorubicin in the conjugate preparation. Moreover, the amount of polymer at the highest dose tested (100 μg/mL) was substantially below the concentration where antiproliferation effects of the polymer were observed. Therefore, the antiproliferation effects of the conjugate were most likely due to the drug that had been released from the polymer in the course of the incubation.

These results are encouraging since the doxorubicin conjugate is less toxic than the free drug yet more toxic than the polymer alone. The question arises as to where the doxorubicin is being released from the polymer. At neutral pH in buffer, drug release is very slow. However, at low pH drug release is substantially faster. Therefore, we examined if the drug−polymer conjugate was internalized by cells.

MDA-MB-431 cells were treated for 1 h and 24 h with the drug−polymer conjugate (**IV**) or the free doxorubicin. The fluorescence of doxorubicin provides a means for monitoring cell uptake of the drug using fluorescence confocal microscopy. Both the cytoplasm and the nuclei were highly fluorescent both at 1 h and 24 h after exposition to free doxorubicin. When cells were exposed to polymeric drug, fluorescence is observed in the cytosol, confirming the cell uptake of the conjugate by endocytosis (Figure 11). However, as also observed with the HPMA derivative of doxorubicin (*46*), little fluorescence was observed in the cell nucleus with the drug−polymer conjugate. This may be due to the slow release of the drug from the carrier at the time of evaluation.

CONCLUSIONS

Various polyester dendritic carriers were evaluated as possible drug carriers. Each of the three drug carriers (**I**, **II**, **III**) are highly water soluble and nontoxic. Model compound **III** exhibited the longest circulatory half-life (72 min) as compared to the lower molecular weight systems **I** and **II** and was selected for further investigation. A doxorubicin−polymer conjugate was synthesized using **III** as the polymeric carrier (**IV**), and the drug was attached by means of an acid-labile hydrazone linkage. The cytotoxicity of the drug was significantly reduced (80−98%) after attaching it to the polymer. However, doxorubicin could be rapidly released from the polymer in an active form at pH values found in the lysosome. Uptake of **IV** by cells in culture was also observed by fluorescence confocal microscopy. In biodistribution experiments, none of these systems accumulated in any organ examined, including the liver, heart, and lungs. The results suggest that this polyester dendritic backbone is a highly water soluble, nontoxic, and biocompatible polymer. However, a higher molecular weight system must be prepared to further increase the circulation half-life to effectively exploit the EPR phenomenon. This new system is a promising polymeric backbone for use as scaffolds in the development of well-defined macromolecular drug carriers.

ACKNOWLEDGMENT

We thank Dr. Nikolay Vladimirov and Dr. Miroslav Janco (UCB) for their significant contribution in the development of the HPLC method for the performance of the drug release studies. We also thank John Andrew MacKay (UCSF) for his valuable assistance in the experiments involving confocal microscopy. Financial support of this research by UC Breast Cancer Research and Development Program (6JB-0137), the National Science Foundation (DMR-9816166), the Department of Energy (Basic Energy Sciences), and the National Institutes of Health (Grant GM 65361) is acknowledged with thanks.

LITERATURE CITED

(1) Langer, R. (1990) New Methods of Drug Delivery. *Science 249*, 1527−1533.

(2) Duncan, R., Dimitrijevic, S., and Evagorou, E. G. (1996) The Role of Polymer Conjugates in the Diagnosis and Treatment of Cancer. *S. T. P. Pharma Sciences 6*, 237−263.

(3) Maeda, H., Seymour, L. W., and Miyamoto, Y. (1992) Conjugates of Anticancer Agents and Polymers: Advantages of Macromolecular Therapeutics in Vivo. *Bioconjugate Chem. 3*, 351−362.

(4) Mehvar, Reza (2000) Dextrans for Targeted and Sustained Delivery of Therapeutic and Imaging Agents. *J. Control. Release 69*, 1−25.

(5) Matsumura, R. B., and Maeda, H. (1986) A New Concept for Macromolecular Therapeutics in Cancer Chemotherapy: Mechanism of Tumoritropic Accumulation of Proteins and the Antitumor Agent SMANCS. *Cancer Res. 46*, 6387−6392.

(6) Ellens, H., Bentz, J., and Szoka, F. C., Jr. (1985) H+-Induced and Ca-2+-Induced Fusion and Destabilization of Liposomes. *Biochemistry 24*, 3099−3106.

(7) Watkins, D. M., Sayed-Sweet, Y., Klimash, J. W., Turro, N. J., and Tomalia, D. A. (1997) Dendrimers with hydrophobic

cores and the formation of supramolecular dendrimer-surfactant assemblies. *Langmuir 12*, 3136−3141.
(8) Hawker, C. J., Wooley, K. L., and Fréchet, J. M. J. (1993) Unimolecular Micelles and Globular Amphiphiles − Dendritic Macromolecules as Novel Recyclable Solubilization Agents. *J. Chem. Soc., Perkin Trans. 1, 12*, 1287−1297.
(9) Eliaz, R., and Szoka, F. C., Jr. (2001) Liposome Encapsulated Doxorubicin Targeted to CD44: a Strategy to Kill CD44-Overexpressing Tumor Cells. *Cancer Res. 61*, 2592−2601.
(10) Duncan, R. (1992) Drug-polymer Conjugates: Potential for Improved Chemotherapy. *Anticancer Drugs 3*, 175−210.
(11) Cuvier, C., Roblot-Treupel, L., Milliot, J. M., Lizard, G., Chevillards, S., Manfait, M., Couvreur, P., and Poupon, M. F. (1992) Doxorubicin-loaded Nanospheres bypass Tumour Cell Multidrug Resistance. *Biochem. Pharmacol. 44*, 509−517.
(12) Omelyanenko, V., Kopečková, P., Gentry, C., and Kopeček, J. (1998) Targetable HPMA Copolymer-Adriamycin Conjugates: Recognition, Internalization, and Subcellular Fate. *J. Control. Release 53*, 25−37.
(13) Maeda, H., Wu, J., Sawa, T., Matsumura, Y., and Hori, K. (2000) Tumor Vascular Permeability and the EPR Effect in Macromolecular Therapeutics: A Review. *J. Control. Release 65*, 271−284.
(14) Seymour, L. W. (1992) Passive Tumor Targeting of Soluble Macromolecules and Drug Conjugates. *Crit. Rev. Ther. Drug 9*, 135−187.
(15) Seymour, L. W., Miyamoto, Y., Maeda, H., Brereton, M., Strohalm, J., Ulbrich, K., and Duncan, R. (1995) Influence of Molecular Weight on Passive Tumour Accumulation of a Soluble Macromolecular Drug Carrier. *Eur. J. Cancer 31A*, 766−770.
(16) Greenwald, R. B., Conover, C. D., and Choe, Y. H. (2000) Poly(Ethylene Glycol) Conjugated Drugs and Prodrugs: A Comprehensive Review. *Crit. Rev. Ther. Drug 17*, 101−161.
(17) Vasey, P. A., Kaye, S. B., Morrison, R., Twelves, C., Wilson, P., Duncan, R., Thomson, A. H., Murray, L. S., Hilditch, T. E., Murray, T., Burtles, S., Fraier, D., Frigerio, E., and Cassidy, J. (1999) Phase I Clinical and Pharmacokinetic Study of PK1 [N−(2-Hydroxypropyl)methacrylamide Copolymer Doxorubicin]: First member of a New Class of Chemotherapeutic Agents-Drug-Polymer Conjugates *Clin. Cancer Res. 5*, 83−94.
(18) Ulbrich, K., Šubr, V., Strohalm, J., Plocavá, D., Jelínkova, M., and Říhová, B. (2000) Polymeric Drugs Based on Conjugates of Synthetic and Natural Macromolecules: I. Synthesis and Physicochemical Characterization. *J. Control. Release 64*, 63−79.
(19) Liu, M., and Fréchet, J. M. J. (1999) Designing Dendrimers for Drug Delivery. *Pharm. Sci. Technol. Today 2*, 393−401.
(20) Liu, M., Kono, K., and Fréchet, J. M. J. (1999) Water-Soluble Dendrimer-Poly(ethylene glycol) Starlike Conjugates as Potential Drug Carriers. *J. Polym. Sci., Polym. Chem. 37*, 3492−3502.
(21) Kono, K., Liu, M., and Fréchet, J. M. J. (1999) Design of Dendritic Macromolecules Containing Folate or Methotrexate Residues. *Bioconjugate Chem. 10*, 1115−1121.
(22) Grayson, S. M., Jayaraman, M., and Fréchet, J. M. J. (1999) Convergent synthesis and 'surface' functionalization of a dendritic analogue of poly(ethylene glycol). *Chem. Commun. 14*, 1329−1330.
(23) Liu, M., Kono, K., and Fréchet, J. M. J. (2000) Water-soluble dendritic unimolecular micelles: Their potential as drug delivery agents. *J. Control. Release 65*, 12−131
(24) Esfand, R., and Tomalia, D. A. (2001) Poly(Amidoamine) (PAMAM) Dendrimers: From Biomimicry to Drug Delivery and Biomedical Applications. *Drug Discovery Today 6*, 427−436.
(25) Plank, C., Mechtler, K., Szoka, F. C., Jr., and Wagner, E. (1996) Activation of the Complement System by Synthetic DNA Complexes: A Potential Barrier for Intravenous Gene Delivery. *Hum. Gene Ther. 7*, 1441−1450.
(26) Tomalia, D. A., and Durst, H. D. (1993) Genealogically Directed Synthesis − Starburst Cascade Dendrimers and Hyperbranched Structures. *Top. Curr. Chem. 165*, 193−313.
(27) Fréchet, J. M. J. (1994) Functional Polymers and Dendrimers − Reactivity, Molecular Architecture, and Interfacial Energy. *Science 263*, 1710−1715.
(28) Newkome, G. R., Moorefield, C. N., and Vögtle, F. (1996) Dendritic Macromolecules: Concepts, Synthesis, Perspectives, VCH: Weinheim, Germany.
(29) Tomalia, D. A., Baker, H., Dewald, J., Hall, M., Kallos, G., Martin, S., Roeck, J., Ryder, J., and Smith, P. (1985) A New Class of Polymers-Starburst-Dendritic Macromolecules. *Polym. J. 17*, 117−132.
(30) Haensler, J., and Szoka, F. C., Jr. (1993) Poliamidoamine Cascade Polymers Mediate Efficient Transfection of Cells in Culture. *Bioconjugate Chem. 4*, 372−379.
(31) Malik, N., Wiwattanapatapee, R., Klopsch, R., Lorenz, K., Frey, H., Weener, J. W., Meijer, E. W., Paulus, W., and Duncan, R. (2000) Dendrimers: Relationship Between Structure and Biocompatibility in Vitro, and Preliminary Studies on the Biodistribution of 125I-Labeled Polyamidoamine Dendrimers in Vivo. *J. Control. Release 65*, 133−148.
(32) Supattapone, S., Wille, H., Uyechi, L., Safar, J., Tremblay, P., Szoka, F. C., Jr., Cohen, F. E., Prusiner, S. B., and Scott, M. R. (2001) Branched Polyamines Cure Prion-Infected Neuroblastoma Cells. *J. Virol. 75*, 3453−3461.
(33) Duncan, R., and Malik, N. (1996) Dendrimers: Biocompatibility and Potential for Delivery of Anticancer Agents. *Proc. Int. Symp. Controlled Release Bioact. Mater. 23*, 105−106.
(34) Hawker, C. J., and Fréchet, J. M. J. (1990) Preparation of Polymers with Controlled Molecular Architecture − A New Convergent Approach to Dendritic Macromolecules. *J. Am. Chem. Soc. 112*, 7638−7647.
(35) Ihre, H. R., Padilla De Jesús, O. L., Szoka, F. C., Jr., and Fréchet, J. M. J. (2002) Polyester Dendritic Systems for Drug Delivery Applications: Design, Synthesis, and Characterization. *Bioconjugate Chem. 13*, 443−452.
(36) Skehan, P., Storeng, R., Scudiero, D., Monks, A., McMahon, J., Vistica, D., Qarren, J. T., Bokesch, H., Kenney, S., and Boyd, M. R. (1990) New colorimetric cytotoxicity assay for anticancer drug screening. *J. Natl. Cancer Inst. (Bethesda) 82*, 1107−1112.
(37) Larwood, D. J., and Szoka, F. C., Jr. (1984) Synthesis, Characterization, and *In Vivo* Disposition of Iodinatable Polyetylene Glycol Derivatives: Differences In Vivo as a Function of Chain Length. *J. Label. Comput. Radiopharmaceut. 21*, 603−614.
(38) Krummeich, C., Holschbach, M., and Stöcklin, G. (1994) Direct nca electrophilic radioiodination of tyrosine analogues; their in vivo stability and brain-uptake in mice. *Appl. Radiat. Isotopes 45*, 929−935.
(39) Meijer, D. K., and Molema, G. (1995) Targeting of drugs to the liver. *Semin. Liver Dis. 15*, 202−56.
(40) Francis, G. E., Delgado, C., Fisher, D, Malik, F., and Agrawal, A. K. (1996) Polyethylene Glycol Modification: Relevance of Improved Methodology to Tumour Targeting. *J. Drug Target. 3*, 321−340.
(41) Kaneko, T., Willner, D., Monkovíc, I., Knipe, J. O., Braslawsky, G. R., Greenfield, R. S., and Vyas, D. M. (1991) New Hydrazone Derivatives of Adriamycin and Their Immunoconjugates- a Correlation between Acid Stability and Cytotoxicity. *Bioconjugate Chem. 2*, 133−141.
(42) Lemieux, G. A., and Bertozzi, C. R. (1998) Chemoselective ligation reactions with proteins, oligosaccharides and cells. *TIBTECH 16*, 506−511.
(43) Melton, R. G., Knox, R. J., Eds. (1999) *Enzyme Prodrug Strategies for Cancer Therapy*, Kluwer Academic/Plenum Publishers, New York.
(44) Takakura, Y., Takagai, A., Hashida, M., and Sezaki, H. (1987) Disposition and tumor localization of mitomycin C-Dextran Conjugates in Mice. *Pharm. Res. 4*, 293−300.
(45) Krishna, R., and Mayer, L. D. (1997) Liposomal doxorubicin circumvents PSC 833-free drug interactions, resulting in effective therapy of multidrug-resistant solid tumors. *Cancer Res. 57*, 5246−5253.
(46) Hovorka, O., Šťastný, M., Etrych, T., Šubr, V., Strohalm, J., Ulbrich, K.; Říhová, B. (2002) Differences in the intracellular fate of free and polymer-bound doxorubicin. *J. Controlled Release 80*, 101−117.

BC010103M

Molecular Vehicles for Targeted Drug Delivery

Marina V. Backer,* Renee Aloise, Kristen Przekop, Konstantin Stoletov,† and Joseph M. Backer

SibTech, Inc., Newington, Connecticut 06111, and Albert Einstein College of Medicine, Bronx, New York 10461.
Received November 7, 2001; Revised Manuscript Received March 4, 2002

Targeted drug delivery by cell-specific cytokines and antibodies promises greater drug efficacy and reduced side effects. We describe a novel strategy for assembly of drug delivery vehicles that does not require chemical modification of targeting proteins. The strategy relies on a noncovalent binding of standardized "payload" modules to targeting proteins expressed with a "docking" tag. The payload modules are constructed by linking drug carriers to an adapter protein capable of binding to a docking tag. Using fragments of bovine ribonuclease A as an adapter protein and a docking tag, we have constructed vascular endothelial growth factor (VEGF) based vehicles for gene delivery and for liposome delivery. Assembled vehicles displayed remarkable selectivity in drug delivery to cells overexpressing VEGF receptors. We expect that our strategy can be employed for targeted delivery of many therapeutic or imaging agents by different recombinant targeting proteins.

INTRODUCTION

The current revolution in drug discovery is driven by functional genomics, proteomics, high throughput screening, and in silico drug design. It is widely expected that these new technologies will yield numerous potent and highly selective drugs. Targeted drug delivery, as opposed to systemic delivery, can dramatically increase drug efficacy while decreasing side effects and the patient's treatment burden. Targeted delivery requires "loading" drugs onto cell-specific cytokines or antibodies. Although initially these targeting proteins were purified from natural sources, now most of them are available as recombinant proteins. Thus, effective technology for loading drugs onto recombinant targeting molecules is crucial for channeling the current revolution in drug discovery into targeted drug delivery.

Currently, several strategies are used for loading drugs onto targeting proteins (*1*). In one approach, drugs (e.g., radionuclides) are directly conjugated to targeting proteins. In another approach, drugs are loaded onto high capacity drug carriers (e.g., liposomes, synthetic polymers, etc.). These carriers are either directly conjugated to targeting proteins or derivatized for interactions with specific adapters that are conjugated to the targeting proteins. Streptavidin/biotin interaction is particularly widely explored for binding various carriers to targeting proteins (*2*). Since both strategies rely on chemical conjugation of drugs, carriers, or adapters directly to targeting proteins, they share common problems such as (i) potential for inactivation of cell binding domains by conjugation, (ii) the inevitable heterogeneity of final products, and (iii) development of custom conjugation procedures for every targeting protein. These problems are the major stumbling blocks in using cell-specific proteins for targeted drug delivery. Recently, heterobifunctional recombinant antibodies recognizing one epitope on the cell surface and another epitope on the drug carrier have been proposed for targeted drug delivery (*3*, *4*). This approach avoids chemical modification of targeting antibody but it requires custom development of heterobifunctional recombinant antibodies, and the prospects of efficient internalization of antibody are uncertain.

We have recently proposed a new strategy for converting targeting proteins into vehicles for drug delivery (*5*). The strategy relies on a modular assembly of drug delivery vehicles and therefore avoids random chemical modification of targeting proteins. We proposed to construct standardized "payload" modules by linking various drug carriers to a special adapter protein (Figure 1). The function of the adapter protein is to bind a payload module to a "docking" tag fused to a targeting protein. In this approach, the assembly of a drug delivery vehicle does not require chemical modification of targeting proteins and relies on standardized components. Here we describe vascular endothelial growth factor (VEGF) based vehicles for delivery of liposome-encapsulated doxorubicin and for gene delivery. To construct these vehicles we have used a 104-aa fragment of bovine ribonuclease A (known as S-protein), as an adapter protein and a 15-aa fragment of bovine ribonuclease A (known as S-peptide) as a docking tag. This tag is incorporated in various pET expression vectors from Novagen (Madison, WI) and is widely used for affinity purification and quantitation of recombinant proteins. Assembled vehicles displayed remarkable selectivity in drug delivery to cells overexpressing VEGF receptors. We expect that our strategy can be employed for targeted delivery of many therapeutic or imaging agents by different recombinant targeting protein.

MATERIALS AND METHODS

Cells. 293 human transformed embryonic kidney cells (CRL-1573) and HL-60 human promyelocytic cells (CCL-240) were from American Type Culture Collection (Rockville, MD). PAE/KDR porcine aortic endothelial cells expressing 2.5×10^5 VEGFR-2/cell and PAE/V control cells were kindly provided by Dr. B. Terman (Albert Einstein School of Medicine, Bronx, NY). 293/KDR cells expressing 2.5×10^6 VEGFR-2/cell and PAE/0.1-KDR

* To whom correspondence should be addressed at SibTech, Inc., 705 North Mountain Road, Newington, CT 06111. Phone: (860) 953-1753; Fax: (860) 953-1317; E-mail: mbacker@sibtech.com.

† Albert Einstein College of Medicine.

10.1021/bc0155770 CCC: $22.00 © 2002 American Chemical Society
Published on Web 04/12/2002

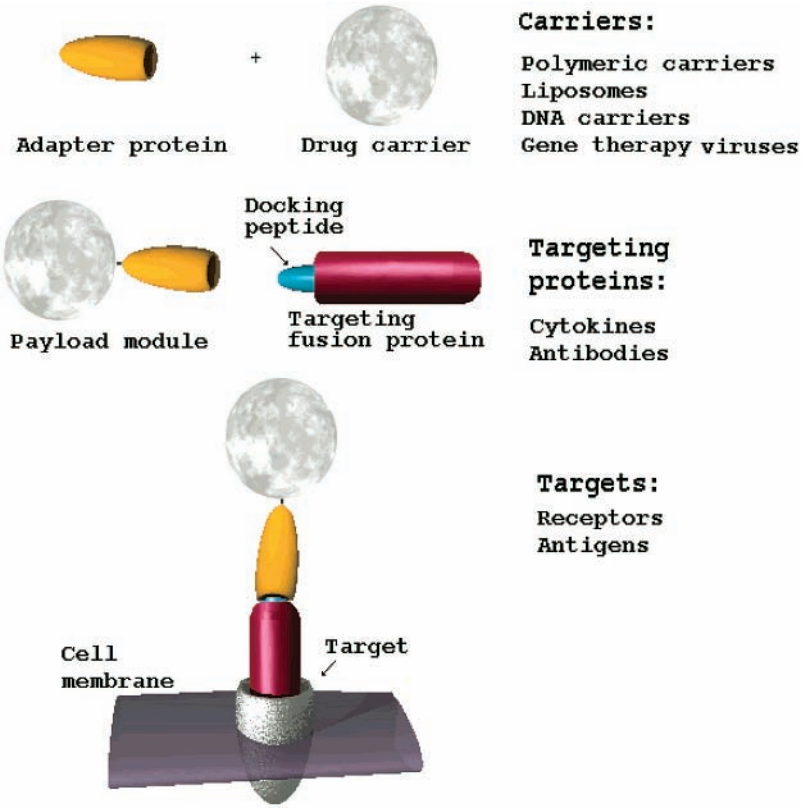


Figure 1. Construction of a molecular delivery vehicle.

expressing 2.5×10^4 VEGFR-2/cell have been developed in SibTech, Inc. (*6*, *7*). HL-60 cells were grown in RPMI 1640 (Gibco Life Technologies, Carlsbad, CA) supplemented with 20% fetal bovine serum (FBS, Gemini, Newton, MA), 4 mM L-glutamine, and antibiotics at 37 °C, 5% CO_2. All other cells were grown in DMEM with 10% FBS, 2 mM L-glutamine, and antibiotics at 37 °C, 5% CO_2.

Plasmids. $VEGF_{121}$ was cloned into pET-32a(+) (Novagen, Madison, WI) containing a coding sequence for a 15-aa fragment of bovine ribonuclease A, known as S-tag, as described previously (*7*). DNA encoding *E. coli* thioredoxin was removed from pET-32/$VEGF_{121}$ plasmid by *Nde*I digestion. The resulting pET/$VEGF_{121}$ plasmid encoded human $VEGF_{121}$ with a 42-aa N-terminus containing S-tag. S-tagged VEGF was expressed in Origami-(DE3)pLysS (Novagen) and purified as described (*8*). The concentration of the purified protein was determined by the S-tag Rapid Assay kit (Novagen) and reflected the concentration of S-tagged VEGF monomers. Human procaspase 8b (Mch5-beta, GenBank accession: AF009620) was amplified by RT-PCR using total RNA of HL-60 cells (RNeasy RNA isolation kit, Qiagen, Valencia, CA) with primers 5′-ac*tctaga*ttggtcacttgaaccttggg and 5′-ac*tcta-ga*agcaccatcaatcagaaggg introducing *Xba*I sites (italic); and cloned into pcDNA3.1/Zeo(+) (Invitrogen, Carlsbad, CA). Cloned cDNAs were confirmed by sequencing. The pGL3 plasmid encoding firefly luciferase was from Promega (Madison, WI).

Liposomes Preparation and Loading. S-protein fragment of bovine ribonuclease A (SP, Sigma, St. Louis, MO) at a concentration of 0.93 mM was modified with 0.7 mM poly(ethylene glycol)-α-distearoyl phosphatidylethanolamine, ω-NHS ester (DSPE-PEG-NHS, average MW 3400, Shearwater Polymers, Huntsville, AL) in 0.1 M NaPi, 0.15 M NaCl, pH 7.2, under argon at 37 °C for 4 h. Dioleoyl phosphatidylcholine (Avanti, Alabaster, AL) and cholesterol (Sigma) were mixed at the molar percent ratio of 65:35, lyophilized from cyclohexane, and hydrated in a buffer containing 10 mM HEPES pH 7.2, 150 mM NaCl, 0.1 mM EDTA, 0.1 mM EGTA, and 0.34 mM doxorubicin (Dox, Sigma, St. Louis, MD), and 13 μM DSPE-SP. After four freeze−thaw cycles, the lipids were extruded for 15 cycles through two stacked 0.08 μm polycarbonate membranes using a miniextruder (Avanti). Free Dox and SP were removed by chromatography on Sepharose CL-4B (Sigma). Lipid content in purified liposomes, named Lip(Dox)−SP, was determined by phosphate assay (Pierce, Rockford, IL), Dox content was determined fluorometrically (excitation at 470 nm, emission at 590 nm), and SP content was determined by micro-BCA protein assay (Pierce). The liposome surface Zeta potential and size were measured by Delsa 440SX Zeta Potential Analyzer (Coulter-Beckman, Miami, FL). Complexes of Lip(Dox)−SP with VEGF had an average size of 139 nm (SD = 26) and a zeta-potential of 0.45 mV (SD = 2.25) indicating that our procedure yielded unilamellar liposomes.

The sensitivity of 293 and 293/KDR cells to free Dox was determined using MTT cell proliferation assay (Promega). Briefly, 293 and 293/KDR cells were seeded on 96-well plate, 10^3 cells/well. Twenty-four hours later cells in quadruplicate wells were treated with Dox at a concentration range of 0.1 pM to 10 μM. After 24 h of treatment, the Dox-containing medium was replaced with fresh culture medium. MTT cell proliferation assay was performed according to the manufacturer's instructions after additional 48 h of incubation under the normal culture conditions.

Preparation of Polyethylenimine/S-Protein Conjugates. Linear 25 kDa polyethylenimine (PEI, Polysciences Inc., Warrington, PA) at concentration of 5 mM was modified with 5 mM Traut's reagent (Pierce) in 50 mM triethanolamine, 0.15 M NaCl, 1 mM EDTA, pH 8.0,

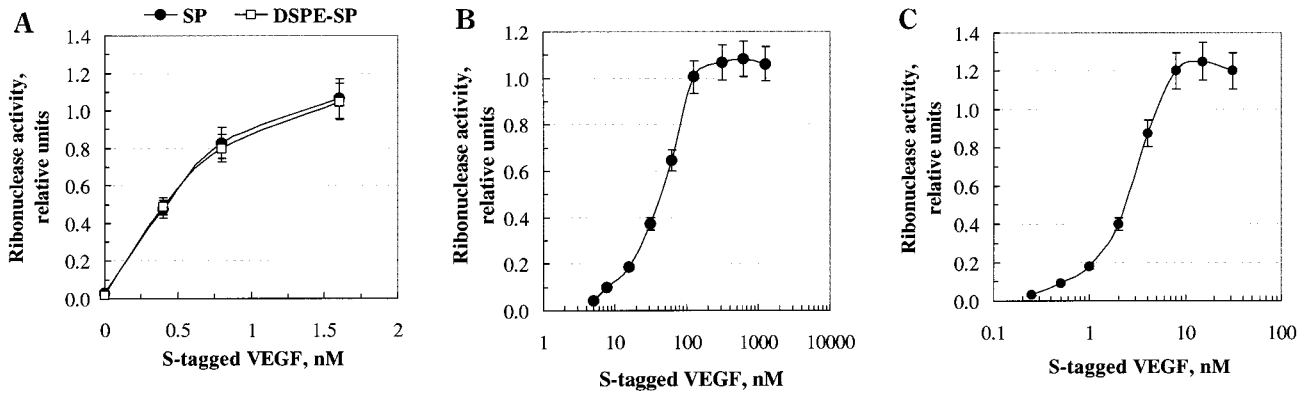


Figure 2. Derivatized S-protein (SP) binds to S-tagged VEGF. Derivatized SP was mixed with varying amounts of S-tagged VEGF. Ribonuclease activity was measured using S-tag Rapid Assay Kit (Novagen). A, DSPE-SP and control SP at concentrations of 4 nM, each. B, Lip(Dox)−SP, at SP concentration of 580 nM. C, PEI−SP, at SP concentration of 6 nM.

under argon at room temperature for 20 min. Concentration of SH groups in modified PEI was determined by Ellman's reagent (Pierce). SP at concentration of 0.66 mM was modified with 1.32 mM sulfo-MBS (Pierce) in conjugation buffer containing 0.1 M NaPi, 0.15 M NaCl, pH 7.2, at room temperature for 30 min. Modified SP and PEI were mixed at the molar ratio of 1:1 in conjugation buffer and incubated at room temperature for 4 h with constant agitation. PEI−SP conjugates were purified by gel-filtration on SE 100/40 (BioRad, Hercules, CA).

Preparation of DNA/PEI−SP−VEGF Complexes. DNA/PEI−SP−VEGF complexes were prepared as described (*5*). The surface zeta potential was measured by a Delsa 440SX Zeta Potential Analyzer (Coulter-Beckman). The ability of all cells to accept and express pGL3 DNA was determined using DNA/PEI complexes at N/P ratio from 5 to 13. The transfectability of VEGFR-2 expressing cells and control cells was found to be similar within 15% experimental error (data not shown).

Measurements of Ribonuclease Activity. Ribonuclease activity was measured with S-tag Rapid Assay Kit (Novagen). A relative unit of ribonuclease activity is 1 OU of acid-soluble material released from polyC incubated with various complexes of S-protein and S-tagged VEGF under the manufacturer's conditions.

RESULTS AND DISCUSSION

Construction of Molecular Drug Delivery Vehicles. The overall design of the modular drug delivery vehicle is shown in Figure 1. In our approach, conjugating the appropriate drug carriers to a universal adapter protein creates standardized payload modules. The role of the adapter protein is to bind with high affinity to a specific peptide fused to a targeting protein. This peptide serves as a "docking tag" for a payload module. In principle, any recombinant targeting protein expressed with such a docking tag can bind a premade adapter−carrier module, and the assembled vehicle can be used for targeted drug delivery.

A number of peptide tags recognized by specific proteins have already been developed for purification and detection of recombinant proteins. Among these, the so-called S-tag system based on interaction between S-peptide and S-protein fragments of bovine ribonuclease A appears to be the best choice for our purposes for the following reasons. First, the 15-aa S-peptide and 104-aa S-protein (SP) fragments form the smallest tag/adapter complex currently available with a K_d of 10^{-9} M^{-1} (*9*). Second, the S-peptide/SP complex is an active ribonuclease (known as RNase S), and therefore association of S-tagged recombinant proteins with SP-carrier modules can be readily detected by the reconstituted ribonuclease activity (*10*). Third, the bovine S-peptide/SP complex has been extensively studied for more than 40 years, detailed information about various aspects of this system is available, and bacterial expression plasmids for production of S-tagged proteins as well as S-protein are commercially available (*9*−*13*). Finally, the complex can be "humanized" by using appropriate fragments of human ribonuclease I (RNase I), thus improving chances for therapeutic success of the proposed strategy.

As a targeting protein we have chosen VEGF, the most specific cytokine for endothelial cells (*14*). The VEGF targeting ability is further narrowed by the evidence that its receptor, VEGFR-2 (KDR/Flk-1), is overexpressed at the sites of pathological angiogenesis (*15*−*17*). This exquisite specificity marks VEGFR-2 as a prominent target for anti-angiogenic therapy. Indeed, several recent reports indicated that VEGF-toxin fusion proteins and anti-VEGFR-2 neutralizing antibodies display highly selective activity in vivo and in vitro (*6*, *18*, *19*). Within VEGF family, $VEGF_{121}$ appears to be the most attractive candidate to be used as a targeting protein for two reasons. First, it has selective affinity to VEGFR-2 and second, it lacks a heparin-binding domain and, therefore, cannot be sequestered in the extracellular matrix. We have expressed $VEGF_{121}$ as a fusion protein containing bovine S-tag as a docking tag (S-tagged VEGF). Using SP as an adapter we have constructed payload modules for liposome delivery and for gene delivery.

Payload Module SP Binds to S-Tagged VEGF. To construct a payload module for liposome delivery, SP was conjugated to distearoyl phosphatidylethanolamine (DSPE) modified with poly(ethylene glycol). Derivatized SP (DSPE−SP) formed catalytically active complexes with S-tagged VEGF as effectively as unmodified SP ($K_d \sim 0.5$ nM), as judged by concentration dependence of ribonuclease activity of these complexes (Figure 2*A*). The fully assembled doxorubicin-loaded, DSPE−SP containing liposomes (Lip(Dox)−SP) also retained the ability to bind S-tagged VEGF (Figure 2B). The enzymatic activity of Lip(Dox)−SP−VEGF complexes was detectable at concentrations 50−100 fold higher than that of DSPE−SP−VEGF (compare Figure 2A and 2B), suggesting lower specific activity of liposome-associated reconstructed ribonuclease. In experiments with Lip(Dox)−SP−VEGF, the total concentration of SP was 580 nM and ribonuclease activity of the complexes reached a plateau at

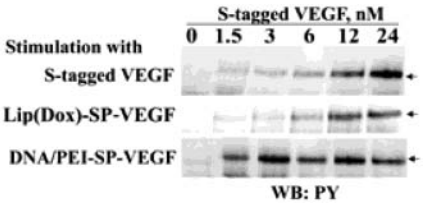


Figure 3. VEGF-based molecular delivery vehicles activate cellular VEGFR-2. Near confluent 293/KDR cells were incubated overnight in DMEM with 0.5% FBS, and then shifted to serum-free DMEM with 0.5 mM sodium vanadate for 5 min at 37 °C. Cells were stimulated with free S-tagged VEGF or VEGF-based delivery vehicles for 5 min at 37 °C, lysed, and analyzed by Western blotting using anti-phosphotyrosine RC20:HRPO conjugate (BD Transduction Labs, San Diego, CA). Arrows indicate positions of VEGFR-2.

~300 nM S-tagged VEGF as expected if SP is randomly distributed between the inner and the outer surfaces of liposomes.

To construct a payload module for gene delivery, SP was conjugated to polyethylenimine (PEI), a well-characterized DNA carrier (*20*−*22*). The conjugation protocol included (i) introduction of SH-group in PEI, (ii) introduction of a maleimide group in SP, and (iii) cross-linking of the modified PEI and SP via a reaction between SH and maleimide groups. We found that SP covalently bound to PEI (PEI−SP) binds S-tagged VEGF with nanomolar (K_d ~2 nM) affinity (Figure 2C).

VEGF Associated with Payload Modules Binds and Activates VEGFR-2. To test the functional activity of S-tagged VEGF in assembled delivery vehicles, we employed a VEGFR-2 tyrosine autophosphorylation assay. As a control we used free S-tagged VEGF. In this assay, assembled doxorubicin-loaded liposome delivery vehicles (Lip(Dox)−SP−VEGF) were as active as S-tagged VEGF alone, suggesting that binding of VEGF to the liposome surface did not affect its interaction with VEGFR-2 (Figure 3).

DNA delivery vehicles (DNA/PEI−SP−VEGF) containing pGL3 DNA at the N/P ratio of 8.4 (where N is the number of amino groups in PEI and P is the number of DNA phosphate groups) induced VEGFR-2 tyrosine autophosphorylation at VEGF concentrations as low as 1.5 nM (Figure 3). Importantly, DNA/PEI−SP−VEGF complexes were more efficient in this assay than free S-tagged VEGF. This effect can be explained by the higher avidity of DNA/PEI−SP−VEGF complexes to cells overexpressing VEGFR-2. Indeed, at the N/P ratio of 8.4 every pGL3 plasmid (5256 bp) is bound to several 25 kDa PEI (~600 monomers per molecule), and the complexes are packaged into highly condensed particles (*20*). Since every PEI−SP carries VEGF, assembled DNA/PEI−SP−VEGF will contain several VEGF molecules per a tightly packed complex and therefore can bind to cellular VEGFR-2 with higher avidity than individual VEGF.

VEGF-Based Targeted Delivery of Therapeutics. Lip(Dox)−SP−VEGF were tested on 293/KDR (2.5×10^6 VEGFR-2/cell) and 293 parental cells. To account for nonreceptor mediated toxicity, 293/KDR and 293 were treated with Lip(Dox)−SP and growth inhibition induced by Lip(Dox)−SP−VEGF was calculated relative to these controls. There were no difference in sensitivity of 293/KDR and 293 cells to Lip(Dox)−SP (data not shown). We found that Lip(Dox)−SP−VEGF did not affect 293, but inhibited growth of 293/KDR in a dose-dependent manner (Figure 4*A*) with IC_{50} of 0.8 nM for equivalent concentration of Dox. 293/KDR and 293 displayed similar sensitivity to free Dox with IC_{50} of 8 nM and 10 nM, respectively

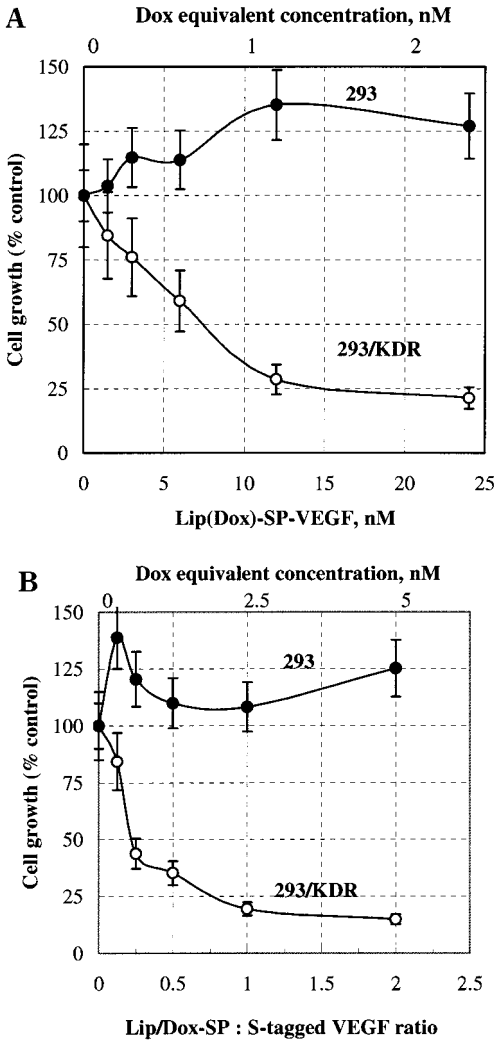


Figure 4. VEGF targets liposomes to cells overexpressing VEGFR-2. 293/KDR and 293 parental cells were plated on 24-well plates, 5×10^3 cells/well 20 h before the experiment. Lip(Dox)−SP were mixed with S-tagged VEGF at varying SP to VEGF molar ratios in serum-free DMEM, incubated on ice for 20 min, and then added to cells in complete culture medium in triplicate wells. After 20 h, cells were shifted to fresh culture medium. Cells were counted in a Coulter Counter (Coulter-Beckman) after 3-day incubations. Control cells were treated with equal amounts of Lip(Dox)−SP without VEGF and growth inhibition induced by Lip(Dox)−SP−VEGF was calculated relative to these controls. Liposome delivery experiments were repeated two times. A, Lip(Dox)−SP−VEGF at liposome SP to VEGF ratio of 1:1. Dox equivalent concentration is indicated. B, Varying amounts of Lip(Dox)−SP and constant 12 nM VEGF.

(data not shown). Thus, a 10-fold decrease in IC_{50} for 293/KDR can be attributed to VEGF-mediated delivery of liposome-encapsulated Dox. Similar decrease in IC_{50} was reported for human umbilical vein endothelial cells (HUVEC) treated with immunoliposome-encapsulated and free Dox (23). Interestingly, effect Lip(Dox)−SP−VEGF on 293/KDR was close to saturation at the liposome SP to S-tagged VEGF monomer ratio of 0.5:1 (Figure 4*B*). The latter result indicated that docking of Lip(Dox)−SP to both S-tags in the VEGF dimer does not significantly improve interaction of the resulting complex with cellular VEGFR-2.

VEGF-based DNA delivery vehicles were tested on three cell lines expressed varying number of VEGFR-2 per cell: PAE/0.1-KDR (2.5×10^4 VEGFR-2/cell), PAE/KDR (2.5×10^5 VEGFR-2/cell), and 293/KDR. PAE/V and 293/V cells transfected with empty vectors served as

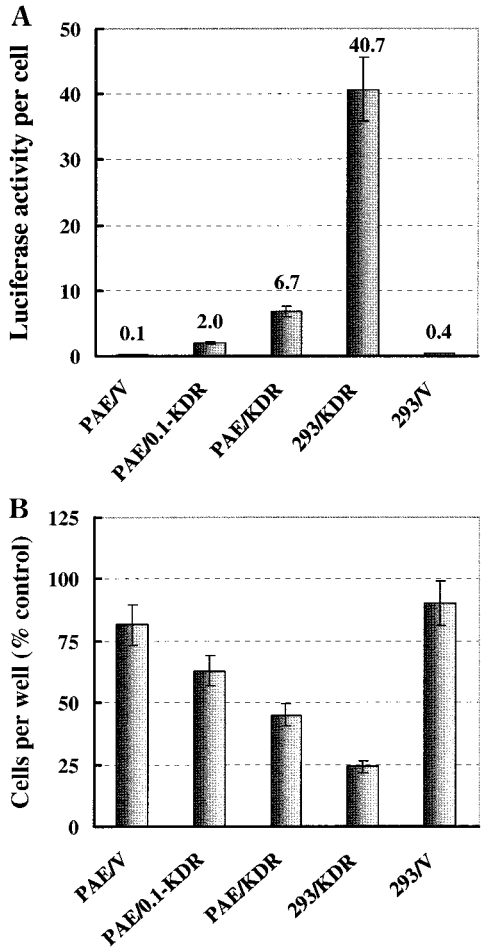


Figure 5. VEGF targets DNA delivery vehicles to cells overexpressing VEGFR-2. Cells were plated on 24-well plates at densities of 4×10^3 cells/well for PAE, PAE/KDR, PAE/0.1-KDR, and 2×10^4 cells/well for 293 and 293/KDR, 20 h before the experiment. PEI−SP was mixed with S-tagged VEGF (SP to VEGF ratio of 1:1.5) in 5% glucose, incubated on ice for 20 min, added dropwise to DNA in 5% glucose (N/P of 8.4), incubated on ice for an additional 20 min, and added to cells in complete culture medium to final concentrations of 12 nM VEGF, 36 nM PEI−SP, and 0.7 μg DNA per well. DNA delivery experiments were repeated three times. A, 40 h after luciferase DNA delivery, cells from triplicate wells were lyzed and assayed for luciferase activity, while cells from duplicate wells were washed with PBS, trypsinized, and counted in a Coulter Counter. B, 70 h after caspase DNA delivery, cells from triplicate wells were washed with PBS, trypsinized, and counted in a Coulter Counter.

controls. To reduce nonspecific DNA delivery, the DNA/PEI−SP−VEGF complexes were assembled with an N/P ratio of 8.4 giving a negative surface charge (zeta-potential of −25.4 mV, SD = 9.4). The efficiency of luciferase DNA delivery to cells depended on the cellular density of VEGFR-2, with the highest luciferase activity detected in 293/KDR cells expressing ~2.5×10^6 VEGFR-2/cell (Figure 5*A*). It should be noted that we have recently found that freshly isolated human circulating endothelial precursor cells express more VEGFR-2 than 293/KDR, indicating that VEGFR-2 may be overexpressed to very high density on certain cells in vivo (manuscript in preparation).

To test whether the VEGF-based vehicle can deliver therapeutically significant quantities of DNA to targeted cells, we have loaded the vehicle with the plasmid expressing human pro-caspase 8b, an apical protease of the apoptotic cascade (*24*). We found that VEGF-based caspase DNA delivery resulted in preferential death of cells expressing VEGFR-2 and that this effect also depended on the level of VEGFR-2 per cell (Figure 5B). Thus, we can expect that VEGF-based delivery vehicles in vivo will more efficiently target cells overexpressing VEGFR-2, such as endothelial cells at the sites of pathological angiogenesis or endothelial progenitor cells.

Our results provide evidence that VEGF-based molecular delivery vehicles can be constructed without random chemical modification of the targeting protein. We believe that molecular vehicles for delivery of therapeutic and imaging agents may be constructed using other targeting proteins, different drug carriers, and new payload modules. We expect that construction of a targeting protein, which can be combined with premade payload modules, would require significantly less effort than development of a customized chemical modification procedure for the same protein or development of a heterobifunctional antibody against the same target. Our recent experiments indicate that adapter/docking tag system can be based on human RNase I, and that random chemical modification of the adapter protein can be avoided by engineering an additional cysteine residue into S-protein fragment of RNase I (manuscript in preparation). Experiments are now in progress to develop novel payload modules based on humanized adapter/docking tag system.

ACKNOWLEDGMENT

This work was supported in part by a grant from National Institutes of Health (# 2 R44 HL61143-02). We thank C. Hamby for critical reading of the manuscript and A. Backer for help with graphic.

LITERATURE CITED

(1) Dubowchik, G. M., and Walker, M. A. (1999) Receptor-mediated and enzyme-dependent targeting of cytotoxic anticancer drugs. *Pharmacol. Ther. 83*, 67−123.

(2) Wilbur, D. S., Pathare, P. M., Hamlin, D. K., Stayton, P. S., To, R., Klumb, L. A., Buhler, K. R., and Vessella, R. L. (1999) Development of new biotin/streptavidin reagents for pretargeting. *Biomol. Eng. 16*, 113−118.

(3) Kriangkum, J., Xu, B.. Nagata, L. P., Fulton, R. E., and Suresh, M. R. (2001) Bispecific and bifunctional single chain recombinant antibodies. *Biomol. Eng. 18*, 31−40.

(4) Zhu, H., Jain, R. K., and Baxter, L. T. (1998) Tumor pretargeting for radioimmunodetection and radioimmunotherapy. *J. Nuclear Med. 39*, 65−76.

(5) Gaidamakova, E. K., Backer, M. V., and Backer, J. M. (2001) Molecular vehicle for target-mediated delivery of therapeutics and diagnostics. *J. Controlled Release 74*, 341−347.

(6) Backer, M. V., and Backer, J. M (2001) Targeting endothelial cells overexpressing VEGFR-2: selective toxicity of Shiga-like toxin-VEGF fusion proteins. *Bioconjugate Chem. 12*, 1066−1073.

(7) Backer, M. V., and Backer, J. M. (2001) Functionally active VEGF fusion proteins. *Prot. Expr., Purif. 23*, 1−7.

(8) Li, B., Fuh, G., Meng, G., Xin, X., Gerritsen, M. E., Cunningham, B., and de Vos A. M. (2000). Receptor-selective variants of human vascular endothelial growth factor. *J. Biol. Chem. 275*, 29823−29828.

(9) Kim, J. S., and Raines, R. T. (1993) Ribonuclease S-peptide as a carrier in fusion proteins. *Protein Sci. 2*, 348−356.

(10) Richards, F. M., and Wyskoff, H. W. (1971) in *The Enzymes* (P. D. Boyer, Ed.) pp 647−806, Academic Press, New York.

(11) Chakshusmathi, G., Girish, S., Ratnaparkhi, S., Madhu, P. K., and Varadarajan, R. (1999) Native-state hydrogen-exchange studies of a fragment complex can provide structural information about the isolated fragments. *Proc. Natl. Acad. Sci. U. S. A. 96*, 7899−7904.

(12) Connelly, P. R., Varadarajan, R., Sturtevant, J. M., and Richards, F. M (1990) Thermodynamics of protein-peptide interactions in the ribonuclease S system studied by titration calorimetry. *Biochemistry 29*, 6108−6114.

(13) Kim, E. E., Varadarajan, R., Wyckoff, H. W., and Richards, F. M. (1992) Refinement of the crystal structure of ribonuclease S. Comparison with and between the various ribonuclease A structures. *Biochemistry 31*, 12304−12314.

(14) Senger, D. R., Van de Water, L., Brown, L. F., Nagy, J. A., Yeo, K. T., Yeo, T. K., Berse, B., Jackman, R. W., Dvorak, A. M., and Dvorak, H. F. (1993) Vascular permeability factor (VPF, VEGF) in tumor biology. *Cancer Metastasis Rev. 12*, 303−324.

(15) Feng, D., Nagy, J. A., Brekken, R. A., Pettersson, A., Manseau, E. J., Pyne, K., Mulligan, R., Thorpe, P. E., Dvorak, H. F., and Dvorak, A. M. (2000) Ultrastructural localization of the vascular permeability factor/vascular endothelial growth factor (VPF/VEGF) receptor-2 (FLK-1, KDR) in normal mouse kidney and in the hyperpermeable vessels induced by VPF/VEGF-expressing tumors and adenoviral vectors. *J. Histochem. Cytochem. 48*, 545−556.

(16) Brown, L., Detmar, M., Claffey, K., Nagy, J., Feng, D., Dvorak, A. M., and Dvorak, H. F. (1997) Vascular permeability factor/vascular endothelial growth factor: a multifunctional angiogenic cytokine, in *Regulation of Angiogenesis* (I. Goldberg, E. Rosen, Eds) pp 233−269, Basel, Birkhouser Verlag.

(17) Detmar, M., Brown, L. F., Claffey, K. P., Yeo, K. T., Kocher, O., Jackman, R. W., Berse, B., and Dvorak, H. F. (1994) Overexpression of vascular permeability factor/vascular endothelial growth factor and its receptors in psoriasis. *J. Exp. Med. 180*, 1141−1146.

(18) Arora, N., Maood, R., Zheng, T., Cai, J., Smith, L., and Gill, P. S. (1999) Vascular endothelial growth factor chimeric toxin is highly active against endothelial cells. *Cancer Res. 59*, 183−188.

(19) Prewett, M., Huber, J., Li, Y., Santiago, A., O'Connor, W., King, K., Overholser, J., Hooper, A., Pytowski, B., Witte, L., Bohlen, P., and Hicklin, D. J. (1999) Antivascular endothelial growth factor receptor (fetal liver kinase 1) monoclonal antibody inhibits tumor angiogenesis and growth of several mouse and human tumors. *Cancer Res. 59*, 5209−5218.

(20) Boussif, O., Lezoualch, F., Zanta, M.-A.,. Mergny, M. D, Scherman, D., Demeneix, B., and Behr, J.-P. (1995) A versatile vector for gene and oligonucleotide transfer into cells in culture and in vivo. *Proc. Natl. Acad. Sci. U. S. A. 92*, 7297−7301.

(21) Zanta, M.-A., Boussif, O., Adib, A., and Behr, J.-P. (1997) In vitro gene delivery to hepatocytes with galactosylated polyethylenimine. *Bioconjugate Chem. 8*, 839−844.

(22) Rolland, A. (1998) From genes to gene medicines: recent advances in nonviral gene delivery. *Crit. Rev. Ther. Drug Carrier Syst. 15*, 143−198.

(23) Spragg, D. D., Alford, D. R., Greferath, R., Larsen, C. E., Lee, K.-D., Gurtner, G. C., Cybulsky, M. I., Tosi P. F., Nicolau, C., and Gimbrone, M. A., Jr. (1997) Immunotargeting of liposomes to activated vascular endothelial cells: A strategy for site-selective delivery in the cardiovascular system. *Proc. Natl. Acad. Sci. U. S. A. 94*, 8795−8800.

(24) Cohen, G. M. (1997) Caspases: the executioners of apoptosis. *Biochem. J. 326*, 1−16.

BC0155770

Utility of Thiol-Cross-Linked Fluorescent Dye Labeled Terminators for DNA Sequencing

Satyam Nampalli, Mark G. McDougall, Katherine Lavrenov, Haiguang Xiao, and Shiv Kumar*

Amersham Biosciences, 800 Centennial Ave, Piscataway, New Jersey 08855-1327. Received December 11, 2001; Revised Manuscript Received March 13, 2002

Dipivaloyl-5-carboxyfluorescein *N*-hydroxysuccinimidyl ester **1** and 5-propargylamino-2′,3′-dideoxyuridine triphosphate **5** were modified with maleimide, haloacetamide, and sulfhydryl reactive functional groups to participate in cross-conjugation reactions via sulfide bonds to generate fluorescently labeled, thioether cross-conjugated terminators **10** and **11**. Their DNA sequencing potential was compared with an amide cross-conjugated terminator **13**, synthesized by directly coupling 5-carboxyfluorescein NHS ester with 18-ddUTP **9**. These terminators (**10**, **11**, and **13**) in combination with the Thermo Sequenase II DNA polymerase, in thermal cycle sequencing experiments, revealed that the thioether cross-conjugated terminator **10** and amide cross-conjugated terminator **13** served as good terminating substrates, generating satisfactory single-color gel images and electropherograms, while the other thioether cross-conjugated and maleimide derived one **11** underwent unexpected pH and temperature induced decomposition without showing fluorescent signatures for incorporation.

INTRODUCTION

The technique of using fluorescent dye-labeled terminators in Sanger (*1*) DNA sequencing has proven very cost-effective and safe over the radioactive isotope-labeled ones. Moreover, the FRET (fluorescence resonance energy transfer) dye-pair labeled terminators (*2*, *3*) or primers (*4*, *5*) are very widely used as part of the kit for high throughput DNA sequencing with a thermostable DNA polymerase. DNA polymerases are very sensitive to the unnatural, dye-labeled dideoxynucleotide terminators in that the rate of incorporation of the terminators and generation of an electropherogram with more evenly distributed peak heights, are highly dependent upon the spacer that serves as a bridge between the fluorescent dyes and nucleotide bases (*6*). To date, the spacers of these fluorescent terminators composed of alkynylamido (*2*, *3*), alkynylethoxyamido (*7*), and the rigidified alkynyl-aryl-alkynylethoxyamido (*8*) functional groups. None of these fluorescent terminators, so far utilized, for sequencing purposes, contained thioether cross-linked spacers interspersed with alkynyl-alkyl-amido functional groups. For achieving thioether cross-linking, between two molecules (e.g., nucleic acids/proteins and fluorescent dyes) of interest, one needs to modify one molecule with a thiol (sulfhydryl) in the disulfide form and the other with an alkyl halide or maleimide. Thiols can be generated in situ by reducing the disulfide-modified molecule with DTT (dithiothreitol, *9*) or TCEP (tris(2-carboxyethlyphosphine, *10*) to react with alkylhalides or maleimides forming thioether bonds. In our continued efforts to provide enzyme friendly fluorescent dye-labeled terminators for improved, high throughput DNA sequencing as well as protein and other nucleic acid detection studies, we have embarked on design and synthesis of the fluorescent dye terminators, involving thioether cross-linking in the ultimate step. These synthetic studies were aimed at investigating the substrate activity of these thiol cross-linked fluorescent ddNTPs with a DNA polymerase, stability to cycle sequencing conditions, and peak uniformity of the labeled amplicons in direct comparison with an amide bond cross-linked fluorescent terminator.

* To whom correspondence should be addressed. Phone: (732) 980-2878; Fax; (732) 457-8353. E-mail: shiv.kumar@am.amershambiosciences.com.

EXPERIMENTAL PROCEDURES

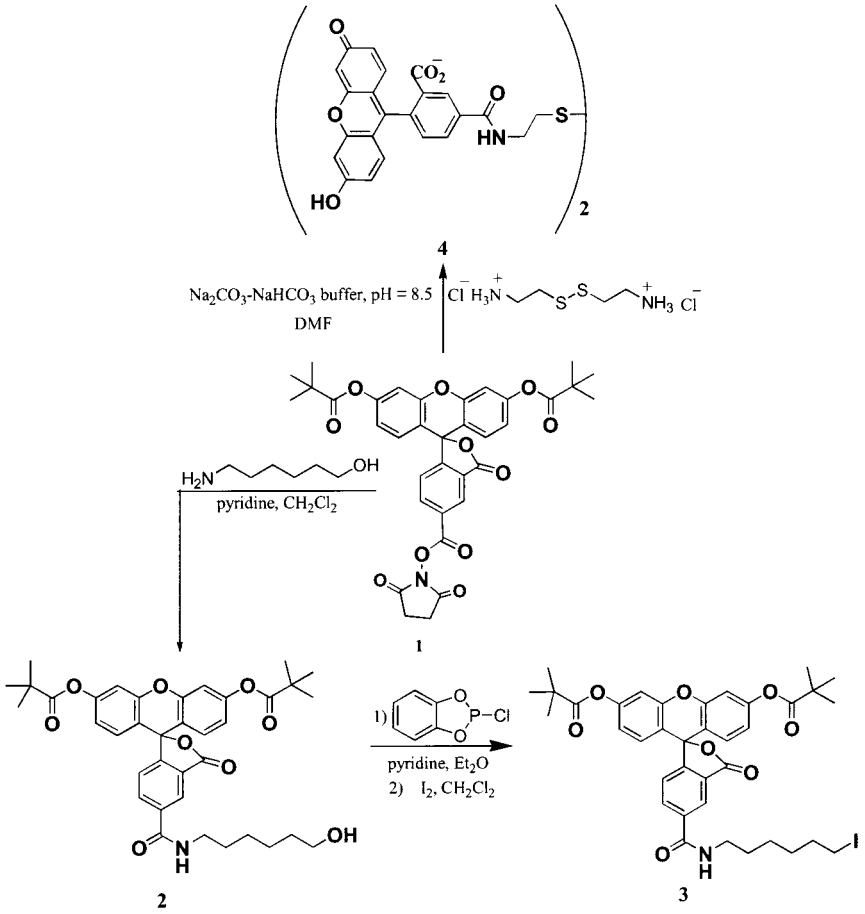
General Remarks. The chemical reagents such as SPDP, TCEP, and 5-FAM-NHS ester were purchased from Molecular Probes, Inc. The DNA polymerase, Thermo Sequenase II was obtained from Amersham Biosciences. NMR spectra were recorded on a Varian 300 MHz spectrometer and are reported in parts per million downfield from TMS. Mass spectra were obtained on a Micromass LC-MS instrument using TOF ES. DNA sequencing analysis and gel images were performed on ABI 377 sequencer. UV/vis spectra were recorded on a Perkin-Elmer Lambda20 spectrometer. The number in 11-ddUTP and 18-ddUTP denotes the number of atoms present in the spacer that connects the nucleotide base with the fluorescent dye or the pendant spacer moiety at the 5-position of the nucleotide base. For convenience, the abbreviation FAM is used for 5-carboxyfluorescein as mentioned in the Molecular Probes catalog.

5-(6-Hydroxyhexanamido)dipivaloylfluorescein (2). To a stirred solution of dipivaloyl-5-carboxyfluorescein *N*-hydroxysuccinimidyl ester **1** (0.5 g) in anhydrous CH_2Cl_2 (10 mL) were added anhydrous pyridine (250 μL) and 6-aminohexanol (100 mg). The reaction mixture was stirred overnight, diluted with 25 mL of CH_2Cl_2, and washed with 10% aqueous citric acid (2 × 15 mL) and brine (2 × 15 mL). The organic layer was dried over anhydrous Na_2SO_4 and evaporated under reduced pressure, and the residue was purified on silica gel column chromatography eluting with 2% MeOH−CH_2Cl_2 to give **2** (438 mg, 89%) as an amorphous solid.

5-(6-Iodohexanamido)dipivaloylfluorescein (3). To a stirred and cooled (0 °C) solution of **2** (322 mg, 0.5 mmol) in anhydrous ether (15 mL) were added anhydrous pyridine (41 μL, 0.5 mmol) and 1,2-phenylene phosphorochloridite (60 μL, 0.5 mmol) dropwise. The reaction

10.1021/bc015591c CCC: $22.00 © 2002 American Chemical Society
Published on Web 04/20/2002

Scheme 1. Synthesis of Fluorescein Disulfide (4) and Alkyl Iodide (3)



mixture was allowed to come to room temperature and to continue stirring overnight. The salt formed was filtered and washed with ether and the filtrate evaporated under reduced pressure to provide the phosphorochloridite derivative, which without purification was treated with I_2 (127 mg, 0.5 mmol) in CH_2Cl_2 (10 mL) for 2 h to afford the crude alkyl iodide. Purification of the crude alkyl iodide on silica gel column, eluting with 1:1 hexanes−ethyl acetate, gave **3** (97%). ^{1}H NMR (300 MHz, $CDCl_3$) δ 8.34 (s, 1H, Ar-*H*), 8.16 (d, J = 8.5 Hz, 1H, Ar-*H*), 7.26 (d, J = 8.5, 1H, Ar-*H*), 7.25 (s, 1H, Ar-*H*), 7.06 (s, 1H, Ar-*H*), 6.77 (bs, 4H, Ar-*H*), 6.59 (bs, 1H, N*H*), 4.40 (m, 2H, CH_2NH), 3.18 (t, 2H, J = 17 Hz, CH_2I), 1.42−1.84 (m, 8H, (CH_2)$_4$), 1.35 (s, 18H, CH_3 × 3).

5-(Cystamido)fluorescein (4). To a stirred solution of **1** (270 mg, 0.42 mmol) in anhydrous DMF (10 mL) was added a 0.1 M Na_2CO_3−$NaHCO_3$ buffer (pH 8.5) solution of cystamine dihydrochloride (45 mg, 0.2 mmol) at room temperature. After stirring the reaction mixture overnight, it was evaporated under reduced pressure and the residue subjected to reversed-phase HPLC on a Delta-Pak C18 column (15 μm, 100 Å) eluting with a gradient of 0.1 M TEAB to 100% CH_3CN in 60 min at 5 mL/min gave compound **4** (27%). ^{1}H NMR (300 MHz, $CDCl_3$) δ 8.45(s, 2H, Ar-*H*), 8.07 (d, J = 8.5 Hz, 2H, Ar-*H*), 7.34 (d, J = 8.5, 2H, Ar-*H*), 7.00 (d, 4H, Ar-*H*), 7.05 (s, 1H, Ar-*H*), 6.66 (bs, 8H, Ar-*H*), 6.59 (bs, 2H, N*H*), 3.69 (t, 4H, J = 5.0 Hz, CH_2S), 3.31 (m, 4H, HNCH_2), 1.06 (s, 18H, CH_3).

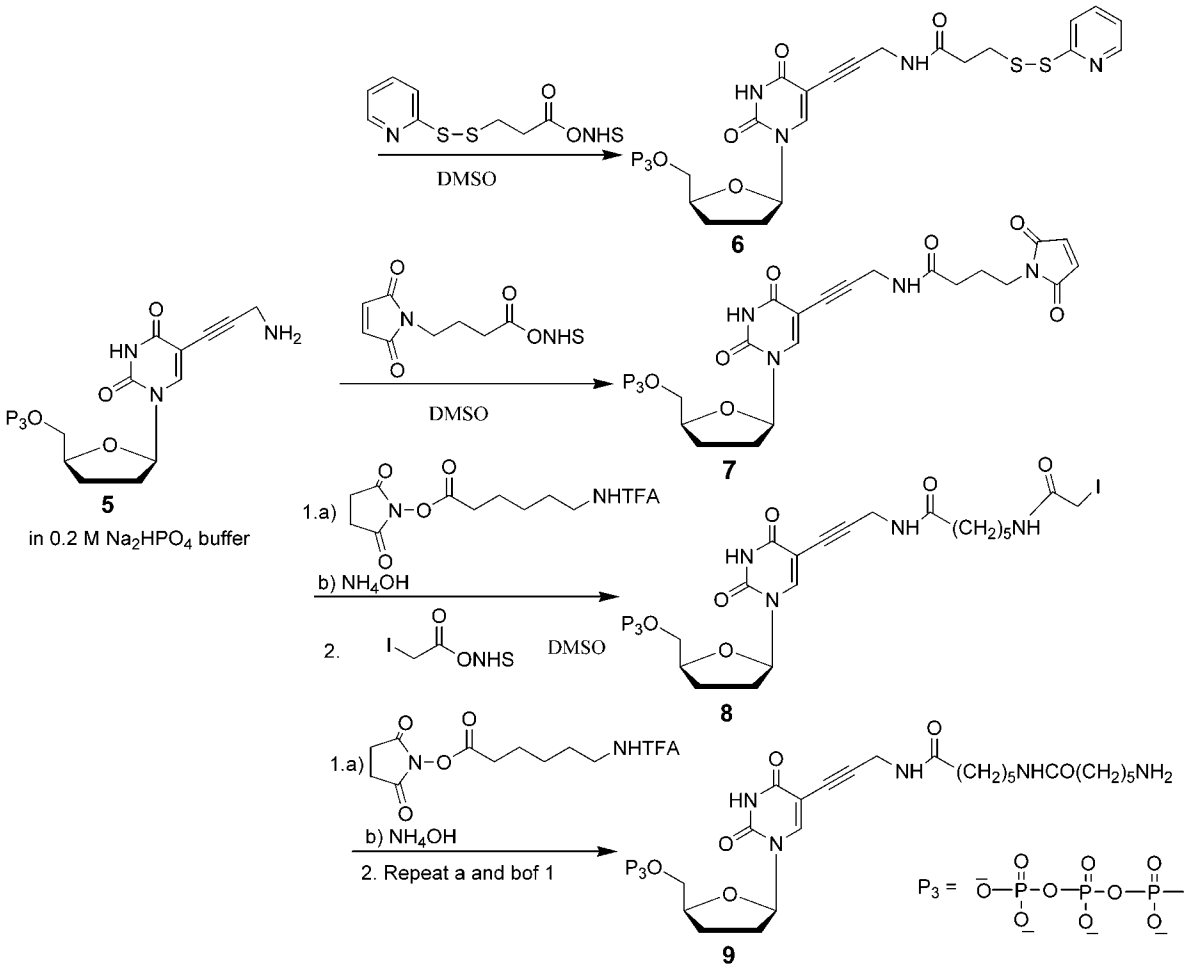
Pyridyldithiopropionamidyl-PA-ddUTP (6). A 0.2 M sodium phosphate buffer (pH 7.2) solution (2.5 mL) of PA-ddUTP **5** (10 mg, 0.012 mmol) was treated with DMSO (0.5 mL) solution of SPDP (16 mg, 0.049 mmol) for 2 h at room temperature. The reaction mixture was subjected to reversed-phase HPLC on a Delta-Pak C18 semiprep column (15 mm, 100 Å, 300 × 19) eluting with 0.1 M TEAB (pH 7.5) to 100% CH_3CN in 60 min at 5 mL/min to provide **6** (8 mg, 60%) after evaporation and lyophilization.

Maleimidobutanamidyl-PA-ddUTP (7). Compound **5** (10 mg, 0.012 mmol) was reacted with SMB (succinimidyl 4-maleimidylbutanoate, 14 mg, 0.049 mmol) and product **7** (9.5 mg, 70%) purified using similar reaction and HPLC conditions as described for **6**. Observed 669.01 TOF MS ES− m/z for $C_{20}H_{24}N_4O_{16}P_3$, 669.00.

Iodoacetamidohexanamidyl-PA-ddUTP (8). In the first step, 11-ddUTP was synthesized from **5** and succinimidyl N-TFA-aminocaproate following the literature procedure. In the second step, 11-ddUTP (1.23 mL of 10 mM solution in phosphate buffer, pH 7.3, 0.012 mmol) was conjugated with succinimidyl iodoacetate (14 mg, 0.049 mmol) in DMSO (1.8 mL) by stirring at room temperature for 2 h. The reaction mixture was loaded onto a reversed-phase C18 HPLC column and purified as described for **6** to give **8** (86% yield based on the concentration determined using λ_{max} 291 nm, absorption (A) 1.33, and extinction coefficient (ϵ) 13000 M^{-1} cm^{-1} with 6.8 min retention time. Observed 784.55 TOF MS m/z ES− in water for $C_{20}H_{28}IN_4O_{15}P_3$, 784.98.

Amino-Terminated 18-ddUTP (9). To a stirred solution of **5** (200 mg, 0.25 mmol) in Na_2CO_3−$NaHCO_3$ buffer (pH 8.5, 7 mL) was added a DMF solution (3 mL) of

Scheme 2. Synthesis of Modified ddNTPs



succinimidyl N-TFA-aminocaproate (205 mg, 0.63 mmol). After 2 h, the reaction mixture was treated with 30% aqueous NH_4OH (2 mL) under sealed conditions for 2 h. After evaporation under reduced pressure, the residue was purified on a reversed-phase HPLC Delta Pak C18 semiprep column (15 μm, 100 Å, 300 × 19 mm), eluting with a gradient of 0.1 M TEAB to 100% CH_3CN 130 mL/min in 60 min to afford 11-ddUTP (165 mg, 71%). This extended 11-ddUTP (100 mg, 0.12 mmol) was further treated with succinimidyl N-TFA-caproate (53 mg, 0.16 mmol) in a mixture of Na_2CO_3−$NaHCO_3$ buffer (pH 8.5, 3 mL) and DMF(2 mL) for 2 h. After treatment with NH_4-OH, the product 18-ddUTP **9** (67 mg, 60%) was isolated using HPLC as described above.

Thioether-Cross-Linked Fluorescent Dye Terminator (10). To a stirred and cooled (5 °C) Na_2CO_3−$NaHCO_3$ solution (pH 8.5) of **6** (0.002 mmol) were sequentially added TCEP·HCl (4.3 mg, 0.015 mmol) and a DMSO solution (1.5 mL) of **3** (1.8 mg, 0.0023 mmol) under Ar gas. After 5 h, the reaction mixture was treated with 30% NH_4OH (200 μL) for 2 h and then loaded on a semiprep Q-Sepharose HPLC column (10 × 16). Elution with a gradient of buffer A (40% CH_3CN in 0.1 M TEAB; 10 min) to buffer B (40% CH_3CN in 1 M TEAB; 60 min) provided **10** (12%; concentration determined in water at 494 nm absorption/68000 extinction coefficient was 0.287 mM) with 70 min retention time. Observed 1049.25 TOF MS ES− *m/z* for $C_{42}H_{44}N_4O_{20}P_3S$, 1049.16.

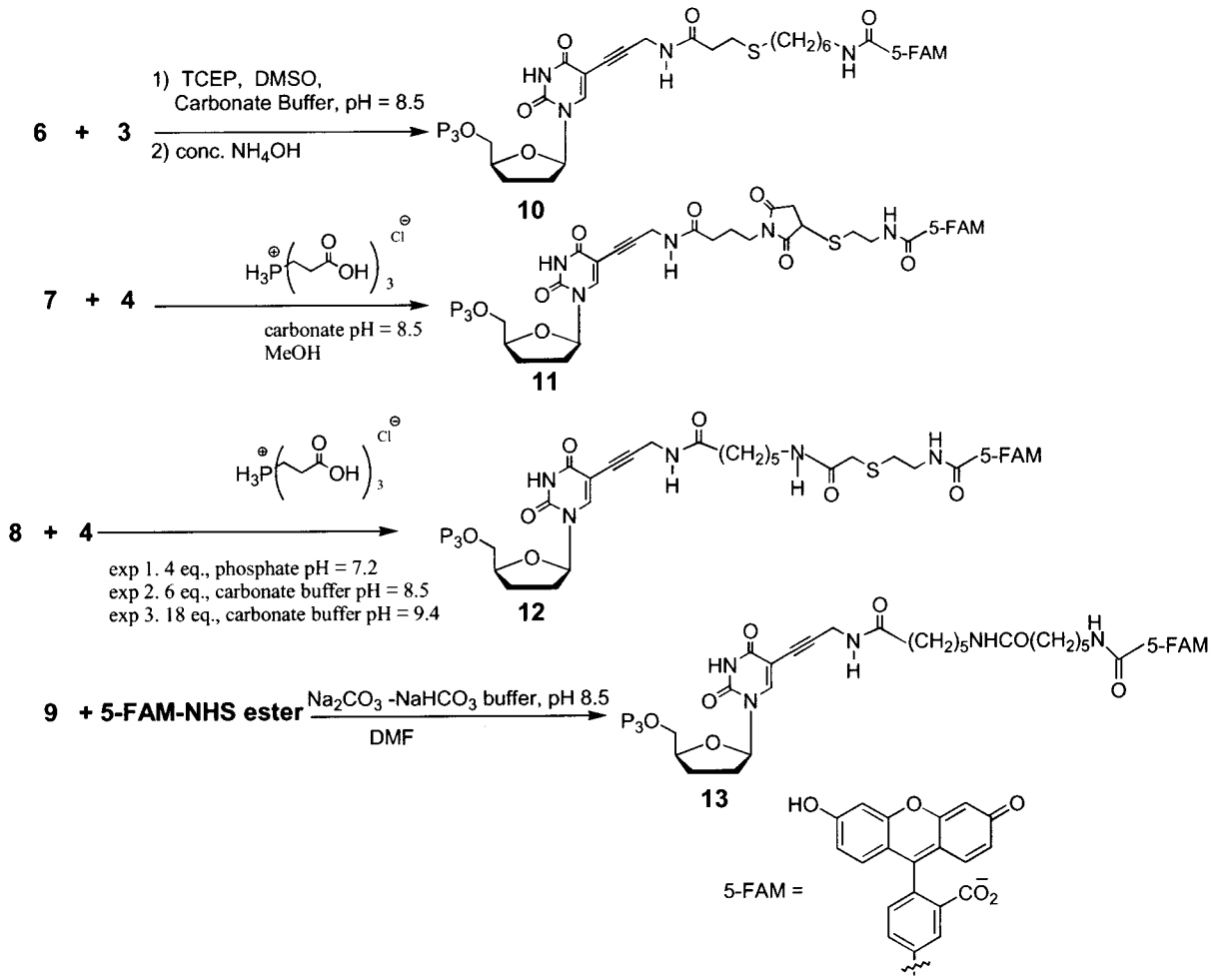
Thioether-Cross-Linked Fluorescent Dye Terminator (11). Compound **4** (1.9 mg, 0.002 mmol) and TCEP·HCl (6.3 mg, 0.022 mmol) were dissolved in a mixture of 2 mM phosphate buffer (0.8 mL; pH 7.3) and MeOH (0.5 mL) and stirred at room temperature. The maleimide-modified-ddUTP **7** (200 μL, 0.002 mmol) was added, and monitoring by HPLC after 1 h indicated completion of the reaction. The reaction mixture was purified using Q-Sepharose HPLC column described for **10** to give **11** (10%, concentration determined in water at λ_{max} 494 nm, with ϵ = 68000). Observed 1171.72 TOF MS ES+ *m/z* for $C_{43}H_{39}N_5Na_3O_{22}P_3S$, 1171.75.

Amide-Cross-Linked FAM-18-ddUTP (13). A 0.1 M Na_2CO_3−$NaHCO_3$ buffer (pH 8.5) solution (1.5 mL) of **9** (10 mg, 0.01 mmol) was reacted with a DMF solution of 5-FAM-NHS ester (5.5 mg, 0.012 mmol) at room temperature for 3 h. Compound **13** (60%) was isolated following the procedure described for **10**.

RESULTS AND DISCUSSION

Synthesis. The electrophilic and nucleophilic fluorescent dyes **3** and **4** (Scheme 1) required for the intended study were synthesized starting from dipivaloyl-5-carboxyfluorescein succinimidyl ester (**1**). Reaction of 6-aminohexanol with **1** in the presence of pyridine in anhydrous CH_2Cl_2 provided **2** (87%), which was converted to the alkyl iodide **3** in 97% yield via the cyclic phosphite in a displacement reaction with I_2. Synthesis of the nucleophilic fluorescent dye, in the form of its disulfide (**4**), was achieved in 27% yield by reacting **1** with cystamine hydrochloride in a mixture of DMF and Na_2-CO_3−$NaHCO_3$ buffer (pH 8.5). On the other hand, the propargylamino functionality in 5-(3-aminopropynyl)-ddUTP **5** (*11*) was suitably modified to generate two each

Scheme 3. Synthesis of Thiol- and Amide-Crosslinked ddNTPs



of nucleo- and electrophilic partners to participate in the final conjugation reaction. Thus, **5** was indirectly thiolated by reacting with SPDP (succinimidyl 3-(2-pyridyldithio)propionate) in a mixture of DMSO and phosphate buffer (pH 7.2) to afford pyridyldithiopropionamidyl-PA-ddUTP (**6**) conjugate, which upon reduction would release the nucleophilic thiol of **6** and 2-pyridinethione (Scheme 2). The maleimidobutanamidyl-PA-ddUTP (**7**) was obtained by reacting **5** with succinimidyl 4-maleimidylbutanoate. Synthesis of the electrophilic terminator, iodoacetamidohexanamidyl-PA-ddUTP (**8**) was accomplished in three steps involving treatment with succinimidyl 6-N-TFA-aminocaproate, ammonolysis with 30% aqueous ammonia followed by iodide displacement reaction with succinimidyl iodoacetate. For preparation of the extended terminator, **9** containing 2-amide bonds and a terminal reactive amino functionality, compound **5** was reacted iteratively with succinimidyl 6-N-TFA-aminocaproate and NH_4OH.

In the ultimate cross-conjugation reactions, the thiol-reactive alkyl iodide **3** was employed to react with in situ generated thiol of **6** upon treatment with tris(2-carboxyethyl)phosphine (TCEP) in a mixture of DMSO and Na_2CO_3−$NaHCO_3$ buffer (pH 8.5) followed by removal of pivaloyl groups with aqueous ammonia provided the thioether-cross-conjugated terminator **10** (12%) (Scheme 3). Under the same reaction conditions (vide supra), the thiol-reactive maleimide **7** was allowed to cross-conjugate with in situ generated thiol of the disulfide **4** to give the fluorescent, thioether-cross-linked terminator **11** (10%). In sharp contrast, the iodoacetamide-modified-ddUTP (**8**) when reacted with thiol of **4** at three different pHs, 7.2, 8.5, and 9.4, produced disappointing yields of unstable, fluorescent thioether-cross-linked terminator **12**. This was due to faster hydrolysis of the iodoacetamide functionality in **8** than the nucleophilic displacement with **4**. HPLC (C18 Delta Pak) analysis of the reactions carried out under different pHs (vide supra) revealed dominant hydrolysis product formation showing 5.45 min retention time to that of **12** at 7.95 min. A small amount of **12** was isolated from the combined reaction mixtures and characterized by mass spectral analysis to show its mass at 1093.92 (TOF MS ES+, exact mass for $C_{43}H_{46}N_5O_{21}P_3S$ is 1093.16) The amino-terminated 18-ddUTP (**9**) was conjugated with 5-carboxyfluorescein succinimidyl ester to give FAM-18-ddUTP (**13**, 60%).

Cycle Sequencing. To test functional outcome of the synthesized thiol-cross-linked, fluorescein-ddUTPs (**10** and **11**) along with the FAM-18-ddUTP (**13**), under a DNA polymerase catalysis, individual cycle-sequencing reactions were performed. A typical cycle-sequencing reaction contained M13 mp18 DNA template, −40 universal primer, Thermo Sequenase II DNA polymerase, dNTPs (dATP, dCTP, dGTP, and dTTP), Tris buffer (50 mM, pH 8.5), $MgCl_2$ (5 mM), and the individual conjugates **10**, **11**, and **13**. For all three reactions, thermal cycling (95 °C, 20 s; 50 °C, 30 s; 60 °C, 2 min) program was used in 25 cycles. Following the PCR postreaction workup (ethanol precipitation), amplicons terminated with the fluorescent ddUTP conjugates were subjected to slab gel electrophoresis and detection on ABI 377 DNA sequencer. The slab gel images from the above three

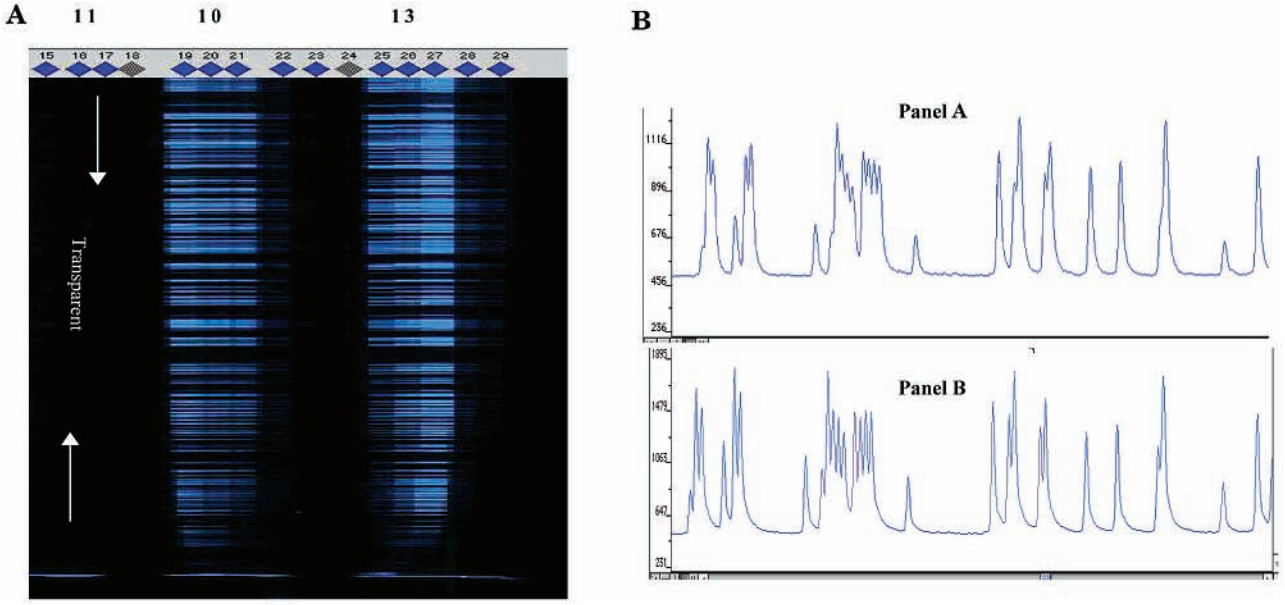


Figure 1. (A) DNA sequencing ladder images of amplicons terminated by thioether (**10**)- and triamide (**13**)-cross-linked terminators. Maleimide-derived, thioether-cross-linked fluorescent terminator (**11**) did not leave any fluorescent images due to cleavage. (B) Partial, one-color electropherogram generated by amplicons terminated by thioether (Panel A: **10**)- and amide (Panel B: **13**)-cross-linked fluorescent terminators.

reactions indicated comparable ladders for **10** and **13** terminated amplicons, while that of **11** being transparent owing to have undergone reversed-Michael reaction under the cycle sequencing conditions (Figure 1).

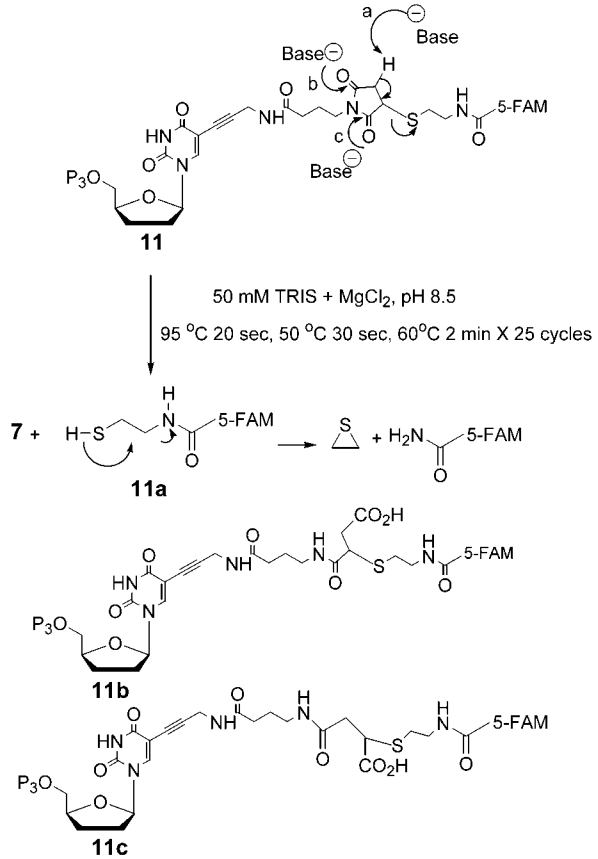
As it was difficult to isolate the suspected, linker-specific cleavage products **7**, **11a**−**c** (Scheme 4), believed to have been formed via a, b, and c mechanistic pathways (*12*), from the PCR reaction mixture for characterization, compound **11** was subjected to mere PCR thermal cycling (vide supra) conditions in the same buffer and pH to see if it would generate cleavage products. Analysis by mass spectrometry of the reversed phase-HPLC-isolated compound revealed the structure for the cleavage product as **7**. Other cleavage products with a fluorescent tag could not be isolated and identified. Despite cleavage of the terminator **11** during thermal cycling, one cannot rule out the possibility of cleavage product **7** or its hydrolyzed version being incorporated into the amplicons, which lacked the ability to leave fluorescent signatures.

Comparative examination of the partial electropherograms, generated by the amplicons terminated by **10** and **13**, suggested that both terminators were equally good substrates for the Thermo Sequenase II DNA polymerase, showing almost the same level of peak intensity and uniformity with somewhat decreased peak resolution in case of **10**. On the other hand, comparison of **10** and **11** with commercial terminators (*3*) with shorter linkers between the nucleotide and the fluorescent dye generally show decreased peak uniformity and resolution.

CONCLUSIONS.

In this paper, we have reported the synthesis of two thiol-cross-linked fluorescent dye terminators (**10** and **11**) and their DNA sequencing potential compared to the amide-cross-linked fluorescent terminator (**13**). The single-color DNA sequencing experiments conducted, using these new terminators, revealed the structural importance of the chain-terminating nucleotides and their effect on the sequencing function. The DNA sequencing information derived from the amplicons of thiol-cross-linked fluorescent terminators serve as a new model and provide useful pointers for designing new terminators.

Scheme 4. Tentative Mechanistic Pathways for pH Dependent, Linker Specific Cleavage Products 7, 11a−c



ACKNOWLEDGMENT

We thank Dr. Anup Sood and Matthew Bull for the mass spectral analysis and Dr. Carl W. Fuller for many helpful discussions.

LITERATURE CITED

(1) Sanger, F., Nicklen, S., and Coulson, A. R. (1977) DNA sequencing with chain-terminating inhibitors. *Proc. Natl. Acad. Sci. U. S. A. 74* (12), 5463−5467.

(2) (a) Nampalli, S., Khot, M., and Kumar, S. (2000) Fluorescence resonance energy transfer terminators for DNA sequencing. *Tetrahedron Lett. 41*, 8867−8871. (b) Rao, T. S., Nampalli, S., Lavrenov, K., Zhang, W., Xiao, H., Nelson, J., and Kumar, S. (2001) Four color FRET dye nucleotide terminators for DNA sequencing. *Nucleosides, Nucleotides Nucleic Acids 20* (4−7), 673−676. (c) Prober, J. M., Trainor, G. L., Dam, R. J., Hobbs, F. W., Robertson, C. J., Zagursky, R. J., Cocuzza, A. J., Jensen, M. A., and Baumeister, K. (1987) A system for rapid DNA sequencing with fluorescent chain-terminating dideoxynucleotides. *Science 238*, 336−341.

(3) (a) Rosenblum, B. B., Lee, L. G., Spurgeon, S. L., Khan, S. H., Menchen, S. M., Heiner, C. R., and Chen, S. M. (1997) New dye-labeled terminators for improved DNA sequencing patterns. *Nucleic Acids Res. 25*, 22, 4500−4504. (b) Lee, L. G., Connell, C. R., Woo, S. L., Cheng, R. D., McArdle, B. F., Fuller, C. W., Halloran, N, D., and Wilson, R. K. (1992) DNA sequencing with dye-labeled terminators and T7 DNA polymerase: effect of dyes and dNTPs on incorporation of dye-terminators and probability analysis of termination fragments. *Nucleic Acids Res. 20*, 2471−2483.

(4) Huang, S.-C., Mathies, R. A., and Glazer, A. N. (1997) Optimization of spectroscopic and electrophoretic properties of energy transfer primers. *Anal. Biochem. 252*, 72−88.

(5) Ju, J., Ruan, C., Fuller, C. W., Glazer, A. N., and Mathies, R. A. (1995) Fluorescence resonance energy transfer dye-labeled primers for DNA sequencing and analysis. *Proc. Natl. Acad. Sci. U. S. A. 92*, 4347−4351.

(6) Duthie, R. Scott., Kalve, I. M., Samols, S. B., Hamilton, S., Livshin, I., Khot, M., Nampalli, S., Kumar, S., and Fuller, C. W. (2002) Novel cyanine dye-labeled dideoxynucleoside triphosphates for DNA sequencing. *Bioconjugate Chem*., in press.

(7) Khan, S. H., et al. (1998) Substituted propargylethoxyamido nucleosides, oligonucleotides and methods for using same. U.S. Patent 5,770,716.

(8) Khan, S. H., et al. (1999) Nucleotide compounds including a rigid linker. U.S. Patent 5,948,648.

(9) Gorman, J. J., Corino, G. L., and Mitchell, S. J. (1987) Fluorescent labeling of cysteinyl residues: Application to extensive primary structure analysis of proteins on a microscale. *Eur. J. Biochem. 168*, 169−179.

(10) Burns, J. A., Butler, J. A., Moran, J., and Whitesides, G. M. (1991) Selective reduction of disulfides by tris(2-carboxyethyl)phosphine. *J. Org. Chem. 56*, 2648−2650.

(11) Hobbs, F. W., Jr., et al. (1991) Alkynylamino-Nucleotides. U.S. Patent 5,047,519.

(12) Lewis, M. R., and Shively, J. E. (1998) Maleimidocysteineamido-DOTA derivatives: New reagents for radiometal chelate conjugation to antibody sulfhydryl groups undergo pH-dependent cleavage reactions. *Bioconjugate Chem. 9*, 72−86.

BC015591C

Total Chemical Synthesis of a 27 kDa TASP Protein Derived from the MscL Ion Channel of *M. tuberculosis* by Ketoxime-Forming Ligation

Gerd G. Kochendoerfer,* Janette M. Tack, and Sonya Cressman

Gryphon Sciences, 250 East Grand Avenue, Suite 90, South San Francisco, California 94080. Received December 19, 2001; Revised Manuscript Received February 19, 2002

A 27-kDa TASP protein, T_5Msc(103−151), that was derived from the cytoplasmic domain (amino acid residues 103−151) of the MscL ion channel of *M. tuberculosis* was synthesized by ketoxime-forming chemoselective ligation between a template molecule carrying five pyruvic acid groups, and linear channel peptides carrying one aminooxyacetic acid group. Ketoxime-forming ligation provided for highly efficient assembly of this large totally synthetic protein construct with yields >90% with modest excess (1.5×) of the aminooxy peptide. Formation of the desired TASP molecule was confirmed by SDS−PAGE analysis and MALDI mass spectrometry. The effect of template attachment on the structure of the peptides constituting the TASP was assessed by circular dichroism spectroscopy. Attachment of the peptides to the topological template induces predominantly helical secondary structure, whereas an analogous peptide that did not bear an aminooxy group, MscL(103−151), does not exhibit significant secondary structure at pH 7 and is found to be monomeric in concentrations up to 65 μM. This observation can be explained by entropic destabilization of the unfolded state of T_5Msc(103−151) due to the attachment to the template and the resulting loss of degrees of freedom. Pyruvic acid-based ketoxime-forming chemoselective ligation may thus prove to be a useful tool for the assembly of large, non-native protein constructs and their biophysical study.

INTRODUCTION

The molecular mechanisms underlying the folding and oligomeric assembly of membrane proteins are not fully understood (*1*, *2*). Membrane proteins are thought to be composed of distinct protein domains that fold independently prior to assembly of the full-length protein (*1*, *3*). For that reason, the study of folding and assembly of small membrane proteins, in particular small ion channels, is useful to understand membrane protein folding on an experimental and theoretical level. Recently, we introduced the application of chemical ligation to the total synthesis of membrane proteins. For instance, we showed that both the cytoplasmic and the membrane-spanning domains of totally synthetic influenza A M2 protein help to stabilize the tetrameric assembly of this protein (*4*). The MscL (mechanosensitive channel large)[1] of *M. tuberculosis* in conjunction with its known crystal structure (*5*) provides another interesting system to understand the assembly of membrane proteins. MscL is one of several channels constituting the stress response of the bacterium and allows the efflux of ions and small molecules in response to osmotic stress (*6*−*8*). The crystal structure of the 151-amino acid full-length channel reveals two membrane-spanning helices that are arranged as a homopentamer (*5*). In addition, this structure indicates that the cytoplasmic residues 103−115-fold into a homopentameric helical pore outside the putative membrane-spanning region (see Figure 1) (*5*). As pointed out by the authors, the crystals are disordered beyond residue 115 in the solved structure, and the crystals were obtained at pH 3.5 which casts doubt about the relevance of this structural motif at physiological pH.

When performing CD (circular dichroism) measurements on a peptide derived from the C-terminal domain (amino acid residues 103−151) of MscL, we observed that this peptide did not display any secondary structural feature in aqueous solution under neutral conditions, but rather displayed predominant random-coil structure (see below). We hypothesized that the folding of the C-terminal domain of MscL was partially driven by the attachment of the peptides to the topological template formed after the transmembrane domains assemble into the helical pore.

Design. In the TASP (template-assembled synthetic protein) approach pioneered by Mutter and co-workers (*9*−*11*), peptide building blocks are covalently linked to a topological template in order to direct folding toward a particular three-dimensional packing arrangement and thus mimicking some of the structural and functional properties of native proteins. To test our hypothesis, we designed a TASP that grafts five copies of the C-terminal peptide of MscL (amino acid residues 103−151) onto a peptidic template to mimic the situation in the full-length

* To whom correspondence should be addressed. E-mail Gkochendoerfer@gryphonsci.com; phone (650) 360 1418; fax (650) 952 3055.

[1] Abbreviations: Aoaa, aminooxyacetic acid; CD circular dichroism, DCM dichloromethane; DIEA, *N*,*N*-diisopropylethylamine; DIC, diisopropycarbodiimide; DMF, dimethylformamide; ESI/MS, electron spray ionization mass spectrometry; HBTU, 2-(1*H*-benzotriazole-1-yl)-1,1,3,3-tetramethyluronium hexafluorophosphate; MALDI−TOF, matrix-assisted laser desorption/ionization time-of-flight; MscL, mechanosensitive channel large; Mtt, 4-methyltrityl; NHS, *N*-hydroxysuccinimide; RP-HPLC, reverse phase high performance liquid chromatography;S-DVB, styrene-divinylbenzene; SDS−PAGE, sodium dodecyl sulfate polyacrylamide gel electrophoresis; SEC, size-exclusion chromatography; SPPS, solid-phase peptide synthesis; TASP, template-assembled synthetic protein; TM, transmembrane; TFA, trifluoroacetic acid.

10.1021/bc010128l CCC: $22.00 © 2002 American Chemical Society
Published on Web 04/09/2002

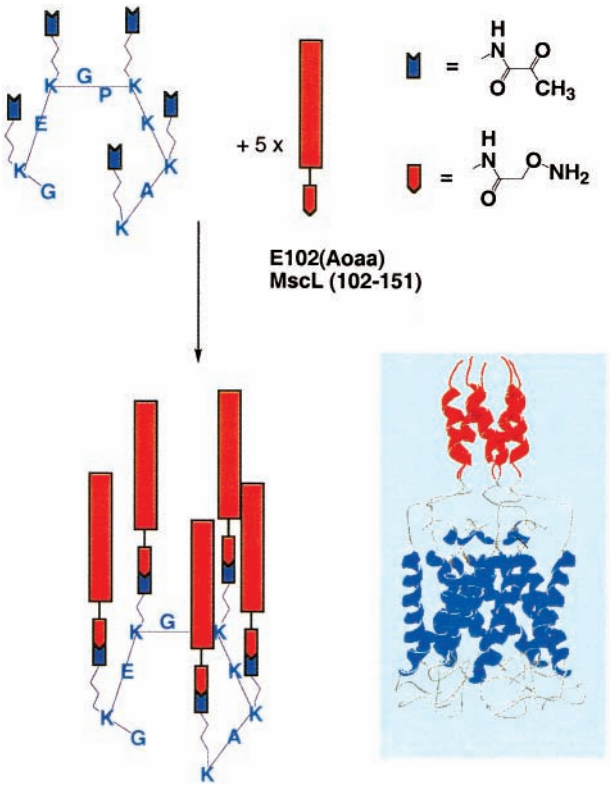


Figure 1. Total chemical synthesis of T_5Msc(103−151): The channel peptide E102(Aoaa) Msc(102−151) is attached to the linear template peptide by chemoselective oxime forming ligation. The inset shows the crystal structure of MscL of *M. tuberculosis* (PDB access code: 1MSL, graphics program: deep view). Amino acid residues 103−115 which comprise the N-terminus of the peptides making up T_5Msc(103−151) are coded in red.

protein (see Figure 1). The amino acid sequence of the template is identical to the sequence employed by Montal and co-workers (*12*) to build a pentameric ion channel TASP. The wild-type like activity of this construct demonstrated that nicotinic acetylcholine receptors assemble to form a pentamer, a finding borne out by electron microscopy and crystallographic analysis (*13*−*15*). We decided to construct a TASP that spans the entire C-terminal domain (starting in the helical region colored in red in Figure 1) beyond the region resolved in the crystal structure to enable future structural work on this protein domain. Our prediction was that attachment of the C-terminal MscL peptide to such a topological template would be sufficient to fold the peptides into a helical pore as observed in the crystal structure.

Synthetic Strategy. The TASP design target represents a formidable synthetic challenge due to its large size and complexity. Previously, TASPs have been synthesized either directly by SPPS (solid-phase peptide synthesis) (*16*, *17*) or by independent SPPS of the template and the peptide building blocks, followed by chemoselective ligation or segment condensation of the peptide building blocks to the template (*18*−*29*). The large size of the target protein precludes the direct assembly by SPPS due to the large expected number of side-products stemming from the assembly of 256 amino acids in one covalent construct. Therefore, chemoselective ligation is preferred because of the ease of synthesis and purification of unprotected synthetic peptides of ∼50 amino acid residue length, followed by the assembly of these segments into the full-length construct. The challenge was to identify a ligation chemistry that yields complete reaction due to the difficulty in chromatographically separating the very similar intermediate trimer and tetramer species from the desired pentameric species. Chemoselective linkage chemistries employed previously for TASP assembly included (a) thioether formation between a thio acid or thiol group and a haloalkyl group (*19*, *24*, *28*) or a thiol group and a maleimide group (*22*, *25*, *27*), (b) aldoxime formation between an aldehyde and an aminooxy group (*18*, *20*, *21*, *23*, *29*) and reductive amination (*26*). Initially, we attempted to form the TASP by reaction of a pentamaleimide or a pentaiodoacetyl template with a MscL(103−151) peptide containing an N-terminal cysteine. However, significant amounts (>30%) of dimer, trimer, and tetramer reaction intermediates remaining after completion of the reaction prevented the purification of large quantities of pure material, even in the presence of a 3-fold excess of peptide relative to template. We then considered ketoxime formation for the TASP (to avoid any additional template oxidation/deprotection steps prior to the oximation reaction which are necessary for aldoxime formation). In the literature, levulinic acid and its derivatives are the preferred ketones for chemoselective ligation of nucleophile-bearing groups to peptides and proteins (*30*−*34*). However, we and others (*33*) experienced incomplete reactions using a levulinic acid-based template for attachments of multiple peptides.

In this paper, we report a strategy for assembly of TASPs that involves the straightforward, efficient, and complete formation of a ketoxime bond between an aminooxy group on a linear peptide synthesized by Boc chemistry and a pentapyruvic acid bearing template synthesized by Fmoc chemistry. Oxime-forming ligation of these constructs not only provides for efficient assembly of the desired 27 kDa TASP protein, but may have general usefulness for the ligation of synthetic and recombinant peptides.

EXPERIMENTAL PROCEDURES

Boc-protected amino acids were obtained from Midwest Biotech (Fishers, IN) and Fmoc-protected amino acids were obtained from Novabiochem (San Diego, CA). Trifluoroacetic acid was obtained from Halocarbon (River Edge, NJ). DIEA (*N*,*N*-diisopropylethylamine) was obtained from Applied Biosystems (Foster City, CA). HBTU (2-(1*H*-benzotriazol-1-yl)-1,1,3,3-tetramethyluronium hexafluorophosphate) was obtained from Spectrum (Gardena, CA). Carbonyl-free acetonitrile was obtained from Burdick & Jackson (Gardena, CA). Other chemicals were from Sigma (St. Louis, MO) or Aldrich (Milwaukee, WI) and were used as received.

Peptide Synthesis and Purification. The sequence of the E102(Aoaa) Msc (102−151) peptide in single-letter code is (Aoaa)-VEQPGDTQ VVLLTEIRDL LAQTNGDSPG RHGGRGTPSP TDGPRASTES Q. The peptide was synthesized at a 0.2 mmol scale on a custom-modified Applied Biosystems 433A peptide synthesizer. The peptide was synthesized on an S−DVB (stryrene−divinylbenzene) resin carrying a $-OCH_2-$PAM linker (Applied Biosystem, Foster City, CA) using an in situ neutralization protocol for machine-assisted Boc (*tert*-butoxycarbonyl) chemistry (*35*). Side-chain protecting groups were: Arg(Tos), Asp(OChx), Asn(Xan), Glu(OChx), His(DNP), Lys-(2ClZ), Ser(Bzl), Thr(Bzl), and Tyr(2BrZ). DMF (*N*,*N*-dimethylformamide) and DCM (dichloromethane) were HPLC grade and used as received. After the final amino acid coupling, the terminal Boc protecting group was removed by treatment with 100% TFA, followed by neutralization with 10% DIEA in DMF for 1 min. A 2 mmol amount of Boc-aminooxyacetic acid was added to

the resin after activation with 2 mmol of DIC (diisopropylcarbodiimide) and 2 mmol NHS (*N*-hydroxysuccinimide) in 3 mL DMF for 30 min. The terminal Boc protecting group was then removed by treatment with 100% TFA for 2 × 1 min. The peptide was deprotected and simultaneously cleaved from the resin support using HF/*p*-cresol according to standard Boc-chemistry procedures (*35*). The peptide was purified by preparative C-4 RP-HPLC with a linear gradient of 20 to 40% Buffer B (acetonitrile containing 0.08% TFA) versus 0.1% aqueous TFA in 80 min.

The sequence of the Msc (103−151) peptide in single-letter code is VEQPGDTQ VVLLTEIRDL LAQTNGD-SPG RHGGRGTPSP TDGPRASTES Q. It was prepared analogously except for the addition of aminooxyacetic acid. The sequence of the linear template is K(Mtt)AK-(Mtt)K(Boc)K(Mtt)PGK(Mtt)E(OtBu)K(Mtt)G. The template was synthesized manually using Fmoc chemistry (*36*) on an S−DVB resin carrying a Rink linker (Novabiochem, San Diego, CA). For a synthesis on a 0.2 mmol scale, 2.1 mmol of amino acid was dissolved in 3.8 mL of DMF containing 1.9 mmol of HBTU and 1 mL of DIEA and activated for 3 min. Coupling was performed for 20 min per cycle, and deprotection was performed with 2 × 3 min batch washes with 20% piperidine in DMF. After the last amino acid coupling step, the Fmoc protecting group was not removed. The Mtt side-chain protecting group was removed by multiple treatments with 2% TFA in DCM. After neutralization with 10% DIEA in DMF, 1 mmol of pyruvic acid was coupled to the resin after activation with 1 mmol of DIC and 1 mmol of NHS in DCM for 45 min. The template was purified by C-4 RP-HPLC with a linear gradient of 15−35% Buffer B versus 0.1% aqueous TFA in 60 min. Fractions containing the desired material were identified by ESI/MS, frozen, and lyophilized.

Analytical RP-HPLC. Analytical RP-HPLC was performed on a Vydac C-4 analytical column (5 μm particle size, 0.46 cm × 15 cm), using a Hewlett-Packard Model 1100 quaternary pump high-pressure mixing system with 214 and 280 nm UV detection.

Oxime-Forming Chemoselective Ligation. A 1.5-fold molar excess (aminooxy acetyl) peptide to pyruvic acid group on the template) of E102(Aoaa) Msc (102−151) was added to a solution of the template in 50% aqueous acetonitrile containing 0.09% TFA. After 15 min reaction time, solvents were evaporated to dryness on a speedvac to drive the reaction to completion, and the dry mix was redissolved in 50% aqueous acetonitrile containing 0.09% TFA. The N-terminal Fmoc-protecting group on the template was removed by addition of a 3-fold excess of 6 M guanidinium chloride, 100 mM acetate, pH 4 buffer, and an equivalent volume of piperidine (final concentration 20%) for 20 min. The solution was acidified with glacial acetic acid, and reactants and products were separated by preparative reverse-phase HPLC with a linear gradient of 20 to 48% Buffer B (acetonitrile containing 0.08% TFA) versus 0.1% aqueous TFA in 80 min. Fractions containing the desired material were identified by SDS−PAGE, frozen, and lyophilized.

Mass Spectrometry. T_5Msc(103−151) was dissolved in a saturated solution of α-cyano-4-hydroxycinnamic acid in 50% aqueous acetonitrile/0.09% TFA acid. A 1 μL aliquot was deposited directly on the sample slide and allowed to air-dry. The sample preparations were analyzed using a Ciphergen Biosystems Massphoresis System time-of-flight mass spectrometer. The spectra were externally calibrated using horseradish peroxidase (MW = 43240 Da) and represent an average of 50 shots.

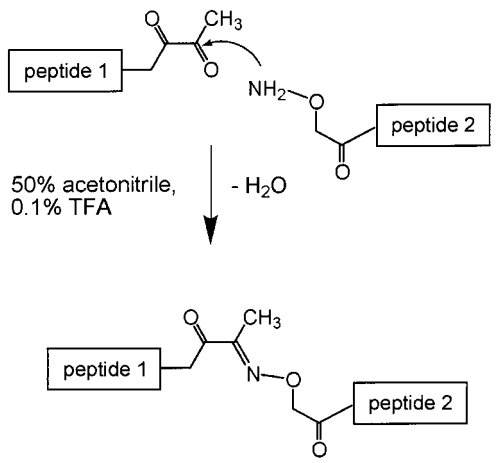
Protein Folding. To induce folding, T_5Msc(103−151) and the Msc (103−151) peptide were dissolved at a concentration of 1 mg/mL in 6 M guanidinium hydrochloride buffer containing 200 mM $H_2PO_4^-$ (counterion sodium), pH 7, respectively. The peptides were dialyzed stepwise O/N against 100× volume into 20 mM $H_2PO_4^-$ (counterion sodium), pH 7, containing 100 mM NaCl, and finally 20 mM $H_2PO_4^-$ ((counterion sodium), pH 7. For folding at low pH, the final buffer was 20 mM glycine (counterion chloride), pH 4.

Circular Dichroism Spectrometry. CD spectra were acquired with a JASCO-J700 CD spectrometer at 20 °C between 190 and 250 nm in 0.4 nm increments (bandwidth: 1 nm, dwell-time: 2 s, averaged over three acquisitions). Quantitative secondary structure modeling was performed by least-squares fitting to a set of proteins of known structure using the CDsstr and Continll algorithms as implemented by the CDPRO software package (http://lamar.colostate.edu/∼sreeram/CDPRO). The basis set employed for modeling the linear peptide also included several unfolded proteins, since the fits in the absence of unfolded proteins in the basis set were unsatisfactory. The Selcon3 algorithm implemented in the same software package did yield significantly worse fits as indicated by more than four times higher RMSD values (experimental − calculated) and was therefore discarded. However, the determined percentage of helicity and disordered structure was comparable.

RESULTS

The channel peptide E102(Aoaa) MscL (102−151) was assembled using Boc chemistry SPPS following standard procedures (*35*). After chain assembly, an aminooxy acetic acid group was coupled to the N-terminus of the peptide to serve as chemoselective linker. The peptide was deprotected, cleaved, and purified using standard methods (*35*). For structural comparison, an analogous peptide that did not bear an aminooxy group (MscL(103−151) was synthesized. The template peptide (*12*) was synthesized by SPPS following the Fmoc strategy as described in the methods section (*36*). After chain assembly, pyruvic acid was coupled to five specific side-chains to serve as chemoselective ligation linkers. The TASP T_5Msc(103−155) was assembled by joining five unprotected, purified channel peptides to the purified template peptide through a chemoselective ketoxime-forming ligation (See Scheme 1). A

Scheme 1. Ketoxime-Forming Ligation by Reaction of a Pyruvic Acid Bearing Peptide (left) with an Aminooxyacetic Acid Bearing Peptide (right). The Newly Formed Oxime Bond Is Stabilized by Electron Resonance



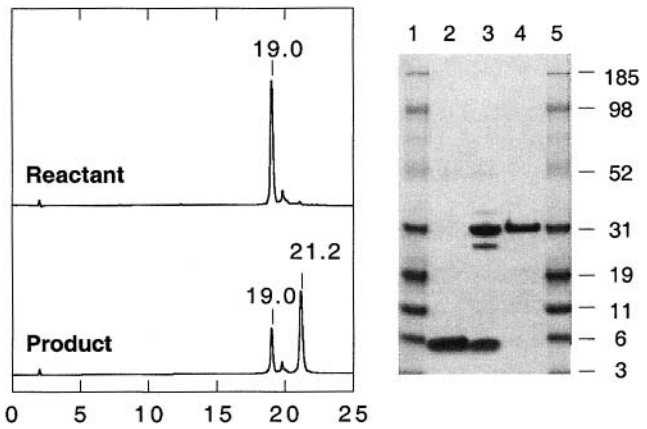


Figure 2. Analysis of oxime-forming ligation: Left: RP-HPLC traces (detected at 214 nm) monitoring the oxime-forming ligation reaction. Analytical reversed-phase HPLC was performed on aliquots with a linear gradient of 5−65% Buffer B (acetonitrile containing 0.08% TFA) versus 0.1% aqueous TFA over 24 min on a Vydac C-4 analytical column. Top: RP-HPLC trace after injection of an aliquot of the reactant peptide E102-(Aoaa)Msc(102−151). Bottom: Equivalent RP HPLC trace after the oximation reaction. Right: NuPAGE Bis-Tris (Mes) SDS−PAGE gel (4−12%) monitoring the synthesis and purification of T_5Msc(103−151). Gels were stained for protein with Coomassie blue. Lane 1 + 5: MW Standard. Lane 2: Reactant (E102Aoaa) Msc(102−151). Lane 3: Crude oximation mix. Lane 4: Purified T_5Msc(103−151).

1.5-fold molar excess (aminooxy peptide to pyruvic acid unit on the template) of E102(Aoaa) MscL (102−151) was added to a solution of the template in 50% aqueous acetonitrile containing 0.09% TFA. Figure 2 presents HPLC traces monitoring the formation of the target TASP, named T_5Msc(103−151). The linear E102(Aoaa) MscL (102−151) peptide exhibits a single dominant peak at 19.0 min. A minor peak at 19.8 min corresponds to an aminooxy-mediated dimer that is intrinsically unreactive and appears after lyophilization of the purified peptide. After the reaction mixture was dried on a Speedvac and redissolved in 50% acetonitrile containing 0.09% TFA, a new peak at 21.2 min appears. The increase of this peak is correlated with a decrease of the reactant peak. To monitor the completeness of the reaction more quantitatively, an SDS−PAGE gel of the reactant, and the product mix after dissolution in SDS sample buffer was obtained. The monomeric starting material in Lane 2 (Figure 2) shows the expected molecular weight of ∼5 kDa. The crude reaction mixture in Lane 3 indicates very high reaction efficiency. In addition to the unreacted starting material and the desired pentamer band at ∼31 kDa, only a weak band for the tetramer (<10%), but no lower oligomers, is detected in the crude reaction mix. In addition, a small population of hexameric compound is detected. Since incomplete reaction may occur at any of the five pyruvic acid sites, this result suggests that the ligation reaction is >98% complete for each aminooxyacetic−pyruvic acid ketone pair even with the modest excess (1.5-fold) of aminooxy peptide employed. After workup, reactants and products were separated by preparative RP-HPLC as described in the methods section. Fractions containing the desired TASP protein, T_5Msc(103−151), were identified by SDS−PAGE, frozen, and lyophilized. Lane 4 in the SDS−PAGE gel in Figure 2 indicates high (>98%) oligomeric purity for the purified pool of T_5Msc(103−151).

Additional analytical data characterizing purified T_5-Msc(103−151) is presented in Figure 3. The RP-HPLC trace of the purified TASP protein shows a single

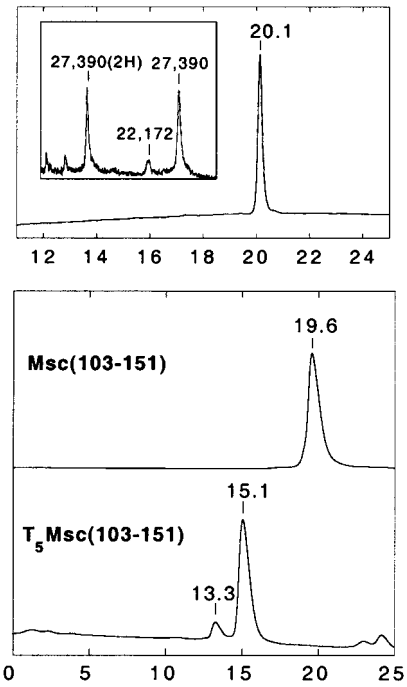


Figure 3. Analytical characterization of T_5Msc(103−151): Top: Reverse-phase HPLC chromatogram of purified T_5Msc-(103−151) construct. Analytical reverse-phase HPLC was performed with a linear gradient of 5−65% Buffer B (acetonitrile containing 0.08% TFA) versus 0.1% aqueous TFA over 24 min on a Vydac C-4 analytical column. The inset shows a MALDI-TOF mass spectrum of purified T_5Msc(103−151). Peaks originating from doubly protonated species are marked as (2H). Bottom: Size-exclusion HPLC chromatogram of the purified and "folded" T_5Msc(103−151) (Top) and Msc(103−151) (Bottom) construct. Analytical SEC HPLC was performed on aliquots using 20 mM $H_2PO_4^-$, pH 7 containing 100 mM NaCl as mobile phase on a Tosoh-Haas G2000 SWXL column (particle size 5 μM, pore size 125 Å). Size exclusion standards eluted at the following retention times: albumin (69 kDa): 14.9 min; ovalbumin (46 kDa): 15.9 min; chymotrypsin (21 kDa): 21.9 min.

dominant peak with a peptidic purity greater than 95%. Formation of the desired pentameric TASP was verified by MALDI-TOF mass spectrometry. The observed molecular weight of T_5Msc(103−151) is 27390 ± 20 Da (theoretical mass = 27389 (average isotope composition)). The impurity observed in the MALDI spectrum at ∼5 kDa below the target molecular weight is attributed to cleavage of the UV-absorbing oxime bond by the excitation laser as well as possibly a slight channel peptide tetramer impurity. The latter interpretation is confirmed by a clear laser power dependence of the relative intensity of this impurity peak.

To induce folding, T_5Msc(103−151) and Msc(103−151) were dissolved in denaturing buffer, followed by dialysis into 20 mM $H_2PO_4^-$, pH 7. Size-exclusion chromatographic analysis (Figure 3, bottom) indicates that the retention time (15.1 min) of "folded" T_5Msc(103−151) lies between the retention times of the molecular weight-standards ovalbumin (∼46 kDa) and albumin (69 kDa). The apparent discrepancy of this apparent weight to the real confirmed molecular weight can be rationalized by the expected nonglobular, possibly rodlike shape of the TASP. Rodlike proteins are expected to be more hindered when entering the pores of the size-exclusion resin, thus exhibiting higher apparent molecular weights (*37*). An alternative explanation is that a significant part of the TASP may be (a) unfolded or only loosely structured, leading to increased apparent molecular weight or (b) completely dimeric. These alternatives, while less likely,

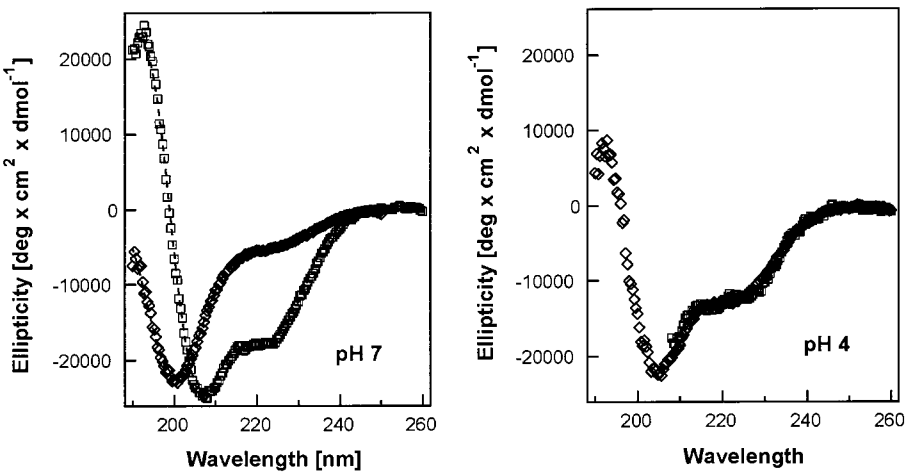


Figure 4. Left: Circular dichroism spectra of Msc(103−151) (diamonds) and T_5Msc(103−151) (squares) in 20 mM $H_2PO_4^-$ (counterion sodium), pH 7. Data fits obtained from the quantitative secondary structure modeling are also shown for the measurements at pH 7 (dashed lines). The concentrations of T_5Msc(103−151) and Msc(103−151) were 42 μg/mL (1.5 μM) and 38 μg/mL (7.4 μM), respectively. Right: Circular dichroism spectra of Msc(103−151) (diamonds) and T_5Msc(103−151) (squares) in 20 mM glycine (counterion chloride), pH 4. The concentrations of T_5Msc(103−151) and Msc(103−151) were 58 μg/mL (2.1 μM) and 84 μg/mL (16.5 μM), respectively.

will be addressed in further studies. In summary, it appears that MscL (103−151) is predominantly monomeric (>90%) with a dimeric species (retention time 13.3 min) representing the major additional population under our assay conditions up the highest concentration (∼65 μM) employed in the CD analysis.

To assess folding of T_5Msc(103−151), CD spectra were acquired of the TASP and MscL (103−151), respectively, in aqueous buffer. The final buffers were 20 mM $H_2PO_4^-$, pH 7, and 20 mM glycine buffer, pH 4, respectively. Figure 4 presents the CD spectrum of the linear Msc (103−151), and the CD spectrum of T_5Msc(103−151), respectively, under comparable total peptide concentrations in 20 mM $H_2PO_4^-$, pH 7. Inspection of the CD trace of Msc(103−151) indicates predominant random coil structure at pH 7. A significant increase in helicity is observed after lowering the pH to 4 for this peptide. SEC (size-exclusion chromatography) reveals that the peptide is monomeric at pH 4 as well (data not shown). Subsequently, the concentration dependence of the helical content was determined since for a pentameric oligomer one expects a strong dependence of the oligomeric state on the concentration. The respective CD spectra do not change significantly over the range from 7.4 to 66 μM for the peptide at pH 7 and 3.5 to 65 μM for the peptide at pH 4. Thus, peptide MscL (103−151) is intrinsically helical in the monomeric state at low pH, but predominantly in a random coil conformation at physiological pH.

By contrast, T_5Msc(103−151) exhibits a CD trace at both pH 7 as well as pH 4 typically observed for proteins with a high helical content and shows a slight decrease in helicity at pH 4 relative to pH 7. The CD spectra of T_5Msc(103−151) and Msc(103−151) at pH 4 are virtually superimposable at higher wavelengths (intrinsic absorption of UV light, most likely by the oxime bond, precluded acquisition of data beyond this region). Quantitative secondary structure modeling of the data obtained at pH 7 revealed that whereas the linear synthetic peptide exhibits ∼15% helical structure and is primarily comprised of disordered structure (61−73%), assembly of the peptides on the peptide template increases the helical content to 60−67%, with only 20% disordered structure. Whereas these numbers should not be taken literally due to the limited accuracy of quantitative CD analysis, they do confirm the trend observed by visual inspection. A small percentage of β-sheet structure (<10%) may be partially attributed to the template peptide. Related template peptides have previously been shown to form a preferred β-sheeted conformation (*38*, *39*). However, the small size of the template peptide (11 amino acid residues) relative to the total size of the T_5Msc(103−151) construct (256 amino acid residues) suggests that the template would only make a minor contribution to the CD spectrum of T_5Msc(103−151).

DISCUSSION

We describe the total chemical synthesis of the 27.3 kDa synthetic TASP protein T_5Msc(103−151) by chemoselective segment condensation of five 49-amino acid residue peptides with a structural template. The ability to synthesize T_5Msc(103−151) underlines the usefulness of using chemoselective ligations of purified, unprotected peptides for the total chemical synthesis of large and complex synthetic protein constructs (*29*, *40*, *41*). We have introduced the use of chemoselective ketoxime-forming ligation between pyruvic acid and aminooxyacetic acid for the highly efficient ligation of six unprotected peptide segments. Some advantages of the use of pyruvic acid−aminooxy acetic acid ketoxime formation are (a) very rapid and efficient ligation chemistry, (b) small linker size, and (c) direct incorporation into peptides without any need for deprotection, or oxidation of aldehyde or amino acid precursors (*23*, *29*, *42*, *43*). Pyruvic acid ketoximes are expected to be much more stable than the related levulinic acid ketoxime since the pyruvic acid ketoxime bond is resonance-stabilized by conjugation with its carbonyl group. In addition, this chemistry is not only applicable to chemoselective ligation of synthetic peptides, but for any situation in which rapid, highly efficient, and stable (oxime) linkages between a peptide/protein and any other chemical moiety are desired. This includes recombinant and natural peptides, and proteins bearing an N-terminal alanine which can be transformed into pyruvic acid by oxidative transamination of its α-amino group using glyoxylic acid/Cu^{2+} (*42*, *44*). Therefore, pyruvic acid-forming ligation may have general use in bioconjugate chemistry. Conceivable applications include the synthesis of peptide dendrimers for vaccine development (*23*, *45*, *46*) and the attachment of polymers or pharmacophores to synthetic peptides and proteins.

The lack of secondary structure in the linear channel peptide Msc(103−151) suggests that the cytoplasmic

helical pore observed in the crystal structure does not constitute a protein domain of MscL as defined by Wetlaufer (*47*). Instead, it appears to be only folded at low pH, or in the context of the full-length channel protein. In the latter case, the folded TM domain of MscL may also support folding of Msc(103−151). These findings are consistent with recent molecular dynamics simulations by Elmore and co-workers predicting that the assembly of the C-terminal domain immediately adjacent to the TM domain is energetically unfavorable at neutral pH due to the mutual repulsion of a large number of negatively charged amino acid residues in this region (*48*).

The folding of the Msc(103−151) helices is not caused by specific steric effects induced by the template. Preliminary experiments using attachment of the Msc(103−151) peptide via the thiol group of a cysteine side-chain to a much larger, cyclical template (*28*) with twice the distance between helix attachment sites showed virtually identical results. Side-chain attachment of the peptides to the helices provides for an uncapped N-terminus, and therefore helix-capping effects are neither responsible for the observed secondary structure features. The dramatic increase in helical structure after attachment of the channel peptides to the template peptide therefore suggests that folding of the C-terminal extension of MscL is at least facilitated by the attachment of the peptides to the topological template.

Our results are similar to findings by Mutter and coworkers who showed that template attachment can overcome charge repulsion in the formation of four-helical bundles of model peptides (*16*). The reduced chain entropy of the channel peptides after template attachment in the *unfolded* state of T_5Msc(103−151) significantly increases its free energy and thereby promotes folding in contrast to the unattached peptides that do not fold spontaneously at neutral pH. In T_5Msc(103−151), this effect appears to be sufficiently strong to overcome the unfavorable enthalpy of assembly of the pentameric helical pore found in the MD study and thus allows the intracellular portion of the channel peptide to acquire secondary structure that is consistent with the formation of a helical pore observed in the crystal structure. However, the large amount of α-helical structure observed in the TASP also suggests that regions beyond the helical pore observed in the crystal structure may exhibit helical secondary structure. These speculations, and the potential role of this pore destabilization in facilitating opening of the pore upon mechanical stress, will have to be verified by detailed structural and thermodynamic analysis of the synthetic TASP protein.

CONCLUSION

The synthesis of the 27.3 kDa synthetic TASP protein T_5Msc(103−151) underlines the strength of using chemoselective ligations of purified, unprotected peptides for the total chemical synthesis of large and complex synthetic protein constructs (*29*, *40*, *41*). Attachment of pyruvic acid to peptides synthesized by Fmoc chemistry is site-specific, straightforward and their rapid oxime-forming ligation yields a very stable interpeptide linkage. This chemistry may thus prove useful in the evolving field of total chemical protein synthesis.

ACKNOWLEDGMENT

This work was supported in part by NIH 1 P01 GM62532-01. We thank Shiah-Yun Chen (Gryphon Sciences) for insightful discussions on protein folding, Keith Rose (Geneprot, Geneva) for suggestions, and many helpful discussions on oxime-forming chemistry, Maia Carnevali (Gryphon Sciences) for automated peptide synthesis, and Stephen Kent (University of Chicago) for critical comments on the manuscript.

LITERATURE CITED

(1) Popot, J. L., and Engelman, D. M. (2000) Helical membrane protein folding, stability, and evolution. *Annu. Rev. Biochem. 69*, 881−922.

(2) Dieckmann, G. R., and DeGrado, W. F. (1997) Modeling transmembrane helical oligomers. *Curr. Opin. Struct. Biol. 7*, 486-494.

(3) Popot, J.-L., and Engelman, D. M. (1990) Membrane protein folding and oligomerization: The two-stage model. *Biochemistry 29*, 4031−4037.

(4) Kochendoerfer, G. G., Salom, D., Lear, J. D., Wilk-Orescan, R., Kent, S. B. H., and DeGrado, W. F. (1999) Total chemical synthesis of the integral membrane protein influenza A virus M2: Role of its C-terminal domain in tetramer assembly. *Biochemistry 38*, 11905−11913.

(5) Chang, G., Spencer, R. H., Lee, A. T., Barclay, M. T., and Rees, D. C. (1998) Structure of the MscL homologue from *Mycobacterium tuberculosis*: a gated mechanosensitive ion channel. *Science 282*, 2220−2226.

(6) Blount, P., Sukharev, S. I., Moe, P. C., Nagle, S. K., and Kung, C. (1996) Towards an understanding of the structural and functional properties of MscL, a mechanosensitive channel in bacteria. *Biol. Cell 87*, 1−8.

(7) Levina, N., Totemeyer, S., Stokes, N. R., Louis, P., Jones, M. A., and Booth, I. R. (1999) Protection of *Escherichia coli* cells against extreme turgor by activation of MscS and MscL mechanosensitive channels: identification of genes required for MscS activity. *EMBO J. 18*, 1730−1737.

(8) Hamill, O. P., and Martinac, B. (2001) Molecular basis of mechanotransduction in living cells. *Physiol. Rev. 81*, 685−740.

(9) Mutter, M., and Vuilleumier, S. A. (1989) A chemical approach to protein design. Template assembled synthetic proteins. *Angew. Chem., Int. Ed. Engl. 28*, 535−554.

(10) Tuchscherer, G., Scheibler, L., Dumy, P., and Mutter, M. (1998) Protein design: on the threshold of functional properties. *Biopolymers 47*, 63−73.

(11) Bayley, H. (1999) Designed membrane channels and pores. *Curr. Opin. Biotechnol. 10*, 94−103.

(12) Montal, M. O., Iwamoto, T., Tomich, J. M., and Montal, M. (1993) Design, synthesis and functional characterization of a pentameric channel protein that mimics the presumed pore structure of the nicotinic cholinergic receptor. *FEBS Lett. 320*, 261−266.

(13) Miyazawa, A., Fujiyoshi, Y., Stowell, M., and Unwin, N. (1999) Nicotinic acetylcholine receptor at 4.6 A resolution: transverse tunnels in the channel wall. *J. Mol. Biol. 288*, 765−786.

(14) Brejc, K., van_Dijk, W. J., Klaassen, R. V., Schuurmans, M., van_Der_Oost, J., Smit, A. B., and Sixma, T. K. (2001) Crystal structure of an ACh-binding protein reveals the ligand-binding domain of nicotinic receptors. *Nature 411*, 269−276.

(15) Smit, A. B., Syed, N. I., Schaap, D., van_Minnen, J., Klumperman, J., Kits, K. S., Lodder, H., van der Schors, R. C., van Elk, R., Sorgedrager, B., Brejc, K., Sixma, T. K., and Geraerts, W. P. (2001) A glia-derived acetylcholine-binding protein that modulates synaptic transmission. *Nature 411*, 261−268.

(16) Mutter, M., Tuchscherer, G. G., Miller, C., Altmann, K., Carey, R., Wyss, D. F., Labhardt, A. M., and Rivier, J. E. (1992) Template-assembled synthetic proteins with four-helix-bundle topology. Total chemical synthesis and conformational study. *J. Am. Chem. Soc. 114*, 1463−1470.

(17) Iwamoto, T., Grove, A., Montal, M. O., Montal, M., and Tomich, J. M. (1994) Chemical synthesis and characterization of peptides and oligomeric proteins designed to form transmembrane ion channels. *Int. J. Pept. Protein Res. 43*, 597−607.

(18) Ernest, I., Villeumier, S., Fritz, H., and Mutter, M. (1990) Synthesis of a 4-helix bundle-like template-assembled protein (TASP) by condensation of a protected peptide on a conformationally constrained cyclic carrier. *Tetrahedron Lett. 31*, 4015−4018.
(19) Dawson, P. E., and Kent, S. B. H. (1993) Convenient Total Synthesis of a 4-Helix TASP Molecule by Chemoselective Ligation. *J. Am. Chem. Soc. 115*, 7263−7266.
(20) Tuchscherer, G. (1993) Template assembled synthetic proteins: condensation of a multifunctional peptide to a topological template via chemoselective ligation. *Tetrahedron Lett. 34*, 8419−8422.
(21) Nyanguile, O., Mutter, M., and Tuchscherer, G. (1994) Synthesis of antiparallel 4-α-helix bundle TASP by chemoselective ligation. *Lett. Pept. Sci. 1*, 9−16.
(22) Nefzi, A. Sun, X. and Mutter, M. (1995) Chemoselective ligation of multifunctional peptides to topological templates via thioether formation for TASP synthesis. *Tetrahedron Lett. 36*, 229−230.
(23) Rose, K. (1994) Facile synthesis of homogeneous artificial proteins. *J. Am. Chem. Soc. 116*, 30−33.
(24) Rau, H., and Haehnel, W. (1998) Design, Synthesis, and Properties of a Novel Cytochrome b Model. *J. Am. Chem. Soc. 120*, 468−476.
(25) Rau, H. K., DeJonge, N., and Haehnel, W. (1998) Modular synthesis of de novo-designed metalloproteins for light-induced electron transfer. *Proc. Natl. Acad. Sci. U.S.A. 95*, 11526−11531.
(26) Tahmassebi, D., and Sasaki, T. (1998) Synthesis of a three-helix bundle protein by reductive amination. *J. Org. Chem. 63*, 728−731.
(27) Rau, H. K., DeJonge, N., and Haehnel, W. (2000) Combinatorial synthesis of four-helix bundle hemoproteins for tuning of cofactor properties. *Angew. Chem., Int. Ed. 39*, 250−253.
(28) De, E., Chaloin, L., Heitz, A., Mery, J., Molle, G., and Heitz, F. (2001) Conformation and ion channel properties of a five-helix Bundle protein. *J. Pept. Sci. 7*, 41−49.
(29) Rose, K., Zeng, W., Regamey, P. O., Chernushevich, I. V., Standing, K. G., and Gaertner, H. F. (1996) Natural peptides as building blocks for the synthesis of large protein-like molecules with hydrazone and oxime linkages. *Bioconjugate Chem. 7*, 552−556.
(30) Canne, L. E., Ferré-D′Amaré, A. R., Burley, S. K., and Kent, S. B. H. (1995) Total chemical synthesis of a unique transcription factor-related protein: cMyc-Max. *J. Am. Chem. Soc. 117*, 2998−3007.
(31) Ayers, B., Blaschke, U. K., Camarero, J. A., Cotton, G. J., Holford, M., and Muir, T. W. (1999) Introduction of unnatural amino acids into proteins using expressed protein ligation. *Biopolymers 51*, 343−354.
(32) Marcaurelle, L. A., and Bertozzi, C. R. (1998) Direct Incorporation of Unprotected Ketone Groups into Peptides During Solid-Phase Synthesis: Application to the One-Step Modification of Peptides with Two Different Biophysical Probes for FRET. *Tetrahedron Lett. 39*, 7279−7282.
(33) Mitchell, J. P., Roberts, K. D., Langley, J., Koentgen, F., and Lambert, J. N. (1999) A direct method for the formation of peptide and carbohydrate dendrimers. *Bioorg. Med. Chem. Lett. 9*, 2785−2788.
(34) Ingallinella, P., Marco, A. D., Taliani, M., Fattori, D., and Pessi, A. (2001) A new method for chemoselective conjugation of unprotected peptides to dauno- and doxorubicin. *Bioorg. Med. Chem. Lett. 11*, 1343−1346.
(35) Schnölzer, M., Alewood, P., Jones, A., Alewood, D., and Kent, S. B. H. (1992) In situ Neutralization in Boc-Chemistry Solid-Phase Peptide Synthesis. *Int. J. Pept. Protein Res. 40*, 180−193.
(36) Fields, C. G., Lloyd, D. H., Macdonald, R. L., Otteson, K. M., and Noble, R. L. (1991) HBTU activation for automated Fmoc solid-phase peptide synthesis. *Pept. Res. 4*, 95−101.
(37) Dubin, P., Kaplan, J. I., Tian, B. S., and Mehta, M. (1990) Size-exclusion chromatography dimension of rodlike macromolecules. *J. Chromatography 515*, 37−42.
(38) Dumy, P., Eggleston, I. M., Esposito, G., Nicula, S., and Mutter, M. (1996) Solution structure of regioselectively addressable functionalized templates: an NMR and restrained molecular dynamics investigation. *Biopolymers 39*, 297−308.
(39) Peluso, S., Rueckle, T., Lehmann, C., Mutter, M., Peggion, P., and Crisma, M. (2001) Crystal structure of a synthetic cyclodecapeptide fo template-assembled synthetic protein design. *CHEMBIOCHEM 2*, 432−437.
(40) Wilken, J., and Kent, S. B. (1998) Chemical protein synthesis. *Curr. Opin. Biotechnol. 9*, 412−426.
(41) Kochendoerfer, G. G. (2001) Chemical protein synthesis methods in drug discovery. *Curr. Opin. Drug Discov. Devel. 4*, 205−214.
(42) Papanikos, A., Rademann, J., and Meldal, M. (2001) Alpha-Ketocarbonyl peptides: a general approach to reactive resin-bound intermediates in the synthesis of peptide isosteres for protease inhibitor screening on solid support. *J. Am. Chem. Soc. 123*, 2176−2181.
(43) Spetzler, J. C., and Hoeg-Jensen, T. (2001) A new amino acid derivative with a masked side-chain aldehyde and its use in peptide synthesis and chemoselective ligation. *J. Pept. Sci. 7*, 537−551.
(44) Cennamo, C. (1954) Nonenzymic transamination between peptides and pyrodoxal. *Naturwissenschaften 41*, 39.
(45) Tam, J. P. (1988) Synthetic peptide vaccine design: synthesis and properties of a high-density multiple antigenic peptide system. *Proc. Natl. Acad. Sci. U.S.A. 85*, 5409−5413.
(46) Shao, J., and Tam, J. P. (1995) Unprotected peptides as building blocks for the synthesis of peptide dendrimers with oxime, hydrazone, and thiazolidine linkages. *J. Am. Chem. Soc. 117*, 3893−3899.
(47) Wetlaufer, D. B. (1973) Nucleation, rapid folding, and globular intrachain regions in proteins. *Proc. Natl. Acad. Sci. 70*, 697−701.
(48) Elmore, D. E., and Dougherty, D. A. (2001) Molecular Dynamics Simulations of Wild-Type and Mutant Forms of the *Mycobacterium tuberculosis* MscL Channel. *Biophys. J. 81*, 1345−1359.

BC010128L

Efficient Calf Thymus DNA Condensation upon Binding with Novel Bile Acid Polyamine Amides

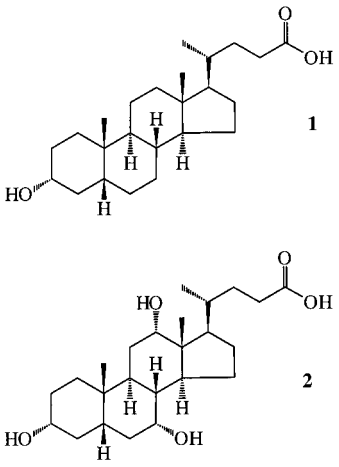
Andrew J. Geall, Dima Al-Hadithi, and Ian S. Blagbrough*

Department of Pharmacy and Pharmacology, University of Bath, Bath BA2 7AY, U.K. Received August 10, 2000

Polyamine amides have been prepared from lithocholic and cholic acids (5β-colanes) by acylation of tri-Boc-protected tetraamines spermine and thermine. These designed ligands for DNA are polyammonium ions at physiological pH. In NMR spectra, they display ^{14}N-^{1}H ^{1}J = 51 Hz, 1:1:1 triplets, due to the symmetry of the $R^{14}NH_3^+$ cations. The binding affinities of these conjugates for calf thymus DNA were determined using an ethidium bromide fluorescence quenching assay and compared with spermine and polylysine. DNA-binding affinities were dependent upon both salt concentration and the hydrophobicity or intermolecular bonding (facial effects) of the lipid moieties in these conjugates. Light scattering at 320 nm was used to determine DNA condensation and particle formation. The observed self-assembly phenomena are discussed with respect to DNA charge neutralization and DNA bending with loss of ethidium cation intercalation sites, ultimately leading to DNA condensation. These polyamine amides are models for lipoplex formation with respect to gene delivery (lipofection), a key first step in gene therapy.

INTRODUCTION

Among polyamine-containing natural products (*1*−*7*), polyamino-steroids form a novel, small group whose members and their analogues display a variety of interesting biological activities. Walker and co-workers have recently reported the DNA-binding affinity and in vitro gene delivery potential of various polyamines conjugated to the steroidal bile acids lithocholic **1** and cholic **2** acids



lithocholic acid **1** and cholic acid **2**

(*8*, *9*). Although most of their transfection agents contained a cationic headgroup (tetraamine spermine **3**, a polyammonium ion at physiological pH) attached to a hydrophobic tail (e.g., cholic acid spermine amide **13**), there were significant differences in the transfection activities across the series (*8*, *9*). Diamino steroids cyclobuxine (*10*), irehdiamine A, and malouetine have long been known to interact with DNA (*10*−*13*). The natural product bufotoxin, isolated from the venom of the European toad *Bufo vulgaris* (*B. bufo bufo* Linné), contains an arginyl guanidine functional group pendant from a steroid (bufotalin) nucleus and displays digitalis-like cardiac effects (*14*−*16*). Recently, Regen and co-workers reported their (so-called) molecular umbrella from cholic acid **2** and triamine spermidine, creating structures that can mask an attached agent (dansyl as a drug mimetic) from the surrounding environment (*17*−*19*). Polyamino-steroid squalamine, isolated from liver and gallbladder tissues of the dogfish shark, *Squalus acanthias*, is a spermidine-containing sterol sulfate which displays antimicrobial and fungicidal properties, and induces osmotic lysis of protozoa (*20*−*23*).

As part of our continuing studies on polyamine-mediated DNA condensation (*24*−*32*), we have synthesized polyamine amide conjugates of lithocholic **1** and cholic acids **2** in order to investigate the effects on changes in hydrophobicity on their binding affinity to DNA. Structure−activity relationships (SAR) for the binding of polyamines to DNA (*13*, *33*−*38*), and the subsequent condensation of DNA (*37*−*41*), indicate that polyammonium ions are suitable for use as gene delivery systems (*42*−*54*). Following DNA-binding studies with a short series of synthetic polyamino-steroids, up to four structural features have been shown to contribute to the strength and type of DNA interactions: cation type, total number of positive charges, regiochemical distribution of the ammonium groups, and steroid hydrophobicity (*55*−*57*). The mechanism by which these compounds cause lipofection is still poorly understood (*50*−*54*). Therefore, it is important to determine their physicochemical properties for the design of lipoplexes capable of efficient lipofection (*58*).

We are investigating how changes in the hydrophobicity of a lipopolyamine affect the condensation of DNA and hence lipoplex formation (*24*−*32*). Herein we report the design and synthesis, using our orthogonal protection strategy, of unsymmetrical polyamine amides from bile acids, two amides of lithocholic acid **1**, **11** and **12** (at position 24), and two of cholic acid **2**, **13**, and **14** (also at

* To whom correspondence should be addressed. Phone: 44-1225-826795. Fax: 44-1225-826114. E-mail: prsisb@bath.ac.uk.

10.1021/bc000093+ CCC: $22.00 © 2002 American Chemical Society
Published on Web 04/26/2002

position 24) (*24*). The 5β-cholane ring structure was chosen as the lipid moiety, it has found previous use in lipoplex formation (*8, 9*), and a variety of derivatives of these bile acids are readily available substituted with differing numbers of hydroxyl groups at varying positions on the ring system. Two readily available polyamines were used as the cationic headgroups: 1,12-diamino-4,9-diazadodecane **3** (spermine, 3.4.3) and 1,11-diamino-4,8-diazaundecane (thermine, norspermine, 3.3.3) **4**. Differences in the distribution of positive charges along these two polyamine headgroups and their effects on binding affinity, including salt-dependent binding of these polyamine amides of lithocholic and cholic acids have been investigated. To investigate the SAR for their binding affinities for calf thymus (CT) DNA, we used a modified ethidium bromide displacement assay (*59, 60*). Changes in binding affinity for CT DNA with respect to variations in the hydroxyl substituents on a lipopolyamine are investigated with respect to the use of bile acids in lipoplex formation, a key first step in gene therapy (*50-58*).

EXPERIMENTAL PROCEDURES

General Details and Reagents. General details, column, RP-HPLC, solvents and other chromatographic details, NMR, MS, and other spectroscopic details are as previously described (*25*, *26*). Poly-L-lysine hydrobromide (RMM 4−15 kDa) was purchased from SAF and had an average RMM of 9.6 kDa (PL 9600) (DP 46) when measured by viscosity and 8.0 kDa (DP 38) measured by LALLS. CT DNA sodium salt and all other reagents and chemicals were obtained from SAF and were of the highest grades available.

General Procedure A: Poly-Boc Protection of Polyamines. To a cold (−78 °C) methanolic solution of the polyamine was added ethyl trifluoroacetate (1 equiv) dropwise over 30 min, and then without isolation, the remaining amino functional groups were protected quantitatively by the dropwise addition of an excess of di-*tert*-butyl dicarbonate in methanol (10 mL). Trifluoroacetyl functional group removal at pH 11 with concentrated aqueous ammonia, workup, and purification as previously reported (*25*−*27*) afforded the title compound as a colorless homogeneous oil.

General Procedure B: Amide Formation. To a solution of the poly-Boc-protected polyamine in CH_2Cl_2 (10 mL) the bile acid, 1-hydroxybenzotriazole (HOBt) (0.2 equiv) and dicyclohexylcarbodiimide (DCC) (1.5 equiv) were added. Then the reaction mixture was stirred at 25 °C, under nitrogen, for 24 h. The precipitate of dicyclohexylurea was then removed by filtration. The filtrate was concentrated in vacuo and the residue purified over silica gel (CH_2Cl_2-MeOH) to afford the title compound as a white foam.

General Procedure C: Boc Removal. To a stirring solution of lipopolyamine dissolved in CH_2Cl_2 (180 mL), under nitrogen at 25 °C, was added TFA (20 mL). After 2 h, the solution was concentrated in vacuo, lyophilized, and purified by semipreparative RP-HPLC over Supelcosil ABZ+Plus (5 μm, 25 cm × 10 mm, MeOH-0.1% aqueous TFA) to afford the title compound as a white solid (poly-TFA salt).

(N^1,N^4,N^9-Tri-*tert*-butoxycarbonyl)-1,12-diamino-4,9-diazadodecane, 5. 1,12-Diamino-4,9-diazadodecane **3** (spermine, 3.4.3) (1.0 g, 5.0 mmol) was reacted according to general procedure A to afford the title compound **5** as a homogeneous oil (1.24 g, 50%). Purified over silica gel (CH_2Cl_2-MeOH-concentrated NH_3(aq) 70:10:1 to 50:10:1 v/v/v), R_f 0.5 (CH_2Cl_2-MeOH-concentrated NH_3(aq) 50:10:1 v/v/v) (*25*).

(N^1,N^4,N^8-Tri-*tert*-butoxycarbonyl)-1,11-diamino-4,8-diazaundecane, 6. 1,11-Diamino-4,8-diazaundecane **4** (thermine, norspermine, 3.3.3) (3.0 g, 16.0 mmol) was reacted according to general procedure A to afford the title compound **6** as a homogeneous oil (3.16 g, 41%). Purified over silica gel [CH_2Cl_2-MeOH-concentrated NH_3(aq) 100:10:1 v/v/v], R_f 0.18 [CH_2Cl_2-MeOH-concentrated NH_3(aq) 100:10:1 v/v/v] (*25*).

***N^1*-(3α-Hydroxy-5β-cholan-24-carbonyl-(*N^4*,*N^9*,*N^{12}*-tri-*tert*-butoxycarbonyl))-1,12-diamino-4,9-diazadodecane, 7.** Polyamine **5** (500 mg, 1.0 mmol) and lithocholic acid (375 mg, 1.0 mmol) were reacted according to general procedure B to afford the title compound **7** as a white foam (610 mg, 71%). Purified by column chromatography over silica gel (CH_2Cl_2-MeOH; 25:1 v/v), R_f 0.22 (CH_2Cl_2-MeOH; 20:1 v/v). ^{1}H NMR, 400 MHz, $CDCl_3$: 0.64 (s, 3 H, 18′-CH_3); 0.83−2.26 (m, 69 H, 2-CH_2, 6-CH_2, 7-CH_2, 11-CH_2, 3 × OC(CH_3)$_3$, 1′-CH_2, 2′-CH_2, 4′-CH_2, 5′-CH, 6′-CH_2, 7′-CH_2, 8′-CH, 9′-CH, 11′-CH_2, 12′-CH_2, 14′-CH, 15′-CH_2, 16′-CH_2, 17′-CH, 19′-CH_3, 20′-CH, 21′-CH_3, 22′-CH_2, 23′-CH_2); 2.84−3.05 (m, 12 H, 1-CH_2, 3-CH_2, 5-CH_2, 8-CH_2, 10-CH_2, 12-CH_2); 3.60−3.70 (m, 1 H, 3′-CH); 6.75−6.90 (br s, 1 H, CH_2-N*H*CO). ^{13}C NMR, 100 MHz, $CDCl_3$: 12.0 (18′-CH_3); 18.3 (21′-CH_3); 20.7 (11′-CH_2); 23.2 (19′-CH_3); 24.1 (15′-CH_2); 25.4, 25.6, 25.9 (6-CH_2, 7-CH_2, overlapping); 26.3 (7′-CH_2); 27.1 (6′-CH_2); 27.6, 28.1, 28.4, 28.7 [2-CH_2, 11-CH_2, 16′-CH_2, 3 × O-C-(*C*H_3)$_3$, overlapping]; 30.4 (2′-CH_2); 31.7 (22′-CH_2); 33.7 (23′-CH_2); 34.5 (10′-C); 35.3, 35.4 (12-CH_2, 20′-CH, 1′-CH_2); 35.8 (8′-CH); 36.3 (4′-CH_2); 37.3 (1-CH_2); 40.1 (12′-CH_2); 40.3 (9′-CH); 42.0 (5′-CH); 42.6 (13′-CH); 43.2, 43.7 (3-CH_2, 10-CH_2, overlapping); 46.6 (5-CH_2, 8-CH_2, overlapping); 56.0 (17′-CH); 56.4 (14′-CH); 71.6 (3′-CH); 79.7 (3 × quaternary OC, overlapping); 156.0, 156.4 (3 × NCOO); 173.7 (CH_2-*C*ON). MS, FAB$^+$ found 861, 20% (M^++1), $C_{49}H_{88}N_4O_8$ requires M^+ = 860.

***N^1*-(3α-Hydroxy-5β-cholan-24-carbonyl-(*N^4*,*N^8*,*N^{11}*-tri-*tert*-butoxycarbonyl))-1,11-diamino-4,8-diazaundecane, 8.** Polyamine **6** (500 mg, 1.0 mmol) and lithocholic acid (385 mg, 1.0 mmol) were reacted according to general procedure B to afford the title compound **8** as a white foam (751 mg, 87%). Purified by column chromatography over silica gel (CH_2Cl_2-MeOH; 25:1 v/v), R_f 0.30 (CH_2Cl_2-MeOH; 20:1 v/v). ^{1}H NMR, 400 MHz, $CDCl_3$: 0.64 (s, 3 H, 18′-CH_3); 0.84−2.24 [m, 67 H, 2-CH_2, 6-CH_2, 10-CH_2, 3 × O-C-(CH_3)$_3$, 1′-CH_2, 2′-CH_2, 4′-CH_2, 5′-CH, 6′-CH_2, 7′-CH_2, 8′-CH, 9′-CH, 11′-CH_2, 12′-CH_2, 14′-CH, 15′-CH_2, 16′-CH_2, 17′-CH, 19′-CH_3, 20′-CH, 21′-CH_3, 22′-CH_2, 23′-CH_2]; 2.84−3.05 (m, 12 H, 1-CH_2, 3-CH_2, 5-CH_2, 7-CH_2, 9-CH_2, 11-CH_2); 3.60−3.70 (m, 1 H, 3′-CH); 6.75−6.90 (br s, 1 H, CH_2-N*H*CO). ^{13}C NMR, 100 MHz, $CDCl_3$: 12.0 (18′-CH_3); 18.3 (21′-CH_3); 20.7 (11′-CH_2); 23.2 (19′-CH_3); 24.1 (15′-CH_2); 26.3 (7′-CH_2); 27.1 (6′-CH_2); 27.6, 28.1, 28.4, 28.7 [2-CH_2, 6-CH_2, 10-CH_2, 16′-CH_2, 3 × OC(CH_3)$_3$, overlapping]; 30.4 (2′-CH_2); 31.7 (22′-CH_2); 33.7 (23′-CH_2); 34.5 (10′-C); 35.3, 35.4 (11-CH_2, 20′-CH, 1′-CH_2, overlapping); 35.8 (8′-CH); 36.4 (4′-CH_2); 37.3 (1-CH_2); 40.1 (12′-CH_2); 40.3 (9′-CH); 42.0 (5′-CH); 42.6 (13′-CH); 43.6, 43.7, 44.2, 44.7 (3-CH_2, 5-CH_2, 7-CH_2, 9-CH_2, overlapping); 56.0 (17′-CH); 56.4 (14′-CH); 71.7 (3′-CH); 79.7 (3 × quaternary OC, overlapping); 155.9, 156.3 (3 × NCOO); 173.7 (CH_2-*C*ONH). MS, FAB$^+$ found 847, 20% (M^++1), $C_{48}H_{86}N_4O_8$ requires M^+ = 846.

***N^1*-(3α,7α,12α-Trihydroxy-5β-cholan-24-carbonyl-(*N^4*,*N^9*,*N^{12}*-tri-*tert*-butoxycarbonyl))-1,12-diamino-4,9-diazadodecane, 9.** Polyamine **5** (500 mg, 1.0 mmol) and cholic acid (406 mg, 1.0 mmol) were reacted according

to general procedure B to afford the title compound **9** as a white foam (532 mg, 60%). Purified by column chromatography over silica gel (CH_2Cl_2-MeOH; 15:1 to 10:1 v/v), R_f 0.17 (CH_2Cl_2-MeOH; 10:1 v/v). ^{1}H NMR, 400 MHz, $CDCl_3$: 0.67 (s, 3 H, 18′-CH_3); 0.88 (s, 3 H, 19′-CH_3); 0.91−2.40 (m, 62 H, 2-CH_2, 6-CH_2, 7-CH_2, 11-CH_2, 3 × O-C-(CH_3)$_3$, 1′-CH_2, 2′-CH_2, 4′-CH_2, 5′-CH, 6′-CH_2, 8′-CH, 9′-CH, 11′-CH_2, 14′-CH, 15′-CH_2, 16′-CH_2, 17′-CH, 20′-CH, 21′-CH_3, 22′-CH_2, 23′-CH_2); 2.80−3.37 (m, 12 H, 1-CH_2, 3-CH_2, 5-CH_2, 8-CH_2, 10-CH_2, 12-CH_2); 3.37−3.50 (m, 1 H, 3′-CH); 3.83 (s, 1 H, 7′-CH); 3.96 (s, 1 H, 12′-CH); 6.75−6.90 (br s, 1 H, CH_2-N*H*CO). ^{13}C NMR, 100 MHz, $CDCl_3$: 12.5 (18′-CH_3); 17.5 (21′-CH_3); 22.5 (19-CH_3); 25.5, 25.7, 26.0 (6-CH_2, 7-CH_2, overlapping); 26.4 (9′-CH_2); 27.6 (16′-CH_2); 27.7, 28.1, 28.2, 28.4, 28.5, 28.7, 28.9 (2-CH_2, 11-CH_2, 11′-CH_2, 3 × OC(CH_3)$_3$, overlapping); 30.5 (2′-CH_2); 31.7 (22′-CH_2); 33.6 (23′-CH_2); 34.7 (6′-CH_2); 34.8 (10′-C); 35.3 (1′-CH_2); 35.5, 35.7 (12-CH_2, 20′-CH, overlapping); 37.4, 37.7 (1-CH_2); 39.5 (8′-CH); 39.6 (4′-CH_2); 41.5, 41.7 (5′-CH, 14′-CH); 43.5, 43.7, 44.2 (3-CH_2, 5-CH_2, 8-CH_2, 10-CH_2, overlapping); 46.4, 46.8 (13′-C, 17′-CH); 68.4 (7′-CH); 71.9 (3′-CH); 73.0 (12′-CH); 79.6, 79.8 (3 × quaternary OC, overlapping); 156.1, 156.4 (3 × NCOO); 174.1 (CH_2-*C*ONH). MS, FAB$^+$ found 893, 40% ($M^+ + 1$), $C_{49}H_{88}N_4O_{10}$ requires $M^+ = 892$.

***N*^{1}-(3α,7α,12α-Trihydroxy-5*β*-cholan-24-carbonyl)-(*N*^{4},*N*^{8},*N*^{11}-tri-*tert*-butoxycarbonyl))-1,11-diamino-4,8-diazaundecane, 10.** Polyamine **6** (500 mg, 1.0 mmol) and cholic acid (418 mg, 1.0 mmol) were reacted according to general procedure B to afford the title compound **10** as a white foam (824 mg, 91%). Purified by column chromatography over silica gel (CH_2Cl_2-MeOH; 20:1 to 15:1 to 10:1 v/v), R_f 0.20 (CH_2Cl_2-MeOH; 10:1 v/v). ^{1}H NMR, 400 MHz, $CDCl_3$: 0.67 (s, 3 H, 18′-CH_3); 0.88 (s, 3 H, 19′-CH_3); 0.91−2.30 [m, 60 H, 2-CH_2, 6-CH_2, 10-CH_2, 3 × O-C-(CH_3)$_3$, 1′-CH_2, 2′-CH_2, 4′-CH_2, 5′-CH, 6′-CH_2, 8′-CH, 9′-CH, 11′-CH_2, 14′-CH, 15′-CH_2, 16′-CH_2, 17′-CH, 20′-CH, 21′-CH_3, 22′-CH_2, 23′-CH_2]; 2.88−3.38 (m, 12 H, 1-CH_2, 3-CH_2, 5-CH_2, 7-CH_2, 9-CH_2, 11-CH_2); 3.38−3.50 (m, 1 H, 3′-CH); 3.83 (s, 1 H, 7′-CH); 3.96 (s, 1 H, 12′-CH); 6.75−6.90 (br s, 1 H, CH_2-N*H*-CO). ^{13}C NMR, 100 MHz, $CDCl_3$: 12.5 (18′-CH_3); 17.5 (21′-CH_3); 22.5 (19-CH_3); 26.4 (9′-CH_2); 27.6 (16′-CH_2); 28.2, 28.5, 28.8, 28.9 [2-CH_2, 6-CH_2, 10-CH_2, 11′-CH_2, 3 × O-C-(*C*H_3)$_3$, overlapping]; 30.5 (2′-CH_2); 31.7 (22′-CH_2); 33.6 (23′-CH_2); 34.7 (6′-CH_2); 34.8 (10′-C); 35.3 (1′-CH_2); 35.5, 35.7 (11-CH_2, 20′-CH, overlapping); 37.4 (1-CH_2, overlapping); 39.5 (8′-CH); 39.6 (4′-CH_2); 41.5, 41.7 (5′-CH, 14′-CH); 43.5, 43.8, 44.8 (3-CH_2, 5-CH_2, 7-CH_2, 9-CH_2, overlapping); 46.4, 46.7 (13′-C, 17′-CH); 68.4 (7′-CH); 71.9 (3′-CH); 73.0 (12′-CH); 79.8 (3 × quaternary OC, overlapping); 156.0, 156.1 (3 × NCOO); 174.1 (CH_2-*C*ONH). MS, FAB$^+$ found 879, 5% ($M^+ + 1$), $C_{48}H_{86}N_4O_{10}$ requires $M^+ = 878$.

***N*^{1}-(3α-Hydroxy-5*β*-cholan-24-carbonyl)-1,12-diamino-4,9-diazadodecane, 11.** Amide **7** (300 mg, 0.34 mmol) was deprotected according to general procedure C. The residue was lyophilized to produce 352 mg of a white powder, 225 mg was purified by RP-HPLC (MeCN-0.1% TFA(aq), 38:62 v/v) to afford the title compound **11** as a white solid (polytrifluoroacetate salt, 61 mg, 27%), t_R 11.5 min by RP-HPLC (Supelcosil ABZ+Plus, 5 μm, 15 cm × 4.6 mm, MeCN-0.1% TFA(aq), 40:60 v/v). ^{1}H NMR, 400 MHz, d_6-DMSO: 0.61 (s, 3 H, 18′-CH_3); 0.82−0.98 (m, 7 H, 1′*β*-CH, 19′-CH_3, 21′-CH_3); 0.98−1.28 (m, 9H, 2′α-CH, 6′α-CH, 7′α-CH, 11′*β*-CH, 14′-CH, 15′α-CH, 16′*β*-CH, 17′-CH, 22′*β*-CH); 1.28−1.44 (m, 7 H, 4′*β*-CH, 5′-CH, 7′*β*-CH, 8′-CH, 9′-CH, 11′α-CH, 20′-CH); 1.44−1.86 (m, 13 H, 6-CH_2, 7-CH_2, 11-CH_2, 1′α-CH, 2′*β*-CH, 4′α-CH, 6′*β*-CH, 15′*β*-CH, 16′α-CH, 22′α-CH); 1.86−2.15 (m, 5 H, 2-CH_2, 12′*β*-CH, 23′α-CH, 23′*β*-CH); 2.84−3.05 (m, 10 H, 3-CH_2, 5-CH_2, 8-CH_2, 10-CH_2, 12-CH_2); 3.05−3.15 (m, 2 H, 1-CH_2); 3.30−3.42 (m, 1 H, 3′-CH); 4.15 [br s, 1 × OH, (+H_2O)]; 7.24 (1:1:1, t, ^1J = 51, ^{14}N-^{1}H); 8.03, 8.71, 8.90 (3 × br s, ammonium signals). ^{13}C NMR, 100 MHz, d_6-DMSO: 11.8 (18′-CH_3); 18.2 (21′-CH_3); 20.3 (11′-CH_2); 22.5, 22.7 (6-CH_2, 7-CH_2); 23.2 (19′-CH_3); 23.7, 23.8 (2-CH_2, 15′-CH_2); 26.0, 26.1 (11-CH_2, 7′-CH_2); 26.8 (6′-CH_2); 27.7 (16′-CH_2); 30.3 (2′-CH_2); 31.5 (22′-CH_2); 32.2 (23′-CH_2); 34.1 (10′-C); 34.9 (20′-CH); 35.1 (1′-CH_2); 35.3 (8′-CH); 35.5 (1-CH_2); 36.1 (4′-CH_2); 36.2 (12-CH_2); 39.6 (12′-CH_2); 39.9 (9′-CH); 41.4 (5′-CH); 42.2 (13′-CH); 43.8 (3-CH_2); 44.6 (10-CH_2); 46.0, 46.1 (5-CH_2, 8-CH_2); 55.5 (17′-CH); 56.0 (14′-CH); 69.8 (3′-CH); 173.1 (CH_2-*C*ONH). MS, FAB$^+$ found 561, 40% ($M^+ + 1$), $C_{34}H_{64}N_4O_2$ requires $M^+ = 560$. High-resolution MS *m*/*z*, FAB$^+$ found 561.5135, (M^++1), $C_{34}H_{65}N_4O_2$ requires $M^+ + 1 = 561.5108$.

***N*^{1}-(3α-Hydroxy-5*β*-cholan-24-carbonyl)-1,11-diamino-4,8-diazaundecane, 12.** Amide **8** (300 mg, 0.36 mmol) was deprotected according to general procedure C. The residue was lyophilized to produce 347 mg of a white powder, 225 mg were purified by RP-HPLC [MeCN-0.1% TFA(aq), 38:62 v/v] to afford the title compound **12** as a white solid (polytrifluoroacetate salt, 71 mg, 32%). t_R 7.0 min by RP-HPLC [Supelcosil ABZ+Plus, 5 μm, 15 cm × 4.6 mm, MeCN-0.1% TFA(aq), 38:62 v/v]. ^{1}H NMR, 400 MHz, d_6-DMSO: 0.61 (s, 3 H, 18′-CH_3); 0.84−0.98 (m, 7 H, 1′*β*-CH, 19′-CH_3, 21′-CH_3); 0.98−1.28 (m, 9H, 2′α-CH, 6′α-CH, 7′α-CH, 11′*β*-CH, 14′-CH, 15′α-CH, 16′*β*-CH, 17′-CH, 22′*β*-CH); 1.28−1.44 (m, 7 H, 4′*β*-CH, 5′-CH, 7′*β*-CH, 8′-CH, 9′-CH, 11′α-CH, 20′-CH); 1.44−1.86 (m, 9 H, 10-CH_2, 1′α-CH, 2′*β*-CH, 4′α-CH, 6′*β*-CH, 15′*β*-CH, 16′α-CH, 22′α-CH); 1.86−2.15 (m, 7 H, 2-CH_2, 6-CH_2, 12′*β*-CH, 23′α-CH, 23′*β*-CH); 2.85−3.05 (m, 10 H, 3-CH_2, 5-CH_2, 7-CH_2, 9-CH_2, 11-CH_2); 3.05−3.14 (m, 2 H, 1-CH_2); 3.30−3.42 (m, 1 H, 3′-CH); 3.63 [br s, 1 × OH, (+H_2O)]; 7.22 (1:1:1, t, ^1J = 51, ^{14}N-^{1}H); 8.01, 8.79, 8.97 (3 × br s, ammonium signals). ^{13}C NMR, 100 MHz, d_6-DMSO: 11.8 (18′-CH_3); 18.2 (21′-CH_3); 20.3 (11′-CH_2); 22.3 (6-CH_2); 23.2 (19′-CH_3); 23.7 (2-CH_2, 15′-CH_2, overlapping); 26.0, 26.1 (10-CH_2, 7′-CH_2); 26.8 (6′-CH_2); 27.6 (16′-CH_2); 30.3 (2′-CH_2); 31.4 (22′-CH_2); 32.2 (23′-CH_2); 34.1 (10′-C); 34.9 (20′-CH); 35.0 (1′-CH_2); 35.2 (8′-CH); 35.4 (1-CH_2); 36.1 (11-CH_2); 36.2 (4′-CH_2); 39.6 (12′-CH_2); 39.8 (9′-CH); 41.4 (5′-CH); 42.2 (13′-CH); 43.8, 43.9 (3-CH_2, 9-CH_2); 44.7 (5-CH_2, 7-CH_2, overlapping); 55.4 (17′-CH); 56.0 (14′-CH); 69.8 (3′-CH); 173.0 (CH_2-*C*ONH). MS, FAB$^+$ found 547, 100% ($M^+ + 1$), $C_{33}H_{62}N_4O_2$ requires $M^+ = 546$. High-resolution MS *m*/*z*, FAB$^+$ found 547.4955, ($M^+ + 1$), $C_{33}H_{63}N_4O_2$ requires $M^+ + 1 = 547.4951$.

***N*^{1}-(3α,7α,12α-Trihydroxy-5*β*-cholan-24-carbonyl)-1,12-diamino-4,9-diazadodecane, 13.** Amide **9** (300 mg, 0.34 mmol) was deprotected according to general procedure C. The residue was lyophilized to produce 345 mg of a white powder, 220 mg was purified by RP-HPLC [MeCN-0.1% TFA(aq), 25:75 v/v] to afford the title compound (*8*, *9*) **13** as a white solid (polytrifluoroacetate salt, 74 mg, 34%). t_R 5.0 min by RP-HPLC [Supelcosil ABZ+Plus, 5 μm, 15 cm × 4.6 mm, MeCN-0.1% TFA(aq), 27:73 v/v]. ^{1}H NMR, 400 MHz, d_6-DMSO: 0.58 (s, 3 H, 18′-CH_3); 0.50−1.00 (m, 8 H, 1′*β*-CH, 15′α-CH, 19′-CH_3, 21′-CH_3); 1.05−1.50 (m, 10 H, 2′α-CH, 2′*β*-CH, 4′*β*-CH, 5′-CH, 6′α-CH, 11′-CH_2, 16′*β*-CH, 20-CH, 22′*β*-CH); 1.50−2.00 (m, 19 H, 2-CH_2, 6-CH_2, 7-CH_2, 11-CH_2, 1′α-CH, 4′α-CH, 6′*β*-CH, 9′-CH, 14′-CH, 15′*β*-CH, 16′α-CH, 17′-CH, 22′α-CH, 23′α-CH, 23′*β*-CH); 2.00−2.25 (m, 3 H, 4′α-CH, 9′-CH, 23α-CH); 2.78−3.01 (m, 10 H, 3-CH_2, 5-CH_2, 8-CH_2, 10-CH_2, 12-CH_2); 3.01−3.12 (m, 2 H, 1-CH_2); 3.12−3.22 (m, 1 H, 3′-CH); 3.43 [br s, 3 × OH, (+H_2O)];

3.61 (s, 1 H, 7′-CH); 3.79 (s, 1 H, 12′-CH); 7.22 (1:1:1, t, ^1J = 51, ^{14}N-^{1}H); 8.01, 8.67, 8.87 (3 × br s, ammonium signals). ^{13}C NMR, 100 MHz, d_6-DMSO: 12.2 (18′-CH_3); 17.0 (21′-CH_3); 22.5, 22.7 (6-CH_2, 7-CH_2, 15′-CH_2, 19′-CH_3, overlapping); 23.7 (2-CH_2); 26.0 (11-CH_2); 26.1 (9′-CH_2); 27.2 (16′-CH_2); 28.5 (11′-CH_2); 30.3 (2′-CH_2); 31.6 (22′-CH_2); 32.3 (23′-CH_2); 34.3 (10′-C); 34.8 (6′-CH_2); 35.1, 35.2 (1′-CH_2, 20′-CH); 35.4 (1-CH_2); 36.1 (12-CH_2); 38.8 (4′-CH_2, 8′-CH); 41.3, 41.4 (5′-CH, 14′-CH); 43.8 (3-CH_2); 44.5 (10-CH_2); 45.6 (13′-C); 46.0, 46.1 (5-CH_2, 8-CH_2, 17′-CH); 66.1 (7′-CH); 70.3 (3-CH); 70.9 (12′-CH); 173.2 (CH_2-*C*ONH). MS, FAB$^+$ found 593, 100% ($M^+ + 1$), $C_{34}H_{64}N_4O_4$ requires $M^+ = 592$. High-resolution MS *m/z*, FAB$^+$ found 593.5010, ($M^+ + 1$), $C_{34}H_{65}N_4O_4$ requires $M^+ + 1 = 593.5006$.

***N*^{1}-(3α,7α,12α-Trihydroxy-5*β*-cholan-24-carbonyl)-1,11-diamino-4,8-diazaundecane, 14.** Amide **10** (300 mg, 0.34 mmol) was deprotected according to general procedure C. The residue was lyophilized to produce 352 mg of a white powder, 225 mg was purified by RP-HPLC [MeCN-0.1% TFA(aq), 27:73 v/v] to afford the title compound **14** as a white solid (polytrifluoroacetate salt, 124 mg, 55%). t_R 6.8 min by RP-HPLC [Supelcosil ABZ+Plus, 5 μm, 15 cm × 4.6 mm, MeCN-0.1% TFA(aq), 30:70 v/v]. ^{1}H NMR, 400 MHz, d_6-DMSO: 0.58 (s, 3 H, 18′-CH_3); 0.50−1.00 (m, 8 H, 1′*β*-CH, 15′α-CH, 19′-CH_3, 21′-CH_3); 1.05−1.50 (m, 10 H, 2′α-CH, 2′*β*-CH, 4′*β*-CH, 5′-CH, 6′α-CH, 11′-CH_2, 16′*β*-CH, 20′-CH, 22′*β*-CH); 1.50−2.05 (m, 17 H, 2-CH_2, 6-CH_2, 10-CH_2, 1′α-CH, 4′α-CH, 6′*β*-CH, 9′-CH, 14′-CH, 15′*β*-CH, 16′α-CH, 17′-CH, 22′α-CH, 23′α-CH, 23′*β*-CH); 2.05−2.28 (m, 3 H, 4′α-CH, 9′-CH, 23α-CH); 2.85−3.05 (m, 10 H, 3-CH_2, 5-CH_2, 7-CH_2, 9-CH_2, 11-CH_2); 3.05−3.15 (m, 2 H, 1-CH_2); 3.15−3.25 (m, 1 H, 3′-CH); 3.60 (s, 1 H, 7′-CH); 3.79 (s, 1 H, 12′-CH); 5.00 [br s, 3 × OH, (+H_2O)]; 7.21 (1:1:1, t, ^1J = 51, ^{14}N-^{1}H); 8.01, 8.78, 8.97 (3 × br s, ammonium signals). ^{13}C NMR, 100 MHz, d_6-DMSO: 12.2 (18′-CH_3); 17.0 (21′-CH_3); 22.4, 22.5, 22.7 (6-CH_2, 15′-CH_2, 19′-CH_3, overlapping); 23.8 (2-CH_2); 26.0 (10-CH_2); 26.2 (9′-CH_2); 27.2 (16′-CH_2); 28.5 (11′-CH_2); 30.3 (2′-CH_2); 31.6 (22′-CH_2); 32.3 (23′-CH_2); 34.3 (10′-C); 34.8 (6′-CH_2); 35.1, 35.2 (1′-CH_2, 20′-CH); 35.5 (1-CH_2); 36.1 (11-CH_2); 39.2 (4′-CH_2, 8′-CH); 41.3, 41.4 (5′-CH, 14′-CH); 43.9, 44.0 (3-CH_2, 9-CH_2); 44.7 (5-CH_2, 7-CH_2); 45.6 (13′-C); 46.0 (17′-CH); 66.1 (7′-CH); 70.3 (3-CH); 70.9 (12′-CH); 173.2 (CH_2-*C*ONH). MS, FAB$^+$ found 579, 100% ($M^+ + 1$), $C_{33}H_{62}N_4O_4$ requires $M^+ = 578$. High-resolution MS *m/z*, FAB$^+$ found 579.4849, ($M^+ + 1$), $C_{33}H_{63}N_4O_4$ requires $M^+ + 1 = 579.4854$. In our hands, all members of this series of polyamine amides **11-14** were water soluble at 1 mg ml^{-1} (*8*, *9*).

RESULTS AND DISCUSSION

Polyamines spermine **3** and thermine **4** were sequentially unsymmetrically protected with di-*tert*-butyl dicarbonate using our orthogonal protection strategy (*24*−*31*). Selective protection of one primary amine group, in each symmetrical polyamine **3** and **4**, by reaction with ethyl trifluoroacetate, afforded the respective monotrifluoroacetamides. Immediately, in these solutions, the remaining amino functional groups were Boc protected, with di-*tert*-butyl dicarbonate, to afford the fully protected polyamines. The trifluoroacetyl protecting group was then cleaved (in situ) by increasing the pH to 11 with concentrated aqueous ammonia, to afford N^1,N^2,N^3-tri-Boc protected polyamines **5** and **6**. Acylation of the free primary amine of these unsymmetrically protected polyamines **5** and **6** with lithocholic **1** and cholic acids **2** (DCC, cat. HOBt), afforded the fully protected polyamine

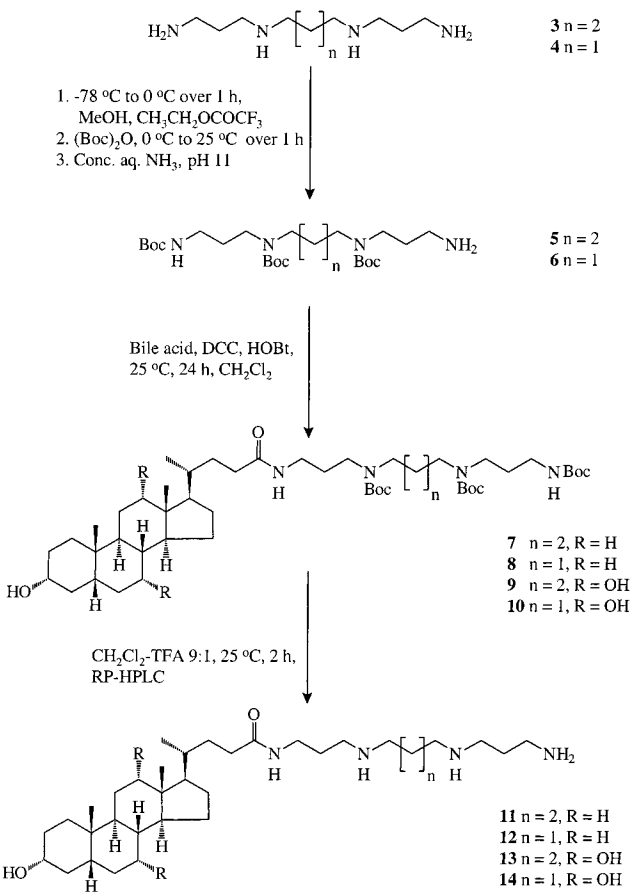
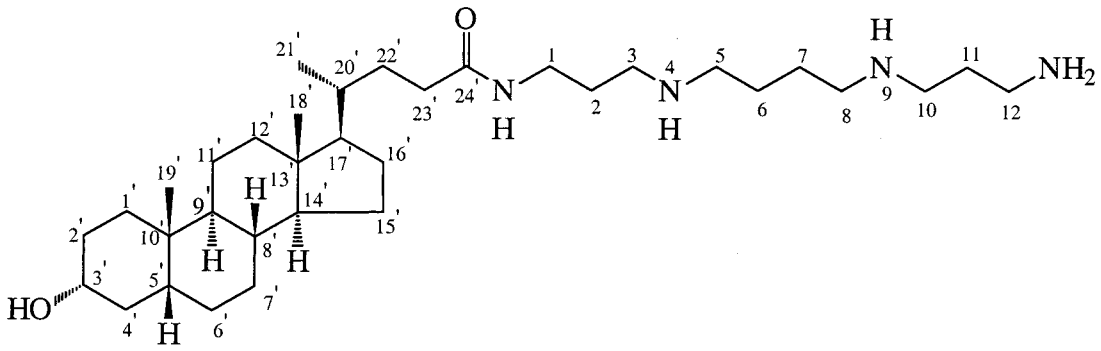


Figure 1. Synthesis of target polyamine amides **11**−**14**.

amides **7-10**. Deprotection (TFA-CH_2Cl_2, 1:9 v/v) and purification to homogeneity by RP-HPLC afforded target polyamine amides **11-14**, as their polytrifluoroacetate salts (Figure 1). The proposed structures were unambiguously assigned using ^{1}H, ^{13}C and HETCOR NMR and accurate FAB-MS.

The pK_as of the polyamine headgroups on polyamino steroids **11**−**14** were assumed to be the same as those measured potentiometrically for the cholesterol carbamates we have previously reported (*29*). The net positive charge was then calculated using the Henderson−Hasselbach equation at pH 7.4. Therefore, polyamine amides **11** and **13** (conjugates of spermine) have been assigned a net positive charge of 2.4 and polyamine amides **12** and **14** (conjugates of thermine) have been assigned a net positive charge of 2.3. We have named the target compounds **11**−**14** as their corresponding polyamine derivatives and have outlined the numbering system we used in the NMR assignments with N^1-(3α-hydroxy-5*β*-cholan-24-carbonyl)-1,12-diamino-4,9-diazadodecane **11** selected as an example.

The complete NMR spectroscopic assignment of the polyamine headgroups in this series of polyamine amides **11**−**14** is based upon calculations using additivity rules (*61*), ^{1}H, ^{13}C chemical shift correlation spectroscopy, and detailed comparisons with cholesterol carbamates previously characterized (*25*, *31*). The assignment of the 5*β*-cholane ring structure is based upon literature assignments (*62*), and the expected changes in the carbon chemical shifts due to substituent effects are entirely consistent with these assignments. Conformational isomers (populations interconverted by *σ*-bond rotation) are observed for the poly-Boc-protected polyamines, and therefore, two signals for each carbon on the methylene



Structure and numbering system for N^1-(3α-hydroxy-5β-cholan-24-carbonyl)-1,12-diamino-4,9-diazadodecane **11**

backbone of the polyamine and for each carbon on the Boc groups were typically observed. Generally ^{14}N-^{1}H couplings are not observed, but in the case of ammonium compounds, the combination of quadrupole relaxation and exchange of NH-protons is not sufficiently large to eliminate completely the coupling across one bond (*61*). Therefore, amides **11**−**14** display broad ammonium signals above δ 7.0 ppm (typically 8.0, 8.8, and 9.0 ppm, exchanged with D_2O). In addition, signals at δ 7.2 (1:1:1 t, $^1J = 51$ Hz, ^{14}N-^{1}H) were observed for these ammonium ions which we interpret as due to the symmetry of the $R^{14}NH_3^+$ cations (*61*).

Ethidium Bromide Displacement Assay. Relative binding affinities for CT DNA of the target compounds **11**−**14** were measured using a modified ethidium bromide fluorescence quenching assay, a refined displacement assay (*59*, *60*), and plotted against charge ratio (CR) as defined in the literature (*58*). The decrease in fluorescence was critically compared against polylysine (PL, average RMM 9.6 kDa, PL 9600) and spermine **3** (Figure 2) for compounds **11**−**14** at 20 mM NaCl as a function of CR (ammonium:DNA phosphate ions) (*58*). At physiological pH, spermine carries a net positive charge of 3.8 (*25*, *29*), PL 9600 a net positive charge in excess of 30. In Figure 2, polyamine amides **11** and **12**, and polycationic PL 9600 exhibit similar binding affinities for DNA. With PL 9600, complete displacement of ethidium bromide occurs as the conjugate−DNA complexes approach a charge ratio of 1. A slight excess of positive charge is required to displace the ethidium cation with the lithocholic acid conjugates **11** and **12**. This fluorescence quenching assay measures the relative binding affinities for DNA between compounds of comparable structure (*59*, *60*). Therefore, compared to spermine **3**, conjugates **11** and **12** have a greater binding affinity for DNA (Figure 2). There was no visible precipitation of the DNA. These data are consistent with complex formation between the DNA and the polyamine amide conjugates. This binding of polyamines and their conjugates to DNA is not a trivial process (*27*−*41*, *55*−*57*, *63*−*68*); they may bind preferentially to GC-rich major groove and to AT-rich minor groove regions (*63*−*66*). Covalent attachment of a lipid moiety, such as an aliphatic chain or a steroid, further enhances polyamine-mediated DNA condensation (*39*−*49*).

Cholic acid **2** is a sterol nucleus with a hydroxylated hydrophilic surface and an all-hydrocarbon hydrophobic surface, possessing the 5β-cholane ring structure (a *cis*-fused A,B-bicycle). Polyamine N^1-acylation with cholic acid **2** affords more hydrophilic polyamine amides **13** and **14** (moreso than **11** and **12**) as they contain three hydroxyl groups (compared to the one alcohol functional group of lithocholic acid) that are all located regiospecifically on the α-face of the 5β-cholane ring system. Amides **13** and **14** have a decreased binding affinity for DNA, compared to their lithocholic acid counterparts **11** and **12** (Figure 2), and they require a large excess of positive charge to displace the ethidium cation from its CT DNA intercalation sites. The differences in binding affinities between the spermine **11** and **13** and thermine **12** and **14** polyamine moieties were small (Figure 2). At 150 mM NaCl salt concentrations the binding affinity for CT DNA of PL 9600 is unaffected, but that of spermine **3** shows marked salt-dependent binding (Figure 3). Spermine amide **11**, which contains the lithocholane ring structure (with one hydroxyl moiety), requires an excess of positive charge (CR approximately 8) to displace the ethidium cation (Figure 3). The binding behavior of spermine amide **13** mimics that of spermine **3** at high salt concentrations, and the displacement of ethidium is almost completely inhibited even at a CR of >10.

DNA Condensation (Light Scattering) Assay. To investigate whether CT DNA is condensed into particles by spermine cholic acid amide **13**, the UV absorbance at 320 nm has been measured (*33*). In Figure 4, we show the apparent increase in UV absorption at 320 nm of DNA as aliquots are added at low and high salt concentrations (20 and 150 mM NaCl, respectively). At low salt concentrations, these data are consistent with particle formation and the absorption reaches a plateau at the same charge ratio (approximately 4) as essentially maximal ethidium bromide exclusion (Figure 2). However, due to the lack of sensitivity of this light-scattering assay, the DNA concentration was in a 10-fold excess compared to that used in the ethidium bromide assay. Significantly, at high salt concentrations, there are no particles formed by DNA condensation and hence no light scattering, with no visible precipitation of the DNA. These data (Figures 3 and 4) are consistent with inhibition of complex formation between the DNA and polyamine amide conjugate **13** at elevated salt concentrations.

From detailed comparisons of light-scattering assay data (Figure 4 and data not shown) together with ethidium bromide fluorescence quenching data (Figure 2 and Figure 3), we conclude that gross morphological changes occur to CT DNA as a result of polyamine amide binding. These effects are sensitive to the number of hydroxyl groups on the lipid moiety (reflecting its hydrophobicity) and are also salt concentration dependent. They are consistent with charge neutralization of CT

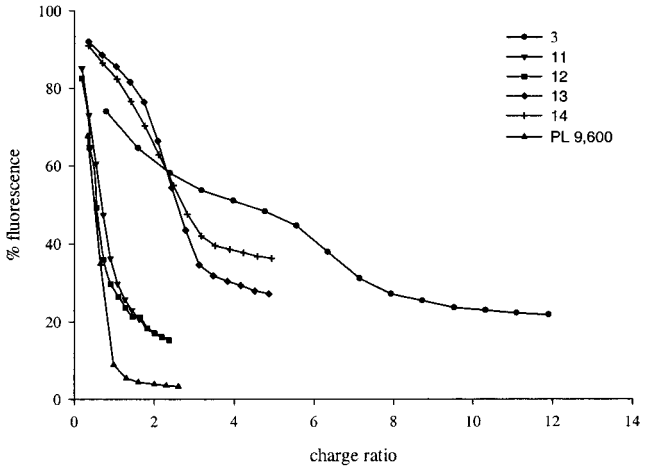


Figure 2. Ethidium bromide displacement assay of spermine **3**, amides **11**−**14**, and polylysine at 20 mM NaCl. CT DNA (6 μg in buffer, 3 mL, 20 mM NaCl, 2 mM HEPES, 10 μM EDTA, pH 7.4) was mixed with ethidium bromide (3 μL of 0.5 mg/mL) and aliquots of compound (5 μL of 0.25 mg/mL, 1 min equilibration time) were added, the fluorescence (%) determined, and plotted against the charge ratio of ammonium:DNA phosphate ions (*58*).

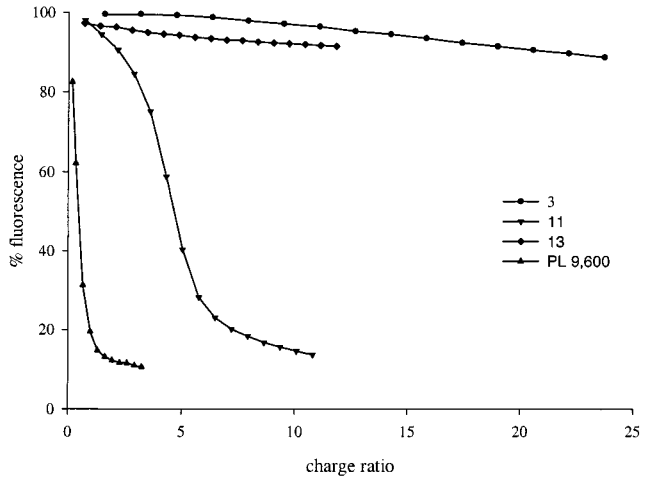


Figure 3. Ethidium bromide displacement assay of spermine **3**, amides **11** and **13**, and polylysine at 150 mM NaCl. CT DNA (6 μg in buffer, 3 mL, 150 mM NaCl, 2 mM HEPES, 10 μM EDTA, pH 7.4) was mixed with ethidium bromide (3 μL of 0.5 mg/mL) and aliquots of compound (5 μL of 0.25 mg/mL, 1 min equilibration time) were added, the fluorescence (%) determined, and plotted against the charge ratio of ammonium:DNA phosphate ions (*58*).

DNA, the loss of ethidium cation binding sites within the DNA double helix, and ultimately with DNA condensation and particle formation. These latter effects are the first key steps in gene therapy for the formation of lipoplexes.

Measurement of the ability of a drug to displace ethidium cation from DNA has been shown to be a valid measurement of DNA binding ability of both intercalative and nonintercalative drugs, including free polyamines and their conjugates (*55*−*57*, *59*, *69*−*74*). Displacement of ethidium cation from DNA provides an indirect method of measuring the binding affinity of drugs that lack a chromophore. It does not provide a direct measure of the binding constant, but offers a qualitative comparison of binding affinities within a series of compounds with similar structures. Molecular modeling studies of ethidium cation intercalation into DNA have shown that binding is accompanied by a helical screw axis displacement (or dislocation) in its structure (*75*). The helical axes are displaced approximately +1.0 Å (for B DNA), base pairs in the immediate region are twisted by 10°, giving rise to an angular unwinding of −26° and the intercalated base pairs are tilted relative to one another by 8°. These changes in DNA conformation mean that intercalation is limited to every other base pair at maximal drug-nucleic acid binding ratios, i.e., a neighbor exclusion model (*75*). These modeling studies also indicate that the conformational flexibility of DNA allows intercalation of the ethidium cation at kinked regions of the double helix. Thus, intercalation of ethidium cation occurs at regions where the base-pairs are unwound (kinked), which induces a conformational change in the double helix, restricting the total number of intercalation sites.

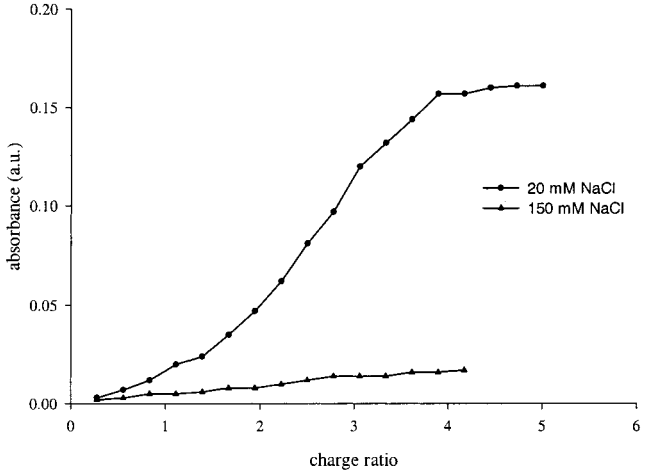


Figure 4. Light-scattering assay of polyamine amide **13** at low (20 mM NaCl) and high (150 mM NaCl) salt concentrations. CT DNA (60 μg in buffer, 3 mL, 20 mM NaCl, 2 mM HEPES, 10 μM EDTA, pH 7.4) was stirred and aliquots of compound (5 μL of 1.0 mg/mL, 1 min equilibration time) were added, the absorption (320 nm) measured, and plotted against the charge ratio of ammonium:DNA phosphate ions (*58*).

DNA collapse, by charge neutralization of cationic lipids, is thought to be a key step in lipoplex formation (*58*). This collapse is termed condensation, and affords compact, highly ordered toroids that have a possible relationship to the packaging of DNA in viruses, in particular they represent models for DNA organization within bacteriophage heads (*76*−*78*). The fluorescent intensity of the intercalated ethidium cation is not affected by increasing concentrations of cationic lipid until a specific lipid:DNA ratio is reached, upon which a large and sharp decrease of the intensity is observed. Härd et al. have demonstrated that the binding constant of ethidium cation is dependent on the molecular flexibility of DNA in linker regions of chromatin and that this flexibility is altered through cationic compaction (*79*). Thus, DNA condensation might be expected to lower the affinity of ethidium cation for DNA, and therefore, its exclusion cannot be considered to be a direct measure of a drug's binding affinity. Basu et al. also concluded that simple polyamine−DNA association was not entirely responsible for the release of ethidium cation, but that there is an associated conformational (DNA bending) change (*33*, *80*). DNA bending, induced by polyamine binding above a critical concentration, caused conformational changes within the double helix that facilitated the release of bound ethidium cation. The model for ethidium cation intercalation proposed by Sobell et al. shows the need for flexibility within the double helix of DNA to allow intercalation (*75*). Ethidium bromide exists in equilibrium between the intercalated sites and free in

solution. Therefore, loss of flexibility in the double-stranded structure of DNA through condensation will result in a shift in the binding equilibrium of ethidium cation into the solution phase, with the resultant loss in fluorescence.

Wilson and Bloomfield predicted (*81*), using the polyelectrolyte theory of Manning (*82*), that when approximately 90% of the negative (phosphate) charge on the DNA is neutralized, condensation will occur (*39*−*41*, *67*, *68*). Thus, if binding affinities of compounds causing DNA condensation are expressed in terms of the CR at which 50% (CR_{50}) of the ethidium cation fluorescence is quenched (*58*), efficient condensing agents will have CR_{50} values below 1. DNA condensation, at low salt concentrations (20 mM NaCl), is clearly an efficient process with lithocholic acid polyamine amides **11** and **12** ($CR_{50} = 0.7$ and 0.6, respectively). However, an excess of positive charges is required for cholic acid polyamine amides **13** and **14** ($CR_{50} = 2.6$ and 2.8 respectively) and for free spermine ($CR_{50} > 4.0$) to condense CT DNA, reflecting their significantly weaker binding affinities for DNA. At high salt concentrations (150 mM NaCl), DNA condensation with lithocholic acid polyamine amide **11** is salt dependent, the CR_{50} has increased from 0.7 to 4.7. The more hydrophilic cholic acid polyamine amide **13** exhibits even greater salt-dependent DNA condensation; the CR_{50} has increased from 2.6 to >12. Basu et al. have previously shown that the association of free polyamines with DNA is more sensitive to change in ionic strength than is the association of ethidium bromide with DNA (*80*). The concentration of polyamine required to release all of the intercalator dye in their studies was too high for experimental use without causing DNA aggregation (*37*, *38*, *80*). Basu and co-workers have also demonstrated that this assay is suitable for the investigation of DNA binding with simple, free polyamines, e.g., spermine **3** and thermine (norspermine) **4** where there was little fluorescence quenching at a CR of 1 (*33*, *73*, *80*). We have obtained similar results with conjugates **13** and **14** and free spermine **3** at low (20 mM NaCl) (Figure 2) and especially at high (150 mM NaCl) salt concentrations (Figure 3). Thus, while hydrophobicity is important for minor groove recognition (*83*), DNA condensation is dependent upon hydrophobicity and distance between positive charges (*84*, *85*) as well as total number of charges (*39*−*41*, *67*, *68*). These data give support to our hypotheses that both DNA binding and DNA condensation are also sensitive functions of the lipid that is covalently bound to the polyamine, as well as functions of the positively charged polyamine moiety itself. Neutral and cationic lipid-DNA interactions are a mature research area (*86*−*90*). The binding interactions between naturally occurring lipids and polynucleotides are important, and they have also been extensively studied with model membranes (*86*). The mechanisms by which these novel complexes are formed between cationic lipids and plasmid DNA have recently gained further significance with the potential of these particles in nonviral gene delivery (*87*−*90*). These new structures, both those involving cationic liposomes and those, like our studies, using cationic lipids have given rise to detailed freeze-fracture electron and atomic force microscopic studies of these particles sometimes described as "spaghetti and meatballs" (*48*, *53*, *60*, *77*, *78*, *88*, *91*−*97*). The formation of these compact particles is also directly related to the displacement of water molecules as a result of polyelectrolyte effects. Record and co-workers (*98*−*101*) have made detailed analytical studies of the effects of oligocationic ligand binding to DNA.

One mechanistic explanation of our observed self-assembly phenomena is that hydrophobic interactions between lithocholic acid moieties within **11** and **12**, but not between the more polar cholic acid moieties in **13** and **14**, cooperatively stabilize the condensed and/or condensing DNA complexes. There is some limited literature support for this possible explanation, in studies of the molecular mechanics of the complex formation of cholic acid micelles (*102*). The complex facial interactions observed with other arch-shaped or concave bile acids have been reviewed by Fuhrhop and Köning (*103*) where "micelle curvature is determined not by the hydrophobic effect, but by the molecular shape of the monomers and strong intermolecular bonding" (*103*). Regen and co-workers have recently reported, in a previous article in Bioconjugate Chem. (*104*), detailed studies on the "cloistering" of cholic acid amides due to facial effects mediated by either hydrogen bonding or van der Waals' forces between nearest-neighbors (*104*). We propose that initial charge neutralization of the polyanionic polynucleic acid by our polycationic lipo-polyammonium ions (*25*, *26*, *105*) is followed by DNA bending (*106*, *107*). After several of these bends (*106*), the induced curve is symmetrical, this is consistent with Hud's constant radius of curvature model (*77*, *78*), and adds further evidence to the microscopy pictures currently available. It has recently been shown that, depending upon the exact conditions, spermine **3** can induce condensation of DNA (*97*). Nevertheless, the key questions about any nucleotide sequence selectivity for the initial bending sites along the duplex CT DNA (*106*, *107*), and the accuracy of the constant radius of curvature model will require further experiments (*77*, *78*), preferably with designed high affinity small molecule probes and also defined DNA sequences (*38*). The polyamine amides designed and prepared herein should therefore contribute to those studies.

ACKNOWLEDGMENT

We thank the EPSRC and Celltech Chiroscience for a CASE studentship (to A.J.G.). We are grateful to a referee for helpful directions with respect to lipid−DNA interactions. We acknowledge useful discussions with Dr. Richard J. Taylor and Dr. Michael A. W. Eaton (Celltech Chiroscience), and with Dr. Ian S. Haworth (University of Southern California). I.S.B. and I.S.H. are recipients of a NATO grant (CRG 970290).

LITERATURE CITED

(1) Ganem, B. (1982) New chemistry of naturally occurring polyamines. *Acc. Chem. Res. 15*, 290−298.
(2) Tabor, C. W., and Tabor, H. (1984) Polyamines. *Annu. Rev. Biochem. 53*, 749−790.
(3) Bergeron, R. J. (1986) Methods for selective modification of spermidine and its homologues. *Acc. Chem. Res. 19*, 105−113.
(4) Behr, J.-P. (1994) Gene transfer with synthetic cationic amphiphiles: prospects for gene therapy. *Bioconjugate Chem. 5*, 382−389.
(5) Marton, L. J., and Pegg, A. E. (1995) Polyamines as targets for therapeutic intervention. *Annu. Rev. Pharmacol. Toxicol. 35*, 55−91.
(6) Blagbrough, I. S., Carrington, S., and Geall, A. J. (1997) Polyamines and polyamine amides as potent selective receptor probes, novel therapeutic lead compounds, and synthetic vectors in gene therapy. *Pharm. Sci. 3*, 223−233.
(7) Cohen, S. S. (1998) *A guide to the polyamines*, Oxford University Press, New York.
(8) Walker, S., Sofia, M. J., Kakarla, R., Kogan, N. A., Wierichs, L., Longley, C. B., Bruker, K., Axelrod, H. R., Midha, S., Babu, S., and Kahne, D. (1996) Cationic facial amphiphiles: a

promising class of transfection agents. *Proc. Natl. Acad. Sci. U.S.A. 93*, 1585−1590.
(9) Walker, S., Sofia, M. J., and Axelrod, H. R. (1998) Chemistry and cellular aspects of cationic facial amphiphiles. *Adv. Drug Delivery Rev. 30*, 61−71.
(10) Mahler, H. R., and Dutton, G. (1964) Nucleic acid interactions. V. Effects of cyclobuxine. *J. Mol. Biol. 10*, 157−175.
(11) Mahler, H. R., Goutarel, R., Khuong-Huu, Q., and Ho, M. T. (1966) Nucleic acid interactions. VI. Effects of steroidal diamines. *Biochemistry 5*, 2177−2191.
(12) Mahler, H. R., Green, G., Goutarel, R., and Khuong-Huu, Q. (1968) Nucleic acid-small molecule interactions. VII. Further characterization of deoxyribonucleic acid-diamino steroid complexes. *Biochemistry 7*, 1568−1582.
(13) Waring, M. J. (1970) Variation of the supercoils in closed circular DNA by binding of antibiotics and drugs: evidence for molecular models involving intercalation. *J. Mol. Biol. 54*, 247−279.
(14) Wieland, H., and Alles, R. (1922) Poisonous substance of toads. *Chem. Ber. 55*, 1789−1798.
(15) Wieland, H., and Behringer, H. (1941) Toad poisons. (XI). Constitution of bufotalin. *Liebigs Ann. 549*, 209−237.
(16) Pettit, G. R., Kamano, Y., Drasar, P., Inoue, M., and Knight, J. C. (1987) Steroids and related natural-products. 104. Synthesis of Bufalitoxin and Bufotoxin. 36. Bufadienolides. *J. Org. Chem. 52*, 3573−3578.
(17) Janout, V., Lanier, M., and Regen, S. L. (1996) Molecular umbrellas. *J. Am. Chem. Soc. 118*, 1573−1574.
(18) Janout, V., Lanier, M., and Regen, S. L. (1997) Design and synthesis of molecular umbrellas. *J. Am. Chem. Soc. 119*, 640−647.
(19) DeLong, R. K., Yoo, H., Alahari S. K., Fisher, M., Short, S. M., Kang, S. H., Kole, R., Janout. V., Regan, S. L., and Juliano, R. L. (1999) Novel cationic amphiphiles as delivery agents for antisense oligonucleotides. *Nucleic Acids Res. 27*, 3334−3341.
(20) Moore, K. S., Wehrli, S., Roder, H., Rogers, M., Forrest, J. N., McCrimmon, D., and Zasloff, M. (1993) Squalamine - an aminosterol antibiotic from the shark. *Proc. Natl. Acad. Sci. U.S.A. 90*, 1354−1358.
(21) Moriarty, R. M., Tuladhar, S. M., Guo, L., and Wehrli, S. (1994) Synthesis of squalamine. A steroidal antibiotic from the shark. *Tetrahedron Lett. 35*, 8103−8106.
(22) Moriarty, R. M., Enache, L. A., Kinney, W. A., Allen, C. S., Canary, J. W., Tuladhar, S. M., and Guo, L. (1995) Stereoselective synthesis of squalamine dessulfate. *Tetrahedron Lett. 36*, 5139−5142.
(23) Sadownik, A., Deng, G., Janout, V., and Regen, S. L. (1995) Rapid construction of a squalamine mimic. *J. Am. Chem. Soc. 117*, 6138−6139.
(24) Geall, A. J., Al-Hadithi, D., and Blagbrough, I. S. (1998) Spermine and thermine conjugates of cholic acid condense DNA, but lithocholic acid polyamine conjugates do so more efficiently. *Chem. Commun.* 2035−2036.
(25) Geall, A. J., Taylor, R. J., Earll, M. E., Eaton, M. A. W., and Blagbrough, I. S. (2000) Synthesis of cholesteryl polyamine carbamates: pK_a studies and condensation of calf thymus DNA. *Bioconjugate Chem. 11*, 314−326.
(26) Geall, A. J., and Blagbrough, I. S. (2000) Homologation of polyamines in the rapid synthesis of lipospermine conjugates and related lipoplexes. *Tetrahedron 56*, 2449−2460.
(27) Blagbrough, I. S., and Geall, A. J. (1998) Practical synthesis of unsymmetrical polyamine amides. *Tetrahedron Lett. 39*, 439−442.
(28) Geall, A. J., and Blagbrough, I. S. (1998) Homologation of polyamines in the synthesis of lipo-spermine conjugates and related lipoplexes. *Tetrahedron Lett. 39*, 443−446.
(29) Geall, A. J., Taylor, R. J., Earll, M. E., Eaton, M. A. W., and Blagbrough, I. S. (1998) Synthesis of cholesterol-polyamine carbamates: pK_a studies and condensation of calf thymus DNA. *Chem. Commun.* 1403−1404 and 1607.
(30) Blagbrough, I. S., Al-Hadithi, D., and Geall, A. J. (1999) DNA condensation by bile acid conjugates of thermine and spermine. *Pharm. Pharmacol. Commun. 5*, 139−144.
(31) Geall, A. J., and Blagbrough, I. S. (1999) DNA condensation by cholesterol polyamine carbamates. *Pharm. Pharmacol. Commun. 5*, 145−150.
(32) Geall, A. J., Eaton, M. A. W., Baker, T., Catterall, C., and Blagbrough, I. S. (1999) The regiochemical distribution of positive charges along cholesterol polyamine carbamates plays significant roles in modulating DNA binding affinity and lipofection. *FEBS Lett. 459*, 337−342.
(33) Basu, H. S., and Marton, L. J. (1987) The interaction of spermine and pentamines with DNA. *Biochem. J. 244*, 243−246.
(34) Thomas, T. J., and Messner, R. P. (1988) Structural specificity of polyamines in left-handed Z-DNA formation: immunological and spectroscopic studies. *J. Mol. Biol. 201*, 463−467.
(35) Thomas, T. J., Gunnia, U. B., and Thomas, T. (1991) Polyamine-induced B-DNA to Z-DNA conformational transition of a plasmid DNA with $(dG\text{-}dC)_n$ insert. *J. Biol. Chem. 266*, 6137−6141.
(36) Schneider, H.-J., and Blatter, T. (1992) Interactions between acyclic and cyclic peralkylammonium compounds and DNA. 33. *Angew. Chem., Int. Ed. Engl. 31*, 1207−1208.
(37) Pelta, J., Livolant, F., and Sikorav, J.-L. (1996) DNA aggregation induced by polyamines and cobalthexamine. *J. Biol. Chem. 271*, 5656−5662.
(38) Saminathan, M., Antony, T., Shirahata, A., Sigal, L. H., Thomas, T., and Thomas, T. J. (1999) Ionic and structural specificity effects of natural and synthetic polyamines on the aggregation and resolubilization of single-, double-, and triple-stranded DNA. *Biochemistry 38*, 3821−3830.
(39) Bloomfield, V. A. (1991) Condensation of DNA by multivalent cations - considerations on mechanism. *Biopolymers 31*, 1471−1481.
(40) Bloomfield, V. A. (1996) DNA condensation. *Curr. Opin. Struct. Biol. 6*, 334−341.
(41) Bloomfield, V. A. (1997) DNA condensation by multivalent cations. *Biopolymers 44*, 269−282.
(42) Behr, J.-P., Demeneix, B., Loeffler, J.-P., and Perez-Mutul, J. (1989) Efficient gene transfer into mammalian primary endocrine cells with lipopolyamine-coated DNA. *Proc. Natl. Acad. Sci. U.S.A. 86*, 6982−6986.
(43) Guy-Caffey, J. K., Bodepudi, V., Bishop, J. S., Jayaraman, K., and Chaudhary, N. (1995) Novel polyaminolipids enhance the cellular uptake of oligonucleotides. *J. Biol. Chem. 270*, 31391−31396.
(44) Lee, E. R., Marshall, J., Siegel, C. S., Jiang, C., Yew, N. S., Nichols, M. R., Nietupski, J. B., Ziegler, R. J., Lane, M. B., Wang, K. X., Wan, N. C., Scheule, R. K., Harris, D. J., Smith, A. E., and Cheng, S. H. (1996) Detailed analysis of structures and formulations of cationic lipids for efficient gene transfer to the lung. *Hum. Gene Ther. 7*, 1701−1717.
(45) Moradpour, D., Schauer, J. I., Zurawski, V. R., Jr., Wands, J. R., and Boutin, R. H. (1996) Efficient gene transfer into mammalian cells with cholesteryl-spermidine. *Biochem. Biophys. Res. Commun. 221*, 82−88.
(46) Bischoff, R., Cordier, Y., Perraud, F., Thioudellet, C., Braun, S., and Pavirani, A. (1997) Transfection of myoblasts in primary culture with isomeric cationic cholesterol derivatives. *Anal. Biochem. 254*, 69−81.
(47) Byk, G., Dubertret, C., Escriou, V., Frederic, M., Jaslin, G., Rangara, R., Pitard, B., Crouzet, J., Wils, P., Schwartz, B., and Scherman, D. (1998) Synthesis, activity, and structure−activity relationship studies of novel cationic lipids for DNA transfer. *J. Med. Chem. 41*, 224−235.
(48) Remy, J.-S., Abdallah, B., Zanta, M. A., Boussif, O., Behr, J.-P., and Demeneix, B. (1998) Gene transfer with lipospermines and polyethylenimines. *Adv. Drug Delivery Rev. 30*, 85−95.
(49) Hebling-Leclerc, A., Scherman, D., and Wils, P. (1999) Cellular uptake of cationic lipid/DNA complexes by cultured myoblasts and myotubes. *Biochim. Biophys. Acta 1418*, 165−175.
(50) Crystal, R. G. (1995) Transfer of genes to humans. Early lessons and obstacles to success. *Science 270*, 404−410.
(51) Felgner, P. L. (1997) Nonviral strategies for gene therapy. *Sci. Am. 276*, 86−90.

(52) O'Driscoll, C. (1997) Gene geniuses. *Chem. Brit. 33*, 66−69.
(53) Mahato, R. I., Rolland, A., and Tomlinson, E. (1997) Cationic lipid-based gene delivery systems: pharmaceutical perspectives. *Pharm. Res. 14*, 853−859.
(54) Verma, I. M., and Somia, N. (1997) Gene therapy - promises, problems and prospects. *Nature 389*, 239−242.
(55) Hsieh, H.-P., Muller, J. G., and Burrows, C. J. (1994) Structural effects in novel steroidal polyamine-DNA binding. *J. Am. Chem. Soc. 116*, 12077−12078.
(56) Hsieh, H.-P., Muller, J. G., and Burrows, C. J. (1995) Synthesis and DNA binding properties of C3-, C12-, and C24-substituted amino-steroids derived from bile acids. *Bioorg. Med. Chem. 3*, 823−835.
(57) Muller, J. G., Ng, M. M. P., and Burrows, C. J. (1996) Hydrophobic vs Coulombic interactions in the binding of steroidal polyamines to DNA. *J. Mol. Recognit. 9*, 143−148.
(58) Felgner, P. L., Barenholz, Y., Behr, J.-P., Cheng, S. H., Cullis, P., Huang, L., Jessee, J. A., Seymour, L., Szoka, F., Thierry, A. R., Wagner, E., and Wu, G. (1997) Nomenclature for synthetic gene delivery systems. *Hum. Gene Ther. 8*, 511−512.
(59) Cain, B. F., Baguley, B. C., and Denny, W. A. (1978) Potential antitumor agents. 28. Deoxyribonucleic acid polyintercalating agents. *J. Med. Chem. 21*, 658−668.
(60) Gershon, H., Ghirlando, R., Guttman, S. B., and Minsky, A. (1993) Mode of formation and structural features of DNA-cationic liposome complexes used for transfection. *Biochemistry 32*, 7143−7151.
(61) *Tables of Spectral Data for Structure Determination of Organic Compounds* (1989) 2nd ed., pp C5−C177 and H15−H80, Springer-Verlag, Berlin.
(62) Waterhous, D. V., Barnes, S., and Muccio, D. D. (1985) Nuclear magnetic resonance spectroscopy of bile acids. Development of two-dimensional NMR methods for the elucidation of proton resonance assignments for five common hydroxylated bile acids, and their parent bile acid, 5β-cholanoic acid. *J. Lipid Res. 26*, 1068−1078.
(63) Adlam, G., Blagbrough, I. S., Taylor, S., Latham, H. C., Haworth, I. S., and Rodger, A. (1994) Multiple binding modes with DNA of anthracene-9-carbonyl-N^1-spermine probed by LD, CD, normal absorption, and molecular modelling compared with those of spermidine and spermine. *Bioorg. Med Chem. Lett. 4*, 2435−2440.
(64) Rodger, A., Blagbrough, I. S., Adlam, G., and Carpenter, M. L. (1994) DNA binding of spermine derivatives: spectroscopic study of anthracene-9-carbonyl-N^1-spermine with poly[d(G−C).d(G−C)] and poly[d(A−T).d(A−T)]. *Biopolymers 34*, 1583−1593.
(65) Rodger, A., Taylor, S., Adlam, G., Blagbrough, I. S., and Haworth, I. S. (1995) Multiple DNA-binding modes of anthracene-9-carbonyl-*N*1 spermine. *Bioorg. Med. Chem. 3*, 861−872.
(66) Blagbrough, I. S., Taylor, S., Carpenter, M. L., Novoselskiy, V., Shamma, T., and Haworth, I. S. (1998) Asymmetric intercalation of *N*1-(acridin-9-ylcarbonyl)spermine at homopurine sites of duplex DNA. *Chem. Commun.* 929−930.
(67) Tam, S. C., and Williams, R. J. P. (1985) Electrostatics and biological systems. *Struct. Bonding 63*, 103−151.
(68) Rowatt, E., and Williams, R. J. P. (1992) The binding of spermine and magnesium to DNA. *J. Inorg. Biochem. 46*, 87−97.
(69) Braithwaite, A. W., and Baguley, B. C. (1980) Existence of an extended series of antitumor compounds which bind to deoxyribonucleic acid by nonintercalative means. *Biochemistry 19*, 1101−1106.
(70) Stewart, K. D. (1988) The effect of structural changes in a polyamine backbone on its DNA-binding properties. *Biochem. Biophys. Res. Commun. 152*, 1441−1446.
(71) Edwards, M. L., Snyder, R. D., and Stemerick, D. M. (1991) Synthesis and DNA-binding properties of polyamine analogues. *J. Med. Chem. 34*, 2414−2420.
(72) Stewart, K. D., and Gray, T. A. (1992) Survey of the DNA binding properties of natural and synthetic polyamino compounds. *J. Phys. Org. Chem. 5*, 461−466.
(73) Delcros, J.-G., Sturkenboom, M. C. J. M., Basu, H. S., Shafer, R. H., Szöllösi, J., Feuerstein, B. G., and Marton, L. J. (1993) Differential effects of spermine and its analogues on the structures of polynucleotides complexed with ethidium bromide. *Biochem. J. 291*, 269−274.
(74) Cai, J., Soloway, A. H., Barth, R. F., Adams, D. M., Hariharan, J. R., Wyzlic, I. M., and Radcliffe, K. (1997) Boron-containing polyamines as DNA targeting agents for neutron capture therapy of brain tumors: synthesis and biological evaluation. *J. Med. Chem. 40*, 3887−3896.
(75) Sobell, H. M., Tsai, C.-C., Jain, S. C., and Gilbert, S. G. (1977) Visualization of drug-nucleic acid interactions at atomic resolution. *J. Mol. Biol. 114*, 333−365.
(76) Widom, J., and Baldwin, R. L. (1980) Cation-induced toroidal condensation of DNA. Studies with $Co^{3+}(NH_3)_6$. *J. Mol. Biol. 144*, 431−453.
(77) Hud, N. V., Downing, K. H., and Balhorn, R. (1995) A constant radius of curvature model for the organization of DNA in toroidal condensates. *Proc. Natl. Acad. Sci. U.S.A. 92*, 3581−3585.
(78) Hud, N. V. (1995) Double-stranded DNA organization in bacteriophage heads: An alternative toriod-based model. *Biophys. J. 69*, 1355−1362.
(79) Härd, T., Nielsen, P. E., and Norden, B. (1988) Molecular flexibility of extended and compacted polynucleosomes - a steady-state fluorescence polarization study. *Eur. J. Biophys. 16*, 231−242.
(80) Basu, H. S., Schwietert, H. C. A., Feuerstein, B. G., and Marton, L. J. (1990) Effects of variation in the structure of spermine on the association with DNA and the induction of DNA conformational changes. *Biochem. J. 269*, 329−334.
(81) Wilson, R. W., and Bloomfield, V. A. (1979) Counterion-induced condensation of deoxyribonucleic acid. A light-scattering study. *Biochemistry 18*, 2192−2196.
(82) Manning, G. S. (1978) The molecular theory of polyelectrolyte solutions with applications to the electrostatic properties of polynucleotides. *Q. Rev. Biophys. 11*, 179−246.
(83) Haq, I., Ladbury, J. E., Chowdhry, B. Z., Jenkins, T. C., and Chaires, J. B. (1997) Specific binding of Hoechst 33258 to the $d(CGCAAATTTGCG)_2$ duplex: calorimetric and spectroscopic studies. *J. Mol. Biol. 271*, 244−257.
(84) Mahler, H. R., and Mehrotra, B. D. (1963) The interaction of nucleic acids with diamines. *Biochim. Biophys. Acta 68*, 211−233.
(85) Yoshikawa, Y., and Yoshikawa, K. (1995) Diaminoalkanes with an odd number of carbon atoms induce compaction of a single double-stranded DNA chain. *FEBS Lett. 361*, 277−281.
(86) Budker, V. G., Godovikov, A. A., Naumova, L. P., and Slepneva, I. A. (1980) Interaction of polynucleotides with natural and model membranes. *Nucleic Acids Res. 8*, 2499−2515.
(87) Smith J. G., Walzem, R. L., and German, J. B. (1993) Liposomes as agents of DNA transfer. *Biochim. Biophys. Acta 1154*, 327−340.
(88) Sternberg, B., Sorgi, F. L., and Huang, L. (1994) New structures in complex formation between DNA and cationic liposomes visualized by freeze-fracture electron microscopy. *FEBS Lett. 356*, 361−366.
(89) Reimer, D. L., Zhang, Y., Kong, S., Wheeler, J. J., Graham, R. W., and Bally, M. B. (1995) Formation of novel hydrophobic complexes between cationic lipids and plasmid DNA. *Biochemistry 34*, 12877−12883.
(90) Bally, M. B., Zhang, Y. P., Wong, F. M. P., Kong, S., Wasan, E., and Reimer, D. L. (1997) Lipid/DNA complexes as an intermediate in the preparation of particles for gene transfer: an alternative to cationic liposome/DNA aggregates. *Adv. Drug Delivery Rev. 24*, 275−290.
(91) Gosule, L. C., and Schellmann, J. A. (1976) Compact form of DNA induced by spermidine. *Nature 259*, 333−335.
(92) Gosule, L. C., and Schellmann, J. A. (1978) DNA condensation with polyamines I. Spectroscopic studies. *J. Mol. Biol. 121*, 311−327.
(93) Chattoraj, D. K., Gosule, L. C., and Schellmann, J. A. (1978) DNA condensation with polyamines II. Electron microscopic studies. *J. Mol. Biol. 121*, 327−337.

(94) Mou, J., Czajkowsky, D. M., Zhang, Y., and Shao, Z. (1995) High-resolution atomic-force microscopy of DNA: the pitch of the double helix. *FEBS Lett. 371*, 279−282.

(95) Hansma, H. G., Golan, R., Hsieh, W., Lollo, C. P., Mullen-Ley, P., and Kwoh, D. (1998) DNA condensation for gene therapy as monitored by atomic force microscopy. *Nucleic Acids Res. 26*, 2481−2487.

(96) Lin, Z., Wang, C., Feng, X., Liu, M., Li, J., and Bai, C. (1998) The observation of the local ordering characteristics of spermidine-condensed DNA: atomic force microscopy and polarizing microscopy studies. *Nucleic Acids Res. 26*, 3228−3234.

(97) Böttcher, C., Endisch, C., Fuhrhop, J.-H., Catterall, C., and Eaton, M. (1998) High-yield preparation of oligomeric C-type DNA toroids and their characterization by cryoelectron microscopy. *J. Am. Chem. Soc. 120*, 12−17.

(98) Anderson, C. F., and Record M. T. (1995) Salt nucleic acid interactions. *Annu. Rev. Phys. Chem. 46*, 657−700.

(99) Zhang, W., Bond, J. P., Anderson, C. F., Lohman, T. M., and Record, M. T. (1996) Large electrostatic differences in the binding thermodynamics of a cationic peptide to oligomeric and polymeric DNA. *Proc. Natl. Acad. Sci. U.S.A. 93*, 2511−2516.

(100) Record, M. T., Zhang, W. T., and Anderson, C. F. (1998) Analysis of effects of salts and uncharged solutes on protein and nucleic acid equilibria and processes: a practical guide to recognizing and interpreting polyelectrolyte effects, Hofmeister effects, and osmotic effects of salts. *Adv. Protein Chem. 51*, 281−353.

(101) Zhang, W. T., Ni, H. H., Capp, M. W., Anderson, C. F., Lohman, T. M., and Record M. T. (1999) The importance of Coulombic end effects: experimental characterization of the effects of oligonucleotide flanking charges on the strength and salt dependence of oligocation (L8+) binding to single-stranded DNA oligomers. *Biophys. J. 76*, 1008−1017.

(102) Jou, W. S., and Chun, P. W. (1991) Molecular mechanics of the formation of cholic acid micelles. *J. Mol. Graphics 9*, 237−246.

(103) Fuhrhop, J.-H., and Köning, J. (1994) in *Membranes and Molecular Assemblies: The Synkinetic Approach*, pp 34−36 and 203−204, RSC, Cambridge, U.K.

(104) Zhang, L.-H., Janout, V., Renner, J. L., Uragami, M., and Regen S. L. (2000) Enhancing the "stickiness" of bile acids to cross-linked polymers: a bioconjugate approach to the design of bile acid sequestrants. *Bioconjugate Chem. 11*, 397−400.

(105) Geall, A. J., Al-Hadithi, D., and Blagbrough, I. S. (2000) Cheno-, urso- and deoxycholic acid spermine conjugates: relative binding affinities for calf thymus DNA. *Tetrahedron 56*, 3439−3447.

(106) Rouzina, I., and Bloomfield, V. A. (1998) DNA bending by small, mobile multivalent cations. *Biophys. J. 74*, 3152−3164.

(107) Shen, M. R., Downing, K. H., Balhorn, R., and Hud, N. V. (2000) Nucleation of DNA condensation by static loops: formation of DNA toroids with reduced dimensions. *J. Am. Chem. Soc. 122*, 4833−4834.

BC000093+

Control of Radioactivity Pharmacokinetics of ^{99m}Tc−HYNIC-Labeled Polypeptides Derivatized with Ternary Ligand Complexes

Masahiro Ono,[†] Yasushi Arano,[‡] Takahiro Mukai,[§] Tsuneo Saga,[§] Yasushi Fujioka,[†] Kazuma Ogawa,[†] Hidekazu Kawashima,[†] Junji Konishi,[§] and Hideo Saji*,[†]

Department of Patho-Functional Bioanalysis, Graduate School of Pharmaceutical Sciences, Kyoto University, Yoshida Shimoadachi-cho, Sakyo-ku, Kyoto 606-8501, Department of Molecular Imaging and Radiotherapy, Graduate School of Pharmaceutical Sciences, Chiba University, 1-33 Yayoi-cho, Inage-ku, Chiba 263-8522, and Department of Nuclear Medicine and Diagnostic Imaging, Graduate School of Medicine, Kyoto University, Shogoin Kawahara-cho, Sakyo-ku, Kyoto 606-8507, Japan. Received March 28, 2001; Revised Manuscript Received October 23, 2001

An enhancement of the target/nontarget ratio of radioactivity levels enables reliable diagnosis and therapy using polypeptide radiopharmaceuticals in nuclear medicine. In the present study, we investigated the effects of the physicochemical properties of radiometabolites on the radioactivity pharmacokinetics after administration of ^{99m}Tc-labeled polypeptides using 6-hydrazinopyridine-3-carboxylic acid (HYNIC). Four ternary ligands (L) [3-benzoylpyridine (BP), 3-acetylpyridine (AP), 3-nicotinic acid (NIC), pyridine (PY)] with different lipophilicity were selected as coligands for the preparation of ^{99m}Tc−HYNIC-polypeptides. Each of the ternary ligands tested provided ^{99m}Tc−HYNIC-labeled galactosyl-neoalbumin (NGA) and Fab fragments of high stability with high radiochemical purity. Moreover, after administration of each ^{99m}Tc−HYNIC-labeled NGA into normal mice, the respective ternary ligand [^{99m}Tc](HYNIC−lysine)(tricine)(L) complexes were generated as final radiometabolites in the hepatic lysosome. The partition coefficients of [^{99m}Tc](HYNIC−lysine)(tricine)-(BP), [^{99m}Tc](HYNIC−lysine)(tricine)(AP), [^{99m}Tc](HYNIC−lysine)(tricine)(NIC), and [^{99m}Tc](HYNIC−lysine)(tricine)(PY) were determined to be −2.21, −2.37, −2.93, and −2.73, respectively. Elimination rates of these radiometabolites from the lysosome were enhanced in the order of increasing lipophilicity of the radiometabolites. After injection of the four ^{99m}Tc−HYNIC-labeled Fab fragments into normal mice, blood clearances of radioactivity were similar while radioactivity elimination rates from the kidney were enhanced in the order of increasing lipophilicity of the radiometabolites. The present study indicated that the lipophilicity of the radiometabolites constitutes one important factor affecting their elimination rates from the tissues. Thus, as ternary ligands facilitate alteration of the physicochemical properties of radiometabolites, the use of ternary ligand complexes might be applicable for controlling the pharmacokinetics of ^{99m}Tc-labeled polypeptides.

INTRODUCTION

Radiopharmaceuticals derived from polypeptides and peptides have been shown to be useful for both diagnostic and therapeutic applications. However, high-level and prolonged retention of radioactivity has been observed in nontarget tissues such as the liver and kidney when these radiopharmaceuticals are administered. This results in a high background radioactivity in imaging diagnosis and also increases the radiation dose to the patients, thus limiting their therapeutic uses.

To decrease the radioactivity levels in nontarget tissues, attempts to conjugate polypeptides with a radiolabel via a metabolizable linkage have been made (*1*−*5*). However, the following criteria should be addressed for application of radiolabeling reagents with a metabolizable linkage to polypeptides. One important point is whether the radiolabeled compound released from the polypeptides by cleavage of the labile bond can rapidly penetrate the lysosomal membrane. Another point to be considered is whether the metabolizable linkage is stable enough in plasma so as not to impair the radioactivity in the target delivered by the polypeptides. Although radiolabeling reagents with a metabolizable linkage satisfy these criteria, they cannot be applied to polypeptides that are internalized within target cells.

Another solution to the high radioactivity levels in nontarget tissues appears to be the chemical modification of polypeptides and peptides. This strategy involves modification of isoelectric points of (poly)peptides by acylating amine residues, attachment of negatively charged polymer, or substitution of N-terminal amino acid with an acidic amino acid (*6*−*9*). Although these methods can be applied to polypeptides that are internalized within target cells, long-term retention of the radioactivity in the target tissues is required for further enhancement of the target/nontarget ratio.

Recent studies on the metabolism of radiolabeled polypeptides have shown that in vivo behaviors of radiometabolites generated after lysosomal proteolysis play a critical role in determining the radioactivity levels in tissues (*10*−*13*). These findings provide the following approaches to enhance the target/nontarget ratio of

* To whom correspondence should be addressed. Telephone: 81−75−753−4567; fax: 81−75−753−4568; e-mail: hsaji@pharm.kyoto-u.ac.jp.

[†] Department of Patho-Functional Bioanalysis, Graduate School of Pharmaceutical Sciences, Kyoto University.

[‡] Chiba University.

[§] Department of Nuclear Medicine and Diagnostic Imaging, Graduate School of Medicine, Kyoto University.

10.1021/bc010043k CCC: $22.00 © 2002 American Chemical Society
Published on Web 04/09/2002

radioactivity level. When applied to polypeptides such as antibodies against solid tumors, which are not or are only slowly internalized within target cells, generation of radiometabolites that are eliminated rapidly from the tissues constitutes one useful approach. Radiolabeled polypeptides remain bound to the surface of target cells, while their radiometabolites generated after lysosomal proteolysis are eliminated rapidly from nontarget tissues. As a consequence, the target/nontarget ratio is increased. On the other hand, when applied to internalizable (poly)-peptides within target cells, generation of radiometabolites that are eliminated slowly from the tissues would be required to prolong radioactivity retention in target tissues. Therefore, it is important for enhancement of the target/nontarget ratio to control the in vivo behaviors of radiometabolites generated after lysosomal proteolysis of polypeptide radiopharmaceuticals regardless of whether the parental molecules are internalized into target cells. However, the relationships between the physicochemical properties of radiometabolites and their elimination rates from the tissues remain unclear.

6-Hydrazinopyridine-3-carboxylic acid (HYNIC) is a representative agent used to prepare technetium-99m (^{99m}Tc)-labeled (poly)peptides with tricine as a coligand (*14*−*18*). However, it was found that the complex [^{99m}Tc]-(HYNIC)(tricine)$_2$, which is not stable and exists as multiple species, could affect the pharmacokinetics of ^{99m}Tc-labeled (poly)peptides and their radiometabolites due to exchange reaction of tricine with protein in the plasma and tissues (*19*−*22*). To decrease the problems associated with ^{99m}Tc−HYNIC-labeled small peptides, Liu et al. exploited several pyridine derivatives as ternary ligands to form ternary ligand complexes, [^{99m}Tc](HYNIC-peptide)(tricine)(pyridine derivative), with high stability and fewer isomers (*23*). On the basis of these findings, we applied a preformed chelate of tetrafluorophenol active ester of the ternary ligand complex [^{99m}Tc](HYNIC)-(tricine)[3-benzoylpyridine (BP)] to prepare ^{99m}Tc-labeled polypeptides (24). Our previous study using galactosyl-neoglycoalbumin (NGA) indicated that [^{99m}Tc](HYNIC−lysine)(tricine)(BP) was generated as a major radiometabolite in the liver and that the binding of this metabolite with lysosomal proteins was low. In addition, little plasma protein binding was observed in ^{99m}Tc−HYNIC-labeled Fab fragment derivatized with this ternary ligand complex. These findings indicated that the pyridine derivatives could serve as highly stable coligands for preparing ^{99m}Tc−HYNIC-labeled polypeptides and that the use of various pyridine derivatives would generate radiometabolites with different physicochemical properties in the tissues.

In the present study, four pyridine derivatives [BP, 3-acetylpyridine (AP), 3-nicotinic acid (NIC) and pyridine (PY)] with different lipophilicity were selected as ternary ligands to prepare ^{99m}Tc−HYNIC-labeled polypeptides. We investigated the effects of lipophilicity of the radiometabolites on the radioactivity pharmacokinetics after injection of ^{99m}Tc−HYNIC-labeled NGA. In addition, the radioactivity elimination from the kidney after injection of four ^{99m}Tc−HYNIC-labeled Fab fragments was also estimated along with the blood clearance.

MATERIALS AND METHODS

Reagents and Chemicals. [^{99m}Tc]Pertechnetate ($^{99m}TcO_4^-$) was eluted in saline solution on a daily basis from Daiichi Radioisotope Laboratory generators (Chiba, Japan). Na[^{125}I] was obtained from the Daiichi Kagaku (Tokyo, Japan) and was diluted with 0.1 M phosphate buffer (pH 7.4) to 3.7 MBq/μL. Reversed phase high performance liquid chromatography (RP-HPLC) was performed with a Cosmosil 5 C_{18}-AR-300 column (4.6 × 150 mm, Nacalai Tesque, Kyoto, Japan) at a flow rate of 1.0 mL/min with a gradient mobile phase starting from 90% A (0.1% aqueous trifluoroacetic acid) and 10% B (acetonitrile with 0.1% trifluoroacetic acid) to 50% A and 50% B at 20 min and to 100% B at 30 min (solvent system 1). RP-HPLC was also performed with a gradient mobile phase starting from 100% A to 100% B in 30 min (solvent system 2). Size-exclusion HPLC (SE-HPLC) was performed using a 5 Diol-300 column (7.5 × 600 mm, Nacalai Tesque) connected to a 5 Diol-300 guard column (7.5 × 50 mm, Nacalai Tesque), eluted with 0.1 M phosphate buffer (pH 6.8) at a flow rate of 1 mL/min. The eluent was collected with a fraction collector (RediFrac; Pharmacia Biotech, Tokyo, Japan) at 30-s intervals, and the radioactivity levels in each fraction (500 μL) were determined with an auto well counter (ARC-2000; Aloka, Tokyo). The radioactivity of liver homogenates was analyzed by gel permeation chromatography (GPC) using a Sephadex G-50 (Pharmacia Biotech) column (18 × 400 mm) equilibrated and eluted with 0.1 M phosphate buffer (pH 6.8) at a flow rate of 1 mL/min. The eluent was collected with a fraction collector at 2.5-min intervals, and the radioactivity levels in each fraction (2.5 mL) were measured with an auto well counter. TLC analyses were performed with silica plates (Merck Art 5553) with a mixture of 10% aqueous ammonium chloride−methanol (1:1) or saline as the developing solvent. Cellulose acetate electrophoresis (CAE) strips were run in veronal buffer (pH 8.6, $I = 0.05$) at a constant current of 0.8 mA for 30 min. Proton nuclear magnetic resonance (^{1}H NMR) spectra were recorded on a Bruker AC-200 spectrometer, and the chemical shifts are reported in ppm downfield from an internal tetramethylsilane standard. Fast atom bombardment mass spectra (FAB-MS) were obtained with a JMS−HX/HX 110 A model (JEOL Ltd., Tokyo, Japan). Tricine, BP, AP, NIC, and PY were purchased from Nacalai Tesque, and other reagents were of reagent grade and used as received. To facilitate collection of urine and feces after administration of radiolabeled polypeptides, mice were housed in metabolic cages (Metabolica, MM type; Sugiyama-Gen Iriki Co. Ltd., Tokyo, Japan).

Synthesis of Galactosyl-neoglycoalbumin (NGA). Cyanomethyl-2,3,4,6-tetra-*O*-acetyl-1-β-galactopyranoside, synthesized according to the procedure of Lee et al. (*25*), was conjugated with human serum albumin (HSA, A-3782; Sigma Co. St. Louis, MO), according to the procedure of Stowell et al. (*26*). The phenol−sulfuric acid reaction (*27*) indicated that 43 galactose units were attached to each HSA molecule.

Tumor and Monoclonal Antibodies. KT005-cloned human osteogenic sarcoma was maintained by serial sc transplantation in athymic mice. Pieces of tumor tissue (~0.5 g) at ~2.5 weeks postimplantation were used for the in vivo study**.** The monoclonal antibody against osteogenic sarcoma (OST7, IgG_1), generated by the standard hybridoma technique, was purified by ammonium sulfate precipitation with subsequent protein A affinity chromatography (Pharmacia Biotech), as reported previously (*28*). The Fab fragment was prepared by the standard procedure using papain (*29*).

Synthesis of ^{99m}Tc−HYNIC Ternary Ligand Complexes. 2,3,5,6-Tetrafluorophenyl 6-hydrazinopyridine-3-carboxylate (HYNIC-TFP) was synthesized according to the procedure described previously (*24*). To a 2 mL vial were added 30 μL of HYNIC-TFP (3 mg/mL in isopropyl

alcohol), 200 μL of tricine solution (30 mg/mL in 10 mM citrate buffer, pH 5.2), 100 μL of ternary ligand solution (10 mg/mL in 10 mM citrate buffer, pH 5.2), 100 μL of $^{99m}TcO_4^-$ solution (10 mCi/mL in saline), and 25 μL of $SnCl_2 \cdot 2H_2O$ solution (1.0 mg/mL in 0.1 N HCl). The reaction mixture was heated at 95 °C for 15 min followed by cooling on ice for 10 min. Then, the reaction mixture was analyzed by RP-HPLC (solvent system 1).

Radiolabeling of Polypeptides. To a solution of NGA 100 μL (5.0 mg/mL in 0.1 M carbonate buffer, pH 9.0) was added an equal volume of ternary ligand [^{99m}Tc](HYNIC−TFP) complex solution, and the mixture was incubated for 1 h at room temperature. [^{99m}Tc]-(HYNIC−NGA) conjugate was purified by the centrifuged column procedure using Sephadex G-50 equilibrated and eluted with 0.1 M phosphate buffer (pH 7.4). Ternary ligand [^{99m}Tc](HYNIC−Fab) conjugates were prepared according to the procedure described above using 100 μL of Fab solution (5.0 mg/mL in 1 M carbonate buffer, pH 10.0) in place of NGA. Radiochemical yields were assessed by SE-HPLC, CAE, and TLC developed with saline. The levels of HYNIC molecules conjugated per NGA and Fab were determined by measuring the hydrazino groups with *p*-nitrobenzaldehyde according to the method of King et al. (*30*). [^{99m}Tc](HYNIC−Fab)(tricine)$_2$ was prepared by conjugation of 6-hydrazinopyridine-3-carboxylate hydrochloride with Fab fragments, followed by ^{99m}Tc radiolabeling with [^{99m}Tc](tricine)$_2$, according to the procedure described previously (*22*). Direct radioiodination of Fab fragments was performed by the chloramine T method according to the procedure described previously (*4*).

Synthesis of Ternary Ligand [^{99m}Tc](HYNIC−Lysine) Complexes. HYNIC−lysine was synthesized according to the method described previously (*21*). To a 2 mL vial was added 30 μL of HYNIC−lysine (3 mg/mL in 10 mM citrate buffer, pH 5.2), 200 μL of tricine solution (30 mg/mL in 10 mM citrate buffer, pH 5.2), 100 μL of ternary ligand solution (10 mg/mL in 10 mM citrate buffer, pH 5.2), 100 μL of $^{99m}TcO_4^-$ solution (370 MBq/mL in saline), and 25 μL of $SnCl_2 \cdot 2H_2O$ solution (1.0 mg/mL in 0.1 N HCl). The reaction mixture was heated at 95 °C for 15 min. After being cooled at room temperature for 10 min, the reaction mixture was analyzed by RP-HPLC (solvent system 2), CAE, and TLC developed with a mixture of 10% aqueous ammonium chloride−methanol (1:1).

Partition Coefficients of Ternary Ligand [^{99m}Tc]-(HYNIC−Lysine) Complexes. The partition coefficient was measured by mixing each ternary ligand [^{99m}Tc]-(HYNIC−lysine) complex with 3 mL each of 1-octanol and 0.1 M phosphate-buffered saline (pH 4.75). These tubes were left for 20 min at room temperature and then centrifuged for 5 min. Two precisely measured samples (1.0 mL each) from the 1-octanol and buffer layers were counted for radioactivity. The partition coefficient was then determined by calculating the ratio of the radioactivity of the octanol layer to that of the buffer layer.

Plasma Stability of ^{99m}Tc-Labeled Polypeptides. [^{99m}Tc](HYNIC−NGA) conjugates or [^{99m}Tc](HYNIC−Fab) conjugates were diluted 20-fold with freshly prepared murine plasma, and the solution was incubated at 37 °C for 24 h. After 24 h incubation, the radioactivity of each [^{99m}Tc](HYNIC−Fab) conjugate was analyzed by SE-HPLC. After 1, 3, 6, and 24 h incubation, the radioactivity of each [^{99m}Tc](HYNIC−NGA) conjugate was analyzed by CAE.

Immunoreactivity Measurement. The immunoreactivity of [^{99m}Tc](HYNIC−Fab)(tricine)$_2$ and [^{99m}Tc]-(HYNIC−Fab)(tricine)(BP) was determined using ^{125}I-Fab as a control, according to the procedure described previously (*5, 31*). Tumor cells (1.75×10^5 to 2.8×10^6) suspended in 100 μL of Dulbecco's PBS were incubated with 100 μL of [^{99m}Tc](HYNIC−Fab)(tricine)$_2$, [^{99m}Tc]-(HYNIC−Fab)(tricine)(BP), and ^{125}I−Fab for 1 h at 4 °C. After centrifugation at 10000*g* for 5 min, the supernatant was discarded and the radioactivity was determined using a well counter.

In Vivo Studies. Animal studies were conducted in accordance with our institutional guidelines and were approved by Kyoto University Animal Care Committee. Biodistribution studies were performed by the intravenous administration of [^{99m}Tc](HYNIC−NGA) conjugates or [^{99m}Tc](HYNIC−Fab) conjugates to 6-week-old male ddY mice (27−30 g) (*32*). The polypeptide concentrations of [^{99m}Tc](HYNIC−NGA) conjugates and [^{99m}Tc](HYNIC−Fab) conjugates were adjusted to 90 μg/mL and 200 μg/mL, respectively, with saline. Groups of five mice each were administered 9 μg (37−74 KBq) of [^{99m}Tc](HYNIC−NGA) conjugates or 20 μg (37−74 KBq) of [^{99m}Tc](HYNIC−Fab) conjugates prior to sacrificing the animals at 10 or 30 min, 1, 3, 6, or 24 h postinjection by decapitation. Tissues of interest were removed and weighed, and the radioactivity counts were determined with an auto well gamma counter. To determine the amounts and routes of excretion of radioactivity from the body, mice were housed in metabolic cages for 24 h after administration of [^{99m}Tc](HYNIC−NGA) conjugates or [^{99m}Tc](HYNIC−Fab) conjugates, and urine and feces were collected and the radioactivity was determined.

The subcellular distribution of radioactivity in the liver after injection of ^{99m}Tc-labeled NGAs into normal mice was investigated by perfusing the organ in situ with cold 0.25 M sucrose buffered with 10 mM phosphate buffer (pH 7.4) at 1 and 6 h postinjection of [^{99m}Tc](HYNIC−NGA) conjugates (133−266 KBq). The liver was treated according to the procedure described previously (*10, 21*). Briefly, the isolated organ was minced with scissors and suspended in 4 volumes of the same buffer prior to homogenization by hand with a Dounce homogenizer (20 strokes). This was followed by two final strokes in an ice-cooled Potter−Elvehjem homogenizer with a Teflon pestle rotated at 800 rpm. The resulting homogenate was centrifuged twice for 5 min at 340*g* at 4 °C. The isolated supernatant was then layered on top of iso-osmotic (0.25 M sucrose) 37.5% Percoll (9 mL; Pharmacia Biotech) at a density of 1.08 g/mL. After centrifugation at 20000*g* (RP 30 rotor; Hitachi Co. Ltd., Tokyo, Japan) for 90 min at 4 °C, the gradients were collected in 14 fractions. β-Galactosidase was used as a marker enzyme for lysosomes (*33, 34*), and its activity in each fraction was determined using *p*-nitrophenyl β-galactopyranoside as the substrate (*35*). The density and radioactivity counts of the respective fractions were also determined.

The radiolabeled species remaining in the liver at 1 and 6 h postinjection of [^{99m}Tc](HYNIC−NGA) conjugates (133−266 KBq) into normal mice were analyzed according to the procedure described previously (*10, 21*). Briefly, the murine liver was perfused in situ with cold 0.1 M Tris-citrate buffer (pH 6.5) containing 0.15 M NaCl, 0.02% sodium azide, 1 TIU/mL aprotinin, 2 mM benzamidine·HCl, 2 mM iodoacetamide, 1 mM phenylmethylsulfonyl fluoride, and 5 mM diisopropyl fluorophosphate before isolation of the hepatic samples (1 g each). Each tissue sample was placed in a test tube and subjected to three cycles of freezing (dry ice−acetone bath) and thawing. After addition of 5 volumes of the same buffer containing an additional 35 mM β-octyl-glucoside, the

samples were homogenized with a Polytron homogenizer (PT 10−35, Kinematica GmbH, Littau, Switzerland) at full speed with three consecutive 30-s bursts prior to centrifugation at 48000*g* for 20 min at 4 °C (Himac CS-120 Centrifuge; Hitachi Co. Ltd.). The supernatant was separated from the pellet, and the radioactivity was counted. The liver homogenate samples were analyzed immediately by SE-HPLC, CAE, and TLC after filtration through a polycarbonate membrane with a pore diameter of 0.45 μm (Nacalai Tesque). Each sample was also analyzed immediately by RP-HPLC (solvent system 2) after ultrafiltration with a 10 kDa cutoff membrane (Microcon-10; Amicon Grace, Tokyo, Japan).

The radiolabeled species excreted in the urine for 6 h postinjection of [^{99m}Tc](HYNIC−Fab) conjugates were analyzed by SE-HPLC and RP-HPLC (solvent system 2) after filtration through a polycarbonate membrane with a pore diameter of 0.45 μm and a 10 kDa cutoff ultrafiltration membrane, respectively.

Biodistribution Studies in Athymic Mice Bearing Osteogenic Sarcoma. Athymic mice bearing osteogenic sarcoma were also treated intravenously with 100 μL of [^{99m}Tc](HYNIC−Fab)(tricine)$_2$ or [^{99m}Tc](HYNIC−Fab)-(tricine)(BP) (20 μg each), and the animals were sacrificed at 3 or 6 h postinjection (five mice each). Mean weights of mice and tumors used in this study were 18.91 ± 0.95 and 0.23 ± 0.08 g, respectively. Organs of interest were removed and weighed, and the radioactivity in each tissue was determined. Tumor/blood and tumor/kidney ratios were then calculated from the corresponding %ID/g values.

Statistical Analysis. Statistical analysis was performed by applying unpaired *t*-test. $P < 0.05$ was considered statistically significant.

RESULTS

Conjugation of Ternary Ligand Complexes with Polypeptides. Ternary ligand [^{99m}Tc](HYNIC−NGA) conjugates and [^{99m}Tc](HYNIC−Fab) conjugates were prepared by conjugation of ternary ligand [^{99m}Tc](HYNIC-TFP) complexes (active esters) with the ϵ-amine residues of polypeptides. Synthesis of the ternary ligand [^{99m}Tc]-(HYNIC-TFP) complexes was accomplished in one step by direct reduction of [^{99m}Tc]pertechnetate with stannous chloride in the presence of HYNIC-TFP, tricine, and ternary ligands. This gives >75% radiochemical yields of the ^{99m}Tc chelated active esters. RP-HPLC analyses of ternary ligand [^{99m}Tc](HYNIC-TFP) complexes indicated that the major impurity in each reaction was a carboxlic acid of the ^{99m}Tc−HYNIC ternary ligand complex produced due to hydrolysis. The inability to conjugate the carboxylic acid of the ternary ligand ^{99m}Tc−HYNIC complex with polypeptides was confirmed. The conjugation of the ^{99m}Tc−HYNIC active ester with polypeptides was prepared by reaction of the active esters of ^{99m}Tc−HYNIC with ϵ-amine residues of polypeptides at room temperature for 1 h and afforded yields from 30 to 40%. After purification by the centrifuged column procedure, [^{99m}Tc](HYNIC−NGA) conjugates and [^{99m}Tc]-(HYNIC−Fab) conjugates were obtained with radiochemical purities over 95% as determined by SE-HPLC, TLC, and CAE analyses. Average numbers of HYNIC molecules conjugated per NGA and Fab were 1.7 and 0.6, respectively, as determined by measuring the hydrazine groups. In addition, we examined the binding of [^{99m}Tc]-(HYNIC−Fab)(tricine)(BP), [^{99m}Tc](HYNIC−Fab)(tricine)$_2$, and ^{125}I−Fab to KT005 cells, and no differences were observed in the cell-bound radioactivity among the three radiolabeled Fab fragments.

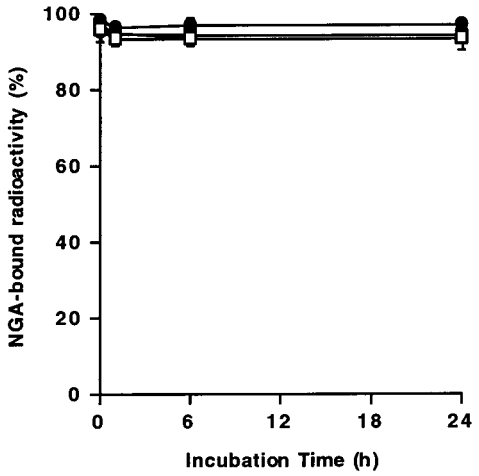


Figure 1. Percent radioactivity in NGA fractions following incubation of [^{99m}Tc](HYNIC−NGA)(tricine)(BP) (●), [^{99m}Tc]-(HYNIC−NGA)(tricine)(AP) (○), [^{99m}Tc](HYNIC−NGA)(tricine)-(NIC) (■), and [^{99m}Tc](HYNIC−NGA)(tricine)(PY) (□) in murine plasma at 37 °C. Values were determined by CAE. Each value represents the mean ± SD of three experiments.

Plasma Stability of [^{99m}Tc](HYNIC−NGA) Conjugates. Percent radioactivity after incubation of [^{99m}Tc]-(HYNIC−NGA) conjugates in freshly prepared murine plasma at 37 °C is shown in Figure 1. The percent radioactivity associated with NGA fractions were unchanged after 24 h incubation in murine plasma.

Biodistribution Study of [^{99m}Tc](HYNIC−NGA) Conjugates in Mice. Radioactivity levels in liver, urine, and feces after intravenous administration of [^{99m}Tc]-(HYNIC−NGA) conjugates are shown in Table 1. At 10 min postinjection, over 90% of the injected radioactivity was accumulated in the liver for all [^{99m}Tc](HYNIC−NGA) conjugates. After this postinjection interval, the radioactivity was gradually eliminated from the liver by hepatobiliary excretion as the major excretion route for the four [^{99m}Tc](HYNIC−NGA) conjugates. ([^{99m}Tc]-(HYNIC−NGA)(tricine)(BP) > [^{99m}Tc](HYNIC−NGA)-(tricine)(AP) > [^{99m}Tc](HYNIC−NGA)(tricine)(NIC) and [^{99m}Tc](HYNIC−NGA)(tricine)(PY)). Low radioactivity levels were observed in tissues other than the liver and intestine throughout the experimental period. No evidence of enterohepatic circulation of the radioactivity was observed.

Analyses of Radioactivity in the Liver. The representative Percoll density gradient centrifugation profiles of radioactivity in the liver at 1 and 6 h postinjection of [^{99m}Tc](HYNIC−NGA)(tricine)(NIC) are shown in Figure 2. Each liver homogenate showed a major radioactivity peak at a density of ca. 1.10 g/mL, which correlated well with the β-galactosidase activity profiles. [^{99m}Tc]-(HYNIC−NGA) conjugates using other ternary ligands (BP, AP, and PY) showed profiles similar to that of [^{99m}Tc](HYNIC−NGA)(tricine)(NIC).

The supernatants of the liver homogenates after injection of all ^{99m}Tc-labeled NGAs were obtained with radiochemical efficiencies of over 90%. Figure 3 shows GPC profiles of the liver supernatants at 1 and 6 h postinjection of [^{99m}Tc](HYNIC−NGA)(tricine)(NIC). These liver supernatants depicted a major radioactivity peak at an elution volume (82.5 mL) close to that of [^{99m}Tc]-(HYNIC−lysine)(tricine)(NIC). The radioactivity peaks in the low molecular weight fractions represented 94.2 and 96.6% of the total radioactivity at 1 and 6 h postinjection, respectively. Under these conditions, the parental [^{99m}Tc](HYNIC−NGA) conjugates had an elution

Table 1. Biodistribution of Radioactivity after Intravenous Administration of ^{99m}Tc-Labeled NGA in Mice[a]

	time after injection					
tissue	10 min	30 min	1 h	3 h	6 h	24 h
			[^{99m}Tc](HYNIC−NGA)(BP)(tricine)			
blood[b]	0.3 ± 0.1	0.4 ± 0.1	0.3 ± 0.0	0.2 ± 0.0	0.1 ± 0.1	0.1 ± 0.0
liver	90.7 ± 1.6	61.0 ± 5.6	43.8 ± 1.9	29.1 ± 3.3	20.3 ± 2.6	12.1 ± 1.1
kidney	0.5 ± 0.2	1.5 ± 0.5	2.0 ± 0.3	0.8 ± 0.2	0.3 ± 0.2	0.2 ± 0.1
intestine	2.6 ± 0.3	19.2 ± 3.9	34.7 ± 1.8	43.9 ± 3.7	33.2 ± 13.3	1.7 ± 0.1
urine						19.0 ± 1.4
feces						53.6 ± 1.8
			[^{99m}Tc](HYNIC−NGA)(AP)(tricine)			
blood[b]	1.0 ± 0.1	0.9 ± 0.1	0.8 ± 0.1	0.4 ± 0.1	0.3 ± 0.0	0.1 ± 0.1
liver	90.5 ± 1.9	72.8 ± 2.5	54.1 ± 2.1	35.8 ± 2.4	25.1 ± 1.8	18.3 ± 1.6
kidney	0.8 ± 0.2	1.6 ± 0.8	1.4 ± 0.8	1.0 ± 0.1	0.5 ± 0.1	0.2 ± 0.0
intestine	1.4 ± 0.2	11.4 ± 1.4	20.8 ± 3.5	33.0 ± 5.5	40.1 ± 6.9	1.5 ± 0.5
urine						26.5 ± 1.9
feces						45.3 ± 1.5
			[^{99m}Tc](HYNIC−NGA)(NIC)(tricine)			
blood[b]	1.1 ± 0.2	0.9 ± 0.2	0.7 ± 0.1	0.5 ± 0.0	0.4 ± 0.1	0.2 ± 0.0
liver	92.6 ± 3.4	71.0 ± 3.4	62.3 ± 1.1	51.1 ± 3.2	47.0 ± 3.5	33.2 ± 1.31
kidney	1.0 ± 0.3	1.0 ± 0.6	1.2 ± 0.5	0.6 ± 0.1	0.5 ± 0.1	0.3 ± 0.0
intestine	1.4 ± 0.2	11.2 ± 1.7	16.4 ± 1.2	23.8 ± 2.6	18.5 ± 3.7	1.8 ± 0.6
urine						22.2 ± 2.3
feces						31.8 ± 1.8
			[^{99m}Tc](HYNIC−NGA)(PY)(tricine)			
blood[b]	1.1 ± 0.1	0.9 ± 0.2	0.7 ± 0.1	0.4 ± 0.0	0.3 ± 0.0	0.2 ± 0.0
liver	91.9 ± 0.5	77.4 ± 1.5	64.3 ± 3.7	52.6 ± 3.8	46.0 ± 3.5	36.0 ± 2.6
kidney	0.7 ± 0.1	0.7 ± 0.3	0.8 ± 0.2	0.8 ± 0.3	0.5 ± 0.1	0.3 ± 0.1
intestine	1.4 ± 0.2	8.0 ± 1.3	15.5 ± 1.4	21.8 ± 2.5	26.7 ± 2.2	1.3 ± 0.2
urine						18.8 ± 1.3
feces						35.2 ± 2.3

[a] Expressed as % injected dose. Each value represents the mean ± SD of five animals. [b] Expressed as % injected dose per gram.

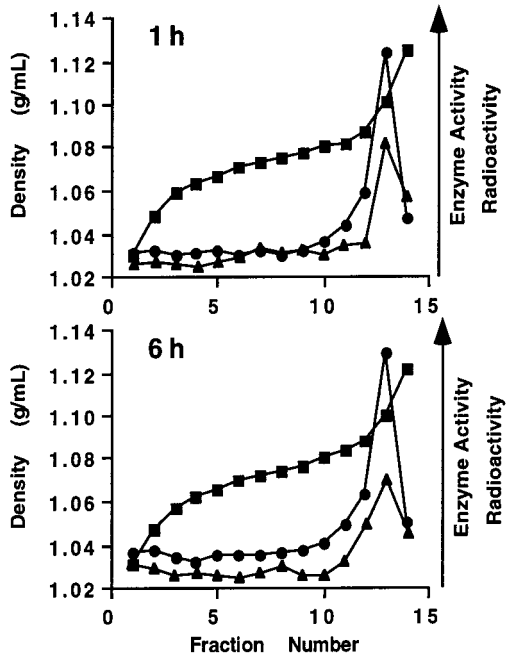


Figure 2. Percoll density gradient centrifugation profiles of liver homogenate at 1 and 6 h postinjection of [^{99m}Tc](HYNIC−NGA)(tricine)(NIC). In both preparations, a single radioactivity peak (●) that coincided with β-galactosidase activity (▲) was detected at a density (■) of ca. 1.10 g/mL.

volume of 32.5 mL. Similar results were obtained when we analyzed the liver supernatants of [^{99m}Tc](HYNIC−NGA) conjugates with the other ternary ligands (BP, AP, and PY). Figure 4 shows RP-HPLC profiles of the liver homogenates at 1 and 6 h postinjection of [^{99m}Tc](HYNIC−NGA)(tricine)(BP), [^{99m}Tc](HYNIC−NGA)(tricine)(AP), [^{99m}Tc](HYNIC−NGA)(tricine)(NIC), and [^{99m}Tc](HYNIC−NGA)(tricine)(PY). All liver supernatants had radiochromatograms identical to the respective ternary ligand [^{99m}Tc](HYNIC−lysine) complexes. These results were also confirmed by co-chromatographic analyses (data not shown). Furthermore, the liver homogenates were analyzed by TLC and CAE, and all liver homogenates showed a single radioactivity peak similar to the respective ternary ligand [^{99m}Tc](HYNIC−lysine) complexes.

Plasma Stability of [^{99m}Tc](HYNIC−Fab) Conjugates. Figure 5 shows SE-HPLC profiles of [^{99m}Tc](HYNIC−Fab) conjugates before and after incubation in freshly prepared murine plasma for 24 h. Although a small peak of radioactivity was observed in large molecular weight fractions (12 and 17 min), each [^{99m}Tc]-(HYNIC−Fab) conjugate showed a major radioactivity peak at the retention time identical to the intact Fab up to 24 h of incubation.

Biodistribution Study of [^{99m}Tc](HYNIC−Fab) Conjugates in Normal Mice. Table 2 shows elimination of radioactivity from the blood and kidneys after administration of [^{99m}Tc](HYNIC−Fab) conjugates. No significant differences were observed in radioactivity levels in the blood among the four Fab conjugates. Radioactivity levels in the kidney reached their peaks at 1 h postinjection for all Fab conjugates, and the radioactivity elimination from the kidney differed with the ternary ligands used. Among the four ternary ligands, [^{99m}Tc](HYNIC−Fab)(tricine)(BP) exhibited the fastest elimination from the kidney. The majority of radioactivity excreted from the body was detected in the urine.

Analyses of Radioactivity in the Urine. Figure 6 shows radiochromatograms of urine samples obtained by 24 h postinjection of [^{99m}Tc](HYNIC−Fab) conjugates. SE-HPLC showed two radioactivity peaks at retention times similar to those of intact [^{99m}Tc](HYNIC−Fab) conjugates (19 min) and low molecular weight compounds (25−28 min). RP-HPLC analyses after filtration with a 10 kDa cutoff membrane showed that the radioactivity in the low

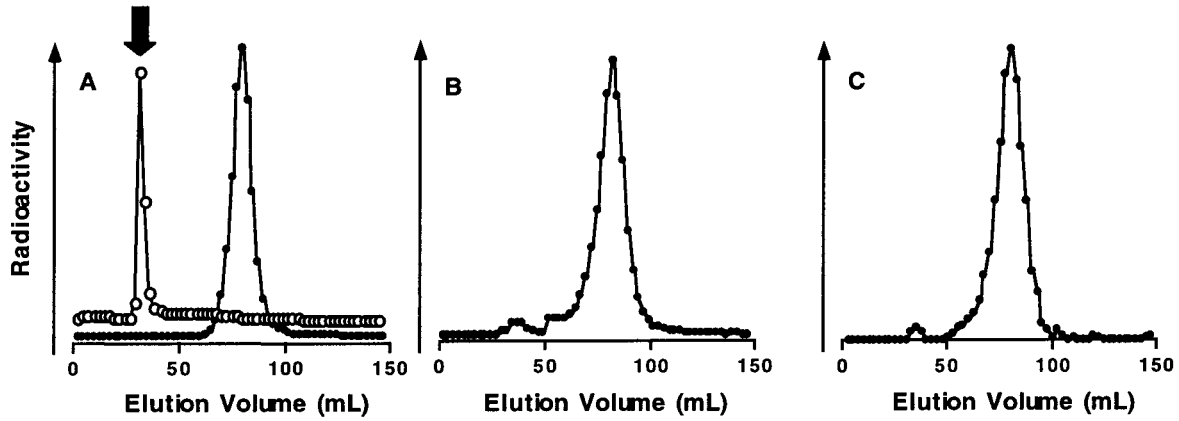


Figure 3. Analyses of liver homogenates at 1 (B) and 6 h (C) postinjection of [^{99m}Tc](HYNIC−NGA)(tricine)(NIC) by GPC. Radiochromatogram of [^{99m}Tc](HYNIC−lysine)(tricine)(NIC) (●) when analyzed by GPC (A). Under these conditions, [^{99m}Tc](HYNIC−NGA)(tricine)(NIC) (○) and blue dextran (↓) eluted at 32.5 mL (A).

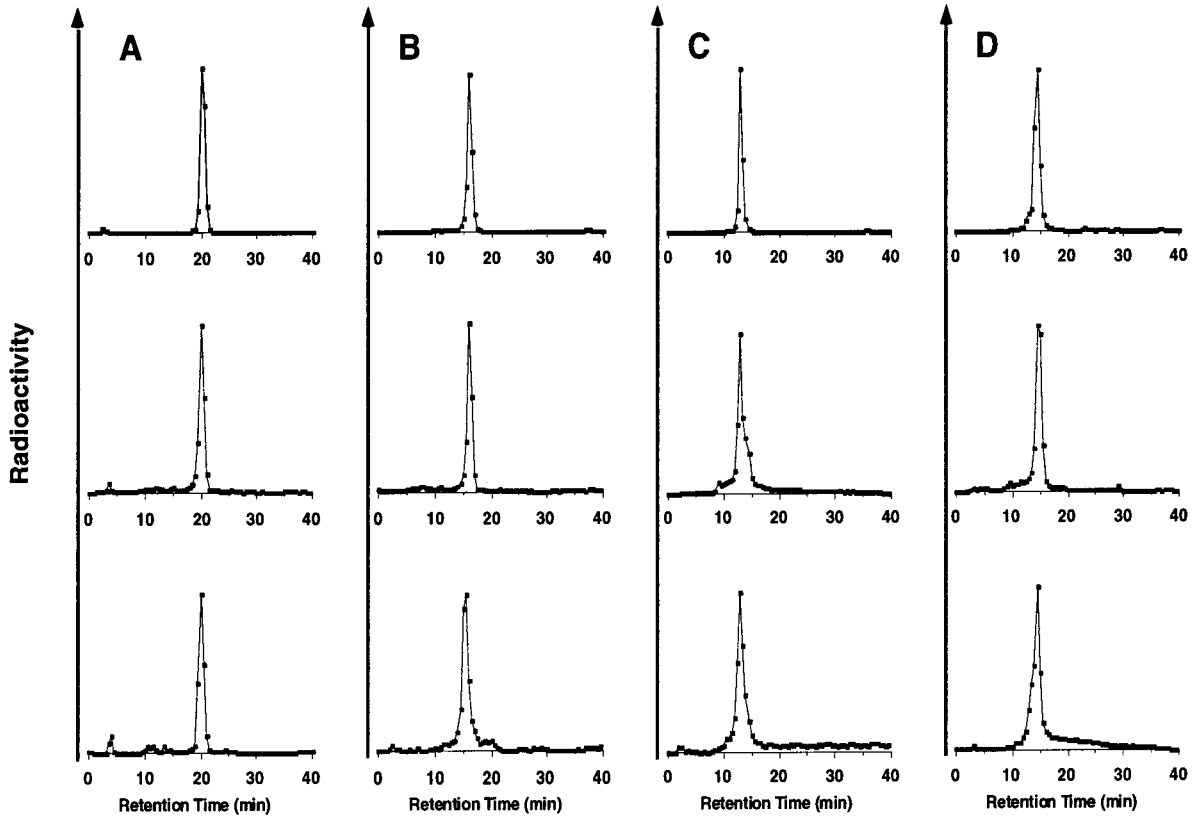


Figure 4. Analyses of liver homogenates at 1 (middle panels) and 6 h (lower panels) postinjection of [^{99m}Tc](HYNIC−NGA)(tricine)-(BP) (A), [^{99m}Tc](HYNIC−NGA)(tricine)(AP) (B), [^{99m}Tc](HYNIC−NGA)(tricine)(NIC) (C) and [^{99m}Tc](HYNIC−NGA)(tricine)(PY) (D) by RP-HPLC using solvent system 2. Radiochromatograms of [^{99m}Tc](HYNIC−lysine)(tricine)(pyridine derivative) when analyzed by RP-HPLC (upper panels).

molecular weight fraction had a retention time identical to that of the respective lysine adduct. These observations were also confirmed by cochromatographic analyses. Furthermore, on TLC, urine samples showed a single radioactivity peak similar to the ternary ligand [^{99m}Tc]-(HYNIC−lysine) complexes.

Partition Coefficients and Retention Times of Ternary Ligand [^{99m}Tc](HYNIC−Lysine) Complexes. The partition coefficients (as log PC values) and the retention times in RP-HPLC of ternary ligand [^{99m}Tc]-(HYNIC−lysine) complexes are summarized in Table 3. The rank order of the lipophilicity of ternary ligand [^{99m}Tc](HYNIC−lysine) complexes was [^{99m}Tc](HYNIC−lysine)(tricine)(BP) > [^{99m}Tc](HYNIC−lysine)(tricine)(AP) > [^{99m}Tc](HYNIC−lysine)(tricine)(PY) > [^{99m}Tc](HYNIC−lysine)(tricine)(NIC).

Biodistribution Study in Athymic Mice Bearing Osteogenic Sarcoma. Figure 7 shows the radioactivity levels in blood, kidney, and tumor at 3 and 6 h after administration of [^{99m}Tc](HYNIC−Fab)(tricine)(BP) and [^{99m}Tc](HYNIC−Fab)(tricine)$_2$ in athymic mice bearing osteogenic sarcoma. [^{99m}Tc](HYNIC−Fab)(tricine)(BP) showed significant reduction of radioactivity levels in the blood and kidney at both postinjection times compared with [^{99m}Tc](HYNIC−Fab)(tricine)$_2$, although [^{99m}Tc]-(HYNIC−Fab)(tricine)(BP) showed lower radioactivity

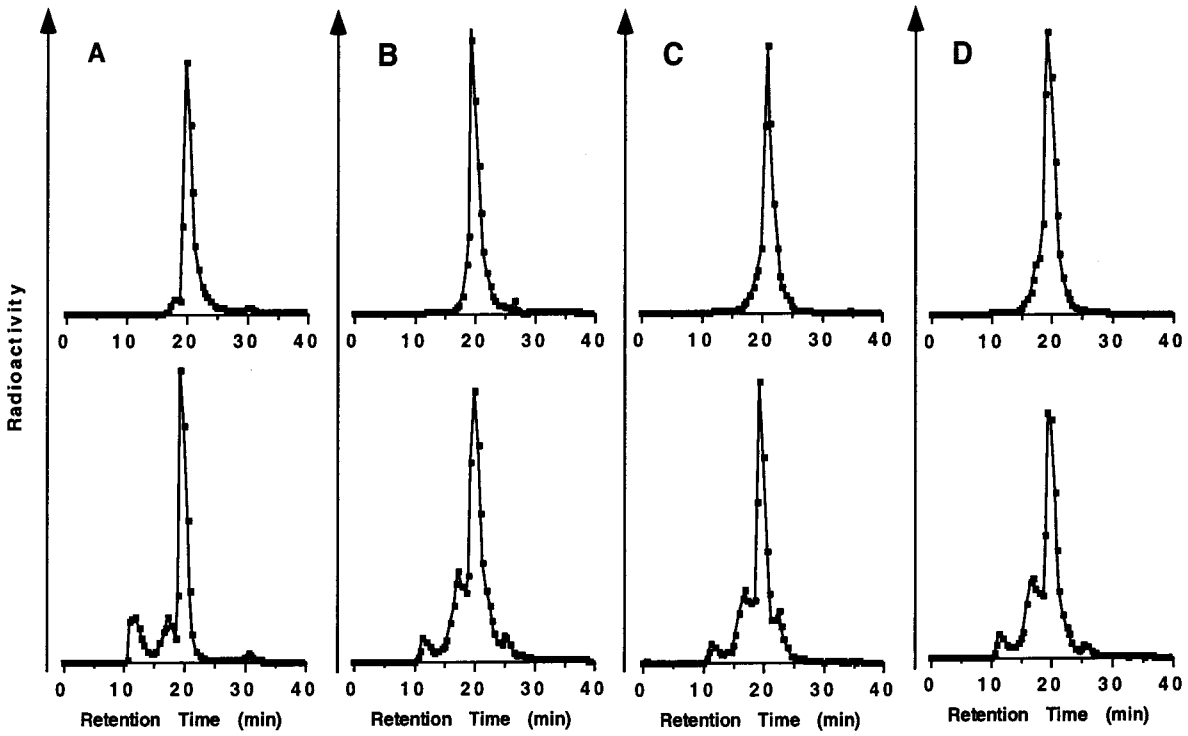


Figure 5. SE-HPLC profiles of radioactivity in murine plasma before (upper panels) and after 24 h incubation (lower panels) at 37 °C of [^{99m}Tc](HYNIC−Fab)(tricine)(BP) (A), [^{99m}Tc](HYNIC−Fab)(tricine)(AP) (B), [^{99m}Tc](HYNIC−Fab)(tricine)(NIC) (C) and [^{99m}Tc](HYNIC−Fab)(tricine)(PY) (D). Under these conditions, thyroglobulin (670 kDa), glutamate dehydrogenase (290 kDa), IgG (150 kDa), bovine serum albumin (68 kDa), Fab fragment (5 kDa) and cytochrome C (13 kDa) had retention times of 12, 14.5, 16, 18, 19, and 21 min, respectively, on SE-HPLC.

Table 2. Biodistributions of Radioactivity after Intravenous Administration of ^{99m}Tc-Labeled Fab in Mice[a]

	time after injection					
tissue	10 min	30 min	1 h	3 h	6 h	24 h
			[^{99m}Tc](HYNIC−Fab)(tricine)(BP)			
blood	21.1 ± 1.2	12.2 ± 2.1	7.8 ± 1.1	3.5 ± 0.6	1.9 ± 0.3	0.4 ± 0.1
liver	7.0 ± 0.4	6.9 ± 1.5	6.7 ± 1.3	6.6 ± 1.4	5.2 ± 1.0	2.8 ± 0.4
kidney	31.5 ± 3.8	52.2 ± 5.4	54.7 ± 5.3	37.1 ± 2.3	22.5 ± 1.9	6.9 ± 1.1
intestine	1.1 ± 0.1	1.3 ± 0.2	1.7 ± 0.4	2.1 ± 0.3	2.9 ± 0.6	0.4 ± 0.1
urine[b]						51.7 ± 3.1
feces[b]						11.6 ± 1.0
			[^{99m}Tc](HYNIC−Fab)(tricine)(AP)			
blood	22.5 ± 0.6	14.1 ± 0.7	8.2 ± 1.1	3.1 ± 0.5	2.1 ± 0.1	0.5 ± 0.2
liver	6.2 ± 0.1	6.2 ± 0.7	5.7 ± 0.8	4.4 ± 0.9	5.0 ± 0.3	3.4 ± 0.5
kidney	36.3 ± 4.4	51.2 ± 3.1	65.9 ± 6.7	47.2 ± 7.9	29.0 ± 2.9	13.1 ± 2.5
intestine	1.0 ± 0.2	1.3 ± 0.2	1.1 ± 0.1	1.2 ± 0.3	1.4 ± 0.3	1.6 ± 1.2
urine[b]						58.1 ± 3.0
feces[b]						8.2 ± 3.0
			[^{99m}Tc](HYNIC−Fab)(tricine)(NIC)			
blood	24.3 ± 1.1	13.4 ± 0.8	7.7 ± 0.7	4.2 ± 0.4	1.8 ± 0.2	0.4 ± 0.2
liver	6.7 ± 0.6	5.7 ± 0.5	6.4 ± 1.3	6.3 ± 0.8	5.3 ± 1.6	4.7 ± 1.1
kidney	30.3 ± 1.0	48.9 ± 2.4	58.5 ± 3.9	50.1 ± 5.9	27.0 ± 2.7	15.2 ± 2.0
intestine	1.1 ± 0.1	1.1 ± 0.1	1.2 ± 0.2	1.4 ± 0.3	1.3 ± 0.2	0.6 ± 0.1
urine[b]						60.7 ± 0.4
feces[b]						5.4 ± 1.2
			[^{99m}Tc](HYNIC−Fab)(tricine)(PY)			
blood	23.7 ± 1.4	14.5 ± 2.4	8.8 ± 1.7	3.9 ± 0.2	2.4 ± 0.3	0.6 ± 0.2
liver	4.3 ± 0.4	4.9 ± 0.6	5.5 ± 0.9	4.6 ± 0.5	4.0 ± 0.5	2.6 ± 0.4
kidney	27.7 ± 2.5	54.8 ± 9.8	73.1 ± 5.8	58.7 ± 3.3	44.0 ± 5.0	15.1 ± 1.9
intestine	0.9 ± 0.1	1.3 ± 0.1	1.4 ± 0.2	1.0 ± 0.1	0.9 ± 0.2	0.7 ± 0.1
urine[b]						57.4 ± 4.2
feces[b]						3.8 ± 1.0

[a] Expressed as % injected dose per gram. Each value represents the mean ± SD of five animals. [b] Expressed as % injected dose.

levels in the tumor than [^{99m}Tc](HYNIC−Fab)(tricine)$_2$. Thus, [^{99m}Tc](HYNIC−Fab)(tricine)(BP) provided significantly higher tumor/blood and tumor/kidney ratios of radioactivity than [^{99m}Tc](HYNIC−Fab)(tricine)$_2$ (Figure 8).

DISCUSSION

Although the relationship between solute lipophilicity and permeation across the cell membrane is well-known, there have been no systematic studies of the effects of

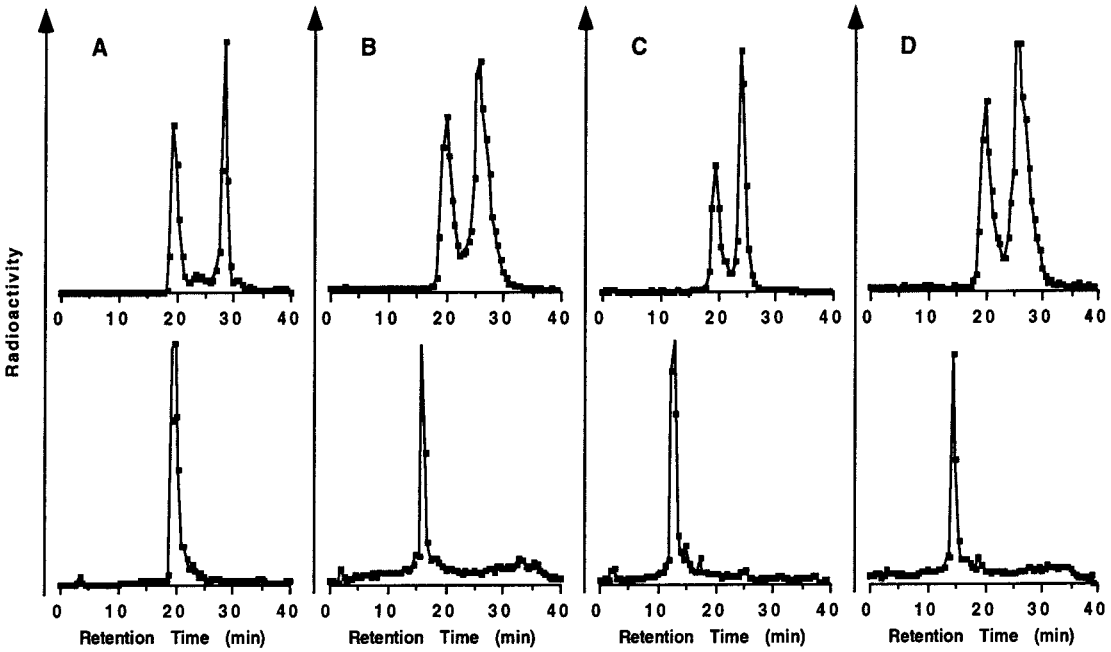


Figure 6. Radiochromatograms of urine samples obtained for 6 h postinjection of [^{99m}Tc](HYNIC−Fab)(tricine)(BP) (A), [^{99m}Tc]-(HYNIC−Fab)(tricine)(AP) (B), [^{99m}Tc](HYNIC−Fab)(tricine)(NIC) (C), and [^{99m}Tc](HYNIC−Fab)(tricine)(PY) (D) by SE-HPLC (upper panels) and RP-HPLC using solvent system 2 (lower panels). Urine samples were analyzed by SE-HPLC after filtration through a polycarbonate membrane with a pore diameter of 0.45 μm and by RP-HPLC after ultrafiltration through a 10 kDa cutoff membrane.

Table 3. Partition Coefficients and RP-HPLC Data of [^{99m}Tc](HYNIC−Lysine) Ternary Ligand Complexes.

radiometabolite	log PC[a]	retention time (min)[b]
[^{99m}Tc](HYNIC−lysine)(BP)(tricine)	−2.21 ± 0.03	20.3
[^{99m}Tc](HYNIC−lysine)(AP)(tricine)	−2.37 ± 0.05	16.1
[^{99m}Tc](HYNIC−lysine)(PY)(tricine)	−2.73 ± 0.06	14.3
[^{99m}Tc](HYNIC−lysine)(NIC)(tricine)	−2.93 ± 0.16	13.2

[a] Octanol/buffer (0.1 M phosphate buffered saline, pH 4.75) partition coefficients. Each value represents the mean ± SD of three experiments. [b] Using solvent system 2.

the lipophilicity of radiometabolites on their elimination rates from the tissue after administration of radiolabeled polypeptides. A previous study in our laboratory indicated that radiometabolites with different lipophilicity should show different permeation rates through the hepatic lysosomal membrane (*11*). As the pyridine derivative coligands could alter the lipophilicity of ^{99m}Tc−HYNIC-labeled metabolites, we used four pyridine derivatives as ternary ligands to prepare ^{99m}Tc−HYNIC-labeled polypeptides for further investigation of the effects of the lipophilicity of radiometabolites on the radioactivity elimination from the tissue.

The procedure for synthesis of ternary ligand complexes and subsequent conjugation with polypeptides has been well established as described previously (*24*). The selective conjugation of ternary ligand [^{99m}Tc](HYNIC-TFP) complexes to the ϵ-amine residues of polypeptides was supported by generating lysine adducts of HYNIC as radiometabolites (Figures 4 and 6). The rapid and quantitative accumulation of all ^{99m}Tc-labeled NGAs (Table 1) and the lack of changes in immunoreactivity of ^{99m}Tc-labeled Fab suggested that the biological reactivity of parental proteins was retained after conjugation of preformed ^{99m}Tc−HYNIC complexes.

The stability of the ^{99m}Tc−HYNIC-labeled polypeptides designed in the present study was evaluated by incubation in murine plasma. After incubation of all [^{99m}Tc]-(HYNIC−NGA) conjugates in murine plasma, almost all radioactivity was observed in the NGA fractions (Figure 1). Plasma incubation of four [^{99m}Tc](HYNIC−Fab) conjugates showed high stability of the ternary ligand ^{99m}Tc complexes against exchange reaction with plasma proteins (Figure 5), whereas [^{99m}Tc](HYNIC−Fab)(tricine)$_2$ showed significantly larger amounts of higher molecular weight radiolabeled species (over 600 kDa) (*22*). The high degree of stability of ^{99m}Tc−HYNIC ternary ligand complex against exchange reaction with plasma proteins was reflected by the faster blood clearance of ternary ligand [^{99m}Tc](HYNIC−Fab) conjugates as compared with [^{99m}Tc](HYNIC−Fab)(tricine)$_2$ (*21*). The lack of significant differences in the blood clearance of radioactivity among the four ^{99m}Tc-labeled Fab fragments indicated that the association of ternary ligand complexes with polypeptides did not affect the pharmacokinetics of the parental Fab.

Stability of radiometabolites was investigated by analysis of radiometabolites generated in hepatocytes after administration of [^{99m}Tc](HYNIC−NGA) conjugates. On GPC and RP-HPLC analyses, all liver homogenates at 1 h postinjection of four [^{99m}Tc](HYNIC−NGA) conjugates showed a single radioactivity peak at a position identical to that of the respective ternary ligand [^{99m}Tc](HYNIC−lysine) complex (Figures 3 and 4). The radiochromatograms were unchanged for up to 6 h postinjection. These findings indicated that the ternary ligand complexes remained stable against exchange reaction with proteins in the lysosomes even after catabolism to lysine adducts. Therefore, elimination rates from the liver after injection of ternary ligand [^{99m}Tc](HYNIC−NGA) conjugates would reflect those of the respective radiometabolites.

Radioactivity elimination from the tissues after administration of ^{99m}Tc−HYNIC-labeled NGAs varied with the ternary ligands used. As shown in Table 1, [^{99m}Tc]-(HYNIC−NGA) conjugates prepared using four ternary ligands were eliminated from the liver in the order of increasing lipophilicity of radiometabolites, ternary ligand [^{99m}Tc](HYNIC−lysine) complexes (Table 3). As almost all radioactivity of the [^{99m}Tc](HYNIC−lysine) complexes existed in the lysosomes of hepatocytes (Figure 2), the

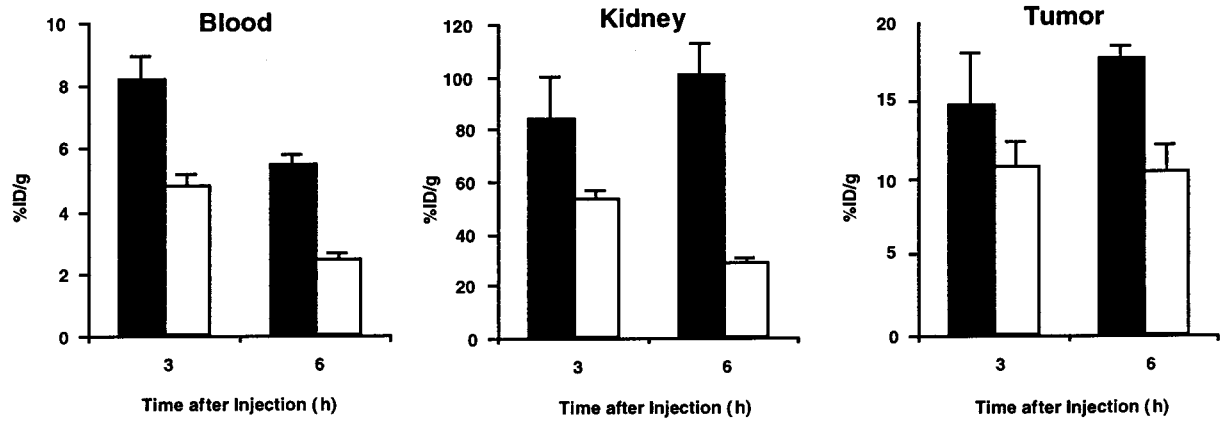


Figure 7. Comparative biodistribution of radioactivity at 3 and 6 h postinjection of [^{99m}Tc](HYNIC−Fab)(tricine)(BP) (open columns) and [^{99m}Tc](HYNIC−Fab)(tricine)$_2$ (closed columns) in athymic mice bearing osteogenic sarcoma. Each value represents the mean ± SD of five animals.

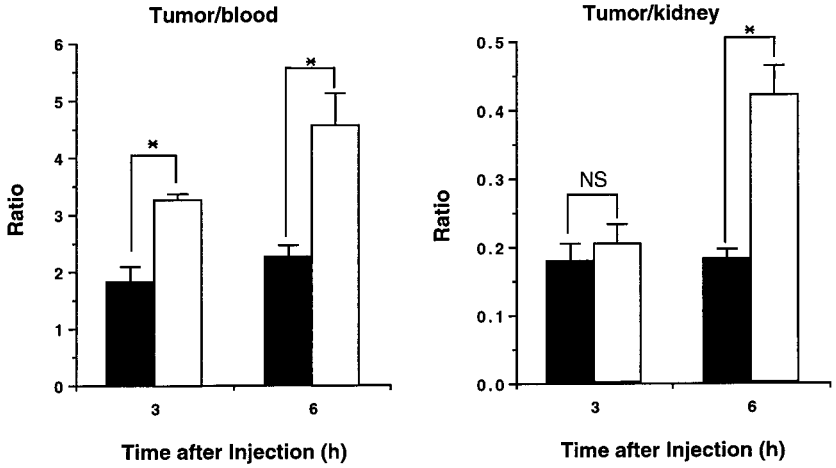


Figure 8. Tumor/blood and tumor/kidney ratios of the radioactivity at 3 and 6 h postinjection of [^{99m}Tc](HYNIC−Fab)(tricine)(BP) (open columns) and [^{99m}Tc](HYNIC−Fab)(tricine)$_2$ (closed columns) in athymic mice bearing osteogenic sarcoma. Significance was determined by unpaired *t*-test (*: $p < 0.01$, NS: not significant). Each value represents the mean ± SD of five animals.

lipophilicy of radiometabolites would affect the permeation rates through the lysosomal membrane.

Radioactivity elimination from the kidney after injection of ternary ligand [^{99m}Tc](HYNIC−Fab) conjugates differed with the ternary ligands used (Table 2). Radioactivity excreted in the urine existed as intact radiolabeled Fab fragments and ternary ligand [^{99m}Tc](HYNIC−lysine) complexes (Figure 6). As elimination of four [^{99m}Tc](HYNIC−Fab) conjugates from the kidney would be similar, the differences in radioactivity elimination from the kidney after injection of the four [^{99m}Tc](HYNIC−Fab) conjugates could reflect differences in elimination rates of the radiometabolites. Indeed, radioactivity elimination from the kidney after injection of ternary ligand [^{99m}Tc](HYNIC−Fab) conjugates increased in the order of increasing lipophilicity of the radiometabolites, ternary ligand [^{99m}Tc](HYNIC−lysine) complexes (Tables 2 and 3).

These findings indicated that the lipophilicity of radiometabolites plays an important role in the radioactivity elimination rates from the tissues after administration of radiolabeled polypeptides. The present findings also suggested that radiolabeling reagents producing lipophilic radiometabolites by lysosomal proteolysis would be useful for the enhancement of the target/nontarget ratio of radioactivity levels when using radiolabeled polypeptides that are not internalized within the target cells. To confirm the usefulness of this approach, the biodistribution study in athymic mice was performed using Fab fragments that are not internalized within tumor cells (Figures 7 and 8). BP was selected as a ternary ligand, as [^{99m}Tc](HYNIC−lysine)(tricine)(BP) exhibited the most rapid elimination from the tissues. Although [^{99m}Tc](HYNIC−Fab)(tricine)(BP) showed lower radioactivity levels in the tumor compared with [^{99m}Tc]-(HYNIC−Fab)(tricine)$_2$, [^{99m}Tc](HYNIC−Fab)(tricine)-(BP) showed significant increases of the tumor/blood and tumor/kidney ratios due to significant reduction of the radioactivity levels in the blood and kidney (Figure 8).

Determination of the relationships between the lipophilicity of radiometabolites and their elimination rates from the tissues would facilitate design of radiolabeling reagents with a metabolizable linkage. However, it is necessary for enhancement of the target/nontarget ratio not only to release the lipophilic radiometabolites in the nontarget tissues but also to stabilize the metabolizable linkage in plasma. As chemical structures of linkages and radiolabels attached to the metabolizable bonds significantly affect the stability of these bonds in radiolabeled polypeptides (*36*), radiolabeling reagents producing lipophilic radiometabolites by lysosomal proteolysis might be more useful than those that require cleavage of a metabolizable linkage.

The present findings also suggested that the reagents to radiolabel polypeptides producing hydrophilic radiometabolites would be required when applied to internalizable (poly)peptides within target cells. Use of chemically modified (poly)peptides in combination with these re-

agents could achieve further enhancement of the target/nontarget ratio.

In conclusion, the present study indicated that the lipophilicity of the radiometabolites derived from radiolabeled polypeptides constitutes one important factor affecting the elimination rate from the tissues. As pyridine derivatives could serve as stable ternary ligands in ^{99m}Tc−HYNIC-labeled polypeptides and alter the physicochemical properties of radiometabolites, the use of pyridine derivatives as ternary ligands for preparation of ^{99m}Tc−HYNIC-labeled polypeptides might be applicable for controlling the radioactivity pharmacokinetics. The findings of the present study will be useful to enhance the target/nontarget ratios of polypeptide radiopharmaceuticals.

LITERATURE CITED

(1) Haseman, M. K., Goodwin, D. A., Meares, C. F., Kaminski, M. S., Wensel, T. G., McCall, M. J., and Levy, R. (1986) Metabolizable ^{111}In chelate conjugated anti-idiotype monoclonal antibody for radioimmunodetection of lymphoma in mice. *Eur. J. Nucl. Med. 12*, 455−460.

(2) Paik, C. H., Quadri, S. M., and Reba, R. C. (1989) Interposition of different chemical linkages between antibody and ^{111}In-DTPA to accelerate clearance from nontarget organs and blood. *Nucl. Med. Biol. 16*, 475−481.

(3) Weber, R. W., Boutin, R. H., Nedelman, M. A., Lister-James, J., and Dean, R. T. (1990) Enhanced kidney clearance with an ester-linked ^{99m}Tc-radiolabeled antibody Fab′-chelator conjugate. *Bioconjugate Chem. 1*, 431−437.

(4) Arano, Y., Wakisaka, K., Ohmomo, Y., Uezono, T., Akizawa, H., Nakayama, M., Sakahara, H., Tanaka, C., Konishi, J., and Yokoyama, A. (1996) Assessment of radiochemical design of antibodies using an ester bond as the metabolizable linkage: evaluation of maleimidoethyl 3-(tri-*n*-butylstannyl)-hippurate as a radioiodination reagent of antibodies for diagnostic and therapeutic applications. *Bioconjugate Chem. 7*, 628−637.

(5) Arano, Y., Inoue, T., Mukai, T., Wakisaka, K., Sakahara, H., Konishi, J., and Yokoyama, A. (1994) Discriminated release of a hippurate-like radiometal chelate in nontarget tissues for target-selective radioactivity localization using pH-dependent dissociation of reduced antibody. *J. Nucl. Med. 35*, 326−333.

(6) Khaw, B. A., Klibanov, A., O'Donnell, S. M., Saito, T., Nossiff, N., Slinkin, M. A., Newell, J. B., Strauss, H. W., and Torchilin, V. P. (1991) Gamma imaging with negatively charge-modified monoclonal antibody: modification with synthetic polymers. *J. Nucl. Med. 32*, 1742−1751.

(7) Gangopadhyay, A., Petrick, A. T., and Thomas, P. (1996) Modification of antibody isoelectric point affects biodistribution of 111-indium-labeled antibody. *Nucl. Med. Biol. 23*, 257−261.

(8) Kim, I. S., Yoo, T. M., Kobayashi, H., Kim, M. K., Le, N., Wang, Q. C., Pastan, I., Carrasquillo, J. A., and Paik, C. H. (1999) Chemical modification to reduce renal uptake of disulfide-bonded variable region fragment of anti-Tac monoclonal antibody labeled with ^{99m}Tc. *Bioconjugate Chem. 10*, 447−453.

(9) Akizawa, H., Arano, Y., Mifune, M., Iwado, A., Saito, Y., Mukai, T., Uehara, T., Ono, M., Fujioka, Y., Ogawa, K., Kiso, Y., and Saji, H. (in press) Effect of molecular charges on renal uptake of ^{111}In-DTPA conjugated peptides. *Nucl. Med. Biol.*

(10) Arano, Y., Mukai, T., Uezono, T., Wakisaka, K., Motonari, H., Akizawa, H., Taoka, Y., and Yokoyama, A. (1994) A biological method to evaluate bifunctional chelating agents to label antibodies with metallic radionuclides. *J. Nucl. Med. 35*, 890−898.

(11) Arano, Y., Mukai, T., Akizawa, H., Uezono, T., Motonari, H., Wakisaka, K., Kairiyama, C., and Yokoyama, A. (1995) Radiolabeled metabolites of protein play a critical role in radioactivity elimination from the liver. *Nucl. Med. Biol. 22*, 555−564.

(12) Akizawa, H., Arano, Y., Uezono, T., Ono, M., Fujioka, Y., Uehara, T., Yokoyama, A., Akaji, K., Kiso, Y., and Saji, H. (1998) Renal metabolism of ^{111}In-DTPA-D-Phe^1-octreotide in vivo. *Bioconjugate Chem. 9*, 662−670.

(13) Mukai, T., Arano, Y., Nishida, K., Sasaki, H., Saji, H., and Nakamura, J. (1999) In-vivo evaluation of indium-111-diethylenetriaminepentaacetic acid labeling for determining the sites and rates of protein catabolism in mice. *J. Pharm. Pharmacol. 51*, 15−20.

(14) Abrams, M. J., Juweid, M., tenKate, C. I., Schwartz, D. A., Hauser, M. M., Gaul, F. E., Fuccello, A. J., Rubin, R. H., Strauss, H. W., and Fischman, A. J. (1990) Technetium-99m-human polyclonal IgG radiolabeled via the hydrazino nicotinamide derivative for imaging focal sites of infection in rats. *J. Nucl. Med. 31*, 2022−2028.

(15) Claessens, R. A., Koenders, E. B., Oyen, W. J. G., and Corstens, F. H. (1996) Retention of technetium-99m in infectious foci in rats after release from technetium-99m labeled human nonspecific polyclonal immunoglobulin G: a dual-label study with hydrazinonicotinamido and iminothiolano immunoglobulin. *Eur. J. Nucl. Med. 23*, 1536−1539.

(16) Ultee, M. E., Bridger, G. J., Abrams, M. J., Longley, C. B., Burton, C. A., Larsen, S. K., Henson, G. W., Padmanabhan, S., Gaul, F. E., and Schwartz, D. A. (1997) Tumor imaging with technetium-99m-labeled hydrazinonicotinamide-Fab′ conjugates. *J. Nucl. Med. 38*, 133−138.

(17) Verbeke, K., Hjelstuen, O., Debrock, E., Cleynhens, B., De Roo, M., and Verbruggen, A. (1995) Comparative evaluation of ^{99}Tc^m-Hynic-HSA and ^{99}Tc^m-MAG$_3$−HSA as possible blood pool agents. *Nucl. Med. Commun. 16*, 942−957.

(18) Fischman, A. J., Rauh, D., Solomon, H., Babich, J. W., Tompkins, R. G., Kroon, D., Strauss, H. W., and Rubin, R. H. (1993) In vivo bioactivity and biodistribution of chemotactic peptide analogues in nonhuman primates. *J. Nucl. Med. 34*, 2130−2134.

(19) Liu, S., Edwards, D. S., Looby, R. J., Harris, A. R., Poirier, M. J., Barrett, J. A., Heminway, S. J., and Carroll, T. R. (1996) Labeling a hydrazino nicotinamide-modified cyclic IIb/IIIa receptor antagonist with ^{99m}Tc using aminocarboxylates as coligands. *Bioconjugate Chem. 7*, 63−71.

(20) Decristoforo, C. and Mather, S. J. (1999) 99m-Technetium-labeled peptide-HYNIC conjugates: effects of lipophilicity and stability on biodistribution. *Nucl. Med. Biol. 26*, 389−396.

(21) Ono, M., Arano, Y., Uehara, T., Fujioka, Y., Ogawa, K., Namba, S., Mukai, T., Nakayama, M., and Saji, H. (1999) Intracellular metabolic fate of radioactivity after injection of technetium-99m-labeled hydrazino nicotinamide derivatized proteins. *Bioconjugate Chem. 10*, 386−394.

(22) Ono, M., Arano, Y., Mukai, T., Uehara, T., Fujioka, Y., Ogawa, K., Namba, S., Nakayama, M., Saga, T., Konishi, J., Horiuchi, K., Yokoyama, A., and Saji, H. (2001) Plasma protein binding of ^{99m}Tc-labeled hydrazino nicotinamide derivatized polypeptides and peptides. *Nucl. Med. Biol. 28*, 155−164.

(23) Liu, S., Edwards, D. S., and Harris, A. R. (1998) A novel ternary ligand system for ^{99m}Tc-labeling of hydrazino nicotinamide-modified biologically active molecules using imine-N-containing heterocycles as coligands. *Bioconjugate Chem. 9*, 583−595.

(24) Ono, M., Arano, Y., Mukai, T., Fujioka, Y., Ogawa, K., Uehara, T., Saga, T., Konishi, J., and Saji, H. (2001) ^{99m}Tc−HYNIC-derivatized ternary ligand complexes for ^{99m}Tc-labeled polypeptides of low in vivo protein binding. *Nucl. Med. Biol. 28*, 215−224.

(25) Lee, Y. C., Stowell, C. P., and Krantz, M. J. (1976) 2-imino-2-methoxyethyl 1-thioglycosides: new reagents for attaching sugars to proteins. *Biochemistry 15*, 3956−3963.

(26) Stowell, C. P. and Lee, Y. C. (1980) Preparation of some new neoglycoproteins by amidination of bovine serum albumin using 2-imino-2-methoxyethyl 1-thioglycosides. *Biochemistry 19*, 4899−4904.

(27) Dubois, M., Gilles, K. A., Hamilton, J. K., Rebers, P. A., and Smith, F. (1956) Colorimetric method for determination of sugars and related substances. *Anal. Chem. 28*, 350−356.

(28) Gorevic, P. D., Prelli, F. C., and Frangione, B. (1985) Purification and characterization of serum immunoglobulins. *Methods Enzymol. 116*, 3−25.
(29) Hosoi, S., Nakamura, T., Higashi, S., Yamamuro, T., Toyama, S., Shinomiya, K., and Mikawa, H. (1982) Detection of human osteosarcoma-associated antigen(s) by monoclonal antibodies. *Cancer Res. 42*, 654−659.
(30) King, T. P., Zhao, S. W., and Lam, T. (1986) Preparation of protein conjugates via intermolecular hydrazone linkage. *Biochemistry 25*, 5774−5779.
(31) Koizumi, M., Endo, K., Kunimatsu, M., Sakahara, H., Nakashima, T., Kawamura, Y., Watanabe, Y., Saga, T., Konishi, J., Yamamuro, T., Hosoi, S., Toyama, S., Arano, Y., and Yokoyama A. (1988) ^{67}Ga-labeled antibodies for immunoscintigraphy and evaluation of tumor targeting of drug-antibody conjugate in mice. *Cancer Res. 48*, 1189−1194.
(32) Imai, S., Morimoto, J., Tsubura, T., Esaki, K., Michalides, R., Holms, R. S., Deimling, O., and Higlgers, J. (1986) Genetic marker patterns and endogenous mammary tumor virus genes in inbred mouse strains in Japan. *Exp. Anim. 35*, 263−276.
(33) Alquier, C., Guenin, P., Munari-Silem, Y., Audebet, C., and Rousset, B. (1985) Isolation of pig thyroid lysosomes. *Biochem. J. 232*, 529−537.
(34) Caimi, L., Marchesini, S., Aleo, M. F., Bresciani, R., Monti, E., Casella, A., Guidici, M. L., and Preti, A. (1989) Rapid preparation of a distinct lysosomal population from myelinating mouse brain using Percoll gradients. *J. Neurochem. 52*, 1722−1728.
(35) Distler, J. and Jourdian, G. W. β-Galactosidase from bovine testes. *Methods Enzymol. 50*, 514−520.
(36) Arano Y, Wakisaka K, Mukai T, Uezono T, Motonari H, Akizawa H, Kairiyama C, Ohmomo Y, Tanaka C, Ishiyama M, Sakahara H, Konishi J, and Yokoyama A. (1996) Stability of a metabolizable ester bond in radioimmunoconjugates. *Nucl. Med. Biol. 23*, 129−136.

BC010043K

Synthesis and Biodistribution of ^{211}At-Labeled, Biotinylated, and Charge-Modified Poly-L-lysine: Evaluation for Use as an Effector Molecule in Pretargeted Intraperitoneal Tumor Therapy

Sture Lindegren,*[,†,§] Håkan Andersson,[‡] Lars Jacobsson,[†] Tom Bäck,[†] Gunnar Skarnemark,[§] and Börje Karlsson[†]

Department of Radiation Physics, Göteborg University, Sahlgrenska University Hospital, SE-413 45 Göteborg, Sweden, Department of Oncology, Göteborg University, Sahlgrenska University Hospital, SE-413 45 Göteborg, Sweden, and Department of Nuclear Chemistry, Chalmers University of Technology, SE-412 96 Göteborg, Sweden. Received April 25, 2001; Revised Manuscript Received October 23, 2001

Poly-L-lysine (7, 21, and 204 kDa) has been evaluated as an effector carrier for use in pretargeted intraperitoneal tumor therapy. For the synthesis, the ϵ-amino groups on the poly-L-lysine were modified in three steps utilizing conjugate biotinylation with biotin amidocaproate *N*-hydroxysuccinimide ester (BANHS), conjugate radiolabeling with ^{211}At using the intermediate reagent N-succinimidyl 3-(trimethylstannyl)benzoate (m-MeATE), and charge modification using succinic anhydride, resulting in an increase in the molecular weight of approximately 80% of the final product. The labeling of the m-MeATE reagent and subsequent conjugation of the polymer were highly efficient with overall radiochemical yields in the range of 60−70%. The in vitro avidin binding ability of the modified polymer was almost complete (90−95%), as determined by binding to avidin beads using a convenient filter tube assay. Following intraperitoneal (ip) injection in athymic mice, the 13 kDa polymer product was cleared mainly via the kidneys with fast kinetics (biological half-live $T_b \approx 2$ h) and with low whole-body retention. The clearance of the 38 kDa polymer was distributed between kidneys and liver, and the 363 kDa polymer was mainly sequestered by the liver with a T_b of 8 h. Increased tissue uptake in the thyroid, lungs, stomach, and spleen following the distribution of the large effector molecules (38 and 363 kDa) suggests that degradation of the polymers by the liver may release some of the label as free astatine/astatide.

INTRODUCTION

Intraperitoneal tumors may arise from disseminated carcinomas, especially those originating from the ovaries. Generally, patients with ovarian cancer have advanced disease at the time of diagnosis (FIGO[1] stage IIB−IV) and, as a rule, tumor dissemination is restricted to the peritoneal surface. The standard treatment for ovarian cancer is surgery followed by chemotherapy. However, despite a high initial curative response, most tumors relapse and the 5-year survival is no higher than 30%. The residual and recurrent tumor cells respond weakly to further chemotherapy, and new, more effective forms of treatment are therefore urgently required.

Endoradiotherapy using radiohalogenated monoclonal antibodies has been investigated in recent years in an effort to improve the therapeutic effect of treatment of ovarian carcinomas (*1, 2*). The halogen of main interest has been the β-emitter ^{131}I, which has also been employed in clinical studies (*3, 4, 5*). Recently, ^{211}At, the heaviest element in the halogen group, has been the focus of attention for use in radioimmunotherapy (RIT) (*6, 7*). ^{211}At is a radionuclide-emitting α-particles (i.e. high-LET radiation) with a range of 50−80 μm in human tissue. As tumor spread in patients with ovarian cancer is primarily in the form of peritoneal micrometastases, ^{211}At may be a suitable choice of nuclide for adjuvant intraperitoneal radioimmunotherapy for this form of malignancy.

Despite some promising clinical reports on RIT of ovarian cancer, the clinical application of radiolabeled antibodies has so far been limited, mainly because of the unfavorable in vivo distribution, resulting in low tumor uptake, low target-to-nontarget ratios, and slow clearance rates from normal tissues (*8*).

Pretargeted radioimmunotherapy (PRIT) in which a tagged antibody is preadministered for tumor targeting, followed by administration of a labeled ligand (effector molecule) as a multistep delivery system, has been proposed to improve the pharmacokinetics of the label in vivo. For this purpose, avidin and biotin are the most commonly used intermediates because of their high-affinity binding characteristics (*9, 10*). It has been shown, utilizing various protocols based on the biotin−avidin system for PRIT that, due to a more favorable in vivo distribution of the labeled effector molecule, significantly improved tumor uptake and tumor-to-normal-tissue ratios could be achieved (*11, 12, 13, 14*). In most cases, the

* To whom correspondence should be addressed. Sture Lindegren, Department of Radiation Physics, Sahlgrenska University Hospital, SE-413 45 Göteborg, Sweden; Fax: +46 31 822 493; E-mail: sture.lindegren@radfys.gu.se.

† Department of Radiation Physics, Göteborg University.

‡ Department of Oncology, Göteborg University.

§ Chalmers University of Technology.

[1] Abbreviations used: BANHS, biotinamidocaproate *N*-hydroxysuccinimide; m-MeATE, *N*-succinimidyl 3-(trimethylstannyl)benzoate; mAb, monoclonal antibody; DMF, dimethylformamide; FPLC, fast protein liquid chromatography; FIGO, International Federation of Gynecology and Obstetrics; HABA, 2-(4′-hydroxyazobenzene)benzoic acid; PBS, phosphate-buffered saline; TNBSA, 2,4,6-trinitrobenzenesulfonic acid; NS[^{125}I]IB, *N*-succinimidyl 3-[^{125}I]iodobenzoate; NS[^{211}At]AtB, *N*-succinimidyl 3-[^{211}At]astatobenzoate.

10.1021/bc010054d CCC: $22.00 © 2002 American Chemical Society
Published on Web 04/17/2002

effector molecule is a conjugate of a biotin and radionuclide, which exhibits rapid in vivo clearance and low uptake in normal tissue (*15, 16*).

In a few investigations, poly-L-lysine has been explored as a multicarrier of biotin and radionuclides for pretargeted radioimmunotherapy (*17, 18*). The advantages of these polymer conjugates are that increased avidity for avidin and higher specific radioactivity may be achieved. Furthermore, the available molecular weight range of poly-L-lysine may allow increased control of the biodistribution compared with the mono-derivative of biotin.

In this study, the synthesis and distribution of biotinylated, astatinated, and charge-modified poly-L-lysine, as a prospective effector molecule for use in pretargeted intraperitoneal tumor therapy, have been investigated. Three different average sizes of the polymer (7, 21, and 204 kDa) were evaluated with respect to radiolysis after astatine exposure, in vitro biotin binding capacity to avidin, and in vivo biodistribution and biological half-life in nude mice.

EXPERIMENTAL PROCEDURES

Materials. Poly-L-lysine (7, 21, and 204 kDa), biotinamidocaproate *N*-hydroxysuccinimide ester, *N*-bromsuccinimide (NBS), and *N*-iodosuccinimide (NIS) were purchased from Sigma Chemical Co. Avidin (ImmunoPure Avidin), Avidin beads (ImmunoPure Immobilized Avidin Gel), 2-(−4-hydroxyazobenzene)benzoic acid (HABA), and 2,4,6-trinitrobenzenesulfonic acid (TNBSA) were obtained from Pierce Chemical Co. All other nonradioactive commercial chemicals and solvents used were of analytical grade or better.

^{211}At was produced by the ^{209}Bi(α,2n)^{211}At reaction (*19*) on the Scanditronic MC32−NI cyclotron at the Cyclotron and PET Unit, Rigshospitalet, Copenhagen, Denmark. Na[^{125}I]I was obtained from NEN Life Science Products Inc.

General. After irradiation, the target was immediately shipped to the Department of Radiation Physics, Göteborg, and the astatine was isolated from the target by dry-distillation, according to the method described previously (*19*). The radioactivity was measured using an ionization chamber (Capintech CRC-15) utilizing proper settings for ^{211}At, cross-calibrated for the 70−90 keV ^{211}Po X-rays in a NaI(Tl) detector (Wizard Wallac γ-well counter, Finland). The biological half-life of the astatinated polymers in athymic mice was determined by measurement of whole-body radioactive content using a NaI(Tl) scintillation detector (Harshaw Chemie B.V.)

High performance liquid chromatography, HPLC, was conducted on a Waters 600/486 system with the Waters Baseline 820 analysis software. Reversed-phase chromatography was performed using a Kromasil C-18 (4.6 × 250 mm) column (EKA-Nobel AB, Sweden), and size-exclusion analysis was carried out on a Superdex-200 FPLC column (Amersham Pharmacia Biotech, Sweden). Preparative gel-permeability chromatography was conducted on disposable Sephadex G-25 PD-10 columns (Amersham Pharamacia Biotech, Sweden). Mass spectral data were obtained by inductively coupled plasma ion source mass spectroscopy (ICP-MS).

Labeling of *N*-Succinimidyl-3-(trimethylstannyl)-benzoate. The labeling of *N*-succinimidyl-3-(trimethylstannyl)benzoate, m-MeATE, was performed using the procedure previously reported (*20*). Briefly, to a 1.3-mL reaction vial containing 20−30 MBq ^{211}At as dry residue were added 0.5 nmol of *N*-iodosuccinimide and 1.0 nmol of m-MeATE in 1% acetic acid/methanol. The m-MeATE was reacted with the halogen for 15 min during gentle agitation at room temperature. The reaction was stopped by the addition of 50 nmol of $Na_2S_2O_5$. Iodination of the precursor was accomplished in essentially the same way as the astatination, except that *N*-bromosuccinimide (NBS) was used as the oxidizing agent.

The labeling efficiency was determined by running an aliquot of the reaction mixture on a reversed-phase C-18 column, isocratically eluted with acetonitrile/2 mM phosphoric acid 60:40 as the mobile phase. The product, *N*-succinimidyl-3-[^{211}At]astatobenzoate (NS[^{211}At]AtB) or *N*-succinimidyl-3-[^{125}I]iodobenzoate (NS[^{125}I]IB), was used immediately, unpurified for conjugation to the biotinylated polymer.

Modification of Poly-L-lysine. *Biotinylation.* Biotinamidocaproate *N*-hydroxysuccinimide ester (BANHS) was dissolved in dimethylformamide (DMF) to a concentration of 5−10 mg/mL. To poly-L-lysine in 0.2 M carbonate buffer pH 8.5 was added a 10−20-fold molar excess of the biotinylation reagent during vigorous agitation, and the reaction was allowed to proceed for 1 h during gentle agitation at room temperature. Further chemistry was conducted on the crude biotinylated product.

Conjugate Labeling. Prior to conjugate labeling of the biotinylated polymer, NIS in the labeling mixture was promptly reduced by the addition of 50 nmol of sodium metabisulfite, and the organic fraction of the solvent was evaporated under a gentle stream of nitrogen. To the labeling mixture was added 200 μg of the crude biotinylated poly-L-lysine to give a final volume of 50 μL, and conjugate labeling was allowed to proceed for 10 min during gentle agitation at room temperature.

Succinylation. The biotinylated and labeled polymer was finally reacted with succinic anhydride, in excess over available amines, to convert the remaining unsubstituted amino groups to carboxylic residues. Following conjugate labeling, solid succinic anhydride, in the form of flakes, was added to the reaction mixture. The pH was adjusted with 1 M carbonate buffer, pH 8.5, during the reaction in order to maintain the amino residues unprotonated. After 10 min reaction time, the polymer fraction was isolated by passage over a G-25 PD-10 column (Pharmacia, Sweden).

The final product was analyzed with respect to unbound radioactivity by methanol precipitation according to the method of Reist et al. (*21*), and the size by gel-filtration chromatography. The biotinylation efficiency was calculated using the HABA dye method (*22*), and degree of succinylation was determined using the TNBSA spectrophotometric method (*23*). The average molecular weights of the modified polylysines were estimated to be 13, 38, and 363 kDa.

Radiolysis of Poly-L-lysine after ^{211}At Exposure. To investigate radiolysis effects during labeling, nonmodified poly-L-lysine (204 kDa) was exposed to increasing activities, i.e., absorbed doses, of ^{211}At. Astatine, in chloroform, was added to Eppendorf tubes in a single point series, and the solvent was evaporated. The activities of the dry astatine residues were 0.80, 1.38, 4.85, and 11.7 MBq. A constant amount of poly-L-lysine (50 μL, 2 mg/mL) in 0.2 M carbonate buffer, pH 8.5, was then added to each tube.

The astatine was allowed to decay during agitation at 4 °C for 120 h (16.7 half-lives), resulting in absorbed doses to the volume of 0.66, 1.1, 4.0, and 9.5 kGy, as determined using basic dosimetry calculations derived from the following equations:

Number of ^{211}At decays (N):

$$N = \frac{A_0}{\lambda}(1 - e^{-\lambda t}) \text{ for complete decay } N = \frac{A_0}{\lambda}$$

where A_0 is the total radioactivity measured at the start of exposure, λ is the decay constant, and t is the total exposure time.

Absorbed dose (D):

$$D = \frac{E_{\text{abs}}}{m_{(\text{volume})}} \approx \frac{N\bar{E}_\alpha(1.6 \times 10^{-13})}{m_{(\text{volume})}}(\text{Gy})$$

where E_{abs} is the absorbed energy in the reaction volume (MeV), $\bar{E}_\alpha \approx 6.8$ MeV is the mean alpha particle energy (*24*), and m_{volume} is the mass of the solution (kg).

After radiation exposure, the polymer was labeled with ^{125}I according to the m-MeATE method and charge modified with succinic anhydride as described above. The effect of the radiation, i.e., fragmentation, was analyzed and compared with nonexposed, iodine-labeled, succinylated polymer by size-exclusion chromatography on a Superdex-200 column.

In Vitro Binding of Modified Polylysine. The biological function of the biotin moiety on the modified polylysine was examined by binding to avidin beads. Fifty microliters of the avidin bead slurry was transferred to Costar spin-x, 45 μm, filter tubes (Corning Inc., NY). An aliquot of the modified polymer (25 ng) was added, and the volume was adjusted to 150 μL with PBS. The effector molecule was reacted with the beads for 30 min at room temperature during agitation. The beads were then washed three times with PBS, and bound radioactivity was measured in a γ-well counter.

Nonspecific binding to avidin was determined by incubating nonbiotinylated, labeled polylysine with the beads, and nonspecific binding to the filter tubes was determined by incubation with the modified polymer in tubes not containing avidin beads.

Animal Experiments. The tissue distribution and whole-body retention of the 13, 38, and 363 kDa polymers were evaluated in female athymic mice (Balb/C nu/nu), 6−8 weeks of age. Following ip administration of the effector molecule (550−800 kBq in 500 μL of PBS) mice were sacrificed by cervical dislocation at 1, 3, 6, 18, and 24 h postinjection, in groups of four animals per point in time. Whole blood was collected by cardiac puncture immediately after the animals had been killed, and tissues including neck, lungs, stomach, liver, small intestine, large intestine, kidneys, spleen, intraperitoneal fat, and muscle were excised and washed in saline. The tissues were blotted dry and accurately weighed, and the radioactivity was measured in a γ-well counter. All tissue data were corrected for radioactive decay and expressed as the percent of injected radioactivity per gram of organ (%ID/g), except for the neck, where it was expressed as the percent of injected activity (%ID).

The biological half-life of the modified polymers was evaluated by following the whole-body radioactive retention in groups of 5 mice for 24, hours measured with a sodium iodide detector.

RESULTS

The radioactivity of the irradiated target was in the range of 200 to 300 MBq ^{211}At upon arrival in Göteborg. Isolation of ^{211}At was conducted by dry-distillation of the target material, and recovery yields of 70−80% of the initial ^{211}At activity were routinely obtained within a 20-min preparation time. Aliquots of the recovered astatine were immediately used for conjugate labeling via the ϵ-amino groups on poly-L-lysine, utilizing the intermediate labeling reagent m-MeATE. Radiohalogenation of the m-MeATE resulted in labeling yields of 85−95% for both the NS[^{125}I]IB and the NS[^{211}At]AtB product. Prior to the conjugate astatine labeling, the poly-L-lysine was biotinylated using biotin amidocaproate *N*-hydroxysuccinimide (BANHS) with an efficiency of 73−85% as determined by the HABA method (*22*). To avoid workup losses of radioactivity in ensuing conjugations, labeling and charge modification of the biotinylated polylysine were conducted in a single pot without purification of the labeling mixture. After conjugate labeling the poly-L-lysine was subjected to charge modification by complete conversion of the remaining unsubstituted primary amines to carboxylic residues using succinic anhydride. Because of the reaction conditions, the molecular weight of the final product was increased by approximately 80% since the modification by means of the number of substitutents per polymer were in the order ^{211}At ≪ biotin ≪ succinic acid. However, charge modification is essential, as it decreases nonspecific adsorption both in vitro and in vivo. Generalized structural formulas of the reacting species and the final product are shown in Figure 1.

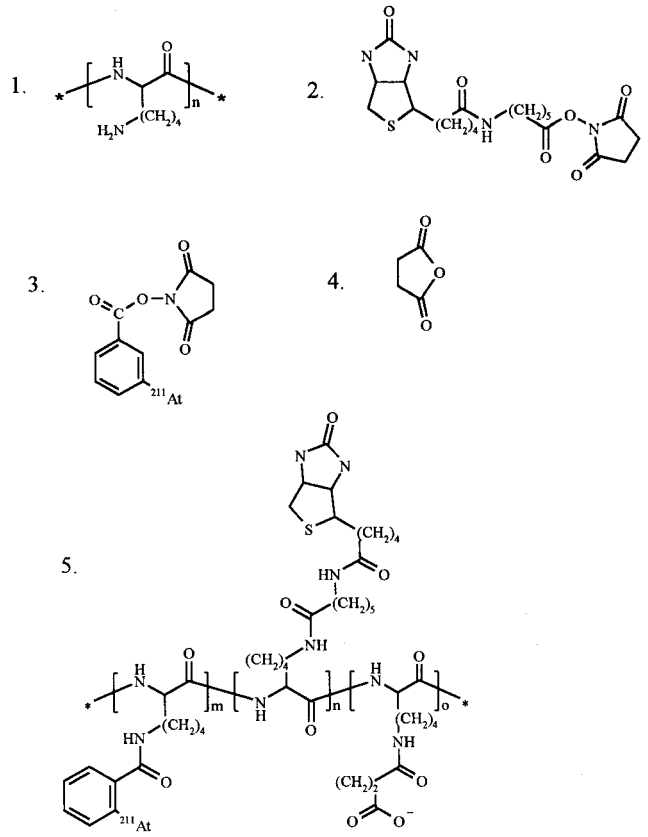


Figure 1. Generalized structural formula for (1) poly-L-lysine, (2) *N*-succinimidyl 3-[^{211}At]astatobenzoate (NS[^{211}At]AtB), (3) biotinamidocaproate *N*-hydroxysuccinimide (BANHS), (4) succinic anhydride, (5) modified poly-L-lysine (^{211}At−PL$_{suc}$−B).

Good conjugation yields of 70 ± 5% were achieved in the coupling of NS[^{211}At]AtB to polylysine, corresponding to a mean radiochemical yield of 63 ± 4%. Since the labeling procedure involved an excess of the m-MeATE reagent over astatine and the labeling reaction mixture is used in unpurified form for conjugation to the polylysine, the precursor may also be present (i.e. conjugate coupled) in the final product. Organic tin, the $Sn(CH_3)_3$

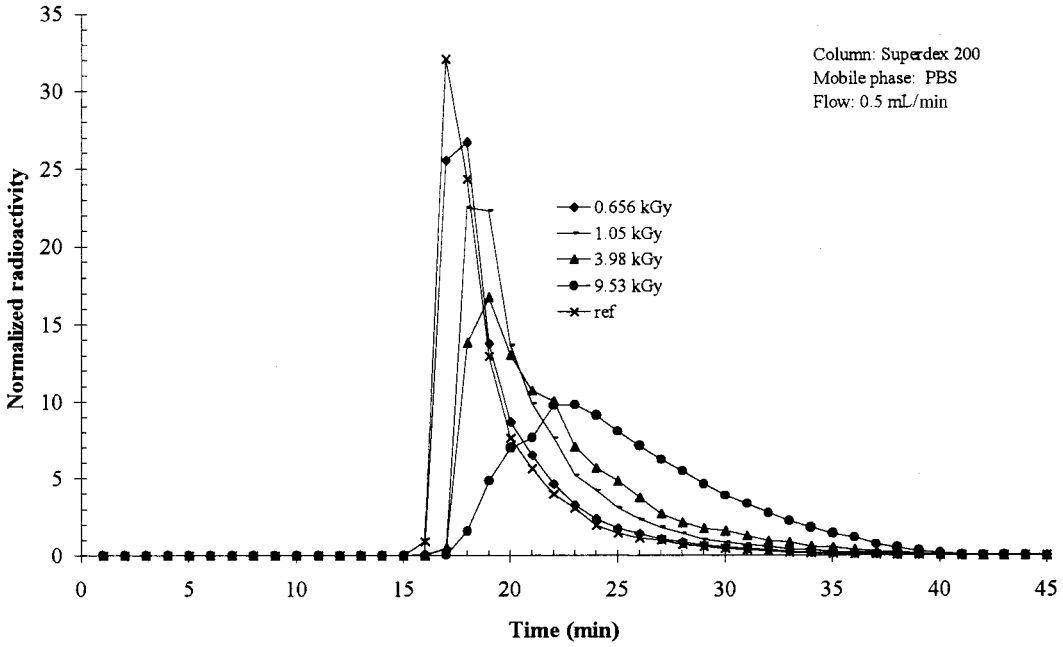


Figure 2. Size-exclusion analysis of poly-L-lysine (204 kDa) exposed to 0.656−9.53 kGy of ^{211}At. Determination were performed on the ^{125}I-labeled and succinylated derivative.

Table 1. Tissue Distribution of ^{211}At Labeled, Biotinylated, and Charge-Modified Poly-L-lysine (386 kDa average molecular weight) in Athymic Mice[a]

	^{211}At−PL_{suc}−B (363 kDa)				
tissue	1 h	3 h	6 h	18 h	24 h
blood	2.02 ± 0.63	2.48 ± 1.03	1.21 ± 0.13	0.49 ± 0.10	0.34 ±0.17
neck[b]	0.09 ± 0.05	0.59 ± 0.18	1.10 ± 0.32	0.92 ± 0.19	0.85 ± 0.53
lung	2.72 ± 0.50	7.48 ± 1.53	6.46 ± 0.38	2.32 ± 0.47	1.65 ± 0.62
liver	5.45 ± 0.71	3.58 ± 0.73	1.18 ± 0.32	0.36 ± 0.09	0.25 ± 0.10
stomach	3.36 ± 1.19	8.69 ± 1.80	9.90 ± 2.67	4.76 ± 1.30	3.88 ± 1.48
small intestine	0.92 ± 0.19	2.50 ± 0.81	1.98 ± 0.50	0.68 ± 0.23	0.56 ± 0.31
large intestine	1.05 ± 0.48	2.01 ± 0.43	1.81 ± 0.37	0.75 ± 0.20	0.61 ± 0.22
kidney	3.00 ± 0.73	3.75 ± 0.73	2.67 ± 0.30	1.17 ± 0.27	0.86 ± 0.40
spleen	6.23 ± 0.38	9.48 ± 2.57	4.71 ± 0.93	1.02 ± 0.50	0.64 ± 0.37
ip fat	3.07 ± 1.54	2.82 ± 0.89	1.72 ± 0.52	0.51 ± 0.07	0.52 ± 0.22
muscle	1.18 ± 0.52	0.84 ± 0.33	0.53 ± 0.19	0.15 ± 0.03	0.14 ± 0.03

[a] Results are given as mean ± standard deviation of the percent of injected dose per gram tissue (%ID/g); n = four animals per time point. [b] Results are expressed as the percent of injected dose (%ID).

group, may be toxic if released in vivo, and the modified polymers were therefore subjected to ICP-MS analysis. Only <10 pg tin, corresponding to <0.0003% of in put amount of the m-MeATE precursor was detected in the spectra. This is probably due to differences in solubility of the precursor and the labeled reagent in the conjugation buffer.

The radiochemical purity of the products was always greater than 95%, as determined by methanol precipitation and by size-exclusion analysis. However, when subjecting the polymer to astatine activities that resulted in a high absorbed dose to the reaction volume, radiolysis effects, i.e., fragmentation, of the polylysine, occurred. As can be seen in Figure 2, the polymer is gradually decomposed when exposed to absorbed doses above 660 Gy, with an initially high degree of large fragments at 1100 Gy and increasingly smaller fragments at higher exposures.

The biotin binding ability of the modified polymer product was examined by means of its reaction with avidin beads using a fast, convenient filter tube assay. Almost complete biotin binding (90−95%) to the beads was achieved with low, nonspecific binding to the tubes. Even when labeling at high absorbed doses, in the range where fragmentation occurred, the degree of biotin binding was high. Low nonspecific binding to avidin beads was demonstrated by subjecting the beads to nonbiotinylated labeled polylysine.

The tissue distribution and whole-body retention of the 13, 38, and 363 kDa molecular weight effector molecules were evaluated in nude mice following intraperitoneal administration. The tissue distribution data for the polymers from one to 24 h are summarized in Tables 1−3. As can be seen, the distributions of the 38 and 363 kDa effector molecule show uptake in stomach (14.74 and 9.90% ID/g), lungs (6.74 and 7.48% ID/g), and spleen (7.64 and (9.48% ID/g) reaching a maximum at 1−3 h and 3−6 h postinjection. The radioactivity was thereafter slowly cleared from the tissues. The thyroid, known to accumulate astatide (*25*), shows increasing uptake at 3 to 6 h (0.65 and 1.1% ID) with a slight decrease over the remaining time of observation. Note that the thyroid was not dissected from the neck, and the results are therefore expressed as the percent of injected dose (% ID). All other organs show low uptake including the blood, which exhibited a maximum uptake of (2.48% ID/g) at 3 h.

Compared with the larger polymers, the tissue distribution of the 13 kDa effector molecule shows lower uptake in all tissues except for the kidneys, 1 h postin-

Table 2. Tissue Distribution of ^{211}At-Labeled, Biotinylated, and Charge-Modified Poly-L-lysine (38 kDa average molecular weight) in Athymic Mice[a]

	^{211}At−PL_{suc}−B (38 kDa)				
tissue	1 h	3 h	6 h	18 h	24 h
blood	3.00 ± 0.88	1.37 ± 0.22	0.83 ± 0.12	0.29 ± 0.06	0.31 ± 0.04
neck[b]	0.21 ± 0.04	0.64 ± 0.09	0.62 ± 0.12	0.50 ± 0.20	0.41 ± 0.07
lung	4.48 ± 1.07	6.74 ± 1.39	4.67 ± 0.74	1.65 ± 0.31	1.69 ± 0.23
liver	3.48 ± 0.47	1.47 ± 0.17	0.88 ± 0.15	0.25 ± 0.05	0.27 ± 0.03
stomach	5.93 ± 2.16	14.74 ± 2.45	8.64 ± 3.90	2.48 ± 0.59	3.34.± 1.22
small intestine	1.93 ± 0.49	1.76 ± 0.14	1.16 ± 0.24	0.53 ± 0.17	0.77 ± 0.14
large intestine	2.00 ± 0.20	1.74 ± 0.20	1.11 ± 0.10	0.40 ± 0.08	0.67 ± 0.12
kidney	14.67 ± 1.58	3.89 ± 0.52	2.32 ± 0.40	0.95 ± 0.31	0.85 ± 0.07
spleen	7.64 ± 1.19	7.37 ± 1.65	4.28 ± 1.28	0.93 ± 0.33	0.64 ± 0.11
ip fat	4.99 ± 0.59	3.20 ± 0.42	1.91 ± 0.30	0.45 ± 0.06	0.61 ± 0.32
muscle	2.22 ± 0.65	0.41 ± 0.08	0.26 ± 0.04	0.11 ± 0.03	0.14 ± 0.01

[a] Results are given as mean ± standard deviation of the percent of injected dose per gram tissue (%ID/g); n = four animals per time point. [b] Results are expressed as the percent of injected dose (%ID).

Table 3. Tissue Distribution of ^{211}At-Labeled, Biotinylated, and Charge-Modified Poly-L-lysine (13 kDa average molecular weight) in Athymic Mice[a]

	^{211}At−PL_{suc}−B (13 kDa)				
tissue	1 h[b]	3 h	6 h	18 h	24 h
blood	3.15 ± 0.95	0.81 ± 0.09	0.51 ± 0.10	0.21 ± 0.04	0.15 ± 0.04
neck[c]	0.36 ± 0.37	0.25 ± 0.07	0.28 ± 0.12	0.16 ± 0.06	0.16 ± 0.07
lung	5.36 ± 0.78	4.53 ± 0.38	3.26 ± 0.67	1.23 ± 0.16	0.93 ± 0.19
liver	1.37 ± 0.19	0.76 ± 0.05	0.55 ± 0.11	0.18 ± 0.03	0.16 ± 0.03
stomach	3.71 ± 0.53	5.55 ± 1.55	3.90 ± 1.02	1.68 ± 0.21	1.85 ± 0.39
small intestine	1.37 ± 0.24	1.15 ± 0.31	0.77 ± 0.18	0.35 ± 0.09	0.40 ± 0.32
large intestine	2.05 ± 0.41	1.19 ± 0.09	0.83 ± 0.12	0.32 ± 0.06	0.27 ± 0.03
kidney	18.53 ± 1.26	2.31 ± 0.23	1.36 ± 0.25	0.54 ± 0.11	0.38 ± 0.04
spleen	4.85 ± 1.11	3.58 ± 0.50	2.58 ± 0.59	0.51 ± 0.06	0.62 ± 0.40
ip fat	4.10 ± 2.40	0.88 ± 0.08	0.65 ± 0.15	0.22 ± 0.05	0.19 ± 0.05
muscle	0.72 ± 0.15	0.41 ± 0.04	0.27 ± 0.06	0.17 ± 0.09	0.13 ± 0.06

[a] Results are given as mean ± standard deviation of the percent of injected dose per gram tissue (%ID/g); n = four animals per time point. [b] n = Three animals. [c] Results are expressed as the percent of injected dose (%ID).

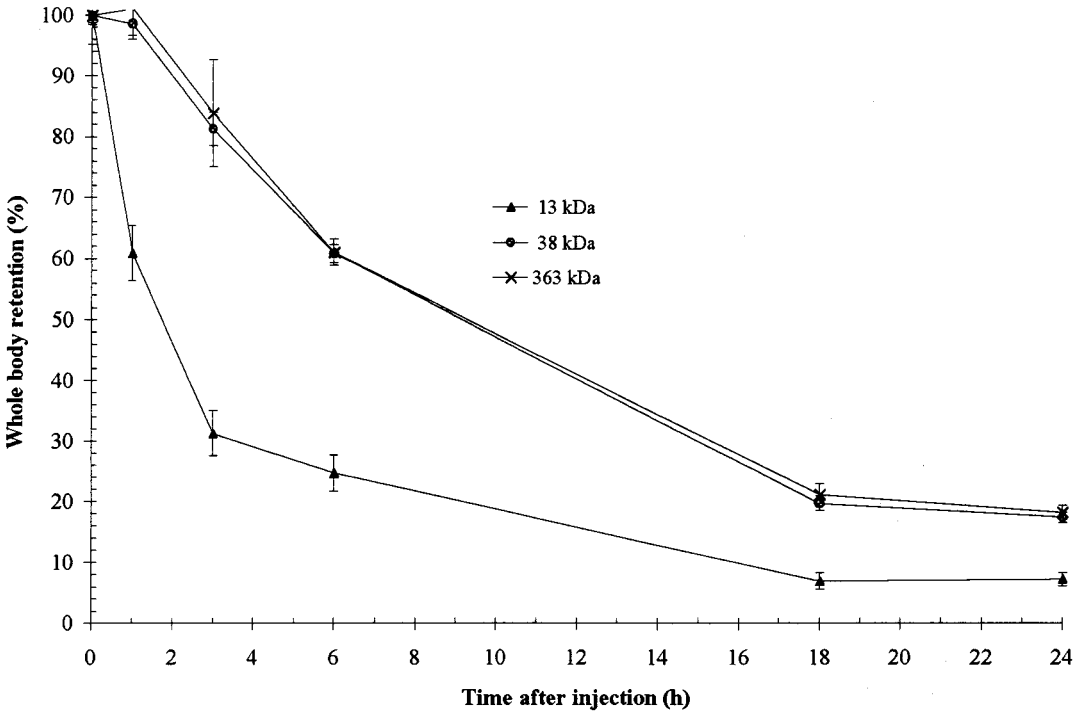


Figure 3. The whole-body retention of the 13, 38, and 363 kDa effector molecule in nude mice, following intraperitoneal administration. Results are given as mean ± SEM for four animals per time point.

jection, which may be due to the rapid clearance mainly through the kidneys. The whole-body retention of the astatinated polymers is presented in Figure 3. The results show that whole-body clearance is fast, with biological half-lives of 2 and 8 h for the low- and high-molecular-weight effector molecules, respectively. This is also reflected in the low tissue content at the later points in time.

DISCUSSION

Since the development of the hybridoma technology (*26*) monoclonal antibodies have been used for a variety of applications. Using this method it is possible to produce monoclonal antibodies specific to virtually any molecule of interest. In vivo, one of the challenges has been to develop a novel radioimmunopharmaceutical for tumor imaging and therapy. However, due to the size and passive distribution processes of in vivo administered antibodies, only a small fraction of the injected activity will bind to tumor cells. The remaining non-tumor-bound antibody is evenly distributed and slowly cleared from the body, causing undesirable background and elevated dose to normal tissue. To circumvent the unfavorable distribution of labeled antibodies, pretargeting strategies utilizing the high-affinity binding characteristics between biotin and avidin as intermediates for multistep administration, have been proposed by several investigators (*12, 13, 14*). Various biotin derivatives have been developed for cross-linking and for labeling with radionuclides to provide effector molecules for pretargeting.

The aim of this study was to produce biotin-polylysine-based effector molecules for use in pretargeted ovarian tumor therapy. Ovarian tumors disseminate primarily to the peritoneal surface as microtumors, and therefore a suitable choice of nuclide may be the α-emitter ^{211}At. Following the decay, the α-particles deposit a considerable amount of energy in a micro-volume, and calculations have shown that only a few astatine decays per cell are required to cause lethal radiation damage (*27*). Previous experiments by our research group have also demonstrated the high cell-killing effect of astatine in vitro (*28*) and in vivo (*7*) when subjecting ovarian cancer cells and microtumors to the astatine-labeled ovarian-tumor-specific monoclonal antibody MOv18. On the basis of the encouraging results of those studies, improvement in the pharmacokinetics to minimize the irradiation of normal tissue was suggested, employing a pretargeting strategy that involves polylysine as an effector carrier. Poly-L-lysine was used since each molecule, depending on the polymerization degree, contains a number of ϵ-amino groups that can readily be derivatized with different *N*-acylation reagents, thus allowing bifunctional conjugate modification. Apart from this facile chemistry, polylysine can be obtained as mono-amino acid- or copolymers of different molecular weights, which may permit increased control of the biodistribution of the effector molecule.

Applications utilizing polylysine as carriers for nuclides have previously been proposed, such as a polychelating agent for high-specific-activity metal-nuclide binding of antibodies, for use in single-photon emission computed tomography (SPECT) and magnetic resonance tomography, and for therapy (*29*). The application of polylysine as an effector carrier for use in PRIT has also been reported (*17, 18*).

In this study, polylysine (7, 21, and 204 kDa) was modified by conjugate coattachment of the biotin reagent (BANHS), the astatine-labeled reagent NS[^{211}At]AtB, and succinic anhydride in a simple three-step procedure. The product could easily be obtained, with the reaction conditions employed, ^{211}At activities of 10−20 MBq (100 kBq/μg), in a short preparation time, and preliminary experiments suggest that the procedure can be scaled up to higher astatine activities, e.g. for clinical applications. However, it should be noted that the polylysine is sensitive to radiolysis from the astatine decay in the reaction volume. The molecule can be subjected to an absorbed dose of about 700 Gy without any apparent damage, as determined by size-exclusion chromatography analysis. Increasing the dose above this level resulted in gradual fragmentation with random molecular breakdown at 700−1000 Gy and almost complete decomposition at higher doses (4000−10000 Gy). This is in good agreement with the observations of Larsen and Bruland who studied α-particle-induced radiolysis effects on antibodies and found that an absorbed dose of 1000 Gy could be tolerated with no or minor affects on the immunoreactivity (*30*).

The only biologically active part of the effector molecule is the biotin moiety which, surprisingly, was not affected to any high extent by the radiation dose, as determined by binding the effector molecule exposed to a high-absorbed dose to avidin beads. We suggest that the radiation resistance is dependent on the size of the molecule, implying that biotin could withstand much higher absorbed doses than the polymers. In this study, biotin substitution was performed with a 10−20-fold excess of reagent over polymer to ensure uniform attachment on a molar basis, which resulted in approximately 8−16 biotin molecules per polymer. Uniform biotinylatation of the low specific radioactive product was confirmed by high binding efficiency to avidin beads. A very high degree of biotin attachment to the polymer is possible, with ultimately complete biotinylation, except for the label, which would give a tremendous increase in avidity for avidin. However, most of the biotin derivatives commercially available have limited aqueous solubility, and this may affect the labeling chemistry and the solubility of the final product (*31*). Moreover, problems associated with cleavage of the biotin nuclide or carrier bond in vivo due to systemic biotinidase activity when utilizing the commercially available reagents have been reported (*32, 33*). To circumvent these problems Foulon et al. have developed new biotin compounds for labeling with radiohalogens, e.g. ^{211}At and iodine isotopes, which are resistant to biotinidase activity (*16*). Several new biotin derivatives for conjugate labeling have also been explored by Wilbur et al. with regard to solubility and avidin binding characteristics, as well as biotinidase resistance to identify the derivative with the best properties for in vivo applications (*31, 34*).

The effector molecules studied in the present work were evaluated regarding the tissue distribution following ip injection in nude mice during 24 h postadministration. Significant differences in tissue uptake between the 13 kDa and the larger polymers were seen, which are related to different clearance routes. All molecules enter the circulation from the peritoneal cavity, and their sizes predetermine that the 13 kDa polymer is cleared mainly via the kidneys, the 38 kDa polymer through liver and kidneys and the 363 kDa polymer is sequestered primarely by the liver. Compared with the 13 kDa polymer, a higher uptake of the 38 and 363 kDa polymers was observed in the thyroid gland, stomach, lungs, and spleen, which may reflect the release of astatine/astatide after degradation in the liver. This might be a limiting factor for prospective clinical use, but the astatine/astatide uptake may be decreased by the use of blocking agents, as proposed by Larsen et al., thus limiting the absorbed dose to these tissues (*35*). The normal tissue at greatest risk is the bone marrow but, because the residence time of the three effector molecules in the circulation following intraperitoneal administration is short, and provided that there are no active uptake mechanisms, the dose to the bone marrow is likely to be limited. Compared with astatinated IgG antibodies, the

radioactive content in the blood is of the order of at least 10 times less for the large polymers and a factor of 20 less for the small polymer (*36*). Therefore, increased absorbed dose to tumor tissue might be achieved in PRIT utilizing polylysine as the effector carrier as higher activities of the astatinated effector molecule can be administered without increasing the radiotoxic effects on normal tissues, i.e., the bone marrow.

In summary, the preparation, in vitro avidin binding characteristics and biodistribution of biotinylated, astatinated, and charged modified poly-L-lysine of different molecular weights for prospective use as an effector molecule in pretargeted intraperitoneal tumor therapy were investigated. Following ip administration, the three modified polymers studied showed low whole-body retention with clearance routes determined by the size of the molecules. Somewhat higher uptakes of radioactivity in normal tissues were observed for the high-molecular-weight effector molecules, suggesting that for clinical applications a low-molecular-weight poly-L-lysine should be used for derivatization. However, application using a complete pretargeted intraperitoneal tumor model may contribute to lowering normal tissue uptake due to reduced escape of the effector molecule from the peritoneal cavity by binding to its mAb−avidin conjugate at the tumor target. Therefore, further investigations will be focused on more homogeneous preparations of both high- and low-molecular-weight poly-L-lysine for the modification, new biotinidase-resistant water-soluble derivatives and scale-up of the labeling procedure to meet the requirements for patient studies.

ACKNOWLEDGMENT

We would like to thank Elisabet Warnhammar (Department Oncology, Göteborg University, Sweden) and Jörgen Elgquist (Department of Radiation Physics, Göteborg University, Sweden) for excellent technical assistance with the animal study. Thanks are due to Dr. Stig Palm (Department of Radiation Physics, Göteborg University, Sweden) for help with the dosimetry evaluation and Arvid Ödegaard-Jensen (Department of Nuclear Chemistry, Chalmers University of Technology) for help with mass spectral analysis. This work was supported by grants from the Swedish Cancer Foundation (Grant 3548) and the King Gustaf V Jubilee Clinic Cancer Research Foundation in Göteborg, Sweden.

LITERATURE CITED

(1) Senekowisch, R., Schmid, p., Möllenstädt, S., Kriegel, H., and Pabst, H. W. (1989) Experimental model for radioimmunotherapy of human ovarian carcinoma with I-131-labeled monoclonal antibody OC125. *Strahlenther onkol. 165*, 564−566.

(2) Molthoff., C. F. M., Pinedo, H. M., Schlüper, H. M. M., and Boven, E. (1992 a) Influence of dose and schedule on therapeutic efficacy of ^{131}I-labeled monoclonal antibody 139H2 in a human ovarian cancer xenograft model. *Int. J. Cancer 51*, 108−115.

(3) Epenetos, A. A., Munro A. J., Stewart, S., Rampling, R., Lambert, H. E., McKenzie, C. G., Soutter, P., Rahemtulla, A., Hooker, G., Sivolapenko, G. B., Snook, D., Courtneay-Luck, N., Dhokia, B., Krausz, T., Taylor-Papadimitriou, J., Durbin, H., and Bodmer, F. (1987) Antibody-guided irradiation of advanced ovarian cancer with intraperitoneally administered radiolabeled monoclonal antibodies. *J. Clin. Oncol. 5*, 1890−1899.

(4) Molthoff, C. F., Buist, R. M., Kenemans, P., Pinedo, H. M., and Boven, E. (1992) Experimental and Clinical Analysis of the Characteristics of a Chimeric Monoclonal Antibody, MOv18, Reactive With an Ovarian Cancer-Associated Antigen. *J. Nucl. Med. 33*, 2000−2005.

(5) Crippa, F., Bolis, G., Seregni, E., Gavoni, N., Scarfone, G., Ferraris, C., Buraggi, G. L., and Bombardieri, E. (1995) Single-dose intraperitoneal radioimmunotherapy with the murine monoclonal antibody I-131 MOv18: Clinical results in patients with minimal residual disease of ovarian cancer. *Eur. J. Cancer 31A*, 686−690.

(6) Zalutsky, M. R., McLendon, R. E., Garg, P. K., Archer, G. E., Schuster, J. M., and Bigner, D. D. (1994) Radioimmunotherapy of neoplastic meningitis in rats using an α-particle-emitting immunoconjugate. *Cancer Res. 54*, 4719−4725.

(7) Andersson H., Lindegren S., Bäck T., Jacobsson L., Leser G., and Horvath G. (2000) Radioimmunotherapy of nude mice with intraperitoneally growing ovarian cancer xenogaft utilizing ^{211}At-labeled monoclonal antibody MOv18. *Anticancer Res. 20*, 459−462.

(8) Halpern, E., and Dillman, R. O. (1987) Problems associated with radioimmunodetection and possibilities for future solutions. *J. Biol. Response Mod. 6*, 235−262.

(9) Stoldt, H. S., Aftab, F., Chinol, M., Paganelli, G., Luca, F., Testori, A., and Geragherty, J. G. (1997) Pretargeting Strategies for Radio-Immunoguided Tumour Localisation And Therapy. *Eur. J. Cancer. 33*, 186−192.

(10) Hnatowich, D. J., Virzi, F., and Ruskowski, M. (1987) Investigation of Avidin and Biotin for Imaging Applications. *J. Nucl. Med. 28*, 1294−1302.

(11) Chinol, M., Casalini, P., Maggiolo, M., Canevari, S., Omodeo, E. S., Caliceti, P., Veronese, F. M., Cremonesi, M., Chiolerio, F., Nardone, E., Siccardi, A. G., and Paganelli, G. (1998) Biochemical modifications of avidin improve pharmacokinetics and biodistribution, and reduce immunogenicity. *Br. J. Cancer 78*, 189−197.

(12) Zhang, M., Yao, Z., Sakahara, H., Saga, T., Nakamoto, Y., Sato, N., Zhao, S., Nakada, H., Yamashina, I., and Kunoshi, J. (1998) Effect of administration route and dose of streptavidin or biotin on the tumor uptake of radioactivity in intraperitoneal tumor with multistep targeting. *Nucl. Med. Biol. 25*, 101−105.

(13) Breitz, H. B., Weiden, P. L., Beaumier, P. L., Axworthy, D. B., Seiler, S. Su, F−M., Graves, S., Bryan, K., and Reno, J. M. (1999) Clinical optimization of pretargeted radioimmunotherapy with antibody-streptavidin conjugated and ^{90}Y-DOTA-biotin. *J. Nucl. Med. 41*, 131−140.

(14) Paganelli, G., Belloni, C., Magnani, P., Zito, F., Pasini, A., Sassi, I., Meroni, M., Mariani, M., Vignali, M., Siccardi, A. G., and Fazio, F. (1992) Two-Step Tumour Targetting in Ovarian Cancer Patients Using Biotinylated Monoclonal Antibodies and Radioactive Streptavidin. *Eur. J. Nucl. Med. 19*, 332−329.

(15) Wilbur, D. S., Hamlin, D. K., Pathare, P. M., and Weerawarna S. A. (1997) Biotin reagents for antibody pretargeting. synthesis radioiodination, and in vitro evaluation of biotinidase resistant biotin derivatives. *Bioconjugate Chem. 8*, 572−584.

(16) Foulon, C. F., Alston, K. L., and Zalutsky, M. R. (1998) Astatine-211-labeled biotin conjugates resistant to biotinidase for use in pretargeted radioimmunotherapy. *Nucl. Med. Biol. 25*, 81−88.

(17) Torchilin V. P. (1999) Biotin-conjugated polychelating agent. *Bioconjugate Chem. 10*, 146−149.

(18) del Rosario R. B., and Wahl R. L. (1992) Biotinylated iodopolylysine for pretargeted radiation delivery. *J. Nucl. Med. 34*, 1147−1151.

(19) Lindegren, S., Bäck, T., and Jensen, H. J. (2001) Dry-distillation of astatine-211 from irradiated bismuth targets: a time-saving procedure with high recovery yields. *Appl. Radiat. Isot. 55*, 157−160.

(20) Lindegren, S., Andersson, H., Bäck, T., Jacobsson, L., Karlsson, B., and Skarnemark, G. (2001) High-efficiency astatination of antibodies using *N*-iodosuccinimide as the oxidising agent in labeling of *N*-succinimidyl 3-(trimethylstannyl)benzoate. *Nucl. Med. Biol. 28*, 33−39.

(21) Reist C. J., Foulon C. F., Alston K., Bigner D. D., and Zalutsky M. R. (1999) Astatine-211 labeling of internalizing

anti-EGFRvIII monoclonal antibody using N-succinimidyl 5-[^{211}At]astato-3-Pyridincarboxylate. *Nucl. Med. Biol. 26*, 405−411.
(22) Green N. M. (1965) A spectrophotometric assay for avidin and biotin based on binding of dyes by avidin. *Biochem. J. 94*, 23c−24c.
(23) Cayot P., and Tainturier G. (1996) The quantification of protein amino groups by the trinitrobenzensulfonic acid method: A reexamination. *Anal. Biochem. 249*, 184−200.
(24) Weber D., Eckerman K., Dillman T., and Ryman J. (1989) *MIRD: Radionuclide data and decay schemes*, The Society of Nuclear Medicine, New York.
(25) Hamilton, J. G., Asling, C. W., Garrison, W. M., and Scott, K. G. (1953) The accumulation, metabolism and biological effects of astatine in rats and monkeys. *Univ. Calif. Publ. Pharmacol. 2*, 283−343.
(26) Köhler, G., and Milstein, C. (1975) Continuous cultures of fused cells secreting antibody of predefined specificity. *Nature 256*, 495−497.
(27) Ritter, R. H., Cleaver, J. E., and Tobias, C. A. (1977) Radiation induce a large proportion of nonrejoining DNA breaks. *Nature 266*, 635−655.
(28) Palm, S., Bäck, T., Claesson, I., Delle, U., Hultborn, R., Jacobsson, L., Köpf, I., and Lindegren, S. (2000) In vitro effects of free ^{211}At, ^{211}At−Albumin, and ^{211}At-monoclonal antibody compared to external photon irradiation for two human cancer cell lines. *Anticancer Res. 20*, 1005−1012.
(29) Torchilin, V. P., Klibanov, A. L., Nossiff, N. D., Slinkin, M. A., Strauss, H. W., Haber; E., Smirnov, V. N., and Khaw, B. A. (1987) Monoclonal Antibody Modification With Chelate-Linked High-Molecular-Weight Polymers: Major Increase in Polyvalent Cation Binding Without Loss of Antigen Binding. *Hybridoma 6*, 229−240.
(30) Larsen, R. H., and Bruland, Ø. S. (1995) Radiolysis of radioimmunoconjugates. Reduction in antigen-binding ability by α-particle radiation. *J. Labeled Compd. Radiopharm. 34*, 1009−1018.
(31) Wilbur, D. S., Pathare, P. M., Hamlin, D. K., Stayton, P. S., To, R., Klumb, L. A., Buhler, K. R., and Vesella, R. L. (1999) Development of new biotin/streptavidin reagents for pretargeting. *Biomol. Eng. 16*, 113−118.
(32) Hymes, J., and Wolf, B. (1996) Biotinidase and its role in biotin metabolism. *Clin. Acta 255*, 1−11.
(33) Foulon, C. F., Shoultz, B. W., and Zalutsky, M. R. (1997) Preparation and Biological Evaluation of Astatine-211 Labeled Biotin Conjugate: Biotinyl-3-[^{211}At]astatoanilide. *Nucl. Med. Biol. 24*, 135−143.
(34) Wilbur, D. S., Chyan, M.-K., Pathare, p. M., Hamlin, M. B., Frownfelter, M. B., and Kegly, B. B. (2000) Biotin reagents for antibody pretargeting. 4. Selection of biotin conjugates for in vivo application based on thier dissociation rate from avidin and streptavidin. *Bioconjugate Chem. 11*, 569−583.
(35) Larsen, R. H., Slade, S., and Zalutsky, M. R. (1998) Blocking [^{211}At]astatide accumulation in normal tissues: Preliminary evaluation of seven potential compounds. *Nucl. Med. Biol. 25*, 351−357.
(36) Garg, P. K., Harrison, C. L., and Zalutsky, M. R. (1990) Comparative tissue distribution of the α-emitter ^{211}At and ^{131}I as labels of a monoclonal antibody and F(ab′)$_2$ fragment. *Cancer Res. 50*, 3514−3520.

BC010054D

In Vitro Gene Transfection Using Dendritic Poly(L-lysine)

Mio Ohsaki,[†] Tatsuya Okuda,[†] Akihiro Wada,[‡] Toshiya Hirayama,[‡] Takuro Niidome,*[,†] and Haruhiko Aoyagi[†]

Department of Applied Chemistry, Faculty of Engineering, Nagasaki University, Nagasaki 852-8521, Japan, and Department of Bacteriology, Institute of Tropical Medicine, Nagasaki University, Nagasaki 852-8523, Japan.
Received July 3, 2001; Revised Manuscript Received February 25, 2002

Monodispersed dendritic poly(L-lysine)s (DPKs) of several generations were synthesized, and their characteristics as a gene transfection reagent were then investigated. The agarose gel shift and ethidium bromide titration assay proved that the DPKs of the third generation and higher could form a complex with a plasmid DNA, and the degree of compaction of the DNA was increased by the increasing number of the generation. The DPKs of the fifth and sixth generation, which have 64 and 128 amine groups on the surface of the molecule, respectively, showed efficient gene transfection ability into several cultivated cell lines without significant cytotoxity. In addition, the transfection efficiency of the DPK of the sixth generation was not seriously reduced even if serum was added at 50% of the final concentration into the transfection medium. Because we can strictly synthesize various DPK derivatives, which have several types of branch units, terminal cationic groups, and so on, they are expected to be a good object of study regarding the basic information on the detailed mechanism of gene transfection into cells. We also expect to be able to easily construct DPK-based functional gene carriers, e.g., DPKs modified by ligands such as a sugar chain, which can enable advanced gene delivery in vivo.

INTRODUCTION

Nonviral gene delivery systems into cells consist of cationic polymers, such as polylysine derivatives (*1*−*3*) and polyethleneimines (*4*), cationic lipids (*5*), or cationic oligopeptides (*6*−*10*) that electrostatically form a complex with the negatively charged DNA that can be taken up by the cells. In 1993, novel gene delivery techniques, in which cationic polyamidoamine (PAMAM[1]) cascade polymers are used as a gene carrier into cells, have been reported by Haensler et al. (*11*). The dendrimers showed high levels of transfection in a wide variety of cultivated cells with less toxicity. They then reported that stringently synthesized and purified, monodispersed PAMAM dendrimers showed low levels of transfection. However, the activity was dramatically enhanced by heat treatment in a solvolytic solvent (*12*, *13*). In those reports, they suggested that the increase in transfection efficiency after the degradation is due to the increase in flexibility that enables the degraded heterodisperse dendrimers to be compacted on forming a complex with the DNA and to swell when released from the DNA.

On the other hand, in 1981, Dankewalter et al. reported the synthesis of dendritic poly(L-lysine) using Boc-L-Lys(Boc)-OH benzhydrylamide as a core (*14*), and the properties were then described by Aharoni et al. in 1982 (*15*). The dendritic molecule is not strictly classified in the original concept of the 'dendrimer' described by Tomalia because it consists of asymmetrical L-lysine residues (*16*); however, the new concept of a dendritic molecule consisting of amino acids is expected to enable us to construct a functional gene carrier in the next generation, which is directed in a different way from a PAMAM-type dendrimer. Dendritic poly(L-lysine) can be synthesized with a well-defined molecule and a precise number of terminal amines per dendrimer. In addition, we expect to easily construct functional gene carriers, e.g., those modified by ligands such as a sugar chain, endosome disrupting agents, and an intracellular targeting signal, by selecting several protecting groups of the lysine, such as Boc, Z, and Fmoc groups (*17*). As a candidate for the gene carrier among several types of dendritic poly(L-lysine)s, block copolymers consisting of poly(ethylene glycol) and poly(L-lysine) dendrimer were reported (*18*, *19*). The copolymers formed about 100 nm of a spherical complex with DNA and did not show any cytotoxity toward NIH3T3 cells even at higher concentration (*19*). Shah et al. also reported that amphipathic asymmetric poly(L-lysine) dendrimers, in which the dendritic structure was attached to an amino group of α-amino myristic acid, had gene transfer ability into cells without significant cytotoxity (*20*).

In this study, we focused on a monodispersed and symmetric dendritic poly(L-lysine) (DPK) made of hexamethylenediamine as an initiator core proposed by Maruo et al. (*17*). To investigate the characteristics of DPK as a gene carrier into cells, we synthesized several

* To whom correspondence and reprint requests should be addressed: Department of Applied Chemistry, Nagasaki University, Nagasaki 852-8521, Japan. Tel. and Fax: 81−958−43−7306; E-mail: tanido@net.nagasaki-u.ac.jp.

[†] Department of Applied Chemistry, Faculty of Engineering, Nagasaki University.

[‡] Department of Bacteriology, Institute of Tropical Medicine, Nagasaki University.

[1] Abbreviations: DCHA, dicyclohexylamine; DMEM, Dulbecco's modified Eagle's medium; DMF, *N*,*N*-dimethylformamide; DPK, dendritic poly(L-lysine); FBS, fetal bovine serum; HBS, 21 mM Hepes-NaOH buffer (pH 7.4) containing 135 mM NaCl, 5.0 mM KCl; HBTU, 2-(1*H*-benzotriazol-1-yl)-1,1,3,3-tetramethyluronium hexafluorophosphate; HOBt, 1-hydroxybenzotriazole; MALDI TOF-MS, matrix-assisted time-of-flight mass spectrometry; MTT, 3-(4,5-dimethyl-2-thiazolyl)-2,5-diphenyl-*2H*-tetrazolium bromide; PAMAM, polyamidoamine; TFA, trifluoroacetic acid.

10.1021/bc015525a CCC: $22.00 © 2002 American Chemical Society
Published on Web 04/11/2002

generations of DPKs, and their binding abilities with a plasmid DNA and the gene transfection abilities into cells were then evaluated.

EXPERIMENTAL PROCEDURES

Chemicals and Instruments. All amino acid derivatives and reagents for peptide synthesis, ethidium bromide and MTT (3-(4,5-dimethyl-2-thiazolyl)-2,5-diphenyl-*2H*-tetrazolium bromide) were purchased from Watanabe Chemical (Hiroshima, Japan), Wako Chemicals (Osaka, Japan), and Dojindo (Kumamoto, Japan), respectively. Mass spectra were obtained on matrix-assisted time-of-flight mass spectrometry (MALDI TOF-MS) using Applied Biosystems, Voyager Linear DE (Tokyo, Japan). Plasmid DNA which contains a luciferase gene and SV40 promoter (PicaGene control vector, PGV−C) was purchased from Toyo Ink (Tokyo, Japan). Plasmid DNA which contains a EGFP gene and CMV promoter (pEGFP−C1) was purchased from CLONTECH (Tokyo, Japan). Closed circular plasmid DNA was purified by ultracentrifugation in CsCl gradients. The plasmid preparations showed a major band of closed circular DNA and a minor amount (<20%) of nicked plasmid. DMEM, RPMI1640, kanamycine sulfate, and heat-inactivated FBS were purchased from IWAKI GLASS (Chiba, Japan). Lipofectin and SuperFect were purchased from Invitrogen (Tokyo, Japan) and Qiagen (Tokyo, Japan), respectively.

Synthesis of Dendritic Poly-L-lysine. DPKs were synthesized from hexamethylenediamine as an initiator core. Boc-L-Lys(Boc)-OH·DCHA (528 mg, 1.0 mmol) and hexamethylenediamine (58 mg, 0.50 mmol) were coupled by HBTU (379 mg, 1.0 mmol) and HOBt·H_2O (153 mg, 1.0 mmol) in 15 mL of DMF containing triethylamine (154 μL, 1.1 mmol). After incubation for 15 h at room temperature, the reaction mixture was evaporated and precipitated with 10% citrate aqueous. The precipitate was isolated by filtration, redissolved in ethanol, and precipitated once more with diethyl ether to give 325 mg (84%) of the Boc-protected DPK of first generation. In addition, we confirmed using the Kaiser Test whether the coupling was completely achieved (*21*). The Boc-protected DPK of first generation (325 mg, 0.42 mmol) was dissolved in 5 mL of TFA. After being stirred for 1 h at room temperature, the mixture was evaporated and precipitated with diethyl ether to give 323 mg (93%) of DPK of first generation.

DPK of second generations was prepared by coupling between DPK of first generation (323 mg, 0.39 mmol) and Boc-L-Lys(Boc)-OH·DCHA (823 mg, 1.6 mmol) in 30 mL of DMF containing triethylamine (238 μL, 1.7 mmol), HBTU (592 mg, 1.6 mmol), and HOBt·DCHA (239 mg, 1.6 mmol). After incubation for 15 h at room temperature, the reaction mixture was evaporated and precipitated with 10% citrate aqueous. The precipitate was collected by filtration and washed by water followed by ethyl acetate and then redissolved in ethanol and precipitated once more with water to give 540 mg (82%) of the Boc-protected DPK of second generation. Deprotection of the Boc group was performed by same manner in the case of DPK of first generation (KG1): yield 557 mg (97%).

DPKs of third to sixth generations were prepared with the same method of synthesis as that used for DPK of second generation (KG2): DPK of third generation (KG3), yield 1.00 g (86%); DPK of fourth generation (KG4), yield 1.60 g (79%); DPK of fifth generation (KG5), yield 2.15 g (67%), DPK of sixth generation (KG6), yield 3.02 g (70%).

Acid−Base Titration. The ability of DPK to protonate and obtain a positive charge over a 10 to 3 pH range was determined by acid−base titration (*22*). A 30 mL solution of 1 mM dendrimer as amino group concentration was prepared. The solution was titrated to a pH of 10 with 1 N NaOH where the pH was measured. The solution was then titrated with 0.1 N HCl given in various volume increments.

Acrylamide Gel Electrophoresis. Acrylamide gel electrophoresis under nondenaturing condition was performed by modified method of Davis (*23*). Slab gel was prepared as follows. Separation gel: 12% acrylamide gel containing 0.32% of *N,N′*-methylene bisacrylamide (Bis) and 320 mM glycine-KOH buffer (pH 7.3); stacking gel: 3% acrylamide gel containing 0.08% of Bis and 80 mM glycine-KOH buffer (pH 10.3). Four micrograms of DPKs were run for 2 h at 50 V in 200 mM glycine/imidazole running buffer (pH 8.3). Gel was stained by 2.5% Coomassie Brilliant Blue R-250 in 50% methanol, 40% water, 10% acetic acid for 1 h. Destaining was accomplished by gentle agitation in the same acid−methanol solution but in the absence of dye.

Agarose Gel Electrophoresis. Complex formation of DPKs and a plasmid DNA was examined by the electrophoretic mobility of the complex on an agarose gel stained with ethidium bromide at the various ratios of peptide to a plasmid DNA. The tests were performed by mixing 0.1 μg of the plasmid DNA (PGV−C) with the peptides in 10 μL of HBS (21 mM Hepes-NaOH buffer containing 135 mM NaCl, 5.0 mM KCl, and 0.76 mM Na_2HPO_4 pH 7.4), in which the amino groups (DPK)/phosphate groups (DNA) ratios (N/P ratios) were 0, 0.10, 0.25, 0.50, 1.0, 2.0, 4.0, and 8.0, respectively. Gel electorophoresis sample buffer was added to each sample, and it was electrophoresed on 1% (w/v) agarose gel for 40 min at 100 V. TBE (45 mM Tris-Borate and 1 mM EDTA, pH 8.0) buffer was used as an electrophoresis buffer. The gel was stained with ethidium bromide (0.5 μg/mL) for 30 min and illuminated with an UV illuminator to show the location of the DNA.

Fluorescence Titration Assay. Binding abilities of DPKs with plasmid DNA were monitored by a fluorescent titration assay (*24*). Ten micrograms of plasmid DNA (PGV−C) was mixed with DPK in 980 μL of HBS, in which the N/P ratios were 0, 0.25, 0.50, 0.75, 1.0, 1.25, 1.5, 1.75, 2.0, 2.5, 3.0, and 4.0, respectively. After standing for 20 min at room temperature, 20 μL of 20 μg/mL of ethidium bromide solution was added to the DPK−DNA mixtures. The fluorescence of the intercalated dye was measured on a spectrofluorometer F-3010 (Hitachi, Japan) by exciting at 530 nm while monitoring emmision at 590 nm, with the slits set at 20 nm. Fluorescence intensity blanks were subtracted from all values before data analysis.

Particle Size Analysis. Samples were prepared by mixing 5.0 μg of plasmid DNA (PGV−C) with DPKs in 500 μL of HBS and analyzed using a Nicomp submicron particle sizer model 370 in the solid particle mode. The mean diameter and population distribution were computed from the diffusion coefficient using functions supplied by the instrument.

Zeta Potential Analysis. Samples were prepared by mixing 10 μg of plasmid DNA (pCMVLuc) with KG6 or poly-L-lysine at N/P ratios of 1, 2, 4, and 8 in 1 mL of DMEM. After incubation for 15 min at room temperature, the zeta potential of the DNA complex was measured with a ELS-8000 (Otsuka Electronics Co., Ltd., Osaka, Japan). The measurement was performed in triplicate.

Cell Culture. CHO cells (a chinese hamster ovary, RCB accession no. RCB0285), COS-7 cells (a monkey kidney cell line, RCB accession no. RCB0539), and HeLa

cells (a human cervix, RCB accession no. RCB0271) were purchased from RIKEN Cell Bank (Tsukuba, Japan). HuH-7 cells (a human hepatoma cell line, JCRB accession no. JCRB0403) were purchased from Health Science Research Resources Bank (Osaka, Japan). CHO, COS-7, and HeLa cells were cultivated in DMEM supplemented with 10% FBS and antibiotics (30 μg/mL kanamycine sulfate) at 37 °C in a humidified atmosphere containing 5% CO_2. HuH-7 cells were cultivated in RPMI1640 supplemented with 5% FBS and the antibiotics at 37 °C in a humidified atmosphere containing 5% CO_2. These cells were plated at a density of 1.0×10^4 cells/well 48 h prior to transfection in a 24-well plate.

DPK-Mediated Gene Transfer. Just before transfection procedure, the cells in the 24-well plate were washed by 1 mL of serum free medium. Ten microliters of DPK solution was added to 240 μL of serum free medium containing plasmid DNA (PGV−C). After standing for 15 min at room temperature, the DPK−DNA mixture was poured gently to the cells. After incubation for 3 h at 37 °C, 1 mL of medium containing FBS was added, and incubation was continued for 24 h at 37 °C. The medium was replaced with 1 mL of a fresh medium containing FBS, and the cells were further incubated for 24 h. Harvesting of cells and luciferase assays were performed as described in the protocol of PicaGene luminescence kit (Toyo Ink; Tokyo, Japan). Luciferase relative light units (RLU) were analyzed by luminometer (Maltibiolumat LB9505, Berthold, Germany). The protein concentrations of the cell lysates were measured by Bradford assay using bovine serum albumin as a standard (*25*). The light unit values shown in the figures represent the specific luciferase activity (RLU/mg protein) which is standardized for total protein content of the cell lysate. The measurement of gene transfer efficiency was performed in triplicate.

Cytotoxic Activities of Peptides. Cytotoxic activities of DPKs were evaluated using MTT assay (*26*). Cells were plated at 1×10^4 cells per well in a 96-well plate and incubated for 24 h at 37 °C. Four microliters of DPK (3.2 mM of amines) solution is added to 96 μL of serum free medium containing 1.0 μg of plasmid DNA (PGV−C; N/P ratio = 4). After standing for 15 min at room temperature, the DPK-DNA mixture was poured gently to the cells. After incubation for 3 h at 37 °C, 100 μL of medium containing FBS was added, and incubation was continued for 24 h at 37 °C. The medium was replaced with 200 μL of a fresh medium containing FBS, and the cells were further incubated for 24 h. The medium was removed and replaced by 100 μL of the MTT solution (0.5 mg/mL of medium). After incubation for 4 h at 37 °C, the cells were washed by 200 μL of HBS, and then 200 μL of 0.04 N HCl/2-propanol was added. The absorbances of lysates at 540 nm were measured by 96-well microplate reader. Results are expressed as the percentage of dye reduction in cells treated with the transfection protocol compared with dye reduction in cells treated with medium only. The measurement was performed in duplicate.

RESULTS

Synthesis of Dendritic Poly-L-lysine. Dendritic poly(L-lysine)s (DPKs) were synthesized from hexamethylenediamine as an initiator core. A DPK of the first generation was synthesized by coupling Boc-L-Lys(Boc)-OH·DCHA to hexamethylenediamine by the HBTU−HOBt method (*27*). DPKs of the second to sixth generations were obtained by coupling Boc-L-Lys(Boc)-OH repeatedly after deprotection with TFA (Figure 1). At every coupling step, a Kaiser Test, which detects residual free amino groups (*21*), was performed. As a result, we confirmed that the coupling was completely achieved. DPKs of the first to sixth generations were named KG1 to KG6, respectively. The final preparations of the DPKs could be identified by MALDI TOF-MS (Table 1). Although the ion peaks of KG5 and KG6 were broad (the width at half-height was about 302 and 1200 *m/z*, respectively), the peak values corresponded to the calculated ones. To evaluate the purity of each DPK, acrylamide gel electrophoresis under nondenaturing conditions was performed (Figure 2). As a result, the KG2 and KG3 generations showed a clear single band. In the case of KG4 to KG6, a main band and its smear at the upper position were observed. However, no smear was observed in the lower position of the main band, indicating that that no small molecule originated by incomplete coupling of Boc-L-Lys(Boc)-OH existed in the final preparation. In the case of the commercially available PAMAM dendrimer of the third and fourth generations, a main band and a wide smear were observed (Figure 2, lanes 1, 2). The reason the smear at the upper position was observed would be that the electrophoresis conditions are not suitable for DPKs yet or that oligomerization of the DPKs occurred in the electrophoresis buffer with high pH.

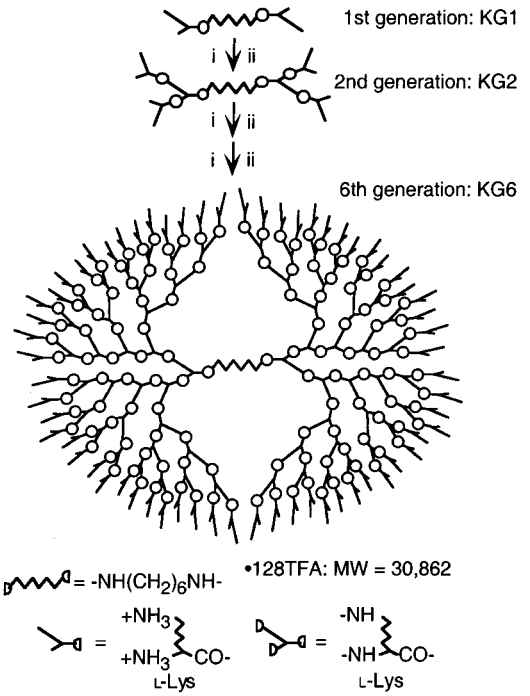


Figure 1. Structure and synthetic route of dendritic poly(L-lysine)s (DPKs). Reagents: (i) Boc-L-Lys(Boc)-OH·DCHA, HBTU, HOBt·H_2O, DIEA; (ii) TFA.

Table 1. Identification of Dendritic Poly(L-lysine)s (DPKs) by MALDI TOF-MS

DPK	formula	calculated	found
KG2	$C_{42}H_{88}N_{14}O_6$	886.3 ($[M + H]^+$)	885.5[a]
KG3	$C_{90}H_{184}N_{30}O_{14}$	1933.6 ($[M + Na]^+$)	1934.8[a]
KG4	$C_{186}H_{376}N_{62}O_{30}$	3984.4 ($[M + Na]^+$)	3985.1[b]
KG5	$C_{378}H_{760}N_{126}O_{62}$	8064.0 ($[M + H]^+$)	8062.4[b]
KG6	$C_{762}H_{1528}N_{254}O_{126}$	16267.1 ($[M + H]^+$)	16137.9[b]

[a] 3-Hydroxypicolinic acid was used as a matrix. [b] α-Cyano-4-hydrocinnamic acid was used as a matrix.

Buffer Effect of DPK. Many cationic polymers possess amines protonated at neutral pH. The acid−base titration profile was obtained for KG6 and is shown in

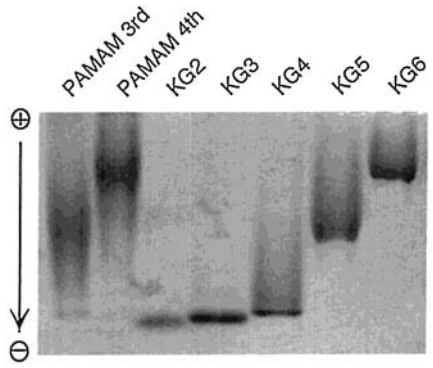


Figure 2. Acrylamide gel electrophoresis of DPKs under nondenaturing conditions. Four microliters of DPKs and commercially available PAMAM dendrimers of the third and fourth generations was applied on the gel as described in Experimental Procedures. After electrophoresis, the gel was stained by 2.5% Coomassie Brilliant Blue R-250.

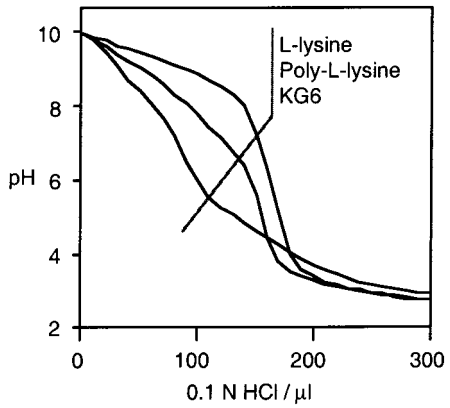


Figure 3. Acid−base titration profiles of L-lysine, poly-L-lysine, and KG6. The solution of pH 10 containing 1 mM amino groups was titrated with 0.1 N HCl given in various volume increments.

Figure 3. The titration curve of KG6 tends to be horizontal at less than pH 6, whereas the curves of L-lysine and poly-L-lysine tend to be horizontal at above pH 8. The initial protonation of the amino group of L-lysine and poly-L-lysine occurred at high pH; however, and that of KG6 showed considerable buffer capacity in a neutral and weakly acidic pH range.

Binding Ability of DPKs to DNA. The formation of the DPK−DNA complexes was examined by their electrophoretic mobility on an agarose at various N/P (amine/phosphate) ratios of DPKs to plasmid DNA (Figure 4). KG3 could completely inhibit the migration of the DNA on the agarose gel at N/P ratios of 2.0, while KG1 and KG2 could not retard the migration of the DNA even if the dendrimers were added to the DNA at an N/P ratio of 8.0. In the cases of KG4, KG5, and KG6, no migration of the plasmid DNA band occurred at an N/P ratio of 1.0, indicating that these molecules had strong binding ability compared with the lower generation ones. The retardation ability of DPK reached a maximum at the fourth generation.

The binding ability was also estimated by the ethidium bromide titration assay (*24*). DPKs bound to DNA lead to exclusion of the ethidium bromide intercalation and a decrease in fluorescence. Increasing the amount of KG3 to KG6 caused a reduction in the fluorescence. The fluorescence intensities versus charge ratio flattened out at N/P ratios above 1.5 and then reached plateaus at 40−25% (Figure 5). The reduction of the fluorescence depended on the generation of DPKs, indicating that DPKs of higher generations have a strong ability to cause

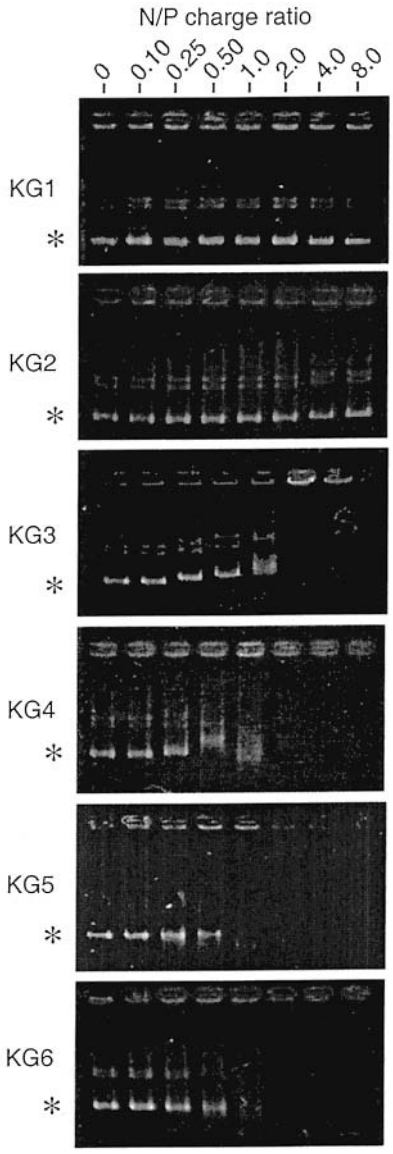


Figure 4. Agarose gel electrophoresis of the complexes of DPKs and plasmid DNA. Plasmid DNA (100 ng) and various amounts of DPKs were mixed, followed by electrophoresis on an agarose gel (1% w/v) stained with ethidium bromide. The N/P ratio (amino groups: phosphate groups) is indicated above each lane. The asterisk on the left of the gel indicates the position of the supercoiled form of the plasmid DNA.

compaction of DNA compared with the DPKs of lower generations. On the other hand, little reduction of the fluorescence was observed by the addition of KG1 and KG2. These data from the ethidium bromide titrations for DPKs correspond to those from the agarose gel shift assay.

Size and Distribution of DPK−DNA Complex. The size distribution of the DPK-plasmid DNA complexes at an N/P ratio of 4.0 was compared using dynamic light scattering data (Table 2). Populations of particles with a mean diameter of 200 to 250 nm were observed for KG3 to KG6. In the range of N/P ratio of 2.0 to 8.0, the size was not altered significantly. In the cases of KG1 and KG2, the sizes could not be estimated due to the limited light scattering of its complex with the DNA. The sizes determined by dynamic light scattering were also confirmed by observation using transmission electron microscopy with negative staining. As a result, whereas KG3 to KG6 formed several sizes of aggregates, aggregates were observed within the ranges of the size

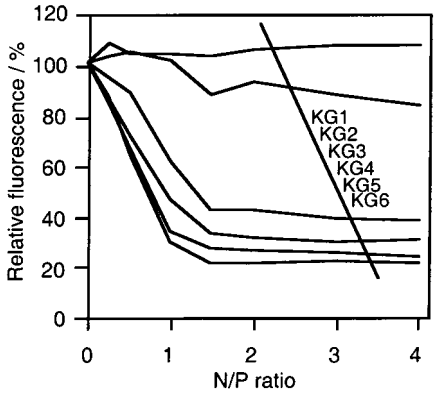


Figure 5. Fluorescence titration assay. Ten microliters of plasmid DNA was mixed with DPKs in 980 μL of HBS at various N/P ratios. After allowing the mixture to stand for 20 min at room temperature, 20 μL of 20 μg/mL of ethidium bromide solution was added to the DPK−DNA mixtures. The fluorescence was measured on a spectrofluorometer by exciting at 530 nm while monitoring emission at 590 nm.

Table 2. Size Distribution of DPK−Plasmid DNA Complexes

DPK−DNA complex[a]	N/P ratio	particle size population	
		diameter (nm)[b]	σ (nm)[c]
KG1	4.0	n.d.[d]	n.d.[d]
KG2	4.0	n.d.[d]	n.d.[d]
KG3	4.0	257	82
KG4	4.0	196	59
KG5	4.0	273	61
KG6	2.0	226	64
KG6	4.0	190	46
KG6	8.0	244	67

[a] DPK−DNA complex was prepared by mixing 0.5 μg of plasmid DNA with DPK in 50 μL of HBS. [b] Represents the mean diameter of particles. [c] Standard deviation of the population. [d] Correct values could not be determined due to little light scattering of the complex.

distributions determined using dynamic light scattering (data not shown).

Gene Transfer Abilities of DPKs in Vitro. The transfection abilities of DPKs into four kinds of cell lines were tested with the plasmid DNA, which contains a reporter gene encoding firefly luciferase (Figure 6). KG5 and KG6 showed significant transfection abilities into all cell lines, and the efficiencies were the same or greater compared with a commercially available transfection reagent, Lipofectin. In the case of KG4, the gene expression was observed in HuH-7 and COS-7 cells, not in CHO and HeLa cells. We considered that the complex of KG4 with the DNA would be different from that of KG5 and KG6 strictly (see Discussion). The difference in the character of the complex, which effects the uptake into cells and transfer to the nucleus, would be the basis for the cell specificity.

Expression of the EGFP gene in CHO cells was also examined by the same protocol as that for the luciferase gene. As a result of transfection using KG6 at an N/P ratio of 4.0, about 20% of the cells expressed the EGFP (date not shown). The efficiency of KG6 was similar to that of SuperFect as a control molecule.

Sufficient Conditions for Gene Transfection Mediated by DPKs. To determine sufficient conditions for gene transfection mediated by DPK, we measured the transfection abilities at various N/P ratios, amounts of complex, and incubation times to CHO cells cultivated in 24-well plate (Figure 7). As a result of a change in the N/P ratio, the gene expression in the case of KG5 and KG6 reached plateaus at an N/P ratio of 4.0 (Figure 7A). At an N/P ratio of 8.0, high expression was observed; however, significant cytotoxity (about 60% of cell viability) simultaneously appeared. The gene expression mediated by KG4 was increased by an increasing N/P ratio; however, the level is still lower than that of KG5 and KG6. KG3 could not show gene transfection ability even if the N/P ratio was increased to 8.0. For the amounts of the DNA complexes with KG5 and KG6, KG6 showed a considerably higher transfection ability at a low amount of complex, corresponding to a range from 0.5 to 1.5 μg of DNA compared with KG5 at an N/P ratio of 4.0 (Figure 7B). Finally, the time-course of the incubation of the complex with the cells was followed (Figure 7C). Incubation for 0.5 and 1 h was insufficient for gene transfection. However, in the case of 3 h incubation, high gene expression was observed, and the level increased gently up to 12 h. To sum up the optimum condition of gene transfection mediated by DPKs into CHO cells cultivated in 24-well plate, sufficient gene expression is observed when the complex composed of 2.5 μg of DNA and KG6 at an N/P ratio of 4.0 is incubated with the cells for 3 h.

Cytotoxic Activities of KG6 and Its DNA Complexes. Cytotoxic activities of KG6 and its complex with the plasmid DNA were also evaluated by MTT assay. Cell viabilities in the presence of KG6 and its DNA complex at an N/P ratio of 4.0 were more than 80% (Figure 8). On the other hand, SuperFect show significant cytotoxity under the conditions optimized for KG6 as described above, indicating that KG6 is advantageous over SuperFect from the point of view of cytotoxity. KG5 also showed weak cytotoxity similar to that of KG6. In contrast, little

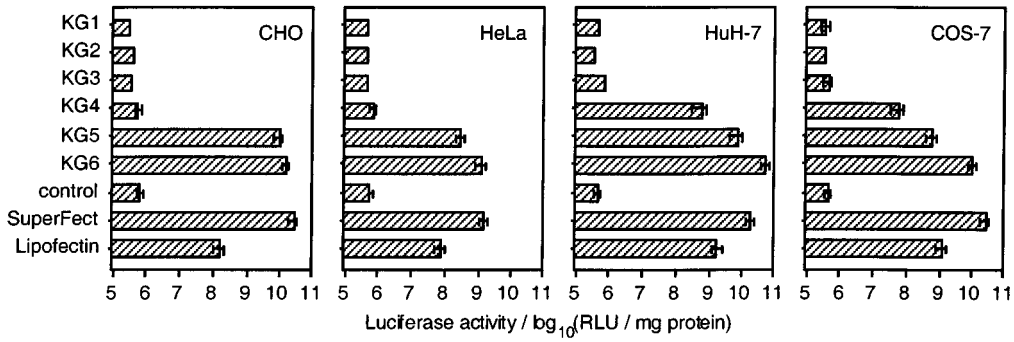


Figure 6. Transfection efficiencies of DPKs into several cell lines. The cells were incubated with DPK−DNA complex containing 2.5 μg of plasmid DNA and DPK at an N/P ratio of 4.0 for 3 h at 37 °C. Harvesting of the cells and luciferase assays were performed 48 h after transfection as described in Experimental Procedures. Data represent the mean value from $n = 3$, and the standard error from the mean.

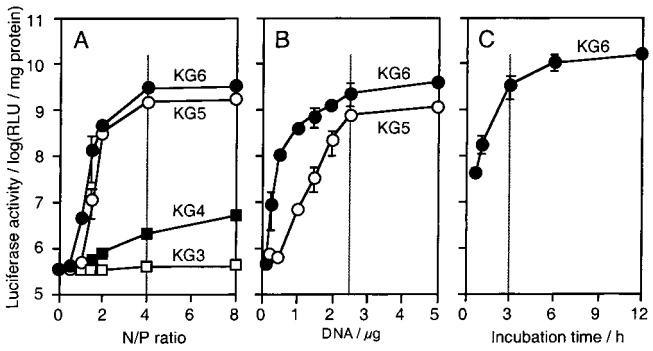


Figure 7. Sufficient conditions of gene transfection mediated by DPK into CHO cells. Transfection efficinecies were measured in various N/P ratios (Panel A), amounts of DNA complex (Panel B), and incubation time (Panel C) to CHO cells cultivated in 24-well plate. The gray lines in the graphs indicate a standard condition, which shows sufficient transfection efficiency. Data represent the mean value from $n = 3$, and the standard error from the mean.

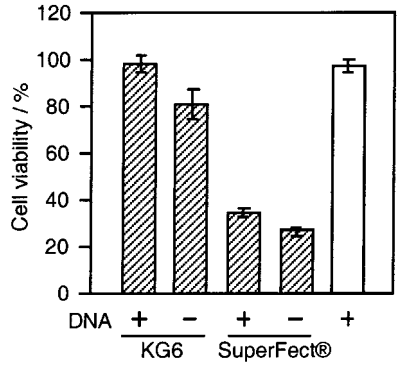


Figure 8. Cytotoxic activities of KG6 and SuperFect alone and their complexes with plasmid DNA at N/P ratio of 4.0. Cell viabilities were evaluated by MTT assay as described in Experimental Procedures. The open bar indicates cell viability in the presence of the plasmid DNA alone. Data represent the mean value from $n = 2$, and the standard error from the mean.

cytotoxities were observed in DPKs of the fourth generation and below (data not shown).

Effect of Serum on the Transfection Efficiency. It is well-known that several components of serum affect the forming of the DNA complex with gene carrier molecules, and the gene expression then generally decreases significantly. We tested the effect of serum added to the transfection medium on the transfection effciency of KG6 (Figure 9). As a result, addition of serum gradually decreased the gene expression; however, the expression in the presence of 50% serum gave 10^9 RLU/mg of cell protein, which was about one-tenth that of KG6 and corresponded to about 50 ng of luciferase protein/mg of cell protein. Concerning the high activity of KG6 still observed in the presence of serum, the surface charge of the complex with DNA is one of the important determinants of interaction with serum components (*28*). To clarify this point, we measured the zeta potential of the DNA complex of KG6 at several N/P ratios (Figure 10). Interestingly, the zeta potential of the complex of KG6 was kept in a neutral or slightly positive level (+3 mV) even when the N/P ratio was increased to 8, while that of poly-L-lysine was positive values (+20 mV) at N/P ratios of 4 and 8. This neutral surface of the complex of KG6 would contribute the inert character in the presence of serum.

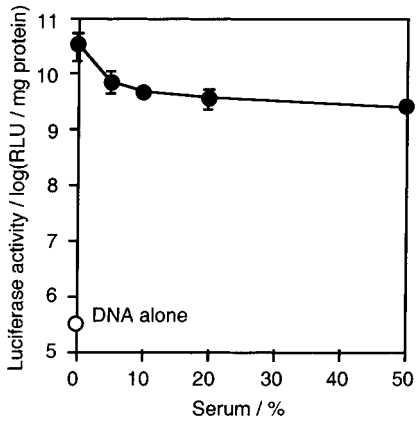


Figure 9. Effect of serum on transfection efficiency of KG6 into CHO cells. Ten microliters of KG6 solution (3.2 mM of amines) was added to serum-free medium containing 2.5 μg of the plasmid DNA (N/P ratio = 4.0), and then an appropriate amount of FBS was added. The mixture, 250 μL, is poured gently onto the cells. Harvesting of the cells and luciferase assays were performed 48 h after transfection as described in Experimental Procedures. Data represent the mean value from $n = 3$, and the standard error from the mean.

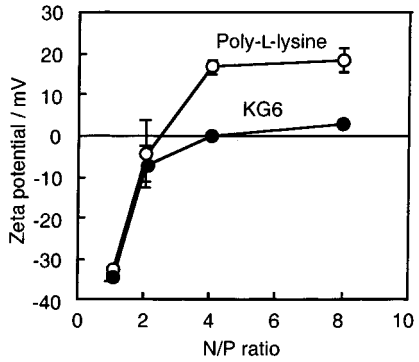


Figure 10. Zeta potentials of DNA complex of KG6 and poly-L-lysine. Closed and open circles indicate zeta potentials of the DNA complex of KG6 and poly-lysine, respectively. Data represent the mean value from $n = 3$, and the standard deviation from the mean.

DISCUSSION

Dendrimer-mediated gene or oligonucleotide delivery into cells was reported from several groups (*11*−*14*, *20*, *29*−*31*). This dendrimer-based nucleic acid-carrier molecule is expected to enable the construction of a unique carrier, which cannot be derived from linear type polymers, because of the spherical and monodispersed structure. It could be designed in response to several purposes, such as alteration of size or shape of the dendrimer, ligand modification, and so on (*17*). In this study, we focused on the dendritic molecules consisting of amino acids, L-lysine residues as a branch unit. Because the peptide-based dendrimer can be synthesized by conventional peptide synthetic chemistry, it is expected that some types of dendrimers could be designed and synthesized conveniently and would provide basic information on the relationship of structure and function as a dendritic gene carrier.

To examine the ability of DPKs to form the complex with the plasmid DNA, we employed the agarose gel shift assay, ethidium bromide titration assay, and dynamic light scattering analysis. DPKs of low generations, KG1 and KG2, showed no binding ability to the DNA. In the cases of KG3 and KG4, a slight retardation of the DNA migration on the agarose gel was observed at an N/P ratios of 0.5, and complete inhibition of the migration

occurred at N/P ratios of 2.0 and 1.0, respectively (Figure 4). For KG5 and KG6, complete inhibition of the migration occurred at N/P ratios of 1.0 without forming the intermediate complex, which was observed as a slight retardation of the DNA migration observed in the cases of KG3 and KG4. This result indicates that the change to compacted globule states from the structure of the elongated coil DNA by addition of KG5 or KG6 was all-or-none (*32*, *33*). As a result of ethidium bromide titration assay, the addition of KG5 or KG6 strongly reduced the fluorescence of the ethidium bromide compared with that of KG3 or KG4 (Figure 5), indicating that the degree of compaction occurring with KG5 or KG6 was stronger than that with KG3 or KG4. From the analysis of the size distribution of the complex, DPKs of the third to sixth generations formed about 200−250 nm of complexes with the plasmid DNA (Table 2). The sizes of the complexes of DPKs were almost the same but were not reflected by strength of the compaction of the DNA.

DPKs, especially KG5 and KG6, showed high transfection abilities into a variety of cell lines (Figure 6). In addition, we could confirm the ability into other cell lines, i.e., Caco-2, HepG2, MKN45, and a human cartilage cell line. For the Caco-2, we already reported the usage as a transfection reagent for the purpose of evaluating promoter activity (*34*). We also tested the transfection abilities of KG7 (DPK of the seventh generation). However, the transfection ability of KG7 was about one-tenth that of KG6 (data not shown). A PAMAM dendrimer showed maximal efficiency at the sixth generation, with 192 terminal amino groups (*11*). KG6 has 128 terminal amino groups; therefore, the optimum generation of DPK for transfection corresponded to that of the PAMAM dendrimer.

How was the DNA complex of DPK internalized into the cells? We have preliminary data as follows: (1) the transfection ability of KG6 was inhibited by the addition of *N*-ethylmaleimide, which inhibits the fusion between endosomes at an early stage of the endocytotic pathway (*35*); (2) that was inhibited by the addition of cytochalasin B, which depolymerizes the microfilaments of actin and blocks the uncoated pit-mediated endocytosis (macropinocytotic process) (*36*); (3) that was not significantly inhibited by the addition of chlorpromazine, an inhibitor of clathrin-dependent, receptor-mediated endocytosis (*37*). These results suggest that the uptake of the DNA complex of DPK is mediated by the endocytosis pathway, especially the macropinocytotic process. Furthermore, KG6 shows a buffering effect in a weak acidic environment (Fingure 3). It is likely that the escape of the DNA complex from the endocytotic vesicle to the cytosol was enhanced by the sponge effect of KG6 itself (*4*). This explanation is not contradictory to the fact that no effect of the addition of chloroquine to the transfection medium was observed (data not shown).

As a result of cytotoxicity measurement, 80% and higher cell viability was observed with the addition of KG6 alone and its DNA complex (Figure 8). It could be said that this cytotoxity of KG6 was sufficiently low; furthermore, its DNA complex showed less cytotoxity. In contrast, a commercially available PAMAM dendrimer-based transfection reagent, SuperFect, showed cytotoxity under our ideal conditions for DPK. Actually, a large number of cells which peeled off and then floated in the medium was observed compared with the case of KG6. Of course, under the optimized condition for SuperFect described in the instruction book, 80% and greater cell viabilities were observed. It is clear that KG6 has the advantage of low cytotoxity compared with the PAMAM dendrimer-based transfection reagent.

In this study, we introduced the usage of DPK for gene transfection in vitro. We can strictly synthesize various DPK derivatives, which have several types of branch units (e.g., lysine, ornithine, aminobutyric acid, and their D-, L-isomer), terminal cationic groups (e.g., amino, imidazole, and guanidino groups), and core structure (e.g., diamines which have several lengths of methylene chains and some triamines). The derivatives will enable us to closely discuss how the complex is advantageous for transfection into cells, what structural features and characteristics of the gene carrier are necessary for efficient transfection, and if the transfection efficiency was low, which stage was the rate-limiting step? This basic information is important for development of the transfection reagent of the next generation. Furthermore, DPK has a serum-tolerant transfection ability. This character would be due to the neutral surface of the DNA complex. From the point of view of the usage in vivo, this character is also advantageous, that is, nonspecific interaction with serum components is reduced and the half-life of circulation of the complex in blood vessel will be extended. This expectation also indicates that when DPK is carefully modified by a ligand molecule such as a sugar chain, the molecules will function as an advanced carrier that realizes highly controlled gene delivery in vivo. Usage of DPK as a gene carrier will give us basic information for the structure−function relationship of gene carriers and let us develop highly efficient and functional gene delivery systems.

ACKNOWLEDGMENT

This research was supported by a Grant-in-aid from the Ministry of Education, Culture, Sports, Science and Technology of Japan (No. 11771471 and No. 12217115), from Foundation Advanced Technology Institute, and from Nagasaki Advanced Technology Development Council. We acknowledge technical support in performing particle size analysis by Drs. Tohru Inoue and Sannamu Lee in the Department of Chemistry, Faculty of Science, Fukuoka University, Fukuoka, Japan. MALDI TOF-MS was performed by Dr. Masayuki Fujii in the Department of Chemistry, Kyushu School of Engineering, Kinki University, Iizuka, Japan; his help is greatly appreciated.

LITERATURE CITED

(1) Wu, G. Y., and Wu, C. H. (1987) Receptor-Mediated in Vitro Gene Transformation by a Soluble DNA Carrier System. *J. Biol. Chem. 262*, 4429−4432.

(2) Wagner, E., Cotton, M., Foiser, R., and Birnstiel, M. L. (1991) Transferrin-Polycation DNA Complexes: the Effect of Polycation on the Structure of the Complex and DNA Delivery to Cells. *Proc. Natl. Acad. Sci. U.S.A. 88*, 4255−4259.

(3) Stankovics, J., Crane, A. M., Andrews, E., Wu, C., Wu, G. Y., and Ledley, F. D. (1994) Overexpression of Human Methylmalonyl CoA Mutase in Mice after in Vivo Gene Transfer with Asialoglycoprotein/Polylysine/DNA Complexes. *Hum. Gene Ther. 5*, 1095−1104.

(4) Boussif, O., Lezoualc'h, F., Zanta, M. A., Mergny, M. D., Scherman, D., Demeneix, B., and Berh, J. P. (1995) A Versatile Vector for Gene and Oligonucleitide Transfer into Cells in Culture and in Vivo Polyethyleneimine. *Proc. Natl. Acad. Sci. U.S.A. 92*, 7297−7301.

(5) Felgner, P. L., Tsai, Y. J., Sukhu, L., Wheeler, C. J., Manthorpe, M., Marshall, J., and Cheng, S. H. (1995) Improved Cationic Lipid Formulations for in Vivo Gene Therapy. *Ann. N. Y. Acad. Sci. 772*, 126−139.

(6) Gottschalk, S., Sparrow, J. T., Hauer, J., Mims, M. P., Leland, F. E., Woo, S. L. C., and Smith, L. C. (1996) A Novel

DNA-Peptide Complex for Efficient Gene Transfer and Expression in Mammalian Cells. *Gene Ther. 3*, 448−457.
(7) Wadha, M. S., Collard, W. T., Adami, R. C., Mckenzie, D. L., and Rice, K. G. (1997) Peptide-Mediated Gene Delivery: Influence of Peptide Structure on Gene Expression. *Bioconjugate Chem. 8*, 81−88.
(8) Wyman, T. B., Nicol, F., Zelphati, O., Scaria, P. V., Plank, C., and Szoka, F. C. (1997) Design, Synthesis, and Characterization of a Cationic Peptide that Binds to Nucleic Acids and Permeabilizes Bilayers. *Biochemistry 36*, 3008−3017.
(9) Niidome, T., Takaji, K., Urakawa, M., Ohmori, H., Wada, A., Hirayama, T., and Aoyagi, H. (1999) Chain Length of Cationic α-Helical Peptide Sufficient for Gene Delivery into Cells. *Bioconjugate Chem. 10*, 773−780.
(10) Niidome, T., Urakawa, M., Sato, H., Takahara, Y., Anai, T., Hatakayama, T., Wada, A., Hirayama, T., and Aoyagi, H. (2000) Gene Transfer into Hepatoma Cells Mediated by Galactose-Modified α-Helical Peptides. *Biomaterials 21*, 1811−1819.
(11) Haensler, J., and Szoka, F. C. (1993) Functionalization of Polyamidoamine Cascade Polymers and Their Use for Efficient Transfection of Cells in Culture. *Bioconjugate Chem. 4*, 372−379.
(12) Tang, M. X., Redemann, C. T., and Szoka, F. C., Jr. (1996) In Vitro Gene Delivery by Degraded Polyamidoamine Dendrimers. *Bioconjugate Chem. 7*, 703−714.
(13) Tang, M. X., and Szoka, F. C. (1997) The Influence of Polymer Structure on the Interactions of Cationic Polymers with DNA and Morphology of the Resulting Complexes. *Gene Ther. 4*, 823−832.
(14) Dankewalter, R. G., Kolc, J., and Lukasavage, W. J. (1981) Macromolecular Hoghly Branched Homogeneous Compound Based on Lysine Units. U.S. Patent 4,289,872, September 15, 1981.
(15) Aharoni, S. M., Crosby, C. R., III, and Walsh, E. K. (1982) Size and Solution Properties of Globular *tert*-Butyloxycarbonyl-Poly(α,ϵ-L-Lysine). *Macromolecules 15*, 1093−1098.
(16) Tomalia, D. A., Baker, H., Dewald, J., Hall, M., Kallos, G., Martin, S., Roeck, J., Ryder, J., and Smith, P. (1985) A New Class of Polymers: Starburst Dendritic Macromolecules. *Polym. J. 17*, 117−132.
(17) Maruo, N., Uchiyama, M., Kato, T., Arai, T., Akisada, T., and Nishino, N. (1999) Hemispherical Synthesis of Dendritic Poly(L-Lysine) Combining Sixteen Free-Base Porphyrins and Sixteen Zinc Porphyrins. *Chem. Commun. 20*, 2057−2058.
(18) Choi, J. S., Lee, E. J., Choi, Y. H., and Park, J. S. (1999) Poly(Ethylene Glycol)-Block-Poly(L-Lysine) Denrimer: Novel Linear Polymer/Dendrimer Block Copolymer Forming Spherical Water-Soluble Polyionic Complex with DNA. *Bioconjugate Chem. 10*, 62−65.
(19) Choi, J. S., Joo, D., Kim, C. H., Kim, K., and Park, J. S. (2000) Synthesis of a Barbell-Like Triblock Copolymer, Poly(L-Lysine) Dendrimer-Block-Poly(Ethylene Glycol)-Block-Poly(L-Lysine) Dendrimer and Its Self- Assembly with Plasmid DNA. *J. Am. Chem. Soc. 122*, 474−480.
(20) Shah, D. S., Sakthivel, T., Toth, I., Florence, A. T., and Wilderspin, A. F. (2000) DNA Transfection and Transfected Cell Viability Using Amphipathic Asymmetric Dendrimers. *Int. J. Pharm. 208*, 41−48.
(21) Kaiser, E., Colescott, R. L., and Bossinger, C. D. (1970) Color Test for Detection of Free Terminal Amino Groups in the Solid-Phase Synthesis of Peptides. *Anal. Biochem. 34*, 595−598.
(22) Benns, J. M., Choi, J. S., Mahato, R. I., Park, J. S., and Kim, S. W. (2000) pH-Sensitive Cationic Polymer Gene Delivery Vehicle: *N*-Ac−Poly(L-Histidine)-Graft-Poly(L-Lysine) Comb Shaped Polymer. *Bioconjugate Chem. 11*, 637−645.
(23) Davis, B. J. (1964) Disk Electrophoresis. II. Method and Application to Human Serum Proteins. *Ann. N. Y. Acad. Sci. 121*, 404−427.
(24) Wadhwa, M. S., Collard, W. T., Adami, R. C., McKenzie, D. L., and Rice, K. G. (1997) Peptide-Mediated Gene Delivery: Influence of Peptide Structure on Gene Expression. *Bioconjugate Chem. 8*, 81−88.
(25) Bradford, M. M. (1976) A Rapid and Sensitive Method for the Quantitation of Microgram Quantities of Protein Utilizing the Principle of Protein-Dye Binding. *Anal. Biochem. 72*, 248−254.
(26) Hansen, M. B., Nielsen, S. E., and Berg, K. (1989) Re-Examination and Further Development of a Precise and Rapid Dye Method for Measuring Cell Growth/Cell Kill. *J. Immun. Methods 119*, 203-210.
(27) Fields, C. G., Lloyd, D. H., Macdonald, R. L., Otteson, K. M., and Noble, R. L. (1991) HBTU Activation for Automated Fmoc Solid-Phase Peptide Synthesis. *Pept. Res. 4*, 95−101.
(28) Li, S., Rizzo, M. A., Bhattacharya, S., and Huang, L. (1998) Characterization of Cationic Lipid-Protamine-DNA (LPD) Complex for Intravenous Gene Delivery. *Gene Ther. 5*, 930−937.
(29) Kukowska-Latallo, J. F., Bielinska, A. U., Johnson, J., Spindler, R., Tomalia, D. A., and Baker, J. R., Jr. (1996) Efficient Transfer of Genetic Material into Mammalian Cells Using Starburst Polyamidoamine Dendrimers. *Proc. Natl. Acad. Sci. U.S.A. 93*, 4897−902.
(30) Bielinska, A., Kukowska-Latallo, J. F., Johnson, J., Tomalia, D. A., and Baker, J. R. Jr. (1996) Regulation of in Vitro Gene Expression Using Antisense Oligonucleotides or Antisense Expression Plasmids Transfected Using Starburst PAMAM Dendrimers. *Nucleic Acids Res. 24*, 2176−82.
(31) Poxon, S. W., Mitchell, P. M., Liang, E., and Hughes, J. A. (1996) Dendrimer Delivery of Oligonucleotides. *Drug Deliv. 3*, 255−261.
(32) Yoshikawa, K., Yoshikawa, Y., Koyama, Y., and Kanbe, T. (1997) Highly Effective Compaction of Long Duplex DNA Induced by Polyethylene Glycol with Pendant Amino Groups. *J. Am. Chem. Soc. 119*, 6473−6477.
(33) (2000) Cooperative vs Phase Transition in a Giant Single DNA Molecule. *J. Am. Chem. Soc. 122*, 9891−9896.
(34) Ogushi, K., Wada, A., Niidome, T., Mori, N., Oishi, K., Nagatake, T., Takahashi, A., Asakura, H., Makino, S., Hojo, H., Nakahara, Y., Ohsaki, M., Hatakeyama, T., Aoyagi, H., Kurazono, H., Moss, J., and Hirayama, T. (2001)*Salmonella Enteritidis* FliC (Flagella Filament Protein) Induces Human β-Defensin-2 (hBD-2) mRNA Production by Caco-2 Cells. *J. Biol. Chem.*, in press.
(35) Rothman, J. E. (1994) Mechanisms of Intracellular Protein Transport. *Nature 372*, 55−63.
(36) Paccaud, J. P., Siddle, K., and Carpentier, J. L. (1992) Internalization of the Human Insulin Receptor. The Insulin-Independent Pathway. *J. Biol. Chem. 267*, 13101−13106.
(37) Orlandi, P. A., and Fishman, P. H. (1998) Filipin-Dependent Inhibition of Cholera Toxin: Evidence for Toxin Internalization and Activation Through Caveolae-Like Domains. *J. Cell Biol. 141*, 905−915.

BC015525A

Methotrexate Conjugate with Branched Polypeptide Influences *Leishmania donovani* Infection in Vitro and in Experimental Animals†

György Kóczán,‡ Asoke C. Ghose,§ Ananda Mookerjee,§ and Ferenc Hudecz*,‡

Research Group of Peptide Chemistry, Hungarian Academy of Sciences, Eötvös L. University, Budapest 112, POB 32, Hungary, H-1518 and Department of Microbiology, Bose Institute, P-1/12 C. I. T. Scheme 7M, Calcutta, 700054, India. Received July 18, 2001

Methotrexate (MTX) has been coupled to various structurally related, polycationic (poly[Lys(DL-Ala$_m$)] (AK), poly[Lys(Ser$_i$-DL-Ala$_m$)] (SAK), poly[Lys(DL-Ala$_m$-Leu$_i$)] (ALK)), or amphoteric (poly[Lys(Glu$_i$-DL-Ala$_m$)] (EAK)) synthetic branched polypeptides containing poly[L-Lys] backbone by the aid of BOP reagent. The average degree of MTX incorporation was found to be dependent on the charge properties of the polymer. Under the experimental conditions used, the molar substitution ratio achieved was higher for polycations (25%) than for the amphoteric polypeptide (10%). We have studied the effect of polycationic polypeptides on *Leishmania donovani* infection. Results demonstrated that MTX conjugates in which the drug is covalently attached to carrier have pronounced leishmanicid activity. In this communication we showed that (a) a branched polypeptide−methotrexate conjugate with a polycationic carrier (ALK) increases the effect of MTX against *Leishmania donovani* infection in mice; (b) the covalent bond between the carrier and methotrexate is essential for both in vivo and in vitro activity; and (c) the number of *Leishmania donovani* parasites in infected macrophages are markedly reduced in conjugate treated animals. In vitro observation might also indicate that the MTX conjugate exhibits an effect through an uptake by macrophages which is different from that of the free drug.

INTRODUCTON

Methotrexate (MTX,[1] L-4-amino-N^{10}-methylpteroyl-glutamic acid), a folate antimetabolite, has been in clinical use for more than 35 years. It is a potent anticancer agent of proven benefit in the treatment of acute leukemia, osteogenic sarcoma (*1*), and of rheumatological disorders (*2*−*4*). Recently its inhibitory potential has been demonstrated against a group of intracellular parasites (*Leishmania*) of macrophages (*5*). Visceral leishmaniasis or kala-azar in man is caused by the protozoan parasite *Leishmania donovani*, which proliferates intracellularly within the mononuclear phagocytes of the infected host (*6*).

Methotrexate has been linked to various macromolecules such as BSA, mannosylated-, galactosylated-, or glucosylated-BSA (*7*, *8*), mannosylated-HSA (*9*), or maleylated-BSA (*10*), for delivery into cells containing *L. donovani* parasites or to polylysine for studying the mechanism of action of cellular uptake by pinocytosis in mice and human tumor cell lines (*11*−*14*).

The methods of conjugation of methotrexate to these carriers have involved predominantly the glutamic acid moiety. Activation of α- and γ-carboxyl groups has been achieved in situ in the presence of the carrier using water soluble carbodiimide like EDC (*15*) or by ester formation with *N*-hydroxysuccinimide (*11*). (None of the above methods reported have been used for selective derivatization of α- or γ-carboxyl groups of MTX (*15*).)

MTX was also one of the first antitumor drug attached covalently to high molecular weight carriers to improve the therapeutic index by site-specific targeting and/or by changing the pharmacological properties of MTX to provide controlled release. It has been demonstrated that the biodistribution of branched polypeptide attached drugs (e.g., MTX, daunomycin, amylorid) can be strongly modified by the charge and side chain structure of the carrier resulting in elevated and more prolonged blood levels, slower drug excretion, and a longer half-life (*16*, *17*).

For the investigation of the conjugate's leishmanicid activity we have prepared a new set of methotrexate-branched polypeptide conjugates (*18*) (Figure 1). In these compounds MTX molecules are attached to polycationic poly[Lys(DL-Ala$_m$)] (AK), poly[Lys(Ser$_i$-DL-Ala$_m$)] (SAK), poly[Lys(DL-Ala$_m$-Leu$_i$)] (ALK) or amphoteric poly[Lys-(Glu$_i$-DL-Ala$_m$)] (EAK) polypeptide carrier by amide bonds. Branched polypeptides with the general formula poly-[Lys(X$_i$-DL-Ala$_m$)] (XAK) or poly[Lys(DL-Ala$_m$-X$_i$)] (AXK), where $i < 1$ and $m \sim 3$, have been used as biodegradable (*19*) macromolecular carriers for targeting antitumor

* To whom correspondence should be addressed: Dr. Ferenc Hudecz, Research Group of Peptide Chemistry, Hungarian Academy of Sciences, Pázmány P. sétány 1A, Budapest, Hungary, H-1117, Fax: 36 1 372 2620, Tel: 36 1 372 2828, e-mail: hudecz@szerves.chem.elte.hu.

† A preliminary account of this work was read at 10th International Congress of Immunology, New-Delhi, India, 1998.

‡ Hungarian Academy of Sciences.

§ Bose Institute.

[1] Abbreviations (in order of appearance in the text): MTX, methotrexate; EAK, poly[Lys(Glu$_i$-DL-Ala$_m$)]; SAK, poly[Lys(Ser$_i$-DL-Ala$_m$)]; ALK, poly[Lys(DL-Ala$_m$-Leu$_i$)]; AK, poly[Lys(DL-Ala$_m$)]; $\overline{DP}_n$, number average of the degree of polymerization; PBS, phosphate-buffered saline, pH 7.3; $\overline{DS}$, average degree of substitution; MTX-SAK, poly[Lys(MTX$_j$-Ser$_i$-DL-Ala$_m$)]; MTX-ALK, poly[Lys(MTX$_j$-DL-Ala$_m$-Leu$_i$)]; MTX-AK, poly[Lys(MTX$_j$-DL-Ala$_m$)]; MTX-EAK, poly[Lys(MTX$_j$-Glu$_i$-DL-Ala$_m$)]; BOP benzotriazol-1-yl-oxytris(dimethylamino)phosphonium hexafluorophosphate; DIEA, *N*,*N*-diisopropylethylamine; DMF, dimethylformamide; DMSO, dimethyl sulfoxide; HOBt, 1-hydroxybenzotriazole.

10.1021/bc015530e CCC: $22.00 © 2002 American Chemical Society
Published on Web 04/30/2002

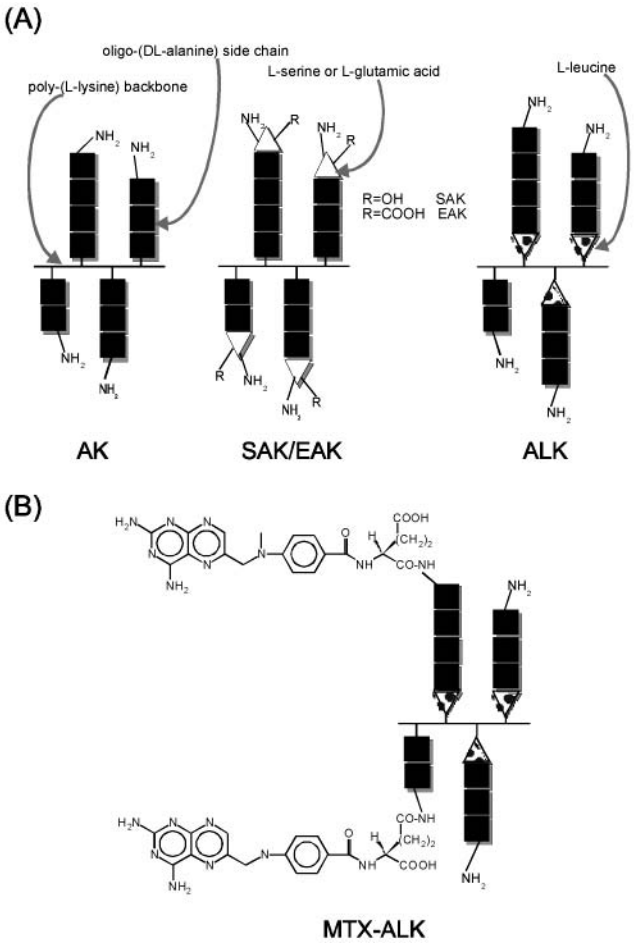


Figure 1. Schematic representation of branched polypeptide−MTX conjugates: poly[Lys(MTX$_j$-DL-Ala$_m$-Leu$_i$)] (MTX−ALK).

agents (*16*−*25*), radioligands (*26*, *27*), immunomodulatory peptides (*28*), or constructing synthetic antigens with T or B cell epitopes (*29*−*31*).

In this paper we describe the improved synthesis of MTX conjugates with selected polycationic and amphoteric polypeptides and the results of comparative studies against *Leishmania donovani* infection using these compounds. These conjugates have been tested and compared with that of the free drug and of free carrier in the control of *L. donovani* infection in BALB/c mice. We have also investigated the mechanism of leishmanicid activity in mouse macrophages in vitro following their treatment with MTX, MTX + branched polypeptide mixture, and MTX-branched polypeptide conjugates.

EXPERIMENTAL PROCEDURES

Abbreviations used in this paper follow the rules of the IUPAC/IUB Commission of Biochemical Nomenclature (*32*) in accord with the recommended nomenclature of graft polymers (*33*).

Materials. Methotrexate was obtained from Lederle Laboratories (Gosport, U.K.); *N*,*N*-diisopropylethylamine (DIEA), 1-hydroxybenzotriazole (HOBt), and trifluoroacetic acid (TFA) were Fluka products (Buchs, Switzerland), while benzotriazol-1-yloxytris(dimethylamino)-phosphonium hexafluorophosphate (BOP) was purchased from Bachem (Bubendorf, Switzerland). Hydroxylamin, glacial acetic acid, diethyl ether, and dimethylformamide (DMF) were purchased from REANAL (Budapest, Hungary). DMF was stored over molecular sieve. Branched polypeptides used in these studies were prepared in our laboratories as described earlier (*19*−*21*). The characteristics of these compounds are summarized in Table 1. Polylysine with $\overline{DP}_n = 60 \pm 2$ or $\overline{DP}_n = 90 \pm 2$ (EAK) and $\overline{M}_w/\overline{M}_n = 1.65 \pm 0.15$ was used.

Table 1. Characteristics of Branched Polypeptides

		amino acid composition[b]			
polypeptide	code[a]	Lys	Ala (m)	Ser/Leu/Glu (i)	$\overline{M}_w$[c] (±5%)
poly[Lys(DL-Ala$_m$)]	AK	1.00	2.06	−	16 700
poly[Lys(Ser$_i$-DL-Ala$_m$)]	SAK	1.00	4.08	0.92	28 800
poly[Lys(Glu$_i$-DL-Ala$_m$)]	EAK	1.00	5.00	0.90	41 500*
poly[Lys(DL-Ala$_m$ -Leu$_i$)]	ALK	1.00	3.00	0.97	34 800

[a] Code of branched polypeptides is based on one letter symbol of amino acids. [b] Determined by amino acid analysis after hydrolysis in 6 M HCl at 105 °C for 24 h. [c] Calculated from the number average degree of polymerization of polylysine ($\overline{DP}_n$ =60 ± 2 or $\overline{DP}_n$ = 90 ± 2*) and from the amino acid composition of branched polypeptides.

Animals. Inbred mice (BALB/c strain) were obtained from the National Institute of Nutrition, Hyderabad, India. Female mice, 6−8 weeks old and of 20−25 g body weight were used in these experiments.

Parasites. The *Leishmania donovani* strain (BI2302) was isolated from the bone marrow material of a kala-azar patient. The strain was maintained in vivo through serial passages in hamsters (*35*).

METHODS

Coupling of Methotrexate to Branched Polypeptides. Coupling was performed with BOP in the presence of 1-hydroxybenzotriazole (HOBt) and DIEA in water−DMF (1:9, v/v) mixture. Briefly: Branched polypeptide ALK (10 mg, 0.24 μmol) was dissolved in 0.5 mL of deionized water, and the clean and viscous solution was diluted with 4.5 mL of DMF (c = 2 mg/mL). Dried methotrexate (5.62 mg, 11.0 μmol) (0.5 mol calculated for amino group of side chains of the polymer), 4.88 mg (11.0 μmol) of BOP reagent, 1.7 mg (11.0 μmol) of HOBt, and 2.75 μL (22 μmol) of *N*,*N*-diisopropylethylamine (DIEA) were dissolved in 2 mL of DMF and the reaction proceeded for 10 min at 4 °C. The solution with preactivated MTX was added to the solution of branched polypeptide. The mixture was stirred at room temperature and allowed to react for 12 h at RT in the dark. The final concentration of polypeptide was 1.53 mg/mL. The input molar ratios of MTX to polypeptide were 0.1:1, 0.3:1, and 0.5:1. Since the relative amounts of α- and γ-coupled material are unknown, the error introduced by assuming no effect of coupling, although probably small, is not known accurately. After conjugation, the solvent was removed in vacuo, and the resulting oil was triturated with 5 mL of diethyl ether three times. The product was dissolved in 1 mL of glacial acetic acid and diluted with 3 mL of water. The solution was placed in Visking tubing (molecular mass cutoff 12000−14000 Da, Fisons, Loughborough, UK) and dialyzed extensively against 1.0% acetic acid for 48 h. The average degree of molar substitution ($\overline{DS}$) was estimated by amino acid analysis and spectrophotometrically at λ = 373 nm assuming that the extinction coefficient of methotrexate at λ = 373 nm is 7800 M^{-1} cm^{-1}. Analytical data on the conjugates are presented in Table 2.

Analysis of Ester Bound Methotrexate to Poly[Lys(Ser$_i$-DL-Ala$_m$)]. Ser-containing conjugate poly[Lys(MTX$_j$-Ser$_i$-DL-Ala$_m$)] (MTX-SAK) was treated with 1.1 M hydroxylamine (0.1 M final concentration) in 0.1 M carbonate buffer (pH 9.0) at 37 °C overnight, similarly

Table 2. Chemical Characterization of MTX-Branched Polypeptide Conjugates

conjugate	code[a]	$\overline{DS_j}$[b] (%)	$\overline{M_w}$[c] (±5%)
poly[Lys(MTX$_j$-DL-Ala$_m$)]	MTX-AK	26.3	24 800
poly[Lys(MTX$_j$-Ser$_i$-DL-Ala$_m$)]	MTX-SAK	25.1	36 200
poly[Lys(MTX$_j$-Glu$_i$-DL-Ala$_m$)]	MTX-EAK	10.2	53 200*
poly[Lys(MTX$_j$ -DL-Ala$_m$-Leu$_i$)]	MTX-ALK	25.0	37 800

[a] Code of conjugates is composed of the abbreviation of branched polypeptide and of methotrexate attached. [b] Average degree of substitution determined from the amino acid analysis after hydrolysis in 6 M HCl at 105 °C for 24 h. [c] Calculated from the number average degree of polymerization of polylysine ($\overline{DP_n} = 60 \pm 2$ or $\overline{DP_n} = 90 \pm 2$*) and from the amino acid composition of conjugates.

to the method of Endo et al. (*34*) with some modifications (*39*). The samples were run on RP-HPLC as described below.

RP-HPLC Analysis of MTX-Branched Polypeptide Conjugates. The HPLC system consisted of one Model 600 ternary gradient pump and controller, a Model 490E programmable multi-wavelength UV−visible detector, a Model 717 autosampler, and an in-line degasser (all from Waters, Milford, MA). All injections were made by the autosampler. Data were recorded and processed with Millenium manager software. A 15 cm × 4.6 mm column with a spherical 5 μm silica (300 Å pore size) with a C18 hydrophobic bonded phase were used (Ultrasphere, Beckman, CA). The mobile phase consisted of 0.1% (v/v) TFA in HPLC grade water (eluent A), and 0.1% (v/v) TFA in 80% (v/v) acetonitrile−water mixture (eluent B). Gradient elution was used at 1 mL/min flow rate; the B content of the eluent was increased from 5% to 60% between 5 and 35 min. All samples were dissolved in distilled water and were filtered before analysis using 0.45 μm Spartan 13 (Schleicher and Schuell, Dassel, Germany) filters. UV absorbance was monitored at $\lambda =$ 373 nm for MTX containing samples and at $\lambda = 214$ nm for free polypeptide samples. The injected volume was selected so that the absorbance value at the peak maximum was below 1.0 absorbance unit. Quantitative analysis of conjugates was performed using peak-area measurement calibrated with appropriate standards. All analyses were carried out at ambient temperature.

Amino Acid Analysis. The amino acid composition of branched polypeptides and their MTX conjugates was determined by amino acid analysis using a Beckman (Fullerton, CA) model 6300 amino acid analyzer. Prior to the analysis, samples were hydrolyzed in 6 M HCl in sealed and evacuated tubes at 110 °C for 24 h.

In Vivo Treatment of *L. donovani* Infected BALB/c Mice with MTX Alone or in Combination with MTX Conjugates. Groups of four to five mice were infected with *L. donovani* amastigotes (about 2×10^7 parasites/0.1 mL/animal) via the intracardial (ic) route. Different groups of animals received different types of treatment as per the following protocol. For initial experiments groups of animals were treated with MTX (50, 100, or 200 μg/injection/animal) by the intraperitoneal (ip) route on every alternate day starting from day 10 following the infection. Five such injections were given and animals were sacrificed on day 28 following the infection, i.e., 10 days after the last injection. The degree of parasitaemia in the sacrificed animals was determined by microscopic counting of the number of amastigotes in their liver impression smears stained with Giemsa. At least 500 nucleated cells were screened for the purpose and results are expressed as the number of amastigotes/100 cells (*36*).

Other groups of infected animals were similarly treated with five doses of MTX covalently coupled to different branched polypeptides (poly[Lys(MTX$_j$-DL-Ala$_m$)] (MTX-AK), MTX-SAK and poly[Lys(MTX$_j$-DL-Ala$_m$-Leu$_i$)] (MTX-ALK)) so that the administered compounds contained equivalent amounts of MTX (100 μg/injection/animal). Whenever required, groups of infected mice were also treated with unconjugated branched polypeptides or with a mixture of MTX and branched polypeptides using a similar protocol. The control group of infected mice received only normal saline (0.9% NaCl) injections. All mice (treated or control) were sacrificed on day 28, and parasitemia in their liver was determined microscopically as described above.

In Vitro Treatment of *L. donovani* Infected Mouse Macrophages with MTX Alone or in Combination with Branched Polypeptides. Antileishmanial activities of MTX or branched polypeptide ALK or their combinations were determined in vitro by using mouse macrophages infected with leishmania parasites (*37*). For this, peritoneal exudate cells were collected from mice pretreated with 2% (w/v) thioglycolate solution. Washed cells were resuspended in RPMI-1640 medium containing 10% heat inactivated fetal calf serum (RPMI−FCS) and overlaid on glass cover slips taken in 35 mm diameter plastic Petri dishes. Dishes were kept at 37 °C in air containing 5% CO_2 for 4 h to allow attachment of cells. Following washing, cells remaining attached to the cover slips were further incubated overnight with RPMI−FCS. Next, *L. donovani* promastigotes freshly harvested from a log phase culture of the parasite grown in a liquid culture medium (*38*) were added to the Petri dishes in a cell-to-parasite ratio of about 1:10. After incubation for 6 h at 37 °C, free parasites were removed by washing and the Petri dishes were incubated with RPMI−FCS containing appropriate doses of MTX (25 μg/mL of incubation medium) or ALK (108 μg/mL) or their mixture or poly[Lys(MTX$_j$-DL-Ala$_m$-Leu$_i$)] (MTX-ALK) conjugate. The control dish (with parasitized macrophages in cover slips) contained neither drug nor conjugates. Following incubation of the dishes for a period of 72 h, cover slips containing parasitized macrophages were taken out, fixed, stained with Giemsa, and examined microscopically to determine the number of intracellular parasites per macrophage. At least, 100 macrophages were screened in each cover slip for the purpose.

RESULTS

Synthesis and Chemical Characterization of MTX-Branched Polypeptide Conjugates. The coupling of MTX to branched polypeptide was achieved by the BOP reagent-based activation method in which one carboxyl group of the molecule was linked to the α amino group of the side chains of branched polypeptide AK, SAK, ALK, or EAK to provide covalent α-amide type bonding (Figure 1). The carboxyl groups of MTX were activated by equimolar BOP and HOBt in situ using a tertiary amine (DIEA). It should be noted that no precipitate was observed during the synthesis of the conjugate under these conditions. The MTX-XAK/AXK preparations were triturated followed by dialysis, and free MTX content was assessed by reversed-phase HPLC. The amino acid composition of purified conjugates was determined by amino acid analysis. Considering the amino acid composition of the free carrier and of the Glu content of MTX the average degree of molar substitution ($\overline{DS}$) was calculated. Characteristic values of the conjugates (MTX content, $\overline{M_w}$) are summarized in Table 2. The results presented in this table indicate that the amount of MTX

incorporation into the polypeptide conjugate depends mainly on the charge properties of the terminal amino acid residue of the side chain. The average molar substitution ratio was in the range of 10.2−26.3% expressed as % of modified side chains in the conjugates. Interestingly enough no marked differences have been observed among the respective $\overline{DS}$ values of polycationic polypeptides ($\overline{DS}$ for MTX-AK 26.0%, for MTX-SAK 25.1%, and for MTX-ALK 25.0%), while in case of MTX conjugate with amphoteric EAK only 10.2% of the side chains were substituted at 0.5:1 input MTX:EAK molar ratio. These values indicate that 10−26% of the free amino groups of branched polypeptide was modified by MTX. Consequently, all MTX conjugates studied still preserved the polycationic or amphoteric character of the branched polypeptide used.

Under these conditions the active ester derivative of MTX could react with the hydroxyl group of the Ser residue producing an ester linkage between MTX and branched polypeptide SAK. The ester bond can be cleaved by hydroxylamine (*34*, *39*). To verify the absence of ester-linked MTX two sets of MTX-SAK conjugate samples were investigated. Conjugates before and after hydroxylamine treatment were analyzed by RP-HPLC using two wavelengths to access free drug in the MTX conjugate preparations. The retention time for MTX, absorbing at $\lambda = 373$ nm, was found to be 10.1 min. Free SAK was detected at $\lambda = 214$ nm at the void volume, whereas the t_R value for MTX-SAK was 14.5 min at both $\lambda = 214$ and 373 nm, indicating the presence of covalently bound MTX. Quantitative analysis, performed on a reversed-phase HPLC column (pore size of 300 Å, gradient elution), indicated that less than 0.01% of free MTX besides the total MTX content in the conjugate samples can be detected using peak-area measurement calibrated with appropriate standards. It should be noted that no free MTX was detected in the MTX-SAK samples before hydroxylamine treatment. These data are in accord with our earlier observation that conditions for the preparation of conjugates highly influence the extent of ester bound formation between OH group and active ester derivative of MTX. The lack of free MTX in MTX-SAK samples suggests that the formation of the amide linkage between MTX and branched polypeptide is favored in a DMF−water 9:1 (v/v) solvent mixture.

After analyzing the purity of freshly synthesized compounds, their stability was investigated. Typical chromatograms of free MTX and of MTX-SAK conjugate containing free MTX as a control are shown in Figure 2. The stability data of conjugate samples obtained after 4−180 days storage at 4 °C. No free MTX was detected (data not shown).

Treatment of *L. donovani* Infected Mice with MTX Alone or in Combination with Branched Polypeptides. In preliminary experiments, different groups of *L. donovani* infected mice were treated with different doses (50−200 μg/injection/animal) of MTX, and their liver parasite load was estimated. About 20%, 36%, and 47% reduction of their liver parasite load was demonstrable following treatment with 50 μg, 100 μg, and 200 μg/injection/animal, respectively (five injections administered as per the protocol described in the Materials and Methods section). A dose of 100 μg of MTX was subsequently chosen for all subsequent experiments for the determination of any additional benefit, which may be derived from the combination therapy of MTX and MTX conjugates.

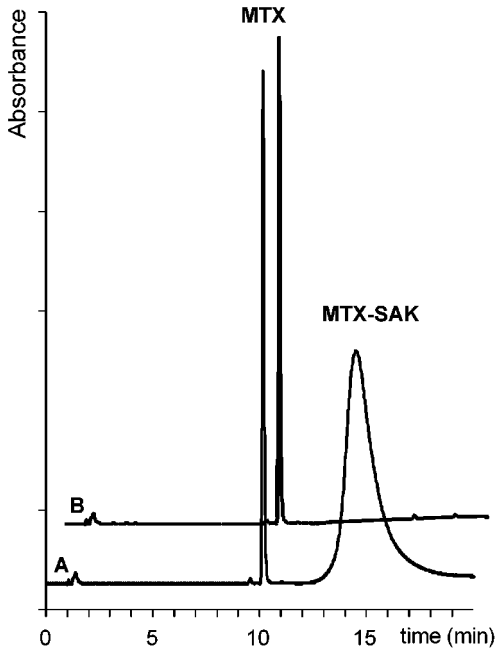


Figure 2. RP-HPLC chromatograms of a mixture of poly[Lys-(MTX$_j$-Ser$_i$-DL-Ala$_m$)] (MTX−SAK) conjugate and MTX (A) and of free MTX (B).

Initially, different groups of *L. donovani* infected mice were treated with MTX branched polypeptide conjugates (MTX-AK, MTX-SAK, and MTX-ALK). It should be noted that due to the high tendency of gel formation under experimental conditions MTX-EAK conjugate was not investigated. All three preparations showed significant levels of antileishmanial activity (data not shown). However, the conjugate MTX-ALK produced most encouraging data (>90% reduction in the number of parasite). Therefore, detailed studies were undertaken with this conjugate and with the corresponding branched polypeptide, ALK.

Table 3 shows the effect of treatment of leishmania infected mice with free MTX as well as in its conjugated form with ALK. About 42% reduction in the liver parasite burden was noted in the MTX treated group of animals as compared to those of untreated control group, and the difference was statistically significant ($0.01 < P < 0.05$). Treatment of animals with MTX-ALK conjugate, however, led to more marked reduction (~95%) of their liver parasite burden as compared to those in the control group and the difference was statistically highly significant ($P < 0.001$). The MTX-ALK conjugate treated group had also significantly ($0.001 < P < 0.01$) less number of liver parasites than that of the MTX alone treated group. Further experiments were carried out to determine the antileishmanial effect of ALK treatment alone or in the form of a mixture with MTX. Results presented in Table 3 demonstrate that treatment of *L. donovani* infected mice with free ALK did not induce any significant ($P > 0.1$) level of reduction of their liver parasite burden. On the other hand, treatment of animals with the MTX+ALK mixture produced about 35% reduction in the parasitemia as compared to that of the control group and the decrease was statistically significant ($0.001 < P < 0.01$). However, the MTX+ALK mixture treated group failed to show any significant difference ($P > 0.1$) in their liver parasitemia as compared to that of the MTX alone treatment group.

Treatment of *L. donovani* Infected Mouse Macrophages in Vitro with MTX Alone or in Combination with the Branched Polypeptide ALK. The effect

Table 3. Reduction of Parasite Burden in the Liver of *L. donovani* Infected Mice Following Treatment with MTX (alone) or in Conjugation with ALK

treatment group[a,b]	no. of parasites/ 100 nucleated cells	mean ± SE	statistical significance[c]
I. control	119.9	115.2 ± 4.5	
(n = 5)	124.3		
	123.1		
	103.9		
	104.6		
II. MTX	89.1	66.2 ± 14.6	0.01 < P* < 0.05
(n = 5)	32.6		
	110.9		
	53.0		
	45.5		
III. ALK	112.4	103.7 ± 5.5	P* > 0.1
(n = 5)	102.2		
	102.6		
	124.1		
	77.6		
IV. ALK+ MTX	84.7	75.6 ± 4.1	0.001 < P* < 0.01
mixture	67.6		P** > 0.1
(n = 5)	92.9		
	62.3		
	51.4		
V. ALK-MTX	12.5	6.0 ± 1.9	P* < 0.001
(n = 5)	4.6		0.001 < P** < 0.01
	7.3		
	1.5		
	3.9		

[a] n = number of animals. [b] Animals were treated with MTX (100 μg/injection/animal), with ALK (432 μg/injection/animal) or ALK+MTX (a mixture of 100 μg of MTX and 432 μg of ALK/injection/animal) or ALK−MTX (100 μg of MTX conjugated to 432 μg of ALK/injection/animal). [c] *Compared to group I. **Compared to group II.

of in vitro treatment of parasite infected mouse macrophages with MTX alone or in combination with ALK was studied, and results are presented in Table 4 and Figure 3. It may be seen that treatment of macrophages with MTX (alone) (Figure 3B) or in the form of a mixture with ALK (Figure 3C) induced only marginally significant (0.05 < P <0.1) reduction in the intracellular parasite level while ALK (alone) failed to show any reduction of this kind (P > 0.1). On the other hand, considerable (about 54%) decrease of the parasite load was noted following MTX-ALK conjugate treatment (Figure 3D vs Figure 3A), and the reduction was significant (0.001 < P < 0.01) as compared to that of the control. The MTX-ALK conjugate was also found to be more efficient than MTX + ALK mixture or MTX alone (0.01 < P <0.05) in reducing the number of amastigotes within the macrophages.

DISCUSSION

Synthetic effort with soluble carriers to discover alternate means to introduce MTX into cells could lead

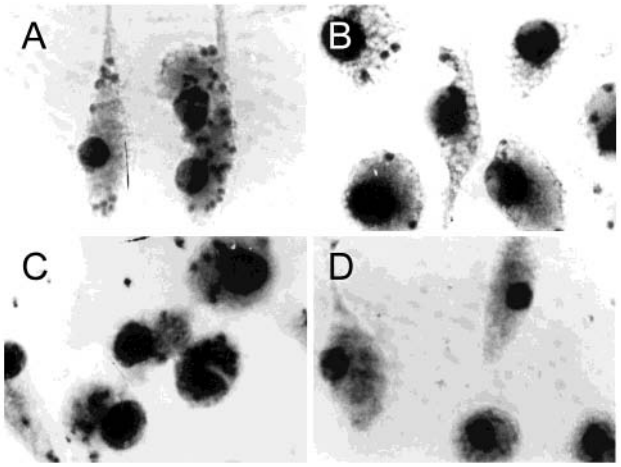


Figure 3. Effect of treatment of *L. donovani*-infected mouse macrophages in vitro with MTX (B), MTX + poly[Lys-(DL-Ala$_m$-Leu$_i$)] (ALK) mixture (C) and poly[Lys-(MTX$_j$-DL-Ala$_m$-Leu$_i$)] (MTX−ALK) conjugate (D). (A) show infected macrophages without any treatment (control). Microscopic magnification: 330×.

increased and selective uptake of the drug and thus more beneficial therapeutic effect. For the construction of macromolecule−drug conjugates it is important to provide rational basis to the selection of the proper carrier. To this end we have previously reported data on the synthesis, biodistribution and in vitro cytotoxicity of the antimetabolite drug methotrexate-branched polypeptide conjugates using osteogenic sarcoma cell line (*16*). In this contribution we extended our studies by investigation of antileishmanial effect of MTX conjugates in experimental animals. For this a new set of branched polypeptide-based conjugates was prepared by an improved synthetic procedure. After covalent coupling of MTX to the α-amino groups of AK, SAK, or ALK conjugates with a similar average degree of molar substitution the overall charge of the compounds remains positive.

It is believed that positive charge density is required for uptake of MTX−linear poly(α-amino acid) (e.g., polylysine, polyornitine) by various mouse or human tumor cells (*11, 13*). A mode of action of the conjugates involves binding to the cell-surface, subsequent endocytic internalization, localization in the lysosomal system, and degradation by lysosomal enzymes to liberate the drug (*12, 13, 40*). This hypothesis was supported by experimental results using polylysine-coupled MTX and L929 mouse fibroblast (*12*) and mouse mammary tumor MM46 cells (*40*) in vitro. MTX attached to poly(D-lysine) directly or through a Leu-Ala-Leu-Ala tetrapeptide spacer between the drug and the ϵ-amino groups of poly(D-lysine) was also investigated. No effect was observed with MTX-poly(D-lysine), while the conjugate containing MTX at the

Table 4. Effect of Treatment of *L. donovani* Infected Mouse Macrophages in Vitro with MTX, ALK, and Their Combinations

	number of parasites/macrophage (after 72 h of treatment)					
treatment group[a]	expt. 1	expt. 2	expt. 3	expt. 4	mean ± SE	statistical significance[c]
I. control	3.9	3.3	3.2	5.0	3.8 ± 0.7	
II. MTX	3.2	2.3	2.2	3.6	2.8 ± 0.3	0.05 < P* < 0.1
III. ALK	3.0	2.8	n.d.[b]	3.9	3.2 ± 0.3	P* > 0.1
IV. ALK+MTX (mixture)	2.8	2.4	n.d.	3.2	2.8 ± 0.2	0.05 < P* < 0.1
V. ALK-MTX	2.1	1.7	1.3	2.2	1.8 ± 0.2	0.001 < P* < 0.01 0.01 < P** < 0.05 0.01 < P*** < 0.05

[a] Macrophages were treated with MTX (25 μg/mL of culture), or ALK (108 μg/mL) or ALK+MTX mixture (25 μg/mL of MTX and 108 μg of ALK/mL) or ALK−MTX (c) (25 μg of MTX conjugated to 108 μg of ALK/mL). [b] n.d. = not determined. [c] *Compared to Group I. **Compared to Group II. ***Compared to Group IV.

N-terminal α-amino group of the Leu-Ala-Leu-Ala unit exhibited potent cytotoxicity, indicating that the spacer is cleaved in the secondary lysosomes (*40*). In addition, the cytotoxicity of a terner conjugate in which MTX-Leu-Ala-Leu-Ala was coupled to monoclonal antibody specific for MM46 cells was not inhibited by TPP, an inhibitor of the membrane active transport system for MTX (*40*). Taken together these data suggest that the transport pathways of MTX and of MTX−carrier conjugates are different and independent (*12*). Trouet et al. (*41*) has demonstrated that a daunorubicin conjugate with Ala-Leu-Ala-Leu spacer and succinylated BSA carrier was stable in serum but was cleaved by lysosomal hydrolases. These findings could be adopted for the speculation on the mechanism of action of MTX-ALK conjugate with marked antileishmania activity observed in vivo and in vito.

It has been described that MTX attached to mannose−BSA strongly inhibits the growth of *Leishmania donovani* inside macrophages. This conjugate was 100 times more active than the free MTX. In contrast MTX conjugated to BSA or other nonspecific neoglycoproteins such as galactose−BSA and glucose−BSA have leishmanicidal effects comparable to that of the free MTX (*7*). Further results indicated that mannose−BSA based MTX conjugate binds specifically to mannose-specific receptor of macrophages and is internalized and degraded in lysosomes, releasing the active drug to act on *Leishmania* parasites (*8, 9, 42*). These data suggest that the uptake mechanism of mannose-containing conjugates is related to the presence of mannose receptor of infected macrophages. On the other hand, our findings clearly indicate that MTX conjugates without a mannose moiety could also be introduced into macrophages.

Recently it has been documented that *Leishmania* and other trypanosomatid protozoa require reduced pteridines (pterins and folates) for growth, suggesting that inhibition of these pathways could be targeted for effective chemotherapy (*43*). Findings suggest that successful antifolate chemotherapy in *Leishmania* will have to target simultaneously both dihydrofolate reductase (DHFR) and pteridine reductase 1 (PTR1). It is attractive to speculate on the mechanism of action of branched polypeptide attached MTX. On the basis of published data outlined above and our own observations reported in this communication, it is likely that MTX released from MTX-branched polypeptide conjugate might act as an inhibitor of enzymes involved in the unusual pteridine metabolism in this lower eukaryote.

CONCLUSION

These studies have indicated that synthetic branched polypeptides can be considered as potential candidates for constructing suitable conjugates for methotrexate delivery into *Leishmania donovani* infected macrophages. In this communication we showed that (a) a branched polypeptide−methotrexate conjugate with a polycationic carrier (ALK) increase the leishmanicid activity of MTX in mice; (b) the covalent bond between the carrier and methotrexate is essential for the effect; and (c) the number of *L. donovani* parasites in infected macrophages are markedly reduced in conjugate treated animals. The latter observation might indicate that the MTX conjugate exhibits its effect throught an uptake by macrophages which is different from that of the free drug. Further comparative studies are in progress to clarify the mechanism of action.

ACKNOWLEDGMENT

These studies were supported by grants from the Hungarian Research Fund (OTKA T-038038), from the Hungarian−Indian Intergovernmental Program (4/1996), from the Hungarian Ministry of Health (T-12/2000), Budapest, and from Hungarian Ministry of Education (MediChem, 047/2001) Hungary.

LITERATURE CITED

(1) Embleton, M. J., and Garnett, M. C. (1985) Antibody targeting of anticancer agents. *Monoclonal antibodies for cancer detection and therapy* (R. W. Baldwin, and V. S. Byers, Eds.) pp 317−344, Academic Press, London.

(2) Furst, D. E., and Kremer, J. M. (1988) Methotrexate in rheumatoid arthritis. *Arthritis Rheum. 31,* 305−314.

(3) Gardner-Medwin, J. M., and Powell, R. J. (1996) One patient, two unusual conditions and three basic lessons. *Ann. Rheum. Dis. 55,* 350−352.

(4) Vardy, D. A., Cohen, A., Kachko, L., Zvulunov, A., and Frankenburg, S. (1999) Relapse of cutaneous leishmaniasis in a patient with an infected subcutaneous rheumatoid nodule. *Br. J. Dermatol. 141,* 914−917.

(5) Mukhopadhyay, A., Chaudhuri, G., Arora, S. K., Sehgal, S., and Basu, S. K. (1989) Receptor mediated drug delivery to macrophages in chemotherapy of leishmaniasis. *Science 244,* 705−707.

(6) Bryceson, A. D. M. (1966) *Manson's Tropical Diseases* (G. C. Cook, Ed.) pp 1213−1245, W. B. Saunders, London.

(7) Chakraborty, P., Bhaduri, A. N., and Das, P. K. (1990) Sugar receptor mediated drug delivery to macrophages in the therapy of experimental visceral leishmaniasis. *Biochem. Biophys. Res. Commun. 166,* 404−410.

(8) Chakraborty, P., Bhaduri, A. N, and Das, P. K. (1990) Neoglycoproteins as carriers for receptor-mediated drug targeting in the treatment of experimental visceral leishmaniasis. *J. Protozool. 37,* 358−364.

(9) Sett, R., Sarkar, H. S., and Das, P. K. (1993) Pharmacokinetics and biodistribution of methotrexate conjugated to mannosyl human serum albumin. *J. Antimicrob. Chemother. 31,* 151−159.

(10) Chaudhuri, G., Mukhopadhyay, A., and Basu, S. K. (1989) Selective delivery of drugs to macrophages through a highly specific receptor. An efficient chemotherapeutic approach against leishmaniasis. *Biochem. Pharmacol. 38,* 2995−3002.

(11) Ryser, H. J. P., and Shen, W. C. (1978) Conjugation of methotrexate to poly(L-Lysine) increases drug transport and overcomes drug resistance in cultured cells. *Proc. Natl. Acad. Sci. U.S.A. 75,* 3867−3870.

(12) Shen, W. C., and Ryser, H. J. P. (1981) Selective protection against the cytotoxicity of methotrexate and methotrexate-poly(lysine) by thiamine pyrophosphate, heparin and leucivorin *Life Sci. 28,* 1209−1214.

(13) McGuire, J. J., and Russell, C. A. (1990) A human leukemia cell culture system for testing new antifols: differential senstivity of lymphoid and nonlymphoid cell lines to unconjugated and methotrexate-conjugated polymers of basic amino acids. *Leukemia 4,* 48−52.

(14) Galivan, J., Balinska, M., and Whiteley, J. M. (1982) Interaction of methotrexate-poly(L-Lys) with transformed hepatic cells in culture. *Arch. Biochem. Biophys. 216,* 544−550.

(15) Upeslacis, J., and Hinman, L. (1988) Chemical modification of antibodies for cancer chemotherapy *Annual Reports in Medicinal Chemistry* (N. Saltzman, Ed.) pp 151−160, Acad. Press, New York.

(16) Hudecz, F., Clegg, J. A., Kajtár, J., Embleton, M. J., Pimm, M. V., Szekerke, M., and Baldwin, R. W. (1993) Influence of carrier on biodistribution and in vitro cytotoxicity of methotrexate-branched polypeptide conjugates. *Bioconjugate Chem. 4,* 25−33.

(17) Hudecz, F., Clegg, J. A., Kajtár, J., Embleton, M. J., Szekerke, M., and Baldwin, R. W. (1992) Synthesis, confor-

mation, biodistribution and in vitro cytotoxicity of daunomycin-branched polypeptide conjugates. *Bioconjugate Chem. 3*, 49−57.

(18) Kóczán, Gy., Ghosh, A. K, Mookherjee, A., Ghose, A. C., and Hudecz, F. (1998) Application of branched chain polymeric polypeptides for methotrexate targeting to macrophages in Leishmania donovani infection. *The Immunologist S1*, 610.

(19) Hudecz, F. (1995) Design of synthetic branched-chain polypeptides as carriers for bioactive molecules. *Anti-Cancer Drugs 6*, 171−193.

(20) Mezö, G., Kajtár, J., Hudecz, F., and Szekerke, M. (1993) Carrier design: conformational studies of amino acid (X) and oligopeptide (X-DL-Alam) substituted poly[L-lysine]. *Biopolymers 33*, 873−883.

(21) Hudecz, F., Pimm, M. V., Rajnavölgyi, É., Mezö, G., Fabra, A., Gaál, D., Kovács, A. L., Horváth, A., and Szekerke, M. (1999) Carrier design: New generation of polycationic branched polypeptides containing OH groups with prolonged blood survival and diminished in vitro cytotoxicity. *Bioconjugate Chem. 10*, 781−790.

(22) Gaál, D., and Hudecz, F. (1998) Low toxicity and high antitumour activity of daunomycin by conjugation to immunpotential amphoteric branched polypeptide. *Eur. J. Cancer 34*, 155−161.

(23) Mezö, G., Sármay, G., Hudecz, F., Kajtár, J., Nagy, Zs., Gergely, J., and Szekerke, M. (1996) Synthesis and characterization of p-borono-Phe − branched polypeptide − monoclonal antibody ternary systems for potential use in boron neutron capture therapy (BNCT) *J. Bioact. Compat. Polym. 11*, 263−285.

(24) Mezö, G., Mezö, I., Seprõdi, A., Teplán, I., Kovács, M., Vincze, B., Pályi, I., Kajtár, J., Szekerke, M., and Hudecz, F. (1996) Synthesis, conformation, biodistribution and hormon related in vitro antitumor effect of a GnRH antagonist-branched polypeptide conjugate. *Bioconjugate Chem. 7*, 642−650.

(25) Pató, J., Ulbrich, K., Baker, P., Mezö, G., and Hudecz, F. (1999) Synthesis of macromolecular conjugates of a urokinase inhibitor. *J. Bioact. Compat. Polym. 14*, 99−121.

(26) Pimm, M. V., and Hudecz, F.(1996) Biodistribution in tumour-bearing mice of polycationic, amphoteric and polyanionic branched polypeptides with poly(L-lysine) backbone labeled with ^{125}I and ^{111}In: Tumour accumulation less than that of labeled serum proteins. *J. Cancer Res. Clin. Oncol. 122*, 45−54.

(27) Perkins, A. C., Frier, M., Pimm, M. V., and Hudecz, F. (1998) Tc^{99m}-branched chain polypeptide (BCP): a potential synthetic radiopharmaceutical. *J. Labelled Compds 41*, 631−638.

(28) Mezö, G., Kajtár, J., Szókán, Gy., Sármay, G., Gergely, J., and Szekerke, M. (1991) Branched polypeptides as carriers of tuftsin analogues: synthesis, structure and immunostimulatory activity. *Peptides 1990* (E. Giralt, and D. Andreu, Eds.) pp 244−245, ESCOM Sci.

(29) Wilkinson, K. A., Vordermeier, M. H., Wilkinson, R., Iványi, J., and Hudecz, F. (1998) Synthesis and in vitro T cell immunogenicity of conjugates with dual specificities: attachment of epitope peptides of 16 kDa and 38 kDa proteins from M. tuberculosis to branched polypeptide. *Bioconjugate Chem. 9*, 539−547.

(30) Wilkinson, K. A., Hudecz, F., Vordermeier, H. M., Ivanyi, J., and Wilkinson R. J. (1999) Enhancement of the T cell response to a mycobacterial peptide by conjugation to synthetic branched polypeptide *Eur. J. Immunol. 29*, 2788−2796.

(31) Mezö, G., Mihala, N, Andreu, D., and Hudecz, F. (2000) Conjugation of epitope peptides to branched chain polypeptides via Cys(Npys). *Bioconjugate Chem. 11*, 484−491.

(32) IUPAC−IUB Commission on Biochemical Nomenclature. (1972) *Biochem. J. 127*, 753−756.

(33) IUPAC−IUB Commission on Biochemical Nomenclature. (1984) *Eur. J. Biochem. 138*, 9−37.

(34) Endo, N., Takeda, Y., Umemoto, N., Kishida, K., Watanabe, K., Saito, M., Kato, Y., and Hara,T. (1988) Nature of linkage and mode of action of methotrexate conjugated with antitumor antibodies: implications for future preparation of conjugates. *Cancer Res. 48*, 3330−3335.

(35) Dasgupta, S., Mookerjee, A., Chowdhury, S. K., and Ghose, A. C. (1999) Immunosuppression in hamsters with progressive visceral leishmaniasis: an evaluation of the role of nitric oxide towards the impairment of lymphoproliferative response. *Parasitol. Res. 85*, 594−596.

(36) Stauber, L. A. (1958) Host resistance to the khartoum strain of Leishmania donovani. *Rice Inst. Pamph. 45*, 80−85.

(37) Ghose, A. C., Mookerjee, A., Sengupta, K., Ghosh, A. K., Dasgupta, S., and Ray, P. K. (1999) Therapeutic and prophylactic uses of the immunomodulator Protein A in the control of Leishmania donovani infection in experimental animals. *Immunol. Lett. 65*, 175−181.

(38) Ghosh, A. K., Dasgupta, S., and Ghose, A. C. (1995) Immunoglobulin G subclass specific antileishmanial antibody responses in Indian kala-azar and post kala-azar dermal leishmaniasis. *Clin. Diagn. Lab. Immunol. 2*, 291−296.

(39) Hudecz, F., Garnett, M. C., Khan, T., and Baldwin, R. W. (1992) The influence of synthetic conditions on the stability of methotrexate-monoclonal antibody conjugates determined by reversed phase high performance liquid chromatography. *Biomed. Chromatogr. 6*, 128−132.

(40) Umemoto, N., Kato, Y., Endo, N., Takeda, Y., and Hara, T. (1989) Preparation and in vitro toxicity of a MTX-anti-MM46 monoclonal antibody conjugate via an oligopeptide spacer. *Int. J. Cancer. 43*, 677−684.

(41) Trouet, A., Masquelier, M., Baurain, R., and Deprez-De Campeneere, D. (1982) A covalent linkage between daunorubicin and proteins that is stable in serum and reversible by lysosomal hydrolases, as required for a lysosomotropic drug-carrier conjugate: in vitro and in vivo studies. *Proc. Natl. Acad. Sci. U.S.A.* 79, 2626−2629.

(42) Basu, N., Sett, R., and Das, P. K (1991) Down-regulation of mannose receptors on macrophages after infection with Leishmania donovani. *Biochem. J. 277*, 451−456.

(43) Nare, B., Luba, J., Hardy, L. W., and Beverley, S. (1997) New approaches to Leishmania chemotherapy: pteridine reductase 1 (PTR1) as a target and modulator of antifolate sensitivity. *Parasitology 114 Suppl.* S101−110.

BC015530E

Synthesis of Antisense Oligonucleotide−Peptide Conjugate Targeting to GLUT-1 in HepG-2 and MCF-7 Cells

Chang-Po Chen,[‡] Xiao-Xu Li,[‡] Liang-Ren Zhang,[‡] Ji-Mei Min,[‡] Judy Yuet-Wah Chan,[†] Kwok-Pui Fung,[†] Sheng-Qi Wang,[#] and Li−He Zhang*[,‡]

School of Pharmaceutical Sciences, Peking University, Beijing 100083, China, Department of Biochemistry, The Chinese University of Hong Kong, Shatin, N.T., Hong Kong, China, Beijing Institute of Radiation Medicine, Beijing 100850, China. Received August 1, 2001; Revised Manuscript Received January 15, 2002

A simple procedure for the preparation of oligonucleotide−peptide conjugate was developed. *p*-Hydroxybenzoic acid was used as a linker for the connection of the fragments of peptide and oligonucleotide. It was found that such formed linkage was stable under the conditions of conjugate synthesis. The designed conjugate targeting to GLUT-1 showed up to 50% inhibition of cell proliferation in HepG-2 and MCF-7 cells. Comparing to the results from the expressed antisense RNA in cancer cells, it was proposed that the conjugate of signal peptide mimic and antisense oligonucleotide could improve the permeability of antisense oligonucleotide through cell membrane.

INTRODUCTION

The selective inhibition of expression of specific genes by oligodeoxynucleotides (ODNs) via an antisense or antigene strategy provides an attractive and elegant approach to drug discovery (*1*). Several requirements must be fulfilled by a potential antisense oligonucleotide including rapid penetration into cells, and stability against the degradation by nuclease (*2*−*4*).

Antisense oligonucleotides with phosphorothioate backbones exhibit several advantages over other forms, including relatively high nuclease resistance as well as the ability to induce degradation of the target sequence by RNase H (*1*, *3*). On the other hand, chemical modifications with kinds of tethered groups that increase the lipophilic properties of the ODNs have also accumulated. The conjugates of ODNs with liphophilic groups such as cholesterol (*5*), lipid, psoralen, acridine, or alkyl chain (*6*−*11*) which associated with increased activity and in some cases with actual increased intracellular concentration have been described. Recently, studies focused on the increase of both the cell uptake and the biological stability toward nuclease involve peptide modification of antisense ODNs. It was reported that several types of peptides, such as nuclear transport signal sequence, viral fusion peptides, hydrophobic peptides, and signal peptides, have shown intrinsic ability to perturb cell membrane (*12*−*17*). It would be interesting to investigate whether such kinds of peptide conjugates could be used for the purpose of improving their cell membrane permeability. It has long been shown that glucose transporter genes (GLUT) are overexpressed in many human cancer cells, providing extra energy for the rapid growth of cancer cells (*18*), and the antisense oligonucleotides with phosphorothioate backbone (5′-CCA TGG CAG CGC TGC-3′) against GLUT-1 gene exhibited about 25% inhibition of proliferation in HL-60 cells (*19*). We have also reported the synthesis of a spin-labeled conjugate of peptide and peptide nucleic acid (*20*). In this paper, we described the synthesis of the conjugate of antisense oligodeoxynuleotide (S-oligos) with a signal peptide mimic and discussed its growth inhibition in cancer cells. In most cases, nucleases digest ODNs in a 3′-exo-cleavage manner (*21*); therefore, it is reasonable to design the conjugate antisense oligonucleotide with a peptide at the 3′-end.

The incompatibility of peptide chemistry and nucleic acid chemistry constitutes the major challenge for the synthesis of an intact peptide−ODNs conjugate. The accumulated data and concepts provided a wider range of methods for preparation of this defined structure (*13*−*16*, *22*−*33*). In this paper, we use *p*-hydroxybenzoic acid as a linker to connect the fragments of peptide and oligonucleotide, the consecutive assembly of the peptide, and then the ODN on a solid support was applied with much concern for a simple, convenient, and efficient preparative procedure.

EXPERIMENTAL SECTION

(1) Synthesis of Peptide on CPG. (*a) Hydroxylation of AP−CPG (22).* To aminopropyl controlled pore glass (AP−CPG, PE product, pore size 500 Å, 0.5 g, amino group loaded: 0.22 mmol/g), 30 mL of γ-butyrolactone and 13 mg of 4-(dimethylamino)pyridine (DMAP) were added, and the mixture was placed in an incubator at 60 °C for 7 days under shaking. The extent of the reaction was monitored by the disappearance of the primary amino groups by the ninhydrin analysis (*34*).

(b) Loading of the First Amino Acid on CPG. The CPG obtained in the previous step was drained and washed with dichloromethane (DCM), methanol, and DCM and then reacted with *N*-α-Fmoc-*N*-ε-Boc-L-lysine (57.4 mg, 0.11 mmol) and DMAP (3 mg) in 2 mL of dimethylformamide (DMF) and DCM (3:1, v/v) for 2 min. To the mixture was added 0.2 mL of dicyclohexylcarbodiimide (DCC) (1 M), and the reaction was performed at 37 °C for 24 h. After the sample was washed with DCM and methanol, a small amount of CPG was deprotected by

* To whom correspondence should be addressed. Phone: +86-10-62091700. Fax: +86-10-62092724. E-mail: zdszlh@mail.bjmu.edu.cn.

[‡] Peking University.

[†] The Chinese University of Hong Kong.

[#] Beijing Institute of Radiation Medicine.

10.1021/bc015540f CCC: $22.00 © 2002 American Chemical Society
Published on Web 04/06/2002

trifluoroacetic acid (TFA) to determine the extent of the reaction by ninhydrin assay; the major CPG were treated with acetic anhydride (Ac_2O) and triethylamine (TEA) in DCM (3 mL, 1:1:2, v/v) for 20 min to protect the residual hydroxyl groups. The CPG was washed with DCM and methanol alternately and finally by DCM.

(c) Elongation of Peptide. The Boc group at the first amino acid on the resulted CPG was removed by treatment with 33% TFA in DCM (v/v) at room temperature for 30 min. The CPG was washed (DCM and MeOH) and neutralized (10% TEA in DCM, v/v 10 min). Further peptide synthesis was carried out on the manual peptide synthesizer using standard Boc chemistry. The coupling reaction was performed sequentially using 2.5-fold molar excess of *N*-α-Boc protected L-amino acids (A, L, L, A and L) (Penisular products) and DCC with the reaction concentration of 0.1 M in DCM at room temperature for 2 h. The extent of the condensation was determined by ninhydrin assay. The yield of each coupling reaction is over 99%. The retained amino groups were acetylated as before. To determine the component of the peptide, partial resulted CPG was treated by 33% TFA followed by concentrated ammonium hydroxide at 55 °C for 14 h. After the sample was purified on HPLC, the peptide was identified by MALDI-TOF MS and amino acid analysis. MALDI-TOF MS *m/z*: 628.07 (M + 1), calculated for $C_{30}H_{57}N_7O_7$: *m/z*: 627.43; amino acid analysis: Lys:Ala:Leu = 1:2:3.

(d) Loading of Linker on CPG. Following the described procedure of Boc-deprotection at the terminal amino acid, the CPG was reacted with *p*-hydroxybenzoic acid (35 mg, 0.25 mmol) in 2 mL of DCM/DMF (1/1, v/v) using DCC (0.25 mmol) as coupling reagent at room temperature for 2 h, and the extent of the reaction was determined by ninhydrin assay using a small amount of washed CPG. After the sample was washed with DCM, MeOH, and DMF alternately, the majority of CPG were drained and dried for the next step.

(2) Synthesis of ODNs on CPG. A total of 30 mg of the resultant CPG obtained from previous reaction was served as the solid phase support and submitted to cartridge of Applied Biosystem 931 DNA synthesizer for the synthesis of the desired sequence of *S*-oligonucleotide. The reaction cycles were carried out in 1−2 μM scale using cyanoethyl protected nucleoside phosphoramidites as coupling blocks, the procedures were set in compliance with the protocols recommended except prolonged 60 s of the capping wait step with the DMAP/Ac_2O solution. Stepwise sulfurization was performed with the standard reagent. The yield of each coupling reaction is 95−97%. The reaction was stopped at DMT-on. Normal cleavage and deprotection were completed with aqueous ammonia to obtain the peptide conjugated oligonucleotide (DMT-on). The oligomer was purified using oligonucleotide purification cartridges (OPC, Applied Biosystems). The DMT-on conjugates were purified by HPLC using Delta-Pak C18 column (Waters, 100 Å, 15 μm, 7.8 × 300 mm). The gradient was 0−40% B in 25 min, 40−100% B in 15 min (mobile phase A is 0.1 M triethylammonium acetate (pH 7.0), and mobile phase B is acetonitrile). The purified DMT-on conjugates were detritylated through OPC. After concentration, the hybrid molecules were purified by HPLC using NUCLEOSIL C18 column (Phenomenex, 100 Å, 10 μm, 4.6 × 250 mm). The gradient was the same as above, but here the mobile phase A is 0.02 M triethylammonium acetate (pH 7.0), and the mobile phase B was 50% acetonitrile in water. The resulting product appeared as a white solid (190 μg) after dried, and the sample was identified by MALDI-TOF MS or ESI-TOF MS. Antisense oligomer *m/z*: calculated 5603.33; found: 5603.58; sense oligomer *m/z*: calculated 5644.87; found: 5643.63.

(3) Effects on the Inhibition of Growth of HepG-2 and MCF-7 Cells by Peptide-ODNs Conjugate. Cells were seeded in 96-well culture plates at a concentration of 5000 cells/well (40−50% confluence). After overnight culture, the complete medium was replaced by plain medium. The peptide−ODNs conjugate was dissolved in sterilized phosphate-buffered saline (PBS). Conjugate and liposome complex was prepared (2.5 μM, DNA: liposome = 1:1) and added into the well. After 5-h incubation at 37 °C, the complex was removed and complete medium was added. For Northern analysis, 6-well culture plate was used instead but the cell confluence, and the conjugate concentration remained unchanged.

MTT assay (*35*): For adherent cells, the medium was first removed before 30 μL of 3-4,5-dimethylthiazol-2,5-diphenyl tetrazolium bromide (MTT) (5 mg/mL in PBS) was added in each well. The cells were incubated at 37 °C for 2 h. Then, 100 μL of DMSO was added and the cells were incubated for 5 min. After all crystal was dissolved, optical density was read by an ELISA plate reader at 540 nm. Northern hybridization was described in ref *19*.

Western hybridization: Total protein was extracted from the cells by lysing the cells with lysis buffer. A total of 30 μg of protein was loaded into each lane of SDS−PAGE with 7.5% separating gel and 5% stacking gel. After the protein was transferred to a PVDF membrane, the membrane was blocked by 5% nonfat milk. Then, it was followed by goat anti-human GLUT-1 antibody (Diagostic Research) and HRP-conjugated anti-goat secondary antibody. Finally, the signal was detected by ECL Western blotting detection reagents (Amersham Pharmacia).

RESULTS AND DISCUSSIONS

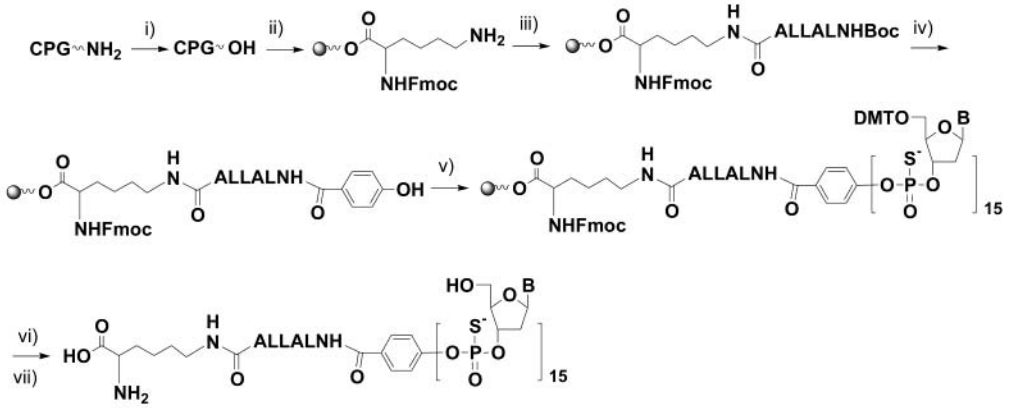
The synthesis of peptide−oligonucleotide conjugate was shown in Scheme 1. The hydroxylation of aminopropyl CPG was completed with γ-butyrolactone and DMAP at a higher temperature. The hydroxyl group can be used to load the first lysine by formation of an ester bond that can also be cleaved under basic conditions in concordance with ordinary ODN synthesis. To fulfill the designed peptide sequence, α-Fmoc-ε-Boc-lysine was selected as the first loaded amino acid on the CPG. The ε-amino group of lysine was used to prolong the peptide sequence, and the α-amino group would play the role of positive charge in the constructed peptide−ODN conjugate. The peptide synthesis was carried out on the CPG with standard solid phase peptide synthesis (SPPS) via Boc strategy. The major concern involved the adverse cleavage of the ester bond between peptide and CPG caused by acidic deprotection procedure. We checked every deprotection and coupling reaction by ninhydrin analysis during the whole process of peptide assembly; fortunately, the adverse cleavage of the ester bond between peptide and CPG did not happen. According to the MALDI-TOF MS, the molecular weight of the final product is concordant with the calculated value of the designed sequence.

The hydroxycarboxylic acid is frequently used as a linker for the connection of peptide and oligonucleotides, and the hydroxyl group from the linker can be reacted for the formation of the phosphate diester bond which could connect with 3′-activated nucleoside blocks by the phosphoramidite or phosphotriester chemistry (*26*, *27*).

Scheme 1[a]

5′-CCATGGCAGCGCTGC-LALLAK (Antisense)

5′-GCAGCGCTGCCATGG-LALLAK (Sense)



[a] (i) γ-Butyrolactone, DMP, 60 °C, 7 days; (ii) α-Fmoc-ε-Boc-Lys-OH, DCC, DMAP/DMF/DCM; (iii) Solid-phase peptide synthesis. (a) Deprotection: TFA/DCM, (b) coupling: Boc-Aa-OH, DCC/DCM, (c) capping: Ac_2O/TEA/DCM, (d) repeating (a), (b), (c); (iv) (a) TFA/DCM, (b) *p*-hydroxy benzoic acid, DCC; (v) Standard DNA synthesis of PS oligonucleotide; (vi) (a) Ammonium cleavage, (b) OPC purification; (vii) 5% CF_3COOH.

But in some cases the phosphate diester bond derived from aliphatic hydroxyl is unstable in basic condition; β elimination is a common reason for the interruption of the synthesis of peptide−oligonucleotide conjugate (*36*, *37*). An alternative approach is incorporation of thiol-containing groups that could serve as the linker for the connection of peptide and oligonucleotide. The thioester is more stable, but the preparation seems more complex to accomplish (*25*, *30*). The phosphate diester bond formed from the aromatic hydroxyl, such as the hydroxyl of tyrosine, is much more stable in the basic conditions (*38*, *39*). For this purpose, we suggested that *p*-hydroxybenzoic acid could be designed for serving as linker with the improved stability. After the condensation of *p*-hydroxybenzoic acid on the N-end of peptide, the resultant CPG was submitted to further synthesis of phosphorothioated ODN and showed the high stepwise loading efficiency of nucleoside phosphoramidites same as that of ordinary CPG. The normal basic condition (aqueous ammonia) was adopted to conduct the cleavage of the conjugate from CPG and the deprotection of nucleobase as well as the removing of Fmoc group of lysine.

The signal peptide mimic was designed according to the common sequence pattern consisting of a stretch of hydrophobic amino acids and a basic residue (Lys) at the end of peptide; the conformation of peptide bears the highest α-helix tendency according to computer-aided design (Insight II/Discover). Compared to the control sample (the conjugate of peptide-sense oligonucleotide), the designed conjugate showed up to 50% inhibition of cell proliferation in HepG-2 and MCF-7 cells as shown in Figure 1 and Figure 2. Also, the expression of mRNA and protein of GLUT-1 were decreased by the analysis of Northern and Western hybridization (Figure 3, Figure 4). In a previous paper, the same antisense oligonucleotide without peptide conjugated only showed a transient inhibition of HL-60 cell proliferation of about 25%. However, when comparing the efficiency between synthetic antisense oligonucleotides and expressed antisense RNA in inhibiting GLUT-1 gene expression, expressed antisense RNA produced over 50% inhibition of HL-60 cell proliferation (*19*). Considering all of the data, the efficiency of the designed peptide−antisense oligonucleotide conjugate in inhibiting proliferation of HepG-2 and MCF-7 cells is same as the expressed antisense RNA in HL-60 cells. It seems that the designed peptide sequence could improve the properties of antisense oligonucleotide for the penetration through the cell membrane.

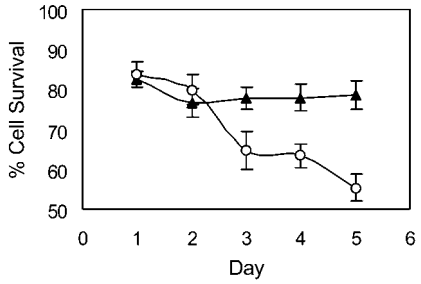


Figure 1. The effect of sense and antisense peptide−oligonucleotide on HepG-2 cell proliferation. Sense (▲); antisense (△). The results are expressed as mean ± SD ($n = 5$).

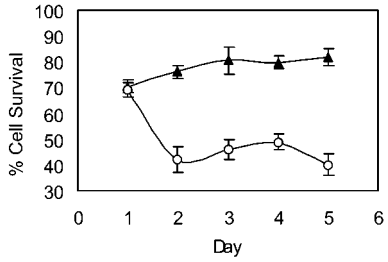


Figure 2. The effect of sense and antisense peptide−oligonucleotide on MCF-7 cell proliferation. Sense (▲); antisense (△). The results are expressed as mean ± SD ($n = 5$).

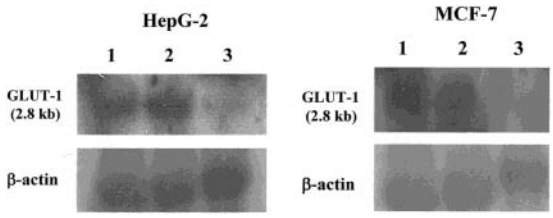


Figure 3. Northern blot analysis of the effect of sense and antisense peptide−oligonucleotide on GLUT-1 gene expression in HepG-2 and MCF-7 cells. Negative control (lane 1); sense (lane 2); antisense (lane 3).

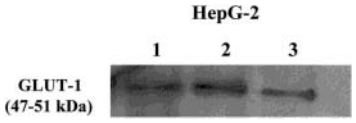


Figure 4. Western blot analysis of the effect of sense and antisense peptide−oligonucleotide on GLUT-1 gene expression in HepG-2 cells. Negative control (lane 1); sense (lane 2); antisense (lane 3).

Signal peptide is an N-terminal extension of premature secretary protein and directs the translocation of protein through the membrane of endoplasmic reticulum of eukaryotes or the inner membrane of prokaryotes. They typically consist of a hydrophobic core consisting of a stretch of hydrophobic amino acids with high tendency of α-helix, basic residues near the N-terminal, and some neutral residues at the C-terminal (*40*, *41*). The cellular mechanism involved in translocation of signal peptide is complex, but it is hypothesized that the transportation of the polypeptide chain is related to the hydrophobic property, conformation, and charge nature of the signal peptide sequence, with the cooperative function of signal peptide on the lipid bilayer membrane (*16*, *17*). It was reported that the long h-region sequence which had been applied as a carrier of certain protein domain enables the whole polypeptide to get through the cell membrane (*41*), and some kind of amphiphilic anionic peptide with over 20 amino acids shows the great potential of mediating cytosol and nuclear delivery of coincubated oligonucleotides with its disturbance effect on the membrane (*42*). In this paper, a short peptide antisense oligonucleotide conjugate was designed, and it may provide a simple method for the modification of antisense oligonucleotides.

In conclusion, a short signal peptide mimic was designed, and a simple procedure for the preparation of peptide−oligonucleotide conjugate was developed. It was found that the designed conjugate could inhibit the proliferation of HepG-2 and MCF-7 cells, and the efficiency is same as the expressed antisense RNA.

ACKNOWLEDGMENT

This study was supported by National Natural Science Foundation of China, and by National Key Project for Basic Research (G1998051103) awarded by The Ministry of Science and Technology, People's Republic of China, and supported by an earmarked grant from Research Grants Council (ref. CUHK 4148/98M), Hong Kong, China.

LITERATURE CITED

(1) Uhlman, E., and Peyman, A. (1990) Antisense oligonucleotides: a new therapeutic principle. *Chem. Rev. 90*, 543−548.
(2) Wagner, R. W. (1994) Gene inhibition using antisense oligonucleotides. *Nature 372*, 333−335.
(3) Crooke, S. T. (1992) Oligonucleotide therapy. *Curr. Opin. Biotechnol. 3*, 656−661.
(4) Vlasov, V. V., Balakireva, L. A., and Yakubov, L. A. (1997) Transport of oligonucleotides across natural and model membrane. *Biochim. Biophys. Acta 1197*, 95−108.
(5) Krieg, A. M., Tonkinson, J., Matson, S., Zhao, Q., Saxon, M., Zhang, L., Bhanja, U., Yakubov, L. and Stein, C. A. (1993) Modification of antisense phosphodiester oligodeoxynucleotides by a 5′-cholesteryl moiety increases cellular association and improved efficacy. *Proc. Natl. Acad. Sci. U.S.A. 90*, 1048−1052.
(6) MacKellar, C. Graham, D., Will, D. W., Burgess, S., and Brown, T. (1992) Synthesis and physical properties of anti-HIV antisense oligonucleotides bearing terminal lipophilic groups. *Nucleic Acids Res. 20*, 3411−3417.
(7) Cumin, F., Asselberg, F., Lartigot, M., and Felder, E. (1993) Modulation of human prorenin gene expression by antisense oligonucleotides in transfected CHO cells. *Eur. J. Biochem. 212*, 347−354.
(8) Wang, L. X., Yang, D. C., Li, Y. Y., Takagi, Y., Taira, K., Tong, L., and Zhang, L. H. (1995) The synthesis and biological activities of oligodeoxynucleotides that are covalently linked to psoralen at their 5′ ends. *Drug Des. Discovery 13*, 109−121.
(9) Verspieren, P., Cornelissen, A. W. C. A., Thuong, N. T., Helene, C., and Toulme, J. J. (1987) An acridine-linked oligodeoxynucleotide targeted to the common 5′ end of trypanosome mRNAs kills cultured parasites. *Gene 61*, 307−315.
(10) Kabanov, A. V., Vinogradov, E. M., Kobetz, N. D., Zarytova, V. F., Ryte, A. S., Yurchenko, L. V., and Vlassov, V. V. (1990) A new class of antivirals: antisense oligonucleotides combined with a hydrophobic substituent effectively inhibit influenza virus reproduction and synthesis of virus-specific proteins in MDCK cells. *FEBS Lett. 259*, 327−330.
(11) Saison-Behmoaras, T., Tocque, B., Rey, I., Chassignol, M., Thuong, N. T., and Helene, C. (1991) Short modified antisense oligonucleotides directed against Ha-ras point mutation induce selective cleavage of the mRNA and inhibit T 24 cells proliferation. *EMBO J. 10*, 1111−1118.
(12) Eritja, R., Pons, A., Escarceller, M., Giralt, E., and Albericio, F. (1991) Synthesis of defined peptide−oligonucleotide hybrids containing a nuclear transport signal sequence. *Tetrahedron 47*, 4113−4120.
(13) Soukchareun, S., Tregear, G. W., and Haralambidis, J. (1995) Preparation and characterization of antisense oligonucleotide−peptide hybrids containing viral fusion peptides. *Bioconjugate Chem. 6*, 43−53.
(14) de la Torre, B. G., Avino, A., Tarrason, G., Piulats, J., Albericio, F., and Eritja, R. (1994) Stepwise solid-phase synthesis of oligonucleotide−peptide hybrids. *Tetrahedron Lett. 35*, 2733−2736.
(15) Ede, N. J., Tregear, G. W., and Haralambidis, J. (1994) Routine preparation of third oligonucleotides: application to the synthesis of oligonucleotide−peptide hybrids. *Bioconjugate Chem. 5*, 373−378.
(16) Tamm, L. K. (1991) Membrane insertion and lateral mobility of synthetic amphilic signal peptides in lipid model membranes. *Biochim. Biophys. Acta 1071*, 123−148.
(17) Batenburg, A. M., Demel, R. A., Verkleij, A. J., and de Kruijff, B. (1988) Penetration of the signal sequence of *Escherichia coli* PhoE protein into phospholipid model membranes leads to lipid-specific changes in signal peptide structure and alterations of lipid organization. *Biochemistry 27*, 5678−5685.
(18) Au, K. K., Liong, E., Li, J. Y., Li, P. S., Liew, C. C., Kwok, T. T., Choy, Y. M., Lee, C. Y., and Fung, K. P. (1997) Increases in mRNA levels of glucose transporters types 1 and 3 in Ehrlich ascites tumor cells during tumor development. *J. Cell. Biochem. 67*, 131−135.
(19) Chan, J. Y.-W., Kong, S.-K., Choy, Y.-M, Lee, C.-Y., and Fung, K.-P. (1999) Inhibition of glucose transporter gene expression by antisense nucleic acids in HL-60 leukemia cells. *Life Sci. 65*, 63−70.
(20) Li, X. X., Cheng, Y. Z., Zhang, L. R., and Zhang, L. H., (1999) Synthesis of spin labeled conjugate of peptide and peptide nucleic acid. *Synth. Commun. 29*, 1519−1525.
(21) Gamper, H. B., Reed, M. W., Cox, T., Virosco, J. S., Adams, A. D., Gall, A. A., Scholler, J. K., and Meyer, R. B., Jr. (1993) Facile preparation of nuclease resistant 3′ modified oligodeoxynucleotides. *Nucleic Acids Res. 21*, 145−150.
(22) Antopolsky, M., Azhayeva, E., Tengvall, U., and Azhayeva, A. (2002) Towards a general method for the stepwise solid-phase synthesis of peptide−oligonucleotide conjugates. *Tetrahedron Lett. 43*, 527−530.
(23) Tung, C.-H., and Stein, S. (2000) Preparation and applications of peptide oligonucleotide conjugates. *Bioconjugate Chem. 11*, 605−618.
(24) Peyrottes, S., Mestre, B., Burlina, F., and Gait, M. J. (1998) The synthesis of peptide−oligonucleotide conjugates by a fragment coupling approach. *Tetrahedron 54*, 12513−12522.

(25) Arar, K., Monsigny, M., and Mayer, R. (1993) Synthesis of oligonucleotide−peptide conjugates containing a KDEL signal sequence. *Tetrahedron Lett. 34*, 8087−8090.
(26) Truffert J.-C., Lorthioir, O., Asseline, U., Thuong, N. T., and Brack, A. (1994) On-line solid-phase synthesis of oligonucleotide−peptide hybrid using silica supports. *Tetrahedron Lett. 35*, 2353−2356.
(27) Haralambidis J., Duncan L., and Tregear G. W. (1987) The solid-phase synthesis of oligonucleotides containing a 3′-peptide moiety. *Tetrahedron Lett. 28*, 5199−5202.
(28) Bergmann F., and Bannwarth W. (1995) Solid phase synthesis of directly linked peptide−oligonucleotide hybrids using standard synthesis protocols. *Tetrahedron Lett. 36*, 1839−1842.
(29) Juby, C. D., Richardson, C. D., and Brousseau, R. (1991) Facile preparation of 3′ oligonucleotide−peptide conjugates. *Tetrahedron Lett. 32*, 879−882.
(30) Soukchareun, S., Haralambidis, J., and Tregear, G. W. (1998) Use of Nα-Fmoc-cystein (S-thiobutyl) derivatized oligodeoxynucleotides for the preparation of oligodeoxynucleotide−peptide hybrid molecules. *Bioconjugate Chem. 9*, 466−475.
(31) Wei, Z., Tung, C. H., Zhu, T. M., and Stein, S. (1994) Synthesis of oligoarginine-oligonucleotide conjugates and oligoarginine-bridged oligonucleotide pairs. *Bioconjugate Chem. 5*, 468−474.
(32) Napoli, L. D., Messere, A., Montesarchio, D. M., Piccialli, G., Benedetti, E., Bucci, E., and Rossi, F. (1999) A new solid-phase synthesis of oligonucleotides 3′-conjugated with peptides. *Bioorg. Med. Chem. 7*, 395-400.
(33) McMinn, D. L., and Greenberg, M. M. (1999) Convergent solution-phase synthesis of a nucleotide using a protected oligonucleotide. *Bioorg. Med. Chem. Lett. 9*, 547−550.
(34) Sarin, V. K., Kent, S. B., Tam, J. P., and Merrifild, R. B. (1981) Quantitative monitoring of solid-phase peptide synthesis by the ninhydrin reaction. *Anal. Biochem. 117*, 147−157.
(35) Twentyman, P. R., and Luscombe, M. (1987) Astudy of some variables in tetrazolium dye (MTT) based assay for cell growth and chemosensitivity. *Br. J. Cancer 56*, 279−285.
(36) Juodka, B. A. (1984) Covalent interaction of proteins and nucleic acids: synthetic and natural nucleotide−peptides. *Nucleosides Nucleotides 3*, 445−483.
(37) Waldmann, H., and Gabold, S. (1997) Chemoenzymatic synthesis of nucleopeptide. *Chem. Commun.*1861−1862.
(38) Schattenkerk, C., Wheesmann, C. T. J., de Graaf, M. J., van der Marel, G. A., and van Boom, J. H. (1984) Synthesis of a naturally occurring nucleopeptide fragment via a phosphotriester approach. *Tetrahedron Lett. 25*, 5197−5200.
(39) Filippov, D., Kuyl-Yehesliely, E., van der Marel, G. A., Tesser, G. I., and van Boom, J. H. (1998) Synthesis of a nucleopeptide fragment from poliovirus genome. *Tetrahedron Lett. 39*, 3597−3600.
(40) von Heijne, G. (1985) Signal sequence: the limits of variation. *J. Mol. Biol. 184*, 99−105.
(41) von Heijne, G. (1990) The signal peptide. *J. Membr. Biol. 115*, 195−201.
(42) Lin, Y. Z., Yao, S. Y., Veach, R. A., Torgerson, T. R., and Hawiger, J. (1995) Inhibition of nuclear translocation factor NF−κB by a synthetic peptide containing a cell membrane-permeable motif and nuclear translocation sequence. *J. Biol. Chem. 270*, 14255−14258.
(43) Pichon, C., Freulon, I., Midoux, P., Mayer, R., Monsigny, M., and Roche, A. C. (1997) Cytosolic and nuclear delivery of oligonucleotides mediated by an amphiphilic anionic peptide. *Antisense Nucleic Acid Drug Dev. 7*, 335−343.

BC015540F

NODAGATOC, a New Chelator-Coupled Somatostatin Analogue Labeled with [$^{67/68}$Ga] and [^{111}In] for SPECT, PET, and Targeted Therapeutic Applications of Somatostatin Receptor (hsst2) Expressing Tumors

Klaus-Peter Eisenwiener,[†,⊥] M. I. M. Prata,[‡,⊥] I. Buschmann,[†] Han-Wen Zhang,[†] A. C. Santos,[§] Sandra Wenger,[∥] Jean Claude Reubi,[∥] and Helmut R. Mäcke*[,†]

Division of Radiological Chemistry, Institute of Nuclear Medicine, Department of Radiology, University Hospital, Petersgraben 4, CH-4031 Basel, Switzerland, Departamento de Bioquímica e CNC, Universidade de Coimbra, Coimbra, Portugal, Faculdade de Medicina, Serviço de Biofísica, Universidade de Coimbra, Coimbra, Portugal, and Division of Cell Biology and Experimental Cancer Research, Institute of Pathology, University of Berne, PO Box 62, Murtenstrasse 31, CH-3010 Berne, Switzerland. Received August 10, 2001; Revised Manuscript Received December 27, 2001

A monoreactive NOTA (1,4,7-triazacyclononane-1,4,7-triacetic acid) derived prochelator (1-(1-carboxy-3-carbo-*tert*-butoxypropyl)-4,7-(carbo-*tert*-butoxymethyl)-1,4,7-triazacyclononane (NODAGA(tBu)$_3$)) was synthesized in five steps with an overall yield of 21%. It is useful for the coupling to the N-terminus of peptides on solid phase and in solution; it was coupled to [Tyr^3]-octreotide (TOC) on solid phase, and the resulting peptide, NODAGA-Tyr^3-octreotide (NODAGATOC), was labeled with the radiometals ^{111}In and ^{67}Ga in high yields and good specific activities. [^{67}Ga]− and [^{111}In]−NODAGA-Tyr^3-octreotide appear to be useful to visualize primary tumors and metastases which express somatostatin receptors subtype 2 (sstr2), such as neuroendocrine tumors, because of their high affinity to this receptor subtype with $IC_{50} = 3.5 \pm 1.6$ nM and 1.7 ± 0.2 nM, respectively. NODAGATOC could be used as a SPECT and PET tracer, when labeled with ^{111}In, ^{67}Ga, or ^{68}Ga, and even for therapeutic applications. Surprisingly, [^{111}In]−NODAGATOC shows 2 times higher binding affinity to sstr2, but also a factor of 4 higher affinity to sstr5 compared to [^{67}Ga]−NODAGATOC. [^{67}Ga]−NODAGATOC is very stable in serum and rat liver homogenate. There is no difference in the rate of internalization into AR4-2J rat pancreatic tumor cells; both radioligands are highly internalized, at 4 h a 3 times higher uptake compared to [^{111}In]−DOTA-Tyr^3-octreotide ([^{111}In]−DOTATOC) was found. The biodistribution of [^{67}Ga]−NODAGATOC in AR4-2J tumor bearing nude mice is very favorable at short times after injection; there is fast excretion from all nontarget organs except the kidneys and high uptake in sst receptor rich organs and in the AR4-2J tumor. Again it is superior to [^{111}In]−DOTATOC in this respect. The results indicate an improved biological behavior which is likely due to the fact that an additional spacer group separates the chelate from the pharmacophoric part of the somatostatin analogue.

INTRODUCTION

Peptides are important regulators of growth and cellular functions in normal tissue but also in tumors. Tumors often overexpress receptors for different regulatory peptides. Certain types of tumors also respond to the growth inhibiting or growth promoting signals of certain peptides. This effect has become important in the treatment of some tumors in man. An important example are analogues of SRIF[1] (somatostatin release inhibiting factor) which are being used in the treatment of symptomatic neuroendocrine tumors and in acromegaly (*1*). A development of the last 10 years or so has been the use of radiolabeled versions of regulatory peptide analogues in the in vivo localization of tumors (*2*−*8*). Of paramount importance is the DTPA-derivatized somatostatin analogue octreotide labeled with [^{111}In] which is commercially available under the trade name OctreoScan (*9*, *10*). As this type of peptide−chelate conjugates show very rapid blood clearance and diffusion into different tissues, the use of short-lived positron emitters becomes feasible. We have introduced a few strategies that use

* To whom correspondence should be addressed: Tel: ++41 61 265 46 99; Fax: ++41 61 265 55 59, E-mail: hmaecke@uhbs.ch.

† Institute of Nuclear Medicine.

‡ Departamento de Bioquímica e CNC, Universidade de Coimbra.

§ Faculdade de Medicina, Serviço de Biofísica, Universidade de Coimbra.

∥ University of Berne.

⊥ K.-P.E. and M.I.M.P contributed equally to these studies.

[1] Abbreviations: SRIF, somatotropin release inhibiting factor; sstr, somatostatin receptor; DIC, diisopropylcarbodiimide; DOTA, 1,4,7,10-tetraazadodecane-1,4,7,10 tetraacetic acid; DTPA, diethylenetriaminepentaacetic acid; octreotide, D-Phe-Cys-Phe-D-Trp-Lys-Thr-Cys-Thr(ol) (disulfide bond); NOTA, 1,4,7-triazacyclononane-1,4,7-triacetic acid; NMP, *N*-methylpyrrolidone; DFO, desferrioxamine; Fmoc, 9-fluorenylmethoxycarbonyl; TFA, trifluoroacetic acid; HATU, *O*-(7-azabenzotriazol-1-yl)-1,1,3,3-tetramethyluronium hexafluorophosphate; TMS, tetramethylsilane; FCS, foetal calf serum; DMEM, Dulbecco's minimal essential medium; MOPS, 3-morpholinopropanesulfonic acid; DIPEA, diisopropylethylamine; HEPES, *N*-(2-hydroxyethyl)-piperazine-*N*′-2-ethanesulfonic acid; Tris, tris(hydroxymethyl)-aminomethane; BSA, bovine serum albumine; TETA, 1,4,8,10-tetraazacyclotetradecane-1,4,8,10-tetraacetic acid.

10.1021/bc010074f CCC: $22.00 © 2002 American Chemical Society
Published on Web 04/23/2002

[^{68}Ga], a 68 min half-life-generator-produced metallic positron emitter coupled to somatostatin analogues (*11*−*13*). Whereas the use of the bifunctional chelator desferrioxamine-B (DFO) led to a radiopeptide which showed very good tumor targeting and visualization in a tumor-bearing rat model, the same conjugate was not very successful in patients because of a slow blood clearance (*14*).

The DOTA monoamide conjugated peptide [Tyr^3]-octreotide (DOTA-Tyr^3-octreotide = DOTATOC) showed very promising in vitro and in vivo properties if labeled with ^{67}Ga, ^{111}In, and ^{90}Y (*11*, *15*). The IC_{50} value of Ga^{III}−DOTATOC, if measured in an assay using a sstr2 receptor expressing cell line, and [^{125}I]-[Leu^8, D-Trp^{22}, Trp^{25}]-somatostatin-28 was 2.5 ± 0.5 nM compared to 11.4 ± 1.7 nM of the corresponding Y^{III}−DOTATOC (*16*). In addition, a Scatchard analysis using rat brain cortex membranes gave a K_d value of 0.46 ± 0.1 nM for [^{67}Ga]−DOTATOC (*16*) and 2.57 ± 0.2 nM for [^{111}In]−DOTATOC, respectively (*15*). The uptake of the respective radioligands in a tumor-bearing mouse model (AR4-2J rat pancreatic tumor cell line) was 13% of the injected dose per g (%ID/g) tumor for [^{111}In]−DOTATOC and 30% ID/g tumor for [^{67}Ga]−DOTATOC at 4 h postinjection. Interestingly, the [^{67}Ga]−DOTATOC showed a lower uptake and shorter residence time in the kidney compared to [^{111}In]−DOTATOC. The respective radioactivities in the kidney at 1, 4, 24, and 48 h for [^{111}In]−DOTATOC were 15, 12.5, 8, and 4% ID/g, whereas for [^{67}Ga]−DOTATOC the radioactivities in the kidneys were 8.5, 7.5, 4, and 2.5% ID/g at the same time points (*11*).

The reason for these differences are not fully understood yet. The metal ion dependence may stem from structural differences within the coordination environment. The X-ray crystal structures of the model peptides Ga^{III}−DOTA-D-PheNH$_2$ and Y^{III}(In^{III}, manuscript in preparation)−DOTA-D-PheNH$_2$ showed remarkable differences. In the Ga^{III} complex, DOTA adopts a cis-pseudooctahedral geometry with a folded macrocyclic unit (2424 conformation) (Figure 1). The equatorial plane is formed by two transannular nitrogens of the macrocyclic ring and the oxygens of the corresponding carboxylate groups. The axial positions are occupied by the remaining two ring nitrogens. Two potential coordination sites of the chelator are free, namely one carboxylate group and the amide carboxy oxygen (*11*). This structural feature may contribute to the somewhat more efficient kidney clearance, and the latter leads to a spacer function between chelate and bioactive peptide (Figure 1). This may consequently introduce less steric strain and improve receptor binding affinity and concomitantly tumor uptake in vivo. Unlike the Ga^{III} structure in Y^{III}(In^{III})−DOTA-D-PheNH$_2$, the coordination number of Y^{III} (In^{III}) is eight and includes the amide carbonyl oxygen. This may lead to some steric scrambling and lower the receptor affinity compared to a chelate which is somewhat remote from the pharmacophoric part of the peptide as in the Ga^{III} complex.

The purpose of this study therefore is to synthesize a NOTA-based [Tyr^3]-octreotide derivative (NODAGA-Tyr^3-octreotide, NODAGATOC) which should allow to carry a spacer function between the ^{67}Ga (^{111}In) complexing chelator and the peptide. This should demonstrate the importance of the spacer for improved receptor binding affinity. The first step was the synthesis of a bifunctional NOTA-derived prochelator which can be conveniently coupled to peptides on solid support and in solution. In addition, we studied SRIF-receptor affinity, biodistribution as well as internalization and externalization of the ^{67}Ga (^{111}In) labeled peptide compared to our "gold standard" of somatostatin receptor scintigraphy [^{111}In]−DOTA-Tyr^3-octreotide in the rat pancreas tumor cell line AR4-2J and a corresponding nude mice tumor model. NOTA was used because of the known high stability of the Ga^{III}−NOTA and In^{III}−NOTA complexes which makes any interference and false interpretation of biological and pharmacological data due to a potential transchelation chemistry rather unlikely.

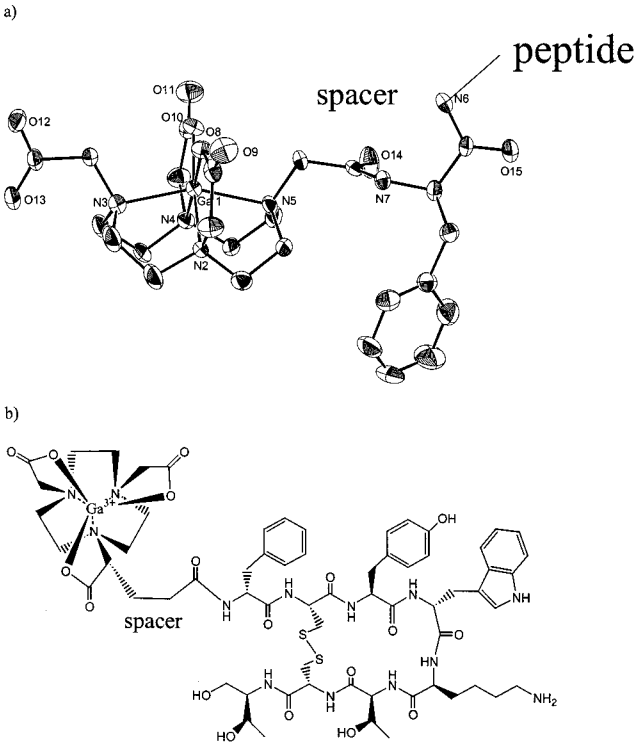


Figure 1. (a) ORTEP plot of the crystal structure of Ga^{III}−DOTA-D-PheNH$_2$. (b) Structural formula of NODAGA-Tyr^3-Octreotide.

The interest in peptide chelator conjugates for labeling with gallium radionuclides comes from their desirable physical properties (*17*, *18*). Three gallium radionuclides exist with decay characteristics that are suitable for γ-scintigraphy, PET imaging, and receptor-mediated radiotherapy: ^{68}Ga is a 68 min half-life-generator-produced positron emitter which is of interest because of the 280 d half-life of the parent ^{68}Ge. This gives the generator a long half-life of more than 1 year and allows PET imaging at institutions without on-site cyclotron.

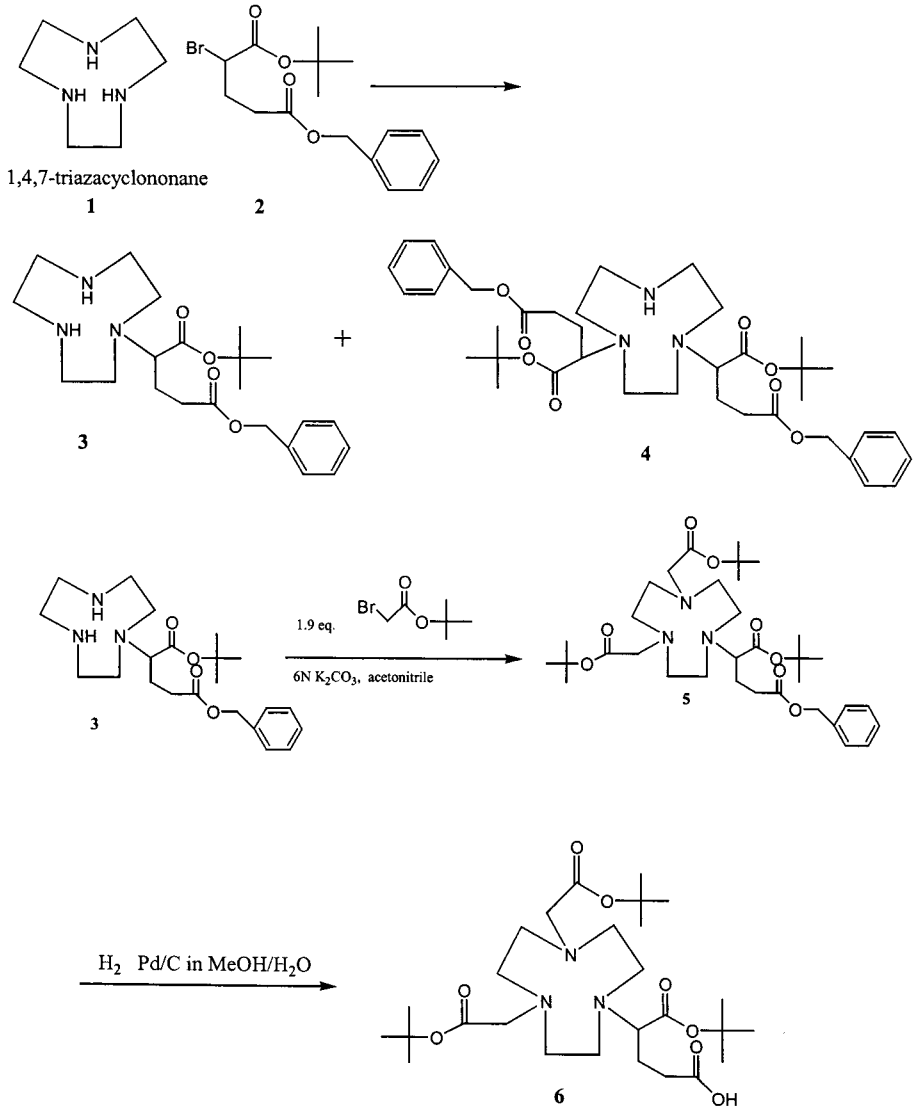
^{67}Ga has a half-life of 78.3 h and decays via electron capture with 3 γ-emissions at 93 keV (38%), 185 keV (24%), and 300 keV (16%) which are useful for planar scintigraphy and single photon emission tomography (SPET). In addition, ^{67}Ga is also a reasonably efficient Auger-emitter for use in internal radiotherapy if the vectors used to bring the radionuclide to the tumor cell are being internalized and the radionuclide comes close to the nucleus.

^{66}Ga again is a positron emitter with an attractive intermediate half-life of 9.5 h which is of current interest because of its longer half-life, more suitable to the pharmacokinetics of a variety of biomolecules (*19*, *20*). It is cyclotron-produced and emits positrons with an abundance of 56% and E_{mean} = 1.7 MeV.

EXPERIMENTAL SECTION

Materials and Methods. *General Methods.* All chemicals were obtained from commercial sources and used

Scheme 1. Synthesis of NODAGA(tBu)$_3$ (6)



without further purification. 1,4,7-Triazacyclononane was commercially available (Macrocyclics, Dallas, TX). Octreotide was commercially available as Sandostatin (Novartis). [^{111}In]Cl_3 and [^{67}Ga]Cl_3 were purchased from Mallinckrodt Med. (Petten, The Netherlands). Chemical reactions were monitored by thin-layer chromatography (TLC) on Merck plates precoated with silica gel 60 F_{254} (0.25 mm). Spots were visualized either by UV light or iodine. Flash chromatography was performed on silica gel 60 (Fluka). Electrospray ionization (ESI) mass spectroscopy was carried out with a Finnigan SSQ 7000 spectrometer or fast atom bombardment (FAB) mass spectroscopy with a VG 70SE spectrometer. Analytical and semipreparative HPLC was performed on a Hewlett-Packard 1050 HPLC system with a multiwavelength detector and a flow-through Berthold LB 506 Cl γ-detector with a Macherey-Nagel Nucleosil 120 C_{18} column and preparative HPLC on a Metrohm HPLC system LC−CaDI 22−14 with a Macherey-Nagel VP 250/21 Nucleosil 100−5 C_{18} column. Quantitative γ-counting was performed on a COBRA 5003 γ-system well counter from Packard Instrument. ^{1}H and ^{13}C NMR was performed with either a Brucker spectrometer at 360/99 MHz or a Varian VXR 400 at 400/101 MHz. Chemical shifts reported are relative to trimethylsilane (TMS). Solid-phase peptide synthesis was performed on a semiautomatic peptide synthesizer commercially available from Rink Combichem (Bubendorf, Switzerland). The cell culture medium was Dulbecco's minimal essential medium (DMEM) from GibcoBRL. DOTA-Tyr^3-octreotide (DOTATOC) was synthesized as described before (*11*).

Synthesis. Starting from the commercially available glutamic acid 5-benzyl ester, α-bromoglutaric acid diester (**2**) (Scheme 1) was synthesized in two steps as described before (*21*).

1-(1-Carbobenzyloxy-3-carbo-*tert*-butoxypropyl)-1,4,7-triazacyclononane (3). A solution of 513 mg (1.44 mmol) of α-bromoglutaric acid 1-*tert*-butyl ester 5-benzyl ester (**2**) in 20 mL of chloroform was added over a period of 3 h to a solution of 557 mg (4.31 mmol) of 1,4,7 triazacyclononane in 20 mL of chloroform. The mixture was stirred over 3 d at room temperature and concentrated to a brown oil. The crude product was purified by column chromatography with silica gel 60 (5 × 20 cm; eluents: 250 mL of ethanol/ammonia 95:5; 300 mL of chloroform/ethanol/ammonia 7:3:0.5). Yield: 404 mg (69.2%) of a colorless oil. Unreacted 1,4,7-triazacyclononane was recovered and can be reused after distillation. ^{1}H NMR [$CDCl_3$, RT]: δ 1.5 (s, 9H, C(CH_3)$_3$); 2.2−1.85 (m, 2H, CHNCH_2); 2.9−2.5 (m, 14H, NCH_2, CH_2COOBzl); 3.25 (dd, 1H, C*H*Br); 5.1 (s, 2H, CH_2Ph); 7.35 (m, 5H, arom); ^{13}C NMR [$CDCl_3$, RT]: δ 24.7, 25.2 (CH_2CHN);

28.1 (C(CH_3)$_3$); 31.0 (CH_2COOBzl); 46.5, 46.6, 49.8 (NCH_2); 65.4, 65.7 (HCNCH_2); 66.1 (COOCH_2Phe); 81.0 (C(CH$_3$)$_3$); 126.6, 126.9, 128.1, 128.2, 128.4 (arom); 135.8 (arom) 172.0, 172.7, 173.0 (*C*OOtBu, *C*OOBzl); IR (KBr, cm^{-1}): 2931 (ν as, CH_2); 2850 (ν sym, CH_2); 1725 (ν as C=O, COOtBu, COOBzl); 1368 (δ C(CH_3)$_3$); 1152 (ν C−O); 753, 699 (arom). EI-MS (*m*/*z* (%)): 406.1 (46, [M + H]$^+$); 350.1 (100, [M − C_4H_9]$^+$).

Analytical data of the side product 1,4-(1-carbobenzyloxy-3-carbo-*tert*-butoxypropyl)-1,4,7-triazacyclononane (**4**): ^{1}H NMR [$CDCl_3$, RT]: δ 1.0 (s, 18H, C(CH_3)$_3$); 1.35−1.7 (m, 4H, CHNCH_2); 1.9−2.45, 2.6−2.8 (2m, 16H, NCH_2, CH_2COOBzl); 3.2 (m, 2H, C*H*Br); 4.6 (s, 4H, CH_2Ph); 6.8 (m, 10H, arom); EI-MS, *m*/*z* (relative intensity): 682.3 (100, [M + H]$^+$); 626.2 (15, [M − C_4H_9]$^+$); 570.1 (10, [M − 2C_4H_9]$^+$).

1-(1-Carbobenzyloxy-3-carbo-*tert*-butoxypropyl)-4,7-bis(carbo-*tert*-butoxymethyl)-1,4,7-triazacyclononane (5). A 390 mg (0.963 mmol) amount of [1-(1-carbobenzyloxy-3-carbo-*tert*-butoxypropyl)-1,4,7-triazacyclononane] (**3**) in 30 mL of dry acetonitrile is cooled to 4 °C. A 255 μL (1.733 mmol) amount *tert*-butylbromoacetic acid was added dropwise over a period of 15 min. The reaction mixture was stirred for additional 15 min before adding 728 mg (5.271 mmol) of dry potassium carbonate and allowed to warm slowly to room temperature over 4 h. The mixture was filtered afterward over Celite and evaporated to dryness to afford the crude product (540 mg, 95%) which can be used for the next step without further purification. Purification was also done by silica gel chromatography (5 × 20 cm; eluents: 80 mL of ethyl acetate; 100 mL of $CHCl_3$/EtOH 20:1; 100 mL of $CHCl_3$/EtOH 4:1). ^{1}H NMR [$CDCl_3$, RT]: δ 1.5 (s, 27H, C(CH_3)$_3$); 1.85−3.6 (m, 21H, C*H*NCH_2, NCH_2, CH_2-COOBzl, CH_2COOtBu); 5.1 (s, 2H, CH_2Ph); 7.35 (m, 5H, arom); ^{13}C NMR [$CDCl_3$, RT]: δ 24.7, 25.3 (*C*H$_2$CHN); 27.3, 27.7, 28.1, 28.3 (C(*C*H$_3$)$_3$); 30.9, 31.0, 31.3 (*C*H$_2$-COOBzl, *C*H$_2$COOtBu)); 50.5, 51.5, 53.1, 58.2 (N*C*H$_2$); 65.4 (H*C*NCH$_2$); 66.4 (COO*C*H$_2$Phe); 81.3, 81.7, 82.1 (*C*(CH$_3$)$_3$); 127.0, 127.5, 128.2, 128.3, 128.7 (arom); 136.0 (arom) 170.7, 171.4, 172.1, 172.8, 173.1 (*C*OOtBu, *C*OOBzl); IR (KBr, cm^{-1}): ν = 2975, 2927 (ν as, CH_2); 2854 (ν sym, CH_2); 1734 (ν as C=O, COOtBu, COOBzl); 1368 (δ C(CH_3)$_3$); 1153 (ν C−O); 753, 699 (arom). EI-MS, *m*/*z* (relative intensity): 635, 634 (100, [M + H]$^+$).

1-(1-Carboxy-3-carbo-*tert*-butoxypropyl)-4,7-(carbo-*tert*-butoxymethyl)-1,4,7-triazacyclononane (NODAGA(tBu)$_3$) (6). A 150 mg (0.237 mmol) of 1-(1-carbobenzyloxy-3-carbo-*tert*-butoxypropyl)-4,7-(carbo-*tert*-butoxymethyl)-1,4,7-triazacyclononane (**5**) was dissolved in 20 mL of 2-propanol and 50 mg 10% Pd/C suspended in 0.5 mL of H_2O was added. The mixture was treated by bubbling hydrogen through the solution over 18 h, filtered over Celite, and evaporated to dryness. The residue was chromatographed on silica gel 60 (2-propanol/ammonia 95:5) to obtain 85 mg (66%) of a yellow oil. ^{1}H NMR [$CDCl_3$, RT]: δ 1.5 (s, 27H, C(CH_3)$_3$); 2.0 (m, 2H, CH_2COOH); 2.5 (m, 2H, NCHCH_2); 2.8−3.2 (m, 12H, NCH_2); 3.45−3.75 (m, 5H, C*H*NCH$_2$, CH_2COOtBu); ^{13}C NMR [$CDCl_3$, RT]: δ 25.1, 25.2 (*C*H$_2$CHN); 27.8, 28.0 (C(*C*H$_3$)$_3$); 32.7 (*C*H$_2$COOH, *C*H$_2$COOtBu)); 49.3, 51.7, 52.6, 57.2 (N*C*H$_2$); 65.5 (H*C*NCH$_2$); 81.1, 82.0 (*C*(CH$_3$)$_3$); 169.4, 171.1 (*C*OOtBu); 176.5 (*C*OOH); IR (KBr, cm^{-1}): ν = 2977, 2932 (ν as, CH_2); 1727 (ν as C=O, COOtBu, COOH); 1368 (δ C(CH_3)$_3$); 1251 (ν C−OH); 1156 (ν C−O). EI-MS, *m*/*z* (relative intensity): 1088 (10, [2M + H]$^{2+}$); 567, 566 (12, [M + Na]$^+$); 545, 544 (100, [M + H]$^+$).

Synthesis of NODAGATOC (8). D-Phe^1-Cys(Acm)^2-Tyr(tBu)^3-D-Trp(Boc)^4-Lys(Boc)^5-Thr(tBu)^6-Cys(Acm)^7-Thr(tBu)^8-ol (**7**) was assembled on a trityl chloride resin (TCP, Pepchem, Tübingen, Germany) using standard Fmoc (9-fluorenylmethoxycarbonyl) strategy (*22*) with diisopropylcarbodiimide (DIC) as coupling reagent. The coupling of the chelator was done as follows: 81 mg of octapeptide (18.3 μmol peptide, 0.9 mmol/g resin) assembled on TCP-resin was incubated for 4 h with a mixture of a 40 min preincubated solution of 30 mg (0.055 mmol) (**6**) and 21 mg (0.055 mmol) of HATU (*O*-(7-azabenzotriazol-1-yl)-*N*,*N*,*N*',*N*'-tetramethyluronium-hexafluoro-phosphate) in 2 mL of NMP (*N*-methylpyrrolidone). The pH was adjusted to 7−8 using DIPEA (diisopropylethylamine, 10 μL, 0.06 mmol). The peptide was cleaved from the resin with 20% acetic acid in dichloromethane (five times 3 mL) and coevaporated three times with toluene (100 mL) to remove the acetic acid. Then it was cyclized with 10 equiv of iodine in methanol/water 9:1, deprotected with TFA/phenol/thioanisole/water 85:5:5:5 for 4−6 h, and purified by preparative HPLC (Macherey-Nagel Nucleosil 100−5 C_{18}, flow: 15 mL/min; eluents: A = 0.1% trifluoroacetic acid (TFA) in water and B = acetonitrile; nonlinear gradient: 0 min, 85% A; 20 min, 70% A). MS ((−)EI, *m*/*z* (%)): 1391.1 (100, [M − H]$^-$); ((+)EI, *m*/*z* (%)): 1392.9 (8, [M + H]$^+$), 697.3 (100, [M + 2H]$^{2+}$). The overall yield based on the first Fmoc cleavage is 31.5%.

Ga−NODAGATOC (9). The ^{69,71}Ga^{III} complex was synthesized according to the methods previously described (*11*, *16*). A mixture of 500 μg (0.34 μmol) (**8**) in 500 μL of 0.4 M sodium acetate buffer (pH 5) was incubated with 102 μL of a 0.01 M aqueous solution of Ga(III) nitrate nonahydrate (1.02 μmol) for 25 min at 95 °C, cooled to room temperature, and purified over a SepPak C_{18} cartridge preconditioned with 10 mL of ethanol and 10 mL of water. The cartridge was eluted with 10 mL of 0.4 M sodium acetate (pH 5) followed by 3 mL of methanol resulting in 400 μg (76%) of Ga−NODAGATOC after evaporation of the methanol. MS ((−)EI, *m*/*z* (%)): 1495 (12, [M − H]$^-$); ((+)EI, *m*/*z* (%)): 1461 (14, [M + H]$^+$), 742 (100, [M + 2H]$^{2+}$).

In−NODAGATOC (10) was synthesized as (**9**) using $InCl_3$·5H_2O.

Radiotracer for Internalization Experiments. [^{111}In]−NODAGATOC was prepared by dissolving 10 μg of NODAGATOC (7.2 nmol) in sodium acetate buffer (100 μL, 0.4 M, pH 5); after the addition of $^{111}InCl_3$ (3.5 mCi), the solution was heated at 95° for 25 min. A 1.5 molar excess of $InCl_3$·5H_2O was added and the final solution heated at 95 °C for 25 min. [^{67}Ga]−NODAGATOC (10 μg of ligand, 3 mCi of $^{67}GaCl_3$) was prepared in the same way, using Ga(III) nitrate nonahydrate. In a modification of this protocol, acetate buffer was replaced by HEPES (150 μL, 0.1 M, pH 5.8). The final labeling solution had a pH 2.5. This protocol gave yields >95% at a specific activity of 40 GBq/μmol^{-1}. Subsequently radiolabeled peptides were purified utilizing a SepPak C_{18} cartridge preconditioned with 10 mL of methanol and 10 mL of water; the cartridge was eluted with 3 mL of water, followed by 2 mL of ethanol, to afford the very pure radioligand with a specific activity ≥15 GBq μmol^{-1}. A quality control was performed by HPLC (eluents: A = 0.1% TFA in water and B = acetonitrile; gradient: 0−30 min, 55% A, 30−36 min, 100% B, 36−40 min, 95% A).

Metal/Ligand Stability Studies. The chemical stability of the radiometal complexes [^{67}Ga]− and [^{111}In]−NODAGATOC was studied by measuring the rate of exchange of the radiometal in the presence of 10^5 molar excess of DTPA at pH 5. Solutions were stored at 37 °C,

and at periods up to 10 days aliquots were removed and analyzed by HPLC using the gradient described above.

Serum Stability. To 3 mL of fresh human serum, previously equilibrated in a 5% CO_2 (95% air) environment at 37 °C, was added 5 μCi of the [^{67}Ga]−NODAGATOC standard solution. The mixture was incubated in a 5% CO_2, 37 °C environment. At appropriate periods of time (0, 30 min, 1, and 4 h), 100 μL aliquots (in triplicate) were removed and treated with 200 μL of ethanol. Samples were then cooled (4 °C) and centrifuged for 15 min at 500*g* and 4 °C to precipitate serum proteins. One hundred microliters of supernatant was removed for activity counting in a γ well-counter. The sediment was washed twice with 1 mL of ethanol and counted. The activity in supernatant was compared with the activity in the pellet to give the percent peptide not bound to proteins.

The peptide structure in the supernatant was checked by HPLC using the equipment mentioned above.

Receptor Autoradiography and Binding Affinity. Determination of peptide conjugate concentrations and receptor autoradiography was described previously (*16*). Concentrations of peptides were determined spectrophotometrically using $\epsilon_{280} = 6800\ M^{-1}\ cm^{-1}$. IC_{50} values using autoradiographic methods were determined as described (*16*).

In brief, cells stably transfected with sst1-sst5 were kindly provided by Drs. T. Reisine and G. Singh (University of Pennsylvania, Philadelphia, PA). They were washed twice with and scraped into ice-cold 0.05 M Tris-HCl (pH 7.4), collected by centrifugation, and homogenized using a rotor/strator slash system (Polytron, Kinematica Inc., Littau, Switzerland) in the same buffer. After centrifugation at 120 g for 5 min at 4 °C, the supernatant was collected and centrifuged again at 48.000 g for 30 min at 4 °C. The resulting pellet was resuspended in ice-cold Tris buffer, transferred into a microfuge tube, and centrifuged at 20.000 g for 15 min at 4 °C. After withdrawal of the supernatant, the membrane pellet was stored at −80 °C.

Receptor autoradiography was performed on 20-μm-thick cryostat (Leitz 1720, Rockleigh, NJ) sections of the membrane pellets, mounted on microscope slides and then stored at −20 °C. For each of the tested compounds, complete displacement experiments were performed with the universal somatostatin radioligand [^{125}I]-[Leu^{8},D-Trp^{22},Trp^{25}]somatostatin 28 using increasing concentrations of the unlabeled peptide ranging from 0.1 to 1000 nM. As a control, somatostatin 28 was run in parallel using the same increasing concentrations. IC_{50} values were calculated after quantification of the data using a computer-assisted image processing system as described previously (*23*). Tissue standards (autoradiographic [^{125}I]-microscales, Amersham), containing known amounts of isotopes, cross-calibrated to tissue-equivalent ligand concentrations, were used for quantification (*24*).

Radiotracers Used in Biodistribution Studies. [^{67}Ga]−NODAGATOC and [^{111}In]−DOTATOC were prepared with the methodology described in the previous section, without addition of cold metal but using lower peptide amounts. If necessary, radioligands were purified by SepPak C_{18} cartridge and after evaporation of ethanol were diluted in NaCl (0.1% BSA, pH 7.4) to afford the very pure radioligands with a specific activity of ca. 40 GBq/μmol conjugate. The radiotracers were subjected to quality control by HPLC as described above.

Cell Culture. AR4-2J (ATCC, Manassas, VA) rat pancreatic tumor cells were cultured in Dulbecco's minimal essential medium (DMEM). DMEM was supplemented with vitamins, essential and nonessential amino acids, L-glutamine, antibiotics (peniciline/streptomycine), fungicide (amprotencine), and 10% fetal calf serum (FCS) as described elsewhere (*25*).

Internalization/Externalization Studies. Internalization and externalization experiments were performed as indicated in previous publications in six-well plates (*25, 26*). Briefly, the cells were washed twice with internalization medium [DMEM supplemented with 0.1% FCS, vitamins, essential and nonessential amino acids, L-glutamine, antibiotic (penicillin/streptomycin), and fungicide (amprotencin)], and they were allowed to adjust to the medium for 1 h at 37 °C. Approximately 3.7 kBq (2.5 pmol) of radioligand were added to the medium, and the cells, 10^6 cells per well, were incubated (in triplicates) for 4 h at 37 °C, 5% CO_2, with or without excess cold octreotide (300 μL of a 1 μM solution) to determine nonspecific internalization. The final volume was 3 mL. At appropriate time periods, the internalization was stopped by removal of the medium and washing the cells with ice-cold phosphate-buffered saline. Cells were then treated with glycine buffer twice for 5 min at room temperature (0.05 M glycine solution, pH adjusted to 2.8 with 1 N HCl) to distinguish between cell surface-bound (acid releasable) and internalized (acid resistant) radioligand. Finally, cells were treated with 1 N NaOH and incubated at 37 °C for 10 min to detach them from plates, and the radioactivity was measured in a γ-counter. For externalization the AR4-2J cells were allowed to internalize the radioligands for periods of 2 and 4 h and then were exposed to an acid wash, as described in the previous section, to dissociate cell-surface-receptor-bound radioligand. Three milliliters of culture medium were added to each well, cells were incubated at 37 °C in a 5% CO_2 environment, and externalization of the cell-incorporated radioactivity was studied during 3 h.

Biodistribution Experiments in AR4-2J Tumor-Bearing Nude Mice. Six to ten week old Swiss female nude mice (IFFA-CREDO, France) were implanted subcutaneously with 5 million AR4-2J rat pancreatic tumor cells, previously expanded in Dulbecco's minimal essential medium (DMEM, GibcoBRL). DMEM was supplemented with vitamins, essential and nonessential amino acids, L-glutamine, antibiotics (penicilline/streptomycine), fungicide (amprotencine), and 10% fetal calf serum (FCS).

Fourteen days after inoculation, the tumors weighed 50−100 mg, and the mice were injected in the lateral tail vein with 5 μCi of [^{67}Ga]−NODAGATOC or [^{111}In]−DOTATOC, diluted in NaCl (0.1% BSA, pH 7.4, total injected volume = 200 μL). For determination of nonspecific uptake in tumor or receptor-positive organs, a group of four animals was injected in the tail vein with 50 μg of cold octreotide in NaCl (injected volume, 200 μL), 30 min before radiotracer injection. At 4, 24, and 48 h mice (in groups of three or four) were sacrificed and organs of interest collected, rinsed of excess blood, weighed, and counted in a γ-counter. The percentage of injected dose per gram (% ID/g) was calculated for each tissue. The total counts injected per animal were determined by extrapolation from counts of an aliquot taken from the injected solution. Urine samples were analyzed for possible metabolites by HPLC.

All animal experiments were performed in compliance with the Swiss regulation for animal treatment (Bundesamt für Veterinärwesen, approval no. 789).

RESULTS

Synthesis and Radiolabeling. An important step toward the synthesis of NOTA-derivatized bioactive

Scheme 2. Synthesis of NODAGATOC (8)

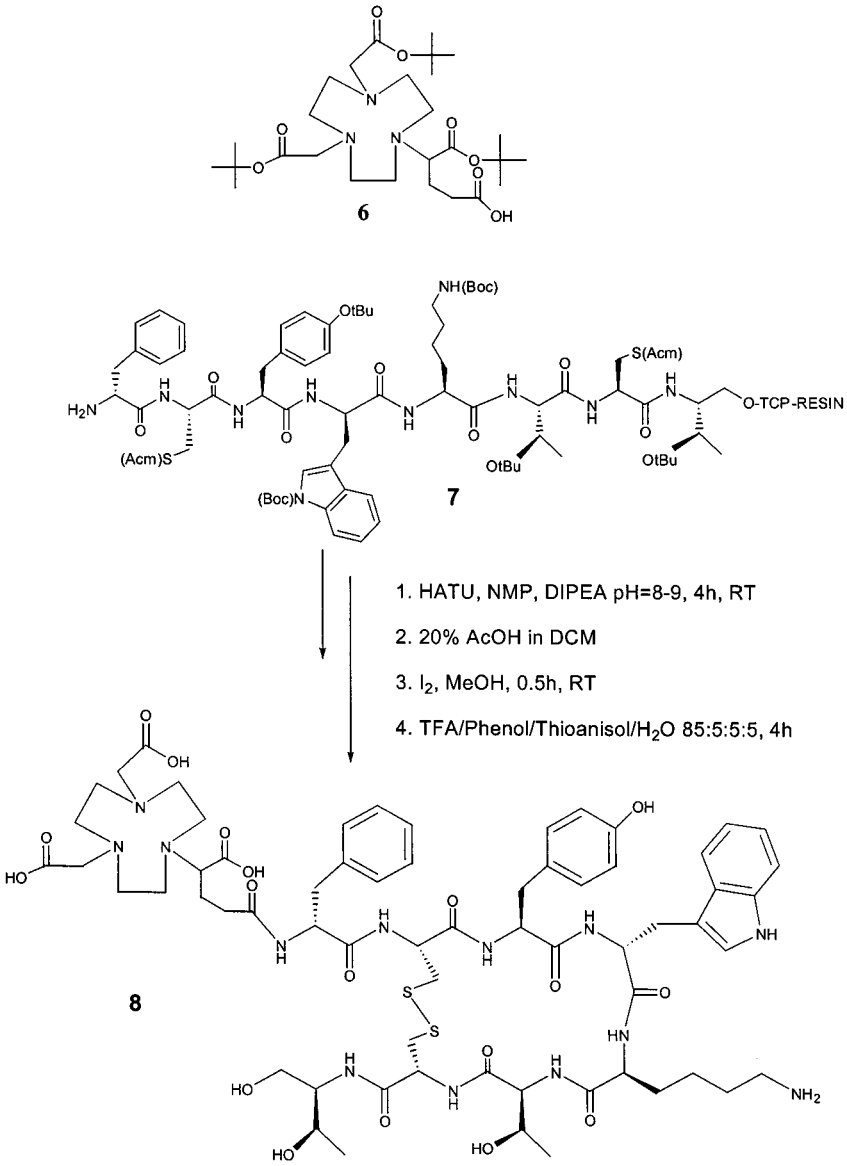


Table 1. Yields of the Monoalkylation of 1,4,7-Triazacyclononane (1) with *β*-Bromoglutaric Acid 1-*tert*-Butyl Ester 5-Benzyl Ester (2)

ratio of **1** to **2**	% yield of monoalkylated product	% yield of dialkylated product
1.3:1	36.9	23
2:1	50.9	20
3:1	69.2	>5

peptides is the development of the corresponding prochelator NODAGA(tBu)$_3$ (**6**) (Scheme 1). The monoreactive NODAGA-prochelator was synthesized in five steps with an overall yield of 21% (Schemes 1 and 2). Two side reactions decreased the yields of steps 3 and 4. The monoalkylation of 1,4,7-triazacyclononane (**1**) with α-bromoglutaric acid 1-*tert*-butyl ester 5-benzyl ester (**2**) gave more than 20% of the dialkylated product 1,4-bis(1-carbobenzyloxy-3-carbo-*tert*-butoxypropyl)-1,4,7-triazacyclononane (**3a**) if the ratio of **1**:**2** was 2. Only the use of a 3-fold excess of **1** over **2** gave yields based on **2** of about 70% (Table 1). In step 4, overalkylation to a quarternary ammonium salt was found even if stoichiometric ratios were used. Therefore only 1.9 equiv of bromoacetic acid *tert*-butyl ester were employed. In addition, cooling to 4 °C appeared to be advantageous to avoid overalkylation.

After these partially optimized synthetic steps, **6** was obtained in a reasonable overall yield of 21%. The linear side chain protected octapeptide D-Phe^1-Cys(Acm)^2-Tyr-(tBu)^3-D-Trp(Boc)^4-Lys(Boc)^5-Thr(tBu)^6-Cys(Acm)^7-Thr-(ol)(tBu)^8 **(7)** was assembled on a TCP resin using Fmoc-strategy (*22*) with DIC as coupling reagent. **6** (3 equiv) was coupled to **7** on the resin with the use of HATU (*O*-(7-azabenzotriazol-1-yl)-*N*,*N*,*N*',*N*'-tetramethyluronium hexafluorophosphate) as coupling reagent. The protected peptide was mildly cleaved from the resin (20% CH_3-COOH), cyclized with I_2 in methanol, deprotected, and purified by preparative HPLC analogous to Arano et al. (*27*) (Scheme 2). Reversed phase HPLC afforded the peptide in ≥95% purity. The composition and structure of NODAGATOC were verified by MS-ESI and by the retention of a high-binding affinity to sstr2. NODAGATOC was labeled with the radiometals of interest (^{67}Ga, ^{111}In) using acetate buffer (pH 5, 0.4 M) by heating (95 °C, 25−30 min); the labeling yields were >99% (^{111}In) and >60% (^{67}Ga) at a specific activity >40 GBq μmol^{-1}. It could be shown by an accidental labeling protocol that using HEPES (pH ≈ 2.5) better labeling yields (≥95% at 40 GBq μmol^{-1}) of [^{67}Ga]NODAGATOC were obtained. We assume that this is due to the lower pH which may

Table 2. Affinity Profiles (IC_{50}) for Human sst1−sst5 Receptors of a Series of Somatostatin Analogues. IC_{50} Values (nM ± SE) Are in Triplicates. Number of Independent Studies in Brackets. Somatostatin-28 Is Used as Internal Control in Each of the Experiments

peptide	hsst1	hsst2	hsst3	hsst4	hsst5
somatostatin-28	4.1 ± 0.3 (15)	2.6 ± 0.2 (16)	5.4 ± 0.6 (13)	4.1 ± 0.3 (16)	3.9 ± 0.4 (17)
DOTA-Tyr^3-octreotide (DOTATOC)	>10000 (7)	13.9 ± 2.8 (6)	816 ± 259 (5)	>1000 (5)	393 ± 85 (6)
Y-DOTA-Tyr^3-octreotide[a]	>10000 (6)	11.4 ± 1.7 (6)	389 ± 135 (5)	>10000 (6)	204 ± 92 (6)
Ga-DOTA-Tyr^3-octreotide	>10000 (6)	2.5 ± 0.5 (7)	607 ± 165 (6)	>1000 (6)	106 ± 37 (7)
NODAGA-Tyr^3-octreotide (NODAGATOC)	>10000 (2)	3.2 ± 1.0 (2)	675 ± 225 (2)	>1000 (2)	305 ± 85 (2)
Ga−NODAGA-Tyr^3-octreotide	>1000 (2)	3.5 ± 1.6 (2)	325 ± 55 (2)	>1000 (2)	185 ± 35 (2)
In−NODAGA-Tyr^3-octreotide	>1000 (3)	1.7 ± 0.2 (3)	293 ± 71 (3)	320 ± 17 (3)	44 ± 8 (3)

[a] In−DOTA-Tyr^3-octreotide was shown to have the same sstr2 receptor affinity as Y^{III}−DOTA-Tyr^3-octreotide using a somewhat different assay *(11)*.

favor the $^{67}Ga^{3+}$ over the metal impurities present. An expansion of this finding was outside the scope of this work.

Receptor Binding. Table 2 shows the newly synthesized NODAGATOC somatostatin analogues investigated and their respective IC_{50} values for the five somatostatin receptor subtypes. As controls, somatostatin 28 (SS28), which binds with high affinity to all five somatostatin receptor subtypes, and our gold standards Ga/Y-DOTATOC were included. Ga−NODAGATOC shows high affinity only to sstr2 with an IC_{50} of 3.5 ± 1.6 nM close to the one of Ga-DOTATOC (2.5 ± 0.5 nM) whereas it binds significantly better to sstr2 than Y-/In-DOTATOC. Measurable affinity was also found to sstr3 and sstr5. Interestingly, In−NODAGATOC binds with higher affinity to sstr2 (1.7 ± 0.2 nM) and also has distinctly higher affinity to sstr4/sstr5 than Ga−NODAGATOC. A remarkably low IC_{50} value was found for sstr5, and no binding affinity was found to sstr1.

Stability of the Radiotracers. Our studies had demonstrated that with both radiolabeled peptides no radiolysis breakdown products were observed and that there is no appreciable release of ^{67}Ga even under extreme conditions (10^5 times excess of DTPA). The pseudo first-order dissociation rate constant for [^{67}Ga]−NODAGATOC was shown to be $<10^{-8}$ s^{-1} compared to 3.5×10^{-6} s^{-1} for [^{111}In]−NODAGATOC.

Stability in Serum. Incubation of [^{67}Ga]−NODAGATOC in fresh human serum shows high metabolic stability as well as high stability with regard to transchelation. At 4 h, 98.3% of the activity remained in the nonproteic fraction. We found also, by HPLC, that the radioactivity present in this fraction, after 4 h of incubation, was still peptide bound and represents intact radioligand indicating that no transchelation or appreciable metabolic decay did take place.

Stability in Rat Liver Homogenate. The possible degradation of [^{67}Ga]−NODAGA-Tyr^3-octreotide was studied in 30% rat liver homogenate, a medium rich in peptidases and proteinases. The analysis was carried out by HPLC and until 4 h of incubation no degradation products were observed.

[^{67}Ga]/[^{111}In]−NODAGATOC Internalization and Externalization Results. The AR4-2J rat pancreatic carcinoma cell line is known to express sstr2 receptors both in vivo and in vitro (*28*). The two radioligands were internalized by AR4-2J cells in a time dependent way, as shown in Figure 2. Both radiopeptides showed a fast and time dependent cell uptake by endocytosis which did not reach a plateau within 4 h of incubation at 37 °C. There was no difference between the two radioligands. Both show about 18% (of the added activity) specific internalization after 2 h compared to only about 6% of [^{111}In]−DOTATOC (Figure 3). Internalization was strongly reduced in the presence of 0.1 μM unlabeled octreotide

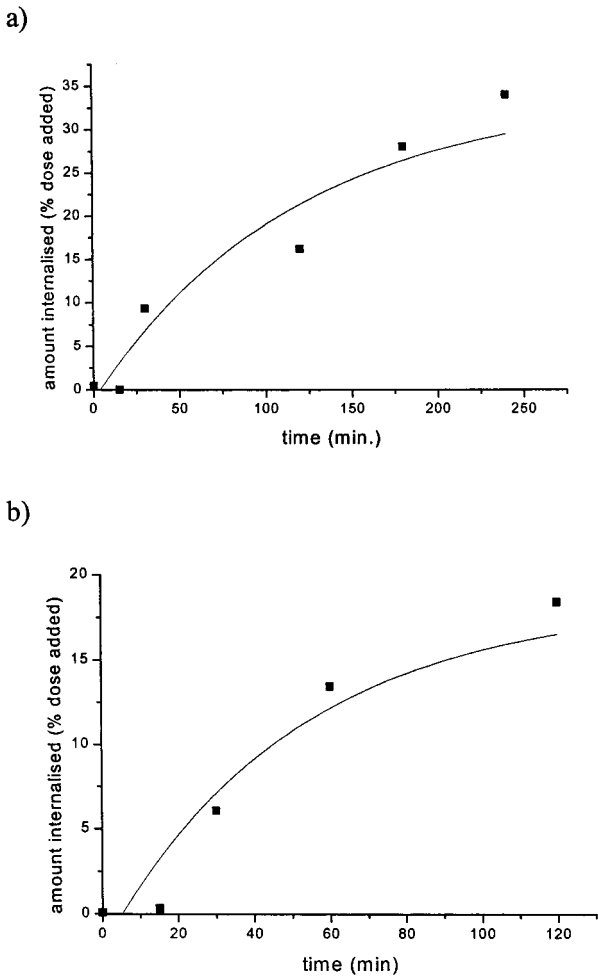


Figure 2. Uptake kinetics on rat pancreatic tumor AR4-2J cells of (a) [^{111}In]−NODAGA-Tyr^3-octreotide and (b) [^{67}Ga]−NODAGA-Tyr^3-octreotide. Data result from two independent experiments with triplicates in each experiment.

(data not shown). In fact, nonspecific internalization was <3% of the added activity. The surface bound peptide (acid removable) was <7% of the added activity. The externalization of both peptides was studied with cells exposed 2 and/or 4 h to the radioligand as described for internalization (Figure 4). Again a time dependent externalization was found which appears to depend somewhat on the time period cells were allowed to internalize as well as on the radioligand studied. Interestingly, the externalized radiopeptides were shown to be intact by HPLC as they coelute with the original radiopeptides.

Animal Biodistribution Studies. Biodistribution data were obtained by comparing [^{67}Ga]−NODAGATOC with our gold standard for sstr2 receptor targeting [^{111}In]−DOTATOC. The biodistribution of the latter was

Table 3. Biodistribution and Tissue Ratios in AR4-2J Tumor-Bearing Nude Mice. Results Are the Mean of Groups of Three or Four Animals

site	[^{67}Ga]−NODAGATOC (4 h)		[^{111}In]−DOTATOC (4 h)		[^{67}Ga]−NODAGATOC (24 h)[b]	[^{111}In]−DOTATOC (24 h)[b]	[^{67}Ga]−NODAGATOC (48 h)[b]
	unblocked	blocked[a]	unblocked	blocked[a]			
	Biodistribution (%ID/g for three or four animals)						
blood	0.05 ± 0.004	0.04 ± 0.01	0.07 ± 0.04	0.06 ± 0.009	0.007 ± 0.0009	0.008 ± 0.002	0.003 ± 0.0005
pancreas	1.25 ± 0.67	0.26 ± 0.06	1.10 ± 0.15	0.14 ± 0.11	0.22 ± 0.26	0.35 ± 0.10	0.02 ± 0.005
s. intest.	0.70 ± 0.08	0.14 ± 0.05	0.29 ± 0.06	0.09 ± 0.03	0.07 ± 0.02	0.07 ± 0.01	0.02 ± 0.006
spleen	0.19 ± 0.04	0.06 ± 0.02	0.16 ± 0.03	0.10 ± 0.02	0.03 ± 0.008	0.08 ± 0.03	0.02 ± 0.005
liver	0.16 ± 0.02	0.18 ± 0.05	0.23 ± 0.04	0.27 ± 0.04	0.02 ± 0.0002	0.09 ± 0.009	0.01 ± 0.003
stomach	4.80 ± 0.67	0.56 ± 0.08	2.77 ± 0.73	0.41 ± 0.35	0.38 ± 0.06	0.78 ± 0.08	0.11 ± 0.01
adrenals	2.90 ± 0.43	0.70 ± 0.17	1.46 ± 0.13	0.35 ± 0.21	0.46 ± 0.13	0.53 ± 0.07	0.42 ± 0.26
kidney	7.08 ± 1.50	18.0 ± 2.95	12.84 ± 0.98	12.55 ± 1.30	0.46 ± 0.05	5.64 ± 0.66	0.22 ± 0.04
lung	0.46 ± 0.03	0.19 ± 0.05	0.28 ± 0.07	0.16 ± 0.03	0.09 ± 0.09	0.12 ± 0.01	0.05 ± 0.07
heart	0.08 ± 0.01	0.05 ± 0.01	0.07 ± 0.02	0.05 ± 0.008	0.02 ± 0.003	0.03 ± 0.003	0.01± 0.003
tumor	21.21 ± 3.55	3.64 ± 1.39	12.50 ± 0.65	6.81 ± 0.03	2.60 ± 0.47	5.60 ± 0.48	0.73 ± 0.20
	Tissue Ratio						
tumor/blood	424		188		321	700	243
tumor/liver	133		54		130	62	37
tumor/kidney	3		0.97		5.7	0.94	3.3

[a] Blocked with 50 μg of octreotide 30 min before injection of radiopeptide. [b] Unblocked.

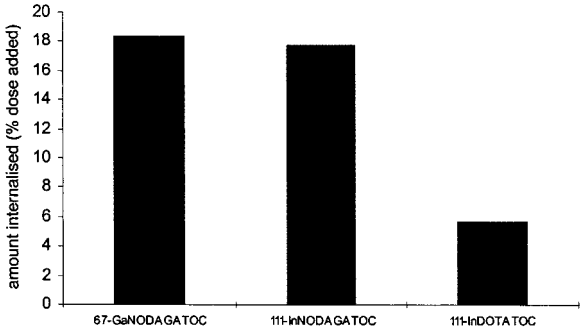


Figure 3. Uptake on rat pancreatic tumor AR4-2J cells of [^{67}-Ga]−NODAGA-Tyr^3-octreotide, [^{111}In]−NODAGA-Tyr^3-octreotide, and [^{111}In]−DOTA-Tyr^3-octreotide, 2 h after incubation with ca. 0.09 μCi of the radiolabeled peptides in a 37 °C, 5% CO_2 environment.

reported before (*11*, *25*, *26*, *28*) and was used as a reference because a new batch of AR4-2J cells was used. Data obtained with nude mice bearing the AR4-2J pancreatic tumor are presented in Table 3 as % of injected dose per gram of tissue (% ID/g) as a function of time.

Both peptides displayed rapid blood clearance with only 0.05−0.07% ID/g remaining in blood at 4 h which can be associated with a fast elimination of radioactivity from the sstr-negative tissues not involved in the excretion process. In accordance with previous results (*28*) using [^{111}In]−DOTATOC and [^{67}Ga]−DOTATOC, [^{67}Ga]−NODAGATOC is excreted mainly by the kidney pathway, leading to very low liver uptake. Moreover, our HPLC studies in mouse urine demonstrated that the [^{67}Ga]−NODAGATOC is excreted unchanged in the first 4 h after radiotracer injection. [^{67}Ga]−NODAGATOC shows high uptake values in sst receptor expressing organs such as adrenals, pancreas, and stomach, and in the AR4-2J tumor. In addition, a very rapid clearance from all other organs and tissues except the kidneys was found. The results of an in vivo competition experiment using large excess of octreotide preinjected iv resulted in a >83% reduction of tumor uptake and also in a reduction of the uptake in the sstr-positive organs (80% in pancreas, 82% in stomach, 76% in adrenals). The injection of the blocking dose had no significant influence on the uptake in nontarget organs except the kidneys where the uptake is increased by a factor of >2.

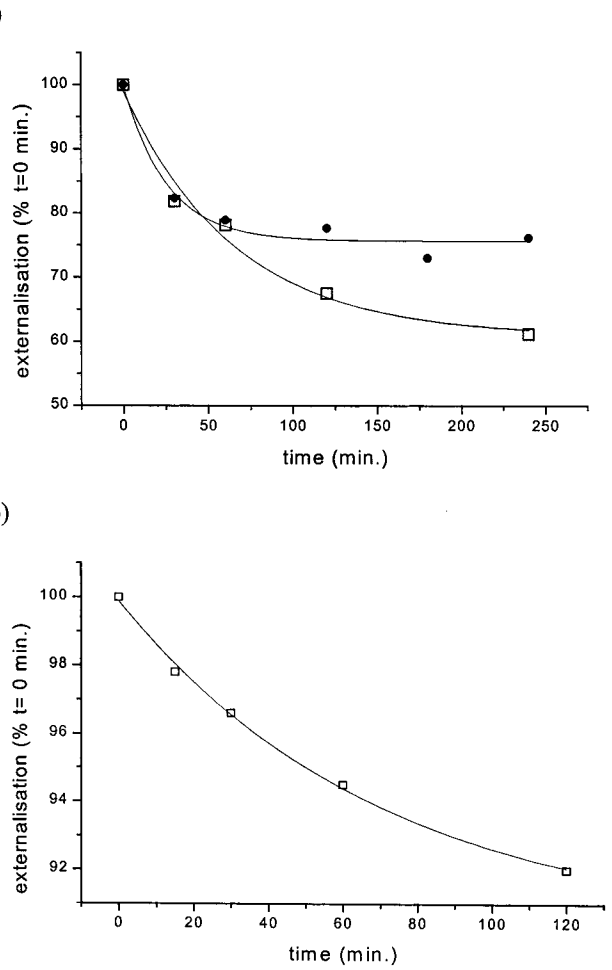


Figure 4. Externalization kinetics of (a) [^{111}In]−NODAGA-Tyr^3-octreotide and (b) [^{67}Ga]−NODAGA-Tyr^3-octreotide, by rat pancreatic AR4-2J tumor cells. Efflux of the radiolabeled peptides is expressed in percentage of radioactivity associated with the cells after acid wash retained in the cell compared with the uptake at 2 h (squares) or 4 h (circles) considered as 100%. After this period, the cells were exposed to an acid wash to remove cell surface bound radioligand. Each point represents two experiments carried out in triplicate.

[^{67}Ga]−NODAGATOC has a higher uptake in all sstr-positive tissues than [^{111}In]−DOTATOC at 4 h (tumor, 21.2 ± 3.5% ID/g vs 12.5 ± 0.65%; pancreas, 1.25 ± 0.67%

ID/g vs 1.1 ± 0.25; stomach, 4.8 ± 0.67% ID/g vs 2.77 ± 0.75% ID/g; adrenals, 2.9 ± 0.43% ID/g vs 1.46 ± 0.35% ID/g). A further remarkable result of the new radiopeptide is the very favorable tumor:kidney ratio which is 3.0 at 4 h compared to 1 for ^{111}In−DOTATOC, the ratio even increases at 24 h to 5.7 whereas it remains 1 at 24 h for ^{111}In−DOTATOC. Additional tumor/unspecific tissue ratios at 4 h can be seen from Table 3. They are as follows (in parentheses the data for ^{111}In−DOTATOC are given): 424 (188) for tumor/blood and 133 (54) for tumor/liver. These very favorable ratios indicate the high potential of this radiopeptide for early time point, highly sensitive diagnostic tumor imaging. An unexpected result is the relatively quick washout from the tumor and receptor-positive organs. In the tumor, the dose dropped from 21.2% ID/g at 4 h to 2.6% ID/g at 24 h and 0.73% ID/g at 48 h. A similar rate of decline is found in the other receptor-positive organs. Somewhat fortunately, this decline is even faster in the kidneys. The residence time of ^{111}In−DOTATOC is distinctly longer in receptor-positive tissues but also in the kidneys.

DISCUSSION

In the past few years several SRIF-derived positron-emitting radiopeptides have been developed (*12, 13, 29*−*32*), and some of them had been or are currently being investigated for PET imaging of SRIF receptor-positive tumors in patients (*33*−*35*). An ideal PET tracer will allow to answer many important questions in the new and rising field of tumor targeting with use of radiopeptides, e.g., receptor regulation due to pharmacologic and chemotherapeutic intervention, receptor quantification and potential receptor downregulation due to receptor mediated radiopeptide therapy. The radiopeptides discussed in this manuscript were designed to answer questions arising from earlier developments in our laboratory and to offer new conjugates for studies with the Ga^{III}, In^{III}, and Cu^{II} (*36*) radioisotopes. The macrocyclic chelator NOTA satisfies the coordination requirements of the respective metal ions in the indicated oxidation states. The NODAGATOC differs from our gold standard DOTA−[Tyr^3]-octreotide (DOTATOC) by the coupling of a new macrocyclic chelator to [tyr^3]-octreotide. We synthesized first a new bifunctional derivative of NOTA which had to fulfill two criteria:

(1) Compatibility with peptide synthesis; in other words, an orthogonally carboxylic acid group protected NOTA derivative has to be synthesized which upon specific deprotection of one carboxylic acid group is soluble in the common solvens used in solid-phase synthesis and may be used as an amino acid surrogate for coupling to the N-terminus of a requested peptide. (2) In addition, three acetate arms should be retained for metal coordination necessitating preparation of a C-functionalized NOTA. Different syntheses of bifunctional NOTA derivatives have been reported before by Parker et al. (overall yield: 7.7%) (*37*), Meares and Studer (yield: 1.34%) (*38*), and McMurray et al. (yield: 6.4%) (*36*). Their syntheses used intra- or intermolecular cyclization strategy as key steps affording NOTA's functionalized on a carbon of the macrocyclic ring. They were not designed for coupling to peptides, and harsh conditions for deprotection and reduction were necessary. Our aim was to introduce the carboxy function for coupling on the methylene group of a carboxymethyl arm, allowing one to start with commercially available triaazacyclononane, thus avoiding a cyclization step. A similar strategy was used by Brechbiel et al. (*39*) to yield a bifunctional NOTA for antibody modification in 9% overall yield. In addition, this strategy was used in the functionalization of DOTA (*21, 40*−*41*). The key steps are the synthesis of an orthogonally protected bromoalkyl dicarboxylic acid diester and the monoalkylation of the triazacyclononane macrocycle. The latter step was performed using 3 equiv of 1,4,7-triazacyclononane over the alkylating diester to give **3** (69.2%). **5** was obtained in 90% yield using somewhat less than 2 equiv of bromoacetic acid *tert*-butyl ester to avoid overalkylation. The overall yield of the five steps was about 21%. The coupling of **6** to the linear octapeptide (appropriately protected) assembled on the TCP-resin was straightforward. The cleavage was followed by oxidative cyclization using I_2 and deprotection in a mixture of TFA/phenol/thioanisole/water. The crude mixture was purified by preparative HPLC.

We have proposed earlier the use of a similar bifunctional chelator (NODASA = 1,4,7-triazacyclononane-1-succinic acid-4,7-diacetic acid) and the use of the radiogallium complex in a prelabeling approach (*42*). Although this approach is very attractive and was proven to work well with model peptides and with the nonradioactive Ga^{III}, it proved not to be practical for larger amounts of radioactivity because of relatively low coupling yields of [^{67}Ga]−NODASA to the peptide due to low solubility. This caused a large waste of radioactivity. The coupling of the present prochelator works well under peptide synthesis conditions and allows the preparation of a kit-formulated version of the conjugate.

Receptor Binding Studies. One of the aims of this study was to probe the hypothesis that the higher sstr2 affinity of [Ga^{III}]−DOTA-Tyr^3-octreotide vs [Y^{III}]−DOTA-Tyr^3-octreotide and [In^{III}]−DOTA-Tyr^3-octreotide can be explained by the different metal complex geometries of the respective metal DOTA-D-Phe coordination compounds which result in a spacer function between the Ga^{III} complex and the pharmacophoric peptide. This is due to the fact that the carboxyamido group connecting the two entities is not participating in the metal coordination contrary to the octadentate nature of the chelate unit in [Y^{III}]−DOTA-D-Phe. If this were true, [Ga^{III}]−NODAGATOC should have a receptor affinity closer to Ga^{III}−DOTATOC than [Y^{III}(In^{III})]DOTATOC. Indeed, we interpret the value of 3.5 ± 1.6 nM, which is very close to the value of [Ga^{III}]−DOTATOC, as originating from the structurally introduced ethylene spacer function. It is remarkable and not foreseen that [In^{III}]−NODAGATOC shows significant differences compared to [Ga^{III}]−NODAGATOC not only with regard to the sstr2 affinity which with 1.7 ± 0.2 nM is significantly higher than the one of [Ga^{III}]−NODAGATOC. Also, the affinity to sst4 and sst5 is significantly higher for the [In^{III}]−NODAGATOC vs [Ga^{III}]−NODAGATOC. The structural factors contributing to this difference are not clear. Both metals fit well into the cavity offered by NOTA. X-ray structural data point at potential differences. Whereas In^{III} (ionic radius = 0.80 Å, CN6; 0.92 Å, CN8) (*43*) prefers coordination number 7 or 8, the smaller Ga^{III} (ionic radius = 0.62 Å) is perfectly satisfied by hexadentate ligands and fits well into the cavity offered by NOTA and functionalized derivatives of it (*42, 44*). In this context, it is interesting to note that in the solid-state In^{III}−NOTA is crystallizing with one Cl^- ion in a pentagonal bipyramidal coordination environment (*44*). We propose as a possible explanation of the above-mentioned affinity differences that in the biological fluids used in our assays either Cl^- or H_2O are being coordinated to In^{III}.

Stability of Tracers. [^{67}Ga]−NODAGATOC and [^{111}In]−NODAGATOC proved to be more or less stable

with regard to radiometal transfer. The ^{67}Ga-labeled peptide is $>10^3$ times more stable than [^{111}In]−NODAGATOC which correlates well with the thermodynamic stability of most of the triaza complexes of these two metals (e.g., log *K* (GaNOTA) = 30.98, log *K* (InNOTA) = 25.9 (*45*). Also, the metabolic stability is very high in fresh human serum and surprisingly in a rat liver homogenate (data not shown).

Cell Uptake and Release. The internalization and release of the two new radiopeptides was studied in the AR4-2J cell line known to express sstr2 receptors (*28*). The cell uptake at 4 h was the same for both radiopeptides but was a factor of 3 higher than for [^{111}In]−DOTATOC at 2 h (18% vs about 6%). The fast internalization indicates that—according to the current knowledge that only agonistic drugs can internalize (*46*)—[^{67}Ga]− and [^{111}In]−NODAGATOC are both powerful agonists for sstr2 and parallel the improved binding affinity of the two radiopeptides over [^{111}In]−DOTATOC. Internalization was inhibited by the addition of excess octreotide. In the time interval of the study (30 min to 4 h) no steady state was reached yet but the distinct leveling-off indicates the close approach to it which can be explained with the beginning efflux.

If the cells upon internalization of the radioligand for 2 and/or 4 h were exposed to the culture medium, again a time-dependent efflux of the radiopeptides could be observed, indicating a rapid recycling of the radiopeptides to the extracellular medium. A steady state is reached already after 2−4 h of release studies. This is due to the reactivation of the receptor by the released radiopeptide which was shown to be intact by HPLC as it coelutes with the original radiopeptides. It appears that already 25−40% of the externalized agonist are enough to stimulate the receptor to undergo reendocytosis. At steady state, about 60−75% of the radioactivity are located inside the cell and can be routed to lysosomes for degradation. The finding that the amount of externalized radiopeptide and the earlier reaching of a steady state appear to depend on the time internalization was allowed (Figure 3) indicates that this mechanism may be valid. On the other hand, it may just reflect that the steady state is reached earlier because the absolute value of 4 h internalization is higher than the one of 2 h internalization. A distinction between the two possibilities can only be made after careful structural analysis of the peptide contained inside the cells. The interpretation above is in keeping with the conclusion of data obtained by Koenig et al. (*47*), using ^{125}I-labeled somatostatin analogues in sstr2-expressing CHO cells.

Biodistribution Studies. The biodistribution studies in AR4-2J-tumor bearing (sstr2-positive) nude mice showed a higher uptake of [^{67}Ga]−NODAGATOC in sstr-bearing organs and the tumor compared to [^{111}In]−DOTATOC by up to a factor of 2 at 4 h postinjection paralleling the higher binding affinity and higher rate of internalization. Compared to [^{67}Ga]−DOTATOC (data published earlier) the new tracer shows almost the same performance, i.e., a somewhat lower tumor uptake but a higher tumor-to-blood, tumor-to-liver, tumor-to-heart, and a comparable tumor-to-kidney ratio.

In addition, using the same animal model it is far superior to ^{111}In-DTPA-octreotide which showed only 3.03% ± 0.26% ID/g in the tumor at 4 h and an inferior tumor-to-normal organ ratio, e.g. tumor/blood = 7.6, tumor/liver = 4 at the same time point (*28*).

Unforeseen is the fast washout (short residence time) of the tumor and sstr2-positive organs. It is faster compared to other somatostatin-based radiopeptides studied in this laboratory. The approximate biological half-life in the tumor is 7 h. The reason for this is not known yet. Our original hypothesis that it is due to metabolic instability of the exposed peptide bond between NODAGA and D-Phe due to the coupling via the carboxy ethyl spacer compared to the DOTA monoamide coupled peptides was not confirmed by studies with liver homogenate and fresh serum. In the latter cases a protection of the same bond is accomplished due to the fact that the amidocarboxy oxygen is involved in the coordination to the metal. The short tumor retention time resembles somewhat the behavior of most of the [^{64}Cu]−TETA−SRIF analogues discussed by Lewis et al. (*48*). Also, as discussed above, internalization and release studies do not give any clue as to the reason for the fast washout.

In conclusion, NODAGATOC most likely is a peptide−chelator conjugate with very promising properties for human studies if labeled with the short-lived positron emitters ^{68}Ga and ^{66}Ga. Because of the relatively fast washout from tumors, its suitability for a potential therapeutic application with the Auger electron emitter ^{67}Ga has to be shown in other animal models and in patients.

In addition, we developed a new chelator−somatostatin analogue for selective tumor targeting which is also suitable for ^{111}In and because of favorable complex stability most likely for ^{64}Cu and ^{55}Co labeling and their use in the targeting of sstr2-positive tumors in patients.

ACKNOWLEDGMENT

We wish to thank the Swiss National Science Foundation (31-52969.97) and Mallinckrodt Med. for financial support of this work and Novartis for analytical support. M.I.M. Prata acknowledges a grant from Fundaçao Calouste Gulbenkian (Portugal). We are grateful to the group of Prof. Krähenbühl for support with the rat liver homogenate experiment.

LITERATURE CITED

(1) Lamberts, S. W. J., Van der Lely, A.-J., De Herder, W. W., and Hofland, L. J. (1996). Octreotide. *N. Engl. J. Med. 25,* 246−254.

(2) Behr, T. M., Béhé, M., and Becker, W. (1999). Diagnostic applications of radiolabeled peptides in nuclear endocrinology. *Q. J. Nucl. Med. 43,* 268−80.

(3) Fischman, A. J., Babich, J. W., and Strauss, H. W. (1993). A Ticket to Ride: Peptide Radiopharmaceuticals. *J. Nucl. Med. 34,* 2253−2263.

(4) Heppeler, A., Froidevaux, S., Eberle, A. N., and Maecke, H. R. (2000). Receptor Targeting for Tumor Localisation and Therapy with Radiopeptides. *Curr. Med. Chem. 7,* 971−994.

(5) Lister-James, J., Moyer, B. R., and Dean, T. (1996). Small peptides radiolabeld with ^{99m}Tc. *Q. J. Nucl. Med. 40,* 221−233.

(6) Liu, S., and Edwards, D. S. (1999). ^{99m}Tc-Labeled Small Peptides as Diagnostic Radiopharmaceuticals. *Chem. Rev. 99,* 2235−2268.

(7) Reubi, J. C. (1995). Neuropeptide Receptors in Health and Disease: The Molecular Basis for In Vivo Imaging. *J. Nucl. Med. 36,* 1825−35.

(8) Thakur, M. L. (1995). Radiolabeled peptides: Now and the future. *Nucl. Med. Commun. 16,* 724−732.

(9) Krenning, E. P., Bakker, W. H., Kooij, P. P., Breeman, W. A., Oei, H. Y., de Jong, M., Reubi, J. C., Visser, T. J., Bruns, C., and Kwekkeboom, D. J., et al. (1992). Somatostatin receptor scintigraphy with indium-111-DTPA-D-Phe-1-octreotide in man: metabolism, dosimetry and comparison with iodine-123-Tyr^3-octreotide. *J. Nucl. Med. 33,* 652−8.

(10) Krenning, E. P., Kwekkeboom, D. J., Bakker, W. H., Breeman, W. A., Kooij, P. P., Oei, H. Y., van Hagen, M., Postema, P. T., de Jong, M., and Reubi, J. C., et al. (1993). Somatostatin receptor scintigraphy with [^{111}In-DTPA-D-Phe^{1}]- and [^{123}I-Tyr^{3}]-octreotide: the Rotterdam experience with more than 1000 patients. *Eur. J. Nucl. Med. 20,* 716−31.

(11) Heppeler, A., Froidevaux, S., Maecke, H. R., Jermann, E., Béhé, M., Hennig, M., and Powell, P. (1999). Radiometal-Labeled Macrocyclic Chelator-Derivatised Somatostatin Analogue with Superb Tumour-Targeting Properties and Potential for Receptor-Mediated Internal Radiotherapy. *Chem. Eur. J. 5,* 1974−1981.

(12) Smith-Jones, P. M., Stolz, B., Bruns, C., Albert, R., Reist, H. W., Friedrich, R., and Maecke, H. R. (1994). Gallium-67/Gallium-68-[DFO]-Octreotide − A Potential Radiopharmaceutical for PET imaging of Somatostatin Receptor-Positive Tumors: Synthesis and Radiolabeling In Vitro and Preliminary In Vivo Studies. *J. Nucl. Med. 35,* 317−325.

(13) Stolz, B., Smith-Jones, P. M., Albert, R., Reist, H., Maecke, H. R., and Bruns, C. (1994). Biological Characterisation of [^{67}Ga] or [^{68}Ga] Labeled DFO−Octreotide (SDZ 216−297) for PET Studies of Somatostatin Receptor Positive Tumors. *Horm. Metab. Res. 26,* 453−459.

(14) Maecke, H. R., Heppeler, A., and Nock, B. (1999). Somatostatin Analogues Labeled with Different Radionuclides, i*n Technetium, Rhenium and Other Metals in Chemistry and Nuclear Medicine* (M. Nicolini, U. Mazzi, Eds.) Vol. 5, pp 77−91, SGE Ditoriali, Padova.

(15) De Jong, M., Bakker, W. H., Krenning, E. P., Breeman, W. A. P., Pluijm, M. E. v. d., Bernard, B. F., Visser, T. J., Jermann, E., Behe, M., Powell, P., and Maecke, H. R. (1997). Yttrium-90 and indium-111 labeling, receptor binding and biodistribution of [DOTA^{0}, D.-Phe^{1}, Tyr^{3}]octreotide, a promising somatostatin analogue for radionuclide therapy. *Eur. J. Nucl. Med. 24,* 368−371.

(16) Reubi, J. C., Schär, J. C., Waser, B., Wenger, S., Heppeler, A., Schmitt, J. S., and Maecke, H. R. (2000). Affinity profiles for human somatostatin receptor subtypes SST1-SST5 of somatostatin radiotracers selected for scintigraphic and radiotherapeutic use. *Eur. J. Nucl. Med. 27,* 273−282.

(17) Anderson, C. J., and Welch, M. J. (1999). Radiometal-Labeled Agents (Non-Technetium) for Diagnostic Imaging. *Chem. Rev. 99,* 2219−2234.

(18) Green, M. A., Welch, and M. J. (1989). Gallium Radiopharmaceutical Chemistry. *Nucl. Med. Biol. 16,* 435−448.

(19) Caraco, C., Aloj, L., and Eckelman, W. C. (1998). The gallium-deferoxamine complex: stability with different deferoxamine concentrations and incubation conditions. *Appl. Radiat. Isot. 49,* 1477−9.

(20) Sharma, V., Beatty, A., Wey, S. P., Dahlheimer, J., Pica, C. M., Crankshaw, C. L., Bass, L., Green, M. A., Welch, M. J., and Piwnica-Worms, D. (2000). Novel gallium(III) complexes transported by MDR1 P-glycoprotein: potential PET imaging agents for probing P-glycoprotein-mediated transport activity in vivo. *Chem. Biol. 7,* 335−43.

(21) Eisenwiener, K.-P., Powell, P., and Mäcke, H. R. (2000). A Convenient Synthesis of Novel Bifunctional Prochelators for Coupling to Bioactive Peptides for Radiometal Labeling. *Bioorg., Med. Chem. Lett. 10,* 2133−2135.

(22) Atherton, E., and Sheppard, R. (1989). Solid phase peptide synthesis—a practical approach, IRL Press, Oxford.

(23) Reubi, J. C., Kvols, L. K., Waser, B., Nagorney, D. M., Heitz, P. U., Charboneau, J. W., Reading, and C. C., Moertel, C. (1990). Detection of somatostatin receptors in surgical and percutaneous needle biopsy samples of carcinoids and islet cell carcinomas. *Cancer Res. 50,* 5969−77.

(24) Reubi, J. C. (1995). In vitro identification of vasoactive intestinal peptide receptors in human tumors: implications for tumor imaging. *J. Nucl. Med. 36,* 1846−53.

(25) Hofland, L. J., Koetsveld, P. M. v., Waaijers, M., Zuydenrwijk, J., Breeman, W. A. P., Krenning, E. P., and Lamberts, S. W. J. (1995). Internalization of the radioiodinated somatostatine analogue [^{125}I-Tyr^{3}]octreotide by mouse and human pituitary tumor cells: increase by unlabeled octreotide. *Endocrinology 136,* 3698−3706.

(26) De Jong, M., Bernard, B. F., Brun, E. d., Gameren, A. v., Bakker, W. H., Visser, T. J., Mäcke, H. R., and Krenning, E. P. (1998). Internalization of radiolabeled [DTPA°]octreotide and [DOTA, Tyr^{3}]octreotide: peptides for somatostatine receptor-targeted scintigraphy and radionuclide therapy. *Nucl. Med. Commun. 19,* 283−288.

(27) Arano, Y., Akizawa, H., Uezono, T., Akaji, K., Ono, M., Funakoshi, S., Koizumi, M., Yokoyama, A., Kiso, Y., and Saji, H. (1997). Conventional and high-yield synthesis of DTPA-conjugated peptides: application of a monoreactive DTPA to DTPA-D-Phe^{1}-octreotide synthesis. *Bioconjugate Chem. 8,* 442−446.

(28) Froidevaux, S., Heppeler, A., Eberle, A. N., Meier, A.-M., Häusler, M., Beglinger, C., Béhé, M., Powell, P., and Mäcke, H. R. (2000). Preclinical Comparison in AR4-2J Tumor Bearing-Mice of Four Radiolabeled 1,4,7,10-Tetraazacyclododecane-1,4,7,10-Tetraacetic Acid-Somatostatin Analogues for Tumor Diagnosis and Internal Radiotherapy. *Endocrinology 141,* 3304−3312.

(29) Anderson, C. J., Dehdashti, F., Cutler, P. D., Schwarz, S. W., Laforest, R., and Bass, L. A., et al. (2001). ^{64}Cu-TETA-octreotide as a PET imaging agent for patients with neuroendocrine tumors. *J. Nucl. Med. 42,* 213−21.

(30) Anderson, C. J., Pajeau, T. S., Edwards, W. B., Sherman, E. L. C., Rogers, B. E., and Welch, M. J. (1995). In Vitro and In Vivo Evaluation of Copper-64-Octreotide Conjugates. *J. Nucl. Med. 36,* 2315−2325.

(31) Lewis, J. S., Srinivasan, A., Schmidt, M. A., and Anderson, C. J. (1999). In vitro and in vivo evaluation of ^{64}Cu-TETA-Tyr^{3}-octreotate. A new somatostatin analogue with improved target tissue uptake. *Nucl. Med. Biol. 26,* 267−73.

(32) Wester, H.-J., Brockmann, J., Rösch, F., Wurz, W., Herzog, H., Smith-Jones, P., Stolz, B., Bruns, C., and Stöcklin, G. (1997). PET-Pharmacokinetics of ^{18}F−Octreotide: A Comparison with ^{67}Ga-DFO and ^{86}Y-DTPA-Octreotide. *Nucl. Med. Biol. 24,* 275−286.

(33) Förster, G. J., Engelbach, M., Brockmann, J., Reber, H., Buchholz, H.-G., Mäcke, H. R., Rösch, F., Herzog, H., and Bartenstein, P. (2001). Preliminary data on biodistribution and dosimetry for therapy planning of somatostatin receptor positive tumours: comparison of ^{86}Y-DOTATOC and ^{111}In-DTPA-octreotide. *Eur. J. Nucl. Med. 28/12,* 1743−1750.

(34) Henze, M., Schuhmacher, J., Hipp, P., Kowalski, J., Becker, D. W., Doll, J., Mäcke, H. R., Hofmann, M., Debus, J., and Haberkorn, U. (2001). PET Imaging of Somatostatin Receptors Using [^{68}Ga]DOTA-D-Phe^{1}-Tyr^{3}-Octreotide: First Results in Patients with Meningiomas. *J. Nucl. Med. 42,* 1053−1056.

(35) Hofmann, M., Maecke, H. R., Börner, A. R., Weckesser, E., Schöffski, P., Oei, M. L., Schumacher, J., Henze, M., Heppeler, A., Meyer, G. J., and Knapp, W. H. (2001). Biokinetics and imaging with the somatostatin receptor PET radioligand ^{68}Ga-DOTATOC: preliminary data. *Eur. J. Nucl. Med. 28/12,* 1751−1757.

(36) McMurry, T. J., Brechbiel, M., Wu, C., and Gansow, O. A. (1993). Synthesis of 2-(p-Thiocyanatobenzyl-1,4,7-triazacyclononane-1,4,7-triacetic Acid: Application of the 4-Methoxy-2,3,6-trimethylbenzenesulfonamide Protecting Group in the Synthesis of Macrocyclic Polyamines. *Bioconjugate Chem. 4,* 236−245.

(37) Cox, J. P. L., Craig, A. S., Helps, I. M., Jankowsi, K. J., Parker, D., Eaton, M. A. W., Millican, A. T., Millar, K., Beeley, N. R. A., and Boyce, B. A. (1990). Synthesis of C- and N−Functionalised Derivatives of 1,4,7-Triazacyclononane-1,4,7-triacetic Acid (NOTA), 1,4,7,10-Tetra-azacyclododecane-1,4,7,10-tetrayltetraacetic Acid (DOTA), and Diethylenetriaminepenta-acetic Acid (DTPA): Bifunctional Complexing Agents for the Derivatisation of Antibodies. *J. Chem. Soc., Perkin Trans. 1* 2567−76.

(38) Studer, M., and Meares, C. F. (1992). Synthesis of Novel 1,4,7-Triazacyclononane-*N*,*N*′,*N*″-triacetic Acid Derivatives Suitable for Protein Labeling. *Bioconjugate Chem. 3,* 337−341.

(39) Brechbiel, M., McMurry, T. J., and Gansow, O. A. (1993). A Direct Synthesis of a Bifunctional Chelating Agent for Radiolabeling Proteins. *Tetrahedron Lett. 34,* 3691−3694.

(40) Chappell, L. L., Rogers, B. E., Khazaeli, M. B., Mayo, M. S., Buchsbaum, D. J., and Brechbiel, M. W. (1999). Improved Synthesis of the Bifunctional Chelating Agent 1, 4,7,10-Tetraaza-N-(1-carboxy-3-(4-nitrophenyl)propyl)-N′,N″,N‴-tris(acetic acid)cyclododecane (PA-DOTA). *Bioorg. Med. Chem. 7,* 2313−2320.

(41) Kruper, W. J., Rudolf, P. R., and Langhoff, C. A. (1993). Unexpected Selectivity in the Alkylation of Polyazamacrocycles. *J. Org. Chem. 58,* 3869−3876.

(42) André, J. P., Mäcke, H. R., Zehnder, M., Macko, L., and Acyel, K. G. (1998). 1,4,7-Triazacyclononane-1-succinic acid-4,7-diacetic acid (NODASA): a new bifunctional chelator for radio gallium-labeling of biomolecules. *Chem. Commun.* 1301−1302.

(43) Shannon, R. D. (1976). Revised Effective Ionic Radii and Systematic Studies of Interatomic Distances in Halides and Chalcogenides. *Acta Crystallogr. 32 A,* 751−767.

(44) Broan, C. J., Cox, J. P. L., Craig, A. S., Kataky, R., Parker, D., Harrison, A., Randall, A. M., and Ferguson, G. (1991). Structure and Solution Stability of Indium and Gallium Complexes of 1,4,7-Triazacyclononanetriacetate and of Yttrium Complexes of of 1,4,7,10-Tetraazacyclododecanetetraacetate and Related Ligands: Kinetically Stable Complexes for Use in Imaging and Radioimmunotherapy. X-ray Molecular Structure of the Indium and Gallium Complexes of 1,4,7-Triazacyclononane-1,4,7-triacetic Acid. *J. Chem. Soc., Perkin Trans. 2,* 87−98.

(45) Clarke, E. T., Martell, A. (1991). Stabilities of the Fe(III), Ga(III) and In(III) chelates of N,N′,N″-triazacyclononanetriacetic acid. *Inorg. Chim. Acta 181,* 273−280.

(46) Koenig, J. A., and Edwardson, J. M. (1997). Endocytosis and recycling of G protein-coupled receptors. *Trends Pharmacol. Sci.* 276−287.

(47) Koenig, J. A., Kaur, R., Dodgeon, I., Edwardson, J. M., and Humphrey, P. P. A. (1998). Fates of endocytosed somatostatin sst2 receptor and associated agonists. *Biochem. J. 336,* 291−298.

(48) Lewis, J. S., Lewis, M. R., Srinivasan, A., Schmidt, M. A., Wang, J., and Anderson, C. J. (1998). Comparison of Four ^{64}Cu-Labeled Somatostatin Analogues in Vitro and in Tumor-Bearing Rat Model: Evaluation of New Derivatives for Positron Emission Tomography Imaging and Targeted Radiotherapy. *J. Med. Chem.* 1341−1347.

BC010074F

Mixed-Phase Hybridization of Short Oligodeoxyribonucleotides on Microscopic Polymer Particles: Effect of One-Base Mismatches on Duplex Stability

Kaisa Ketomäki, Harri Hakala,† and Harri Lönnberg*

Department of Chemistry, University of Turku, FIN-20014 Turku, Finland. Received September 5, 2001; Revised Manuscript Received December 27, 2001

Hybridization of short oligonucleotides (10- and 11-mers) to complementary probes immobilized to microscopic polymer particles was quantified by a sandwich type mixed-phase hybridization assay based on a time-resolved fluorometric measurement of a photoluminescent europium(III) chelate from the surface of a single particle. Among the 54 sequences that were studied, 21 were fully complementary to the particle-bound probes, while 33 contained an internal one-base mismatch. The observed affinities were compared to those predicted by the nearest-neighbor model. In addition, various factors, such as the pore size of the particle, the linker structure, the charge type of the probe, and the efficiency of agitation, that might be expected to affect the kinetics of mixed-phase hybridization have been examined.

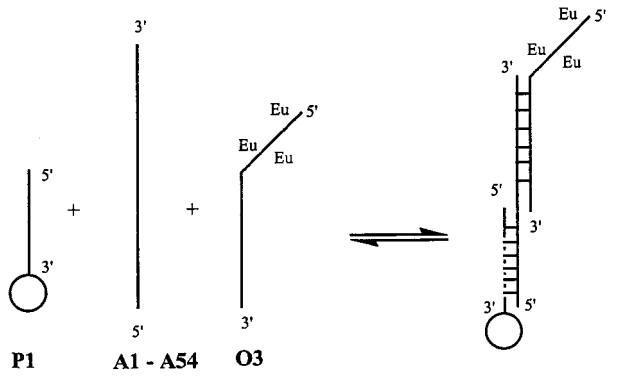
INTRODUCTION

We have recently described a mixed-phase hybridization assay that is based on the use of a mixture of categorized polymer microparticles as the solid phase (*1*). The method allows simultaneous screening of several potential base mutations or deletions from a single PCR-amplified sample, and it hence offers an alternative for the widely used oligonucleotide microarrays (*2*−*6*). Each particle bears, in addition to a given oligonucleotide probe, prompt fluorophores that allow recognition of the particle category when the particles after hybridization are subjected one by one to the fluorescence measurement. The hybridization is, in turn, quantified by time-resolved fluorometry. On application of a sandwich type protocol, the PCR-amplified oligonucleotide forms first in solution a duplex with an appropriately designed oligonucleotide probe labeled with a photoluminescent lanthanide chelate, and hybridizes then with the particle-bound probe (Scheme 1). The lanthanide ion emission is measured directly from a single particle after complete quenching of the emission of the prompt fluorophores (*7*). The photoluminescent lanthanide chelates exhibit as markers one major advantage over organic dyes; the Stokes shift, i.e., the difference between the wavelengths of emission and excitation, is large, and hence, the concentration quenching is negligible. Accordingly, the intensity of the emission signal measured from an individual particle is strictly linearly related to the number of chelates on the particle over 5−6 orders of magnitude (*8*−*10*). For this reason, the method suits quantitative analysis of the concentration of oligonucleotides in the sample exceptionally well (*1*).

All mixed-phase hybridization assays, using either microarrays or categorized microparticles, are eventually based on the dependence of the stability of solid-supported duplexes on the sequence. It has been well established (*11*−*17*) that the stability of oligodeoxyribonucleotide duplexes in aqueous salt solutions may be rather reliably predicted by applying the so-called nearest-neighbor model for helix propagation. The same approach has more recently been used to determine the nearest-neighbor parameters for all possible internal point mismatches (*16*, *18*−*21*). Since the applicability of a mixed-phase hybridization assay is largely determined by the selectivity of hybridization, it is important to know how well the nearest-neighbor parameters referring to hybridization in solution may be used to predict the affinity for particle-bound probes.

We have shown previously (*1*, *8*) that the microparticle approach described above allows, at least in favorable cases, unequivocal detection of a point mutation or deletion, provided that the length of the complementary region is carefully optimized. For example, a single AG or CT mismatch in the middle of a 12-mer complementary sequence has been shown to decrease the affinity for the particle-bound probe by 2 orders of magnitude (*8*). Deletion of a single internal A or C has also been shown to retard the hybridization of a 12−14-mer probe by up to 2 orders of magnitude, although the destabilization

Scheme 1. Principle of the Sandwich Type Hybridization Assay[a]



[a] **P1**, particle-bound oligonucleotide probe; **A1**−**A54**, target oligonucleotides studied; **O3**, fluorescently tagged oligonucleotide probe.

† Present address: Wallac Oy, P.O. Box 10, FIN-20101 Turku, Finland.

10.1021/bc0100859 CCC: $22.00 © 2002 American Chemical Society
Published on Web 03/28/2002

appears to be rather sequence dependent (*1*, *8*). It is, however, known that all base mismatches are not as strongly destabilizing in solution. In fact, the so-called linearly independent nearest-neighbor $\Delta G°$ parameters for dimeric 5′-NX-3′ fragments, where X stands for a mismatched nucleoside, range from −1.1 to 1.3 kcal/mol (*16*, *18*−*21*), while those for the corresponding fully Watson−Crick bonded fragments fall between −2.2 and −0.6 kcal/mol (*17*). To find out how much various internal one-base mismatches in various molecular environments decrease the affinity of oligonucleotides for particle-bound probes, 21 fully complementary short oligonucleotides (10- and 11-mers) and 33 oligonucleotides having one internal point mismatch have been subjected to the sandwich type mixed-phase hybridization assay described in Scheme 1. The observed affinities are compared to those predicted by the nearest-neighbor model. In addition to these equilibrium studies, various factors, such as the pore size of the particle, the linker structure, the charge type of the probe, and the efficiency of agitation, that might be expected to affect the kinetics of mixed-phase hybridization have been examined.

EXPERIMENTAL PROCEDURES

Preparation of Oligonucleotide-Coated Microparticles. The polymer particles used to immobilize the oligonucleotide probes were the products of SINTEF. They were made of a copolymer of glycidyl methacrylate (40%) and ethylene dimethylacrylate (60%), and functionalized with primary amino groups (1 mmol/g) obtained by reacting the particle-bound epoxy groups with diethylenetriamine. The particles were uniformly sized, having a diameter of either 50 (**P1**) or 59 μm (**P2**). The smaller particles (**P1**) had an average pore size of 30 nm, a total pore volume of 0.822 mL/g, and a surface area of 137 m^2/g, and the larger ones (**P2**) had a pore size of 50 nm, a total pore volume of 1.469 mL/g, and a surface area of 92 m^2/g. A desired proportion (10−30 μmol/g, i.e., 1−3%) of the amino groups of **P1** and **P2** was acylated with (4,4′-dimethoxytrityloxy)acetic acid, and the rest of the groups were carefully capped by repeated acetylations (*22*). The oligonucleotide probes were assembled on these supports via a normal phosphoramidite strategy, as described previously (*10*) in detail.

Oligonucleotides and Their Fluorescently Tagged Conjugates. Oligonucleotides were assembled via a normal phosphoramidite strategy and purified by ion-exchange HPLC. Preparation of the fluorescently tagged oligonucleotides, **O1**−**O3**, has been described previously (*8*, *9*).

Hybridization Assays. The hybridization assays in kinetic measurements were carried out by shaking 50 particles (**P1** or **P2**) in 10 μL of Tris buffer (50 mM, pH 7.5, containing 0.5 M NaCl and 0.01% Tween 20) that contained **O1** at a concentration of 17 nmol/L (*9*). The reaction temperature was 25 °C, and aliquots were withdrawn from 15 min to 24 h. The particles were thoroughly washed, and a single particle was subjected to a time-resolved fluorescence measurement (*7*).

The sandwich type hybridization assays used to study the dependence of the duplex stability on sequence were carried out by shaking 50 particles (**P1**) in 10 μL of the Tris buffer described above. The concentration of both the target oligonucleotide (**A1**−**A54**) and the fluorescently tagged oligonucleotide (**O3**) was 17 nmol/L. The reaction temperature was 25 °C and the reaction time 24 h. The particles were washed, and the fluorescence emission was quantified by the single-particle technique (*7*). Typically, 10 individual particles were measured, the standard deviation ranging from 5 to 20%.

Calibration. To convert the fluorescence emission measured from a single particle to the number of fluorescently tagged oligomers attached to this particle, two sets of particles **P1a** were subjected to hybridization with tagged oligomer **O1** or **O3**, the initial concentration of which was varied from 5.1 to 51 nmol/L. After incubation for 20 h, one set of the particles was subjected to fluorescence measurement by the single-particle technique (*7*), while from the other set, europium(III) ion was released to solution and quantified according to the DELFIA protocol (*25*). Additionally, the concentration of **O1** or **O3** in solution before and after the hybridization was determined by the DELFIA protocol. The calibration line was measured separately for every particle that was employed.

RESULTS AND DISCUSSION

Preparation of Oligonucleotide-Coated Microparticles and Characterization of Their Hybridization Properties. Two different types of uniformly sized porous particles made of a copolymer of glycidyl methacrylate (40%) and ethylene dimethylacrylate (60%) and functionalized with amino groups were used as the solid support in the mixed-phase hybridization assays. Usually, 50 μm particles (**P1**) having an average pore size of 30 nm and a surface area of 137 m^2/g were employed. However, slightly larger (59 μm) particles (**P2**) having a larger pore size (50 nm) and a smaller surface area (92 m^2/g) were also used for comparative purposes.

To allow the assembly of oligonucleotides on the particles according to the normal phosphoramidite protocol, a desired proportion of the amino functions was acylated with (4,4′-dimethoxytrityloxy)acetic acid (DMTrOCH$_2$COOH), while the rest were carefully capped by repeated acetylations (*22*). The level of *N*-(DMTrOCH$_2$CO) loading of the particles, when determined by the DMTr cation assay (*23*), ranged from 12 to 28 μmol/g. The oligonucleotide chains were then assembled on the deprotected hydroxy function. The amide linker that was employed turned out to be entirely resistant to deprotection of the base moieties by ammonolysis. We have previously shown that oligonucleotide synthesis on similar polymer particles gives full-length 16-mer sequences in an only 30% yield, the rest of the sequences being truncated (*10*). Despite this heterogeneity of the oligonucleotide probe, the hybridization efficiency and selectivity of such particles have been demonstrated to be comparable to those obtained by postsynthetic immobilization by purified fully homogeneous probes (*10*).

A fluorescently tagged 42-mer oligodeoxyribonucleotide, 5′-d(**CTATATTCATCATAGG**AAACACCAAAGATGATAATTX$_5$C)-3′ (**O1**), was used to elucidate the hybridization properties of the oligonucleotide-coated particles. Here, X stands for N^4-(6-aminohexyl)-2′-deoxycytidine tethered to a photoluminescent europium(III) chelate, {2,2′,2″,2‴-[(4′-{4‴-[(4,6-dichloro-1,3,5-triazin-2-yl)amino]phenyl}-2,2′:6′,2″-terpyridine-6,6″-diyl)bis(methylenenitrilo)]}tetrakis(acetato)europium(III) (*24*). The sequence complementary to the particle-bound 16-mer is indicated in bold. The kinetics of the binding of **O1** to the particles was followed by shaking 50 particles in 10 μL of Tris buffer (50 mM, pH 7.5, containing 0.5 M NaCl and 0.01% Tween 20) that contained **O1** at a concentration of 17 nmol/L at 25 °C. The particles were thoroughly washed, and a single particle was subjected to a time-resolved fluorescence measurement (*7*). To

Table 1. Effect of the Oligo(T) Linker on the Efficiency and Kinetics of the Hybridization of the Fluorescently Tagged Oligonucleotide (O1) to a Complementary Oligonucleotide Probe Assembled on Microparticles P1 and P2

particle	sequence	$\tau_{1/2}$ (h)[a]	*n*(bound)/ *n*(total)
P1a	3′-T_3-[oligo]-5′ [b]	7	0.6
P1b	3′-T_{15}-[oligo]-5′	7	0.6
P1c	3′-T_{30}-[oligo]-5′	7	0.6
P1d	3′-T_{50}-[oligo]-5′	7	0.3
P1e	3′-T_3-[oligo]-5′ [c]	7	0.05
P1f	3′-T_3-[oligo]-5′ [d]	7	0.6
P1g	3′-T_3-[TATAAGTAGTATCC]-5′	7	0.6
P2a	3′-T_3-[oligo]-5′	7	0.6
P2b	3′-T_{50}-[oligo]-5′	7	0.6
P2c	3′-T_{100}-[oligo]-5′	7	0.6

[a] The half-life for hybridization at 25 °C. [b] The abbreviation [oligo] stands for the common hybridizing sequence 3′-d(GATATAAGTAGTATCC)-5′. [c] A methylphosphonate oligodeoxyribonucleotide. [d] A2′-*O*-Methylribonucleotide oligomer.

estimate the contribution of unspecific adsorption of the labeled oligomer to the particles, a comparative study with a noncomplementary fluorescently tagged 32-mer, 5′-d(X_{20}ATCATCTTTGGT)-3′ (**O2**), was carried out. Consistent with previous results (*8*−*10*), the unspecific binding was in all cases almost negligible; less than 1% of the **O2** was attached to the particles. The fluorescence emission of a single particle was converted to the number of fluorescently tagged oligomers (**O1**) attached to the particle with the aid of a calibration line, which was obtained by plotting the emission intensities measured from a single particle against the amount of europium(III) released to solution and quantified by the DELFIA protocol (*25*). The amount of europium(III) in solution before and after the hybridization, i.e., the concentration of **O1**, was determined similarly. The decrease in the concentration of **O1** upon hybridization always agreed with the amount of europium(III) released from the particles after hybridization, which lent considerable support to the reliability of the determination. The calibration line that was obtained was essentially similar to that reported earlier for a closely related system (*8*).

We have shown previously that the mixed-phase hybridization assays described above suffer from one major shortcoming, viz., slow binding of oligonucleotides from the solution phase to the particle-bound probes (*8*−*10*). On using five particles per 1 μL sample, the half-life of the equilibration is on the order of hours at 25 °C. The half-life is inversely proportional to the number of particles in a unit volume of the sample, and the process may hence simply be accelerated by using more particles (*9*). This, however, leads to decreased sensitivity; the analyte is distributed among a larger number of particles, and the emission from an individual particle is reduced. Accordingly, faster kinetics of hybridization is highly desirable.

One might a priori assume that insertion of a long hydrophilic spacer between the hybridizing oligonucleotide sequence and the solid support accelerates the hybridization. To test this assumption, oligonucleotide probes consisting of a 16-nucleotide 5′-terminal hybridizing sequence, 3′-d(GATATAAGTAGTATCC)-5′, and a 3−100-nucleotide 3′-terminal oligo(T) spacer were assembled on **P1** and **P2**. Unfortunately, introduction of such a spacer did not result in the desired acceleration. As seen from Table 1, the kinetics was not markedly affected either by the length of the spacer or by the pore size of the particle. Within the limits of experimental errors, the half-life remained constant (7 h) with both particles. In contrast, the hybridization efficiency, i.e., the mole fraction of **O1** bound to the particle, seemed to be moderately affected by these factors. With porous particles **P2**, having a large pore size (50 nm), the hybridization efficiency (60%) did not depend on the length of the spacer, but with particles **P1** having smaller pores (30 nm), the efficiency was decreased to less than half of the original value when the spacer was longer than 30 nucleotide units.

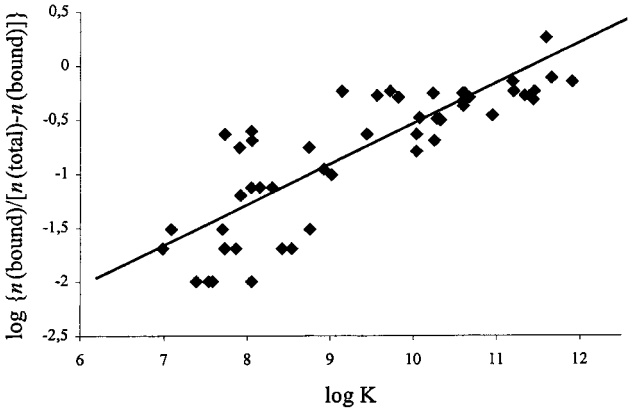


Figure 1. Logarithmic equilibrium constants, log{*n*(bound)/[*n*(total) − *n*(bound)]}, for the binding of oligonucleotides **A1**−**A54** to their complementary particle-bound probes (see Table 2) plotted vs the logarithmic stability constants of the respective duplexes in solution.

Addition of a detergent to the hybridization buffer also had some effect on the efficiency but not on the kinetics of hybridization. In the presence of 0.01% Tween 20, the hybridization efficiency was slightly increased, when the concentration of the target oligonucleotide was low. At high concentrations, the influence remained negligible.

The chemical nature of the support-bound probe did not have any effect on the hybridization kinetics. In addition to oligodeoxyribonucleotide probes, deoxyribonucleotide methylphosphonate and 2′-*O*-methylribonucleotide oligomers were assembled on particles **P1**, and their ability to bind **O1** was studied. The methylphosphonate probes exhibited a markedly reduced hybridization efficiency (5%) compared to the unmodified deoxynucleotide probes (60%), while the 2′-*O*-methylribonucleotide oligomers exhibited a slightly enhanced affinity for **O1**. Unfortunately, no positive effect on the hybridization kinetics could be observed in either case.

The only factor that, in addition to the number of particles in a unit volume, had any influence on the hybridization kinetics was the efficiency of agitation. When the solution of **O1** containing five particles (**P1**) in 1 μL was mixed by rotating a sealed tube at a rate of 20 rpm, the half-life of hybridization was ∼7 h at 25 °C. Ultrasonic mixing reduced the half-life to ∼3 h and efficient agitation with a planar shaker (Vortex) to ∼1 h (data not shown). This observation, together with the fact that the hybridization is accelerated with the increasing number of particles in the sample, strongly suggests that the rate of hybridization is limited by the diffusion of the oligonucleotide in solution, and not by the binding event itself.

Dehybridization of **O1** from support **P1g**, bearing a 14-mer sequence complementary to **O1**, was also studied. At 25 °C, the half-life for the release of **O1** from **P1g** was ∼15 h. Accordingly, the particles may well be rapidly washed without any loss of the hybridized oligonucleotide. However, at 40 °C, the dehybridization was surprisingly fast, the half-life being <1 h.

Table 2. Hybridization Efficiencies, *n*(bound)/*n*(total), of Oligonucleotides (A1−A54) with Their Solid-Supported (P1) Complementary Probes at 25 °C (pH 7.5; $I = 0.5$ M with NaCl)[a]

	oligonucleotide in solution[b]	sequence on particle **P1**[c]	*n*(bound)/*n*(total)[d]
		fully complementary sequences	
A1	5′-**ACCACAACCC**-[oligo]-3′	**S**-3′-T_6GGT**TGGTGTTGGG**T_3-5′	0.44 (−15.75)
A2	5′-**AACCACAACC**-[oligo]-3′	**S**-3′-T_6GG**TTGGTGTTGG**GT_3-5′	0.32 (−14.91)
A3	5′-**CAACCACAAC**-[oligo]-3′	**S**-3′-T_6G**GTTGGTGTTG**GGT_3-5′	0.27 (−14.47)
A4	5′-**CCAACCACAA**-[oligo]-3′	**S**-3′-T_6**GGTTGGTGTT**GGGT_3-5′	0.30 (−14.92)
A5	5′-**ACCAACCACA**-[oligo]-3′	**S**-3′-T_5**TGGTTGGTGT**TGGGT_3-5′	0.26 (−15.41)
A6	5′-**AACCAACCAC**-[oligo]-3′	**S**-3′-T_4**TTGGTTGGTG**TTGGGT_3-5′	0.36 (−14.91)
A7	5′-**AAACCAACCA**-[oligo]-3′	**S**-3′-T_3**TTTGGTTGGT**GTTGGGT_3-5′	0.27 (−14.52)
A8	5′-**ATGCAGTACG**-[oligo]-3′	**S**-3′-T_3ATACG**TACGTCATGC**GT_3-5′	0.36 (−14.94)
A9	5′-**GCATGCAGTA**-[oligo]-3′	**S**-3′-T_3ATA**CGTACGTCAT**GCGT_3-5′	0.34 (−15.02)
A10	5′-**ATGCATGCAG**-[oligo]-3′	**S**-3′-T_3A**TACGTACGTC**ATGCGT_3-5′	0.24 (−14.53)
A11	5′-**ATGCACAGCT**-[oligo]-3′	**S**-3′-T_3**TACGTGTCGA**T_2-5′	0.37 (−15.77)
A12	5′-**ATGCACATCT**-[oligo]-3′	**S**-3′-T_3**TACGTGTAGA**T_2-5′	0.17 (−14.43)
A13	5′-**CTGCACAGCT**-[oligo]-3′	**S**-3′-T_3**GACGTGTCGA**T_2-5′	0.37 (−16.12)
A14	5′-**CATGCAGTAC**-[oligo]-3′	**S**-3′-T_3ATAC**GTACGTCATG**CGT_3-5′	0.25 (−14.18)
A15	5′-**TGCAGTACGC**-[oligo]-3′	**S**-3′-T_3ATACGT**ACGTCATGCG**T_3-5′	0.65 (−16.30)
A16	5′-**TGCATGCAGT**-[oligo]-3′	**S**-3′-T_3AT**ACGTACGTCA**TGCGT_3-5′	0.35 (−15.94)
A17	5′-**GCTAAGTAACG**-[oligo]-3′	**S**-3′-T_3**CGATTCATTGC**T_3-5′	0.34 (−14.97)
A18	5′-**TGCAAGTACGA**-[oligo]-3′	**S**-3′-T_3**ACGTTCATGCT**T_3-5′	0.44 (−16.41)
A19	5′-**TAGCAGTCGAA**-[oligo]-3′	**S**-3′-T_3**ATCGTCAGCTT**T_3-5′	0.33 (−16.10)
A20	5′-**TAAGCGCGTAA**-[oligo]-3′	**S**-3′-T_3**ATTCGCGCATT**T_3-5′	0.42 (−16.76)
A21	5′-**GCTAATTAACG**-[oligo]-3′	**S**-3′-T_3**CGATTAATTGC**T_3-5′	0.19 (−14.13)
		sequences containing one mismatch[e]	
A22	5′-**ACCACAAC**A**C**-[oligo]-3′	**S**-3′-T_6GGT**TGGTGTTGGG**T_3-5′	0.10 (−12.56)
A23	5′-**ACCACAAC**G**C**-[oligo]-3′	**S**-3′-T_6GGT**TGGTGTTGGG**T_3-5′	0.19 (−13.29)
A24	5′-**ACCACAAC**T**C**-[oligo]-3′	**S**-3′-T_6GGT**TGGTGTTGGG**T_3-5′	0.15 (−12.31)
A25	5′-**TGCAGTAC**T**C**-[oligo]-3′	**S**-3′-T_3ATACGT**ACGTCATGCG**T_3-5′	0.02 (−10.87)
A26	5′-**TGCAGTAC**A**C**-[oligo]-3′	**S**-3′-T_3ATACGT**ACGTCATGCG**T_3-5′	0.01 (−10.67)
A27	5′-**TGCAGTAC**C**C**-[oligo]-3′	**S**-3′-T_3ATACGT**ACGTCATGCG**T_3-5′	0.01 (−10.40)
A28	5′-**TGCAT**T**CAGT**-[oligo]-3′	**S**-3′-T_3ATACGT**ACGTACGTCA**T_3-5′	0.00 (−12.04)
A29	5′-**TGCA**C**GCAGT**-[oligo]-3′	**S**-3′-T_3ATACGT**ACGTACGTCA**T_3-5′	0.00 (−12.04)
A30	5′-**CAACC**C**CAAC**-[oligo]-3′	**S**-3′-T_6G**GTTGGTGTTG**GGT_3-5′	0.03 (−9.98)
A31	5′-**CAAC**T**A**C**AAC**-[oligo]-3′	**S**-3′-T_6G**GTTGGTGTTG**GGT_3-5′	0.02 (−11.07)
A32	5′-**GCTAA**C**TAACG**-[oligo]-3′	**S**-3′-T_3**CGATTAATTGC**T_3-5′	0.01 (−10.60)
A33	5′-**GCTAA**T**TAACG**-[oligo]-3′	**S**-3′-T_3**CGATTCATTGC**T_3-5′	0.02 (−10.88)
A34	5′-**TGCAA**T**TACGA**-[oligo]-3′	**S**-3′-T_3**ACGTTCATGCT**T_3-5′	0.03 (−12.32)
A35	5′-**TAGCA**T**TCGAA**-[oligo]-3′	**S**-3′-T_3**ATCGTCAGCTT**T_3-5′	0.02 (−12.01)
A36	5′-**TAAGC**T**CGTAA**-[oligo]-3′	**S**-3′-T_3**ATTCGCGCATT**T_3-5′	0.01 (−11.33)
A37	5′-**G**T**TAA**T**TAACG**-[oligo]-3′	**S**-3′-T_3**CGATTAATTGC**T_3-5′	0.02 (−9.83)
A38	5′-**A**G**ACCAACCA**-[oligo]-3′	**S**-3′-T_3**TTTGGTTGGT**GTTGGGT_3-5′	0.07 (−11.47)
A39	5′-**A**C**ACCAACCA**-[oligo]-3′	**S**-3′-T_3**TTTGGTTGGT**GTTGGGT_3-5′	0.15 (−11.13)
A40	5′-**A**T**ACCAACCA**-[oligo]-3′	**S**-3′-T_3**TTTGGTTGGT**GTTGGGT_3-5′	0.06 (−11.15)
A41	5′-**G**A**TAATTAACG**-[oligo]-3′	**S**-3′-T_3**CGATTAATTGC**T_3-5′	0.03 (−10.84)
A42	5′-**G**G**TAATTAACG**-[oligo]-3′	**S**-3′-T_3**CGATTAATTGC**T_3-5′	0.02 (−11.85)
A43	5′-**G**A**TAAGTAACG**-[oligo]-3′	**S**-3′-T_3**CGATTCATTGC**T_3-5′	0.07 (−11.68)
A44	5′-**G**G**TAAGTAACG**-[oligo]-3′	**S**-3′-T_3**CGATTCATTGC**T_3-5′	0.09 (−12.69)
A45	5′-**G**T**TAAGTAACG**-[oligo]-3′	**S**-3′-T_3**CGATTCATTGC**T_3-5′	0.07 (−11.33)
A46	5′-**T**A**CAAGTACGA**-[oligo]-3′	**S**-3′-T_3**ACGTTCATGCT**T_3-5′	0.20 (−11.33)
A47	5′-**T**C**CAAGTACGA**-[oligo]-3′	**S**-3′-T_3**ACGTTCATGCT**T_3-5′	0.19 (−10.88)
A48	5′-**T**T**CAAGTACGA**-[oligo]-3′	**S**-3′-T_3**ACGTTCATGCT**T_3-5′	0.17 (−11.34)
A49	5′-**T**G**GCAGTCGAA**-[oligo]-3′	**S**-3′-T_3**ATCGTCAGCTT**T_3-5′	0.14 (−14.13)
A50	5′-**T**C**GCAGTCGAA**-[oligo]-3′	**S**-3′-T_3**ATCGTCAGCTT**T_3-5′	0.37 (−12.87)
A51	5′-**T**T**GCAGTCGAA**-[oligo]-3′	**S**-3′-T_3**ATCGTCAGCTT**T_3-5′	0.37 (−13.68)
A52	5′-**T**G**AGCGCGTAA**-[oligo]-3′	**S**-3′-T_3**ATTCGCGCATT**T_3-5′	0.36 (−14.41)
A53	5′-**T**C**AGCGCGTAA**-[oligo]-3′	**S**-3′-T_3**ATTCGCGCATT**T_3-5′	0.35 (−13.46)
A54	5′-**T**T**AGCGCGTAA**-[oligo]-3′	**S**-3′-T_3**ATTCGCGCATT**T_3-5′	0.34 (−13.82)

[a] Refers to equilibration of 50 particles with 10 μL of a 17 nmol/L solution of **A1**−**A54**. [b] The abbreviation [oligo] stands for the sequence 5′-GT*ACACCAAAGATGATA*TT-3′, in which the italic nucleotides were used to bind the fluorescently tagged oligonucleotide **O3**. [c] The sequence engaged in duplex formation indicated in bold. [d] The Gibbs free energies of duplex formation calculated from the nearest-neighbor parameters reported in the literature (*16*−*21*). [e] The mismatched base underlined.

Relationship between the Sequence and Duplex Stability in Mixed-Phase Hybridizations. The binding of 54 oligonucleotides having a 10- or 11-nucleotide 5′-terminal region complementary to the solid-supported probe was quantified by the sandwich type assay depicted in Scheme 1. Among these oligonucleotides, 21 (**A1**−**A21**) were fully complementary to the support-bound probe over this 10−11-nucleotide sequence, while the remaining 35 (**A22**−**A54**) contained one internal point mismatch. Each of these oligonucleotides contained in its 3′-terminus the same 16-nucleotide sequence used to bind a fluorescently tagged probe, 5′-d(CX_5ATATCATCTTTGG-TGT)-3′ (**O3**). The complementarity over 16 nucleotides is sufficient to warrant virtually quantitative duplex

Table 3. Effect of One-Base Mismatches on the Affinity for the Particle-Bound Probes

mismatch	fully complementary sequence	mismatched sequence	remaining affinity (%)[a]
C·T	5′-TGCATGCAGT-3′	5′-TGCAT**T**CAGT-3′	<1 (+3.9)
	5′-GCTAAGTAACG-3′	5′-GCTAA**T**TAACG-3′	6 (+4.1)
	5′-TGCAAGTACGA-3′	5′-TGCAA**T**TACGA-3′	7 (+4.1)
	5′-TAGCAGTCGAA-3′	5′-TAGCA**T**TCGAA-3′	6 (+4.1)
	5′-TAAGCGCGTAA-3′	5′-TAAGC**T**CGTAA-3′	2 (+5.4)
	5′-TGCAAGTACGA-3′	5′-T**T**CAAGTACGA-3′	39 (+5.1)
	5′-TGCAGTACGC-3′	5′-TGCAGTAC**T**C-3′	3 (+5.4)
	5′-CAACCACAAC-3′	5′-CAACC**C**CAAC-3′	3 (+3.4)
	5′-TCATCATAGG-3′	5′-TCATC**C**TAGG-3′	6[b] (+3.7)
	5′-AAACCAACCA-3′	5′-A**C**ACCAACCA-3′	40 (+3.4)
	5′-TAAGCGCGTAA-3′	5′-T**C**AGCGCGTAA-3′	83 (+3.3)
	5′-TAGCAGTCGAA-3′	5′-T**C**GCAGTCGAA-3′	>100 (+3.2)
G·T	5′-CAACCACAAC-3′	5′-CAAC**T**ACAAC-3′	3 (+4.5)
	5′-ACCACAACCC-3′	5′-ACCAC AAC**T**C-3′	17 (+3.4)
	5′-GCTAAGTAACG-3′	5′-G**T**TAAGTAACG-3′	21 (+3.6)
	5′-GCTAATTAACG-3′	5′-G**T**TAATTAACG-3′	11 (+3.6)
	5′-AAACCAACCA-3′	5′-A**G**ACCAACCA-3′	13 (+3.1)
	5′-TAGCAGTCGAA-3′	5′-T**G**GCAGTCGAA-3′	42 (+2.0)
	5′-TAAGCGCGTAA-3′	5′-T**G**AGCGCGTAA-3′	86 (+2.4)
A·C	5′-TGCATGCAGT-3′	5′-TGCA**C**GCAGT-3′	<1 (+3.9)
	5′-GCTAATTAACG-3′	5′-GCTAA**C**TAACG-3′	5 (+3.5)
	5′-TGCAGTACGC-3′	5′-TGCAGTAC**A**C-3′	2 (+5.6)
	5′-TGCAAGTACGA-3′	5′-T**A**CAAGTACGA-3′	45 (+5.1)
A·G	5′-ATTCATCATAGG-3′	5′-ATTCAT**A**ATAGG-3′	<1[b] (+3.9)
	5′-ACCACAACCC-3′	5′-ACCACAAC**A**C-3′	8 (+3.2)
	5′-GCTAATTAACG-3′	5′-G**A**TAATTAACG-3′	16 (+3.3)
	5′-GCTAAGTAACG-3′	5′-G**A**TAAGTAACG-3′	21 (+3.3)
C·C	5′-TGCAGTACGC-3′	5′-TGCAGTAC**C**C-3′	2 (+5.9)
	5′-TGCAAGTACGA-3′	5′-T**C**CAAGTACGA-3′	43 (+5.5)
T·T	5′-AAACCAACCA-3′	5′-A**T**ACCAACCA-3′	9 (+3.4)
	5′-TAAGCGCGTAA-3′	5′-T**T**AGCGCGTAA-3′	81 (+2.9)
	5′-TAGCAGTCGAA-3′	5′-T**T**GCAGTCGAA-3′	>100 (+2.4)
G·G	5′-ACCACAACCC-3′	5′-ACCACAAC**G**C-3′	25 (+2.5)
	5′-GCTAATTAACG-3′	5′-G**G**TAATTAACG-3′	16 (+2.3)
	5′-GCTAAGTAACG-3′	5′-G**G**TAAGTAACG-3′	26 (+2.3)

[a] Given as *n*(bound)/*n*(total) for the mutated sequence compared to the corresponding value for the fully complementary sequence. The values in parentheses are the changes in $\Delta G°$ in kilocalories per mole expected on the basis of the nearest-neighbor parameters referring to aqueous salt solutions. [b] Taken from ref *8*.

formation between **O3** and the target oligonucleotide (**A1**−**A54**) (*8*). Table 2 lists all the sequences that were employed. The table also records the hybridization efficiencies, *n*(bound)/*n*(total), obtained by equilibrating 50 particles with 10 μL of 17 nmol/L oligonucleotide (**A1**−**A54**) solution. In Figure 1, the logarithmic distribution coefficients, log{*n*(bound)/[*n*(total) − *n*(bound)]}, are plotted against the logarithmic equilibrium constant of the duplex formation in aqueous salt solution. The latter values have been calculated from the Gibbs free energies of duplex formation obtained in an additive manner from the linearly independent nearest-neighbor $\Delta G°$ parameters reported for the formation of fully complementary duplexes (*16*) and point-mutated (*16*, *18*−*21*) sequences in solution phase. While these two quantities expectedly correlate, the individual points are vastly scattered, the correlation coefficient being only 0.7. In other words, the nearest-neighbor parameters referring to aqueous salt solutions allow only a rough estimation of the affinity for particle-bound probes. The slope of the correlation line in Figure 1 is 0.4 ± 0.1, which means that mixed-phase hybridization is less sensitive to the sequence than that in solution. When the equilibrium constant for the duplex formation in solution is decreased by 1 order of magnitude, the mixed-phase distribution coefficient is diminished by a factor of only 2.5.

Table 3 summarizes the effects of various one-base mismatches on the particle-supported duplex stability. The data suggest that a single-point mismatch reduces the hybridization efficiency by 1−2 orders of magnitude when present in the central part of a 10−12-mer complementary region. This appears to be the case at least with C·T, G·T, A·C, and A·G mismatches. As indicated in Table 3, the destabilization (change in $\Delta G°$) expected for these mismatches on the basis of the nearest-neighbor parameters ranges from 3.4 to 5.4 kcal/mol. This means that the equilibrium constant for duplex formation in solution may be expected to be decreased by a factor of 260−7000. Accordingly, the observed 14- to >100-fold diminution of the affinity for particle-bound probes is expected on the basis of the relationship shown in Figure 1; a 60−1800-fold drop in affinity is predicted by this relationship.

If the mutated base is in the penultimate position at the 3′-end, the nearest neighbors seem to play a more dominant role. An almost 100-fold decrease in the affinity is observed with base triplets that in solution destabilize the duplex by more than 5 kcal/mol: 5′-C**T**C-3′/3′-G**C**G-5′, 5′-C**A**C-3′/3′-G**C**G-5′, and 5′-C**C**C-3′/3′-G**C**G-5′. In cases where the destabilizing effect of the base triplet is on the order of 3 kcal/mol, the affinity is decreased by only ≤1 order of magnitude: 5′-C**A**C-3′/3′-G**G**G-5′ (8%), 5′-C**T**C-3′/3′-G**G**G-5′ (17%), and 5′-C**G**C-3′/3′-G**G**G-5′ (25%). Since the particle-bound probe is immobilized through its 3′-end, the mismatched base pair in the support-bound duplex is situated rather distant from the particle surface. In contrast, a mismatch at the penultimate site at the 5′-end of the target oligonucleotide in solution leads

to a support-bound duplex containing the mismatched base pair close to the particle surface. This appears to result in markedly reduced selectivity. All 5′-mutated oligonucleotides listed in Table 3 show only moderately reduced affinity compared to their fully complementary counterpart, and in some cases, the mismatch appears even to increase the affinity. This appears to be the case, in particular, when the 5′-terminal and the penultimate nucleotides of the fully complementary sequence are either A or T. Accordingly, when solid-supported oligonucleotide arrays or particle libraries are constructed and used to screen sequences in solution, one should bear in mind that the discriminating ability of the solid-supported probes may be markedly impaired at the end through which the probe is tethered to the support.

LITERATURE CITED

(1) Hakala, H., Virta, P., Salo, H., and Lönnberg, H. (1998) Simultaneous detection of several oligonucleotides by time-resolved fluorometry: the use of a mixture of categorized microparticles in a sandwich type mixed-phase hybridization assay. *Nucleic Acids Res. 26*, 5581−5588.

(2) Mir, K. U., and Southern, E. M. (1999) Determining the influence of structure on hybridization using oligonucleotide arrays. *Nat. Biotechnol. 17*, 788−792.

(3) Hacia, J. G. (1999) Resequencing and mutational analysis using oligonucleotide microarrays. *Nat. Genet. Suppl. 21*, 42−47.

(4) Lipshutz, R. J., Fodor, S. P. A., Gingeras, T. R., and Lockhart, D. J. (1999) High-density synthetic oligonucleotide arrays. *Nat. Genet. Suppl. 21*, 20−24.

(5) Milner, N., Mir, K. U., and Southern, E. M. (1997) Selecting effective antisense reagents on combinatorial oligonucleotide arrays. *Nat. Biotechnol. 15*, 537−541.

(6) Sohail, M., Akhtar, S., and Southern, E. M. (1999) The folding of large RNAs studied by hybridization to arrays of complementary oligonucleotides. *RNA 5*, 646−655.

(7) Lövgren, T., Heinonen, P., Hakala, H., Heinola, J., Harju, R., Takalo, H., Mukkala, V.-M., Schmid, R., Lönnberg, H., Pettersson, K., and Iitiä, A. (1997) Sensitive bioaffinity assays on individual microparticles using time-resolved fluorometry. *Clin. Chem. 43*, 1937−1943.

(8) Hakala, H., Mäki, E., and Lönnberg, H. (1998) Detection of oligonucleotide hybridization on a single microparticle by time-resolved fluorometry: quantitation and optimization of a sandwich type assay. *Bioconjugate Chem. 9*, 316−321.

(9) Hakala, H., and Lönnberg, H. (1997) Time-resolved fluorescence detection of oligonucleotide hybridization on a single microparticle: covalent immobilization of oligonucleotides and quantitation of a model system. *Bioconjugate Chem. 8*, 232−237.

(10) Hakala, H., Heinonen, P., Iitiä, A., and Lönnberg, H. (1997) Detection of oligonucleotide hybridization on a single microparticle by time-resolved fluorometry: hybridization assays on polymer particles obtained by direct solid phase assembly of oligonucleotide probes. *Bioconjugate Chem. 8*, 232−237.

(11) Breslauer, K. J., Frank, R., Blocker, H., and Marky, L. A. (1986) Predicting DNA duplex stability from the base sequence. *Proc. Natl. Acad. Sci. U.S.A. 83*, 3746−3750.

(12) Delcourt, S. G., and Blake, R. D. (1991) Stacking energies in DNA. *J. Biol. Chem. 266*, 15160−15169.

(13) Doktycz, M. J., Goldstein, R. F., Paner, T. M., Gallo, F. J., and Benight, A. S. (1992) Studies of DNA dumbbells. I. Melting curves of 17 DNA dumbbells with different duplex stem sequences linked by T4 endloops: evaluation of the nearest-neighbor stacking interactions in DNA. *Biopolymers 32*, 849−864.

(14) SantaLucia, J., Jr., Allawi, H. T., and Seneviratne, P. A. (1996) Improved nearest-neighbor parameters for predicting DNA duplex stability. *Biochemistry 35*, 3555−3562.

(15) Sugimoto, N., Nakano, S., Yoneyama, M., and Honda, K. (1996) Improved thermodynamic parameters and helix initiation factor to predict stability of DNA duplexes. *Nucleic Acids Res. 24*, 4501−4505.

(16) Allawi, H. T., and SantaLucia, J., Jr. (1997) Thermodynamics and NMR of internal GT mismatches in DNA. *Biochemistry 36*, 10581−10594.

(17) SantaLucia, J., Jr. (1998) A unified view of polymer, dumbbell, and oligonucleotide DNA nearest-neighbor thermodynamics. *Proc. Natl. Acad. Sci. U.S.A. 95*, 1460−1465.

(18) Allawi, H. T., and SantaLucia, J., Jr. (1998) Thermodynamics of internal CT mismatches in DNA. *Nucleic Acids Res. 26*, 2694−2701.

(19) Allawi, H. T., and SantaLucia, J., Jr. (1998) Nearest-neighbor thermodynamic parameters for internal GA mismatches in DNA. *Biochemistry 37*, 2170−2179.

(20) Allawi, H. T., and SantaLucia, J., Jr. (1998) Nearest-neighbor thermodynamics of internal AC mismatches in DNA: sequence dependence and pH effects. *Biochemistry 37*, 9435−9444.

(21) Peyret, N., Seneviratne, P. A., Allawi, H. T., and SantaLucia, J., Jr. (1999) Nearest-neighbor thermodynamics and NMR of DNA sequences with internal AA, CC, GG, and TT mismatches. *Biochemistry 38*, 3468−3477.

(22) Hovinen, J., Guzaev, A., Azhayev, A., and Lönnberg, H. (1994) Novel solid supports for the preparation of 3′-derivatized oligonucleotides: introduction of 3′-alkylphosphate tether groups bearing amino, carboxy, carboxamido, and mercapto functionalities. *Tetrahedron 50*, 7203−7218.

(23) Atkinson, T., and Smith, M. (1984) in *Oligonucleotide Synthesis: A Practical Approach* (M. J. Gait, Ed.) p 48, IRL Press, Oxford, U.K.

(24) Mukkala, V.-M., Helenius, M., Hemmilä, I., Kankare, J., and Takalo, H. (1993) Development of luminescent europium(III) and terbium(III) chelates of 2,2′:6′,2″-terpyridine derivatives for protein labelling. *Helv. Chim. Acta 76*, 1361−1378.

(25) Hemmilä, I., Dakabu, S., Mukkala, V.-M., Siitari, H., and Lövgren, T. (1984) Europium as a label in time-resolved immunofluorometric assays. *Anal. Biochem. 137*, 335−343.

BC0100859

Aliphatic Ionenes as Gene Delivery Agents: Elucidation of Structure−Function Relationship through Modification of Charge Density and Polymer Length

Alexander N. Zelikin,[†,‡] David Putnam,[§] Prasad Shastri,[§] Robert Langer,*[,§] and Vladimir A. Izumrudov*[,†]

M. V. Lomonosov Moscow State University, Chemistry Department, Vorob'evi Gori V-234, 119899, Moscow, Russia; Massachusetts Institute of Technology, Division of Health Sciences and Technology, E25-342, Cambridge, Massachusetts, 02139; and Massachusetts Institute of Technology, Chemical Engineering Department, E25−342, Cambridge, Massachusetts, 02139. Received September 6, 2001; Revised Manuscript Received November 29, 2001

Polycation-based gene delivery agents are generally polydisperse populations whose properties are averaged among the different molecular weight species. Therefore, to understand the physicochemical properties of polycations and their relationships to cellular gene transfer, one needs to control the molecular weight of the polymer as well as its cationic charge density. To investigate the structure−function correlation of polycations with respect to the degree of polymerization (DP) and charge density, a series of model materials based on aliphatic ionenes was synthesized and fractionated into distinct molecular weight fractions with DP range from 14 to 32. The aliphatic ionene fractions and their polyelectrolyte complexes (PEC) with DNA were studied using physicochemical and biological methods. Ionene polymers were shown to possess low cytotoxicity (minimal viability of the P388D1 murine macrophage cells 80%). DP and charge density of the ionenes were shown to be the factors of effective control of PEC dissociation in water−salt solutions, with a diminished role of charge density upon lengthening the ionene chain. These polymer characteristics were also important for DNA−ionene PEC resistivity to DNase activity and the ability of ionenes to serve as gene delivery vectors in vitro and exhibited good correlation with the results of salt-induced dissociation of PEC. These data may be useful for developing correlations and mathematical models to predict synthetic gene delivery vector efficiency.

INTRODUCTION

With the advent of modern molecular biology and the potential to not only identify the genetic basis of disease, but also potentially treat diseases at the genetic level, came the promising field of gene therapy. However, while new targets for gene therapy are discovered at an extraordinary pace, the discovery of safe and effective gene delivery vehicles has lagged behind. Currently, there are approximately 400 gene therapy protocols in clinical trials worldwide (see http://www.wiley.co.uk/genetheraphy/clinical/coutries.html) and the success of these clinical trials is directly influenced by the efficiency of the delivery system.

The most effective vectors for transfection are those based on viruses and viral peptide sequences (*1*). However utilization of these agents is substantially hindered by immunologic issues. Therefore attempts are being made to create nonviral gene-delivery agents, such as liposomes and polycations (*1*). The latter effectively bind to negatively charged DNA, which results in substantial DNA compaction. Moreover, if the polyelectrolyte complex (PEC) has an overall positive charge it significantly increases the interaction of PEC with negatively charged cell membranes. Different groups have studied DNA−polycation interactions with respect to the delivery of DNA in vitro and in vivo. The structure of the polycation and its affinity to DNA has a substantial influence on transfection level (*1*−*3*).

While the field of gene transfer with polycationic agents is maturing, to date, general data reporting the correlation between macromolecular characteristics, such as degree of polymerization (DP) and charge density, on the transfection capacity of the polycation are unavailable in the literature. In fact, there is discrepancy in the literature regarding polymer structure and transfection capacity. Godbey et al. (*4*) studied transfection with complexes of DNA with polyethylenimine (PEI) and found that the level of reporter gene expression increases with increasing PEI molecular weight. Similar results were obtained by Wolfert et al. (*5*) for systems based on methacrylate-derived polycations. This was also true in the case of polymers with quaternary ammonium ions as positive moieties in the side chain, although the observed transfection levels were rather low (*5*). In contrast, Schaffer et al. (*6*) showed that the dependence of transfection efficiency as a function of polylysine DP has a maximum at DP ≈ 36. Other properties of polycations were also shown to be dependent on DP and charge density and sometimes contrast with the efficiency of transfection. For example cytotoxicity of polycations

* To whom all correspondence should be addressed: phone (+ 7 095) 9393117, fax (+7 095) 9390174, email: izumrud@genebee.msu.su and phone (671) 2533413, fax (617) 2588827, email: rlanger@mit.edu.

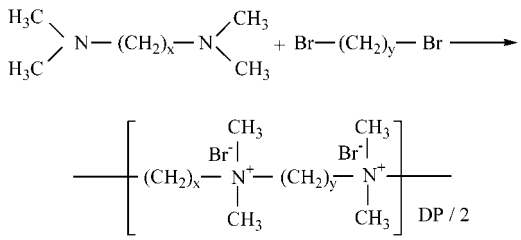
[†] M. V. Lomonosov Moscow State University.

[‡] Massachusetts Institute of Technology, Division of Health Sciences and Technology.

[§] Massachusetts Institute of Technology, Chemical Engineering Department.

10.1021/bc015553t CCC: $22.00 © 2002 American Chemical Society
Published on Web 03/22/2002

Scheme 1



x,y-Ionene

increased with growing polymer charge density (*7*). Plank et al. (*8*) showed that activation of the complement system by synthetic DNA complexes is a potential barrier for gene delivery and that long chain polylysines are much stronger activators compared to short chain samples.

One approach to the design of better polycation-based vectors is to describe the steps of complexation in physicochemical terms. In other words there is a need for mathematical descriptions of the kinetics and thermodynamics of the vector pathway from administration to gene expression, and efforts have been made to create such models (*9*, *10*). However, to date, no model can fully predict the efficiency of a novel vector. Thus detailed studies of the connection between the physicochemical and biological properties of the DNA-containing PEC could be useful.

The goal of this study was to investigate the influence of DP and charge density of polymeric quaternary ammonium salts upon complexing with DNA and biological properties of PEC formed in order to correlate physicochemical features of the polycations and its biological activity.

To accomplish this we used model polycations with charged quaternized nitrogen atoms in the polymer backbone (Scheme 1). Such polymers constitute the family of polyelectrolytes called ionenes (*11*). These polymers are attractive in the scope of this study, as the charge density of ionenes is solely determined by the choice of starting materials for synthesis and thus can be changed at will in a wide range. Moreover, with these materials it is possible to vary one parameter while keeping the other constant. For example, it is possible to obtain samples with the same degree of polymerization but different charge density, or to keep the intercharge spacing constant and alter the polymer chain length.

EXPERIMENTAL SECTION

3-(4,5-Dimethylthiazol-2-yl)-2,5-diphenyltetrazolium bromide (MTT), ethidium bromide, TAE, and HEPES buffer were purchased from Sigma (St. Louis, MO). DNAse I was purchased from USB Corporation.

P388D1 mouse macrophage cell line was a kind gift from Zycos (Cambridge, MA). Cell culture was grown in RPMI medium 1640 with 10 vol % of FBS, and the medium also contained penicillin (100 units/mL) and streptomycin (100 μg/mL). Immortalized African green monkey kidney fibroblasts (COS7) were purchased from American Type Culture Collection (Manassas, VA) and grown in Dubelco's Eagle Modified Medium (DMEM) containing 10 vol % FBS, 100 units/mL penicillin, 100 μg/mL streptomycin. All cell culture growth and incubation was conducted at 37 °C in 5% CO_2 atmosphere.

Sodium salt of highly polymerized calf thymus DNA (~10000 base pairs) was purchased from Sigma and used without purification. Concentration of DNA phosphate groups was determined by UV absorbance measurements at 260 nm assuming molar extinction coefficient $\epsilon_{260} = 6500$ L mol^{-1} cm^{-1}. pCMV−Luciferase was purchased from Elim Biopharmaceuticals, Inc. (San Francisco, CA).

Polymer Synthesis. 2,4-, 2,8-, and 2,10 ionenes were synthesized, fractionated, and purified as described elsewhere (*12*).

Gel Retardation. DNA−ionene complexes were formed by mixing 50 μL of pCMV−Luciferase DNA solution (0.2 mg/mL in 10 mM HEPES buffer, pH 7.2) and 50 μL of solution of ionene at a desired concentration with vortexing. Complexes were allowed to form for 30 min at room temperature. After that, 20 μL of the solution was loaded onto 1% agarose gel in TAE buffer and ran at 90 V for 60 min. The gels were visualized with ethidium bromide.

Complex Size and Zeta-Potential Measurement. Polyelectrolyte complexes were formed as described above for the gel retardation assay. The mixture was diluted to 1.6 mL with HEPES buffer. Complex particle size and zeta potentials were measured at room temperature using Zeta-pals dynamic light scattering detector (Brookhaven Instruments, Holtsville, NY) with a 15 mV laser and incident laser beam at 676 nm. Correlation functions were collected at a scattering angle of 90°. Particle sizes were calculated using multiple angle sizing option of the instruments particle-sizing software. Particle sizes are expressed as effective diameters assuming log-normal distribution. Zeta potentials were calculated using the Smolukowsky model for aqueous suspensions.

DNAse Resistivity. Stoichiometric DNA−polycation complexes, prepared as described above, were placed into 1 mL of 10 mM PBS buffer containing 5 mM $MgCl_2$ at 25 °C. To this solution was added 10 units of DNAse I, and optical density of the solution at 260 nm was recorded for 30 min.

Fluorescence Quenching. Fluorescence intensity was measured using Jobin-Yvon-3CS Spectrofluorimeter (France) in a water-thermostatic stirred cell holder. The measurements were performed in a quartz fluorescence cell with continuous stirring. The excitation and emission wavelengths were 535 and 595 nm, respectively. Concentration of calf thymus DNA, expressed in concentration of phosphate groups, was $[P] = 4 \times 10^{-5}$ base-mol L^{-1} in all experiments. Solutions of polyelectrolyte complexes were prepared directly in the fluorimetric cell by mixing of definite volumes of stock solutions of the polymers. Fluorimetric titration was performed by successive addition of 4 M NaCl solution and measuring the intensity of fluorescence. Time interval between the additions was 5 min.

Cytotoxicity. Cytotoxicity of the polymers was evaluated using the MTT assay (*13*). P388D1 cells were grown in 96-well plates at initial cell density of 10000 cells per well in 0.2 mL of growth medium for 24 h, after which time the media was replaced with growth medium containing polymers at various concentrations and incubated at 37 °C for 24 h. At this time 25 μL of MTT solution (5 mg/mL) in sterile PBS buffer was added to each well and incubated for 2 h, after which 100 μL of extraction buffer (20% w/v SDS in 50:50 v/v DMF−water, pH 4.7) was added to each well and incubated for 24 h at 37 °C. The optical densities were measured using a microplate reader (Dynatech MR5000) at 560 nm. The results are expressed as percent relative to the control (no polymer added) cells.

Transfection. Immortalized African monkey kidney fibroblasts (COS-7) were grown in six-well plates at initial densities of 200000 cell per well in 2 mL of growth media for 24 h. After this the growth medium was

replaced with 2 mL of reduced serum media and polymer complexes were added to the corresponding wells. Polymer complexes were prepared as described for the gel assay analysis. Each sample contained 10 μg of DNA. After 4 h of incubation the media was changed to DMEM and cells were allowed to grow for 36 h. At this time growth media was removed, and cell lysates were formed and analyzed for luciferase activity (Promega luciferase assay kit) and total protein content (BCA assay, Pierce).

RESULTS AND DISCUSSION

The first report of ionenes dates back to the 1930s (*14*). In the 1940s Rembaum et al. (*11*) conducted an extensive research on ionene formation kinetics and thermodynamics. In 1961 Kimura et al. (*15*) isolated three samples of hexadimethrine bromide, 3,6-ionene, with different molecular weights and studied toxicity of these samples on mice. They found that LD_{50} significantly decreases with the lengthening of the ionene chain length. Efimov et al. (*16*) performed similar experiments and showed that the LD_{50} is also dependent on the charge density of ionenes: the longer the intercharge spacing along the ionene chain the lower the value of LD_{50}. To the best of our knowledge, the only report of the use of ionene polymers for gene delivery is that of Aubin et al. who used *3,6*-ionene for DMSO-assisted transfection (*17*). However this study was focused on optimization of DMSO-assisted transfection, rather than influence of the ionene characteristics on its ability to induce gene delivery. Yet until recently there was no efficient way to fractionate polydisperse ionene samples. Thus the experimental results could be masked by broad molecular weight distribution of ionene samples.

Recently (*12*) we described a method of effective fractionation of polydisperse samples of ionenes, which allowed us to obtain samples of 2,4-, and 2,8-ionenes in the range of DP 10 to 30 and study the physicochemical properties of ionene-containing polyelectrolyte complexes with poly(methacrylic acid). In this paper we investigate the physicochemical properties of DNA-containing PEC with ionenes and correlate them to ability of the ionenes to serve as gene delivery agents. For simplicity a sample of *x,y*-ionene with a certain DP will be denoted as ionene-[*x,y*/DP], where DP equals to the number of charged nitrogen atoms per ionene chain. In all cases the charge ratio of the polyelectrolytes is expressed in the ratio of the base-mole concentrations of charged moieties, $\varphi \equiv [+]/[-]$.

Complexes of plasmid DNA (pCMV−Luciferase) with ionenes were formed at different charge ratios of polyelectrolytes, and agarose gel electrophoresis was subsequently performed. This method allows visualization of the interaction of DNA and polycations. Uncomplexed or incompletely neutralized DNA, $\varphi < 1$, migrates in the electric field toward the anode, whereas stoichiometric complexes or complexes with an excess of positive charges do not migrate. Staining the gel with ethidium bromide (EB) provides a picture of the complexes' position on the gel. A representative picture for different ionenes is presented in Figure 1. As anticipated, in all the studied cases the complete retardation of DNA migration is observed at $\varphi \geq 1$.

The same complexes were analyzed for size using dynamic light scattering. The complex particle size as a function of ionene−DNA charge ratio for ionene-[2,4/20] is plotted in Figure 2. The increase of ionene content is accompanied by a substantial decrease in PEC particle size. This is true up to the charge ratio of unity, where the particles are neutral and form aggregates. With

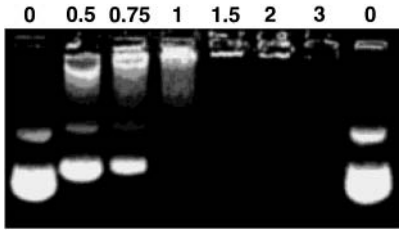


Figure 1. Electrophoretic retardation of pCMV−luciferase by ionene-[2,4/20]. Numbers signify the ionene−DNA charge ratios.

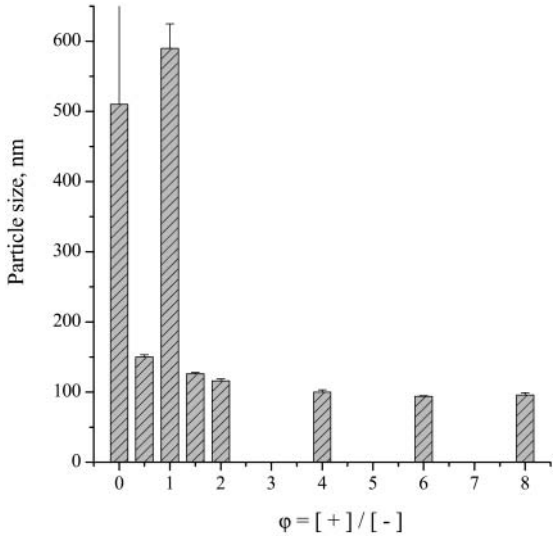


Figure 2. Dependence of the DNA−ionene-[2,4/20] complex particle size on the charge ratio of the polyelectrolytes.

excess polycation, charged complex particles do not aggregate, and at charge ratios of the polymers 2:1 the particle size is ~100 nm. This means that DNA−ionene-[2,4/20] complexes meet the requirement to form complexes less than 150 nm diameter, making endocytosis feasible (*18*).

Analogous dependencies were obtained for all utilized ionene samples (data not shown). All ionenes formed complexes with DNA with a particle size about 100 nm at charge ratios of the polymers greater than 2:1 regardless of charge density or chain length of the polycation. This correlates well with the results of Wolfert et al. (*5*), who showed, that regardless of DP and the nature of the charged moiety, polycations can complex DNA into small particles.

With excess polycation, soluble complex particles are thought to have an overall positive charge. To investigate this with ionenes, zeta potentials of the complex particles were determined (Figure 3). At $\varphi > 1$ the surface charge of DNA−ionene complex particles is positive, as is the case for all studied samples of ionenes regardless of polycation chain length and charge density.

The incorporation of DNA into a PEC can substantially hinder its accessibility to DNAse and thus dramatically decrease nuclease activity. Figure 4 shows the results of experiments in which DNA (curve 1) and DNA−ionene [2,8/29] complex $\varphi = 1$ (curve 2) were treated with DNAse I. Nuclease activity was monitored by the change in optical density at 260 nm (*19*). These data show that accessibility of nucleic acid to DNAse is much lower in the case of PEC compared to uncomplexed DNA.

Dependencies analogous to those presented in Figure 4 were obtained for each DNA−ionene complex and the ΔA_{260} ($\Delta t = 30$ min) was calculated (Figure 5). On this plot the greater the value of $1/\Delta A_{260}$, the more stable the

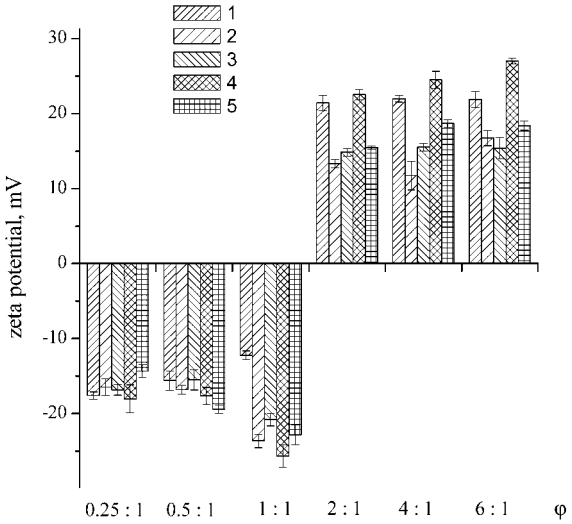


Figure 3. Zeta potentials of DNA-containing complexes with ionene-[2,4/20] (1), [2,8/14] (2), [2,8/20] (3), [2,8/29] (4) and [2,10/20] (5) at different charge ratios of the polyelectrolytes, $\varphi = [+]/[-]$.

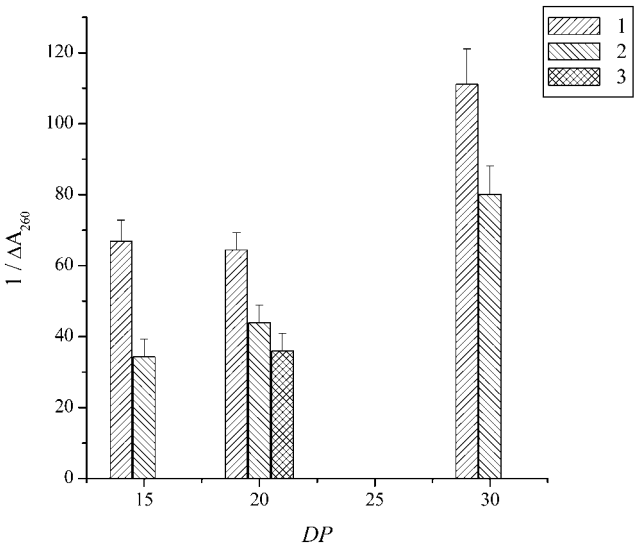


Figure 5. DNAse resistivity for stoichiometric DNA-containing complexes as a function of ionene DP for 2,4-ionene (1), 2,8-ionene (2), and 2,10-ionene (3).

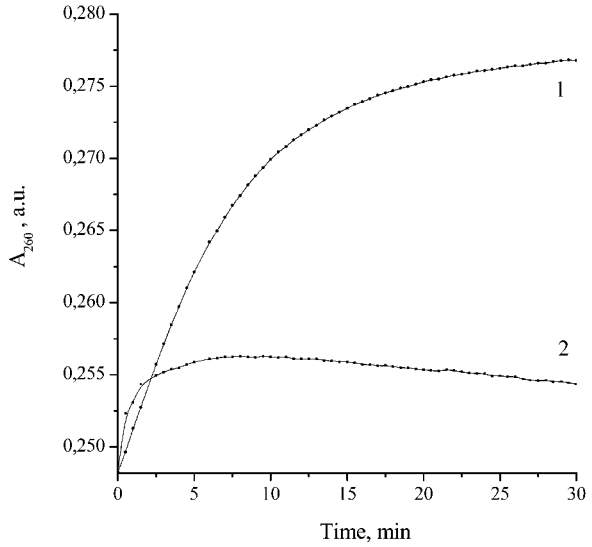


Figure 4. Dependence of optical density at 260 nm in solutions of DNAse I and DNA (1) and DNA−ionene-[2,4/29] PEC, $\varphi = 1$ (2); PBS buffer, 0.005 M $MgCl_2$.

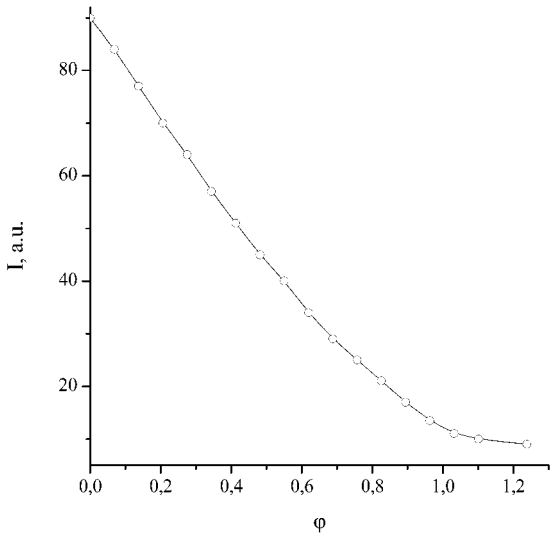


Figure 6. Dependence of fluorescence intensity I of the DNA−ionene-[2,4/20] solution on charge ration of the polymers, $\varphi = [+]/[-]$. $[P] = 4 \times 10^{-5}$ M; [P]/[EB] = 20/1; Tris buffer, pH 9.0; 25 °C.

complex upon DNAse treatment. Comparing data for different ionenes with the same DP shows that a decrease of ionene charge density is followed by a decrease in the resistance of its complex with DNA to nuclease activity. The increase of ionene chain length increases the ionene's ability to shield DNA from nuclease.

The stability of polyelectrolyte complexes formed by calf thymus DNA and ionenes in water−salt solutions was studied using a fluorescence quenching technique (*5, 20*) employing ethidium bromide as a fluorescent probe. The results of titration of DNA with ionene-[2,4/20] are presented in Figure 6. As seen, the introduction of ionene into the solution of DNA−EB complex leads to a pronounced decrease of fluorescence intensity, I, which suggests the formation of a PEC (*20*). This is true up to the charge ratio of the polymers equal to unity, where quenching ceases.

The dissociation of DNA−ionene complex ($\varphi = 1.2$) in water−salt solutions was determined by NaCl titration in the presence of EB. The fluorescence intensity of the polyelectrolyte mixture I was normalized by I_0: intensity of fluorescence of DNA−EB complex at the same salt concentration. In all experiments the ratio of DNA (expressed in concentration of phosphate groups, [P]) to EB was [P]/[EB] = 20/1. As a quantitative measure of the stability of PEC to dissociation in water−salt solution, we define the value C^*_{NaCl}, which is the value of C_{NaCl} that corresponds to the midpoint of the curve of fluorescence ignition. Figure 7 presents the dependence of C^*_{NaCl} vs DP of the ionene for complexes of DNA with 2,4-ionene (curve 1) and 2,8-ionene (curve 2).

As follows from curve 1, the stability of DNA-containing complexes with 2,4-ionene significantly increases with the lengthening of the chain of polycation. Likewise, C^*_{NaCl} for the complex DNA−ionene-[2,4/8] is 0.13 mol L^{-1}, whereas for the complex with ionene-[2,4/20] this value is equal to 0.27 mol L^{-1}. It is noteworthy that in the region of the shortest chains of 2,4-ionene the stability of DNA-containing complexes decreases particularly rapidly. This correlates well with the concept that the value of cooperative binding length for most

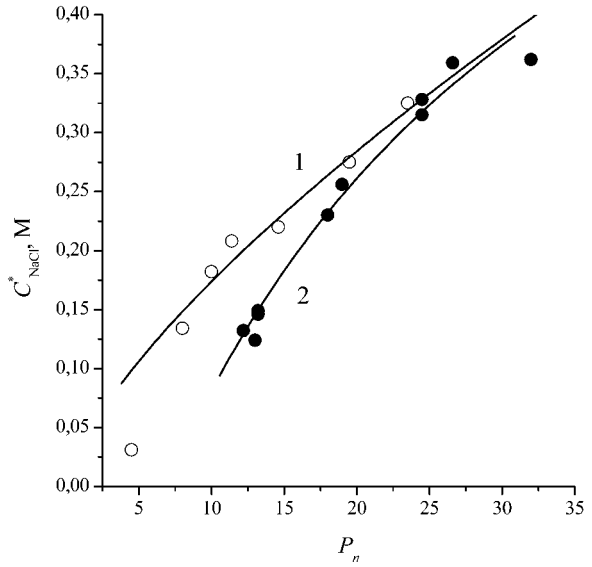


Figure 7. Dependence of C^*_{NaCl}, M on the degree of polymerization of the ionene in solutions of PEC formed by DNA with 2,4-ionene (1) and 2,8-ionene (2). $\varphi = 1{,}2$; other conditions as in Figure 6.

examined pairs of polyelectrolytes lies in the range 4 to 7 monomer units (*21*).

The dependence obtained for the complexes of DNA with 2,8-ionenes of different DP (Figure 7, curve 2) is similar to that for DNA−2,4-ionenes. In this case the growth of the stability of the complex with the increase of polycation chain length is even more pronounced. For short chains of ionenes the stability of 2,4-ionene containing complexes is higher than for the complexes with 2,8-ionene, as would be expected from higher charge density of 2,4-ionene (*12, 20*). Strikingly, upon lengthening of the ionenes chains the difference in stability of the complexes decreases, and on attainment of 20−25 monomer units, the difference between the ionenes as partners for complexation with DNA becomes vanishingly small. In other words, the charge density proved to be the factor controlling stability of DNA-containing PEC only in the case of the ionenes with relatively low DPs.

The cytotoxicity of the ionenes was studied using P388D1 macrophages (Figure 8). The minimum viability of the cells exposed to solutions of ionenes at various concentrations of polycation is 80% relative to controls, indicating low cytotoxicity of ionenes compared to polyethyleneimine and polylysine (*22*), which is critical to normalize the polymer effects in the cell-based transfection assays.

As the whole range of viability of cells treated with different ionenes is within experimental error, it is difficult to deduce the influence of the DP and intercharge spacing of ionenes on their toxicity. However, our data indicate that the influence of these parameters on sample cytotoxicity in vitro is substantially lower than that found in vivo (*15, 16*). The data obtained also suggest that the cytotoxicity is a function of the nature of the polycation charged moiety (primary, secondary, tertiary, or quaternary amine group) rather than the DP of the macromolecule or its charge density.

Polymeric quaternary ammonium salts possess little activity as gene delivery agents. While most of the polycations with different types of charged moieties are able to condense DNA into small particles with an overall positive surface charge, the efficiency of transfection dramatically drops from polylysine-based vectors to quaternary ammonium polymers (*5*).

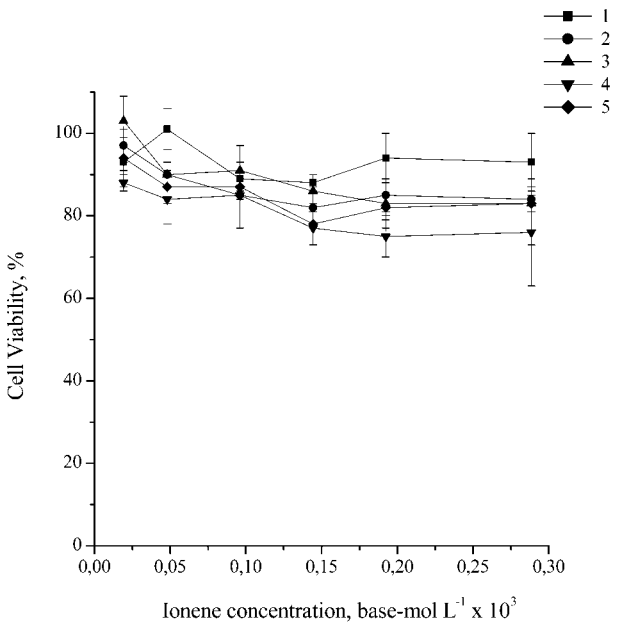


Figure 8. In vitro cytotoxicity as a function of ionene base-mole concentration for ionenes [2,4/20] (1), [2,8/14] (2), [2,8/20] (3), [2,8/29] (4) and [2,10/20] (5).

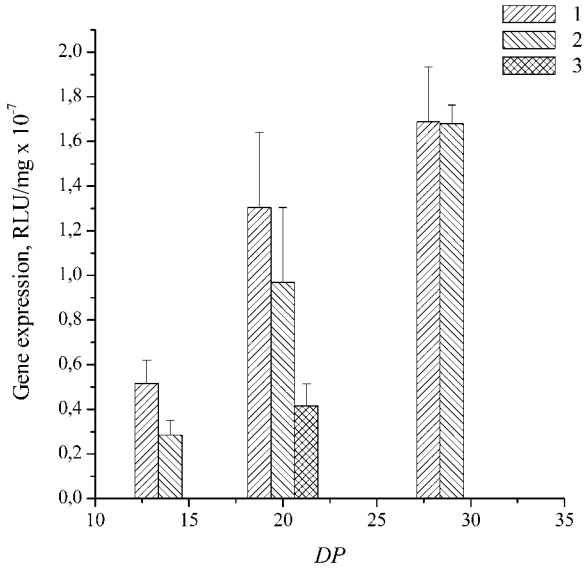


Figure 9. pCMV-Luciferase expression as a function of ionene DP for 2,4-ionene (1), 2,8-ionene (2), and 2,10-ionene (3).

Nevertheless, even this relatively low activity allows examining the ability of ionenes to induce nucleic acid delivery with respect to the influence of polycation macromolecular characteristics. It is well documented that most polymer properties change rapidly in the region of low DP values, while at a certain DP one would expect a property−structure plateau (*23*). For this reason we studied low DP trends using aliphatic ionenes (Figure 9).

To determine the optimal charge ratio of the polymers for transfection, COS-7 cells were exposed to DNA−ionene-[2.4/20] complexes with different ionene contents. These experiments showed that the highest levels of reporter gene expression are observed at a charge ratio 4:1 (data not shown). In all further experiments, cells were treated with DNA−ionene complexes at $\varphi = 4$.

Using samples of ionenes with the same charge density and different chain lengths revealed the influence of polycation chain length on the transfection level. Figure

9 shows that increase of chain length of the ionene leads to a pronounced increase of reporter gene expression. This observation is true for both 2,4- and 2,8-ionene. This result corresponds well with those obtained for synthetic gene delivery vectors based on polyethyleneimine (*4*) and other polycations (*5*). It is also consistent with the data obtained by Schaffer et al. (*6*), who showed that the transfection level as a function of polylysine DP has a maximum at DP $\approx$ 36. As stability of DNA−ionene complexes is lower than that with polylysine (*20*), one can expect the appearance of such maximum in case of ionene-based vectors at DPs higher than 36 monomer units. Unfortunately, we could not isolate ionene samples with DP higher than 30; this is a subject of ongoing research.

To scrutinize the influence of polymer charge density we performed transfections with complexes of DNA with ionenes of the same chain length but different intercharge distance, ionenes [2.4/20], [2.8/20], and [2.10/20]. Data, presented in Figure 9, show that the increase of ionene charge density is followed by a pronounced increase in transfection level. Likewise, in the case of 2,4-ionene, the observed value of RLU/mg is ~1,5 times higher than for 2,8-ionene. For the latter, in turn, it is 2 times higher than for 2,10-ionene, for which the level of transfection is only slightly higher than that observed for uncomplexed DNA.

Another interesting notion comes from comparing the data in Figures 5, 7, and 9. The influence of ionene charge density and chain length on PEC stability in water−salt solutions and tolerance to DNAse action correlate well with transfection efficiency. Moreover, it can be observed that different ionenes which complexes with DNA possess similar stability to dissociation in water−salt solutions induce equivalent DNA expression.

This finding shows the strong influence of polymer microstructure and molecular weight on the PEC properties. According to the revealed correlation, physicochemical results may be useful for predictions of PEC applicability for transfection. The revealed extraordinary correlation between the results obtained by different approaches (stability of the complexes toward dissociation in water−salt solutions, resistivity toward DNase restriction and transfection efficiency) certainly does not imply that the results of different approaches are directly transferable, yet it shows that physicochemical evaluation of the system can give a reasonable prediction of the biological usefulness of the system and can be used for creating mathematical models for prediction of a novel vector.

ACKNOWLEDGMENT

Authors would like to thank Dr. D. Lynn, Dr. D. Anderson, Dr. C. Gentry, and D. Ting for significant contribution to the work. Financial support of the study by NIH grant # 2-R01-6M26698-21, BPEC grant # EEC-9843342 and Russian Fund of Fundamental Research 99-03-33399a are gratefully acknowledged.

LITERATURE CITED

(1) Kabanov, A. V., Felgner, P. L., and Seymour, L. W. (1998) *Self-Assembling Complexes for Gene Delivery: From Laboratory to Clinical Trial,* John Wiley and Sons, Inc., New York,.
(2) Varga, C. M., Wickham, T. J., and Lauffenburger, D. A. (2000) *Biotechnol. Bioeng. 70*, 593−605.
(3) Luo, D., and Saltzman, W. M. (2000) *Nature Biotechnol. 18*, 33−37.
(4) Godbey, W. T., Wu, K. K., and Mikos, A. G. *J. Biomed. Mater. Res.* (1999) *45*, 268−275.
(5) Wolfert, M. A., Dash, P. R., Nazarova, O., Oupicky, D., Seymour, L. W., Smart, S., Strhalm, J., and Ulbrich, K. (1999) *Bioconjugate Chem. 10*, 993−1004.
(6) Schaffer, D. V., Fidelman, N. A., Dan, N., and Lauffenburger, D. A. (2000) *Biotechnol. Bioeng. 67*, 598−606.
(7) Plank, C., Zatloukal, K., Cotton, M., Mechtler, K., and Wagner, E. (1992) *Bioconjugate Chem. 3*, 533−539.
(8) Plank, C., Mechtler, K., Szoka, F. C., and Wagner, E. (1996) *Human Gene Therapy 7*, 1437−1446.
(9) Ledley, T. S., and Ledley, F. D. (1994) *Human Gene Therapy 5*, 679−691.
(10) Dee, K. U., and Shuler, M. L. (1997) *Biotechnol. Bioeng. 54*, 468−490.
(11) Rembaum, A., Baumgartner, W., and Eisenberg, A. (1968) *Polym. Lett. 6*, 159−171.
(12) Zelikin, A. N., Akritskaya, N. I., and Izumrudov, V. A. (2001) *Macromol. Chem. Phys. 202* (15), 3018−3026.
(13) Hansen, M. B., Neilsen, S. E., and Berg, K. (1989) *J. Immunol. Methods 22*, 203-210.
(14) Littmann, E. R., and Marvel, C. S. **(**1930) *J. Am. Chem. Soc. 52*, 287−294.
(15) Kimura, E. T., Young, P. R., and Barlow, G. H. (1962) *Proc. Soc. Exp. Biol. Med. 111*, 37−41.
(16) Efimov, V. S., Gulaeva, J. G., Menshova, G. I., Razvodovskiy, E. V., Zezin, A. B., and Lakin, K. M. **(**1974**)** *Pharmakologiya 6*, 688.
(17) Aubin, R. A., Weinfeld, M., Mirzayans, R., and Paterson, M. C. **(**1994) *Mol. Biotechnol. 1*, 29−48.
(18) McGraw, T. E., and Maxfield, F. R. In *Targeted Drug Delivery*, Juliano, R. L. Ed.; Springer: New York, 1991; p 11−41.
(19) Katayose, S., and Kataoka, K. (1997) *Bioconjugate Chem. 8*, 702−707.
(20) Izumrudov, V. A., Zhiryakova, M. V., and Kudaibergenov, S. E. (2000) *Biopolymers 52*, 94−108.
(21) Papisov, I. M., and Litmanovich, A. A. (1988) *Adv. Polym. Sci. 90*, 139−179.
(22) Putnam, D., Gentry, C. A., Pack, D. W., and Langer, R. (2001) *Proc. Nat. Acad. Sci. U.S.A. 98*, 1200−1205.
(23) Odian, G. *Principles of Polymerization*, 3rd ed., John Wiley and Sons, Inc., New York, 1991.

BC015553T

Near-Infrared Fluorescent Nanoparticles as Combined MR/Optical Imaging Probes

Lee Josephson,* Moritz F. Kircher, Umar Mahmood, Yi Tang, and Ralph Weissleder

Center for Molecular Imaging Research, Massachusetts General Hospital, Charlestown, Massachusetts. Received September 14, 2001; Revised Manuscript Received December 21, 2001

A number of quantitative three-dimensional tomographic near-infrared fluorescence imaging techniques have recently been developed and combined with MR imaging to yield highly detailed anatomic and molecular information in living organisms (*1, 2*). Here we describe magnetic nanoparticle based MR contrast agents that have a near-infrared fluorescence (NIRF) that is activated by certain enzymes. The probes are prepared by conjugation of arginyl peptides to cross-linked iron oxide amine (amino-CLIO), either by a disulfide linkage or a thioether linker, followed by the attachment of the indocyanine dye Cy5.5. The NIRF of disulfide-linked conjugate was activated by DTT, while the NIRF of thioether-linked conjugate was activated by trypsin. Fluorescent quenching of the attached fluorochrome occurs in part due to the interaction with iron oxide, as evident by the activation of fluorescence with DTT when nanoparticles that have less than one dye attached per particle. With a SC injection of the probe, axillary and brachial lymph nodes were darkened on MR images and easily delineated by NIRF imaging. The probes may provide the basis for a new class of so-called smart nanoparticles, capable of pinpointing their position through their magnetic properties, while providing information on their environment by optical imaging techniques.

INTRODUCTION

Magnetic nanoparticles are now well established as magnetic resonance (MR) reporters for detecting pathologies in the liver, spleen, and lymph nodes where, after phagocytosis, their presence is evident primarily by a darkening effect on T2 weighted images. After injection, magnetic nanoparticles accumulate in target tissues and are degraded over a period of several days, providing a convenient time interval to determine nanoparticle disposition. MR is now capable of providing high spatial resolution images (on the order of tens of microns per voxel resolution) of nanoparticle disposition in vitro, in small animals, and in humans. Nanoparticles can be identified in normal human lymph nodes, generally less than about 10 millimeters in diameter, and millimeter-sized metastases can be visualized within the node (*3*−*5*). Current magnetic nanoparticles, while providing superb information on their spatial disposition, are not designed to provide information on the molecular environment surrounding the nanoparticle.

We have recently developed novel enzyme-activated near-infrared fluorescent (NIRF) probes that can image the activity of specific proteases in the local environment of the probe in vivo (*6*−*8*). Probes have been synthesized by the attachment of the NIRF dye Cy5.5 to a poly-lysine derivatized with PEG, a material termed poly(ethylene glycol) graft copolymer Cy5.5-PGC (PGC, PEG graft copolymer) (*7, 9*). In vivo the polylysine backbone is cleaved by cathepsin B, while in vitro it can be cleaved by trypsin. However, current optical imaging methods acquire the NIRF signal against a nonfluorogenic background and hence provide little spatial/anatomic information. The development of optical tomographic imaging techniques offers the prospect of providing a lower detection limit for fluorochromes, and a higher spatial resolution, but a second imaging modality will still be required to obtain anatomical background.

In this communication, we report on a new type of magnetic nanoparticle that acts as an MR contrast agent providing information on the location of the probe and, as a probe for optical imaging, providing information on the molecular environment of the probe. Contrast enhancement by MR results from a core of superparamagnetic iron oxide, while the NIRF signal results from cleavable Cy5.5-derivatized peptides attached to the surface of the nanoparticle. Amino-CLIO, a magnetic nanoparticle with a surface of aminated, cross-linked dextran, has been used to attach a variety of biological molecules, including the tat peptide of the HIV tat protein (*10*), transferrin (*11*), and oligonucleotides (*12*), and provides a convenient platform for the attachment of Cy5.5 peptides.

Two chimeric nanoparticle probes are described. The first exhibits NIRF fluorescence when activated by a reducing environment, while the second exhibits NIRF fluorescence when activated by proteases. These novel probes may provide the basis for a new class of so-called smart nanoparticle probes, whose position can be ascertained by MR imaging and which provide information on their molecular environment through NIRF.

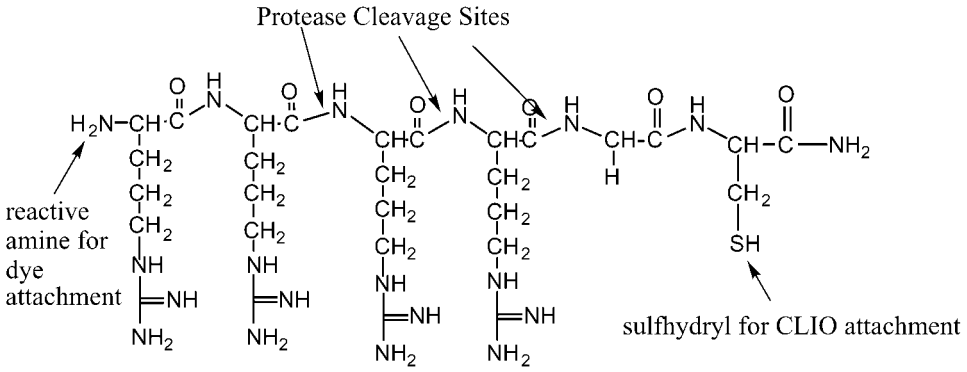
EXPERIMENTAL PROCEDURES

Two dye−arginyl peptide nanoparticle conjugates were synthesized according to Figure 1 and are denoted Cy5.5-R4−SS−CLIO and Cy5.5-R4−SC−CLIO. The designation "SS" denotes a disulfide linkage between the peptide and the iron oxide while "SC" denotes a thioether linkage, while the R4 stands for four arginyl peptides in the L configuration. The primary amine of a dextran-coated

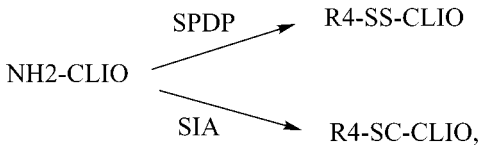
Corresponding author: Lee Josephson, Ph.D., Center for Molecular Imaging Research, Massachusetts General Hospital, Bldg. 149 13th Street, #5406, Charlestown, MA 02129. Tel.: (617) 726 5788. Fax: (617) 726 5708. E-mail: josephso@helix.mgh.harvard.edu.

10.1021/bc015555d CCC: $22.00 © 2002 American Chemical Society
Published on Web 04/02/2002

1. Design of R4, a protease cleavable peptide



2. Synthesis of Arginyl peptide-CLIO Conjugates



3. Synthesis of Cy5.5-arginyl peptide -CLIO Conjugates

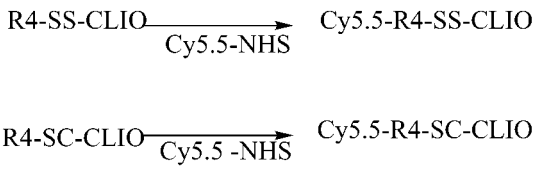


Figure 1. Scheme for synthesis of Cy5.5-arginyl-CLIO conjugates.

cross-linked iron oxide (amino-CLIO) was reacted with one of two activating agents, either *N*-succinimidyl 3-(2-pyridyldithio)propionate (SPDP) or succinimidyl iodoacetate (SIA), to produce two reactive forms of CLIO as shown in Figure 1. The L-arginyl peptide R−R−R−R−G−C ("R4") is attached to the activated CLIO's through a C-terminal cysteine residue to the SPDP or succinimidyl iodoacetate CLIO, followed by the N terminal residue with *N*-hydroxylsuccinimidyl (NHS) ester of Cy5.5 to yield Cy5.5-R4−SS−CLIO and Cy5.5-R4−SC−CLIO.

Synthesis of Aminated-CLIO. Aminated CLIO was prepared as described (*10, 11*). It consists of a core of superparamagnetic iron oxide, a cross-linked coating of dextran with amino groups.

Peptide Synthesis. Peptides were synthesized on an automatic synthesizer (PS3, Rainin, Woburn, MA) at a 0.1 mmol scale using Fmoc chemistry with HBTU and HOBT. They were cleaved from Rink amide HBHA resin (Novabiochem, San Diego, CA) with 5 mL of TFA/thioanisole/ethanedithiol/anisole (90/5/3/2) and purified by C18 reversed phase chromatography. Peptides were the L-arginyl peptide R−R−R−R−G−C−NH_2 ("R4") and the d-arginyl peptide r−r−r−r−G−C−NH_2 ("r4"). By MALDI-MS R4 was 802.93 calculated versus 803.3 found (M + 1). For the peptide r4 M + 1 was 803.63.

Synthesis of Cy5.5 Nanoparticle Conjugates. To synthesize the thioether-bonded conjugate R4−SC−CLIO, amino-CLIO (22 mg Fe, 1.5 mL) was added to 0.5 mL of 0.1M Na_2HPO_4 and 0.5 mL of 150 mM SIA in DMSO. The reaction was allowed to sit for 1 h at room temperature and the addition of succinimidyl-iodoacetate repeated. Iodoacetyl-CLIO was separated from iodoacetic acid using a Sephadex G-25 column equilibrated with 0.025 M Citrate pH 6.5 at 4 °C. To the void volume, 5 mL, was added 6−7 mg of R4 in 0.6 mL of citrate buffer and the reaction incubated overnight at room temperature. Unreacted peptide was removed by dialysis against 3 L of 0.025 M citrate pH 8.2 using a 14 kDa cutoff membrane.

To synthesize the disulfide linked conjugate R4−SS−CLIO, amino-CLIO was activated with SPDP as described (*10*) and reacted with R4 as above except that the pH of the citrate buffer was 8.2 for chromatography and storage (Figure 1).

To attach Cy5.5 to arginyl-CLIO conjugates, 200 μL of 1 M $NaHCO_3$ (pH 8.3) was added to 2 mL of R4−SC−CLIO (7.2 mg Fe). Four hundred forty microliters was then added to each of the five tubes of lyophilized Cy5.5 (Amersham Pharmacia, Piscataway, NJ). After 2 h at room temperature, unreacted dye was removed using PD-10 columns run in a spin separation mode. Columns were washed with 0.025 M citrate pH 8.2 and spun dry. A one milliliter sample was added to columns that were spun at 2500*g* for 7 min.

To synthesize Cy5.5-R4−SS−CLIO conjugates with varying ratios of dye attached, various amounts of dye

Table 1. Physical Properties of Cy5.5-arginyl-CLIO Conjugates

conjugate	size (nm)	R1 (s^{-1} mM^{-1})	R2 (s^{-1} mM^{-1})	peptides per particle	fluorochromes per particle
Cy5.5-R4−SS−CLIO	68 ± 13	27.8	91.2	11.9	1.19
Cy5.5-R4−SC−CLIO	62 ± 7	29.9	92.5	15.5	1.79

were reacted with a fixed amount of conjugate. R4−SS−CLIO (0.1 mg) was added to between 10 and 160 μL of a tube of NHS−Cy5.5 reconstituted with 500 μL of water immediately before use. Additional water and buffer was added so that the reaction with dye occurred in a volume of 275 μL of 0.05 M $NaHCO_3$. After 2 h at room-temperature, unreacted dye was removed using PD-10 columns as above.

Physical Properties of Nanoparticles. The number of peptides per CLIO was determined as the number of reactive primary amino groups using fluorescamine (*13, 14*). Five to fifty microliters of arginyl-CLIO nanoparticles or various amounts of the standard peptide (R4) were diluted into 500 μL of 0.1 M borate, pH 8.5. The weight of R4 was determined by amino acid analysis. Two hundred fifty microliters of fluorescamine (4 mg in 20 mL of acetyl nitrile) was added, and the mixture was allowed to stand overnight at room temperature. Fifty microliters of trypsin (1 mg/mL in 0.1 M phosphate) was added, and samples were allowed to stand for 2 h at room temperature. Fluorescamine fluorescence, ex 390, em 475, was measured after separating the iron oxide from low molecular weight materials by ultrafiltration (*10*). Iron concentration was determined by absorbance (*11*). The peptide-to-crystal ratio was obtained from concentrations of peptide and iron, assuming 2064 iron atoms per crystal (*15*).

Dye/Particle Ratios. Spectra of conjugates were taken using a Hitachi 3500 spectrophotometer. The number of dyes per crystal attached was taken from the absorption at 675 nm and an extinction coefficient of 250000 $M^{-1}cm^{-1}$ and assuming 2064 iron atoms per crystal.

Activation of NIRF. For Cy5.5-R4−SS−CLIO or Cy5.5-R4−SC−CLIO, activation by trypsin or DTT was determined in a microtiter plate with volume of 350 μL of 0.01 M phosphate pH 7.4 with a concentration conjugate of approximately 80 μg Fe/mL. Either trypsin (10 μg/mL, Sigma Chemical St. Louis, MO) or DTT (5 mM) were present. The plate was incubated at room temperature for various times up to 200 min and Cy5.5 fluorescence determined (ex 660, em 695) using a fluorescent microtiter plate reader (Spectra Max, Molecular Devices, Sunnyvale, CA). Activation was defined as a dimensionless number obtained by dividing fluorescence obtained with trypsin (or DTT) by fluorescence obtained without trypsin (or DTT), after subtraction of background fluorescence (*16*).

Magnetic and Size Measurements. The R1 and R2 relaxivities were measured using a 0.47 T tabletop relaxometer as described (*10, 11*). Size was determined by laser light scattering using a Coulter N4 particle size analyzer.

MR and Optical Imaging. For the determination of tissue signal intensities after intravenous (iv) injection (Figure 4), C57 BL/6 mice (National Cancer Institute) were injected through the tail vein with Cy5.5-R4−SC−CLIO (5.1 mg Fe/kg, 2 nmoles dye, 150μL). After 18 h, animals were euthanized with pentobarbital sodium (200 mg/kg, ip), and tissues (approximately 200 mg) were placed in a 96-well microtiter plate. MR imaging was performed on a clinical GE Signa 1.5T imager using a standard 3 in. surface coil to acquire signal. A T2 weighted pulse sequence TR/TE 3000/100 was used (1.0 mm slice thickness, 256 × 256 matrix, 8 cm FOV).

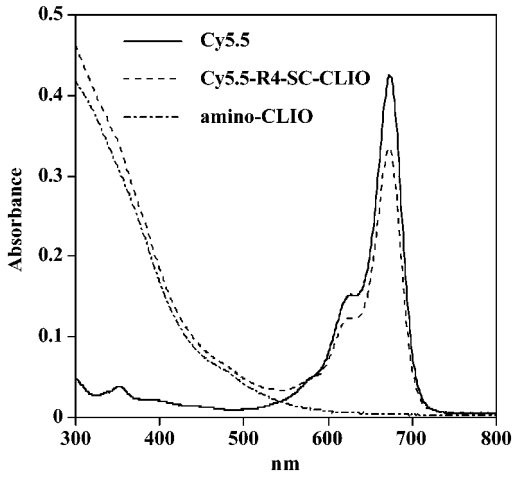


Figure 2. Absorption spectra of Cy5.5, amino-CLIO and Cy5.5-R4−SC−CLIO.

For imaging lymph nodes after subcutaneous (SC) injection (Figure 5), a nu/nu nude mouse (Taconic Farms, Tarrytown, NY) was injected with Cy5.5-R4−SC−CLIO (2.2 mg Fe/kg, 0.85 nmol dye, 30 μL) under the skin of the left front extremity. After 24 h, animals were anesthetized with ketamine/xylazine (80/10 mg/kg, ip) and imaged in the magnet with the coil above. A T1 weighted pulse sequence (TR/TE 500/17) was used (1.5 mm slice thickness, 256 × 256 matrix, 6 cm FOV).

Optical imaging was performed using a whole mouse imaging system, a modification of a commercially available chemiluminescence system, as described (*17*). Cy5.5 fluorescence was obtained with a band-pass filter at 630 ± 20 nm (model # 630RDF30 Omega Optical, Brattleboro, VT) and a 700 nm long pass filter (700 EFLP; Omega Optical). Animals were handled according to institutional guidelines.

RESULTS

The physical properties of Cy5.5-R4−SC−CLIO and Cy5.5-R4−SS−CLIO are summarized in Table 1. The nanoparticles are similar in size and have the high relaxivity characteristics of superparamagnetic iron oxides (*15*).

The absorption spectrum of Cy5.5-R4−SS−CLIO is shown in Figure 2. Cy5.5-R4−SS−CLIO had an absorption maximum of 680 nm, which is slightly shifted from the maximum of 675 nm for Cy5.5. The spectrum of amino-CLIO is also shown, which is dominated by the absorption of iron oxide in the ultraviolet region of the spectrum and which shows little absorption in the near-infrared portion of the spectrum. The distinct spectral properties of amino-CLIO and Cy5.5 suggest that the iron oxide would have little effect on the NIRF of Cy5.5 though evidence for such an interaction is presented below.

Figure 3A shows the effect of treating the nanoparticle conjugates Cy5.5-R4−SS−CLIO and Cy5.5-R4−SC−CLIO with DTT. DTT cleaves disulfide bonds and provides gentle conditions for separating intact molecules from the surface of magnetic nanoparticles (*11, 12*).

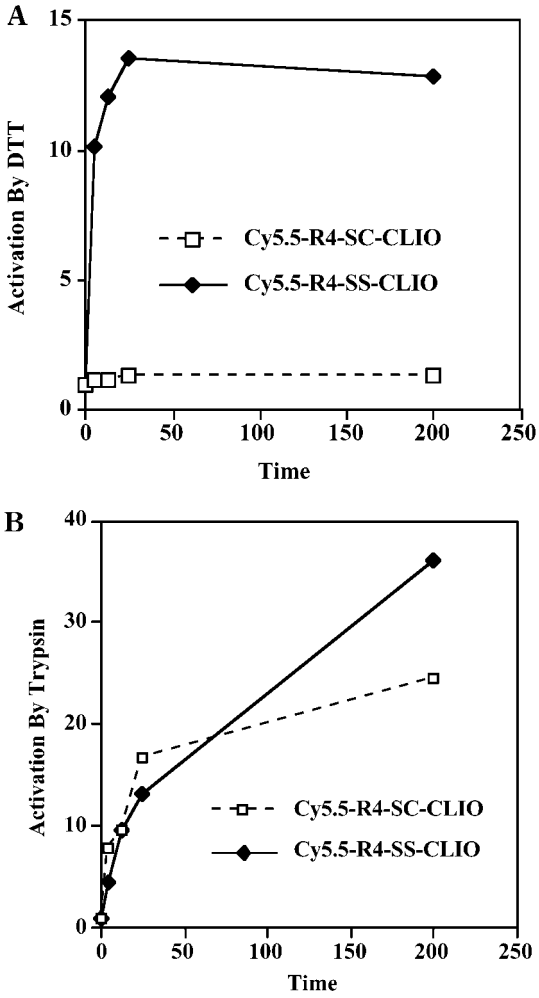


Figure 3. Activation of optical magnetic nanoparticle conjugates by DTT (A) or trypsin (B).

Incubation of Cy5.5-R4−SS−CLIO with DTT resulted in a 12.8-fold increase in NIRF. On the other hand, the NIRF of the thioether-linked nanoparticle Cy5.5-R4−SC−CLIO was not activated by DTT. Trypsin incubation activated the near-infrared fluorescence of Cy5.5-R4−SS−CLIO and Cy5.5-R4−SS−CLIO 36.2 and 27.4-fold (Figure 3B), respectively, by cleaving peptide bonds and releasing a number of degradation products (Cy5.5-R−R, Cy5.5-R−R−R−). Activation by trypsin was notably slower than that with DTT presumably because the concentration of DTT employed (5 mM) was high enough to produce a nearly instantaneous cleavage of disulfide bonds. Activation was notably higher with trypsin than with DTT (36.2 versus 12.8), which may reflect intramolecular interactions between the negatively charged Cy5.5 dye and positively charged peptide obtained when Cy5.5-R4−SS−CLIO is treated with DTT (Cy5.5-R−R−R−R−G−C−NH_2). To further prove the specificity of conjugate activation, a conjugate denoted Cy5.5-r4-SS−CLIO was synthesized, where r4 indicates a peptide identical to "R4" but with all amino acids in the protease-resistant D configuration. Cy5.5-r4-SS−CLIO was activated by DTT but was resistant to activation by trypsin (Josephson, unpublished observations).

Enzyme-activatable Cy5.5 probes generate signals when exposed to proteases primarily because multiple fluorochromes attached to a single carrier molecule quench due to interactions with each other (*3, 8, 17*). Proteolysis cleaves bonds between fluorochromes, increasing the distance between them and activating the

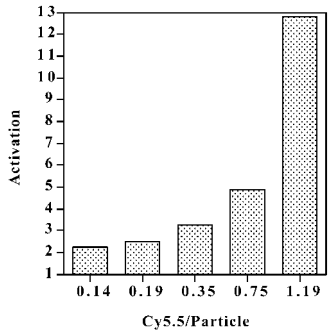


Figure 4. Activation of the disulfide linked nanoparticle conjugate Cy5.5-R4−SS−CLIO with different numbers of fluorochromes (Cy5.5) attached. Activation was with DTT.

NIRF signal. The quenching/activation attained with less than two dye molecules per nanoparticles suggests that quenching may result from an interaction of Cy5.5 with CLIO rather than between Cy5.5 molecules, an interaction which if present occurs despite the lack of spectral overlap between iron oxide and Cy5.5.

To further analyze the activation of fluorescence obtained, a series of Cy5.5-R4−SS−CLIO conjugates were made at different ratios of Cy5.5 to iron oxide. Figure 4 shows the activation of Cy5.5-R4−SS−CLIO conjugates ranging from 0.14 Cy5.5 molecules per particle to 1.19 Cy5.5 molecules per particle. Remarkably, fluorescence increased 2.28-fold with a conjugate that had an average of 0.14 mol of Cy 5.5 per particle, suggesting that quenching is occurring, at least in part, from an interaction between the dye and the iron oxide. Activation increased to 12.8-fold as the number of Cy5.5 molecules was increased to 1.19 Cy5.5's per particle.

To demonstrate the ability of Cy5.5-R4−SC−CLIO to act as a combined MR/optical imaging probe, we injected the agent into mice by the IV and SC routes of administration and obtained MR images and NIRF images. With the IV injection (Figure 5), the animal was sacrificed and MR and NIRF images were obtained from tissues after dissection. Uptake of Cy5.5-R4−SC−CLIO, through the presence of magnetic iron oxide in the spleen and lung, is evident from the lower signal intensity (darkening) of those tissues on MR images, compared to tissues from an uninjected animal. With NIRF fluorescence, no signal was obtained with tissues from an uninjected animal, reflecting the absence of fluorochromes in the range of 610 to 650 nm used to excite Cy5.5. With the injected animal on the other hand, a high intensity NIRF signal was obtained from the liver and spleen and a weak NIRF signal was obtained from the kidney. The low intensity signal from the kidney probably results from proteolytic degradation of the conjugate and excretion of low molecular degradation products.

With the SC injection (Figure 6), MR imaging and NIRF images were obtained on a single live mouse. Figure 6A shows transverse MR images of the axillary and brachial nodes after injection into the front extremity. Axillary and brachial nodes are evident as points of very low signal intensity in two different transverse planes. The darkening of the axillary node due to Cy5.5-R4−SC−CLIO is further shown in the coronal view in Figure 6B. Similar points of low signal intensity are not evident for the contralateral, uninjected side of the animal. Figure 6C shows a white light, reflectance image determined by the surface topography of the animal. However, with the corresponding NIRF image (Figure 6D) background light is negligible, and fluorescent signal

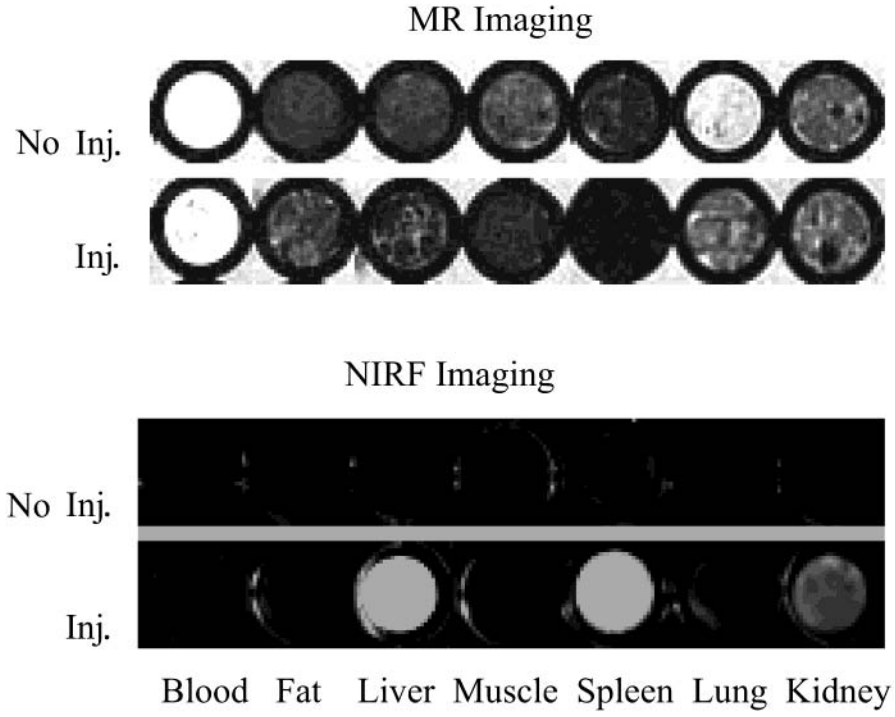


Figure 5. MR and NIRF images from tissues of animals injected iv with Cy5.5-R4−SC−CLIO.

from the brachial and axillary nodes passes through the skin, permitting the nodes to be seen as bright centers or points of light.

DISCUSSION

We have designed magnetic nanoparticles that serve both as magnetic resonance contrast agents and NIRF optical probes. With SC administration the conjugate denoted Cy5.5-R4−SC−CLIO produced contrast-enhanced MR images of lymph nodes that were free of the susceptibility artifact that can accompany the use of iron oxide based contrast agents (*18, 19*). The procedure also provided a NIRF signal sufficiently strong to be seen with our simple imaging equipment consisting of a relatively low power halogen lamp and CCD camera described in detail elsewhere (*17*). However, SC administration used here is a technique that allows nanoparticles to concentrate at high doses in lymph nodes, such as the brachial and axillary nodes, that drain the injection sites of the front extremity (*20*). More sensitive means of visualizing fluorochrome distribution, such as diffuse optical tomography (*1, 21*), may enable the detection of far lower tissue concentrations of Cy5.5 than possible with our equipment.

It has recently been recognized that colloidal materials, rather than organic molecules, can act as efficient quenchers of fluorescence. For example molecular beacons based on the hybridization of target oligonucleotides to single stranded hairpins use a pair of organic molecules (EDANS/DABCYL) as a donor/quencher pair (*22*). However, 1.4 nm colloidal gold can replace DABCYL for hairpin-based molecular beacons (*23*). In this example oligonucleotides are attached to gold through a 5′ terminal phosphate through a $(CH_2)_6-SH$ group, while a dye couple is coupled to a 3′ hydroxyl group through a $(CH_2)_6-NH_2$ linker. Fluorescence is quenched until the hairpin opens due to hybridization, which increases the distance between gold and the fluorophore. With magnetic nanoparticles, treatment with DTT or trypsin cleaves covalent bonds between the fluorophore and the

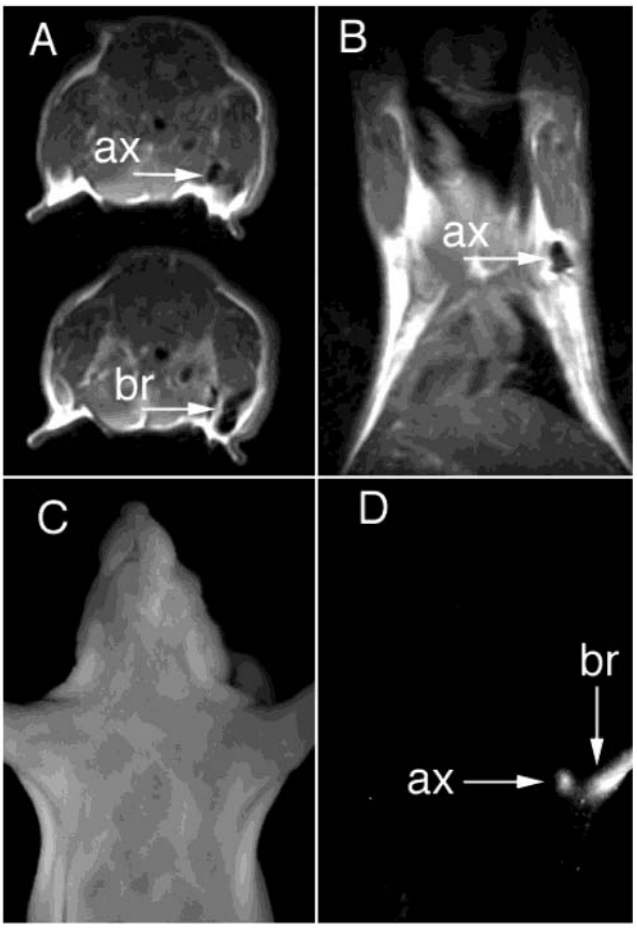


Figure 6. MR and NIRF images from tissues animals injected with Cy5.5-R4−SC−CLIO after SC injection. A. Contrast enhanced MR images of lymph nodes where ax = axillary and br = brachial. B. Contrast enhanced coronal image of the axillary node. C and D. White light and NIRF images, respectively, showing intense regions of NIRF in axillary and brachial nodes.

nanoparticle, permitting the fluorophore to leave the local environment of the nanoparticle and distribute through the bulk media. Interestingly, fluorophores ranging from fluorescein (ex 494, em 520) to Cy 5 (ex 649, em 670) were highly quenched by colloidal gold (*23*). We have noted that the attachment of fluorescein to magnetic nanoparticles is associated with a profound quenching effect (Josephson, unpublished observations). The fluorescence quenching of magnetic nanoparticles may be due to nonradiative energy transfer between the dye and iron oxide or to collisions between the Cy5.5 and the nanoparticle. In the case of colloidal gold nonradiative energy transfer is believed to be the dominant mechanism of fluorescence quenching (*23*).

The chemistry we have employed (Figure 1) offers many options for the design of optically activatable nanoparticles. It can be used to synthesize nanoparticles designed for activation by any protease by selecting peptides that are selective substrates for any protease. The method requires only that the peptide have a C-terminal cysteine, a reactive N-terminal amino that reacts with the *N*-hydroxysuccinimide esters of *fluorochromes* and a lack of primary amino groups elsewhere on the peptide. The R4 peptide meets these *requirements*, since the guanidyl groups of the arginine are unreactive NHS esters (*24*).

The optical nanoparticle probes we have designed utilize polyarginyl peptides to link the fluorophore Cy5.5 to the nanoparticle. Sequences of basic amino acids such as polyarginine can be cleaved by trypsin, a convenient protease for in vitro studies with specificity for basic amino acids. In vivo Cy5.5-R4−SC−CLIO can be activated by proteases with a specificity for basic amino acids such as cathepsin B, which cleaves optical probes such as Cy5.5-PGC which has a polylysine backbone (*7, 17*). Cathepsin B is a widely distributed enzyme found in high concentrations in the organs of the reticuloendothelial system (RES) (*25, 26*). It has been proposed to play a role in tumor invasiveness (*27, 28*) and been examined as a prognostic marker in breast cancer (*29, 30*) and small cell lung carcinomas (*31, 32*).

The attachment of polyarginyl nanoparticles to nanoparticles may result in particles with membrane translocating properties similar to tat-CLIO (*10, 33*). Positively charged peptides derived from the tat protein of HIV (GRKKRRQRRRPPQ) or from homeoprotein transcription factors (RQIKIWFQNRRMKWKK) act as internalization signals for a wide variety of cells (*33*−*35*). We have recently demonstrated that after iv injection a Tat-CLIO nanoparticle is translocated into cells and concentrated in the nucleus, in a manner similar to that obtained when the reagent is incubated with cells in culture (Wunderbaldinger, Josephson and Weissleder, in preparation). Since the guanidine headgroup of arginine seems to be all that is required for a substantial degree of membrane translocating activity (*36, 37*) nanoparticles with simple polyarginyl peptides may be able to efficiently enter cells other than macrophages.

The importance of macrophage activation for a variety of medically important conditions, the association of macrophage activation with elevated levels of proteases, and the ability of macrophages to concentrate nanoparticles after intravenous injection suggest that the optical magnetic nanoparticle probes described here might initially be employed to measure macrophage activation in vivo. The activation state of macrophages is a key element in a wide range of diseases, ranging from the host defense against cancer cells (*38*) to the response to infectious microorganisms (*39*). Immunological activation of macrophages in response to stimuli such as mineral oil, thioglycolate and gamma-interferon is associated with increased levels of proteases such as cathepsins B and D (*40, 41*). The development of macrophage-targeted optically active nanoparticles is aided by the fact that similar particles are in clinical use and accumulate in macrophages of the liver, spleen, and lymph nodes (*4, 5, 42*). Following the chemistry developed here, nanoparticle probes might be designed which reveal the location of macrophages that clear nanoparticles from circulation, while providing a fundamentally new type of information on the immunological activation state of the macrophages that have sequestered them. The ability to obtain satisfactory MR and optical images with the nanoparticle/optical probe described here, together with use of more sensitive and sophisticated equipment for fluorochrome detection in vivo, suggests that future materials of this type might be developed for eventual clinical use.

ACKNOWLEDGMENT

M.F.K. was supported by the German Research Foundation (DFG).

LITERATURE CITED

(1) Ntziachristos, V., and Weissleder, R. (2001) Experimental three-dimensional fluorescence reconstruction of diffuse media by use of a normalized Born approximation. *Optics Lett. 26,* 893−895.

(2) Wind, R. A., Minard, K. R., Holtom, G. R., Majors, P. D., Ackerman, E. J., and Colson, S. D., et al. (2000) An integrated confocal and magnetic resonance microscope for cellular research. *J. Magn. Reson. 147,* 371−7.

(3) Harisinghani, M. G., Saini, S., Weissleder, R., Hahn, P. F., Yantiss, R. K., and Tempany, C., et al. (1999) MR lymphangiography using ultrasmall superparamagnetic iron oxide in patients with primary abdominal and pelvic malignancies: radiographic- pathologic correlation. *AJR Am. J. Roentgenol. 172,* 1347−51.

(4) Anzai, Y., McLachlan, S., Morris, M., Saxton, R., and Lufkin, R. B. (1994) Dextran-coated superparamagnetic iron oxide, an MR contrast agent for assessing lymph nodes in the head and neck. *AJNR Am. J. Neuroradiol. 15,* 87−94.

(5) Harisinghani, M. G., Saini, S., Hahn, P. F., Weissleder, R., and Mueller, P. R. (1998) MR imaging of lymph nodes in patients with primary abdominal and pelvic malignancies using ultrasmall superparamagnetic iron oxide (Combidex). *Acad. Radiol. 5 Suppl 1,* S167−9, discussion S183−4.

(6) Bremer, C., Tung, C. H., and Weissleder, R. (2001) In vivo molecular target assessment of matrix metalloproteinase inhibition. *Nat. Med. 7,* 743−8.

(7) Weissleder, R., Tung, C. H., Mahmood, U., and Bogdanov, A., Jr. (1999) In vivo imaging of tumors with protease-activated near-infrared fluorescent probes. *Nat. Biotechnol. 17,* 375−8.

(8) Tung, C. H., Mahmood, U., Bredow, S., and Weissleder, R. (2000) In vivo imaging of proteolytic enzyme activity using a novel molecular reporter. *Cancer Res. 60,* 4953−8.

(9) Bogdanov, A. A., Jr., Martin, C., Bogdanova, A. V., Brady, T. J., and Weissleder, R. (1996) An adduct of cis-diamminedichloroplatinum(II) and poly(ethylene glycol)poly(L-lysine)-succinate: synthesis and cytotoxic properties. *Bioconjugate Chem. 7,* 144−9.

(10) Josephson, L., Tung, C. H., Moore, A., and Weissleder, R. (1999) High-efficiency intracellular magnetic labeling with novel superparamagnetic-Tat peptide conjugates. *Bioconjugate Chem. 10,* 186−91.

(11) Hogemann, D., Josephson, L., Weissleder, R., and Basilion, J. P. (2000) Improvement of MRI probes to allow efficient detection of gene expression. *Bioconjugate Chem. 11,* 941−6.

(12) Josephson, L., Perez, J. M., and Weissleder, R. (2001) Magnetic nanosensors for the detection of oligonucleotide sequences. *Angew. Chem., Int. Ed. 40,* 3204−3206.

(13) Udenfriend, S., Stein, S., Bohlen, P., Dairman, W., Leimgruber, W., and Weigele, M. (1972) Fluorescamine: a reagent for assay of amino acids, peptides, proteins, and primary amines in the picomole range. *Science 178,* 871−2.
(14) Long, W. (1985) Evaluation of fluorescamine as a phosphogenic derivatizing reagent of primary amines. *Anal. Lett. 18,* 543−553.
(15) Shen, T., Weissleder, R., Papisov, M., Bogdanov, A., Jr., and Brady, T. J. (1993) Monocrystalline iron oxide nanocompounds (MION): physicochemical properties. *Magn. Reson. Med. 29,* 599−604.
(16) Tung, C. H., Bredow, S., Mahmood, U., and Weissleder, R. (1999) Preparation of a cathepsin D sensitive near-infrared fluorescence probe for imaging. *Bioconjugate Chem. 10,* 892−6.
(17) Mahmood, U., Tung, C. H., Bogdanov, A., Jr., and Weissleder, R. (1999) Near-infrared optical imaging of protease activity for tumor detection. *Radiology 213,* 866−70.
(18) Liebig, T., Stoupis, C., Ros, P. R., Ballinger, J. R., and Briggs, R. W. (1993) A potentially artifact-free oral contrast agent for gastrointestinal MRI. *Magn. Reson. Med. 30,* 646−9.
(19) Harika, L., Weissleder, R., Poss, K., and Papisov, M. I. (1996) Macromolecular intravenous contrast agent for MR lymphography: characterization and efficacy studies. *Radiology 198,* 365−70.
(20) Bengele, H. H., Palmacci, S., Rogers, J., Jung, C. W., Crenshaw, J., and Josephson, L. (1994) Biodistribution of an ultrasmall superparamagnetic iron oxide colloid, BMS 180549, by different routes of administration. *Magn. Reson. Imag. 12,* 433−42.
(21) Ntziachristos, V., Yodh, A. G., Schnall, M., and Chance, B. (2000) Concurrent MRI and diffuse optical tomography of breast after indocyanine green enhancement. *Proc. Natl. Acad. Sci. U.S.A. 97,* 2767−72.
(22) Tyagi, S., and Kramer, F. R. (1996) Molecular beacons: probes that fluoresce upon hybridization. *Nat. Biotechnol. 14,* 303−8.
(23) Dubertret, B., Calame, M., and Libchaber, A. J. (2001) Single-mismatch detection using gold-quenched fluorescent oligonucleotides. *Nat. Biotechnol. 19,* 365−70.
(24) Hermanson, G. T. (1996) *Bioconjugate Techniques*, San Diego, Academic Press, p 139.
(25) Howie, A. J., Burnett, D., and Crocker, J. (1985) The distribution of cathepsin B in human tissues. *J. Pathol. 145,* 307−314.
(26) Qian, F., Chan, S. J., Gong, Q. M., Bajkowski, A. S., Steiner, D. F., and Frankfater, A. (1991) The expression of cathepsin B and other lysosomal proteinases in normal tissues and tumors. *Biomed. Biochim. Acta 50,* 531−540.
(27) Yan, S., Sameni, M., and Sloane, B. F. (1998) Cathepsin B and human tumor progression. *Biol. Chem. 379,* 113−23.
(28) Krepela, E., Vicar, J., and Cernoch, M. (1989) Cathepsin B in human breast tumor tissue and cancer cells. *Neoplasma 36,* 41−52.
(29) Lah, T. T., Kalman, E., Najjar, D., Gorodetsky, E., Brennan, P., and Somers, R., et al. (2000) Cells producing cathepsins D, B, and L in human breast carcinoma and their association with prognosis. *Human Pathol. 31,* 149−60.
(30) Lah, T. T., Cercek, M., Blejec, A., Kos, J., Gorodetsky, E., and Somers, R., et al. (2000) Cathepsin B, a prognostic indicator in lymph node-negative breast carcinoma patients: comparison with cathepsin D, cathepsin L, and other clinical indicators. *Clin. Cancer Res. 6,* 578−84.
(31) Werle, B., Kraft, C., Lah, T. T., Kos, J., Schanzenbacher, U., and Kayser, K., et al. (2000) Cathepsin B in infiltrated lymph nodes is of prognostic significance for patients with nonsmall cell lung carcinoma. *Cancer 89,* 2282−91.
(32) Werle, B., Lotterle, H., Schanzenbacher, U., Lah, T. T., Kalman, E., and Kayser, K., et al. (1999) Immunochemical analysis of cathepsin B in lung tumours: an independent prognostic factor for squamous cell carcinoma patients. *Br. J. Cancer 81,* 510−9.
(33) Lewin, M., Carlesso, N., Tung, C. H., Tang, X. W., Cory, D., and Scadden, D. T., et al. (2000) Tat peptide-derivatized magnetic nanoparticles allow in vivo tracking and recovery of progenitor cells. *Nat. Biotechnol. 18,* 410−4.
(34) Prochiantz, A. (1999) Homeodomain-derived peptides. In and out of the cells. *Ann. N.Y. Acad. Sci. 886,* 172−9.
(35) Lindgren, M., Hallbrink, M., Prochiantz, A., and Langel, U. (2000) Cell-penetrating peptides. *Trends Pharmacol. Sci. 21,* 99−103.
(36) Mitchell, D. J., Kim, D. T., Steinman, L., Fathman, C. G., and Rothbard, J. B. (2000) Polyarginine enters cells more efficiently than other polycationic homopolymers. *J. Pept. Res. 56,* 318−325.
(37) Rothbard, J. B., Garlington, S., Lin, Q., Kirschberg, T., Kreider, E., and McGrane, P. L., et al. (2000) Conjugation of arginine oligomers to cyclosporin A facilitates topical delivery and inhibition of inflammation. *Nat. Med. 6,* 1253−7.
(38) Fidler, I. J. (1994) Therapy of cancer metastasis by systemic activation of macrophages. *Adv. Pharmacol. 30,* 271−326.
(39) Seljelid, R., and Busund, L. T. (1994) The biology of macrophages: II. Inflammation and tumors. *Eur. J. Haematol. 52,* 1−12.
(40) Lesser, M., Chang, J. C., and Orlowski, M. (1985) Cathepsin B and D activity in stimulated peritoneal macrophages. *Mol. Cell Biochem. 69,* 67−73.
(41) Lafuse, W. P., Brown, D., Castle, L., and Zwilling, B. S. (1995) IFN-gamma increases cathepsin H mRNA levels in mouse macrophages. *J Leukocyte Biol. 57,* 663−9.
(42) Weissleder, R., Heautot, J. F., Schaffer, B. K., Nossiff, N., Papisov, M. I., and Bogdanov, A., Jr., et al. (1994) MR lymphography: study of a high-efficiency lymphotrophic agent. *Radiology 191,* 225−30.

BC015555D

In Vitro and in Vivo Evaluation of a Technetium-99m-Labeled Cyclic RGD Peptide as a Specific Marker of $\alpha_V\beta_3$ Integrin for Tumor Imaging

Zi-Fen Su, Guozheng Liu, Suresh Gupta, Zhihong Zhu, Mary Rusckowski, and Donald J. Hnatowich*

Division of Nuclear Medicine, Department of Radiology, University of Massachusetts Medical School, Worcester, Massachusetts 01655. Received September 20, 2001; Revised Manuscript Received March 11, 2002

Three amino acids residues, Arg-Gly-Asp (RGD), in vitronectin and fibronectin show affinity for $\alpha_V\beta_3$ integrins expressed in vascular endothelial cells. That tumor growth can upregulate the expression of these integrins on tumor cells for invasion and metastasis and in tissue neovasculature suggests the potential of developing radiolabeled RGD peptides as antagonists of $\alpha_V\beta_3$ integrins for broad spectrum tumor specific imaging. The polypeptide RGD-4C, which contains four cysteine residues for cyclization, has shown preferential localization on integrins at sites of tumor angiogenesis. Both RGD-4C and RGE (Arg-Gly-Glu)-4C (as control) were purchased and conjugated with 6-hydrazinopyridine-3-carboxylic acid (HYNIC) for ^{99m}Tc radiolabeling. After purification of the conjugated peptides by a C18 Sep-Pak cartridge with 20% methanol, both peptides were radiolabeled using tricine. For cell binding studies, both ^{99m}Tc peptides were further purified by SE HPLC. High specific radioactivity of labeled cyclized RGD/E (cyclized RGD/E will be simplified as RGD/E through out the text) of about 20 Ci/μmol was achieved. Both ^{99m}Tc complexes were stable in the labeling solution for over 24 h at room temperature. In the human umbilical vein endothelial (HUVE) cell studies, the binding at 1 h of radiolabeled RGD/E was determined at 4 °C and at concentrations in the picomolar to nanomolar range. Under these conditions, cell accumulation of ^{99m}Tc in the case of RGD was as much as 16 times greater than the control RGE. As a check on specificity, 7 nM of native cyclized RGD blocked 50% of the binding of ^{99m}Tc-labeled RGD to cells. The binding percentage of ^{99m}Tc-labeled RGD to purified $\alpha_V\beta_3$ integrin protein, as determined by SE HPLC, increased with the concentration of the integrin while ^{99m}Tc-labeled RGE showed no binding. The association constant for ^{99m}Tc-RGD was modest at 7×10^6 M^{-1}. In both human renal adenocarcinoma (ACHN) and human colon cancer cell line (LS174T) nude mouse tumor models, the accumulation of ^{99m}Tc-labeled RGD/E exhibited no statistical difference. In conclusion, possibly because of limited numbers of $\alpha_V\beta_3$ integrin receptors per tumor cell and low binding affinity, radiolabeled RGD peptides may have limitations as tumor imaging agents.

INTRODUCTION

Tumors must establish a neovasculature to grow. To do so, the endothelial cells need to organize themselves into capillaries anchored to the extravascular matrix. The organization of the vascular endothelial cells is accomplished by an interaction of dimerized single-transmembrane glycoproteins (vitronectin, fibronectin, and von Willebrand factor), named $\alpha_V\beta_3$ integrin, with triplet peptides Arg-Gly-Asp (RGD) sequenced in the proteins of the extracellular matrix (*1*, *2*). The $\alpha_V\beta_3$ integrins are also expressed on cancer cells (*3*, *5*) and therefore play an important role in the invasion (*6*), metastasis (*7*, *8*), proliferation (*9*), and apoptosis of cancer (*10*, *11*). Because the expression of $\alpha_V\beta_3$ integrins is reported to be strong on activated endothelial cells but restricted on normal cells (*12*, *13*), synthetic RGD containing small peptides have been proposed as antagonists (*14*, *15*) against vascular endothelial cell and tumor growth. The RGD peptides, by binding to $\alpha_V\beta_3$ integrin of either endothelial or tumor cells, are capable of inhibiting cell−matrix interaction (*16*), interrupting signal transmission (*17*), affecting cell migration (*18*, *19*), and causing tumor cell regression (*20*, *21*) or apoptosis (*22*, *23*).

The detection of early stage cancer is important in preventing cancer cell metastasis. However, the sensitivity and specificity of current methods for cancer detection especially in early stages are not ideal (*24*). Radiolabeled RGD peptides could be used as a class of tumor (i.e. tumor angiogenesis) specific markers in cancer detection (*25*, *26*). Haubner et al. (*27*) have prepared two ^{125}I-labeled RGD peptides, [^{125}I]-3-iodo-D-Tyr^4-cyclo(-Arg-Gly-Asp-D-Tyr-Val-) and [^{125}I]-3-iodo-D-Tyr^5-cyclo(−Arg-Gly-Asp-D-Phe-Tyr-), as tumor $\alpha_V\beta_3$ integrins antagonists. The accumulation of the ^{125}I-RGD in xenotransplanted melanoma M21 tumors in mice was 1.3−2% ID/g at 1 h postinjection and decreased with time. To improve the tumor uptake, a sugar group was introduced into the cyclic peptides (*28*). The tumor uptake of the glycosylated ^{125}I-RGD remained at 3% ID/g 1 to 4 h postinjection.

It has been reported that the aspartic acid residue of RGD is highly susceptible to chemical degradation leading to the loss of biological activity (*29*). This degradation was prevented when the RGD-containing peptide was cyclized via disulfide linkage (*29*, *30*). In addition to improved stability, these cyclic peptides show higher potency than the linear peptides in inhibiting the attachment of vitronectin (*31*) to cells. Peptide RGD-4C contains four cysteine residues forming two disulfide

* Author for correspondence: Division of Nuclear Medicine, Department of Radiology, University of Massachusetts Medical School, 55 Lake Avenue North, Worcester, MA 01655. Phone: (508) 856-4256; fax: (508) 856-4572; e-mail: donald.hnatowich@umassmed.edu.

10.1021/bc0155566 CCC: $22.00 © 2002 American Chemical Society
Published on Web 04/20/2002

linkages in the molecule. In phage display studies, only phage carrying the RGD-4C peptide accumulated in tumor whereas phage carrying another linear RGD peptide did not (*31*, *32*). Preliminary xenotransplanted tumor imaging studies from this laboratory suggested that ^{99m}Tc-labeled cyclic RGD-4C, (Cys^1-Cys^9, Cys^3-Cys^7) H_2N-Cys-Asp-Cys-Arg-Gly-Asp-Cys-Phe-Cys-COOH, may localize on integrins at sites of tumor angiogenesis (unpublished data). However, high specific radioactivity labeling would be required for $\alpha_V\beta_3$ integrin imaging if the number of integrins expressed on tumor vascular cells was low as reported by others (*33*). In this study, we prepared purified ^{99m}Tc-labeled RGD-4C as positive and RGE-4C, (Cys^1-Cys^9, Cys^3-Cys^7)H_2N−Cys-Asp-Cys-Arg-Gly-Glu-Cys-Phe-Cys-COOH, as negative control peptides at high specific radioactivity, carried out an in vitro $\alpha_V\beta_3$ positive human umbilical vein endothelial (HUVE) cell (*34*, *35*) binding test, and imaged the biodistributions of the ^{99m}Tc complexes in nude mice bearing either xenotransplanted human ACHN or LS174T tumors.

EXPERIMENTAL PROCEDURES

Materials and Methods. RGD/E peptides were purchased from Advanced ChemTech (Louisville KY). Succinimidyl 6-hydrazinopyridine-3-carboxylate (NHS−HYNIC) was synthesized as described (*36*). *N*-tris-(hydroxymethyl)methylglycine (tricine), *N*-[2-hydroxylethyl]piperazine-*N*′-[2-ethanesulfonic acid] (HEPES), trifluroacetic acid (TFA), dimethyl sulfoxide (DMSO), and d_6-DMSO were purchased from Aldrich (Milwaukee, WI) or Sigma (St. Louis, MO). Na^{99m}TcO$_4$ was obtained from ^{99}Mo/^{99m}Tc generator (DuPont Pharma, Billerica, MA). C18 Sep-Pak cartridges were produced by Waters Corporation (Milford, MA). The human $\alpha_V\beta_3$ integrin protein (MW 237 kDa, stored in a solution of 20 mM Tris-HCl, pH 7.5, 150 mM NaCl, 2 mM $MgCl_2$, 0.1 mM $CaCl_2$, 0.2% Triton X-100) was obtained from Chemicon International, Inc. (Temecula, CA). Human umbilical vein endothelial (HUVE) cells, endothelial cell basal medium (EBM), and endothelial cell growth medium (EGM) were provided by Clonetics (Walkersville, MD). Human renal adenocarcinoma (ACHN) cell line and human colon cancer cell line (LS174T) were obtained from American Type Culture Collection (Manassas, VA). Minimum essential medium (MEM) and fetal bovine serum (FBS) were purchased from Gibco BRL Products (Gaithersburg, MD). NIH Swiss nude mice were provided by Taconic Labs (Germantown, NY). Nembutal was from Abbott Laboratories (North Chicago, IL).

Zorbax SB300 C18 reversed phase (RP) column (4.6 × 250 mm, 5 μm) was manufactured by Agilent Technologies (Palo Alto, CA). Size exclusion (SE) Superdex Peptide HR 10/30 column (1.0 × 30 cm) was produced by Pharmacia Biotech AB (Uppsala, Sweden). The high performance liquid chromatography (HPLC) system consisted of a 501 and a 510 pump and a 2487 dual channel UV detector (Waters, Milford, MA) fitted with a homemade in-line radiation detector. Radioactive samples were counted in a Packard Cobra II well counter. The centrifuge (Biofuge fresco) was produced by Kendro Laboratory Products (Newtown, CT). Fast-atom-bombardment (FAB-MS) and electrospray ionization (ESI-MS) mass spectra were measured by a JEOL JMS-AX505HA mass spectrometer (JEOL USA, Inc., Peabody, MA).

NHS−HYNIC Conjugation. The RGD/E peptides (1 mg, ∼1 μmol) dissolved in 1 mL of 0.1 M pH 8.0 HEPES buffer were stirred at room temperature. To each solution

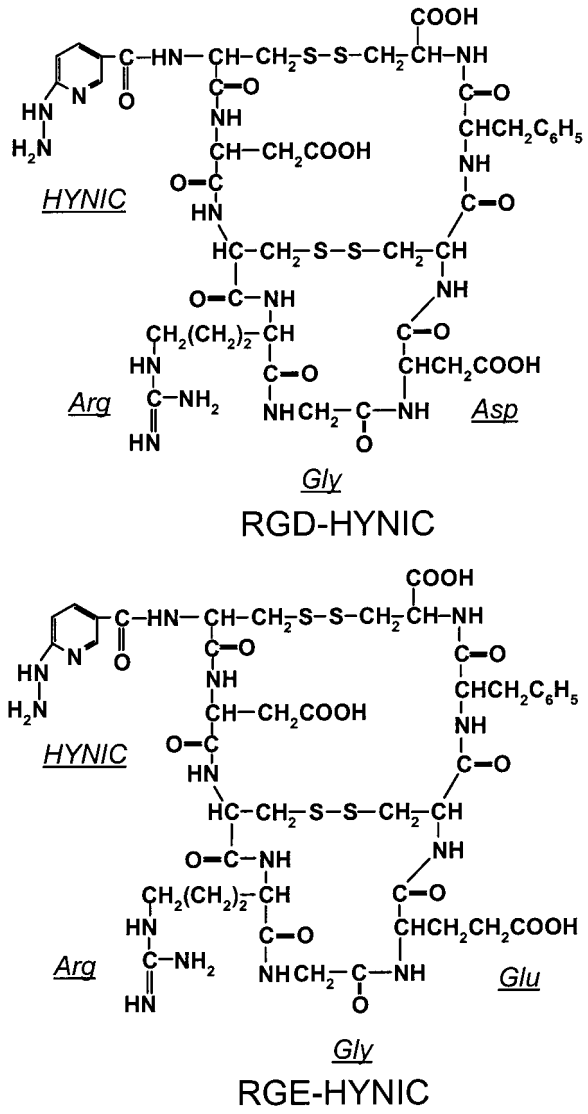


Figure 1. Proposed structures of RGD−HYNIC and RGE−HYNIC.

was added 5 μmol (1.4 mg) of NHS−HYNIC dissolved in 50 μL of dry *N*,*N*-dimethylformamide (DMF, dried over 4 Å molecular sieve). After 1−2 h, the coupling solution was loaded on a C18 Sep-Pak cartridge, preconditioned with 5 mL of methanol followed by 5 mL of water. The loaded cartridge was first washed with 5 mL of water, and 0.3 mL fractions were collected using 20% of MeOH as eluant. Each fraction was analyzed by RP (reversed phase) HPLC with water/acetonitrile solvents pair containing 0.1% TFA as mobile phase with gradient from 100% water to 10% water over 25 min. The fractions with the highest concentration of RGD or RGE, as indicated by UV absorption at 240 and 254 nm, were pooled and lyophilized. Approximately 70% of the theoretical yields were obtained in both cases. The expected structures of RGD/E-HYNIC are shown in Figure 1 and differ only in the extra methylene group of RGE (Glu vs Asp).

Technetium-99m Labeling. The influence of pH values and concentrations of all reagents on the ^{99m}Tc labeling efficiency of RGD/E was investigated. The percentage of pertechnetate and reduced ^{99m}Tc oxide colloid were determined by thin layer and paper chromatography, such as ITLC−SG with saline and Whatman No. 1 paper strip with acetone as developing solvent. The radiochemical purity, recovery, and stability of the ^{99m}Tc-labeled peptides were evaluated by RP HPLC with

either water/acetonitrile or water/acetonitrile containing 0.1% TFA as mobile phase. In this way, labeling conditions were optimized.

The general procedure for ^{99m}Tc labeling of the conjugated peptides was as follows: 0.05 μg to 0.2 μg (0.043−0.17 nmol) of RGD/E-HYNIC in 5 to 20 μL of water, 15 μL of 100 mg/mL tricine in water, 50 μL of 0.25 M pH 5.2 NH_4OAc buffer, 1 to 5 mCi of ^{99m}Tc pertechnetate generator eluant, and 4 to 8 μg of $SnCl_2$ in 10 μL 0.04 N HCl solution were mixed. After incubation at room temperature for 20 min, the labeling solution was analyzed. For in vivo and in vitro tests, the ^{99m}Tc-labeled peptides were purified by SE HPLC collecting every 0.7 mL. The purity of the fraction with the highest radioactivity was tested before use by reanalysis on SE HPLC with 0.1 M pH 7.2 phosphate buffer (PB). The ^{99m}Tc-labeled native RGD/E and NHS−HYNIC were used to identify HPLC peaks due to the radiochemical impurities. Fractions containing the major peaks off RP and SE HPLC for both ^{99m}Tc-labeled peptides were collected separately. The collected fractions were reinjected into both HPLC systems as a check on retention times, radiochemical purity, recovery, and stability.

Binding of Labeled RGD/E to $\alpha_V\beta_3$ Integrin. To establish whether ^{99m}Tc-labeled RGD, like native RGD, shows binding affinity to the $\alpha_V\beta_3$ integrin, both SE HPLC purified labeled RGD and RGE were separately mixed with purified $\alpha_V\beta_3$ integrin protein and analyzed by SE HPLC. Before mixing, the $\alpha_V\beta_3$ integrin protein appeared as a sharp single peak in the UV with retention time of 10.4 min, and the purified ^{99m}Tc complexes of RGD/E appeared in the radioactivity profile as a single peak at 22 min. Purified ^{99m}Tc-RGD ($1.7-2.6 \times 10^{-14}$ mol) along with $2-3 \times 10^{-12}$ mol of unlabeled conjugated RGD and the purified ^{99m}Tc-RGE ($1.9-3.3 \times 10^{-14}$ mol) along with $2-3 \times 10^{-12}$ mol of unlabeled conjugated RGE were mixed with various amounts of the $\alpha_V\beta_3$ integrin protein (5 μg, 10 μg, and 15 μg, $2.1-6.3 \times 10^{-11}$ mol) and analyzed by SE HPLC.

HUVE, ACHN, and LS174T Cells. HUVE cells are known to express $\alpha_V\beta_3$ integrin.[35,37] This cell line was cultured in EGM (500 mL of EBM with supplements of 0.5 mL of 10 ng/mL human recombinant epidermal growth factor (hEGF), 0.5 mL of 1.0 μg/mL of hydrocortisone, and 2.0 mL of a 3 mg/mL solution of bovine brain extract (BBE), 0.5 mL of 50 μg/mL gentamicin, 0.5 mL of 50 ng/mL amphotericin B) containing 10% FBS in a 37 °C incubator with 5% CO_2. The cells were harvested in 0.05% trypsin/0.02% EDTA. After cell counting using a trypan blue dye exclusion assay, the cells were suspended in either EGM, EBM, or PBS at a concentration of 2 to 3×10^6 cells/mL for use. It is assumed that the volume of 500 million HUVE cells is roughly 1 mL.

ACHN and LS174T cell lines were grown in MEM containing 2 mM L-glutamine, 1.5 g/L sodium bicarbonate, 0.1 mM nonessential amino acids, 1.0 mM of sodium pyruvate, 10% FBS, and 100 mg/mL of penicillin−streptomycin. After being harvested and rinsed with trypsin/EDTA, the cells were suspended in MEM with 0.1% human serum albumin (HSA) to a concentration of about 10^7 cells/mL for animal implanting.

Binding of Labeled RGD/E to HUVE Cells. HUVE cells were cultured in EGM containing 10% FBS. After being harvested, the cells were washed in PBS and suspended in either PBS, EBM, or EGM at a concentration of 2 to 3×10^6 cells/mL. To the cell suspension was added 0.01−15 μCi of the SE HPLC purified labeled RGD or RGE. The cell suspension was incubated at 4 °C for 30 min and then centrifuged at 2000 rpm for 4 min. A 30 μL volume of the supernatant was transferred to a plastic tube for radioactivity counting. The cell pellets were washed with cold fresh medium three times and separated from the supernatant for counting. The count (*38*) of the cell pellet was defined as C_{cell}. The count of an equal volume of the supernatant was defined as C_{medium}.

Binding Competition of Labeled RGD and Native RGD to HUVE Cells. Various amounts (final concentration between 50 pM to 58 μM) of native RGD was added to Eppendorf vials containing $2-3 \times 10^6$ HUVE cells suspended in EGM. After incubation at 4 °C for 30 min, the labeled RGD (0.17 μCi) was added, and the cells were incubated for a further 1 h at 4 °C. The vials were centrifuged, and 30 μL of supernatant was transferred for counting. After being washed three times with cold fresh EGM, the cell pellet in the Eppendorf tip was placed in a plastic test tube for counting.

In Vivo Biodistribution of Labeled RGD/E in Tumor-Bearing Mice. LS174T cells (10^6) in MEM containing 0.1% HSA were implanted in one thigh in each of four nude mice. After the tumor grew to approximate 1 cm in any dimension, two animals each received approximately 0.17 μg (0.16 nmol, 24 μCi) of the purified ^{99m}Tc-RGD or RGE. Animals were imaged at 6 h postinjection and were then sacrificed for biodistribution. Radioactivity of the tissue samples was measured against a standard of each injectate.

Each of 10 nude mice was implanted with 10^6 ACHN cells in one thigh. After the tumor size was 1 cm in any dimension, each animal received approximately 4.7 ng (4.1 pmol, 24 μCi) of the purified labeled RGD or RGE. Thus each ACHN-bearing animal received only about 3% of the peptide dosage received by each of the LS174T-bearing animals. The animals were imaged at 6 h postinjection and sacrificed.

Imaging. Mice anesthetized with Nembutal (1.5 mg/25 g mouse) were placed horizontally on the face of the upright collimator. Scintigrams were taken with an Elscint (Hackensack, NJ) APEX 409 M portable large field of view scintillation camera equipped with a parallel hole, medium-energy collimator and an Elscint APEX F1 computer. Images were acquired for a preset time using a 256 × 256 matrix with a 30% energy window set at 140 keV.

RESULTS

HYNIC Conjugation. The molecular mass of RGD measured by FAB-MS was 1017.2714 ($[M + H]^+$, $C_{37}H_{53}N_{12}O_{14}S_4$), calcd 1017.2687, while that of RGE was 1031.2850 ($[M + H]^+$, $C_{38}H_{55}N_{12}O_{14}S_4$), calcd 1031.2843. The errors of the measurements were 2.6 and 0.6 ppm, respectively. The molecular mass of HYNIC-coupled RGD detected by ESI-MS was 1152.3 ($[M + H]^+$, $C_{43}H_{58}N_{15}O_{15}S_4$), calcd 1152.3, whereas the molecular ion of the RGE−HYNIC was not seen on the spectrum. The RGE−HYNIC was then further purified by RP HPLC, lyophilized, and measured by ESI-MS, ES-MS, and FAB-MS, but no expected molecular ion was detected. This may possibly be due to the instability of RGE−HYNIC. C18 Sep-Pak cartridges were used as a simple and effective method to separate the labeled peptides from most of the impurities, such as NHS−HYNIC, hydrated HYNIC, HEPES, and solvents such as DMF. After the purification, the ratio of peptide-HYNIC to uncoupled peptides was in the range of 6 to 10 as indicated by UV absorbance on RP HPLC. Neither native RGD/E exhibited a maximum absorption in the range of 240 nm to 600 nm, while both of the coupled peptides revealed

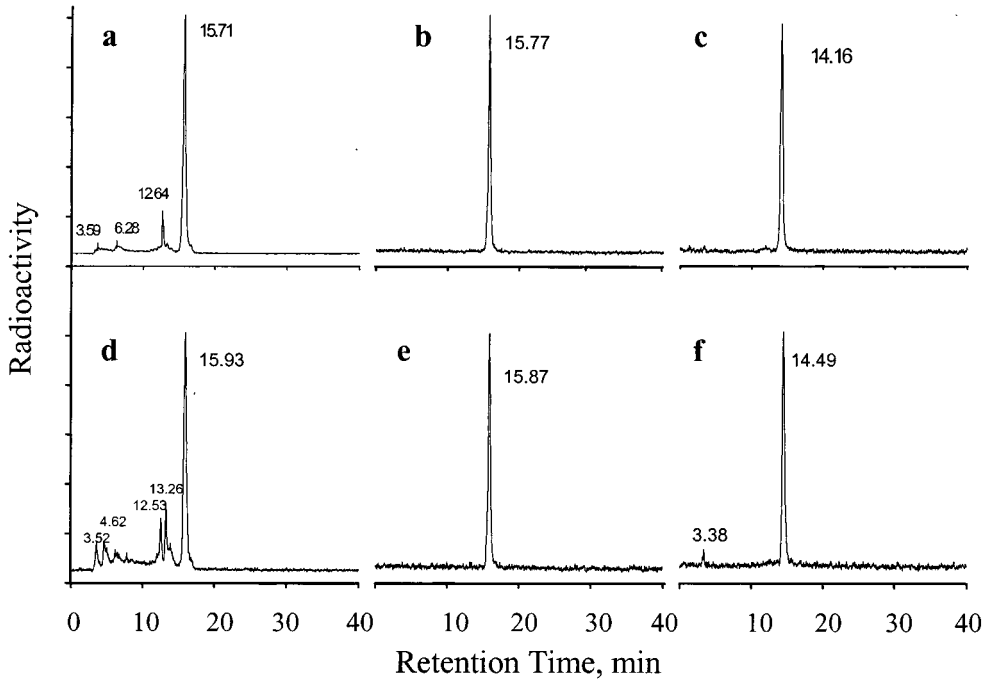


Figure 2. RP HPLC radiochromatograms of ^{99m}Tc-labeled RGD (panel a) and ^{99m}Tc-labeled RGE (panel d) with water/acetonitrile containing 0.1% TFA as mobile phase. The major peak of panels a and d was isolated, re-injected, and analyzed by RP HPLC with (panel b for ^{99m}Tc-RGD and panel e for ^{99m}Tc-RGE) and without 0.1%TFA in the eluant (panel c for ^{99m}Tc-RGD and panel f for ^{99m}Tc-RGE, respectively).

maximum absorption at 283 nm with extinction coefficient of 1.1×10^4 cm^2/mol. The retention times of the native RGD/E on RP HPLC were 15.0 and 15.2 min, respectively. When coupled with HYNIC, the peptides became less hydrophilic than the native peptides and the retention times increased to 15.5 and 15.7 min, respectively. The presence of unlabeled peptides did not significantly affect the ^{99m}Tc labeling of the coupled peptides.

Technetium-99m Labeling. The labeling efficiency of both HYNIC-coupled RGD/E was identical at about 85−90% compared to 10−30% for native, uncoupled RGD/E. Figures 2a and 2d show RP HPLC radiochromatograms (with water/acetonitrile containing 0.1% TFA as mobile phase) of ^{99m}Tc-labeled RGD (retention time 15.7 min) and RGE (15.9 min), respectively. The major peak in Figure 2a was isolated and reinjected into the RP column with (Figure 2b) or without (Figure 2c) 0.1% TFA in the mobile phase. Similarly, the major peak in Figure 2d was isolated and reanalyzed by RP HPLC with (Figure 2e) or without (Figure 2f) 0.1% TFA in the mobile phase. The reanalysis indicated that the purified radiolabeled peptides were pure and stable in the two solvent systems. The ^{99m}Tc labeling of RGD/E without HYNIC produced broad peaks (retention times from 12 to 17 min) on RP HPLC not seen in the labeling of HYNIC coupled RGD/E. Free NHS−HYNIC did not show significant ^{99m}Tc labeling under the same conditions (data not shown). When the labeling was carried out in neutral media, such as water or 0.1 M PB pH 7.2, the impurity peaks at 12.6 to 13.3 min (Figure 2a, 2d) could be as high as 44% but were much lower at 11−22% when the labeling was carried out in 0.25 M acetate buffer pH 5.2. Little pertechnetate remained but approximately 10−15% of ^{99m}Tc was present as radiocolloids. Presumably for this reason, approximately 30−50% of ^{99m}Tc was retained on the RP or SE column during the HPLC purification of the labeled peptides. The formation of radiocolloids could be reduced through the use of ^{99m}Tc-gluconate or ^{99m}Tc-tartrate as transfer ligands, but the labeling efficiency then decreased possibly because of competition of these transfer ligands with tricine. It was primarily to remove ^{99m}Tc colloids that the labeled RGD (Figure 3a) and labeled RGE (data not shown) were purified by SE HPLC before use. The purified ^{99m}Tc peptides were reanalyzed by RP HPLC, which showed a major sharp peak at 15.4 min in the radiochromatograms identical to that of the unpurified sample. This indicated that the major peak on both RP and SE HPLC was due to the desired ^{99m}Tc complexes.

The radiochemical purity, recovery, and the percentage of ^{99m}Tc colloid remained unchanged on standing for the unpurified labeled peptides over 20 h. After the HPLC purification, the radiochemical purity and recovery of both labeled RGD/E were over 95% by RP HPLC with or without 0.1% TFA in the mobile phase. Reanalysis by SE HPLC showed a single peak in both cases with a retention time of 23 min and recovery of 78−85% (Figure 3b). This indicated that the ^{99m}Tc-labeled peptides are stable in either acidic or neutral media (e.g. water or 0.1 M pH 7.2 PB).

High Specific Activity Preparation of Labeled RGD/E. High specific radioactivity could be achieved by labeling as little as 0.4 pmol to 4.3 nmol of both peptides with a large excess of ^{99m}Tc. The minimum molarity providing adequate radiolabeling by RP HPLC was about 4.3 pmol (5 ng), and in this case the labeling efficiency was only 10%. Labeling of higher amounts of peptide generally resulted in higher radiochemical yield, but the radiochemical recovery from RP HPLC remained unchanged (52−55%) due to ^{99m}Tc colloid formation. To optimize specific radioactivity, especially for cell binding studies, labeling of 43 pmol (50 ng) RGD/E with increasing amounts of ^{99m}Tc was investigated. The results, illustrated in Figure 4, show that the maximum specific radioactivity was approximately 20−30 Ci/μmol for both peptides (depending somewhat on the quality of ^{99m}Tc pertechnetate generator eluant). Therefore, in practice, 43 to 86 pmol (50 to 100 ng) of the peptide was labeled

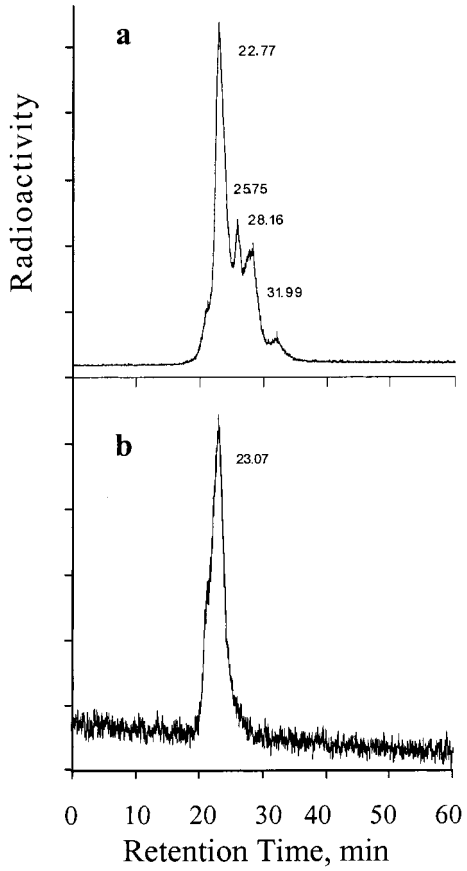


Figure 3. SE HPLC radiochromatograms of ^{99m}Tc-labeled-RGD before (panel a) and after the major peak was isolated and re-injected (panel b).

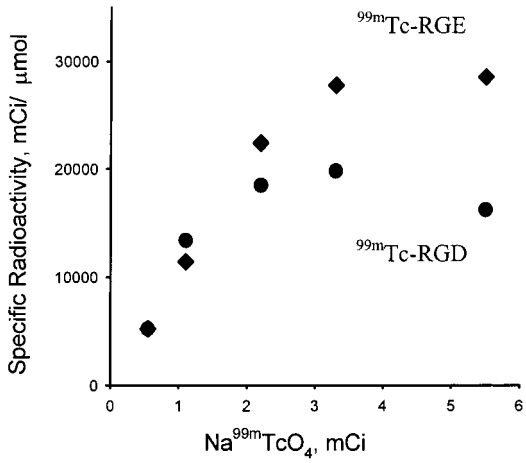


Figure 4. Influence on specific radioactivity of ^{99m}Tc-RGD (circles) or -RGE (squares) with increasing ^{99m}Tc radioactivity ranging from 0.5−5.5 mCi.

for both cell binding and animal studies. To ensure sufficient quantities of purified labeled peptides (100−300 μCi in 0.7 mL of phosphate buffer) for five animal injections, 86 to 129 pmol (0.1−0.15 μg) of peptide was used for each of the labelings.

Integrin Protein Binding. Figure 5 illustrates the UV chromatogram of 15 μg of $\alpha_V\beta_3$ integrin protein (top panel), the radiochromatograms of the mixture of 15 μg of integrin protein with 13 μCi of purified RGD (middle panel) or with 17 μCi of RGE (bottom panel). By comparison with labeled RGE, the ^{99m}Tc complex of RGD exhibited a shift with $\alpha_V\beta_3$ integrin protein on the chromatogram indicating specific binding. The binding

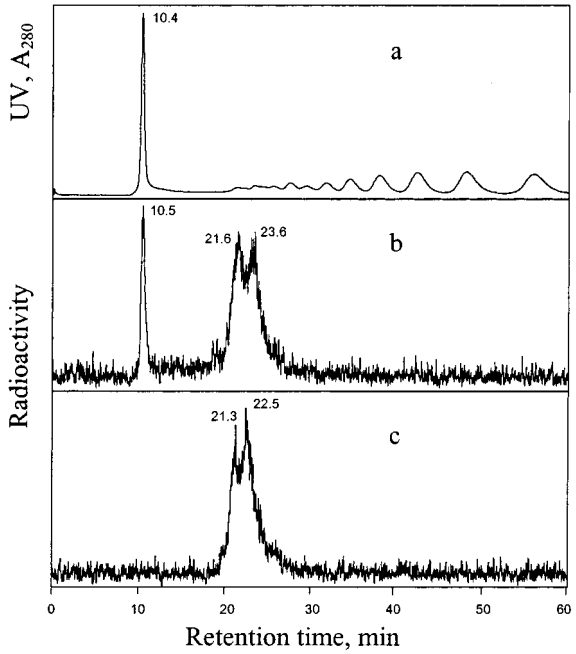


Figure 5. SE HPLC chromatograms of the $\alpha_V\beta_3$ integrin protein at 10.4 min in the UV (panel a) and the radioactivity profiles resulting from the addition to the $\alpha_V\beta_3$ integrin protein of ^{99m}Tc-RGD (panel b) and ^{99m}Tc-RGE (panel c) under similar conditions. A shift in the radioactivity profile to the retention time of the integrin is seen only in the case of RGD.

percentage of labeled RGD to $\alpha_V\beta_3$ integrin protein increased from 7.5% to 20.4% with a corresponding increase in the concentration of the integrin (0.2−0.5 μmol). By contrast, no significant binding was seen for labeled RGE. It is interesting that the majority of the label remained unbound even though the molarity of the integrin used was greater than the sum of the labeled and unlabeled RGD. This implies a weak association constant of RGD−HYNIC with the integrin. It may be assumed that one molecule of RGD binds with one integrin, and the binding equilibrium can be described by eq 1:

$$^{99m}\text{Tc-RGD} + \text{Integrin} = \text{Integrin} - (^{99m}\text{Tc-RGD}) \quad (1)$$

Then, if K is the equilibrium constant, eq 1 can be rewritten as eq 2:

$$\log\{[^{99m}\text{Tc-RGD}]_b/[^{99m}\text{Tc-RGD}]_f\} = \log K + \log[\text{Integrin}]_f \quad (2)$$

where $[^{99m}\text{Tc-RGD}]_b$ and $[^{99m}\text{Tc-RGD}]_f$ are the concentrations of the bound and the free ^{99m}Tc-RGD, respectively, while $[\text{Integrin}]_f$ is the concentration of the free $\alpha_V\beta_3$ integrin protein. The $[\text{Integrin}]_f$ was estimated from the difference of the total integrin used minus the integrin bound. Assuming that the labels, free or bound, and the unlabeled RGD were not decomposed when passing through the SE HPLC, the association constant K (eq 2) can be estimated from a log−log plot of the ratio of bound to free ^{99m}Tc-RGD, as detected by SE HPLC, vs the concentration of the free integrin. The plot (data not shown) exhibited a straight line with a slope of 1.17 (correlation coefficient $r = 0.98$) and an intercept of 6.8. The slope suggested that roughly one RGD was bound to each integrin protein, whereas the intercept indicated that the association constant of ^{99m}Tc-RGD−HYNIC with $\alpha_V\beta_3$ integrin protein was modest ($\sim 7 \times 10^6$ M^{-1}).

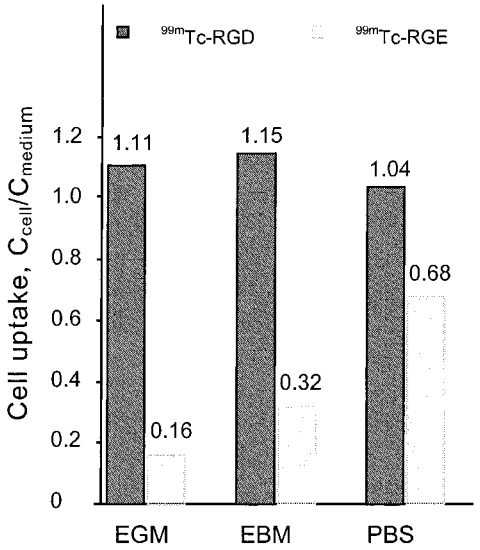


Figure 6. Histograms showing the ratio of counts in the pellet to counts in the supernatant i.e., C_{cell}/C_{medium}) for ^{99m}Tc-RGD and ^{99m}Tc-RGE added to HUVE cell incubated in three different media.

Table 1. The Relationship of the HUVE Cell Binding Ratios with the Specific Radioactivity of the Labeled RGD and RGE[a]

^{99m}Tc-RGD−HYNIC		^{99m}Tc-RGE−HYNIC		
specific activity, mCi/μmol	C_{cell}/C_{medium}	specific activity, mCi/μmol	C_{cell}/C_{medium}	cell uptake differentials, RGD/RGE
54	0.73	44	0.047	16
122	0.46	85	0.081	5.7
11000	1.11	17000	0.16	6.9
18000	1.38	35000	0.26	5.3

[a] The RGD and RGE radiolabels were purified by SE HPLC before use.

Cell Binding. SE HPLC purified labeled RGD/E were used as positive and control for HUVE cells binding, respectively. The results revealed that the ^{99m}Tc complexes exhibited important differences in cell binding as expected. For example, labeled RGD showed 5- to 16-fold higher binding than that of the control (Table 1). Cell uptake of both ^{99m}Tc complexes improved slightly when the specific radioactivity increased. However, this improvement in C_{cell}/C_{medium} was surprisingly small in comparison to the large change in specific radioactivity. Furthermore, the type of media influenced the binding of ^{99m}Tc-RGE but not ^{99m}Tc-RGD. The C_{cell}/C_{medium} ratios of ^{99m}Tc-RGD in HUVE cells in the three media were similar, while those of ^{99m}Tc-RGE varied with the media (Figure 6).

It was important in this research to estimate the average number of $\alpha_V\beta_3$ integrin expressed per cell since this value is a direct determinant of the potential of tumor imaging with ^{99m}Tc-labeled RGD. Scatchard plot is a common method used in determining the number of binding sites per cell by using ^{125}I-labeled macro molecules (*39*). However, an excessive molarity of peptide is usually required for the labeling with ^{99m}Tc (the ratio can be 100:1 or larger), and thus the unlabeled peptide would compete with the label for $\alpha_V\beta_3$ integrin protein binding. For this reason, using Scatchard plots to determine the cell-binding site with ^{99m}Tc-labeled peptide was assumed to be inappropriate (*40*). However, it was advisable to test the dependence of cell uptake on the concentration of labeled RGD in the medium. After 30 min incubation

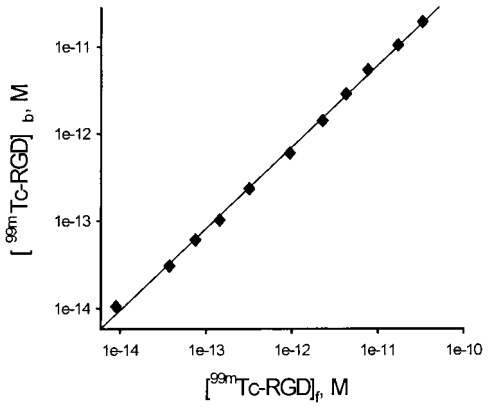


Figure 7. Log−log plot of concentration of ^{99m}Tc-RGD bound vs the complex present in supernatant. The subscript "b" stands for "bound" whereas "f" for "free".

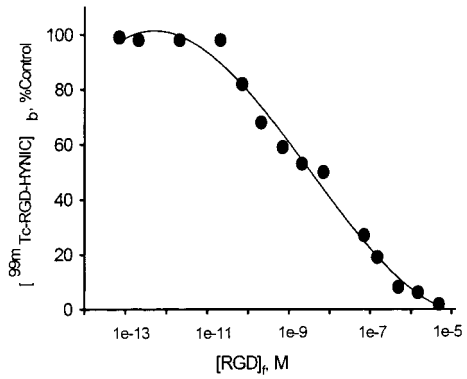


Figure 8. Semilog plot showing increasing inhibition of binding of purified ^{99m}Tc-RGD to HUVE cells with increasing concentrations of native RGD. Plotted as the percentage of bound ^{99m}Tc-RGD vs concentration of unlabeled RGD in supernatant. The subscript "b" stands for "bound" whereas "f" for "free".

with labeled RGD at temperatures close to 4 °C, the HUVE cells were isolated from the medium; the radioactivity in the cell pellets and in the supernatant was measured separately and expressed in terms of concentration (assuming 500 million HUVE cells have a volume of 1 mL). Figure 7 illustrates the log−log plot of concentration of the labeled RGD bound to HUVE cells vs that of the free drug in the medium. That a straight line with a slope of unity resulted suggested that the ^{99m}Tc-RGD was partitioned almost equally between cells and the medium. Accordingly, the uptake of labeled RGD in these cells under this experimental condition might not be generated from the binding with $\alpha_V\beta_3$ integrin protein but rather by a mechanism of passive diffusion or internalization. This diffusion might happen at the lowest concentration (10^{-14} M) of ^{99m}Tc-RGD tested. If this diffusion occurred after the saturation of the $\alpha_V\beta_3$ integrin by RGD, the number of binding sites on the cell must then be small and easily saturated.

Binding Competition Test. The above results show that $\alpha_V\beta_3$ binding sites on HUVC cells can be easily saturated. Since unlabeled RGD will compete with labeled RGD for a limited number of binding sites, a specific radioactivity as high as possible was necessary for the cell binding tests and for the animal imaging. After purification, 0.4 pmol of labeled RGD was added to 2.1×10^6 HUVE cells preincubated with increasing amounts of native RGD. Figure 8 shows the percent of labeled RGD bound vs the concentration of the native RGD added. The binding decreased with increasing

Table 2. Biodistribution of ^{99m}Tc-RGD and ^{99m}Tc-RGE in Nude Mice Bearing Xenotransplanted LS174T Tumors 6 h Postinjection[a]

	^{99m}Tc-RGD, $n = 2$		^{99m}Tc-RGE, $n = 2$	
organs	% ID/g	range	% ID/g	range
liver	2.00	0	1.70	0.10
heart	0.85	0.05	0.55	0.05
kidney	3.25	0.05	2.80	0.40
lung	1.10	0	0.90	0.10
spleen	1.35	0.05	0.45	0.05
stomach	2.60	0.60	0.95	0.05
sm. intestine	1.35	0.15	0.85	0.15
lg. intestine	2.20	0.10	2.10	0
muscle	0.35	0.05	0.30	0
tumor	0.75	0.05	0.60	0
blood	0.95	0.05	1.05	0.05
tumor/muscle	2.2	0.2	2.0	0
tumor/blood	0.8	0	0.6	0

[a] Each mouse received either 24 μCi of purified ^{99m}Tc-RGD or 24 μCi of ^{99m}Tc-RGE for the tests.

Table 3. Biodistributions of ^{99m}Tc-RGD−HYNIC and ^{99m}Tc-RGE−HYNIC in Nude Mice Bearing Xenotransplanted ACHN Tumors 6 h Postinjection[a]

	^{99m}Tc-RGD, (n=5)		^{99m}Tc-RGE, (n=5)		
organs	% ID/g	±SD	% ID/g	±SD	P values
liver	0.89	0.25	1.1	0.21	0.08
heart	0.45	0.06	0.51	0.15	0.20
kidney	3.5	0.96	4.6	0.83	0.04
lung	0.72	0.19	1.0	0.28	0.03
spleen	0.80	0.10	0.48	0.12	0.001
stomach	0.89	0.42	1.1	0.36	0.26
sm. intestine	1.0	0.37	0.44	0.07	0.005
lg. intestine	1.9	0.76	1.6	0.29	0.23
muscle	0.23	0.05	0.24	0.05	0.41
tumor	0.59	0.10	0.60	0.02	0.40
blood	0.36	0.06	1.1	0.25	0.0001
tumor/muscle	2.6	0.33	2.5	0.8	
tumor/blood	1.6	0.20	0.5	0.2	

[a] Each mouse received either 24 μCi of purified ^{99m}Tc−RGD or 24 μCi of ^{99m}Tc−RGE for the tests.

concentration of native RGD as expected with 50% binding blocked by approximately 7×10^{-9} M of native RGD.

In Vivo Animal Tests. Both LS174T and ACHN tumors were used for in vivo studies. While approximately the same radioactivity (24 μCi) was injected in each animal, each LS174T animal received 170 ng of labeled RGD/E while each ACHN animal received only 4.7 ng of these peptides. Images were taken 3 and 6 h postinjection. The biodistribution results at 6 h are listed in Table 2 (LS174T tumor) and in Table 3 (ACHN tumor). The accumulation in both tumors for both peptides was similar at 0.6−0.8% ID/g. Thus, the higher specific radioactivity used in the ACHN mice did not result in improved accumulations over that used in the LS174T mice.

DISCUSSION

Current methods of detecting cancer have both low specificity and sensitivity. There is, therefore, a pressing need for a widely available, noninvasive test for the diagnosis of cancer. It is likely that further gains in specificity and sensitivity can be achieved by using receptor-based imaging agents that target specific features of cancer tissue such as its neovasculature. In all neoplastic diseases, tumor growth and metastasis require persistent new blood vessels without which tumor cells become necrotic or apoptotic (41−45). Among the molecular markers associated with neovascular angiogenesis is the $\alpha_V\beta_3$ integrin, a protein that is absent or barely detectable in established blood vessels but is concentrated in forming blood vessels (*46*). Thus, the early and highly selective appearance of this integrin in tumor makes it a useful target for tumors imaging.

The cysteine-rich (*47*) cyclic polypeptide RGD-4C molecules were designed as $\alpha_V\beta_3$ integrin specific marker for tumor angiogenesis imaging. However, as reported (*33*), the number of $\alpha_V\beta_3$ integrin proteins expressed on endothelia or tumor cells may be limited. If the number of target integrins is limited, then a high specific radioactivity will be required to prevent saturation of integrin binding during imaging. Technetium may be complexed by ligands attached to biological molecules; however, thermodynamically, excessive chelator has to be applied for adequate chelation of ^{99m}Tc. It is thus difficult to achieve high specific radioactivity although there are examples. A unique method has been reported by Baidoo et al. (*48*). After the radiolabeling of a peptide containing a diaminedithiol chelator, the unlabeled peptide was removed on a iodoacetamide-derivatized gel resulting in a specific radioactivity of at least 100 Ci/μmol (the remaining unlabeled peptide was below the UV detection limit). Another successful approach to achieving high specific activity of ^{99m}Tc-labeled peptides used HYNIC as chelator and was reported by Liu et al. (*49*). A specific radioactivity of 20 Ci/mol was achieved by labeling 4.7 nmol of HYNICtide with 100 mCi of pertechnetate.

The coupling of NHS−HYNIC to RGD and RGE was convenient (*50*), and the purification of RGD−HYNIC and RGE−HYNIC by C18 Sep-Pak cartridge was simple and reproducible. Only 43−129 pmol of RGD/E (about 1% to 0.1% the amount of peptides usually used for ^{99m}Tc labeling) was successfully labeled in this laboratory at a specific radioactivity of approximately 20−30 Ci/μmol (the free RGD/E in the labeling solution was undetectable by UV) and therefore similar to the highest values reported by others (*48*, *49*). Despite the unavoidable formation of ^{99m}Tc colloids, a radiochemically pure ^{99m}Tc complex was produced as shown by a single major peak on RP and SE HPLC. When combined with SE HPLC purification, the purity and specific activity of the ^{99m}Tc-labeled peptide was suitable for cell binding and in vivo animal imaging.

The major radioactivity peak shown on both RP and SE HPLC was believed to be the desired complex for several reasons. First, the ^{99m}Tc labeling of the coupled RGD/E always showed the same single sharp peaks on RP HPLC radiochromatograms. Second, the retention times of the ^{99m}Tc-labeled RGD/E peptides on RP HPLC were always greater than those of the unlabeled peptides, indicating the labels were more lipophilic. Third, the nonspecific ^{99m}Tc-labeled RGD and RGE showed broad peaks and a lower labeling efficiency on RP HPLC and were unstable in acidic solvents, whereas the ^{99m}Tc complexes were stable either in acidic or neutral solvents.

The labeled RGD/E were purified by SE HPLC with 0.1 M pH 7.2 PB as eluant. The purity and stability of the purified ^{99m}Tc complexes were tested by reinjection to RP and SE HPLC. The results confirmed that the major peaks in both systems were due to the same complexes, that the purification was successful and reproducible, and that the complexes were stable in either acidic solution and phosphate buffer and therefore probably stable in cell binding and in vivo animal tests.

The uptake percentage of the labeled RGE to HUVE cells was always smaller than that of the labeled RGD

almost certainly because the former does not specifically bind to the $\alpha_V\beta_3$ integrin.

The ^{99m}Tc complexes of RGD/E also showed the expected differences in $\alpha_V\beta_3$ integrin protein binding. The binding percentage of the labeled RGD rose from 7.5% to 20.4% when the concentration of the integrin increased from 0.2 to 0.5 μM while no significant increase was detected in the case of labeled RGE. This indicates a specific association of labeled RGD but not RGE with the $\alpha_V\beta_3$ integrin. That the percentage shift on SE HPLC of the labeled RGD by the addition of a molar excess of the $\alpha_V\beta_3$ integrin protein (the molar ratios of the integrin protein to the total labeled and unlabeled RGD/E peptides were 14−18) is small may be due to the weak association constant (7×10^6 M^{-1}) since the manufacturer of the integrin protein guarantees the absence of significant contamination of the integrin with matrix binding proteins.

It was seen that the binding difference of ^{99m}Tc complexes on the $\alpha_V\beta_3$ integrin protein was consistent with that seen in the HUVE cell binding tests. The data in Table 1 show a slight increase in cell binding of the labeled RGD with a large increase in the specific radioactivity, suggesting the number of the specific binding sites may be small and saturation could occur even at this low concentration of RGD peptide. The binding of antigen−antibody or receptor−ligand normally shows an increase with dosage until saturating concentrations are reached (*51*−*53*). However, the straight line of Figure 7 implies nonspecific binding even when 3×10^6 cells were incubated with lowest concentration of labeled RGD. At that point, approximately 1.7×10^7 labeled RGD molecules (3×10^{-14} M) along with 3×10^9 molecules (4.8×10^{-12} M) of unlabeled RGD were incubated with 3 million cells. If this is the case, the upper limit of the concentration of the $\alpha_V\beta_3$ integrin may be by calculation as small as 4.8×10^{-12} M. This corresponds to only one $\alpha_V\beta_3$ protein expressed on each HUVE cell. A limited $\alpha_V\beta_3$ integrin expression on HUVE (*34*, *35*, *16*) and ACHN (*54*) cell types has been confirmed but not quantified.

Taken together, the labeled RGD peptides may have limited utility as markers for tumor imaging because the binding constant of ^{99m}Tc-RGD−HYNIC to the integrin is modest (7×10^6 M^{-1}) and because of the small number of the $\alpha_V\beta_3$ integrins expressed on each tumor cell. For example the concentration of labeled RGD specifically bound to the $\alpha_V\beta_3$ integrin may be estimated: when 20 μCi purified labeled RGD ($\sim 4 \times 10^{-14}$ mol, 2.8×10^{-11} M) is injected into a mouse with a 0.2 mL xenotransplanted tumor (approximately 10^8 tumor cells) and with a blood volume of approximately 1.4 mL, it may be calculated that only one molecule of labeled RGD would get bound to 1000 tumor cells. Any accumulation exceeding this value would then be nonspecific. This assumption is in agreement with the results of our in vivo animal tests showing minimal tumor uptake of radioactivity. The fact that the tumor uptake of labeled RGE was similar to that of RGD (Tables 2 and 3) and that increasing the specific radioactivity of labeled RGD/E did not significantly improve the tumor accumulations in vivo is evidence that the uptake in endothelial or tumor cells was nonspecific.

As discussed above, the in vivo tumor uptake showed no significant difference for labeled RGD and RGE. This seemed very likely due to the small number of $\alpha_V\beta_3$ integrins expressed on either tumor capillary cells or on the tumor cells being limited and easily saturated. If this is the case, it could be difficult to use ^{99m}Tc-labeled RGD as the tumor imaging agent because the percentage of ^{99m}Tc-RGD complex bound would be extremely low with a weak association constant.

CONCLUSION

Despite the use of RGD labeled at high specific activity, the tumor uptake of ^{99m}Tc-RGD−HYNIC in $\alpha_V\beta_3$ positive tumors growing in nude mice was marginal. These results are therefore in agreement with other investigators attempting to image this receptor with cyclic RGD peptides (*28*). In this investigation, we were able to confirm that the poor imaging results are probably a result of limited numbers of these receptors on the tumor used in this investigation and probably other tumors as well.

ACKNOWLEDGMENT

We wish to thank Ms. Loretta Lee and Dr. Yumin Zhang for providing the cells used in this study. We are grateful to Dr. Bruce Line for suggesting RGE as a control peptide and for other helpful suggestions. We thank Dr. A. Mike Rauth (Ontario Cancer Institute, Toronto, ON) for kind advice and helpful suggestions to this paper. This research was funded in part by DOD grant DAMD17-00-1-03326.

LITERATURE CITED

(1) DePasquale, J. A. (1998) Cell matrix adhesions and localization of the vitronectin receptor in MCF-7 human mammary carcinoma cells. *Histochem. Cell Biol. 110* (5), 485−94.

(2) Germer, M., Kanse, S. M., Kirkegaard, T., Kjoller, L., Felding-Habermann, B., Goodman, S., and Preissner, K. T. (1998) Kinetic analysis of integrin-dependent cell adhesion on vitronectin−the inhibitory potential of plasminogen activator inhibitor-1 and RGD peptides. *Eur. J. Biochem. 253* (3), 669−74.

(3) Vartanian, R. K., and Weidner, N. (1994) Correlation of intratumoral endothelial cell proliferation with microvessel density (tumor angiogenesis) and tumor cell proliferation in breast carcinoma. *Am. J. Pathol. 144* (6), 1188−94.

(4) Weidner, N. (1999) Tumour vascularity and proliferation: clear evidence of a close relationship. *J. Pathol. 189* (3), 297−9.

(5) Li, C., Guo, B., Bernabeu, C., and Kumar, S. (2001) Angiogenesis in breast cancer: The role of transforming growth factor beta and CD105. *Microsc. Res. Tech. 52* (4), 437−49.

(6) Zheng, D. Q., Woodard, A. S., Fornaro, M., Tallini, G., and Languino, L. R. (1999) Prostatic carcinoma cell migration via alpha(v)beta3 integrin is modulated by a focal adhesion kinase pathway. *Cancer Res. 59*(7), 1655−64.

(7) Felding-Habermann, B., O'Toole, T. E., Smith, J. W., Fransvea, E., Ruggeri, Z. M., Ginsberg, M. H., Hughes, P. E., Pampori, N., Shattil, S. J., Saven, A., Mueller, B. M. (2001) Integrin activation controls metastasis in human breast cancer. *Proc. Natl. Acad. Sci. U. S. A. 98* (4), 1853−8.

(8) Wong, N. C., Mueller, B. M., Barbas, C. F., Ruminski, P., Quaranta, V., Lin, E. C., Smith, J. W. (1998) Alpha(V) integrins mediate adhesion and migration of breast carcinoma cell lines. *Clin. Exp. Metastasis 16* (1), 50−61.

(9) Petitclerc, E., Stromblad, S., von Schalscha, T. L., Mitjans, F., Piulats, J., Montgomery, A. M., Cheresh, D. A., and Brooks, P. C. (1999) Integrin alpha(v)beta3 promotes M21 melanoma growth in human skin by regulating tumor cell survival. *Cancer Res. 59* (11), 2724−30.

(10) van der Zee, R., Murohara, T., Passeri, J., Kearney, M., Cheresh, D. A., and Isner, J. M. (1998) Reduced intimal thickening following alpha(v)beta3 blockade is associated with smooth muscle cell apoptosis. *Cell Adhes. Commun. 6*(5), 371−9.

(11) Chen, X., Wang, J., Fu, B., and Yu, L. (1997) RGD-containing peptides trigger apoptosis in glomerular mesangial cells of adult human kidneys. *Biochem. Biophys. Res. Commun. 234* (3), 594−9.

(12) Natali, P. G., Hamby, C. V., Felding-Habermann, B., Liang, B., Nicotra, M. R., Di Filippo, F., Giannarelli, D., Temponi, M., and Ferrone, S. (1997) Clinical significance of alpha(v)-beta3 integrin and intercellular adhesion molecule-1 expression in cutaneous malignant melanoma lesions. *Cancer Res. 57* (8), 1554−60.

(13) Hendrix, M. J., Seftor, E. A., Kirschmann, D. A., and Seftor, R. E. (2000) Molecular biology of breast cancer metastasis Molecular expression of vascular markers by aggressive breast cancer cells. *Breast Cancer Res. 2* (6), 417−22.

(14) Goligorsky, M. S., Noiri, E., Kessler, H., and Romanov, V. (1998) Therapeutic effect of arginine-glycine-aspartic acid peptides in acute renal injury. *Clin. Exp. Pharmacol. Physiol. 25* (3−4), 276−9.

(15) Sheu, J. R., Yen, M. H., Kan, Y. C., Hung, W. C., Chang, P. T., and Luk, H. N. (1997) Inhibition of angiogenesis in vitro and in vivo: comparison of the relative activities of triflavin, an Arg-Gly-Asp-containing peptide and anti-alpha(v)beta3 integrin monoclonal antibody. *Biochim. Biophys. Acta. 1336* (3), 445−54.

(16) Gawaz, M., Neumann, F. J., Dickfeld, T., Reininger, A., Adelsberger, H., Gebhardt, A., and Schomig, A. (1997) Vitronectin receptor (alpha(v)beta3) mediates platelet adhesion to the luminal aspect of endothelial cells: implications for reperfusion in acute myocardial infarction. *Circulation 96* (6), 1809−18.

(17) Tennant, T. R., Rinker-Schaeffer, C. W., and Stadler, W. M. (2000) Angiogenesis inhibitors. *Curr. Oncol. Rep. 2* (1), 11−6.

(18) Koyama, T., Nakajima, Y., Miura, K., Yamazaki, M., Shinozaki, M., Kumagai, T., and Sakaniwa, M. (1997) Analysis of extracellular matrix proteins in malignant chicken cell lines. *J. Vet. Med. Sci. 59* (5), 405−8.

(19) Maheshwari, G., Brown, G., Lauffenburger, D. A., Wells, A., Griffith, L. G. (2000) Cell adhesion and motility depend on nanoscale RGD clustering. *J. Cell Sci. 113* (Pt 10), 1677−86.

(20) Brooks, P. C., Montgomery, A. M., Rosenfeld, M., Reisfeld, R. A., Hu, T., Klier, G., and Cheresh, D. A. (1994) Integrin alpha v beta 3 antagonists promote tumor regression by inducing apoptosis of angiogenic blood vessels. *Cell 79* (7), 1157−64.

(21) Kang, I. C., Lee, Y. D., and Kim, D. S. (1999) A novel disintegrin salmosin inhibits tumor angiogenesis. *Cancer Res. 59* (15), 3754−60.

(22) Buckley, C. D., Pilling, D., Henriquez, N. V., Parsonage, G., Threlfall, K., Scheel-Toellner, D., Simmons, D. L., Akbar, A. N., Lord, J. M., and Salmon, M. (1999) RGD peptides induce apoptosis by direct caspase-3 activation. *Nature 397* (6719), 534−9.

(23) Ravi, D., Ramadas, K., Mathew, B. S., Panikkar, K. R., Nair, M. K., and Pillai, M. R. (2001) Apoptosis, angiogenesis and proliferation: trifunctional measure of tumour response to radiotherapy for oral cancer. *Oral Oncol. 37* (2), 164−71.

(24) Khalkhali, I., Villanueva-Meyer, J., Edell, S. L., Connolly, J. L., Schnitt, S. J., Baum, J. K., Houlihan, M. J., Jenkins, R. M., and Haber, S. B. (2000) Diagnostic accuracy of 99mTc-sestamibi breast imaging: multicenter trial results. *J. Nucl. Med. 41* (12), 1973−9.

(25) Arap, W., Pasqualini, R., and Ruoslahti (1998) Cancer treatment by targeted drug delivery to tumor vasculature in a mouse model. *Science 279*, 377−380.

(26) Pasqualini, R., Koivunen, E., and Ruoslahti (1997) α_V integrin as receptors for tumor targeting by circulating ligands. *Nature Biotech. 15*, 542−546.

(27) Haubner, R., Wester, H. J., Reuning, U., Senekowitsch-Schmidtke, R., Diefenbach, B., Kessler, H., Stocklin, G., and Schwaiger, M. (1999) Radiolabeled alpha(v)beta3 integrin antagonists: a new class of tracers for tumor targeting. *J. Nucl. Med. 40* (6), 1061−71.

(28) Haubner, R., Wester, H. J., Burkhart, F., Senekowitsch-Schmidtke, R., Weber, W., Goodman, S. L., Kessler, H., and Schwaiger, M. (2001) Glycosylated RGD-containing peptides: tracer for tumor targeting and angiogenesis imaging with improved biokinetics. *J. Nucl. Med. 42* (2), 326−36.

(29) Bogdanowich-Knipp, S. J., Jois, D. S., and Siahaan, T. J. (1999) The effect of conformation on the solution stability of linear vs cyclic RGD peptides. *J. Pept. Res. 53* (5), 523−9.

(30) Bogdanowich-Knipp, S. J., Chakrabarti, S., Williams, T. D., Dillman, R. K., and Siahaan, T. J. (1999) Solution stability of linear vs cyclic RGD peptides. *J. Pept. Res. 53* (5), 530−41.

(31) Koivunen, E., Wang, B., and Ruoslahti, E. (1995) Phage libraries displaying cyclic peptides with different ring sizes: ligand specificities of the RGD-directed integrins. *Biotechnology* (*NY*) *13* (3), 265−70.

(32) Ruoslahti, E. (1996) RGD and other recognition sequences for integrins. *Annu. Rev. Cell Dev. Biol. 12*, 697−715.

(33) van Hagen, P. M., Breeman, W. A., Bernard, H. F., Schaar, M., Mooij, C. M., Srinivasan, A., Schmidt, M. A., Krenning, E. P., and de Jong, M. (2000) Evaluation of a radiolabeled cyclic DTPA-RGD analogue for tumour imaging and radionuclide therapy. *Int. J. Cancer. 90* (4), 186−98.

(34) Kosugi, S., Tomiyama, Y., Honda, S., Kashiwagi, H., Shiraga, M., Tadokoro, S., Kiyoi, T., Kurata, Y., and Matsuzawa, Y. (2001) Anti-alphavbeta3 antibodies in chronic immune thrombocytopenic purpura. *Thromb. Haemost. 85* (1), 36−41.

(35) Pollman, M. J., Naumovski, L., and Gibbons, G. H. (1999) Vascular cell apoptosis: cell type-specific modulation by transforming growth factor-beta1 in endothelial cells versus smooth muscle cells. *Circulation 99* (15), 2019−26.

(36) Abrams, M. J., Juweid, M., TenKate, C. I., Schwartz, D. A., Hauser, M. A., Gaul, F. E., Fuccello, A. J., Rubin, R. H., Strauss, H. W., and Fischman, A. (1990) Technetium-99m-Human Polyclonal IgG Radiolabeled via the Hydrazino Nicotinamide Derivative for Imaging Focal Sites of Infection in Rats. *J. Nucl. Med. 31*, 2022−2028.

(37) Kosugi, S., Tomiyama, Y., Honda, S., Kashiwagi, H., Shiraga, M., Tadokoro, S., Kiyoi, T., Kurata, Y., and Matsuzawa, Y. (2001) Anti-alphavbeta3 antibodies in chronic immune thrombocytopenic purpura. *Thromb. Haemost. 85*(1), 36−41.

(38) Su, Z. F., Zhang, X., Ballinger, J. R., Rauth, A. M., Pollak, A., and Thornback, J. R. (1999) Synthesis and Evaluation of Two Technetium-99mTc-Labeled Peptidic 2-Nitroimidazoles for Imaging Hypoxia. *Bioconjugate Chem. 10*, 897−904.

(39) Renner, C., Stehle, I., Lee, F. T., Hall, C., Catimel, B., Nice, E. C., Mountain, A., Rigopoulos, A., Brechbiel, M. W., Pfreundschuh, M., and Scott, A. M. (2001) Targeting properties of an anti-CD16/anti-CD30 bispecific antibody in an in vivo system. *Cancer Immunol. Immunother. 50* (2), 102−8.

(40) Liu, S., and Edwards, D. S. (1999) ^{99m}Tc-Labeled Small Peptides as Diagnostic Radiopharmaceuticals. *Chem. Rev. 99* (9), 2235−2268.

(41) MacDonald, T. J., Taga, T., Shimada, H., Tabrizi, P., Zlokovic, B. V., Cheresh, D. A., and Laug, W. E. (2001) Preferential susceptibility of brain tumors to the antiangiogenic effects of an alpha(v) integrin antagonist. *Neurosurgery 48* (1), 151−7.

(42) Weidner, N. (1999) Tumour vascularity and proliferation: clear evidence of a close relationship. *J. Pathol. 189* (3), 297−9.

(43) Liu, W., Ahmad, S. A., Reinmuth, N., Shaheen, R. M., Jung, Y. D., Fan, F., and Ellis, L. M. (2000) Endothelial cell survival and apoptosis in the tumor vasculature. *Apoptosis 5* (4), 323−8.

(44) Kumar, C. C., Malkowski, M., Yin, Z., Tanghetti, E., Yaremko, B., Nechuta, T., Varner, J., Liu, M., Smith, E. M., Neustadt, B., Presta, M., and Armstrong, L. (2001) Inhibition of angiogenesis and tumor growth by SCH221153, a dual alpha(v)beta3 and alpha(v)beta5 integrin receptor antagonist. *Cancer Res. 61* (5), 2232−8.

(45) Pollman, M. J., Naumovski, L., and Gibbons, G. H. (1999) Endothelial cell apoptosis in capillary network remodeling. *J. Cell Physiol. 178* (3), 359−70.

(46) Brooks, P. C., Clark, R. A., and Cheresh, D. A. (1994) Requirement of vascular integrin alpha v beta 3 for angiogenesis. *Science 264* (5158), 569−71.

(47) Yeh, C. H., Peng, H. C., Yih, J. B., Huang, T. F. (1998) A new short chain RGD-containing disintegrin, accutin, inhibits

the common pathway of human platelet aggregation. *Biochim. Biophys. Acta 1425* (3), 493−504.

(48) Baidoo, K. E., Scheffel, U., Stathis, M., Finley, P., Lever, S. Z., Zhan, Y., and Wagner, H. N., Jr. (1998) High-affinity no-carrier-added 99mTc-labeled chemotactic peptides for studies of inflammation in vivo. *Bioconjugate Chem. 9* (2), 208−17.

(49) Liu, S., Edwards, D. S., Looby, R. J., Harris, A. R., Poirier, M. J., Barrett, J. A., Heminway, S. J., and Carroll, T. R. (1996) Labeling a hydrazino nicotinamide-modified cyclic IIb/IIIa receptor antagonist with 99mTc using aminocarboxylates as coligands. *Bioconjugate Chem. 7*(1), 63−71.

(50) Hnatowich, D. J., Chang, F., Lei, K., Qu, T., and Rusckowski, M. (1997) The influence of temperature and alkaline pH on the labeling of free and conjugated MAG3 with technetium-99m. *Appl. Radiat. Isot. 48* (5), 587−94.

(51) Hu, D. D., Hoyer, J. R., and Smith, J. W. (1995) Ca2+ suppresses cell adhesion to osteopontin by attenuating binding affinity for integrin alpha v beta 3. *J. Biol. Chem. 270* (17), 9917−25.

(52) Pelletier, A. J., Kunicki, T., and Quaranta, V. (1996) Activation of the integrin alpha v beta 3 involves a discrete cation-binding site that regulates conformation. *J. Biol. Chem. 271* (3), 1364−70.

(53) Kunicki, T. J., Annis, D. S., and Felding-Habermann, B. (1997) Molecular determinants of arg-gly asp ligand specificity for beta3 integrins. *J. Biol. Chem. 272* (7), 4103−7.

(54) Korhonen, M., Sariola, H., Gould, V. E., Kangas, L., and Virtanen, I. (1994) Integrins and laminins in human renal carcinoma cells and tumors grown in nude mice. *Cancer Res. 54* (16), 4532−8.

BC0155566

Evaluation of Different α-Galactosyl Glycoconjugates for Use in Xenotransplantation

Guerard W. Byrne,*,† Alexander Schwarz,†,§ Joanna R. Fesi,† Patrick Birch,† Anna Nepomich,† Ivona Bakaj,† Margaret A. Velardo,† Cong Jiang,†,|| Adriana Manzi,†,|| Howard Dintzis,‡ Lisa E. Diamond,† and John S. Logan†

Nextran Inc., 303B College Road, Princeton, New Jersey; Johns Hopkins University School of Medicine, Department of Biophysics, Baltimore, Maryland; and Baxter Healthcare Corporation, Chicago, Illinois. Received October 12, 2001; Revised Manuscript Received February 12, 2002

Porcine organs are rapidly rejected after transplantation into primate recipients due to the presence of preexisting immunoglobulins that bind to terminal galactose α1,3 galactose residues (α-galactosyl) present on porcine glycoproteins and glycolipids. Currently available immunosuppressive reagents have been largely ineffective at controlling the synthesis of these anti-Gal antibodies. Nonantigenic hapten polymers have been shown to be effective materials for blocking humoral immune responses in various model systems. We have developed a series of α-galactosyl glycoconjugate polymers and tested their ability to block anti-Gal antibody binding in vitro and in vivo. A galactose α1,3 galactose *β* 1,4 GlcNAc trisaccharide free acid (TRFA) with a hexanoic acid spacer, containing five methylene groups and a carboxylic acid, was produced and coupled to a variety of polymeric backbones including dextran, branched poly(ethylene glycol) (PEG), and poly-L-lysine. The ability of monomeric TRFA and the α-galactosyl conjugates to block anti-Gal IgG and IgM binding was determined using a competition ELISA assay on defined HSA−Gal glycoconjugates and porcine microvascular endothelial cell substrates. We show that branched PEG carriers, with a TRFA sugar attached to each branch, exhibit enhanced antibody blocking ability compared to TRFA, but at higher target antigen densities these simple PEG conjugates are no more effective then an equivalent amount of TRFA in blocking anti-Gal IgM antibody interactions. In contrast, polymers of the branched PEG conjugates and linear conjugates made using dextran and poly-L-lysine were 2000 to 70000-fold more effective inhibitors of anti-Gal antibodies. In a study using nonhuman primates, a single dose infusion of polymeric PEG or dextran glycoconjugates dramatically reduced the level of circulating anti-Gal antibodies in cynomologus monkeys for at least 72 h. Glycoconjugates similar to these might be useful both to block anti-Gal interactions in vivo and to specifically control the induced anti-Gal immune response.

INTRODUCTION

Organ transplantation is now widely viewed as the preferred treatment for end stage organ failure, on both a quality of life and overall cost basis. The demand for organs, however, is much greater than the number of people on the transplant waiting list and the availability of human organs is not likely to increase in any significant way over the next few years (Evans et al. 1992; Orians et al. 1993). The shortage of human organs has led to increased interest in both mechanical alternatives and in the use of animals to provide organs for human transplantation, the field of xenotransplantation.

For xenotransplantation, the pig, due to availability, size, and suitability for molecular engineering, is the preferred source of organs. Porcine organs, however, are rapidly rejected after transplantation into primates due to the presence of preexisting primate immunoglobulins that bind to terminal galactose α1,3 galactose residues (α-galactosyl[1]) on porcine glycoproteins and glycolipids (Good et al. 1992; Lin et al. 1997; Neethling et al. 1994; Sandrin et al. 1993; Taniguchi et al. 1996). These antibodies are responsible for initiating hyperacute rejection (HAR), and under conditions that block HAR, the strong induction of anti-Gal antibodies may contribute to the process of acute vascular xenograft rejection (Cotterell et al. 1995; Galili et al. 1997; Kozlowski et al. 1998b; McCurry et al. 1997). The immunosuppressive regimes currently used in transplantation have been largely ineffective at controlling this immune response (Alwayn et al. 1999), suggesting that alternative approaches will need to be developed.

One potential methodology to control preexisting and induced anti-Gal antibodies is through the use of nonantigenic hapten polymers. Peptide and haptens conjugated to immunoglobulins (Borel 1971; Borel and Borel 1988; Borel et al. 1996; Galanaud et al. 1975; Waldschmidt et al. 1983; Zambidis et al. 1997; Zambidis and Scott 1996), lymphocytes (Borel 1980; Cowdery et al. 1982; Li and Scott 1980), and polymeric carrier molecules (Desaymard 1977; Dintzis et al. 1990; Dintzis et al. 1989; Jones et al.

* To whom correspondence should be addressed. Phone: 609-243-0009. Fax: 609-520-1235. E-mail: gbyrne@nextran.com.
† Nextran Inc.
‡ Johns Hopkins University School of Medicine.
§ Present address: Biosphere Medical, Rockland, MA.
|| Baxter Healthcare Corp.

[1] Abbreviations: α-galactosyl, terminal galactose α 1,3 galactose residues; PMVEC, porcine microvascular endothelial cell; TRFA, a galactose α1,3 galactose *β* 1,4 GlcNAc trisaccharide free acid with a five-carbon spacer arm; HAR, hyperacute rejection; HSA, human serum albumin; HSA−Gal, human serum albumin conjugated to α-galactosyl trisaccharide; OVA, ovalbumin.

10.1021/bc015565e CCC: $22.00 © 2002 American Chemical Society
Published on Web 03/26/2002

1994) have been used to establish humoral tolerance in small animal models. Dintzis and colleagues (Dintzis et al. 1990; Symer et al. 1995) demonstrated that dextran−hapten conjugates can block humoral immune responses if the conjugate density and size were carefully controlled. Although the conjugate backbone may vary, this general approach has also been applied clinically to reduce the circulation of anti-dsDNA in patients with systemic lupus erythematosus (Furie et al. 2001; Weisman et al. 1997). As a first step toward exploring the suitability of this approach in xenotransplantation, we have synthesized a series of α-galactosyl glycoconjugates and tested their ability to block anti-Gal antibody binding. A galactose α1,3 galactose β 1,4 GlcNAc trisaccharide with a five-carbon spacer arm and terminal carboxylic acid group (referred to as an hexanoic acid spacer) was coupled to a variety of polymeric backbones including dextran, branched poly(ethylene glycol) (PEG), and poly-L-lysine. All these α-galactosyl conjugates blocked anti-Gal IgG and IgM binding to an HSA−Gal glycoconjugate substrate in an ELISA assay, but the linear dextran, lysine, and polymeric PEG forms exhibited far greater activity than the simpler multivalent PEG conjugates. The in vivo effect of polymeric PEG and dextran conjugates was tested in nonhuman primates. Infusion of these conjugates was well tolerated and resulted in a dramatic reduction of the apparent titer for circulating anti-Gal IgG and IgM for up to 14 days. Compounds similar to these may be an effective method of blocking anti-Gal antibody in vivo, and these materials may have tolerative effects on anti-Gal B-cells that might lead to more profound suppression of the anti-Gal immune response.

MATERIALS AND METHODS

Synthesis of TRFA. Galactose α(1,3) galactose β(1,4) *N*-acetylglucosamine trisaccharide containing a hexanoic acid spacer (TRFA) was produced from glucosamine hydrochloride through a three-step chemoenzymatic synthesis (Figure 1). The overall synthesis consisted of two main steps, the first step being the chemical synthesis of 5-methoxycarbonylpentyl 2-acetamido-2-deoxy-β-D-glucopyranoside and the second step the enzymatic addition of galactose residues to produce 5-methoxycarbonylpentyl-α-D-galactosyl (1,3) β-D-galactosyl (1,4) 2-acetamido-2-deoxy-β-D-glucopyranoside (referred to as the trisaccharide ester). The trisaccharide ester was saponified to produce the final trisaccharide free acid (TRFA).

Synthesis of 5-Methoxycarbonylpentyl 2-Acetamido-2-deoxy-β-D-glucopyranoside. The hydroxyl groups of glucosamine hydrochloride (compound **1**) were protected by acetylation with sodium acetate and acetic anhydride in 1,2-dichloroethane. The peracetylated derivative was a mixture of the two anomers (compounds **2**). This product was not isolated but rather treated in situ with hydrogen chloride gas by bubbling for up to 7 days. The chlorine substitution proceeds with inversion of configuration, reacting only with the β-anomer for steric reasons. The mutarrotation is thus favored and equilibrium displaced until reaction completion resulting in a product with α configuration. The reaction was sequentially extracted with cold sodium bicarbonate and cold water and the organic phase dried with anhydrous magnesium sulfate. The filtrate was washed with 1,2-dichloroethane, dried, dissolved in dichloromethane, and mixed with ethyl ether and hexane. This mixture was cooled and left to crystallize. The solid was washed with hexane and dried under vacuum to give 2-acetamido-2-deoxy-α-D-glucopyranosyl chloride (compound **3**). The identity of this intermediate was confirmed by ^{1}H NMR

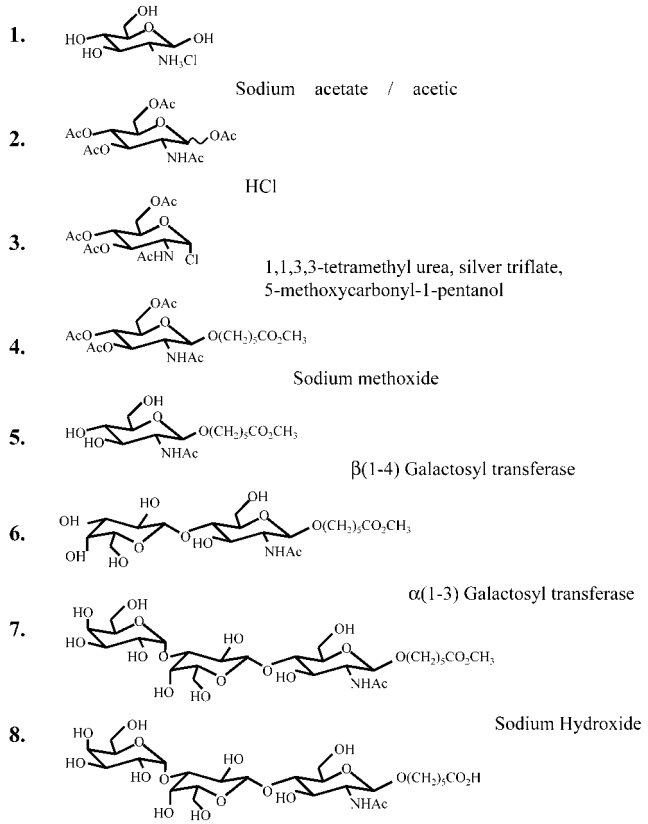


Figure 1. The starting material, glucosamine hydrochloride (compound **1**), and intermediate compounds (**2**−**7**) produced during the synthesis of galactose α(1,3) galactose β(1,4) *N*-acetylglucosamine trisaccharide containing a hexanoic acid spacer are depicted. The primary reactants used in each successive reaction are also indicated.

($CDCl_3$): δ 6.18 (1H, d, $J_{1,2}$ = 3.67 Hz, H-1), 5.32 (1H, t, $J_{3,4}$, $J_{4,5}$ = 10.62 Hz, H-4), 5.21 (1H, t, $J_{2,3}$, $J_{3,4}$ = 9.89 Hz, H-3), 2.10, 2.05, 1.98 (9H, 3s, OCOCH_3). The hexanoic acid spacer was added to the intermediate using 5-methoxycarbonyl-1-pentanol with 1,1,3,3-tetramethylurea and silver triflate in dichloromethane under the conditions of the Koenigs−Knorr glycosylation method. The reaction was filtered through a Celite 521 filter agent, and the filter cake was washed with dichloromethane. The filtrate was sequentially washed with concentrated HCl, sodium bicarbonate, and deionized water, and the organic phase was dried over sodium sulfate overnight. After filtration, the solids were dissolved in dichloromethane and mixed with ethyl ether and hexane for crystallization at −20 °C for 36−72 h. This intermediate glycoside (compound **4**) was analyzed by ^{1}H NMR where the conjugation of the hexanoic spacer was confirmed by the multiple peaks between 1.3 and 1.8 ppm. This material was deacetylated in methanol using sodium methoxide and neutralized with a Dowex 50 WX 8−200 resin to produce the monosaccharide ester 5-methoxycarbonylpentyl 2-acetamido-2-deoxy-β-D-glucopyranoside (compound **5**). The regiospecificity of the reaction was confirmed by checking the purity of compound **5** by ^{1}H NMR spectroscopy. The spectrum was compared to that of model compounds found in the literature, and the identity of this product was confirmed by ^{1}H NMR (D_2O): δ 4.45 (1H, d, $J_{1,2}$ = 8.06 Hz, H-1), 3.64 (3H, s, OCH_3), 2.38 (2H, t, CH_2CH_2-COOMe), 1.98 (3H, s, OCOCH_3), 1.56 [6H, m, $(CH_2)_3$]. The conversion of glucosamine hydrochloride (compound **1**) to the monosaccharide ester (compound **5**) results in an overall yield of 18−23% on a 2.0 kg scale.

Enzymatic Addition of Galactose. Galactose was added to monosaccharide ester by coupled enzymatic addition using β-(1,4)-galactosyltransferase, UDP-galactose-4-epimerase, pyruvate kinase, UDP-glucose pyrophosphorylase, phosphoenol pyruvate, glucose-1-phosphate, and UDP to produce the disaccharide (compound **6**). This β-galactosyltransferase cycle continued for 6−8 days until 90−95% complete as determined by TLC on silica gel. After this reaction, the material was filtered through an Alsop pad, a 1.0 mm filter, and a 10K spiral wound membrane. The pH of the solution was adjusted to 7.3−7.6 and supplemented with additional glucose-1-phosphate, UDP, pyruvate kinase, UDP-glucose pyrophosphorylase, UDP-galactose-4-epimerase, and α(1,3)-galactosyltransferase to initiate formation of the α-galactosyl trisaccharide ester (compound **7**). After this enzymatic reaction, the material was treated as described above, diafiltered over a polysulfone membrane against water, and treated with Dowex 50 WX8−200 to remove salts and ions, and the identity of compound **7** was confirmed by ^{1}H NMR in D_2O: δ 1.20−2.30 (m, 6H, $(CH_2)_3$); 2.01 (s, 3H, OAc); 2.39 (t, 2H, $CH_2C{=}O$); 3.68 (s, 3H, OCH_3); 4.47 (d, 1H J = 10.3 Hz, β-anomeric); 4.50 (d, 1H, J = 10.1 Hz, β-anomeric); 5.13 (d, 1H, J = 3.9 Hz, α-anomeric). The trisaccharide ester was converted to the final trisaccharide free acid (TRFA, compound **8**) by reacting with a molar excess of 6 N sodium hydroxide.

The enzymes β (1,4)-galactosyltransferase (secreted bovine form expressed in mouse myeloma), α (1−3)-galactosyltransferase (recombinant form from murine source expressed in mouse myeloma cells), and UDP-Gal-4-epimerase (recombinant form from *Streptococcus termophilus* overexpressed in *E. coli*) were produced at Nextran (San Diego, CA). Pryuvate kinase was obtained from Roche (Indianapolis, IN) and UDP-glucose pyrophosphorylase (from bakers' yeast) from Sigma (St. Louis, MO). The D-glucose-1-phosphate disodium salt was from Genzyme (Boston, MA). All other chemicals were obtained from commercial sources in reagent pure grade.

^{1}H Nuclear Magnetic Resonance Spectroscopy. The α-galactosyl trisaccharide acid was repeatedly exchanged in D_2O (99.96%, Aldrich Chemical Co.) with intermediate lyophilization, and finally dissolved in 500 μl of 99.996% D_2O. Spectra were recorded on a Varian JEOL 400 MHz NMR spectrometer at Acorn Inc. (Livermore, CA). Line-broadening (0.2 Hz) was applied to 1D spectra. Chemical shifts were measured relative to the residual HOD peak at 4.80 ppm. Spectral peak assignments were made by comparing the results with data in the literature and with the standard compounds. Determination of TRFA content by NMR was done by adding a known quantity of 1,2-*O*-isopropylidene-α-D-glucofuranose as internal standard and the area of the doublet at ∼5.16 ppm, corresponding to H-1 of α-galactofuranose, compared to that of the doublet of the anomeric proton of TRFA, to calculate their relative molar ratio.

HPLC Chromatography. Evaluation of TRFA content and purity was done by hydrophilic interaction chromatography using a Polyglycoplex column. The TRFA was resolved from sample impurities using 100% of solvent A (20% of 37.5 mM ammonium acetate buffer (pH 6.0) in acetonitrile, v/v) for 5 min, followed by a 5 min linear gradient to 20% of solvent A/80% of solvent B (37% of 20.3 mM ammonium acetate buffer (pH 6.0) in acetonitrile, v/v), and a final isocratic step maintaining the previous concentration for 20 min. The column was washed and reequilibrated to yield a total run time of 40 min. An injection volume of 50 μL was used at a nominal concentration of 100 mg/mL. The flow rate was 1 mL/min. Detection was accomplished using an Alltech ELSD 500 detector (temp = 95 °C; nitrogen flow = 2.00 slpm; ATTN = 1). The limit of quantitation of this method was 50 μg on column.

Fast-Atom Bombardment and Electrospray-Ionization Mass Spectrometry. The molecular weight of TRFA was evaluated by FAB-MS and ESI-MS (M-Scan Inc). FAB-MS was done using a VG Analytical ZAB 2SE high field mass spectrometer. A cesium ion gun was used to generate primary ions used to bombarded the sample dissolved in distilled water and contained in the stainless steel probe mixed with glycerol/thioglycerol as the matrix. Secondary ions were recorded in the positive mode. Mass calibration was done using cesium iodide. ESI-MS was performed using a VG Biotech Bio-Q mass spectrometer with quadrupole analyzer.

Synthesis of α-Galactosyl Conjugates. All conjugates were produced using the α-galactosyl trisaccharide acid (TRFA). The Dex40 conjugate was produced using Dextran-amine (Molecular Probes) and TRFA in 100 mL reactions containing 100 mM MES (pH 5.5) 12.5 mg/mL TRFA, 10 mg/mL dextran-amine and 25 mg/mL 1-(3-dimethylaminopropyl)-3-ethylcarbodiimide hydrochloride (EDC). The reaction mixture was incubated at room temperature overnight and then extensively dialyzed to distilled water, lyophilized, and resuspended at 50 mg/mL in sterile saline. Synthesis of a poly-L-lysine conjugate (PLL300) was performed in a similar manner using 20 mL of 100 mM MES (pH 5.5) 15 mg/mL TRFA, 10 mg/mL poly-L-lysine (Sigma), and 70 mg/mL of EDC. The reaction mixture was incubated at room temperature overnight and then extensively dialyzed to distilled water, lyophilized, and resuspended at 50 mg/mL in sterile saline.

An eight-branched poly(ethylene glycol) conjugate (Nex1205) was produced using TRFA and EDC. A reaction mixture containing 100 mg/mL of branched PEG-amine (Shearwater), 106 mg/mL of TRFA, and 80 mg/mL EDC in MES (pH 5.5) was stirred for 1 h at room temperature. Additional EDC was added for a final concentration of 160 mg/mL and incubated overnight. Synthesis of the four branched PEG conjugate (Nex8507) was the same except that half the concentration of TRFA and EDC was used. The reaction was dialyzed through a 3K membrane against distilled water, lyophilized, and resuspended at 50 mg/mL in saline. Polymerized branched PEG conjugates (Nex8587 and Nex1285) were produced in a reaction containing 50 mg/mL of four or eight branched PEG amine, 28 mg/mL of *N*-hydroxysulfosuccinimide (NHSS), 250 mg/mL EDC, and 60 mg/mL of TRFA. The reaction was shaken overnight on a rotary shaker and dialyzed, lyophilized, and resuspended at 50 mg/mL in saline.

HSA glycoconjugates with variable TRFA densities were produced by conjugating TRFA to HSA using NHSS and EDC. The general reaction conditions consisted of mixing 16 mL of cold 200 mM Tris (pH 6.5) containing 1 g of HSA (Sigma) with 4 mL of 100 mM MES (pH 5.5) containing 80 mg/mL NHSS and 37.5 mg/mL EDC. The mixture was reacted at 4 °C temperature for 4 h on a rotory shaker, and the reaction was stopped by the addition of 4 mL of 1 M Tris (pH 8,5). The conjugates were dialyzed through 10K membranes against distilled water and lyophilized. Increased TRFA densities were produced by increasing the amount of EDC in the reaction. The average TRFA density in each conjugate was determined by mass spectroscopy, and each conjugate was examined by SDS−PAGE silver stained gels

and anti-Gal western blots to detect the presence of intermolecular cross linking.

Light Scattering Determination of Molecular Weight. Glycoconjugate samples containing 10−20 mg/mL in 0.15 M phosphate buffer, pH 7.2 were injected into a Superose 12 HR 10/30 high-resolution gel filtration column (Amersham Pharmacia Biotech, Piscataway, NJ). The column was pumped at 0.5 mL/min with the same phosphate buffer. The effluent flowed online directly into a capillary light-scattering cell of a Wyatt Dawn DSP light-scattering instrument (Wyatt Technology Corp. Santa Barbara, CA) and from there directly into a Hewlett-Packard 1037A refractive index detector. Data from both the light-scattering detectors (measured at 15 different angles by separate diode detectors) and the refractive index detector were recorded online by a Dell Optiplex GX1 microcomputer, using Wyatt Astra software for Windows version 4.723. The same system was calibrated against monomeric bovine serum albumin (Sigma) as a standard for determining absolute molecular weight distributions of the glycoconjugates.

Determination of α-Galactose Content. The ratio of galactose and *N*-acetylglucosamine in TRFA was determined after exhaustive acid hydrolysis using a DX500 HPLC equipped with an ED40 pulsed amperometer (Dionex Corp., Sunyvale, CA). Acid hydrolysis was performed on 100 μL of 0.1 M TRFA mixed with an equal volume of 4 M trifluoroacetic acid and hydrolyzed at 100 °C for 3 h. The material was evaporated to dryness in a Speed Vac, and residual TFA was removed by adding 100 μL of methanol and then drying in the Speed Vac. Finally the sample was resuspended in 1 mL of Nanopure water. A high-pH anion-exchange chromatography method using a CarboPac PA1 column (Dionex) coupled to the pulsed amperometer detector (HPAEC_PAD) was developed to resolve galactose and *N*-acetylglucosamine. The column was run at 1 mL/min, and the sample was eluted by an isocratic step with 40 mM sodium hydroxide. This system provided excellent resolution of the samples and could typically detect 5−10 pmol of each carbohydrate.

The amount of α-linked galactose present in the TRFA and glycoconjugates was also determined using α-galactosidase (Sigma) and galactose dehydrogenase (Roche). The assay was adapted from a commercially available kit (Boehringer) for quantifying lactose levels (Huber et al. 1975). The α-linked galactose residues are hydrolyzed by α-galactosidase to release D-galactose. In the presence of NAD and galactose, galactose dehydrogenase produces galactonic acid and NADH. The amount of NADH produced is determined by absorbance at 340 nm and is stoichiometric to the amount of galactose in the reaction.

Inhibition and Competition ELISA Assay. To estimate the ability of TRFA and glycoconjugates to block anti-Gal antibody binding, an ELISA-based assay measuring inhibition of nonhuman primate anti-Gal antibody was developed. Pooled baboon serum was diluted 1:120 into phosphate-buffered saline (PBS) with 1% HSA containing serial dilutions of TRFA or glycoconjugates and incubated for 30 min at room temperature. Samples were then placed in 96-well microtiter plates previously coated with 30 μg/mL of an HSA−Gal conjugates with the specified antigen density. For most of our analysis the HSA−Gal ELISA substrates contained on average four ($HSA-Gal_{(4)}$) or eight ($HSA-Gal_{(8)}$) TRFA epitopes for each protein monomer. Serum samples containing α-galactosyl conjugates were incubated in 96-well plates for 1.5 h at 4 °C and washed, and the amount of anti-Gal binding was determined by colorometric assay using biotin-conjugated goat anti-Human IgM or IgG (Zymed) and alkaline phosphatase-conjugated streptavidin. The degree of inhibition was determined by the formula $(OD_{total} - \text{sample } OD_{inh})/OD_{total}) \times 100$ where the OD_{total} is the optical density observed in the absence of inhibitor and the OD_{inh} is the optical density measured in the presence of TRFA or the glycoconjugate.

Antibody inhibition was also determined using 96-well plates containing porcine microvascular endothelial cells (PMVEC) as described (Platt et al. 1990). Cells were grown in Medium 199 (Gibco) supplemented with endothelial cell growth supplement (30 mg/mL), Heparin (4000 U/mL), and 10% FBS (Hyclone). At confluence the cells were fixed with 1% gluteraldehyde for 5 min, washed with PBS, and stored at −80 °C until used. To measure antibody inhibition, plates were blocked in PBS with 1% ovalbumin (OVA) and 0.1% Tween 20 at room temperature. Serum samples were preincubated for 30−60 min at room temperature in 1% OVA/PBS, with serial dilutions of TRFA or α-galactosyl conjugates in 1%OVA/PBS. Samples were added to the PMVEC ELISA plates in duplicate, and the plates were incubated for 90 min at 4 °C. Biotin-conjugated goat anti-human IgM or IgG (Zymed) diluted 1:1000 in 1% OVA /PBS was used to label bound antibody and alkaline phosphatase-conjugated streptavidin (Zymed 43−4322) diluted 1:3000 to quantify the level of activity.

An assay to detect the presence of the Nex1285 conjugate in serum was also developed. This assay measured the inhibition by Nex1285-containing serum of biotinylated human anti-Gal antibody binding to $HSA-Gal_{(8)}$-coated ELISA plates. The amount of biotinylated human anti-Gal antibody was selected to give an optical density reading of approximately 1.0 in the absence of any inhibition. A reference standard of Nex1285 (200 μg/mL) and serum samples containing Nex1285 were serially diluted into PBS containing 1% HSA. Equal volumes of serum and biotinylated human anti-Gal antibody (5 μg/mL) were mixed, incubated for 30 min at ambient temperature, and transferred to $HSA-Gal_{(8)}$-coated plates. After 1 h incubation, the plates were washed and the amount of anti-Gal antibody binding determined using alkaline phosphatase-conjugated streptavidin. The amount of Nex1285 was calculated by comparison to the reference standard.

Conjugate Infusion Studies. Groups of three cynomologus monkeys (*Macaca fascicularis*) were infused with the α-galactosyl conjugates Nex8507, Nex8587, Nex1285, and Gal−Dex−FITC or with unconjugated PEG or dextran controls at a dose of 100 mg/kg. All animals were previously equipped with surgically implanted chronic venous catheters and vascular access ports to facilitate infusion and blood collection. The test materials were prepared in normal saline and infused over a 15−60 min period. Blood samples were collected prior to the start of the infusion and at 5 and 10 min after the beginning the infusion. Additional samples were collected at 5, 10, 20, and 30 min and 1, 2, 4, 6, 8, 12, 24, 48, 72, and 336 h after completion of the infusion. Animals were individually housed and observed for clinically relevant abnormalities during infusions and at each sample collection. The experiments were conducted in accordance with NIH guidelines for Care and Use of Laboratory Animals.

RESULTS

Characterization of TRFA. An α-galactosyl trisaccharide free acid (TRFA) containing a five-carbon spacer with a carboxy terminus was prepared following the

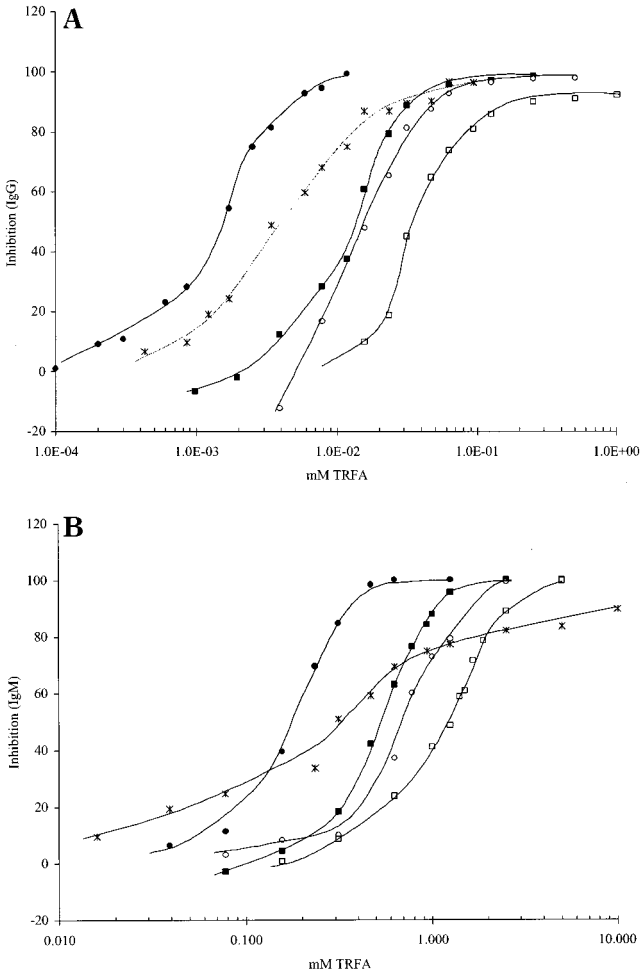


Figure 2. The inhibition of anti-Gal IgG and IgM by free α-galactosyl trisaccharide. The inhibitory effects of TRFA was determined in a competition ELISA using PMVEC cells (*) and HSA−Gal substrates containing an average α-galactosyl content of four (●), eight (■), 13 (○), and 21 (□) residues per mole. Baboon serum diluted 1:120 was mixed with α-galactosyl trisaccharide for 30 min at room temperature and then applied to the ELISA plate. A. Inhibition of anti-Gal IgG. B. Inhibition of anti-Gal IgM. Lines for this and other graphs are freehand approximations to the data.

described chemoenzymatic synthesis. This material was lyophilized, and samples were characterized by NMR, FAB-MS, ESI-MS, HPLC, and hydrolysis with α-galactosidase. The TRFA was a white powder with typical moisture content of 2.8−5.5%. Structural analysis done using ^{1}H NMR identified characteristic protons including the α-anomeric proton of galactopyranose (5.135 ppm; d, 1H, $J = 3.9$ Hz), the β-anomeric protons of galactopyranose, and 2-acetamido-2-deoxy-D-glucopyranose, at 4.47 ppm (d, 1H, $J = 10.3$ Hz) and 4.50 ppm (d, 1H, $J = 10.1$ Hz), respectively. The presence of the alkyl chain was confirmed by the methylene multiplet at ∼1.59 ppm corresponding to the internal methylene groups in the chain, by the triplet at 2.368 ppm corresponding to the methylene group contiguous to the ester, and by the multiplet at ∼1.34 ppm corresponding to the methylene group directly attached to the monosaccharide. The methyl signal of the *N*-acetyl group was at 2.023 ppm. The expected molecular weight of TRFA was 660 Da, and this was confirmed by FAB-MS and ESI-MS analysis that showed a quasimolecular ion cluster, $(M + H)^+$ at *m*/*z* 660 with the corresponding $(M + Na)^+$ cluster at *m*/*z* 682. This analysis also detected ions at *m*/*z* 336, 399, 498, and 528, and these may be associated fragments. On the basis of hydrophilic interaction chromatography using a Polyglycoplex column, with comparison to known reference standards, TRFA synthesis typically yielded material with a purity between 98% and 100%. The ratio of galactose to *N*-acetylglucosamine in TFRA was analyzed by HPAEC−PAD after complete acid hydrolysis and indicated the expected Gal:GlcNAc ratio of 2:1. Consistent with this finding, TRFA was readily hydrolyzed by α-galactosidase and yielded 1.49 mM of hydrolyzed galactose per gram of TRFA. This value was slightly less than the 1.51 mM per gram expected from a pure preparation but was entirely consistent with our physical analysis and the estimated purity of 98%.

Table 1. Inhibition of Anti-Gal Antibody on PMVEC and Variable Density HSA Conjugates[a]

conjugate density	IgG IC_{50} (mM TRFA)	IgG fold change	IgM IC_{50} (mM TRFA)	IgM fold change	IC_{50} ratio IgM/IgG
4	0.0016	1.0	0.184	1.0	118.2
8	0.0138	8.8	0.528	2.9	38.3
9	0.0129	8.2	0.490	2.6	38.1
13	0.0166	10.6	0.713	3.9	43.0
17	0.0338	21.7	1.078	5.9	31.9
21	0.0352	22.6	1.272	6.9	36.2
PMVEC	0.00367	2.4	0.308	1.7	84.0

[a] The table presents the concentration of α-Gal trisaccharide free acid (TRFA) required to inhibit 50% of anti-Gal IgG and IgM binding in baboon serum to a series of human serum albumin conjugates with different levels of α-Gal incorporation and to fixed porcine microvascular endothelial cells. Inhibition of IgG and IgM is also presented as a normalized fold change and as an IC_{50} ratio to illustrate the increased amounts of sugar required to inhibit antibody binding to higher density antigen substrates and to compete different antibody isotypes.

Inhibition of Anti-Gal Antibodies on Glycoconjugates and PMVECs. Anti-Gal antibodies binding from baboon serum in the presence of serial dilutions of TRFA was measured on HSA−Gal conjugates with 4 to 21 sugar residues per mole of protein and on fixed porcine microvascular endothelial cells (PMVEC). The amount of TRFA required to block antibody binding depended on the antibody isotype and the antigen density in the ELISA (Figure 2 and Table 1). At low antigen density anti-Gal IgG and IgM were more easily blocked compared to higher density substrates. For example, in an ELISA using the HSA−$Gal_{(4)}$ conjugate, half the anti-Gal IgG binding was inhibited by 1.6 μM of TRFA, but equivalent inhibition at higher antigen density required approximately 20-fold more TRFA. Similarly blocking anti-Gal IgM binding to high density substrates required approximately 7-fold more TRFA than needed to block antibody binding to HSA−$Gal_{(4)}$. A ratio of the TRFA concentrations required to inhibit 50% of the anti-Gal IgM and IgG binding illustrates the effects of isotype on anti-Gal inhibition. Anti-Gal IgM required more TRFA to inhibit binding than did IgG. Although this was most apparent at low antigen density, where over 100 fold more TRFA was required to block anti-Gal IgM compared to IgG, inhibition of anti-Gal IgM required 30−40-fold more TRFA at all of the antigen densities tested.

Anti-Gal antibody binding to PMVEC cells could also be blocked using TRFA and showed the same isotype dependence observed using the synthetic HSA conjugates. Blocking anti-Gal IgG binding to PMVEC cells was more sensitive to TRFA inhibition than IgM which required more then 80-fold more sugar to inhibit antibody binding. Half of the anti-Gal binding to PMVEC cells could be blocked by 3.7 μM TRFA for IgG or 0.31 mM of

Table 2. Characterization of α-Galactosyl Sugar and Sugar Conjugates[a]

material	structure	mM α-Gal (gram)	MW	IC_{50}(4) IgG	IC_{50}(8) IgG	IC_{50}(4) IgM	IC_{50}(8) IgM
TRFA	monomer	1.49 (1.5)	660 (99.0)	0.0044 (1.0)	0.0175 (1.0)	0.1906 (1.0)	0.6220 (1.0)
Nex8507	branched	0.32 (0.316)	5000−30000 (98.7)	1.0×10^{-4} (44.2)	2.1×10^{-3} (8.4)	0.0516 (3.7)	0.825 (0.7)
Nex1205	branched	0.48 (0.523)	5000−50000 (97.6)	8.2×10^{-5} (53.6)	4.7×10^{-4} (37.5)	6.3×10^{-3} (30.1)	0.655 (0.9)
Gal-PLL(300)	linear	0.42 (na)	15000−300000 (98.3)	1.0×10^{-5} (443.8)	8.8×10^{-5} (198.0)	1.4×10^{-5} (13484)	6.2×10^{-5} (10010)
Dex40	linear	0.24 (na)	30000−1000000 (97.7)	5.2×10^{-6} (848.7)	5.6×10^{-5} (313.4)	2.7×10^{-6} (71784)	1.1×10^{-4} (5825)
Nex8587	branched polymerized	0.23 (na)	5000−100000 (98.6)	4.8×10^{-5} (91.5)	7.9×10^{-4} (21.9)	1.3×10^{-3} (148.6)	0.249 (2.5)
Nex1285	branched polymerized	0.28 (na)	10000−1000000 (98.7)	2.2×10^{-5} (202.3)	2.2×10^{-4} (79.0)	2.5×10^{-6} (77104)	8.6×10^{-5} (7270)

[a] The table lists each conjugate, its general structure, α-galactosyl content molecular weight distribution, and IC_{50}. The α-galactosyl content (mM α-galactosyl TRFA per gram) was determined using α-galactosidase. This value was used to standardize all of the antibody blocking studies. For the branched PEG conjugates (Nex8507 and Nex1205) the expected amount of α-galactosyl is based on an idealized molecule of 10kDa with four or eight branches. The molecular weight distributions are based on light scatter analysis. The range in molecular weight and the percentage of the conjugate that falls in that range (parenthesis) is given. The IC_{50} values were calculated from ELISA assays using HSA−$Gal_{(4)}$ and HSA−$Gal_{(8)}$. The fold change in IC_{50}, in parentheses, relative to TRFA is indicated for each conjugate.

TRFA for IgM. These values were similar to the amounts of TRFA required to block IgG and IgM binding to HSA−Gal conjugates containing four or eight sugar residues per mole of protein. While these conjugates may be a good average estimation of antibody binding to PMVEC cells, the broad inhibition profile observed for PMVEC cells compared to the sharper sigmoidal profiles for the conjugates (Figure 2) suggests that the cell display a wide variety of antigen densities. This was particularly evident for anti-Gal IgM where the glycoconjugate substrates may underestimate the influence of high density α-galactosyl epitopes present on PMVEC cells. Persistent anti-PMVEC IgM binding in the presence of high amounts of TRFA is likely due to the presence of non-Gal antibodies in our pooled serum samples.

Characterization of α-Gal Conjugates. A series of α-galactosyl glycoconjugates were produced to investigate the effects of α-galactosyl density and oligomerization on the ability to block antibody binding. The conjugates used different chemical backbone structures and ranged widely in molecular weight. Three broad classes of α-galactosyl conjugates were produced. To examine the effects of multimeric TRFA, simple branched PEG conjugates containing four or eight branches with each branch capped by a TRFA molecule were produced. A second class of conjugates used the linear backbones of dextran or poly-L-lysine. These linear conjugates were produced to examine the effects of increased molecular size and highly repetitive presentation of TRFA on antibody blocking. Finally polymerized versions of the branched PEG conjugates were produced to directly compare the effects of increased conjugate size on antibody blocking. To gauge the activity of each α-galactosyl conjugate relative to monomeric TRFA, all of the materials were standardized based on the amount of trisaccharide available for hydrolysis by α-galactosidase. We focused our in vitro antibody inhibition analysis on ELISAs using HSA−Gal conjugates that contain four or eight sugars per mole of protein, since these conjugates reasonably estimated antibody binding to PMVEC cells.

Simple poly(ethylene glycol) based glycoconjugates with four or eight branches were produced by coupling the carboxylic acid group of TRFA to primary amines on the terminus of each PEG branch. This conjugation produced a peptide bond attaching an α-Gal trisaccharide sugar to each branch of the PEG backbone. Light scattering analysis of glycoconjugates containing four or eight branches (Nex8507 and Nex1205) exhibited an average molecular weight distribution consistent with the expected conjugation of one TRFA sugar to each branch of the carrier. The polydispersity (Mz/Mn) of the Nex8507 and Nex1205 conjugates was similar to the distribution of the starting material, consistent with the absence of polymerization (data not shown). Hydrolysis of these conjugates with α-galactosidase yielded 0.32 and 0.48 mM TRFA per gram of Nex8507 and Nex1205, respectively (Table 2), similar to the expected molar concentration of TRFA in an idealized conjugate.

On the basis of available free trisaccharide, the branched PEG conjugates were 40- to 50-fold more effective at inhibiting anti-Gal IgG compared to TRFA when assayed against the low antigen density HSA−$Gal_{(4)}$ (Figure 3A, Table 2). The effectiveness of anti-Gal IgG blocking was reduced, however, at higher antigen density particularly for the four-branched conjugate Nex8507 which blocked anti-Gal IgG only 8-fold more effectively than TRFA (Figure 3C). Anti-Gal IgM binding was more difficult to inhibit and like TRFA, the branched PEG conjugates required more material to effectively block anti-Gal IgM (Figure 4A and C). Although the NEX1205 conjugate with eight branches was up to 30-fold more effective at blocking anti-Gal IgM in the HSA−$Gal_{(4)}$ ELISA at higher antigen density this conjugate and the four-branched conjugate (NEX8507) were indistinguishable from TRFA (Figure 4C, Table 2).

To investigate the role that larger glycoconjugate structures with more repetitive presentation of TRFA might have on antibody inhibition, we produced linear α-galactosyl conjugates using dextran (Dex40) and poly-L-lysine (PLL300) as the backbone. The sugar was coupled to these long linear conjugates through a peptide bond, resulting in an average of one TRFA epitope every 12 (PLL300) or 19 (Dex40) residues, similar to the overall TRFA content present in the branched PEG conjugates. Due to their increased size, however, the linear conjugates contained a far greater number of sugar epitopes per molecule than the four- and eight-branched PEG conjugates. The linear conjugates inhibited anti-Gal IgG binding to both HSA−$Gal_{(4)}$ and HSA−$Gal_{(8)}$ (Figure 3B and 3D). The effectiveness of this inhibition was approximately 16-fold greater than the inhibition observed for Nex1205 (Table 2) with the larger Dex40 exhibiting

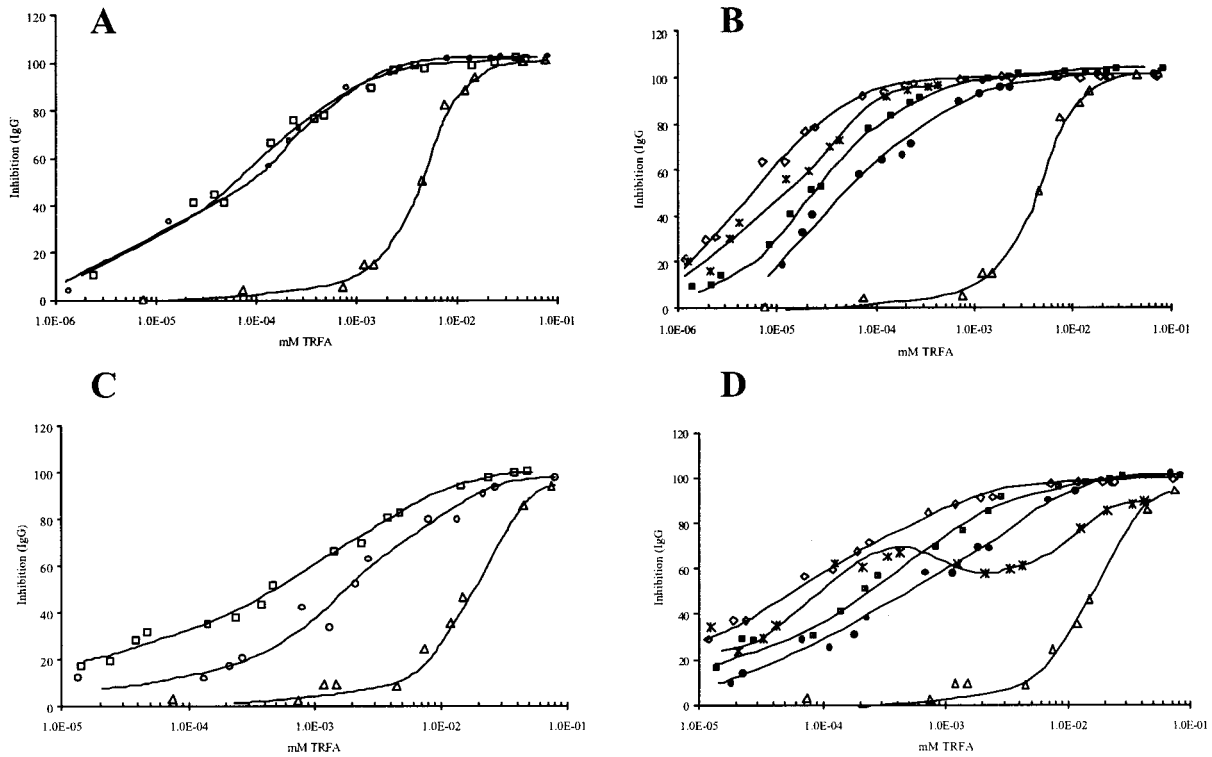


Figure 3. Inhibition of anti-Gal antibodies by TRFA and α-galactosyl conjugates. Anti-Gal IgG inhibition was determined using an HSA−$Gal_{(4)}$ (A and B) or HSA−$Gal_{(8)}$ (C and D) ELISA substrate for TRFA (△) and conjugates NEX8507 (○), NEX1205 (□), PLL300 (*), Dex40 (◇), NEX8587 (●), and NEX1285 (■). For clarity, the inhibition profiles for the simple branched conjugates (A and C) are separated from the linear and polymeric conjugates (B and D). The concentration of trisaccharide sugar and each conjugate was standardized based on their α-galactosyl content as determined by α-galactosidase hydrolysis. Each test sample was added to a 1:120 dilution of normal baboon serum and incubated at room temperature for 30 min. The mixtures were assayed for antibody binding on ELISA plates containing an HSA−Gal conjugate with four TRFA molecules per protein. Inhibition is expressed as the percentage of antibody binding relative to serum without added α-galactosyl sugar of conjugated materials.

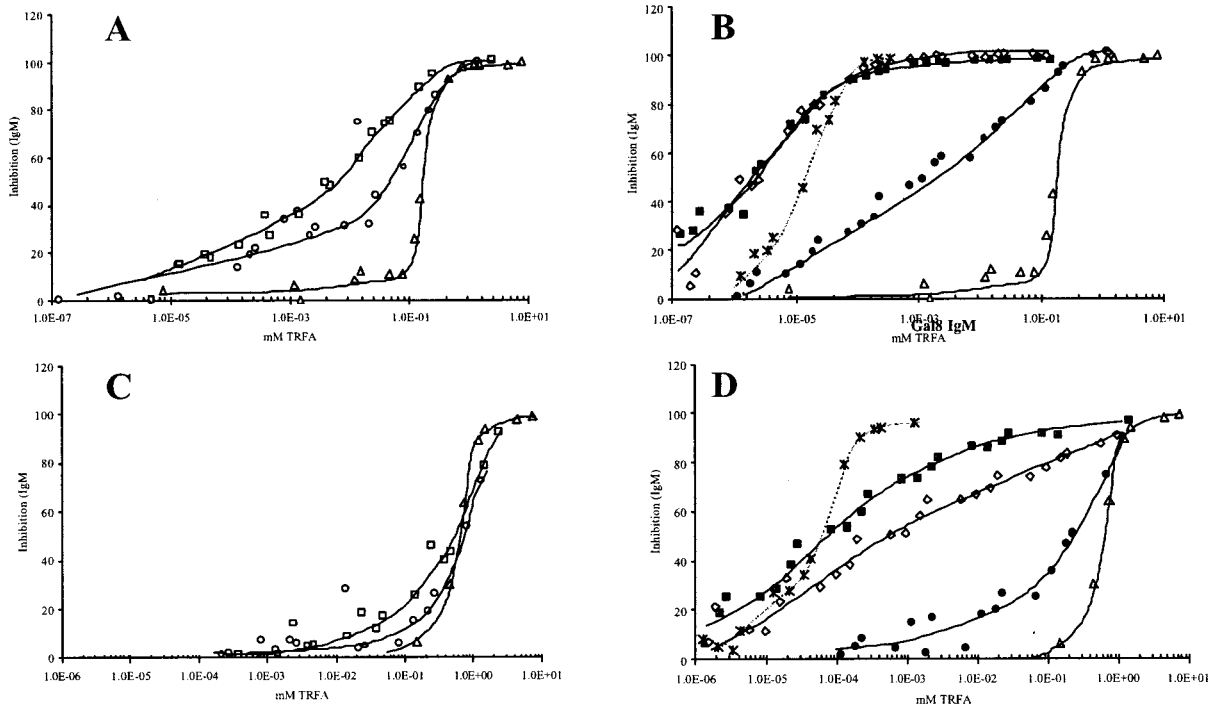


Figure 4. Inhibition of anti-Gal IgM antibodies by TRFA and α-galactosyl conjugates. Symbols are the same as described in Figure 2. Inhibition was determined using an HSA−$Gal_{(4)}$ (A and B) of HSA−$Gal_{(8)}$ (C and D) ELISA substrates. As in Figure 2 the branched conjugates (A and C) are shown separate from the linear and polymeric conjugates (B and D).

the highest inhibition at either antigen density. Both the Dex40 and PLL300 were highly effective inhibitors of anti-Gal IgM, exhibiting 13000 to 70000-fold greater inhibition than TRFA at low antigen density and 5000 to 10000-fold greater activity against the higher antigen density (Figure 4B and 4D; Table 2). Although the

α-galactosyl content of Dex40 was approximately half that observed for eight-branched Nex1205, Dex40 was 2000 to 6000-fold more effective than Nex1205 at inhibiting anti-Gal IgM (Table 2). The PLL300 conjugate was also highly effective at blocking anti-Gal IgM antibody in our ELISA assays, and this conjugate, perhaps due to the higher content of α-galactosyl residues, maintained its ability to block anti-Gal IgM, even at the higher antigen density. Unlike the other conjugates, however, antibody inhibition by PLL300 often exhibited erratic effects at concentrations above 1.2 μM TRFA (approximately 3.0 μg/mL of polymer).

The linear α-galactosyl conjugates were clearly much more effective at blocking anti-Gal IgM than the smaller branched PEG conjugates. Since both types of conjugates had a similar content of α-galactosyl sugar, we thought that the enhanced ability of linear conjugates to block IgM was likely to result from the structural difference between the conjugate types. For example, the linear conjugates might more effectively engage the pentameric anti-Gal IgM binding sites whereas the smaller branched conjugates might only bind to one or two antigen binding sites within an antibody. To investigate this further we polymerized the branched PEG conjugates into higher order structures using EDC and NHSS. Details of this reaction are under investigation but there is evidence of Peg-to-Peg, Peg-to-TRFA and TRFA-to-TRFA cross-linking in the final polymerized products, Nex8587 and Nex1285. Due to this intermolecular cross-linking, these conjugates exhibited much wider size distributions than either the original PEG amine or the simple branched Nex8507 and Nex1205 conjugates (Table 2). The Nex8587 and Nex1285 conjugates had comparable α-galactosyl content but were approximately half that observed in Nex1205 and essentially equal to the level of Dex40. These polymerized conjugates inhibited anti-Gal IgG binding at a level that was 20−200-fold more effective than TRFA (Figure 3B and 3D). The Nex1285 conjugate was similar to Dex40 in its ability to block anti-Gal IgM exhibiting 7000−70000-fold more effective antibody inhibition than TRFA depending on the ELISA substrate. In contrast the Nex8587 conjugate behaved more like the branched Nex1205 conjugate and was only 2-fold more effective than TRFA at inhibiting anti-Gal IgM against the high-density substrate (Figures 4B and 4D).

Antibody Inhibition in Primates. The polymerized PEG and linear α-galactosyl conjugates exhibited a dramatic improvement in antibody inhibition in our inhibition ELISA. To investigate if these conjugates would be effective at blocking antibody in vivo, we administered a single bolus infusion (100 mg/kg) to sets of three cynomologus monkeys for each conjugate (Figure 5A and 5B). The conjugates were infused over a 15−60 min period and serum samples were taken over a three-day period to estimate the clearance rate of the conjugate and to examine the effects on anti-Gal antibody. A follow-up serum sample, 14 days after infusion was also examined. To facilitate our analysis, a Gal−Dex−FITC conjugate was used in this study. This material contained just less than one FITC fluorochrome per mole and had an α-galactosyl density of one sugar every eight residues. This material had a smaller size distribution (97% within 10000 to 100000 Da) than the Dex40 previously described and was not as effective an inhibitor of anti-Gal IgM. All of the PEG conjugates were the same as described in Table 2. Infusion of control unconjugated PEG or dextran had no effect on circulating anti-Gal antibody levels (data not shown). In contrast, from the onset of infusion and for up to 30 min postinfusion all of the conjugates

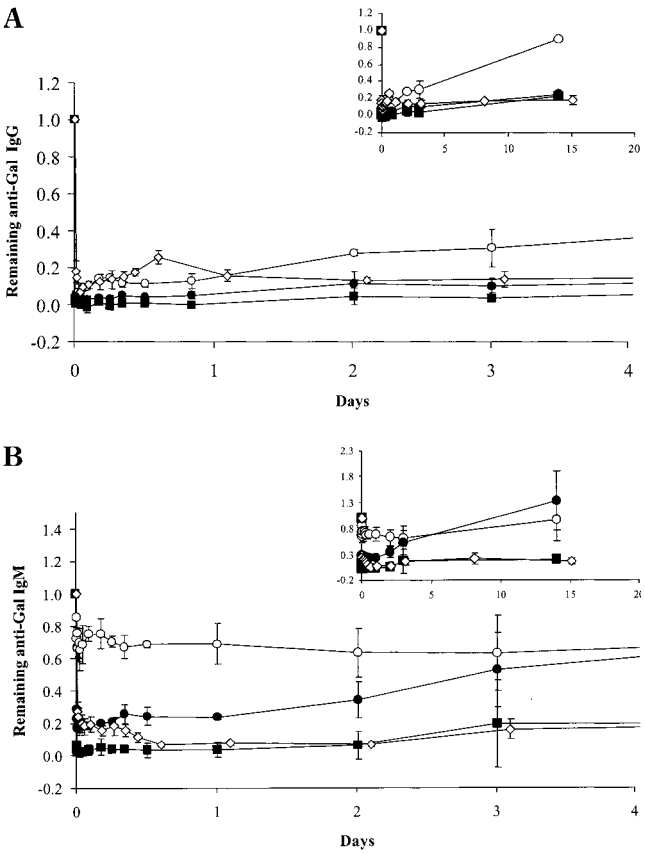


Figure 5. In vivo effects of α-galactosyl conjugates in cynomologus monkeys. The level of circulating anti-Gal IgG (A) and IgM (B) in cynomologus monkeys after a single dose infusion (100 mg/kg) of Nex8507 (○), Nex8587 (●), Nex1285 (■), and Gal−Dex−FITC (◇) was determined. Conjugates were infused at time zero. Antibody levels prior to infusion were set to 1.0. The graphs illustrate the fractional reduction of anti-Gal IgG and IgM in circulation after infusion. The Gal−Dex−FITC conjugate used in this experiment was a separate preparation, different from the Dex40 listed in Table 2. For this experiment the Gal−Dex−FITC material included a FITC moiety at a level of just less than one FITC molecule per dextran to facilitate detection. Compared to Dex40, this conjugate was not as effective at inhibiting anti-Gal antibodies in our in vitro assay exhibiting an IC50 value approximately 120-fold higher than Dex40 for inhibiting anti-Gal IgM using the HSA−$Gal_{(4)}$ substrate. Over 97% of the Gal−Dex−FITC was between 10000 and 100000 Da, smaller than Dex40, and had a substitution ratio of one α-galactosyl sugar every eight glucose residues. Error bars represent standard deviation. The insert shows the data on an expanded axis and includes the 14 day time point.

(Nex8507, Nex8587, Nex1285, and Gal−Dex−FITC) produce a 95% or greater apparent reduction in detectable anti-Gal IgG. Greater than 80% inhibition of IgG was maintained for the duration of the study (14 days) for all of the polymeric conjugates, except the simpler branched PEG conjugate (Nex8507) which showed a return to baseline levels between 7 and 14 days postinfusion (Figure 5A and insert). The effects on anti-Gal IgM were more varied (Figure 5B). The polymerized eight-branched PEG conjugate Nex1285 and the Gal−Dex−FITC conjugate effectively blocked anti-Gal IgM throughout the study period, showing more than 75% inhibition 7 and 14 days after infusion. The polymerized four-branched PEG conjugate Nex8587 conjugate was effective during the early part of the experiment, reducing apparent anti-Gal IgM by approximately 80% for the first 24 h; however, monkeys infused with NEX8587 exhibited a returned to baseline anti-Gal levels by 7−14 days postinfusion. In contrast, infusion of Nex8507 was minimally

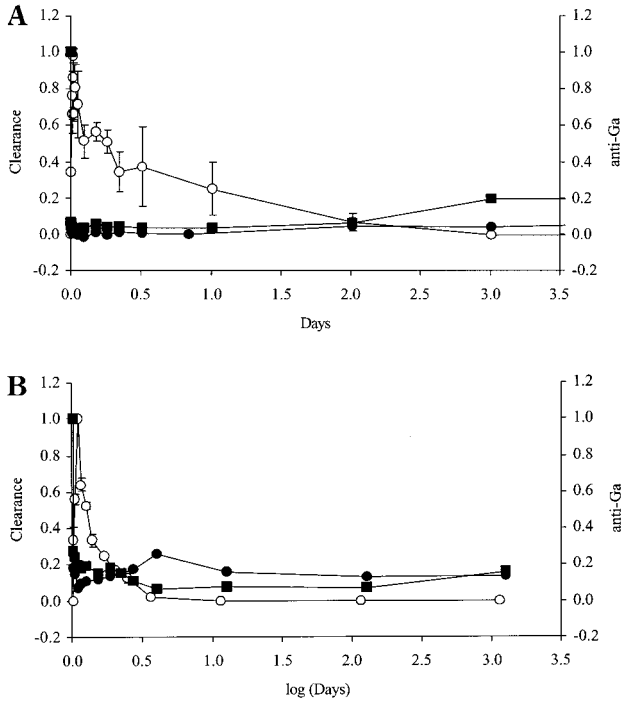


Figure 6. Clearance profiles for Nex1285 (A) and Gal−Dex−FITC (B) after infusion into cynomologus monkeys. The serum concentration of NEX1285 was determined by competition ELISA and the concentration of Gal−Dex−FITC by measuring FITC fluorescence. Each graph shows the clearance profile for the α-galactosyl conjugate (○) and the average serum anti-Gal IgG (●) and IgM (■) levels during the first 3 days postinfusion.

effective, initially reducing anti-gal IgM levels by approximately 35% with a rapid return to near baseline anti-Gal values within the first 24 h postperfusion.

These results show that the more effective conjugates can largely eliminate anti-Gal antibody activity for up to 14 days. Although we might have expected a first dose effect, due to the formation of antigen:antibody complexes, infusion of these conjugates was well tolerated with only a mild reddening of mucosal membranes noted in some animals. The slow rate of infusion may have helped to limit any first dose effect. We noted no significant changes in serum chemistry or hematological measurements during the course of the experiment.

The effects of α-galactosyl conjugates on serum anti-Gal activity in cynomologus monkeys was in broad agreement with our in vitro inhibition studies where the larger polymerized PEG and linear conjugates were more effective antibody inhibitors than the multimeric branched PEG conjugates. Antibody blocking activity may also be related to the in vivo clearance rates of the conjugates. Since anti-Gal antibody concentrations are roughly 10−50 μg/mL, our infusion protocol created a reservoir of excess α-galactosyl conjugate. This excess material might interfere with our ELISA analysis of serum anti-Gal levels. To investigate this, we examined the serum clearance of both Nex1285 and Gal−Dex−FITC since these conjugates appeared to have prolonged inhibitory effects. Clearance of Nex1285 was estimated by measuring the ability of postinfusion serum to block exogenous biotinylated human anti-Gal antibody binding to HSA−$Gal_{(8)}$-coated ELISA plates (Figure 6A). Clearance of the Gal−Dex−FITC conjugate was determined by measuring FITC fluorescence in the serum (Figure 6B). Peak inhibitory effects (Nes1285) or serum concentration (Gal−Dex−FITC) were achieved at the end of or within 20 min after the infusion. By 24 h postinfusion serum inhibition by Nex1285 was substantially reduced from the peak activity and fluorescence from Gal−Dex−FITC was no longer detectable. Serum from Nex1285 treated monkeys lost the ability to block exogenous human anti-Gal antibody by 3 days postinfusion. An analysis of these clearance profiles indicated a terminal half-life of 12 and 16 h for Gal−Dex−FITC and Nex1285, respectively. These values are similar to the serum half-life reported by Nagasaka in rats (Nagasaka et al. 1997) for linear PEG α-galactosyl conjugates. The extended in vivo circulation of the polymerized PEG and dextran conjugates may contribute to the efficiency of inhibition early after infusion; however, clearance of these materials suggests that the reduced level of serum anti-Gal antibodies observed at 7 and 14 days after infusion was not due to residual α-galactosyl conjugate but was likely due to a more prolonged inhibition of anti-Gal antibody production.

DISCUSSION

Anti-Gal antibody is the dominant specificity in human serum that binds to porcine cells, initiating hyperacute rejection, and likely contributing to acute vascular xenograft rejection. In agreement with previous publications (Neethling et al. 1996; Romano et al. 1999; Simon et al. 1998) we show here that these antibodies can be effectively blocked by incubation with carbohydrates that contain terminal Gal α1,3-Gal structures. The measured effectiveness of this inhibition was dependent on the isotype of the anti-Gal antibody and on the density of the α-galactosyl antigens. We report here the initial characterization of a series of α-galactosyl conjugates. An α-galactosyl trisaccharide sugar, which was the basis for all of the α-galactosyl conjugates, inhibits anti-Gal antibody at approximately 15 μM for IgG and 600 μM for IgM. More effective inhibition of IgG was achieved with defined oligomeric conjugates containing four or eight α-galactosyl residues per mole, but these conjugates showed only marginal improvement in inhibition of IgM. In contrast heterogeneous polymeric conjugates, using several different carrier structures, exhibited an enhanced ability to block both anti-Gal IgG and IgM. Enhanced IgM inhibition appeared to be most dependent on the size of the conjugate. These characteristics defined by in vitro inhibition assays were paralleled in a single dose infusion study in nonhuman primates. Infusion of a branched PEG conjugate with four α-galactosyl residues per carrier resulted in a greater than 80% inhibition of circulating anti-Gal IgG; however, the IgG levels returned to baseline values within 7−14 days. This same conjugate showed only marginal and transitory inhibition of IgM. In contrast, the larger heterogeneous polymeric PEG or dextran conjugates produced a profound reduction in circulating anti-Gal IgG and IgM which persisted for 14 days.

Several defined α-galactosyl oligomers and conjugates have been described previously. Nagasaka et al. (Nagasaka et al. 1997) have reported on the development of linear α-galactosyl PEG conjugates, and Rieben et al. (Rieben et al. 2000) have reported the development of oligomeric α-galactosyl molecules. These materials and the simple four- and eight-branched PEG conjugates we developed are attractive due to their defined structures; unfortunately these conjugates show rather weak ability to block antibody probably due to the low number of sugar residues and the overall small size of the conjugate. Highly repetitive conjugates of α-galactosyl sugars similar to Nex1285, PLL300, and Dex40 have also been reported (Rieben et al. 2000). These materials are usually much more effective inhibitors, but due to the more

heterogeneous nature of the carrier moiety, these polymers exhibit much wider size distribution and structural variability. Although polymeric conjugates such as these may be difficult to molecularly define, our data suggests that effective inhibition requires a large conjugate able to provide multiple α-galactosyl domains necessary to inhibit IgM.

Several groups have used α-galactosyl sugar to develop immunoabsoption methods to remove anti-Gal antibody from the circulation (Kozlowski et al. 1998a; Lin et al. 1997). This method can be highly effective and prolong xenograft survival but the depletion of anti-Gal antibody is temporary and antibody levels rebound to baseline levels within a few days (Watts et al. 2000). Our analysis of Nex1285 and Gal−Dex−FITC in cynomologus monkeys indicates that these materials have a dramatic immediate impact on circulating anti-Gal antibody and, unlike antibody absorption, suggests that infusion of α-Gal conjugates may lead to a more prolonged antibody inhibition. Pharmacokinetic analysis of Nex1285 and Gal−Dex−FITC shows that these materials have a prolonged terminal serum half-life, but that this half-life is not sufficient to account for an extended 80% reduction of IgG and IgM for 7 and 14 days after infusion. At this time we do not know if antibody:conjugate interactions leads to opsonization, and clearance of the complex or if blocked antibody continues to circulate. It is clear, however, that 3 days after infusion of Nex1285 there is no longer material in circulation that can block exogenous human anti-Gal antibody. This suggests that the reduction in anti-Gal titer observed at 7 and 14 days postinfusion results from a more long-lasting impact on the immune system.

Prolonged immunological inhibition of B-cells by haptenated conjugates has been reported previously by Dintzis and colleagues (Dintzis et al. 1976; Dintzis et al. 1985; Reim et al. 1996; Symer et al. 1995). These studies examined in detail the structural characteristics of hapten−polymer conjugates that lead to tolerogenic or immunogenic materials and suggest that haptenated polymers act directly on antigen specific B-cells to inhibit formation of antibody secreting cells. There are significant differences, however, between anti-Gal immune responses in xenotransplantation and the anti-hapten work described above. The α-Gal immune response is derived from a population of natural antibodies that probably developed in response to gut microflora. Anti-Gal B cells appear to be from the B1 or marginal zone B cell lineage (Ohdan et al. 2000) and tend to produce antibody with relatively low affinity interactions as is typical of natural anti-carbohydrate antibodies. In contrast Dintzis's work was mainly on high affinity immune responses from conventional B-cells after immunization with artificial haptens. Due to these differences the tolerogenic parameters defined for immune responses to high affinity haptens may differ from those for the anti-Gal antibodies. Interestingly, although the Gal−Dex−FITC polymer used in the infusion study was much less effective in the in vitro assay compared to Dex40 it still exhibited remarkable antibody blocking activity in cynomologus monkeys. This may suggest that smaller polymers or lower doses may be just as effective at blocking antibody in vivo. Additional primate studies will be required to determine the optimal method of using these materials and to determine if these materials are able to induce a prolonged reduction in anti-Gal antibodies. Also detailed characterization of the effects that polymeric α-galactosyl conjugates have on circulating antibody and on anti-Gal B-cells should help clarify the mechanism of action. Nevertheless, these results suggest that a high degree of anti-Gal antibody inhibition can be achieved using α-galactosyl conjugates capable of polymeric interactions. These conjugates were well tolerated in nonhuman primates, do not appear to induce a strong immune reaction and should be an effective method of controlling anti-Gal antibody during xenotransplantation.

ACKNOWLEDGMENT

Funding for the study described in this article was provided by Nextran, Inc. Under a licensing agreement between the Johns Hopkins University and Nextran, Dr. Dintzis is entitled to a share of payments received by the University from development of the licensed technology. The terms of this arrangement are being managed by the University in accordance with its conflict of interest policies.

LITERATURE CITED

Alwayn, I. P., Basker, M., Buhler, L., and Cooper, D. K. (1999) The problem of anti-pig antibodies in pig-to-primate xenografting: current and novel methods of depletion and/or suppression of production of anti-pig antibodies. *Xenotransplantation 6*, 157−168.

Borel, Y. (1971) Induction of immunological tolerance by a hapten (DNP) bound to a nonimmunogenic protein carrier. *J. Exp. Med. 230*, 180−182.

Borel, Y. (1980) Haptens bound to self-IgG induce immunologic tolerance, while when coupled to syngeneic spleen cells they induce immune suppression. *J. Immunol. 50*, 71−104.

Borel, Y., and Borel, H. (1988) Oligonucleotide linked to human gammaglobulin specifically diminishes anti-DNA antibody formation in cultured lymphoid cells from patients with systemic lupus erythematosus. *Immunol. Res. 82*, 1901−1907.

Borel, Y., Fritsche, R., Borel, H., Dahlgren, U., Dalhman-Hoglund, A., and Hanson, L. A. (1996) Parenteral and oral administration of tolerogens: protein-IgG conjugates. *Ann. N. Y. Acad. Sci. 778*, 80−87.

Cotterell, A. H., Collins, B. H., Parker, W., Harland, R. C., and Platt, J. L. 1995. The humoral immune response in humans following cross-perfusion of porcine organs. *Transplantation 60*, 861−8.

Cowdery, J. S., Laskin, C. A., and Steinberg, A. D. (1982) The specificity of in vivo tolerance to haptens in NZB and normal mice after exposure to hapten-modified syngeneic spleen cells. *J. Immunol. 128*, 1571−1576.

Desaymard, C. (1977) Role of epitope density in the induction of immunity and tolerance with thymus-independent antigens. IV. Selective tolerance and IgE response by DNP-levan conjugates. *Eur. J. Immunol. 7*, 646−649.

Dintzis, H. M., Dintzis, R. Z., and Vogelstein, B. (1976) Molecular determinants of immunogenicity: the immunon model of immune response. *Proc. Natl. Acad. Sci. U. S. A. 73*, 3671−3675.

Dintzis, R. Z., Middleton, M. H., and Dintzis, H. M. (1985) Inhibition of anti-DNP antibody formation by high doses of DNP− polyacrylamide molecules; effects of hapten density and hapten valence. *J. Immunol. 135*, 423−427.

Dintzis, R. Z., Okajima, M., Middleton, M. H., and Dintzis, H. M. (1990) Inhibition of antibody formation by receptor cross-linking: the molecular characteristics of inhibitory haptenated polymers. *Eur. J. Immunol. 20*. 229−232.

Dintzis, R. Z., Okajima, M., Middleton, M. H., Greene, G., and Dintzis, H. M. (1989) The immunogenicity of soluble haptenated polymers is determined by molecular mass and hapten valence. *J. Immunol. 143*, 1239−1244.

Evans, R. W., Orians, C. E., and Ascher, N. L. (1992) The potential supply of organ donors. An assessment of the efficacy of organ procurement efforts in the United States. *JAMA 267*, 239−246.

Furie, R. A., Cash, J. M., Cronin, M. E., Katz, R. S., Weisman, M. H., et al. (2001) Treatment of systemic lupus erythematosus with LJP 394. *J Rheumatology 28*, 257−265.

Galanaud, P., Aldo-Benson, M., and Borel, Y. (1975) Carrier-determined tolerance in vitro. *J. Immunol. 114*, 141−144.

Galili, U., LaTemple, D. C., Walgenbach, A. W., and Stone, K. R. (1997) Porcine and bovine cartilage transplants in cynomolgus monkey: II. Changes in anti-Gal response during chronic rejection. *Transplantation 63*, 646−651.

Good, A. H., Cooper, D. K., Malcolm, A. J., Ippolito, R. M., Koren, E., et al. (1992) Identification of carbohydrate structures that bind human antiporcine antibodies: implications for discordant xenografting in humans. *Transplant. Proc. 24*, 559−562.

Huber, R. E., Wallenfels, K., and Kurz, G. (1975) The action of beta-galactosidase (*Escherichia coli*) on allolactose. *Can. J. Biochem. 53*, 1035−1038.

Jones, D. S., Hachmann, J. P., Osgood, S. A., Hayag, M. S., Barstad, P. A., et al. (1994) Conjugates of double-stranded oligonucleotides with poly(ethylene glycol) and keyhole limpet hemocyanin: a model for treating systemic lupus erythematosus. *Bioconjugate Chem. 5*, 390−399.

Kozlowski, T., Ierino, F. L., Lambrigts, D., Foley, A., Andrews, D., et al. (1998a) Depletion of anti-Gal(alpha)1−3Gal antibody in baboons by specific alpha-Gal immunoaffinity columns. *Xenotransplantation 5*, 122−131.

Kozlowski, T., Monroy, R., Xu, Y., Glaser, R., Awwad, M., et al. (1998b) Anti-Gal(alpha)1−3Gal antibody response to porcine bone marrow in unmodified baboons and baboons conditioned for tolerance induction. *Transplantation 66*, 176−182.

Li, J. T., and Scott, D. W. (1980) Role of self-carriers in the immune response and tolerance. VI. Induction and reversal of TNP-modified self-unresponsiveness in vitro. *J. Immunol. 125*, 2380−2384.

Lin, S. S., Kooyman, D. L., Daniels, L. J., Daggett, C. W., Parker, W., et al. (1997) The role of natural anti-Gal alpha 1−3Gal antibodies in hyperacute rejection of pig-to-baboon cardiac xenotransplants. *Transpl. Immunol. 5*, 212−218.

McCurry, K. R., Parker, W., Cotterell, A. H., Weidner, B. C., Lin, S. S., et al. (1997) Humoral responses to pig-to-baboon cardiac transplantation: implications for the pathogenesis and treatment of acute vascular rejection and for accommodation. *Hum. Immunol. 58*, 91−105.

Nagasaka, T., Kobayashi, T., Muramatsu, H., Fujimoto, H., Matsuo, I., et al. (1997) alpha-Galactosyl oligosaccharides conjugated with poly(ethylene glycol) as potential inhibitors of hyperacute rejection upon xenotransplantation. *Artif. Organs 232*, 731−736.

Neethling, F. A., Joziasse, D., Bovin, N., Cooper, D. K., and Oriol, R. (1996) The reducing end of alpha Gal oligosaccharides contributes to their efficiency in blocking natural antibodies of human and baboon sera. *J. Biomech. 9*, 98−101.

Neethling, F. A., Koren, E., Ye, Y., Richards, S. V., Kujundzic, M., et al. (1994) Protection of pig kidney (PK15) cells from the cytotoxic effect of anti-pig antibodies by alpha-galactosyl oligosaccharides. *Transplantation 57*, 959−963.

Ohdan, H., Swenson, K. G., Kruger Gray, H. S., Yang, Y. G., Xu, Y., et al. (2000) Mac-1-negative B-1b phenotype of natural antibody-producing cells, including those responding to Gal alpha 1, 3Gal epitopes in alpha 1,3-galactosyltransferase-deficient mice. *J. Immunol. 165*, 5518−5529.

Orians, C. E., Evans, R. W., and Ascher, N. L. (1993) Estimates of organ-specific donor availability for the United States. *Transplant. Proc. 25*, 1541−1542.

Platt, J. L., Turman, M. A., Noreen, H. J., Fischel, R. J., Bolman, R. M. d., and Bach, F. H. (1990) An ELISA assay for xenoreactive natural antibodies. *Transplantation 49*, 1000−1001.

Reim, J. W., Symer, D. E., Watson, D. C., Dintzis, R. Z., and Dintzis, H. M. (1996) Low molecular weight antigen arrays delete high affinity memory B cells without affecting specific T-cell help. *Mol. Immunol. 33*, 1377−1388.

Rieben, R., Bovin, N. V., Korchagina, E. Y., Oriol, R., Nifant'ev, N. E., et al. (2000) Xenotransplantation: in vitro analysis of synthetic alpha-galactosyl inhibitors of human anti-Galalpha1→3Gal IgM and IgG antibodies. *Glycobiology 10*, 141−148.

Romano, E., Neethling, F. A., Nilsson, K., Kosanke, S., Shimizu, A., et al. (1999) Intravenous synthetic alphaGal saccharides delay hyperacute rejection following pig-to-baboon heart transplantation. *Xenotransplantation 6*, 36−42.

Sandrin, M. S., Vaughan, H. A., Dabkowski, P. L., and McKenzie, I. F. (1993) Anti-pig IgM antibodies in human serum react predominantly with Gal(alpha 1−3)Gal epitopes. *Proc. Natl. Acad. Sci. U. S. A. 90*, 11391−11395.

Simon, P. M., Neethling, F. A., Taniguchi, S., Goode, P. L., Zopf, D., et al. (1998) Intravenous infusion of Galalpha1−3Gal oligosaccharides in baboons delays hyperacute rejection of porcine heart xenografts. *Transplantation 65*, 346−353.

Symer, D. E., Reim, J., Dintzis, R. Z., Voss, E. W., Jr., and Dintzis, H. M. (1995) Durable elimination of high affinity, T cell-dependent antibodies by low molecular weight antigen arrays in vivo. *J. Immunol. 155*, 5608−5616.

Taniguchi, S., Neethling, F. A., Korchagina, E. Y., Bovin, N., Ye, Y., et al. (1996) In vivo immunoadsorption of antipig antibodies in baboons using a specific Gal(alpha)1−3Gal column. *Transplantation 62*, 1379−1384.

Waldschmidt, T. J., Borel, Y., Vitetta, E. S. (1983) The use of haptenated immunoglobulins to induce B cell tolerance in vitro. The roles of hapten density and the Fc portion of the immunoglobulin carrier. *J Immunol 131*, 2204−2209.

Watts, A., Foley, A., Awwad, M., Treter, S., Oravec, G., et al. (2000) Plasma perfusion by apheresis through a Gal immunoaffinity column successfully depletes anti-Gal antibody: experience with 320 aphereses in baboons. *Xenotransplantation 7*, 181−185.

Weisman, M. H., Bluestein, H. G., Berner, C. M., and de Haan, H. A. (1997) Reduction in circulating dsDNA antibody titer after administration of LJP 394. *J. Rheumatol. 24*, 314−318.

Zambidis, E. T., Barth, R. K., Scott, D. W. (1997) Both resting and activated B lymphocytes expressing engineered peptide-Ig molecules serve as highly efficient tolerogenic vehicles in immunocompetent adult recipients. *J. Immunol. 158*, 2174−2182.

Zambidis, E. T., and Scott, D. W. (1996) Epitope-specific tolerance induction with an engineered immunoglobulin. *Proc. Natl. Acad. Sci. U. S. A. 93*, 5019−5024.

BC015565E

Inhibitory Effect of Supramolecular Polyrotaxane−Dipeptide Conjugates on Digested Peptide Uptake via Intestinal Human Peptide Transporter

Nobuhiko Yui,*,† Tooru Ooya,† Tomokatsu Kawashima,† Yoshimasa Saito,‡ Ikumi Tamai,‡ Yoshimichi Sai,‡ and Akira Tsuji*,‡

School of Materials Science, Japan Advanced Institute of Science and Technology, 1-1 Asahidai, Tatsunokuchi, Ishikawa 923-1292, Japan and Faculty of Pharmaceutical Sciences, Kanazawa University, 13-1 Takara-Machi, Kanazawa, Ishikawa 920-0934, Japan. Received October 17, 2001; Revised Manuscript Received March 13, 2002

The effect of polyrotaxane−dipeptide (Val-Lys) conjugates on the uptake of a model dipeptide (Gly-Sar) was examined via human peptide transporter (hPEPT1) on HeLa cells. Here, Val-Lys groups are introduced to α-CDs, which are threaded onto a poly(ethylene oxide) chain capped with bulky end-groups (polyrotaxane). The Gly-Sar uptake via hPEPT1 was significantly inhibited in the polyrotaxane conjugates, and this inhibitory effect was not explained by the sum of interaction between hPEPT1 and α-CD−Val-Lys conjugates. Further, the inhibition was significantly greater than those observed in dextran−Val-Lys conjugates. Therefore, our data clearly suggests that supramolecular structure in the polyrotaxane conjugates contributes considerably to the inhibitory effect via multivalent binding of Val-Lys groups with hPEPT1.

INTRODUCTION

Proteins are enzymatically digested to di- or tripeptides and/or amino acids, and these protein-digestive products are absorbed via specific transporters from the small intestine. Multiple transporters are involved in intestinal membrane transports for amino acids, while di- and tripeptides are transported only via peptide transporter, PEPT1. Besides, in terms of the intake of proteins and the absorption of some drugs, peptide transporter is expected to be more important than amino acid transporters. In particular, conjugation of poorly absorbable drugs with PEPT1-recognizable molecules such as di- or tripeptides is a powerful approach to exploit the substrate affinity of PEPT1. Kamo et al. synthesized dipeptide analogues conjugated at the ϵ-amino group of Lys in Val-Lys or Lys-Sar with fluorescent dyes as model hydrophobic drugs (*1*). They also reported that the hydrophobicity of dipeptide conjugates was an important parameter recognized by PEPT1 (*2*). The objective of their study was to enhance drug absorption through PEPT1, and thus conjugates of lower molecular weight were a minimum requirement. Dietary protein restriction is now recommended for patients of chronic renal disease (CRD),[1] but compliance is not typically high due to the effect on quality of life (QOL). In this sense, it is logical to temporarily inhibit the absorption of digested proteins via PEPT1 to improve QOL of patients. The inhibitor should be recognized by PEPT1 and have nonabsorbable properties so as to preclude kidney damage. In these points of view, multivalent ligands that display multiple sites of recognition by PEPT1 on intestinal surfaces are advantageous. Such multivalent ligands maycooperatively interact with PEPT1 and inhibit their absorption.

Cooperative affinity of ligands using synthetic or natural polymers such as tabacco mosaic virus (*3*), sugarballs (*4*), and comb-branched or dendrigraft neoglycopolymers (*5*) has been proposed as a new drug design strategy. The important factors that control the binding features include valency, architecture of the scaffolds, and orientation of the ligands. Such multivalent ligands can act as inhibitors of receptor−ligand interactions and activators of biological systems (*6*). For example, Baker, Jr. et al. studied the effect of ligand architecture, including dendrimers, comb-branched copolymers, dendrigraft copolymers, and linear-dendron architectural copolymers, on inhibitory activity and specificity (*5*). Arimoto et al. reported that a multivalent polymer of vancomycin, synthesized by ring-opening metathesis polymerization (ROMP), showed enhanced antibacterial activity against vancomycin-resistant bacteria (*7*), suggesting that multivalent ligands might be promising tools in the fight against multiresistant bacteria. Accordingly, the design of the scaffold structure is important not only for clarifying the multivalent mechanism in nature but also for designing new drugs, such as multivalent viral and toxin inhibitors.

* To whom correspondence should be addressed. N. Yui: Phone: +81-761-51-1640. Fax: +81-761-51-1645. E-mail: yui@jaist.ac.jp. A. Tsuji: Phone: +81-76-234-4479. Fax: +81-76-234-4477. E-mail: tsuji@kenroku.kanazawa-u.ac.jp.

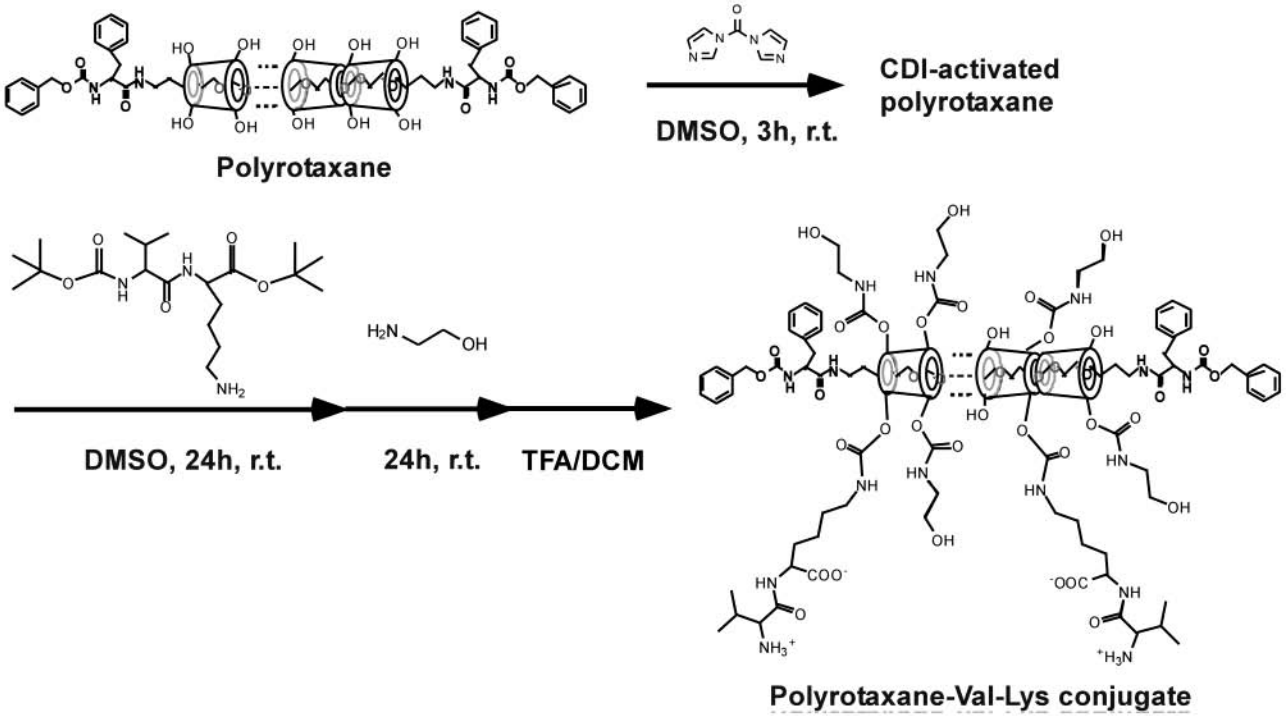
† Japan Advanced Institute of Science and Technology.

‡ Kanazawa University.

[1] Abbreviations: CRD, chronic renal disease; QOL, quality of life; ROMP, ring-opening metathesis polymerization; α-CDs, α-cyclodextrins; Gly-Sar, glycylsarcosine; PEO-BA, α-(3-aminopropyl)-ω-(3-aminopropyl)polyoxyethylene, CDI, *N*,*N*′-carbonyldiimidazole; DIPEA, *N*,*N*′-diisopropylethylamine, HOBt, 1-hydroxybenzotriazole; WSC·HCl, water-soluble carbodiimide [1-ethyl-3-(dimethylamino)carbodiimide]; DMAP, (dimethylamino)pyridine; DMEM, Dulbecco's modified Eagle's medium; FCS, fetal calf serum; HBSS, Hanks balanced salt solution; MES, 2-(*N*-morpholino)ethanesulfonic acid; HEPES, 2-[4-(2-hydroxyethyl)-1-piperazinyl]ethanesulfonic acid.

10.1021/bc015567z CCC: $22.00 © 2002 American Chemical Society
Published on Web 04/17/2002

Scheme 1. Synthesis of Polyrotaxane−Val-Lys Conjugates



We have systematically studied the design of supramolecular-structured polymers as new biomaterials and drug carriers. One of the representatives is a biodegradable polyrotaxane, in which a lot of chemically modified α-cyclodextrins (α-CDs) are threaded onto a poly(ethylene oxide) (PEO) chain capped with an amino acid or an oligopeptide (*8*). The biodegradable polyrotaxanes may have a variety of ligands, which can simultaneously bind to multivalent receptors on a cell surface, because many hydroxyl groups are available for introducing ligands on the α-CDs located along the polyrotaxane structure. In our previous study, polyrotaxane−biotin conjugates were synthesized to demonstrate the potential of multivalent ligands (*9*, *10*). On the basis of this architectural design, we have proposed the development of multivalent ligands using the polyrotaxanes as a specific inhibitor of PEPT1. In this study, polyrotaxane−dipeptide (valyllysine, Val-Lys) conjugates are synthesized and characterized, and the inhibitory effect of the conjugates on [^{3}H]glycylsarcosine ([^{3}H]Gly-Sar, a model peptide transported by PEPT1) transport in HeLa cells stably expressing human PEPT1 (hPEPT1) is evaluated in comparison with α-CD−Val-Lys and dextran−Val-Lys conjugates. Our final goal is to inhibit absorption of digested peptides in the intestinal tract via hPEPT1 transporter through multivalent binding of PEPT1-recognizable polymers.

MATERIALS AND METHODS

Materials. α-CD was purchased from Bio-Research Corporation of Yokohama (Yokohama, Japan). α-(3-Aminopropyl)-ω-(3-aminopropyl)polyoxyethylene (PEO-BA: $M_n = 4000$) was kindly supplied by Sanyo Chemical Co. (Kyoto, Japan). Benzyloxycarbonyl-L-phenylalanine (Z-L-Phe), 2-aminoethanol, *N*,*N*′-carbonyldiimidazole (CDI), and *N*,*N*′-diisopropylethylamine (DIPEA) were purchased from Wako Pure Chemical Co. Ltd., (Osaka, Japan). *N*-Hydroxysuccinimide, 1-hydroxybenzotriazole (HOBt), and Boc-Val were purchased from Peptide Institute, Inc. (Osaka, Japan). Lys-(Cbz)-O*t*Bu·HCl was purchased from BACHEM (Bubendorf, Switzerland). Water-soluble carbodiimide (1-ethyl-3-(dimethylamino)carbodiimide, WSC·HCl) and (dimethylamino)pyridine (DMAP) were purchased from DOJINDO Labs (Kumamoto, Japan). Dextran from *Leuconostoc mesenteroids* (M_n = 15000−20000) and Gly-Sar were purchased from Sigma Chemical Co. (St. Louis, MO). *N*,*N*-Dimethylformamide (DMF) and dimethyl sulfoxide (DMSO) were purchased from the Wako Pure Chemical Co. Ltd. and distilled by the usual method. All other chemicals used were of reagent grade. [^{3}H]Glycylsarcosine ([^{3}H]Gly-Sar) was purchased from Moravek Biochemicals Inc. (Brea, CA). Other chemaicals used were of the highest purity available.

Synthesis of Polyrotaxane−Val-Lys Conjugates (Scheme 1). Boc-Val-Lys-O*t*Bu·HCl was synthesized and characterized according to the previous report by Kamo et al. (*1*). A polyrotaxane, in which many α-CDs are threaded onto a PEO-BA ($M_n = 4000$) capped with Z-L-Phe, was prepared according to our method (*9*, *11*). Briefly, an inclusion complex of α-CDs and PEO-BA was prepared by simply mixing a saturated aqueous solution of α-CDs with a PEO-BA aqueous solution (1/44 equiv of α-CD). Then the succinimide ester of Z-L-Phe, prepared by a condensation reaction of Z-L-Phe and *N*-hydroxysuccinimide, was allowed to heterogeneously react with the terminal amino groups in the inclusion complex in DMSO. The chemical structure was characterized by 750 MHz ^{1}H NMR using a FT-NMR spectrometer (Varian FT-NMR Gemini750, Palo Alto, CA). The number of α-CDs was determined to be ca. 23 from the ^{1}H NMR spectra based on the comparison of integration of the signals at 4.75 (C_1H of α-CD) with those at 3.49 (CH_2CH_2O of PEO). The obtained polyrotaxane (0.17 mmol) and CDI (e.g., 15.6 mmol) were dissolved in dry DMSO (10 mL) and stirred at room temperature for 3 h. The reaction mixture was poured into excess ether, and the resulting precipitate was filtered and dried in vacuo to obtain CDI-activated polyrotaxanes. The number of *N*-acylimidazole groups per polyrotaxane molecule was determined by

Table 1. Synthesis of CDI-Activated Polyrotaxanes

sample code[a]	OH groups in polyrotaxane (mmol)	CDI (mmol)	CDI-activation (%)[b]
27aIM-α/E4-PHE-Z	3.1	3.1	27
46aIM-α/E4-PHE-Z	3.1	6.1	46
54aIM -α/E4-PHE-Z	3.1	9.2	54
57aIM -α/E4-PHE-Z	3.1	15.4	57

[a] aIM = *N*-acylimidazole group, α/E4-PHE-Z = polyrotaxane. [b] Calculated from the equation (A).

measuring the absorbance at 207 nm after hydrolysis of *N*-acyl carbonate groups using 2 M NaOH aqueous solution. Degree of the activation was calculated by the following equation (A):

$$\text{CDI-activation (\%)} = [\text{Im}]/[\text{OH}]_{\text{prx}} \times 100 \quad \text{(A)}$$

where [Im] and $[OH]_{prx}$ are, respectively, concentrations of the *N*-acylimidazole groups and total hydroxyl groups in the polyrotaxanes. The synthetic conditions and results were summarized in Table 1.

The CDI-activated polyrotaxane (*N*-acylimidazole groups per polyrotaxane molecule: 0.97 mmol), Boc-Val-Lys-O*t*Bu·HCl (e.g., 3.3 mmol), and DIPEA (1.1 equiv of Boc-Val-Lys-O*t*Bu·HCl) were dissolved in DMSO (2 mL) and stirred at room temperature for 24 h. The feed ratio of the CDI-activated polyrotaxane and Boc-Val-Lys-O*t*Bu·HCl was varied (Table 2). After that, 2-aminoethanol (33 mmol) was added to the solution and further stirred for 24 h. The solution was dialyzed against water and lyophilized to obtain a polyrotaxane−Boc-Val-Lys-O*t*Bu conjugate as white powder. Finally, the protecting groups of Boc and *t*-Bu were removed in the mixture of dichloromethane and trifluoroacetic acid (7:3), precipitated in excess ether, and dried in vacuo to obtain a polyrotaxane−Val-Lys conjugate as white powder.

Yield: ∼10%. ^{1}H NMR D_2O + NaOD, ppm: δ 7.35−7.18 (aromatics of Z-L-Phe), 7.15−6.80 (−OCONH− of carbamoyl linkages), 5.02 (C_1H of α-CD), 4.25−3.30 (C_3H, C_5H, C_6H_2, C_4H, and C_2H of α-CD), 4.19 (α-CH of Lys), 3.62 (CH_2CH_2O of PEO), 3.75 (α-CH of Val), 3.17 (CH_2 of hydroxyethyl carbamoyl groups), 2.15 (β-CH of Val), 1.38 (β-, γ-, and δ-CH_2 of Lys), 0.98 (CH_3 of Val).

Synthesis of α-CD−Val-Lys Conjugates. α-CD (0.31 mmol) and CDI (5.56 mmol) were dissolved in dry DMF (5 mL), and the solution was stirred at room temperature for 3 h. Boc-Val-Lys-O*t*Bu·HCl (0.62 mmol) and DIPEA (1.1 equiv of Boc-Val-Lys-O*t*Bu·HCl) were added to the solution and stirred at room temperature for 24 h. Then, 2-aminoethanol (5.6 mmol) was added to the solution and further stirred for 24 h. The solution was dialyzed against water and lyophilized to obtain an α-CD−Boc-Val-Lys-O*t*Bu conjugate as white powder. Finally, the protecting groups of Boc and *t*-Bu were removed in a manner similar to the polyrotaxane−Val-Lys conjugates.

Yield: ∼80%. ^{1}H NMR D_2O, ppm: δ 7.10−6.81 (−OCONH− of carbamoyl linkages), 4.93 (C_1H of α-CD), 4.00−3.33 (C_3H, C_5H, C_6H_2, C_4H, and C_2H of α-CD), 4.35 (α-CH of Lys), 3.67 (α-CH of Val), 3.13 (CH_2 of hydroxyethylcarbamoyl groups), 2.01 (β-CH of Val), 1.32 (β-, γ-, and δ-CH_2 of Lys), 0.91 (CH_3 of Val).

Synthesis of Dextran−Val-Lys Conjugates. Hydroxyl groups of dextran were activated using *p*-nitrophenyl chloroformate according to our previous method (*12*). The activated dextran (0.01 mmol, the number of *p*-nitrophenyl carbonate group per 100 glucose units: 20) was dissolved in dry DMSO (10 mL), and then Boc-Val-Lys-O*t*Bu·HCl (e.g., 0.4 mmol) was added to the solution. The reaction mixture was stirred at room temperature for 48 h. The feed ratio of the activated dextran and Boc-Val-Lys-O*t*Bu·HCl was varied according to the reaction conditions (Table 2). Then, the solution was dialyzed against water and lyophilized to obtain a dextran−Boc-Val-Lys-O*t*Bu conjugate as white powder. Finally, the protecting groups of Boc and *t*-Bu were removed in a manner similar to the polyrotaxane−Val-Lys conjugates.

Yield: ∼50%. ^{1}H NMR DMSO-d_6, ppm: δ 4.91−4.76 (O_2H, O_3H of dextran), 4.64 (C_1H of dextran), 4.59−4.40 (O_4H of dextran), 4.19 (α-CH of Lys), 3.92−3.19 (C_3H, C_5H, C_6H_2, C_2H, and C_4H of dextran), 3.75 (α-CH of Val), 2.13 (β-CH of Val), 1.33 (β-, γ-, and δ-CH_2 of Lys), 0.98 (CH_3 of Val).

Characterization. Purity of the conjugates was confirmed by gel permeation chromatography (GPC) using a column of Sephadex G-75, 0.1 M phosphate buffer, pH 7.4 as an eluent. The peaks on the GPC were detected by refractive index. The structure of the conjugates was characterized by 750 MHz ^{1}H NMR using the FT-NMR spectrometer. The number of α-CDs in the polyrotaxane was determined by the ^{1}H NMR spectra. The number of Val-Lys per one conjugate molecule was determined by the following equation (B):

$$N_{\text{VK}} = [\text{Val}]/[\text{polyrotaxane}],$$
$$[\text{polyrotaxane}] = [\text{Phe}]/2 \quad \text{(B)}$$

where N_{VK} is the number of Val-Lys per one conjugate molecule, [Val] the concentration of Val in the conjugate, [polyrotaxane] the concentration of the polyrotaxane, and [Phe] the concentration of the terminal Z-L-Phe in the polyrotaxane, which were determined by amino acid analysis using an amino acid analyzer (Hitachi L-8500A, Tokyo, Japan).

Cell Culture and Uptake Experiments Using HeLa-hPEPT1. HeLa cells that were stably transfected with human peptide transporter PEPT1-cDNA (HeLa-hPEPT1) or vector DNA (pcDNA3, Invitrogen, San Diego, CA) alone (HeLa-pcDNA3) were grown in Dulbecco's modified Eagle's medium (DMEM), supplemented with 10% FCS, 2mM glutamine and 1.0 mg/mL geneticine (G418, Sigma Chemicals, St. Louis, MO), as described previously (*13*). For the uptake study, each cell line was seeded at a density of 10^5 cells/cm^2 on multidishes (NUNC, Multidish 4 wells, Denmark) and were grown for 4 days. Uptake of [^{3}H]Gly-Sar (0.48 μM) by the cultured cells was examined at 37 °C according to our previous study (*13*).

The uptake of [^{3}H]Gly-Sar by the cells was usually measured using Hanks balanced salt solution (HBSS) consisting of 0.952 mM $CaCl_2$, 5.36 mM KCl, 0.441 mM KH_2PO_4, 0.812 mM $MgSO_4$, 136.7 mM NaCl, 0.385 mM Na_2HPO_4, 25 mM D-glucose, and 10 mM MES adjusted to pH 6.0 by HEPES. The cells cultured on the dishes were washed by HBSS and preincubated with HBSS for 5 min. Then, the uptake was initiated by changing the medium with HBSS containing radiolabeled Gly-Sar and each test compound. The uptake was terminated by removing the uptake solution and three times washing with ice-cold HBSS. The cells were dissolved in 0.25 mL aliquots of 5 N NaOH for 2 h, neutralized by 5 N HCl (0.25 mL), and mixed with the scintillation fluid Cleasol-I (Nacalai tesque, Kyoto, Japan), and then the associated radioactivities were measured with a liquid scintillation counter (LSC-5100, Aloka, Tokyo, Japan). Protein was measured by the protein-dye binding method (*14*).

Table 2. Synthesis of Polyrotaxane−Val-Lys Conjugates

sample code[a]	feed ratio ([VK]/[activated compd])	no. of Val-Lys/mol[b]	no. of α-CD/mol[c]	no. of HE/mol[c]	total M_n[c]
111HE-α/E4-PHE-Z	0	0	23	111	33200
1VK71HE-α/E4-PHE-Z	88	1	22	71	30560
2VK57HE-α/E4-PHE-Z	97	2	16	57	24100
11VK36HE-α/E4-PHE-Z	153	11	9	36	18240
46VK98HE-α/E4-PHE-Z	683	46	21	98	43200
3VK-Dextran	3	3	−	0	17900
6VK-Dextran	13	6	−	0	18800
10VK-Dextran	23	10	−	0	20000
36VK-Dextran	40[d]	36	−	0	26600
16VK8HE-Dextran	40	16	−	8	21800
1VK3HE-αCD	2	1	−	3	1400

[a] VK = Boc-Val-Lys-O*t*Bu·HCl, HE = hydroxyethylcarbamoyl groups, α/E4-PHE-Z = polyrotaxane. [b] Calculated from amino acid analysis. [c] Calculated from 750 MHz ^{1}H NMR spectra for the polyrotaxane−Val-Lys and α-CD−Val-Lys conjugates, and from GPC with a calibration using pullulan standard. [d] The reaction was carried out at 40 °C.

RESULTS AND DISCUSSION

Synthesis. To introduce Val-Lys groups using the hydroxyl groups of α-CDs in the polyrotaxane, the ϵ-amino group of lysine in Val-Lys was used because the α-carboxyl group and α-amino group of Val-Lys are essential for better recognition of PEPT1 (*1*). The hydroxyl groups of α-CDs in the polyrotaxane were activated by CDI. As shown in Table 1, the percentage of the activation increased with the amount of CDI. The IR spectrum of the sample displayed a strong peak around 1700 cm^{-1} after activation. These results indicate that *N*-acylimidazole groups were actually introduced to the polyrotaxane. Maximum number of the activation was found to be nine per α-CD molecule in the polyrotaxane.

From the ^{1}H NMR spectrum of the product after coupling Val-Lys with the CDI-activated polyrotaxane, the peaks attributed to Z-L-Phe, α-CDs, PEO, hydroxyethylcarbamoyl group, and Val-Lys were confirmed. There were no peaks attributed to *N*-acylimidazole groups in the spectrum, suggesting that the coupling reaction and the following washing procedure were successful. Similarly, all the peaks attributed to the Val-Lys conjugates were confirmed with regard to the α-CD−Val-Lys conjugate and the dextran−Val-Lys conjugate. Table 2 summarizes the synthesis of the polyrotaxane−Val-Lys, the α-CD−Val-Lys, and the dextran−Val-Lys conjugates. The number of Val-Lys per polyrotaxane molecule increased with the amount of Val-Lys in the feed. The maximum number of Val-Lys was ca. 46 per polyrotaxane molecule, indicating that two Val-Lys groups were introduced to every α-CD molecule. Figure 1 shows GPC chromatograms of the polyrotaxane−Val-Lys conjugate and the polyrotaxane (a), the α-CD−Val-Lys conjugate and α-CD (b), and the dextran−Val-Lys conjugate and dextran (c), respectively. It was found that the elution volume of the polyrotaxane−Val-Lys conjugate was similar to that of the hydroxyethylcarbamoyl−polyrotaxane, and there was no peak attributed to α-CD. This result indicates that free α-CD and its derivatives are not contaminated in the polyrotaxane−Val-Lys conjugate. The elution time of the α-CD−Val-Lys conjugate was shorter than that of α-CD, presumably due to association of the conjugates. Such an association behavior was not observed in the polyrotaxane−Val-Lys conjugate. Perhaps, due to the rodlike structure of the polyrotaxane, the association may be reduced. The association property of either the polyrotaxane or a drug−polyrotaxane conjugate was studied by light scattering measurements in our previous studies (*15*, *16*). The association number of the polyrotaxane molecules decreases with increasing the number of α-CDs in the polyrotaxane. Our previous study suggests that the rodlike structure of polyrotaxanes in physiological environments contribute to their reduced association. As for the dextran−Val-Lys conjugate, the elution time was found to be a little bit shorter than the peak of dextran (Figure 1c). M_n of the dextran calculated from GPC with a calibration using pullulan standard was ca. 17100, and M_n of all the dextran−Val-Lys conjugates (Table 2) was larger than that of the dextran. These results indicate that the dextran−Val-Lys conjugate exhibits an association under buffered conditions.

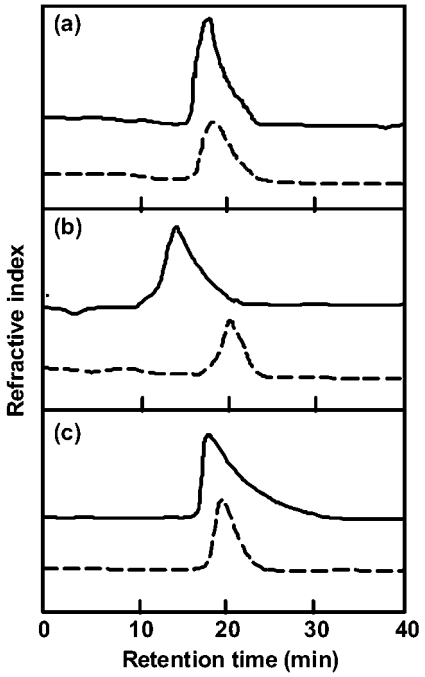


Figure 1. GPC traces of the conjugates. (a) Polyrotaxane−Val-Lys conjugate (46VK98HE-α/E4-PHE-Z, solid line) and hydroxyethyl carbamoyl polyrotaxane (dashed line), (b) α-CD−Val-Lys conjugate (1VK8HE-α-CD, solid line) and α-CD (dashed line), and (c) dextran−Val-Lys conjugate (16VK8HE-Dextran, solid line) and dextran (dashed line). Column: Sephadex G-70, Eluent: 0.1 M phosphate buffer, pH 7.4.

Inhibition of PEPT1-Mediated Transport of [^{3}H] Gly-Sar by the Conjugates. In vitro efficacy of the polyrotaxane−Val-Lys conjugates as an inhibitor of peptide transporter was evaluated by the uptake of Gly-Sar by HeLa cells stably expressing hPEPT1. Figure 2 shows the inhibitory effect of the polyrotaxane−Val-Lys conjugate and the α-CD−Val-Lys conjugate (46VK98HE-α/E4-PHE-Z and 1VK3HE-αCD in Table 2, respectively) on the uptake of [^{3}H]Gly-Sar. In Figure 2,

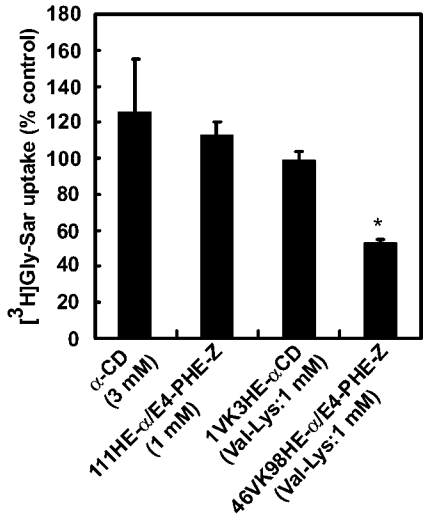


Figure 2. Inhibition of [^{3}H]Gly-Sar uptake via hPEPT1 by polyrotaxane−Val-Lys conjugate (46VK98HE-α/E4-PHE-Z), α-CD−Val-Lys conjugate (1VK3HE-αCD), hydroxyethylcarbamoyl-polyrotaxane (111HE-α/E4PHE-Z) and α-CD. Mean ± SEM (n = 4). * Significantly different (p < 0.05) from 111HE-α/E4PHE-Z.

hydroxyethylcarbamoyl-polyrotaxane (111HE-α/E4-PHE-Z) and α-CD were used as references, and the concentration was calculated based on Val-Lys residue. The uptake of [^{3}H]Gly-Sar was strongly reduced in the presence of the polyrotaxane−Val-Lys conjugate, while such a reduction was not observed for the polyrotaxane itself (111HE-α/E4-PHE-Z). The α-CD−Val-Lys conjugate showed a slight inhibitory effect with increasing Val-Lys concentration (data not shown), while α-CD itself did not. These results indicate that Val-Lys moiety immobilized on the polyrotaxane or α-CD is actually recognized by hPEPT1. Interestingly, the inhibitory effect of the polyrotaxane−Val-Lys conjugates was much greater than predicted from the Val-Lys dependency of the α-CD conjugates. The α-CD−Val-Lys conjugate can interact with one hPEPT1. On the other hand, Val-Lys moieties introduced to the polyrotaxane backbone has potential to interact with multiple hPEPT1s expressed on HeLa cells. Thus, it is considered that Val-Lys introduced to the polyrotaxane cooperatively interacts with hPEPT1. Since the molecular size of the polyrotaxane−Val-Lys conjugates is much larger than that of the α-CD−Val-Lys conjugate, the kinetics of Val-Lys−PEPT1 binding may be an important issue in the cooperative interactions. To examine this issue, the conjugates were incubated with HeLa cells at 37 °C for 30 min, prior to the measurement of [^{3}H]Gly-Sar uptake. The inhibitory potency of the polyrotaxane−Val-Lys conjugate increased by the preincubation, as opposed to not using preincubation (Figure 3). On the contrary, the preincubation of the α-CD−Val-Lys conjugate reduced the inhibitory effect. Kiessling et al. reported the enhanced interaction of neoglycopolymers with concanavalin A by preincubation (*17*). In our case, the polyrotaxane conjugate is considered to rebind with PEPT1 during the incubation, which has been kinetically proved using a model ligand and binding protein (*10*). Therefore, our results suggest the multivalent binding and/or cooperative interaction of the polyrotaxane−Val-Lys conjugates with hPEPT1.

A key feature of our designed polyrotaxane conjugates is the contribution of the supramolecular structure to the inhibitory effect. Figure 4 summarizes the inhibitory effect of the polyrotaxane−Val-Lys conjugates in comparison with the dextran−Val-Lys conjugates. The

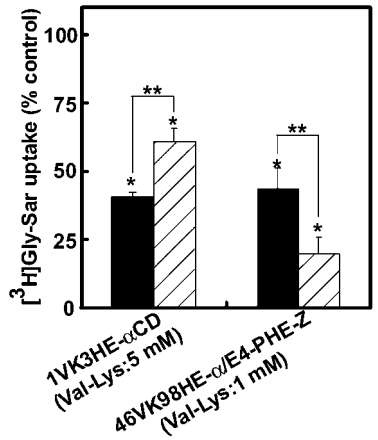


Figure 3. Effect of preincubation on the inhibition of [^{3}H]Gly-Sar uptake via hPEPT1. Mean ± SEM (n = 4). * Significantly different (p < 0.05) from control. ** Significantly different (p < 0.05) from nonpreincubation. Black bar: simultaneous addition. Slash bar: preincubation of 30 min.

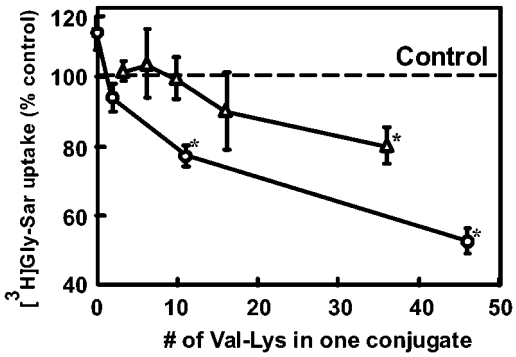


Figure 4. Inhibition of [^{3}H]Gly-Sar uptake via hPEPT1 as a function of the number of Val-Lys in one conjugate molecule. The concentration of each conjugate is 1 mM as Val-Lys basis. The polyrotaxane−Val-Lys conjugates (circle) and dextran−Val-Lys conjugate (triangle). Mean ± SEM (n = 4). * Significantly different (p < 0.05) from control.

concentration of Val-Lys in each conjugate was adjusted to be 1 mM. [^{3}H]Gly-Sar uptake in both conjugates decreased with increasing the number of Val-Lys in one conjugate molecule. The inhibition of [^{3}H]Gly-Sar uptake with the polyrotaxane−Val-Lys conjugates was significantly greater than those of the dextran−Val-Lys conjugates. In the case of conjugates between the oligopeptide and the water-soluble polymer, such as dextran−Val-Lys conjugates, the hydrophobic oligopeptide (Val-Lys) groups are likely to associate each other, owing to the flexibility of the polymer backbones, which is related with the result in Figure 1. Such association may prevent access of PEPT1 toward the Val-Lys moieties. In contrast, the Val-Lys moieties introduced in the polyrotaxane are expected to be well arrayed along the supramolecular rodlike backbone, as to easily face PEPT1 on the membrane, considering the result of Figure 1 and our previous studies. Therefore, it is suggested that the supramolecular structure of polyrotaxanes has a suitable architecture for designing polymeric inhibitors capable of multivalent binding between Val-Lys and hPEPT1.

CONCLUSIONS

The polyrotaxane−Val-Lys conjugates were found to exhibit great inhibitory effect on the uptake of a model oligopeptide, Gly-Sar, via hPEPT1. Special interest should be paid to the facts that this inhibitory effect was not explained from the monovalent interaction of hPEPT1

with Val-Lys moiety and that the polyrotaxane was superior to dextran as a conjugate pair. These results strongly suggest both the multivalent interaction of the polyrotaxane conjugate with hPEPT1 and the contribution of the supramolecular structure to this effect. The polyrotaxane−Val-Lys conjugates have been confirmed not to be absorbed from the intestine in the alternative in vivo study (*18*), suggesting that reabsorption in renal epithelial cells via PEPT2 kidney can be avoided. The polyrotaxane used in this study was not specially designed aiming at the practical use but prepared for the first fundamental research, and the in vivo efficacy of the polyrotaxane−Val-Lys conjugates is not so high (data not shown). As mentioned before, in the polyrotaxane−Val-Lys conjugates, the α-CD−Val-Lys conjugate and a linear PEO chain are noncovalently bound via mechanical locking. Sliding and rotational motion of concentrated Val-Lys groups along the polyrotaxane might contribute to the inhibitory effect reported in this study. The solubility of the polyrotaxane is also an important issue because the introduction of Val-Lys groups into the polyrotaxane reduced the solubility. Our recent study succeeded to prepare carboxyethyl ester-introduced polyrotaxanes as a calcium-chelating agent for peptide drug delivery, and these polyrotaxanes displayed excellent solubility in PBS (*19*). In this point of view, to clarify the relation of the inhibitory effect with the specific structure of the polyrotaxane, a variation of the polyrotaxane−Val-Lys conjugates is now being prepared in terms of the molecular weight of PEO, the number of α-CDs, the number of Val-Lys groups, and the degree of carboxyethyl ester groups. Therefore, our design approach on the conjugation of PEPT1-recognizable oligopeptides with supramolecular-structured polyrotaxanes is expected to be useful for retarding the progression of chronic renal disease that requires dietary protein restriction .

ACKNOWLEDGMENT

The authors are grateful to Mr. Koichi Higashimine (Japan Advanced Institute of Science and Technology) for 750 MHz ^{1}H NMR measurements. A part of this study was financially supported by Grants-in-Aid from Micromachine Center, Japan, from NOVARTIS Foundation for the Promotion of Science, Japan, and for Scientific Research on Priority Areas “Molecular Synchronization for Design of New Materials System” from the Ministry of Education, Science, Sports and Culture, Japan.

LITERATURE CITED

(1) Abe, H., Satoh, M., Miyauchi, S., Shuto, S., Matsuda, A., and Kamo, N. (1999) Conjugation of dipeptide to fluorescent dyes enhances its affinity for PepT1 in human intestinal Caco-2 cells. *Bioconjugate Chem. 10*, 24−31.

(2) Takeoka, R., Abe, H, Miyauchi, S., Shuto, S., Matsuda, A., Kobayashi, M., Miyazaki, K., and Kamo, N. (2001) Significance of substrate hydrophobicity for recognition by an oligopeptide transporter (PEPT1). *Bioconjugate Chem. 12*, 485−492.

(3) Schwyzer, R., and Kriwaczek, V. K. (1981) Tabaco mosaic virus as a carrier for small molecules: Artificial receptor antibodies and superhormones. *Biopolymers 20*, 2011−2020.

(4) Aoi, K., Itoh, K., and Okada, M. (1995) Globular carbohydrate macromolecule “Sugar Balls”. 1. Synthesis of novel sugar-persubstituted poly(amido amine) dendrimers. *Macromolecules 28*, 5391−5393.

(5) Reuter, J. D., Myc, A., Hayes, M. M., Gan, Z., Roy, R., Qin,D., Yin, R., Piehler, L. T. Esfand, R., Tomalia, D. A., and Baker, J. R., Jr. (1999) Inhibition of viral adhesion and infection by sialic-acid-conjugated dendritic polymers. *Bioconjugte Chem. 10*, 271−278.

(6) Kiessling, L. L., and Pohl, N. L. (2000) Synthetic multivalent ligands in the exploration of cell-surface interactions. *Curr. Opin. Chem. Biol. 4*, 696−703.

(7) Arimoto, H., Nishimura, K., Kinumi, T., Hayakawa, I., and Uemura, D. (1999) Multivalent polymer of vancomycin: enhanced antibacterial activity against VRE. *Chem. Commun*. 1361−1362.

(8) Ooya, T., Eguchi, M., and Yui, N. (2001) Enhanced accessibility of peptide substrate toward a membrane-bound metalloexopeptidase by supramolecular structure of polyrotaxane. *Biomacromolecules 2*, 200−203.

(9) Ooya, T., Kawashima, T., and Yui, N.(2001) Synthesis of polyrotaxane-biotin conjugates and surface plasmon resonance analysis of streptavidin recognition. *Biotechnol. Bioprocess Eng. 6*, 293−300.

(10) Ooya, T., and Yui, N. (2002) Multivalent interactions between biotin-polyrotaxane conjugates and streptavidin as a model of new targeting for transporters. *J. Controlled Release 80*, 219−228.

(11) Yui, N., Ooya, T., and Kumeno, T. (1998) Effect of biodegradable polyrotaxane on platelet activation. *Bioconjugate Chem. 9*, 118−125.

(12) Huh, K. M., Kumashio, Y., Ooya, T., and Yui, N. (2001) A new synthetic route for dextran graft copolymers containing thermo-responsive polymers. *Polym. J. 33*, 108−111.

(13) Nakanishi, T., Tamai, I., Takaki, A., and Tsuji, A. (2000) Cancer cell-targeted drug delivery utilizing oligopeptide transport activity. *Int. J. Can. 88*, 274−280.

(14) Bradford, M. M. (1976) A rapid and sensitive method for the quantitation of microgram quantities of protein utilizing the principle of protein-dye binding. *Anal. Biochem. 72*, 248−254.

(15) Ooya, T., and Yui, N. (1998) Supramolecuar dissociation of biodegradable polyrotaxanes by enzymatic terminal hydrolysis. *Macromol. Chem. Phys. 199*, 2311−2320.

(16) Ooya, T., and Yui, N. (1999) Synthesis of a theophylline-polyrotaxane conjugate and its drug release via supramolecular dissociation. *J. Controlled Release 58*, 251−269.

(17) Mann, D. A., Kanai, M., Maly, D. J., and Kiessling, L. L. (1998) Probing low affinity and multivalent interactions with surface plasmon resonance: Ligand for Concanavarin A. *J. Am. Chem. Soc. 120*, 10575−10582.

(18) Tamai, I., Saito, Y., Sai, Y., Kawashima, T., Ooya, T., Yui, N., and Tsuji, A. (2001) Retardation of progressive chronic retinal disease by polyrotaxane-dipeptide conjugates that inhibit intestinal peptide transporter PEPT1. *Proc. Int. Symp. Controlled Release Bioact. Mater. 28*, 7115.

(19) Ooya, T., Eguchi, M., Ozaki, A., and Yui, N. (2002) Carboxyethylester-polyrotaxanes as a new calcium chelating polymer: Synthesis, calcium binding and mechanism of trypsin inhibition. *Int. J. Pharm*., in press.

BC015567Z

A Streptavidin−Biotin Binding System That Minimizes Blocking by Endogenous Biotin

Kevin J. Hamblett,[†] Brian B. Kegley,[‡] Don K. Hamlin,[‡] Ming-Kuan Chyan,[‡] David E. Hyre,[†] Oliver W. Press,[§,#] D. Scott Wilbur,[‡] and Patrick S. Stayton[†,*]

Departments of Bioengineering, Medicine, and Radiation Oncology, University of Washington, Seattle, Washington 98195 and The Fred Hutchinson Cancer Research Center, Seattle, Washington 98109-1024. Received October 17, 2001

Pretargeted radioimmunotherapy specifically targets radiation to tumors using antibody−streptavidin conjugates followed by radiolabeled biotin. A potential barrier to this cancer therapy is the presence of endogenous biotin in serum, which can block the biotin-binding sites of the antibody−streptavidin conjugate before the administration of radiolabeled biotin. Serum-derived biotin can also be problematic in clinical diagnostic applications. Due to the extremely slow dissociation of the biotin−streptavidin complex, this endogenous biotin can irreversibly block the biotin-binding sites of streptavidin and reduce therapeutic efficacy, as well as reduce sensitivity in diagnostic assays. We tested a streptavidin mutant (SAv-Y43A), which has a 67-fold lower affinity for biotin than wild type streptavidin, and three bivalent bis-biotin constructs as replacements for wild-type streptavidin and biotin used in pretargeting and clinical diagnostics. Biotin dimers were engineered with certain parameters including water solubility, biotinidase resistance, and linker lengths long enough to span the distance between two biotin-binding sites of streptavidin. The bivalent biotins were compared to biotin in exchange, retention, and off-rate assays. The faster off-rate of SAv-Y43A allowed efficient exchange of prebound biotin by the biotin dimers. In fluorescent competition experiments, the biotin dimer ligands displayed high avidity binding and essentially irreversible retention with SAv-Y43A. The off-rate of a biotinidase-stabilized biotin dimer from SAv-Y43A was 4.36×10^{-6} s^{-1}, over 640 times slower compared to biotin. These findings strongly suggest that employing a mutant streptavidin in concert with a bivalent biotin can mitigate the deleterious impact of endogenous biotin, by allowing exchange of bound biotin and retention of the biotin dimer carriers.

INTRODUCTION

The high affinity streptavidin (SAv[1])−biotin binding system is widely utilized in clinical diagnostic applications (*1*) and is under evaluation as a molecular component in tumor-targeted cancer therapeutics. In diagnostics, SAv is used as "molecular velcro" to bind biotinylated antibodies or other proteins that specifically capture the desired target for diagnosis. For cancer therapeutics, the biotin/SAv binding pair is being used in chemical reagents designed to optimize the targeting of radionuclides to cancer cells for therapy (*2*−*8*). In this application, termed "pretargeting", a monoclonal antibody (mAb)−SAv conjugate is injected into a patient, allowed to localize at the tumor over 24−48 h, followed by the clearing of excess reagent from blood and administration of the radiolabeled biotin derivative. The excess radiolabeled biotin is rapidly excreted via the renal system. Very encouraging results have been obtained with the pretargeting approach in preclinical therapy studies using human tumor xenografts in athymic mice (*9*, *10*).

While the high affinity of the streptavidin−biotin system is a central feature of both diagnostic and pharmaceutical applications, this tight interaction can paradoxically present a serious limitation when naturally occurring "endogenous" biotin blocks the biotin binding sites of SAv. Biotin is involved in intermediary metabolism (*11*−*13*) and is present in blood at 0.6−3.0 nM (*14*). Axworthy et al. determined that the biotin binding sites of SAv are partially blocked by endogenous biotin in pretargeting applications, impairing its efficacy (*10*). Similarly, tissue slices and blood samples used for clinical diagnostics can also contain significant levels of endogenous biotin that reduce the efficacy of biotin/SAv based detection systems (*15*−*18*).

Strategies that circumvent the blocking of the biotin-binding sites of streptavidin by endogenous biotin may therefore offer therapeutic advantages. The intrinsic challenge is to engineer a decrease in streptavidin affinity for endogenous biotin, while preserving high affinity for the biotinylated radiation carriers in the case of therapeutics, or biotinylated macromolecules (e.g., antibodies, oligonucleotides) in the case of clinical diagnostics. We

* Address correspondence to: Patrick S. Stayton, Ph.D., Department of Bioengineering, 351721, University of Washington, Seattle, WA 98195. Phone: 206-685-8148, Fax: 206-685-8256, stayton@u.washington.edu.

[†] Department of Bioengineering.

[#] Department of Medicine.

[‡] Department of Radiation Oncology.

[§] The Fred Hutchinson Cancer Research Center.

[1] Abbreviations: Av, avidin; cpm, counts per minute; EDC, 1-(3-dimethylaminopropyl)-3-ethylcarbodiimide; HABA, 2-(4-hydroxyphenylazo)benzoic acid; mAb−SAv, monoclonal antibody−streptavidin conjugate; NCS, *N*-chlorosuccinimide; NHS, *N*-hydroxysuccinimide; SAv, streptavidin; SAv-Y43A, streptavidin mutant having the tyrosine at residue 43 replaced with an alanine, SAv-WT, wild-type streptavidin; *t*-Boc, *tert*-butyloxycarbonyl; TCDI, thiocarbonyldiimidazole; TFA, trifluoroacetic acid; TFP, tetrafluorophenyl; TFP-OAc, tetrafluorophenyl trifluoroacetate;

10.1021/bc010087t CCC: $22.00 © 2002 American Chemical Society
Published on Web 04/30/2002

describe here how site-directed SAv binding pocket mutants can be used to achieve this goal in concert with appropriately designed bivalent biotin ligands and radiation carriers. We have utilized previously described site-directed streptavidin mutants (*19*−*22*) and bivalent biotin ligands designed to effectively reach the two adjacent biotin binding pockets of streptavidin (*23*, *24*). The lower affinities and faster biotin off-rates of the SAv mutants allows prebound endogenous biotin to quickly dissociate, while the dual binding of the bis-biotin ligand results in a striking avidity effect that leads to high affinity capture of the modified bivalent ligands. These ligands can be readily designed as biotinidase-stabilized ligands and jointly as radiation carriers.

EXPERIMENTAL PROCEDURES

General. All chemicals purchased from commercial sources were analytical grade or better and were used without further purification unless noted. Most reagents were obtained from Aldrich Chemical Co. (Milwaukee, WI). Biotin was obtained from Sigma Chemicals (St. Louis, MO). 4,7,10-Trioxa-1,13-tridecanediamine was obtained from Fluka (St. Louis, MO). biotin-4-fluorescein was obtained from Molecular Probes (Eugene, OR). 2,3,5,6-Tetrafluorophenyl trifluoroacetate (TFP-OTFA) was prepared as previously described (*25*). L-Aspartic acid α-*tert*-butyl ester was obtained from Calbiochem-Novabiochem Corp. (San Diego, CA). Solvents for HPLC analysis were obtained as HPLC grade and were filtered (0.2 μm) prior to use. Silica gel chromatography was conducted with 70−230 mesh 60 Å silica gel (Aldrich Chemical Co.). Melting points were obtained in open capillary tubes on a Mel-Temp II apparatus with a Fluka 51 K/J electronic thermometer and are uncorrected.

Radioactive Materials. Standard methods for safely using radionuclides of iodine were employed (*26*). Na[^{125}I]I was purchased from NEN/Dupont (Billerica, MA) as high pH, high concentration solutions in 0.1 N NaOH. Measurement of ^{125}I was accomplished on the Capintec CRC-15R or a Capintec CRC-7 Radioisotope Calibrator.

Spectral Analyses. ^{1}H NMR spectra were obtained on a Bruker AC-200 (200 MHz), Bruker AC 300 (300 MHz), or Bruker AC 500 (500 MHz) instrument. Chemical shifts are expressed as ppm using tetramethylsilane as internal standard ($\delta = 0.0$ ppm). Mass spectral data (both low resolution and high resolution) of most compounds prepared in this study were obtained on a PerSeptive Biosystems Mariner electrospray time-of-flight mass spectrometer (ESI-TOF). For analysis, the samples were dissolved in 50/50 MeOH/H_2O and were introduced by an integral syringe infusion pump. Some mass spectral data (low resolution) were obtained on a VG Analytical (Manchester, England) VG-70 SEQ mass spectrometer with associated 11250J Data System. These mass spectral data were obtained by fast atom bombardment (FAB^+) in a matrix of 2-hydroxyethyl disulfide (2HEDS) and poly(ethylene glycol) 300 or 600 containing thioglycolate. High resolution mass spectral data were used for compound identification. Compounds containing Sn isotopes had five matching isotopic masses, but only one is provided as identification. ^{1}H NMR and HPLC were used to assess purity of nonradioactive compounds (these data are provided in the Supporting Information).

Chromatography. HPLC separations of nonradioactive compounds were obtained on Hewlett-Packard quaternary 1050 gradient pumping system with a variable wavelength UV detector (254 nm) and a Varex ELSD MKIII evaporative light-scattering detector. Analysis of the HPLC data were conducted on Hewlett-Packard HPLC ChemStation software. All reactions were monitored by HPLC. Reversed-phase HPLC chromatography was carried out using an Alltech Altima C-18 column (5 μm, 250 mm × 4.6 mm) using a gradient solvent system at a flow rate of 1 mL/min. A gradient of MeOH and H_2O/0.1% HOAc was used. Starting with 40% MeOH, the initial solvent mixture was held for 2 min; then the gradient was increased to 100% MeOH over the next 10 min and then held at 100% MeOH for 8 min. Retention times (t_R) under these conditions for biotin conjugates are provided with the experimental procedures.

HPLC separations of radioiodinated biotin derivatives were conducted using a gradient system which consisted of two Beckman model 110B pumps, a Beckman 420 controller, a Beckman model 153 UV detector (254 nm), and a Beckman model 170 radioisotope detector. The separations were obtained using HPLC conditions described above, except the gradient was started with 30% MeOH.

Compound Preparation. The following compounds were prepared as previously described: **1**, **4** (*23*); **8** (*27*); **11**, **12** (*24*); **13**, **14**, [^{125}I]**13** (*28*); **17** (*29*); **21**, and **22** (*30*).

***N*-(*tert*-Butyloxycarbonyl)-5-aminoisophthalate Bis-tetrafluorophenyl Ester (3).** To 236 mL of a 1:1 mixture of DMF/H_2O containing 5-aminoisophthalic acid (25.28 g, 140 mmol) and NaOH (12.3 g, 307 mmol) at ice/H_2O temperature was added di-*tert*-butyl dicarbonate (32.1 g, 147 mmol). The reaction was allowed to come to room temperature while stirring for 30 h. The reaction mixture was acidified slowly with 3 N HCl (111 mL), and the mixture was diluted with an additional 100 mL of H_2O. The precipitate was collected, washed with water, and dried to yield 28.8 g (73%) of the *t*-Boc protected aminoisophthalic acid mp > 300 °C. ^{1}H NMR (DMSO-d_6, 200 MHz): δ 1.50 (s, 9H), 8.08 (t, $J = 1.5$ Hz, 1H), 8.31 (d, $J = 1.5$ Hz, 2H), 9.80 (s, 1H). HRMS calcd for $C_{13}H_{16}NO_6$ $(M + H)^+$: 282.0977. Found: 282.0981. HPLC: t_R =11.3 min.

A quantity (5 g, 18 mmol) of the *t*-Boc protected 5-aminoisophthalic acid was dissolved in 40 mL of DMF, and tetrafluorophenol (6.5 g, 39 mmol) was added. To this mixture was added a solution containing EDC in 30 mL of DMF. The reaction was stirred at room temperature for 16 h, and the DMF was removed under vacuum. The crude product was divided into two portions, and each portion was purified on a silica column (200 g) eluting with 5% EtOAc/hexanes. The fractions containing product (by HPLC) were evaporated under vacuum and combined to provide 6.8 g (67%) of 3 as a white solid, mp 159.7−161.8 °C dec ^{1}H NMR ($CDCl_3$, 200 MHz): δ 1.55 (s, 9H), 6.83 (s, 1H), 7.08 (m, 1H), 8.54 (d, $J = 1.5$ Hz, 2H), 8.67 (t, $J = 1.5$ Hz, 1H). HRMS calcd for $C_{25}H_{15}F_8NNaO_6$ $(M + Na)^+$: 600.0669. Found: 600.0674. HPLC: $t_R = 16.3$ min.

***N′*,*N″*-Bis(8-biotinamido-3,6-dioxaoctanylamino)-5-(*N*-*tert*-butyloxycarbonyl)aminoisophthalamide (5).** A quantity of **4** (321 mg, 0.86 mmol) was dissolved in 4 mL of DMF, and Et_3N (60 μL, 0.43 mmol) was added. In a separate flask, a quantity of **3** (50 mg, 0.086 mmol) was dissolved in 10 mL of DMF. The solution of **3** was dripped slowly into the solution of **4** over a 1 h period. The solvent was removed under vacuum, and the crude product was dissolved into a minimal amount of MeOH. This solution was loaded onto a silica gel column (8 g) and was eluted using EtOAc (400 mL) and then MeOH/EtOAc mixtures increasing in the percentage of MeOH. The product eluted using a mixture of 60% EtOAc/40% MeOH. Fractions containing product were taken to dryness under

vacuum to yield 65 mg (79%) of **5** as a colorless solid, mp 94−95 °C; ^{1}H NMR (MeOH-d_4, 200 MHz) 1.0−1.6 (br m, 10H), 1.4 (s, 9H), 2.0 (m, 4H), 2.5 (m, 2H), 2.8 (m, 2H), 3.0 (m, 2H), 3.2 (m, 8H), 3.4 (m, 16H), 4.1 (m, 2H), 4.3 (m, 2H), 4.5 (s, 2H), 7.7 (m, 1H), 7.9 (m, 2H); HRMS calcd for $C_{45}H_{72}N_9O_{12}S_2$ (M + H) 994.4749 found 994.4742; HPLC: t_R= 10.9 min.

***N′,N″*-Bis(8-biotinamido-3,6-dioxaoctanylamino)-5-((*N*-*tert*-butoxycarbonyl)-13-amino-4,7,10-trioxatridecane-thioureido)isophthalamide (9).** A quantity of **5** (356 mg, 0.36 mmol) was dissolved in 1 mL of TFA. The reaction was allowed to stir for 10 min, and the excess TFA was removed under a gentle stream of argon (in a fume hood). The residue was dissolved in a minimal amount of MeOH, and an excess of Et_3N (1 mL) was added. The mixture was stirred for 10 min, and the excess Et_3N and solvent were removed under vacuum. The crude amino-biotin dimer, **6**, was further dried under vacuum to yield 302 mg (94%). HRMS calcd for $C_{40}H_{63}N_9O_{10}NaS_2$ (M + Na) 916.4041, found 916.4043; HPLC: t_R= 7.5 min.

The isolated **6** was added to a solution of thiocarbonyldiimidazole (66 mg, 0.37 mmol) in 4 mL of DMF. The reaction was stirred at room temperature for 0.5 h and then taken to dryness under a stream of argon to yield **7** which was directly used in the following step. A quantity of the *t*-Boc-protected trioxadiamine **8** (113 mg, 0.35 mmol) was added to the solution, and the reaction was stirred for 0.5 h at room temperature. The reaction mixture was then triturated with 50 mL of ether and stirred for 1 h until the solution became clear. The ether was decanted, and the crude product was dissolved in a minimal amount of MeOH. The crude material was loaded onto silica gel column (40 g). The column was eluted with EtOAc (100 mL) and then with increasing concentration of MeOH in EtOAc until the product eluted (50% MeOH). Fractions containing product (by HPLC) were taken to dryness to yield 125 mg (31%) of **9** as a tacky solid; ^{1}H NMR (MeOH-d_4, 200 MHz) 1.4 (s, 9H), 1.6 (m, 8H), 1.9 (m, 2H), 2.2 (t, J = 7.3 Hz, 4H), 2.7 (d, J = 12.5 Hz, 4H), 2.9 (dd, J = 5.1, 12.8 Hz, 2H), 3.1 (t, J = 6.9 Hz, 1H), 3.2 (m, 2H), 3.3 (m, 8H), 3.3 (m, 4H), 3.6 (m, 28H), 4.2 (m, 2H), 4.4 (m, 2H) 4.5 (s, 2H), 8.0 (d, J = 1.4 Hz, 2H), 8.0 (t, J = 1.4 Hz, 1H); HRMS calcd for $C_{56}H_{93}N_{11}O_{15}NaS_3$ (M + Na) 1278.5929 found 1278.5912; HPLC: t_R= 11.2 min.

***N′,N″*-Bis(8-biotinamido-3,6-dioxaoctanylamino)-5-((13-amino-4,7,10-trioxatridecane)thioureido)-isophthalamide (10).** A quantity of **9** (125 mg, 0.1 mmol) was dissolved in 1 mL of TFA. The reaction was stirred for 10 min, and the excess TFA was removed under a gentle stream of argon. The product was dissolved in a minimal amount of MeOH, and an excess of Et_3N (1 mL) was added and was allowed to stir for 10 min. Excess Et_3N and solvent were removed under vacuum, and the product was dried under vacuum to yield 107 mg (93%) of **10**. HRMS calcd for $C_{51}H_{86}N_{11}O_{13}S_3$ (M + H) 1156.5560 found 1156.5569; HPLC: t_R= 7.5 min. This material was of sufficient purity (>95% by HPLC) to be used directly in subsequent reactions.

***N′,N″*-Bis(8-biotinamido-3,6-dioxaoctanylamino)-5-((13-(*N*-(*p*-iodo)benzamido-4,7,10-trioxatridecane)-thioureido)isophthalamide (15).** A quantity of **10** (50 mg, 0.04 mmol) was dissolved in 4 mL of DMF. Et_3N (15 μL, 0.08 mmol) and *p*-iodobenzoate TFP ester **11** (18 mg, 0.04 mmol) were added, and the reaction was stirred for1 h at room temperature. The mixture was triturated with 50 mL of ether and stirred for an additional 1 h. The ether was decanted, and the product was dried under vacuum to yield 54 mg (90%) of **15** as a tacky solid; ^{1}H NMR (MeOH-d_4, 500 MHz) 1.4 (s, 4H), 1.6 (m, 8H), 1.9 (m, 4H), 2.2 (t, J = 7.4 Hz, 4H), 2.7 (d, J = 12.9 Hz, 2H), 2.9 (dd, J = 4.9, 12.9 Hz, 2H), 3.2 (m, 4H), 3.3 (m, 4H), 3.3 (m, 20H), 3.6 (m, 12H), 3.7 (m, 8H), 4.3 (m, 2H), 4.5 (m, 2H) 4.6 (s, 4H), 7.5 (d, J = 8.6 Hz, 2H), 7.8 (d, J = 8.6 Hz, 2H), 8.0 (s, 2H), 8.0 (s, 1H); HRMS calcd for $C_{58}H_{88}N_{11}O_{14}NaS_3I$ (M + Na) 1408.4612 found 1408.4617; HPLC: t_R= 12.0 min.

***N′,N″*-Bis(8-biotinamido-3,6-dioxaoctanylamino)-5-((13-(*N*-(*p*-tri-*n*-butylstannyl)benzamido-4,7,10-trioxatridecane)thioureido))isophthalamide (16).** This compound was prepared as described for **15** (above) except the stannylbenzoate TFP ester, **12** (25 mg, 0.04 mmol) was added in the place of **11**. The reaction yielded 48 mg (77%) of **16** as a tacky solid; ^{1}H NMR (MeOH-d_4, 500 MHz) 0.9 (t, J = 6.8 Hz, 9H), 1.1 (m, 4H), 1.3 (m, 8H), 1.6 (m, 12H), 1.9 (m, 6H), 2.2 (t, J = 7.4 Hz, 8H), 2.7 (d, J = 12.3 Hz, 4H), 2.8 (s, 4H), 2.9 (dd, J = 4.9, 12.3 Hz, 2H), 3.0 (s, 2H), 3.2 (m, 4H), 3.3 (m, 8H), 3.4 (m, 4H), 3.6 (m, 12H), 3.6 (m, 8H), 4.3 (m, 2H), 4.5 (m, 2H), 7.5 (d, J = 8.0 Hz, 2H), 7.7 (d, J = 0.80 Hz, 2H), 8.0 (s, 2H), 8.1 (s, 1H); LRMS calcd for $C_{70}H_{115}N_{11}O_{14}NaS_3Sn$ (M + Na) 1571 found 1571; HPLC: t_R= 16.0 min.

Preparation of [^{125}I]15. To a solution containing *p*-tri-*n*-butylstannybenzoate NHS ester **13** (50 μg in 1 mg/mL solution MeOH/5%AcOH) and Na[^{125}I]I (3 μL in 0.1 N NaOH, 977 μCi) was added NCS (10 μL in 1 mg/mL solution MeOH). The reaction mixture was stirred for 5 min at room temperature. Sodium metabisulfite (10 μL in 1 mg/mL solution H_2O) was then added to quench the reaction. The reaction mixture was dried under a stream of air (through charcoal filter), and a solution containing **10** (200 μL of 1 mg/mL solution in DMF) and Et_3N (10 μL) was added. This mixture was stirred for 0.5 h at room temperature, and the product was purified by HPLC to give a 75% radiochemical yield of [^{125}I]**15**.

***N*-(Biotinyl)-α-*tert*-butyl-*β*-*N*-(8-amino-3,6-dioxaoctanyl)aspartamide (19).** A quantity (100 mg, 0.18 mmol) of **17** was dissolved into 2 mL of anhydrous DMF. This solution was added slowly (1 h) into a solution of dioxadiamine **18** (260 μL, 1.78 mmol) in 2 mL of anhydrous DMF. After the addition was complete, the reaction was allowed to stir for an additional 1 h at room temperature. The reaction mixture was then triturated with 100 mL of ether, and this mixture was stirred for 1 h. The ether was decanted, and an additional 100 mL of ether was added and stirred for another 1 h. After that time, the ether was decanted, and the product was dried under vacuum to yield 74 mg (76%) of **19** as a tacky solid; ^{1}H NMR (MeOH-d_4, 200 MHz) 1.4 (s, 9H), 1.6 (m, 4H), 2.2 (t, J = 7.3 Hz, 2H), 2.6 (m, 4H), 2.9 (m, 2H), 3.23 (m, 1H), 3.3 (m, 4H), 3.5 (m, 4H), 3.6 (m, 4H), 4.3 (dd, J = 4.4, 8.0 Hz, 1H), 4.4 (dd, J = 4.4, 7.7 Hz, 1H), 4.6 (t, J = 6.2, 1H); HRMS calcd for $C_{24}H_{43}N_5O_7NaS$ (M + Na) 568.2810, found 568.2781; HPLC: t_R= 6.5 min.

***N′,N″*-Bis(*N*-(biotinyl)-*β*-*N*-(8-amino-3,6-dioxaoctanyl)aspartamidyl-5-*N*-(*p*-iodobenzamido)aminoisophthalamide (23).** A quantity of **19** (500 mg, 0.77 mmol) was dissolved in 3 mL of TFA. The reaction was stirred for 10 min and the excess TFA was removed under a gentle stream of argon. The residue was washed several times with 5 mL portions of ether to remove any remaining TFA. The residue was then dried under vacuum to yield **20** as the TFA salt. The isolated **20** was >95% pure (by HPLC) and was used directly in next reaction step. HPLC: t_R = 3.0 min.

Quantities of **20** (370 mg, 0.757 mmol), **21** (267 mg, 0.378 mmol), and Et_3N (160 μL, 1.13 mmol) were dis-

solved in 5 mL of DMF. This mixture was stirred for 0.5 h and then triturated with 100 mL of ether. The resultant solid was collected by filtration and dried on vacuum. A yield of 350 mg (68%) **23** was obtained as a white solid; mp 80−81 °C; ^{1}H NMR (MeOH-d_4, 200 MHz) 1.4 (m, 4H), 1.6 (m, 6H), 2.2 (t, J = 7.3 Hz, 4H), 2.6 (m, 4H), 2.8 (s, 2H), 2.9 (dd, J = 4.7, 12.8 Hz, 2H), 3.3 (m, 6H), 3.5 (t, J = 5.1 Hz, 8H), 3.6 (m, 12H), 4.2 (m, 2H), 4.4 (m, 2H), 4.5 (m, 2H), 7.7 (d, J = 8.7 Hz, 2H), 7.9 (d, J = 8.4 Hz, 2H), 8.0 (t, J = 1.4 Hz, 1H), 8.3 (d, J = 1.4 Hz, 2H); HRMS calcd for $C_{55}H_{75}N_{11}O_{17}Na_2S_2I$ (M−H+2Na) 1398.3628, found 1398.3624; HPLC: t_R = 11.2 min.

***N′,N″*-Bis(*N*-(biotinyl)-*β*-*N*-(8-amino-3,6-dioxaoctanyl)aspartamidyl-5-*N*-(*p*-(tri-*n*-butylstannyl)benzamido)aminoisophthalamide (24).** A quantity (300 mg, 0.613 mmol) of **20** (prepared as described above), **22** (266 mg, 0.306 mmol), and Et_3N (130 μL, 0.92 mmol) was dissolved in 5 mL of DMF. That solution was stirred at room temperature for 0.5 h and then triturated with 100 mL of ether. The precipitate was collected by filtration, dissolved in minimal amount of MeOH, and loaded onto silica gel column (20 g). The column was first eluted using EtOAc (300 mL), and then MeOH was added to the eluant in increasing proportions until the product eluted (50% methanol). The solvent was removed from fractions containing product (determined by HPLC). The residue was dried under vacuum to yield 149 mg (32%) of **24** as a white solid; mp 174−176 °C; ^{1}H NMR (DMSO-d_6, 300 MHz) 0.8 (t, J = 7.2 Hz, 9H), 1.0(t, J = 7.7 Hz, 6H), 1.3 (m, 10H), 1.5 (m, 12H), 2.0 (t, J = 6.7 Hz, 4H), 2.3 (m, 2H), 2.5 (s, 2H), 2.5 (s, 2H), 2.8 (dd, J = 4.6, 12.9 Hz, 2H), 3.0 (m, 2H), 3.1 (m, 4H), 3.2−3.7 (m, 20H), 4.1 (m, 2H), 4.2 (m, 2H), 4.3 (m, 2H), 7.5 (d, J = 7.2 Hz, 2H), 7.5 (d, J = 7.2 Hz, 2H), 8.0 (d, J = 8.3 Hz, 2H), 8.2 (s, 1H), 8.3 (s, 2H), 8.5 (s, 2H), 8.9 (s, 2H), 10.7 (d, J = 9.8 Hz, 1H); HRMS calcd for $C_{67}H_{101}N_{11}O_{17}Na_3S_2Sn$ (M − 2H + 3Na) 1584.5426, found 1584.5533; HPLC: t_R= 15.7 min.

Preparation of [^{125}I]23. To a 50 μL solution of **24** (1 mg/mL in 5%AcOH/MeOH) was added 7 μL of Na^{125}I (2.8 mCi) in 0.1 N NaOH. To the resultant solution was added 15 μL of a 1 mg/mL solution of NCS in MeOH. The reaction was quenched after 5 min with 15 μL of a 1 mg/mL solution of sodium metabisulfite in H_2O. Radio-HPLC analysis indicated that the reaction gave >75% radiochemical yield, and 1.5 mCi (54%) [^{125}I]**23** was isolated from the HPLC effluent; t_R= 15.6 min.

Streptavidin. The production and purification of streptavidin, SAv-WT and the site-directed mutant, SAv-Y43A, has been previously described (*22*). Briefly, SAv was expressed in BL21(DE3) cells containing the pET-21a plasmid with the SAv gene. Cells were grown in 3 L of 2xYT media until an OD_{600} between 0.6 and 0.9 was reached, at which time induction was initiated by the addition of isopropyl beta-D-thiogalactoside to a final concentration of 0.1 mM. Cells were grown for 3 h and harvested by centrifugation. Cells were lysed to liberate the inclusion bodies, followed by washing of the inclusion bodies. The inclusion bodies were solubilized using 6 M Gdn-HCl and refolded by dilution in Tris-Saline at 4 °C. SAv-WT and SAv-Y43A were purified using an iminobiotin column. All experiments performed report SAv concentration as the monomer concentration not the standard tetramer concentration.

Molecular Modeling. Simulations of the distances between biotin carboxylate carbons were obtained from the computer program ChemDraw 3D (CambridgeSoft Corporation, Cambridge, MA) after the structures were energy minimized in their fully extended, planar conformation.

Binding Stoichiometry Determination. SAv-Y43A monomer concentration was determined by spectrophotometric analysis at 280 nm (ϵ = 34000 $M^{-1}cm^{-1}$). 2-(4-Hydroxyphenylazo)benzoic acid (HABA) was added, and the absorbance was measured at 500 nm. Biotin, biotin dimer **1**, biotin dimer **15**, or biotin dimer **23** were titrated separately and the OD_{500} was measured to determine the percent change in HABA occupied biotin binding sites. The ratio of biotin moieties to biotin sites was calculated as the cumulative concentration of biotin added to the sample divided by the total concentration of biotin binding sites (*31*).

Fluorescence Assays of Ligand-Binding Kinetics. Quantitation of ligand binding kinetics and ligand exchange with biotin-4-fluorescein were performed on a Hitachi spectrophotofluorometer F4500 with excitation at 494 nm and emission monitored at 525 nm, 5 nm excitation and emission slit widths. The off-rate of biotin-4-fluorescein (Molecular Probes, Eugene OR) from SAv-Y43A was determined at 37 °C by adding equimolar amounts of mutant to biotin-4-fluorescein at 380 nM, followed by addition of a 1000-fold excess of biotin. The fluorescence was measured continuously for 1 h after the addition of the biotin. The off-rate of biotin-4-fluorescein was determined to be 7.6 × 10^{-4} s^{-1} at 37 °C. Ligand exchange experiments were performed in which biotin, biotin dimer **1**, biotin dimer **15**, and biotin dimer **23** were competed with biotin-4-fluorescein. Five equiv of competitor (biotin, biotin dimer **1**, biotin dimer **15**, or biotin dimer **23**) were added to prebound SAv-Y43A, and the fluorescence emission was measured continuously for 1 h. The experiment was also performed with SAv-WT.

^{3}H-Biotin Ligand Competition Experiments. Competition assays were performed as previously described (*22*) in which biotin, biotin dimer **1**, biotin dimer **15**, and biotin dimer **23** were directly compared to ^{3}H-biotin (Amersham Pharmacia). SAv-Y43A at a subunit concentration of 10 nM was mixed with 10 nM ^{3}H-biotin. Unlabeled competitor (biotin, biotin dimer **1**, biotin dimer **15**, or biotin dimer **23**) at defined concentrations between 0 and 500 nM was added to the mixture, and the reactions were incubated at 37 °C for 2.5 h. A 100 μL volume of the reaction was added to 200 μL of 0.2 M $ZnSO_4$, followed by the addition of 200 μL of 0.2 M NaOH. The mixture was vortexed for 15 s to precipitate the protein and any bound ligand. Samples were centrifuged at 14000 rpm for 1−3 min to pellet the precipitate. Radioactivity of 200 μL of the supernatant was quantified using a scintillation counter.

^{125}I-Biotin Dimer Off-Rate Assay. The biotin dimer **23**[^{125}I] was used to determine the dissociation rate from SA-Y43A. Biotin dimer **23**[^{125}I] was mixed with a 100-fold excess of SA-Y43A. Separation of the unbound biotin dimer **23**[^{125}I] from biotin dimer **23**[^{125}I] bound to SA-Y43A was achieved by using ultrafiltration concentrators (Millipore, Bedford, MA) with a 10000 molecular weight cutoff. Prerinsing concentrators with biotin dimer **23** was necessary to prevent nonspecific binding of biotin dimer **23**[^{125}I] to the membrane. The unbound biotin dimer **23** at time zero was roughly 5% of the total activity present in the sample. This mixture was allowed to equilibrate at 37 °C for 45 min, and 30 μL of the reaction was removed to measure the total radioactivity in cpm. A 200 μL volume of the reaction was then removed and filtered through a concentrator for 2 min at 10000 rpm. A 30 μL volume of the flow-through was removed and the radioactivity measured as the zero time point. A 2800-fold excess of biotin dimer **23** was added to the mixture to start the assay, and at various time points 200 μL was

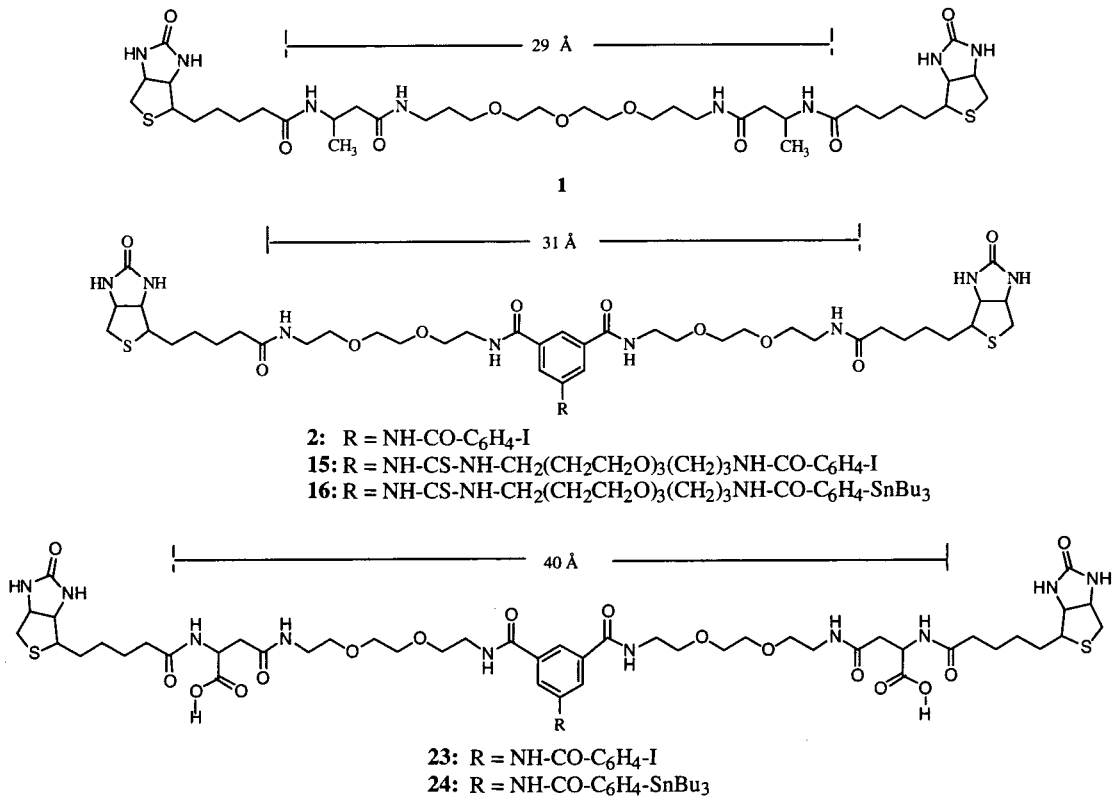


Figure 1. Structures of biotin dimers with the estimated distance between biotin carboxylate carbons.

removed and filtered through the concentrator. A 30 μL volume of the flow-through was removed and the radioactivity measured.

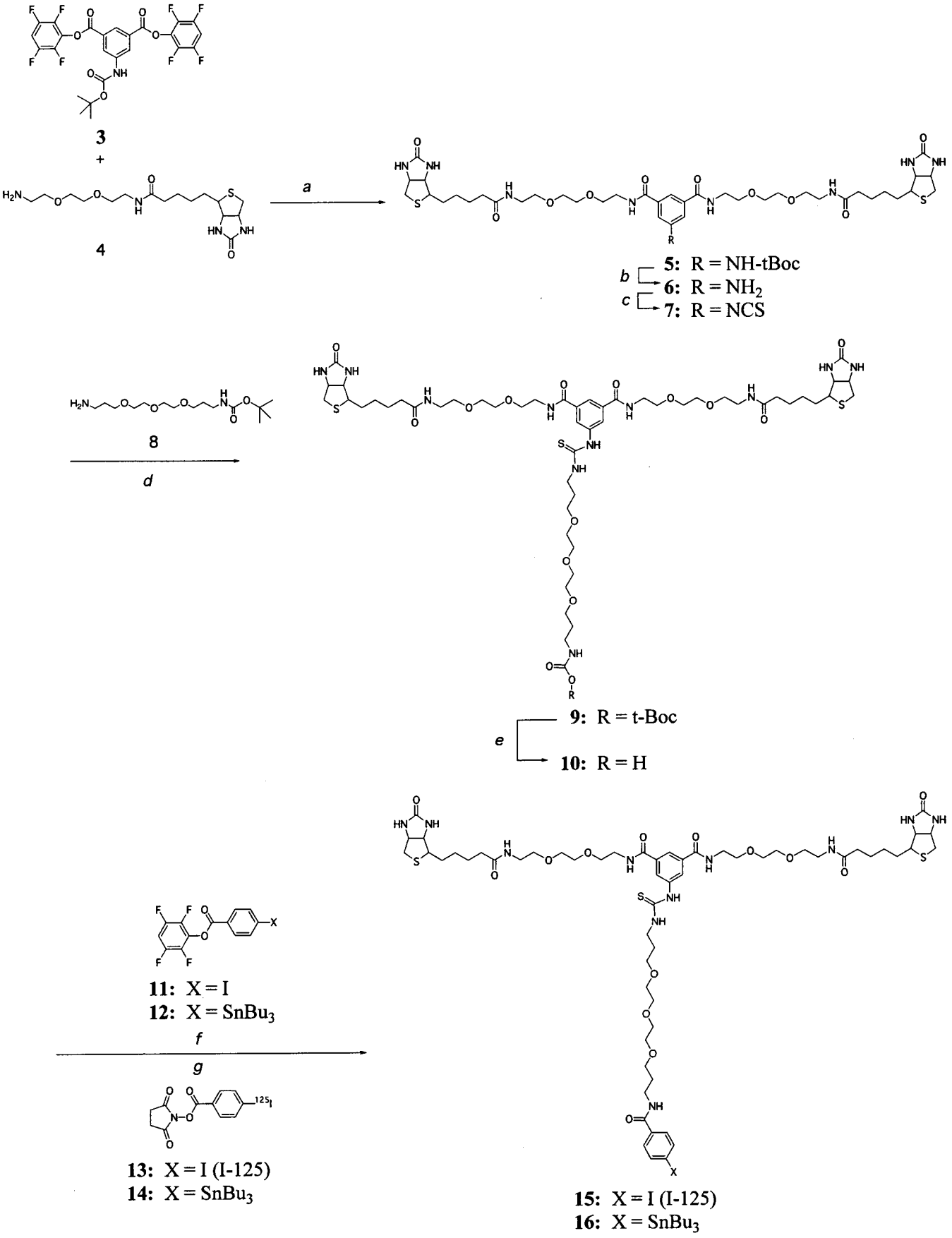
Data Analysis. Linear regression to determine off-rates were performed using GraphPad Prism version 3.02 for Windows, GraphPad Software, San Diego, CA, www.graphpad.com.

RESULTS

Biotin Dimer Synthesis. The structures of the biotin dimers, **1**, **15**, and **23**, prepared for these studies are shown in Figure 1. The first biotin dimer used in the studies, **1**, was prepared by reaction of 2 equiv of 3-(biotinamide)butyrate tetrafluorophenyl ester with 4,7,10-trioxa-1,13-tridecanediamine in DMF as previously described (*23*). The second biotin dimer used in the studies, **15**, was prepared as depicted in Scheme 1. Reaction of the trifunctional cross-linking reagent, *N*-Boc-5-aminoisophthalate bis-TFP ester, **3**, with the dioxaoctanediamine adduct of biotin, **4**, and triethylamine in DMF provided the *t*-Boc protected biotin dimer **5** in 79% purified yield. Deprotection of the *t*-Boc group with trifluoroacetic acid (TFA) was nearly quantitative, and the anilino product was pure enough to be used directly for the preparation of the isothiocyanate, **7**. The aryl isothiocyanate containing biotin dimer, **7**, was prepared by reaction of **6** with thiocarbonyldiimidazole in DMF at room temperature. Biotin dimer **7** was converted to the thiourea adduct **9** in 31% purified yield by reaction with mono-*t*-Boc-protected trioxatridecanediamine **8**. The *t*-Boc group was removed from **9** in nearly quantitative yield in neat TFA to yield **10**, and that material was reacted with the benzoate TFP esters **11** and **12** to prepare the desired biotin dimers, **15** (90%) and **16** (77%), respectively. The third biotin dimer used in the studies, **23**, was prepared as depicted in Scheme 2. In that synthesis, the TPF ester of the α-amino adduct of biotin and aspartic acid β-*tert*-butyl ester, **17**, was first prepared as previously described (*29*). Reaction of **17** with the dioxaoctanediamine **18** provided the adduct **19** in 76% purified yield. Due to a concern that the tri-*n*-butylstannyl group would not be stable to TFA, the deprotection step was carried out on **19**. The deprotection provided **20** in nearly quantitative yield. Reaction of **20** with the iodobenzoyl- and stannylbenzoylaminoisophthalate bis-TFP esters, **21** and **22**, provided the targeted iodobenzoyl-biotin dimer **23** and the stannylbenzoylbiotin dimer **24** in 68% and 32% isolated yields.

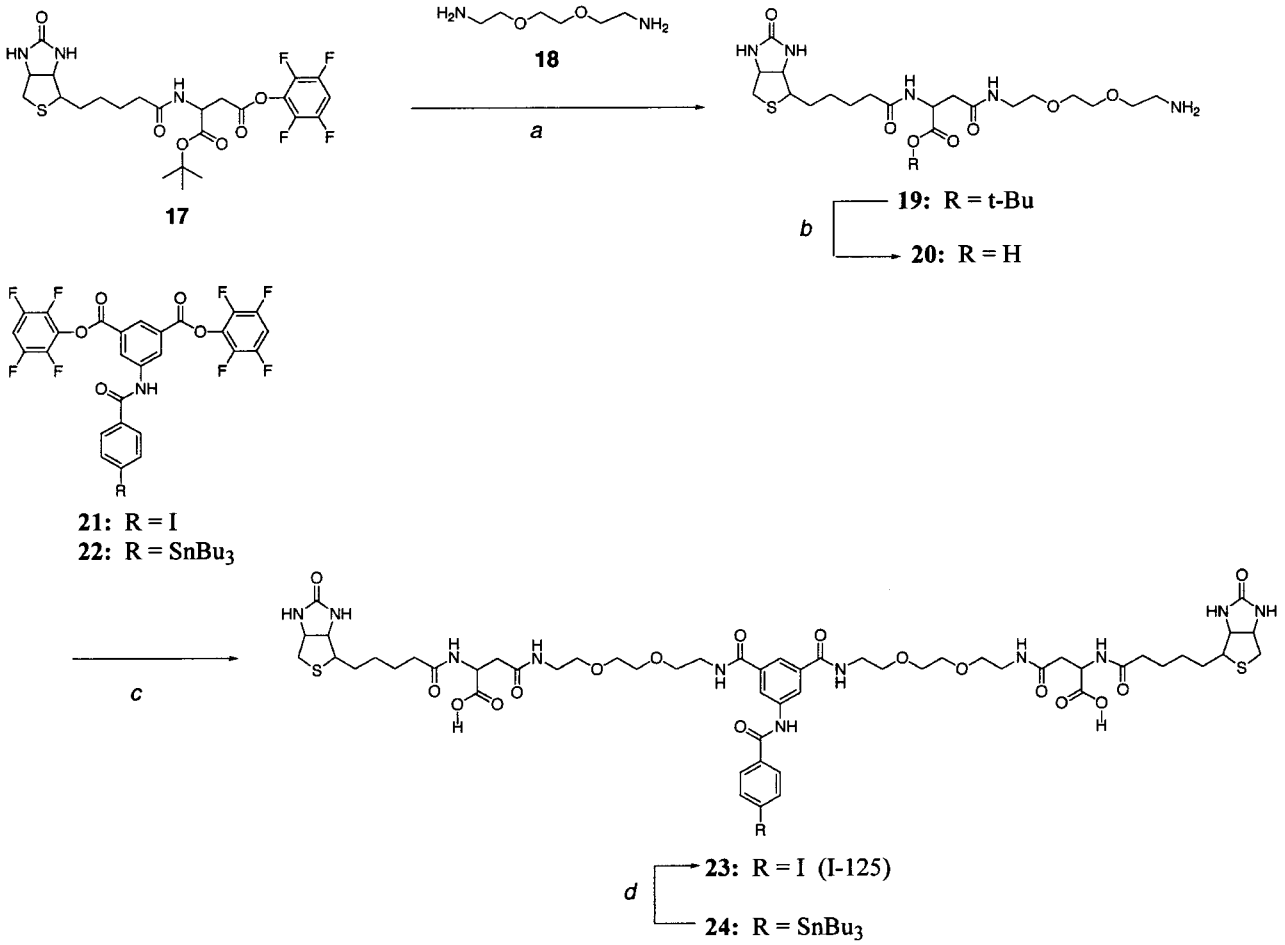
Preparation of Radioiodinated Biotin Dimers, [^{125}I]15 and [^{125}I]23. Arylstannane intermediates have been shown to efficiently introduce radioiodine into a variety of molecules (*32*, *33*). Therefore, we chose to prepare biotin dimers **16** and **24** to use as intermediates for the preparation of [^{125}I]**15** and [^{125}I]**23**. The corresponding iodobenzoyl-biotin dimers **15** and **23** were prepared for binding studies with ^{3}H-biotin and as HPLC reference standards for the radioiodinated compounds. In initial radioiodination studies, the arylstannane **16** was reacted with *N*-chlorosuccinimide (NCS) in a mixture of methanol and acetic acid. Although radioiodination of arylstannanes are generally very facile under those conditions, very low radiolabeling yields were obtained with **16**. We are uncertain of the reason for this, but believe that the thiourea functionality in **16** may interfere with the radioiodination. We have obtained similar results with other compounds that contain thiourea functionalities (*34*). After several radioiodination attempts with **16**, we decided to prepare [^{125}I]**15** via an alternative route. In the alternative route, the aminobiotin dimer **10** was reacted with *p*-[^{125}I]iodobenzoate *N*-hydroxysuccinimide (NHS) ester, **13**, which was prepared from *p*-tri-*n*-butylstannylbenzoate NHS ester, **14**, as previously described (*28*). This provided the desired

Scheme 1. Synthetic Route for Preparation of Biotin Dimer 15 and Radioiodination Methods To Produce [^{125}I]15[a]



[a] (a) Et_3N, DMF, 1 h, rt, 79%; (b) TFA, 10 min, rt, 94%; (c) TCDI, DMF, 30 min; (d) **8**, DMF, 30 min, rt, 31%; (e) TFA, 10 min, rt, 93%; (f) **11** or **12**, DMF, Et_3N, 1 h, rt, 90% or 77%; (g) [^{125}I]**13**, Et_3N, DMF, 30 min, rt, 75%.

Scheme 2. Synthetic Route for Preparation Biotin Dimer 23 and Radioiodination To Form [^{125}I]23[a]



[a] (a) **18**, DMF, 1 h, rt, 76%; (b) TFA, 10 min, rt, 95%; (c) **21** or **22**, DMF, Et_3N, 30 min, rt, 68% or 32%; (d) Na[^{125}I], NCS, MeOH, HOAc, 5 min, 75%.

[^{125}I]**15** in good yield (75%). Contrary to the thiourea containing **16**, direct radioiodination of stannylbenzoyl-biotin dimer **24** with NCS in a methanol/acetic acid solution provided high yields of the desired [^{125}I]**23**.

Stoichiometry of Bis-Biotin Ligand Binding. The binding stoichiometry of the bivalent bis-biotin ligands was determined with a HABA displacement assay (*31*). Biotin and the bivalent biotin ligands were titrated into a solution containing HABA-saturated SAv-Y43A, which permits the determination of the quantity of HABA displaced per quantity of ligand added. The HABA displacement assays are plotted as the percent change in HABA occupied biotin binding sites versus the ratio of biotin moiety added to the biotin binding-site concentration (Figure 2). As expected, a ratio of one biotin moiety per one streptavidin binding site was obtained for biotin, i.e., 4 equiv of biotin was needed to displace 4 equiv of HABA per SAv-Y43A tetramer. The HABA assay revealed that one of the bivalent biotins did not bind to SAv in a true bivalent fashion. Biotin dimer **1** bound the streptavidin tetramer at an average of three bis-biotin molecules per streptavidin tetramer at saturation (i.e., one bis-biotin ligand bound bivalently and two bis-biotin ligands bound through one biotin moiety), compared to the expected ratio of two molecules per streptavidin tetramer observed with biotin dimer **15** and biotin dimer **23**. This finding emphasizes that the distance between biotin groups and the steric properties of the spacer arms play an important role in determining the binding properties of the bis-biotin ligands.

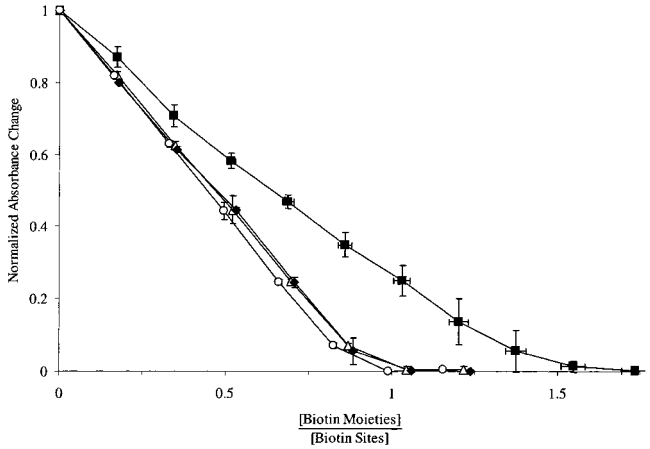


Figure 2. Bis-biotin binding stoichiometry determination. SAv-Y43A was mixed with HABA and the OD_{500} measured. Competitor was added in fixed aliquots and the OD_{500} measured. The percent change in the OD_{500} is plotted versus the ratio of the competitor biotin moiety concentration to the concentration of biotin binding sites. The competitors are biotin (diamonds), biotin dimer **1** (filled squares), biotin dimer **15** (filled triangles), and biotin dimer **23** (circles).

Exchange of Bound Biotin Ligands with Bis-Biotin Ligands. Previous thermodynamic and kinetic characterization of site-directed SAv mutants (*19*−*22*) led to the selection of the SAv-Y43A mutant as one that would allow exchange of bound endogenous biotin at 37 °C, while retaining sufficiently high affinity to efficiently

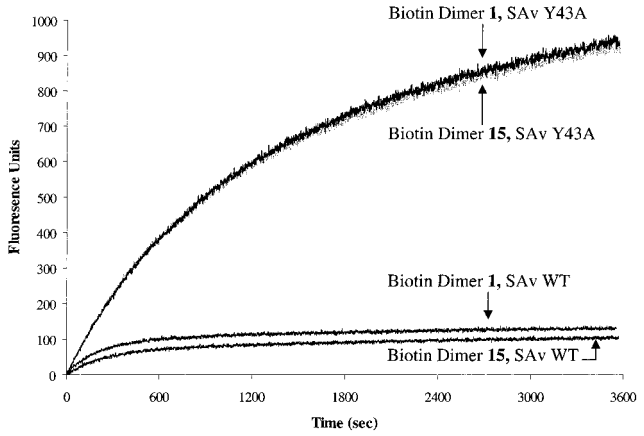


Figure 3. Bis-biotin exchange properties. SAv-Y43A and SAv-WT were incubated with an equimolar amount of biotin-4-fluorescein. A 5-fold molar excess of competitors was added and the fluoresence measured for 1 h. For each protein two competitors are shown (biotin dimer **1** and biotin dimer **15**). The biotin dimer **15**/SAv-Y43A experiment is shown in gray due to its close proximity to biotin dimer **1**/SAv-Y43A.

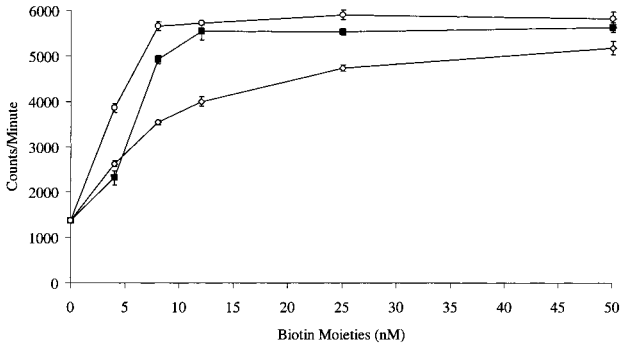


Figure 4. Ligand competition assay. SAv-Y43A was incubated with an equimolar concentration of ^{3}H-biotin and various concentrations of competitor. The free ^{3}H-biotin was separated from protein and bound ligand and the radioactivity measured. Free ^{3}H-biotin is plotted versus the competitor biotin moiety concentration. The competitors are biotin (diamonds—bottom line), biotin dimer **1** (filled squares—middle line), and biotin dimer **23** (circles—top line).

capture bis-biotin ligands. The biotin off-rate from SAv-Y43A is $28 \times 10^{-4} s^{-1}$ at 37 °C and the K_a is reduced by 67-fold from SAv-WT (*22*). The impact of this faster off-rate on ligand exchange can be observed by comparing the exchange of prebound biotin-4-fluorescein from SAv-WT versus SAv-Y43A by the bis-biotin ligands. This kinetic exchange was followed by the appearance of biotin-4-fluorescein fluorescence in the unbound state. Representative curves for the exchange with biotin dimers **1** and **15** are shown in Figure 3. Over the time period of 1 h, corresponding to four half-lives, there is no significant exchange of the bound biotin-4-fluorescein for SAv-WT, while nearly 100% of expected ligand exchange is observed with SAv-Y43A, based on the stoichiometry of biotin-4-fluorescein to added free biotin. The kinetic approach to equilibrium with the SAv-Y43A mutant proceeds with the expected off-rate of 7.7×10^{-4} s^{-1} for biotin-4-fluorescein at 37 °C. A direct comparison of the biotin derivatives to biotin was performed with ^{3}H-biotin ligand competition experiments. At equivalent competitor concentrations (in biotin moieties), biotin dimers **1**, **15**, and **23** (data not shown) displace more ^{3}H-biotin than biotin does, indicating that they all have a significantly higher affinity for SAv-Y43A than biotin (Figure 4).

Retention Properties of Bis-Biotin Ligands. While the kinetic exchange properties of bound biotin are a direct function of its off-rate, the retention properties of the bis-biotin ligand are dependent on its affinity and kinetic parameters. The retention of the biotin dimers **1** and **15** was directly tested by pre-binding them to SAv-Y43A and then adding a 1-fold equivalent of biotin-4-fluorescein. When biotin was pre-bound to SAv-Y43A, the fluorescence of added biotin-4-fluorescein was quenched by 73% at this 1:1 stoichiometry due to the exchange with biotin and binding of this modified ligand to SAv-Y43A (Figure 5). However, there was only 8% quenching of fluorescence upon addition of biotin-4-fluorescein after 1 h when biotin dimer **1** or **15** is prebound to SAv-Y43A, within experimental error of zero exchange. To directly quantitate the off-rate properties of the bis-biotin ligands, the biotin dimer [^{125}I]**23** was prebound with SAv-Y43A at 37 °C and the unbound fraction monitored as a function of time after addition of excess biotin (Figure 6). The off-rate was determined to be 4.36×10^{-6} s^{-1} which is approximately 640-fold slower than biotin from SAv-Y43A. This places the likely K_a for the biotin dimer **23** as higher than biotin for SAv-WT, and thus a very high affinity protein—ligand couple.

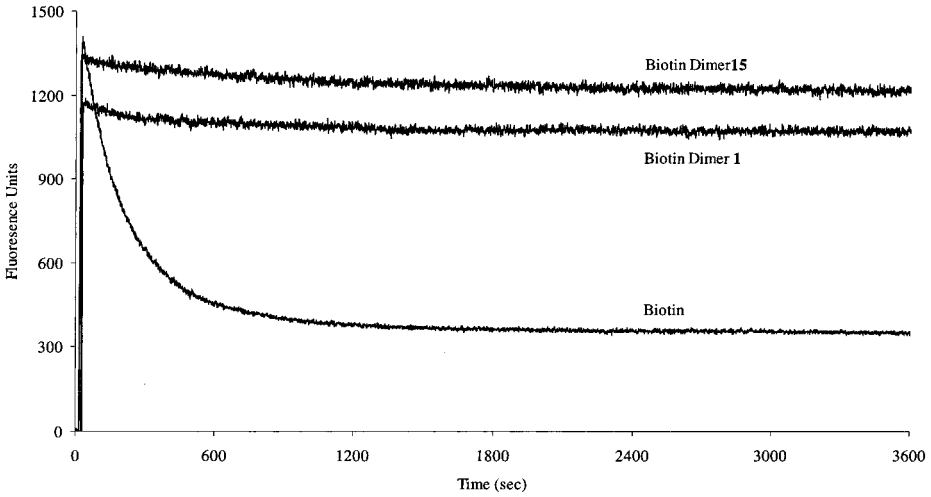


Figure 5. Bis-biotin retention properties. The biotin dimers **1** and **15** and biotin were prebound to SAv-Y43A, followed by the injection of 1 equiv of biotin-4-fluorescein. Fluorescence was measured continuously for roughly 1 h.

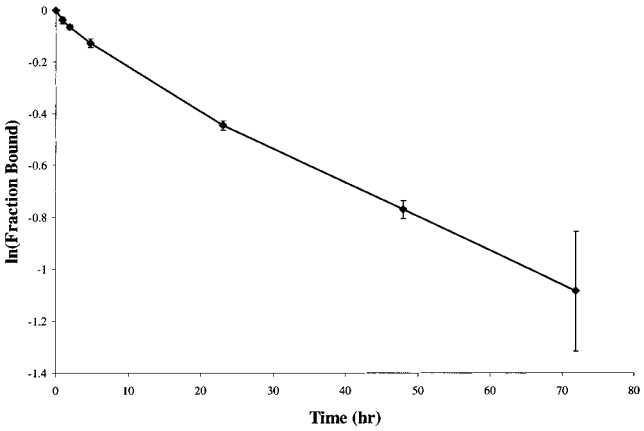


Figure 6. Determination of bis-biotin ligand off-rate. SAv-Y43A was incubated with [^{125}I]biotin dimer **23**, and at time = 0 a 2800-fold molar excess of nonradioactive biotin dimer was added. Radioactivity of the unbound [^{125}I]biotin dimer **23** was measured at various time points and the natural log of the fraction bound [^{125}I]biotin dimer **23** plotted against time. Data points are connected by lines.

DISCUSSION

The very high binding affinity of biotin with avidin (Av) and streptavidin (SAv) has led to the use of these binding pairs in a wide variety of in vitro and in vivo applications. A potential limitation of this system in clinical diagnostic and therapeutic applications is the significant level of endogenous biotin present in serum and tissues (*14*). In cancer therapeutics, the endogenous biotin can bind with SAv prior to injection of the radiolabeled biotin and effectively block its binding due to the slow dissociation rate (*35*). To circumvent this problem in animal studies, mice are placed on avidin-supplemented diet for two weeks (*36*) or biotin deficient diets for 5−7 days (*10*). However, this does not completely remove endogenous biotin, as it can be released from storage in the liver (*37*). Therefore, a large quantity of mAb−SAv is injected (300−400 μg/mouse) such that endogenous biotin does not block a significant amount of the radiolabeled biotin at the tumor. Although the concentration of biotin present in serum and tissue in humans is lower than found in mice (*35*, *38*), large amounts of mAb−SAv conjugate have also been used in clinical studies (i.e., 125 μg conjugate/mL plasma volume, or approximately 400 mg/average size patient) (*39*). In addition to decreasing the amount of radioactivity delivered to the cancer cells, the large quantities of injected mAb−SAv are likely to increase the immunogenicity of that reagent and increase the cost of the materials significantly.

We have thus investigated the dual use of a site-directed streptavidin mutant with a modified biotin ligand to circumvent the limitation of endogenous biotin in clinical diagnostics and therapeutics. The general design criteria for a streptavidin/bis-biotin ligand-binding system requires that endogenous biotin be exchangeable, while the modified biotin ligand remains strongly bound and retained to SAv. These criteria were met with the SAv-Y43A mutant that displayed an accelerated biotin off-rate, and the bis-biotin ligands that displayed high affinity for the mutant due to the ligand bivalency and concomitant avidity effect. Previous work in the Wilbur group on the structural design of biotin derivatives has shown that they should (1) have linkers which provide adequate space between the biotin and the attached moiety to retain the high affinity binding, (2) have good water solubility, and (3) have structural features which result in blockage of the enzyme biotinidase without decreasing the binding affinity (*24*, *29*, *40*). For cancer therapeutics, the radionuclide carrying moiety was designed such that the length did not become too long (i.e. >50 Å).

A great advantage of a repertoire of modified biotins and affinity mutants is the ability to engineer the system for a specific application. Bivalent biotin can be designed for specific applications, where for example, a biotinidase-resistant bis-biotin ligand (e.g., biotin dimer **23**) is needed for therapeutic or clinical applications. For other in vitro applications, other biotin dimers might suffice. A SAv affinity mutant can be selected to obtain a specific exchange rate of endogenous biotin. The intrinsic challenge is to engineer a decrease in streptavidin affinity for endogenous biotin to the proper range for a specific application, given the situational conditions of protein/ligand concentrations and potentially of flow kinetics, while preserving high affinity for the bis-biotin ligands. In therapeutic applications, over 95% of ^{90}Y-DOTA−biotin is cleared from the blood within 2 h (*41*). At 37 °C the half-life of biotin binding to SAv is 6.5 h. Any endogenous biotin bound to mAb−SAv is unlikely to be exchanged with the ^{90}Y-DOTA−biotin given the quick pharmacokinetics of the therapeutic and the slow dissociation of any endogenous biotin. Improving the exchange rate of biotin can be achieved using a SAv affinity mutant such as SAv-Y43A in lieu of SAv-WT. However, in many applications this would not prove useful without increasing the retention of a therapeutic molecule compared to endogenous biotin. In these studies, bivalent biotins were shown to bind to SAv-Y43A more tightly than biotin to SAv-WT, and this general approach should be applicable to either therapeutic or diagnostic systems where endogenous biotin acts as an interference.

ACKNOWLEDGMENT

This work was supported by the NIH (NCI Grant CA76287 and DK49655), the Whitaker Foundation (Graduate Fellowship for K.J.H.) and the Department of Energy, Medical Applications and Biophysical Research Division, Office of Biological and Environmental Research under grant number DE-FG03-98ER62572.

Supporting Information Available: HPLC chromatograms, ^{1}H NMR spectra, LRMS, and HRMS of the new compounds prepared (**3**, **5**, **9**, **15**, **16**, **19**, **23**, and **24**) in the research described in this manuscript. This material is available free of charge via the Internet at http://pubs.acs.org.

LITERATURE CITED

(1) Wilchek, M., and Bayer, E. A. (1990) Avidin−Biotin Technology. *Methods Enzymology 184*, 746−784.

(2) Gautherot, E., Rouvier, E., Daniel, L., Loucif, E., Bouhou, J., Manetti, C., Martin, M., Le-Doussal, J. M., and Barbet J. (2000) Pretargeted Radioimmunotherapy of Human Colorectal Xenografts with Bispecific Antibody and 131I-Labeled Bivalent Hapten. *J. Nuclear Med. 41*(3), 480−487.

(3) Goodwin, D. A., Meares, C. F., Watanabe, N., McTigue, M., Chaovapong, W., Ransone, C. M., Renn, O., Greiner, D. P., Kukis, D. L., and Kronenberger, S. I. (1994) Pharmacokinetics of pretargeted monoclonal antibody 2D12.5 and ^{88}Y-Janus-2-(*p*-nitrobenzyl)-1,4,7,10-tetraazacyclododecanetetraacetic acid (DOTA) in BALB/c mice with KHJJ mouse adenocarcinoma: a model for ^{90}Y radioimmunotherapy. *Cancer Res. 54* (22), 5937−46.

(4) Karacay, H., Sharkey, R. M., Govindan, S. V., McBride, W. J., Goldenberg, D. M., Hansen, H. J., and Griffiths, G. L. (1997) Development of a Streptavidin-Anti-Carcinoembryonic Antigen Antibody, Radiolabeled Biotin Pretargeting Method

for Radioimmunotherapy of Colorectal Cancer. Reagent Development. *Bioconjugate Chem. 8*, 585−594.

(5) Gasparri, A., Moro, M., Curnis, F., Sacchi, A., Pagano, S., Veglia, F., Casorati, G., Siccardi, A. G., Dellabona, P., and Corti, A. (1999) Tumor pretargeting with avidin improves the therapeutic index of biotinylated tumor necrosis factor alpha in mouse models. *Cancer Res. 59* (12), 2917−23.

(6) Knox, S. J., Goris, M. L., Tempero, M., Weiden, P. L., Gentner, L., Breitz, H., Adams, G. P., Axworthy, D., Gaffigan, S., Bryan, K., Fisher, D. R., Colcher, D., Horak, I. D., and Weiner, L. M. (2000) Phase II trial of yttrium-90-DOTA-biotin pretargeted by NR-LU-10 antibody/streptavidin in patients with metastatic colon cancer. *Clin. Cancer Res. 6* (2), 406−14.

(7) Paganelli, G., Malcovati, M., and Fazio, F. (1991) Monoclonal antibody pretargetting techniques for tumour localization: the avidin−biotin system. International Workshop on Techniques for Amplification of Tumour Targeting. *Nuclear Med. Commun. 12* (3), 211−34.

(8) Cremonesi, M., Ferrari, M., Chinol, M., Stabin, M. G., Grana, C., Prisco, G., Robertson, C., Tosi, G., and Paganelli, G. (1999) Three-step radioimmunotherapy with yttrium-90 biotin: dosimetry and pharmacokinetics in cancer patients. *Eur. J. Nuclear Med. 26* (2), 110−20.

(9) Press, O., Corcoran, M., Subbiah, K., Hamlin, D. K., Wilbur, D. S., Johnson, T., Theodore, L., Yau, E., Mallett, R., Meyer, D. L., and Axworthy, D. (2001) A Comparative Evaluation of Conventional and Pretargeted Radioimmunotherapy of CD20-Expressing Lymphoma Xenografts. *Blood 98* (8), 2535−2543.

(10) Axworthy, D. B., Reno, J. M., Hylarides, M. D., Mallett, R. W., Theodore, L. J., Gustavson, L. M., Su, F.-M., Hobson, L. J., Beaumier, P. L., and Fritzberg, A. R. (2000) Cure of Human Carcinoma Xenografts by a Single Dose of Pretargeted Yttrium-90 with Negligible Toxicity. *Proc. Natl. Acad. Sci. 97* (4), 1802−1807.

(11) Hymes, J., and Wolf, B. (1999) Human Biotinidase Isn't Just for Recycling Biotin. *J. Nutr. 129*, 485s−489s.

(12) Hymes, J., and Wolf, B. (1996) Biotinidase and its Roles in Biotin Metabolism. *Clin. Chim. Acta 255*, 1−11.

(13) Dakshinamurti, K., and Chauhan, J. (1989) Biotin. *Vitamins Hormones 45*, 337−385.

(14) Baker, H. (1985) Assessment of Biotin Status: Clinical Implications. *Ann. N. Y. Acad. Sci. 447*, 129−132.

(15) Bussolati, G., Gugliotta, P., Volante, M., Pace, M., and Papotti, M. (1997) Retrieved Endogenous Biotin: A Novel Marker and Potential Pitfall in Diagnostic Immunohistochemistry. *Histopathology 31*, 400−407.

(16) McQuaid, S., McMahon, J., and Allan, G. M. (1995) A Comparison of Digoxigenin and Biotin Labeled DNA and RNA Probes for in Situ Hybridization. *Biotech. Histochem. 7* (3), 147−154.

(17) Kohler, A., Lauritzen, B., and Van Noorden, J. F. (2000) Signal Amplification in Immunohistochemistry at the Light Microscopic Level Using Biotinylated Tyramide and Nonogold−Silver Staining. *J. Histochem. Cytochem. 48* (7), 933−941.

(18) Wang, H., and Pevsner, J. (1999) Detection of Endogenous Biotin in Various Tissues: Novel Functions in the Hippocampus and Implications for its Use in Avidin−Biotin Technology. *Cell Tissue Res. 296*, 511−516.

(19) Hyre, D. E., Le Trong, I., Freitag, S., Stenkamp, R. E., and Stayton, P. S. (2000) Ser45 plays an important role in managing both the equilibrium and transition state energetics of the streptavidin−biotin system. *Protein Sci. 9*, 878−885.

(20) Chu, V. F. S., Le Trong, I., Stenkamp, R. E., and Stayton, P. S. (1998) Thermodynamic and structural consequences of flexible loop deletion by circular permutation in the streptavidin−biotin system. *Protein Sci. 7*, 848−859.

(21) Chilkoti, A., Tan, P. H., and Stayton, P. S. (1995) Site-directed mutagenesis studies of the high-affinity streptavidin−biotin complex: contributions of tryptophan residues 79, 108, and 120. *Proc. Natl. Acad. Sci. 92* (5), 1219−24.

(22) Klumb, L., Chu, V., and Stayton, P. S. (1998) Energetic Roles of Hydrogen Bonds at the Uriedo Oxygen Binding Pocket Streptavidin−Biotin Complex. *Biochemistry 37* (21), 7657−7663.

(23) Wilbur, D., Pathare, P. M., Hamlin, D. K., and Weerawarna, S. A. (1997) Biotin Reagents for Antibody Pretargeting. 2. Synthesis and in Vitro Evaluation of Biotin Dimers and Trimers for Cross-Linking of Streptavidin. *Bioconjugate Chem. 8*, 819−832.

(24) Wilbur, D., Hamlin, D. K., Pathare, P. M., and Weerawarna, S. A. (1997) Biotin reagents for Antibody Pretargeting. Synthesis, Radioiodination, and in Vitro Evaluation of Water Soluble, Biotinidase Resistant Biotin Derivatives. *Bioconjugate Chem. 8*, 572−584.

(25) Gamper, H. B., Reed, M. W., Cox, T., Virosco, J. S., Adams, A. D., Gall, A. A., Scholler, J. K., and Meyer, R. B. (1993) Facile Preparation of Nuclease Resistant 3′ Modified Oligodeoxynucleotides. *Nucleic Acids Res. 21*, 145−150.

(26) Wilbur, D. S., Hamlin, D. K., Vessella, R. L., Stray, J. E., Buhler, K. R., Stayton, P. S., Klumb, L. A., Pathare, P. M., and Weerawarna, S. A. (1996) Antibody fragments in tumor pretargeting. Evaluation of biotinylated Fab′ colocalization with recombinant streptavidin and avidin. *Bioconjugate Chem. 7*, 689−702.

(27) Wilbur, D. S., Hamlin, D. K., Buhler, K. R., Pathare, P. M., Vessella, R. L., Stayton, P. S., and To, R. (1998) Streptavidin in antibody pretargeting. 2. Evaluation of methods for decreasing localization of streptavidin to kidney while retaining its tumor binding capacity. *Bioconjugate Chem. 9*, 322−330.

(28) Wilbur, D. S., Hadley, S. W., Hylarides, M. D., Abrams, P. G., Beaumier, P. A., Morgan, A. C., Reno, J. M., and Fritzberg, A. R. (1989) Development of a stable radioiodinating reagent to label monoclonal antibodies for radiotherapy of cancer. *J. Nuclear Med. 30*, p 216−226.

(29) Wilbur, D. S., Chyan, M. K., Pathare, P. M., Hamlin, D. K., Frownfelter, M. B., and Kegley, B. B. (2000) Biotin reagents for antibody pretargeting. 4. Selection Of biotin conjugates for in vivo application based on their dissociation rate from avidin and streptavidin. *Bioconjugate Chem. 11*, p 569−583.

(30) Pathare, P. M., Wilbur, D. S., Hamlin, D. K., Heusser, S., Quadros, E. V., McLoughlin, P., and Morgan, A. C. (1997) Synthesis of Cobalamin Dimers Using Isophthalate Crosslinking of Corrin Ring Carboxylates and Evaluation of Their Binding to Transcobalamin II. *Bioconjugate Chem. 8*, 161−172.

(31) Green, N. (1965) A spectrophotometric Assay for Avidin and Biotin Based on Binding of Dyes by Avidin. *Biochem. J. 94*, 23c−24c.

(32) Wilbur, D. S. (1992) Radiohalogenation of proteins: an overview of radionuclides, labeling methods, and reagents for conjugate labeling. *Bioconjugate Chem. 3*, p 433−470.

(33) Kabalka, G. W., and Varma, R. S. (1989) The Synthesis of Radiolabeled Compounds Via Organometallic Intermediates. *Tetrahedron 45*, 6601−6621.

(34) Wilbur, D. S., Hamlin, D. K., Kegley, B. B., Chyan, M. K., Pathare, P. M., and Wan, F. (2001) Studies Which Indicate That Thiourea Bonds Interfere With Radioiodination Reactions. *J. Labeled Cpd. Radiopharm 44*, S973−S975.

(35) Rusckowski, M., Fogarasi, M., Fritz, B., and Hnatowich, D. J. (1997) Effect of endogenous biotin on the applications of streptavidin and biotin in mice. *Nuclear Med. Biol. 24* (3), p 263−8.

(36) Rosebrough, S., and Hartley, D. F. (1995) Quantification and Lowering of Serum Biotin. *Lab. Anim. Sci. 45* (5), p 554−557.

(37) Shriver, B., Roman-Shriver, C., and Allred, J. B. (1993) Depletion and Repletion of Biotinyl Enzymes in Liver of Biotin-Deficiet Rats: Evidence of a Biotin Storage System. *J. Nutr. 123*, 1140−1149.

(38) Mock, D. M., and DuBois, D. B. (1986) A sequential, solid-phase assay for biotin in physiologic fluids that correlates with expected biotin status. *Anal. Biochem. 153* (2), 272−278.

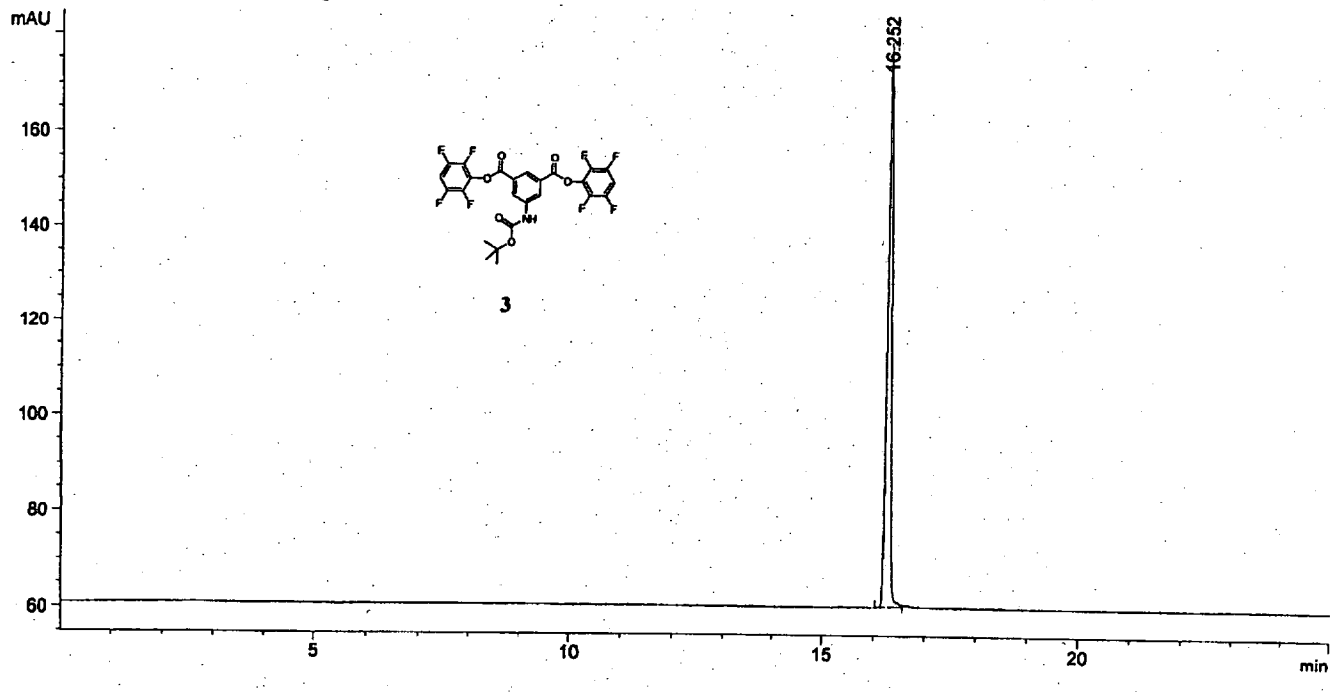
(39) Theodore, L. J., Fritzberg, A. R., Schultz, J. E., and Axworthy, D. B. (2000) Evolution of a Pretarget Radio-

immunotherapeutic Regimen, in *Radioimmunotherapy of Cancer* (Abrams, P. G., and Fritzberg, A. R., Eds.) pp 195−221, Marcel Dekker, New York.

(40) Wilbur, D. S., Hamlin, D. K., Chyan, M. K., Kegley, B. B., and Pathare, P. M. (2001) Biotin reagents for antibody pretargeting. 5. Additional studies of biotin conjugate design to provide biotinidase stability. *Bioconjugate Chem*. *12*, 616−623.

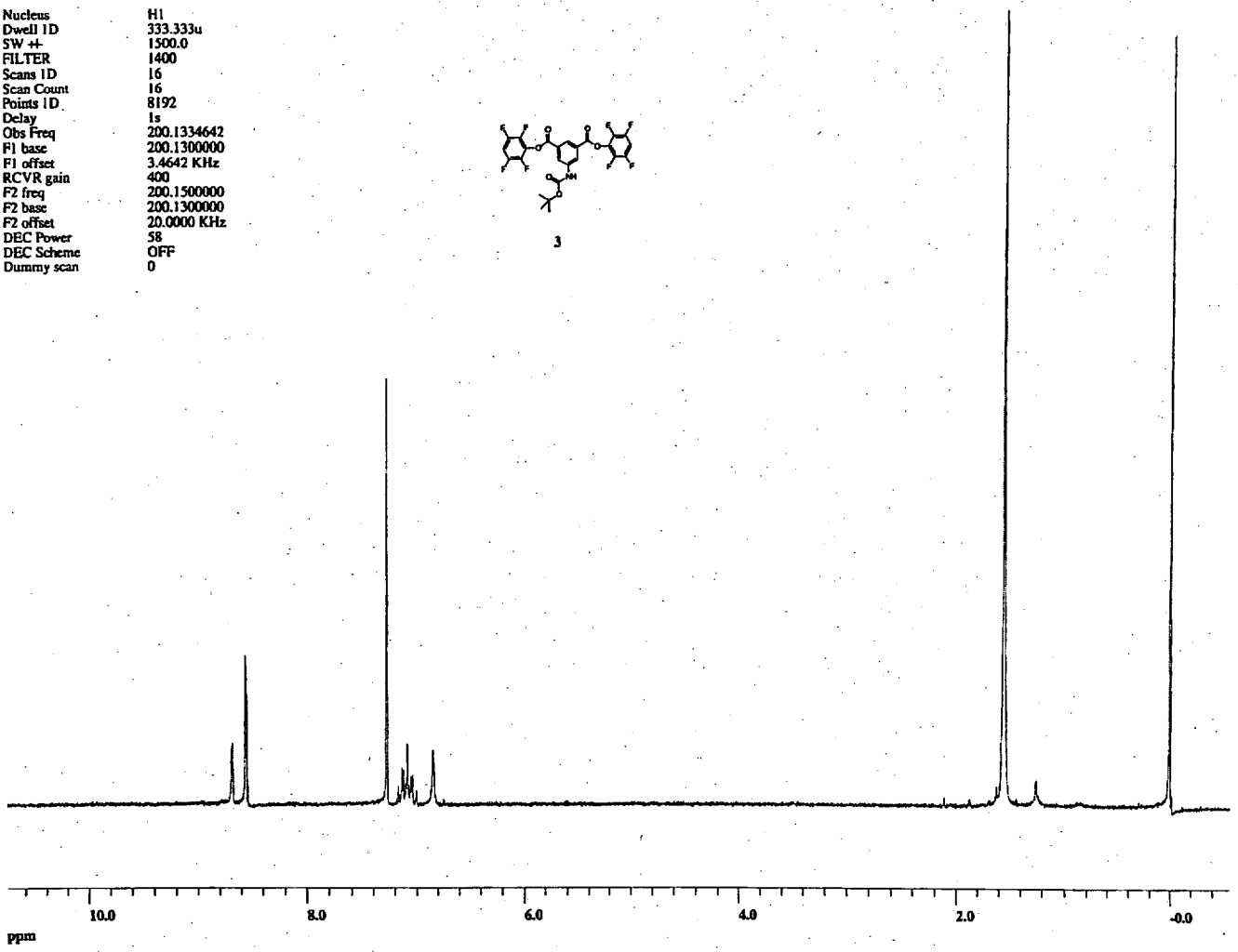
(41) Weiden, P. L., Breitz, H. B., Press, O., Appelbaum. J. W., Bryan, J. K., Gaffigan, S., Stone, D., Axworthy, D., Fisher, D., and Reno, J. (2000) Pretargeted radioimmunotherapy (PRIT) for treatment of non-Hodgkin's lymphoma (NHL): initial phase I/II study results. *Cancer Biother. Radiopharm*. *15* (1), 15−29.

BC010087T


mAU
160
140
120
100
80
60
16.252
5
10
15
20
min
3

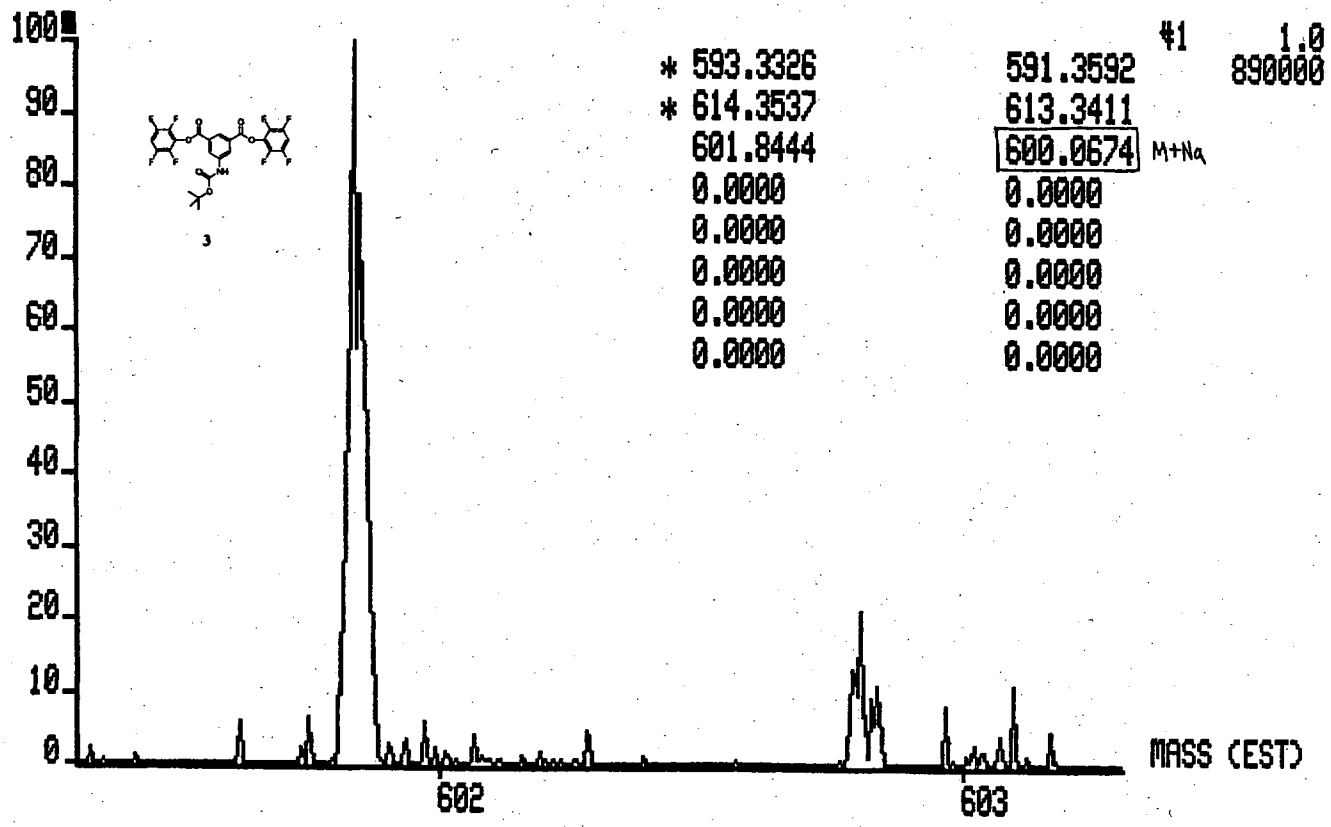
Nucleus	H1
Dwell 1D	333.333u
SW +/-	1500.0
FILTER	1400
Scans 1D	16
Scan Count	16
Points 1D	8192
Delay	1s
Obs Freq	200.1334642
F1 base	200.1300000
F1 offset	3.4642 KHz
RCVR gain	400
F2 freq	200.1500000
F2 base	200.1300000
F2 offset	20.0000 KHz
DEC Power	58
DEC Scheme	OFF
Dummy scan	0

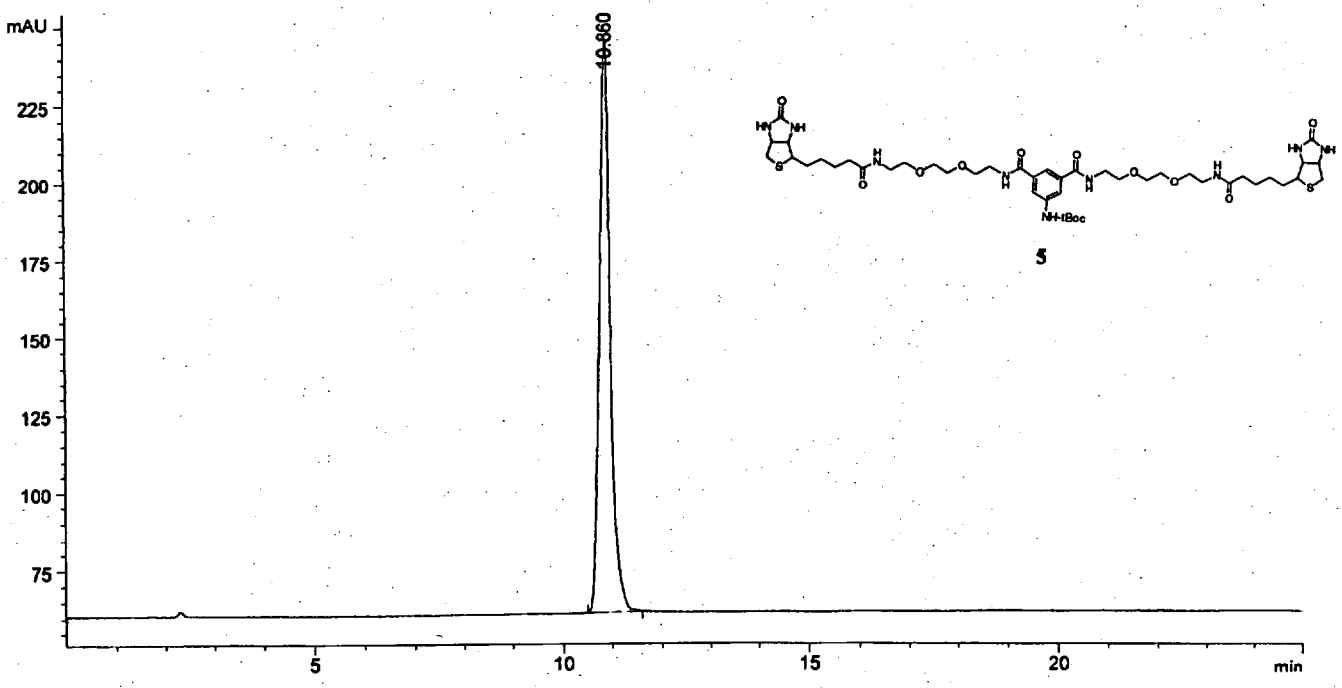
3



© 2002 American Chemical Society, Bioconjugate Chem., Hamblett bc010087t Supporting Info Page 3

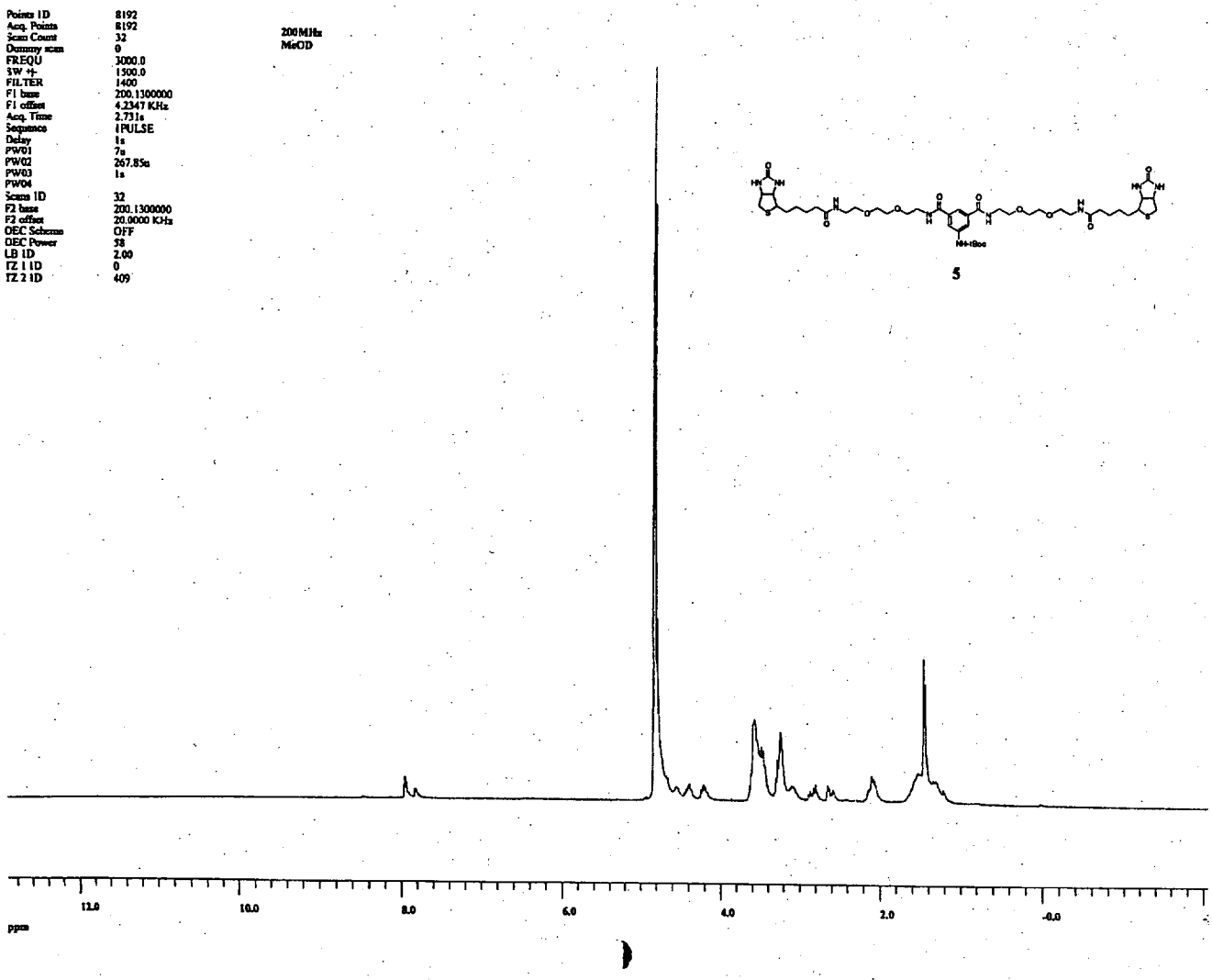
3



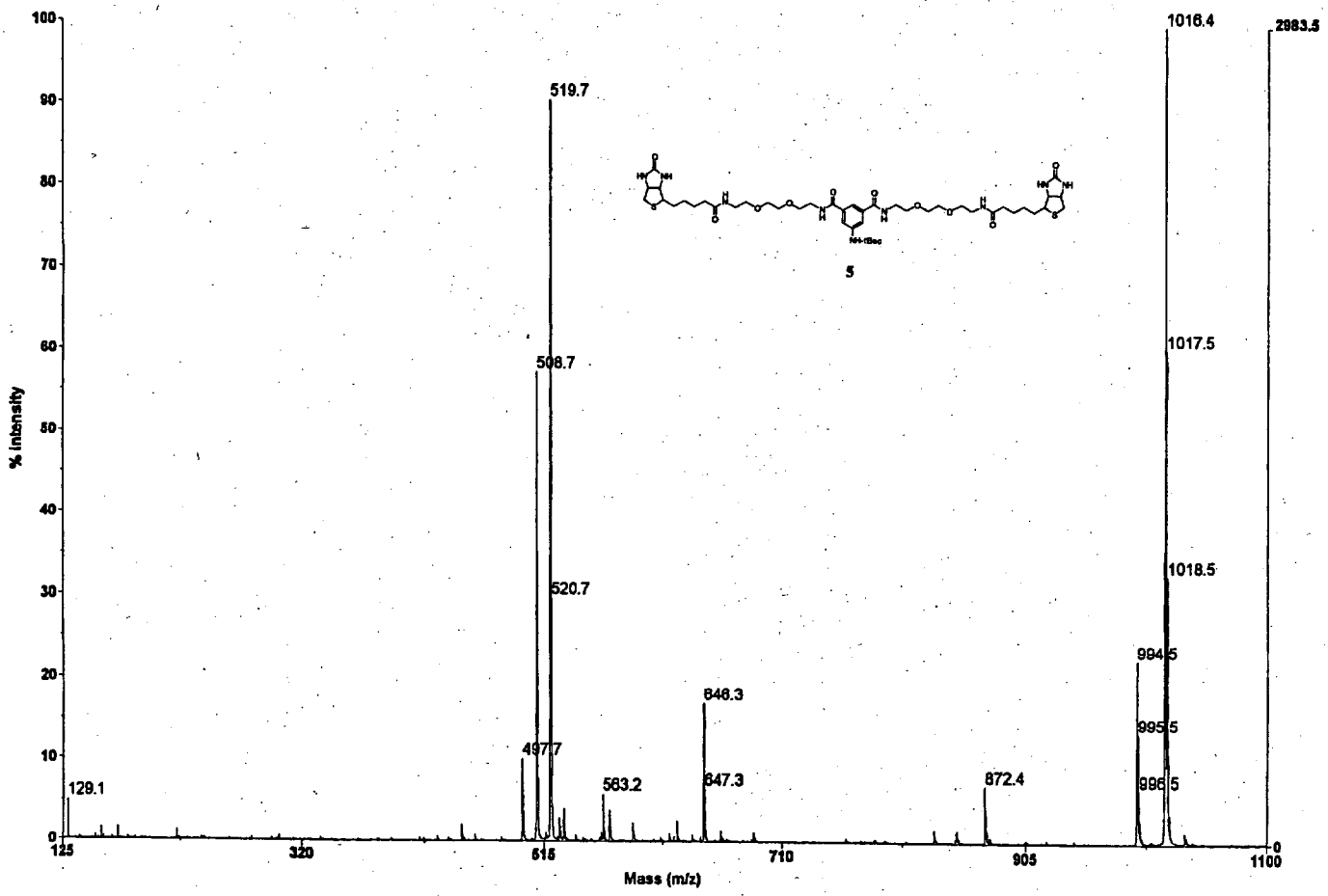


5

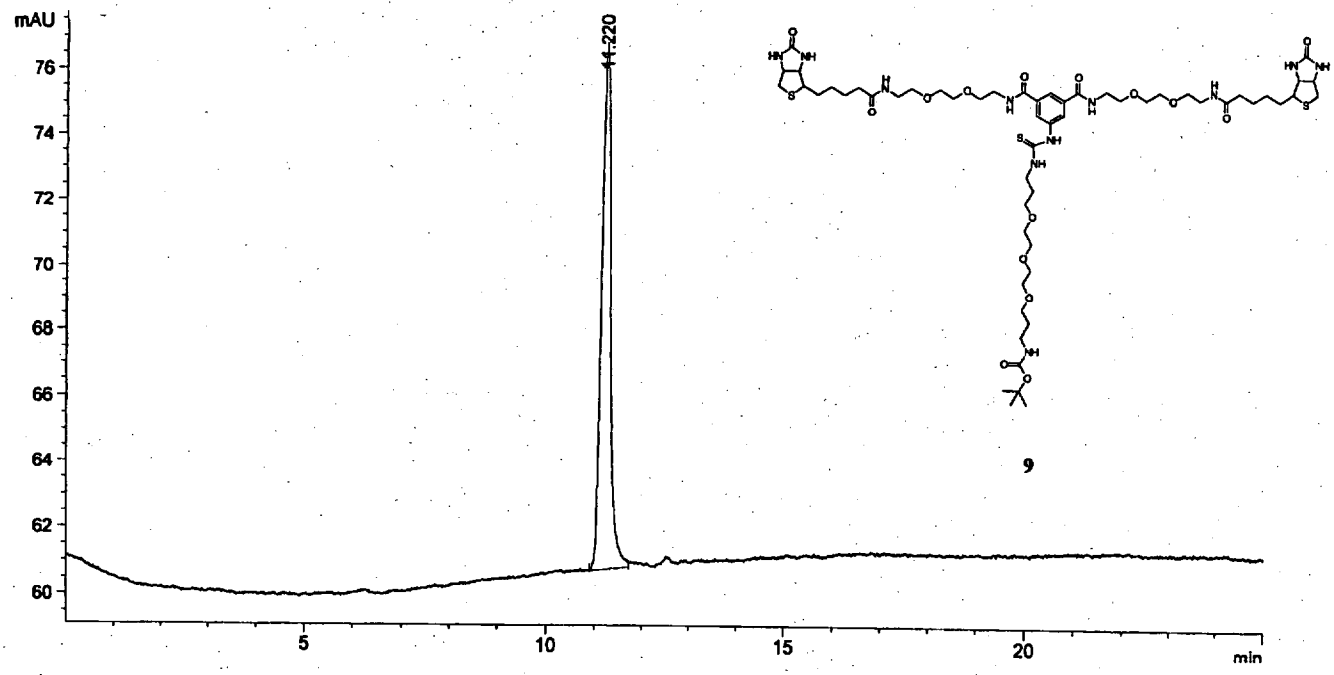
© 2002 American Chemical Society, Bioconjugate Chem., Hamblett bc010087t Supporting Info Page 5



© 2002 American Chemical Society, Bioconjugate Chem., Hamblett bc010087t Supporting Info Page 6

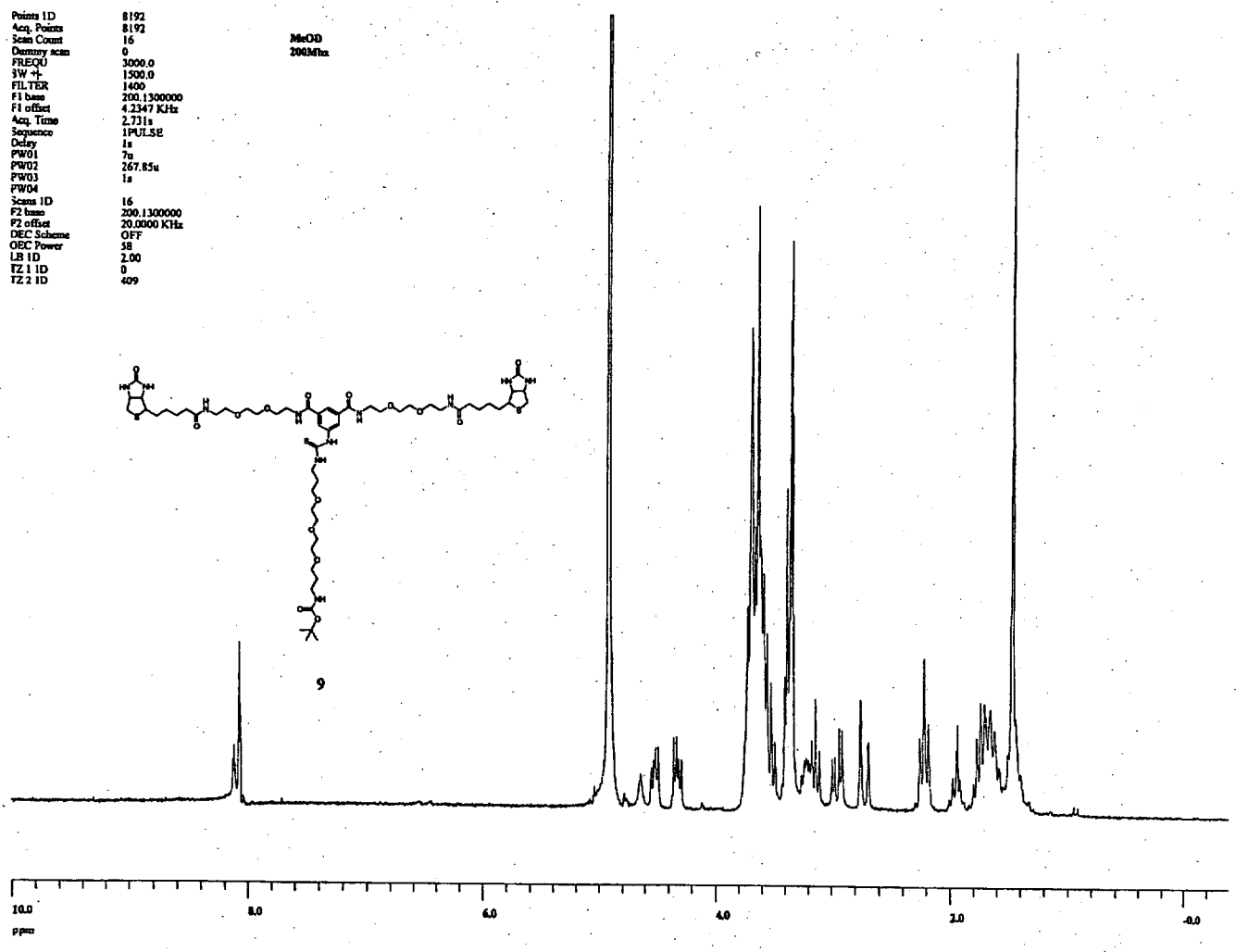


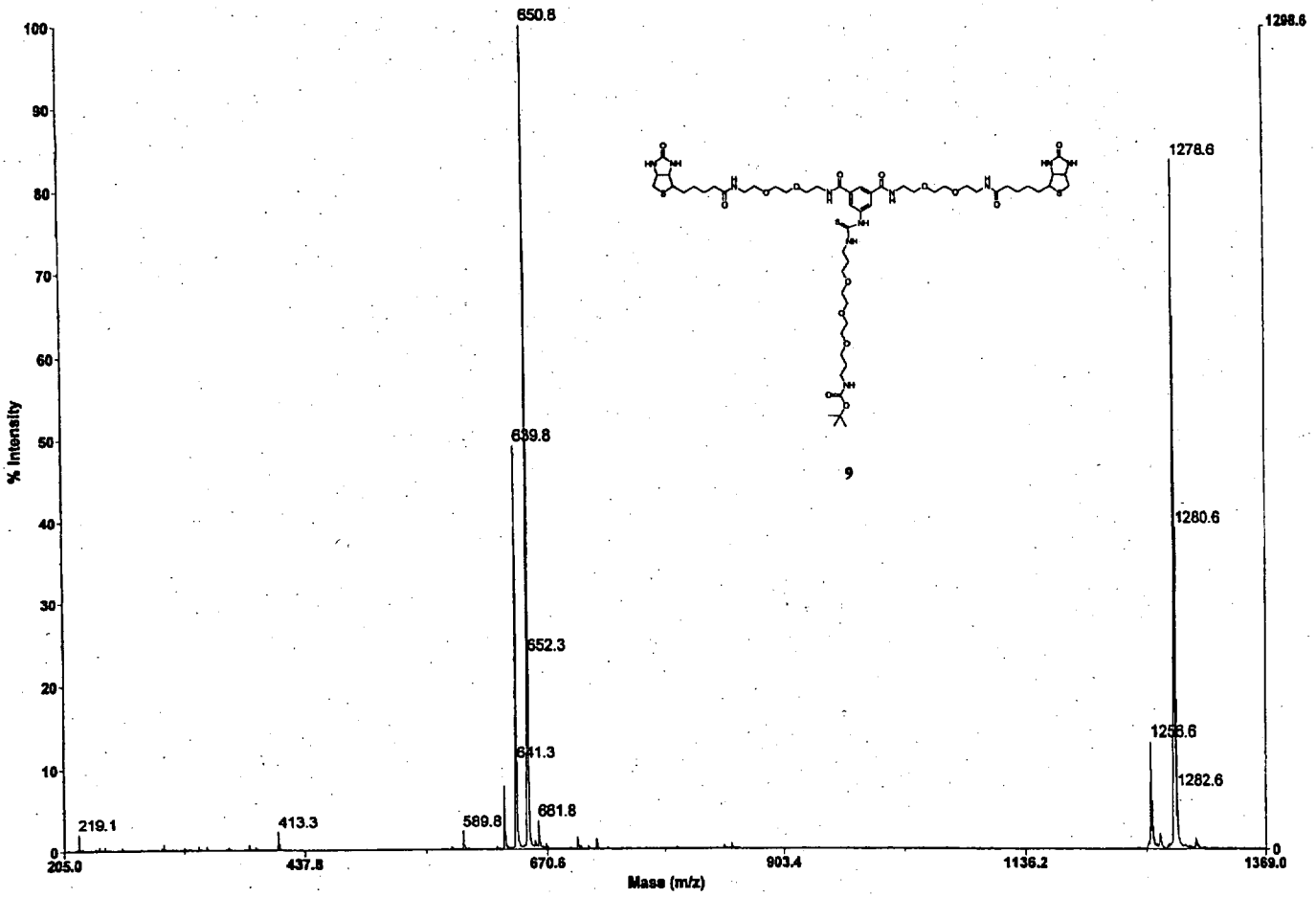
© 2002 American Chemical Society, Bioconjugate Chem., Hamblett bc010087t Supporting Info Page 7

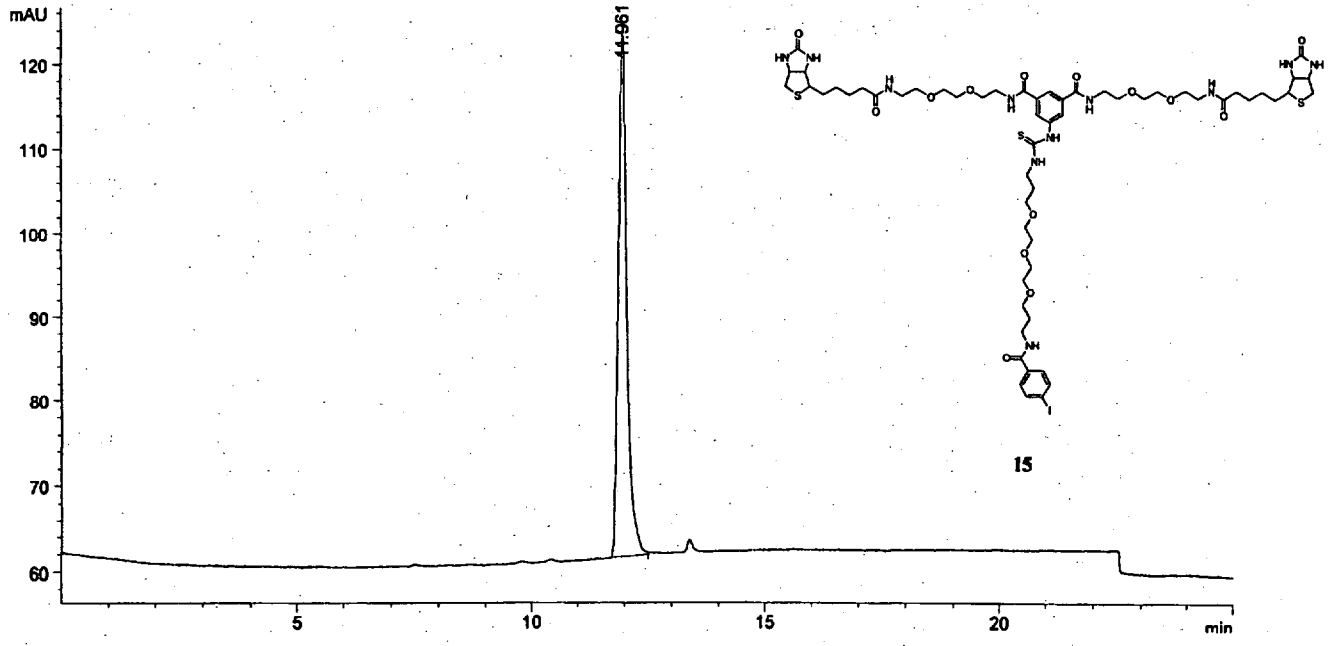


9

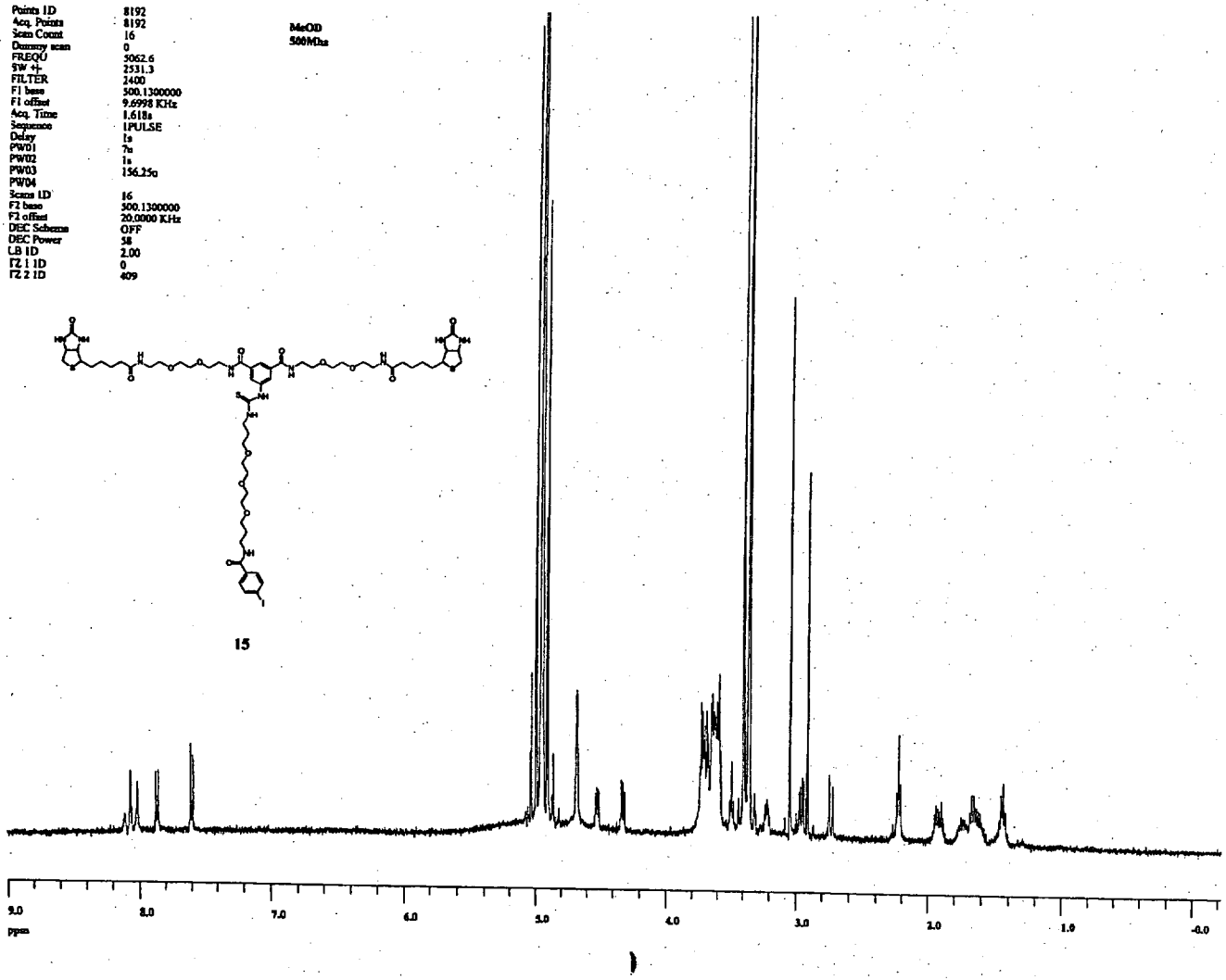
© 2002 American Chemical Society, Bioconjugate Chem., Hamblett bc010087t Supporting Info Page 8



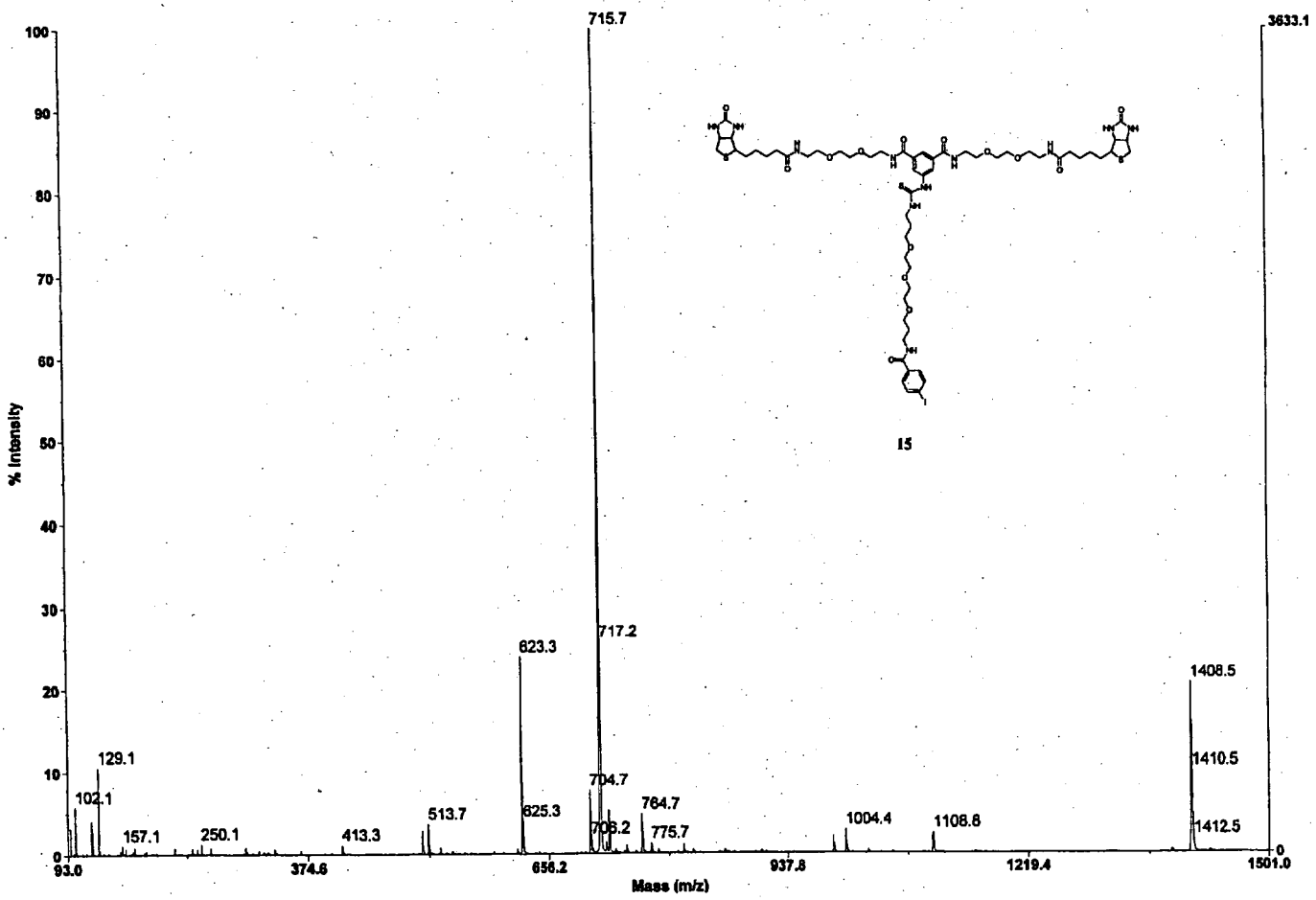

650.8
1298.6
1278.6
639.8
652.3
641.3
681.8
589.8
413.3
219.1
1280.6
1256.6
1282.6
% Intensity
Mass (m/z)
205.0
437.8
670.6
903.4
1136.2
1369.0
9



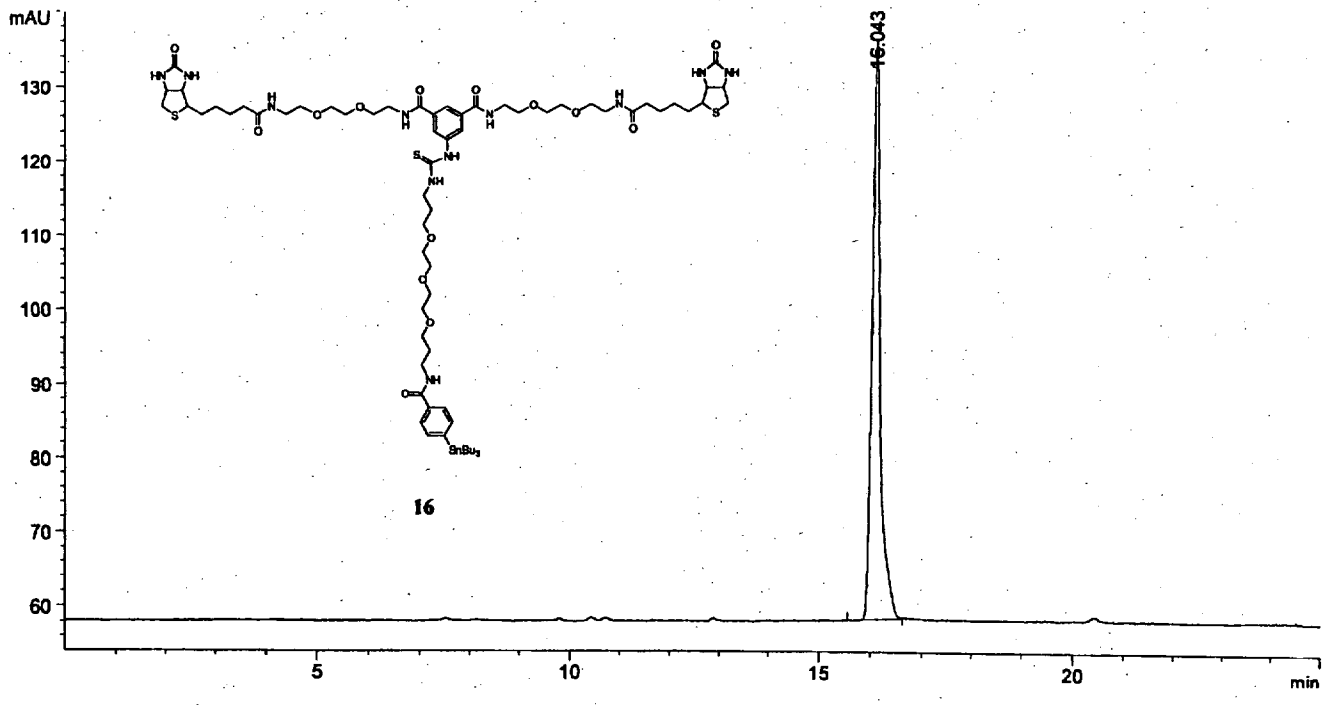
15


Points 1D 8192
Acq. Points 8192
Scan Count 16
Dummy scan 0
FREQU 5062.6
SW 44. 2531.3
FILTER 2400
F1 base 500.1300000
F1 offset 9.6998 KHz
Acq. Time 1.618s
Sequence 1PULSE
Delay 1s
PW01 7u
PW02 1s
PW03 156.25u
PW04
Scans 1D 16
F2 base 500.1300000
F2 offset 20.0000 KHz
DEC Scheme OFF
DEC Power 58
LB 1D 2.00
FZ 1 1D 0
FZ 2 1D 409
MeOD
500Mhz
9.0
8.0
7.0
6.0
5.0
4.0
3.0
2.0
1.0
-0.0
ppm

15

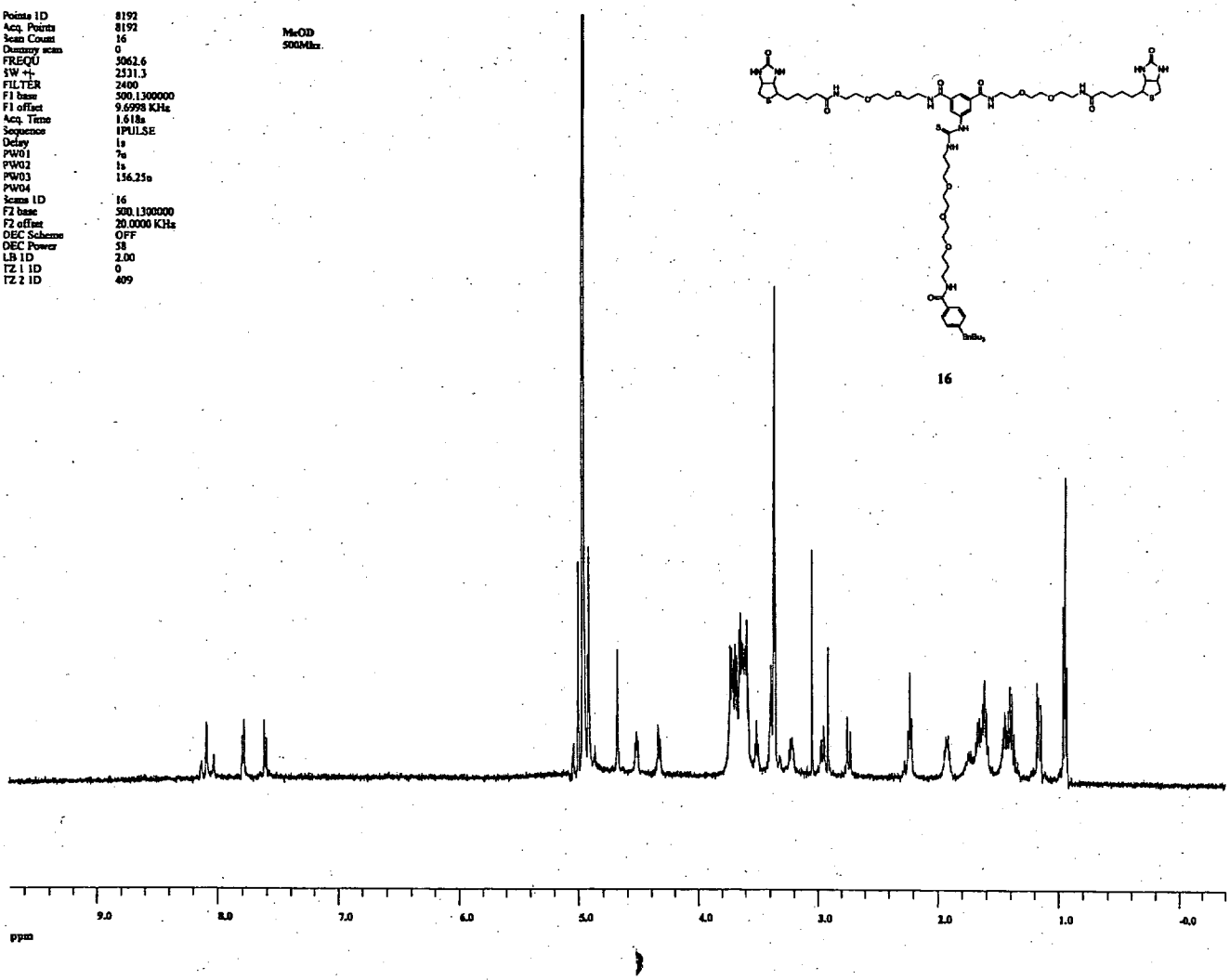

% Intensity
Mass (m/z)
715.7
3633.1
623.3
717.2
1408.5
129.1
1410.5
102.1
704.7
764.7
513.7
625.3
1004.4
1108.6
157.1
250.1
413.3
775.7
1412.5
15

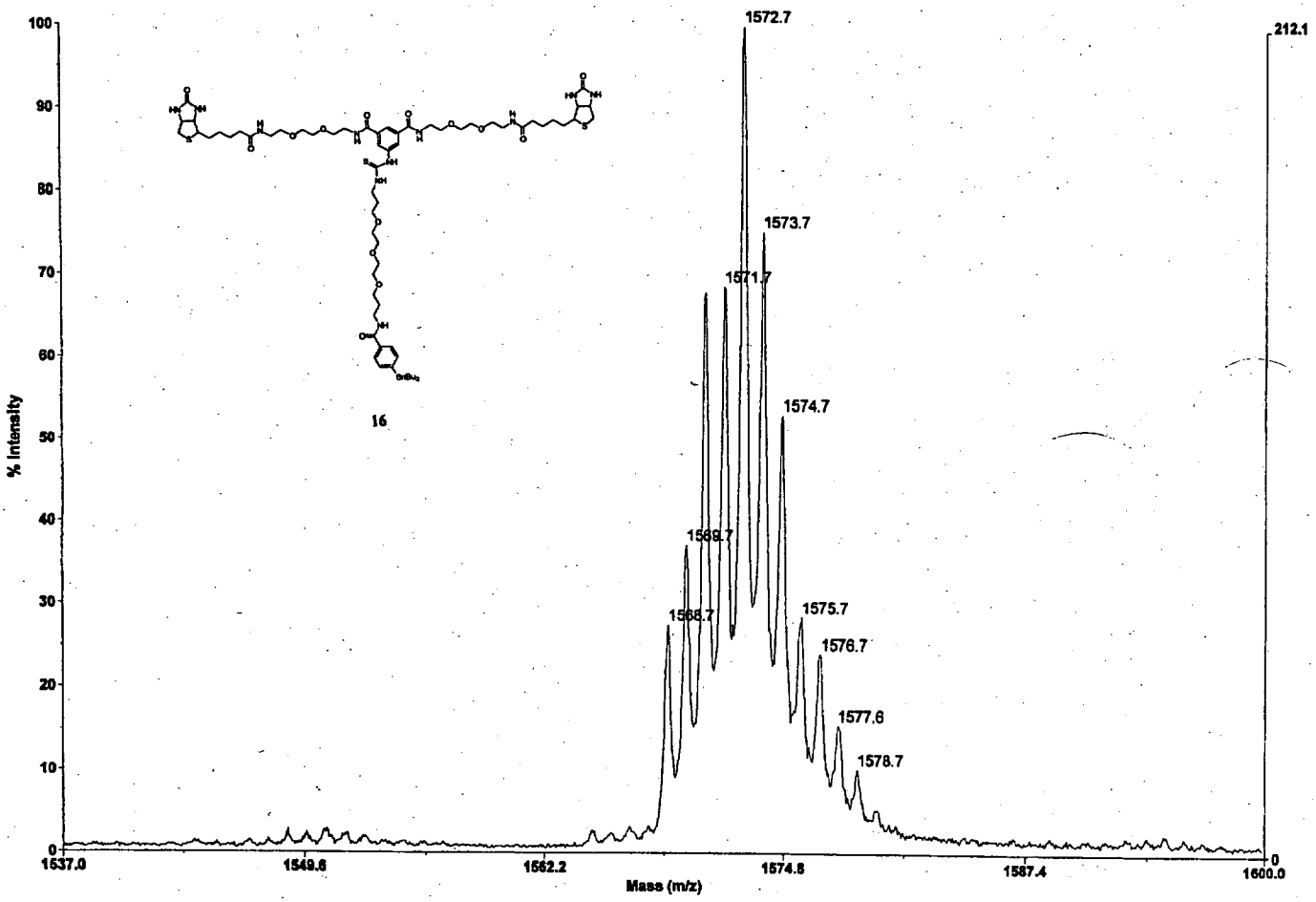
© 2002 American Chemical Society, Bioconjugate Chem., Hamblett bc010087t Supporting Info Page 13

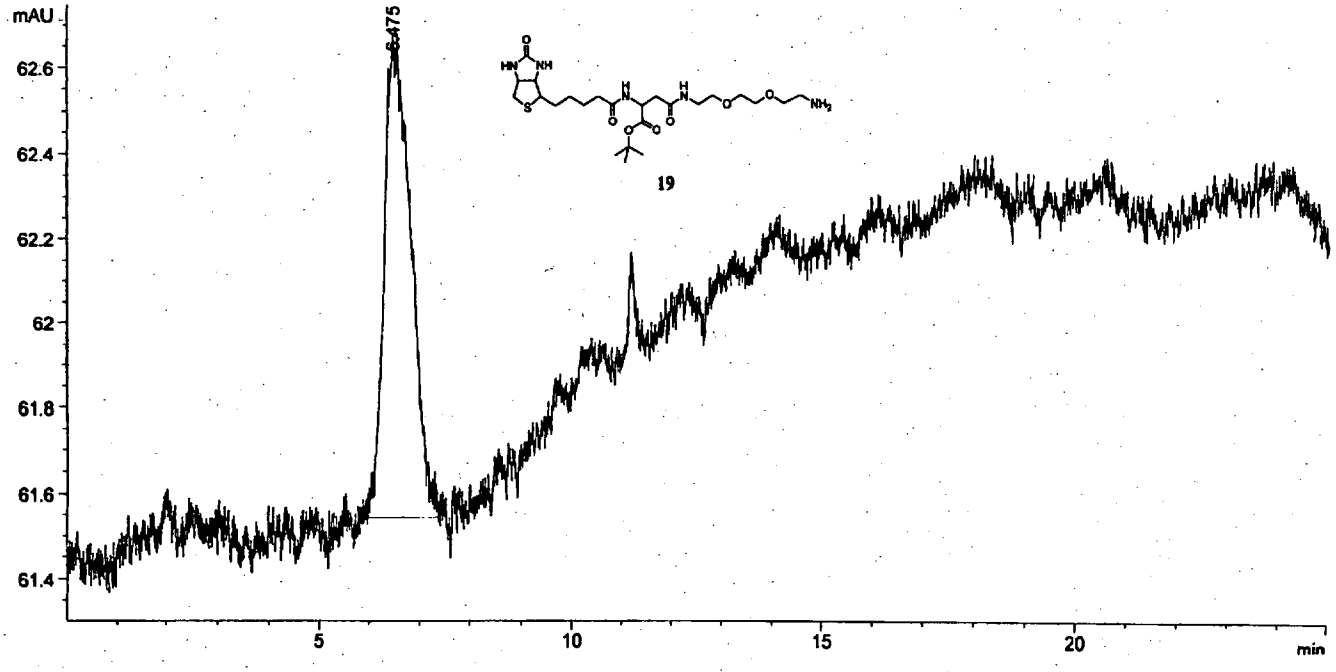


16

© 2002 American Chemical Society, Bioconjugate Chem., Hamblett bc010087t Supporting Info Page 14

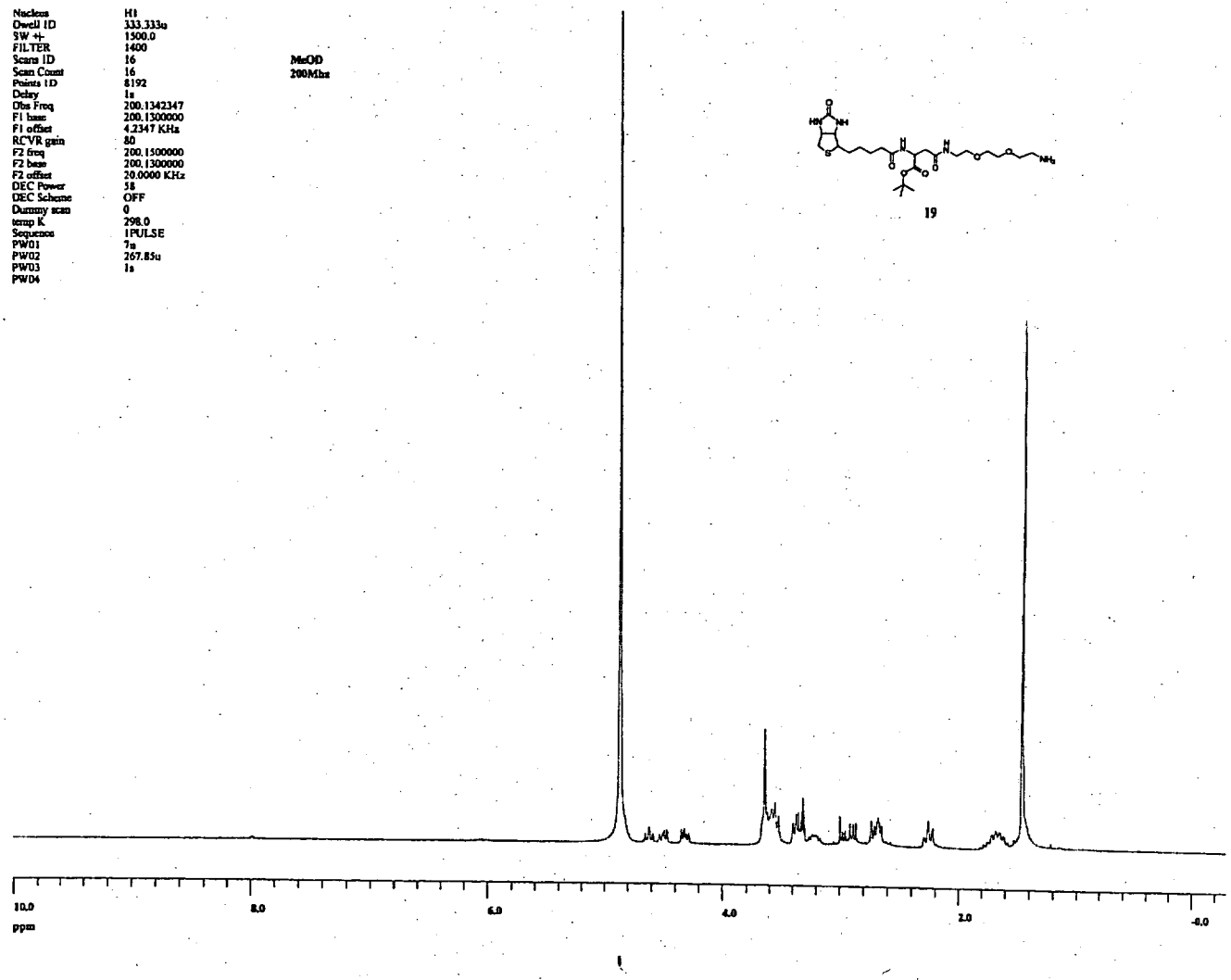


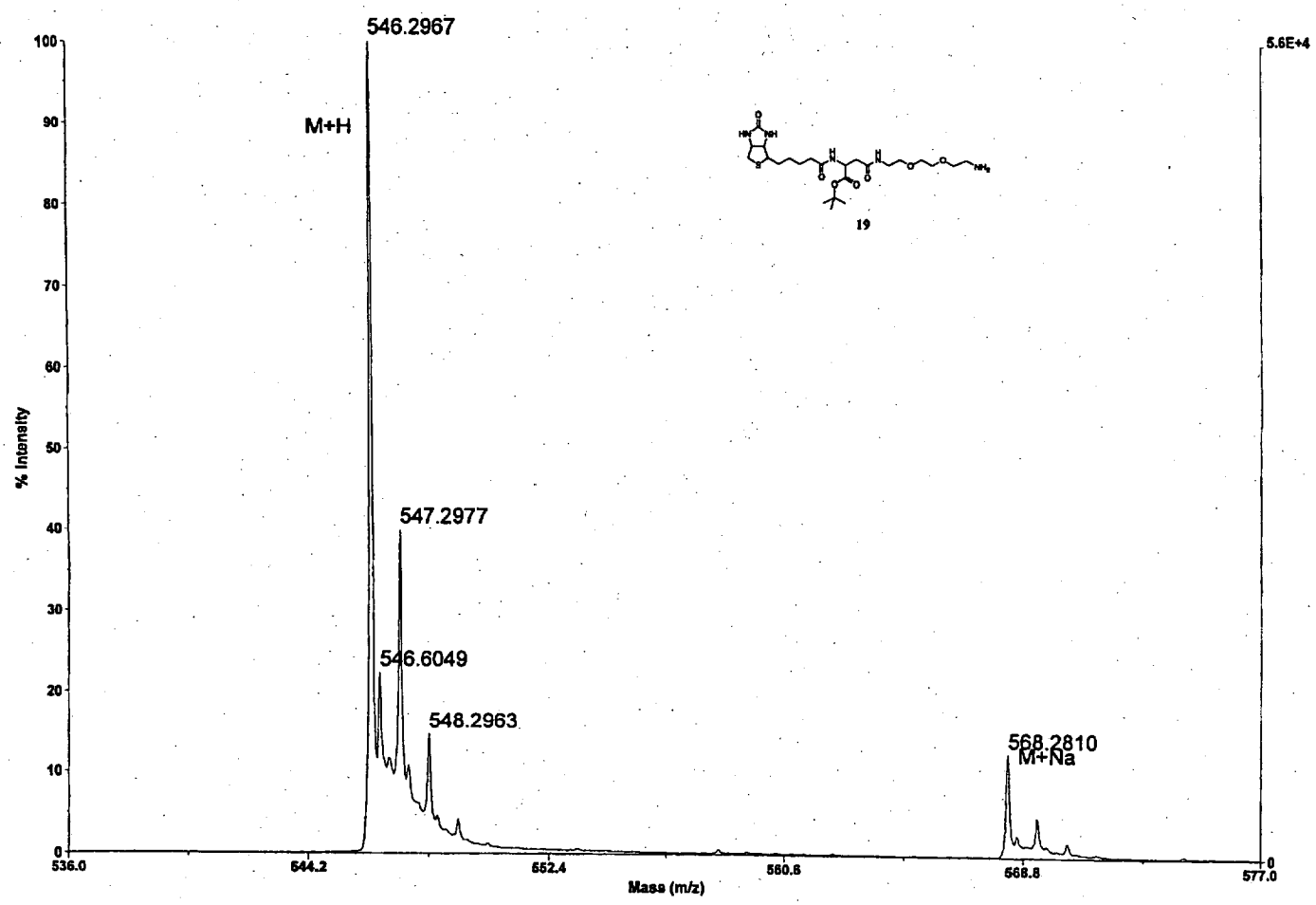

16
% Intensity
Mass (m/z)
1572.7
212.1
1573.7
1571.7
1574.7
1569.7
1568.7
1575.7
1576.7
1577.6
1578.7
100
90
80
70
60
50
40
30
20
10
0
1537.0
1549.8
1562.2
1574.8
1587.4
1600.0

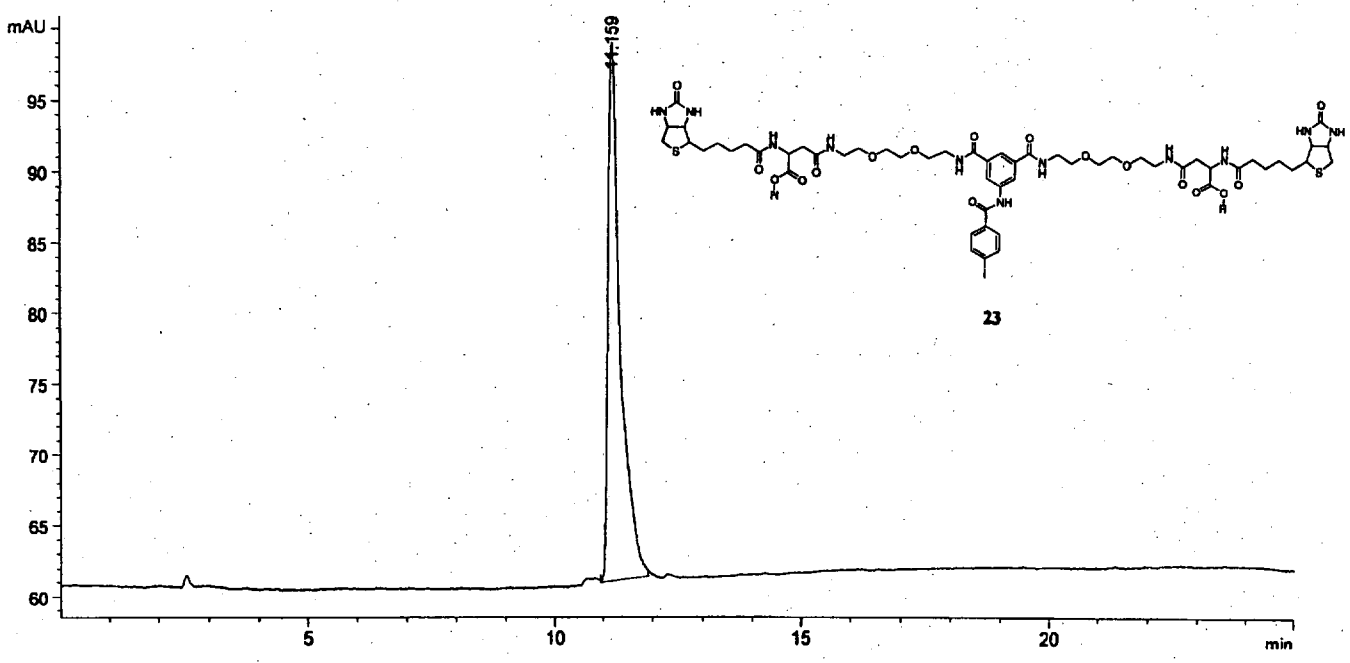


19

© 2002 American Chemical Society, Bioconjugate Chem., Hamblett bc010087t Supporting Info Page 17




546.2967
M+H
547.2977
546.6049
548.2963
568.2810
M+Na
% Intensity
Mass (m/z)
5.6E+4
100
90
80
70
60
50
40
30
20
10
0
536.0
544.2
552.4
560.6
568.8
577.0
19



23

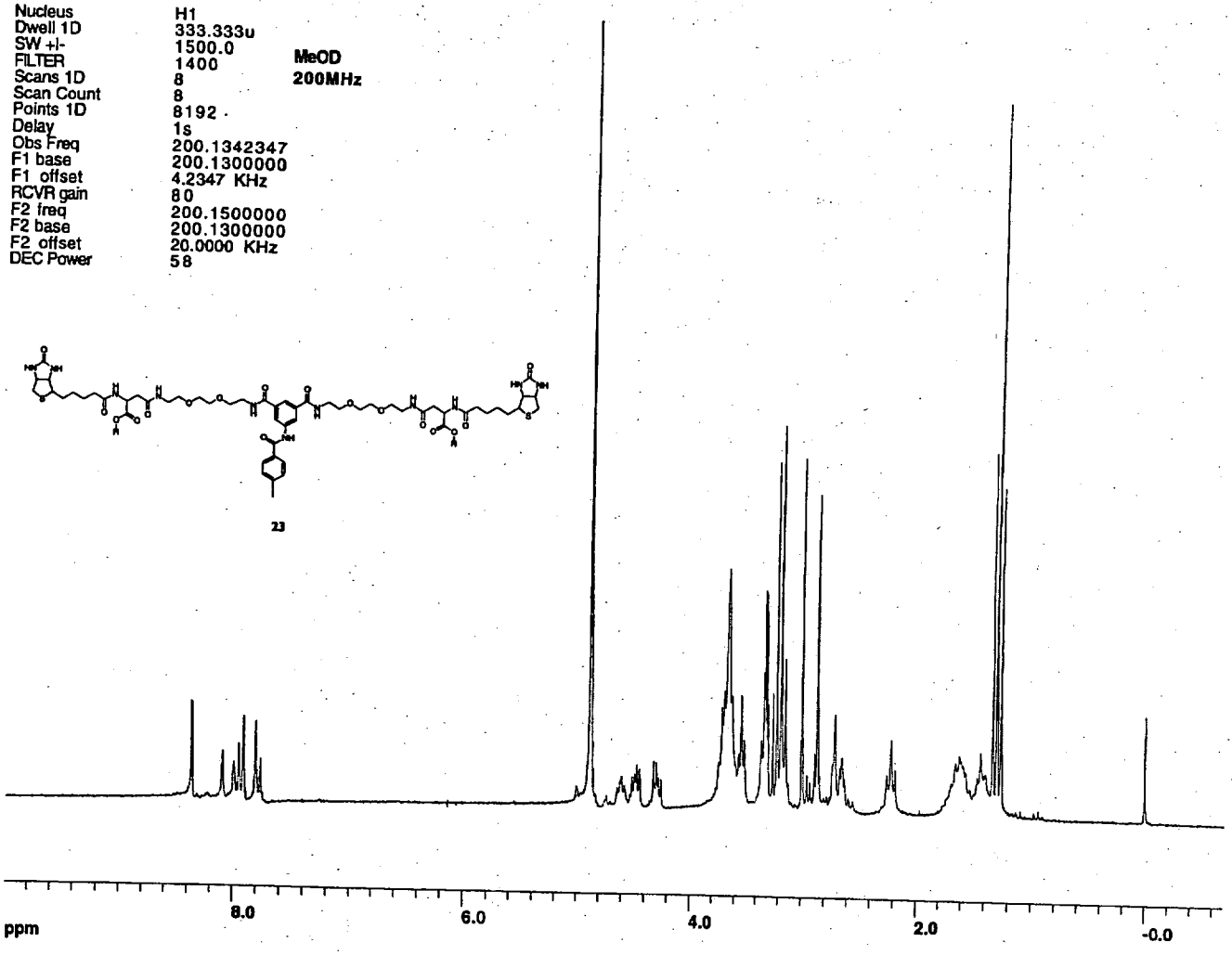
© 2002 American Chemical Society, Bioconjugate Chem., Hamblett bc010087t Supporting Info Page 20

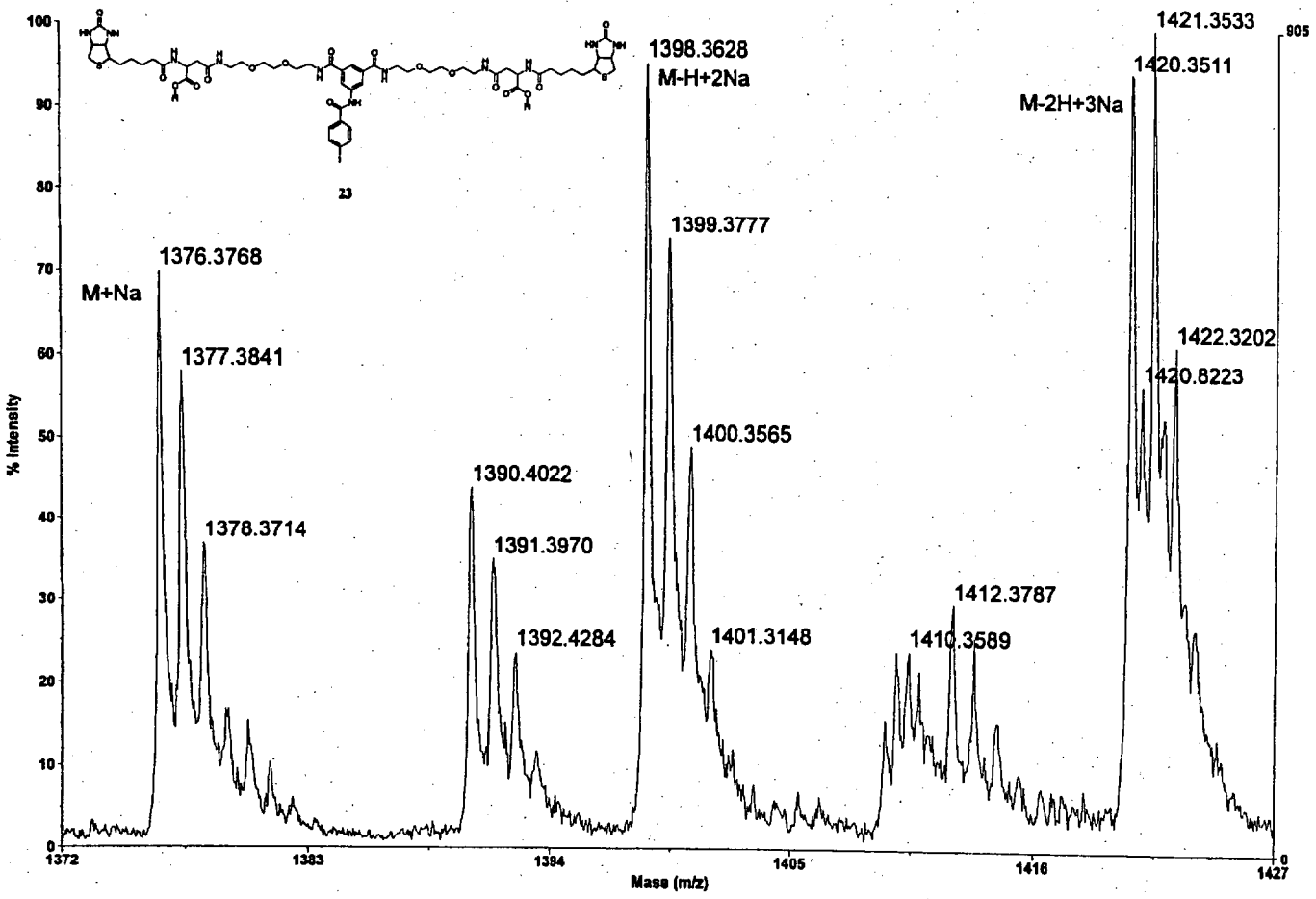
20

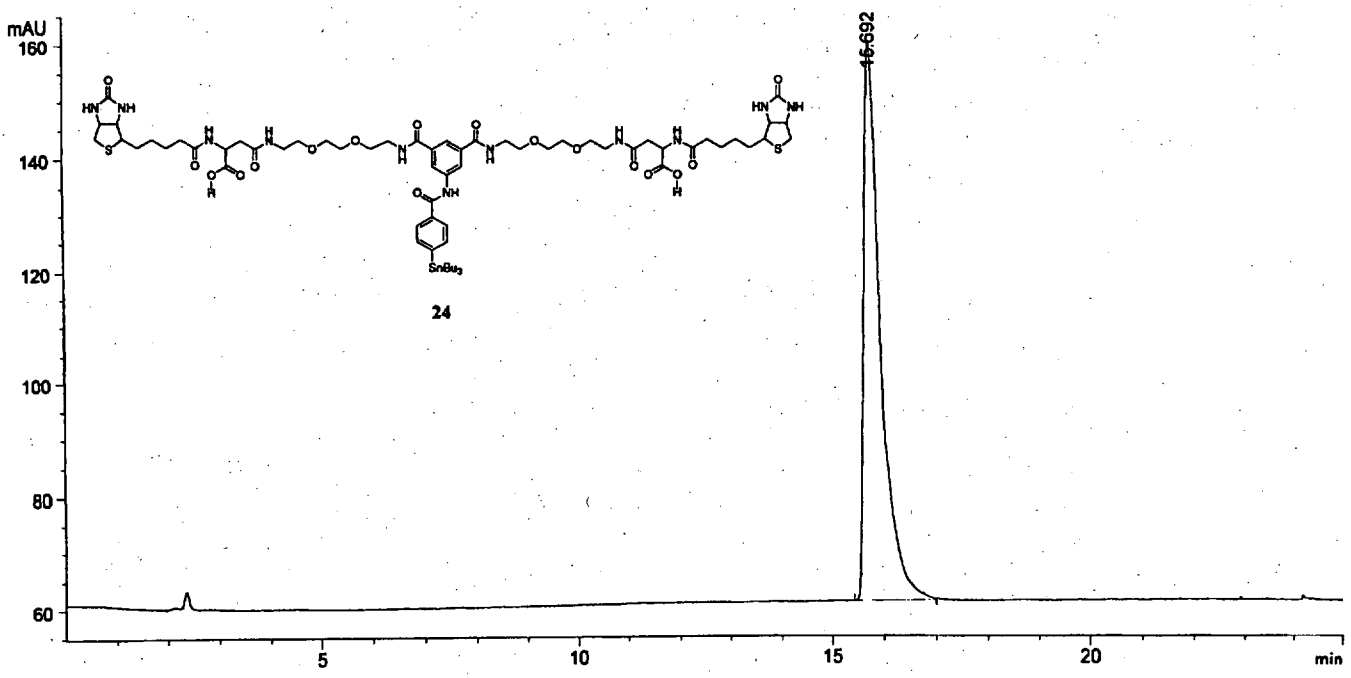
Nucleus	H1
Dwell 1D	333.333u
SW +/-	1500.0
FILTER	1400
Scans 1D	8
Scan Count	8
Points 1D	8192
Delay	1s
Obs Freq	200.1342347
F1 base	200.1300000
F1 offset	4.2347 KHz
RCVR gain	80
F2 freq	200.1500000
F2 base	200.1300000
F2 offset	20.0000 KHz
DEC Power	58

MeOD
200MHz

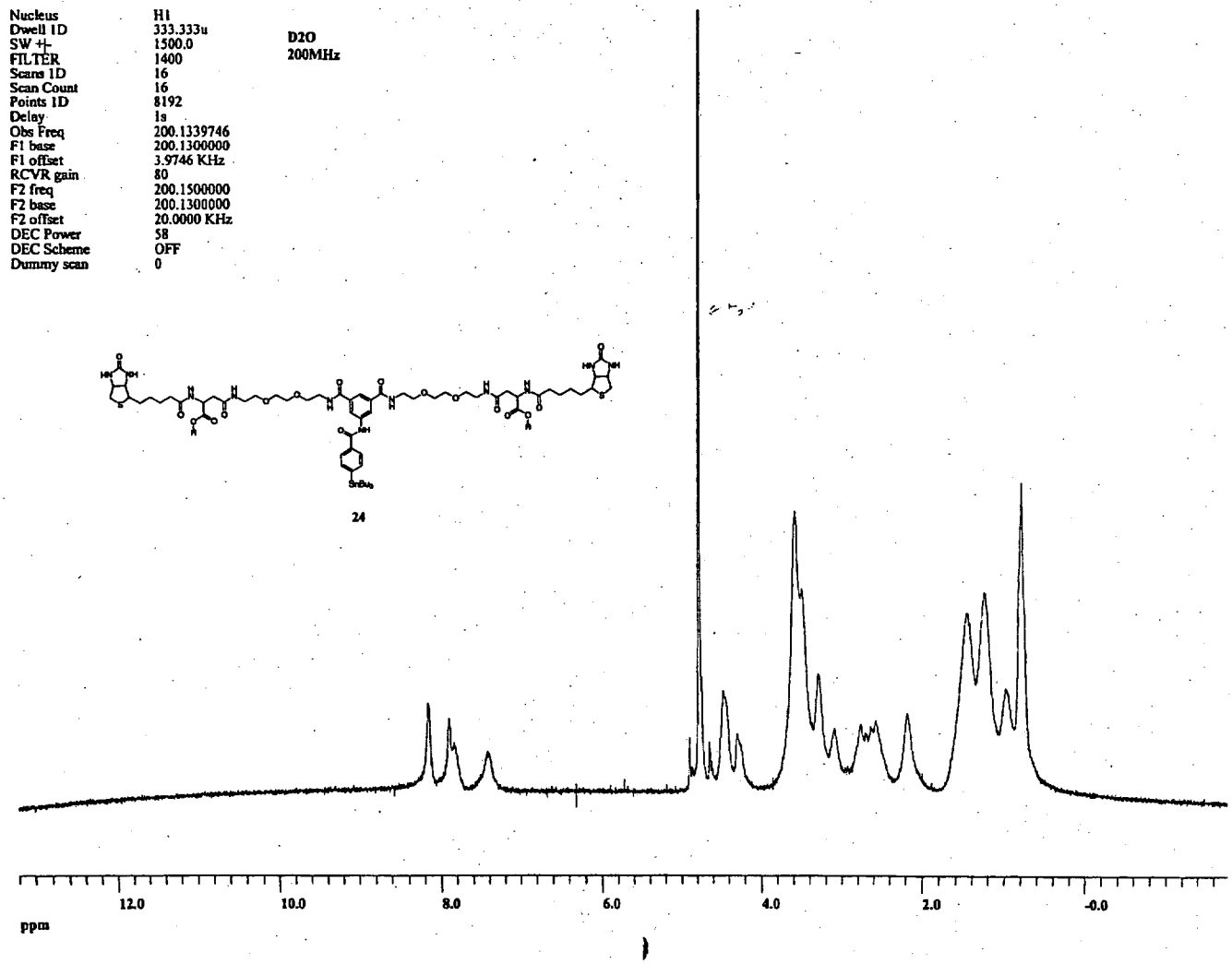
23



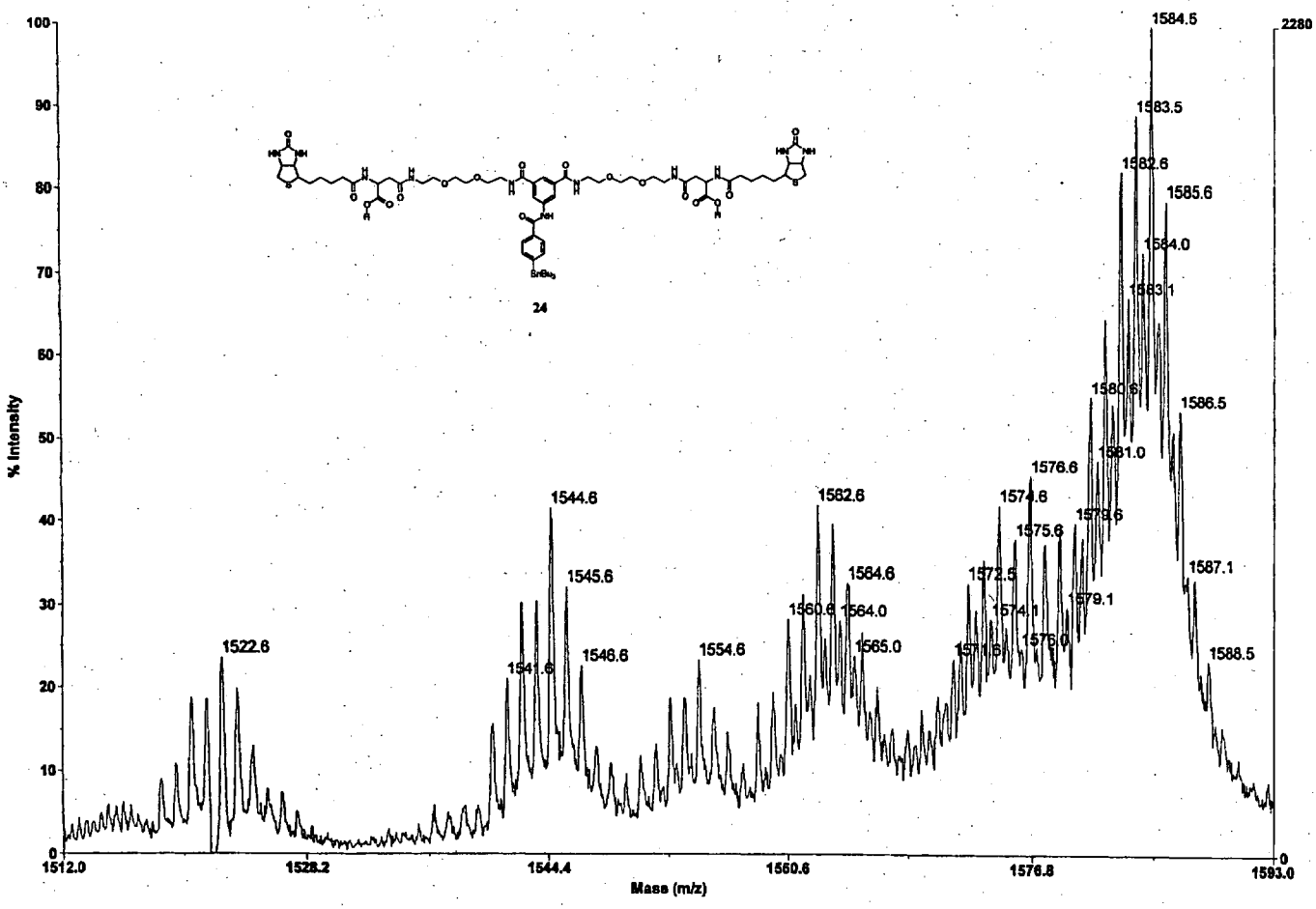

23
1376.3768
M+Na
1377.3841
1378.3714
1390.4022
1391.3970
1392.4284
1398.3628
M-H+2Na
1399.3777
1400.3565
1401.3148
1412.3787
1410.3589
1421.3533
1420.3511
M-2H+3Na
1422.3202
1420.8223
% Intensity
Mass (m/z)
1372
1383
1394
1405
1416
1427


mAU
160
140
120
100
80
60
16.692
5
10
15
20
min
24

© 2002 American Chemical Society, Bioconjugate Chem., Hamblett bc010087t Supporting Info Page 23



© 2002 American Chemical Society, Bioconjugate Chem., Hamblett bc010087t Supporting Info Page 24



A ^{99m}Tc(I)-Postlabeled High Affinity Bombesin Analogue as a Potential Tumor Imaging Agent

R. La Bella,[†,‡] E. Garcia-Garayoa,*[,†] M. Bähler,[‡] P. Bläuenstein,[†] R. Schibli,[†] P. Conrath,[§] D. Tourwé,[§] and P. A. Schubiger[†,‡]

Center for Radiopharmaceutical Science, Paul Scherrer Institute, CH-5232 Villigen, Switzerland, Department of Applied Biosciences, Swiss Federal Institute of Technology, CH-8057 Zurich, Switzerland, and Department of Organic Chemistry, Vrije Universiteit Brussels, B-1050 Brussels, Belgium. Received October 26, 2001; Revised Manuscript Received March 22, 2002

The overexpression of neuropeptide receptors observed in many cancers provides an attractive target for tumor imaging and therapy. Bombesin is a peptide exhibiting a high affinity for the gastrin releasing peptide (GRP) receptor, which is overexpressed by a variety of tumors such as breast or prostate cancer. In the present study, we have evaluated if the bombesin analogue [N_α-histidinyl acetate]-bombesin(7−14), radiolabeled with the novel $[^{99m}Tc(OH_2)_3(CO)_3]^+$, has the potential to be used as a diagnostic radiopharmaceutical. Receptor saturation studies, carried out on the GRP receptor-expressing PC-3 human prostate cancer cell line, revealed for [^{99m}Tc(CO)$_3$−N_α-histidinyl acetate]-bombesin(7−14) K_d values in the subnanomolar range. Competitive binding assays, using the cold rhenium(I)-labeled analogue as a surrogate for the ^{99m}Tc-conjugate, also showed high affinity binding. Incubation of the radioconjugate with PC-3 cells resulted in a rapid temperature- and time-dependent specific internalization. At 37 °C more than 70% was internalized within the first 15 min and remained constant up to 2 h. Despite the weak proteolytic stability of [^{99m}Tc(CO)$_3$−N_α-histidinyl acetate]bombesin-(7−14) in vitro, biodistribution studies, performed in PC-3 tumor-bearing mice, showed low uptake in the tumor (0.89 ± 0.27% ID/g 30 min pi) but high uptake into the pancreas (7.11 ± 3.93% ID/g 30 min pi), a GRP receptor-positive organ. Blockade experiment (coinjection of 300 μg bombesin/mouse with the radioligand) showed specificity of the uptake. Despite the low tumor uptake, tumor-to-blood ratios of 2.0 and 2.7 and tumor-to-muscle ratios of 8.9 and 8.0 were obtained at 30 min and 1.5 h postinjection, respectively. The promising results merit the future in vivo investigation of ^{99m}Tc/^{188}Re-tricarbonyl-labeled bombesin analogues.

INTRODUCTION

The discovery that certain tumor types overexpress receptors for neuropeptides dates back to the mid 1980s (*1*). To date, radiolabeled receptor binding peptides emerged as a new class of radiopharmaceuticals (*2*). Peptides show some favorable characteristics: they are readily synthesized, inexpensive, and can withstand harsh chemical conditions for modifications and radiolabeling. Furthermore, they offer several advantages over antibodies: they are less likely to induce immunogenic responses and they are expected to have a better pharmacokinetic profile inherent in a faster blood clearance, a better tissue penetration, a higher tumor uptake and therefore more favorable tumor-to-background ratios. The amphibian 14-amino acid peptide bombesin (BB) is part of the superfamily of bombesin-like peptides that also includes the mammalian homologue gastrin releasing peptide (GRP) and the related neuromedin B (NMB). These neuropeptides effect a broad range of physiological responses through G protein-coupled receptors with seven transmembrane domains. Besides being naturally localized in the central nervous system and in peripheral tissue (*3*, *4*), the GRP receptor is also expressed in a number of neuroendocrine tumors. Prostate and breast cancer might be of clinical significance as recent findings indicated a massive receptor overexpression in neoplastic transformed prostate and breast tissue (*5*, *6*). Bombesin has been shown to cause through the GRP receptor a tumor growth effect in cancer cell lines in culture or as xenografts in nude mice (*7*−*9*). The mechanism by which tumor growth stimulation occurs does not appear to be constant but in general seems to involve transactivation and up-regulation of epidermal growth factor receptors (*10*, *11*). Importantly, the tumor growth-stimulating effect of bombesin can be blocked by GRP receptor antagonists (*9*, *12*, *13*). Therefore, the use of GRP receptor antagonists and/or GRP receptor-targeting cytotoxic peptide conjugates could be an efficient chemotherapeutic approach. In nuclear medicine, ^{99m}Tc-labeled bombesin analogues could probably allow early noninvasive diagnosis of GRP receptor-positive tumors by γ-scintigraphy. Application of therapeutic radionuclides likes the β^--emitting rhenium-186 and rhenium-188 might even allow radiotherapy of these types of tumors.

The aim of the present work was the in vitro and in vivo characterization of a new bombesin analogue functionalized with a N_α-histidinyl acetate bifunctional chelator (BFC) and radiolabeled with the organometallic precursor $[^{99m}Tc(OH_2)_3(CO)_3]^+$. The study involved the synthesis of [^{99m}Tc(CO)$_3$−N_α-histidinyl acetate]bombesin-(7−14), **1**, as well as the pharmacological evaluation in

* To whom correspondence should be addressed: Telephone: ++41−56−310−2817, Fax: ++41−56−310−2849, E-mail: elisa.garcia@psi.ch.

† Paul Scherrer Institute.

‡ Swiss Federal Institute of Technology.

§ Vrije Universiteit Brussel.

10.1021/bc015571a CCC: $22.00 © 2002 American Chemical Society
Published on Web 04/17/2002

vitro and in vivo including binding properties, internalization, chemical stability, metabolic stability, and biodistribution of the radioconjugate in nude mice bearing PC-3 prostate adenocarcinoma xenografts.

MATERIAL AND METHODS

Reagents and materials were obtained from following sources: Fmoc-protected amino acids and 4-(2′,4′-dimethoxyphenyl-Fmoc-aminoethyl)-phenoxy resin were purchased from NovaBiochem (Läufelingen, Switzerland). Bombesin and Neuromedin B were obtained from Bachem (Bubendorf, Switzerland). [^{125}I-Tyr^4]bombesin was purchased from NEN Life Science Products (Zaventem, Belgium). The ^{99}Mo/^{99m}Tc generator was obtained from Mallinckrodt (Petten, The Netherlands). Culture medium Dulbeccos's MEM with GLUTAMAX I, fetal bovine serum, antibiotic/antimycotic solution, trypsin/EDTA, bovine serum albumin and soybean trypsin inhibitor were obtained from GIBCO BRL Life Technologies AG (Basel, Switzerland). HEPES, chymostatin, and bacitracin were from Sigma (Buchs, Switzerland). The cold binding buffer contained 50 mM Hepes, 125 mM NaCl, 7.5 mM KCl, 5.5 mM $MgCl_2$, 1 mM EGTA, 5 g/l BSA, 2 mg/L chymostatin, 100 mg/L soybean trypsin inhibitor, 50 mg/L bacitracin, pH 7.4. Further chemicals were obtained from Fluka (Buchs, Switzerland). The peptides were synthesized on a semiautomated Labortec peptide synthesizer SP640B. Correct mass was identified by electron spray-mass spectrometry (Micromass VG Trio 2000, Manchester, England). RP-HPLC analyses were performed on a Merck-Hitachi L-7000-system equipped with an L-7400 tunable absorption detector and a Berthold LB 506 B radiometric detector. For analyses and purification a Macherey-Nagel CC Nucleosil 100−5 C18 reverse phase column (10 μm, 250 × 4.6 mm) was used. HPLC solvents consisted of (A) water with 0.1% trifluoroacetic acid and (B) acetonitrile with 0.1% trifluoroacetic acid. The HPLC system started with a linear gradient 95% A/5% B to 40% A/60% B from 0 to 30 min. The gradient remained at 40% A/60% B for 5 min before switching back to 95% A/5% B for another 5 min. The flow rate was 1.5 mL/min. Radioactive samples from in vitro and in vivo experiments were measured with a NaI-γ-counter (Packard Canberra Cobra II).

Cell Culture. The human PC-3 adenocarcinoma cell line was obtained from European Collection of Cell Cultures (Salisbury, United Kingdom). Cells were maintained in Dulbecco's MEM with GLUTAMAX I supplemented with 1% fetal bovine serum, 100 units/mL penicilline G sodium, 100 μg/mL streptomycin sulfate and 0.25 μg/mL amphotericin B. Cells were cultured at 37 °C in a humidified incubator under an atmosphere containing 7.5% CO_2 and passaged weekly.

Peptide Synthesis. Solid-phase synthesis of [N_α-histidinyl acetate]bombesin(7−14) was carried out using Fmoc-strategy. The cold rhenium(I)-labeled conjugate was obtained by mixing 100 μL of 1 mM [N_α-histidinyl acetate]bombesin(7−14), 20 μL of 5.5 mM $(TEA)_2Re(CO)_3Br_3$, 20 μL of 15 mM NaOH, and adding up to 200 μL with water. The mixture was heated for 6 h at 75 °C. The peptides were analyzed by ES-MS and RP-HPLC.

Radiolabeling. $[^{99m}Tc(OH_2)_3(CO)_3]^+$ was prepared according to earlier descriptions (*14*). Depending on the needs, 0.1 to 0.3 mL of the neutralized technetium-99m tricarbonyl solution were mixed with 10−30 μL of 1 mM [N_α-histidinyl acetate]bombesin(7−14) and again heated to about 75 °C for 1 h. The product was analyzed and purified (for determination of K_d) by RP-HPLC.

Receptor Binding Studies. Inhibition assays with PC-3 cells were performed as previously described (*15*). In brief, cells were placed at confluence in 48-well plates with 25000 cpm of [^{125}I-Tyr^4]bombesin in the presence of increasing concentrations of the different bombesin analogues (0−3000 nM). After 1 h at 37 °C, cells were washed twice with cold binding buffer and then solubilized with 1 N NaOH. Radioactivity was determined using a NaI-γ-counter. For saturation studies, cells were incubated in triplicate with increasing concentrations (1 to 500 pM, equivalent to 2 to 1000 kBq of ^{99m}Tc activity) of the ^{99m}Tc(I)-labeled bombesin analogue for 1 h at 37 °C. The concentrations of active ^{99m}Tc were calculated as described by Bauer and Pabst (*16*) and Hill et al. (*17*). After two washing steps with binding buffer, cells were solubilized with 1 N NaOH at 37 °C. Nonspecific binding was determined with 1 μM bombesin.

Internalization Studies. Internalization of the ^{99m}Tc(I)-labeled bombesin analogue was performed as previously described (*18*, *19*). Briefly, PC-3 cells were incubated in six-well plates in triplicate with about 200000 cpm of compound **1** with or without excess of 1 μM cold bombesin for 2 h at 4 °C. Then they were washed three times with ice-cold culture medium to discard free peptide and incubated with previously warmed culture medium for 0, 5, 15, 30, and 120 min at 37 °C for internalization. After these times, cell-surface bound radioligand was removed by two steps of acid wash (50 mM glycine-HCl/100 mM NaCl, pH 2.8) at room temperature for 5 min. Subsequently, the cells were solubilized by incubation with 1 N NaOH at 37 °C to determine internalized radioligand. Release of internalized radioconjugated peptide was determined by incubating PC-3 cells at confluence in tissue culture dishes (60 × 15 mm) with about 2 × 10^5 cpm of **1** for 1 h at 37 °C. The cells were then washed three times with ice-cold culture medium and cell-surface bound radioligand was removed by two steps of acid wash. After having washed twice with culture medium, the cells were incubated for different time periods at 37 °C. At each time point (30 min, 1, 2.5, 5, and 24 h) the radioactivity present in the medium (released) as well as the acid wash (cell-surface bound) and the acid wash resistant (internalized) were determined with a NaI-γ-counter. Results were expressed as percentage of total activity in the wells (released + cell-surface bound + internalized).

Histidine and Cysteine Challenge. Challenging assays were done according to the method of Stalteri et al. (*20*) with some modifications. A 10 μL amount of the ^{99m}Tc(I)-labeled peptide were added to 90 μL of 0.01 M histidine or cysteine (1000-fold molar excess of challenging agents). The resulted solutions were incubated at 37 °C, and progress of the reaction was followed by RP-HPLC with radiometric detection.

In Vitro Stability. Studies of metabolic stability were performed with compound **1** in human plasma and whole blood. Plasma and blood from healthy donors were incubated at 37 °C with the ^{99m}Tc(I)-labeled peptide at a concentration of 0.2 pmol peptide/mL for different time periods. After incubation, plasma samples were precipitated with acetonitrile/ethanol and then centrifuged (4 °C, 2 × 10^4 g), whereas the blood samples were centrifuged previously to the precipitation to remove first blood cells. After repeated precipitation and centrifugation, the supernatants were then analyzed by RP-HPLC.

In Vivo Stability. To evaluate the in vivo degradation of the conjugate, blood of sacrificed PC-3 xenografted CD-1 nu/nu mice (1.5 h pi) was collected. The samples were centrifuged, and the supernatant was precipitated

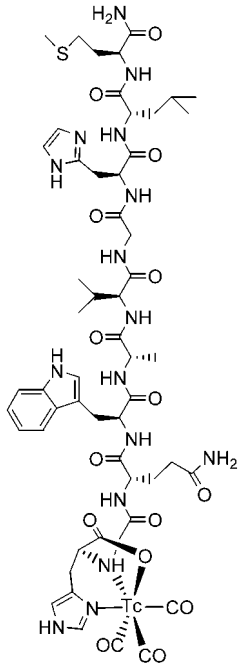


Figure 1. Proposed structure of [^{99m}Tc(CO)$_3$−N_α-histidinyl acetate]bombesin(7−14).

with acetonitrile/ethanol (1:1) and centrifuged again at 4 °C. The final supernatants were analyzed by RP-HPLC.

Animal Studies. Biodistribution of the radioconjugate was estimated in female CD-1 nu/nu mice (6- to 8-weeks old). Human PC-3 prostate adenocarcinoma xenografts were induced by subcutaneous injection of 8×10^6 cells/mouse. Ten days after the tumor induction the mice received the ^{99m}Tc(I)-labeled bombesin analogue (3.5−4 MBq/mouse) intravenously into the tail vein. Organs and tissue (blood, heart, lung, spleen, kidneys, stomach, pancreas, ileum, colon, liver, muscle, bone, brain, and tumor) were excised from the sacrificed animals at 30 min, 1.5, and 24 h postinjection. All tissues were weighed, and the radioactivity was determined by γ-counting. Results were expressed as percentage of injected dose per gram (% ID/g) of tissue. An in vivo receptor blocking study was also carried out. In this study, each animal received 300 μg of cold bombesin by coinjection with the radiolabeled bombesin analogue (in 95% saline/5% ethanol). The animals were sacrificed at 30 min postinjection, all tissues were removed, weighed, and γ-counted, and the % ID/g tissue was calculated.

RESULTS

Radiolabeling. HPLC analyses revealed a single main peak (>95% of total activity) after the labeling, which corresponded to the ^{99m}Tc−peptide conjugate (Figure 1). Generally, pertechnetate and free ^{99m}Tc(I)-tricarbonyl represented only 0−5% and 0−1%, respectively, of the total radioactivity after 1 h of labeling.

Receptor Binding Studies. All bombesin analogues tested showed the typical sigmoid curves in the displacement assays (Figure 2). The synthesized conjugates inhibited the binding of [^{125}I-Tyr^4]bombesin in the same concentration range as the natural peptide itself (Table 1).

In saturation studies, receptor binding of [^{99m}Tc−N_α-histidinyl acetate]bombesin(7−14) to intact PC-3 cells was found to be saturable (Figure 3, A). Specific binding rapidly increased in the concentration range of 1 to 100 pM radioconjugate and reached a plateau at 250 pM.

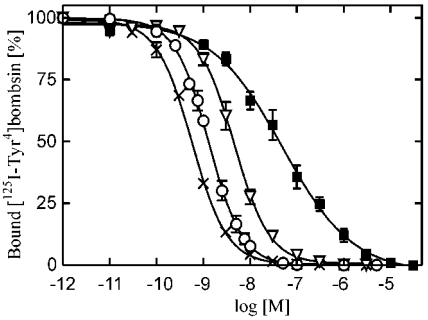


Figure 2. Displacement curves of [^{125}I-Tyr^4]bombesin binding to GRP receptors on the human prostate cancer cell line PC-3 by bombesin (○), [N_α-histidinyl acetate]bombesin(7−14) (▽), [Re(I)-N_α-histidinyl acetate]bombesin(7−14) (×), and neuromedin B (■).

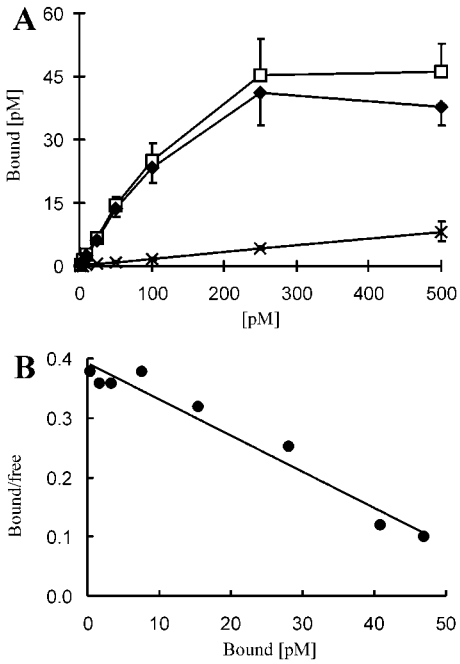


Figure 3. A: Binding of [^{99m}Tc(CO)$_3$−N_α-histidinyl acetate]-bombesin(7−14) to PC-3 cells as a function of ligand concentration. The cells were incubated with 1 to 500 pM [^{99m}Tc(CO)$_3$−N_α-histidinyl acetate]bombesin(7−14) in the absence (□, total binding) or presence (×, nonspecific binding) of 1 μM bombesin for 1 h at 37 °C. Specific binding (◆) was calculated as the difference between total and nonspecific binding. B: Scatchard analysis of these data. Each point means the value of triplicate determinations.

Table 1. Inhibition of [^{125}I-Tyr^4]Bombesin Binding to PC-3 Cells by Different Bombesin Analogues

compound	IC_{50} [nM]
bombesin	1.5
[N_α-histidinyl acetate]bombesin(7−14)	4.3
[Re(I)-N_α-histidinyl acetate]bombesin(7−14)	0.6
neuromedin B	73.9

Scatchard analysis of the binding data indicated the presence of a homogeneous population of binding sites with high affinity for the used cell line (Figure 3, B). At 37 °C, the calculated dissociation constant (K_d) was 2.1×10^{-10} M.

Internalization Studies. The rate of internalization of [^{99m}Tc(CO)$_3$−N_α-histidinyl acetate]bombesin(7−14) was time and temperature dependent (Figure 4). At 4 °C, cell-surface binding toward GRP receptors occurred but no internalization (<1%).

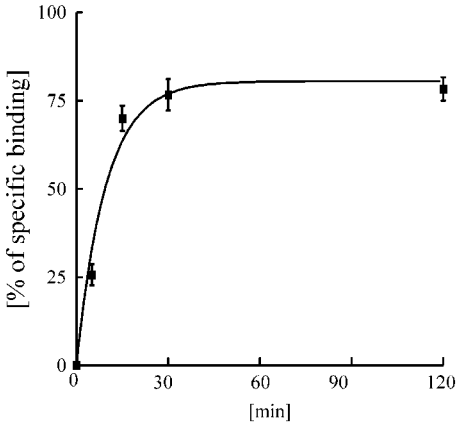


Figure 4. Time course internalization of [^{99m}Tc(CO)$_3$−N_α-histidinyl acetate]bombesin(7−14) in PC-3 cells at 37 °C. Data are percentage of acid-resistant (internalized) radioactivity in the cells.

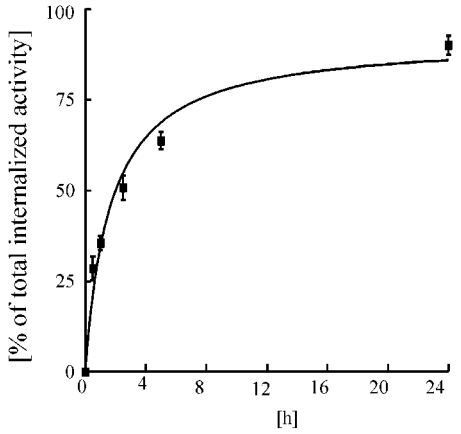


Figure 5. Time-dependent release of internalized radioactivity from PC-3 cells at 37 °C, after incubation with [^{99m}Tc(CO)$_3$−N_α-histidinyl acetate]bombesin(7−14) for 1 h at 37 °C.

Table 2. Percentage of ^{99m}Tc(I)-tricarbonyl Remaining Bound to the Bombesin Analogue after Incubation with 1000× Molar Excess of Histidine and Cysteine at 37 °C

	intact conjugate [%] after		
reagent	1 h	4 h	24 h
histidine	97 ± 3	94 ± 5	90 ± 3
cysteine	99 ± 2	97 ± 4	95 ± 4

After incubation at 37 °C bound radioligand was rapidly transformed from an acid-strippable (cell-surface bound) to an acid-resistant form (internalized). Specifically, after 5 min at 37 °C, 25 ± 3% of cell-associated radioactivity was internalized, and the maximum was reached at 30 min with 70 ± 4% internalized radioactivity. Despite this high internalization rate, there was no long-term retention of radioactivity in the cells (Figure 5).

The internalized radioactivity was quickly released. After 30 min at 37 °C, 27 ± 3% of internalized radioconjugate was already released. More than 50 ± 2% was released after 2.5 h and about 90 ± 4% after 24 h.

Histidine and Cysteine Challenge. Stability of the labeled peptide at pH 7 and 37 °C to a challenge with histidine and cysteine at a molar ratio of 1/1000 was analyzed by RP-HPLC (Table 2).

There was only insignificant reoxidation of the radioconjugate to [^{99m}TcO$_4$]$^-$ after 24 h at 37 °C (<1%). In general, only little ligand exchange occurred, whereby with an excess of histidine, the ligand was slightly more displaced than in the presence of excess cysteine.

Table 3. Stability of [^{99m}Tc(CO)$_3$−N_α-histidinyl acetate]bombesin(7−14) in Human Plasma and Whole Human Blood after Incubation at 37 °C[a]

incubation time [min]	intact radioconjugate [%] in	
	human plasma	human blood
0	100	100
5	83	70
15	76	55
30	46	30
60	22	9
120	7	2

[a] Data are expressed as percentage of intact radioconjugate.

Table 4. Biodistribution in Nude Mice Bearing PC-3 Human Prostate Adenocarcinoma Cell Xenografts at Different Time Points after iv Injection of [^{99m}Tc(CO)$_3$-N_α-histidinyl acetate]bombesin(7−14) (3.5−4 MBq/mouse)[a]

organ	0.5 h	1.5 h	24 h
blood	0.45 ± 0.06	0.12 ± 0.02	0.06 ± 0.03
heart	0.16 ± 0.04	0.06 ± 0.02	0.04 ± 0.02
lung	0.45 ± 0.08	0.20 ± 0.05	0.10 ± 0.04
spleen	0.37 ± 0.04	0.18 ± 0.04	0.08 ± 0.11
kidneys	9.47 ± 2.06	0.98 ± 0.24	0.49 ± 0.24
stomach	0.96 ± 0.32	0.58 ± 0.09	0.42 ± 0.06
pancreas	7.11 ± 3.93	1.77 ± 0.03	0.49 ± 0.06
ileum	3.04 ± 3.54	1.88 ± 0.38	0.07 ± 0.04
colon	1.30 ± 0.24	0.61 ± 0.52	0.09 ± 0.04
liver	3.33 ± 0.28	0.63 ± 0.22	0.60 ± 0.18
muscle	0.10 ± 0.02	0.04 ± 0.02	0.02 ± 0.01
bone	0.17 ± 0.10	0.08 ± 0.02	0.07 ± 0.03
brain	0.04 ± 0.01	0.02 ± 0.01	0.00 ± 0.00
tumor	0.89 ± 0.27	0.32 ± 0.10	0.10 ± 0.04

[a] Data are percentage of injected dose per gram (% ID/g) of tissue ± SD by reference of total injected dose (n = 3).

In Vitro Stability. The stability of the radioconjugate was tested both in human plasma and whole blood. The results are summarized in Table 3.

The peptide was rapidly metabolized when incubated in human plasma. After 5 min, about 80% remained intact and only 20% were intact after 1 h. Using whole blood, the enzymatic degradation was even quicker. Only 70% of the radioconjugate was intact after 5 min of incubation. After 60 min, less than 10% remained intact, and after 2 h of incubation, the radiolabeled peptide was almost totally degraded. However, reformation of free ^{99m}TcO$_4^-$ during incubation in plasma and blood could not be detected.

In Vivo Stability. The metabolism of **1** was also estimated in vivo. The analyzed blood (from 1.5 h postinjection sacrificed mice) still contained about 7% intact radioconjugate (identified by coinjection with the reference). Besides the intact radiopeptide there were five main metabolites, from which three seemed to be identical with those found in the in vitro stability studies.

Animal Studies. In the biodistribution study, performed with **1**, a rapid distribution and clearance was observed in PC-3 xenografted nude mice (Table 4). High uptake was observed in the kidneys and the liver (9.47 ± 2.06% ID/g and 3.33 ± 0.28% ID/g, 30 min pi). However, there was a rapid clearance of the radioactivity from all organs (e.g., 0.49 ± 0.24% ID/g kidney and 0.60 ± 0.18% ID/g liver 24 h after iv injection). Second highest uptake was observed in the pancreas, a GRP receptor-positive organ (7.11 ± 3.93% ID/g, 30 min pi). In the tumor, only low uptake was found (0.89 ± 0.27% ID/g 30 min after iv injection).

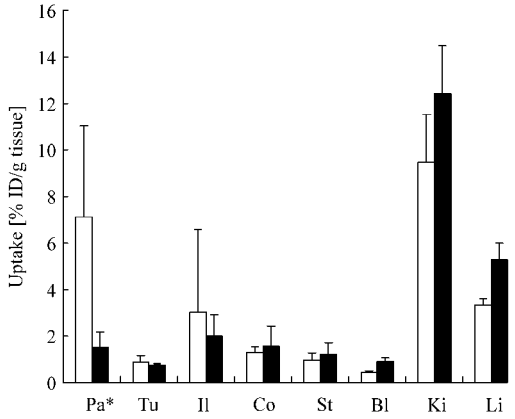


Figure 6. Receptor blockade study: biodistribution of [^{99m}Tc-(CO)$_3$−N_α-histidinyl acetate]bombesin(7−14) 0.5 h pi with (black bars) and without (white bars) coinjection of 300 μg of bombesin/mouse for blocking the GRP receptors. Data are percentage of injected dose per gram (% ID/g) of tissue ± SD by reference of total injected dose (n = 4). Pa = pancreas, Tu = tumor, Il = ileum, Co = colon, St = stomach, Bl = blood, Ki = kidneys, Li= liver. * P < 0.01, t-test.

In the study of GRP receptor blockade, a dose of 300 μg bombesin/mouse was able to reduce specifically the uptake of the radioconjugate (Figure 6). However, the uptake was significantly reduced only in the pancreas. A partial reduction could be observed in the ileum. No reduction was obtained in the tumor as well as in all other organs tested.

DISCUSSION

Radiolabeling of the BFC-derived 8-amino acid sequence of bombesin was very effective. The N-terminal introduction of N_α-histidinyl acetate as BFC made general post labeling yields of more than 95% possible. Despite the fact that bombesin(7−14) has one endogenous histidine in the peptide sequence (a potential anchor group for [^{99m}Tc(OH$_2$)$_3$(CO)$_3$]$^+$), the formation of a single radiolabeled species has been observed under the applied labeling conditions. This proved suitability of tridentate N_2O structures, like N_α-histidinyl acetate, as BFCs for the [^{99m}Tc(OH$_2$)$_3$(CO)$_3$]$^+$ (*21*) even in the presence of competing functionalities within the peptide/protein sequence. In addition, challenging assays with histidine (N_2O ligand) and cysteine (NOS ligand) revealed only little ligand exchange and/or decomposition and therefore confirmed the kinetic inertness of the built complex (*21, 22*). Only little reoxidation to [^{99m}TcO$_4$]$^-$ (less than 5%) took place.

Maintenance of GRP receptor-affinity was tested in the PC-3 human prostate adenocarcinoma cell line. The bioconjugate retained high affinity binding (Table 1). [Re-(CO)$_3$−N_α-histidinyl acetate]bombesin(7−14) even revealed higher GRP receptor-affinity than the natural ligand probably due to the lipophilicity of the "Re(CO)$_3$"-core. However, in receptor saturation experiments the higher GRP receptor affinity could not be confirmed, as the Scatchard plot analysis revealed for [^{99m}Tc(CO)$_3$−N_α-histidinyl acetate]bombesin(7−14) a similar K_d value as for the native (iodinated) peptide (*23*). Internalization studies with the ^{99m}Tc(I)-labeled bombesin derivative revealed a time- and temperature-dependent uptake into PC-3 cells, 70 ± 4%, after 30 min at 37 °C (Figure 4). This uptake into the target cells is highly desired, as it should result in increased tumor-to-background ratios. Furthermore, as internalization of G protein-coupled receptor ligands is mostly specific for agonists (*24*), it is believed that the radioconjugate **1** is an agonist. Internalization of ligand/GRP receptor complexes involves the final entrapment of the ligands in lysosomes, where—in case of peptides—they are quickly degraded (*25, 26*). Due to this immediate lysosomal degradation, no long-term retention of radioactivity in the cells is to be expected. Studies of radioactivity release from PC-3 cells confirmed this prediction, as 2.5 h after internalization of the radiopeptide, already 50 ± 2% was released, and after 24 h, 90 ± 4% (Figure 5).

Obviously, for longer entrapment of the radioconjugate in the cell, stabilization of the peptide might be needed. Therefore, metabolic stability of **1** was tested in vitro as well as in vivo. Degradation in vitro was quick with a half-life of 28 min in human plasma (Table 3). An even faster in vitro degradation was obtained when incubated in human blood ($t_{1/2}$ = 18 min), comparable to the in vivo stability in mouse blood, which did confirm comparability of in vitro and in vivo stability testing at least. In terms of desired stabilization, this may be achieved by replacement of glycine at position 11 by a D-alanine (*27*).

Biodistribution studies were performed in PC-3 xenografted CD-1 nu/nu mice to evaluate pharmacokinetics and specificity of in vivo GRP receptor targeting. There was a rapid clearance from blood and all nontargeted tissues (Table 4). Uptake into the GRP receptor-bearing pancreas was highest at 30 min pi, with 7.11 ± 3.93% ID/g tissue. The difference in the uptake of compound **1** into the pancreas with and without coinjection of 300 μg of bombesin was significant (7.11 ± 3.93% ID/g and 1.51 ± 0.68% ID/g, respectively), demonstrating the ability of the radioconjugate to specifically target in vivo GRP-expressing cells (Figure 6). However, only low uptake was observed in the tumor (0.89 ± 0.27% ID/g tissue). An explanation might be that the GRP receptor-bearing acini cells in the pancreas were well accessible to the blood stream, whereas the PC-3 tumors were weakly vascularized.

CONCLUSION

We could show that bombesin derivatives can readily be functionalized with relatively small, tridentate BFC for the radiolabeling with the organometallic precursor [^{99m}Tc(OH$_2$)$_3$(CO)$_3$]$^+$. The radioactive label reveals a high in vitro and in vivo stability. The labeled peptide retained fully the biological activity. The simple and organometallic labeling approach will allow the effective labeling of small peptides under mild conditions. Therefore, it can potentially be useful for therapeutic application of receptor avid substances in the future using the rhenium isotopes Re-186/188.

ACKNOWLEDGMENT

This work has been partly funded by Biomed 2 project, No. BMH4-CT98-3198, and by the FWO grant G.0116.97.

LITERATURE CITED

(1) Reubi, J. C., Maurer, R., von Werder, K., Torhorst, J., Klijn, J. G., and Lamberts, S. W. (1987) Somatostatin receptors in human endocrine tumors. *Cancer Res. 47*, 551−558.

(2) Boerman, O. C., Oyen, W. J. G., and Corstens, F. H. M. (2000) Radio-labeled receptor-binding peptides: A new class of radiopharmaceuticals. *Sem. Nucl. Med. 30*, 195−208.

(3) Katsuno, T., Pradhan, T. K., Ryan, R. R., Mantey, S. A., Hou, W., Donohue, P. J., Akeson, M. A., Spindel, E. R., Battey, J. F., Coy, D. H., and Jensen, R. T. (1999) Pharmacology and cell biology of the bombesin receptor subtype 4 (BB4−R). *Biochemistry 38*, 7307−7320.

(4) Jensen, R. T., Moody, T., Pert, C., Rivier, J. E., and Gardner, J. D. (1978) Interaction of bombesin and litorin with specific membrane receptors on pancreatic acinar cells. *Proc. Natl. Acad. Sci. 75*, 6139−6143.

(5) Markwalder, R., and Reubi, J. C. (1999) Gastrin-releasing peptide receptors in the human prostate: relation to neoplastic transformation. *Cancer Res. 59*, 1152−1159.

(6) Gugger, M., and Reubi, J. C. (1999) Gastrin-releasing peptide receptors in nonneoplastic and neoplastic human breast. *Am. J. Pathol. 155*, 2067−2076.

(7) Nelson, J., Donnelly, M., Walker, B., Gray, J., Shaw, C., and Murphy, R. F. (1991) Bombesin stimulates proliferation of human breast cancer cells in culture. *Br. J. Cancer 63*, 933−936.

(8) Moody, T. W., and Cuttitta, F. (1993) Growth factor and peptide receptors in small cell lung cancer. *Life Sci. 52*, 1161−1173.

(9) Cuttitta, F., Carney, D. N., Mulshine, J., Moody, T. W., Fedorko, J., Fischler, A., and Minna, J. D. (1985) Bombesin-like peptides can function as autocrine growth factors in human small-cell lung cancer. *Nature 316*, 823−826.

(10) Koppan, M., Halmos, G., Arencibia, J. M., Lamharzi, N., and Schally, A. V. (1998) Bombesin/gastrin-releasing peptide antagonists RC-3095 and RC-3940-II inhibit tumor growth and decrease the levels and mRNA expression of epidermal growth factor receptors in H-69 small cell lung carcinoma. *Cancer 83*, 1335−1343.

(11) Szepeshazi, K., Halmos, G., Schally, A. V., Arencibia, J. M., Groot, K., Vadillo Buenfil, M., and Rodriguez Martin, E. (1999) Growth inhibition of experimental pancreatic cancers and sustained reduction in epidermal growth factor receptors during therapy with hormonal peptide analogues. *J. Cancer Res. Clin. Oncol. 125*, 444−452.

(12) Aprikian, A. G., Tremblay, L., Han, K., and Chevalier, S. (1997) Bombesin stimulates the motility of human prostate-carcinoma cells through tyrosine phosphorylation of focal adhesion kinase and of integrin-associated proteins. *Int. J. Cancer 72*, 498−504.

(13) Bologna, M., Festuccia, C., Muzi, P., Biordi, L., and Ciomei, M. (1989) Bombesin stimulates growth of human prostatic cancer cells in vitro. *Cancer 63*, 1714−1720.

(14) Alberto, R., Schibli, R., Egli, A., Schubiger, P. A., Abram, U., and Kaden, T. A. (1998) A novel organometallic aqua complex of technetium for labeling of biomolecules: synthesis of $[^{99m}Tc(OH_2)_3(CO)_3]^+$ from $[^{99m}TcO_4]^-$ in aqueous solution and its reaction with a bifunctional ligand. *J. Am. Chem. Soc. 120*, 7987−7988.

(15) Garcia-Garayoa, E., Allemann-Tannahill, L., Bläuenstein, P., Willimann, M., Carrel-Rémy, N., Tourwé, D., Iterbeke, K., Conrath, P., and Schubiger, P. A. (2001) In vitro and in vivo evaluation of new radiolabeled neurotensin(8−13) analogues showing high affinity for NT1 receptors. *Nucl. Med. Biol. 28*, 75−84.

(16) Bauer, R., and Pabst, H. W. (1982) Tc-generators − yield of ^{99m}Tc and ratio to 'inactive' ^{99}Tc. *Eur. J. Nucl. Med. 7*, 35−36.

(17) Hill, D. M., Barnes, R. K., Wong, H. K., and Zawadzki, A. W. (2000) The quantification of technetium in generator-derived pertechnetate using ICP-MS. *Appl. Radiat. Isot. 53*, 415−419.

(18) Casalini, P., Luison, E., Menard, S., Colnaghi, M. I., Paganelli, G., and Canevari, S. (1997) Tumor pretargeting: role of avidin/streptavidin on monoclonal antibody internalization. *J. Nucl. Med. 38*, 1378−1381.

(19) De Jong, M., Bernard, B. F., De Bruin, E., Van Gameren, A., Bakker, W. H., Visser, T. J., Macke, H. R., and Krenning, E. P. (1998) Internalization of radiolabeled [$DTPA^0$]octreotide and [$DOTA^0$, Tyr^3]octreotide: peptides for somatostatin receptor-targeted scintigraphy and radionuclide therapy. *Nucl. Med. Commun. 19*, 283−288.

(20) Stalteri, M. A., Bansal, S., Hider, R., and Mather, S. J. (1999) Comparison of the stability of technetium-labeled peptides to challenge with cysteine. *Bioconjugate Chem. 10*, 130−136.

(21) Schibli, R., La Bella, R., Alberto, R., Garcia-Garayoa, E., Ortner, K., Abram, U., and Schubiger, P. A. (2000) Influence of the denticity of ligand systems on the in vitro and in vivo behavior of ^{99m}Tc(I)-tricarbonyl complexes: a hint for the future functionalization of biomolecules. *Bioconjugate Chem. 11*, 345−351.

(22) Egli, A., Alberto, R., Tannahill, L., Schibli, R., Abram, U., Schaffland, A., Waibel, R., Tourwé, D., Jeannin, L., Iterbeke, K., and Schubiger, P. A. (1999) Organometallic ^{99m}Tc-aquaion labels peptide to an unprecedented high specific activity. *J. Nucl. Med. 40*, 1913−1917.

(23) Reile, H., Armatis, P. E., and Schally, A. V. (1994) Characterization of high-affinity receptors for bombesin/gastrin releasing peptide on the human prostate cancer cell lines PC-3 and DU-145: internalization of receptor bound [^{125}I-Tyr^4]bombesin by tumor cells. *Prostate 25*, 29−38.

(24) Van de Wiele, C., Dumont, F., Van Belle, S., Slegers, G., Peers, S. H., and Dierckx, R. A. (2001) Is there a role for agonist gastrin-releasing peptide receptor radioligands in tumour imaging? *Nucl. Med. Commun. 22*, 5−15.

(25) Grady, E. F., Slice, L. W., Brant, W. O., Walsh, J. H., Payan, D. G., and Bunnett, N. W. (1995) Direct observation of endocytosis of gastrin releasing peptide and its receptor. *J. Biol. Chem. 270*, 4603−4611.

(26) Slice, L. W., Yee, H. F., Jr., and Walsh, J. H. (1998) Visualization of internalization and recycling of the gastrin releasing peptide receptor-green fluorescent protein chimera expressed in epithelial cells. *Receptors Channels 6*, 201−212.

(27) Coy, D. H., Mungan, Z., Rossowski, W. J., Cheng, B. L., Lin, J. T., Mrozinski, J. E., Jr., and Jensen, R. T. (1992) Development of a potent bombesin receptor antagonist with prolonged in vivo inhibitory activity on bombesin-stimulated amylase and protein release in the rat. *Peptides 13*, 775−781.

BC015571A

Novel Near-Infrared Cyanine Fluorochromes: Synthesis, Properties, and Bioconjugation

Yuhui Lin, Ralph Weissleder, and Ching-Hsuan Tung*

Center for Molecular Imaging Research, Massachusetts General Hospital, Harvard Medical School, Charlestown, Massachusetts 02129. Received October 29, 2001; Revised Manuscript Received January 31, 2002

Recently, near-infrared (NIR) fluorescence light has been applied to image various biological events in vivo, because it penetrates tissue more efficiently than light in the visible spectrum. Compounds exhibiting fluorescent properties in the NIR range are key elements for this upcoming optical imaging technology. In this paper, we report the synthesis of four new, water-soluble NIR cyanine fluorochromes which have superior chemical stability and optical properties. Each fluorochrome was designed with a monoreactive carboxyl group for labeling purposes. When multiple fluorochromes were attached to a single macromolecule, fluorescence quenching was observed. On the basis of this property, a novel autoquenched enzyme sensitive NIR fluorescence probe was prepared.

INTRODUCTION

Noninvasive imaging with light photons represents an intriguing avenue for extracting biological information from living subjects. While light in the visible range is routinely used for intravital microscopy, imaging of deeper tissues (>500 μm to cm) requires the use of near-infrared (NIR) light, as hemoglobin and water, the major absorbers of visible and infrared light, respectively, have their lowest absorption coefficient in the NIR region (650−900 nm). Light photons can be used to measure different native parameters of tissue through which they travel, such as absorption, scattering, polarization, spectral characteristics, and fluorescence. Near-infrared fluorescence imaging in particular is expected to have a major impact in biotechnology and medicine because of its high sensitivity and the fact that no radiation is necessary for acquisition and the versatility of different reporter probes. The recent descriptions of targeted NIR fluorochromes (*1*, *2*), activatable NIR fluorochromes (*3*), red-shifted fluorescent proteins (*4*), and bioluminescent probes (*5*) has lent further credence to the field. Conversely, a number of reflectance (*6*) and tomographic imaging systems have recently been developed to detect NIR fluorescence in deep tissues (*7*) including patients (*8*, *9*).

At the heart of NIR imaging lies the need for biocompatible fluorochromes. While indocyanine green (ICG) has been used clinically for over 20 years with few side effects (*10*), its use in designing targeted agents is limited primarily because of the nonavailability of monoderivatized activated precursors. Additional disadvantages are its hydrophobicity, high albumin binding, nonlinear fluorescence, and other intrinsic properties (*11*). Recently, several new derivatives such as tricarbocyanines (*2*) and cyptates (*12*) have been described and synthesized by different groups.

General problems with the synthesis of NIR fluorochromes compared to visible light fluorochromes are (1) significant spectral broadening as the wavelength increases, (2) low quantum yield, (3) photoinstability, (4) chemical instability with increasing red-shift, and (5) the tendency to aggregate because of hydrophobicity. The ideal NIRF reporters for in vivo imaging should have the following characteristics: (1) a peak fluorescence close to "700−900 nm", (2) high quantum yield, (3) narrow excitation/emission spectrum, (4) high chemical and photostability, (5) nontoxicity, (6) good biocompatibility, biodegradability and excretability, (7) availability of monofunctional derivatives as platform technology, and (8) commercial viability and scalable production for large quantities required for human use.

We describe here the synthesis of a number of highly stable NIR fluorochromes designed with the above prerequisites in mind. The agents contain multiple hydrophilic groups and have been prepared as monohydroxy succinimide esters for binding to biomolecules such as peptides, metabolites, proteins, and other affinity ligands.

MATERIALS AND METHODS

Chemicals. 6-Amino-1,3-naphthalene disulfonic acid disodium salt, 1,4-butanesultone, 4-hydrazinobenzoic acid, 3-methyl-2-butanone, iodoethane, diisopropylcarbodiimide (DIPCDI), and *N*-hydroxysuccinimide (NHS) were purchased from Aldrich (Milwaukee, WI). Glutaconaldehyde dianil hydrochloride, malconaldehyde dianil hydrochloride, and *p*-hydrazinobenzenesulfonic acid were purchased from TCI America (Portland, OR). All other reagents and solvents were purchased from Aldrich and were used as received.

Purification and Spectroscopic Analysis. Purification of dyes was performed on a Rainin preparative HPLC instrument (Woburn, MA) using a C18−RP preparative column (Vydac, Hesperia, CA; flow rate = 6 mL/min; eluant A, water with 0.1% TFA; eluant B, 90% of acetonitrile and 10% of eluant A; starting at 90% A for 5 min and then a linear gradient over 40 min to 50% A). The dual HPLC detector was set at 240 and 360 nm. Dyes were collected, and solvent was removed by Speed-vac concentrator (Savant, Holbrook, NY). Absorbance spectra were measured on a U-3000 spectrophotometer (Hitachi, San Jose, CA). Fluorescence spectra were recorded using

* To whom correspondence should be addressed. Ching H. Tung, Ph.D., Center for Molecular Imaging Research, Massachusetts General Hospital, 149 13th St., Rm. 5406, Charlestown, MA 02129. (tel): (617) 726-5779. (fax): (617) 726-5708. e-mail: tung@helix.mgh.harvard.edu.

10.1021/bc0155723 CCC: $22.00 © 2002 American Chemical Society
Published on Web 04/17/2002

a F-4500 fluorophotometer (Hitachi). The proton NMR spectra were recorded in D_2O in a 400 MHz FT-NMR spectrometer.

Synthesis of Cyanine Dyes. 1,1,2-Trimethylbenzindoleninium 1,3-disulfonate (*13*), 5-carboxy-1-(4-sulfobutyl)-2,3,3-trimethyl-3*H*-indolenine **2** (*14*), and 1-(4-sulfonatobutyl)-2,3,3-trimethylindoleninium-5-sulfonate **5** (*15*) were synthesized according to the literature. All compounds were used in crude form because conventional chromotagraphy and/or recrystalization proved to be difficult for the highly hydrophilic compounds.

***N*-Ethyl-2,3,3-trimethylbenzindoleninium 5,7-Disulfonate 1.** In a 50 mL round-bottomed flask were placed 4.7 g of 1,1,2-trimethylbenzindoleninium 1,3-disulfonate dipotassium salt, 8 mL of ethyl iodide, and 50 mL of 1,2-dichlorobenzene. The mixture was heated under argon atmosphere at 90 °C for 12 h and then at 125 °C for another 10 h. After being cooled to room temperature, 1,2-dichlobenzene was decanted and the solid was washed three times with an acetone/ether mixture. The solid was filtered off and dried under vacuum to result in 4.1 g of crude **1**.

Intermediate 3. In a 50 mL round flask were placed 1.92 g of **1**, 1.12 g of glutaconaldehyde dianil hydrochloride, 20 mL of acetic anhydride, and 5 mL of glacial acetic acid. The mixture was heated at 120 °C for 3 h and was then precipitated from ethyl acetate upon cooling. After filtration, the solid was washed twice with ethyl acetate and dried under vacuum to yield 2.2 g of crude intermediate **3**.

NIR1. A mixture of 0.60 g of intermediate **3**, 0.33 g of 5-carboxy-1-(4-sulfobutyl)-2,3,3-trimethyl-3*H*-indolenine **2**, 0.49 g of potassium acetate, 12 mL of acetic anhydride, and 5 mL of glacial acetic acid was stirred and heated at 120 °C under argon atmosphere for 30 min. After being cooled to room temperature, the mixture was poured into 200 mL of ethyl acetate and the precipitate was collected by centrifugation and then dried to result in 0.86 g of crude NIR1. The crude product was further purified by reverse phase HPLC to give 14% (based on the crude product) of pure NIR1. ^{1}H NMR (D_2O): δ 1.24 (6H, s), 1.28 (3H, t), 1.54 (6H, s), 1.80 (4H, broad m), 2.90 (2H, broad t), 3.86 (2H, broad), 4.12 (2H, broad q), 5.76 (1H, broad), 6.03 (2H, broad), 7.04 (2H, broad), 7.21 (1H, d), 7.33 (1H, broad), 7.53 (1H, broad), 7.58 (1H, s), 7.65 (1H, d), 7.73 (1H, d), 8.19 (1H, s), 8.52 (1H, s), 8.71 (1H, d).

Intermediate 4. In a 50 mL round flask were placed 1.70 g of **1**, 0.93 g of malonaldehydedianil hydrochloride, 20 mL of acetic anhydride, and 5 mL of glacial acetic acid. The mixture was then heated at 120 °C for 3 h. Upon being cooled, the mixture was precipitated in ethyl acetate. After filtration the solid was washed twice with ethyl acetate and dried under vacuum to yield 1.5 g of crude intermediate **4**.

NIR2. A mixture of 0.58 g of intermediate **4**, 0.35 g of 5-carboxy-1-(4-sulfobutyl)-2,3,3-trimethyl-3*H*-indolenine **2**, 0.49 g of potassium acetate, 12 mL of acetic anhydride, and 5 mL of glacial acid was stirred and heated at 120 °C under argon atmosphere for 30 min. After being cooled to room temperature, the mixture was poured into 200 mL of ethyl acetate. The precipitate was collected by centrifugation and dried to result in 0.9 g of crude NIR2. The crude product was then purified by reversed phase HPLC to give 21% (based on the crude product) of pure NIR2. ^{1}H NMR (D_2O): δ 1.19 (3H, t), 1.24 (6H, s), 1.52 (6H, s), 1.80 (4H, broad m), 2.90 (2H, broad t), 3.90 (2H, broad m), 4.02 (2H, broad q), 5.82 (1H, broad d), 5.85 (1H, broad d), 6.14 (2H, t), 7.08 (1H, d), 7.56 (1H, s), 7.61−7.77 (4H, m), 8.19 (1H, s), 8.51 (1H, s), 8.70 (1H, d).

Intermediate 6. In a 50 mL round flask were placed 0.80 g of 1-(4-sulfonatobutyl)-2,3,3-trimethylindoleninium-5-sulfonate **5**, 0.50 g of glutaconaldehyde dianil hydrochloride, 10 mL of acetic anhydride, and 5 mL of glacial acetic acid. The mixture was then heated at 120 °C for 3 h. Upon cooling, the mixture was precipitated from ethyl acetate. After filtration the solid was washed twice with ethyl acetate and dried under vacuum to yield 0.88 g of crude intermediate **6**.

NIR3. A mixture of 0.88 g of intermediate **6**, 0.55 g of 5-carboxy-1-(4-sulfobutyl)-2,3,3-trimethyl-3*H*-indolenine **2**, 0.85 g of potassium acetate, 12 mL of acetic anhydride, and 5 mL of glacial acetic acid was stirred and heated at 120 °C under argon atmosphere for 30 min. After being cooled to room temperature, the mixture was poured into 200 mL of ethyl acetate. The precipitate was collected by centrifugation and dried to result in 0.9 g of crude NIR3. The crude product was then purified by reverse phase HPLC to give 6.7% (based on the crude product) of pure NIR4. ^{1}H NMR (D_2O): δ 1.36 (6H, s), 1.42 (6H, s), 1.56−1.81 (6H, broad m), 1.81−1.89 (2H, broad m), 2.84−2.90 (4H, m), 3.92 (2H, broad t), 4.06 (2H, broad t), 5.85 (1H, broad d), 6.10 (2H, broad), 6.28 (1H, broad t), 7.17 (2H, broad m), 7.26 (1H, d), 7.45 (1H, broad), 7.53 (1H, broad), 7.67−7.77 (4H, m).

Intermediate 7. In a 50 mL round flask were placed 0.80 g of 1-(4-sulfonatobutyl)-2,3,3-trimethylindoleninium-5-sulfonate **5**, 0.45 g of malonaldehydedianil hydrochloride, 10 mL of acetic anhydride, and 5 mL of glacial acetic acid. The mixture was then heated at 120 °C for 3 h. Upon cooling, the mixture was precipitated from ethyl acetate. After filtration the solid was washed twice with ethyl acetate and dried under vacuum to yield 0.74 g crude intermediate **7**.

NIR4. A mixture of 0.74 g of intermediate **7**, 0.45 g of 5-carboxy-1-(4-sulfobutyl)-2,3,3-trimethyl-3*H*-indolenine **2**, 0.70 g of potassium acetate, 12 mL of acetic anhydride, and 5 mL of glacial acid were stirred and heated at 120 °C under argon atmosphere for 30 min. After being cooled to room temperature, the mixture was poured into 200 mL of ethyl acetate. The precipitate was collected by centrifugation and dried to result in 0.9 g of crude NIR4. The crude product was then purified by reverse phase HPLC to give 8.1% (based on the crude product) of pure NIR3. ^{1}H NMR (D_2O): δ 1.29 (6H, s), 1.39 (6H, s), 1.71−1.78 (6H, broad m), 1.84−1.88 (2H, broad m), 2.79−2.87 (4H, m), 3.92 (2H, broad t), 4.04 (2H, broad t). 5.82 (1H, d), 6.06 (1H, d), 6.23 (1H, t), 7.20 (1H, d), 7.25 (1H, d), 7.60−7.75 (6H, m).

Determination of the Extinction Coefficients and Fluorescence Quantum Yield. All NIR dyes were purified by preparative HPLC twice as described above. The K^+ ions were replaced with H^+ by ion-exchange chromatography in deionized water (cation-exchange resin, Dowex-50, 8% cross-link, 100−200 mesh). About 20 mg of a dye was dissolved in 100 mL of deionized water. The absorbance was measured individually in three dilutions of the stock solution in deionized water or in ethanol (95%). The fluorescence emission maxima and intensities of the dyes were obtained using dilute solutions in water and exciting at both the main absorption peak as well the short-wavelength shoulder of the main absorption peak. In cases of NIR2 and NIR4, the quantum yields were calculated relative to a standard solution of Cy5.5 (Amersham-Pharmacia, Piscataway, NJ) with quantum yield of 0.29, whereas in cases of NIR1 and NIR3. The calculations were performed relative to a standard solution of Cy7 (Amersham-Pharmacia) with a quantum yield of 0.28.

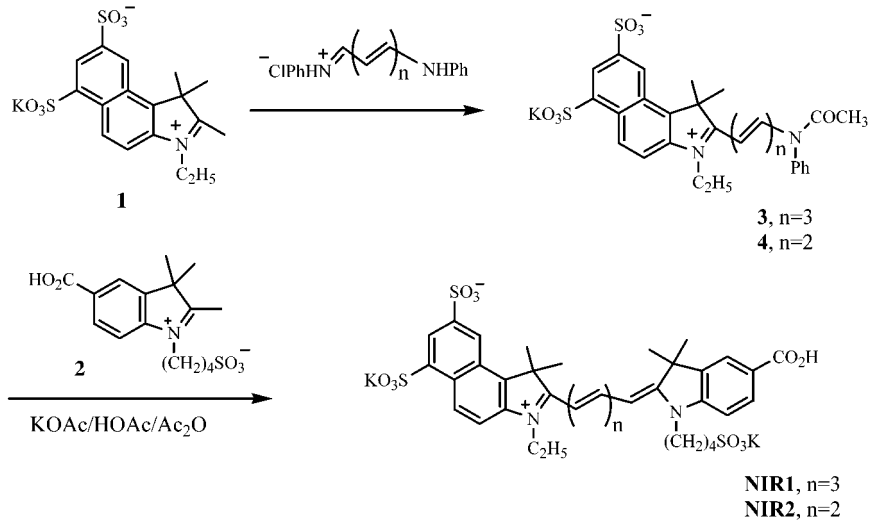


Figure 1. Synthetic scheme of NIR1 and NIR2.

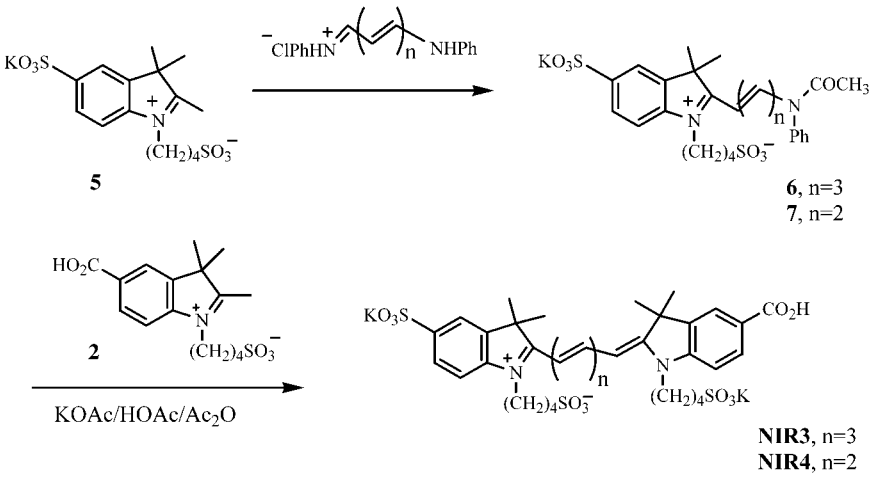


Figure 2. Synthetic scheme of NIR3 and NIR4.

Activation of Cyanine Dyes. In a typical experiment, 10 mg of dye, 30 μL of diisopropylcarbodiimide, 50 μL of *N*-methylmorpholine, 22.0 mg of NHS, and 0.5 mL of dry DMF were placed in a small round-bottomed flask under argon atmosphere. The mixture was stirred at room temperature for 3 h and then precipitated in ether. After centrifugation, the ether was decanted and the solid was washed four more times with ether and dried in a vacuum. The HPLC result indicated that more than 98% of dye was converted to active ester.

Imaging of NIR Dyes. Imaging was performed using a previously developed NIRF reflectance imaging system (*6*). Briefly, the system consisted of a light-tight chamber equipped with a halogen white light source and excitation band-pass filters providing the excitation wavelengths of 610−650 nm or 750−770 nm (Omega Optical, Brattlebore, VT). Equalmolar NIR dyes and ICG were loaded to individual wells (0.16 nmol in 200 μL) in a clear-bottom 96-well plate (Corning, Corning, NY). Fluorescence was detected by a 12-bit monochrome CCD camera (Kodak, Rochester, NY) equipped with a 12.5−75 mm zoom lens and emission band-pass filters at 680−720 nm or 800−820 nm (Omega Optical, Brattlebore, VT). Exposure time was 10 s per image. Images were analyzed using commercially available software (Kodak Digital Science 1D software, Rochester, NY).

Synthesis of Enzyme Sensitive Probe with Various Amounts of NIR2. The enzyme sensitive probes were synthesized similar to the described protocol (*3*). Briefly, partially PEGylated polylysine (0.1 mg, MW = 500000 Da. (*16*)) was reacted with various amounts of NIR2−NHS ester, whose concentration was 0.4, 2, 4, 8, 20, 40, or 80 μM in 20 mM $NaHCO_3$, at room temperature for 3 h. The NIR2-labeled polymers were then separated from excess low molecular weight reagents using a 50 kDa cutoff microconcentrators (Amicon, Beverly, MA). Based on NIR2 absorption measurement at 662 nm, the average numbers of NIR2 fluorochrome per PGC are 0.2, 0.8, 1.4, 2.4, 4.3, 5.7, and 7.0, respectively.

Trypsin Activation of NIR2−PGC Probes. The activation of the NIRF probe was done in a 96-well plate with various NIR2−PGC probes. In each well, NIR2−PGC (40 pmole) in 200 μL of PBS was incubated with 10 μL of trypsin solution (0.05% trypsin, 0.53 mM EDTA, Mediatech, Herndon, VA). The reactions were monitored using a fluorescence microplate reader (Spectramax, Molecular Devices, Sunnyvale, CA) with excitation and emission wavelength at 662 and 684 nm, respectively. The reactions were purformed in duplicate.

RESULTS AND DISCUSSION

Synthesis of Nonsymmetrical Cyanine Dyes. The synthetic pathways for the four new cyanine dyes are outlined in Figures 1 and 2. The synthesis of NIR1 and NIR2 was carried out starting from 1,1,2-tri-

methylbenzindoleninium 1,3-disulfonate dipotassium salt, which was converted to **1** by treating with ethyl iodide. Reaction of **1** with malconaldehyde dianil hydrochloride or glutaconaldehyde dianil hydrochloride resulted in the intermediates **3** and **4**. Intermediates **3** and **4** were stable at room temperature and in aqueous solution, and no significant decomposition could be observed over more than two weeks. The asymmetrical dyes NIR1 and NIR2 were assembled by reacting **3** or **4** with 5-carboxy-1-(4-sulfobutyl)-2,3,3-trimethyl-3*H*-indolenine **2**. Similarly, the synthesis of NIR3 and NIR4 was started with 1-(4-sulfonatobutyl)-2,3,3-trimethylindoleninium-5-sulfonate **5**, which was converted to intermediates **6** or **7** by the reaction with malconaldehyde dianil hydrochloride or glutaconaldehyde dianil hydrochloride. Like intermediates **3** and **4**, intermediates **6** and **7** were also stable at room temperature. Reaction of intermediate **6** or **7** with 5-carboxy-1-(4-sulfobutyl)-2,3,3-trimethyl-3*H*-indolenine **2** yielded the asymmetrical dyes NIR3 and NIR4, respectively.

The multistep synthesis of the described compounds showed several peculiarities. First, the intermediateries were difficult to purify, leading us to use mixtures for subsequent reactions followed by final HPLC purification. We assume that purification of the intermediaries was difficult because of their extremely high water solubility. Irrespective of this step, we showed that the final products were >98% pure as determined by HPLC. Clean NMR spectra were obtained, except for the integration of one or two bridged methine protons, which might be due to the resonance structure of the cyanine dyes. Indeed similar finding about NMR spectra of cyanine dyes have been reported (*17*).

Unlike previously described and commercially available near-infrared cyanine dyes (*2*, *13*, *18*), the ones reported here bear two different heterocyclic ring systems including a 3-ring and a 2-ring heterocyclic system. The rationale for this design is severalfold, including the ability to fine-tune spectral properties for imaging compounds and the improvement in the typically mitigating self-aggregation of large planar dyes. The latter is of particular concern since self-aggregating fluorochromes may be poorly soluble, as is the case for ICG. To further improve solubility, we chose to also include a constant and large number of sulfonate groups in all dyes.

Spectral Properties of Dyes. The absorption spectra of NIR1−4 are shown in Figure 3A. As in other cyanine dyes, the difference in absorbance maximum between indodicarbocyanine dye and indotricarbocyanine dye was about 100 nm. The terminal ring system contributes very little to the absorbance maximum compared to that of the bridging methine unit. The difference in absorbance maximum between 3/2 ring systems (e.g., NIR2) compared to 2/2 homocycles (e.g., NIR4) was only 10 nm. Excitation and emission spectra of NIR1 and NIR2 are shown in Figure 3B. Indodicarbocyanine dyes had a 20 nm Stokes shift of the fluorescence emission maximum, while indotricarbocyanine dyes exhibited a 30 nm Stokes shift of the fluorescence maximum. The dyes had high molar extinction coefficient above 250000, similar as the range published for other compounds. Quantum yields of the different fluorochromes varied from 0.23 to 0.43. Optical properities of the compounds were summarized on Table 1.

Activation of Dyes. The cyanine dyes were converted to reactive *N*-hydroxysuccinimide esters by DICPDI and NHS in the presence of *N*-methylmorpholine in DMF (Figure 4). An almost quantitative yield (typically >98%) was observed using reversed phase HPLC (Figure 4). As

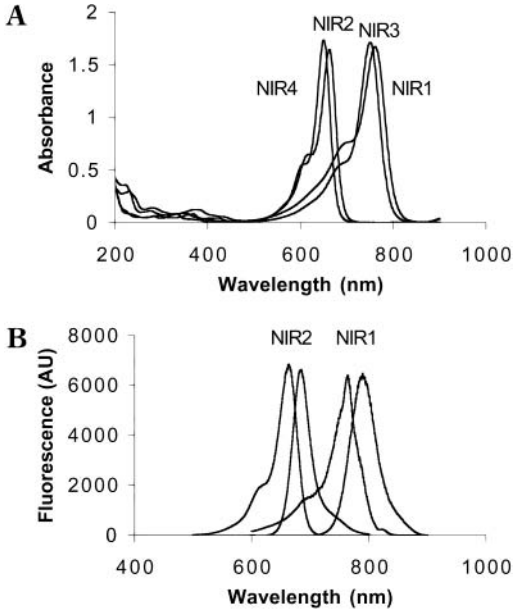


Figure 3. Absorption (A) and fluorescence (B) spectra of NIR fluorochromes.

Table 1. Optical Properties of NIR Fluorochromes

compd	solvent	$\lambda_{max,abs}$ (nm)	$\lambda_{max,em}$ (nm)	Stokes shift (nm)	ϵ (L mol^{-1} cm^{-1})	QY
NIR1	H_2O	761	796	35	268000	0.23
	EtOH	769				
NIR2	H_2O	662	684	22	250000	0.34
	EtOH	667				
NIR3	H_2O	750	777	27	275000	0.28
	EtOH	756				
NIR4	H_2O	650	671	21	260000	0.43
	EtOH	654				

seen in Figure 4, the elution times for NIR2 and its active ester were 27.1 and 29.0 min, respectively. The active ester was remarkably stable. Even in water, less than 10% of the active ester was hydrolyzed over a period of 20 days (4 °C), based on HPLC analysis. A test reaction was done by reacting NIR2−NHS active ester with benzylamine. The resultant NIR2−benzylamine conjugate showed an elution time of 32.1 min (HPLC results not shown).

Imaging of NIR Dyes. In subsequent studies we utilized a home-built imaging system (*6*) to image the newly synthesized NIR dyes and compared them to ICG. The images were acquired with two sets of filters. One has 610−650 nm excitation and 680−720 nm emission; the other has 750−770 nm excitation and 800−820 nm emission. As shown in Figure 5, the fluorescence signals of NIRs are well resolved in this fluorescence imaging system. At 700 nm, only NIR2 and NIR4 were detectable, while NIR1 and NIR 3 were detectable at 800 nm. Moreover, the NIR1 and NIR3 showed significantly better optical property than ICG. The signal intensity of NIR1 and NIR3, as compared to ICG, were 7- and 12-fold higher, respectively.

Enzyme Activatable NIRF Probe. Recently, we have developed a panel of biocompatible molecular probes for the in vivo detection of specific protease activity, particularly for those proteases that play key roles in different aspects of cancer growth, metastases formation, and angiogenesis (*3*, *19*, *20*). In those studies, a commercially available fluorochrome (Cy5.5) was used as the fluorescence reporter. In this study the newly synthesized

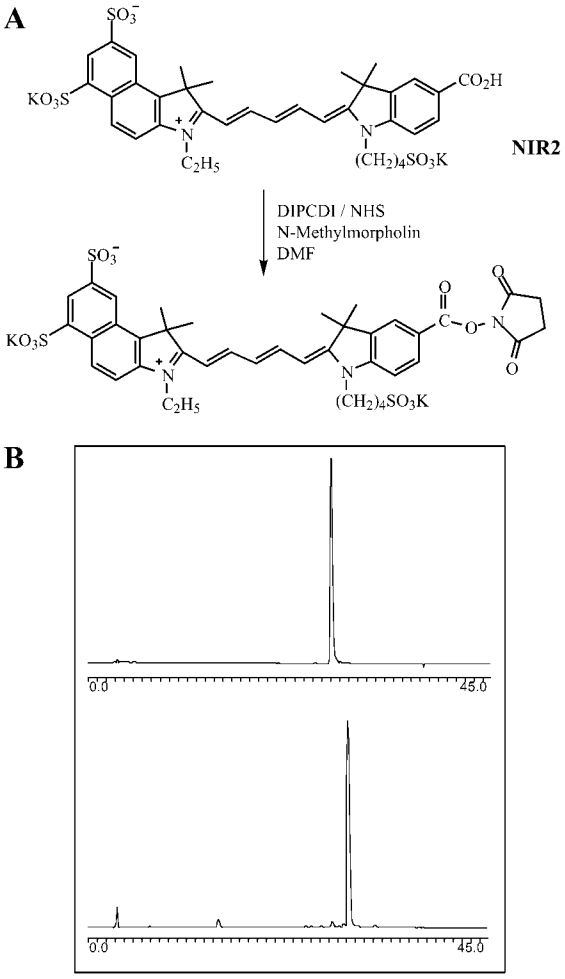


Figure 4. A. Activation of NIR2. B. HPLC traces before (top) and after modification (bottom).

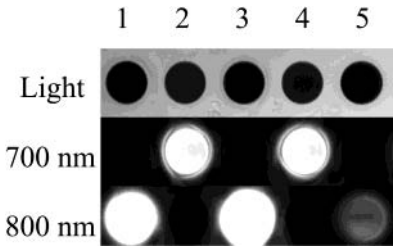


Figure 5. NIR fluorescence and white light images of probes at equimolar concentration. Well 1 to 5 is NIR1, NIR2, NIR3, NIR4, and indocyanine green, respectively. Note the bright fluorescence of the new dyes compared to ICG.

NIR fluorochromes as alternative reporters was tested. The fluorochromes were attached to a partially peglyated graft coplymer (PGC), which has a polylysine backbone (*21*). The probes were designed to have minimum fluorescence signal in their native states and become highly fluorescent after enzyme-mediated release of fluorochromes, resulting in signal amplification. To reduce the initial fluorescence signal, a high local concentration of fluorochromes was desired to have significant self-quenching. Since the lysine residues on PGC were only partially pegylated, free amino groups on the unmodified lysine side chain could be used for fluorochrome attachment. Nevertheless, additional free lysine residues were also needed for trypsin recognition. As a consequence, the number of fluorochromes per polymer had to be optimized in order to maximize the fluorescence increase after enzymatic cleavage.

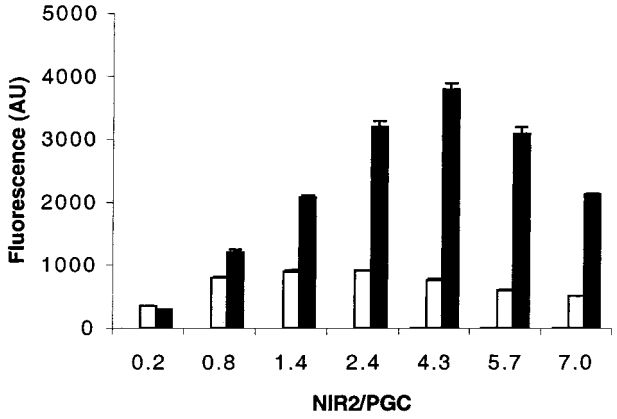


Figure 6. Fluorescence measurement of NIR−PGC probes before (white bars) and after (black bars) cleavage by trypsin for 3 h.

For this purpose, PGC probes were labeled with different amounts of NIR2. Overall, seven conjugates with 0.2, 0.8, 1.4, 2.4, 4.3, 5.7, and 7.0 NIR2 residues per PGC molecule were prepared. The white bars in Figure 6 shows the fluorescent signal of the labeled polymers before trypsin treatment. As expected, there is an increase in the signal from 0.2 to 0.8 dyes/polymer, while at higher dye/polymer ratio, considerable self-quenching is observed. The black bars in Figure 6 show the fluorescence signals obtained after 3 h of tryptic cleavage. Maximum recovery was found for 4.3 NIR2 per PGC. At this ratio, the fluorescence signal increased 5-fold in 3 h and 9-fold in 24 h. Interestingly, recovery was lower when more NIR2 was attached to the backbone, presumably due to the less enzyme-accessible cleavage sites on the backbone. These studies demonstrate the importance of the proposed optimization studies which are required to maximize the dequenching effect upon enzymatic cleavage.

The self-quenching phenomenon of NIRF cyanine dyes was not only shown by NIR2, as similar results were obtained when NIR1 was used in the preparation (data not shown). Extensive self-quenching was also reported with Cy5, Cy5.5, and Cy7 (*22*). The fluorescence signal was not enhanced by attaching multiple labels onto one molecule; on the contrary, it was significantly reduced due to serious self-quenching. We have applied this negative effect in a positive way to design several quenched probes as previously described and used them to imaging tumor-associated protease activity in vivo (*3*, *19*, *20*).

In summary, we describe the synthesis and properties of a number of nonsymmetrical cyanine dyes. The dyes are characterized by high stability, high quantum yield, and water solubility. Likewise, the monoactivated hydroxysuccinimide esters of the fluorochromes were exceptionally stable, yet fully reactive with primary amines. We are currently testing the use of fluorochrome-tagged molecules for imaging of tumors and other diseases in vivo. It is anticipated that the developed fluorochromes have a range of biotech applications extending beyond imaging.

ACKNOWLEDGMENT

This research was supported by NIH CA86355, CA88365, CA79443, CO97065, and NSF BES-0119382.

LITERATURE CITED

(1) Neri, D., Carnemolla, B., Nissim, A., Leprini, A., Querze, G., Balza, E. et al. (1997) Targeting by affinity-matured

recombinant antibody fragments of an angiogenesis associated fibronectin isoform. *Nat. Biotechnol. 15*, 1271−5.
(2) Licha, K., Hessenius, C., Becker, A., Henklein, P., Bauer, M., Wisniewski, S. et al. (2001) Synthesis, Characterization, and Biological Properties of Cyanine- Labeled Somatostatin Analogues as Receptor-Targeted Fluorescent Probes. *Bioconjugate Chem. 12*, 44−50.
(3) Weissleder, R., Tung, C. H., Mahmood, U., and Bogdanov, A. (1999) In vivo imaging of tumors with protease-activated near-infrared fluorescent probes. *Nature Biotech. 17*, 375−8.
(4) Gross, L. A., Baird, G. S., Hoffman, R. C., Baldridge, K. K., and Tsien, R. Y. (2000) The structure of the chromophore within DsRed, a red fluorescent protein from coral. *Proc. Natl. Acad. Sci. U.S.A. 97*, 11990−5.
(5) Contag, P. R., Olomu, I. N., Stevenson, D. K., and Contag, C. H. (1998) Bioluminescent indicators in living mammals. *Nat. Med. 4*, 245−7.
(6) Mahmood, U., Tung, C., Bogdanov, A., and Weissleder, R. (1999) Near-infrared optical imaging system to detect tumor protease activity. *Radiology 213*, 866−870.
(7) Ntziachristos, V., Weissleder, R. (2001) Experimental three-dimensional fluorescence reconstruction of diffuse media by use of a normalized Born approximation. *Opt. Lett. 26*, 893−895.
(8) Ntziachristos, V., Yodh, A. G., Schnall, M., and Chance, B. (2000) Concurrent MRI and diffuse optical tomography of breast after indocyanine green enhancement. *Proc. Natl. Acad. Sci. U.S.A. 97*, 2767−72.
(9) Ntziachristos, V., Ripoll, J., and Weissleder, R., (2002) Can near-infrared fluorescence propagate through human organs for noninvasive clinical examinations? *Opt. Lett. 27*, 333−335.
(10) Hope-Ross, M., Yannuzzi, L. A., Gragoudas, E. S., Guyer, D. R., Slakter, J. S., Sorenson, J. A., et al. (1994) Adverse reactions due to indocyanine green. *Ophthalmology 101*, 529−33.
(11) Mordon, S., Devoisselle, J. M., Soulie-Begu, S., and Desmettre, T. (1998) Indocyanine green: physicochemical factors affecting its fluorescence in vivo. *Microvasc. Res. 55*, 146−52.
(12) Achilefu, S., Dorshow, R. B., Bugaj, J. E., and Rajagopalan, R. (2000) Novel receptor-targeted fluorescent contrast agents for in vivo tumor imaging. *Invest. Radiol. 35*, 479−85.
(13) Mujumdar, S. R., Mujumdar, R. B., Grant, C. M., and Waggoner, A. S. (1996) Cyanine-labeling reagents: sulfobenzindocyanine succinimidyl esters. *Bioconjugate Chem. 7*, 356−62.
(14) Terpetschnig, E., Szmacinski, H., Ozinskas, A., and Lakowicz, J. R. (1994) Synthesis of squaraine-N-hydroxysuccinimide esters and their biological application as long-wavelength fluorescent labels. *Anal. Biochem. 217*, 197−204.
(15) Mujumdar, R. B., Ernst, L. A., Mujumdar, S. R., Lewis, C. J., and Waggoner, A. S. (1993) Cyanine dye labeling reagents: sulfoindocyanine succinimidyl esters. *Bioconjugate Chem. 4*, 105−11.
(16) Bogdanov, A., Jr., Wright, S. C., Marecos, E. M., Bogdanova, A., Martin, C., Petherick, P. et al. (1997) A long-circulating copolymer in "passive targeting" to solid tumors. *J. Drug Target. 4*, 321−30.
(17) Ernst, L. A., Gupta, R. K., Mujumdar, R. B., and Waggoner, A. S. (1989) Cyanine dye labeling reagents for sulfhydryl groups. *Cytometry 10*, 3−10.
(18) Oswald, B., Patsenker,L., Duschl, J., Szmacinski, H., Wolfbeis, O. S., and Terpetschnig, E. (1999) Synthesis, spectral properties, and detection limits of reactive squaraine dyes, a new class of diode laser compatible fluorescent protein labels. *Bioconjugate Chem. 10*, 925−31.
(19) Tung, C., Mahmood, U., Bredow, S., and Weissleder, R. (2000) In vivo imaging of proteolytic enzyme activity using a novel molecular reporter. *Cancer Res. 2000*, 4953−4958.
(20) Bremer, C., Tung, C. H., and Weissleder, R. (2001) In vivo molecular target assessment of matrix metalloproteinase inhibition. *Nat. Med. 7*, 743−8.
(21) Bogdanov, A., Weissleder, R., and Brady, T. (1995) Long-circulating blood pool imaging agents. *Adv. Drug Deliv. Rev. 16*, 335−348.
(22) Gruber, H. J., Hahn, C. D., Kada, G., Riener, C. K., Harms, G. S., Ahrer, W. et al. (2000) Anomalous fluorescence enhancement of Cy3 and cy3.5 versus anomalous fluorescence loss of Cy5 and Cy7 upon covalent linking to IgG and noncovalent binding to avidin. *Bioconjugate Chem. 11*, 696−704.

BC0155723

Streptavidin in Antibody Pretargeting. 3. Comparison of Biotin Binding and Tissue Localization of 1,2-Cyclohexanedione and Succinic Anhydride Modified Recombinant Streptavidin

D. Scott Wilbur,*,† Donald K. Hamlin,† Damon L. Meyer,‖,⊥ Robert W. Mallett,‖ Janna Quinn,‡ Robert L. Vessella,‡ and Oliver W. Press§

Departments of Radiation Oncology and Urology, University of Washington, Seattle, Washington 98195, and Fred Hutchinson Cancer Research Center, Seattle Washington 98109, and NeoRx Corporation, Seattle, Washington 98119. Received November 1, 2001; Revised Manuscript Received February 1, 2002

Recombinant streptavidin (rSAv) is of interest as a carrier of α-emitting radionuclides in pretargeting protocols for cancer therapy. Due to the inherently high kidney localization of rSAv, modification of this protein is required before it can be useful in pretargeting. Previous studies (Wilbur, D. S., Hamlin, D. K. et al. (1998) *Bioconjugate Chem*. *9*, 322−330) have shown that succinylation of rSAv using succinic anhydride decreases the kidney localization appreciably. In continuing studies, the biotin binding characteristics and biodistribution in mice of rSAv modified by reaction with succinic anhydride (amine modification) or 1,2-cyclohexanedione (arginine modification) have been compared. Modification of rSAv was conducted using 5−50 mol equiv of succinic anhydride and 60−200 mol equiv of 1,2-cyclohexanedione. Most studies were conducted using rSAv modified with the highest quantities of reagents. Succinylation of rSAv did not alter binding with biotin derivatives, but a small increase in the biotin derivative dissociation rate was noted for arginine-modified rSAv. Amino acid analysis of 1,2-cyclohexanedione-treated rSAv indicated about 40% of the arginine residues, or an average of 1.6 residues per subunit, were modified, whereas none of the lysine residues were modified. IEF analyses showed that the pI of the arginine-modified rSAv was 5.3−6, whereas the pI for the succinylated rSAv was approximately 4. Electrospray mass spectral analyses indicated that one to three conjugates of 1,2-cyclohexanedione, and two to three conjugates of succinic anhydride, were obtained per subunit. Both modification reactions resulted in greatly decreasing the kidney localization of rSAv (normally 20−25% ID/g at 4, 24, and 48 h pi). However, the kidney concentration for the succinylated rSAv continued to decrease (5% ID/g to 1.5% ID/g) from 4 to 48 h pi, whereas the concentration (5% ID/g) remained constant over that period of time for the arginine-modified rSAv. In contrast to this, the liver concentration appeared to be slightly higher (3% ID/g vs 2% ID/g) at the later time points for the succinylated rSAv. When less than 50 mol equiv of succinic anhydride were employed in the modification of rSAv, a correlation between increasing kidney localization with decreasing equivalents reacted was observed. Although the differences in the two modified rSAv are not substantial, succinylated rSAv appears to have more favorable properties for pretargeting studies.

INTRODUCTION

Selective targeting of therapeutic radionuclides to cancer cells in patients, termed "Targeted Radiotherapy" or "Endoradiotherapy" holds great potential for cancer therapy, particularly in the killing of disseminated cancer cells present in metastatic disease. Radiolabeled monoclonal antibodies (mAbs[1]) have been shown to be very effective at targeting cancer cells, but inherent problems have, thus far, limited their use in cancer therapy (*1*−*6*). To circumvent the problems associated with directly labeled mAbs, alternative approaches utilizing the cancer cell targeting of mAbs are under investigation. One particularly promising approach is termed "pretargeting" (*7*,*8*). In that approach, a mAb conjugate is used to target cancer cells and a separate molecule that binds with the mAb conjugate is used to carry the therapeutic radionuclide. Although this alternative approach involves multiple administrations of reagents, it permits optimization of important parameters, such as pharmacokinetics, route of excretion, and stabilization of the radionuclide-carrying molecule from metabolic processes. Indeed, promising therapy results have been obtained with the pretargeting approach (*9*−*11*).

In our previous studies, a pretargeting approach which uses biotinylated mAb Fab′ fragments with radiolabeled recombinant streptavidin (rSAv) was investigated (*12*). Those studies demonstrated that each biotinylated Fab′ bound in the tumor xenograft captured one radiolabeled rSAv molecule. However, an inherently high kidney localization of SAv molecules (*13*) was problematic with

* Address correspondence to D. Scott Wilbur, Ph.D., Department of Radiation Oncology, University of Washington, 2121 N. 35th Street, Seattle, WA 98103-9103, Phone: 206-685-3085, FAX: 206-685-9630, E-mail: dswilbur@u.washington.edu.

† Department of Radiation Oncology, University of Washington.

‡ Department of Urology, University of Washington.

§ Fred Hutchinson Cancer Research Center.

‖ NeoRx Corporation.

⊥ Current address for D. Meyer is Seattle Genetics, Inc. Bothell, WA.

[1] Abreviations: ChT, chloramine-T; cpm, counts per minute; IEF, isoelectric focusing; mAb, monoclonal antibody; %ID/g, percent injected dose per gram; PBS, phosphate-buffered saline; pi, postinjection; rSAv, recombinant streptavidin; rt, room temperature, SAv, streptavidin.

10.1021/bc015574n CCC: $22.00 © 2002 American Chemical Society
Published on Web 04/23/2002

the approach. It has been hypothesized that the kidney localization observed comes from specific recognition of a surface RYD (Arg, Tyr, Asp) amino acid sequence which is similar to the fibronectin binding RGD (Arg, Gly, Asp) sequence (*14*,*15*) and results in a specific localization in the renal cortex (*16*). Studies in this laboratory demonstrated that the kidney localization could be alleviated by succinylation of rSAv (*17*). This result is thought to due to the high anionic surface charge produced on rSAv and not to an alteration in the RYD sequence on the surface of the protein.

Our continued interest in the use of rSAv as a carrier of radionuclides in pretargeting protocols led us to further investigate methods of decreasing kidney localization of this protein. We were particularly interested in the chemical modification of the RYD sequence in rSAv investigated by personnel at NeoRx Corporation.[2] They found that specific chemical modification of arginine residues using 1,2-cyclohexanedione (*18*−*20*) decreased the kidney localization. Those results prompted us to conduct an investigation comparing the biotin binding properties and tissue distributions of rSAv modified using succinic anhydride and 1,2-cyclohexanedione. The results of that investigation are reported herein.

EXPERIMENTAL PROCEDURES

General. All chemicals purchased from commercial sources were analytical grade or better and were used without further purification. Chloramine-T (ChT) and phosphate-buffered saline (PBS) were obtained from Sigma (St. Louis, MO). 1,2-Cyclohexanedione, and most other chemicals, were obtained from Aldrich Chemical Co. (Milwaukee, WI). Recombinant streptavidin was obtained from Boehringer Mannheim (Indianapolis, IN). Solvents for HPLC analysis were obtained as HPLC grade and were filtered (0.2 μm) prior to use. The biotin derivatives **1**−**3**, containing the cyanocobalamin chromophore, were obtained as previously described (*21*). Biotin-deficient diet chow with 10% egg white solids (TD 96343) was obtained from Harlan Teklad (Madison, WI, www.harlan.com). Centricon-10 centrifugation concentrators were obtained from Amicon (Beverly, MA).

Na[^{125}I]I and Na[^{131}I]I were purchased from NEN/Dupont (Billerica, MA) as high concentration/high specific activity radioiodide in 0.1 N NaOH. Measurement of ^{125}I and ^{131}I was accomplished on the Capintec CRC-15R. Tissue samples were counted in a Wallac 1480 Wizard gamma counter with the following window settings: 15−85 keV for I-125 and 260−430 keV when ^{125}I and ^{131}I are counted together. The ^{125}I counts are compensated for spillover counts from the ^{131}I in the calculations.

Chromatography. HPLC separations of the modified rSAv were obtained on Hewlett-Packard isocratic system consisting of a Model 1050 pumping system and a Model 1050 Multiple Wavelength Detector (280 nm). Proteins were evaluated on a Protein Pak 300 SW glass size exclusion column (10 μm, 8 mm × 30 cm, Waters Corporation, Milford, MA) run at 0.75 or 1.0 mL/min eluting with 50 mM sodium phosphate buffer (pH 6.8) which contained 300 mM NaCl, 1 mM EDTA, and 1 mM sodium azide. Analysis of the HPLC data was conducted on Hewlett-Packard HPLC ChemStation software. Retention times (t_R) for rSAv, arginine-modified rSAv, and succinylated rSAv were 27.6−27.8 min (0.75 mL/min flow) or 15.4−15.6 min (1.0 mL/min flow).

[2] Mallett, R., and Meyer, D. NeoRx Corporation, Seattle, WA, unpublished results.

Radiolabeled Proteins. Size-exclusion chromatography was also used to evaluate radioiodinated rSAv. HPLC separations of radioiodinated proteins were conducted on a system that consisted of a Waters Model 510 pump, a Waters Lambda-Max UV detector, and a Beckman model 170 radioisotope detector. The detectors were connected to a computer through a Hewlett-Packard Model 35900 interface, and data from the chromatograms was obtained on a computer running Hewlett-Packard ChemStation Software. The proteins were separated on a BioSelect SEC250−5 size exclusion column (7.8 mm × 300 mm, BioRad, Hercules, CA), eluting with a solvent mixture of 25 mM Tris-HCl, 75 mM NaCl, and 1 mM EDTA, pH 7.2, at a flow rate of 0.70 mL/min. Retention time (t_R) for rSAv was 13.4 min on this system.

Mass Spectral Analyses. Electrospray mass spectra were obtained by atmospheric pressure chemical ionization on a Micromass Quattro II Tandem Quadrupole Mass Spectrometer (Micromass Ltd., Manchester, U.K.). The sample was introduced directly. The mass spectral data was obtained on a PC running Windows NT based Micromass MaxEnt software.

Arginine Modification of Streptavidin. Two experimental procedures for modification of rSAv were used in the studies. All studies used modified rSAv produced by Method A, except for the amino acid analyses.

Method A. To 0.8 mL of rSAv (24.2 mg/mL, 19.4 mg, 0.37 μmol) in PBS was added 0.2 mL 1.0 M NaOH. To this mixture was added 8.6 mg (77 μmol) of solid 1,2-cyclohexanedione. The mixture was stirred for 1 h and then eluted through a Sephadex G-25 column using a 20 mM sodium phosphate, 60 mM NaCl, pH 7.0 solution. The protein gained a slight yellow coloration during the modification.

Method B. To 0.4 mL of 25.4 mg/mL solution of rSAv (10.2 mg, 0.19 μmol) in PBS was added 8 μL of 10 M NaOH to prepare a final concentration of 0.2 M. To that solution was added 1.3 mg (11.4 μmol) 1,2-cyclohexanedione, and the reaction was allowed to proceed for 5 h at ambient temperature. The modified rSAv solution was exchanged into PBS using a G-25 size exclusion column. From this procedure, 8.3 mg (81%) of modified rSAv was obtained following the buffer exchange.

Succinylation of Streptavidin. The succinylation reactions were conducted in a manner similar to that previously described (*17*). Briefly, a 200 μL aliquot of a 5 mg/mL solution of rSAv (1 mg, 1.9×10^{-2} μmol) was added to 370 μL of 50 mM $NaHCO_3$ buffer (pH 8.5). To this solution was added varying quantities [5 equiv: 9.4 μg (9.4×10^{-2} μmol); 10 equiv: 19 μg (19×10^{-2} μmol); 25 equiv: 47 μg (4.7×10^{-2} μmol); 50 equiv: 94 μg (94×10^{-2} μmol)] of succinic anhydride in 2−20 μL DMSO. After 30 min at room temperature, the contents were transferred to a Centricon-10 and concentrated to 50 μL. PBS (500 μL) was added, and the solution was again concentrated to 50 μL. This wash step was repeated five times. The final concentrations of protein (2.4−3.6 mg/mL) and recovery yields (92−100%) were determined for each succinylation reaction.

Electrophoresis. Two electrophoresis instruments and methods were used in the studies. The IEF gel shown in Figure 1 was obtained on a Novex PowerEase 500 instrument with the XCell II chamber using Invitrogen (Novex) precast gels, pH 3−10 (1.0 mm × 12 well) running under the standard IEF Program. The protein was stained with GelCode Blue Stain (Pierce). IEF standards were from Serva Electrophoresis GmbH: pH 10.7, cytochrome C; 9.5, ribonuclease A; 8.3, 8.0, 7.8, lectin; 7.4, 6.9, myoglobin; 6.0, carbonic anhydrase; 5.3,

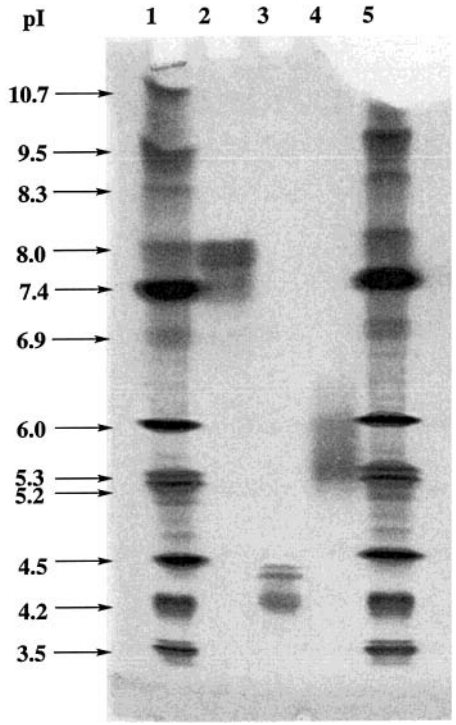


Figure 1. Digitized image of IEF gel comparing pI of unmodified rSAv with succinylated and arginine-modified rSAv. Lanes 1 and 5: IEF standards (Serva IEF markers 3−10). Lane 2: unmodified rSAv (control). Lane 3: succinylated rSAv. Lane 4: arginine-modified rSAv.

5.2, β-lactoglobulin; 4.5, trypsin inhibitor; 4.2, glucose oxidase; 3.5, amyloglucosidase. The IEF gels shown in Figures 5A and 5B were obtained on a PhastSystem electrophoresis apparatus (Pharmacia LKB, Uppsala, Sweden) using the optimized method for IEF described in "Separation Technique File #100". The IEF were run using PhastGel IEF 3−9 precast gels. Protein staining was accomplished by the silver stain method described in "Development Technique File #210". IEF was conducted with samples running in opposite directions. The electrophoresis standards were from the Broad pI Kit (pI 3.5−9.3) (Amersham Pharmacia Biotech, NJ) and are composed of: pI 9.30, trypsinogen; 8.65, 8.45, 8.15, lentil lectin; 7.35, 6.85, myoglobin; 6.55, 5.85, carbonic anhydrase B; 5.20, lactoglobulin A; 4.55, trypsin inhibitor; 3.75, methyl red; 3.50, amylglucosidase.

Amino Acid Analysis. Amino acid analyses of hydrolyzed 1,2-cyclohexanedione-modified and -unmodified rSAv were conducted according to the procedure described by Heinrikson R. L. et al. (*22*). The modified rSAv samples were hydrolyzed with 6 N HCl in the vapor phase at 200 °C for 75 min and then derivatized with phenyl isothiocyanate (PTC) using an Applied Biosystems Model 420 H automated hydrolyzer/derivatizer. The PTC-AA mixture was next injected onto a reversed-phase C-18 column configured on an Applied Biosystems Model 130A HPLC system. The column effluent was monitored at 254 nm and the chromatogram analyzed using the Applied Biosystems Model 610 data acquisition system.

Biotin Binding Studies. Biotin derivative binding studies were conducted as previously described (*21*). Briefly, to 300 μL of a 1 mg/mL solution (300 μg; 5.65 nmol) of rSAv, arginine-modified rSAv, or succinylated rSAv in a plastic microcentrifuge vial was added 4 equiv (22.6 nmol) of a biotin conjugate (**1**−**3**) dissolved in 30 μL of a 10% aqueous DMSO solution. The rSAv/biotin derivative mixture was incubated for 1 h at room temperature, and 100 μL of the solution was assayed on the HPLC. To the remaining rSAv/biotin derivative solution was added 40 μL of a 1 mg/mL solution (40 μg; 164 nmol) of biotin in 10% aqueous DMSO. That solution was incubated for 3 h, and 100 μL was removed for analysis by HPLC. Areas under the peaks for bound and unbound biotin derivative provided the relative dissociation values in Table 1. In some examples, there was a slight excess (<10%) of the biotin derivative (**1**−**3**) that was not bound prior to the addition of excess biotin. The percent dissociation was adjusted for that material.

Table 1. Relative Dissociation of Biotin Derivatives from rSAv and Modified rSAv[a]

biotin derivative	rSAv, %	succinylated rSAv, %	arginine-modified rSAv, %
biotin-CN-Cbl, **1**	96	99	85
biotin-sarcosine-CN-Cbl, **2**	9	58	8
biotin-aspartate-CN-Cbl, **3**	91	91	80

[a] Values represent the percent of biotin derivative remaining bound after 3 h at room temperature in the presence of a large excess of biotin. Structures of biotin derivatives are shown in Figure 3.

Radioiodination of Proteins. Radioiodination reactions were conducted using chloramine-T as previously described (*23*). Radioiodination yields of 90−96% were obtained for ^{125}I-labeled rSAv and succinylated rSAv. Radioiodination yield of ^{125}I-labeled arginine-modified rSAv was 31%. Radioiodination yield of ^{131}I-labeled rSAv was 84% and of ^{131}I-labeled succinylated SAv was 95%.

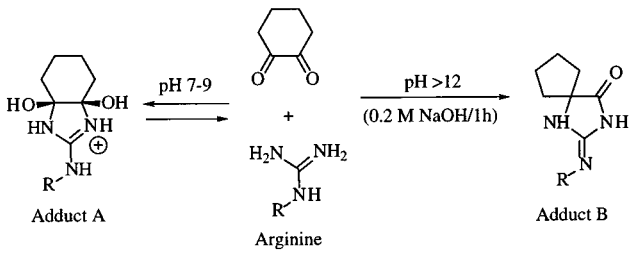
Biodistributions. *General.* Animal use and procedures were approved by the University of Washington's Institutional Animal Care and Use Committee (IACUC). Animal care and use was conducted in accordance with the NIH guidelines.[3] Male athymic mice (BALB/c nu/nu), 4−5 weeks of age were obtained from Charles River Laboratories (Hollister, CA). All injections of reagents were administered to mice in a total volume of approximately 100 μL (injectate weighed) via the lateral tail vein. Injections and sacrifice of the animals were done at predetermined times. The tissues excised are listed in Figures 4A, 4B, and 6, and in Tables 2 and 3 in Supporting Information. Blood samples were obtained by cardiac puncture immediately before sacrifice. Urine samples were obtained by syringe bladder tap at the time the tissues were excised. Excised tissues were blotted free of blood, weighed, and counted. Calculation of the percent injected dose (%ID) and percent injected dose per gram (%ID/g) in the tissues was based on internal standards containing 1 μL of the injected dose. Total blood volume was estimated to be 8% of body weight for the calculations (*24*).

Comparison of Modified rSAv. In the experiment, 15 mice, which had been placed on biotin-free diets for 7 days prior to beginning the study, were used. Each mouse was injected with a mixture containing 50 μg of succinylated [^{131}I]rSAv and 50 μg of arginine-modified [^{125}I]-rSAv, prepared as described above. The specific activity of the succinylated [^{131}I]rSAv was 0.12 μCi/μg and of the arginine-modified [^{125}I]rSAv was 0.13 μCi/μg. Groups of five mice each were sacrificed at 4, 24, and 48 h postinjection, and the tissue distribution of radioactivity was obtained as described above.

Succinylated rSAv. In the experiment, 20 mice were used. rSAv that had been reacted with 5, 10, 25, or 50

[3] NIH guidelines are described in NIH Publication 86-23: *Guide for the Care and Use of Laboratory Animals.*

Scheme 1: Reaction of Arginine with 1,2-Cyclohexanedione Showing the Two Different Product Pathways at pH 7−9 vs pH >12



equiv of succinic anhydride were radiolabeled with ^{125}I (four preparations). The specific activities of ^{125}I-labeled succinylated rSAv preparations were: 5 equiv, 0.74 μCi/μg; 10 equiv, 0.79 μCi/μg; 25 equiv, 0.84 μCi/μg; 50 equiv, 0.93 μCi/μg. A control that contained unmodified radiolabeled [^{131}I]rSAv was prepared for coinjection. The control ^{131}I-labeled rSAv had a specific activity of 1.49 μCi/μg. Each mouse was injected with a mixture containing 15 μg succinylated [^{125}I]rSAv and 15 μg [^{131}I]rSAv. Tissue biodistributions were obtained at 24 h postinjection as described above.

RESULTS

Modification of rSAv. Modification of rSAv was conducted by its reaction with either succinic anhydride in $NaHCO_3$ buffer at pH 8.5 or with 1,2-cyclohexanedione in PBS containing 0.2 M NaOH, pH 12. Succinic anhydride can react with a number of protein functional groups (e.g., amines, thiols, phenols, and imidazoles). All of the succinic anhydride reactions with protein side chain functional groups are reversible in the basic media (*19*) except for the reaction of amine to form amide bonds, making this modification selective for amino groups on proteins. Reaction of proteins with 1,2-cyclohexanedione is highly selective for guanidine functionality of arginine. There are two reaction products that can be obtained, depending on the pH of the reaction solution. As depicted in Scheme 1, reaction of cyclohexanedione with arginine at pH 7−9 produces a bicyclic chemical adduct (adduct A). However, this reaction is not desirable for our application as the formation of that adduct is reversible, potentially resulting in some, or all, of the arginine residues being unmodified when tested in vivo. The syndiol, adduct A, may be stabilized by boric acid (*18*), but this reaction is also reversible making the stability in vivo still an issue. At high pH, a reaction occurs which results in the irreversible formation of a spiro-bicyclic compound (adduct B). Fortunately, rSAv is like avidin in that it is quite stable to highly alkaline conditions (*25*,*26*), making this reaction useful for our application.

Characterization of Modified rSAv. The modified rSAv was analyzed by size-exclusion HPLC. Although there were small differences in retention times noted (e.g., 0.1−0.2 min), no reproducible link could be made for a modification resulting in a longer or shorter retention time. Because the modification reactions alter the charges on the protein, IEF analyses were conducted. An IEF comparing rSAv, succinylated rSAv and arginine-modified rSAv is shown in Figure 1. The unmodified rSAv (lane 2) has two primary bands with pI of around 7.6−7.8. The succinylated rSAv (lane 3) has a primary band with a pI around 4.2 and two small bands with pI around 4.5. The arginine-modified rSAv (lane 4) has a primary band with a pI around 5.3 and a diffuse area between pI 5.3−6.0.

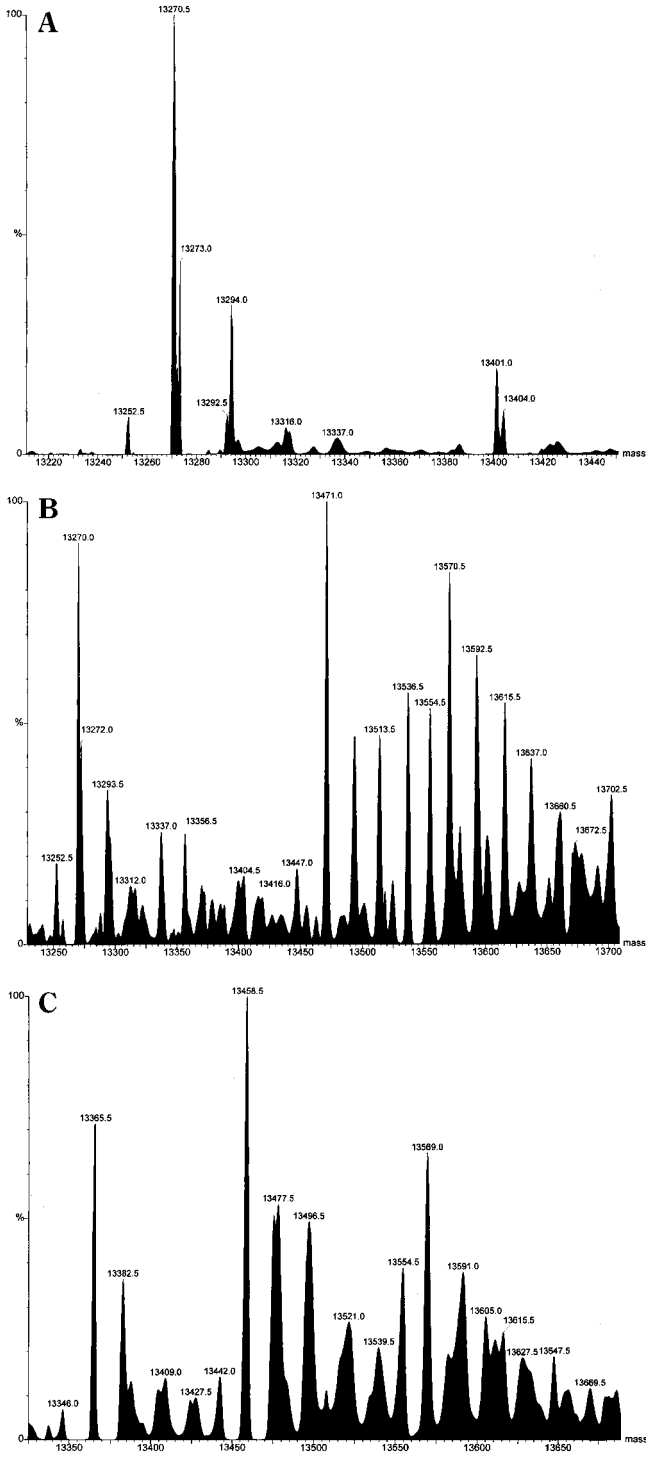


Figure 2. Digitized images of electrospray mass spectra of unaltered rSAv (2A), succinylated rSAv (2B), and arginine-modified rSAv (2C). Note that in Figure 2B, unaltered rSAv has been added as an internal reference.

Electrospray mass spectral data was obtained on samples of rSAv, succinylated rSAv, and arginine-modified rSAv to obtain information on the number of conjugates per subunit. Mass spectra for these materials are shown as Figures 2A−C. The mass spectrum of unaltered wild-type rSAv (Figure 2A) shows the mass of a subunit is 13270.5 amu (total mass of tetramer is 53082 amu). The mass spectrum for succinylated rSAv is shown in Figure 2B. Note that rSAv was added as an internal standard (i.e., peaks at 13270 amu and 13294 amu). Aside from peaks for the rSAv standard, the major peaks for the modified rSAv subunits reacted with 50 equiv of

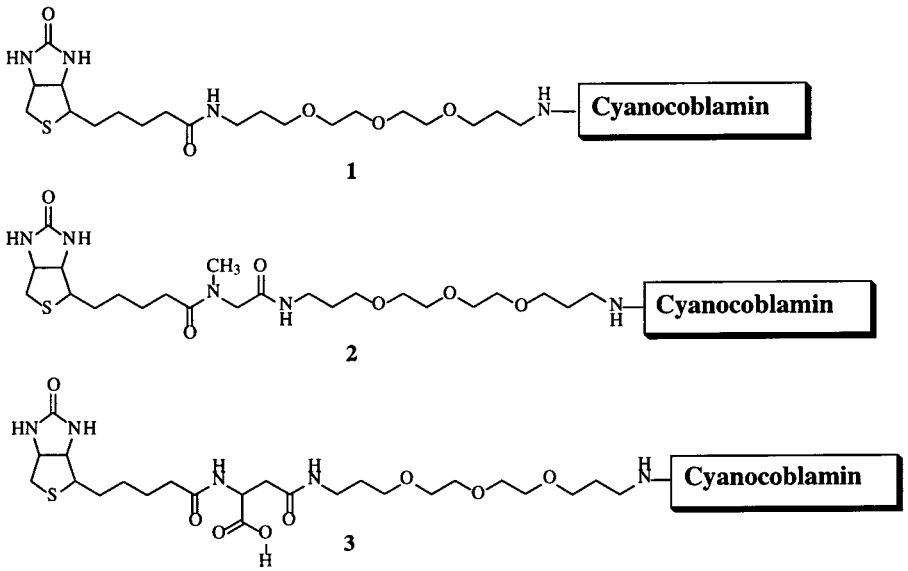


Figure 3. Structures of biotin derivatives **1**−**3** used in rSAv binding studies. The cyanocobalamin chromophore (360 nm) allows UV quantification without interference from protein absorbance (i.e., 280 nm). The biotin derivatives were obtained as previously described (*21*).

succinic anhydride have masses of 13471 amu (100%;+200 amu over rSAv) and 13571 amu (85%; +300 amu) with a number of additional peaks present being due to sodium adducts. Since conjugation of a succinic anhydride adds a mass of 100 amu to the protein, the mass spectral data indicates that the majority of subunits have two or three succinic anhydride molecules conjugated. The mass spectrum for arginine-modified rSAv is shown in Figure 2C. Conjugation of 1,2-cyclohexanedione to form adduct A (Scheme 1) increases the mass of the protein by 112 amu, but rearrangement to form adduct B (Scheme 1) results in a mass increase of only 94 amu. Reaction of 200 equiv of 1,2-cyclohexanedione with rSAv produces a mixture of modified proteins with mass peaks for modified subunits of 13366 amu (72%; +95 amu), 13383 (46%; +112 amu; B), 13459 (100%; + 188 amu), 13478 (53%; +207 amu), 13497 amu (48%; +226 amu); 13555 amu, (38%; +284 amu), 13569 amu (63%; + 299 amu) and 13569 (37%; +320 amu). The mass spectral data indicate that both adducts (A and B) are obtained under the conjugation conditions employed in this investigation. The data indicate that there were one to three adducts per rSAv subunit, and the molecular weight increases correlate with the two types of adducts being present on rSAv (from the listing above) in the following combinations; rSAv plus: B (+94 amu), A (+112 amu), BB (+188 amu), BA(+206 amu), AA(+224 amu), BBB(+282 amu), BBA(+300 amu), and BAA(+318 amu).

The specificity for arginine versus lysine residues in the conjugation with 1,2-cyclohexanedione was assessed by conducting amino acid analyses. Unmodified rSAv was run as a control. The analyses indicated that about 40% of the arginine residues were modified (i.e., amount of arginine decreased) by reaction with 1,2-cyclohexanedione. This implies that an average of 1.6 arginine residues per subunit reacted. Importantly, no change in the quantity of lysine was found, confirming that the cyclohexanedione reaction was specific for arginine residues.

The biotin binding of modified rSAv was of interest. Although it is important to diminish the kidney localization of rSAv for in vivo pretargeting application, it is most desirable that this is done with the retention of the very high biotin binding affinity. Three biotin derivatives containing the cyanocobalamin chromophore (compounds **1**−**3**, Figure 3) were prepared as previously described (*21*), and their binding with rSAv, succinylated rSAv, and 1,2-cyclohexanedione modified rSAv was evaluated. All rSAv samples displayed similar association kinetics for the three biotin derivatives (data not shown). Of more interest were the relative rates of dissociation of rSAv-bound biotin derivatives. In that assay, 4 equiv of the biotin derivative are bound with the rSAv, a large excess of biotin is added, and the amount of released (dissociated) biotin derivative is measured at a 3 h time point (*27*). The relative dissociation rates obtained in this investigation are listed in Table 1. The results indicate that succinylated rSAv retains a slow dissociation rate for the biotin−cyanocobalamin adduct **1**, but arginine-modified rSAv appears to have a slightly faster dissociation rate. In our previous studies, it was shown that biotin adducts containing a sarcosine (*N*-methylglycine) moiety (e.g., **2**) have an increased dissociation rate. It was of interest to determine if the modified rSAv showed similar relative dissociation rates. Indeed, arginine-modified rSAv displayed similar dissociation kinetics to that of unaltered rSAv. Interestingly, the succinylated rSAv appeared to have a slower dissociation rate. The α-aspartate adduct of biotin, **3**, was also evaluated as biotin derivatives currently under investigation incorporate this structural feature to block the biotinamide cleaving action of biotinidase (*28*). Importantly, only a small decrease was noted for the dissociation of **3** from rSAv and succinylated rSAv. Binding of **3** with arginine-modified rSAv showed a somewhat faster dissociation rate.

Comparative Tissue Distribution Studies. A tissue distribution study was conducted to compare succinylated rSAv with arginine-modified rSAv. In the study, the proteins were labeled (^{125}I or ^{131}I) and were coinjected into athymic mice so that a direct comparison could be made. Unlike most proteins, direct radioiodination of rSAv provides a radiolabel that is not susceptible to in vivo deiodination (*23*), presumably because the rSAv is highly resistant to protease degradation. Importantly, use of radioiodination methods that employ conjugates, such as [I*]iodobenzoates (*29*), was not an attractive alternative for these studies, as a decrease in kidney localization had been previously observed when rSAv was radioiodinated with a *p*-[I*]]iodobenzoyl labeling moiety (*23*). Thus,

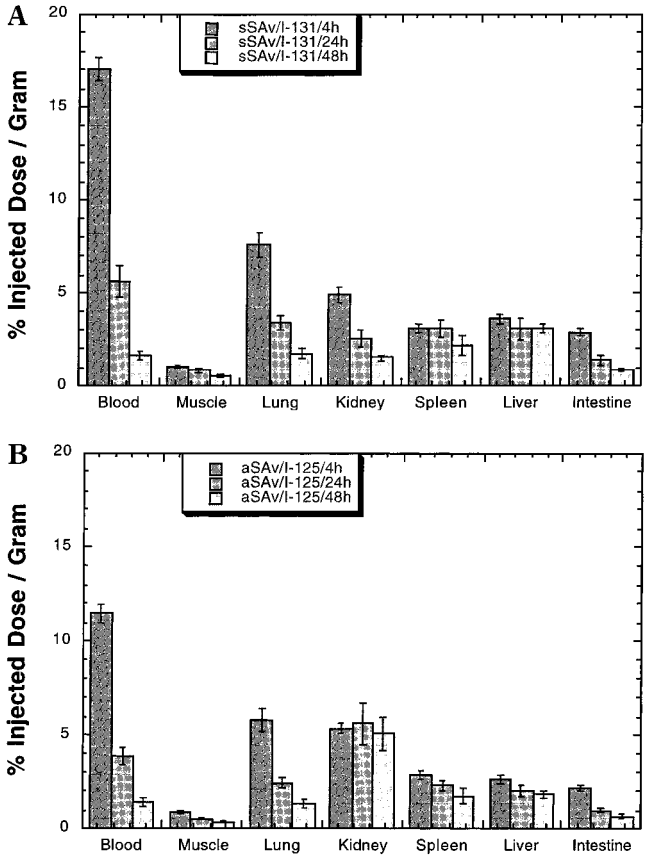


Figure 4. Graphs of the data obtained from the biodistribution of (coinjected) arginine-modified [^{125}I]rSAv and succinylated [^{131}I]rSAv in 15 athymic mice. The data obtained for each reagent (radionuclide) is shown in a separate graph for simplicity. Graph 4A shows the tissue distribution of succinylated (50 equiv) [^{131}I]SAv at 4, 24, and 48 h pi. Graph 4B shows the plotted data for arginine-modified [^{125}I]rSAv at 4, 24, and 48 h pi. The mice were placed on biotin-free diets for 7 days prior to the initiation of the experiment. Five animals were used per time point.

methods of radiolabeling that modified the surface amine groups could not be used because that would complicate the interpretation of the effect of arginine modification on the kidney localization.

We chose to use athymic mice, to place them on biotin-free diets for 7 days prior to the study, and to administer a total of 100 μg of rSAv to each mouse so that the results would reflect their distribution in the athymic mouse xenograft model used in our pretargeting studies. The results of the biodistribution of succinylated [^{131}I]rSAv and arginine-modified [^{125}I]rSAv at 4, 24, and 48 h pi are shown graphically in Figures 4A and 4B, respectively (full data provided as Tables 2 and 3 in Supplemental Information). While kidney localization at 4 h pi is similar for the two modified rSAvs, kidney retention of radioactivity at 24 and 48 h pi is much higher for arginine-modified rSAv. As noted in previous studies (*17*), the retention of the succinylated rSAv in blood is higher than that of the arginine-modified rSAv. It also appears that there are higher concentrations of succinylated rSAv in the liver and spleen than for the arginine-modified rSAv, but this may be due in part to the higher blood concentration.

Varying Levels of Succinylation. An evaluation was conducted to determine how the extent of rSAv modification with succinic anhydride affected kidney localization. In the experiment, 5, 10, 25, and 50 equiv of succinic anhydride were reacted with rSAv. As an initial step in

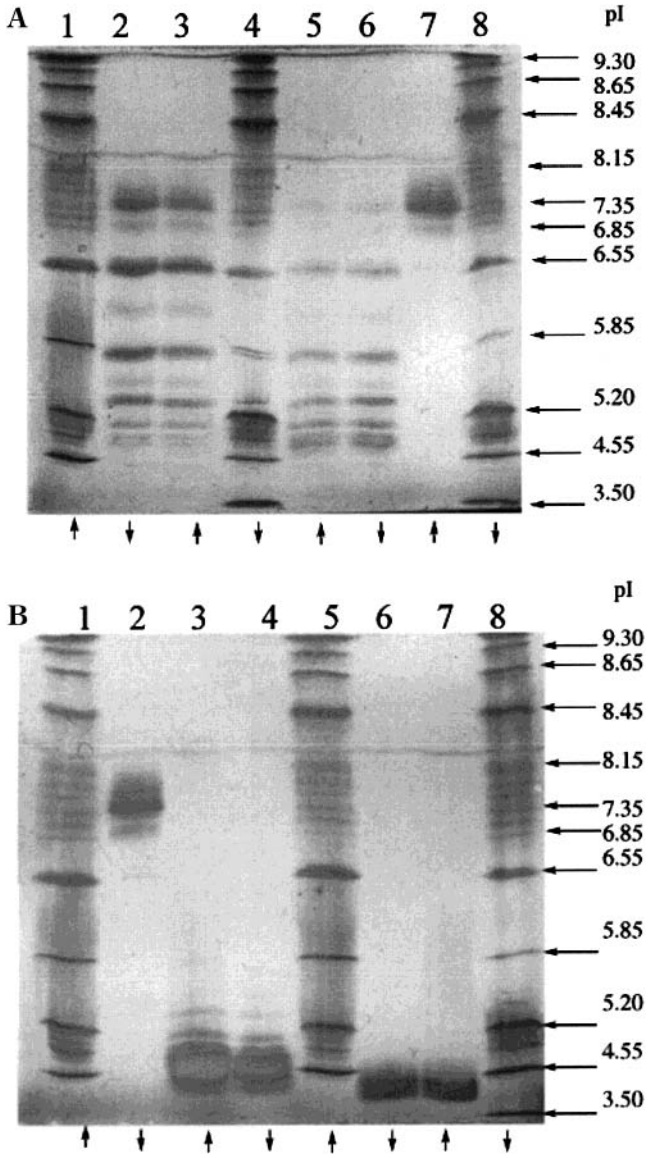


Figure 5. Digitized images of IEF gels (A and B) showing the rSAv products obtained when modified with various quantities of succinic anhydride. Samples were placed on opposing sides of the gel and run in two different directions to ensure equilibrium was reached. Arrows at bottom of lanes depict direction of sample movement. (A) Lanes 1, 4, and 8: IEF standards (isoelectric calibration kit, broad pI; 3−10) run in opposite direction to application of the adjacent sample. Lanes 2 and 3: rSAv succinylated with 5 equiv of succinic anhydride. Lanes 5 and 6: rSAv succinylated with 10 equiv of succinic anhydride. Lane 7: rSAv which has not been succinylated (control). (B) Lanes 1, 5, and 8: IEF standards (isoelectric calibration kit, broad pI; 3−10) run in opposite direction to application of the adjacent sample. Lane 2: rSAv which has not been succinylated (control). Lanes 3 and 4: rSAv succinylated with 25 equiv of succinic anhydride. Lanes 6 and 7: rSAv succinylated with 50 equiv of succinic anhydride.

the evaluation, the product of each of these reactions was evaluated by IEF. The IEF obtained are shown in Figure 5A and 5B. Modification of rSAv by reaction with 5 equiv of succinic anhydride yielded a major component (pI ∼6.6) and four minor components (pI ∼6.0, 5.8 5.3, 5), but left 50% of the rSAv unmodified (pI ∼7.4−7.8). The modified rSAv from the reaction of 10 equiv of succinic anhydride contained only a trace of unaltered rSAv and a small quantity of the component at pI ∼6.6, but had four major components (pI ∼5.8, 5.3, 5, and 4.7). The modified rSAv from the reaction of 25 equiv had all components in a

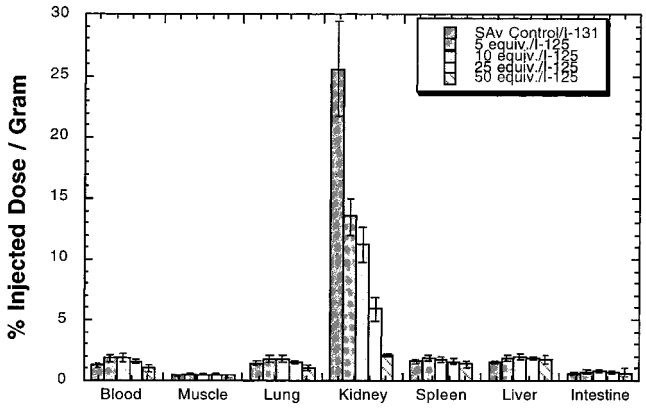


Figure 6. Graph of the biodistribution of [^{125}I]rSAv that has been modified with 5, 10, 25, or 50 equiv of succinic anhydride. A control [^{131}I]rSAv was coinjected with each of the preparations, and an example is shown for comparison in the graph. The biodistribution was obtained in 20 athymic mice (five per time point) at 24 h pi.

broad band (pI $\sim$ 4−5). The modified rSAv obtained in the reaction of 50 equiv of succinic anhydride was very acidic, with all components merging in a broad band at pI $\sim$3.8−4.5.

Biodistributions were determined for each of the rSAv preparations that had been modified with varying amounts of succinic anhydride. In contrast to the direct comparison of 1,2-cyclohexanedione and succinic anhydride modified rSAv, (1) the mice were not placed on biotin free diets, (2) smaller quantities of protein were administered (i.e., 30 μg/mouse), and (3) the distributions were examined at only one time point (i.e., 24 h pi). These changes were made to simplify the study, as it was believed that the conditions in the previous study were not required for this evaluation. The results of the study are shown graphically in Figure 6. The data indicate that the level of succinylation dramatically influences the kidney concentration of streptavidin. Although lower absolute concentrations (%ID/g) were observed in the blood in this study, a similar increase in concentration of succinylated rSAv over the unmodified rSAv was noted. The lower blood concentrations are believed to be due to the smaller amount of protein administered, but may also be due to the fact that the mice were not placed on biotin-free diets prior to conducting the biodistribution, or due to other factors that are not obvious.

DISCUSSION

The purpose of this investigation was to compare succinic anhydride-modified rSAv with arginine-modified rSAv, both being potential reagents for use as carriers of radionuclides in "two-step" pretargeting protocols. Although a number of studies have been conducted to evaluate the use of SAv as a carrier of radionuclides in pretargeting protocols (*30*−*36*), more recently most pretargeting studies have been focused on using biotin derivatives as carriers of the radionuclide. Our laboratory is particularly interested in the application of α-particle emitting radionuclides, such as At-211 and Bi-213, to therapy of metastatic cancer. At present it appears that the most promising approach to deliver these radionuclides to cancer cells in vivo is to use a monoclonal antibody-based pretargeting protocol. Thus, we have been developing new biotin and SAv pretargeting reagents for this application (*37*). While we are investigating the use of biotin derivatives as radionuclide carriers in pretargeting, we are also interested in using rSAv as a carrier. The rationale for using rSAv as a carrier molecule is based on the fact that it is cleared much more slowly from the blood than biotin derivatives (*24*), its slow degradation may provide stability to the radiolabel, and its increased blood circulation time may permit injection of smaller quantities of these expensive isotopes. Further, we believe that the toxicity of α-emitting radionuclides that decay while circulating in the blood stream will be minimal due to the short path length of the α particle. Preliminary studies involving the use of monoclonal antibodies labeled with α-emitters for bone marrow conditioning in transplantation seem to support that belief (*38*).

SAv has an inherently high and sustained kidney localization (*13*,*30*). This fact could preclude its use as a carrier of radionuclide in pretargeting protocols, so methods of decreasing the kidney localization have been of interest. The ideal rSAv for carrying radionuclides in pretargeting protocols would circulate freely in the blood without localization to tissues other than tumor sites. While kidney localization is dramatically decreased after modification, inspection of the biodistributions of succinylated rSAv (Figure 4A) and arginine-modified rSAv (Figure 4B) indicates that neither of these proteins are ideal carriers. This statement is made, as the concentration of radioactivity in spleen and liver of the mouse model does not diminish as the blood concentration decreases in the distribution of either modified rSAv. Perhaps more troubling is the fact that the kidney concentration of the arginine-modified rSAv does not decrease, suggesting that the radioactivity is trapped there. The biotin binding characteristics of an ideal rSAv molecule for pretargeting is less obvious. It seems likely that the 10−15% faster dissociation rates observed for biotin derivative, **1** or **3**, binding with arginine-modified rSAv versus succinylated rSAv would have little effect when short half-lived (α-emitting) radionuclides are used for in vivo applications. A factor that supports use of succinylated rSAv over arginine-modified rSAv is the fact that it is less heterogeneous (by mass spectral analysis, Figure 2B and 2C).

While the properties of succinylated rSAv may be only marginally better than arginine-modified rSAv, we will continue to use it in the development of pretargeting protocols for α-emitting radionuclides. To improve succinylated rSAv's properties, it will need to be optimized. Evaluation of the amount of succinylation required to attain low levels of kidney localization was conducted by studying the products obtained from reaction of 5, 10, 25, and 50 equiv of succinic anhydride. The results obtained from that evaluation clearly indicate that high levels of succinylation are required to eliminate the inherent kidney localization. The IEF (Figures 5A/5B) and biodistributions (Figure 6) of modified rSAv obtained from varying levels of succinylation show that the pI must be lower than 4.5 to diminish the kidney concentration to blood levels. This can be contrasted to the observation that the pI of arginine-modified rSAv is higher (5.2−6), but achieves a similar level of kidney localization at 4 h pi (Figure 4). Although these data provide the basis for using high levels of succinic anhydride to modify the lysine residues, it is interesting to assess the number lysine amines modified in rSAv. The gene for streptavidin encodes for a protein that has eight lysine residues per subunit (*39*); however, postsecretory modification of SAv (*40*) provides a "core" protein that is truncated at both the C and N termini, resulting in a protein that has only four lysine residues per subunit (*41*). Recombinant "core" streptavidin, depending on the

termini chosen, may have three or four lysine residues per subunit (*42*, *43*). In the rSAv studied, there are three lysine residues. The mass spectral data indicates that two to three lysines per subunit are modified when 50 equiv of succinic anhydride are reacted for 30 min at room temperature.

Our goal for this research was to evaluate whether one method provided a more optimal rSAv for use in pretargeting; however, some interesting observations can be made pertaining to kidney localization of SAv. It has been hypothesized by Wilcheck et al. that the high kidney localization of SAv is due to a surface sequence of amino acids, RYD, which they propose is close enough to the fibronectin binding sequence RGD to bind receptors (*14*,*15*). It appeared that a simple test of this hypothesis might be to modify one of the amino acids in the RYD sequence. Arginine was thought to be the best candidate for modification, as it appeared to be the easiest to selectively modify. Fortunately, the amino acid sequences for SAv and rSAv are known (*39*,*42*), and crystal structures for many SAv variants are available from the Brookhaven Protein Data Bank. For recombinant SAv, molecular modeling has indicated that one of the four arginine residues (R53) present per subunit is on the surface formed by the amino terminal sequence in residues ~13−57, and another arginine residue (R84) is on a loop between β-strands in a buried section of the surface (*43*). Both of these arginine residues appear to be solvent accessible, making it likely that they could be modified. The other two arginine residues (R59 and R103) appear to be in the buried hydrophobic regions. Interestingly, the RYD sequence is present as R59,Y60,D61, of which the aspartic acid residue (D61) appears to be surface-exposed whereas the arginine and tyrosine are not. However, it is possible this sequence could become exposed to the surface at the high pH used in the modification reaction after ionization of the carboxylate of the aspartic acid and the phenol of the tyrosine residues. Therefore, one might predict that 1−3 arginine residues could be modified in the reaction with 1,2-cyclohexanedione, and that is what was found.

Despite the data presented herein that suggests a modification of a minimum of two lysine residues per subunit are required to alleviate kidney localization, other data seem to indicate that modification of as few as one lysine, or one arginine, per subunit may be all that is required. For example, mass spectral data from the modification of arginine with 1,2-cyclohexanedione that displayed low kidney concentrations had only one arginine residue blocked. This would seem to indicate that modification of one specific arginine (per subunit) is required to diminish kidney localization. Additionally, it was noted that minimal derivatization of rSAv with succinic anhydride (e.g., 5 equiv offered per SAv tetramer) decreased the kidney localization by 50% (Figure 6). In that preparation, the IEF indicated that about 50% of the rSAv subunits were not modified, and the remainder of rSAv subunits may have only a single modification site. Further, previous studies have shown that conjugation of only one [^{125}I]iodobenzoate[4] to the SAv tetramer resulted in a decrease in the kidney concentration by 25% (*17*). These results seem to indicate that a single (solvent accessible) lysine amine per subunit is required for kidney localization. Even if modification of only one residue is required, complete modification of the four identical lysine or arginine residues in the tetrameric SAv requires an excess of reagents, and it can be expected that other lysine amines or arginine residues would be modified under those conditions. Interestingly, the lysine and arginine modification results are consistent with both the RYD binding hypothesis and another hypothesis put forth by Mogensen and Solling (*44*). They hypothesized that tubular reabsorption of proteins comes about by binding between a free positive amino or guanidinium group in the protein molecule and a negative site on the tubular cell surface. Our results appear to be consistent with this hypothesis as well. The results obtained indicate that modification of either lysine or an arginine residue greatly diminishes kidney localization over that of rSAv that is not modified. Whether a combination of these functionalities in close proximity is required for kidney localization has not been delineated.

These studies have not provided adequate evidence to state that a specific amino acid sequence, such as the RYD sequence, or that a specific amino or guanidinium functionality is required for kidney localization. We previously proposed that altering the charge on the rSAv to be highly negative with succinylation blocked its ability to cross the glomerular wall (*17*). This possibility has not been substantiated or refuted in these studies. Based on the observation that radioiodinated rSAv is retained in cells when internalized, the fact that the kidney concentration of succinylated rSAv continues to decrease with time may indicate that it is not internalized by the proximal tubular cells in the kidney. Since the kidney concentration in the arginine-modified rSAv does not change with time, it seems likely that it is internalized by the proximal tubular cells. Perhaps the best method to determine whether specific amino acids or amino acid sequences are responsible for kidney localization is to conduct site-directed amino acid substitutions of arginine and/or lysine found at the surface of the rSAv structure and examine the biodistributions of those proteins. We hope to undertake such studies at a later time.

Summary. rSAv was modified by reaction with succinic anhydride and 1,2-cyclohexanedione. The reaction of succinic anhydride is selective for conversion of amine functionalities to succinamide derivatives. The modified rSAv obtained after succinylation was found to bind biotin derivatives with nearly the same affinity as unaltered rSAv. The reaction of 1,2-cyclohexanedione is selective for conversion of guanidinium functionalities on arginine residues to produce a mixture of adducts at high pH. From the biotin derivative binding studies, it appears that biotin binding with arginine-modified rSAv has slightly lower affinity. Differences in the in vivo data were not striking. In both reactions, the modified rSAv was found to have relatively low concentration in kidneys of mice. However, the kidney concentration of the succinylated rSAv continued to decrease with time, whereas it remained constant in the arginine-modified rSAv. Additional studies demonstrated that high levels of succinylation were required to obtain the lowest kidney concentrations. The data obtained from these studies indicate that succinylated rSAv has properties that make it a better choice as a radionuclide carrier in pretargeting protocols than arginine-modified rSAv.

ACKNOWLEDGMENT

We would like to thank personnel at NeoRx Corporation for their discussion of the arginine modification approach. That discussion led to the investigation de-

[4] It is probable that only one [^{125}I]iodobenzoate group was conjugated per SAv tetramer because of the very small quantity of high specific activity radiolabeled compound used in the conjugation reaction.

scribed herein. We are grateful for the financial support provided by the Department of Energy, Medical Applications and Biophysical Research Division, Office of Health and Environmental Research under grant number DE-FG03-98ER62572, DOD Prostate Cancer Research Program DAMD17-98-1-8500, and National Institutes of Health RO1 CA76287.

Supporting Information Available: Tables containing the complete biodistribution data for arginine-modified and succinylated rSAv (Table 2) and modification of rSAv with varying quantities of succinic anhydride (Table 3). This material is available free of charge via the Internet at http://pubs.acs.org.

LITERATURE CITED

(1) Verhaar Langereis, M. J., Zonnenberg, B. A., de Klerk, J. M. H., and Blijham, G. H. (2000) Radioimmunodiagnosis and therapy. *Cancer Treatment Rev.. 26*, 3−10.

(2) Press, O. W. (1999) Radiolabeled antibody therapy of B-cell lymphomas. *Seminars Oncol. Oct 26*, 58−65.

(3) Chatal, J.-F., Peltier, P., Bardiès, M., Chétanneau, A., Thedrez, P., Faivre-Chauvet, A., and Gestin, J.-F. (1992) Does Immunoscintigraphy serve clinical needs effectively? Is there a future for radioimmunotherapy? *Eur. J. Nucl. Med. 19*, 205−213.

(4) Buchsbaum, D. J., and Lawrence, T. S. (1991) Tumor Therapy with Radiolabeled Monoclonal Antibodies. *Antibodies, Immunoconjugates, Radiopharm. 4*, 245−272.

(5) Larson, S. M. (1991) Radioimmunology: Imaging and Therapy. *Cancer 67*, 1253−1260.

(6) Hnatowich, D. J. (1990) Antibody Radiolabeling, Problems and Promises. *Nucl. Med. Biol. 17*, 49−55.

(7) Paganelli, G., Riva, P., Deleide, G., Clivio, A., Chiolerio, F., Scassellati, G. A., Malcovati, M., and Siccardi, A. G. (1988) In Vivo Labeling of Biotinylated Monoclonal Antibodies by Radioactive Avidin: A Strategy to Increase Tumor Radiolocalization. *Int. J. Cancer 2*, 121−125.

(8) Chinol, M., Grana, C., Gennari, R., Cremonesi, M., Geraghty, J. G., and Paganelli, G. (2000) Pretargeted Radioimmunotherapy of Cancer, in *Radioimmunotherapy of Cancer* (P. G. Abrams, and A. R. Fritzberg, Eds.) pp 169−193, Marcel Dekker, New York.

(9) Theodore, L. J., Fritzberg, A. R., Schultz, J. E., and Axworthy, D. B. (2000) Evolution of a Pretarget Radioimmunotherapeutic Regimen, in *Radioimmunotherapy of Cancer* (P. G. Abrams, and A. R. Fritzberg, Eds.) pp 195−221, Marcel Dekker, New York.

(10) Axworthy, D. B., Reno, J. M., Hylarides, M. D., Mallett, R. W., Theodore, L. J., Gustavson, L. M., Su, F., Hobson, L. J., Beaumier, P. L., and Fritzberg, A. R. (2000) Cure of human carcinoma xenografts by a single dose of pretargeted yttrium-90 with negligible toxicity. *Proc. Natl. Acad. Sci. U.S.A. 97*, 1802−1807.

(11) Press, O. W., Corcoran, M., Subbiah, K., Hamlin, D. K., Wilbur, D. S., Johnson, T., Theodore, L. J., Yau, E., Mallett, R., Meyer, D. L., and Axworthy, D. (2001) A comparative evaluation of conventional and pretargeted radioimmunotherapy of CD20 expressing lymphoma xenografts. *Blood 98*, 2535−2543.

(12) Wilbur, D. S., Hamlin, D. K., Vessella, R. L., Stray, J. E., Buhler, K. R., Stayton, P. S., Klumb, L. A., Pathare, P. M., and Weerawarna, S. A. (1996) Antibody fragments in tumor pretargeting. Evaluation of biotinylated Fab′ colocalization with recombinant streptavidin and avidin. *Bioconjugate Chem. 7*, 689−702.

(13) Wilbur, D. S., Stayton, P. S., To, R., Buhler, K. R., Klumb, L. A., Hamlin, D. K., Stray, J. E., and Vessella, R. L. (1998) Streptavidin in antibody pretargeting. Comparison of a recombinant streptavidin with two streptavidin mutant proteins and two commercially available streptavidin proteins. *Bioconjugate Chem. 9*, 100−107.

(14) Alon, R., Bayer, E. A., and Wilchek, M. (1990) Streptavidin Contains an RYD Sequence Which Mimics the RGD Receptor Domain of Fibronectin. *Biochem. Biophys. Res. Commun. 170*, 1236−1241.

(15) Alon, R., Bayer, E. A., and Wilchek, M. (1992) Cell-adhesive properties of streptavidin are mediated by the exposure of an RGD-like RYD site. *Eur. J. Cell Biol. 58*, 271−279.

(16) Schechter, B., Arnon, R., Colas, C., Burakova, T., and Wilcheck, M. (1995) Renal accumulation of streptavidin: Potential use for targeted therapy of the kidney. *Kidney Int. 47*, 1327−1335.

(17) Wilbur, D. S., Hamlin, D. K., Buhler, K. R., Pathare, P. M., Vessella, R. L., Stayton, P. S., and To, R. (1998) Streptavidin in antibody pretargeting. 2. Evaluation Of methods for decreasing localization of streptavidin to kidney while retaining its tumor binding capacity. *Bioconjugate Chem. 9*, 322−330.

(18) Atassi, M. Z. (1977) Chemical Modification and Cleavage of Proteins and Chemical Strategy in Immunochemical Studies of Proteins, in *Immunochemistry of Proteins* (M. Z. Atassi, Ed.) pp 1−161, Plenum Press, New York.

(19) Feeney, R. E., Yamasaki, R. B., and Geoghegan, K. F. (1982) Chemical Modification of Proteins: an Overview. In: *Modification of Proteins. Food, Nutritional, and Pharmacological Aspects.* (R. E. Feeney, and J. R. Whitaker, Eds.) pp 3−55, American Chemical Society, Washington D. C.

(20) Lundblad, R. L. (1995) The Modification of Arginine, in *Techniques in Protein Modification*, pp 163−186, CRC Press, Boca Raton.

(21) Wilbur, D. S., Chyan, M. K., Pathare, P. M., Hamlin, D. K., Frownfelter, M. B., and Kegley, B. B. (2000) Biotin reagents for antibody pretargeting. 4. Selection Of biotin conjugates for in vivo application based on their dissociation rate from avidin and streptavidin. *Bioconjugate Chem. 11*, 569−583.

(22) Heinrikson, R. L., and Meredith, S. C. (1984) Amino acid analysis by reverse-phase high-performance liquid chromatography: precolumn derivatization with phenylisothiocyanate. *Anal. Biochem 136*, 65−74.

(23) Wilbur, D. S., Stayton, P. S., To, R., Buhler, K. R., Klumb, L. A., Hamlin, D. K., Stray, J. E., and Vessella, R. L. (1998) Streptavidin in Antibody Pretargeting. Comparison of a Recombinant Streptavidin with Two Streptavidin Mutant Proteins and Two Commercially Available Streptavidin Proteins. *Bioconjugate Chem. 9*, 100−107.

(24) Fritzberg, A. R., Beaumier, P. L., Bottino, B. J., and Reno, J. M. (1994) Approaches to improved antibody- and peptide-mediated targeting for imaging and therapy of cancer. *J. Controlled Release 28*, 167−173.

(25) Green, N. M. (1963) Avidin. 4. Stability at Extremes of pH and Dissociation into Subunits by Guanidine Hydrochloride. *Biochem. J. 89*, 609-620.

(26) Green, N. M. (1975) Avidin. *Adv. Prot. Chem. 29*, 85−133.

(27) Wilbur, D. S., Pathare, P. M., Hamlin, D. K., Frownfelter, M. B., Kegley, B. B., Leung, W. Y., and Gee, K. R. (2000) Evaluation of biotin-Dye conjugates for use in an HPLC assay To assess relative binding of biotin derivatives with avidin and streptavidin. *Bioconjugate Chem. 11*, 584−598.

(28) Wilbur, D. S., Hamlin, D. K., Chyan, M. K., Kegley, B. B., and Pathare, P. M. (2001) Biotin reagents for antibody pretargeting. 5. Additional studies of biotin conjugate design to provide biotinidase stability. *Bioconjugate Chem. 12*, 616−623.

(29) Wilbur, D. S., Hadley, S. W., Hylarides, M. D., Abrams, P. G., Beaumier, P. A., Morgan, A. C., Reno, J. M., and Fritzberg, A. R. (1989) Development of a stable radioiodinating reagent to label monoclonal antibodies for radiotherapy of cancer. *J. Nucl. Med. 30*, 216−226.

(30) Pimm, M. V., Fells, H. F., Perkins, A. C., and Baldwin, R. W. (1988) Iodine-131 and indium-111 labeled avidin and streptavidin for pre-targetted immunoscintigraphy with biotinylated anti-tumour monoclonal antibody. *Nucl. Med. Commun. 9*, 931−941.

(31) Paganelli, G., Pervez, S., Siccardi, A. G., Rowlinson, G., Deleide, G., Chiolerio, F., Malcovati, M., Scassellati, G. A., and Epenetos, A. A. (1990) Intraperitoneal Radio-Localization of Tumors Pre-Targeted by Biotinylated Monoclonal Antibodies. *Int. J. Cancer 45*, 1184−1189.

(32) Khawli, L. A., Alauddin, M. M., Miller, G. K., and Epstein, A. L. (1993) Improved Immunotargeting of Tumors with Biotinylated Monoclonal Antibodies and Radiolabeled Streptavidin. *Antibodies, Immunoconjugates, Radiopharm. 6*, 13−27.

(33) Muzykantov, V. R., Atochina, E. N., Gavriljuk, V., Danilov, S. M., and Fisher, A. B. (1994) Immunotargeting of Streptavidin to the Pulmonary Endothelium. *J. Nucl. Med. 35*, 1358−1365.

(34) Saga, T., Weinstein, J. N., Jeong, J. M., Heya, T., Lee, J. T., Le, N., Paik, C. H., Sung, C., and Neumann, R. D. (1994) Two-Step Targeting of Experimental Lung Metastases with Biotinylated Antibody and Radiolabeled Streptavidin. *Cancer Res. 54*, 2160−2165.

(35) Zhang, M., Sakahara, H., Yao, Z., Saga, T., Nakamoto, Y., Sato, N., Nakada, H., Yamashina, I., and Konishi, J. (1997) Intravenous Avidin Chase Improved Localization of Radiolabeled Streptavidin in Intraperitoneal Xenograft Pretargeted with Biotinylated Antibody. *Nucl. Med. Biol. 24*, 61−64.

(36) Zhang, M., Yao, Z., Saga, T., Sakahara, H., Nakamoto, Y., Sato, N., Nakada, H., Yamshina, I., and Konishi, J. (1998) Improved Intratumoral Penetration of Radiolabeled Streptavidin in Intraperitoneal Tumors Pretargeted with Biotinylated Antibody. *J. Nuclear Med. 39*, 30−33.

(37) Wilbur, D. S., Pathare, P. M., Hamlin, D. K., Stayton, P. S., To, R., Klumb, L. A., Buhler, K. R., and Vessella, R. L. (1999) Development of new biotin/streptavidin reagents for pretargeting. *Biomol. Eng. 16*, 113−118.

(38) Sandmaier, B. M., Bethge, W., Wilbur, D. S., Hamlin, D. K., Santos, E. B., Brechbiel, M. W., Fisher, D. R., and Storb, R. (2002) Evaluation of Nonmyeloablative Bone Marrow Transplantation Using a Bismuth-213 Labeled Anti-CD45 Radioimmunoconjugate for Conditioning in the Dog Model. *Blood*, in press.

(39) Argarana, C. E., Kuntz, I. D., Birken, S., Axel, R., and Cantor, C. R. (1986) Molecular cloning and nucleotide sequence of the streptavidin gene. *Nucl. Acids Res. 14*, 1871−1882.

(40) Bayer, E. A., Hen-Hur, H., Hiller, Y., and Wilchek, M. (1989) Postsecretory modifications of streptavidin. *Biochem. J. 259*, 369−376.

(41) Pahler, A., Hendrickson, W. A., Kolks, M. A. G., Argarana, C. E., and Cantor, C. R. (1987) Characterization and Crystallization of Core Streptavidin. *J. Biol. Chem. 262*, 13933−13937.

(42) Sano, T., Pandori, M. W., Chen, X., Smith, C. L., and Cantor, C. R. (1995) Recombinant Core Streptavidins. A Minimum-Sized Core Streptavidin Has Enhanced Structural Stability and Higher Accessibility to Biotinylated Macromolecules. *J. Biol. Chem. 270*, 28204−28209.

(43) Meyer, D. L., Schultz, J., Lin, Y., Henry, A., Sanderson, J., Jackson, J. M., Goshorn, S., Rees, A. R., and Graves, S. S. (2001) Reduced antibody response to streptavidin through site-directed mutagenesis. *Protein Sci. 10*, 491−503.

(44) Mogensen, C. E., and Sølling, K. (1977) Studies on Renal Tubular Protein Reabsorption: Partial and Near Complete Inhibition by Certain Amino Acids. *Scand. J. Clin. Lab. Invest. 37*, 477−486.

BC015574N

Table 2: Distribution of Radioactivity for Co-injected arginine modified [^{125}I]rSAv and succinylated [^{131}I]rSAv in BALB/c mice.[a]

Tissues	4 h[b,c]		24 h		48 h	
	I-125	I-131	I-125	I-131	I-125	I-131
blood	11.47 ± 0.46	17.03 ± 0.59	3.86 ± 0.46	5.61 ± 0.84	1.38 ± 0.21	1.63 ± 0.26
muscle	0.83 ± 0.06	1.04 ± 0.05	0.51 ± 0.05	0.82 ± 0.09	0.36 ± 0.04	0.58 ± 0.06
lung	5.80 ± 0.56	7.61 ± 0.65	2.42 ± 0.27	3.39 ± 0.42	1.35 ± 0.21	1.73 ± 0.27
kidney	5.37 ± 0.29	4.93 ± 0.43	5.65 ± 1.12	2.56 ± 0.46	5.07 ± 0.91	1.50 ± 0.17
spleen	2.87 ± 0.22	3.12 ± 0.25	2.32 ± 0.27	3.07 ± 0.45	1.75 ± 0.41	2.19 ± 0.53
liver	2.62 ± 0.26	3.64 ± 0.27	1.99 ± 0.28	3.07 ± 0.56	1.87 ± 0.18	3.10 ± 0.27
intestine	2.14 ± 0.15	2.88 ± 0.16	0.97 ± 0.15	1.36 ± 0.25	0.64 ± 0.11	0.87 ± 0.12
neck	11.15 ± 2.39	3.34 ± 0.83	9.42 ± 8.73	5.97 ± 2.93	2.24 ± 0.35	3.36 ± 0.46
stomach	12.88 ± 10.28	3.55 ± 1.98	1.93 ± 0.18	2.54 ± 0.27	1.36 ± 0.33	1.83 ± 0.34
urine[d]	44.40 ± 14.76	9.28 ± 4.03	8.21 ± 1.94	14.43 ± 3.21	4.15 ± 0.22	8.06 ± 0.66

[a]Values shown are % injected dose / gram ± standard deviation. [b]Time of sacrifice from injection of iodinated rSAv. [c]Data were obtained for $n = 5$ mice; average animal weight, 31.35 ± 1.89 g; Injectate for each animal had 50 µg/6.5 µCi of arginine modified [^{125}I]rSAv and 50 µg/6.0 µCi of succinylated [^{131}I]rSAv in approximately 100 µL of 0.9% sterile saline. [d]Urine was collected by syringe bladder tap after sacrifice.

© 2002 American Chemical Society, Bioconjugate Chem., Wilbur bc015574n Supporting Info Page 1

Table 3: Distribution of Radioactivity for Co-injected succinylated [^{125}I]rSAv and unmodified [^{131}I]rSAv in BALB/c mice at 24 h pi[a]

Tissues	5 equivalents[b,c]		10 equivalents		25 equivalents		50 equivalents	
	I-125	I-131	I-125	I-131	I-125	I-131	I-125	I-131
blood	1.87 ± 0.25	1.24 ± 0.16	1.89 ± 0.29	1.08 ± 0.16	1.60 ± 0.18	1.09 ± 0.09	1.02 ± 0.28	1.16 ± 0.25
muscle	0.57 ± 0.09	0.45 ± 0.08	0.55 ± 0.08	0.42 ± 0.04	0.54 ± 0.09	0.47 ± 0.04	0.41 ± 0.15	0.46 ± 0.11
lung	1.81 ± 0.27	1.44 ± 0.19	1.80 ± 0.26	1.32 ± 0.23	1.53 ± 0.19	1.38 ± 0.16	1.08 ± 0.22	1.36 ± 0.24
kidney	13.50 ± 1.48	25.55 ± 3.90	11.21 ± 1.38	26.57 ± 3.90	5.91 ± 0.99	25.47 ± 3.70	2.08 ± 0.11	27.46 ± 2.16
spleen	1.85 ± 0.19	1.65 ± 0.17	1.79 ± 0.24	1.45 ± 0.14	1.62 ± 0.22	1.49 ± 0.14	1.36 ± 0.31	1.55 ± 0.26
liver	1.85 ± 0.21	1.55 ± 0.17	1.97 ± 0.23	1.51 ± 0.23	1.87 ± 0.11	1.49 ± 0.04	1.82 ± 0.31	1.62 ± 0.23
intestine	0.77 ± 0.13	0.66 ± 0.11	0.86 ± 0.10	0.71 ± 0.12	0.73 ± 0.06	0.68 ± 0.11	0.68 ± 0.39	0.78 ± 0.42
neck	4.93 ± 1.72	5.85 ± 2.58	3.87 ± 1.93	4.34 ± 2.91	3.57 ± 0.77	3.95 ± 1.25	4.00 ± 0.52	4.89 ± 0.86
stomach	1.48 ± 0.15	1.37 ± 0.14	1.61 ± 0.26	1.53 ± 0.33	1.47 ± 0.25	1.57 ± 0.31	1.13 ± 0.27	1.37 ± 0.32
urine[d]	14.70 ± 6.42	15.08 ± 6.21	11.75 ± 2.85	11.91 ± 2.60	13.14 ± 2.17	11.97 ± 1.95	12.90 ± 4.93	13.34 ± 4.21

[a]Values shown are % injected dose / gram ± standard deviation. [b]Number of equivalents of succinic anhydride used in reaction with rSAv. [c]Data were obtained for n = 5 mice; average animal weight, 26.70 ± 1.81 g; Injectate for each animal had one of the succinylated [^{125}I]rSAv preparations: (1)15 μg/11.1 μCi of (5 equiv) succinylated [^{125}I]rSAv, (2) 15 μg/11.9 μCi of (10 equiv) succinylated [^{125}I]rSAv, (3) 15 μg/12.6 μCi of (25 equiv) succinylated [^{125}I]rSAv, or (4) 15 μg/14 μCi of (50 equiv) succinylated [^{125}I]rSAv, in a mixture with 15 μg/22 μCi of unmodified [^{131}I]rSAv in approximately 100 μL of 0.9% sterile saline. [d]Urine was collected by syringe bladder tap after sacrifice.

© 2002 American Chemical Society, Bioconjugate Chem., Wilbur bc015574n Supporting Info Page 2

Surface-Tethered DNA Complexes for Enhanced Gene Delivery

Tatiana Segura[†] and Lonnie D. Shea[†,‡,*]

Departments of Chemical Engineering and Biomedical Engineering, Northwestern University, 2145 Sheridan Road E156, Evanston, Illinois 60208-3120. Received November 2, 2001; Revised Manuscript Received February 6, 2002

Overcoming the barriers to efficient gene transfer is a fundamental goal of biotechnology. A versatile approach to enhance the delivery of nonviral DNA involves complexation with cationic polymers, which can be designed to overcome the barriers to effective gene transfer. More recently, DNA release from a polymer substrate or scaffold has been shown to enhance gene transfer, likely by increasing DNA concentrations in the cell microenvironment. We propose a novel approach that combines these two strategies in which cationic polymer/DNA complexes are tethered to a substrate that supports cell adhesion. The cationic polymers package the DNA for efficient internalization and the surface tethering functions to maintain elevated concentrations in the cell microenvironment for cells adhered to the substrate. The cationic polymer polylysine (degree of polymerization equal to 19 or 150) was modified with biotin groups, which was confirmed by mass spectrometry and biochemical analysis. Complex formation of DNA with biotinylated-polylysine, or mixtures of biotinylated and nonbiotinylated polylysines, was confirmed by gel electrophoresis. Plasmid DNA encoding for the reporter gene β-galactosidase was complexed with different mixtures of biotinylated and nonbiotinylated polylysine and incubated on neutravidin (nonglycosylated avidin)-coated surfaces. DNA surface densities ranging from 0.1 to 4.3 μg/cm^2 were observed and found to be a function of the number of biotin groups, the molecular weight of the polylysine, and the amount of DNA. HEK293T or NIH/3T3 cells were then seeded onto the DNA-modified surfaces, and transfection was quantified at 48 and 96 h. Transfection by the DNA surfaces was observed with both cell lines, and expression levels up to 100 fold greater than bulk delivery of the complexes was obtained. Transfection was found to be a function of the surface DNA quantities and the number of tethers on the complex. Transfected cells were observed only in the region in which DNA complexes were tethered, suggesting that the location of transfected cells can be specifically controlled. Surface tethering of DNA represents a promising approach to enhancing gene transfer and spatially controlling gene delivery, which may have applications to a multitude of fields ranging from tissue engineering to functional genomics.

INTRODUCTION

Developing systems capable of controlled and efficient gene transfer is a fundamental goal of biotechnology, with applications ranging from basic science to clinical medicine. In the area of basic science, increasing or decreasing the expression level of a gene within a cell has the power to reveal or confirm the roles of specific components of signaling pathways and can lead to a mechanistic understanding of cell behavior, disease pathogenesis, and drug action (*1*, *2*). Assays based on cellular responses to altered gene expression allow gene function to be examined within a biological context that is more representative of the physiological situation (*3*, *4*). The growing collection of gene sequences and cloned cDNAs has led to the development of microarrays of cell clusters expressing gene products as a high-throughput approach to screen for a phenotype of interest (*5*). Alternatively, therapeutic strategies using gene delivery are under development for inherited genetic disorders, cancer, and tissue regeneration (*6*, *7*). The successful application of gene transfer for basic science and clinical medicine requires the ability to manipulate the expression of target genes in the desired cell population. Numerous techniques are under development to overcome the barriers to gene transfer, which includes processes such as cellular internalization, endosomal escape, and nuclear trafficking.

Cationic polymers provide a versatile approach for gene transfer, as the polymers can be designed or modified to overcome the barriers to gene transfer (*8*, *9*). Complexation with cationic polymers functions to condense DNA, to produce a complex with a less-negative surface charge, to enhance cellular internalization of DNA, and to protect the DNA from degradation. Although many types of cationic polymers have been explored (*10*−*13*), polymers based on poly(L-lysine) (PLL) (*14*−*16*), poly(ethylenimine) (PEI) (*17*−*19*), and poly(amidoamine) (PAMAM) (*20*, *21*) are among the most commonly utilized. Numerous studies have examined the relationship between the physical properties of the cationic polymer (e.g., molecular weight) with the ability to condense DNA and to efficiently transfer the DNA to cells (*17*, *22*). Complexes are formed at nitrogen:phosphate ratios ranging from 0.5:1 to 20:1 and typically produces complexes with sizes ranging from 50 to 150 nm (*23*−*25*). An advantage of the cationic polymers is that functional domains can be covalently incorporated to design a synthetic vector capable of overcoming the barriers to gene transfer. Fusogenic peptides and other functional groups have been attached to enhance endosomal escape of the DNA complexes (*26*,

* Address correspondence to Lonnie D. Shea, Department of Chemical Engineering, Northwestern University, 2145 Sheridan Rd./E156, Evanston, IL 60208-3120. Phone: 847-491-7043. Fax: 847-491-3728. E-mail: l-shea@northwestern.edu.

[†] Department of Chemical Engineering.

[‡] Department of Biomedical Engineering.

10.1021/bc015575f CCC: $22.00 © 2002 American Chemical Society
Published on Web 03/15/2002

27). Alternatively, ligands that bind to specific cell surface receptors have been attached to increase binding of the DNA complexes to the cell surface and can enhance cellular internalization (*28*−*31*).

Recently, the polymeric systems that were developed to deliver biologically active proteins have been adapted to deliver nonviral DNA. Polymeric scaffolds have been fabricated from a variety of materials, both natural (e.g., collagen) and synthetic (e.g., poly(lactide-*co*-glycolide)), which function as a support for cell adhesion and migration (*7*). These scaffolds act to increase the local concentration of DNA within the cellular microenvironment either by providing a sustained release of DNA (*32*) or by maintaining the DNA locally (*33, 34*). Enhanced gene transfer by these polymer scaffolds in vivo likely results from an increased concentration at the cell surface, which has been shown to enhance gene transfer in vitro (*35*).

We present a novel approach toward enhancing DNA delivery that combines DNA complexation with polymeric delivery. DNA is complexed with a cationic polymer and subsequently tethered to a substrate the supports cell adhesion. The cationic polymer polylysine is covalently modified with biotin groups, complexed with DNA, and the resulting complexes are bound to a neutravidin-coated surface. The quantity and location of DNA on the surface can be controlled and cells cultured on the surface are transfected by the surface-associated DNA.

EXPERIMENTAL PROCEDURES

Materials. Plasmid DNA encoding for β-galactosidase (pNGVL1-β-gal) was purified from bacteria culture using Quiagen (Santa Clara, CA) reagents and stored in Tris-EDTA buffer solution (10 mM Tris, 1 mM EDTA, pH = 7.4). Fluorescein tagged β-galactosidase vector (Fl-β-gal) was purchased from Gene Therapy Systems (San Diego, CA). Two polylysine (PLL) peptides were used for DNA complexation: Cys-Trp-Lys_{19} (K_{19}, BioPeptide, San Diego, CA) and Lys_{150} (K_{150}, average molecular weight of 20000, Sigma, St Louis, MO). Avidin and biotin reagents for peptide modification and surface tethering were purchased from Pierce (Rockford, IL). All other reagents were obtained from Fisher Scientific (Fairlawn, NJ) unless otherwise noted.

Synthesis of Biotinylated Polylysine. The peptide K_{19} was modified with a biotin group through the terminal cysteine residue by reaction of the sulfhydryl group with the iodoacetyl group of the biotinylation reagent, EZ-link-PEO-iodoacetyl-biotin. The peptide K_{19} (10 mg) was dissolved in 850 μL of buffer (50 mM Tris, 5 mM EDTA, pH = 8.3) that was previously bubbled with nitrogen gas. The EZ-link-PEO-iodoacetyl-biotin (3.8 mg) was also dissolved in 150 μL of buffer (0.1 M sodium phosphate, 5 mM EDTA, pH = 6.0). The biotin solution was added dropwise to the peptide solution, mixed gently, covered with aluminum foil, and incubated for 90 min. The starting peptide solution and the reaction mixture were analyzed by HPLC to determine if the reaction had gone to completion. The starting peptide solution and the reaction mixture were resolved by injecting 20 μg through a C18 RP-HPLC column eluted with water (0.1% trifluoroacetic acid (TFA)) and an acetonitrile gradient (0.1% TFA, 0 to 95% over 50 min at 60 °C) while detecting the absorbance at 260 nm. For purification, sephadex (G15) was equilibrated in deionized water for 30 min prior to packing in a glass column (2 cm diameter × 12 cm height). The reaction mixture was passed though the column using deionized water. Twenty fractions were collected, and the presence of the tryptophan side chain was examined by measuring the absorbance at 260 nm (Beckman Instruments Inc., Fullerton, CA). The fractions with the greatest absorbance at 260 nm were lyophilized (Labconco Corp., Kansas City, MO) and analyzed by mass spectrometry. The purified biotinylated peptide (K_{19}-B) was stored as a powder at −20 °C.

The peptide K_{150} was biotinylated using succinimide ester (NHS)/amine chemistry. K_{150} (10 mg) was dissolved in 1 mL of phosphate buffered saline (PBS, pH = 7) and EZ-link-Sulfo-NHS-LC-biotin (2.8 mg) was added directly to the solution, mixed gentlyb and incubated for 2 h at 4 °C. The reaction mixture was purified using dialysis cassettes immersed in deionized water. The dialyzed product was further purified using a monomeric avidin column to separate the biotinylated components from nonbiotinylated species. The biotinylated product was eluted with 10 mL of a 10 mM biotin solution and dialyzed to remove the unconjugated biotin. The purified biotinylated peptide (K_{150}-B) was then lyophilized and stored as a powder at −20 °C. The degree of biotinylation of K_{150}-B was determined by quantifying the mole ratio of biotin to K_{150} using 2-(4′-hydroxyazobenzene)benzoic acid (HABA). The absorbance at 500 nm of a HABA/avidin solution in PBS was recorded before and after the addition of the K_{150}-B and used to calculate the molar ratio of biotin to K_{150}.

Complex Formation and Surface Tethering. The ability of the biotinylated and nonbiotinylated polylysine (K_{150}, K_{150}-B, K_{19}, K_{19}-B) to condense DNA was assessed by gel electrophoresis. Biotinylated and nonbiotinylated peptides were mixed and added in a stepwise manner (1 μL of 1 mg/mL) to a DNA solution (200 μL of 20 μg/mL). After each addition step, the solution was vortexed for 4 s and incubated for 10 min and a sample (10 μL) removed. Upon complete addition of peptide, trypsin was added to digest the polylysine. Gel electrophoresis was performed to assess the extent of complex formation for the samples and the trypsin-digested DNA solution.

DNA/PLL complexes were incubated on surfaces to specifically tether the complexes through the biotin−neutravidin binding. DNA (90 μL of 44.4 μg/mL) was complexed at a charge ratio (±) of 5.5:1 with the four peptides (K_{150}, K_{150}-B, K_{19}, or K_{19}-B) individually or with mixtures of biotinylated and nonbiotinylated peptides. The number of tethers on each complex is varied by mixing biotinylated and nonbiotinylated PLLs prior to complexation with DNA. Complexes were incubated after mixing for 30 min at room temperature and then allowed to bind to prewashed neutravidin coated surfaces for 2 h. The unbound complexes were then removed from the wells and washed with tris-buffered saline (TBS). The surface quantities of DNA were determined by incubating with trypsin (100 μL) at 37 °C for 2 h to degrade the PLL and release the DNA into solution. The quantity of DNA was measured with a fluorometer (Turner Designs TD-360) using the Hoechst dye. Tethered DNA complexes were visualized by fluorescence microscopy using the Fl-tagged β-galactosidase vector before and after washing with TBS.

Cell Culture and Transfection. Transfection of cells on the DNA-modified surfaces was examined using a β-galactosidase plasmid and two cell lines (HEK293T and NIH/3T3). Polyethyleneimine (PEI, 22 kDa, MBI−Fermentas, Hanover, MD, 0.5 μL of 10 μM) was added to DNA-modified surfaces and incubated for 5 min. Cells were then plated and cultured on the surfaces for 48−96 h and then lysed for assay of the β-galactosidase enzyme activities (Promega, Madison, WI) and protein levels (BioRad, Hercules, CA). Alternatively, cells were

stained with X-gal to determine the location of transfected cells. HEK293T and NIH/3T3 were cultured at 37 °C and 5% CO_2 in Dubelcco's modified eagle medium (DMEM, Life Technologies, Gaithersburg, MD) supplemented with 10% heat inactivated FBS and 1% penicillin/streptomycin.

Control experiments to characterize the effectiveness of surface-mediated delivery were performed by using bulk delivery of DNA complexed with the nonbiotinylated K_{150} or K_{19}. For bulk delivery of K_{150}/DNA complexes, the quantity of DNA delivered was determined based on the amount of surface associated DNA obtained when DNA was complexed only with K_{150}-B. For bulk delivery of K_{19}/DNA, the quantity of DNA delivered was determined based on the amount of surface-associated DNA obtained when DNA was complexed with a mixture of K_{150}-B/K_{19}, which had a predominance of K_{19} over K_{150}-B. Upon formation of the K_{150}/DNA and K_{19}/DNA complexes, PEI was added at the same molar ratio of DNA:PEI that was used for the substrate-mediated delivery. For the bulk delivery experiments, HEK293T and NIH/3T3 cells were plated at 1 day prior to transfection and cultured in complete media.

RESULTS

PLL Biotinylation and DNA Complexation. Polylysine was covalently modified with biotin residues either through an N-terminal cysteine side chain (K_{19}) or through an amine (K_{150}). HPLC analysis of the initial peptide (K_{19}) and the peptide reaction mixture (K_{19}-B) demonstrated that the reaction proceeded to completion (Figure 1a), as evidenced by the increase in molecular weight in the reaction mixture and the absence of the lower molecular weight K_{19} peak. Mass spectrometry (Figure 1b) suggests that the approach for modifying the peptide K_{19} results in the attachment of a single biotin group. A good correspondence was found between the theoretically expected molecular weight for K_{19} modified with a single biotin (3158 Da) and the experimentally obtained molecular weight (3157.66 ± 0.77 Da). Alternatively, the chemistry employed for modification of K_{150} allows for multiple biotin residues to be attached per PLL. The K_{150}-B synthesis resulted in a 3.1:1 molar ratio of biotin to K_{150} by using a 10:1 molar ratio of biotinylation reagent to K_{150} in the reaction mixture.

Biotinylated and nonbiotinylated peptides were subsequently analyzed for their ability to complex with DNA using gel electrophoresis. The nonbiotinylated peptides (K_{19}, K_{150}) completely eliminate the electrophoretic mobility at charge ratios of 3.1 and 1.2, respectively (Figure 2a,c). However, the presence of the biotin group on the peptide affected the charge ratio at which the mobility is eliminated, which is 4.6 and 4.9 for K_{19}-B and K_{150}-B, respectively (Figure 2b,d). Mixtures of K_{150}-B with K_{19} were also examined by gel electrophoresis for DNA complexation at a charge ratio of 5.5:1. The inhibition of mobility was observed for all combinations of the two peptides (Figure 2e−g). The results of Figure 2 illustrate that the biotinylated peptides, nonbiotinylated peptides, and mixtures of biotinylated and nonbiotinylatd peptides are capable of electrostatically neutralizing plasmid DNA and eliminating its electrophoretic mobility.

Surface Tethering of DNA/PLL Complexes. DNA complexed with biotinylated PLL was examined to determine if the biotin groups on the PLL were available for tethering to a surface using the affinity of biotin for neutravidin (nonglycosylated avidin). Surface-associated DNA was visualized for DNA complexed with K_{150}-B.

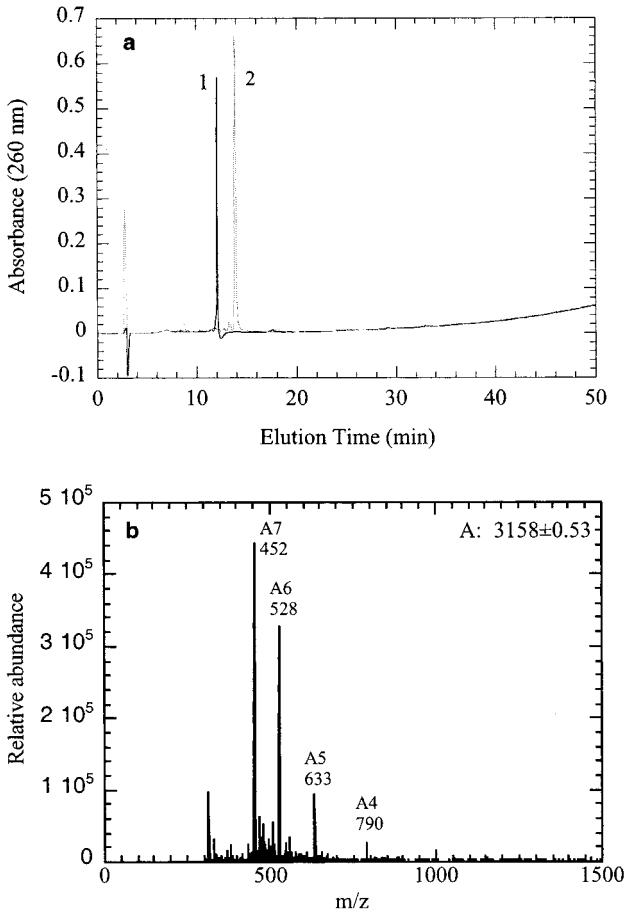


Figure 1. HPLC and mass spectrometry confirm the formation of biotyinylated K_{19}. (a) HPLC of the K_{19} starting material **1** and the reaction mixture **2**. The shift in molecular weight between **1** and **2** and absence of the low molecular weight peak in **2** confirmed that the reaction went to completion. (b) Mass spectrometry of the purified reaction mixture.

Fluorescence images taken after the initial incubation on the surface and before the wash demonstrates the presence of complexes across the entire surface (Figure 3a). Thorough washing of the surfaces resulted in a reduction of the quantity of surface-associated DNA (Figure 3b). All subsequent studies used surfaces that were thoroughly washed to ensure binding specificity of the complexes.

The quantity of surface associated DNA was subsequently measured as a function of the PLL peptides and the number of biotin groups per complex. Nonbiotinylated peptides used for DNA condensation resulted in low surface densities (<0.1 μg DNA/cm^2) due to nonspecific adsorption. The use of biotinylated peptides for DNA complexation increased the surface density of DNA relative to the conditions lacking biotin groups ($p < 0.05$), suggesting that biotin groups are available on the DNA complexes for interactions with the surface-associated neutravidin. The maximal amount of surface-associated DNA was observed for DNA complexes formed solely with biotinylated peptides ($p < 0.001$), with densities of 2.9 and 4.3 μg DNA/cm^2 obtained for K_{150}-B and K_{19}-B, respectively (Figure 4a,b). Complexes formed from either K_{150}-B or K_{19}-B are calculated to have an average number of biotin groups equal to 1705 and 4342, respectively. These surface densities correspond to a tethering efficiency (mass DNA on surface/mass DNA added) of 24% (K_{150}) and 35% (K_{19}). For the K_{150}-B and K_{19}-B, decreasing the amount of DNA incubated on the surface was found

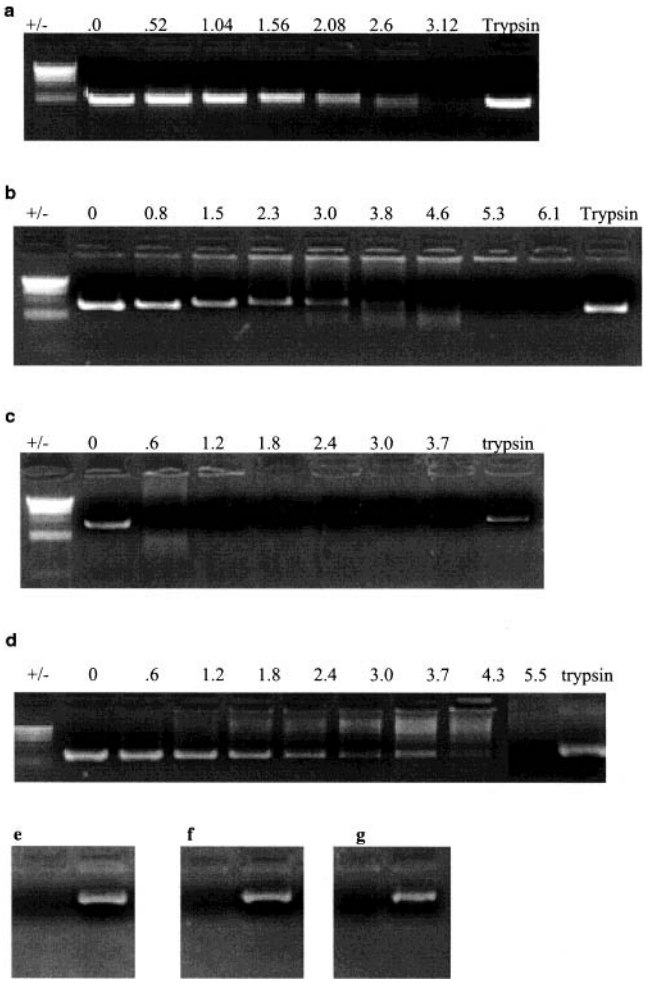


Figure 2. Electrophoretic retardation of DNA complexed with mixture of biotinylated and nonbiotinylated polylysine. (a) Nonbiotinylated K_{19}, (b) biotinylated K_{19}, (c) nonbiotinylated K_{150}, and (d) biotinylated K_{150} were examined at a range of charge ratios. Condensation of DNA with mixtures of K_{150}-B and K_{19} were examined at a charge ratio of 5.5:1. The conditions examined were (e) 50% K_{150}-B/50%K_{19}, (f) 25%K_{150}-B/75%K_{19}, and (g) 5% K_{150}-B/95%K_{19}, where the percentages indicate the amount of each component based on the number of amine groups.

to decrease the amount of surface-associated DNA (data not shown). The quantity of surface-associated DNA was also found to decrease as the number of biotin groups in the DNA/PLL complex decreased. The molecular weight of polylysine, both biotinylated and nonbiotinylated also affected the quantity of surface-associated DNA. For the biotinylated peptide K_{150}-B, fewer numbers of biotin groups were required to obtain an equivalent amount of surface associated DNA as for the peptide K_{19}-B. However, the use of the nonbiotinylated peptide K_{19} for complexation resulted in increased DNA surface densities relative to the use of K_{150}.

Transfection. Culture of HEK293T and NIH/3T3 cells on the DNA-modified surfaces led to cellular transfection at 48 h, with levels of protein production equal to or greater than that obtained by bulk delivery. The transfection experiments used mixtures of K_{150}-B and K_{19} for DNA complexation because this combination had an increased amount of surface associated DNA relative to the other peptide mixtures, particularly when the complexes had few numbers of biotin groups. Quantification of protein expression levels for HEK293T demonstrated that complexes with 28 and 426 biotin groups produced

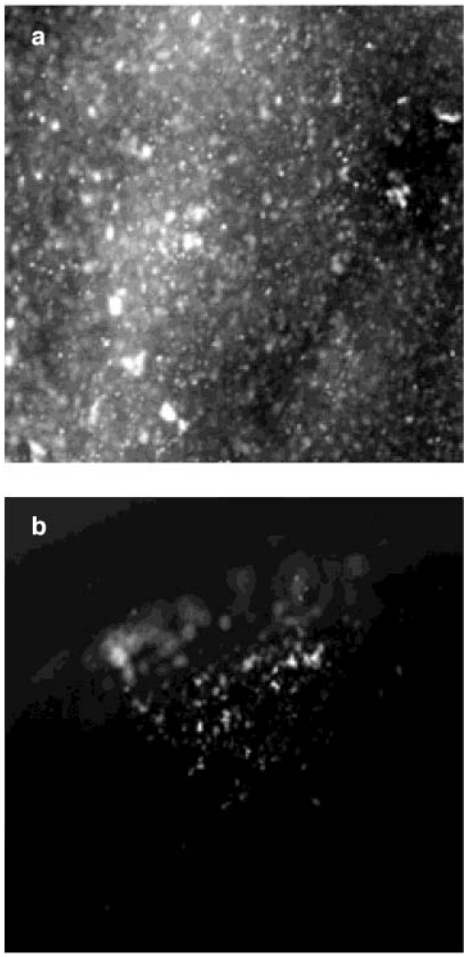


Figure 3. Fluorescence photomicrograph of surface-associated DNA. Fluorescence images taken (a) immediately after surface incubation and (b) after thorough washing.

the maximal transfection (Figure 5a), which was statistically greater ($p < 0.05$) than other conditions with greater numbers of biotin groups. Expression levels obtained for surface-associated complexes with 1705 and 853 biotin groups were not significantly different from the control conditions, which consisted of bulk delivery of DNA complexes formed from either K_{150} or K_{19}. For bulk delivery, the amount of DNA added in complexes with K_{150} or K_{19} corresponded to the surface quantities of DNA for K_{150}-B (1705 biotin groups) and K_{150}-B/K_{19} (28 biotin groups), respectively. These conditions were chosen as the control conditions to represent the limiting cases of surface associated delivery regarding DNA quantities (0.7 μg and 0.16 μg) and PLL composition (K_{150}, K_{19}). For the NIH/3T3 cells, expression levels obtained by surface associated complexes with 28, 426, and 853 biotin were significantly greater than those obtained with complexes containing 1705 biotin residues ($p < 0.05$). No significant difference between complexes with 28 biotin groups and its bulk control ($p > 0.05$) and 1705 biotin groups and its bulk control ($p > 0.05$) were found. The distribution of transfected cells throughout the cell population also differed between the delivery mechanisms. For bulk delivery, transfected cells were seen throughout the cell population (not shown); however, surface-mediated delivery resulted in cells that were transfected in clusters (Figure 6). Additionally, the location of transfected cells on the surface was consistent with the location of surface-associated DNA seen with the fluorescently tagged plasmid (Figure 3b).

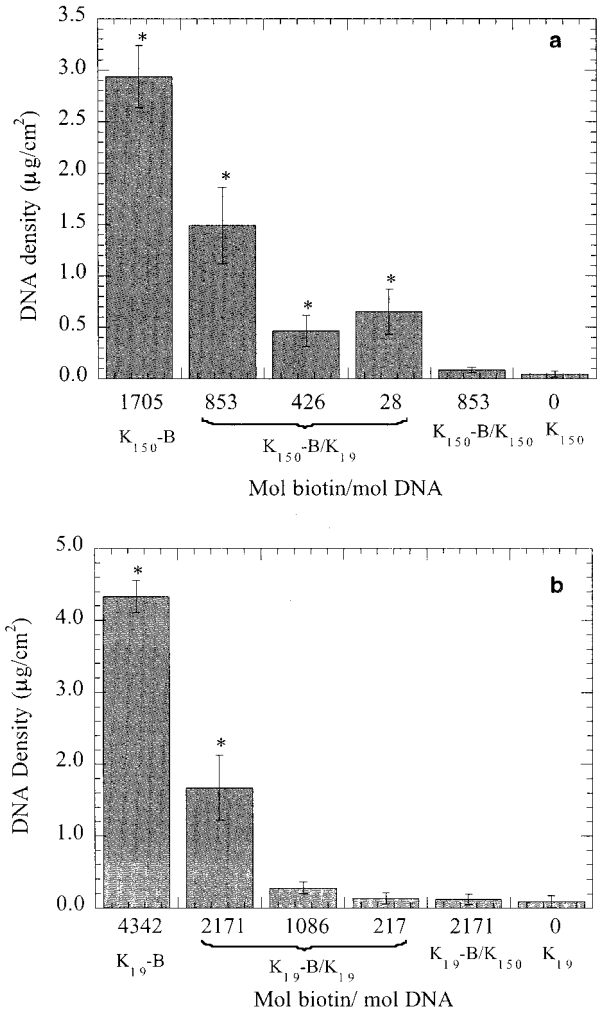


Figure 4. Density of surface-associated DNA. Complexes were formed by mixing DNA with (a) K_{150}-B or (b) K_{19}-B with either K_{19} or K_{150} at a charge ratio of 5.5. The moles of biotin per mole DNA (i.e., average number of biotin groups per complex), which varied from 28 to 1705 for K_{150}-B and 217 to 4342 for K_{19}-B, are listed beneath each bar. The symbol * indicates statistical significance ($p < 0.05$) in the surface densities relative to complexes without biotin.

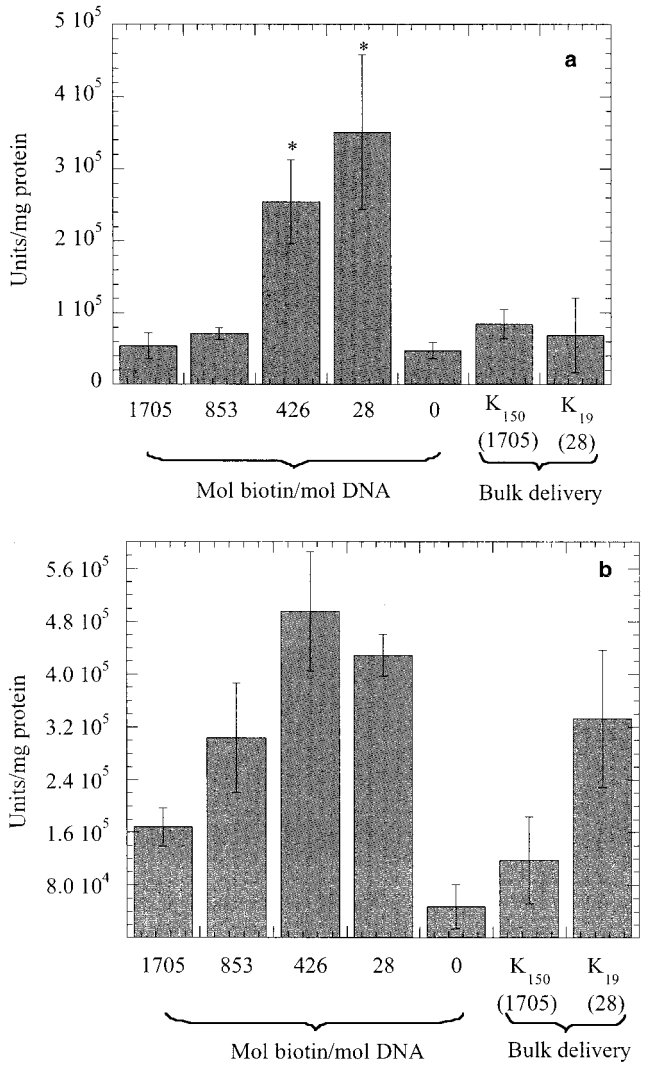


Figure 5. Expression levels by surface mediated transfection after 48 h of incubation. The expression levels for (a) HEK293T and (b) NIH/3T3 cells were determined using an assay for β-galactosidase activity. Bulk delivery of complexes resembling the limiting conditions for surface-associated DNA, 1705 and 28 biotin groups, respectively, were used as a control. For bulk delivery of K_{150}/DNA complexes, the quantity of DNA delivered was determined based on the amount of surface-associated delivery for K_{150}-B that has 1705 biotin groups. For bulk delivery of K_{19}/DNA complexes, the quantity of DNA delivered was determined based on the amount of surface-associated DNA for K_{150}-B/K_{19} that has 28 biotin groups, which has a predominance of K_{19} over K_{150}. The symbol * indicates statistical significance in transfection levels ($p < 0.05$) relative to both bulk delivery conditions.

The expression levels of protein at 96 h by cells cultured on DNA-modified surfaces increased relative to the that observed at 48 h and, for all biotinylated DNA complexes, was greater than that obtained by bulk delivery. Maximal expression levels by HEK293T cells was obtained for the complexes containing 28 biotin groups and was statistically significant from all other conditions tested ($p < 0.05$) (Figure 7a). The expression level decreased as the average number of biotin groups on the complex increased ($p < 0.05$). The complexes formed with K_{150}-B (1705 biotin groups) had the lowest transfection level of the surface associated delivery; however, the expression level was significantly greater than the bulk control ($p < 0.01$). The expression levels for the NIH/3T3 cells were less dependent on the number of biotin groups, yet the decreasing expression levels for increasing numbers of biotin groups was again observed. For all conditions tested with surface associated delivery of DNA complexes tethered to the surface with biotin groups, an increased level of transfection was observed relative to the delivery of nonbiotinylated DNA complexes and the bulk delivery of DNA complexes ($p < 0.01$).

DISCUSSION

This report presents a novel approach to DNA delivery that combines DNA condensation with polymeric delivery by tethering DNA complexes to a surface that supports cell adhesion in order to enhance gene transfer by increasing the concentration of DNA in the cellular microenvironment. In the first step of the process, cationic peptides are covalently modified with a functional group. A mixture of modified and unmodified cationic peptides are then complexed with nonviral DNA, and the resulting complexes are tethered to a substrate, which can support cell adhesion, through the functional group on the cationic peptide. Surface densities of DNA ranging from 0.1 to 4.3 μg DNA/cm^2 were obtained with coupling efficiencies up to 35%. The density of surface-associated DNA was determined to be a function of the

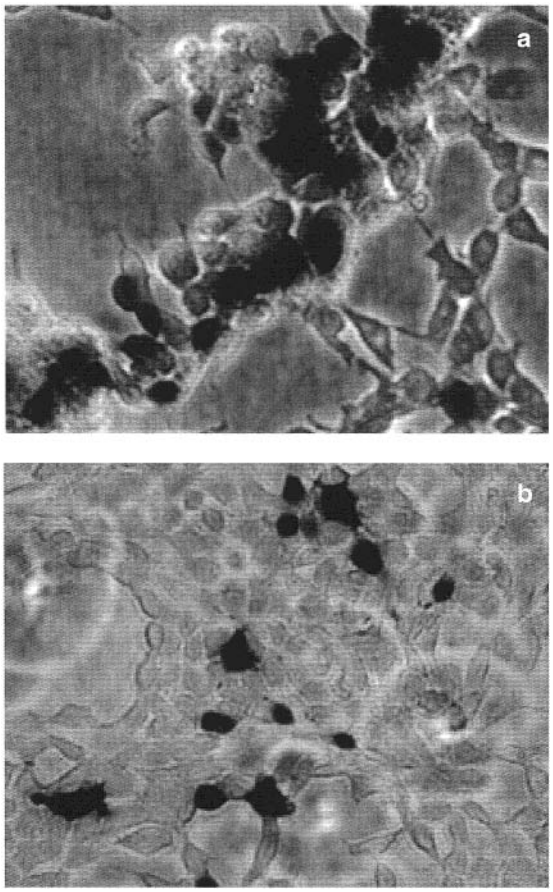


Figure 6. Photomicrograph of cells transfected by surface-associated delivery. (a) HEK293T and (b) NIH/3T3 were stained with X-gal after incubation on surfaces for 48 h.

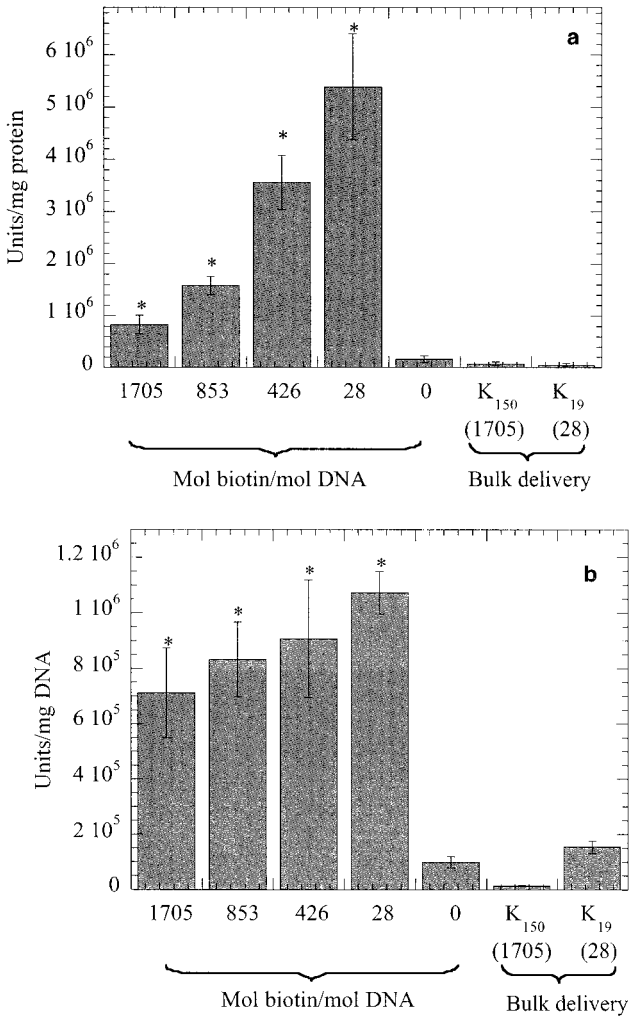


Figure 7. Expression levels by surface-mediated transfection after 96 h of incubation. The expression levels for (a) HEK293T and (b) NIH/3T3 were determined using an assay for β-galactosidase activity. The bulk controls were performed as previously described. The symbol * indicates statistical significance in transfection levels ($p < 0.05$) relative to both bulk delivery conditions.

number of tethers, the molecular weight of the cationic peptide, and the initial amount of DNA. Cells cultured on these surfaces express the transgene, and the level of transgene expression is dependent upon the exposure time of cells to the DNA and the surface tethering. At 96 h of culture, surface-mediated delivery resulted in significantly greater expression of the transgene than that obtained by bulk delivery of similar DNA complexes. Interestingly, the location of transfected cells was consistent with the location to which DNA was tethered.

Cationic polymers are a leading class of transfection reagents, which results from their ability to complex DNA, and their molecular diversity enables the physicochemical properties of the DNA complexes to be manipulated. PLL has been shown capable of condensing DNA into toroidal nanostructures with a radius of gyration less than 150 nm (*23, 24*). However, PLL does not generally produce extensive transfection, and several approaches have been undertaken to enhance its gene transfer efficiency. The internalization of PLL/DNA complexes can be enhanced by the covalent attachment of ligands, such as transferrin (*29*), folate (*36*), lectins (*37*), epidermal growth factor (EGF) (*30*), and RGD peptides (*38*). The ligand functions to direct the DNA complex to the cell surface by specifically binding to a receptor, thus increasing the quantity of DNA at the cell microenvironment (*30*). The approach described in this report utilizes a similar philosophy to enhance the concentration of DNA at the cell surface, with the primary difference being that the "ligand" in our system binds to a substrate, onto which cells can adhere. This strategy of nucleic acid complexes binding to the extracellular matrix to enhance gene transfer has been employed by retroviruses. The different domains of fibronectin can separately support the binding of cells (through integrin receptors) and retroviruses, which results in colocalization of the target cell and the virion and may lead to an enhancement of gene transfer (*39*). Synthetic systems have also been developed that increase cell-surface concentrations of DNA by adsorbing DNA complexes to the surface (*35, 40, 41*) or by releasing or entrapping DNA within a polymeric scaffold (*32, 34*).

The molecular weight of the cationic polymer impacts the ability of the polymer to complex with DNA and, ultimately, the ability of complexes to bind to the surface. Previous reports with polylysine have identified that the optimal molecular weight of the unmodified polymer represents a balance between effective condensation and cytotoxicity. Relative to low-molecular weight, the high-molecular weight PLL forms tighter and smaller condensates that are more resistant to the effects of salt concentration and sonication (*24, 42*). However, cytotoxicity has been found to be inversely related to particle size, potentially due to the high molecular weight PLL (*22*). Our results with the peptides K_{150} and K_{19} on DNA condensation and the electrophoretic mobility are con-

sistent with these reports and suggest that the peptide K_{150} has a higher affinity for DNA than does K_{19}. The attachment of biotin groups affected the ability of polylysine to complex with DNA, as evidenced by the change in the amount of polylysine required to completely eliminate the electrophoretic mobility of the DNA (Figure 2a,c).

For complexes formed with low numbers of biotin groups (28 mol biotin/mol DNA), the mixture of biotinylated, high-molecular weight PLL (K_{150}-B) and nonbiotinylated low molecular weight PLL (K_{19}) proved to be most effective combination for the binding of DNA to the substrate. The increased binding of DNA complexes to the substrate with K_{150}-B as the source of biotin groups was hypothesized to result from the degree of polymerization increasing the probability that the biotin groups are incorporated into the complex and that the incorporated biotins are available for binding. The studies on the elimination of electrophoretic mobility suggest that K_{150}-B and K_{19} have a similar binding affinity for DNA (Figure 2a,d); thus, mixtures of the two peptides with DNA are not expected to favor either peptide for DNA complexation. The increased binding of the K_{150}-B/K_{19}/DNA complexes to the substrate relative to either K_{150}/DNA or K_{19}/DNA suggests that both the biotinylated and nonbiotinylated peptides were incorporated into the complex. The complexes are completely condensed, indicating that K_{19} is involved with complexation (Figure 2g). Additionally complexes are bound to the substrate at levels greater than control, suggesting that biotinylated K_{150} is present in the complex. Our results are consistent with previous studies with EGF modified polylysine (*30*). EGF was attached to a high molecular weight polylysine with the inclusion of a spacer arm, which produced a more nativelike EGF-receptor binding. Conversely, the nonbiotinylated peptide employed had a low degree of polymerization (K_{19}), which was thought to have a reduced affinity for DNA and was thus less likely to displace the biotinylated polylysine.

The number of functional groups incorporated into the DNA complex was found to determine the surface densities of DNA and influence the ability of cells to internalize the DNA. The number of tethers within the complex was regulated through combinations of biotinylated and nonbiotinylated peptide. Increases in the number of tethers per complex led to more surface-associated DNA; however, greater transfection was observed with fewer tethers per complex. This observed relationship between the number of functional groups, the surface quantities of DNA, and the transfection may be explained by the strength of adhesion between the complexes and the surface. Insight regarding the binding of DNA complexes to the surfaces can be obtained from the models that have been developed to describe the binding of multivalent ligands to multivalent receptors (*43, 44*). An increased number of functional groups in the complex would provide more sites for surface-association and thus an increase in the adhesion strength relative to complexes with fewer functional groups. The increased adhesion strength would likely increase the amount of DNA that would remain following the washing procedure. Nevertheless, the increased adhesion strength between the complex and the surface may limit cellular internalization. The DNA must be internalized by the cell and transported to the nucleus for transfection, which may be inhibited if the DNA complex is tightly associated with the surface.

The ratio of lysine/nucleotide that has been used for DNA complexation can range from approximately 0.5 to 6.0. An increase in this ratio produces a more complete condensation of the DNA (e.g., Figure 2) for improved protection against degradation. Additionally, nonspecific adsorption of the complexes to the cell surface has been shown to increase as the lysine/nucleotide ratio increased (*30*). Ratios between 0.9 and 1.3 are expected to have minimal effects due to charge interaction and are more effective for studies with specific cell targeting through attached ligands. The charge ratio used for these studies (5.5) takes advantage of the nonspecific interaction between the DNA complex and the cell. In addition to complexing the DNA, the polylysine may act to modulate the cellular interactions with the surface. Polylysine coating is a commonly used surface treatment for in vitro cell culture experiments. An additional advantage of the increased lysine/nucleotide ratio is the increased number of biotin groups that could associate with the complex and tether the complexes to the surface. The increased lysine/nucleotide ratio may also reduce the strength of interaction between the surface bound polylysine and the DNA complex, which could facilitate cellular internalization.

An interesting result from these studies is that the expression levels increased significantly between 48 and 96 h for the surface mediated DNA delivery but not for the bulk delivery. This result suggests that the DNA is not internalized only at the initial exposure to the DNA, but increasing amounts may be internalized as the cells are adhered to the surface. These effects may result from either a decrease in the number of tethers with time, which would enable more complexes to be internalized over time, or from an increased stability of the complexes. The number of tethers per complex may decrease due to release of the complex from the surface, such as by dissociation of the DNA complex from the biotinylated PLL that is surface bound, or by degradation of polylysine by cell-secreted proteases. Alternatively, the increased gene expression may arise from an increased stability of the complexes over time. DNA complexed with polylysine is known to aggregate over time in the presence of serum (*45, 46*), which may decrease the transfection competence of the complex over time. However, complexes tethered to the surface would be prevented from aggregating and would thus retain their transfection competence. The concept of increased stability due to surface tethering has been demonstrated for proteins, where the tethering of transferrin or insulin to poly(methyl methacrylate) resulting in higher levels of activity that either soluble or physically adsorbed proteins (*47*). Additionally, tethering of EGF to poly(ethyleneoxide)-based hydrogels has also been found to increase its stability and activity when compared to physically absorbed EGF (*48*).

In conclusion, we have described a process to enhance gene transfer through a surface-mediated delivery of DNA complexes. DNA complexes are tethered to surfaces that support cell adhesion through functional groups attached to the cationic polymers. Cells cultured on these surfaces are transfected by the surface-associated DNA and express the transgene. Importantly, transfected cells are localized to the sites at which DNA is tethered, potentially providing a mechanism to spatially regulate gene delivery. This approach may be applied to the development of microarrays of living cells expressing predefined genes for research into functional genomics or to the field of tissue engineering as a means to precisely direct cellular functions within a developing tissue.

ACKNOWLEDGMENT

The authors gratefully acknowledge the efforts of Felicia M. Bogdan for technical assistance and Terry L. Sheppard for helpful discussions. Funding for this project was provided by a grant from the NSF (BES-0092701). T.S. was supported by Northwestern University's NIH Predoctoral Training Grant (5-T32 6M 08449-06).

LITERATURE CITED

(1) Rohrer, D. K., and Kobilka, B. K. (1998) G protein-coupled receptors: functional and mechanistic insights through altered gene expression. *Physiol Rev. 78,* 35−52.

(2) Stark, G. R., and Gudkov, A. V. (1999) Forward genetics in mammalian cells: functional approaches to gene discovery. *Hum. Mol. Genet. 8,* 1925−1938.

(3) Silverman, L., Campbell, R., and Broach, J. R. (1998) New assay technologies for high-throughput screening. *Curr. Opin. Chem. Biol. 2,* 397−403.

(4) Schena, M., Heller, R. A., Theriault, T. P., Konrad, K., Lachenmeier, E., and Davis, R. W. (1998) Microarrays: biotechnology's discovery platform for functional genomics. *Trends Biotechnol. 16,* 301−306.

(5) Ziauddin, J., and Sabatini, D. M. (2001) Microarrays of cells expressing defined cDNAs. *Nature 411,* 107−110.

(6) Anderson, W. F. (1998) Human gene therapy. *Nature 392,* 25−30.

(7) Bonadio, J., Goldstein, S. A., and Levy, R. J. (1998) Gene therapy for tissue repair and regeneration. *Adv. Drug Del. Rev. 33,* 53−69.

(8) Segura, T., and Shea, L. D. (2001) Materials for Non-Viral Gene Delivery, in *Annual Review of Materials Research* (S. I. Stupp, Ed.), pp 25−46, Palo Alto.

(9) Brown, M. D., Schatzlein, A. G., and Uchegbu, I. F. (2001) Gene delivery with synthetic (non viral) carriers. *Int. J. Pharm. 229,* 1−21.

(10) Boussif, O., Delair, T., Brua, C., Veron, L., Pavirani, A., and Kolbe, H. V. (1999) Synthesis of polyallylamine derivatives and their use as gene transfer vectors in vitro. *Bioconjugate Chem. 10,* 877−883.

(11) Gonzales, H., Hwang, S. J., and Davis, M. E. (1999) New class of polymers for the delivery of macromolecular therapeutic. *Bioconjugate Chem. 10,* 1068−1074.

(12) Murphy, J. E., Uno, T., Hamer, J. D., Cohen, F. E., Dwarki, V., and Zuckermann, R. N. (1998) A combinatorial approach to the discovery of efficient cationic peptoid reagents for gene delivery. *Proc. Natl. Acad. Sci. U.S.A. 95,* 1517−1522.

(13) van de Wetering, P., Moret, E. E., Schuurmans-Nieuwenbroek, N. M., van Steenbergen, M. J., and Hennink, W. E. (1999) Structure−activity relationships of water-soluble cationic methacrylate/methacrylamide polymers for nonviral gene delivery. *Bioconjugate Chem. 10,* 589−597.

(14) McKenzie, D. L., Kwok, K. Y., and Rice, K. G. (2000) A potent new class of reductively activated peptide gene delivery agents. *J. Biol. Chem. 275,* 9970−9977.

(15) Katayose, S., and Kataoka, K. (1997) Water-soluble polyion complex associates of DNA and poly(ethylene glycol)-poly(L-lysine) block copolymer. *Bioconjugate Chem. 8,* 702−707.

(16) Choi, J. S., Lee, E. J., Choi, Y. H., Jeong, Y. J., and Park, J. S. (1999) Poly(ethylene glycol)-*block*-poly(L-lysine) dendrimer: novel linear polymer/dendrimer block copolymer forming a spherical water-soluble polyionic complex with DNA. *Bioconjugate Chem. 10,* 62−65.

(17) Fischer, D., Bieber, T., Li, Y., Elsasser, H. P., and Kissel, T. (1999) A novel nonviral vector for DNA delivery based on low molecular weight, branched polyethylenimine: effect of molecular weight on transfection efficiency and cytotoxicity. *Pharm. Res. 16,* 1273−1279.

(18) Boussif, O., Lezoualc'h, F., Zanta, M. A., Mergny, M. D., Scherman, D., Demeneix, B., and Behr, J. P. (1995) A versatile vector for gene and oligonucleotide transfer into cells in culture and in vivo: polyethylenimine. *Proc. Natl. Acad. Sci. U.S.A. 92,* 7297−7301.

(19) Blessing, T., Kursa, M., Holzhauser, R., Kircheis, R., and Wagner, E. (2001) Different strategies for formation of pegylated EGF-conjugated PEI/DNA complexes for targeted gene delivery. *Bioconjugate Chem. 12,* 529−537.

(20) Zhang, Z. Y., and Smith, B. D. (2000) High-generation polycationic dendrimers are unusually effective at disrupting anionic vesicles: membrane bending model. *Bioconjugate Chem. 11,* 805−814.

(21) Qin, L., Pahud, D. R., Ding, Y., Bielinska, A. U., Kukowska-Latallo, J. F., Baker, J. R., Jr., and Bromberg, J. S. (1998) Efficient transfer of genes into murine cardiac grafts by Starburst polyamidoamine dendrimers. *Hum. Gene Ther. 9,* 553−560.

(22) Duguid, J. G., Li, C., Shi, M., Logan, M. J., Alila, H., Rolland, A., Tomlinson, E., Sparrow, J. T., and Smith, L. C. (1998) A physicochemical approach for predicting the effectiveness of peptide-based gene delivery systems for use in plasmid-based gene therapy. *Biophys. J. 74,* 2802−2814.

(23) Golan, R., Pietrasanta, L. I., Hsieh, W., and Hansma, H. G. (1999) DNA toroids: stages in condensation. *Biochemistry 38,* 14069−14076.

(24) Wadhwa, M. S., Collard, W. T., Adami, R. C., McKenzie, D. L., and Rice, K. G. (1997) Peptide-mediated gene delivery: influence of peptide structure on gene expression. *Bioconjugate Chem. 8,* 81−88.

(25) Goula, D., Remy, J. S., Erbacher, P., Wasowicz, M., Levi, G., Abdallah, B., and Demeneix, B. A. (1998) Size, diffusibility and transfection performance of linear PEI/DNA complexes in the mouse central nervous system. *Gene Ther. 5,* 712−717.

(26) Midoux, P., Mendes, C., Legrand, A., Raimond, J., Mayer, R., Monsigny, M., and Roche, A. C. (1993) Specific gene transfer mediated by lactosylated poly-L-lysine into hepatoma cells. *Nucleic Acids Res. 21,* 871−878.

(27) Putnam, D., Gentry, C. A., Pack, D. W., and Langer, R. (2001) Polymer-based gene delivery with low cytotoxicity by a unique balance of side-chain termini. *Proc. Natl. Acad. Sci. U.S.A. 98,* 1200−1205.

(28) Baatz, J. E., Bruno, M. D., Ciraolo, P. J., Glasser, S. W., Stripp, B. R., Smyth, K. L., and Korfhagen, T. R. (1994) Utilization of modified surfactant-associated protein B for delivery of DNA to airway cells in culture. *Proc. Natl. Acad. Sci. U.S.A. 91,* 2547−2551.

(29) Wagner, E., Zenke, M., Cotten, M., Beug, H., and Birnstiel, M. L. (1990) Transferrin-polycation conjugates as carriers for DNA uptake into cells. *Proc. Natl. Acad. Sci. U.S.A. 87,* 3410−3414.

(30) Schaffer, D. V., and Lauffenburger, D. A. (1998) Optimization of cell surface binding enhances efficiency and specificity of molecular conjugate gene delivery. *J. Biol. Chem. 273,* 28004−28009.

(31) Harbottle, R. P., Cooper, R. G., Hart, S. L., Ladhoff, A., McKay, T., Knight, A. M., Wagner, E., Miller, A. D., and Coutelle, C. (1998) An RGD-oligolysine peptide: a prototype construct for integrin-mediated gene delivery [see comments]. *Hum. Gene Ther. 9,* 1037−1047.

(32) Shea, L. D., Smiley, E., Bonadio, J., and Mooney, D. J. (1999) DNA delivery from polymer matrixes for tissue engineering. *Nat. Biotechnol. 17,* 551−554.

(33) Fang, J., Zhu, Y. Y., Smiley, E., Bonadio, J., Rouleau, J. P., Goldstein, S. A., McCauley, L. K., Davidson, B. L., and Roessler, B. J. (1996) Stimulation of new bone formation by direct transfer of osteogenic plasmid genes. *Proc. Natl. Acad. Sci. U.S.A. 93,* 5753−5758.

(34) Bonadio, J., Smiley, E., Patil, P., and Goldstein, S. (1999) Localized, direct plasmid gene delivery in vivo: prolonged therapy results in reproducible tissue regeneration. *Nat. Med. 5,* 753−759.

(35) Luo, D., and Saltzman, W. M. (2000) Enhancement of transfection by physical concentration of DNA at the cell surface. *Nat. Biotechnol. 18,* 893−895.

(36) Gottschalk, S., Cristiano, R. J., Smith, L. C., and Woo, S. L. (1994) Folate receptor mediated DNA delivery into tumor cells: potosomal disruption results in enhanced gene expression. *Gene Ther. 1,* 185−191.

(37) Stewart, A. J., Pichon, C., Meunier, L., Midoux, P., Monsigny, M., and Roche, A. C. (1996) Enhanced biological activity of antisense oligonucleotides complexed with glycosylated poly-L-lysine. *Mol. Pharmacol. 50,* 1487−1494.

(38) Harbottle, R. P., Cooper, R. G., Hart, S. L., Ladhoff, A., McKay, T., Knight, A. M., Wagner, E., Miller, A. D., and Coutelle, C. (1998) An RGD-oligolysine peptide: a prototype construct for integrin-mediated gene delivery. *Hum. Gene Ther. 9*, 1037−1047.

(39) Williams, D. A. (1999) Retroviral-fibronectin interactions in transduction of mammalian cells. *Ann. N.Y. Acad. Sci. 872*, 109−113; discussion 113−104.

(40) Bielinska, A. U., Yen, A., Wu, H. L., Zahos, K. M., Sun, R., Weiner, N. D., Baker, J. R., Jr., and Roessler, B. J. (2000) Application of membrane-based dendrimer/DNA complexes for solid-phase transfection in vitro and in vivo. *Biomaterials 21*, 877−887.

(41) Zheng, J., Manuel, W. S., and Hornsby, P. J. (2000) Transfection of cells mediated by biodegradable polymer materials with surface-bound polyethyleneimine. *Biotechnol. Prog. 16*, 254−257.

(42) Adami, R. C., Collard, W. T., Gupta, S. A., Kwok, K. Y., Bonadio, J., and Rice, K. G. (1998) Stability of peptide-condensed plasmid DNA formulations. *J. Pharm. Sci. 87*, 678−683.

(43) Perelson, A. S., Macken, C. A., Grimm, E. A., Roos, L. S., and Bonavida, B. (1984) Mechanism of cell-mediated cytotoxicity at the single cell level. VIII. Kinetics of lysis of target cells bound by more than one cytotoxic T lymphocyte. *J. Immunol. 132*, 2190−2198.

(44) Lauffenburger, D. A., and Lindermam, J. J. (1993) *Receptors Models for binding, trafficking, and signaling*, Oxford Unversity Press, New York.

(45) Tang, M. X., and Szoka, F. C. (1997) The influence of polymer structure on the interactions of cationic polymers with DNA and morphology of the resulting complexes. *Gene Ther. 4*, 823−832.

(46) Lucas, P., Milroy, D. A., Thomas, B. J., Moss, S. H., and Pouton, C. W. (1999) Pharmaceutical and biological properties of poly(amino acid)/DNA polyplexes. *J. Drug Target. 7*, 143−156.

(47) Ito, Y., Liu, S. Q., and Imanishi, Y. (1991) Enhancement of cell growth on growth factor-immobilized polymer film. *Biomaterials 12*, 449−453.

(48) Kuhl, P. R., and Griffith-Cima, L. G. (1996) Tethered epidermal growth factor as a paradigm for growth factor-induced stimulation from the solid phase. *Nat. Med. 2*, 1022−1027.

BC015575F

Development of a Nonviral Gene Delivery Vehicle for Systemic Application

Suzie Hwang Pun[†,‡] and Mark E. Davis*[,†]

Chemical Engineering, California Institute of Technology, Pasadena, California 91125 and Insert Therapeutics Inc., 2585 Nina Street, Pasadena, California 91107. Received November 2, 2001; Revised Manuscript Received January 30, 2002

Polycation vehicles used for in vitro gene delivery require alteration for successful application in vivo. Modification of polycations by direct grafting of additional components, e.g., poly(ethylene glycol) (PEG), either before or after DNA complexation, tend to interfere with polymer/DNA binding interactions; this is a particular problem for short polycations such as linear, β-cyclodextrin-containing polycations (βCDPs). Here, a new method of βCDP polyplex (polycation/DNA composite structures) modification is presented that exploits the ability to form inclusion complexes between cyclodextrins and adamantane. Surface-PEGylated βCDP polyplexes are formed by self-assembly of the polyplexes with adamantane−PEG conjugates. While unmodified polyplexes rapidly aggregate and precipitate in salt solutions, the PEGylated βCDP polyplexes are stable at conditions of physiological salt concentration. Addition of targeting ligands to the adamantane−PEG conjugates allows for receptor-mediated delivery; galactosylated βCDP-based particles reveal selective targeting to hepatocytes via the asialoglycoprotein receptor. Galactosylated particles transfect hepatoma cells with 10-fold higher efficiency than glucosylated particles (control), but show no preferential transfection in a cell line lacking the asialoglycoprotein receptor. Thus, surface modification of βCDP-based polyplexes through the use of cyclodextrin/adamantane host/guest interactions endows the particles with properties appropriate for systemic application.

Cationic polymers are routinely used as transfection reagents for DNA delivery to cultured cells (*1*−*3*). These polycations self-assemble with and condense DNA into small particles termed polyplexes (*4*). When formulated with a net positive charge, polyplexes bind to cell surfaces and are internalized (*5*). Despite laboratory success with polyplexes, cationic polymers are often highly toxic and therefore currently not used in human trials for gene delivery. In addition, polyplex formulations optimized for in vitro delivery are typically not amenable for in vivo use because successful systemic delivery requires very different particle characteristics. After intravenous injection, cationic polyplexes interact with serum proteins and are quickly eliminated from the bloodstream by phagocytic cells (*6*, *7*). Additionally, these polyplexes rapidly aggregate at physiological ionic strengths (150 mM salt concentration). Finally, gene delivery vehicles should ideally target specific cells in the body while cationic polyplexes tend to be primarily taken up by liver Kupffer cells (*8*, *9*). Therefore, cationic polyplexes require modification before they can be successfully applied for systemic gene delivery.

One method of preventing polyplex self-aggregation and undesired interactions with non-self-entities employs steric stabilization of polyplexes with hydrophilic polymers. Poly(ethylene glycol) (PEG) has been conjugated to different nonviral gene carriers, and the resulting PEGylated particles have demonstrated increased salt and serum stability (*10*−*14*). PEG can be grafted onto the reactive primary amine functional groups of cationic polymers. This method has been used for PEGylating polyethylenimine (PEI) and poly(L)lysine (PLL) in order to impart steric stabilization to the particles thus formed (*11*, *15*). In doing so, the charge density of the polymers is reduced. Therefore, this method is often ineffective for short polymers that have lower DNA binding constants, i.e., the polymer−DNA condensation interactions are disrupted (*16*, *17*). An alternative PEGylation approach requires complexation of the cationic polymer with DNA followed by reaction of surface-available amines with activated PEG (*14*). While postcomplexation PEG grafting successfully stabilizes PEI-based polyplexes, PEGylation of low molecular weight polymers by this method may result in disruption of polyplex structure.

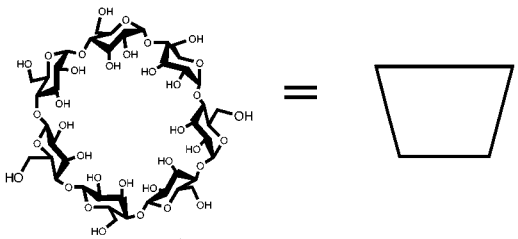
Stabilized particles may be directed to the desired organ or cells of interest by the attachment of a ligand for receptor-mediated targeting. For example, conjugation of galactose or other ligands for the asialoglycoprotein receptor can result in targeting to hepatocytes (*6*, *18*−*20*).

A family of β-cyclodextrin-containing polymers (βCDPs) suitable for DNA delivery has been described (*21*, *22*). These polymers contain β-cyclodextrins (cyclic oligomers of glucose) in the polymer backbone and are cationic due to repeating amidine groups. βCDP-based polyplexes show low in vitro (IC_{50} = 1.1 mM) and in vivo (LD_{40} = 200 mg/kg of polymer alone in mice) toxicity and are therefore promising in vivo agents. These polyplexes are subject to the same aggregation and nonspecific interactions noted above for other polyplexes. The goal of our work is to develop a method of modifying βCDP-based polyplexes for in vivo use that mitigates nondesirable

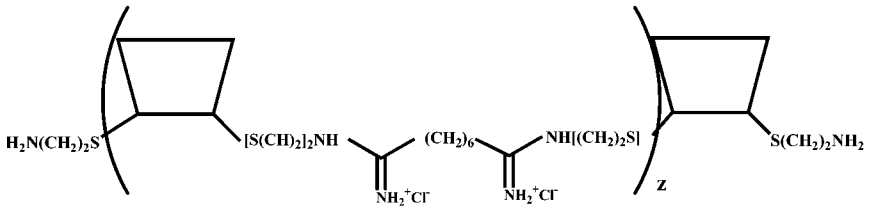
* To whom correspondence should be addressed. E-mail: mdavis@cheme.caltech.edu.
† California Institute of Technology.
‡ Insert Therapeutics Inc.

10.1021/bc0155768 CCC: $22.00 © 2002 American Chemical Society
Published on Web 04/20/2002

Chart 1

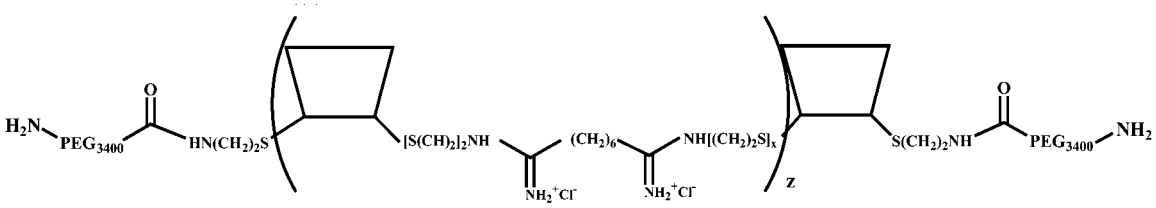


β-Cyclodextrin



βCDP6

Chart 2



βCDP6-PEG$_{3400}$

interactions that would be encountered after i.v. administration.

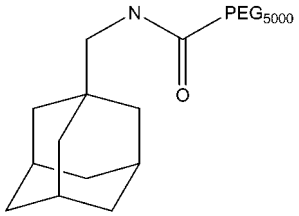
Cyclodextrins have the capability of forming inclusion compounds with hydrophobic moieties. With some molecules, this association can be quite strong. For example, adamantane derivatives have *β*-cyclodextrin association constants (K_a) on the order of 10^4-10^5 (*23*). Complexes between adamantane end-capped poly(ethylene oxide) and cyclodextrin copolymers have also been described (*24*, *25*). Here, we exploit cyclodextrin/guest compound complexation to develop a new method for modifying *β*CDP-based polyplexes. Adamantane is conjugated to a desired polyplex modifier such as PEG, and the resulting compounds are exposed to *β*CDP-based polyplexes for self-assembly between adamantanes and cyclodextrins. This method is applied to *β*CDP-based polyplexes to provide particles that are stable in salt solutions and to formulate galactose-modified particles that demonstrate targeted delivery to hepatoma cells.

EXPERIMENTAL PROCEDURES

Polycation Synthesis. *βCDP6.* *β*CDP6 (6 denotes the number of methylene groups separating the charges) was synthesized according to previously described procedures and is shown in Chart 1 (*21*, *22*). The average molecular weight of the polycation corresponds to a "z" of approximately 4 (*21*, *22*).

βCDP6−PEG$_{3400}$. *β*CDP6 (20.3 mg, 3 *μ*mol) and FMOC−PEG$_{3400}$−NHS (10 equiv, 190 mg, 60 *μ*mol, Shearwater Polymers) were added to a glass vial equipped with a magnetic stirbar and dissolved in 1 mL of 50 mM $NaHCO_3$, pH 8.5. The solution was stirred in the dark at room temperature for 20 h and then lyophilized. The solid was dissolved in 0.5 mL of 20% piperidine in DMF and stirred for 30 min for FMOC deprotection. The solvent was removed in vacuo and the remaining viscous liquid dissolved in water and the pH brought below 6.0 with 0.1 M HCl. Complete PEG coupling and FMOC deprotection was verified by TNBS amine quantification (*26*). The polymer was separated from unreacted PEG by anion-exchange chromatography and lyophilized to yield a white fluffy powder (Chart 2).

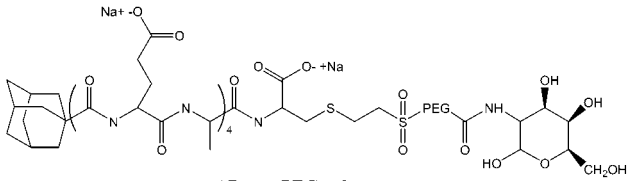
Synthesis of Adamantane Conjugates. *Adamantane−PEG$_{5000}$* (*AD−PEG$_{5000}$*). PEG$_{5000}$−SPA (674 mg, 135 *μ*mol, Shearwater Polymers) was added to a glass vial equipped with a magnetic stirbar. 1-Adamantanemethylamine (5 equiv, 675 *μ*mol, Aldrich) dissolved in 10 mL of dichloromethane was then added and the solution stirred overnight at room temperature. The solvent was removed in vacuo, and water was added to the remaining solution. The solution was centrifuged at 20K rcf for 10 min, whereupon the adamantanemethylamine phase separated as a denser liquid. The aqueous portion was collected and dialyzed for 24 h (Slide-A-Lyzer, MWCO = 3500) against water. The solution was lyophilized to yield 530 mg of a white, fluffy powder (75% yield, structure of product shown below). The product was analyzed on a Beckman Gold HPLC system equipped with a Richards Scientific ELS detector and a C18 column and found to be pure (retention time of PEG$_{5000}$−NHS: 10.7 min; retention time of product: 12.0 min; acetonitrile/water gradient). AD−PEG$_{3400}$ was synthesized using a similar protocol (56% yield; product confirmed by Maldi-TOF analysis).



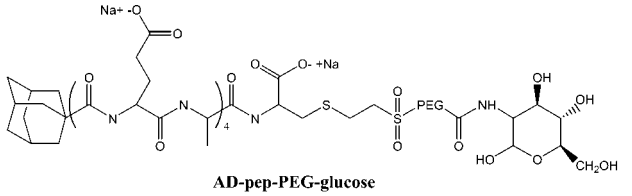
Adamantane-PEG_{5000}

Adamantane−Anionic Peptide−PEG_{3400}−Galactose/Glucose (*AD−pep−PEG−gal/glc*). An anionic peptide (sequence: E-A-E-A-E-A-E-A-C) was synthesized by the Biopolymer Synthesis Facility (Beckman Institute, California Institute of Technology) using an automatic synthesizer. Before cleaving the peptide from the resin, adamantanecarboxylic acid (ACA, Aldrich) was conjugated to the N-terminal end of the peptide with DCC coupling chemistry. The resulting peptide (AD-E-A-E-A-E-A-E-A-C, MW 1084) was cleaved from the resin and analyzed by Maldi-TOF.

Galactose− and glucose−PEG_{3400}−vinyl sulfone (gal/glc-PEG_{3400}−VS) were prepared with approximately 95% yield by reacting NHS− PEG_{3400}−VS (Shearwater Polymers) with 20 equiv of glucosamine or galactosamine (Sigma) in phosphate-buffered saline, pH 7.2, for 2 h at room temperature. The solution was dialyzed extensively against water and then lyophilized. The thiols of the anionic peptide (2 equiv) were reacted with galactose−PEG_{3400}−VS or glucose−PEG_{3400}−VS in 50 mM sodium borate buffer (pH 9.5) containing 10 mM TCEP. The solution was acidified, and the precipitated peptide (insoluble below pH 9.0) was removed by centrifugation. The supernatant was collected, dialyzed extensively, and lyophilized. The desired products were confirmed by Maldi-TOF analysis (schematic shown below).



AD-pep-PEG-galactose



AD-pep-PEG-glucose

Polyplex Preparation and Characterization. *Plasmids.* Plasmid pGL3-CV (Promega, Madison, WI), containing the luciferase gene under the control of the SV40 promoter, was amplified by *Esherichia coli* and purified using Qiagen's Endotoxin-free Megaprep kit (Valencia, CA).

Physicochemical Characterization. pGL3-CV (2 μg) in 600 μL of dH_2O was mixed with an equal volume of βCDP6 (in dH_2O) at a charge ratio of 5+/−. Particle size and zeta potential were measured using a ZetaPals dynamic light scattering detector (DLS, Brookhaven Instruments Corporation, Holtsville, NY).

Post-DNA-Complexation PEGylation by Grafting. The procedure used was modified from Ogris et al. (*14*). pGL3-CV (5 μg) in 500 μL of dH_2O was mixed with an equal volume of PEI (in dH_2O) at 3+/− or 6+/− (stage 1). βCDP6 complexes were prepared in the same manner at a charge ratio of 5+/−. The polyplex diameters were measured by DLS. After complex formation, 10 mg/mL of PEG_{5000}−SPA in DMF (Shearwater Polymers) was added to the solution and mixed at room temperature for 2 h (stage 2). After particle size determination, 500 μL of PBS, pH 7.2, were added to the solution. The solution was incubated for 30 min at room temperature before final particle sizes were measured by DLS (stage 3). A schematic of this procedure is illustrated in Scheme 1.

Post-DNA-Complexation PEGylation by Inclusion Compound Formation. pGL3-CV (2 μg) in 600 μL of dH_2O was mixed with an equal volume of βCDP6 (in dH_2O) at a charge ratio of 5+/−. The desired amount of AD−PEG (10 mg/mL in dH_2O) was added and particle size determined by DLS. PBS (600 μL), pH 7.2, was added to the solution and particle size monitored in 1 min intervals for 10 min. For serum stability determination, polyplexes (0.05 mg/mL DNA, CDP at 3+/−) and polyplexes PEGylated by inclusion compound formation (CDP at 3+/−, 100% adamantane to cyclodextrin by mol %) containing 5 μg of plasmid DNA were prepared by adding equal volumes of polymer solutions (50 μL) to DNA solutions. An aliquot of MEM media containing 10% fetal bovine serum (900 μL) was added to the polyplex solutions and allowed to incubate for 5 min before centrifuging at 14000 rpm for 100 min. Media was then removed, and the remaining pellet was washed with water and then resuspended in 1 mL of dH_2O. The amount of DNA in the pellet was quantified by UV adsorbance at 260 nm.

Formulation of Glycosylated Particles. Cyclodextrin-based polyplexes were prepared as described previously (*22*) at 5+/−. Adamantane-conjugated modifier was dissolved in dH_2O at the desired concentrations and added to the polyplexes at 5 μL of AD−pep−PEG−sugar/μg DNA. For physicochemical characterization, glycosylated particles containing 2 μg of pGL3-CV plasmid were prepared as described and diluted with the addition of 1.2 mL of dH_2O. Particle size and zeta potential of the modified polyplexes were determined by DLS.

Transmission Electron Microscopy. Polyplexes, PEGylated polyplexes, and glycosylated polyplexes were prepared as described in the previous sections in 10 μL final volume. For salt stability studies, 5 μL of PBS was added to the solutions and used 10 min after salt addition. Grids were prepared and visualized as described previously (*21*).

Cell Culture and Transfection Experiments. *Cells.* HepG2 (hepatoma) and HeLa (cervical carcinoma) cells were purchased from the ATCC, and HuH-7 cells (hepatoma) were purchased from the Japan Health Sciences Foundation. Cells were cultured according to recommended procedures. Media and supplements were purchased from Gibco BRL (Gaithersburg, MD).

Transfections. HepG2, HeLa, and HuH-7 cells were transfected in the presence of serum with modified and unmodified βCDP6-based particles containing the pGL3-CV plasmid as described previously for other adherent cell lines (*22*). Determination of cell viability and total protein concentration was conducted by Lowry protein assay, also described previously (*22*). For inhibition studies, transfections were conducted following a similar protocol except cells were preincubated for 15 min at 4 °C with 1 mg/mL asialofetuin (Sigma), after which polyplexes were added directly to the AF-containing media. Transfection media was removed after 1 h and replaced with 1 mL complete media/well.

Scheme 1

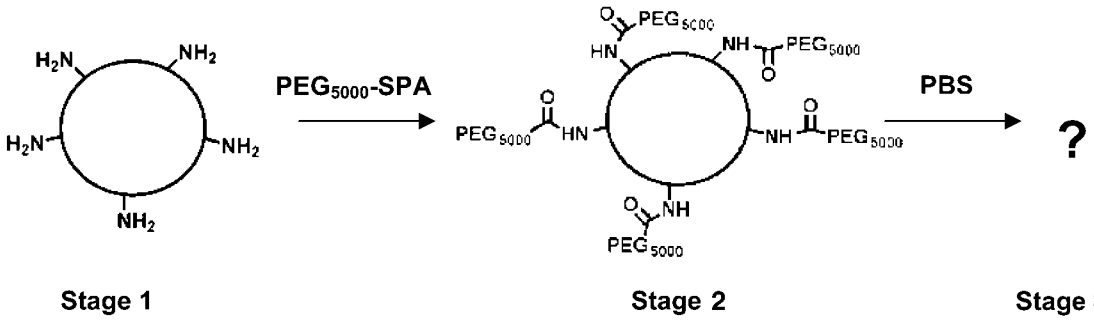


Table 1. Particle Sizes of PEI and βCDP6 Polyplexes during Post-DNA-Complexation Pegylation by Grafting[a,b]

polyplex	PEG	stage 1 (nm)	stage 2 (nm)	stage 3 (nm)
PEI 3+/−	10:1	58	65	115
PEI 6+/−	10:1	55	60	78
βCDP6 5+/−	100%	70	67.4	303
βCDP6 5+/−	150%	70	X*	N/A
βCDP6 5+/−	200%	70	X*	N/A
βCDP6 5+/−	100% PEG**	67	81	700

[a] For stage 1, 5 μg of DNA plasmid (in 500 μL of dH_2O) was mixed with PEI or βCDP6 (in 500 μL of dH_2O) at the indicated ratios. PEG_{5000}−SPA (10 mg/mL in DMF) was then added to the polyplexes in stage 2. The PEG_{5000}−SPA was allowed to react with the polymer primary amines. After 2 h, 500 μL of PBS, pH 7.2, was added to solution. The solution was incubated for 30 min before particle size measurement. All particle sizes were determined by dynamic light scattering and reported as the mean of three measurements. [b] *Poor correlation function; no size measurements possible. **PEG_{10000} added instead of PEG_{5000}−SPA.

RESULTS

Salt Stabilization by PEGylation. The following PEGylation approaches to the βCDP6 polycation were examined: pre-DNA-complexation PEGylation, post-DNA-complexation PEGylation by grafting, and post-DNA-complexation PEGylation by inclusion compound formation. The results from each method are provided below.

Pre-DNA-Complexation PEGylation. PEG_{3400}−NHS was coupled to the βCDP6 amine end groups to give the polymer CDP6−PEG_{3400}. The PEGylated polymer was mixed with plasmid DNA for particle size measurements. While βCDP6 condenses plasmid DNA to uniform particles with hydrodynamic diameter, ∼130 nm, PEGylated βCDP6 is unable to condense DNA.

Post-DNA-Complexation PEGylation by Grafting. Ogris et al. PEGylated transferrin/PEI (polyethylenimine) and PEI after complexation with plasmid DNA by reacting some of the primary amino groups of PEI with PEG_{5000}−SPA (*14*). PEI polyplexes were formulated at 3+/− and 6+/− while the βCDP6 polyplexes were formulated at 5+/− for stage 1. PEG_{5000}−SPA was added to PEI at 10:1 w/w according to the procedure published by Ogris et al. (*14*). βCDP6 was PEGylated with 100%, 150%, and 200% PEG:amine (mol %). As a control, PEG_{10000} (terminated with hydroxyl groups) was also added to βCDP6 at 100%. The particle diameters obtained at each stage are presented in Table 1. The PEI polyplexes increased slightly in size upon PEGylation (58 nm to 65 nm for 3+/− and 55 nm to 60 nm for 6+/−). PEGylation protected the PEI polyplexes against salt-induced aggregation. Although unmodified PEI particles increase in diameter to ∼800 nm after salt addition, PEGylated PEI polyplexes increased slightly in size to 78 nm (for 6+/−) and 115 nm (for 3+/−).

The particle size of CDP-based polyplexes was maintained at 67 nm after PEGylation with 100% PEG_{5000}−SPA. However, the monitoring of particle size as a function of time revealed that the particles were disrupted for approximately 30 s after PEG addition. The small particles were again observed after that time. Therefore, the addition of 100% PEG_{5000}−SPA may PEGylate a fraction of the βCDP6. Because the polycation is added in excess with respect to the DNA (at a 5+/−), the particles could then rearrange such that the unmodified polycations form polyplexes with the plasmid DNA while most of the PEGylated polycation remains free in solution. Salt addition to these particles results in particle aggregation (300 nm), although not to the extent of unmodified βCDP6 polyplexes (700 nm). The addition of 150% and 200% PEG_{5000}−SPA to βCDP6-based polyplexes results in particle disruption; particle counts drop drastically and no consistent correlation function was observed.

Post-DNA-Complexation PEGylation by Inclusion Compound Formation. The approach to post-complexation PEGylation developed here is to use the ability of cyclodextrins to form inclusion complexes with guest molecules, and the method is schematically illustrated in Figure 1A. Adamantane was conjugated to various PEG molecules. The adamantane−PEG (AD−PEG) molecules were added to solutions of preformed polyplexes at 100% adamantane to cyclodextrin (mol %). A schematic of this self-assembly process for post-DNA-complexation PEGylation by inclusion compound formation is depicted in Figure 1B. PBS was then added to the solutions and the particle size monitored by DLS in 1 min intervals (Figure 2A). The average diameter of βCDP6 polyplexes increases from 58 to 272 nm within 10 min after salt addition. The presence of free PEG_{5000} in solution does not prevent aggregation (average diameter of 278 nm after salt addition). However, PEGylation with AD−PEG molecules reduces particle aggregation in a length dependent matter. Ten minutes after salt addition, particles PEGylated with AD−PEG_{3400} aggregate to 204 nm in diameter while particles PEGylated with AD−PEG_{5000} only increased in diameter to 95 nm 10 min after salt addition. Additionally, the particles PEGylated with AD−PEG_{5000} demonstrate sustained stability in physiological salt concentration (150 mM). The stabilization also occurs in a PEG density-dependent manner (Figure 2B). The average particle diameter measured 10 min after salt addition increases by 4.7-fold for unmodified polyplexes (58 nm to 272 nm) but only 1.2-fold for polyplexes modified with the addition of 150% or 200% PEG−adamantane to cyclodextrin.

The stabilization in salt by PEGylation of βCDP6 polyplexes via inclusion compound formation was verified by transmission electron microscopy. βCDP6-based polyplexes formulated in water appear as discrete, uniform

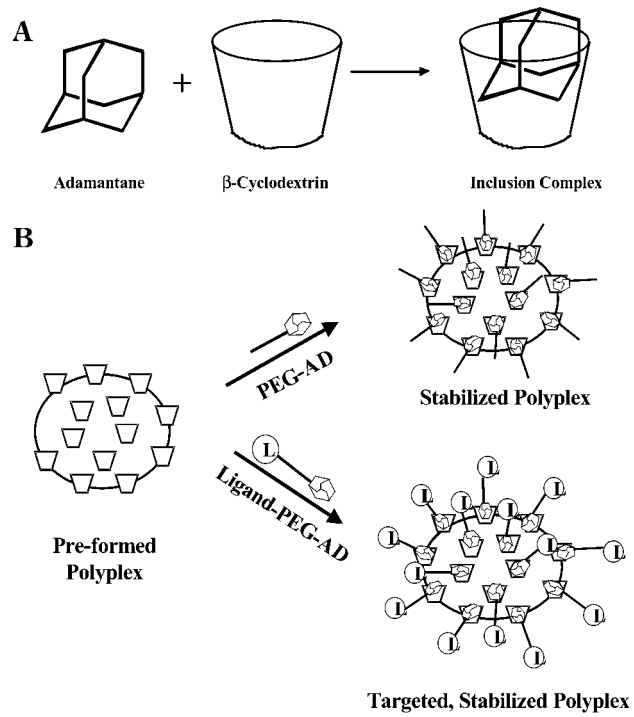


Figure 1. (A). Schematic of inclusion compound formation. (B). Schematic for post-DNA-complexation PEGylation by inclusion compound formation by PEG−AD and ligand−PEG−AD. PEG is conjugated to adamantane. Adamantane forms an inclusion complex with β-cyclodextrin on the polyplex surface and brings with it PEG or PEG−L to decorate the polyplex and provide steric stabilization and targeting.

particles with diameters around 100 nm (Figure 3A). PEGylated βCDP6-based polyplexes (100% PEG:CD by mole) formulated in water are also uniform particles with diameters around 100 nm (Figure 3B). An aliquot of PBS (150 mM salt concentration) was then added to the polyplexes to give a final salt concentration of 50 mM. After 10 min, the solutions were loaded onto a grid and visualized by electron microscopy. Unmodified polyplexes in 50 mM salt aggregated; no discrete particles were observed (Figure 3C). Electron micrographs similar to Figure 3C have been observed previously by Goula et al. for PEI-based polyplexes (*27*). To the contrary, βCDP6-based polyplexes modified with AD−PEG_{5000} were resistant to salt-induced aggregation. Electron microscopy revealed discrete particles (~110 nm in diameter, Figure 3D). Thus, successful stabilization of βCDP6-based polyplexes by AD−PEG_{5000} modification is demonstrated by both DLS measurements and electron microscopy.

The PEGylated polyplexes are also stable in culture media containing 10% serum. Unmodified and PEGylated polyplexes were exposed to serum-containing media for 10 min and then centrifuged to pellet aggregated complexes. The pellets were resuspended in water and the amount of DNA in the pellet was quantified by UV adsorption. All of the DNA from the unmodified polyplexes were recovered in the pellets, indicating that the polyplexes aggregate rapidly in the presence of physiological salt and serum. In addition, proteins were precipitated with the unmodified polyplexes (on average 6 μg protein/μg DNA). However, only ~18% of the DNA from PEGylated polyplexes was recovered in the pellets, demonstrating increased stabilization in the presence of serum.

Galactose-Mediated Delivery to Hepatocytes. *Preparation and Characterization of Galactose and Glucose-Modified Polyplexes.* βCDP6-based polyplexes require formulation at a net positive charge for complete condensation of DNA (*21*). However, these positively charged polyplexes indiscriminately transfect cultured cells. To differentiate between charge-mediated transfection and receptor-mediated transfection, the polyplexes should ideally possess neutral or negative zeta potentials and contain a targeting ligand directed at the receptor of interest. Adamantane−anionic peptide−PEG_{3400}−galactose (AD−pep−PEG−gal) was prepared for βCDP6 polyplex modification. The adamantane serves as the guest for forming inclusion complexes with the βCDP6-based polyplexes, the anionic peptide increases the binding affinity of the AD−pep−PEG−gal compound for the cationic polyplex while also decreasing the zeta potential of the polyplex to eliminate charge-mediated entry, and the PEG provides steric stabilization and serves as a spacer between the polyplex and the galactose molecules that act as the targeting ligands to hepatocytes. A glucose analogue (AD−pep−PEG−glc) was prepared as a control.

The zeta potentials of βCDP6 polyplexes (prepared at 5+/−) modified with various amounts of AD−pep−PEG−gal/glc were determined and are shown in Figure 4A. Unmodified polyplexes are positively charged, with zeta potential around +10 mV. The addition of the glycosylated adamantane compounds to the complexes decreases the zeta potential of the particles. The alteration of charge plateaus at around 50% AD−pep−PEG−gal/glc (% PEG to CD by mole) with zeta potential approximately −7 mV. Little differences between the zeta potentials of the galactose and glucose-modified polyplexes are observed. The size of the two types of particles is also very similar. Electron micrographs of the galactosylated particles (50% galactose:CD by mole) show particles with average diameters around 100 nm (Figure 4B), while measurements by DLS reveal particles with diameters around 120 nm (data not shown). Although these particles are negatively charged, the particles look similar to the unmodified polyplexes (Figure 3A), demonstrating that modification by inclusion compound formation does not significantly affect polyplex morphology.

Galactosylated and glucosylated βCDP6 particles containing the luciferase gene were prepared at 0, 20, 40, 60, 80, and 100% PEG and exposed to HepG2 (hepatoma) cells (Figure 5A). Unmodified polyplexes yielded the highest transfection (2×10^8 RLU/mg protein). At 20% PEG, the galactosylated and glucosylated particles have reduced but positive zeta potentials and gave similar transfection efficiencies. At 40% PEG, the particles are anionic (~−5 mV) and the transgene activity from glucosylated polyplexes is reduced by 2 orders of magnitude from that of the polyplex alone, while activity from galactosylated polyplexes is reduced by 1 order of magnitude. As the PEG concentration increases to 100%, the luciferase activity of glucosylated polyplexes continues to decrease; however, activity of galactosylated polyplexes remains 1 order of magnitude higher than the glucosylated polyplexes. Another hepatoma cell line, HuH-7, was transfected with the modified polyplexes and the same trend is observed. The glycosylated polyplexes transfect HuH-7 cells with the same efficiency when formulated at net positive charges. However, when formulated at net negative charges, galactosylated polyplexes consistently transfect with higher efficiencies, with up to 15-fold higher luciferase activity (at 50% PEG). HeLa cells that do not express the asialogylcoprotein receptor were transfected with the modified polyplexes. No preferential transfection of galactosylated polyplexes to HeLa cells was observed (Figure 5B).

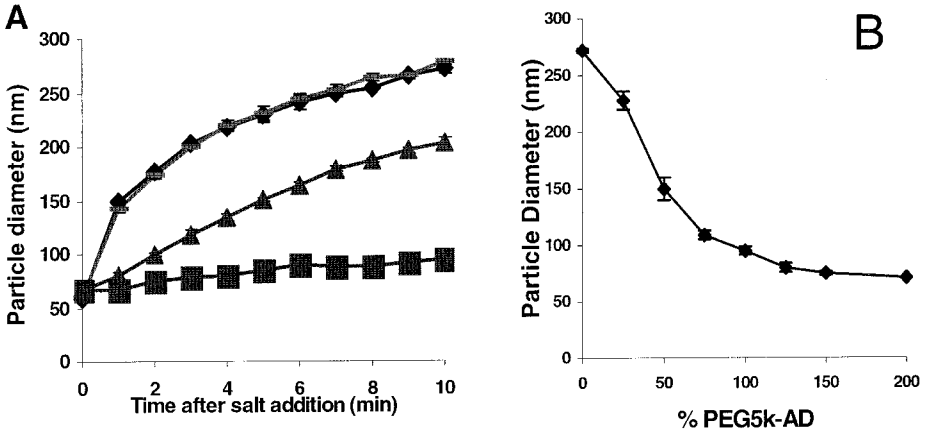


Figure 2. Salt stabilization of polyplexes by PEGylation. Plasmid DNA was mixed with βCDP6 at 5+/−, and then PEG compounds were added to the complexes for a total volume of 1.2 mL. PBS (600 μL) was added to the solutions, and the particle sizes were monitored by dynamic light scattering. (A) The effect of PEG length on salt stabilization. Polyplexes were mixed with various PEG compounds. Particle sizes were monitored by dynamic light scattering for 10 min after salt addition. (♦: polyplex, —: polyplex + PEG_{5000}, ▲: polyplex + AD−PEG_{3400}, ■: polyplex + AD−PEG_{5000}). (B). The effect of AD−PEG_{5000} concentration of salt stabilization. Various amounts of AD−PEG_{5000} were added to polyplexes before exposure to 50 mM PBS. Particle sizes were measured 10 min after salt addition.

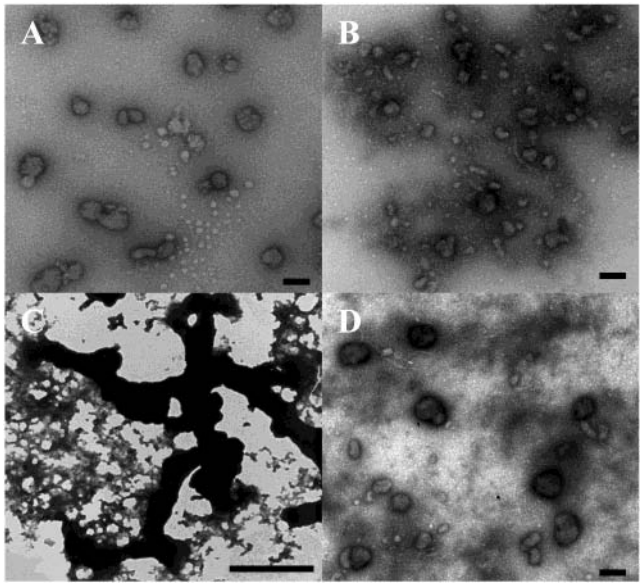


Figure 3. Transmission electron micrographs of (A) unmodified βCDP6 polyplexes, (B) βCDP6 polyplexes PEGylated by AD−PEG_{5000} modification, (C) unmodified βCDP6 polyplexes in 50 mM salt, and (D) PEGylated βCDP6 polyplexes in 50 mM salt. (Bar is 100 nm for A, B, D and 1000 nm for C).

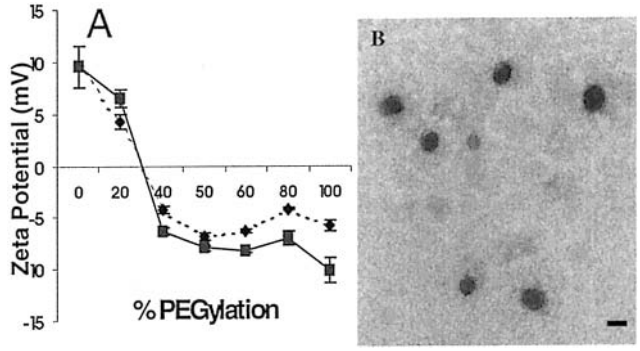


Figure 4. (A). Zeta potential of glycosylated polyplexes. Polyplexes were prepared at 5+/− in water and modified with various amounts of AD−pep−PEG−gal or AD−pep−PEG−glc (100% PEG = 1 mol PEG/1 mol CD). Polyplexes were diluted in water to 2 μg DNA/1.2 mL dH_2O and zeta potential determined by DLS measurements. (Solid line, galactosylated polyplexes; dashed line, glucosylated polyplexes.) (B). Transmission electron micrograph of galactosylated particles modified with 50% AD−pep−PEG−gal (bar is 100 nm).

To verify cell entry via the asialoglycoprotein receptor, transfections were performed in the presence of an excess of asialofetuin, a high affinity ligand for the asialoglycoprotein receptor (Figure 6). Asialofetuin did not affect polyplex or glucosylated polyplex transfection but decreased transfection with galactosylated polyplexes by 4-fold.

The toxicities of the βCDP polyplexes and modified particles were measured by determining total cellular protein 48 h after transfection. βCDP-based polyplexes have been shown to be well-tolerated to high doses both in vitro and in vivo (*21*, *22*). The adamantane-based compounds do not impart significant added toxicity to the βCDP particles (93% cell survival with galactosylated polyplexes vs 96% survival with unmodified polyplexes).

DISCUSSION

This work describes the development of a new method for modifying the surface properties of βCDP-based polyplexes that will now allow for their study as systemic, in vivo, gene delivery agents. Two features necessary for a successful systemic carrier are stability at physiological conditions and selective delivery to sites of interest (*28*). These issues are addressed here by PEGylation of the βCDP-based polyplexes and by the attachment of a galactose ligand for delivery to hepatocytes.

PEGylation has been shown to stabilize colloidal particles (*28*). Three different approaches to βCDP-based polyplex PEGylation were assessed: pre-DNA-complexation PEGylation, post-DNA-complexation PEGylation by grafting, and post-DNA-complexation PEGylation by inclusion compound formation. PEG was covalently conjugated to the amine termini of βCDP6. While βCDP6 self-assembles with and condenses DNA to small particles (*21*, *22*), the presence of PEG_{3400} at the polymer termini inhibits DNA condensation. Choi et al. report successful albeit reduced DNA binding with PEGylated PLL (*11*). However, they used PLL with MW 25000, that contains on average 170 amines/polymer strand. The long polycation provides for strong DNA binding. The βCDP6 possesses approximately 10 charges/polymer strand, and PEGylation doubles the molecular weight. Therefore, it

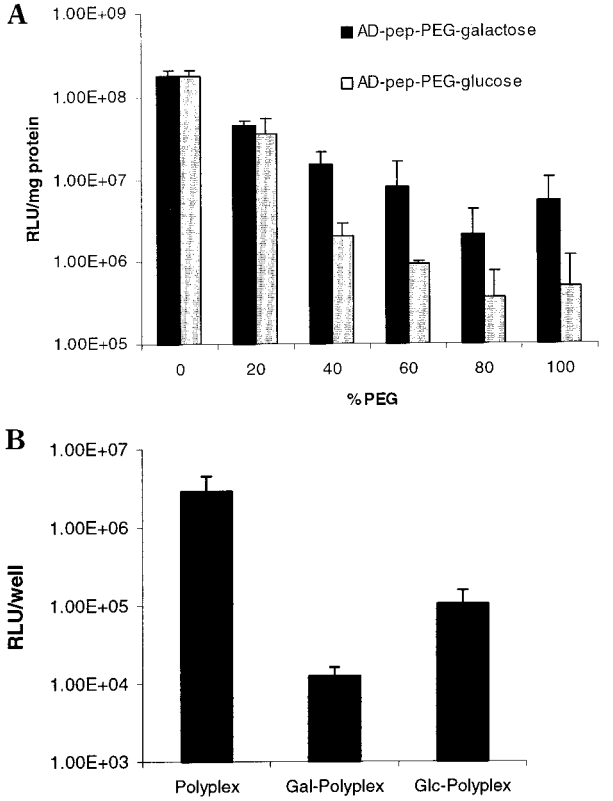


Figure 5. A. Galactose- and glucose-mediated transfection of HepG2 hepatoma cells. Cells were transfected with 1 μg of luciferase gene-containing plasmid complexed with βCDP6 at 5+/− and modified with various amounts of AD−pep−PEG−galactose or AD−pep−PEG−glucose (100% PEG = 1 mol PEG/1 mol CD). Luciferase protein activity is reported as the mean +/− SD of three samples in RLU/mg of total protein (protein concentration determined by Lowry protein assay). Black bars, galactosylated polyplexes; hatched bars, glucosylated polyplexes. DNA alone = 1,000 RLU/mg protein. B. Galactose- and glucose-mediated transfection of HeLa cells that do not express the asialoglycoprotein receptor. Cells were transfected with 1 μg of luciferase gene-containing plasmid complexed with βCDP6 at 5+/− and modified with various amounts of AD−pep−PEG−galactose (Gal-Polyplex) or AD−pep−PEG−glucose (Glc−Polyplex, 100% PEG = 1 mol PEG/1 mol CD). Luciferase protein activity is reported as the mean ± SD of three samples in RLU/mg of total protein (protein concentration determined by Lowry protein assay).

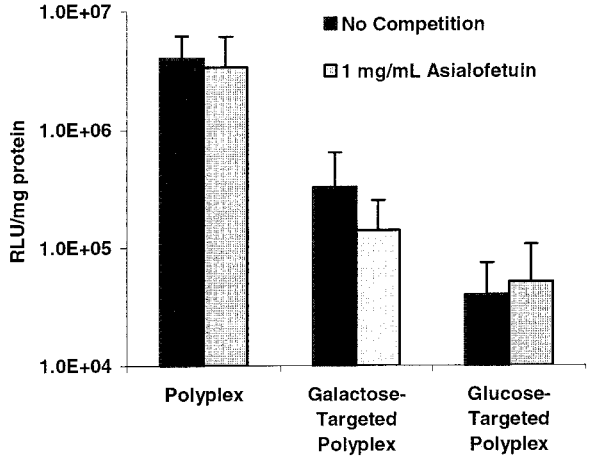


Figure 6. HepG2 cells were transfected with polyplexes (unmodified or modified with 50% AD−pep−PEG−galactose/glucose) prepared at 5+/−. Luciferase protein activity was determined 48 h after transfection and reported as RLU/mg total protein (total protein determined by Lowry assay). Data are presented as mean ± SD of three samples. Competitive inhibition of galactose-mediated delivery. HepG2 cells were transfected in the presence (hatched bars) and absence (black bars) of asialofetuin (amounts larger than 1 mg/mL significantly altered cell proliferation behavior and therefore were not used).

is not surprising that PEGylation of the βCDPs eliminates its ability to condense to plasmid DNA.

Post-complexation PEGylation as described by Ogris et al. (*14*) and Oupicky et al. (*29*) first requires the formation of the polyplex followed by PEGylation of the particles. This method involves the conjugation of surface-available, primary amines and thus reduces polyplex instability that can result from the interference in the DNA condensation process when using PEG−grafted polycations. This approach is effective for polymers such as PEI and HPMA but results in particle disruption for βCDP6-based polyplexes (Table 1). Thus, post-DNA-complexation PEGylation by reaction with accessible polymer functional groups is likely to be effective for high molecular weight polymers with high charge densities. However, reaction with low molecular weight βCDP6 destabilizes the polyplex structure.

The approach to surface modification developed here involves the use of PEG conjugated to moieties that are in turn exploited as anchors to the polyplex surface by inclusion compound formation in cyclodextrins (Figure 1). We hypothesized that use of the cyclodextrin cups for the site of modification would cause minimum disturbance to preformed polyplexes. This is because the βCDPs bind to DNA via electrostatic interactions of the cationic amidine groups on the βCDP and the anionic phosphate groups on the DNA. The cyclodextrin cups should therefore be available on the polyplex surface for complexation. Adamantane−PEG conjugates were added to βCDP6-based polyplexes, and the resulting particles remained small and disperse with only slightly increased diameters (Figures 2 and 3A). PEGylation introduced salt stability to the polyplexes in a PEG length and PEG density-dependent manner (Figure 2).

The salt stability of PEGylated βCDP6-based polyplexes was confirmed by electron microscopy. While unmodified polyplexes form large aggregates in 50 mM salt, PEGylated βCDP6-polyplexes remain discrete and condensed (Figure 3A−D). In addition, PEGylated βCDP6-based polyplexes have increased stability in the presence of serum. Other investigators have reported interference of polymer/DNA condensation by PEGylation. For example, PEGylation of PEI (MW 2000) results in thick thread and donut morphologies rather than densely compacted structures (*16*) and PEGylation of PLL (MW 4000) altered polyplex structure from toroids to rods (*12*). Here, it is shown that PEGylation by inclusion compound formation stabilizes βCDP6-based polyplexes without disrupting the polyplex structure.

The PEGylated particles maintained small sizes in the presence of 150 mM salt for hours. The adamantane is integral to forming protected polyplexes; the addition of free PEG_{5000} has no effect on salt stabilization. The addition of adamantane (in DMSO) eliminates the salt stability of the modified polyplexes by displacing the AD−PEG from the polyplexes. Thus, it is clear that the adamantane in the AD−PEG_{5000} forms an inclusion complex with the β-cyclodextrins on the surface of the polyplexes.

PEGylation of polyplexes alleviates salt-induced aggregation by providing a steric layer around the particles. The steric layer prevents close contact between particles by keeping the van der Waals attraction forces, that are dependent on the interparticle distance, lower than the

thermal energy of the particles. Therefore, there should be a critical polymer length greater than the range of van der Waals attraction between particles that results in polymer stabilization. For many colloidal systems, the necessary distance is ~5 nm (*30*). The lengths of PEG_{3400} and PEG_{5000} are estimated to be 3.5 and 4.3 nm, respectively (*30*). PEG_{5000} is long enough to stabilize βCDP6 polyplexes in salt while PEG_{3400} does not provide enough steric stabilization under the experimental conditions. Interestingly, Gref et al., working with PEG-coated poly(lactic acid) (PLA) nanoparticles of 160−270 in diameter, also found 5000 to be the minimum PEG molecular weight necessary for significant reductions in the plasma protein binding to the nanoparticles (*31*).

The association between the AD−PEG molecules and the βCDP6 polyplexes was empirically found to be very strong. PEGylated particles with DNA concentrations as dilute as 1 μg/mL remained stable under physiological salt conditions. The high association may be a result of decreased diffusional mobility of the adamantane away from the cyclodextrin because it is tethered to the PEG molecule and the high local concentration of cyclodextrin molecules on the polyplex surface, i.e., when an adamantane molecule exits one cyclodextrin cup, it is likely to go back in the same or a nearby cyclodextrin rather than going into solution (distances between cyclodextrins is very small relative to what they would be for individual cyclodextrins in solution).

Based on the success of PEGylating βCDP-based polyplexes by inclusion compound formation, an anionic, galactosylated adamantane compound was evaluated as a modifier to target βCDP-based polyplexes to hepatocytes. These adamantane modifiers contain four elements: (i) the adamantane, to attach the compound to the polyplex surface, (ii) an anionic peptide to change the polyplex surface charge and thereby reduce nonspecific transfection due to charge, (iii) PEG to serve as a tether for the ligand and as a stabilizing agent, and (iv) galactose as a targeting ligand to the asialoglycoprotein receptor (ASGP−R) or glucose as a low affinity ligand as a control. As demonstrated by the data shown in Figure 4A, the addition of these compounds to polyplexes causes the zeta potential to decrease. The drop in surface charge confirms modification of polyplexes. Additionally, the zeta potentials and particle sizes of the galactose and glucose-modified polyplexes are very similar (approximately −7 mV, 120 nm). Electron microscopy reveals that the galactosylated particles, although having different surface charge, retain approximately the same morphology and size as the unmodified polyplexes (Figures 3 and 4B). Therefore, differences in transfection ability between these particles are due to the ligand rather than physicochemical differences in the particles.

The glycosylated particles were exposed to the HepG2 cell line for uptake and transgene expression experiments. Uptake experiments were conducted at a variety of conditions (different degrees of polyplex modification, polyplex charge, and polyplex exposure time to cells) using fluorescently labeled plasmid DNA for analysis by flow cytometry. As expected, uptake efficiency was dependent on several parameters. However, uptake of galactosylated polyplexes into the hepatoma cells was consistently higher than uptake of glucosylated polyplexes. When formulated at positive zeta potentials (0, 10, or 20% PEG), no difference in transfection efficiency is observed between glucosylated and galactosylated polyplexes. This is not surprising because when the polyplexes are positively charged, they are efficiently and indiscriminantly internalized by nonspecific interactions with proteoglycans (*5*). When the particles are formulated at net negative charges (PEG−pep ≥ 40%), selective transfection by the galactosylated formulation is observed. In fact, the luciferase activity from galactose-mediated transfection is consistently an order of magnitude higher than from glucosylated polyplexes.

The glucosylated polyplexes also demonstrate a AD−pep−PEG−glc-dependent response to surface modification. Addition of the anionic adamantane derivative reduces the surface charge, resulting in a precipitous drop in transfection ability beyond 20% PEGylation. In contrast, the effect of PEGylation on transfection observed with galactosylated polyplexes is not so pronounced most likely because the cells continue to internalize these particles by receptor-mediated endocytosis via the ASGP−R. The gene expression from galactosylated polyplexes is approximately 1 order of magnitude lower than that of unmodified polyplexes. Other investigators report increased transfection to hepatocytes upon galactosylation of polyplexes (*18*, *32*, *33*). However, in those systems, charged-mediated delivery is not eliminated upon galactosylation, and uptake should occur by both charge and receptor-mediated delivery. Here, charge-mediated delivery of galactosylated βCDP particles is minimized by formulating anionic βCDP6 particles with the galactose ligand. Galactosylated βCDP particles are mainly endocytosed by the ASGP−R-mediated pathway. The reduction in expression from galactosylating the βCDP particles is therefore not surprising as uptake studies with unmodified and galactosylated polyplexes demonstrated that receptor-mediated endocytosis provides for less cellular uptake than nonspecific, charge-mediated uptake (data not shown). Reduction of nonspecific, charge-mediated uptake and gene expression is likely to be essential for effective, systemic, in vivo application.

Delivery via the ASGP−R is confirmed by two methods. First, transfection in the presence of asialofetuin, a high affinity ligand to the receptor, specifically decreases transfection of galactosylated polyplexes without affecting transfections with unmodified and glucosylated polyplexes (Figure 6). Second, luciferase activity is not observed for transfections of HeLa cells (do not express the ASGP−R) with galactosylated polyplexes (Figure 5B). Luciferase activity is observed only with unmodified polyplexes. The targeted delivery system demonstrates no toxicity over the unmodified polyplex. The low toxicity of these particles make them attractive for in vivo delivery applications.

For future work, receptor−ligand interactions can be further optimized by using different conjugation chemistries between the galactose ligand and the PEG. In this study, galactosamine was conjugated to the adamantane modifier via the C2 position. David et al. report that conjugation via the galactose C1 position results in higher uptake into hepatoma cells than conjugation via the C2 position (*34*). In addition, asialofetuin, a natural ligand for the ASGP−R binds to the receptor via a triantennary galactose residue. In fact, the affinity constants for the ASGP−R has been established with tri- ≫ bi- ≫ monoantennary galactose with affinity constants of about 10^{-9}, 10^{-6}, and 10^{-3} M, respectively (*35*). Therefore, incorporation of a C1-conjugated galactose residue or a multiantennary galactose ligand into the adamantane−PEG modifier could further improve the targeting ability of the galactosylated polyplexes.

In conclusion, a new method of modifying the surface of βCDP-based polyplexes through the use of cyclodextrin/adamantane host/guest interactions is presented. The inclusion complex formation is not restricted to adaman-

tane and β-cyclodextrin, as a multitude of guest/host materials are known. Also, the method should be applicable to other cyclodextrin-containing polymers that should be capable of forming of forming polyplexes, e.g., polyamidoamine dendrimers (*36*), polyallylamines (*37*), PEI (*38*), and chitosan (*39*). Here, we have demonstrated stabilization and galactose-mediated targeting of surface-modified particles without any increase in cell-associated toxicity. This method of adapting polyplexes for in vivo use imposes no interference with polyplex formation, occurs by self-assembly, and is modularly adaptable for various applications including the addition of agents that effect intracellular trafficking, codelivery of small molecules, different targeting agents, or combinations thereof (*40*). This system is currently being studied in animal models.

ACKNOWLEDGMENT

S.J.H. thanks the Whitaker Foundation for financial support for the portion of research conducted at the California Institute of Technology. S.J.H. is also grateful for helpful discussions with Dr. Nathalie Bellocq (Insert Therapeutics) and Prof. John Brady (Caltech). M.E.D. is a consultant to and has financial interest in Insert Therapeutics.

LITERATURE CITED

(1) Behr, J.-P. (1993) Synthetic Gene-Transfer Vectors. *Acc. Chem. Res. 26*, 274−278.

(2) Bielinska, A., Kukowska-Latallo, J., and Baker, J. (1997) The interaction of plasmid DNA with polyamidoamine dendrimers: mechanism of complex formation of analysis of alterations induced in nuclease sensitivity and transcriptional activity of the complexed DNA. *Biochim. Biophys. Acta 1353*, 180−190.

(3) Boussif, O., Lezoualcl′h, F., Zanta, M., Mergny, M., Scherman, D., Demeneix, B., and Behr, J.-P. (1995) A versatile vector for gene and oligonucleotide transfer into cells in culture and in vivo: Polyethylenimine. *Proc. Natl. Acad. Sci. U.S.A. 92*, 7297−7301.

(4) Felgner, P., Barenholz, Y., Behr, J.-P., Cheng, S., Cullis, P., Huang, L., Jessee, J., Seymour, L., Szoka, J., FC, Thierry, A., Wagner, E., and Wu, G. (1997) Nomenclature for Synthetic Gene Delivery Systems. *Hum. Gene Ther. 8*, 511−512.

(5) Mislick, K., and Baldeschwieler, J. (1996) Evidence for the role of proteoglycans in cation-mediated gene transfer. *Proc. Natl. Acad. Sci. U.S.A. 93*, 12349−12354.

(6) Nishikawa, M., Takemura, S., Takahara, Y., and Hashida, M. (1998) Targeted delivery of plasmid DNA to hepatocytes in vivo: Optimization of the pharmacokinetics of plasmid DNA galactosylated poly(L-lysine) complexes by controlling their physicochemical properties. *J. Pharm. Exp. Ther. 287*, 408−415.

(7) Dash, P., Read, M., Barrett, L., Wolfert, M., and Seymour, L. (1999) Factors affecting blood clearance and in vivo distribution of polyelectrolyte complexes for gene delivery. *Gene Ther. 6*, 643−650.

(8) Ward, C. M., Read, M. L., and Seymour, L. W. (2001) Systemic circulation of poly(L-lysine)/DNA vectors is influenced by polycation molecular weight and type of DNA: differential circulation in mice and rats and the implications for human gene therapy. *Blood 97*, 2221−2229.

(9) Collard, W., Yang, Y., Kwok, K., Park, Y., and Rice, K. (2000) Biodistribution, Metabolism, and In Vivo Gene Expression of Low Molecular Weight Glycopeptide Polyethylene Glycol Peptide DNA Co−Condensates. *J. Pharm. Sci. 89* (4), 499−512.

(10) Woodle, M. (1998) Controlling liposome blood clearance by surface-grafted polymers. *Biochim. Biophys. Acta 1113*, 171−199.

(11) Choi, Y., Liu, F., Kim, J.-S., Choi, Y., Park, J., and Kim, S. (1998) Poly(ethylene glycol)-grafted poly-L-lysine as polymeric gene carrier. *J. Controlled Rel. 54*, 39−48.

(12) Kwoh, D., Coffin, C., Lollo, C., Jovenal, J., Banaszczyk, M., Mullen, P., Phillips, A., Amini, A., Fabrycki, J., Bartholomew, R., Brostoff, S., and Carlo, D. (1999) Stabilization of poly-L-lysine/DNA polyplexes for in vivo gene delivery to the liver. *Biochim. Biophys. Acta 1444*, 171−190.

(13) Wolfert, M., Schacht, E., Toncheva, V., Ulbrich, K., Nazarova, O., and Seymour, L. (1996) Characterization of Vectors for Gene Therapy Formed by Self-Assembly of DNA with Synthetic Block Co−Polymers. *Hum. Gene Ther. 7*, 2123-2133.

(14) Ogris, M., Brunner, S., Schüller, S., Kircheis, R., and Wagner, E. (1999) PEGylated DNA/transferrin−PEI complexes: reduced interaction with blood components, extended circulation in blood and potential for systemic gene delivery. *Gene Ther. 6*, 595−605.

(15) Erbacher, P., Bettinger, T., Belguise-Valladier, P., Zou, S., Coll, J.-L., Behr, J.-P., and Remy, J.-S. (1999) Transfection and Physical Properties of Various Saccharide, Poly(ethylene glycol), and Antibody-Derivatized Polyethylenimines (PEI). *J. Gene Med. 1*, 210−222.

(16) Nguyen, H.-K., Lemieux, P., Vinogradov, S., Gebhart, C., Guerin, N., Paradis, G., Bronich, T., Alakhov, V., and Kabanov, A. (2000) Evaluation of polyether-polyethyleneimine graft copolymers as gene transfer agents. *Gene Ther. 7*, 129−138.

(17) Garrett, S., Davies, O., Milroy, D., Wood, P., Pouton, C., and Threadgill, M. (2000) Synthesis and Characterisation of Polyamine-Poly(ethylene glycol) Constructs for DNA Binding and Gene Delivery. *Bioorg. Med. Chem. 8*, 1779−1797.

(18) Bettinger, T., Remy, J.-S., and Erbacher, P. (1999) Size Reduction of Galactosylated PEI/DNA Complexes Improves Lectin-Mediated Gene Transfer into Hepatocytes. *Bioconjugate Chem. 10*, 558−561.

(19) Wadhwa, M., Knoell, D., Young, A., and Rice, K. (1995) Targeted Gene Delivery with a Low Molecular Weight Glycopeptide Carrier. *Bioconjugate Chem. 6*, 283−291.

(20) Nishikawa, M., Yamauchi, N., Morimoto, K., Ishida, E., Takakura, Y., and Hashida, M. (2000) Hepatocyte-targeted in vivo gene expression by intravenous injection of plasmid DNA complexed with synthetic multi-functional gene delivery system. *Gene Ther. 7*, 548−555.

(21) Gonzalez, H., Hwang, S., and Davis, M. (1999) New class of polymers for the delivery of macromolecular therapeutics. *Bioconjugate Chem. 10*, 1068−1074.

(22) Hwang, S., Bellocq, N., and Davis, M. (2001) Effects of Structure of Beta-Cyclodextrin-Containing Polymers on Gene Delivery. *Bioconjugate Chem. 12* (2), 280−290.

(23) Cromwell, W., Bystrom, K., and Eftink, M. (1985) Cyclodextrin adamantanecarboylate inclusion complexes-studies of the variation in cavity size. *J. Phys. Chem.-US 89*, 326−332.

(24) Amiel, C., and Sébille, B. (1999) Association between amphiphilic poly(ethylene oxide) and β-cyclodextrin polymers: aggregation and phase separation. *Adv. Colloid Interf. Sci. 79*, 105−122.

(25) Sandier, A., Brown, W., and Mays, H. (2000) Interaction between an Adamantane End-Capped Poly(ethylene oxide) and a β-Cyclodextrin Polymer. *Langmuir 16*, 1634−1642.

(26) Hermanson, G. T. (1996) In: p. 132, Academic Press, Rockford, IL.

(27) Goula, D., Remy, J.-S., Erbacher, P., Wasowicz, M., Levi, G., Abdallah, B., and Demeneix, B. (1998) Size, diffusibility and transfection performance of linear PEI/DNA complexes in the mouse central nervous system. *Gene Ther. 5*, 712−717.

(28) Hwang, S., and Davis, M. (2001) Cationic polymers for gene delivery: Designs for overcoming barriers to systemic administration. *Curr. Op. in Mol. Ther. 3*(2), 183−191.

(29) Oupicky, D., Howard, K., Konák, C., Dash, P., Ulbrich, K., and Seymour, L. (2000) Steric Stabilization of poly-L-Lysine/DNA Complexes by the Covalent Attachment of Semitelechelic poly[*N*-(2-Hydroxypropyl)methacrylamide]. *Bioconjugate Chem. 11*, 492−501.

(30) Napper, D. (1983) *Polymeric Stabilization of Colloidal Dispersions*, Academic Press, London.

(31) Gref, R., Lück, M., Quellec, P., Marchand, M., Dellacherie, E., Harnisch, S., Blunk, T., and Müller, R. (2000) 'Stealth' corona-core nanoparticles surface modified by poly(ethylene glycol) (PEG): influences of the corona (PEG chain length and surface density) and of the core composition on phagocytic uptake and plasma protein adsorption. *Colloids Surf. B: Biointerfaces 18*, 301−313.

(32) Lim, D., Yeom, Y., and Park, T. (2000) Poly(DMAEMA-NVP)-*b*-PEG−galactose as Gene Delivery Vector for Hepatocytes. *Bioconjugate Chem. 11*, 688−695.

(33) Midoux, P., Mendes, C., Legrand, A., Raimond, J., Mayer, R., Monsigny, M., and Roche, A. (1993) Specific gene transfer mediated by lactosylated poly-L-lysine into hepatoma cells. *Nuc. Acids Res. 21* (4), 871−878.

(34) David, A., Kopeckova, P., Rubinstein, A., and Kopecek, J. (2001) Enhanced biorecognition and internalization of HPMA copolymers containing multiple or multivalent carbohydrate side-chains by human hepatocarcinoma cells. *Bioconjugate Chem. 12*, 890−899.

(35) Brietfeld, P. P., Charles, F., Simmons, J., Strous, G. J. A. M., Geuze, H. J., and Schwartz, A. L. (1985) Cell biology of the asialoglycoprotein receptor system: A model of receptor-mediated endocytosis. *Int. Rev. Cytol. 97*, 47−95.

(36) Arima, H., Kihara, F., F., H., and Uekama, K. (2001) Enhancement of Gene Expression by Polyamidoamine Dendrimer Conjugates with a-, b-, and g-cyclodextrins. *Bioconjugate Chem. 12*, 476−484.

(37) Hollas, M., Chung, M. A., and Adams, J. (1998) Complexation of pyrene by poly(allylamine) with pendent b-cyclodextrin side groups. *J. Phys. Chem. B 102*, 2947−2953.

(38) Suh, J., Lee, S. H., and Zoh, K. D. (1992) A novel host containing both binding site and nucleophile prepared by attachment of β-cyclodextrin to poly(ethylenimine). *J. Am. Chem. Soc. 114*, 7916−7917.

(39) Tanida, F., Tojima, T., Han, S. M., Nishi, N., Tokura, S., Sakairi, N., Seino, H., and Hamada, K. (1998) Novel synthesis of a water soluble cyclodextrin-polymer having a chitosan skeleton. *Polymer 39*, 5261−5267.

(40) Hwang, S. (2001) In *Chemical Engineering*, p 167, California Institute of Technology, Pasadena.

BC0155768

Formation of Fibrinogen-Based Hydrogels Using Phototriggerable Diplasmalogen Liposomes

Zhi-Yi Zhang,[†] Pochi Shum,[†] Melinda Yates,[†] Phillip B. Messersmith,[‡] and David H. Thompson[†,*]

Department of Chemistry, Purdue University, West Lafayette, Indiana 47907-1393, and Biomedical Engineering Department, Northwestern University, 2145 Sheridan Road, Evanston, Illinois 60208. Received November 22, 2001; Revised Manuscript Received December 4, 2001

We report the triggered release of Ca^{2+} from liposomal compartments to induce rapid gelation of protein-based hydrogels. Phototriggerable liposomes were designed by entrapping $CaCl_2$ within liposomes composed of 38:57:5 diplasmenylcholine (DPPlsC):disteroylphosphatidylcholine (DSPC): bacteriochlorophyll (Bchl). These liposomes release >80% of their entrapped Ca^{2+} within 15 min when irradiated at 800 nm (800 mW/cm^2). A precursor solution, containing liposomes suspended in aqueous human fibrinogen and transglutaminase (TGase), remained fluid for several hours in the dark, but gelled rapidly when exposed to 800 nm excitation, as a result of photosensitized Ca^{2+} release and TG-induced fibrinogen cross-linking. TGase and hrFXIII activities, determined using a fluorimetric dansylcadaverine assay, were found to depend strongly on irradiation time and reaction temperature. SDS−PAGE of the photolyzed reaction mixture revealed that gelation arises from enzyme-catalyzed cross-linking of predominately the α and γ chains of fibrinogen. This approach to the phototriggered formation of protein hydrogels creates new opportunities for biomaterials applications in drug delivery, tissue engineering, and wound healing.

INTRODUCTION

Development of new strategies and materials to facilitate rapid and efficient wound healing and localized drug delivery are major thrusts of biomaterials research. Fibrinogen hydrogels are potentially important biomaterials for drug delivery applications. Protein-based hydrogels such as these can be created by exploiting various Ca^{2+}-dependent enzymes to catalyze the enzyme-mediated cross-linking of polypeptide precursors (*1*, *2*). One such family of Ca^{2+}-dependent enzymes are the transglutaminases, which promote the formation of cross-links between glutamine and lysine residues on neighboring proteins (*3*−*7*) (Figure 1a). An area of considerable interest is the development of injectable biomaterials that undergo a rapid sol−gel transformation in-situ to form semisolid hydrogels. These materials may be potentially useful for site-directed drug delivery, wound healing, and in the emerging field of tissue engineering (*8*). Light activation is a particularly promising way to achieve in-situ formation of biomaterials since it provides a very broad range of adjustable parameters (e.g. pulse duration, intensity, pulse cycle, and wavelength) that can be optimized for biological compliance and clinical efficacy. Moreover, fiber optic light sources are common clinical devices that can offer a convenient means for triggering useful chemical reactions within confined regions. For example, UV and visible light activated photopolymerization systems have been developed for rapid in vivo gelation of monomeric liquids for drug delivery and tissue repair (*9*−*11*).

Efforts in our laboratories have been aimed at developing stimuli-responsive liposome strategies for site-specific drug delivery (*12*−*21*) and in-situ formation of resorbable biomaterials (*22*−*27*). The ability of stimuli-responsive liposomes to release sequestered reagents in response to an applied stimulus (temperature, light, pH, etc. (*15*, *16*)) can be exploited to trigger in-situ formation of mineral-, polymer-, and peptide-based biomaterials.

In this work, we use phototriggered release of liposomal Ca^{2+} as an initiator of enzyme-mediated formation of fibrinogen hydrogels. The basic strategy of this approach is to utilize calcium-loaded phospholipid vesicles to physically isolate calcium ions from Ca^{2+}-dependent enzymes contained within the surrounding aqueous medium (Figure 1b); photoactivated release of Ca^{2+} converts the enzyme from an inactive to an active state. Previously, Wymer et al. used this concept to photochemically control the activity of a calcium-dependent phospholipase A_2 in a cascade triggering approach (*20*). This work employs Ca^{2+}-dependent transglutaminase (TGase)[1] enzymes (protein−glutamine:amine γ-glutamyltransferase, EC 2.3.2.13), which catalyze an acyltransfer reaction between the γ-carboxamide groups of peptide-bound glutamine residues and the ϵ-amino groups of lysine residues in proteins (*3*−*7*). In this case, photoactivated release of Ca^{2+} from liposomes results in the cross-linking of a soluble protein (fibrinogen) through the formation of ϵ-(γ-glutamyl)lysine isopeptide side-chain bridges as shown in Figure 1. This paper describes a method for producing transglutaminase-cross-linked hydrogels based on photooxidative triggering of Ca^{2+} release from diplasmalogen (DPPlsC) liposomes, with subsequent

* Corresponding author: Voice: 765-494-0386; FAX, 765-496-2592; Email, davethom@purdue.edu.

[†] Purdue University.

[‡] Northwestern University.

[1] Abbreviations used: Bchl, bacteriochlorophyll *a*; Ca−FTE, calcium-loaded freeze−thaw-extruded vesicles; Ca−IFV, calcium-loaded interdigitation fusion vesicles; DPPlsC, 1,2-Di-(1′-*Z*-*O*-hexadecenyl)-*sn*-glycero-3-phosphocholine; DSPS, 1,2-Disteroyl-*sn*-glycero-3-phosphocholine; hrFXIII, human recombinant Factor XIII; HBS, HEPES-buffered saline, (10 mM HEPES, 0.3 M NaCl, 1 mM EDTA, pH 7.4); TGase, tissue transglutaminase.

10.1021/bc015580j CCC: $22.00 © 2002 American Chemical Society
Published on Web 04/04/2002

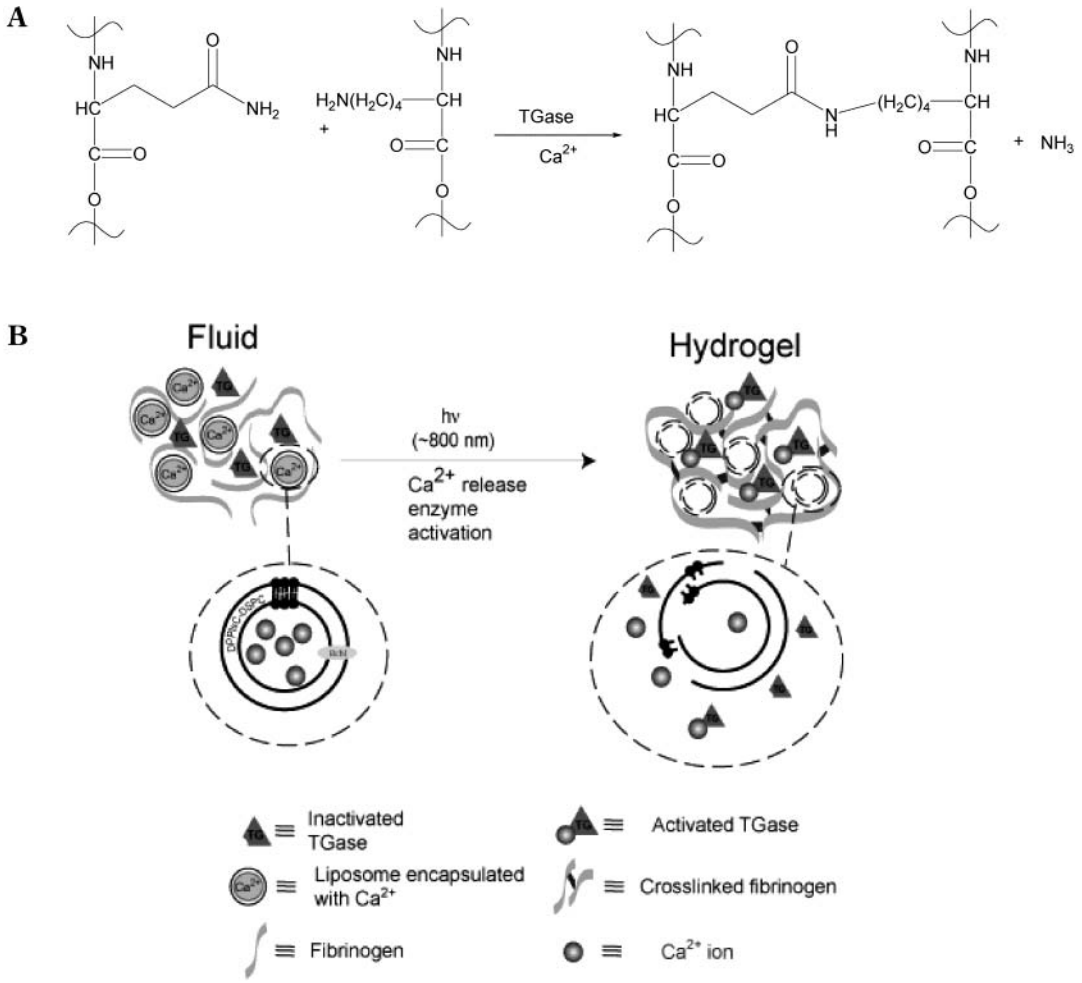


Figure 1. A: Glutamine-lysine cross-linking reaction catalyzed by calcium-dependent transglutaminase (TGase). B: Conceptual illustration of the photoinduced fibrinogen gelation process.

activation of transglutaminase-catalyzed cross-linking of fibrinogen. The gelation rate and physical properties of these hydrogels have been characterized by dansylamine fluorescence assay, SDS−PAGE, and cryogenic scanning electron microscopy (C−SEM) to determine the rate and extent of protein cross-linking.

MATERIALS AND METHODS

Materials. Diplasmenylcholine (DPPlsC) was synthesized as described (*21*). Human recombinant Factor XIII (hrFXIII) was generously supplied by ZymoGenetics Corporation (Seattle, WA). 1,2-Disteroyl-*sn*-glycerol-3-phosphatidylcholine (DSPC), bacteriochlorophyll *a* (Bchl), Arsenazo III (AIII), NaCl, $CaCl_2$, human fibrinogen (93% clottable), tissue transglutaminase (TGase), dithiothreitol (DTT), HEPES, and EDTA were all used as received.

Preparation of Liposomes. Calcium chloride-loaded phospholipid vesicles were prepared by the interdigitation−fusion approach as previously described (*23*, *28*). A lyophilized powder of 38:57:5 (mol %) DPPlsC:DSPC:Bchl was hydrated in the presence of 0.2 M $CaCl_2$ for 15 min at 65 °C with occasional vortexing. The resulting vesicle suspension was sonicated under an inert atmosphere at 65 °C for 30 min, cooled to room temperature, and then centrifuged at 3000*g* for 3 min to remove metal particles released from the sonicator probe tip. Absolute ethanol was added to the supernatant to achieve a final ethanol concentration of 4 M. The solution was mixed vigorously and then incubated at 22 °C for 15 min. Ca^{2+}-encapsulated interdigitation−fusion vesicles (Ca−IFVs) were obtained by flushing the suspension with dry Ar at 65 °C for 60 min and at 23 °C for an additional 30 min to remove the remaining EtOH. Extravesicular Ca^{2+} was removed from the liposome suspension by repeated centrifugation (20000*g*) for 3 min with isotonic 0.3 M NaCl solution (containing 1 mM EDTA in 10 mM HEPES at pH 7.4, HBS) and decanting of the supernatant. This process was repeated until Ca^{2+} was no longer detected in the supernatant using the Arsenazo III spectrophotometric assay (see below) (*29*). The Ca−IFV's were resuspended in isotonic HBS solution to a final lipid concentration of 20 mg/mL and then stored at 4 °C until use. The average Ca−IFV diameter, determined via quasielastic light scattering using a Coulter N4−Plus instrument and the manufacturers' analysis software, was approximately 1.9 μm.

The amount of Ca^{2+} encapsulated within the Ca−IFV was determined using the calcium sensitive dye, Arsenazo III (AIII, $\lambda_{max} = 560$ nm), which undergoes a color change upon complexation with Ca^{2+} (Ca^{2+}-AIII, $\lambda_{max} = 656$ nm) (*29*). A 5 μL aliquot of Ca−IFV suspension was added to 3 mL of AIII solution (0.2 mM AIII in 20 mM HEPES, 0.3 M NaCl, pH 7.4) in a 1 × 1 cm cuvette. The mixture was vigorously stirred for 30 s with a micromagnetic stir bar and then the UV absorption at 656 nm measured. Subsequent addition of 10% Triton X-100 (30 μL) to this mixture leads to vesicle disruption and complete release of Ca^{2+}. Control experiments showed that this assay was linear over 5−100 μM calcium concentration ranges.

Light-Triggered Ca^{2+} Release from Ca−IFV. Liposome solutions (1.5 mL in 13 × 100 mm culture tubes) were illuminated using a SDL 820 Al−Ga−As diode laser (Spectro Diode Labs, San Jose, CA, $\lambda_{em} = 800$ nm) coupled to a 1 mm diameter optical fiber, the emitting end of which was mounted perpendicular to the side plane of an irradiation cuvette. Incident light intensities were measured using a MAX 5100 power meter (Molectron Detector, Portland, OR). A 10 μL aliquot of liposome sample was added to 3 mL of AIII solution. Release of Ca^{2+} from the liposomes was followed as a function of time by measuring the absorption intensity at 656 nm before and after the addition of 10% Triton X-100 solution and the amount of Ca^{2+} released calculated as previously described (*27*).

Light-Activation of hrFXIII and Liver TGase via Ca−IFVs. The activity of hrFXIII and liver TGase in the presence of Ca−IFV's was determined using the fluorometric dansylcadaverine assay (*30*), modified to account for the presence of Ca−IFVs (see below). Sample temperature control was provided by a water-jacketed cell holder, which was connected to a thermostated water bath. Bicine buffer (50 mM in 0.29 mM NaCl, pH 9.0; 1.2 mL), Tris buffer (50 mM in 0.175 mM NaCl, pH 7.5; 1.0 mL), and monodansylcadaverine (2 mM in 50 mM Tris buffer, pH 7.5; 40 μL) were combined in a 1 cm × 1 cm quartz fluorescence cuvette. After temperature equilibration, 0.2 mL of dimethylcasein (2% in distilled H_2O, cooled to 5 °C) was added. The solution temperature initially dropped by approximately 1 °C, but returned to the set temperature within 1−2 min. Thrombin (500 units/mL; 20 μL) was then diluted with 0.1 mL of distilled water and immediately combined with 10 μL of hrFXIII (10 mg/mL), and the entire volume transferred to the monodansylcadaverine-containing cuvette.[2] DTT (50 μL in 50% glycerol) was then added, followed by a volume of the Ca−IFV suspension (35 mM Ca^{2+}; 60 μL). Time-dependent fluorescence data collection was then started ($\lambda_{ex} = 360$ nm; $\lambda_{em} = 500$ nm; slit widths = 20 nm). After 5 min incubation in the dark, the samples were illuminated at 800 nm as described above. The distance between the end of optical fiber and the solution surface was approximately 3 cm. Incident light power was measured at the surface of the suspension.

Light Triggered Gelation of Precursor Suspensions. Fluid hydrogel precursor solutions were prepared by suspending Ca−IFV in a solution containing TGase and fibrinogen. The hydrogel precursor solution was produced by first combining 200 μL of human fibrinogen solution (50 mg/mL in HBS), 10 μL of TGase (0.02 units/μL), and 10 μL of 0.5 M DTT in a 10 × 13 cm culture tube, followed by addition of 200 μL of Ca−IFV solution with mixing. The culture tube was immersed in a water bath held at 37 °C and the tip of the laser fiber positioned 3 cm away from the surface of the precursor solution. The laser power was then adjusted to give the desired power density without introducing heating effects.

Transglutaminase-catalyzed cross-linking of fibrinogen was detected by sodium dodecyl sulfate polyacrylamide gel electrophoresis (SDS−PAGE) according to the method of Laemmli (*31*). TGase solution (10 μL) was combined with Ca−IFV's (200 μL) and fibrinogen solution (at 2 mg/mL in HBS; 200 μL), and the samples were irradiated for 40 min at 37 °C. Aliquots of the reaction mixture were withdrawn at 10 min intervals during the irradiation and immediately analyzed by SDS−PAGE.

[2] Alternatively, tissue-TG (2 units) was diluted into 0.1 mL of H_2O, but otherwise treated in the same manner.

Cryogenic Scanning Electron Microscopy (C−SEM). Samples were frozen by plunging into N_2 slush. The samples were then fractured and sublimated at −70 °C for 30 min prior to sputter-coating for 4 min with Au at approximately −160 °C. Samples were imaged at −140 °C in a JEOL JSM-840 SEM using a 4 kV accelerating voltage. The structures observed were consistent in numerous areas viewed.

RESULTS

Thompson et al. have previously shown that Ca-loaded DPPlsC:Bchl liposomes can rapidly release Ca^{2+} upon irradiation at 800 nm (*20*, *32*). This study employed the same photooxidatively based triggering chemistry, except that DSPC was used as the major membrane lipid component to keep the dark leakage rates low and minimize the amount of DPPlsC required (Figure 2). Phototriggered calcein release experiments showed that formulations containing 38% DPPlsC were capable of releasing more than 80% of their cargo when irradiated for 30 min at 800 nm, 1 W/cm^2 (Figure 3). To further reduce the lipid requirements of this system, we used the interdigitation fusion technique to make large vesicles that were capable of very high trapping efficiencies. This approach enabled 53 mM Ca^{2+} encapsulation efficiencies using only 20 mg/mL of total lipid. By comparison, liposomes prepared by conventional freeze−thaw-extrusion (FTE) methods were capable of encapsulating only 13 mM of Ca^{2+} at the same lipid concentration.[3] As shown in Figure 4, more than 90% of the entrapped Ca^{2+} was released upon irradiation of 38:57:5 DPPlsC:DSPC:Bchl Ca−IFV at 800 nm for 45 min.

Our approach to photoinitiated triggering of hydrogel formation is based on the well-known dependence of TGase activity on free Ca^{2+} concentrations (*7*). We first sought to verify this dependence using Ca−IFV to initiate hrFXIII and TGase activity by photooxidative triggering. For this purpose, the fluorescence based assay that monitors monodansylcadaverine incorporation into casein (*30*) was employed. This assay is based on fluorescence intensity increases that result when the dansyl group becomes enzymatically coupled to casein via amide bond formation. Figures 5 and 6 show the fluorescence intensity increases as a function of time for reaction mixtures containing *N*′,*N*′-dimethylcasein, Ca−IFV, and either liver TGase (Figure 5) or hrFXIII (Figure 6) at both 24 °C and 37 °C. At 24 °C with 100 s irradiation time, the fluorescence intensity of both enzymes rises only slowly during the first 60 min (Figure 5 and 6). However, the fluorescence intensity rises rapidly at 37 °C, indicating that hrFXIII and TGase more efficiently catalyze the incorporation of monodansylcadaverine into *N*′,*N*′-dimethylcasein via a photoinitiated release of Ca^{2+} at higher temperature.

To test the concept of phototriggerable TGase-catalyzed fibrinogen gelation, Ca−IFV were mixed with fibrinogen and liver TGase to form a precursor solution which did not gel in the dark at 37 °C for 120 min. Mild irradiation (0.4 W/cm^2) of these samples at 37 °C, however, led to the formation of a dense gel within 40 min (Figure 7a). Gelation time could be reduced to 15 min by increasing the laser power to 0.8 W/cm^2 or by increasing the TGase concentration to 0.6 units (data not shown). Cryo-SEM analysis (Figure 7b and 7c) of the irradiated sample from

[3] The Ca^{2+} concentrations reported here, 53 mM and 13 mM, for Ca−IFV and Ca−FTE, respectively, refer to the *bulk* Ca^{2+} concentrations (i.e., after complete escape of Ca^{2+} from the inner vesicle compartment due to Triton X-100 addition).

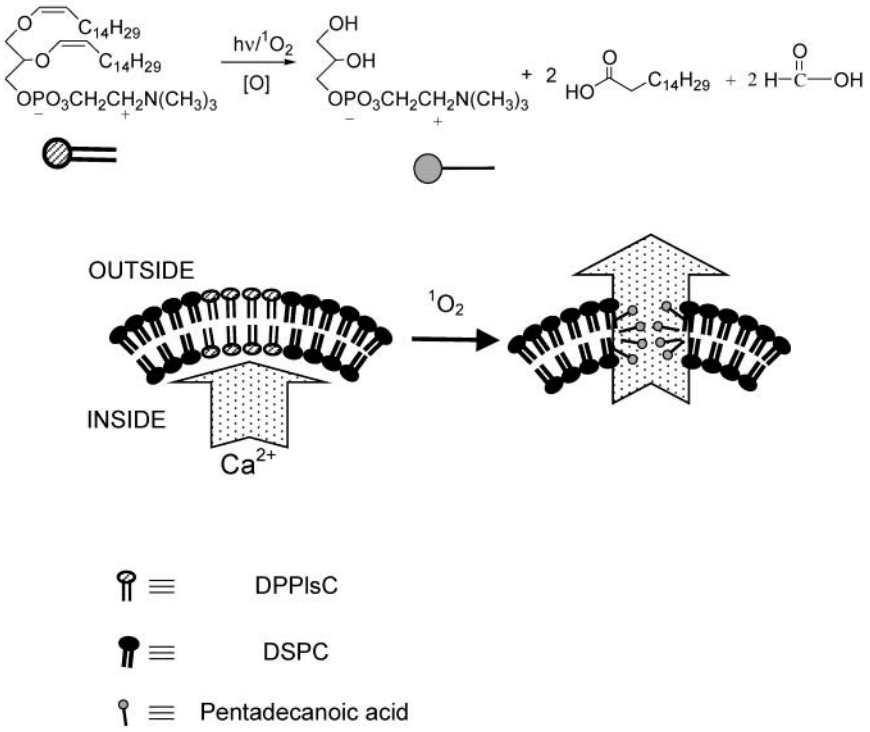


Figure 2. Diplasmalogen photooxidation reaction (top) that controls Ca^{2+} ion availability in bulk solution via creation of liposomal membrane defects (bottom).

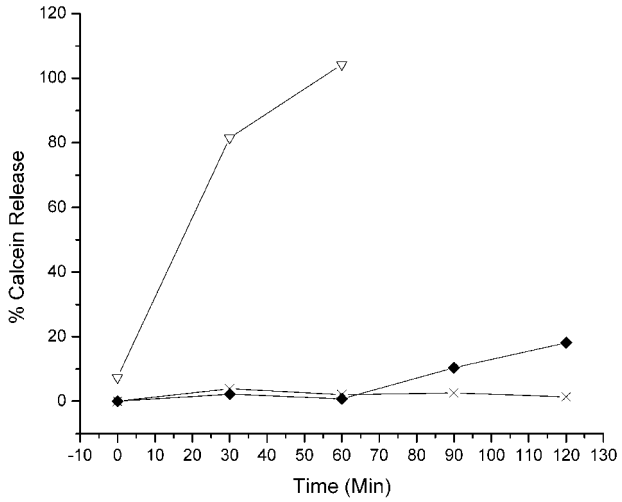


Figure 3. Photoinduced calcein release from various formulations of DSPC:DPPlsC:Bchl liposomes at 37 °C. DPPlsC:DSPC:Bchl, ▽, 38:57:5; ◆, 18:77:5; ×, 20:79.5:0.5. Total lipid concentration, 10 mM in HBS, pH 7.4; laser source intensity, 800 nm Al/Ga/As diode laser at 1 W/cm^2.

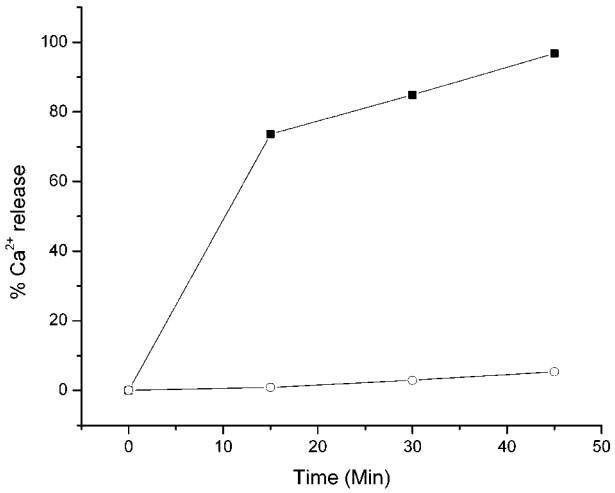


Figure 4. Photoinduced Ca^{2+} release from interdigitation−fusion vesicles at 37 °C. ■, 1.3 W/cm^2; ○, dark. Total lipid concentration, 1.5 mg/mL in HBS; laser intensity, 1.3 W/cm^2 @ 800 nm; bulk Ca^{2+} concentration when completely released, 3.25 mM.

Figure 7a reveals the formation of a microporous network structure whose pores are approximately the diameter of the Ca−IFV. The pores of this hydrogel material may be imprinted by the vesicle precursors, i.e., the vesicles themselves may serve as both the Ca^{2+} source and as a template for the TGase-catalyzed cross-linking reaction.

SDS−PAGE analysis of photoinitiated Ca−IFV/TGase/fibrinogen samples was performed as a function of irradiation time to observe the TGase-induced changes in protein MW upon cross-linking (Figure 8). For samples incubated in the dark at 37 °C, SDS−PAGE revealed no observable protein cross-linking through 40 min, as indicated by the persistence of the fibrinogen α-, β-, and γ-bands. By contrast, irradiation of the samples at 800 nm (400mW/cm^2, 37 °C) resulted in extensive loss of both the α and γ chains of fibrinogen within 10 min, as well as a gradual loss of the β-band over 40 min. At the same time, weakly staining higher molecular weight bands emerged, along with a densely stained, very high molecular weight band which did not penetrate the gel.

DISCUSSION

The goal of this project is to formulate aqueous protein solutions, which can expeditiously gelate upon transglutaminase catalysis in the presence of Ca^{2+} ions. Our method employs phototriggered liposomal release of Ca^{2+} to initiate the rapid enzymatic cross-linking of fibrinogen solutions to form hydrogels. Phototriggerable liposomes were designed by entrapping $CaCl_2$ within liposomes composed of 38:57:5 DPPlsC:DSPC:Bchl. These liposomes

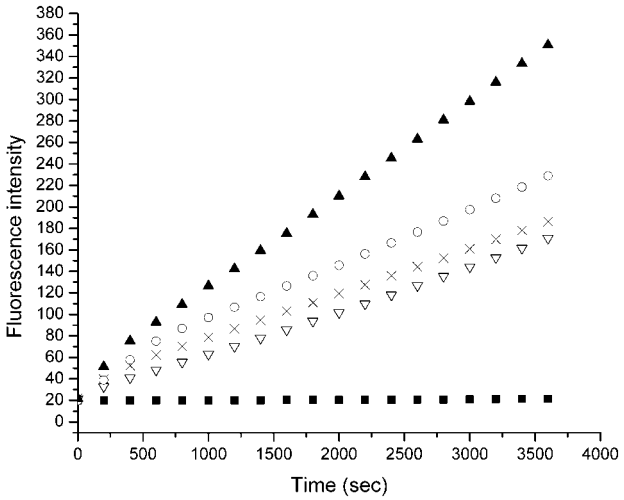


Figure 5. Fluorescence intensity increase versus time for the photoinitiated reaction between TGase, *N′*,*N′*-dimethylcasein, monodansylcadaverine, and photoresponsive Ca−IFV's. ■, dark at 24 °C; ▽, 100 seconds irradiation at 24 °C and 800 nm (1.3 W/cm^2); ▲, 100 seconds irradiation at 37 °C and 800 nm (1.3 W/cm^2). ×, 200 s irradiation at 24 °C and 800 nm (1.3 W/cm^2); ○, 400 s irradiation at 24 °C and 800 nm (1.3 W/cm^2); 1.2 mL of Bicine buffer (50 mM in 0.29 M NaCl, pH 9.0); 1.0 mL of Tris buffer (50 mM in 0.175 M NaCl, pH 7.5); 40 μL of monodansylcadaverine (2 mM in 50 mM Tris buffer, pH 7.5); 0.2 mL of dimethylcasein; 10 μL TGase (0.02 units/mL); final Ca^{2+} concentration 1 mM; final lipid concentration 0.2 mg/mL.

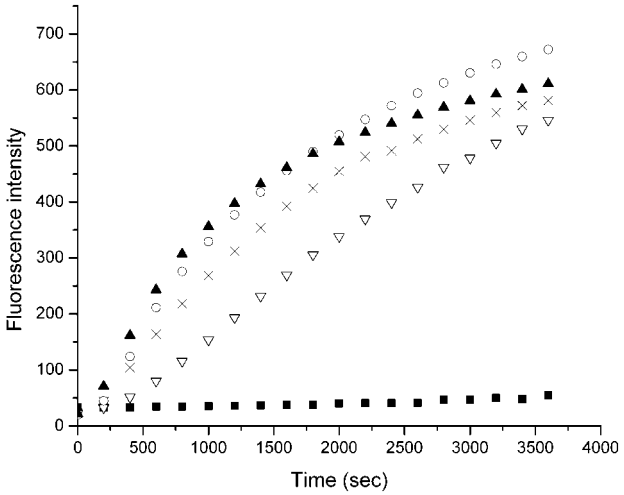


Figure 6. Fluorescence intensity increase versus time for the photoinitiated reaction between hrFXIII/thrombin, *N′*,*N′*-dimethylcasein, monodansylcadaverine, and photoresponsive Ca−IFV's. ■, dark at 24 °C; ▽, 100 seconds irradiation at 24 °C and 800 nm (1.3 W/cm^2), ▲, 100 seconds irradiation at 37 °C and 800 nm (1.3 W/cm^2). ×, 200 s irradiation at 24 °C and 800 nm (1.3 W/cm^2); ○, 400 s irradiation at 24 °C and 800 nm (1.3 W/cm^2); 1.2 mL of Bicine buffer (50 mM in 0.29 M NaCl, pH 9.0); 1.0 mL of Tris buffer (50 mM in 0.175 M NaCl, pH 7.5); 40 μL of monodansylcadaverine (2 mM in 50 mM Tris buffer, pH 7.5); 0.2 mL of dimethylcasein; 20 μL of thrombin (500 units/mL); 10 μL of hrFXIII (10 mg/mL); final Ca^{2+} concentration 1 mM; final lipid concentration 0.2 mg/mL.

could release ∼90% of entrapped Ca^{2+} when irradiated at 800 nm for 30 min (Figure 4). Photochemical control of TGase enzyme and FXIII activity was clearly demonstrated using the dansylcadaverine enzyme assay as shown in Figures 5 and 6. When Ca−IFV's were used as the sole source of Ca^{2+}, virtually no enzyme activity was observed in the dark control sample (i.e., nonirradiated). FXIII and TGase became active, however, in the presence of the millimolar concentrations of Ca^{2+} that were

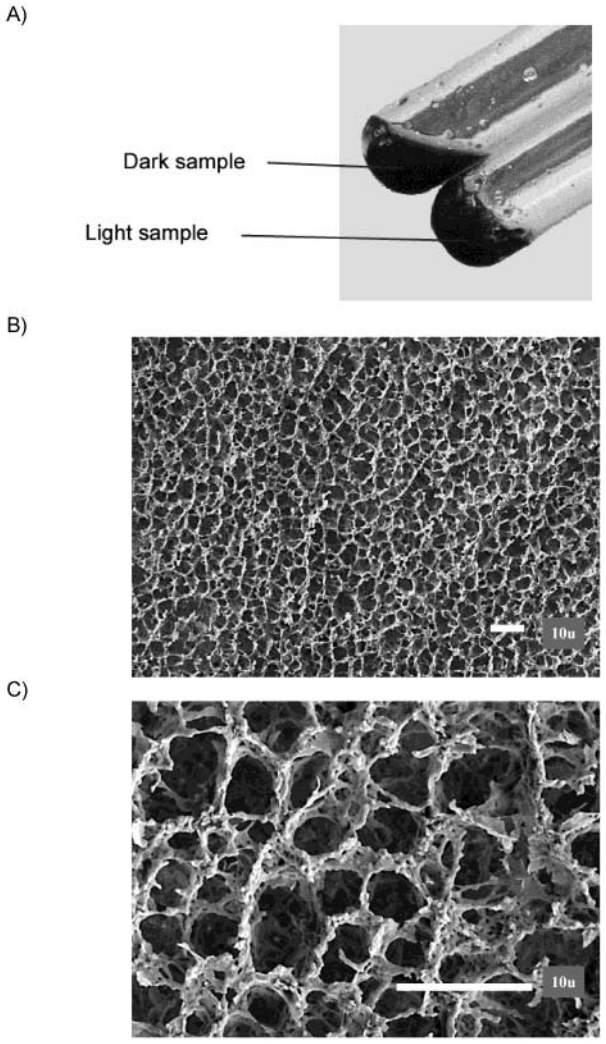


Figure 7. A: Macroscopic appearance of fibrinogen precursor solutions without (top) and with (bottom) exposure to 800 nm excitation (40 min @ 0.4 W/cm^2). B and C: C−SEM of cryofractured sample of phototriggered fibrinogen hydrogel.

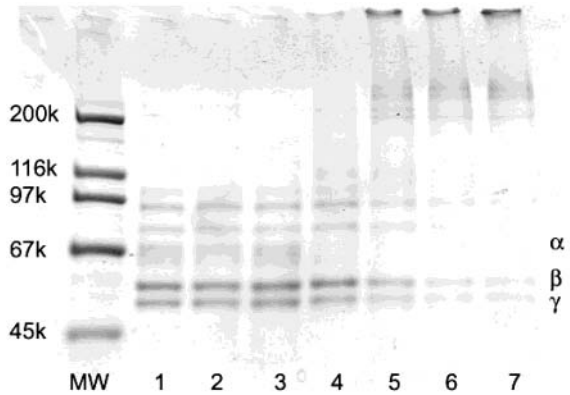


Figure 8. SDS−PAGE of fibrinogen solutions sampled at various irradiation times. MW, molecular weight marker lane; lanes 1−4 dark control samples at 0, 10, 20, and 40 min, respectively; lanes 5−7 irradiated samples (800 nm, 400 mW/cm^2, 37 °C), respectively at 10, 20, and 40 min.

released by the Ca−IFV after irradiation at 800 nm for only 100 sec at 24 °C. As expected, higher enzyme activities were observed after irradiation of the suspensions at 800 nm for 100 sec at 37 °C.

The phototriggered Ca^{2+} release from Ca−IFV was used to activate enzyme-catalyzed cross-linking of pro-

teins to form hydrogels within 40 min, as confirmed by visual observations and SDS−PAGE experiments. Figure 8 showed that the intensity of the α- and γ-bands decreased when the suspensions were irradiated at 800 nm for 10 min. Densely stained wells at the origins of lanes 5−7 indicate the formation of macromolecules in the cross-linking reaction that cannot penetrate into the gel. When higher laser power or TGase concentrations were applied to the precursor solution at 800 nm and at 37 °C, gelation time was reduced to 15 min.

Commercially available, fibrin-based adhesives produce strong, biodegradable gels very quickly (<10 min) and are used as surgical glues, tissue sealants, and drug delivery devices (*33*). These materials consist of fibrinogen, FXIII, thrombin, and Ca^{2+} and are typically delivered via a dual syringe device that separates fibrinogen and FXIII from Ca^{2+} and thrombin during storage. Mixing of the components during discharge from the syringe results in thrombinolysis of fibrinogen to create fibrin, which self-assembles into a gel that is later cross-linked by Ca^{2+}-activated FXIII. This sequence of reactions closely mimics the manner in which fibrin and activated FXIII are formed in vivo (*4*). Through extensive cross-linking of the protein substrate by FXIII, resistance to both mechanical and enzymatic degradation is imparted to the material (*34*). Our approach relies on Ca^{2+}-activation of FXIII as well; however, there are several key differences between the fibrinogen hydrogels described in this paper and conventional fibrin tissue adhesives. For example, our formulations do not contain thrombin, which plays a key role in formation of both fibrin and activated FXIII in vivo. Because of this, the molecular (and supramolecular) structure of the fibrinogen gels are expected to be distinctly different from fibrin gels. Furthermore, the absence of thrombin could be an advantage in clinical use, since many current fibrin tissue formulations utilize bovine thrombin, which can induce anaphylactic and autoimmune responses in patients (*35*).

CONCLUSIONS

We recently reported the use of near-infrared (NIR) sensitive liposomes to trigger gelation of a self-assembling peptide (*26*); however, to the best of our knowledge, this is the first example of triggered protein hydrogel formation using NIR light. Since NIR has good tissue penetration relative to visible or UV light, one can conceivably (1) trigger the gelation of these suspensions in a noninvasive fashion using an external NIR source, (2) temporospatially modulate the release of drugs from NIR-sensitive liposomes entrapped within an implanted hydrogel, (3) produce hydrogels that possess unique gradient or microstructural properties. These experiments demonstrate that this approach to the phototriggered formation of protein hydrogels creates new opportunities for biomaterials applications in drug delivery, tissue engineering and wound healing. Experiments to explore these opportunities are currently in progress.

ACKNOWLEDGMENT

This work was supported by grants from NIH GM55266 & DE 13030. The authors thank ZymoGenetics, Inc. for their generous donation of hrFXIII.

LITERATURE CITED

(1) Sperinde, J. J., and Griffith, L. G. (1997) Synthesis and characterization of enzymatically cross-linked poly(ethylene oxide) hydrogels. *Macromolecules 30*, 5255−5264.

(2) Schense, J. C., and Hubbell, J. A. (1999) Cross-linking exogenous bifunctional peptides into fibrin gels with factor XIIIa. *Bioconjugate Chem. 10*, 75−81.

(3) Clarke, D. D., Mycek, M. J., Neidle, A., and Waelsch, H. (1959) Incorporation of amines into protein. *Arch. Biochem. Biophys. 79*, 338−354.

(4) Folk, J. E., and Finlayson, J. S. (1977) The ϵ-(γ-glutamyl)-lysine cross-link and the catalytic role of transglutaminases. *Adv. Protein Chem. 31*, 1−133.

(5) Greenberg, C. S., Birckbichler, P. J., and Rice, R. H. (1991) Transglutaminases: multifunctional cross-linking enzymes that stabilize tissues. *FASEB J. 5*, 3071−7.

(6) Aeschlimann, D., and Paulsson, M. (1994) Transglutaminases: protein cross-linking enzymes in tissues and body fluids. *Thromb. Haemost. 71*, 402−15.

(7) Lorand, L., and Conrad, S. M. (1984) Transglutaminases. *Mol. Cell Biochem. 58*, 9−35.

(8) Ritter-Jones, M. and Messersmith, P. B. (2002) *Oral and Maxillofacial Clinics of North America*, Vol. 14, pp 1−10.

(9) Hubbell, J. A. (1996) Hydrogel systems for barriers and local drug delivery in the control of wound healing. *J. Controlled Release 39*, 305−313.

(10) Anseth K. S., Shastri V. R., and Langer R. (1999) Photopolymerizable degradable polyanhydrides with osteocompatibility. *Nature Biotech. 17*, 156−159.

(11) Kim, B. S., Hrkach, J. S., and Langer, R. (2000) Biodegradable photocrosslinked poly(ether-ester) networks for lubricious coatings. *Biomaterials 21*, 259−265.

(12) Anderson, V. C., and Thompson, D. H (1992) Triggered release of hydrophilic agents from plasmalogen liposomes using visible light or acid. *Biochim. Biophys. Acta 1109*, 33−42.

(13) Thompson, D. H., Gerasimov, O. V., Wheeler, J. J., Rui, Y., and Anderson, V. C. (1996) Triggerable plasmalogen liposomes: improvement of system efficiency. *Biochim. Biophys. Acta 1279*, 25−34.

(14) Gerasimov, O. V., Schwan, A. and Thompson, D. H. (1997) Acid-catalyzed plasmenylcholine hydrolysis and its effect on bilayer permeability: a quantitative study. *Biochim. Biophys. Acta 1324*, 200−14.

(15) Thompson, D. H., Rui, Y., and Gerasimov, O. V. (1996) Triggered release from liposomes mediated by physically- and chemically induced phase transitions in *Vesicles*, Surfactant Science Series, Vol. 62, (Rosoff, M., Ed.), pp 679−746.

(16) Shum, P., Kim, J.-M, and Thompson, D. H. (2001) Phototriggering of liposomal drug delivery systems. *Adv. Drug Del. 53*, 273−284.

(17) Kim, J.-M., and Thompson, D. H., Acid- and oxidatively labile vinyl ether surfactants: synthesis and drug delivery applications, in *Reactions and Synthesis in Surfactant Systems*, Surfactant Science Series, Vol. 100 (Texter, J., Ed.), pp 145−154.

(18) Rui, Y., Wang, S., Low, P., and Thompson, D. H. (1998) Diplasmenylcholine-folate liposomes: an efficient vehicle for intracellular drug delivery. *J. Am. Chem. Soc. 120*, 11213−11218.

(19) Qualls, M. M., and Thompson, D. H. (2001) Chloroaluminum phthalocyanine tetrasulfonate delivered via acid-labile diplasmenylcholine-folate liposomes: intracellular localization and synergistic phototoxicity. *Int. J. Cancer 93*, 384−392.

(20) Wymer, N. J., Gerasimov, O. V., and Thompson, D. H. (1998) Cascade liposomal triggering: light-induced Ca^{2+} release from diplasmenylcholine liposomes triggers PLA_2-catalyzed hydrolysis and contents leakage from DPPC liposomes. *Bioconjugate Chem. 9*, 305−308.

(21) Boomer, J. A., and Thompson, D. H. (1999) Synthesis of acid-labile diplasmenyl lipids for drug and gene delivery applications. *Chem. Phys. Lipids 99*, 145−153.

(22) Messersmith, P. B., and Starke, S. (1998) Thermally triggered calcium phosphate formation from calcium-loaded liposomes. *Chem. Mater. 10*, 117−124.

(23) Messersmith, P. B., Vallabhaneni, S., and Nguyen, V. (1998) Preparation of calcium-loaded liposomes and their use in calcium phosphate formation. *Chem. Mater. 10*, 109−116.

(24) Murphy, W., and Messersmith, P. B. (2000) Compartmental control of mineral formation: adaptation of a biomineralization strategy for biomedical use. *Polyhedron 19*, 359−363.
(25) Cui, H., and Messersmith, P. B. (1998) *Tailored polymeric materials for controlled delivery systems*, ACS Symposium Series, Vol. 709 (McCullough, I., Shalaby, S., Eds.), pp 203−211.
(26) Collier, J. H., Hu, B. H., Ruberti, J. W., Zhang, J., Shum, P., Thompson, D. H. and Messersmith, P. B. (2001) Thermally and photochemically triggered self-assembly of peptide hydrogels. *J. Am. Chem. Soc. 123*, 9463−9464.
(27) Westhaus, E., and Messersmith, P. B. (2001) Triggered release of calcium from lipid vesicles: a bioinspired strategy for rapid gelation of polysaccharide and protein hydrogels. *Biomaterials 22*, 453−462.
(28) Ahl, P. L. (1994) Interdigitation-fusion: a new method for producing lipid vesicles of high internal volume. *Biochim. Biophys. Acta 1195*, 237−244.
(29) Sokolove, P. M., and Kester, M. B. (1989) Quantitation of Ca^{2+} uptake by Arsenazo III-loaded liposomes. *Anal. Biochem. 177*, 402−406.
(30) Lorand L., Siefring, G. E., Tong, Y. S., Bruner-Lorand J., and Gray, A. J. (1979) Dansylcadaverine specific staining for transamidating enzymes. *Anal. Biochem.* 93, 453−458.
(31) Laemmli, U. K. (1970) Cleavage of structural proteins during the assembly of the head of bacteriophage T4. *Nature 227*, 680−685.
(32) Gerasimov, O. V., Wymer, N., Miller, D., Rui, Y., and Thompson, D. H. (1999) *Intelligent materials for controlled release*, ACS Symposium Series, Vol. 728 (Dinh, S., DeNuzzo, Comfort, A., Eds.), pp 164−178.
(33) Sierra, D., and Saltz, R (1996) *Surgical adhesives and sealants: Current technology and applications*, Technomic Publishing Company, Inc., Basel.
(34) Lewis, K., Teller, D., Fry, J., Lasser, G., and Bishop P. (1997) Cross-linking kinetics of the human transglutaminase, Factor XIII [A_2], acting on fibrin gels and γ-chain peptides. *Biochemistry 36*, 995−1002.
(35) MacPhee, M. J. Commercial and pooled source fibrin sealant, in *Surgical adhesives and sealants: Current technology and applications* (D. Sierra and R. Saltz, Eds.) pp 13−18.
(36) Rapaport, S., Zivelin, A., Minow, R., Hunter, C., and Donnelly, K., (1992) Clinical significance of antibodies to bovine and human thrombin and factor V after surgical use of bovine thrombin, *Am. J. Clin. Path. 97*, 84−91.

BC015580J

Dendrimers as Carrier Protein Mimetics for IgE Antibody Recognition. Synthesis and Characterization of Densely Penicilloylated Dendrimers

Francisco Sánchez-Sancho,[†] Ezequiel Pérez-Inestrosa,*[,†] Rafael Suau,[†] Cristobalina Mayorga,[‡] María J. Torres,[‡] and Miguel Blanca[§]

Departamento de Química Orgánica, Facultad de Ciencias, Universidad de Málaga, Campus de Teatinos, E-29071 Málaga, Spain, Research Unit for Allergic Diseases, Hospital Carlos Haya, Málaga, Spain, and Allergic Service, Hospital Universitario La Paz, Madrid, Spain. Received November 26, 2001; Revised Manuscript Received February 4, 2002

The synthesis of benzylpenicilloyl-containing dendrimers has been achieved by a convenient procedure involving quantitative functionalization of the terminal amino groups of the three Starbust PAMAM generations used (**G$_n$**; $n = 0, 1, 2$). All these densely penicilloylated dendrimers (**G$_n$P**) exhibit similar, simple NMR spectroscopic data suggesting highly symmetric structures and a monodisperse nature, and the results obtained from MALDI-TOF-MS demonstrate their exact chemical composition. The use of PAMAM dendrimers has allowed us to synthesize, for the first time, carrier benzylpenicilloyl conjugates (**G$_n$P**) of precisely defined chemical structure. The attempts to synthesize **G$_2$P** show that forced experimental conditions are not always useful for the functionalization of the dendrimer, especially in introducing bulky groups. The initial results with sera from patients with different RAST levels were positive and thus suggestive that inhibition occurs, so recognition exists; we can therefore conclude that the hapten−carrier (dendrimer) conjugates studied mimic recognition with natural hapten−carrier (protein) conjugates.

INTRODUCTION

In contrast to linear polymers, dendrimers are highly branched macromolecules with a regular treelike structure of well-defined three-dimensional architecture (*1*). Dendrimers are promising polymeric materials to be used as skeleton building blocks for the development of clusters by virtue of their precisely defined structure (*2*). At the molecular level, dendrimers are potential diagnostic agents thanks to the ease with which they can incorporate multiple functionalities leading to a high activity through multiple interactions that result in increased sensitivity (*3*). Dendritic substances have provided crucial advances; they have already been tested in preclinical studies, particularly as contrast media for magnetic resonance applications (*4*). Dendrimers containing multiple identical ligands are very attractive from the pharmacochemical point of view, since these structures can exhibit amplified substrate binding. Enhanced substrate binding originates either from statistical or cooperativity effects (*5*).

The idea of using a dendritic multifunctional platform to amplify substrate binding has also been exploited to generate antibodies, the improved immunoresponse of which has been ascribed to their high antigen content (*6*). Poly(amidoamine) dendrimers (PAMAM) (*7*) have been used for drug delivery and biomedical applications (*8a*) such as coupling to antibodies to develop immunoassays combining the advantages of hetero- and homogeneous immunoassays (*8b*). The synthesis of several saccharide residues attached to the periphery of preformed PAMAM dendritic cores has been reported, and an increased binding affinity for certain proteins when compared with the individual monomeric sugar unit was demonstrated (*9*).

Current projects in our laboratories are focused on the development of β-lactam hapten−carrier conjugates for quantifying IgE antibodies to penicillins (*10*). Evaluation of subjects with an immediate allergic reaction requires an adequate clinical history plus in vivo and/or in vitro tests (*11*). β-Lactams need to be conjugated with a protein carrier to induce specific IgE antibodies (*12*), and the nature of this molecule is important in the sensitivity of the in vitro test used to detect these antibodies. Since the in vitro tests for detecting specific IgE antibodies to β-lactams are not so sensitive as skin tests, an improvement of in vitro techniques is needed to enhance diagnosis in allergic patients. In this paper we report on the preparation and properties of PAMAM dendrimers functionalized with peripheral benzylpenicilloyl (BPO) units. The benzylpenicilloyl group is the major determinant responsible for the allergic response to β-lactam antibiotics (*13*).

The general aim of this research was to design and synthesize a sequence of precisely defined molecular structures to achieve hapten−carrier conjugates of increasing benzylpenicilloyl density at the periphery of preformed PAMAM dendritic cores and exploiting their exo-receptor properties.

Conventional peptide carrier conjugates, human serum albumin (HSA) or poly-L-lysine (PLL), have the disadvantage of a nonprecise density of haptens in their structure; also, the haptens are randomly distributed in the large protein or peptide carriers. Although tradition-

* To whom correspondence should be addressed. Phone: (+34) 952 13 20 23. Fax: (+34) 952 13 19 41. E-mail: inestrosa@uma.es.

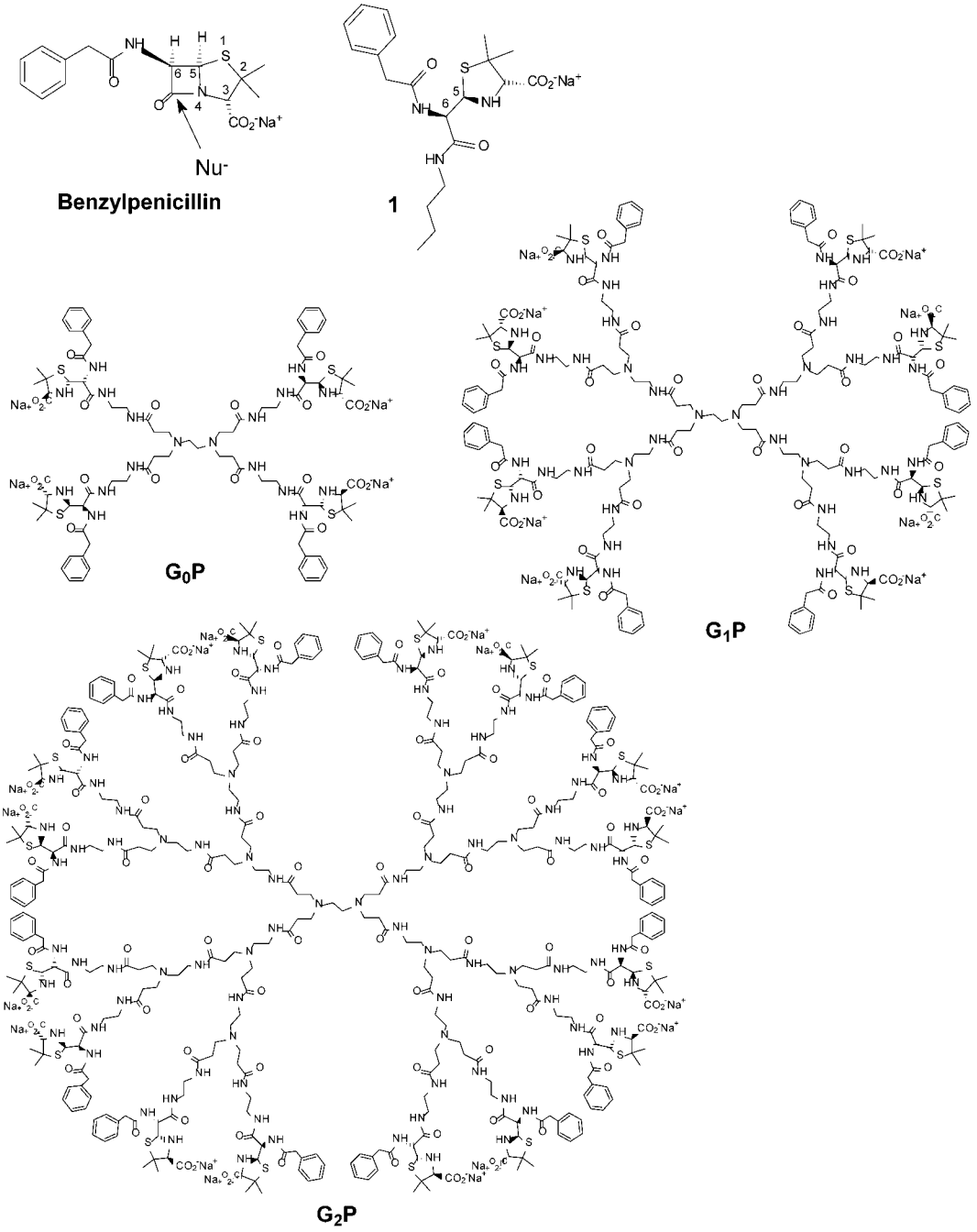
[†] Universidad de Málaga.

[‡] Hospital Carlos Haya.

[§] Hospital Universitario La Paz.

10.1021/bc0155824 CCC: $22.00 © 2002 American Chemical Society
Published on Web 04/03/2002

Chart 1. Structures for Model Compound 1 and the Synthesized Dendrimers G_0P, G_1P, and G_2P



ally considered the natural globular carrier, HSA has the limitation of its intrinsic low hapten−carrier density, in addition to the difficulty of establishing the exact structure of its conjugates (*10a*). On the other hand, PLL conjugates—even those with increased hapten−carrier ratios—actually consist of a combination of several structures because PLL is always an average of heterogeneous molecular weight peptides. As a result, this type of conjugate features low reproducibility and reliability in antibody recognition tests (*10b*). Furthermore, the flexibility of polymer chains makes the three-dimensional structures rather variable and difficult to predict. However, the surface and interior of dendrimers are considered segregated (*14*) so all the peripheral haptenic ligands of the conjugates obtained from them should be accessible for binding. Conversely, linear polymers, depending on their conformations, may envelop a substantial fraction of appended ligands.

We chose PAMAM dendrimers due to their availability, generally globular shape and solubility for all molecular sizes. The novel *functional dendritic molecules* (*15*) synthesized from them, reported herein, are part of our program to develop a new in vitro test to quantify *IgE* antibodies to specific β-lactam conjugates with a view to improving the existing methods for diagnosing allergy to this type of antibiotics.

The dendrimers studied, $\mathbf{G_0}$ to $\mathbf{G_2}$, are shown in Chart 1. The chemical properties of the penicilloylated dendrimers were studied and compared with those of the model monomer compound **1** (Chart 1). Covalent coupling of benzylpenicillin to the dendrimers produces novel compounds with unique properties of solubility, high charge density, and specificity. Moreover, these compounds have the ability to remain in an aqueous solution throughout an analytical process (a property considered to be particularly important) (*16*). The structural recogni-

tion of the new compounds from IgE antibodies has been evaluated and compared with that of classical BPO−PLL conjugates.

EXPERIMENTAL PROCEDURES

General. Starburst PAMAM dendrimers (generations zero to two) were purchased from Aldrich as 20 wt % solutions in methyl alcohol. Penicillin G sodium salt was purchased from CEPA, S. L. Standard chemicals were from Aldrich or Merck and used without further purifications. SephadexTM G-10 was purchased from Amersham Pharmacia Biotech AB. The compound **1** was prepared according to the previously reported procedure (*17*). ^{1}H and ^{13}C NMR spectroscopic measurements were carried out on a Bruker WP200 SY or DRX400 BB spectrometer, and chemical shifts (δ) are given in ppm relative to the residual solvent peak. All NMR spectra were recorded using D_2O as solvent (with Na_2CO_3 to ensure a basic pD $\cong$ 11) at room temperature. The MALDI-TOF mass spectra were acquired using a PE Biosystems Voyager System 2081 and were recorded by dissolving the product in 1:1 H_2O/CH_3CN containing 0.1% trifluoroacetic acid (TFA) and using 2,4,6-trihydroxyacetophenone (THAP) (**G_0P** and **G_1P**) or 3,5-dimethoxy-4-hydroxycinnamic acid (sinapinic acid) (**G_2P**) as the matrix. The FAB-MS spectrum was obtained using a VG Quattro mass spectrometer and was recorded by using 3-nitrobenzyl alcohol (3-NBA) as the matrix.

General Procedure for the Synthesis of Dendrimers G_nP (n = 0, 1, 2). Penicillin G sodium salt, was added to a stirred solution of the corresponding Starburst PAMAM dendrimer, in 0.02 M aqueous carbonate buffer, pH 10.8, at 20 °C (**G_0P** and **G_1P**) or 4 °C (**G_2P**). The mixture was stirred for the time stated in each case and then purified by gel filtration, using Sephadex G-10 as stationary phase and distilled water as eluent. The solvent was then evaporated in vacuo to obtain the corresponding pure product.

RAST Inhibition Studies. Three sera from patients allergic to penicillins were collected, and specific IgE antibodies were determined by radioallergosorbent tests (RAST) as reported (*17*) using in the solid-phase benzylpenicillin conjugated to PLL (BPO−PLL). Results, expressed as a percentage of maximum label uptake, were considered positive when higher than 2.5%, this being the mean + 2SD of the negative control group (*17*). To study the capacity of the different dendrimers to bind specific IgE antibodies and compare them with the classical monomer used in different studies bound to butylamine **1**, RAST inhibition studies were made as described (*17*). This was carried out using the same solid phase, BPO−PLL. In the fluid phase the sera from patients allergic to penicillin were incubated with three different penicilloylated dendrimers at three 10-fold concentrations, ranging from 25 mM to 0.25 mM for **G_0P**, from 12.5 mM to 0.125 mM for **G_1P**, from 6.25 mM to 0.0625 for **G_2P**, and from 100 mM to 1 mM for **1**. The results were expressed as inhibition percentages.

RESULTS AND DISCUSSION

Penicillins are reactive to a variety of nucleophilic reagents such as alcohols, amines and thiols. The result of this nucleophilic attack is the cleavage of the β-lactam amide bond, which yields penicilloic acid derivatives such as **1**. The rate of reaction of the β-lactam ring in penicillins with amines and other nucleophiles resembles carboxylic acid anhydrides in their acylating capability (*18*). We used this reactivity as the strategy to functionalize the amino terminal groups on the periphery of PAMAM dendrimers. To determine the reaction rate, we previously reacted benzylpenicillin sodium salt with butylamine at NMR scale using D_2O as solvent. The characteristic ^{1}H chemical shifts for protons H-6 and H-5 in the β-lactam ring of benzylpenicillin were used to monitor the progress of the reaction. These two protons resonate at 5.53 and 5.41 ppm ($J_{5,6}$ = 3.9 Hz) in benzylpenicillin, and at 4.85 and 4.30 ppm ($J_{5,6}$ = 8.5 Hz) when the β-lactam ring is open. The reaction was very fast and completed within 15 min. Furthermore, only the product corresponding to the aminolysis of the β-lactam ring was detected (compound **1**). The efficiency and rate of this coupling reaction encouraged us to use the same procedure to synthesize the functionalized dendrimers (**G_nP**).

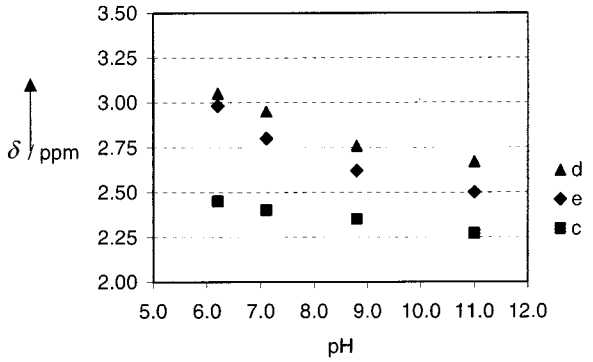


Figure 1. Influence of pH on δ for the inner protons in **G_0P** (for assignments, see Chart 1).

Three different generations of dendrimers were employed (n = 0−2), the reactions being carried out in an aqueous carbonate buffer at pH 10.8 (to ensure that every terminal amino group in the PAMAM dendrimer was deprotonated), using excess benzylpenicillin and controlling the temperature, which turned out to be a strongly influential factor. All products were purified by size-exclusion chromatography and provided essentially pure dendrimers (**G_0P**−**G_2P**) the chemical structure of which was unequivocally assigned by mass spectrometry and ^{13}C and ^{1}H NMR spectroscopy.

The reaction of the zero-generation dendrimer (**G_0**) was monitored by ^{1}H NMR in D_2O, using basic pD obtained by addition of Na_2CO_3. Under these conditions, the ^{1}H NMR spectrum was very clear and contained a single set of signals each of which integrated correctly with the expected number of protons, according to the chemical structure. The resonances for the methylene protons directly bonded to the terminal amino groups were very useful as they clearly reflected deshielding of this signal from 2.70 to 3.22 ppm as the coupling reaction developed. On the other hand, the ^{1}H NMR spectrum recorded in D_2O containing no Na_2CO_3 exhibited two sets of signals that can be assigned to the presence of protonated species (*19*). Therefore, recording the NMR spectra at a basic pD was crucial with a view to evaluating the synthesized dendrimers. Figure 1 shows the influence of pH on the ^{1}H chemical shift (δ) of the inner protons in dendrimer **G_0P**.

The ^{13}C NMR spectrum (Figure 2) was very useful to confirm the structural homogeneity of this compound. While carbons (a) and (b) appeared at 42.78 and 40.82 ppm, respectively, in the zeroth-generation PAMAM dendrimer, they resonated at virtually the same frequency (39.50 and 39.61 ppm) in **G_0P**. The absence of signals for carbons bonded to unsubstituted amino groups confirmed the efficiency of the coupling process.

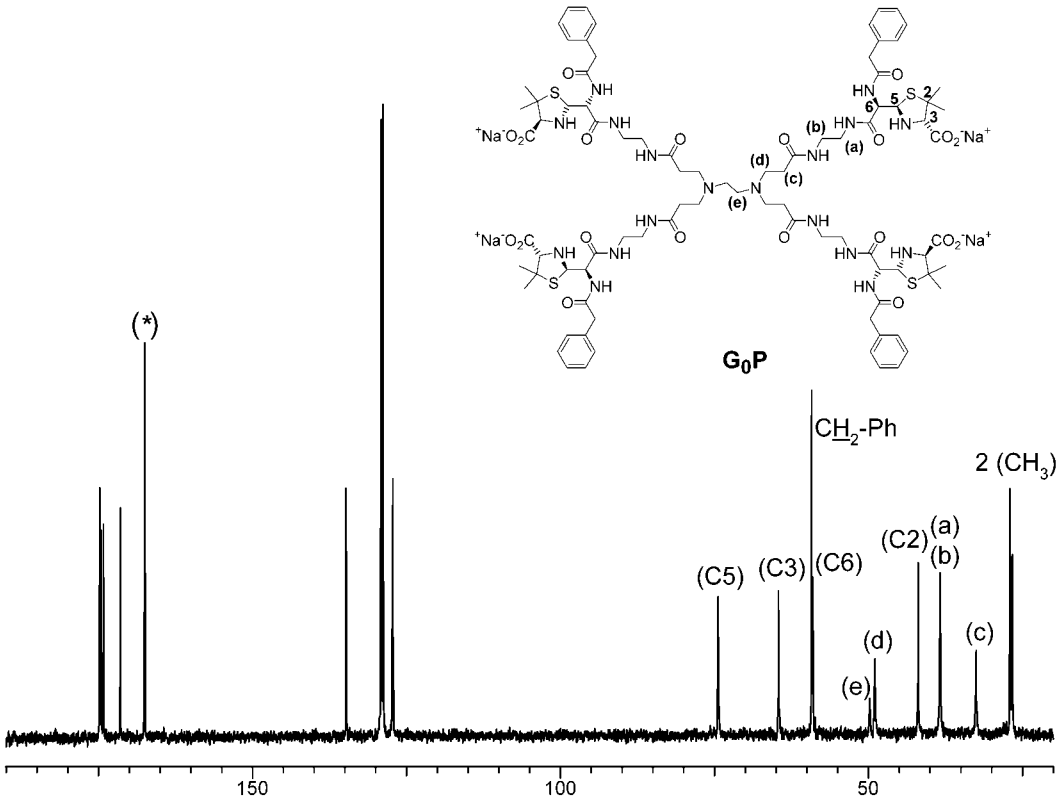


Figure 2. ^{13}C NMR spectrum [100 MHz, D_2O + Na_2CO_3(*)] for dendrimer **G_0P**.

Table 1. Molecular Masses for the Synthesized Dendrimers

		molecular weight	
compound	molecular formula	calculated	observed
G_0P(Na)	$C_{86}H_{116}N_{18}O_{20}S_4Na_4$	1942	1943 $[M+H]^+$ [a]
G_0P(H)	$C_{86}H_{120}N_{18}O_{20}S_4$	1854	1855 $[M+H]^+$ [b]
G_1P(H)	$C_{190}H_{272}N_{42}O_{44}S_8$	4105	4106 $[M+H]^+$ [b]
G_2P(H)	$C_{398}H_{576}N_{90}O_{92}S_{16}$	8606	8607 $[M+H]^+$ [b]

[a] FAB-MS. [b] MALDI-TOF-MS.

Mass spectrometry analysis was carried out using the fast atom bombardment (FAB) and matrix-assisted laser-desorption ionization time of flight (MALDI-TOF) techniques (Table 1). The zeroth-generation dendrimer (**G_0P-(Na)**) was analyzed by FAB-MS, which afforded a molecular ion at $m/z = 1943$ in the spectrum, corresponding to its $[M + H]^+$ adduct. The best conditions for recording the MALDI-TOF mass spectrum for this compound were dissolving the product in 1:1 H_2O/CH_3CN containing 0.1% trifluoroacetic acid (TFA) and using 2,4,6-trihydroxyacetophenone (THAP) as matrix. Under these conditions, the carboxylic moieties in **G_0P** are expected to be protonated (**G_0P(H)**), so a peak corresponding to this structure was found at higher m/z values in the spectrum ($[M + H]^+$).

The first-generation penicilloylated dendrimer (**G_1P**) was synthesized in the same manner, starting from first generation PAMAM dendrimer and using excess benzylpenicillin. The ^1H NMR and ^{13}C NMR spectra were very similar to those for the zeroth-generation dendrimer; the mass spectrometry analysis was performed by using the MALDI-TOF technique under the above-described conditions. A peak matching $[M + H]^+$ for **G_1P(H)** was found in the molecular ion region corresponding to the dendrimer with carboxylic acid moieties in the penicilloyl portions (Table 1).

All attempts at obtaining the functionalized second-generation dendrimer (**G_2P**) under the same conditions as **G_0P** and **G_1P** failed; the result was the second-generation dendrimer with incomplete peripheral substitution. The ^{13}C NMR spectrum showed small signals that could be assigned to carbons bonded to unsubstituted amino groups, as later confirmed by the MALDI-TOF-MS analysis. Attempts involving more drastic conditions (e.g., a higher temperature, an increased concentration of benzylpenicillin, a prolonged reaction time), starting either from the second generation PAMAM dendrimer or the isolated, partially functionalized dendrimer, provided no improvement.

The dendritic structure is a dynamic system (*20*) and, as such, due to the apparent conformational mobility (*21*) it might result in a statistically higher spatial volume engaged with every bulky terminal penicilloyl group. This fact could introduce additional steric hindrance in benzylpenicillin approach to unsubstituted terminal amino groups. However, this restrictive factor could be reduced decreasing the mobility of the partially functionalized dendrimer. Similar observations were reported for a completely different dendrimer family (*9b*) in whitch formation of a "sugar ball" dendrimeric precursor was attempted by terminating the reaction at low temperature.

Bearing in mind this consideration, and the proven efficiency of the coupling process employed, we synthesized **G_2P** at a low temperature (4 °C) to ensure complete peripheral substitution. The penicilloylated dendrimer obtained with this method **G_2P** exhibited ^1H NMR and ^{13}C NMR spectra similar to those for **G_0P** and **G_1P**. The mass spectrometry analysis of the second generation dendrimer, performed using the MALDI-TOF technique and 3,5-dimethoxy-4-hydroxycinnamic acid as matrix, revealed the expected peak at $m/z = 8607$ ($[M + H]^+$,

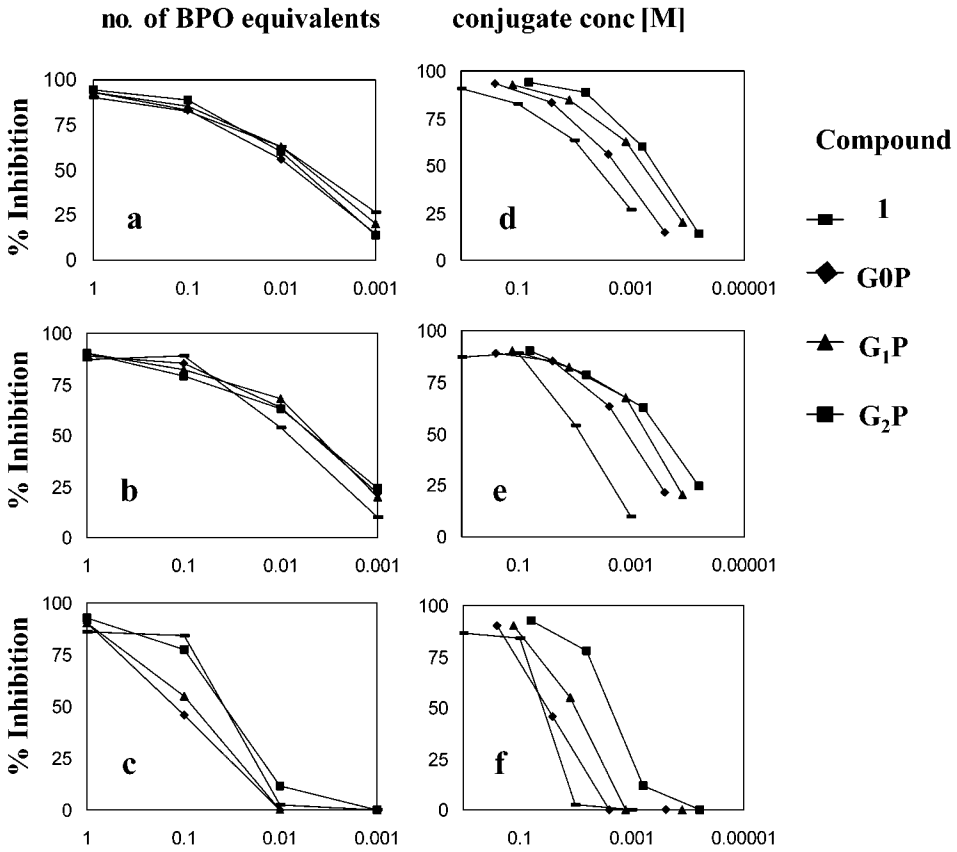


Figure 3. RAST inhibition assay. Sera from patients allergic to penicillins with different specific IgE antibody levels were tested. Specific IgE antibody levels were 7.24 for sera of low affinity (a/d), 9.14 for sera of medium affinity (b/e), and 13.41 for sera of high affinity (c/f). BPO−PLL disks were used in the solid phase. Different dendrimers conjugated to benzylpenicillin **G_0P**, **G_1P**, and **G_2P** and butylamine conjugated to benzylpenicillin **1** were used as inhibitors in the fluid phase.

$G_2P(H)$, Table 1), which confirmed the complete peripheral functionalization of this compound.

To compare the capacity of different dendrimers conjugated to penicillin to bind specific IgE antibodies, RAST inhibition studies were carried out using sera from patients allergic to penicillin. Figure 3 shows the inhibition curves obtained with sera from three patients with different specific IgE antibody levels (ranging from 7 to 13%) determined previously by RAST. As seen, these dendrimers are recognized by the specific IgE antibody from patients allergic to penicillin. We first compared the results obtained with the different conjugates using the same number of penicillin equivalents (Figures 3a, 3b, and 3c). For this, different concentrations of the inhibitors were used, but as they had the same number of penicillin equivalents, there were no differences between the dendrimers and the monomer of butylamine, the pattern being similar in all the sera studied. When we compared these results in terms of conjugate concentrations (Figures 3d, 3e, and 3f), there were clear differences in the capacity of the different dendrimers and butylamine conjugate to bind to specific IgE antibodies. The maximum inhibition in all three cases studied was with **G_2P**, followed by **G_1P**, **G_0P**, and finally **1**. This indicates that a concentration of **1** approximately 100 fold higher than that for **G_2P** is needed to obtain the same percentage inhibition. The differences with the other dendrimers are less clear, although there was a direct correlation between the molecular weight of the dendrimer and the specific IgE antibody binding capacity.

In summary, we synthesized and characterized a series of densely penicilloylated dendrimers (**G_nP**, $n = 0-2$) with precisely defined chemical structures. These dendrimers exhibit very similar, simple ^{1}H NMR and ^{13}C NMR spectra that are suggestive of highly symmetric structures and of the monodisperse nature of these compounds. Furthermore, the mass spectrometry analysis of these functional dendrimers confirmed their exact chemical composition. This constitutes significant progress compared with conventional benzylpenicilloyl conjugates (BPO−HSA and BPO−PLL).

The proposed approach to the synthesis of dendrimer **G_2P** can be a useful tool for the functionalizing of this type of dendrimer provided the coupling process employed is efficient enough. As noted earlier, the use of "forcing conditions" led to no improved results.

Preliminary RAST inhibition studies have confirmed the usefulness of penicilloylated dendrimers as conjugates for the recognition of IgE antibodies from patients allergic to penicillin. We are now ready to evaluate the relevance of the size of the hapten−carrier conjugate and hapten density profile in recognition, simply by changing the generation of the starting dendrimer (in our study there was an increase in the percent RAST inhibition from generation 0 to 2). Thus, presenting many penicillin determinants to specific IgE antibodies using structures able to carry many hapten molecules would increase in vitro sensitivity. Consequently, these compounds can be considered promising candidates for use in the development of a new in vitro test, with increased sensitivity for the diagnosis of allergy to β-lactam antibiotics compared to the test used until now. Work is in progress in our laboratories.

ACKNOWLEDGMENT

This work was supported by funds granted for the realization of the FEDER Project 1FD97-0516. F.S-S is grateful for the award of a fellowship related to this project. The authors are also grateful to Prof. E. Giralt (Departamento de Química Orgánica, Universidad de Barcelona, Spain) for recording the MALDI-TOF-MS spectra and to Dr. M. Maestro (SXAIN, Universidad de La Coruña, Spain) for the FAB-MS spectrum.

Supporting Information Available: Preparation procedure, chemical structure, ^{1}H and ^{13}C NMR data, and MALDI-TOF-MS data and spectra for **G_0P**, **G_1P**, and **G_2P**; FAB-MS data for **G_0P**. This material is available free of charge via the Internet at http://pubs.acs.org.

LITERATURE CITED

(1) For general recent reviews on dendrimers, see: (a) Newkome, G. R., Moorefield, C. N., and Vögtle, F. (1996) *Dendritic Molecules: Concepts, Syntheses, Perspectives*, VCH, Weinheim. (b) Matthews, O. W., Shipway, A. N., and Stoddart, J. F. (1998) Dendrimers-branching out from curiosities into new technologies. *Prog. Polym. Sci. 23*, 1−56. (c) Archut, A., and Vögtle, F. (1998) Functional Cascade Molecules. *Chem. Soc. Rev. 27*, 233−240. (d) Narayanan, V. V., and Newkome, G. R. (1998) Supramolecular Chemistry within Dendritic Structures. *Top. Curr. Chem. 197*, 19−77. (e) Fischer, M., and Vögtle, F. (1999) Dendrimers: From Design to Application − A Progress Report. *Angew. Chem., Int. Ed. 38*, 884−905.

(2) Roy, R., Zanini, D., Meunier, S. J., and Romanowska, A. (1993) Solid-Phase Synthesis of Dendritic Sialoside Inhibitors of Influenza-A Virus Hemagglutinin. *J. Chem. Soc., Chem. Commun.* 1869−1872.

(3) (a) Service, R. F. (1995) Chemistry − Dendrimers − Dream Molecules Approach Real Applications. *Science 267*, 458−459. (b) Twyman, L. J., Beezer, A. E., Esfand, R., Hardy, M. J., and Mitchell, J. C. (1999) The Synthesis of Water Soluble Dendrimers, and their Application as Possible Drug Delivery Systems. *Tetrahedron Lett. 40*, 1743−1746.

(4) (a) Lauffer, R. B. (1987) Paramagnetic metal complexes as water proton relaxation for NMR imagin: theory and design. *Chem. Rev. 87*, 901−927. (b) Caravan, P., Ellison, J. J., McMurry, T. J., and Lauffer, R. B. (1999) Gadolinium(III) Chelates as MRI Contrast Agents: Structure, Dynamics, and Applications. *Chem. Rev. 99*, 2293−2352.

(5) Mammen, M., Choi, S.-K., and Whitesides, G. M. (1998) Polyvalent Interactions in Biological Systems: Implications for Design and Use of Multivalent Ligands and Inhibitors. *Angew. Chem., Int. Ed. 37*, 2754−2794.

(6) (a) Tam, J. P. (1988) Synthetic peptide vaccine design: synthesis and properties of a high-density multiple antigenic peptide system. *Proc. Nat. Acad. Sci. U.S.A. 85*, 5409−5413. (b) Posnett, D. N., McGrath, H., and Tam, J. P. (1988) A novel method for producing anti-peptide antibodies. Production of site-specific antibodies to the T cell antigen receptor beta-chain. *J. Biol. Chem. 263*, 1719−1725.

(7) PAMAM dendrimers were first developed by Tomalia and co-workers: (a) Tomalia, D. A., Baker, H., Dewald, J. R., Hall, M., Kallos, G., Martin, S., Roeck, J., Ryder, J., and Smith, P. (1985) A new class of polymers: starburst-dendritic macromolecules. *Polym. J. (Tokyo) 17*, 117−132. (b) Tomalia, D. A., Baker, H., Dewald, J. R., Hall, M., Kallos, G., Martin, S., Roeck, J., Ryder, J., and Smith, P. (1986) Dendritic macromolecules: synthesis of starburst dendrimers. *Macromolecules 19*, 2466−2468. (c) Tomalia, D. A., Naylor, A. M., and Goddart, W. A., III. (1990) Starburst dendrimers: molecular-level control of size, shape, surface chemistry, topology, and flexibility from atoms to macroscopic matter. *Angew. Chem., Int. Ed. 29*, 138−175. (d) Tomalia, D. A., and Durst, H. D. (1993) Genealogically Directed Synthesis − Starburst Cascade Dendrimers and Hyperbranched Structures. *Top. Curr. Chem.* 192−313. (e) Frechet, J. M. J., and Tomalia, D. A. (2001) Dendrimers and Other Dendritic Polymers (Frechet, J. M. J., and Tomalia, D. A., Eds.) J. Wiley & Sons Ltd, West Sussex.

(8) (a) For a recent review, see: Esfand, R., and Tomalia, D. A. (2001) Poly(amidoamine) (PAMAM) dendrimers: from biomimicry to drug delivery and biomedical applications. *Drug Discov. Today 6*, 427−436. (b) Singh, P., Moll, F., Lin, S. H., Ferzli, C., Yu, S. K., Koski, R. K., Saul, R. G., and Cronin, P. (1994) Starburst Dendrimers − Enhanced Performance and Flexibility for Immunoassays. *Clin. Chem. 40*, 1845−1849 and refs 24, 25 in 8a.

(9) (a) Aoi, K., Itoh, K., and Okada, M. (1995) Globular Carbohydrate Macromolecule Sugar Balls 0.1. Synthesis of Novel Sugar-Persubstituted Poly(Amido Amine) Dendrimers. *Macromolecules 28*, 5391−5393. (b) Aoi, K., Tsutsumiuchi, K., Yamamoto, A., and Okada, M. (1997) Globular Carbohydrate Macromolecule "Sugar Balls" 3. "Radial-Growth Polymerization" of Sugar-Substituted α-Amino Acid *N*-Carboxyanhydrides (GlycoNCAs) with a Dendritic Initiator. *Tetrahedron 53*, 15415−15427.

(10) (a) Blanca, M., Mayorga, C., Pérez, E., Suau, R., Juárez, C., Vega, J. M., Carmona, M. J., Pérez-Estrada, M., and García, J. (1992) Determination of IgE antibodies to the benzylpenicilloyl determinant: A comparison betweend poly-L-lysine and human serum albumin as carrier. *J. Immunol. Methods 153*, 99−105. (b) Blanca, M., Moreno, F., Mayorga, C., García, J., Fernández, M., Pérez, E., Juárez, C., and Suau, R. (1994) The nature of the carrier in the RAST assay influences the capacity for detecting IgE antibodies to penicillins. *J. Clin. Immunoassay 17*, 166−170.

(11) De Weck, A. L. (1983) Penicillin and cephalosporins, in *Allergic Reaction to Drugs* (De Weck, A. L., and Bundgaard, H., Eds.) pp 423−482, Springer-Verlag, Berlin.

(12) Dewdeney, J. M. (1977) Immunology of the antibiotics, in *The Antigens* (Sela, M., Ed.) vol. 5, pp 73−245, Academic Press, New York.

(13) Weiss, M. E., and Adkinson, N. F. (1988) Immediate hypersensitivity reactions to penicillins related antibiotics. *Clin. Allergy 18*, 515−540.

(14) Zeng, F., and Zimmerman, S. C. (1997) Dendrimers in Supramolecular Chemistry: From Molecular Recognition to Self-Assembly. *Chem. Rev. 97*, 1681−1712.

(15) The term "functional dendrimer" is used to describe dendritic molecules which have useful or reactive functional groups that can take part in chemical/physical processes without degrading the dendritic matrix. For reviews on functional dendrimers, see: (a) Issberner, J., Moors, R., and Vögtle, F. (1995) Dendrimers − From Generations and Functional-Groups to Functions. *Angew. Chem., Int. Ed. 33*, 2413−2420. (b) Smith, D. K., and Diederich, F. (1998) Functional Dendrimers: Unique Biological Mimics. *Chem. Eur. J. 4*, 1353−1361. (c) Chow, H. F., Mong, T. K.-K., Nongrum, M. F., and Wan, C.-W. (1998) The Synthesis and Properties of Novel Functional Dendritic Molecules. *Tetrahedron 54*, 8543−8660. (d) Bosman, A. W., Janssen, H. M., and Meijer, E. W. (1999) About Dendrimers: Structure, Physical Properties, and Applications. *Chem. Rev. 99*, 1665−1688. (e) Vögtle, F., Gestermann, S., Hesse, R., Schwierz, H., and Windisch, B. (2000) Functional dendrimers. *Prog. Polym. Sci. 25*, 987−1041.

(16) Blanca, M., Torres, M. J., Mayorga, C., Romano, A., Pérez-Inestrosa, E., and Suau, R. (1999) In−Vitro Methods for Quantifying IgE Antibodies to Beta-Lactams. *Allergy 54*, 8−12.

(17) Moreno, F., Blanca, M., Mayorga, C., Terrados, S., Moya, M. C., Pérez, E., Suau, R., Vega, J. M., García, J., Miranda, A., and Carmona, M. J. (1995) Studies of the Specificities of IgE Antibodies Found in Sera from Subjects with Allergic Reactions to Penicillins. *Int. Arch. Allergy Immunol. 108*, 74−81.

(18) McGregor D. N. (1984) *Comprehensive Heterocyclic Chemistry* (Lwowski, W., Ed.) pp 299−339, Vol. 7, Pergamon Press, Oxford.

(19) PAMAM dendrimers are known to be positively charged at physiological pH. See: Poxon, S. W., Mitchell, P. M., Liang, E., and Hughes, J. A. (1996) Dendrimer delivery of oligonucleotide. *Drug Delivery 3*, 255−261. On the other hand, Tomalia and co-workers have studied the protonation of PAMAM dendrimers as a function of pH. See ref 7d, p 287.

(20) Ashton, P. R., Anderson, D. W., Brown, C. L., Shipway, A. N., Stoddart, J. F., and Tolley, M. S. (1998) The Synthesis and Characterization of a New Family of Polyamide Dendrimers. *Chem. Eur. J. 4*, 781−795.

(21) Chaumette, J.-L., Laufersweiler, M. J., and Parquette, J. R. (1998) Synthesis and Chiroptical Properties of Dendrimers Elaborated from a Chiral, Nonracemic Central Core. *J. Org. Chem. 63*, 9399−9405.

BC0155824

Improved Tumor Selectivity of Radiolabeled Peptides by Receptor and Antigen Dual Targeting in the Neurotensin Receptor Model

Marc Hillairet de Boisferon,[§,†,||] Olivier Raguin,[§,†,||] Cynthia Thiercelin,[†,||] Monique Dussaillant,[†,||] William Rostène,[†] Jacques Barbet,[‡,||] André Pélegrin,[#,||] and Anne Gruaz-Guyon*[,†,||]

INSERM U339, Faculté de Médecine et Hôpital Saint-Antoine, Paris, France; INSERM U463, Nantes, France; EA2989 CRLC Val d'Aurelle-Paul Lamarque, Montpellier, France; CNRS GDR 2352, Immunociblage des tumeurs, France. Received November 28, 2001; Revised Manuscript Received March 1, 2002

Radiolabeled peptides are emerging tools for diagnosis and therapy of tumors overexpressing receptors. However, binding to receptors expressed by nontumor tissues may cause toxicity. The objective of this study was to specifically enhance the binding affinity of labeled peptides to tumor cells, as opposed to receptor-positive nontumor cells, to ensure targeting selectivity. This was achieved by the simultaneous binding of hapten-bearing peptides to their receptor and to a tumor-associated antigen, mediated by a bispecific antibody directed to the tumor antigen and to the hapten. Binding of labeled neurotensin analogues bearing the DTPA(indium) hapten (NT−DTPA(^{111}In)) to human colorectal carcinoma cells (HT29), which express the neurotensin receptor (NTR1) and carcinoembryonic antigen (CEA), was studied in the presence of a bispecific antibody (BsmAb) directed to CEA and to DTPA-(indium). In vitro dual binding of NT−DTPA in the presence of BsmAb was about 6.5-fold higher than monovalent binding to NTR1 and 3.5-fold higher than the sum of the monovalent bindings to NTR1 or to CEA, suggesting cooperativity. Increased binding under bivalent conditions translated into increased internalization. In vivo pretargeting with BsmAb enhanced tumor uptake and tumor retention. Hapten bearing peptides binding simultaneously an overexpressed cell-surface receptor and a tumor antigen show increased selectivity to target tumor cells as compared to cells only expressing the cell surface receptor. Better resistance to enzymatic degradation and optimized administration protocols should further enhance in vivo targeting selectivity and may allow the development of radiopharmaceuticals labeled with isotopes suitable for radiotherapy such as ^{131}I or ^{90}Y.

INTRODUCTION

Many tumors overexpress receptors for small biologically active peptides, such as hormones or neuromediators. Their radiolabeled analogues are potential tools for tumor targeting. Their fast diffusion in tumor tissue offers a major pharmacokinetic advantage as compared to antibodies. In addition, internalization of receptor-bound ligands offers an opportunity for isotope accumulation in target cells. The potential of peptide radiopharmaceuticals is illustrated by the successful development of somatostatin analogues to visualize tumors and more recently by therapeutic applications (*1*, *2*). Labeled analogues of peptide ligands for several other receptors, overexpressed by tumors (*3*), such as CCK (*4*, *5*), gastrin (*4*), vasoactive intestinal peptide (*6*), melanocyte stimulating hormone (*7*), and neurotensin (*8*) are under investigation. However, the background due to receptor-positive nontumor tissues contributes to decrease tumor to normal tissue uptake ratios and is expected to cause toxicity (*9*).

Enhancement of the affinity of a peptide for tumor cell surface, as opposed to receptor-positive nontumor tissue, would increase targeting selectivity and might be a key step to the development of more efficient therapeutic agents. It is well-known that affinity is enhanced by the cooperativity of multivalent binding. The aim of the present study was to evaluate the feasibility of increasing the binding affinity of a labeled peptide for receptor-positive tumor cells by the simultaneous targeting of an endogenous receptor and an antigen at the tumor cell surface. With an adequate choice of the antigen and of the receptor, no affinity enhancement will occur on nontumor tissue expressing only one of these targets. Hence, double targeting will enhance selectivity for tumor cells.

The binding of an anti-hapten x anti-antigen bispecific antibody (BsmAb) to a selected tumor-associated antigen provides hapten-binding sites at the tumor cell surface. Then a labeled hapten-bearing ligand can bind simultaneously to a tumor-overexpressed receptor and to the bispecific antibody (Figure 1).

To evaluate this approach we have chosen carcinoembryonic antigen (CEA) and type 1 neurotensin receptor (NTR1) dual targeting as a model. CEA and NTR1 expression is encountered on some colorectal carcinomas, breast, small cell lung carcinoma, and pancreatic carcinoma cells. The HT29 colorectal carcinoma cell line was used to investigate this approach (*10*, *11*). The diethyl-

* Correspondence to Anne Gruaz-Guyon INSERM U.339, Biophysique, Faculté de Médecine Saint-Antoine, 27 Rue Chaligny, 75012 Paris, France. (Tel: (33) 1 40 01 14 66, Fax: (33) 1 43 43 89 46). e-mail: gruaz@adr.st-antoine.inserm.fr.

† INSERM U339, Faculté de Médecine et Hôpital Saint-Antoine.

‡ INSERM U463, Nantes.

EA2989 CRLC Val d'Aurelle-Paul Lamarque.

|| CNRS GDR 2352, Immunociblage des tumeurs.

§ The contributions of Marc Hillairet de Boisferon and Olivier Raguin are to be considered as equal.

10.1021/bc015585g CCC: $22.00 © 2002 American Chemical Society
Published on Web 04/25/2002

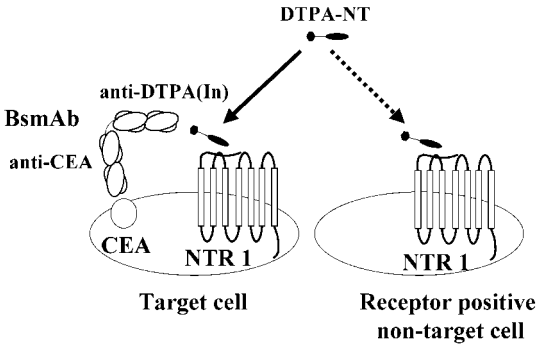


Figure 1. Schematic representation of enhanced tumor targeting specificity of a hapten-bearing peptide by dual targeting of a receptor and an antigen. At the tumor cell surface the dual binding of DTPA(indium)−NT analogue to NTR1 and to the BsmAb bound to CEA will provide affinity enhancement. This will not occur at the surface of receptor-positive antigen-negative nontumor cells. (DTPA: diethylenetriaminepentaacetic acid, NT: neurotensin, BsmAb: anti-CEA x anti-DTPA(indium) bispecific antibody).

enetriaminepentaacetic acid (DTPA)−indium complex (DTPA(indium)) was used as a hapten. Two neurotensin analogues bearing the DTPA(indium) hapten (DTPA−NT) were synthesized. Their dual binding to NTR1 and to CEA at HT29 cell surface, in the presence of anti-CEA x anti-DTPA(indium) BsmAb, was studied in vitro and in vivo.

MATERIAL AND METHODS

Cells. HT29 cells (ATCC, Rockville, MD) are human colorectal carcinoma cells that express the high affinity neurotensin receptor (NTR1) (*10*) and CEA (*11*) at their surface. These cells were grown in DMEM medium (Gibco, France) supplemented with 10% fetal calf serum (FCS), 1% glutamine, and 0.1% gentamycin at 37 °C in 5% CO_2.

For binding experiments, cells were treated as described by Velcich et al. (*11*) in order to increase CEA expression. Briefly, cells were distributed into 12-well Corning dishes (6×10^5 cells per well in 1 mL) and incubated at 37 °C for 24 h using the culture conditions described above. Culture medium was then replaced by 1 mL of low serum medium (0.05% FCS). Twenty-four hours later, cells were treated with low serum medium supplemented with 10 μg/mL forskolin (Sigma, France).

Synthesis of the DTPA−NT Analogues. DTPA-dianhydride (Aldrich, France) was reacted with the lysine ϵ-NH_2 of neurotensin (pGlu-Leu-Tyr-Glu-Asn-Lys-Pro-Arg-Arg-Pro-Tyr-Ile-Leu) (Neosystem, France) or with the α-NH_2 of a neurotensin analogue (Gly-Glu-Leu-Tyr-Glu-Asn-Lys(Ac)-Pro-Arg-Arg-Pro-Tyr-Ile-Leu) (Neosystem, France) to obtain, respectively, pGlu-Leu-Tyr-Glu-Asn-Lys(DTPA)-Pro-Arg-Arg-Pro-Tyr-Ile-Leu (hereafter referred to as [Lys(DTPA)]−NT) and DTPA−Gly-Glu-Leu-Tyr-Glu-Asn-Lys(Ac)-Pro-Arg-Arg-Pro-Tyr-Ile-Leu (DTPA−Gly−NT).

Briefly, 1.8 μmol of a neurotensin solution (220 μL) in HEPES buffer (0.6 M, pH 8.2, filtered through Chelex 100 (Biorad, France)) was added with stirring to 14.5 μmol of DTPA dianhydride (Aldrich, France) in solution in DMSO (220 μL). The pH was maintained at 8.2 until the reaction was completed. After evaporation of the solvents, the crude product was dissolved in water and trifluoroacetic acid to reach pH 2. The solution was filtered through Chelex 100. DTPA−NT analogues were purified by C18 reverse phase chromatography (Nucleosil, Shandon, France) using a linear 15-min gradient (A: H_2O/TFA(0.05%), B: acetonitrile) from 0% to 26% B and a linear 20-min gradient from 26% to 30%. Purity was checked by C18 reverse phase chromatography under isocratic conditions (acetonitrile 30%, H_2O/TFA 0.05%). Both peptides were purified to at least 95% purity. The DTPA−NT analogues were characterized by mass spectrometry 2048.16 found, 2048.32 calculated for [Lys-(DTPA)]−NT, 2165.50 found and 2165.37 calculated for DTPA−Gly−NT using a Nermag R10−10 mass spectrometer with an electrospray ion source (Analytica of Branford) equipped with an iron guide.

Antibodies. All antibodies used in this work were kindly provided by Immunotech S.A., France. The anti-CEA (clone F6) is a mouse $IgG_{1,\kappa}$ monoclonal antibody specific for human CEA (*12*). The antibody directed to the DTPA(indium) complex is an $IgG_{1,\lambda}$ (*13*).

The anti-DTPA(indium) Fab′ fragment was biotinylated and immobilized on avidin-coated tubes (Immunotech S.A., France) to determine DTPA(indium)−NT immunoreactivity (1 μg per tube) or equilibrium affinity constants (0.1 μg per tube). The anti-CEA x anti-DTPA-(indium) BsmAb was prepared as already described (*14*) by chemical coupling of the two reduced Fab′ fragments using *o*-phenylenedimaleimide. Equilibrium affinity constant (K_a) for the binding of anti-CEA x anti-DTPA-(indium) BsmAb to CEA expressed at HT29 cell surface was determined as $2.6 \pm 1.4 \times 10^8$ M^{-1} by competition binding experiments between ^{125}I-labeled Bsmab (prepared by the iodogen method (*15*)) and increasing concentrations of unlabeled Bsmab (1×10^{-10} M to 1×10^{-8} M). Nonspecific binding was evaluated in the presence of excess unlabeled anti-CEA IgG (2×10^{-7} M). The number of binding sites per HT29 cell was $2.1 \pm 0.1 \times 10^4$ after a 24-h treatment by forskolin, about 6-fold higher than that determined without forskolin treatment ($3.5 \pm 0.7 \times 10^3$). All subsequent experiments were performed on forskolin-treated HT29 cells. The anti-CEA immunoreactivity of the BsmAb was 87% (*16*) and the anti-DTPA(indium) immunoreactivity of the BsmAb determined by incubating trace amounts of ^{125}I-labeled BsmAb in DTPA(indium)-coated tubes was 85%.

Radiolabeling. The DTPA−NT analogues (0.2 nmol) were labeled with indium-111 ($^{111}InCl_3$, 11.1 MBq, CIS bio international, France) in 100 mM acetate−10 mM citrate buffer pH 5.0 during 22 h at room temperature. Then, since the anti-DTPA(indium) antibody is specific to the DTPA(indium) complex, free DTPA groups were saturated with nonradioactive $InCl_3$ (2 nmol) in the same buffer. Excess free indium was removed on a Sep-Pak cartridge (Waters, Milford, MA) in acetate−citrate buffer, followed by elution of the labeled DTPA−NT analogues in acetate−citrate buffer/ethanol (50/50, v/v). ^{111}In-labeling of both DTPA−NT analogues led to a chelation of indium-111 of 88 ± 5% for ^{111}In-labeled [Lys(DTPA)]−NT and 85 ± 4% for DTPA(^{111}In)−Gly−NT. Their specific activities were very similar: 179 ± 16 and 177 ± 12 MBq/nmol, respectively.

Computer Simulations. Delaage and co-workers (*17*, *18*) have introduced several years ago a methodology to calculate binding equilibrium under complex situations. This methodology has been implemented as an add-in to Microsoft Excel 97 run on an ordinary PC (*19*). The multiple equilibrium system is described by a partition function, and the program calculates the free concentrations of all interacting species by minimizing the partition function for a given set of parameters. Then parameter estimation is obtained by variance-weighted nonlinear least-squares regression. Results are given as the best-fit estimation ± SD. This program allowed us to deter-

mine unknown parameters such as binding affinity, receptor density, or accessibility factors to interpret binding experiments. In addition it allowed us to test for the cooperativity of peptide-binding to target cells (*19*). This program is available on request to J. B. (Jacques.Barbet@nantes.inserm.fr).

Briefly, steps to model the multiple binding system are described as follows. F1 is the free NT-DTPA(In) concentration, F2 the free BsmAb concentration, F3 the NTR concentration, F4 the CEA concentration, P1 the affinity binding constant (K_a) of NT-DTPA to the antibody, P2 the K_a for binding of the antibody to CEA, P3 the K_a for binding of NT-DTPA to NTR, P4 an accessibility factor (taking into account a loss in affinity for a simultaneous binding of NT−DTPA to the receptor and the BsmAb), and P5 a cooperativity factor (reflecting the enhanced binding in dual binding condition). The concentrations of the various complexes formed are [NT-DTPA-(In)+BsmAb]:F1.F2.P1; [BsMAb+CEA]: F2.F4.P2; [NTR+NT-DTPA(In)]: F1.F3.P3; [NTR+NT-DTPA(In)+ BsmAb]:F1.F3.P3. F2.P1.P4; [NTR+NT-DTPA(In)+ BsmAb+CEA]:F1.F3.P3. F2.P1.P4.F3.P3.P5. Binding affinity constants were set to the values determined in independent experiments, and the number of CEA and NTR binding sites and the accessibility and cooperativity factors were estimated, from experimental data, by the program.

NT−DTPA Analogues Binding Parameters Determination. Equilibrium affinity binding constant (K_a) and immunoreactivity of ligands were evaluated from binding experiments on cells or on antibody-coated tubes. Binding parameters were then determined from experimental results by curve-fitting to experimental bound-to-total ratios for all available data using the program described above. Every result is expressed as mean ± standard deviation.

Determination of DTPA−NT Analogues Binding Affinities to the Anti-DTPA(Indium) Antibody. Affinity constants of each ^{111}In-labeled DTPA−NT analogue for anti-DTPA(indium) antibody were determined by incubating trace amounts of the ^{111}In-labeled [Lys-(DTPA)]−NT and increasing concentrations of unlabeled DTPA−NT analogue saturated with nonradioactive $InCl_3$ (5.1×10^{-11} M to 10^{-6} M) in anti-DTPA(indium)-coated tubes (0.1 μg) in a final volume of 1 mL of phosphate-buffered saline (PBS) supplemented with 0.2% bovine serum albumin (BSA) for 2.5 h at 37 °C under shaking. Then 100 μL of supernatant were collected and counted. Tubes were washed twice with 0.9% NaCl and 0.002% Tween 20 and counted. Nonspecific binding was evaluated in the presence of excess unlabeled DTPA−NT analogues (saturated with nonradioactive indium, 10^{-6} M) (two experiments in duplicate).

Determination of DTPA−NT Analogues Binding Affinities to NTR1. Neurotensin (NT) was labeled with iodine-125 by the lactoperoxidase method (*20*) and purified by ion-exchange chromatography. Cells were incubated in the presence of trace amounts of ^{125}I-neurotensin and increasing concentrations of unlabeled DTPA−NT analogues saturated with nonradioactive indium (4×10^{-10} M to 1×10^{-6} M) in 500 μL of binding medium (DMEM/0.2% BSA/0.8 mM 1,10-phenanthroline). For each experiment, nonspecific binding was evaluated in the presence of an excess of unlabeled neurotensin (1×10^{-6} M). After 1 h at 37 °C, 50 μL of the supernatant were taken off. Cells were washed twice with ice-cold DMEM/BSA 0.2% and removed from the wells by addition of 900 μL 0.1 M NaOH and counted. An aliquot of the supernatant was counted (three experiments in triplicate).

Binding of DTPA−NT Analogues to HT29 Cells in the Presence of Anti-CEA x Anti-DTPA(Indium) Bispecific Antibody. As HT29 cells simultaneously express CEA and NTR1, monovalent binding of DTPA−NT analogues to CEA, mediated by the BsmAb, was evaluated in the presence of excess unlabeled neurotensin in order to saturate NTR1 at cell surface. This condition mimics cells expressing CEA alone. Monovalent binding of DTPA−NT analogues to NTR1 in the presence of BsmAb was studied using excess anti-CEA IgG to saturate CEA at cell surface, mimicking cells expressing NTR1 alone. Dual binding was studied in parallel in absence of neurotensin or anti-CEA IgG.

The following protocol (protocol 1) was used in most experiments unless otherwise stated. A solution of BsmAb (300 μL, binding medium) was preincubated on the cells. After 2 h of incubation at 37 °C, ^{111}In-labeled-DTPA−NT analogues (200 μL binding medium) were added without washing. Then, the cells were incubated for 1 h at 37 °C. Final concentrations: DTPA(^{111}In)−NT 0.15×10^{-9} M, BsmAb as indicated. The cells and the supernatant were counted as above. For NTR1 monovalent binding experiments, the BsmAb solution contained excess anti-CEA IgG (2×10^{-7} M, final concentration), and for CEA monovalent binding experiments, the ^{111}In-labeled-DTPA−NT analogue solution contained excess neurotensin (1×10^{-6} M, final concentration).

In protocol 2, BsmAb was preincubated as above, and after 2 h at 37 °C, cells were washed once with ice-cold DMEM/0.2% BSA and incubated with 500 μL of ^{111}In-labeled-DTPA−NT analogues for 1 h at 37 °C. In protocol 3, the ^{111}In-labeled-DTPA−NT analogues were incubated with BsmAb in 500 μL of binding medium for 30 min at 37 °C before a 1-h incubation with the cells.

Binding kinetics and internalization experiments were performed with a 2-h pretargeting of the BsmAb without washing (protocol 1), with a final BsmAb concentration of 6×10^{-9} M and of 0.15×10^{-9} M ^{111}In-labeled-DTPA−NT analogues. At selected time intervals (15, 30, 60, 120, and 240 min), supernatant and cells were removed and counted as above for binding determination. The internalized fraction was evaluated by treating the cells for 15 min at 4 °C with DMEM/0.2% BSA adjusted to pH 2.0 with 1 M HCl. This last procedure dissociated surface-bound ligands. Cells were then washed twice with ice-cold DMEM/0.2% BSA. The radioactivity of the cells was counted. Internalization was expressed as the percentage of the total incubated activity that remained associated with the cells after acid wash. As above, for each condition the monovalent binding to CEA or NTR1 was determined in the presence of excess neurotensin or anti-CEA IgG, respectively.

In Vivo Experiments. Animal experiments were performed in compliance with the regulations of the institution and with generally accepted guidelines governing such work.

Animals. Female SWISS nu/nu mice, 6−8 weeks old (Iffa Credo, France), were grafted by subcutaneous injection in the flank with 2×10^6 HT29 human colorectal carcinoma cells. Biodistribution studies were performed two weeks later.

Biodistribution. Mice were given anti-CEA x anti-DTPA(indium) or an irrelevant anti-CD20 x anti-DTPA-(indium) BsmAb (40 pmol in 150 μL of PBS) or vehicle only by intravenous injection. Twenty-four hours later, ^{111}In-labeled [Lys(DTPA)]−NT (15−30 pmol, 25 MBq/

nmol) or an irrelevant ^{111}In-DTPA-bearing peptide AG5.1 (Ac-Lys(DTPA)-GABA-D-Tyr-GABA-Lys(Gly succinyl-histamine)-NH_2) (*19*) (15 pmol, 25 MBq/nmol) was injected iv. Mice were weighed and sacrificed at selected time intervals (1, 3, and 24 h). Tumor, organs, and blood were collected, and the radioactivity in these samples was determined. The injected doses were corrected for losses during injection and subcutaneously injected material remaining in the animal tail.

Tumor Imaging. For imaging studies, mice were administered with relevant BsmAb (40 pmol) or vehicle 24 h before ^{111}In-labeled [Lys(DTPA)]−NT (30 pmol) as described above. Images of the two groups were recorded simultaneously at 3, 6, and 24 h after injection of the labeled analogue. Mice were anesthetized and positioned on the head of the gamma-camera (Picker Prism2000XP). Acquisition was performed for 15 min with 163−183 keV and 237−257 keV energy windows.

Statistical Analysis. Student t test was used to evaluate the significance of in vitro results. For in vivo experiments, statistical analysis of differences in the tissue uptake values and tumor-to-organ ratios was performed using ANOVA variance analysis followed by the Newman−Keuls test. Differences at $p < 0.05$ were considered significant.

RESULTS

Synthesis of the DTPA−NT Analogues. Two neurotensin analogues, pGlu-Leu-Tyr-Glu-Asn-Lys(DTPA)-Pro-Arg-Arg-Pro-Tyr-Ile-Leu ([Lys(DTPA)]−NT) and DTPA−Gly-Glu-Leu-Tyr-Glu-Asn-Lys(Ac)-Pro-Arg-Arg-Pro-Tyr-Ile-Leu (DTPA−Gly−NT), bearing the hapten DTPA, which is a chelating agent suitable for ^{111}In-labeling, have been synthesized by coupling DTPA to an NH_2 group as described in Materials and Methods. Both peptides were purified to at least 95% purity and identified by mass spectrometry.

Equilibrium Affinity Constants of DTPA−NT Analogues Binding to Anti-DTPA(Indium) Antibody. Equilibrium affinity constants for the binding of DTPA−NT analogues to anti-DTPA(indium) antibody were determined by competition experiments. The affinity constant of [Lys(DTPA)]−NT for binding to anti-DTPA-(indium) antibody was $8.4 \pm 0.7 \times 10^8$ M^{-1}, which is in agreement with K_a values determined for peptides bearing DTPA coupled to the ϵ-NH_2 of a lysine (*19*). The K_a binding value decreased when DTPA was coupled to the α-NH_2 of the glycine residue ($1.6 \pm 0.1 \times 10^8$ M^{-1} for DTPA−Gly−NT).

Affinity Constants of DTPA−NT Analogues Binding to NTR1. Affinity parameters for the binding of DTPA−NT analogues to NTR1 were determined by competition experiments. The affinity constants were similar for both DTPA−NT analogues ($1.0 \pm 0.4 \times 10^8$ M^{-1} for [Lys(DTPA)]−NT and $8.7 \pm 3.4 \times 10^7$ M^{-1} for DTPA−Gly−NT) and about 10-fold lower than that of neurotensin ($9.7 \pm 3.0 \times 10^8$ M^{-1}) determined in the same experiment. The number of binding sites was $4.9 \pm 1.1 \times 10^4$ per cell.

Monovalent Binding of DTPA−NT Analogues to NTR1 at HT29 Cell Surface in the Presence of Anti-CEA x Anti-DTPA(Indium) Bispecific Antibody. To study the monovalent binding of DTPA−NT analogues to NTR1 in the presence of BsmAb, CEA at cell surface was saturated with 2×10^{-7} M anti-CEA IgG (no difference was observed between 2×10^{-7} M and 1×10^{-6} M). Increasing the BsmAb concentration (7.2×10^{-11} M to 5.4×10^{-8} M) decreased the binding of DTPA−NT analogues to NTR1 by about 75% (from 1189 ± 234 to 256 ± 5 molecules per cell, $P < 0.001$) for [Lys(DTPA)]−NT (Figure 2A) and about 62% (from 1231 ± 159 to 428 ± 41 molecules per cell, $P = 0.001$) for DTPA−Gly−NT (Figure 3A) at the highest BsmAb concentration tested. This reduced binding was interpreted in terms of accessibility factors (0.13 ± 0.02 for [Lys(DTPA)]−NT and 0.11 ± 0.04 for DTPA−Gly−NT expressing steric hindrance in the simultaneous binding of the relatively small hapten-bearing peptide to the NT receptor and the anti-hapten antibody.

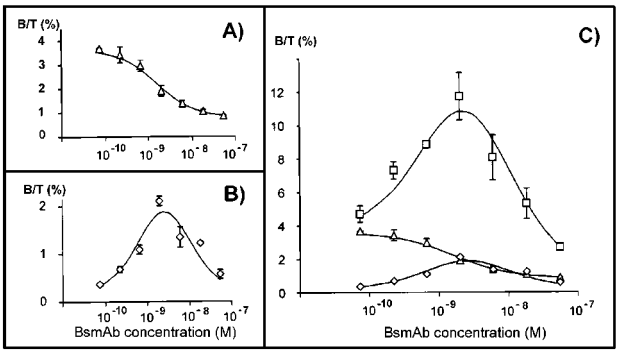


Figure 2. Binding of [Lys(DTPA)]−NT to CEA and NTR1 in the presence of increasing concentrations of pretargeted anti-DTPA(indium) x anti-CEA BsmAb. A: monovalent binding to NTR1 in the presence of excess anti-CEA IgG (2×10^{-7} M) (△: experimental, curve: computer simulation), B: monovalent binding to CEA determined in the presence of excess NT (1×10^{-6} M) (◇: experimental, curve: computer simulation), C: dual binding (□: experimental, curve: computer simulation). Final concentration of [Lys(DTPA)]−NT: 0.15×10^{-9} M. Fraction of radioactivity associated to the cells (B/T%) was counted. The mean of triplicate determinations are plotted ± standard deviation unless smaller than the point as plotted.

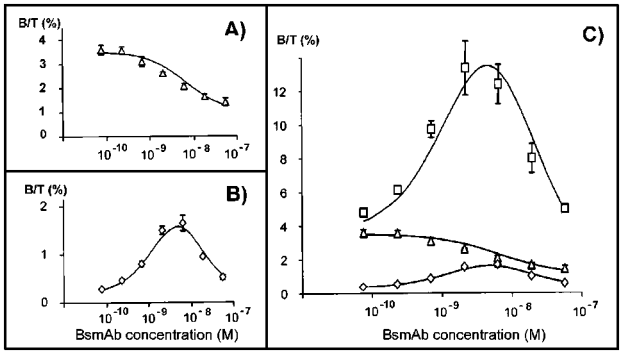


Figure 3. Binding of DTPA−Gly−NT to CEA and NTR1 in the presence of increasing concentrations of pretargeted anti-DTPA(indium) x anti-CEA BsmAb. A: monovalent binding to NTR1 in the presence of excess anti-CEA IgG (2×10^{-7} M) (△: experimental, curve: computer simulation), B: monovalent binding to CEA determined in the presence of excess NT (1×10^{-6} M) (◇: experimental, curve: computer simulation), C: dual binding (□: experimental, curve: computer simulation). Final concentration of DTPA−Gly−NT: 0.15×10^{-9} M. Fraction of radioactivity associated to the cells (B/T%) was counted. The mean of triplicate determinations are plotted ± standard deviation unless smaller than the point as plotted.

Monovalent Binding of DTPA−NT Analogues to HT29 Cell Surface CEA. The monovalent binding of the labeled DTPA−NT analogues to CEA was monitored in the presence of increasing concentrations of BsmAb (7.2×10^{-11} M to 5.4×10^{-8} M). As HT29 cells simultaneously express NTR1 and CEA, the binding to CEA was evaluated in the presence of excess neurotensin (1×10^{-6} M) to saturate NTR1. Binding increased with increasing concentrations of BsmAb to reach a maximum of 535 ±

173 molecules bound per cell at a BsmAb concentration of 2×10^{-9} M for [Lys(DTPA)]−NT (Figure 2B) and of 493 ± 42 at a BsmAb concentration of 6×10^{-9} M for DTPA−Gly−NT (Figure 3B). Then, at higher BsmAb concentrations, labeled DTPA−NT analogues were trapped by excess antibody in the supernatant and binding to cells decreased.

Bivalent Binding of DTPA-NT Analogues to CEA and NTR1. The dual binding of the ^{111}In-labeled DTPA−NT analogues to NTR1 and CEA was studied in the presence of increasing bispecific antibody concentrations (7.2×10^{-11} M to 5.4×10^{-8} M). It was compared to monovalent binding to NTR1 and to CEA in experiments run in parallel. Dual binding exhibited a bell-shaped curve, as expected from the increasing concentration of free antibody in the supernatant (Figure 2C, 3C). Maximal bivalent binding of [Lys(DTPA)]−NT was observed at a bispecific antibody concentration of 2×10^{-9} M, and of DTPA−Gly−NT at a BsmAb concentration of 6×10^{-9} M.

Bivalent binding was greater than each monovalent binding to NTR1 or to CEA ($p < 0.001$) except for DTPA−Gly−NT binding to NTR at a 7.2×10^{-11} M BsmAb concentration (Figures 2 and 3). In addition, it was higher than the sum of monovalent bindings in a large range of BsmAb concentration (2.2×10^{-10} M to 5.4×10^{-8} M, $p < 0.001$). The highest ratio between bivalent binding and the sum of the monovalent bindings was observed at a BsmAb concentration of 6×10^{-9} M. At this BsmAb concentration, 3123 ± 406 molecules of [Lys(DTPA)]−NT were bound per cell versus 461 ± 44 for monovalent binding to NTR1 and 507 ± 108 for monovalent binding to CEA, and 4218 ± 135 molecules of DTPA−Gly−NT versus 640 ± 41 for monovalent binding to NTR1 and 493 ± 42 for monovalent binding to CEA.

Because incubation time is not sufficient for receptor and antigen reexpression, the bound/internalized fractions should reflect the formation of bivalent complexes at the cell surface. Thus, binding on HT 29 cells was evaluated by computer simulation of the binding curves and nonlinear least-squares regression to estimate cooperativity factors. Affinity constants calculated in independent experiments were used to analyze experimental results. Typical curve fits are presented in Figures 2 and 3. Cooperativity factors were estimated to 1090 ± 15 for [Lys(DTPA)]−NT and 2440 ± 668 for DTPA−Gly−NT. Cooperativity far exceeded steric hindrance represented in equilibrium calculations by the accessibility factors determined above. Without the assumption of cooperative binding, satisfactory curve fitting could not be obtained in the bivalent situation.

Kinetics of Bivalent Binding and Internalization of DTPA−NT Analogues to CEA and NTR1. Kinetic experiments were performed with a 2-h pretargeting of the BsmAb (6×10^{-9} M). Binding of [Lys(DTPA)]−NT (Figure 4A) and DTPA−Gly−NT (Figure 4B) increased over the 4-h incubation under the monovalent NTR1 binding condition and bivalent binding condition. However, the ratios between bivalent binding and the sum of monovalent bindings were similar for both analogues and were not significantly increased between 2 and 4 h of incubation (3.2 ± 0.01 at 2 h and 3.7 ± 0.4 at 4 h for [Lys(DTPA)]−NT and 3.5 ± 0.01 and 3.8 ± 0.7, respectively, for DTPA−Gly−NT).

A high fraction of the peptide bound to NTR1 was internalized (86 ± 4% and 79 ± 2% for [Lys(DTPA)]−NT and DTPA−Gly−NT, respectively). A similar fraction of the bound peptide was internalized when bivalent binding was allowed (94 ± 6% and 89 ± 10%, respectively). The amount of internalized radioactivity under bivalent conditions was higher than that observed after binding to NTR1 ($p < 0.001$) for both analogues (7.7 ± 1.1-fold for [Lys(DTPA)]−NT and 6.3 ± 0.9 for DTPA−Gly−NT).

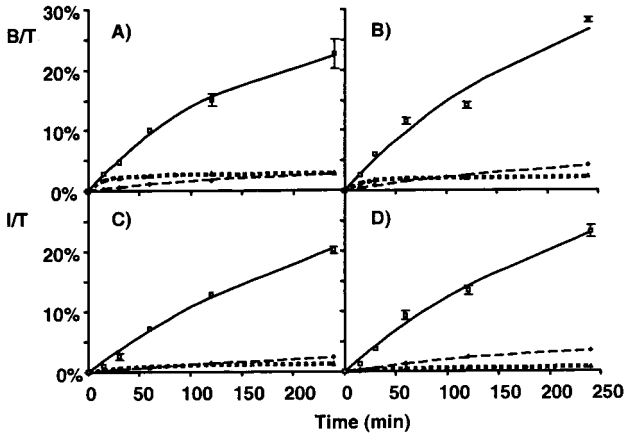


Figure 4. Binding kinetics and kinetics of internalization of DTPA−NT analogues at 37 °C in the presence of pretargeted BsmAb. Binding kinetics [Lys(DTPA)]−NT (A) and DTPA−Gly−NT (B) and kinetics of internalization of [Lys(DTPA)]−NT (C) and DTPA−Gly−NT (D) (final concentrations: 0.15×10^{-9} M DTPA−NT analogues and 6×10^{-9} M BsmAb). Bivalent binding to CEA and NTR1 (solid line) was performed after a 2 h pretargeting of the BsmAb. Monovalent binding to CEA was evaluated in the presence of excess NT (1×10^{-6} M) (dotted line) and monovalent binding to NTR1 in the presence of excess anti-CEA IgG (2×10^{-7} M) (broken line). Fraction of radioactivity associated to the cells (B/T%) or inside the cells (I/T%) was counted. The mean of triplicate determinations are plotted ± standard deviation unless smaller than the point as plotted.

Influence of the Protocol. Pretargeting of the BsmAb without a wash prior to the incubation of the peptide (protocol 1), which was performed in the above-described experiments, was compared to two other experimental conditions using a fixed BsmAb concentration (6×10^{-9} M). Protocol 2 was performed similarly except for a wash of the cells prior to the incubation of the peptide. In protocol 3, the ^{111}In-DTPA−NT analogues were mixed with the BsmAb and incubated 30 min at 37 °C before incubation (1 h) with the cells.

Monovalent binding to NTR1 or to CEA were performed in parallel in the presence of excess anti-CEA IgG or excess neurotensin as described above. Whatever the protocol used, when simultaneous binding to NTR1 and to CEA was allowed, the fraction of peptide bound to cells was increased compared to each monovalent binding conditions (Table 1). In addition, for the three protocols, the bivalent binding was higher than the sum of the monovalent bindings to NTR1 and to CEA suggesting that cooperativity is not dependent on the experimental conditions.

Biodistribution Studies in Human Colorectal Cancer Xenografted Nude Mice. In vivo dual targeting of NTR1 and CEA was studied in nude mice grafted with HT29 cells and preinjected with anti-DTPA(indium) x anti-CEA BsmAb 24 h before ^{111}In-labeled [Lys(DTPA)]−NT injection (Table 2). Radioactivity persistence in blood was increased in mice pretargeted with BsmAb (1.6 ± 0.4 at 1 h, versus 0.32 ± 0.31% ID/g, $p < 0.01$). Pretargeting with BsmAb increased tumor uptake of ^{111}In-labeled [Lys(DTPA)]−NT at 1, 3, and 24 h post peptide injection ($p < 0.01$). In addition, BsmAb pretargeting protracted tumor retention (with BsmAb 20% decrease of tumor activity between 1 h and 3 h postinjection, versus 57% in the absence of BsmAb). Dual

Table 1. Bivalent and Monovalent Bindings of DTPA−Gly−NT and [Lys(DTPA)−NT] to HT29 Cells: Comparison of Three Different Protocols[a]

B/T %	protocol	bivalent binding	monovalent binding to NTR1	monovalent binding to CEA
DTPA−Gly−NT	1	6.1 ± 0.2	1.3 ± 0.1	0.61 ± 0.04
	2	13 ± 1	3.5 ± 0.2	1.9 ± 0.1
	3	2.9 ± 0.2	1.1 ± 0.1	0.23 ± 0.02
[Lys(DTPA)−NT]	1	5.3 ± 0.2	0.62 ± 0.03	1.7 ± 0.1
	2	16 ± 1	2.6 ± 0.1	5.4 ± 1.1
	3	2.3 ± 0.2	0.56 ± 0.04	0.84 ± 0.04

[a] Protocol 1: after 2 h preincubation of BsmAb, ^{111}In-labeled-DTPA−NT analogues were incubated for 1 h; protocol 2 was performed as protocol 1 except for a wash of the cells prior to peptide incubation; protocol 3: the ^{111}In-labeled-DTPA−NT analogues were incubated with BsmAb for 30 min before a 1-h incubation with the cells. Final concentrations: BsmAb 6×10^{-9} M, DTPA(^{111}In)−NT 0.15×10^{-9} M, 37 °C. (Fraction of radioactivity associated to the cells: B/T%, mean ± standard deviation).

targeting (^{111}In-labeled [Lys(DTPA)]−NT and BsmAb) enhanced tumor to organ uptake ratios, particularly for the gastrointestinal tract at 3 and 24 h ($p < 0.01$) (stomach $p < 0.01$ at 3 and 24 h, colon and small intestine $p < 0.05$ at 3 h and $p < 0.01$ at 24 h) in comparison with NTR1 targeting (^{111}In-labeled [Lys(DTPA)]−NT, without BsmAb). Tumor-to-kidney ratios were also improved ($p < 0.01$ at 3 h and $p < 0.05$ at 24 h). Pretargeting with an irrelevant BsmAb (anti-DTPA x anti-CD20), able to bind to DTPA but not to CEA was compared to pretargeting with the relevant BsmAb. Tumor-to-organ ratios at 3 h post labeled NT−DTPA injection was significantly improved by relevant BsmAb pretargeting as compared to irrelevant for organs known to express NT receptors (stomach: $p < 0.01$, colon: $p < 0.01$ and small intestine: $p < 0.05$), while no significant difference was observed for other organs.

In mice pretargeted with the relevant BsmAb 3 h after injection of ^{111}In-labeled [Lys(DTPA)]−NT tumor uptake was higher ($p < 0.01$) than tumor uptake (0.65 ± 0.09% ID/g) of a ^{111}In-DTPA bearing peptide with no affinity for NTR1 (irrelevant-DTPA peptide: Ac-Lys(DTPA)-GABA-D-Tyr-GABA-Lys(Gly succinyl-histamine)-NH_2 (*19*)).

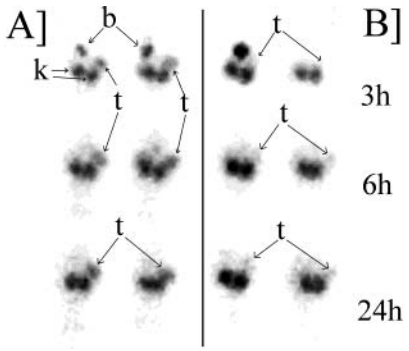


Figure 5. Tumor imaging in mice with pretargeted^{111}In-labeled [Lys(DTPA)]−NT. Images (ventral views) were recorded at 3, 6, and 24 h postinjection (Picker Prism 2000XP gamma-camera). Subcutaneously HT29-xenografted nude mice were injected with A: anti-CEA x anti-DTPA(indium) BsmAb (40 pmol) (tumor weights: left 355.6 mg, right 497.9 mg) or B: vehicle (tumor weights: left 481.7 mg, right 358.8 mg), 24 h before ^{111}In-labeled [Lys(DTPA)]−NT (30 pmol). t: tumor, b: bladder, k: kidney.

At 3, 6, and 24 h post [Lys(DTPA)]−NT injection, tumors were visualized in relevant BsmAb-pretargeted mice whereas tumors were hardly or not detected in vehicle preinjected mice. Kidneys and bladder were the major radioactivity accumulation sites in normal organs, indicating that the major route of excretion was renal.

DISCUSSION

Within the past few years, the use of low molecular weight radiolabeled peptides, which exhibit a faster clearance than antibodies and provide a higher accessibility to tumor cells, has been described. Taking advantage of the overexpression of numerous peptide receptors by various tumor cells, labeled peptides (somatostatin, MSH, VIP, neurotensin, CCK, and gastrin analogues, for example) have been developed for diagnosis and therapeutic purposes (*1*−*8*), but binding also

Table 2. Biodistribution Studies of ^{111}In-Labeled-[Lys(DTPA)]−NT in Nude Mice Grafted with Human Colon Carcinoma Cells[a,b]

	[Lys(DTPA)]−NT			[Lys(DTPA)]−NT + relevant BsmAb, 40 pmol			[Lys(DTPA)]−NT + irrelevant BsmAb, 40 pmol		irrelevant (DTPA)−peptide + relevant BsmAb, 40 pmol
	1 h* ($n = 3$)	3 h* ($n = 7$)	24 h** ($n = 4$)	1 h* ($n = 3$)	3 h* ($n = 7$)	24 h** ($n = 4$)	3 h* ($n = 7$)	24 h** ($n = 4$)	3 h* ($n = 4$)
					Uptake (% ID/g)				
tumor	1.7 ± 0.5	0.72 ± 0.22	0.54 ± 0.13	2.9 ± 0.6	2.4 ± 0.3	1.3 ± 0.2	1.1 ± 0.4	0.74 ± 0.15	0.65 ± 0.11
blood	0.32 ± 0.31	0.043 ± 0.007	0.021 ± 0.003	1.6 ± 0.4	0.15 ± 0.03	0.034 ± 0.004	0.062 ± 0.011	0.044 ± 0.008	0.15 ± 0.03
kidneys	8.4 ± 3.7	9.8 ± 1.8	6.4 ± 2.9	11.7 ± 0.7	12.5 ± 2.0	5.8 ± 1.1	8.2 ± 0.6	7.2 ± 4.2	1.6 ± 0.1
					Tumor (T)/Organ Ratio				
T/blood	12.0 ± 11.8	17.6 ± 6.6	26.0 ± 4.2	1.92 ± 0.22	16.8 ± 4.5	39.2 ± 7.9	17.2 ± 4.4	17.1 ± 2.0	4.3 ± 0.6
T/heart	16.2 ± 11.1	19.6 ± 5.6	11.8 ± 3.9	6.84 ± 0.95	27.4 ± 3.4	22.9 ± 4.7	21.5 ± 4.9	13.9 ± 1.5	9.7 ± 0.6
T/lung	4.45 ± 4.20	9.80 ± 3.46	9.80 ± 3.76	4.02 ± 0.17	14.8 ± 2.1	20.8 ± 6.9	13.3 ± 4.6	10.4 ± 1.6	4.2 ± 0.8
T/liver	13.2 ± 7.1	9.01 ± 1.82	5.14 ± 1.11	6.75 ± 0.44	8.51 ± 3.95	8.25 ± 1.44	8.72 ± 1.55	4.40 ± 0.66	4.8 ± 0.9
T/spleen	10.4 ± 9.0	9.38 ± 1.44	4.06 ± 2.06	8.28 ± 1.41	16.0 ± 2.2	6.79 ± 1.42	12.8 ± 2.6	6.46 ± 4.47	8.8 ± 0.8
T/kidneys	0.24 ± 0.15	0.073 ± 0.014	0.10 ± 0.06	0.25 ± 0.06	0.19 ± 0.04	0.24 ± 0.07	0.13 ± 0.05	0.12 ± 0.04	0.41 ± 0.05
T/muscle	6.17 ± 9.1	14.6 ± 8.2	20.2 ± 3.9	9.99 ± 2.55	33.4 ± 11.8	35.1 ± 7.4	24.0 ± 8.3	20.0 ± 8.7	24.8 ± 2.1
T/GIT	5.44 ± 1.60	2.79 ± 1.43	3.07 ± 1.34	6.10 ± 1.98	7.54 ± 3.68	9.79 ± 1.10	3.52 ± 0.89	4.29 ± 0.88	5.53 ± 2.090
T/stomach	nd	19.1 ± 4.6	9.85 ± 6.45	nd	42.6 ± 5.6	32.6 ± 12.8	14.8 ± 8.3	15.3 ± 6.2	24.4 ± 9.9
T/colon	nd	3.37 ± 0.40	3.23 ± 1.92	nd	6.91 ± 1.26	10.3 ± 2.8	2.50 ± 0.89	3.46 ± 1.00	2.94 ± 0.89
T/small intestine	nd	3.50± 0.36	2.33 ± 0.74	nd	8.14 ± 2.04	7.93 ± 0.50	4.06 ± 0.51	3.84 ± 0.77	8.69 ± 4.70

[a] Nude mice, grafted with HT29 cells in the flank, were given anti-CEA x anti-DTPA(indium) or vehicle or irrelevant BsmAb by iv injection. Twenty-four hours later 15 (*) or 30 (**) pmol of ^{111}In-labeled [Lys(DTPA)]−NT or 15 pmol of an irrelevant ^{111}In-DTPA-bearing peptide (Ac-Lys(DTPA)-GABA-D-Tyr-GABA-Lys(Gly succinyl-histamine)-NH_2) was injected iv. Mice were sacrificed at selected time intervals. Tumor, organs, and blood were collected, and the radioactivity in these samples was determined. Tissue radioactivity is expressed as percentage injected dose/g tissue (% ID/g mean in bold ± standard deviation). [b] Number of animals (n) indicated, except for stomach, colon, and small intestine, $n = 4$.

occurs in nontumor tissues expressing the receptors, which is expected to cause toxicity (*9*).

We have shown that bispecific antibody-mediated dual binding enhances radiolabeled bivalent hapten binding in vitro (*13, 21*) and in vivo targeting in animal models (*13*) and in the clinic (*14, 22, 23*) and that it can also provide an improved selectivity of antigen targeting (*19, 21*). Our objective is to specifically enhance the binding affinity of peptides to receptor-positive tumor cells, as opposed to receptor-positive nontumor cells, to ensure a higher targeting selectivity. The dual binding of a radiolabeled peptide to a receptor and to an antigen on tumor cell surface should enhance the binding to these cells in comparison with a monovalent binding to receptor-positive antigen-negative cells. Numerous tumor cells simultaneously bear receptors and antigens at their surface.

In the present paper, we chose neurotensin receptor (NTR1) and CEA dual targeting as a model to test the feasibility of this approach. NTR1 (*24, 25*) and CEA (*26*) are present on breast, small cell lung carcinoma, pancreatic carcinoma cells, and some colorectal carcinomas. HT29 cells were selected as a model of NTR1 and CEA coexpression. A BsmAb formed by the covalent linking of two Fab′, one directed to CEA and the other one to the DTPA(indium) hapten, was used. Binding of the BsmAb to CEA provided DTPA(indium) binding sites to the HT29 cell surface, allowing the simultaneous binding of DTPA(indium) bearing neurotensin analogues to two sites (NTR1 and CEA) at the target cell surface. All in vitro experiments with HT29 cells were performed after a 24-h forskolin treatment as this increases CEA levels at the cell surface (*11*) with no modification of the binding affinity to the CEA or to the NTR1 (data not shown). Under these conditions, expression of CEA and NTR1 was of the same order of magnitude, which is the optimal condition to evaluate the feasibility of dual binding.

Two neurotensin analogues bearing the hapten DTPA were synthesized: [Lys(DTPA)]−NT and DTPA−Gly−NT. The affinity of DTPA−Gly−NT for the anti-DTPA-(indium) antibody was about 5-fold lower than that of [Lys(DTPA)]−NT in agreement with our previous observation that the highest K_a values are obtained when the DTPA is coupled to the ϵ-NH_2 of a lysine as it is in the immunogen (*19*).

Affinity constant for the binding of [Lys(DTPA)]−NT to the neurotensin receptor NTR1 was 10-fold lower than that of neurotensin itself, determined in the same experimental conditions, in agreement with the observation of a decreased affinity of neurotensin derivatives substituted on the ϵ-amino group of the lysine (*27*). Unexpectedly the affinity constant of DTPA−Gly−NT was similar to that of [Lys(DTPA)]−NT.

As both DTPA−NT analogues were able to bind to NTR1 and to anti-DTPA(indium) antibody, we evaluated both the ability of the anti-CEA x anti-DTPA(indium) BsmAb to target DTPA−NT analogues to CEA, and the influence of BsmAb on the binding of these peptides to NTR1. The ^{111}In-labeled DTPA−NT analogues were efficiently targeted to CEA by the BsmAb. Binding in the presence of increasing concentrations of antibody followed a bell-shaped curve, due to trapping of ^{111}In-labeled DTPA−NT by excess antibody in the supernatant at high BsmAb concentrations. The BsmAb concentration necessary for maximal binding of the peptide was higher for DTPA−Gly−NT in agreement with its lower affinity for the anti-DTPA(indium) as compared to [Lys(DTPA)]−NT. The presence of BsmAb dramatically decreased but did not abrogate the monovalent binding of DTPA−NT analogues to NTR1 (more than 60% inhibition at the highest antibody concentration tested). This result suggested that the affinity of the BsmAb-DTPA(^{111}In)−NT complex for NTR1 was lower than that of the free DTPA-(^{111}In)−NT, probably due to steric hindrance.

The simultaneous binding of DTPA(^{111}In)−NT analogues to NTR1 and to CEA (bivalent binding) in the presence of BsmAb was tested using different incubation protocols with controls of monovalent binding to CEA or NTR1 performed in parallel. Whatever the operating procedure, the incubation time, and BsmAb concentration dual, binding was higher than binding to NTR1 (with a 6×10^{-9} M BsmAb concentration 6.6-fold for DTPA−Gly−NT and about 6.8-fold for [Lys(DTPA)]−NT, after 2 h incubation of the peptides). These results demonstrated the feasibility of enhanced selectivity of radioisotopes targeting to tumor cells bearing simultaneously one receptor and one antigen, compared to nontarget cells bearing only the targeted receptor.

The bivalent binding was higher than the monovalent binding to CEA (8.6-fold for DTPA−Gly−NT and 6.2-fold for [Lys(DTPA)]−NT in the same conditions). The increased selectivity toward receptor-positive/antigen-positive target cells, compared to receptor-negative/antigen-positive cells, may allow nontumor specific antigens, such as clusters of differentiation, to be considered in this context.

In addition, the binding enhancement provided by dual binding was higher than the sum of the monovalent bindings for both DTPA−NT analogues in a wide range of bispecific antibody concentrations (2.2×10^{-10} M to 1.8×10^{-8} M). Fitting these binding curves required the assumption of cooperativity for the simultaneous binding of the DTPA−NT analogues to NTR1 and to anti-CEA x anti-DTPA(indium) BsmAb bound to cell surface CEA. These results suggest that, as previously observed for double antigen targeting (*19, 21, 28*), dual targeting to a receptor and an antigen provides an affinity enhancement due to the cooperativity of dual binding. Cooperativity factors far exceeded steric hindrance, represented in calculations by an accessibility factor. Thus, the decreased binding of DTPA−NT analogues to NTR1 observed in the presence of BsmAb should translate into reduced uptake in receptor-positive antigen-negative tissues and cooperativity should restore or even provide an enhanced binding on receptor positive antigen-positive tumor cells.

In in vivo pretargeting approaches, unlabeled bispecific antibodies are injected first, and the labeled derivative is injected a few days later to allow tumor uptake and clearance of the bispecific antibody. However, at this time a significant fraction of the circulating antibody remains in the circulation. This was better reproduced in vitro by incubating the peptide without washing the BsmAb. As expected, the specific binding of the ^{111}In-labeled DTPA−NT analogue was lower under these conditions, due to trapping of the peptide by excess antibody in the supernatant, but the ratios of dual binding to the sum of the monovalent bindings were higher.

Binding of neurotensin analogues to NTR1 results in the internalization of the ligand. Bivalent binding did not prevent analogues from internalization. In fact, increased binding under bivalent conditions translated into increased internalization. This property is of major interest, as internalization is an important factor for internal radiotherapy since it may result in the accumulation of the radioisotope in the tumor and allow the use of short-range emitting isotopes such as α emitters. In this

respect, dual binding to a receptor and an antigen could afford a major advantage compared to single receptor targeting.

The method was evaluated in nude mice grafted with HT29 human colorectal cells in the flank. [Lys(DTPA)]−NT was labeled with indium-111 in order to perform biodistributions and imaging studies. The clearance of the hapten-bearing peptide was reduced in the presence of the BsmAb due to trapping in the plasma by excess antibody, as we demonstrated earlier for pretargeted bivalent DTPA haptens (*13*). Dual targeting (in the presence of BsmAb) enhanced tumor uptake in comparison with NTR1 targeting (without BsmAb). Tumor uptake was also increased by dual targeting in comparison with CEA targeting (irrelevant ^{111}In labeled-DTPA−peptide and BsmAb). In addition tumor to normal organ uptake ratios were enhanced particularly for the gastrointestinal tract (stomach, colon, and small intestine) where NT receptors are located (*29*), demonstrating that uptake increase provided by the BsmAb is higher in the tumor than in NTR1-positive tissues. Thus the targeting selectivity for tumor cells is enhanced by simultaneous targeting of NT receptor and CEA compared to monovalent targeting (NTR or CEA). Pretargeting with a relevant BsmAb (anti-CEA x anti-DTPA(indium)) provided a significant enhancement of tumor to NTR-positive organ ratios as compared to irrelevant BsmAb pretargeting (pretargeting with an anti-CD20 x anti-DTPA-(indium) unable to bind to CEA). Thus tumor to NTR1-positive organ ratios may be attributed to dual binding rather than to reduced clearance due to binding of the NT-DTPA(indium) analogue to a BsmAb.

In vitro, the analysis of NT-DTPA binding to target cells in the presence and absence of BsmAb and inhibitors allowed us to conclude that NT-DTPA binds simultaneously cooperatively to NTR1 and CEA via the BsmAb. In vivo, pretargeting with BsmAb of NT-DTPA increased tumor uptake, protracted tumor retention, and enhanced tumor to organ uptake ratios, particularly for the gastrointestinal tract, but cooperativity could not be demonstrated. One reason is the reduced clearance of hapten-bearing−NT in the presence of BsmAb, which improves tumor uptake even if the BsmAb does not bind the target cells. Other reasons are the enzymatic degradation of the peptide (in in vitro experiments 1,10-phenanthroline was added to prevent enzymatic degradation) and the possible use of nonoptimal doses of bispecific antibody and peptide. ^{111}In-labeling of NT-DTPA analogues were used in this study to evaluate the feasibility of simultaneous targeting of a receptor and an antigen. To optimize the in vivo targeting selectivity to tumor cells and to develop radiopharmaceuticals suitable for therapy, new hapten bearing receptor−ligands resistant to enzymatic degradation must be developed. Tumor-to-kidneys ratios were also improved, but peptides exhibiting a low renal accretion, such as those described by Chavatte K. et al. (*8*), labeled with isotopes suitable for internal radiotherapy, such as ^{131}I or ^{90}Y, will be necessary.

In conclusion, the double targeting of a receptor and an antigen at the tumor cell surface may be beneficial to peptide targeting of radioisotopes by increasing targeting specificity, tumor uptake, and isotope residence time in the tumor. DTPA−NT analogues, resistant to enzymatic degradation, in combination with an anti-CEA x anti-DTPA(indium) bispecific antibody, might be used in several clinical situations, including pancreatic tumors, small cell lung carcinoma, or colon carcinoma expressing both CEA and a neurotensin receptor (*24*−*26*). Successful targeting of radioactive isotopes to MTC has been performed using either anti-CEA antibodies (*22, 30*) or gastrin or CCK analogues (*4, 5*). Tumor uptake and contrast ratios in this disease could be improved by means of dual targeting. This approach might be of interest for radiopeptide therapy in many other cases of tumors overexpressing peptide receptors. For example VIP/PACAP receptors are expressed by most of human tumors such as breast, colon, or small cell lung carcinomas (*9*). These receptors are potentiel targets for VIP/PACAP ligands in vivo. The limitations for a radiotherapy using such agents include the destruction by irradiation of receptor-positive normal target tissues (*9*). Enhancing the selectivity by dual targeting of the VIP/PACAP receptor and a selected antigen may provide tumor to normal tissue uptake ratios suited for therapy. Antigens such as MDR P-glycoproteins, expressed on multidrug resistant tumors, CEA, or MUC1 expressed by various carcinomas, might be used for dual targeting of VIP/PACAP receptor positive tumors.

Numerous other receptor and antigens might be selected for dual targeting of tumors, but the antigen should not be internalizing for successful BsmAb pretargeting. With internalizing antigens, simultaneous injection of the labeled analogue and the BsmAb may be considered (*21*).

Very often antigen and receptor expression differs among tumors of the same type. Nevertheless, it is expected that a set of radiopharmaceuticals recognizing different receptors and bearing the same hapten, combined with a set of BsmAb directed to various antigens and to the hapten, will allow combinations of one radiopharmaceutical and one BsmAb able to perform dual targeting on a wide range of tumors.

ACKNOWLEDGMENT

The authors gratefully acknowledge Pr. G. Milhaud and Dr. D. Pelaprat for helpful discussions, Pr. S. Askienazy for research facilities, and M. Brissac, B. Vinson, and S. Hermant for in vivo experiments. This work was supported in part by the Association pour la Recherche contre le Cancer through Grant 4042 allocated to A.G.G. The authors thank the Ligue Nationale Contre le Cancer for awarding a fellowship to O.R.

LITERATURE CITED

(1) Breeman, W. A. P., de Jong, M., Kwekkeboom, D. J., Valkema, R., Bakker, W. H., Kooij, P. P. M., Visser, T. J., and Krenning, E. P. (2001) Somatostatin Receptor-Mediated Imaging and Therapy: Basic Science, Current Knowledge, Limitations and Future Perspectives. *Eur. J. Nucl. Med. 28*, 1421−1429.

(2) Kwekkeboom, D. J., Krenning, E. P., and de Jong, M. (2000) Peptide Receptor Imaging and Therapy. *J. Nucl. Med. 41* (10), 1704−1713.

(3) Boerman, O. C., Oyen, W. J. G., and Corstens, F. H. M. (2000) Radio-Labeled Receptor-Binding Peptides: A New Class of Radiopharmaceuticals. *Semin. Nucl. Med. 30* (3), 195−208.

(4) Behr, T. M., Jenner, N., Behe, M., Angerstein, C., Gratz, S., Raue, F., and Becker, W. (1999) Radiolabeled peptides for targeting cholecystokinin-B/Gastrin receptor-expressing tumors. *J. Nucl. Med. 40*, 1029−1044.

(5) De Jong, M., Bakker, W. H., Bernard, B. F., Valkema, R., Kwekkeboom, D. J., Reubi, J. C., Srinivasan, A., Schmidt, M., and Krenning, E. P. (1999) Preclinical and initial clinical evaluation of ^{111}In-labeled nonsulfated CCK_8 analog: a peptide for CCK−B receptor-targeted scintigraphy and radionucleide therapy. *J. Nucl. Med. 40*, 2081−2087.

(6) Virgolini, I., Raderer, M., Kurtaran, A., Angelberger, P., Banyal, S., Yang, Q., Shuren, L., Banyai, M., Pidlich, J.,

Niederle, B., Scheithauer, W., and Valent, P. (1994) Vasoactive intestinal peptide-receptor imaging for the localization of intestinal adenocarcinomas and endocrine tumors. *N. Engl. J. Med. 331,* 1116−1121.

(7) Bard, D. R. (1995) An improved imaging agent for malignant melanoma, based on [Nle[4], D-Phe[7]]α-melanocyte stimulating hormone. *Nucl. Med. Commun. 16,* 860−866.

(8) Chavatte, K., Terriere, D., Jeannin, L., Iterbeke, K., Briejer, M., Schuurkes, J., Mertens, J. J. R., Bruyneel, E., Tourwé, D., Leysen, J. E., and Bossuyt, A. (1999) Labelling and evaluation of new stabilised neurotensin (8-13) analogues for single photon emission tomography (SPET). *J. Labelled Compd. Radiopharm. 42,* 423−435.

(9) Reubi, J. C. (2000) In vitro evaluation of VIP/PACAP receptors en healthy and diseased human tissues. Clinical implications. *Ann. N. Y. Acad. Sci. 921,* 1−25.

(10) Evers, B. M., Ishizuka, J., Chung, D. H., Townsend, C. M., and Thompson, J. C. (1992) Neurotensin expression and release in human colon cancers. *Ann. Surg. 216* (4), 423−431.

(11) Velcich, A., Palumbo, L., Jaury, A., Laboisse, C., Racevskis, J., and Augenlicht, L. (1995) Patterns of expression of lineage-specific markers during the in vitro-induced differenciation of HT29 colon carcinoma cells. *Cell Growth Differ. 6,* 749−757.

(12) Chetanneau, A., Baum, R. P., Lehur, P. A., Liehn, J. C., Perkins, A. C., Bares, R., Bourguet, P., Herry, J. Y., Saccavini, J. C., and Chatal, J. F. (1990) Multi-centre immunoscintigraphic study using indium-111-labeled CEA-specific and/or 19−9 monoclonal antibody F(ab′)2 fragments. *Eur. J. Nucl. Med. 17,* 223−229.

(13) Le Doussal, J. M., Gruaz-Guyon, A., Martin, M., Gautherot, E., Delaage, M., and Barbet, J. (1990) Targeting of indium-111-labeled bivalent hapten to human melanoma mediated by bispecific monoclonal antibody conjugates: imaging of tumors hosted in nude mice. *Cancer Res. 50,* 3445−3452.

(14) Le Doussal, J. M., Chetanneau, A., Gruaz-Guyon, A., Martin, M., Gautherot, E., Lehur, P. A., Chatal, J. F., Delaage, M., and Barbet, J. (1993) Bispecific monoclonal antibody-mediated targeting of an indium-111-labeled DTPA dimer to primary colorectal tumors: pharmacokinetics, biodistribution, scintigraphy and immune response. *J. Nucl. Med. 34* (10), 1662−1671.

(15) Salacinsky, P. R., McLean, C., Sykes, J. E., Clement-Jones, V. V., and Lowry, P. J. (1981) Iodination of proteins and peptides using a solide phase oxidizing agent 1,3,4,6-tetrachloro-3,6-diphenylglycoluryl (iodogen). *Anal. Biochem. 117,* 136−141.

(16) Gautherot, E., Le Doussal, J. M., Bouhou, J., Manetti, C., Martin, M., Rouvier, E., and Barbet, J. (1998) Delivery of therapeutic doses of radioiodine using bispecific antibody-targeted bivalent haptens. *J. Nucl. Med. 39* (11), 1937−1943.

(17) Bellon, B., Jelsch, J., and Delaage, M. (1973) Théorie des équilibres multiples pour les polymères. *Biochimie 55,* 1159−1162.

(18) Barbet J., Le Doussal, J. M., Gruaz-Guyon, A., Martin, M., Gautherot, E., and Delaage, M. (1993) Computer calculation of multiple binding equilibrium isotherms: application to the binding of bivalent ligands to antibodies interacting with cell surface Fc-receptor. *J. Theor. Biol. 165,* 321−340.

(19) Hillairet de Boisferon, M., Raguin, O., Dussaillant, M., Rostène, W., Barbet, J., and Gruaz-Guyon, A. (2000) Enhanced targeting specificity to tumor cells by simultaneous recognition of two antigens. *Bioconjug. Chem. 11,* 452−460.

(20) Mazella, J., Poustis, C., Labbe, C., Checler, F., Kitabgi, P., Granier, C., van Rietschoten, J., and Vincent, J. P. (1983) Monoiodo-(trp[11]) neurotensin, a highly radioactive ligand of neurotensin receptors. Preparation, biological activity, and binding properties to rat brain synaptic membranes. *J. Biol. Chem. 258* (6), 3476−3481.

(21) Hillairet de Boisferon, M., Manetti, C., Raguin, O., Gautherot, E., Rostène, W., Barbet, J., and Gruaz-Guyon, A. (1997) Pretargeted radioimmunotherapy using iodine-131-labeled bivalent hapten-bearing peptides. *Lett. Pept. Sci. 4,* 331−339.

(22) De Labriolle-Vaylet, C., Cattan, P., Sarfati, E., Wioland, M., Billotey, C., Brochériou, C., Rouvier, E., de Roquancourt, A., Rostene, W., Askienazy, S., Barbet, J., Milhaud, G., and Gruaz-Guyon, A. (2000) Successful surgical removal of occult metastases of medullary thyroid carcinoma recurrences with the help of immunoscintigraphy and radioimmunoguided surgery. *Clin. Cancer Res. 6* (2), 363−371.

(23) Kraeber-Bodere, F., Bardet, S., Hoefnagel, C. A., Vieira, M. R., Vuillez, J. P., Murat, A., Ferreira, T. C., Bardies, M., Ferrer, L., Resche, I., Gautherot, E., Rouvier, E., Barbet, J., and Chatal, J. F. (1999) Radioimmunotherapy in medullary thyroid cancer using bispecific antibody and iodine 131-labeled bivalent hapten: preliminary results of a phase I/II clinical trial. *Clin. Cancer. Res. 5* (10 Suppl), 3190s−3198s.

(24) Reubi, J. C., Waser, B., Schaer, J. C., and Laissue, J. A. (1999) Neurotensin receptors in human neoplasms: high incidence in Ewing's sarcomas. *Int. J. Cancer 82,* 213-218.

(25) Reubi, J. C., Waser, B., Friess, H., Büchler, M., and Laissue, J. (1998) Neurotensin receptor: a new marker for human ductal pancreatic adenocarcinoma. *Gut 42,* 546−550.

(26) Behr, T. M., Sharkey, R. M., Juweid, M. E., Dunn, R. M., Vagg, R. C., Ying, Z., Zhang, C. H., Swayne, L. C., Vardi, Y., Siegel, J. A., and Goldenberg, D. M. (1997) Phase I/II clinical radioimmunotherapy with an iodine-131-labeled anti-carcinoembryonic antigen murine monoclonal antibody IgG. *J. Nucl. Med. 38* (6), 858−870.

(27) Gaudriault, G., and Vincent, J. P. (1992) Selective labeling of α- or ϵ-amino groups in peptides by the Bolton-Hunter reagent. *Peptides 13,* 1187−1192.

(28) Le Doussal, J. M., Gautherot, E., Martin, M., Barbet, J., and Delaage, M. (1991) Enhanced in vivo targeting of an asymmetric bivalent hapten to double-Ag-positive mouse B cells, using mAb conjugate cocktails. *J. Immunol. 146* (1), 169−175.

(29) Kitabgi, P., Checler, F., Mazella, J., and Vincent, J. P. (1985) Pharmacology and biochemistry of neurotensin receptors. *Rev. Clin. Basic. Pharm. 5,* 397−486.

(30) Juweid, M., Sharkey, R. M., Behr, T., Swayne, L. C., Herskovic, T., Pereira, M., Rubin, A. D., Hanley, D., Dunn, R., Siegel, J., and Goldenberg, D. M. (1996) Radioimmunotherapy of medullary thyroid cancer with iodine-131-labeled anti-CEA antibodies. *J. Nucl. Med. 37* (6), 905−911.

BC015585G

Profiling Solid-Phase Synthesis Products by Free-Solution Conjugate Capillary Electrophoresis

Wyatt N. Vreeland,[†] Gary W. Slater,[‡] and Annelise E. Barron*[,†]

Department of Chemical Engineering, Northwestern University, Evanston, Illinois, and Department of Physics, University of Ottawa, Ottawa, Ontario, Canada. Received November 30, 2001; Revised Manuscript Received February 7, 2002

Solid-phase synthesis of oligomers, both natural and nonnatural, has proved to be invaluable for the development of many areas of biotechnology. A critical step in the solid-phase synthesis of any oligomer is determining the number and concentration of different constituents present in the product mixture resulting from the synthesis, both before and after purification. Most typically, this analysis is performed by reversed-phase high performance liquid chromatography (RP-HPLC), with the separated components detected by UV absorbance. Recently, we described a novel technique, free-solution conjugate electrophoresis (FSCE), for the high-resolution separation and sensitive laser-induced fluorescence (LIF) detection of uncharged, synthetic polymers, PEG in particular. In this report, we apply this bioconjugate capillary electrophoresis technique to analyze products of the solid-phase synthesis of oligomeric polyamides, namely poly(*N*-substituted glycines), or polypeptoids. When compared to more traditional RP-HPLC analysis, FSCE analysis of oligomeric peptoids results in separation resolutions that are approximately five times higher and separation efficiencies that are increased by 150%. Moreover, when FSCE with LIF detection is applied to the analysis of oligomeric polyamides after HPLC purification, impurities that are not detectable in RP-HPLC analysis are readily separated and detected. With the advent of capillary array electrophoresis (CAE), which allows for automated, parallel analysis of many different samples, we believe that FSCE will be especially applicable to the analysis of combinatorial synthesis products, by allowing researchers to evaluate many different samples in a single, highly parallel, fully automated analysis. This is in contrast to RP-HPLC analysis, in which samples must be analyzed in series.

INTRODUCTION

The solid-phase synthesis of polypeptides (*1*) has, over the past several decades, proven to be an invaluable tool for the study of molecular biology. For example, chemically synthesized polypeptides have allowed biochemists to determine the high-resolution structures of many proteins (*2*−*4*), enabling the elucidation of important biological pathways. In some cases, solid-phase peptide synthesis (SPPS) has allowed the study of proteins or protein fragments that were previously unobtainable in sufficient quantity, if at all, from natural preparations.

More recently, synthetic routes have been developed to various classes of nonnatural, sequence-specific, biomimetic oligomers, including poly-*N*-substituted glycines or "polypeptoids" (*5*−*10*), β-peptides (*11*−*14*), γ-peptides (*15*), oligoureas (*16*), and peptide nucleic acids (*17*). These biomimetic oligomers, based on backbones which are variants of the natural polypeptide (polyamide) structure, with differences also in their side chain chemistries, are of interest for their abilities to adopt stable secondary structures, and for their potential to shed light on factors that endow natural polypeptides with bioactivity (*18*−*21*). It is hoped that nonnatural oligomers can be developed as bioactive, structured peptide mimics, as well as useful materials for other applications in biotechnology such as gene therapy, genetic analysis, and bioseparations.

The ability to synthesize polypeptides on solid-phase support allows the per-monomer coupling efficiencies to be pushed to >99.9%, providing a route to the creation of long oligomers (>40 monomers in length) (*1*). Since the addition of any given monomer in the sequence never goes to 100%, when the final peptide preparation is cleaved from the solid support it represents a mixture of the desired full-length sequence with various deletion products, or if there was incomplete protection of any reactive side chains, even some branched oligomers. A critical step in the production of chemically synthesized polypeptides is the evaluation of the composition of the crude products as they are cleaved from the solid-phase resin. This is typically done by analytical, reversed-phase (RP) HPLC in small-bore columns packed with fine-mesh resin. The level of resolution of the full-length peptide sequence from deletion fragments and side products is generally quite good under the best conditions. HPLC profiling of the crude products of SPPS allows researchers to assess the success of the synthesis, and can be used on intermediary samples to track the coupling efficiency as a function of the length of the growing polypeptide chain. Generally, the predominant peak will be the desired polypeptide if the synthesis has gone well, and can be isolated by preparative RP-HPLC.[1] The final, purified polypeptide preparation will generally be characterized again by analytical RP-HPLC, as well as by

* Correspondence: Annelise E. Barron, Assistant Professor, Northwestern University, Department of Chemical Engineering, 2145 Sheridan Rd., Rm E136, Evanston, IL 60208-3120. Phone: (847) 491-2778. Fax: (847) 491-3728. E-mail: a-barron@northwestern.edu.

[†] Northwestern University.

[‡] University of Ottawa.

10.1021/bc0155871 CCC: $22.00 © 2002 American Chemical Society
Published on Web 03/12/2002

electrospray ionization mass spectrometry (ESI-MS) to assess its level of purity. For nonnatural oligomers such as polypeptoids and β-peptides, similar approaches to profiling crude products of synthesis and purification are also taken, i.e., RP-HPLC is still the critical and most widely used technique (*6*, *22*).

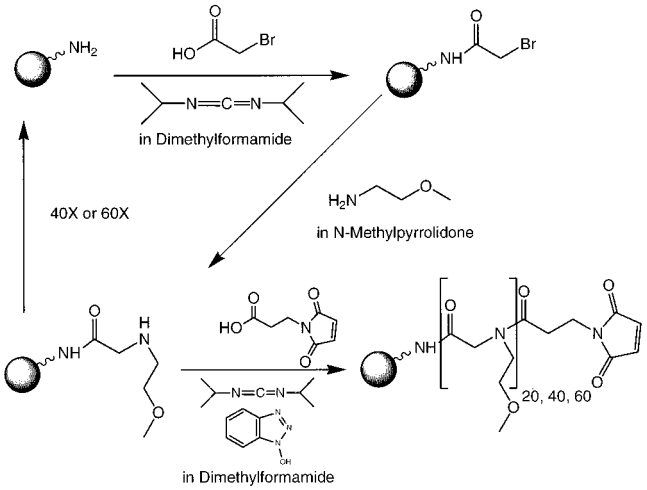
To analyze the overall quality of a crude or purified chemically synthesized polyamide, the different components of the biopolymer sample must be sufficiently separated from one another. These separated components may be quantified according to their relative abundance, their molecular mass, and/or another indicative, quantitative parameter (e.g., UV absorbance at a particular wavelength). When separation is carried out by RP-HPLC, a sample is separated by partitioning between a solid-phase packing contained in the HPLC column and a mobile liquid phase that flows through voids in the packing (*23*). The composition of the liquid mobile phase is often changed throughout the analysis, so that the sample mixture components will each elute in order of increasing hydrophobicity, and are subsequently detected by a UV absorbance detector (*24*).

RP-HPLC results in the oligomer of interest being separated based on the strength of its interaction with the solid phase. The selection of liquid mobile phase and of the chemistry of the column packing determines, in large part, the quality of the separation and of the analysis. For samples that are extremely hydrophilic or hydrophobic, the identification of an appropriate solid phase and method of solvent composition programming to achieve high resolution can be challenging (*25*).

When coupled to a UV absorbance detector, as is typical, the limit of detection (LOD) of the sample in the mobile liquid-phase of an HPLC separation is relatively high when compared to the LOD of highly sensitive laser-induced fluorescence (LIF) detectors that are currently available (*26*). Also, the use of mobile phases with appreciable UV extinction coefficients can severely limit the sensitivity of detection of sample in the eluent of an HPLC column, especially for the UV detection of extremely dilute species in a given sample. Finally, in the analysis of biopolymers that lack a unique chromophore, one must rely on detection of the chromophore of the polymer backbone (214 nm in the case of polyamides). Detecting a chromophore in the polymer backbone, which yields a chain-length dependent molar extinction coefficient, complicates the quantification of sample species, since peak area is then dependent upon both relative abundance and upon chain length.

In the past few years, capillary electrophoresis (CE) has become increasingly popular as a high-resolution, high-sensitivity technique for the separation and analysis of molecules of chemical and biochemical interest including chiral molecules (*27*), proteins (*28*), carbohydrates (*29*), and DNA (*30*−*33*). We recently reported a new capillary electrophoresis technique, which we call free-solution conjugate electrophoresis (FSCE), for the separation and effective mass spectrometry of uncharged poly(ethylene glycol) (PEG) samples (*34*). In that work, molar mass profiling of several different PEG samples was achieved via end-on conjugation of these polydisperse polymers to monodisperse, fluorescently labeled DNA oligomers, followed by free-solution electrophoretic separation of the bioconjugates in a long capillary (*34*). We show here that this technique can be extended to the separation and analysis of both crude and purified solid-phase synthesis products.

Scheme 1



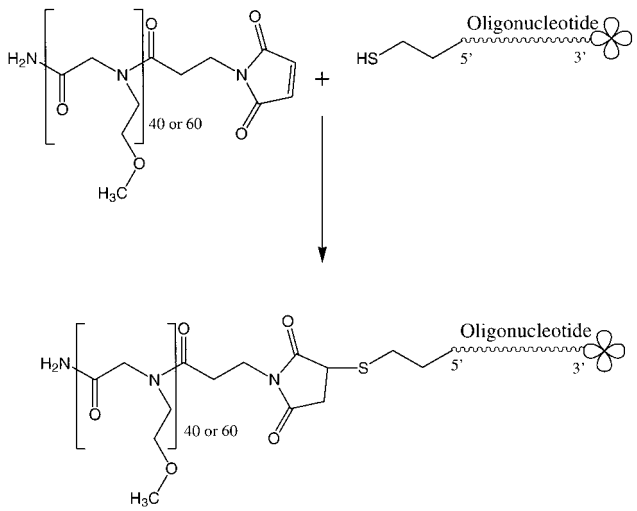
In particular, we describe the application of FSCE to the analysis of both unpurified and purified oligomers produced via chemical synthesis. This method, we believe, provides an interesting alternative to HPLC for the characterization of chemically produced polyamides. The novel separation mode that we demonstrate is accomplished by end-on conjugation of each of the species present in a complex oligomer mixture with a monodisperse, fluorescently labeled DNA oligomer. The resulting DNA−oligomer conjugates are then separated by free-solution capillary electrophoresis. Specifically, we apply FSCE to a class of biomimetic molecules that are remarkably similar to polypeptides, called poly-*N*-substituted glycines, or *polypeptoids*. Exploiting the extreme sensitivity of LIF detection and the excellent resolving power of capillary electrophoresis, FSCE allows for accurate and sensitive separation of various species present in a complex sample mixture resulting from a solid-phase synthesis.

EXPERIMENTAL SECTION

Polypeptoid Synthesis. The synthesis of the oligomer samples of interest, in particular the poly-*N*-substituted glycines or "polypeptoids" used in this study, has been described elsewhere (*5*). The synthetic protocol for the particular molecules studies here is depicted in Scheme 1. All reactions were carried out on an ABI 433A automated peptide synthesizer (Applied Biosystems, Foster City, CA) with in-house modifications to the control software. Briefly, 0.25 mmol of Fmoc-rink amide resin (Nova Biochem, San Diego, CA) were deprotected by treatment with 20% (v/v) piperidine (Applied Biosystems, Foster City, CA) in dimethyformamide (DMF) (Fisher Scientific, Itasca, IL), in two consecutive 15-min treatments. The oligomer chain was then assembled with alternating cycles of bromoacetylation step and amine displacement of the bromine from the *N*-terminal alkyl halide. The bromoacetylation was accomplished by mixing 4.3 mL of 1.2 M bromoacetic acid (Aldrich, Milwaukee, WI) in DMF and 1 mL of diisopropylcarbodiimide

[1] Abbreviations: CAE, capillary array electrophoresis; CE, capillary electrophoresis; ESI-MS, electrospray ionization mass spectrometry; epoxy-pDMA, poly(dimethylacrylamide-*co*-allyl glycidyl ether); FSCE, free-solution conjugate electrophoresis; LIF, laser-induced fluorescence; LOD, limit of detection; MALDI-TOF, matrix-assisted laser desorption ionization−time-of-flight; PEG, poly(ethylene glycol); RP-HPLC, reversed-phase high performance liquid chromatography; SPPS, solid-phase peptide synthesis.

Scheme 2



(Aldrich, Milwaukee, WI) with the resin. The mixture was then vortexed for 45 min, the liquid drained, and the resin rinsed 4 times with 7 mL of DMF. Next, the resin was mixed with 4 mL of 1 M methoxyethylamine (Aldrich, Milwaukee, WI) in *N*-methylpyrrolidone and vortexed for 45 min to introduce the methoxyethyl side-chain moiety. The liquid was then drained, and the resin was again rinsed four times with 7 mL of DMF. These two reaction cycles were then alternated until the polypeptoid was of the desired length.

A reactive *N*-terminal maleimide functionality was attached to the amino terminus of the polypeptoid while it was still on the resin, to allow for facile conjugation to DNA oligomers, as depicted in Scheme 2. This was accomplished by mixing the resin with 500 μL of 1.2 M maleimidopropionic acid (Fluka, Buchs Switzerland) in DMF and 144 μL of diisopropylcarbodiimde, vortexing the resin slurry for 45 min, and rinsing the resin four times with 3 mL of DMF. Finally, the polypeptoid was cleaved from the solid support by treatment with 95% (v/v) trifluoroacetic acid (Aldrich, Milwaukee, WI) in water for 30 min. The polypeptoid-containing liquid was then passed through a filter to separate it from the solid support. Next, the crude polypeptoid solution was extracted with a water−diethyl ether mixture, and the aqueous layer retained, frozen, and lyophilized to yield a golden, viscous oil.

RP-HPLC Analysis Conditions. Unpurified and purified peptoids were dissolved in water and analyzed by RP-HPLC on C18 packing (Vydac, 5 μm, 300 Å, 2.1 × 250 mm). A linear gradient of 10−60% B in A was run over 50 min at a flow rate of 0.1 mL/min (solvent A = 0.1% TFA in water, solvent B = 0.1% TFA in acetonitrile) at 60 °C; peaks were detected by UV absorbance at 214 nm. Preparative HPLC was performed on a Vydac C18 column (Vydac, 15 μm, 300 Å, 22 × 250 mm) using the same solvent and detection systems; peaks were eluted with a linear gradient of 10−60% B in A over 50 min at 12 mL/min.

Polypeptoid−DNA Conjugation Conditions. Prior to conjugation with a monodisperse, fluorescently labeled DNA oligomer, each polypeptoid was purified from non-peptoid impurities remaining from the cleavage reaction by preparative HPLC. This was necessary because the particular solubility properties of this peptoid sequence prevented us from using ether precipitation to remove small-molecule contaminants of the cleavage products. We intend to develop a one-step, on-resin conjugation with the DNA label that will allow this step to be bypassed in the future. To accomplish the necessary purification for this study, several milligrams of unpurified polypeptoid were loaded onto the preparative HPLC column; after the elution of the initial void volume peak, the entire eluent of the HPLC analysis was collected for FSCE analysis of unpurified polypeptoids. For the FSCE analysis of HPLC-purified polypeptoids, only the desired peak, representing the full-length product, was collected. Subsequently, each sample was frozen and lyophilized from the HPLC buffer to yield a light gold, viscous oil.

Poly(*N*-methoxyethyl)glycines 40 and 60 monomers in length were each conjugated end-on to poly(thymidine)-deoxyribonucleic acid 20 bases in length (Oligos, Etc., Wilsonville, OR). DNA samples had been prepurified using gel electrophoresis by the vendor, to ensure that each DNA oligomer was monodisperse. Moreover, each DNA oligomer included a fluorescein dye on its 3′ terminus to allow for LIF detection, and a thiol (SH) functionality on its 5′ terminus to allow for conjugation with the maleimide functionality of the amino terminus of the polypeptoid. This conjugation forms a stable thioether linkage between the DNA and the polypeptoid (Scheme 2).

To ensure that the 5′-thiol terminus of the DNA was optimally reactive with the maleimide terminus of the polypeptoid, the DNA was first chemically reduced, as recommended by the vendor and previously described (*34*).

The conjugation reaction was accomplished by dissolving a given polypeptoid sample to a concentration of 12.8 mM in 0.1 M sodium phosphate buffer, 0.15 M NaCl, pH = 7.2, and adding 10 μL of each of the 12.8 mM polypeptoid solutions to the lyophilized DNA powder from the above reduction protocol. This solution was incubated at room temperature for 24 h. Finally, the resultant mixture was diluted 1:300 in distilled, deionized H_2O immediately prior to capillary injection and analysis.

Capillary Electrophoresis Analysis Conditions. All capillary electrophoretic separations were conducted in 25-μm inner-diameter fused silica capillaries, 100 cm in total length (95.4 cm effective length) (Polymicro Technologies, Phoenix, AZ), and filled with one of two buffers. For the analysis of unpurified polypeptoids, 1X TTE + 7 M urea (50 mM *N*-tris[hydroxymethyl]methyl-3-aminopropanesulfonic acid, 50 mM Tris, 2 mM ethylenediaminetetraacetic acid, 7 M urea), pH = 8.5 (Amresco, Solon, OH) buffer was used, whereas for the analysis of purified polypeptoids, 1X TTE buffer was used. All buffers were prepared with 18 MΩ distilled, deionized water (E-pure, Barnstead, Dubuque, IA). The internal surface of the capillary was dynamically coated with an adsorbed layer of a poly(dimethylacrylamide-*co*-allyl glycidyl ether) (epoxy-pDMA) to reduce electroosmotic flow mobility to negligible levels (*35*). All analyses were performed using a BioFocus 3000 Capillary Electrophoresis system equipped with a laser-induced fluorescence detector (BioRad, Hercules, CA). At the beginning of each day of analysis, the capillary was flushed for 15 min with 1 M NaOH, followed by a 5-min water rinse, and then flushed for 20 min with a 0.1% (w/v) solution of epoxy-pDMA in water. All capillary rinses were done with a syringe pump at a flow rate of 100 μL/h. Electroosmotic flow after capillary coating by this method was measured to be 3.0×10^{-10} m^2/(V·s) by the method of Williams and Vigh (*36*).

Prior to each analysis, the capillary was flushed with several column volumes of the electrophoresis buffer. Immediately prior to sample injection, the injection end

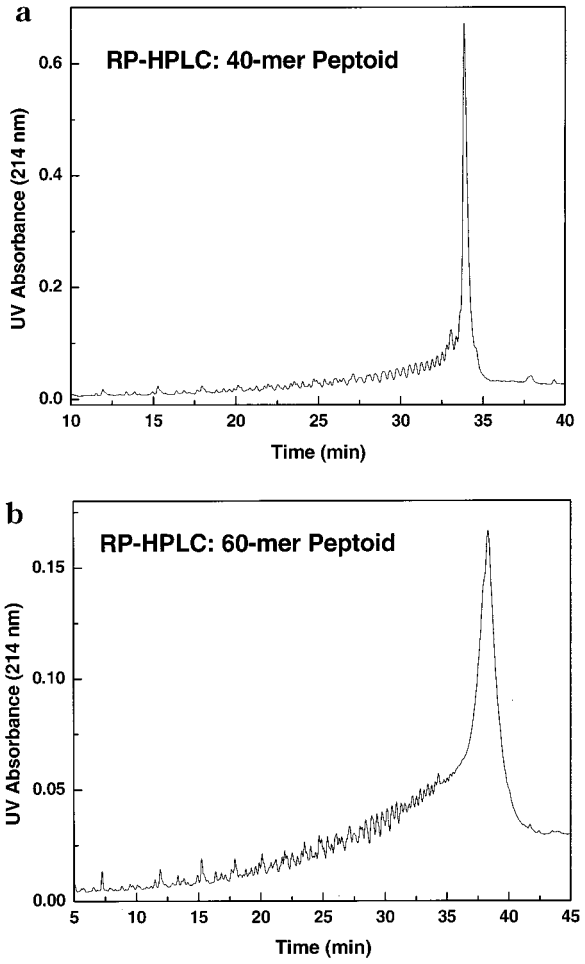


Figure 1. (a) RP-HPLC separation of a crude (unpurified) 40-monomer poly(*N*-methoxyethyl glycine). Conditions: C18 packing (Vydac, 5 μm, 300 Å, 2.1 × 250 mm). A linear gradient of 10−60% B in A was run over 50 min at a flow rate of 0.1 mL/min (solvent A = 0.1% TFA in water, solvent B = 0.1% TFA in acetonitrile) at 60 °C; peaks were detected at 220 nm. (b) RP-HPLC separation of an unpurified 60-monomer poly(*N*-methoxyethyl glycine). Conditions as in Figure 1a.

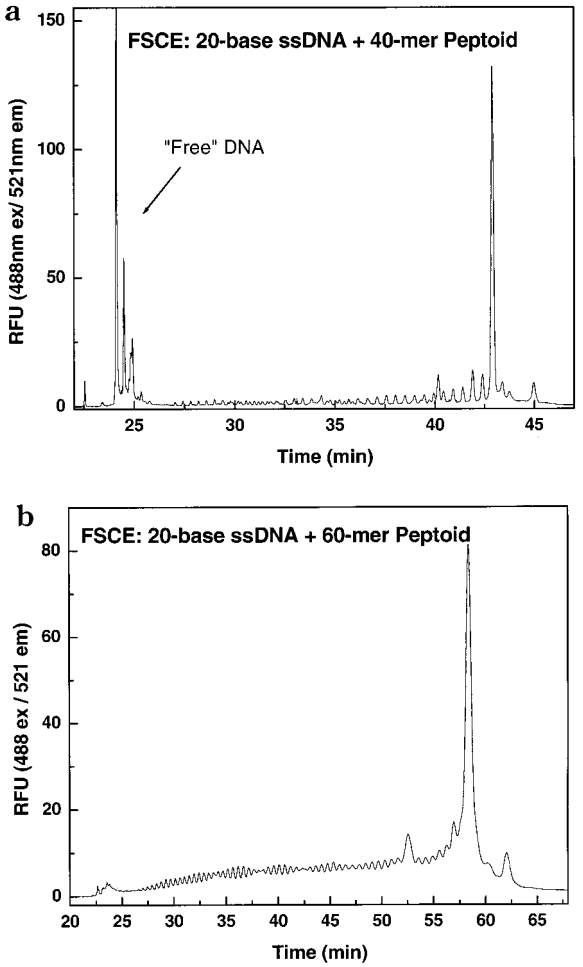


Figure 2. (a) FSCE separation of an unpurified 40-monomer poly(*N*-methoxyethyl glycine) using a 20-base ssDNA "engine". Conditions: buffer 1X TTE + 7 M urea, pH 8.5. Field Strength 300 V/cm, current ~ 4 μA. Capillary 100 cm × 25 μm (95.4 cm effective length). LIF detection, 488 nm excitation, 521 nm emission. Injection: 150 V/cm, 2 s. (b) FSCE separation of an unpurified 60-monomer poly(*N*-methoxyethyl glycine) using a 20-base ssDNA "engine". Conditions are as in Figure 2a.

of the capillary was briefly dipped into deionized water to remove residual buffer salts from the outer surface of the capillary. Sample was introduced into the capillary by an electrokinetic injection at 150 V/cm for 2 s. Electrophoresis was conducted at 300 V/cm until all peaks had eluted. Detection of the analytes was achieved with excitation of the 3′-fluorescein DNA label using the 488 nm line of an argon-ion laser, and emission detected at 521 nm.

Data Analysis. All peak parameters and migration times were determined with the PeakFit software package (SPPS, Inc., Chicago, IL).

RESULTS AND DISCUSSION

The separation mechanism of FSCE derives from the different bioconjugate properties created by the covalent linkage of the polyamide molecules to monodisperse DNA oligomers. The highly charged DNA oligomer component of the conjugate endows each molecule with an equal electromotive force during electrophoresis, while the less charged polyamide component gives each molecule a unique amount of hydrodynamic drag. Hence, the electrophoretic mobility of each bioconjugate is a precise function of the length and nature of the polyamide "tail", allowing for free-solution electrophoretic separation of each of the conjugates. The advantages of this approach can be illustrated by carrying out a direct comparison of the results of RP-HPLC and FSCE analysis of a set of model peptoid−DNA conjugates. For this study, we selected a very simple model polypeptoid molecule for illustrative purposes, composed of N-substituted glycine monomers with an uncharged, hydrophilic methoxyethyl side-chain moiety.

Electropherograms and Chromatograms for the Analysis of Unpurified Polypeptoids. Figure 1a and 1b show the results of RP-HPLC analyses of 40-mer unpurified peptoid and 60-mer unpurified peptoid oligomers prepared by solid-phase synthesis, respectively. In RP-HPLC analysis, the constituents of the complex samples are separated on the basis of their effective hydrophobicity. For peptoids composed of this particular monomer (*N*-methoxyethyl glycine), the effective hydrophobicity of the molecule increases as the peptoid chain increases in length. Thus RP-HPLC, in this case, separates the different constituents of the complex sample in order of increasing chain length. The major peak in each figure, while not fully resolved from other sample components, represents the full-length sequence (as confirmed by electrospray mass spectrometry of the material in this peak).

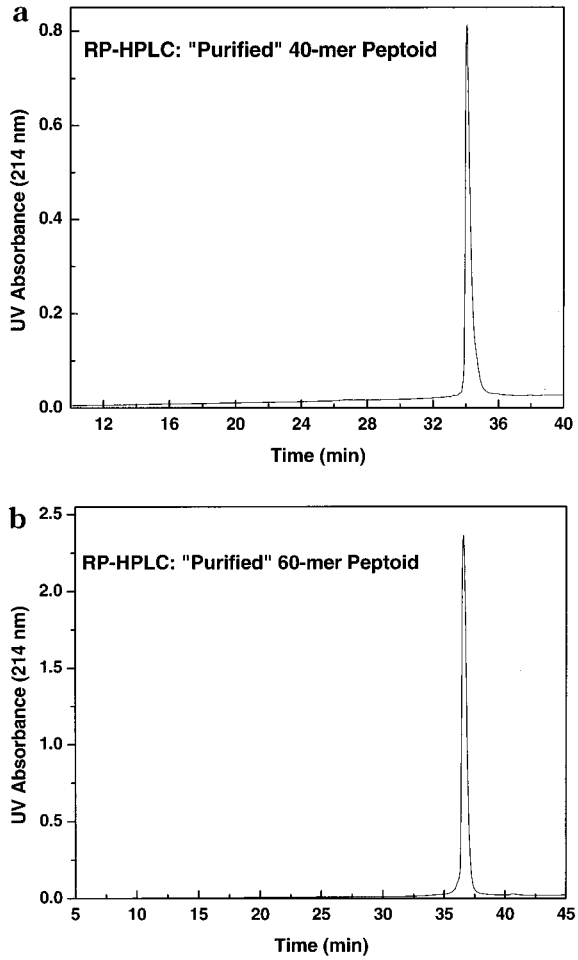


Figure 3. (a) RP-HPLC analysis of a RP-HPLC-purified 40-monomer poly(*N*- methoxyethyl glycine). Conditions as in Figure 1a. (b) RP-HPLC analysis of a RP-HPLC-purified 60-monomer poly(*N*-methoxyethyl glycine). Conditions as in Figure 1a.

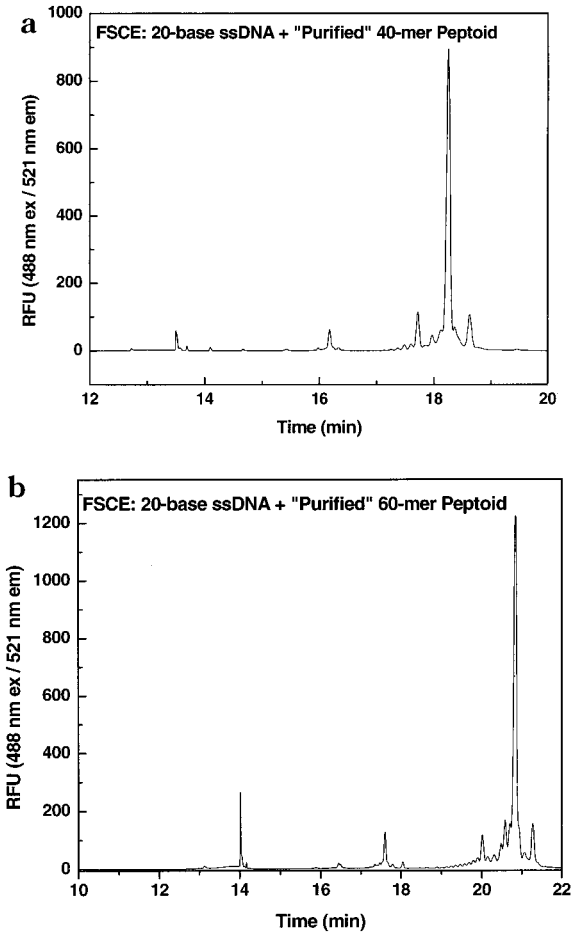


Figure 4. (a) FSCE analysis of the sample seen in Figure 3a using a 20-base ssDNA "engine". Conditions: Buffer 1X TTE, pH 8.5, other conditions as in Figure 2a. (b) FSCE analysis of the sample seen in Figure 3b using a 20-base ssDNA "engine". Conditions as in Figure 4a.

Figures 2a and 2b present the results of the FSCE analyses of a 20-base DNA + 40-mer unpurified peptoid conjugate, and of a 20-base DNA + 60-mer unpurified peptoid conjugate, respectively. Although HPLC and FSCE separate the constituents of the complex sample via different mechanisms, the qualitative results of the two separation mechanisms are similar. The FSCE analyses, however, result in the constituents of the complex sample mixture being resolved more fully when compared to RP-HPLC analyses of the same molecules. This is a result of the high selectivity of capillary electrophoresis and the exquisite sensitivity of LIF detection. The initial group of peaks in Figure 2a eluting at approximately 24 min represents various "free" residual DNA species from the conjugation reaction that were not conjugated to any peptoid oligomers. This peak is not present in Figure 2b, as the concentrations were adjusted in this reaction so that there was virtually no residual, unreacted DNA. In both Figures 2a and 2b, numerous small peaks representing DNA−peptoid conjugates, eluting in order of increasing peptoid chain length, follow the initial "free DNA" peak. The latest eluting, major peak represents the conjugate with the largest peptoid, which is the full-length desired product (confirmed by mass spectrometry).

The presence of a single fluorophore on the 3′ terminus of each of the DNA−peptoid conjugates allows one to calculate the molar percentage of each component in the original peptoid sample, simply as the ratio of the area of the peak representing that particular peptoid component to the area of all DNA−peptoid conjugate peaks in the electropherogram. Thus, the percent yield of the full-length product is simply the ratio of the area under the last eluting major peak to the sum of the areas under all DNA−peptoid conjugate peaks. Electrokinetic injections, which were used in this study, can cause a bias in the amount of higher-mobility sample components introduced into the capillary. Higher-mobility species (i.e., conjugates with short peptoid components) will tend to be injected to a greater extent than lower-mobility fragments. Formally, one must correct for this bias to obtain accurate quantitation of the relative abundance of each species present in the sample. However, in previous FSCE studies, we have determined this bias to be negligible (*34*).

Chromatograms and Electropherograms for the Analysis of Purified Polypeptoids. Figures 3a and 3b show the analytical HPLC chromatograms obtained for 40- and 60-mer polypeptoids *after* preparative HPLC purification. Notice that both RP-HPLC analyses show a single, large, relatively Gaussian peak, leading to the conclusion that the polypeptoid samples are essentially pure after the preparative HPLC purification step. That is, virtually no impurities can be detected by RP-HPLC with UV absorbance detection.

These HPLC results are in contrast to Figures 4a and 4b, which show the results of the FSCE analysis of the same, purified 40- and 60-mer peptoid samples after conjugation to 20-base DNA oligomers. Comparison of

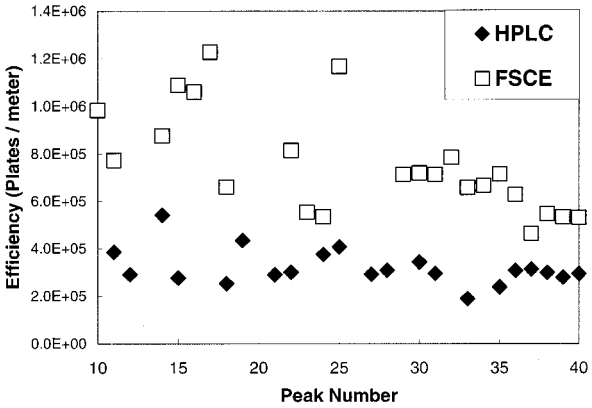


Figure 5. Plot of separation efficiency as a function of peak number for the FSCE separation (open squares) and RP-HPLC separation (filled diamonds) of the 40 monomer poly(*N*-methoxyethyl glycine) seen in Figures 1a and 2a. Peak data obtained with PeakFit software.

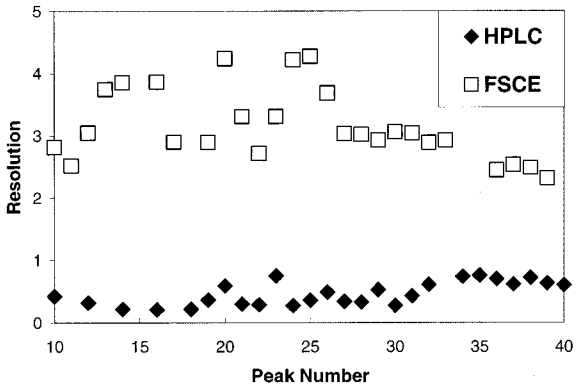


Figure 6. Plot of separation resolution as a function of peak number for the FSCE separation (open squares) and RP-HPLC separation (closed diamonds) of the 40 monomer poly(*N*-methoxyethyl glycine) seen in Figures 1a and 2a. Peak data obtained using PeakFit software.

Figures 3a and 3b with Figures 4a and 4b shows the superior separation performance and sensitivity of FSCE with LIF detection for the detection of sample impurities, when compared to standard RP-HPLC with UV detection. Impurities that are present in purified polypeptoid samples are not observed in HPLC analysis, yet are readily detected by FSCE analysis and represent substantial contamination of the desired peptoid (41% and 47%, as determined by peak integration, in Figures 4a and 4b, respectively). Thus, FSCE can lead to a more accurate and sensitive characterization of the absolute purity of a polyamide sample than is possible with standard RP-HPLC. This may be important for the evaluation of polypeptide or polypeptoid purity for applications, such as peptidomimetic pharmaceuticals, where the ultimate purity of an oligomer sample can impact not only its performance, but also the side effects it engenders.

Plate Heights. The number of theoretical plates achievable in a given separation length provides a quantitative measure of the efficiency of the separation. For separation techniques such as HPLC and CE, which are configured in a "finish-line" detection configuration in which the analytes migrate through a stationary detector, separation efficiency is manifested as the peak width. A low number of theoretical plates indicates that the separation technique or hardware has effects that are limiting the separation of the individual components in the complex sample mixture. A plot of the number of theoretical plates as a function of peptoid size, for both the HPLC and FSCE separations, is presented in Figure 5, for the 40-mer polypeptoid. In both FSCE and HPLC analyses, the last major eluting peak was assumed to be the full-length synthesis product and is assigned a peak number corresponding to the number of monomers in the polypeptoid (e.g., 40 for the 40-mer polypeptoid, 60 for the 60-mer polypeptoid). Peaks were then counted backward (i.e., decreasing in time) and assigned a peak number of one less than the peak that eluted immediately after it. Plate efficiencies were determined using the method described by Ren et al. (*37*). As can be seen in the figure, the average plate efficiency of the FSCE analysis is 2.5 times greater than that of an RP-HPLC, with several peaks displaying efficiencies well over 1×10^6 plate per meter. Higher average plate efficiency indicates that FSCE analysis produces peaks that are narrower than in HPLC; hence, we can conclude that fewer dispersive effects are limiting the FSCE separation when compared to more traditional RP-HPLC chromatographic separation techniques. Further, this shows that a greater number of species can be resolved in a given time window due to their narrower representative peaks.

Resolution. Resolution provides an overall, quantitative measure of how well each of the components in the complex sample is separated. Resolution of neighboring peaks can be calculated as:

$$R = \frac{1.18(t_b - t_a)}{(\mathrm{FWHM}_a + \mathrm{FWHM}_b)} \qquad (1)$$

where t_a and t_b are the elution times of peaks two adjacent peaks a and b, respectively, and FWHW_a and FWHW_b are the full temporal width at half the peak height of peaks a and b, respectively (*37*). Figure 6 presents the resolution of both HPLC and FSCE separations methods as a function of peptoid size for the 40mer polypeptoid. Peaks were assigned using the methodology explained in the Plate Heights section. As can be seen, the average resolution of the FSCE analysis is approximately 5 times that of RP-HPLC analysis and allows components of the complex sample mixture to be more fully resolved. Increased resolution means that the peaks are further separated from one and other and therefore are less likely to overlap in a given analysis. Peak separation leads to more accurate quantitation of each species present and thereby a more precise evaluation of the composition of the sample mixture.

The application of free-solution conjugate electrophoresis (FSCE) to the analysis of chemically synthesized oligomers, as we have demonstrated it here with maleimide−thiol linking of the DNA to the analyte, should be directly applicable to virtually any chemically synthesized oligomer, in particular polypeptides. As long as those peptides do not contain reactive thiols (cysteines), and the cleavage conditions to remove the polyamide from the solid support do not require the use of chemical that will react with the terminal maleimide, FSCE should be applicable. The addition of the maleimide functionality to the terminus of the oligomer is accomplished with standard chemicals for the synthesis of polyamides, such as peptides and peptoids and is therefore compatible with existing synthesis chemistries and protocols. However, the peptoid sequence chosen for this study did not require the use of side-chain protecting strategies, simplifying the compatibility of the maleimide linking protocol with the cleavage conditions. If more complicated and diverse side-chain chemistries are present in the polyamide analyte, alternative linking strategies will have to be

implemented to actualize FSCE profiling. Additionally, the solubility properties of this particular peptoid sequence prevented the use of standard ether precipitation workup techniques; thus, FSCE analysis was preceded by an RP-HPLC semipurification to remove small molecule contaminants. However, with optimization of chemical linking strategies to be insensitive to these contaminants, this procedure could be obviated.

CONCLUSIONS

FSCE analysis, when applied to chemically produced oligomers, results in high-resolution and high-efficiency separations. The average separation efficiency is 2.5 times greater and resolutions are 5 times higher than those obtained with RP-HPLC. When applied to HPLC-purified oligomer samples, FSCE allows for the separation and detection of impurities that are not observed in the HPLC analysis of the same samples. Thus, FSCE offers an attractive alternative for the analysis of chemically produced oligomers that may be challenging to analyze via more traditional chromatographic methods. With further development and optimization it seems likely that FSCE, with its orthogonal separation mechanism, could serve as a useful complement to HPLC that will allow for extremely sensitive and accurate characterization of polyamide samples including polypeptides of therapeutic interest. Moreover, with the advent of capillary array electrophoresis (CAE) instruments, now available commercially, FSCE with a modified conjugation strategy could allow the products of combinatorial solid-phase peptide synthesis to be analyzed in parallel. This would be impossible by HPLC, where typically only a single column is available and samples must be analyzed in series.

ACKNOWLEDGMENT

W.N.V. was supported by Northwestern University's NIH Predoctoral Biotechnology Training Grant (5-T32 GM 08449-06). G.W.S. acknowledges financial support from Applied Biosystems and the Natural Science and Engineering Research Council of Canada (NSERC). A.E.B. and W.N.V. acknowledge support from the U.S. Department of Energy, Office of Biological and Environmental Research Grant DE-FG02-99ER62789. A.E.B. and W.N.V. acknowledge helpful discussions with Dr. Ronald N. Zuckermann, as well as the generous gift of the epoxy-pDMA wall coating polymer by Dr. Marcella Chiari.

LITERATURE CITED

(1) Kochendoerfer, G. G., and Kent, S. B. H. (1999) Chemical protein synthesis. *Curr. Opin. Chem. Biol. 3*, 665−671.

(2) Jardetzky, T. S., Brown, J. H., Gorga, J. C., Stern, L. J., Urban, R. G., Chi, Y. I., Stauffacher, C., Strominger, J. L., and Wiley, D. C. (1994) 3-Dimensional Structure of a Human Class-II Histocompatibility Molecule Complexed With Superantigen. *Nature 368*, 711−718.

(3) Baker, K. A., Dutch, R. E., Lamb, R. A., and Jardetzky, T. S. (1999) Structural basis for paramyxovirus-mediated membrane fusion. *Mol. Cell 3*, 309−319.

(4) Brubaker, K., Cowley, S. M., Huang, K., Loo, L., Yochum, G. S., Ayer, D. E., Eisenman, R. N., and Radhakrishnan, I. (2000) Solution structure of the interacting domains of the Mad-Sin3 complex: Implications for recruitment of a chromatin-modifying complex. *Cell 103*, 655−665.

(5) Zuckermann, R. N., Kerr, J. M., Kent, S. B. H., and Moos, W. H. (1992) Efficient method for the preparation of peptoids [oligo(*N*-substituted glycines)] by submonomer solid-phase synthesis. *J. Am. Chem. Soc. 114*, 10646−10647.

(6) Wu, C. W., Sanborn, T. J., Zuckermann, R. N., and Barron, A. E. (2001) Peptoid oligomers with alpha-chiral, aromatic side chains: Effects of chain length on secondary structure. *J. Am. Chem. Soc. 123*, 2958−2963.

(7) Wu, C. W., Sanborn, T. J., Huang, K., Zuckermann, R. N., and Barron, A. E. (2001) Peptoid oligomers with alpha-chiral, aromatic side chains: Sequence requirements for the formation of stable peptoid helices. *J. Am. Chem. Soc. 123*, 6778−6784.

(8) Simon, R. J., Kania, R. S., Zuckermann, R. N., Huebner, V. D., Jewell, D. A., Banville, S., Ng, S., Wang, L., Rosenberg, S., Marlowe, C. K., Speilmeyer, D. C., Tan, R., Frankel, A. D., Santi, D. V., Cohen, F. E., and Bartlett, P. A. (1992) Peptoids: A modular approach to drug discovery. *Proc. Natl. Acad. Sci. U.S.A. 89*, 9367−9371.

(9) Kirshenbaum, K., Barron, A. E., Goldsmith, R. A., Armand, P., Bradley, E. K., Truong, K. T. V., Dill, K. A., Cohen, F. E., and Zuckermann, R. A. (1998) Sequence-specific polypeptoids: A diverse family of heteropolymers with stable secondary structure. *Proc. Natl. Acad. Sci. U.S.A. 95*, 4303−4308.

(10) Figliozzi, G. M., Goldsmith, R., Ng, S. C., Banville, S. C., and Zuckermann, R. N. (1996) In *Combinatorial Chemistry*, Academic Press Inc., San Diego, Vol. 267, pp 437−447.

(11) Appella, D. H., Christianson, L. A., Karle, I. L., Powell, D. R., and Gellman, S. H. (1996) beta-peptide foldamers: Robust Helix formation in a new family of beta-amino acid oligomers. *J. Am. Chem. Soc. 118*, 13071−13072.

(12) Seebach, D., Ciceri, P. E., Overhand, M., Jaun, B., Rigo, D., Oberer, L., Hommel, U., Amstutz, R., and Widmer, H. (1996) Probing the helical secondary structure of short-chain beta-peptides. *Helv. Chim. Acta 79*, 2043−2066.

(13) Seebach, D., Overhand, M., Kuhnle, F. N. M., Martinoni, B., Oberer, L., Hommel, U., and Widmer, H. (1996) beta-peptides: Synthesis by Arndt-Eistert homologation with concomitant peptide coupling. Structure determination by NMR and CD spectroscopy and by X-ray crystallography. Helical secondary structure of a beta-hexapeptide in solution and its stability towards pepsin. *Helv. Chim. Acta 79*, 913−941.

(14) Appella, D. H., Christianson, L. A., Klein, D. A., Richards, M. R., Powell, D. R., and Gellman, S. H. (1999) Synthesis and structural characterization of helix-forming beta-peptides: *trans*-2-aminocyclopentanecarboxylic acid oligomers. *J. Am. Chem. Soc. 121*, 7574−7581.

(15) Hintermann, T., Gademann, K., Jaun, B., and Seebach, D. (1998) gamma-peptides forming more stable secondary structures than alpha-peptides: Synthesis and helical NMR-solution structure of the gamma-hexapeptide analog of H-(Val-Ala-Leu)(2)-OH. *Helv. Chim. Acta 81*, 983−1002.

(16) Wilson, M. E., and Nowick, J. S. (1998) An efficient synthesis of N,N′-linked oligoureas. *Tetrahedron Lett. 39*, 6613−6616.

(17) Egholm, M., Buchardt, O., Nielsen, P. E., and Berg, R. H. (1992) Peptide Nucleic-Acids (Pna) − Oligonucleotide Analogs With an Achiral Peptide Backbone. *J. Am. Chem. Soc. 114*, 1895−1897.

(18) Barron, A. E., and Zuckermann, R. N. (1999) Bioinspired polymeric materials: in-between proteins and plastics. *Curr. Opin. Chem. Biol. 3*, 681−687.

(19) Gellman, S. H. (1998) Foldamers: A manifesto. *Acc. Chem. Res. 31*, 173−180.

(20) Kirshenbaum, K., Zuckermann, R. N., and Dill, K. A. (1999) Designing polymers that mimic biomolecules. *Curr. Opin. Struct. Biol. 9*, 530−535.

(21) Stigers, K. D., Soth, M. J., and Nowick, J. S. (1999) Designed molecules that fold to mimic protein secondary structures. *Curr. Opin. Chem. Biol. 3*, 714−723.

(22) Arnold, U., Hinderaker, M. P., Nilsson, B. L., Huck, B. R., Gellman, S. H., and Raines, R. T. (2001) Semisynthesis of proteins containing nonnatural modules. *Biochemistry 40*, 97.

(23) F. Lottspeich, A. H., Hupe, K.-P. (1981) *High performance liquid chromatography in protein and peptide chemistry: proceedings, international symposium*, Walter de Gruyter, New York.

(24) Engelhardt, H. (1979) *High performance liquid chromatography*, 2nd ed., Springer-Verlag, Berlin, 1979.

(25) Seipke, G., Mullner, H., and Grau, U. (1986) High-Pressure Liquid-Chromatography (HPLC) of Proteins. *Angew. Chem., Int. Ed. Engl. 25*, 535−552.
(26) Dovichi, N. J., Martin, J. C., Jett, J. H., and Keller, R. A. (1983) Attogram Detection Limit for Aqueous Dye Samples by Laser- Induced Fluorescence. *Science 219*, 845−847.
(27) Vespalec, R., and Bocek, P. (1999) Chiral separations in capillary electrophoresis. *Electrophoresis 20*, 2579−2591.
(28) Lopez, M. (2000) Better approaches to finding the needle in a haystack: Optimizing proteome analysis through automation. *Electrophoresis 21*, 1082−1093.
(29) Hong, M., Sudor, J., Stefansson, M., and Novotny, M. V. (1998) High-Resolution studies of hyaluronic acid mixtures through capillary gel electrophoresis. *Anal. Chem. 70*, 568−573.
(30) Slater, G. W., Kist, T. B. L., Ren, H. J., and Drouin, G. (1998) Recent developments in DNA electrophoretic separations. *Electrophoresis 19*, 1525−1541.
(31) Schmalzing, D., Koutny, L., Salas-Solano, O., Adourian, A., Matsudaira, P., and Ehrlich, D. (1999) Recent developments in DNA sequencing by capillary and microdevice electrophoresis. *Electrophoresis 20*, 3066−3077.
(32) Viovy, J. L. (2000) Electrophoresis of DNA and other polyelectrolytes: Physical mechanisms. *Rev. Mod. Phys. 72*, 813−872.
(33) Albarghouthi, M. N., and Barron, A. E. (2000) Polymeric matrices for DNA sequencing by capillary electrophoresis. *Electrophoresis 21*, 4096−4111.
(34) Vreeland, W. N., Desruisseaux, C., Karger, A. E., Drouin, G., Slater, G. W., and Barron, A. E. (2001) Molar mass profiling of synthetic polymers by free-solution capillary electrophoresis of DNA−polymer conjugates. *Anal. Chem. 73*, 1795−1803.
(35) Chiari, M., Cretich, M., Damin, F., Ceriotti, L., and Consonni, R. (2000) New adsorbed coatings for capillary electrophoresis. *Electrophoresis 21*, 909−916.
(36) Williams, B. A., and Vigh, C. (1996) Fast, accurate mobility determination method for capillary electrophoresis. *Anal. Chem. 68*, 1174−1180.
(37) Ren, H., Karger, A., Oaks, F., Menchen, S., Slater, G. W., and Drouin, G. (1999) Separating DNA sequencing fragments without a sieving matrix. *Electrophoresis 20*, 2501.

BC0155871

Synthesis and Properties of Novel Tetraalkyl Cationic Lipids

Jérôme Gaucheron,*[,†] Tabitha Wong,[†] Kim F. Wong,[†] Norbert Maurer,[†] and Pieter R. Cullis[†,‡]

Department of Biochemistry and Molecular Biology, University of British Columbia, 2146 Health Sciences Mall, Vancouver, BC, Canada V6T 1Z3 and Inex Pharmaceuticals Corporation, 100-8900 Glenlyon Parkway, Glenlyon Business Park, Burnaby, BC, Canada V5J 5J8. Received December 20, 2001

The synthesis, physical properties, and transfection potencies of two representives of a new class of divalent, tetraalkyl cationic lipids is described. These cationic lipids are dimers of *N*,*N*-Dioleyl-*N*,*N*-dimethylammonium chloride (DODAC) joined by a hydrocarbon tether three or six carbons in length (TODMAC3 and TODMAC6, respectively). It is shown that TODMAC6 can display improved transfection properties in comparison to DODAC when formulated into plasmid DNA−cationic lipid complexes. These improved transfection potencies are observed at cationic lipid to DNA charge ratios of two or higher. It is also shown that TODMAC6 exhibits equivalent or improved ability (as compared to DODAC) to induce nonbilayer structure in mixtures with anionic lipid. This is consistent with the hypothesis that the ability of cationic lipids to induce nonbilayer structures when mixed with anionic lipids is correlated to their transfection potency. Complexes containing TODMAC3 on the other hand exhibit lower transfection potencies than achieved with DODAC, behavior that is consistent with steric effects limiting the formation of ion pairs with anionic lipids. It is concluded that TODMAC6 exhibits potential as a transfection agent for in vitro and in vivo use and that the design of cationic lipids according to their ability to induce nonbilayer structure provides a useful guide for synthesis of new cationic lipids.

INTRODUCTION

Plasmid DNA-cationic lipid complexes are the leading nonviral gene therapy vectors used in the clinical setting (*1*−*4*). However the levels of gene expression that can be achieved using these complexes are substantially lower than can be achieved using viral vectors. Considerable effort has therefore been devoted to synthesizing new cationic lipids that have improved transfection properties over those currently available (*5*−*10*). These efforts are largely phenomenological due to the lack of understanding of the mechanism whereby cationic lipids facilitate the intracellular delivery of macromolecules such as plasmid DNA. In this regard recent work from this laboratory suggests that the ability of cationic lipids to facilitate intracellular delivery is related to their ability to induce the nonbilayer hexagonal H_{II} phase in combination with anionic lipids (*11*). In particular this proposal suggests that the most potent cationic lipids are those that are the most effective inducers of H_{II} phase organization.

The ability of lipids to adopt the H_{II} phase has been related to their dynamic "molecular shape" properties. Within this framework lipids with a small cross-sectional area in the headgroup region and a larger acyl chain cross-sectional area exhibit a "cone" shape compatible with H_{II} phase organization (*12*). In this regard a direct method to increase the cone-shaped character of a given lipid is to increase the number of alkyl chains associated with the headgroup. In this work we describe the synthesis and transfection properties of a new class of cationic lipids that contain four alkyl chains. It is shown that these cationic lipids can exhibit improved transfection properties compared to dialkyl cationic lipids.

Earlier studies have shown *N*,*N*-dioleyl-*N*,*N*-dimethylammonium chloride (DODAC) to be quite an effective DNA transfection agent (*13*, *14*). We thus chose a synthetic route to generate a molecule with two quaternary ammonium groups and four oleyl chains, essentially a DODAC dimer. The procedure involved alkylating dimethylamines with oleyl bromide. The polymorphic phases of these new cationic lipids were monitored by ^{31}P NMR of these lipid mixtures containing 1,2-dipalmitoyl-sn-glycero-3-[phospho-L-serine] (DPPS). The in vitro transfection potency was measured and compared with that of DODAC.

EXPERIMENTAL PROCEDURES

Materials and Reagents. All organic solvents and reagents including the Dragendorff reagent and ninhydrin reagent were obtained from Sigma-Aldrich Canada (Oakville, ON). DOPE and DPPS were purchased from Avanti Polar Lipids (Alabaster, AL). The cationic lipid DODAC was a gift from Dr. Steven Ansell of Inex Pharmaceuticals (Vancouver, BC). The plasmid pCMV-luc (5650 bp, CMV promoter, coding for luciferase) was a gift from Inex Pharmaceuticals (Vancouver, BC).

Analytical Techniques. The cationic lipids were purified by column chromatography using silica gel 60 (Merck, 70−230 mesh) and dichloromethane (CH_2Cl_2)/methanol (MeOH) mixtures. Unless stated otherwise, the ratios describing the composition of solvent mixtures represent relative volume fractions. The reaction progress was followed by thin-layer chromatography (TLC) on silica plates F_{254} (Merck). The following developing systems were used: UV light, H_2SO_4/EtOH (1/1 v/v), Dragendorff reagent (Sigma), ninhydrin reagent (Sigma). ^{1}H, ^{13}C, and ^{31}P NMR spectra were obtained employing a Bruker MSL 200 spectrometer operating at 200.13,

* To whom correspondence should be addressed. Phone: (604) 822−2649. Fax: (604) 822−4843. E-mail: jerome_gaucheron@yahoo.fr.

† University of British Columbia.

‡ Inex Pharmaceuticals Corporation.

10.1021/bc0101259 CCC: $22.00 © 2002 American Chemical Society
Published on Web 04/05/2002

50.3, and 81.02 MHz, respectively. Deuterated chloroform ($CDCl_3$) was used as the solvent in the NMR experiments. Chemical shifts were measured relative to $CHCl_3$ (δ 7.24 ppm) for ^1H, relative to $CDCl_3$ (δ 77.16 ppm) for ^{13}C. The following abbreviations are used to describe the signal multiplicities: s (singlet), d (doublet), t (triplet), q (quadruplet), and m (multiplet). Chemical shifts are expressed in ppm and listed as follows: shift in ppm (multiplicity, coupling, integration and assignment). Elemental analyses were carried out by Microanalytical Service (Department of Chemistry, University of British Columbia).

Synthesis of *N,N,N′,N′*-Tetraoelyl-*N,N′*-dimethyl-1,3-propanediammonium Chloride (TODMAC3). A solution of *N,N′*-dimethyl-1,3-propanediamine (0.253 g, 2.5 mmol) and oleyl bromide (5 g, 15.1 mmol) in toluene (20 mL) and a solution of tetrabutylammonium hydrogensulfate (0.4 g, 1.2 mmol) in 1 M sodium hydroxide (20 mL) were stirred under reflux. After 4 days, 2.5 g oleyl bromide (7.5 mmol) was added and the reaction continued for another 5 days. The water phase was extracted two times with toluene. The combined organic phases were evaporated. The residue was dissolved in CH_2Cl_2 and washed six times with 3% hydrochloric acid and three times with saturated aqueous NaCl. The organic phase was evaporated and the remaining material purified by silica gel chromatography (CH_2Cl_2/MeOH from 10/0 to 9/1). **TODMAC3** was obtained as a pale yellow oil at a yield of 1.15 g (0.98 mmol, 39%). The product was washed six times with 3% hydrochloric acid and three times with saturated aqueous NaCl again.

TLC (CH_2Cl_2/MeOH 9/1, H_2SO_4/EtOH): $R_f = 0.43$. ^1H NMR ($CDCl_3$): δ 0.87 (t, $^3J = 6.6$ Hz, 12H, CH_3); 1.08−1.48 (broad s, 88H, $CH_3(CH_2)_6CH_2CH{=}CHCH_2(CH_2)_5$); 1.48−1.77 (m, 10H, CH_2CH_2N); 1.80−2.12 (m, 16H, $=CHCH_2$); 3.22−3.80 (m, 18H, CH_3, CH_2N); 5.20−5.45 (m, 8H, =CH). ^{13}C NMR ($CDCl_3$): δ 14.1 (CH_3CH_2); 22.7 (CH_3CH_2); 27.2 ($=CHCH_2$); 22.5, 26.4, 29.1, 29.2, 29.3, 29.5, 29.7 ($CH_3(CH_2)_2(CH_2)_4CH_2CH{=}CHCH_2(CH_2)_6$, $NCH_2CH_2CH_2N$); 31.9 ($CH_3CH_2CH_2$); 49.0 (NCH_3); 61.5 (NCH_2); 129.6, 130.1 (=CH). Anal. ($C_{77}H_{152}N_2Cl_2$) H, N, C: calcd, 78.58; found, 79.50.

Synthesis of *N,N,N′,N′*-Tetraoelyl-*N,N′*-dimethyl-1,6-hexanediammonium chloride (TODMAC6). TODMAC6 was synthesized using the same procedure as described above for TODMAC3 by substituting *N,N′*-dimethyl-1,6-hexanediamine for *N,N′*-dimethyl-1,3-propanediamine.

TLC (CH_2Cl_2/MeOH 9/1, H_2SO_4/EtOH): $Rf = 0.61$. ^1H NMR ($CDCl_3$): δ 0.85 (t, $^3J = 6.6$ Hz 12H, CH_3); 1.00−1.46 (broad s, 92H, $CH_3(CH_2)_6CH_2CH{=}CHCH_2(CH_2)_5$, $N(CH_2)_2(CH_2)_2(CH_2)_2N$); 1.46−1.74 (m, 10H, CH_2CH_2N); 1.80−2.12 (m, 16H, $=CHCH_2$); 3.14−3.75 (m, 18H, CH_3, CH_2N); 5.20−5.45 (m, 8H, =CH). ^{13}C NMR ($CDCl_3$): δ 14.1 (CH_3CH_2); 22.7 (CH_3CH_2); 27.2 ($=CHCH_2$); 21.0, 22.5, 23.9, 26.4, 29.4, 29.6, 29.8 ($CH_3(CH_2)_2(CH_2)_4CH_2CH{=}CHCH_2(CH_2)_6$, $NCH_2(CH_2)_4CH_2N$); 31.9 ($CH_3CH_2CH_2$); 49.0 (NCH_3); 61.2, 62.7 (NCH_2); 129.7, 130.2 (=CH). Anal. ($C_{80}H_{158}N_2Cl_2$)·H_2O C, H, N.

^{31}P Nuclear Magnetic Resonance Spectroscopy. Lipid mixtures containing 40−50 mg DPPS and appropriate molar ratios of cationic lipids (DODAC, TODMAC3, TODMAC6) were prepared by drying from chloroform solution, placed in 10 mm NMR tubes, and hydrated with 1.5 mL of distilled water. Free induction decays (FIDs) corresponding to 1000 scans were obtained by using a 3.0 μs 60° pulse with a 1 s interpulse delay and a spectral width of 25000 Hz. A gated two-level proton decoupling was used to ensure sufficient decoupling with minimum sample heating. An exponential multiplication corresponding to 50 Hz of line broadening was applied to the FIDs prior to Fourier transformation. The sample temperature (±1 °C) was regulated using a Bruker B−VT1000 variable temperature unit. Chemical shifts were referenced to 85% phosphoric acid as an external standard.

Preparation of Large Unilamellar Vesicles (LUV). Mixtures of cationic lipids and DOPE in chloroform were dried under a stream of nitrogen gas, and the residual solvent was removed under high vacuum for 2 h. The resulting lipid films were hydrated with distilled water. LUVs were obtained by extruding the lipid dispersions 10 times through two stacked 100-nm pore size polycarbonate filters (Costar Nuclepore polycarbonate membrane, Northern Lipids Inc. extruder) (*15*). Phospholipid concentrations were determined by the inorganic phosphorus assays according to Fiske and Subbarow (*16*).

Preparation of Lipoplexes. Lipoplexes were prepared in distilled water at pDNA concentrations ranging from 12.5 to 25 μg pDNA/ml at positive-to-negative charge ratios between 0.5 and 5. Plasmid DNA was added under vortexing to cationic LUVs (cationic lipid/DOPE 1:1). In the absence of the helper lipid DOPE, lipoplexes were prepared by addition of the cationic lipids from ethanol solutions to an aqueous solution containing the pDNA. The amount of ethanol in these formulations was between 0.4 and 2.3%. The lipoplexes were incubated at room temperature for 30 min, diluted to a final concentration of 2.5 μg pDNA/mL with serum-free media (Dulbecco's Modified Eagle's Medium, DMEM), and subsequently applied to BHK cells.

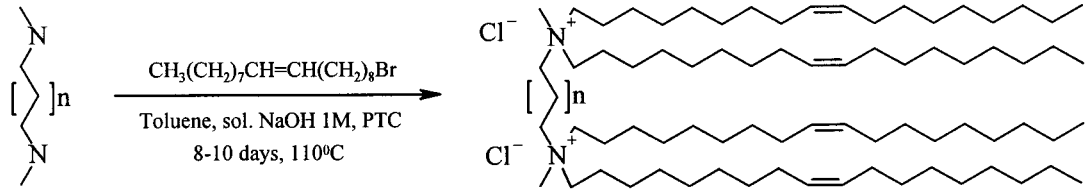
In Vitro Transfection of BHK Cells. BHK cells, grown in DMEM supplemented with 10% fetal calf serum (FCS), 100 U/mL of penicillin, and 100 μg/mL of streptomycin, were seeded in 96-well plates at a density of 1×10^4 cells per well 24 h before transfection. The next day media was removed and replaced with 100 μL of lipoplexes dispersed in serum-free DMEM (0.25 μg pDNA/100 μL). After 4 h, lipoplexes were replaced with serum-containing DMEM and cells further incubated for 20 h. After that the culture medium was aspirated, the cells washed twice with 100 μL of PBS and then lysed through addition of 50 μL of lysis buffer (0.1% Triton X-100 in PBS). Luciferase activity was measured with a Dynex luminometer (Dynex model ML3000) using the Luciferase Assay Kit from Promega. The total protein concentration per well was determined using the BCA assay from Pierce. Means and standard deviations were calculated from three independent experiments.

Statistical Analyses. Statistical analyses were performed using a Student t test. The difference between two means was considered as significant when the probability p is 0.05.

RESULTS

Rationale for and Synthesis of the Cationic Lipids TODMAC3 and TODMAC6. As indicated in the Introduction, cationic lipids with a small cross-sectional area in the headgroup region would be expected to give rise to improved transfection properties compared to lipids with larger headgroup areas, assuming the cross-sectional area in the alkyl chain region remains constant (*11*). One method to vary the headgroup area is to create a dimer of cationic lipids joined together in the headgroup region by a tether of variable length. We chose to work with DODAC, a cationic lipid with excellent transfection properties, and construct dimers joined by hydrocarbon

Scheme 1. Chemical Structure, Code Name, and Synthetic Route of the Tetraalkyl Cationic Lipids



n = 1 TODMAC3
n = 4 TODMAC6

tethers three and six carbons long (TODMAC3 and TODMAC6, respectively).

These cationic lipids were synthesized by nucleophilic substitution of secondary amines using oleyl bromide under phase-transfer catalytic condition as outlined in Scheme 1. The reaction was performed in toluene and 1 M sodium hydroxide in the presence of a phase-transfer catalyst for 10 days at 100 °C. The strongly basic amines required high alkaline reaction conditions so that they remained deprotonated to react with oleyl bromide. The yields were 39 and 85% for TODMAC3 and TODMAC6, respectively. The lower yield for TODMAC3 is probably due to steric hindrance as a result of the close proximity of the two positive charges. The diquaternary ammonium chlorides were characterized by ^{1}H and ^{13}C NMR as well as by elemental analysis. The NMR resonances are consistent with the diquaternary structure of the cationic lipids (see above Experimental Procedures).

Polymorphic Phase Properties of Mixtures of TODMAC3 and TODMAC6 with DPPS. The ability of cationic lipids to induce the hexagonal H_{II} phase in combination with anionic lipids correlates well with their transfection properties in plasmid DNA−cationic lipid complexes. The relative ability of cationic lipids to induce the H_{II} phase can be ascertained by measuring the bilayer-to-nonbilayer transition temperature (T_C) of the cationic lipid in equimolar mixtures (with respect to charge) with an anionic phospholipid such as DPPS. The bilayer-to-nonbilayer transition can be conveniently monitored employing ^{31}P NMR techniques (*12*). Briefly, phospholipids that are in a bilayer organization exhibit a broad (≥40 ppm) aymmetric ^{31}P NMR line shape with a low field shoulder and a high field peak whereas phospholipids in the hexagonal H_{II} phase exhibit a line shape with reversed asymmetry that is a factor of 2 narrower. Phospholipids in nonbilayer cubic phases that often occur in conjunction with H_{II} phase formation exhibit narrow "isotropic" ^{31}P NMR spectra. It should be noted that small (diameter ≤ 200 nm) phopholipid vesicles also exhibit isotropic spectra; however, in the results presented here the presence of such spectra will be attributed to nonbilayer structures as the temperature-dependent phase behavior was reversible.

In the first series of experiments the temperature-dependent polymorphism of TODMAC6/DPPS mixtures was compared to the behavior of DODAC/DPPS mixtures. As shown in Figure 1, at 25 °C both mixures exhibited ^{31}P NMR line shapes indicative of bilayer structure. However at 30 °C the mixture containing TODMAC6 has largely adopted the H_{II} phase or a structure giving rise to a narrow isotropic ^{31}P NMR peak, whereas the dispersion containing DODAC remains in a bilayer organization at 35 °C, adopting the structure giving rise to the "isotropic" ^{31}P NMR peak at 30 °C. On the basis of this behavior it would be expected that TODMAC6 should exhibit transfection properties that are comparable to or slightly better than DODAC when used in plasmid DNA−cationic lipid complexes.

The ^{31}P NMR behavior of dispersions of TODMAC3/DPPS (0.5:1; mol:mol) is illustrated in Figure 2A. At temperatures as low as 15 °C an H_{II} component is clearly visible; however, the large bulk of the phospholipid remains in the bilayer organization and the proportion in the H_{II} phase does not increase as the temperature is raised. This behavior is consistent with a limited solubility of the TODMAC3 in the DPPS component in the lipid mixture. This may be due to steric constraints associated with the need to form ion pairs between the cationic lipid and two DPPS molecules in order to form the H_{II} phase. For example, if only one DPPS molecule was able to form an ion pair with each TODMAC3, 50% of the DPPS would be unpaired and thus remain in the bilayer organization. If this is the case it would be expected that TODMAC3/DPPS systems containing higher proportions of TODMAC3 should exhibit increased preference for nonbilayer structure. The phase properties of a mixture containing equimolar proportions of TODMAC3 and DPPS were therefore investigated and, as shown in Figure 2B, this system exhibited an increased preference for H_{II} phase structure. On the basis of this behavior TODMAC3 would not be expected to be as effective a transfection agent as DODAC on a charge for charge basis.

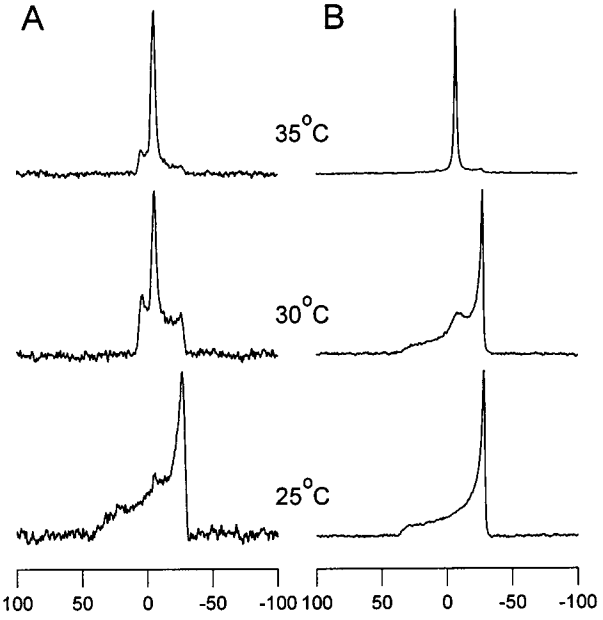


Figure 1. ^{31}P NMR spectrum obtained from an aqueous dispersion of TODMAC6/DPPS (0.5 molar ratio) (A) and of DODAC/DPPS (1 molar ratio) (B). The temperatures are indicated. Sample parameters and NMR parameters are described in Experimental Procedures.

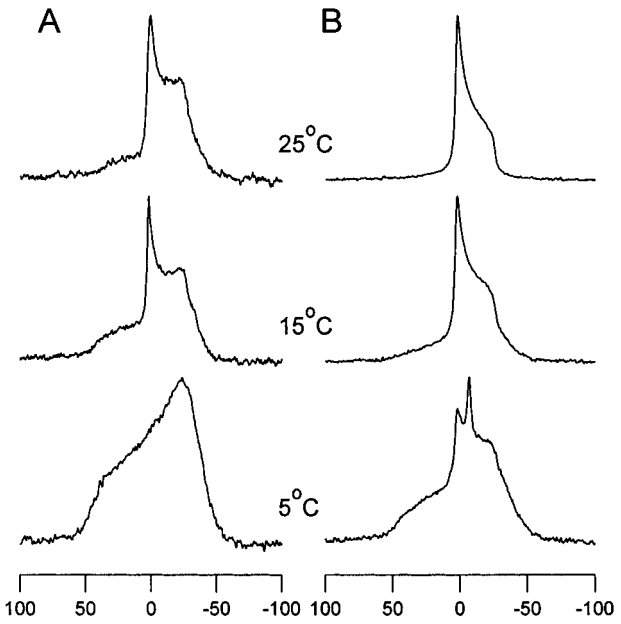


Figure 2. ^{31}P NMR spectrum obtained from an aqueous dispersion of TODMAC3/DPPS (0.5 molar ratio) (A) and of TODMAC3/DPPS (1 molar ratio) (B). The temperatures are indicated. Sample parameters and NMR parameters are described in Experimental Procedures.

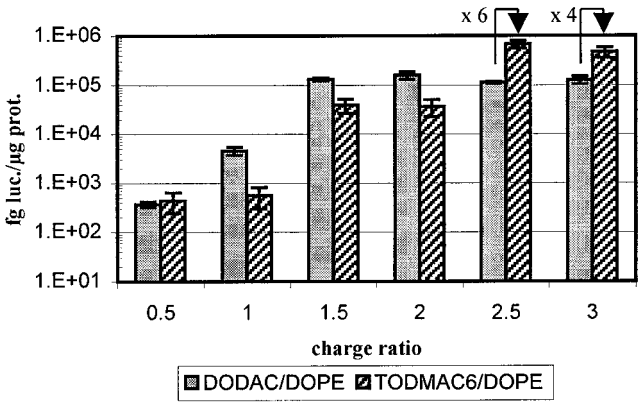


Figure 3. Transfection efficiency in BHK cells of the TODMAC6/DOPE lipoplexes, as compared with, DODAC/DOPE lipoplexes. The data presented correspond to a concentration of 0.25 μg DNA/well. The given means ± SEM were calculated from three independent experiments.

In Vitro Transfection Properties of Plasmid DNA−Cationic Lipid Complexes Containing TODMAC3 and TODMAC6. Plasmid DNA cationic lipid complexes are usually formed by mixing plasmid DNA with preformed vesicles containing the cationic lipid mixed with equimolar amounts of the "helper" lipid dioleoylphosphatidylethanolamine (DOPE) (*17*, *18*). However, it was found that vesicles could not be prepared consisting of TODMAC3/DOPE mixtures, as lipid films prepared of this lipid mixture were extremely difficult to hydrate and formed clumps that could not be extruded. Vesicles of TODMAC6/DOPE could be readily prepared, and the transfection properties of complexes formed employing TODMAC6 and DODAC and containing the L018 plasmid coding for the luciferase gene were tested in vitro using baby hamster kidney (BHK) cells. Figure 3 illustrates the transfection properties of complexes prepared at cationic lipid-to-DNA charge ratios (positive to negative) ranging from 0.5 to 5. It may be observed that the transfection potency of complexes containing TODMAC6 are comparable to or slightly lower than complexes

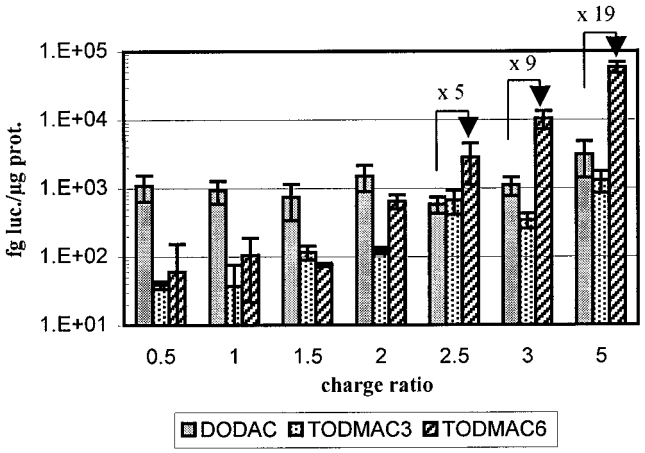


Figure 4. Transfection efficiency in BHK cells of the TODMAC6 and TODMAC3 lipoplexes, as compared with, DODAC lipoplexes. The data presented correspond to a concentration of 0.25 μg DNA/well. The given means ± SEM were calculated from three independent experiments.

containing DODAC at charge ratios or two or lower, but are greater at higher charge ratios.

To test the relative transfection potencies of DODAC, TODMAC6, and TODMAC3 a different procedure was used to associate the cationic lipid with the plasmid to form the complexes. In this method the cationic lipid dissolved in ethanol is introduced into an aqueous solution of the plasmid and DOPE is not present. The transfection properties of complexes formed in this manner are shown in Figure 4. It may be noted that at charge ratios of two and lower DODAC exhibits superior tranfection properties; however, at charge ratios above two TODMAC6 exhibits transfection properties that are superior to both DODAC and TODMAC3. Specifically, for charge ratios ≥2.5, TODMAC6 complexes gave rise to luciferase expression levels 5−20-fold higher than could be achieved with DODAC or TODMAC3.

DISCUSSION

This study describes the synthesis and transfection properties of a new class of tetraalkyl cationic lipids designed to increase the ability of cationic lipids to induce the hexagonal H_{II} phase. There are three points of interest, the first of which concerns the physical properties of these lipids in relation to their molecular shape characteristics. A second area concerns the correlation between the ability to induce H_{II} organization and the observed transfection properties. Finally, it is of interest to discuss the utility of the TODMAC3 and TODMAC6 cationic lipids and their derivatives as transfection agents. We discuss these points in turn.

The physical properties of TODMAC3 and TODMAC6 are quite different. TODMAC6 readily forms bilayer structures, both in the presence and absence of DOPE, on dispersion in an aqueous medium, whereas TODMAC3 does not. Further, when mixed with equimolar (with respect to charge) amounts of DPPS, TODMAC6 forms a homogeneous dispersion that collectively adopts nonbilayer structure in the region of 30 °C. TODMAC3 on the other hand is able to interact with only a limited subset of the DPPS but is able to induce the H_{II} phase for that subset at temperatures as low as 15 °C. At higher TODMAC3/DPPS ratios (2:1 on a charge basis), TODMAC3 is able to induce apparently complete H_{II} organization at temperatures of 25 °C or higher. These results are consistent with steric effects that limit the ability of

TODMAC3 to interact with more than one DPPS molecule due to the small size of the TODMAC3 headgroup.

The correlation between the ability of TODMAC6 and TODMAC3 to induce nonbilayer structure and their transfection properties is of obvious interest for the design of cationic lipids with optimized transfection capabilities. TODMAC6/DPPS and DODAC/DPPS liposomes exhibit bilayer−nonbilayer transitions that are close together, in the region of 30−35 °C. On this basis it would be expected that plasmid DNA−cationic lipid complexes containing TODMAC6 or DODAC should exhibit roughly equivalent transfection properties. For the complexes containing DOPE this is largely true, although somewhat higher transfection potency is observed for the complexes containing TODMAC6 at higher charge ratios. For the complexes prepared in the absence of DOPE the TODMAC6, complexes are not as effective transfection agents at charge ratios less than two but can be substantially more potent at charge ratios above two. In the case of TODMAC3 the tranfection potency of the complexes (prepared in the absence of DOPE) only become comparable to complexes containing DODAC at charge ratios above two. This could be interpreted as reflecting a need for increased amounts of TODMAC3 in order to bind to endogenous anionic lipid due to steric effects inhibiting these interactions. Overall these results suggest that while the ability to induce nonbilayer structure correlates roughly with transfection potency, other factors can also influence transfection potencies substantially. These other effects include the method of constructing the complexes, steric barriers inhibiting the formation of neutral ion pairs between cationic and anionic lipids, the ability of the cationic lipid to dissociate from the plasmid DNA following uptake into the cell, and the lipid composition of the endosomal membrane.

The final area of discussion concerns the utility of TODMAC6 and TODMAC3 as transfection agents. It would appear that TODMAC3 has limited advantages over currently available cationic lipid such as DODAC. The utility of TODMAC3 is further compromised by the inability to incorporate DOPE into complexes containing TODMAC3 due to the inability to form vesicular structures. However, TODMAC6 appears to have interesting potential, particularly at charge ratios above two. Current work is focused on exploring this potential when incorporated into "stabilized plasmid-lipid particles" (SPLP) (*19*−*21*) for in vivo applications for treatment of systemic disease.

ACKNOWLEDGMENT

This research was supported by the Canadian Institutes of Health Research.

LITERATURE CITED

(1) Nishikawa, M., and Huang, L. (2001) Nonviral vectors in the new millennium: delivery barriers in gene transfer. *Hum. Gene Ther. 20*, 861−70.

(2) Pedroso de Lima, M. C., Simoes, S., Pires, P., Faneca, H., and Duzgunes, N. (2001) Cationic lipid-DNA complexes in gene delivery: from biophysics to biological applications. *Adv. Drug Deliv. Rev. 47*, 277−94.

(3) Welsh, M. J., and Zabner, J. (1999) Cationic lipid mediated gene transfer of CFTR: safety of a single administration to the nasal epithelia. *Hum. Gene Ther. 10*, 1559−72.

(4) Maurer, N., Fenske, D. B., and Cullis, P. R. (2001) Developments in liposomal drug delivery systems. *Expert Opin. Biol. Ther. 1*, 1−25.

(5) Felgner, P. L., Gadek, T. R., Holm, M., Roman, R., Chan, H. W., Wenz, M., Northrop, J. P., Ringold, G. M., and Danielsen, M. (1987) Lipofection: a highly efficient, lipid-mediated DNA-transfection procedure. *Proc. Natl. Acad. Sci. U.S.A. 84*, 7413−7417.

(6) Miller, A. D. (1998) Cationic Liposomes for gene therapy. *Angew. Chem., Int. Ed. 37*, 1768−1785.

(7) Felgner, J. H., Kumar, R., Sridhar, C. N., Wheeler, C. J., Tsai, Y. J., Border, R., Ramsey, P., Martin, M., and Felgner, P. L. (1994) Enhanced gene delivery and mechanism studies with a novel series of cationic lipid formulations. *J. Biol. Chem. 269*, 2550−2561.

(8) Wang, J., Guo, X., Xu, Y., Barron, L., and Szoka, F. C., Jr. (1998) Synthesis and characterization of long chain alkyl acyl carnitine esters. Potentially biodegradable cationic lipids for use in gene delivery. *J. Med. Chem. 41*, 2207−2215.

(9) Gao, H., and Hui, K. M. (2001) Synthesis of a novel series of cationic lipids that can act as efficient gene delivery vehicles through systematic heterocyclic substitution of cholesterol derivatives. *Gene Ther. 8*, 855−63.

(10) Hyvonen, Z., Plotniece, A., Reine, I., Chekavichus, B., Duburs, G., and Urtti, A. (2000) Novel cationic amphiphilic 1,4-dihydropyridine derivatives for DNA delivery. *Biochim. Biophys. Acta 1509*, 451−66.

(11) Hafez, I. M., Maurer, N., and Cullis, P. R. (2001) On the mechanism whereby cationic lipids promote intracellular delivery of polynucleic acids. *Gene Ther. 8*, 1188−96.

(12) Cullis, P. R., and de Kruijff, B. (1979) Lipid polymorphism and the functional roles of lipids in biological membranes. *Biochim. Biophys. Acta 559*, 399−420.

(13) Schoen, P., Chonn, A., Cullis, P. R., Wilschut, J., and Scherrer, P. (1999) Gene transfer mediated by fusion protein hemagglutinin reconstituted in cationic lipid vesicles. *Gene Ther. 6*, 823−32.

(14) Lam, A. M., and Cullis, P. R. (2000) Calcium enhances the transfection potency of plasmid DNA−cationic liposome complexes. *Biochim. Biophys. Acta 1463*, 279−90.

(15) Mayer, L. D., Hope, M. J., and Cullis, P. R. (1986) Vesicles of variable sizes produced by a rapid extrusion procedure. *Biochim. Biophys. Acta 858*, 161−8.

(16) Fiske, C. H., Subbarow, Y. (1925) The colorimetric determination of phosphorus. *J. Biol. Chem. 66*, 375−379.

(17) Farhood, H., Serbina, N., and Huang, L. (1995) The role of dioleoyl phosphatidylethanolamine in cationic liposome mediated gene transfer. *Biochim. Biophys. Acta 1235*, 289−295.

(18) Hui, S. W., Langner, M., Zhao, Y., Ross, P., Hurley, E., and Chan, K. (1996) The role of helper lipids in cationic liposome-mediated gene transfer. *Biophys. J. 71*, 590−599.

(19) Tam, P., Monck, M., Lee, D., Ludkovski, O., Leng, E. C., Clow, K., Stark, H., Scherrer, P., Graham, R. W., and Cullis, P. R. (2000) Stabilized plasmid-lipid particles for systemic gene therapy. *Gene Ther. 7*, 1867−74.

(20) Zhang, Y. P., Sekirov, L., Saravolac, E. G., Wheeler, J. J., Tardi, P., Clow, K., Leng, E., Sun, R., Cullis, P. R., and Scherrer, P. (1999) Stabilized plasmid-lipid particles for regional gene therapy: formulation and transfection properties. *Gene Ther. 6*, 1438−47.

(21) Wheeler, J. J., Palmer, L., Ossanlou, M., MacLachlan, I., Graham, R. W., Zhang, Y. P., Hope, M. J., Scherrer, P., and Cullis, P. R. (1999) Stabilized plasmid-lipid particles: construction and characterization. *Gene Ther. 6*, 271−81.

BC0101259

TECHNICAL NOTES

New Fmoc Pseudoisocytosine Monomer for the Synthesis of a Bis-PNA Molecule by Automated Solid-Phase Fmoc Chemistry

Philippe Neuner* and Paolo Monaci

Istituto di Ricerche di Biologia Molecolare P. Angeletti, Via Pontina Km 30,600, 00040 Pomezia (Roma), Italy .
Received August 10, 2001; Revised Manuscript Received December 5, 2001

The synthesis of *N*-[2-(*N*-9-fluorenylmethoxycarbonyl)aminoethyl]-*N*-(2-*N*-(benzyloxycarbonyl)isocytosin-5-ylacetyl)glycine monomer and its incorporation into a PNA molecule via automated Fmoc solid-phase chemistry is described.

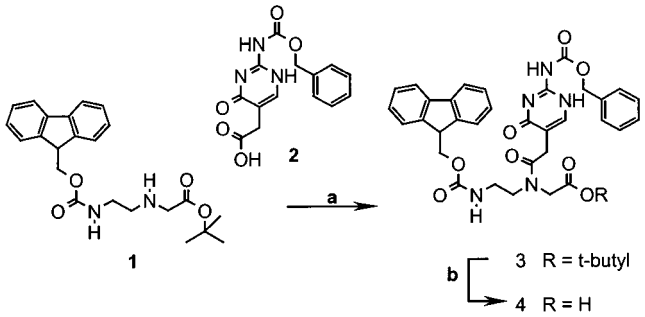
INTRODUCTION

Peptide nucleic acid (PNA) is a polynucleic acid consisting of natural or modified nucleobases linked to a peptide backbone (*1*). PNA exhibits a remarkable specificity and very high affinity in recognizing complementary DNA or RNA strands (*2*). Here we focus on a dimeric PNA molecule (bis-PNA) consisting of a homopyrimidine PNA oligomer (C/T) connected via a flexible linker (2-aminoethoxy-2-ethoxyacetic acid) to a second PNA sequence (J/T, where J is pseudoisocytosine). This bis-PNA has been shown to form highly stable triple helix conjugates $(PNA)_2$/DNA by strand invasion in a P-loop structure form. The formation and stability of the triple strand complex is only slightly influenced by pH in the neutral range, mainly due to the stabilizing effect of the protonated N1 position of the J residue at physiological pH (*3*). Early synthesis of PNA was essentially based on the manual assembly of monomers via *tert*-butyloxycarbonyl (Boc) chemistry on solid support (*4*). More recently, the design and preparation of sets of fluorenylmethoxycarbonyl (Fmoc)/acid labile PNA building blocks, the development of instrumentation, and optimization of synthesis protocols have led to the rapid and efficient synthesis of PNA probes by the mild and well-known Fmoc chemistry (*5*, *6*). However, the only reported strategy for synthesising a bis-PNA-containing pseudoisocytosine still relies on the Boc chemistry (*7*). The lack of an Fmoc automated synthesis procedure for the preparation of this molecule led us to attempt the synthesis of the *N*-[2-(*N*-9-fluorenylmethoxycarbonyl)aminoethyl]-*N*-(2-*N*-(benzyloxycarbonyl)isocytosin-5-ylacetyl)glycine monomer, which is fully compatible with Fmoc chemistry, commercial PNA building blocks, and synthesizer.

EXPERIMENTAL PROCEDURES

Synthesis of the required *tert*-butyl *N*-[2-(*N*-9-fluorenylmethoxycarbonyl)aminoethyl]glycine **1** and N^2-(benzyloxycarbonyl)isocytosin-5-ylacetic acid **2** were carried out as described in the literature (*5*, *7*). The base acetic acid **2** was reacted with **1**, leaving the intermediate **3** in good yield after flash chromatography (*8*). Removal of the *tert*-butyl ester with TFA in DCM gave **4** (Scheme 1) without significant loss of the N^2-benzyloxycarbonyl-protecting group (*9*).

Scheme 1[a]



[a] Reagents: (a) *N*-methylmorpholine, HOBt, HBTU/DMF; (b) TFA/DCM.

A key aspect of the synthesis of the bis-PNA using Fmoc (J^{Cbz}) was removal of the N^2-benzyloxycarbonyl protecting group of the pseudoisocytosine. In a standard protocol, treatment of the synthesis resin with a TFA/*m*-cresol (4:1) mixture efficiently released the polymer from the solid support and cleaved the cytosine benzhydryloxycarbonyl (Bhoc) blocking group. In a preliminary experiment, this deprotection 'cocktail' proved to be too mild to cleave the pseudoisocytosine benzyloxycarbonyl (Cbz), even after overnight treatment of the polymer (data not shown). Thompson et al. chose hydrogen fluoride (HF) in their work to cleave the *N*-benzyloxycarbonyl group (5). As an alternative, we chose a single treatment with a mixture of TFMSA/TFA/*m*-cresol to release and efficiently cleave the blocking group from the polymer.

RESULTS AND DISCUSSION

The solid-phase synthesis of the bis-PNA (NH2-LL-TCTCTCTC-LLL-JTJTJTJT-CONH2) was performed on a PerSeptive Biosystems Expedite 8909 automated synthesizer using the manufacturer's protocols. All reagents including Fmoc C (Bhoc), Fmoc T, Fmoc AEEA spacer (L = 2-aminoethoxy-2-ethoxyacetic acid), and HATU were

* Correponding author. Tel: + 39 6 91 093 335; fax: + 39 6 91 093 225; e-mail: philippe_neuner@merck.com.

10.1021/bc0100758 CCC: $22.00 © 2002 American Chemical Society
Published on Web 04/04/2002

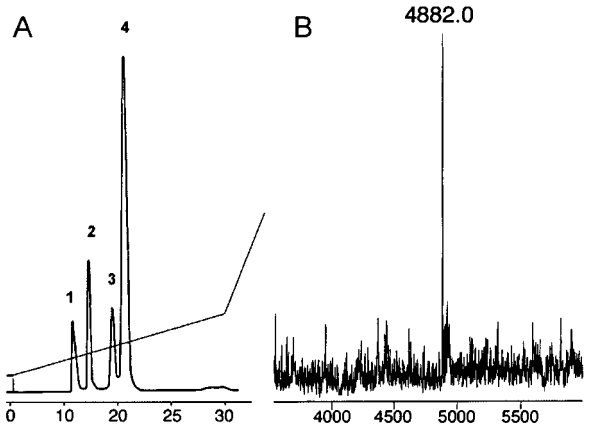


Figure 1. A. Preparative RP-HPLC trace of the crude products from bis-PNA synthesis. Peaks 1, 2, and 3 correspond to the products of the unsuccessful synthesis (data not shown). Peak 4 corresponds to the expected bis-PNA (H_2N-LL-TCTCTCTC-LLL-JTJTJTJT-$CONH_2$). B. MS analysis of peak 4. M (calcd) for $C_{198}H_{274}N_{78}O_{71}$ = 4882.87, M (experimental) = 4882.00.

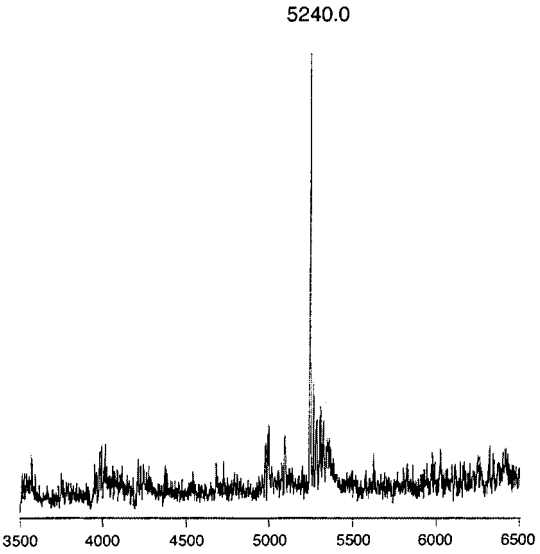


Figure 2. Mass spectrum of bis-PNA Fluo-HN-LL-TCTCTCTC-LLL-JTJTJTJT-$CONH_2$ (L = 2-aminoethoxy-2-ethoxyacetic acid). M (calcd) for $C_{219}H_{284}N_{78}O_{77}$ = 5241.18; M (experimental) = 5240.00.

obtained from PerSeptive Biosystems. The PNA monomers were dissolved in NMP at a 0.2 M concentration. Synthesis using either XAL or PAL columns synthesis (2 μmol scale) were investigated and showed no significant difference in yield. After oligomerization, the resin was dried and transferred to a screw-cap vial. The vial was cooled on ice, and 200 μL of a mixture TFMSA/TFA/*m*-cresol (18:73:9) was added. Reaction proceeded at room temperature for 90 min. Solid support was separated by filtration and the filtrate poured into 10 volumes of ice-cold Et_2O. Centrifugation gave a pellet, which was purified by HPLC.

Preparative RP C18 HPLC purification was performed using a SymmetryPrep C18 (7.8 × 150 mm) reverse-phase column (Waters). Eluant A: 99.9% water, 0.1% TFA; eluant B: 10% water, 89.9% acetonitrile, 0.1% TFA; a linear gradient of 5−30% eluant B over 25 min at a flow rate of 2.0 mL/min monitored at 260 nm (Figure 1). The expected bis-PNA eluted at 21.8 min. The average yield was usually 20−25% (1−1.25 mg) of purified oligomer

Final product was analyzed for purity by mass determination on a LCQ quadrupole ion trap mass spectrometer Finningan-MAT (San Jose, CA).

Labeling of the Bis-PNA in Solution. The bis-PNA synthesized above was routinely labeled in solution with various dyes (Biotin, Fluorescein, Rhodamine) according to the general protocol described here:

To 12 OD (optical density) units of bis-PNA in ultrapure water was added a solution of 1 mg of *N*-succinimidyl ester dye (Fluka) in 100 μL of DMF, followed by 20 μL of a 10% NMM (aq). The solution was thoroughly vortexed, and the reaction proceeded for 3 h in the dark. The volume was taken to 0.5 mL by adding ultrapure water, and the reaction mixture was purified by RP-HPLC using conditions described above. An average yield of 40−60% of the labeled PNA was easily obtained.

In conclusion, we have described the synthesis of a new PNA pseudoisocytosine building block with orthogonal protecting groups (Fmoc/Cbz) and its use in the synthesis of a bis-PNA on an automated synthesizer. It was our experience that the versatile and economical automated assembly of the bis-PNA molecule described here facilitates the collinear synthesis of PNA−peptide chimeras by standard Fmoc chemistry (*6*). To our knowledge, no detailed description of the synthesis of the monomer and its incorporation into a PNA fragment by Fmoc chemistry has been previously reported. Until now, our attempts to protect the N2 exocyclic of the pseudoisocytosine with a mild acid-labile protecting group (Boc and Bhoc) using the standard methodologies have resulted in poor yields (*10*). We are currently investigating other strategies and new blocking groups.

ACKNOWLEDGMENT

We wish to thank J. Clench for linguistic editing and G. Bifolchetti for photographic work.

LITERATURE CITED

(1) Nielsen, P. E.; Egholm, M.; Berg, R. H.; Buchardt, O. (1991)-Sequence-selective recognition of DNA by strand displacement with a thymine-substituted polyamide. *Science 254*, 1497−1500.

(2) Knudsen, H.; Nielsen, P. E. (1996) Antisense properties of duplex and triplex forming PNAs. *Nucleic Acid Res. 24*, 495−500.

(3) Huhn, H.; Demidov, V. V.; Nielsen, P. E.; Frank-Kamenetskii, M. D. (1999) An experimental study of mechanism and specificity of peptide nucleic acid (PNA) binding to duplex DNA. *J. Mol. Biol. , 286*, 1337−1345.

(4) Dueholm, L. K.; Egholm, M.; Berhens, C.; Christensen, L.; Hansen, H. F.; Vulpius, T.; Petersen, K. H.; Berg, H. R.; Nielsen, E. P.; Buchardt, O. (1994) Synthesis of peptide nucleic acid monomers containing the four natural nucleobases: Thymine, cytosine, adenine and guanine and their oligomerization. *J. Org. Chem. 59*, 5767−5773.

(5) Thompson, S. A.; Josey, J. A.; Cadilla, R.; Gaul, M. D.; Hassman, C. F.; Luzzio, M. J.; Pipe, A. J.; Reed, J. L.; Ricca, D. J.; Wiethe, R. W.; Noble, S. A. (1995) Fmoc mediated synthesis of peptide nucleic acids. *Tetrahedron 22*, 6179−6194.

(6) Mayfield, L. D.; Corey, D. R. (1999) Automated synthesis of peptide nucleic acids and peptide nucleic acid-peptide conjugates. *Anal. Biochem. 268*, 401−404.

(7) Egholm, M.; Christensen, L.; Dueholm, K. L.; Buchardt, O.; Coull, J.; Nielsen, P. E. (1995) Efficient pH-independent equence-sepcific DNA binding by pseudoisocytosine-containing bis-PNA. *Nucleic Acid Res. 23*, 217−222.

(8) To a stirred solution of **2** in DMF (1.5 mmol/10 mL) were added 1.5 equiv of *N*-methylmorpholine, 1.5 equiv of *N*-hydroxybenzotriazole (HOBt), followed by 1 equiv of 2-(1*H*-benzotriazole-1-yl)-1,1,3,3-tetramethyluronium hexafluoro-

phosphate (HBTU) at 0 °C. After 10 min, 0.9 equiv of **1** was added in one portion, and the mixture was stirred overnight after which dichloromethane was added. The organic layer was washed with half-saturated aqueous sodium bicarbonate, half-saturated aqueous potassium hydrogen sulfate, and brine, dried (Na_2SO_4), filtered, and evaporated under reduce pressure. The crude product was purified on silica gel flash chromatography using a gradient of 2−6% methanol in dichloromethane. Average synthetic yield: 55−65% of **3** as a white solid. ^{1}H NMR ($CDCl_3$) (two rotamers) δ: 1.30 (s, 4.5H), 1.40 (s, 4.5H), 3.15 (s, 1.2H), 3.25 (s, 0.8H), 3.40−3.70 (m, 4H), 3.95 (s, 1H), 4.15−4.45 (m, 4H), 5.20 (s, 2H), 7.25−7.35 (m, 10H), 7.45 (s, 0.45H), 7.50 (s, 0.55H), 7.60 (m, 2H), 7.75 (m, 2H). MS (FAB+) *m*/*z*: 682.20 (M + H).

(9) To a stirred solution of **3** was added (10 mL/mmol of **3**) trifluoroacetic acid (TFA) dropwise at 0 °C. The reaction was followed by TLC and completed after 5−6 h. The solvent was evaporated under reduce pressure and coevaporated twice with acetonitrile and freeze-dried. Average synthetic yield: 85% of **4** as a white solid. ^{1}H NMR (DMSO) (two rotamers) δ: 3.20−3.50 (m 6H), 3.95 (s 1H) 4.30 (m 3H), 5.25 (s 2H), 7.25−7.40 (m 10H), 7.55 (s 0.45H), 7.60 (s 0.55H), 7.65 (d, J = 7 Hz, 2H), 7.90 (d, J = 7 Hz, 2H). MS (FAB+) *m*/*z*: 626.15 (M + H).

(10) Coull, J. M.; Egholm, M.; Hodge, R. P.; Ismail, M.; Rajur, S. Patent application WO 96/40685.

BC0100758

A Simple Two-Step Approach for Introducing a Protected Diaminedithiol Chelator during Solid-Phase Assembly of Peptides

Jean Gariépy,* Sandrine Rémy, Xiuguo Zhang, James R. Ballinger,† Eleonora Bolewska-Pedyczak, Michael Rauth, and Stuart K. Bisland

Department of Medical Biophysics, University of Toronto, and Division of Molecular and Structural Biology, Ontario Cancer Institute, Princess Margaret Hospital, 610 University Avenue, Toronto, Ontario, Canada M5G 2M9. Received August 27, 2001; Revised Manuscript Received December 10, 2001

A simple synthetic strategy is described to incorporate a protected diaminedithiol (N_2S_2) chelator during Fmoc solid-phase synthesis of short peptides. The resulting constructs could be efficiently labeled with technetium-99m (^{99m}Tc). The chelator was assembled at the N-terminus of peptides in a two-step procedure where the deprotected terminal amino group was first reacted with di-Fmoc-diaminopropionic acid (Fmoc-DAP-[Fmoc]-OH). The two protected amino groups were then simultaneously deprotected and subsequently reacted with *S*-benzoylthiolglycolic acid (TGA) to generate a protected N_2S_2 chelator. This metal binding site was introduced into di- and tripeptides. Each peptide construct was composed of a C-terminal lysine residue and an N-terminal diaminopropionic moiety modified to create the chelator site. The ϵ-amino group at the C-terminal lysine was further derivatized with a nitroimidazole group to facilitate cellular retention. The resulting constructs were then cleaved from the resin support, purified, and labeled with [^{99m}Tc]pertechnetate. Six constructs were prepared differing by a single amino acid inserted between the diaminopropionic acid and lysine residues. Optimal labeling yields of >70% were achieved around neutral pH and heating at 75 °C for 10 min. Purified ^{99m}Tc-labeled constructs were found to accumulate in Chinese hamster ovary (CHO) cells in vitro as a function of charge and hydrophobicity.

INTRODUCTION

Technetium-99m (^{99m}Tc) is the most commonly used radionuclide in nuclear medicine (*1*). Its short half-life (~6 h) and ease of production and the advent of ^{99m}Tc chelators that can be covalently linked to peptides, proteins, and other biologically active molecules represent key features promoting its use in diagnostic imaging. More importantly, peptides and related peptidomimetics can now be rapidly assembled by solid-phase synthesis approaches, offering the prospect of developing new and powerful classes of ^{99m}Tc-labeled radiopharmaceuticals. Peptides can be designed to incorporate specific sequences enabling them to achieve a desired biodistribution (i.e., targeted to receptors) or pharmacokinetic response (a function of their mass, charge, or lipophilicity). Short peptides are also less immunogenic than proteins such as monoclonal antibodies. Strategies for labeling peptides with ^{99m}Tc (*2*−*11*) and their application in medicine have recently been reviewed (*12*−*14*). At the present time, most technetium chelators are thiol-containing agents, which are susceptible to oxidation events if left unprotected prior to labeling. Histidine tags have also been suggested as potentially useful ^{99m}Tc chelators when introduced into recombinant proteins (*15*). More importantly, differences in chelators as well as peptides have been shown to influence the in vivo properties of the resulting ^{99m}Tc-labeled peptides (*16*, *17*). Most approaches used to date do not provide a systematic design strategy to incorporate a well-established protected thiol-containing chelator anywhere into peptides. The present report describes a simple strategy for assembling a diamidedithiol (N_2S_2)[1] chelator during solid-phase peptide synthesis. The N_2S_2 group was incorporated at the N-terminus of six peptide constructs containing a C-terminal 2-nitroimidazole group.

EXPERIMENTAL PROCEDURES

Chemicals and Reagents. Benzoyl chloride, L-2,3-diaminopropionic acid hydrochloride (DAPA), 1,4-dioxane, 2-bromoethyl acetate (BEA), and 2-nitroimidazole were purchased from Sigma-Aldrich Fine Chemicals (St. Louis, MO). 9-Fluorenylmethyl choroformate (Fmoc-Cl) was obtained from Advanced ChemTech (Louisville, KY). Di-Fmoc-aminopropionic acid can now be directly purchased from Chem-Impex International (Wood Dale, IL) or Bachem BioScience Inc. (King of Prussia, PA). Thioglycolic acid (TGA; mercaptoacetic acid) was obtained from Fischer Scientific (Cedarlane Laboratories Ltd., Hornby, ON). SepPak C_{18} solid-phase extraction cartridges (1.5 mL capacity) were purchased from Waters (Milford, MA). Sodium [^{99m}Tc]pertechnetate was obtained from Mallinckrodt Medical Inc. (Mississauga, ON) or from a ^{99}Mo/^{99m}Tc radionuclide generator (Dupont, Billerica, MA).

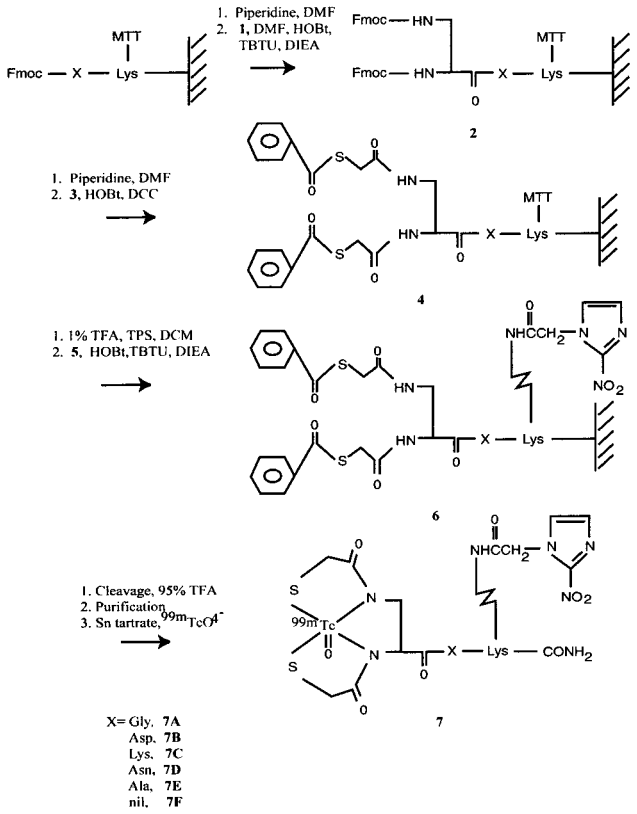
* To whom correspondence should be addressed at the Ontario Cancer Institute, Princess Margaret Hospital, 610 University Ave., Toronto, Ontario, Canada M5G 2M9. Phone: 416-946-2967; Fax: 416 946-6529; Electronic mail: gariepy@uhnres.utoronto.ca.

† Present address: Department of Nuclear Medicine, Addenbrooke's Hospital, Cambridge, UK.

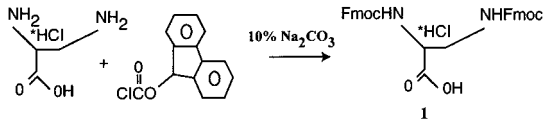
[1] Abbreviations: DAPA, L-diaminopropionic acid; 2-NIAA, 2-nitroimidazole acetic acid; N_2S(benzoyl)$_2$, *S*-benzoyl-protected diaminedithiol chelator assembled at the N-terminus of each peptide during solid-phase peptide synthesis; Peptide A, N_2S(benzoyl)$_2$-**Gly**-Lys(2-NIAA)-amide; Peptide B, N_2S(benzoyl)$_2$-**Asp**-Lys(2-NIAA)-amide; Peptide C, N_2S(benzoyl)$_2$-**Lys**-Lys(2-NIAA)-amide; Peptide D, N_2S(benzoyl)$_2$-**Asn**-Lys(2-NIAA)-amide; Peptide E, N_2S(benzoyl)$_2$-**Ala**-Lys(2-NIAA)-amide; Peptide F, N_2S(benzoyl)$_2$-Lys(2-NIAA)-amide.

10.1021/bc0100814 CCC: $22.00 © 2002 American Chemical Society
Published on Web 03/08/2002

Scheme 1. Synthetic Scheme for the Preparation of N_2S(benzoyl)$_2$-Containing Peptides



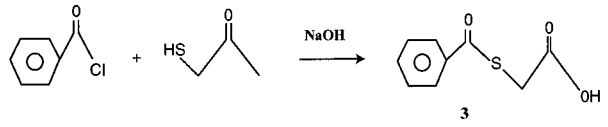
Scheme 2



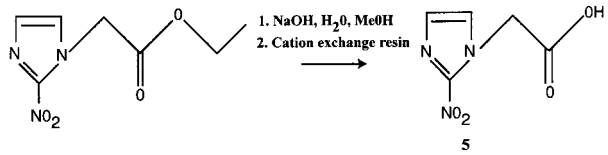
Peptide Synthesis Reagents. *N*-α-9-Fluorenylmethyloxycarbonyl (Fmoc) protected amino acids, peptide-amide linker (PAL) resin, [2-(1*H*-benzotriazol)-1-yl]-1,1,3,3-tetramethyluronium tetrafluoroborate (TBTU), and *N*-hydroxybenzotriazole·H_2O (HOBt) were obtained from Calbiochem-NovaBiochem Corp. (San Diego, CA). 1,3-Dicyclohexylcarbodiimide (DCC), diisopropylethylamine (DIEA), trifluoroacetic acid (TFA), triisopropylsilane (TPS), *N*,*N*-dimethylformamide (DMF), and dichloromethane (DCM) were purchased from Schweizerhall Pharma (Piscataway, NJ). HPLC-grade acetonitrile (ACN) was purchased from BDH Inc. (Toronto, ON). Other buffers and inorganic salts and reagent chemicals were purchased from Sigma-Aldrich (St. Louis, MO).

Synthesis of Di-Fmoc-diaminopropionic Acid (Scheme 2). The two amino groups of L-diaminopropionic acid (DAPA) were protected with 9-fluorenylmethyl (Fmoc) groups following a standard protocol utilizing 9-fluorenylmethyl choroformate (Fmoc-Cl; ref *18*). Briefly, DAPA (4.18 g, 30 mmol) was dissolved in 100 mL of 10% Na_2CO_3 in water. Fifty milliliters of dioxane (peroxide-free) was then added to the solution, and the resulting mixture was stirred in an ice−water bath. Fmoc-Cl (15.6 g, 60.24 mmol) dissolved in 75 mL of dioxane was then added in small portions to the DAPA solution. The reaction mixture was subsequently stirred for 1 h at 0 °C followed by an additional 12 h period at room temperature. Dioxane was evaporated on a rotary evaporator and the reaction mixture poured into 1.5 L of distilled water. The aqueous solution was washed twice with 200 mL of ethyl acetate to remove unreacted Fmoc-Cl and

Scheme 3



Scheme 4



cooled to 0 °C. Ethyl acetate (800 mL) was further added to the aqueous phase, and the suspension was acidified to pH 2 under vigorous stirring with concentrated HCl. The organic phase was recovered and washed with water to pH 7 and finally dried over anhydrous Mg_2SO_4. The ethyl acetate was evaporated and the oily residue macerated with hexane. The resulting solid crude product was recrystallized from ethyl acetate/hexane. Thin-layer chromatography (Analtech Uniplate silica gel GF plates; solvent system, 90:8:2 $CHCl_3$:MeOH:AcOH), pure product: R_f 0.52 (79% yield). Analyses for di-Fmoc-diaminopropionic acid (**1**): MS *m*/*z* observed 549 [M+H$^+$], calcd 549; melting point 178−180 °C. Di-Fmoc-aminopropionic acid can now be purchased directly from Chem-Impex International (Wood Dale, IL) or Bachem BioScience Inc. (King of Prussia, PA).

Synthesis of *S*-Benzoylthioglycolic Acid (Scheme 3). *S*-Benzoylthioglycolic acid (**3**) was synthesized according to the protocol of Schneider et al., 1984 (*19*). Sodium hydroxide pellets (3.05 g; 75 mmol) and thioglycolic acid (7 g, TGA; 75.9 mmol) were mixed and dissolved into a 50 mL solution of toluene/water (1:2.5) at 5 °C. Benzoyl chloride (8.82 mL; 62.7 mmol) was then added to this solution over 30 min, maintaining the temperature between 5 and 15 °C. The reaction was allowed to proceed for an additional 30 min at room temperature. The mixture was then diluted to twice its volume with water and the aqueous phase washed twice with benzene (100 mL). The organic phase was discarded, and the aqueous layer was subsequently chilled to 4 °C and acidified to pH 1.0−1.5 with HCl (6 N). The precipitate was filtered off, washed in cold distilled water, and finally dried under vacuum. The precipitate was recrystallized from ethyl acetate (EtOAc): yield 7.5 g (76.5%), white crystalline product; melting point 102−103 °C. Analyses for *S*-benzoylthioglycolic acid [$\varnothing COS(CH_2)_nCO_2H$]: MS *m*/*z* observed 197 [M+H$^+$], calcd 197; ^{1}H NMR ($CDCl_3$/tetramethylsilicone): 7.99 (d, 2H$^+$, ortho position of benzoyl ring), 7.61 (t, 1H, ρ position of benzoyl ring), 7.48 (t, 2H$^+$, meta position of benzoyl ring), 3.92 (S, 2H$^+$, SCH_2CO).

Synthesis of 2-Nitroimidazole Ethyl Acetate (2-NIEA). 2-Bromoethyl acetate (BEA; 1.08 mL, 6.46 mmol) was added to a solution of 2-nitroimidazole (2-NI; 1 g, 8.84 mmol) and potassium carbonate (6 g) in dry acetonitrile (50 mL). The mixture was reacted with constant stirring for 36 h at room temperature, and the resulting precipitate was filtered and washed with acetone. Evaporation of the organic filtrate under reduced pressure yielded a yellow oil (1.8 g). Analytical TLC revealed a major product combined with two other side products; R_f 0.66 (CH_2Cl_2/MeOH/NH_3, 50:7:1). The pure product was isolated from the crude oil using flash chromatography (silica gel) eluted with CH_2Cl_2/MeOH/NH_3 (50:7:1) as yellowish oil: 1.05 g (60% yield); TLC, one spot, R_f 0.66. Analyses for 2-nitroimidazole ethyl acetate: MS *m*/*z*

observed 200 [M+H$^+$], calcd 200; ^{1}H NMR ($CDCl_3$/tetramethylsilicone) δ_H ($CDCl_3$): 7.202 (d, 1H, *H*-imidazole ring), 7.095 (d, 1H, *H*-imidazole ring), 5.12 (s, 2H, NCH_2COO), 4.28 (q, 2H, OCH_2CH$_3$), 1.30 (t, 3H, OCH2CH_3); δ_c ($CDCl_3$): 166.0 (C═O), 128.5 (*C*H-imidazole ring), 126.5 (*C*H-imidazole ring), 62.6 (NCH_2COO), 50.9 (OCH_2CH$_3$), 14.0 (OCH$_2$CH_3).

Preparation of 2-Nitroimidazole Acetic Acid (2-NIAA; Scheme 4). The purified oil of nitroimidazole ethyl acetate (0.9 g) was mixed into a solution of NaOH (4 N, 2.5 mL), water (10 mL), and MeOH (10 mL). The resulting solution was stirred at room temperature until no ester derivative was evident by TLC (~30 min), at which point a cation-exchange resin (H$^+$, Bio-Rad, 4 g), which had been protonated by washing with H_2SO_4 (1 N; 30 mL) and distilled water, was used to convert the basic solution to its acetic derivative (**5**; pH 2.5). Subsequent filtration and drying of the filtrate yielded a dark yellow paste (1.16 g). Chromatography of crude product on silica gel [eluent, CH_2Cl_2/CH_3CN/HCOOH (30:10:1)] yielded a white crystal: 0.28 g; mp >140 °C (decomposed); R_f 0.30 (CH_2Cl_2/CH_3CN/HCOOH, 30:10:1), 0.61 (CH_2Cl_2/CH_3CN/HCOOH (10:10:1)]. Analyses for 2-nitroimidazole acetic acid: MS *m*/*z* observed 172 [M+H$^+$], calcd 172. ^{1}H NMR ($CDCl_3$/tetramethylsilicone) (DMSO-d_6): δ_H 7.55 (1H, d, *H*-imidazole ring), 7.17 (1H, d, *H*-imidazole ring), 5.15 (2H, s, NCH_2COO), 3.90 (1H, broad, COOH); δ_c (DMSO-d_6): 169.1 (C═O), 129.0 (*C*H-imidazaole ring), 128.3 (*C*H-imidazole ring), 51.3 (NCH2COOH).

Synthesis, Purification, and Characterization of Peptides (Scheme 1). Peptides were assembled using standard Fmoc chemistry protocols and a peptide-amide linker (PAL) resin support. Briefly, 2.2 g (1.5 mmol) of peptide-amide linker (PAL) resin with a substitution of 0.69 mmol/g was deprotected with 20% piperidine in *N*,*N*-dimethylformamide (DMF) for 20 min. Two equivalents (3 mmol) of Fmoc-Lys-(Mtt)-OH was then coupled to the deprotected resin using molar equivalents of *N*-hydroxybenzotriazole·H_2O (HOBt) and [2-(1*H*-benzotriazol)-1-yl]-1,1,3,3- tetramethyluronium tetrafluoroborate (TBTU) in 10 mL of DMF for 5 min at room temperature with constant rocking. Two milliliters of diisopropylethylamine (DIEA) was then added to the slurry and the reaction allowed to continue for a further 40 min. The resin was deprotected and washed as described above and subsequently dried overnight under vacuum. The resulting resin was then dispensed into six equivalent (0.2 mmol) portions. Each resin fraction was then reacted with 5 equiv of either Fmoc-Gly (A), Fmoc-Asp(OtBu) (B), Fmoc-Lys(Boc) (C), Fmoc-Asn (D), or Fmoc-Ala (E) or left untreated (F; no amino acid added). Coupling was conducted in the presence of 1 mmol of HOBt and 1 mmol of TBTU, as described above. The reaction was completed after 2 h at room temperature (>99% coupling) as confirmed by the lack of ninhydrin color (absence of remaining free amino groups; ref *20*). Each peptide-resin sample was then deprotected in 20% piperidine in DMF and Fmoc-DAP-(Fmoc)-OH (**1**; 1.3 g; 0.4 mmol) prepared in 10 mL of DMF as well as 0.2 mmol of HOBt and TBTU dispensed into each slurry. DIEA (0.3 mL) was dispensed into each slurry, and the reactions were allowed to proceed for 2 h. All coupling reactions went to completion as confirmed by ninhydrin tests (*20*). The Fmoc groups on DAP (**2**) were then removed, and 4 equiv (8 mmol) of *S*-benzoylthiolglycolic acid (**3**), HOBt, and dicyclohexylcarbodiimide (DCC) was added to each resin sample to complete the scaffold of the protected diaminedithiol chelator (**4**). Following the coupling of 2-nitroimidazole acetic acid (**5**) to the ϵ-amino group at the C-terminal lysine residue of each construct (next paragraph, **6**), the peptides were cleaved from their resin support, analyzed, and purified to homogeneity by reverse-phase HPLC on a Zorbax SB-C_{18} column (5 μm, 0.94 cm × 25 cm) prior to ^{99m}Tc radiolabeling (**7A**−**7F**). The column was equilibrated in 0.1% trifluoroacetic acid (TFA)/20% acetonitrile in water (eluent A), and the peptides were separated using a 40 min linear gradient going from 0% to 100% eluent B [where eluent B was 0.1% TFA/70% acetonitrile containing 0.1% (v/v) trifluoroacetic acid]. All peptides eluted at around 40% acetonitrile/water. Peptide peaks were detected at 214 nm, and the flow rate was 1 mL/min. A Waters HPLC apparatus (model 510) equipped with a Lambda-Max variable-wavelength detector was used for the purification steps. Analytical HPLC profiles of the ^{99m}Tc-labeled peptides were recorded using a Beckman HPLC (Fullerton, CA) system incorporating a radiometric detection set on a ^{99m}Tc window (Beckman 171 radioisotope detector with a modified yttrium silicate scintillant). The Vydac reversed-phase (R-P) C_{18} column (5 μm, 0.46 cm × 25 cm) was first equilibrated in 10% acetonitrile/90% water/0.1% TFA, and the peptides were eluted using a 25 min gradient increasing from 0 to 100% of eluent B (90% acetonitrile/10% water/0.1% TFA). The column flow rate was 1.5 mL/min. ^{1}H NMR (δ_H) and ^{13}C NMR (δ_C) spectra were recorded on a Bruker 300AC spectrometer at 500 and 126 MHz, respectively. Electrospray mass spectra (ESMS) were obtained on a Sciex API(N°3) mass spectrometer in the positive ion mode. Radioactivity of syringes and vials was measured in a Capintec CRC-15R dose calibrator while radioactivity in in vitro samples was measured in a Picker Pace II automatic gamma counter.

Coupling of 2-Nitroimidazole Acetic Acid to the N_2S(benzoyl)$_2$-Containing Peptides and Release of Constructs from the Solid Support. The 4-methyltrityl (Mtt) protecting the ϵ-amino group at the C-terminal lysine residue was removed by treating the resin samples with 1% trifluoroacetic acid (TFA)/5% triisopropylsilane (TPS) in dichloromethane for 20 min at room temperature. The nitroimidazole group (**5**) was then coupled to this site by dispensing 0.5 mmol of NIAA, HOBt, and TBTU prepared in 0.3 mL of DIEA into each peptide-resin reaction vessel. The coupling reaction was completed within 3 h at room temperature. *S*-Benzoyl-protected peptides were cleaved from their solid support in the presence of 95% TFA/2.5% H_2O, 2.5% TPS. Total yields of product ranged from 20 to 30%. The peptides were purified to homogeneity by reverse-phase HPLC using a linear gradient as described earlier in this section (Figure 1). MS: *m*/*z* Peptide A: X = Gly, observed 798 [M+H$^+$], calcd 798; Peptide B: X = Asp, observed 839 [M+H$^+$], calcd 839; Peptide C: X = Lys, observed 869 [M+H$^+$], calcd 869; Peptide D: X = Asn, observed 855 [M+H$^+$], calcd 855; Peptide E: X = Ala, observed 812 [M+H$^+$], calcd 812; Peptide F: observed 741 [M+H$^+$], calcd 741.

Labeling N_2S(benzoyl)$_2$-Containing Constructs with Technetium-99m. Initial conditions to label the N_2S_2-containing peptides were based on methods described elsewhere (*21*, *22*). In brief, N_2S(benzoyl)$_2$-containing peptides were first dissolved in 2% DMSO/water to give a final stock concentration of 0.4 mg/mL. Aliquots (100 μL) of each solution were dispensed into test tubes, together with 100 μL of a stannous tartrate solution [composed of 1 mL of disodium tartrate (13 mg/mL in water) and 10 μL of a stock solution of stannous chloride (20 mg/mL in 1 N HCl)]. These mixtures were defined as composed of a 1:1 volume ratio of Sn tartrate to peptide. The final pH of these solutions (either pH 2, 7.5, or 9) was adjusted by a dropwise addition of either 1 N HCl or sodium bicarbonate (42 mg/mL prepared in

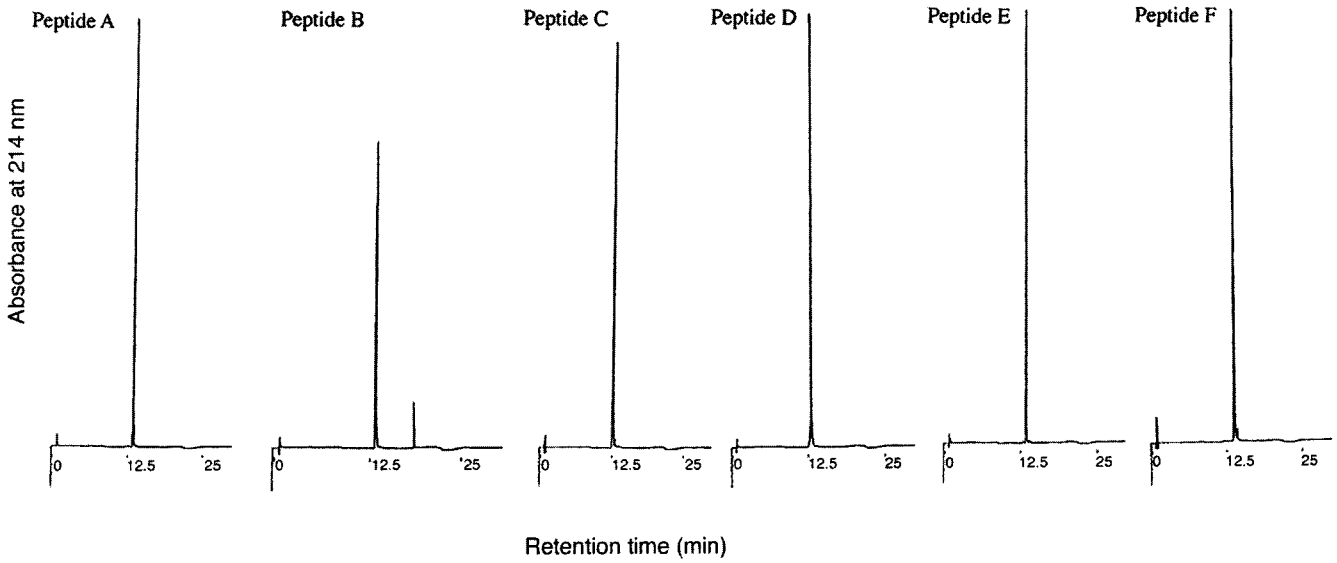


Figure 1. Elution profiles of purified N_2S(benzoyl)$_2$-containing peptides. Peptides were injected onto an analytical Zorbax SB-C_{18} column and eluted using a linear gradient going from 0 to 100% eluent B over a 25 min period. Eluent A: 0.1% TFA in 10% acetonitrile/water. Eluent B: 0.1% TFA in 90% acetonitrile/water. The column flow rate was 1.5 mL/min. All peptides eluted with a similar retention time near 12.5 min. Peptide A, N_2S(benzoyl)$_2$-**Gly**-Lys(2-NIAA)-amide, MW = 797. Peptide B, N_2S(benzoyl)$_2$-**Asp**-Lys(2-NIAA)-amide, MW = 838. Peptide C, N_2S(benzoyl)$_2$-**Lys**-Lys(2-NIAA)-amide, MW = 868. Peptide D, N_2S(benzoyl)$_2$-**Asn**-Lys(2-NIAA)-amide, MW = 854. Peptide E, N_2S(benzoyl)$_2$-**Ala**-Lys(2-NIAA)-amide, MW = 811. Peptide F, N_2S(benzoyl)$_2$-Lys(2-NIAA)-amide, MW = 740.

0.75 M ammonium hydroxide). An aliquot (100 μL) of sodium [^{99m}Tc]pertechnetate ($^{99m}TcO_4^-$; 50−80 MBq) was finally added to each tube, and each tube was then sealed and heated at 75 °C for 10−20 min. Parameters such as the volume ratio of Sn tartrate to peptide (3:1, 1:1, 1:4, and 1:10) and the reaction temperature (50, 75, 90, and 100 °C) were also modified to optimize the labeling procedure. Samples were purified using disposable C_{18} SepPak cartridges (Waters). The SepPak columns were equilibrated in distilled water. The radiolabeled samples were then injected into the cartridges and the columns subsequently washed with distilled water to remove unbound [^{99m}Tc]pertechnetate and [^{99m}Tc]tartrate. Labeled peptides were eluted from the SepPak with ethanol (3 fractions; 0.5, 0.5, and 1 mL, respectively). The extent of ^{99m}Tc-labeling was expressed as the percentage of radioactivity in the ethanol fractions (eluent) divided by the total radioactivity in all of the fractions combined.

In Vitro Cellular Uptake of ^{99m}Tc-Labeled N_2S_2-Containing Peptides. Chinese hamster ovarian (CHO) cells (subclone AA 8-4) were grown at 37 °C and 5% CO_2 as a suspension in α-minimal essential medium containing 10% (v/v) fetal calf serum. A 45 mL solution of cells (1×10^6 cells/mL of growth media) was prepared, from which 9.7 mL aliquots were dispensed into each of four sterile glass vials. Cells were allowed to equilibrate for 40 min in glass vials as stirred cell suspensions before being exposed to labeled peptide. All cell cultures were maintained at 37 °C. ^{99m}Tc-labeled peptide samples were initially diluted with water to a final radioactive concentration of 10 MBq/mL. Three hundred (300) microliters of each ^{99m}Tc-labeled peptide sample was then dispensed into each cell suspension using a syringe. Duplicate aliquots (300 μL) of cell suspensions were removed at selected time intervals following the addition of labeled peptides to cells (5 min, 1 h, 2 h, 3 h, and 4 h) and placed into microcentrifuge tubes containing 1 mL of ice-cold saline. Collected samples were then centrifuged (12000*g* for 2 min), and 100 μL of each supernatant was transferred into 5 mL polypropylene tubes. The radioactivity of the supernatant gives a measure of ^{99m}Tc-labeled peptide that had not been internalized into the CHO cells (C_{out}). The remaining supernatant was removed and the cell pellet washed again with ice-cold saline. The radioactivity of the cell pellet indicates the amount of intracellular ^{99m}Tc-labeled peptide (C_{in}). The overall amount of internalized radiolabeled sample is expressed as the ratio C_{in}/C_{out} (*7*).

RESULTS AND DISCUSSION

Solid-Phase Assembly of N_2S(benzoyl)$_2$-Containing Peptides. The objective of this study was to provide a simple synthesis strategy for incorporating a protected form of a diaminedithiol chelator into peptide constructs. Six peptides (Peptide A to Peptide F; **7A**−**7F**, Scheme 1) were assembled on a 431A peptide synthesizer (Applied Biosystems) using standard Fmoc solid-phase peptide synthesis protocols (Experimental Procedures). The chelator was assembled at the N-terminus of each peptide while a nitroimidazole group was introduced on the side chain of their C-terminal lysine residue. Chromatograms confirming the purity of each final construct are presented in Figure 1.

Concurrent Removal of Protecting Groups and Labeling of the Chelator with ^{99m}Tc Can Be Achieved in the Presence of Stannous Chloride and Disodium Tartrate. *S*-Benzoyl-protected peptides were simultaneously deprotected and radiolabeled using an exchange reaction with [^{99m}Tc]tartrate. Several parameters relating to pH, temperature, and the volume ratio of stannous tartrate to peptide used were evaluated for Peptide F to establish appropriate labeling conditions (Figure 2). Conditions which proved useful for radiolabeling the constructs were as follows: temperature of 75 °C for 10 min, pH 7.5, and a 1:1 volume ratio of stannous tartrate [100 μL of a stock solution composed of 1 mL of disodium tartrate (13 mg/mL in water) and 10 μL of a stock solution of stannous chloride (20 mg/mL in 1 N HCl)] to peptide (100 μL; 40 μg). Under these conditions, ^{99m}Tc-labeling of >70% could be consistently attained for Peptides A, B, C, D, and F, when quantified by reverse-phase HPLC (gradient from 10% to 90% acetonitrile in 25 min at a flow rate of 1.5 mL/min;

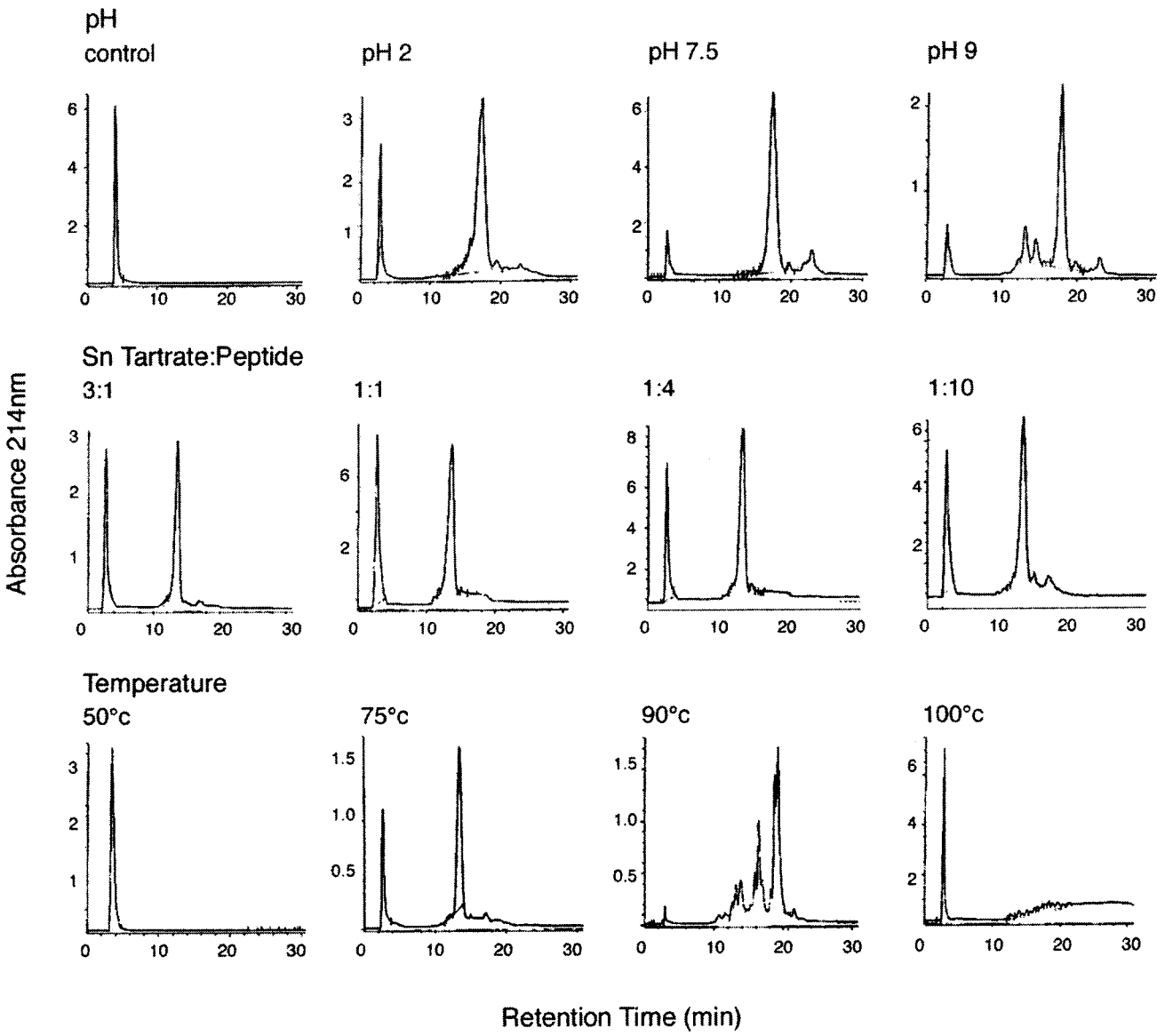


Figure 2. Reversed-phase HPLC profiles showing the effect of pH, temperature, and stannous tartrate to peptide ratio on the ^{99m}Tc labeling of Peptide F. Top Row: Effect of altering pH conditions. The top left chromatogram depicts the elution profile of tartrate/[^{99m}Tc]tartrate complex in the absence of peptide. Peptide F was treated for 10 min at 75 °C with a 1:1 volume ratio of stannous tartrate to peptide (100 μL of Sn tartrate stock solution to 100 μL of 0.4 mg/mL peptide solution). Middle Row: Effect of changing the stannous tartrate to peptide volume ratio. Peptide F was treated for 10 min at 75 °C and pH 7.5. Lower Row: Effect of changing the reaction temperature. Peptide F was treated for 10 min at pH 7.5 with a 1:1 volume ratio of stannous tartrate to peptide. Chromatograms of the radiolabeled peptides were obtained on a Vydac reversed-phase C_{18} column (5 μm, 0.46 cm × 25 cm), using a linear gradient going from 10 to 90% acetonitrile in 25 min. The flow rate was 1.5 mL/min, and radioactive peaks were recorded on a Beckman 171 radioisotope detector. Eluent A: 0.1% TFA/10% acetonitrile/water; eluent B: 0.1 TFA/90% acetonitrile in water.

radioactive detection). Other conditions increased the heterogeneity of the final labeled products (Figure 2: pH >7.5, temperatures above 75 °C) or resulted in poor labeling (temperatures below 75 °C). The specific activity of the constructs typically ranged in values from 2 to 10 Ci/mmol. The resulting ^{99m}Tc-labeled peptides were purified and subsequently tested for their ability to accumulate in mammalian cells in vitro. Cellular uptake measurements performed on Chinese hamster ovary cells indicated that the insertion of charged or polar amino acids (Asp, Asn, Lys) at position X results in labeled constructs harboring a weak ability to enter cells (C_{in}/C_{out} values ranging from 0.4 to 1.8 with a value of 1.0 representing free diffusion in and out of cells). In contrast, peptides with a hydrophobic residue (Ala) at position X or simply lacking residue X (Peptide F) accumulated more readily into CHO cells (C_{in}/C_{out} values ranging from 2.9 to 3.2).

Positioning a Diaminedithiol Chelator at Selected Sites within Peptides. This study describes the insertion of a protected chelator at the N-terminus of peptides during Fmoc-based solid-phase peptide synthesis. A simple strategy to incorporate this chelator elsewhere into peptide constructs is to make use of Fmoc-Lys(Dde) or its homologue, Fmoc-Lys(ivDde) (*23*−*25*). These lysine derivatives have an ϵ-amino protecting group [(4,4-dimethyl-2,6-dioxocyclohex-1-ylidene)ethyl, **Dde**; (4,4-dimethyl-2,6-dioxocyclohex-1-ylidene)-3-methylbutyl, **ivDde**; Calbiochem-Novabiochem Corp., San Diego, CA) which can be removed in the presence of 2% hydrazine. Fmoc-Lys(Dde) or (ivDde) can be positioned at a nonessential site in any peptide during solid-phase peptide synthesis. An important step in this approach is to insert a tBoc-protected amino acid as the last residue in the peptide prior to the removal of the Dde or ivDde-protecting group on the lysine side chain with hydrazine.

The free ϵ-amino group can then be modified with Fmoc-DAP-(Fmoc)-OH followed by *S*-benzoylthiolglycolic acid as described in this paper to create the protected diaminedithiol chelator. The peptide can then be released from the support in the presence of trifluoroacetic acid, which also removes the N-terminal tBoc group.

CONCLUSION

A simple and reproducible method for introducing a benzoyl-protected N_2S_2 chelator into peptides was developed using standard protocols for Fmoc solid-phase peptide synthesis (Scheme 1). The thiol-protecting benzoyl groups are stable under the acidic conditions (trifluoroacetic acid) associated with the cleavage of synthetic peptides from resins following Fmoc-based peptide assembly. Six peptides containing the protected N_2S_2 chelator at their N-terminus were prepared and purified to homogeneity by reverse-phase chromatography prior to labeling with ^{99m}Tc (Figure 1). The benzoyl groups were efficiently removed following heating (75 °C for 10 min) at neutral pH in the presence of a stannous tartrate solution (Figure 2). Ligand exchange between [^{99m}Tc]-pertechnetate and the deprotected diaminedithiol chelator also occurs under these conditions, yielding ^{99m}Tc-labeled peptides.

Note Added in Proof: Technetium labeling efficiencies of >97% have recently been achieved by Drs. Mathew Thakur (Thomas Jefferson University) and Mick Welling (Leiden University Medical Center, The Netherlands) for two different peptides assembled by our group using the procedure stated in this paper.

ACKNOWLEDGMENT

This work was supported by a grant from the Canadian Breast Cancer Research Initiative (to J.G.).

LITERATURE CITED

(1) Srivastava, S. C. (1996) Is there life after technetium: what is the potential for developing new broad-based radionuclides? *Semin. Nucl. Med. 26*, 119−131.

(2) Lister-James, J., Knight, L. C., Maurer, A. H., Bush, L. R., Moyer, B. R., and Dean, R. T. (1996) Thrombus imaging with a technetium-99m-labeled activated platelet receptor-binding peptide. *J. Nucl. Med. 37*, 775−781.

(3) Lister-James, J., Moyer, B. R., and Dean, T. (1996) Small peptides radiolabeled with ^{99m}Tc. *J. Nucl. Med. 40*, 221−233.

(4) Liu, S., Edwards, D. S., and Barrett, J. A. (1997) ^{99m}Tc labeling of highly potent small peptides. *Bioconjugate Chem. 8*, 621−636.

(5) Hnatowich, D. J., Qu, T., Chang, F., Ley, A. C., Ladner, R. C., and Rusckowski, M. (1998) Labeling peptides with technetium-99m using a bifunctional chelator of a N-hydroxysuccinimide ester of mercaptoacetyltriglycine. *J. Nucl. Med. 39*, 56−64.

(6) Luyt, L. G., Jenkins, H. A., and Hunter, D. H. (1999) An N_2S_2 bifunctional chelator for technetium-99m and rhenium: complexation, conjugation, and epimerization to a single isomer. *Bioconjugate Chem. 10*, 470−479.

(7) Su, Z. F., Zhang, X., Ballinger, J. R., Rauth, A. M., Pollak, A., and Thornback, J. R. (1999) Synthesis and evaluation of two technetium-99m-labeled peptidic 2-nitroimidazoles for imaging hypoxia. *Bioconjugate Chem. 10*, 897−904.

(8) Rusckowski, M., Qu, T., Pullman, J., Marcel, R., Ley, A. C., Ladner, R. C., and Hnatowich, D. J. (2000) Inflammation and infection imaging with a 99mTc-neutrophil elastase inhibitor in monkeys. *J. Nucl. Med. 41*, 363−374.

(9) Zhang, X., Su, Z. F., Ballinger, J. R., Rauth, A. M., Pollak, A., and Thornback, J. R. (2000) Targeting hypoxia in tumors using 2-nitroimidazoles with peptidic chelators for technetium-99m: effect of lipophilicity. *Bioconjugate Chem. 11*, 401−407.

(10) Thakur, M. L., Marcus, C. S., Saeed, S., Pallela, V., Minami, C., Diggles, L., Le Pham, H., Ahdoot, R., and Kalinowski, E. A. (2000) 99mTc-labeled vasoactive intestinal peptide analogue for rapid localization of tumors in humans. *J. Nucl. Med. 41*, 107−110.

(11) Thakur, M. L., Pallela, V. R., Consigny, P. M., Rao, P. S., Vessileva-Belnikolovska, D., and Shi, R. (2000) Imaging vascular thrombosis with 99mTc-labeled fibrin alpha-chain peptide. *J. Nucl. Med. 41*, 161−168.

(12) Thakur, M. L. (1995) Radiolabeled peptides: now and the future. *Nucl. Med. Commun. 16*, 724−732.

(13) Schneider, R. F., Subramanian, G., Feld, T. A., McAfee, J. G., Zapf-Longo, C., Palladino, E., and Thomas, F. D. (1984) *N*,*N*′-bis(*S*-Benzoylmercaptoacetamido) Ethylenediamine and Propylenediamine ligands as renal function imaging agents. 1. Alternate synthetic methods. *J. Nucl. Med. 25*, 223−229.

(14) Liu, S., and Edwards, D. S. (1995) New N_2S_2 diamidedithiol and N_3S triamidethiols as bifunctional agents for labeling small peptides with technetium-99m. In *Technetium and rhenium in chemistry and nuclear medicine* (Nicolini, M., Bandoli, G., and Mazzi, U., Eds.) Vol. 4, pp 383−393, SG Editoriali, Padova, Italy.

(15) Waibel, R., Alberto, R., Willuda, J., Finnern, R., Schibli, R., Stichelberger, A., Egli, A., Abram, U., Mach, J. P., Pluckthun, A., and Schubiger, P. A. (1999) Stable one-step technetium-99m labeling of His-tagged recombinant proteins with a novel Tc(I)-carbonyl complex. *Nat. Biotechnol. 17*, 897−901.

(16) Qu, T., Wang, Y., Zhu, Z., Rusckowski, M., and Hnatowich, D. J. (2001) Different chelators and different peptides together influence the in vitro and mouse in vivo properties of 99Tcm. *Nucl. Med. Commun. 22*, 203−215.

(17) Rao, T. N., Adhikesavalu, D., Camerman, A., and Fritzberg, A. R. (1990) Technetium (V) and rhenium (V) complexes of 2,3-bis(mercaptoacetamido) propanoate. Chelate ring stereochemistry and influence on chemical and biological properties. *J. Am. Chem. Soc. 112*, 5798−5804.

(18) Bodansky, M., and Bodansky, A. (1984) in *The Practise of Peptide Synthesis: Reactivity & Structure Concepts in Organic Chemistry*, Vol. 21, pp 24−25, Springer/Verlag, New York.

(19) Schneider, R. F., Subramanian, G., Feld, T. A., McAfee, J. G., Zapf-Longo, C., Palladino, E., and Thomas, F. D. (1984) N,N′-bis(S-Benzoylmercaptoaccetamido) Ethylenediamine and propylenediamine ligands as renal function imaging agents. 1. Alternate synthetic methods. *J. Nucl. Med. 25*, 223−229.

(20) Kaiser, E., Colescott, R. L., Bossinger, C. D., and Cook, P. I. (1970) Color test for detection of free terminal amino groups in the solid-phase synthesis of peptides. *Anal. Biochem. 34*, 595−598.

(21) Fritzberg, A. R., Kuni, C. C., Klingensmith, W. C., III, Stevens, J., and Whitney, W. P. (1982) Synthesis and biological evaluation of Tc-99m N,N′-bis(mercaptoacetyl)-2,3-diaminopropanoate: a potential replacement for [^{131}I]*o*-iodohippurate. *J. Nucl. Med. 23*, 592−598.

(22) Chang, F., Qu, T., Rusckowski, M., and Hnatowich, D. J. (1999) NHS-MAS3: a bifunctional chelator alternative to NHS-MAG3. *Appl. Radiat. Isot. 50*, 723−732.

(23) Ahlborg, N. (1995) Synthesis of a diepitope multiple antigen peptide containing sequences from two malaria antigens using Fmoc chemistry. *J. Immunol. Methods 179*, 269−275.

(24) Hoogerhout, P., Stittelaar, K. J., Brugghe, H. F., Timmermans, J. A., ten Hove, G. J., Jiskoot, W., Hoekman, J. H., and Roholl, P. J. (1999) Solid-phase synthesis and application of double-fluorescent-labeled lipopeptides, containing a CTL-epitope from the measles fusion protein. *J. Pept. Res. 54*, 436−443.

(25) Chhabra, S. R., Hothi, B., Evans, D. J., White, P. D., Bycroft, B. W., and Chan, W. C. (1998) An appraisal of new variants of Dde amine protecting group for solid-phase peptide synthesis. *Tetrahedron Lett. 39*, 1603−1606.

BC0100814

Preparation and Tumor Cell Uptake of Poly(*N*-isopropylacrylamide) Folate Conjugates

Denis Dubé,[‡] Mira Francis,[†] Jean-Christophe Leroux,[†,§] and Françoise M. Winnik*[,‡,†]

Department of Chemistry and Faculty of Pharmacy, Université de Montréal, C. P. 6128, succursale Centre Ville Montréal QC Canada H3C 3J7. Received September 3, 2001; Revised Manuscript Received January 7, 2002

Folate conjugates (PNIPAM-NH−FA) of a copolymer of *N*-isopropylacrylamide (NIPAM) and amino-*N*′-ethylenedioxy-bis(ethylacrylamide) were prepared by an efficient synthesis leading to random grafting, via a short dioxyethylene spacer, of ∼7 folic acid residues per macromolecule. The chemical composition of the copolymer was characterized by ^{1}H NMR and UV/vis spectroscopy. A fluorophore-labeled folate PNIPAM conjugate was tested by in vitro assays performed with cultured KB-31 cells overexpressing the folate receptor. The cellular uptake of the copolymer was found to be temperature dependent and was competitively decreased by free folic acid, indicating that the polymer uptake is mediated specifically by the folate receptor. Hydrophobically modified folate conjugates of NIPAM, amino-*N*′-ethylenedioxy-bis(ethylacrylamide) copolymers, bearing a small number of *n*-octadecyl groups were prepared following a modified synthetic procedure for use in future studies of FA-targeted liposomes.

INTRODUCTION

The modification of liposomes with synthetic polymers is a promising approach toward the development of new highly efficient drug carriers. By coating the surface of liposomes with carefully designed water soluble polymers, several major improvements may be achieved, such as increase in liposome circulation time, responsiveness to external stimuli, and specific targeting. For example, it has been recognized several years ago that poly(ethylene glycol) (PEG)-modified liposomes are endowed of exceptional stability in vivo (*1*). Formulations incorporating small PEG-coated vesicles are used clinically (*2*). In these systems, the brushlike coat of PEG chains that covers the lipid bilayer is believed to act as a sterically repulsive shield against nonspecific opsonization by plasma proteins. While the PEG chains are particularly effective in this role, other water-soluble polymers have been shown to offer some level of protection, together with additional enabling functions, such as temperature- or pH-responsiveness. Extensively studied systems include complexes between liposomes and the pH-sensitive polyelectrolyte poly(2-ethylacrylic acid) (*3*) and the temperature-responsive neutral polymer, poly(*N*-isopropylacrylamide) (PNIPAM) (*4*). The performance of polymer-modified liposomes as drug carriers depends, to a large extent, on the reliable anchoring of the polymer within the lipid bilayer. In the case of PNIPAM, anchoring of the polymer on the bilayer is effected via a small number of long alkyl chains attached to the polymer backbone, an approach pioneered by Ringsdorf and co-workers (*5*), and employed effectively by several research teams (*6*, *7*, *8*). Anchoring PNIPAM chains onto liposome bilayers results in a decrease of the adsorption of serum proteins, at least below the lower critical solution temperature of PNIPAM (*9*) and increases the liposome circulation times in vivo (*10*). The cytotoxicity of PNIPAM and its derivatives still remains to be assessed in depth. Toxicity data on this polymer are scarce. Matsumaru et al. (*11*) showed that PNIPAM did not present any sign of acute toxicity after intravenous administration to mice. Recently, Fujimoto and co-workers (*12*) reported that a copolymer of NIPAM and *N*-methacryloyloxysuccinimide displayed no cytotoxicity toward U-937 cells below 4 mg/mL. We also observed that copolymers of NIPAM, octadecylacrylate, and methacrylic acid generated no acute local and systemic inflammatory response in rat following subcutaneous injection (*13*).

For efficient drug delivery, a carrier system should also promote tumor or lesion targeting and intracellular access. Internalization of the drug carrier may be achieved by coupling to the carrier a normally endocytosed ligand, taking advantage of natural endocytosis pathways. Using this strategy, a variety of ligands, such as antibodies, growth factors, or cytokines, are used to facilitate the uptake of carriers inside target cells (*14*). In the work reported here, we have sought to take advantage of the mechanism of folic acid (FA) uptake by cells to promote targeting and internalization, a methodology exploited previously to facilitate entry of attached drugs (*15*, *16*), antibodies (*17*), imaging agents (*18*), macromolecules (*19*, *20*, *21*), or liposomes (*22*, *23*) into cells. Folic acid is transported into cells via potocytosis, a receptor-mediated endocytosis (*24*, *25*, *26*). In this process, the ligand-bound receptor is sequestered in caveolae, internalized into postcaveolar plasma vesicles, released from the receptor via an intravesicular reduction in pH, and subsequently transported into the cytoplasm. The ligand-free receptor is then recycled to the cell surface by reopening of the caveolae. The folate receptor is known to be overexpressed on the surface of cancer cells in the case of epithelial malignancies, such as ovarian, colorectal, and breast cancer, whereas in most normal tissue it is expressed in very low levels (*27*, *28*, *29*).

We are currently assessing applications of folate−PNIPAM conjugates as coating of liposomes internalized via receptor-enhanced cellular uptake. We designed a

* To whom correspondence should be addressed. Phone (514) 343 6123; fax (514) 343 2362; e-mail francoise.winnik@umontreal.ca.

† Faculty of Pharmacy.

‡ Department of Chemistry.

§ Canada Research Chair in Drug Delivery.

10.1021/bc010084g CCC: $22.00 © 2002 American Chemical Society
Published on Web 03/30/2002

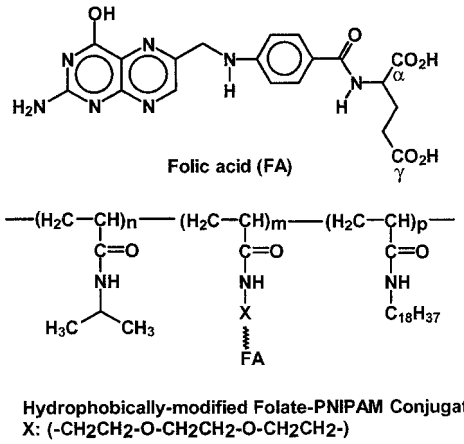


Figure 1. Chemical structure of folic acid and of the hydrophobically modified folate polymeric conjugate

family of *N*-isopropylacrylamide (NIPAM) copolymers carrying a small number of octadecyl groups and folic acid residues grafted along the chain via a short ethylenedioxy chain (Figure 1). The FA conjugates were obtained by amidation, with folic acid, of an aminated precursor copolymer. The folic acid molecule (Figure 1) possesses two carboxyl groups, termed α and γ, which can act as handles for covalent attachment. It has been demonstrated that folate linked via its γ-carboxyl group retains a strong affinity toward its receptor, whereas its α-carboxyl derivatives are not recognized as readily (*30*, *31*). We chose to attach the folate to the distal end of a short ethylenedioxy chain in order to increase the range of accessible receptor sites. We report here the synthesis and characterization of folate−PNIPAM conjugates and a preliminary in vitro evaluation of their targeting potential, using fluorescently labeled folate−PNIPAM conjugates that do not carry hydrophobic chains, which may interfere with the selected assays. Cytotoxicity assays confirmed that the folate−PNIPAM conjugates bind specifically to KB cells without harming the cells. Direct competition experiments with free folate demonstrated that the PNIPAM−folate conjugates effectively target the cells even at folate concentration above normal serum levels.

EXPERIMENTAL PROCEDURES

Materials. Water was deionized using a Milli Q water purification system (Millipore). *N*-Isopropylacrylamide, obtained from Fisher Scientific (Pittsburgh, PA), was recrystallized from acetone/heptane 2/3 v/v. *N*,*N*-Azobis(isobutyronitrile), trifluoroacetic acid, 2,2′-(ethylenedioxy)-bis(ethylamine), di-*tert*-butyl dicarbonate, acryloyl chloride, 1-(3-dimethylaminopropyl)-3-ethylcarbodiimide hydrochloride (EDC), folic acid dihydrate, and 2,4,6-trinitrobenzenesulfonic acid (TNBS), were purchased from Aldrich Chemical Co (Milwaukee, WI). *N*-*n*-Octadecylacrylamide was prepared as described previously (*32*). Fluorescein dichlorotriazine (5-DTAF), sodium chloride, dibasic sodium phosphate, monobasic sodium phosphate, Triton X-100, and 3-(4,5-dimethylthiazol-2-yl)-2,5-diphenyltetrazolium bromide (MTT) were obtained from Sigma Chemical Co (St Louis, MO). Bicinchoninic acid (BCA) was obtained from Pierce Co (Rockford,IL). N−BOC-ethylenedioxy-bis(ethylamine) was prepared as described previously (*33*). Dioxane and tetrahydrofuran (THF) were dried by distillation over sodium. Triethylamine was dried by distillation over potassium hydroxide, Dichloromethane was dried by distillation over calcium hydride. All other solvents were reagent grade and used as received. Phosphate buffers of pH 4.7 [20 mM NaH_2PO_4 + HCl (0.1M)], pH 7.4 (50 mM KH_2PO_4, NaOH 3.91 mmol), and a borate buffer of pH 9.5 (12.5 mM Borax, 0.8 mM NaOH) were prepared from the corresponding salts. Phosphate buffered saline pH 7.2 (PBS) was prepared from 75 mM NaCl, 53 mM Na_2HPO_4 and 13 mM NaH_2PO_4. Silica gel (60−200 mesh) was purchased from Baker. The ion-exchange resin AG 501-X8(D) and DOWEX 2 × 8−400 were obtained from BioRad Laboratories and Supelco, respectively. Spectra/Por membranes (3500 MW cutoff) were employed for dialysis.

Instrumentation. NMR spectra were recorded on a Bruker ARX-400 400 MHz spectrometer. Infrared spectra were recorded on a Bomem Hartmann & Braun IR spectrometer fitted with a Bomem Grams/32 data analysis software. UV/Visible spectra were measured with a Hewlett-Packard 8452A photodiode array spectrometer. Viscometry measurements were carried out with an Ubbelhode semi-microdilution viscometer at 27 °C.

Monomer and Polymer Synthesis. *N-BOC-N′-(Ethylenedioxy-bis(ethylacrylamide) (EDBE).* A solution of acryloyl chloride (0.7 mL, 8.5 mmol) in dichloromethane (10 mL) was added dropwise into a solution of *N*-BOC-ethylenedioxy-bis(ethylamine) (1.94 g, 8.0 mmol) and triethylamine (2.35 mL, 17 mmol) in dichloromethane (40 mL) kept at 0 °C. At the end of the addition, the mixture was kept at 0 °C for 1 h and allowed to warm to room temperature. The mixture was washed with water, 1 N aqueous acetic acid, aqueous saturated sodium bicarbonate, and brine. The organic layer was dried over anhydrous sodium sulfate, filtered, and concentrated in vacuo. The yellow viscous oil which was purified by flash chromatography over silica eluted with hexane/ethyl acetate 1/3 v/v yielding *N*-BOC-*N′*-(ethylenedioxy-bis(ethylacrylamide) (1.20 g, 50% yield) as a pale yellow viscous oil. ^{1}H NMR ($CDCl_3$, δ): 1.38 (s, 9H, $(CH_3)_3C$), 3.26 (q, 2H, J = 5 Hz, CH_2NHCOO), 3.52 (m, 10 H, CH_2 of ethylenedioxy), 4.95 (br s, 1H, N*H*), 5.58 (dd, 1H, J = 0.6, 10 Hz, *H*(*Z*)HC═), 6.10 (dd, 1H, J = 10, 17 Hz, H_2C═C*H*), 6,26 (dd, 1H, J = 0.6, 17 Hz, *H*(*E*)HC═) ppm; FTIR ($\bar{\nu}$, cm^{-1}) 1170 (O−$C(CH_3)_3$ stretching), 1527 (CONHR carbonyl stretching), 1711 (urethane carbonyl stretching), 2930 (alkene stretching).

Copolymerization of N-Isopropylacrylamide (NIPAM) and N-BOC-N′-Ethylenedioxy-bis(ethylacrylamide). A solution of NIPAM (0.456 g, 4.0 mmol) and *N*-BOC-*N′*-ethylenedioxy-bis(ethylacrylamide) (0.270 g, 1.0 mmol) in dioxane (10 mL) was degassed for 30 min by vigorous bubbling of nitrogen. The mixture was heated to 60 °C. AIBN (3.4 mg, 0.021 mmol) was added at once. The polymerization mixture was stirred at 60 °C for 18 h. It was cooled to room temperature. The polymer, PNIPAM-NHBOC, was isolated by precipitation into diethyl ether (500 mL) and further purified by two precipitations from THF into diethyl ether. It was dried in vacuo (yield: 72 (%); ^{1}H NMR ($CDCl_3$, δ) 1.13 (br s, $(CH_3)_2CHNH$), 1.44 (s, $(CH_3)_3C$), 3.30−3.62 (m, CH_2 of ethylenedioxy group and main chain), 3.99 (br s, $(CH_3)_2CHNH$) ppm.

Deprotection of PNIPAM-NHBOC. Trifluoroacetic acid (0.18 mL, 2.4 mmol, 10 equiv per BOC equiv) was added to a solution of PNIPAM-NHBOC (150 mg) in dichloromethane (6.0 mL) cooled in an ice/water bath. The reaction mixture was warmed to room temperature and stirred for 18 h. The solvent was evaporated. The polymer, PNIPAM-$NH_3^+CF_3COO^-$, was purified by two precipitations from THF into diethyl ether and dried in vacuo (yield: ∼100%). Dowex 2 × 8−400 (100 mg) was added to a solution of PNIPAM-NH_2 (130 mg) in water. The mixture was stirred at room temperature for 2 h.

The resin was separated by filtration. The polymer was isolated by lyophilization (70 mg, yield: 63%). ^{1}H NMR (D_2O, δ) 1.17 (s, $(CH_3)_2CHNH$), 3.19−3.74 (m, CH_2 of ethylenedioxy group and of main chain), 3.90 (s, $(CH_3)_2$-CHNH) ppm.

Preparation of PNIPAM-NH−FA. A solution of EDC (53 mg, 0.28 mmol) and folic acid (59 mg, 0.12 mmol) in anhydrous DMSO (2 mL) was prepared and stirred at room temperature for 1 h. It was then added to a solution of PNIPAM-NH (100 mg, 0.165 mmol amine groups) in phosphate buffer (25 mL, pH 4.7). The resulting mixture was stirred at room temperature and in the dark for 16 h. It was brought to pH 9.0 by dropwise addition of diluted aqueous NaOH and dialyzed first against pH 7.4 phosphate buffer for 3 days and then against water for 3 days. The polymer was isolated by lyophilization (115 mg, 80%). ^{1}H NMR (D_2O, δ) 1.14 (s, $(CH_3)_2CHNH$), 3.19−3.76 (m, CH_2 of ethylenedioxy and main chain), 3.90 (1H, $(CH_3)_2CHNH$), 6.75 (d, $J = 7$ Hz, 3′, 5′ H of folate group), 7.63 (d, $J = 7$ Hz, 2′, 6′ H of folate group), 8.77 (s, C_7-H of folate group) ppm; UV/vis (phosphate buffer pH 7.4) 363 nm; folate content: 0.336 mmol g^{-1} polymer).

PNIPAM-NH−DTAF. A solution of fluorescein dichlorotriazine (3.9 mg, 0.0071 mmol) in aqueous borate buffer (5 mL, pH 9.5) was added to a solution of PNIPAM-NH (85 mg, 0.140 mmol amine) in the same buffer (25 mL). The reaction mixture was stirred at room temperature for 2 h. It was dialyzed against pH 9.5 borate buffer for 16 h and against water for 3 days. The polymer was isolated by lyophilization (70 mg, 71%). ^{1}H NMR (D_2O, δ) 1.08 (s, $(CH_3)_2CHNH$), 3.19−3.76 (m, CH_2 of ethylenedioxy and main chain), 3.90 (1H, $(CH_3)_2CHNH$) ppm; UV/vis (pH 9.5 borate buffer) 490 nm; DTAF content: 0.095 mmol g^{-1} polymer).

PNIPAM-NH−FA−DTAF. The polymer was prepared as described for the preparation of PNIPAM-NH−DTAF, starting from PNIPAM-NH−FA (83 mg); 72% yield; 1.10 (s, $(CH_3)_2CHNH$), 3.08−3.64 (m, CH_2 of ethylenedioxy), 3.85 (1H, $(CH_3)_2CHNH$), 6.74 (d, $J = 7$ Hz, folate aromatic protons), 7.62 (d, $J = 7$ Hz, folate aromatic protons) ppm; UV/vis (borate buffer pH 9.5) 492 nm; DTAF content: 0.043 mmol g^{-1} polymer).

Preparation of PNIPAM-NH−FA−ODA. The copolymer was prepared following the three-step procedure outlined for the preparation PNIPAM-NH−FA, starting from NIPAM (0.574 g, 4.84 mmol), *N*-BOC-*N*′-ethylenedioxy-bis(ethylacrylamide) (0.780 g, 2.5 mmol) and *N*-octadecylacrylamide (101 mg, 0.308 mmol).

PNIPAM-N-t-BOC−ODA: yield: 77%; ^{1}H NMR ($CDCl_3$, δ) 0.87 (t, $J = 17$ Hz, $H_3CC_{17}H_{34}$), 1.14 (br s, $(CH_3)_2$-CHNH), 1.45 (s, $(CH_3)_3C$), 2.10 (br, main chain protons and CH_2 of octadecyl group), 3.31−3.63 (m, CH_2 of ethylenedioxy), 3.99 (br s, $(CH_3)_2CHNH$) ppm.

PNIPAM-NH−ODA: yield: 59%; ^{1}H NMR (D_2O, δ) 0.89 (br t, $H_3CC_{17}H_{34}$), 1.14 (br s, $(CH_3)_2CHNH$), 3.19−3.76 (m, CH_2 of ethylenedioxy), 3.90 (br s, $(CH_3)_2CHNH$) ppm.

PNIPAM-NH−FA−ODA: yield: 50%; ^{1}H NMR (D_2O, δ) 0.89 (br t, $H_3CC_{17}H_{34}$), 1.14 (br s, $(CH_3)_2CHNH$), 3.19−3.3.76 (m, CH_2 of ethylenedioxy), 3.90 (br s, $(CH_3)_2CHNH$) ppm.; UV/vis (phosphate buffer, pH 7.4) 363 nm; folate content 0.196 mmol g^{-1} polymer.

UV/Vis Analysis. *Folate Content.* The content of folate in the conjugates was determined by quantitative UV spectrophotometry of polymer solutions in aqueous phosphate buffer (pH 7.4) using the molar extinction coefficient value of 6197 mol^{-1} cm^{-1} at $\lambda = 363$ nm (*34*).

DTAF Content. The content of DTAF in the conjugates was determined by quantitative UV spectrophotometry of polymer solutions in aqueous borate buffer (pH 9.2) using the molar extinction coefficient value of 70000 mol^{-1} cm^{-1} at $\lambda = 490$ nm (*35*).

Colorimetric Determination of the Free Amine Groups (*36*). A known amount of polymer (5 mg) was dissolved in a solution of excess TNBS (0.01 M) in sodium hydrogen carbonate (2.0 mL, 20 g L^{-1}, pH 8.2). The solution was kept for 2 h at 40 °C. It was cooled to room temperature and made up to 10 mL with a water/THF solution (v/v). The amount of TNBS-derivatized amines in a sample was determined from the absorbance at λ 345 nm, using TNBS-derivatized *N*-BOC-ethylenedioxy-bis(ethylamine) ($\epsilon_{345\ nm} = 8700$ L mol^{-1} cm^{-1}) as reference compound. A solution of TNBS without added polymer was treated under the same conditions. Its absorbance at 345 nm was subtracted from that of the TNBS-derivatized polymers to correct for its residual absorbance at this wavelength.

Cell Culture, Cytotoxicity, and FA Uptake Studies. *Cell Lines.* KB-31 cells, a human nasopharyngeal epidermal carcinoma cell line overexpressing surface receptors for folic acid (a gift from Dr. Daryl Drummond, Research Institute, California Pacific Medical Center, San Francisco, CA), were maintained in a monolayer culture in folate-free RPMI 1640 medium containing L-glutamine (Gibco laboratories). The medium was supplemented with 10% (v/v) heat-inactivated fetal bovine serum (FBS, Gibco laboratories) and 1% (v/v) penicillin−streptomycin antibiotics (10000 U mL^{-1} penicillin G and 10000 μg mL^{-1} streptomycin, Gibco laboratories) solution (100 U mL^{-1} penicillin G, 100 μg mL^{-1} streptomycin). Cultured cells were incubated at 37 °C in a humidified atmosphere containing 5% CO_2.

Cytotoxicity Assay. KB-31 cells were seeded in triplicate in 96-well plates at 5×10^4 cells/well. Cells were allowed to adhere for 4 h at 37 °C in a humidified atmosphere of 5% CO_2 in air. Solutions of PNIPAM-NH−FA−DTAF or PNIPAM-NH−DTAF in culture medium (0−1 mg mL^{-1}) were added to the cells. After several different incubation times (2−24 h), cell viability was determined by a MTT test, according to the procedure described by Mosmann (*37*). The test is based on mitochondrial dehydrogenase cell activity as an indicator of cell viability. Ten microliter aliquots of a MTT solution in PBS (5 mg mL^{-1}) were added to each well. After incubation for an additional 4 h at 37 °C, a 2-propanol solution of HCl (100 μL, 0.4 N HCl) was added to each well to ensure solubilization of formazan crystals. The optical density values were determined using a multiwell-scanning spectrophotometer (Bio-Tek Instruments Inc.) at 570 nm.

Fluorescence Microscopy. Cells were plated at a concentration of 5×10^5 cells per 35 mm dish in a six-well plastic culture plate 24 h prior to the assay. They were then incubated for 1 h at 37 °C with a solution of PNIPAM-NH−FA−DTAF or PNIPAM-NH−DTAF in culture medium (0.2 mg mL^{-1}). For free folate competition studies, 1 mM folic acid was added to the incubation medium. After incubation, the cells were washed five times with 2 mL of PBS to remove free polymer. Cell-associated fluorescence was viewed with an Axiovert inverted fluorescence microscope (Zeiss) equipped with a filter set that produces excitation in the range 465−495 nm and allows observation of fluorescence emission in the range 515−555 nm with a long wave path dichroic mirror and barrier filter. Cells were photographed using a 1310C DVC digital camera (DVC Company Inc.).

Quantitation of the Uptake of PNIPAM-NH−FA−DTAF by KB-31 Cells. Cells were plated at a concentration of 5×10^5 cells per 35 mm dish in a six-well plastic

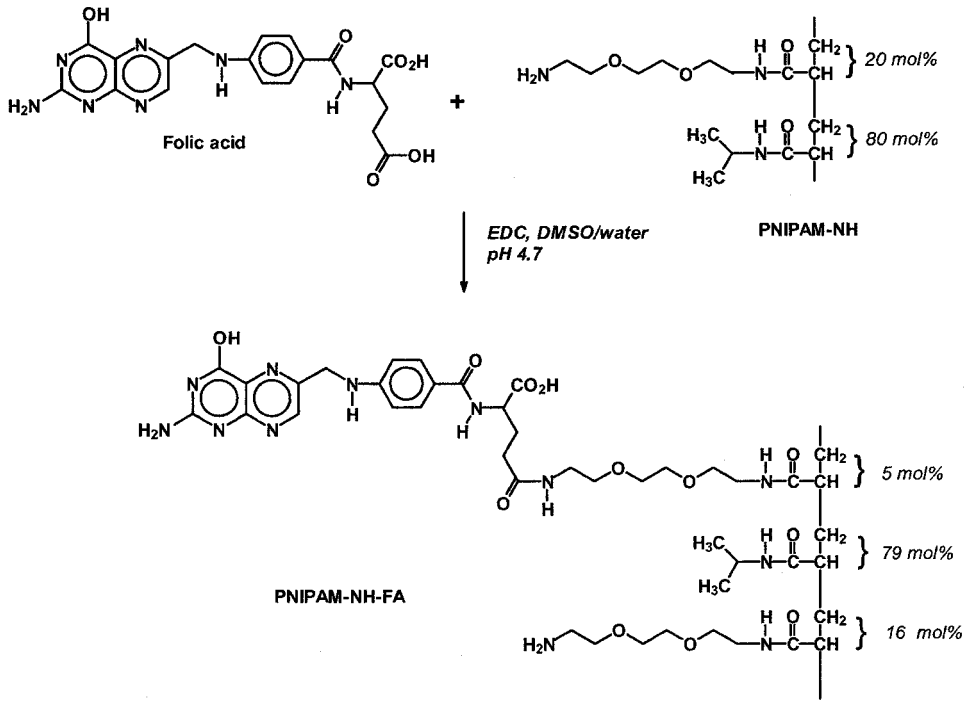


Figure 2. Synthetic sequence for the preparation of the copolymer PNIPAM-NH−FA

culture plate 24 h prior to the assay. They were then incubated for 1 h at 37 °C and 2 h at 4 °C with PNIPAM-NH−FA−DTAF or PNIPAM-NH−DTAF (0.2 mg mL^{-1} in culture medium). For free folate competition studies, 1 mM folic acid was added to the incubation medium. After incubation, the cells were washed five times with 2 mL of PBS. The cells were then solubilized in Triton X-100 solution (2 mL, 1% w/v final concentration in PBS). Cell-associated fluorescence was measured using a series 2 Aminco Bowman (Spectronic Instruments Inc.) fluorescence spectrometer. Samples were excited at 492 nm, and fluorescence emission intensity was monitored at 516 nm. The amount of cell-associated polymer was calculated using a predetermined standard curve and calibrated with protein cell content determined by a bicinchoninic acid (BCA) protein assay (Pierce).

RESULTS AND DISCUSSION

Preparation and Characterization of Folate Conjugates. Folate−PNIPAM conjugates were prepared by postmodification of a copolymer of *N*-isopropylacrylamide (NIPAM) and amino-*N′*-ethylenedioxy-bis(ethylacrylamide) as shown in Figure 2. The copolymer PNIPAM-NH was obtained by free radical copolymerization in dioxane of NIPAM and *N*-BOC-*N′*-ethylenedioxy-bis-(ethylacrylamide) followed by deprotection of the terminal primary amine groups. The composition of the BOC-protected copolymer was determined by ^{1}H NMR spectroscopy, using the singlet at δ 1.14 ppm, assigned to the resonance of the *tert*-butyl protons of the BOC units, and the broad singlet at δ 3.90 ppm, assigned to the resonance of the methine NIPAM protons, to calculate the molar ratio of EDBE and NIPAM units, respectively (Figure 3). The disappearance of the signal at δ 1.14 ppm in the ^{1}H NMR spectrum of PNIPAM-NH confirmed that the deprotection step went to completion. A primary-amine-specific colorimetric assay was performed with PNIPAM-NH to ascertain the composition of the deprotected copolymer. This copolymer is soluble in water and in PBS at all temperatures between 0 and 60 °C, unlike the homopolymer PNIPAM, which in aqueous solution exhibits a cloud point at 31 °C. This enhanced water solubility is attributed to the presence of the hydrophilic ethylenedioxy-containing residues along the polymer chain.

Coupling of the folate residue to the polymer was achieved via an EDC-mediated reaction of folic acid and the primary amine functions linked to the polymer. The success of the linkage was confirmed by the presence of signals at δ 6.75−8.77 ppm in the ^{1}H NMR spectrum of PNIPAM-NH−FA and by an absorbance at $\lambda = 363$ nm in the UV spectrum of the copolymer. It is known that carbodiimide-activated folic acid can couple either via the α or the γ carboxyl group of its glutamate residue, although EDC has been shown to favor linkage of the distal γ carboxyl residue. Wang et al. (*31*) used ^{1}H NMR spectral data to ascertain the regiochemistry of the linkage of folate derivatives and ethylenediamine. Unfortunately, in the ^{1}H NMR spectrum of PNIPAM-NH−FA (Figure 3), the relevant signals are masked by broad and strong signals due to the resonances of the protons associated to the polymer residues. Thus, we were unable to determine the regiochemistry of the folate linkage in PNIPAM-NH−FA. It is expected to consist mostly of the γ-linked isomer, due to the reaction conditions selected and also to the steric constraints imposed by the polymer chain.

Hydrophobically modified PNIPAM−folate conjugates were obtained via the same synthetic sequence, starting with a copolymer of NIPAM, amino-*N′*-ethylenedioxy-bis-(ethylacrylamide), *N*-*n*-octadecylacrylamide (Figure 2). The level of hydrophobic group incorporation in the HM−folate conjugate could not be determined on the basis of the ^{1}H NMR spectrum of its aqueous solution, which exhibited significant line broadening indicative of the formation of micellar structures and concomitant motional restriction of the alkyl chains (*38*). The octadecyl group content of the precursor, PNIPAM-N-t-BOC−ODA, could be determined accurately from the ^{1}H NMR spectrum of its solution in $CDCl_3$, using the triplet at δ 0.87 ppm, attributed to the resonance of the terminal methyl protons of the octadecyl chain and the broad singlet at δ

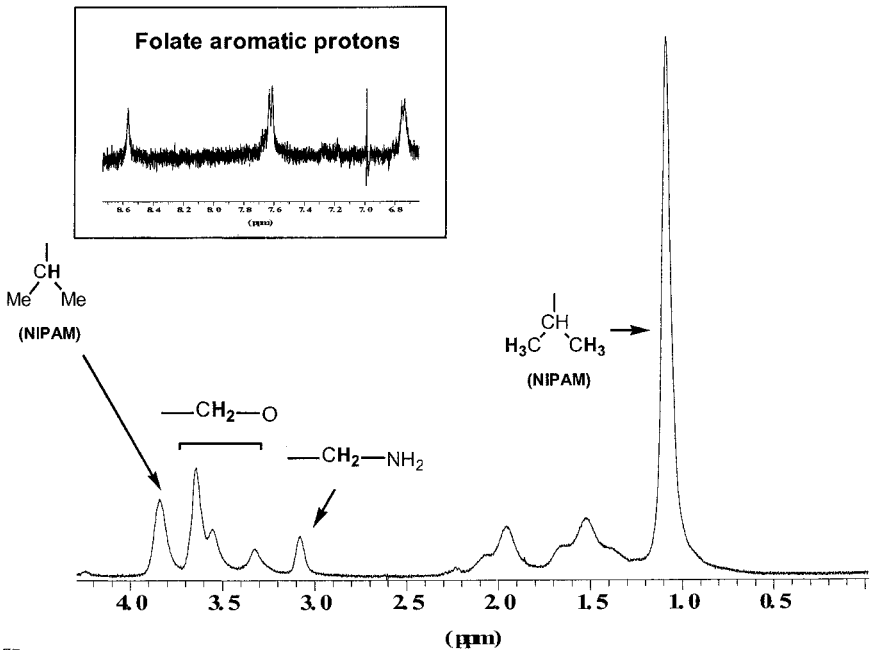


Figure 3. ^{1}H NMR spectrum of PNIPAM-NH−FA in D_2O.

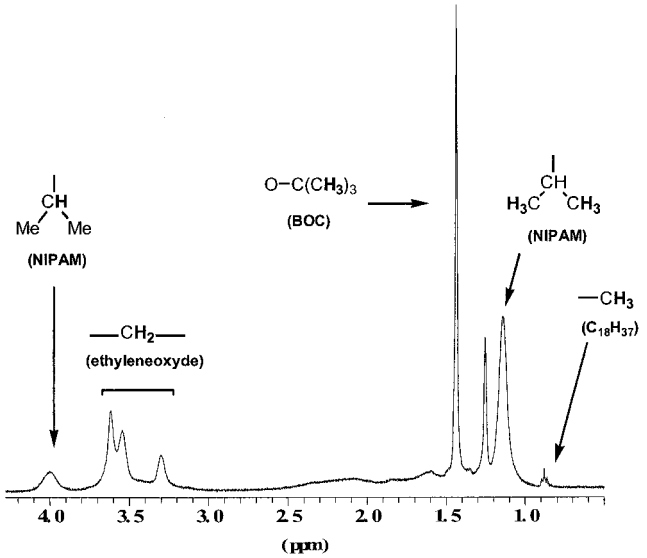


Figure 4. ^{1}H NMR spectrum of PNIPAM-NBOC−ODA in $CDCl_3$.

Table 1. Composition and Physical Properties of the Polymers

	composition (mol %)				
polymer	NIPAM[a]	EDBE[a,b]	ODA[a]	FA[c]	M_{vis}[d]
PNIPAM-NH	79	21			20000
PNIPAM-NH−FA	79	16		5	20000
PNIPAM-NH−ODA	63	33	4		20000
PNIPAM-NH−ODA−FA	63	30	4	3	20000

[a] From ^{1}H NMR spectra. [b] From quantitative analysis of primary amine groups (see text). [c] From UV/vis spectra. [d] From viscometry in THF, 27 °C, using the relationship $[\eta] = 10^{-3.307} M_{vis}^{0.79}$ (Ganachaud, F., et al. (2000) *Macromolecules 18*, 6738).

4.0 ppm, attributed to the resonance of the NIPAM methine proton (Figure 4). The physical properties and the composition of the PNIPAM−FA−ODA are listed in Table 1.

Cellular Uptake of PNIPAM−Folate Conjugates. The cytotoxicity of PNIPAM-NH−FA−DTAF and PNIPAM-NH−DTAF on KB-31 cells was evaluated after

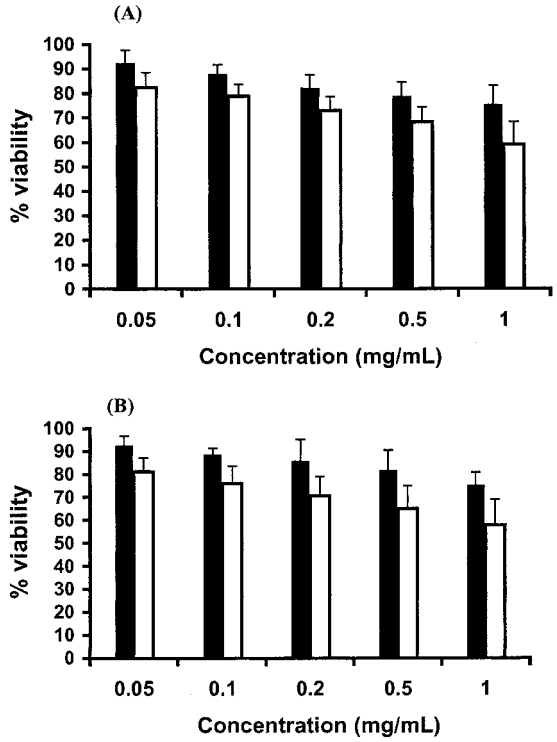


Figure 5. Effect of PNIPAM-NH−FA−DTAF (A) and PNIPAM-NH−DTAF (B) concentration on KB-31 cell viability determined by MTT assay after a 2-h (closed columns) or 24-h (open columns) incubation time. Mean ± SD (n = 3).

incubation at 37 °C for 2 and 24 h (Figure 5). The two polymers exhibited nearly identical toxicity profiles. Cell viability reached a value of approximately 75% and 60% after incubation of 2 and 24 h, respectively, for the highest polymer concentration tested (1 mg/mL). These results corroborate our previous results on the cytotoxicity on macrophage-like J774 cells where a pH-sensitive NIPAM copolymer was evaluated (*39*) which exhibited an LD_{50} in excess of 1 mg/mL after a 24-h incubation period.

To assess the uptake of PNIPAM-NH−FA by cells overexpressing the folate receptor, the fluorescently

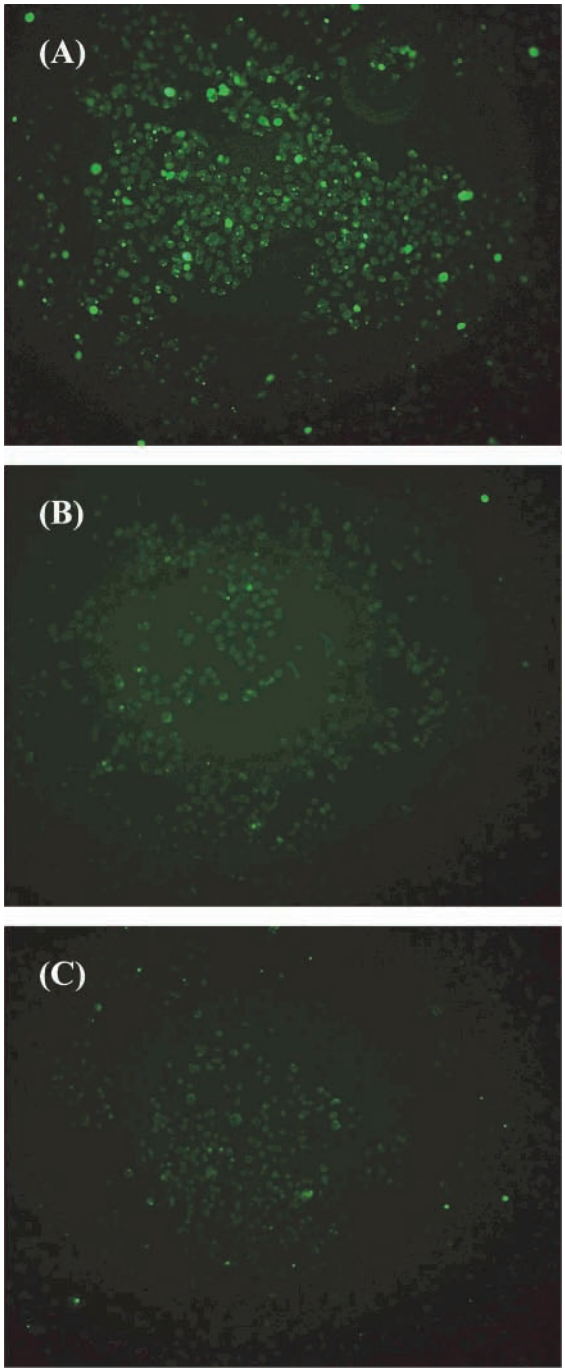


Figure 6. Fluorescence micrographs of KB-31 cells incubated at 37 °C for 1 h with PNIPAM-NH−FA−DTAF (A, B) or PNIPAM-NH−DTAF (C) (0.2 mg/mL). Cells were incubated in the absence (A, C) or presence (B) of 1 mM free folic acid.

labeled polymer and its precursor were incubated for 1 h at 37 °C with KB-31 cells. Fluorescence micrographs of cells exposed to the folate-bearing polymer PNIPAM-NH−FA−DTAF displayed an intensive and diffuse fluorescence indicating binding of the polymer on the cell membrane (Figure 6A). Some cells displayed a punctuated fluorescence pattern suggesting that the polymer was localized also in endocytic vesicles. In contrast, cells incubated with the fluorescently labeled nontargeted polymer PNIPAM-NH−DTAF displayed only very weak fluorescence attributed to low nonspecific uptake of the polymer (Figure 6B). The role of cell surface folate receptors in polymer binding was assessed further by incubating KB-31 cells with PNIPAM-NH−FA−DTAF in the presence of 1 mM free folic acid used as competitive

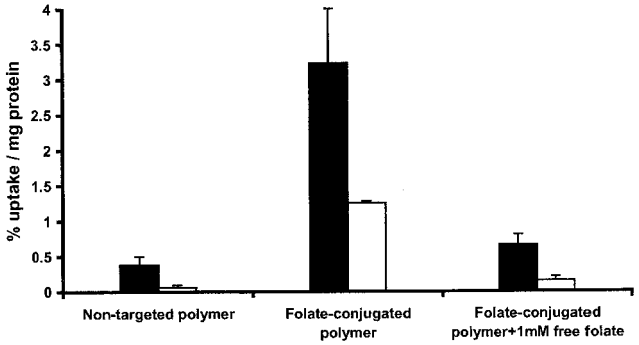


Figure 7. Uptake of PNIPAM-NH−FA−DTAF or PNIPAM-NH−DTAF (0.2 mg/mL) by KB-31cells in the absence or presence of 1 mM folic acid. The cells were incubated at 37 °C for 1 h (closed columns) or 4 °C for 2 h (open columns). Mean ± SD ($n = 3$).

inhibitor of cellular uptake. Fluorescence micrographs of the cells incubated for 1 h (Figure 6C) show that the presence of free folic acid effectively inhibited uptake of PNIPAM-NH−FA−DTAF by the cells.

The uptake of folate-conjugated and nontargeted polymer by KB-31 cells was quantified by fluorescence spectroscopy. The cells were incubated with each copolymer for 1 h at 37 °C and for 2 h at 4 °C (Figure 7). After incubation at 37 °C, the uptake of PNIPAM-NH−FA−DTAF was 8.5 times higher than that of PNIPAM-NH−DTAF. The level of uptake of the folate-conjugated polymer was reduced by 80% in the presence of 1 mM free folic acid. Incubation at 4 °C resulted in a 2.5-fold decrease in cell association of PNIPAM-NH−FA−DTAF, compared to the uptake upon incubation at 37 °C. The uptake of the nontargeted polymer upon incubation at 4 °C was barely detectable by fluorescence. As the endocytic process is strongly inhibited at 4 °C, fluorescence of cells incubated at this temperature in the presence of labeled polymer can be attributed only to polymer bound on the cell surface. The folate-conjugated polymer still displayed a 19-fold increase in uptake versus its nontargeted counterpart. The addition of 1 mM free folic acid resulted in an 88% decrease of fluorescence, demonstrating the specific receptor-mediated binding of PNIPAM-NH−FA−DTAF. The fact that 100% inhibition was not achieved upon addition of free folic acid may be an indication of some level of nonspecific uptake of the copolymer. It may also reflect the stronger avidity of the copolymer as a result of multivalent interaction (*9*, *16*), as each polymer chain bears several folic acid residues (*40*) with an average of seven folic acid molecules.

CONCLUSIONS

In this report, we described an efficient and flexible synthesis of noncytotoxic PNIPAM folate conjugates. We have demonstrated that selective recognition of the conjugates by the folate receptors is maintained upon linking of folate to the macromolecule. We recently demonstrated that pH-sensitive amphiphilic NIPAM copolymers could facilitate the transfer of liposomal content from the endosomes/lysosomes to the cytoplasm (*39*). Therefore, by combining the tumoral targeting ability of folic acid with the unique physicochemical properties of NIPAM copolymers, one could design highly efficient liposomal systems for the cytoplasmic delivery of a variety of active compounds. Indeed, it is now clearly established that folate mediates endocytosis of macromolecules, drugs, and colloidal carriers into vesicles that become rapidly acidified to a pH of about 5 (*41*). Although

the folate-targeting approach has been successful in a number of studies (16), endosomally targeted materials, which do not cross easily cell membranes, do not escape from the endosome in the absence of a triggerable membrane destabilization/fusion pathway. Therefore, for the delivery of macromolecules, such as DNA, or of highly hydrophilic drugs, inefficient translocation into the cytosol may compromise the folate targeting approach. To circumvent this problem, folic acid can be conjugated to a copolymer exhibiting endosomolytic properties (e.g., polyethylenimine) (*16*) or attached to fusiogenic liposomes (*42*). Future investigations will focus on the design of delivery systems consisting of serum-stable liposomes modified with a pH- and/or temperature-sensitive folate-conjugated NIPAM copolymer and their uptake in various cell models overexpressing the folate receptor.

ACKNOWLEDGMENT

This work was supported by grants of the Canadian Institutes of Health Research (CIHR) to J.C.L. and of the Natural Sciences and Engineering Research Council of Canada (NSERC) to F.M.W. J.C.L. and M.F. acknowledge scholarships from the Fonds de la Recherche en Santé du Québec and the Canadian International Development Agency, respectively.

LITERATURE CITED

(1) Lasic, D., Martin, F., Eds. (1995) *Stealth Liposomes,* CRC Press, Boca Raton, FL.

(2) Drummond, D. C., Meyer, O., Hong, K., Kirpotin, D., and Papahadjopoulos, D. (1999) Optimizing liposomes for delivery of chemotherapeutic agents to solid tumors. *Pharmacol. Rev. 51,* 691−743.

(3) Thomas, J. L., and Tirrell, D. A. (1992) Polyelectrolyte-sensitized phospholipid vesicles. *Acc. Chem. Res. 25,* 336−342.

(4) Schild, H. G. (1992) Poly (N-Isopropylacrylamide): experiment, theory, and application. *Prog. Polym. Sci. 17,* 163−249.

(5) Ringsdorf, H., Venzmer, J., and Winnik, F. M. (1991) Interaction of hydrophobically modified poly-N-(isopropylacrylamides) with model membranes or playing a molecular accordion. *Angew. Chem., Int. Ed. Engl. 30,* 315−319.

(6) Hayashi, H., Kono, K., and Takagishi, T. (1996) Temperature-controlled release properties of phospholipid vesicles bearing a thermo-sensitive polymer. *Biochim. Biophys. Acta 1280,* 127−134.

(7) Kim. J.-C., Bae, S. K., and Kim, J.-D. (1997) Temperature sensitivity of liposomal lipid bilayers mixed with poly-(N-isopropylacrylamide-*co*-acrylic acid). *J. Biochem. 121,* 15−19.

(8) Meyer, O., Papahadjopoulos, D., and Leroux, J. C. (1998) Copolymers of N-isopropylacrylamide can trigger pH sensitivity to stable liposomes. *FEBS Lett. 42,* 61−64.

(9) Yamazaki, A., Winnik, F. M., Cornelius, R. M., and Brash, J. L. (1999) Modification of liposomes with *N*-substituted polyacrylamides: identification of proteins adsorbed from plasma. *Biochim. Biophys. Acta 1421,* 103−115.

(10) Roux, E., Stomp, R., Giasson, S., Pézolet, M., Moreau, P., and Leroux, J. C. (2001) Steric stabilization of liposomes by pH-responsive N-isopropylacrylamide copolymer. *Pharm. Res.* (submitted).

(11) Matsumaru, Y., Hyodo, A., Nose, T., Ito, S., Hirano, T., and Ohashi, S. (1996) Applications of thermosensitive polymers as a new embolic material for intravascular neurosurgery. *J. Biomater. Sci. Polym. Ed. 7,* 795−804.

(12) Fujimoto, F., Iwasaki, C., Arai, C., Kuwako, M., and Yasugi, E. (2000) Control of cell death by the smart polymeric vehicle. *Biomacromolecules 1,* 515−518.

(13) Molinaro, G., Adam, A., Zignani, M., Taillefer, J., Schwach-Abdellaoui, K., Gurny, R., and Leroux, J. C. (1999) Evaluation of the local and systemic inflammatory responses induced by the subcutaneous injection of different biopolymers. *Proceed. Intern. Symp. Control. Relat. Bioact. Mater. 26,* 607−608.

(14) Duncan, R., and Connors, T., Eds. (1996) Drug targeting in cancer therapy. *J. Drug Targeting 3,* 317−410.

(15) Ladino, C. A., Chari, R. V., Bourret, L. A., Kedersha, N. L., and Goldmacher, V. S. (1997) Folate-maytansinoids: target-selective drugs of low molecular weight. *Int. J. Cancer 73,* 859−864.

(16) Sudimack, J., and Lee, R. J. (2000) Targeted drug delivery via the folate receptor. *Adv. Drug Delivery Rev. 41,* 147−162.

(17) Coney, L. R., Tomasetti, A., Carayannopoulos, L., Frasca, V., Kamen, B. A., Colnaghi, M. L., and Zurawski, V. R. Jr. (1991) Cloning of a tumor-associated antigen: MOv18 and MOv19 antibodies recognize a folate-binding protein. *Cancer Res. 51,* 6125−6132.

(18) Luo, J., Smith, M. D., Lantrip, D. A., Wang, S., and Fuchs, P. L. (1997) Efficient syntheses of pyrofolic acid and pteroyl azide, reagents for the production of carboxyl-differentiated derivatives of folic acid. *J. Am. Chem. Soc. 119,* 10004−10013.

(19) Leamon, C. P., and Low, P. S. (1991) Delivery of macromolecules into living cells: a method that exploits folate receptor endocytosis. *Proc. Natl. Acad. Sci. U.S.A. 88,* 5572−5576.

(20) Mislick, K. A., Baldeschwieler, J. D., Kayyem, J. F., and Meade, T. J. (1995) Transfection of folate-polylysine DNA complexes: evidence for lysosomal delivery. *Bioconjugate Chem. 6,* 512−515.

(21) Kono, K., Liu, M., and Fréchet, J. M. J. (1999) Design of dendritic macromolecules containing folate or methotrexate residues. *Bioconjugate Chem. 10,* 1115−1121.

(22) Gabizon, A., Horowitz, A. T., Goren D., Tzemach, D., Mandelbaum-Shavit, F., Qazen, M. M. and Zalipsky, S. (1999) Targeting folate receptor with folate linked to extremities of poly(ethylene glycol)-grafted liposomes: in-vitro studies *Bioconjugate Chem. 10,* 289−298 (and references therein).

(23) Anderson, K. E., Stevenson, B. R., and Rogers, J. A. (1999) Folic acid-PEO-labeled liposomes to improve gastrointestinal absorption of encapsulated agents. *J. Controlled Release 60,* 189−198.

(24) Rothberg, K. G., Ying, Y., Kolhouse, J. F., Kamen, B. A., and Anderson, R. G. W.(1992) The glycophospholipid-linked folate receptor internalizes folate without entering the clathrin-coated endocytic pathway. *J. Cell. Biol. 110,* 637−649.

(25) Kamen, B. A., and Capdevilla, A. (1986) Receptor-mediated folate accumulation is regulated by the cellular folate content. *Proc. Natl. Acad. Sci. U.S.A. 83,* 5983−5987.

(26) Anderson, R. G. W., Kamen, B. A., and Rothberg, K. G. (1992) Potocytosis sequestration and transport of small molecules. *Science 255,* 410−411.

(27) Campbell, I. G., Jones, T. A., Foulkes, W. D., and Trowsdale, J. (1991) Folate-binding protein is a marker for ovarian cancer. *Cancer Res. 51,* 5329−5338.

(28) Ross, J. F., Chaudhuri, P. K., and Ratnam, M. (1994) Differential regulation of folate receptor isoforms in normal and malignant tissues in vivo as in established cell lines-physiological and clinical applications. *Cancer 73,* 2432−2443.

(29) Weitman, S. D., Lark, R,. H., Coney, L. R., Fort, D. W., Frasca, V., Zurawski, V. R., Jr., and Kamen, B. A. (1992) Distribution of the folate receptor GP38 in normal and malignant cell lines and tissues. *Cancer Res. 52,* 3396−3401.

(30) Leamon, C. P., Pastan, I., and Low, P. S. (1993) Cytotoxicity of folate-Pseudomonas exotoxin conjugates towards tumor cells. Contribution of translocation domain. *J. Biol. Chem. 269,* 24847−24854.

(31) Wang, S., Luo, J., Lantrip, D. A., Waters, D. J., Mathias, C. J., Green, M. A., Fuchs, P., and Low, P. S. (1997) Design and synthesis of [^{111}In]DTPA-Folate for use as a tumor-targeted radiopharmaceutical. *Bioconjugate Chem. 8,* 673−679.

(32) Ringsdorf, H., Venzmer, J., and Winnik, F. M. (1991) Fluorescence studies of hydrophobically modified poly-(N-isopropylacrylamides). *Macromolecules 24,* 1678−1686.

(33) Krapcho, A. P., and Kuell, C. S. (1990) Monoprotected diamines. N-tert-Butoxycarbonyl-α,*ω*-alkanediamines from α,*ω*-alkanediamine. *Synth. Commun. 20,* 2559−2564.

(34) Reddy, J. A., and Low, P. S. (1998) Folate-mediated targeting of therapeutic and imaging agents to cancers. *Crit. Rev. Ther. Drug Carrier Syst. 15*, 587−627.
(35) Blakeslee, D. (1977) Immunofluorescence using trichlorotriazine-fluorescein (DTAF). *J. Immunol. Methods 17*, 361−364.
(36) Kuijpers, A. J., Engbers, G. H. M., Meyvis, T. K., de Smedt, S. S. C., Demeester, J., Krijgsveld, J., Zaat, S. A. J., Dankert, J., and Feijen, J. (2000) Combined gelatin-chondroitin sulfate hydrogels for controlled release of cationic antibacterial proteins. *Macromolecules 33*, 3705−3713.
(37) Mosmann, T. (1983) Rapid colorimetric assay for cellular growth and survival: Application to proliferation and cytotoxicity assays. *J. Immunol. Methods 65*, 55−63.
(38) Dubé, D. MSc Thesis, Université de Montréal (2001).
(39) Francis, M. F., Dhara, G., Winnik, F. M., and Leroux, J. C. (2001) In vitro evaluation of pH-sensitive polymer/niosome complexes. *Biomacromolecules 2*, 741−749.
(40) The number of folic acid groups per chain, estimated from the viscosity averaged molecular weight of the polymer and the UV-determined folic acid polymer content, is approximately 7.
(41) Lee, R. J., Wang, S., and Low, P. S. (1996) Measurement of endosome pH following receptor-mediated endocytosis. *Biochim. Biophys. Acta 1312*, 237−242.
(42) Reddy, J. A., and Low, P. S. (2000) Enhanced folate receptor mediated gene therapy using a novel pH-sensitive lipid formulation. *J. Control. Release 64*, 27−37.

BC010084G

Transition Metal−Carbonyl Labeling of Biotin and Avidin for Use in Solid-Phase Carbonyl Metallo Immunoassay (CMIA)

Michèle Salmain,[†] Nathalie Fischer-Durand,[†] Laure Cavalier,[†] Bogna Rudolf,[‡] Janusz Zakrzewski,[‡] and Gérard Jaouen[†,*]

Ecole Nationale Supérieure de Chimie de Paris, Laboratoire de Chimie et Biochimie des Complexes Moléculaires (UMR CNRS 7576), 11 rue Pierre et Marie Curie, 75231 Paris Cedex 05, France, and University of Lodz, Department of Organic Chemistry, 90-136 Lodz, Narutowicza 68, Poland. Received October 25, 2001; Revised Manuscript Received December 7, 2001

The preparation of several transition metal−carbonyl tracers of biotin and avidin is described. Multiple labeling of avidin was achieved by acylation of some of its amine-bearing residues with *N*-succinimidyl 4-pentynoate (dicobalt hexacarbonyl). By varying the initial amount of this complex, protein conjugates with the extent of derivatization of up to 13 were obtained. Biotin was labeled with one (η^5-cyclopentadienyl)manganese tricarbonyl moiety by reaction of biotin hydrazide, whereas multiple labeling was reached by successive conjugation of biotin and *N*-succinimidyl 4-pentynoate (dicobalt hexacarbonyl) or (η^5-cyclopentadienyl)iron dicarbonyl (η^1-*N*-maleimidato) to poly-L-lysine or fourth generation Starburst dendrimer. All the conjugates displayed a good to excellent bioaffinity toward their respective counterparts, as measured by competitive enzymatic assays.

INTRODUCTION

The biotin−avidin system is now widely exploited as a bioanalytical tool, particularly in immunoassays (*1*). It takes advantage of the exceptionally high affinity constant of the biotin−avidin association ($K_a = 1 \times 10^{15}$ M^{-1}) and the fact that biomacromolecules can be biotinylated without loss of activity. Furthermore, the protein avidin is a tetramer with four biotin binding sites arranged in two pairs on opposed faces of the molecule, allowing up to four biotinylated species to be bound to a single avidin molecule (*2*). The biotin−avidin system is particularly useful to mediate the binding of the reporter group (enzyme, fluorophore, etc.) to the antibody (*3*). The three basic designs are the labeled avidin−biotin (LAB)[1], the bridged avidin−biotin (BRAB), and the avidin−biotin complex (ABC) systems. These three systems allow the amplification of the detection signal in ELISA techniques as compared to the direct enzyme-antibody labeled methods (*4*).

Labeling of (strept)avidin and biotin with conventional reporter groups has been reported several times in the literature. Regarding (strept)avidin, most of the labeling methods involve their lysine residues (*5*), whereas biotin is exclusively derivatized from its carboxylic acid function with the addition of a spacer arm to enhance the efficiency of formation of the complex between the biotinylated molecule and avidin (*6*).

We have described an immunoassay method named Carbonyl Metallo ImmunoAssay (CMIA) that associates transition metal−carbonyl reporter groups and Fourier transform infrared (FTIR) spectroscopy as the detection method. The principle of this immunoassay consists so far in labeling the antigen (in our case a hapten) with a transition metal−carbonyl complex unit which is then involved in a competitive liquid-phase immunoassay with specific polyclonal antibodies and the analyte. Following extraction of the free fraction of tracer with an organic solvent, its amount is quantitated by taking advantage of the specific and intense absorption bands of the transition metal carbonyl complex unit in the mid-infrared spectral range (1800−2150 cm^{-1}). Assay of the major antiepileptic drugs and cortisol has been described (*7*−*10*). However, this format just described is unsuitable for the assay of high molecular weight molecules (antigens) and is not readily automated. Furthermore, most of the immunoassays are based on the immobilization of the capture system onto a solid-phase to facilitate separation steps. Among the most popular solid phases are 96-well microtiter plates made of plastic (polystyrene). These are compatible with colorimetric detection. Other plates (white or black) are well suited for fluorescence detection. We had tried to adapt polystyrene microtiter plates to direct IR transmission measurement of transition metal−carbonyl tracers but, even though this material presents a transmission window in the range of absorption of these tracers, the sensitivity of detection was far above the level suited for typical immunoassays (*11*). Thus, the need for signal amplification is obvious and the biotin−avidin system appears very attractive for this purpose as seen above. We have set about to synthesize transition metal−carbonyl derivatives of both biotin and avidin in view of using them in a solid-phase amplified CMIA based on the LAB, BRAB, or especially the ABC systems.

* To whom correspondence should be addressed. Telephone: +33 (0)1 44 27 66 97. Fax: +33 (0)1 43 26 00 61. e-mail: jaouen@ext.jussieu.fr.

[†] Ecole Nationale Supérieure de Chimie de Paris.

[‡] University of Lodz.

[1] Abbreviations used: LAB, labeled avidin−biotin; BRAB, bridged avidin−biotin; ABC, avidin−biotin complex; CMIA, Carbonyl Metallo Immunoassay; FTIR, Fourier transform infrared; PL, poly-L-lysine; Fp, (η^5-cyclopentadienyl)iron dicarbonyl; PAMAM, polyamidoamine; NAV, neutravidin ; TFE, 2,2,2-trifluoroethanol; TSTU, *N*,*N*,*N*′,*N*′-tetramethyl-(*O*)-(*N*-succinimidyl)uronium tetrafluoroborate.

10.1021/bc015570i CCC: $22.00 © 2002 American Chemical Society
Published on Web 03/21/2002

EXPERIMENTAL PROCEDURES

Materials. *N*-Succinimidyl 4-pentynoate (dicobalt hexacarbonyl) **1** was synthesized as previously described (*12*). Complex (η^5-cyclopentadienyl carboxaldehyde)manganese tricarbonyl **2** was synthesized as previously described (*13*). (η^5-cyclopentadienyl)iron dicarbonyl (η^1-*N*-maleimidato) **5** was synthesized according to a previously published procedure (*14*). Avidin, poly-L-lysine hydrobromide (PL, average molecular weight = 235 kDa, average polymerization degree = 1125), biotin, biotin hydrazide, horseradish peroxidase biotinamidocaproyl (HRP-biotin), 4′-hydroxyazobenzene-2-carboxylic acid (HABA) orthophenylene diamine (OPD) and *N*,*N*-diisopropylethylamine (DIPEA) were purchased from Sigma. PAMAM Starburst dendrimer fourth generation was purchased from Aldrich. Neutravidin (NAV) was purchased from Pierce Chemicals, *N*,*N*,*N*′,*N*′-tetramethyl-(*O*)-(*N*-succinimidyl)uronium tetrafluoroborate (TSTU) and 2,2,2-trifluoroethanol (TFE) were purchased from Fluka.

Instrumentation. ^{1}H NMR spectra were recorded on an AM 200 FT spectrometer (Bruker) operating at 200 MHz. Infrared spectra were recorded on an MB100 FT spectrometer equipped with an MCT detector. UV−visible spectra were recorded on an UV/mc^2 spectrometer (Safas). The ESI mass spectrum was recorded at the "Service de spectrométrie de masse" of the Université Pierre et Marie Curie, Paris, France.

Methods. *Preparation of Cymantrenyl Biotin Hydrazone **3**.* Biotin hydrazide (0.08 g, 0.3 mmol) was dissolved in 10 mL of TFE. Complex **2** (0.07 g, 0.32 mmol) was added to the mixture that was stirred 24 h at room temperature in the dark. The yellow-brown solution was concentrated under vacuum and chromatographed on an alumina column (50−160 μm particle diameter). Excess compound **2** was eluted with dichloromethane, and compound **3** was eluted with dichloromethane/methanol 3/2. After workup, 0.06 g of **3** was obtained as a brown solid (yield = 60%). ^{1}H NMR (methanol-d_4) δ in ppm/TMS 1.4−1.8 (m, 6H) -$(CH_2)_3$, 2.30 (t, 2H, 7.9 Hz) CH_2−CO, 2.71 (d, 1H, 12 Hz) CH_2−S, 2.94 (dd, 1H, 4.2 and 12 Hz) CH_2−S, 3.25 (br m, 1H) CH−S, 4.32 (m, 1H) CH, 4.50 (m, 1H) CH, 5.49 and 5.39 (s, 4H) Cp, 7.74 and 7.57 (s, 1H) CH=N. IR (KBr) ν in cm^{-1} 2020, 1935 $\nu_{C\equiv O}$, 1700 $\nu_{C=O}$. MS (MeOH) *m*/*z* 495 (M + Na), 357 (M + Na − Mn-$(CO)_3$)

*Preparation of Biotin−PL−Dicobalt Hexacarbonyl **4**.* A solution of biotin (0.11 mg/mL, 0.46 mM) in anhydrous DMF was treated with 1.1 mol equiv of DIPEA and TSTU. The mixture was stirred 2 h at room temperature. A solution of PL (1 mg/mL, 4.2 μM) was prepared in borate buffer pH 9.3. To 9 volumes of this solution was added 1 volume of the solution of activated biotin. In these conditions, the initial biotin-to-PL ratio was 12 (initial biotin/NH_2 functions = 0.01). This mixture was stirred overnight at room temperature. To 9 parts of this solution was added 1 part of a freshly prepared 14 mM solution of **1** in acetonitrile. In these conditions the initial **1** to PL ratio was 400 (initial **1** to NH_2 functions ratio = 0.35). The reaction mixture was stirred 14 h in the dark, centrifuged 30 min at 4000 rpm, and dialyzed in 2 L of PBS overnight at 4 °C to remove unreacted biotin and **1**.

*Preparation of Biotin−Dendrimer−Fp **6**.* Fourth generation PAMAM Starburst dendrimer (43 μL, 10% solution in MeOH) was added to a 0.01 M solution of the *N*-succinimidyl ester of biotin in DMF prepared as above (0.2 mL). The mixture was stirred 2 h at room temperature, 0.35 mL of a 0.04 M solution of compound **5** in methanol was added, and the mixture incubated 18 h at 35 °C. The solvent was evaporated under vacuum, and the residue was dissolved in 2 mL of water and washed with 10 mL of chloroform. The aqueous phase was passed on a 10-mL gel filtration column (Kwiksep dextran, Pierce chemicals), and the dendrimer conjugate was eluted with water.

Preparation of NAV−Dicobalt Hexacarbonyl Conjugate. A solution of neutravidin (2 mg/mL, 33 μM) was prepared in borate buffer pH 8.5. To 1 mL of this solution was added 0.05 mL of a 6.6 mM solution of **1** in acetonitrile. The initial **1**-to-protein ratio was 10. The reaction mixture was stirred 1 h at room temperature, centrifuged 10 min at 4000 rpm, and dialyzed overnight in 2 × 0.5 L of 25 mM HEPES buffer pH 7.4 containing 0.1% NaN_3 at 4 °C. This experiment was repeated with 13.2 or 19.8 mM solutions of **1** (20 and 30 mol equiv, respectively).

Analysis of the Conjugates. The concentration of accessible biotin fragments bound to **4** and **6** was assayed by the HABA dye assay (*15*). The concentration of dicobalt hexacarbonyl probes $[Co_2(CO)_6]_f$ bound to tracer **4** was assayed by FTIR at 2054 cm^{-1} (k = A/[**1**] = 39 M^{-1}) as previously described (*11*). The concentration of Fp (Fp = (η^5-cyclopentadienyl)iron dicarbonyl) probes bound to tracer **6** was measured spectroscopically at 370 nm (ϵ_{370} = 1000 M^{-1} cm^{-1}). The concentration of dendrimer residual amino groups was measured colorimetrically by the trinitrobenzene sulfonic acid assay (*16*). The concentration of neutravidin $[NAV]_f$ was assayed by the Coomassie Blue assay taking neutravidin solutions as standards (*17*).

*Competitive Binding Assay of **3**.* Standard solutions of biotin and **3** in PBS−1% BSA in the range 0−20 μM were applied to two series of Micronic tubes (0.4 mL per tube), and then 0.4 mL of a 10 ng/mL solution of HRP-biotin was added to each tube. A 0.2 mL amount of each solution was added in triplicate to streptavidin-coated polystyrene microtiter plates (Combiplate streptavidin, Labsystems). Plates were incubated 50 min at 4 °C in the dark and washed five times with PBS−0.05% Tween 20, and 0.2 mL of OPD solution (0.7 mg/mL in citrate buffer pH 5 + 0.16% H_2O_2 v/v) was added to the wells. After 20 min, the enzymatic reaction was stopped by 0.05 mL of 2.5 M H_2SO_4, and the absorbance at 490 nm was read with a microtiter plate reader (Biorad).

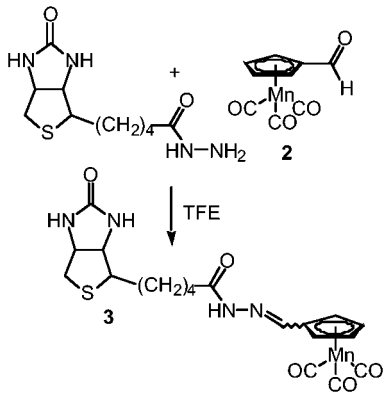
*Competitive Binding Assay of **4**.* The procedure was essentially the same as for **3** except that the streptavidin-coated plates were preincubated with a 10 μM solution of PL in PBS and that BSA was omitted in the incubation buffer.

Competitive Binding Assay of NAV−Dicobalt Hexacarbonyl Conjugate. A 0.1 mL amount of standard solutions of NAV or NAV conjugate in the range 0−1.8 μM made up in PBS−1% BSA was applied in duplicate to streptavidin-coated microtiter plates, followed by addition of HRP−biotin (0.1 mL of a 10 ng/mL solution). Plates were incubated 50 min at 4 °C in the dark. Washing and revelation steps were similar as above.

RESULTS AND DISCUSSION

Several synthetic pathways were tried to prepare a transition metal−carbonyl tracer of biotin. First, commercially available biotin hydrazide was added to a solution of compound **1** in TFE, a powerful solvent to dissolve both biotin hydrazide and **1**. No coupling adduct was formed as monitored by reverse phase HPLC and addition of activators such as 1-hydroxybenzotriazole

Scheme 1. Synthesis of Biotin Tracer 3

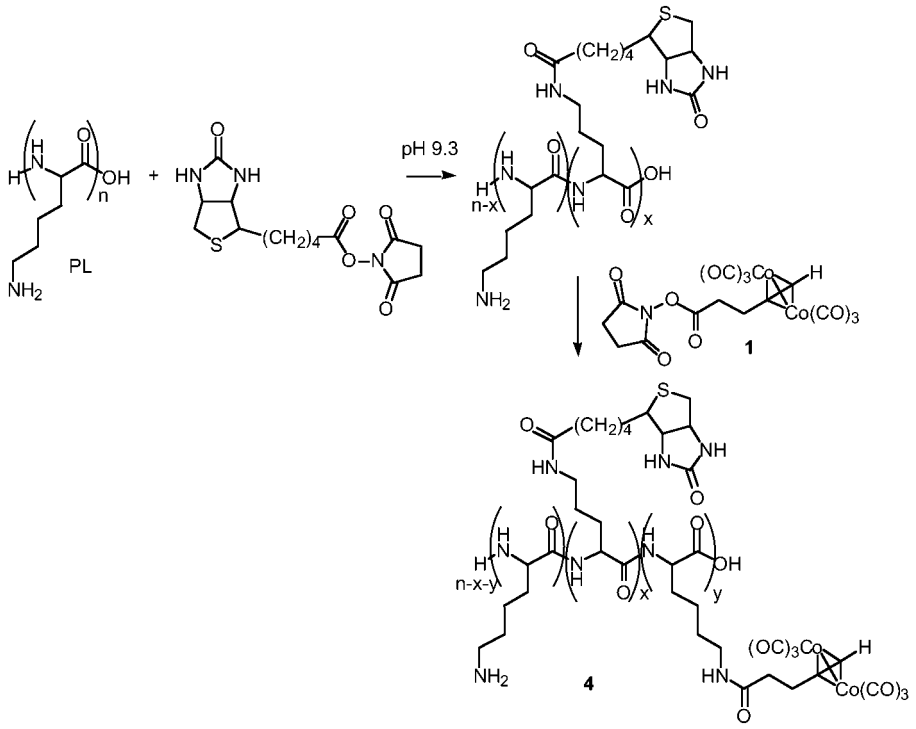


and/or DIPEA had no effect on the reaction. Instead, degradation of the activated ester was observed at length. It was concluded that the *N*-succinimidyl ester **1** was not reactive enough to acylate biotin hydrazide, conversely to the *N*-succinimidyl ester of cortisol 3-(*O*)carboxymethyl)oxime (*18*). As biotin hydrazide is a common reagent to biotinylate antibodies through their oxidized carbohydrate sites, we decided to use (η^5-cyclopentadienyl carboxaldehyde) manganese tricarbonyl **2** as transition metal−carbonyl labeling agent. Biotin hydrazide was allowed to react with a slight excess of **2** in TFE and after purification by chromatography on alumina, the hydrazone **3** was obtained in 60% yield (Scheme 1). ^{1}H NMR analysis of **3** showed two singlets at 7.57 and 7.74 ppm for the CH of the hydrazone, indicating that this compound was a mixture of two stereoisomers of the *E* and *Z* configurations at the C−N double bond. IR spectroscopy of **3** showed the presence of two intense $\nu_{C\equiv O}$ bands at 2020 and 1935 cm^{-1}, which are characteristic of the (η^5-cyclopentadienyl) manganese tricarbonyl moiety.

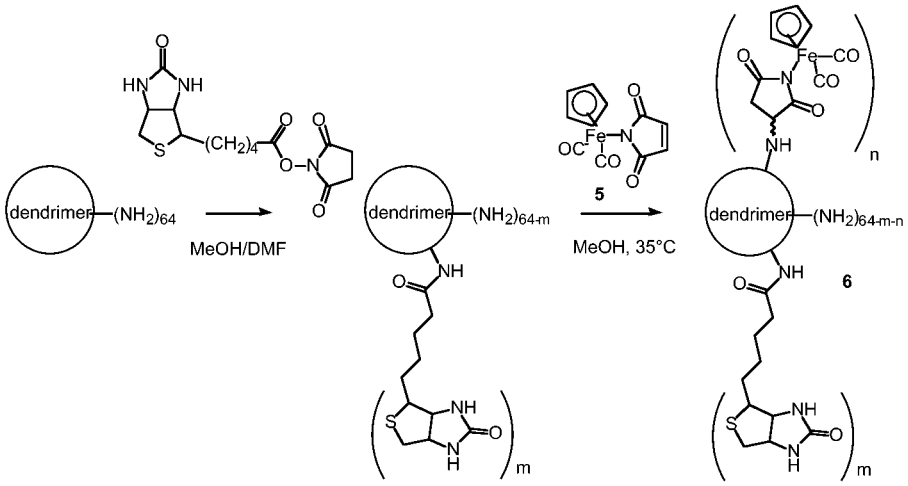
One way to amplify the IR signal of the biotin tracer would be to attach several transition metal−carbonyl units to it. As biotin is a small molecule with few functions, it is not straightforward. Nevertheless, some authors suggested use of poly-L-lysine (PL) to covalently bind both biotin and the reporter groups with a chosen ratio (*19, 20*). Other hapten tracers have been prepared in this manner (*21*−*23*). High molecular weight polypeptides and polyvinylamine have also been used in this purpose (*24*−*27*). We applied this principle to synthesize in a one-pot procedure the biotin tracer **4** with a favorable biotin to transition metal−carbonyl label ratio, as illustrated in Scheme 2. PL of average polymerization degree of 1125 was first reacted with a 12 molar excess of biotin *N*-succinimidyl ester in aqueous buffer at pH 9.3 and then with a molar ratio of **1** to PL of 400. The PL conjugate **4** was purified by extensive dialysis in phosphate buffer to remove any unbound or loosely bound biotin and transition metal−carbonyl complex. The concentration of biotin bound to PL was measured by the HABA dye assay and the concentration of bound transition metal−carbonyl units by IR spectroscopy. The calculated final label-to-biotin ratio *y*/*x* was 115. This tracer is characterized by the presence of 3 intense $\nu_{C\equiv O}$ bands at 2094, 2050, 2018 cm^{-1} (KBr pellet).

Full generation PAMAM Starburst dendrimers are another type of molecule with a high content of primary amine functional groups. For example, the commercially available fourth generation PAMAM dendrimer has a total of 64 surface amine groups for conjugation to biotin and a suitable transition metal−carbonyl reagent. The synthesis of the biotin−dendrimer−Fp conjugate **6** was achieved by first reacting fourth generation Starburst dendrimer with biotin *N*-succinimidyl ester followed by reaction with maleimide **5** at 35 °C (Scheme 3). Indeed we have previously shown that alkylation of **5** by amines occurred at basic pH and high temperature (*28*). The dendrimer conjugate **6** was purified by aqueous gel filtration chromatography and its homogeneity proved by reverse phase HPLC. Spectroscopic measurements indicated that **6** contained 45 Fp groups, 4 biotin entities, and 15 residual amine functions. Therefore, the Fp-to-biotin ratio *m*/*n* was found equal to ca. 11. This tracer is

Scheme 2. Synthesis of Biotin Tracer 4



Scheme 3. Preparation of Biotin Tracer 6



Scheme 4. Synthesis of Neutravidin−Dicobalt Hexacarbonyl Conjugates.

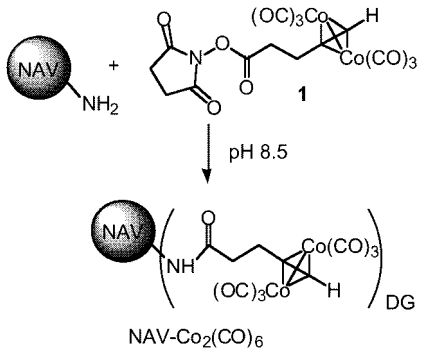


Table 1. Labeling of NAV with Complex 1

initial NAV-to-**1** ratio	$[NAV]_f$ (μM)[a]	$[Co_2(CO)_6]_f$ (μM)[b]	DG[c]	yield, %
10	23.3	175	7.5	75
20	30.8	308	10.0	50
30	31.9	432	13.5	45

[a] The protein concentration $[NAV]_f$ was measured by the Coomassie blue assay. [b] The concentration of transition metal−carbonyl units $[Co_2(CO)_6]_f$ was measured by IR spectroscopy at 2054 cm^{-1} by deposition of 10 μL samples on nylon membranes and subsequent air drying ($[Co_2(CO)_6]_f = A_{2054}/39$). [c] Degree of conjugation DG = $[Co_2(CO)_6]_f/[Nav]_f$ of the protein conjugates.

characterized by the presence of two intense $\nu_{C\equiv O}$ bands at 2050 and 2000 cm^{-1}.

Labeling of neutravidin (NAV), a commercially available deglycosylated form of avidin with an isoelectric point of 6.3 ± 0.3 with transition metal−carbonyl units was also achieved by reacting the protein in borate buffer pH 8.5 with compound **1** (Scheme 4). The initial ratio between metal−carbonyl complex **1** and NAV was varied from 10 to 30 in a similar manner as previously described (*11*). After 1 h, the protein conjugates were purified by gel filtration chromatography and analyzed by spectroscopic methods to measure their degree of conjugation DG = $[Co_2(CO)_6]_f/[NAV]_f$. Results are summarized in Table 1.

Thus, chemical modification of NAV by complex **1** allowed a maximum of ca. 13 transition metal−carbonyl units to be covalently bound to the protein molecule. We suspect that higher degrees of conjugation are not reachable because some binding sites (i.e. lysine residues) may be more sterically demanding or highly derivatized conjugates may become insoluble in aqueous medium.

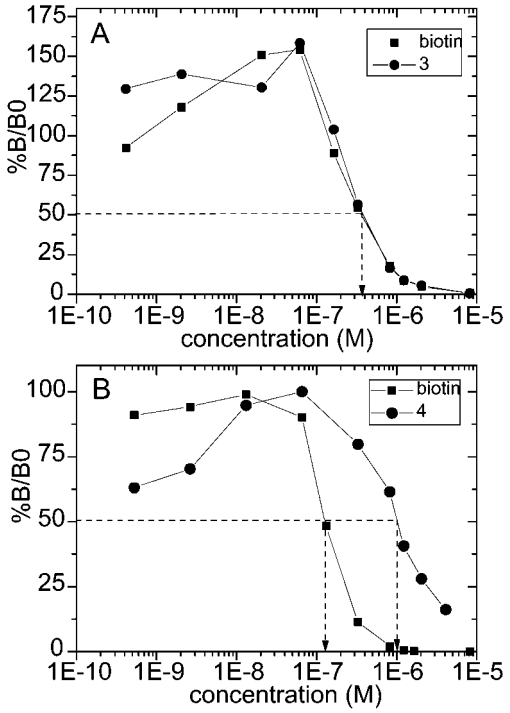


Figure 1. Competitive binding assay of biotin tracers. A. **3**. B. **4**.

The avidin tetramer contains 32 lysine residues (+ 4 N-terminal sites), i.e., a total of 36 potential sites for covalent binding of **1**. These amines are all located at the surface of the protein and away from the biotin binding sites as seen from the X-ray structure of the avidin/biotin complex (*29*). Thus the second explanation is the most probable, as we have observed protein precipitation at length.

To assess the usefulness of such transition metal−carbonyl tracers in bioassays, we performed competitive enzymatic binding assays using commercially available streptavidin-coated microtiter plates and HRP−biotin as tracer. For biotin metal−carbonyl conjugates, the assay consisted of competing biotin or biotin conjugate with HRP−biotin for the binding to immobilized streptavidin (Figure 1). For the NAV−$Co_2(CO)_6$ conjugate with a degree of conjugation of 10, the assay consisted in the competition between NAV or NAV−$Co_2(CO)_6$ conjugate and immobilized streptavidin for the binding of HRP−biotin (Figure 2). The amount of surface bound HRP−

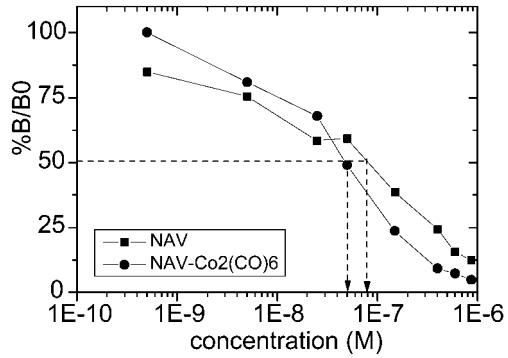


Figure 2. Competitive binding assay of neutravidin−dicobalt hexacarbonyl conjugate.

biotin was quantified with OPD/H_2O_2 as substrates. In the conditions of assay, the IC_{50} of NAV was 0.05 mM while that of the NAV−$Co_2(CO)_6$ conjugate was 0.085 μM. The conjugation of 10 transition metal−carbonyl entities altered very slightly the molecular recognition of the NAV conjugate by HRP−biotin. On the other hand, biotin and biotin tracer **3** had identical IC_{50} (0.4 μM in the assay), indicating that the conjugation of the (η^5-cyclopentadienyl) manganese tricarbonyl to the hydrazide function of biotin hydrazide did not alter in the least its binding affinity to streptavidin. Conversely, the polymeric tracer **4** had an IC_{50} eight times higher than that of biotin (IC_{50} = 1 μM versus 0.13 μM in the assay). Two factors may be put forward to explain this discrepancy. Either covalent binding of biotin to PL decreased its affinity toward streptavidin or not all biotin molecules are accessible for binding to immobilized streptavidin because of steric hindrance. The latter explanation seems more plausible so we anticipate that one biotin out of eight is accessible to binding to immobilized streptavidin.

In conclusion, we have prepared and characterized three transition metal−carbonyl labeled biotin tracers and several avidin conjugates. These tracers were shown to display good to excellent bioactivities toward streptavidin and biotin, respectively. Amplification of the IR signal is anticipated for the conjugates with a favorable reporter group-to-ligand ratio (10-to-1 for neutravidin, 115-to-1 or 11-to-1 for biotin), as no quenching occurs for IR detection. Their use in a solid-phase CMIA is under way, as we have recently shown that the binding of a NAV−$Co_2(CO)_6$ conjugate to self-assembled monolayers of biotin molecules on gold substrates could be successfully transduced by FT-IR spectroscopy in the reflection−absorption mode (*30, 31*).

ACKNOWLEDGMENT

The Centre National de la Recherche Scientifique is gratefully acknowledged for its financial support. This research was in part supported by the Polish State Committee for scientific research (Grant PZB-KBN-15/T09/99). The French-Polish exchange program "Polonium" is also gratefully acknowledged for travels funding.

LITERATURE CITED

(1) Diamandis, E. P., and Christopoulos, T. K. (1991) The biotin-(strept)avidin system: principles and applications in biotechnology. *Clin. Chem. 37*, 625−636.

(2) Green, N. M. (1990) Avidin and streptavidin. *Methods Enzymol. 184*, 51−67.

(3) Christopoulos, T. K., and Diamandis, E. P. (1996) Immunoassay configurations. *Immunoassay* (T. K. Christopoulos, and E. P. Diamandis, Eds.) pp 227−236, Academic Press, San Diego, CA.

(4) Bayer, E. A., and Wilchek, M. (1996) The avidin−biotin system. *Immunoassay* (T. K. Christopoulos, and E. P. Diamandis, Eds.) pp 237−267, Academic Press, San Diego, CA.

(5) Haugland, R. P., and Bhalgat, M. K. (1998) Preparation of avidin conjugates. *Methods Mol. Biol. 80*, 185−196.

(6) Haugland, R. P., and You, W. W. (1998) Coupling of antibodies with biotin. *Methods Mol. Biol. 80*, 173−183.

(7) Salmain, M., Vessières, A., Brossier, P., Butler, I. S., and Jaouen, G. (1992) Carbonylmetalloimmunoassay (CMIA) a new type of nonradioisotopic immunoassay. Principles and application to phenobarbital assay. *J. Immunol. Methods 148*, 65−75.

(8) Philomin, V., Vessieres, A., and Jaouen, G. (1994) New applications of carbonylmetalloimmunoassay (CMIA): a non-radioisotopic approach to cortisol assay. *J. Immunol. Methods 171*, 201−210.

(9) Varenne, A., Vessières, A., Salmain, M., Brossier, P., and Jaouen, G. (1995) Production of specific antibodies and development of a nonisotopic immunoassay for carbamazepine by the carbonylmetallo-immunoassay (CMIA) method. *J. Immunol. Methods 186*, 195−204.

(10) Vessières, A., Kowalski, K., Zakrzewski, J., Stepien, A., Grabowski, M., and Jaouen, G. (1999) Synthesis of CpFe(CO)-(L) complexes of hydantoin anions (Cp = eta5-C_5H_5, L = CO, PPh_3), and the use of the 5,5-diphenylhydantoin anion complexes as tracers in the nonisotopic immunoassay CMIA of this antiepileptic drug. *Bioconjugate Chem. 10*, 379−385.

(11) Varenne, A., Salmain, M., Brisson, C., and Jaouen, G. (1992) Transition metal carbonyl labeling of proteins. A novel approach to a solid-phase two-site immunoassay using Fourier transform infrared spectroscopy. *Bioconjugate Chem. 3*, 471−476.

(12) Salmain, M., Vessières, A., Butler, I., and Jaouen, G. (1991) N-Succinimidyl (4-pentynoate)hexacarbonyldicobalt: a transition-metal carbonyl complex having similar uses to the Bolton−Hunter reagent. *Bioconjugate Chem. 2*, 13−15.

(13) Kolobova, N. E., Valueva, Z. P., and Solodova, M. Y. (1980) *Izv. Akad. Nauk SSSR, Ser. Khim.*, 2387−2391.

(14) Rudolf, B., and Zakrzewski, J. (1994) *Tetrahedron Lett. 35*, 9611.

(15) Hermanson, G. T. (1996) *Bioconjugate techniques*. Academic Press, San Diego, CA.

(16) Sashidhar, R. B., Capoor, A. K., and Ramana, D. (1994) Quantitation of e-amino group using amino acids as reference standards by trinitrobenzene sulfonic acid. *J. Immunol. Methods 164*, 121−127.

(17) Bradford, M. M. (1976) A rapid and sensitive method for the quantitation of microgram quantities of protein utilizing the principle of protein-dye binding. *Anal. Biochem. 72*, 248−254.

(18) Dressendorfer, R. A., Kirschbaum, C., Rohde, W., Stahl, F., and Strasburger, C. J. (1992) Synthesis of a cortisol-biotin conjugate and evaluation as a tracer in an immunoassay for salivary cortisol measurement. *J. Steroid Biochem. Mol. Biol. 43*, 683−692.

(19) del Rosario, R. B., and Wahl, R. L. (1993) Biotinylated iodopolylysine for pretargeted radiation delivery. *J. Nucl. Med. 34*, 1147−1151.

(20) Torchilin, V. P. (1999) Biotin-conjugated polychelating agent. *Bioconjugate Chem. 10*, 146−149.

(21) Luke, F. J., and Schlegel, W. (1990) A time-resolved fluoroimmunoassay for the determination of prostaglandin F2 alpha. *Clin. Chim. Acta 189*, 257−265.

(22) Claassen, E., and Van Rooijen, N. (1985) A trinitrophenyl (TNP)-poly-L-lysine-horseradish peroxidase conjugate for the detection of anti-TNP antibodies in vivo. *J. Histochem. Cytochem. 33*, 840−844.

(23) Gonzalez, R. R., Maentausta, O., Solyom, J., and Vihko, R. (1990) Direct solid-phase time-resolved fluoroimmunoassay of 17 alpha-hydroxyprogesterone in serum and dried blood spots on filter paper. *Clin. Chem. 36*, 1667−1672.

(24) Baxter, A. B., Melnikoff, S., Stites, D. P., and Brasch, R. C. (1991) AUR Memorial Award 1991. Immunogenicity of gadolinium-based contrast agents for magnetic resonance

imaging. Induction and characterization of antibodies in animals. *Invest. Radiol. 26*, 1035−1040.
(25) Qin, Q. P., Lovgren, T., and Pettersson, K. (2001) Development of highly fluorescent detection reagents for the construction of ultrasensitive immunoassays. *Anal. Chem. 73*, 1521−1529.
(26) Trubetskoy, V. S., and Torchilin, V. P. (1995) Fast and specific labeling of antibody fragments with multiple atoms of heavy metal radioisotopes. *Anal. Biochem. 229*, 345−347.
(27) Lamture, J. B., and Wensel, T. G. (1995) Intensely luminescent immunoreactive conjugates of proteins and dipicolinate-based polymeric Tb(III) chelates. *Bioconjugate Chem. 6*, 88−92.
(28) Rudolf, B., Zakrzewski, J., Salmain, M., and Jaouen, G. (1998) Metallo-carbonyl complexes based on the $CpFe(CO)_2$-(η^1-*N*-imidato) system as protein labeling reagents: reactivity and selectivity studies using bovine serum albumin as a model protein. *New J. Chem.*, 813−818.
(29) Pugliese, L., Coda, A., Malcovati, M., and Bolognesi, M. (1993) Three-dimensional structure of the tetragonal crystal form of egg-white avidin in its functional complex with biotin at 2.7 A resolution. *J. Mol. Biol. 231*, 698−710.
(30) Pradier, C.-M., Salmain, M., Zheng, L., and Jaouen, G. (accepted) Specific binding of avidin to biotin immobilised on modified gold surfaces: Fourier transform infrared reflection absorption spectroscopy (FT-IRRAS) analysis. *Surf. Sci.*
(31) Yam, C.-M., Pradier, C.-M., Salmain, M., Fischer-Durand, N. and Jaouen, G. (2002) Molecular recognition of avidin on biotin-functionalized gold surfaces detected by FT-IRRAS and use of metal−carbonyl probes. *J. Coll. Interface Sci. 245*, 204−207.

JULY/AUGUST 2002
Volume 13, Number 4

© Copyright 2002 by the American Chemical Society

Bioconjugate Chemistry

ARTICLES

Novel Cyanine Dye-Labeled Dideoxynucleoside Triphosphates for DNA Sequencing

R. Scott Duthie, Inta M. Kalve,† Sui Bi Samols,‡ Scott Hamilton, Inna Livshin,‡ Mahesh Khot, Satyam Nampalli, Shiv Kumar,* and Carl W. Fuller*

Amersham Biosciences, 800 Centennial Avenue, Piscataway, New Jersey 08855. Received June 27, 2001; Revised Manuscript Received March 24, 2002

Single color cyanine dye-labeled (Cy 5.0 and Cy 5.5) dideoxynucleoside-5′-triphosphates, or 'terminators', containing different spacer lengths were synthesized and evaluated for efficacy in DNA sequencing methods using a modified thermally stable DNA polymerase. The single color cyanine dye terminators were formulated into two separate sets of sequencing mixes, one for Cy 5.0 and the other for Cy 5.5, and evaluated on different automated sequencing platforms. Each set of mixes included two pyrimidine terminators with 17-atom linkers and two purine terminators with 10-atom linkers between the dye and the nucleotide. The two sets of cyanine dye-labeled terminators chosen for this cycle sequencing study produced improved band patterns with band uniformity similar to that obtained with dye-primer sequencing methods.

INTRODUCTION

Fluorescent sequencing was first reported using dye-labeled primers (*1*), but methods using dye-labeled dideoxynucleoside triphosphates (ddNTPs; terminators) (*2*, *5*) have also gained acceptance in recent years. The advantage of using dye-labeled ddNTPs instead of labeled primers is that only properly terminated fragments are labeled (*2*). Strong stops associated with polymerase pausing or falling off the template without proper termination of the nascent DNA strand is not seen. Use of dye-labeled ddNTPs in automated sequencing has helped reduce the need to resequence problematic areas where polymerase stops are prevalent. Additionally, synthesis of labeled, specific primers is not required for the sequencing reactions. One major weakness of using dye-labeled terminators is the unevenness of the resulting sequencing peak heights or areas with cycle sequencing methods (*4*−*6*).

Most of the fluorescent dyes used for dye-terminator DNA sequencing have been applied to the four-color instruments of Applied Biosystems and E. I. Du Pont (*2*, *5*). These instruments have 488 nm lasers, so the dyes were all chosen for excitation at this wavelength. Most of these dyes have been either fluorescein or rhodamine derivatives. Since the instruments must distinguish four colors of fluorescence at once, there have even been attempts to use fluorescence energy transfer to obtain efficient four-color sets of dyes that can all be excited at 488 nm (*7*−*9*). These approaches have required the use

* To whom correspondence should be addressed. Fax: (732) 457-8353, E-mail: carl.fuller@am.amershambiosciences.com or shiv.kumar@am.amershambiosciences.com.

† Present address: Pel-Freez Clinical Systems, LLC, 9099 N. Deerbrook Trail, Brown Deer, WI 53223.

‡ Present address: USB Corporation, 26111 Miles Rd., Cleveland, OH 44128.

10.1021/bc015522y CCC: $22.00 © 2002 American Chemical Society
Published on Web 06/26/2002

of complex, multiccolor optics for fluorescence detection. The use of fluorescein and rhodamine dyes has also been limited by their extinction coefficients (approximately 80000 M^{-1} cm^{-1}). Furthermore, it is desirable to use longer wavelength light for excitation because background fluorescence is considerably lower with 635 or 675 nm excitation than it is with 488 nm excitation (*12*−*14*).

We have instead focused on the use of simpler, single-color instruments, such as ALFexpress and SEQ4X4 (Amersham Biosciences, Piscataway, NJ) and Clipper and Long-Read Tower (Visible Genetics, Toronto, Canada). These instruments use inexpensive 635 and 675 nm lasers, which are ideally suitable for excitation of the cyanine dyes—Cy 5.0 and Cy 5.5 (*12*). While these instruments require 2−4 lanes for determination of a single DNA sequence, they are much simpler and less expensive than the four-color instruments that need only a single lane per sequence. Additionally, the cyanine dyes have significantly higher extinction coefficients (250000 M^{-1} cm^{-1}) than the fluorescein and rhodamine dyes, so they act as more efficient collectors of the excitation light.

To produce fully functional sets of cyanine-labeled dideoxynucleotides, a number of criteria had to be met. Preliminary experiments indicated that direct coupling of the cyanine dye NHS esters with simple propargylamino-modified pyrimidine nucleotides resulted in dye-labeled nucleotides that were relatively poor substrates for DNA polymerases. In addition, dyes with different charges resulted in labeled fragments that had widely differing mobilities upon electrophoresis through gels. After considerable experimentation with many combinations of dyes, linkers and nucleotides (*10*, *11*), we have come up with two optimal sets of novel labeled dideoxynucleotides for DNA sequencing on single-color instruments (vide supra). Herein, we describe these two sets of dye-labeled terminators and show their performance with Thermo Sequenase DNA polymerase (*15*, *16*) as monitored using the single-color sequencing instruments. These sequences have remarkably even band intensities for dye-terminator sequencing methods (*18*). In fact, they rival better dye-primer sequences for high data quality.

MATERIALS AND METHODS

The following reagents were obtained from Amersham Biosciences: Thermo Sequenase DNA polymerase, M13mp18(+) strand DNA, four-color dye terminators, HLA DRB*plus* Typing Kit, GFX PCR DNA and Gel Band Purification Kit.

Genomic DNA from immortalized B-lymphocyte cell lines AMAI and WT51 was obtained from ProtoProbe, Inc., Milwaukee, WI.

Synthesis of Dye-Labeled ddNTPs. The propargylamino dideoxy nucleotides **1**−**6** (Scheme 1), required for synthesis of Cy 5.5 and Cy 5.0 conjugates **7**−**14** (Scheme 2), were prepared following the procedure described by Hobbs and Cocuzza (*3*). Cy 5.5- and Cy 5.0-NHS esters used in these conjugation reactions were purchased from Amersham Biosciences (Piscataway, NJ). Preceding the name of each ddNTP are numbers which denote how many atoms are between the dye moiety and the attachment site on the base, either the C5 position of pyrimidines or the C5 position of pyrrolopyrimidines. Yields of the dye−nucleotide conjugates were determined by UV−vis spectrophotometer readings in TE buffer, pH 7.5, using a λ_{max} of 648 nm for Cy 5.0 conjugates (ϵ = 250000 M^{-1} cm^{-1}) or 675 nm for Cy 5.5 conjugates (ϵ = 250000 M^{-1} cm^{-1}). The formula for this determination was the following:

Concentration = (absorbance at either λ_{648} for Cy 5.0 or λ_{675} for Cy 5.5 ÷ extinction coefficient of 250000)-(dilution factor). Micro Mass LCT was used to analyze the dye−nucleotide terminators.

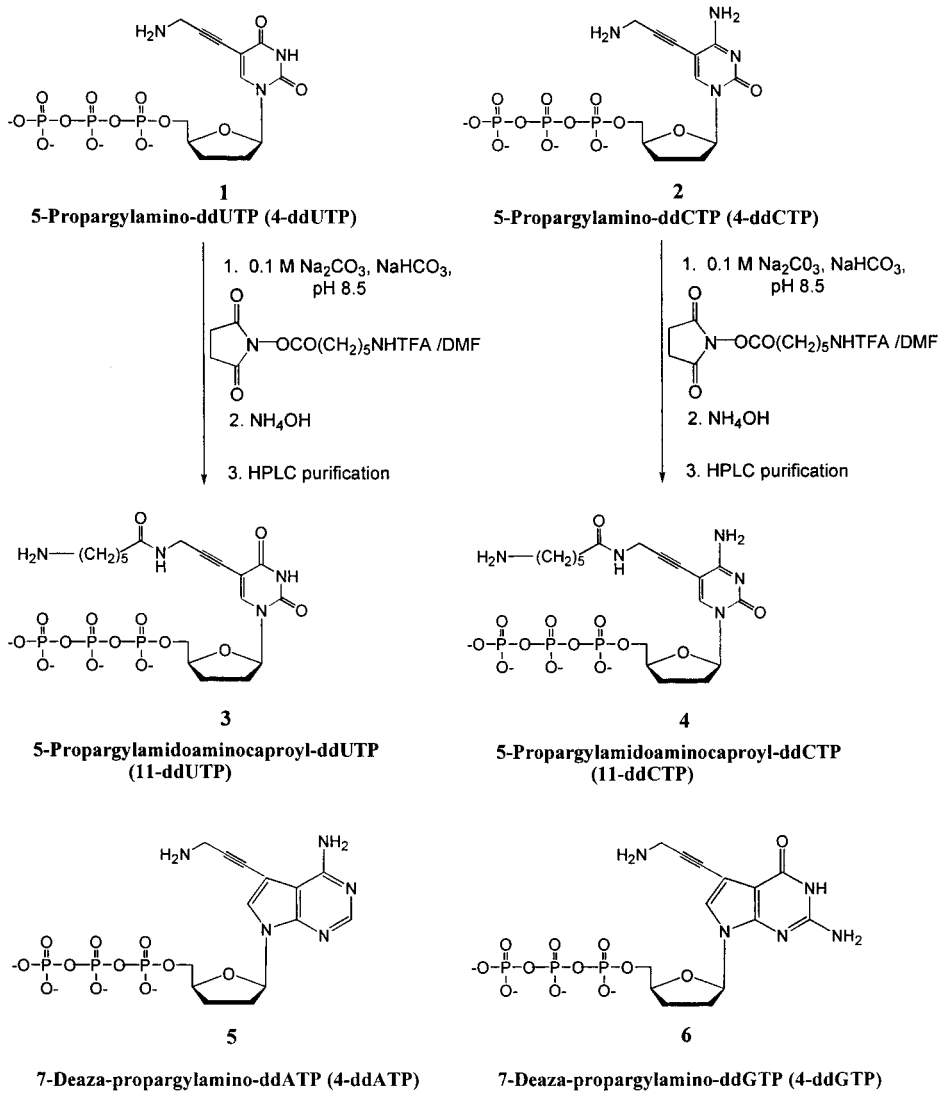
Synthesis of 11-ddUTP (3) 11-ddCTP (4). A 50 mg (63 μmol) amount of 5-propargylamino-ddUTP (4-ddUTP, **1**) (*10*) or 5-propargylamino-ddCTP (4-ddCTP, **2**) in 3 mL of 0.1 M Na_2CO_3−$NaHCO_3$ (pH 8.5) was stirred individually at room temperature with 2.5 equiv of N-TFA-aminocaproic acid-NHS ester (51 mg; 160 μmol) in 1 mL of anhydrous DMF. After 1 h of stirring, the solutions were evaporated under reduced pressure. The resulting residues were treated with 5 mL of 30% aqueous NH_4OH for 2 h at RT to remove the TFA group and then dried as before. The products were purified by HPLC using a Delta Pak (Waters) C18 column (5 cm × 30 cm, 15 μm, 100 Å) eluted with a gradient of 0.1 M TEAB (buffer A, pH 7.0) and 3:1 0.1 M TEAB:CH_3CN (buffer B, pH 7.0) in 30 min with a flow rate of 130 mL/min. Identical fractions were pooled and evaporated under reduced pressure to obtain 11-ddUTP, **3** (40 mg, 70%), and 11-ddCTP, **4** (30 mg, 52%).

Conjugation of 11-ddUTP (3) with Cy 5.5-NHS ester: Formation of Cy 5.5−17-ddUTP (7, Scheme 2). To a magnetically stirred solution of 11-ddUTP (12 μmol) in 0.1 M Na_2CO_3−$NaHCO_3$ (1 mL, pH 8.5) at room temperature was added 1 mL of an anhydrous DMF solution of Cy 5.5-NHS ester (20 mg, 18 μmol, 1.6 equiv). After 1 h, the reaction mixture was evaporated under reduced pressure and the product purified by silica gel column (32 cm × 2 cm) chromatography. Excess dye and unwanted byproducts were eluted with 1:1 MeOH/$CHCl_3$ (3 × 30 mL) followed by neat MeOH (2 × 30 mL). The desired Cy 5.5−17-ddUTP (**7**) was then eluted with 6:3:1 iso-PrOH:NH_4OH:H_2O (4 × 40 mL). Identical fractions were pooled and evaporated, and the resulting residue was further purified by HPLC using a Delta Pak (Waters) C18 column (19 mm × 30 cm, 15 μm, 100 Å) using a gradient of 0.1 M TEAB (buffer A, pH 7.0) and 1:1 0.1 M TEAB:CH_3CN (buffer B, pH 7.0) in 30 min at a flow rate of 20 mL/min. The HPLC retention time for this compound was 19 min. Identical fractions were pooled and evaporated under reduced pressure to obtain 4.36 μmol (39%) of Cy 5.5−17-ddUTP (**7**). TOF MS ES-, *m*/*z* in water, MS 1516.25, observed M^{-1} 1515.24.

Synthesis of Cyanine Dye−Nucleotide Conjugates (Scheme 2). Following the same methods used for Cy 5.5−17-ddUTP, syntheses of Cy 5.5−17-ddCTP (**8**), Cy 5.5−10-ddATP (**9**), and Cy 5.5−10-ddGTP (**10**) were accomplished with yields ranging from 30 to 45%. HPLC retention times for these compounds were 19, 22, and 23 min, respectively. **8**: TOF MS ES-, *m*/*z* in water, MS 1515.26, observed M^{-1} 1514.25; **9**: TOF MS ES-, *m*/*z* in water, MS 1425.19, observed M^{-1} 1424.19; **10**: TOF MS ES-, *m*/*z* in water, MS 1441.19, observed M^{-1} 1440.18.

Nucleotide derivatives 11-ddUTP, 11-ddCTP, 4-ddATP, and 4-ddGTP were also conjugated with Cy 5-NHS ester to synthesize their conjugates, Cy 5.0−17-ddUTP (**11**), Cy 5.0−17-ddCTP (**12**), Cy 5.0−10-ddATP (**13**), and Cy 5.0−10-ddGTP (**14**). Yields from these reactions were in the range of 30−50%. HPLC retention times for these compounds were 20, 7, 9, and 10 min, respectively. **11**: TOF MS ES-, *m*/*z* in water, MS 1256.30, observed M^{-1} 1255.29; **12**: TOF MS ES-, *m*/*z* in water, MS 1255.32, observed M^{-1} 1254.31; **13**: TOF MS ES-, *m*/*z* in water,

Scheme 1. Synthesis of 5-Propargylamidoaminocaproic-ddUTP (11-ddUTP) and 5-Propargylamidoaminocaproic-ddCTP (11-ddCTP)



MS 1165.25, observed M^{-1} 1164.24; **14**: TOF MS ES-, *m*/*z* in water, MS 1181.24, observed M^{-1} 1180.24.

Polymerase Chain Reactions. Typical reaction volumes were 25−50 μL containing 15 mM Tris-HCl, pH, 8.3, 200 μM each dATP, dCTP, dGTP, and dTTP (Amersham Biosciences), 1.5−2.5 units of *Taq* DNA polymerase (Amersham Biosciences), 1−200 ng of template, and 1−10 pmol of primers. Typical thermal cycling conditions consisted of a 1−2 min initial heat denaturation step at 95 °C and then 25−30 cycles, each consisting of the following steps:

95 °C for 30 s, 45− 60 °C for 30 s, 72 °C for 120 s. Reactions were held at 4 °C once thermal cycling had been completed. PCR products were purified using GFX PCR DNA and Gel Band Purification Kit.

Sequencing Reactions. The basic procedure involved mixing 10−20 units of Thermo Sequenase DNA polymerase, 1−10 pmol of primer, 50−500 ng of template, deoxynucleoside triphosphates (dNTPs; Amersham Biosciences), and a specific dye-labeled ddNTP in a total volume of 6−8 μL. Four separate reactions were required to sequence a template, each reaction containing a different dye-labeled ddNTP. Reactions were subjected to a thermal cycling protocol followed by postreaction workup of the cyanine dye terminator-labeled Sanger fragments by either ethanol precipitation or column chromatography. Purified products were then analyzed on an automated DNA sequencing instrument. A typical Cy 5.0 dye-labeled terminator sequencing reaction contained the following mixture:

14.6 mM Tris-HCl, pH 9.5; 3.4 mM $MgCl_2$; 150 μM each of dATP, dCTP, dGTP, and dTTP; and either 0.2 μM Cy 5.0−10-ddATP, 0.16 μM Cy 5.0−17-ddCTP, 0.4 μM Cy 5.0−10 ddGTP, or 0.325 μM Cy 5.0−17-ddUTP.

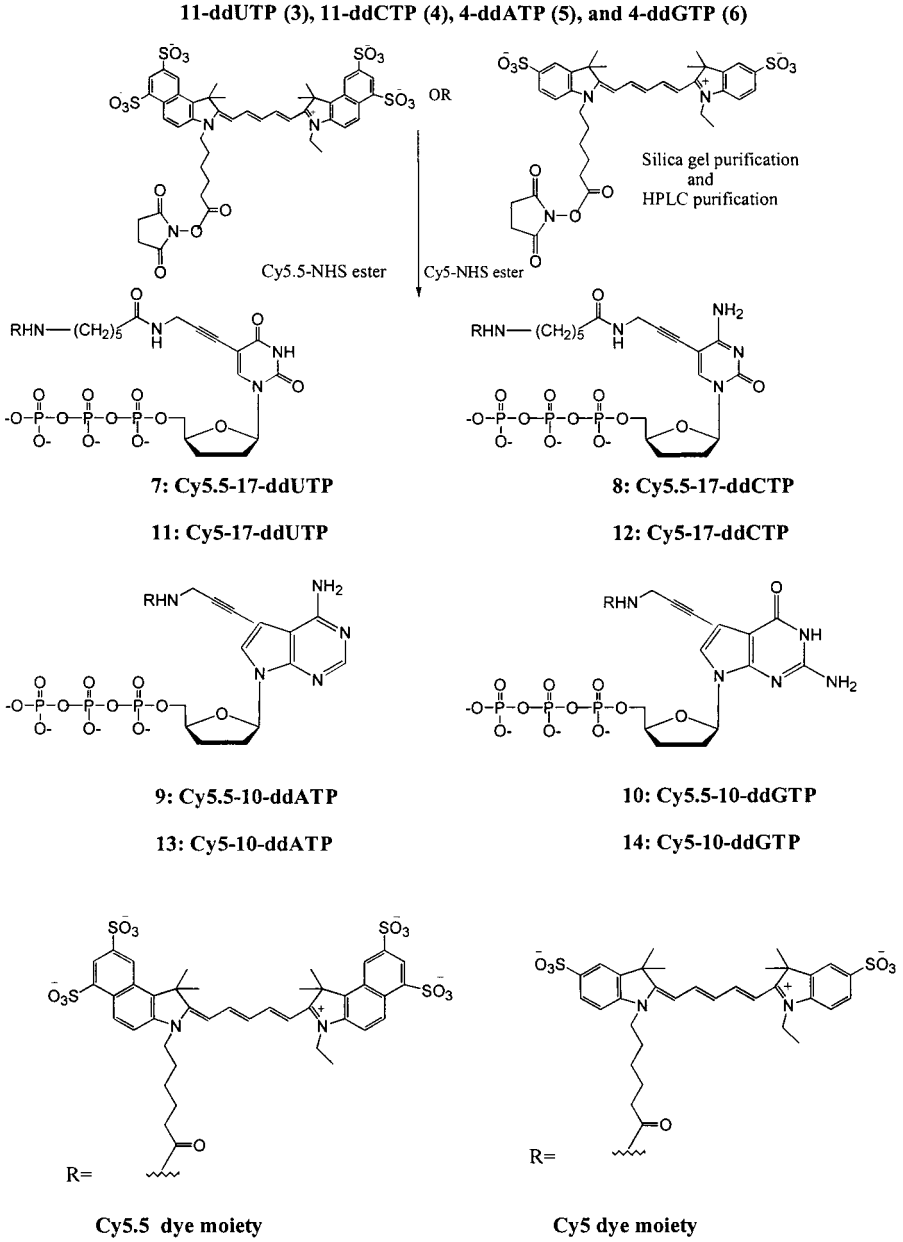
A typical DNA sequencing reaction using Cy 5.5 dye-labeled terminators contained the following mixture:

14.6 mM Tris-HCl, pH 9.5; 3.4 mM $MgCl_2$; 75 μM each of dATP, dCTP, dGTP, and dTTP; and either 1.5 μM Cy 5.5−10-ddATP, 1.5 μM Cy 5.5−17-ddCTP, 1.5 μM Cy 5.5−10-ddGTP, or 1.5 μM Cy 5.5−17-ddUTP.

Typical thermal cycling conditions consisted of a 1−2 min initial heat denaturation step at 95 °C, and then 25−30 cycles each consisting of 95 °C for 30 s, 45−60 °C for 30 s, and 72 °C for 120 s. Reactions were held at 4 °C until purification and analysis.

Reaction products were purified by precipitation with the addition of 2 μL of 7.5 M ammonium acetate and 30 μL of chilled absolute ethanol. After being mixed and incubated on ice for 20 min, DNA was pelleted by centrifugation at room temperature for 15 min using a standard lab bench microcentrifuge set on high speed (10000−16000*g*). Supernatants were carefully removed

Scheme 2. Synthesis of Cy-Dye Conjugates



by aspiration, and each DNA pellet was rinsed with 200 μL of ice-cold 70% ethanol. The tubes were recentrifuged for 5 min, and supernatants were again removed. DNA pellets were stripped of liquid under vacuum at room temperature for about 2 min without taking them to complete dryness. Each tube had 6−8 μL of formamide loading dye (95% formamide, 50 mM EDTA, pH 8.0, 0.2 mg/mL new fuchsin) added and was then mixed, using a vortex mixer fitted with a tube holder, for 10−15 min at room temperature. Resuspended DNA was denatured at 70−72 °C for 2.5−3 min, and the tubes were immediately quenched on ice. Aliquots, 1.5−8 μL, were then loaded in wells of sequencing gels for analysis.

Alternatively, sequencing reaction products were purified using AutoSeq G-50 columns (Amersham Biosciences). In this alternative procedure, each completed reaction mixture was diluted with distilled water to a volume of 15−25 μL and the entire sample loaded on a prespun column. The separate column effluents were stripped of liquid using a speed-vac, treated, and loaded on sequencing gels for analysis (vide supra).

Primers. Various primers were employed during the course of this study for both PCR and cycle sequencing reactions. Their sequences and how they are defined in the body of the text are as follows:

M13−40 primer, 5′-d[CGC CAG GGT TTT CCC AGT CAC GAC]-3′.

Reverse sequence primer (RSP), 5′−d[CAG GAA ACA GCT ATG AC]-3′.

M13 Universal primer, 5′−d[GTA AAA CGA CGG CCA GT]-3′.

Universal cycle primer, 5′-d[GTT TTC CCA GTC ACG ACG TTG TA]-3′.

Sequencing Instruments. The following DNA sequencing instruments were used in this study: ALFexpress DNA Analysis System (Cy 5.0 dye; Amersham Biosciences, Piscataway, NJ), SEQ4X4 Personal Sequencing System (Cy 5.5 dye; Amersham Biosciences, Piscataway, NJ), and both Clipper and Long-Read Tower System (Visible Genetics, Inc., Toronto, Ontario, Canada; both Cy 5.0 and Cy 5.5 dyes) (*17*).

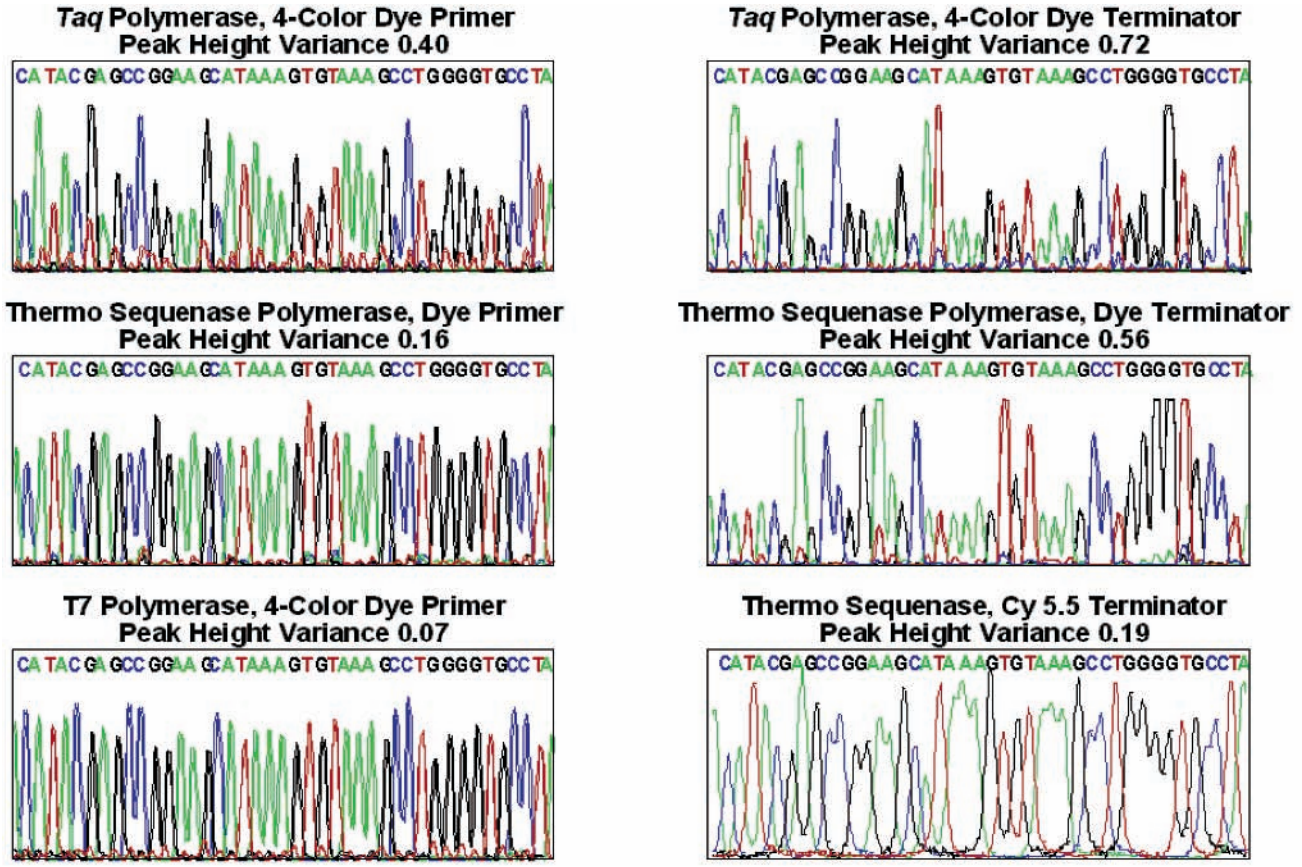


Figure 1. Visual representation of peak height variation using different dye terminators and DNA polymerases.

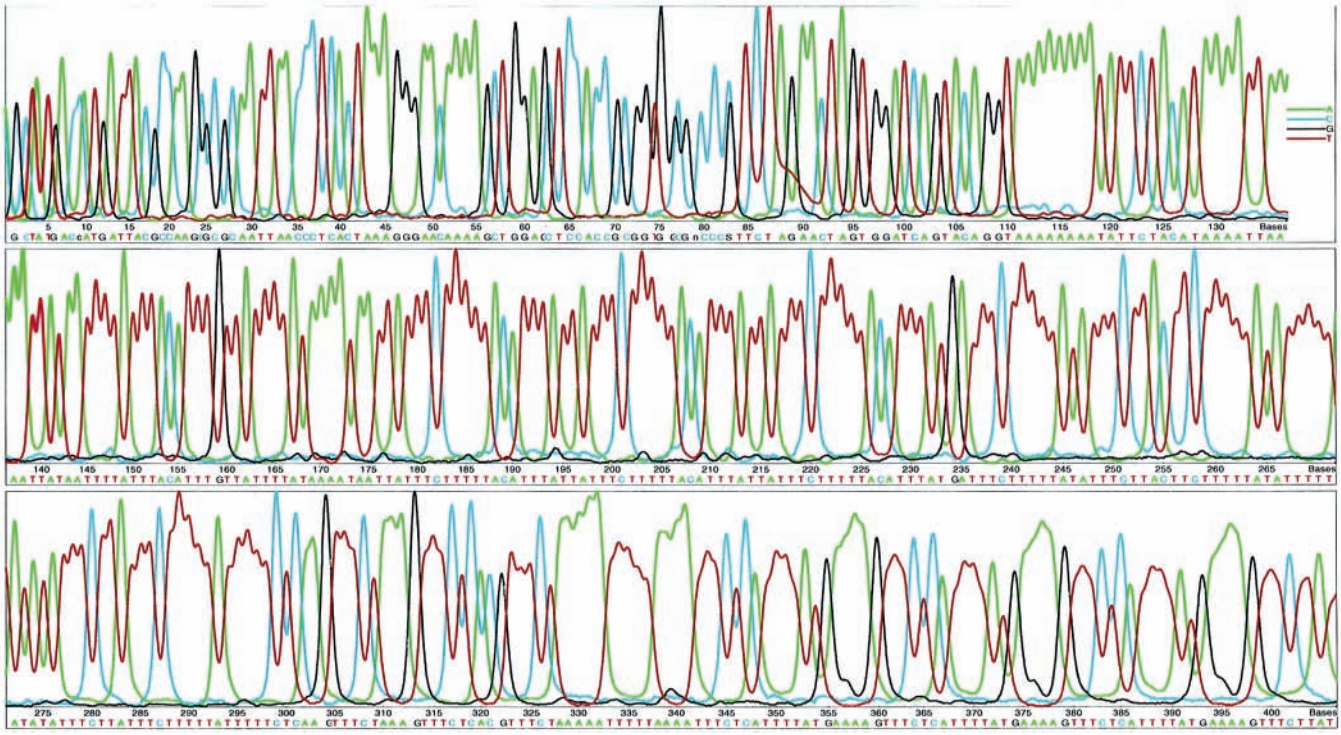


Figure 2. A 600-base PCR product generated by amplification of a pUC18 clone containing a 385-base insert of AT rich *Tetrahymena thermophilia* genomic DNA. The product was gel-purified and 300 ng of the resulting material sequenced using Thermo Sequenase DNA polymerase and Cy 5.0 dye terminators with detection on the ALF*express* DNA Analysis System.

RESULTS AND DISCUSSION

Thermo Sequenase DNA polymerase (Amersham Biosciences) contains a single amino acid modification which increases the rate of ddNTP incorporation by more than 1000-fold (*15*). When used in cycle sequencing reactions with unmodified ddNTPs, DNA polymerases containing this amino acid modification produce band patterns with

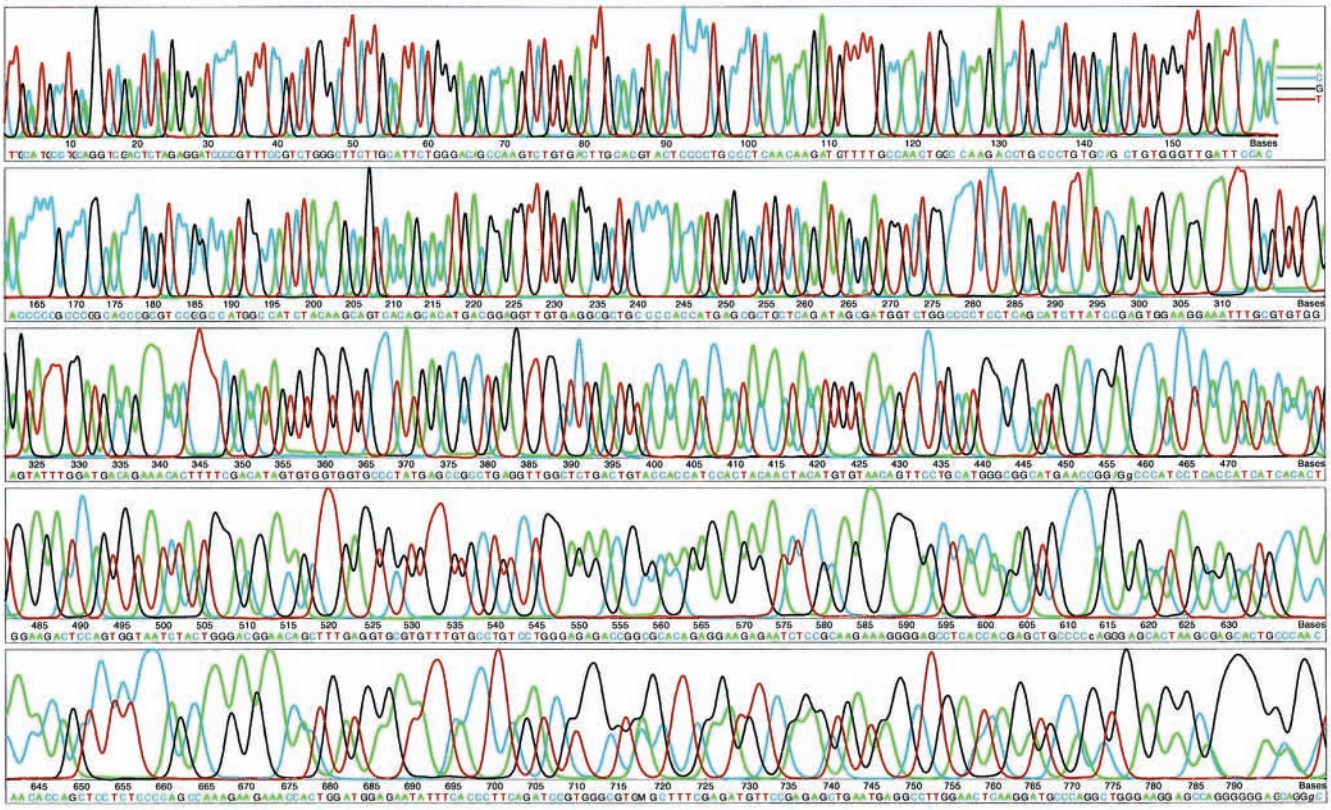


Figure 3. Sequence of pUC18 containing about an 800-base insert of p53 DNA using Thermo Sequenase DNA polymerase and Cy 5.0 dye terminators with detection on ALF*express* DNA Analysis System.

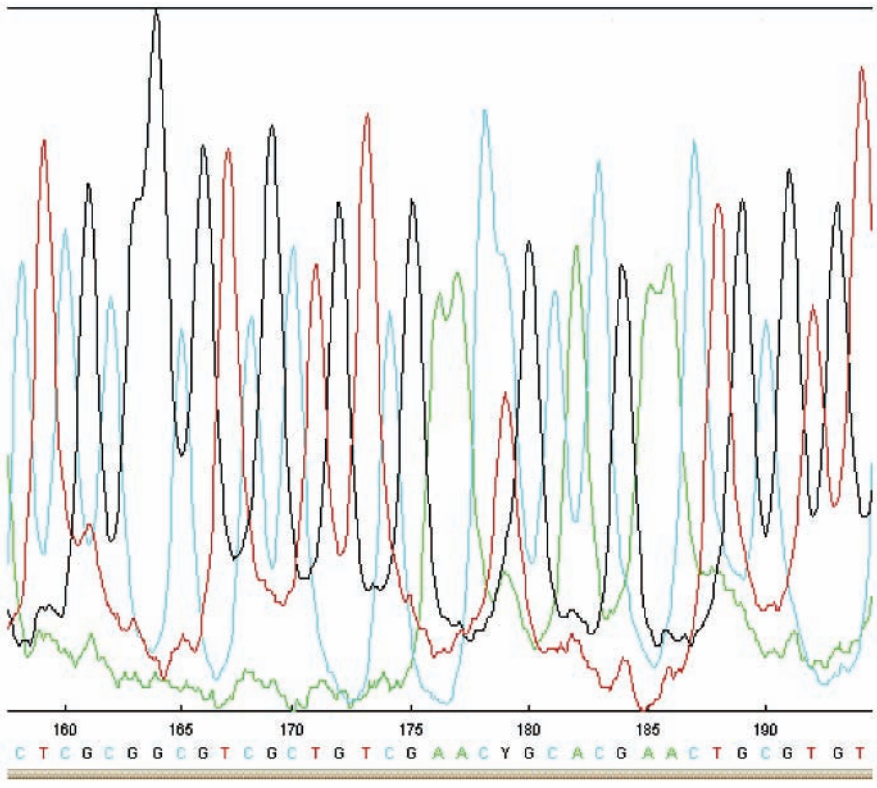


Figure 4. Heterozygote determination using Cy 5.0 dye terminators and Thermo Sequenase DNA polymerase with detection on ALF*express* DNA Analysis System.

very uniform peak intensities. In contrast, when performing similar reactions with dye-labeled ddNTPs, the same DNA polymerases generate peak heights that can fluctuate over approximately a 20-fold range in intensity (*18*).

A comparative peak height variation study (*5*) was performed between the Cy 5.5 terminators and other fluorophore reporting systems used in DNA sequencing. The peak height variation was standardized using bases between 50 and 350 of M13mp18(+) DNA sequenced with

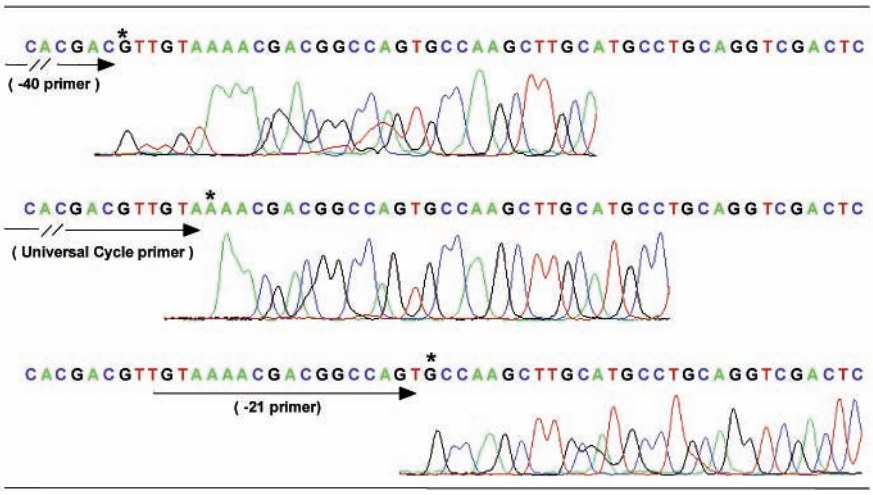


Figure 5. PCR products of M13mp18(+) strand sequenced with the indicated primers. Note that the first base of each product is readable using SEQ4X4 Personal Sequencing System.

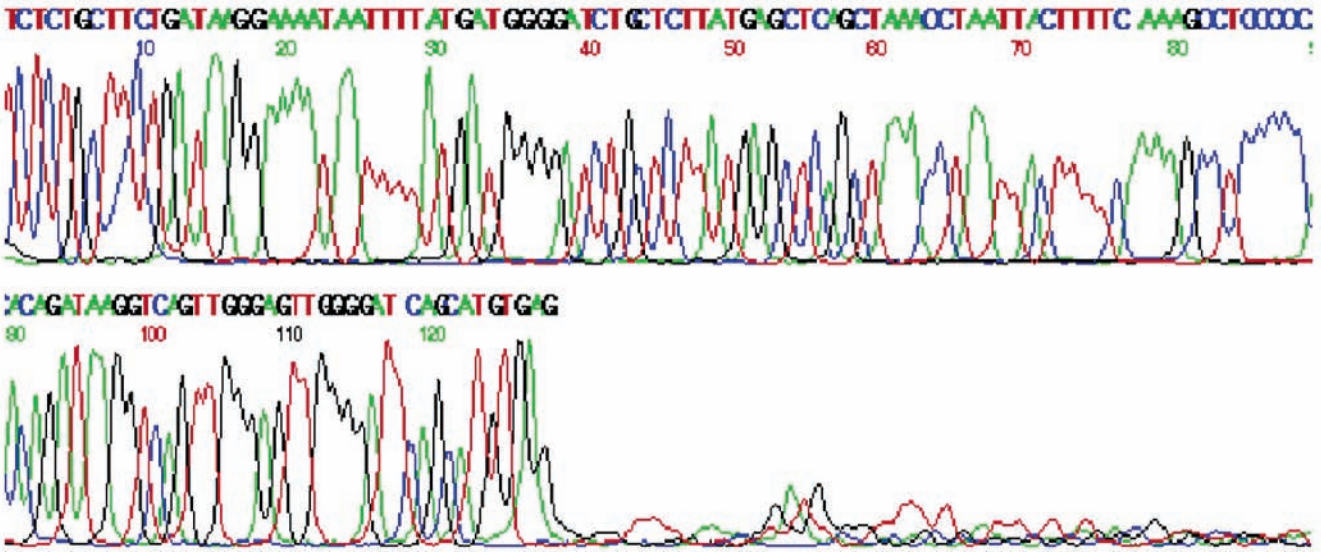


Figure 6. Last base determination of a PCR product of human β-globin DNA using Cy 5.5 dye terminators with SEQ4X4 Personal Sequencing System.

the M13−40 primer. Sequence data within this region was examined prior to peak variation analysis to ensure that the sequence was correct. Briefly, peak height data were fit to a second-degree polynomial equation comparing height to scan plot position. This corrected for the normal systematic variation in intensities found in DNA sequences. The data were then normalized by dividing the peak height at a given scan position by the polynomial estimate at that same position. The values reported are the variance of the normalized peak heights. Thus, smaller values indicate better, more uniform band intensities. Figure 1 represents some examples showing peak height variation obtained with different terminators and different DNA polymerases. Sequencing reactions using dye-primers and T7 DNA polymerase had the best peak height variation with a value of 0.07. Peak height variation for the Cy 5.5 terminators was found to be considerably better than the value (approximately 0.3) found for the four-color dye terminators currently used in the majority of high throughput sequencing facilities (*8*, *9*).

We investigated the ability of four new dye terminators to resolve stretches of either GC- or AT-rich base pairs. The Cy 5.0 dye-terminator protocol was tested with two plasmid constructs, one highly AT-rich that was used as a template to generate a 600-base pair PCR product for sequencing, and the other GC-rich where the plasmid was itself sequenced. Figure 2 presents sequence data from a 600-base pair PCR product containing *Tetrahymena thermophilia* DNA cloned into pUC18. A PCR product was first generated with this template using both the M13−40 primer and RSP. The purified material (∼300 ng) was sequenced using the M13 universal primer. Between bases (Figure 2**)** 110 and 298 the number of AT base pairs compared with the total number of base pairs is 91%, with the entire fragment comprising 76% AT. Of the 406 bases of sequence data (Figure 2), only one ambiguity at position 83 was observed to be caused by the base-calling software, and that may be resolved with manual intervention as a 'G'. Also notice that the base-calling software has added an extra base at position 79 (n).

Figure 3 presents sequence data from an 807-base insert in pUC18 of a p53 cDNA clone covering part of exon 4, all of exons 5 through 9, and part of exon 10. Between base 163 and 285 in Figure 3 is an area that is 71% GC-rich, with an overall GC content of the presented sequence at 58%. The first ambiguity was identified at base 718 and could not be resolved by manual intervention because of gel resolution.

Another important characteristic of these dye-terminator systems is unambiguous and reliable detection of heterozygotes. PCR products of separate amplifications of AMAI and WT51 genomic DNA were performed according to the manufacturer's instructions found in the HLA DRB*plus* Typing Kit. These products were purified with GFX PCR DNA and Gel Band Purification Kit and the concentration determined by spectrophotometer measurement. A mix of two of the PCR products was then sequenced using Cy 5.0 terminators. Figure 4 demonstrates heterozygote determination when 120 ng of WT51 and 80 ng of AMAI PCR products were mixed and sequenced. The 'Y' at position 179 in Figure 4 represents either a 'C' or 'T'. With this mixture of genomic DNA templates both a 'C' and a 'T' would be expected at this position as observed.

We also investigated the ability of our sequencing system to elucidate either the first base following the primer or the last base of an amplicon. For the first base determination 50 ng of M13mp18(+) strand DNA was amplified and then sequenced using three different M13 primers: −40, Universal Cycle, or Universal. Figure 5 demonstrates that the first base following the primer is visible in each reaction, even when the primer was immediately followed by a multiplet of the same base. Last base determination was accomplished using a PCR product of the human beta globin locus purified by Exo/SAP treatment. All sequence from the 128 base pair fragment is visible in Figure 6, demonstrating our system has the capability of elucidating as much sequence data as possible from a PCR template.

CONCLUSIONS

In this paper we have reported the synthesis of cyanine dye-labeled dideoxynucleoside triphosphates and their utility in single-color DNA sequencing methods. We have also demonstrated the ability of these two sets of cyanine dye-labeled terminators, when combined with a suitable DNA polymerase, to generate excellent quality sequencing data using simple and inexpensive instrumentation.

ACKNOWLEDGMENT

The authors thank Dr. Kathy Karrer, Marquette University, Milwaukee, WI, for the kind gift of *Tetrahymena thermophilia* DNA, Dr. Maria Ortiz-Rivera and Steve Marshall for their technical assistance, and Dr. Anup Sood for mass spectral analysis.

LITERATURE CITED

(1) Smith, L. M., Sanders, J. Z., Kaiser, R. J., Hughes, P., Dodd, C., Connell, C. R., Heiner, C., Kent, S. B. H., and Hood, L. E. (1986) Fluorescence detection in automated DNA sequence analysis. *Nature 321*, 674−679.

(2) Prober, J. M., Trainor, G. L., Dam, R. J., Hobbs, F. W., Robertson, C. W., Zagursky, R. J., Cocuzza, A. J., Jensen, M. A., and Baumeister, K. (1987) A system for rapid DNA sequencing with fluorescent chain-terminating dideoxynucleotides. *Science 238*, 336−341.

(3) Hobbs, F. W., Jr., and Cocuzza, A. J. (1991) Alkynylaminonucleotides. United States Patent No. 5047519.

(4) Innis, M. A., Myambo, K. B., Gelfand, D. H., and Brow, M. A. (1988) DNA sequencing with *Thermus aquaticus* DNA polymerase and direct sequencing of polymerase chain reaction-amplified DNA. *Proc. Natl. Acad. Sci. U.S.A. 85*, 9436−9440.

(5) Lee, L. G., Connell, C. R., Woo, S. L., Cheng, R. D., McArdle, B. F., Fuller, C. W., Halloran, N. D., and Wilson, R. K. (1992) DNA sequencing with dye-labeled terminators and T7 DNA polymerase: effect of dyes and dNTPs on incorporation of dye-terminators and probability analysis of termination fragments. *Nucleic Acids Res. 20*, 2471−2483.

(6) Parker, L. T., Deng, Q., Zakeri, H., Carlson, C., Nickerson, D. A., Kwok, P. Y. (1995) Peak Height variations in automated sequencing of PCR products using Taq dye-terminator chemistry. *Biotechniques 19*, 116−121

(7) Ju, J., Ruan, C., Fuller, C. W., Glazer, A. N., and Mathies, R. A. (1995) Fluorescence resonance energy transfer dye-labeled primers for DNA sequencing and analysis. *Proc. Natl. Acad. Sci. U.S.A. 92*, 4347−4351. (b) Huang, S.-C., Mathies, R. A., and Glazer, A. N. (1997) Optimization of spectroscopic and electrophoretic properties of energy transfer primers. *Anal. Biochem. 252*, 72−88.

(8) Nampalli, S., Khot, M., and Kumar, S. (2000) Fluorescence resonance energy transfer terminators for DNA sequencing. *Tetrahedron Lett.. 41*, 8867−8871. (b) Nampalli, S., Khot, M., Nelson, J. R., Flick, P. K., Fuller, C. F., and Kumar, S. Fluorescence resonance energy transfer dye nucleotide terminators: A new synthetic approach for high-throughput DNA sequencing. (2001) *Nucleosides, Nucleotides Nucleic Acids 20* (4−7), 361−367.

(9) Rosenblum., B. B., Lee, L. G., Spurgeon, S. L., Khan, S. H., Menchen, S. M., Heiner, C. R., and Chen, S. M. (1997) New dye-labeled terminators for improved DNA sequencing patterns. *Nucleic Acids Res. 25* (22), 4500−4504.

(10) Kumar, S., Fuller, C. W., Nampalli, S., Khot, M., Livshin, I., Sun, L., Hamilton, S., Samols, S. B., Mamone, J. A., Hujer, K. M., McArdle, B. F., Nelson, J. R., and Duthie, S. (1999) Uniform band intensities in fluorescent dye terminator sequencing. *Nucleosides Nucleotides 18*, 1101−1103.

(11) Kumar, S., Nampalli, S., McArdle, B. F., Fuller, C. W. (1999) Dideoxy dye terminators. PCT WO 99/40223.

(12) Southwick, P. L., Ernst, L. A., Tauriello, E. W., Parker, S. R., Mujumdar, R. B., Mujumdar, S. R., Clever, H. A., and Waggoner, A. S. (1990) Cyanine dye labeling reagents-carboxymethylindocyanine succinimidyl esters. *Cytometry 11*, 418−430.

(13) Waggoner, A. (2000) Cyanine dyes as labeling reagents for detection of biological and other materials by luminescence methods. United States Patent No. 6048982.

(14) Middendorf, L. R., and Patonay, G. (1994) Sequencing near-infrared and infrared fluorescence labeled DNA for detecting using laser diodes. United States Patent No. 5366603.

(15) Tabor, S., and Richardson, C. C. (1995) A single residue in DNA polymerases of the *Escherichia coli* DNA polymerase I family is critical for distinguishing between deoxy- and dideoxyribonucleotides. *Proc. Natl. Acad. Sci. 92*, 6339−6343.

(16) Vander Horn, P. B., Davis, M. C., Cunniff, J. J., Ruan, C., McArdle, B. F., Samols, S. B., Szasz, J., Hu, G., Hujer, K. M., Domke, S. T., Brummet, S. R., Moffett, R. B., and Fuller, C. W. (1997) Thermo Sequenase DNA polymerase and T. acidophilum pyrophosphatase: New thermostable enzymes for DNA sequencing. *Biotechniques 22*, 758−765

(17) Yager, T. D., Dunn, J. M., and Stevens, J. K. (1997) High-speed DNA sequencing in ultrathin slab gels. *Curr. Opin. Biotechnol. 8*, 107−113.

(18) Fuller, C., and Reeve, M. (1995) A novel thermostable polymerase for DNA sequencing. *Nature, 376*, 796−797.

BC015522Y

Establishment of Intein-Mediated Protein Ligation under Denaturing Conditions: C-Terminal Labeling of a Single-Chain Antibody for Biochip Screening

Jens R. Sydor, Maria Mariano, Steve Sideris, and Steffen Nock*

Zyomyx, Inc., 26101 Research Road, Hayward, California 94545. Received March 26, 2002; Revised Manuscript Received June 3, 2002

Intein-mediated protein ligation is a recently developed method that enables the C-terminal labeling of proteins. This technique requires a correctly folded intein mutant that is fused to the C-terminus of a target protein to create a thioester, which allows the ligation of a peptide with an N-terminal cysteine (*1*, *2*). Here we describe the establishment of this method for the labeling, under denaturing conditions, of target proteins that are expressed insolubly as intein fusion proteins. A GFPuv fusion protein with the *Mycobacterium xenopi gyrA* intein was expressed in inclusion bodies in *Escherichia coli* and initially used as a model protein to verify intein cleavage activity under different refolding conditions. The intein showed activity after refolding in nondenaturing and slightly denaturing conditions. A construct of the same intein with an anti-neutravidin single-chain antibody was also expressed in an insoluble form. The intein-mediated ligation was established for this single chain antibody−intein fusion protein under denaturing conditions in 4 M urea to prevent significant precipitation of the fusion protein during the first refolding step. Under optimized conditions, the single-chain antibody was labeled with a fluorescent peptide and used for antigen screening on a biochip after final refolding. This screening procedure allowed the determination of binding characteristics of the scFv for avidin proteins in a miniaturized format.

INTRODUCTION

Inteins are self-splicing protein elements that excise themselves out of a precursor protein, ligating the flanking polypeptide sequences together. Since their discovery in 1990 (*3*, *4*), inteins have been used for a variety of protein engineering techniques including the C-terminal ligation of proteins to peptides or protein fragments (*5*−*8*). In this case, the C-terminus of a target protein is fused to an intein mutant that is unable to splice itself out of the precursor protein, but is still capable of generating a thioester at the C-terminus of the target protein. An N-terminal cysteine-containing peptide or protein fragment is then ligated to the C-terminal thioester of the target protein (Figure 1). This is usually achieved by the aid of another thiol compound that releases the target protein from the intein in a transthioesterification reaction. This C-terminal thioester is then reacted with a peptide containing an N-terminal cysteine, the thiol of which exchanges with the low molecular weight thiol compound. Finally, the thioester formed between the target protein and the peptide spontaneously rearranges to generate a native amide bond (*1*, *2*). This technique has proven useful in protein engineering to incorporate unnatural modifications such as fluorophores or isotope labels into proteins (*9*−*11*).

An important prerequisite for intein-mediated protein ligation (IPL) is that the fusion protein is in a correctly folded conformation to allow the intein-mediated formation of the thioester. Unfortunately, a significant number of proteins, including those fused to inteins, can only be obtained in insoluble form in inclusion bodies when expressed in *E. coli*. The protein isolation from inclusion bodies generally requires a denaturation and refolding step. So far, there are only a limited number of examples that describe the refolding of intein fusion proteins into active conformations. For example, the refolding of intein fusions into nondenaturing buffer has been performed, although with a low yield of refolded protein and intein cleavage activity (*12*). Additionally, low concentrations of denaturants such as guanidine hydrochloride have been added to increase the solubility of peptides during the ligation without affecting intein activity (*10*). A general method that could be applied to a variety of

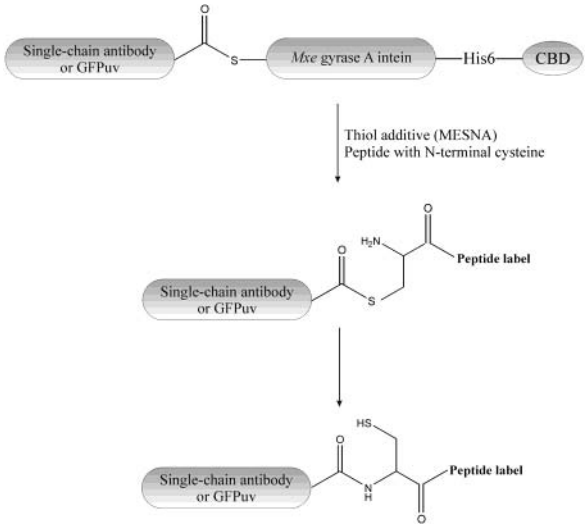


Figure 1. Schematic description of the intein fusion constructs and the intein-mediated protein ligation.

* To whom correspondence should be addressed: Zyomyx, Inc., 26101 Research Road, Hayward, CA 94545. Tel: +1−510-266-7504, fax: +1−510-266-7792, e-mail: snock@zyomyx.com.

10.1021/bc025534z CCC: $22.00 © 2002 American Chemical Society
Published on Web 06/28/2002

proteins expressed as insoluble intein fusions would, therefore, expand the applicability of the IPL.

One application of this technique could be the C-terminal site-specific labeling of single-chain antibodies, which are very important binding reagents used for the detection of biomolecules (*13*−*15*). The expression and isolation of active single-chain antibodies is usually problematic, however, due in part to the reducing environment in the cytoplasm, which inhibits the formation of the disulfide bonds within these antibody fragments. Production of active scFv's[1] is usually accomplished by expressing them in the periplasm, which is an oxidizing environment, or in inclusion bodies, with a subsequent refolding and oxidation step (*16*−*19*). The amount of scFv's isolated from the periplasm is usually low, however, and refolding of scFv's from inclusion bodies is usually unsuccessful.

To overcome these limitations, we describe a method that results in a high yield of functional scFv's that have been labeled by IPL. The basis of this method is to first express the scFv as an insoluble intein-fusion protein. The protein is then fully resolubilized and denatured, after which it is transferred into a mildly denaturing buffer in which the intein is functional, but where the denaturant allows the partially folded scFv to remain soluble. Correctly folded fusion proteins then undergo IPL, becoming labeled in the process. IPL under mildly denaturing conditions was tested on two unrelated proteins fused to the gyrase A intein from *Mycobacterium xenopi*. We also describe the utilization of scFv's with a C-terminal fluorescent tag for antigen screening in a biochip format.

This strategy also offers a variety of other possibilities for the C-terminal labeling of scFv's, such as the introduction of other unnatural modifications for oriented capture agent immobilization on surfaces.

EXPERIMENTAL PROCEDURES

Materials. For the cloning procedures, oligonucleotides were supplied by MWG (High Point, NC) and enzymes and chitin beads by New England Biolabs (Beverly, MA). Denaturants, urea and guanidine-hydrochloride, were purchased from Fisher Scientific (Pittsburgh, PA). Roche Molecular Biochemicals was the supplier of the 1,4-dithiothreitol (Inidianapolis, IN). Ethanethiol was purchased from Fluka (Milwaukee, WI). 2-Mercaptoethanesulfonic acid, sodium salt (MESNA), and all other inorganic salts were obtained from Sigma Chemical Company (St. Louis, MO). Pierce Chemical Company (Rockford, IL) was the supplier of neutravidin, avidin, and streptavidin.

Cloning and Expression of Intein Fusion Constructs. The DNA sequence of the target proteins was cloned into pTXB1 (New England Biolabs, Beverly, MA) that was modified by the introduction of a His-tag between the intein and the chitin-binding domain as well as SfiI and NotI restriction sites in the MCS for cloning of the scFv or GFPuv in frame with the *Mxe* gyrA intein (Figure 1). The sequence for GFPuv was obtained from Clontech (Palo Alto, CA), and the sequence for the scFv was published elsewhere (*20*).

Transformation of this plasmid into *E. coli* BL21(DE3) was done by electroporation according to the manufacturer's instructions (Stratagene, La Jolla, CA). BL21-(DE3) cells contain a chromosomal copy of the T7 RNA polymerase gene under the control of the IPTG-inducible lacUV5 promoter. Expression was induced by the addition of 0.1 mM IPTG. Six hours after induction and incubation at 30 °C, cells were harvested by centrifugation at 4 °C, which yielded ∼8 to10 g of wet cell pellet per liter cell culture. The cells were stored at −80 °C until further use.

Synthesis of the myc Peptide with and without Rhodamine Label. Solid-phase peptide synthesis (*21*) was performed manually or on a CS536 peptide synthesizer from CSBio (San Carlos, CA), using in situ neutralization/2-(1*H*-benzotriazol-1-yl)-1,1,3,3-tetramethyluronium hexafluorophosphate activation protocols for stepwise Boc-chemistry chain elongation on an MBHA resin (*22*). The rhodamine derivative 5-(and 6)-carboxytetramethylrhodamine (TAMRA) was coupled to the lysine side chain with the following procedure. The ϵ-amino group of the lysine side chain was protected with an Fmoc group. After chain elongation, the amino group was deprotected by two 5 min incubations of the resin with 20% piperidine in DMF and subsequent washing with DMF. TAMRA was then activated and coupled like other amino acids, described in the general protocol (*22*). After HF cleavage, the peptides were purified with a C18-column from Vydac (Hesperia, CA) by using linear gradients of buffer B (acetonitrile, 0.1% trifluoroacetic acid) in buffer A (H_2O, 0.1% trifluoroacetic acid) and UV detection at 215 nm.

Isolation and Solubilization of Inclusion Bodies. Cells were resuspended in cell lysis buffer (200 mM NaCl, 20 mM sodium phosphate, pH 7.3, 1 mM EDTA) and lysed in a microfluidizer (Microfluidics International Corporation, Newton, MA). The crude inclusion body (IB) fraction was isolated by centrifugation at 31000 g for 10 min at 4 °C and resuspended in 0.1 M Tris, pH 7, 1mM EDTA. A 0.5 volume of 60 mM EDTA, 6% Triton X-100, 1.5 M NaCl, pH 7, was added and the suspension incubated at 4°C for 30 min with stirring. The IB fraction was isolated by centrifugation as described above and resuspended in wash buffer (50 mM sodium phosphate, pH 7.3, 1 mM EDTA). Centrifugation was repeated to isolate the IB pellets, which were subsequently stored at −20 °C (2 weeks) or −80 °C (>2 weeks). From a 1L culture, 1.5−2 g of IB were typically obtained. Inclusion bodies were solubilized in wash buffer plus 6 M GuHCl and 100 mM DTT for 2 h at RT with constant stirring. The pH was adjusted to 3−4 by the dropwise addition of 1 N HCl. Finally, the sample was centrifuged at 10000 g for 30 min at 4 °C to remove the insoluble cellular debris from the solubilized protein, which was then filtered.

Partial Refolding and IPL under Denaturing Conditions. The solubilized protein sample (10 mg/mL) in 6 M GuHCl was rapidly diluted at a rate of 0.1 mL/min into refolding buffer (wash buffer plus 4 M urea) at RT to give a final 1:10 dilution. The diluted sample was dialyzed against refolding buffer overnight at RT and then centrifuged at 10000 g for 30 min at 4 °C. The target protein-*Mxe*gyrA-His6-CBD fusion in the supernatant was purified by binding to a chitin resin at RT and

[1] Abbreviations: Boc, *tert*-butyloxycarbonyl; BSA, bovine serum albumin; CBD, chitin-binding domain; DMF, dimethylformamide; EDTA, ethylenediaminetetraacetic acid; ELISA, enzyme-linked immunosorbent assay; Fmoc, 9-fluorenylmethoxycarbonyl; GFPuv, variant of the green fluorescent protein optimized for higher bacterial expression and higher fluorescence when excited by UV light; GuHCl, guanidine hydrochloride; His6, Histidine-tag consisting of six histidines; HRP, horseradish peroxidase; IPL, intein-mediated protein ligation; MESNA, 2-mercaptoethanesulfonic acid; OPD, *O*-phenylenediamine; PBS, phosphate-buffered saline; PLL-*g*-PEG-B30%, poly(L-lysine)-grafted-poly(ethylene glycol) with 30% biotin content; scFv, single-chain variable fragment of an antibody; TAMRA, 5-(and 6)-carboxytetramethylrhodamine.

washing with 5 column volumes of refolding buffer. The IPL was induced by the addition of 1 volume of 200 mM MESNA and 4 mM of peptide to 1 volume of the chitin beads containing the intein fusion protein in the same buffer and incubated for 36 h at RT. The supernatant was isolated, and the beads were washed with the refolding buffer. The wash fractions were combined with the supernatant, and the sample was dialyzed using one of the following methods: (1) directly into PBS with 10% glycerol, (2) directly into PBS, 10% glycerol, 3 mM/0.3 mM reduced/oxidized glutathione and then into PBS, 10% glycerol, or (3) stepwise dialysis into 2 M urea, 50 mM sodium phosphate, pH 7.3, 1 mM EDTA, 3 mM/0.3 mM reduced/oxidized glutathione, and then into 1 M urea in the same buffer and finally into PBS, 10% glycerol.

Determination of scFv Activity by ELISA. The wells of a Nunc-Immuno Plate Maxisorp Surface (Nalge Nunc International, Denmark) were coated with 100 μL of 2 μg/mL neutravidin (or 5 μg/mL BSA as a negative control) in 0.1 M sodium carbonate, pH 9.6, overnight at 4 °C. The wells were then blocked with 200 μL of 3% w/v nonfat dried milk in PBS, 0.1% v/v Tween-20, followed by the addition of 100 μL of scFv-myc in PBS, 0.1% v/v Tween-20, and incubated for 1 h at 37 °C. The wells were washed three times with PBS, 0.1% v/v Tween-20, followed by the addition of 100 μL of anti-myc antibody at a 1:1000 dilution in 3% w/v nonfat dried milk in PBS, 0.1% v/v Tween-20, with incubation for 1 h at 37 °C. The wash step described earlier was repeated, and an HRP-conjugated goat anti-mouse IgG (Jackson ImmunoResearch Laboratories, Inc., West Grove, PA) was added at a 1:2000 dilution in 3% w/v nonfat dried milk in PBS, 0.1% v/v Tween-20, and incubated at 37 °C for 1 h. After repeating the same washing step, OPD peroxidase substrate (SigmaFast *o*-phenylenediamine dihydrochloride tablets; Sigma, St. Louis, MO) was added first and then 3 N HCl to deactivate the enzyme. The optical density readings at 490 nm were recorded as relative units.

Antigen Screening on Protein Biochips. The preparation of the protein microarray surfaces was performed with an in-house microarrayer as described elsewhere (*23*). Briefly, a silicon chip with a 20 nm layer of TiO_2 was incubated with a solution of PLL-*g*-PEG-B30% for 1 h at room temperature to form the biotin surface. Neutravidin, avidin, and streptavidin (Pierce, Rockford, IL) were arrayed at varying concentrations onto the biotin-activated chip. After being washed, a microfluidic channel array was positioned onto the TiO_2 surface to create individual channels on the chip. The surface in the channels was then incubated with 100 nM scFvE9-myc-TAMRA in PBS, 0.05% Tween-20, 1% (w/v) BSA, and washed with PBS and then with H_2O.

The chips were scanned in a confocal fluorescence scanner (ScanArray 5000; GSI Lumonics, Billerica, MA) with a 543 nm excitation laser and a 578 nm emission filter.

Signal intensities for given spot sizes were determined with the program QuantArray Version 3.0 (Packard BioScience, Billerica, MA).

RESULTS AND DISCUSSION

Initial Refolding Studies for the *Mxe* gyrA Intein with GFPuv as a Model Protein. In a first set of experiments, we chose GFPuv as a model protein to test the refolding capability of the *Mxe* gyrA intein in a target protein-intein-His6-CBD fusion (Figure 1). This GFPuv−intein construct can be expressed as a soluble or insoluble intein fusion protein in *E. coli*, depending on the growth conditions, and its refolding can be monitored by the intrinsic fluorescence properties. We made the observation in our experiments that, in contrast to expression at 15 °C, expression of a GFPuvK238Y-*Mxe*gyrA-His6-CBD intein fusion protein at 30 °C in *E. coli* gave mostly insoluble fusion protein (Figure 2). This construct gave us the opportunity to test whether we could regain activity of this particular intein from *Mycobacterium xenopi* after refolding. The inclusion bodies were isolated and solubilized in 6 M GuHCl by a procedure which is similar to the one published by Rudolph et al. (*24*, *25*).

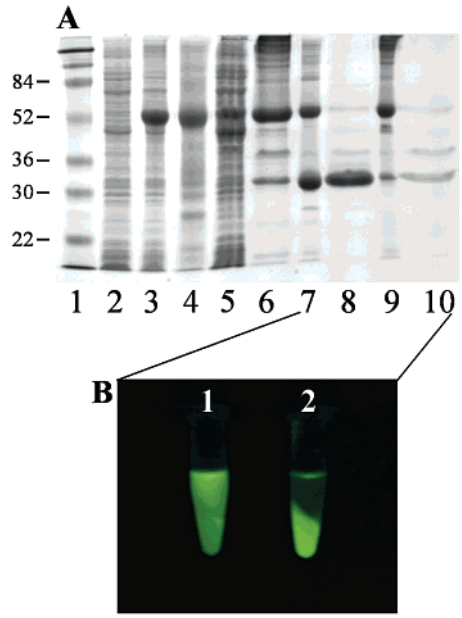


Figure 2. SDS−PAGE and fluorescence analysis of expression and intein-mediated cleavage of the GFPuvK238Y-*Mxe*gyrA-H6-CBD construct. The fusion protein was isolated from inclusion bodies after expression and refolded in nondenaturing PBS buffer containing 10% glycerol. Cleavage was performed after binding to chitin beads for 36 h at 4 °C with 2% ethanethiol. A, SDS−PAGE analysis. Lane 1: Protein marker (molecular weight in kDa). Lane 2: Cell lysate before induction. Lane 3: Cell lysate after induction with 0.1 mM IPTG and expression for 6 h at 30 °C. Lane 4: Insoluble fraction after lysis with a microfluidizer. Lane 5: Soluble fraction after lysis. Lane 6: Protein fraction bound to the chitin beads before cleavage. Lane 7: Protein fraction bound to the chitin beads after 36 h incubation with 2% ethanethiol at 4 °C. Lane 8: Supernatant fraction after 36 h incubation with 2% ethanethiol at 4 °C. Lane 9: Protein fraction bound to the chitin beads in the control incubation without ethanethiol. Lane 10: Supernatant fraction of the control incubation without ethanethiol. B, Fluorescence analysis. UV irradiation of the microcentrifuge tubes containing the intein-mediated cleavage samples after centrifugation. Tube 1 contains the reaction with 2% ethanethiol, tube 2 contains the control reaction without ethanethiol. Lane 7−10 in the SDS−PAGE analysis represent the chitin beads fractions and supernatants of these reaction tubes.

The GFPuv−intein fusion protein was refolded by dialysis into nondenaturing PBS buffer containing 10% glycerol. The solubilized protein in denaturing buffer showed no fluorescence upon irradiation with UV light whereas the refolded sample clearly showed GFPuv fluorescence which indicated a correct folding of the soluble fraction. There was, however, also a significant amount of precipitated protein in the dialyzed sample. After centrifugation, the supernatant was loaded onto chitin beads and incubated with 2% ethanethiol for 36 h at 4 °C.

The results presented in Figure 2 show that a fraction of the gyrase A intein mutant is able to generate a thioester at its N-terminus after refolding, which leads

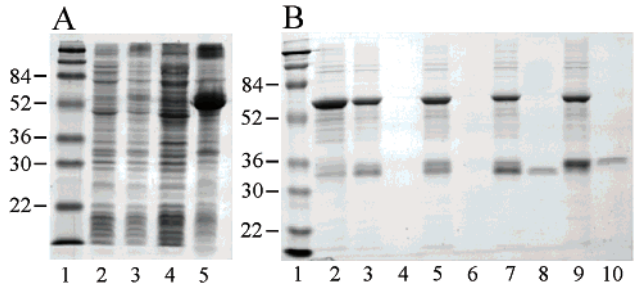


Figure 3. SDS−PAGE analysis of expression and optimized intein-mediated protein ligation under denaturing conditions with an scFv−intein fusion protein. A, Lane 1: Protein marker (molecular weight in kDa). Lane 2: Cell lysate before induction. Lane 3: Cell lysate after induction with 0.1 mM IPTG and expression for 6 h at 30 °C. Lane 4: Soluble fraction after lysis with a microfluidizer. Lane 5: Insoluble fraction after lysis. B, Lane 1: Protein marker (molecular weight in kDa). Lane 2: Protein fraction bound to the chitin beads before cleavage. Lane 3: Protein fraction bound to the chitin beads after 36 h incubation with 2% ethanethiol at RT. Lane 4: Supernatant fraction after 36 h incubation with 2% ethanethiol at RT. Lane 5: Protein fraction bound to the chitin beads after 36 h incubation with 2% ethanethiol and 2 mM myc peptide at RT. Lane 6: Supernatant fraction after 36 h incubation with 2% ethanethiol and 2 mM myc peptide at RT. Lane 7: Protein fraction bound to the chitin beads after 36 h incubation with 100 mM MESNA at RT. Lane 8: Supernatant fraction after 36 h incubation with 100 mM MESNA at RT. Lane 9: Protein fraction bound to the chitin beads after 36 h incubation with 100 mM MESNA and 2 mM myc peptide at RT. Lane 10: Supernatant fraction after 36 h incubation with 100 mM MESNA and 2 mM myc peptide at RT.

to the cleavage of GFPuv from the beads by an attack of the thioester with ethanethiol. GFPuv accumulates in the supernatant of the reaction with ethanethiol whereas there is only a minor cleavage of GFPuv in the control reaction without ethanethiol. This might be due to some hydrolysis of the thioester (Figure 2). About 50% of the refolded construct contains an active intein, estimated from the relative protein concentrations in the SDS−PAGE, which gives reasonable amounts of target protein in the supernatant. In this case, several milligrams of GFPuv could be obtained from 1 L of cell culture by this procedure, which proves that a *Mxe* gyrA intein fusion protein can be successfully refolded to an active intein conformation.

Intein-Mediated Ligation under Denaturing Conditions for the C-Terminal Labeling of an scFv. As mentioned above, the refolding of the GFPuv−intein fusion protein led to significant amounts of protein loss due to precipitation. Also, unlike GFPuv, which is relatively easy to refold, more challenging proteins, such as scFv's, largely precipitated as intein fusion proteins during this refolding step.

For this reason, we wished to establish a refolding and cleavage procedure that could be applied for target proteins that are difficult to refold into active conformations.

As a model system to develop such a procedure, we constructed a vector which directs the cytoplasmic expression of a fusion construct of the *Mxe* gyrA intein with a single-chain Fv against neutravidin (*20*). This fusion protein, like that of the GFPuv construct, was expressed in an insoluble form in *E. coli* (Figure 3A). The inclusion body fraction containing the fusion protein was isolated and solubilized in 6 M GuHCl.

Instead of a direct transfer of the fusion protein into physiological buffer conditions, we first diluted it into an intermediate buffer that is mildly denaturing. This was intended to allow partial refolding of the intein and the chitin-binding domain to active conformations, thus allowing for protein immobilization and intein-mediated protein ligation. At the same time, it was intended to prevent the precipitation of the fusion protein that was observed when dialyzing directly into physiological buffer conditions. We first tried to perform the IPL in buffers with varying concentrations of GuHCl. Although the CBD was still able to bind to the chitin beads to some extent at low GuHCl concentrations, the intein showed no cleavage activity (data not shown). Ayers et al. have shown that intein cleavage activity in a soluble fusion protein can be mostly retained upon addition of up to 2 M GuHCl (*10*). In our case, however, the fusion protein had already been insoluble and needed to be solubilized in 6 M GuHCl before a transfer to lower GuHCl concentrations, and so the conditions are not directly comparable.

In our next experiments, we transferred the fusion protein from 6 M GuHCl to a buffer containing the milder denaturant urea in order to prevent precipitation of the fusion protein and regain activity of the intein by the same time. A variety of different transfer protocols were compared, and the best results regarding intein activity were achieved by a stepwise dilution approach into 4 M urea (*24*, *25*). In this case, 10 mL of a 10 mg/mL solution of the scFv−intein−CBD fusion protein was slowly added to 90 mL of a 4 M urea buffer at room temperature with a flow rate of 0.1 mL/min with constant stirring. This stepwise dilution approach lowers the concentration of the denatured protein during the refolding process and therefore prevents aggregation of folding intermediates (*24*, *25*). The dilution was followed by another dialysis step into 4 M urea overnight at room temperature to ensure the removal of GuHCl.

The protein sample was then bound to 1 mL chitin beads for the purification of the intein fusion protein. We then added the thiol additive and the peptide with the N-terminal cysteine. The IPL releases the target protein coupled to the modifying peptide into the supernatant while retaining the intein−CBD fusion protein on the beads. The ligation was carried out for 36 h at RT with a 50% chitin beads suspension in 4 M urea containing 100 mM MESNA and 2 mM peptide.

The SDS−PAGE analysis of this reaction, performed with the scFv against neutravidin and a myc peptide with an N-terminal cysteine (NH_2-CGGEQKLISEEDLN-$CONH_2$), showed results that were consistently seen in our investigations (Figure 3). The use of MESNA as a thiol additive improves the cleavage of the target protein from the intein fusion on the chitin beads in comparison to ethanethiol. The ligations at room temperature gave slightly higher amounts of product than ligations at 4 °C, without affecting the activity of the scFv (as measured by ELISA, see below). The addition of the peptide slightly increased the fraction of the fusion protein that cleaves from the intein, but also increased the amount of precipitated byproduct, as can be seen in the chitin bead fraction, which appears to contain some insoluble product. This approach, however, yielded significant amounts of ligated scFv in the supernatant. The yield of the intein cleavage was up to 20% under these conditions, based on the estimation of protein concentrations, using the protein standards of the SDS−PAGE analysis. The overall yield was approximately 2 mg of labeled scFv per liter of culture. In comparison, the amounts of scFv obtained from an *E. coli* periplasmic expression system is usually in the microgram range. The additional label-

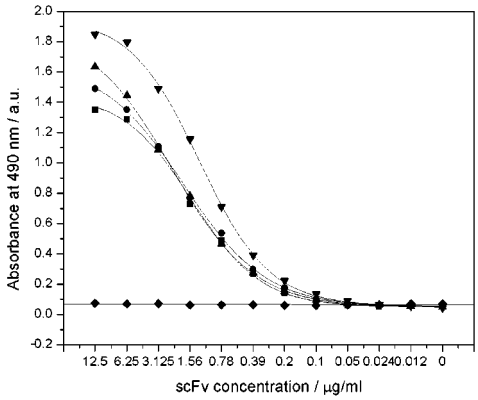


Figure 4. ELISA with the scFv E9 against the antigen neutravidin after different final refolding conditions. ELISA signals for the (▲) myc peptide labeled scFv E9 after stepwise dialysis from 4 M urea to PBS, 10% glycerol buffer with an oxido-shuffling system, (●) direct dialysis in PBS, 10% glycerol buffer with an oxido-shuffling system, and (■) direct dialysis in PBS, 10% glycerol buffer. (▼) ELISA signal of the same scFv expressed with a C-terminal myc tag in a soluble form in the periplasm of *E. coli* as a positive control and (◆) ELISA signal for the negative control with BSA as an antigen.

ing of the antibody fragment makes this procedure particularly useful.

In the last step, we used different final dialysis procedures to transfer the labeled scFv into nondenaturing PBS buffer and compared these products by ELISA to the same scFv that was solubly expressed in the *E. coli* periplasm with the same C-terminal myc tag. This ensures that a given dialysis protocol leads to a correctly folded and site-specifically labeled scFv with a specific activity, which is comparable to an scFv obtained from soluble periplasmic expression. We used the following three dialysis protocols to transfer the IPL products from the 4 M urea buffer into physiological buffer: (1) directly into PBS, 10% glycerol with reduced/oxidized glutathione as an oxido-shuffling system to ensure proper formation of disulfide bonds. (2) PBS, 10% glycerol without an oxido-shuffling system. (3) Stepwise dialysis into 2 M urea in PBS, and then into 1 M urea in PBS, and finally into PBS, 10% glycerol with reduced/oxidized glutathione. The ELISA assay was performed on neutravidin-coated plates (BSA as a negative control) in which the myc-tagged scFv's were detected by a mouse anti-myc antibody, followed by an HRP-conjugated goat anti-mouse IgG.

The final transfer protocol of the IPL-labeled antibody fragment does not have a significant effect on the specific activity, as the three different dialysis conditions led to about the same activity in the ELISA assay (Figure 4). The comparison with the myc-tagged scFv that was solubly expressed in the *E. coli* periplasm shows that the activity is in the same range. The slightly lower signal for the myc-tagged scFv's that were obtained from the IPL under denaturing conditions is probably due to the fact that the conditions of the IPL usually lead to some cleavage of the scFv without ligation of the peptide, so the total signal resulting from the peptide label of the scFv is slightly reduced.

The periplasmic expression of the scFv-myc construct, however, led to much lower overall yields and does not allow the labeling of the antibody fragment with unnatural modifications such as fluorophores.

The expression and isolation of scFv's in a soluble form usually shows limited success, and the yields are very low. On the other hand, the expression in inclusion bodies

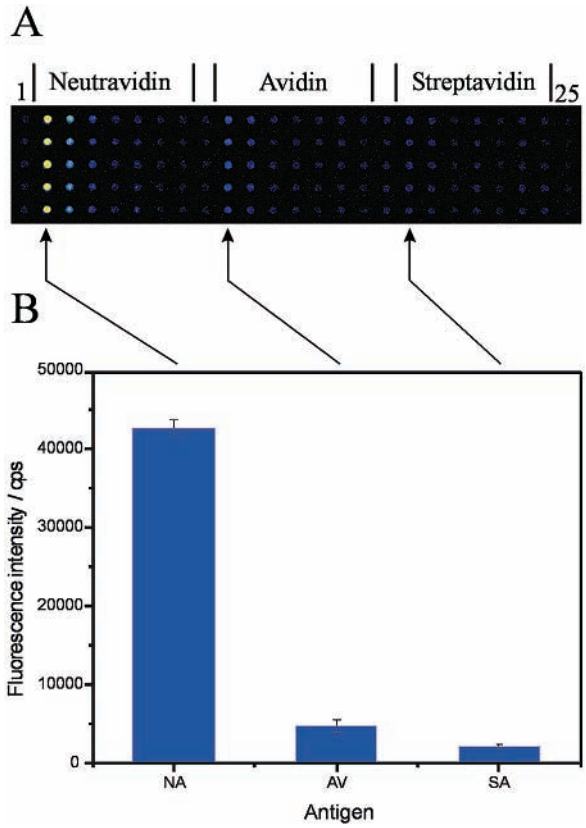


Figure 5. Biochip screening of the fluorescently labeled scFv E9 with different surface-immobilized antigens. A, Microarray surface with 50 μm spots containing different concentrations of the analytes and additional spots with no analyte as a control. Column 1: no analyte; columns 2−8: neutravidin spotted at concentrations of 500, 250, 125, 65, 31, 16, and 8 μg/mL; column 9: no analyte; column 10−16: avidin spotted at concentrations of 500, 250, 125, 65, 31, 16, and 8 μg/mL; column 17: no analyte; column 18−24: streptavidin spotted at concentrations of 500, 250, 125, 65, 31, 16, and 8 μg/mL; column 25: no analyte. B, Averaged fluorescence signals from the five spots with the highest concentration of the antigens (indicated by arrows), NA = neutravidin, AV = avidin, SA = streptavidin. Error bars represent the standard deviations of the averaged signals from the five replicates in each column. The averaged signals were not background subtracted.

results in higher expression yields, but the refolding to an active conformation is generally very difficult and also of limited success. Our technique circumvents these problems and adds the additional opportunity of C-terminal labeling of a single-chain antibody with unnatural modifications such as fluorophores.

Antigen Screening with a Fluorescently Labeled scFv in a Biochip Format. This advantage was further demonstrated by site-specific intein-mediated labeling of the scFv with a rhodamine-containing myc peptide (NH_2-CGGEQKLISEEDLNGGK(TAMRA)-$CONH_2$) using an identical protocol to that described above. To test the utility of the resulting fluorescent scFv, we used a biochip assay. The preparation of the surface was published elsewhere (*23*). The analyte neutravidin and two control proteins, avidin and streptavidin, were microarrayed on a TiO_2 chip containing a biotin-derivatized poly(L-lysine)-poly(ethylene glycol) copolymer (PLL-*g*-PEG-B30%), and the chips were then incubated with a 100 nM solution of the scFv-myc-TAMRA by interfacing the chip with a microfluidic channel array. After the chips were washed, the fluorescence on the chips was analyzed with a fluorescence scanner (Figure 5). The fluorescence intensity was quantified and averaged for five spots in each

row containing the antigens at varying concentrations. The results clearly show the binding properties of the fluorescently labeled scFv in a chip assay format. The specific binding of neutravidin compared to streptavidin and the weak cross-reactivity with avidin are in good correlation with BIAcore experiments that we performed (data not shown).

In contrast to ELISA's, chip-based assays can be performed in a more miniaturized format to ensure higher throughput and smaller sample consumption (*23*). The microfluidic channels interfacing the microarray have a volume of about 10 μL and contain 250 features with a 50 μm diameter. Therefore, the assay can be performed on a significantly smaller scale compared to other immunoassay formats.

In conclusion, the site-specific intein-mediated labeling of single-chain antibodies under denaturing conditions for biochip assays offers new possibilities in the work with antibody fragments. This technique can produce large amounts of active and site-specifically labeled scFv for different applications. The antibody fragment can initially be labeled with a fluorophore for antigen screening in a chip assay format. The same fusion protein can then also be used to introduce other modifications for an oriented immobilization of the antibody fragment on surfaces.

ACKNOWLEDGMENT

We thank Walter Khu and Zhenni Ding for the synthesis of the peptides. In addition, we thank David Wilson and Hans Beernink for critical reading of the manuscript.

LITERATURE CITED

(1) Muir, T. W., Sondhi, D., and Cole, P. A. (1998) Expressed protein ligation: A general method for protein engineering. *Proc. Natl. Acad. Sci. U.S.A. 95*, 6705−6710.

(2) Severinov, K., and Muir, T. W. (1998) Expressed Protein Ligation, a Novel Method for Studying Protein−Protein Interactions in Transcription. *J. Biol. Chem. 273*, 16205−16209.

(3) Kane, P. M., Yamashiro, C. T., Wolczyk, D. F., Neff, N., Goebl, M., and Stevens, T. H. (1990) Protein Splicing Converts the Yeast *TFP1* Gene Product to the 69-kD Subunit of the Vacuolar H^+-Adenosine Triphosphatase. *Science 250*, 651−657.

(4) Hirata, R., Ohsumi, Y., Nakano, A., Kawasaki, H., Suzuki, K., and Anraku, Y. (1990) Molecular Structure of a Gene, *VMA1*, Encoding the Catalytic Subunit of H^+- Translocating Adenosine Triphosphatase from Vacuolar Membranes of *Saccharomyces cerevisiae*. *J. Biol. Chem. 265*, 6726−6733.

(5) Noren, C. J., Wang, J., and Perler, F. B. (2000) Dissecting the Chemistry of Protein Splicing and Its Applications. *Angew. Chem., Int. Ed. 39*, 450−466.

(6) Perler, F. B., and Adam, E. (2000) Protein splicing and its applications. *Curr. Opin. Biotechnol. 11*, 377−383.

(7) Blaschke, U. K., Silberstein, J., and Muir, T. W. (2000) Protein Engineering by Expressed Protein Ligation. *Methods Enzymol. 328*, 478−496.

(8) Giriat, I., Muir, T. W., and Perler, F. B. (2001) Protein Splicing and Its Applications. *Genet. Eng. 23*, 171−199.

(9) Cotton, G. J., and Muir, T. W. (2000) Generation of a dual-labeled fluorescence biosensor for Crk-II phosphorylation using solid-phase expressed protein ligation. *Chem. Biol. 7*, 253−261.

(10) Ayers, B., Blaschke, U. K., Camarero, J. A., Cotton, G. J., Holford, M., and Muir, T. W. (1999) Introduction of Unnatural Amino Acids into Proteins Using Expressed Protein Ligation. *Biopolymers 51*, 343−354.

(11) Iakovenko, A., Rostkova, E., Merzlyak, E., Hillebrand, A. M., Thomä, N. H., Goody, R. S., and Alexandrov, K. (2000) Semi-synthetic Rab proteins as tools for studying intermolecular interactions. *FEBS Lett. 468*, 155−158.

(12) Kawasaki, M., Makino, S.-I., Matsuzawa, H., Satow, Y., Ohya, Y., and Anraku, Y. (1996) Folding-Dependent in Vitro Protein Splicing of the *Saccharomyces cerevisiae VMA1* Protozyme. *Biochem. Biophys. Res. Comm. 222*, 827−832.

(13) Raag, R., and Whitlow, M. (1995) Single-chain Fvs. *FASEB J. 9*, 73−80.

(14) Jackson, H., Bacon, L., Pedley, R. B., Derbyshire, E., Field, A., Osbourn, J., and Allen, D. (1998) Antigen specificity and tumor targeting efficiency of a human carcinoembryonic antigen-specific scFv and affinity-matured derivatives. *Br. J. Cancer 78*, 181−188.

(15) Hanes, J., Schaffitzel, C., Knappik, A., and Plückthun, A. (2000) Picomolar affinity antibodies from a fully synthetic naive library selected and evolved by ribosome display. *Nature Biotechnol. 18*, 1287−1292.

(16) Houston, J. S., Mudgett-Hunter, M., Tai, M.-S., McCartney, J., Warren, F., Haber, E., and Oppermann, H. (1991) Protein Engineering of Single-Chain Fv Analogues and Fusion Proteins. *Methods Enzymol. 203*, 46−88.

(17) Glockshuber, R., Schmidt, T., and Plückthun, A. (1992) The Disulfide Bonds in Antibody Variable Domains: Effects on Stability, Folding in Vitro, and Functional Expression in *Escherichia coli*. *Biochemistry 31*, 1270−1279.

(18) Skerra, A. (1993) Bacterial expression of immunoglobulin fragments. *Curr. Opin. Immunol. 5*, 256−262.

(19) Kurucz, I., Titus, J. A., Jost, C. R., and Segal, D. M. (1995) Correct Disulfide Pairing and Efficient Refolding of Detergent-Solubilized Single-Chain Fv Proteins From Bacterial Inclusion bodies. *Mol. Immunol. 32*, 1443−1452.

(20) Phipps, M. L., Xu, X., Nock, S., and Kassner, P. D. (2000) Detection of antibody display phage without clearing of bacterial culture. *Biotechniques 29*, 739−740.

(21) Merrifield, R. B. (1986) Solid-phase synthesis. *Science 232*, 341−347.

(22) Schnölzer, M., Alewood, P., Jones, A., Alewood, D., and Kent, S. B. H. (1992) In situ neutralization in Boc-chemistry solid-phase peptide synthesis. *Int. J. Pept. Protein Res. 40*, 180−193.

(23) Ruiz-Taylor, L. A., Martin, T. L., Zaugg, F. G., Witte, K., Indermuhle, P., Nock, S., and Wagner, P. (2001) Monolayers of derivatized poly(L-lysine)-grafted poly(ethylene glycol) on metal oxides as a class of biomolecular interfaces. *Proc. Natl. Acad. Sci. U.S.A. 98*, 852−857.

(24) Rudolph, R., and Lilie, H. (1996) In vitro folding of inclusion body proteins. *FASEB J. 10*, 49−55.

(25) Rudolph, R., Böhm, G., Lilie, H., and Jaenicke, R. (1997) Folding proteins. *Protein Function: A practical Approach* (Creighton, T. E., Ed.) pp 57−99, IRL Press, Oxford, UK.

BC025534Z

Peptide Arrays for Highly Sensitive and Specific Antibody-Binding Fluorescence Assays

Oleg Melnyk,*,† Xavier Duburcq,*,‡,§ Christophe Olivier,§ Florence Urbès,§ Claude Auriault,‡ and Hélène Gras-Masse†

UMR CNRS 8525, UMR CNRS 8527, and Sedac-Therapeutics, Biological Institute of Lille, 1 rue du Pr Calmette, 59021 Lille, France. Received November 27, 2001; Revised Manuscript Received March 6, 2002

We report a novel generation of peptide arrays fabricated by site-specific ligation of glyoxylyl peptides onto glass slides covered by a semicarbazide sol−gel layer. These arrays allowed the highly sensitive and specific detection of antibodies in very small blood samples from infected individuals using three model peptidic epitopes (HCV Core and NS4, EBV Capsid) in an immunofluorescence assay. Comparison with standard enzyme-linked immunosorbent assays (ELISAs) demonstrated a large gain in sensitivity and specificity. These unique properties, combined with the possibility to immobilize glycoproteins such as antibodies, offer the possibility to perform sandwich immunofluorescent assays in a highly parallel format.

INTRODUCTION

Today, the miniaturization of biological assays is at the origin of crucial biological research and medical advances. In this respect, the design of miniaturized devices for the simultaneous highly sensitive and specific detection of antibodies from complex biological samples should represent a breakthrough. Over the past decade, the trends toward miniaturization of high-throughput screening systems have generated a great deal of interest in the scientific community. Microfabricated analytical devices have found applications in the field of gene expression profiling (*1*) or large-scale functional analysis of peptides (*2*−*4*) or proteins (*5*−*7*). Owing to the possibility to implement simultaneously a large variety of assays based on antibody or antigen detection, microarrays may revolutionize the diagnostic of infections. So far, applications of protein arrays to the detection of antibodies have displayed high background levels, low signal intensities, and cross-reactivities (*8*−*12*). As a result, the design of miniaturized devices for the highly sensitive and specific detection of antibodies from complex biological samples has not been achieved to date (*13*).

Here we report that a novel generation of peptide arrays, assembled by site-specific semicarbazone ligation of medium-sized peptides onto glass slides, allows the highly sensitive and specific detection of antibodies in very small blood samples from infected individuals. Three model peptidic epitopes (HCV Core and NS4, EBV Capsid) were used for antibody detection studies based on an immunofluorescent assay. The peptide arrays were analyzed with a fluorescence array scanner. A collection of referenced sera permitted demonstration of a large gain in sensitivity and specificity for our arrays as compared to the standard ELISA tests.

* To whom correspondence should be addressed. O.M. and X.D. contributed equally to this work. Oleg Melnyk: Tel: 33(0)3 20 87 12 15, fax: 33(0)3 20 87 12 33, e-mail: oleg.melnyk@pasteur-lille.fr.

† UMR CNRS 8525.

‡ UMR CNRS 8527.

§ Sedac-Therapeutics.

EXPERIMENTAL PROCEDURES

Peptide Synthesis. The peptides were synthesized in an automated peptide synthesizer (model Pioneer, Perseptive Biosystems Inc., MA) using the Fmoc/*tert*-butyl strategy (*14*).

Peptides **3** and **5**−**7** were synthesized on a poly(ethylene glycol) polyacrylamide copolymer (amino PEGA resin (*15*), Novabiochem, Meudon, France) derivatized with an isopropylidene tartrate linker as described in refs *27*−*29*. The peptides were purified by preparative RP-HPLC (C18−VYDAC, buffer A: deionized water containing 0.05% TFA; buffer B: acetonitrile/deionized water: 4/1 by vol. containing 0.05% TFA).

Peptide **3**, yield 21%, MALDI-TOF $[M + H]^+$ calcd 3587.0 found 3587.0. Peptide **5**, yield 21%, MALDI-TOF $[M + H]^+$ calcd 3733.1, found 3732.7. Peptide **6**, yield 25%, MALDI-TOF $[M + H]^+$ calcd 2755.4, found 2755.7. Peptide **7**, yield 34%, MALDI-TOF $[M + H]^+$ calcd 2606.3, found 2606.5.

For peptide **8** (0.1 mmol scale), peptide elongation was followed by acylation with diglycolic anhydride/DIEA: 4 equiv/4 equiv in DMF during 30 min. The peptidyl resin was washed with DMF (4 × 2 min) and then treated successively with 10 equiv of 4,7,10-trioxa-1,13-tridecanediamine (TTD), 3 equiv of DIEA, and 2 equiv of PyBOP (Novabiochem, Meudon, France) in DMF. After 30 min of reaction, the beads were washed with DMF (4 × 2 min) and acylated with Fmoc-L-Ser(O*t*Bu)-OH/HBTU/HOBt/DIEA: 10 equiv/10 equiv/10 equiv/30 equiv in DMF during 45 min. The resin was washed with DMF (4 × 2 min) and deprotected with DMF/piperidine: 4/1 by vol. The resin was washed with DMF (4 × 2 min) and CH_2Cl_2 (4 × 2 min) and dried. Deprotection and cleavage from the solid support was performed with TFA/H_2O/TIS: 95/2.5/2.5 by vol (2 h). The peptide was precipitated in cold ether, redissolved in aqueous acetic acid, and lyophilized. Periodic oxidation was performed in a pH 7.0 0.1 M phosphate buffer with 2 equiv of $NaIO_4$ (5 min). The peptide was purified by RP-HPLC on a C18 Nucleosil 320 × 12 mm column (100 Å, 5 μm), detection at 220 nm, 50 °C, 3 mL/min, 0−20% B in 20 min. Peptide **8**, yield 25%, MALDI-TOF $[M + H]^+$ calcd 2722.4, found 2722.5.

10.1021/bc015584o CCC: $22.00 © 2002 American Chemical Society
Published on Web 06/04/2002

For peptide **4** (0.1 mmol scale), peptide elongation was followed by acylation with Fmoc-L-Lys(Mtt)-OH. Removal of the Mtt group (*16*) with 1% TFA in CH_2Cl_2 (*17*) was followed by acylation with Fmoc-L-Ser(O*t*Bu)-OH as described for peptide **8**. The peptide was deprotected, cleaved with TFA/phenol/H_2O (10 mL/0.5 mL/0.75 g) (2 h), and precipitated in cold diethyl ether. The crude peptide was then oxidized with periodate as described for peptide **8**. Peptide **4** was purified by RP-HPLC on a C3 Zorbax 250 × 15 mm column, detection at 225 nm, 60 °C, 4 mL/min, 0−80% B in 60 min. Peptide **4**, yield 18%, MALDI-TOF $[M + H]^+$ calcd 3544.0, found 3543.8.

Amino acid composition of all the peptides was determined on a Beckman amino acid analyzer (model 7300, ninhydrin detection) following hydrolysis of aliquots in 6 N HCl/phenol (10/1 by vol) (48 h at 110 °C).

Semicarbazide Slides. Full details of semicarbazide glass slide optimization, characterization, and preparation will be reported elsewhere. Rapidly, glass slides (Esco, 114 slides at a time) cleaned with a H_2SO_4/H_2O_2 (1/1 by vol) solution were silanized with 3-aminopropyltrimethoxysilane. The amino slides were treated with triphosgen/diisopropylethylamine in 1,2-dichloroethane and Fmoc-$NHNH_2$ in DMF, respectively, to install the semicarbazide functions. Finally, removal of the Fmoc groups was performed with piperidine/DBU in dimethylformamide. Four slides were used for the quality control. Three slides were immersed 1 h at 37 °C in a 10^{-4} M solution of Rho-Lys-Arg-$NH(CH_2)_3NH-CO-CHO$ (synthesized according to ref 27−28, where Rho is (5)-6-carboxytetramethylrhodamine). One slide was treated with the control peptide Rho-Lys-Arg-NH_2. The fluorescence intensity of the slides was quantified using an Affymetrix 418 Array Scanner (MWG). Typically, the mean fluorescence intensity of semicarbazide slides treated with the glyoxylyl-rhodaminated probe was found to be 36260 (SD 3940) at L35, PMT50 scanner sensitivity (control slide: mean fluorescence 3450, SD 486). Both fluorescent probes were found to adsorb similarly on untreated slides (mean fluorescence for the glyoxylyl probe: 7790, SD 670, mean fluorescence for the amide probe: 5270, SD 930, L35, PMT50).

Human Sera. Sera were collected from the clinical laboratory of the Centre Hospitalier Régional (Lille, France). The reactivity of HCV-referenced sera was determined with the AxSYM HCV version 3.0 Abbott ELISA kit (30 HCV-negative and 100 HCV-positive individuals). The reactivity of EBV-referenced sera (36 HCV-positive and 15 HCV-negative individuals) was determined using an immunofluorescence assay (anti-VCA IFA, Immunoconcept).

ELISAs. Microtiter plate wells (Carbo-bind, Costar, Corning Inc., NY) were coated 60 min at 37 °C with the peptide (5 μg/mL in 0.1 M acetate buffer pH 5.5). The wells were washed and then saturated with 2.5% milk in PBS (0.01 M phosphate buffer supplemented with 1.8% NaCl pH 7.4) at 37 °C. After four washings with PBS 0.05% Tween 20 (PBS-T, Sigma-Aldrich, Saint Quentin Fallavier, France), human sera diluted 1/100 in PBS plus 0.5% Tween 20 plus 2.5% milk were incubated in coated wells for 120 min at 37 °C. After four washings, the peroxidase-conjugated goat antibodies to human IgG-A-M (Diagnostic Pasteur, Marnes la Coquette, France), diluted 1/10000 in PBS plus 0.5% Tween 20 plus 2.5% milk, were incubated for 60 min at 37 °C. Bound conjugated antibodies were detected using *o*-phenylenediamine dihydrochloride substrate (Sigma) plus H_2O_2 in 0.05 M citrate buffer pH 5.5, for 30 min in the dark at room temperature. The reaction was blocked by addition of 2 N H_2SO_4. The absorbance was recorded against a blank at 492 nm through a multichannel automatic plate-reader (M_R 5000, Dynatech, Grafton, Ohio). Mean at 492 nm + 3 standard deviation (SD) of HCV-sera were used as cutoff values in the ELISAs. The ELISAs were performed at least twice to assess their reproducibility.

Peptide Arrays. A manual arrayer (Microarray Printer XMM 47832, Xenopore, Hawthorne, NJ) equipped with 32 pins was used to print the slides. Similar results were obtained using an Affymetrix 417 arrayer. The printed slides were incubated overnight at 37 °C in a humid chamber and stored until use at room temperature for a period ranging from days to several months. The slides were washed and incubated during 120 min at 37 °C under microscope slide with 50 μL of human sera diluted 1/50 in PBS plus 0.5% Tween 20 plus 2.5% milk. After four washings, 50 μL of the rhodamine(TRITC)-conjugated goat antibodies to human IgG-A-M (Jackson ImmunoResearch Laboratories, Baltimore, MD), diluted 1/100 in PBS plus 0.5% Tween 20 plus 2.5% milk, were incubated for 60 min at 37 °C under cover glass. The slides were then washed, dried, and scanned with an Affymetrix 418 Array Scanner (MWG). The data where analyzed using the ScanAlyse software (Stanford University).

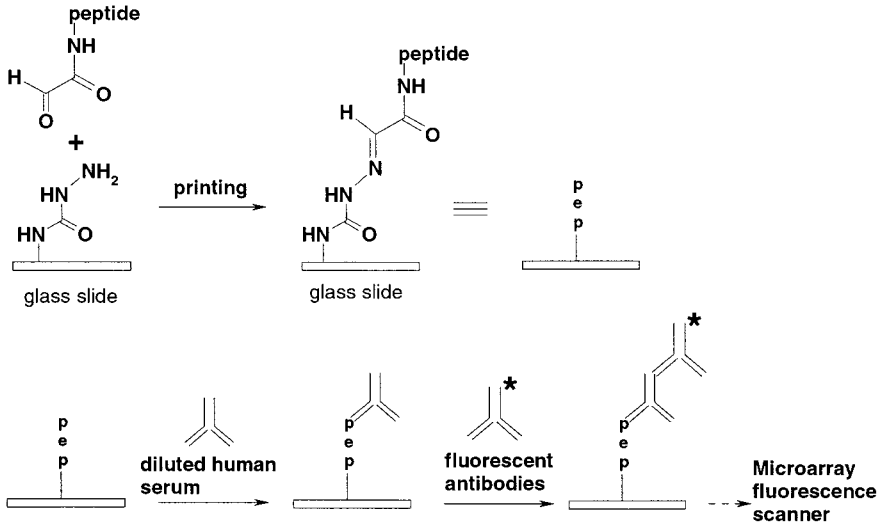
Immobilization of Antibodies on Semicarbazide Slides. The antibodies (donkey IgG anti-goat IgG F(c), Rockland, Gilbertsville, PA, or goat IgG anti-human Ig G−A-M, Jackson ImmunoResearch Laboratories, Baltimore, MD) were oxidized as described in ref 32. Following oxidation, the antibodies (600 μg) were dialyzed (nanosep tubes, Pall Gelman Laboratory, Ann Arbor, MI) against acetate buffer pH 5.5 0.1 mM (six washings), solubilized in 40 μL of acetate buffer pH 5.5 0.1 mM and placed in a 384-well plate. Ten slides were printed using a manual Xenopore XMM 47832 printer and incubated one night at 37 °C in a humid chamber. The slides were washed and incubated under cover glass with 50 μL of rhodamine conjugated goat IgG F(c) fragment (Rockland, Gilbertsville) diluted 1/100 in PBS plus 0.5% Tween 20 plus 2.5% milk (60 min at 37 °C). The slides were washed, dried in air, and analyzed with an Affymetrix 418 Array Scanner. The data were processed with the ScanAlyse software.

RESULTS AND DISCUSSION

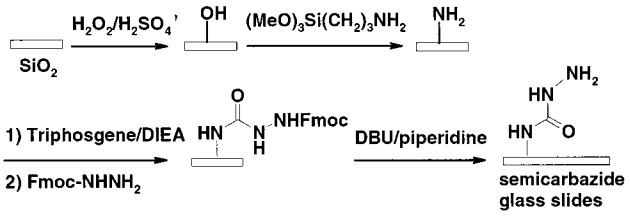
Glass Slide Design and Preparation. The design of miniaturized devices for the highly sensitive and specific detection of antibodies from complex biological samples represents a challenge which, besides the selection of the probes, relies mainly upon the surface properties of the array. We first hypothesized that the optimal surface for antibody detection would be uncharged at neutral pH and highly hydrated. Indeed, neutral hydrophilic polymers have been found to reduce protein adsorption on different surfaces (*18, 19*). Second, the surface should be chemically inert toward immunoglobulins but should allow the covalent site-specific and dense immobilization of synthetic polypeptides so as to favor the antigen accessibility and to reach high signal-to-noise ratios. Glass slides covered by a semicarbazide sol−gel layer were found to meet all these criteria, and in conjunction with the well developed chemistry of glyoxylyl peptides (*20*) were used to elaborate a novel generation of peptide arrays assembled by semicarbazone site-specific ligation (Scheme 1).

The optimization, characterization, and preparation of semicarbazide glass slides will be reported in a paper devoted to the fabrication of oligodeoxynucleotide mi-

Scheme 1. Semicarbazone Assembled Peptide Arrays



Scheme 2. Preparation of Semicarbazide Glass Slides



croarrays using a similar immobilization strategy (*21*, *22*). Very rapidly as shown in Scheme 2, microscope glass slides were cleaned with H_2SO_4/H_2O_2 (piranha solution) and silanized with 3-aminopropyltrimethoxysilane. The amino slides were then treated successively with triphosgen/DIEA and Fmoc-$NHNH_2$ (*23*) in DMF to install the semicarbazide groups. Finally, removal of the Fmoc groups was performed with piperidine/DBU in dimethylformamide. The density and homogeneity of the semicarbazide sol−gel layer was evaluated by immersing the slides in a solution of a glyoxylyl dipeptide labeled with (5)-6-carboxytetramethylrhodamine (Rho-Lys-Arg-NH-$(CH_2)_3$NH−CO−CHO, peptide **1**) followed by quantification of the fluorescence using the Cy3 channel of a DNA microarray scanner. Immobilization through site-specific semicarbazone formation was demonstrated by several control experiments using either underivatized dipeptide **2** Rho-Lys-Arg-NH_2 on semicarbazide slides or glyoxylyl peptide **1** on slides lacking the semicarbazide functionality (see Experimental Section).

Synthesis of Model Glyoxylyl Peptide Antigens. The three model sequences selected for our study are derived from immunodominant and conserved regions of hepatitis C virus (HCV, core p21 15−45 (*24*), NS4 1925−1947 (*25*)) and Epstein−Barr virus (EBV, VCAp18 153−176 (*26*)). The corresponding glyoxylyl peptides are shown in Figure 1. For the HCV core p21 antigen, the glyoxylyl group was placed either at the N-terminus at the extremity of a Lys side-chain (peptide **4**) or at the C-terminus. In this later case, two different spacers were used to document the influence of the distance between the peptide and the glass surface upon the detection of antibodies (peptides **3** and **5**). N- or C-glyoxylyl derivatives were also synthesized for the EBV VCAp18 peptide (peptides **7** and **8**). Only one derivative was evaluated for the HCV NS4 peptide (peptide **6**).

HCV p21 NTNRRPQDVKFPGGGQIVGGVYLLPRRGPRLG

HCV NS4 AFASRGNHVSPTHYVPESDAAARG

EBV VCAp18 **AVDTGSGGGGQPHDTAPRGARKKQG**

Peptide 3 H-HCV p21

Peptide 4 HCV p21-NH_2

ecneuqes

Peptide 5 : H-HCV p21
Peptide 6 : H-HCV NS4
Peptide 7 : H-EBV VCAp18

Peptide 8 EBV VCAp18-OH

Figure 1. Model glyoxylyl peptide antigens used in this study.

Peptides **3**, **5**−**7** were synthesized on the solid phase using an isopropylidene tartrate-based linker and the Fmoc/*t*Bu strategy as described elsewhere (*27*, *28*, *29*). Peptides **4** and **8** were obtained from the corresponding seryl precursors by treatment with $NaIO_4$ according to Geoghegan et al. (*30*). For H-Lys(Ser)−HCV core p21 15−45, the peptide elongation step using the Fmoc/*t*Bu strategy was followed by coupling with Boc-L-Lys(Fmoc)-OH. The Fmoc group was removed with piperidine and the ϵ-amino group was acylated with Fmoc-L-Ser(O*t*Bu)-OH. The peptidyl resin was deprotected and cleaved from the solid support as usual with concentrated trifluoroacetic acid. For the seryl precursor of peptide **8**, the peptidyl resin was treated with diglycolic (DG) anhydride to introduce a carboxylic acid function on the N-terminus.

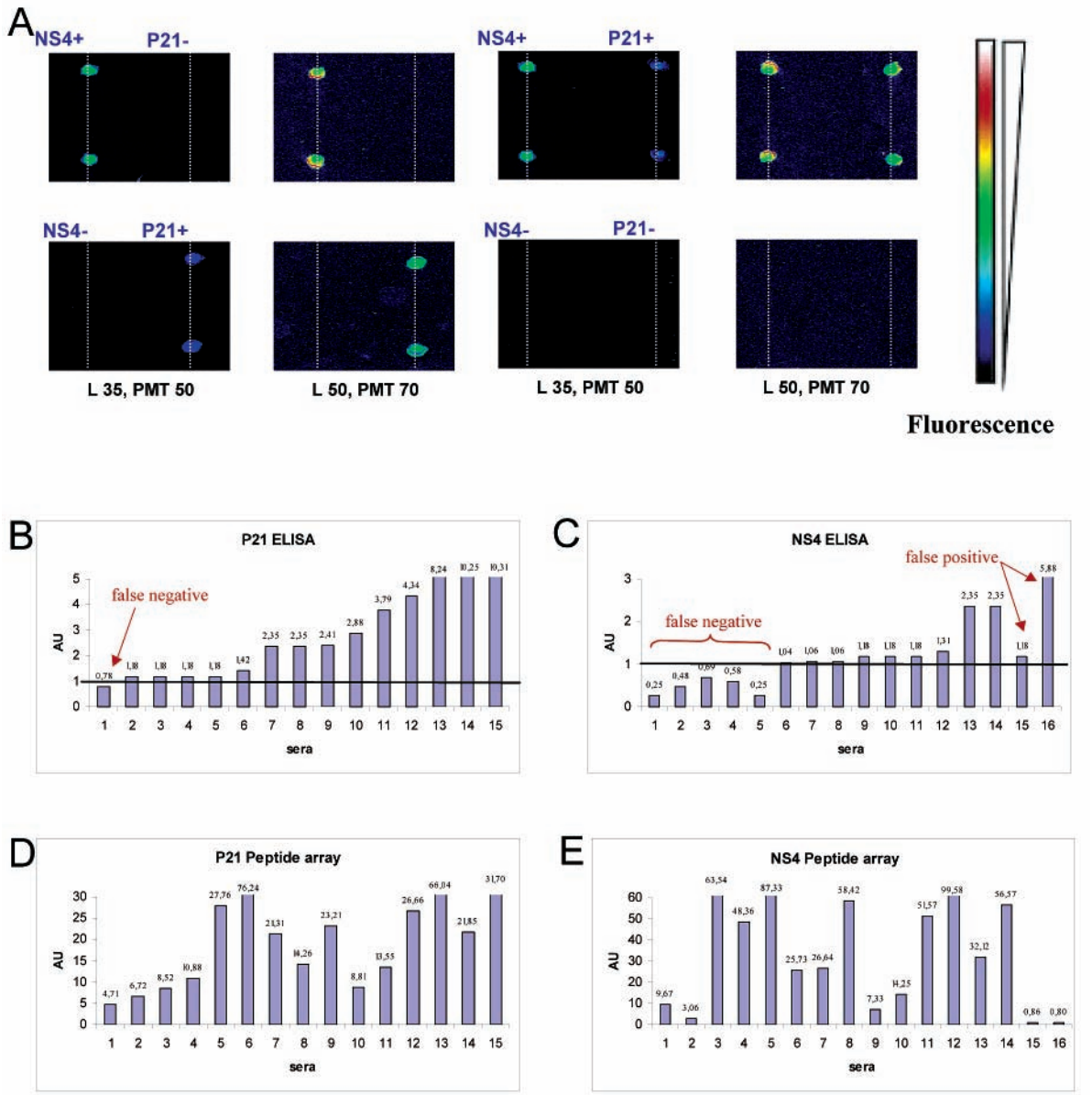


Figure 2. Detection of antibodies to peptides **5** (HCV p21) and **6** (HCV NS4) expressed in arbitrary units (AU). AU = signal value/cutoff. (Cutoff = 1 AU = mean of the background + 3 SD). (a) Scanning image of HCV+ (NS4+P21+, NS4+P21-, NS4−P21+) and HCV− sera at a low (L35, PMT50) or high (L50, PMT70) scanner sensitivity. (b) Detection of antibodies to peptide **5** by ELISA for 15 sera. (c) Detection of antibodies to peptide **6** by ELISA for 16 sera. (d) Peptide **5** array fluorescence for the same sera as b. (e) Peptide **6** array fluorescence for the same sera as c.

In situ activation of the carboxylic acid group with PyBOP in the presence of 4,7,10-trioxa-1,13-tridecanediamine (TTD) was followed by acylation with Fmoc-L-Ser-(O*t*Bu)-OH. Deprotection and cleavage from the support afforded H-Ser-TTD-DG-EBV VCAp18 peptide.

Peptide Array Spotting. The glyoxylyl peptides were printed using a manual arrayer from Xenopore, which led to a spot diameter of about 550 μm. Similar results were obtained using an Affymetrix 417 arrayer (spot diameter of 160 μm) showing that the data did not depend on the printing technology. As for rhodaminated probe **1**, the presence of a glyoxylyl group on the HCV p21 peptide is essential for an efficient immobilization on semicarbazide slides. The glyoxylyl antigens were printed at a concentration of 10^{-4} M in a pH 5.5 acetate buffer. HCV p21 and NS4 peptides were also printed as a 1/1 mixture using the same experimental conditions. The slides were incubated overnight in a humid chamber at 37 °C and then directly used for antibody detection. Importantly, no further chemical treatment for the capping of the remaining semicarbazide groups was found to be necessary before the incubation with the sera.

Detection of Antibodies by an Immunofluorescent Assay. Comparison with Enzyme-Linked Immunosorbent Assays. The peptide arrays were utilized for the detection of antibodies as shown in Scheme 1. Incubation with diluted human sera was followed by detection of immobilized antibodies with a rhodamine-labeled anti-human Ig-G-A-M antibodies. These two steps were performed under a cover glass and required minutes quantities of sera (1μL) and labeled antiboby (1 μg). The slides were imaged using the Cy-3 channel of a DNA microarray scanner.

A referenced collection of 130 sera of HCV infected (100) or not (30) individuals was analyzed using the peptide array technology and by ELISA (AxSYM HCV version 3.0 Abbott, or ELISA with p21 or NS4 antigens coated on carbo-bind plates). The background noise of the arrays, defined as the fluorescence signal between the printed spots, was found to be very low for all the tested

Table 1. Comparison between ELISAs and Peptide Arrays for HCV Antibodies Detection

		ELISAs			peptide array			Western-blot[b]			remarks	
entry	Nb of sera	reference test[a]	Carbobind[c] p21	NS4	p21	NS4	p21+NS4	core	NS4	NS3		
1	73	+	+	+	+	+	+	nd	nd	nd		
2	14	+	+	−	+	−	+	nd	nd	nd		
3	1	+	+	+	−	−	−	−	−	−	false ELISAs	positive
4	1	+	−	+	−	−	−	−	−	−	false ELISAs	positive
5	5	+	−	−	−	−	−	−	−	−	false ELISAs	positive
6	2	+	−	−	−	+	+	−	+	+	false ELISAs	negative
7	4	+	+	−	+	+	+	+	+	+	false ELISAs	negative
8	30	−	−	−	−	−	−	nd	nd	nd		

[a] AxSYM HCV version 3.0, Abbott. [b] CHIRON RIBA HCV 3.0 SIA, Ortho-Clinical Diagnostics. [c] Carbo-bind plates, Costar, Corning Incorporated.

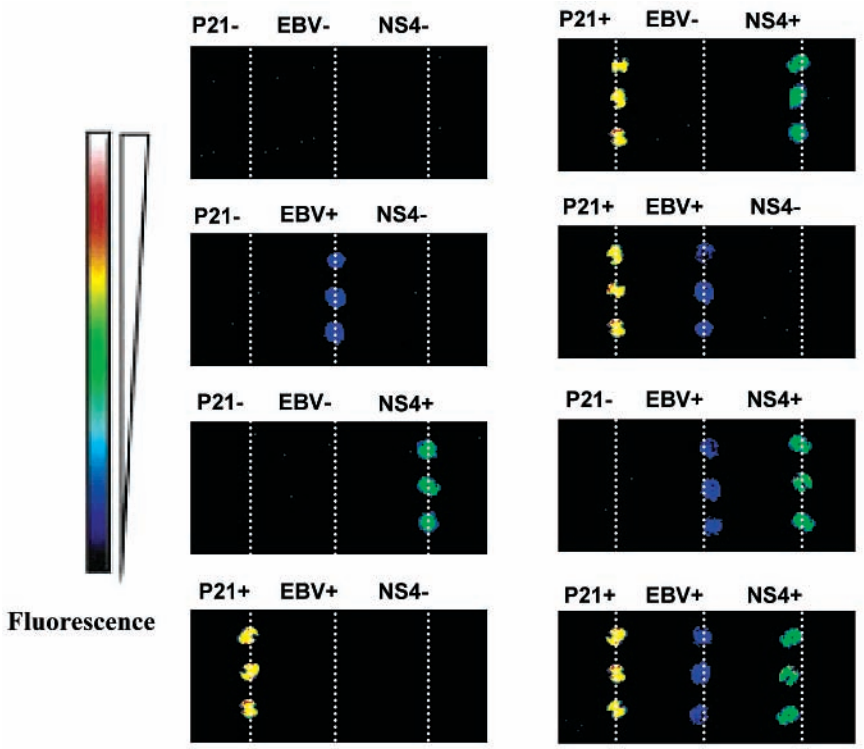


Figure 3. Scanning image of HCV+ (NS4+P21+, NS4+P21−, NS4−P21+), HCV−, and EBV VCAp18+ or EBV VCA p18- sera at a L35, PMT50 scanner sensitivity (peptides **5**, **6**, and **8**).

sera and corresponded to 0.1% of the highest signal observed. Interestingly, the fluorescence obtained with the sera of noninfected individuals was always found to be below the mean of the background + 3 SD, even at a high scanner sensitivity (Figure 2A).

Analogously, no fluorescence was observed for HCV+p21- or HCV+NS4- sera with p21 or NS4 peptides, respectively. Thus, to the contrary of ELISAs, no nonspecific binding could be detected with peptide arrays. Consequently, the cutoff value of positivity was defined as the mean of the background + 3 SD. The data collected in Table 1 show that peptide arrays and ELISAs were in agreement for 117 sera (entries 1, 2, and 8).

For the 13 sera, where discrepancies were observed between the different tests (entries 3−7, Table 1), an additional analysis was performed using a western-blot assay (CHIRON RIBA HCV 3.0 SIA, Ortho-Clinical Diagnostics), which is the most sensitive and specific test for HCV antibodies detection. The western-blot assay confirmed the peptide array results, and that these sera were false positive or false negative by ELISA. Thus, at least for the selected model epitopes, peptide arrays displayed 100% of sensitivity and specificity. In addition, the arrays were found to be much more sensitive than ELISAs, since comparison of ELISA and peptide array data indicated an average gain in sensitivity of about 8. Figure 2b−e detail the fluorescence and absorbance values for HCV+p21+ or HCV+NS4+ sera just above the cutoff value in ELISA, expressed in arbitrary units (AU) as defined in the legend of Figure 2. The consequence of this gain in sensitivity is that false negative sera or sera just above the ELISA cutoff were detected without ambiguity using the peptide arrays.

The same sensitivity and specificity levels were reached with the VCAp18 EBV peptides **7** or **8**. Indeed, 36 EBV-positive sera were found positive with the peptide array technology, whereas the fluorescence values associated with the 15 EBV-negative sera were always below the cutoff value of positivity (as for HCV sera, background + 3SD). Interestingly, when peptides **5**, **6**, and **8** were printed on the same slide, no cross-reaction was observed between a particular peptide and antibodies specific for the two others (Figure 3). These data illustrate the high specificity of this peptide array technology, an essential characteristic to permit the application of the array format for the simultaneous detection of different antibodies.

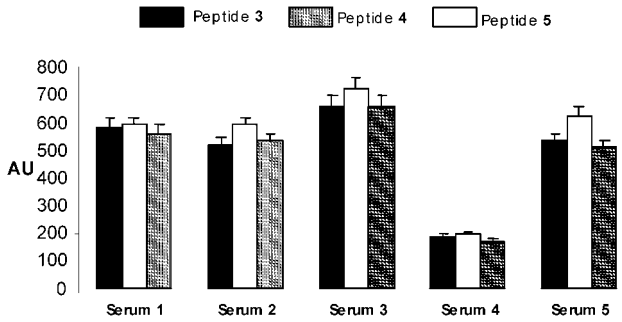


Figure 4. Influence of the spacer and of the glyoxylyl group position upon the detection of antibodies directed against HCV core p21 15−45 antigen, HCV+ sera, L35, PMT 50.

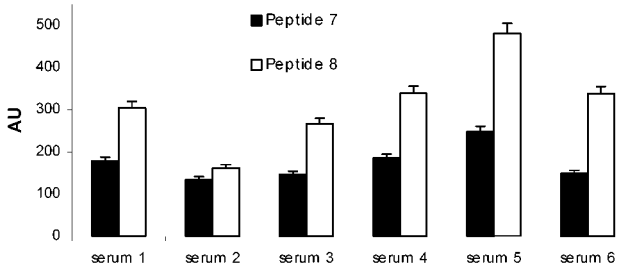


Figure 5. Influence of the glyoxylyl group position upon the detection of antibodies directed against EBV VCAp18 antigen, data expressed in arbitrary units (AU), HBV+ sera, L35, PMT50.

Influence of the Spacer and of the Glyoxylyl Group Position. Peptides **3**−**5** permitted us to evaluate both the influence of the spacer separating the peptide from the glass surface and of the site of immobilization for the HCV p21 antigen. The data presented in Figure 4 show that no significant difference could be observed between these three peptides. For the site-specific immobilization through the C-terminus, the size of the spacer seemed to have little or no effect on antigen recognition.

To the contrary of HCV p21, detection of antibodies directed against EBV VCAp18 antigen was found to be highly dependent upon the site of attachment to the glass surface (Figure 5). Indeed, peptide **8** permitted to improve significantly the detection of antibodies in the cases where peptide **7** displayed low ratios. Nevertheless, both peptides displayed the same levels of sensibility and specificity for the serodetection of EBV infections, at least for the tested sera.

Quality Control, Reproducibility, Stability upon Storage. An important aspect of antibody detection is the reproducibility of the assay. To document the spot to spot reproducibility, peptide **5** was spotted 600 times on the same slide. The array was incubated with an HCV p21 + serum and treated as described before (Figure 6a). The standard deviation (SD) of the fluorescence for 600 spots was found to be 5.1%. Figure 6b details the fine structure of a spot and shows that the fluorescence inside the spot was uniform, an essential characteristic for the automation of fluorescence measurements.

Another important aspect of the peptide array methodology is the possibility to reach high slide to slide reproducibility levels. To check this point, 12 slides were spotted with peptide **5** (600 spots) and treated with the same HCV+ serum. The SD between the mean fluorescence of the spots and of the background for the different slides was found to be only 4.5%.

Finally, the peptide arrays were also tested for their stability upon storage. For peptides **5**−**7**, no significant variation in fluorescence intensity of the spots and of the background was observed following up to 6 months of aging at 37 °C in a humid chamber (Figure 7). This feature can be attributed to the high chemical stability of the semicarbazone linkage and of the sol−gel layer.

Site-Specific Immobilization of Antibodies. To broaden the utility of this methodology, we have also shown that semicarbazide slides allow the immobilization of glycoproteins and thus can be used for the preparation of protein arrays or mixed peptide−proteins arrays. Indeed, periodic oxidation is a well established and mild method for generating aldehyde groups on glycoproteins (*31*, *32*). The reaction of these aldehyde groups with semicarbazide functionalized slides leads to the covalent immobilization of the proteins. For example, oxidized donkey IgG anti goat IgG Fc and goat IgG anti human

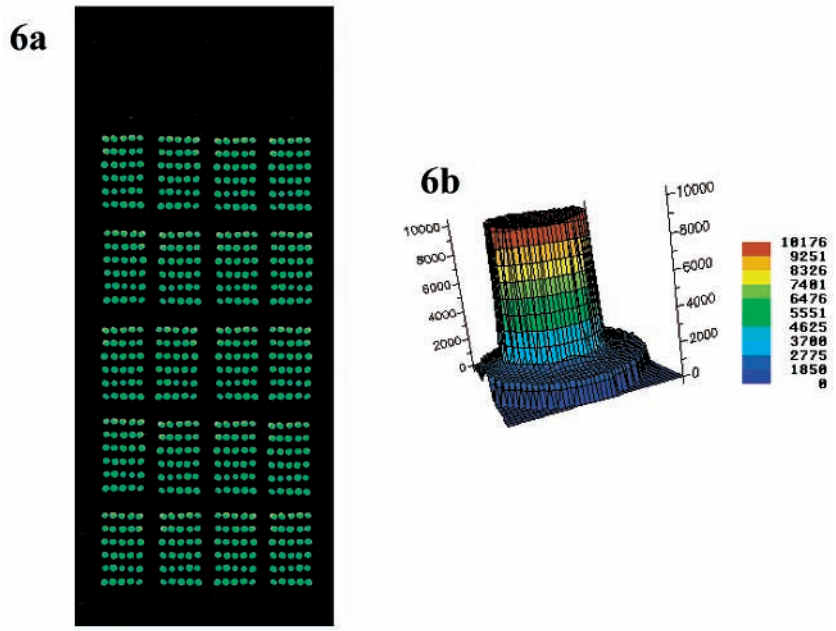


Figure 6. (a) Spot to spot reproducibility, peptide **5**, Affymetrix 418 Array Scanner, scanner sensitivity L35, PMT50; (b) fine structure of a spot, same slide as in a, array WoRx microarray scanner, Applied Precision, Issaquah, Washington.

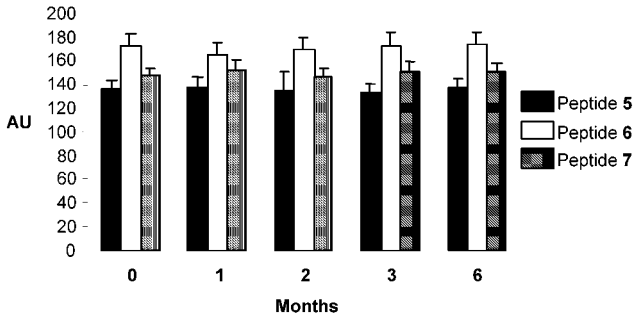


Figure 7. Stability of peptide arrays upon accelerated aging, peptides **5**−**7**, HCV+ and EBV+ referenced sera, data expressed in arbitrary units (AU), L35, PMT50.

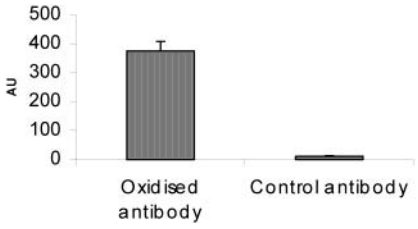


Figure 8. Site-specific immobilization of oxidized antibodies, scanner sensitivity L35, PMT50.

IgG-A−M were immobilized on semicarbazide slides and incubated with goat IgG Fc fragment labeled with rhodamine. Figure 8 shows that the fluorescence associated with donkey antibodies was found to be high, whereas fluorescence associated with the control goat antibodies corresponded to the background. Importantly, the slides were printed, washed, and incubated using the procedures employed for peptide arrays. Since these conditions retained the binding capacity and the specificity of immobilized antibodies, the simultaneous detection of antibodies and of circulating antigens on the same slide seems conceivable.

CONCLUSION

At the origin, microarrays were developed to utilize the huge amount of information provided by genome projects, but they have clear potential for many other fields where multiple tests have to be performed using very small biological samples. We have demonstrated that arrays, assembled by semicarbazone site-specific ligation of synthetic polypeptides to glass slides, displayed very high sensitivities and specificities for antibodies directed toward several model peptidic epitopes. These unique properties combined with the possibility to immobilize glycoproteins should find many applications such as sandwich immunofluorescent assays, detection of circulating antigens, epitope mapping, and high throughput screenings.

ACKNOWLEDGMENT

We thank CNRS, Université de Lille 2, Institut Pasteur de Lille and Sedac-Therapeutics for financial support, Rémi Desmet, Annick Blanpain, and Eric Diesis for technical assistance, Frédéric Malingue for data studies, David Hot and Ludovic Huot for fluorescence measurements, Thomas Heim for AFM studies, and Steven Brooks for proofreading the manuscript. We thank Pr Yves Lemoine for giving us an access to the Affymetrix 418 array scanner and Affymetrix 417 arrayer.

LITERATURE CITED

(1) Schena, M., Shalon, D., Davis, R. W., and Brown, P. O. (1995) Quantitative monitoring of gene expression patterns with a complementary DNA microarray. *Science 270*, 467−470.

(2) Emili, A. Q., and Cagney, G. (2000) Large-scale functional analysis using peptide or protein arrays. *Nat. Biotechnol. 18*, 393−397.

(3) Fodor, S. P. A., Read, J. L., Pirroung, M. C., Stryer, L., Tsai Lu, A., and Solas, D. (1991) Light-directed, spacially addressable parallel chemical synthesis. *Science 251*, 767−773.

(4) Falsey, J. R., Renil, M., Park, S., Li, S., and Lam, K. S. (2001) Peptide and small molecule microarray for high throughput cell adhesion and functional assays. *Bioconjugate Chem. 12*, 346−353.

(5) Irwing, R. A., and Hudson, P. J. (2000) Proteins emerge from disarray. *Nat. Biotechnol. 18*, 932−933.

(6) MacBeath, G., and Schreiber, S. L. (2000) Printing proteins as microarrays for high-throughput function determination. *Science 289*, 1760−1763.

(7) Zhu, H., and Snyder, M. (2001) Protein arrays and microarrays. *Curr. Opin. Chem. Biol. 5*, 40−45.

(8) Joos, T. O. et al. (2000) A microarray enzyme-linked immunosorbent assay for autoimmune diagnostics. *Electrophoresis 21*, 2641−2650.

(9) Mendoza, L. G. et al. (1999) High-throughput microarray-based enzyme-linked immunosorbent assay (ELISA). *Biotechniques 27*, 778−788.

(10) DeWildt, R. M. T., Mundy, C. R., Gorick, B. D., and Tomlinson, I. A. (2000) Antibody arrays for high-throughput screening of antibody−antigen interactions. *Nat. Biotechnol. 18*, 989−994.

(11) Arenkov, P. et al. (2000) Protein microchips: use for immunoassay and enzymatic reactions. *Anal. Biochem. 278*, 123−131.

(12) Haab, B. B., Dunham, M. J., and Brown, P. O. (2001) Protein microarrays for highly parallel detection and quantitation of specific proteins and antibodies in complex solutions. http://genomebiology.com/2001/2/2/research/0004.1.

(13) Petrik, J. (2001) Microarray technology: the future of blood testing? *Vox Sang. 80*, 1−11.

(14) Fields, G. B., and Noble, R. L. (1990) Solid-phase peptide synthesis utilizing 9-fluorenyl methoxycarbonyl amino acids. *J. Pept. Protein Res. 35*, 161−214.

(15) Meldal, M. (1993) In *Peptides 1992, Proceedings of the European Peptide Symposium* (C. Schneider, and A. N. Eberle, Eds.) p 61, Escom, Leiden.

(16) Aletras, A., Barlos, K., Gatos, D., Koutsogianni, S., and Mamos, P. (1995) Preparation of the very acid-sensitive Fmoc-Lys(Mtt)-OH. *Int. J. Pept. Protein Res. 45*, 488−496.

(17) Bourel, L., Carion, O., Gras-Masse, H., and Melnyk, O. (2000) The deprotection of Lys(Mtt) revisited. *J. Pept. Sci. 6*, 264−270.

(18) Bergström, K., et al. (1994) Effects of branching and molecular weight of surface-bound poly(ethylene oxide) on protein rejection. *J. Biomater. Sci., Polym. Ed. 6*, 123−132.

(19) Giacomelli, C., Bremer, M. G. E. G., and Norde, W. (1999) ATR-FTIR study of IgG adsorbed on different silica surfaces. *J. Colloid Interface Sci. 220*, 13−23.

(20) Tam, J. P., and Spetzler, J. C. (1995) Chemoselective approaches to the preparation of peptide dendrimers and branched artificial proteins using unprotected peptides as building blocks. *Biomed. Pept., Proteins Nucleic Acids 1*, 123−132.

(21) Melnyk, O., Gras-Masse, H., and Lemoine, Y. (2001) Produits comprenant un support sur lequel sont fixés des acides nucléiques et leur utilisation comme puce à ADN. *Bull. Off. Propr. Ind. 23*, publication number 2 801 904.

(22) Olivier, C., Ollivier, N., Hot, D., Huot, L., Lemoine, Y., Huynh-Dinh, T., Gouyette, C., Gras-Masse, H., Melnyk, O. (2001) A novel generation of DNA microarrays fabricated using semicarbazone ligation, presented at the 7th Interna-

tional Symposium on Solid Phase Synthesis & Combinatorial Chemical Libraries, University of Southampton, England, UK, 18−22 Sept. 2001, poster number 22.

(23) Zhang, R.-E., Cao, Y.-L., and Hearn, M. W. (1991) Synthesis and application of Fmoc-hydrazine for the quantitative determination of saccharides by reversed-phase high-performance chromatography in the low and subpicomole range. *Anal. Biochem. 195*, 160−167.

(24) Jolivet-Reynaud, C. et al. (1998) HCV core immunodominant region analysis using mouse monoclonal antibodies and human sera: characterisation of major epitopes useful for antigen detection. *J. Med. Virol. 56*, 300−309.

(25) Longombardo, G. et al. (1998) Immune response to an epitope of the NS4 protein of hepatitis C virus in HCV related disorders. *Clin. Immunol. 87*, 124−129.

(26) Van Grunsven, W. M. J., Spaan, W. S. M., and Middeldorp, J. M. (1994) Localization and diagnostic application of immunodominant domains of the BFR3 encoded Epstein−Barr virus capsid protein. *J. Infect. Dis. 170*, 13−19.

(27) Melnyk, O., Fruchart, J.-S., Grandjean, C., and Gras-Masse, H. (2001) Tartric acid-based linker for the solid-phase synthesis of C-terminal peptide α-oxo aldehyde. *J. Org. Chem. 66*, 4153−4160.

(28) Fruchart, J.-S., Gras-Masse, H., and Melnyk, O. (1999) A new linker for the synthesis of C-terminal peptide α-oxo aldehydes. *Tetrahedron Lett. 40*, 6225−6228.

(29) Fruchart, J.-S., Urbès, F., Gras-Masse, H., and Melnyk, O. (2002) Site-specific immobilisation of glyoxylyl peptides for more sensitive and specific enzyme-linked immunosorbent assays. *Lett. Pept. Sci.*, accepted for publication.

(30) Geoghegan, K. F., and Stroh, J. G. (1992) Site-directed conjugation of nonpeptide groups to peptides and proteins via periodate oxidation of a 2-amino alcohol. Application to modification at N−Terminal serine *Bioconjugate Chem. 3*, 138−146.

(31) Rodwell, J. D., Alvarez, V. L., Lee, C., Lopes, A. D., Goers, J. W. F., King, H. D., Powsner, H. J., and McKearn, T. J. (1986) Site-specific covalent modification of monoclonal antibodies: *In vitro* and *in vivo* evaluations. *Proc. Natl. Acad. Sci. U.S.A. 83*, 2632−2636.

(32) Wolfe, C. A. C., Hage, D. S. (1995) Studies on the rate and control of antibody oxidation by periodate. *Anal. Biochem. 231*, 123−130.

BC015584O

DOTA−D-Tyr[1]-Octreotate: A Somatostatin Analogue for Labeling with Metal and Halogen Radionuclides for Cancer Imaging and Therapy

Wen Ping Li,[†] Jason S. Lewis,[†] Joonyoung Kim,[†] Joseph E. Bugaj,[‡] Michael A. Johnson,[‡] Jack L. Erion,[‡] and Carolyn J. Anderson*[,†]

Mallinckrodt Institute of Radiology, Washington University School of Medicine, St. Louis, Missouri 63110 and Mallinckrodt, Inc. 675 McDonnell Blvd., St. Louis, Missouri 63134. Received December 10, 2001; Revised Manuscript Received April 25, 2002

The goal of this study was to evaluate a somatostatin receptor ligand, DOTA−D-Tyr[1]-octreotate (DOTA-DY1-TATE), that has the chelator 1,4,7,10-tetraazacyclotetradecane-*N*,*N*′,*N*″,*N*‴-tetraacetic acid (DOTA) attached to the D-Tyr[1] residue, allowing radiolabeling with both radiohalogens and radiometals. A potential advantage of having a chelator attached to the Tyr[1] residue is that halogen radiolabels may residualize or remain trapped in tumor cells rather than clear from the tumor. DOTA-DY1-TATE was synthesized by solid-phase methods and radiolabeled with ^{61}Cu, ^{64}Cu, and ^{125}I in high radiochemical purity and specific activity. A competitive binding assay demonstrated that ^{nat}Cu-DOTA-DY1-TATE and DOTA-^{nat}I-DY1-TATE had comparable affinity to ^{nat}In-DTPA-OC in AR42J rat pancreatic tumor cells membranes. ^{61}Cu-DOTA-DY1-TATE had a dissociation constant (K_d) of 176.4 pM and a receptor concentration (B_{max}) of 244.4 fmol/mg. A tumor uptake of 1.515 %ID/g was determined for ^{64}Cu-DOTA-DY1-TATE and 0.814 %ID/g for DOTA-^{125}I-DY1-TATE in AR42J tumor bearing Lewis rats at 1 h postinjection. DOTA-^{125}I-DY1-TATE remained in the tumor at a higher concentration out to 4 h postinjection, suggesting that the iodine may have residualized in the tumor cells. MicroPET imaging of ^{64}Cu-DOTA-DY1-TATE in AR42J tumor bearing rats and SCID mice at 2 h postinjection showed significant uptake and good contrast in the thigh tumors in the rat model and in the neck and thigh tumors of the mouse. This study demonstrates that DOTA-DY1-TATE is a somatostatin analogue that can be labeled with both metal and halogen radionuclides, and its ^{64}Cu- and ^{125}I-radiolabeled compounds showed somatostatin receptor-mediated uptake in normal and tumor tissues.

INTRODUCTION

Over the last 15 years, considerable progress has been made in the investigation of radiolabeled somatostatin analogues as radiotherapeutic agents for somatostatin receptor-positive tumors. A number of studies have focused on improving the target tissue uptake of radiolabeled somatostatin analogues. It has been shown that changing the C-terminus from an alcohol to a carboxylic acid increases uptake of the peptide in somatostatin subtype 2 receptor (SSTR2)-positive tissues (*1*−*3*). It has further been shown that replacing the N-terminal D-Phe in octreotide with D-Tyr allows iodination of the N-terminus and subsequent residualization of the iodinated D-amino acid (*4*). Therefore, in this current study we synthesized DOTA−D-Tyr[1]-octreotate (DOTA-DY1-TATE, Figure 1) to allow both radiolabeling with halogens (e.g., ^{124}I, ^{125}I, ^{131}I, ^{76}Br, ^{77}Br), as well as radiometals (e.g., ^{86}Y, ^{90}Y, ^{68}Ga, ^{177}Lu, ^{111}In, ^{64}Cu). One of our goals is to achieve higher somatostatin receptor binding affinity and better target tissue uptake as well as allow halogen radionuclides to residualize in target tissues.

The use of positron-emitting halogen radionuclides, specifically ^{124}I ($t_{1/2}$ = 4.2 d) and ^{76}Br ($t_{1/2}$ = 16 h), to label radiopharmaceuticals for PET imaging has increased greatly over the past decade. For example, ^{76}Br has been labeled to octreotide (*5*) and ^{76}Br-labeled bromodeoxyuridine has been investigated as a tumor and brain imaging agent (*6*, *7*). Iodine-124 is currently used to produce [^{124}I]-5-iodo-2′-fluoro-1-β-D-arabinofuranosyl-uracil (FIAU) which has been used to image gene expression (*8*). Copper-64 [$t_{1/2}$ = 12.8 h; 40% β^- (0.656 MeV); 19% β^+ (0.6 MeV); 38% EC] has diverse applications in radiopharmaceutical chemistry for PET imaging as well as therapy (*9*, *10*). Copper-61 [$t_{1/2}$ = 3.35 h; 60% β^+ (1.21 MeV); 40% EC] is another cyclotron-produced positron-emitting radionuclide that is made at Washington University using the same targetry system as is used for ^{64}Cu (*11*). Moreover, ^{61}Cu and ^{64}Cu can be produced on demand in high yield and in high specific activity on a small biomedical cyclotron (*11*, *12*).

The AR42J rat pancreatic carcinoma cell line is known to express SSTR2 both in vitro and in vivo (*13*, *14*). AR42J cells grown in culture were utilized to evaluate the in vitro binding affinity and were implanted in

* Corresponding author: Carolyn J. Anderson, Ph.D., Mallinckrodt Institute of Radiology, Washington University School of Medicine, 510 S. Kingshighway Blvd., Campus Box 8225, St. Louis, MO 63110. Phone: (314) 362-8427; fax: (314) 362-9940, e-mail: andersoncj@mir.wustl.edu.

† Washington University School of Medicine.

‡ Mallinckrodt, Inc.

[1] Abbreviations used: DTPA, diethylenetriaminepentaacetic acid; DOTA, 1,4,7,10-tetraazacyclododecane-*N*,*N*′,*N*″,*N*‴-tetraacetic acid; TETA, 1,4,8,11-tetraazacyclotetradecane-*N*,*N*′,*N*″,*N*‴-tetraacetic acid; Y3, tyrosine-3; OC, octreotide; TATE, octreotate; D-Tyr[1], DY1; somatostatin subtype 2 receptor, SSTR2; positron emission tomography, PET; confidence interval, CI.; region of interest, ROI.

10.1021/bc015590k CCC: $22.00 © 2002 American Chemical Society
Published on Web 05/25/2002

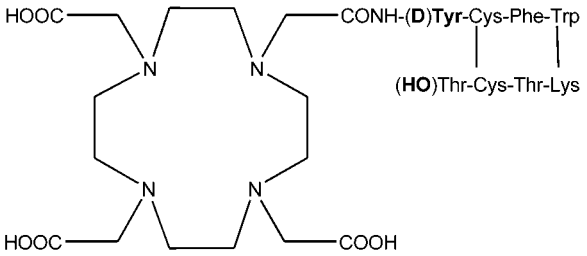


Figure 1. Structure of DOTA−D-Tyr[1]-octreotate (DOTA-DY1-TATE).

immature, normal Lewis rats for in vivo biodistribution and microPET imaging. In this study, we determined the in vitro binding affinity of copper-labeled DOTA-DY1-TATE to AR42J tumor cell membranes and investigated the in vivo biodistribution of ^{64}Cu-DOTA-DY1-TATE and DOTA-^{125}I-DY1-TATE in AR42J tumor bearing rats. MicroPET imaging studies of ^{64}Cu-DOTA-DY1-TATE were carried out in the AR42J tumor-bearing SCID mice and immature Lewis rats.

MATERIALS AND METHODS

Materials and Analyses. ^{61}Cu and ^{64}Cu were produced on a Cyclotron Corporation CS-15 biomedical cyclotron at Washington University of School of Medicine, using previously reported methods (*11*, *12*). Sodium[^{125}I]-iodide was purchased from NEN LifeScience (Boston, MA). Indium-111-chloride ($^{111}InCl_3$) was obtained from Mallinckrodt, Inc. (St. Louis, MO). IODO-GEN precoated iodination tubes were purchased from Pierce (Rockford, IL). Reversed-phase extraction C-18 SepPak Light cartridges were obtained from Waters (Milford, MA). Ammonium acetate (NH_4OAc) was purchased from Fluka Chemical Co. (Ronkonkoma, NY); Copper acetate (99.99%) and indium acetate (99.95%) were purchased from Alfa Morton Thiokol Inc. (Danvers, MA). Trifluoroacetic acid (TFA) was obtained from J. T. Baker (Chicago, IL). All other chemicals were purchased from Aldrich Chemical Co., Inc. (Milwaukee, WI). All solutions were prepared using ultrapure water (18 MΩ-cm resistivity). Thin-layer chromatography (TLC) was performed using Whatman $MKC_{18}F$ reversed phase plates with 10% ammonium acetate:methanol (30:70) as the mobile phase. Radio-TLC detection was accomplished using a BIOSCAN System 200 Imaging Scanner (Washington, DC). Analytical reversed-phase HPLC was accomplished on a Waters (Milford, MA) 600E chromatography system with a Waters 991 photodiode array detector and an Ortec Model 661 (EG&G Instruments, Oak Ridge, TN) radioactive detector. Millenium 32 software (Waters, Milford, MA) was used to quantify chromatograms by integration. All HPLC samples were analyzed on a Vydac Protein & Peptide C-18 column (2.2 × 25 cm). The mobile phase was H_2O (0.1% TFA) (solvent A) and 90% acetonitrile (ACN) (0.1% TFA) (solvent B). The gradient consisted of 5% B to 75% B in 25 min (1.0 mL/min flow rate). Radioactive samples were counted using a Beckman 8000 automated well-type counter (Fullerton, CA).

Preweaned (21-day old, 40−50 g) male Lewis rats were purchased from Charles River Laboratories (Boston, MA) and Female SCID-Fox Chase CB-17 mice (29−35 days old, 25−30 g) were purchased from Taconic Farms Inc (Germantown, NY). The AR42J tumor line was obtained from American Type Culture Collection (ATCC, Rockville, MD).

Synthesis of DY1-TATE and DOTA-DY1-TATE. The synthesis of DYI-TATE and DOTA-DY1-TATE were accomplished by using similar methods previously described (*3*). Briefly, solid-phase peptide synthesis (SPPS) was carried out on an Applied Biosystems model 432A "Synergy" peptide synthesizer using the Fmoc (9-fluorenylmethoxy-carbonyl) methodology. Activated Fmoc-protected amino acids (25 μmol) were required by the instrument protocol. Activation was performed by combining 1-hydroxybenzotriazole (HOBt) and 2-(1*H*-benzotriazol-1-yl)-1,1,3,3-tetramethyluronium hexafluorophosphate (HBTU). DOTA-tris(*tert*-butyl ester) (Macrocyclics, Dallas, TX) was activated and coupled to Fmoc-protected amino acid. Final purifications of the peptides were accomplished by reversed-phase HPLC, employing a Vydac Protein & Peptide C-18 column (2.2 × 25 cm).

Preparation of Radiolabeled Somatostatin Analogues. DTPA-OC was labeled with ^{111}In as previously described (*15*). Radiolabeling with ^{61}Cu and ^{64}Cu was carried out by addition of 1−5 mCi (37−185 MBq) of ^{61}Cu or ^{64}Cu in 0.1 M ammonium acetate (pH 6.5) to 1−5 μg of the peptide in 0.1 M ammonium acetate followed by 30 min incubation at 65 °C as previously reported (*16*). The $^{64/61}$Cu-labeled DOTA-DY1-TATE was purified on a C-18 SepPak Light cartridge, using 100% ethanol as the elution solvent, and radiochemical purity was determined by radio-TLC or radio-HPLC.

Radioiodinated DOTA-DY1-TATE was synthesized using the IODO-GEN method (*17*, *18*). Briefly, Na[^{125}I] [300−400 μCi (11.1−14.8 MBq)] was added to 10 μg of DOTA-DY1-TATE diluted with 0.01 M PBS (100 μL) in a glass vial coated with IODO-GEN (50 μg). The reaction mixture was removed from the reaction vessel following 25 min of incubation at room temperature. The solution was then diluted with 3 mL of water. The resulting solution was eluted through a C-18 reversed-phase extraction cartridge, which was preconditioned with 5 mL of 70% ethanol and subsequently activated with 5 mL of 2-propanol. The cartridge was rinsed successively with 5 mL of distilled water and 5 mL of 0.5 M acetic acid. The radioiodinated peptide was eluted in 5 mL of 96% ethanol, and the solvent was evaporated at room temperature under a gentle stream of nitrogen. The dry residue was reconstituted in 1−3 mL of 0.9% NaCl.

The cold copper and indium agents (^{nat}Cu-DOTA-DY1-TATE, ^{nat}Cu-DOTA-Y3-TATE, ^{nat}In-DTPA-OC) for the receptor binding assays were prepared by the reaction of copper and indium acetate using the same procedure described above for radiolabeling of DOTA-DY1-TATE with ^{61}Cu, ^{64}Cu, and ^{111}In. DOTA-^{nat}I-DY1-TATE was synthesized by following the same procedure as for DOTA-^{125}I-DY1-TATE, and the reaction yield was confirmed by HPLC.

In Vitro Receptor Binding Assay. The binding affinity of Cu-DOTA-DY1-TATE was measured in AR42J rat pancreatic tumor membranes using methods previously described with minor modifications (*9*). Briefly, ^{61}Cu-DOTA-DY1-TATE was displaced with increasing concentrations of ^{nat}Cu-DOTA-DY1-TATE. A competitive binding assay was performed by displacing ^{111}In-DTPA-OC with the competing ligands ^{nat}Cu-DOTA-DY1-TATE, ^{nat}Cu-DOTA-Y3-TATE, ^{nat}In-DTPA-OC and DOTA-^{nat}I-DY1-TATE. Assays were carried out using the Millipore Multiscreen system (Bedford, MA) (*9*). The best-fit IC_{50} values, the dissociation constant (K_d), and the number of SSTR2 binding sites (B_{max}) for the AR42J cells were calculated using PRISM (Graphpad, San Diego, CA).

Animal Models. All animal experiments were performed in compliance with the Guidelines for the Care and Use of Research Animals established by Washington

University's Animal Studies Committee. For AR42J tumor-bearing mice, AR42J cells were grown as xenografts in female SCID mice. Briefly, AR42J cells (1×10^7), grown in F-12K Nutrient mixture medium containing 20% fetal calf serum (FCS) were injected subcutaneously, bilaterally, into flanks and necks of female SCID mice (*19*). The tumors were allowed to grow 10−12 days until 0.5−0.9 g in size. Male Lewis rats (21 d old) were implanted with AR42J tumors in the necks or/and left legs from tumor obtained from Mallinckrodt, Inc (St. Louis, MO) (passage 36) and maintained by serial passage in animals. Tumor was excised from euthanized rats and was rinsed with sterile saline and placed on ice in a Petri dish containing Gibco Media 199 (Sigma Chemical Co., St. Louis, MO). Connective and necrotic tissue were removed, and the material was diced into small pieces (2×2 mm). The freshly dissected pieces were delivered to the left flank of the animal via a 13-gauge trocar inserted subcutaneously. AR42J tumor growth was observed for 2 weeks after implantation, and tumors achieved a solid, palpable mass of 1.0−1.5 g in size by ∼14 days postimplantation.

Biodistribution of ^{64}Cu-DOTA-DY1-TATE and DOTA-^{125}I-DY1-TATE. Biodistribution studies were carried out using immature (∼33 day old) male Lewis rats bearing AR42J tumors (12 days post-implant) in the left flank. Anesthetized animals received a coinjection of ^{64}Cu-DOTA-DY1-TATE and DOTA-^{125}I-DY1-TATE (32 μCi for ^{64}Cu, 5 μCi for ^{125}I, 0.68 μg peptide for each compound) via the tail vein. The animals were euthanized at 1, 4, 24, and 72 h postinjection. A group of 5 rats were coinjected with a blocking dose of DY1-TATE (150 μg) and sacrificed 1 h postinjection. Following euthanization, the tissues and organs of interest were removed and weighed, and the radioactivity was measured in a gamma counter. Standards ($n = 5$) were prepared to verify the counting efficiency of the gamma counter for each radionuclide. Samples were first counted for ^{64}Cu using a specific energy window that did not have detectable crossover for ^{125}I. After allowing for complete decay of the ^{64}Cu (>12 half-lives), the samples were then counted using the energy window specific for ^{125}I. The percent injected dose per gram (% ID/g) and percent injected dose per organ (% ID/organ) were calculated by comparison with standards representing the injected dose per animal. A group of five rats that were sacrificed at 72 h postinjection were housed in individual metabolism cages for the collection of urine and feces at various time points from 1 to 72 h for determination of the %ID excreted.

MicroPET Images. Positron emission tomography (PET) imaging was performed on the first commercially available microPET (Concorde Microsystems, Knoxville, TN) which was based on the design of Cherry and colleagues (*20*). Imaging studies were carried out on four SCID mice and four male Lewis rats carrying AR42J tumors. Two mice bearing tumors on the neck and left leg and four rats (two rats had tumors on neck and left leg, the other two rats had tumors on left legs only) were imaged on the microPET at selected times postinjection. Two tumor-bearing mice were each injected with 1 mCi ^{64}Cu-DOTA-DY1-TATE (1 mCi/μg for control, 1 mCi/50 μg for blocked) and imaged at 10 min, 1, 2, and 4 h postinjection. The two mice were imaged side by side and remained in the same bed position for all time points. Four rats were each injected with 2.5 mCi ^{64}Cu-DOTA-DY1-TATE (2.5 mCi/μg for control, 2.5 mCi/150 μg for blocked) and imaged at 10 min, 1, 2, and 4 h. Each rat was imaged in two bed positions. Immediately after imaging, the %ID/g of tumor from the rats was determined by measuring the dissected tumors in a dose calibrator (Capintec, Ramsey, NJ). Tumor, kidney, and liver activities of ^{64}Cu were generated by measuring regions of interest (ROIs) that encompassed the entire organ from the microPET images in AR42J tumor-bearing SCID mice and Lewis rats after 2 and 4 h postinjection.

Statistical Methods. To compare differences between the data, a student's t-test was performed using Prism (Graphpad, San Diego, CA). Differences at the 95% confidence level ($p < 0.05$) were considered significant.

RESULTS

Chemistry and Radiochemistry. The DY1-TATE and DOTA-DY1-TATE were analyzed by analytical reversed-phase HPLC (UV detection 214 nm) using conditions described in the Methods section and by LC-MS. DY1-TATE: HPLC retention time = 17.9 min; MS, *m/z* calculated for $C_{49}H_{64}N_{10}O_{12}S_2$ $(M + H)^+ = 1048.4$, found 1049.3. DOTA-DY1-TATE: HPLC retention time = 20.4 min; MS, *m/z* calculated for $C_{65}H_{90}N_{14}O_{19}S_2$ $(M + H)^+ = 1434.7$, found 1435.6. ^{111}In-DTPA-OC and $^{61/64}$Cu-DOTA-DY1-TATE were prepared in ≥98% radiochemical purity. Specific activities for both ^{111}In- and $^{61/64}$Cu-labeled conjugates ranged from 1500 to 3500 Ci/mmol (56000 to 111000 GBq/mmol). The radiochemical purity of DOTA-^{125}I-DY1-TATE was confirmed to be greater than 98% by radio-HPLC. DOTA-DY1-TATE was typically labeled with ^{125}I to a specific activity of 300 Ci/mmol (11000 GBq/mmol). The reaction yields for "cold" somatostatin analogues were greater than 98% as confirmed by radio-TLC of an exchange reaction between natural Cu^{2+} or In^{3+} with ^{64}Cu or ^{111}In, respectively.

In Vitro Receptor Binding Assay. A homogeneous competitive binding assay was performed using AR42J tumor membranes, where ^{61}Cu-DOTA-DY1-TATE was challenged with increasing concentrations of ^{nat}Cu-DOTA-DY1-TATE. The IC_{50} value for ^{nat}Cu-DOTA-DY1-TATE was determined to be 1.35 nM, with a 95% confidence interval (CI) of 1.02 to 1.8 nM (Figure 2A). Scatchard analysis of the data showed a K_d of 176.4 pM (95% CI 158.4 to 201.3 pM) and a somatostatin B_{max} in the AR42J membranes of 244.4 fmol/mg (95% CI 219.7 to 274.1 fmol/mg) of membrane protein (Figure 2B).

A competitive binding assay was performed between four somatostatin analogues vs ^{111}In-DTPA-OC. The concentration of the radioligand in the binding assays was 0.05 nM. The IC_{50} values were 1.78 nM for Cu-DOTA-Y3-TATE, 4.62 nM for Cu-DOTA-DY1-TATE, 4.8 nM for DOTA-I-DY1-TATE, and 4.87 nM for In-DTPA-OC (Figure 3 and Table 1). These results suggest that Cu-DOTA-DY1-TATE and DOTA-I-DY1-TATE have similar binding affinity to AR42J cells as In-DTPA-OC, while the analogue with Tyr in the 3-position has somewhat higher binding affinity.

Biodistribution Studies. Summaries of the biodistribution data are shown in Figure 4. Rapid clearance of the radioactivity from the blood circulation was observed for both compounds. At all times of analysis the average uptake of ^{64}Cu activity in tumors was approximately twice as high as ^{125}I activity ($p < 0.03$). The highest tumor uptake of ^{64}Cu-DOTA-DY1-TATE (1.515 ± 0.154 %ID/g) was found after 1 h postinjection, and was 1.247 ± 0.250 %ID/g at 4 h postinjection, suggesting that the ^{64}Cu was residualized in the tumor out to at least 4 h postinjection. A similar trend was observed for DOTA-^{125}I-DY1-TATE (0.814 ± 0.058%ID/g at 1 h, 0.543 ± 0.016

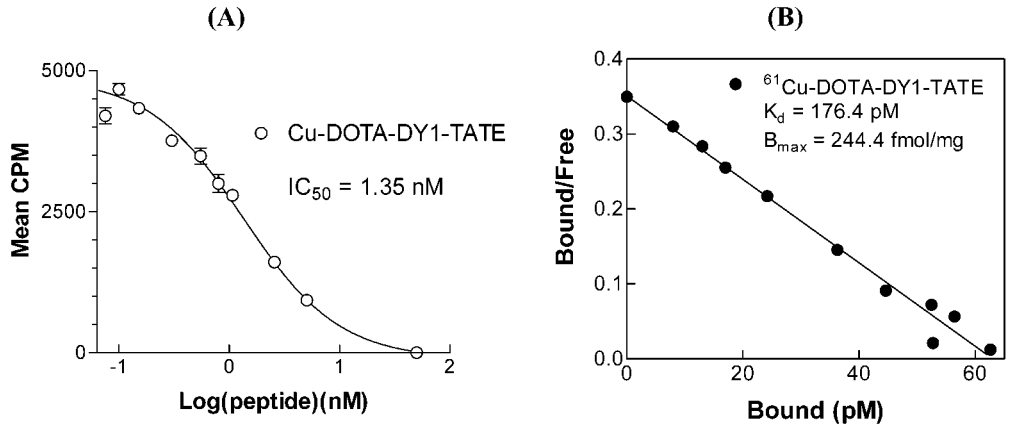


Figure 2. The in vitro binding affinity of ^{61}Cu-DOTA-DY1-TATE to AR42J rat pancreatic tumor membranes blocked with increasing concentrations of unlabeled Cu-DOTA-DY1-TATE ($n = 6$ for each data point).

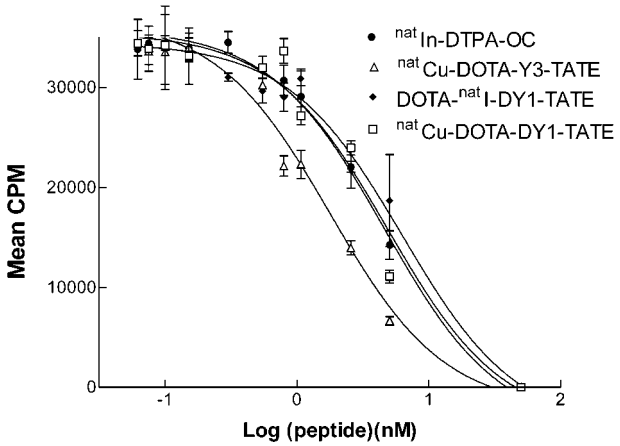


Figure 3. Competitive binding assay of Cu-DOTA-DY1-TATE, DOTA-I-DY1-TATE, Cu-DOTA-Y3-TATE, and In-DTPA-OC displacing ^{111}In-DTPA-OC in AR42J tumor membranes ($n = 3$ for each data point).

Table 1. IC_{50} Values for Competitive Binding Assay of ^{nat}Cu-DOTA-DY1-TATE, DOTA-^{nat}I-DY1-TATE, ^{nat}Cu-DOTA-Y3-TATE, and ^{nat}In-DTPA-OC Displacing ^{111}In-DTPA-OC in AR42J Tumor Membranes ($n = 3$ for each data point)

competing ligand	IC_{50} (nM)	95% CI (nM)
^{nat}Cu-DOTA-Y3-TATE	1.78	1.29−2.46
^{nat}Cu-DOTA-DY1-TATE	4.62	3.28−6.52
DOTA-^{nat}I-DY1-TATE	4.58	3.13−6.69
^{nat}In-DTPA-OC	4.87	3.98−5.96

%ID/g at 4 h) in the tumors. In the rats that received the co-injected blocking dose, the uptake in the tumor of ^{64}Cu-DOTA-DY1-TATE (0.468 ± 0.046 %ID/g) and DOTA-^{125}I-DY1-TATE (0.323 ± 0.016 %ID/g) was significantly lower at 1 h postinjection ($p < 0.02$) (Table 2). The higher uptake of ^{64}Cu-labeled conjugate in the tumor compared to ^{125}I-labeled conjugate may be due to a greater degree of retention of ^{64}Cu-DOTA-DY1-TATE in the tumor compared to DOTA-^{125}I-DY1-TATE. Since time points earlier than 1 h were not evaluated for the biodistribution studies, it is difficult to know whether the uptake of DOTA-^{125}I-DY1-TATE in the tumor peaked prior to 1 h.

The uptake in the pituitary and the pancreas at 1 h postinjection was significantly higher with ^{64}Cu-DOTA-DY1-TATE (1.985 ± 0.334 %ID/g for pituitary, 1.490 ± 0.337 %ID/g for pancreas) compared with DOTA-^{125}I-DY1-TATE (1.246 ± 0.160 %ID/g for pituitary, 0.850 ± 0.203 %ID/g for pancreas) ($p < 0.05$). Uptake in the SSTR2-rich pituitary, adrenals, and pancreas was blocked with unlabeled DY1-TATE for both the ^{125}I and ^{64}Cu-labeled peptides, suggesting receptor-mediated uptake of both compounds in these tissues (Table 2). No appreciable differences were observed for non-somatostatin-receptor-positive tissues between rats that received a coinjection of blocking dose and unblocked rats.

Liver uptake for DOTA-^{125}I-DY1-TATE at all times of analysis was lower than for ^{64}Cu-DOTA-DY1-TATE. However, the kidney uptake of DOTA-^{125}I-DY1-TATE (9.761 ± 1.036 %ID/g at 1 h, 9.450 ± 0.255 %ID/g at 4 h, 8.190 ± 0.646 %ID/g at 24 h, 5.921 ± 0.880 %ID/g at 72 h) was 3-fold higher than that of ^{64}Cu-DOTA-DY1-TATE (2.888 ± 0.187 %ID/g at 1 h, 2.389 ± 0.202 %ID/g at 4 h, 1.740 ± 0.061 %ID/g at 24 h, 1.206 ± 0.158 %ID/g at 72 h). The kidney clearance of DOTA-^{125}I-DY1-TATE maintained a level of 5.921 ± 0.880 %ID/g even after 72 h postinjection. This high kidney uptake and longer retention time of DOTA-^{125}I-DY1-TATE was similar to that of ^{125}I-DY1-TATE and DTPA-^{125}I-DY1-TATE (*4*). This is most likely due to the longer residence time of the DOTA-^{125}I-DY1 residue in the kidneys compared to ^{125}I-L-amino acids. Except for ^{125}I activity in thyroid, normal tissue uptake of DOTA-^{125}I-DY1-TATE decreased throughout the period.

The highest tumor:blood ratios were found at 4 h postinjection for both ^{64}Cu- and ^{125}I-labeled DOTA-DY1-TATE in AR42J tumor-bearing Lewis rats (7.8 ± 1.5 and 8.8 ± 0.9, respectively). For DOTA-^{125}I-DY1-TATE, the tumor-to-blood ratio maintained at high levels out to 24 h postinjection (6.4 ± 1.0), while for ^{64}Cu-DOTA-DY1-TATE the ratio dropped to 2.6 ± 0.6. Tumor:muscle ratios were similar for ^{64}Cu- and ^{125}I-labeled DOTA-DY1-TATE, with the peak ratio occurring at 4 h (19.2 ± 3.8 and 21.9 ± 2.5, respectively).

The excretion data demonstrated that 59.18 ± 21.05 %ID for ^{64}Cu and 64.22 ± 19.93 %ID for ^{125}I was excreted from the urine by 4 h postinjection. By 24 h postinjection, ∼75 %ID of ^{64}Cu-DOTA-DY1-TATE activity was found in the urine and feces, and ∼85 %ID of DOTA-^{125}I-DY1-TATE activity was excreted (Table 3).

MicroPET Images. Figure 5A shows the coronal microPET images of AR42J tumor-bearing SCID mice, 2 h postadministration of ^{64}Cu-DOTA-DY1-TATE, with and without a coinjected blocking dose of DY1-TATE. Uptake in the neck and thigh tumors was visible at 2 h postinjection for the control mouse (left). Conversely, the other mouse (right) that received a blocking dose showed reduced uptake at both tumor sites. Prominent uptake was observed in the liver and kidneys in both animals.

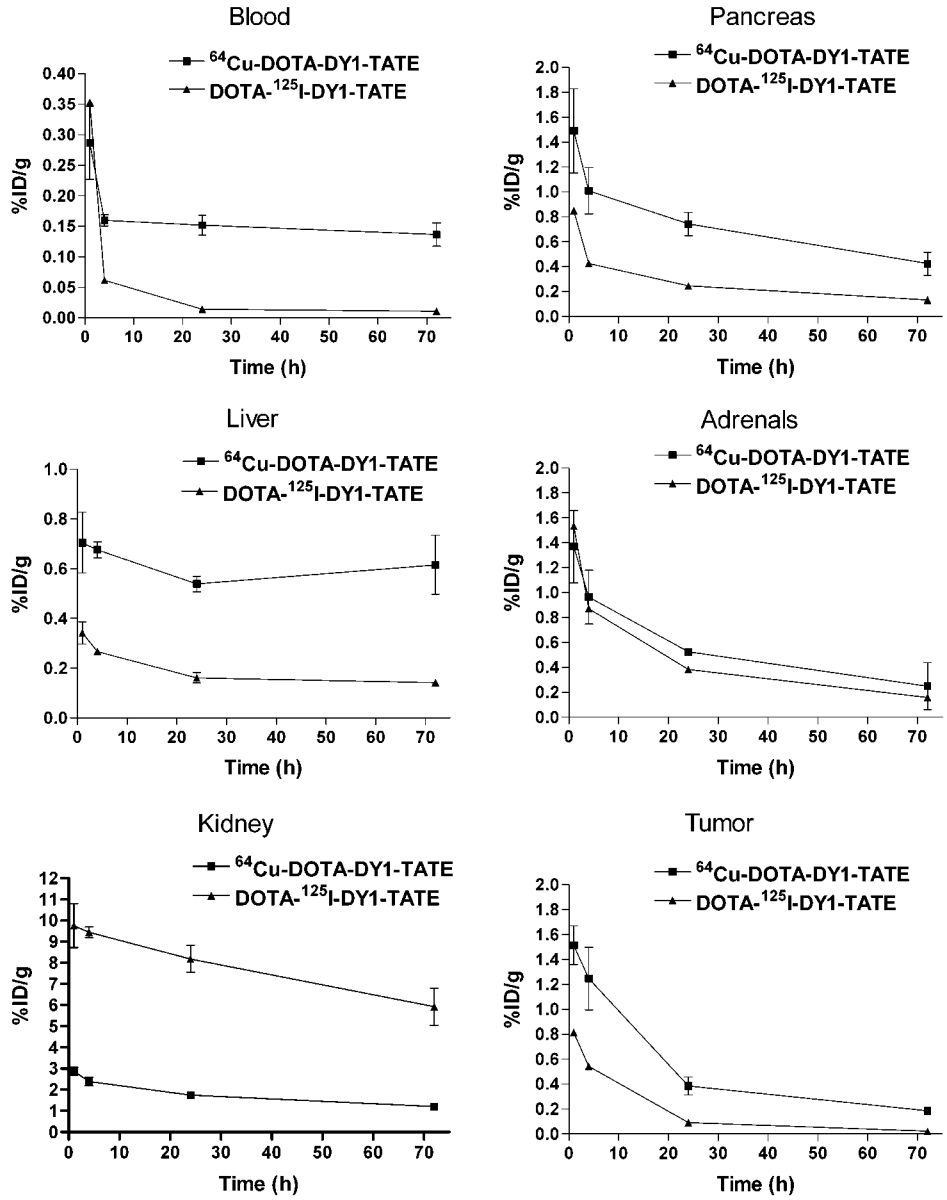


Figure 4. Biodistribution data of ^{64}Cu-DOTA-DY1-TATE and DOTA-^{125}I-DY1-TATE in normal and SSTR2 positive tissues (blood, liver and kidneys, pancreas, adrenals, tumor). Data are presented as %ID/g ± SD, $n = 5$ for each time point.

Table 2. Biodistribution of ^{64}Cu-DOTA-DY1-TATE and DOTA-^{125}I-DY1-TATE in AR42J Tumor Bearing Lewis Rats at 1 h, with and without a Coadministration of Blocking Agent[a]

tissue	^{64}Cu, 1 h	^{64}Cu, 1 h block	^{125}I, 1 h	^{125}I, 1 h block
blood	0.287 ± 0.060	0.361 ± 0.065	0.354 ± 0.073	0.434 ± 0.064
liver	0.705 ± 0.122	0.981 ± 0.199	0.342 ± 0.045	0.352 ± 0.036
kidney	2.888 ± 0.187	3.626 ± 0.176	9.761 ± 1.036	10.895 ± 0.863
pituitary	1.985 ± 0.334	0.516 ± 0.456	1.246 ± 0.160	0.325 ± 0.208
adrenals	1.369 ± 0.291	0.234 ± 0.066	1.534 ± 0.351	0.212 ± 0.036
pancreas	1.490 ± 0.337	0.409 ± 0.059	0.850 ± 0.203	0.270 ± 0.024
tumor	1.515 ± 0.154	0.468 ± 0.046	0.814 ± 0.058	0.323 ± 0.016
thyroid	0.307 ± 0.040	0.388 ± 0.083	1.357 ± 0.131	1.234 ± 0.023

[a] Data are presented as % ID/g ± SD ($n = 5$).

Four hours after administration of ^{64}Cu-DOTA-DY1-TATE, both tumor sites in the nonblocked animal could still be easily identified, as well as showing higher uptake than other normal organs.

Figure 5B shows the microPET images in Lewis rats bearing AR42J tumors of ^{64}Cu-DOTA-DY1-TATE obtained after 2 h postinjection with and without the addition of DY1-TATE as a blocking agent. Imaging was performed at 1, 2, and 4 h postinjection. Similar to the AR42J tumor-bearing mice images, tumor uptake was also observed in the tumor-bearing rats. The most prominent region of ^{64}Cu-DOTA-DY1-TATE uptake was the bladder, due to the rapid excretion of this compound into the urine. In addition, significant uptake in the SSTR2-rich pituitary was observed.

Uptake of radioactivity in the tumor, kidney, and liver measured from the microPET images in the AR42J tumor-bearing SCID mice and Lewis rats after 2 and 4

Table 3. Excretion of ^{64}Cu-DOTA-DY1-TATE and DOTA-^{125}I-DY1-TATE in AR42J Tumor-Bearing Lewis Rats[a]

	^{64}Cu-DOTA-DY1-TATE			DOTA-^{125}I-DY1-TATE		
	4 h	24 h	48 h	4 h	24 h	48 h
urine	59.18 ± 21.05	65.36 ± 19.88	66.29 ± 20.35	64.22 ± 19.93	74.93 ± 21.77	77.76 ± 20.34
feces	<0.1	9.08 ± 9.45	11.12 ± 9.87	<0.1	9.79 ± 8.97	12.39 ± 5.42

[a] All data are reported as % ID ± SD (n = 5).

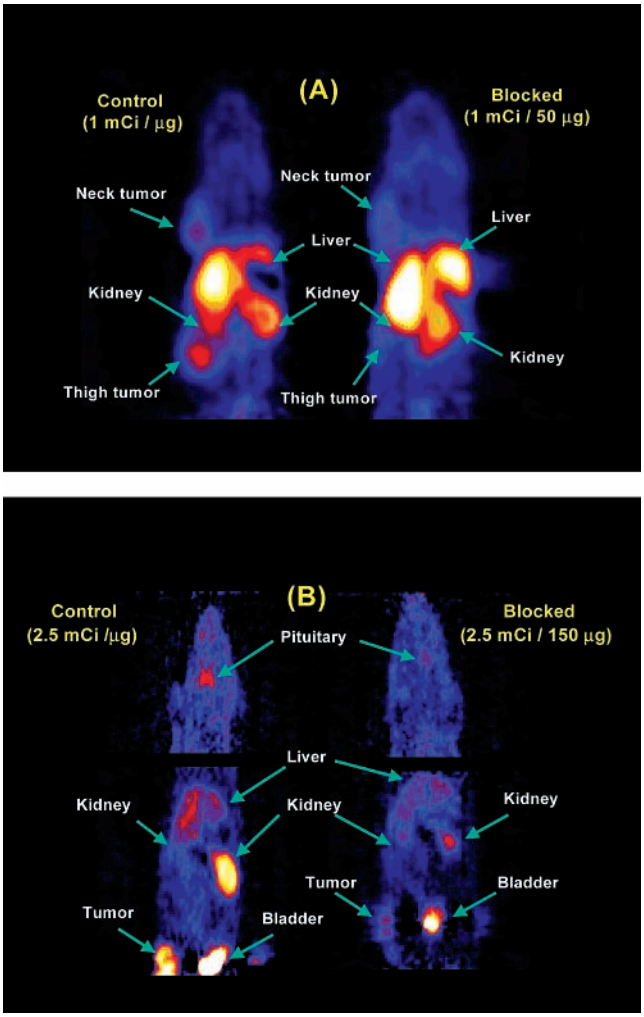


Figure 5. (A) Coronal microPET images of AR42J tumor-bearing SCID mice after 2 h postadministration of ^{64}Cu-DOTA-DY1-TATE, with and without a coinjected blocking dose (2.5 mCi/μg, left; 2.5 mCi/μg coinjected with 50 μg of DY1-TATE, right). (B) Coronal microPET images of AR42J tumor-bearing Lewis rats (2 bed positions) after 2 h postadministration of ^{64}Cu-DOTA-DY1-TATE, with and without a coinjected blocking dose (2.5 mCi/μg, left; 2.5 mCi/μg coinjected with 150 μg of DY1-TATE, right).

h postinjection are given in Figures 6A and 6B. In the SCID mice, the results suggested tumor activity in the control mice (0.02 μCi/μL at 2 h pi, 0.02 μCi/μL at 4 h pi) was about 2-fold higher than in blocked mice (0.01 μCi/μL for 2 h pi, 0.01 μCi/μL for 4 h pi). In SCID mice, the tumor activity was similar at both 2 and 4 h postinjection. In the 'blocked' Lewis rats, a similar reduction in activity was observed compared to control Lewis rats. Tumor activity in the control rats (0.03 μCi/μL for 2 h pi, 0.02 μCi/μL for 4 h pi) was 2−3-fold higher than in 'blocked' rats (0.01 μCi/μL for 2 h pi, 0.01 μCi/μL for 4 h pi). These results agreed with tumor uptake measurements that were determined by measuring the activity of the dissected tumor in a dose calibrator, where 4.14 ± 0.01 %ID/g was found in the control tumor and 1.46 ± 0.00 %ID/g was in the tumor of the rat coinjected with blocking agent. These data confirmed that tumor uptake was blocked with an excess of DY1-TATE. Moreover, blocking of tumor activity in the rats appeared to be more effective than in mice, which probably reflects the crossover activity from liver/kidney in mice that obscures the tumor, especially in the blocked mice when measuring regions of interest (ROIs) that encompassed the entire organ.

DISCUSSION

The utility of radiolabeled somatostatin analogues for imaging and therapy of cancer is well described in the literature. The majority of newly developed somatostatin analogues were specifically designed for labeling radiometals (*1*−*3*). The goal of this research was to design a somatostatin analogue for labeling both radiometals and halogens, with the added feature of having the halogen residualized in target tissue. Here we investigated DOTA-DY1-TATE, where the *C*-terminal alcohol of octreotide was replaced with a *C*-terminal acid (TATE). This analogue was labeled with ^{64}Cu and ^{125}I and compared in in vitro receptor binding assays and in vivo somatostatin-receptor-positive tumor-bearing animal models. Having a somatostatin analogue that allows the ability for labeling both metals and halogens will allow direct comparisons of these analogues with the only modification being the radionuclide used for labeling.

Receptor binding experiments using AR42J rat pancreatic tumor membranes were performed to verify the IC_{50} values of the new somatostatin analogues compared to ^{111}In-DTPA-OC. Scatchard analysis was performed with $^{61/nat}$Cu-DOTA-DY1-TATE to determine the K_d of this analogue. The unlabeled iodinated and copper complexed DOTA-DY1-TATE analogues had binding affinity that were comparable to In-DTPA-OC while the IC_{50} for Cu-DOTA-Y3-TATE was about 2−3-fold lower. These data are encouraging, since it demonstrates that the binding affinity was not compromised with the DY1-TATE analogues compared to the DTPA-OC and DOTA-Y3-TATE analogues. Another DY1 analogue (DTPA-^{125}I-DY1−OC) was described by Breeman et al. (*4*); however, this analogue had an IC_{50} value vs ^{125}I-Y3-OC that was 200-fold higher than ^{125}I-Y3-OC itself.

The biodistribution of ^{64}Cu- and ^{125}I-labeled DOTA-DY1-TATE were performed in one coinjection experiment in AR42J tumor-bearing Lewis rats. This model has several advantages compared to the typically utilized animal models, AR42J tumor-bearing nude/SCID mice, and CA20948-tumor bearing rats. AR42J cells grow both in cell culture and in animal models, which allows the advantage of comparing in vitro receptor binding studies and tumor-bearing animal studies using the same tumor cell line. The use of young rats (21 d) also allows the AR42J tumor cells to be implanted into immunocompetent rodents, rather than immunocompromised nude or SCID mice.

Greater somatostatin-receptor-mediated uptake was observed with ^{64}Cu-DOTA-DY1-TATE than DOTA-^{125}I-DY1-TATE in the pancreas as well as the AR42J tumor (p < 0.02), whereas the uptake was similar in the

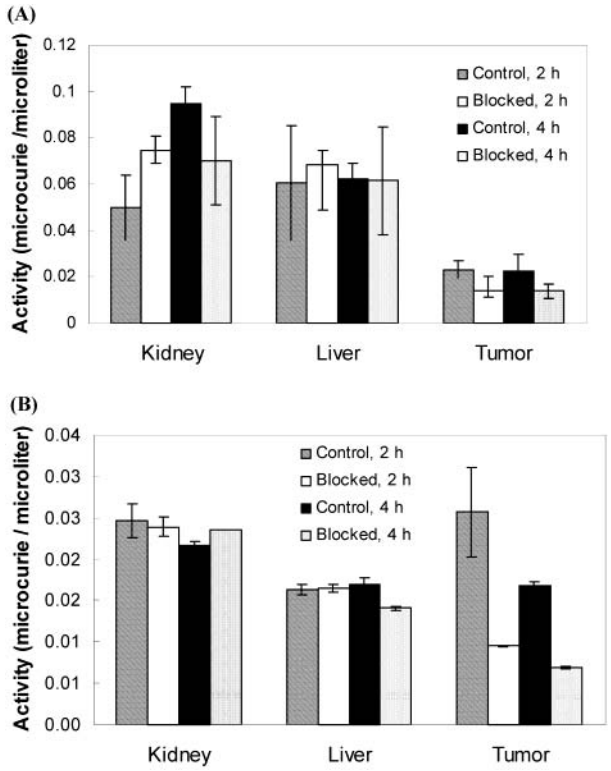


Figure 6. Tumor, kidney, and liver activity of ^{64}Cu after 2 and 4 h postadministration of ^{64}Cu-DOTA-DY1-TATE generated by measuring ROIs from microPET images in control and blocked AR42J tumor-bearing SCID mice (A) and Lewis rats (B). Each bar presents two animals.

adrenals. However, the liver and blood uptake of ^{64}Cu-DOTA-DY1-TATE were significantly greater than for DOTA-^{125}I-DY1-TATE ($p < 0.01$). The high uptake in the blood at longer time points and the increasingly high uptake in the liver was problematic for ^{64}Cu-DOTA-DY1-TATE, suggesting that ^{64}Cu dissociated from the DOTA chelator (*21*). Research is ongoing to develop more stable chelators for copper radionuclides that have greater kinetic stability, and these will eventually be conjugated to somatostatin analogues (*22*). It is predicted that conjugating a chelator to DY1-TATE that forms a more stable Cu(II) complex than DOTA will significantly decrease accumulation in the blood, liver and kidneys.

The uptake of ^{64}Cu- and ^{125}I-labeled DOTA-DY1-TATE was not as high in somatostatin-receptor positive tissues as has been observed for other radiolabeled somatostatin analogues. Comparisons between the AR42J tumor-bearing rat model can only be made with CA20948 tumor-bearing rats, since to the best of our knowledge, uptake of radiolabeled somatostatin analogues has not yet been reported for the AR42J tumor-bearing rat model. Therefore, comparisons with other somatostatin-receptor positive tissues are presented here. For example, the uptake of ^{64}Cu-TETA-Y3-TATE in the rat pancreas was 9.35 ± 1.66 %ID/g in Lewis rats (*19*) at 1 h postinjection, compared to 1.49 ± 0.34 %ID/g for ^{64}Cu-DOTA-DY1-TATE and 0.85 ± 0.20 %ID/g for DOTA-^{125}I-DY1-TATE. A biodistribution study of ^{177}Lu-DOTA-Y3-TATE in Lewis rats showed a pancreas uptake of 10.49 ± 1.91 %ID/g (*23*). However, the uptake of the DOTA-DY1-TATE analogues in the pancreas was comparable or greater than ^{64}Cu-TETA-OC (0.86 ± 0.14 %ID/g) and ^{111}In-DTPA-OC (0.42 ± 0.09 %ID/g) (*15*). Compared to DTPA-^{125}I-DY1−OC (*4*), the pancreas and adrenal uptakes of DOTA-^{125}I-DY1-TATE were somewhat higher (pancreas: 0.85 vs ∼0.5 %ID/g, respectively; adrenal: 1.5 vs ∼1.0 %ID/g, respectively). This suggests that the octreotate analogues may be superior to the octreotide analogues, which has been previously been reported (*2*, *3*).

Although the radiometal-labeled DOTA/TETA-Y3-TATE analogues showed superior receptor-mediated uptake, these analogues do not allow the ability to label via a residualizing label with radiohalogens. Therefore, the use of the DY1 analogues opens possibilities for the radiotherapeutic application of radioiohalogened ligands in patients with somatostatin receptor-positive tumors.

MicroPET imaging of ^{64}Cu-DOTA-DY1-TATE in AR42J tumor-bearing mice and rats at 2 h postinjection showed higher amounts of activity in the liver and kidneys compared to other normal tissues (Figure 6). The tumor also had significant uptake and showed good contrast compared with receptor-negative background tissue in the neck and thigh tumors of the mouse, and the thigh tumors in the rat model. In the AR42J-tumor bearing Lewis rats, the somatostatin receptor-positive pituitary was visualized, whereas it was not visualized in the rat coinjected with a blocking dose. Quantification of the activity in the rat tumor, liver, and kidney was comparable to the relative amounts determined by traditional biodistribution. The quantification of the microPET images also demonstrated that the activity in the tumor was significantly blocked, and this decrease in uptake corresponded to the visual decrease in uptake delineated in the images. These data suggest that microPET may be used as an alternative to traditional multiple animal biodistribution studies for screening new positron-emitting radiopharmaceuticals.

CONCLUSIONS

The study presented here demonstrates that DOTA-DY1-TATE is a peptide that can be labeled with both metal and halogen radionuclides. The IC_{50} values for ^{64}Cu- and ^{125}I-labeled DOTA-DY1-TATE were comparable to ^{111}In-DPTA-OC, and these analogues showed somatostatin receptor-mediated uptake in normal and tumor tissues in vivo. DOTA-^{125}I-DY1-TATE appeared to remain in the tumor out to 4 h postinjection, suggesting that the iodine was possibly residualized in the tumor cells. Future studies include microPET imaging in the AR42J tumor-bearing rat model with DOTA-DY1-TATE labeled with other positron-emitting radionuclides such as ^{76}Br, ^{124}I, and ^{86}Y.

ACKNOWLEDGMENT

The authors wish to thank Lynne Jones, Nicole Mercer, Mu Wang, Virginia Richey, and John Engelbach for technical assistance, and W. Barry Edwards, Ph.D. (MetaPhore Pharmaceuticals) for helpful discussions. This research was supported by NIH Grant R01 CA64475 (C.J.A.). The production of copper radionuclides at Washington University is supported by a grant from the National Cancer Institute (R24 CA86307 − M. J. Welch, P. I.). MicroPET imaging is supported by NIH/NCI SAIRP grant (1R24 CA83060). We would also like to thank the Small Animal Imaging Core of the Alvin J. Siteman Cancer Center at Washington University and Barnes Jewish Hospital in St. Louis, MO for additional support of the microPET imaging. The core is supported by a NCI Cancer Center Support Grant (1P30 CA91842).

LITERATURE CITED

(1) de Jong, M., Bakker, W. H., Breeman, W. A. P., Bernard, B. F., Hofland, L. J., Visser, T. J., Srinivasan, A., Schmidt, M., Behe, M., Maecke, H., and Krenning, E. P. (1998) Pre-

Clinical Comparison of [DTPA^0]Octreotide, [DTPA^{0}Tyr^3]-Octreotide and [DOTA^{0}Tyr^3]Octreotide as Carriers for Somatostatin Receptor-Targeted Scintigraphy and Radionuclide Therapy. *Int. J. Cancer 75*, 406−411.

(2) de Jong, M., Breeman, W. A. P., Bakker, W. H., Kooij, P. P. M., Bernard, B. F., Hofland, L. J., Visser, T. J., Srinivasan, A., Schmidt, M., Erion, J. L., Bugaj, J. E., Maecke, H. R., and Krenning, E. P. (1998) Comparison of ^{111}In-Labeled Somatostatin Analogues for Tumor Scintigraphy and Radionuclide Therapy. *Cancer Res. 58*, 437−441.

(3) Lewis, J. S., Lewis, M. R., Srinivasan, A., Schmidt, M. A., Wang, J., and Anderson, C. J. (1999) Comparison of Four ^{64}Cu-labeled Somatostatin Analogues in vitro and in a Tumor-bearing Rat Model: Evaluation of New Derivatives for PET Imaging and Targeted Radiotherapy. *J. Med. Chem. 42*, 1341−1347.

(4) Breeman, W. A. P., de Jong, M., Bernard, B., Hofland, L. J., Srinivasan, A., Vanderpluijm, M., Bakker, W. H., Visser, T. J., and Krenning, E. P. (1998) Tissue Distribution and Metabolism of Radioiodinated DTPA(0), D.-Tyr(1) and Tyr-(3) Derivatives of Octreotide in Rats. *Anticancer Res. 18*(*1A*), 83−89.

(5) Yngve, U., Khan, T. S., Bergstrom, M., and Langstrom, B. (2001) Labeling of Octreotide using Br-76-prosthetic Groups. *J. Lab. Compd. Radiopharm. 44*, 561−573.

(6) Gardelle, O., Roelcke, U., Vontobel, P., Crompton, N. E. A., Guenther, I., Blauenstein, P., Schubiger, P. A., Blattmann, H., Ryser, J. E., Leenders, K. L., and Kaser-Hotz, B. (2001) [Br-76]bromodeoxyuridine PET in Tumor-bearing Animals. *Nucl. Med. Biol. 28*, 51−57.

(7) Ryser, J. E., Blauenstein, P., Remy, N., Weinreich, R., Hasler, P. H., Novak-Hofer, I., and Schubiger, P. A. (1999) [Br-76]bromodeoxyuridine, a Potential Tracer for the Measurement of Cell Proliferation by Positron Emission Tomography, in vitro and in vivo Studies in Mice. *Nucl. Med. Biol. 26*, 673−679.

(8) Bennett, J. J., Tjuvajev, J., Johnson, P., Doubrovin, M., Akhurst, T., Malholtra, S., Hackman, T., Balatoni, J., Finn, R., Larson, S. M., Federoff, H., Blasberg, R., and Fong, Y. M. (2001) Positron Emission Tomography Imaging for Herpes Virus Infection: Implications for Oncolytic Viral Treatments of Cancer. *Nat. Med. 7*, 861−865.

(9) Anderson, C. J., Jones, L. A., Bass, L. A., Sherman, E. L. C., McCarthy, D. W., Cutler, P. D., Lanahan, M. V., Cristel, M. E., Lewis, J. S., and Schwarz, S. W. (1998) Radiotherapy, Toxicity and Dosimetry of Copper-64-TETA-Octreotide in Tumor-Bearing Rats. *J. Nucl. Med. 39*, 1944−1951.

(10) Anderson, C. J., Dehdashti, F., Cutler, P. D., Schwarz, S. W., Laforest, R., Bass, L. A., Lewis, J. S., and McCarthy, D. W. (2001) Copper-64-TETA-octreotide as a PET Imaging Agent for Patients with Neuroendocrine Tumors. *J. Nucl. Med. 42*, 213−221.

(11) McCarthy, D. W., Shefer, R. E., Klinkowstein, R. E., Bass, L. A., Margenau, W. H., Cutler, C. S., Anderson, C. J., and Welch, M. J. (1997) The Efficient Production of High Specific Activity Cu-64 Using a Biomedical Cyclotron. *Nucl. Med. Biol. 24*, 35−43.

(12) McCarthy, D. W., Bass, L. A., Cutler, P. D., Shefer, R. E., Klinkowstein, R. E., Herrero, P., Lewis, J. S., Cutler, C. S., Anderson, C. J., and Welch, M. J. (1999) High Purity Production and Potential Applications of Copper-60 and Copper-61. *Nucl. Med. Biol. 26*, 351−358.

(13) Rosewicz, S., Vogt, D., Harth, N., Grund, C., Franke, W. W., Ruppert, S., Schweitzer, E., Riecken, E.-O., and Wiedenman, B. (1992) An Amphicrine Pancreatic Cell Line: AR42J Cells Combine Exocrine and Neuroendocrine Properties. *Eur. J. Cell Biol. 59*, 80−91.

(14) Christophe, J. (1994) Pancreatic Tumoral Cell Line AR42J: An Amphicrine Model. *Am. J. Physiol.* (*Gastrointest. Liver Physiol.*) *266*(*29*), G963-G971.

(15) Anderson, C. J., Pajeau, T. S., Edwards, W. B., Sherman, E. L. C., Rogers, B. E., and Welch, M. J. (1995) In vitro and in vivo Evaluation of Copper-64-Labeled Octreotide Conjugates. *J. Nucl. Med. 36*, 2315−2325.

(16) Lewis, J. S., Laforest, R., Lewis, M. R., and Anderson, C. J. (2000) Comparative Dosimetry of Copper-64 and Yttrium-90-labeled Somatostatin Analogues in a Tumor-bearing Rat Model. *Cancer Biother. Radiopharm. 15*, 593−604.

(17) Breeman, W. A. P., Hofland, L. J., Bakker, W. H., van der Pluijm, M., van Koetsveld, P. M., de Jong, M., Setyono-Han, B., Kwekkeboom, D. J., Visser, T. J., Lamberts, S. W. J., and Krenning, E. P. (1993) Radioiodinated Somatostatin Analogue RC-160: Preparation, Biological Activity, in vivo Application in Rats and Comparison with [^{123}I-Tyr^3]octreotide. *Eur. J. Nucl. Med. 20*, 1089−1094.

(18) Foulon, C. F., Reist, C. J., Bigner, D. D., and Zalutsky, M. R. (2000) Radioiodination via D-amino Acid Peptide Enhances Cellular Retention and Tumor Xenograft Targeting of an Internalizing Anti-epidermal Growth Factor Receptor Variant III Monoclonal Antibody. *Cancer Res. 60*, 4453−4460.

(19) Lewis, J. S., Srinivasan, A., Schmidt, M. A., and Anderson, C. J. (1998) In vitro and in vivo Evaluation of ^{64}Cu-TETA-Tyr^3-Octreotate. A New Somatostatin Analogues with Improved Target Tissue Uptake. *Nucl. Med. Biol. 26*, 267−273.

(20) Cherry, S. R., Shao, Y., Silverman, R. W., Meadors, K., Siegel, S., Chatziioannou, A., Young, J. W., Jones, W. F., Moyers, J. C., Newport, D., Boutenouchet, A., Farquhar, T. H., Andreaco, M., Paulus, M. J., Binkley, D. M., Nutt, R., and Phelps, M. E. (1997) MicroPET: a High-Resolution PET Scanner for Imaging Small Animals. *IEEE Trans. Nucl. Sci. 44*, 1161−1166.

(21) Bass, L. A., Wang, M., Welch, M. J., and Anderson, C. J. (2000) In vivo Transchelation of Copper-64 from TETA-octreotide to Superoxide Dismutase in Rat Liver. *Bioconjugate Chem. 11*, 527−532.

(22) Sun, X., Wuest, M., Weisman, G. R., Wong, E. H., Reed, D. P., Boswell, C. A., Motekaitis, R., Martell, A. E., Welch, M. J., and Anderson, C. J. (2002) Radiolabeling and in vivo Behavior of Copper-64-labeled Cross-Bridged Cyclam Ligands. *J. Med. Chem. 45*, 469−477.

(23) Lewis, J. S., Wang, M., Laforest, R., Wang, F., Erion, J. L., Bugaj, J. E., Srinivasan, A., and Anderson, C. J. (2001) Toxicity and Dosimetry of ^{177}Lu-DOTA-Y3-octreotate in a Rat Model. *Int. J. Cancer 94*, 873−877.

BC015590K

Quantitation of the Tumor-Targeting Properties of Antibody Fragments Conjugated to Cell-Permeating HIV-1 TAT Peptides

Uwe Niesner,[†,‡] Cornelia Halin,[†,‡] Luisa Lozzi,[§] Maja Günthert,[‡] Paolo Neri,[§] Heidi Wunderli-Allenspach,[‡] Luciano Zardi,[||] and Dario Neri*[,‡]

Institute of Pharmaceutical Sciences, Swiss Federal Institute of Technology Zurich, Winterthurerstrasse 190, CH-8057 Zurich, Switzerland, Department of Molecular Biology, University of Siena, Via Fiorentina 1, I-53'100 − Siena, Italy, and Laboratory of Cell Biology, National Cancer Research Institute, Largo Rosanna Benzi 10, I-16'132 − Genova, Italy. Received February 22, 2002; Revised Manuscript Received April 4, 2002

Human monoclonal antibodies are promising agents for the development of more selective anticancer therapeutics. However, the tumor-targeting efficiency of most anticancer antibodies is severely limited by their poor penetration into the tumor mass. Recent studies have shown that a peptide derived from the HIV TAT protein could improve the distribution of cytoplasmic reporter proteins when administered systemically as fusion proteins or cross-linked chimeras. In this article, we tested by quantitative biodistribtution analysis whether conjugation to TAT peptides could improve the tumor targeting properties of scFv(L19)-Cys: an engineered human antibody fragment specific for the ED-B domain of fibronectin, a marker located in the modified extracellular matrix surrounding tumor neovasculature. Our results show that TAT peptides, consisting either of L-amino acids or D-amino acids, can efficiently transduce target cells when conjugated to fluorophores and/or antibody fragments, suggesting a receptor-independent cell entry mechanism. However, conjugation of scFv(L19)-Cys to TAT peptides resulted in a severely reduced tumor targeting performance compared to the unconjugated antibody, as measured in murine F9 teratocarcinoma-bearing mice, after intravenous injection of the radiolabeled antibody preparations. Our results outline the usefulness of TAT peptides for the efficient in vitro transduction of cells with globular proteins. In particular, the use of TAT peptides composed of D-amino acids may significantly reduce proteolytic degradation. At the same time, the poor biodistribution properties of antibody−TAT conjugates cast doubts over the applicability of this methodology for the delivery of biopharmaceuticals in vivo.

INTRODUCTION

The development of better chemotherapeutic drugs for the treatment of solid tumors needs to address two main issues, which are currently limiting therapeutic efficacy. First, most anticancer drugs interfere with cell replication and consequently exhibit toxicity toward normal proliferating tissues. Thus, it would be desirable to increase the selectivity of chemotherapeutic agents, i.e., their preferential killing of tumor cells rather than normal cells (*1*). Second, low molecular weight cytotoxic drugs often localize more efficiently in normal tissues, rather than in tumors (*2*). This undesired property, which significantly limits the in vivo efficacy of promising drugs, may be attributed to the high interstitial pressure and to unfavorable blood flow properties within rapidly growing solid tumors (*3*−*5*).

The delivery of biocidal agents to the tumor by means of specific monoclonal antibody−drug conjugates may reverse the biodistribution properties of anticancer drugs and therefore result in improved anticancer selectivity. Indeed, Mylotarg (a monoclonal antibody specific for CD33, conjugated to calicheamicin) has been approved by the American Food and Drug Administration for the treatment of acute myeloid leukemia. Furthermore, Bexxar and Zevalin (two radiolabeled monoclonal antibodies specific for CD20) are expected to be approved by the FDA soon (*6*), while more than 700 antibody-based biopharmaceuticals are currently in clinical development by some 200 biotech companies (*7*). However, despite these promising developments, solid tumors have often proven to be relatively resistant to antibody-based therapies. Typically, antibodies penetrate tumors slowly, displaying good tumor:blood ratios only several hours after intravenous injection (*8*). Furthermore, the so-called "antigen barrier" may sequester the antibody in perivascular regions, preventing a homogeneous distribution within the tumor mass (*9*, *10*). In fact, in patients, typically, only 0.001−0.01% of the injected antibody dose accumulates per gram of solid tumor.

Vascular targeting, i.e., the selective delivery of therapeutic agents (e.g., antibody conjugates) to the tumor neovasculature, has been proposed as an avenue for overcoming the limitations of the antibody-mediated targeting of tumor cells (*11*, *12*). Markers on the tumor neovasculature should be readily accessible to intravenously administered antibody derivatives. There is a growing evidence that the selective damage of tumor neovasculature may lead to massive death of tumor cells, which rely on blood vessels for their supply of nutrients

* Corresponding author: Prof. Dr. Dario Neri, Institute of Pharmaceutical Sciences, Swiss Federal Institute of Technology Zurich, Building 36 M14, Winterthurerstrasse 190, CH-8057 Zurich, Switzerland. Tel: +41−1−635 60 63; Fax: +41−1−635 68 86; e-mail: neri@pharma.anbi.ethz.ch.

[†] Both authors contributed equally.

[‡] Swiss Federal Institute of Technology Zurich.

[§] University of Siena.

[||] National Cancer Research Institute.

10.1021/bc025517+ CCC: $22.00 © 2002 American Chemical Society
Published on Web 06/14/2002

and oxygen to satisfy their metabolic needs. It is estimated that more than 100 tumor cells rely on one endothelial cell for survival. Furthermore, angiogenesis (i.e., the formation of new blood vessels from preexisting ones) is a general feature in aggressive solid tumors, and a vascular targeting agent should be effective with different tumor types. Notably, angiogenesis plays an important role in relevant diseases other than cancer, including rheumatoid arthritis, psoriasis, and ocular disorders such as the exudative form of age-related macular degeneration and diabetic retinopathy (*13*).

Recently, we have reported on the tumor targeting properties of human monoclonal antibody fragments specific for the ED-B domain of fibronectin, a marker of angiogenesis (*14*−*17*). Antibodies specific to ED-B-containing fibronectin (B-FN) selectively target the neovasculature in vivo, as shown in animal models and in patients, thus opening the possibility to selectively deliver therapeutic molecules to new blood vessels.

The scFv(L19) antibody fragment, with picomolar affinity for the ED-B domain, was chemically coupled to a photosensitizer and mediated the selective and complete occlusion of ocular neovasculature in a rabbit model, after irradiation with near-infrared light (*18*). Nilsson et al. reported that the fusion protein of L19 with the extracellular domain of tissue factor mediates the selective thrombosis of new blood vessels, in different types of murine tumor models (*19*). Furthermore, promising therapeutic results have been obtained in rodents with scFv(L19)-cytokine fusion proteins (*20*, *21*).

B-FN is a marker of the modified ECM associated with the tumor enovasculature. Biodistribution studies have shown that crossing the endothelial cell layer of tumor blood vessels is a slow process and in fact limits the absolute tumor uptake of anti-ED-B antibody fragments, which are typically cleared from blood with half-lives of approximately 30 min (*17*, *35*).

Recently, the transacting transcriptional activater protein (TAT) has been described as a protein with the ability to enter and leave cells in by unconventional manner (classical cell entry mechanisms can be excluded), in a process termed protein transduction (*22*−*24*). TAT is a viral regulatory protein, isolated from human immunodeficiency virus 1 (HIV-1), which binds the viral nascent 5′ leader RNA hairpin transactivation response element (TAR) (*25*, *26*). The TAT sequence responsible for the transduction properties has been identified as the basic domain comprising residues 49−57 (RKKRRQRRR) (*27*), which contains a nuclear localization signal and is involved in the binding of TAR RNA.

In vitro studies with TAT peptides, labeled with fluorescein or magnetic beads, have demonstrated a rapid cell internalization of this peptide, with predominant nuclear localization (*27*, *28*). Furthermore, the intraperitoneal injection of mice with β-galactosidase fused to a TAT peptide resulted in the delivery of the biologically active fusion protein to all tissues in mice, including the brain (*29*). However, the X-Gal detection method used in this article did not allow a quantitative evaluation of targeting efficacy, but only a relative comparison with mice treated with unconjugated β-galactosidase. Nonetheless, these experiments generated excitement in the field of protein-based therapeutics (*30*), since epithelial structures and brain have proven rather impermeable to most proteins.

When an adenovirus was used to continuously express β-glucuronidase, fused to TAT peptide, only a modest increase of enzymatic activity was observed in tissues, as compared to the uptake properties of unmodified β-glucuronidase (*31*). Furthermore, quantitative biodistribution studies performed with ^{99m}Tc-labeled TAT peptide (GRKKRRQRRR) showed an initial whole body distribution, followed by rapid clearance by both renal and hepatobiliary excretion, with low uptake [<1% injected dose per gram of tissue; (%ID/g)] in normal organs not involved in the clearance process (*32*).

The aim of this work was to test whether a site-specific conjugation of TAT peptides to the high-affinity anti-ED-B antibody fragment scFv(L19) would result in improved crossing of endothelial barriers and, consequently, in enhanced tumor uptake. In this article, we show that both TAT peptides with the sequence CGISYGRKKRRQRRR (TAT), made of D- or L-amino acids, exhibited rapid uptake in cells. This peptide sequence corresponds to residues 44−57 of the TAT protein, to which an N-terminal cysteine residues had been appended to facilitate chemical modification. The peptides could be readily conjugated to cysteine-tagged scFv(L19), allowing for a site-specific modification of the antibody with full retention of immunoreactivity. Cell uptake studies of the scFv(L19)−TAT conjugate confirmed that this antibody derivative is taken up by cells, though with a different subcellular pattern. However, quantitative biodistribution experiments performed with radioiodinated scFv(L19)−TAT showed a significantly lower tumor uptake of the immunoconjugate (compared to the unmodified antibody), raising doubts on the usefulness of TAT sequence for the efficient transport of proteins to perivascular regions of tissues in vivo.

EXPERIMENTAL PROCEDURES

Cell Lines and Genes. F9 murine teratocarcinoma were used for the grafting of subcutaneous tumors (*17*)**.** The anti-ED-B human antibody fragment scFv(L19) has been described elsewhere (*16*). The human embryonic kidney (HEK) 293 cell line was obtained from American Type Culture Collection (ATCC; Rockville, MD).

Peptide Synthesis. Peptides (CGISYGRKKRRQRRR) were synthesized as described (*33*) using either all amino acids in L configuration or all D amino acids and amidation at the C-terminus. Peptides were analyzed and purified by C_{18} reversed-phase HPLC at a flow rate of 2 mL/min using as eluent 0.1% trifluoroacetic acid in water modified by a linear gradient of 20−100% methanol over 40 min. A single HPLC peak was observed for each peptide. Peptide identity was confirmed by MALDI-TOF (Protein Service Labor, ETH Zürich, Switzerland).

Cloning of scFv(L19)-Cys. To append residues GGGC at the C-terminus of scFv(L19), the gene coding for scFv(L19) was amplified with the primers *L19Xho1back* (5′ gta tct ctc gag aaa aga gag gtg cag ctg ttg gag tct ggg 3′) and *L19CNot1for* (5′ tta att cgc ggc cgc tca tta aca ccc gcc ccc ttt gat ttc cac ctt ggt ccc ttg 3′). The PCR product was cloned into the yeast *Pichia pastoris* expression vector pPIC9K (Invitrogen, Groningen, The Netherlands), using the *Xho*I/*Not*I sites of the vector.

Expression and Purification of L19Cys. *Pichia pastoris* cells were electroporated with the vector and plated on Minimal Dextrose histidine deficient (MD; Invitrogen) agar plates. The resulting colonies were plated on yeast extract peptone dextrose (YPD; Invitrogen) agar plates with increasing concentrations of G418 (neomycin). Clones of G418-resistant cells (>2 mg/mL) were screened for scFv(L19)-Cys expression by ELISA using biotinylated recombinant ED-B domain of fibronectin as antigen (*34*) and protein A conjugated to HRP as detection reagent (Sigma, Buchs, Switzerland). The

protein was produced in 2 L shaker flasks, using buffered methanol−complex medium (BMMY; Invitrogen) as expression medium and purified from the supernatant by affinity chromatography over antigen columns as previously described (*34*). After dialysis in 10 mM HEPES, pH 6.7, the protein was loaded onto a Resource-S cation exchange column (Amersham Pharmacia Biotech, Dübendorf, Switzerland) and eluted with a linear salt gradient. The homodimeric antibody fraction was collected, and the protein was analyzed by SDS−PAGE (both in reducing and nonreducing conditions) and in native conditions by fast protein liquid chromatography gel filtration on a Superdex S75 column (Amersham Pharmacia Biotech).

Antibody Conjugation. Tat-peptides were dissolved at 0.05 mg/mL in 50 mM phosphate, 100 mM NaCl (phosphate-buffered saline, PBS), at pH 6.5, and treated with a 8-fold molar excess of bis-maleimidohexane (BMH; Pierce, Bezons, France) in dimethylfomamide (DMF) (final concentration 10% (v/v) DMF) for 2 h at 4 °C. The mixture was applied to a small carboxymethyl (CM) sepharose cation exchange column (Amersham Pharmacia Biotech), and the peptide conjugate was eluted with 1 M NaCl. Prior to cross-linking, scFv(L19)-Cys (1 mg/ml) was reduced for 1 h at room temperature with 10 mM dithioerythritol (DTE; Sigma) in PBS, pH 7.4. After desalting on a PD-10 gel filtration column (Amersham Pharmacia Biotech), the reduced antibody was incubated for 2 h at 4 °C in PBS, pH 6.5, with a 10-fold molar excess of the peptide−BMH conjugate. ScFv(L19)−TAT conjugates were purified from unconjugated antibody and peptide on a CM-sepharose cation exchange column. ScFv(L19)-Cys−TAT conjugate was eluted at 50mM phosphate, 300 mM NaCl at pH 7.4. The conjugate was >95% pure as judged by SDS−PAGE.

Fluorescent Labeling of TAT Peptides. Fluorescein-5-maleimide (Molecular Probes, Leiden, The Netherlands) at 100 μM in 10% (v/v) dimethylformamide in PBS, pH 7.4, was incubated with 400 μM of TAT peptides or reduced glutathione as control for 60 min at room temperature. The reaction mixtures were analyzed by reversed-phase HPLC. A single fluorescent peak of equivalent intensity was detected in the reaction mixtures, and no unreacted fluorescein-5-maleimide could be detected. The reaction mixtures were used at 4 μM concentration (corresponding to 1 μM of fluorescently labeled peptide) for cell uptake experiments without further purification. Glutathione was labeled in a similar manner.

Fluorescent Labeling of scFv(L19)-Cys−TAT Immunoconjugates. ScFv(L19)-Cys was reacted with one vial of Cy5 monofunctional reactive dye (Amersham Pharmacia Biotech) according to the manufacturer's instructions, followed by a PD-10 gel filtration column. A portion of the fluorescently labeled antibody (antibody: Cy5 ratio = 0.6:1) was used as control in cell uptake experiments; the remaining portion was conjugated to TAT peptides as described in the section Antibody Conjugation. Immunoreactivity of the labeled antibody was measured by affinity chromatography as described (*17*) and was, in all cases, >89%. Furthermore, dilution series of conjugated and unconjugated antibody gave similar results in ELISA, using biotinylated ED-B as antigen. Cy5-labeled scFv(L19)-Cys and scFv(L19)-Cys−TAT conjugates were diluted with PBS to a final concentration of 0.1 mg/mL and used as 7-fold stock solution for cell uptake experiments. The protein concentration was determined by measurement of the absorbance at 280 and 650 nm and by Coomassie blue staining following SDS−PAGE.

Fluorescence Microscopy. HEK cells were grown on glass cover slips to 30−50% confluency. Fluorescently labeled peptides (1 μM), scFv(L19)-Cys (0.5 μM) or scFv(L19)-Cys−TAT conjugates (0.5 μM) were added to the culture medium. Cells were incubated for 15−30 min at 37 °C. After being washed three times with PBS, cells were fixed in 3% paraformaldehyde in PBS for 10 min at room temperature. Cells were rinsed with PBS and treated with 0.1M glycine in PBS, and nuclei were then stained with Dapi (Hoechst 33342) at 100 ng/mL. The cells were washed again, and then preparations were mounted in Mowiol (Calbiochem, Laufelfingen, Switzerland) and analyzed by confocal laser microscopy on a Zeiss LSM 410 inverted microscope (lasers: HeNe 633 nm, HeNe 543 nm, Ar 488/514 nm and ArUV 364 nm). Images were processed on a Silicon Graphics workstation using IMARIS, a 3D multichannel image processing software for confocal microscopic images (Bitplane, Zurich, Switzerland).

Biodistribution Experiments. Biodistribution experiments in mice bearing F9 tumors were performed as described (*17*). Briefly, scFv(L19)-Cys and purified scFv(L19)-Cys−TAT^{D} conjugates were radioiodinated with iodine-125, and approximately 2 mg (2−4 mCi) were injected into the tail vein of 12−14 weeks old, female SV129 mice (M&B A/S, Ry, Denmark) bearing subcutanously implanted F9 murine teratocarcinoma. Mice were sacrificed 1 h or 24 h after injection, the organs were weighed, and the radioactivity was counted. Targeting results of representative organs are expressed as percent injected dose per gram of tissue (%ID/g). Experiments were performed in agreement with Swiss regulations and under a "Tumor targeting" Project license issued to D. N. by the "Kantonales Veterinäramt des Kantons Zürich" (Bewilligung 80/2000). No free peptide was detectable in the injected solution as determined by radiography of dried SDS−PAGE gels. The immunoreactivity of the radiolabeled antibodies was determined by a radioimmunoassay, using ED-B as antigen and measuring the bound radioactivity. Blood and urine of the animals were collected at 1 h after injection to assess the serum stability of the injected scFv(L19)-Cys−TAT^{D} conjugate in vivo. Cells were spun down, and the supernatant was analyzed by SDS−PAGE, followed by radiography.

RESULTS

Localization of B-FN in Tumors. Quantitative biodistribution studies performed with the L19 antibody, specific to the ED-B domain of fibronectin, have shown that different antibody formats deliver different amounts of antibody to the tumor. In particular, antibody fragments with longer half-life in serum (e.g., diabodies, minibodies, IgG) mediate a higher accumulation in the tumor, as compared to scFv(L19) preparations (*16*, *35*). While these data suggest that B-FN is mainly localized in the subendothelial ECM and is therefore separated from the blood stream by a layer of endothelial cells, a formal demonstration has still been missing.

We investigated sections of murine F9 teratocarcinoma by confocal laser immunofluorescence microscopy using the L19 antibody. Figure 1A,B shows that B-FN (red) is located in the abluminal aspects of the tumor blood vessels (stained in green with an anti-actin antibody).

TAT Peptides and Cell Transduction. At the beginning of our work, it was not known whether TAT peptides, composed of D-amino acids rather than L-amino acids, would be capable of cell transduction. For practical

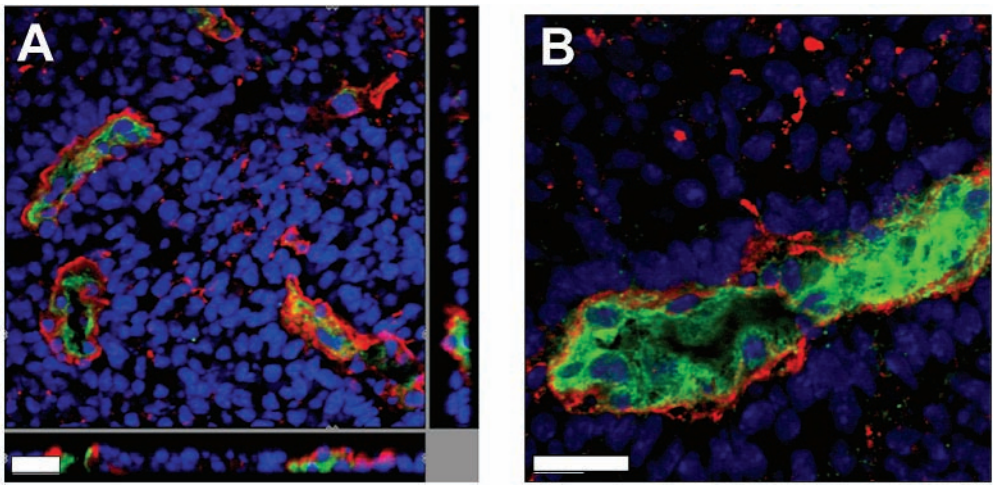


Figure 1. Three-color confocal fluorescence microscopic images of a murine F9 teratocarcinoma section stained with the L19 antibody (red) specific to the ED-B domain of fibronectin, a marker of angiogenesis. Cell nuclei are stained with DAPI (blue) while actin staining (green) outlines the endothelial cells of the tumor blood vessels. Bars: 20 mm.

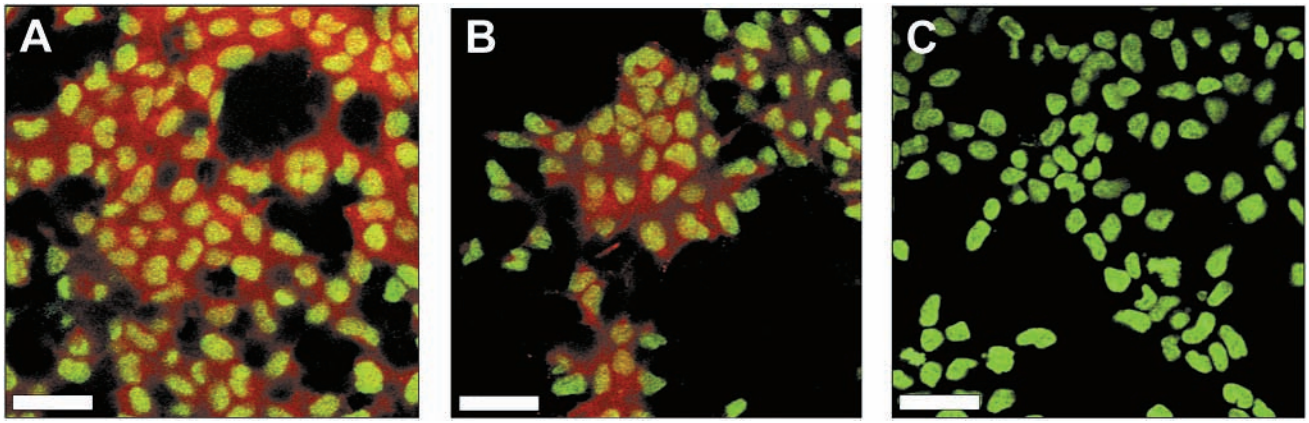


Figure 2. Confocal micrograph of intracellular accumulation of fluorescein labeled TAT peptides and fluorescein-labeled glutathione in HEK 293 cells. Cells were incubated for 15 min at 37 °C with either fluorescein−TAT^L (A), with fluorescein−TAT^D (B), or with fluorescein-labeled glutathione (C), all at 1 mM concentration. Panels show double staining of cells with fluorescein (red) and DAPI for visualization of cell nuclei (green). Bars: 40 mm.

applications, the resistance to proteolysis of TAT peptides composed of D-amino acids would offer significant advantages.

We synthesized the peptide CGISYGRKKRRQRRR (TAT), using either L- or D-amino acids (hereafter termed TAT^L and TAT^D). This peptide sequence had previously been shown to efficiently enter cells (*29*). The thiol group of the N-terminal cysteine residue was used for the stable conjugation of the peptide to maleimido-5-fluorescein. Figure 2A and 2B shows the results of cell uptake experiments, performed on human embryonic kidney cells (HEK 293) using fluorescein−peptide conjugates. Cell incubation with 1 μM fluorescein−TAT^L and fluorescein−TAT^D yielded a strong and homogeneous fluorescent cell staining within the cytoplasm and the nuclei, similar to the one previously reported for the L-peptide. Simultaneous confocal laser microscopic detection of DAPI staining of cell nuclei (Figure 2A−C) confirmed that virtually all the HEK 293 cells had taken up the peptide conjugates. By contrast, cell incubation with fluorescein−glutathione (used as negative control peptide) did not show a significant peptide uptake (Figure 2C).

The fact that fluorescein−TAT^L and fluorescein−TAT^D are taken up by cells with similar efficiency indicates a receptor-independent cell entry mechanism.

Antibody−TAT Peptide Conjugates and Cell Transduction. We used 1,6-bis-maleimidohexane as a homobifunctional cross-linker, to mediate the coupling of TAT^D to scFv(L19)-Cys (Figure 3A). A C-terminal cysteine residue had been appended to this antibody fragment, specific for the ED-B domain of fibronectin, a marker of angiogenesis (*14*, *15*), to allow its site-specific chemical modification, without loss of immunoreactivity (*36*−*38*). Similar to what has recently been described for other antibody fragments (*39*), we expressed scFv(L19)-Cys in *Pichia pastoris*, since this expression system provided yields which were significantly higher, compared to *E. coli*. The antibody fragment was purified to homogeneity by affinity chromatography, using an ED-B resin (*40*).

Figure 3B shows a nonreducing SDS−PAGE analysis of the scFv(L19)-Cys before and after conjugation to TAT^D. Lane 1 shows that approximately 50% of scFv-(L19)-Cys was present as a disulfide-bonded homodimer, which could be reduced using dithioerythritol (lane 2). Incubation of reduced scFv(L19)-Cys with an excess of the reaction product between TAT and a molar excess of 1,6-bis-maleimidohexane (TAT-BMH) resulted in the complete coupling of both TAT^L and TAT^D to the antibody fragment (lane 3). Unreacted TAT-BMH and antibody were separated from the scFv(L19)-Cys-TAT conjugates

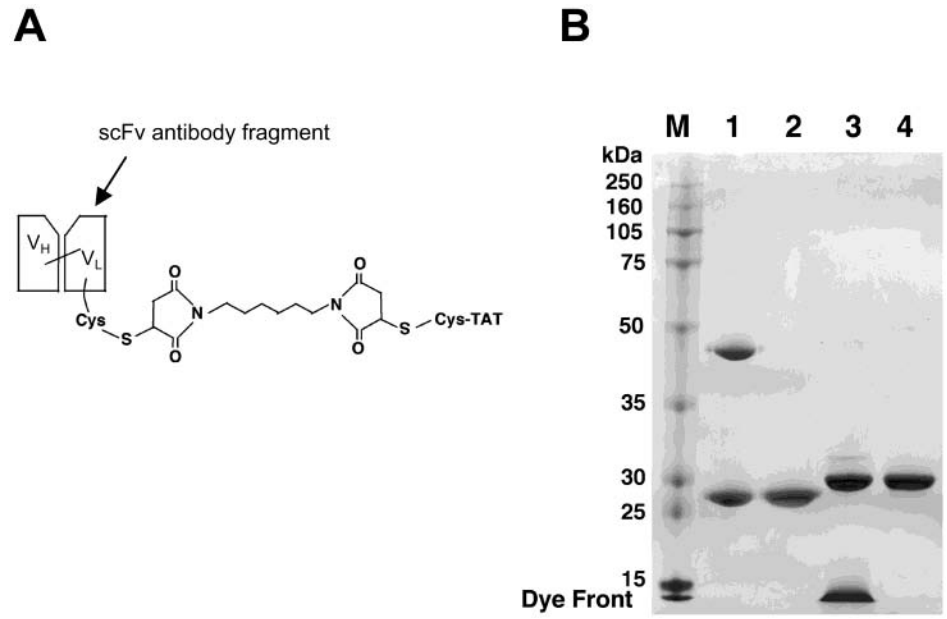


Figure 3. (A) Schematic representation of scFv(L19)-Cys conjugated to a TAT peptide by means of a bis-malimidohexane (BMH) cross-linker. The thioether bonds of cysteine residues are indicated. (B) Nonreducing SDS−PAGE analysis documenting the conjugation of scFv(L19)-Cys to TAT-peptides, using bis-maleimidohexane (BMH) as cross-linker. M: Molecular weight marker; Lane 1: scFv-(L19)-Cys; Lane 2: reduced scFv(L19)-Cys; Lane 3: Reaction mix after incubation of scFv(L19)Cys with TAT-BMH conjugate showing the band of the reacted scFv(L19)-Cys−TAT and the one of the unreacted TAT-BMH (used in molar excess); Lane 4: purified scFv-(L19)-Cys−TAT conjugate.

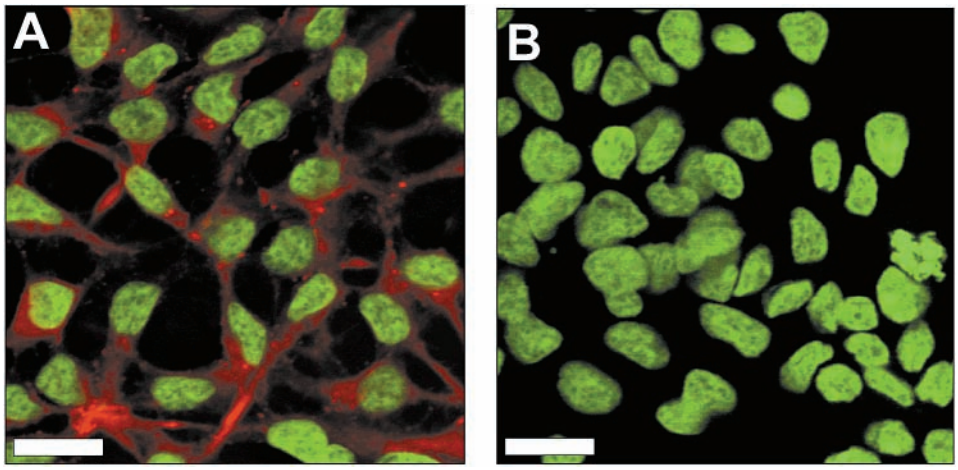


Figure 4. Confocal micrograph showing the intracellular accumulation of Cy5-labeled scFv(L19)-Cys−TAT^D as compared to the one of unconjugated, Cy5 labeled scFv(L19)-Cys. HEK 293 cells were incubated for 30 min at 37 °C with either Cy5-labeled scFv-(L19)-Cys−TAT^D or Cy5-labeled scFv(L19)-Cys (B). Panels show double labeling of cells with Cy5 (red) and the DAPI (green). Bars: 20 mM

by CM-sepharose cation exchange chromatography, yielding a pure antibody−peptide conjugate (lane 4).

To assay the cell transduction activity of the scFv(L19)-Cys-TAT, the scFv(L19)-Cys was labeled with the red fluorophore Cy5, prior to coupling to TAT. Fluorescence microscopic analysis of HEK 293 cells exposed to either Cy5-scFv(L19)-Cys−TAT^D (Figure 4A) or Cy5-scFv(L19)-Cys (Figure 4B) reveals that only the TAT-modified antibody is taken up by the cells. When compared to unconjugated TAT peptides (Figure 2), Cy5-scFv(L19)-Cys−TAT^D shows a compartmentalized cell uptake, which does not overlap with the nuclei.

Tumor Targeting Experiments. To test whether conjugation to TAT peptides could improve the tumor targeting properties of scFv(L19)-Cys, we performed quantitative biodistribution studies in in immunocompetent Sv129 mice, bearing a subcutaneously grafted syngeneic F9 teratocarcinoma. On the basis of the similar cell transduction properties of TAT^D and TAT^L, we decided to use TAT^D for all the following experiments, since this peptide is resistant to proteolysis. ScFv(L19)-Cys and scFv(L19)-Cys−TAT^D were radiolabeled with iodine-125 using the Iodogen method, to a specific activity of 0.5−1 μCi/μg. The labeled antibodies retained >86% immunoreactivity, as assessed by affinity chromatography and by radioimmunoassay (RIA) (*16*, *17*).

Mice were injected intravenously with 2 μg of fusion protein and sacrificed at an early and a late time point (1 h or 24 h) after injection. The in vivo stability of the radiolabeled proteins was confirmed by SDS−PAGE, followed by radiography, of blood and urine samples collected 1 h after injection. Table 1 shows the biodistribution results, expressed as percent injected dose per gram of tissue or fluid (%ID/g) for tumor, blood, and relevant organs. Unconjugated scFv(L19)-Cys showed a significant accumulation in tumors (tumor:blood ratio =

Table 1. Biodistribution of scFv(L19)-TAT^D and scFv(L19)-Cys[a]

	ScFv(L19)-Cys, %ID/g	ScFv(L19)-Cys-TAT^D, %ID/g
	1 Hour	
tumor	11.8 ± 1.4	4.1 ± 1.1
spleen	4.2 ± 0.3	11.8 ± 2.0
kidney	24.1 ± 3.6	16.0 ± 6.7
liver	3.2 ± 0.2	43.9 ± 12.8
lung	6.1 ± 1.0	5.5 ± 1.8
heart	4.6 ± 0.7	2.1 ± 0.6
intestine	3.9 ± 0.3	4.3 ± 3.5
blood	11.0 ± 1.9	4.9 ± 2.9
	24 Hours	
tumor	8.1 ± 3.2	0.5 ± 0.0
spleen	0.3 ± 0.0	2.8 ± 0.4
kidney	0.8 ± 0.1	1.5 ± 0.2
liver	0.3 ± 0.0	5.5 ± 0.9
lung	0.7 ± 0.1	1.0 ± 0.0
heart	0.3 ± 0.1	0.1 ± 0.0
intestine	1.0 ± 0.2	0.3 ± 0.2
blood	1.0 ± 0.1	0.2 ± 0.0

[a] Biodistribution results of SV129 mice bearing the F9 teratocarcinoma at 1 h and 24 h after injection with 2 mg of radioiodinated ScFv(L19)-Cys or ScFv(L19)-Cys−TAT^D conjugate. Antibody doses in the different organs are expressed as percent injected dose/gram tissue (%ID/g).

9.1:1 at 24 h), similar to what had previously been observed for scFv(L19) devoid of the C-terminal Cys residue (*16*, *17*, *41*). However, conjugation of scFv(L19)-Cys to TAT^D resulted in a severely reduced tumor targeting performance compared to the unconjugated antibody (with tumor:blood ratio = 2.5: 1 at 24 h).

Similar to scFv(L19) (*17*), scFv(L19)-Cys was cleared from circulation through the kidneys (Table 1). By contrast, scFv(L19)-Cys−TAT^D showed a rapid uptake in the liver at early time points, similar to the one reported in biodistribution studies for unconjugated TAT peptides (*32*). High liver, kidney, and spleen values persisted up to 24 h, whereby tumor values followed the levels of normal organs (Table 1). In summary, site-specific conjugation of scFv(L19)-Cys to TAT^D abolishes the tumor-targeting properties of this antibody fragment, while enhancing antibody uptake in the liver and in the spleen, without affecting the other normal organs.

DISCUSSION

In this article, we show for the first time that TAT^D and TAT^L have similar cell transduction behavior (Figure 2). This observation strongly supports the existence of a receptor-independent uptake mechanism, consistent with findings reported by other groups (*30*, *42*). The cell uptake of TAT^D may have practical consequences, since peptides made of D-amino acids are not proteolyzed, thus facilitating both in vitro and in vivo applications. Furthermore, D-peptides are not presented by MHC Class II molecules and should not elicit a cellular immune response (*43*).

Our experiments show that TAT also facilitates the uptake of chemically modified antibody fragments (Figure 4), compared to unmodified antibodies. However, the transduction of TAT-conjugated antibody fragments leads to a compartmentalized cell uptake, thus potentially limiting the applicability of TAT-based cell transduction technology either to smaller molecules or to highly bioactive macromolecules.

The most surprising finding of our study was the fact that TAT^D completely abolished the tumor targeting properties of scFv(L19), a human antibody fragment specific for a marker of angiogenesis. ScFv(L19) has previously shown excellent biodistributions in animal tumor models and has entered clinical trials for the immunoscintigraphic detection of tumors in patients with cancer. The inability of scFv(L19)-Cys−TAT^D to target tumors has to be attributed to an inefficient crossing of the endothelial cell layer lining tumor blood vessels (acting as a physical barrier to B-FN, located in the perivascular ECM), since this site-specific conjugate retains full immunoreactivity. The rapid liver uptake of scFv(L19)-Cys−TAT^D may further contribute to the observed lower tumor values (Table 1). Similar findings have been reported for an unconjugated radiolabeled TAT^L peptide, which have recently been investigated in quantitative biodistribution studies in mice (*32*).

The ability of scFv(L19) to target tumors has not been affected by conjugation of this antibody fragment to radionuclides (*16*, *17*), or small organic molecules (*18*, *40*, *41*). Furthermore, excellent biodistribution results in tumor-bearing mice were observed with scFv(L19) fused to a procoagulant protein domain (*19*) and to the cytokines interleukin-2 (*21*) and interleukin-12 (*20*), demonstrating the versatility of scFv(L19) as a tumor targeting vehicle.

However, we have recently found that fusion of scFv(L19) to the proangiogenic cytokine VEGF-165 (but not to the shorter isoformVEGF-121) completely abolished the tumor-targeting property of the antibody, while not significantly affecting blood clearance (*44*). VEGF-165 and VEGF-121 differ by a positively charged heparin-binding peptidic moiety, which is inserted in the VEGF-165 molecule by a mechanism of alternative splicing at the level of the pre-mRNA. The observation that the addition of positively charged moieties (such as TAT^D or VEGF-165) impair the tumor-targeting properties of antibody fragments prompts more quantitative investigations on the interplay between protein charge and vascular permeability.

The poor efficiency of TAT-mediated cell transduction in vivo has recently also been reported by other groups. Tremblay and co-workers showed that the direct delivery of a TAT−eGFP fusion protein to muscle tissue, using subcutaneous or intraarterial injections, only led to few positive fibers in the muscle periphery or surrounding the blood vessels (*45*). As mentioned previously, another study revealed that the continuous in vivo production of TAT−β-glucuronidase from adenovirally transduced hepatocytes only lead to moderately increased uptake of the enzyme in certain tissues (*31*). Some authors have suggested that misfolded proteins may be more amenable to TAT-mediated cell transduction (*46*, *47*). However, this avenue appears to be of little practical utility in biomedical applications, since it may no be able to meet Good Manufacturing Practice standards, required by regulatory authorizations.

The poor in vivo performance of TAT-modified antibodies suggests that other methodologies (such as fusion to vasoactive cytokines) may be more general avenues for improving antibody uptake in the tumor environment (*48*). In a broader perspective, the present article (and a previous related study, performed with unmodified TAT peptides (*32*)) underlines the need to perform quantitative biodistribution studies in animal models, when assessing the potential of TAT peptides and other cell transducing agents, as vehicles for crossing membrane barriers in vivo.

ACKNOWLEDGMENT

Financial support from the Schweizerischer Nationalfonds [TANDEM and Project No. 31-64912; D.N.], the

ETH Zürich [D.N., H.W.A.], the Bundesamt für Bildung und Wissenschaft [D.N.], and the Associazione Italiana Ricerca sul Cancro [L.Z.] is gratefully acknowledged.

LITERATURE CITED

(1) Torrance, C. J., Agrawal, V., Vogelstein, B., and Kinzler, K. W. (2001) Use of isogenic human cancer cells for high-throughput screening and drug discovery. *Nat. Biotechnol. 19*, 940−5.

(2) Bosslet, K., Straub, R., Blumrich, M., Czech, J., Gerken, M., Sperker, B., Kroemer, H. K., Gesson, J. P., Koch, M., and Monneret, C. (1998) Elucidation of the mechanism enabling tumor selective prodrug monotherapy. *Cancer Res. 58*, 1195−1201.

(3) Jain, R. K. (1991) Haemodynamic and transport barriers to the treatment of solid tumours. *Int. J. Radiat. Biol. 60*, 85−100.

(4) Jain, R. K., and Baxter, L. T. (1988) Mechanisms of heterogeneous distribution of monoclonal antibodies and other macromolecules in tumours: significance of elevated interstitial pressure. *Cancer Res. 48*, 7022−7032.

(5) Jain, R. K. (1998) Delivery of molecular and cellular medicine to solid tumors. *J. Controlled Release 53*, 49−67.

(6) Petryk, M., and Grossbard, M. L.(2001) Hematologic malignancies. *Oncologist 6*, 317−326.

(7) Walsh, G. (2000) Biopharmaceutical benchmarks. *Nature Biotechnology 18*, 831−833.

(8) Wu, A. M., and Yazaki, P. Y. (2000) Designer genes: recombinant antibody fragments for biological imaging. *Q. J. Nuclear Medicine 44*, 268−283.

(9) Adams, G. P., Schier, R., Marshall, K., Wolf, E. J., McCall, A. M., Marks, J. D., and Weiner, L. M. (1998) Increased affinity leads to improved selective tumour delivery of scFv antibodies. *Cancer Res. 58*, 485−490.

(10) Juweid, M., Neumann, R., Paik, C., Perez-Bacete, M. J., Sato, J., van Osdol, W., and Weinstein, J. N. (1992) Micropharmacology of monoclonal antibodies in solid tumors: direct experimental evidence for a binding site barrier. *Cancer Res. 52*, 5144−53.

(11) Thorpe, P. E., and Burrows, F. J. (1995) Antibody-directed targeting of the vasculature of solid tumors. *Breast Cancer Res. Treat. 36*, 237−251.

(12) Halin C., and Neri, D. (2001) Antibody-Based targeting of angiogenesis. *Crit. Rev. Ther. Drug Carrier Syst. 18*, 299−339.

(13) Folkman, J. (1995) Angiogenesis in cancer, vascular, rheumathoid and other disease. *Nature Med. 1*, 27−31.

(14) Castellani, P., Viale, G., Dorcaratto, A., Nicolo′, G., Kazmarek, J., Querze, G., and Zardi, L. (1994) The fibronectin isoform containing the ED-B oncofetal domain: a marker of angiogenesis. *Int. J. Cancer 59*, 612−618.

(15) Neri, D., Carnemolla, B., Nissim, A., Balza, E., Leprini, A., Querze', G., Pini, A., Tarli, L., Halin, C., Neri, P., Zardi, L., and Winter, G. (1997) Targeting by affinity-matured recombinant antibody fragments of an angiogenesis associated fibronectin isoform. *Nature Biotechnol. 15*, 1271−1275.

(16) Viti, F., Tarli, L., Giovannoni, L., Zardi, L., and Neri, D. (1999) Increased binding affinity and valence of recombinnat antibody fragments lead to improved targeting of tumoral angiogenesis. *Cancer Res. 59*, 347−352.

(17) Tarli, L., Balza, E., Viti, F., Borsi, L., Castellani, P., Berndorff, D., Dinkelborg, L., Neri, D., and Zardi, L. (1999) A high affinity human antibody that targets tumoural blood vessels. *Blood 94*, 192−198.

(18) Birchler, M., Viti, F., Zardi, L., Spiess, B., and Neri, D. (1999) Selective targeting and photocoagulation of ocular angiogenesis mediated by a phage-derived human antibody fragment. *Nature Biotechnol. 17*, 984−988.

(19) Nilsson, F., Koshmehl, H., Zardi, L., and Neri, D. (2001) Targeted delivery of tissue factor to the ED-B domain of fibronectin, a marker of angiogenesis, mediates the infarction of solid tumours in mice. *Cancer Res. 61*, 711−716.

(20) Halin, C., Rondini, S., Nilsson, F., Berndt, A., Kosmehl, H., Zardi, L., and Neri, D. (2002) Enhancement of the antitumor activity of interleukin-12 by targeted delivery to the neo-vasculature. *Nature Biotechnol. 20*, 264−269.

(21) Carnemolla, B., Borsi, L., Balza, E., Castellani, P., Meazza, R., Berndt, A., Ferrini, S., Kosmehl, H., Neri, D., and Zardi, L. (2002) Enhancement of the antitumor properties of Interleukin-2 by its targeted delivery to the tumor blood vessel extracellular matrix. *Blood 99*, 1659−1665.

(22) Frankel , A.D., and Pabo, C. O. (1988) Cellular uptake of the tat protein from human immunodeficiency virus. *Cell 55*, 1189−93.

(23) Green, M., and Loewenstein, P. M. (1988) Autonomous functional domains of chemically synthesized human immunodeficiency virus tat trans-activator protein. *Cell 55*, 1179−88.

(24) 0 Mann, D. A., and Frankel, A. D. (1991) Endocytosis and targeting of exogenous HIV-1 Tat. *EMBO 10*, 1733−1739.

(25) Fisher, A. G., Feinberg, M. B., Josephs, S. F., Harper, M. E., Marselle, L. M., Reyes, G., Gonda, M. A., Aldovini, A., Debouk, C., Gallo, R. C., et al. (1986) The trans-activator gene of HTLV−III is essential for virus replication. *Nature 320*, 367−71.

(26) Gaynor, R. B. (1995) Regulation of HIV-1 gene expression by the transactivator protein Tat. *Curr. Top. Microbiol. Immunol. 193*, 51−77.

(27) Vives, E., Brodin, P., and Lebleu, B. A. (1997) truncated HIV-1 Tat protein basic domain rapidly translocates through the plasma membrane and accumulates in the cell nucleus. *J. Biol. Chem. 272*, 16010−7.

(28) Lewin, M., Carlesso, N., Tung, C. H., Tang, X. W., Cory, D., Scadden, D. T., and Weissleder, R. (2000) Tat peptide-derivatized magnetic nanoparticles allow in vivo tracking and recovery of progenitor cells. *Nat. Biotechnol. 18*, 410−4.

(29) Schwarze, S. R., Ho, A., Vocero-Akbani, A., and Dowdy, S. F. (1999) In vivo protein transduction: delivery of a biologically active protein into the mouse. *Science 285*, 1569−1572.

(30) Prochiantz A. (2000) Messenger proteins: homeoproteins, TAT and others. *Curr. Opin. Cell Biol. 12*, 400−6.

(31) Xia, H., Mao, Q., and Davidson, B. L. (2001) The HIV Tat protein transduction domain improves the biodistribution of beta-glucuronidase expressed from recombinant viral vectors. *Nature Biotechnol. 19*, 640−4.

(32) Polyakov, V., Sharma, V., Dahlheimer, J. L., Pica, C. M., Luker, G. D., and Piwnica-Worms, D. (2000) Novel Tat-peptide chelates for direct transduction of technetium-99m and rhenium into human cells for imaging and radiotherapy. *Bioconjugate Chem. 11*, 762−71.

(33) Montigiani, S., Neri, G., Neri, P., and Neri, D. (1996) Alanine substitutions in calmodulin binding peptides result in unexpected affinity enhancement. *J. Mol. Biol. 258*, 6−13.

(34) Pini, A., Viti, F., Santucci, A., Carnemolla, B., Zardi, L., Neri, P., and Neri, D. (1998) Design and use of a phage-display library: human antibodies with subnanomolar affinity against a marker of angiogenesis eluted from a two-dimensional gel. *J. Biol. Chem. 273*, 1769−21776.

(35) Borsi, L., Balza, E., Bestagno, M., Castellani, P., Biro, A., Leprini, A., Sepulve, J., Burrone, O., Neri, D., Zardi, L. (2002) Selective targeting of tumoral vasculature: comparison of different formats of an antibody (L19) to the ED-B domain of fibronectin. *Cancer Res.*, submitted.

(36) Liberatore, M., Neri, D., Neri, G., Pini, A., Iurilli, A. P., Ponzo, F., Spampinato, G., Padula, F., Pala, A., and Colella, A. C. (1995) Efficient one-step direct labeling of recombinant antibodies with technetium-99m. *Eur. J. Nucl. Med. 22*, 1326−9.

(37) George, A. J., Jamar, F., Tai, M. S., Heelan, B. T., Adams, G. P., McCartney, J. E., Houston, L. L., Weiner, L. M., and Oppermann, H., Peters, A. M. (1995) Radiometal labeling of recombinant proteins by a genetically engineered minimal chelation site: technetium-99m coordination by single-chain Fv antibody fusion proteins through a C-terminal cysteinyl peptide. *Proc. Natl. Acad. Sci. U. S. A. 92*, 8358−62.

(38) Verhaar, M. J., Keep, P. A., Hawkins, R. E., Robson, L., Casey, J. L., Pedley, B., Boden, J. A., Begent, R. H., and Chester, K. A. (1996) Technetium-99m radiolabeling using a phage-derived single-chain Fv with a C-terminal cysteine. *J. Nucl. Med. 37*, 868−72.

(39) Marty, C., Scheidegger, P., Ballmer-Hofer, K., Klemenz, R., and Schwendener, R. A. (2001) Production of functionalized single-chain Fv antibody fragments binding to the ED-B domain of the B-isoform of fibronectin in Pichia pastoris. *Protein Expr. Purif. 21*, 156−64.

(40) Fattorusso, R., Pellecchia, M., Viti, F., Neri, P., Neri, D., and Wuthrich, K. (1999) NMR structure of the human oncofoetal fibronectin ED-B domain, a specific marker for angiogenesis. *Struct. Fold. Des. 7*, 381−90.

(41) Demartis, S., Tarli, L., Borsi, L., Zardi, L., and Neri, D. (2001) Selective targeting of tumour neovasculature by a radiohalogenated human antibody fragment specific for the ED-B domain of fibronectin. *Eur. J. Nucl. Med. 28*, 534−539.

(42) Derossi, D., Chassaing, G., Prochiantz, A. (1998) Trojan peptides: the penetratin system for intracellular delivery. *Trends Cell Biol. 8*, 84−7.

(43) Schumacher, T. N., Mayr, L. M., Minor, D. L. Jr., Milhollen, M. A., Burgess, M. W., and Kim, P. S. (1996) Identification of D-peptide ligands through mirror-image phage display. *Science 271*, 854−7.

(44) Halin, C., Niesner, U., Villani, M. E., Zardi, L., and Neri, D. Tumor targeting properties of antibody-VEGF fusion proteins. Submitted.

(45) Caron, N. J., Torrente, Y., Camirand, G., Bujold, M., Chapdelaine, P., Leriche, K., Bresolin, N., and Tremblay, J. P. (2001) Intracellular delivery of a Tat-eGFP fusion protein into muscle cells. *Mol. Ther. 3*, 310−8.

(46) Nagahra, H., Vocero-Akbani, A. M., Snyder E. L., Ho, A., Latham, D. G., Lissy, N. A., Becker-Hapak, M., Ezhevsky, S. A., and Dowdy, S. F. (1998) Transduction of full-length TAT fusion proteins into mammalian cell: TAT-p27Kip1 induces cell migration. *Nature Med. 4*, 1449−1452.

(47) Kwon, H. Y., Eum, W. S., Jang, H. W., Kang, J. H., Ryu, J., Ryong Lee, B., Jin, L. H., Park, J., and Choi, S. Y. (2000) Transduction of Cu, Zn-superoxide dismutase mediated by an HIV-1 Tat protein basic domain into mammalian cells. *FEBS Lett. 485*, 163−7.

(48) Hornick, J. L., Khawli, L. A., Hu, P., Sharifi, J., Khanna, C., and Epstein, A. L. (1999). Pretreatment with a monoclonal antibody/interleukin-2 fusion protein directed against DNA enhances the delivery of therapeutic molecules to solid tumors. *Clin. Cancer Res. 5*, 51−60.

BC025517+

Development of EGF-Conjugated Liposomes for Targeted Delivery of Boronated DNA-Binding Agents

Erika Bohl Kullberg,*,† Nill Bergstrand,‡ Jörgen Carlsson,† Katarina Edwards,‡ Markus Johnsson,‡ Stefan Sjöberg,§ and Lars Gedda†

Division of Biomedical Radiation Sciences, Department of Oncology, Radiology and Clinical Immunology, Rudbeck Laboratory, Uppsala University. S− 751 85 Uppsala, Sweden. Received September 21, 2001; Revised Manuscript Received January 23, 2002

Liposomes are of interest as drug delivery tools for therapy of cancer and infectious diseases. We investigated conjugation of epidermal growth factor, EGF, to liposomes using the micelle-transfer method. EGF was conjugated to the distal end of PEG−DSPE lipid molecules in a micellar solution and the EGF−PEG−DSPE lipids were then transferred to preformed liposomes, either empty or containing the DNA-binding compound, water soluble acridine, WSA. We found that the optimal transfer conditions were a 1-h incubation at 60 °C. The final conjugate, ^{125}I-EGF−liposome−WSA, contained approximately 5 mol % PEG, 10−15 EGF molecules at the liposome surface, and 10^4 to 10^5 encapsulated WSA molecules could be loaded. The conjugate was shown to have EGF-receptor-specific cellular binding in cultured human glioma cells.

INTRODUCTION

Liposomes have gained considerable interest as drug delivery tool for therapy of cancer and infectious diseases. They have therapeutic advantages, such as the ability to deliver large amounts of drugs to specific sites, spare healthy tissue from toxic effects, and increase the systemic circulation time of the drug (*1*−*6*). However, one problem with liposomes is their poor stability in the circulatory system. To improve this, poly(ethylene glycol), PEG, is frequently used as a component in the lipid bilayer. PEG stabilizes the liposomes sterically and also effectively protects the liposomes from degradation by the reticuloendothelial system (RES) (*7*−*9*).

Specific accumulation of liposomal substances in tumor cells may be achieved by attachment of targeting agents to the liposomal surface. One way to gain both stability and specificity is to use PEG as a spacer and conjugate the targeting agent to the terminus of the polymer (*10*). We chose this approach and developed a conjugate of epidermal growth factor (EGF) attached to PEG-stabilized liposomes. EGF can be used as a tumor-seeking agent since the EGF receptor is overexpressed in many tumor cells including gliomas and squamos carcinomas (*11*). EGF is a stable protein with well-defined reaction sites for conjugation. It is also known that EGF undergoes receptor-mediated endocytosis, which brings the ligand−receptor complex inside the cell.

The compound Water-Soluble Boronated Acridine-1 (WSA) is a candidate drug for boron neutron capture therapy, BNCT (*12*), and can be actively loaded into liposomes using a pH-gradient procedure (*13*). WSA consists of a boron cage with 10 boron atoms coupled to a DNA intercalating acridine analogue and spermidine to achieve high water solubility. The compound is primarily developed for BNCT, and the stable nuclide, ^{10}B, produces a helium and a lithium ion after neutron capture-induced fission (*14*). Healthy tissue can potentially be saved since only the cells that take up the compound are affected by the ion particles (*15*).

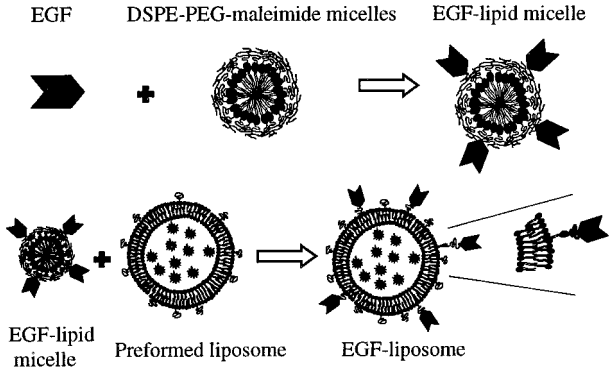


Figure 1. Schematic drawing of the micelle-transfer method. EGF is attached to DSPE−PEG−maleimide lipids in micelles via a thiol linkage. The EGF lipids, in the form of micelles, are mixed with preformed liposomes, and the EGF−PEG−DSPE molecules are thereby incorporated into the liposome membranes

We investigated the possibility to attach EGF to DSPC/cholesterol/DSPE−PEG liposomes, empty or loaded with the drug WSA, using the micelle transfer method (Figure 1). EGF was coupled to maleimide−PEG−DSPE molecules in micelles to achieve a protocol that can easily be adjusted to new targeting agents and new drugs (*16*). The EGF-conjugated micellar lipids were then incorporated into preformed liposomes (*17*). This approach is appealing since the development of new formulations can be reduced to only redesigning the conjugation or the loading step.

Optimizations of the micelle transfer conditions, i.e., time, temperature, and concentration, were performed. We studied the stability of the formulation regarding

* To whom correspondence should be addressed. Erika.Bohl@bms.uu.se, Fax +46 18 471 3432.

† Division of Biomedical Radiation Sciences, Department of Oncology, Radiology and Clinical Immunology.

‡ Department of Physical Chemistry.

§ Department of Organic Chemistry.

10.1021/bc0100713 CCC: $22.00 © 2002 American Chemical Society
Published on Web 05/10/2002

ligand attachment and leakage of the encapsulated compound. The receptor specificity was analyzed by incubating the EGF liposome conjugate with U-343 MGa glioma cells (*18*) with either blocked or nonblocked receptors.

MATERIALS AND METHODS

Murine EGF, obtained from Chemicon International , was labeled with ^{125}I from Amersham Pharmacia Biotech, Uppsala, Sweden. The protein was modified with 2-iminothiolane (Traut's Reagent from Sigma, St. Louis, MO) to obtain thiol groups for conjugation. The Sephadex G-25 columns (NAP-5 columns), the Sephadex G-150 and Sepharose CL-4B gels used for separation, and the empty PD-10 columns were purchased from Amersham Pharmacia Biotech, Uppsala, Sweden. NHS-PEG(3400)-maleimide was purchased from Shearwater Polymers, Huntsville, AL, and 1,2-disteaoryl-*sn*-glycero-3-phosphatidylethanoleamine (DSPE) was obtained from Avanti Polar Lipids, Alabaster, AL. The lipids forming the liposomes 1,2 disteaoryl-*sn*-glycero-3-phosphatidylcholine (DSPC) and 1,2-disteaoryl-*sn*-glycero-3-phosphatidylethanolamine-*N*-[poly(ethylene glycol)-2000] (DSPE−PEG) were purchased from Avanti Polar Lipids. Cholesterol (Cho) was obtained from Sigma Aldrich (Stockholm, Sweden). The DNA binding compound, 1,8-diamino-4-*N*-3-[12-(*N*-9-acridinyl-3-aminopropyl)-*p*-carborane-1-yl]propyl-4-azo-octane hydrogen chloride (WSA, Water-Soluble Acridine Derivative) was produced as described (*12*).

The cell line, U-343 MGaCl2:6 (a subclone of U-343MG, hereafter referred to as U-343 MGa), was grown in Ham's F-10 medium supplemented with 10% FCS and PEST (penicillin 100 IU/mL and streptomycin 100 μg/mL), L-glutamine (2 mM), and amphotericin B (2.5 μg/mL) (all from Biochrom KG, Berlin, Germany). The cells were incubated at 37 °C in humidified air containing 5% CO_2.

Micelles. The micelles were composed of DSPE−PEG−maleimide lipids. NHS−PEG(3400)−maleimide was coupled to the phospholipid DSPE as described (*19*) and dried to form a lipid film. The micelles were formed by hydrating the dried lipid DSPE−PEG−maleimide film in Hepes buffer (20 mM with 150 mM NaCl pH 7.4) at a concentration above the critical micelle concentration, approximately 5 μM (*20*).

Liposomes. The liposomes were composed of DSPC: Cho (60:40 molar ratio), and they contained additionally 0, 3, or 5 mol % DSPE−PEG compared to total lipid. The liposomes were prepared by freeze thawing and extrusion (*13*). Mostly unilamellar liposomes with 100 nm diameter were produced. Liposomes loaded with the DNA binding agent WSA were identical to the above. The loading of WSA was performed using a pH gradient as described (*13*). Briefly, liposomes with an acidic interior (citrate buffer, 300 mM pH 4) were created, and the pH on the outside of the liposomes was raised to 7.8 with sodium carbonate. This pH gradient caused the WSA molecules to enter the liposomes actively and be trapped inside with a concentration up to 300 mM, which gives approximately 10^5 to 10^6 boron atoms per liposome (*13*). Liposomes with an acidic interior, but without WSA, were used in a control experiment.

Radiolabeling of EGF. EGF, diluted in 0.1 M sodium phosphate buffer (0.1 M NaCl, pH 7.5) (25−75 μL, 1 μg EGF/μL) was labeled with 2−7 MBq ^{125}I by the chloramine-T method. The desired amount of ^{125}I (1−5 μL) was added to the EGF solution and 10 μL chloramine-T (2 μg/μL in 0.1 M sodium phosphate buffer 0.1 M NaCl, pH 7.5) was added and mixed for 1 min. The reaction was stopped by 25 μL sodium metabisulfite 25 μL (2 μg/μL in 0.1 M sodium phosphate buffer 0.1 M NaCl, pH 7.5). The labeled protein was separated from reagents by gel filtration on a Sephadex G-25 column (NAP-5) and eluted in 500−600 μL with Traut's buffer (50 mM triehanolamine 0.15 M NaCl, 1 mM EDTA, pH 8).

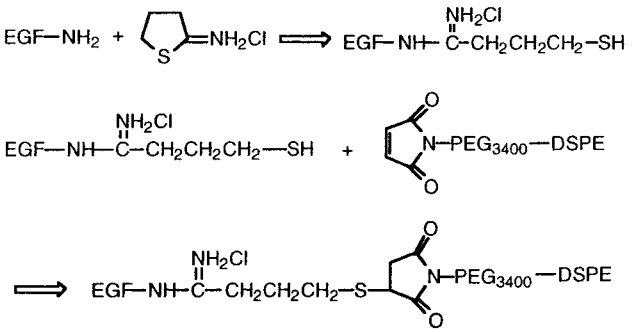


Figure 2. Scheme of the reactions of thiolation of EGF with Traut's reagent (2-iminothiolane) and the thiol conjugation of EGF−SH to maleimide−PEG−DSPE.

Conjugation of ^{125}I-EGF to Maleimide−PEG−DSPE in Micelles (Figure 2). The labeled protein was modified with an excess of Traut's reagent (300−700 μg) for 1h in room temperature (20−23 °C) under argon. Excess reagent was removed by gel filtration on a NAP-5 column eluted with 0.1 M sodium phosphate buffer (0.1 M NaCl, pH 7.5). The thiolated ^{125}I-EGF was mixed with the micelle solution at room-temperature overnight (16−24 h) at either 1:100 or 1:30, EGF: phospholipid molar ratio (PL concentration 0.35 to 0.12 mM). To remove unbound EGF, the sample was separated by gel filtration on a small (PD-10 size) column with Sephadex G-150 gel and eluted with HEPES buffer in 600 μL fractions. The fractions were measured on a gamma counter (1480 Wizard 3, Wallac, Turku, Finland), and the fraction of EGF conjugated to the micellar lipids was determined.

Transfer of ^{125}I-EGF−PEG−DSPE to Liposomes. The influence of various parameters on the rate and the amount of incorporated lipid was studied. The parameters were temperature (room temperature (RT), 37 °C, and 60 °C), lipid concentration (0.5−2.5 mM total lipid), the ratio of liposomal lipid to micellar lipid (1−5% micellar lipid:liposomal lipid), and concentration of PEG-DSPE in the preformed liposomes (0%, 3%, and 5% PEG). The amount of ^{125}I-EGF−PEG−DSPE incorporated was studied after 1, 4, and 24 h, and the same procedure was used for all experiments: ^{125}I-EGF−PEG−DSPE micelles were mixed with the liposome solution under the varying conditions and for the desired time. The transfer was performed in a heating block. After, EGF−liposomes were purified by gel filtration on a small column (PD-10 size) with Sepharose CL-4B gel, eluted with HEPES buffer. The fraction of ^{125}I-EGF−PEG−DSPE incorporated into the liposomes was determined by measuring the eluted fractions (0.5 mL) on a gamma counter. The final conjugates are hereafter referred to as ^{125}I-EGF−liposome−WSA for the loaded liposomes and ^{125}I-EGF−liposome for the unloaded.

Stability and Leakage. The stability of the conjugate was tested by incubation of the ^{125}I-EGF−liposome conjugate diluted in culture medium for up to 3 weeks in 4 °C or 1 week in 37 °C. After incubation, the sample was separated by gel filtration on a CL-4B column. The amount of ^{125}I found in the liposome fraction was determined and was assumed to constitute intact conjugate, and a comparison was made with the total amount of ^{125}I eluted from the column. The leakage of the

encapsulated compound was determined as described (*13*). Briefly, the liposomal sample was separated on a gel filtration column (NAP-5), and the absorbance of lysed separated sample was compared with the absorbance of the lysed initial sample.

Stability of EGF at Different Temperatures and Times. EGF (2.5 μg) was labeled with 10 MBq ^{125}I (as described above) and after purification incubated in HEPES buffer at RT, 37 °C, and 60 °C for 1 and 24 h. The binding activity was examined with U-343 MGa cells grown in small cell dishes (3 cm) with approximately 600000 cells in each dish. The cell dishes were first washed with serum-free medium and the ^{125}I-EGF samples were added (approximately 10 ng/dish). As a control, preincubated dishes with an excess of unlabeled EGF were used. After 30 min, the incubation media was removed, and the cells were washed 6 times with serum-free medium. The cells were trypsinized for 15 min and then resuspended in medium to a total volume of 1.5 mL per cell dish. Of this, 0.5 mL was used for cell counting and 1 mL was measured in a gamma counter to determine the bound radioactivity. The amount of bound ligand was determined and compared to untreated ^{125}I-EGF.

Displacement Test. A displacement study was made to analyze the specificity of the EGF–liposome conjugate. U-343 MGa cells were grown in 3-cm cell dishes, approximately 10^6 cells per dish. Loaded liposome conjugate, 0.5 mL (^{125}I-EGF–liposome–WSA), or unloaded liposome conjugate (^{125}I-EGF–liposome) was added to dishes with 0.5 mL of nonradioactive EGF at the concentration 0, 0.001, 0.01, 0.1, 1, 10, 100, 1000, or 10,000 ng/mL. The cells were incubated with the liposomes for 4 h, the incubation media was removed, and cells were washed six times with cold serum-free medium, trypsinized (trypsin EDTA), and resuspended (total volume 1.5 mL/dish). A volume of 0.5 mL was used for cell counting, and 1 mL was measured in the gamma counter to determine the amount of liposome conjugate bound to the cells. In the displacement study, the liposomal compounds were prepared as described above, and the following composition was used: 3% DSPE-PEG liposomes, 25 μg of EGF labeled with 50 MBq ^{125}I, conjugation overnight, transfer of micellar lipids at 60 °C for 16 h, 3% micellar lipid:liposomal lipid ratio for the unloaded liposomes, 5% micellar lipid:liposomal lipid ratio for the loaded liposomes (to compensate for the lower incorporation level, see Results).

RESULTS

Conjugation of ^{125}I-EGF to Maleimide–PEG–DSPE in Micelles. The coupling efficiency was determined by separating the ^{125}I-EGF micelle conjugate from free ^{125}I-EGF by gel filtration on a Sephadex G-150 column (Figure 3). Approximately 30% of the added ^{125}I-EGF was coupled to the micelles for both 1:100 and 1:30 molar ratio. The figure shows the 1:30 case; a similar pattern was obtained for the 1:100 case. This gives approximately 1 EGF /100 lipids for the highest molar ratio. The conjugation of thiolated ^{125}I-EGF to the maleimide groups on the lipids was shown to be thiol-specific (Figure 3).

Transfer of ^{125}I-EGF–PEG–DSPE to Liposomes. The ^{125}I-EGF–PEG–DSPE transfer efficiency into both WSA-loaded and -unloaded liposomes was examined during the conditions described below.

Temperature and Time. Three different temperatures were studied: RT, 37 °C, and 60 °C (Figure 4). We found

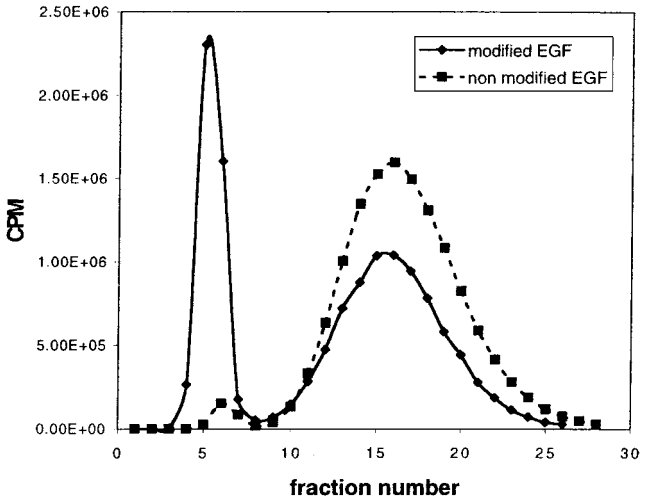


Figure 3. Gel filtration chromatogram for purification of ^{125}I-EGF–PEG micelles. The peak in fraction 4–8 represents the ^{125}I-EGF–PEG-lipid micelles. Fraction 10–25 is ^{125}I-EGF and ^{125}I. The solid line is the elution curve for ^{125}I-EGF modified with Traut's reagent to obtain a thiol group for conjugation to the maleimide group of the maleimide–PEG–DSPE lipid. The dotted line is the elution curve for unmodified ^{125}I-EGF and only a limited unspecific attachment (see fractions 6 and 7) to the maleimide group is seen.

that 60 °C was the best of the tested temperatures for the incorporation of EGF lipids into liposomes. At this temperature no further increase in the amount of incorporated ^{125}I-PEG–DSPE could be seen after 1 h. For RT and 37 °C, the amount incorporated increased with time, but was after 24 h still not as much as 60 °C at 1 h. A smaller amount of lipid was incorporated into the liposomes when the liposomes were loaded with the DNA binding compound WSA (Figure 4). After 1 h at 60 °C, about 30% of the added micellar lipid (Figure 4D) had entered in WSA-loaded liposomes whereas in empty liposomes, with the same PEG amount, this value was about 60% (Figure 4B). To test whether the acidic interior, pH 4, of the loaded liposomes affected their ability to incorporate EGF–lipids, unloaded liposomes with a similar acidic interior were used in control experiments. The level of incorporation at 60 °C (50%) was about the same as for nonacidic unloaded liposomes (data not shown), indicating that the lower level of incorporation in the loaded liposomes was not due to their acidic interior.

Different PEG–Lipid Concentrations in the Liposomes. The PEG–lipid ratio in the liposomes before transfer did not seem to affect the incorporation of ^{125}I-EGF–DSPE at 60 °C or RT (Figure 4A,B,C). Somewhat lower incorporation was seen at 60 °C for 1 and 4 h with 5% PEG, but this increased with time (Figure 4C). Transfer at 37 °C with 0% PEG gave lower incorporation than with 3% and 5% PEG during all studied times (Figure 4A,B,C). The overall transfer with WSA-loaded liposomes was much lower than for liposomes with no load (Figure 4D), as mentioned above. For the loaded liposomes, we chose to continue with 3% PEG since PEG–lipid is needed for the stability and at least after shorter transfer times, the larger amount, 5%, might reduce the incorporation of ^{125}I-EGF–PEG–DSPE.

Concentration Effects. The incorporation of ^{125}I-EGF–DSPE was analyzed as a function of the amount of added ^{125}I-EGF–DSPE. Three different concentrations of ^{125}I-EGF–DSPE were applied. A saturation effect could be seen since 3% and 5% ^{125}I-EGF–DSPE to liposomal lipid gave about the same incorporation, about twice the

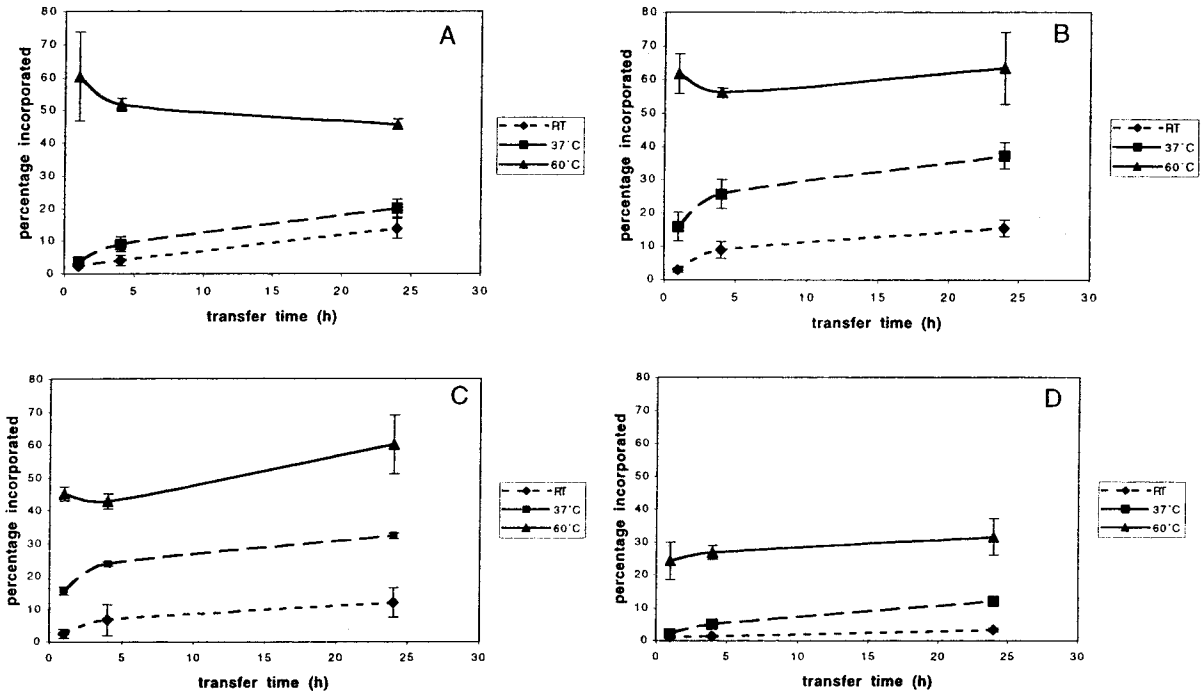


Figure 4. Incorporation ability of ^{125}I-EGF−PEG−DSPE lipid molecules into preformed liposomes. The percentage of added lipid incorporated in the liposome membrane was measured using the ^{125}I-label on EGF. The amount of added EGF lipid was 2.7% to total liposomal lipid. A: 0% PEG in the preformed liposomes, B: 3% PEG-DSPE to total lipid, C: 5% PEG-DSPE to total lipid, D: WSA loaded liposomes with 3% PEG-DSPE, to total lipid. Error bars represent maximal errors from double experiments.

Table 1. Micelle Transfer to Liposomes as a Function of the Percentage Micellar EGF−Lipid, ^{125}I-EGF−PEG−DSPE, to Liposome Lipid[a]

^{125}I-EGF−PEG−DSPE to liposome lipid, ratio	% incorporated	nmol EGF/ mmol lipid
0.01	66 ± 1	19 ± 1
0.03	52 ± 1	42 ± 2
0.05	35 ± 2	46 ± 1

[a] Incorporation was performed for 1 h in 60 °C and with an initial concentration of 3% PEG in the liposomes.

Table 2. Stability of the ^{125}I-EGF−Liposome−WSA Conjugate after Storage in Complete Culture Medium at Either 4 or 37 °C[a]

time	4 °C	37 °C
2 days	97%	90%
5 days	nd	85%
1 week	nd	79%
3 weeks	90%	nd

[a] The result is given as the percentage of total radioactivity that remained in the liposome fraction. nd = not determined.

amount of EGF incorporated compared to 1% (Table 1). The total lipid concentration in the reaction tube did not affect the incorporation of micelles when 3% ^{125}I-EGF−DSPE to liposomes was applied. No difference regarding the transfer could, in this case, be seen for 2.5 mM, 1 mM, and 0.5 mM total lipid (data not shown).

Stability and Leakage. The stability was rather good since 79% of the radioactivity remained in the liposome fraction after 1 week of incubation at 37 °C with ^{125}I-EGF−liposome−WSA diluted in complete culture medium (Table 2). Samples incubated for 3 weeks at 4 °C had 90% radioactivity in the liposome fraction. The leakage of WSA from the liposomes was about 12% at 60 °C after 1 h. At 37 °C, the leakage was about 10% after 24 h. No extra leakage due to the transfer process was observed for either temperature.

Stability of EGF at Different Temperatures and Times. The cell tests showed that the binding ability and receptor specificity of ^{125}I-EGF was almost unaltered for all studied times and temperatures during the micelle transfers. A slight decrease was however detected for 24 h in 60 °C (Figure 5).

Displacement Test. By adding high concentrations of EGF, it was possible to displace the binding of ^{125}I-EGF−liposomes almost completely (Figure 6) proving receptor specific binding. Specificity was also seen for ^{125}I-EGF−liposome−WSA. However, the fraction of nonreceptor specific binding of radioactivity increased to about 30% in the latter case. The reason for this increase in nonspecific binding is at present not clear, but it appears likely that the WSA in some way modifies the properties of the liposomes.

DISCUSSION

Here, we showed that EGF can be coupled to PEG-stabilized liposomes using the micelle transfer method. A transfer temperature of 60 °C produces higher amounts of liposome incorporated ^{125}I-EGF−PEG−DSPE than at room temperature or 37°C. This is not unexpected since the bilayer fluidity increases with increasing temperature. EGF loses nearly no biological activity at 60 °C. The leakage of WSA at 60 °C was higher than at 37 °C, but it was not severe enough to defend the use of 37 °C as transfer temperature.

The optimization studies included investigations of how the amount of PEG−lipid in the initial liposome preparation affected the incorporation of EGF-conjugated PEG−lipid. Three different PEG−lipid concentrations were tested in the preformed liposomes, and only small differences were observed between them. At short time scales, a somewhat lower level of incorporation was observed for the preparation containing the highest amount of PEG−lipid, i.e., 5 mol %. The incorporated amount increased, however, with time and reached after

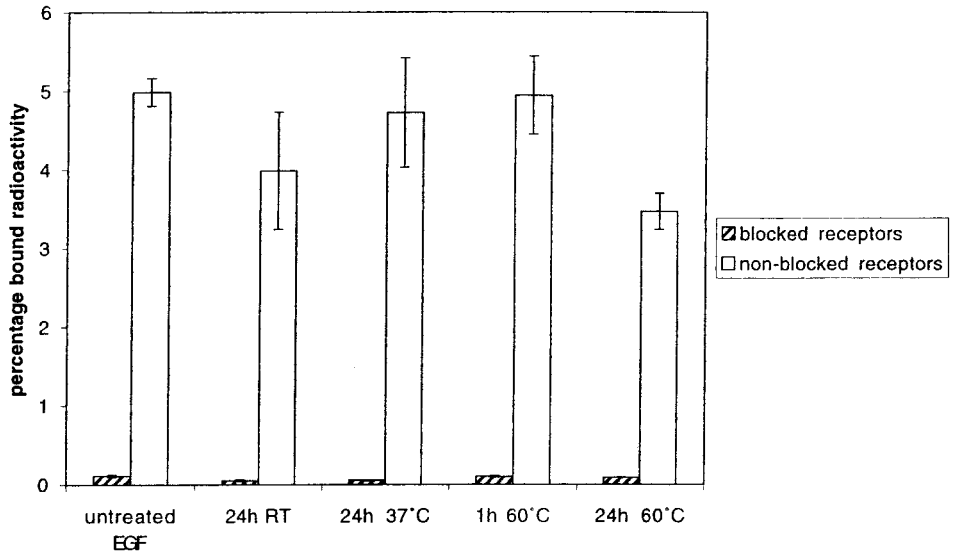


Figure 5. Test of the binding ability of temperature pretreated ^{125}I-EGF to cultured glioma cells. Binding was also tested on blocked receptors to ensure that receptor specificity did not change. An excess of unlabeled EGF was used to block the receptors in those cases. The cells were incubated with EGF for 30 min. Each bar corresponds to three cell dishes. Error bars represent maximal errors.

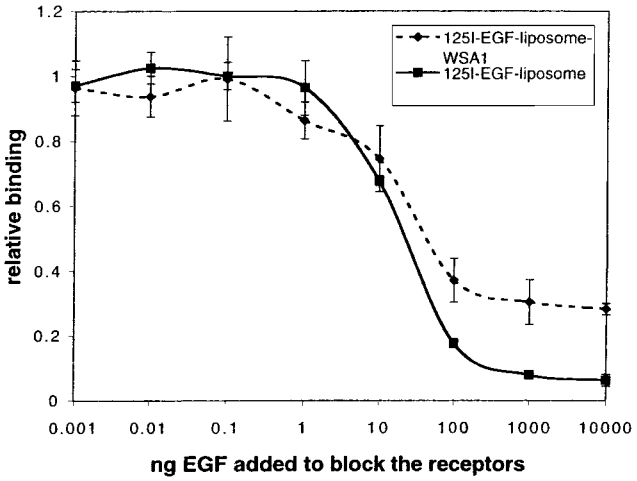


Figure 6. Test of binding specificity of ^{125}I-EGF–liposome–WSA conjugate and ^{125}I-EGF–liposome conjugate. The added amount of conjugate was the same, and increasing concentrations of unlabeled EGF displaced the binding to the EGF receptor. The incubation time was 4 h for both conjugates. For all studies the amount bound without blocking was normalized to unity. Error bars represent maximal errors; ^{125}I-EGF–liposome–WSA, $n = 6$, ^{125}I-EGF–liposome, $n = 3$.

24 h the same level as observed for 0 mol % and 3 mol %. Since an initial PEG–lipid concentration of 3 mol % gave the preferred final PEG–lipid content, we chose this concentration for our further experiments.

A clear difference in the transfer was observed between empty and WSA-loaded liposomes. The amount of incorporated EGF-conjugated PEG–lipid was significantly lower for liposomes containing WSA than for unloaded liposomes with the same PEG–lipid content. A similar study published by Ishida et al. (*16*) reported that the amount of DSPE–PEG in the preformed liposomes affects the ability of lipids to incorporate into liposomes. Ishida et al. also studied coupling of antibody to Caelyx/Doxil liposomes with the micelle transfer method. The results indicated a much lower transfer for liposomes loaded with drug than for empty liposomes with slightly lower PEG-lipid content (4% PEG–lipid vs 5% PEG–lipid). We do not rule out the possibility that the PEG–lipid concentration in the preformed liposomes may influence the amount of incorporation but believe that, at least in our case, the decrease in the transfer is mainly due to the content of the liposomes.

A final concentration of about 5 mol % PEG–lipid is desired for prolonged liposome circulation in vivo (*21*). With the unloaded liposomes, this can be achieved by using 3 mol % PEG–lipid in the liposomes before transfer and 3% micellar lipid to total lipid the transfer. With the loaded liposomes, we obtained about 4 mol % total PEG–lipid in the final conjugate. One way to increase the final PEG–lipid amount, and also the EGF amount, is to slightly increase the micelle lipid to total lipid ratio.

We studied liposomes with a radius of about 100 nm and such liposomes contain approximately 75000–80000 phospholipids per liposome (*19*). For these liposomes we managed to obtain about 10–15 EGF molecules /liposome. This amount is assumed to be enough to achieve a satisfactory cellular uptake of antibody-targeted liposomes (*10, 19*). However, the optimal amount of EGF molecules on the liposome surface needed for a high cell uptake, and desirable clearance from the systemic circulation, has to be studied in future in vitro and in vivo experiments.

In two earlier studies, direct coupling of EGF to phospholipids via disulfide bonds was used (*22, 23*). This approach would for our PEG-stabilized, long-circulating liposomes probably lead to lower binding to tumor cells since the ligand would be "buried" within the PEG-layer (*24*). Instead, we conjugated EGF to the PEG-part of the lipids, ending up with the targeting agent outside the PEG-layer of the liposomes. We chose to conjugate EGF to maleimide–PEG–DSPE, thereby also avoiding the problem of unstable disulfide bonds within the circulation.

The stability of the ^{125}I-EGF–liposome–WSA conjugate was good; besides, it could be stored at 4 °C for weeks. The stability at 37 °C was also acceptable and high enough for us to be sure that no significant spontaneous degradation occurred during the in vitro tests with cultured tumor cells.

The ^{125}I-EGF–liposome conjugate showed mainly EGF-receptor-specific binding to cultured glioma cells, as proven by displacement of the conjugate with increasing

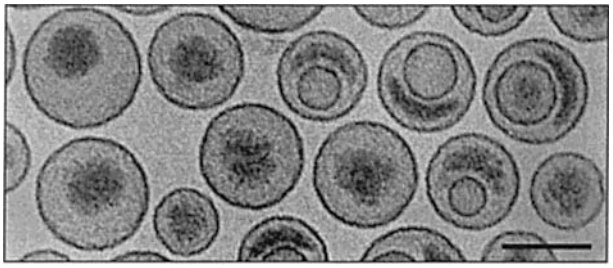


Figure 7. Cryo-Tem analysis picture of liposomes loaded with WSA. Bar represents 100 nm.

amounts of nonradioactive EGF. We cannot, at present, explain why the nonspecific binding of conjugates loaded with WSA was higher than that of the conjugate without WSA. There seems to be no disturbance of the liposome bilayer due to the load as shown in previous studies based on Cryo-TEM(*13*). The Cryo-TEM analyses showed intact liposomes with WSA crystals in the middle (Figure 7).

More studies on the cellular uptake, retention kinetics, and fate of the load are currently in progress.

CONCLUDING REMARKS

Although the problem with high uptake of liposomes by the RES system has been widely addressed during the last years (*7*−*9*), the dose-limiting organ for radionuclide therapy of malignancies using liposomes is still thought to be the liver (*25*). Further improvements are needed and one important factor is the tumor cell specificity of the liposomes. An active tumor targeting approach using antibodies, antibody fragments, or receptor ligands coupled to liposomes can hopefully increase the tumor specificity and decrease the dose to the liver. A binary system, such as BNCT, would give the opportunity to choose the area of neutron activation of boron and thereby further decrease the liver dose. Earlier reports on liposomes for BNCT lack specific tumor targeting ability (*3, 27*−*30*). Here, we presented a liposomal delivery vehicle for specific tumor targeting. We loaded about 10^5 to 10^6 boron atoms in each liposome, which is enough to make the liposomes interesting for therapy. It is known that 10^8 to 10^9 boron atoms are needed per tumor cell for therapeutic effect (*26*), and with the achieved number of boron atoms per liposome, it is realized that only 10^2 to 10^4 receptor interactions are needed per cell. The targeting ability will hopefully give the liposomes a much higher potential to find, bind, and inactivate tumor cells.

The procedure of the micelle-transfer method is attractive since the load and the targeting agent can be easily exchanged. We are currently developing DNA-binding compounds for halogen labeling, such as ^{211}At and ^{125}I, which may be exchanged for WSA used in this study. The use of EGF as a targeting molecule is at present being evaluated at our laboratory in a clinical study on bladder cancer patients. In this study, EGF−dextran (*31*) is used, but EGF-labeled liposomes might be applied if the penetration properties are found to be satisfactory.

ACKNOWLEDGMENT

Financial support was given by the Swedish Cancer Society grant 4141-B00-03XAB.

LITERATURE CITED

(1) Gabizon, A., and Papahadjopoulos, D. (1988) Liposome formulations with prolonged circulation time in blood and enhanced uptake by tumors. *Proc. Natl. Acad. Sci. U.S.A. 85*, 6949−6953.

(2) Gabizon, A. A. (1992) Selective tumor localization and improved therapeutic index of anthracyclines encapsulated in long-circulating liposomes. *Cancer Res. 52* (*4*), 891−6.

(3) Feakes, D. A., Shelly, K., and Hawthorne, M. F. (1995) Selective boron delivery to murine tumors by lipophilic species incorporated in the membranes of unilamellar liposomes. *Proc. Natl. Acad. Sci. U. S.A. 92* (*5*), 1367−70.

(4) Forssen, E. A., Coulter, D. M., and Proffitt, R. T. (1992) Selective in vivo localization of daunorubicin small unilamellar vesicles in solid tumors. *Cancer Res. 52* (*12*), 3255−61.

(5) Bakker-Woudenberg, I. A., Lokerse, A. F., ten Kate, M. T., Mouton, J. W., Woodle, M. C., and Storm, G. (1993) Liposomes with prolonged blood circulation and selective localization in Klebsiella pneumoniae-infected lung tissue. *J. Infect. Dis. 168* (*1*), 164−71.

(6) Papahadjopoulos, D., Allen, T. M., Gabizon, A., Mayhew, E., Matthay, K., Huang, S. K., Lee, K. D., Woodle, M. C., Lasic, D. D., Redemann, C., and et al. (1991) Sterically stabilized liposomes: improvements in pharmacokinetics and antitumor therapeutic efficacy. *Proc. Natl. Acad. Sci. U.S.A. 88* (*24*), 11460−4.

(7) Maruyama, K., Yuda, T., Okamoto, A., Kojima, S., Suginaka, A., and Iwatsuru, M. (1992) Prolonged circulation time in vivo of large unilamelar liposomes composed of distearoyl phosphatidylcholine and cholesterol containing amphipathic poly(ethylene glycol). *Biochim. Biophys. Acta 1128* (*1*), 44−9.

(8) Klibanov, A. L., Maruyama, K., Torchilin, V. P., and Huang, L. (1990) Amphipathic poly(ethylene glycol)s effectively prolong the circulation time of liposomes. *FEBS Lett. 268* (*1*), 235−7.

(9) Allen, T. M., Hansen, C., Martin, F., Redemann, C., and Yau-Young, A. (1991) Liposomes containing synthetic lipid derivatives of poly(ethylene glycol) show prolonged circulation half-lives in vivo. *Biochim. Biophys. Acta 1066* (*1*), 29−36.

(10) Allen, T. M., Brandeis, E., Hansen, C. B., Kao, G. Y., and Zalipsky, S. (1995) A new strategy for attachment of antibodies to sterically stabilized liposomes resulting in efficient targeting to cancer cells [published erratum appears in *Biochim. Biophys. Acta* 1995, Dec 13; *1240* (*2*), 285]. *Biochim. Biophys. Acta 1237* (*2*), 99−108.

(11) Collins, V. P. (1993) Amplified genes in human gliomas. *Semin. Cancer Biol. 4* (*1*), 27−32.

(12) Ghaneolhosseini, H., Tjarks, W., and Sjöberg, S. (1998) Synthesis of novel Boronated Acridines- and Spermidines as possible agents for BNCT. *Tetrahedon 54*, 3877−3884.

(13) Johnsson, M., Bergstrand, N., and Edwards, K. (1999) Optimization of drug loading procedures and characterization of liposomal formulations of two novel agents intended for boron neutron capture therapy (BNCT). *J. Liposome Res. 9* (*1*), 53−79.

(14) Locher, G. L. (1936) Biological effects and therapeutic possibilities of neutrons. *Am. J. Roentgenol. Radium Ther. 36* (*1*), 1−13.

(15) Barth, R. F., Soloway, A. H., and Brugger, R. M. (1996) Boron Neutron Capture Therapy of brain tumors: Past history, current status and future potential. *Cancer Invest. 14* (*6*), 534−550.

(16) Ishida, T., Iden, D. L., and Allen, T. M. (1999) A combinatorial approach to producing sterically stabilized (Stealth) immunoliposomal drugs. *FEBS Lett. 460* (*1*), 129−33.

(17) Uster, P. S., Allen, T. M., Daniel, B. E., Mendez, C. J., Newman, M. S., and Zhu, G. Z. (1996) Insertion of poly(ethylene glycol) derivatized phospholipid into preformed liposomes results in prolonged in vivo circulation time. *FEBS Lett. 386*, 243−246.

(18) Ponten, J., and Westermark, B. (1978) Properties of human malignant glioma cells in vitro. *Med. Biol. 56*, 184−193.

(19) Kirpotin, D., Park, J. W., Hong, K., Zalipsky, S., Li, W. L., Carter, P., Benz, C. C., and Papahadjopoulos, D. (1997) Sterically stabilized anti-HER2 immunoliposomes: design and targeting to human breast cancer cells in vitro. *Biochemistry 36* (*1*), 66−75.

(20) Johnsson, M., Hansson, P., and Edwards, K. (2001) Spherical micelles and other self-assembled structures in dilute aqueous mixtures of poly(ethylene glycol) -lipids. *J. Phys. Chem. B. 105*, 8420−8430.

(21) Silvander, M., Johnsson, M., and Edwards, K. (1998) Effects of PEG-lipids on permeability of phosphatidylcholine/cholesterol liposomes in buffer and in human serum. *Chem. Phys. Lipids 97* (*1*), 15−26.

(22) Ishii, Y., Aramaki, Y., Hara, T., Tsuchiya, S., and Fuwa, T. (1989) Preparation of EGF labeled liposomes and their uptake by hepatocytes. *Biochem. Biophys. Res. Commun. 160* (*2*), 732−6.

(23) Kikuchi, A., Sugaya, S., Ueda, H., Tanaka, K., Aramaki, Y., Hara, T., Arima, H., Tsuchiya, S., and Fuwa, T. (1996) Efficient gene transfer to EGF receptor overexpressing cancer cells by means of EGF-labeled cationic liposomes.. *Biochem. Biophys. Res. Commun. 227* (*3*), 666−671.

(24) Blume, G., Cevc, G., Crommelin, M. D. J. A., Bakker-Woudenberg, I. A., Kluft, C., and Storm, G. (1993) Specific targeting with poly(ethylene glycol)-modified liposomes: coupling of homing devices to the ends of the polymeric chains combines effective target binding with long circulation times. *Biochim. Biophys. Acta. 1149*, 180−184.

(25) Emfietzoglou, D., Kostarelos, K., and Sgouros, G. (2001) An analytic dosimetry study for the use of radionuclide-liposome conjugates in internal radiotherapy. *J. Nuclear Med. 42* (*3*), 499−504.

(26) Hartman, T., Carlsson, J. (1994) Radiation dose heterogeneity in receptor and antigen mediated boron neutron capture therapy. *Radiother. Oncol. 31* (*1*), 61−75.

(27) Shelly, K., Feakes, D. A., Hawthorne, M. F., Schmidt, P. G., Krisch, T. A., and Bauer, W. F. (1992) Model studies directed toward the boron neutron-capture therapy of cancer: boron delivery to murine tumors with liposomes. *Proc. Natl. Acad. Sci. U.S.A. 89* (*19*), 9039−43.

(28) Hawthorne, M. F., and Shelly, K. (1997) Liposomes as drug delivery vehicles for boron agents. *J. Neurooncol. 33* (*1*−*2*), 53−8.

(29) Mehta, S. C., Lai, J. C., and Lu, D. R. (1996) Liposomal formulations containing sodium mercaptoundecahydrododecaborate (BSH) for boron neutron capture therapy. *J. Microencapsul. 13* (*3*), 269−79.

(30) Moraes, A. M., Santana, H. A., and Carbonell, R. G. (1999) Preparation and characterization of liposomal systems entrapping the boronated compound o-carboranylpropylamine. *J. Microencapsul. 16* (*5*), 647−664.

(31) Carlsson, J., Blomquist, E., Gedda, L., Liljegren, Å, Malmström, P.-U., Sjöström, A., Sundin, A., Westlin, J.-E., Zhao, Q., Tolmachev, V., and Lundqvist, H. (1999) Conjugate chemistry and cellular processing of EGF-Dextran. *Acta Oncol. 38*, 313−321.

BC0100713

Cholesterol Inclusion in Liposomes Affects Induction of Antigen-Specific IgG and IgE Antibody Production in Mice by a Surface-Linked Liposomal Antigen

Yoshio Nakano,[†] Masahito Mori,[†] Hiroyuki Yamamura,[†] Seishiro Naito,[‡] Hiroshi Kato,[‡] Maiko Taneichi,[‡] Yuriko Tanaka,[‡] Katsutoshi Komuro,[‡] and Tetsuya Uchida*[,‡]

DDS Development Division, NOF Corporation, Tokyo, Japan, and Department of Safety Research on Blood and Biological Products, National Institute of Infectious Diseases, Tokyo, Japan. Received October 15, 2001; Revised Manuscript Received April 24, 2002

In the previous study, we investigated the induction of ovalbumin (OVA)-specific antibody production in mice by OVA−liposome conjugates made using four different lipid components, including unsaturated carrier lipid and three different saturated carrier lipids. All of the OVA−liposome conjugates tested induced IgE-selective unresponsiveness. The highest titer of anti-OVA IgG was observed in mice immunized with OVA−liposomes made using liposomes with the highest membrane fluidity, suggesting that the membrane fluidity of liposomes affects their adjuvant effect. In this study, liposomes with five different cholesterol inclusions, ranging from 0% to 43% of the total lipid, were made, and the induction of OVA-specific antibody production by OVA−liposome conjugates was compared among these liposome preparations. In contrast to the results in the previous study, liposomes that contained no cholesterol and possessed the lowest membrane fluidity demonstrated the highest adjuvant effect for the induction of IgG antibody production. In addition, when the liposomes with four different lipid compositions were used, OVA−liposome conjugates made using liposomes that did not contain cholesterol induced significantly higher levels of anti-OVA IgG antibody production than did those made using liposomes that contained cholesterol and, further, induced significant production of anti-OVA IgE. These results suggest that cholesterol inclusion in liposomes affects both adjuvanticity for IgG production and regulatory effects on IgE synthesis by the surface-coupled antigen of liposomes.

INTRODUCTION

Vaccines are undoubtedly the most efficient tool for control or elimination of severe infectious diseases. Over the course of development of modern vaccines, weak immunogenicity presented a major difficulty (*1*). Consequently, the use of adjuvants became indispensable. Aluminum-containing compounds are, at present, the only adjuvants approved for clinical use. However, they are not active with all immunogens, and they are known to induce production of IgE antibodies, which can cause allergic reactions in the vaccinee (*2*). To date, many adjuvant formulations have been developed, but only a few have been evaluated in clinical trials, mainly due to their toxicity and side effects (*3*). Among the candidates for adjuvants, liposomes have garnered recent attention for their capacity as carriers of vaccines (*4*−*8*). Most of the liposomal vaccines proposed have been made by antigen entrapment within the liposomal compartment (*5*). However, encapsulated and surface-linked liposomal antigens are known to induce differential immune responses (*9*). The capability to induce cellular immune response by a surface-linked, but not by encapsulated, liposomal antigen has been reported (*8*).

We previously reported that surface-linked liposomal antigen induced antigen-specific IgG, but not IgE, antibody production (*10*). This antigen modification was expected to serve as a novel protocol for the development of vaccines that would induce minimal allergic response. IgE-selective unresponsiveness was induced regardless of the coupling procedure of antigen and liposomes (*11*). In addition, differential adjuvant effects were obtained with antigen−liposome conjugates including differentially formulated liposomes, whereas IgE antibody production was not induced by the prepared conjugates (*12*).

Inclusion of cholesterol in the liposome formulation is known to affect the stability and adjuvanticity of liposomes (*7*, *13*). In this study, liposomes with different cholesterol inclusions were prepared and then coupled with antigens in order to investigate the induction of antigen-specific IgG and IgE antibody production. The aim of this study was to determine the correlation between cholesterol inclusion in liposomes and the induction of antibody production by surface-linked liposomal antigens.

MATERIALS AND METHODS

Experimental Animals. BALB/c mice (8 weeks of age, female) were purchased from Charles River (Yokohama, Kanagawa, Japan).

Chemicals. All phospholipids were obtained from NOF Co., Tokyo, Japan. Reagent grades of cholesterol and 1,6-diphenyl-1,3,5-hexatriene (DPH) were purchased from Wako Pure Chemical Co., Osaka, Japan.

* To whom correspondence should be addressed: National Institute of Infectious Diseases, 4−7−1 Gakuen, Musashimurayama City, Tokyo 208-0011, Japan. Phone: +81 425 61 9724. Fax: +81 425 61 9722. E-mail: tuchida@nih.go.jp.

[†] NOF Corporation.

[‡] National Institute of Infectious Diseases.

10.1021/bc0155667 CCC: $22.00 © 2002 American Chemical Society
Published on Web 06/27/2002

Table 1. Liposomes with Different Cholesterol Inclusions

cholesterol inclusion (%)	liposome formulation	molar ratio
0	dipalmitoyl phosphatidyl choline (DPPC)	8.0
	dipalmitoyl phosphatidyl ethanolamine (DPPE)	6.0
	dimyristoyl phosphatidyl glycerol (DMPG)	2.0
	cholesterol	0.0
10	dipalmitoyl phosphatidyl choline (DPPC)	7.1
	dipalmitoyl phosphatidyl ethanolamine (DPPE)	5.3
	dimyristoyl phosphatidyl glycerol (DMPG)	2.0
	cholesterol	1.6
20	dipalmitoyl phosphatidyl choline (DPPC)	6.2
	dipalmitoyl phosphatidyl ethanolamine (DPPE)	4.6
	dimyristoyl phosphatidyl glycerol (DMPG)	2.0
	cholesterol	3.2
30	dipalmitoyl phosphatidyl choline (DPPC)	5.3
	dipalmitoyl phosphatidyl ethanolamine (DPPE)	3.9
	dimyristoyl phosphatidyl glycerol (DMPG)	2.0
	cholesterol	4.8
43	dipalmitoyl phosphatidyl choline (DPPC)	4.0
	dipalmitoyl phosphatidyl ethanolamine (DPPE)	3.0
	dimyristoyl phosphatidyl glycerol (DMPG)	2.0
	cholesterol	7.0

Table 2. Liposomes Made Using Four Different Carrier Lipids with or without Cholesterol

name	liposome formulation	molar ratio
oleoyl (+CHO)	dioleoyl phosphatidyl choline (DOPC)	4
	dioleoyl phosphatidyl ethanolamine (DOPE)	3
	dioleoyl phosphatidyl glycerol (DOPG)	2
	cholesterol	7
oleoyl (−CHO)	dioleoyl phosphatidyl choline (DOPC)	8
	dioleoyl phosphatidyl ethanolamine (DOPE)	6
	dioleoyl phosphatidyl glycerol (DOPG)	2
	cholesterol	0
myristoyl (+CHO)	dimyristoyl phosphatidyl choline (DMPC)	4
	dimyristoyl phosphatidyl ethanolamine (DMPE)	3
	dimyristoyl phosphatidyl glycerol (DMPG)	2
	cholesterol	7
myristoyl (−CHO)	dimyristoyl phosphatidyl choline (DMPC)	8
	dimyristoyl phosphatidyl ethanolamine (DMPE)	6
	dimyristoyl phosphatidyl glycerol (DMPG)	2
	cholesterol	0
palmitoyl (+CHO)	dipalmitoyl phosphatidyl choline (DPPC)	4
	dipalmitoyl phosphatidyl ethanolamine (DPPE)	3
	dipalmitoyl phosphatidyl glycerol (DPPG)	2
	cholesterol	7
palmitoyl (−CHO)	dipalmitoyl phosphatidyl choline (DPPC)	8
	dipalmitoyl phosphatidyl ethanolamine (DPPE)	6
	dipalmitoyl phosphatidyl glycerol (DPPG)	2
	cholesterol	0
stearoyl (+CHO)	distearoyl phosphatidyl choline (DSPC)	4
	distearoyl phosphatidyl ethanolamine (DSPE)	3
	distearoyl phospatidyl glycerol (DSPG)	2
	cholesterol	7
stearoyl (−CHO)	distearoyl phosphatidyl choline (DSPC)	8
	distearoyl phosphatidyl ethanolamine (DSPE)	6
	distearoyl phospatidyl glycerol (DSPG)	2
	cholesterol	0

Liposomal Antigen. Ovalbumin (OVA, Grade VII) was purchased from Sigma (St. Louis, MO).

Liposomes. The liposomes with different cholesterol inclusions used in this study are listed in Table 1. The liposomes consisting of four different components, with or without cholesterol, are listed in Table 2. The crude liposome solution was passed through a membrane filter (Nucleopore polycarbonate filter, Coster, Cambridge, MA) with a pore size of 0.2 μm. The diameter of liposomes was analyzed using a NICOMP 370 submicron particle sizer (Pacific Scientific, Silver Springs, MD). After filtration, the mean size and SE of liposomes listed in Tables 1 and 2 were 222.8 ± 10.1 and 224.0 ± 14.3 nm, respectively.

Preparation of Fluorescence-Labeled Liposomes. Fluorescence-labeled liposomes containing phospholipids were prepared as follows: DPPC, DPPE, DMPG, and cholesterol with the indicated molar ratio (Table 1) were dissolved in a mixture of solvents (chloroform/methanol/water = 65/25/4 by volume), and then 4.3 M DPH in chloroform solution was added. After vigorous mixing, solvents were removed completely under reduced pressure, followed by the addition of 1 mM phosphate buffer (pH 6.0) containing 8.5% sucrose to create a lipid vesicle suspension. The suspension was then extruded through a polycarbonate filter (0.2 μm) to adjust the liposome size. Fluorescence-labeled liposomes containing phospholipids that included a myristoyl group, palmitoyl group, or stearoyl group acting as the acyl chain were prepared by the same method.

Fluorescence Measurement. Fluorescence depolarization of DPH was measured according to the method described by Lents et al. (*14*) using a Hitachi F-2000 spectrophotometer equipped with a temperature-controlled cuvette holder. DPH was excited at 360 nm and its fluorescence was measured at 428 nm using an UV-

39 instrument filter UV-39 to cutoff wavelengths below 390 nm. The degree of fluorescence polarization was calculated from the formula

$$P = (I_{VV} - I_{VH}G)/(I_{VV} + I_{VH}G)$$

where I_{VV} and I_{VH} are the observed fluorescence intensities measured with polarizers parallel and perpendicular to the vertically polarized exciting beam, respectively, and G is a correction factor for the transmission efficiency of vertically and horizontally polarized light. A 3-mL portion of 1 mM phosphate buffer (pH 6.0) containing 8.5% sucrose was mixed well with 0.3 mL of the liposome suspension prepared as described previously. The mixture was then allowed to stand at 37 °C for 5 min before measurement. Samples from each liposome suspension were prepared in triplicate.

Coupling of OVA to Liposomes. Liposomal conjugates with OVA (OVA−liposome) via glutaraldehyde were prepared as follows: to a mixture of 90 mg of liposomes and 6 mg of OVA in 2.5 mL phosphate buffer (pH 7.2), 0.5 mL of 2.5% glutaraldehyde solution was added in drops. The mixture was stirred gently for 1 h at 37 °C, and then 0.5 mL of 3 M glycine-NaOH (pH 7.2) was added to block the excess aldehyde groups. The mixture was then incubated overnight at 4 °C. The liposome-coupled OVA and uncoupled OVA in the resulting solution were separated using CL-4B column chromatography (Pharmacia Fine Chemical Co., Upsala, Sweden). The amount of lipid in the liposomal fraction was measured using a phospholipid content assay kit (Phospholipid-Test-Wako, Wako Pure Chemical Co., Osaka, Japan). The OVA−liposome solution was adjusted to 10 mg lipid/mL and kept at 4 °C until use. For the measurement of OVA coupled to liposome, radiolabeled OVA ([methyl-^{14}C], purchased from New England Nuclear, Boston, MA) was mixed with cold OVA and then used for coupling with liposome and for determining the calibration curve. The radioactivity of the resulting OVA−liposome solution was counted using a calibration curve. The mean and SE of OVA coupled to liposomes listed in Tables 1 and 2 were 47.0 ± 2.2 and 47.8 ± 2.5 μg/mg of lipid, respectively. These results suggested that the variation in moles of phosphatidyl choline (4−8), phosphatidyl ethanolamine (3−6), and differential cholesterol inclusion in liposomes did not result in the differential coupling efficiency of OVA to liposomes.

Immunization. Mice were immunized intraperitoneally (ip) with OVA−liposome at a dose of 2 mg of lipid/200 μL/mouse. Four weeks after primary immunization, mice were boosted in the same manner as that used for primary immunization. For the measurement of serum antibodies, mice were bled from the tail vein.

Measurement of Serum Antibodies. Six weeks after primary immunization, serum anti-OVA IgG and IgG isotypes were determined by enzyme-linked immunosorbent assay (ELISA) using HRP-labeled goat anti-mouse IgG (Zymed Lab., San Francisco, CA). OVA-specific IgE was determined by monoclonal antibody-captured ELISA using monoclonal antibody against murine IgE produced by clone B1E3.

Preparation of SAC and CD4$^+$ T Cells. Spleen cell suspensions were prepared in RPMI-1640 containing 10% fetal calf serum (FCS). Cells (5×10^7) in 5 mL of medium containing 10% FCS were plated into 50-mm plastic tissue culture dishes (No. 3002, Becton-Dickinson Labware, Franklin Lakes, NJ) and incubated at 37 °C in a humidified 5% CO_2 atmosphere for 2 h. After culture, nonadherent cells were removed by vigorous washing in warm media, and adherent cells were then harvested with a cell scraper. CD4$^+$ T cell purification from SC of mice immunized with OVA−liposome was performed with the magnetic cell sorter system MACS, according to the manufacturer's protocol using anti-CD4 antibody-coated microbeads (Miltenyi Biotec GmbH, No. 492-01). CD4$^+$ T cells were suspended in RPMI-1640 containing 10% FCS at a cell density of 2×10^6/mL. In the preliminary examinations, OVA at a final concentration of 1 mg/mL, 24 h (Th1) and 96 h (Th2) culture period, respectively, were found to be optimal for cytokine production. The cell suspension was plated at 250 μL per well onto a 48-well culture plate (No. 3047, Becton-Dickinson Labware, Franklin Lakes, NJ), and 500 μL of 2 mg/mL OVA solution and 250 μL of 8×10^5/mL SAC in the same media was added. After incubation in a CO_2 incubator, the culture supernatants were collected and assayed for cytokines.

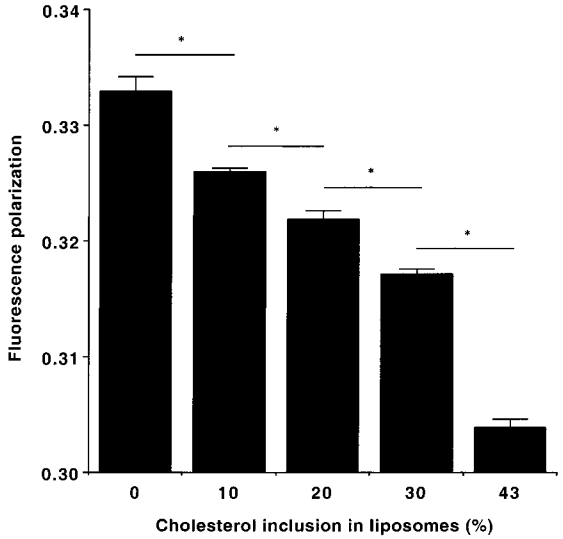


Figure 1. Degree of fluorescence polarization in the liposomes with five different cholesterol inclusions. The degree of fluorescence polarization at 37 °C was calculated as described in Materials and Methods. Data represent mean and SE of the triplicate measurements. (*) Significant ($p < 0.01$).

Cytokine Assays. IL-4 in the culture supernatant was measured using the Biotrak mouse ELISA system (Amersham International, Buckinghamshire, U.K.). All test samples were assayed in duplicate, and the standard error in each test was always less than 5% of the mean value.

Statistical Analysis. The Student's *t*-test was employed for the statistical analysis.

RESULTS

Membrane Fluidity of Liposomes. Figure 1 shows the degree of fluorescence polarization of the liposome preparations listed in Table 1. A significant difference was observed in the degree of fluorescence polarization among liposomes with different cholesterol inclusions. The increase in fluorescence polarization values can be interpreted as the result of a decrease in mobility of the hydrophobic region of phospholipid bilayers in the membranes. The results suggest that the membrane fluidity of liposomes correlated well with the amount of cholesterol contained, and liposomes containing no cholesterol showed the lowest membrane fluidity.

Anti-OVA Antibody Production in Mice Immunized with OVA−Liposome Prepared Using Liposomes with Different Cholesterol Inclusions. Lipo-

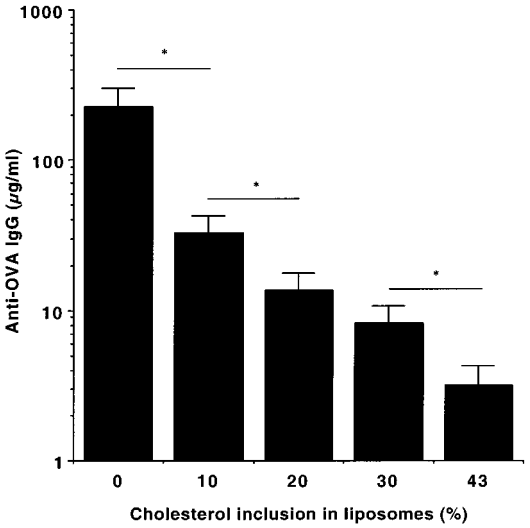


Figure 2. Anti-OVA antibody production in mice immunized with OVA−liposome made using liposomes with five different cholesterol inclusions. Six weeks after primary immunization, mice were bled from the tail vein, and serum anti-OVA IgG were measured. Data represent mean and SE of five mice per group. (*) Significant ($p < 0.01$).

somes in Figure 1 were coupled with OVA and inoculated into mice as described in Materials and Methods. Anti-OVA IgE antibody production was not observed in any of the groups of mice throughout the observation period (data not shown). On the other hand, anti-OVA IgG antibody production was induced in correlation with cholesterol inclusion in liposomes (Figure 2), and OVA−liposome prepared using liposome that contained no cholesterol induced the highest level of anti-OVA IgG antibody production.

Anti-OVA Antibody Production in Mice Immunized with OVA−Liposomes Made Using Liposomes with Four Different Lipid Formulations with or without Cholesterol. Liposomes of four different lipid formulations were prepared in the presence or absence of cholesterol as listed in Table 2, and the induction of anti-OVA IgG antibody production by OVA−liposome was investigated. OVA−liposome prepared using liposome consisting of unsaturated carrier lipids ("oleoyl" liposomes) induced the highest titer of anti-OVA IgG. Among OVA−liposomes prepared using liposomes consisting of saturated carrier lipids, the preparation using liposomes possessing the longest carbon chain ("stearoyl" liposomes) induced the lowest IgG antibody production when cholesterol was included in the liposomes (Figure 3a). On the other hand, OVA−liposome prepared using liposomes that did not contain cholesterol induced a significantly higher level of anti-OVA IgG antibody production than did those prepared using liposomes that contained cholesterol, except in the case of "oleoyl" liposomes. Interestingly, significant anti-OVA IgE antibody production was observed in mice immunized with OVA−liposome made using liposomes that did not contain cholesterol, except in the case of "palmitoyl" liposomes (Figure 3b).

Cytokine Production by Splenic CD4$^+$ T Cells of Mice Immunized with OVA−Liposome. Splenic CD4$^+$ cells were taken from mice in the previous experimental groups (Figure 3), and in vitro cytokine production was investigated. Because no cytokine production was observed in the absence of OVA under the culture conditions described in Materials and Methods, data shown in Figure 4 is considered to represent antigen-specific cytokine production. Significant levels of IL-4 production were observed in all groups of mice, and no correlation was found between in vitro T cell IL-4 production and in vivo anti-OVA IgE antibody production (Figure 3b). Similar results were obtained when production of IL-13 was monitored (data not shown).

DISCUSSION

In the present study, liposomes with five different cholesterol inclusions (Table 1) were used to make OVA−liposome conjugates, and induction of antigen-specific antibody production was monitored. All of the conjugates induced IgE-selective unresponsiveness. Among liposomes with five different cholesterol inclusions, membrane fluidity changed relative to the amount of cholesterol contained (Figure 1). The induction of IgG antibody production by OVA−liposome conjugates prepared using these liposomes correlated well with the membrane

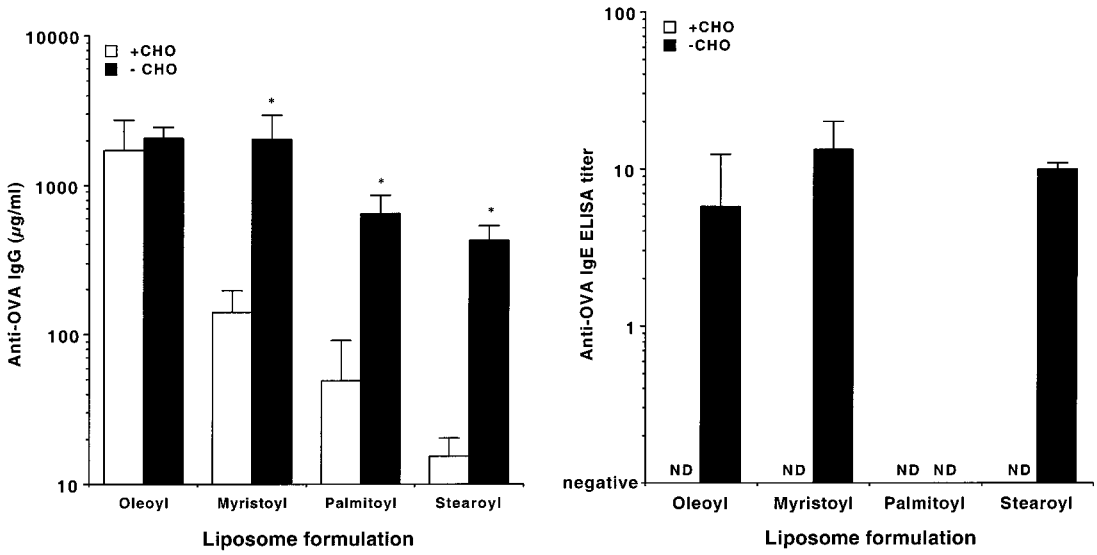


Figure 3. Anti-OVA antibody production in mice immunized with OVA−liposome made using liposomes with four different lipid formulations with (□) or without (■) cholesterol. Six weeks after primary immunization, mice were bled from the tail vein, and serum anti-OVA antibodies were measured: (a) IgG; (b) IgE. Data represent mean and SE of five mice per group. (*) Significant ($p < 0.01$) difference as compared with liposomes of the same formulation containing cholesterol. ND, not detected.

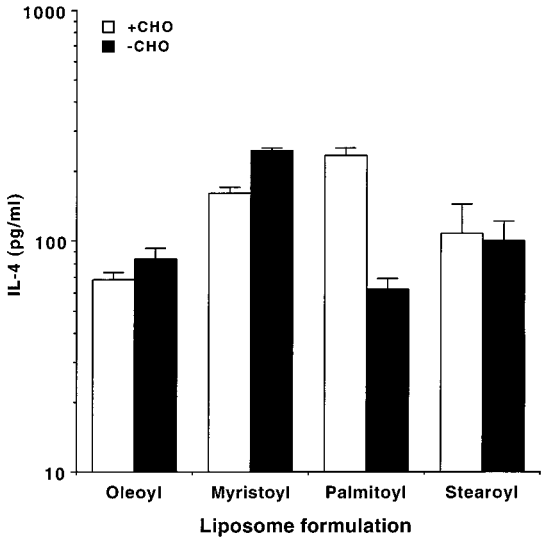


Figure 4. OVA-specific cytokine production by splenic $CD4^+$ T cells of mice immunized with OVA−liposome. Splenic $CD4^+$ T cells in the experiment shown in Figure 3 were stimulated with OVA as described in Materials and Methods, and IL-4 in the culture supernatants was monitored. Data represent mean IL-4 (pg/mL) and SE of five mice per group.

fluidity or with cholesterol inclusion in liposomes; OVA−liposome conjugates prepared using liposome that contained no cholesterol and possessed the lowest membrane mobility induced the highest level of anti-OVA IgG antibody production (Figure 2).

The results obtained in the present study differ from those obtained in the previous study (*12*); in the previous study, among liposomes with four different lipid components, the one possessing the highest membrane mobility displayed the highest adjuvant effect for the induction of IgG antibody production when cholesterol was included in all liposome preparations. We then prepared the same panel of liposomes as those used in the previous study in the presence or absence of cholesterol (Table 2) and investigated the induction of anti-OVA antibody production by OVA−liposome conjugates prepared using these liposome preparations. The results obtained using cholesterol-containing liposomes well-confirmed the results of the previous study (Figure 3a). On the other hand, in the cases of "myristoyl", "palmitoyl", and "stearoyl" liposomes, liposomes containing no cholesterol displayed significantly higher adjuvant effects than identically formulated liposomes containing cholesterol. Unexpectedly, OVA−liposome conjugates made using liposomes containing no cholesterol induced a significant production of anti-OVA IgE, except in the "palmitoyl" liposome group (Figure 3b). It is unlikely that IgE production was induced in those groups in relation to the induction of high titers of IgG antibody production, because in mice immunized with OVA−liposome prepared using "oleoyl" liposomes, IgE antibody production was induced only in the group of no-cholesterol liposomes, although a similar level of IgG antibody production was induced in both groups, regardless of the presence or absence of cholesterol in liposomes. Interestingly, among liposomes without cholesterol, IgE antibody production was not induced only in the group of mice immunized with "palmitoyl" liposomes. The results were in agreement with those shown in Figure 2; the liposome consisted mainly of palmitic acid (Table 1), and IgE production was not induced regardless of the inclusion of cholesterol. Although, at present, the mechanism of the induction of IgE-selective unresponsiveness by antigen−liposome conjugates remains unclear, the differential induction of IgE antibody production by OVA−liposome conjugates among liposomes with different lipid formulations, in the absence of cholesterol, could provide an insight into the mechanism. By the inclusion of cholesterol, liposomes are made more resistant to disintegration and biological degradation (*7*). Perhaps the change in the stability of liposomes caused by cholesterol inclusion affects both adjuvanticity and the capacity to induce IgE-selective unresponsiveness by antigen-coupled liposomes. Both IL-4 and IL-13 are known to play a key role in the induction of IgE antibody production (*15*). However, $CD4^+$ T cells of mice immunized with OVA−liposome produced IL-4 upon in vitro stimulation with OVA (Figure 4), regardless of in vivo IgE production (Figure 3b), showing that antigen-specific IL-4 production by T cells did not participate in the regulation of IgE production in mice immunized with OVA−liposome.

Thus, in the present study, liposomes with different cholesterol inclusions were used to prepare OVA−liposome conjugates, and the induction of anti-OVA antibody production was investigated in mice. The liposomal adjuvanticity for IgG and IgE antibody production was strikingly different among liposomes with different cholesterol inclusions. These results suggest that the cholesterol inclusion in liposomes affects adjuvanticity for IgG production and exerts regulatory effects on IgE synthesis by the surface-coupled antigen of liposomes.

ACKNOWLEDGMENT

This work was supported in part by a grant from The Japan Health Sciences Foundation (Research on Health Sciences focusing on Drug Innovation).

LITERATURE CITED

(1) Audibert, F. M., and Lise, D. (1993) Adjuvants: current status, clinical perspectives and future prospects. *Immunol. Today 14*, 281−284.

(2) Mark, A., Bjorksten, B., and Granstrom, M. (1995) Immunoglobulin E responses to diphtheria and tetanus toxoids after booster with aluminum-adsorbed and fluid DT-vaccines. *Vaccine 13*, 669−673.

(3) Gupta, R. K., and Siber, G. R. (1995) Adjuvants for human vaccines—current status, problems and future prospects. *Vaccine 13*, 1263−1276.

(4) Wassef, N. M., Alving, C. R., and Richards, R. L. (1994) Liposomes as carriers for vaccines. *ImmunoMethods 4*, 217−222.

(5) Gregoriadis, G. (1994) Liposomes as immunoadjuvants and vaccine carriers: antigen entrapment. *ImmunoMethods 4*, 210−216.

(6) Gluck, R. (1995) Liposomal presentation of antigens for human vaccines. *Pharmacol. Biotechnol. 6*, 325−345.

(7) Green, S., Fortier, J. D., Madsen, J., Swartz, G., Einck, L., Gubish, E., and Nacy, C. (1995) Liposomal vaccines, in *Immunology of Proteins and Peptides VIII* (M. Z. Atassi, and G. S. Bixler, Eds.), pp 83−92, Plenum Press, New York.

(8) Alving, C. R., Koulchin, V., Glenn, G. M., and Rao, M. (1995) Liposomes as carriers of peptide antigens: induction of antibodies and cytotoxic T lymphocytes to conjugated and unconjugated peptides. *Immunol. Rev. 145*, 5−31.

(9) Fortin, A., Shaum, E., Krzystyniak, K., and Therien, HM. (1996) Differential activation of cell-mediated immune functions by encapsulated and surface-linked liposomal antigens. *Cell Immunol. 169*, 208−217.

(10) Naito, S., Horino, A., Nakayama, M., Nakano, Y., Nagai, T., Mizuguch, J., Komuro, K., and Uchida, T. (1996) Ovalbumin-liposome conjugate induces IgG but not IgE antibody production. *Int. Arch. Allergy Immunol. 109*, 223−228.

(11) Nakano, Y., Mori, M., Nishinohara, S., Takita, Y., Naito, S., Horino, A., Kato, H., Taneichi, M., Ami, Y., Suzaki, Y., Komuro, K., and Uchida, T. (1999) Antigen-specific, IgE selective unresponsiveness induced by antigen-liposome conjugates. *Int. Arch. Allergy Immunol. 120*, 199−208.

(12) Nakano, Y., Mori, M., Nishinohara, S., Takita, Y., Naito, S., Kato, H., Taneichi, M., Komuro, K., and Uchida, T. (2001) Surface-linked liposomal antigen induces IgE-selective unresponsiveness regardless of the lipid components of liposomes. *Bioconjugate Chem. 12,* 391−395.

(13) Hashimoto, K., Inoue, K., Nojima, S., Tadakuma, T., and Yasuda, T. (1982) Immunogenicity of liposomal model membranes sensitized with spin-labeled haptens and topographical distribution of haptens on the membranes. *J. Biochem. 92*, 1813−1821.

(14) Lentz, B. R., Barenholz, Y., and Thompson, T. E. (1976) Fluorescence depolarization studies of phase transitions and fluidity in phospholipid bilayers. 1. Single component phosphatidylcholine liposomes. *Biochemistry 5*, 4521−4528.

(15) Corry, D. B., and Kheradmand, F. (1999) Induction and regulation of the IgE response. *Nature 402*, B18−B23.

BC0155667

Steps toward High Specific Activity Labeling of Biomolecules for Therapeutic Application: Preparation of Precursor $[^{188}Re(H_2O)_3(CO)_3]^+$ and Synthesis of Tailor-Made Bifunctional Ligand Systems

Roger Schibli,*[,†] Rolf Schwarzbach,[†] Roger Alberto,[§] Kirstin Ortner,[§] Helmut Schmalle,[§] Cécile Dumas,[†] André Egli,[†] and P. August Schubiger[†,‡]

Center for Radiopharmaceutical Science, Paul Scherrer Institute, CH-5232 Villigen PSI, Switzerland, Department of Applied Biosciences, Swiss Federal Institute of Technology, CH-8057 Zurich, Switzerland, and Department of Inorganic Chemistry, University of Zurich, CH-8057 Zurich, Switzerland. Received October 18, 2001; Revised Manuscript Received February 25, 2002

Two kit preparations of the organometallic precursor $[^{188}Re(H_2O)_3(CO)_3]^+$ in aqueous media are presented. Method A uses gaseous carbon monoxide and amine borane ($BH_3{\cdot}NH_3$) as the reducing agent. In method B CO(g) is replaced by $K_2[H_3BCO_2]$ that releases carbon monoxide during hydrolysis. Both procedures afford the desired precursor in yields >85% after 10 min at 60 °C. HPLC and TLC analyses revealed 7 ± 3% of unreacted $^{188}ReO_4^-$ and <5% of colloidal $^{188}ReO_2$. Solutions of up to 14 GBq/mL Re-188 have been successfully carbonylated with these two methods. The syntheses of two tailor-made bifunctional ligand systems for the precursor $[^{188}Re(H_2O)_3(CO)_3]^+$ are presented. The tridentate chelates consist of a bis[imidazol-2-yl]methylamine or an iminodiacetic acid moiety, respectively. Both types of ligand systems have been prepared with alkyl spacers of different length and a pendent primary amino or carboxylic acid functionality, enabling the amidic linkage to biomolecules. The tridentate coordination of the ligands to the rhenium-tricarbonyl core could be elucidated on the macroscopic level by X-ray structure analyses and 1D and 2D NMR experiments of two representative model complexes. On the nca level, the ligands allow labeling yields >95% with $[^{188}Re(H_2O)_3(CO)_3]^+$ under mild reaction conditions (PBS buffer, 60 °C, 60 min) at ligand concentrations between 5×10^{-4} M and 5×10^{-5} M. Thus, specific activities of 22−220 GBq per μmol of ligand could be achieved. Incubation of the corresponding Re-188 complexes in human serum at 37 °C revealed stabilities between 80 ± 4% and 45 ± 10% at 24 h, respectively, and 63 ± 3% and 34 ± 3% at 48 h postincubation in human serum depending on the chelating system. Decomposition product was mainly $^{188}ReO_4^-$. The routine kit-preparation of the precursor $[^{188}Re(H_2O)_3(CO)_3]^+$ in combination with tailor-made ligand systems enables the organometallic labeling of biomolecules with unprecedented high specific activities.

INTRODUCTION

In the past years, the bioinorganic chemistry of rhenium has been developed toward novel applications in therapeutic nuclear medicine (*1*, *2*). Interests in this field origin from the fact, that the two particle emitting radioisotopes Re-186 and Re-188 have excellent physical decay properties for therapeutic applications (Re-186: $t_{1/2}$ = 89 h, β^- 1.07 MeV, γ 137 keV; Re-188: $t_{1/2}$ = 18 h, β^- 2.12 MeV, γ 155 keV). Furthermore, due to the generator technique, Re-188 is nowadays readily available carrier-free and at any time (*3*). In analogy to Tc-99m, most of the currently applied Re-186/188 labeling techniques use precursors or complexes in higher oxidation states (*4*, *5*). However, it is a fact that rhenium needs harsher conditions to be reduced from its original oxidation state +VII to lower oxidation states typically +V/+III. It is also frequently observed, that these rhenium complexes have a higher tendency reoxidize, than their technetium analogues. Therefore, kinetically more inert complexes containing technetium and rhenium in the low oxidation state +I have received more attention, recently (*6*−*10*). Soft metal centers show an increased kinetic inertness and a low affinity for hard nitrogen and oxygen donor groups, readily present in the blood serum. This characteristic protects the complexes in vivo against ligand dissociation and ligand exchange.

Our group has developed a fully aqueous-based kit preparation of the organometallic technetium precursor $[^{99m}Tc(H_2O)_3(CO)_3]^+$ under mild reaction conditions in the presence of gaseous carbon monoxide and sodium borohydrate (*11*). The formulation could be optimized in terms of kit-stability and commercial production due to substitution of both gaseous CO and $NaBH_4$ by $K_2[H_3BCO_2]$ (*12*). However, till today the corresponding Re-186/188 precursor $[^*Re(H_2O)_3(CO)_3]^+$ **1** was obtained only in low yields via the above-mentioned methods.

In the present work we describe two simple and fully aqueous-based synthetic routes to obtain the precursor $[^{188}Re(H_2O)_3(CO)_3]^+$ in high yields and with high specific activities. To translate the excellent specific activities on the labeling of biomolecules, tridentate bifunctional

* To whom correspondence should be addressed: Telephone: ++41−56−310−2837, Fax: ++41−56−310−2849, E-mail: roger.schibli@psi.ch.

† Paul Scherrer Institute.

‡ Swiss Federal Institute of Technology.

§ University of Zurich.

10.1021/bc015568r CCC: $22.00 © 2002 American Chemical Society
Published on Web 05/11/2002

ligand systems tailor-made for the precursors $[^{188}Re(H_2O)_3(CO)_3]^+$ have been synthesized. The first ligand system consists of bis[imidazol-2yl]methylamine chelate originally developed for copper(II) (*13*). To our knowledge this chelate system has never been tested and reacted with a soft, organometallic precursor. The second type of ligands consists of an iminodiacetic acid (IDA) moiety, which is well-known to form complexes with almost any metal of the fist and second transition row. Both chelating systems proved to be good candidates for facile bifunctionalization with spacers of different chain length bearing a terminal amino or carboxylic acid group for amidic linkage to carboxylic acid or primary amino group of biomolecules. On the other hand, they offer three potential coordination sites, forming multiple stable chelating rings with the rhenium-tricarbonyl center. The X-ray structures of two model complexes exemplify the coordinative features of these new ligand systems. In vitro plasma stabilities of the corresponding Re-188 complexes will be discussed.

MATERIALS AND METHODS

Solvents for syntheses were purchased from Aldrich Chemical Co. or Fluka, Buchs, Switzerland and were dried according to standard methods. Glycine **2**, 5-aminopentanoic acid **3**, and 10-aminoundecanoic acid **4** were purchased from Fluka. The precursor $(NEt_4)_2[ReBr_3(CO)_3]$ (*14*), *N-tert*-butyloxycarbonyldiaminopropane **5**, and *N-tert*-butyloxycarbonyldiaminohexane **6** (*15*), bis(imidazol-2-yl)nitromethane **7** (*16*), bis(imidazol-2-yl)-carboxymethylaminomethane **8a** (*13*), and $K_2[H_3BCO_2]$ (*12*) were synthesized according to the literature. Na-$[^{188}ReO_4]$ was eluted from a $^{188}W/^{188}Re$ generator (Oak Ridge National Laboratories, Oak Ridge, TN) using 0.9% saline. The elution volume (approximately 30 mL) was reduced to a total of 5 mL (max. 14 GBq/mL) using the method of Blower (*17*). HPLC analyses were performed on a Merck-Hitachi L-7000-system equipped with an L-7400 tunable absorption detector and a Berthold LB 506 B radiometric detector. HPLC solvents consisted of aqueous 0.05 M TEAP (triethylammonium phosphate) buffer, pH = 2.25 (solvent A) and methanol (solvent B). For the radiochemical analyses, a Macherey-Nagel C-18 reversed phase column (10 μm, 150 × 4.1 mm) was used. The HPLC system started with 100% of A from 0 to 3 min. The eluent switched at 3 min to 75% A and 25% B and at 9 min to 66% A and 34% B followed by a linear gradient 66% A/34% B to 100% B from 9 to 20 min. The gradient remained at 100% B for 2 min before switching back to 100% A. The flow rate was 1 mL/min. The thin-layer chromatography (TLC) system was performed using glass-backed silica gel plates (Merck $60F_{254}$, mobile phase of 99% methanol 1% concentrated HCl) and paper (Whatman No.1, mobile phase 99.5% methanol, 0.5% 6 M aqueous HCl). The plates were scanned with a Burkard RAYTEST RITA-3200 radioanalyzer. Radioactive samples were counted in a Camberra Packard COBRA II auto gamma well counter. Reactions with activities >500 MBq/mL have been performed in specially equipped lead-boxes with manipulators. Nuclear magnetic resonance spectra were recorded on a 300 MHz Varian Gemini 2000 spectrometer. The ^1H and ^{13}C chemical shifts are reported relative to residual solvent protons as a reference. IR spectra were recorded on a Perkin-Elmer FT-IR 16PC using KBr pellets. Elementary analyses were performed at the department of inorganic chemistry of the university of Zurich.

Preparation of Precursor $[^{188}Re(H_2O)_3(CO)_3]^+$, 1. Method A. A 5 mg amount of $BH_3{\cdot}NH_3$ was placed in 10 mL glass vial. The vial was sealed with an aluminum capped rubber stopper and flushed with CO for 20 min. The generator eluate (1 mL, 3−14 GBq/mL) was mixed with 6 μL of concentrated H_3PO_4 (98%) prior to the injection in the reaction vial. The vial was incubated at 60 °C for 15 min. Pressure from the evolving H_2 gas was balanced with a 20 mL syringe. The reaction was cooled on an ice bath. The final pH of the reaction solution was neutral. Yield: 85 ± 5% determined by means of HPLC and TLC. **Method B.** A 5 mg amount of $BH_3{\cdot}NH_3$ and 3 mg of $K_2[H_3BCO_2]$ were placed in 10 mL glass vial and flushed with nitrogen. The generator eluate (1 mL, 3−14 GBq/mL) was mixed with 6 μL of concentrated H_3PO_4 (98%) prior to the injection in the reaction vial. The vial was incubated at 60 °C for 15 min. Pressure from the evolving H_2 gas was balanced with a 20 mL syringe. The reaction was cooled on an ice bath. The final pH of the reaction solution was neutral. Yield: 80 ± 5% determined by means of HPLC and TLC.

Radiolabeling. The radioactive complexes were prepared according to the following general procedure: 450 μL of a solution of $[^{188}Re(H_2O)_3(CO)_3]^+$ and 50 μL of a 10^{-3} M, and 10^{-4} M, respectively, 950 μL of a solution of $[^{188}Re(H_2O)_3(CO)_3]^+$ and 50 μL of a 10^{-2} M, 10^{-3} M, and 10^{-4} M solution of the corresponding ligand in PBS buffer (0.1 M NaCl/0.05 M sodium phosphate buffered, pH = 6.5−7.5) were placed in a 10-mL glass vial under nitrogen. The vial was sealed and the reaction heated to 60 °C for 60 min and cooled on an ice bath.

In Vitro Plasma Stability. The solutions of the ^{188}Re complexes were adjusted with physiological saline to a concentration of 370 MBq/mL. Aliquots of 100 μL of these solutions were added to 400 μL human plasma and incubated at 37 °C. Aliquots were taken and analyzed after 1 h, 4, 24, and 48 h.

Preparation of Compound 8c and 8d. The ligands **8c/d** were synthesized according to the procedure described for **8a** (*13*) starting from the corresponding aminoalkyl carboxylic acid (n = 4, 10). Yields: 50−70%. Analytical data for ligand **8c** (n = 4): Calculated for $C_{12}H_{17}N_5O_2{\cdot}1.6$ HCl: C 44.81; H 5.83; N 21.77. Found C 44.91; H 5.95; N 22.35. ^1H NMR (D_2O): δ 7.41 (s, 4 H), 6.68 (s, 1 H), 3.51 (t, 2 H), 2.33 (t, 2 H) 1.82 (m, 2 H), 1.69 (m, 2 H). ^{13}C NMR (D_2O): δ 177.9, 143.3, 122.7, 53.7, 42.0, 34.2, 25.6, 23.2. MS (ES): m/z (%) 264 (60) [M + 1]. Analytical data for ligand **8d** (n = 10): Calculated for $C_{18}H_{29}N_5O_2{\cdot}1.7$ HCl: C 52.80; H 7.56; N 17.10. Found: C 52.63; H 7.03; N 17.27. ^1H NMR (D_2O): δ 7.50 (s, 4 H), 6.30 (s, 1 H), 2.82 (t, 2 H), 2.23 (t, 2 H), 1.6−1.4 (m, 4 H), 1.2−1.1 (broad m, 12 H). ^{13}C NMR (D_2O): δ 179.1, 135.9, 122.9, 66.8, 47.8, 35.6, 34.0, 28.5, 25.7, 24.4, 23.3. MS (ES): m/z (%) 348 (100) [M + 1].

Preparation of Compounds 9a and 9b. The compounds **9a/b** were synthesized according to the following, general procedure starting from the corresponding *N-tert*-butyloxycarbonyldiamines (n = 3, **5**, and n = 6, **6**). Bis-[imidazol-2-yl]nitromethane (500 mg, 2.2 mmol) was dissolved in 2.6 mL of 2 M NaOH. One equivalent of the corresponding mono Boc-protected diaminoalkane was added under vigorous stirring. The suspension was heated at 80 °C for 20 min, in which a clear orange solution was formed. After cooling on an ice bath, the almost colorless product precipitated. The pure product was filtered and dried under vacuum. Yields: 50−70%. Analytical data for compound **9a** (n = 3): Calculated for $C_{15}H_{24}N_6O_2$: C 56.23; H 7.55; N 26.23: Found: C 55.96; H 6.95; N 26.71. ^1H NMR (MeOH-d_4): δ 6.91 (s, 4 H), 4.99 (s, 1 H), 3.06 (t, 2 H), 2.46 (t, 2 H), 1.56 (q, 2 H), 1.33 (s, 9 H). ^{13}C NMR (MeOH-d_4): δ 162.3, 143.4, 121.5,

70.6, 51.6, 40.5, 33.8, 25.6, 24.2, 23.7. MS (ES): *m/z* (%) 321 (100) [$M + 1$]. Analytical data for compound **9b** ($n = 6$): Calculated for $C_{18}H_{30}N_6O_2$: C 59.64; H 8.34; N 23.19: Found: C 59.08; H 7.24; N 22.91. ^{1}H NMR (MeOH-d_4): δ 7.12 (s, 4 H), 5.01 (s, 1 H), 3.33 (t, 2 H), 2.53 (t, 2 H), 1.63 (m, 4 H), 1.40 (s, 4 H), 1.34 (s, 9 H). ^{13}C NMR (MeOH-d_4): δ 160.2, 144.4, 120.8, 66.2, 50.4, 42.5, 34.2, 28.6, 25.5, 25.1 23.4, 22.3, 20.1. MS (ES): *m/z* (%) 363 (100) [$M + 1$].

Preparation of Compounds 10a and 10b. Compounds **10a/b** were deprotected in 3 M HCl at 50 °C for 20 min. After removal of the solvent, the products could be obtained almost quantitatively in the hydrochloride form as pale rose powder. Yields >95%. Analytical data for ligand **10a** ($n = 3$): Calculated for $C_{10}H_{16}N_6 \cdot 4.5$ HCl: C, 31.0; H, 6.1; N, 21.7. Found: C, 31.1; H, 5.95; N, 21.5. ^{1}H NMR (MeOH-d_4): δ 7.58 (s, 4 H), 5.94 (s, 1 H), 3.16 (t, 2 H, 9 Hz), 2.81 (t, 2 H, 6 Hz), 1.95 (m, 2 H). ^{13}C NMR (MeOH-d_4): δ 139.6, 117.8, 57.7, 42.5, 39.4, 25.6. MS (ES): *m/z* (%) 221 (100) [$M + 1$]. Analytical data for ligand **10b** ($n = 6$): Calculated for $C_{13}H_{22}N_6 \cdot 4$ HCl: C, 38.3; H, 6.4; N, 20.6. Found: C, 37.9; H, 6.1; N, 20.2. ^{1}H NMR (MeOH-d_4): δ 7.51 (s, 4 H), 6.04 (s, 1 H), 2.96 (t, 2 H), 2.73 (t, 2 H), 1.62 (m, 2 H), 1.58 (m, 2 H), 1.33 (m, 4 H). ^{13}C NMR (MeOH-d_4): δ 140.4, 117.7, 56.7, 42.5, 34.2, 28.6, 25.7,23.6, 20.4. MS (ES): *m/z* (%) 263 (80) [$M + 1$].

Preparation Compounds 11a and 11b. The compounds **11a/b** were synthesized according to the following, general procedure using the corresponding amino alkyl carboxylic acid ($n = 4$, **3** and $n = 10$, **4**). A 1 g amount of 5-aminopentanoic acid **3** or 11-aminoundecanoic acid **4**, respectively, was dissolved in 100 mL of methanol together with 2.5 equiv of triethylamine. Methyl bromoacetate (2.1 equiv) was added over a period of 2 h at room temperature. The reaction was refluxed overnight. After removal of the solvent, the oily residue was purified by column chromatography (CH_2Cl_2/ethyl acetate: 4:1). The esters were saponified with 2 M NaOH under reflux for 60 min. The solution was neutralized with concentrated HCl and the solvent evaporated under reduced pressure. The residue was extracted twice with 5 mL of methanol to separate NaCl. After evaporation of the methanol the products were obtained as white solids. Yield: 40−60%. Analytical data for compound **11a** ($n = 4$): Calculated for $C_9H_{15}NO_6$: C 46.35; H 6.48; N 6.01. Found: C 45.85; H 5.53; N 5.92. ^{1}H NMR (MeOH-d_4): δ 3.38 (t, 2 H), 3.15 (s, 4 H), 3.04 (t, 2 H), 2.88 (q, 4 H). ^{13}C NMR (MeOH-d_4): δ 179.9, 171.5, 66.8, 56.2, 50.3, 33.1, 28.0. MS (ES): *m/z* (%) 234 (100) [$M + 1$]. Analytical data for compound **11b** ($n = 10$): Calculated for $C_{15}H_{27}NO_6$: C 56.77; H 8.57; N 4.41. Found: C 56.45; H 6.97; N 4.21.^{1}H NMR (D_2O): δ 3.41 (t, 2 H), 3.21 (s, 4 H), 2.62 (t, 2 H), 1.77 (m, 2 H), 1.6−1.1 (m, 14 H). ^{13}C NMR (D_2O): δ 177.0, 171.0, 56.0, 51.1, 35.3, 33.2, 33.0, 28.6, 28.3, 26.8, 25.0, 23.3. MS (ES): *m/z* (%) 318 (100) [$M + 1$].

Preparation of Compounds 12a/b and 13a/b. The compounds **13a/b** were synthesized according to the following, general procedure using the corresponding *N-tert*-butyloxycarbonyldiamines ($n = 3$, **5** and $n = 6$, **6**). The *N-tert*-butyloxycarbonyldiamines were dissolved in 50 mL of methanol together with 2 equiv of triethylamine. Methyl bromoacetate (2.1 equiv) was added over a period of 2 h at room temperature. The reaction was refluxed overnight. After removal of the solvent the oily residue was diluted with water and extracted three times with ethyl acetate. The organic layers were combined and dried over Na_2SO_4. After filtration and evaporation of the solvent, the crude products **12a/b** were checked by means of NMR and processed without purification. The crude products were dissolved in 3 M HCl and heated at 50 °C for 30 min. After removal of the solvent the residues were dissolved in 2 M NaOH and refluxed for 60 min. The solution was neutralized with concentrated HCl and the solvent evaporated under reduced pressure. The residue was extracted twice with 5 mL of methanol to separate NaCl. After evaporation of the methanol, the products were obtained as white solids. Yield: 40−60%. Analytical data for ligand **13a** ($n = 3$): Calculated for $C_7H_{14}N_2O_4 \cdot 0.3$NaCl: C 40.47; H 6.79; N 13.49. Found: C 40.64; H 7.21; N 13.91. ^{1}H NMR (D_2O): δ 3.53 (s, 4 H), 2.83 (t, 2 H), 2.74 (t, 2 H), 1.87 (q, 2 H). ^{13}C NMR (D_2O): δ 176.1, 94.3, 64.1, 60.5, 51.7 40.0, 33.8. MS (ES): *m/z* (%) 191 (100) [$M + 1$]. Analytical data for ligand **13b** ($n = 6$): Calculated for $C_{10}H_{20}N_2O_4 \cdot 0.2$NaCl: C 49.23; H 8.26; N 11.48. Found: C 49.11; H 7.38; N 11.96. ^{1}H NMR (D_2O): δ 3.53 (s, 4 H), 2.83 (t, 2 H), 2.74 (t, 2 H), 1.87 (q, 2 H), 1.4−1.2 (m, 6 H). ^{13}C NMR (D_2O): δ 179.0, 95.1, 60.2, 58.1, 53.9, 42.3, 34.4, 29.6. MS (ES): *m/z* (%) 233 (100) [$M + 1$].

Preparation of Compound 8b. Compound **8a** (200 mg, 0.9 mmol) was dissolved in 10 mL of methanol. The solution was cooled to 0 °C on an ice bath before adding 60 μL (0.9 mmol) of $SOCl_2$. To the reaction solution was added 500 mg of molecular sieve, and the reaction was stirred overnight at room temperature. After filtration, the solvent was removed under reduced pressure to obtain the product. Yield 190 mg (90%). Analytical data: Calculated for $C_{10}H_{13}N_5O_2$: C 51.06; H 5.57; N 29.77. Found: C 51.12; H 4.98; N 29.24. ^{1}H NMR (D_2O): δ 7.12 (s, 4 H), 5.30 (s, 1 H), 3.67 (s, 3 H), 3.51 (s, 2 H). ^{13}C NMR (D_2O): 174.3, 138.1, 135.8 116.4, 56.7, 42.5. MS (ES): *m/z* (%) 236 (100) [$M + 1$].

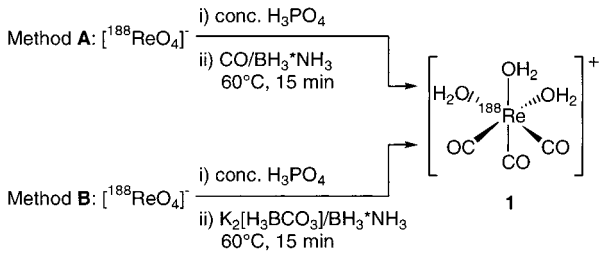
Preparation [Re(8b)(CO)$_3$]Br. $(NEt_4)_2[ReBr_3(CO)_3]$ (100 mg, 0.12 mmol) was dissolved in 5 mL of methanol. One equivalent of **8a** (30 mg) was added and the reaction stirred overnight at room temperature. The reaction was concentrated to 1 mL and layered with diethyl ether. The products crystallized completely after 3 days. Yield: 47 mg (65%). Analytical data: Calculated for $C_{13}H_{13}N_5O_5$-ReBr: C 26.67; H 2.24; N 11.96. Found: C 26.12; H 2.98; N 11.24. ^{1}H NMR (MeOH-d_4): δ 7.40 (d, 1 H, 1.5 Hz), 7,33(d, 1 H, 1.5 Hz), 7.22 (d, 1 H, 1.5 Hz), 7.20 (d, 1 H, 1.5 Hz), 6.20 (s, 1 H), 3.78 (s, 3H), 3.61 (s, 2 H). IR (KBr, cm^{-1}): 3420 (w), 2028 (vs), 1922 (vs), 1904 (vs), 1758 (m), 1290 (w), 1138 (m), 858 (w).

Preparation of [Re(13aH$^+$)(CO)$_3$]. $(NEt_4)_2[ReBr_3(CO)_3]$ (82 mg, 0.11 mmol) was dissolved in 5 mL of H_2O. Ligand **13a** (25 mg, 0.13 mmol) was added and the reaction heated at 70 °C for 2 h. Immediately after cooling to room temperature, the product crystallized almost quantitatively from the reaction solution. Yield: 48 mg (95%). Analytical data: Calculated for $C_{10}H_{13}N_2O_7Re \cdot 0.9H_2O$: C 25.25; H 3.14; N 5.89. Found: C 26.73; H 3.31; N 5.64. ^{1}H NMR (DMSO-d_6): δ 3.76 (d, 2 H, 16 Hz), 3.40 (d, 2 H, 16 Hz), 3.30 (t, 2 H), 3.28 (m, 2 H), 2.80 (t, 2 H). IR (KBr, cm^{-1}): 3446 (w), 2362 (w), 2018 (vs), 1902 (vs), 1870 (vs), 1654 (s), 1622 (s), 1394 (m), 548 (w).

RESULTS AND DISCUSSION

Contrary to the almost quantitative reductive carbonylation of $^{99m}TcO_4^-$ in the presence of BH_4^-, CO, and Na_2CO_3 in aqueous media, only traces of the desired Re-188 precursor were detected under these reaction conditions. Failure of this approach can presumably be explained by several facts: (i) Rhenium has a lower redox potential than technetium. (ii) Rhenium +V and/or +III intermediates presumably formed during the reductive

Scheme 1



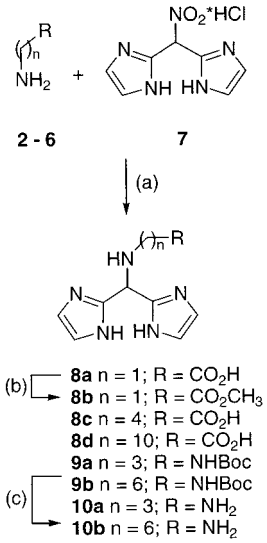
carbonylation are unstable at basic pH. (iii) Under neutral/acidic conditions rhenium(III/IV) intermediates are stable but BH_4^- hydrolyzes fast. Thus, BH_4^- is not available for reduction of the metal center. To circumvent these problems, the water-soluble aminoborane, $BH_3{\cdot}NH_3$, was used instead of BH_4^-. Aminoborane is sufficiently stable under neutral/acidic conditions and is highly reducing.

The organometallic precursor $[^{188}Re(H_2O)_3(CO)_3]^+$ **1** was synthesized via two routes starting from $^{188}ReO_4^-$ in saline. Method A uses solid $BH_3{\cdot}NH_3$ as the reducing agent and gaseous carbon monoxide as the source of CO ligands. The perrhenate solution was acidified with concentrated phosphoric acid prior to injection in the reaction vial to maintain an acidic/neutral pH during the reaction. After 15 min at 60 °C, the reaction was completed (Scheme 1). The HPLC γ-trace revealed beside the peak of the desired product **1** (70 ± 10%; RT = 5 min) and remaining $^{188}ReO_4^-$ (7 ± 3%; RT = 10 min) a third peak of a byproduct with a retention time of 10.5 min (10 ± 5%). This byproduct of unknown composition can be converted into the precursor **1** by acidifying the carbonyl solution to pH < 2. TLC analysis of the carbonyl solution revealed only the peak of precursor **1** (85 ± 5%; $R_f = 0.4$) and $^{188}ReO_4^-$ (10 ± 2%; $R_f = 0.7$). Less than 5% colloidal $^{188}ReO_2$ was detected at the origin.

In method B, $K_2[H_3BCO_2]$ was used as a solid source of CO and $BH_3{\cdot}NH_3$ as the reducing agent. The perrhenate solution was also acidified with concentrated phosphoric acid previous to injection in the reaction vial. After 15 min at 60 °C, the yields and product distribution were similar to those in method A (Scheme 1). The amount of $BH_3{\cdot}NH_3/K_2[H_3BCO_2]$ and acid (concentrated H_3PO_4) was carefully balanced, to avoid fast hydrolysis of the boranes and to maintain a sufficient low pH to stabilize reduced rhenium intermediates. Using exclusively $K_2[H_3BCO_2]$ instead of $BH_3{\cdot}NH_3$ and CO(g) did not yield the desired precursor even if applied in large excess (10−50 mg per reaction vial). Furthermore, it was observed that, when reaction volume was increased (>1 mL), the yields of **1** dropped significantly. Since a concerted mechanism, where the reduction of the metal center and the CO addition take place almost simultaneously, is proposed for the carbonylation reaction (*12*), the availability of reducing agent and CO are limiting factors. Thus, a fast saturation of the aqueous solution with carbon monoxide can only be guaranteed if the volume of the solution is relatively small. Yet, solutions of up to 14 GBq/mL Re-188 could be successfully carbonylated with both methods.

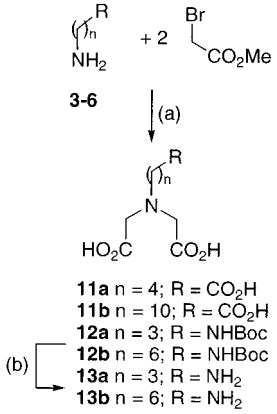
The free precursor **1** is stable (>90%) for approximately 3 h at pH = 7−5. After this time, decomposition of the precursor and reformation of $^{188}ReO_4^-$ was observed in the absence of effectively coordinating and stabilizing ligands. Addition of radical scavenging coligand such as gentisic acid or ascorbic acid did not significantly improve the half-life of the precursor.

Scheme 2[a]



[a] Reagents and conditions: (a) 2 M NaOH, 80 °C; (b) MeOH, $SOCl_2$; (c) 3 M HCl, 50 °C.

Scheme 3[a]

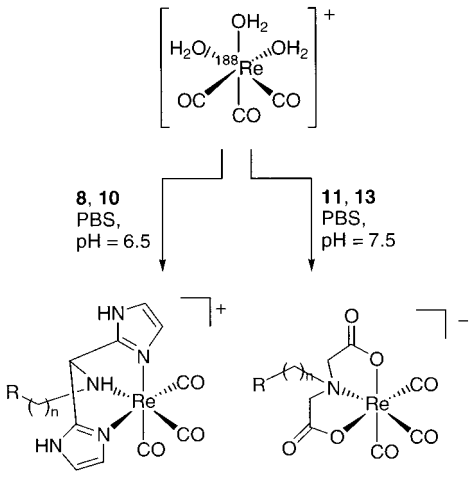


[a] Reagents and conditions: (a) MeOH, NEt_3, reflux, 15 h; 2 M NaOH; (b) 3 M HCl, 50 °C.

To translate the excellent yields and specific activities of precursor **1** on the radiolabeling of biomolecules such as peptides and proteins, novel, bifunctional ligand systems have been developed. Ligands **8** and **10** could be produced in a straightforward synthetic approach. Bifunctionalization of the chelate system was achieved by reacting the previously *mono N*-Boc-protected diamines or commercially available amino alkyl carboxylic acids with bis(imidazol-2-yl)nitromethane in the presence of aqueous NaOH (Scheme 2). Under these conditions, the nitro group is displaced by the nucleophilic amino group forming the corresponding N_α-substituted 2,2′-bis-(imidazolyl)methanes. Deprotection of the Boc group was accomplished in 3 M HCl at 50 °C (Scheme 3). The $^1H/^{13}C$ NMR and mass spectra and elemental analyses confirmed the composition and the symmetric structure of the ligands. In all compounds the four C−H protons of the imidazole rings are chemically equivalent, forming singlets around 7 ppm.

Ligands **11** and **13** could be produced in two and three steps, respectively. The chelating moiety was built up by a double alkylation of the primary amino group with methyl bromoacetate in the presence of triethylamine in good yields. Subsequent saponification of the ester groups and/or deprotection of the *N*-Boc group afforded the bifunctional IDA derivatives (Scheme 3). The $^1H/^{13}C$ NMR

Scheme 4



and mass spectra and elemental analyses confirmed the composition and the structures of the ligands.

Radiolabeling and in Vitro Stability. Radiolabeling of ligands **8/10** and **10/13** with precursor **1** was performed in PBS buffer at pH 6.5−7.5 (Scheme 4). Different labeling conditions have been tested. Short incubation at higher temperature (10 min, 100 °C) or longer incubation at lower temperature (37 °C, 3 h) revealed almost complete consumption of **1**, but it was observed that under these conditions the reformation of perrhenate prohibits labeling yields better than 40% of the initial activity. The best conditions for radiolabeling were found to be 60 °C for 60 min in PBS. All tested ligand systems formed single species with the precursor **1**.

Plotting the labeling yields of the different chelate systems as a function of ligand concentration revealed steep sigmoid curves (Figure 1). Generally the 2,2′-diimidazolylmethylamine chelates (**8**/**10**) yielded the corresponding Re-188 complexes at 1 order of magnitude lower concentration (5×10^{-5}M) than the IDA-chelates (5×10^{-4}M for **11**/**13**). At these concentrations, labeling yields >95% in respect to $[^{188}Re(OH_2)_3(CO)_3]^+$ and specific activities of up to 220 GBq/μmol ligand (based on initial activity of 14 GBq/mL $^{188}ReO_4^-$) could be achieved. The pendent additional functional groups (CO_2H or NH_2) did not seem to have an influence on the labeling yields.

Stability of the Re-188 complexes was evaluated in human serum at 37 °C over a period of 48 h (Table 1). The $^{188}Re(CO)_3$ complexes with ligands **8**/**10** showed generally a higher stability (80 ± 4% 24 h and 63 ± 3% 48 h postincubation in human serum) than those with ligands **11**/**13** (45 ± 10% 24 h and 34 ± 3% 48 h postincubation in human serum). The TLC and HPLC analyses of aliquots of the incubated plasma samples revealed beside the intact complexes decomposition predominantly to $^{188}ReO_4^-$. Only minor transchelation and aggregation to plasma proteins have been observed (>4% of total activity).

Preparation and Analysis of Rhenium Complexes. To determine the coordinative features of the novel ligand systems, two representative rhenium model complexes with ligand **8b** and **13a** have been prepared and fully characterized including the X-ray structures. The complexes revealed almost identical retention times on the HPLC column ($[Re(\mathbf{8b})(CO)_3]^+$: 19.8 min; $[Re(\mathbf{13a})(CO)_3]$: 20.4 min) as the corresponding radioactive complexes ($[^{188}Re(\mathbf{8b})(CO)_3]^+$: 19.9 min; $[^{188}Re(\mathbf{13a})(CO)_3]$: 20.2 min) proving the identity of the complexes on the macroscopic and the nca level. Analysis of the ^{1}H NMR

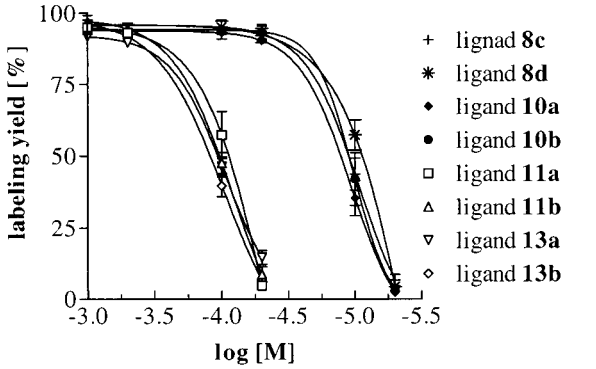


Figure 1. Labeling yield as a function of the ligand concentration in PBS buffer pH = 6.5 (ligands **8**/**10**) and pH = 7.5 (ligands **11**/**13**) 60 min, 60 °C.

Table 1. Stability (%[a]) of $^{188}Re(CO)_3$ Complexes with Ligands 8/10 and 11/13 in Human Serum Albumin at 37 °C

time/ligand	1 h	4 h	24 h	48 h
8a	96 ± 1	95 ± 1	85 ± 5	63 ± 10
8c	95 ± 1	85 ± 6	80 ± 5	65 ± 3
8d	94 ± 6	92 ± 2	76 ± 5	61 ± 10
10a	98 ± 4	94 ± 3	83 ± 7	68 ± 6
10b	92 ± 5	81 ± 7	78 ± 4	60 ± 4
11a	90 ± 6	68 ± 4	50 ± 7	33 ± 5
11b	95 ± 6	62 ± 7	52 ± 2	38 ± 8
13a	92 ± 6	58 ± 6	48 ± 7	35 ± 12
13b	93 ± 8	68 ± 9	40 ± 14	30 ± 10

[a] Values represent the means ± SD (n = 3).

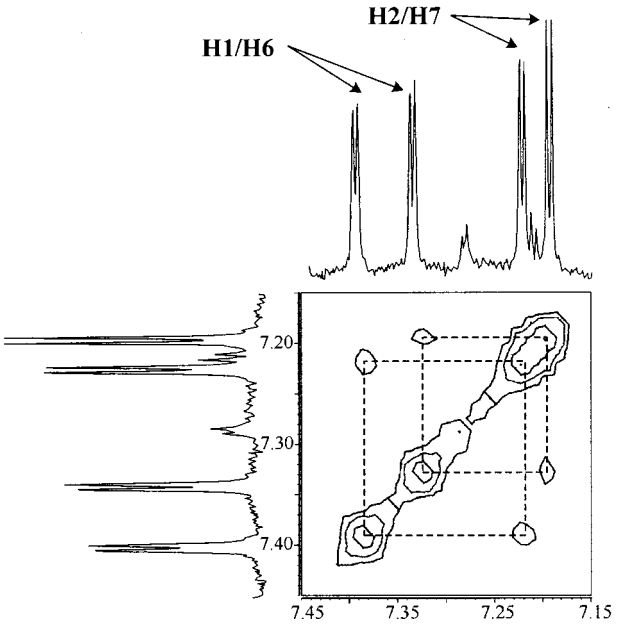


Figure 2. 2D proton NMR (COSY) of the aromatic region (imidazole protons) of complex $[Re(\mathbf{8b})(CO)_3]Br$. For proton numbering, see Figure 3.

spectrum of complex $[Re(\mathbf{8b})(CO)_3]Br$ showed four doublets with an intensity of one proton each. Two-dimensional NMR experiments (^{1}H/^{1}H COSY) revealed coupling between two pairs of protons (Figure 2) indicating an unsymmetrical coordination or structure of the complex.

A concluding explanation for this observation could be found after analysis of the X-ray structure. Crystals of X-ray quality could be grown by exchange of the bromide in complex $[Re(\mathbf{8b})(CO)_3]Br$ with the more bulky perchlorate anion. The ligand coordinates tridentately via the two imidazole rings and the secondary amino group

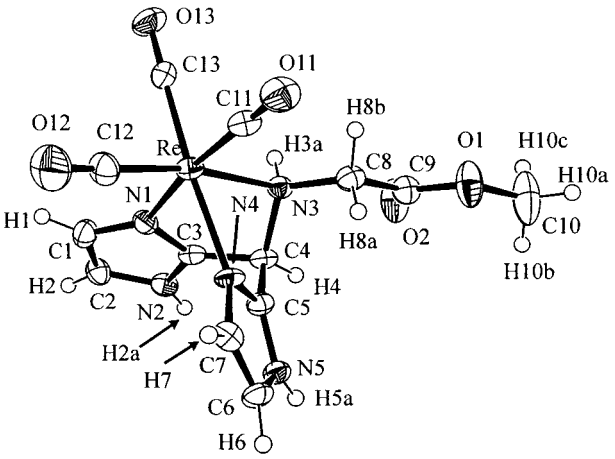


Figure 3. ORTEP (*18*) of the complex cation $[Re(\mathbf{8b})(CO)_3]^+$. Re−C(13) 1.950(6) Å; Re−N(1) 2.194(6) Å; N(3)−C(8) 1.470(8) Å; N(3)−C(4) 1.522(7) Å; C(3)−C(4) 1.491(9) Å; C(4)−C(5) 1.518-(8) Å; C(12)−Re−C(13) 89.8(3)°; C(12)−Re−N(1) 98.5(3)°; N(1)−Re−N(4) 81.00(19)°; N(1)−Re−N(3) 74.93(19)°; N(4)−Re−N(3) 73.68(18)°; C(8)−N(3)−C(4) 115.1(4)°; C(3)−C(4)−C(5) 104.2(5)°.

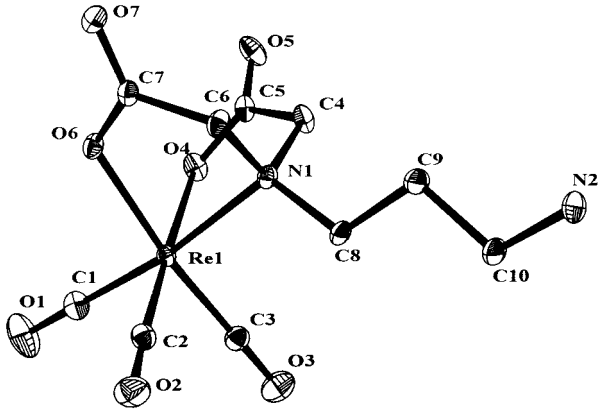


Figure 4. ORTEP (*18*) of the complex $[Re(\mathbf{13aH}^+)(CO)_3]$. H-atoms are omitted for clarity. Re(1)−C(1) 1.919(4) Å; Re(1)−O(4) 2.114(3) Å; Re(1)−O(6) 2.153(3) Å; Re(1)−N(1) 2.239(3) Å; C(2)−Re(1)−C(1) 87.74(17)°; C(3)−Re(1)−C(1) 88.40(17)°; C(2)−Re(1)−O(4) 173.96(13)°; O(4)−Re(1)−O(6) 78.19(11)°; O(4)−Re-(1)−N(1) 78.69(11)°; O(6)−Re(1)−N(1) 76.78(11)°.

as expected, forming two five-membered and one six-membered ring with the metal center (Figure 3). The structure clearly reveals the asymmetry of the ligand/complex after complexation. In respect to the N(3)−C(4) bond one of the imidazole rings is *trans* and one is *cis* oriented in respect to the acetyl methyl ester group (Figure 3). Clearly the orientation of the residue at the coordinated secondary amino group must be the reason for the chemical nonequivalence of the imidazole rings. The fact, that this NMR pattern was observed for all complexes with an N_α-substituted 2,2′-diimidazolylmethane amine ligand but not with the unsubstituted is a further evidence for this assumption. Temperature-dependent NMR experiments (20−90 °C) did not show a significant change of these patterns, proving the rigid and inert coordination of the ligand to the metal center. The IR spectrum of compound $[Re(\mathbf{8b})(CO)_3]Br$ showed the typical *fac*-$M(CO)_3$ pattern for the CO ligands at 2028 and 1922 cm^{-1}/1904 cm^{-1}. This is significantly blue-shifted, compared to the educt $(NEt_4)_2[ReBr_3(CO)_3]$ (2000 cm^{-1}, 1868 cm^{-1}).

The neutral complex $[Re(\mathbf{13aH}^+)(CO)_3]$ crystallized directly as colorless needles from the reaction medium (H_2O). Analysis of the ^1H NMR spectrum of complex $[Re(\mathbf{13aH}^+)(CO)_3]$ revealed a typical pattern of an AB system for the four protons of the coordinated IDA moiety. The previously identical NCH_2COO protons of the IDA moiety became nonequivalent upon rigid coordination to the metal center by virtue of their different chemical environment. The same spectroscopic features have been observed for all complexes with ligands **11** and **13** and were also reported for rhenium-tricarbonyl complexes of IDA-functionalized desoxyglucose and glucose derivatives (*19*). The IR spectrum of compound $[Re(\mathbf{13aH}^+)(CO)_3]$ showed M−CO stretch frequencies at 2018 and 1902 cm^{-1}. The X-ray structure confirmed the tridentate coordination of the ligand via the two carboxylates and the tertiary amino group (Figure 4).

CONCLUSION

The organometallic precursor $[^{188}Re(H_2O)_3(CO)_3]^+$ can now be prepared in a simple one-step synthesis in good yields and high specific activities. These procedures will allow the easy performance of therapeutic studies using the organometallic labeling approach. In fact in vitro experiments with Re-188 tricarbonyl-labeled antibodies against bladder cancer have shown the superior characteristic of the carbonyl technology compared to "classical" Re(V) methods (*20*). The novel, tridentate, bifunctional chelating systems presented in this work are versatile and offer the possibility to insert presumably any type (e.g. alkyl, poly(ethylene glycol), benzene) and length of spacer adaptable to different biomolecules. Particularly with ligands containing a bis(imidazole-2-yl)methylamine moiety high labeling yields should be possible at low ligand concentration.

ACKNOWLEDGMENT

We thank Judith Stahel, for her assistance in preparing the Re-188 complexes and Prof. Horst Bruchertseifer and Dr. Bernd Jäckel for generously providing Na-$[^{188}ReO_4]$. This work was supported by Mallinckrodt-Tyco Inc.

Supporting Information Available: Tables of crystal data, structure solution and refinement, atomic coordinates, bond lengths and angles and anisotropic thermal parameters for $[Re(\mathbf{8b})(CO)_3]ClO_4$ and $[Re(\mathbf{13aH}^+)(CO)_3]$ in CIF-format. This material is available free of charge via the Internet at http://pubs.acs.org.

LITERATURE CITED

(1) Volkert, W. A., and Hoffman, T. J. (1999) Therapeutic Radiopharmaceuticals. *Chem. Rev. 99*, 2269−2292.
(2) Liu, S., and Edwards, E. S. (2001) Bifunctional Chelators for Therapeutic Lanthanide Radiopharmaceuticals. *Bioconjugate Chem. 12*, 7−34.
(3) Coursey, B. M., J. M., C., Cessa, J., Hoppes, D. D., Schima, F. J., Unterweger, M. P., Golas, D. B., Callahan, A. P., Mirzadeh, S., and Knapp, F. F. (1990) Assay of the Eluent from the Alumina-Based Tungsten-188-Rhenium-188 Generator. *Radioact. Radiochem.* 38−49.
(4) Ferro-Flores, G., Pimentel Gonzalez, G., Gonzales-Zavala, M. A., Artega de Murphy, C., Melendez Alafort, L., Tendilla, J. I., and Croft, B. Y. (1999) Preparation, Biodistribution, and Dosimetry of 188Re Labeled MoAb or cea1 and Its F(ab′)2 Fragments by Avidin−Biotin Strategy. *Nucl. Med. Biol. 26*, 57−62.
(5) Karacay, H., McBride, W. J., Griffiths, G. L., Sharkley, R. M., Barbet, J., Hansen, H. J., and Goldenberg, D. M. (2000) Experimental Pretargeting Studies of Cancer with Humanized anti-CEAXMurine anti-[In-DTPA] Bispecific Antibody Constructs and a 99mTc-/188Re-Labeled Peptide. *Bioconjugate Chem. 11*, 842−854.

(6) Wenzel, M., and Saidi, M. (1993) Esters of Tc-99m Labeled Cytectrenecarboxylic Acid with Alcohols of Cyclic Amines as Cerebral Radiodiagniostic Agents. *J. Labelled Compd. Radiopharm. 33*, 77−80.

(7) Minutolo, F., and Katzenellenbogen, J. A. (1998) A Convenient Three-Component Synthesis of Substituted Cyclopentadienyl Tricarbonyl Rhenium Complexes. *J. Am. Chem. Soc. 120*, 4514−4515.

(8) Prakash, S., Went, M. J., and Blower, P. J. (1996) Cyclic and Acyclic Polyamines as Chelator of Rhenium-186 And Rhenium-188 For Therapeutic Use. *Nucl. Med. Biol. 23*, 543−549.

(9) Top, S., Morel, P., Pankowski, M., and Jaouen, G. (1996) Rapid and mild synthesis of $[Re_2(CO)_{10}]$ by reduction of $[NH_4][ReO_4]$ at atmospheric CO pressure. *J. Chem. Soc., Dalton Trans.* 3611−3612.

(10) Mullen, G. E. D., Blower, P. J., Price, D. J., Powell, A. K., Howard, M. J., and Went, M. J. (2000) Trithiacyclononane as a Ligand for Potential Technetium and Rhenium Radiopharmaceuticals: Synthesis of $[M(9S3)(SC_2H_4SC_2H_4S)][BF_4]$ (M = ^{99}Tc, Re, ^{188}Re) via C−S Cleavage. *Inorg. Chem. 39*, 4093−4098.

(11) Alberto, R., Schibli, R., Egli, A., Schubiger, P. A., Abram, U., and Kaden, T. A. (1998) A Novel Organometallic Aqua-complex of Technetium for the Labeling of Biomolecules: Synthesis of $[^{99m}Tc(OH_2)_3(CO)_3]^+$ from $[^{99m}TcO_4]^-$ in Aqueous Solution and its Reaction with Bifunctional Ligands. *J. Am. Chem. Soc. 120*, 7987−7988.

(12) Alberto, R., Ortner, K., Wheatley, N., Schibli, R., and Schubiger, P. A. (2001) Synthesis and Properties of Boranocarbonate: A Convenient in Situ CO Source for the Aqueous Preparation of $[^{99m}Tc(H_2O)_3(CO)_3]^+$. *J. Am. Chem. Soc. 123*, 3135−3136.

(13) Campell, C. J., Driessen, W. L., Reedijk, J., Smeets, W., and Spek, A. L. (1998) Glycine coupled to bis(imidazole): a tetradentate ligand rendering dinuclear copper(II) compounds through ligand sharing. *J. Chem. Soc., Dalton Trans.* 2703−2706.

(14) Alberto, R., Schibli, R., Schubiger, P. A., Abram, U., and Kaden, T. A. (1996) Reactions with the Technetium and Rhenium Carbonyl Complexes $[NEt_4]_2[MX_3(CO)_3]$. Synthesis and Structure of $[Tc(CN\text{-}^tBu)_3(CO)_3][NO_3]$ and $[NEt_4][Tc_2(\mu\text{-}SCH_2CH_2OH)_3(CO)_6]$. *Polyhedron 15*, 1079−1089.

(15) Pons, J.-F., Fauchère, J.-L., Lamaty, F., Molla, A., and Lazaro, R. (1998) A Constrained Diketopiperazine as a New Scaffold for the Synthesis of Peptidometics. *Eur. J. Org. Chem.* 853−859.

(16) Joseph, M., Leigh, T., and Swain, M. L. (1977) Synthesis of and Novel Reactions with Bis[imidazol-2-yl]nitromethane. *Synthesis* 459−461.

(17) Blower, P. J. (1993) Extending the life of a 99Tcm generator: a simple an convenient method for concentrating generator eluate for clinical use. *Nucl. Med. Commun. 14*, 995−997.

(18) Farrugia, L. J. (1997) ORTEP-3 for Windows − a version of ORTEP−III with a Graphical User Interface (GUI). *J. Appl. Crystallogr. 30*, 565−566.

(19) Petrig, J., Schibli, R., Dumas, C., Alberto, R., and Schubiger, P. A. (2001) Derivatization of glucose and 2-deoxyglucose for transition metal complexation: Substitution reactions with organometallic ^{99m}Tc and Re precursors and fundamental NMR investigations. *Chem. Eur. J. 7*, 1868−1873.

(20) Murray, A., Scholfield, D. F., Schibli, R., Novak, I., Waibel, R., Vincent, R. M., and Perkins, A. C. (2001) A Preliminary Comparison of Methods for Production of 188Re−C595 Antibodies for Radioimmunotherapy of Bladder Cancer. *J. Labeled Comp. Radiopharm. 44*, S573−S575.

BC015568R

Novel Poly(ethylene glycol) Derivatives for Preparation of Ribosome-Inactivating Protein Conjugates

Silvia Arpicco,[†] Franco Dosio,[†] Andrea Bolognesi,[‡] Chiara Lubelli,[‡] Paola Brusa,[†] Barbara Stella,[†] Maurizio Ceruti,[§] and Luigi Cattel*[,†]

Dipartimento di Scienza e Tecnologia del Farmaco, Via Pietro Giuria 9, 10125 Torino, Italy, Dipartimento di Patologia Sperimentale, Via S. Giacomo 14, 40126 Bologna, Italy, and Dipartimento Farmacochimico, Tossicologico e Biologico, Via Archirafi 32, 90123 Palermo, Italy. Received November 12, 2001; Revised Manuscript Received May 9, 2002

This study describes the synthesis, characterization, and reactivity of new methoxypoly(ethylene glycol) (mPEG) derivatives containing a thioimidoester reactive group. These activated polymers are able to react with the lysyl ϵ-amino groups of suitable proteins, generating an amidinated linkage and thereby preserving the protein's positive charge. mPEG derivatives of molecular weight 2000 and 5000 Da were used, and two spacer arms were prepared, introducing chains of different lengths between the hydroxyl group of the polymer and the thioimidate group. These mPEG derivatives were used to modify gelonin, a cytotoxic single-chain glycoprotein widely used in preparation of antitumoral conjugates, whose biological activity is strongly influenced by charge modification. The reactivity of mPEG thioimidates toward lysil ϵ-amino groups of gelonin was evaluated, and the results showed an increased degree of derivatization in proportion to the molar excesses of the polymer used and to the length of the alkyl spacer. Further studies showed that the thioimidate reactive is able to maintain gelonin's significant biological activity and immunogenicity. On the contrary, modification of the protein with N-hydroxysuccinimide derivative of mPEG strongly reduces the protein's cytotoxic activity. Evaluation of the pharmacokinetic behavior of native and PEG-grafted gelonin showed a marked increase in plasma half-life after protein PEGylation; in particular, the circulating life of the conjugates increased with increased molecular weight of the polymer used. The biodistribution test showed lower organ uptake after PEGylation, in particular by the liver and spleen.

INTRODUCTION

Ribosome-inactivating proteins (RIPs)[1] are a group of naturally occurring plant and fungal proteins that have been widely studied for their potential applications, especially as anticancer agents (*1*).

All RIPs exhibit RNA N-glycosidase activity, depurinating rRNA at a specific universally conserved position (i.e., cleavage of N-glycosidic bond of a specific adenine of 28S rRNA) (*2*). More recently, it has appeared that RIPs are also capable of inactivating many nonribosomal nucleic acid substrates (*3*) and hence can be considered polynucleotide:adenosine glycosidases. These insights have renewed interest in RIPs because understanding the enzymatic activity enhances exploitation of the properties and activities of RIPs for diverse applications. Indeed, such biomolecules are being exploited for designing immunotoxins/hormonotoxins obtained by chemical conjugation or by production of chimeric proteins using gene splicing DNA techniques (*4*, *5*). Other applications of therapeutic potential for nonconjugated RIPs lie in the treatment of some cancers (*5*) and AIDS (*6*, *7*) and as abortifaciens (*8*).

Gelonin, a protein extracted from the seeds of *Gelonium multiflorum*, is one of the most interesting RIPs and has been widely used in the preparation of conjugates directed against tumor epitopes (*9*, *10*) or as antiviral agent (*11*, *12*). Recently, it has also been suggested that gelonin has DNA-damaging activity, which may be responsible for the elimination of the parasite 6 kb extrachromosomal mitochondrial DNA of *Plasmodium falciparum*-infected erythrocytes (*13*−*15*).

Gelonin has been used by our group particularly in the preparation of conjugates with monoclonal antibodies using both new heterobifunctional linkers and noncovalent systems (*16*−*19*). Indeed, one favorable aspect of using gelonin is its low systemic toxicity (LD_{50} 40 mg/Kg body weight) and its low toxicity on intact cells (IC_{50} > 33 μM on HeLa) due to its incapability of penetrating cell membranes. Furthermore, it is rapidly removed from the bloodstream by kidney filtration (*20*). Clinical use of RIPs and related immunotoxins may be limited by the host immune response observed in patients after injection of RIPs, as reported in Lambert et al. (*21*). Allergic reaction and occasional anaphylactic response have, for example, been described for trichosanthin (*22*, *23*), and the same behavior has been found for gelonin (*24*). Specific antibodies against immunotoxins containing gelonin have been observed after infusion in monkeys;

* Corresponding author. Phone: ++39.011.6707697. Fax: ++39.011.6707695. E-mail: luigi.cattel@unito.it.

[†] Dipartimento di Scienza e Tecnologia del Farmaco.

[‡] Dipartimento di Patologia Sperimentale.

[§] Dipartimento Farmacochimico.

[1] Abbreviations: RIPs, ribosome-inactivating proteins; mPEG, methoxypoly(ethylene glycol); PEG, poly(ethylene glycol); SPDP, N-succinimidyl-3-(2-pyridyldithio)-propionate; SS-5PEG, methoxypoly(ethylene glycol) succinimidyl succinate with M_r of 5 kDa; SS-20PEG, methoxypoly(ethylene glycol) succinimidyl succinate with M_r of 20 kDa; TNBS, 2,4,6-trinitrobenzenesulfonic acid; THF, tetrahydrofuran; SDS−PAGE, sodium dodecyl sulfate polyacrylamide gel electrophoresis; ELISA, enzyme-linked immunosorbent assay; FCS, fetal calf serum.

10.1021/bc015578s CCC: $22.00 © 2002 American Chemical Society
Published on Web 06/19/2002

high-titer antibody responses developed quickly, and sera from the infused monkeys were able to block the cytotoxicity of the immunotoxin (*24*).

To improve the behavior and thus the therapeutic efficacy of gelonin, alone or conjugated with a targeting moiety, we considered an approach to surface modification using a covalent coupling reaction with poly(ethylene glycol) (PEG) derivatives.

PEG is used to modify various proteins. PEG-grafted proteins exhibit increased stability, decreased immunogenicity, and increased circulating lives (*25*−*27*). Furthermore, PEG conjugates are more resistant to proteolysis, and in vivo activity can sometimes be enhanced despite a reduction in in vitro activities (*28*). The major problem of PEG conjugation of RIPs is their sensitivity to lysine modification. Some authors have reported a rapid decrease in the ability of several RIPs, and in particular gelonin, to inhibit protein synthesis after modification with SPDP or other reactives able to modify charge (*29*−*31*).

To obtain polymer conjugates with almost unaltered gelonin activity, we prepared novel derivatives of mPEG containing a thioimidoester reactive group. This reactive group is able to react with the protein lysyl ϵ-amino groups in physiological conditions (pH 7.5), generating an amidinated linkage and thus preserving the positive charge of the protein.

This paper describes the synthesis and chemical characterization of mPEG-thioimidates, with different molecular weights and different spacers between mPEG and thioimidate group**.** These reactives were applied to prepare different conjugates with gelonin. The conjugates were then purified and characterized in terms of molecular mass, in vitro activity, and immunogenicity. The pharmacokinetics and organ distribution were also studied.

EXPERIMENTAL PROCEDURES

Materials. mPEG 2000 and 5000 and mPEG succinimidyl succinate with M_r of 5 kDa (SS-5PEG) were purchased from Sigma Chemical Co. (St. Louis, MO). mPEG succinimidyl succinate with M_r of 20 kDa (SS-20PEG) was from Shearwaters Corp. (Huntsville, AL). Gelonin was extracted from seeds of Gelonium multiflorum and purified to mass homogenicity (M_r = 30 kDa) and characterized (*32, 33*). 2,4,6-trinitrobenzenesulfonic acid (TNBS) was from Serva (Heidelberg, Germany). All other reagents were purchased from Aldrich (Milwaukee, WI). Diethyl ether and tetrahydrofuran (THF) were dried over sodium benzophenone ketyl.

General Procedures. ^{1}H NMR spectra were recorded on a Bruker AC 200 instrument, operating at 200 MHz, with tetramethylsilane as internal standard. Ultraviolet spectra were recorded on a Beckman DU-70 spectrophotometer. The reactions were monitored by TLC on F_{254} silica gel precoated sheets (Merck, Milan, Italy); after development, the sheets were exposed to iodine vapor. Flash column chromatography was performed on 230−400 mesh silica gel (Merck).

Preparation of Sodium Naphthalene Solution. Naphthalene 2.6 g (20 mmol) was dissolved in 20 mL of dry THF under a nitrogen atmosphere dried by passing it through concentrated sulfuric acid and NaOH platelets in two washing bottles. About 0.5 g (22 mmol) of small clean pieces of sodium was then rapidly added, and the mixture was stirred for 2 h at room temperature under dry nitrogen.

Preparation of mPEG(CH$_2$)$_2$CN (1, 2). Five grams of mPEG 2000 (2.5 mmol) or 5000 (1 mmol) was dissolved in 100 mL of toluene and dried by removal of the water−toluene azeotrope. The solution was cooled to room temperature, concentrated, and then dissolved in 50 mL of dry THF. The sodium naphthalene solution prepared previously was added dropwise to the mPEG solution under dry nitrogen and stirring; addition continued until a persistent pale green solution was obtained. A solution of 3-bromopropionitrile (2 mL, 25 mmol in the case of mPEG 2000 or 830 μL, 10 mmol in the case of mPEG 5000) dissolved in 5 mL of dry THF was slowly added to the solution, and the reaction mixture was allowed to stand overnight at room temperature under dry nitrogen. The reaction mixture was concentrated under reduced pressure and filtered, and the filtrate was added dropwise into 100 mL of diethyl ether under stirring; the resulting solid was collected by filtration and purified. Derivative **1**, prepared from mPEG 2000, was purified by flash chromatography with elution in dichloromethane/methanol (96:4). The pure product was obtained with a yield of 60% (3 g): ^{1}H NMR ($CDCl_3$) 3.6 (s, mPEG backbone methylene), 3.3 (s, 3H, terminal mPEG methoxy), 2.6 (t, 2H, −O−CH$_2$−*CH$_2$*−CN). We obtained 2 g (40%) of derivative **2** after crystallization from diethyl ether; ^{1}H NMR ($CDCl_3$) 3.6 (s, mPEG backbone methylene), 3.3 (s, 3H, terminal mPEG methoxy), 2.5 (t, 2H, −O−CH$_2$−*CH$_2$*−CN).

Preparation of mPEG(CH$_2$)$_6$CN (3, 4). The same procedure used to prepare **1** and **2** was followed, using 7-bromoheptanenitrile (25-fold molar excess respect to mPEG). The crude products were purified by flash chromatography (dichoromethane/methanol, 93:7) to give **3** (85%): ^{1}H NMR ($CDCl_3$) 3.55 (s, mPEG backbone methylene), 3.4 (s, 3H, terminal mPEG methoxy), 2.34 (t, 2H, −CH$_2$−CN), 1.59 (m, 4H, −O−CH$_2$−*CH$_2$*−CH$_2$−CH$_2$−*CH$_2$*−CH$_2$−CN), 1.4 (m, 4H,-O−CH$_2$−CH$_2$−*CH$_2$*−*CH$_2$*−CH$_2$−CH$_2$−CN).

Derivative **4** was purified by flash chromatography with elution in dichloromethane/methanol 92:8 (yield 95%). The NMR spectrum was similar to that of compound **3**.

Preparation of mPEG−Thioimidate ester hydrochlorides (5−8). The thioimidate ester hydrochlorides **5**−**8** were obtained from the corresponding nitriles **1**−**4** by the Pinner synthesis (*34*). Hydrogen chloride gas, dried by being passed through concentrated sulfuric acid in two washing bottles, was bubbled through ice-cold ethanthiol (560 μL, 7.5 mmol). The nitrile (0.25 mmol) dissolved in anhydrous dichloromethane was quickly added to the cold solution under stirring; the flask was tightly stoppered and left overnight at 0 °C. Anhydrous cold diethyl ether was then added to the reaction mixture, which was left at −20 °C until a crystalline solid formed. The supernatant was decanted, and the precipitate was washed 3 times with anhydrous cold diethyl ether under argon and dried under reduced pressure at room temperature.

Compounds **5** (yield 85%) and **6** (yield 75%): ^{1}H NMR ($CDCl_3$) 3.6 (s, mPEG backbone methylene), 3.4 (s, 3H, terminal mPEG methoxy), 3.1 (t, 2H, −O−CH$_2$−*CH$_2$*−C=NH_2^+), 1.4 (t, 3H, S−CH$_2$−*CH$_3$*).

Compounds **7** and **8** (yield 95%): ^{1}H NMR ($CDCl_3$) 3.64 (s, mPEG backbone methylene), 3.4 (s, 3H, terminal mPEG methoxy), 2.9 (t, 2H, −*CH$_2$*−C=NH_2^+), 1.8 (m, 4H, −O−CH$_2$−*CH$_2$*−CH$_2$−CH$_2$−*CH$_2$*−CH$_2$−C=NH_2^+), 1.6−1.4 (m, 7H −O−CH$_2$−CH$_2$−*CH$_2$*−*CH$_2$*−CH$_2$−CH$_2$−C=NH_2^+, −S−CH$_2$−*CH$_3$*).

Polymers−Gelonin Conjugate Preparation. A solution of gelonin (5 mg/mL, 500 μL) in PBS-EDTA (100 mM sodium phosphate, 100 mM NaCl, 1 mM EDTA, pH 7.4), deaerated and flushed with argon, was added to

different molar excesses of the mPEG−thioimidate ester hydrochlorides (**5**−**8**). The solution was left for 1 h at room temperature under stirring. The molar ratio of activated mPEG to protein ranged from 2- to 50-fold. For comparison, gelonin was also modified with increasing excesses (from 2- to 50-fold) of the commercially available SS-5PEG, methoxypoly(ethylene glycol) succinimidyl succinate with a M_r of 5 kDa.

The unreacted PEG was removed using an Amicon system (Danvers, MA) with YM membranes (cutoff, 10 and 30 kDa). The crude conjugates were separated on a Zorbax Bio Series GF 250 column (250 × 9.4 mm) (Du Pont, Newtown, Connecticut) that was equilibrated and eluted with 0.01 M sodium phosphate, 0.1 M sodium sulfate, pH 7.0, eluting buffer, and flow rate 0.5 mL/min. The chromatographic procedures were performed at 20 °C. All the chromatograms were generated on a Merck-Hitachi 655A-12 Liquid Chromatographer equipped with a L5000 LC Controller (Merck), and the eluting fractions were monitored at 280 nm using a L4000 UV detector. Peak heights and areas were recorded and processed on a CBM-10A Shimadzu interface (Shimadzu, Milan, Italy).

The protein concentration was evaluated spectrophotometrically at 280 nm and also determined by a biuret assay.

The extent of protein modification was evaluated colorimetrically following the Habeeb's method (*35*). The sample solution (1 mL) at protein concentration between 0.7 and 1 mg/mL was diluted with 1 mL of 4% sodium bicarbonate solution, and 1 mL of 0.1% 2,4,6-trinitrobenzenesulfonic acid (TNBS) solution was added. After 2 h at 40 °C, the reaction was stopped by the addition of sodium dodecyl sulfate and HCl. The absorption at 341 nm was correlated with the number of free amino groups ($\epsilon = 12400$).

Gelonin−PEG conjugates were analyzed by sodium dodecyl sulfate polyacrylamide gel electrophoresis (SDS−PAGE) using 4−15% precast gels (Bio-Rad, Hercules, CA) in nonreducing conditions. Coomassie blue staining was used to visualize the proteins.

Protein Synthesis Inhibition Assay. The inhibitory activity of gelonin−PEG derivatives on cell-free protein synthesis was evaluated with a rabbit reticulocyte lysate prepared as described by Allen and Schweet (*36*). Gelonin, appropriately diluted, was added to a reaction mixture containing, in a final volume of 62.5 μL: 10 mM Tris/HCl buffer, pH 7.4, 100 mM ammonium acetate, 2 mM magnesium acetate, 1 mM ATP, 0.2 mM GTP, 15 mM phosphocreatine, 3 μg of creatine kinase, 0.05 mM amino acids (minus leucine), 3.3 kBq of L-^{14}C-leucine (Amersham International, Bucks, U.K.), and 25 μL of a rabbit reticulocyte lysate. Incubation was at 28 °C for 5 min. The reaction was arrested with 1 mL of 0.1 M potassium hydroxide, and two drops of hydrogen peroxide and 1 mL of 20% (w/v) of trichloroacetic acid were added. Precipitated proteins were collected on glass-fiber disks, and the radioactivity incorporated was measured with a β-counter (Beckman, Fullerton, CA) after addition of 5 mL of Ready Gel scintillation cocktail (Beckman) containing 0.7% acetic acid. Each experiment was carried out in duplicate. The concentration of RIP causing 50% inhibition of leucine incorporation (IC_{50}) was calculated by linear regression analysis. All tests were repeated three times.

Production of Antigelonin mAbs. Antigelonin mAbs were produced according to a standard immunization/fusion protocol using P3U1 myeloma cells (*37*). Hybrid cells were selected by culture in HAT (hypoxanthine aminopterin thymidine) medium 18 h after fusion. Hybridoma supernatants were screened by the enzyme-linked immunosorbent assay (ELISA) using gelonin-coated microtiter plates. For this study, we mixed three mAbs (B 3.1, A12, E17) that strongly reacted in ELISA assay with native gelonin. The culture medium for hybrids was RPMI 1640 supplemented with 10% FCS and 2 mM L-glutamine.

Immunoreactivity. The immunoreactivity was determined using a modification of the ELISA assay (*38*). Enzyme microtitration plates were coated with antigen (4 μg/well of RIP) solubilized in 50 mM sodium bicarbonate buffer, pH 9.6, and left overnight at 4 °C. The plates were washed 3 times with 0.14 M NaCl/5 mM sodium phosphate buffer, pH 7.5, containing 0.05% (v/v) Tween 20 (PBS-Tween), blocked with 200 μL/well of PBS-Tween containing 0.5 mg/mL bovine serum albumin for 60 min at 37 °C, and washed 3 times as described above. Specific mouse antisera mix was serially diluted in PBS-Tween, added to the antigen coated plates, and incubated for 3 h at 37 °C. Plates were washed 3 times and incubated with 200 μL of appropriately diluted secondary antibody (goat antimouse IgG conjugated with alkaline phosphatase, Sigma) in PBS-Tween for 1 h at 37 °C. Plates were washed 3 times as described above and incubated with 200 μL of 1 mg/mL 4-nitrophenyl phosphate disodium salt in diethanolamine buffer, pH 9.8, for 30 min a 37 °C. Absorbance was measured in a Bio-Rad microtiter plate reader at 405 nm.

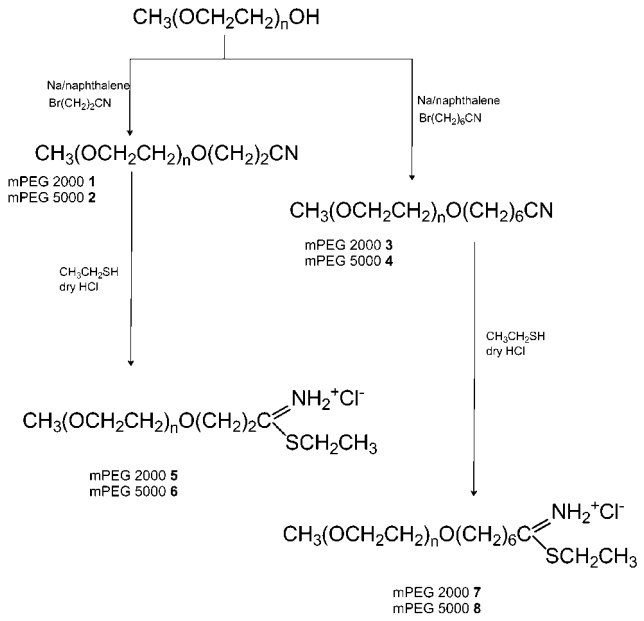
Pharmacokinetics and Biodistribution. To evaluate the in vivo behavior of gelonin and mPEG modified protein, we prepared different conjugates using ^{125}I gelonin as tracer. The protein was labeled with ^{125}I by the iodogen method (*39*), and 250 MBq of ^{125}I gelonin (specific activity 166.15 MBq/μg) was added to a solution of unlabeled protein (10 mg/mL). The conjugates were prepared as previously described, reacting gelonin with a 5-fold molar excess of thioimidate derivatives **7** and **8** and with a 3-fold molar excess of SS-20PEG.

Pharmacokinetic studies were performed using female Balb/c mice (1 month old, 18−20 g; Charles River Italia, Milan, Italy), the mice drank water plus 0.2% (v/v) Lugol solution 3 days before and during the experiment to block thyroid iodine uptake. The animals were injected intravenously into the tail vein (groups of three animals each) with a single dose of ^{125}I-gelonin and of the mPEG−^{125}I-gelonin conjugates ranging from 7.5 to 9.1 MBq. The samples were diluted in a carrier solution of PBS pH 7.4 to a volume of 100 μL. Blood samples were taken from the retroorbital plexus and withdrawn into heparin-containing tubes at various times (0, 10, 15, 20, 30, 60, 90, 120, and 240 min and 24 h for conjugates and 0, 5, 10, 15, 30, and 45 min for gelonin). Experiments were repeated 3 times. The blood samples were precipitated rapidly with 1 mL of cold trichloroacetic acid (12.5%, w/v). The samples were counted directly in a gamma counter (L'ACN, Milan, Italy) and then centrifuged; the resultant pellets were counted and used to determine the pharmacokinetic parameters.

Pharmacokinetic parameters were determined from a two-compartmental model analysis using the Software KINETICA 2.00.200 (InnaPhase, Champs Sur Marne, France). Data were fitted using a compartmental open model. Elimination and distribution were represented by the following parameters: mean residence time (MRT), total body clearance (Cl), volume of distribution at steady state (V_{ss}), distribution, and elimination phases ($t_{1/2}^{\alpha}$, $t_{1/2}^{\beta}$).

Other groups of five animals each were similarly injected, and the liver, kidney, and spleen, were removed at different times (10, 30, 60, and 120 min, and 24 h).

Scheme 1



The organs were washed twice in physiological solution, wiped, weighed, and γ-counted. The counting was performed on intact organs and also after mechanical shattering to correctly measure radioactivity. The monitored radioactivity was recorded as concentration, in percent injected dose per gram of organ versus time and represented through histograms. The experiments were repeated 3 times.

Care and handling of the animals were in accordance with the provisions of the European Economic Community Council Directive 86/209 recognized and adopted by the Italian Government (approval Decree No. 230/95 B).

RESULTS

Chemistry. The mPEG−thioimidate ester hydrochlorides **5**−**8** were obtained as shown in Scheme 1. These activated polymers were prepared starting from mPEG of molecular weight 2000 and 5000 Da and were characterized by the presence of spacers of different lengths between the polymer chain and the reactive group.

Initially, the sodium naphthalene solution was prepared by stirring clean pieces of sodium with a slight excess of naphthalene in dry THF under nitrogen at room temperature (*40*). Then mPEG 2000 or 5000 was converted to the corresponding nitrile **1** or **2** by titration with sodium naphthalene to generate the alkoxide, followed by treatment with 3-bromopropionitrile. Derivative **1**, obtained from mPEG 2000, was easily purified by flash chromatography, but it was not possible to purify the corresponding nitrile **2** prepared from mPEG 5000 in the same way because it was impossible to discriminate the starting product from the obtained nitrile by TLC. Derivative **2** was thus purified by crystallization from diethyl ether. Compounds **3** and **4** were obtained in a similar way, using 7-bromoheptanenitrile instead of 3-bromopropionitrile and were easily purified by flash chromatography. Probably in this case, the presence of a hexamethylenic spacer between the PEG backbone and the nitrile group allowed better discrimination of derivatives **3** and **4** on gel chromatography. The corresponding thioimidates **5**−**8** were prepared throught the Pinner synthesis by addition of the nitrile to a solution of ethanthiol previously saturated with dry hydrogen chloride. The yield of activation was usually above 90% and was ascertained by NMR (integration of the peaks corresponding to the terminal mPEG−methoxy and to the methylene in α position to the thioimidate). The thioimidates required storage under very anhydrous conditions and were stored at −20 °C under dry argon. To maintain their reactivity unmodified, it is important to reduce exposure to atmospheric humidity because of the hygroscopicity of the compounds. Under these conditions they are stable for several months.

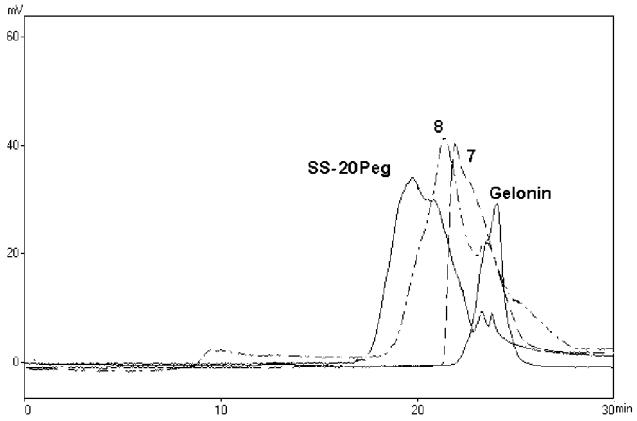


Figure 1. Molecular exclusion chromatographic profiles of gelonin and crude conjugates obtained by reaction with 5-fold molar excesses of compounds **7**, **8**, and SS-20PEG on gel-filtration column Zorbax Bio Series GF 250.

Reaction of mPEG−Thioimidate with Gelonin. The reactivity of the activated polymers **5**−**8** toward the protein lysyl ϵ−amino groups of gelonin, a 30 kDa cytotoxic single-chain glycoprotein, was evaluated. Gelonin was found to be composed of 258 amino acids and contains 21 lysine residues (*41*). The mPEG−thioimidate was added in various molar excesses (from 2- to 50-fold) to the solution of the protein (5 mg/mL) for 1 h at room temperature; the conjugates were then purified from the excess of mPEG by ultrafiltration. To remove the unreacted gelonin, we submitted the conjugates to molecular exclusion chromatography (Figure 1). This purification is necessary before submitting the samples to characterization assays and to in vitro tests.

The concentration of native or PEG-grafted protein was evaluated either spectrophotometrically at 280 nm or using biuret reaction.

The derivatization degree was estimated by titration of free amino groups by TNBS method. Figure 2 shows the number of modified amino groups of gelonin versus the different excesses of mPEG−thioimidates. From the figure, it is evident that the derivatization degree increases in proportion to the molar excess of mPEG used. This is particularly evident for derivatives **7** and **8**, characterized by the presence of a hexamethylenic spacer between the polymer backbone and the thioimidate reactive group, which was found to be more reactive toward the protein than derivatives **5** and **6**, characterized by a dimethylenic spacer. This behavior is more evident when the mPEG−thioimidate excess was increased from 10- to 50-fold. At 50-fold excess of **8**, for instance, 12 lysine residues were derivatized with compound **8** and only six with compound **6**. We also compared the reactivity of the thioimidates with that of the commercially available SS-5PEG (M_r, 5 kDa) characterized by the presence of a highly reactive succinimidyl ester reactive group, which generates an amidic bond by reaction with protein amino groups. As shown in Figure 2, compound **8** and SS-5PEG demonstrated a similar

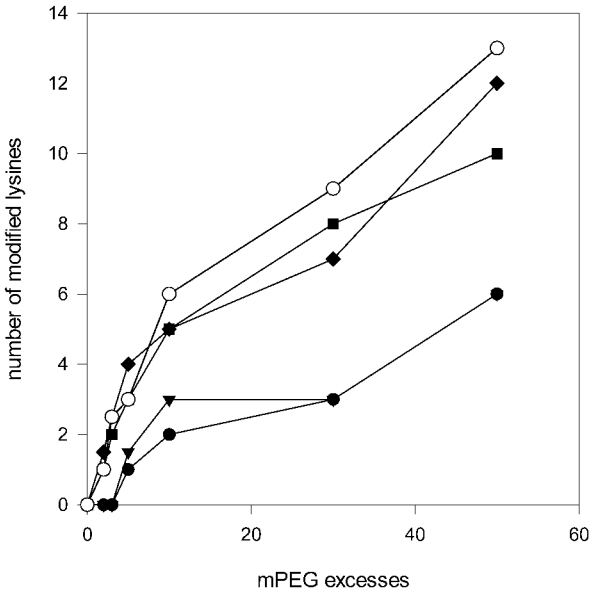


Figure 2. Reactivity of different mPEG−thioimidates toward gelonin. The activated polymer was added in molar excesses from 2- to 50-fold to solutions of the protein. The extent of protein modification was evaluated by titration of free amino groups by the TNBS method after purification from excess mPEG. The points represents the arithmetic means of three determinations; SDs (not reported) were <10% of the means. Solid circle compound, **5**; solid triangle pointing down, **6**; solid square, **7**; solid diamond, **8**; and outline circle, SS-5PEG.

behavior using excesses of polymer, modifying up to 50% of the total lysines of gelonin.

To analyze the molecular weight of the protein after derivatization with the different mPEG-thioimidates, we analyzed the conjugates by SDS−PAGE electrophoresis.

Figure 3 shows the SDS−PAGE of the gelonin−PEG conjugates obtained by modifying the protein with different excesses of compound **7** and **8** and SS-20PEG (M_r, 20 kDa). The gel shows that, on increasing the number of mPEG molecules attached to gelonin, the size of the protein increased although a clear distribution in molecular weight was evident only for lower derivatization degrees. On increasing the linked PEG molecules, broader bands appeared. Bands relative to unreacted gelonin were evident only when lower mPEG excess was used.

Protein Synthesis Inhibition Activity and Immunoreactivity. Table 1 summarizes the characteristics of PEGylated gelonin in terms of derivatization degree, IC_{50} in a reticulocyte lysate cell free protein synthesis system, and antigelonin antiserum recognition.

The thioimidate linkers are able to maintain a higher activity than the N-hydroxysuccinate analogues. Gelonin

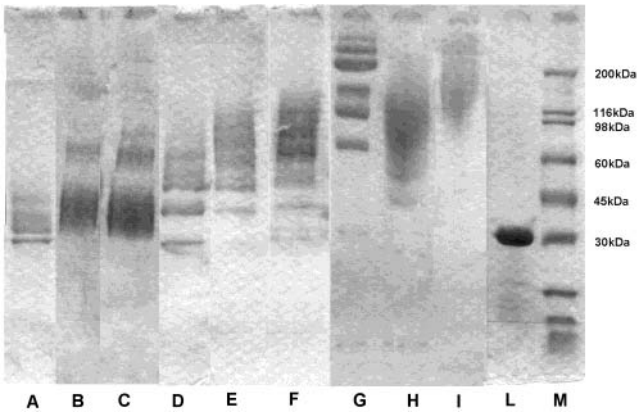


Figure 3. SDS−PAGE analysis of gelonin and conjugates obtained with increasing excesses of mPEG−thioimidates **7** and **8** and SS-20PEG. Samples were run on a 4−15% polyacrylamide gel under nonreducing conditions and Coomassie blue staining. Lanes A−C, conjugates obtained with molar excesses (5, 10, and 20) of compound **7**; lanes D−F, conjugates prepared using increasing excesses of compound **8** (5, 10, and 20); lanes G−I, conjugates prepared using increasing excesses of SS-20PEG (5, 10, and 20); lane L, gelonin; lane M, molecular markers. Molecular masses are expressed in kDa.

is a highly basic protein (pI, >9), and thus direct evaluation of surface charge modification (e.g., by IEF) is not realizable, but as demonstrated in a previous paper (*31*), a direct relationship between charge modification and loss of cell-free activity exists. Gelonin appeared very sensitive to modification of its RNA N-glycosidase activity; on increasing the derivatization degree over two lysyl groups, activity rapidly decreases. From the results in Table 1, the thioimidate linkage appears able to maintain 50% of native activity for a derivatization degree of three groups, while only 18% was evident using N-hydroxysuccinate analogue under the same conditions. An increase in M_r over 5 kDa is responsible for a rapid fall of gelonin activity: in fact, just one PEG group of 20 kDa can reduce the toxic activity to 12% of initial values.

Immunoreactivity is strongly affected by PEG length; a PEG 2 kDa chain is not able, in any of the conditions tested, to reduce antibody recognition by more than 68% (compounds **5**, **7**), while an increase in M_r to 5 kDa reduces recognition to 37%. A further increase in M_r (SS-20 PEG) give not a detectable reaction at any antiserum dilution.

Pharmacokinetic Studies and Organ Disposition. The influence of the PEG protein modification on circulation time was studied after intravenous bolus administration of native and modified gelonin to Balb/c mice. The RIP was radiolabeled with ^{125}I and the samples injected i.v. to groups of mice; blood samples were collected at

Table 1. Inhibition of Protein Synthesis in a Cell-Free System and Immunoreactivity of Gelonin and PEG Derivatives[a]

PEG reactive	modified[b] Lys	IC_{50}[c]	% immunoreactivity[d]	PEG reactive	modified[b] Lys	IC_{50}[c]	% immunoreactivity[d]
5	2	0.41	76	**6**	2	0.33	60
	4	0.57	72		3	0.89	55
	6	3.73	70		6	3.9	45
7	2	0.36	76	**8**	2	0.35	64
	4	1.13	70		3	0.66	54
	6	3.82	70		6	2.63	43
	10	>5.33	68		10	>5.33	37
SS-5 PEG	3	1.73	53	SS-20 PEG	1	2.62	n.d.
	6	>5.3	40		2	4.50	n.d.
	10	>5.33	38		4	>5.33	n.d.

The points represent the means of three separate determinations. [a] n.d. not detectable. [b] The degree of derivatization was detected by the TNBS method and electrophoresis. [c] The IC_{50} (concentration giving 50% inhibition of protein synthesis) expressed in nM was assayed on rabbit reticulocyte lysate. Gelonin has a IC_{50} value of 0.31 nM. [d] The relative immunoreactivity (100% for pure gelonin) was obtained using a specific antiserum and assayed on ELISA test.

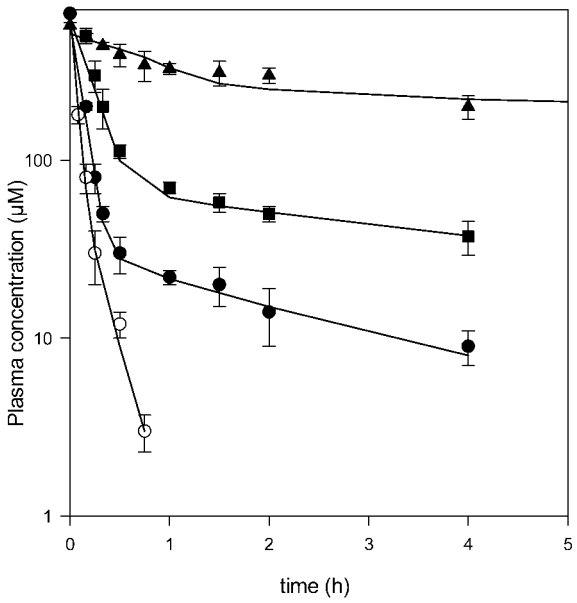


Figure 4. Pharmacokinetic profiles following an intravenous bolus injection of radiolabeled gelonin and mPEG conjugates in mice. The reported data are the arithmetic means of three determinations, and SDs are indicated. Outline circle, gelonin; solid circle, conjugate obtained with compound **7**; solid square, conjugate obtained with compound **8**; solid triangle, conjugate obtained with SS-20PEG.

intervals and radioactivity determined. Since similar behavior in in vitro tests of compounds **5** and **6** versus compounds **7** and **8** was found, the analysis on animals were performed only on thioimidate **7** and **8** and with SS-PEG 20 kDa in order to have a comparison for the highest M_r.

Figure 4 shows the pharmacokinetic profiles of gelonin and conjugates obtained with compound **7**, **8**, and SS-20PEG. The gelonin rapidly disappears from blood circulation ($t_{1/2}^{\alpha}$ is 2 min and $t_{1/2}^{\beta}$ is 13 min, see Table 2), while an increase in molecular mass and hydrophilic radius (from 30 kDa for gelonin to 36, 45, and 70 kDa for conjugates with **7**, **8**, and SS-20PEG, respectively) increases survival time. Following a bicompartmental model for 2 and 5 kDa PEG conjugates, the distribution phase appears rapid ($t_{1/2}^{\alpha}$ of 4 and 7 min), but a progressive decrease in elimination is evident ($t_{1/2}^{\beta}$ from 70 to 273 min). Different behavior appeared when the conjugate M_r increased above the glomerular sieving threshold: the $t_{1/2}^{\alpha}$ increased to 44 min and the $t_{1/2}^{\beta}$ up to 25 h. The mean residence time also reflects the slow elimination from the body due to PEGylation; MRT increases in a quadratic mode, from 10 min for gelonin to 94, 324, and 2073 min for the conjugates.

The levels of accumulation of native and PEG modified gelonin sampled in the organs involved in toxin removal (liver kidney and spleen) after i.v. administration of conjugates are shown in Figure 5. These values are expressed as percentages of the dose per gram of tissue and were sampled up to 24 h after injection. The pattern of biodistribution confirms the pharmacokinetic profiles; gelonin is rapidly removed from the body by kidney filtration, and an increase in molecular mass proportionally decreases kidney uptake and increases liver and spleen uptake. Specific accumulation in these RES organs is reduced progressively for 5 kDa and for 20 kDa mPEG conjugates, with a proportional increase in blood survival time.

DISCUSSION

Targeting of toxins is one of the approaches to the selective removal of cancer or viruses. The major problems encountered in the use of toxin as therapeutic agents are due to nonspecific toxicity, low blood-residence time, and immunogenicity induced by the toxin moiety. The main way to solve these problems is to construct recombinant RIPs or in to use soluble hydrophilic masking polymers (*42*, *43*).

The present study aimed to evaluate the characteristics of mPEG derivatives able to generate a stable linkage and to increase the immunological and pharmacokinetic properties of the RIP gelonin, chosen as model protein sensitive to surface modification. This RIP has been exploited in therapeutic application both in immunotoxin preparation and as such: several interesting studies have recently been reported (*9*, *42*, *44*) as well as other relevant applications of gelonin in the treatment of tumors, involving the use of new techniques such as shock wave permeabilization or photochemical internalization (*45*−*47*).

Several methods of activating PEG to obtain protein conjugates have been described (*48*), but some of them change the total charge of the modified protein, in some cases reducing its biological activity. In contrast, the imido ester derivatives of mPEG, described in a patent (*49*), after reaction with the amino groups of proteins, lead to a charged amidine group without altering the positive charge of the protein.

Several amidination experiments, using, for example, alcohol dehydrogenase, carbonic anhydrase, trypsin, or lysozime, have demonstrated that retention of the surface charge distribution favors preservation of the tertiary and quaternary structure of proteins, and thus retention of their biological activities (*50*).

By studying the amidination mechanism of proteins, it has been found that the imidic esters lead to the desired amidinated proteins at a pH > 9, while for pH values below 8, the formation of cross-linked products is favored (*51*). At pH values normally used for the modification of proteins, the imidic ester generated a mixture of reaction products. On the contrary, using a thioimidate derivative such as S-methylthioacetimidate (*52*), it has been shown that amidination of a standard protein can be obtained even at pH 6 without any side reaction or cross-linking. At this pH, complete modification of all gelonin accessible lysines can be achieved. It has been suggested that reaction of the imidoester RX−C(R)═NH2$^+$ (X = O or S) with protein amino groups leads to a tetrahedral intermediate. Using imidic esters (X = O)

Table 2. Pharmacokinetic Parameters[a]

	$t_{1/2}^{\alpha}$ (min)	$t_{1/2}^{\beta}$ (min)	MRT (min)	V_{ss} (ml)	Cl (ml h^{-1})
gelonin	2.25 ± 0.22	13.27 ± 1.2	10.16 ± 2	0.129 ± 0.02	0.76 ± 0.12
conjugate with compound **7**	4.40 ± 0.8	70.67 ± 3.5	94.05 ± 8.1	0.308 ± 0.11	0.196 ± 0.2
conjugate with compound **8**	7.58 ± 1.5	273.18 ± 15.2	324.98 ± 32	0.063 ± 0.01	0.0118 ± 0.004
conjugate with SS-20 PEG	43.91 ± 4.7	1489.16 ± 23.9	2073.06 ± 45	0.017 ± 0.013	$4.9\ 10^{-4} \pm 3.5\ 10^{-5}$

[a] Pharmacokinetic parameters (means ± S.D.) of gelonin and conjugates obtained with mPEG of different molecular mass obtained after i.v. administration in mice (n = 3 each). The values were obtained by adopting a two-compartment open pharmacokinetic model.

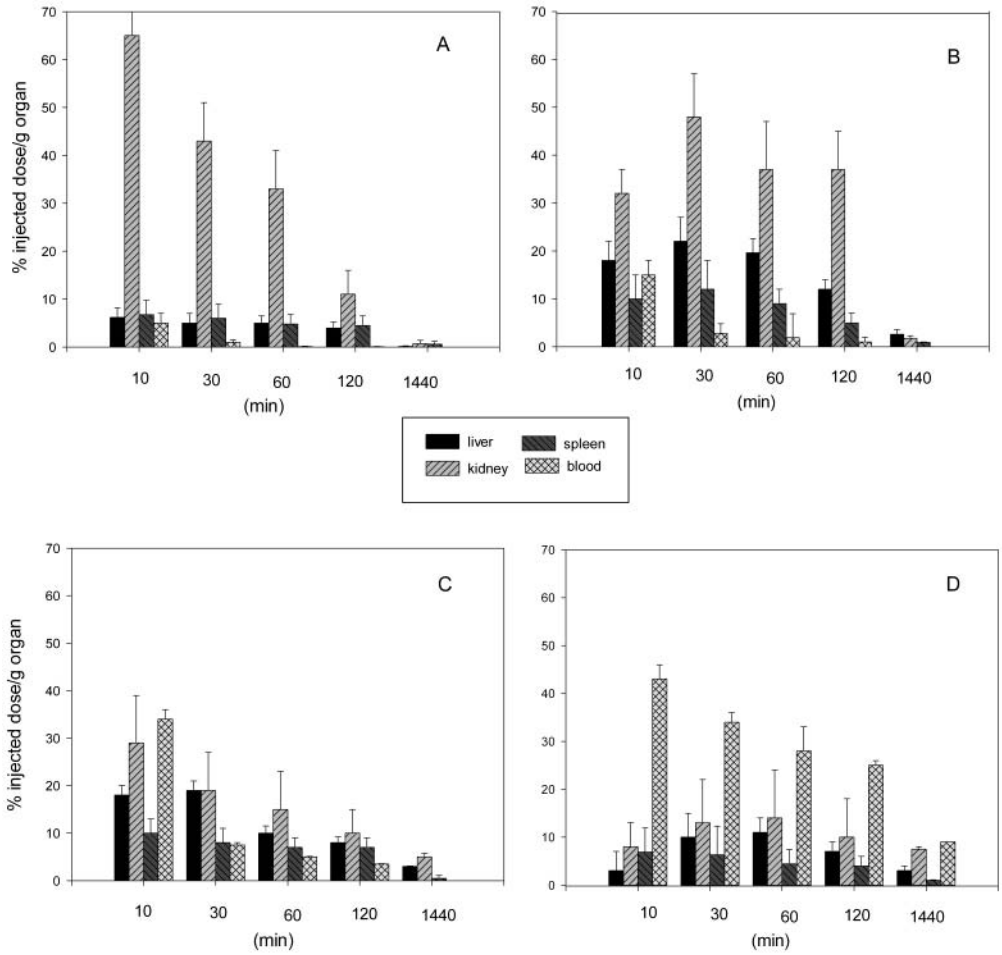


Figure 5. Disposition profiles in elimination organs after intravenous administration in mice: native gelonin (panel A); conjugates with compounds **7**, **8**, and SS-20PEG are shown in panel B, C, and D, respectively. SDs values are reported.

below pH 8, the protonation and elimination of the amino group leading to protein cross-linked derivatives prevails. A better leaving group, such as the thioimidate reagents (X = S), should favor elimination of the alkanethiolated group even at a low pH (pH 7.5−8), preferentially giving the desired amidinate protein (*52*).

Our thioimidate derivatives of mPEG have shown good reactivity at neutral pH, quite similar to that of commercially available mPEG−SS. This was particularly evident for compounds **7** and **8**, which have a hexamethylene spacer group between mPEG and the reactive moiety. The length of this lipophilic and flexible arm is also very important, since the PEG−hexamethylene−thioimidate derivative is much more reactive than the dimethylene ones toward the exposed amino groups of the protein.

Although PEGylation of proteins usually leads to a decrease in the in vitro activity, due to charge or surface modification, in vivo activity can sometimes be enhanced. This is probably due to the increase in blood circulation and thus the increased diffusion in the perfused organs. This behavior is confirmed by the PEGylation of the RIP trichosanthin (*23*). In this case, native RIP and mutants were linked by a thioether linkage on specific cystein groups. In all cases, and both with 5 and with 20 kDa mPEGs, a drastic decrease in enzymatic activity appeared (10−20-fold) with a marked decrease in immunogenicity. In our hands, the N-hydroxysuccinimide derivatives 5 kDa PEG also strongly reduce gelonin activity, and this confirms our and other authors' results (*31*, *53*). Thioimidate reactives, on the contrary, are able to maintain the activity of gelonin at least three times better than N-hydroxysuccinimide reactives.

The results also show that a polymeric chain of high M_r is not suitable because, even at lower derivatization degree, the length of mPEG 20 kDa is sufficient to completely inhibit accessibility to the catalytic site. The hindrance induced by this chain toward specific antiserum is complete in all conditions, and the pharmacokinetics and tissue distribution confirm the longest retention in the blood circulation. The better candidate appears to have a 5 kDa PEG chain that, as reviewed by the authors (*54*), has been extensively used for many proteins of therapeutic interest. A mean of three groups of compound **8** allows significant biological activity to be maintained, reduces immunogenicity to one-half of the initial value, and greatly extends circulatory life (MRT of 5.4 h vs 10 min for gelonin). This value is confirmed by a lower RES organs uptake.

In conclusion, we have shown that novel PEG derivatives are able to increase the behavior of RIPs, maintaining RNA N-glycosidase activity at high levels. This may make gelonin a better therapeutic candidate; in particular, the improvement in immunological properties makes it possible for a panel of toxin/immunotoxin to be administered. This approach has been applied in treating both tumors and HIV, with an evident increase in therapeutic results (*21*, *55*−*57*). In order not to reduce the activity of gelonin with other derivatization steps, conjugation with targeting molecules could utilize the noncovalent interaction, as described by the author elsewhere (*18*).

ACKNOWLEDGMENT

This work was supported by MURST 40−60% (Progetto Nazionale "Tecnologie Farmaceutiche"). We wish to thank Mr. Daniele Zonari for contributing valuable technical assistance to this project.

LITERATURE CITED

(1) Peumans, W. J., Hao, Q., and Van Damme, E. J. M. (2001) Ribosome-inactivating proteins from plants: more than RNA N-glycosidases? *FASEB J. 15*, 1493−1506.

(2) Endo, Y., Mitsui, K., Motizuki, M., and Tsurugi, K. (1987) The mechanism of action of ricin and related toxic lectins on eukaryotic ribosomes. The site and the characteristics of the modification in 28 S ribosomal RNA caused by the toxins. *J. Biol. Chem. 262*, 5908−5912.

(3) Barbieri, L., Valbonesi, P., Bonora, E., Gorini, P., Bolognesi, A., and Stirpe F. (1997) Polynucleotide:adenosine glycosidase activity of ribosome-inactivating proteins: effect on DNA, RNA and poly(A). *Nucleic Acids Res. 25*, 518−522.

(4) Frankel, A. E., Kreitman, R. J., and Sausville E. A. (2000) Targeted toxins. *Clin. Cancer Res. 6*, 326−334.

(5) Kreitman, R. J. (1999) Immunotoxins in cancer therapy. *Curr. Opin. Immunol. 11*, 570−578.

(6) Zarling, J. M., Moran, P. A., Haffar, O., Sias, J., Richman, D. D., Spina, C. A., Myers, D. E., Kuebelbeck, V., Ledbetter, J. A., and Uckun, F. M. (1990) Inhibition of HIV replication by pokeweed antiviral protein targeted to CD4+ cells by monoclonal antibodies. *Nature 347*, 92−95.

(7) Byers, V. S., Levin, A. S., Malvino, A., Waites, L., Robins, R. A., and Baldwin, R. W. (1994) A phase II study of effect of addition of trichosanthin to zidovudine in patients with HIV disease and failing antiretroviral agents. *AIDS Res. Hum. Retrov. 10*, 413−420.

(8) Yeung, H. W., Li, W. W., Feng, Z., Barbieri, L., and Stirpe, F. (1988) Trichosanthin, alpha-momorcharin and beta-momorcharin: identity of abortifacient and ribosome-inactivating proteins. *Int. J. Pept. Protein Res. 31*, 265−268.

(9) Rosenblum, M. G., Shawver, L. K., Marks, J. W., Brink, J., Cheung, L., and Langton-Webster, B. (1999) Recombinant immunotoxins directed against the c-erb-2/HER2/neu oncogene product: in vitro cytotoxicity, pharmacokinetics, and in vivo efficacy studies in xenograft models. *Clin. Cancer Res. 5*, 865−874.

(10) Pagliaro, L. C., Liu, B., Munker, R., Andreeff, M., Freireich, E. J., Scheinberg, D. A., and Rosenblum, M. G. (1998) Humanized M195 monoclonal antibody conjugated to recombinant gelonin: an anti-CD33 immunotoxin with antileukemic activity. *Clin. Cancer Res. 4*, 1971−1976.

(11) Smee, D. F., Sidwell, R. W., and Barnett, B. B. (1996) Combination of antiviral immunotoxin and ganciclovir or cidofovir for the treatment of murine cytomegalovirus infections. *Antivir. Res. 32*, 165−171.

(12) Au, T. K., Collins, R. A., Lam, T. L., Ng, T. B., Fong, W. P., and Wan, D. C. (2000) The plant ribosome inactivating proteins luffin and saporin are potent inhibitors of HIV-1 integrase. *FEBS Lett. 471*, 169−172.

(13) Surolia, N., and Misquith S. (1996) Cell surface receptor directed targeting of toxin to human malaria parasite, Plasmodium falciparum. *FEBS Lett. 396*, 57−61.

(14) Nicolas, E., Beggs, J. M., and Taraschi, T. F. (2000) Gelonin is an unusual DNA glycosylase that removes adenine from single-stranded DNA, normal base pairs and mismatches. *J. Biol. Chem. 275*, 31399−31406.

(15) Nicolas, E., Beggs, J. M., Haltiwanger, B. M., and Taraschi, T. F. (1998) A new class of DNA glycosylase/apurinic/apyrimidinic lyases that act on specific adenines in single-stranded DNA. *J. Biol. Chem. 273*, 17216−17220.

(16) Arpicco, S., Dosio, F., Brusa, P., Crosasso, P., and Cattel, L. (1997) New coupling reagents for the preparation of disulfide cross-linked conjugates with increased stability. *Bioconjugate Chem. 8*, 327−337.

(17) Dosio, F., Brusa, P., Crosasso, P., Fruttero, C., Bolognesi, A., and Cattel, L. (1996) Synthesis of different immunotoxins composed by ribosome inactivating proteins non-covalently bound to monoclonal antibody. *Il Farmaco 51*, 477−482.

(18) Dosio, F., Brusa, P., Delprino, L., Grosa, G., Ceruti, M., and Cattel, L. (1994) A new approach in the synthesis of immunotoxins: ribosome inactivating protein noncovalently bound to monoclonal antibody. *J. Pharm. Sci. 83*, 206−211.

(19) Delprino, L., Giacomotti, M., Dosio, F., Brusa, P., Ceruti, M., Grosa, G., and Cattel, L. (1993) Toxin-targeted design for anticancer therapy. II: Preparation and biological comparison of different chemically linked gelonin-antibody conjugates. *J. Pharm. Sci. 82*, 699−704.

(20) Barbieri, L., Battelli, M. G., and Stirpe, F. (1990) Blood clearance and organ distribution and tissue concentration of native, homopolymerized and IgG-conjugated ribosome-inactivating proteins. *Xenobiotica 20*, 1331−1341.

(21) Lambert, J. M., Blattler, W. A., McIntyre, G. D., Goldmacher, V. S., and Scott, C. F., Jr. (1988) Immunotoxins containing single-chain ribosome-inactivating proteins. *Cancer Treat. Res. 37*, 175−209.

(22) He, X. H., Shaw, P. C., and Tam, S. C. (1999) Site-directed poly(ethylene glycol) modification of trichosanthin: effects on its biological activities, pharmacokinteics, and antigenicity. *Life Sci. 64*, 1163−1175.

(23) He, X. H., Shaw, P. C. and Tam, S. C. (1999) Reducing the immunogenicity and improving the in vivo activity of trichosanthin by site-directed pegylation. *Life Sci. 65*, 355−368.

(24) Reimann, K. A., Turner, S., Lambert, J. M., Reed, M. H., Schlossman, S. F., and Letvin, N. L. (1989) In vivo administration of lymphocyte-specific monoclonal antibodies in nonhuman primates. V. Evidence that humoral immune response to monoclonal antibodies and immunotoxin conjugates abrogates their cytotoxic activity. *Transplantation 48*, 906−912.

(25) Delgrado, C., Francis, G. E., and Fisher, D. (1992) The uses and properties of PEG-linked proteins. *Crit. Rev. Ther. Drug Carrier Syst. 9*, 249−304.

(26) Katre, N. V. (1993) The conjugation of proteins with polyethylene glycol and other polymers: Altering properties of protein to enhance their therapeutic potential. *Adv. Drug Delivery Rev. 10*, 91−114.

(27) Zalipsky, S., and Lee, C. (1992) Use of functionalized polyethylene glycols for modification of polipeptides. *Poly-(Ethylene Glycol) Chemistry: Biotechnical and Biomedical Applications* (J. M. Harris, Ed.) pp 347−370, Plenum Press, New York.

(28) Clark, R., Olson, K., Fuh, G., Marian, M., Mortensen, D., Teshima, G., Chang, S., Chu, H., Mukku, V., Canova-Davis, E., Somers, T., Cronin, M., Winkler, M., and Wells, J. A. (1996) Long-acting growth hormones produced by conjugation with polyethylene glycol. *J. Biol. Chem. 271*, 21969−21977.

(29) Thorpe, P. E., Brown, A. N., Ross, W. C., Cumber, A. J., Detre, S. I., Edwards, D. C., Davies, A. J., and Stirpe, F. (1981) Cytotoxicity acquired by conjugation of an anti-Thy1.1 monoclonal antibody and the ribosome-inactivating protein, gelonin. *Eur. J. Biochem. 116*, 447−454.

(30) Lambert, J. M., Senter, P. D., Yau-Young, A., Blattler, W. A., and Goldmacher, V. S. (1985) Purified immunotoxins that are reactive with human lymphoid cells. Monoclonal antibodies conjugated to the ribosome-inactivating proteins gelonin and the pokeweed antiviral proteins. *J. Biol. Chem. 260*, 12035−12041.

(31) Dosio, F., Brusa, P., Delprino, L., Ceruti, M., Grosa, G., Cattel, L., Bolognesi, A., and Barbieri, L. (1993) A new 'solid phase' procedure to synthesize immunotoxins (antibody-ribosome inactivating protein conjugates). *Il Farmaco 48*, 105−115.

(32) Stirpe, F., Olsnes, S., and Pihl, A. (1980) Gelonin, a new inhibitor of protein synthesis, nontoxic to intact cells. Isolation, characterization, and preparation of cytotoxic complexes with concanavalin A. *J. Biol. Chem. 255*, 6947−6953.

(33) Barbieri, L., Stoppa, C., and Bolognesi, A. (1987) Large-scale chromatographic purification of ribosome-inactivating proteins. *J. Chromatogr. 408*, 235−243.

(34) Roger, R., and Neilson, D. G. (1961) The chemistry of imidates. *Chem. Rev. 61*, 179−211.

(35) Habeeb, A. F. S. A. (1966) Determination of free amino groups in proteins by trinitrobenzenesulfonic acid. *Anal. Biochem. 14*, 328−336.
(36) Allen, E. H., and Schweet, R. S. (1962) Synthesis of hemoglobin in a cell free system. Properties of the complete system. *J. Biol. Chem. 237*, 760−767.
(37) Tazzari, P. L., Zhang, S., Chen, Q., Sforzini, S., Bolognesi, A., Stirpe, F., Xie, H., Moretta, A., and Ferrini, S. (1993) Targeting of saporin to CD25-positive normal and neoplastic lymphocytes by an anti-saporin/anti-CD25 bispecific monoclonal antibody: in vitro evaluation. *Br. J. Cancer 67*, 1248−1253.
(38) Engvall, E., and Perlmann, P. (1971) Enzyme-linked immunosorbent assay, ELISA. Quantitation of specific antibodies by enzyme labeled anti immunoglobulin in antigen-coated tubes. *Immunology 109*, 129−132.
(39) Fraker, P. J., and Speck, J. D. (1978) Protein and cell membrane iodinations with a sparingly soluble chloroamide, 1,2,4,6-tetrachloro-3a,6a-diphenylglycouril. *Biochem. Biophys. Res. Commun. 80*, 849−857.
(40) Fradet, A., and Marechal, E. (1981) Synthesis of monocarboxylic polyoxyethylenes. *Polym. Bull. 4*, 205−210.
(41) Rosenblum, M. G., Kohr, W. A., Beattie, K. L., Beattie, W. G., Marks, W., Toman, P. D., and Cheung, L. (1995) Amino acid sequence analysis, gene construction, cloning, and expression of gelonin, a toxin derived from *Gelonium multiflorum*. *J. Interferon Cytokine Res. 15*, 547−555.
(42) Rosenblum, M. G., Marks, J. W., and Cheung, L. H. (1999) Comparative cytotoxicity and pharmacokinetics of antimelanoma immunotoxins containing either natural or recombinant gelonin. *Cancer Chemoth. Pharm. 44*, 343−348.
(43) Tsutsumi, Y., Onda, M., Nagata, S., Lee, B., Kreitman, R. J., and Pastan, I. (2000) Site-specific chemical modification with polyethylene glycol) of recombinant immunotoxin anti-Tac(Fv)-PE38 (LMB-2) improves antitumor activity and reduces animal toxicity and immunogenicity. *Proc. Natl. Acad. Sci. U.S.A. 97*, 8548−8553.
(44) Bolognesi, A., Polito, L., Tazzari, P. L., Lemoli, R. M., Lubelli, C., Fogli, M., Boon, L., de Boer, M., and Stirpe, F. (2000) In vitro anti-tumour activity of anti-CD80 and anti-CD86 immunotoxins containing type 1 ribosome-inactivating proteins. *Br. J. Haematol. 110*, 351−361.
(45) Selbo, P. K., Sandvig, K., Kirveliene, V., and Berg, K. (2000) Release of gelonin from endosomes and lysosomes to cytosol by photochemical internalization. *Biochim. Biophys. Acta 1475*, 307−313.
(46) Selbo, P. K., Sivam, G., Fodstad, O., Sandvig, K., and Berg, K. (2000) Photochemical internalisation increases the cytotoxic effect of the immunotoxin MOC31-gelonin. *Int. J. Cancer 87*, 853−859.
(47) Delius, M., and Adams, G. (1999) Shock wave permeabilization with ribosome inactivating proteins: a new approach to tumor therapy. *Cancer Res. 59*, 5227−5232.
(48) Zalipsky, S. (1995) Functionalized poly(ethylene glycol) for preparation of biologically relevant conjugates. *Bioconjugate Chem. 6*, 150−165.
(49) Ueno, H., and Fujino, M. (1987) Chemically modified protein and production thereof. Eur. Patent Appl. 0 236 987.
(50) Hunter M. J., and Ludwig M. L. (1972) Amidination. *Methods Enzymol. 54*, 585−597.
(51) Browne, D. T., and Kent, S. B. H. (1975) Formation of nonamidine products in the reaction of primary amine with imido esters. *Biochem. Biophys. Res. Commun. 67*, 126−132.
(52) Thum, M., Hoenes, J., and Pfleiderer, G. (1987) S-Methylthioacetidate is a new reagent for amidination of proteins at low pH. *Biochim. Biophys. Acta 923*, 263−267.
(53) Atkinson, S. F., Bettinger, T., Seymour, L. W., Behr, J. P., and Ward, C. M. (2001) Conjugation of folate via gelonin carbohydrate residues retains ribosomal-inactivating properties of the toxin and permits targeting to folate receptor positive cells. *J. Biol. Chem. 276*, 27930−27935.
(54) Monfardini, C., and Veronese, F. M. (1998) Stabilization of substances in circulation. *Bioconjugate Chem. 9*, 418−450.
(55) Oijen, M. G., and Preijers, F. W. (1998) Rationale for the use of immunotoxins in the treatment of HIV-infected humans. *J. Drug Targeting 5*, 75−91.
(56) Wawrzynczak, E. J., Cumber, A. J., Henry, R. V., May, J., Newell, D. R., Parnell, G. D., Worrell, N. R., and Forrester, J. A. (1990) Pharmacokinetics in the rat of a panel of immunotoxins made with abrin A chain, ricin A chain, gelonin, and momordin. *Cancer Res. 50*, 7519−7526.
(57) Deonarain, M. P., and Epenetos, A. A. (1998) Design, characterization and anti-tumour cytotoxicity of a panel of recombinant, mammalian ribonuclease-based immunotoxins. *Br. J. Cancer 77*, 537−546.

BC015578S

Identification of Two Tamoxifen Target Proteins by Photolabeling with 4-(2-Morpholinoethoxy)benzophenone

Fabienne Mésange,[†] Mohamed Sebbar,[†] Joël Capdevielle,[‡] Jean-Claude Guillemot,[‡] Pascual Ferrara,[‡] Francis Bayard,[†] Marc Poirot,[†] and Jean-Charles Faye*[,†]

INSERM U397 Institut Claudius Regaud 20-24 rue du pont Saint Pierre 31052 Toulouse Cedex, France, and Laboratoire de biochimie des protéines, Sanofi Synthélabo, Labège Innopole, BP 137, 31676 Labège Cedex, France. Received December 3, 2001; Revised Manuscript Received April 9, 2002

Our quest to identify target proteins involved in the activity of tamoxifen led to the design of photoaffinity ligand analogues of tamoxifen able to cross-link such proteins. A new tritiated photoprobe, 4-(2-morpholinoethoxy)benzophenone (MBoPE), was synthesized and used to identify proteins involved in tamoxifen binding in rat liver. MBoPE, which has structural features in common with the potential antagonist of the intracellular histamine receptor (*N*,*N*-diethyl-2-[(4-phenylmethyl)phenoxy]ethanamine HCl: DPPE) is unable to bind the estrogen receptor although it does compete with tamoxifen for an antiestrogen binding site (AEBS). This tritiated benzophenone derivative was obtained by metal-catalyzed halogen−tritium replacement reaction. Because of its high specific activity, four target proteins could be photolabeled, three of which were identified with M_r of 60 000, 49 500, and 14 000, while the fourth at 27 500 was in too low an amount and could not be sequenced. The 49.5 kDa protein corresponded by mass spectrometry to the microsomal epoxide hydrolase already identified with an aryl azide photoprobe [Mesange, F., et al. (1998) *Biochem. J. 334,* 107−112]. The 60 and 14 kDa proteins were identified as the carboxylesterase (ES10) and the liver fatty acid binding protein (L-FABP), respectively. The inhibitory effect of tamoxifen on carboxylesterase activity and the competitive efficacy of oleic acid on [^{3}H]tamoxifen binding suggest that both proteins are AEBS subunits. Moreover, treatment of hepatocytes with antisense mRNA directed against ES10 or L-FABP abolished both tamoxifen and MBoPE binding. On the basis of previous pharmacological arguments, the 27.5 kDa protein might correspond to the sigma I receptor. Altogether, these results confirm that the microsomal epoxide hydrolase is a target for tamoxifen and provide evidence of two new target proteins implicated in cell lipid metabolism.

INTRODUCTION

The antiestrogen tamoxifen has few known noxious side effects and has become the world's second most widely used antitumor drug. It was initially designed as an antagonist of binding of the steroid hormone estradiol to the estrogen receptor (ER). Given the ubiquitous presence of antiestrogen binding sites (AEBS) that specifically bind triphenylethylenic antiestrogens such as tamoxifen with high affinity ($K_D = 10^{-9}$ M), several group (*1*−*5*) have focused attention on the potential existence of a protein or proteins that are different from ER and mediate several of the biological activities of tamoxifen (*6*, *7*). By developing specific AEBS-targeted ligands based on the tamoxifen backbone but without ER affinity, we (*8*, *9*) and others (*5*, *10*) have hypothesized that AEBS mediates estrogen receptor-independent biological activities of tamoxifen. Moreover, the AEBS prototypical ligand DPPE (*N*,*N*-diethyl-2-[(4-phenylmethyl)phenoxy]ethanamine HCl), which was expected to be a specific ligand of a new intracellular histamine receptor (*11*) has been shown to potentiate the chemotherapeutic index of cytotoxic drugs in vitro (*12*, *13*). Clinical trials have shown that DPPE, in association with cyclophosphamide or doxorubicin, is successful in the treatment of metastatic prostate cancer (*14*) and metastatic breast cancer (*15*). Further, this product has been shown, by acting in the liver by an estrogen receptor-independent pathway, to modulate the serum lipids in a manner similar to tamoxifen (*16*) Identification and characterization of the proteins is important to understand the side effects of tamoxifen and to design new drugs. For this reason, our group has worked to identify and purify AEBS using photolabeling strategies (*9*). On the basis of the structure of DPPE described by Brandes (*17*), an azido-photoaffinity tritiated ligand was used to identify microsomal epoxide hydrolase as a component of AEBS (*18*). Because of the low specific activity (2 Ci/mmol) obtained with this ligand, a tritiated photoactivable ligand, 4-(2-morpholinoethoxy)benzophenone, also named morpholino-benzoylphenoxy-ethanamine (MBoPE), was prepared having high specific activity (40 Ci/mmol). This photoactivable aryl ketone (*19*) was chemically more stable than the aryl azide previously used, was activated at 360 nm (with less protein damage), and inserted into unreactive C−H bonds in the presence of water. This tamoxifen-competing ligand could be employed after electrofocusing prepurification. By these techniques, specific photolabeling (competed by either tamoxifen or unlabeled MBoPE) of microsomal epoxide hydrolase was obtained, as previously reported (*18*), as well as the fatty acid binding protein L-FABP and the carboxylesterase ES10.

* To whom correspondence shoud be sent: Jean-Charles Faye, INSERM U397 Institut Claudius Regaud 20-24 rue du pont Saint Pierre 31052 Toulouse Cedex, France. Phone: 33561424646. Fax: 33561424631. E-mail: faye@icr.fnclcc.fr.

[†] INSERM U397 Institut Claudius Regaud.

[‡] Sanofi Synthélabo, Labège Innopole.

10.1021/bc015588t CCC: $22.00 © 2002 American Chemical Society
Published on Web 06/19/2002

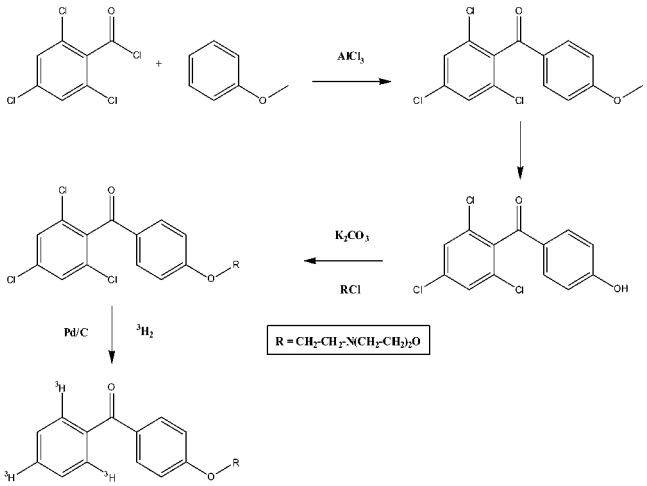


Figure 1. Outline of synthesis of [^{3}H] MBoBPE.

MATERIALS AND METHODS

Chemicals. [^{3}H]-Tamoxifen (specific activity 84 Ci/mmol) was from Amersham, and unlabeled steroids were from Steraloïd. Tamoxifen was a gift from Imperial Chemical Industries. Tris, KCl, sodium azide, glycerol, EDTA, dimethylformamide, and other reagents were obtained from Sigma.

Synthesis of Photosensitive Ligand MBoPE (Figure 1). *Synthesis of 2,4,6-Trichloro- 4′-methoxybenzophenone.* $AlCl_3$ (4 g, 30 mmol) was progressively added to a solution of anisole (2.2 g, 20 mmol) and 2,4,6-trichlorobenzoyl chloride (5 g, 20 mmol) in 50 mL of anhydrous dichloromethane at −80 °C in an inert atmosphere, and the reaction was monitored by TLC. The reaction mixture was gradually brought to ambient temperature and poured into a mixture of crushed ice and 0.1 N HCl (150 mL). The organic layer was collected, washed with water, dried (Na_2SO_4), and concentrated to yield 5.5 g of a white solid (87% yield, mp = 110−111 °C). Mass spectrum (70 eV) *m/e* (relative intensity) 315.6. ^{1}H NMR (100 MHz, DMSO-d_6), δ; 3.83 (s, 3H, OCH_3); 6.87 (d, 2H, arom); 7.26 (d, 2H, arom), 7.59 (d, 2H, arom). Anal. ($C_{14}H_9Cl_3O_2$) C, H, N, Cl.

Synthesis of 4-Hydroxyphenyl 2,4,6-Trichlorophenyl Ketone. One equivalent of 4-methoxyphenyl 2,4,6-trichlorophenyl ketone was heated to melting point at 250 °C with 10 equiv of pyridinium chloride. After 4 h, 30 mL of water were added followed by 30 mL of ether. The ether phase was washed with a 0.1 N solution of HCl, dried over Na_2SO_4, and evaporated. The phenolic product was recrystallized in 2-propanol (yield 70%). Mass spectrum (70 eV) *m/e* (relative intensity) 302.6. ^{1}H NMR (100 MHz, DMSO-d_6) δ; 6.82−7.59 (m, 6H, arom); 12.4 (s, 1H, OH phenolic, exchangeable with ^2H_2O). Anal. ($C_{14}H_9ClO_2$) C, H, N, Cl.

Synthesis of 4-(2-Morpholinoethoxy)phenyl 2,4,6-Trichlorophenyl Ketone. 4-Hydroxyphenyl 2,4,6-trichlorophenyl ketone was added (0.5 g, 1.6 mmol) to a solution of NaOH (200 mg, 4.8 mmol) in 15 mL of water. The mixture was boiled for 1 h. A total of 1.1 equiv of 2-morpholinoethyl chloride was added gradually to the mixture. After the sample was refluxed for 12 h, the reaction mixture was cooled and extracted with 30 mL of diethyl ether. The organic layer was washed with 3 × 10 mL of 0.1 N NaOH, and then with 3 × 10 mL of brine. The organic layer was extracted with 1.5 mL of 6 N HCl. The aqueous layer was evaporated, dried over P_2O_5, and recrystallized from ethanol (75% yield, mp = 110−111 °C). Mass spectrum (70 eV) *m/e* (relative intensity) 415.9. ^{1}H NMR (100 MHz, DMSO-d_6) δ; 3.47 (m, 4H, -N(CH_2-CH_2)$_2$O); 4.01 (m, 4H, -N(CH_2CH_2)$_2$O); 3.65−3.69 (t, 2H, J = 6.8 Hz) Ar−O−CH_2−CH_2−N; 4.40−4.53 (t, 2H, J = 6.05 Hz, Ar−O−CH_2−CH_2−N-); 6.93−6.96 (m, 2H, arom); 6.99−7.05 (m, 2H, arom), 7.23−7.41 (m, 2H, arom). Anal. ($C_{19}H_{19}Cl_4NO_3$) C, H, N, Cl.

Synthesis of 4-(2-Morpholinoethoxy)phenyl 2,4,6-^{3}H Phenyl Ketone. The tritiation was performed at the Commissariat à l'Energie Atomique (Saclay, France) by catalytic tritium exchange with $^3H_2$ over Pd/C (5%) in ethanol. The chemical and radiochemical purity of 4-(2-morpholinoethoxy) phenyl (2,4,6-^{3}H phenyl) ketone ([^{3}H]-MBoPE) was determined by HPLC under the following conditions: isocratic elution on a C18 RP column (254 × 4.6) licrosorb (Bishof, Germany) coupled to UV detection at 220 nm using 60% acetonitrile in ammonium acetate, pH 8. The specific activity of this compound, determined by quantitative HPLC, was 40 Ci/mmol. The mass of an injected sample was determined by comparing the integrated area of the eluted peak with an area calibration curve generated by injecting known weights of unlabeled MBoPE, and the activity of the eluting peak was determined by scintillation counting.

Preparation and Solubilization of Rat Liver Microsomes. Sprague−Dawley rats were ovarectomized by dorsal route at least three weeks before sacrifice by cervical dislocation. Livers were removed and the microsomes prepared and solubilized as previously described (*20*).

Preparation and Solubilization of Microsomes from Cultured Cells. All procedures were performed at 4 °C; 5 × 10^6 cells were pelleted by centrifugation at 1500 rpm for 15 min and washed with PBS. Homogenization was carried out by sonication in TTE buffer pH 7.4 (Tris-HCl 50 mM, EDTA 1.5 mM, thioglycerol 12 mM). The homogenate was centrifuged at 10000*g* for 20 min, and AEBS measurements obtained from the supernatant as previously described (*18*). The protein concentration was determined by the Bradford method (*21*).

Binding Studies. Binding studies were routinely performed with 200 μL aliquots of solubilized material. For the K_I determination, [^{3}H]tamoxifen or [^{3}H]MBoPE were incubated in the presence or absence of various concentrations of unlabeled compounds and in the presence of 1 μM estradiol to block ligand binding to estrogen receptors. After incubation (16 h at 4 °C), the bound and free radioligands were separated on Sephadex LH-20 columns (*20*). No-specific binding was determined in the presence of 1 μM tamoxifen, and its value was corrected according to the method of Rosenthal (*22*). The equilibrium dissociation constant (K_D) was determined with increasing tritiated ligand and calculated with the EBDA Ligand computer program (*23*).

Photoinactivation of the Tamoxifen Binding Capacity. After incubation of the soluble preparation for 18 h at 4 °C with 150 nM MboPE into 800 μL aliquots, the samples were UV-irradiated for various periods of time (8 W) at 365 nm. The residual [^{3}H]tamoxifen binding capacity was measured as described above, after elimination of the noncovalent bound ligand by passage through a Sephadex G25 column (Pharmacia). A control experiment was carried out in the absence of MBoPE to determine the UV induced protein degradation.

Electrofocusing. Solubilized microsomal proteins were subjected to liquid electrofocusing in a Rotofor Cell (Biorad). The 20 mM CHAPS supernatant of the microsomal extraction was mixed with 3 mL of pH 3−10 ampholytes and 2 mL of pH 5−8 ampholytes. Electrofocusing was performed for 6 h at 4 °C with power 12 W,

and the solution of each of 20 compartments was collected. After the pH was measured and adjusted to 7.4 with 100 mM Tris, each fraction was checked for [^{3}H]-tamoxifen and [^{3}H]MBoPE binding.

Photolabeling. The electrofocused fraction pH 6.7 was incubated for 18 h at 4 °C with [^{3}H]MBoPE (150 nM) in the presence or absence of tamoxifen (1 μM). UV irradiation was carried out for 45 min and the photolinked proteins precipitated with 10% TCA. After centrifugation at 12000*g*, the pellet was washed twice with ethanol/ether (v/v: 1/2), dried, and dissolved in electrophoresis sample buffer (50 mM Tris, pH 6.8, 100 mM dithiotreitol, 8% glycerol, 2% SDS). The radioactivity was determined before loading onto a polyacrylamide gel.

SDS−PAGE and Autoradiography. Samples were subjected to electrophoresis as described by Laemmli (*24*). Following protein migration, the gel was either rapidly stained (*25*) and cut in 5-mm slices, which were then crushed and proteolyzed with proteinase k (the radioactivity contained in 10000*g* supernatant was determined), or dried in the presence of Amplify (Amersham) and autoradiographed.

Proteolyses, Peptide Purifications, and Sequences. In-gel trypsinisation of the radioactive bands revealed by the autoradiogram was performed as previously described by Rosenfeld et al. (*25*). The peptides eluted from the polyacrylamide matrix were purified on a Brownlee Labs microgradient system on a C18 Ultrasphere column (250 × 2.1 mm). Elution was performed with a linear gradient of 5 to 70% acetonitrile, 0.1% TFA at a flow rate of 300 μL/min, and the peaks detected at 218 nm were manually collected.

Sequence analysis was performed on a gas-phase sequencer (470A, Applied Biosystems).

ORF Subcloning of Human Liver Fatty Acid Binding Protein. Total RNA from the hepato-carcinoma cell line SKHep-1 was obtained by a rapid guanidinium thiocyanate procedure (*26*). The cDNA encoding for the human L-FABP was acquired by RT-PCR of total RNA using the superscript preamplification system (GIBCO-BRL) with random hexamers for the reverse transcription step. Oligonucleotides with *Eco*RI and *Bam*HI restriction sites, matching the first 15 and last 16 bases of the ORF cDNA encoding the human L-FABP, respectively (*27*), were used for PCR. The amplification product was cloned in the *Eco*RI, *Bam*HI restriction sites of pSG5 vector (*28*) and sequenced by the dideoxy chain-termination technique (*29*).

Rat Liver Carboxylesterase. (ES10) cDNA (*30*) was a generous gift from Dr. M. Robbi (University of Brussels, Belgium). It should be subcloned in the pSG5 vector at the *Eco*RI restriction site.

Overproduction of Human L-FABP and ES10. Plasmids (1 μg) were transiently transfected in COS-7 cells using the DEAE-Dextran methodology, as previously described (*18*). Cells were harvested by scraping 48 h after transfection and sonicated in TTE buffer.

Enzyme ES10 Assays. Carboxylesterase activity was measured colorimetrically at 30 °C, using *p*-nitrophenylacetate as substrate, according to the procedure previously reported by Hosokawa (*31*). Assays were carried out on the solubilized microsomal subfraction of transiently transfected COS-7 cells. Increasing concentrations, up to 10^{-4} M, of tamoxifen were added and the concentration that inhibited 50% of the enzyme activity (IC_{50}) was determined.

Inhibition of Specific Protein Syntheses in SKHep-1 Cells. Inhibition of the synthesis of specific proteins was obtained by using an oligonucleotide antisense strategy

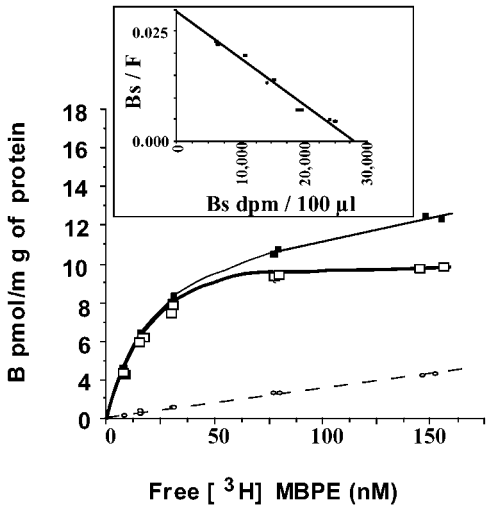


Figure 2. [^{3}H]MBoPE saturation binding curve on solubilized microsomes. Increasing concentrations of [^{3}H]MBoPE were incubated with 100 μL of solubilized microsomes as described in Materials and Methods (■) total binding (◇) unspecific binding in the presence of a 100-fold excess of either MBoPE or Tx (□) specific binding. The graph shown is representative of five independent experiments. The corresponding Scatchard representation of specific binding is shown in the inset.

with 18-mer oligonucleotides matching with the first 5′ translated codons of a protein encoding mRNA (*32*, *33*). The following oligodeoxynucleotides (ODN) were made: 3′-TACTCAAAGAGGCCGTT-5′ and 3′-TGCTACAC CGAGGCAG-5′ for human L-FABP and human carboxylesterase, respectively. Controls were carried out with randomized bases contained in the antisense ODN and with the 5′/3′ base inverted sequence of the antisense ODN.

The transfections of SKHep-1 with oligonucleotides (final concentration = 20 μM) were carried out using the cationic liposome lipofectin system according to the manufacturer's recommendations (Gibco BRL).

RESULTS

Binding Studies and Photoinactivation. As previously reported (*19*), MBoPE is able to compete with [^{3}H]-tamoxifen on AEBS of solubilized microsomes. The inhibitory efficacy of MBoPE on tamoxifen binding (K_I = 1.3 10^{-7} M) was determined by Dixon plots and was, in good agreement with the affinity of [^{3}H]MBoPE (K_D = 1.1 10^{-7} M), calculated from the results in Figure 2, with the EBDA ligand computer program (*23*).

The ability of MBoPE to inactivate photochemically tamoxifen binding was investigated on solubilized microsomes of rat liver as previously described (*9*). After as little as 5 min, MBoPE produces a covalent irreversible linkage to AEBS that inhibits [^{3}H]tamoxifen binding (Figure 3). In the absence of MBoPE, 100% of the tamoxifen binding is conserved for up to 30 min, showing that UV irradiation at 365 nm does not destroy the proteins but activates the photoprobe since only 50% of the sites remained accessible in its presence. The progressive decrease in residual tamoxifen binding indicates that the photolinkage of MBoPE is time dependent, thus enhancing the usefulness of this photoprobe for tamoxifen target labeling.

Purification of the Photolabeled Proteins. Because of its high specific activity, MBoPE has an advantage over the previous azido photoprobe (*9*) in that it can be used in the presence of free ligands to provide a nonspecific estimation and in binding studies after solubilization and

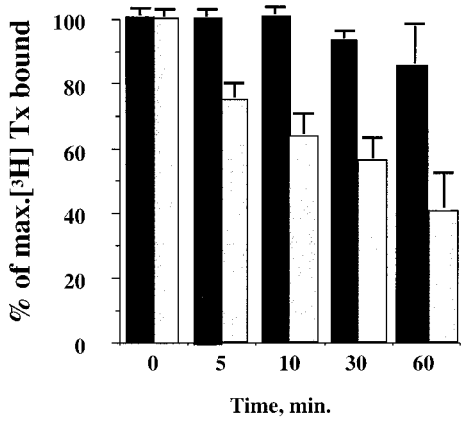


Figure 3. Photoinactivation of solubilized AEBS. Unlabeled MBoPE (500 nM) were incubated with solubilized AEBS extracts and subjected (grey bars) or not (black bars) to UV irradiation for 45 min. The residual [^{3}H]tamoxifen binding was determined after removal of free ligand on a PD10 column.

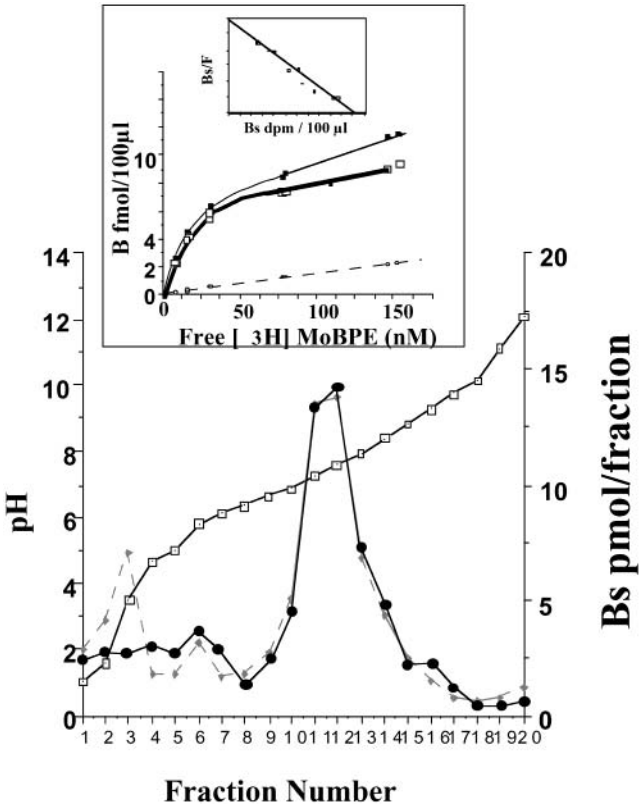


Figure 4. Specific binding studies after iso-electrofocusing. Isoelectrofocusing was performed with a rotofore on solubilized microsomal protein as described in Materials and Methods. Binding was carried out either with (●) [^{3}H]Tx (3 nM) or (♦) [^{3}H]MBoPE (100 nM) in the presence or absence of 1 μM unlabeled Tx. Inset: Scatchard analysis of the fraction 12.

electrofocusing. Similar binding patterns were found for tritiated tamoxifen and MBoPE (Figure 4), and the affinity parameters for tamoxifen and MBoPE (Figure 4; inset) were determined on fraction numbers 3 (pH = 3.2) and 12 (pH = 6.7). We were not able to obtain a saturation curve of binding with fraction 3, although K_D values similar to those observed in the crude extract were found for [^{3}H]Tx ($K_D = 3 \times 10^{-9}$ M) and [^{3}H]MBoPE ($K_D = 1 \times 10^{-7}$ M) with fraction 12 (Figure 4). This result is in good agreement with previous observations (*9*), which gave a pI of about 6.4 for AEBS when photolabeling, with another azido ligand, was carried out before chromatofocusing. The fraction with a pI = 6.7 was therefore used

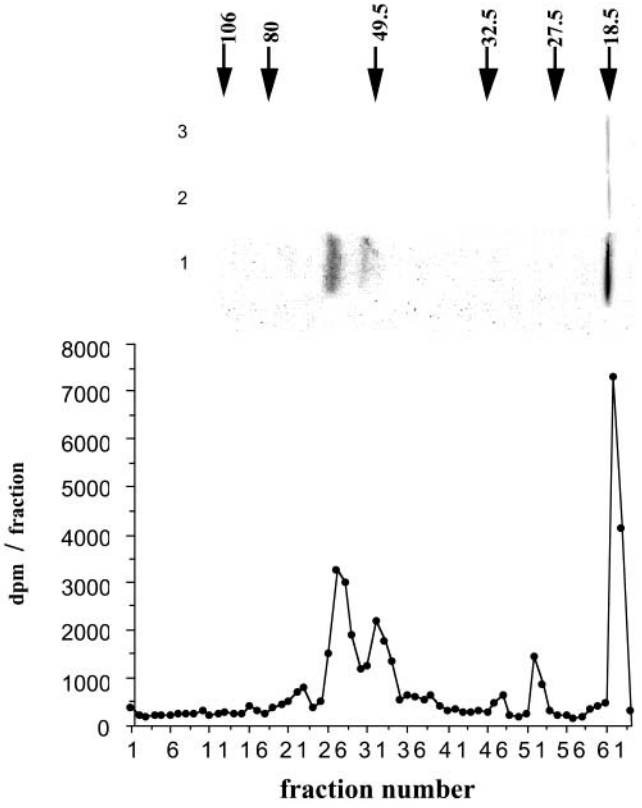


Figure 5. Photolabeling with [^{3}H]MBoPE after electrofocusing. The pH 6.7 fraction was incubated for 18 h at 4 °C with [^{3}H]-MBoPE (100 nM) in the absence (lane 1) or presence of unlabeled (lane 2) 10 μM MBoPE, (lane 3) 1 μM Tx. After UV irradiation at 360 nm, samples were TCA precipitated, solubilized with sample buffer, and subjected to SDS−PAGE on 10% gel. Bottom: specific radioactivity (lane 1 minus lane 3) determined by counting. Upper: the gel was fixed, incubated with Amplify, dried, and exposed for 23 days to the obtained autoradiogram.

for photolabeling and further purification steps. Acid-precipitable proteins were subjected to SDS−PAGE, and photolabeling was evaluated either by autoradiography or counting (Figure 5). Radioactive peaks were extracted and loaded onto polyacrylamide gels of 12 or 18% for bands corresponding to M_r of 60 000 and 49 500, or 14 000, respectively. The proteins were lightly fixed, stained, and directly trypsinized in the gel as described in Materials and Methods and in ref 27. The radioactive peak at M_r 49 500 corresponds, according to mass spectroscopy analyses, to the microsomal epoxide hydrolase previously reported (*18*). Eluted peptides, corresponding to the protein with apparent M_r of 60 000, were simultaneously analyzed by mass spectroscopy and purified by C18 reverse phase column HPLC. Two distinct peptides were sequenced according to the Edman method. The detected amino acid sequences were NLFHR, DAGAPTFMYEFEYR, corresponding to amino acids 220−224 and 418−431 of the rat carboxylesterase (ES-10) identified by Robbi et al. (*30*).

The theoretical molecular masses of these amino acid sequences correspond to two peaks observed in mass spectroscopy. These amino acid series exhibited 100% homology with sequences from the rat carboxylesterase ES 10.

The same experimental procedures were performed for the M_r 14 000 protein and two peptides were sequenced, namely, the MVTTFK and AMGLPEDLIQK amino acid sequences which exhibit 100% homology with sequences 91−96 and 21−31 of the rat liver fatty acid protein (L-

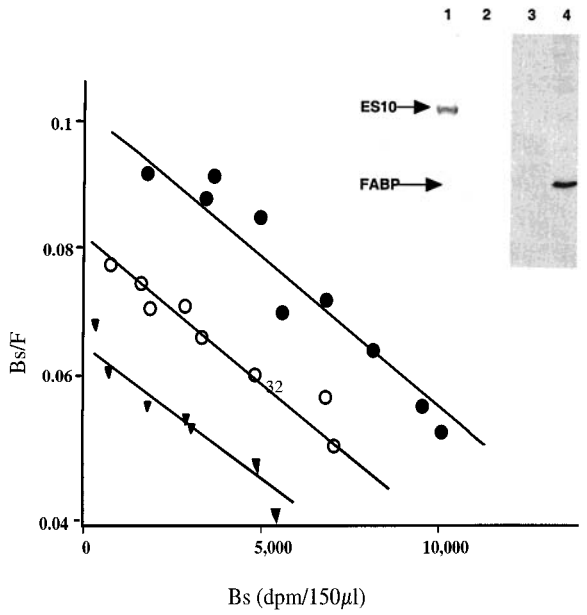


Figure 6. FABP and ES10 overexpressions: [^{3}H]Tx binding analyses of COS-7 transfected cells. FABP and ES10 corresponding cDNA were transiently transfected and microsomal membranes incubated at 4 °C with increasing concentrations of [^{3}H]tamoxifen (0.05−10 nM). (▼) control cells (○) FABP, (●) ES10. The equilibrium dissociation constant (K_D) was calculated with the EBDA Ligand computer program (*24*). Western blot analyses of solubilized microsomes (20 μg of protein loaded) with antibodies directed against ES10 (lanes 1 and 2) or FABP (lanes 3 and 4). Lane 1: transfected cells with ES10 cDNA (5 μg). Lanes 2 and 3 mock transfected cells. Lane 4: transfected cells with liver FABP cDNA (5 μg).

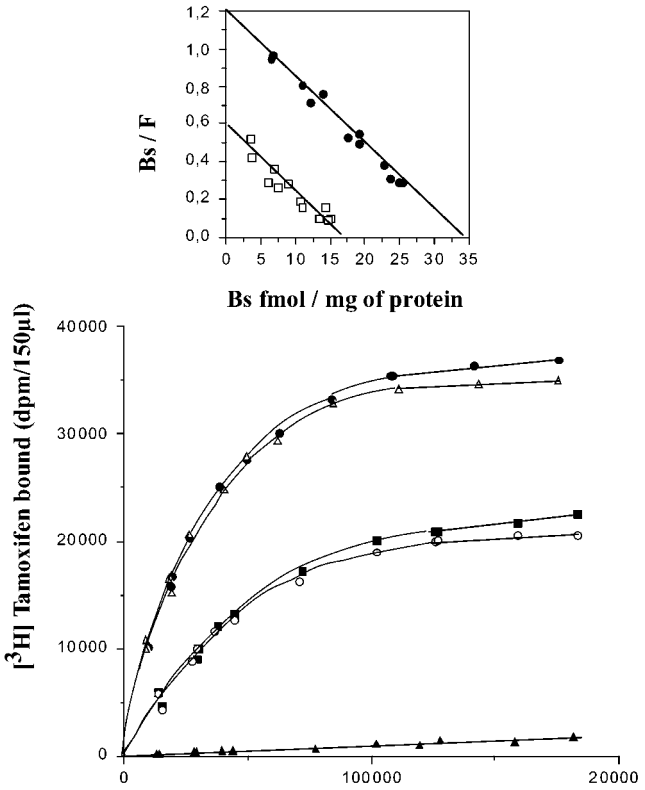


Figure 7. [^{3}H]Tx binding displacement with oleic acid. Competitions were performed on liver microsomal membrane proteins incubated with increasing concentrations of [^{3}H]Tx in the (●) absence and in the (□) presence of oleic acid (30 μM).

FABP), the full-length cDNA of which was isolated by Gordon et al. (*34*).

The radioactive peak seen at 27 500 (Figure 5) could not be further purified. We have previously shown that AEBS ligands exhibit structural similarities with sigma receptor ligands and bind with high affinity to the sigma I receptor (*35*) for which the reported molecular mass in the liver is 28 kDa (*36*).

Protein Overexpression. Binding Studies. To ensure that carboxylesterase and FABP belonged to the AEBS complex, their cDNA open reading frames were subcloned in the pSG5 vector and transiently transfected in COS-7 cells. The specific increase of AEBS was determined by [^{3}H]Tx Scatchard analyses and by binding studies of [^{3}H]-MBoPE at the single concentration of 150×10^{-9} M. As seen in Figure 6, although the protein overexpressions determined by Western blots were increased at least 10-fold, the endogenous proteins were not detected by antibodies under our conditions, and the increase in Tx binding to solubilized microsomes of transfected cells with carboxylesterase overexpression was 1.85-fold, and 1.4-fold in the case of FABP. As shown by Scatchard analysis, the overexpresion of each protein does not change the K_D of tamoxifen binding. Similar increases in binding site numbers were observed with tritiated MBoPE: 2.5−5.9 pmol/mg of protein for carboxylesterase and 2.5−5 pmol/mg of protein for FABP.

Competition for [^{3}H]Tx Binding by the p-Nitrophenylacetate and Oleic Acid Subtrates of Carboxylesterase and FABP, Respectively. Increasing concentrations of [^{3}H]Tx in the presence or absence of *p*-nitrophenylacetate or oleic acid were used to determined the competitive activities of these products. The solubilized microsomal fractions of the respective transfected cells were used as biological supports (rat liver and SKHep1 cells were also used without any modification of the results). Although the carboxylesterase substrate (*p*-nitrophenylacetate) did not compete with tamoxifen up to 10^{-3} M, the oleic acid at 3×10^{-8} M was able to significantly displace tamoxifen. As seen in Figure 7 the B_{max} decreased, whereas the K_D was unchanged by the competitor evidencing a inhibitory effect of the oleic acid on the tamoxifen binding. However, *p*-nitrophenylacetate, at concentrations exceeding 10^{-3} M, induced various problems of solubility (formation of aggregates in the test tube), binding saturability and reproducibility. To ensure that carboxylesterase was a tamoxifen target, its catalytic activity was therefore estimated in the presence of tamoxifen or MBoPE. Tamoxifen and MBoPE were apparently able to inhibit the catalysis of *p*-nitrophenylacetate by carboxylesterase with $IC_{50} = 20 \times 10^{-6}$ and 60×10^{-6} M, respectively.

Inhibition of Protein Expression by Antisense Oligonucleotides. Following our previous studies with the human hepatoma cell line SKHep1 for which the half-life (26 ± 2 h) and concentration of AEBS had previously been estimated (*18*), an antisense oligonucleotides strategy, directed against the corresponding human liver mRNA of the characterized proteins was chosen. Figure 8 shows the Scatchard plots of [^{3}H]Tx binding following various cell treatments. Controls were carried out with the corresponding scrambled and 5′/3′ inverted sequence oligonucleotides at the same concentration (20 μM). Antisense ODNs against L-FABP and ES10 were able to inhibit [^{3}H]Tx binding to a similar extent (50%) without any effect on the K_D, whereas the scrambled and inverted oligonucleotides had no effect, thus demonstrating the specificity of the inhibition. Binding of [^{3}H]-MBoPE at a single concentration (150×10^{-9} M) gave similar inhibition results (data not shown).

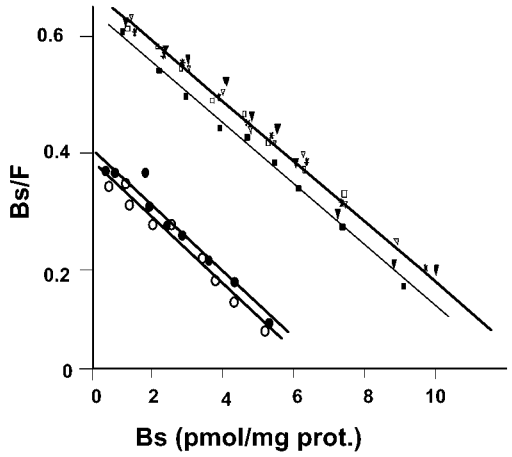


Figure 8. Inhibition of [^{3}H]Tx binding with oligonucleotides. Scatchard analyses of [^{3}H]Tx binding in SKHep-1 cells were carried out as in Figure 6. (▼) Control cells, (○) FABP antisense, (*) FABP scrambled ODN, (□) FABP inverted ODN, (●) ES10 antisense, (■) ES10 scrambled ODN, and (▽) ES10 inverted ODN.

DISCUSSION

Identifying the intracellular target proteins of tamoxifen constitutes an important step in understanding the mechanism of action of this antiestrogen. We have for several years been using a specific photolabeling strategy based on the highest affinity site for tamoxifen binding (AEBS). Microsomal epoxide hydrolase was the first protein shown to be a member of the AEBS (*18*). However, the low specific activity of the previous photoprobe has prevented the determination of other potential protein targets of tamoxifen in the protein complex with molecular mass between 100 and 700 kDa (*6*, *37*, *38*). Using products of the intestinal metabolism of triarylethylene antiestrogen (*39*), we synthesized a new radioactive photoprobe, named MBoPE, with a specific activity 20-fold higher than the former. This photoprobe has, in addition to epoxide hydrolase, led to the determination of two new proteins involved in tamoxifen binding. Although the overexpression of these proteins obtained by transient transfection of their ORF does not substantially increase the maximal binding (B_{max}) of tritiated tamoxifen, their inhibition with the antisense strategy suggests that the liver fatty acid binding protein (L-FABP) and liver carboxylesterase ES10 also belong to the heteropolypeptide AEBS. Moreover, while in both experiments only B_{max} was modified and the affinity (K_D) did not change, a tamoxifen interaction with the same binding site could be observed in each case. L-FAPB is widely expressed in liver, and photolabeling of this protein might be nonspecific. However, L-FABP is a cytosolic protein, and its concentration in the microsomal subcellular fraction is low. The involvement of FABP in AEBS has already been suggested by Hwang (*40*). We show here that the competition of [^{3}H]Tx with oleic acid in binding studies is noncompetitive, which would suggest different binding domains for tamoxifen and fatty acid. Altogether, the results obtained here show that L-FABP is a protein target of tamoxifen. Although its precise function remains unknown, it is assumed to be involved in the uptake, intracellular transport, compartmentalization, and metabolism of fatty acids. It is also involved in peroxisome proliferation and has been described as a specific mediator of the mitogenesis induced by two classes of carcinogenic peroxisome proliferators (*41*).

The microsomal carboxylesterase ES 10 is the second new protein we have shown to be a tamoxifen target. Its catalytic inhibition by tamoxifen and MBoPE accord with its belonging to AEBS. This protein is included in a family of at least four enzyme isoforms. All are glycoproteins of the high-mannose type, which are able to cleave simple aliphatic and aromatic esters (*42*). It has been suggested hat the enzyme might correspond to the activity of acyl coenzyme A cholesterol acyltransferase (ACAT) (*43*). In agreement with this hypothesis, we recently observed that tamoxifen was an inhibitor of ACAT in vitro and in vivo (C. Danthier, unpublished data), and the enzymatic activity of ES10 might require FABP as a cofactor.

Taken together, these data indicate that FABP and ES 10 are possible components of the antiestrogen binding site and suggest that one mode of action of tamoxifen would be to interfere with lipid metabolism in an estrogen receptor-independent mechanism. Moreover, it has recently been reported in yeast that sigma I receptor corresponds to the C7/C8 sterol isomerase implied in tamoxifen binding and activity (*36*, *44*), suggesting that this enzyme would be a part of AEBS. All these results suggest that tamoxifen interacts with a large heteroprotein complex, the molecular mass of which is probably about 700 kDa. Most of the proteins in this complex interfere with cholesterol biosynthesis, since we have shown that they are inhibited by tamoxifen. These results could explain the cholesterol downregulation reported in various experimental and therapeutic treatments (*45*).

ACKNOWLEDGMENT

This work was supported in part by grants from INSERM, ARC, Ligue nationale contre le cancer and Institut Claudius Regaud. (ES10) cDNA and antibodies are from Dr. M. Robbi (University of Brussels, Belgium).

LITERATURE CITED

(1) Faye, J. C., Lasserre, B., and Bayard, F. (1980) Antiestrogen specific, high affinity saturable binding sites in rat uterine cytosol. *Biochem. Biophys. Res. Commun. 93*, 1225−31.

(2) O'Brian, C. A., Liskamp, R. M., Solomon, D. H., and Weinstein, I. B. (1985) Inhibition of protein kinase C by tamoxifen. *Cancer Res. 45*, 2462−5.

(3) Lam, H. Y. (1984) Tamoxifen is a calmodulin antagonist in the activation of cAMP phosphodiesterase. *Biochem. Biophys. Res. Commun. 118*, 27−32.

(4) Sutherland, R. L., Murphy, L. C., San Foo, M., Green, M. D., Whybourne, A. M., and Krozowski, Z. S. (1980) High-affinity anti-oestrogen binding site distinct from the oestrogen receptor. *Nature 288*, 273−5.

(5) Brandes, L. J., and Hermonat, M. W. (1984) A diphenylmethane derivative specific for the antiestrogen binding site found in rat liver microsomes. *Biochem. Biophys. Res. Commun. 123*, 724−8.

(6) Faye, J. C., Jozan, S., Redeuilh, G., Baulieu, E. E., and Bayard, F. (1983) Physicochemical and genetic evidence for specific antiestrogen binding sites. *Proc. Natl. Acad. Sci. U.S.A. 80*, 3158−62.

(7) Sudo, K., Monsma, F. J., Jr., and Katzenellenbogen, B. S. (1983) Antiestrogen-binding sites distinct from the estrogen receptor: subcellular localization, ligand specificity, and distribution in tissues of the rat. *Endocrinology 112*, 425−34.

(8) Faye, J. C., Fargin, A., Valette, A., and Bayard, F. (1987) Antiestrogens, different sites of action than the estrogen receptor? *Horm. Res. 28*, 202−11.

(9) Poirot, M., Chailleux, C., Fargin, A., Bayard, F., and Faye, J. C. (1990) A potent and selective photoaffinity probe for the anti-estrogen binding site of rat liver. *J. Biol. Chem. 265*, 17039−43.

(10) Taylor, F. R., Saucier, S. E., Shown, E. P., Parish, E. J., and Kandutsch, A. A. (1984) Correlation between oxysterol

binding to a cytosolic binding protein and potency in the repression of hydroxymethylglutaryl coenzyme A reductase. *J. Biol. Chem. 259*, 12382−7.

(11) Brandes, L. J., Macdonald, L. M., and Bogdanovic, R. P. (1985) Evidence that the antiestrogen binding site is a histamine or histamine-like receptor. *Biochem. Biophys. Res. Commun. 126*, 905−10.

(12) Brandes, L. J., LaBella, F. S., and Warrington, R. C. (1991) Increased therapeutic index of antineoplastic drugs in combination with intracellular histamine antagonists. *J. Natl. Cancer Inst. 83*, 1329−36.

(13) Jones, J. A., Albright, K. D., Christen, R. D., Howell, S. B., and McClay, E. F. (1997) Synergy between tamoxifen and cisplatin in human melanoma cells is dependent on the presence of antiestrogen-binding sites. *Cancer Res. 57*, 2657−60.

(14) Brandes, L. J., Bracken, S. P., and Ramsey, E. W. (1995) *N*,*N*-Diethyl-2-[4-(phenylmethyl)phenoxy]ethanamine in combination with cyclophosphamide: an active, low-toxicity regimen for metastatic hormonally unresponsive prostate cancer. *J. Clin. Oncol. 13*, 1398−403.

(15) Brandes, L. J., and Bracken, S. P. (1998) The intracellular histamine antagonist, *N*,*N*-diethyl-2-[4-(phenylmethyl)phenoxy] ethamine HCL, may potentiate doxorubicin in the treatment of metastatic breast cancer: Results of a pilot study. *Breast Cancer Res. Treat. 49*, 61−8.

(16) Lazier, C. B., and Breckenridge, W. C. (1990) Comparison of the effects of tamoxifen and of a tamoxifen analogue that does not bind the estrogen receptor on serum lipid profiles in the cockerel. *Biochem. Cell Biol. 68*, 210−7.

(17) Brandes, L. J. (1984) A diphenylmethane derivative selective for the anti-estrogen binding site may help define its biological role. *Biochem. Biophys. Res. Commun. 124*, 244−9.

(18) Mésange, F., Sebbar, M., Kedjouar, B., Capdevielle, J., Guillemot, J. C., Ferrara, P., Bayard, F., Delarue, F., Faye, J. C., and Poirot, M. (1998) Microsomal epoxide hydrolase of rat liver is a subunit of the anti-oestrogen-binding site. *Biochem J. 334*, 107−12.

(19) Delarue, F., Kedjouar, B., Mesange, F., Bayard, F., Faye, J. C., and Poirot, M. (1999) Modifications of benzylphenoxy ethanamine antiestrogen molecules: influence affinity for antiestrogen binding site (AEBS) and cell cytotoxicity. *Biochem. Pharmacol. 57*, 657−61.

(20) Chailleux, C., Poirot, M., Mesange, F., Bayard, F., and Faye, J. C. (1994) Characterization of the membranous antiestrogen binding protein: I. Partial purification of the protein in its active state. *J. Recept. Res. 14*, 23−35.

(21) Bradford, M. M. (1976) A rapid and sensitive method for the quantitation of microgram quantities of protein utilizing the principle of protein-dye binding. *Anal. Biochem. 72*, 248−54.

(22) Rosenthal, R. E. (1967) A graphic method for the determination and presentation of binding parameters in a complexe system. *Anal. Biochem. 20*, 522−532.

(23) McPherson, G. A. (1985) Analysis of radioligand binding experiments. A collection of computer programs for the IBM PC. *J. Pharmacol. Methods 14*, 213−28.

(24) Laemmli, U. K. (1970) Cleavage of structural proteins during the assembly of the head of bacteriophage T4. *Nature 227*, 680−5.

(25) Rosenfeld, J., Capdevielle, J., Guillemot, J. C., and Ferrara, P. (1992) In-gel digestion of proteins for internal sequence analysis after one- or two-dimensional gel electrophoresis. *Anal. Biochem 203*, 173−9.

(26) Chomczynski, P., and Sacchi, N. (1987) Single-step method of RNA isolation by acid guanidinium thiocyanate-phenol-chloroform extraction. *Anal. Biochem 162*, 156−9.

(27) Lowe, J. B., Boguski, M. S., Sweetser, D. A., Elshourbagy, N. A., Taylor, J. M., and Gordon, J. I. (1985) Human liver fatty acid binding protein. Isolation of a full length cDNA and comparative sequence analyses of orthologous and paralogous proteins. *J. Biol. Chem. 260*, 3413−7.

(28) Green, S., Issemann, I., and Sheer, E. (1988) A versatile in vivo and in vitro eukaryotic expression vector for protein engineering. *Nucleic Acids Res. 16*, 369.

(29) Sanger, F., Nicklen, S., and Coulson, A. R. (1977) DNA sequencing with chain-terminating inhibitors. *Proc. Natl. Acad. Sci. U.S.A. 74*, 5463−7.

(30) Robbi, M., Beaufay, H., and Octave, J. N. (1990) Nucleotide sequence of cDNA coding for rat liver pI 6.1 esterase (ES-10), a carboxylesterase located in the lumen of the endoplasmic reticulum. *Biochem. J. 269*, 451−8.

(31) Hosokawa, M., Hirata, K., Nakata, F., Suga, T., and Satoh, T. (1994) Species differences in the induction of hepatic microsomal carboxylesterases caused by dietary exposure to di(2-ethylhexyl)phthalate, a peroxisome proliferator. *Drug Metab. Dispos. 22*, 889−94.

(32) Thierry, A. R., and Dritschilo, A. (1992) Intracellular availability of unmodified, phosphorothioated and liposomally encapsulated oligodeoxynucleotides for antisense activity. *Nucleic Acids Res. 20*, 5691−8.

(33) Erickson, R. P. (1993) The use of antisense approaches to study development. *Dev. Genet. 14*, 251−7.

(34) Gordon, D. A., Shelness, G. S., Nicosia, M., and Williams, D. L. (1988) Estrogen-induced destabilization of yolk precursor protein mRNAs in avian liver. *J. Biol. Chem. 263*, 2625−31.

(35) Kedjouar, B., Daunes, S., Vilner, B. J., Bowen, W. D., Klaebe, A., Faye, J. C., and Poirot, M. (1999) Structural similitudes between cytotoxic antiestrogen-binding site (AEBS) ligands and cytotoxic sigma receptor ligands. Evidence for a relationship between cytotoxicity and affinity for AEBS or sigma-2 receptor but not for sigma-1 receptor. *Biochem. Pharmacol. 58*, 1927−39.

(36) Hanner, M., Moebius, F. F., Flandorfer, A., Knaus, H. G., Striessnig, J., Kempner, E., and Glossmann, H. (1996) Purification, molecular cloning, and expression of the mammalian sigma 1 binding site. *Proc. Natl. Acad. Sci. U.S.A. 93*, 8072−7.

(37) Fargin, A., Faye, J. C., le Maire, M., Bayard, F., Potier, M., and Beauregard, G. (1988) Solubilization of a tamoxifen-binding protein. Assessment of its molecular mass. *Biochem. J. 256*, 229−36.

(38) Matin, A., Hwang, P. L., and Kon, O. L. (1987) Murine antiestrogen-binding protein: characterization, solubilization and modulation by lipids. *Biochim. Biophys. Acta 931*, 364−75.

(39) Ruenitz, P. C., and Bagley, J. R. (1986) Metabolism of nitromiphene (CI 628) in the immature female rat: role of gastrointestinal microflora in the biotransformation of a triarylethylene antiestrogen. *Cancer Res. 46*, 6255−9.

(40) Hwang, P. L. (1990) High-affinity binding sites for oxygenated sterols in rat liver microsomes: possible identity with antiestrogen binding sites. *Biochim. Biophys. Acta 1033*, 154−61.

(41) Khan, S. H., and Sorof, S. (1994) Liver fatty acid-binding protein: specific mediator of the mitogenesis induced by two classes of carcinogenic peroxisome proliferators. *Proc. Natl. Acad. Sci. U.S.A. 91*, 848−52.

(42) Mentlein, R., Suttorp, M., and Heymann, E. (1984) Specificity of purified monoacylglycerol lipase, palmitoyl-CoA hydrolase, palmitoyl-carnitine hydrolase, and nonspecific carboxylesterase from rat liver microsomes. *Arch. Biochem. Biophys. 228*, 230−46.

(43) Becker, A., Bottcher, A., Lackner, K. J., Fehringer, P., Notka, F., Aslanidis, C., and Schmitz, G. (1994) Purification, cloning, and expression of a human enzyme with acyl coenzyme A: cholesterol acyltransferase activity, which is identical to liver carboxylesterase. *Arterioscler. Thromb. 14*, 1346−55.

(44) Labit-Le Bouteiller, C., Jamme, M. F., David, M., Silve, S., Lanau, C., Dhers, C., Picard, C., Rahier, A., Taton, M., Loison, G., Caput, D., Ferrara, P., and Lupker, J. (1998) Antiproliferative effects of SR31747A in animal cell lines are mediated by inhibition of cholesterol biosynthesis at the sterol isomerase step. *Eur. J. Biochem. 256*, 342−9.

(45) Jordan, V. C., and Morrow, M. (1999) Tamoxifen, raloxifene, and the prevention of breast cancer. *Endocr. Rev. 20*, 253−78.

BC015588T

Polyethylene Glycol Conjugates of Methotrexate Varying in Their Molecular Weight from MW 750 to MW 40000: Synthesis, Characterization, and Structure−Activity Relationships in Vitro and in Vivo

Katja Riebeseel,[†,‡] Elfi Biedermann,[§] Roland Löser,[§] Norbert Breiter,[§] Ralf Hanselmann,[‡] Rolf Mülhaupt,[‡] Clemens Unger,[†] and Felix Kratz*[,†]

Tumor Biology Center, Department of Medical Oncology, Clinical Research, Breisacher Strasse 117, 79106 Freiburg, Germany, Institute for Macromolecular Chemistry, Stefan-Meier-Strasse 31, 79104 Freiburg, Germany, and Klinge Pharma - Fujisawa Group, Weihenstephaner Strasse 28, 81673 Munich, Germany. Received December 14, 2001; Revised Manuscript Received February 18, 2002

Poly(ethylene glycol)s (PEGs) are potential drug carriers for improving the therapeutic index of anticancer agents. In this work, the anticancer drug methotrexate (MTX) was activated with *N*,*N*′-dicyclohexylcarbodiimide (DCC) and coupled to amino group bearing PEGs of MW 750, 2000, 5000, 10 000, 20 000, and 40 000. First, the activation process of MTX with DCC in the presence and absence of *N*-hydroxysuccinimide was analyzed through HPLC. Preincubation of methotrexate with DCC alone at 0 °C proved to be favorable with respect to the amount of activated species and the formation of byproducts. MTX−PEG conjugates were synthesized according to this procedure, isolated through size-exclusion chromatography, and characterized through analytical HPLC, MALDI-TOF spectrometry, and gel permeation chromatography. In a cell-free assay, all of the drug polymer conjugates inhibited the target enzyme of MTX, dihydrofolate reductase (DHFR), to a similar extent, but were not as active as free MTX. Additionally, incubation of the MTX−PEG40000 conjugate for 6 days at 37 °C in phosphate buffered saline (pH 7.4), in cell-conditioned medium, or in human serum revealed no significant release of methotrexate. These results, taken together, indicate that release of MTX from polymer conjugates is not necessary for an effective interaction with the active site of dihydrofolate reductase. Evaluation of the in vitro cytotoxicity of the MTX−PEG conjugates in two adherent and three suspension human tumor cell lines revealed that the IC_{50} values of the tested compounds increased with the size of the drug−polymer conjugates. The most effective compound tested in these assays was the free drug MTX itself (IC_{50} value ranging from ∼0.01 to 0.05 μM), while the IC_{50} values of the polymer conjugates were higher (IC_{50} value for MTX−PEG750, 2000 and 5000: ∼0.6−3 μM; for MTX-PEG10000 and 20000: ∼2−7 μM; and for MTX−PEG40000: > 6 μM). Subsequently, MTX−PEG5000, MTX−PEG20000, and MTX−PEG40000 were evaluated in a human mesothelioma MSTO-211H xenograft model, and their antitumor effects were compared with free methotrexate and the albumin conjugate MTX−HSA, a conjugate that is currently in phase II clinical trials. In contrast to the in vitro results, the high molecular weight MTX−PEG conjugates exhibited the highest in vivo antitumor activity: At a dose of 40 and 80 mg/kg MTX−PEG5000 was less active than MTX at its optimal dose of 100 mg/kg; MTX−PEG20000 at a dose of 40 mg/kg showed antitumor efficacy comparable to MTX, but MTX−PEG40000 at a dose of 20 mg/kg was superior to MTX and demonstrated antitumor activity of the same order as MTX−HSA (20 mg/kg).

INTRODUCTION

Methotrexate (MTX), a folic acid antagonist, is a widely used agent for the treatment of certain human cancers (*1*). The drug acts as an inhibitor of dihydrofolate reductase (DHFR), an essential enzyme in the biosynthesis of thymidylate, which is required for DNA replication (*2*).

The efficacy of MTX in anticancer chemotherapy is hampered by its very short plasma half-life. It is administered in relatively high doses, which often leads to drug resistance and causes nonspecific toxicities in normal proliferating cells, limiting the permissible dose of the drug. Adverse side effects may be minimized by targeted delivery of the drug directly to the tumor site. Various attempts have been made to enhance tumor selectivity of MTX by conjugating the anticancer agent to monoclonal antibodies that recognize tumor-associated antigens (*3*−*7*). However, this strategy of "active tumor targeting" is limited by an immune response against the employed murine antibodies as well as the presence of antigens in normal tissue and in the circulation. "Passive targeting" of the tumor can be achieved by coupling antineoplastic drugs to macromolecules because high molecular weight conjugates generally accumulate at the tumor site due to the "enhanced permeability and retention" (EPR) effect (*8*−*11*). Methotrexate has previously

* To whom correspondence should be addressed: Dr. Felix Kratz, Tumor Biology Center, Department of Medical Oncology, Clinical Research, Breisacher Strasse 117, 79106 Freiburg, Germany. Tel: +49−761−2062176; fax: +49−761−2061899; e-mail: felix@tumorbio.uni-freiburg.de.

† Tumor Biology Center.

‡ Institute for Macromolecular Chemistry.

§ Klinge Pharma - Fujisawa Group.

10.1021/bc010098m CCC: $22.00 © 2002 American Chemical Society
Published on Web 05/02/2002

been coupled to the biological polymers fibrinogen (*12*, *13*), gelatin (*14*), and serum albumin (*15*−*17*). The most promising of these compounds is a methotrexate albumin conjugate that exhibits excellent antiproliferative properties in vivo, while its systemic toxicity compared to the free drug is significantly reduced (*18*−*20*). The MTX−HSA conjugate has successfully been evaluated in phase I clinical studies (*21*, *22*) and is currently undergoing phase II clinical trials in Germany.

In recent years, the potential of synthetic macromolecules as carriers of cytotoxic drugs has attracted wide interest (*23*, *24*). Conjugates of various anticancer agents with soluble polymers such as dextrans (*25*), polypeptides (*26*, *27*), and especially with *N*-(2-hydroxypropyl)methacrylamide copolymer (HPMA) (*9*, *28*) and poly(ethylene glycol) (*29*) have been extensively investigated. MTX conjugates with poly(L-lysine) (*30*, *31*), dextran (*32*), or HPMA (*33*) have been synthesized demonstrating in vitro cytotoxicity against human tumor cell lines.

Among synthetic polymers, high molecular weight poly(ethylene glycol) (PEG) plays an outstanding role as a drug carrier. As a water-soluble, biocompatible, nontoxic, and nonimmunogenic material, it exhibits favorable pharmacokinetics and tissue distribution (*34*, *35*). A wide variety of biologically relevant molecules including proteins, enzymes, lipids, and low molecular weight drugs have been coupled to PEG to take advantage of these properties (*36*). PEG conjugates of the anticancer agents paclitaxel, camptothecin (*29*), and doxorubicin (*37*) have been designed to enhance the water-solubility and plasma half-life of the drugs. The camptothecin PEG conjugate Prothecan has recently been evaluated in a phase I clinical trial (*38*).

In this paper, we report on the synthesis, characterization, in vitro and in vivo evaluation of MTX−PEG conjugates ranging in their molecular weight from MW 750 up to MW 40 000.

EXPERIMENTAL SECTION

General. Methotrexate was provided by Klinge-Pharma GmbH, (Munich, FRG); mPEG-NH_2 (MW 750 and 2000) and H_2N-PEG-NH_2 (MW 10 000 and 20 000) were purchased from Rapp-Polymers (Tübingen, FRG); mPEG-NH_2 (MW 5000) was obtained from Shearwater-Polymers (Huntsville, USA); H_2N-PEG-NH_2 (MW 40000) was supplied by Richard B. Greenwald (ENZON Inc., New Jersey, USA); all other chemicals used were at least reagent grade and obtained from Sigma-Aldrich (Deisenhofen, FRG) or Merck (Darmstadt, FRG) and used without further purification. PBS buffer contained 0.004 M sodium phosphate and 0.15 M NaCl and was adjusted to pH 7.4. All the employed buffers were vacuum-filtered through a 0.2 μm membrane (Sartorius, Göttingen, FRG) before use.

Instrumentation. TLC analysis was performed on silica coated plates 60 F_{254} from Merck (Darmstadt, FRG); spots were visualized under UV light (254 and 366 nm). Column chromatography was carried out on silica gel (0.040−0.063 mm) from Merck (Darmstadt, FRG). NMR spectra were obtained on a Bruker ARX 300 (300 MHz) and a Bruker ARC (75.4 MHz) with TMS as internal standard. Mass spectra (ESI) were recorded on a Finnigan MAT 312. Reported M + 1 peaks were the major species in each case. If not otherwise indicated, HPLC analysis was performed on an apparatus consisting of a Kontron 422 pump and a Kontron 535 detector (at 370 nm). For peak integration, KromaSystem 2000 software (version 1.83 by Kontron BioTEK) was used.

Analysis of the Activation Process. Method A. A total of 4.54 mg of MTX (10 μmol) and 11.5 mg of NHS (10 mmol) were dissolved in 225 μL of dry DMF. The reaction was started by adding 200 μL of dry methanol and a solution of 2.06 mg of DCC (10 μmol) in 75 μL of DMF and stirring at room temperature for 18 h. Before HPLC analysis, the white precipitate was removed by centrifugation. **Method B:** 4.54 mg of MTX (10 μmol) were dissolved in 132.5 μL of dry DMF and cooled to 0 °C. The reaction was started by adding an ice-cold solution of 2.27 mg of DCC (11 μmol, 1.1 equiv) in 82.5 μL of DMF and stirring at 0 °C for 18 h. The white precipitate was removed by centrifugation. The supernatant was added to 200 μL of dry methanol or 2-methoxyethylamine, and the solution was stirred for 3 h at room temperature.

The product profiles of the above-described reactions were monitored by analytical HPLC on a Lichrosorb-CN column ([250 × 4], 5 μm, Merck, Darmstadt, FRG) with 30% methanol (v/v) in ammonium phosphate (pH 5.0) and a flow of 1 mL/min. A 50 μL sample of the reaction mixture was centrifuged to remove the white precipitate. The clear yellow supernatant was precipitated with 1 mL of diethyl ether. After centrifugation, the yellow precipitate was washed twice with 1 mL of diethyl ether and dissolved in 500 μL mobile phase.

General Procedure for the Preparative Scale Synthesis of MTX Derivatives. A solution of 454 mg of MTX (1.0 mmol) in 14 mL of dry DMF was kept at 0 °C and added to an ice-cold solution of 227 mg of DCC (1.1 mmol, 1.1 equiv) in 1 mL of dry DMF. After the sample was stirred at 0 °C for 18 h, the white precipitate was removed by centrifugation (4000 rpm, 4 °C, 10 min) and subsequent filtration over celite. The filtrate (∼15 mL) was added to an excess of the respective nucleophile to yield MTX esters or amides.

Synthesis of MTX Methylesters. The filtered solution of activated MTX was added to dry methanol (50 mL, gradient grade) and stirred at room temperature for 3 h. Methanol was removed by rotary evaporation (200 mbar, 40 °C), the crude product was precipitated with diethyl ether and dried in vacuo. Column chromatography on silica gel with 95:5 (v/v) THF/H_2O yielded some mixed fractions and three products: **MTX α-methylester 1** (108 mg); retention time (R_t) on analytical HPLC (Lichrosorb-CN column): 4.2 min, purity >98%; MS (ESI) m/z (M + 1) = 469.3; ^{1}H NMR (DMSO-d_6): δ(ppm) = 1.86−2.09 (m, 2H, β-CH_2), 2.28 (t, 2H, J = 6.4 Hz, γ-CH_2), 3.21 (s, 3H, NCH_3), 3.61 (s, 3H, OCH_3), 4.36 (m, 1H, α-CH), 4.78 (s, 2H, 9-CH_2), 6.61 (bs, 2H, 4-NH_2), 6.82 (d, 2H, J = 8.7 Hz, 3′-H, 5′-H), 7.42 (bs, 1H, 2-NH_2), 7.53 (bs, 1H, 2-NH_2), 7.74 (d, 2H, J = 8.7 Hz, 2′-H, 6′-H), 8.57 (s, 1H, 7-H), 8.70 (d, 1H, J = 6.0 Hz, 8′-NH); ^{13}C NMR (DMSO-d_6): δ(ppm) = 25.96 (C-β), 31.15 (C-γ), 38.97 (C-11), 51.54 (C-α), 52.24 (O-CH_3), 54.71 (C-9), 110.94 (C-3′, C-5′), 120.76 (C-1′), 121.27 (C-4a), 128.81 (C-2′, C-6′), 145.83 (C-6), 149.03 (C-7), 150.85 (C-4′), 155.05 (C-8a), 162.56 (C-4), 162.71 (C-2), 166.18 (C-7′), 171.10 (C-carboxyl), 174.75 (C-carboxyl). **MTX γ-methylester 2** (85 mg); HPLC (Lichrosorb-CN column): R_t = 3.3 min, purity >98%; MS (ESI) m/z (M + 1) = 469.2; ^{1}H NMR (DMSO-d_6): δ (ppm) = 1.86−2.17 (m, 2H, β-CH_2), 2.33−2.42 (m, 2H, γ-CH_2), 3.21 (s, 3H, NCH_3), 3.55 (s, 3H, OCH_3), 4.29 (m, 1H, α-CH), 4.80 (s, 2H, 9-CH_2), 6.63 (bs, 2H, 4-NH_2), 6.83 (d, 2H, J = 8.7 Hz, 3′-H, 5′-H), 7.50 (bs, 1H, 2-NH_2), 7.71 (d, 2H, J = 8.7 Hz, 2′-H, 6′-H; superimposed by one proton of 2-NH_2, bs, 1H), 8.02 (d, 1H, J = 7.5 Hz, 8′-NH), 8.57 (s, 1H, 7-H); ^{13}C NMR (DMSO-d_6): δ (ppm) = 26.71 (C-β), 30.27 (C-γ), 39.28 (C-11), 51.45 (C-α), 52.45 (γ-

OCH_3), 54.93 (C-9), 111.27 (C-3′, C-5′), 121.32 (C-4a), 121.55 (C-1′), 128.91 (C-2′, C-6′), 146.48 (C-6), 149.32 (C-7), 151.06 (C-4′), 155.00 (C-8a), 162.79 (C-4), 162.84 (C-2), 166.34 (C-7′), 173.29 (C-carboxyl), 174.24 (C-carboxyl).

MTX-Dimethylester 3 (12 mg); HPLC (Lichrosorb-CN column): $R_t = 10.2$ min, purity >96%; MS (ESI) m/z (M + 1) = 483.2; ^{1}H NMR (DMSO-d_6): δ (ppm) = 1.90−2.17 (m, 2H, β-CH_2), 2.43 (t, 2H, $J = 7.5$ Hz, γ-CH_2), 3.22 (s, 3H, NCH_3), 3.58 (s, 3H, α-OCH_3), 3.62 (s, 3H, γ-OCH_3), 4.41 (m, 1H, α-CH), 4.79 (s, 2H, 9-CH_2), 6.64 (bs, 2H, 4-NH_2), 6.83 (d, 2H, $J = 8.7$ Hz, 3′-H, 5′-H), 7.45 (bs, 1H, 2-NH_2), 7.73 (d, 2H, $J = 8.7$ Hz, 2′-H, 6′-H; superimposed by one proton of 2-NH_2, bs, 1H), 8.36 (d, 1H, $J = 7.5$ Hz, 8′-NH), 8.58 (s, 1H, 7-H); ^{13}C NMR (DMSO-d_6): δ (ppm) = 25.70 (C-β), 29.87 (C-γ), 39.05 (C-11), 51.25 (C-α), 51.67 (α-OCH_3), 51.73 (γ-OCH_3), 54.75 (C-9), 110.97 (C-3′, C-5′), 120.64 (C-1′), 121.31 (C-4a), 128.87 (C-2′, C-6′), 145.89 (C-6), 149.09 (C-7), 150.94 (C-4′), 155.08 (C-8a), 162.62 (C-4), 162.74 (C-2), 166.33 (C-7′), 172.50 (C-carboxyl), 172.64 (C-carboxyl).

Synthesis of MTX 2-Methoxyethylamides. The filtrate of the activated MTX solution was added to an excess of 2-methoxyethylamine (265 μl, 3 equiv) and stirred at room temperature for 3 h. The crude product was precipitated with diethyl ether from the DMF solution and dried in vacuo. Column chromatography on silica gel with 2:1 (v/v) ethyl acetate/methanol yielded three products: **MTX α-2-methoxyethylamide 4** (115 mg); HPLC (Lichrosorb-CN column): $R_t = 3.6$ min, purity > 98%; MS (ESI) m/z (M + 1) = 512.3; ^{1}H NMR (DMSO-d_6): δ (ppm) = 1.78−1.93 (m, 2H, β-CH_2), 1.98−2.19 (m, 2H, γ-CH_2), 3.18 (s, 3H, OCH_3), 3.20 (s, 3H, NCH_3), 3.22 (m, 2H, C$\underline{H}_2$O), 3.30 (t, 2H, $J = 5.7$ Hz, C$\underline{H}_2$−NH″), 4.17 (m, 1H, α-C$\underline{H}$), 4.77 (s, 2H, 9-CH_2), 6.63 (bs, 2H, 4-NH_2), 6.80 (d, 2H, $J = 8.7$ Hz, 3′−H, 5′−H), 7.43 (bs, 1H, 2-NH_2), 7.73 (bs, 1H, 2-NH_2), 7.78 (d, 2H, $J = 8.7$ Hz, 2′−H, 6′−H), 7.85 (t, 1H, $J = 5.7$ Hz, NH″), 8.55 (s, 1H, 7-H), 9.73 (bs,1H, 8′-NH); ^{13}C NMR (DMSO-d_6): δ (ppm) = 27.72 (C-β), 34.24 (C-γ), 38.14 C$\underline{H}_2$−NH″), 38.94 (C-11), 54.63 (C-α), 54.75 (C-9), 57.80 (O-C$\underline{H}_3$), 70.47 (C$\underline{H}_2$O), 110.98 (C-3′, C-5′), 121.32 (C-4a), 121.65 (C-1′), 128.84 (C-2′, C-6′), 145.90 (C-6), 149.01 (C-7), 150.60 (C-4′), 155.08 (C-8a), 162.59 (C-4), 162.75 (C-2), 165.85 (C-7′), 172.35 (C-carboxyl), 176.80 (C-carboxyl). **MTX γ-2-methoxyethylamide 5** (70 mg); HPLC (Lichrosorb-CN column): $R_t = 2.9$ min, purity >96%; MS (ESI) m/z (M + 1) = 512.4; ^{1}H NMR (DMSO-d_6): δ (ppm) = 1.78−2.19 (m, 2H, β-CH_2, γ-CH_2), 3.18 (s, 3H, OC$\underline{H}_3$), 3.19 (s, 3H, NCH_3), 3.11−3.16 (m, 2H, C$\underline{H}_2$O), 3.27 (t, 2H, $J = 5.7$ Hz, C$\underline{H}_2$−NH″), 3.99 (m, 1H, α-CH), 4.77 (s, 2H, 9-CH_2), 6.65 (bs, 2H, 4-NH_2), 6.83 (d, 2H, $J = 9.0$ Hz, 3′−H, 5′−H), 7,45 (bs, 1H, 2-NH_2), 7.60 (d, 1H, $J = 6.4$ Hz, 8′-NH), 7.63 (d, 2H, $J = 8.7$ Hz, 2′−H, 6′−H), 7.73 (bs, 1H, 2-NH_2), 8.01 (t, 1H, $J = 5.7$ Hz, NH″), 8.57 (s, 1H, 7-H); ^{13}C NMR (DMSO-d_6): δ (ppm) = 25.21 (C-β), 34.24 (C-γ), 38.14 (C$\underline{H}_2$−NH″), 38.94 (C-11), 54.63 (C-α), 54.75 (C-9), 57.80 (O-CH$_3$), 70.54 (C$\underline{H}_2$O), 111.16 (C-3′, C-5′), 121.33 (C-4a), 122.18 (C-1′), 128.10 (C-2′, C-6′), 145.91 (C-6), 149.01 (C-7), 150.57 (C-4′), 155.10 (C-8a), 162.61 (C-4), 162.76 (C-2), 164.80 (C-7′), 172.54 (C-carboxyl), 173.92 (C-carboxyl). **MTX bis-2-methoxyethylamide 6** (10 mg); HPLC (Lichrosorb-CN column): $R_t = 11.2$ min; purity >98%; MS (ESI) m/z (M + 1) = 569.4; ^{1}H NMR (DMSO-d_6): δ (ppm) = 1.74−2.20 (m, 4H, β-CH_2, γ-CH_2), 3.16−3.42 (m, 17H, NCH_3, C$\underline{H}_2$−NH″, C$\underline{H}_2$O, OC$\underline{H}_3$), 4.32 (m, 1H, α-CH), 4.79 (s, 2H, 9-CH_2), 6.62 (bs, 2H, 4-NH_2), 6.81 (d, 2H, $J = 8.7$ Hz, 3′−H, 5′−H), 7.45 (bs, 1H, one proton of 2-NH_2), 7.61−7.78 (m, 4H, 2′−H, 6′−H, one proton of 2-NH_2, NH″), 7.91 (t, 1H, $J = 5.1$ Hz, NH″), 8.04 (d, 1H, $J = 7.9$ Hz, 8′-NH), 8.56 (s, 1H, 7-H); ^{13}C NMR (DMSO-d_6): δ (ppm) = 24.45 (C-β), 27.63 (C-γ), 38.26 (C$\underline{H}_2$−NH″), 38.99 (C-11), 54.77 (C-9), 57.80 (OC$\underline{H}_3$), 70.40 (C$\underline{H}_2$O), 110.89 (C-3′, C-5′), 121.13 (C-1′), 121.31 (C-4a), 128.82 (C-2′, C-6′), 145.96 (C-6), 149.04 (C-7), 150.76 (C-4′), 155.05 (C-8a), 162.59 (C-4), 162.72 (C-2), 165.86 (C-7′), 170.61 (C-carboxyl), 171.87 (C-carboxyl).

Racemization Analysis of MTX Derivatives. The amount of D- and L- enantiomers of the isolated α- and γ-MTX derivatives (methylesters and 2-methoxyethylamides) synthesized according to the described procedure, was determined on the following chiral HPLC system: Nucleodex-β-OH column (Macherey & Nagel, Düren, FRG), mobile phase: 20% (v/v) acetonitrile in aqueous triethanolamine (10 g/L in water) adjusted to pH 7.0 with acetic acid, flow: 1 mL/min.

Preparation and Characterization of the MTX−PEG Conjugates. All conjugates were synthesized using the same procedure. Data for one experiment is described below. The final concentration of the conjugates was between 2 and 5 mM (with respect to MTX) as determined through the absorption at 372 nm with a UV−Vis spectrophotometer U-2000 from Hitachi ($\epsilon_{372} = 7400$ cm^{-1} M^{-1}). The conjugates were stored at −20 °C. The amount of free MTX in the conjugate solutions was < 2% as determined through analytical HPLC at 370 nm on a Nucleogel aqua-OH [40−8] column (300 × 7.7 mm, Macherey & Nagel, Düren, FRG) under isocratic conditions with 1 mL/min PBS buffer as mobile phase.

Synthesis of MTX−PEG40000. A total of 150 mg of MTX (0.33 mmol) and 75 mg of DCC (0.36 mmol; 1.1 equiv) were dissolved in 5.0 mL of DMF. The clear yellow solution was stirred for 18 h at 0 °C. The formed white precipitate was subsequently removed by centrifugation (4000 rpm, 10 min, 4 °C) and filtration over celite. The filtrate was added to 2200 mg of H_2N-PEG40000-NH_2 (0.11 mmol of NH_2 groups) and stirred at room temperature for 3 h. DMF was subsequently removed in high vacuo. The residue was dissolved in 30 mL of PBS buffer and purified through preparative FPLC performed on Sephadex G25 superfine (Pharmacia) with PBS buffer as mobile phase. Peak elutions were monitored at 280 nm using a LKB 8300-UVCORD monitor controlled by FPLC-Detector software (version 1.03, Pharmacia Biotech, Uppsala, Sweden). Concentration of the conjugate to a volume of approximately 25 mL to a final concentration of 5 mM was carried out with CENTRIPREP-10-concentrators from Amicon, FRG (30 min at 4 °C and 4500 rpm).

MALDI-TOF Spectrometry of the Conjugates MTX−PEG750−5000 and the Respective Free PEG Carriers. MALDI-TOF mass spectrometry was performed on a Bruker Reflex II spectrometer operating in the reflection mode at 21.50 kV. As matrix, α-cyano-4-hydroxycinnamic acid (10 mg/mL in methanol) was used. Calibration was performed using a standard of linear PEGs in THF (10 mg/mL). Polymeric samples were dissolved in methanol (5 mg/mL) and added to the matrix solution (1 μL each). After 1 μL of potassium chloride solution (1 mg/mL) was added, the mixture was placed on the stainless steel sample probe and allowed to dry.

Stability of MTX−PEG40000. The stability of MTX−PEG40000 at 37 °C was investigated in different media: (a) phosphate buffered saline (PBS buffer at pH 7.4), (b) cell-conditioned medium, and (c) human serum. The cell-conditioned medium was prepared by growing MCF-7 human breast cancer cells in RPMI 1640 medium (Bio Whittaker, Europe) containing 10% FCS at 37 °C for 48 h. After centrifugation, the supernatant was removed and

stored at −20 °C. A 5 mM stock solution of MTX−PEG40000 in PBS was diluted with the respective medium to a final concentration of 100 μM. The samples were incubated at 37 °C and then analyzed through anion-exchange chromatography on a BioLogic DuoFlow 1082 HPLC apparatus (Biorad Laboratories, Munich, FRG): HR − 5/20 column (Pharmacia Biotech, Uppsala, Sweden) filled with POROS 20 PI weak anion-exchanger (Perseptive Biosystems, Framingham, USA). The injection volume was 1 mL and the flow was 4 mL/min with 10 mM Tris-HCl and increasing NaCl concentration [buffer A: 10 mM Tris HCl (pH 7.5), buffer B: buffer A + 140 mM NaCl; buffer C: buffer A + 1 M NaCl)] according to the following method: 0−1.0 min (buffer A, isocratic); 1.0−7.0 min (linear gradient 100% buffer A to 100% buffer B); 7.0−18.0 min (linear gradient 100% buffer B to 100% buffer C); 18−21 min (buffer C, isocratic); 22−25 min (buffer A, isocratic). Peak elutions were detected at 370 nm with a Bischoff-Lambda1010 detector (Bischoff, Leonberg, FRG). The decrease in the height of the conjugate peak was monitored over 144 h in triplicate.

Cell Free Dihydrofolate Reductase (DHFR) Assay. The assay was adapted for 96 well-plates, and all solutions were freshly prepared. β-NADPH was dissolved in assay buffer (50 mM potassium phosphate, pH 7.5 containing 0.1% BSA) yielding the reaction buffer with a final concentration of 1×10^{-3} M β-NADPH. The bovine enzyme DHFR was dissolved in reaction buffer at a final concentration of 0.018 U/mL. A total of 100 μL of this assay solution containing β-NADPH and DHFR were transferred into each well, and then 13 μL of test compound (or assay buffer in the case of control) were added followed by 10 μL of tetrazolium salt (MTT, stock solution: 5 mg/mL in assay buffer). The enzymatic reaction was started by adding 10 μL of the substrate solution (10^{-2} M dihydrofolic acid in assay buffer). The plate was transferred immediately to the plate reader (Bio-Tek EL340, Deelux, Gödenstorf, FRG) to monitor the initial velocity of the kinetic process.

At room temperature, the increase of the absorption exhibits a plateau over a period of 10 min. This process is characterized by the initial velocity ($V_0 = dp/dt$) of the enzymatic reaction, which can be reduced by various inhibitors of the target enzyme DHFR. For dose−response curves, V_0 was plotted versus the concentration of MTX derivative. All experiments were performed in triplicate. Standard deviation was < 5%.

Cell Lines and Cytotoxic Assays. The leukemic cell lines HL-60 and THP-1 were purchased from the American Type Culture Collection (ATCC Rockville, Maryland, USA). The CCRF−CEM cell line was generously made available by Dr. G. Jansen (University Hospital Vrije Universiteit, Amsterdam, NL). The MCF-7 cell line was kindly provided by Prof. Dietel (Humboldt University Hospital Charité, Berlin, FRG) and the prostate cancer cell line DU-145 was obtained from the Cell Line Service (CLS, Heidelberg, FRG). Cell lines were maintained by weekly passages in their recommended medium supplemented with 10% fetal calf serum, FCS (Life Technologies, Eggenstein-Leopoldshafen, FRG). The leukemic cell lines, growing as suspension cultures, as well as the adherent prostate cancer cell line DU-145 were grown in RPMI 1640 medium, whereas the adherent cancer cell line MCF-7 was maintained in IMEMZO medium. The cytotoxicity experiments were performed in MEM medium. All basal media were supplemented with 10% FCS, 2 mM Glutamax I (Gibco, Paisly, UK), 100 IU/mL penicillin and 100 μg/mL streptomycin. RPMI 1640 and MEM medium were purchased from Sigma (Deisenhofen, FRG) and IMEMZO was obtained from Life Technologies (Eggenstein-Leopoldshafen, FRG). Cells were cultured at 37°C in a humidified atmosphere and gassed continuously with 5% CO_2 in air. All further ingredients were of reagent grade and purchased from Sigma (Deisenhofen, FRG). The WST-1 ready-to-use solution was obtained from Roche Diagnostics (Mannheim, FRG) and the BCA reagent for protein determination was purchased from Pierce, distributed by Bender & Hobein (Munich, FRG).

Adherent Cells. For the cytotoxicity experiments, growth medium was removed, and the cell layer was washed once with 2 mL of trypsin/EDTA solution before adding 1 mL of trypsin solution. After 5 min at 37 °C, cell detachment was almost complete, and the trypsinization process was stopped by adding 5 mL of medium containing 10% FCS. The cell number within the obtained cell suspension was determined by electronic cell volume measurements using a CASY 1 Cell counter + analyzer system, model TTC (Schärfe System, Reutlingen, FRG) equipped with a 60 μm capillary. Finally, cells were seeded at a density of approximately 5000 cells in 200 μL per well in 96-well flat bottom culture dishes (Greiner, Frickenhausen, FRG). The plates were incubated at 37 °C in a humidified atmosphere and gassed continuously with 5% CO_2 in air. After 1 day, when the cells were adherent to the dishes, the cultures were replenished with fresh medium containing the test substances at concentrations between 0.01 and 10 μM. The plates were incubated for the specified period of time (see Table 3) without further medium change. Within each assay, samples were prepared and measured for each concentration in triplicate or quadruplicate.

Protein Determination (BCA Assay). The two reagent solutions, A (bicinchoninic acid) and B (cupric sulfate), were mixed in a ratio of 1:50 directly before use to give the working solution. The medium was removed from the plates, the cells were carefully washed once with phosphate-buffered saline, and then 200 μL of working solution was transferred into each well. After the samples were incubated for 30 min at 37 °C, the absorption at 562 nm was determined. The mean value of each compound-treated group was calculated as a percentage of the control.

Suspension Cells. Suspension cells were grown in their recommended medium supplemented with 10% FCS. For the experiment, cells were centrifuged at 1200 rpm for 5 min at room temperature. The cell pellet was resuspended in growth medium, and the cell number was determined by electronic cell volume measurements using a CASY 1 Cell counter. A total of 100 μL of the cell suspensions were finally seeded at a density of approximately 5000 or 40 000 cells per well in 96-well, flat bottom culture dishes (Greiner, Frickenhausen, FRG). A total of 100 μL medium containing the test substances (final concentration 0.01−1 μM) were added immediately after seeding. The plates were incubated at 37 °C in a humidified atmosphere and gassed continuously with 5% CO_2 in air for the indicated growth period (see Table 3). All samples were prepared and measured in triplicate or quadruplicate for each concentration. Methotrexate was dissolved in 0.9% NaCl to obtain a final stock solution of 10^{-2} M, which was stored at −20 °C. All PEG derivatives of methotrexate were provided as 2 mM solution in PBS buffer (pH 7.4).

Cellular Dehydrogenase Activity (WST-1 Assay). The assay was carried out according to the manufacturer's instructions (Roche Diagnostics GmbH, Mannheim, FRG). Briefly, 20 μL of WST-1 reagent was added to the

cultures (200 μL/well) in the microtiter plates (96-wells) and incubated in a humidified atmosphere containing 5% CO_2 at 37 °C. The amount of formed formazan was quantified after 4 h by measuring the optical density in each well at 450 nm against a background control (absorption of culture medium plus WST-1 ready-to-use solution in the absence of cells) using a microtiter plate reader (Bio-Tek EL340, Deelux, Gödenstorf, FRG). The mean value of each treated group was calculated as percentage of the untreated control group.

Human Tumor Xenografts. For the in vivo testing of the conjugates in comparison with MTX and MTX−HSA, female NMRI nu/nu mice (M&B A/S, Denmark) were used. Mice were held in laminar flow shelves under sterile and standardized environmental conditions (25 ± 1 °C room temperature, 70 ± 3% relative humidity, 12-h light/dark cycle). They received autoclaved food and bedding (Ssniff Granulat S8/15', J. Rettenmaier & Söhne Faserstoffwerke, Ellwangen-Holzmühle, FRG) and acidified drinking water (pH 3.0) ad libitum. All animal experiments were performed under the auspices of the German Animal Protection Law.

The human mesothelioma MSTO-211H cells (Cell Lines Service, Heidelberg, FRG) were cultured in sterile tissue culture flasks with IMEMZO medium, supplemented with 10% FCS at 37 °C in a humidified atmosphere of 5% CO_2. The cells were passaged and expanded in number by trypsinization of cell monolayers, followed by replating an aliquot of cell suspension every 7 days. The culture medium was changed every 3−4 days. Cells in log-phase growth were harvested by trypsinization.

The cell number was determined with a cell counter (Beckmann-Coulter, Krefeld, FRG). The cells were centrifuged for 5 min at 1000 rpm, resuspended in sterile Ca^{2+}-, Mg^{2+}-free PBS-buffer and adjusted to 15 million cells/mL of buffer. Tumor cells were inoculated subcutaneously into the left flank of the animals using an inoculation volume of 0.2 mL. Each of the mice received 3×10^6 cells. In the control group the animals received 0.9% sterile saline solution.

The treatment was started when tumor sizes had reached 20−50 mm^2. Between 6 and 8 mice were treated per dose group. Changes in tumor size and side effects were recorded. The tumor volume was calculated using the formula $(ab^2)/2$ (a = larger diameter of the tumor, b = smaller diameter of the tumor). Antitumor activity was assessed comparing the relative tumor volume of the treated (Tx/To; Tx = tumor volume on any given day, To = initial tumor volume) and the control group (C); the ratio between the mean of the relative tumor volumes of treated and that of control tumors × 100 resulted in T/C values (in %). The experiment was completed when tumor regrowth or severe side effects were observed.

In a first series, the experimental setting consisted of seven groups including one control group. Six animals were allocated to each group. The animals in control group 1 were treated with 0.9% saline solution. The animals in groups 2 and 3 were treated with MTX−PEG5000 a dose of 40 and 80 mg/kg, and in groups 4 and 5 the animals were treated with MTX−PEG20000 at a dose of 20 and 40 mg/kg, respectively. In group 6, the animals received 20 mg/kg of MTX-HSA, in group 7 MTX was administered at a dose of 100 mg/kg. All dosages are expressed in terms of MTX. Because of the high dose volumes in groups 3, 5, and 6, the application volume was split into two injections with an interval of 2 h. The animals in groups 1−5 were treated on day 1, 8, and 15, the animals in groups 6 and 7 were only treated on day 1 and 8 (because of the poor condition of the animals). Tumor size was measured on day 1, 4, 6, 8, 11, 13, 15, 18, and 20. The individual body weight of all animals was determined at study initiation and on day 1, 4, 6, 8, 11, 13, 15, 18, and 20. After a posttreatment observation period of 5 days, all animals were killed by CO_2 asphyxiation (day 20).

In a second series, the experimental setting consisted of five groups including one control group. Eight animals were allocated to each group. The animals in control group 1 were treated with 0.9% saline solution. The animals in groups 2 and 3 were treated with MTX−PEG40000 at doses of 10 and 20 mg/kg. In group 4, the animals received 20 mg/kg MTX−HSA and in group 5 MTX was administered at a dose of 100 mg/kg. Because of the high dose volume in group 4 the application volume of MTX−HSA was split into two injections with an interval of 2 h inbetween. The intravenous treatment was performed on day 1, 8, and 15. Tumor size was measured on day 0, 4, 6, 11, 13, 18, 20, 25, 27, 29, and 32. The individual body weight of all animals was determined at study initiation and on day 1, 4, 6, 8, 11, 13, 15, 18, 20, 22, 25, 27, 29, and 32. After a posttreatment observation period of 16 days the surviving animals in groups 2, 3, 4, and 5 were killed by CO_2 asphyxiation (day 32). The animals in the control group were killed on day 28 due to the size of the tumor.

CHEMISTRY

Activation of the carboxyl groups of methotrexate with *N,N'*-dicyclohexylcarbodiimide (DCC) and *N*-hydroxysuccinimide (NHS) for coupling the drug covalently to amino bearing molecules, such as peptides or proteins, is an established technique (*39*, *40*). Furthermore, the first macromolecular prodrug of methotrexate that has reached the clinic, the MTX−HSA conjugate, is synthesized using this procedure (*41*). The initially formed carbodiimide adducts react directly with *N*-hydroxysuccinimide to yield activated NHS esters that react with nucleophiles, e.g., amines, to stable amide derivatives (see Scheme 1).

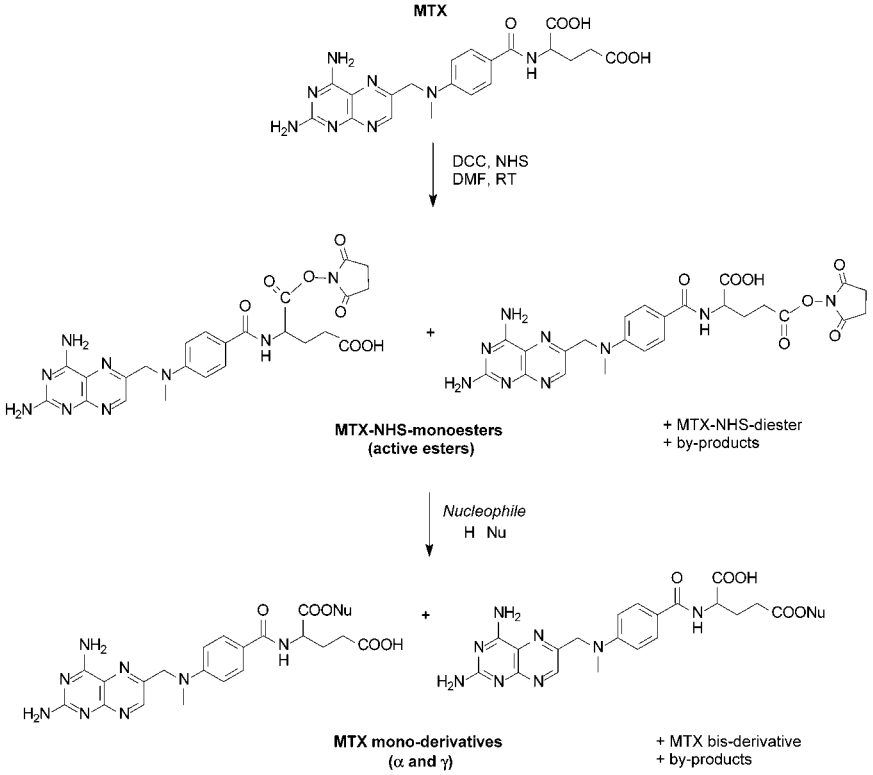
Although frequently used, this active ester method not only yields the desired methotrexate α- and γ-isomers but also bis-derivatives and several byproducts due to rearrangement reactions (e.g., formation of *N*-acylisourea derivatives) (*39*). Especially the activated bis-derivatives of MTX are unfavorable compounds because they can lead to cross-linking of the carrier protein in the subsequent conjugation reaction.

Furthermore, optically pure *N*-benzoyl α-amino acids form oxazolone derivatives after activation of their α-carboxyl group, followed by racemization (*42*). Because the L-glutamic acid moiety in MTX is acylated by a benzoic acid derivative, the drug is postulated to undergo racemization whenever its α-carboxyl group is activated (*39*, *43*) resulting in the formation of the less active D-isomer of MTX (*44*).

Thus, our first goal was to understand the activation process in more detail and subsequently optimize the reaction conditions for obtaining better defined coupling products with macromolecular carriers.

Initially, several attempts were made to isolate the α- and γ- MTX−NHS active esters, but failed due to their high reactivity. In a second approach, methotrexate was reacted in DMF for 18 h at ambient temperature with 1 equiv of DCC and 1 equiv of NHS, and an excess of methanol was added to yield the stable methyl esters in situ. The reaction products were identified using analytical HPLC; reference samples of the MTX α-, γ- and dimethylester were obtained by preparative scale syn-

Scheme 1. Reaction Pathway of the Activation Process of Methotrexate (MTX) with *N,N′*-Dicyclohexylcarbodiimide (DCC) and *N*-Hydroxysuccinimide (NHS) in DMF[a]



[a] Active ester intermediates react immediately with nucleophiles to yield stable α- and γ- monoderivatives of MTX. In addition, the MTX bis-derivative and several byproducts are formed in small amounts.

thesis (as described in the Experimental Section) and characterized by NMR and mass spectrometry.

Not surprisingly, the product profile of this reaction was quite complex (see Figure 1a). Besides a high amount of unreacted MTX (∼55%, values determined through peak integration), we found the monoesters to be the predominant products (∼13% α- and ∼23% γ-derivative). Smaller amounts of MTX dimethylester were produced (∼4%) and also several byproducts (∼5%). At 0 °C, more than 75% MTX remained unchanged, while the amount of dimethylester was not significantly reduced (data not shown). In summary, this reaction cannot be considered to be ideal for a controlled coupling of MTX to macromolecular carriers. The rate of MTX-activation is below 50% and about 9% unfavorable byproducts are produced.

In a next step, the activation procedure was modified according to Kato et al. (*45*), who described a different mechanistic pathway for the reaction of methotrexate with DCC (see Scheme 2). In the absence of NHS and any other nucleophile, the formation of a cyclic anhydride is postulated when MTX is preincubated with DCC in DMF at 0 °C. The activated intermediate can then react with an added nucleophile (e.g., an alcohol or amine) to give stable MTX monoderivatives. MTX was incubated with 1.1 equivalents of DCC in DMF and stirred at 0 °C for 18 h. In contrast to the published procedure (*45*), the addition of tertiary amines (e.g., pyridine or triethylamine) was avoided because no influence of the base on the reaction progress could be detected (data not shown).

The white precipitate (probably *N,N′*-dicyclohexylurea) was removed, and the activated MTX was reacted with an excess of methanol for 3 h at room temperature. HPLC analysis of the crude product is shown in Figure 1b. In this case, only ∼35% of MTX remained unchanged. MTX α-methylester was the main product (∼37%), while ∼26% of the γ-methylester was formed. The amount of diester was reduced to ∼2%, and no other byproducts could be detected.

To reproduce these results, the above experiment was repeated with 2-methoxyethylamine acting as a nucleophilic model compound for methoxy-PEG-amines (mPEG-NH_2). Activated MTX was reacted with 3 equiv of the amine to yield ∼30% unchanged drug, ∼46% α-amide, ∼23% γ-amide, and ∼2% byproduct (see Figure 2).

The extent of racemization of L-MTX during the latter activation process was examined by chiral HPLC of the isolated α- and γ-methylesters as well as the α- and γ-2-methoxyethylamides. For the MTX α-methylester and both amides, we found complete racemization with almost 50% of each isomer, while the γ-methylester showed only approximately 35% D-isomer (chromatograms are shown in the supporting material).

PEG conjugates of L-methotrexate were prepared by coupling the drug to α-methoxy-poly(ethylene glycol)-ω-amine, mPEG-NH_2 (MW 750, 2000, and 5000), or α,ω-bis-amino poly(ethylene glycol) NH_2-PEG-NH_2 (MW 10 000, 20 000, and 40 000) according to the preincubation procedure (Scheme 3). The carboxyl groups of MTX were activated by preincubating MTX with 1.1 equivalents of DCC in dry DMF for 18 h at 0 °C. The activated intermediate (MTX*), presumably the cyclic MTX−anhydride, reacts with nucleophilic amino-PEGs yielding MTX−PEG conjugates that were isolated through preparative size-exclusion chromatography over Sephadex G-25 in phosphate buffered saline (pH 7.4). Analytical size-exclusion HPLC showed that the amount of free MTX in the conjugate solutions was <2%. Representative chromatograms are shown in the Supporting Information.

To obtain information about the loading ratio of the purified MTX−PEG conjugates, MALDI-TOF spectrometry was performed. A comparison of the MALDI-TOF

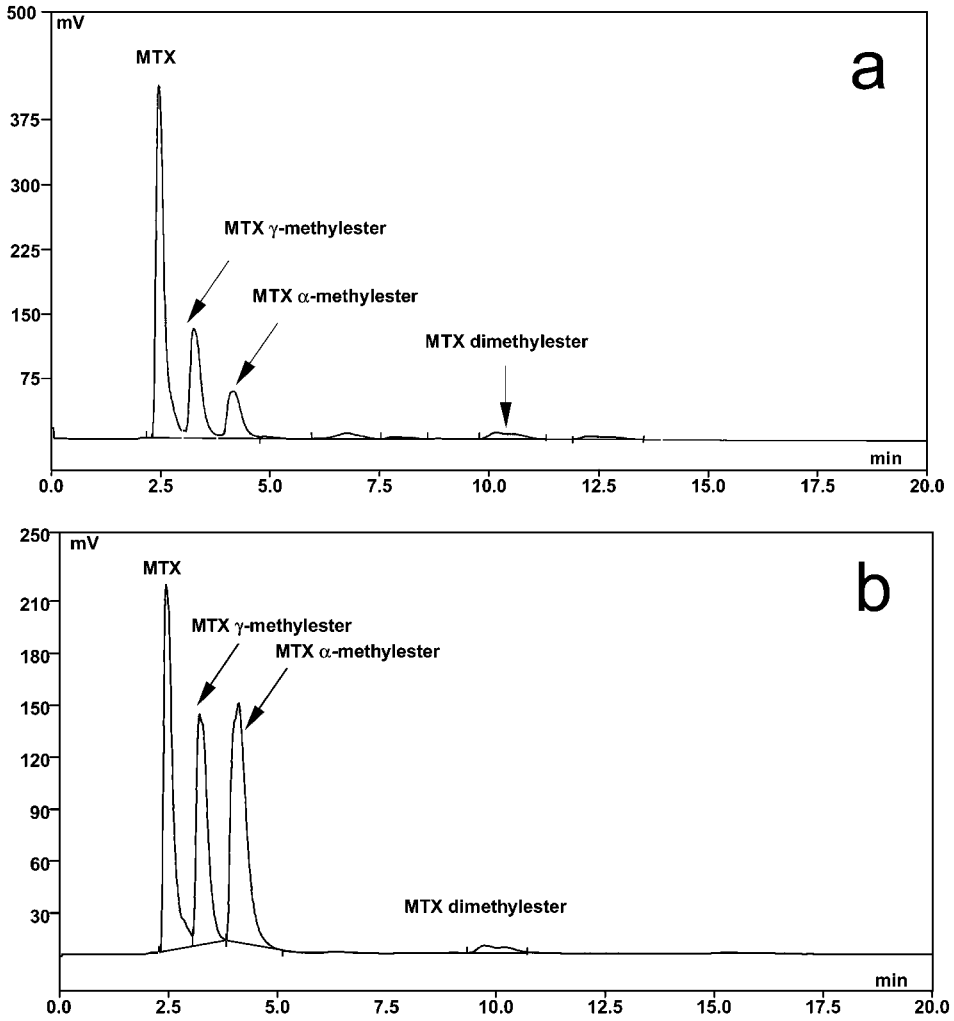


Figure 1. HPLC analysis of the product profile of the reaction of activated methotrexate (MTX) with methanol (Lichrosorb-CN column). (a) MTX reacted with 1 equiv of DCC, 1 equiv of NHS, and an excess of methanol for 18 h at ambient temperature. The crude product contains ~55% unchanged MTX, ~13% α-methylester, ~23% γ-methylester, ~4% dimethylester, and ~5% byproducts. (b) MTX preincubated with 1.1 equiv of DCC for 18 h at 0 °C and then reacted with an excess of methanol for 3 h at ambient temperature. The crude product contains ~35% unchanged MTX, ~37% α-methylester, ~26% γ-methylester, ~2% dimethylester. No byproducts were detected.

spectra of the low molecular weight MTX-PEG conjugates (MW 750−5000) with those of the respective amino-PEG carriers revealed a shift of 436 Da in the single mass peaks, indicating that the polymer conjugates carried exactly one MTX molecule (see mass spectra in the Supporting Information). Additionally, no subdistribution of unreacted PEG was observed in the mass spectra of the MTX−PEG conjugates confirming that the conjugate solutions contained no free amino-PEG. The calculated molecular weight Mw and Mn of the conjugates and the respective free carriers are summarized in Table 1.

Because MALDI-TOF spectrometry was not suitable for determining the mass distribution of modified high-molecular weight PEGs, we examined the high molecular weight conjugates (MTX−PEG10000−40000) through gel permeation chromatography (GPC). Unfortunately, the very polar compounds interacted strongly with the employed size-exclusion column (PLGel, Mixed-B, 5 μm; Polymer Laboratories, Darmstadt, FRG) so that their retention times could not be compared with any reference standards.

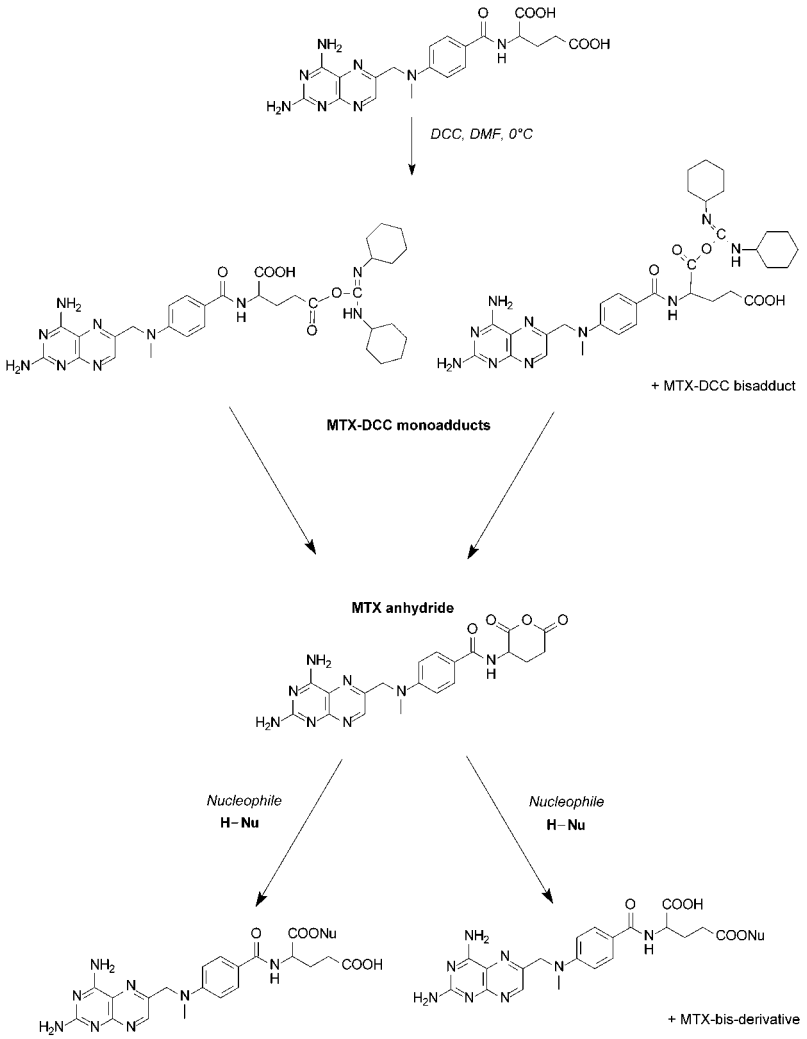
BIOLOGY

Inhibition of Dihydrofolate Reductase, DHFR. The inhibitory effect of MTX, MTX−PEG conjugates, and the respective free PEG carriers on the target enzyme DHFR was evaluated in a cell-free assay, which is based on the reduction of dihydrofolate to tetrahydrofolate by the enzyme DHFR in the presence of NADPH. The formed tetrahydrofolate is utilized simultaneously for the reduction of the tetrazolium salt MTT to formazan. During the reaction, the amount of formazan generated is monitored spectrophotometrically by determining the absorption at $\lambda = 595$ nm using a kinetic plate reader.

As expected, the free drug MTX showed a steep concentration response curve with an IC_{50} value of approximately 2 μM, while none of the amino-PEGs had an influence on enzyme activity (see Figure 3a). In contrast, all of the tested MTX−PEG conjugates inhibited the target enzyme DHFR (IC_{50} values in the range of 4−8 μM). Surprisingly, the molecular weight of the conjugates had no significant influence on the extent of enzyme inhibition (Figure 3b).

In vitro Cytotoxicity of MTX-PEG Conjugates. The in vitro efficacy of the MTX−PEG conjugates was tested in five human tumor cell lines: suspension CCRF−CEM, HL-60, and THP-1 human leukemia cells as well as adherent MCF-7 (human breast cancer) and DU-145 (human prostate cancer) cells. The metabolic activity of the suspension cells was determined using a WST-1

Scheme 2. Reaction Pathway of the Activation Process of MTX with DCC in DMF[a]



[a] The activation product is probably a cyclic MTX-anhydride that reacts with nucleophiles to yield stable α- and γ-monoderivatives of MTX. As a by-product, the MTX bis-derivative was produced in small amounts.

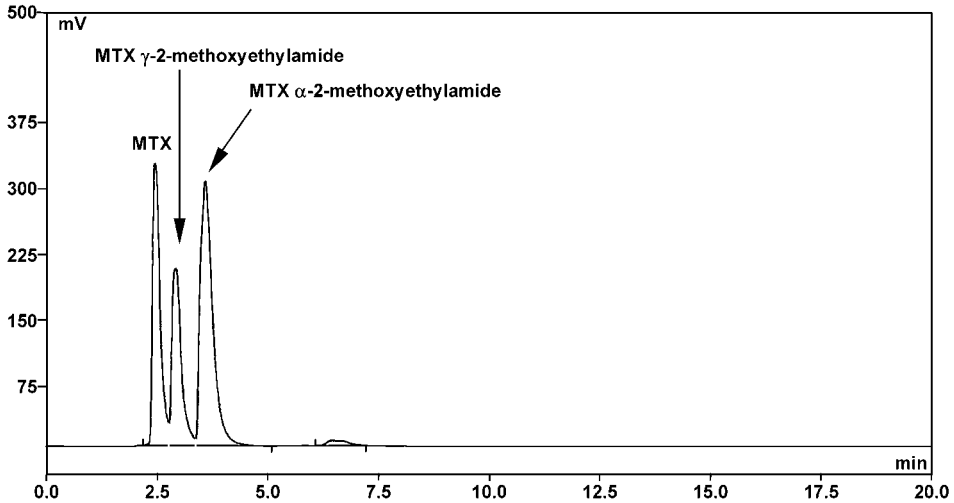
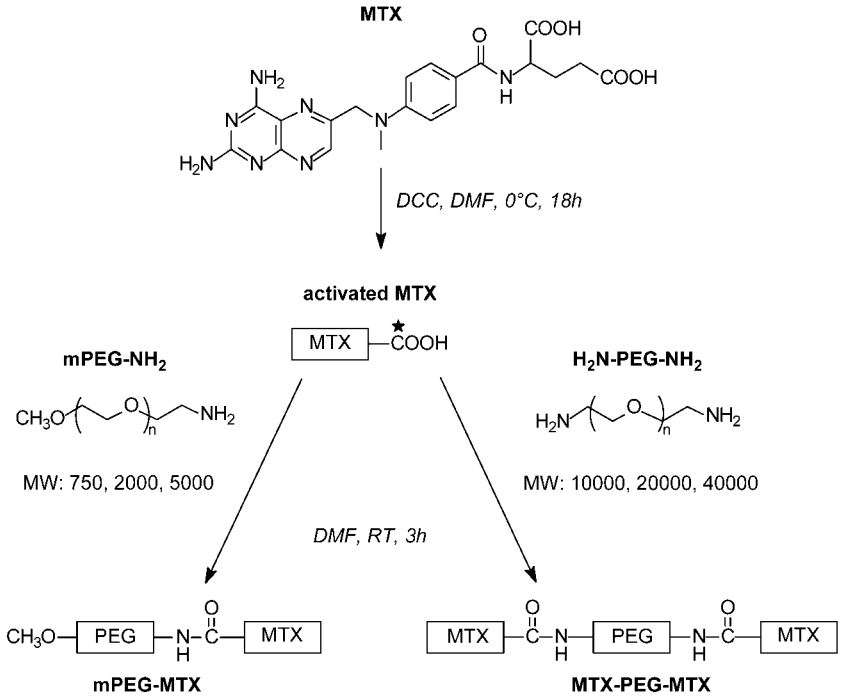


Figure 2. HPLC analysis of the product profile of the reaction of activated methotrexate (MTX) with 2-methoxyethylamine (Lichrosorb-CN column). MTX was preincubated with 1.1 equiv of DCC for 18 h at 0 °C and then reacted with an excess of 2-methoxyethylamine for 3 h at ambient temperature. The crude product contains ∼30% unchanged MTX, ∼46% MTX α-2-methoxyethylamide, ∼23% MTX γ-2-methoxyethylamide, and ∼2% byproduct.

assay, which is a colorimetric assay for the quantification of cell proliferation based on the cleavage and reduction of a water-soluble, stable tetrazolium salt WST-1 to formazan by cellular dehydrogenases. For the adherent cancer cell lines, the commercially available BCA (bicinchoninic acid) assay was performed to determine the total protein content per well as a parameter for overall vitality. This assay is based on the reduction of Cu^{2+} to

Scheme 3. Reaction Pathway for the Synthesis of MTX-PEG Conjugates: the Drug Is Activated with DCC in DMF[a]



[a] In a second step, the activated species reacts with the nucleophilic amino-PEGs to yield MTX−PEG amides.

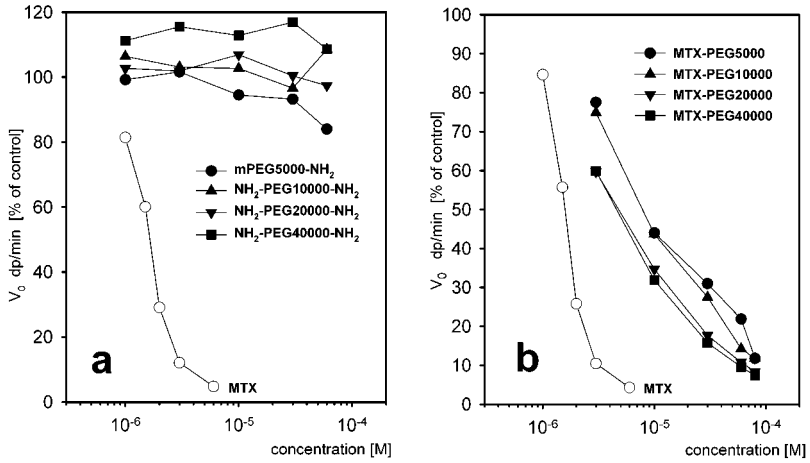


Figure 3. Effect of MTX and MTX−PEG conjugates on isolated dihydrofolate reductase in a cell-free assay. MTX, the unconjugated PEG carriers MW 5000−40000 (a) and the respective MTX-PEG conjugates (b) were tested for their ability to inhibit dihydrofolate reductase (DHFR) in a cell-free assay using 0.0180 U of DHFR per well.

Table 1. Molecular Weight Mw and Mn of Amino-PEG Carriers (MW 750−2000) and the Respective MTX−PEG Conjugates as Determined by MALDI-TOF Spectrometry

compound	Mw	Mn	Mw/Mn
mPEG750-NH_2	991	1024	1.03
mPEG2000-NH_2	2157	2183	1.01
mPEG5000-NH_2	5096	5167	1.01
mPEG750-MTX	1387	1403	1.01
mPEG2000-MTX	2334	2402	1.03
mPEG5000-MTX	5716	5763	1.03

Table 2. Stability of MTX-PEG40000 Conjugate in Various Media at 37°C Determined through Weak Anion-Exchange HPLC[a]

time (days)	PBS buffer (pH 7.4) %	cell-conditioned medium %	human serum %
0	100.0 ± 3.4	100.0 ± 1.2	100.0 ± 2.7
3	95.3 ± 2.6	93.0 ± 4.1	90.8 ± 0.8
6	94.4 ± 1.9	94.3 ± 2.9	91.2 ± 2.4

[a] The decrease of the conjugate peak was monitored in triplicate.

Cu^+ by proteins in an alkaline medium (biuret reaction) and the highly sensitive and selective complexation of Cu^+ by bicinchoninic acid.

The results of the cell culture experiments are summarized in Table 3. The IC_{50} value for the free drug MTX ranged from 0.008 to 0.052 μM in the tested cell lines; cytotoxicity of the MTX-PEG conjugates was dependent on their molecular weight: IC_{50} values of the small conjugates (MW 750−5000) were between 0.5 and 2 μM, while the IC_{50} values for the high-molecular weight compounds (MW > 10000) were in the range of 3−10 μM or higher.

In Vivo Activity of MTX-PEG Conjugates in the MSTO-211H Mesothelioma Model in Nude Mice. In a first series of experiments, the antitumor effect of MTX−PEG5000 (at a dose of 40 and 80 mg/kg) and MTX−PEG20000 (20 and 40 mg/kg) was evaluated in a

Table 3. In Vitro Cytotoxicity of Methotrexate and MTX−PEG Conjugates against Various Human Tumor Cell Lines[a]

	IC_{50} (μM)				
	suspension cell lines			adherent cell lines	
compound	CCRF−CEM[b]	THP-1[b]	HL-60[b]	MCF-7[c]	DU-145[d]
MTX	0.020	0.008	0.010	0.022	0.052
MTX−PEG750	0.57[e]	n.d.	n.d.	n.d.	2.27
MTX−PEG2000	0.64	n.d.	n.d.	n.d.	2.88
MTX−PEG5000	0.69	0.64	0.84	0.93	2.08
MTX−PEG10000	3.01	4.16	2.25	5.24	6.96
MTX−PEG20000	1.95	1.97	2.44	1.85	5.11
MTX−PEG40000	6.83	6.07	7.35	>10[f]	>10[f]

[a] The results obtained with either the WST-1 (suspension cultures) or BCA (adherent cell lines) assay were expressed in concentration−response-curves (CRC) relative to untreated controls (see Supporting Information). To determine the individual sensitivity of each cell line toward MTX or the different MTX conjugates, the IC_{50} value was read from the CRC. The IC_{50} value was defined as the concentration that caused a 50% reduction in cell numbers. [b] Incubation time: 3 days. [c] Incubation time: 7 days. [d] Incubation time: 6 days. [e] Incubation time: 5 days; n.d. = not determined. [f] IC_{50} value not reached.

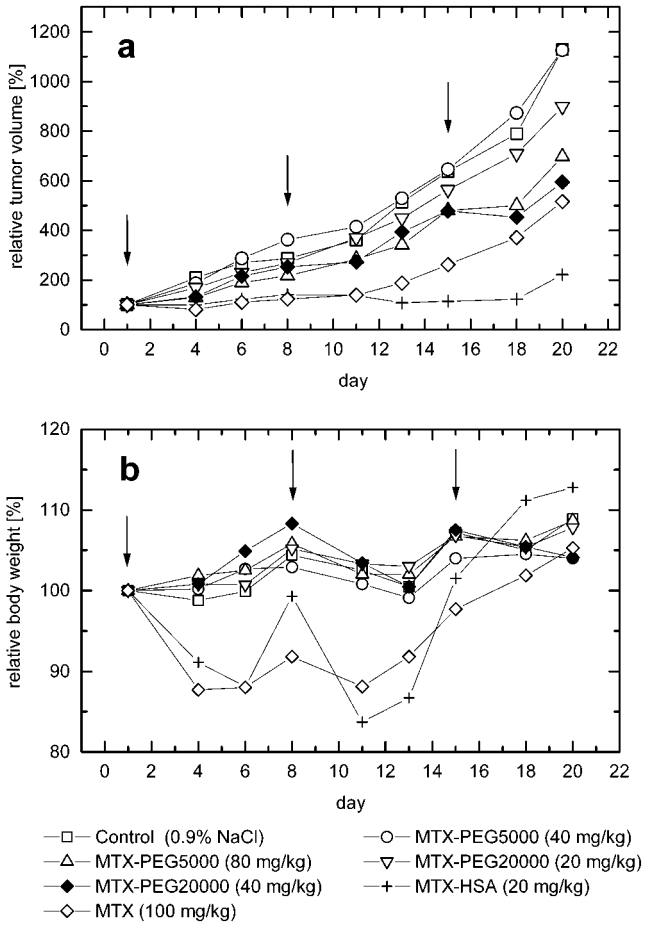


Figure 4. Tumor growth inhibition (a) and body weight loss (b) of subcutaneously inoculated human mesothelioma xenografts (MSTO-211H) in NMRI nu/nu mice treated on day 1, 8, and 15 with MTX, MTX-HSA, MTX-PEG5000, and MTX-PEG20000, respectively. Arrows indicate the days of treatment.

MSTO-211H mesothelioma model in nude mice in comparison to free MTX at the maximum tolerated dose (MTD) of 100 mg/kg and the reference conjugate MTX−HSA (20 mg/kg, MTD). The results of this study are summarized in Figure 4. MTX−PEG5000 exhibited a marginal effect on tumor growth even at a dose of 80 mg/kg. At 40 mg/kg, MTX−PEG20000 showed a tumor growth inhibition similar to free MTX at a dose of 100 mg/kg (MTD), while body weight loss was negligible indicating that the MTD of the MTX−PEG conjugate was not yet reached. A higher dose of MTX−PEG20000 conjugate could not be administered due to the high viscosity of the solution. In this experiment, therapy with MTX−HSA at 20 mg/kg (MTD) showed the highest antitumor effect.

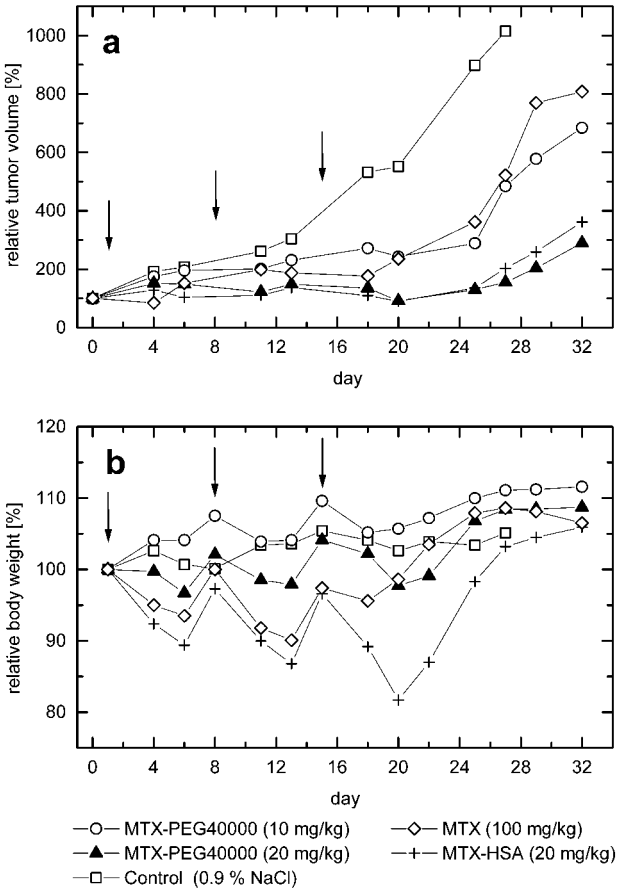


Figure 5. Tumor growth inhibition (a) and body weight loss (b) of subcutaneously inoculated human mesothelioma xenografts (MSTO-211H) in NMRI nu/nu mice treated on day 1, 8, and 15 with MTX, MTX−HSA, and MTX-PEG40000, respectively. Arrows indicate the days of treatment.

In a second series, we evaluated MTX−PEG40000 in the same human tumor xenograft model and compared its activity with MTX and MTX−HSA (Figure 5). Due to the high viscosity of the MTX−PEG40000 solution, the highest administered dose was limited to 20 mg/kg. MTX−PEG40000 at this dose demonstrated a good antitumor effect, which was significantly higher than under therapy with free MTX. Efficacy was comparable to MTX−HSA at its MTD (20 mg/kg), but no significant influence on body weight was observed (Figure 5b), indicating that the conjugate was well tolerated.

DISCUSSION

Methotrexate has frequently been coupled to macromolecular carriers such as antibodies or synthetic polymers by activation of its carboxyl groups using *N*,*N*′-dicyclohexylcarbodiimide (DCC) and/or *N*-hydroxysuccinimide (NHS) (*5*, *40*, *43*). However, the stereochemistry of the activation process and its implication for the composition of the resulting drug conjugates has not been adequately addressed.

A series of experiments revealed that activating MTX with DCC in the absence or presence of NHS followed by reaction with a nucleophile (methanol or 2-methoxyethylamine) produces a mixture of α- and γ-MTX derivatives as the main products with concomitant formation of byproducts such as the diester or diamide derivatives of MTX and probably *N*-acylurea derivatives that are commonly formed when activating carboxylic acids with DCC (*39*). Minimizing the formation of byproducts and maximizing yields is best achieved by preincubating MTX with DCC in the cold and in the absence of NHS and then directly adding the nucleophile.

As shown by chiral HPLC, racemization of the L-glutamate moiety of MTX takes place when activating the carboxyl groups with DCC in accord with the literature (*43*, *46*). Analysis of the isolated model compounds, i.e., the α- and γ-methylester as well as the α- and γ-2-methoxyethylamide derivatives of MTX, showed complete racemization of the MTX α-derivatives and the MTX-γ-amide. The MTX γ-methylester contained only ∼35% of the D-isomer.

Due to the observed stereochemical properties of the MTX model compounds, we can safely predict that the MTX−PEG conjugates, synthesized according to the same activation procedure, are mixtures of α- and γ-isomers and L- and D-enantiomers.

In our in vitro studies, we first examined to what extent the different MTX−PEG were able to inhibit the target enzyme dihydrofolate reductase (DHFR). Interestingly, the MTX−PEG conjugates showed very similar IC_{50} values in the DHFR assay demonstrating that the length of the polymer backbone does not have a significant influence on the inhibition of the target enzyme (see Figure 3). The lower activity of the MTX−PEG conjugates compared with free MTX is probably due to the partial derivatization of the alpha-carboxyl group of MTX; this free carboxyl group has shown to be important for the binding to DHFR. Derivatization at the γ-position is usually well tolerated, while the blocked α-carboxyl group leads to decreased cellular uptake and reduced enzyme inhibition (*47*, *48*). This explanation is supported by our results with α- and γ-methylester in the DHFR assay which show that the γ-methylester is more active than the α-methylester (see Supporting Information).

Although the ability of inhibiting the isolated cellular enzyme, DHFR, is very similar for all the tested MTX−PEG conjugates, cell culture experiments in five human tumor cell lines show a different picture: The molecular weight of the carrier molecule has a significant influence on the cytotoxic activity of the conjugates. Low-molecular weight conjugates (MW ≤ 5000) exhibit an IC_{50} value of around 0.5−3 μM, while conjugates of higher molecular weight are less active in the tested cell lines with IC_{50} values in the range of 2−7 or >10 μM. Free MTX is approximately 20- to 1000-fold more active than the MTX−PEG conjugates (see Table 3).

These differences are likely to be due to different rates of cellular uptake which occurs either by diffusion through the cell membrane, by active transport through the MTX specific amino acid carrier (*49*) or by endocytosis (*50*).

A noteworthy result of our studies was that the MTX−PEG conjugate with the lowest activity in vitro (MTX−PEG40000) was the most active compound in subsequent in vivo experiments in a mesothelioma xenograft model. At a dose of 20 mg/kg MTX−PEG40000 showed superior efficacy compared to free MTX at its optimal dose (100 mg/kg) but similar activity to the methotrexate albumin conjugate MTX−HSA (also at 20 mg/kg, MW of human serum albumin ∼66 500) (see Figure 5). Even at a tenth of the dose (10 mg/kg) compared to the free drug (100 mg/kg), MTX−PEG40000 was as active as MTX in this animal model. In contrast, MTX−PEG conjugates of MW 5000 (at 40 and 80 mg/kg) and MW 20 000 (at 20 and 40 mg/kg) were significantly or slightly less active than free MTX.

These results, taken together, emphasize the importance of the molecular weight of the drug polymer conjugate with respect to in vivo antitumor efficacy. As recently emphasized by Greenwald and coworkers for drug conjugates with PEGs, improved efficacy of the drug conjugates compared to the free drug is observed in vivo once the molecular weight of the PEG backbone exceeds MW 20 000 (*29*). The pathophysiology of tumor tissue, characterized by angiogenesis, hypervasculature, a defective vascular architecture and an impaired lymphatic drainage (known in the literature as enhanced permeability and retention of macromolecules, "EPR-effect") serves as a working model for explaining the targeting potential of macromolecules with MW > 20 000 for solid tumors (*11*).

An open issue regarding the mode of action of MTX polymer conjugates is the cleavability of the amide bond between the glutamate moiety of MTX and the amino group of PEG. Our stability studies show that less than 10% of MTX are released after 6 days when MTX−PEG40000 is incubated at 37 °C in PBS buffer, cell-conditioned medium or human serum indicating that large amounts of MTX are unlikely to be cleaved from the polymer extracellularly. A reasonable assumption is that a lysosomal enzyme, such as γ-glutamyl hydrolase (γ-GH, EC 3.4.19.9), cleaves the amide bond considering that this enzyme efficiently hydrolyzes the γ-glutamyl tail of folate and antifolate polyglutamates (*51*, *52*). Unfortunately, this enzyme is not commercially available to date. It will, however, be important to elucidate the cleavage mechanism of MTX−PEG and MTX−HSA conjugates in future work considering that the level of expression of lysosomal enzymes in solid tumors has a decisive effect on the efficacy of enzymatically cleavable drug polymer conjugates. This has recently been emphasized by Duncan et al.: PK1, a doxorubicin−HPMA copolymer, is stable in the bloodstream but releases doxorubicin through cleavage of a tetrapeptide bond by intracellularly or extracellularly secreted cysteine proteases such as cathepsin B. The in vivo activity of this conjugate is correlated with the amounts of cathepsin B levels found in tumor cells and tumor tissue (*53*).

In summary, the structure−activity relationships elaborated in this study emphasize that in the field of drug polymer conjugates a systematic comparison of in vitro and in vivo data is a critical step for selecting drug candidates for further preclinical assessment.

Supporting Information Available: Chromatograms of chiral HPLC showing the racemization of various MTX compounds (Figure 6); HPLC analysis and MALDI−TOF spectra of MTX−PEG conjugates (Figures 7 and 8); inhibitory effect of MTX compounds on DHFR (Figure 9); and dose−response curves of MTX PEG conjugates in various cells (Figures 10−12). This material is available free of charge via the Internet at http://pubs.acs.org.

LITERATURE CITED

(1) Bertino, J. R. Ode to methotrexate. *J. Clin. Oncol.* **1993**, *11*, 5−14.

(2) Hitchings, G. H., and Smith, S. L. Dihydrofolate reductases as targets for inhibitors. *Adv. Enz. Regul.* **1980**, *18*, 349−371.

(3) Ballantyne, K. D., Perkins, A. C., Pimm, M. V., Garnett, M. C., Clegg, J. A., Armitage, N. C., Baldwin, R. W., and Hardcastle, J. D. Biodistribution of a monoclonal antibody-methotrexate conjugate (791T/36-MTX) in patients with colorectal cancer. *Int. J. Cancer (Suppl. 2).* **1988**, *41*, 103−108.

(4) Kralovec, J. A., Spencer, G., Blair, A. H., Mammen, M., Singh, M., and Ghose, T. I. Synthesis of methotrexate-antibody conjugates by regiospecific coupling and assessment of drug and antitumor activities. *J. Med. Chem.* **1989**, *32*, 2426−2431.

(5) Kralovec, J. A., Singh, M., Mammen, M., Blair, A. H., and Ghose, T. I. Synthesis of site-specific methotrexate IgG conjugates. Comparison of stability and antitumor activity with active-ester-based conjugates. *Cancer Immunol. Immunother.* **1989**, *29*, 293−302.

(6) Elias, D. J., Hirshowitz, L., Kline, L. E., Kroener, J. F., Dillman, R. O., Walker, L. E., Robb, J. A., and Timms, R. M. Phase I clinical comparative study of monoclonal antibody KS1/4 and KS1/4-methotrexate immunoconjugate in patients with nonsmall cell lung carcinoma. *Cancer Res.* **1990**, *50*, 4154−4159.

(7) Elias, D. J., Kline, L. E., Robbins, B. A., Johnson, H. C. L., Pekny, K., Benz, M., Robb, J. A., Walker, L. E., Kosty, M., and Dillman, R. O. Monoclonal antibody KS1/4-methotrexate immunoconjugate studies in nonsmall cell lung carcinoma. *Am. J. Resp. Crit. Care Med.* **1994**, *150*, 1114−1122.

(8) Maeda, H., Seymour, L. W., and Miyamoto, Y. Conjugates of anticancer agents and polymers: advantages of macromolecular therapeutics in vivo. *Bioconjugate Chem.* **1992**, *3*, 351−362.

(9) Seymour, L. W., Miyamoto, Y., Maeda, H., Brereton, B. M., Strohalm, J., Ulbrich, K., and Duncan, R. Influence of molecular weight on passive tumor accumulation of a soluble macromolecular drug carrier. *Eur. J. Cancer.* **1995**, *31A*, 766−770.

(10) Takakura, Y., and Hashida, M. Macromolecular drug carrier systems in cancer chemotherapy: Macromolecular prodrugs. *Crit. Rev. Oncol. Hematol.* **1995**, *18*, 207−231.

(11) Maeda, H., Wu, J., Sawa, T., Matsumura, Y., and Hori, K. Tumor vascular permeability and the EPR effect in macromolecular therapeutics: A review. *J. Controlled Release* **2000**, *65*, 271−284.

(12) Dyr, J. E., Slavic, K., and Vodrazka, Z. Chemical binding of folic acid and methotrexate to bovine fibrinogen. *Thrombosis Res.* **1983**, *31*, 737−746.

(13) Boratynski, J., Opolski, A., Wietrzyk, J., Gorski, A., and Radzikowski, C. Cytotoxic and antitumor effect of fibrinogen-methotrexate conjugate. *Cancer Lett.* **2000**, *148*, 189−195.

(14) Kosasih, A., Bowman, B. J., Wigent, R. J., and Ofner, C. M., III. Characterization and in vitro release of methotrexate from gelatin/methotrexate conjugates formed using different preparation variables. *Int. J. Pharm.* **2000**, *204*, 81−89.

(15) Bures, L., Bostik, J., Motycka, K., Spundova, M., and Rehak, L. The use of protein as a carrier of methotrexate for experimental cancer chemotherapy. III. Human serum albumin-methotrexate derivative, its preparation and basic testing. *Neoplasma* **1988**, *35*, 329−342.

(16) Kim, C.-K., and Hwang, S. J. Pharmacokinetics and organ-distribution of 3H-methotrexate and 3H-methotrexate-human serum albumin conjugates in mice. *Drug Dev. Ind. Pharm.* **1993**, *19*, 961−970.

(17) Stehle, G., Sinn, H., Wunder, A., Schrenk, H. H., Stewart, J. C. M., Hartung, G.;, Maier-Borst, W., and Heene, D. L. Plasma protein (albumin) catabolism by the tumor itself-implications for tumor metabolism and the genesis of cachexia. *Crit. Rev. Oncol. Hematol.* **1997**, *26*, 77−100.

(18) Stehle, G., Wunder, A., Sinn, H., Schrenk, H. H.;, Schütt, S.;, Frei, E., Hartung, G., Maier-Borst, W., and Heene, D. L. Pharmacokinetics of methotrexate-albumin conjugates in tumor-bearing rats. *Anti-Cancer Drugs* **1997**, *8*, 835−844.

(19) Wunder, A., Stehle, G., Schrenk, H. H., Hartung, G., Heene, D. L., Maier-Borst, W.;, and Sinn, H. Antitumor activity of methotrexate-albumin conjugates in rats bearing a Walker-256 carcinoma. *Intern. J. Cancer.* **1998**, *76*, 884−890.

(20) Stehle, G., Wunder, A., Schrenk, H. H., Hartung, G., Heene, D. L., and Sinn, H. Methotrexate-albumin conjugate causes tumor growth delay in Dunning R3327 HI prostate cancer bearing rats. *Anti-Cancer Drugs* **1999**, *10*, 405−411.

(21) Hartung, G., Stehle, G., Sinn, H., Schrenk, H. H., Heeger, S., Kränzle, M., Fiebig, H. H., Maier-Borst, W., Heene, D. L., and Queisser, W. Phase I-trial of a methotrexate-albumin conjugate (MTX-HSA) in cancer patients. *Eur. J. Cancer* **1997**, *33*, S249−250.

(22) Hartung, G., Stehle, G., Sinn, H., Wunder, A., Schrenk, H. H., Heeger, S., Kränzle, M., Edler, L., Frei, E., Fiebig, H. H., Heene, D. L., Maier-Borst, W., and Queisser, W. Phase I trial of methotrexate-albumin in a weekly intravenous bolus regimen in cancer patients. *Clin. Cancer Res.* **1999**, *5*, 753−759.

(23) Duncan, R. Drug-Polymer conjugates: Potential for improved chemotherapy. *Anti-Cancer Drugs* **1992**, *3*, 175−210.

(24) Seymour, L. W. Passive tumour targeting of soluble macromolecules and drug conjugates. *Crit. Rev. Ther. Drug Carrier Syst.* **1992**, *9*, 125−187.

(25) Mehvar, R. Dextrans for targeted and sustained delivery of therapeutic and imaging agents. *J. Controlled Release* **2000**, *69*, 1−25.

(26) Hudecz, F. Design of synthetic branched-chain polypeptides as carriers for bioactive molecules. *Anti-Cancer Drugs* **1995**, *6*, 171−193.

(27) Hoste, K., Schacht, E. H., and Seymour, L. W. New derivatives of polyglutamic acid as drug carrier systems. *J. Controlled Release* **2000**, *64*, 53−61.

(28) Ulbrich, K., Subr, V., Strohalm, J., Plocova, D., Jelinkova, M., and Rìhová, B. Polymeric drugs based on conjugates of synthetic molecules and natural macromolecules. I. Synthesis and physicochemical characterisation. *J. Controlled Release* **2000**, *64*, 63−79.

(29) Greenwald, R. B., Conover, C. D., and Choe, Y. H. Poly(ethylene glycol) conjugated drugs and prodrugs: A comprehensive review. *Crit. Rev. Ther. Drug Carrier Syst.* **2000**, *17*, 101−161.

(30) Ryser, H. J.-P., and Shen, W.-C. Conjugation of methotrexate to poly(L-lysine) increases drug transport and overcomes drug resistance in cultured cells. *Proc. Natl. Acad. Sci. U.S.A.* **1978**, *75*, 3867−3870.

(31) Shen, W.-C., and Ryser, H. J.-P. Poly (L-lysine) and poly (D-lysine) conjugates of methotrexate: Different inhibitory effect on drug resistant cells. *Mol. Pharmacol.* **1979**, *16*, 614−622.

(32) Dang, W., Colvin, O. M., Brem, H., and Salzman, W. M. Covalent coupling of methotrexate to dextran enhances the penetration of cytotoxicity into a tissue-like matrix. *Cancer Res.* **1994**, *54*, 1729−1735.

(33) Subr, V., Strohalm, J., Hirano, T., Ito, Y., and Ulbrich, K. Poly[N−(2-hydroxypropyl)methacrylamide] conjugates of methotrexate − Synthesis and in vitro drug release. *J. Controlled Release* **1997**, *49*, 123−132.

(34) Yamaoka, T., Tabata, Y., and Ikada, Y. Distribtion and tissue uptake of poly(ethylene glycol) with different molecular weights after intravenuous administration to mice. *J. Pharm. Sci.* **1994**, *83*, 601−606.

(35) Murakami, Y., Tabata, Y., and Ikada, Y. Tumor accumulation of poly(ethylene glycol) with different molecular weights after intravenous injection. *Drug Delivery* **1997**, *4*, 23−31.

(36) Zalipsky, S. Chemistry of poly(ethylene glycol) conjugates with biologically active molecules. *Adv. Drug Delivery Rev.* **1995**, *16*, 157−182.

(37) Rodrigues, P. C. A., Beyer, U., Schumacher, P., Roth, T., Fiebig, H., Unger, C., Messori, L., Orioli, P., Paper, D. H., Mülhaupt, R., and Kratz, F. Acid-sensitive poly(ethylene glycol) conjugates of doxorubicin: Preparation, in vitro efficacy and intracellular distribution. *Bioorg. Med. Chem.* **1999**, *7*, 2517−2524.

(38) Enzon Inc., Products under development (http://www.enzon.com/develop.html), 2001.

(39) Rosowsky, A., and Yu, C.-S. Methotrexate Analogues. 10. Direct coupling of methotrexate and diethyl-L-glutamate in the presence of peptide-forming reagents. *J. Med. Chem.* **1978**, *21*, 170−175.

(40) Kulkarni, P. N., Blair, A. H., and Ghose, T. I. Covalent binding of methotrexate to immunoglobulins and the effect of antibody-linked drug on tumor growth in vivo. *Cancer Res.* **1981**, *41*, 2700−2706.

(41) Stehle, G., Sinn, H., Wunder, A., Schrenk, H. H., Schütt, S., Maier-Borst, W., and Heene, D. L. The loading rate determines tumor targeting properties of methotrexate-albumin conjugates in rats. *Anti-Cancer Drugs* **1997**, *8*, 677−685.

(42) Bodanszky, M. *Principles of Peptide Synthesis*; Springer: Heidelberg; **1984**.

(43) Kueffner, U., Esswein, A., Lohrmann, U., Montejano, Y. D., Vitols, K. S., and Huennekens, F. M. Occurrence and significance of diastereomers of methotrexate-α-peptides. *Biochemistry* **1990**, *29*, 10540−10545.

(44) Cramer, S. M., Schornagel, J. H., Kalghatgi, K. K., Bertino, J. R., and Horváth, C. Occurrence and significance of D-methotrexate as a contaminant of commercial methotrexate. *Cancer Res.* **1984**, *44*, 1843−1846.

(45) Kato, Y., Endo, N., Takeda, Y., and Hara, T. Production of conjugate of methotrexate with protein. *J*apanese Patent Application No. 60-277817, 1987.

(46) Nagy, A., Czoke, B., and Schally, A. V. Selective coupling of methotrexate to peptide hormone carriers through a gamma-carboxamide linkage of its glutamic acid moiety: Benzotriazol-1-yloxytris(dimethylamino)phosphonium hexafluorophosphate activation in salt coupling. *Proc. Natl. Acad. Sci. U.S.A.* **1993**, *90*, 6373−6376.

(47) Rosowsky, A., Forsch, R. A., Uren, J., and Wick, M. M. Methotrexate Analogues. 14. Synthesis of new γ-substituted derivatives as dihydrofolate reductase inhibitors and potential anticancer agents. *J. Med. Chem*. **1981**, *24*, 1450−1455.

(48) Rosowsky, A. Chemistry and biological activity of antifolates. *Prog. Med. Chem*. **1989**, *26*, 1−252.

(49) Sirotnak, F. M., and Tolner, B. Carrier-mediated membrane transport of folates in mammalian cells. *Annu. Rev. Nutr.* **1999**, *19*, 91−122.

(50) Mukherjee, S., Ghosh, R. N., and Maxfield, F. R. Endocytosis. *Physiol. Rev*. **1997**, *77*, 759−803.

(51) Galivan, J., Ryan, T., Rhee, M., Yao, R., and Chave, K. Glutamyl hydrolase: Properties and pharmacologic impact. *Sem. Oncol.* **1999**, *26*, 33−37.

(52) Galivan, J., Ryan, T. J., Chave, K., Rhee, M., Yao, R., and Yin, D. Glutamyl hydrolase. Pharmacological role and enzymatic characterization. *Pharmacol. Ther.* **2000**, *85*, 207−215.

(53) Loadman, P. M., Bibby, M. C., Double, J. A., Al-Shakhaa, W. M., and Duncan, R. Pharmacokinetics of PK1 and doxorubicin in experimental colon tumor models withn differing responses to PK1. *Clin. Cancer Res.* **1999**, *5*, 3682−3688.

BC010098M

© 2002 American Chemical Society, Bioconjugate Chem., Riebeseel bc010098m Supporting Info Page 1

Supporting Information
-contents-

Figure 6:

Chromatograms of chiral HPLC showing the racemization of MTX α-methylester (a), MTX-γ-methylester (b), MTX α-2-methoxyethylamide (c), MTX γ-2-methoxy-ethylamide (d).

Figure 7:

HPLC analysis of MTX-PEG conjugates on a Nucleogel® column.

Figure 8a-d:

MALDI-TOF Spectra of MTX-PEG conjugates (MW 750, 2000 and 5000) and the respective unconjugates amino-PEG carriers.

Figure 9:

Inhibitory effect of MTX, MTX-α-methylester and MTX-γ-methylester on DHFR.

Figure 10:

Dose-response curves of MTX, MTX-PEG750 and MTX-PEG2000 on CCRF-CEM and DU-145 cells.

Figure 11:

Dose-response curves of MTX, MTX-PEG5000, MTX-PEG10000, MTX-PEG20000 and MTX-PEG40000 on CCRF-CEM, HL-60 and THP-1 leukemia cells.

Figure 12:

Dose-response curves of MTX, MTX-PEG5000, MTX-PEG10000, MTX-PEG20000 and MTX-PEG40000 on MCF-7 and DU-145 cells.

Figure 6

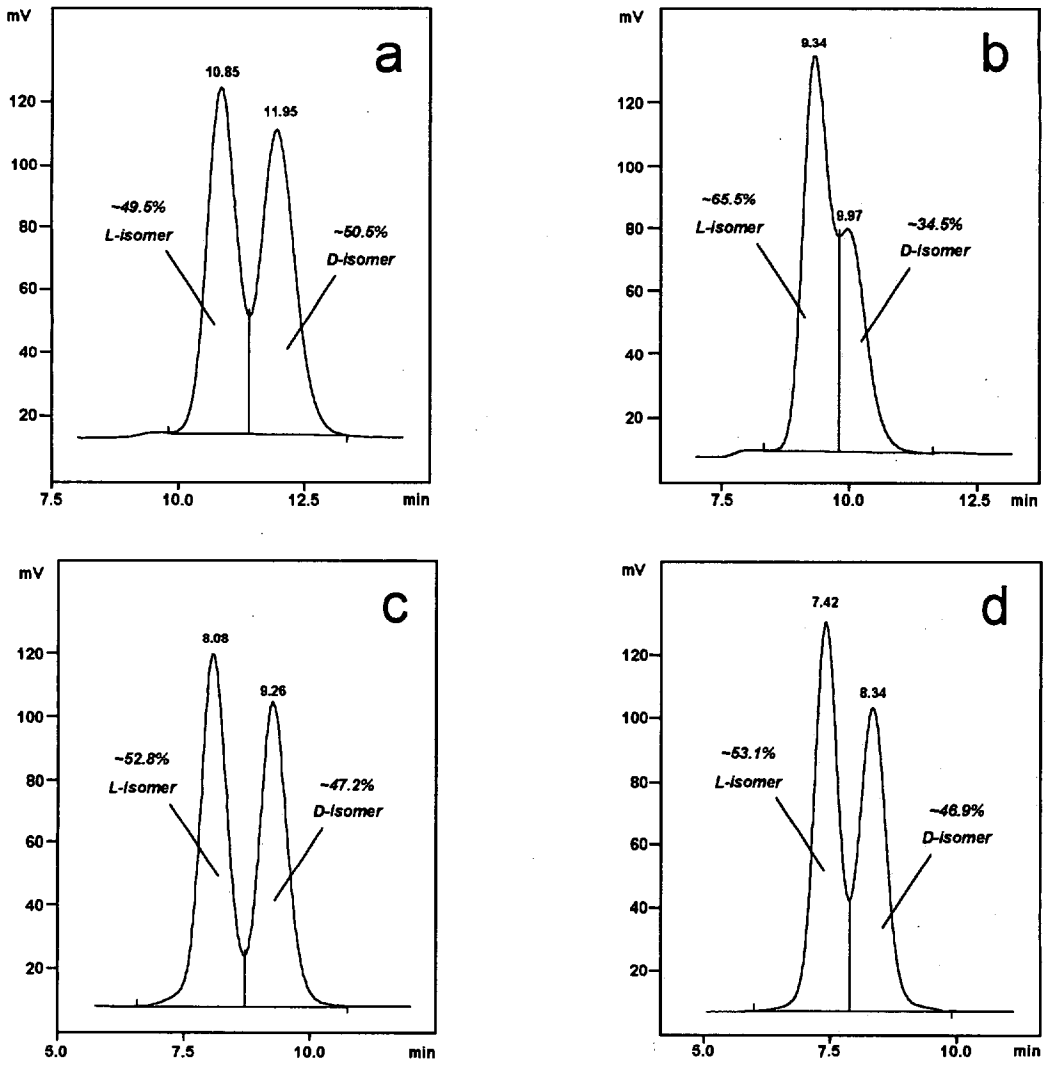


Figure 6: HPLC analysis of the purified MTX-derivatives on a chiral Nucleodex®-β-OH-column: (a) MTX α-methylester, (b) MTX γ-methylester, (c) MTX α-2-methoxy-ethylamide, (d) MTX γ-2-methoxyethylamide.

Figure 7

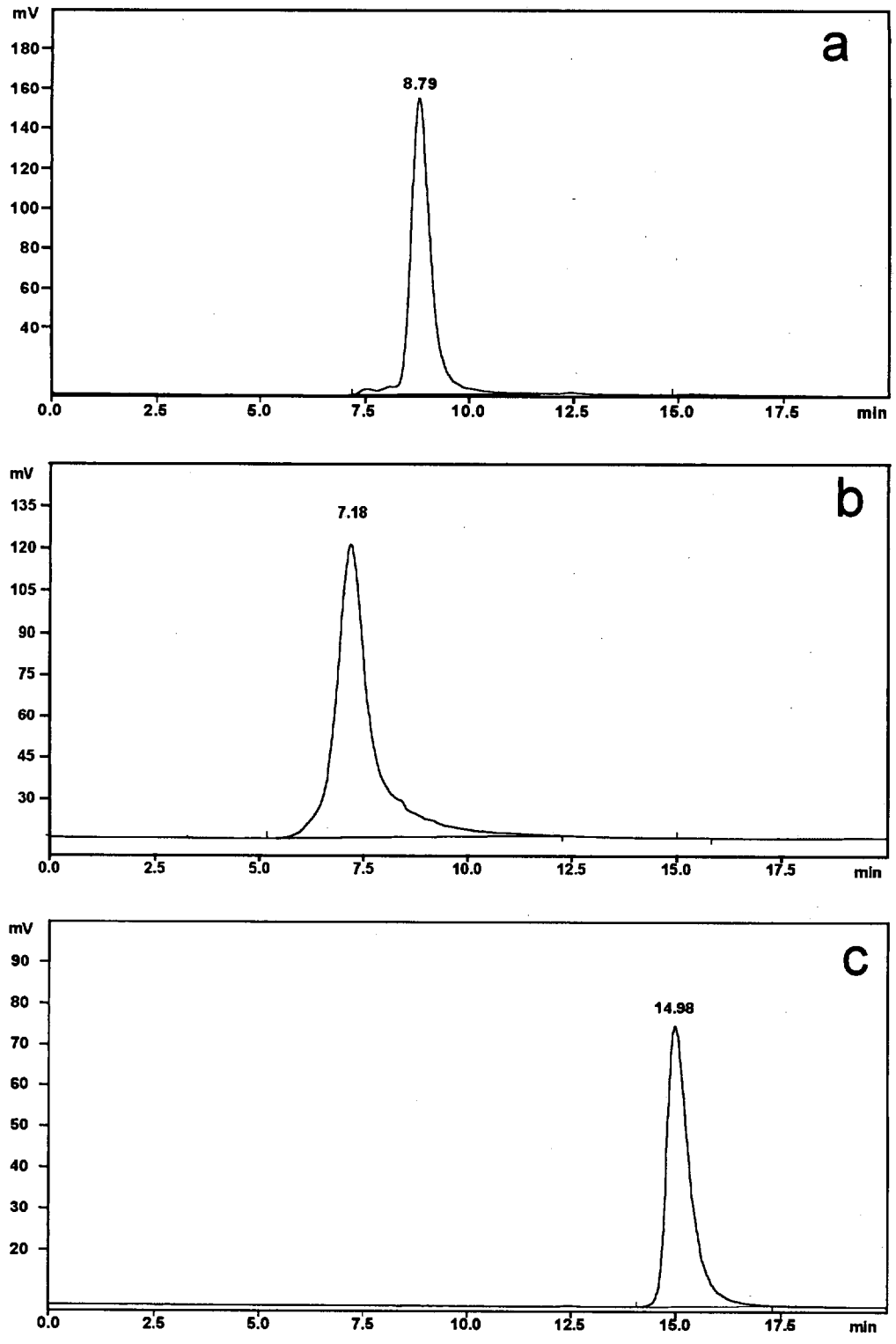


Figure 7: Analytical HPLC of MTX-PEG5000 conjugate **(a)**, MTX-PEG40000 conjugate **(b)** and free MTX **(c)** on a Nucleogel®-aqua-OH column with PBS (pH 7.4) as eluent. The conjugate solutions contain only traces of free MTX.

Figure 8a

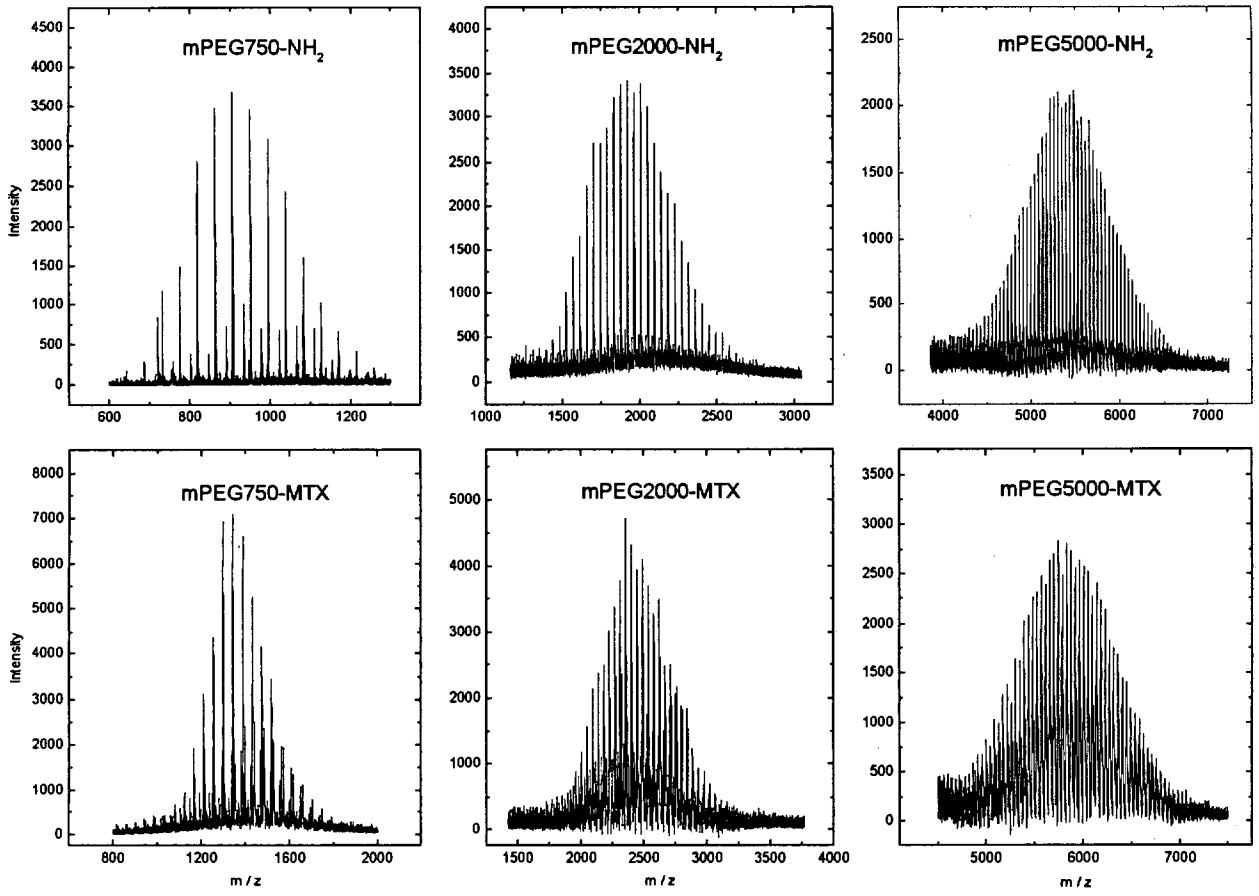


Figure 8a: MALDI-TOF spectra of the unconjugated amino-PEG carriers (MW 750-5000, top) and the respective MTX-PEG conjugates (bottom).

Figure 8b

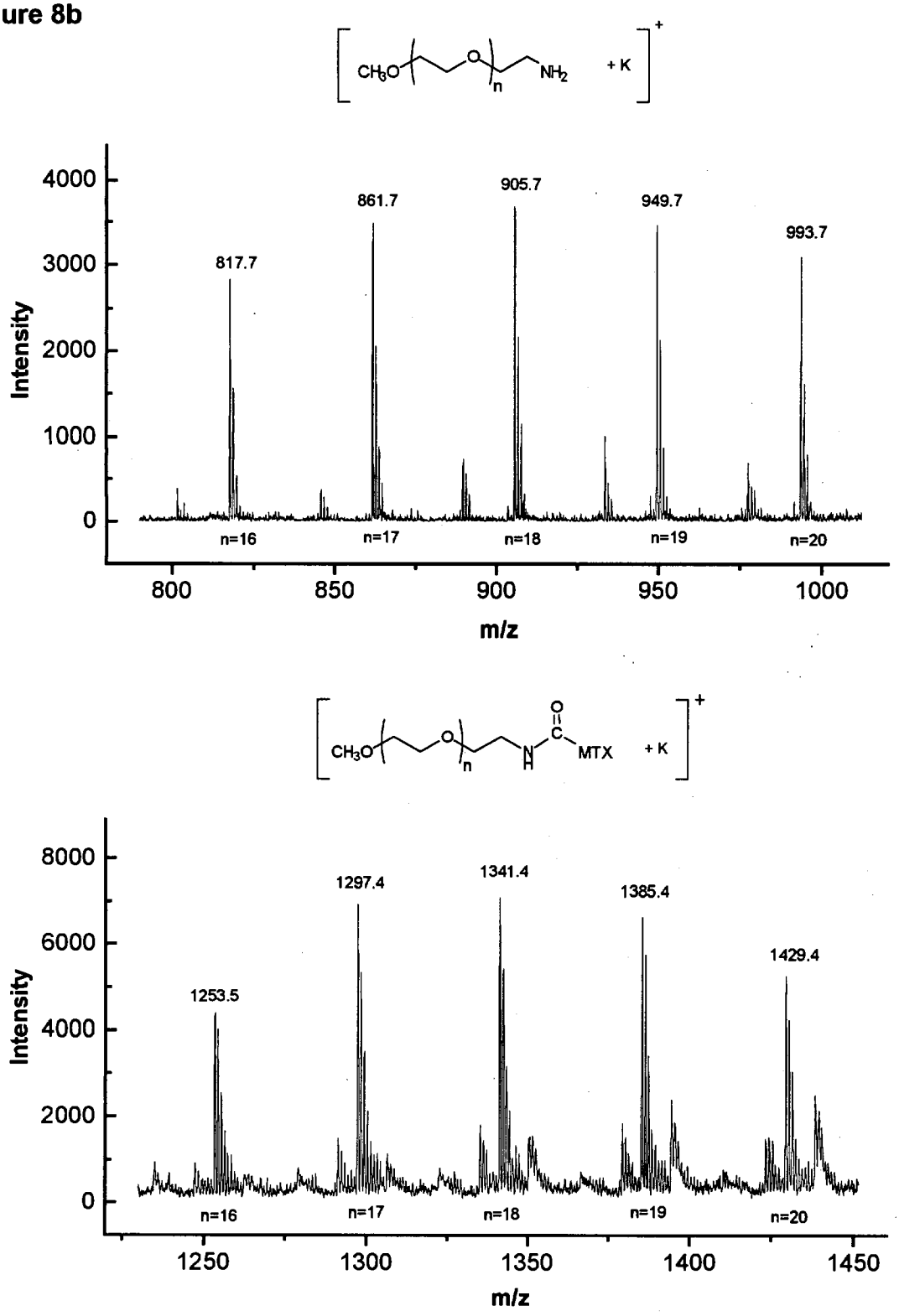


Figure 8b: Detailed MALDI-TOF spectra: The single mass peaks of the MTX-PEG750 (bottom) are shifted by a factor of approximately 436 Da, equivalent to one MTX molecule.[a]

[a] $MW_{(mPEG\text{-}MTX)} = MW_{(mPEG\text{-}NH_2)} + MW_{(MTX)} - MW_{(H_2O)} = MW_{(mPEG\text{-}NH_2)} + 436$

Figure 8c

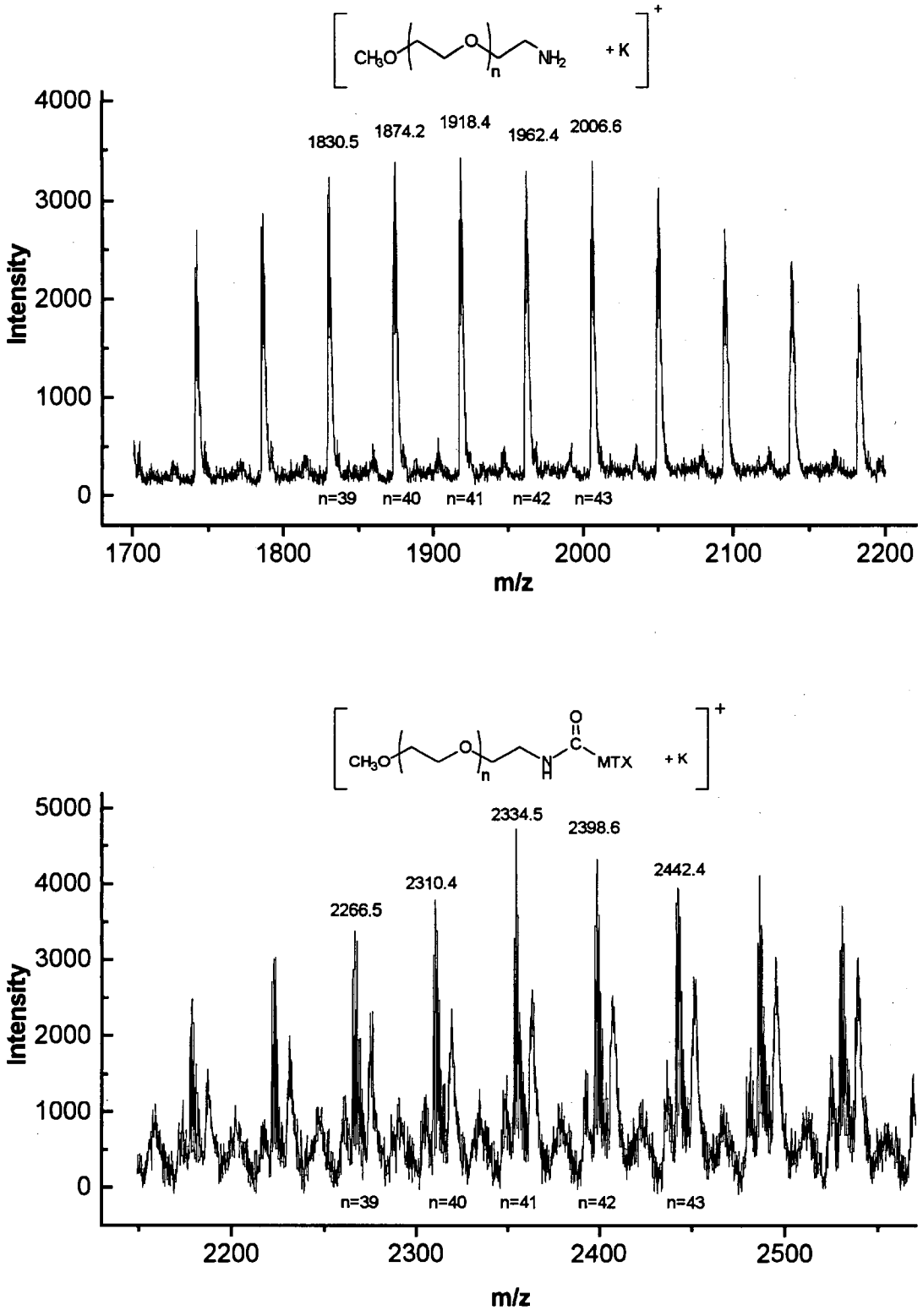


Figure 8c: Detailed MALDI-TOF spectra: The single mass peaks of the MTX-PEG2000 (bottom) are shifted by a factor of approximately 436 Da, equivalent to one MTX molecule.[a]

[a] $MW_{(mPEG\text{-}MTX)} = MW_{(mPEG\text{-}NH_2)} + MW_{(MTX)} - MW_{(H_2O)} = MW_{(mPEG\text{-}NH_2)} + 436$

Figure 8d

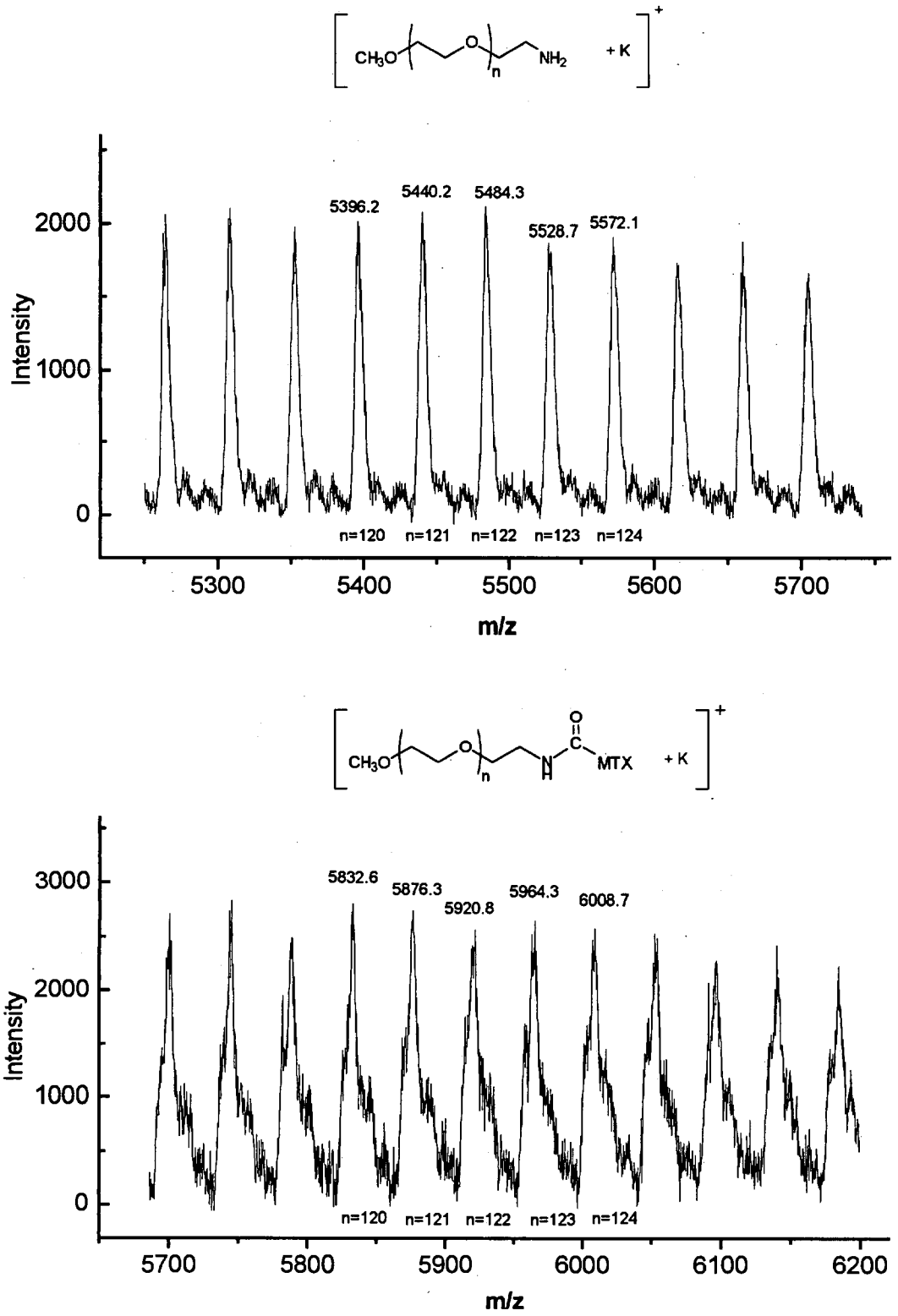


Figure 8c: Detailed MALDI-TOF spectra: The single mass peaks of the MTX-PEG5000 (bottom) are shifted by a factor of approximately 436 Da, equivalent to one MTX molecule.[a]

[a] $MW_{(mPEG\text{-}MTX)} = MW_{(mPEG\text{-}NH_2)} + MW_{(MTX)} - MW_{(H_2O)} = MW_{(mPEG\text{-}NH_2)} + 436$

Figure 9

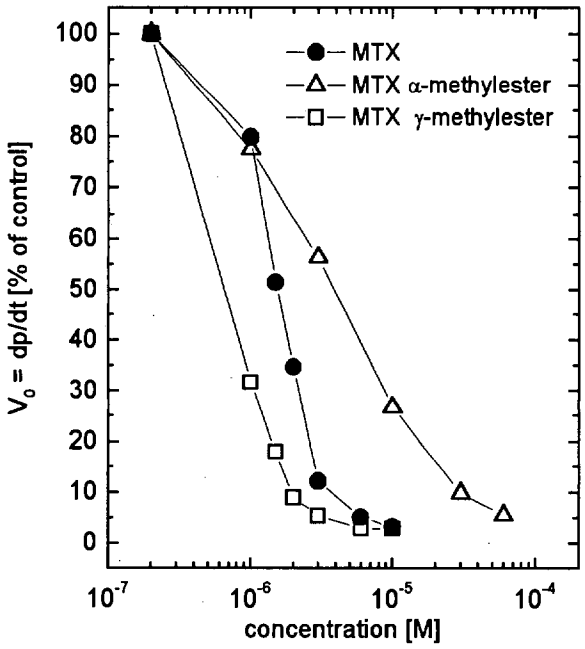


Figure 9: Effect of MTX and the isolated MTX α- and γ-methylesters on dihydrofolate reductase determined in a cell free assay using 0.018 U enzyme per well.

Figure 10

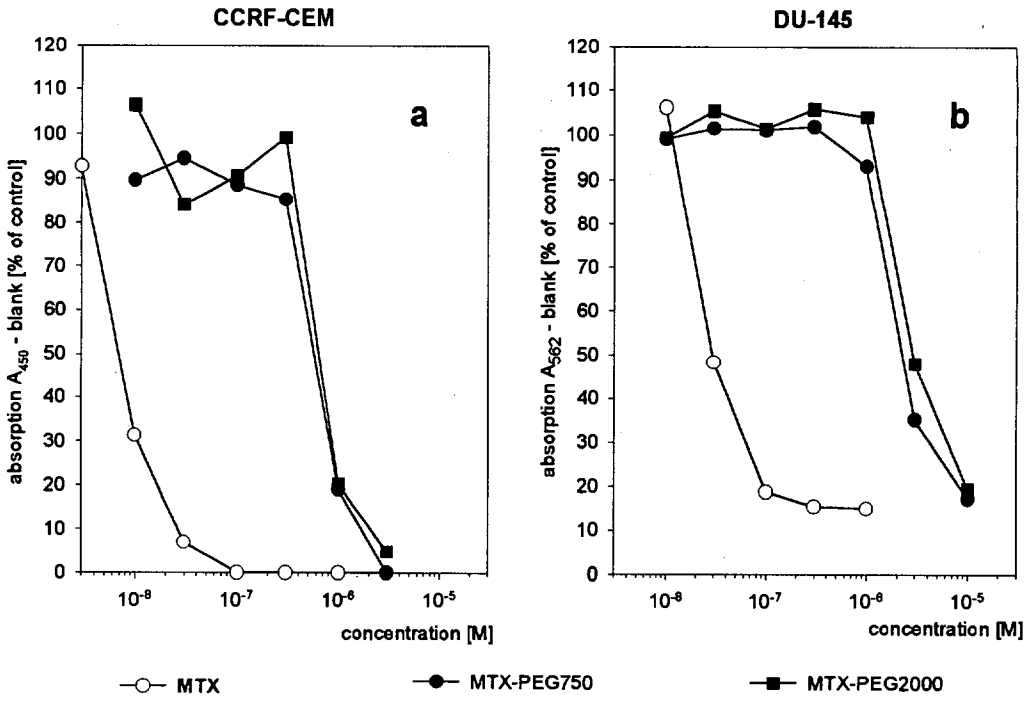


Figure 10: Dose-response curves for MTX, MTX-PEG750 and MTX-PEG2000 in the CCRF-CEM and DU145 cell line. CCRF-CEM **(a)** and DU-145 cells **(b)** were continuously incubated for 5 or 6 days (seeding density: 5000 cells in 200 µL) with different concentrations of MTX and MTX-conjugates. The growth inhibitory effect of the compounds was determined by measuring the total protein content using the BCA assay (DU-145 cells) or determining the metabolic activity by using the WST-1 assay (CCRF-CEM cells).

Figure 11

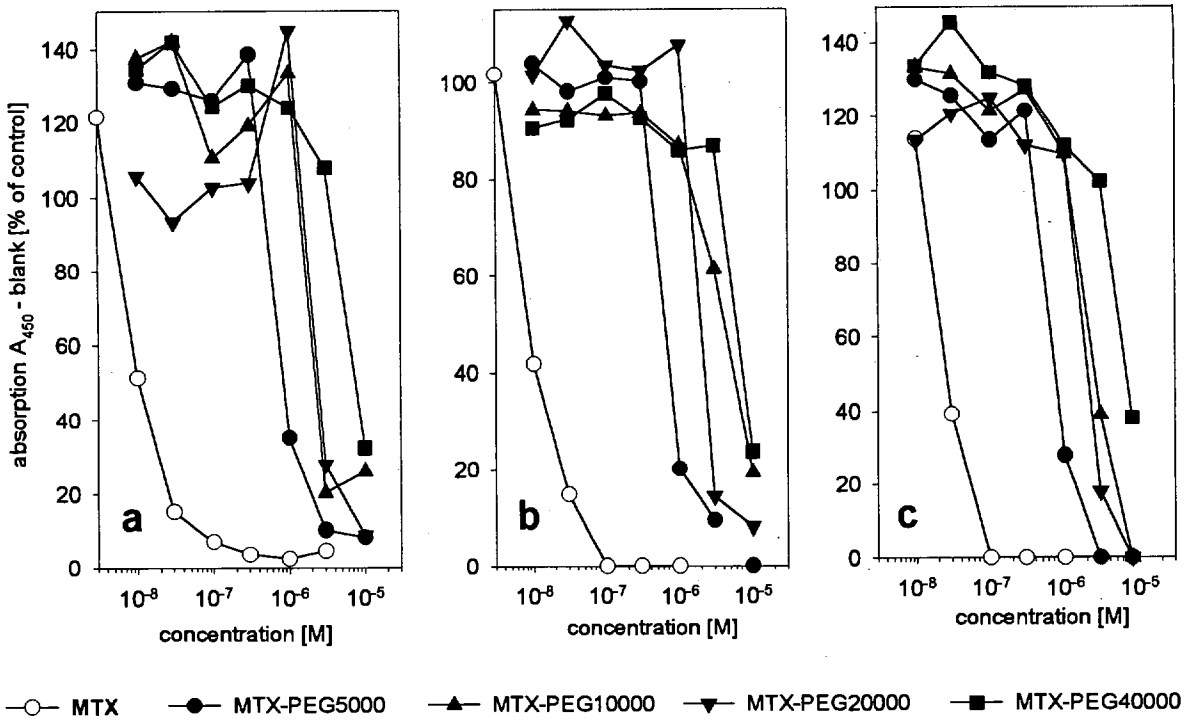


Figure 11: Dose-response curves for MTX, MTX-PEG5000, MTX-PEG10000, MTX-PEG20000 and MTX-PEG40000 in the HL-60, the THP-1 and the CCRF-CEM cell line. HL-60 **(a)**, THP-1 cells **(b)** and CCRF-CEM cells **(c)** were continuously incubated for 3 days (seeding density: 40000 cells in 200 µL) with different concentrations of MTX and MTX-conjugates. The growth inhibitory effect of the compounds was determined by measuring the metabolic activity of the cells using the WST-1 assay.

Figure 12

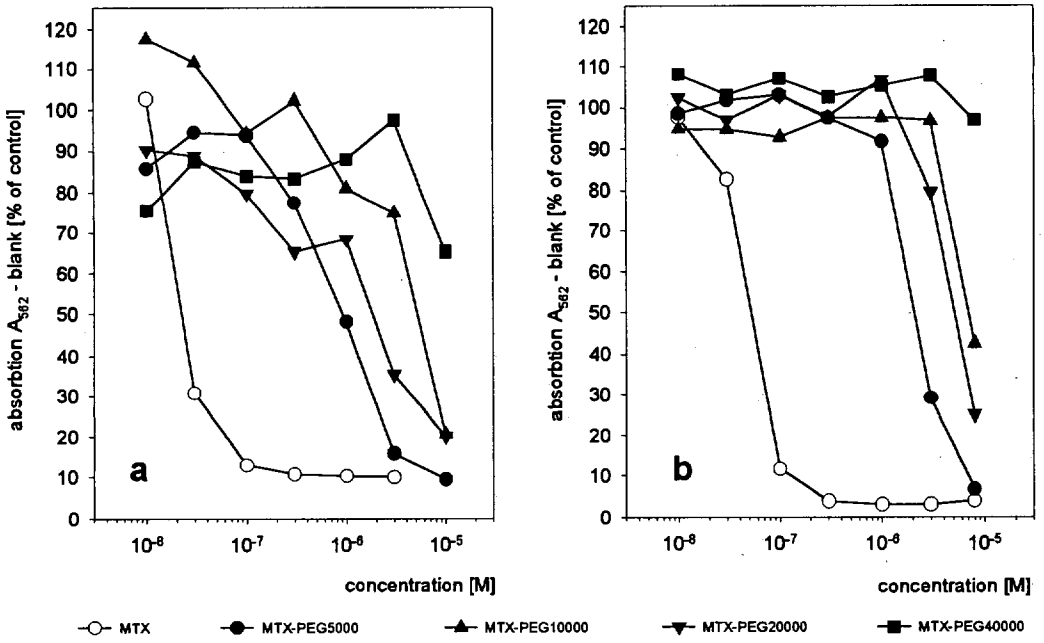


Figure 12: Dose-response curves for MTX, MTX-PEG5000, MTX-PEG10000, MTX-PEG20000 and MTX-PEG40000 in the MCF-7 and the DU-145 cell line. MCF-7 human breast cancer cells **(a)** and DU-145 human prostate cancer cells **(b)** were continuously incubated for 7 or 6 days respectively (seeding density: 5000 cells in 200 µL) with different concentrations of MTX and MTX-conjugates. The growth inhibitory effect of the compounds was determined by measuring the total protein content using the BCA assay.

Modifications in Synthesis Strategy Improve the Yield and Efficacy of Geldanamycin−Herceptin Immunoconjugates

Raya Mandler,[†] Hisataka Kobayashi,[†] Marie Y. Davis,[†] Thomas A. Waldmann,[†] and Martin W. Brechbiel*[,‡]

Metabolism Branch and the Chemistry Section, Radiation Oncology Branch, National Cancer Institute, NIH, Bethesda, Maryland 20982-1002. Received December 26, 2001; Revised Manuscript Received April 15, 2002

Geldanamycin (GA) was modified with *N*-*tert*-butyloxycarbonyl-1,3-diaminopropane to introduce a latent primary amine. After deprotection, this primary amine provided a site for introduction of a maleimide group that enabled linkage to proteins. This maleimido derivative of geldanamycin (GMB-APA-GA) was linked to the monoclonal antibody Herceptin after the antibody had been modified with Traut's reagent to introduce thiol groups. By this sequence, a new immunoconjugate (H:APA-GA) was generated that showed greater antiproliferative activity than the previously reported analogous immunoconjugate created with a 1,4-diaminobutane spacer derivative of geldanamycin to form an immunoconjugate, H:ABA-GA. Both immunoconjugates inhibited in vitro the growth of MDA-361/DYT2 cells, a cell line overexpressing the HER2 antigen, while Herceptin alone was ineffective. However, H:APA-GA showed better efficacy than H:ABA-GA (IC_{50} = 0.2 vs 0.58 mg/mL and cell doubling time >12 vs 6 days, respectively). Results of the in vivo therapy experiments in a xenograft model were consistent with the in vitro findings. Treatment with Herceptin prolonged the survival of the tumor-bearing mice when compared with the control group, but H:ABA-GA and H:APA-GA were each more efficacious than unmodified Herceptin. However, unlike H:ABA-GA, the immunoconjugate H:APA-GA caused stable tumor regression (in 25% of the recipients), showing a qualitative improvement with potential clinical relevance.

INTRODUCTION

Geldanamycin (GA)[1] (Figure 1) is a benzoquinoid ansamycin produced by the actinomycete *Streptomyces hygroscopicus* that is related to herbimycin A with a known cellular target being the cytosolic protein chaperone hsp90 (*1*). Upon binding to hsp90, GA inhibits its ability to protect cellular enzymes from proteasomal degradation and disrupting in this way many crucial cellular processes (*2*). Consequently, this molecule is extremely cytotoxic to a wide variety of cells, including neoplastic cells. While the antitumor potential of GA has long been recognized, clinical use of native GA has not been pursued due to the drug's severe toxicity and difficulties with aqueous formulation (*3*). Numerous GA analogues have been synthesized and studied in an effort to develop derivatives with improved therapeutic indices (*4*). These studies indicated that modifications at the 17 position on the quinone ring maintained anticancer activity at nanomolar range while reducing the overall toxicity (*3*, *4*). One of these derivatives, 17-allylamino-GA (Figure 1), is currently entering Phase II clinical trials to treat a variety of solid tumors (*5*, *6*).

Further reduction of GA systemic toxicity could potentially be achieved by selectively targeting and delivering an active GA species into malignant cells using a monoclonal antibody (mAb) as the targeting vehicle. Clearly, internalization is a prerequisite for successful application of such immunoconjugates (*7*). With the advances of therapeutic mAbs into clinical use, it is conceivable that mAbs that internalize efficiently could also be used as the targeting vehicle in such an application (*8*). Several tumor-targeting mAb's armed with small toxic compounds have already been clinically evaluated and one has been approved for therapy of AML in elderly patients (*9*, *10*).

In our present studies, Herceptin was chosen as the targeting mAb. This mAb was the first to be approved by the FDA for therapy of solid tumors (*11*). Herceptin specifically targets the membrane receptor HER2, a member of the epidermal growth factor receptor family. HER2 is overexpressed in approximately 30% of human gastric, lung, and breast carcinomas and is associated with poor prognosis. Blocking of HER2 activity or interfering with its expression was shown to inhibit proliferation and reduce tumor growth (*11*−*13*). Because HER2 stability and function depends on hsp90, this protein is highly sensitive to and is efficiently eliminated by GA (*14*). Herceptin has been previously shown to internalize upon binding to HER2. The conjugation with GA is through an acid-labile bond that should release the GA derivative once the endocytosed conjugate is shuttled into the lysosomes. In fact, our laboratories have already reported that such conjugates do deliver a more potent selective cytotoxic impact than use of just Herceptin (*15*−*17*).

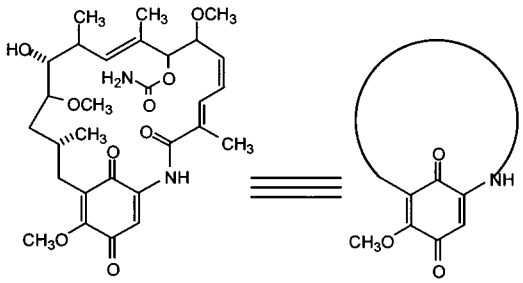
* To whom correspondence should be addressed: NIH, Chemistry Section, 10 Center Drive, Building 10, Room B3B69, Bethesda, MD 20892-1002. E-mail: martinwb@mail.nih.gov.

[†] Metabolism Branch, National Cancer Institute.

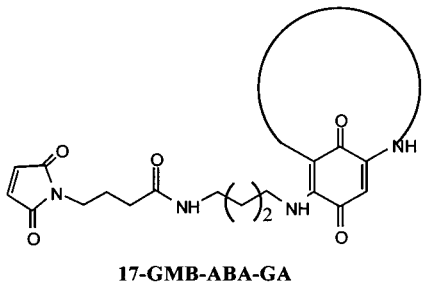
[‡] Chemistry Section, National Cancer Institute.

[1] Abbreviations: BOC, *tert*-butyuloxycarbonyl; GA, geldanamycin; mAb, monoclonal antibody; H:ABA-GA, Herceptin conjugated with 17-(3-[4-maleimidobutyrcarboxamido]butylamino)-geldanamycin; H:APA-GA, Herceptin conjugated with 17-(3-[4-maleimidobutyrcarboxamido]propylamino)geldanamycin; GMB, 4-maleimidobutyric acid *N*-hydroxysuccinimidyl ester; GMB-ABA-GA, 17-(3-[4-maleimidobutyrcarboxamido]butylamino)-geldanamycin; GMB-ABA-GA, 17-(3-[4-maleimidobutyrcarboxamido]propylamino)geldanamycin.

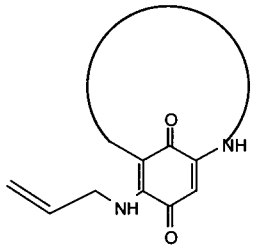
10.1021/bc010124g Not subject to U.S. Copyright. Published 2002 by American Chemical Society
Published on Web 06/19/2002



Geldanamycin



17-GMB-ABA-GA



17-Allylamino-GA

Figure 1. Structures of geldanamycin, 17-GMB-ABA-GA, 17-allylamino-GA.

Conjugation of mAb's with GA has not been a straightforward process because GA lacks a suitable functional group for direct covalent linkage to protein. As recently reported by our laboratories, introduction of a primary amine group originating from modification at the 17 position has been successful and permitted subsequent addition of a heterobifunctional cross-linking reagent for conjugation of the modified GA to mAb's (*15*, *16*). By use of this chemistry, 17-GMB-ABA-GA (Figure 1) could be conjugated to Herceptin efficiently and reproducibly. The product immunoconjugate, H:ABA-GA, subsequently demonstrated a higher antiproliferative effect on HER2 overexpressing cells than unmodified Herceptin. H:ABA-GA was also shown to be specific for HER2-positive, but not for HER2-negative, cells. The choice of 17-GMB-ABA-GA rather than the more potent 17-GMB-APA-GA, butyl spacer versus propyl spacer, respectively, was the result of a compromise between activity and availability of the required GA derivative (*15*, *16*). While 17-APA-GA had higher antiproliferative activity than 17-ABA-GA, the preparation of 17-GMB-APA-GA has been problematic. Simple introduction of the amine via direct aminolysis with 1,3-diaminopropane yielded a complex mixture of byproducts (*15*). Exposure to silica during chromatography aggravated this condition, efficiently catalyzing the formation of a seven-membered imine ring from the distal amine and the quinone carbonyl, further complicating access to this derivative. Insertion of an additional methylene into the amine chain eliminated this cyclization (*15*) and thus provided 17-GMB-ABA-GA in excellent yield. This synthesis ultimately allowed for the synthesis of a very pure and active GA-mAb immunoconjugate. (*15*)

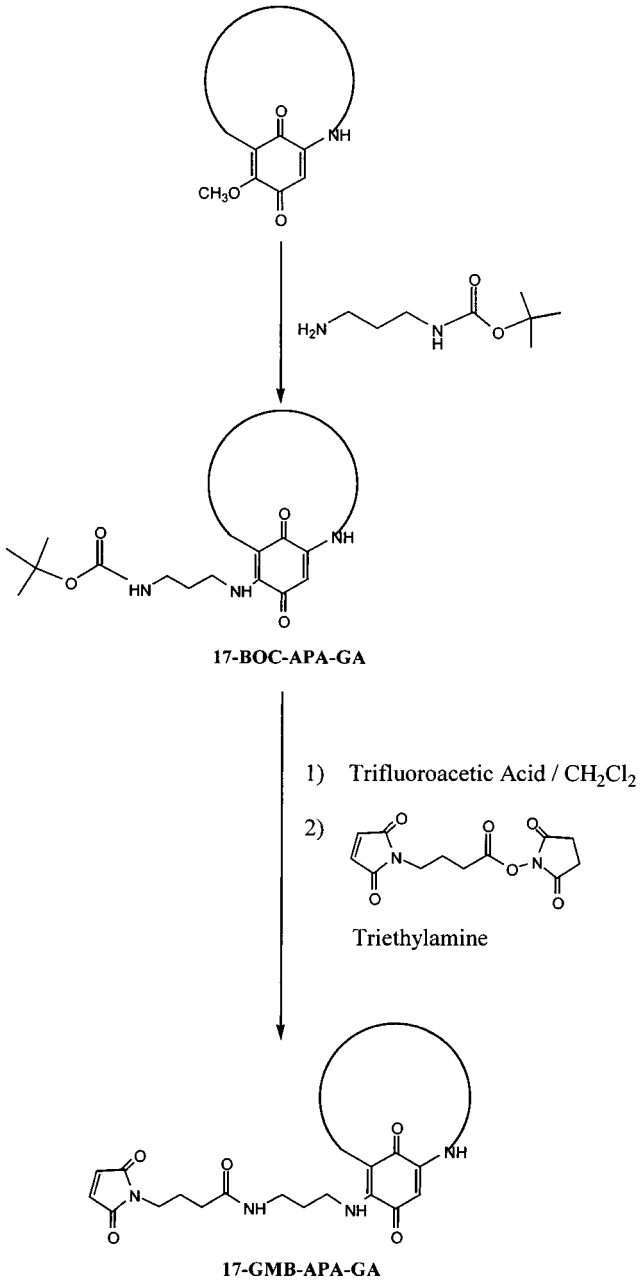


Figure 2. Synthesis of 17-GMB-APA-GA.

However, this strategy compromised the potency of the final immunoconjugate, prompting re-examination of the chemical strategies that had been employed.

Herein, we report on a successful modified synthesis strategy of 17-GMB-APA-GA (Figure 2), its conjugation to Herceptin, and an evaluation of this immunoconjugate's efficacy in vitro as well as in tumor-bearing mice.

EXPERIMENTAL PROCEDURES

Materials and Methods. All anhydrous solvents and reagents except where noted otherwise were obtained from Aldrich, Sigma, or Fluka and were used as received. The *N*-hydroxysuccinimidyl ester of 4-maleimidobutyric acid (GMB) was prepared by modification of a literature method (*18*). Geldanamycin (GA) was generously supplied by Edward A. Sausville and Gordon Cragg, NPG, DTP, DCTD, NCI. Triethylamine was distilled from CaH_2 prior to use.

^1H and ^{13}C NMR were obtained using a Varian Gemini 300 instrument, and chemical shifts are reported in ppm

on the δ scale relative to TMS, TSP, or solvent. Proton chemical shifts are annotated as follows: ppm (multiplicity, integral, coupling constant (Hz)). Chemical ionization mass spectra (CI-MS) were obtained on a Finnegan 3000 instrument. Fast atom bombardment mass spectra (FAB-MS) were obtained on an Extrel 4000 in the positive ion detection mode. Elemental analyses were performed by Atlantic Microlabs (Norcross, GA).

The MDA-361/DYT2 cell line was generously provided by Drs. Dajun Yang and Marc E. Lippman of The Lombardi Cancer Center, Georgetown University (Washington, DC) (*19*). The NIH3T3/HER cell line was generously provided by Dr. S. Aaronson, NIH (*20*). ^{125}I was obtained in the NaI form from Amersham Biosciences Corp. (Piscataway, NJ).

Caution: ^{125}I ($t_{1/2}$ = 59.4 day) is a γ-emitting radionuclide. Appropriate shielding and handling protocols should be in place when using this isotope. All protocols in which animals were used have been approved by the National Cancer Institute Animal Care and Use Committee.

17-(3-*tert*-Butyloxycarbonyl(aminopropyl)amino)-geldanamycin (17-*N*-BOC-APA-GA). GA (0.5 g, 0.89 mmol) was dissolved in $CHCl_3$ (300 mL), and *N*-*tert*-butyloxcarbonyl-1,3-diaminopropane (250 mg, 1.44 mmol) was added. The reaction was stirred shielded from light for 48 h, during which the initial golden yellow solution grew darker and an additional 100 mg (0.575 mmol) of the monoprotected diamine was added. After 96 h, the reaction was assayed by thin-layer chromatography (TLC) on silica (5% MeOH/$CHCl_3$). Despite the now dark purple appearance of the reaction, a distinct yellow component corresponding to GA was still evident by TLC, and another 100 mg of the protected diamine was added. After 120 h, the amount of GA remaining was deemed minimal by TLC, the reaction solution was concentrated to ca. 25 mL, and hexanes (ca. 450 mL) was added to precipitate the crude product. The suspension was placed at −20 °C for 24 h, after which the dark purple solid was collected on a Buchner funnel, washed with hexanes, and dried in vacuo in the absence of light. The pure 17-*N*-BOC-APA-GA was cleanly isolated by flash chromatography on silica (2.5 × 35 cm column) eluting with 1:99 MeOH/$CHCl_3$ (470 mg, 75%). ^{1}H NMR (300 MHz, $CDCl_3$, δ): 0.991 (br, d, 6H, J = 5.7 Hz), 1.432 (m, 1H), 1.456 (s, 9H), 1.803 (s, 3H), 1.835 (m, 2H), 2.028 (s, 3H), 2.410 (dd, 1H, J = 12.9, 10.8 Hz), 2.61−2.82 (m, 3H), 3.239 (m, 1H), 3.276 (s, 3H), 3.366 (s, 3H), 3.40−3.70 (m, 6H), 4.309 (d, 1H, J = 9.9 Hz), 4.693 (t, 2H, J = 6.3 Hz), 4.837 (br, s, 2H), 5.185 (s, 1H), 5.81−5.95 (m, 2H), 6.586 (t, 2H, J = 11.7 Hz, one proton obscured), 6.955 (d, 1H, J = 11.7 Hz), 7.267 (s, 1H), 9.167 (s, 1H). FAB-MS (nba/CsI) *m*/*e*: 704 (M^+). Anal. Calcd for $C_{36}H_{56}N_4O_{10}$: C, 61.33; H, 8.02; N, 7.95. Found: C, 61.45; H, 8.37; N, 7.72.

17-(3-(4-Maleimidobutyrcarboxamido)propyl-amino)geldanamycin (17-GMB-APA-GA). The 17-*N*-BOC-APA-GA (100 mg, 0.142 mmol) was dissolved in CH_2Cl_2 (100 mL) and treated with trifluoroacetic acid (10 mL) at room temperature for 1 h, after which TLC indicated that starting material was no longer present. The solution was rotary-evaporated at ambient temperature until near dry. The residue was taken up in CH_2Cl_2 (ca. 50 mL) and rotary-evaporated until near dry 3 times and then finally dried in vacuo for 24 h. The crude protonated amine was taken up in ethyl acetate (100 mL), and GMB (80 mg, 0.286 mmol) was added to the solution. Immediately thereafter, triethylamine (100 μL) was added, and the reaction was stirred in the dark for 24 h. At this point, TLC on silica with 10% MeOH/$CHCl_3$ indicated one major component, and the solvent was removed by rotary evaporation at ambient temperature. The product was isolated by flash chromatography on silica as described previously, eluting with 2% MeOH/$CHCl_3$ (90 mg, 83%). ^{1}H NMR (300 MHz, $CDCl_3$, δ): 0.990 (t, 6H, J = 7.5 Hz), 1.77−1.60 (m, 3H), 1.802 (s, 3H), 1.99−1.84 (m, 3H), 2.029 (s, 3H), 2.184 (t, 2H, J = 7.2 Hz), 2.44−2.32 (m, 2H), 2.61−2.80 (m, 3H), 3.275 (s, 3H), 3.48−3.38 (m, 2H), 3.367 (s, 3H), 3.38−3.66 (m, 6H), 4.314 (d, 1H, J = 9.9 Hz), 5.191 (s, 1H), 5.81−5.95 (m, 2H), 6.044 (t, 1H, J = 5.7 Hz), 6.588 (t, 1H, J = 11.4 Hz), 6.626 (t, 1H, J = 5.7 Hz), 6.726 (s, 2H), 6.956 (d, 1H, J = 12.0 Hz), 7.263 (s, 1H), 9.164 (s, 1H). FAB-MS (nba/prg/CsI) *m*/*e*: 767 (M^+). HR-FAB-MS *m*/*e*: 767.3742, error = −0.7 ppm. Anal. Calcd for $C_{39}H_{53}N_5O_{11}$: C, 60.99; H, 6.97; N, 9.12. Found: C, 61.18; H, 7.04; N, 8.97.

Conjugation of GA Derivatives (17-GMB-ABA-GA, 17-GMB-APA-GA) to Herceptin (H:ABA-GA, H:APA-GA). The conjugation was performed as previously reported (*15*, *16*). Herceptin was reacted with Traut's reagent at a molar ratio of 1:13. Excess Traut's reagent was removed by buffer exchange into conjugation buffer (50 mM HEPES, 150 mM NaCl, 10 mM EDTA (pH 7.0)). The molarity of the SH functionality groups after thiolation was determined by the method of the Ellman reaction at A_{412} (*16*). When compared with the molarity of the mAb itself, this value allowed calculation of the average reaction ratio of GA:mAb. The reaction conditions employed yielded an average of three thiol groups per protein molecule. Thereafter, 17-GMB-APA-GA (or 17-GMB-ABA-GA) was dissolved in DMSO (2 mg/mL) and was reacted with the mAb at ≥5-fold the concentration of the mAb's SH groups. The reaction mixture was kept in the dark at 25 °C for 1 h and then was dialyzed extensively (3 × 1 L during 48 h) against PBS without Ca^{2+}/Mg^{2+} at 4 °C. The presence of the GA moiety on the mAb was confirmed by spectrophotometric reading at A_{334}, as previously reported (*15*, *16*). All conjugates were filtered for sterility and were kept at 15−20 mg/mL, at 4 °C. Humanized anti-CD25 mAb (Zenapax, Hoffman-LaRoche) was similarly treated to produce a comparable immunoconjugate as previously reported (*16*).

Immunoreactivity and Cell Binding Assay. To establish that the conjugation did not compromise the mAb, antigen recognition and cell binding of the immunoconjugates were compared to native Herceptin. MDA-361/DYT2 cells as well as the HER2-transfectant cell line NIH3T3/HER were used as a source of HER2 for these assays. The transfectant cells were employed because they expressed a much higher receptor/cell number than MDA-361/DYT2 cells (2.3×10^6 vs 0.18×10^6 receptor/cell, respectively, as determined by Scatchard plot analysis) and thus provided conditions for a more accurate evaluation of antigen binding. Herceptin and H:APA-GA were each labeled using ^{125}I (7 mCi/mg of protein) employing a modified Chloramine-T method. Immunoreactivity was determined by a modified cell-binding assay (*21*, *22*). Aliquots of the ^{125}I-labeled H:APA-GA or parental Herceptin (2 ng/100 μL) were incubated in parallel with 5.0×10^5 to 2.0×10^6 NIH3T3/HER cells or 1.0×10^6 MDA-361/DYT2 cells for 2 h at 4 °C. Nonspecific binding was determined under conditions of excess antibody (25 μg of nonradiolabeled Herceptin). The K_d values for Herceptin and the GA immunoconjugate were obtained from the Scatchard plot analysis.

Evaluation of In Vitro Efficacy of H:APA-GA. MDA-361/DYT2 cells were seeded into six-well, flat-bottom plates at 5×10^4 cells/mL and allowed to adhere. Herceptin and the two GA immunoconjugates were each

added to the wells at 0.5 mg/mL (2 mL). Control treatments were PBS only (vehicle) and 1 μM BOC-APA-GA (2 mL). To calculate cell doubling times, cells were detached and counted every 48 h, for 12 days.

To establish an IC_{50} for the conjugates, MDA-361/DYT2 cells were seeded into 96-well plates and were treated with increasing concentrations of Herceptin and either of the two conjugates, as described previously (*15*, *16*). Cultures were allowed to grow until the PBS-treated controls reached 80% confluency. Cell growth was measured after fixing the cultures in all wells, staining the fixed cells with Crystal Violet, and reading the eluted dye at A_{540} (*15*).

Evaluation of Therapeutic Efficacy of the H:APA-GA with Human Xenografts in Athymic Mice. Six-week old athymic female mice (NCI, Frederick, MD) were inoculated sc with MDA-361/DYT2 cells (2×10^6/0.1 mL). These tumors are estrogen-dependent; therefore, E2 pellets (Innovative Research of America, Sarasota, FL) were inserted under the skin 24 h prior to tumor transplanation (0.72 β-estradiol, constant release for 60 days). When tumors reached 15−20 mm^3, the mice were randomly divided into groups ($n = 8$) and treatment was initiated. The treatment regimen was an ip dose of the immunoconjugate at 4 mg/Kg in PBS (0.2 mL) every 3 days for 120 days. The size of the tumors and their appearance was monitored and recorded during that time. Mice were terminated when the tumors reached ~1200 mm^3, if the tumor became necrotic, or if the animals showed signs of severe stress and illness.

RESULTS AND DISCUSSION

The synthesis of the 17-GMB-APA-GA (Figure 2) was performed using the mono-BOC-protected 1,3-diaminopropane. This completely eliminated the competing formation of the seven-membered ring that occurred with use of just the diamine. Thus, treatment of GA with *N-tert*-butyloxcarbonyl-1,3-diaminopropane (Figure 2) produced a dark purple solid that was isolated by precipitation with hexane and then easily purified by column chromatography on silica gel. The most effective reaction conditions involved a careful titration of the GA with the protected amine over several days while carefully following the progress of the reaction by TLC. Regardless of this care, isolation of a minor product that appeared to have added two equivalents of protected diamine (as determined by mass spectrometry) was still observed. This product was presumed to form from the addition of a second equivalent of the monoprotected diamine to the quinone carbonyl, forming an imine.

The rationale for using the *tert*-butylcarbamate (BOC) protecting group was that the formed primary amine would be efficiently protonated upon acidic removal of the BOC group and would effectively continue to inhibit the competing cyclization reaction. Although acidic deprotonation and interception of the amine was expected to lead to the desired product, this was not altogether assured. Deprotection with trifluoroacetic acid appeared to be extremely efficient. However, initial attempts to first directly generate the free amine and subsequently perform reactions with the *N*-hydroxysuccinic ester of γ-maleimidobutyric acid (GMB) led to capricious results. In contrast, reproducible results were only obtained by generating the free amine in situ as the final component of this reaction, concomitantly trapping the amine with the GMB. As such, routine production of the GA derivative, 17-GMB-ABA-GA, suitable for conjugation to proteins or peptides in reasonably large amounts was achieved in good yield and excellent purity.

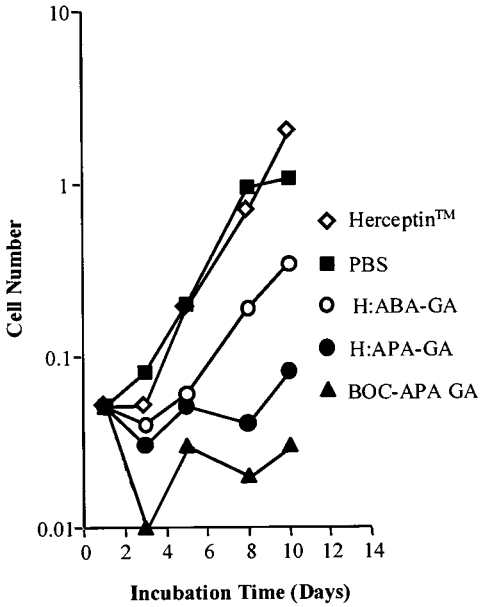


Figure 3. Effect of GA immunoconjugates on cellular growth rate of HER2-overexpressing cells. MDA-361/DYT2 cells were treated with 0.5 mg/mL Herceptin or GA immunoconjugate. Cell numbers were determined every 48 h, for 12 days. Cell doubling times for the PBS, Herceptin, H:ABA-GA, and H:APA-GA-treated cultures were 1.4, 1.6, 6.2, and greater than 12 days, respectively.

This product, as well as the previously reported 17-GMB-ABA-GA, were each conjugated to Herceptin, as described in the Experimental Procedures (*15*, *16*). Previously, the purity of the 17-GMB-ABA-GA had been assessed by analytical SE-HPLC and shown to be essentially congruent with Herceptin (*15*). This observation was duplicated by sodium dodecyl sulfate−polyacrylamide gel electrophoresis (SDS−PAGE). Thus, in this current study, SDS−PAGE was employed to confirm the absences of conjugation reaction byproducts. All of the conjugates employed herein were found to be comparable to Herceptin as determined by SDS−PAGE (data not shown).

The immunoreactivity of H:APA-GA was not compromised by this conjugation process to any detectable level as measured in binding assays. The absolute amount of bound immunoconjugate to MDA-361/DYT2 cells was 13% ± 1% for both H:APA-GA and parental Herceptin using 1.0×10^6 cells. Binding was even higher (~91 ± 2% for Herceptin and H:APA-GA) when the assay was performed with NIH3T3/HER cells, consistent with the fact that the amount of HER2 antigen was higher on the surface of these cells. To support the characterization of the immunoconjugate, the K_d values for Herceptin and the H:APA-GA, as obtained from Scatchard plot analysis, were determined. The K_d values clearly were not significantly different, 4.2 ×and 3.8×10^{-9} M for H:APA-GA and Herceptin, respectively, and were consistent with previously reported values for Herceptin (*23*).

The biological activity of 17-APA-GA was reported to be approximately 3-fold higher than that of 17-ABA-GA (*16*). Thus, the immunoconjugate formed with 17-GMB-APA-GA, H:APA-GA, was expected to exert a stronger inhibitory activity compared with H:ABA-GA. The antiproliferative activity of the two immunoconjugates was evaluated using MDA-361/DYT2 cells and is displayed in Figure 3. Cell growth rate was measured in cultures treated with either 0.5 mg/mL of Herceptin, H:ABA-GA, or H:APA-GA. The effect of Herceptin alone was marginal

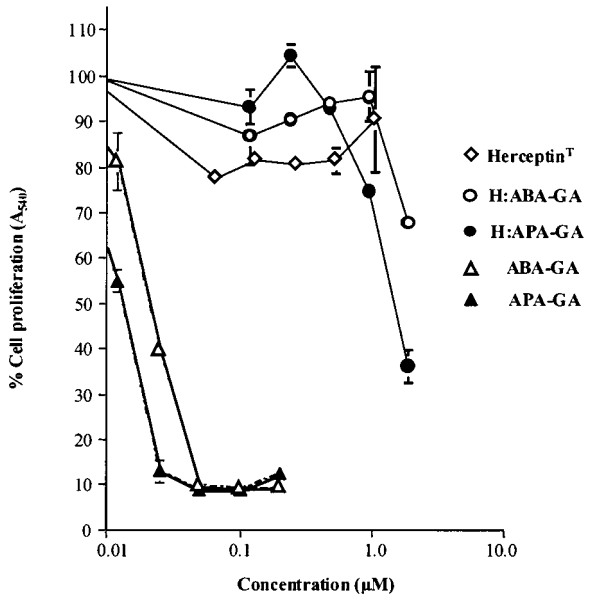


Figure 4. Dose−response curves obtained from MDA-361/DYT2 cultures treated with increasing concentrations of either Herceptin, GA immunoconjugates, or GA derivatives alone. Doses are expressed in molarity of GA moeity, other than in the Herceptin alone samples. All samples were run in duplicate and are presented with SD bars.

while both immunoconjugates inhibited cellular growth. As expected, the H:APA-GA showed higher efficacy than H:ABA-GA, maintaining the cultures at no apparent growth for 8 days. Cell doubling times for the control (PBS) and Herceptin-treated cultures were 1.4 and 1.6 days, respectively, while for H:ABA-GA this was 6.2 days. In contrast, the doubling time of the H:APA-GA-treated cultures exceeded 12 days. The IC_{50} values of H:APA-GA and H:ABA-GA were determined from seven separate experiments to be 0.2 ± 0.03 and 0.58 ± 0.02 mg/mL, respectively, and a representative experiment is shown in Figure 4. In contrast, IC_{50} values for native Herceptin could not be determined because the maximal inhibition of unmodified Herceptin reached only 25%, even at concentrations higher than 10 mg/mL (Figure 4).

The specificity of cell targeting was addressed in our earlier publications on GA immunoconjugates (*15*−*17*). In brief, anti-HER2:GA immunoconjugates were demonstrated to not inhibit proliferation of HER2-negative cells, such as the lymphocytic cell line HuT102. These immunoconjugates also did not inhibit the proliferation carcinoma cells with normal HER2 expression, such as A431 or MCF-7 cells. The inverse condition was also demonstrated, that is, that GA immunoconjugates comprised of irrelevant mAbs did not affect HER2-positive cells and that, in all cases, selective internalization was crucial for efficacy.

Concurrent with our ongoing studies, Kasuya et al. reported a similar finding concerning the isolable nature of the propylamine-derivatized GA via a protonation procedure that was used postreaction between GA and 1,3-diaminopropane (*24*). The procedure provided here is believed to offer some advantages in that complete obviation of the competing cyclization reaction was achieved and that both the carbamate-protected GA and protonated-deprotected GA are then readily available for subsequent chemical modification. While chromatographic separation steps were required to obtain the carbamate-protected GA as well as the 17-GMB-APA-GA in high purity, these operations were not difficult. In the case of the former compound, this did eliminate the consistently present impurity that arose from addition of a second molecule of reagent to GA.

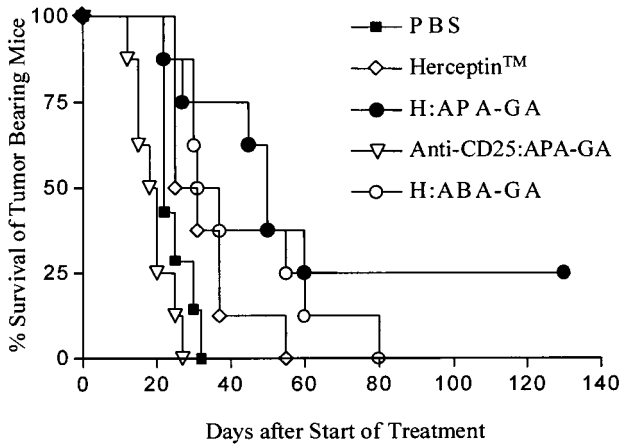


Figure 5. Effect of GA immunoconjugates on survival of MDA-361/DYT2 sc xenograft (15−20 mm^3) bearing athymic mice (n = 8/group). Reagents were given ip at 3 day intervals at 4 mg/kg and were continued for 3 months.

Recently, Kasuya et al. also reported the preparation of a GA immunoconjugate that targets ovarian cancer cells (*25*). They employed different chemistry creating a polymeric form of APA-GA with *N*-(2-hydroxyproply)-methacrylamide (HPMA) that could be conjugated to the anti-OA-3 mAb, OV-TL16. This conjugation strategy was designed to form a lysosomally degradable linkage that efficiently releases GA intracellularly. The linkage of 17-APA-GA to HPMA significantly reduced the antiproliferative activity, with a 40-fold increase of the IC_{50} value (19 μM in A2780 cells) and the final product (anti-OA-3:GA immunoconjugate) had modest activity, similar to the nonspecific conjugate of GA with bovine serum albumin.

H:ABA-GA and H:APA-GA were then tested for their in vivo efficacy in a xenograft model of MDA-361/DYT2 tumors that were transplanted sc into athymic mice. Therapy was initiated when tumors had reached a detectable size (15−20 mm^3) as described in the Experimental Procedures. The administration regimen was chosen to mimic a dose used in patients (4 mg/Kg) and corresponded to $t_{1/2}$ (*17*) (i.e., ip injections every 3 days through 120 days). Efficacy was determined on the basis of survival and tumor progression. As shown in Figure 5, the survival of Herceptin-treated recipients was prolonged compared with that of the placebo group. The H:ABA-GA and H:APA-GA conjugates prolonged survival even further, but neither Herceptin nor the H:ABA-GA were able to induce a complete, stable tumor regression. However, treatment with the H:APA-GA immunoconjugate induced permanent tumor regression in 2/8 recipients. No tumors were detectable by visual inspection, even after 4 months had elapsed, 1 month after the ip injection treatment had been halted. Thus, H:APA-GA was qualitatively superior to H:ABA-GA because this immunoconjugate could cure a fraction of the recipient mice while H:ABA-GA, in repeated experiments, was only able to retard tumor growth.

In this study, we have demonstrated that the strategy of BOC protecting and acid deprotection allowed production of large quantities of the desired 17-GMB-APA-GA in excellent purity. Thus, the previously encountered technical obstacles to larger-scale production of 17-APA-GA immunoconjugates have been eliminated. Conjugation of 17-GMB-APA-GA to the anti-HER2 mAb Herceptin resulted in an immunoconjugate with enhanced

antiproliferative action when compared with that of the native mAb. More importantly, this immunoconjugate is superior to the previously studied immunoconjugate, H:ABA-GA, and shows significantly improved efficacy in vivo.

ACKNOWLEDGMENT

The authors thank Robert Cohen and Mark Sliwkowski, Genentech Inc., for their generous supply of Herceptin, and the Laboratory of Analytical Chemistry, NIDDK, for their assistance in obtaining detailed mass spectra data for all of the geldanamycin derivatives.

LITERATURE CITED

(1) DeBoer, C., Meulman, P. A., Wnuk, R. J., and Peterson, D. H. (1970) Geldanamycin, a new antibiotic. *J. Antibiot. 23*, 442−447.

(2) Neckers, L., Schulte, T. W., and Mimnaugh, E. (1999) Geldanamycin as a potential anti-cancer agent: Its molecular target and biochemical activity. *Invest. New Drugs 17*, 361−373

(3) Sausville, E. A. (2001) Combining Cytotoxics and 17-Allylamino, 17-Demethoxygeldanamycin: Sequence and Tumor Biology Matters. *Clin. Cancer Res. 7*, 2155−2158.

(4) Schnur, R. C., Corman, M. L., Gallaschun, R. J., Cooper, B. A., Dee, M. F., Doty, J. L., Muzzi, M. L., Moyer, J. D., DiOrio, C. I., Barbacci, E. G., Miller, P. E., O'Brien, A. T., Motin, M. J., Foster, B. A., Polack, V. A., Savage, D. M., Sloan, D. E., Pustilnik, L. R., and Moyer, M. P. (1995) Inhibition of the Oncogene Product $p185^{erbB-2}$ in Vitro and in Vivo by Geldanamycin and Dihydrogeldanamycin. *J. Med. Chem. 38*, 3806−3812.

(5) Wilson, R. H., Takimoto, C. H., Agnew, E. B., Morrison, G., Grollman, F., Thomas, R. R., Saif, M. W., Hopkins, J., Allegra, C., Grochow, L., Szabo, E., Hamilton, J. M., Monahan, B. P., Neckers L., and Grem, J. L. (2001) Phase I pharmacologic study of 17-(allylamino)-17-demethoxygeldanamycin (AAG) in adult patients with advanced solid tumors. *Proc. Am. Soc. Clin. Oncol., 37th Annual Meeting*, San Francisco, CA, May 11−16, 2001.

(6) Munster, P. N., Tong, W., Schwartz, L., Larson, S., Kenneson, K., De La Cruz, A., Rosen, N., and Scher, H. (2001) Phase I trial of 17-(allylamino)-17-demethoxygeldanamycin (17-AAG) in patients with advanced solid malignancies. *Proc. Am. Soc. Clin. Oncol., 37th Annual Meeting*, San Francisco, CA, May 11−16, 2001.

(7) Preijers, F. W. M. B., Tax, W. J. M., De Witte, T., Janssen, A., Heijden, H. V. D., Vidal, H., Wessels, J. M. C., and Capel, P. J. A. (1988) Relationship between internalization and cytotoxicity of ricin A-chain immunotoxins. *Br. J. Haematol. 70*, 289−294.

(8) King, D. J. (1998) *Applications and Engineering of Monoclonal Antibodies*, Chapter 4, pp 119−160, Taylor and Francis Inc., Philadelphia, PA.

(9) Tolcher, A. W., Ochoa, L., Patnaik, A., Hammond, L., Hildalgo, M., Edwards, T., Drengler, R., Erickson, J., DeWitte, M., Desai, K., Chari, R., Lambert, J., and Rowinsky, E. K. (2001) SB-408075, a tumor-activated prodrug maytansinoid immunoconjugate directed to the C242 antigen: a phase I pharmacokinetic and biologic correlative study. *Proc. Am. Soc. Clin. Oncol., 37th Annual Meeting*, San Francisco, CA, May 11−16, 2001.

(10) Frankel, A. E., Sievers, E. L., and Scheinberg, D. A. (2000) Cell Surface Receptor-Targeted Therapy of Acute Myeloid Leukemia: A Review. *Cancer Biother. Radiopharm. 15*, 459−476.

(11) Baselga, J. (2001) Clinical Trials of Herceptin. *Eur. J. Cancer 37*, S18−S24.

(12) Slamon, D. J., Clark, G. M., Wong, S. G., Levin, W. J., Ullrich, A., and McGuire, W. L. (1987) Human Breast Cancer: Correlation of Relapse and Survival with Amplification of the HER-2/neu Oncogene. *Science 235*, 177−182.

(13) Muss, H. B., Thor, A. D. Berry, D. A., Kute, T., Liu, E. T., Koerner, F., Cirrincione, C. T., Budman, D. R., Wood, W. C., Barcos, M., and Henderson, I. C. (1994) c-erbB-2 Expression and Response to Adjuvant Therapy in Women with Node-Positive Early Breast Cancer. *N. Engl. J. Med. 330*, 1260−1266.

(14) Zheng, F. F., Kuduk, S. D., Chiosis, G., Munster, P. N., Sepp-Lorenzino, L., Danishefsky, S. J., and Rosen, N. (2000) Identification of a geldanamycin dimer that induces the selective degradation of HER-family tyrosine kinases. *Cancer Res. 60*, 2090−2094.

(15) Mandler, R, Dadachova, E., Brechbiel, J. K., and Brechbiel, M. W. (2000) Synthesis and Evaluation of Anti-Proliferative Activity of a Geldanamycin-Herceptin Immunoconjugate. *Bioorg. Med. Chem. Lett. 10*, 1025−1028.

(16) Mandler, R., Wu, C., Sausville, E. A., Roettinger, A. J., Newman, D. J., Ho, D. K., King, C. R., Yang, D., Lippman, M. E., Landolphi, N. F., Dadachova, E., Brechbiel, M. W., and Waldmann, T. A. (2000) Immunoconjugates of Geldanamycin and Anti-HER2 Monoclonal Antibodies: Antiproliferative Activity on Human Breast Carcinoma Cell Lines. *J. Natl. Cancer Inst. 92*, 1573−1581.

(17) Mandler, R., Hinson, E. R., Davis, M. Y., Sausville, E. A., Newman, D. J., Yang, D., Roettinger, A. J., Brechbiel, M. W., and Waldmann, T. A. (2001) Herceptin: geldanamycin immunoconjugates augment the efficacy of Herceptin in mice bearing HER2-overexpressing xenografts. *Clin. Cancer Res. 7*, 3786S−3786S.

(18) Kitagawa, T., Kawasaki, T., and Munechik, H. (1982) Enzyme immunoassay of blasticidin S with high selectivity: A new and convenient method for preparation of immunogenic (hapten-protein) conjugates. *J. Biochem. 92*, 585−590.

(19) Yang, D., Kuan, C. T., Payne, J., Kihara, A., Murray, A., Wang, L. M., Alimandi, M., Pierce, J. H., Pastan, I., and Lippman, M. E. (1998) Recombinant heregulin-Pseudomonas exotoxin fusion proteins: interactions with the heregulin receptors and antitumor activity in vivo. *Clin. Cancer Res. 4*, 993−1004.

(20) Heidaran, M. A., Fleming, T. P., Bottaro, D. P., Bell, G. I., Di Fiore, P. P., and Aaronson, S. A. (1990) Transformation of NIH3T3 fibroblasts by an expression vector for the human epidermal growth factor precursor. *Oncogene 5*, 1265−1270.

(21) Kobayashi, H., Sakahara, H., Saga, T., Hosono, M., Shirato, M., Kanda, H., Ishibashi, K., Watanabe, T., Endo, K., Ishiwata, I., and Konishi, J. (1993) A human/mouse chimeric monoclonal antibody against CA125 for radioimmunoimaging of ovarian cancer. *Cancer Immunol. Immunother. 37*, 143−149.

(22) Kobayashi, H., Le, N., Kim, I. S., Kim, M.-K., Pie, J.-E., Drumm, D., Paik, D. S., Waldmann, T. A., Paik, C. H., and Carrasquillo, J. A. (1999) The pharmacokinetic characteristics of glycolated humanized anti-Tac Fabs are determined by their isoelectric points. *Cancer Res. 59*, 422−430.

(23) Carter, P., Presta, L., Gorman, C. M., Ridgway, J. B. B., Henner, D., Wong, W. L. T., Rowland, A. M., Kotts, C., Carver, M. E., and Shepard, H. M. (1992) Humanization of an anti-$p^{185/HER2}$ antibody for human cancer therapy. *Proc. Natl. Acad. Sci. U.S.A. 89*, 4285−4289.

(24) Kasuya, Y., Lu, Z.-R., Kopeckova, P., and Kopecek, J. (2001) Improved synthesis and evaluation of 17-substituted aminoalkylgeldanamycin derivatives applicable to drug delivery systems *Bioorg. Med. Chem. Lett. 11*, 2089−2091.

(25) Kasuya, Y., Lu, Z.-R., Kopeckova, P., Minko, T., Tabibi, S. E., and Kopecek, J. (2001) Synthesis and characterization of HPMA copolymer-aminopropylgeldanamycin conjugates. *J. Controlled Release 74*, 203−211.

BC010124G

Selective Adsorption of Serum Albumin on Biomedical Polyurethanes Modified by a Poly(ethylene oxide) Coupling-Polymer with Cibacron Blue (F3G-A) Endgroups

Dong-an Wang,*[,†,‡] Bao-lin Chen,[†,§] Jian Ji,[†] and Lin-xian Feng[†,||]

Department of Polymer Science and Engineering, Zhejiang University, Hangzhou, 310027, P. R. China, Department of Pharmaceutical Sciences, University of Tennessee Health Science Center, Memphis, Tennessee 38163, and Department of Chemistry, Inner Mongolia Hulunbeier Collage, Hailaer, 021008, P. R. China . Received January 22, 2002; Revised Manuscript Received April 3, 2002

A tri-*block*-coupling polymer, "PEO−MDI−PEO" ["poly(ethylene oxide)−4,4′-methylene diphenyl diisocyanate−poly(ethylene oxide)", abbreviated "MPEO"], was used to react with a triazine dye, Cibacron Blue F3G-A (ciba), in an alkaline environment. The product of this nucleophilic reaction was a penta-*block*-coupling polymer, "ciba-PEO-MDI-PEO-ciba" (abbreviated "cibaMPEO"). The cibaMPEO-modified poly(ether urethane) (PEU) surfaces were prepared by dip-coating and detected by XPS. The surface enrichment of both ciba endgroups and poly(ethylene oxide) spacer-arms was revealed. On the modified surfaces, bovine serum albumin (BSA)-adsorbing experiments were carried out, respectively, in the low and high BSA bulk-concentration solutions, and accordingly, the methods of radioactive ^{125}I-probe and ATR-FTIR were, respectively, employed for the characterization. The competitive adsorption of BSA and bovine serum fibrinogen (Fg) in the BSA−Fg binary solutions was also studied using a ^{125}I-probe, and through which the reversibly BSA-selective adsorption on cibaMPEO-modified PEU surfaces was confirmed. Finally, the improvement of blood-compatibility on the modified surfaces was verified by the plasma recalcification time (PRT) test.

INTRODUCTION

The implantable biomedical devices made of polymeric materials, such as blood-contacting intravascular catheters, have been extensively utilized for the interventional treatments in clinical practice. However, the surfaces of these devices may promote the in situ blood coagulation, microbial infections, and consequent inflammatory reactions (*1*, *2*). It is believed that these iatrogenic effects are likely to be mediated by adsorbed host proteins on the device surfaces (*3*, *4*). It is also widely accepted that albumin-coated surfaces can minimize those harmful effects (*5*, *6*). Thus, a series of novel surface-modifying additives (SMA) were specially designed to develop surfaces that would selectively bind the host albumin.

In our study, a triazine dye, Cibacron Blue F3G-A (abbreviated "ciba") (Schemes 1, 2) and the polymeric material poly(ethylene oxide) (PEO) were employed as the two main components of the SMA. Ciba possesses the capacity to selectively bind the host albumin. It is proposed that the binding of ciba to human serum albumin (HSA) is at the bilirubin-binding sites and ciba's binding to bovine serum albumin (BSA) is at the fatty acid-binding sites (*7*, *8*). PEO is a well-known and very useful biomaterial. Under aqueous physiological conditions, hydrophilic PEO has high kinetic chain mobility and large thermodynamical steric volume (*9*), leading to the repulsion of almost all kinds of foreign adherence and adsorption. Accordingly, for the SMA in our study, ciba was introduced as the functional endgroup, and the PEO chains were employed as the spacer-arms. We hypothesize that on the modified surface, ciba will selectively bind the host albumin, while the PEO will be resistant to the adsorption of the tangible humoral (particularly haemal) components such as proteins and cells. As the endgroup, ciba's presence on the blood−polymer interface would depend on the support from the hydrophilic PEO backbones, and the activity of ciba would also be provided by the mobility of PEO chains. Because of this proposed cooperative effect between the PEO spacer and ciba endgroup of SMA, the biocompatibility of the medical device was expected to be improved.

The SMA in our study is a penta-*block*-coupling polymer of "ciba−PEO−4,4′-methylene diphenyl diisocyanate (MDI)−PEO−ciba" (abbreviated "cibaMPEO") (Schemes 1, 2), which was a product of the nucleophilic reaction between ciba and the preproduct, a tri-*block*-coupling polymer of "PEO−MDI−PEO" (abbreviated "MPEO") (Scheme 1) (*10*, *11*). The matrix material of the medical device in this paper was poly(ether urethane) (PEU). The expedient dip-coating method of surface modification was selected. According to the conclusions from our earlier studies (*10*, *11*), H-bonds will be formed between the middle MDI-blocks of cibaMPEO and the "hard" blocks of PEU chains (Scheme 2), by which the stability of the coating can be ensured.

The adsorbing experiments of BSA and/or fibrinogen (Fg) were carried out on the modified surfaces. The systemic quantitative analysis was performed using attenuated total reflection (ATR) FT-IR spectroscopy (*12*, *13*) for the experiments with high BSA-bulk-concentra-

* Current address of the corresponding author: Dong-an Wang, Ph.D., Department of Pharmaceutical Sciences, University of Tennessee Health Science Center, 26 South Dunlap St., Room 406, Memphis, TN 38163, Tel: (901) 448-6848, Fax: (901) 448-6092, E-mail: danielwda@netzero.net.

† Zhejiang University.

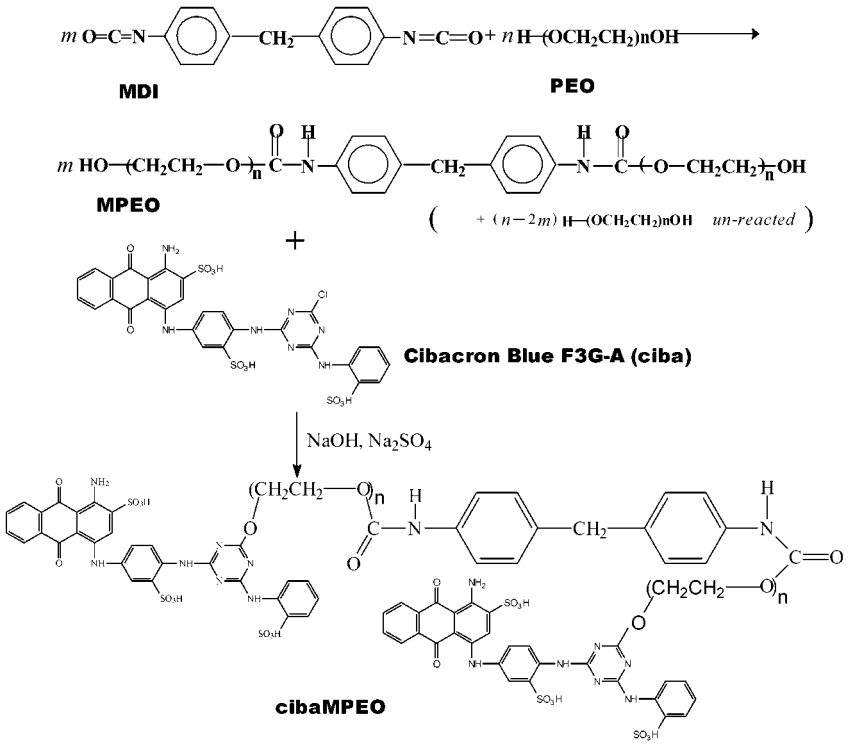
‡ University of Tennessee Health Science Center.

§ Inner Mongolia Hulunbeier Collage.

|| Deceased on July 26, 2001.

10.1021/bc0255079 CCC: $22.00 © 2002 American Chemical Society
Published on Web 06/22/2002

Scheme 1. Synthesis Routes of MPEOs and CibaMPEOs



tion solutions and using a radioactive ^{125}I-labeled probe (*8*) for the experiments with low BSA- and/or Fg-bulk-concentration solutions. Finally, for characterization of anticoagulation, measurements of plasma recalcification time (PRT) (*14*) were carried out.

EXPERIMENTAL SECTION

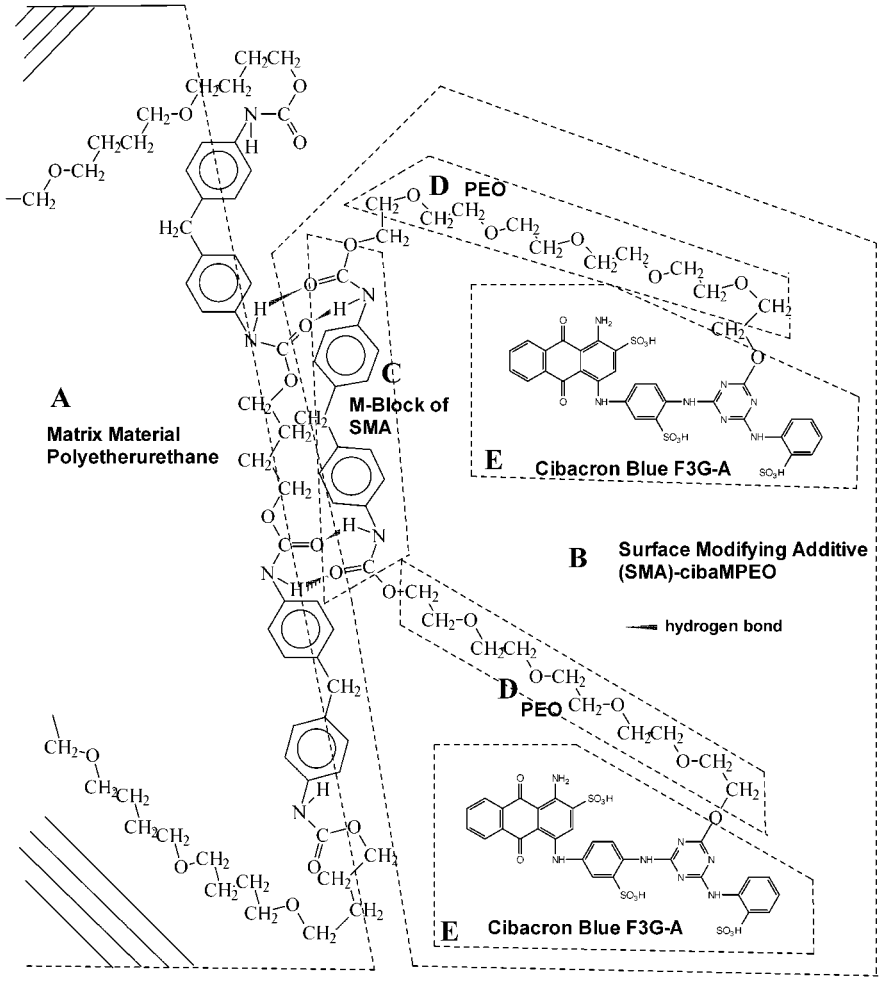
Preparation of SMA−CibaMPEO and Modified PEU Surfaces. *Preparation of MPEO and CibaMPEO.*The synthesis and purification of MPEO (PEO MW 1000, 2000, 6000, and 10000; the corresponding MPEO were named MPEO1k, -2k, -6k, and -10k) were reported previously (*10*). The preparation of SMA−cibaMPEO (Scheme 1) was based on the nucleophilic substitution of the Cl^- on ciba (Cibacron Blue; purchased from Sigma Chemical Co., St. Louis, MO, C9534) by MPEO's hydroxyl endgroup (*15*). MPEO (MPEO1k, -2k, -6k, and 10k, respectively, 5.0 g) and ciba (accordingly 1.00, 0.5, 0.33, and 0.10 g) were dissolved in deionized water (10 mL) with NaOH (1.12 g) and anhydrous Na_2SO_4 (0.48 g). The mixture was moderately stirred at room temperature for 12 h. Ice-cold acetic acid (1.6 mL) was added to terminate the reaction by neutralizing the medium. The product was dried over magnesium sulfate and concentrated in vacuo. The residue was further dried under high vacuum overnight at 60 °C. The resulting blue powders were washed and filtered with tetrahydrofuran to remove the insoluble salts and unreacted ciba. Finally, graded precipitation was carried out with ethyl ether to isolate the desired blue products from the unreacted MPEO, which was monitored by the resulting color and GPC (Baseline 810 method, Waters). The corresponding final products were respectively named cibaMPEO1k, -2k, -6k, and 10k. ^{1}H NMR spectroscopy (500 MHz, AVANCE DMX500, Bruker; solvent DMSO-d_6, Aldrich) and XPS (ADXPS, VG Instruments) were used for characterization.

Preparation of CibaMPEO-Modified PEU Surfaces. The sheets (80 mm × 10 mm × 2 mm) of poly(ether urethane) (PEU, Pellethane 2363−80AE, Dow Chemical) were used as the matrix material, and the PEU pellets were used as the film-building additive (FBA) for coating. FBA−PEU has been extracted with alcohol in a soxhlet extractor for 72 h to remove the processing aid (stearamide additive) (*16*). The coating solution was obtained by dissolving SMA−cibaMPEO and FBA−PEU together into tetrahydrofuran and then diluting with equal volume of alcohol. The dosage ratio of cibaMPEO/PEU was 3:2 (w/w), and the concentration of cibaMPEO was 4% (w/v). The dip-coating process was performed on an electric lifter. The matrix-PEU sheets were vertically dipped into and then lifted out of the coating solution with constant speed followed by drying in a vacuum for 30 min. The process was repeated three times. Two kinds of control sample, which was respectively coated only with the FBA−PEU or only with MPEO/FBA−PEU, were also prepared. XPS was used to analyze the modified PEU surfaces (PEU-control, ctMPEO2k, ct-cibaMPEO1k, -2k, -6k, and -10k).

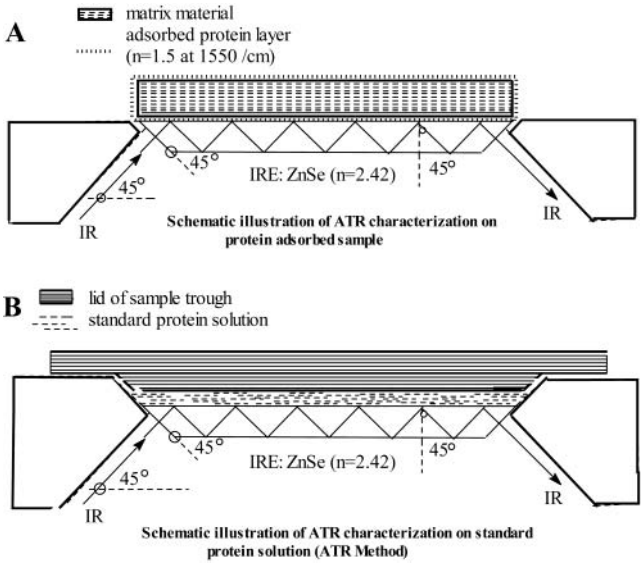
Preparation of Protein-Adsorbed Surfaces. *Proteins and Buffers.* Bovine serum albumin (BSA) was provided by Sigma (A-2153, protein content 96−99%, M_n 66,210, refraction index $n_2 = 1.5$ at infrared absorbance 1550 cm^{-1} (*12*)). Bovine serum fibrinogen (Fg) was also from Sigma (F-8630, protein content 74% (Biuret), clottable protein 87%, 10% sodium citrate, 15% NaCl). Fg was purified by dialysis with dialysis sacks (Sigma 250-7U, retains proteins with $M_n > 12000$) and stored under −20 °C. The tris(hydroxyethyl)methylaminomethane (A.R., abbreviated "Tris") and glycine (A.R., abbreviated "Gly") were from Shanghai Bio-Chem. Co. The buffers of "Tris-HCl" solution (6.057 g Tris/water 1000 mL, pH 7.35−7.40) and "Gly-NaOH" solution (6 g Gly/water 80 mL, pH 8.80) were prepared. The Gly-NaOH buffer was stored under 4 °C. All the water used was double-distilled deionized water.

Radioactive Protein Probe. Radioactive Na^{125}I (25 mCi, original radiointensity 160−180 mCi/mL, without reductives, $t_{1/2}$ = 59.7 d) was provided by the Institute of

Scheme 2. Schematic Representation of the H Bond Incorporation between CibaMPEO and PEU



Scheme 3. Methods of Quantitative Characterization of (a) Protein-Adsorbed Samples and (b) Standard Protein Solutions by ATR-FT-IR



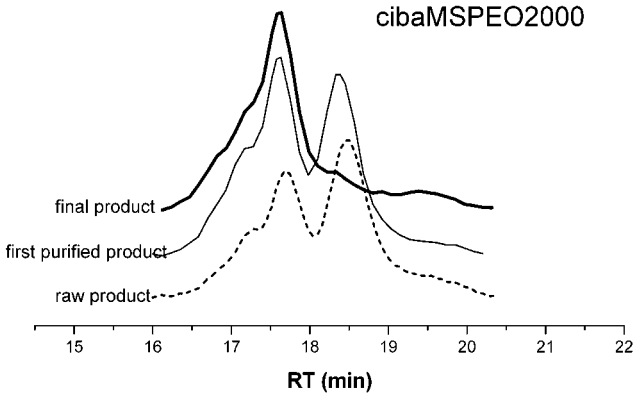


Figure 1. GPC spectra of cibaMPEO(2k) for the purification. The chromatographic peaks at approximately 17.5 min (RT) represent the product cibaMPEO; the peaks at approximately 18.5 min (RT) represent the unreacted MPEO.

Atomic Energy of China and was used within the first half of $t_{1/2}$. The preparation of ICl solution and the following ^{125}I-labeling of the protein were reported elsewhere (*17*). The radioactive protein probe was acquired by mixing the solution of protein (4 mg/0.1 mL) in Gly-NaOH into the solution of 0.01 mL of ICL/0.5 of mL Gly-NaOH/Na^{125}I (Na^{125}I dosage for BSA 0.2 mCi, for Fg 0.1 mCi) and then eluting with Tris-HCl through an alkali PS anion exchanger column (Shanghai Chemical Co.).

Protein Solutions. As for the protein-bulk-solution for adsorption and/or the protein-standard-solution for the calculation, the BSA, Fg, and the BSA−Fg binary solutions were respectively prepared in Tris-HCl buffer. The radioactive bulk solution was prepared by adding the radioactive protein probe into the solution containing 9 times as much non-radioiodine-labeled protein. The de-

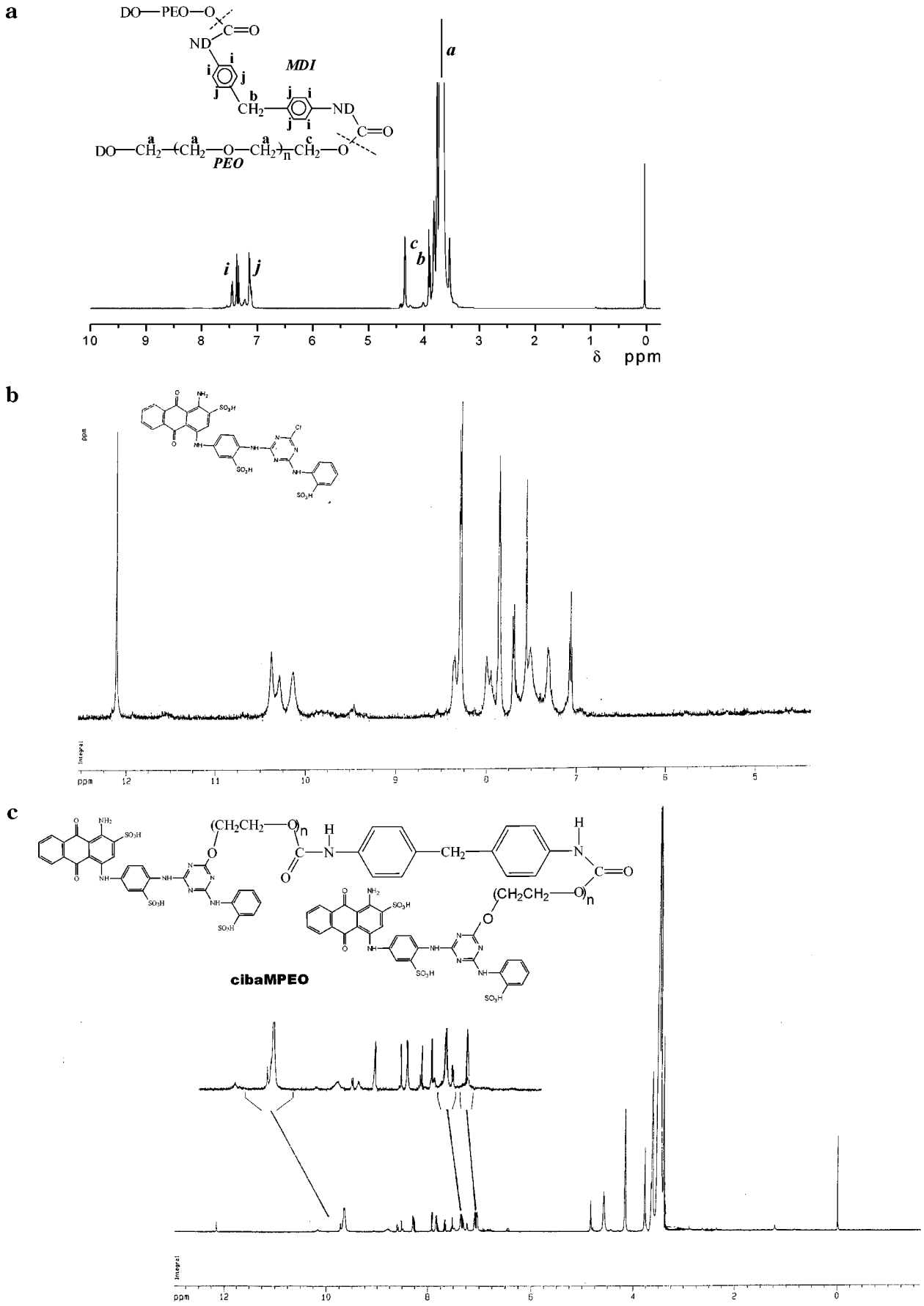


Figure 2. ^{1}H NMR spectra: (a) MPEO(2k), (b) Cibacron Blue F3G-A and (c) cibaMPEO(2k).

termination of concentration was performed through an ultraviolet (Beckman DU-50) method (*18*).

Adsorption Experiment. The modified sheets were previously equilibrated in water for 2 h, and the method

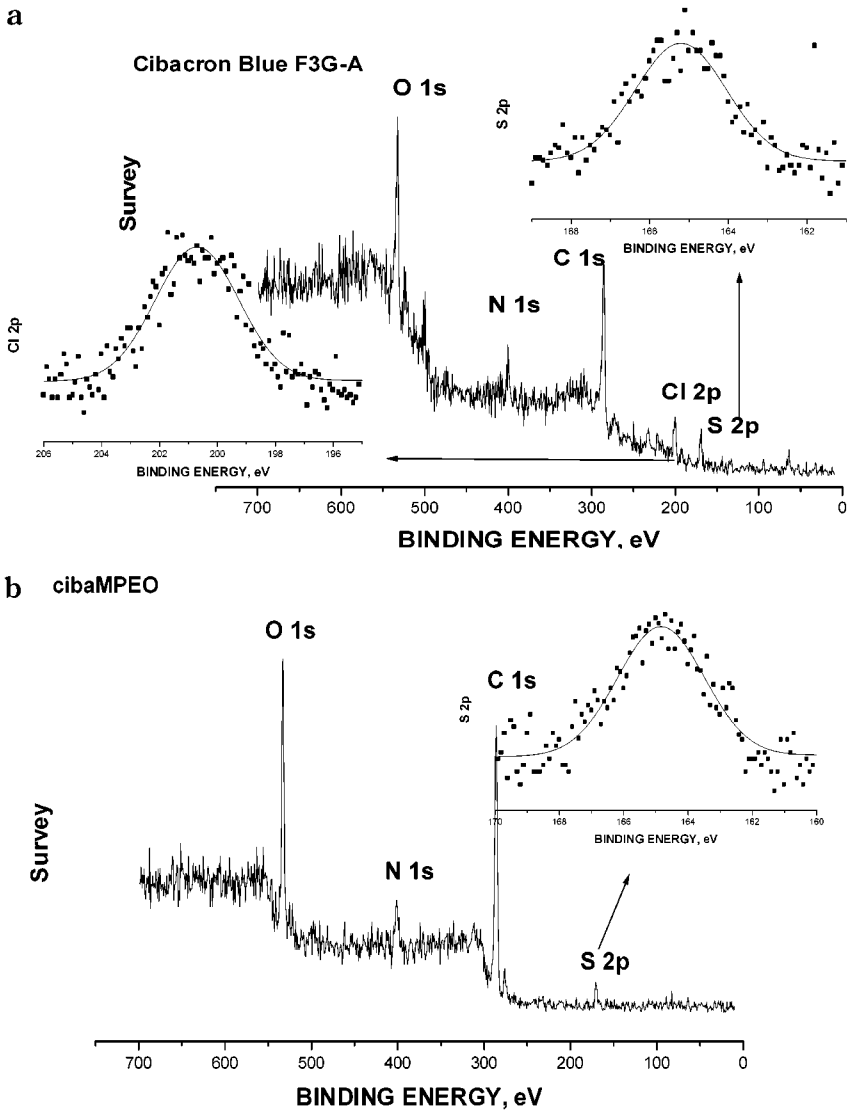


Figure 3. Survey XPS spectra of the powders: (a) Cibacron Blue F3G-A and (b) cibaMPEO(2k).

of adsorption followed a static immersing process in the protein-bulk-solution at 37 °C. After immersion, the residual solution on the surface of the samples was thoroughly removed by a centrifugal method instead of the popular rinsing method with protein-free buffer, to avoid the undesirable protein desorption by leaching and to maintain the original status on the polymer surfaces in the protein solution.

ATR-FTIR Analysis of BSA-Adsorbed Surfaces. ATR-FTIR (E.S.P., MAGNA-IR560, Nicolet; two types of ATR fittings respectively for solid samples (Scheme 3a) and solution (Scheme 3b); IRE crystal: ZnSe, sampling interface 80 mm × 10 mm, refractive index $n_1 = 2.42$, infrared internal reflecting angle *(θ)* 45°) was used to quantitatively characterize the adsorbed proteins (non-radioiodine-labeled). Thirty-two scans were performed. The blank sheet without BSA (or the solvent) was prescanned in a referenced infrared path to yield the background data, the corresponding BSA-adsorbed sample (or the protein solution) was scanned, and the nonprotein background was subtracted off automatically. The correct subtraction should make the region 1900−1720 cm^{-1} flat (*12*). BSA solutions (10.4 mg/mL and 30.6 mg/mL) were used as the parallel standard solution.

Static Isothermal Adsorption. The 5.0 mg/mL, 10.4 mg/mL, and 30.6 mg/mL BSA solutions were employed, and the time of adsorption was 30 min.

Static Adsorption Kinetics. The 30.6 mg/mL BSA solution was employed, and data at six time-points (0.5, 1, 5, 10, 30, and 60 min) were collected.

Adsorption Analysis of ^{125}I-Labeled Proteins A scintillation γ-ray counter (SN 682, Shanghai Institute of Atomic Nucleus) was used to quantitatively characterize the adsorbed proteins (radioiodine-labeled), and the data at six time-points (5, 10, 15, 30, 60, and 90 min) were respectively collected. The standard curve was obtained according to the radiocount from the standard ^{125}I-labeled protein solution.

Adsorption of ^{125}I-Labeled Proteins. The 0.4 mg/mL BSA solution and the 0.04 mg/mL Fg solution were respectively employed.

Selective Binding of Albumin in BSA−Fg Binary Protein System. Parallel adsorption on the same samples was carried out at the same time respectively in radioiodine-labeled BSA/nonlabeled Fg and nonlabeled BSA/radioiodine-labeled Fg binary solutions with the same protein concentrations. The compound results indicated the information of competitive adsorption. Two systems

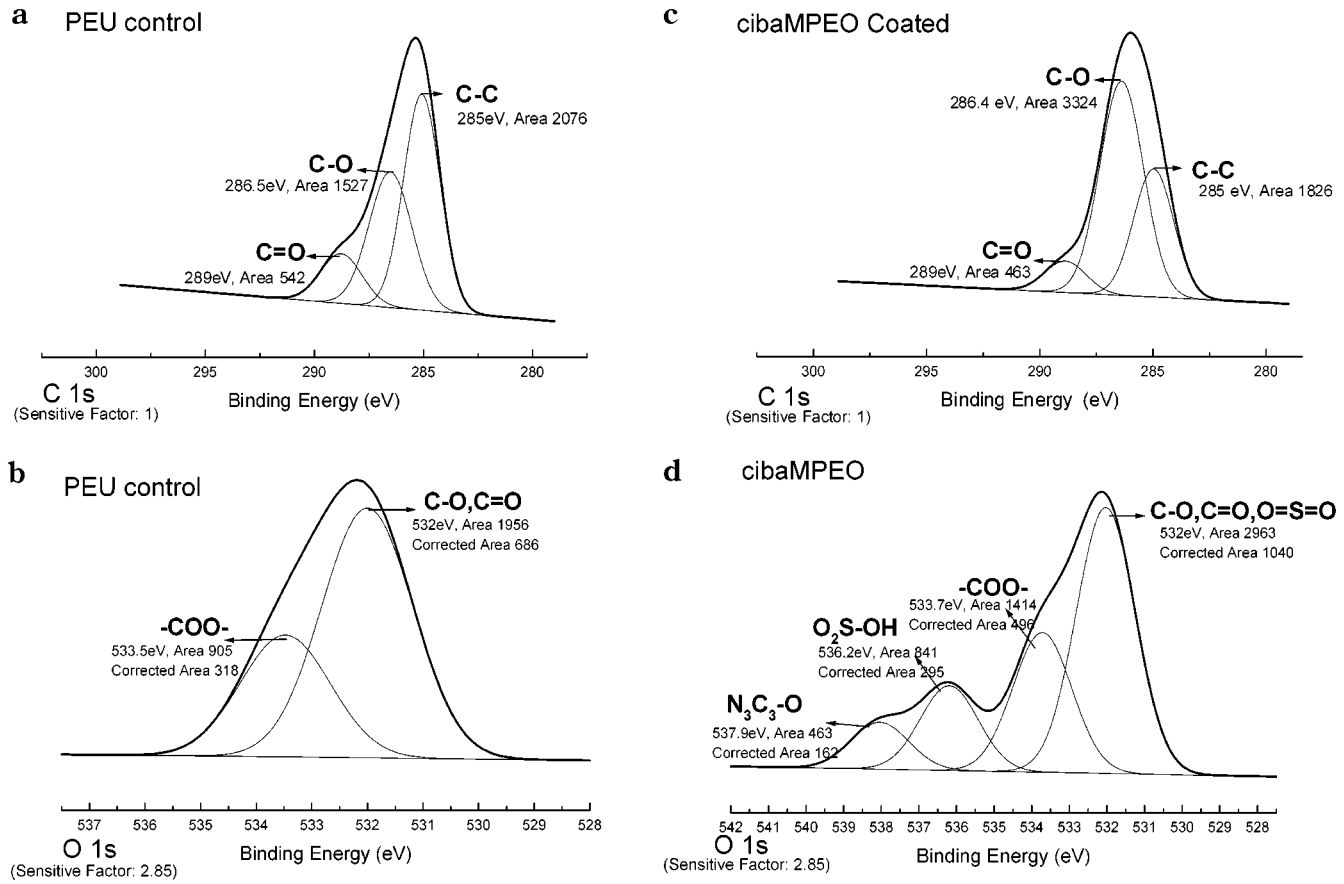


Figure 4. Curve-fit data of the XPS spectra: (a) and (b) respectively C 1s and O 1s peaks of PEU-control; (c) and (d) respectively C 1s and O 1s peaks of ct-cibaMPEO(2k).

of BSA−Fg binary solutions with the concentration of 0.8−0.02 and 0.8−0.06 (mg/mL) were employed, respectively.

Reversibility of Albumin Binding. After the samples had been immersed in 0.4 mg/mL radioiodine-labeled BSA solution for 60 min, the radioactive solution was replaced by non-radioiodine-labeled BSA solution with the same concentration. Then the data at three time-points, 5, 30, and 60 min (65, 90, and 120 min) were collected, respectively.

Plasma Recalcification Time Tests. Human plasma (0.1 mL, blood type B, Central Blood Bank of Hangzhou; containing ACD anticoagulant, without Ca^{2+}) and $CaCl_2$ solution (0.1 mL 0.025 mol/L) were respectively warmed to 37 °C and then were mixed in a test tube whose inner wall had been coated with the SMAs. At the same time, we began to stir the recalcified plasma with a small stainless steel hook and started to time it until the silky fibrin appeared. The duration was recorded as the plasma recalcification time (PRT).

RESULTS AND DISCUSSION

SMA−CibaMPEO and CibaMPEO-Modified PEU Surfaces. *Synthesis and Purification of SMA−CibaMPEO.* As described by Burton et al.,[15] following synthesis, the product was purified several times with ion exchanger. Finally, the dark blue polymeric powder of cibaMPEO was obtained. The GPC data (Figure 1, cibaMPEO2k) indicates that the ciba endgroups have changed the hydromechanical size of whole molecule dramatically, although the M_n of ciba is relatively small. The gradual flatting of the unreacted MPEOs' GPC peak at RT 18.4 min indicates that the product was purified. Figures 2a, 2b, and 2c are the ^1H NMR spectra of MPEO2k, ciba, and cibaMPEO2k, respectively, from which it can be observed that the spectrum of cibaMPEO combines all the typical peaks of ciba and MPEO. Moreover, when the XPS spectrain Figures 3a and 3b are compared, ciba powder and cibaMPEO2k powder, respectively, in the cibaMPEO2k spectrum (Figure 3b) the Cl-2p peak at approximately 201 eV has been eliminated, while the S-2p peak at approximately 165 eV is still present. All the data above indicate that the Cl^- of ciba has been nucleophilically substituted by the hydroxyl endgroup of MPEO and that the synthesis shown in Scheme 1 has been accomplished.

Surface Analysis on Modified PEU by XPS. From Figures 4a and 4c, the XPS C-1s region of PEU-control and ct-cibaMPEO2k, respectively, the ratio of C−O (286.5 eV)/C−C (285 eV) increases from 0.736 to 1.820. This ratio on PEU (on the soft blocks, poly(tetramethylene glycol)) is 2/3, while on cibaMPEO (on PEO segments) it is approximately 2; thus, the increase indicates the enrichment of PEO chains on the ct-cibaMPEOs. From Figures 4b and 4d, the XPS O-1s region of PEU-control and ct-cibaMPEO2k, respectively, it is indicated that the components of ciba have been introduced. Furthermore, the radiocount of O/C (has been corrected with the sensitive factor of oxygen 2.85) also has increased from 0.2422 to 0.3551. All of the data confirm the surface-content of both PEO and ciba.

ATR-FTIR Analysis of BSA-Adsorbed Surfaces. Due to the sensitivity and the operating conditions, the quantitative method of ATR-FTIR was specially used to deal with the BSA adsorption in the solution with a high BSA-bulk-concentration. In this paper, the concentration

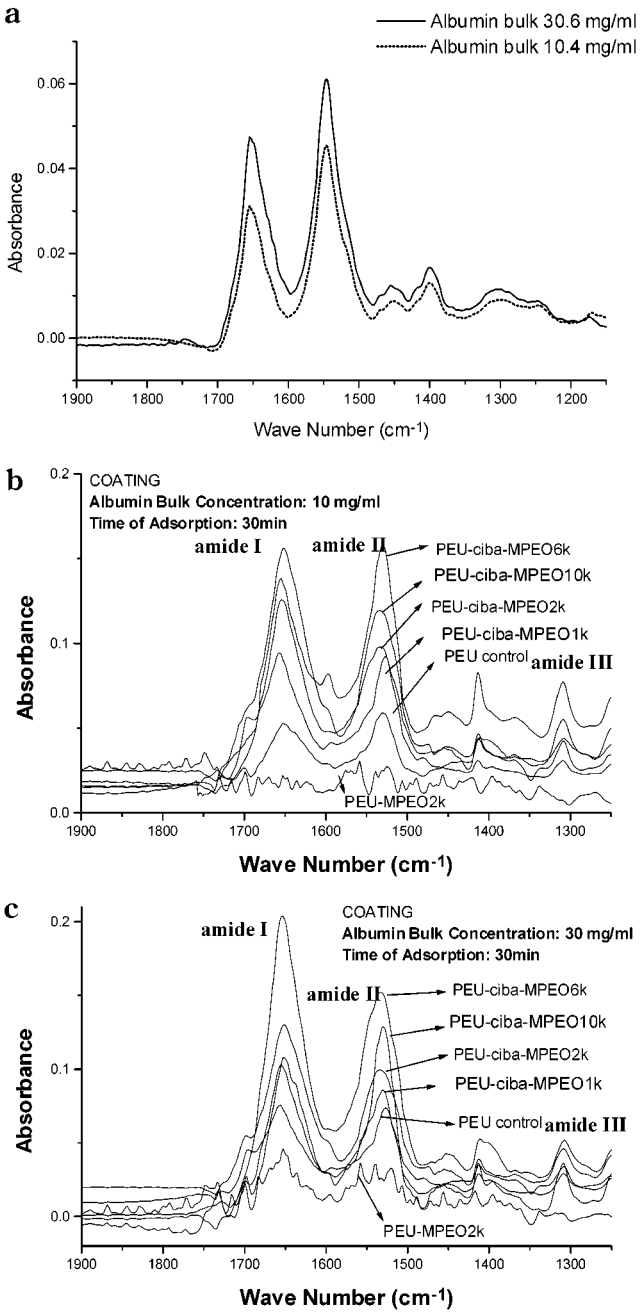


Figure 5. ATR−FT-IR spectra: (a) 30.6 mg/mL and 10.4 mg/ml standard BSA solution; ct-cibaMPEO(2k) from (b) 10.4 mg/mL BSA-bulk-solution and (c) 30.6 mg/ml BSA-bulk-solution.

was as high as 5.0−30.6 mg/mL. On the IR spectra, the integrated area of the protein-typical amide II band at 1550 cm^{-1} was obtained because its peak area can be related to the total amount of protein adsorbed at the interface (*19*, *20*). The horizontal baseline for integration was 1720−1480 cm^{-1}, and the region for integration was 1600−1480 cm^{-1} (*12*). The integrated area A_2 for BSA-adsorbed samples and A_s for standard solution is the average value of six parallel data.

The calculation of the adsorbing density on the modified PEU surfaces is based on the Tompkin equation (*21*),

$$\frac{A}{N}\frac{n_{21}E_0^2\epsilon}{\cos\theta}\int_0^\infty C(z)\exp\left(\frac{-2z}{d_p}\right)dz$$

where A is the integrated absorbance, N is the number of internal reflections, n_{21} is the index of refraction

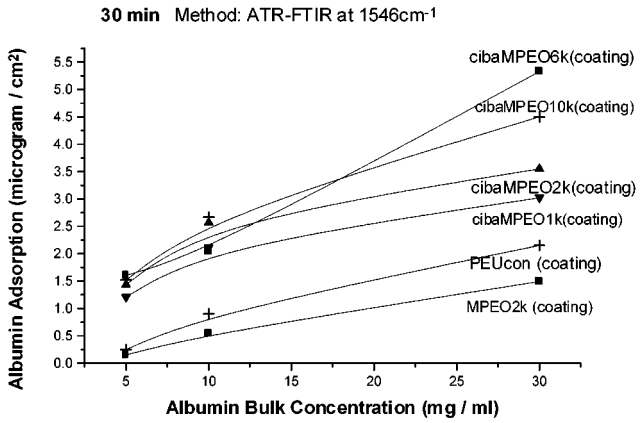


Figure 6. Curves of static isothermal BSA-adsorption: PEU-control, ctMPEO2k, and ct-cibaMPEOs, characterized by ATR-FTIR.

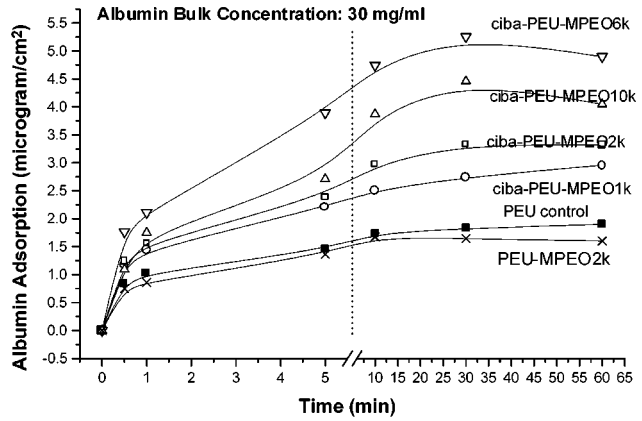


Figure 7. Curves of static BSA-adsorbing kinetics: PEU-control, ctMPEO2k, and ct-cibaMPEOs, characterized by ATR-FTIR.

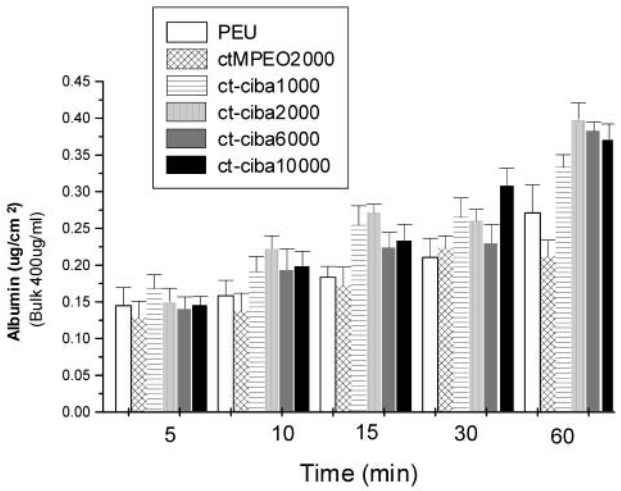


Figure 8. Static BSA-adsorbing data of PEU-control, ctMPEO2k, and ct-cibaMPEOs, characterized by radioactive ^{125}I-probe.

n_2/n_1, ϵ is the integrated molar absorptivity, θ is the incidence angle, $C(z)$ is the concentration as a function of distance z from the interface, E_0 is the electric field amplitude, d_p is the depth of penetration, $d_p = \lambda/[2\pi(n_1^2 \sin^2\theta - n_2^2)^{1/2}]$ (*21*), and λ is the infrared wavelength (6.45 μm, 1550 cm^{-1}). According to the results reported (*5*), besides the dimensions of the PEU sheet surface are exactly equal to that of the IRE testing interface, the

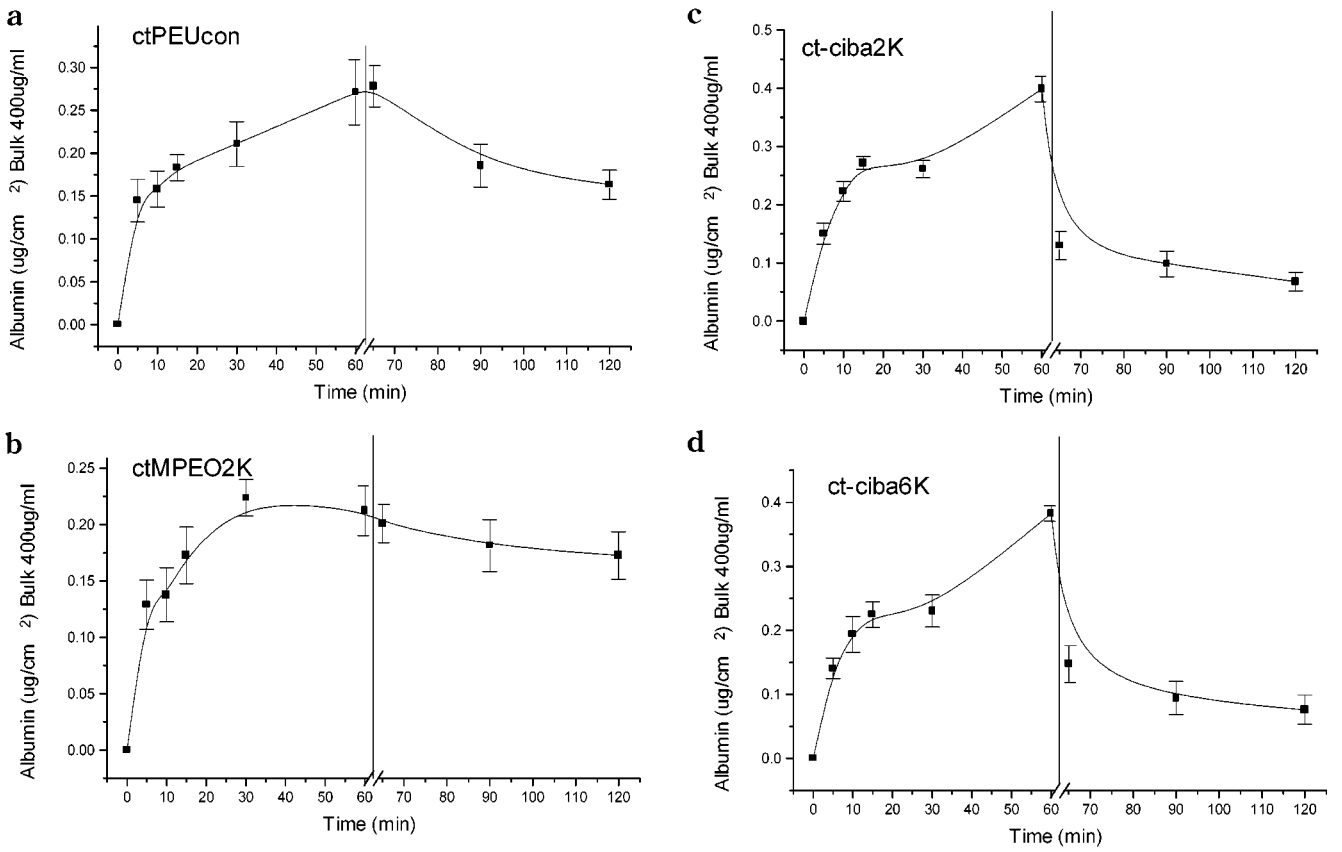


Figure 9. Curves of static BSA-adsorbing kinetics: (a) PEU-control, (b) ctMPEO2k, (c) ct-cibaMPEO2k, and (d) ct-cibaMPEO6k, characterized by radioactive ^{125}I-probe.

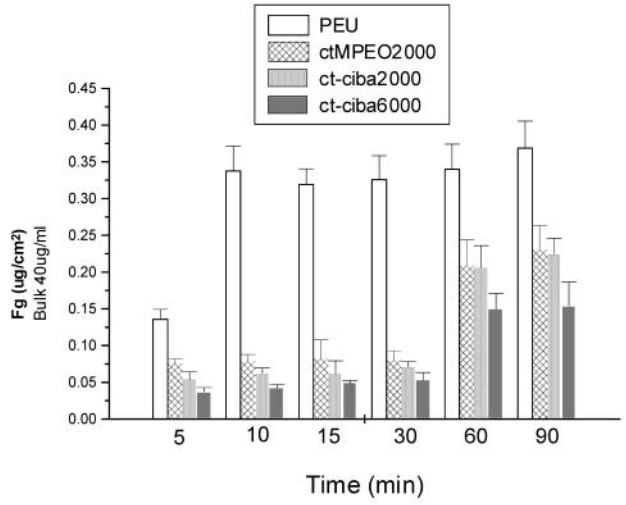


Figure 10. Static Fg-adsorption data of PEU-control, ctMPEO2k, and ct-cibaMPEOs, characterized by radioactive ^{125}I-probe.

equation can be simplified as $\Gamma = A_2C_sd_p/(2A_s)$, where Γ is the density of protein adsorption (μg/cm^2) and C_s is the concentration of standard protein solution.

Figure 5 shows the examples of ATR-FTIR spectra. Figures 5a, 5b, and 5c are respectively the spectra of BSA standard solutions, adsorbed BSA on the sample surfaces in 10.4 mg/mL bulk solution and that in 30.6 mg/mL bulk solution. Figure 6 is the isothermal curves of BSA-adsorption. It is observed that for all the samples, the relation between the amount of adsorbed BSA and the concentration of BSA-bulk-solution (5.0−30.6 mg/mL) is generally a linearly incremental change. In addition, the amount of adsorbed BSA on PEU-control was lower than that on the ct-cibaMPEOs, but higher than that on ctMPEO2k, which indicates the repulsion of the bare PEO chains to the BSA-adsorption and simultaneously demonstrated the outstanding BSA-binding capacity of ciba. The ascending BSA-adsorption from that on ct-cibaMPEO1k to that on ct-cibaMPEO6k indicates that the longer PEO chain is able to provide better support and higher mobility to ciba endgroups, which is due to the intrinsic property of PEO in aqueous environments (*9*). For ciba endgroups, better support from PEO will lead to a higher surface enrichment, and higher mobility means higher activity for BSA-binding. This cooperative effect between PEO spacer and ciba endgroup was approximately best achieved under a PEO-chain-length of 6000. Longer PEO chains such as in PEO10000 cannot significantly produce any more positive effects; on the contrary, the amount of ciba endgroups will inevitably decrease, which is the reason for less BSA-adsorption on ct-cibaMPEO10k than that on ct-cibaMPEO6k. Figure 7 shows the curves for static adsorption kinetics. In the case of 30.6 mg/mL BSA-bulk-concentration, the fast BSA-adsorption happens in the first minute, and then the adsorption slows down; for different samples, a larger amount of adsorbed BSA is obtained, the later the adsorbing saturation is reached.

Adsorption Analysis of ^{125}I-Labeled Proteins. *Adsorption and Reversible Binding of ^{125}I-Labeled BSA.* The amount of adsorbed BSA on each sample is shown in Figure 8. According to the comparison with the case of PEU-control, the PEO chains' repulsive performance and the ciba's BSA-binding capacity, as well as the PEO−ciba cooperative effect, are respectively confirmed by the BSA-adsorbing performances on the ctMPEO and ct-cibaMPEOs. The curves of adsorption under low BSA-

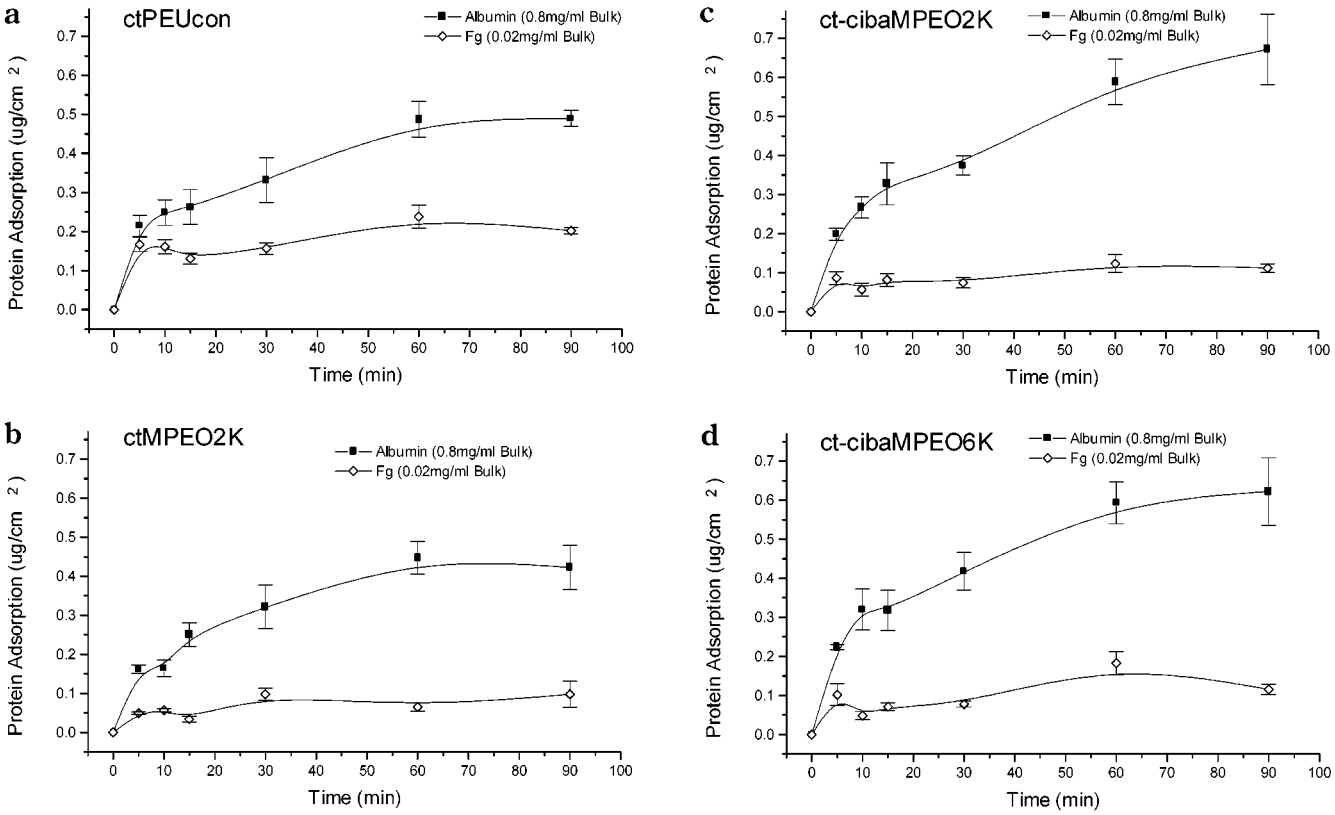


Figure 11. Static BSA−Fg (BSA: 0.8 mg/mL, Fg: 0.02 mg/mL) binary competitive adsorbing kinetics: (a) PEU-control, (b) ctMPEO2k, (c) ct-cibaMPEO2k, and (d) ct-cibaMPEO6k, characterized by radioactive ^{125}I-probe.

bulk-concentration (0.4 mg/ml, shown in Figure 9) demonstrate a similar kinetic adsorbing behavior to that in the high concentration solutions characterized by ATR-FTIR, whereas the difference of BSA-binding capacity between the various samples exhibited under low bulk concentration is not so dramatic as that under high bulk concentration.

The desired effective protein-adsorption is a dynamic equilibrium of adsorption and desorption. Thus, adsorbed proteins with activity can be displaced by the proteins in the bulk solution by probability. Proteins that remain adherent to the polymeric surface permanently are considered irreversibly bound (*22*). Figures 9a and 9b indicate that approximately 41% and 19% of previously bound BSA (radioiodine-labeled) respectively on PEU-control and ctMPEO2k could be displaced in 60 min. From Figures 9c and 9d, it is indicated that approximately 83% and 80% of previously bound BSA (radioiodine-labeled) respectively on ct-cibaMPEO2k and ct-cibaMPEO6k could be displaced within 60 min. Therefore, BSA was reversibly bound to ct-cibaMPEOs, and for ctMPEO2k, despite the high repulsion of PEO, the bound BSA was mostly unrenewable.

Adsorption of ^{125}I-Labeled Fg. Fg was used as a competitive protein because it is known to readily adsorb to implant surfaces and because surfaces that avidly adsorb fibrinogen may be highly thrombogenic (*22*). The amount of adsorbed Fg (bulk-concentration 0.04 mg/mL) on each sample is shown in Figure 10. Within 90 min, the ctMPEO2k and ct-cibaMPEOs bound approximately from 30% to 70% as much ^{125}I-labeled Fg as did PEU-control. The weakest Fg adsorption took place on ct-cibaMPEO6k, and the amounts of the adsorbed Fg on ctMPEO2k and ct-cibaMPEO2k were quite close to each other. All the results listed above indicate that ciba has little special capacity for Fg-binding, while the PEO chains' repulsion to Fg-adsorption has been largely exhibited, and as the dominant factor, the longer the PEO chain length, the higher the repulsion.

Selectivity and Homogeneity of Surface BSA Binding. The direct determination of the extent of preferential binding of BSA to the modified surfaces in the presence of Fg-competition was also performed. The results from the binary BSA−Fg solution with the concentration of 0.8−0.02 (mg mL^{-1}, 40:1 w/w, Bi−Sys I) are shown in Figures 11 and 12, and the results from the 0.8−0.06 system (mg mL^{-1}/mg mL^{-1}, 40:3 w/w, Bi−Sys II) are shown in Figures 13 and 14. The bulk-concentration ratio of BSA to Fg in Bi−Sys II agrees with that ratio in plasma (*23*). From Figures 12b and 14b, it is observed that in the presence of competing Fg, the BSA-adsorbing kinetics on all the surfaces, including PEU-control, ctMPEO2k, and ct-cibaMPEOs, was similar to that in the BSA−one-protein system. As for Bi−Sys I, the curves of competitive adsorbing kinetics (shown in Figure 11) and the ratios of adsorbed-BSA amount to adsorbed-Fg amount (shown in Figure 12a) already can exhibit preferential binding of BSA to the ct-cibaMPEOs. Yet as for Bi−Sys II, the case of more Fg binding than SMA binding on PEU-control was even completely reversed on the ct-cibaMPEOs (shown in Figures 13 and 14a), which can indicate a further dramatic predominance of the homogeneous albumin binding brought by SMA-cibaMPEO.

Plasma Recalcification Time Tests. The results of the PRT tests are shown in Figure 15. Compared with the case of glass and PEU-control, the anticoagulative performance of the modified surfaces was improved, in which the best performance was exhibited on the surfaces modified by cibaMPEO2k-6k. The antithrombogenicity

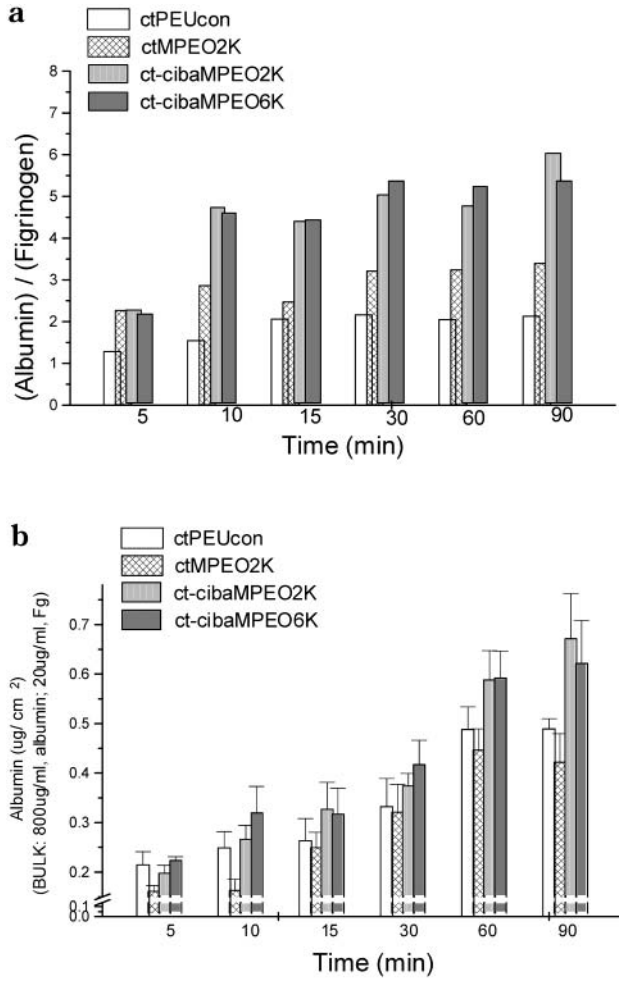


Figure 12. Static BSA−Fg (BSA: 0.8 mg/mL, Fg: 0.02 mg/mL) binary competitive adsorption data of PEU-control, ctMPEO2k, ct-cibaMPEO2k and -6k: (a) ratio of adsorbed BSA amount to adsorbed Fg amount, (b) amount of adsorbed BSA, characterized by radioactive ^{125}I-probe.

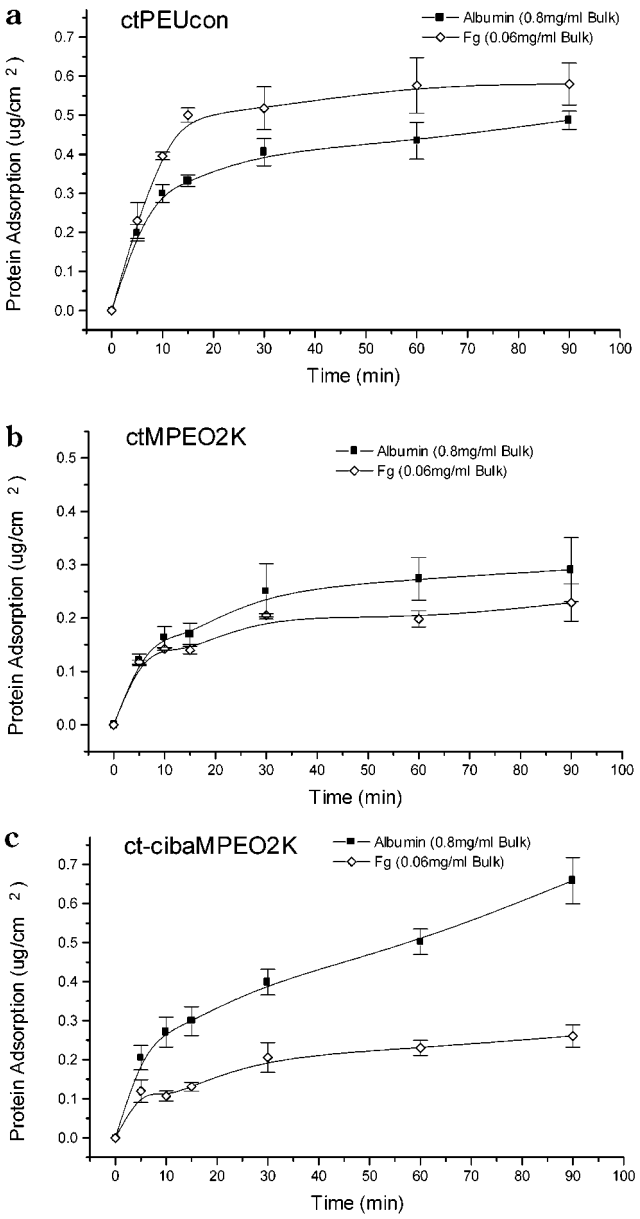


Figure 13. Static BSA−Fg (BSA: 0.8 mg/mL, Fg: 0.06 mg/mL) binary competitive adsorbing kinetics: (a) PEU-control, (b) ctMPEO(2k), and (c) ct-cibaMPEO(2k), characterized by radioactive ^{125}I-probe.

of ct-cibaMPEO1k was similar to that of ctMPEO2k. Along with enlargement of the PEO-chain size from 6k to 10k, the capacity of anti-coagulation decreased. Up to ct-cibaMPEO10k, the anti-coagulative performance was also down to the level of ctMPEO2k. The PRT of the samples is related to the corresponding demonstration of protein adsorption under the competition of albumin−fibrinogen binding. The antithrombogenicity of the cibaMPEOs is originated from the cooperation between ciba endgroups and the PEO spacer, which is due to the coeffect of the exclusion of the thrombogenic proteins and cells plus the selective binding of the inert and biocompatible albumin. While for MPEO2k, it is only from the nonspecifically repulsive function of PEO. On one hand, too long a PEO spacer would make the surface ciba-content limited and the albumin binding would be limited, but on the other hand too short a PEO spacer would immobilize the ciba endgroups and make them less active. Therefore, the cooperative effect between ciba and PEO would finally act on the antithrombogenicity of the modified surfaces.

CONCLUSIONS

In this study, the SMA−cibaMPEOs were synthesized, and the cibaMPEO-modified PEU surfaces were prepared by dip-coating. The surface analysis by XPS revealed the surface enrichment of both ciba and PEO. On the modified surfaces, the quantitative analysis of serum proteins' adsorption was performed. The BSA-adsorption respectively in the low and high BSA bulk-concentration solutions was correspondingly characterized by the methods of radioactive ^{125}I-probe and ATR-FTIR. The Fg-adsorption in the Fg bulk solution and the BSA−Fg competitive adsorption in the BSA−Fg binary solutions were also characterized utilizing the radioactive ^{125}I-probe. Finally the blood compatibility of the modified surfaces was examined by PRT tests.

According to the results of the two independent methods, the BSA-adsorbing kinetics curves of the samples both in the low and high BSA-bulk-concentration solutions, as well as including that in the BSA−Fg binary solutions, were respectively exhibited to be similar to each other. The only difference observed was the higher BSA adsorption in the high BSA-bulk-concentration solution. The comparison between the protein-adsorbing results on PEU-control, ctMPEO2k, and the ct-cibaMPEOs indicates that ciba has a high capacity of selectively

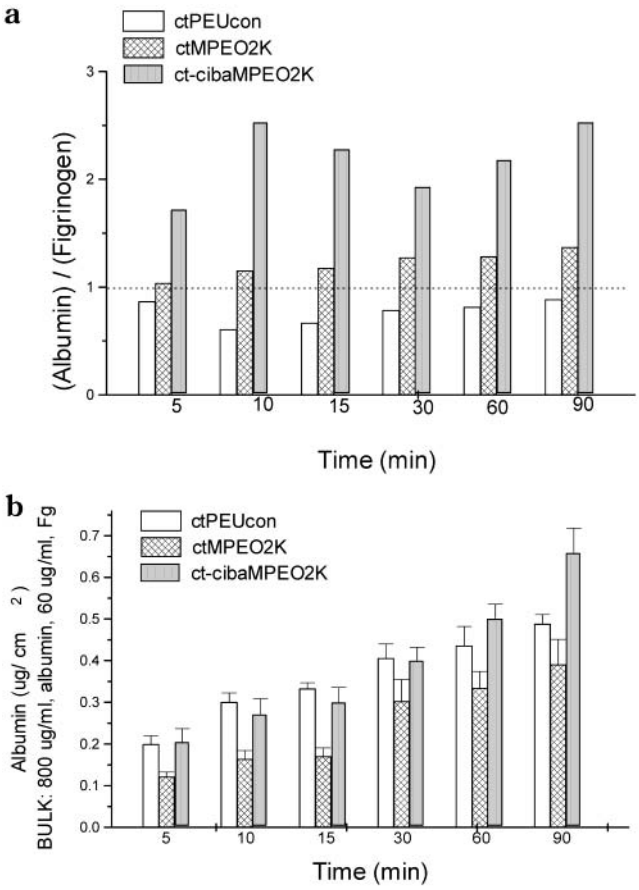


Figure 14. Static BSA-Fg (BSA: 0.8 mg/mL, Fg: 0.02 mg/mL) binary competitive adsorption data of PEU-control, ctMPEO-(2k), and ct-cibaMPEO(2k): (a) ratio of adsorbed BSA amount to adsorbed Fg amount, (b) amount of adsorbed BSA, characterized by radioactive ^{125}I-probe.

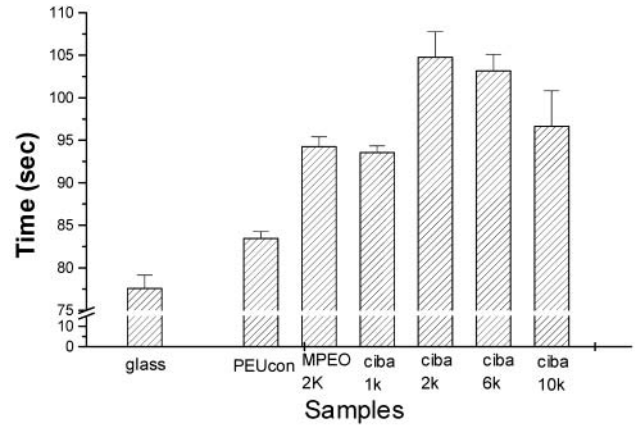


Figure 15. Plasma recalcification time data of glass, PEU-control, ctMPEO(2k), ct-cibaMPEOs.

binding albumin, while PEO can nonspecifically repulse both of the protein adsorption. Whether in a competitive binary protein system or in a one-protein system, the achievement of the albumin-coated surface depends on the demonstration of the cooperative effects between the functional endgroup ciba and the PEO spacer. If the hydrophilic and mobile PEO spacer is too short like PEO1k, it could not sufficiently support and activate the ciba endgroup in the aqueous environment. If the PEO spacer is too long like PEO10k, the surface content of ciba endgroups will inevitably be reduced and the folding of long-chain PEO will also decrease the chain mobility. The results indicate that the remarkable coeffect between the nonspecific repulsion by PEO spacer and the reversibly selective albumin-binding by ciba endgroups is achieved on cibaMPEO2k and -6k, and accordingly, good blood compatibility was also obtained.

ACKNOWLEDGMENT

This research is financially supported by Ministry of Education, National Natural Science Foundation (NSFC 29804009) and National Basic Science Research and Development Grants (No. G1999054305) of the People's Republic of China.

LITERATURE CITED

(1) Lelah, M. D., and Cooper, S. L. (1986) *Polyurethanes in Medicine*, p 57, CRC Press, Boca Raton, FL.
(2) Ikada, Y. (1984) *Advances in Polymer Science*, Vol. 57, p 103, Springer, Berlin.
(3) Han, D. K., Park, K. D., Rug, G. H., Kim, U. Y., Min, B. G., and Kim, Y. H. (1996) Plasma protein adsorption to sulfonated poly(ethylene oxide) grafted polyurethane. *J. Biomed. Mater. Res. 30*, 23−30.
(4) Aldenhoff, Y. B. (1995) Studies on a new strategy for surface modification of polymeric biomaterials. *J. Biomed. Mater. Res. 29*, 917−928.
(5) Pitt, W. G., and Cooper, S. L. (1988) Albumin adsorption on alkyl chain derivatized polyurethanes: I. The effect of C-18 alkylation. *J. Biomed. Mater. Res. 22*, 359−382.
(6) Pitt, W. G., Grasel, T. G., Cooper, and S. L. (1988) Albumin adsorption on alkyl chain derivatized polyurethanes, II. The effect of alkyl chain length. *Biomaterials 9*, 36−43.
(7) He, M. X., and Carter, D. C. (1992) Atomic structure and chemistry of human serum albumin. *Nature 358*, 209−214.
(8) Keogh, J. R., and Eaton, J. W. (1994) Albumin binding surfaces for biomaterials. *J. Lab. Clin. Med. 124*, 537−545.
(9) Llanos, G. R., and Sefton, M. V. (1993) Does poly(ethylene oxide) possess a low thrombogenicity. *J. Biomater. Sci. Polym. Edn. 4*, 381−400.
(10) Wang, D. A., Ji, J., and Feng, L. X. (2000) Surface analysis of poly (ether urethane) blending stearyl poly (ethylene oxide) coupling-polymer. *Macromolecules 33*, 8472−8478.
(11) Wang, D. A., Ji, J., and Feng, L. X. (2000) Various-sized stearyl poly (ethylene oxide) coupling-polymer blending Poly (ether urethane) material for surface study and biomedical applications. *Macromol. Chem. Phys. 201*, 1574−1584.
(12) Chittur, K. K. FTIR/ATR for protein adsorption to biomaterial surface. (1998) *Biomaterials 19*, 357−369.
(13) Fink, D. J., Hutson, T. B., Chittur, K. K., and Gendreau, R. M. Quantitative surface studies of protein adsorption by infrared spectroscopy II. quantification of adsorbbed and buik proteins. *Anal. Biochem.* **1987**, *165*, 147−154.
(14) Wang, Z. Y., Li, J. Z., and Ruan, C. G. (1996) *Thrombogenic and Haemostatic Fundamental Theoretics and Clinical Practice*, 2nd ed., p 280, Shanghai Sci., & Technol Press, Shanghai.
(15) Burton, S. J., McLoughlin, S. B., Stead, C. V., and Lowe, C. R. (1988)Design and applications of biomimetic anthraquinone dyes I. Synthesis and characterization of terminal ring isomers of C. I. reactive blue 2. *J. Chromatogr. 435*, 127−137.
(16) Ratner, B. D., Yoon, S. C., Kaul, A., and Rahman, R. (1987) *Polyurethanes in Biomedical Engineering II* (H. Planck, I. Syre, M. Dauner, and G. Egbers, Eds.) p 231, Elsevier, Amsterdam.
(17) Brash, J. L., and Davidoson, V. J. (1976) Adsorption of glass and polyethylene from solutions of fibrinogen and albumin. *Thromb. Res. 9*, 249−259.
(18) Lin, J. C. (1988) *Haemo-Biochemistry*, p 409, People's Health Press, Beijing.
(19) Miyazawa, T. (1980) *Infrared Spectra and Helical Conformation in Poly-α-Amino Acids* (G. D. Fasman, Ed.) p 1, Marcel Dekker, New York.
(20) Jeon, J. S., Sperline, R. P., and Raghavan, (1992) S. Quantitative Analysis of Adsorbed Serum Albumin on Seg-

mented Polyurethane Using FT-IR/ATR Spectroscopy. *Appl. Spectrosc. 46*, 1644−1648.
(21) Harrick, N. J. (1967) *Internal reflection spectroscopy*, Interscience, New York.
(22) Chinn, J. A., Horbett, T. A., and Ratner, B. D. (1992) Baboon fibrinogen adsorption and platelet adhesion to polymeric materials. *Thromb Haemost. 65*, 608−617.
(23) Elbert, D. L., and Hubbell, J. A. (1996) Surface treatments of polymers for biocompatibility. *Annu. Rev. Mater. Sci. 26*, 365−394.

BC0255079

Chemical Coupling of a Monoclonal Antisurfactant Protein-B Antibody to Human Urokinase for Targeting Surfactant-Incorporating Alveolar Fibrin

Clemens Ruppert,[†] Reinhold Schmidt,[†] Friedrich Grimminger,[†] Yasuhiro Suzuki,[‡] Werner Seeger,[†] Claus-Michael Lehr,[§] and Andreas Günther*,[†]

Department of Internal Medicine, Justus-Liebig-University Giessen, Giessen, Germany, Department of Ultrastructural Research, Institute for Frontier Medical Sciences, Kyoto University, Kyoto, Japan, and Department of Biopharmaceutics and Pharmaceutical Technology, Saarland University, Saarbrücken Germany.
Received January 24, 2002

Intraalveolar fibrin formation is a common histopathological finding in acute inflammatory and chronic interstitial lung diseases. Incorporation of hydrophobic surfactant components into polymerizing fibrin results in a severe loss of surface activity, altered mechanical and structural clot properties, and a reduced susceptibility toward fibrinolytic degradation. Such events have been implicated in atelectasis formation, impairment of gas exchange, and provocation of fibroproliferative changes. In an effort to address the unique features of alveolar fibrin, we designed a hybrid molecule consisting of a monoclonal antibody against surfactant protein SP-B (8B5E) and the catalytic domain of urokinase (B-chain), which was termed MABUC. The urokinase B-chain was prepared by limited reduction of human two-chain-urokinase and subsequent affinity purification and coupled to the antibody using a heterobifunctional cross-linker. Purification of the chimeric protein included gel filtration chromatography and affinity chromatography. An ELISA-like microtiter plate assay, based on the immunological detection of the SP-B moiety and the fibrinolytic activity of the u-PA domain, was developed for the detection of the hybrid molecule. Chromogenic substrate assays, ^{125}I-based fibrin plate assays, and active site titration were performed to analyze the specific fibrinolytic activity of the conjugate. MABUC was found to fully retain the ability of SP-B binding and the fibrinolytic activity of u-PA. In addition, MABUC was noted to be 1.5−2-fold more effective in the dissolution of surfactant embedding clots and to be ∼3-fold more resistant against PAI-1, the predominant fibrinolysis inhibitor in the alveolar compartment, as compared to the native u-PA. The superiority of MABUC was particularly prominent (>5-fold efficacy) when investigating clot material incorporating both PAI-1 and surfactant, as a mimicry of alveolar fibrin. We conclude that urokinase and 8B5E can be cross-linked chemically, thus yielding a fibrinolytic enzyme with enhanced substrate specificity for surfactant-containing clots and higher PAI-1 resistance as compared to native u-PA.

INTRODUCTION

Intraalveolar accumulation of fibrin-rich material ("hyaline membranes") is a hallmark of acute inflammatory lung diseases such as the adult respiratory distress syndrome (ARDS[1]), but also of chronic interstitial pulmonary diseases such as idiopathic lung fibrosis (IPF) (*1*−*6*). Under a variety of inflammatory conditions, the alveolar hemostatic balance is shifted toward a predominance of procoagulant activity, which is mainly attributable to the extrinsic pathway enzymes tissue factor and FVII (*7*−*15*). In contrast, the fibrinolytic activity in the alveolar space is often markedly reduced under these circumstances. Concentrations of urokinase, representing the predominant plasminogen activator within the alveolar compartment, were found to be decreased in lavage fluids from patients with ARDS and those suffering from IPF. In addition, highly elevated activities of plasminogen activator inhibitor 1 (PAI-1) and α_2-antiplasmin were consistently encountered in these patients (*8*−*10*, *12*, *15*, *16*). Under these conditions, fibrinogen leaking into the alveolar space due to an impaired capillary−endothelial and alveo−epithelial barrier function must be assumed to be rapidly converted into fibrin.

The role of alveolar fibrin formation is presently largely unsettled. Although probably helpful in limiting events of pulmonary hemorrhage, in reducing transepithelial fluid flux, and in promoting repair processes after lung tissue injury, it may also have major disadvantages:

First, in ARDS (*17*, *18*), severe pneumonia (*19*), and interstitial lung diseases (*20*), the ability of pulmonary surfactant to reduce the alveolar surface tension is markedly impaired. Changes in the surfactant composi-

* Corresponding author: Andreas Günther, M.D., Medizinische Klinik II; Klinikstrasse 36, D-35385 Giessen, Germany. Phone: +49/641/99/42350; FAX: +49/641/99/42359; e-mail: andreas.guenther@innere.med.uni-giessen.de.

[†] Justus-Liebig-University Giessen.

[‡] Kyoto University.

[§] Saarland University.

[1] Abbreviations: APSAC, activated anisoylated-streptokinase−plasminogen-activator complex; ARDS.; adult respiratory distress syndrome; CYS, cysteine; DTT, dithiothreitol; HMW/LMW tc-u-PA, high molecular weight/low molecular weight two-chain-urokinase-type plasminogen activator; LYS, lysine; MES, 2-(*N*-morpholino)ethansulphonic acid; MUGB, 4-methylumbelliferyl-*p*-guanidinobenzoate hydrochloride; PAI-1, plasminogen-activator-inhibitor 1; PEG, poly(ethylene glycol); PL, phospholipids; SDS−PAGE, sodium dodecyl sulfate−polyacrylamide gel electrophoresis; SP-B, surfactant protein B; S-SMPB, sulfosuccinimidyl 4-(*p*-maleidophenyl)butyrate.

10.1021/bc0255081 CCC: $22.00 © 2002 American Chemical Society
Published on Web 06/19/2002

tion including altered phospholipid and fatty acid profiles and reduced content of the surfactant proteins SP-A, SP-B, and SP-C serve as one explanation for this consistent finding (*19*−*21*). In addition, inhibition of surfactant properties by inflammatory mediators and plasma-derived proteins including albumin, C-reactive protein, hemoglobin, and fibrinogen has been reported (*22*−*25*). Furthermore, fibrin polymerization in vitro in the presence of pulmonary surfactant was shown to result in a nearly complete incorporation of all hydrophobic surfactant compounds, such as phospholipids and surfactant protein SP-B and SP-C (*26*). In this regard, polymerizing fibrin was found to represent the most effective surfactant inhibitory mechanism hitherto described.

Second, in vitro experiments revealed that fibrin clots embedding natural surfactant compounds display markedly altered mechanical properties (*27*) and are less susceptible to proteolytic attack by plasmin, trypsin, or elastase (*28*). This may be advantageous to meet lung physiological demands, but hinders the removal of alveolar fibrin once it is established.

Third, by inactivation of the pulmonary surfactant system, alveolar fibrin formation may seriously deteriorate gas exchange and lung compliance. This has recently been directly demonstrated in rabbit lungs, in which selective alveolar generation of fibrin by sequential aerosolization of fibrinogen and thrombin forwarded a marked increase in pulmonary shunt flow due to severe atelectasis formation (*29*).

Last, alveolar fibrin formation may provide a provisional matrix for subsequent invasion of fibroblasts and may thus promote the fibroproliferative response in late ARDS and in fibrotic lung diseases (*30*−*35*). It was, indeed, observed in morphological studies that atelectatic and fibrin-adherent alveoli may serve as nidus for the fibroblast activation (*3*).

Interestingly, complete lysis of such surfactant incorporating fibrin clots in vitro was recently noted to result in the liberation of intact surfactant material, alongside with a marked improvement in surface tension properties (*27*). In this regard, the plasminogen activators u-PA and t-PA were shown to be the more effective agents as compared to plasmin or activated anisoylated-streptokinase−plasminogen-activator complex (APSAC) (*36*). It is in line with these findings that the markedly increased shunt flow in the above-mentioned model of alveolar fibrin formation was reversed by subsequent nebulization of surfactant plus urokinase. Therapeutic dissolution of alveolar fibrin may thus represent an interesting approach to recruit alveolar units and to prevent lung fibrotic events in prolonged pulmonary inflammatory states. To this end, any tool would be welcomed that might enhance selectivity and potency of the fibrinolytic attack toward surfactant-containing fibrin, a structure unique to the alveolar space. Following this line, we presently constructed and characterized a monoclonal anti-SP-B-antibody−urokinase-conjugate (MABUC) that was obtained by chemical cross-linking of the B-chain of u-PA and a monoclonal antibody against SP-B (8B5E, (*37*)). We report that this hybrid molecule indeed shows an increased fibrinolytic activity toward surfactant-containing clots, as compared to native urokinase, and a clearly increased resistance against the predominant antagonist of fibrinolyis in the alveolar compartment, plasminogen-activator-inhibitor (PAI)-1. Moreover, due to the antibody-dependent targeting of the surfactant-specific protein SP-B, the volume of distribution of this new tool may be expected to be largely restricted to the alveolar space when aerosol is administered to this compartment.

MATERIALS AND METHODS

Bovine SP-B was purified by LH-60-chromatography as described previously (*38*); human high molecular weight two-chain urokinase (HMW-tc-u-PA) and purified human fibrinogen were kindly provided by Prof. N. Heimburger (Behringwerke, Marburg, Germany). Thrombin (30 IU/mL) was purchased from Behring (Marburg, Germany), and benzamidine, PEG 8000, 4-methylumbelliferyl-*p*-guanidinobenzoate hydrochloride (MUGB), methylumbelliferone, and Tween 20 were received from Sigma (Munich, Germany). Sulfosuccinimidyl 4-(*p*-maleidophenyl)butyrate (S-SMPB) was obtained from Pierce (via KMF Laborchemie, St. Augustin, Germany). The anti SP-B antibody (8B5E) was a kind gift from Y. Suzuki (*37*) (Chest Disease Research Institute, Kyoto University, Kyoto, Japan). HMW-tc-u-PA (activity standard with 2860U/mg protein) was a product from ADI (via Loxo, Dossenheim, Germany), and ^{125}I-labeled human fibrinogen was obtained from Amersham (Braunschweig, Germany). Immuno plates (Maxisorp, Polysorp) were purchased from Nunc (Wiesbaden, Germany). BSA was obtained from Paesel & Lorei (Frankfurt, Germany), and the chromogenic substrates (S2251, S2444) and plasminogen were products from Chromogenix (Mölndal, Sweden). Benzamidine-Sepharose-6B, Sephadex-G-100, HiTrap-Protein-G, and the HiPrep-desalting column were obtained from Amersham Pharmacia (Freiburg, Germany). AB-complex was from Dako (Hamburg, Germany). Mutant, recombinant PAI-1 was obtained from Calbiochem (Bad Soden, Germany). Alveofact was a kind gift from Thomae (Biberach, Germany). All other chemicals were obtained from Merck AG (Darmstadt, Germany).

Preparation and Isolation of B-Chain of Urokinase. HMW-tc-u-PA (98 mg) was reduced at room temperature for 60 min in 40 mL of 0.6 M sodium acetate, containing a 3000-fold molar excess of benzamidine (1 g) and a 350-fold molar excess of DTT (98 mg). The mixture was immediately desalted by gel filtration on a HiPrep desalting column (2.6 × 10 cm), equilibrated with 0.1 M sodium acetate/5 mM EDTA, pH 6.8. The protein fractions were pooled and applied to a benzamidine-sepharose column (1.6 × 7.5 cm). After the column was washed with pH 6.8 acetate/EDTA buffer to remove nonadsorbed A-chain, B-chain was eluted with 0.1 M sodium acetate/0.5 M sodium chloride/5 mM EDTA, pH 4.0. It was stored frozen at −80 °C until use.

Protein-G Affinity Chromatography for Isolation of Anti SP-B. For removal of non IgG components possibly interfering with the coupling reagent, 8B5E was further purified by means of affinity chromatography. The lyophilized antibody was dissolved in phosphate-buffered saline (PBS) containing 0.5M NaCl, pH 7.4, and applied to a HiTrap-Protein-G column (bed volume 1 mL). The column was washed with PBS containing 0.5 M NaCl, pH 7.4 until the baseline was stable. Desorption of bound IgG was achieved with 0.2 M acetic acid, pH 2.8. For buffer exchange, the eluted protein was passed through a HighPrep desalting column (2.6 × 10 cm), equilibrated with PBS, pH 8.2. It was stored frozen at −80 °C until use.

Coupling Protocol. 8B5E and the B-chain of urokinase were conjugated with the heterobifunctional cross-linker sulfosuccinimidyl 4-(*p*-maleidophenyl)butyrate (S-SMPB) (Figure 1): In the first step, 8B5E dissolved in

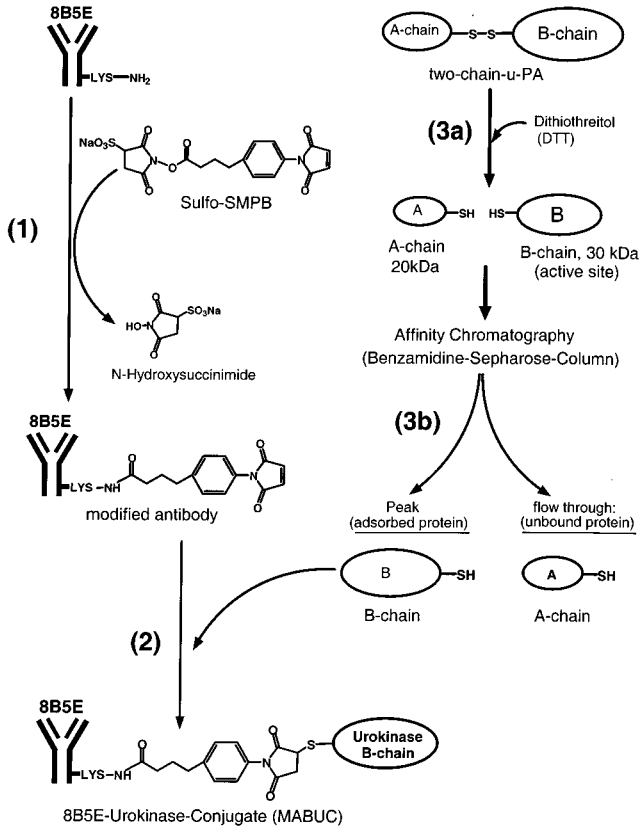


Figure 1. Scheme for the conjugation of monoclonal anti SP-B antibody (8B5E) with urokinase B-chain. In a first step, 8B5E was incubated with Sulfo-SMPB. The *N*-hydroxysuccinimide residues of the heterobifunctional cross-linkers react with lysine-amino groups of the antibody, forming a covalent amide bond (1). After removal of unbound linker molecules (gel filtration on HiTrap desalting column), the modified protein was reacted with urokinase B-chain. Free thiol groups (most likely CYS 279) of the B-chain react with maleimide groups of the activated antibodies, forming a stable thioether linkage (2). Urokinase B-chain was obtained by limited reduction of tc-u-PA in the presence of benzamidine (3a) and subsequent purification by affinity chromatography (3b).

PBS, pH 8.2, at a concentration of 1 mg/mL, was reacted with a 20-fold molar excess of S−SMPB for 45 min at 37 °C. The mixture was then applied to a HiPrep-desalting column (2.6 × 10 cm) for removal of excess uncoupled linker molecules and eluted with PBS/5 mM EDTA, pH 6.8. In the second step, the pooled protein fractions were mixed at a 1:1 molar ratio with the purified B-chain of urokinase preincubated with a 2000× molar excess of benzamidine for protection of the catalytic site, and the mixture was allowed to react for 3 h at room temperature. The reaction was terminated by the addition of iodoacetamide (1 μM final).

Detection of MABUC ("Hybrid-ELISA"). MABUC was identified employing an ELISA-like, microtiter plate-based assay by modification of a solid-phase adsorption-ELISA protocol for quantification of SP-B as previously described (*39*). For this purpose, Polysorp microtiter plates were coated with bovine SP-B dimer (400ng/well) and free binding sites were saturated with BSA (1% BSA/50 mM Tris, pH 7.4, 200 μL/well). Next, samples (150 μL/well) were applied and incubated overnight. Upon triple washing (50 mM Tris/0.5% Tween20, pH 7.4, 200 μL/well) conjugates were detected using S-2444 (2 mM, 200 μL/well), a chromogenic substrate for urokinase. Absorbance was read at 405 nm.

Purification of the Conjugate. The reaction mixture (3 mL aliquots) was first applied to a Sephadex-G100 gelfiltration column 2.6 × 16 cm) equilibrated with 0.1 M sodium acetate, pH 6.8, at a flow rate of 1.5 mL/min. Fractions from the eluted first peak, containing both the conjugate and uncoupled antibody, were loaded onto a benzamidine-Sepharose column (1.6 × 7.5 cm), equilibrated with 0.1 M sodium acetate, pH 6.8, and extensively washed with the same buffer. The adsorbed conjugate was eluted with 0.1 M sodium acetate/0.5 M sodium chloride, pH 4.0.

Fibrin Plate Assay. Proteolysis of fibrin clot was assayed by use of microtiter plates as previously reported (*40*). The final volume in each well was 150 μL. All concentrations refer the final clot volume of 50 mL, and all components were dissolved in 3 mM Ca^{2+} containing saline. First, unlabeled (4 mg/mL) and labeled (≈5 kBq/mL) fibrinogen and plasminogen (4 μg/mL) were introduced into the wells at a volume of 30 μL. Complete clotting was achieved by incubation with thrombin predissolved in 20 μL of buffer fluid (0.12 U/mL, 37 °C, 1.5 h). The plates were spun with 1485*g* for 10 min (Univapo 150H centrifuge) for further consolidation of the clot material in the wells. Next, 100 μL saline/Ca^{2+} without protease or containing u-PA or MABUC were carefully layered onto the surface of the clot and incubated for various time intervals at 37 °C.

To address lysis of fibrin strands embedding surfactant and/or PAI-1, respectively, Alveofact (10−30 mg/mL final volume) and/or PAI-1 (400 ng/mL) was admixed to the fibrinogen solution prior to induction of clotting. Control experiments ascertained complete conversion to fibrin by the protocol of thrombin incubation used. Moreover, this procedure was ascertained to cause >95% incorporation of the surfactant phospholipids into the insoluble fibrin matrix.

After incubation of the clot material with u-PA or MABUC, 75 μL of the supernatant was aspirated, and counts were measured in a Canberra Packard γ-counter. For each time point, the liberation of radiolabel in the presence of the fibrinolytic agent was corrected for baseline release of ^{125}I activity detected in the parallel control experiments with incubation of saline. This baseline release of tracer persistently ranged at <15% of total radioactivity. All data of protease-induced liberation of radiolabel from the insoluble clot are given in percent of total activity applied to each well.

Assay of Amidolytic Activity. The amidolytic activity of the conjugate and urokinase was measured using the chromogenic substrate S-2251. Samples or standards were diluted in 50 mM Tris/0.1 M NaCl, pH 7.4, to a final volume of 50 μL, to which 100 μL of a diluted plasminogen solution (50 mg/mL) was added. Finally, 100 μL S-2251 (2 mM) dissolved in 50 mM Tris/0.1 M NaCl, pH 7.4, was admixed. After incubation, the reaction was stopped by addition of 50 μL of acetic acid (50% aqueous solution), and the absorbance was measured at 405 nm. Sample activity was determined by interpolation from a calibration curve of human tc-u-PA. In some experiments, the amidolytic activity of urokinase was assayed using S-2444. Test samples (50 μL) were incubated with 100 μL buffer (50 mM Tris, pH 8.8) and 100 μL S-2444 (2 mM in distilled water). Reactions were terminated by adding 50 μL of acetic acid (50% solution), and the absorbance was determined at 405 nm against a blank.

To determine the influence of the serine protease inhibitor benzamidine on the enzymatic activity of urokinase during reduction, urokinase (20 μg) was incubated with excess amounts of DTT in the presence or absence

of bezamidine (2500× molar excess) for 1 h at 37 °C. Upon removal of reductant and benzamidine, the remaining activity was assessed by the chromogenic substrate S-2444 and related to the initially employed activity and is given in percent.

Active Site Titration. The active site titration of the conjugate and native urokinase was performed by titration with the fluorogenic substrate 4-methylumbelliferyl-*p*-guanidinobenzoate hydrochloride (MUGB) according to Geiger et al. (*41*). MUGB (1 μM final concentration) was added to urokinase or MABUC, respectively, in 0.1 M barbital-Na−HCl buffer, pH 8.3 (final volume 1 mL), at 25 °C in a spectrofluorometer (Perkin-Elmer). The change in fluorescence intensity was recorded in relative units over time and compared with that of a control containing no enzyme (excitation wavelength 363 nm, emission wavelength 450 nm). The reaction was continuously monitored until a linear increase of the cleavage product (4-methylumbelliferone) occurred. The linear portion of the curve was extrapolated to zero time, and the displacement of the nonlinear portion from the extrapolated linear region of the experimental curve was employed as a measure of the "initial burst" reaction. Active sites of MABUC and urokinase were calculated by interpolation from a calibration curve obtained by recording the relative fluorescence intensity of different known concentrations of 4-methylumbelliferone in the sample buffer.

PAI-1 Inhibition Assay. Inhibition of the plasminogen activators by PAI-1 was investigated using the chromogenic substrate assay as described above and a human recombinant PAI-1 mutant with higher stability as compared to natural PAI-1. In brief, a stock solution of PAI-1 was prepared in 5 mM MES, pH 6.0, containing 0.12 M NaCl, 1 mM EDTA, and 0.1% PEG 8000. The amidolytic activity of urokinase and MABUC was adjusted to 8U/mL, and the proteins were incubated with increasing concentrations of PAI-1 (31.25−500 ng/mL final concentration). After 30 min incubation, 100 μL plasminogen and 100 μL S-2251 were added, and the residual amidolytic activity was determined by reading the absorbance at 405 and by interpolation from a calibration curve of human tc-u-PA.

RESULTS

Preparation and Purification of Urokinase B-Chain. The B-chain of urokinase and thus the active moiety was obtained upon limited reduction of tc-u-PA in the presence of benzamidine. The presence of this low molecular weight serine protease inhibitor preserved the enzymatic activity of urokinase during reduction with DTT over a large dose range (up to 1000-fold molar excess), whereas in the absence of benzamidine the enzyme activity rapidly declined and was completely lost at DTT concentrations surpassing a 700-fold molar excess (Table 1). After application of the incubation mixture onto a HiPrep desalting column for removal of DTT and benzamidine, the resulting B-chain containing one free sulfhydryl moiety was easily isolated from other reduction products (A-chain) by application on a benzamidine-Sepharose column. The islolated B-chain ran as a single band on SDS−PAGE (data not shown). The yield of B-chain was 50.5 mg out of 98 mg HMW-u-PA applied, which corresponds to a 93% recovery.

Preparation and Detection of Anti-SP-B-Antibody-Urokinase Conjugates. First, the maleimide residues of the heterobifunctional linker S-SMPB were introduced into the antibody molecule (8B5E) by induction of an amide bond, resulting in a modified protein being activated for the following coupling reaction. In a second step, the B-chain of urokinase was linked to the maleimide residues via its free sulfhydryl group. Conjugates were detected by means of a "hybrid-ELISA" of the reaction mixture. This assay is based on the functional properties of both SP-B binding by the antibody and fibrinolytic activity of the urokinase B-chain, i.e., only enzymatically active 8B5E−u-PA conjugates are detected (Figure 2). The uncoupled proteins 8B5E and B-chain, lacking the respective complementary component, showed no color development at 405 nm.

Table 1. Influence of Benzamidine on u-PA Stability in Presence of DTT[a]

concentration of DTT [*x*-fold molar excess]	reduction in the absence of benzamidine [% amidolytic activity]	reduction in the presence of benzamidine [% amidolytic activity]
0	100	100
175	29.52 ± 0.8	83.9 ± 1.49
350	5.4 ± 0.08	80.29 ± 2.06
700	0.0 ± 0.0	68.31 ± 0.42
1000	0.0 ± 0.0	64.15 ± 0.25

[a] Enzymatic activity of u-PA was assessed in the presence of increasing concentrations of DTT (*x*-fold molar excess given), in the presence or absence of benzamidine, using the chromogenic substrate S-2444. Mean ± SE of four independent experiments each are given.

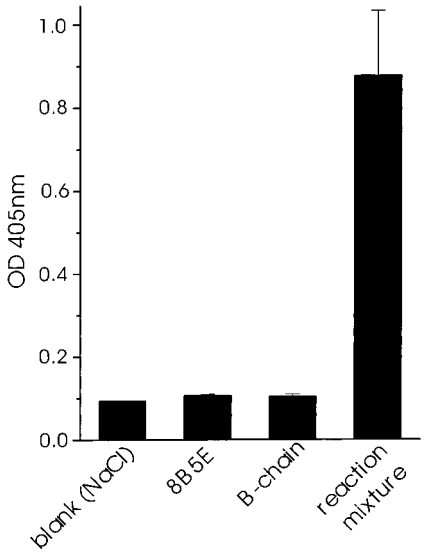


Figure 2. Identification of an anti-SP-B-antibody−u-PA hybrid molecule. Microtiterplate based "Hybrid-ELISA" of the reaction mixture and the uncoupled components B-chain and 8B5E. Samples were transferred to the wells of a microtiter plate coated with SP-B and allowed to bind. After removal of unbound proteins, conjugates were detected using S-2444, a chromogenic substrate for urokinase.

Purification of the Conjugates. Isolation of the conjugates from the reaction mixture required a two-step purification procedure consisting of a gel filtration and an affinity chromatography. To separate uncoupled B-chain from the residual reaction mixture, we chose a Sephadex G-100 column (fractionation range 4−100 kDa). Molecules > 100 kDa (uncoupled antibodies, conjugates) were eluted within the void volume (~15−22 mL), whereas the smaller B-chain appeared later in a second peak (~25−35 mL) (Figure 3a). In addition, the separation of uncoupled B-chain from the residual components was documented by means of SDS−PAGE (not given in detail). Using urokinase affinity chromatography, MABUC could be separated from the remaining uncoupled antibody (Figure 3b) by application of the

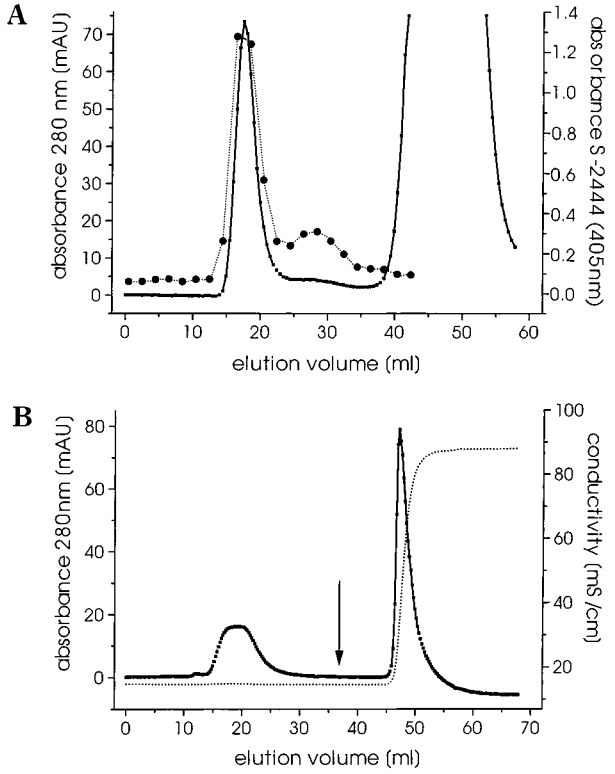


Figure 3. A/B: Chromatographic separation of MABUC from side products. A. 1 mL of the reaction mixture employed for synthesis of the SP-B-u-PA hybrid molecule was loaded onto a Sephadex-G-100 gelfiltration column (2.6 × 16 cm) equilibrated with 0.1 M sodium acetate, pH 6.8. The online recording of the absorbance at 280 nm (squares, solid line) is given. Furthermore, eluted fractions were analyzed for enzymatic activity by means of S-2444, a chromogenic substrate for u-PA (circles, dashed line). B. Pooled fractions of the first chromatographic step (first peak, 15−22 mL) were loaded onto a benzamidine-Sepharose column (1.6 × 7.5 cm), equilibrated with 0.1 M sodium acetate, pH 6.8, and washed with the same buffer to remove uncoupled antibody. The adsorbed conjugate was eluted with 0.1 M sodium acetate/0.5 M sodium chloride, pH 4.0. The online recordings of the absorbance at 280 nm and the conductivity (dashed line) are given. The switch to the elution buffer is indicated by an arrow.

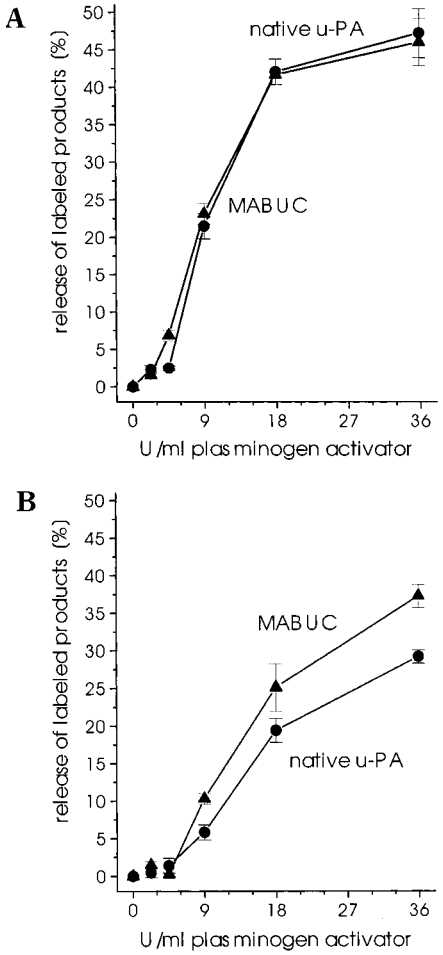


Figure 4. A/B: Fibrinolytic properties of native u-PA or MABUC in absence or presence of clot-embedded surfactant. ^{125}I-labeled fibrinogen was clotted in a microtiter plate in the presence (B, right panel) or absence (A, left panel) of surfactant (Alveofact, 20 mg/mL final). Fibrinolysis was induced by addition of increasing activities of native u-PA or MABUC, and the release of radiolabeled split products was measured after 4 h and is given in percent of the initially provided radioactivity. Mean ± SE of four independent experiments each are given.

pooled fractions of the first chromatographic step. Elution from the benzamidine-Sepharose-column resulted in a single peak. The yield of purified conjugate was 139 μg (13.6% of the originally employed protein).

Fibrinolytic Properties of the 8B5E−B-Chain Conjugate. Incubation of a preformed radiolabeled fibrin clot with increasing activities of native u-PA or MABUC resulted in a dose-dependent release of radioactivity into the soluble phase (Figure 4). Concentrations of the proteolytic enzymes were chosen to surpass baseline liberation of tracer manifold and to achieve release of labeled scisson products in the range of 30−50% of total radioactivity within 4 h. In the absence of surfactant, both native u-PA and MABUC displayed a similar, dose-dependent fibrinolytic activity (Figure 4a). In contrast, a marked retardation of the fibrinolysis kinetics was noted when a fixed dose of calf lung surfactant extract was admixed to fibrinogen prior to coagulation (Figure 4b). Concerning such surfactant-containing clots, MABUC turned out to be the more effective fibrinolytic agent as compared to native u-PA. This was true for both the overall extent of fibrinolyis in this assay (Figure 4b) and the initial kinetics of fibrin-split product release (not shown in detail).

Similarly, at a constant activity of MABUC or native u-PA, incubation of fibrin clots with increasing concentrations of the calf lung surfactant extract resulted in a dose-dependent inhibition of fibrinolysis (Figure 5); however, this effect was markedly less pronounced in case of MABUC-induced fibrinolysis as compared to native u-PA-induced lysis of the fibrin clot. In contrast to clots containing preembedded surfactant, fibrinolysis was not influenced by Alveofact when this natural surfactant was administered simultaneously with native u-PA or MABUC (not shown in detail).

PAI-1 Resistance. When tested using the synthetic substrate S-2444, incubation of native u-PA and MABUC with increasing concentrations of a mutant and thus a more stable form of recombinant human PAI-1 resulted in a dose-dependent inhibition of the enzymatic activity of both agents (Figure 6). MABUC was, however, shown to be markedly less susceptible toward inhibition by PAI-1 than by native u-PA. In addition, this increased PAI-1 resistance was demonstrated in clot lysis experiments employing preformed fibrin clots with embedded PAI-1 (Figure 7).

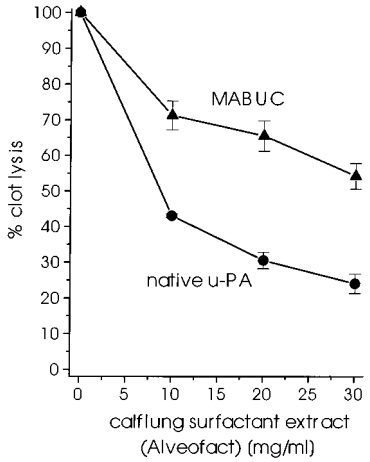


Figure 5. Influence of the concentration of clot-embedded surfactant on fibrinolysis by urokinase and MABUC. Alveofact (10−30 mg/mL, final) was admixed to the fibrinogen solution before performing clotting. The clot material was then incubated with native u-PA or MABUC (1 pmol active enzyme/mL each). After 4 h, the release of labeled products was measured and related to the relative amount of split products released in the absence of surfactant. Mean ± SE of eight independent experiments each are given.

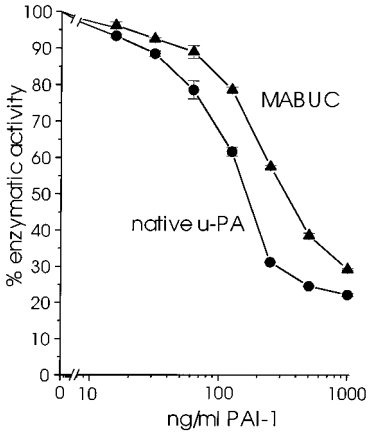


Figure 6. Influence of PAI-1 on the enzymatic activity of native u-PA or MABUC. Native u-PA and MABUC, at an activity of 20 U/mL, were incubated with increasing concentrations of PAI-1 (15.625−1000 ng/mL), and the enzymatic activity was assayed using a chromogenic substrate (related to the activity in the absence of PAI-1). Mean ± SE of three independent experiments each are given.

DISCUSSION

In the current study we have constructed and characterized a hybrid molecule consisting of the B-chain of urokinase and 8B5E, a monoclonal antisurfactant protein SP-B antibody. Using a chemical cross-linking technology as described similarly for conjugation of urokinase with an antibody directed against a fibrin neoantigen (*42*), we manufactured enzymatically active conjugates of 8B5E and urokinase B-chain (MABUC) by use of the heterobifunctional linker sulfosuccinimidyl-4-(*p*-maleidophenyl)butyrate (S-SMPB). Prerequisite for this coupling procedure was the limited reduction of HMW-tc-u-PA and isolation of the B-chain. Care had to be taken not to impair the catalytic property of u-PA during the limited reduction of urokinase necessary for generation and isolation of the B-chain. For this purpose, the enzyme was stabilized by the presence of benzamidine, a known competitive inhibitor targeting the active moiety of u-PA during the reduction process as recently suggested (*43*). Isolation of the B-chain was forwarded by affinity chromatography as also published previously (*43*, *44*) and yielded highly active B-chain at high purity (>93%).

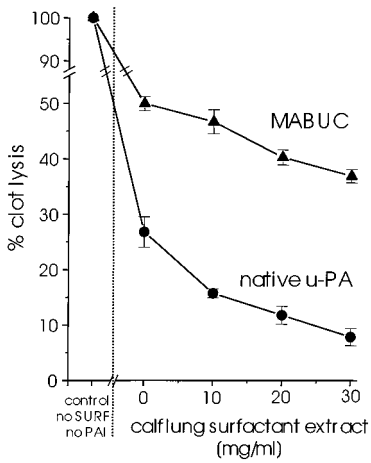


Figure 7. Influence of clot-embedded PAI-1 and various concentrations of surfactant on fibrinolysis by urokinase and MABUC. Alveofact (10−30 mg/mL, final) and PAI-1 (400 ng/mL) were admixed to the fibrinogen solution before performing clotting. The clot material was then incubated with native u-PA or MABUC (1 pmol active enzyme/mL each). After 4 h, the release of labeled products was measured and related to the relative amount of split products released in the absence of surfactant and PAI-1. Mean ± SE of eight independent experiments each are given.

The obtained 8B5E/u-PA-B chain conjugates, named "MABUC", were identified and characterized by a "hybrid-ELISA" based on the functional properties of both the antibody (binding to the solid-phase-adsorbed SP-B) and the B chain of u-PA (scission of the chromogenic substrate). A sequentially performed chromatographic procedure, consisting of gel filtration chromatography for removal of native B-chain followed by affinity chromatography for removal of native antibody, turned out to be suitable for the isolation of MABUC at high purity (>95% by SDS−PAGE).

The precise structure or amino acid sequence of the novel conjugate is not known, as the cross-linker reacts in a random fashion preferentially with the ϵ-amino group of lysine residues, which are present in large number in the antibody molecule. However, according to the coupling protocol the following speculations can be made: Concerning the coupling of the reduced B-chain to the maleimide group of the activated antibody, thioether-based bondage may be expected for Cys 279, and can be assumed to represent the only free thiol group of the B-chain. This view is based on the observation that absence of benzamidine during the reduction process would result in a loss of u-PA activity, suggesting reduction of some important disulfid bonds in close proximity to the catalytic triad. The results obtained with the "hybrid-ELISA" showed that MABUC fully retained the ability of antigen binding suggesting that coupling did not interfere with the antigen binding region of the antibody.

The presently employed coupling protocol was chosen because it greatly reduced the size of possible conjugates. Other protocols, in which native urokinase (HMW-tc-u-PA, 54 kDa) is first modified by the cross-linker and then connected to the antibody, would result in larger hybrid molecules and might affect the enzymatic activity, as the cross-linker could also be linked to lysine residues within or close to the active site of u-PA.

The purified hybrid molecule was shown to possess distinct advantages that could make it a preferable

plasminogen activator for induction of fibrinolysis in the alveolar compartment. First, the SP-B binding ability was fully maintained and might thus be operative to limit the action of this hybrid molecule to the alveolar space, preventing substantial leakage into the systemic circulation. The underlying reason is that SP-B is a unique protein of this compartment and due to its extreme hydrophobicity and intimate interaction with the alveolar phospholipid pool may not be expected to pass into the vascular space in substantial quantities, even under conditions of alveolo−epithelial barrier damage, as, for example, noted for the hydrophilic SP-A. This assumption was, however, not directly addressed in the present study, but will demand additional pharmacokinetic investigations in intact animals. Second, when adjusted to a similar activity as native u-PA using the fibrin plate and the chromogenic substrate assay in absence of surfactant, MABUC was shown to be ∼1.5−2 times more effective in fibrinolysis of surfactant embedding clots. These investigations were performed at concentrations of surfactant and fibrin realistically assumed to exist in vivo under conditions of extensive alveolar clotting (*26*). Third, when analyzing the sensitivity toward inhibition by PAI-1, the predominant fibrinolysis inhibitor of the alveolar compartment, MABUC turned out to be more resistant as compared to the native molecule, with approximately 2-fold concentrations of PAI-1 being necessary to gain the same degree of inhibition. Last, the difference between u-PA and MABUC became particularly apparent when analyzing their efficacy toward fibrin clots incorporating both natural surfactant and PAI-1, a condition representing the most realistic mimicry of alveolar fibrin arising in inflamed lung tissue. Under these circumstances, the lytic capacity of u-PA was largely lost, but that of MABUC was still maintained on a lower yet appreciable level (when probing clots containing 30 mg/mL surfactant and 400 ng/mL PAI-1, the lytic effect of MABUC surpassed that of u-PA > 5-fold).

The following drawbacks of the hybrid molecule of urokinase B-chain and the monoclonal SP-B antibody are imaginable when targeting fibrinolysis in the alveolar comparment. (i) The antibody might interfere with surfactant function, as previously described upon delivery of high concentrations of 8B5E into the alveolar space (*45*). However, such an anti-SP-B effect is clearly dose-dependent, and calculations taking into consideration the lytic capacity of MABUC and the dose-inhibition curves of anti-SP-B on surfactant function do suggest that such an effect might not be relevant. However, this aspect has to be addressed in a detailed fashion when delivering MABUC to the alveolar space of intact lungs. (ii) The antibody binding to the antigen (SP-B) in the alveolar compartment might provoke immunological sequelae that may not be foreseen from in vitro experiments. Even if the present body of knowledge on conjugates of u-PA with antibodies detecting a fibrin neoantigen does not suggest major relevance of such phenomena, the immunological responsiveness of the alveolar space might differ from that of the intravasular space, thus making detailed analysis of this aspect mandatory when delivering MABUC to intact lungs. (iii) The hybrid molecule migh be seriously damaged when undergoing aerosolization; however, pilot experiments addressing this issue rather suggest that this is not the case.

In view of the pathogenetic relevance of alveolar fibrin formation and accumulation of surfactant-rich fibrin clots in the lung for impairment of surfactant function, gas exchange properties and—still hypothetically—fibroproliferative changes in late ARDS and inflammatory lung disease, selective fibrinolysis in the alveolar compartment might offer as new therapeutic approach. Coaerosolation of native urokinase and natural surfactant material was, indeed, recently shown to improve gas exchange and to limit lung fibrosis in experimental models of acute and chronic inflammatory injury (*29*, *46*). A properly designed fibrinolytic agent, addressing the unique nature of alveolar fibrin, might be an interesting tool for such a purpose, and the data of the present study render the anti-SP-B−u-PA-B-chain conjugate an interesting candidate in this context.

ACKNOWLEDGMENT

This work was supported by the Deutsche Forschungsgemeinschaft (Sonderforschungsbereich SFB 547 "Kardiopulmonales Gefässsystem"). This paper includes parts of the thesis of C. Ruppert.

LITERATURE CITED

(1) Ashbaugh, D. G., Bigelow, D. B., Petty T. L., and Levine, B. E. (1967) Acute respiratory distress in adults. *Lancet 2*, 319−323.

(2) Bachofen, M., and Weibel, E. R. (1982) Structural alterations of lung parenchyma in the adult respiratory distress syndrome. *Clin. Chest. Med. 3*, 35−56.

(3) Burkhardt, A. (1989) Alveolitis and collapse in the pathogenesis of pulmonary fibrosis. *Am. Rev. Respir. Dis. 140*, 513−524.

(4) Chapman, H. A., Allen, C. L., and Stone, O. L. (1986) Abnormalities in pathways of alveolar fibrin turnover among patients with interstitial lung disease. *Am. Rev. Respir. Dis. 133*, 437−443.

(5) Hallman, M., Maasilta, P., Kivisaari, L., and. Mattson, K. (1990) Changes in surfactant in bronchoalveolar lavage fluid after hemithorax irradiation in patients with mesothelioma. *Am. Rev. Respir. Dis. 141*, 998−1005.

(6) Jackson, L. K. (1982) Idiopathic pulmonary fibrosis. *Clin. Chest Med. 3*, 579−592.

(7) Gross, T. J., Simon, R. H., and Sitrin, R. G. (1992) Tissue factor procoagulant expression by rat alveolar epithelial cells. *Am. J. Respir. Cell Mol. Biol. 6*, 397−403.

(8) Hasday, J. D., Bachwich, P. R., Lynch, J. P., and Sitrin, R. G. (1988) Procoagulant and plasminogen activator activities of bronchoalveolar fluid in patients with pulmonary sarcoidosis. *Exp. Lung Res. 14*, 261−278.

(9) Idell, S., Koenig, K. B., Fair, D. S., Martin, T. R., McLarty, J., and Maunder, R. J. (1991) Serial abnormalities of fibrin turnover in evolving adult respiratory distress syndrome. *Am. J. Physiol. 261*, L240-L248.

(10) Idell, S., Gonzalez, K., Bradford, H., MacArthur, C. K., Fein, A. M., Maunder, R. J., Garcia, J. G., Griffith, D. E., Weiland, J, Martin, T. R. et al. (1987) Procoagulant activity in bronchoalveolar lavage in the adult respiratory distress syndrome. Contribution of tissue factor associated with factor VII. *Am. Rev. Respir. Dis. 136*, 1466−1474.

(11) Idell, S.,. James, K. K, Levin, E. G., Schwartz, B. S., Manchanda, N., Maunder, R. J., Martin, T. R., McLarty, J., and Fair, D. S. (1989) Local abnormalities in coagulation and fibrinolytic pathways predispose to alveolar fibrin deposition in the adult respiratory distress syndrome. *J. Clin. Invest. 84*, 695−705.

(12) Nakstad, B., Lyberg, T., Skjonsberg, O. H., and Boye, N. P. (1990) Local activation of the coagulation and fibrinolysis systems in lung disease. *Thromb. Res. 57*, 827−838.

(13) Nakstad, B., Boye, N. P., and Lyberg, T. (1987) Procoagulant activities in human alveolar macrophages. *Eur. J. Respir. Dis. 71*, 459−471.

(14) Günther, A., Mosavi, P., Ruppert, C., Heinemann, S., Temmesfeld-Wollbrück, B., Velcovsky, H. G., Morr, H., Grimminger, F., Walmrath, D., and Seeger, W. (2000) Enhanced tissue factor pathway activity and fibrin turnover in the alveolar compartment of patients with interstitial lung disease. *Thromb. Haemost. 83*, 853−860.

(15) Günther, A, Mosavi, P., Heinemann, S., Ruppert, C., Muth, H., Markart, P., Grimminger, F., Walmrath, D., Temmesfeld-Wollbrück, B., and Seeger, W. (2000) Alveolar fibrin formation due to enhanced procoagulant and depressed fibrinolytic capacities in severe pneumonia − comparison with the acute respiratory distress syndrome. *Am. J. Respir. Crit. Care Med. 161*, 454−462.

(16) Bertozzi, P., Astedt, B., Zenzius, L., Lynch, K., LeMaire, F., Zapol, W., and Chapman, H. A., Jr. (1990) Depressed bronchoalveolar urokinase activity in patients with adult respiratory distress syndrome. *N. Engl. J. Med. 322*, 890−897.

(17) Lewis, J. F., and Jobe, A. H. (1993) Surfactant and the adult respiratory distress syndrome. *Am. Rev. Respir. Dis. 147*, 218−233.

(18) Günther, A., Ruppert, C., Schmidt, R., Markart, P., Walmrath, D., Grimminger, F., and Seeger, W. (2001) Surfactant alteration and replacement in acute respiratory distress syndrome. *Respir. Res. 2*: 353−364, 2001.

(19) Günther, A., Siebert, C., Schmidt, R., Ziegler, S., Grimminger, F., Yabut, M., Temmesfeld, B., Walmrath, D., Morr, H., and Seeger, W. (1996) Surfactant alterations in severe pneumonia, acute respiratory distress syndrome, and cardiogenic lung edema. *Am. J. Respir. Crit. Care Med. 153*, 176−184.

(20) Günther, A., Schmidt, R., Nix, F., Yabut Perez, M., Guth, C., Rosseau, S., Siebert, C., Grimminger, F., Morr, H., Velcovsky, H. G., and Seeger, W.(1999) Surfactant abnormalities in idiopathic pulmonary fibrosis, hypersensitivity pneumonitis and sarcoidosis. *Eur. Respir. J. 14*, 565−573.

(21) Gregory, T. J., Longmore, W. J., Moxley, M. A., Whitsett, J. A., Reed, C. R., Fowler, A. A., Hudson, L. D., Maunder, R. J., Crim, C., and Hyers, T. M. (1991) Surfactant chemical composition and biophysical activity in acute respiratory distress syndrome. *J. Clin. Invest. 88*, 1976−1981.

(22) Fuchimukai, T., Fujiwara, T., Takahashi, A., and Enhorning, G. (1987) Artificial pulmonary surfactant inhibited by proteins. *J. Appl. Physiol. 62*, 429−437.

(23) Holm, B. A., and Notter, R. H. (1987) Effects of hemoglobin and cell membrane lipids on pulmonary surfactant activity. *J. Appl. Physiol. 63*, 1434−1442.

(24) Seeger, W., Thede, C., Günther, A., and Grube, C. (1991) Surface properties and sensitivity to protein-inhibition of a recombinant apoprotein C-based phospholipid mixture in vitro − comparison to natural surfactant. *Biochim. Biophys. Acta 1081*, 45−52.

(25) Seeger, W., Stöhr, G., Wolf, H. R., Neuhof, H. (1985) Alteration of surfactant function due to protein leakage: special interaction with fibrin monomer. *J. Appl. Physiol. 58*, 326−338.

(26) Seeger, W. Elssner, A., Günther, A., Krämer, H. J., and Kalinowski, H. O. (1993) Lung surfactant phospholipids associate with polymerizing fibrin: loss of surface activity. *Am. J. Respir. Cell Mol. Biol. 9*, 213−220.

(27) Günther, A., Kalinowski, M., Rosseau, S., and Seeger, W. (1995) Surfactant incorporation markedly alters mechanical properties of a fibrin clot. *Am. J. Respir. Cell Mol. Biol.* 13, 712−718.

(28) Günther, A., M. Kalinowski, Elssner, A., and Seeger, W. (1994) Clot-embedded natural surfactant: kinetics of fibrinolysis and surface activity. *Am. J. Physiol. 267*, L618-L624.

(29) Schermuly, R. T., Günther, A., Ermert, M., Ermert, L., Ghofrani, H. A., Weissmann, N., Grimminger, F., Seeger, W., Walmrath, D. (2001) Conebulization of surfactant and urokinase restores gas exchange in perfused lungs with alveolar fibrin formation. *Am. J. Physiol. Lung Cell Mol. Physiol. 280*, L792−800.

(30) Akiyama, S. K., Hasegawa, E., Hasegawa, T., and Yamada, K. M. (1985) The interaction of fibronectin fragments with fibroblastic cells. *J. Biol. Chem. 260*, 13256−13260.

(31) Aota, S., Nagai, T., Olden, K., Akiyama, S. K., and Yamada, K. M. (1991) Fibronectin and integrins in cell adhesion and migration. *Biochem. Soc. Trans. 19*, 830−835.

(32) Bitterman, P. B., Rennard, S. I., Adelberg, S., and Crystal, R. G. (1983) Role of fibronectin as a growth factor for fibroblasts. *J. Cell. Biol. 97*, 1925−1932.

(33) Campbell, E. J., Senior, R. M., and Welgus, H. G. (1987) Extracellular matrix injury during lung inflammation. *Chest 92*, 161−167.

(34) Couchman, J. R., Austria, M. R., and Woods, A. (1990) Fibronectin-cell interactions. *J. Invest. Dermatol. 94*, 7S−14S.

(35) Yamada, K. M. (1991) Adhesive recognition sequences. *J. Biol. Chem. 266*, 12809−12812.

(36) Günther, A., Markart, P., Kalinowski, M., Ruppert, C., Grimminger, F., and Seeger, W. (1999) Cleavage of surfactant-incorporating fibrin by different fibrinolytic agents − kinetics of lysis and rescue of surface activity. *Am. J. Respir. Cell Mol. Biol. 21*, 738−745.

(37) Suzuki, Y., Kogishi, K., Fujita, Y., Kina, T., and Nishikawa, S. (1986) A monoclonal antibody to the 15, 000 dalton protein associated with porcine pulmonary surfactant. *Exp. Lung Res. 11*: 61−73.

(38) Hawgood, S., Benson, B. J., Schilling, J., Damm, D., Clements, J. A., and White, R. T. (1987) Nucleotide and amino acid sequences of pulmonary surfactant protein SP 18 and evidence for cooperation between SP 18 and SP 28−36 in surfactant lipid adsorption. *Proc. Natl. Acad. Sci. U.S.A. 84*, 66−70.

(39) Krämer, H. J., Schmidt, R., Günther, A., Becker, G., Suzuki, Y., and Seeger, W. (1995) ELISA technique for quantification of surfactant protein B (SP-B) in bronchoalveolar lavage fluid. *Am. J. Respir. Crit. Care Med. 152*, 1540−1544.

(40) Unkeless, J. C., Gordon, S., and Reich, E. (1974) Secretion of plasminogen activator by stimulated macrophages. *J. Exp. Med. 139*, 834−850.

(41) Geiger, M. and Binder, B. R. (1987) Tissue-type plasminogen activator and urokinase: differences in the reaction pattern with the active-site titrant 4-methylumbelliferyl-p-guanidinobenzoate hydrochloride. *Biochim. Biophys. Acta 912*, 34−40.

(42) Bode, C., Runge, M. S., Newell, J. B., Matsueda, G. R., and Haber, E. (1987) Characterization of an antibody-urokinase conjugate. A plasminogen activator targeted to fibrin. *J. Biol. Chem. 262*, 10819−10823.

(43) Tanaka, K., Einaga, K., Tsuchiyama, H., Tait, J. F., and Fujikawa, K. (1996) Preparation and characterization of a disulfide-linked bioconjugate of annexin V with the B-chain of urokinase: an improved fibrinolytic agent targeted to phospholipid-containing thrombi. *Biochemistry 35*, 922−929.

(44) Robbins, K. C., and Tanaka, Y (1986) Covalent molecular weight approximately 92 000 hybrid plasminogen activator derived from human plasmin amino-terminal and urokinase carboxyl-terminal domains. *Biochemistry 25*, 3603−3611.

(45) Grossmann, G., Suzuki, Y, Robertson, B., Kobayashi, T., Berggren, P.,. Li, W. Z, Song, G. W., and Sun, B. (1997) Pathophysiology of neonatal lung injury induced by monoclonal antibody to surfactant protein B. *J. Appl. Physiol. 82*, 2003−2010.

(46) Günther, A, Lübke, N., Weissmann, N., Quanz, K., Weimar, B., Schermuly, R., Ruppert, C., Muth, H., Grimminger, F., and Seeger, W. (2000) Restoration of lung compliance and prevention of lung fibrosis in a rabbit model of bleomycin induced lung fibrosis upon aerosol application of heparin and urokinase. *Am. J. Respir. Crit. Care Med. 161*, A 751 (Abstr.).

BC0255081

Poly(ethylenimine-*co*-L-lactamide-*co*-succinamide): A Biodegradable Polyethylenimine Derivative with an Advantageous pH-Dependent Hydrolytic Degradation for Gene Delivery

Holger Petersen, Thomas Merdan, Klaus Kunath, Dagmar Fischer, and Thomas Kissel*

Department of Pharmaceutics and Biopharmacy, Philipps-University of Marburg, Ketzerbach 63, D-35032 Marburg, Germany. Received February 7, 2002; Revised Manuscript Received April 24, 2002

A biodegradable gene transfer vector has been synthesized by linking several low molecular weight (MW) polyethylenimine (PEI, 1200 Da) blocks using an oligo(L-lactic acid-*co*-succinic acid) (OLSA, 1000 Da). The resulting copolymer P(EI-*co*-LSA) (8 kDa) is soluble in water and degrades via base-catalyzed hydrolytic cleavage of amide bonds. With regard to its application as a gene transfer agent, the polymer showed an interesting pH dependency of degradation. At pH 5, when DNases are highly active, the degradation proceeds at a slower rate than at a physiological pH of 7.4. PEI and P(EI-*co*-LSA) spontaneously formed complexes with plasmid DNA. Whereas the complexes formed with PEI were not stable and aggregated, forming particles of up to 1 μm hydrodynamic diameter, P(EI-*co*-LSA) formed complexes, which were about 150 nm in size and of narrow size distribution. The latter complexes were stable, due to their high surface charge (ζ-potential + 18 mV). Similar to low MW PEI, the copolymer exhibited a low toxicity profile. At the same time, the copolymer showed a significant enhancement of transfection activity in comparison to the low MW PEI. This makes P(EI-*co*-LSA) a promising candidate for long-term gene therapy where biocompatibility and biodegradability become increasingly important.

INTRODUCTION

Over the past decade, charged macromolecules have found considerable interest as drug carrier systems. Whereas anionic polymers have often been reported to adsorb proteins (*1*), polycations (*2*) have shown promise as interpolyelectrolyte complexes containing nucleic acids in the field of nonviral gene transfer. Nevertheless, several requirements have to be fulfilled by these polymers used for in vivo gene delivery. One of the most important demands on macromolecular drug carriers is that they must not accumulate in the human body. The elimination of the polycation as a function of time is very important. Almost all types of polycations have already been studied as gene delivery vehicles (for a review see ref *3*). It is has been reported that cationic macromolecules and their drug complexes accumulate mostly in the liver or kidney (*4*). Furthermore, it is well-known that hydrophilic low molecular weight (MW[1]) substances can be eliminated by the kidney, when their MW is lower than 30 kDa. Therefore, high MW polymers must be degraded or metabolized before they can be eliminated. In the case of natural polymers this metabolic process can be performed by enzymes. However, synthetic polymers are often resistant to enzymatic degradation. Thus, their application as a component of a drug delivery system is limited, especially in the case of chronic or multiple administrations. Whereas in specific indications, such as a terminal cancer, a higher dose of polycations might be tolerable, special care must be taken when treating young patients with inherited genetic disorders. In this case, accumulation of polycations over years might cause severe organ damage.

Therefore, one aim of further development in the field of polymeric gene delivery should be the development of biodegradable polycations. Surprisingly, only scant information about water-soluble, biodegradable polymers for gene transfer is available in the literature. For example, Lim et al. (*5*) reported a biodegradable aliphatic polyester poly[α-(4-aminobutyl)-L-glycolic acid)] (PAGA), which initially degraded very rapidly within the first 100 min and then gradually degraded to its monomers within 6 months. The polymer showed approximately a 2-fold higher transfection efficiency than its structural amide analogue poly(L-lysine). Putnam et al. (*6*) synthesized another amino group bearing aliphatic polyester poly(4-hydroxy-L-proline ester), which were of low toxicity. However, results of degradation studies or transfection experiments have not been reported as of yet. Apart from their biodegradability, these polymers need to be optimized with respect to transfection efficiency.

* Address for correspondence: Prof. Dr. Thomas Kissel, Department of Pharmaceutics and Biopharmacy, Philipps-University of Marburg, Ketzerbach 63, D-35032 Marburg, Germany. Phone: +49-6421-282-5881. FAX: +49-6421-282-7016. E-mail: kissel@mailer.uni-marburg.de.

[1] Abbreviations: MW, molecular weight; MWD, molecular weight distribution; M_n, number-average molecular weight; M_w, weight-average molecular weight; η_{inh}, inherent viscosimetry; PEI, polyethylenimine; OLSA, oligo(L-lactic acid-*co*-succinic acid); P(EI-*co*-LSA), poly(ethylenimine-*co*-L-lactamide-*co*-succinamide); PAGA, poly[α-(4-aminobutyl)-L-glycolic acid)]; PAMAM, polyamidoamine; PL, polylysine; N/P ratio, polycation-nitrogen/polyanion-phosphorous ratio; FTIR, Fourier transform infrared spectroscopy; SEC-MALLS, size exclusion chromatography−multiple angle laser light scattering; DLS, dynamic light scattering; PDI, polydispersity index; RI, refractive index; EDTA, ethylenediamine tetraacetate; Tris HCl, tris(hydroxymethyl)aminomethane hydrochloric acid; MTT, 3-(4,5-dimethylthiazol-2-yl)-2,5-diphenyltetrazolium bromide; DMSO, dimethyl sulfoxide; IC_{50}, inhibitory concentration 50%.

10.1021/bc0255135 CCC: $22.00 © 2002 American Chemical Society
Published on Web 06/01/2002

Our strategy was to use polycations well-known for their high transfection activity and render this polymer degradable. We selected polyethylenimine (PEI) since it has already been widely and successfully used for gene delivery both under in vitro (*7*, *8*) and in vivo (*9*, *10*) conditions.

It has been reported (*11*, *12*) that PEI with high MW (≥25 kDa) is characterized by a high transfection activity, but unfortunately by a high cytotoxicity, as well. In contrast, low MW PEI (≤2 kDa) shows almost no transfection, but seems to be less toxic (*13*). Our concept was to combine the good transfection efficiency of high MW PEI and the low toxicity of low MW PEI by linking several low MW PEIs with an appropriate spacer to form a biodegradable, high MW polycation.

All of the published biodegradable polycationic gene transfer systems exhibited ester bonds as degradable linkages. Here, we report the first synthesis of a biodegradable PEI derivative and its degradation mechanism based on the hydrolytic cleavage of amide bonds. This novel polycation exhibited a degradation profile with a favorable pH dependency.

Finally, it should be noted that Gosselin et al. (*14*) very recently published a concept, which is similar to ours. They coupled several PEIs with a MW of 800 Da together. In contrast to our work, they used a linker chemistry involving disulfide bonds so that the resulting polymer is expected to be degraded via intracellular reduction and not by hydrolysis.

MATERIALS AND METHODS

Polymer Synthesis. *Synthesis of the Oligo(*L*-lactic acid-co-succinic acid) (OLSA)* **3**. The oligomer was prepared by polycondensation of 40.51 g of L-(+) lactic acid **1** (Fluka, 90% in water, 0.405 mol, 20 equiv) in the presence of 2.39 g of succinic acid **2** (Fluka, ≥99.5%, 20 mmol, 1 equiv). The reaction was carried out in vacuo (20 mbar) at 160 °C for 4 h and resulted in a clear, colorless, and highly viscous material. The amount of condensed water (11 g, 0.386 mol condensation product, 19 equiv) corresponds to a conversion of the polycondensation of 90%, which is related to the formation of decamers. Thus, the MW of OLSA is approximately 1000 Da. Determination of the MW by end group analysis from ^{1}H NMR spectra is not possible due to very similar chemical shifts of the methyl protons and the methine protons adjacent to an acid or ester group. ^{1}H NMR ($CDCl_3$): δ = 5.11 (m, OC*H*, 1H), 4.33 (m, HOC*H*, terminal, 0.2 H), 2.64 (m, C(O)CH_2CH_2C(O), 0.2 H), 1.51 (m, CH_3, 3 H), 1.41 (m, CH_3, terminal, 0.6 H) ppm. ^{13}C NMR ($CDCl_3$): δ = 174.9 (*C*═O, lactic acid (LA) terminal), 171.5 (*C*═O, succinic acid (SA)), 169.5 (*C*═O, LA), 68.9 (*C*H, LA), 66.6 (*C*H, LA terminal), 28.5 (*C*H_2*C*H_2, SA), 20.2 (*C*H_3, LA terminal), 16.5 (*C*H_3, LA) ppm.

*Synthesis of Poly(ethylenimine-co-*L*-lactamide-co-succinamide) [P(EI-co-LSA)]* **6**. Amounts of 2.34 g of PEI **4** (1200 Da, Polyscience, 99%, 1.95 mmol, 1.2 equiv) and 1.66 g of OLSA **3** (1000 Da, 1.66 mmol, 1 equiv) were dissolved in 25 mL of absolute ethanol. After 1 h, the solvent was removed under reduced pressure at 40 °C, and the product was isolated as a clear, colorless, and highly viscous material in quantitative yield. This isolated product is referred to as intermediate **5** in this report and was treated at 160 °C for 2 h in vacuo (1 mbar). The resulting polymer was dissolved in ethanol and precipitated in diethyl ether. Solvent residues were removed in vacuo. The orange-red-colored polymer was isolated with a yield of 81%.

Polymer Characterization. *Nuclear Magnetic Resonance Spectroscopy (NMR).* ^{1}H NMR and ^{13}C NMR spectra were recorded in d_6-DMSO (Merck) at 35 °C or $CDCl_3$ (Merck) at an ambient temperature on a Eclipse+ 500 spectrometer from JEOL, Tokyo, Japan, at 500 MHz for ^{1}H NMR and 125 MHz for ^{13}C NMR spectra, respectively. Spectra were evaluated with the NMR data processing program MestRe-C Version 2.2.

Fourier Transform Infrared Spectroscopy (FTIR). FTIR spectroscopy was conducted with a FT-IR 510P spectrometer from Nicolet with PC/IR v. 3.20 software using KBr (for IR spectroscopy, Uvasol, Merck) disks. The waxy and oily samples were smeared on the KBr disk.

Capillary Viscosimetry. The polymers were characterized by capillary viscosimetry (Ubbelohde, Schott, type No. 50101/0a) at 25.0 °C in filtered water (0.22 μm, 0,-055 μS/cm). The polymer concentration was 0.5 g/dL. Inherent viscosity (η_{inh}) was calculated using the equation: $\eta_{inh} = \ln(t/t_0)/c$, where t is the flow time of the polymer solution, t_0 the flow time of the solvent, and c the polymer concentration. The η_{inh} listed in Table 1 and Figure 4A is the mean of five measurements.

Degradation Study. Degradation was studied with the polymer solution used for viscosimetry, incubated for several days in a slowly rotating heating block (Rotatherm, Liebisch, Bielefeld, Germany) at 37.2 °C. Solutions of P(EI-*co*-LSA) at a concentration of 0.5 g/dL exhibited a pH of 9. Solutions with a pH of 7 and 5 were prepared by adding the appropriate amount of HCl. To compare the degradation process at different pH values, relative η_{inh} values were plotted in Figure 8A. Absolute MW determination of these samples were carried out using SEC-MALLS.

Size Exclusion Chromatography in Combination with Multiple Angle Laser Light Scattering (SEC-MALLS). The SEC setup consisted of a HPLC Pump L-6000 from Merck-Hitachi, Darmstadt, Germany, a Merck-Hitachi autosampler AS-200A, and a Merck column thermostat T-6300. Polymers were detected by a differential refractive index (RI) detector RI-71 from Merck and an 18 angle laser light scattering detector from Wyatt Technologies, Santa Barbara, CA (DAWN EOS, GaAs Laser 690 nm, 30 mW, K5 cell). SEC column Novema 3000 was from Polymer Standard Service, Mainz, Germany. As an eluent, 1% formic acid (Riedel-de Haen, 98−100%) was used. The eluent was prepared with pure reagent water (0.22 μm, 0.055 μS/cm, USF Seral, Seradest BETA 25 and Serapur DELTA UV/UF), filtered through 0.2 μm sterile filter, and degassed with a four-channel online vacuum degasser DDG-75 from Duratec, Reilingen, Germany. Additionally, an inline filter (0.45 μm, stainless steel, Rheodyne, Cotati, CA) was set between the columns and MALLS detector. A flow rate of 1 mL/min was applied. Polymer concentration was 5 g/L and 20 μL were injected for each run. MWs were calculated by Astra for Windows Software, version 4.73.04, using Zimm plots. We have evaluated our SEC-MALLS with an commercially available PEI 25 kDa (Aldrich) and found following standard deviations (n = 5). dn/dc: 0.64%. M_n: 4.16%. M_w: 1.67%. M_w/M_n: 3.48%. Similar errors can be expected for the PEI and the PEI derivatives used in this study.

Formation of the Polymer−DNA Complexes. All complexes of DNA and polymer were prepared freshly before use. Plasmid DNA pGL3 control (luciferase reporter vector, 3.5 MDa, 5256 bp) was from Promega, Heidelberg, Germany, and was amplified with a competent *E. coli* strain JM 109 (Promega) according to a protocol from QIAGEN, Hilden, Germany (*15*). Plasmid DNA was used for all experiments except for the MTT

assay, in which DNA from herring testes (Type XIV, Sigma, Steinheim, Germany, 0.3−6.6 MDa, 400−10000 bp) was used.

The polymer solutions were added to DNA solutions in equal volumes, mixed by vortexing, and incubated for 1 min (physicochemical experiments) or 10 min (biological experiments) before use. DNA stock solutions were diluted to a concentration of 40 μg/mL with 150 mM NaCl at pH 7.4. The polymer stock solutions were also diluted with 150 mM NaCl (pH 7.4) to the appropriate concentration depending on the required polycation-nitrogen/polyanion-phosphorus ratio (N/P ratio) and filtered through 0.22 μm pore sized filters. DNA stock solutions were composed of 1 mg/mL pGL3 plasmid in 10 mM tris(hydroxymethyl)aminomethane hydrochloride (Tris HCl) (pH 8) and 1 mM ethylenediaminetetraacetic acid (EDTA). Polymer stock solutions exhibited a concentration of 0.9 mg/mL. Polymer concentration was based on the PEI content in the copolymer only; the lactic acid and succinic acid is ignored in this calculation. Thus, all polymer stock solutions contain the same polycation concentration for a better comparability of the results.

Physicochemical Characterization of Copolymer−DNA Complexes. *Dynamic Light Scattering (DLS).* Complex size measurements were carried out with a Zetasizer 3000 HS from Malvern Instruments, Worcs., UK, at 25 °C (10 mW HeNe laser, 633 nm). Scattered light was detected at a 90° angle through a 400 μm pinhole. Measurements yielding hydrodynamic diameters (*Z* average mean) and polydispersity indices (PDI) were performed with count rates of about 100−400 kCps in form of 10 runs of 60 min duration each and analyzed in the CONTIN mode. The viscosity (0.8905 mPas) and refractive index (1.333) of pure water at 25 °C were used for data analysis. The instrument was calibrated with Nanosphere Size Standards (polymer microspheres in water, 220 nm ± 6 nm) from Duke Scientific, Palo Alto, CA.

Laser Doppler Anemometry. ζ-Potential (zeta-potential) measurements of the complexes were carried out in the standard capillary electrophoresis cell of the Zetasizer 3000 HS from Malvern Instruments at position 17.0 and at 25 °C. Measurement duration was set to automatic. Average values of the ζ-potential were calculated with the data from eight runs. The instrument was calibrated with DTS5050 Electrophoresis Standards from Malvern Instruments.

Biological Characterization of the Polymers and the Polymer−DNA Complexes. *MTT Cytotoxicity Assay.* In vitro cytotoxicity was studied on L929 mouse fibroblasts by MTT assay according to the method of Mosmann (*16*). The cells were incubated with the polymers for 3, 12, and 24 h (8000 cells/well, 96-well microtiter plates) as described in detail earlier (*17*). Each point in Figure 10 represents the mean ± SD of seven determinations.

Transfection Experiments. Transfection activity of the polymers was also studied on L929 mouse fibroblasts using a Luciferase Kit from Promega. Measurements of relative light units (RLU) were conducted on a Sirius Luminometer from Berthold, Pforzheim, Germany. Protein quantification was performed with freshly prepared bicinchoninic acid (BCA) reagent (Pierce, Rockford, IL) and was carried out with an ELISA plate reader from Dynatech MR 5000, Denkendorf, Germany, at 570 nm. Experiments were performed in triplicates as described in more detail in a previous report (*18*).

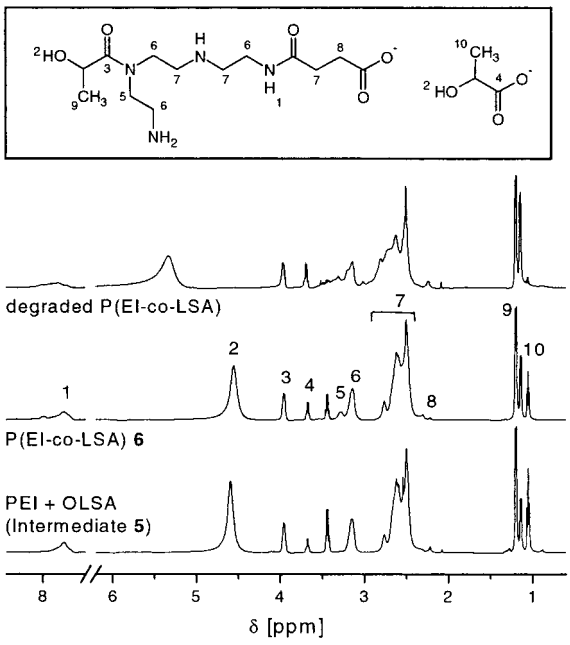


Figure 1. ^{1}H NMR spectra (500 MHz, d_6-DMSO) of polymers **5**, **6**, and the degraded P(EI-*co*-LSA) **6′** after 500 days. The structure shown in this figure is only a part of the macromolecules. Signals at δ = 1.05 and 3.45 ppm are derived from residues of ethanol in the product.

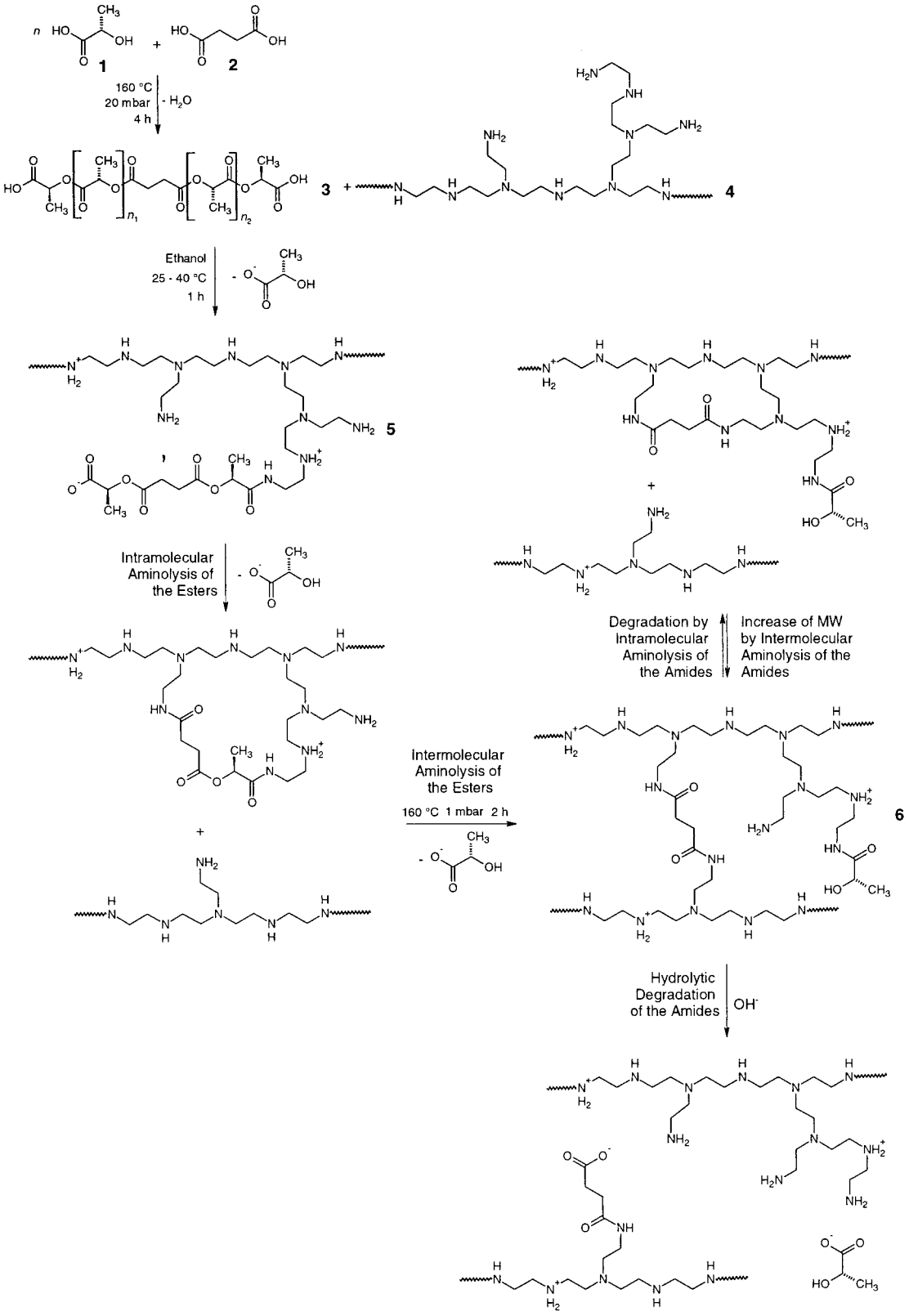
RESULTS AND DISCUSSION

Synthesis and Characterization of P(EI-*co*-LSA). To link several macromolecular PEI units together, we chose the simple bifunctional succinic acid, which had to be activated for the reaction with the amino groups of PEI. It is well-known that primary amines react with many esters just upon mixing and sometimes even at room temperature to yield amides (*19*). Therefore, an easy way to activate succinic acid for the reaction with PEI was to transform the acid into an ester. We used the α-hydroxy acid L-lactic acid as an alcohol. The use of this alcohol for esterification had at least two advantages: On one hand, this alcohol allows the formation of a polyester, which incorporates the succinic unit. As a consequence, there are not only two ester bonds per linker which can react with PEI, but a large number of ester bonds instead. This should improve the conversion of the coupling reaction. On the other hand, it does not matter if not all of the ester bonds of this polyester react with PEI. In this case, the linker will contain amide and ester bonds, so that hydrolytic degradation is guaranteed in every case.

In a first step, we synthesized the polyester to activate the succinic acid (Scheme 1). Polycondensation of succinic acid and L-lactic acid were carried out in bulk. As a result, the conversion of this polycondensation reaction was 90%, which implied that a decamer (10mer) with a MW of about 1000 Da was formed. Because of the low degree of polymerization the polyester will be referred to as oligo(L-lactic acid-*co*-succinic acid) (OLSA) in this article. Due to the incorporated succinic unit, the oligomer did not crystallize, but remained in its glassy state.

PEI and OLSA are highly viscous substances and cannot be mixed easily in bulk. Therefore, in preparation for the next reaction step, a blend of these homopolymers was prepared by dissolving the two components in ethanol and removing the solvent again under reduced pressure. During this process the first reactions took place. The ^{13}C NMR (175 ppm, signal 2 in Figure 2) and

Scheme 1. Synthesis Route and Degradation Mechanism of P(EI-*co*-LSA) 6



the FTIR (1653 cm^{-1}, signal E in Figure 3) spectra verified the formation of amide bonds. Signals of the ester groups (169 ppm, 1761 cm^{-1}, signal D_1 in Figure 3) disappeared. Only in the FTIR spectrum did a weak signal of the ester bond remain. Due to H-bonding between N−H of PEI and the C═O of OLSA, the ester signal had shifted to 1733 cm^{-1} (signal D_2 in Figure 3). In the ^1H NMR spectrum a new signal (6 in Figure 1) at 3.05 ppm appeared and was assigned to methylene protons of the PEI, which are neighbored to an amide bond. Hence, aminolysis of the ester bonds yielded an intermediate of the structure **5** shown in Scheme 1. Only a slight MW increase occurred at this step. While viscosimetry does not indicate any increase of MW, SEC-MALLS revealed an MW (M_w) increase from 1116 to 2853 (Table 1). This suggests that OLSA most likely reacted

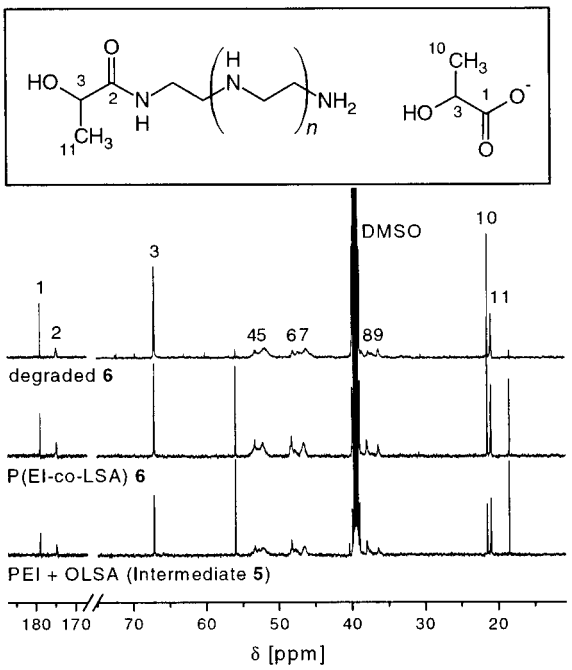


Figure 2. ^{13}C NMR spectra (125 MHz, d_6-DMSO) of polymers **5**, **6**, and the degraded P(EI-*co*-LSA) **6′** after 500 days. The structure shown in this figure is only a part of the macromolecules. Signals at δ = 18.9 and 56.5 ppm are derived from residues of ethanol in the product. Signals 4−9 are derived from the methylene carbons of PEI.

with PEI only to modify and graft the polycation, but did not link different PEI macromolecules together. In this case, a theoretical MW of about 2000 Da is expected for **5** which is in good agreement with M_n = 1795 Da found by SEC-MALLS. Since the reactants were in diluted solution the aminolysis will most likely occur *intra*molecularly. This also explains why the inherent viscosity did not increase, but instead slightly decreased (from 0.050 to 0.042 dL/g, Table 1). Despite the grafting of new blocks onto PEI, the density of the macromolecule remained constant or was even enlarged by the intramolecular linkages. Since density and viscosity are antiproportional to each other (Einstein's viscosity law: $\eta_{sp}/c = 2.5/\rho$, where η_{sp} is the specific viscosimetry [$\eta_{sp} = (t - t_0)/t_0$]) and ρ is the equivalent coil density), the viscosity of the polymer solution is expected to decrease in this case even if MW increases.

In a second reaction step the intermediate **5** was allowed to react at high temperatures (160 °C) and at maximum concentration (in bulk). Under these conditions, the aminolysis of the ester bonds was completed (no remaining ester absorptions in FTIR for **6**) and two additional processes began: Aminolysis of amides (amine−amide interchange reaction) and transamidification (amide−amide interchange reaction) (*20*). The latter reaction most likely played only a minor role, while the predominant reaction was the aminolysis of the amides (*21*). Aliphatic primary amines and, under forced reaction conditions secondary amines as well, can react with the amides (*22*−*24*). Hence, a new signal (signal 5 in Figure 1) appears in the ^1H NMR spectrum at 3.3 ppm. This signal was attributed to methylene protons of PEI adjacent to an *N*,*N*-disubstituted amide, which was formed by the reaction of a secondary amine with an N-monosubstituted amide. The formation of *N*,*N*-disubstituted amides was also verified by the decreased intensity of the N−H amide II absorption in the FTIR spectrum (signal G in Figure 3) from **5** to **6**. While during the first step most reactions probably occurred *intra*molecularly, due to the relatively high dilution, this step favors *inter*molecular reactions, because of the extremely high polymer concentration in bulk. These rearrangements toward intermolecular linkages are responsible for the large MW increase up to 8000 observed by SEC-MALLS. At the same time, inherent viscosity increased from 0.05 dL/g to almost 0.1 dL/g by a factor of 2.

Finally, the solubility behavior of oligomers and polymers are compatible with the proposed reaction scheme. OLSA is soluble in organic solvents, such as ethanol, chloroform, and dimethyl sulfoxide (DMSO), but insoluble in water. In contrast, the intermediate **5** and the resulting polymer **6** are insoluble in chloroform, but soluble in water, ethanol, and DMSO. This also is a measure for the progress of the reaction between PEI and OLSA at ambient temperature after as little as 1 h.

We are aware that copolymer synthesis can be further optimized. Especially, the optimum ratio between lactic acid and succinic acid in the oligomer OLSA has still to be determined. With less lactic acid in OLSA, more amino groups of the PEI will remain unsubstituted, which will probably affect the toxicity of the polymer and the DNA complexation. Copolymers with higher MW can be achieved when the ratio OLSA to PEI is increased. However, this ratio is probably limited. A larger amount of succinic acid linker could lead to cross-linking and would result in loss of solubility of the polymeric network. This optimization process is currently being carried out in our laboratories.

Polymer−DNA Complexes. PEI 1200 Da **4** and copolymer P(EI-*co*-LSA) **6** spontaneously formed complexes with plasmid DNA upon mixture of the solutions. These complexes were studied by DLS, which determined the hydrodynamic diameters and the polydispersity indices (PDI). The results are shown in Figures 4 and 5. The low MW PEI generated complexes of 350 nm in size with a PDI of 0.15, indicating a narrow complex size distribution. However, within 10 min the complexes aggregated to particle diameters of more than 700 nm. Furthermore, the PDI also increased significantly up to 0.5, implying an extreme broad size distribution. Thus, DNA complexes formed with low MW PEI were prone to aggregation. Surprisingly, a decisive enhancement of DNA condensation was observed in the case of copolymer P(EI-*co*-LSA), where the tendency toward aggregation was significantly reduced. In this case, size and stability of the complexes were strongly dependent on the N/P ratio. At N/P 10 complexes were not stable and aggregated from 320 to 570 nm within 10 min. Even at N/P 20 complexes were not quite stable, although the aggregation process (from 220 to 380 nm) was reduced significantly. However, stable complexes were obtained with N/P 50. In this case, no aggregation was observed at all. Complexes were found to be very small in size (150 nm). Also, the size distribution of the P(EI-*co*-LSA) complexes was considerably narrower (PDI < 0.1) in comparison to the PEI 1200 Da complexes. The large difference in complex size distribution between the homopolymer (PDI = 0.601) and copolymer (PDI = 0.077) is exemplarily presented in Figure 8 for N/P 20 after 10 min incubation.

These results could be explained by the differences in ζ-potential of the complexes (Figure 6). Complexes formed with PEI 1200 Da were only of moderate ζ-potential (4−13 mV), which apparently was not sufficient to electrostatically stabilize the complexes against aggregation. In

Table 1. Synthesis and Degradation of P(EI-*co*-LSA): Molecular Weight M_n, M_w and Molecular Weight Distribution M_w/M_n of the Polymers 4, 5, and 6 As Determined by SEC-MALLS

polymer sample	degradation time [d]	d*n*/d*c* [mL/g]	M_n [g/mol]	M_w [g/mol]	M_w/M_n	η_{inh} [dL/g]
PEI 1200 Da **4**	-	0.359	713	1116	1.57	0.050
intermediate **5**	-	0.199	1795	2853	1.59	0.042
		pH 9				
copolymer P(EI-*co*-LSA) **6**	0	0.195	3284	7906	2.41	0.096
	3	-	-	-	-	0.086
	7	0.219	2775	6115	2.20	0.072
	21	0.217	2360	4455	1.89	0.061
	46	0.219	2097	3449	1.65	-
	61	0.217	2112	3112	1.47	-
6′	500	0.221	1593	1789	1.12	0.053
		pH 7				
	0	-	-	-	-	0.1421
	3	-	-	-	-	0.1326
	7	0.219	3412	7017	2.06	0.1217
	28	0.235	2595	5124	1.97	0.1057
	43	0.224	2478	4181	1.69	-
		pH 5				
	0	-	-	-	-	0.1242
	3	-	-	-	-	0.1247
	7	0.218	3473	7563	2.18	0.1206
	28	0.234	3114	6463	2.08	0.1016
	43	0.219	3241	6360	1.96	-

[a] The refractive index increment d*n*/d*c* was determined by a refractive index detector and the inherent viscosity η_{inh} by capillary viscosimetry. Degradation was studied at pH 9, 7, and 5.

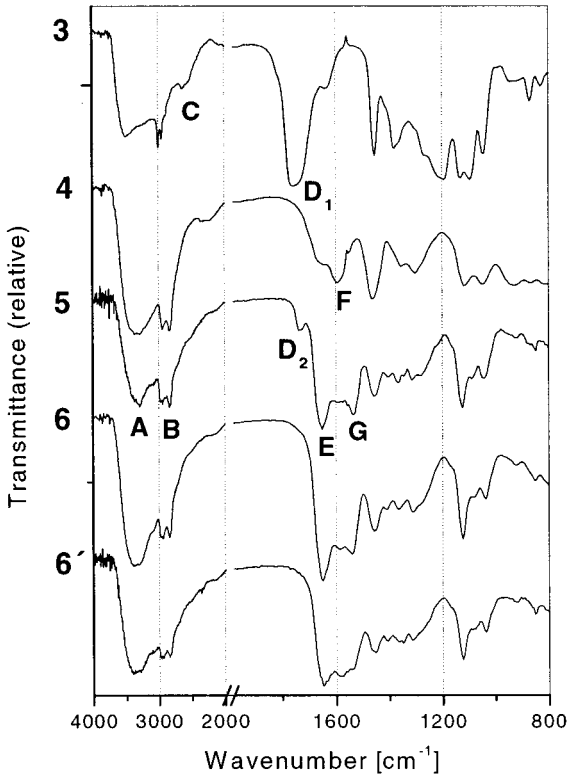


Figure 3. FTIR spectra (from top to bottom, KBr): oligo(lactic acid-*co*-succinic acid) (OLSA) **3**, PEI 1200 Da **4**, intermediate **5**, copolymer P(EI-*co*-LSA) **6**, degraded copolymer **6′**. Characteristic stretching absorptions: (A) N−H amines 3300 cm^{-1}, (B) C−H 2921 cm^{-1}, (C) COOH 2634 cm^{-1}, (D_1) C═O ester 1761 cm^{-1}, (D_2) C═O···H−N ester, (E) C═O amide I 1653 cm^{-1}. Bending absorptions: (F) N−H amines 1594 cm^{-1}, (G) N−H amide II 1541 cm^{-1}.

contrast, the stable complexes of P(EI-*co*-LSA) exhibited highly positive ζ-potentials of about 18 mV for N/P 20 and 50.

Transfection Experiments. Transfection experiments were performed with L929 mouse fibroblasts, as opposed to 3T3 cells, which are more widely used in

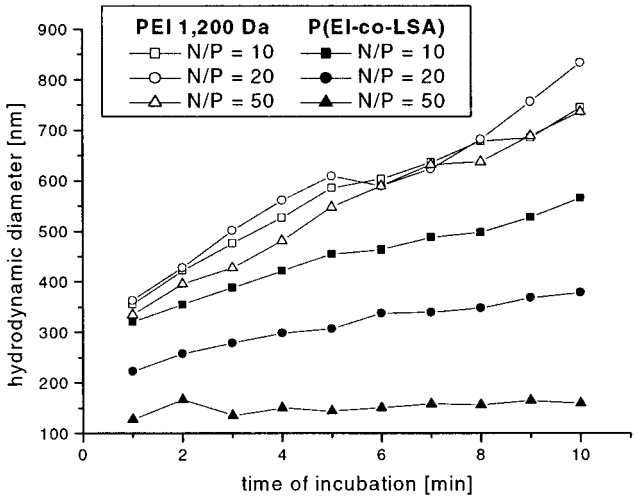


Figure 4. Hydrodynamic diameter of the polymer−DNA complexes as determined by dynamic light scattering at different N/P ratios in 150 mM NaCl at 25 °C.

transfection studies. However, we used the L929 cells in order to provide results which could be correlated with the cytotoxicity data raised from the MTT assay for which this cell line is recommended (see below). In previous experiments using PEI and its derivatives, we found that the transfection activities with L929 cells are similar to the results with 3T3 fibroblasts (data not shown). Results of the transfection experiments are shown in Figure 7. At N/P ratios 10 and 20 no significant differences in transfection activity could be observed between the homopolymer **4** and the copolymer **6**. However, at N/P ratio 50 a 10-fold higher reporter gene expression was found for copolymer P(EI-*co*-LSA) as compared to the homopolymer PEI. This high transfection activity can be attributed to the highly positive surface charge of the complexes (ζ-potential +18 mV) which favors a strong interaction with the negatively charge cell membrane, as well as to the small complex size (150 nm) which allows an easier cellular uptake by endocytosis.

For an efficient gene delivery with polymeric transfer agents it seems to be important that the polycation has

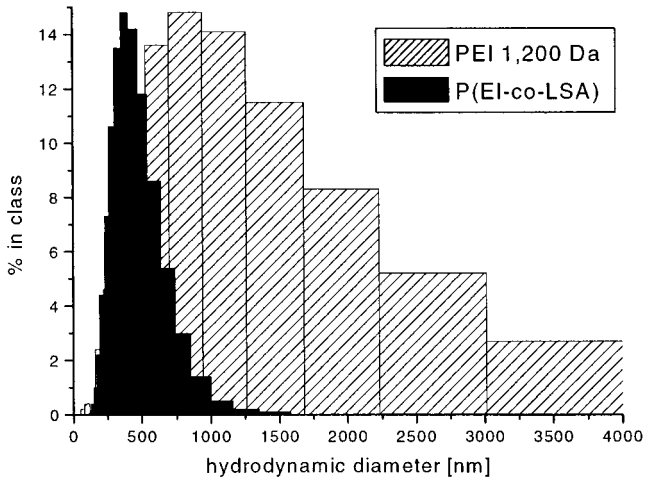


Figure 5. Size distributions of polymer−DNA complexes at N/P = 20 and after 10 min incubation as determined by dynamic light scattering in 150 mM NaCl at 25 °C.

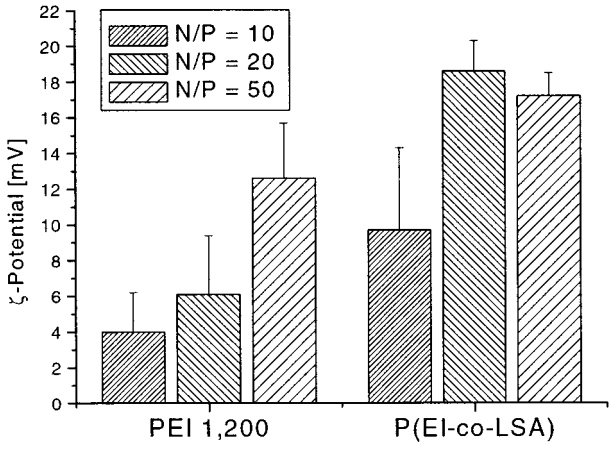


Figure 6. ζ-Potential of the complexes formed with plasmid DNA and PEI 1200 Da and copolymer P(EI-*co*-LSA) as determined by laser Doppler anemometry at different N/P ratios in 150 mM NaCl at 25 °C.

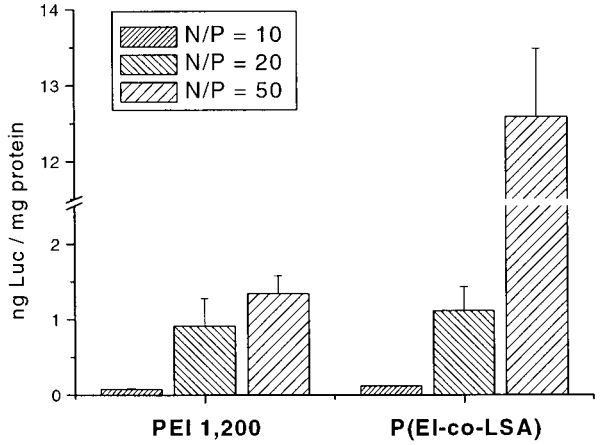


Figure 7. Transfection efficiency of PEI 1200 Da and copolymer P(EI-*co*-LSA) on L929 mouse fibroblasts at different N/P ratios.

a MW > 2000 Da. It has already been reported that low MW PEIs (≤2000 Da) do not transfect efficiently and sometimes not at all (*11*, *12*). Herein, we give an explanation for this poor transfection activity: The instability of the complexes, due to the relatively low ζ-potential, resulted in the formation of aggregates, which might be too large (>800 nm) for a nonspecific uptake into the cells. Apart from increasing the MW of the polycation by optimized polymerization methods, we demonstrate that improved transfection activity can also be achieved by linking low MW polycation units together. These conjugates of higher MW form stable and small complexes with DNA and, therefore, exhibit higher transfection efficiencies.

Degradation of P(EI-*co*-LSA). Biodegradable polymers, especially those for implants or other medical devices, have, in the past, been based on aliphatic polyesters, such as poly(lactic acid), poly(glycolic acid), or poly(ϵ-caprolactone). Creating a degradable polycation with cleavable ester bonds is difficult, since almost all polycations are based on amines, which can easily react with esters. This also is the reason the amino group bearing polyester, PAGA, reported by Lim et al. (*5*) degraded very quickly. The initial MW is reduced to 1/3 after only 100 min. The authors explained the rapid degradation as being a result of self-degradation of the polymer's own ester linkages by the ϵ-amino groups. Generally, ester bonds are easily cleaved if the polymer and the degradation products are water-soluble. Thus, a polycation linked with ester bonds would possibly degrade too fast and is not able to delivery the therapeutic gene efficiently before degradation. A very rapid degradation might be just tolerable in the case of cell culture experiments since only a few hours are required to yield a maximum transfection of the cells. In the case of in vivo gene delivery, however, the gene has to be protected for several hours or more, due to longer circulation times of the complexes in the blood system. A degradable polymeric network based on amides might be more appropriate for an in vivo gene delivery since it shows a higher stability as compared to a system with ester bonds, however, is still degradable, as we will show here.

The degradation pattern of our copolymer was studied in aqueous solutions at pH 5, 7, and 9 at 37 °C. The results of the viscosity measurements (Figure 8A) and MW determination by SEC-MALLS (Figure 8B and 9, Table 1) demonstrated that P(EI-*co*-LSA) had degraded within months and that degradation was accelerated with increasing pH. This finding is compatible with a degradation process which is base-catalyzed by the amino-groups of PEI. Table 1 displays the absolute MW during the degradation process. At pH 9 the copolymer **6** is degraded from M_w 8000 to the MW of the starting material **5** (M_w 3000) within 2 month. At the same time, the MWD is reduced to the original distribution of the PEI homopolymer. This is reasonable because the degradable copolymer P(EI-*co*-LSA) is cleaved into parts of the nondegradable PEI macromolecules with their narrower distribution. While the copolymer **6** is degraded after 1.5 month to a M_w of 3449 Da at pH 9, it is degraded to M_w = 4181 Da at pH 7 and M_w = 6360 Da at pH 5, respectively. Hence, at neutral and physiological pH the copolymer still degrades relatively fast, whereas under acidic conditions (pH 5) the degradation process is remarkably inhibited. We think that this pH dependency is quite favorable for a biodegradable gene delivery system, since it should protect the DNA against enzymatic degradation, especially at the pH at which DNAses are extremely active, as is true for the acidic conditions found in lysosomes (pH 5).

Two possible degradation mechanisms have to be discussed (see Scheme 1). On one hand, since the degradation process is performed in diluted solution, *intra*molecular aminolysis might cleave the *inter*molecular linkages, which would results in a decrease of MW.

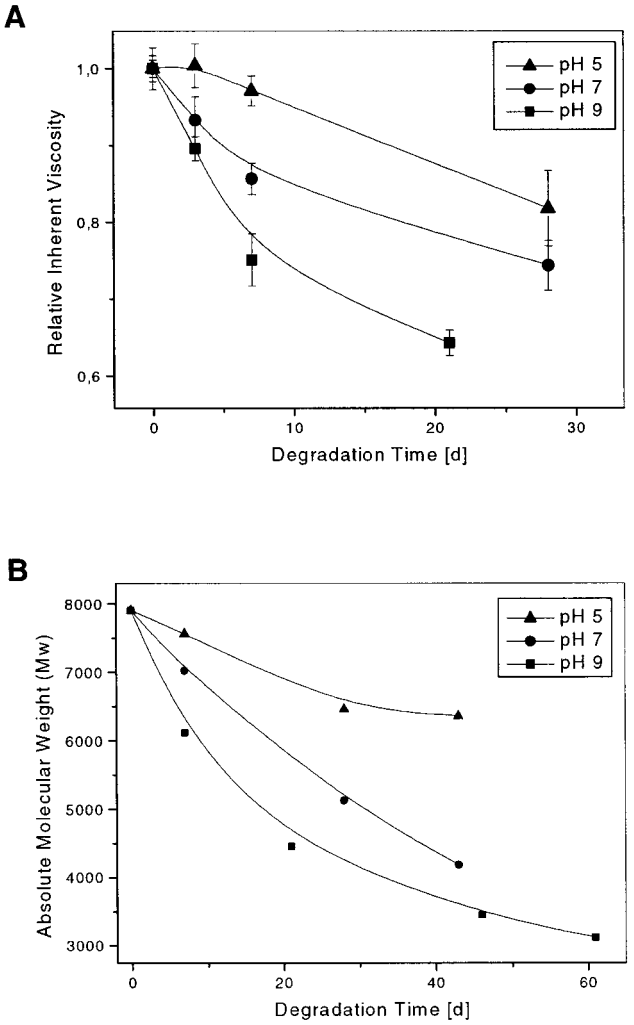


Figure 8. Degradation experiments with P(EI-*co*-LSA) **6** in aqueous solution at 37.2 °C and pH 5, 7, and 9. (A) Change of inherent viscosity during the degradation process as determined by an Ubbelohde viscosimeter. Relative values are presented in this plot. (B) Absolute MW (M_w) during degradation process as determined by SEC-MALLS.

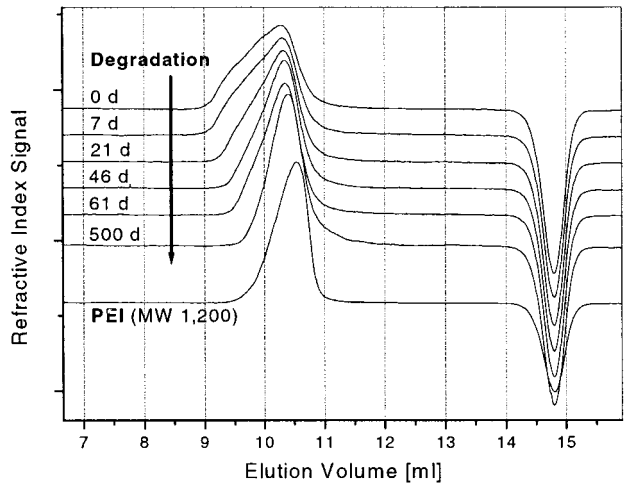


Figure 9. Degradation of P(EI-*co*-LSA):SEC eluograms of PEI 1200 Da **4** and its biodegradable derivative P(EI-*co*-LSA) **6** as detected by a refractive index detector. The degradation study was performed at pH 9 and 37.2 °C.

Still, it remains questionable if the aminolysis of amides really occurs under these mild conditions. On the other hand, the large number of primary amino groups in the vicinity of the amide bonds might facilitate this reaction. The second possible degradation process is the hydrolytic cleavage of the amides. It is generally assumed that the amide bond is rather stable against hydrolysis under mild conditions and that hydrolysis of amides only occurs at extreme pH and temperatures. Nevertheless, three points should be taken into account. First, to significantly decrease the MW of polyamides only a few amide bonds have to be cleaved. Second, the basic environment of the amides in our copolymer caused by the amino groups of PEI probably accelerates the hydrolytic cleavage. Third, several authors (e.g., *25*, *26*) reported the hydrolysis of polyamides under mild conditions and demonstrated that polyamide degradation can be observed after a few days. For instance, it has been reported that even water-*in*soluble aliphatic polyamides made from D- and L-tartaric acids and 1,6-hexamethylenediamine showed a weight loss between 10 and 30% and decays in the MW of nearly 50% after 2 months upon incubation in water under physiological conditions (pH 7.3, 37 °C) (*25*). In contrast, our P(EI-*co*-LSA) and all its degradation products are water-soluble. Thus, in our case the contact of the polymer with water is optimized which favors the amide hydrolysis.

The spectroscopic data support the theory of hydrolytic cleavage of amide bonds. A comparison of the NMR spectra of intermediate **5**, the copolymer **6** and the degraded copolymer **6′** (see Figures 1 and 2) showed an increase in the intensities of free lactic acid (^{1}H: signals 4 and 10, ^{13}C: signals 1 and 10) and a decrease in the intensities of polymer bound lactamide (^{1}H: signals 3 and 9, ^{13}C: signals 2 and 11) is clearly observed. During the reaction from **5** to **6**, aminolysis of the remaining ester bonds led to the release of additional lactic acid. The degradation process from **6** to **6′** released even more lactic acid, which is only possible by hydrolytic cleavage. A decrease of amide bonds by hydrolysis was also detectable by FTIR (Figure 3). Compared to the spectrum of **6**, the intensity of the carbonyl amide I absorption (signal E) was decreased in the spectrum of **6′**, while the intensity of the amino N−H bending absorption (signal G) had increased, thus, indicating an increasing number of free amino groups.

Consequently, if our copolymer is degradable two other polycations known for their application as gene delivery vehicles should also degrade via hydrolytic cleavage of its amide bonds since they also exhibit neighboring amido bonds and amino groups: poly(L-lysine) (PLL) (*27*) and polyamidoamine dendrimers (PAMAM) (*28*). In the case of polylysine, Oppermann et al. (*26*) states that almost nothing is known about the degradation behavior of this poly(amino acid). However, Kunioka et al. (*29*) reported that the similar polyamide poly(ϵ-lysine) had slightly degraded at its amide bonds (2% weight loss after 17 h at 40 °C) in water. In the case of PAMAM dendrimers, it was found that a short heat treatment of aqueous polymer solutions caused hydrolysis of some of the amide bonds, which surprisingly resulted in an even better transfection activity (*30*). Ranucci et al. (*31*) studied the hydrolysis of PAMAMs under physiological conditions and found that, after incubation for 24 h, polymer intrinsic viscosity was decreased by approximately 50%. Interestingly, they also pointed out that hydrolytic degradation progressed much more slowly at pH 5.5 which is in good agreement with our pH−rate profile for polyamide hydrolysis.

Cytotoxicity of the Polymers. The cytotoxicity of the copolymer **6** was studied using the same cell line as in the transfection experiments. As recommended by many

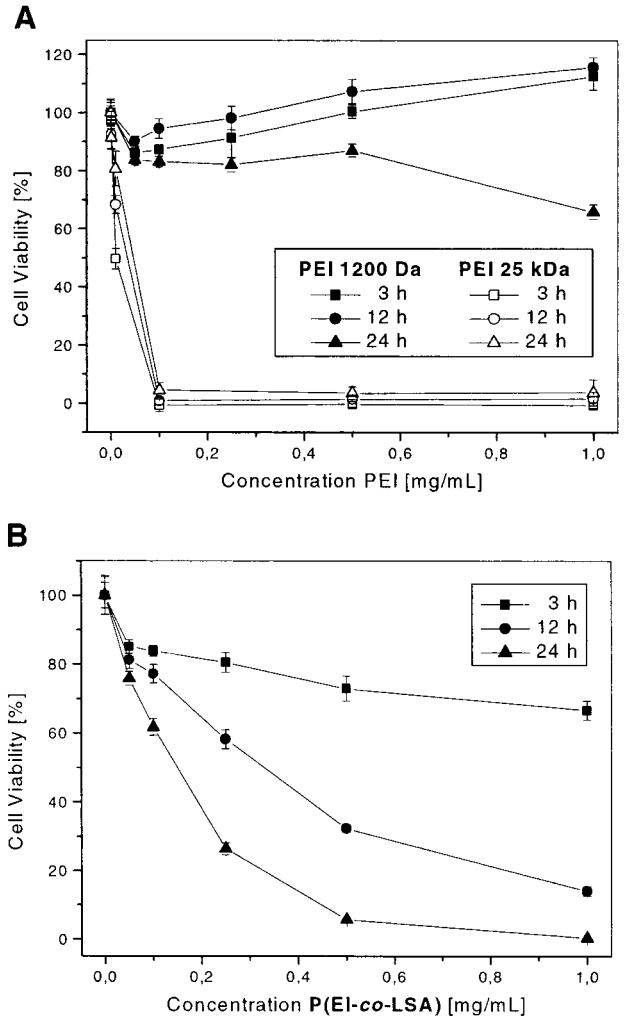


Figure 10. Dose- and time-dependent effects of PEI **4** 1200 Da in comparison to PEI 25 kDa (A) and copolymer **6** P(EI-*co*-LSA) (B) on L929 mouse fibroblasts determined by MTT-assay. Each point represents the mean ± SD of seven determinations.

standard institutions, L929 mouse fibroblasts were used as cell line to test the cytotoxicity of the polymers (*32*, *33*). PEI **4** was also studied as a reference (Figure 10A) and was found to be nontoxic up to a concentration of 0.5 mg/mL for 24 h. Only a slight decrease of cell viability (70%) was found at 1 mg/mL after a 24 h incubation time. IC_{50} values (>1.0 mg/mL) could not be determined in this case. The copolymer **6** (Figure 10B) also showed only a slight decrease in cell viability (67%) after 3 h incubation (IC_{50} > 1.0 mg/mL). At 12 and 24 h incubation time, an increase in toxicity with increasing polymer concentrations was observed (IC_{50}: 0.34 and 0.16 mg/mL, respectively). However, in comparison to commercially available high MW PEI, such as PEI 800 kDa from Fluka or PEI 25 kDa from Aldrich [IC_{50} approximately 0.01 mg/mL, see Figure 10A and (*13*)], the copolymer **6** was still of relative low toxicity. Its toxicity is comparable with the low MW PEI that is described in the literature as a highly effective gene transfer reagent with a low toxicity profile (*17*). Thus, the results of this cytotoxicity assay indicate a good biocompatibility of the biodegradable copolymer. A positive contribution toward the low toxicity profile of the copolymer might have the lactamide units with their terminal hydroxy groups which are generally assumed to have a positive influence on the biocompatibility of drug carrier systems (*34*). Furthermore, biocompatibility should even increase when degradation proceeds. With progressive degradation, copolymer **6** is expected to show a decrease in cytotoxicity, since the degradation products are nontoxic low MW PEI and lactic acid, whose acidity is neutralized by the basic PEI. Finally, it should be emphasized that we measured cytotoxicity of the free polymers. When applied as a gene transfer vehicle, the polymer is complexed with DNA. These complexes are generally less toxic compared to the free polymer (*35*, *36*). Therefore, the results of our cytotoxicity study represent the maximum toxic effect of the polymers.

CONCLUSIONS

A new type of copolymer has been prepared by linking several low MW PEI macromolecules using an oligomer of lactic acid and succinic acid. The resulting copolymer of high MW spontaneously formed complexes with plasmid DNA. Compared to low MW PEI the complexes were much smaller in size and more stable against aggregation which resulted in a 10-fold higher transfection activity of the copolymer. However, the decisive advantage is the biodegradability of this new copolymer which is based on hydrolytic cleavage of amide bonds. It was found that degradation was strongly dependent on pH. Keeping in mind the fact that DNAses are highly active under acidic conditions, as seen in lysosomes (pH 5), biodegradable gene transfer agents should be stable under acidic conditions in order to sufficiently protect the therapeutic gene. On the other hand, the polycation should be degradable under physiological conditions (pH 7.4) where the DNA should be released from the system. Our copolymer fulfils these demands and degrades within a reasonable time period that is long enough to secure gene transfer, but as short as necessary to prevent accumulation in the human body. Additionally, a low toxicity profile was observed for the new copolymer, which indicates its good biocompatibility.

These results demonstrate that the copolymer, P(EI-*co*-LSA), formed by a new synthesis method is a promising candidate for in vivo gene therapy applications. Further development will focus on the modification of the synthesis to improve the MW of the copolymer. It is expected that the transfection efficiency can be even enhanced by this process.

ACKNOWLEDGMENT

We would like to thank C. Selignow for the technical assistance and gratefully acknowledge support of the Deutsche Forschungsgemeinschaft (DFG).

LITERATURE CITED

(1) Jung, T., Breitenbach, A., and Kissel, T. (2000) Sulfobutylated poly(vinyl alcohol)-graft-poly(lactide-*co*-glycolide) facilitate the preparation of small negatively charged biodegradable nanospheres for protein delivery. *J. Controlled Release 67*, 157−169.

(2) De Smedt, S. C., Demeester, J., and Hennink, W. E. (2000) Cationic polymer based gene delivery. *Pharm. Res. 17*, 113−126.

(3) Garnett, M. C. (1999) Gene-delivery systems using cationic polymers. *Crit. Rev. Ther. Drug Carrier Syst. 16*, 147−207.

(4) Takakura, Y., Fujita, T., Hashida, M., and Sezaki, H. (1990) Disposition characteristics of macromolecules in tumor-bearing mice. *Pharm. Res. 7*, 339−346.

(5) Lim, Y. B., Han, S. O., Kong, H. U., Lee, Y., Park, J. S., Jeong, B., and Kim, S. W. (2000) Biodegradable polyester, poly [alpha-(4-aminobutyl)-L-glycolic acid] as a nontoxic gene carrier. *Pharm. Res. 17*, 811−816.

(6) Putnam, D., and Langer, R. (1999) Poly(4-hydroxy-L-proline ester): Low-temperature polycondensation and plasmid DNA complexation. *Macromolecules 32*, 3658−3662.

(7) Pollard, H., Remy, J.-S., Loussouarn, G., Demolombe, S., Behr, J.-P., and Escande, D. (1998) Polyethylenimine but not cationic lipids promotes transgene delivery to the nucleus in mammalian cells. *J. Biol. Chem. 273*, 7507−7511.
(8) Godbey, W. T., Wu, K. K., and Mikos, A. G. (1999) Poly-(ethylenimine) and its role in gene delivery. *J. Controlled Release 60*, 149−160.
(9) Bragonzi, A., Boletta, A., Biffi, A., Muggia, A., Sersale, G., Cheng, S. H., Bordignon, C., and Assael, B. M. (1999) Comparison between cationic polymers and lipids in mediating systemic gene delivery to the lungs. *Gene Ther. 6*, 1995−2004.
(10) Turunen, M. P., Hiltunen, M. O., Ruponen, M., Virkamäki, L., Szoka, F. C., Urtti, A., and Ylä-Herttuala, S. (1999) Efficient adventitial gene delivery to rabbit carotid artery with cationic polymer-plasmid complexes. *Gene Ther. 6*, 6−11.
(11) Godbey, W. T., Wu, K. K., and Mikos, A. G. (1999) Size matters: Molecular weight affects the efficiency of poly-(ethylenimine) as a gene delivery vehicle. *J. Biomed. Mater. Res. 45*, 268−275.
(12) Remy, J.-S., Abdallah, B., Zanta, M. A., Boussif, O., Behr, J.-P., and Demeneix, B. (1998) Gene Transfer with lipospermines and polyethylenimins. *Adv. Drug Delivery Rev. 30*, 85−95.
(13) Fischer, D., Harpe, A. v., Kissel, T. (2000) Polyethylenimine: Polymer structure influences the physicochemical and biological effects of plasmid/PEI complexes. *Biomaterials and Drug Delivery toward New Mellinium* (Park, K. D., Kwon, I. C., Yui, N., Jeong, S. Y., Park, K., Eds.) pp 195−211, Han Rim Wam Publishing Co., Seoul, Korea.
(14) Gosselin, M. A., Guo, W., and Lee, R. J. (2001) Efficient gene transfer using reversibly cross-linked low molecular weight polyethylenimine. *Bioconjugate Chem. 12*, 989−994.
(15) QIAGEN Plasmid Purification Handbook; QIAGEN, Hilden, Germany, 1997.
(16) Mosmann, T. (1983) Rapid colorimetric assay for cellular growth and survival: application to proliferation and cytotoxicity assay. *J. Immunol. Methods 65*, 55−63.
(17) Fischer, D., Bieber, T., Li, Y., Elsässer, H.-P., and Kissel, T. (1999) A novel nonviral vector for DNA delivery based on low molecular weight, branched polyethylenimine: Effect of molecular weight on transfection efficiency and cytotoxicity. *Pharm. Res. 16*, 1273−1279.
(18) Merdan, T., Kunath, K., Fischer, D., Kopecek, J., and Kissel, T. (2002) Intracellular processing of PEI/ribozym complexes can be observed in living cells using CSLM and inhibitor experiments. *Pharm. Res.* (in press).
(19) See organic chemistry textbooks, i.e., Grossman, R. B. (1999) *The art of writing reasonable organic reaction mechanisms*, p 65, Springer, New York.
(20) Flory, P. J. (1992) *Principles of Polymer Chemistry*, p 89, 15th ed., Cornell University Press, Ithaca.
(21) Elias, H.-G. (1990) *Makromoleküle, Band 1, Grundlagen*, p 555, 5th ed., Hüthig u. Wepf, New York.
(22) Kraus, A. M. (1973) The formylation of aliphatic amines by dimethylformamide. *Synthesis* 361−362.
(23) Jaunin, R. (1952) Sur l'aminolyse des amides. I. Aminolyse de l'acetanilide. *Helv. Chim. Acta 35*, 1414−1418.
(24) Galat, A., and Elion, G. (1943) The interaction of amides with amines: A general method of acylation. *J. Am. Chem. Soc. 65*, 1566−1567.
(25) Marques, M. S., Regano, C., Nyugen, J., Aidanpa, L., and Munoz-Guerra, S. (2000) Hydrolytic and fungal degradation of polyamides derived from tartaric acid and hexamethylenediamine. *Polymer 41* (8), 2765−2772.
(26) Oppermann, F. B., Pickartz, S., and Steinbuchel, A. (1998) Biodegradation of polyamides. *Polymer Degrad. Stab.* (special issue SI) *59* (1−3), 337−344.
(27) Zauner, W., Ogris, M., and Wagner, E. (1998) Polylysine-based transfection systems utilizing receptor-mediated delivery. *Adv. Drug Delivery Rev. 30*, 97−113.
(28) Haensler, J., and Szoka, F. C. (1993) Polyamidoamine cascade polymers mediate efficient transfection of cells in culture. *Bioconjugate Chem. 4*, 372.
(29) Kunioka, M., and Choi, H. J. (1998) Hydrolytic degradation and mechanical properties of hydrogels prepared from microbial poly(amino acid)s. *Polymer Degrad. Stab.* (special issue SI) *59* (1−3), 33−37.
(30) Tang, M. X., Redemann, C. T., and Szoka, F. C. (1996) In vitro gene delivery by degraded polyamidoamine dendrimers. *Bioconjugate Chem. 7*, 703.
(31) Ranucci, E., Spagnoli, G., Ferruti, P., Sgouras, D., and Duncan R. (1991) Poly(amidoamine)s with potential as drug carriers: degradation and cellular toxicity. *J. Biomater. Sci., Polym. Ed. 2* (4), 303−315.
(32) U. S. Pharmacopeia 25/NF 20 (2002) Biological reactivity tests, in vitro, p 1893, U. S. Pharmacopeia, Rockville, MD.
(33) Brown, S. A., Ed. (1990) Cell-culture test methods, in *Standard test method for agar diffusion cell culture screening for cytotoxicity*, pp 306−309, ASTM, Philadelphia.
(34) Hudecz, F., Pimm, M. V., Rajnavölgyi, E., Mezo, G., Fabra, A., Gaal, D., Kovacs, A. L., Horvath, A., and Szekerke, M. (1999) Carrier design: New generation of polycationic branched polypeptides containing OH groups with prolonged blood survival and diminished in vitro cytotoxicity. *Bioconjugate Chem. 10*, 781−790.
(35) Fechner, P. M. (2001) Poly(ethylenglykol)-Poly(ethylenimin)-Blockcopolymere (PEI−PEG) als nicht-virale Vektoren für die Gentherapie. Diploma thesis, University of Marburg, Germany.
(36) Petersen, H., Fechner, P. M., Martin, A. L., Kunath, K., Stolnik, S., Roberts, C. J., Tendler, S. J. B., Fischer, D., Davies, M. C., and Kissel, T. Poly(ethylenimine-*graft*-ethylene glycol) Copolymers: Influence of Copolymer Block Structure on DNA complexation and Biological Activities as Gene Delivery System. In preparation.

BC0255135

Synthesis of Peptide−Oligonucleotide Conjugates with Single and Multiple Peptides Attached to 2′-Aldehydes through Thiazolidine, Oxime, and Hydrazine Linkages

Timofei S. Zatsepin,[†] Dmitry A. Stetsenko,[‡] Andrey A. Arzumanov,[‡] Elena A. Romanova,[†] Michael J. Gait,*[,‡] and Tatiana S. Oretskaya*[,†]

Chemistry Department and A. N. Belozersky Institute of Physico-Chemical Biology, M. V. Lomonosov Moscow State University, Moscow, 119899, Russia, and Medical Research Council, Laboratory of Molecular Biology, Hills Road, Cambridge CB2 2QH, UK. Received February 16, 2002; Revised Manuscript Received April 23, 2002

2′-Deoxyoligonucleotides and 2′-*O*-methyloligoribonucleotides carrying one or more 2′-aldehyde groups were synthesized and coupled to peptides containing an N-terminal cysteine, aminooxy, or hydrazide group to give peptide−oligonucleotide conjugates incorporating single or multiple peptides in good yield. The facile conjugation method allows specific coupling in aqueous solution of unprotected oligonucleotides containing aldehyde groups to unprotected N-terminally modified peptides and other small molecules. A 12-mer 2′-*O*-methyloligoribonucleotide complementary to the HIV-1 TAR RNA stem-loop and containing two conjugated copies of an 8-mer model laminin peptide was hardly affected in TAR RNA binding and showed a similar level of inhibition of HIV-1 Tat-dependent in vitro transcription compared to the unconjugated 2′-*O*-methyloligoribonucleotide. Advantages of this conjugation method include (1) the ability to attach more than one peptide or other small molecule to oligonucleotide at defined nucleoside residue locations; (2) a conjugation route that does not affect significantly oligonucleotide binding to RNA structures; and (3) three alternative, facile, and mild conjugation reaction types that do not require use of a large excess of peptide reagent.

INTRODUCTION

Oligonucleotides and their analogues have been studied for more than two decades as specific inhibitors of gene expression. Oligonucleotides can be used to target mRNA by antisense (*1*) or RNAi (*2*) mechanisms, double-stranded DNA by triplex formation (*3*), or proteins by aptamer selection (*4*). Oligonucleotides conjugated to certain peptides have been found to possess improved cell-specific targeting, cellular uptake efficiency, or stability to degradation in comparison to unmodified oligonucleotides (*5*−*7*). In some cases improved binding strength to RNA and target specificity has been achieved (*8*).

Several methods of chemical synthesis of peptide−oligonucleotide conjugates have been developed to date (*5*). The two most popular synthetic approaches are total stepwise solid-phase synthesis and coupling in solution of separately prepared peptide and oligonucleotide fragments. In total synthesis, the same solid support is used for both peptide and oligonucleotide assemblies. Peptide synthesis may be followed by oligonucleotide synthesis (*9*), or vice versa (*10*), or a branched linker is attached to the support permitting independent growth of both peptide and oligonucleotide chains (*11*). Unfortunately, the chemistries of peptide and oligonucleotide synthesis have been poorly compatible up to now. Attempts to solve these problems include modification of the solid support (*12*), base protecting groups of nucleoside components (*13*), side-chain amino acid building blocks (*14*), or deprotection conditions (*15*). Some recent advances in total solid-phase synthesis look promising (*16*), but so far no routine procedure has emerged.

Fragment coupling of peptides to oligonucleotides has found particular utility in the case of longer peptides. One method involves coupling of a protected peptide segment to a support-bound, protected, or partially unprotected oligonucleotide (*17*). A particular advantage of this method is that, as for regular solid-phase synthesis, the excess of reagents is removed easily by filtration. However, coupling yields have been found to be poor in the case of long or "difficult" peptides. A more general approach is the separate solid-phase assembly of oligonucleotide and peptide fragments, deprotection (and purification if necessary) followed by a solution-phase chemoselective ligation mediated by mutually reactive groups introduced into each component during solid-phase assembly or postsynthetically. These methods include formation of disulfide (*18*), thioether (*19*), amide (*20*), oxime (*21*, *22*), thiazolidine (*22*), or imine (*23*) linkages.

An alternative route to synthesis of peptide−oligonucleotide conjugates is by an addition−elimination reaction of a nucleophile to an electrophilic aldehyde group. Here, weakly basic nucleophiles attached to the N-terminus of a peptide should be suitable because they would be expected to have a pK_a lower than that of peptide side chain amino groups (such as of Lys and Arg) and thus should react with aldehydes at pH near or below 7, where aliphatic amino groups of peptide should be

* To whom correspondence should be addressed. M. Gait: Phone 01223-248011; Fax 01223-402070; e-mail mgait@mrc-lmb.cam.ac.uk. T. Oretskaya: Phone (095) 939-5411; Fax (095) 939-3181; e-mail oretskaya@belozersky.msu.ru.

[†] Moscow State University.

[‡] Medical Research Council.

10.1021/bc020016+ CCC: $22.00 © 2002 American Chemical Society
Published on Web 06/25/2002

largely protonated. The use of unprotected peptide fragments has several advantages. First, unprotected peptides are usually water-soluble or can be solubilized by addition of organic cosolvents, such as DMF, or denaturing agents, such as urea or guanidinium chloride. Second, products of conjugation reactions may be readily purified by PAGE or HPLC, do not require additional deprotection steps, and thus may be used directly for biological assays. Appropriate nucleophiles which may react with aldehyde groups include *O*-alkyl hydroxylamines, arylhydrazines, acyl- and sulfonylhydrazides, and carbazates. The linkages thus formed are correspondingly oxime and hydrazone, which are sufficiently stable, yet are prone to cleavage by hydrolysis under forcing conditions. Further, 1,2-aminothiols react with carbonyl groups to form thiazolidines, which are also stable over a wide pH range (*24*). Normally, such conjugation reactions are conducted at a slightly acidic pH.

The advantages of an aldehyde group include the possibility of a reversible additive-free conjugation with a range of nucleophiles without an additional preactivation step that is required for other carboxylic groups. There are two well-known ways to introduce an aldehyde group into oligonucleotides through use of solid-phase phosphoramidite chemistry. One route involves use of a masked aldehyde moiety (*25*) such as an acetal. A second approach involves use of a precursor incorporating a suitably protected 1,2-diol group (*26*). Here an aldehyde can be generated under the more convenient and mild conditions of periodate oxidation (*26*), whereas demasking conditions of an aldehyde group can sometimes be harsh (*25*). 1,2-Diols can be obtained by OsO_4-catalyzed hydroxylation of alkenes (*27*). We described recently a new phosphoramidite reagent for incorporation of 1,2-diol groups into oligonucleotides using 2′-modification (*28*). Conjugation of the subsequently generated 2′-aldehydes may be effected through use of any of three alternative chemistries and thus provides the possibility of introducing multiple peptides into defined positions within an oligonucleotide sequence.

The formation of thiazolidines using N-terminal cysteinyl peptides has been used widely for protein ligation and peptide dendrimer formation (*29*). Cysteine residues can also be introduced at the N-terminus of oligonucleotides by use of phosphoramidite reagents developed recently (*30, 31*). A cysteinyl group has been used frequently for peptide–oligonucleotide conjugation through disulfide or thioether formation (*5*), or more recently for native ligation of peptide (*30*) or oligonucleotide thioesters (*32*). Use of organic cosolvents and elevated temperature leads to consistently better results than aqueous buffer alone (*33*). However, the most common polar aprotic solvents DMF and DMSO are not suitable in the case of thiazolidine formation. DMF use results in side reactions, e.g., formylation of peptide amino groups, and DMSO is a mild oxidizing agent that can cause disulfide formation of cysteine peptides (*29*). Use of NMP or acetonitrile as cosolvents usually gives better results.

An *O*-alkyl hydroxylamino group, more specifically an aminooxyacetyl group, has been widely used for peptide ligation (*29, 34, 35*). Recently aminooxy groups have been incorporated into oligonucleotides (*21*) and used in conjugation reactions with reporter groups (*36, 37*) or modified peptides (*21, 22*). Not only is an oxime linkage stable over a wide pH range (*33*), but aminooxyacetic acid per se or Boc-protected is commercially available. The latter can be used directly in the final coupling step in solid-phase peptide synthesis.

Hydrazone formation seems to be a favorite method for coupling of various groups in carbohydrate and protein chemistry (*38*). Sometimes, a reduction by $NaBH_3CN$ is needed to increase the stability of such conjugates to acidic or basic treatment. Peptide hydrazides can be easily generated from esters by hydrazinolysis. An alternative approach that is better suited for solid-phase synthesis is to introduce Fmoc-4-hydrazinobenzoic acid on to the N-terminus of a peptide (*29*). However, since this method seemed not to be altogether successful, we have used our previously developed thiosuccinate reagent, pentafluorophenyl *S*-benzylthiosuccinate (*30*), to generate a succinic acid monohydrazide on the N-terminus of a peptide after a mild hydrazine treatment.

A few papers describe the synthesis of peptide–oligonucleotide conjugates where a peptide is attached to the 2′-position via a 2′-aminonucleoside (*39–41*), but this route can suffer from low yields (*40, 41*). Further, the incorporation of 2′-aminonucleosides and their acyl derivatives strongly decreases duplex stability (*42*).

2′-*O*-Alkyloligonucleotides are widely used in antisense research. As described in a recent review (*43*), 2′-*O*-alkyloligonucleotides in general show improved binding affinity to target mRNA, a large increase in nuclease resistance, and added stability against depurination compared to unmodified oligodeoxyribonucleotides. Incorporation of multiple 2′-*O*-alkylnucleotides is known to preserve an A-type duplex structure when bound to an RNA strand, since, in contrast to 2′-aminonucleosides, 2′-*O*-alkyl-modified nucleosides adopt a sugar conformation similar to that of ribonucleotides. Pendant peptides conjugated through a 2′-*O*-alkyl modification would be expected to be positioned on the minor groove side of an oligonucleotide–RNA duplex. Considering these potential benefits for peptide–oligonucleotide conjugates, we now report the highly efficient conjugation of peptides, either singly or multiply through 2′-aldehydes, to oligodeoxynucleotides and to 2′-*O*-methyloligoribonucleotides. Further, we show that such conjugates are not impaired significantly in their ability to bind to complementary RNA, and in some cases binding is enhanced. We also report that a 12-mer 2′-*O*-methyloligoribonucleotide complementary to the HIV-1 TAR RNA stem-loop and containing two conjugated copies of an 8-mer model laminin peptide was able to inhibit HIV-1 Tat-dependent in vitro transcription as well as the umodified 2′-*O*-methyloligoribonucleotide, suggesting that such conjugation routes should be suitable in principle for attachment of single or multiple cell-penetrating or cell-targeting peptides.

EXPERIMENTAL SECTION

General. Materials were obtained from commercial suppliers and used without further purification unless otherwise noted. Polystyrylmethyl trimethylammonium metaperiodate (loading 2.17 mmol/g) and polystyrylmethyl trimethylammonium borohydride (loading 3.65 mmol/g) were purchased from Novabiochem, creatine phosphate, creatine kinase, poly[d(I-C)] (Boehringer Mannheim), RNAsin, transcription plasmid phRL-CMV (Promega). Analytical HPLC of peptides was carried out with dual wavelength (215 and 230 nm) UV detection using a Vydac RP-C8 column (4.6 × 250 mm). Preparative peptide HPLC was carried out using a Vydac RP-C8 column (25 × 300 mm) and 215 nm UV detection. A gradient of acetonitrile in 0.1% aq TFA from 10 to 90%

in 30 min was used for the HPLC analysis and purification of peptides. HPLC analysis and purification of 5′-O-Dmt-protected oligonucleotides and conjugates were carried out on a Tracor instrument using 4 × 250 mm DIAKS-130-CETYL column; buffer A: 0.1 M ammonium acetate (pH 7); buffer B: 0.1 M ammonium acetate, 40% MeCN, (pH 7); gradient of B from 0 to 100% in 60 min; flow rate 1 mL/min; temperature 45 °C. Oligonucleotides and conjugates were analyzed by a reversed phase HPLC (ion-pair mode) (Waters) on a DIAKS-130-CETYL column (4 × 250 mm) using a logarithmic gradient: 0−45.9% B (1 min); 45.9−49.2% B (1 min); 49.2−53.6% B (3 min); 53.6−56.9% B (5 min); 56.9−60.2 B (10 min); 60.2−62.1% B (10 min); 62.1−63.5% B (10 min). Separation of oligomers with a retention time step of 1 min/unit was carried out; mobile phase A: H_2O-MeCN (95:5 v/v), 2 mM tetrabutylammonium dihydrogen phosphate, 48 mM KH_2PO_4, pH 7; mobile phase B: H_2O-MeCN (60:40 v/v), 2 mM tetrabutylammonium dihydrogen phosphate, 48 mM KH_2PO_4, pH 7; flow rate 1 mL/min, and temperature 45 °C. MALDI-TOF mass spectra were run on a Voyager DE workstation (PE Biosystems) in a freshly prepared 1:1 v/v mixture of 2,6-dihydroxyacetophenone (40 mg/mL in MeOH), and aq diammonium hydrogen citrate (80 mg/mL) as a matrix. Denaturing gel electrophoresis of oligonucleotides was performed in 15% PAGE containing 2 M urea in Tris-borate buffer (50 mM Tris HCl, 50 mM boric acid, 1 mM EDTA, pH 7.5).

Peptide Synthesis and Characterization. Peptides **6** and **7** were purchased from Bachem. Solid-phase peptide synthesis of peptides **8** and **9** was carried out by the solid-phase Fmoc/*tert*-butyl procedure (*44*) on a PE Biosystems Pioneer peptide synthesizer on a 0.05 mmol scale using HATU/DIEA in situ activation protocol (*45*) and Rink amide NovaGel HL support (Novabiochem). Boc-Aminooxyacetic acid for **8** and *S*-benzyl thiosuccinic acid (*30*) for **9** were placed at the last amino acid position and incorporated at the end of normal Fmoc-on solid-phase synthesis protocol by a standard coupling cycle. In the case of **9**, the resin was removed from a column, treated with 0.5 M hydrazine hydrate solution in dioxane for 2 h at room temperature, filtered, washed by DMF, MeOH, and diethyl ether, and finally dried in vacuo. Both peptides **8** and **9** were subjected to normal acidolytic cleavage and deprotection procedure by TFA−phenol−1,2-ethanedithiol−triisopropylsilane−water (900:25:25:25:25 v/v/v/v/v). Resulting peptides were analyzed by RP-HPLC, their respective molecular masses confirmed by a MALDI-TOF analysis; matrix: 10 mg/mL α-cyano-4-hydroxycinnamic acid, 3% (v/v) TFA in H_2O/MeCN (1:2 v/v).

Oligonucleotide Synthesis and Characterization. Oligodeoxyribonucleotides and 2′-*O*-methyloligonucleotides were assembled on a ABI 380B DNA synthesizer by the cyanoethyl phosphoramidite method (*46*) following manufacturer's recommendations. Protected 2′-deoxy- and 2′-*O*-methylnucleoside phosphoramidites were purchased from Glen Research. Prepacked 0.4 μmol columns were used throughout. For couplings with modified phosphoramidite (*28*), 0.15 M concentration in anhydrous acetonitrile was used, and the coupling time was increased to 15 min. Oligonucleotides were cleaved from the support and deprotected using concentrated aq ammonia overnight at 55 °C.

Synthesis of 2′-Aldehyde Oligonucleotides. *Method A (for subsequent thiazolidine conjugation).* To a solution of 2′-diol oligonucleotide (5 A_{260} units, 43 nmol) in 50 mL of 0.2 M acetate buffer, pH 4.5, were added a few granules of polystyrylmethyl trimethylammonium metaperiodate. After 1 h of shaking, the solution was decanted and polymer washed by H_2O (2 × 20 mL). The solution was evaporated in vacuo to remove volatiles.

Method B (other cases). To a solution of 2′-diol oligonucleotide (5 A_{260} units, 43 nmol) in 50 mL of 0.2 M acetate buffer, pH 4.5, was added 5 mL of 0.1 M $NaIO_4$. After 30 min, the reaction mixture was evaporated in vacuo.

Coupling of N-Terminal Cysteine Peptides to 2′-Aldehyde Oligonucleotide. A solution of peptide **6** or **7** (50−70 nmol) in a mixture of 0.4 M acetate buffer, pH 4.5, and acetonitrile (3:7−7:3 v/v, 50 mL) was added to the oligonucleotide **I**. The reaction mixture was incubated at 37 °C for 0.3−18 h and then evaporated in vacuo and purified by PAGE.

Coupling of *O*-Alkylhydroxylamine Derivatives to 2′-Aldehyde Oligonucleotides. A solution of *O*-alkylhydroxylamine derivative (100 nmol of **2** and **5** or 60−70 nmol of **8**) in 50 mL of the mixture of 0.4 M acetate buffer, pH 4.7, and DMSO (3:7−7:3 v/v) was added to an oligonucleotide. The reaction mixture was incubated at 37 °C for 0.3−5 h, depending on the molecular weight of the conjugated molecule and purified by PAGE in the case of peptide conjugates. Other conjugates were precipitated by addition of 0.1 mL of 2 M $LiClO_4$ and 1 mL of acetone and purified by RP-HPLC.

Coupling of Hydrazines and Hydrazides to 2′-Aldehyde Oligonucleotides. A solution of hydrazine or hydrazide (100 nmol of **3** or 60−70 nmol of **9**) in 50 mL of the mixture of 0.4 M acetate buffer, pH 4.7, and DMSO (3:7−7:3 v/v) was added to an oligonucleotide. The reaction mixture was incubated at 37 °C for 0.3−5 h, and then a few granules of polystyrylmethyl trimethylammonium borohydride were added. The reaction mixture was incubated for 30 min more and purified by PAGE in the case of **9**. In the case of **3**, the conjugate was precipitated by addition of 0.1 mL of 2 M $LiClO_4$ and 1 mL of acetone and purified by RP-HPLC.

Analysis of Hydrolytical Stability of Thiazolidine and Oxime Conjugates. Conjugates (0.2 A_{260} units) were dissolved in 20 mL of 0.2 M acetate buffer, pH 2.0, 3.0, or 4.0, or 0.2 M phosphate buffer, pH 8.0, 9.0, or 10.0. After 24 h, conjugates were precipitated by addition of 0.1 mL of 2 M $LiClO_4$ and 1 mL of acetone.

Analysis and Characterization of Peptide−Oligonucleotide Conjugates. Product elution from gel was performed with 0.5 M aq sodium acetate for 12 h at 4 °C. Conjugates were precipitated by addition of 1 mL of EtOH followed by cooling at −70 °C for 1 h. RP-HPLC (ion-pair mode) analyses were carried out as described previously (*28*). Purified conjugates were then analyzed by MALDI-TOF mass spectrometry.

Thermal Melting Experiments. Absorbance vs temperature profiles were measured on a Varian Cary 50 spectrophotometer in a buffer containing 100 mM NaCl, 10 mM Na_2HPO_4, 1 mM EDTA, pH 7.0. Oligonucleotides, conjugates, and their complementary templates were combined at 4 μM of each strand, heated at 90 °C, and cooled at a rate of 0.5 °C/min in a 1 cm path length cell and then heated back to confirm reversibility and lack of evaporation.

In Vitro Transcription Inhibition. Cell-free transcription reactions with DNA template derived from plasmid p10SLT carrying the wild-type HIV-1 LTR (strain NL4-3) were carried out as described previously (*47*, *54*). Briefly, the reaction mixtures (40 μL) containing 15 μL of HeLa cell nuclear extract (*48*), 10 nM −345 to +524 fragment (*Eco*RV-Xba I) of plasmid p10SLT, 80 mM KCl, 3.5 mM $MgCl_2$, 20 mM HEPES (pH 7.9), 2 mM DTT,

10 μM $ZnSO_4$, 10 mM creatine phosphate, 100 μg mL^{-1} creatine kinase, 1 μg of poly[d(I-C)], 50 μM ATP, GTP, and CTP, 5 μM UTP, [α-^{32}P]-UTP (10 μCi), 1 unit mL^{-1} RNAsin, 200 ng of recombinant Tat protein (*48*), and increasing concentrations of inhibitor oligonucleotide were incubated at 30 °C for 20 min and then stopped by addition of 50 μL of 150 mM sodium acetate solution, 0.5% SDS, 10 mM EDTA, and 20 μg mL^{-1} tRNA. After phenol/chloroform extraction and ethanol precipitation, the reaction products were analyzed by 6% PAGE containing 7 M urea followed by autoradiography. The autoradiographs were scanned densitometrically using a Personal SI (Molecular Dynamics, Inc.), and the resulting digitized images were analyzed by Geltrak software (*49*).

For HIV Tat-independent in vitro transcription plasmid phRL-CMV was linearized using Nhe I. Transcription reactions were carried out essentially as in Tat-dependent transcription with minor differencies. The amount of DNA template was 200 ng, the concentration of KCl was decreased to 50 mM and the HIV Tat protein was not added to the reaction mixture. Tat-independent transcription inhibition was assessed at 0.5 and 2 μM concentrations of the inhibitor.

RESULTS AND DISCUSSION

We have described recently the introduction into oligonucleotides of 2′-*O*-(2,3-dihydroxypropyl)uridine as a suitable precursor of an aldehyde group (*28, 50*). The hydroxyl functions of the 1,2-diol in the modified residue were protected by benzoyl groups, which are removable during standard oligonucleotide deprotection with ammonia solution (Scheme 1). For peptide conjugation studies, we chose to introduce 2′-diol-modified uridine in place of thymidine or uridine residues within oligonucleotides complementary to the HIV-1 TAR RNA apical stem-loop, the target sequence for the HIV-1 trans-activator protein Tat (*51*). We have already shown that such oligonucleotides inhibit Tat binding to TAR RNA in vitro (*52, 53*) and that a 12-mer 2′-*O*-methyloligoribonucleotide inhibits Tat-dependent in vitro transcription (*54*). Both oligodeoxynucleotides (**I**, **II**, **III**, and **VII**) and 2′-*O*-methyloligoribonucleotides (**IV**, **V**, and **VI**) were synthesized containing diol modifications.

Sequence, 5′-3′:

CTCCCAGGCU̲CA **(I)**

CU̲CCCAGGCTCA **(II)**

CU̲CCCAGGCU̲CA **(III)**

cucccaggcU̲ca **(IV)**

cU̲cccaggcuca **(V)**

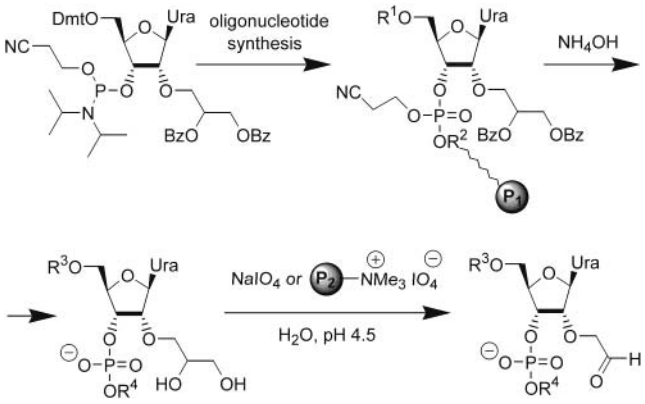
cU̲cccaggcU̲ca **(VI)**

GCU̲CCCAGGCTCAAA **(VII)**

where U̲ is 2′-*O*-(2,3-dihydroxypropyl)uridine, 2′-deoxynucleotides are capitalized, and 2′-*O*-methyl nucleotidesare in lower case

Oxidation of the 1,2-diol group was carried out under mild conditions, namely a 2-fold excess of $NaIO_4$ in acetate buffer, pH 4.5, 30 min. Polymer-supported periodate may also be used, in which case the reaction time was extended to 1 h (Scheme 1). The latter method is especially suitable for a subsequent thiazolidine conjugation, since it requires just a simple filtration step to remove the excess of periodate. The reaction is not very sensitive to pH, thus allowing a variety of buffers to be used. Subsequent conjugations can be carried out without purification of the aldehyde, except for thiol-containing compounds, which may be oxidized to disulfides by an excess of periodate.

Scheme 1[a]



[a] R^1, R^2 = protected oligonucleotide chain; R^3, R^4 = unprotected oligonucleotide chain; P_1 = controlled pore glass, P_2 = macroporous polystyrene.

For initial conjugation experiments (Scheme 2), we have chosen several model compounds and short peptides (Table 1). Peptide **6** is a glycoprotein hormone α (32−46) receptor binding domain (*55*). Peptide **7** incorporates SV-40 large T antigen NLS sequence (*56*). N-Terminally functionalized peptides **8** and **9** include residues 926−933 of laminin B1 chain. This sequence is known to bind laminin receptors and inhibits angiogenesis and tumor growth (*57*). We have studied the effects of pH, stoichiometry, organic solvent addition, and temperature on the reaction efficiency.

When the pH was increased from 3.5 to 6.0, the time of complete reaction (>95%) was also increased, in the case of L-cysteine ethyl ester from less than 5 min to 20 min. In the case of *O*-benzylhydroxylamine and 4-hydrazinobenzoic acid better results were obtained at pH 4.5−5.0, since after 3 h at pH 3.0 traces of degraded oligonucleotide were observed (data not shown). Therefore, thiazolidine formation was carried out at the safer pH 4.5. The effect of stoichiometry was less significant. Use of a 10-fold excess of nucleophile resulted in reaction proceeding twice as fast as when a nearly equimolar ratio was used. The reaction was therefore routinely carried out in the presence of 1.2−1.8 equiv of nucleophilic peptide.

As previously mentioned, DMF and DMSO are unsuitable for use during thiazolidine formation. Acetonitrile, which can be removed easily by evaporation, and NMP provided the best results, while formamide strongly decreased the efficiency of the reaction (data not shown). The best cosolvent for oxime and hydrazone conjugation was DMSO. At elevated temperature (37 °C) the efficacy of all reactions was increased also. In the case of hydrazinobenzoic acid, the resultant hydrazone was reduced to the corresponding hydrazine linkage by use of polystyryl trimethylammonium borohydride.

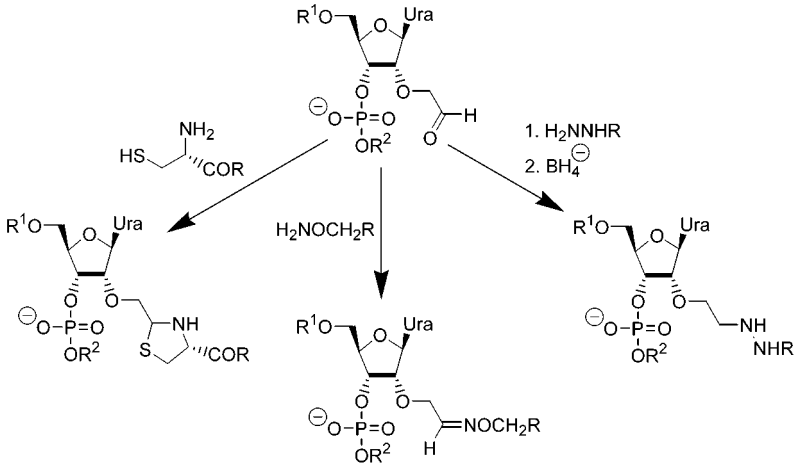
Conjugates of 2′-aldehyde-containing oligonucleotides with *O*-benzylhydroxylamine showed two peaks (Figure 1b, peaks *2* and 3) with close retention times on reversed-phase HPLC in ion-pair mode. After reduction by $NaBH_3CN$, only one peak (Figure 1c, peak 4) on the HPLC trace was observed. We therefore conclude that the two peaks represent oxime syn- and anti-isomers.

Table 1. Oligonucleotide 2′-Conjugates Synthesized, Yields of Crude Products and Isolated Yields (figure following oblique lines)

			oligonucleotide						
type[a]		conjugated molecule/peptide	**I**	**II**	**III**	**IV**	**V**	**VI**	**VII**
T	**1**	H-Cys-OEt	>90	>90	-	-	-	-	-
O	**2**	H_2NOCH_2Ph	>90	>90	-	-	-	-	90
H	**3**	$4\text{-}NH_2NHC_6H_4CO_2H$	85	85	70	-	-	-	-
T	**4**	H-Cys-Gly-OH	>90	>90	90	>90/70	90/65	90/70	-
O	**5**	$H_2NOCH_2CO_2H$	>90	>90	85	-	-	-	-
T	**6**	H-CFSRAYPTPLRSKKT-OH	90/35	-	-	-	-	-	-
T	**7**	H-CGYGPKKKRKVGG-OH	90/25	-	-	-	-	-	-
O	**8**	$H_2NOCH_2CO\text{-}DPGYIGSR\text{-}NH_2$	-	>90/65	90/45	>90/50	90/55	80/45	-
H	**9**	$H_2NNHCO(CH_2)_2CO\text{-}DPGYIGSR\text{-}NH_2$	-	90/62	85/50	-	-	-	-

[a] Type of linkage between oligonucleotide and conjugated moiety: **T** = thiazolidine, **O** = oxime, **H** = hydrazine.

Scheme 2[a]



[a] R^1, R^2 = unprotected oligonucleotide chain; R = conjugated moiety (Table 1).

The hydrolytic stabilities of thiazolidine and oxime conjugates were studied as a function of pH. Purified conjugates were incubated in a suitable buffer for 24 h and then analyzed by RP-HPLC in ion-pair mode (Table 2). Conjugates proved to be stable over a wide pH range, thiazolidine being more stable than oxime.

Initially, we chose to use 4-hydrazinobenzoic acid as a model compound and N-terminal hydrazine modification of peptides (*24*, *29*). However, use of 4-Fmoc-hydrazinobenzoic acid, which is commercially available, may give rise to side-products involving acylation of unprotected nitrogen atoms during solid-phase peptide synthesis under forcing conditions. Therefore, we decided to use our recently developed *S*-benzyl thiosuccinate reagent originally proposed for Fmoc-based solid-supported peptide N-terminal thioester synthesis (*30*). *S*-Benzyl thiosuccinic acid was coupled at the end of normal Fmoc-on solid-phase synthesis by the same HATU-mediated coupling cycle as used for a standard Fmoc amino acid. Then, the resin was treated manually with 0.5 M hydrazine hydrate solution in dioxane for 2 h at room temperature, and, after washing and drying, subjected to normal TFA cleavage. The resulting peptide N-terminal succinyl monohydrazide **9** was analyzed by RP-HPLC and found to be >95% pure and had the correct mass as judged by MALDI-TOF mass spectrometry.

Peptides were conjugated to oligonucleotides under the conditions reported above that were optimized for conjugation of small molecules. The main problem during conjugate synthesis was found to be product isolation and purification, especially in the case of cationic peptides **6** and **7**. Various methods were tried, such as NAP-5 desalting, precipitation by acetone, ethanol, or *n*-butanol, and dialysis, but all of these methods led often to considerable losses of final product. Also we were unable to purify conjugates of peptides **6** and **7** by direct RP-HPLC. In general, the best results were obtained by use of denaturing PAGE, and therefore this method of initial purification was adopted routinely for all conjugates. Analyses of PAGE-purified conjugates by RP-HPLC (ion-pair mode) and by MALDI-TOF MS are presented in Table 3, and a typical HPLC trace is shown in Figure 2.

Table 2. % Hydrolysis of Thiazolidine and Oxime Conjugates at Various pH

	pH					
conjugate[a]	2.0	3.0	4.0	8.0	9.0	10.0
I.1	100	5	<5	<5	10	55
I.2	100	10	<5	<5	30	>90

[a] Oligonucleotides are designated by roman numbers, conjugated molecules by arabic (Table 1).

In the case of the doubly modified 2′-deoxyoligonucleotide III, we were unable to isolate conjugates with cationic peptides (conjugates **III.6** and **III.7)** since during the reaction a white precipitate was formed. This precipitate was insoluble in 4 M NaCl or 2 M $LiClO_4$ and only marginally soluble in DMSO. Further studies will be required to identify more suitable solvent conditions for conjugation of these more demanding peptides. However, conjugates of the singly modified 2′-deoxyoligonucleotide **I** with cationic peptides **6** and **7** were isolated in reasonable yield. Further, good yields were obtained for both singly and doubly modified oligonucleotides **II** and **III** and for singly and doubly modified 2′-*O*-methyloligoribonucleotides **IV**, **V**, and **VI** in conjugation with a model laminin peptides through either oxime or hydrazine linkages (peptides **8** and **9**).

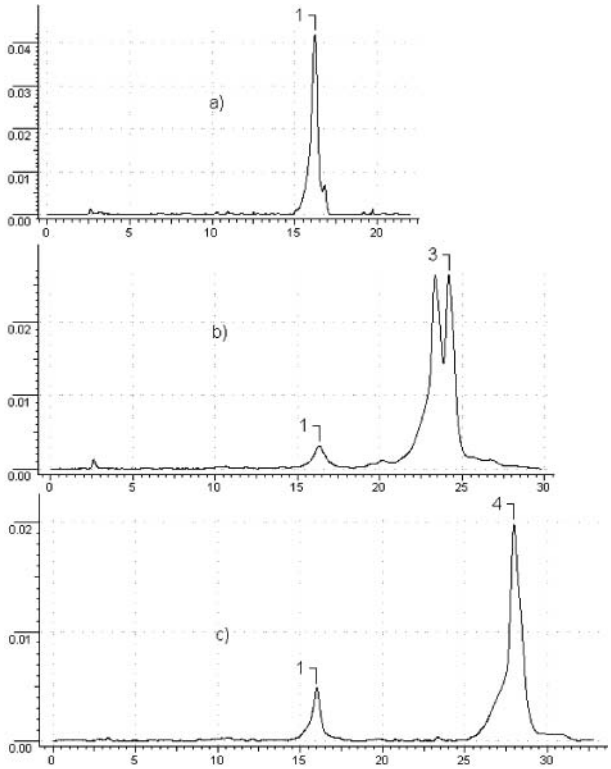


Figure 1. (a) Starting oligonucleotide **VII** (1); (b) reaction mixture of **VII** with *O*-benzylhydroxylamine **2**, peaks 2 and 3 are likely *E*,*Z*-isomers of the conjugate **VII.2**; (c) $NaBH_3CN$ reduction of **VII.2**, peak 4 is the reduced conjugate.

Table 3. RP-HPLC (ion-pair mode) and MALDI-TOF MS Analysis of Oligonucleotides and Conjugates

compound[a]	HPLC retention time,[b] min	calcd mass	found mass
I	13.1	3642.4	3644.6
I.6	14.3	4970.0	4972.7
I.7	14.0	5346.4	5349.3
II	13.1	3642.4	-
II.8	15.5	4528.3	-
II.9	14.9	4571.4	4570.6
III	12.9	3718.4	3717.4
III.8	17.5	5490.3	5486.8
III.9	16.0	5576.4	5575.3
IV	15.7	3972.7	3965.0
IV.4	15.9	4100.8	-
IV.8	18.9	4845.6	4844.8
V	15.6	3972.7	3967.6
V.4	16.0	4100.8	-
V.8	19.7	4845.6	4843.3
VI	15.0	4018.7	4014.3
VI.4	15.7	4275.0	-
VI.8	22.1	5806.5	5802.6

[a] Oligonucleotides are designated by roman numbers, conjugated molecules by arabic (Table 1). [b] RP-HPLC in ion-pair mode (for details, see Experimental Section).

A number of conjugates with various hydrazides, hydrazines, and carbazates were synthesized (Table 4), including reporter group (biotin), marker groups (acridine, pyrene), terephthalic dihydrazide that can be used for oligonucleotide cross-linking, and several lipophilic groups.

We have also studied the influence of 2′-modification and 2′-peptide conjugation on the stability of duplexes formed with complementary DNA and RNA targets. It has been shown previously that incorporation of a similarly modified 2′-*O*-(2,3-dihydroxypropyl)thymidine (*58*,*59*) decreased duplex stability with complementary

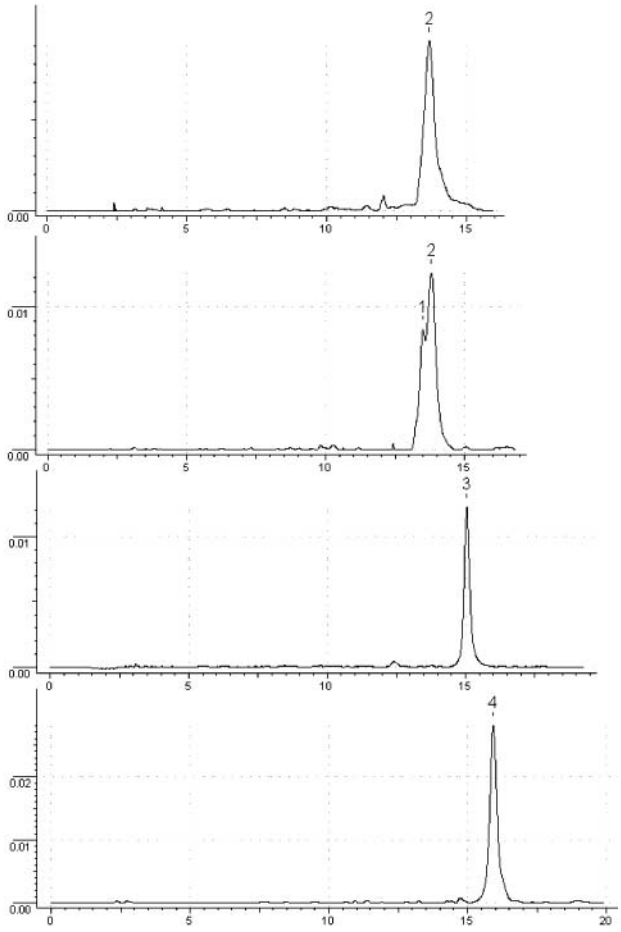


Figure 2. (a) 2′-Aldehyde **III** (2); (b) coinjection of 2′-aldehyde **III** (2) with parent 1,2-diol (1); (c) purified conjugate **II.9** (3); (d) purified conjugate **III.9** (4).

DNA (ΔT_m/mod = −2.2 °C) but increased stability with complementary RNA (ΔT_m/mod = +0.8−1.5 °C). It should be noted that here we have used the corresponding modified U derivative and that replacement of thymidine by uridine of itself would be expected to lead to a duplex T_m decrease of about 0.5 °C (*59*). With this in mind, the thermal melting results of duplexes formed with complementary DNA and RNA targets are summarized in Table 5. In general, the results are in accordance with published data (*5*, *8*). Thus in the case of a DNA target, diol (lines 2−4) or aldehyde modification (lines 5−7) resulted in moderate destabilization of about 3 to 4 °C per residue modified. Very similar destabilizations were found for conjugates with a dipeptide Cys-Gly (lines 8−10), aminooxyacetic acid (lines 11−13) and with a model laminin peptide conjugated through either oxime (lines 14 and 15) or hydrazine linkages (lines 16 and 17). Conjugation of two peptides (**III.8**, **III.9**) decreased duplex stability by about twice the amount seen for conjugation with a single peptide (**II.8**, **II.9**). By contrast in the case of the RNA target, diol modifications were slightly stabilizing (lines 2−4), whereas aldehyde modifications were broadly neutral (lines 5−7, taking into consideration the U for T substitution). Slight stabilization was seen for dipeptide (lines 8−10) and acetic acid conjugates (lines 11−13). Single laminin peptide conjugation (lines 14 and 16) resulted in duplexes melting some 2.8 to 3.1 °C higher, but slightly less stabilization per modification was seen for the double laminin peptide conjugates (lines 15 and 17). The nature of the linkage between peptide and oligonucleotide fragments had little or no influence on

Table 4. Examples of Oligonucleotide II Hydrazine Conjugates with Small Molecules

conjugate[a]	conjugated molecule	MALDI-TOF MS, calcd/found	HPLC retention time,[b] min	yield, %
II.10	semicarbazide	3708.5/3709.4	14.05	79
II.11	methyl carbazate	3723.5/3725.1	14.71	85
II.12	4-hydroxyphenyl hydrazide	3785.6/3787.3	15.08	93
II.13	biotin hydrazide	3853.7/3853.4	14.01	87
II.14	2-aminophenyl hydrazide	3784.6/3784.6	18.14	92
II.15	benzyl hydrazide	3731.5/3729.4	16.41	89
II.16	4-methoxyphenyl hydrazide	3799.6/3799.7	17.74	75
II.17	*n*-pentanoic hydrazide	3763.6/3763.6	21.36	95
II.18	9-hydrazinoacridine	3804.6/3802.3	18.69	80
II.19	1-pyrenebutyric hydrazide	3935.8/3939.2	-[c]	84
II.20	benzyl carbazate	3761.5/3761.9	19.37	70
II.21	3-hydroxy-2-naphthydrazide	3835.7/3839.8	21.74	72
II.22	terephthalic dihydrazide	3789.6/3787.5	14.74	81
II.23	terephthalic dihydrazide acetone adduct	3829.6/3831.2	16.14	74

[a] Oligonucleotides are designated by roman numbers, conjugated molecules by arabic (Table 1). [b] RP-HPLC in ion-pair mode (for details see Experimental Section). [c] Compound **II.19** was purified by RP-HPLC due to high lipophilicity.

Table 5. Thermal Stabilities of Duplexes Formed by 2′-Modified Oligonucleotides and Conjugates with Complementary DNA and RNA Targets

		DNA d(TGAGCCTGGAG)		RNA r(UGAGCCUGGGAG)	
	oligonucleotide or conjugate	$T_m \pm 0.2$, °C	ΔT_m/mod,[a] °C	$T_m \pm 0.2$, °C	ΔT_m/mod[a], °C
1	d(CTCCCAGGCTCA)	56.0	-	58.6	-
2	**I**[b]	52.3	−3.7	59.0	+0.4
3	**II**[b]	52.9	−3.1	59.2	+0.6
4	**III**[b]	49.5	−3.3	59.7	+0.6
5	**I**	51.0	−5.0	58.2	−0.4
6	**II**	51.7	−4.3	58.3	−0.3
7	**III**	46.9	−4.6	57.7	−0.5
8	**I.4**	52.9	−3.1	58.5	−0.1
9	**II.4**	53.1	−2.9	58.7	+0.1
10	**III.4**	50.1	−3.0	58.7	−0.1
11	**I.5**	52.5	−3.5	59.0	+0.4
12	**II.5**	52.1	−3.9	59.1	+0.5
13	**III.5**	48.6	−3.7	59.9	+0.7
14	**II.8**	54.1	−1.9	61.7	+3.1
15	**III.8**	50.6	−2.7	60.6	+1.0
16	**II.9**	53.9	−2.1	61.4	+2.8
17	**III.9**	50.6	−2.7	60.5	+1.0

[a] $\Delta T_m/\text{mod} = [T_m(n) - T_m(1)]/m$, where m is the number of modifications in a duplex. [b] Modified oligonucleotide containing 2′-*O*-(2,3-dihydroxypropyl)uridine.

duplex stability (compare lines 14 with 16 and 15 with 17).

Finally, we have studied the influence of 2′-peptide conjugation on binding of a 12-mer 2′-*O*-methyloligoribonucleotide to its complementary sequence in the apical stem-loop of the HIV-1 TAR RNA (*53, 54*). Under the buffer conditions of transcription (see Experimental Section), single laminin conjugates **IV.8** and **V.8** were insignificantly affected in K_d of binding to the structured TAR RNA target (3.1 ± 0.2 and 4.3 ± 0.9 nM, respectively) compared to the unmodified 2′-*O*-methyloligoribonucleotide (3.2 ± 0.7 nM) (*54*). The double laminin conjugate was only about 2-fold increased in K_d (6.5 ± 0.7 nM). Single and double laminin conjugates of 12-mer 2′-*O*-methyloligoribonucleotides (**IV.8**, **V.8**, and **VI.8**) were tested also for their ability to inhibit Tat-dependent in vitro transcription on an HIV-1 DNA template in the presence of HeLa cell nuclear extract (*54*). The results showed (Figure 3) that the two single laminin conjugates were almost identical in their ability to inhibit Tat-dependent transcription compared to the unconjugated 2′-*O*-methyloligoribonucleotide. For the double laminin conjugate, the inhibition was a little less pronounced at the lower concentrations, but at higher concentrations above 600 nM there was an increased inhibitory power. Control in vitro transcription using a CMV promoter showed that this double laminin conjugate also had significant nonspecific inhibition of constitutive transcriptional activity, particularly above 600 nM, but single laminin conjugates showed only a small nonspecific inhibitory activity (data not shown). It should be borne in mind that the laminin peptide sequence was chosen only as a model and not for any other property. Thus, the nonspecific transcriptional inhibition activity is likely to be inadvertent.

In conclusion, we have shown that oligonucleotides containing 2′-aldehydes generated from 2′-*O*-(2,3-dihydroxypropyl)uridine residues may be conjugated singly or multiply with unprotected peptides by nucleophilic addition−elimination reactions to form thiazolidine, oxime, or hydrazone linkages. Reactions are carried out at pH 4.0−4.5 for thiazolidine and 4.5−5.0 for oxime and hydrazone. The peptide excess can be reduced to 1.2 to 1.8 equiv, and reaction is best carried out at 37 °C in the presence of an organic cosolvent. Similar oxime and thiazolidine conjugation chemistry has been reported recently for the attachment of peptides to 5′-aldehyde-substituted oligonucleotides (*22*). The advantage of our 2′-aldehyde conjugation route is the ability in principle to conjugate more than one peptide at specific locations along the oligonucleotide chain. Further, the 5′- and 3′-termini of the oligonucleotide remain free for attachment of other labels, such as fluorescent or radioactive, or enzyme-catalyzed transformations. In addition, we have

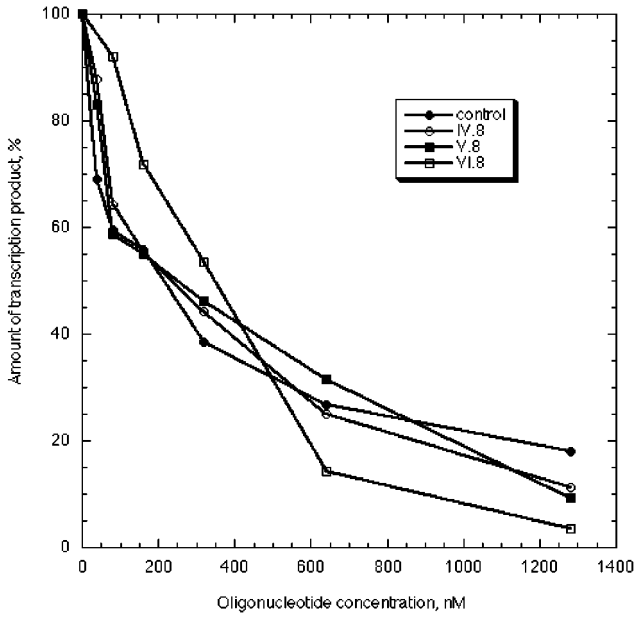


Figure 3. 2′-*O*-Methyloligonucleotide–peptide conjugate inhibition od Tat-dependent in vitro transcription in HeLa cell nuclear extract. Amount of full-length transcript is depicted as a function of oligomer concentration (see inset for key). Control is 2′-*O*-methyldodecamer CUCCCAGGCUCA.

explored a third conjugation procedure by formation of hydrazone linkages, which may be conveniently reduced to hydrazine linkages by use of a solid-supported borohydride reagent.

We have found that for the peptide and small molecule models studied, the resultant peptide–oligonucleotide conjugates generally bind to complementary RNA targets with equally high or better affinity than the corresponding unmodified, unconjugated oligonucleotides. Further, single and double model laminin peptide conjugates of 2′-*O*-methyloligoribonucleotides retained their ability to bind to a structured TAR RNA target and to inhibit HIV-1 Tat-dependent in vitro transcription. Therefore, this 2′-aldehyde conjugation route should be suitable for general use in the design of conjugates of oligonucleotide analogues antisense to RNA targets. We are now exploring these conjugation routes for the attachment of cell-penetrating and cell-targeting peptides in single or multiple copies for cell delivery studies.

ACKNOWLEDGMENT

The authors thank A. V. Kachalova, E. M. Volkov, and Dr. E. M. Zubin for their suggestions and helpful discussions. This work was supported by Wellcome Trust grant 057361, and partially by RFBR grant 00-04-48260.

LITERATURE CITED

(1) Ma, D. D., Rede, T., Naqvi, N. A., and Cook, P. D. (2000) Synthetic oligonucleotides as therapeutics: the coming of age. *Biotechnol. Annu. Rev. 5*, 155–196.

(2) Tuschl, T. (2001) RNA interference and small interfering RNAs. *ChemBioChem. 2*, 239–245.

(3) Praseuth, D., Guieysse, A. L., and Hélène, C. (1999) Triple helix formation and the antigene strategy for sequence-specific control of gene expression. *Biochim. Biophys. Acta 1489*, 181–206.

(4) Hermann, T., and Patel, D. J. (2000) Adaptive recognition by nucleic acid aptamers. *Science 287*, 820–825.

(5) Tung, C.-H., and Stein, S. (2000) Preparation and applications of peptide–oligonucleotide conjugates. *Bioconjugate Chem. 11*, 605–618.

(6) Stetsenko, D. A., Arzumanov, A. A., Korshun, V. A., and Gait, M. J. (2000) Peptide–oligonucleotide conjugates as a new generation of antisense elements. *Mol. Biol. (Mosk.) 34*, 998–1006.

(7) Fischer, P. M., Krausz, E., and Lane, D. V. (2001) Cellular delivery of impermeable effector molecules in the form of conjugates with peptides capable of mediating membrane translocation. *Bioconjugate Chem. 12*, 825–841.

(8) de La Torre, B. G., and Albericio, F., Saison-Behmoaras, E., Bachi, A., Eritja, R. (1999) Synthesis and binding properties of oligonucleotides carrying nuclear localization sequences. *Bioconjugate Chem. 10*, 1005–12.

(9) Robles, J., Pedroso, E., and Grandas, A. (1994) Stepwise solid-phase synthesis of the nucleopeptide Phac-Phe-Val-Ser(p$^{3'}$ACT)-Gly-OH. *J. Org. Chem. 59*, 2482–2486.

(10) Bergmann, F., and Bannwarth, W. (1995) Solid phase synthesis of directly linked peptide-oligodeoxynucleotide hybrides using standard synthesis protocols. *Tetrahedron Lett. 36*, 1839–1842.

(11) Antopolsky, M., and Azhayev, A. (1999) Stepwise solid-phase synthesis of peptide–oligonucleotide conjugates on new solid supports. *Helv. Chim. Acta 82*, 2130–2140.

(12) Basu, S., and Wickstrom, E. (1995) Solid-phase synthesis of a D-peptide-phosphorothioate oligodeoxynucleotide conjugate from two arms of a poly(ethylene glycol)-polystyrene support. *Tetrahedron Lett. 36*, 4943–4946.

(13) Sakakura, A., and Hayakawa, Y. (2000) A novel synthesis of oligonucleotide–peptide conjugates with a base-labile phosphate linker between the two components according to the allyl-protected phosphoramidite strategy. *Tetrahedron 56*, 4427–4435.

(14) Truffert, J. C., Lorthioir, O., Asseline, U., Thuong, N. T., and Brack, A. (1994) On-line solid-phase synthesis of oligonucleotide–peptide hybrids using silica supports. *Tetrahedron Lett. 35*, 2353–2356.

(15) Ueno, Y., Saito, R., and Hata, T. (1993) Studies on the synthesis of nucleotidyl-peptides. II. The preparation of a nucleotidyl-peptide having a 5′-nucleotidyl-(P–O)-serine phosphodiester bond**.** *Nucleic Acids Res. 21*, 4451–4457.

(16) Antopolsky, M., and Azhayev, A. (2000) Stepwise solid-phase synthesis of peptide–oligonucleotide phosphorothioate conjugates employing Fmoc peptide chemistry. *Tetrahedron Lett. 41*, 9113–9117.

(17) Peyrottes, S., Mestre, B., Burlina, F., and Gait, M. J. (1998) The synthesis of peptide–oligonucleotide conjugates by a fragment coupling approach. *Tetrahedron 54*, 12513–12522.

(18) Antopolsky, M., Azhayeva, E., Tengvall, U., Auriola, S., Jääskeläinen, I., Rönkkö, S., Honkakoski, P., Urtti, A., Lönnberg, H., and Azhayev, A. (1999) Peptide–oligonucleotide phosphorothioate conjugates with membrane translocation and nuclear localization properties. *Bioconjugate Chem. 10*, 598–606.

(19) Harrison, J. G., and Balasubramanian, S. (1998) Synthesis and hybridization analysis of a small library of peptide–oligonucleotide conjugates. *Nucleic Acids Res. 26*, 3136–3145.

(20) McMinn, D. L., and Greenberg, M. M. (1999) Convergent solution-phase synthesis of a nucleopeptide using a protected oligonucleotide. *Bioorg. Med. Chem. Lett. 9*, 547–550.

(21) Cebon, B., Lambert, J. N., Leung, D., Mackie, K., McCluskey, K. L., Nguyen, H., and Tassone, C. (2000) New DNA Modification Strategies Involving Oxime Formation. *Austr. J. Chem. 53*, 333–340.

(22) Forget, D., Boturyn, D., Defrancq, E., Lhomme, J., and Dumy, P. (2001) Highly efficient synthesis of peptide–oligonucleotide conjugates: chemoselective oxime and thiazolidine formation. *Chem. Eur. J. 7*, 3976–3984.

(23) Geromel, V., Cao, A., Briane, D., Vassy, J., Rotig, A., Rustin, P., Coudert, R., Rigaut, J. P., Munnich, A., and Taillandier, E. (2001) Mitochondria transfection by oligonucleotides containing a signal peptide and vectorized by cationic liposomes. *Antisense Nucleic Acid Drug Dev. 11*, 175–180.

(24) Spetzler, J. C., and Tam, J. P. (1995) Unprotected peptides as building blocks for branched peptides and peptide dendrimers. *Int. J. Pept. Protein Res. 45*, 78–85.

(25) Matsuda, A., Inada, M., Nara, H., Ohtsuka, E., and Ono, A. (1993) Nucleosides and nucleotides. 126. Incorporation of a mutagenic nucleoside, 5-formyl-2′-deoxyuridine, into an oligodeoxyribonucleotide. *Bioorg. Med. Chem. Lett. 3*, 2751−2754.

(26) Ermolinskii, B. S., and Mikhailov, S. N. (2000) Periodate oxidation in chemistry of nucleic acid. Dialdehyde derivatives of nucleosides, nucleotides, and oligonucleotides. *Russ. J. Bioorg. Chem. 26*, 483−504.

(27) Scroder, M. (1980) Osmium tetraoxide in cis hydroxylation of unsaturated substrates. *Chem. Rev. 80*, 187−213.

(28) Kachalova, A. V., Zatsepin, T. S., Romanova, E. A., Stetsenko, D. A., Gait, M. J., and Oretskaya, T. S. (2000) Synthesis of modified nucleotide building blocks containing electrophilic groups in the 2′-position. *Nucleosides, Nucleotides Nucleic Acids 19*, 1693−1707.

(29) Tam, J. P., and Spetzler, J. C. (1995) Chemoselective approaches to the preparation of peptide dendrimers and branched artificial proteins using unprotected peptides as building blocks. *Biomedical Peptides, Proteins & Nucleic Acids 1*, 123−132.

(30) Stetsenko, D. A., and Gait, M. J. (2000) Efficient conjugation of peptides to oligonucleotides by "native ligation". *J. Org. Chem. 65*, 4900−4908.

(31) Stetsenko, D. A., and Gait, M. J. (2000) New phosphoramidite reagents for the synthesis of oligonucleotides containing a cysteine residue useful in peptide conjugation. *Nucleosides, Nucleotides Nucleic Acids 19*, 1751−1764.

(32) McPherson, M. C., Wright, M., and Lohse, P. A. (1999) Synthesis of an RNA-peptide conjugate by orthogonal ligation. *Synlett S1*, 978−980.

(33) Shao, J., and Tam, J. P. (1995) Unprotected peptides as building blocks for the synthesis of peptide dendrimers with oxime, hydrazone, and thiazolidine linkages. *J. Am. Chem. Soc. 117*, 3893−3899.

(34) Rose, K. (1994) Facile synthesis of homogeneous artificial proteins. *J. Am. Chem. Soc. 116*, 30−33.

(35) Canne, L. E., Ferré-D'Amare, A. R., Burley, S. K., and Kent, S. B. H. (1995) Total chemical synthesis of a unique transcription factor-related protein: cMyc-Max. *J. Am. Chem. Soc. 117*, 2998−3007.

(36) Salo, H., Virta, P., Hakala, H., Prakash, T. P., Kawasaki, A. M., and Manoharan, M., Lönnberg, H. (1999) Aminooxy functionalized oligonucleotides: preparation, on-support derivatization, and postsynthetic attachment to polymer support. *Bioconjugate Chem. 10*, 815−823.

(37) Defrancq, E., and Lhomme, J. (2001) Use of an aminooxy linker for the functionalization of oligodeoxyribonucleotides. *Bioorg. Med. Chem. Lett. 11*, 931−933.

(38) Bergbreiter, D. E., and Momongan, M. R. (1991) Lithiated Hydrazone Anions, in *Comprehensive Organic Synthesis: Selectivity, Strategy, and Efficiency in Modern Organic Chemistry* (B. M. Trost, and J. Flemming, Eds.) Vol. 2, pp 503−526, Pergamon Press, New York.

(39) Zubin, E. M., Romanova, E. A., Volkov, E. M., Tashlitsky, V. N., Korshunova, G. A., Shabarova, Z. A., and Oretskaya, T. S. (1999) Oligonucleotide−peptide conjugates as potential antisense agents. *FEBS Lett. 456*, 59−62.

(40) Hwang, J.-T., and Greenberg, M. M. (1999) Synthesis of modified oligodeoxyribonucleotides on a solid-phase support via derivatization of a selectively revealed 2′-amino-2′-deoxyuridine. *Org. Lett. 1*, 2021−2024.

(41) Hwang, J.-T., and Greenberg, M. M. (2001) Synthesis of 2′-modified oligodeoxynucleotides via on-column conjugation. *J. Org. Chem. 66*, 363−369.

(42) Hendrix, C., Devreese, B., Rozenski, J., van Aershot, A., De Bruyn, A., van Beeumen, J., and Herdewijn, P. (1995) Incorporation of 2′-amidonucleosides in oligodeoxynucleotides and oligoribonucleotides as a model for 2′-linked conjugates. *Nucleic Acids Res. 23*, 51−57.

(43) Manoharan, M. (1999) 2′-Carbohydrate modifications in antisense oligonucleotide therapy: importance of conformation, configuration and conjugation. *Biochim. Biophys. Acta 1489*, 117−130.

(44) Atherton, E., and Sheppard, R. C. (1989) *Solid-Phase Peptide Synthesis: A Practical Approach*, IRL Press at Oxford University Press, Oxford, UK.

(45) Carpino, L. A., El-Faham, A., Minor, C. A., and Albericio, F. (1994) Advantageous applications of azabenzotriazole (triazolopyridine)-based coupling reagents to solid-phase peptide synthesis. *J. Chem. Soc. Chem. Commun.*, 201−202.

(46) Brown, T., and Brown, D. J. S. (1991) Modern machine-aided methods of oligodeoxyribonucleotide synthesis. *Oligonucleotides and Analogues: A Practical Approach* (F. Eckstein, Ed.) pp 1−24, OUP: Oxford.

(47) Keen, N. J., Gait, M. J., and Karn, J. (1996) Human immunodeficiency virus type-1 Tat is an integral component of the activated transcription-elongation complex. *Proc. Natl. Acad. Sci. U.S.A. 93*, 2505−2510.

(48) Rittner, K., Churcher, M. J., Gait, M. J., and Karn, J. (1995) The human immunodeficiency virus long terminal repeat includes a specialised initiator element which is required for Tat-responsive transcription. *J. Mol. Biol. 248*, 562−580.

(49) Smith, J., and Singh, M. (1996) System for accurate one-dimensional gel analysis including high-resolution quantitative footprinting. *BioTechniques 20*, 1082−1087.

(50) Zatsepin, T. S., Kachalova, A. V., Romanova, E. A., Stetsenko, D. A., Gait, M. J., and Oretskaya, T. S. (2001) Synthesis and characteristics of modified oligodeoxyribonucleotides containing 2′-O-(2,3-dihydroxypropyl)uridine and 2′-O-(2-oxoethyl)uridine. *Russ. J. Bioorg. Chem. 27*, 45−51.

(51) Karn, J. (1999) Tackling Tat. *J. Mol. Biol. 293*, 235−254.

(52) Mestre, B., Arzumanov, A., Singh, M., Boulme, F., Litvak, S., and Gait, M. J. (1999) Oligonucleotide inhibition of the interaction of HIV-1 Tat protein with the trans-activation responsive region (TAR) of HIV RNA. *Biophys. Biochim. Acta 1445*, 86−98.

(53) Arzumanov, A., Walsh, A. P., Liu, X., Rajwanshi, V. K., Wengel, J., and Gait, M. J. (2001) Oligonucleotide analogue interference with the HIV-1 Tat protein-TAR RNA interaction. *Nucleosides, Nucleotides Nucleic Acids 20*, 471−480.

(54) Arzumanov, A., Walsh, A. P., Rajwanshi, V. K., Kumar, R., Wengel, J., and Gait, M. J. (2001) Inhibition of HIV-1 Tat-dependent trans activation by steric block chimeric 2′-O-methyl/LNA oligoribonucleotides. *Biochemistry 40*, 14645−14654.

(55) Leng, N., Grasso, P., Deziel, M. R., and Reichert, L. T., Jr. (1995) A synthetic peptide corresponding to glycoprotein hormone alpha subunit residues 32−46 inhibits gonadotropin binding to receptor. *Pept. Res. 8*, 272−277.

(56) Kalderon, D., Roberts, B. L., Richardson, W. D., and Smith, A. E. (1984) A short amino acid sequence able to specify nuclear location. *Cell 39*, 499−509.

(57) Sakamoto, N., Iwahana, M., Tanaka, N. G., and Osada, Y. (1991) Inhibition of angiogenesis and tumor growth by a synthetic laminin peptide, CDPGYIGSR−NH_2. *Cancer Res. 51*, 903−906.

(58) Martin, P. (1995) A new access to 2′-O-alkylated ribonucleosides and properties of 2′−O-alkylated oligoribonucleotides. *Helv. Chim. Acta 78*, 486-504.

(59) Freier, S. M., and Altmann, K.-H. (1997) The ups and downs of nucleic acid duplex stability: structure−stability studies on chemically modified DNA: RNA duplexes. *Nucleic Acids Res. 25*, 4429−4443.

BC020016+

Intracellular Delivery of Nanometric DNA Particles via the Folate Receptor

Emmanuel Dauty, Jean-Serge Remy, Guy Zuber, and Jean-Paul Behr*

Laboratoire de Chimie Génétique associé CNRS/Université Louis Pasteur de Strasbourg, Faculté de Pharmacie BP 24, 67401 Illkirch, France. Received February 22, 2002

The size of condensed DNA particles is a key determinant for both diffusion to target cells in vivo and intracellular trafficking. The smallest complexes are obtained when each DNA molecule collapses individually. This was achieved using a designed cationic thiol-detergent, tetradecyl-cysteinyl-ornithine (C_{14}COrn). The resulting particles were subsequently stabilized by air-induced dimerization of the detergent into a disulfide lipid on the DNA template. Particles are anionic (zeta potential = −45 mV), and their size (30 nm) corresponds to the volume of a single plasmid DNA molecule. The electrophoretic mobility of the condensed DNA, though quasi-neutralized, was found higher than that of the extended DNA. Moreover, the dimerized $(C_{14}COrn)_2$ lipid was found to be an efficient transfection reagent for various cell lines. In an attempt to achieve extended circulation times and to target tumors by systemic delivery, we have coated the particles with PEG−folate residues. Plasmid DNA was condensed into monomolecular particles as described above and coated by simple mixing with DPPE−PEG−folate. Physicochemical measurements showed particles coated with 2% of DPPE−PEG_{3400}−folate remain monomolecular and are stable in the cell-culture medium. Caveolae-mediated cell entry was demonstrated by ligand-dependence, by competition with excess folic acid as well as by confocal microscopy.

INTRODUCTION

Gene delivery with synthetic DNA vehicles remains an attractive approach to gene therapy. Nonviral systems are essentially based on gene compaction by cooperative electrostatic interaction between DNA phosphates and cationic lipids or polymers (*1*−*4*). Their efficacy depends on their ability to overcome several extra- and intracellular barriers the particles encounter between the site of delivery and the nucleus of the target cells. An ideal synthetic vector should (i) condense DNA into neutral or negatively charged complexes, thus avoiding interaction with anionic plasma and extracellular matrix proteins, (ii) form the smallest possible particles to facilitate diffusion, (iii) mediate cell-specific internalization, and (iv) provide vectorial intracellular trafficking to the nucleus.

A small particle size is considered to be a critical parameter for delivery because of known physiological barriers, such as extravasation through blood vessels (*5*), diffusion through mucus (*6*, *7*) or a tumor mass (*8*). Ligand-mediated cellular uptake may be size-dependent as well (*9*, *10*). It was for instance shown that glycolipid-containing liposomes with a size of 30−70 nm were effectively taken up by the asialoglycoprotein receptor of hepatocytes in vitro and in vivo, whereas 90 nm particles were not (*11*). The next step, intracellular trafficking, is also a size-restricted process. Cytoplasmic diffusion of microinjected fluorescent DNA was measured by fluorescence recovery after photobleaching (*12*). It was found that DNA molecules with size > 1 kbp are essentially immobile. Finally, active nuclear pore crossing of nucleoplasmin-coated gold particles was reported to be restricted to particles with size < 25 nm (*13*). These multiple observations highlight the prime importance of controlling the size of the DNA complexes.

Unfortunately, DNA condensation by cationic lipids or polymers generally leads to large polydisperse aggregates containing many DNA molecules. We therefore developed an alternative two-step technique where plasmid DNA molecules were individually condensed with a designed cationic thiol-detergent. The nanometric particles were then stabilized by air oxidation of the detergent into a disulfide lipid on the DNA template (Figure 1) (*14*, *15*). Clean monomolecular DNA collapse was shown to occur for detergent concentrations below the detergent critical micelle concentration (cmc). Recently, we investigated the properties of a series of novel dimerizable cationic detergents made of various combinations of aliphatic chains and headgroups. The tetradecyl-ornithinyl-cysteine (C_{14}COrn) derivative was found capable of both monomolecular DNA condensation and efficient 3T3 cells transfection (*16*). Here, we present additional physical and biological properties of C_{14}COrn, and we explore surface modification of monomolecular DNA particles as a means to increase both intravenous half-life and cell targeting. It is well-known that grafting of flexible water-soluble poly(ethylene glycol) (PEG) chains to the surface of liposomes increases their intravenous circulation time (*17*, *18*). This is thought to be mainly a consequence of the conformational flexibility of PEG chains. Rather than derivatizing our detergent directly with a cell-specific ligand, we attached the ligand to the distal end of a lipid-conjugated PEG molecule. In this way, surface modification of the particle is simply achieved by mixing with the lipid, and so the ligand extends flexibly away from the particle where it can randomly probe the cell surface (*19*). We chose folic acid as the targeting moiety (Figure 1),

* To whom correspondence should be adressed: Jean-Paul Behr. Fax: +33-0390244306; tel: +33-0390244173; e-mail: behr@bioorga.u-strasbg.fr.

10.1021/bc0255182 CCC: $22.00 © 2002 American Chemical Society
Published on Web 06/19/2002

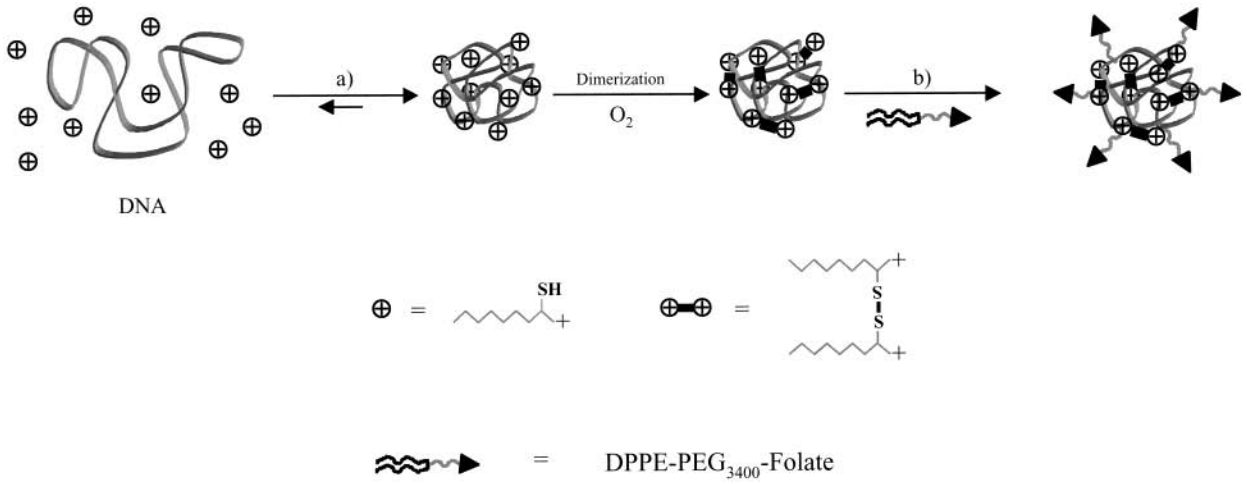


Figure 1. Formation of folate-bearing DNA particles. (a) Plasmid DNA is condensed by a thiol-containing detergent, and the resulting particles are stabilized by template-assisted oxidation of the thiol functions into disulfides. (b) Monomolecular DNA complexes are subsequently coated with PEG−folate residues by means of hydrophobic anchoring.

because certain cancer cells express large amounts of the folic acid receptor.

MATERIALS AND METHODS

Materials. *N*-Hydroxysuccinimidyl-poly(ethyleneglycol)-maleimide (NHS−PEG$_{3400}$−Mal) was purchased from Shearwater Polymers (Huntsville, USA). Dipalmitoylphosphatidylethanolamine (DPPE) and triethylamine (TEA) were from Fluka (St Quentin Fallavier, France). Acetonitrile (ACN), dichloromethane (DCM), *N*,*N*-dimethylformamide (DMF), ethanol (EtOH), methanol (MeOH), and chloroform ($CHCl_3$) were from Carlo Erba (Val de Reuil, France). YOYO-1 and Lissamine rhodamine B-DPPE (DPPE−rhodamine) were from Molecular Probes (Eugene, USA). Transfectam was from Promega (Madison, USA), and JetPEI was from Polyplus (Illkirch, France). The pCMV−Luc plasmid (5.5 kbp) was propagated and purified as described (*20*, *21*). Three additional purification steps were carried out by ultrafiltration (Centricon-100 filter devices, Millipore). Matrix-assisted, laser desorption/ionization time-of-flight spectroscopy (MALDI-TOF-MS) was performed in the positive ion mode using α-cyano-4-hydroxycinnamic acid matrix.

SYNTHESIS

DPPE−PEG$_{3400}$−Mal. DPPE (11.4 mg, 17 μmol) was added to a solution of NHS−PEG$_{3400}$−Mal (50 mg, 14 μmol) in $CHCl_3$ (500 μL), followed by TEA (11 μL, 85 μmol). The resulting suspension was vigorously stirred and maintained at 40 °C for 1 h. The solvent was rotatory evaporated, and the residue was taken up in ACN (2 mL). After being kept for 1 h at −20 °C, the solution was centrifuged to remove traces of insoluble unreacted DPPE and evaporated. The ACN precipitation step was repeated once, and the product was dried in vacuo. Yield: 55.5 mg (96%). TLC ($CHCl_3$/MeOH 85:15) R_f: 0.55. ^{1}H NMR ($CDCl_3$) ∂ 0.88 (t, J = 6 Hz, CH_3, 6H); 1.21−1.35 (s, 48H); 1.57−1.59 (m, CH_2CH_2C=O, 4H); 2.26−2.32 (m, CH_2CH_2C=O, 4H); 3.39−3.48 (m, CH_2NH, 4H); 3.64 (s, PEG, ≈ 300H); 3.82−3.99 (overlapping m, CH_2O−P, $CHCH_2OP$, CH_2−NMal, 6H); 4.13−4.4 (dd, CH_2OC=O, 2H); 5.22 (m, CH, 1H); 6.7 (s, CH_{Mal}, 2H); mass spectrum (MALDI-TOF-MS) The spectrum exhibited a distribution of 44 Da-spaced lines centered at 4345 Da (calculated molecular mass of 4375 Da).

DPPE−PEG$_{3400}$−Folate. Cysteamine-folate (*22*) (2.6 mg, 5.5 μmol) was added to a solution of DPPE−PEG$_{3400}$−Mal (11 mg, 2.5 μmol) in DMF (100 μL), followed by TEA (3.8 μL, 27.5 μmol). The resulting suspension was stirred and maintained at 40 °C for 24 h. The solvent was rotary evaporated, and the residue was taken up in $CHCl_3$ (1 mL). Mass spectrum (MALDI-TOF-MS) The spectrum exhibited a distribution of 44 Da-spaced lines centered at 4825 Da (calculated molecular mass of 4875 Da).

Particle Formation. C_{14}COrn/DNA complexes were prepared by adding the desired amount of detergent (from a 5 mM EtOH stock solution) to 20 μg of pCMV−Luc plasmid DNA in 1 mL of Hepes buffer (15 mM, pH 7.4) under constant stirring. C_{14}COrn/DNA/DPPE−rhodamine complexes were prepared by mixing 36 nmol of C_{14}COrn (N/P = 1.2) and 0.72 nmol (2%) of DPPE−rhodamine in EtOH prior to addition to 20 μg of pCMV−Luc plasmid DNA (60 nmol of phosphates) in 1 mL of Hepes buffer (15 mM, pH 7.4). The DNA concentration was checked by measuring the absorbance at 260 nm before addition of the detergent. The complexes were kept at room temperature to allow cross-linking to occur prior to further characterization. Complexes that were subsequently PEGylated were prepared in advance. Twenty-four hours after mixing plasmid DNA and C_{14}COrn (N/P = 1.2), the desired amount of DPPE−PEG$_{3400}$−folate (from a 0.18 mM solution in EtOH) was added to the complexes. For flow cytometry experiments, plasmid DNA was labeled with YOYO (1 molecule/150 base pairs) before condensation with C_{14}COrn and PEGylation.

Monitoring Complex Formation by Gel Electrophoresis. Twenty microliter samples containing 0.4 μg of pCMV−Luc plasmid DNA in Hepes buffer (15 mM, pH 7.4) were loaded onto a 0.8% agarose gel. The gel was run for 90 min at 8 V/cm in Tris-acetate buffer (40 mM, pH 8). The location of DPPE−rhodamine was assessed by fluorescence spectroscopy (λ_{ex} = 532 nm, λ_{em} = 580 nm) with a Typhoon 8600 apparatus (Amersham Pharmacia Biotech, Orsay, France), and the gel was stained with ethidium bromide to reveal DNA.

Light Scattering Measurements. After overnight oxidation, the particle size and zeta potential were determined by dynamic light scattering using a Zetamaster 3000 (Malvern instruments, Paris, France) with the following specifications: sampling time, 30 s; medium viscosity, 1.054 cP; refractive index, 1.45 (typical liposome RI); scattering angle, 90°; temperature, 25 °C. Data were

analyzed using the multimodal number distribution software included with the instrument. Zeta potentials were measured with the following specifications: sampling time, 30 s; 10 measurements per sample; medium viscosity, 1.054 cP; medium dielectric constant, 80; temperature, 25 °C; beam mode F(Ka) = 1.5 (Smoluchowsky).

Transmission Electron Microscopy. Samples were prepared by adding 36 nmol of C_{14}COrn (N/P = 1.2) to 20 μg of pCMV−Luc plasmid DNA (60 nmol of phosphates) in Hepes buffer (15 mM pH 7.4) and leaving the solution in aerobic condition during 24 h. Carbon films were prepared by sublimation on freshly cleaved mica and recovered by flotation on Cu/Rh grids (300 mesh, Touzard & Matignon, Courtaboeuf, France). After overnight drying, grids were kept on blotting paper in a Petri dish. Immediately before sample addition, grids were glow-discharged (110 mV, 25 s, 25 μA). A drop (5 μL) of sample was left on the grid for 1 min. Complexes were stained with 30 μL of aqueous uranyl acetate (2 % wt/wt) for 20 s, and excess liquid was removed with blotting paper. Observations were performed at 80 kV with a Philips EM 410 transmission electron microscope. Size was determined taking into account the length (L) and the width (l) of each particle (($L + l$)/2).

Cell Culture and Transfection. 3T3 murine fibroblast were grown in Dulbecco's modified Eagles medium (DMEM) (Gibco BRL, Paris, France), BNL CL2 murine hepatocytes in DMEM high glucose (4.5 g/L), HeLa human cervix epitheloid carcinoma in modified Eagles medium (MEM) with Earle's salt (PolyLabo, Strasbourg, France), CHO hamster ovary cells in Ham F-12 (Gibco BRL, Paris, France), and BHK-21 hamster kidney in BHK-21 medium (Gibco BRL). All cell culture media were supplemented with 10% heat-inactivated fetal calf serum (FCS, D. Dutcher, Brumath, France), 2 mM glutamine (Gibco BRL), 100 units/mL penicillin (Gibco BRL), and 100 μg/mL streptomycin (Gibco BRL). Cells were maintained at 37 °C in a 5% CO_2 humidified atmosphere. Complexes were formed by adding at once the desired amount of detergent from the concentrated ethanolic stock solution to the plasmid solution (60 μM phosphate) in Hepes buffer (15 mM, pH 7.4). The solution was kept for 24 h to ensure cross-linking to be completed. Complexes (100 μL of solution corresponding to 2 μg of plasmid per well) were added to the cells maintained in serum-free medium. FCS was added to a final concentration of 10% v/v 3 h later. Transfectam and JetPEI were used as positive controls (*23*, *24*). Cells were lysed 24 h post-transfection, and luciferase gene expression was quantified using a commercial kit (Promega, Cergy Pontoise, France) and a luminometer (Mediators PhL, Wien, Austria). Results were expressed as relative light units (RLU) integrated over 10 s per milligram of cell protein lysate (RLU/mg of protein) using the bicinchoninic acid assay (Pierce, Paris, France). The errors bars represent standard deviation derived from triplicate transfection experiments (± S.D., $n = 3$).

Flow Cytometry. KB cells, a human nasopharyngeal cancer cell line that expresses elevated levels of folate receptors, were cultured in MEM containing 10% heat-inactivated fetal calf serum, 2 mM glutamine, 100 units/mL penicillin, and 100 μg/mL streptomycin, at 37 °C in a 5% CO_2 humidified atmosphere. As described by others (*25*), before each experiment, the cells were grown for two passages in folate-deficient modified Eagle's medium (FDMEM) containing the above-mentioned supplements. Cells were seeded in 24-well plates 24 h before incubation. Immediately prior to incubation with the fluorescent complexes (see "particle formation" paragraph), cells were washed with 1 mL of serum-free FDMEM and incubated for 4 h at 37 °C with particles in 300 μL of serum-free FDMEM (20 μg of plasmid DNA/mL). For the inhibition experiment, incubation was carried out in the presence of 1 mM of free folic acid. After incubation, cells were washed with 1 mL of serum-free FDMEM and incubated 15 min with 100 μg of calf thymus DNA in 0.5 mL of serum-free DMEM to account for any nonspecific electrostatic binding (I. Kopatz, unpublished result). After incubation, the cells were harvested by trypsinization, washed with phosphate-buffer saline (PBS) (centrifugation, 5 min, 500*g*) and suspended in PBS 1% BSA.

Flow cytometric analysis was performed with a FACStar^{Plus} (Becton Dickinson, San Jose, USA) using an argon laser (400 molecular mass power at a wavelength of 488 nm). Sorting windows were used on forward and side scatter to eliminate debris. Granulation, size, and fluorescence (λ_{em} 515 nm) intensity were recorded at a rate of 300 cells/s. Data were analyzed using CellQuest software (Becton Dickinson) and were expressed as mean fluorescence.

Confocal Microscopy. For the confocal microscopy experiments, the cells were cultured on 4-well-chambered cover glass dishes (Lab-Tek, Merck, France) at room temperature. Transfections were done as described above, and the images were taken 24 h post-transfection from living cells on a A MRC-1024ES (Bio-Rad/Elexience, Verrières-le-Buisson, France) confocal laser scanning imaging system equipped with an Eclipse TE 300 (Nikon) inverted microscope, using a 60× water immersion objective. YOYO-labeled DNA was imaged using the 488 nm excitation line of an argon/krypton laser. Confocal sections were taken every 0.8 μm. Digital image recording was performed using the LaserSharp 2.3 software (Bio-Rad).

RESULTS AND DISCUSSION

Synthesis of the Amphiphiles. C_{14}COrn was synthesized as previously described (*16*). To equip the DNA particles with a targeting ligand, we first synthesized a lipid−PEG conjugate capable of inserting within the particle and bearing a maleimide group at its distal end. DPPE−PEG_{3400}−Mal was synthesized from DPPE and the commercially available bifunctional reagent *N*-hydroxysuccinimidyl-poly(ethylene glycol)-maleimide with average molecular mass of 3400 Da. The cysteamine-folate ligand (*22*) was covalently attached to the maleimide group to give DPPE−PEG_{3400}−folate. At the end of the reaction, the desired product was solubilized in $CHCl_3$ and the unreacted cysteamine-folate was simply removed by centrifugation. Sample purity was checked by TLC, and MALDI-TOF analysis of DPPE−PEG_{3400}−folate showed a broad peak centered at $m/z = 4825$ that was consistent with formation of the conjugate (Figure 2).

Monomolecular DNA Condensation. As schematically depicted in Figure 1 path a), anionic DNA molecules were individually condensed with the cationic detergent. Detergents are water-soluble and upon addition of the complexes to cells, their fast exchange with the medium or cell membranes would lead to DNA unfolding (*26*), hence their poor transfection properties (*27*). The particles were therefore stabilized by chemically converting the thiol detergent to a gemini lipid on the template DNA (*14*). In practice, complexes were prepared by adding the desired amount of dimerizable cationic detergent to plasmid DNA, under constant stirring. For each condition, the DNA concentration was determined by measur-

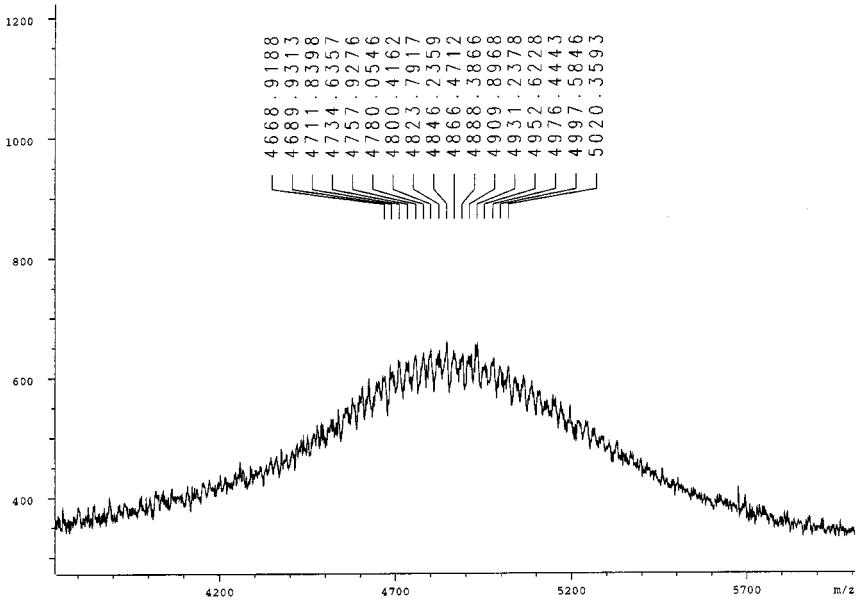


Figure 2. MALDI-TOF spectrum of DPPE−PEG_{3400}−folate.

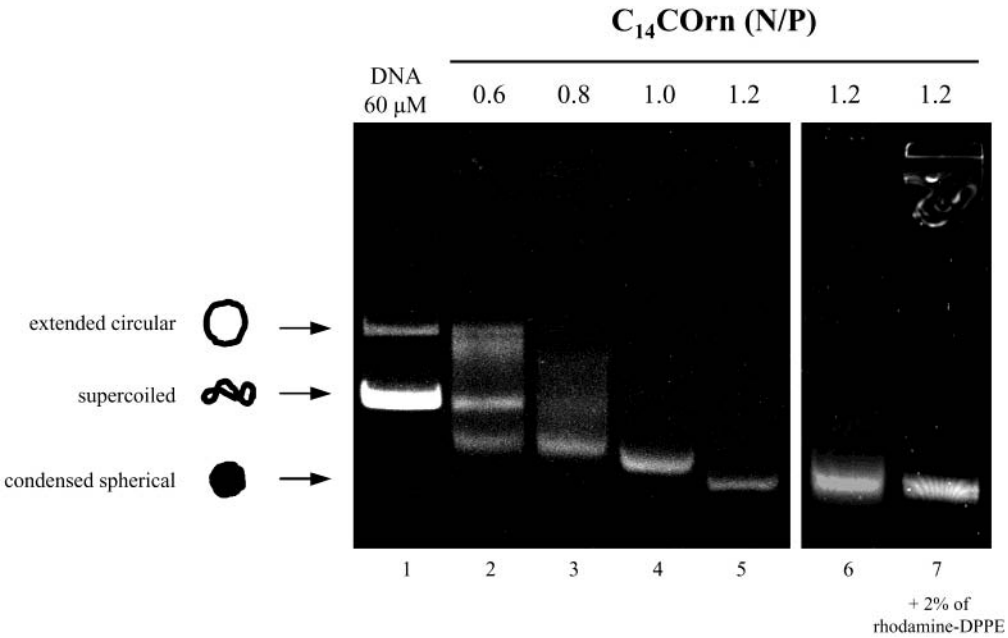


Figure 3. Complex formation as visualized by gel electrophoresis. Free DNA (lane 1) and its complexes with C_{14}COrn for various N/P ratios (lanes 2−5). The gel was stained with ethidium bromide to visualize DNA. The presence of lipid in the particles (N/P 1.2, lane 6) was revealed by addition of 2% of rhodamine-labeled DPPE to the initial mixture (lane 7; fluorescence $\lambda_{ex/em}$: 538/580 nm). Twenty microliter samples containing 0.4 μg of pCMV−Luc plasmid DNA in Hepes buffer (15 mM, pH 7.4), and concentrations of C_{14}COrn detergent as indicated were loaded onto the gel after 6 h incubation.

ing the absorbance at 260 nm before addition of the detergent and complexes were kept at room temperature for at least 4 h to allow cross-linking to occur prior gel electrophoretic analysis. Figure 3 shows the electrophoretic migration pattern observed for plasmid DNA mixed with increasing initial concentrations of C_{14}COrn. For cationic lipids, it is well-known that DNA complexes are too large to migrate into the gel. Here, we found lipid/DNA particles to be fully mobile when formed by oxidation of the detergent in the presence of DNA. At low charge ratios (N/P < 1), the coexistence of free DNA with the complexes showed dimerizable cationic detergent-mediated DNA condensation to be an all-or-nothing process. For a stoichiometric ratio (N/P = 1.0), condensation was completed and particles moved in the gel faster than free plasmid DNA, albeit most DNA phosphate residues were neutralized by the cationic amphiphile. To fully characterize the nature of this surprisingly fast-moving band, its lipidic component was revealed by addition of a 2% rhodamine-labeled DPPE to the initial mixture. The position of rhodamine-labeled DPPE was examined under fluorescence illumination ($\lambda_{ex/em}$: 538/580 nm) before the gel was stained with ethidium bromide to visualize DNA. As shown in Figure 3, the fluorescence of rhodamine colocalized with that of ethidium bromide-intercalated DNA. Stokes diffusion of condensed DNA particles through the agarose gel thus appears to be easier than reptation of the extended micrometric DNA polymer. As already discussed in the introduction, favorable in vivo diffusion and intracellular trafficking properties may thus be expected from the fast migration of the complexes.

The size and surface charge of the $(C_{14}COrn)_2$/DNA particles (N/P = 1.2) were measured by laser light

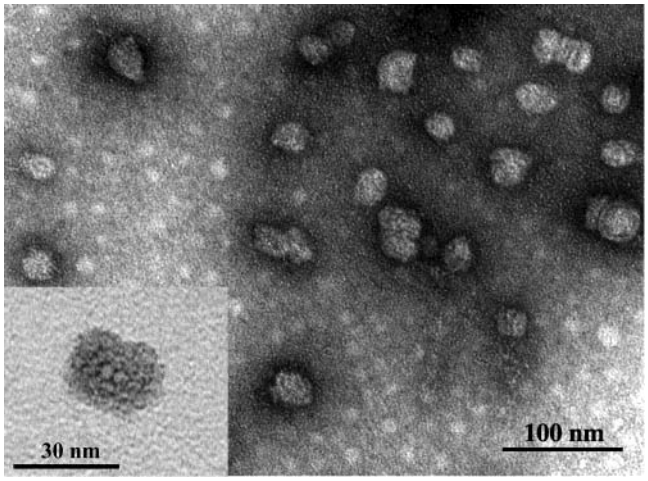


Figure 4. Transmission electron microscopy of $(C_{14}COrn)_2$/DNA particles at N/P = 1.2 in Hepes buffer (15 mM, pH 7.4).

scattering. The average size of the particles and their zeta potential were found to be 39 ± 4 nm and −45 ± 5 mV, respectively. To visualize their morphology and to confirm their size and dispersity, the particles were observed by transmission electron microscopy. A single population of particles with size of 28 ± 4 nm (n = 20) was found (Figure 4). The significantly smaller size found by transmission electronic microscopy may be due to the dehydration process which occurs during sample preparation. According to typical plasmid DNA and amphiphile molecular dimensions, the volume of a monomolecular DNA particle should correspond to a 31 nm sphere. The actual size of the particles thus provides strong evidence for monomolecular collapse of plasmid DNA. Uranyl acetate staining also suggested an internal supramolecular organization consistent with a compacted tubular or micellar phase (Figure 4, inset). This type of packing was previously observed with complexes prepared with Transfectam, a potent cationic lipid transfection reagent (*28*). The similarity of both structures was a good sign that $C_{14}COrn$ would be able to transfect cells.

Cell Transfection Properties of $(C_{14}COrn)_2$. The gene delivery properties of $(C_{14}COrn)_2$/DNA particles were tested on cells of various origins. The transfection

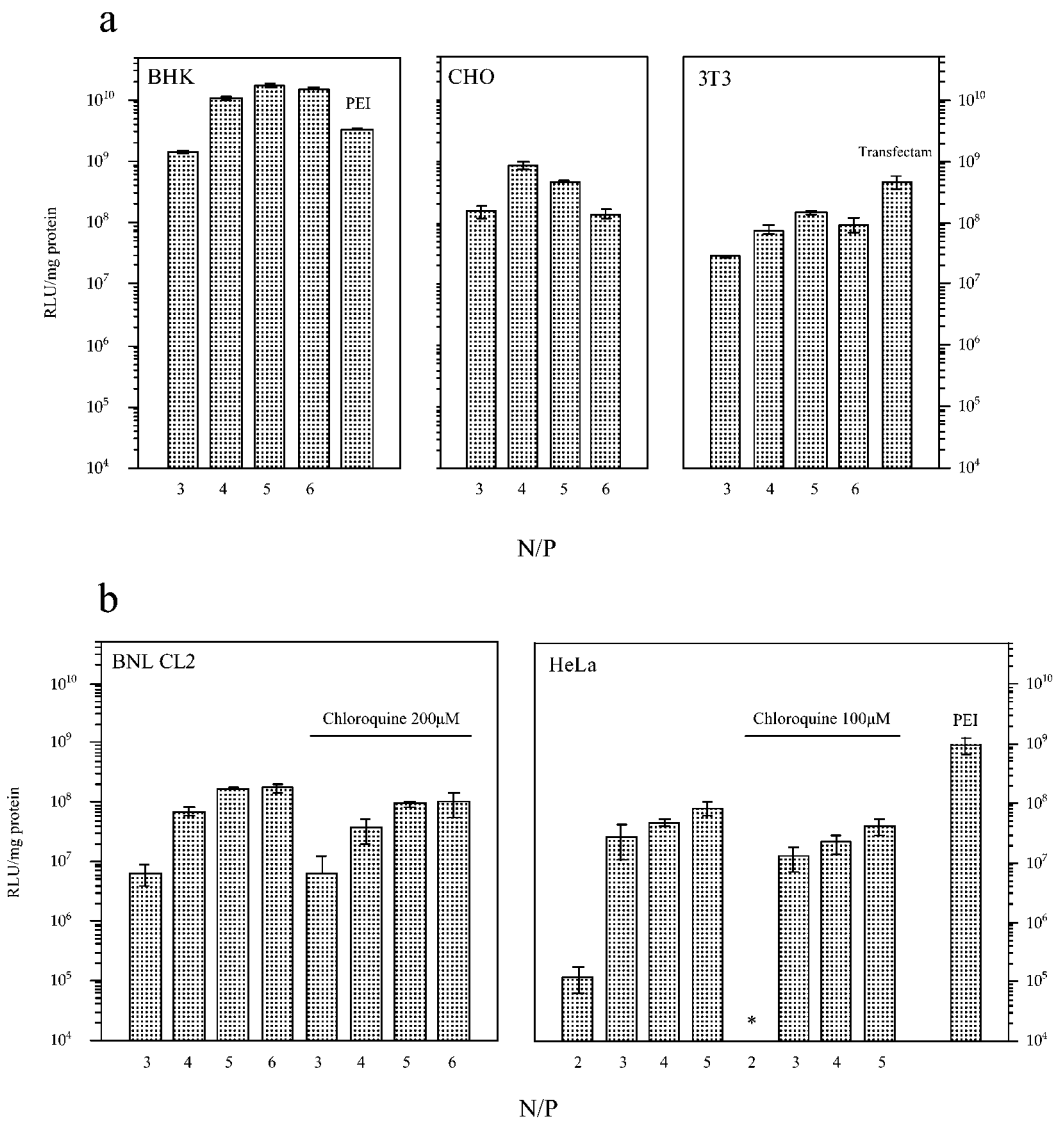


Figure 5. Transfection of BHK, CHO, 3T3, BNL CL2, and HeLa cells. (a) BHK, CHO and 3T3 cells were transfected with pCMV−Luc (2 μg/well) complexed with increasing amounts of $C_{14}COrn$. After 3 h, the transfection medium was completed with 10% FCS, and cells were cultured for an additional 21 h (b) BNL CL-2 and HeLa cells were transfected with pCMV−Luc (2 μg/well) complexed with increasing amounts of $C_{14}COrn$ in the presence or absence of chloroquine. After 3 h, the transfection medium was replaced with fresh culture medium, and cells were cultured for an additional 21 h. Luciferase activity was measured as described in Experimental Procedures. Transfections were carried out in triplicate; error bars indicate standard deviations.

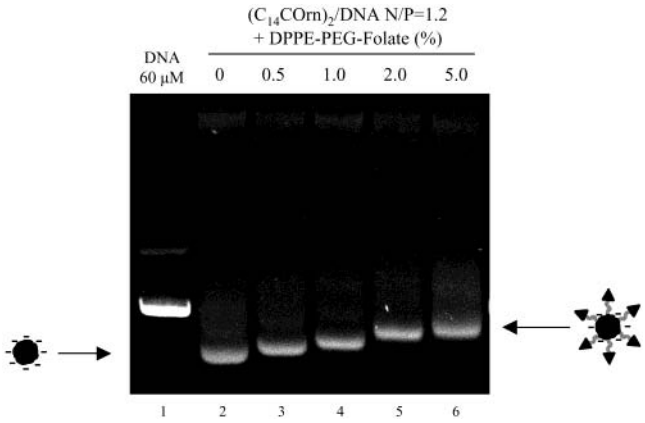


Figure 6. Characterization of $(C_{14}COrn)_2$/DNA/DPPE−PEG_{3400}−folate complexes by agarose gel electrophoresis. The minigel shows plasmid DNA (lane 1) and its complexes with $C_{14}COrn$ 1.2 eq (N/P) with various amounts of DPPE−PEG_{3400}−folate (%): 0, 0.5, 1.0, 2.0, and 5.0 (lanes 2−6). Twenty microliter samples containing 0.4 μg of pCMV−Luc and amphiphile(s) in Hepes buffer (15 mM, pH 7.4) were loaded onto the gel after 24 h incubation.

efficiency of the monomolecular complexes was only slightly above that of naked DNA. Indeed, being devoid of a cationic surface charge (zeta potential of −45 mV), these particles are unable to bind their internalizing receptors, namely, heparan sulfate polyanions (*28*, *29*). Larger cationic particles were therefore prepared with higher N/P ratios, i.e., standard conditions for cationic lipids, and tested in vitro using the luciferase reporter gene. The magnitude of gene expression varied with cell type (Figure 5). However, $(C_{14}COrn)_2$ was always found close to potent transfection reagents such as Transfectam and JetPEI (*23*, *24*). Optimal transfection was observed for N/P = 4−5, which corresponds to the formation of cationic particles. Beyond this optimum, luciferase activity eventually decreased as the N/P ratio was further raised, a possible sign of toxicity. Taken together, these results show that, provided the cationic $(C_{14}COrn)_2$/DNA complexes are able to bind to the cell membrane, they follow the typical intracellular fate of synthetic gene delivery vectors.

Gene expression was not enhanced in the presence of 100 μM (HeLa) or 200 μM (BNL CL2) chloroquine. The $(C_{14}COrn)_2$/DNA complexes must therefore be released from the endosomal compartment by an intrinsic membrane disrupting activity. Treatment of the complexes with a biologically relevant concentration of glutathione (5−20 mM) (*30*, *31*) caused a partial DNA release as seen by electrophoresis (data not shown). Although the cellular compartments in which glutathione is present are not clearly identified, there is some evidence for the presence of glutathione within endosomes (*32*). The cationic disulfide lipid $(C_{14}COrn)_2$ may thus be reduced back into a cationic detergent that causes endosome disruption (*33*, *34*).

PEG-Coated Monomolecular DNA Particles. Systemic delivery through the blood circulation is the most attractive route for transferring genes to nonlocalized tumor metastases. Poly(ethylene glycol) is being extensively used to enhance the stability and the life span of liposomes in the bloodstream, via the so-called "steric-stabilization" mechanism (*17*). Several publications have also described the synthesis of PEG-containing polymers designed to create an inert hydrophilic layer at the surface of DNA condensates, with the aim of improving their solubility and in vivo performances (*35*−*38*). As PEG will also inhibit the ionic interaction between the

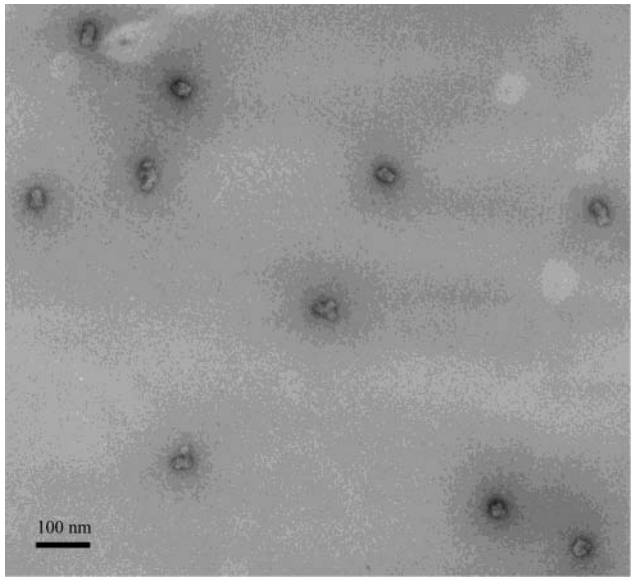


Figure 7. Transmission electron microscopy of $(C_{14}COrn)_2$/DNA/2% DPPE−PEG_{3400}−folate particles at N/P = 1.2 in Hepes buffer (15 mM, pH 7.4).

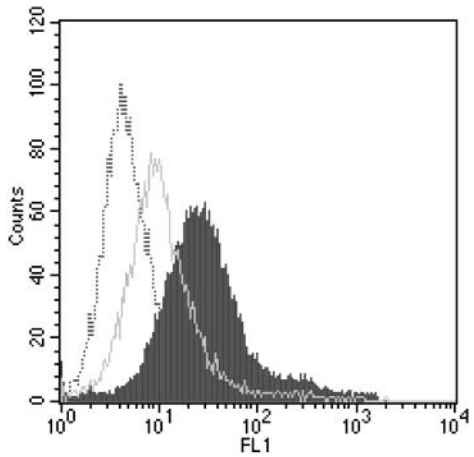


Figure 8. Folate-coated particles adhere to KB cells. Flow cytometry of KB cells exposed for 4 h to 2%-coated DPPE−PEG_{3400}−folate monomolecular YOYO-DNA particles (grey peak). Continuous line: plus 1 mM folic acid. Dotted line: autofluorescence of the cells. *X* axis, fluorescence intensity; *Y* axis, number of cells.

DNA complexes and the cell membrane that leads to cell entry, we coupled folic acid to the remote end of the PEG chain. This vitamin interacts with nanomolar affinity with the folate receptor overexpressed on tumor cells, and is able to trigger receptor-mediated endocytosis of the complexes (*39*). Accordingly, we synthesized a DPPE−PEG_{3400}−folate derivative that may anchor itself into the hydrophobic core particle (Figure 1). Since it was shown that grafting PEG molecules on the condensing agent may interfere with DNA compaction (*40*), we chose a postgrafting strategy. Plasmid DNA was first condensed by the cationic detergent. The monomolecular particles were subsequently coated with the lipid−PEG derivative by simple addition to the aqueous dispersion. The insertion equilibrium was reached within minutes as previously reported by Sou and co-workers in the case of liposomes (*41*). Incorporation was monitored by electrophoresis as a function of the DPPE−PEG_{3400}−folate/C_{14}-COrn ratio (Figure 6). Particles containing 0.5−5% DPPE−PEG_{3400}−folate were stable and able to migrate through the gel. However, their mobility decreased as the

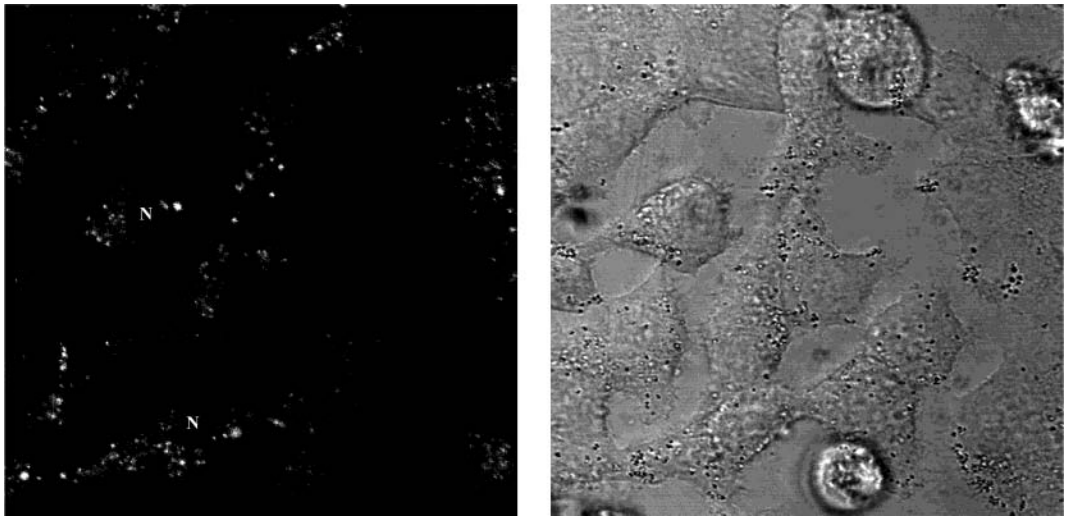


Figure 9. Folate-coated particles are taken up by KB cells. Cells were exposed to 2%-coated DPPE−PEG_{3400}−folate monomolecular YOYO-labeled complexes for 4 h. The medium was subsequently replaced by cell culture medium and cells incubated for an additional 20 h before analysis. Images were taken from living cells. The picture in the left panel corresponds to the fluorescence overlay of z-sections between 2 and 8 μm from the bottom of the cell. The corresponding transmission image is presented in the right panel. N indicates nucleus.

amount of DPPE−PEG_{3400}−folate increased, possibly due to diffusional hindrance brought about by the poly(ethylene glycol) calix (Figure 6).

The optimal in vivo formulation of PEG-grafted liposomes was shown to be reached using 3−7% of DSPE−PEG_{2000} in the lipid mixture (*42*). Since the lipid−PEG was distributed among the two bilayer leaflets, half this percentage should in principle be sufficient to cover a solid particle. The surface of a spherical 35 nm $(C_{14}COrn)_2$/DNA particle is approximately 4000 nm^2. Assuming a PEG_{3400} residue covers roughly 80 nm^2 (*43*), the insertion of ca. 50 molecules DPPE−PEG_{3400}−folate in the particule (i.e., 1%) should be sufficient for effective protection, in rough agreement with the liposome data. Experimentally, particle migration profiles became identical above 2% DPPE−PEG_{3400}−folate. Electron microscopy confirmed that the PEG-coated particles remained compact (Figure 7). Importantly, electrophoresis also showed that coated monomolecular particles did not aggregate in cell-culture medium (data not shown).

Entry into Folate Receptor-Expressing Cells. We finally examined the ability of the particles to carry genes into carcinoma cells overexpressing the folate receptor. The $(C_{14}COrn)_2$/DNA/2%DPPE−PEG_{3400}−folate particles were labeled with the fluorescent DNA-intercalating dye YOYO-1. Particles binding and entry into KB cells was studied by flow cytometry following a 4 h incubation period in folate-free cell culture medium. As shown in Figure 8, virtually all cells took up similar, yet moderate, amounts of the fluorescent complexes. This is to be compared to cationic lipid/DNA complexes, where cellular uptake was shown to be both higher and more heterogeneous (*44*, *45*). Control experiments performed with anionic $(C_{14}COrn)_2$/DNA as well as with $(C_{14}COrn)_2$/DNA/2%DPPE−PEG particles, both lacking the folic acid ligand, confirmed this shift to be significant. Competition experiments in the presence of 1 mM folic acid decreased the amount of particle binding (Figure 8). Effective competition required a large excess of ligand, as a single particle may form multiple tethers with a cluster of receptors on the cell surface. Taken together, these results clearly show that cell binding occurred via the folate receptor.

Unfortunately, transfection results were very disappointing: luciferase activity was found ca. 5 orders of magnitude lower than using JetPEI as a vector. We thus followed the fate of the particles by confocal microscopy (Figure 9). Tiny fluorescent spots were found beneath the cell surface or spread throughout the cytoplasm at 4 h. At 24 h, they were somewhat larger and spread ramdomly. The cytometry (see above) and microscopic observations contrast with typical cationic lipid-mediated transfection, where large clumps of DNA complexes sediment onto the cells, are taken up by heparan sulfate proteoglycan ligation (*46*) and accumulate in a perinuclear compartment (*44*, *45*).

Unsuccessful transfection may thus arise from either (or from a combination) of several factors: (i) 35 nm particles do not sediment well onto the cells; (ii) the number of folate receptors is certainly well below that of ubiquitous anionic proteoglycans; (iii) caveolae are thought to be folic acid-storing organelles and vehicles for transcytosis (*47*). All functions may be nonproductive for gene delivery.

CONCLUSION

This work was meant to be an extension of encouraging results described in the literature that showed that grafting of poly(ethylene glycol)−folic acid residues to DNA complexes led to selective expression of foreign genes in folate-expressing cells in vitro (*35*, *39*, *48*). To our knowledge, these results have had no in vivo developments so far. The size of DNA complexes being a key factor for successful delivery in vivo, we applied our recently developed technique of monomolecular DNA condensation to this goal. The reason we failed up to now is not clear, yet it precludes in vivo experiments. Additional in vitro experiments are being performed.

ACKNOWLEDGMENT

This work was supported by grants and a fellowship (to E.D.) from Vaincre la Mucoviscidose. We warmly thank Dr. Przemyslaw Godzina for help with the mass spectrometer and Liliane Italiano for her skillful technical help.

NOTE ADDED AFTER ASAP POSTING

The sentence "The pCMV−Luc plasmid was linearized with *Xmn* I, according to standard protocols (*21*)" was deleted from Materials and Methods.

LITERATURE CITED

(1) Behr, J. P. (1993) Synthetic gene transfer vectors. *Acc. Chem. Res. 26*, 274−278.

(2) Felgner, P. L., Heller, M. J., Lehn, P., Behr, J. P., and Szoka, F. C. E. (1996) *Artificial Self-Assembling Systems for Gene Delivery*. American Chemical Society, Washington, D. C.

(3) Rolland, A. P. (1998) From genes to gene medicines: recent advances in nonviral gene delivery. *Crit. Rev. Ther. Drug Carrier Syst. 15*, 143−198.

(4) Nishikawa, M., and Huang, L. (2001) Nonviral vectors in the new millennium: delivery barriers in gene transfer. *Hum. Gene Ther. 12*, 861−870.

(5) Wisse, E., De Zanger, R. B., Charels, K., Van Der Smissen, P., and McCuskey, R. S. (1985) The liver sieve: considerations concerning the structure and function of endothelial fenestrae, the sinusoidal wall and the space of Disse. *Hepatology 5*, 683−692.

(6) Sanders, N. N., De Smedt, S. C., Van Rompaey, E., Simoens, P., De Baets, F., and Demeester, J. (2000) Cystic fibrosis sputum: a barrier to the transport of nanospheres. *Am. J. Respir. Crit. Care Med. 162*, 1905−1911.

(7) Olmsted, S. S., Padgett, J. L., Yudin, A. I., Whaley, K. J., Moench, T. R., and Cone, R. A. (2001) Diffusion of macromolecules and virus-like particles in human cervical mucus. *Biophys. J. 81*, 1930−1937.

(8) Reddy, J. A., and Low, P. S. (1998) Folate-mediated targeting of therapeutic and imaging agents to cancers. *Crit. Rev. Ther. Drug Carrier Syst. 15*, 587−627.

(9) Kolb-Bachofen, V., Schlepper-Schafer, J., and Kolb, H. (1983) Receptor-mediated particle uptake by liver macrophages. The galactose- particle receptor mediates uptake via coated and also noncoated structures. *Exp. Cell Res. 148*, 173−182.

(10) Bijsterbosch, M. K., Ziere, G. J., and Van Berkel, T. J. (1989) Lactosylated low-density lipoprotein: a potential carrier for the site- specific delivery of drugs to Kupffer cells. *Mol. Pharmacol. 36*, 484−489.

(11) Rensen, P. C., Sliedregt, L. A., Ferns, M., Kieviet, E., van Rossenberg, S. M., van Leeuwen, S. H., van Berkel, T. J., and Biessen, E. A. (2001) Determination of the upper size limit for uptake and processing of ligands by the asialoglycoprotein receptor on hepatocytes in vitro and in vivo. *J. Biol. Chem. 276*, 37577−37584.

(12) Lukacs, G. L., Haggie, P., Seksek, O., Lechardeur, D., Freedman, N., and Verkman, A. S. (2000) Size-dependent DNA mobility in cytoplasm and nucleus. *J. Biol. Chem. 275*, 1625−1629.

(13) Feldherr, C. M., and Akin, D. (1991) Signal-mediated nuclear transport in proliferating and growth-arrested BALB/c 3T3 cells. *J. Cell. Biol. 115*, 933−939.

(14) Blessing, T., Remy, J. S., and Behr, J. P. (1998) Monomolecular collapse of plasmid DNA into stable virus-like particles. *Proc. Natl. Acad. Sci. U.S.A. 95*, 1427−1431.

(15) Blessing, T., Remy, J.-S., and Behr, J.-P. (1998) Template Oligomerization of DNA-Bound Cations Produces Calibrated Nanometric Particles. *J. Am. Chem. Soc. 120*, 8519−8520.

(16) Dauty, E., Remy, J. S., Blessing, T., and Behr, J. P. (2001) Dimerizable Cationic Detergents with a Low cmc Condense Plasmid DNA into Nanometric Particles and Transfect Cells in Culture. *J. Am. Chem. Soc. 123*, 9227−9234.

(17) Woodle, M. C., and Lasic, D. D. (1992) Sterically stabilized liposomes. *Biochim. Biophys. Acta 1113*, 171−199.

(18) Allen, T. M., Hansen, C., Martin, F., Redemann, C., and Yau-Young, A. (1991) Liposomes containing synthetic lipid derivatives of poly(ethylene glycol) show prolonged circulation half-lives in vivo. *Biochim. Biophys. Acta 1066*, 29−36.

(19) Jeppesen, C., Wong, J. Y., Kuhl, T. L., Israelachvili, J. N., Mullah, N., Zalipsky, S., and Marques, C. M. (2001) Impact of polymer tether length on multiple ligand−receptor bond formation. *Science 293*, 465−468.

(20) Zanta, M. A., Boussif, O., Adib, A., and Behr, J. P. (1997) In vitro gene delivery to hepatocytes with galactosylated polyethylenimine. *Bioconjugate Chem. 8*, 839−844.

(21) Sambrook, J., Fritsch, E. F., and Maniatis, T. (1989) *Molecular Cloning: A Laboratory Manual*, 2nd ed., Cold Spring Harbor, New York.

(22) Atkinson, S. F., Bettinger, T., Seymour, L. W., Behr, J. P., and Ward, C. M. (2001) Conjugation of folate via gelonin carbohydrate residues retains ribosomal-inactivating properties of the toxin and permits targeting to folate receptor positive cells. *J. Biol. Chem. 276*, 27930−27935.

(23) Behr, J. P., Demeneix, B., Loeffler, J. P., and Perez-Mutul, J. (1989) Efficient gene transfer into mammalian primary endocrine cells with lipopolyamine-coated DNA. *Proc. Natl. Acad. Sci. U.S.A. 86*, 6982−6986.

(24) Boussif, O., Zanta, M. A., and Behr, J. P. (1996) Optimized galenics improve in vitro gene transfer with cationic molecules up to 1000-fold. *Gene Ther. 3*, 1074−1080.

(25) Leamon, C. P., and Low, P. S. (1991) Delivery of macromolecules into living cells: a method that exploits folate receptor endocytosis. *Proc. Natl. Acad. Sci. U.S.A. 88*, 5572−5576.

(26) Lleres, D., Dauty, E., Behr, J., Mely, Y., and Duportail, G. (2001) DNA condensation by an oxidizable cationic detergent. Interactions with lipid vesicles. *Chem. Phys. Lipids 111*, 59−71.

(27) Remy, J. S., Sirlin, C., Vierling, P., and Behr, J. P. (1994) Gene transfer with a series of lipophilic DNA-binding molecules. *Bioconjugate Chem. 5*, 647−654.

(28) Labat-Moleur, F., Steffan, A. M., Brisson, C., Perron, H., Feugeas, O., Furstenberger, P., Oberling, F., Brambilla, E., and Behr, J. P. (1996) An electron microscopy study into the mechanism of gene transfer with lipopolyamines. *Gene Ther. 3*, 1010−1017.

(29) Mislick, K. A., and Baldeschwieler, J. D. (1996) Evidence for the role of proteoglycans in cation-mediated gene transfer. *Proc. Natl. Acad. Sci. U.S.A. 93*, 12349−12354.

(30) Meister, A., and Anderson, M. E. (1983) Glutathione. *Annu. Rev. Biochem. 52*, 711−760.

(31) Bellomo, G., Vairetti, M., Stivala, L., Mirabelli, F., Richelmi, P., and Orrenius, S. (1992) Demonstration of nuclear compartmentalization of glutathione in hepatocytes. *Proc. Natl. Acad. Sci. U.S.A. 89*, 4412−4416.

(32) Collins, D. S., Unanue, E. R., and Harding, C. V. (1991) Reduction of disulfide bonds within lysosomes is a key step in antigen processing. *J. Immunol. 147*, 4054−4059.

(33) McKenzie, D. L., Kwok, K. Y., and Rice, K. G. (2000) A potent new class of reductively activated peptide gene delivery agents. *J. Biol. Chem. 275*, 9970−9977.

(34) Byk, G., Dubertret, C., Escriou, V., Frederic, M., Jaslin, G., Rangara, R., Pitard, B., Crouzet, J., Wils, P., Schwartz, B., and Scherman, D. (1998) Synthesis, activity, and structure−activity relationship studies of novel cationic lipids for DNA transfer. *J. Med. Chem. 41*, 229−235.

(35) Leamon, C. P., Weigl, D., and Hendren, R. W. (1999) Folate copolymer-mediated transfection of cultured cells. *Bioconjugate Chem. 10*, 947−957.

(36) Katayose, S., and Kataoka, K. (1997) Water-soluble polyion complex associates of DNA and poly(ethylene glycol)-poly(L-lysine) block copolymer. *Bioconjugate Chem. 8*, 702−707.

(37) Nguyen, H. K., Lemieux, P., Vinogradov, S. V., Gebhart, C. L., Guerin, N., Paradis, G., Bronich, T. K., Alakhov, V. Y., and Kabanov, A. V. (2000) Evaluation of polyether-polyethyleneimine graft copolymers as gene transfer agents. *Gene Ther. 7*, 126−138.

(38) Ogris, M., Brunner, S., Schuller, S., Kircheis, R., and Wagner, E. (1999) PEGylated DNA/transferrin-PEI complexes: reduced interaction with blood components, extended circulation in blood and potential for systemic gene delivery. *Gene Ther. 6*, 595−605.

(39) Lee, R. J., and Low, P. S. (1994) Delivery of liposomes into cultured KB cells via folate receptor- mediated endocytosis. *J. Biol. Chem. 269*, 3198−3204.

(40) Erbacher, P., Bettinger, T., Belguise-Valladier, P., Zou, S., Coll, J. L., Behr, J. P., and Remy, J. S. (1999) Transfection and physical properties of various saccharide, poly(ethylene

glycol), and antibody-derivatized polyethylenimines (PEI). *J. Gene Med. 1,* 210−222.
(41) Sou, K., Endo, T., Takeoka, S., and Tsuchida, E. (2000) Poly(ethylene glycol)-modification of the phospholipid vesicles by using the spontaneous incorporation of poly(ethylene glycol)-lipid into the vesicles. *Bioconjugate Chem. 11,* 372−379.
(42) Allen, T. M. (1994) The Use of Glycolipids and Hydrophilic Polymers in Avoiding Rapid Uptake of Liposomes by the Mononuclear Phagocyte System. *Adv. Drug Deliv. Rev. 13,* 285−309.
(43) Needham, D., McIntosh, T. J., and Lasic, D. D. (1992) Repulsive interactions and mechanical stability of polymer-grafted lipid membranes. *Biochim. Biophys. Acta 1108,* 40−48.
(44) Ruponen, M., Ronkko, S., Honkakoski, P., Pelkonen, J., Tammi, M., and Urtti, A. (2001) Extracellular glycosaminoglycans modify cellular trafficking of lipoplexes and polyplexes. *J. Biol. Chem. 276,* 33875−33880.
(45) Zabner, J., Fasbender, A. J., Moninger, T., Poellinger, K. A., and Welsh, M. J. (1995) Cellular and molecular barriers to gene transfer by a cationic lipid. *J. Biol. Chem. 270,* 18997−19007.
(46) Zuber, G., Dauty, E., Nothisen, M., Belguise, P., and Behr, J. P. (2001) Towards synthetic viruses. *Adv. Drug Deliv. Rev. 52,* 245−253.
(47) Gumbleton, M. (2001) Caveolae as potential macromolecule trafficking compartments within alveolar epithelium. *Adv. Drug Deliv. Rev. 49,* 281−300.
(48) Reddy, J. A., Dean, D., Kennedy, M. D., and Low, P. S. (1999) Optimization of folate-conjugated liposomal vectors for folate receptor- mediated gene therapy. *J. Pharm. Sci. 88,* 1112−1118.

BC0255182

Differential Conjugation of Tat Peptide to Superparamagnetic Nanoparticles and Its Effect on Cellular Uptake

Ming Zhao,*,† Moritz F. Kircher,† Lee Josephson, and Ralph Weissleder

Center for Molecular Imaging Research, Harvard Medical School, Room 5404, Building 149, 13th Street, Charlestown, Massachusetts 02169. Received February 27, 2002; Revised Manuscript Received April 19, 2002

Surface modification of superparamagnetic contrast agents with HIV-1 tat peptide has emerged as a promising means for intracellular magnetic labeling and noninvasive tracking of a large number of cell types with MRI. To achieve efficient intracellular delivery of the nanoparticles, we investigated the effect on cellular uptake of superparamagnetic iron oxide particles by varying the number of attached tat peptides. First, we report here a modified P2T method in measuring the numbers of surface attachments per particle through disulfide linkage. The method was shown to have desirable simplicity and reproducibility. With the P2T method as a tool, conjugates with progressively higher ratios of peptide-to-particle were synthesized. We were able to demonstrate that higher numbers of tat peptide facilitate the cellular uptake of iron oxide nanoparticles in a nonlinear fashion. Cells labeled with these optimized preparations were readily detectable by MR imaging. The increase in sensitivity could allow in vivo tracking of 100-fold lower cell concentration than currently described.

INTRODUCTION

Magnetic resonance imaging (MRI) has emerged as a potentially powerful tool in the investigation of cell migration in vivo (*1*). With a growing array of cell labeling techniques, cells tagged with various monocrystalline MR probes have been evaluated in the past in their detection both in vitro and in vivo (*1*−*4*).

Among these, HIV-1 tat peptide, which carries a transmembrane and a nuclear localization signal within its sequence (*5*), is capable of translocating exogenous molecules into cells (*6*−*10*). Due to its membrane translocation function, tat peptide has been used to derivatize the surface of magnetic pharmaceuticals and substantially facilitated their uptake into target cells. For instance, using tat conjugated 1,4,7,10-tetraazacyclododecane-*N*,*N*′*N*″*N*‴-tetraacetic acid (DOTA), paramagnetic chelates were delivered to intracellular compartments (*2*). In addition, tat-derivatized CLIO (cross-linked superparamagnetic iron oxide), which consists of dextran-coated superparamagnetic iron oxide nanoparticles and is a potent T_2 shortening agent, has been shown to achieve high loading and allowed ex vivo tracking of progenitor cells to bone marrow (*1*).

In a continuous effort to further improve cell labeling conditions and to achieve maximum detectability of labeled cells, it has become necessary to understand how the number of tat peptide per CLIO particle may influence cellular uptake of the complex. To do so, it is imperative to have a method which can accurately and conveniently determine the peptide-to-CLIO ratio. Here we report such a protocol adapted to measure the degree of conjugation on CLIO through disulfide linkage with simplicity, reliability, and reproducibility. Subsequently, a series of CLIO−tat conjugates with progressively higher numbers of tat peptide per CLIO particle were synthesized based on the assumption that higher numbers of peptides would facilitate cellular targeting with greater density of affinity ligands and/or multivalency effects. We observed that high (above 10 per CLIO) numbers of tat peptide increased the intracellular accumulation of CLIO−tat (up to 100-fold) compared to prior preparations, and that this greatly enhanced the detection threshold of labeled cells.

* Corresponding author. E-mail: mingzhao@helix.mgh.harvard.edu.

† These authors made an equal contribution to the study.

MATERIALS AND METHODS

General. A modified tat peptide was synthesized and purified as previously described (*3*), with a sequence GRKKRRQRRRGYK(FITC)C-NH_2. The inclusion of FITC in the peptide sequence is essential for measuring peptide-to-CLIO ratios using the fluorescent absorption method, which is to be compared with the new P2T method (see below). The iodination site (tyrosine), FITC modified lysine, and site of attachment to the nanoparticle (cysteine) are at the C terminal end and separated from the residues involved in membrane translocation by a spacer glycine. The synthesis of amino-CLIO and reaction with *N*-succinimidyl 3-(2-pyridyldithio)propionate (SPDP) have been described elsewhere (*3*).

Measuring the Degree of Conjugation Using the P2T Method. Tat peptide of appropriate amount was dissolved in DMSO (Fisher) to make a concentrated stock. 37.5 μL of tat solution was mixed with 500 μL of CLIO−P2T (1.5 mg/mL Fe). The mixture was allowed to stand for 2 h at room temperature. At the end of the incubation, 70 μL of the reaction mixture was withdrawn for the measurement of pyridine-2-thione (P2T). A microconcentrator (50 kDa molecular weight cut off, Amicon, Beverly, MA) was used to remove CLIO, and the fraction containing P2T was collected as flow-through. A 50 μL amount of the P2T fraction was diluted to 400 μL using 1 × PBS, pH 7.4. The absorbance of P2T was determined at 343 nm on a spectrophotometer, and its concentration was calculated using an extinction coefficient of 8100 $M^{-1}cm^{-1}$. Tat-to-CLIO ratio was subsequently deduced with known iron concentration in the reaction mixture.

To validate the P2T method, the degree of conjugation was also quantified using fluorescent absorption from

10.1021/bc0255236 CCC: $22.00 © 2002 American Chemical Society
Published on Web 06/08/2002

FITC. Briefly, for a suspension of CLIO−tat, the absorbance was determined at 494 nm and the concentration of FITC was calculated using an extinction coefficient of 73000 M^{-1} cm^{-1}.

Synthesis of CLIO−tat Series with Progressively Higher Ratios. A calibration curve was constructed by setting up a series of reactions in smaller scale with a range of peptide concentrations, while keeping all other conditions constant. In detail, 7.5 μL of each peptide stock solution was mixed with 100 μL aliquots of CLIO−P2T (1.5 mg/mL Fe). The reactions were allowed to proceed as above. In due course, tat-to-CLIO ratios were determined to establish a relationship between the amount of peptide used and the resulting ratios. According to the calibration curve, CLIO−tat conjugates of expected ratios were synthesized and characterized. The products were cleaned of unreacted free peptide and low molecular weight impurities using 1.5 × 5 cm gel filtration column (Sephadex G-50) equilibrated with 1 × PBS, pH 7.4.

Control conjugates were synthesized using a peptide (Gly-Arg-Arg-Lys(FITC)-Cys-NH_2) that lacks the transmembrane and nuclear localization sequence of tat. Two control conjugates were synthesized with 9.7 and 12.9 peptides per CLIO particle, respectively. The products were treated with Bolton−Hunter reagent, SHPP (Pierce) to introduce a phenolic group for iodination (see below). In detail, 50 μL of 8 mg/mL of SHPP was mixed with 500 μL of conjugates at pH 8.0. The reaction was allowed to proceed for 2 h at room temperature. The modified product was purified with 1.5 × 5 cm gel filtration column (Sephadex G-50) equilibrated with 1 × PBS, pH 7.4.

Isolation of Lymphocytes. Lymphocytes were obtained from the spleen of C57 Bl/6 mice (National Cancer Institute, Bethesda, MA). Donor animals were sacrificed by inhalation of an overdose of Halothane, and their spleens were removed using aseptic procedures. The spleens were disrupted between frosted histology slides and dispersed in RPMI 1640 medium (Cellgro; Mediatech, Washington, DC) supplemented with 10% fetal bovine serum (FBS; Cellgro; Mediatech). Cells were filtered through a cell-strainer with 30 μm mesh size (Miltenyi Biotech, Auburn, CA) and washed. Erythrocytes were lysed by resuspending the cell pellet in 0.83% ammonium chloride in distilled water. After being washed further, the cells were incubated in RPMI 1640 supplemented with 10% FBS in 175 cm^2 tissue culture flasks (Falcon; Becton Dickinson Labware, Bedford, MA). To remove the majority of the monocyte/macrophage population, the nonadherent cell population was transferred into a new flask after 1 h. This method yielded a cell population containing about 95% lymphocytes, as described (*11*).

Preparation of ^{125}I-Labeled CLIO−tat. Radioactive labeling of CLIO−tat was performed according to the Chizzonite indirect method using IODO-GEN precoated tubes (Pierce, Rockford, IL) following closely the protocol of the manufacturer (Pierce). Briefly, for each sample of CLIO−tat with different tat-to-CLIO ratios 1 mCi ^{125}I was activated for 7 min at RT in IODO-GEN tubes in 100 μL of Tris iodination buffer. The activated ^{125}I was added to 100 μg of CLIO−tat and reacted for 10 min, followed by a reaction with scavenging buffer (50 μL/sample) for 5 min. The samples were added to 1.5 × 5 cm gel filtration columns (Sephadex G-50) and centrifuged at 400*g* for 5 min and the eluates collected. Immediately before performing cell uptake assays, the labeled samples were again purified and equilibrated to the culture conditions with 1.5 × 5 cm gel filtration columns (Sephadex G-50) equilibrated with RPMI-1640 supplemented with 10% FBS.

Cell Uptake Assay. To quantify the cellular uptake of the different CLIO−tat conjugates, 20 μg ^{125}I−CLIO−tat was added to lymphocytes in RPMI-1640 supplemented with 10% FBS at a final concentration of 10^6 cells/ml. Cells were incubated for 2 h in coated (1% BSA in Hanks' balanced salt solution (HBSS; Cellgro; Mediatech)) 5 mL polystyrene culture tubes (Fisher Scientific, Pittsburgh, PA) and incubated at 37 °C, 5% CO_2 in a humidified atmosphere. After an initial washing step with 4 mL HBSS cells were washed 3 times by centrifugation through a step gradient of 40% Histopaque-1077 (Sigma; St. Louis, MO) in HBSS. The cell-pellets were then transferred to a new set of culture tubes and washed again in HBSS. Cell numbers per tube and numbers of viable lymphocytes were determined by trypan blue stain exclusion in a hemocytometer (Fisher Scientific). After aspiration of the supernatant, cell pellets were counted in a gamma counter (Model 1282 Compugamma CS; LKB Wallac, Turku, Finland). Background counts were subtracted, and cell uptake was calculated by scaling cpm/tube to the number of cells/tube. All experiments were performed in triplicate.

Conjugates with thioether (SC) linkage were synthesized using a heterobifunctional cross linker *N*-succinimidyl iodoacetate (SIA). Briefly, CLIO-NH_2 was treated with SIA to introduce iodoacetyl groups, which then reacted with free SH on tat peptides to form SC bonds. The conjugates were purified, radiolabeled, and tested for cellular uptake as described above.

MR Imaging. Phantoms were prepared by immobilizing 10 million cells in 0.8% low-melting agarose (Bio-Rad, Hercules, CA) in small plastic tubes in a final volume of 100 μL per sample. The tubes were embedded in 1% agarose (Bio-Rad) and imaged with a 1.5 T superconducting magnet (Signa 5.0; GE Medical Systems, Milwaukee, WI) using a 3-in. surface coil. A T_2-weighted spin−echo sequence with the timing parameters 3000/60 (TR/TE) was used. Slice thickness was 1 mm, field of view (FOV) 7 × 7 cm, imaging matrix 256 × 256, and number of excitations (NEX) 2.

RESULTS AND DISCUSSION

Noninvasive cell tracking using MRI is being established as a powerful tool in monitoring cell migration in real time in vivo and native environments. Surface modification with HIV-1 tat peptide on a number of MR probes has resulted in substantially enhanced uptake and hence improved MR detection of labeled cells in tissue. In the current study, we set out to optimize CLIO−tat preparations by systematically altering the degree of tat attachment on the surface of CLIO, a potent nanometer T_2/T_2* contrast agent.

To meet this goal, a P2T method was adapted and evaluated in measuring the degree of conjugation on CLIO through disulfide linkage. Instead of directly assaying for the amount of attached peptide, the method determines the average number of pyridine-2-thione (P2T) groups released during conjugation reaction (Figure 1) (*12*). The number of displaced P2T is strictly equal to that of disulfide bonds formed, which in turn reflects the amount of peptide covalently attached on the surface of CLIO.

The usefulness of the P2T method can be summarized as follows. First, P2T is relatively stable, and the absorbance of P2T at 343 nm varied less than 5% within a 24-hour period in aqueous solution, at room temperature

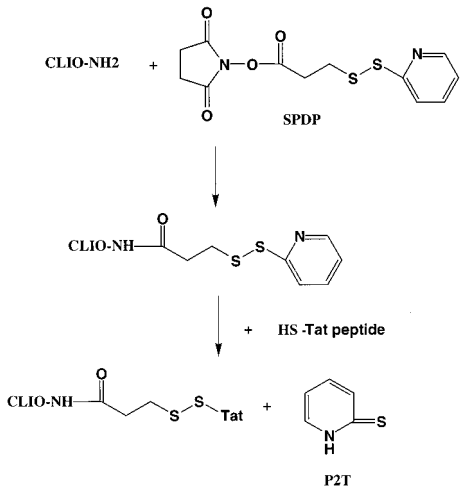


Figure 1. Synthesis of CLIO−tat with disulfide linkage, with P2T as a measurable byproduct.

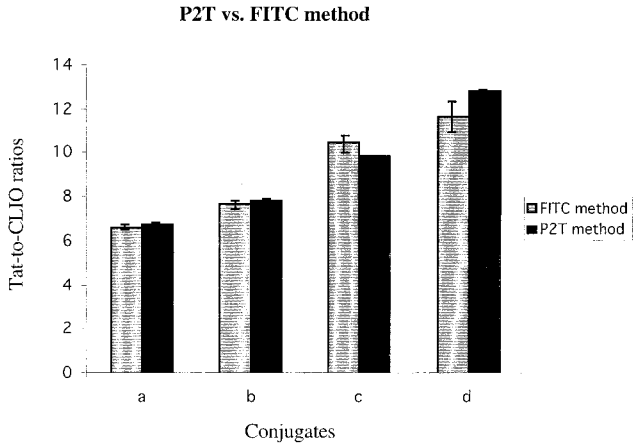


Figure 2. Direct comparison between fluorescent absorption and 2 PY method. Tat-to-CLIO ratios were determined for four conjugates, a, b, c, and d, using the fluorescent absorption method (gray) and P2T method (black), respectively. Error bars indicate the SD ($n = 3$).

(data not shown), whereas the conjugation reaction approaches completion in minutes. Thus uncertainties arisen from P2T degradation are negligible. Second, a distinct absorbance of P2T at 343 nm is well resolved from other chemical components in the reaction. The absorbance of peptides occurs over wavelength below 300 nm, creating little or no interference with P2T measurement. In the same sense, the P2T method could be applied equally well in the conjugation of proteins and nucleic acids, where both are commonly known to have absorbance at below 300 nm. In addition, the method measures the degree of conjugation by determining the number of disulfide bond formation, therefore eliminating the need to tag the peptide or protein solely for quantification purposes.

To evaluate the effectiveness of the P2T method, the degree of conjugation determined using this method was compared with that quantified from FITC absorbance at 494 nm. Figure 2 illustrates the comparison from two preparations. The average numbers of tat peptide per CLIO particle as determined by the two methods have good agreement and are within ±10% variation of each other. Quantification using FITC absorbance directly measures the number of peptide carried on CLIO and thus serves as an authentic standard in the evaluation

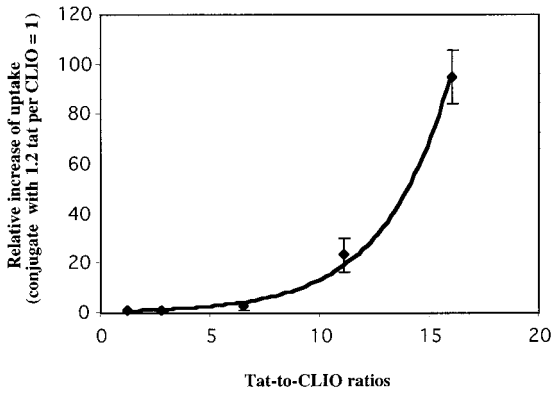


Figure 3. Cellular uptake of radio-labeled CLIO−tat as a function of tat-to-CLIO ratio. The uptake levels of different conjugates are expressed in relative to the conjugate with the lowest tat-to-CLIO ratio. Error bars indicate the SD ($n = 3$).

of the P2T method. By doing so, the latter was shown to have excellent accuracy, reliability, and reproducibility.

With a reliable method to determine the degree of conjugation, a series of CLIO−tat conjugates were designed for cell uptake studies, carrying a progressively increasing number of tat per particle. A calibration curve was constructed between the amount of tat peptide used in the reaction mixture and the resultant tat-to-CLIO ratios. On the basis of the calibration curve, conjugates were synthesized with progressively higher tat/CLIO ratios. The maximum number of peptide which can be attached to CLIO is ultimately limited by the reactive sites on the surface of CLIO particles, where CLIO−NH_2 carries 20−30 amine groups in average per particle. In addition, the degree of conjugation is influenced by the size and hydrophobicity of the peptide. We have observed that the solubility of CLIO can be severely lowered when attached with high number of larger, more hydrophobic peptides.

With a series of CLIO−tat conjugates, the effect of increasing numbers of tat per CLIO particle on cellular uptake could be demonstrated with radiolabeled ^{125}I-CLIO−tat using mouse lymphocytes. As expected, a substantial increase in radioactivity uptake is associated with progressively higher tat-to-CLIO ratios (Figure 3). This effect was clearly not linear, and the observed exponential pattern suggested a role of multivalency. Overall, an increase of 15 tat per CLIO resulted in an elevation of radioactivity uptake of roughly 100 folds. While the current studies used a SS linkage between tat and CLIO, it could be argued that this instability would offset cellular uptake by degradation in serum, our results indicated that this was not the case during the relatively short incubation periods. In addition, comparative studies using similar CLIO−tat preparations containing SC linkage resulted in similar cellular uptake curves. These observations suggested a less important role of the linker type in cellular uptake. In control experiments, where CLIO was attached to similar degrees with a short peptide lacking the transmembrane and nuclear localization sequences, the uptake was near background level. This result indicated that neither the disulfide linker nor FITC contributes to the internalization of CLIO−tat complex.

A dramatically elevated cellular uptake at high tat-to-CLIO ratios is further demonstrated using T_2 weighted MRI (Figure 4). After a 2-h incubation in 20 ng/mL Fe with each of the conjugates, the cells were washed thoroughly and fixed in a phantom, and T_2-weighted MR images were acquired. Changes in signal intensity from

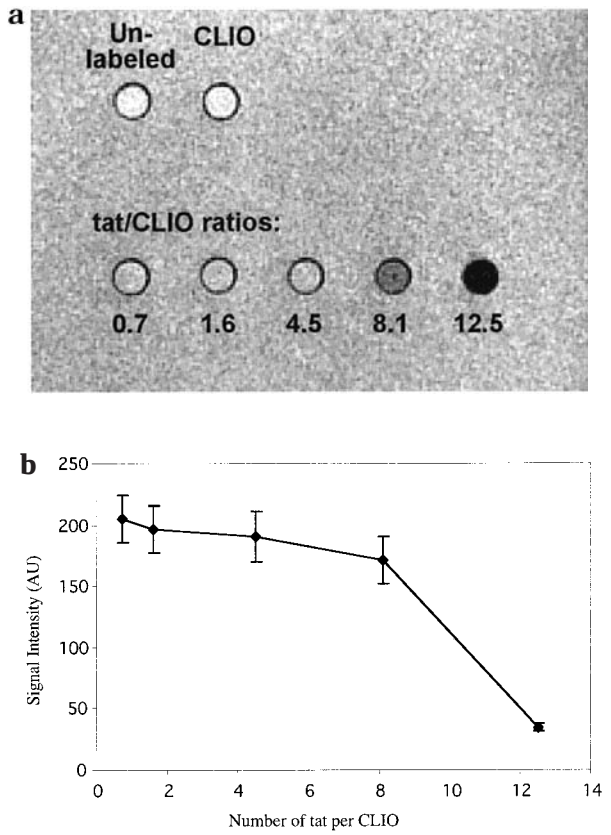


Figure 4. T_2 weighted spin–echo images of cells incubated with a series of CLIO–tat conjugates of progressively increasing tat-to-CLIO ratios. A, 10 million cells were immobilized in 0.8% agar in 100 μL volume. The top row includes images of unlabeled cells (left) and plain CLIO (right). Images in the bottom row were from cells incubated with identical iron concentration of CLIO–tat with increasing tat-to-CLIO ratios. B, relative signal intensities were averaged and plotted as a function of tat-to-CLIO ratios.

cells labeled with plain CLIO were barely detectable compared with unlabeled cells. Magnetic effects from the low tat-to-CLIO conjugates produced little detectable effect. In particular, one to three tat peptides per CLIO generated little difference upon visual inspection of the images. With increasing numbers of tat, the magnetic effect becomes significantly more prominent. At the highest ratio, there were no signs of toxic effects observed with trypan blue exclusion staining.

Finally, the MRI data is consistent with the result from radioactivity uptake experiments in that the loss in signal intensity is clearly associated with progressively increasing tat-to-CLIO ratios. A cluster of basic amino acids in tat peptide is thought to be crucial for membrane translocation (*13*). In addition, the GRKKR nuclear localization signal within its sequence may play a role in the rapid accumulation in the nuclear regions (*13*). Indeed, using a monoclonal antibody against dextran, which is the polysaccharide coating of CLIO, it has been demonstrated that CLIO–tat particles are internalized and localized in and through the nucleus (*3*). These reports confirmed that the observed elevation in radioactivity uptake and the loss of MR signal intensity are caused by the intracellular accumulation of CLIO–tat particles, and that the number of tat peptide on the surface of CLIO dramatically influences uptake of the contrast agent. Once internalized, CLIO–tat is distributed to daughter cells during cell divisions. This can be seen in flow cytometric studies of CLIO–tat labeled cells where cell proliferation is accompanied by a decrease of mean signal intensity and increase in signal heterogeneity (Weissleder, unpublished observations). In addition, the material is clearly biodegradable as demonstrated in nondividing cells and by experiments in vivo (data not shown). We had previously shown that the iron from a CLIO precursor gradually enters global iron metabolism. This is evident from observed decrease in the apparent T_2 effect from injected iron oxide contrast agent over a period of days in vivo and that ^{59}Fe radio tracer became incorporated into hemoglobin of red blood cells (*14*).

In conclusion, we describe a P2T method adapted to determine the degree of conjugation in peptide/protein and CLIO complex with disulfide linkage. The method was shown with simplicity, accuracy, and reproducibility. Using a series of conjugates with progressively increasing numbers of tat peptide per CLIO particle, we demonstrated the multivalent effect of peptide conjugation on cellular uptake, which led to a vastly improved CLIO–tat preparation with 100-fold increase in cell labeling efficiency. This would translate directly into lower detection thresholds of labeled cells in vivo, where imaging of individual, magnetically labeled cells has been a long cherished goal, particularly in tracking immune cells and stem cells.

ACKNOWLEDGMENT

We thank Alexander Petrovski for assistance with MR imaging. This work was funded in part by NIH P50 CA86355. M.Z. was supported by T32 CA 79443. M.F.K. was supported by Deutsche Forschungsgemeinschaft (DFG).

LITERATURE CITED

(1) Lewin, M., Carlesso, N., Tung, C. H., Tang, X. W., Cory, D., Scadden, D. T., and Weissleder, R. (2000) Tat peptide-derivatized magnetic nanoparticles allow in vivo tracking and recovery of progenitor cells. *Nat. Biotech. 18*, 410–414.

(2) Bhorade, R., Weissleder, R., Nakakoshi, T., Moore, A., and Tung, C. H. (2000) Macrocyclic chelators with paramagnetic cations are internalized into mammalian cells via a HIV-tat derived membrane translocation peptide. *Bioconjugate Chem. 11*, 301–305.

(3) Josephson, L., Tung, C. H., Moore, A., and Weissleder, R. (1999) High-efficiency intracellular magnetic labeling with novel superparamagnetic-Tat peptide conjugates. *Bioconjugate Chem. 10*, 186–191.

(4) Weissleder, R., Cheng, H. C., Bogdanova, A., and Bogdanov, A., Jr. (1999) Magnetically labeled cells can be detected by MR imaging. *J. Magn. Reson. Imag. 7*, 258–63.

(5) Vives, E., Brodin, P., and Lebleu, B. (1997) A truncated HIV-1 Tat protein basic domain rapidly translocates through the plasma membrane and accumulates in the cell nucleus. *J. Biol. Chem. 27*, 16010–16017.

(6) Caron, N. J., Torrente, Y., Camirand, G., Bujold, M., Chapdelaine, P., Leriche, K., Bresolin, N., and Tremblay, J. P. (2001) Intracellular delivery of a Tat-eGFP fusion protein into muscle cells. *Mol. Ther. 11*, 301–308.

(7) Eguchi, A., Akuta, T., Okuyama, H., Senda, T., Yokoi, H., Inokuchi, H., Fujita, S., Hayakawa, T., Takeda, K., Hasegawa, M., and Nakanishi, M. (2001) Protein transduction domain of HIV-1 Tat protein promotes efficient delivery of DNA into mammalian cells. *J. Biol. Chem. 276*, 26204–26210.

(8) Kim, D. T., Mitchell, D. J., Brockstedt, D. G., Fong, L., Nolan, G. P., Fathman, C. G., Engleman, E. G., and Rothbard, J. B. (1997) Introduction of soluble proteins into the MHC class I pathway by conjugation to an HIV tat peptide. *J. Immunol. 159*, 1666–1668.

(9) Fawell, S., Seery, J., Daikh, Y., Moore, C., Chen, L. L., Pepinsky, B., and Barsoum, J. (1994) Tat-mediated delivery of heterologous proteins into cells. *Proc. Natl. Acad. Sci. U.S.A. 91*, 664–668.

(10) Wender, P. A., Mitchell, D. J., Pattabiraman, K., Pelkey, E. T., Steinman, L., and Rothbard, J. B. (2000) The design, synthesis, and evaluation of molecules that enable or enhance cellular uptake: peptoid molecular transporters. *Proc. Natl. Acad. Sci. U.S.A. 97*, 13003−13007.
(11) Schoepf, U., Marecos, E. M., Melder, R. J., Jain, R. K., and Weissleder, R. (1998) Intracellular magnetic labeling of lymphocytes for in vivo trafficking studies. *Biotechniques 24*, 642−6, 648−51.
(12) Ngo, T. T. (1986) A simple spectrophotometric determination of solid supported amino groups. *J. Biochem. Biophys. Methods 12*, 349−354.
(13) Efthymiadis, A., Briggs, L. J., Jans, D. A. (1998) The HIV-1 Tat nuclear localization sequence confers novel nuclear import properties. *J. Biol. Chem. 273*, 1623−1628.
(14) Weissleder, R., Stark, D. D., Engelstad, B. L., Bacon, B. R., Compton, C. C., White, D. L., Jacobs, P., and Lewis, J. (1989) Superparamagnetic iron oxide: pharmacokinetics and toxicity. *AJR Am. J. Roentgenol. 152*, 167−73.

BC0255236

Polyethylenimine-*graft*-Poly(ethylene glycol) Copolymers: Influence of Copolymer Block Structure on DNA Complexation and Biological Activities as Gene Delivery System

Holger Petersen,[†] Petra M. Fechner,[†] Alison L. Martin,[‡] Klaus Kunath,[†] Snjezana Stolnik,[‡] Clive J. Roberts,[‡] Dagmar Fischer,[†] Martyn C. Davies,[‡] and Thomas Kissel*[,†]

Department of Pharmaceutics and Biopharmacy, Philipps University, Ketzerbach 63, D-35032 Marburg, Germany, and School of Pharmaceutical Sciences, University of Nottingham, University Park, Nottingham, NG7 2RD, United Kingdom . Received March 18, 2002; Revised Manuscript Received April 25, 2002

For two series of polyethylenimine-*graft*-poly(ethylene glycol) (PEI-*g*-PEG) block copolymers, the influence of copolymer structure on DNA complexation was investigated and physicochemical properties of these complexes were compared with the results of blood compatibility, cytotoxicity, and transfection activity assays. In the first series, PEI (25 kDa) was grafted to different degrees of substitution with PEG (5 kDa) and in the second series the molecular weight (MW) of PEG was varied (550 Da to 20 kDa). Using atomic force microscopy, we found that the copolymer block structure strongly influenced the DNA complex size and morphology: PEG 5 kDa significantly reduced the diameter of the spherical complexes from 142 ± 59 to 61 ± 28 nm. With increasing degree of PEG grafting, complexation of DNA was impeded and complexes lost their spherical shape. Copolymers with PEG 20 kDa yielded small, compact complexes with DNA (51 ± 23 nm) whereas copolymers with PEG 550 Da resulted in large and diffuse structures (130 ± 60 nm). The ζ-potential of complexes was reduced with increasing degree of PEG grafting if MW ≥ 5 kDa. PEG 550 Da did not shield positive charges of PEI sufficiently leading to hemolysis and erythrocyte aggregation. Cytotoxicity (lactate dehydrogenase assay) was independent of MW of PEG but affected by the degree of PEG substitution: all copolymers with more than six PEG blocks formed DNA complexes of low toxicity. Finally, transfection efficiency of the complexes was studied. The combination of large particles, low toxicity, and high positive surface charge as in the case of copolymers with many PEG 550 Da blocks proved to be most efficient for in vitro gene transfer. To conclude, the degree of PEGylation and the MW of PEG were found to strongly influence DNA condensation of PEI and therefore also affect the biological activity of the PEI-*g*-PEG/DNA complexes. These results provide a basis for the rational design of block copolymer gene delivery systems.

INTRODUCTION

Surface modification of drug delivery systems with PEG[1] has met with increasing interest to enhance biocompatibility (*1*), increase systemic circulation times (*2*), and alter their biodistribution (*3*). For instance, nanoparticles (*4*), liposomes (*5*), and also adenoviruses (*6*) have been "PEGylated" mainly to obtain long-circulating particulate delivery systems, based on the so-called "stealth" effect. Recently, PEGylation methodology has been reviewed (*7*). PEGylation of polycations for gene delivery has also been realized leading to block or graft copolymers as summarized in refs *8* and *9*. Among other polycations, PLL has been modified by PEGylation (*10*−*12*) most extensively with the result of reduced complement activation and an increase of DNA complex stability. However, PLL requires endosome disruptive reagents such as chloroquine (*13*) to attain sufficient transgene expression. As compared to PLL, PEI has successfully been used for gene delivery both under in vitro (*14*, *15*) and in vivo (*16*, *17*) conditions. PEI offers a high positive charge density and exhibits a strong proton buffer capacity over a broad pH range (*18*). The latter characteristic is advantageous for PEI since the proton-sponge effect (*19*) allows sufficient gene transfer without endosome disruptive reagents.

PEGylated PEIs have been studied by several authors as potential gene delivery systems. For instance, PEI 25 kDa was grafted with three and 10 PEG 3400 Da blocks carrying a terminal galactose ligand for hepatocyte targeting (*20*). Kabanov and co-workers modified PEI 25 kDa with 37 and 61 PEG 5 kDa blocks and PEI 2 kDa with two blocks of PEG 8 kDa and one block of PEG 10 kDa (*21*, *22*) to study the influence of PEG on oligonucleotide and plasmid DNA complexation. Instead, Choi et al. grafted PEI 25 kDa with 40 and 133 short blocks of PEG 550 Da (*23*) and applied this copolymer for in vitro gene transfer. While all of these groups grafted the PEG onto PEI first and formed the DNA complexes in a subsequent step, Wagner and co-workers first condensed

* To whom correspondence should be addressed. Tel: +49-6421-282-5881. Fax: +49-6421-282-7016. E-mail kissel@mailer.uni-marburg.de.

[†] Philipps University.

[‡] University of Nottingham.

[1] Abbreviations: bPEI, (branched) polyethylenimine; lPEG, (linear) poly(ethylene glycol); mPEG, PEG-monomethyl ether; PLL, poly(L-lysine); MW, molecular weight; HMDI, hexamethylene diisocyanate; AFM, atomic force microscopy; N/P ratio, polycation-nitrogen/polyanion-phosphorous ratio; DLS, dynamic light scattering; PDI, polydispersity index; EtBr, ethidium bromide; LDH, lactate dehydrogenase.

10.1021/bc025529v CCC: $22.00 © 2002 American Chemical Society
Published on Web 06/22/2002

DNA with PEI 800 kDa and subsequently grafted the complex with more than 1600 blocks of PEG 5 kDa (*24*, *25*).

Nevertheless, PEGylation of PEI has not been studied varying both the degree of substitution and the MW of PEG under similar experimental conditions to our knowledge. A retrospective comparison of literature data obtained with PEI of different MW and different experimental conditions is notoriously difficult. Therefore, our investigations were aimed at providing a PEI-*g*-PEG block copolymer sample set in which PEI is kept constant but the extent of PEGylation and the MW of the PEG is varied. Here, we use two series of PEI-*g*-PEG block copolymers in an effort to elucidate the influence of copolymer block structure on DNA condensation (copolymer structure/complex property relationship) and in a second step to compare the physicochemical properties of the complexes with their biological activity revealed in cell culture experiments (complex property/biological activity relationship).

MATERIALS AND METHODS

Materials. bPEI with a MW of 25 kDa (Polymin water free, 99%) was a gift of BASF, Ludwigshafen, Germany. mPEG 550 Da and mPEG 5 kDa were obtained from Aldrich, Milwaukee, WI. Monoamino-mPEG (mPEG-NH_2) 20 kDa was purchased from Rapp Polymere, Tübingen, Germany. All polymers were thoroughly dried in vacuo before use. HMDI (≥99%) was from Fluka, Deisenhofen, Germany. Chloroform (Riedel-de Haën, Seelze, Germany, ≥99%) was treated with HMDI for 4 h at 60 °C and distilled to remove any traces of water and ethanol. Diethyl ether (≥99.5%) from Merck, Darmstadt, Germany, was distilled before use. Light petrol (≥99%, 40−60 °C) was from Riedel-de Haën.

Three different types of DNA were used in this work. DNA from herring testes (Type XIV, 0.3−6.6 MDa, 400−10 000 bp) and plasmid DNA pBR322 (2.9 MDa, 4363 bp) were from Sigma, Steinheim, Germany. Plasmid pGL3 control, luciferase reporter vector (3.5 MDa, 5256 bp) was from Promega, Heidelberg, Germany, and was amplified with a competent *Escherichia coli* strain JM 109 (Promega) according to a protocol from QIAGEN, Hilden, Germany (*26*).

Block Copolymer Synthesis. Synthesis and characterization of the block copolymers has been described in detail elsewhere (*27*, *28*). Briefly, PEG dissolved in anhydrous chloroform ($c = 200$ g/L) was activated for the reaction with the amino groups of PEI with a 10−100-fold excess of HMDI at 60 °C for 8−72 h depending on the MW of PEG (higher MW required longer reaction times). Unreacted HMDI was carefully removed by repetitive extraction with light petrol. Activated PEGs were reacted with PEI at concentrations of 10 g/L in anhydrous chloroform at 60 °C for 8−72 h. The reaction solutions were concentrated to 100 g/L by evaporation of the solvent and dropped into a 20-fold larger volume of diethyl ether to obtain the copolymer by precipitation. Finally, the products were dried in vacuo. Polymers were characterized by ^{1}H and ^{13}C nuclear magnetic resonance (NMR) spectroscopy, which verified the structure of the copolymers and allowed calculation of the composition of ethylenimine and ethylene glycol units in the copolymer. Size exclusion chromatography demonstrated the absence of unreacted PEG and PEI homopolymers. Thus, no further purification steps were necessary.

Formation of the Copolymer−DNA Complexes. All complexes of DNA and polymer were prepared freshly before use. Polymer solutions were added to the DNA solutions in equal volumes, mixed by vortexing, and incubated for 10 min before use unless otherwise stated. DNA stock solutions were diluted to a concentration of 20 μg/mL with 10 mM NaCl at pH 7.4 (AFM experiments) or to 40 μg/mL (all other experiments) with 150 mM NaCl at pH 7.4. The polymer stock solutions were diluted with the same medium as above to the appropriate concentration depending on the required N/P ratio and filtered through 0.22 μm. DNA stock solutions were 2 mg/mL pGL3 plasmid in 10 mM TRIS HCl (pH 8) and 1 mM EDTA, 100 μg/mL pBR322 plasmid in pure reagent water, and 1.11 mg/mL herring testes DNA in 10 mM TRIS HCl (pH 7.4). Homopolymer and copolymer stock solutions were 0.5 mg PEI/mL (AFM experiments) and 0.9 mg PEI/mL (all other experiments) so that all polymer solutions contained the same PEI concentration.

Physicochemical Characterization of Copolymer−DNA Complexes. *AFM.* AFM images were conducted on a Dimension3000 Scanning Probe Microscope from Digital Instruments (Santa Barbara, CA) with a Nanoscope IIIa controller. The solution of polymer−DNA complex was prepared as described above and incubated for 5 min before it was deposited onto freshly cleaved mica and imaged under 10 mM NaCl solution. Immobilization was achieved using electrostatic forces between the opposite charges of the mica and polymer−DNA complexes. All imaging was carried out in the tapping mode at a scan speed of approximately 2 Hz with 512 × 512 pixel data acquisition. V-shaped cantilevers with a pyramidal tip of silicon nitride were used (Park Scientific, CA). The experiments were repeated twice, and the observed structures were found to be reproducible. To determine the mean complex size from these images, the diameter at about half-height of 30 complexes was measured.

DLS. Complex size measurements were carried out with a Zetasizer 3000 HS from Malvern Instruments, Worcs., U.K. at 25 °C (10 mW HeNe laser, 633 nm). Scattering light was detected at 90° angle through a 400 μm pinhole. Measurements yielding hydrodynamic diameters (Z average mean) and PDI were performed with count rates of about 100−400 kCps in the form of 10 runs of 60 min duration each and analyzed in the CONTIN mode. For data analysis, the viscosity (0.8905 mPas) and refractive index (1.333) of pure water at 25 °C were used. The instrument was calibrated with Nanosphere Size Standards (polymer microspheres in water, 220 ± 6 nm) from Duke Scientific, Palo Alto, CA.

Laser Doppler Anemometry (LDA). The ζ-potential measurements of the complexes were carried out in the standard capillary electrophoresis cell of the Zetasizer 3000 HS from Malvern Instruments at position 17.0 and at 25 °C. Measurement duration was set to automatic. Average values of the ζ-potential were calculated with the data from eight runs. The instrument was calibrated with DTS5050 Electrophoresis Standards from Malvern Instruments.

Agarose Gel Retardation Assay. Amounts of 40 μL aliquots of the complex solution were mixed with 4 μL of loading buffer [glycerol (85%) and TAE (40 mM Tris/HCl, 1% acetic acid, 1 mM EDTA, pH 7.4) in equal parts] and loaded onto an EtBr containing 1% agarose gel. Electrophoresis (Blue Marine 200, Serva, Heidelberg, Germany) was carried out at a voltage of 80 V (LKB Bromma 2197 Power Supply, Pharmacia, Freiburg, Germany) for 2 h in TAE running buffer solution. UV light (254 nm) detection was conducted with a Video Copy Processor P67E from Mitsubishi, Japan.

Biological Characterization of PEI-PEG-Copolymer-DNA Complexes. *Hemolysis Assay*. For hemolysis, fresh blood (700 g) from 6 month old rats (Fischer 344 rats, Institute for Pharmacology and Toxicology, University of Marburg) collected in heparinized tubes was centrifuged at 4 °C for 10 min and washed several times with phosphate-buffered saline (PBS) until the supernatant was colorless. A 500 μL amoount of a 2.5% (v/v) suspension of erythrocytes was mixed with 500 μL of complex solution in Eppendorf cups. After it was incubated for 2 and 60 min at 37 °C in a shaking water bath, the blood cells were removed by centrifugation and the supernatant was investigated spectroscopically at 540 nm for the release of hemoglobin. Experiments were performed in triplicate. As controls, PBS (negative = 0%) and 0.2% Triton X-100 solution (positive = 100%) were used.

Aggregation of Erythrocytes. To study polymer/DNA complex-induced aggregation of erythrocytes, rat blood (see hemolysis test) was applied. Ringer's solution (with the addition of sodium citrate, pH 7.4) was used to prevent coagulation. The blood was washed several times with Ringer's solution until the supernatant was colorless as described above. Finally, the erythrocytes were diluted with Ringer's solution 1:50. A 200 μL amount of this cell suspension was treated with 100 μL of polymer solution in 24 well plates (Nunc). After it was incubated for 2 h at 37 °C, pictures were taken of the cells with a Contax RTS 2 camera from AGFA (ASA 100) fitted to a reverse phase contrast microscopy (Nikon TMS) at 40 times magnification. Experiments were performed in triplicate.

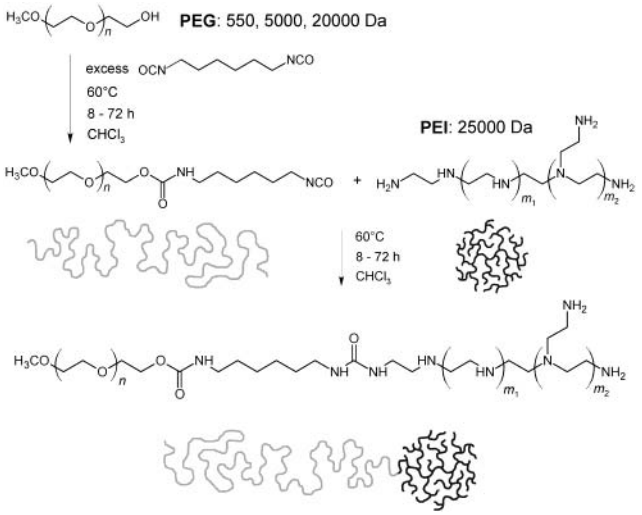
LDH Assay. In vitro cytotoxicity of the complexes with herring testes DNA was evaluated using an LDH assay with 3T3 mouse fibroblasts (500 000 cells/well, 4 h incubation). As reference, PBS (negative, 0%) and 0.1% (w/w) Triton X-100 solution (ICN, Eschwege, Germany) in PBS (positive, 100%) were applied. The LDH content was measured photometrically (340 nm) using a commercial test kit (DQ 1340-K, Sigma) as described in more detail earlier (*28*). Experiments were performed in triplicate.

Transfection Experiments. Transfection activity of the copolymer complexes was studied on 3T3 mouse fibroblasts (NIH 3T3, Swiss mouse embryo, ATCC, Rockville, Maryland) using a Luciferase assay kit from Promega. Measurements of relative light units (RLU) were conducted on a Sirius Luminometer from Berthold, Pforzheim, Germany. Protein quantification was performed with freshly prepared bicinchonic acid (BCA) reagent (Pierce, Rockford, IL) and was carried out with an enzyme-linked immunosorbent assay (ELISA) plate reader from Dynatech MR 5000, Denkendorf, Germany, at 570 nm. Experiments were performed in triplicate as described in more detail in ref *30*.

RESULTS AND DISCUSSION

Two series of block copolymers were prepared by grafting lPEG onto bPEI using a straightforward synthesis route (Scheme 1). Diisocyanate HMDI was used as a linker generating hydrolytically stable urethane bonds between PEG and linker and urea bonds between PEI and linker. In the first series (Scheme 2, horizontal), the PEI (25 kDa) was grafted with different degrees of substitution using PEG blocks all of MW 5 kDa in order to study the quantitative effect of PEG blocks. As a result, the polycationic domain of the copolymers was increasingly surrounded by PEG blocks in this series. The second series (Scheme 2, vertical) was arranged with copolymers all containing an equal weight percent of PEG and PEI (about 50:50%) but with PEGs of different molecular weights (MW 550−20 000 Da). Thus, we varied the copolymer structure in such a way that on one extreme PEG is homogeneously distributed in short blocks within the PEI domain, whereas in the other extreme a clear separation of the PEG and the PEI domain is realized. In other words, the copolymer structure is varied from multiarm grafting to a diblock structure.

Scheme 1. Synthesis of bPEI(25*k*)-*g*-lPEG Copolymers[a]



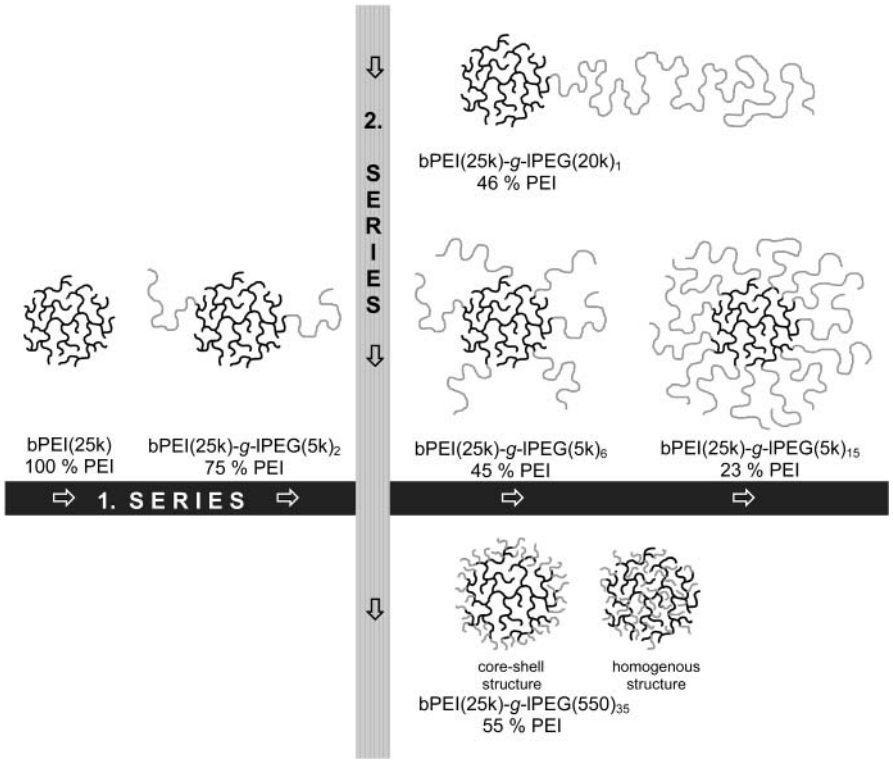
[a] The PEG has a linear structure, and the PEI has a hyperbranched structure.

For these graft (*g*) copolymers, we chose following nomenclature: bPEI(25*k*)-*g*-lPEG(*x*)$_n$ where b and l denote a branched or linear structure. The numbers in brackets (25*k* or *x*, where *x* = 550, 5*k*, or 20*k*) represent the MW of the PEI or the PEG block and the index *n* is the average number of PEG blocks per one PEI macromolecule. The index *n* was calculated from integration of the ^{1}H NMR signals with the MW values of the homopolymers given by the suppliers.

Size and Morphology of the Complexes. To study the influence of copolymer structure on size and shape of the complexes formed with plasmid DNA, we performed AFM experiments in aqueous solution. While transmission electron microscopy (TEM) has been frequently used to characterize DNA/polycation complexes (*20*−*22*), the advantage of AFM stems from the direct observation of these complexes in aqueous solution. Samples for TEM are visualized in vacuo and need to be pretreated and stained, e.g., with zinc uranyl acetate. Therefore, dimensions and structure of DNA/polycation complexes determined in aqueous media using AFM and by TEM could be different. In this study, physiological salt concentrations (150 mM NaCl) as used for the biological experiments were not feasible technically due to formation of salt crystals during the AFM imaging process. Therefore, a low salt concentration of 10 mM NaCl and pH 7.4 was selected. Because immobilization was based on electrostatic forces between the negative charge of mica substrate and the complex, the latter had to exhibit a distinct positive net charge. Therefore, we chose the N/P ratio 9 for this study (compare with ζ-potential measurements below).

The homopolymer PEI showed images of spherical and compact complexes of 142 ± 59 nm diameter (Figure 1A and Figure 2). The first copolymer series (images A−D)

Scheme 2. Schematic of the bPEI(25*k*)-*g*-lPEG Copolymer Sample Set[a]



[a] The black part of the structure represents the cationic branched PEI, and the gray part represents the nonionic linear PEG blocks. It should be remarked that the structures are reduced to two dimensions. Thus, the density of the PEG shield in (3D) reality is smaller than it appears in this scheme. The copolymer bPEI(25*k*)-*g*-lPEG(550)$_{35}$ has two possible structures; however, PEG is more likely homogenously distributed within the PEI than concentrated at the outer sphere of the PEI (core−shell structure).

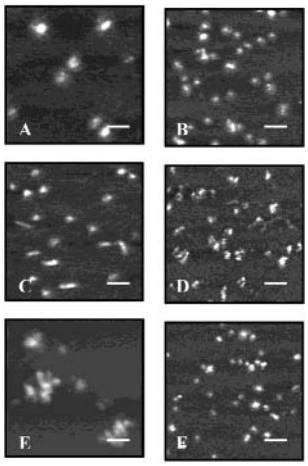


Figure 1. AFM images of polymer/plasmid DNA complexes at N/P ratio 9. Image A shows PEI 25 kDa homopolymer DNA condensates. Images B−D show DNA−polymer condensates produced with plasmid DNA and bPEI(25*k*)-*g*-lPEG(5*k*)$_n$ where n = 2, 6, and 15, respectively. Images E and F show DNA condensates produced with bPEI(25*k*)-*g*-lPEG(550)$_{35}$ and PEI-(25*k*)-*g*-PEG(20*k*)$_1$, respectively. Scale bars are equivalent to 250 nm. The color-encoded height scale extends 15 nm.

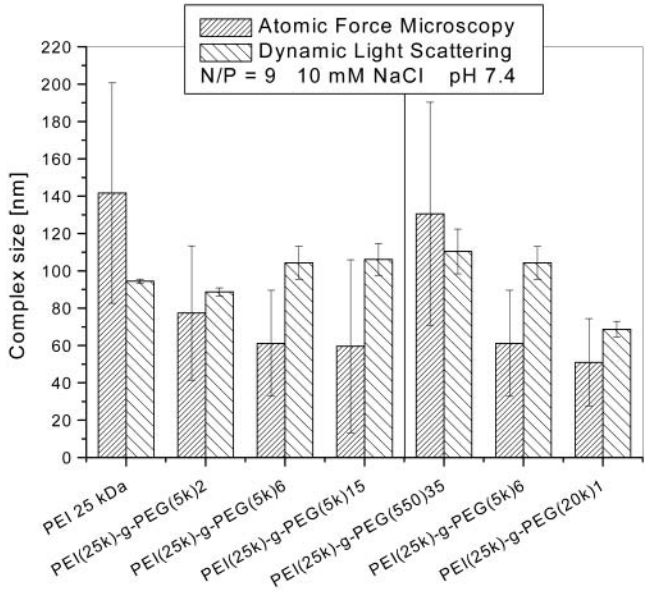


Figure 2. DNA−polymer complex size as determined by AFM (n = 30) and DLS (n = 10) at N/P ratio 9 in 10 mM NaCl. The error bars indicate the standard deviation (SD). In the case of the AFM results, the SD reflects the size distribution.

demonstrated that PEG 5 kDa significantly reduced the diameter of the complexes from 142 nm to about 60 nm, but with an increasing number of PEG blocks, DNA condensation was affected and complexes lost their spherical shape. Whereas the copolymer containing 2 PEG blocks gave spherical complexes with diameters of 77 ± 36 nm, bPEI(25*k*)-*g*-lPEG(5*k*)$_6$ showed a mixture of spherical and rodlike particles (diameter 61 ± 28 nm). When PEI was grafted with 15 PEG blocks, complexes of ill-defined shape were found (diameter 60 ± 46 nm). Furthermore, some of the complexes exhibited stringy structures, which can be attributed to poorly condensed DNA.

Complex size was also determined by DLS in the same medium as used for AFM (10 mM NaCl, pH 7.4). Hydrodynamic diameters are shown in Figure 2 in comparison with the results of the AFM experiments. Differences in complex size were much smaller as compared to the AFM results, and no specific trend could be

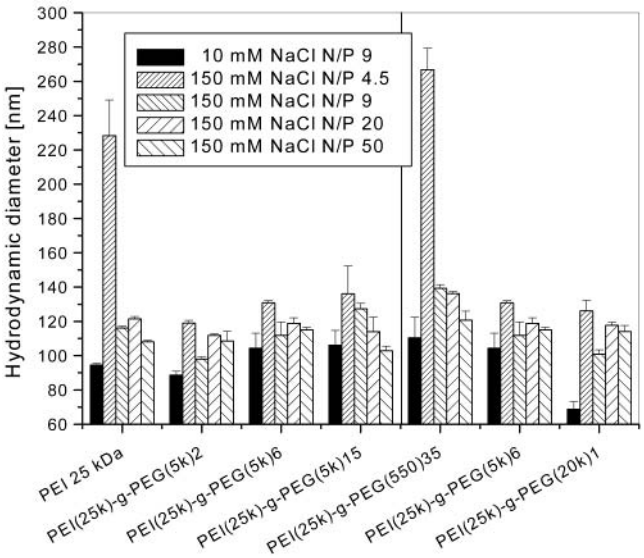


Figure 3. Hydrodynamic diameters of complexes assembled by plasmid DNA with bPEI 25 kDa and bPEI-*g*-lPEG copolymers at different ionic strength and different N/P ratios as determined by DLS.

observed for the first series. The trend found by AFM that PEG 5 kDa reduces the size of the complex was observed by DLS only for bPEI(25*k*)-*g*-lPEG(5*k*)$_2$. Their complexes (88.7 ± 2.2 nm) were on average slightly smaller than complexes formed by the homopolymer PEI (94.5 ± 1.1 nm). However, copolymers with 6 and 15 PEG blocks formed complexes with slightly larger average diameters of about 105 nm probably due to the rodlike shape of some of the complexes as observed in AFM.

In the second series, another trend is observed in AFM (Figure 1C,E,F): Complexes gradually lose their compact and spherical shape with decreasing MW of PEG. Copolymers with one long PEG 20 kDa formed small (51 ± 23 nm) and clearly spherical complexes, whereas copolymers with many short PEG 550 Da gave rather large complexes (131 ± 60 nm), which were fluffy or diffuse and almost shapeless. For this series, DLS measurements revealed the same trend: For bPEI(25*k*)-*g*-lPEG(20*k*)$_1$, a small complex diameter of 68.7 ± 4.3 nm was found, whereas in the case of bPEI(25*k*)-*g*-lPEG(550)$_{35}$ larger diameters (110.4 ± 12.0 nm) were determined.

The results of both the AFM experiments and the DLS measurements demonstrated that DNA complexation with PEI-*g*-PEG is strongly dependent on the block copolymer structure. In the case of PLL-*g*-PEG copolymers, a negative influence of PEG and other hydrophilic polymers on the condensation of DNA was observed (*11*, *31*). Similar disadvantageous effects were anticipated for PEI; therefore PEGylation of the PEI/DNA complex was carried out as a second step after condensation (*25*). This procedure may, however, be impractical in a clinical setting. Here, we demonstrated that PEG does not necessarily interfere with the condensation process of DNA. Attaching only one or two PEG blocks to PEI can even enhance DNA condensation forming compact and spherical complexes with smaller sizes as compared to homopolymer PEI complexes.

Using DLS, complexes were also studied at high ionic strength (150 mM NaCl, pH 7.4) and at different N/P ratios (Figure 3). Under these (more physiological) conditions, all polymers formed larger complexes as compared to low salt concentration. However, with an increasing N/P ratio, the complex size was reduced again. Two exceptional polymers were found. At a low N/P ratio (4.5),

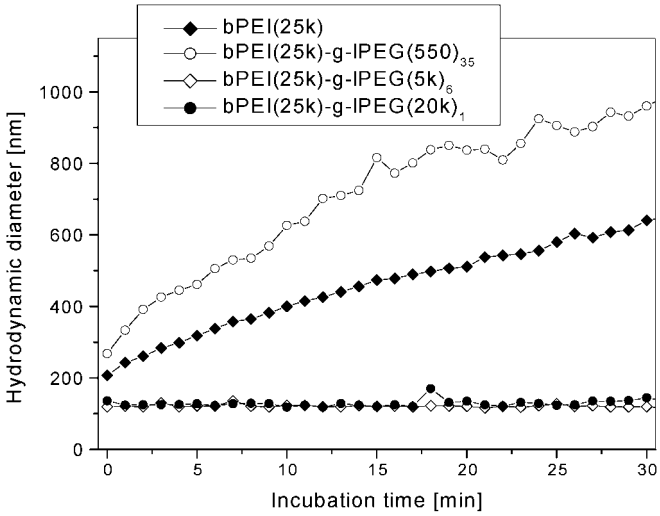


Figure 4. Stabilization study of the complexes assembled by plasmid DNA with bPEI 25 kDa and bPEI-*g*-lPEG at N/P 4.5 and 150 mM NaCl. Complex size (diameter) is as a function of incubation time as determined by DLS.

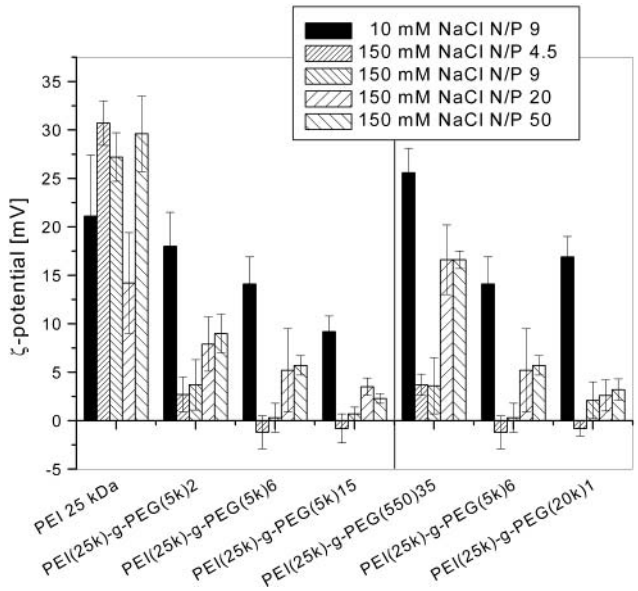


Figure 5. ζ-Potential of plasmid DNA complexes with PEI 25 kDa and bPEI-*g*-lPEG block copolymers at different ionic strength and at different N/P ratios as determined by laser Doppler anemometry.

PEI and bPEI(25*k*)-*g*-lPEG(550)$_{35}$ did not give stable complexes. Over a period of 30 min, complex size increased from 200 to 600 nm and from 270 to 900 nm, respectively (Figure 4). In contrast, all copolymers with PEG of 5 and 20 kDa formed stable complexes at N/P 4.5 (copolymers bPEI(25*k*)-*g*-lPEG(5*k*)$_n$ where *n* is 2 or 15 are not shown in Figure 4). A stabilizing effect of PEG against aggregation of PEI/DNA complexes has been noted previously (*21*, *25*). Short PEG blocks seem to provide little stabilization, and a MW of PEG ≥ 5 KDa is necessary to obtain this effect. At higher N/P ratios (≥9), all homo- and copolymers formed stable complexes, which are probably stabilized electrostatically under these conditions by a larger excess of polycations present.

Surface Charge of the Complexes. To estimate the surface charge of the complexes, we measured the ζ-potential of the complexes by LDA. The results are shown in Figure 5. In the first series of bPEI(25*k*)-*g*-lPEG(5*k*)$_n$ copolymers, the ζ-potential is reduced with an

increasing number *n* of PEG blocks. This is true for different salt concentrations and different N/P ratios. Thus, PEG 5 kDa blocks seem to orientate toward the surface of the complex and shield its core with the cationic net charge. In the case of the copolymers, the ζ-potential increases with increasing N/P ratios. The ζ-potential did not increase further from N/P 20 to 50 since free copolymer was present at N/P 50. In the case of homopolymer PEI, even at low N/P ratio 4.5, ζ-potential is highly positive and is found in the range of +25 to +35 mV. Similar values have been reported by others (*24*, *25*, *32*). A ζ-potential of +35 mV seems to be the maximum surface charge of the PEI−DNA complexes. PEI was reported to possess a ζ-potential of +37 mV (*33*).

In the second series with the copolymers containing about 50% PEG, the ζ-potential is reduced with increasing MW of PEG. Therefore, PEG 5 kDa and especially PEG 20 kDa are able to shield the charged core of the complex. The high ζ-potential of complexes formed with bPEI(25*k*)-*g*-lPEG(550)$_{35}$ points to the poor shielding properties. As we have previously shown using differential scanning calorimetry (*28*), bPEI(25*k*)-*g*-lPEG-(550)$_{35}$ probably did not form a simple core−shell structure in which the PEG blocks surrounded the positively charged PEI core. During the synthesis, the short PEG blocks might penetrate into the branched PEI structure and react also with the inner amino groups. This would yield a copolymer where PEG is more homogeneously distributed over the PEI macromolecule as schematically shown in Scheme 2. This structure could explain the high ζ-potential of the complex.

DNA Complexation and Condensation. Finally, to study DNA complexation and condensation as a function of N/P ratio, agarose gel retardation assays were performed. The gels are shown in Figure 6. No difference was found for the copolymers from the first series with PEG 5kDa: Complete retardation of DNA (indicating complete DNA complexation) was achieved at N/P = 2.0−2.2 whereas for complete exclusion of EtBr (indicating complete DNA condensation) a further excess of the polycation was needed (N/P = 4.5, data not shown). In the case of homopolymer PEI, DNA was complexed completely at N/P = 1.6 and condensed at 3.0. Thus, grafting PEI with PEG 5 kDa slightly hindered the interaction with DNA. When PEI was grafted with short PEG blocks as in the case of copolymer bPEI(25*k*)-*g*-lPEG(550)$_{35}$, the complexation was hindered slightly (N/P = 2.0) but condensation was realized at the same N/P ratio (N/P = 3.0). Here again, we found that short PEG blocks behaved differently than longer PEG chains: PEG 550 Da did not stabilize the complex against aggregation, it did not reduce the positive surface charge, and here, it did not affect DNA condensation. However, the most interesting result from the agarose gel retardation assay is the enhanced DNA condensation observed for copolymer bPEI(25*k*)-*g*-lPEG(20*k*)$_1$ already at N/P = 2.6. This is in line with the results from AFM images where small and compact particles were found. The excellent DNA condensation might be attributed to the special copolymer structure. With only one PEG block on average, this is a diblocklike copolymer and there might be a PEI domain and a PEG domain clearly separated from each other. Thus, the DNA seems to interact with the PEI domain without interference from PEG. Furthermore, some authors reported the DNA condensation ability of PEG (*34*, *35*). Therefore, PEG might additionally participate in the condensation process in a synergistic manner.

Hemocompatibility of the Complexes. The blood compatibility of PEI-*g*-PEG/DNA complexes was screened

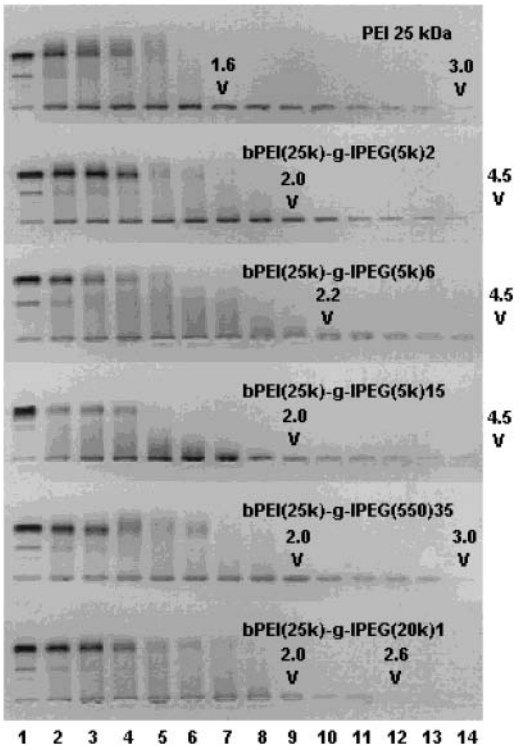


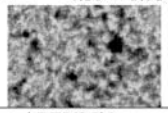
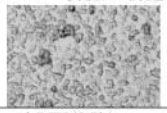
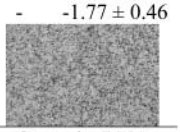
Figure 6. Agarose gel electrophoresis of the complexes of plasmid DNA with bPEI 25 kDa and bPEI-*g*-lPEG block copolymers. Lane 1, N/P = 0 (plasmid only); lanes 2−14, N/P 0.6−3.0 with increments of 0.2. N/P ratios of completed DNA retardation (left mark) and of completed ethidium bromide exclusion (right mark) sign the appropriate lanes. N/P ratio 4.5 was determined with another gel experiment (data not shown).

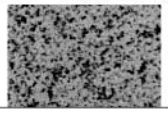
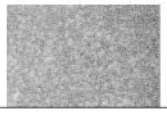
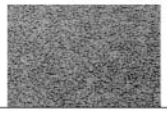
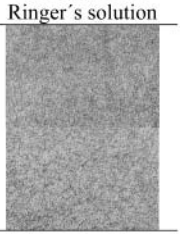
using a hemolysis and an aggregation of erythrocytes under in vitro conditions. These assays are a prerequisite for the intravenous administration of PEI-*g*-PEG/DNA complexes in animals or humans.

The results of the hemolysis assay are presented in Table 1. In a short term experiment (incubation time with erythrocytes, 2 min; data not shown), the acute phase of an intravenous administration is reflected. No hemolysis was observed after short incubation time for any of the PEI-*g*-PEG preparations. Complexes with PEI 25 kDa showed a slight hemolytic activity (1−2%). The long term experiment (60 min incubation) still showed only negligible hemolysis for the complexes of PEI and most copolymers. PEI, bPEI(25*k*)-*g*-lPEG(5*k*)$_2$, and bPEI(25*k*)-*g*-lPEG(550)$_{35}$ caused more hemolysis (up to 5%) after 60 min in comparison with the results after 2 min of incubation. Only bPEI(25*k*)-*g*-lPEG(550)$_{35}$ exhibited a remarkable value of 12% at very high N/P ratios, which is still tolerable since substances are classified as non-hemolytic when hemolysis remains <15% (*36*).

The erythrocyte aggregation assay allowed only semiquantitative estimations about the hemocompatibility of the complexes. Results of this study are given in Table 1. Exemplarily, microscopic images of the erythrocytes are shown in this table for N/P ratio 20. Ringer's solution and free DNA did not show any aggregation (control experiment). In the case of the complexes, aggregation tendency was found as a function of N/P ratio: the larger the excess of polycation in the complex, the stronger the aggregation. Complexes of PEI, bPEI(25*k*)-*g*-lPEG(5*k*)$_2$, and bPEI(25*k*)-*g*-lPEG(550)$_{35}$ showed strong to very strong aggregation of the red blood cells. Because aggregation is often caused by electrostatic interactions between the anionic cell membranes and a cationic object,

Table 1. Erythrocyte Aggregation and Hemolysis Induced by Complexes Formed with Herring Testes DNA and bPEI(25*k*)-*g*-lPEG Copolymers at Different N/P Ratios[a]

N/P ratio	PEI 25 kDa	bPEI(25k)-*g*-lPEG(5k)$_2$	bPEI(25k)-*g*-lPEG(5k)$_6$	bPEI(25k)-*g*-lPEG(5k)$_{15}$
4.5	+ -0.73 ± 0.63	- 0.15 ± 0.48	- -2.44 ± 0.21	- -1.55 ± 0.28
9	++ 1.40 ± 0.26	++ 1.25 ± 0.10	- -1.91 ± 0.34	- -1.45 ± 0.51
20	+++ 4.42 ± 0.22	+++ 1.99 ± 0.51	- -1.50 ± 0.15	- -1.86 ± 0.43
50	++++ 4.59 ± 0.95	++++ 3.09 ± 0.02	+ -1.02 ± 0.07	- -1.77 ± 0.46
20				

N/P ratio	bPEI(25k)-*g*-lPEG(550)$_{35}$	bPEI(25k)-*g*-lPEG(5k)$_6$	bPEI(25k)-*g*-lPEG(20k)$_1$	Controls: DNA Ringer´s solution
4.5	- 0.49 ± 0.62	- -2.44 ± 0.21	- -0.71 ± 0.25	
9	+ 3.24 ± 0.83	- -1.91 ± 0.34	- -0.23 ± 0.25	
20	++ 6.06 ± 0.05	- -1.50 ± 0.15	+ 0.14 ± 0.18	
50	+++ 11.80 ± 0.78	+ -1.02 ± 0.07	++ 1.11 ± 0.07	
20				

[a] Semiquantitative results of the erythrocyte aggregation. Classification: −, no aggregation; +, weak aggregation; ++, medium aggregation; +++, strong aggregation; ++++, very strong aggregation. Images were taken by phase contrast light microscopy and are exemplarily shown for N/P 20. Quantitative results (%) of the hemolysis assay after incubation of 60 min.

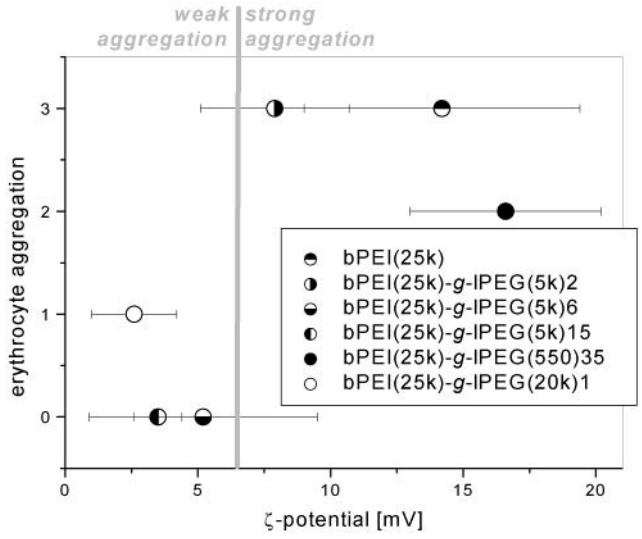


Figure 7. Plot of polymer/DNA complex-induced erythrocyte aggregation (N/P 20) against ζ-potential of the complexes (N/P 20, 150 mM NaCl). Erythrocyte aggregation is given semiquantitatively as follows: 0, no aggregation; 1, weak aggregation; 2, strong aggregation; 3, very strong aggregation.

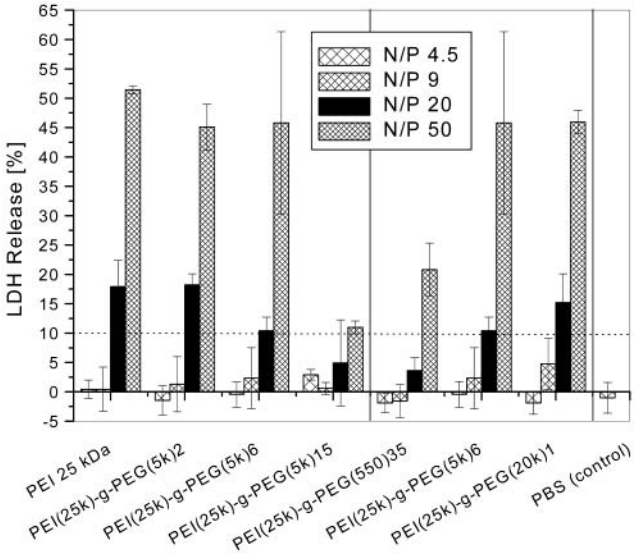


Figure 8. LDH assay of bPEI 25 kDa and bPEI-*g*-lPEG copolymer complexes with herring testes DNA at different N/P ratios after an incubation of 4 h. The experiment was performed with 3T3 mouse fibroblast cell line. A release of less than 10% can be understand as nontoxic.

the surface charge of the complexes was an important key to interpret these results. When the extent of aggregation is plotted against the ζ-potential (Figure 7), a threshold at a ζ-potential of about 6 mV is observed. Below this value, no or only weak aggregation was observed, whereas above this ζ-potential strong aggregation occurred. In all cases where PEGylation reduced ζ-potential of the complexes below 6 mV, no erythrocyte aggregation was observed. This was achieved by grafting six PEG 5 kDa blocks or one 20 kDa block. Because the three polymers showing strong aggregation also induced a relatively strong hemolytic activity, it is likely that high ζ-potentials also affect hemolysis.

Cytotoxicity of the Complexes. The cytotoxicity of the complexes was studied using the LDH assay, which provides information on the destructive interaction of the complexes with cell membranes. It was found that with increasing N/P ratio, the cytotoxicity of the complexes increased (Figure 8). In the first series with the bPEI-(25*k*)-*g*-lPEG(5*k*)$_n$ copolymers, toxicity is reduced with an increasing number *n* of PEG blocks. Another trend is observed for the second copolymer series: Toxicity is reduced with decreasing MW of PEG. Consequently, there are two copolymers that formed complexes with a low toxicity profile: bPEI(25*k*)-*g*-lPEG(550)$_{35}$ and bPEI-(25*k*)-*g*-lPEG(5*k*)$_{15}$. Because their LDH release is <10%, DNA complexes with these copolymers can be regarded as relatively nontoxic (*37*). These two copolymers have two features: First, they both form complexes of ill-defined and more diffuse complex shape. Severe cell membrane damage is often observed when many charges are locally concentrated on the cell membrane (*37*). In contrast, the charges of a diffuse complex are more distributed over a wider area of the cell membrane in comparison with compact complexes. Second, both copolymers are characterized by a high degree of PEG substitution ($n = 15$ and 35, respectively). The toxic sites

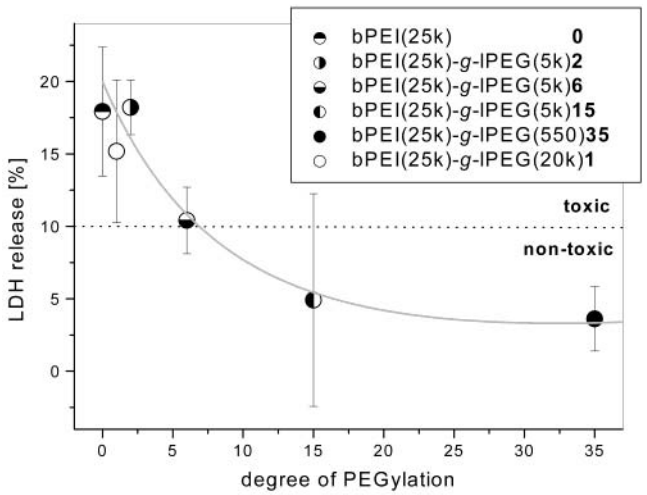


Figure 9. Correlation of degree of PEG grafting (average number of PEG blocks per one PEI molecule) with cytotoxicity of the polymer/DNA complexes as determined by LDH assay (LDH release at N/P = 20).

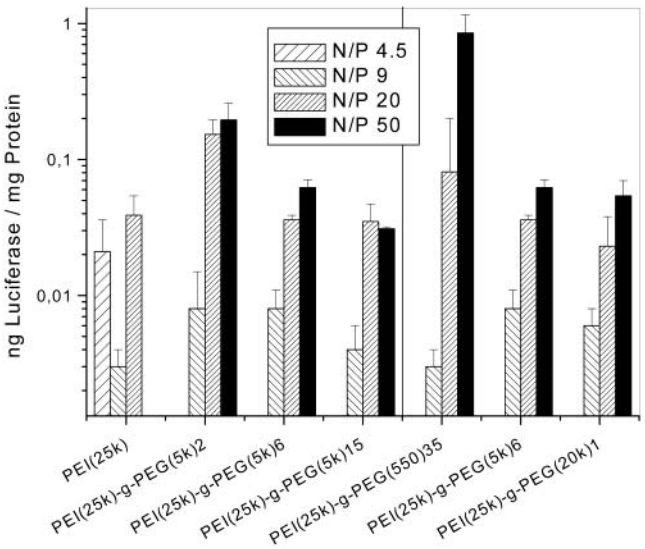


Figure 10. Transfection efficiency of polymer/plasmid DNA complexes with bPEI 25 kDa and bPEI-*g*-lPEG block copolymers at different N/P ratios. The experiment was performed with 3T3 mouse fibroblast cell line.

of the copolymers are the amino groups of PEI. If they are substituted with PEG, the basic amino groups are transformed into neutral urea bonds (according to our synthesis route). Thus, the reduction of the toxicity of PEI is expected to be a function of degree of PEG substitution. Indeed, a plot of percent LDH release against the degree of PEGylation (Figure 9) clearly shows this function, which seems to be independent of the MW of the PEG.

Transfection Efficiency of the Complexes. Finally, the transfection activity of the complexes was studied using the same cell line as in the cytotoxicity assay. The transfection efficiency expressed by amount of luciferase per amount protein was measured at three different N/P ratios for each polymer. As a consequence of the results from preliminary experiments, not every N/P ratio was repeatedly measured for all polymers. Because of the high toxicity of the homopolymer PEI, all cells died at N/P = 50 and a transfection experiment was not feasible. No perceptible transfection could be observed at N/P = 4.5. Therefore, the experiments were run only at higher N/P ratios. The results are presented in Figure 10.

Despite PEGylation, all copolymers showed transfection activity at least as high as homopolymer PEI. Furthermore, at higher N/P ratios, the copolymers turned out to be even more efficient than PEI. This is quite remarkable since most other groups found a significant decrease in transfection activity for the PEG-modified PEIs (*20*, *21*, *23*). All polymers showed higher transfection activities with increasing N/P ratios. In the first series with bPEI(25*k*)-*g*-lPEG(5*k*)$_n$ copolymers, transfection efficiency decreases with increasing number of PEG blocks. Complexes of copolymer with $n = 2$ were even more efficient in gene transfer than complexes of homopolymer PEI. In the case of the second series, copolymer bPEI(25*k*)-*g*-lPEG(20*k*)$_1$ gave similar results as the other 50% PEG copolymer bPEI(25*k*)-*g*-lPEG(5*k*)$_6$. Remarkable results were found for bPEI(25*k*)-*g*-lPEG(550)$_{35}$ even with a high N/P ratio of 50.

The complexity of the gene transfer process prevents the correlation of transfection data with a single physicochemical or biological parameter. For instance, ζ-potential or complex size alone cannot explain why the two polymers with high ζ-potential and large complex size (PEI and bPEI(25*k*)-*g*-lPEG(550)$_{35}$) transfected differently, the first very poorly and the latter very strongly. Also, the cytotoxicity alone did not give a reasonable relationship with transfection activity. Here again, the two polymers with high LDH release (PEI and bPEI(25*k*)-*g*-lPEG(5*k*)$_2$) transfected differently, the first poorly and the latter strongly. Furthermore, the two copolymers of low cytotoxicity (bPEI(25*k*)-*g*-lPEG(5*k*)$_{15}$ and bPEI(25*k*)-*g*-lPEG(550)$_{35}$) also showed quite different transfection activities. Therefore, the results of the transfection experiments could be explained only by a combination of physicochemical and biological parameters. Cytotoxicity and ζ-potential turned out to be the key factors for the explanation of the results of the gene transfer experiments. Whereas a strong cytotoxicity was unwanted, a high ζ-potential is generally assumed to be advantageous for in vitro gene delivery since it enhances the adhesion of the cationic complex with the negatively charged cell membrane (*38*). In Figure 11, the cytotoxicity in means of LDH release is plotted against ζ-potential and the transfection efficiency is represented semiquantitatively by the size of the polymer symbols. The six polymer/DNA complexes could be divided into four groups of different transfection activities. First, in the case of low toxicity and of low ζ-potential, the complexes showed only poor gene expression. These complexes are probably too inert due to the thoroughly shielding PEG blocks and do not interact with the cells. Second, when the ζ-potential was relatively low but the LDH release was high, medium transfection activities were observed for the appropriate complexes. Because of the low ζ-potential, the concentration of cell-adherent complexes might remain low; therefore, the cells survived the treatment of these toxic complexes. Third, the combination of high ζ-potential and high LDH release yielded poor transfection possibly due to a strong interaction of the highly toxic complexes with the cells that did not survive. Fourth and finally, complexes with high ζ-potential but with low cytotoxicity showed high transfection activities and seemed to be most efficient as in vitro gene transfer vectors. Here, highly positive surface charge is not accompanied by toxic side effects. The representative copolymer of this group is bPEI(25*k*)-*g*-lPEG(550)$_{35}$. Also another explanation for the good transfection activity of this copolymer can be put forward. It has been reported for in vitro gene delivery that large complexes more easily reach the cells

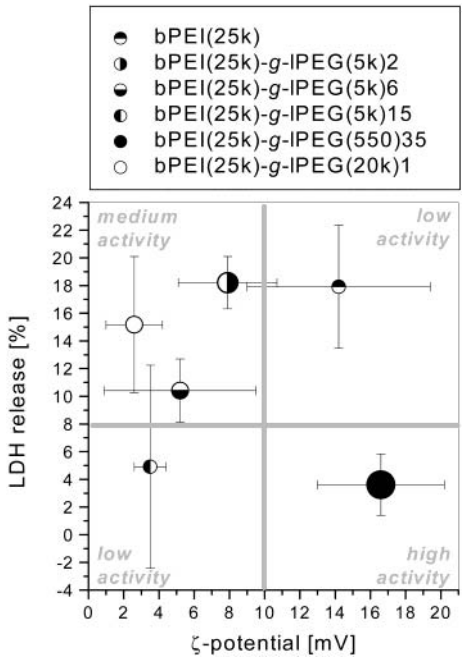


Figure 11. Transfection efficiency in correlation to ζ-potential (N/P 20, 150 mM NaCl) and cytotoxicity as determined by LDH assay (N/P 20) on 3T3 fibroblast. The size of the dot indicates semiquantitatively the transfection efficiency (the larger the symbol, the higher transfection activity).

due to sedimentation (*39*). Thus, the large complexes formed by bPEI(25*k*)-*g*-lPEG(550)$_{35}$ could show higher sedimentation.

CONCLUSIONS

By variation of the degree of substitution and the MW of PEG, we have obtained a set of PEI-*g*-PEG copolymers, which represent a broad range of different block copolymer structures. We have demonstrated that copolymer structure has a strong influence on the shape of the polycation/DNA complex and its surface charge. Copolymers with many short PEG blocks formed large and diffuse complexes of high positive surface charge. Copolymers with only a few but long PEG blocks self-assembled to small and compact condensates of low surface charge. Copolymers with many long PEG blocks generated complexes of ill-defined shape and of almost no surface charge. Furthermore, the physicochemical parameters have a decisive impact on the interaction of the complexes with cells. A high positive ζ-potential of the complexes resulted in a strong erythrocyte aggregation and hemolysis. However, cytotoxicity monitored with fibroblasts was a function of the degree of PEGylation independent of the MW of the PEG. Sufficient in vitro gene expression was realized with the copolymer that formed large complexes with a high positive surface charge and a low toxicity profile, as it was found for the copolymer with many short PEG 550 Da blocks.

ACKNOWLEDGMENT

A.L.M. acknowledges the Royal Pharmaceutical Society of Great Britain for funding. We also thank C. Culmsee (Institute of Pharmacology, University of Marburg) for the rat blood used in this study.

LITERATURE CITED

(1) Kidane, A., Lantz, G. C., Jo, S., and Park, K. (1999) Surface modification with PEO-containing triblock copolymers for improved biocompatibility: In vivo and ex vivo studies. *J. Biomater. Sci., Polym. Ed. 10*, 1089−1105.

(2) Monfardini, C., and Veronese, F. M. (1998) Stabilization of Substances in Circulation. *Bioconjugate Chem. 9*, 418−450.

(3) Dams, E. T. M., Laverman, P., Oyen, W. J. G., Storm, G., Scherphof, G. L., Van der Meer, J. W. M., Corstens, F. H. M., and Boerman, O. C. (2000) Accelerated blood clearance and altered biodistribution of repeated injections of sterically stabilized liposomes. *J. Pharmacol. Exp. Ther. 292*, 1071−1079.

(4) Perrachia, M. T., Fattal, E., Desmaele, D., Besnard, M., Noel, J. P., Gomis, J. M., Appel, M., d'Angelo, J., and Couvreur, P. (1999) Stealth PEGylated polycyanoacrylate nanoparticles for intravenous administration and splenic targeting. *J. Controlled Release 60*, 121−128.

(5) Woodle, M. C. (1998) Controlling liposome blood clearance by surface-grafted polymers. *Adv. Drug Delivery Rev. 32*, 139−152.

(6) O'Riordan, C. R., Lachapelle, A., Delgado, C., Parkes, V., Wadsworth, S. C., Smith, A. E., and Francis, G. E. (1999) PEGylation of adenovirus with retention of infectivity and protection form neutralizing antibody in vitro and in vivo. *Hum. Gene Ther. 10*, 1349−1358.

(7) Bhadra, D., Bhadra, S., Jain, P., and Jain, N. K. (2002) Pegnology: a review of PEG-ylated systems. *Pharmazie 57*, 5−29.

(8) Kabanov, A. V., and Kabanov, V. A. (1998) Interpolyelectrolyte and block ionomer complexes for gene delivery: physicochemical aspects. *Adv. Drug Delivery Rev. 30*, 49−60.

(9) Lemieux, P., Vinogradov, S. V., Gebhart, C. L., Guerin, N., Paradis, G., Nguyen, H.-K., Ochietti, B., Suzdaltseva, Y. G., Bartakova, E. V., Bronich, T. K., St.-Pierre Y., Alakhov, V. Yu., and Kabanov, A. V. (2000) Block and Graft Copolymers and Nanogel Copolymer Networks for DNA Delivery into Cell. *J. Drug Targeting 8*, 91−105.

(10) Choi, Y. H., Lui, F., Kim, J.-S., Choi, Y. K., Park, J. S., and Kim, S. W. (1998) Poly(ethylene glycol)-grafted poly-L-lysine as polymeric gene carrier. *J. Controlled Release 54*, 39−48.

(11) Toncheva, V., Wolfert, M. A., Dash, P. R., Oupicky, D., Ulbrich, K., Seymour, L. W., and Schacht, E. H. (1998) Novel vectors for gene delivery formed by self-assembly of DNA with poly(L-lysine) grafted with hydrophilic polymers. *Biochim. Biophys. Acta 1380*, 354−368.

(12) Katayose, S., and Kataoka, K. (2000) Water-soluble polyion complex associates of DNA and poly(ethylene glycol)-poly(L-lysine) block copolymer. *Gene Ther. 7*, 126−138.

(13) Cotton, M., Längle-Rouault, F., Kirlappos, H., Wagner, E., Mechtler, K., Zenke, H., Berg, H., and Birnstiel, M. L. (1990) Transferrin-polycation-mediated introduction of DNA into human leukemic cells: stimulation by agents that effect the survival of transfected DNA or modulate transferrin receptor levels. *Proc. Natl. Acad. Sci. U.S.A. 87*, 4033−4037.

(14) Pollard, H., Remy, J.-S., Loussouarn, G., Demolombe, S., Behr, J.-P., and Escande, D. (1998) Polyethylenimine but not cationic lipids promotes transgene delivery to the nucleus in mammalian cells. *J. Biol. Chem. 273*, 7507−7511.

(15) Boussif, O., Lezoualćh, F., Zanta, M. A., Mergny, M. D., Scherman, D., Demeneix, B., and Behr, J.-P. (1995) A versatile vector for gene and oligonucleotide transfer into cells in culture and in vivo: polyethylenimine. *Proc. Natl. Acad. Sci. U.S.A. 92*, 7297−7301. (b) For reviews, see Remy, J.-S., Abdallah, B., Zanta, M. A., Boussif, O., Behr, J.-P., and Demeneix, B. (1998) Gene Transfer with lipospermines and polyethylenimins. *Adv. Drug Deliv. Rev. 30*, 85−95. (c) Godbey, W. T., Wu, K. K., and Mikos, A. G. (1999) Poly-(ethylenimine) and its role in gene delivery. *J. Controlled Release 60*, 149−160.

(16) Bragonzi, A., Boletta, A., Biffi, A., Muggia, A., Sersale, G., Cheng, S. H., Bordignon, C., and Assael, B. M. (1999) Comparison between cationic polymers and lipids in mediating systemic gene delivery to the lungs. *Gene Ther. 6*, 1995−2004.

(17) Turunen, M. P., Hiltunen, M. O., Ruponen, M., Virkamäki, L., Szoka, F. C., Urtti, A., and Ylä-Herttuala, S. (1999)

Efficient adventitial gene delivery to rabbit carotid artery with cationic polymer-plasmid complexes. *Gene Ther. 6*, 6−11.
(18) Harpe, A. v., Petersen, H., Li, Y., and Kissel, T. (2000) Characterisation of commercially available and synthesized polyethylenimines for gene delivery. *J. Controlled Release 69*, 309−322.
(19) Behr, J. P. (1997) The proton sponge: a trick to enter cells the viruses did not exploit. *Chimia 51*, 34−36.
(20) Erbacher, P., Bettinger, T., Belguise-Valladier, P., Zou, S., Coll, J.-L., Behr, J.-P., and Remy, J.-S. (1999) Transfection and physical properties of various saccharide, poly(ethylene glycol), and antibody-derivatized polyethylenimines (PEI). *J. Gene Med. 1*, 210−222.
(21) Ngyugen, H.-K., Lemieux, P., Vinogradov, S. V., Gebhart, C. L., Guerin, N., Paradis, G., Bronich, T. K., Alakhov, V. Y., and Kabanov, A. V. (2000) Evaluation of polyether-polyethylenimine graft copolymers as gene transfer agents. *Gene Ther. 7*, 126−138.
(22) Vinogradov, S. V., Bronich, T. K., and Kabanov, A. V. (1998) Self-assembly of polyamine-poly(ethylene glycol) copolymers with phosphorothioate oligonucleotides. *Bioconjugate Chem. 9*, 805−812.
(23) Choi, J. H., Choi, J. S., Suh, H., and Park, J. S. (2001) Effect of poly(ethylene glycol) grafting on polyethylenimine as a gene transfer vector in vitro. *Bull. Korean Chem. Soc. 22*, 46−52.
(24) Kircheis, R., Schuller, S., Brunner, S., Orgris, M., Heider, K. H., Zauner, W., and Wagner E. (1999) Polycation-based DNA complexes for tumor-targeted gene delivery in vivo. *J. Gene Med. 1*, 111−120.
(25) Ogris, M., Brunner, S., Schüller, S., Kircheis, R., and Wagner, E. (1999) PEGylated DNA/transferrin-PEI complexes: reduced interaction with blood components, extended circulation in blood and potential for systemic gene delivery. *Gene Ther. 6*, 595−605.
(26) QIAGEN plasmid purification handbook; QIAGEN, 1997.
(27) Kissel, T., Petersen, H., Fischer, D., Kunath, K., and von Harpe, A. (1999) Kationische Blockcopolymere; DE 199 33 024 A 1 (EP 00/06214/WO 01/05875 A1).
(28) Petersen, H., Fechner, P. M., Fischer, D., and Kissel, T. (2002) Synthesis, characterization and biocompatibility of polyethylenimine-graft-poly(ethylene glycol) block copolymers. *Macromolecules*, accepted.
(29) Fischer, D., Bieber, T., Li, Y., Elsässer, H.-P., and Kissel, T. (1999) A novel nonviral vector for DNA delivery based on low molecular weight, branched polyethylenimine: Effect of molecular weight on transfection efficiency and cytotoxicity. *Pharm. Res. 16*, 1273−1279.
(30) Merdan, T., Kunath, K., Fischer, D., Kopecek, J., and Kissel, T. (2002) Intracellular processing of PEI/ribozym complexes can be observed in living cells using CSLM and inhibitor experiments. *Pharm. Res. 19*, 140−146.
(31) Wolfert, M. A., Schacht, E. H., Toncheva, V., Ulbrich, K., Nazarova, O., and Seymour, L. W. (1996) Characterization of vectors for gene therapy formed by self-assembly of DNA with synthetic block copolymers. *Hum. Gene Ther. 7*, 2123−2133.
(32) Kircheis, R., Wightman, L., and Wagner, E. (2001) Design and gene delivery activity of modified polyethylenimines. *Adv. Drug Delivery Rev. 53*, 341−358.
(33) Godbey, W. T., Wu, K. K., Hirasaki, G. J., and Mikos, A. G. (1999) Improved packing of poly(ethylenimine)/DNA complexes increases transfection efficiency. *Gene Ther. 6*, 1380−1388.
(34) Kleideiter, G., and Nordmeier, E. (1999) Poly(ethylene glycol)-induced DNA condensation in aqueous/methanol containing low-molecular-weight electrolytes solutions. Part II. Comparison between experiment and theory. *Polymer 40*, 4025−4033.
(35) Bloomfield, V. A. (1996) DNA condensation. *Curr. Opin. Struct. Biol. 6*, 334−341.
(36) Richardson, S. C. W., Kolbe, H. V. J., and Duncan, R. (1999) Potential of low molecular mass chitosan as a DNA delivery system: body distribution and ability to complex and protect DNA. *Int. J. Pharm. 178*, 231−243.
(37) Choksakulnimitr, S., Masuda, S., Tokuda, H., Takakura, Y., and Hashida, M. (1995) In vitro cytotoxicity of macromolecules in different cell culture systems. *J. Controlled Release 34*, 233−241.
(38) Mislick, K. A., and Baldeschwieler, J. D. (1996) Evidence for the role of proteoglycans in cation-mediated gene transfer. *Proc. Natl. Acad. Sci. U.S.A. 93*, 12349−12354.
(39) Ogris, M., Steinlein, P., Kursa, M., Mechtler, K., Kircheis, R., and Wagner, E. (1998) The size of DNA/transferrin-PEI complexes is an important factor for gene expression in cultured cells. *Gene Ther. 5*, 1425−1433.

BC025529V

Cathepsin B-Labile Dipeptide Linkers for Lysosomal Release of Doxorubicin from Internalizing Immunoconjugates: Model Studies of Enzymatic Drug Release and Antigen-Specific In Vitro Anticancer Activity

Gene M. Dubowchik,* Raymond A. Firestone,*,† Linda Padilla, David Willner, Sandra J. Hofstead, Kathleen Mosure, Jay O. Knipe, Shirley J. Lasch,§ and Pamela A. Trail§

Bristol-Myers Squibb Pharmaceutical Research Institute, P.O. Box 5100, Wallingford, Connecticut 06492. Received April 2, 2002; Revised Manuscript Received April 30, 2002

The anticancer drug doxorubicin (DOX) has been linked to chimeric BR96, an internalizing monoclonal antibody that binds to a Lewis^y-related, tumor-associated antigen, through two lysosomally cleavable dipeptides, Phe-Lys and Val-Cit, giving immunoconjugates **72** and **73**. A self-immolative *p*-aminobenzyloxycarbonyl (PABC) spacer between the dipeptides and the DOX was required for rapid and quantitative generation of free drug. DOX release from model substrate Z-Phe-Lys-PABC-DOX **49** was 30-fold faster than from Z-Val-Cit-PABC-DOX **42** with the cysteine protease cathepsin B alone, but rates were identical in a rat liver lysosomal preparation suggesting the participation of more than one enzyme. Conjugates **72** and **73** showed rapid and near quantitative drug release with cathepsin B and in a lysosomal preparation, while demonstrating excellent stability in human plasma. Against tumor cell lines with varying levels of BR96 expression, both conjugates showed potent, antigen-specific cytotoxic activity, suggesting that they will be effective in delivering DOX selectively to antigen-expressing carcinomas.

INTRODUCTION

Effective cancer treatment using macromolecular or small molecule prodrugs of cytotoxic agents requires systemic stability as well as selective drug release at the target tissue (*1*, *2*). The chimeric MAb[1] BR96 binds specifically to a Lewis^y-related, tumor-associated antigen expressed on the cell surface of many human carcinomas, and the resulting complex is internalized through the endosome/lysosome pathway (*3*). The DOX-containing immunoconjugate BR96−DOX depends on a hydrazone link for selective hydrolysis inside tumor cell lysosomes (pH ca. 5, $t_{1/2} = 4$ h) and a thioether linker to the MAb to achieve relative stability in circulation (pH ca. 7, $t_{1/2} =$ 120 h) (*4*). Besides its limited hydrolytic stability, the hydrazone can be used to carry only ketone-containing drugs such as DOX or its close analogues (*5*). We sought to replace the hydrazone with cathepsin B-sensitive peptides as they can be used to deliver a greater variety of drugs, they should release those drugs quickly upon internalization into lysosomes, and they do not spontaneously hydrolyze. Cathepsin B (*6*, *7*) is a ubiquitous cysteine protease whose properties do not differ very much from species to species. It is never found extracellularly, except in pathological conditions such as metastatic tumors (*8*) or in areas of tissue destruction in rheumatoid arthritis (*9*). Therefore, conjugates produced with cathepsin B-cleavable linkers are likely to be stable in circulation.

Lysosomally cleavable peptides such as Gly-Phe-Leu-Gly (*10*) and Ala-Leu-Ala-Leu (*11*, *12*) that have been used by others as drug carrier linkers were considered to have significant potential liabilities for our particular targeting vehicle for two reasons: (i) drug release is relatively slow and (ii) the hydrophobic nature of those tetrapeptides would probably cause precipitation or aggregation of a BR96 immunoconjugate carrying a maximal load of eight drug molecules. Because Z-Phe-Arg-X (where X is a fluorogenic moiety) is a general substrate for the assay of cathepsins B and L (*13*), we decided to use this simple sequence as a starting point for substrate design. We first prepared a series of model compounds to determine structural requirements for efficient enzyme-mediated drug release and plasma stability (*14*). In these,

* To whom correspondence should be addressed. Tel: (203)-677-7539. Fax: (203)677-7702. E-mail: Gene.Dubowchik@bms.com.

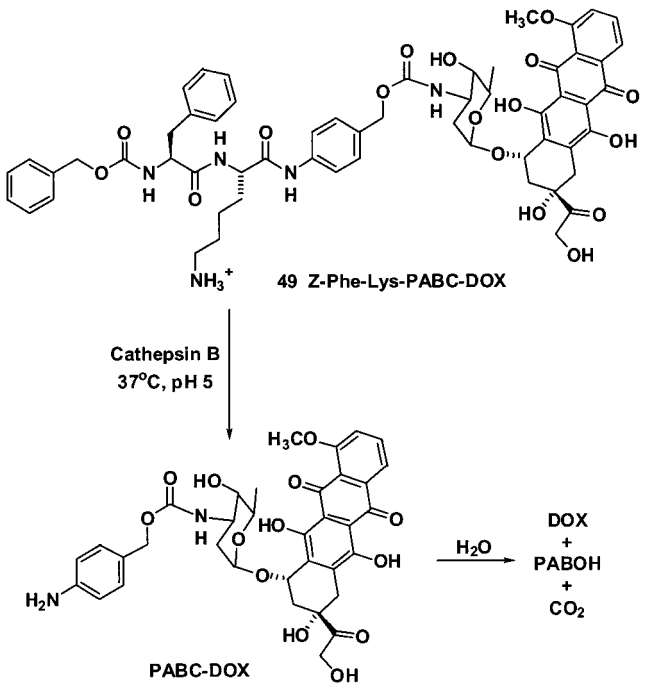
† Present address: Boehringer Ingelheim Pharmaceuticals Inc., 900 Ridgebury Rd., P.O. Box 368, Ridgefield, CT 06877-0368.

§ Present address: Bayer Research Center, 400 Morgan Lane, West Haven, CT, 06516-4175.

[1] Abbreviations: AA, amino acid; Ala, L-alanine; Alloc, allyloxycarbonyl; Arg, L-arginine; Boc, *tert*-butyloxycarbonyl; BSA, bovine serum albumin; Cit, L-citrulline; CPM, counts per minute; DCC, dicyclohexylcarbodiimide; DIEA, diisopropylethylamine; DME, dimethoxyethane; DMF, dimethylformamide; DOX, doxorubicin; DTT, dithiothreitol; EDTA, ethylenediaminetetraacetic acid; EEDQ, 2-ethoxy-1-ethoxycarbonyl-1,2-dihydroquinoline; FAB, fast atom bombardment; FCS, fetal calf serum; FI, fluorescence intensity; Fmoc, 9-fluorenylmethyloxycarbonyl; Gly, glycine; HOSu, *N*-hydroxysuccinimide; HPLC, high-performance liquid chromatography; IgG, immunoglobulin γ; Ile, L-isoleucine; Leu, L-leucine; Lys, L-lysine; MAb, monoclonal antibody; MC, maleimidocaproyl; MMT, monomethoxytrityl; MR, mole ratio; NMP, *N*-methylpyrrolidinone; NMR, nuclear magnetic resonance; PABC, *p*-aminobenzylcarbonyl; PABOH, *p*-aminobenzyl alcohol; PBS, phosphate-buffered saline; Phe, phenylalanine; PNP, *p*-nitrophenyl; SC, succinimidylcaproyl; TFA, trifluoroacetic acid; THF, tetrahydrofuran; Trp, L-tryptophan; Ts, *p*-toluenesulfonyl; Val, L-valine; Z, benzyloxycarbonyl.

10.1021/bc025536j CCC: $22.00 © 2002 American Chemical Society
Published on Web 06/18/2002

Scheme 1



Arg was replaced by Lys and modified Arg at P_1 for synthetic ease as well as potential systemic stability (*15*). We also investigated Cit, which is isosteric and isoelectronic with Arg but much less basic (*16*). Concern that sterically demanding drugs such as DOX would be excluded from the active site of cathepsin B or would otherwise interfere with dipeptide binding led us to incorporate a self-immolative PABC spacer (*17*), which hydrolytically decomposes upon deacylation, spontaneously releasing free drug (Scheme 1). Elaboration of two exemplary dipeptide substrates into linker compounds followed by conjugation with chimeric BR96 gave immunoconjugates that demonstrated excellent in vitro stability and potent cytotoxic activity against antigen-expressing tumor cells.

EXPERIMENTAL SECTION

Chemistry. Protected AAs were purchased from Bachem (Torrance, CA). Cathepsin B, DTT, and EDTA were purchased from Sigma (St. Louis, MO). Tributyltin hydride, trichloromethyl chloroformate (diphosgene), diallyl dicarbonate, and PABOH were purchased from Fluka (St. Louis, MO). All other reagents were purchased from Aldrich Chemical Co. (Milwaukee, WI). Dry solvents were Aldrich Sure Seal grade except for methylene chloride, which was distilled from calcium hydride. All other solvents were reagent grade and were used as received. Sodium sulfate was used as the drying agent for extractive workup unless otherwise indicated. HPLC was carried out on a Varian Star System using a model 9010 solvent delivery system, a 9050 variable wavelength UV−vis detector, and a Micropak C-18 column. Preparative flash chromatography was carried out using Merck grade 9385, 230−400 mesh silica gel. All NMR spectra were run on a Varian Gemini 300 spectrometer (300 MHz). Centrifugation was done with a Tomy Capsule microcentrifuge model HF-120 (Peninsula Laboratories, Belmont, CA).

Boc-Lys(alloc) (1). A stirred solution of Boc-Lys (5.22 g, 21.2 mmol) and $NaHCO_3$ (1.87 g, 1.05 equiv) in water (30 mL) at room temperature was treated with diallyl dicarbonate (3.52 mL, 1.05 equiv) in DME (30 mL). After 16 h, the mixture was poured into a 15% aqueous citric acid solution and the resulting suspension was extracted with ethyl acetate (3 × 150 mL). The combined organic phases were washed with water and brine, dried, and evaporated to give a white solid, which was carried on without further purification (6.99 g, 99%). ^{1}H NMR ($CDCl_3/CD_3OD$): δ 1.41 (9H, s), 1.49 and 1.70 (6H, m), 3.13 (2H, m), 4.25 (1H, m), 4.52 (2H, d), 5.24 (2H, q), 5.87 (1H, m). MS (DCI): *m/e* 331 $(MH)^+$, 275 $(MH - C_4H_8)^+$.

Lys(alloc)·CF_3CO_2H (2). Boc-Lys(alloc) **1** (9.94 g, 30 mmol) in CH_2Cl_2 (50 mL) at room temperature was treated with TFA (19 mL). The mixture was sonicated for several minutes and then left to stand at room temperature for 1 h. The solvents were evaporated at 40 °C, and the gummy solid residue was triturated with ether (75 mL), giving a white solid that was collected by filtration, washed with ether, and dried in vacuo (8.58 g, 83%). ^{1}H NMR (D_2O): δ 1.46 and 1.87 (4H and 2H, m), 3.11 (2H, m), 3.80 (1H, t), 4.51 (2H, br s), 5.22 (2H, q), 5.90 (1H, m). MS (DCI): *m/e* 231 $(MH)^+$. Anal. Calcd for $C_{12}H_{19}N_2O_6F_3$: C, 41.86; H, 5.56; N, 8.14. Found: C, 42.30; H, 5.52; N, 8.29.

Preparation of HOSu-Activated Esters 3−8. A stirred solution of the Z-protected AA (40 mmol) and HOSu (1.1 equiv) in THF (100 mL) at 0 °C was treated with DCC (1.05 equiv). After 15 min, the mixture was allowed to warm to room temperature and was stirred for 16 h. The solid DCU byproduct was filtered off, and the filtrate was evaporated. The thick, colorless oil was dissolved in CH_2Cl_2 (80 mL). The mixture was allowed to stand for 1 h and then was filtered to remove more DCU. The filtrate was evaporated, and the resulting colorless glass was dried in vacuo for 3 h, giving a solid foam that was carried on without further purification. Representative ^{1}H NMR of **3**: ($CDCl_3/CD_3OD$): δ 2.88 (4H, s), 3.27 (2H, m), 4.70 (1H, m), 5.13 (2H, s), 7.27 (10H, m).

Z-Phe-Lys(alloc) (9). A vigorously stirred solution of Z-Phe-OSu **3** (2.783 g, 7.021 mmol) in DME (30 mL) at room temperature was treated with a solution of Lys(alloc)·CF_3CO_2H **2** (2.54 g, 1.05 equiv) and $NaHCO_3$ (1.24 g, 2.1 equiv) in water (30 mL). The temperature was maintained below 25 °C with a cold water bath for the first 30 min. The mixture was stirred at room temperature for 14 h. A small amount of DCU was removed by filtration, and the filtrate was diluted with water (50 mL) and then acidified to pH 3 with 15% aqueous citric acid. The resulting suspension was extracted with ethyl acetate (3 × 80 mL), and the combined organic layers were washed with water and brine, dried, and evaporated to give a glassy solid. This was treated with ether (150 mL), sonicated, and heated in a water bath (50 °C). After it was cooled, the white solid product was collected by filtration and washed with ether (2.79 g, 78%). ^{1}H NMR ($CDCl_3/CD_3OD$): δ 1.25, 1.43, 1.74 and 1.81 (6H, m), 3.00 (2H, m), 3.08 (2H, m), 4.43 (2H, m), 4.48 (2H, d), 5.02 (2H, m), 5.20 (2H, q), 5.84 (1H, m), 7.22 (10H, m). MS (FAB): *m/e* 512 $(MH)^+$, 534 $(M + Na)^+$, 550 $(M + K)^+$. Anal. Calcd for $C_{27}H_{33}N_3O_7$: C, 63.39; H, 6.50; N, 8.21. Found: C, 62.98; H, 6.48; N, 8.21.

Z-Val-Lys(alloc) (10). Compound **10** was prepared as described above for **9** in 82% yield. ^{1}H NMR ($CDCl_3/CD_3OD$): δ 0.89 (6H, 2 x d), 1.30, 1.42, 1.62 and 1.81 (6H, m), 2.03 (1H, m), 3.07 (2H, m), 3.92 (1H, AB q), 4.42 (1H, m), 4.49 (2H, d), 5.06 (2H, s), 5.19 (2H, q), 5.82 (1H, m), 7.28 (5H, m). MS (FAB): *m/e* 949 $(MH)^+$, 971 $(M + Na)^+$,

987 $(M + K)^+$. Anal. Calcd for $C_{23}H_{33}N_3O_7$: C, 59.60; H, 7.18; N, 9.07. Found: C, 59.84; H, 7.31; N, 8.90.

Z-Ala-Lys(alloc) (11). Compound **11** was prepared as described above for **9** in 76% yield. ^{1}H NMR ($CDCl_3/CD_3OD$): δ 1.09 (3H, 2 x d), 1.25, 1.40, 1.67 and 1.80 (6H, m), 3.04 (2H, m), 4.26 (1H, m), 4.40 (1H, m), 4.46 (2H, d), 4.95 (2H, s), 5.13 (2H, q), 5.79 (1H, m), 7.21 (5H, brs). MS (FAB): *m/e* 436 $(MH)^+$, 459 $(M + Na)^+$, 475 $(M + K)^+$. Anal. Calcd for $C_{21}H_{29}N_3O_7$: C, 53.15; H, 6.16; N, 8.85. Found: C, 52.99; H, 6.12; N, 8.78.

Z-Val-Cit (12). To a solution of Z-Val-OSu **4** (2.98 g, 8.566 mmol) in DME (25 mL) at room temperature was added a solution of Cit (2.25 g, 1.5 equiv) and $NaHCO_3$ (1.08 g, 1.5 equiv) in water (25 mL). The temperature was maintained below 25 °C with a cold water bath for the first 30 min. The mixture was stirred vigorously for 16 h. Water (20 mL) containing 2 mL of saturated $NaHCO_3$ was added, and the mixture was washed with ethyl acetate and then acidified to pH 3 with 10% HCl. The resulting suspension was extracted with 10% *n*-butanol/ethyl acetate (3×). The combined organic layers were dried and concentrated in vacuo to give a white solid (3.39 g, 97%). ^{1}H NMR ($CDCl_3/CD_3OD$): δ 0.73 (6H, q), 1.31, 1.46 and 1.63 (4H, m), 1.87 (1H, m), 2.88 (2H, m), 3.72 (1H, AB q), 4.17 (1H, m), 4.86 (2H, s), 7.10 (5H, m). MS (FAB): *m/e* 409 $(MH)^+$, 431 $(M + Na)^+$, 447 $(M + K)^+$. HRMS calcd for $C_{19}H_{29}N_4O_6$, *m/e* 409.2087; found, *m/e* 409.2086. Anal. Calcd for $C_{19}H_{28}N_4O_6 \cdot 0.5H_2O$: C, 54.66; H, 7.00; N, 13.42. Found: C, 54.50; H, 6.86; N, 13.55.

Z-Phe-Cit (13). Compound **13** was prepared as described above for **12** in 78% yield. ^{1}H NMR ($CDCl_3/CD_3OD$): δ 1.39 (2H, m), 1.59 and 1.86 (each 1H, m), 2.81 (1H, q), 3.01 (3H, m), 4.34 (2H, m), 4.92 (2H, ABq), 6.20 (1H, d), 7.15 (10H, m), 7.61 (1H, d). MS (FAB): *m/e* 455.2 $(M - H)^-$. Anal. Calcd for $C_{23}H_{28}N_4O_6 \cdot 0.5H_2O$: C, 59.35; H, 6.28; N, 12.04. Found: C, 59.40; H, 5.99; N, 12.05.

Z-Leu-Cit (14). Compound **14** was prepared as described above for **12** in 75% yield. ^{1}H NMR ($CDCl_3/CD_3OD$): δ 0.91 (6H, ABq), 1.15 (1H, m), 1.45 (2H, m), 1.79 and 1.97 (each 1H, m), 3.04 (2H, t), 4.15 and 4.37 (each 1H, m), 5.08 (2H, s), 7.30 (5H, m), 8.21 (1H, d). MS (FAB): *m/e* 421.2 $(M - H)^-$. Anal. Calcd for $C_{20}H_{30}N_4O_6 \cdot 0.5H_2O$: C, 55.67; H, 7.24; N, 12.98. Found: C, 55.32; H, 6.87; N, 12.82.

Z-Ile-Cit (15). Compound **15** was prepared as described above for **12** in 78% yield. ^{1}H NMR ($CDCl_3/CD_3OD$): δ 0.80 (3H, t), 0.89 (5H, d and m), 1.11 (1H, m), 1.46 (2H, m), 1.77 (2H, m), 3.05 (2H, m), 3.98 and 4.33 (each 1H, m), 5.02 (2H, s), 6.53 (1H, d), 7.27 (5H, m), 7.97 (1H, d). MS (FAB): *m/e* 421.3 $(M - H)^-$. Anal. Calcd for $C_{20}H_{30}N_4O_6 \cdot 0.5H_2O$: C, 55.67; H, 7.24; N, 12.98. Found: C, 55.50; H, 6.92; N, 12.89.

Z-Trp-Cit (16). Compound **16** was prepared as described above for **12** in 87% yield. ^{1}H NMR ($CDCl_3/CD_3OD$): δ 1.37 (2H, m), 1.60 and 1.81 (each 1H, m), 3.02 (2H, t), 3.15 (2H, ABq), 4.33 (1H, m), 4.46 (1H, ABq), 4.97 (2H, s), 6.96 (1H, t), 7.04 (4H, m), 7.22 (5H, m), 7.53 (1H, d). MS (FAB): *m/e* 494.3 $(M - H)^-$. Anal. Calcd for $C_{25}H_{29}N_5O_6 \cdot 0.5H_2O$: C, 59.51; H, 5.99; N, 13.88. Found: C, 59.70; H, 5.78; N, 13.85.

Z-Phe-Arg(NO_2) (17). Compound **17** was prepared as described above for **12** in 88% yield. ^{1}H NMR ($CDCl_3/CD_3OD$): δ 1.51 (2H, m), 1.63 and 1.80 (each 1H, m), 2.87 (1H, m), 3.09 (3H, m), 4.43 (1H, m), 4.66 (1H, m), 4.97 (2H, ABq), 6.00 (1H, brd), 7.05−7.30 (10H, m), 7.51 (1H, brd). MS (FAB): *m/e* 499.2 $(M - H)^-$. Anal. Calcd for $C_{23}H_{27}N_6O_7 \cdot 0.5H_2O$: C, 54.33; H, 5.55; N, 16.53. Found: C, 54.22; H, 5.48; N, 16.61.

Z-Phe-Arg(Ts) (18). Compound **18** was prepared as described above for **12** in 82% yield. ^{1}H NMR ($CDCl_3/CD_3OD$): δ 1.42 (2H, m), 1.62 and 1.77 (each 1H, m), 2.23 (3H, s), 2.84 (1H, m), 3.05 (3H, m), 4.42 and 5.53 (each 1H, m), 4.83 (2H, ABq), 5.99 (1H, br), 7.07 (10H, brs), 7.13 (2H, brs), 7.52 (1H, br), 7.63 (2H, d). MS (FAB): *m/e* 608.3 $(M - H)^-$. Anal. Calcd for $C_{30}H_{34}N_5O_7S \cdot 0.5H_2O$: C, 64.15; H, 6.28; N, 12.47. Found: C, 64.22; H, 6.24; N, 12.53.

Z-Phe-Lys(alloc)-PABOH (19). A stirred solution of Z-Phe-Lys(alloc) **9** (524.7 mg, 1.026 mmol) and PABOH (133 mg, 1.05 equiv) in THF (10 mL) at room temperature was treated with EEDQ (266.3 mg, 1.05 equiv). After 16 h, the mixture was evaporated to dryness at 30 °C, and the residue was triturated with ether (15 mL). The resulting white solid product was collected by filtration, washed with ether, and dried in vacuo (591.6 mg, 94%). ^{1}H NMR ($CDCl_3/CD_3OD$): δ 1.25, 1.42, 1.59 and 1.77 (6H, m), 2.97 (2H, m), 3.06 (2H, m), 4.37 (2H, m), 4.46 (2H, d), 4.55 (2H, s), 4.98 (2H, m), 5.18 (2H, q), 5.81 (1H, m), 7.08 and 7.43 (4H, 2 × d), 7.11 and 7.23 (10H, m). MS (FAB): *m/e* 617 $(MH)^+$, 639 $(M + Na)^+$, 655 $(M + K)^+$. Anal. Calcd for $C_{34}H_{40}N_4O_7$: C, 66.22; H, 6.54; N, 9.08. Found: C, 65.72; H, 6.43; N, 8.92.

Z-Val-Lys(alloc)-PABOH (20). Compound **20** was prepared as described above for **19** in 82% yield. ^{1}H NMR ($CDCl_3/CD_3OD$): δ 0.86 (6H, m), 1.24−1.67 (6H, m), 2.03 (1H, m), 3.08 (2H, m), 4.00 (1H, m), 4.47 (3H, m), 4.57 (2H, s), 5.05 (2H, s), 5.19 (2H, q), 5.81 (1H, m), 7.26 and 7.43 (4H, m), 7.30 (5H, s). MS (FAB): *m/e* 569 $(MH)^+$, 591 $(M + Na)^+$, 607 $(M + K)^+$. Anal. Calcd for $C_{30}H_{40}N_4O_7 \cdot 0.5H_2O$: C, 62.38; H, 7.15; N, 9.70. Found: C, 62.40; H, 7.22; N, 9.79.

Z-Ala-Lys(alloc)-PABOH (21). Compound **21** was prepared as described above for **19** in 88% yield. ^{1}H NMR ($CDCl_3/CD_3OD$): δ 1.18 (3H, 2 x d), 1.28, 1.45, 1.73 and 1.84 (6H, m), 3.08 (2H, m), 4.06 (1H, m), 4.49 (3H, m), 4.56 (2H, s), 5.05 (2H, s), 5.17 (2H, q), 5.81 (1H, m), 7.28 (7H, m), 7.45 (2H, m). MS (FAB): *m/e* 542 $(MH)^+$, 564 $(M + Na)^+$, 580 $(M + K)^+$. Anal. Calcd for $C_{28}H_{36}N_4O_7 \cdot 0.5H_2O$: C, 61.19; H, 6.78; N, 10.19. Found: C, 61.04; H, 6.64; N, 10.27.

Z-Val-Cit-PABOH (22). Z-Val-Cit **12** (1.0397 g, 2.545 mmol) and PABOH (470.2 mg, 1.5 equiv) in THF (10 mL) at room temperature were treated with EEDQ (944.2 mg, 1.5 equiv) with stirring. After 16 h, the mixture was diluted with 10% 2-propanol/ethyl acetate (100 mL) and the solution washed with 10% aqueous citric acid, water, and brine, dried, and evaporated in vacuo. The residue was sonicated in ether for 15 min, and the crude solid product was collected by filtration and dried in vacuo (954.2 mg, 73%). ^{1}H NMR ($CDCl_3/CD_3OD$): δ 0.79 (6H, q), 1.37, 1.53 and 1.72 (4H, m), 1.92 (1H, m), 3.00 (2H, m), 3.85 (1H, m), 4.41 (1H, m), 4.45 (2H, s), 4.95 (2H, m), 7.08−7.40 (9H, m). MS (FAB): *m/e* 514 $(MH)^+$, 536 $(M + Na)^+$, 552 $(M + K)^+$. Anal. Calcd for $C_{26}H_{35}N_5O_6 - H_2O$: C, 58.74; H, 7.01; N, 13.17. Found: C, 59.01; H, 6.62; N, 13.06.

Z-Phe-Cit-PABOH (23). A stirred solution of Z-Phe-Cit **13** (1.2005 g, 2.630 mmol) and PABOH (356.1 mg, 1.1 equiv) in THF (25 mL) at room temperature was treated with EEDQ (715.1 mg, 1.1 equiv). A heavy precipitate was formed overnight. Ether (50 mL) was added, and the suspension was sonicated at room temperature for several minutes. The solid was collected by filtration, washed with ether, and air-dried overnight (1.2665 g, 86%). ^{1}H NMR ($CDCl_3/CD_3OD$): δ 1.18 (2H, m), 1.39 (1H, m), 1.56 (1H, m), 2.60 (1H, q), 2.84 (3H, m), 4.16 (1H, m), 4.46 (3H, m and s), 4.79 (2H, ABq), 6.01

(1H, d), 7.11 (12H, m), 7.38 (2H, d). MS (FAB): *m/e* 561.3 $(MH)^+$. Anal. Calcd for $C_{30}H_{35}N_6O_6 \cdot 0.5H_2O$: C, 63.14; H, 6.36; N, 12.27. Found: C, 62.85; H, 6.26; N, 12.35.

Z-Leu-Cit-PABOH (24). Compound **24** was prepared as described above for **23** in 81% yield. ^{1}H NMR ($CDCl_3$/CD_3OD): δ 0.74 (6H, m), 1.36 (5H, m), 1.51 (2H, m), 1.71 (1H, m), 2.94 (2H, m), 4.02 (1H, q), 4.37 (1H, q), 4.41 (2H, s), 4.91 (2H, s), 7.13 (7H, m), 7.36 (2H, d). MS (FAB): *m/e* 528.4 $(MH)^+$, 550.3 $(M + Na)^+$. Anal. Calcd for $C_{27}H_{37}N_5O_6$-$0.5H_2O$: C, 60.43; H, 7.14; N, 13.05. Found: C, 60.50; H, 6.91; N, 13.02.

Z-Ile-Cit-PABOH (25). Compound **25** was prepared as described above for **23** in 76% yield. ^{1}H NMR ($CDCl_3$/CD_3OD): δ 0.72 (6H, m), 0.98 (2H, m), 1.32 (2H, m), 1.50 (1H, m), 1.63 (2H, m), 2.96 (2H, m), 3.82 (1H, m), 4.40 (3H, m and s), 4.90 (2H, s), 7.13 (7H, m), 7.45 (2H, d). MS (FAB): 526.4 $(M - H)^-$. Anal. Calcd for $C_{27}H_{37}N_5O_6 \cdot 0.5H_2O$: C, 60.43; H, 7.14; N, 13.05. Found: C, 59.94; H, 6.95; N, 13.05.

Z-Trp-Cit-PABOH (26). Compound **26** was prepared as described above for **23** in 98% yield. ^{1}H NMR ($CDCl_3$/CD_3OD): δ 1.12 (2H, m), 1.39 (1H, m), 1.62 (1H, m), 2.91 (2H, m), 3.11 (2H, m), 4.27 (1H, m), 4.48 (1H, m), 4.45 (2H, s), 4.91 (2H, ABq), 6.89 (1H, t), 6.98 (1H, t), 7.16 (9H, m), 7.31 (2H, d), 7.44 (1H, d), 9.42 (1H, br). MS (FAB): *m/e* 599.3 $(M - H)^-$. Anal. Calcd for $C_{32}H_{36}N_6O_6 \cdot 0.5H_2O$: C, 63.04; H, 6.12; N, 13.78. Found: C, 63.24; H, 6.19; N, 13.55.

Z-Phe-Arg(NO_2)-PABOH (27). Compound **27** was prepared as described above for **23** in 65% yield. ^{1}H NMR ($CDCl_3$/CD_3OD): δ 1.46 (2H, m), 1.58 and 1.74 (each 1H, m), 2.86 (m, 1H), 3.08 (3H, m), 4.32 (1H, q), 4.41 (1H, m), 4.51 (2H, s), 4.92 (2H, ABq), 5.99 (1H, d), 7.00−7.28 (12H, m), 7.38 (2H, d), 7.67 (1H, d), 9.14 (1H, br). MS (FAB): *m/e* 606.4 $(MH)^+$. Anal. Calcd for $C_{30}H_{35}N_7O_7 \cdot 0.5H_2O$: C, 58.62; H, 5.90; N, 15.95. Found: C, 58.29; H, 5.70; N, 15.81.

Z-Phe-Arg(Ts)-PABOH (28). Compound **28** was prepared as described above for **23** in 74% yield. ^{1}H NMR ($CDCl_3$/CD_3OD): δ 1.36 (2H, m), 1.52 and 1.71 (each 1H, m), 2.22 (3H, s), 2.86 (1H, m), 3.03 (3H, m), 4.50 (4H, m and s), 4.87 (2H, ABq), 5.97 (1H, br), 6.39 (1H, br), 6.95−7.25 (14H, m), 7.39 (2H, brs), 7.64 (2H, brs), 9.13 (1H, brs). MS (FAB): *m/e* 715.4 $(MH)^+$, 737.5 $(M + Na)^+$. Anal. Calcd for $C_{37}H_{42}N_6O_7S \cdot 0.5H_2O$: C, 61.40; H, 5.99; N, 11.61. Found: C, 61.28; H, 5.84; N, 11.40.

Z-Phe-Lys(alloc)-PABC-PNP (29). A stirred solution of Z-Phe-Lys(alloc)-PABOH **19** (269.6 mg, 0.4372 mmol) in dry THF (8 mL) at room temperature was treated with PNP chloroformate (106.0 mg, 1.2 equiv) and dry pyridine (0.0425 mL, 1.2 equiv). After 6 h, TLC (silica, 25:1 CH_2Cl_2/CH_3OH) indicated completion. Ethyl acetate (25 mL) and 10% aqueous citric acid (25 mL) were added. The organic layer was washed with water and brine, dried, and evaporated to give a yellow solid, which was purified by flash chromatography on silica gel, eluting with 30:1 CH_2Cl_2/CH_3OH, to give the product as an off-white solid (297.4 mg, 87%). ^{1}H NMR ($CDCl_3$/CD_3OD): δ 1.24, 1.42, 1.59 and 1.78 (6H, m), 2.97 (2H, m), 3.04 (2H, m), 4.38 (2H, m), 4.46 (2H, d), 5.01 (2H, s), 5.17 (2H, q), 5.21 (2H, s), 5.37 and 5.80 (each 1H, m), 5.83 (1H, m), 7.11 and 7.56 (4H, 2 × d), 7.13 and 7.25 (10H, m), 7.35 and 8.10 (each 2H, d), 9.23 (1H, br s). MS (FAB): *m/e* 782 $(MH)^+$, 804 $(M + Na)^+$, 820 $(M + K)^+$. Anal. Calcd for $C_{41}H_{43}N_5O_{11}$: C, 62.99; H, 5.54; N, 8.96. Found: C, 62.75; H, 5.49; N, 8.86.

Z-Val-Lys(alloc)-PABC-PNP (30). Compound **30** was prepared as described above for **29** in 71% yield. ^{1}H NMR ($CDCl_3$/CD_3OD): δ 0.91 (6H, m), 1.33−1.87 (6H, m), 2.02 (1H, m), 3.08 (2H, m), 3.95 (1H, m), 4.41 (1H, m), 4.48 (2H, d), 5.06 (2H, s), 5.17 (2H, q), 5.20 (2H, s), 5.82 (1H, m), 7.23 and 7.58 (4H, m), 7.30 (5H, m), 7.38 and 8.31 (4H, m). MS (FAB): *m/e* 734 $(MH)^+$, 756 $(M + Na)^+$, 772 $(M + K)^+$. HRMS calcd for $C_{37}H_{44}N_5O_{11}$, *m/e* 734.3037; found, *m/e* 734.3036.

Z-Ala-Lys(alloc)-PABC-PNP (31). Compound **31** was prepared as described above for **29** in 74% yield except that the eluting solvent for chromatographic purification was 20:1 CH_2Cl_2/CH_3OH. ^{1}H NMR ($CDCl_3$/CD_3OD): δ 1.09 (3H, 2 x d), 1.28, 1.40, 1.66 and 1.79 (6H, m), 3.08 (2H, m), 4.06 (1H, m), 4.38 (1H, m), 4.47 (2H, d), 5.02 (2H, s), 5.13 (2H, q), 5.23 (2H, s), 5.80 (1H, m), 7.25 and 7.60 (4H, m), 7.33 (5H, m), 7.42 and 8.35 (4H, m). MS (FAB): *m/e* 707 $(MH)^+$, 729 $(M + Na)^+$, 745 $(M + K)^+$. HRMS calcd for $C_{35}H_{40}N_5O_{11}$, *m/e* 706.2724; found, *m/e* 706.2722.

Z-Val-Cit-PABC-PNP (32). A stirred solution of Z-Val-Cit-PABOH **32** (383.0 mg, 0.7457 mmol) and PNP chloroformate (225.5 mg, 1.5 equiv) in THF (10 mL) in CH_2Cl_2 (5 mL) was treated at room temperature with pyridine (0.091 mL, 1.5 equiv). Workup as described above for **29** gave a crude, pale yellow solid, which was purified by flash chromatography on silica gel, eluting with (i) 30:1 and (ii) 12:1 CH_2Cl_2/CH_3OH, to give the product as an off-white solid (440.3 mg, 87%). ^{1}H NMR ($CDCl_3$/CD_3OD): δ 0.88 (6H, m), 1.42, 1.61 and 1.80 (4H, m), 2.02 (1H, m), 3.08 (2H, m), 3.99 (1H, m), 4.51 (1H, m), 5.00 (2H, m), 7.20−7.57 (9H, m), 7.30 and 8.20 (each 2H, m). MS (FAB): *m/e* 679 $(MH)^+$, 701 $(M + Na)^+$, 717 $(M + K)^+$. HRMS calcd for $C_{33}H_{39}N_6O_{10}$, *m/e* 679.2728; found, *m/e* 679.2720.

Z-Phe-Cit-PABC-PNP (33). Compound **33** was prepared as described above for **32** in 86% yield. ^{1}H NMR ($CDCl_3$/CD_3OD): δ 1.40 (2H, m), 1.59 and 1.78 (each 1H, m), 2.89 (1H, m), 3.03 (3H, m), 4.39 and 4.46 (each 1H, m), 4.95 (2H, brs), 5.19 (2H, s), 7.00−7.37 (14H, m), 7.55 (2H, d), 8.18 (2H, d). MS (FAB): *m/e* 727 $(MH)^+$, 765 $(M + K)^+$. HRMS calcd for $C_{37}H_{39}N_6O_{10}$, *m/e* 715.2728; found, *m/e* 715.2718.

Z-Leu-Cit-PABC-PNP (34). Compound **34** was prepared as described above for **32** in 83% yield. ^{1}H NMR ($CDCl_3$/CD_3OD): δ 0.73 (6H, m), 1.38 (4H, m), 1.52 (2H, m), 1.73 (1H, m), 2.91 (2H, m), 4.01 (1H, m), 4.38 (1H, m), 4.90 (2H, s), 5.09 (2H, s), 7.05−7.30 (9H, m), 7.44 (2H, d), 7.84 (1H, br), 8.11 (2H, d), 9.52 (1H, br). MS (FAB): *m/e* 693 $(MH)^+$, 715 $(M + Na)^+$, 731 $(M + K)^+$. HRMS calcd for $C_{34}H_{41}N_6O_{10}$, *m/e* 693.2884; found, *m/e* 693.2876.

Z-Ile-Cit-PABC-PNP (35). Compound **35** was prepared as described above for **32** in 83% yield. ^{1}H NMR ($CDCl_3$/CD_3OD): δ 0.72 (6H, m), 0.85 (2H, m), 1.20−1.90 (5H, m), 2.95 (2H, m), 3.94 (1H, m), 4.32 (1H, m), 4.89 (2H, s), 5.03 (2H, s), 7.05−7.30 (9H, m), 7.44 (2H, d), 8.05 (2H, d), 9.39 (1H, br). MS (FAB): *m/e* 715 $(M + Na)^+$, 731 $(M + K)^+$. HRMS calcd for $C_{34}H_{40}N_6O_{10}Na$, *m/e* 715.2704; found, *m/e* 715.2695.

Z-Trp-Cit-PABC-PNP (36). Compound **36** was prepared as described above for **32** in 72% yield. ^{1}H NMR ($CDCl_3$/CD_3OD): δ 1.11 (2H, m), 1.40 (1H, m), 1.63 (1H, m), 2.89 (2H, m), 3.05 (2H, m), 4.06 (1H, m), 4.40 (1H, m), 4.92 (2H, s), 5.09 (2H, s), 6.88 (1H, t), 6.94 (1H, t), 7.05−7.25 (10H, m), 7.34 (2H, d), 7.46 (1H, d), 8.04 (2H, d), 9.52 (1H, br). MS (FAB): *m/e* 766 $(MH)^+$, 788 $(M + Na)^+$, 804 $(M + K)^+$. HRMS calcd for $C_{39}H_{40}N_7O_{10}$, *m/e* 766.2837; found, *m/e* 766.2825.

Z-Phe-Arg(NO_2)-PABC-PNP (37). Compound **37** was prepared as described above for **32** in 84% yield. ^{1}H NMR ($CDCl_3$/CD_3OD): δ 1.35−1.85 (4H, m), 2.99 (2H, m), 3.17

(2H, m), 4.50 (1H, brt), 4.66 (1H, m), 4.92 (2H, ABq), 5.16 (2H, s), 7.00−7.32 (14H, m), 7.51 (2H, d), 8.18 (2H, d), 9.30 (1H, brs). MS (FAB): *m/e* 771 $(MH)^+$, 793 $(M + Na)^+$, 809 $(M + K)^+$. Anal. Calcd for $C_{37}H_{38}N_8O_{11}$: C, 57.66; H, 4.97; N, 14.54. Found: C, 57.53; H, 4.61; N, 14.77.

Z-Phe-Arg(Ts)-PABC-PNP (38). Compound **38** was prepared as described above for **32** in 99% yield. ^{1}H NMR ($CDCl_3$): δ 1.54 (3H, m), 1.82 (1H, m), 2.31 (3H, s), 2.91 (1H, q), 3.13 (3H, m), 4.55 (2H, m), 4.91 (2H, ABq), 5.18 (2H, s), 6.39 (1H, br), 7.02−7.35 (16H, m), 7.60 (2H, d), 7.69 (2H, d), 8.20 (2H, d). MS (FAB): *m/e* 880 $(MH)^+$, 918 $(M + K)^+$. Anal. Calcd for $C_{44}H_{45}N_7O_{11}S$: C, 60.06; H, 5.15; N, 11.14. Found: C, 59.89; H, 5.12; N, 11.31.

Z-Phe-Lys(alloc)-PABC-DOX (39). Z-Phe-Lys(alloc)-PABC-PNP **29** (337.2 mg, 0.4313 mmol) and DOX·HCl (275.2 mg, 1.1 equiv) in NMP (8 mL) at room temperature were treated with Et_3N (0.066 mL, 1.1 equiv). The mixture was allowed to stand in the dark for 2 d. The mixture was then diluted with 10% 2-propanol/ethyl acetate (100 mL) and washed with water (3 × 100 mL) and brine, dried, and evaporated to give an orange solid. This was purified by flash chromatography on silica gel, eluting with (i) 25:1 and (ii) 15:1 CH_2Cl_2/CH_3OH, to give the product as an orange solid (496.3 mg, 77%). ^{1}H NMR ($CDCl_3/CD_3OD$): δ 1.18 (3H, d), 1.22, 1.38, 1.56 and 1.77 (6H, m), 1.74 (2H, m), 2.23 (2H, m), 2.95 (2H, m), 3.02 (2H, m), 3.53 (1H, s), 3.80 (1H, m), 3.99 (3H, s), 4.06 (1H, m), 4.39 (2H, m), 4.43 (2H, d), 4.70 (2H, s), 4.89 (2H, m), 4.92 (1H, m), 4.96 (2H, d), 5.15 (2H, q), 5.11 and 5.39 (each 1H, s), 5.41 (1H, br), 5.60 and 5.92 (each 1H, m), 5.79 (1H, m), 7.08 and 7.23 (10H, m), 7.13 and 7.40 (4H, 2 x d), 7.50, 7.68 and 7.90 (each 1H, m), 9.15 (1H, brs). MS (FAB): *m/e* 1209 $(M + Na)^+$, 1224 $(M + K)^+$. HRMS calcd for $C_{62}H_{67}N_5O_{19}$, *m/e* 1186.4509; found, *m/e* 1186.4463.

Z-Val-Lys(alloc)-PABC-DOX (40). Compound **40** was prepared as described above for **39** in 69% yield. ^{1}H NMR ($CDCl_3/CD_3OD$): δ 0.83 (6H, m), 1.18 (3H, d), 1.29, 1.41, 1.63 and 1.79 (6H, m), 1.72 (2H, m), 1.98 (1H, m), 2.14 (2H, brs), 3.03 (2H, q), 3.02 (2H, m), 3.52 (1H, m), 3.76 (1H, m), 3.94 (1H, m), 3.99 (3H, s), 4.39 (1H, m), 4.42 (2H, d), 4.69 (2H, s), 4.88 (2H, m), 5.01 (2H, d), 5.14 (2H, q), 5.18 (1H, m), 5.41 (1H, br), 5.80 (1H, m), 7.13 and 7.40 (4H, 2 x d), 7.26 (5H, s), 7.32, 7.70 and 7.93 (each 1H, m), 9.25 (1H, br). MS (FAB): *m/e* 1160 $(M + Na)^+$, 1176 $(M + K)^+$. HRMS calcd for $C_{58}H_{67}N_5O_{19}$, *m/e* 1160.4328; found, *m/e* 1160.4358.

Z-Ala-Lys(alloc)-PABC-DOX (41). Compound **41** was prepared as described above for **39** in 67% yield. ^{1}H NMR ($CDCl_3/CD_3OD$): δ 1.08 (3H, m), 1.20 (3H, d), 1.28, 1.40, 1.60 and 1.81 (6H, m), 1.74 (2H, m), 2.19 (2H, brs), 3.02 (4H, m), 3.53 (1H, m), 3.79 (1H, m), 3.92 (1H, m), 3.97 (3H, s), 4.41 (1H, m), 4.45 (2H, d), 4.72 (2H, s), 4.89 (2H, m), 4.99 (2H, d), 5.08 (2H, q), 5.17 (1H, m), 5.39 (1H, br), 5.78 (1H, brs), 7.15 and 7.44 (4H, m), 7.27 (5H, s), 7.35, 7.73 and 7.94 (each 1H, m), 9.19 (1H, br). MS (FAB): *m/e* 1111 $(MH)^+$, 1133 $(M + Na)^+$, 1149 $(M + K)^+$. HRMS calcd for $C_{56}H_{64}N_5O_{19}$, *m/e* 1110.4196; found, *m/e* 1110.4178.

Z-Val-Cit-PABC-DOX (42). Z-Val-Cit-PABC−PNP **32** (126.9 mg, 0.187 mmol) and DOX·HCl (119.3 mg, 1.1 equiv) in NMP (5 mL) at room temperature were treated with Et_3N (0.029 mL, 1.1 equiv). The mixture was stirred in the dark at room temperature for 2 d. Workup as described above for **39** gave a crude orange solid. This was purified by flash chromatography on silica gel, eluting with (i) 12:1, (ii) 8:1, and (iii) 5:1 CH_2Cl_2/CH_3OH, to give the product as a red-orange solid (158.0 mg, 45%). HPLC (15 cm C-18 column, 4:1 CH_3OH /50 mM Et_3N/HCO_2H buffer (pH 2.8), flow rate: 1 mL/min, λ = 495 nm): retention time 3.70 min. ^{1}H NMR ($CDCl_3/CD_3OD$): δ 0.74 (6H, m), 1.07 (3H, d), 1.28−1.88 (4H, m), 1.64 and 2.08 (each 2H, m), 1.88 (1H, m), 2.87 (2H, m), 3.42 (1H, brs), 3.95 (1H, m), 4.11 (3H, s), 4.38 (2H, m), 4.58 (2H, s), 4.78 (2H, s), 4.90 (2H, s), 5.04 (1H, brs), 5.30 (1H, brs), 7.00−7.86 (12H), 9.31 (1H, brs). MS (FAB): *m/e* 1083 $(MH)^+$, 1105 $(M + Na)^+$, 1121 $(M + K)^+$. HRMS calcd for $C_{54}H_{63}N_6O_{18}$, *m/e* 1083.4199; found, *m/e* 1083.4161. Anal. Calcd for $C_{54}H_{62}N_6O_{18}\cdot 3.5H_2O$: C, 56.59; H, 6.07; N, 7.33. Found: C, 56.59; H, 5.79; N, 7.54.

Z-Phe-Cit-PABC-DOX (43). Compound **43** was prepared as described above for **42** in 35% yield. HPLC (15 cm C-18 column, 4:1 CH_3OH /50 mM Et_3N/HCO_2H buffer (pH 2.8), flow rate: 1 mL/min, λ = 495 nm): retention time 4.55 min. ^{1}H NMR ($CDCl_3/CD_3OD$): δ 1.19 (3H, d), 1.40 (3H, m), 1.59 (1H, m), 1.75 (3H, m), 2.18 (2H, ABq), 2.76−3.20 (6H, m), 3.51 (1H, s), 3.80 (1H, m), 3.97 (4H, m and s), 4.10 (1H, q), 4.38 (2H, m), 4.69 (2H, s), 4.92 (4H, m), 5.12 (1H, brs), 5.39 (1H, brs), 6.10 (1H, d), 6.98−7.25 (12H, m), 7.40 (3H, m), 7.71 (1H, t), 7.89 (1H, t). MS (FAB): *m/e* 1169 $(M + K)^+$. HRMS calcd for $C_{58}H_{62}N_6O_{18}K$, *m/e* 1169.3758; found, *m/e* 1169.3740.

Z-Leu-Cit-PABC-DOX (44). Compound **44** was prepared as described above for **42** in 38% yield. HPLC (15 cm C-18 column, 4:1 CH_3OH /50 mM Et_3N/HCO_2H buffer (pH 2.8), flow rate: 1 mL/min, λ = 495 nm): retention time 4.90 min. ^{1}H NMR ($CDCl_3/CD_3OD$): δ 0.72 (6H, m), 1.10 (6H, m), 1.35−1.60 (4H, m), 1.72 (3H, m), 2.09 (2H, m), 2.83 (2H, m), 3.05 (2H, m), 3.46 (1H, brs), 3.73 (1H, m), 3.95 (1H, m), 4.01 (3H, s), 4.41 (1H, m), 4.64 (2H, s), 4.78 (2H, m), 4.93 (2H, s), 5.06 (1H, brs), 5.36 (1H, brs), 6.98−7.90 (12H). MS (FAB): *m/e* 1119 $(M + Na)^+$, 1135 $(M + K)^+$. HRMS calcd for $C_{55}H_{61}N_6O_{18}Na$, *m/e* 1116.3940; found, *m/e* 1116.3911.

Z-Ile-Cit-PABC-DOX (45). Compound **45** was prepared as described above for **42** in 44% yield. HPLC (15 cm C-18 column, 4:1 CH_3OH /50 mM Et_3N/HCO_2H buffer (pH 2.8), flow rate: 1 mL/min, λ = 495 nm): retention time 4.62 min. ^{1}H NMR ($CDCl_3/CD_3OD$): δ 0.74 (6H, m), 0.98 (1H, m), 1.11 (2H, m), 1.20 (3H, d), 1.38 (3H, m), 1.71 (2H, m), 2.13 (2H, m), 2.82 (2H, m), 3.02 (2H, m), 3.48 (1H, brs), 3.75 (1H, m), 3.97 (3H, s), 4.01 (1H, m), 4.39 (1H, m), 4.64 (2H, s), 4.79 (2H, m), 4.93 (2H, s), 5.07 (1H, brs), 5.37 (1H, brs), 6.95−7.95 (12H). MS (FAB): *m/e* 1095 $(MH)^+$, 1133 $(M + K)^+$. HRMS calcd for $C_{55}H_{62}N_6O_{18}$, *m/e* 1094.4121; found, *m/e* 1094.4105.

Z-Trp-Cit-PABC-DOX (46). Compound **46** was prepared as described above for **42** in 48% yield. HPLC (15 cm C-18 column, 4:1 CH_3OH /50 mM Et_3N/HCO_2H buffer (pH 2.8), flow rate: 1 mL/min, λ = 495 nm): retention time 3.80 min. ^{1}H NMR ($CDCl_3/CD_3OD$): δ 1.22 (6H, m and d), 1.48 (1H, m), 1.75 (3H, m), 2.13 (2H, ABq), 2.70−3.17 (6H, m), 3.51 (1H, s), 3.79 (1H, m), 3.91 (3H, s), 4.10 (1H, q), 4.32 (1H, m), 4.38 (1H, m), 4.69 (2H, s), 4.91 (2H, m), 4.93 (2H, s), 5.04 (1H, brs), 5.37 (1H, brs), 5.91 (1H, br), 6.23 (1H, d), 6.89 (1H, t), 6.98 (1H, t), 7.16 (9H, m), 7.31 (1H, d), 7.36 (2H, d), 7.43 (1H, d), 7.64 (1H, t), 7.78 (1H, d). MS (FAB): *m/e* 1192 $(M + Na)^+$, 1208 $(M + K)^+$. Anal. Calcd for $C_{60}H_{63}N_7O_{18}\cdot 3.5H_2O$: C, 58.43; H, 5.72; N, 7.95. Found: C, 58.17; H, 5.57; N, 8.08.

Z-Phe-Arg(NO_2)-PABC-DOX (47). Compound **47** was prepared as described above for **42** in 65% yield. HPLC (15 cm C-18 column, 4:1 CH_3OH /50 mM Et_3N/HCO_2H buffer (pH 2.8), flow rate: 1 mL/min, λ = 495 nm): retention time 4.45 min. ^{1}H NMR ($CDCl_3/CD_3OD$): δ 1.18 (3H, d), 1.49 (3H, m), 1.72 (3H, m), 2.02 (1H, m), 2.21 (1H, m), 2.61 (1H, m), 2.87 (2H, m), 3.06 (4H, m), 3.52 (1H, brs), 3.74 (1H, m), 3.93 (3H, s), 4.03 (1H, m), 4.42

(2H, m), 4.68 (2H, s), 4.87 (2H, m), 5.11 (1H, br), 5.39 (1H, brs), 5.66 (1H, brd), 6.97−7.78 (15H, m), 7.65 (1H, brt), 7.87 (1H, m)9.13 (1H, brs). MS (FAB): *m/e* 1173.7 $(M-H)^-$. Anal. Calcd for $C_{58}H_{62}N_8O_{19}$-$3H_2O$: C, 56.67; H, 5.57; N, 9.11. Found: C, 56.75; H, 5.28; N, 8.92.

Z-Phe-Arg(Ts)-PABC-DOX (48). Compound **48** was prepared as described above for **42** (74%). HPLC (15 cm C-18 column, 4:1 CH_3OH /50 mM Et_3N/HCO_2H buffer (pH 2.8), flow rate: 1 mL/min, λ = 495 nm): retention time 5.96 min. ^1H NMR ($CDCl_3/CD_3OD$): δ 1.16 (3H, d), 1.39 (3H, m), 1.53 (1H, m), 1.71 (3H, m), 2.01 (1H, d), 2.24 (3H, s), 2.82 (3H, m), 3.02 (5H, m), 3.52 (1H, s), 3.76 (1H, q), 3.92 (3H, s), 4.02 (1H, m), 4.40 (1H, m), 4.48 (1H, m), 4.68 (2H, s), 4.84 (2H, m), 5.08 (1H, brs), 5.38 (1H, brs), 5.61 (1H, brd), 5.98 (1H, brd), 6.37 (1H, br), 6.96−7.20 (14H, m), 7.25 (1H, d), 7.32 (2H, d), 7.64 (3H, m), 7.88 (1H, d), 9.11 (1H, brs). MS (FAB): *m/e* 1306 $(M + Na)^+$, 1322 $(M + K)^+$. HRMS calcd for $C_{65}H_{69}N_7O_{19}SNa$, *m/e* 1306.4269; found, *m/e* 1306.4251.

Z-Phe-Lys-PABC-DOX•HCl (49). Z-Phe-Lys(alloc)-PABC-DOX **39** (34.9 mg, 29.4 mmol) and $(PPh_3)_2PdCl_2$ (0.6 mg, 3 mol %) in dry THF (1 mL) under argon at room temperature were treated with acetic acid (0.0035 mL, 2 equiv) and then with Bu_3SnH (0.01 mL, 1.2 equiv). The reaction was stirred at room temperature for 1.5 h and then treated with 1 M HCl in ether (0.06 mL, 2 equiv). The mixture was stored in the freezer for 1 h, and then, the crude orange solid was collected by filtration and washed repeatedly with ether. The solid was washed through the glass frit with 5:1 CH_2Cl_2/CH_3OH, and then, the filtrate was evaporated. The residue was sonicated in CH_3OH (5 mL) to dissolve as much as possible and then filtered to remove an insoluble red byproduct. The filtrate was evaporated to give an orange-red solid (25.1 mg, 75%). HPLC (15 cm C-18 column, 4:1 CH_3OH /50 mM Et_3N/HCO_2H buffer (pH 2.8), flow rate: 1 mL/min, λ = 495 nm): retention time 7.09 min. ^1H NMR ($CDCl_3/CD_3OD$): δ 1.18 (2H, d), 1.34, 1.65 and 1.73 (6H, m), 2.14 (2H, m), 2.81 (2H, m), 3.76 (1H, m), 3.98 (3H, s), 4.05 (1H, m), 4.38 and 4.45 (each 1H, m), 4.67 (2H, s), 4.85 (1H, m), 7.04 and 7.20 (10H, m), 7.14 and 7.43 (4H, m), 7.30, 7.69 and 7.92 (each 1H, m). MS (FAB): *m/e* 1102 $(MH)^+$, 1124 $(M + Na)^+$. HRMS calcd for $C_{58}H_{64}N_5O_{17}$, *m/e* 1102.4297; found, *m/e* 1102.4290. Anal. Calcd for $C_{58}H_{64}N_5O_{17}$·$0.5H_2O$: C, 60.70; H, 5.71; N, 6.10. Found: C, 60.66; H, 5.93; N, 6.02.

Z-Val-Lys-PABC-DOX·HCl (50). Z-Val-Lys(alloc)-PABC-DOX **40** (84.3 mg, 0.0741 mmol) in THF (2 mL) under argon at room temperature was treated with $Pd(PPh_3)_4$ (0.22 mL of a solution of Pd_2dba_3 (4.7 mg, 5.13 mmol) and PPh_3 (13.5 mg, 10 equiv) in THF (1 mL) under argon, acetic acid (0.011 mL, 2.5 equiv), and tributyltin hydride (0.030 mL, 1.5 equiv). The mixture was stirred at room temperature in the dark for 1 h during which time an orange solid began to form. The mixture was diluted with ether (25 mL) followed by 1 M HCl in ether (1 mL). The resulting suspension was sonicated briefly and then filtered. The orange solid was washed repeatedly with ether and then dissolved in 5:1 CH_2Cl_2/CH_3OH. To this was added Celite (2 g), and the solvents were evaporated. The resulting solid was dry-loaded on a Celite column (from a slurry in 100:1 CH_2Cl_2/CH_3OH). The column was eluted with (i) 100:1 and (ii) 10:1 CH_2Cl_2/CH_3OH, to give the product as an orange solid (58.5 mg, 72%). HPLC (15 cm C-18 column, 4:1 CH_3OH /50 mM Et_3N/HCO_2H buffer (pH 2.8), flow rate: 1 mL/min, λ = 495 nm): retention time 6.03 min. ^1H NMR ($CDCl_3/CD_3OD$): δ 0.83 (6H, m), 1.20 (3H, d), 1.41 (2H, m), 1.73 (1H, m), 1.79 (2H, m), 2.02 (1H, m), 2.12 (2H, m), 2.92 (3H, m), 3.17 (1H, d), 3.52 (1H, s), 3.73 (1H, m), 3.92 (1H, m), 4.01 (3H, s), 4.04 (1H, m), 4.44 (1H, m), 4.70 (2H, s), 4.88 (2H, m), 5.11 (3H, m), 5.42 (1H, s), 7.10−7.30 (7H, m), 7.41 (2H, d), 7.32, 7.72 and 7.91 (each 1H, m). MS (FAB): *m/e* 1054 $(MH)^+$. HRMS calcd for $C_{54}H_{64}N_5O_{17}$, *m/e* 1054.4297; found, *m/e* 1054.4283. Anal. Calcd for $C_{54}H_{56}N_5O_{17}$·H_2O: C, 58.51; H, 6.00; N, 6.32. Found: C, 58.74; H, 6.03; N, 6.29.

Z-Ala-Lys-PABC-DOX·HCl (51). Compound **51** was prepared as described above for **50** in 68% yield. HPLC (15 cm C-18 column, 4:1 CH_3OH /50 mM Et_3N/HCO_2H buffer (pH 2.8), flow rate: 1 mL/min, λ = 495 nm): retention time 4.52 min. ^1H NMR ($CDCl_3/CD_3OD$): δ 1.28 (5H, 2 x d and m), 1.49 (2H, m), 1.67 (1H, m), 1.85 (4H, m), 2.91 (2H, m), 3.00 (1H, d), 3.22 (1H, d), 3.61 (1H, s), 3.80 (1H, m), 4.03 (3H, s), 4.11 (1H, m), 4.39 (2H, m), 4.74 (2H, s), 4.92 (2H, m), 5.09 (2H, m), 5.22 (1H, brs), 5.49 (1H, brs), 7.05−7.35 (8H, m), 7.45 (12H, d), 7.77 (1H, t), 7.99 (1H, d), 9.02 (1H, br). MS (FAB): *m/e* 1027 $(MH)^+$, 1049 $(M + Na)^+$. HRMS calcd for $C_{52}H_{60}N_5O_{17}$, *m/e* 1026.3984; found, *m/e* 1026.3967. Anal. Calcd for $C_{52}H_{60}N_5O_{17}$·$2H_2O$: C, 56.85; H, 5.87; N, 6.38. Found: C, 56.51; H, 5.99; N, 6.35.

Z-Phe-Lys(alloc)-DOX (52). A stirred solution of Z-Phe-Lys(alloc) **9** (127.5 mg, 0.2492 mmol), DOX·HCl (159.0 mg, 1.1 equiv), and HOSu (34.4 mg, 1.2 equiv) in NMP (7.5 mL) at 0 °C was treated with DCC (61.7 mg, 1.2 equiv) and Et_3N (0.038 mL, 1.1 equiv). After 30 min, the mixture was allowed to gradually warm to room temperature. After a further 16 h, the mixture was filtered and the filtrate was diluted with ethyl acetate (100 mL). The solution was washed with water (3×) and brine, dried, and evaporated in vacuo. The residue was purified by flash chromatography on silica gel, eluting with 15:1 CH_2Cl_2/CH_3OH, to give an orange solid (196.1 mg, 76%). ^1H NMR ($CDCl_3/CD_3OD$): δ 1.20 (5H, m and d), 1.36 (2H, m), 1.47 (1H, m), 1.64 (2H, m), 1.82 (1H, brt), 2.14 (2H, ABq), 2.81 (1H, d), 3.01 (2H, m), 3.09 (1H, d), 3.54 (1H, s), 3.73 (1H, m), 3.93 (3H, s), 4.06 (1H, q), 4.21 (1H, q), 4.31 (1H, m), 4.43 (2H, d), 4.70 (2H, s), 4.89 (2H, s), 5.17 (3H, q and s), 5.40 (2H, m and s), 5.79 (1H, m), 6.90−7.40 (11H, m), 7.64 (1H, t), 7.87 (1H, d). MS (FAB): *m/e* 1036 $(M - H)^-$. HRMS calcd for $C_{54}H_{60}N_4O_{17}$-Na, 1059.3851; found, 1059.3856.

Z-Val-Cit-DOX (53). This was prepared as described above for **52** in 68% yield, except that 10% *n*-butanol/ethyl acetate was used in place of ethyl acetate, and the eluting solvents in the chromatographic purification were (i) 20:1, (ii) 10:1, and (iii) 5:1 CH_2Cl_2/CH_3OH. HPLC (15 cm C-18 column, 4:1 CH_3OH /50 mM Et_3N/HCO_2H buffer (pH 2.8), flow rate: 1 mL/min, λ = 495 nm): retention time 3.49 min. ^1H NMR ($CDCl_3/CD_3OD$): δ 0.72 (6H, 2 x d), 1.18 (3H, d), 1.32 (2H, m), 1.46 (1H, m), 1.71 (2H, m), 1.83 (2H, m), 2.13 (2H, ABq), 2.81 (1H, d), 2.98 (2H, m), 3.09 (1H, d), 3.50 (1H, s), 3.87 (1H, m), 3.92 (3H, s), 4.02 (1H, m), 4.27 (1H, q), 4.69 (2H, s), 4.92 (2H, m), 5.05 (1H, brs), 5.33 (1H, brs), 6.02 (1H, d), 7.17 (5H, brs), 7.28 (1H, t), 7.62 (2H, t and d), 7.83 (1H, d). MS (FAB): *m/e* 932.6 $(M - H)^-$. Anal. Calcd for $C_{46}H_{55}N_5O_{16}$·$1.5H_2O$: C, 57.49; H, 6.08; N, 7.29. Found: C, 57.36; H, 6.10; N, 7.27.

Z-Phe-Lys-DOX·HCl (54). Compound **54** was prepared as described above for **50** in 77% yield. HPLC (15 cm C-18 column, 4:1 CH_3OH /50 mM Et_3N/HCO_2H buffer (pH 2.8), flow rate: 1 mL/min, λ = 495 nm): retention time 5.88 min. ^1H NMR ($CDCl_3/CD_3OD$): δ 1.15 (3H, d), 1.33 (2H, m), 1.63 (2H, m), 1.74 (2H, m), 2.03 (2H, m), 2.91 (4H, m), 3.19 (1H, d), 3.51 (1H, s), 3.73 (1H, m), 3.98 (3H, s), 4.02 (1H, m), 4.37 (1H, m), 4.43 (1H, m), 4.68 (2H, s), 4.95 (2H, m), 5.18 (1H, brs), 5.40 (1H, brs), 7.00−

7.30 (10H, m), 7.32 (1H, d), 7.69 (1H, t), 7.92 (1H, m). MS (FAB): *m/e* 953 $(MH)^+$, 975 $(M + Na)^+$, 991 $(M + K)^+$. HRMS calcd for $C_{50}H_{57}N_4O_{15}$, *m/e* 953.3820; found, *m/e* 953.3802. Anal. Calcd for $C_{50}H_{57}N_4O_{15}\cdot H_2O$: C, 59.61; H, 5.90; N, 5.56. Found: C, 59.54; H, 5.87; N, 5.40.

Fmoc-Lys(MMT) (55). A stirred suspension of Fmoc-Lys·HCl (23.78 g, 56.42 mmol) in dry CH_2Cl_2 (250 mL) under argon at room temperature was treated with trimethylsilyl chloride (15 mL, 2.1 equiv) and DIEA (10.3 mL, 1.05 equiv). The mixture was heated at reflux for 1 h, during which time it became homogeneous, and then cooled to 0 °C. DIEA (31 mL, 3.1 equiv) was added, followed by *p*-anisyldiphenylmethyl chloride (18.29 g, 1.05 equiv). The reaction was stirred at room temperature for 14 h. The solvent was evaporated, and the residue was partitioned between ethyl acetate and pH 5 buffer (0.05 M biphthalate). The organic phase was washed with more pH 5 buffer, water, and brine, dried, and evaporated to give a pale yellow foam (34.71 g, 96%). ^{1}H NMR ($CDCl_3$): δ 1.26 and 1.68 (2H and 4H, m), 2.45 (2H, m), 3.71 (3H, s), 4.05−4.40 (4H, m), 6.81 (2H, d), 7.15−7.77 (20H, m). MS (FAB): *m/e* 641 $(MH)^+$, 663 $(M + Na)^+$, 679 $(M + K)^+$. HRMS calcd for $C_{41}H_{41}N_2O_5$, *m/e* 641.3015; found, *m/e* 641.3001.

Lys(MMT) (56). Fmoc-Lys(MMT) **55** (5.25 g, 8.19 mmol) in 1:1 CH_2Cl_2/CH_3CN (80 mL) at room temperature was treated with diethylamine (80 mL). After 1.5 h, the solvents were evaporated. The residue was flushed with CH_3CN (2 × 50 mL) at 60 °C and then triturated with ether (80 mL). The resulting solid was collected by filtration, washed with ether, and then dissolved as far as possible in 1:1 CH_2Cl_2/CH_3OH. Some solid byproduct was removed by filtration, and the filtrate was concentrated in vacuo. The resulting light tan solid was dried in vacuo for 4 h (3.2221 g, 94%). ^{1}H NMR (DMSO-d_6): δ 1.34, 1.57 and 1.72 (m, 6H), 2.05 (m, 2H), 3.38 (m, 1H), 3.68 (s, 3H), 3.71 (d, 2H), 7.03−7.40 (m, 12H). MS (FAB): *m/e* 419.2 $(MH)^+$, 441.4 $(M + Na)^+$, 457.4 $(M + K)^+$. Anal. Calcd for $C_{26}H_{30}N_2O_3\cdot 0.5H_2O$: C, 73.04; H, 7.31; N, 6.55. Found: C, 73.12; H, 7.39; N, 6.56.

Fmoc-Phe-OSu (57). Fmoc-Phe (5.1043 g, 13.17 mmol) and HOSu (1.592 g, 1.05 equiv) in CH_2Cl_2 (100 mL) at 0 °C were treated with DCC (2.854 g, 1.05 equiv). The ice bath was allowed to warm to room temperature, and the mixture was stirred for 14 h. DCU was removed by filtration, and the filtrate was evaporated in vacuo. The resulting material was used without further purification.

Fmoc-Val-OSu (58). Fmoc-Val (5.060 g, 14.91 mmol) and HOSu (1.72 g, 1 equiv) in THF (50 mL) at 0 °C were treated with DCC (3.080 g, 1 equiv). The mixture was stirred at room temperature for 16 h, and then, the solid DCU byproduct was filtered off and washed with THF. The solvent was removed on the rotovap, and the resulting glassy solid was used without purification in the next step.

Fmoc-Phe-Lys(MMT) (59). A stirred suspension of Lys(MMT) **56** (4.686 g, 11.20 mmol) and $NaHCO_3$ (941.0 mg, 1 equiv) in water (100 mL) and DME (50 mL) was treated with a solution of Fmoc-Phe-OSu 57 (11.20 mmol) in DME (50 mL). THF (25 mL) was added to aid solubility. The mixture was stirred at room temperature for 2 d and then as much DME as possible was removed in vacuo at 30 °C. The resulting gummy suspension was partitioned between ethyl acetate and pH 5 buffer. The organic phase was washed with water and brine, dried, and evaporated to give a pale yellow foam. This was flushed with CH_2Cl_2 (100 mL). TLC showed the product to be pure enough to carry on without further purification (8.559 g, 97%). ^{1}H NMR ($CDCl_3/CD_3OD$): δ 1.10−1.93 (6H, m), 2.31 (2H, t), 3.00 (2H, m), 3.71 (3H, s), 4.02−4.48 (5H, m), 6.79 (2H, d), 7.00−7.75 (25H, m). MS (FAB): *m/e* 788.2 $(MH)^+$, 810.4 $(M + Na)^+$, 826 $(M + K)^+$.

Fmoc-Val-Cit (60). Fmoc-Val-OSu **58** (14.91 mmol) in DME (40 mL) was added to a solution of Cit (2.743 g, 1.05 equiv) and $NaHCO_3$ (1.315 g, 1.05 equiv) in water (40 mL). THF (20 mL) was added to aid solubility, and the mixture was stirred at room temperature for 16 h. Aqueous citric acid (15%, 75 mL) was added, and the mixture was extracted with 10% 2-propanol/ethyl acetate (2 × 100 mL). The solid product began to precipitate but remained in the organic layer. The suspension was washed with water (2 × 150 mL), and the solvents were evaporated. The resulting white solid was dried in vacuo for 5 h and then treated with ether (80 mL). After brief sonication and trituration, the white solid product was collected by filtration (5.801 g, 78%). ^{1}H NMR (DMSO-d_6): δ 0.87 (6H, q), 1.40, 1.59 and 1.69 (4H, m), 1.97 (1H, m), 2.94 (2H, q), 3.92 (1H, t), 4.10−4.35 (2H, m), 4.23 (2H, t), 5.37 (2H, brs), 5.92 (1H, t), 7.28−7.90 (8H, m), 8.15 (1H, d). MS (FAB): *m/e* 497 $(MH)^+$, 519 $(M + Na)^+$, 535 $(M + K)^+$. HRMS calcd for $C_{26}H_{33}N_4O_6$, 497.2400; found, 497.2394. Anal. Calcd for $C_{26}H_{32}N_4O_6$: C, 62.89; H, 6.50; N, 11.28. Found: C, 62.92; H, 6.67; N, 11.07.

Fmoc-Phe-Lys(MMT)-PABOH (61). Fmoc-Phe-Lys-(MMT) **59** (7.728 g, 9.808 mmol) and PABOH (1.450 g, 1.2 equiv) in CH_2Cl_2 (100 mL) at room temperature were treated with EEDQ (3.640 g, 1.5 equiv). The mixture was stirred at room temperature for 20 h, and then, the solvent was evaporated (water bath at 30 °C). The solid residue was triturated with ether (200 mL), and the resulting suspension was sonicated for 15 min and left to stand at room temperature for 2 h. The resulting solid was collected by filtration, washed well with ether, and dried in vacuo (7.6140 g, 87%). ^{1}H NMR ($CDCl_3/CD_3$-OD): δ 0.98−1.91 (6H, m), 2.06 (2H, t), 2.97 (2H, m), 3.71 (3H, s,), 4.12 (1H, t), 4.20−4.41 (4H, m), 4.59 (2H, s), 6.72 (2H, d), 7.00−7.73 (29H, m). MS (FAB): *m/e* 891.4 $(MH)^+$, 916.7 $(M + Na)^+$, 931 $(M + K)^+$. Anal. Calcd for $C_{57}H_{56}N_4O_6\cdot H_2O$: C, 75.14; H, 6.42; N, 6.15. Found: C, 75.25; H, 6.42; N, 6.19.

Fmoc-Val-Cit-PABOH (62). Fmoc-Val-Cit **60** (1.0443 g, 2.103 mmol) and PABOH (518.0 mg, 2 equiv) in 2:1 CH_2Cl_2/CH_3OH (35 mL) were treated with EEDQ (1.0402 g, 2 equiv). The mixture was stirred in the dark at room temperature for 1.5 d. The solvents were removed on the rotovap at 40 °C, and the white solid residue was triturated with ether (75 mL). The resulting suspension was sonicated for 5 min and then left to stand for 30 min. The solid was collected by filtration, washed with ether, and dried in vacuo (1.0070 g, 80%). ^{1}H NMR (DMSO-d_6): δ 0.88 (6H, t), 1.41 and 1.65 (4H, m), 2.00 (1H, m), 2.99 (2H, m), 3.92 (1H, t), 4.24 (2H, d), 4.19−4.50 (2H, m), 4.43 (2H, d), 5.11 (1H, t), 5.42 (2H, brs), 5.98 (1H, t), 7.15−7.92 (12H, m), 8.12 (1H, d), 9.99 (1H, brs). MS (FAB): *m/e* 602 $(MH)^+$, 624 $(M + Na)^+$, 640 $(M + K)^+$. HRMS calcd for $C_{33}H_{40}N_5O_6$, *m/e* 602.2979; found, *m/e* 602.2977. Anal. Calcd for $C_{33}H_{39}N_5O_6$: C, 65.87; H, 6.53; N, 11.64. Found: C, 65.61; H, 6.49; N, 11.73.

Phe-Lys(MMT)-PABOH (63). Fmoc-Phe-Lys(MMT)-PABOH **61** (4.286 g, 4.80 mmol) in CH_2Cl_2 (35 mL) at room temperature was treated with diethylamine (50 mL). The mixture was sonicated briefly and stirred at room temperature for 4 h after which time no starting material was observed by TLC (15:1 CH_2Cl_2/CH_3OH). The solvents were evaporated, and the residue was flushed with CH_2Cl_2 and purified by flash chromatography on silica gel, eluting with (i) 2%, (ii) 3%, and (iii) 4% CH_3-OH /CH_2Cl_2, to give the product as a colorless foam (2.230

g, 69%). ^{1}H NMR ($CDCl_3$): δ 1.26−2.00 (6H, m), 2.12 (2H, t), 2.75 and 3.21 (each 1H, ABq), 3.68 (1H, ABq), 3.76 (3H, s,), 4.42 (1H, q), 4.66 (2H, brs), 6.79 (2H, d), 7.10−7.42 (21H, m), 7.81 (1H, d), 8.71 (1H, s). MS (FAB): *m/e* 693.4 $(M + Na)^+$, 709 $(M + K)^+$. Anal. Calcd for $C_{42}H_{46}N_4O_4 \cdot 0.5H_2O$: C, 74.20; H, 6.97; N, 8.24. Found: C, 74.28; H, 7.00; N, 8.34.

Val-Cit-PABOH (64). Fmoc-Val-Cit-PABOH **62** (245.2 mg, 0.4075 mmol) in NMP (4 mL) at room temperature was treated with diethylamine (0.8 mL). The mixture was left to stand at room temperature for 16 h, and then, the solvents were removed on the rotovap at 40 °C. The thick, oily residue was treated with CH_2Cl_2 (15 mL), and the mixture was sonicated at room temperature. The resulting solid was collected by filtration, washed with CH_2Cl_2, and dried in vacuo (141.6 mg, 92%). ^{1}H NMR (DMSO-d_6): δ 0.82 (6H, 2 x d), 1.39, 1.59 and 1.66 (4H, m), 1.92 (1H, m), 2.98 (1H, m), 3.03 (2H, d), 4.45 (2H, d), 4.48 (1H, m), 5.10 (1H, brt), 5.41 (2H, brs), 5.99 (1H, brt), 7.21 and 7.52 (each 2H, d), 8.12 (1H, brd), 10.03 (1H, brs). MS (FAB): *m/e* 380 $(MH)^+$, 402 $(M + Na)^+$, 418 $(M + K)^+$. HRMS calcd for $C_{18}H_{30}N_5O_4$, *m/e* 380.2298; found, *m/e* 380.2290. Anal. Calcd for $C_{18}H_{29}N_5O_4$: C, 56.98; H, 7.70; N, 18.46. Found: C, 56.83; H, 7.63; N, 16.31.

MC-Phe-Lys(MMT)-PABOH (65). A stirred solution of Phe-Lys(MMT)-PABOH **63** (448.1 mg, 0.668 mmol) and DIEA (0.128 mL, 1.1 equiv) in CH_2Cl_2 (7 mL) at room temperature was treated with MC-OSu (230.4 mg, 1.12 equiv). The mixture was stirred at room temperature for 3 d. Ethyl acetate (60 mL) was added, and the mixture was washed with pH 5 buffer (2×), water, and brine, dried, and evaporated. The residue was triturated with ether (60 mL), and the resulting solid was collected by filtration and washed with ether (563.8 mg, 98%). ^{1}H NMR ($CDCl_3$): δ 1.05−1.96 (12H, m), 2.07 (2H, t), 2.18 (2H, t), 3.02 (2H, m), 3.39 (2H, t), 3.71 (3H, s), 4.64 (3H, s and m), 4.99 (1H, q), 6.61 (2H, s), 6.71 (2H, d), 6.89 (1H, m), 7.00−7.55 (21H, m), 8.97 (1H, brs). MS (FAB): *m/e* 864 $(MH)^+$, 886 $(M + Na)^+$, 902.4 $(M + K)^+$. Anal. Calcd for $C_{52}H_{57}N_5O_7 \cdot H_2O$: C, 70.81; H, 6.74; N, 7.94. Found: C, 71.15; H, 7.20; N, 8.27.

MC-Val-Cit-PABOH (66). A solution of Val-Cit-PABOH **64** (136.8 mg, 0.3605 mmol) and MC-OSu (122.3 mg, 1.1 equiv) in NMP (5 mL) was stirred at room temperature for 16 h. The NMP was removed under high vacuum on the rotovap (bath temperature, 40 °C), and the thick, oily residue was triturated with ether (20 mL). The solid product was collected by filtration and washed repeatedly with ether (205.7 mg, 99.6%). ^{1}H NMR (DMSO-d_6): δ 0.82 (6H, ABq), 1.10−1.90 (10H, m), 1.92 (1H, m), 2.16 (2H, t), 2.98 (2H, m), 3.33 (2H, t), 4.19 (1H, t), 4.38 (1H, m), 4.42 (2H, brd), 5.10 (1H, brt), 5.42 (2H, brs), 5.97 (1H, brt), 6.99 (2H, s), 7.21 and 7.52 (each 2H, d), 7.82 and 8.07 (each 1H, d), 9.90 (1H, brs). MS (FAB): *m/e* 573 $(MH)^+$, 595 $(M + Na)^+$, 611 $(M + K)^+$. HRMS calcd for $C_{28}H_{41}N_6O_7$, *m/e* 573.3037; found, *m/e* 573.3016. Anal. Calcd for $C_{28}H_{40}N_6O_7 \cdot 2H_2O$: C, 55.25; H, 7.28; N, 13.81. Found: C, 55.31; H, 6.98; N, 14.03.

MC-Phe-Lys(MMT)-PABC-PNP (67). MC-Phe-Lys-(MMT)-PABOH **65** (679.3 mg, 0.786 mmol) and bis-PNP carbonate (1.196 g, 5 equiv) under argon at room temperature were dissolved in CH_2Cl_2 (25 mL) and treated with DIEA (0.41 mL, 3 equiv). After 3 d, TLC indicated completion. The volume was reduced to ca. 5 mL on the rotovap, and the residue was diluted with ethyl acetate (80 mL) and washed with pH 5 buffer, water, and brine, dried, and evaporated. The resulting solid was triturated with ether (80 mL), and the solid was collected by filtration, washed with ether, and purified by flash chromatography on silica gel, eluting with (i) 1:1 and (ii) 8:1 ethyl acetate/hexane, to give the product as a pale yellow glass (670.7 mg, 83%). ^{1}H NMR ($CDCl_3$): δ 1.10−1.95 (12H, m), 2.04 (2H, t), 2.13 (2H, t), 3.04 (2H, m), 3.39 (2H, t), 3.72 (3H, s), 4.58 (1H, q), 4.86 (1H, q), 5.27 (2H, s), 6.58 (1H, d), 6.61 (2H, s), 6.72 (2H, d), 7.03−7.62 (27H, m), 8.22 (2H, d), 8.86 (1H, brs). MS (FAB): *m/e* 1029 $(MH)^+$, 1051.5 $(M + Na)^+$, 1069.4 $(M + K)^+$. HRMS calcd for $C_{59}H_{61}N_6O_{11}$, *m/e* 1029.4398; found, *m/e* 1029.4422. Anal. Calcd for $C_{59}H_{60}N_6O_{11}$: C, 68.86; H, 5.88; N, 8.17. Found: C, 68.68; H, 5.88; N, 8.04.

MC-Phe-Lys(MMT)-PABC-DOX (68). MC-Phe-Lys-(MMT)-PABC-PNP **67** (126.6 mg, 0.123 mmol) and DOX·HCl (71.3 mg, 1 equiv) in NMP (5 mL) at room temperature were treated with DIEA (0.021 mL, 1 equiv). After 2 d standing in the dark at room temperature, the mixture was diluted with ethyl acetate (60 mL) and washed with water (4×) and brine, dried, and evaporated. The residue was purified by flash chromatography on silica gel, eluting with (i) 25:1 and (ii) 20:1 CH_2Cl_2/CH_3OH, to give the product as an orange glass (149.0 mg, 85%). ^{1}H NMR ($CDCl_3$): δ 1.10−1.95 (14H, m), 1.27 (3H, d), 2.10 (4H, m), 2.23 (2H, m), 3.03 (2H, m), 3.20 (2H, m), 3.41 (2H, t), 3.67 (1H, brs), 3.77 (3H, s), 4.08 (3H, s), 4.13 (1H, m), 4.40 (1H, m), 4.56 (2H, m), 4.76 (2H, brs), 4.99 (2H, m), 5.29 (1H, brs), 5.51 (1H, brs), 5.18, 6.02 and 6.38 (each 1H, m), 6.62 (2H, s), 6.77 (2H, d), 7.00−7.60 (22H, m), 7.78 and 8.03 (each 1H, m), 8.22 (1H, brs). MS (FAB): *m/e* 1433.8 $(MH)^+$, 1456.0 $(M + Na)^+$, 1471.8 $(M + K)^+$. HRMS calcd for $C_{80}H_{85}N_6O_{19}$, *m/e* 1433.5870; found, *m/e* 1433.5813.

MC-Phe-Lys-PABC-DOX·Cl_2CHCO_2H (69). A stirred solution of MC-Phe-Lys(MMT)-PABC-DOX **68** (1.1520 g, 0.804 mmol) in CH_2Cl_2 (50 mL) and anisole (8.73 mL, 100 equiv) was treated with dichloroacetic acid (0.66 mL, 10 equiv). After 1 h, ethyl acetate (80 mL) was added and the resulting suspension was stored in the freezer for 1.5 h. The solid was collected by filtration, washed with ethyl acetate, and dried in vacuo (1.0092 g, 97%). HPLC (15 cm C-18 column, 4:1 CH_3OH /50 mM Et_3N/HCO_2H buffer (pH 2.8), flow rate: 1 mL/min, λ = 495 nm): retention time: 4.52 min. ^{1}H NMR ($CDCl_3/CD_3OD$): δ 1.10−1.90 (14H, m), 1.21 (3H, d), 2.10 (2H, t), 2.20 (2H, m), 2.88 (2H, m), 3.02 (2H, m), 3.12 (2H, m), 3.38 (2H, t), 3.52 (1H, brs), 3.79 (1H, m), 4.02 (3H, s), 4.10 (1H, m), 4.43 and 4.54 (each 1H, m), 4.72 (2H, s), 4.92 (2H, m), 5.24 (1H, br s), 5.44 (1H, br s), 5.84 (1H, s), 6.67 (2H, s), 7.10 (5H, brs), 7.21 and 7.48 (each 2H, d), 7.38, 7.77 and 7.99 (each 1H, d, t, and d). MS (FAB): *m/e* 1159 $(M - H)^-$. HRMS calcd for $C_{60}H_{68}N_6O_{18}Na$, *m/e* 1183.4488; found, *m/e* 1183.4457. Anal. Calcd for $C_{62}H_{70}N_6O_{20}Cl_2 \cdot 2H_2O$: C, 56.15; H, 5.62; N, 6.34. Found: C, 55.87; H, 5.68; N, 6.05.

MC-Val-Cit-PABC-PNP (70). MC-Val-Cit-PABOH **66** (112.4 mg, 0.1963 mmol) under argon at room temperature was dissolved in dry pyridine (3 mL). The solution was cooled to 0 °C, and PNP chloroformate (119 mg, 3 equiv) in CH_2Cl_2 (2 mL) was added all at once. After 10 min at 0 °C, the ice bath was removed and the mixture was stirred at room temperature for 2 h. Ethyl acetate (50 mL) and 15% aqueous citric acid (75 mL) were added. The organic phase was washed with more citric acid, water, and brine, dried, and evaporated to give a light yellow gum. This was purified by flash chromatography on silica gel, eluting with (i) 20:1 and (ii) 15:1 CH_2Cl_2/CH_3OH, to give the product as a white solid (21.5 mg, 15%). ^{1}H NMR ($CDCl_3/CD_3OD$): δ 0.90 (6H, d), 1.16−1.95 (10H, m), 2.12 (1H, m), 2.23 (2H, t), 3.17 (2H, m), 3.48 (2H, t), 4.20 (1H, m), 4.59 (1H, m), 5.22 (2H, s), 6.66

(2H, s), 6.91 and 7.79 (each 1H, d), 7.34 and 7.60 (each 2H, d), 7.34 and 8.23 (each 2H, d), 9.49 (1H, brs). MS (FAB): *m/e* 738 $(MH)^+$, 760 $(M + Na)^+$, 776 $(M + K)^+$. Anal. Calcd for $C_{35}H_{43}N_7O_{11}$: C, 56.98; H, 5.87; N, 13.29. Found: C, 56.68; H, 5.82; N, 12.93.

MC-Val-Cit-PABC-DOX (71). MC-Val-Cit-PABC-PNP **70** (21.2 mg, 0.0287 mmol) and DOX·HCl (18.3 mg, 1.1 equiv) in NMP (1.5 mL) at room temperature were treated with DIEA (0.055 mL, 1.1 equiv). The mixture was left to stand in the dark at room temperature for 2 d, and then, CH_2Cl_2 (25 mL) was added. The resulting suspension was stored in the freezer overnight, and then, the solid was collected by filtration and washed with CH_2Cl_2. The undissolved material was purified by flash chromatography on silica gel, eluting with (i) 15:1, (ii) 10:1, and (iii) 5:1 CH_2Cl_2/CH_3OH (the sample was loaded in a minimum amount of 2:1 CH_2Cl_2/CH_3OH), to give the product as an orange solid (22.4 mg, 68%). HPLC (15 cm C-18 column, 4:1 CH_3OH /50 mM Et_3N/HCO_2H buffer (pH 2.8), flow rate: 1 mL/min, $\lambda = 495$ nm): retention time 3.49 min. ^1H NMR ($CDCl_3/CD_3OD$): δ 0.83 (6H, d), 1.18 (3H, d), 1.20−1.86 (12H, m), 1.93 (1H, m), 2.12 (2H, m), 2.17 (2H, t), 2.90−3.20 (4H, q and m), 3.39 (2H, t), 3.50 (1H, brs), 3.98 (3H, s), 4.02 (1H, m), 4.05 (1H, m), 4.46 (1H, m), 4.68 (2H, s), 4.88 (2H, q), 5.16 (1H, brs), 5.39 (1H, brs), 6.62 (2H, s), 7.13 and 7.42 (each 2H, d), 7.32, 7.71 and 7.92 (each 1H; d, t and d). MS (FAB): *m/e* 1141 $(MH)^+$, 1164.6 $(M + Na)^+$, 1180 $(M + K)^+$. HRMS calcd for $C_{56}H_{67}N_7O_{19}Na$, *m/e* 1164.4389; found, *m/e* 1164.4363. Anal. Calcd for $C_{56}H_{67}N_7O_{19}\cdot H_2O$: C, 57.97; H, 5.99; N, 8.45. Found: C, 58.23; H, 5.97; N, 8.18.

Preparation of Immunoconjugates. *BR96-SC-Phe-Lys-PABC-DOX (72).* A solution of the MAb BR96 in 0.025 M citrate buffer (400 mL, 8.52 mg/mL, ca. 0.057 mM, concentration determined by UV absorption at 280 nm, 1 mg/mL of MAb equals 1.4 absorbance units) was diafiltered in two Amicon model 8400 stirred ultra filtration cells fitted with a YM30 ultrafilter (MW cutoff 30 000) to exchange the citrate buffer with 0.01 M phosphate-buffered 0.9% sodium chloride solution (PBS, pH 7.4). The solution was then incubated at 37 °C under nitrogen with gentle stirring and then treated with 10 mM DTT in 0.01 M PBS (16.6 mL, freshly prepared, 7.0 equiv), giving a final DTT concentration of 0.40 mM. After 3 h, the solution was transferred to two Amicon cells and diafiltration was carried out against 0.01 M PBS at pH 6 until the effluent was free of SH groups (as detected by Ellman reagent). The antibody solutions were transferred to a sterile container and kept at 0 °C under nitrogen. The concentration of protein was determined by the UV absorbance at 285 nm and that of thiol by the method of Ellman (*18*) (9.01 mg/mL, and 0.468 mM, respectively; MR (SH/protein) = 8.31). To the stirred antibody solution was added 1 mol of MC-Phe-Lys-PABC-DOX·Cl_2CHCO_2H **69** (57.6 mL of a 5 mg/mL solution in DMF) per mole of free thiol generated on the antibody. After it was stirred at 4 °C for 30 min, the mixture was left to stand for 16 h at 4 °C and then filtered through a 0.22 μm cellulose acetate membrane. The filtrate was chromatographed on a 10 cm × 30 cm gel filtration column (Cellufine GH25, Amicon), and the product-containing fractions were combined. The conjugate solution was filtered again through a 0.22 μm cellulose acetate membrane (final volume, 475 mL). The concentration of DOX was determined using the UV absorbance at 495 nm ($\epsilon_{495} = 8030$ cm^{-1} M^{-1}; 328 mM, 67.9 mg/mL) and that of the MAb at 280 nm with a correction for DOX absorbance at 280 nm according to the formula (*19*)

$$[\text{MAb}]\ (\text{mg/mL}) = (A_{280} - (0.724 \times A_{495}))/1.4$$

where *A* is the observed absorbance at noted wavelength.

The MR of DOX conjugated to the antibody was 8.2. Human IgG (Rockland Inc., Gilbertsville, PA) was used to prepare a nonbinding control IgG-SC-Phe-Lys-PABC-DOX conjugate **74** as described above.

BR96-SC-Val-Cit-PABC-DOX (73). This was prepared essentially as described above for **72** giving an immunoconjugate with MR = 4.4. Human IgG was used to prepare a nonbinding control IgG-SC-Val-Cit-PABC-DOX conjugate **75**.

Drug Release by Cathepsin B. Assay conditions were chosen to approximate the lysosomal medium as a model for intracellular drug release. A stock solution of bovine spleen cathepsin B (EC 3.4.22.1, M_W ca. 40 000) was prepared by dissolving the lyophilized solid (1.2 mg, ca. 36% protein) in 1 mL of a 25 mM sodium acetate/1 mM EDTA buffer (pH 5.0). The enzyme solution was found to be stable at 4 °C for at least 8 h and was stored overnight at −80 °C. Stock solutions were discarded within 2 weeks of preparation. For each assay, a portion of the enzyme solution (0.006 mL) was activated at room temperature with a solution of 30 mM DTT/15 mM EDTA (0.012 mL) for 15 min. The activated cathepsin B was then diluted with 2 mL of a 25 mM acetate/1 mM EDTA buffer (pH 5.0, preincubated at 37 °C) (*20*).

For dipeptide model compounds, 0.008 mL of a 10 mM solution of the substrate in CH_3OH was added to the enzyme solution, giving the following approximate initial concentrations: [cathepsin B] = 30 nM and [substrate] = 0.04 mM. The mixture was incubated at 37 °C, and aliquots were removed at various time points and injected into the HPLC (15 cm C-18 column, 4:1 CH_3OH /50 mM Et_3N-HCO_2H buffer (pH 2.8), flow rate: 1 mL/min, $\lambda =$ 495 nm). The time between injections was varied depending on the speed of drug release. The ratios of DOX/substrate peak areas were used to calculate half-lives ($t_{1/2}$) of release. At 495 nm, the appearance of DOX correlated precisely with the disappearance of substrate. When Z-Phe-Lys-PABC-DOX **49** was run at higher concentrations (≥5 mM), a small, transient peak was observed between the substrate and the DOX peaks that might have been the intermediate PABC-DOX (Figure 1 and Scheme 1). Substrate stabilities were also measured in the pH 5 buffer solution in the absence of cathepsin B. No measurable release of DOX was ever observed within 6−7 h.

For testing of immunoconjugates, 0.3 mL of a 10 mg/mL solution of the substrate in PBS (pH 7.0) was diluted to 1 mL with the pH 5.0 acetate/EDTA buffer at 37 °C (final pH, 5.3). This solution was added to the cathepsin B, activated as described above. The mixture was incubated at 37 °C. Periodically, 0.025 mL aliquots were removed and diluted with ice-cold CH_3OH (0.05 mL) to precipitate protein. The samples were centrifuged, and the supernatants were injected into the HPLC (configured as described above). Half-lives were calculated by calibration of DOX peak areas with a standard curve of known DOX concentrations. For each immunoconjugate, >90% of the theoretical release of DOX was observed.

Drug Release in Rat Liver Lysosomes. Rat liver lysosomes were isolated by differential centrifugation according to the method of Lardeux (*21*). The protein concentration in the lysosomal pellets was determined by the Bradford assay (Bio-Rad Protein Assay Kit II, Bio-Rad, Hercules, CA). For a typical incubation, a known concentration of linker was added to a pH 5.5 sucrose/phosphate buffer mixture containing 0.1% Triton-X and

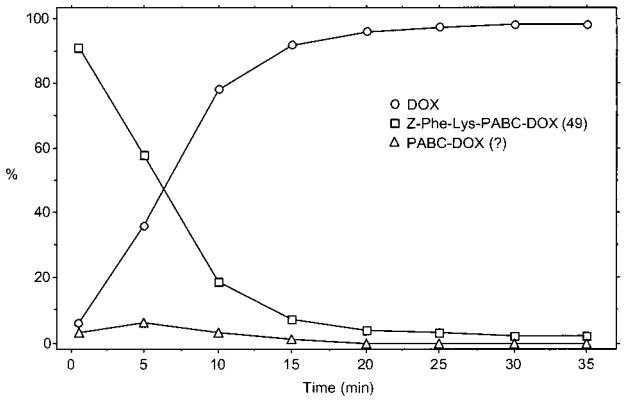


Figure 1. Cathepsin B-mediated release of free DOX from Z-Phe-Lys-PABC-DOX **49** at pH 5.0, 37 °C.

6 mg of lysosomal protein. The mixtures were incubated at 37 °C, and at specific time points, aliquots were removed and the protein was precipitated. The supernatant solution was then extracted and analyzed for free DOX by HPLC. In some experiments, the DOX-containing model substrates and immunoconjugates were incubated with the potent cathepsin B, H, and L inhibitor, E-64 (L-*trans*-epoxysuccinyl-L-leucylamido-(4-guanidino)-butane; final concentration, 0.010 mg/mL) (*22*).

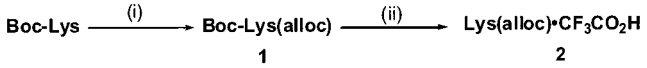
Human Plasma Stability Assays. For each dipeptide model compound assay, a portion (0.004 mL) of a 10 mM solution of the substrate in CH_3OH was injected into freshly drawn human plasma (1 mL, preincubated at 37 °C). For the immunoconjugate, 0.3 mL of a 10 mg/mL solution in PBS (pH 7.0) was diluted to 1 mL with plasma. Each sample was incubated at 37 °C. Aliquots (0.05 mL) were periodically removed and diluted with ice-cold CH_3OH (0.1 mL) to precipitate proteins. The samples were centrifuged for 10 min, and the supernatants were injected into the HPLC (configured as described above). Half-lives were calculated as described above. Enough free DOX was added to a separate plasma sample to give a theoretical release of 1%. This was successfully detected using the same methods.

Human Tumor Cell Lines. L2987 is a lung adenocarcinoma line obtained from I. Hellstrom (Bristol-Myers Squibb, Seattle, WA), HCT116 is a colorectal tumor line obtained from M. Brattain (Baylor Institute, TX), and A2780 is an ovarian carcinoma line obtained from K. Scanlon (National Cancer Institute).

Binding Assays. Binding assays were performed by indirect immunofluorescence. Briefly, target cells were harvested in logarithmic phase using trypsin/EDTA (GIBCO, Grand Island, NY) in PBS. The cells were washed twice in PBS containing 1% BSA (Sigma Chemical Co.) and resuspended to 1×10^7/mL in PBS containing 1% BSA and 0.1% sodium azide. Cells (0.1 mL) were mixed with various antibodies (0.1 mL at 0.040 mg MAb/mL) and incubated for 45 min at 4 °C. The cells were washed twice and resuspended in 0.1 mL of an appropriate concentration of rabbit antihuman IgG (Cappel Laboratories, Cochranville, PA, Fab′2 fragment). Cells were incubated for 30 min at 4 °C, washed twice, and kept on ice until analyzed on a Coulter EPICS 753 fluorescence-activated cell sorter. Data are expressed as FI: the mean channel number of specific minus control antibody.

In Vitro Cytotoxicity. Antigen-specific cytotoxicity was evaluated as described previously (*2*). Briefly, monolayer cultures of various human carcinoma cells were harvested and the cells were counted and resuspended to 1×10^5/mL in RPMI-1640 containing heat-inactivated FCS (RPMI-10% FCS). Cells (0.1 mL/well) were added to each well of 96 well microtiter plates and incubated overnight at 37 °C in a humidified atmosphere of 5% CO_2. Media was removed from the plates, and serial dilutions of DOX or MAb-DOX conjugates were added to the wells. All dilutions were performed in quadruplicate. Cells were exposed to DOX or MAb-DOX conjugates for 2 h, at 37 °C, in a humidified atmosphere of 5% CO_2. Plates were then centrifuged (200*g*, 5 min), the drug or conjugate was removed, and the cells were washed three times and cultured in RPMI-10% FCS (37 °C, 5% CO_2). Approximately 48 h after the addition of conjugates or DOX, the cells were pulsed for 2 h with 1.0 mCi/well of ^{3}H-thymidine (New England Nuclear, Boston, MA). Cells were harvested onto glass fiber mats (Skatron Instruments Inc., Sterling, VA), and dried, and filter-bound ^{3}H radioactivity was determined (β-plate scintillation counter, Pharmacia LKB Biotechnology, Piscataway, NJ). Inhibition of ^{3}H-thymidine uptake was determined by comparing the mean CPM for treated samples with that of the untreated control.

Scheme 2[a]



[a] Conditions: (i) $(Alloc)_2O$, Et_3N, 0 °C to room temperature. (ii) TFA, CH_2Cl_2, room temperature.

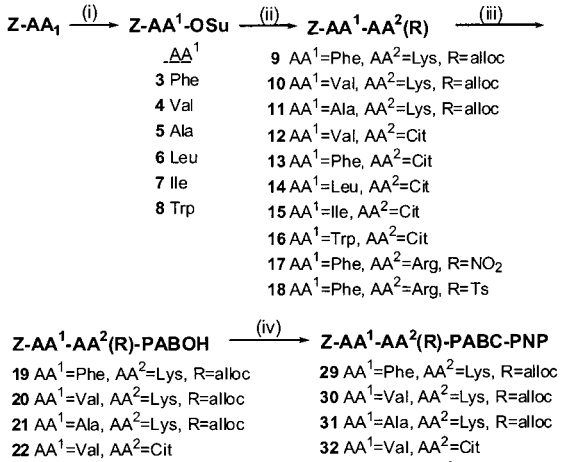
RESULTS AND DISCUSSION

Dipeptide Model Substrate Preparation. The Z-protected dipeptide model substrates were prepared as outlined in Schemes 2−4, for the most part using modifications of well-known methods in peptide chemistry. The self-immolative PABC spacer was introduced by coupling PABOH to the dipeptide using EEDQ (**19**−**28**) followed by reaction with PNP chloroformate to give the activated carbonates (**29**−**38**). Alloc was used for protection of the side chain amino group of Lys (Scheme 2). Deprotection of compounds **39**−**41** and **52** was effected by treatment with $Pd(PPh_3)_4$ or $(PPh_3)_2PdCl_2$ followed by quenching of the allyl−Pd complex with Bu_3SnH (*23*). Triethylsilane was also tried as a hydride source but was found to be too sluggish. Careful addition of either 1 M HCl/ether precipitated the crude ammonium salts (**49**−**51** and **54**). Satisfactory purification usually involved simply dissolving the solid as far as possible in methanol and filtering off insoluble byproducts but could also be carried out by chromatography on Celite, eluting with progressively more polar mixtures of CH_3OH/CH_2Cl_2.

Immunoconjugate Preparation. Chimeric BR96 is a human IgG_1 MAb directed against a Lewis^y-related, tumor-associated antigen. The MAb contains four interchain disulfides that can be opened under mild reducing conditions (i.e., titrated DTT at 37 °C) giving eight free thiol groups that can be functionalized with maleimides and other thiophiles and leaving 12 intrachain disulfides intact (*24*). DOX-peptide substrates **69** and **71** that possess a thiophilic maleimide ring for conjugation to BR96 were prepared as shown in Schemes 5−8. The Val-Cit dipeptide sequence was included because we did not want to rely solely on the in vivo stability of AA[1]-Lys-containing substrates. The six-carbon caproyl spacer used in BR96-DOX was retained to provide space between the dipeptide and the large antibody.

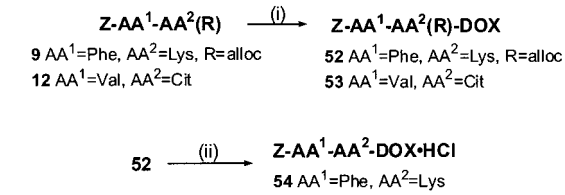
For the preparation of **69** and **71**, two major modifications had to be made to the syntheses shown for the model substrates. In both cases, an N-terminal protecting

Scheme 3[a]



[a] Conditions: (i) HOSu, DCC, 0 °C to room temperature. (ii) $AA^2(R)$, $NaHCO_3$, DME/water, room temperature. (iii) PABOH, EEDQ, THF, room temperature. (iv) PNPOCOCl, pyridine, CH_2Cl_2, room temperature. (v) DOX-HCl, DIEA, DMF, room temperature. (vi) (1) $Pd(PPh_3)_4$ or $(PPh_3)_2PdCl_2$, Bu_3SnH, AcOH, THF, room temperature; (2) 1 M HCl/ether.

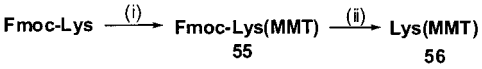
Scheme 4[a]



[a] Conditions: (i) DOX-HCl, HOSu, DCC, DIEA, DMF, 0 °C to room temperature. (ii) (1) $Pd(PPh_3)_4$ Bu_3SnH, THF, room temperature; (2) 1 M HCl/ether.

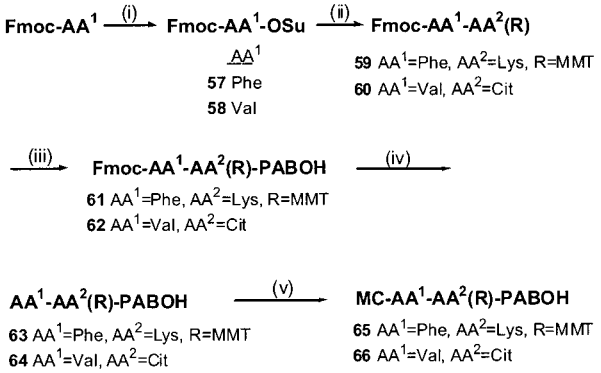
group was required for the P_2 AA until the PABOH was installed (**65** and **66**) since we found that the presence of the maleimide caused nonproductive consumption of EEDQ. For MC-Phe-Lys-PABC-DOX **69**, a new side chain amino protecting group was needed for Lys as maleimides were found to be unstable under all conditions used to remove the alloc group. The selection of protecting groups is very restricted in this case because DOX is labile to all but very mild acids (including TFA) as well as reducing agents, while the maleimide is sensitive to

Scheme 5[a]



[a] Conditions: (i) (1) TMSCl, DIEA, CH_2Cl_2, reflux; (2) MMT chloride; (3) CH_3OH, reflux. (ii) Et_2NH, CH_3CN/CH_2Cl_2, room temperature.

Scheme 6[a]



[a] Conditions: (i) HOSu, DCC, 0 °C to room temperature. (ii) AA^2, $NaHCO_3$, DME/water, room temperature. (iii) PABOH, EEDQ, THF, room temperature. (iv) Et_2NH, NMP or CH_2Cl_2, room temperature. (v) MC-OSu, DIEA, NMP or CH_2Cl_2.

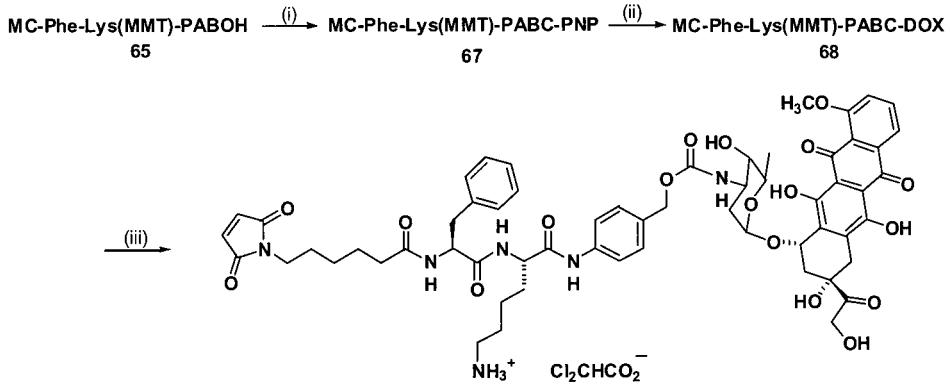
nucleophiles and reduction. We first used Boc and Fmoc as the N-terminal and Lys side chain protecting groups, respectively (synthesis not shown). In this sequence, Fmoc was removed in the final step by very brief (<1 min) treatment with 1% DBU in THF, followed by protonation with 1M HCl/ether. Yields of **69**, as the HCl salt, ranged from 30 to 50% and included large amounts of oligomeric byproducts probably resulting from addition of the Lys amino group to the maleimide. Purification on either LH-20 lipophilic Sephadex or Celite was cumbersome, and the whole procedure was not easily amenable to large-scale synthesis.

Substantial improvement resulted from the use of MMT as the Lys protecting group, with Fmoc blocking the N terminus of the P_2 AA (*25*). MMT was introduced through TMS activation/protection of Fmoc-Lys (Scheme 5) (*26*). Although MMT-protected amines are unreactive under normal conditions with the typical moderately activated carbonates and esters used in peptide-related synthesis, MC-Phe-Lys(MMT)-PABOH (**65**) overreaction with PNP chloroformate did occur at 0 °C, resulting in formation of the Lys-PNP carbamate with loss of MMT. However, we were able to replace the chloroformate with bis-PNP carbonate to provide the activated carbonate **67** in good yield. MMT was removed from the DOX-containing intermediate **68** by treatment with dichloroacetic acid/anisole in CH_2Cl_2 in nearly quantitative yield. The dichloroacetate salt **69** was precipitated out of solution by the addition of ether. Filtration, washing with ether, and thorough drying resulted in analytically pure product.

MC-Val-Cit-PABC-DOX **71** was prepared in a similar manner (Scheme 8). In subsequent work on other Cit-containing linkers, we found that the PNP carbonates (i.e., **70**) are also more efficiently made using bis-PNP carbonate as shown in Scheme 7.

DOX-peptide substrates **69** and **71** were conjugated with thiolated BR96 by a modification of the procedure used for BR96-DOX (*24*) as shown in Scheme 9, affording the immunoconjugates BR96-Phe-Lys-PABC-DOX **72** and BR96-Val-Cit-PABC-DOX **73**. The process involves the reduction of four interchain disulfide bonds in the hinge

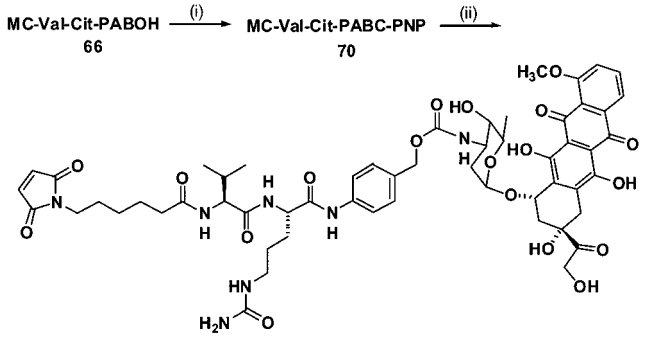
Scheme 7[a]



69 MC-Phe-Lys-PABC-DOX • Cl_2CHCO_2H

[a] Conditions: (i) $(PNPO)_2CO$, DIEA, CH_2Cl_2, room temperature. (ii) DOX-HCl, DIEA, DMF, room temperature. (iii) Dichloroacetic acid, anisole, CH_2Cl_2, room temperature, 1 h.

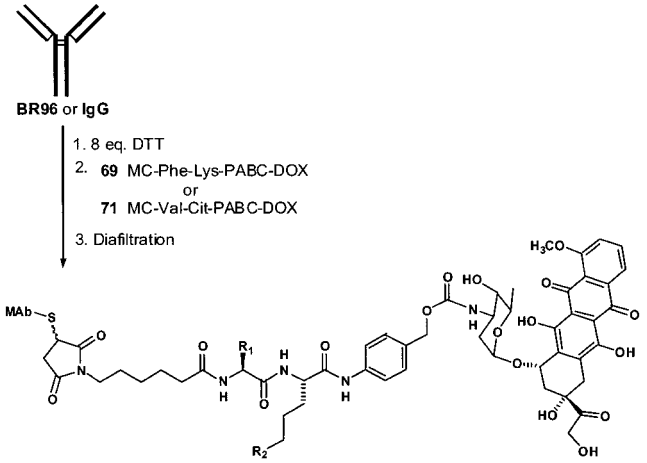
Scheme 8[a]



71 MC-Val-Cit-PABC-DOX

[a] Conditions: (i) PNPOCOCl, pyridine, CH_2Cl_2, room temperature. (ii) DOX-HCl, DIEA, DMF, room temperature.

Scheme 9



72 MAb = BR96, R_1 = Bn, R_2 = CH_2NH_2: BR96-SC-Phe-Lys-PABC-DOX
73 MAb = BR96, R_1 = iPr, R_2 = $NHCONH_2$: BR96-SC-Val-Cit-PABC-DOX
74 MAb = IgG, R_1 = Bn, R_2 = CH_2NH_2: IgG-SC-Phe-Lys-PABC-DOX
75 MAb = IgG, R_1 = iPr, R_2 = $NHCONH_2$: IgG-SC-Val-Cit-PABC-DOX

region of the antibody to give eight free thiol groups. Protein yields for both immunoconjugates were nearly quantitative. The DOX/MAb MR of 8 for the Phe-Lys conjugate **72** represents maximal drug loading. The lower MR of 4.4 for the Val-Cit conjugate **73** probably resulted from the limited aqueous solubility of **71**. Subsequent experiments showed that even very hydrophobic linker compounds could be conjugated to give high MRs by careful manipulation of conditions (i.e., pH, rate of stirring, etc.) during addition. Nonbinding human IgG conjugates (**74** and **75**) were prepared or each dipeptide linker as a control.

Table 1. Half-Lives ($t_{1/2}$) of Cathepsin B-Mediated Release of DOX from Dipeptide Model Substrates at 37 °C, pH 5.0

substrate	no.	$t_{1/2}$ (min)
Z-Phe-Lys-PABC-DOX	**49**	8
Z-Phe-Lys-DOX	**54**	NH[a]
Z-Val-Lys-PABC-DOX	**50**	9
Z-Ala-Lys-PABC-DOX	**51**	60
Z-Val-Cit-PABC-DOX	**42**	240
Z-Val-Cit-DOX	**53**	NH
Z-Phe-Cit-PABC-DOX	**43**	630
Z-Leu-Cit-PABC-DOX	**44**	528
Z-Ile-Cit-PABC-DOX	**45**	918
Z-Trp-Cit-PABC-DOX	**46**	2040
Z-Phe-Arg(NO_2)-PABC-DOX	**47**	1980
Z-Phe-Arg(Ts)-PABC-DOX	**48**	1980

[a] NH = not hydrolyzed (no observed change over 6−7 h).

Enzymatic DOX Release and Plasma Stability. Cathepsin B-mediated DOX release data for these substrates are shown in Table 1. Drug release from representative examples lacking the PABC spacer (**53** and **54**) was not observed over 6−7 h. Steric crowding around the P_1 amide carbonyl and/or the inability of the cathepsin B active site, which is located in a deep cleft in the protein (*6*), to include the bulky DOX moiety are the most probable explanations. Enhanced reactivity of the PABC anilide can be ruled out as the explanation even though aniline pK_a values are low (ca. 4), since cathepsin B released Gly-DOX from a substrate containing Val-Cit-Gly-DOX (synthesis not shown) with $t_{1/2}$ = 2 h, and the pK_a values of the DOX amino group (8.2) (*27*) and Gly-Ala-Ala (8.1) (*28*) are very similar. Therefore, Gly serves as an adequate steric, but not self-immolative, spacer for DOX.

Other trends are evident in the cathepsin B half-life data. At the P_1 site, the protonatable Lys is more readily attacked than Cit, whose side chain can only form hydrogen bonds. Substrates containing nitro- and tosyl-protected Arg (**47** and **48**) are very slowly cleaved. On the basis of the limited variety of side chains tested, the preference at the P_2 site is for a sizable hydrophobic residue. Cathepsin B also accepts basic AAs at P_2, but these sequences would probably be targets of other proteases in vivo (*6*). In the AA^1-Cit series (**42**−**46**), differences in release rates are seen when AA^1 is varied, with Val giving the best results. When P_1 = Lys, there

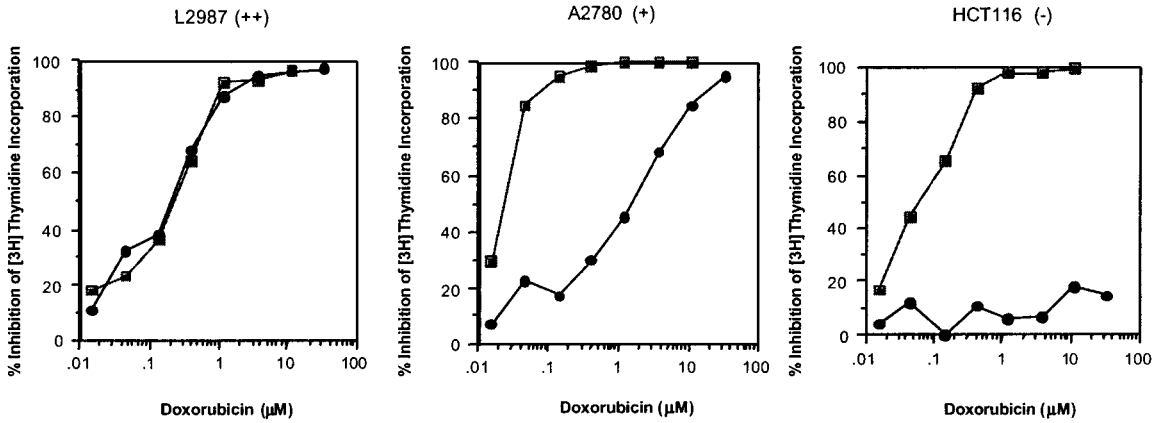


Figure 2. Cytotoxicities of BR96-SC-Phe-Lys-PABC-DOX **72** (●) and DOX (■) against human carcinoma lines L2987 (lung), A2780 (ovarian), and HCT116 (colon) that express different densities of the BR96-defined antigen.

Table 2. Half-Lives (min) of Release of DOX from Dipeptide Model Substrates and Immunoconjugates at 37 °C

substrate	no.	cathepsin B	rat liver lysosomes	human plasma
Z-Phe-Lys-PABC-DOX	**49**	8	29	NH
Z-Phe-Lys-DOX	**54**	NH[a]	NH	
Z-Val-Cit-PABC-DOX	**42**	240	29	NH
Z-Val-Cit-DOX	**53**	NH	NH	
BR96-SC-Phe-Lys-PABC-DOX	**72**	180	55	NH
BR96-SC-Val-Cit-PABC-DOX	**73**	285	159	NH

[a] NH = not hydrolyzed (no observed change over 6−7 h).

Table 3. Cytotoxicity of BR96-Phe-Lys-PABC-DOX 72, a Nonbinding IgG-SC-Phe-Lys-PABC-DOX Conjugate 74 and Unconjugated DOX Against Human Carcinoma Lines Expressing Varying Levels of the BR96 Antigen

		inhibition of proliferation (IC_{50} μM equivalent DOX)			specificity ratio[a]
cell line	BR96 antigen expression	**72**	**74**	DOX	IgG/BR96
L2987	+++	0.2	>33	0.2	>220
A2780	+	1.5	ND[b]	0.02	ND
HCT116	−	>33	>33	0.06	N/A[c]

[a] IC_{50} of **74**/**72**. [b] Not determined. [c] Not applicable.

is no measurable difference between Phe and Val at P_2. However, DOX release is so fast for these substrates that it is unlikely that a difference would have been seen. This P_2 selectivity in the Cit series may reflect different active site binding modes for Cit and Lys at P_1 resulting in somewhat different substrate orientations.

Representative model compounds were tested in a preparation of rat liver lysosomal enzymes (Table 2). Whereas Z-Phe-Lys-PABC-DOX **49** was cleaved much more quickly than Z-Val-Cit-PABC-DOX **42** by cathepsin B alone, in the lysosomal mixture the two showed no difference in their release rates. In addition, DOX release from both was completely inhibited by the cysteine protease inhibitor E-64 (*22*) (data not shown). These results suggest that other lysosomal cysteine proteases that are inhibited by E-64 (cathepsins L and H) may be involved in drug release from **42**. As was seen with cathepsin B, the two substrates that lack the self-immolative PABC spacer (**53** and **54**) are not hydrolyzed in the lysosomal mixture.

Importantly, the AA[1]-Lys substrates **49**−**51** and Z-Val-Cit-PABC-DOX **53** were found to be unchanged in freshly drawn human plasma at 37 °C over 6−7 h (Table 2), demonstrating the stability of these dipeptides to plasma proteases and the PABC spacer to plasma esterases and proteases.

Immunoconjugates **72** and **73** were tested for drug release with cathepsin B (Table 2) as described above for the model substrates. In both cases, DOX was released more slowly from the conjugate in comparison with the corresponding model substrate, perhaps reflecting the greater steric barrier that the antibody presents to the protease. However, the difference in rates between the two immunoconjugates was not of the same magnitude as was seen for the model compounds. DOX release was nearly quantitative (>90%) from both conjugates. In the rat liver lysosome preparation, both **72** and **73** released DOX more quickly than with cathepsin B alone, and release was completely inhibited by E-64, again implicating other lysosomal proteases acting along with cathepsin B, perhaps more effectively. No free DOX was detected from either conjugate upon incubation in freshly drawn human plasma over 7 h (Table 2).

Antigen-Specific Cytotoxicity of BR96-Phe-Lys-PABC-DOX and BR96-Val-Cit-PABC-DOX Conjugates. The L2987, A2780, and HCT116 human carcinoma cell lines were evaluated for their expression of the BR96 antigen using direct immunofluorescence. The L2987 lung tumor line expressed the greatest density of the BR96 antigen (FI = 172.8), the A2780 ovarian line expressed BR96 at a lower density (FI = 103.2), and the HCT116 colon line did not express the antigen (FI = 0). The in vitro potency of BR96-Phe-Lys-PABC-DOX **72** against these three lines was evaluated in comparison with a nonbinding IgG-Phe-Lys-PABC-DOX conjugate **74** and unconjugated DOX (Table 3 and Figure 2). The potency of **72** was directly related to the level of antigen expression on the various cell lines. The L2987 lung carcinoma line that expresses the highest level of BR96 antigen was the most sensitive to **72** (IC_{50} = 0.15 μM) whereas the conjugate was not active against the antigen negative HCT166 carcinoma line (IC_{50} > 33 μM). The antigen-specific activity of **72** was also shown by the lack of activity of the nonbinding conjugate **74**. Against L2987, the line expressing the highest level of the BR96 antigen, **72** was >220-fold more potent than **74** evaluated in parallel. The activity of **72** in comparison with DOX is shown for the three carcinoma lines in Figure 2. The potency of **72** was equivalent to that of unconjugated DOX against the high antigen-expressing line L2987, approximately 75-fold less potent than DOX against the low-expressing A2780 line, and >550-fold less potent than DOX against the antigen negative HCT116 line.

The activity of the BR96-Val-Cit-PABC-DOX conjugate

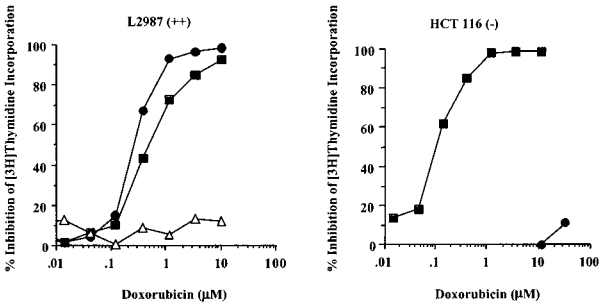


Figure 3. Cytotoxicities of BR96-SC-Val-Cit-PABC-DOX **73** (●), IgG-SC-Val-Cit-PABC-DOX **75** (△), and DOX (■) against human carcinoma lines L2987 (lung) and HCT116 (colon) that express different densities of the BR96-defined antigen.

73 (Figure 3) was also related to the density of BR96 antigen expressed by the L2987 and HCT116 carcinoma lines. The potency of **73** (IC_{50} = 0.4 μM) was similar to that of free DOX (IC_{50} = 0.2 μM) against the high-expressing L2987 line. In contrast, **73** was not active against the antigen negative HCT116 carcinoma line (IC_{50} > 33 μM), even though this line was quite sensitive to free DOX (IC_{50} = 0.1 μM). Both dipeptide-containing immunoconjugates showed superior potency to the hydrazone-linked BR96-DOX (IC_{50} (L2987) = 2.8 μM vs 0.15 μM for **72**) as well as greatly enhanced selectivity (specificity ratio = 8 vs >220 for **72**) (*29*).

In summary, the robust human plasma stability and the potent, antigen-specific cytotoxicity of **72** and **73** suggest that these dipeptide linkers may improve both the efficacy and the therapeutic index of MAb-directed delivery. Indeed, immunoconjugates **72** and **73** proved to be highly active in vivo. Those results will be the subject of a later paper.

NOTE ADDED AFTER ASAP POSTING

The units for a number of IC_{50} values in the text were corrected to micromolar (μM) from millimolar (mM). The corrected version was posted on June 27, 2002.

LITERATURE CITED

(1) Dubowchik, G. M., and Walker, M. A. (1999) Receptor-mediated and enzyme-dependent targeting of cytotoxic anticancer drugs. *Pharmacol. Ther. 83*, 67−123.

(2) Trail, P. A., Willner, D., Knipe, J., Henderson, A. J., Lasch, S. J., Zoeckler, M. E., TrailSmith, M. D., Doyle, T. W., King, H. D., Cassazza, A. M., Braslawsky, G. R., Brown, J., Hofstead, S. J., Greenfield, R., Firestone, R. A., Mosure, K., Kadow, K., Yang, M. B., Hellström, K. E., and Hellström, I. (1997) Effect of Linker Variation on the Stability, Potency and Efficacy of Carcinoma-reactive BR64-Doxorubicin Immunoconjugates. *Cancer Res. 57*, 100−105.

(3) Hellström, I., Garrigues, H. J., Garrigues, U., and Hellström, K. E. (1990) Highly tumor-reactive, internalizing, mouse monoclonal antibodies to Le^y-related cell surface antigens. *Cancer Res. 50*, 2183-2190.

(4) Trail, P. A., Willner, D., Lasch, S. J., Henderson, A. J., Hofstead, S., Casazza, A. M., Firestone, R. A., Hellström, I., and Hellström, K. E. (1993) Cure of xenografted human carcinomas by BR96-doxorubicin immunoconjugates. *Science 261*, 212−215.

(5) Mueller, B. M., Wrasidlo, W. A., and Reisfeld, R. A. (1990) Antibody conjugates with morpholinodoxorubicin and acid-cleavable linkers. *Bioconjugate Chem. 1*, 325−330.

(6) Kirschke, H., Barrett, A. J., and Rawlings, N. D. (1995) Cathepsin B. in *Protein Profile—Proteinases 1: Lysosomal Cysteine Proteinases* (P. Sheterline, Ed.) pp 1587−1643, Academic Press, London.

(7) Otto, H.-H., and Schirmeister, T. (1997) Cysteine proteases and their inhibitors. *Chem. Rev. 97*, 133−172.

(8) Sinha, A. A., Jamuar, M. P., Wilson, M. J., Rozhin, J., and Sloane, B. F. (2001) Plasma membrane association of cathepsin B in human prostate cancer: biochemical and immunogold electron microscopic analysis. *Prostate 49*, 172−184.

(9) Hashimoto, Y., Kakegawa, H., Narita, Y., Hachiya, Y., Hayakawa, T., Kos, J., Turk, V., and Katunuma, N. (2001) Significance of cathepsin B accumulation in synovial fluid of rheumatoid arthritis. *Biochem. Biophys. Res. Commun. 283*, 334−339.

(10) Kovar, M., Strohalm, J., Etrych, T., Ulbrich, K., and Rihova, B. (2002) Star structure of antibody-targeted HPMA copolymer-bound doxorubicin: a novel type of polymeric conjugate for targeted drug delivery with potent antitumor effect. *Bioconjugate Chem. 13*, 206−215.

(11) Versluis, A. J., Rump, E. T., Rensen, P. C., Van Berkel, T. J., and Bijsterbosch, M. K. (1998) Synthesis of a lipophilic daunorubicin derivative and its incorporation into lipidic carriers developed for LDL receptor-mediated tumor therapy. *Pharm. Res. 15*, 531−537.

(12) Studer, M., Kroger, L. A., DeNardo, S. J., Kukis, D. L., and Meares, C. F. (1992) Influence of a peptide linker on biodistribution and metabolism of antibody-conjugated benzyl EDTA. Comparison of enzymatic digestion in vitro and in vivo. *Bioconjugate Chem. 3*, 424−429.

(13) Barrett, A. J. (1980) Fluorometric assays for cathepsin B and cathepsin H with methylcoumarylamide substrates. *Biochem. J. 187*, 909−912.

(14) Dubowchik, G. M., and Firestone, R. A. (1998) Cathepsin B-sensitive dipeptide prodrugs. 1. A model study of structural requirements for efficient release of doxorubicin. *Bioorg. Med. Chem. Lett. 8*, 3341−3346.

(15) Pattabiraman, T. N., and Kumar, R. S. (1994) Protease-Like Activities in Plasma of Different Animals. *Biochem. Arch. 10*, 51−57.

(16) Haney, D. N. (August 16, 1984) Kimberly-Clark Corp., Belgian Patent No. 899,539; Haney, D. N. (1985) *Chem. Abstr. 102*, 20376.

(17) Carl, P. L., Chakravarty, P. K., and Katzenellenbogen, J. A. (1981) A novel connector linkage applicable in prodrug design. *J. Med. Chem. 24*, 479−480.

(18) Riddles, P. W., Blakely, R. L., and Zerner, B. (1979) Ellman's reagent: 5,5′-dithiobis(2-nitrobenzoic acid)—a re-examination. *Anal. Biochem. 94*, 75−81.

(19) Greenfield, R. S., Kaneko, T., Daues, A., Edson, M. A., Fitzgerald, K. A., Olech, L., Grattan, J. A., and Braslawsky, G. R. (1990) Evaluation in vitro of adriamycin immunoconjugates synthesized using an acid sensitive hydrazone linker. *Cancer Res. 50*, 6600−6607.

(20) Bajkowski, A. S., and Frankfater, A. (1975) Specific spectrophotometric assays for cathepsin B. *Anal. Biochem. 68*, 119−127.

(21) Lardeux, B., Gouhot, B., and Forestier, R. A. (1983) Improved recovery of rat liver fractions enriched in lysosomes by specific alteration of the sedimentation properties of mitochondria. *Anal. Biochem. 131*, 160−165.

(22) Barrett, A. J., Kembhavi, A. A., Brown, M. A., Kirschke, H., Knight, C. G., Tamai, M., and Hanada, K. (1982) L-*trans*-Epoxysuccinyl-leucylamido(4-guanidino)butane (E-64) and its analogues as inhibitors of cysteine proteinases including cathepsins B, H and L. *Biochem. J. 201*, 189−198.

(23) Dangles, O., Guibe, F., Balavoine, G., Lavielle, S., and Marquet, A. (1987) Selective cleavage of the allyl and allyloxycarbonyl groups through palladium-catalyzed hydrostannolysis with tributyltin hydride. Application to the selective protection-deprotection of amino acid derivatives and in peptide synthesis. *J. Org. Chem. 52*, 4984−4993.

(24) Willner, D., Trail, P. A., Hofstead, S. J., Lasch, S. J., Braslawsky, G. R., Greenfield, R. S., Kaneko, T., and Firestone, R. A. (1993) (6-Maleimidocaproyl)hydrazone of doxorubicin: a new derivative for the preparation of immunoconjugates of doxorubicin. *Bioconjugate Chem. 4*, 521−527.

(25) Dubowchik, G. M., and Radia, S. (1997) Monomethoxytrityl as a versatile amino protecting group for complex prodrugs of anti-cancer compounds sensitive to strong acids, bases and nucleophiles. *Tetrahedron Lett. 38*, 5257−5260.

(26) Barlos, K., Papaioannou, D., and Theodoropoulos, D. (1982) Efficient "one-pot" synthesis of N-trityl amino acids. *J. Org. Chem. 47*, 1324−1326.
(27) Vigevani, A., and Williamson, M. J. Doxorubicin. (1980) *Anal. Profiles Drug Subst. 9*, 245−273.
(28) Ellenbogen, E. (1952) Dissociation constants of peptides. I. A survey of the effect of optical configuration. *J. Am. Chem. Soc. 74*, 5198−5201.
(29) King, H. D., Yurgaitis, D., Wilner, D., Firestone, R. A., Yang, M. B., Lasch, S. J., Hellstrom, K. E., and Trail, P. A. (1999) Monoclonal antibody conjugates of doxorubicin prepared with branched linkers: a novel method for increasing the potency of doxorubicin immunoconjugates. *Bioconjugate Chem. 10*, 279−288.

BC025536J

Introduction of Lanthanide(III) Chelates to Oligopeptides on Solid Phase

Jari Peuralahti, Harri Hakala, Veli-Matti Mukkala, Kristiina Loman, Pertti Hurskainen, Outi Mulari, and Jari Hovinen*

PerkinElmer Life Sciences, Wallac Oy, P.O. Box 10, FIN-20101 Turku, Finland. Received February 26, 2002.

The synthesis of oligopeptide building blocks for the introduction of nonluminescent and luminescent lanthanide(III) chelates to the oligopeptide structure on the solid phase is described. The oligopeptide conjugates synthesized were used in DELFIA-based receptor binding assay (motilin) as well as in LANCE time-resolved fluorescence quenching assay (caspase-3).

INTRODUCTION

Because of their unique luminescence properties, lanthanide(III) chelates are often used as nonradioactive markers in a wide variety of routine and research applications (*1*−*4*). Because lanthanide(III) chelates give strong, long decay-time luminescence, they are ideal labels for assays where high sensitivity is required. Time-resolved fluorometric assays based on lanthanide chelates have found increasing applications in diagnostics, research, and high throughput screening. The heterogeneous DELFIA technique is applied in assays requiring exceptional sensitivity, robustness, and a multilabel approach. Development of highly luminescent stable chelates extends the use of time resolution to homogeneous assays, based on fluorescence resonance energy transfer (TR-FRET), fluorescence quenching (TR-FQA), or changes in the luminescence properties of a chelate during a binding reaction.

Most commonly, the conjugation reaction is performed in solution between an amino or mercapto group of a bioactive molecule (such as a protein, a peptide, a nucleic acid, an oligonucleotide, or a hapten) and the isothiocyanato, haloacetyl, 3,5-dichloro-2,4,6-triazinyl derivatives of lanthanide(III) chelates (*5*), as well as other reporter groups. Because, in all of the cases, the labeling reaction is performed with an excess of an activated label, laborious purification procedures cannot be avoided. Especially, when attachment of several label molecules, or site-specific labeling in the presence of several functional groups of similar reactivities is required, the isolation and characterization of the desired biomolecule conjugate is extremely difficult and often practically impossible.

Quite recently, we reported our strategy for the introduction of lanthanide(III) chelates to an oligonucleotide structure on a solid phase (*6*). We extend here our approach of biomolecule derivatization to oligopeptides. We describe the synthesis of oligopeptide building blocks that allow for the introduction of nonluminescent and luminescent lanthanide(III) chelates to synthetic oligopeptides using standard machine-assisted chemistry. Also, the suitability of these blocks to oligopeptide derivatization as well as some application data is demonstrated.

* To whom correspondence should be addressed. Phone: + 358 2 2678 513. Fax: + 358 2 2678 380. E-mail: jari.hovinen@perkinelmer.com.

EXPERIMENTAL PROCEDURES

General Methods. Adsorption column chromatography was performed on columns packed with silica gel 60 (Merck). Reagents for oligopeptide synthesis were purchased from Nova Biochem, Molecular Probes, and Applied Biosystems. The oligopeptides were assembled on an Applied Biosystems 433A instrument in 10 μmol scale using Fmoc chemistry and recommended protocols (Fmoc-Off synthesis). The time-resolved fluorometer (Victor^{2}V), DELFIA assay buffer, DELFIA wash solution, DELFIA enhancement solution, and the caspase buffer were from PerkinElmer Life Sciences. NMR spectra were recorded on a Brucker 250 or a JEOL GX-400 spectrometers operating at 250.13 MHz and 399.8 for ^{1}H, respectively. The signal of TMS was used as an internal reference. Coupling constants are given in hertz. Electrospray ionization time-of-flight mass spectra (ESI-TOF-MS) were recorded on an Applied Biosystems Mariner instrument. HPLC analyses were performed on a PerkinElmer LC 2000 instrument. The mobile phase used was the following: (Buffer A) 0.02 M TEAA (pH 7.5); (Buffer B) A in 50% (v/v) acetonitrile. IR spectra were recorded on a PerkinElmer Spectrum One spectrophotometer.

Tetra-*tert*-butyl-1-(4-nitrobenzyl)diethylenetriaminetetrakis(acetate), 2. 1-(4-Nitrobenzyl)diethylenetriamine (5.0 g, 21.0 mmol) was dissolved in dry dimethylformamide (DMF) (120 mL). DIPEA (34 mL), potassium iodide (3 g), and *tert*-butylbromoacetate (22 mL, 0.15 mol) were added, and the mixture was stirred for 2 h at ambient temperature and concentrated in vacuo. The residue was partitioned between water and diethyl ether. The organic phase was washed with water and brine and was dried. After concentration, the crude product was purified on silica gel column (eluent MeOH/CH_2Cl_2, 5:95, v/v). Yield was 17.2 g (95%) of compound **2**. ^{1}H NMR ($CDCl_3$, δ): 8.17 (2H, d, J = 8.5 Hz), 7.56 (2H, d, J = 8.5), 3.94 (2H, s), 3.75 (2H, s), 3.43 (4H, s), 3.32 (2H, br s), 2.79 (7H, br s), 1.46 (9H, s), 1.44 (18H, s), 1.43 (9H, s). IR (film): 1731, 1552, 1367, 1345, 1152 cm^{-1}. ESI-TOF-MS mass for $C_{35}H_{59}N_4O_{10}$ $(M + H)^+$: calcd, 695.42; found, 695.42.

Tetra-*tert*-butyl-1-(4-aminobenzyl)diethylenetriaminetetrakis(acetate), 3. Compound **2** (12.0 g, 17.2

10.1021/bc025521l CCC: $22.00 © 2002 American Chemical Society
Published on Web 06/21/2002

mmol) was dissolved in dry methanol (240 mL) containing Pd/C (10%, 1.2 g). $NaBH_4$ (0.72 g, 19.0 mmol) was added portionwise (caution: exothermic reaction with foaming), and the reaction was allowed to proceed for 3 h at ambient temperature. The reaction mixture was filtered through Celite and neutralized with aq HCl. The filtrate was diluted with dichloromethane, washed with saturated $NaHCO_3$, and dried. Purification was performed on silica gel (eluent MeOH/CH_2Cl_2, 1:9, v/v) giving 10.0 g (87%) of compound **3**. ^{1}H NMR ($CDCl_3$, δ): 7.09 (2H, d, J = 8.5 Hz), 6.61 (2H, d, J = 8.5 Hz), 3.66 (2H, s), 3.45 (4H, s), 3.34 (2H, s), 3.20 (2H, s), 2.78 (8H, br s), 1.45 (36H, 2 s). ESI-TOF-MS mass for $C_{35}H_{61}N_4O_8$ $(M + H)^+$: calcd, 665.45; found, 665.44.

Tetra-*tert*-butyl-1-[4-(fluorenylmethyloxycarbonylaminoacetamido)benzyl]diethylenetriaminetetrakis(acetate), **4.** Compound **3** (9.8 g, 14.7 mmol) was dissolved in CH_2Cl_2 (100 mL) and deaerated with argon. Dicyclohexylcarbodiimide (DCC) (3.34 g, 16.2 mmol), DMAP (184 mg, 1.47 mmol), and Fmoc-Gly-OH (4.37 g, 14.7 mmol) were added, and the mixture was stirred at room temperature for 4 h. Precipitation formed was removed by filtration, and the filtrate was evaporated to dryness to give 11.4 g (81%) of the Fmoc derivative. Compound **4** was used in the next step without further purification. ^{1}H NMR ($CDCl_3$, δ): 7.97 (1H, s), 7.75 (4H, m), 7.59 (2H, m), 7.38 (3H, m), 7.30 (3H, m), 5.61 (1H, s), 4.48 (2H, d, J = 6.9 Hz), 4.24 (1H, t, J = 6.8 Hz), 4.00 (2H, d, J = 4.0 Hz), 3.75 (2H, s), 3.43 (4H, m), 3.33 (2H, m), 3.22 (2H, m), 2.76 (8H, s), 1.45 (36H, 3 s). ESI-TOF-MS mass for $C_{52}H_{74}N_5O_{11}$ $(M + H)^+$: calcd, 944.54; found, 944.56.

Tetra-*tert*-butyl-1-[4-(aminoacetamido)benzyl]diethylenetriaminetetrakis(acetate), **5.** Compound **4** (10 g, 10 mmol) was dissolved in the mixture of piperidine and DMF (300 mL; 20%, v/v), stirred at room temperature for 3 h, and evaporated to dryness. Purification was performed on silica gel (eluent initially petroleum ether/ethyl acetate/triethylamine, 5:2:1, v/v/v, and then MeOH/CH_2Cl_2, 1:4, v/v). Yield was 6.0 g (79%) of compound **5**. ^{1}H NMR ($CDCl_3$, δ): 9.43 (1H, br s), 7.55 (2H, d, J = 8.4 Hz), 7.29 (2H, d, J = 8.4 Hz), 3.75 (2H, s), 3.48 (4H, s), 3.44 (2H, s), 3.33 (2H, s), 3.21 (2H, s), 2.77 (8H, m), 1.70 (36H, s). ESI-TOF-MS mass for $C_{37}H_{64}N_{45}O_9$ $(M + H)^+$: calcd, 722.47; found, 722.47.

Tetra-*tert*-butyl-4′-{2-[4-allyloxycarbonyl-4-(fluorenylmethyloxycarbonylamino)-1-oxo-1-butylamino]-1-oxo-1-ethylamino}benzyldiethylenetriaminetetrakis(acetate), 6. Compound **5** (3.2 g, 4.38 mmol) was dissolved in dichloromethane (80 mL) and deaerated with argon. DCC (1.0 g, 4.67 mmol) and Fmoc-Glu-OAll (1.8 g, 4.25 mmol) were added, and the mixture was stirred at room temperature for 2 h. DCU formed was removed by filtration, and the filtrate was concentrated in vacuo. The allyl derivative was purified by flash chromatography using petroleum ether/ethyl acetate (2:5, v/v) as the eluent. Yield was 4.9 g (67%) of compound **6**. ^{1}H NMR ($CDCl_3$, δ): 8.39 (1H, s), 7.76 (2H, m), 7.56 (2H, m), 7.46 (2H, m), 7.40 (2H, m), 7.31 (2H, m), 7.24 (2H, m), 6.55 (1H, m), 5.89 (1H, m), 5.69 (1H, d, J = 7.9 Hz), 5.29 (2H, m), 4.64 (2H, d, J = 5.6 Hz), 4.41 (2H, m), 4.18 (1H, t, J = 6.8 Hz), 3.73 (2H, s), 3.43 (4H, m), 2.77 (8H, m), 2.32 (2H, m), 2.05 (4H, m), 1.91 (1H, m), 1.74 (4H, m), 1.44 (36 H, 2s). ESI-TOF-MS mass for $C_{60}H_{85}N_6O_{14}$ $(M + H)^+$: calcd, 1113.12; found, 1113.61.

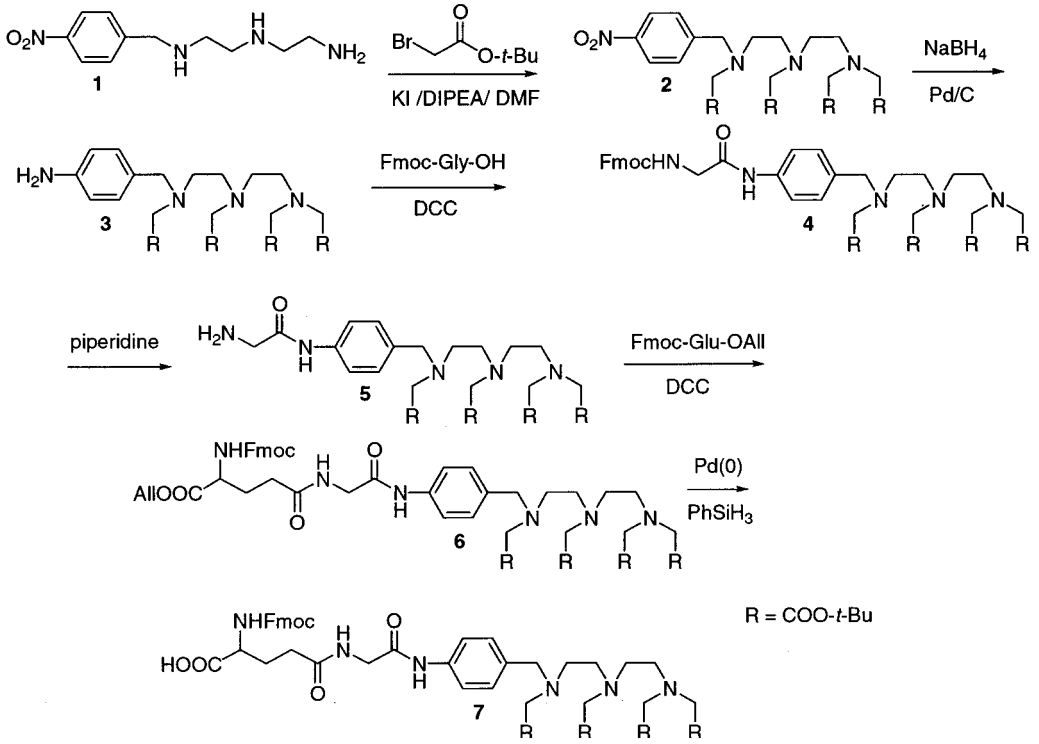
Tetra-*tert*-butyl-4′-{2-[4-carboxy-4-(fluorenylmethyloxycarbonylamino)-1-oxo-1-butylamino]-1-oxo-1-ethylamino}benzyldiethylenetriaminetetrakis(acetate), 7. Compound **6** (2.0 g, 1.8 mmol) was dissolved in dichloromethane (120 mL) and deaerated for 10 min with argon. $Pd(PPh_3)_4$ (41.5 mg, 35.9 μmol) and $PhSiH_3$ (0.5 mL, 3.6 mmol) were added, and the mixture was stirred at room temperature for 1 h. The solution was washed with citric acid (100 mL, 10%, w/v), dried over 4 Å molecular sieves, and evaporated to dryness. Yield of compound **7** was quantitative. ESI-TOF-MS mass for $C_{57}H_{81}N_6O_{14}$ $(M + H)^+$: calcd, 1073.58; found, 1073.57.

Tetra-*tert*-butyl-2,2′,2″,2‴-{[4′-(4″-bromophenyl)-2,2′:6′,2″-terpyridine-6,6″-diyl]bis(methylenenitrilo)}tetrakis(acetate), 9. Compound **8** (3.3 g, 5.25 mmol, pentahydrochloride) was suspended in dry DMF (25 mL). Diisopropylethylamine (13.7 mL), *tert*-butylbromoacetate (7 mL, 47.4 mmol), and potassium iodide (1.0 g, 6.0 mmol) were added, and the mixture was stirred overnight at room temperature and concentrated. The residue was dissolved in dichloromethane (150 mL), washed with saturated $NaHCO_3$ (3 × 40 mL), and dried. Purification was performed on silica gel (eluent petroleum ether/ethyl acetate/triethylamine, 5:1:1, v/v/v). Yield of compound **9** was 3.8 g (80%). ^{1}H NMR ($CDCl_3$, δ): 8.70 (2H, s), 8.55 (2H, dd, J = 1.0 and 7.8 Hz), 7.86 (2H, t, J = 7.8 Hz), 7.77 (2H, d, J = 8.6 Hz), 7.70 (2H, dd, J = 1 and 7.6 Hz), 7.64 (2H, d, J = 8.6 Hz), 4.17 (4H, s), 3.56 (8H, s), 1.44 (36H, s). ESI-TOF-MS mass for $C_{47}H_{61}BrN_5O_8$ $(M + H)^+$: calcd, 902.38; found, 902.41.

Tetra-*tert*-butyl-2,2′,2″,2‴-{[4′-(4″-(3-amino-1-propyn-1-yl)phenyl)-2,2′:6′,2″-terpyridine-6,6″-diyl]bis(methylenenitrilo)}tetrakis(acetate), 10. A mixture of compound **9** (1.0 g, 1.1 mmol), bis(triphenylphosphine)-palladium(II) chloride (15 mg, 0.022 mmol), and CuI (9 mg, 0.16 mmol) in dry THF (6 mL) and triethylamine (4 mL) was deaerated with argon. 3-(Methoxytrityl)aminopropyne was added, and the mixture was stirred overnight at 55 °C. The cooled solution was filtered, and the filtrate was evaporated and redissolved in dichloromethane. The solution was washed with water, dried, and concentrated. It was then dissolved in dichloromethane containing 1% (v/v) of TFA, stirred for 30 min at room temperature, and concentrated. The residue was dissolved in dichloromethane, washed with saturated $NaHCO_3$, dried, and concentrated. Purification on silica gel (eluent petroleum ether/ethyl acetate/triethylamine, 3:5:1, v/v/v) gave the title compound (compound **10**) (45%) as an oil. ^{1}H NMR ($CDCl_3$, δ): 8.70 (2H, s), 8.55 (2H, d, J = 8 Hz), 7.87 (2H, t), 7.77 (2H, d, J = 7.5 Hz), 7.70 (2H, d, J = 7.5 Hz), 7.55 (2H, d, J = 7.5 Hz), 4.17 (4H, s), 3.71 (2H, s), 3.55 (8H, s), 1.46 (36H, s). ESI-TOF-MS mass for $C_{50}H_{64}N_6O_8Na$ $(M + Na)^+$: calcd, 899.47; found, 899.51.

Tetra-*tert*-butyl-4′-{3-[4-allyloxycarbonyl-4-(fluorenylmethyloxycarbonylamino)-1-oxo-1-butylamino]-1-propyn-1-yl}-2,2′:6′,2″-terpyridine-6,6″-diyl]bis(methylenenitrilo)}tetrakis(acetate), 11. Compound **10** (200 mg, 0.23 mmol) and Fmoc-Glu-OAll (104 mg, 0.25 mmol) were dissolved in dichloromethane (6 mL). DCC (52 mg, 0.25 mmol, predissolved in 1 mL of dichloromethane) was added, and the mixture was stirred overnight at room temperature. DCU formed was removed by filtration, and the filtrate was concentrated in vacuo. The residue was filtered through silica gel using diethyl ether as eluent and concentrated to give the allyl derivative (compound **11**) (yield 250 mg, 90%). ^{1}H NMR ($CDCl_3$, δ): 8.71 (2H, s), 8.54 (2H, d, J = 8 Hz), 7.87−7.30 (tot, 16H), 6.15 (1H, br s), 5.67 (1H, br s), 5.64 (1H, br s), 5.36 (1H, m), 5.30 (2H, m), 5.27 (1H, m), 4.65 (2H, m), 4.45 (2H, m), 4.32 (2H, m), 4.25 (1H, m), 4.17 (4H, s), 3.55 (8H, s), 2.33 (2H, m), 1.46 (36H, s). ESI-TOF-MS mass for $C_{73}H_{84}N_7O_{13}$ $(M - H)^-$: calcd, 1266.61; found, 1266.61.

Scheme 1. Synthesis of the Nonluminescent Block



Tetra-*tert*-butyl-4′-{3-[4-carboxy-4-(fluorenylmethyloxycarbonylamino)-1-oxo-1-butylamino]-1-propyn-1-yl}-2,2′:6′,2″-terpyridine-6,6″-diyl]bis(methylenenitrilo)}tetrakis(acetate), 12. Cleavage of the allyl group from compound **11** and workup was performed as described for compound **7**. (Compound **12**) ESI-TOF-MS: mass for $C_{70}H_{80}N_7O_{13}$ $(M - H)^-$: calcd, 1226.58; found, 1226.61.

Synthesis of the Oligopeptide Conjugates. Oligopeptides were assembled on an Applied Biosystems 433A instrument in 10 μmol scale using Fmoc chemistry and recommended protocols (coupling time 30 min for natural amino acid analogues, and 2 h for blocks **7** and **12**). In the synthesis of the caspase-3 substrate, a commercial ϵ-dabsyl Fmoc-lysine block (Molecular Probes) was used to introduce the quencher and Fmoc-hexanoic acid (Fluka) as a spacer at the C-terminus. When the chain assembly was completed, the resin was treated with the mixture of crystalline phenol (75 mg), ethanedithiol (25 μL), thioanisole (50 μL), water (50 μL), and trifluoroacetic acid (1 mL) for 2−4 h. The resin was removed by filtration, and the solution was concentrated in vacuo. The crude oligopeptide was precipitated with diethyl ether. The precipitate was redissolved in water and treated with aqueous europium(III) citrate (5 equiv). Purification was performed on HPLC techniques (column, LiChrocart 125-3 Purospher RP-18e 5 μm; gradient, from 95% to 0% A in 30 min; flow rate was 0.6 mL min^{-1}).

Motilin Assay. Eu-motilin prepared using the ligand building block, **7**, was tested in saturation binding assay using human motilin receptor. All of the reagents were diluted in 50 mM Tris-HCl buffer (pH 7.5) containing 10 mM $MgCl_2$, 0.2% bovine serum albumin, and 25 μM EDTA. Human motilin receptor membrane preparate (0.5 μg/well; PerkinElmer Life Sciences) was incubated in the presence of Eu-motilin (0.25, 1, 4, and 16 nM) in an AcroWell filtration plate (Pall Life Sciences) in the total volume of 100 μL/well at room temperature for 90 min. To determine nonspecific binding, the assay was performed also in the presence of 800 nM motilin. Next, the wells were washed with 50 mM Tris-HCl and 10 mM $MgCl_2$ (pH 7.5) 4 times (300 μL/well) using a manifold (Millipore) and a vacuum pump. After washing, DELFIA enhancement solution was added (200 μL/well), and the plate was shaken for 15 min. Europium fluorescence was measured using a VICTOR^{2}V multilabel counter.

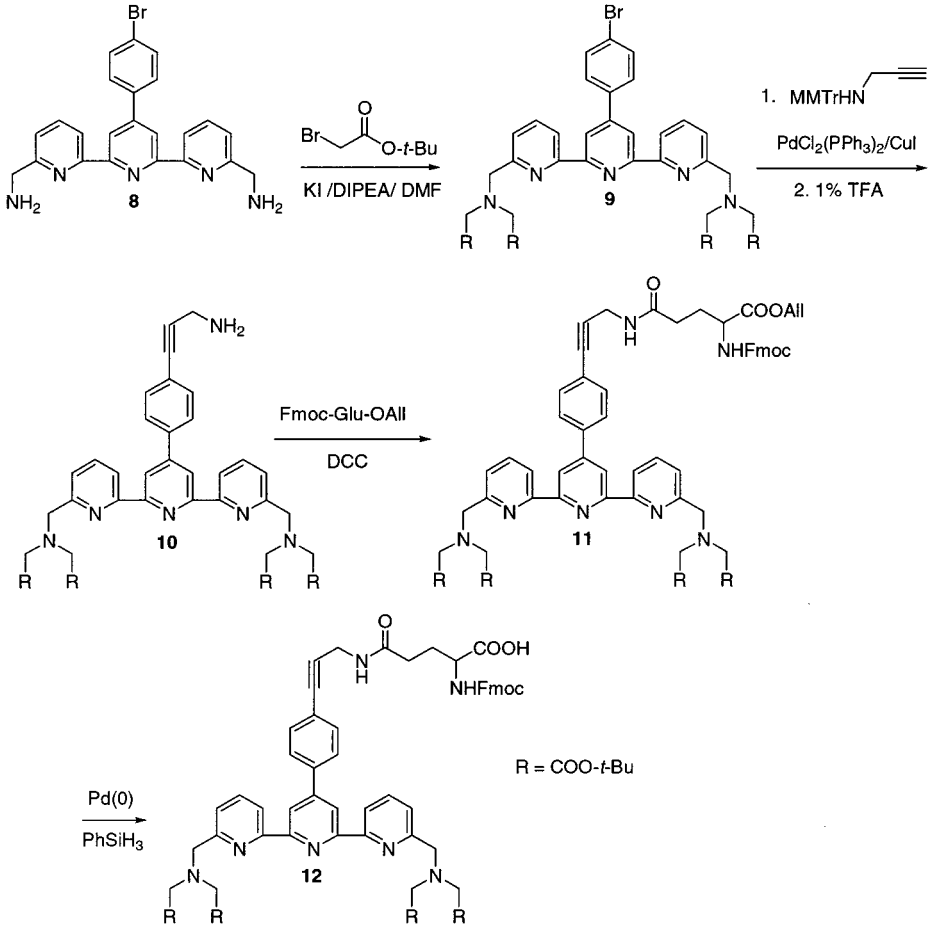
Caspase Assay. The performance of the caspase-3 substrate prepared using the building block **12** was tested in time-resolved fluorescence quenching assay (TR-FQA). The assay was performed in a Wallac 384-plate. Accordingly, caspase buffer (18 μL), substrate (2 μL, 200 pM−2 μM; final concentrations), and caspase-3 enzyme (1 μL, 5 pg/well) were pipetted to a well. In blank wells, there was buffer instead of enzyme. The plate was incubated at 37 °C. Europium fluorescence was measured with VICTOR^{2}V multilabel counter in 15 min time intervals.

RESULTS AND DISCUSSION

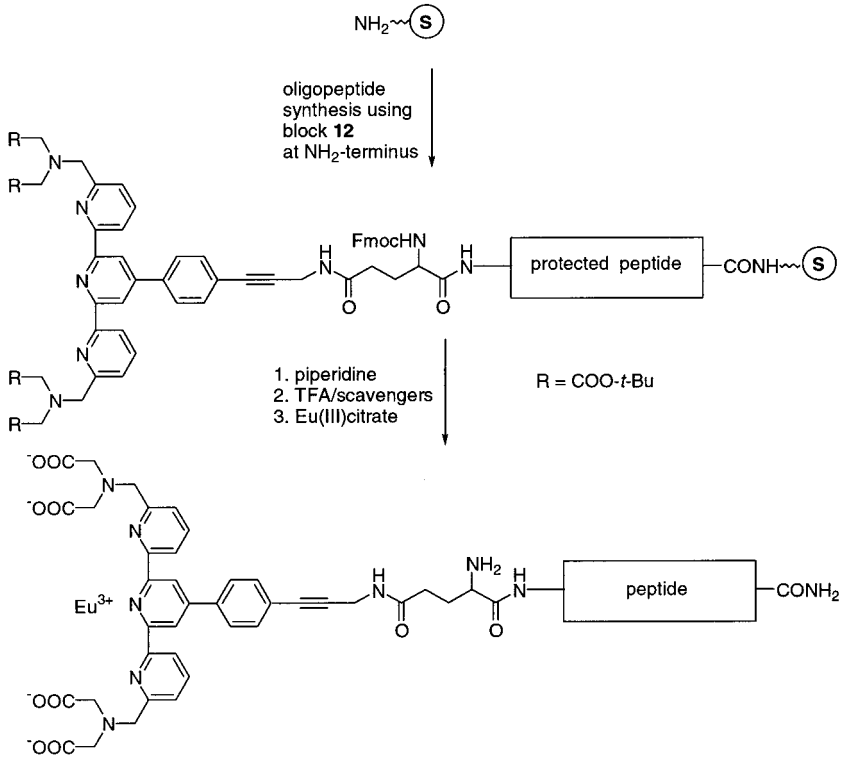
Synthesis of the Nonluminescent Oligopeptide Block. The synthesis of a nonluminescent oligopeptide building block for the introduction of lanthanide(III) chelates to the oligopeptide structure is shown in Scheme 1. Initially, 1-(4-nitrobenzyl)diethylenetriamine (**1**; *7*) was allowed to react with bromoacetic acid *tert*-butyl ester in the presence of potassium iodide as a catalyst to give the corresponding tetraester (**2**) in high yield. Reduction of the nitro group to the amino function gave **3**. It was then converted to the corresponding oligopeptide building block, **7**, by attachment of the spacer arm and the appropriately protected amino acid to the amine function. It is worth noting that elongation of the spacer arm with the glycine residue was essential to reach acceptable coupling efficiency. Transient protection of the glutamic acid residue, in turn, considerably simplified the purification procedures. Palladium-catalyzed allyl cleavage using phenylsilane as allyl scavenger (*8*) gave the final product quantitatively after washing with aq citric acid without need of further purification.

Synthesis of the Luminescent Block. The oligopeptide building block for the introduction of luminescent

Scheme 2. Synthesis of the Luminescent Block



Scheme 3. Introduction of a Luminescent Europium(III) Chelate to an Oligopeptide in the Aid of Block 12



lanthanide(III) chelates to the oligopeptide structure, **12**, was synthesized as shown in Scheme 2. In general, synthesis of the protected ligand was analogous to that published for the corresponding oligonucleotide building block (*6*). Accordingly, alkylation of the amine, **8**, with bromoacetic acid *tert*-butyl ester yielded **9**, the reaction of which with MMTr-protected propargylamine in the presence of Pd(II) and Cu(I) gave, after removal of the

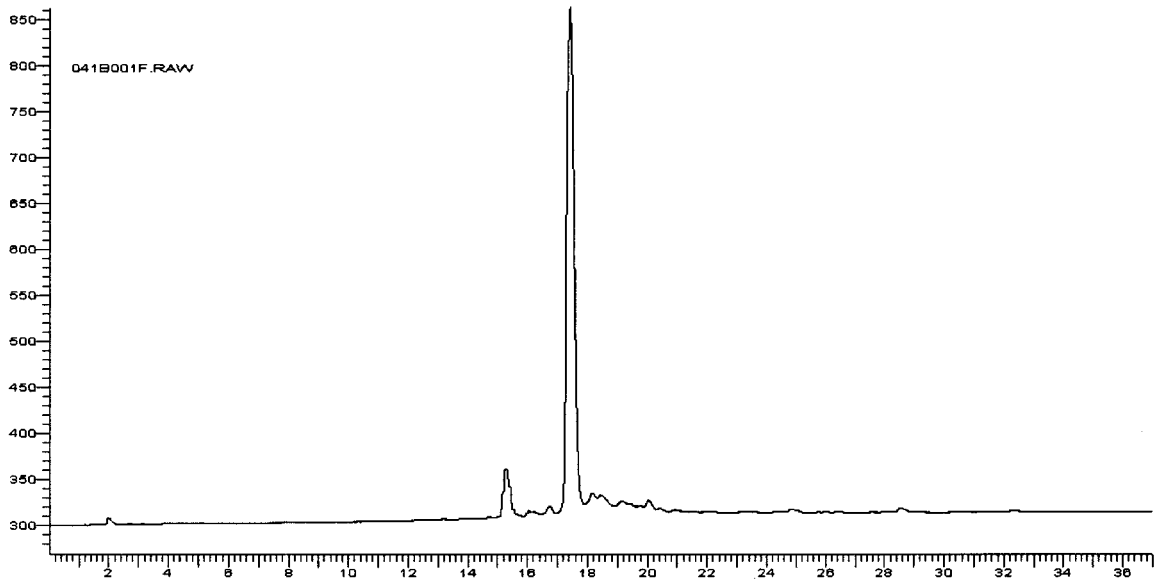


Figure 1. Reversed-phase HPLC trace of an oligopeptide conjugate X_2-Ser-Ile-Glu-Thr-Asp-Lys-$CONH_2$ labeled with a luminescent europium(III) chelate synthesized in the aid of block **12** (crude reaction mixture) detected at 270 nm. X_2 is the position of the label. For chromatographic conditions, see Experimental Procedures.

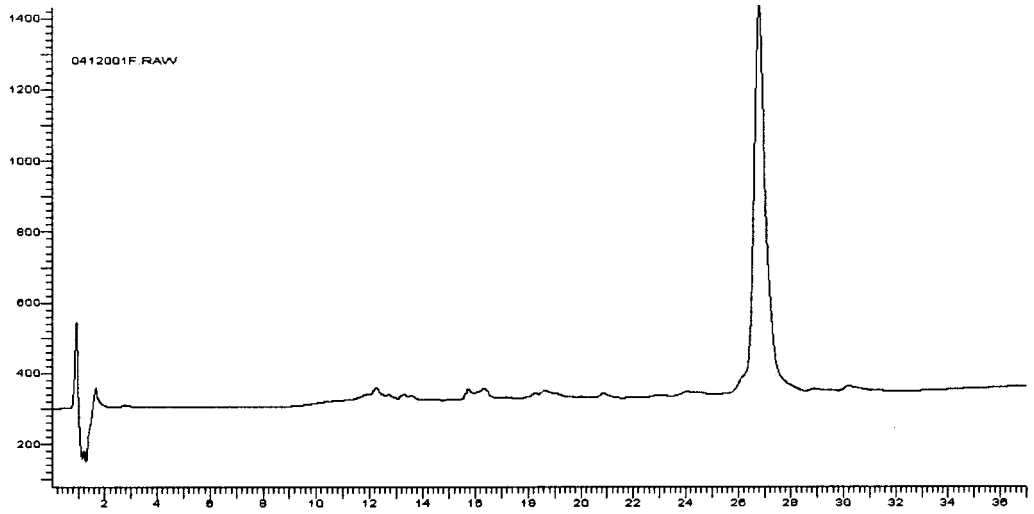


Figure 2. Reversed-phase HPLC trace of an oligopeptide conjugate Phe-Val-Pro-Ile-Phe-Thr-Tyr-Gly-Glu-Leu-Gln-Arg-Met-Gln-Glu-Lys-Glu-Arg-Asn-Lys-Gly-Gln-X_1-$CONH_2$ (motilin) labeled with a nonluminescent europium(III) chelate synthesized in the aid of block **7** (crude reaction mixture) detected at 220 nm. X_1 is the position of the label. For chromatographic conditions, see Experimental Procedures.

amine protection, the ligand **10**. It was then converted to the oligopeptide building block, **12**, as described previously for **7** but by omitting the now unnecessary glycine spacer unit from the linker arm.

Synthesis of the Oligopeptide Conjugates. To demonstrate the applicability of the building blocks **7** and **12** for oligopeptide derivatization, model sequences (e.g., motilin, substance-P, neurokinin-A, and caspase-3) were synthesized in 10 μmol scale using Fmoc chemistry. The blocks **7** and **12** were coupled either to the amino or carboxyl terminus or to the internal position of the coding sequence using prolonged coupling time (2 h instead of 30 min) but otherwise standard conditions (5 equiv of blocks; HBTU/HOBt as an activator). According to fulvene-piperidine assay, coupling efficiencies of **7** and **12** were comparable to natural amino acid analogues. After completion of the oligopeptide synthesis, the oligopeptides were released from the resin and deprotected followed by precipitation from ether. Treatment of the deblocked oligomers with europium(III) citrate converted the oligopeptide conjugates to the corresponding europium chelates (Scheme 3).

Table 1. Oligopeptide Conjugates Synthesized and Their Observed and Calculated Molecular Weights

sequence[a]	$[M - H]^-$ calculated	$[M - H]^-$ observed
X_1-RPKPEEFFGLM-$CONH_2$ (substance P)	2103.87	2103.86
X_2-SIETDK-$CONH_2$ (Ser-caspase-8)	1602.51	1602.40
H-X_1-TDSFVGLM-$CONH_2$ (neurokinin A)	1761.62	1761.59
X_1-HKTDSFVGLM-$CONH_2$ (neurokinin A)	1889.71	1889.59
X_2-DEVD-dabcyl-hex-$CONH_2$ (caspase-3)	1879.63	1879.23
FVPIFTYGELQRMQEKERNKGQ-X_1-$CONH_2$ (motilin)	1728.26[b]	1728.29[b]

[a] X = position of the chelate; X_1 = synthesized in the aid of block **7**; X_2 = synthesized in the aid of block **12**; dabcyl = quencher synthesized in the aid of ϵ-dabcyl-Fmoc-lysine; hex = aminohexanoic acid residue. [b] $[M + 2\ H]^{2+}/2$.

The oligopeptides synthesized were purified on reversed-phase HPLC and characterized on ESI-TOF mass spectrometry. Typical HPLC profiles (crude reaction mix-

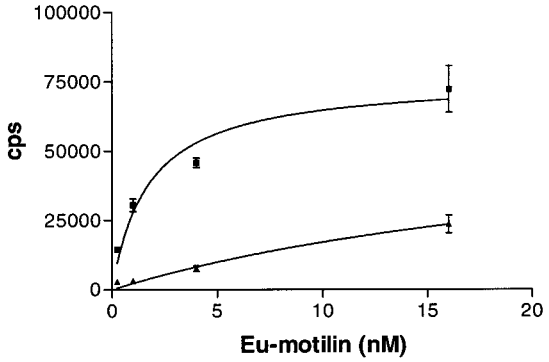


Figure 3. Saturation binding assay using Eu-motilin. Binding curves show total binding (squares) and nonspecific binding (triangles).

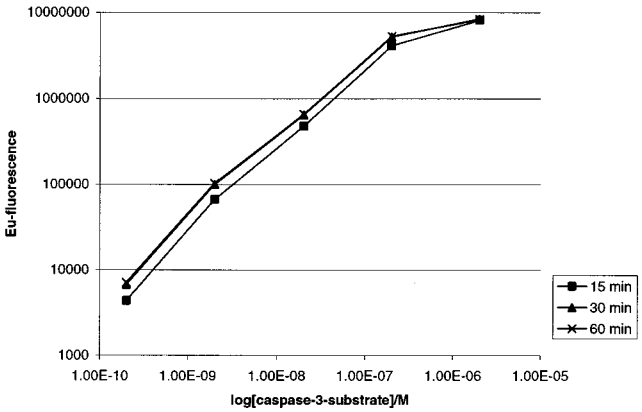


Figure 4. Concentration curve of caspase-3 substrate.

tures) are shown in Figures 1 and 2 as illustrative examples. In all of the cases, the observed molecular weights were in accordance with the proposed structures (Table 1).

Assays. Two of the oligopeptide conjugates synthesized were used in a DELFIA-based binding assay as well as in a LANCE fluorescence quenching assay. Accordingly, the motilin conjugate prepared using the ligand building block, **7**, was tested in saturation binding assay using human motilin receptor (Figure 3). Analysis of data gave a K_d value of 1.7 nM. The performance of the caspase-3 substrate prepared using the building block, **12**, in turn, was tested in TR-FQA. The substrate was cleaved by caspase-3 enzyme. The cleavage separates the quencher and the chelate and thus recovers the europium fluorescence. The results showed that the linear range of the assay is from 200 pM to 200 nM (Figure 4).

ACKNOWLEDGMENT

We thank Mrs. Mirja Koski, Ms. Jenni Degerholm, and Mr. Lassi Jaakkola for skillful technical assistance.

LITERATURE CITED

(1) Hemmilä, I., Dakubu, S., Mukkala, V.-M., Siitari, H., and Lövgren T. (1984) Europium as a label in time-resolved immunofluorometric assays. *Anal. Biochem. 137*, 335−343.
(2) Hemmilä, I., and Mukkala, V.-M. (2001) Time-resolution in fluorometry technologies, labels, and applications. *Crit. Rev. Clin. Lab. Sci. 38*, 441−519.
(3) Hemmilä, I. (1999) LANCE: Homogeneous assay platform for HTS. *J. Biomol. Screening 4*, 303−307.
(4) Mathis, G. (1993) Rare earth cryptates and homogeneous fluoroimmunoassays with human sera. *Clin. Chem. 39*, 1953−1959.
(5) Takalo, H., Mukkala, V.-M., Mikola, H., Liitti, P., and Hemmilä, I. (1994) Synthesis of europium(III) chelates suitable for labeling of bioactive molecules. *Bioconjugate Chem. 5*, 278−282.
(6) Hovinen, J., and Hakala, H. (2001) Versatile strategy for oligonucleotide derivatization. Introduction of lanthanide(III) chelates to oligonucleotides. *Org. Lett. 3*, 2473−2476.
(7) Mukkala, V.-M., Mikola, H., and Hemmilä, I. (1989) The synthesis and use of activated *N*-benzyl derivatives of diethylenetriaminetetraacetic acids: alternative reagents for labeling of antibodies with metal ions. *Anal. Biochem. 176*, 319−325.
(8) Dessolin, M, Guillerez, M.-G, Thieriet, N., Guibe, F., and Loffet, A. (1995) New allyl group acceptors for palladium catalyzed removal of allylic protections and transacylation of allyl groups. *Tetrahedron Lett. 36*, 5741−5744.

BC025521L

TECHNICAL NOTES

Synthesis of Nonluminescent Lanthanide(III) Chelates Tethered to an Aminooxy Group and Their Applicability to Biomolecule Derivatization

Jari Peuralahti, Katri Puukka, Harri Hakala, Veli-Matti Mukkala, Outi Mulari, Pertti Hurskainen, and Jari Hovinen*

PerkinElmer Life Sciences, Wallac Oy, P.O. Box 10, FIN-20101 Turku, Finland. Received January 3, 2002; Revised Manuscript Received May 2, 2002

Synthesis of nonluminescent lanthanide(III) chelates tethered to an aminooxy group (i.e., 1-[4-(6-aminooxyhexamido)benzyl]diethylenetriaminetetraacetic acid lanthanides(III), **6a**−**d**, where Ln^{3+} is Eu, Dy, Sm, and Tb) is described. Their applicability to biomolecule derivatization is demonstrated by allowing them to react with a synthetic oligopeptide, a protein, two synthetic drugs, and a steroid. The oligopeptide and protein were linked to **6** after preoxidation of their *N*-terminal serine residues, while the drugs and the steroid reacted via their ketone functionality. Also some application data is included.

INTRODUCTION

Ketones and aldehydes are known to react with hydroxylamines under mild conditions giving stabile oximes in high yield (*1*). This reaction has been exploited in biomolecule derivatization, e.g., for the introduction of tether arms and label molecules to ketosteroids (*2*, *3*) and for detection of abasic sites of DNA (*4*−*7*). Oligopeptides and proteins, in turn, react smoothly with hydroxylamines after periodate oxidation of their *N*-terminal serine and threonine residues (*8*−*10*). Aminooxy conjugation has also been applied to cell-surface ketone modification (*11*) as well as to the modification of native peptides (*11*) and nucleic acids and oligonucleotides (*12*, *13*).

The labeling reactants described in the literature are most commonly organic dyes. Although organic chromophores can be utilized for several applications, they suffer from many drawbacks, such as Raman scattering, low water solubility, and concentration quenching. Because of their unique fluorescence properties, lanthanide(III) chelates are often used as nonradioactive markers in a wide variety of routine and research applications (*14*, *15*). Since lanthanide(III) chelates give strong long-decay-time fluorescence, they are ideal labels for assays where high sensitivity is required. Time-resolved fluorometric assays based on lanthanide chelates have found increasing applications in diagnostics, research, and high-throughput screening. The heterogeneous DELFIA (dissociation-enhanced lanthanide fluorescence immunoassay) technique is applied in assays requiring exceptional sensitivity, robustness, and multilabel approach (*14*). Development of highly fluorescent stable chelates extends the use of time resolution to homogeneous assays, based on time-resolved energy transfer (TR−FRET), time-resolved fluorescence quenching (TR−FQ), or changes in the chelate's fluorescence properties during a binding reaction (*14*−*20*).

We describe here a simple method for the preparation of nonluminescent lanthanide(III) chelates tethered to an aminooxy group. Also their applicability for biomolecule labeling is demonstrated.

EXPERIMENTAL PROCEDURES

General. Adsorption column chromatography was performed on columns packed with silica gel 60 (Merck). Reagents for oligopeptide synthesis were purchased from Nova Biochem and Applied Biosystems. The oligopeptide was assembled on an Applied Biosystems 433A instrument in 10 μmol scale using Fmoc chemistry and recommended protocols. IL-8 (human) was purchased from PeproTech, and naltrexone, naloxone, and testosterone from Sigma. The time-resolved fluorometer (Victor^{2}V), DELFIA Assay Buffer, DELFIA Wash Solution, and DELFIA Enhancement Solution were obtained from PerkinElmer. NMR spectra were recorded on a Brucker 250 spectrometer operating at 250.13 MHz for ^{1}H. The signal of TMS was used as an internal reference. ESI-TOF mass spectra were recorded on an Applied Biosystems Mariner instrument. HPLC analyses were performed on a Merck-Hitachi Instrument consisting of L-7400 detector, 7100 gradient pump, and D-7500 integrator. Mobile phase used was the following: buffer A: 0.02 M TEAA (pH 7.5); buffer B: A in 50% (v/v) acetonitrile.

6-Aminooxyhexanoic Acid Hydrobromide (1). *N*-Hydroxyphthalimide (7.13 g, 43.7 mmol) and ethyl 6-bromohexanoate (12.28 g, 55 mmol) were dissolved in DMF (45 mL). Triethylamine (9.2 mL, 66 mmol) was added, and the mixture was stirred for 2 d at RT. The precipitate formed was filtered and washed with DMF (5 mL). The

* Address of correspondence: Dr. Jari Hovinen, PerkinElmer Life Sciences. Wallac Oy, P.O. Box 10, FIN-20101 Turku, Finland. Tel + 358 2 2678 111. Fax + 358 2 2678 380. e-mail: jari.hovinen@perkinelmer.com.

10.1021/bc025502b CCC: $22.00 © 2002 American Chemical Society
Published on Web 06/21/2002

filtrate was poured slowly into ice−water (300 mL) and the product separated as an oil. The aqueous layer was decanted, and the remaining oil was washed with ice−water (100 mL). The remaining water was removed using a rotavapor. The residue was dissolved in the mixture of acetic acid (23 mL) and hydrobromic acid (48%, 38 mL) and refluxed for 2 h. The mixture was cooled on an ice bath, and the precipitate formed was removed by filtration. All volatile material was evaporated off in vacuo. The residue was coevaporated twice with water. The solid material was washed with ether and collected by filtration. The residue was suspended in ice−water (15 mL), and the remaining phthalic acid was removed by filtration. The filtrate was concentrated and treated with ether as above. Yield was 9.41 g (94%). It was used for the next step without further purification. ^{1}H NMR (D_2O): δ 3.88 (t, J = 6.4 Hz, 2H); 2.20 (t, J = 7.4 Hz, 2H); 1.50 (p, J = 6.8 Hz, 2H); 1.43 (p, J = 7.5 Hz, 2H); 1.23 (m, 2H). $[M + H]^+$ obsd 148.096, calcd for $C_6H_{14}NO_3^+$: 148.098.

6-(4-Methoxytrityl)aminooxyhexanoic Acid (2). 6-Aminooxyhexanoic acid hydrobromide (**1**; 5.0 g, 21.9 mmol) was dried by coevaporations with dry pyridine and dissolved in the same solvent (50 mL). Triethylamine (5 mL) and 4-methoxytrityl chloride (7.44 g, 24 mmol) were added, and the reaction was allowed to proceed overnight at ambient temperature. All volatile materials were removed in vacuo. The residue was suspended in methylene chloride, washed with sat. $NaHCO_3$, dried over Na_2SO_4, and concentrated. Purification was performed on a silica gel column (eluent CH_2Cl_2:MeOH, 9:1, v/v). Yield was 6.0 g (65%). ^{1}H NMR ($CDCl_3$): δ 8.65 (br s, 1H); 7.30 (m, 12H); 6.81 (d, J = 9.0 Hz, 2H); 3.79 (s, 3H); 3.64 (t, J = 6.3 Hz, 2H); 2.25 (t, J = 7.3 Hz, 2H); 1.49 (m, 4H); 1.25 (m, 2H). $[M - H]^-$ obsd 418.21, calcd for $C_{26}H_{28}NO_4^-$: 418.20.

1-[4-(6-(4-Methoxytrityl)aminooxyhexamido)benzyl)]diethylenetriaminetetraacetic Acid Tetra-*tert*-butyl Ester (4). Compounds **2** (0.42 g, 1.0 mmol) and **3** (0.66 g; 1.0 mmol) were dissolved in methylene chloride (10 mL). DCC (227 mg; 1.10 mmol; predissolved in 2 mL of CH_2Cl_2) was added, and the mixture was stirred for 4 h at room temperature after which dicyclohexyl urea formed was filtered off. Purification was performed on a silica gel column (eluent CH_2Cl_2:MeOH, 9:1, v/v). Yield was 0.45 g (42%). ^{1}H NMR ($CDCl_3$): δ 10.13 (br s, 1H); 8.62 (br d, 1H); 7.44 (d, J = 8.2 Hz, 2H); 7.32−7.24 (m, 14H;) 6.81 (d, J = 8.6 Hz, 2H); 3.79 (s, 3H); 3.74 (s, 2H); 3.65 (t, J = 6.4 Hz, 2H); 3.43 (s, 4H); 3.34 (s, 2H); 3.21 (s, 2H); 2.77 (s, 8H); 2.22 (t, J = 6.4 Hz, 2H); 1.51 (m, 4H); 1.45 (s, 27 H); 1.43 (s, 9H); 1.26 (m, 2H). $[M - H]^-$ obsd 1066.64, calcd for $C_{61}H_{87}N_5O_{11}^-$: 1066.37.

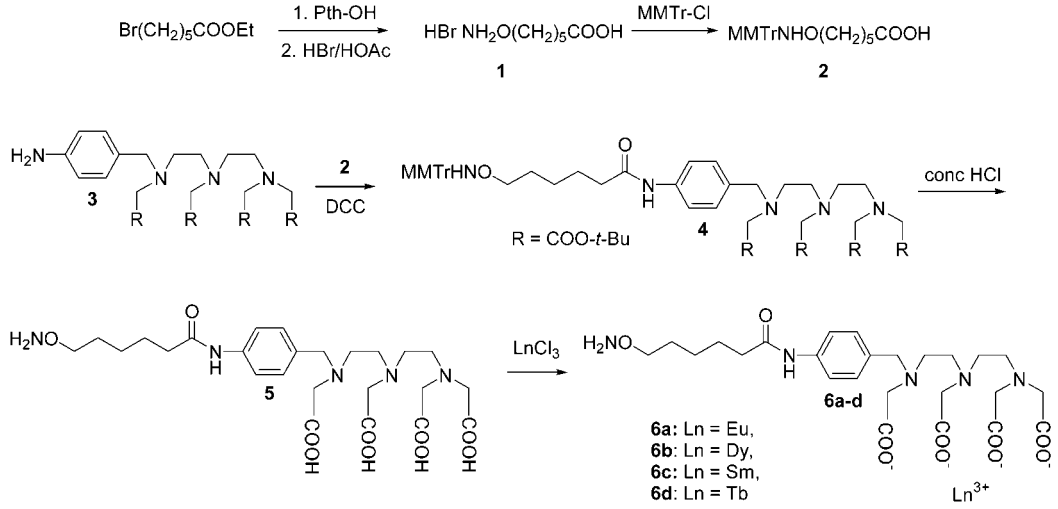
1-[4-(6-Aminooxyhexamido)benzyl]diethylenetriaminetetraacetic Acid Tetrahydrochloride (5). Compound **4** (150 mg, 0.14 mmol) was dissolved in concd HCl (5 mL) and stirred for 2 h at room temperature. All volatile materials were removed in vacuo. Precipitation from diethyl ether yielded the title compound as a solid. It was used for the next step without further purification. ^{1}H NMR (DMSO-d_6): δ 11.08 (br s, 4H); 10.38 (s, 1H); 7.72 (d, J = 8.2 Hz, 2H); 7.47 (d, J = 8.2 Hz, 2H); 4.35 (s, 2H); 4.00 (2 s, 4H); 3.93 (s, 2H); 3.83 (s, 2H); 3.43 (m, 2H); 3.39 (m, 2H); 3.32 (m, 2H); 3.20 (m, 2H); 2.37 (t, J = 7.0 Hz, 2H); 2.22 (t, J = 7.1 Hz, 2H); 1.61 (m, 4H); 1.34 (m, 2H). $[M - H]^-$ obsd 568.26, calcd for $C_{25}H_{39}N_5O_{10}^-$: 568.26.

1-[4-(6-Aminooxyhexamido)benzyl]diethylenetriaminetetraacetic Acid Lanthanide(III) (6a−d). Compound **5** (56.5 mg, 0.079 mmol) was dissolved in water (1.5 mL), and the pH was adjusted to 6.5 with solid $NaHCO_3$. Lanthanide(III) chloride hexahydrate (ca. 35 mg, predissolved in 0.5 mL of water) was slowly added, and the mixture was stirred for 1 h at ambient temperature, after which pH was adjusted to 8.5 with 0.1 M NaOH. Lanthanide hydroxide precipitated was removed by centrifugation, and the solvent was evaporated off in vacuo. The residue was dissolved in water (1 mL) and extracted with phenol (0.5 g). The aqueous layer was removed, after which phenol and the product were partitioned between water (1 mL) and diethyl ether (8 mL). The organic phase was removed, and the aqueous phase was washed with diethyl ether (3•5 mL) and concentrated. Precipitation from THF yielded the title compounds as solids in ca. 70% yield. Their homogenities were judged on HPLC. Gradient 0−1 min 95% A, from 1 to 31 min from 95% A to 100% B, from 31 to 36 min 100% B. Flow rate was 0.6 mL min^{-1}, wavelength 270 nm. Column: LiChrocart 125−3 Purospher RP-18, 5 μm. t_R (**6a−d**) 15.3 min. ESI-TOF MS: The europium(III) chelate, **6a**: $[M - H]^-$ obsd 742.152 calcd for $C_{25}H_{35}N_5O_{10}Eu^-$: 742.157; The dysprosium(III) chelate, **6b**: $[M - H]^-$ obsd 728.08 calcd for $C_{25}H_{35}N_5O_{10}Dy^-$: 728.07; The samarium(III) chelate, **6c**: $[M - H]^-$ obsd 715.07 calcd for $C_{25}H_{35}N_5O_{10}Sm^-$: 715.07. The terbium(III) chelate, **6d**: $[M - H]^-$ obsd 724.09 calcd for $C_{25}H_{35}N_5O_{10}Tb^-$: 724.16.

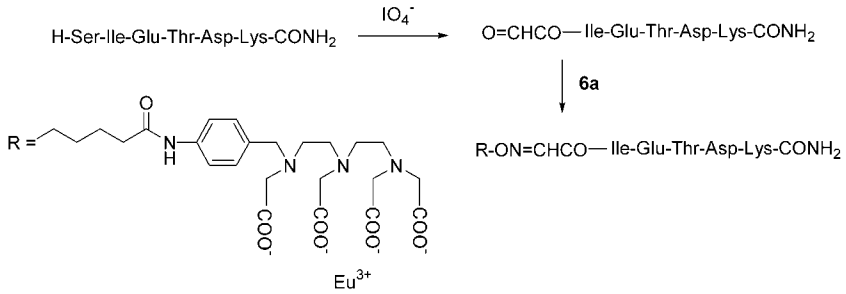
Labeling of H-Ser-Ile-Glu-Thr-Asp-Lys-CONH$_2$ with the Nonluminescent Aminooxychelate (6a). The oligopeptide (3 μmol) predissolved in a phosphate buffer (0.02 M, pH 7.7; 1 mL) was added to a solution of $NaIO_4$ (2 mL, 17.5 mM) in the same buffer solution. The mixture was stirred at room temperature for 30 min, and the reaction was stopped by adding ethylene glycol (2 equiv over sodium periodate). The reaction mixture was applied to a C18 Sep-Pak cartridge. The cartridge was initially washed with 10% CH_3CN containing 0.1% TFA (5 mL). The product was eluted with 80% CH_3CN containing 0.1% TFA (8 mL). The fraction containing the oxidized product was concentrated and purified by HPLC. Column: LiChrocart 250-4 Purospher RP-18, 5 μm and buffer solutions were as above. Gradient: 0 to 10 min 98% A, from 10 to 30 min from 98% A to 100% B, from 30 to 35 min 100% B. Flow rate 1.0 mL min^{-1}. t_R (oxidized product) 22.68 min. The α-*N*-glyoxolyl derivative was dissolved in HEPES-buffer (0.5 M, pH 7.5; 100 μL). The chelate **6a** (ca. 2 equiv) was added, and the mixture was stirred overnight at room temperature. Purification was performed on a HPLC Column: LiChrocart 125-3 Purospher RP-18, 5 μm. Gradient 0−1 min 95% A, from 1 to 31 min from 95% A to 100% B, from 31 to 36 min 100% B. Flow rate was 0.6 mL min^{-1}, t_R (product) 20.23 min.

Labeling of IL-8 with the Nonluminescent Aminooxychelate (6a). IL-8 (0.1 mg) was dissolved in TEAA buffer (pH 7.5, 35 μL; 50 mM) containing methionine as a scavenger (50-fold excess). Sodium metaperiodate (2.4 μL; 50 mM in water; 10-fold excess) was added, and the pH of the solution was adjusted to pH 7.5 with NaOH. The solution was incubated at room temperature for 13 min, after which the reaction was stopped with ethylene glycol (60 μL; 10 M; 10000-fold excess). The oxidation product was purified on NAP-5 column equilibrated with sodium acetate (25 mM; pH 5). Then a 10-fold excess of compound **6a** predissolved in water was added to the oxidized IL-8 solution. The solution was concentrated in SpeedVac until the concentration of IL-8 was ca. 1.3 mg mL^{-1}. After concentration the pH was readjusted to pH 4.7 with aq HCl. The solution was incubated at +4 °C overnight. The pH of the solution was adjusted to 6.5 with

Scheme 1



Scheme 2



1 M Tris-HCl (pH 7.5) and was further incubated for 1 h at +4 °C. The product was purified by gel filtration (Column: Sephadex G-25, grade fine, diameter 0.7 cm, length 50 cm). The column was equilibrated with Tris-HCl buffer, pH 7.8, containing 0.9% NaCl and 0.05% NaN_3. Eu-concentration was 6.5 μM.

The Interaction between Receptor and Ligand. Eu-IL-8, prepared using the chelate **6a**, was tested in saturation binding assay using receptor membrane preparation (CXCR2). All the reagents were diluted in 50 mM Tris-HCl buffer, pH 7.5, containing 10 mM $MgCl_2$, 0.2% bovine serum albumin, and 25 μM EDTA. Receptor preparate (0.5 μg/well; PerkinElmer Life Sciences) was incubated in the presence Eu-IL-8 (0.25, 1, 4, and 16 nM) in an AcroWell filtration plate (Pall Life Sciences) in the total volume of 100 μL per well at room temperature for 90 min. To determine nonspecific binding, the assay was performed also in the presence of 100 nM unlabeled IL-8. Next the wells were washed with 50 mM Tris-HCl, 10 mM $MgCl_2$, pH 7.5, four times (300 μL/well) using a manifold (Millipore) and a vacuum pump. After the wells were washed, DELFIA Enhancement Solution was added (200 μL/well) and the plate was shaken for 15 min. Europium fluorescence was measured using VICTOR^{2}V multilabel counter.

Labeling of Ketones with the Nonluminescent Aminooxychelate, 6a. General Procedure. The ketone (i.e., naltrexone hydrochloride, naloxone hydrochloride, or testosterone; 9.9 μmol; testosterone predissolved in DMF) and compound **6a** (7.3 mg, 9.9 μmol) were dissolved in HEPES-buffer (0.5 M, pH 7.5; 200 μL), and the mixture was stirred overnight at room temperature and precipitated with acetone. The precipitate was dissolved in 0.05 M TEAA (pH 7.5; 0.5 mL) and purified on HPLC. Mobile phase: buffer A: 0.05 M TEAA; buffer B: A in 50% v/v acetonitrile. Gradient 0−1 min 95% A, from 1 to 31 min to 100% B, from 31 to 36 min 100% B, flow rate 0.6 mL min^{-1}, wavelength 270 nm. Column: XTerra MS C-8, 5 μm, 4.6 × 150 mm. Pure fraction was concentrated in vacuo and characterized on ESI-TOF MS. Naloxone conjugate (**7**) $[M - H]^-$ obsd 1027.3, calcd for $C_{44}H_{55}EuN_6O_{13}^-$: 1027.9. Naltrexone conjugate (**8**) $[M - H]^-$ obsd 1041.3, calcd for $C_{45}H_{56}EuN_6O_{13}^-$: 1040.9. Testosterone conjugate (**9**) $[M - H]^-$ obsd 988.3, calcd for $C_{44}H_{61}EuN_5O_{11}^-$: 988.4.

RESULTS AND DISCUSSION

Synthesis of nonluminescent lanthanide(III) chelates tethered to an aminooxy group is outlined in Scheme 1. Initially, 6-aminooxyhexanoic acid, **1**, was prepared by allowing ethyl 6-bromohexanoate to react with *N*-hydroxyphthalimide in the presence of triethylamine followed by acidic hydrolysis. It was then converted to the corresponding MMTr-protected derivative, **2**, reaction of which with 1-(4-aminobenzyl)diethylenetriaminetetraacetic acid tetra-*tert*-butyl ester (**3**; *21*) in the presence of DCC resulted in **4** in moderate yield. Deprotection of the aminooxy and carboxylic acid functions with concd HCl gave the free acid, **5**, which was finally converted to the corresponding europium, terbium, samarium, and dysprosium(III) chelates, **6a**−**d**, by treatment with the appropriate lanthanide(III) chloride at pH 6.5. The chelates were purified by phenol extraction. Their homogenities were judged on HPLC, and their structures were verified by mass spectrometry. It is worth noting that Eu^{3+}, Sm^{3+}, Dy^{3+}, and Tb^{3+} are those four lanthanides routinely used in assays based on DELFIA technology.

The DELFIA Principle (*14*). In dissociative fluorescence enhancement assays polycarboxylate-based non-

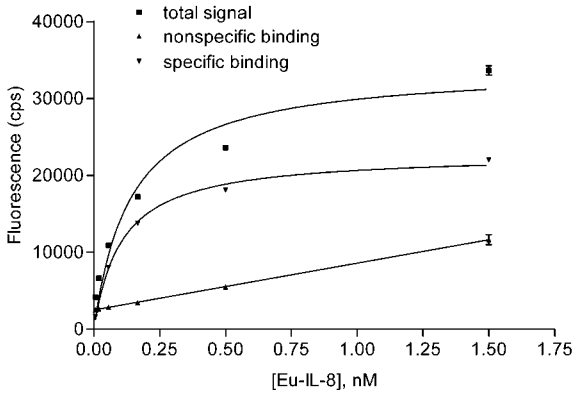
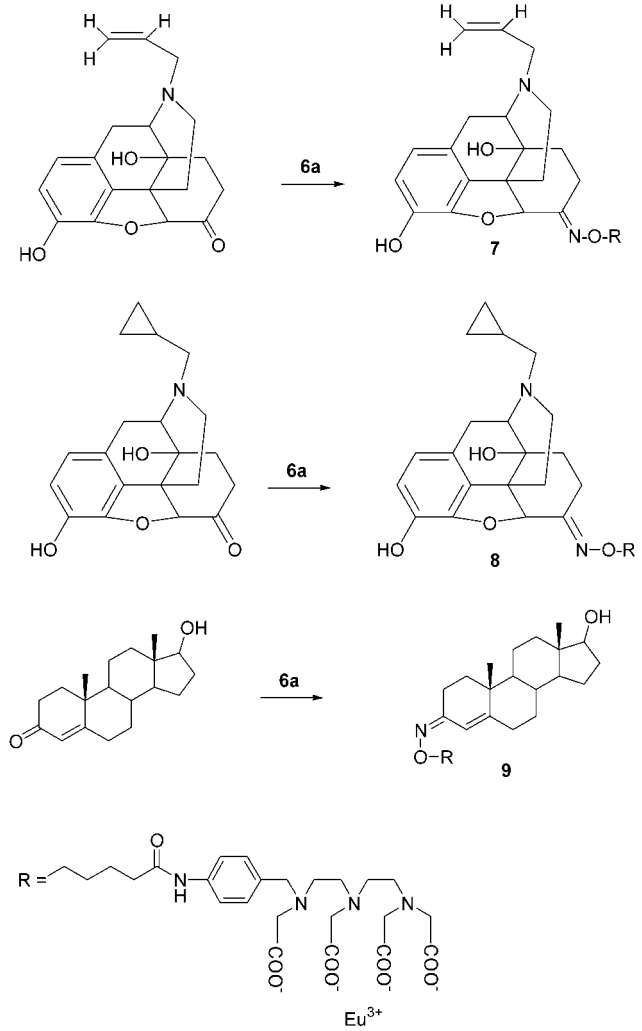


Figure 1. Saturation binding assay of IL-8 labeled with the chelate **6a**. Saturation binding experiments were performed with 0−1.5 nM Eu-interleukin-8 with 2 μg of membrane preparation (CXCR2). Nonspecific binding was determined in the presence of 100 nM unlabeled IL-8. Detection was performed by measuring europium fluorescence.

Scheme 3



fluorescent lanthanide(III) chelates are used as labels. These chelates are applied as carriers of the lanthanide ions through the assay. After perfoming the assay, fluorescence is developed by dissociation of chelated ions and creating new fluorescent chelates in solution. This is achieved by decreasing conditional stability of the complexones by reduction of pH to 3.2. Fluorinated β-diketones present in excess are able to form lanthanide complexes rapidly at the pH used. One lanthanide binds

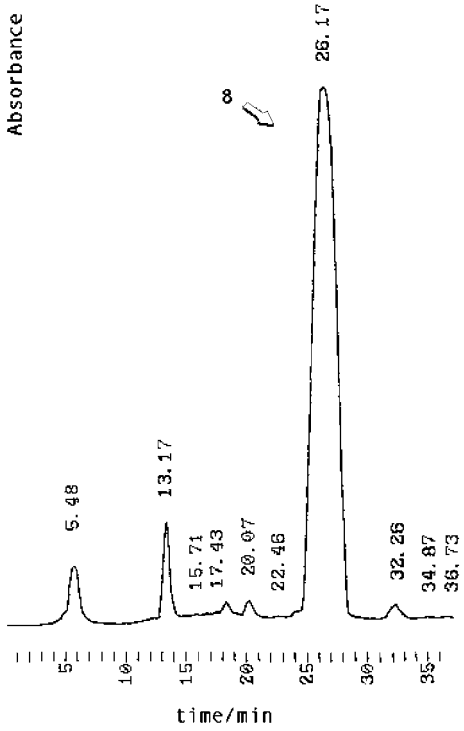


Figure 2. HPLC trace of the reaction of **6a** with naloxone (crude reaction mixture). The major peak (t_R 26.17 min) is the desired product **8** as judged on MS analysis. For chromatographic conditions, see Experimental Procedures.

three diketones to form the light-harvesting group in the chelate. The remaining water molecules are removed with a synergistic agent, TOPO, and the newly formed complex is solubilized with detergents. Finally, lanthanide content is measured fluorometrically. DELFIA is an ultrasensitive assay working well even in picomolar range. As a heterogeneous assay, DELFIA technology is used almost exclusively with solid-phase (microtitration plate) immobilized reagents. It has wide applications as a diagnostic test system, in DNA hybridizations, research immunoassays, receptor−ligand assays, end-point detection of enzymatic reactions, and cytotoxicity assays.

Conjugation to Bioactive Molecules. To demonstrate the applicability of the aminooxychelates synthesized for biomolecule derivatization, one of them, **6a**, was allowed to react with a model peptide, a protein, and two synthetic drugs having a ketone function in their structure, and a ketosteroid. The key steps are discussed below.

A synthetic oligopeptide H-Ser-Ile-Glu-Thr-Asp-Lys-$CONH_2$ was oxidized at its amino terminal serine to the corresponding aldehyde using a standard literature procedures (*8*−*10*), and the reaction was followed on HPLC-MS techniques (Scheme 2). The starting peptide gave a single peak on HPLC with an observed $[M - H]^-$ of 689.3 (calcd 689.3). Its reaction with periodate gave initially the expected α-*N*-glyoxolyl derivative with an observed $[M - H]^-$ of 658.3 (calcd 658.3). Prolonged reaction time gave an additional product with longer t_R on HPLC with an $[M - H]^-$ of 656.3. The undesired product can be attributed to result from oxidation of the threonine residue of the oligopeptide. Its existence could be suppressed by reducing the reaction time and performing the reaction at 0 °C. Finally, the desired α-*N*-glyoxolyl derivative was allowed to react with the europium(III) chelate, **6a**, and the desired site-specifically labeled oligopeptide derivative, with an observed [M −

H]$^-$ of 1359 (calcd 1359), was formed quantitatively. The same labeling strategy was also applied to attachment of **6a** to Interleukin-8 (IL-8).

Saturation Binding Assay. The IL-8 protein labeled with aminooxy-Eu chelate was tested in saturation binding assay based on DELFIA technology using receptor membrane preparation (CXCR2). Saturation binding experiments were performed with 0−1.5 nM Eu-interleukin-8 with 2 μg of membrane preparation. Nonspecific binding was determined in the presence of 100 nM unlabeled IL-8. The ligand binded to receptor specifically, which was detected by measuring europium fluorescence. The K_d-value of Eu−IL-8 for CXCR2 receptor was 0.10 nM (Figure 1).

The applicability of aminooxychelates for hapten labeling was demonstrated by allowing two synthetic drugs, naltrexone and naloxone, and one ketosteroid, testosterone, to react with **6a** at neutral pH (Scheme 3). In all the cases, the desired conjugates were formed quantitatively. The HPLC trace of the reaction of **6a** with naloxone is shown in Figure 2 as an illustrative example.

In summary, nonluminescent europium(III), terbium(III), dysprosium(III), and samarium(III) chelates tethered to an aminooxy group were synthesized, and their applicability to biomolecule derivatization was demonstrated.

LITERATURE CITED

(1) Jencks, W. P. (1964) Mechanism and catalysis of simple carbonyl group reactions. *Prog. Phys. Org. Chem. 2*, 63−128.

(2) Janoski, A. H., Shulman, F. C, and Wright, G. E. (1974) Selective 3-(*O*-carboxymethyl)oxime formation in steroidal 3,-20-diones for hapten immunospecificity. *Steroids 23*, 49−64.

(3) Mikola, H., and Hänninen, E. (1992) Introduction of aliphatic amino and hydroxy groups to keto steroids using *O*-substituted hydroxylamines. *Bioconjugate Chem. 3*, 182−6.

(4) Kubo, K., Ide, H., Wallace, S. S., and Kow, Y. W. (1992) A novel, sensitive and specific assay of abasic sites, the most commonly produced DNA lesions. *Biochemistry 31*, 3703−8.

(5) Boturyn, D., Boudali, A., Constant, J., Defrancq, E., and Lhomme, J. (1997) Synthesis of fluorescent probes for the detection of abasic sites in DNA. *Tetrahedron 53*, 5485−92.

(6) Trevisiol, E., Renard, A., Defrancq, E., and Lhomme, J. (1997) The oxyamino-aldehyde coupling reaction: an efficient method for the derivatization of oligonucleotides. *Tetrahedron Lett. 38*, 8687−90.

(7) Sun, H. B., and Yokota, H. (2001). Detection of abasic sites on individual DNA molecules using atomic force microscopy. *Anal. Chem. 73*, 2229−2232.

(8) Gaertner H. F., Rose K., Cotton, R., Timms, D., Camble, R., and Offord, R. E. (1992) Construction of protein analogues by site-specific condensation of unprotected fragments. *Bioconjugate Chem. 3*, 262−268.

(9) Alouani, S., Gaertner, H. F., Mermod, J., Power, C. A., Bacon, K. B., Wells, T. N. C., and Proudfoot A. E. I. (1995) A fluorescent interleukin-8 receptor probe produced by targetted labeling at the amino terminus. *Eur. J. Biochem. 227*, 328−334.

(10) Geoghegan K. F., and Stroh J. G. (1992) Site-directed conjugation of nonpeptide groups to peptides and proteins via periodite oxidation of a 2-amino alcohol. Application to modification at *N*-terminal serine. *Bioconjugate Chem. 3*, 138−146.

(11) Lemieux, G. A., and Bertozzi, C. R. (1998) Chemoselective ligation reactions with proteins, oligosaccharides and cells. *TIBTECH 16*, 506−513.

(12) Adarichev, v. A., Kalachnikov, S. M., Kiseliova, A. V., and Dymshits, G. M. (1998) Molecular hybridization probes prepared with 4-aminooxybutylamine. *Bioconjugate Chem. 9*, 671−5.

(13) Salo, H., Virta, P., Hakala, H., Prakash, T. P., Kawasaki, A. M., Manoharan, M., and Lönnberg, H. (1999) Aminooxy functionalized oligonucleotides: preparation, on-support derivatization and postsynthetic attachment to polymer support. *Bioconjugate Chem. 10*, 815−23.

(14) Hemmilä, I., and Mukkala, V.-M. (2001) Time-resolution in fluorometry technologies, labels, and applications in bioloanalytical assays. *Crit. Rev. Clin. Lab. Sci. 38*, 441−519.

(15) Hemmilä, I., Ståhlberg, T., and Mottram, P. (1994) *Bioanalytical Applications of Labeling Technologies*, Perkin Elmer, Wallac Oy.

(16) Hemmilä, I. (1991) Applications of fluorescence in immunoassays, in *Chemical Analysis: A series of Monographs on Analytical Chemistry and Its Applications* (J. D. Winefordner, Ed.) Vol. 117, John Wiley & Sons, Inc., New York.

(17) Pope, A. J. (1999) LANCE vs HTRF technologies (or vice versa) *J. Biomol. Screen. 6*, 301−302.

(18) Hemmilä, I. (1999) LANCE: homogeneous assay platform for HTS. *J. Biomol. Screen. 6*, 303−307.

(19) Mathis, G. (1999) HTRF technology *J. Biomol. Screen. 6*, 309−313.

(20) Mathis, G. (1993) Rare earth cryptates and homogeneous fluoroimmunoassays with human sera. *Clin. Chem. 39*, 1953−1959.

(21) Peuralahti, J., Hakala, H., Mukkala, V.-M., Loman, K., and Hovinen, J. (2002) Introduction of lanthanide(III) chelates to oligopeptides on solid phase. *Bioconjugate Chem. 13*, 870−875.

BC025502B

^{99m}Tc-Labeling of a Hydrazinonicotinamide-Conjugated LTB_4 Receptor Antagonist Useful for Imaging Infection and Inflammation

Shuang Liu,* Anthony R. Harris, Neal E. Williams, and D. Scott Edwards

Bristol-Myers Squibb Medical Imaging,† 331 Treble Cove Road, North Billerica, Massachusetts 01862.
Received September 23, 2001; Revised Manuscript Received January 23, 2002

This report describes the ^{99m}Tc labeling of a hydrazinonicotinamide (HYNIC)-conjugated LTB_4 receptor antagonist (SG380). The ternary ligand technetium complex [^{99m}Tc(SG38)(tricine)(TPPTS)] (RP517) was prepared using a non-$SnCl_2$-containing formulation ((2001) *J. Pharm. Sci. 90*, 114−123). Unlike other HYNIC-conjugated small biomolecules, SG380 is lipophilic and has low solubility in the kit matrix. Using a combination of a solubilizing agent (Lysolecithin) and a cosolvent (ethanol), we have developed a new formulation for routine preparation of RP517. Using this formulation, RP517 can be prepared in high radiochemical purity (RCP > 90%) and remains stable in the kit matrix for at least 6 h. We also prepared the corresponding ^{99}Tc analogue, [^{99}Tc]RP517. An HPLC concordance experiment using RP517 and [^{99}Tc]RP517 showed that the same technetium complex was prepared at both the tracer and macroscopic levels. The LC-MS data are completely consistent with the 1:1:1:1 composition for Tc:SG380:tricine:TPPTS.

INTRODUCTION

Accurate and rapid detection of infectious and inflammatory foci is of great importance for elucidation of the cause of the disease, early prevention of the onset of complications, and rapid implementation of a tailored therapeutic regimen. While in some cases infections are diagnosed on the basis of clinical history, physical examination of the patient, in others it is more difficult because they are asymptomatic or cause nonspecific symptoms. Numerous imaging procedures have been developed for visualization of infectious and inflammatory lesions (*1*−*14*). These include ultrasonography, computed tomography (CT), magnetic resonance imaging (MRI), and nuclear medicine procedures. Ultrasonography, CT, and MRI provide details of morphological changes, variations in density, and differences in proton content in tissues (*13*). Nuclear medicine procedures can be used for in vivo characterization of cellular structure and function and for monitoring biological changes in the infectious tissues at the molecular level.

Various ^{99m}Tc-labeled small biomolecules that bind to receptors on inflammatory cells have been studied as potential new radiopharmaceuticals for scintigraphic imaging of infection and inflammation. These include include ^{99m}Tc-labeled chemotactic peptides (*15*−*23*), tuftsin receptor antagonists (*24*−*27*), antimicrobial peptides (*28*−*30*), and a fragment of human platelet factor 4 (*31*, *32*). Although animal studies show that the ^{99m}Tc-labeled chemotactic peptides bind to leukocytes and localize at sites of infection, the use of ^{99m}Tc-labeled agonists as radiopharmaceuticals suffers a major drawback, severe reduction of peripheral leukocyte count. This problem can be avoided by using antagonist peptides as targeting molecules. Unfortunately, the receptor binding affinity of the antagonists tested to date appear to be much lower than that of the agonists.

Leukotriene B_4 (LTB_4) is a proinflammatory mediator, which is derived from the action of 5-lipoxygenase on arachidonic acid and is synthesized primarily by PMNLs, monocytes, and macrophages. LTB_4 is known to stimulate degranulation, aggregation, chemotaxis, and chemokinesis of PMNLs, as well as promote superoxide generation. LTB_4 also promotes the adhesion of neutrophils to the vascular endothelium. LTB_4 receptors are highly expressed on a number of inflammatory cells such as neutrophils, monocytes, macrophages, and lymphocytes. Numerous LTB_4 receptor antagonists have been evaluated for their potential in the treatment of various infectious and inflammatory diseases.

In our previous communication (*33*), we reported a non-$SnCl_2$-containing formulation useful for the ^{99m}Tc-labeling of hydrazinonicotinamide-conjugated small biomolecules (HYNIC−BM[1]). In the non-$SnCl_2$ formulation, each lyophilized vial contains 20 μg of HYNIC−BM, 5 mg of TPPTS (trisodium triphenylphosphine-3,3′,3″-trisulfonate), 6.5 mg of tricine, 40 mg of mannitol, 38.5 mg of disodium succinate hexahydrate, 12.7 mg of succinic acid, and 0.1 mg of pluronic acid (Poloxamer-188, 0.1%). HYNIC is the bifunctional coupling agent for ^{99m}Tc-labeling. Tricine and TPPTS are used as coligands to stabilize the [^{99m}Tc]HYNIC core. The combination of HYNIC−BM, tricine, and TPPTS produces a versatile ternary ligand system which forms technetium complexes, [^{99m}Tc(HYNIC−BM)(tricine)(TPPTS)], with high solution stability. We have been able to use the non-$SnCl_2$ formulation for the ^{99m}Tc-labeling of many small biomolecules, including a GPIIb/IIIa receptor antagonist for thrombus imaging (*33*−*35*), a chemotactic peptide (*23*) for imaging infection and inflammation, and vitronectin receptor antagonists for tumor imaging (*36*).

* To whom correspondence should be addressed: Tel: 978-671-8696 (S.L.); FAX: 978-436-7500; E-mail: shuang.liu@bms.com.

† Formerly Medical Imaging Division, DuPont Pharmaceuticals Company.

[1]Abbreviations: RCP: radiochemical purity; HYNIC−BM: 6-hydrazinonicotinamide-conjugated biomolecule; TPPTS: trisodium triphenylphosphine-3,3′,3″-trisulfonate.

10.1021/bc010120b CCC: $22.00 © 2002 American Chemical Society
Published on Web 06/28/2002

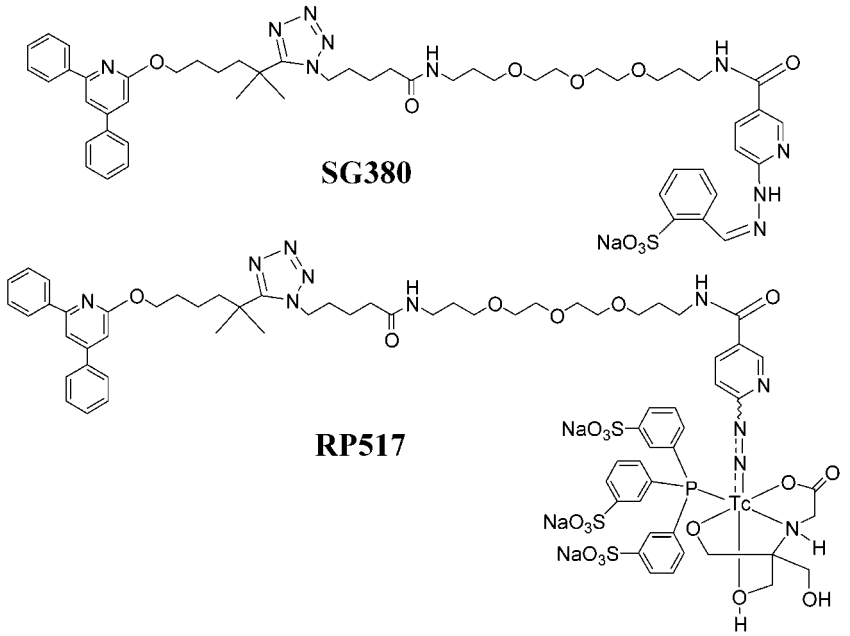


Figure 1. Structures of the HYNIC-conjugated LTB_4 receptor antagonist (SG380) and its ternary ligand technetium complex (RP517).

SG380 is an HYNIC-conjugated LTB_4 antagonist. Theoretically, we should be able to use the non-$SnCl_2$-containing formulation for the ^{99m}Tc-labeling of SG380. To our surprise, direct substitution of 20 μg of SG-380 for HYNIC−BM in the non-$SnCl_2$–containing formulation gave very low yields (60−70%) for RP517 even though the radiolabeling conditions are the same as those used for preparation of the ^{99m}Tc-labeled GPIIb/IIIa receptor antagonist (*33*) and vitronectin receptor antagonists (*36*). The goal of this study is to explore the factors influencing the yield of RP517 and to develop a formulation that provides RCP ≥ 90% for routine preparation of RP517.

EXPERIMENTAL SECTION

Materials. *N,N*-Dimethylacetamide (DMA), L-α-lysophosphatidylcholine (Lysolecithin), Tween-80, mannitol, pluronic acid (Poloxamer-188), succinic acid, TPPTS (trisodium triphenylphosphine-3,3′,3″-trisulfonate), and tricine were purchased from Aldrich or Sigma. Synthesis of SG380 will be published as a separate communication (*37*). $Na^{99m}TcO_4$ was obtained from a commercial DuPont Pharma ^{99}Mo/^{99m}Tc generator, N. Billerica, MA. The generator eluant was collected into a dry and clean 30 mL vial and diluted to the required concentration before use.

Analytical Methods. The HPLC method used a HP-1090 system, a homemade NaI radiometric detector, and a heated (50 °C) Cosmosil C_{18} column (4.6 mm × 250 mm) at a flow rate of 1 mL/min. The gradient mobile phase started from 100% solvent A (75:25 0.025 M succinate buffer, pH = 5.0/acetonitrile) to 30% solvent A and 70% solvent B (acetonitrile) at 35 min. The mobile phase was isocratic at 35−45 min using 30% solvent A and 70% solvent B. LC-MS spectral data were collected using a HP1100 LC/MSD system with an API-electrospray interface. The LC-MS method used a Zorbax C_{18} column (4.6 mm × 150 mm, 3.5 μm particle size) and a mobile phase gradient starting from 92% solvent A (10 mM ammonium acetate buffer, pH 7.0) and 8% solvent B (methanol) to 100% B at 23 min at a flow rate of 1 mL/min. The ITLC method used Gelman Sciences silica gel ITLC paper strips and a 1:1 mixture of acetone and saline as eluant. Using this ITLC method, RP517 and [^{99m}Tc]-pertechnetate migrate while the [^{99m}Tc]colloid remains at the origin.

A General Procedure for Radiolabeling. RP517 was prepared according to the published procedure (*33*) with a slight modification. Briefly, to a lyophilized vial containing 5 mg of TPPTS, 6.5 mg of tricine, 40 mg of mannitol, 38.5 mg of disodium succinate hexahydrate, 12.7 mg of succinic acid, and 0.1 mg of pluronic acid (0.1%); pH = 4.8) was added 1.0 mL of SG380 solution (20 μg/mL in an appropriate solvent or mixture of solvents). The vial was placed into a lead pig, and to the vial was added 0.5 mL of Na[$^{99m}TcO_4$] solution (100 mCi/mL) in saline. The reconstituted vial was heated at 100 °C for 10−40 min in a lead-shielded water bath. After being cooled to room temperature, the reaction mixture was analyzed by radio-HPLC and ITLC. The radiochemical purity (RCP) was calculated as the percentage of integrated area for the radiometric peak of RP517 versus the total area. Since the [^{99m}Tc]colloid formation is negligible (<0.5%), no correction is needed for the HPLC data.

[^{99}Tc]RP517. To a clean 10 mL vial was added 1.5 mg of SG380, 84 mg of tricine, 49 mg of TPPTS, 1.2 mg of NH_4[$^{99}TcO_4$] in 0.4 mL of H_2O, and 1.5 mL of 25 mM succinate buffer (pH = 5.0). The reaction mixture was heated in a 100 °C water bath for 30 min. After being cooled to room temperature, the product was separated by HPLC. The collections of the peak due to RP517 were combined, and volatiles were removed under reduced pressure. The product, [^{99}Tc]RP517, was then desalted using the same HPLC method using water as mobile phase A. The HPLC concordance experiment showed the same retention time for RP517 and [^{99}Tc]RP517. LC-MS: m/z = 1627.2 for $(M + 1)^+$ ($[C_{70}H_{86}N_{11}O_{20}PS_3Tc]^+$) and m/z = 813.7 for $(M + 2)^{2+}$.

RESULTS AND DISCUSSIONS

Recently, we reported a series of the ^{99m}Tc-labeled LTB_4 receptor antagonists for imaging infection and inflammation (*38*−*42*). RP517 (Figure 1) was evaluated in two animal (guinea pig and rabbit) models of focal infection. In the guinea pig peritonitis model (*38, 39*), RP517 showed uptake of 0.6 ± 0.05% ID/g at the site of infection

1 h postinjection. The radioactivity was retained with uptake of 0.5 ± 0.08% ID/g at 4 h postinjection. RP517 is excreted mainly via the hepatobiliary route (*42*). In the rabbit infection model, RP517 showed similar uptake at the infection site with the target-to-background (infected muscle/normal muscle) ratio of 16:1, 1 h postinjection. A primate dosimetry study indicates that the dose-limiting organ is the gall bladder. RP517 is under clinical investigation as a new imaging agent for acute infection and inflammation.

Discovery of a new radiolabeled biomolecule for the intended receptor is just the first step in a long process of the radiopharmaceutical development. In addition to its biological efficacy, the new radiopharmaceutical must have high radiochemical purity (RCP ≥ 90%) and solution stability (≥6 h). A kit formulation is also required due to the 6 h half-life of ^{99m}Tc. The kit components are often dissolved in a buffer system and then lyophilized to form a white powder in a "cake" form. A buffer is used to control the pH in the kit, which is extremely important during manufacturing and radiolabeling processes. A bulking agent is needed so that the kit components can crystallize on the well-formed crystal frameworks of the agent during the lyophilization process. Injection of the whole or part of the reconstituted kit should not cause any significant biological effect, such as neutropenia.

To support clinical studies, we have to develop a formulation for routine preparation of RP517. Recently, we reported a non-$SnCl_2$-containing formulation for the ^{99m}Tc-labeling of HYNIC−BM (*33*). The non-$SnCl_2$ formulation has been successfully used for the ^{99m}Tc-labeling of a HYNIC-conjugated GPIIb/IIIa receptor antagonist for imaging thrombi (*33*) and a HYNIC-conjugated vitronectin receptor antagonist for imaging tumors (*36*). Since SG380 is also an HYNIC-conjugated biomolecule, we decided to use the non-$SnCl_2$ formulation as the platform for the ^{99m}Tc-labeling of SG380. However, it was soon found out that the direct substitution of 20 μg of SG380 for HYNIC−BM in the non-$SnCl_2$ formulation gave fairly low yields (60−70%) of RP517 under the same radiolabeling conditions used for the preparation of other ^{99m}Tc-labeled biomolecules (*33*−*36*).

During our initial radiolabeling studies, we noticed that unlike other HYNIC-conjugated small biomolecules, SG380 is lipophilic and has low solubility in the kit matrix. Even though a surfactant (Poloxamer-188, 0.1%) is used in the non-$SnCl_2$ formulation, both SG380 and its ternary ligand ^{99m}Tc complex RP517 showed significant adsorption on the glass surface of reaction vials. When the solution containing RP517 was filtered through a 0.22 μm filter, only ∼70% of radioactivity was recovered. We hypothesized that the low yield of RP517 is caused by poor water solubility of SG380 in the kit matrix.

The glass surface adsorption of SG380 imposes a significant problem in the manufacturing process and during radiolabeling. In the manufacturing process, the formulation has to be filtered into individual vials to remove any particles. If SG380 shows a significant adsorption on glass surface or in the filter, it will be very difficult to maintain the reproducibility of the whole process. On the other hand, the glass-surface adsorption of SG380 means that there will not be sufficient SG380 available for reaction with ^{99m}Tc. Therefore, the first objective of our formulation efforts was to find an appropriate solubilizing agent or cosolvent to reduce glass-surface adsorption and to increase the solubility of SG380 in the kit matrix.

Table 1. Effect of the Solubilizing Agent or Cosolvent on RCP of RP517.

solubilizing agent or cosolvent concentration[a]	RCP (%)
13.3% EtOH (A)	91.3 ± 0.9/n = 4
0.07% Tween-80 (B)	65.6 ± 0.5/n = 4
0.07% Lysolecithin (D)	86.1 ± 0.9/n = 5
13.3% DMA (E)	91.9 ± 0.9/n = 5
13.3% EtOH + 0.07% Lysolecithin (F)	92.4 ± 0.3/n = 4
water only	81.2 ± 0.4/n = 4

[a] Each lyophilized vials contains 5 mg of TPPTS, 6.5 mg of tricine, 40 mg of mannitol, 38.5 mg of disodium succinate hexahydrate, 12.7 mg of succinic acid, and 0.1 mg of pluronic acid (0.1% Poloxamer-188). This is the concentration after addition of 0.5 mL of [^{99m}Tc]pertechnetate solution.

Screening of Solubilizing Agents and Cosolvents. There are several ways to improve solubility and to reduce the glass-surface adsorption of SG380. These include the use of a solubilizing agent such as Lysolecithin, Tween-80, or a cosolvent such as ethanol or *N*,*N*-dimethylacetamide (DMA). To study the effect of the solubilizing agent or cosolvent on the RCP of RP517, we performed a radiolabeling study using lyophilized vials containing 5 mg of TPPTS, 6.5 mg of tricine, 40 mg of mannitol, 38.5 mg of disodium succinate hexahydrate, 12.7 mg of succinic acid, and 0.1 mg of pluronic acid (Poloxamer-188, 0.1%). In this study, SG380 (∼20 μg) was dissolved in 1 mL of the following solutions: 20% EtOH (A), 0.1 wt % Tween-80 in water (B), 0.1 wt % Lysolecithin in water (C), 20% *N*,*N*-dimethylacetamide (D), 20% EtOH with 0.1 wt % Lysolecithin (E), and water (G). Lyophilized vials were reconsitituted by adding 1 mL of the SG-380 solution and 0.5 mL of Na[$^{99m}TcO_4$] solution (100 mCi/mL). The total volume for each vial was 1.5 mL. After addition of Na[$^{99m}TcO_4$], the actual concentration of the solubilizing agent or cosolvent becomes two-thirds of the original concentration. The reconstituted vials were heated at 100 °C for 30 min. After being cooled to room temperature, they were analyzed by HPLC. Four vials were tested for each condition, and the experiment was repeated using a different generator or the same generator on a different date. Table 1 summarizes the RCP data of RP517. Ethanol (13%) and *N*,*N*-dimethylacetamide (13%) alone or a combination 13% ethanol with 0.07% lysolecithin gave average RCP values ∼90% for RP517. Water by itself gave a RCP value of only 81%. Tween-80 did not give satisfactory yields for RP517.

Ethanol Concentration versus RCP. A radiolabeling study was performed using the same lyophilized vials as in the previous experiment. SG380 was dissolved in aqueous ethanol (0−30% EtOH) to give a concentration of 20 μg/mL. Reconstitution of the vials was achieved by adding 1 mL of the SG380 solution and 0.5 mL of Na[$^{99m}TcO_4$] solution (100 mCi/mL). The reconstituted vials were heated at 100 °C for 30 min, and samples of the reaction mixtures were characterized by HPLC and ITLC. Four vials were tested for each condition, and the experiment was repeated using a different generator or the same generator on a different date. Figure 2 shows the histogram of RCP versus EtOH concentration. The optimal ethanol concentration range is 5−15%.

Heating Time versus RCP. Heating time is another factor influencing the RCP of RP517. In SG380, the hydrazine moiety is protected as a hydrazone of 2-sulfonatobenzylaldehyde. For SG380 to bond to the Tc, hydrolysis of the hydrazone group has to occur. The yield of RP517 depends largely on the amount of hydrazine groups available for Tc-binding and the kinetics of in situ hydrolysis of the hydrazone functionality. The greater the

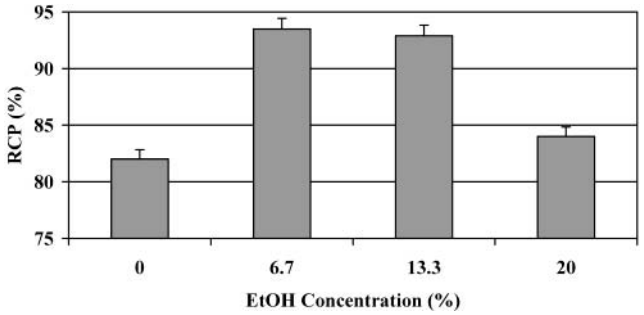


Figure 2. Effect of ethanol concentration on RCP of RP517. Four vials were tested for each condition, and the experiment was repeated using a different generator or the same generator on a different date.

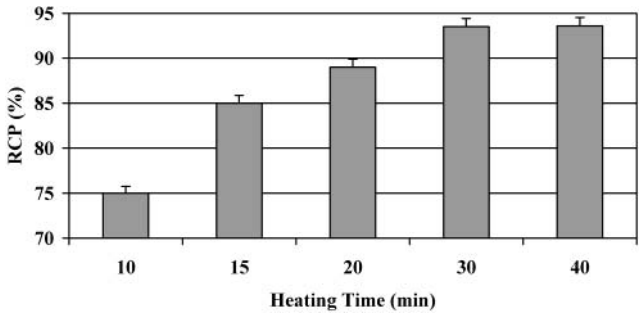


Figure 3. Heating time versus RCP. Four vials were tested for each condition, and the experiment was repeated using a different generator or the same generator on a different date.

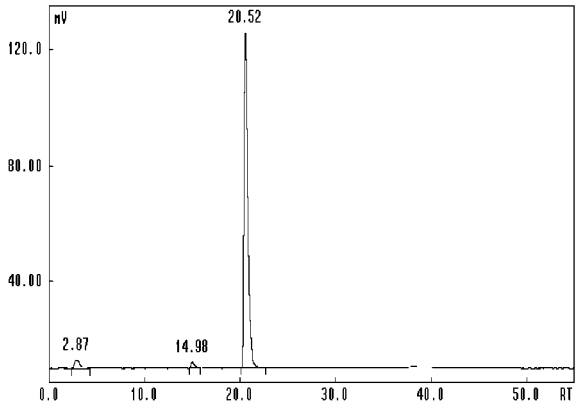


Figure 4. Radio-HPLC chromatogram of RP517.

hydrolysis of the hydrazone group, the more the free hydrazine groups available for Tc-binding; thereby the higher the radiolabeling yield of RP517.

To find an optimal heating time for the preparation of RP517, we performed a radiolabeling study using the same lyophilized vials as in the previous experiments. In this experiment, SG380 was dissolved in 1 mL of 10% EtOH to give a concentration of 20 μg/mL. To each lyophilized vial were added 1.0 mL of SG380 solution and 0.5 mL of Na[$^{99m}TcO_4$] solution (100 mCi/mL). The ethanol concentration was ~6.7%. Reconstituted vials were heated at 100 °C for 10, 15, 20, 30, and 40 min. Figure 3 shows the histogram of heating time versus RCP of RP517. Longer heating time gives better RCP for RP517; but there is no significant difference in RCP between the vials heated 100 °C for 30 min and vials heated 100 °C for 40 min.

HPLC Characterization. Figure 4 shows a typical radio-HPLC chromatogram of RP517. The small peak at ~3 min is due to a combination of several radioimpurities. Since most of radioimpurities in the RP517 kit are less than 1.0%, no further characterization was performed. The LTB_4 targeting moiety contains no chiral center. The technetium chelate is formed as an equal mixture of D and L enantiomers due to the tricine ligand being prochiral. These enantiomers are not separable using the chromatographic conditions described in this study. Thus, RP517 shows only one radiometric peak in its radio-HPLC chromatogram.

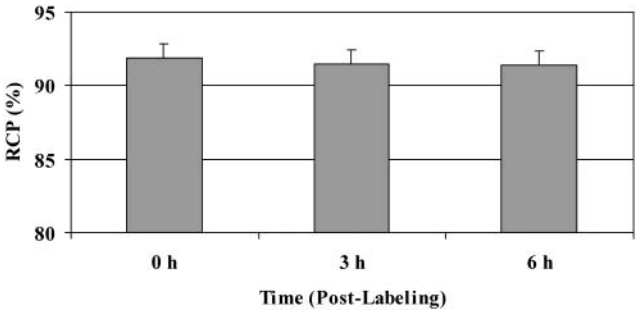


Figure 5. Solution stability of RP517 in the kit matrix.

Solution Stability Studies. We also examined the solution stability of RP517. Each lyophilized vial was reconstituted by adding 1.0 mL of SG380 solution (20 μg/mL in 18% EtOH) and 0.5 mL of Na[$^{99m}TcO_4$] solution (100 mCi/mL). The final ethanol concentration was 12%. Reconstituted vials were heated at 100 °C for 30 min. Samples of the resulting solutions were analyzed by radio-HPLC at $t = 0$, 3, and 6 h post-labeling. The results are shown in Figure 5. RP517 is stable for at least 6 h in the kit matrix.

Synthesis and Characterization of [^{99}Tc]RP517. [^{99}Tc]RP517 was prepared in one step by reacting [NH_4][$^{99}TcO_4$] with SG380 in the presence of excess tricine and TPPTS. The yield for [^{99}Tc]RP517 is relatively low (<30% by UV). After HPLC purification and desalting, [^{99}Tc]RP517 was obtained only in milligram quantities, which is sufficient for the HPLC concordance experiment and LC-MS characterization. The HPLC concordance experiment showed that the same complexes were prepared at the tracer (^{99m}Tc) and macroscopic (^{99}Tc) levels. The LC-MS spectrum of [^{99}Tc]RP517 showed both the monoprotonated molecular ion, $(M + 1)^+$, peak at $m/z = 1627.2$ for $[C_{70}H_{86}N_{11}O_{20}PS_3Tc]^+$ and the diprotonated molecular ion, $(M + 2)^{2+}$, peak at $m/z = 813.7$. The LC-MS data support the proposed structure (Figure 1) and is completely consistent with the 1:1:1:1 composition for Tc:SG380:tricine:TPPTS.

CONCLUSIONS

In this report, we described the synthesis and characterization of a ternary ligand complex [^{99m}Tc(SG380)(tricine)(TPPTS)] (RP517). RP517 was prepared using a non-$SnCl_2$-containing formulation. Unlike other HYNIC-conjugated small biomolecules, SG380 is lipophilic and has low solubility in the kit matrix. To reduce the glass-surface adsorption and to increase the solubility of TA138 in the kit formulation, we have to use a solution containing both Lysolecithin (solubilizing agent) and ethanol (cosolvent) for the radiolabeling. Using this formulation, RP517 can be prepared in high radiochemical purity (>90%) and remains stable in the kit matrix for at least 6 h. The chromatographic and spectroscopic data of the corresponding ^{99}Tc analogue, [^{99}Tc]RP517, are completely consistent with the 1:1:1:1 composition for Tc:SG380:tricine:TPPTS.

Acknowledgment is made to Dr. Thomas D. Harris for the synthesis of hydrazinonicotinamide-conjugated LTB_4 receptor antagonist (SG380).

LITERATURE CITED

(1) Stumpe, K. D. M., Dazzi, H.; Schaffner, A., and von Schilthess, G. K. (2000) Infection imaging using whole-body FDG-PET. *Eur. J. Nucl. Med. 27*, 822−832.
(2) Ercan, M. T., and Kostakolu, L. (2000) Radiopharmaceuticals for the visualization of infectious and inflammatory lessions. *Curr. Pharm. Des. 6*, 1159−1177.
(3) Boerman, O. C., Oyen, W. J. G., and Corstens, F. H. M. (2000) Radio-labeled receptor-binding peptides: a new class of radiopharmaceuticals. *Semin. Nucl. Med. 30*, 195−208.
(4) Liu, S., and Edwards, D. S. (1999) ^{99m}Tc-labeled small peptides as diagnostic radiopharmaceuticals. *Chem. Rev. 99*, 2235−2268.
(5) Okarvi, S. M. (1999) Recent developments of Tc-99m-labeled peptide-based radiopharmaceuticals: a review. *Nucl. Med. Commun. 20*, 1093−1112.
(6) Weiner, R. E., and Thakur, M. L. (1999) Imaging infection/inflammations. *Q. J. Nucl. Med. 43*, 2−8.
(7) Corstens, F. H. M., and van der Meer, J. W. M. (1999) Nuclear Medicine's role in infection and inflammation. *Lancet 354*, 765−770.
(8) Chianelli, M., Mather, S. J., Martin-Comin, J., and Singnore, A. (1997) Radiopharmaceuticals for the study of inflammatory processes: a review. *Nucl. Med. Commun. 18*, 437−455.
(9) Lister-James, J., Moyer, B. R., and Dean, R. T. (1996) Small peptides radiolabeled with ^{99m}Tc. *Q. J. Nucl. Med. 40*, 221−233.
(10) Oyen, W. J. G., Boerman, O. C., van der Laken, C. J., Claessens, R. A. M. J., van deer Meer, J. W. M., and Corstens, F. H. M. (1996) The uptake mechanisms of inflammation- and infection-localizing agents. *Eur. J. Nucl. Med. 23*, 459−465.
(11) Peters, A. M. (1996) The choice of an appropriate agent for imaging inflammation. *Nucl. Med. Commun. 17*, 455−458.
(12) Thakur, M. L. (1995) Radiolabeled peptides: now and future. *Nucl. Med. Commun. 6*, 724−732.
(13) Fischman, A. J., Babich, J. W., and Rubin, R. H. (1994) Infection imaging with technetium-99m-labeled chemotactic peptide analogues. *Semin. Nucl. Med. 24*, 154−168.
(14) McAfee, J. G. (1990) What is the best method for imaging focal infections? *J. Nucl. Med. 31*, 413−416.
(15) Babich, J. W., Solomon, H., Pike, M. C., Kroon, D., Graham, W., Abrams, M. J., Tompkins, R. G., Rubin, R. H., and Fischman, A. J. (1993) Technetium-99m-labeled hydrazino nicotinamide derivatized chemotactic peptide analogues for imaging focal sites of bacterial infection. *J. Nucl. Med. 34*, 1967−1974.
(16) Babich, J. W., and Fischman, A. J. (1995) Effect of "co-ligand" on the biodistribution of ^{99m}Tc-labeled hydrazino nicotinic acid derivatized chemotactic peptides. *Nucl. Med. Biol. 22*, 25−30.
(17) Fischman, A. J., Babich, J. W., and Strauss, H. W. (1993) A ticket to ride: peptide radiopharmaceuticals. *J. Nucl. Med. 34*, 2253−2263.
(18) Fischman, A. J., Rauh, D., Solomon, H., Babich, J. W., Tompkins, R. G., Kroon, D., Strauss, H. W., and Rubin, H. R. (1993) In vivo bioactivity and biodistribution of chemotactic peptide analogues in nonhuman primates. *J. Nucl. Med. 34*, 2130−2134.
(19) Babich, J. W., Graham, W., Barrow, S. A., and Fischman, A. J. (1995) Comparison of the infection imaging properties of a ^{99m}Tc labeled chemotactic peptide with ^{111}In IgG. *Nucl. Med. Biol. 22*, 643−648.
(20) Babich, J. W., Graham, W., Barrow, S. A., Dragotakes, S. C., Tompkins, R. H., Rubin, R. H., and Fischman, A. J. (1993) Technetium-99m-labeled chemotactic peptides: comparison with Indium-111-labeled white blood cells for localizing acute bacterial infection in the rabbit. *J. Nucl. Med. 34*, 1964−1974.
(21) Baidoo, K. E., Scheffiel, U., Stathis, M., Finley, P., Lever, S. Z., and Wagner, H. N., Jr. (1998) High-affinity no-carrier-added ^{99m}Tc-labeled chemotactic peptides for study of inflammation in vitvo. *Bioconjugate Chem. 9*, 208−217.
(22) van der Laken, C. J., Boerman, O. C., Oyen, W. J. G., van de Ven, M, T. P., Edwards, D. S., Barrett, J. A., van der Meer, J. W., and Corstens, F. H. (1997) Technetium-99m-labeled chemotactic peptides in acute infection and sterile inflammation. *J. Nucl. Med. 38*, 1310−1315.
(23) Edwards, D. S., Liu, S., Ziegler, M. C., Harris, A. R., Crocker, A. C., Heminway, S. J., Barrett, J. A., Bridger, G. J., Abrams, M. J., and Higgins, J. D., Jr. (1999) RP463: A stabilized technetium-99m complex of a hydrazino nicotinamide conjugated chemotactic peptide for infection imaging. *Bioconjuate Chem. 10*, 884−891.
(24) Pollak, A., Goodbody, A. E., Ballinger, J. R., Duncan, G. S., Tran, L. L., Dunn-Dufault, R., Meghji, K., Lau, F., Andrey, T. W., Boxen, I., and Summer-Smith, M. (1996) Imaging inflammation with Tc-99m labeled chemotactic peptides: analogues with reduced neutropenia. *Nucl. Med. Commun. 17*, 132−139.
(25) Goodbody, A. E., Ballinger, J., Tran, L. L., Sumner-Smith, M., Lau, F., Meghji, K., and Pollak, A. (1994) A new Tc-99m labeled peptide inflammation imaging agent. *Eur. J. Nucl. Med. 21*, 790 (abstract 262).
(26) Peers, S. H., Tran, L. L., Eriksson, S. J., Ballinger, J., and Goodbody, A. E. (1995) Imaging a model of colitis with RP128, a Tc-99m-chelated tuftsin antagonist. *J. Nucl. Med. 36*, 114P.
(27) Cavelier, V., Goodbody, A. E., Tran, L. L., Bossuyt, A., and Thornback, J. (1996) Human dosimetry of Tc-99m-RP128, a potential inflammation imaging agent. *Eur. J. Nucl. Med. 23*, 1131.
(28) Nibbering, P. H., Welling, M. M., van den Broek, P. J., van Wyngaarden, K. E., Pauwels, E. K. J., and Calame, W. (1998) Radiolabeled antimicrobial peptides for imaging of infections: A review. *Nucl. Med. Commun. 19*, 1117−1121.
(29) Welling, M. M., Nibbering, P. H., Paulusma-Annema, A., Hiemstra, P. S., Pauwels, E. K. J., and Calame, W. Imaging of bacterial infection with (1999) ^{99m}Tc-labeled human neutrophil peptide-1. *J. Nucl. Med. 40*, 2073−2080.
(30) Welling, M. M., Paulusma-Annema, A., Balter, H. S., Pauwels, E. K. J., and Nibbering, P. H. (2000) Technetium-99m labeled antimicrobial peptides discriminate between bacterial infections and sterile inflammations. *Eur. J. Nucl. Med. 27*, 292−301.
(31) Moyer, B. R., Vallabhajosula, S., Lister-James, J., Bush, L. R., Cyr, J. E., Snow, D. A., Bastidas, D., Lipszyc, H., and Dean, R. T. (1996) Technetium-99m-white blood cell-specific imaging agent developed from platelet factor 4 to detect infection. *J. Nucl. Med. 37*, 673−679.
(32) Palestro, C. J., Tomas, M. B., Bhargava, K. K., and et al. (1999) Tc-99m P483H for imaging infection: phase 2 multicenter trial results. *J. Nucl. Med. 40*, 15P.
(33) Liu, S., Edwards, D. S., Harris, A. R., Ziegler, M. C., Poirier, M. J., Ewels, B. A., DiLuzio, W. R., and Hui, P. (2001) Towards developing a non-$SnCl_2$ formulation for DMP444: a new radiopharmaceutical for thrombus imaging. *J. Pharm. Sci. 90*, 114−123.
(34) Edwards, D. S., Liu, S., Harris, A. R., and Ewels, B. A. (1999) ^{99m}Tc-labeling hydrazones of a hydrazinonicotinamide conjugated cyclic peptide. *Bioconjugate Chem. 10*, 803−807.
(35) Edwards, D. S., Liu, S., Barrett, J. A., Harris, A. R., Looby, R. J., Ziegler, M. C., Heminway, S. J., and Carroll, T. R. (1997) A new and versatile ternary ligand system for technetium radiopharmaceuticals: water soluble phosphines and tricine as coligands in labeling a hydrazino nicotinamide-modified cyclic glycoprotein IIb/IIIa receptor antagonist with ^{99m}Tc. *Bioconjugate Chem. 8*, 146−154.
(36) Liu, S., Edwards, D. S., Ziegler, M. C., Harris, A. R., Hemingway, S. J., and Barrett, J. A. (2001) ^{99m}Tc-Labeling of a hydrazinonictotinamide-conjugated vitronectin receptor antagonist. *Bioconjugate Chem. 12*, 624−629.
(37) Harris, T. D. Unpublished results.
(38) Barrett, J. A., Harris, T. D., Hemingway, S. J., McKay, L., Vining, M., Crocker, A. C., Rajopadhye, M., Liu, S., and Edwards, D. S. (1999) Novel technetium-99m labeled leukotriene B4 antagonists as potential inflammation/infection imaging agents. *J. Nucl. Med. 39*, 215P.
(39) Harris, T. D., Glowacka, D., Kalogeropoulos, S. A., Edwards, D. S., Liu, S., Barrett, B. A., Heminway, S. J., and

Vining, M. (1999) The rapid detection of inflammation and infection using Tc-99m labeled LTB_4 antagonists. *J. Labelled Compd. Radiopharm. 42*, S576−S578.

(40) Rajopadhye, M., Overoye, K. L., Nguyen, H. M., Barrett, J. A., Heminway, S. J., Vining, M., McKay, L., Liu, S., and Edwards, D. S. (1999) Leukotriene B_4 antagonists modified with amino acid "east end" and technetium-99m chelators for imaging of sites of inflammation and infection. *J. Labelled Compd. Radiopharm. 42*, S576−S578.

(41) Cheesman, E. H., Liu, S., Edwards, D. S., Heminway, S. J., McKay, L., Vining, M., and Barrett, J. A. (1999) Preparation of a radiolabeled LTB_4 antagonist which incorporates the ligand into the binding site. *J. Labelled Compd. Radiopharm. 42*, S164−S166.

(42) Brouwers, A. H., Laverman, P., Boerman, O. C., Oyen, W. J. G., Barrett, J. A., Harris, T. D., Edwards, D. S., and Corstens, F. H. M. (2000) A ^{99m}Tc-labeled leukotriene B_4 receptor antagonist for scintigraphic detection of infection in rabbits. *Nucl. Med. Commun. 21*, 1043−1051.

BC010120B

Combined Thioether/Hydrazone Chemoselective Ligation Reactions for the Synthesis of Glycocluster−Antigen Peptide Conjugates

Cyrille Grandjean,*,† Valérie Santraine,† Jean-Sébastien Fruchart,‡ Oleg Melnyk,‡ and Hélène Gras-Masse‡

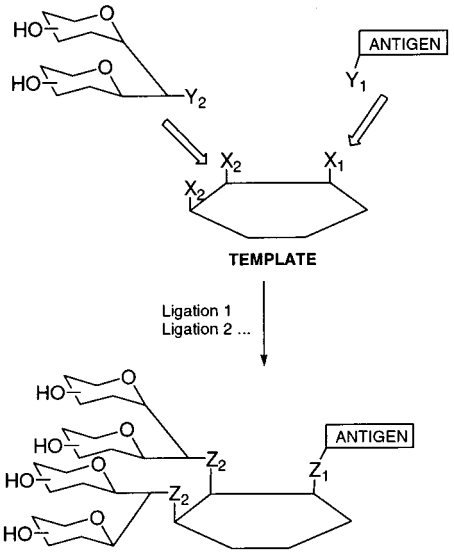
SEDAC−Therapeutics, Parc Eurasanté - Le Galenis, Bâtiment B, 85, rue Nelson Mandela, 59120 Loos, France and UMR 8525 CNRS, Université de Lille II, Institut de Biologie et Institut Pasteur de Lille, 1, rue du Prof Calmette, BP447, 59021 Lille Cedex, France. Received January 16, 2002; Revised Manuscript Received March 21, 2002

Hydrazone/thioether ligation reactions show promise for the synthesis of clustered glycosides−antigen conjugates. Due to its propensity to aggregate, tetanus toxoid-derived epitopic peptide $TT^{830-846}$ was elected to further evaluate this three-component ligation process. This difficult sequence was supplemented by a hydrazine or a glyoxylyl group either at its C- or N-terminus. The peptide-hydrazines or peptide-aldehydes thus obtained were coupled with glyoxylyl- (or hydrazino-) *N*-chloroacetylated-L-lysinyl trees and 2-thioethyl-α-D-mannopyranoside. As anticipated the ligations were controlled by the nature of the peptide and proved difficult for the C-terminal aldehyde derivative. However, when the process was performed in absence of buffer and using mannitol as a dispersing agent, all combinations finally led to the expected glycoconjugates in 40−60% purified yields.

INTRODUCTION

The chemoselective ligation, which refers to the coupling of fully deprotected molecular fragments through two mutually and uniquely reactive functional groups in aqueous media, has become a powerful tool in the synthesis of peptides, proteins, bioconjugates, and even engineered cells (*1*−*5*). Iteration of a single ligation reaction has allowed the assembly of peptide conjugates from more than two segments, but this strategy is hampered by the need for additional steps to remove impurities, excess reagents, and temporary protective groups (*6*−*13*). Elegant solutions have been proposed by adapting the native and the expressed protein ligations on the solid phase which simplifies these processes (*14*−*16*). For solution-phase synthesis, *true orthogonal ligation reactions*, performed sequentially or in a one-pot procedure, are required and examples thereof remain exceedingly rare. One can cite the synthesis of an RNA−peptide conjugate (*17*), the preparation of a heterodimeric transcription factor (*18*), and more recently the synthesis of analogues of chemokines and somatostatins (*19*), by means of thioether/native chemical ligation, thioester/oxime, or pseudoproline/native chemical ligation reactions, respectively. Combination of thioether/oxime ligations has also been envisioned for the Template Assembled Synthetic Proteins approach (*20*), or the synthesis of glycoproteins (*21*, *22*), proof of principle of this strategy being demonstrated (*23*). Finally, our laboratory has proposed a thioether/hydrazone ligation strategy (Scheme 1) (*24*) for the preparation of antigen-clustered glycosides conjugates for the selective targeting of the human dendritic cells' mannose receptor (*25*).

Scheme 1. General Strategy for the Synthesis of Oligoglycosides−Antigen Peptides Conjugates[a]



[a] CTL epitopes, T helper epitopes and (oligo)glycosides or clusters thereof are assembled on a template through one pot or combination of orthogonal ligations. Present study: X_1 = CHO (or $NHNH_2$); Y_1 = $NHNH_2$ (or CHO); X_2 = $ClCH_2CO$; Y_2 = SH.

This approach seems to compete favorably with stepwise oligomannosides−antigen peptides conjugate synthesis, which, among others, requires finely devised protective group manipulations (*26*, *27*). However, our process was (a) dependent on the nature of the antigen and was somewhat troublesome for difficult sequences which tend to aggregate: A more generally applicable procedure would be highly desirable; (b) limited to the conjugation of antigen peptides via their *N*-terminus: The corresponding antigens modified at their C-terminus would be useful to document whether the conjugation site has an impact on the antigen processing by the dendritic

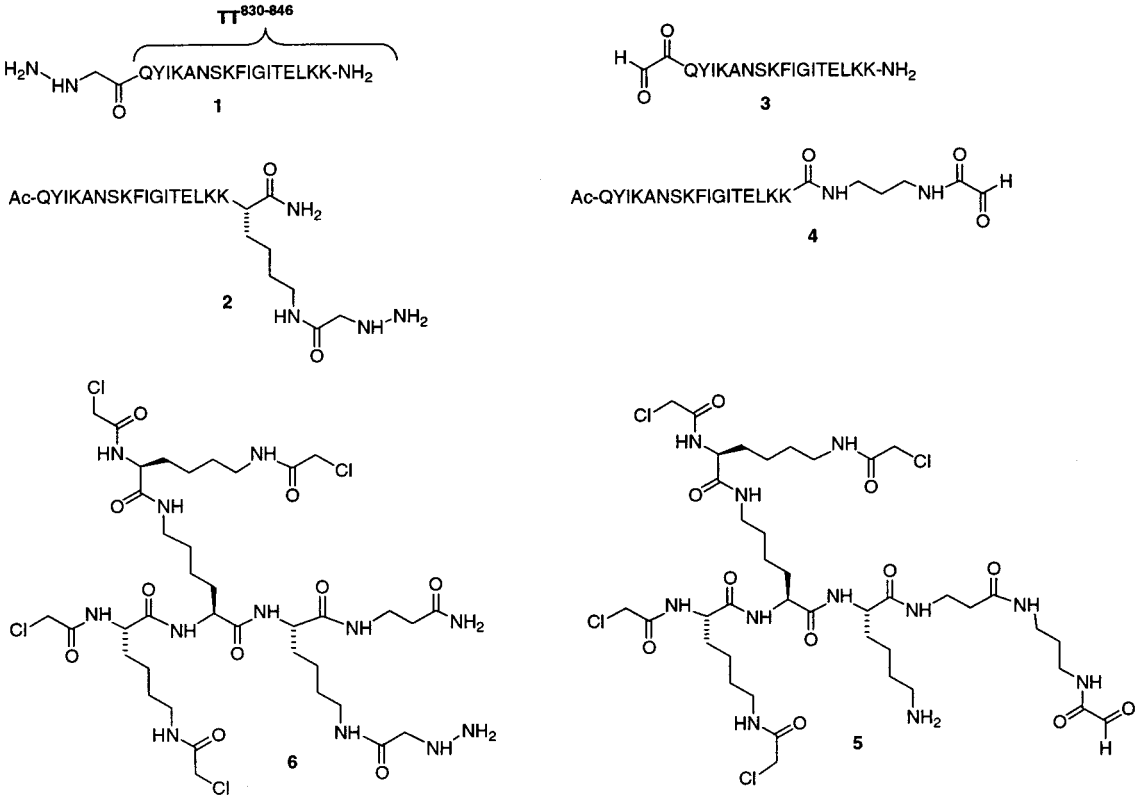
* To whom correspondence should be addressed. Phone (+33) 3 20 87 12 18. Fax: (+33) 3 20 87 12 33. E-mail: Cyrille.Grandjean@sedac-therapeutics.com.

† SEDAC-Therapeutics.

‡ Laboratoire de Synthèse, Structure et Fonction des Biomolécules, UMR 8525 CNRS.

10.1021/bc025505o CCC: $22.00 © 2002 American Chemical Society
Published on Web 06/08/2002

Chart 1. Glyoxylyl and Hydrazino Peptides Evaluated in This Study



cells; and (c) mainly successful using templates bearing the two types of electrophilic groups namely glyoxylyl-poly-*N*-chloroacetylated-L-lysinyl trees: Scope of the hydrazone ligation (and probably those of the ligation strategies) would be extended if one was able to prepare and use hydrazino chloroacetylated templates, i.e., templates bearing a priori uncompatible electrophile/nucleophile groups (*28*).

We now report methodologies and experimental conditions which alleviate most of the above-mentioned limitations. These achievements allow the convenient incorporation of hydrazine and glyoxylyl groups on both template and antigen peptide, either at its N- or C-terminus, and the successful couplings of the fragments thus obtained.

RESULTS AND DISCUSSION

To further examine the hydrazone/thioether ligation, we planned to synthesize and condense compounds **1**−**4**, derived from the tetanus toxin $TT^{830-846}$ epitope, representative of a difficult sequence, with pendant tetravalent-L-lysinyl trees **5** or **6** and 2-thioethyl α-D-mannopyranoside **7** (*29*), (Chart 1).

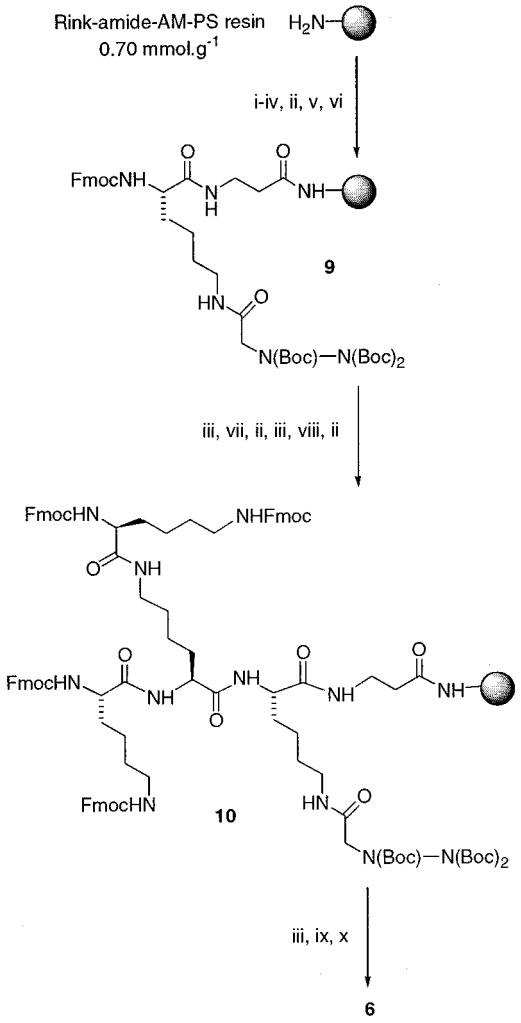
Compounds **1**−**6** were obtained by using the Fmoc[1]/*tert*-butyl solid-phase peptide synthesis strategy (*30*). Syntheses of compounds **1**−**5** were reported previously: Briefly, derivatives **4** and **5** were elaborated on a tartaric acid-derived linker which generates the glyoxylyl function upon cleavage from the solid support, in 15 and 31% yield, respectively (*31*). Glyoxylyl peptide **3** was attained after solution-phase periodic oxidation (*32*) of a $TT^{830-846}$ sequence, augmented with an *N*-terminal serine in 5% overall yield (*28*). Bromine displacement of an *N*-bromoacetylated $TT^{830-846}$-derived peptidyl resin by *tert*-butyl carbazate (*33*) led to the hydrazino peptide **1** in an actual 40% yield following acidic deprotection and cleavage from the resin (*24*). For compounds **2** and **6** (Scheme 2), a Fmoc-L-Lys(Mtt)-OH residue was introduced near the C-terminus. Following selective removal of the 4-methyltrityl group (*34*), the lysinyl side chain amine was coupled with [*N*,*N*′-tri(*tert*-butyloxycarbonyl)hydrazino]-acetic acid **8** using HOBt/HBTU/DIEA activation to install the hydrazine moiety. Full protection of the α-hydrazinoacetic acid was necessary to avoid self-condensation of the corresponding activated ester (*35*). Rest of the syntheses were then completed to give **2** and **6** in 17 and 25% yield, respectively.

Contrasting with our previous attempt to synthesize the hydrazino-tetra-*N*-chloroacetylated lysinyl tree (*28*), we did not detect the presence of any cyclic compound which arises from intramolecular substitution of one chlorine atom by the hydrazine. Hydrazino peptides **1**, **2**, and **6** proved to be stable during RP-HPLC purification (provided mixtures of CH_3CN/TFA were not used as solvent) (*35*) and upon storage at −30 °C. Glyoxylyl derivative **3** was stored as a hydrochloride salt to prevent it from noncovalent aggregation. Glyoxylyl peptide **4** exhibited even more propensity to aggregate. Noncovalent aggregation was partially avoided when the RP-HPLC purification was performed following the cleavage step, and the pure fractions were lyophilized without dilution; the noncovalent aggregation was totally suppressed by adding about a 10-fold excess of mannitol to the fractions, prior to the freeze-drying step (*31*).

When all the partners were available, the combined hydrazone/thioether ligation was next investigated. We decided to perform the hydrazone ligation, the most

[1]Abbreviations: Fmoc, 9-fluorenylmethoxycarbonyl; Mtt, 4-methyltrityl; HOBt, 1-hydroxybenzotriazole; HBTU, *N*-[1*H*-benzotriazol-1-yl)-(dimethylamino)methylene]-*N*-methylmethanaminium hexafluorophosphate; TNBS, 2,4,6-trinitrobenzenesulfonic acid; DIC, diisopropylcarbodiimide; TIS, triisopropylsilane; RP-HPLC, reverse phase-high-pressure liquid chromatography.

Scheme 2. Solid Phase Synthesis of Lysinyl Core 6[a]



[a] Reagents and conditions: i, 4 equiv of Fmoc-*β*-Ala-OH, HBTU−HOBt−DIEA (4:4:12 equiv), DMF,, 45 min; ii, Ac_2O−DIEA−CH_2Cl_2 (5:10:85), 10 min; iii, piperidine−DMF (20:80), 20 min; iv, 4 equiv Fmoc-L-Lys(Mtt)-OH, HBTU−HOBt−DIEA (4:4:12 equiv), DMF, 45 min; v, TFA−CH_2Cl_2 (1:99), seven times; vi, 4 equiv of **8**, HBTU−HOBt−DIEA (4:4:12 equiv), DMF, 45 min; vii, 4 equiv of Fmoc-L-Lys(Fmoc)-OH, HBTU−HOBt−DIEA (4:4:12 equiv), DMF, 45 min; viii, 8 equiv of Fmoc-L-Lys(Fmoc)-OH, HBTU−HOBt−DIEA (8:8:24 equiv), DMF, 45 min; ix, $ClCH_2COOH$ (32 equiv), DIC (16 equiv), DMF, 40 min; x, TFA−H_2O−TIS (95:2.5:2.5), 0 °C, 1 h 30 min.

challenging of the two reactions since involving sensitive material, at once. Moreover, in the reverse strategy, the hydrazine group of compound **5** would have competed with thiols for the chlorine substitution. Thus, L-lysinyl core **5** was reacted at room temperature with hydrazino peptides **1** and **2** in a 95:5 mixture of degassed 2-methyl-2-propanol/water. This solvent was selected for its ability to increase the reaction rate compared to other systems, based on mixtures of organic solvent and aqueous buffer (*36*), and to delay noncovalent aggregation (*28*). L-Lysinyl tree **6** was reacted similarly with glyoxylyl derivatives **3** and **4**. The latter compound was used dispersed in mannitol or partially aggregated in two distinct experiments. As expected, the reactions were almost driven to completion after 10 min (as monitored by RP-HPLC, see for examples Figures 1a and 1b), with the exception of the one conducted with "aggregated" **4** (Figure 1c).

The second ligation was performed after 5 h, a period over which any unreacted α-hydrazinoacetyl peptide tends to evolve with decomposition of the hydrazine group. 2-Thioethyl-α-D-mannopyranoside **7** in degassed 2-methyl-2-propanol/water (1:1) was introduced into each reaction vessel, the apparent pH being adjusted to 8−8.5 (pH paper) by addition of solid potassium carbonate. Formation of the conjugates **11**−**13** was readily observed by RP-HPLC monitoring (see, for example, Figure 1d). By contrast, compound **14** was only obtained cleanly in the presence of mannitol which acts like a dispersing reagent. In its absence, noncovalent aggregation prevailed resulting in incomplete ligations and complex crude mixture (compare Figures 1b, 1e and 1c, 1f). Conjugates **11**−**14**, which appeared very hydrophilic, were actually obtained in 48, 55, 41, and 40% purified yields, respectively (Charts 2 and 3).

In summary, we have shown that hydrazine or aldehyde could equally be introduced at the C- or N-terminus of a peptide. The mild experimental conditions developed were applied for the synthesis of a hydrazino-tetra-*N*-chloroacetylated tree otherwise difficult to obtain. These methodologies allowed study of four combinations of hydrazone chemoselective ligation for the preparation of glycocluster−peptide conjugates using $TT^{830-846}$ as a model. Solution behavior of this difficult sequence was either improved or impaired when modified by a hydrazine group or an aldehyde. However, all permutations were eventually successful and permitted its linkage to be at least four glycosides.[2] Altogether, these achievements confer further flexibility and robustness to the hydrazone/thioether ligation strategy.

EXPERIMENTAL SECTION

General. Analytical reverse-phase high performance liquid chromatography (RP-HPLC), separations were performed upon a Beckman system Gold system using a TSK gel super ODS (TosoHaas) (110 Å, 2 μm, 4.6 × 50 mm) column at a flow rate of 1.5 mL min^{-1} (monitoring and analysis), with detection at 215 nm at 50 °C. Gradient: 0% B for 5 min, 0−100% B over 10 min, 100% B for 1 min, 0% B for 2 min. Semipreparative RP-HPLC separations were performed on a Shimadzu LC-4A systems, on an Hypersil hyperprep C-18 (300 Å, 8 μm, 10 × 260 mm), column at a flow rate of 3 or 5 mL min^{-1}, with detection at either 215 or 230 nm at 50 °C. Solvent system A: 0.05% TFA in water; solvent system B: 0.05% TFA in 40% *i*PrOH-60% water. MALDI-TOF-MS spectra were recorded on a Finnigan Vision 2000 mass spectrometer.

Solid-Phase Peptide Synthesis. Syntheses of compounds **1**−**5** have been reported in references 28, 37, 28, 31, and 31, respectively.

Hydrazino-*N*-chloroacetylated-L-lysinyl Tree 6. This compound was synthesized manually on an rink amide-AM-PS resin (substitution, 0.70 mmol g^{-1}) (Senn Chemicals) using the Fmoc/*tert*-butyl strategy at a 0.1 mmol scale. The coupling steps were performed using a 4-fold excess of amino acid per amine to be reacted via HBTU−HOBt−DIEA activation in DMF and monitored by the TNBS test (*38*): typically, HBTU dissolved in DMF (4 equiv) was added to a mixture of the amino acid (4 equiv), HOBt (4 equiv), and DIEA (12 equiv) in DMF. After stirring for 1 min, the mixture was added to the peptidyl resin (1 equiv), swollen in DMF, and mechani-

[2]Tetravalency seems sufficient to confer specific dendritic cells' mannose receptor recognition, at least in vitro: see ref 25. It is indeed anticipated that the nature and the site of attachment of antigen peptides to the template will modify their behavior and reactivity and affect their processing by the dendritic cells.

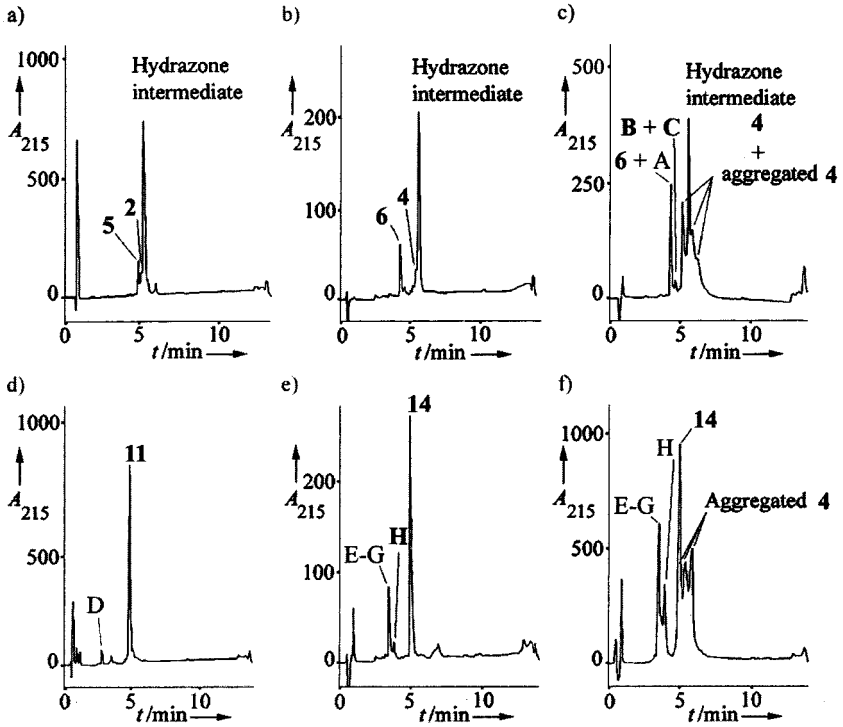
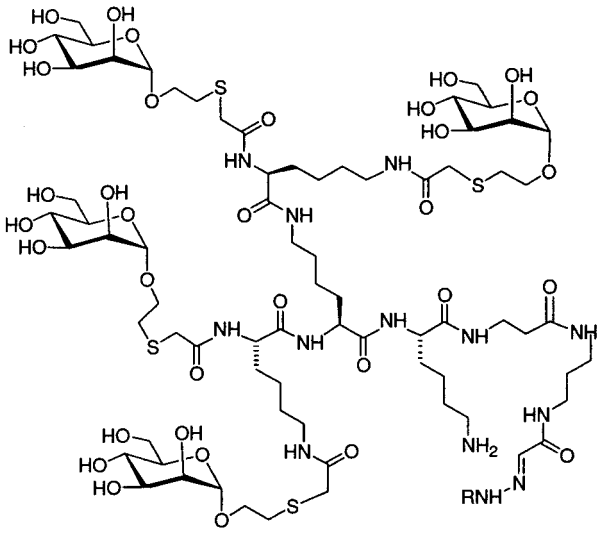


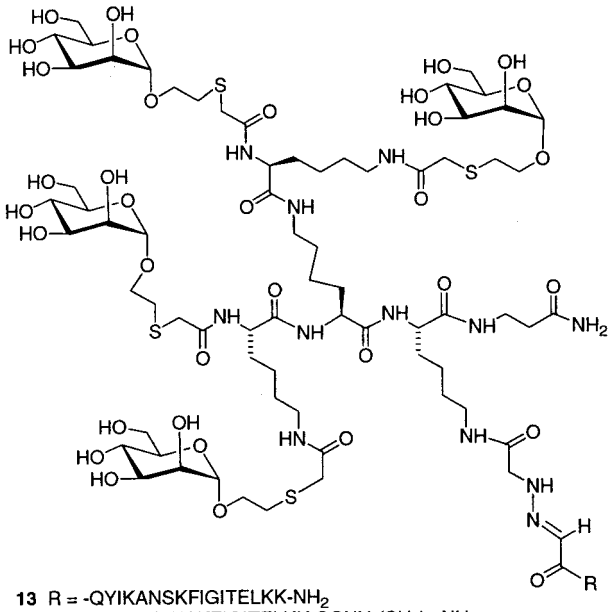
Figure 1. RP-HPLC chromatograms of crude mixtures from the hydrazone ligations after 10 min a) and b) or 5 h c), and following the second thioether ligations d)-f); a) and d) ligations between core **5** and hydrazinopeptide **2**; b) and e) ligations between core **6** and hydrazinopeptide **4** dispersed in mannitol; c) and f) ligations between core **6** and hydrazinopeptide **4** partially aggregated. We previously observed that an antigen and its corresponding tetra-mannosylated derivative usually possess close RP-HPLC retention time. Thus, excess L-lysinyl tree was used in every experiment to fully consume the antigen peptide and facilitate the purification step. The excess tree is transformed into hydrophilic side-products during the thioether ligation, easily separated from the desired conjugate. Side-products formed: Compound A: *m/z* 986.6 $(M + Na)^+$, 1002.4 $(M + K)^+$ (loss of amino group on **6**); Compound B: *m/z* 971.3 $(M + Na)^+$, 988.3 $(M + K)^+$ (loss of hydrazine on **6**); Compound C: *m/z* 1945.8 $(M + Na)^+$, 1961.7 $(M + K)^+$ (dimeric structure derived from **6**); Compound D: *m/z* 1859.3 $(M + Na)^+$ (tetra-mannosylated tree derived from **5**); Compound E: *m/z* 1794.1 $(M + H)^+$, 1817.8 $(M + Na)^+$, 1832.9 $(M + K)^+$ (tetra-mannosylated tree derived from **6**); Compound F: *m/z* 1801.8 $(M + Na)^+$, 1818.7 $(M + K)^+$ (loss of amino group on D); Compound G: *m/z* 1787.7 $(M + Na)^+$, 1802.7 $(M + K)^+$ (loss of hydrazine on D); Compound H: *m/z* 3576.6 $(M + Na)^+$, 3592.2 $(M + K)^+$ (dimeric structure derived from **6**). Chromatographic conditions, see Experimental Section.

Chart 2. Products of Orthogonal Hydrazone/ Thioether Ligation Reactions with L-Lysinyl Core 5



11 R = -CH_2-CO-QYIKANSKFIGITELKK-NH_2
12 R = Ac-QYIKANSKFIGITELKKK($COCH_2$-)-NH_2

Chart 3. Products of Orthogonal Hydrazone/ Thioether Ligation Reactions with L-Lysinyl Core 6



13 R = -QYIKANSKFIGITELKK-NH_2
14 R = Ac-QYIKANSKFIGITELKK-CONH-$(CH_2)_3$-NH-

cally shaken for 45 min. Following filtration, the peptidyl resin was washed with DMF (3 × 2 min) and CH_2Cl_2 (3 × 2 min). Each coupling was followed by a capping with Ac_2O−DIEA−CH_2Cl_2 10:5:85 for 10 min, followed by washing with CH_2Cl_2 (3 × 1 min). Cleavage of the Fmoc protecting groups was achieved by treatment with 20% piperidine in DMF (1 × 2 min, 1 × 20 min), followed by washing with DMF (2 × 2 min), and washing with CH_2Cl_2 (2 × 1 min). Fmoc-β-Ala-OH was first anchored to the resin. Chain protection of the first lysinyl residue

introduced was secured by 4-methyltrityl (Mtt). Following the coupling, the Mtt group of the ϵ-NH_2 of the first lysine residue was removed by treatment with a solution of 1% TFA in CH_2Cl_2 (seven times). Monitoring the deprotection was realized as described in reference 34. [*N*,*N*′-Tri(*tert*-butyloxycarbonyl)hydrazino]acetic acid **8** (4 equiv) was then introduced onto the peptidyl resin, swollen in DMF, via HBTU−HOBt−DIEA activation (4/4/12 equiv). The other lysinyl residues were added as their Fmoc-L-Lys-(Fmoc)-OH derivatives. After the second coupling step, the peptidyl resin was deprotected and acylated using an 4-fold excess of preformed chloroacetic anhydride, prepared via a DIC activation to provide the tetravalent core. The core was then cleaved from the resin and deprotected by TFA−H_2O−$^i Pr_3SiH$ 95:2.5:2.5 (10 mL per g of peptidyl resin), for 1.30 h at 0 °C, precipitated in cold diethyl ether−heptane 1:1, centrifugated, dissolved in H_2O−AcOH 95:5, and freeze-dried.

Compound **6** (27 mg, 25%) was obtained as a white powder after RP-HPLC purification [gradient: 90:10 to 50:50 (A/B), 35 min], followed by freeze-drying; *m*/*z* (positive MALDI-TOF-MS) 1003.5 $(M + Na)^+$, 979.4 $(M + H)^+$.

General Procedure for the Hydrazone/Thioether Ligation. All solvents were degassed by bubbling N_2 before use. *N*-Chloroacetylated core **5** or **6** (1 mg, 0.88 and 0.91 μmol, respectively) is reacted with the modified antigen **1**−**3** (0.9 equiv) or **4** [0.9 equiv, dispersed in mannitol, 6.6% (w/w) as determined by total acid hydrolysis (*31*)], in *tert*-BuOH−H_2O 95:5 (400 μL) for 5 h at room temperature under nitrogen.

In parallel, 2-thioethyl α-D-mannopyranoside disulfide (4 equiv), dissolved in *tert*-BuOH−H_2O 50:50 (200 μL), was reacted with tri-*n*-butylphosphine (1 equiv/disulfide) at room temperature under nitrogen, and the reduction was monitored by RP−HLPC. On completion, the reaction mixture is transferred to the crude lysinyl tree−antigen peptide conjugate and the apparent pH adjusted to 8−8.5 (paper) by addition of solid potassium carbonate. The reaction mixture was stirred at room temperature under nitrogen and monitored by RP-HPLC. After completion of the reaction, the crude mixture was diluted with H_2O, frozen, and freeze-dried. Compounds were obtained as white powders following semipreparative RP-HPLC purifications and freeze-drying.

Compound 11 (1.65 mg, 48%) was obtained as a white powder after RP-HPLC purification [gradient: 100:0 to 60:40 (A/B), 70 min], followed by freeze-drying; *m*/*z* (positive MALDI-TOF-MS) 3892.9 $(M + Na)^+$, 3870.8 $(M + H)^+$.

Compound 12 (2.42 mg, 55%) was obtained as a white powder after RP-HPLC purification [gradient: 100:0 to 80:20 (A/B), 10 min, then 80:20 to 70:30 (A/B), 25 min, then isocratic], followed by freeze-drying; *m*/*z* (positive MALDI-TOF-MS) 4077.9 $(M + K)^+$, 4061.9 $(M + Na)^+$, 4039.9 $(M + H)^+$.

Compound 13 (1.43 mg, 41%) was obtained as a white powder after RP-HPLC purification [gradient: 100:0 to 78:22 (A/B), 10 min, then 78:22 to 68:32 (A/B), 30 min, then isocratic], followed by freeze-drying; *m*/*z* (positive MALDI-TOF-MS) 3850.8 $(M + K)^+$, 3834.8 $(M + Na)^+$, 3812.9 $(M + H)^+$.

Compound 14 (1.43 mg, 40%) was obtained as a white powder after RP-HPLC purification [gradient: 100:0 to 80:20 (A/B), 10 min, then 80:20 to 65:35 (A/B), 30 min], followed by freeze-drying; *m*/*z* (positive MALDI-TOF-MS) 3934.0 $(M + Na)^+$, 3911.9 $(M + H)^+$.

ACKNOWLEDGMENT

We are grateful to H. Drobecq for recording mass spectra.

LITERATURE CITED

(1) Hang, H. C., and Bertozzi, C. R. (2001). Chemoselective approaches to glycoprotein assembly. *Acc. Chem. Res. 34*, 727−736.
(2) Muir, T. W. (2001) Development and application of expressed protein ligation. *Synlett 6*, 733−740.
(3) Tam, J. P., Yu, Q., and Xu, M.-Q. (2000) Orthogonal ligation strategies for peptide and protein. *Biopolymers (Pept. Sci.) 51*, 311−332.
(4) Dibowski, H., and Schmidtchen, F. P. (1998) Bioconjugation of peptides by palladium-catalyzed C−C cross-coupling in water. *Angew. Chem., Int. Ed. Engl. 37*, 476−478.
(5) Bong, D. T., and Ghadiri, M. R. (2001) Chemoselective Pd-(0)-catalyzed peptide coupling in water. *Org. Lett. 3*, 2509−2511.
(6) Wei, Z., Tung, C.-H., Zhu, T., and Stein, S. (1994) Synthesis of oligoarginine−oligonucleotide conjugates and oligoarginine-bridged oligonucleotide pairs. *Bioconjugate Chem. 5*, 468−474.
(7) Futaki, S., Aoki, M., Ishikawa, T., Kondo, F., Asahara, T., Niwa, M., Nakaya, Y., Yagami, T., and Kitagawa, K. (1999) Chemical ligation to obtain proteins comprising helices with individual amino acid sequences. *Bioorg. Med. Chem. 7*, 187−192.
(8) Rau, H. K., and Haehnel, W. (1998) Design, synthesis and properties of a novel cytochrome *b* model. *J. Am. Chem. Soc. 120*, 468−476.
(9) Vilaseca, L. A., Rose, K., Werlen, R., Meunier, A., Offord, R. E., Nichols, C. L., and Scott, W. L. (1993) Protein conjugates of defined structure: Synthesis and use of a new carrier molecule. *Bioconjugate Chem. 4*, 515−520.
(10) Cervigny, S. E., Dumy, P., and Mutter, M. (1996) Synthesis of glycopeptides and lipopeptides by chemoselective ligation. *Angew. Chem., Int. Ed. Engl. 35*, 1230−1232.
(11) Mathieu, M., Lehmann, C., Razaname, A., and Tuchscherer, G. (1997) Engineering of zinc finger and MHC motifs to locked-in tertiary folds. *Lett. Pept. Sci. 4*, 95−100.
(12) Tuchscherer, G., Lehman, C., and Mathieu, M. (1998) New protein mimetics: The zinc finger motif as a locked-in tertiary fold. *Angew. Chem., Int. Ed. 37*, 2990−2993.
(13) Lelièvre, D., Buré, C., Laot, F., and Delmas, A. (2001) Synthesis of pepdide di-aldehyde precursor for stepwise chemoselective ligations via oxime bonds. *Tetrahedron Lett. 42*, 235−238.
(14) Canne, L. E., Botti, P., Simon, R. J., Chen, Y., Dennis, E. A., and Kent, S. B. H. (1999) Chemical protein synthesis by solid-phase ligation of unprotected peptide segments. *J. Am. Chem. Soc. 121*, 8720−8727.
(15) Camarero, J. A., Cotton, G. J., Adeva, A., and Muir, T. W. (1998) Chemical ligation of unprotected peptides directly from a solid support. *J. Pept. Res. 51*, 303−316.
(16) Cotton, G. J., Ayers, B., Xu, R., and Muir, T. W.(1999) Insertion of a synthetic peptide into a recombinant protein framework: A protein biosensor. *J. Am. Chem. Soc. 121*, 1100−1101.
(17) McPherson, H., Wright, M. C., and Lohse, P. A. (1999) Synthesis of an RNA-peptide conjugate by orthogonal ligation. *Synlett* 978−980.
(18) Canne, L. E., Ferré-D'Amaré, A. R., Burley, S. K., and Kent, S. B. H. (1995) Total chemical synthesis of a unique transcription factor-related protein: cMyc-Max. *J. Am. Chem. Soc. 117*, 2998−3007.
(19) Tam, J. P., Yu, Q., and Yang, J.-L. (2001) Tandem ligation of unprotected peptides through thiaprolyl and cysteinyl bonds in water. *J. Am. Chem. Soc. 123*, 2487−2494.
(20) Mutter, M., Dumy, P., Garrouste, P., Lehmann, C., Mathieu, M., Peggion, C., Peluso, S., Razaname, A., and Tuchscherer, G. (1996) Template assisted synthetic proteins (TASP) as functional mimetics of proteins. *Angew. Chem., Int. Ed. Engl. 35*, 1482−1485.

(21) Marcaurelle, L. A., and Bertozzi, C. R. (1999) New directions in the synthesis of glycopeptide mimetics. *Chem. Eur. J. 5*, 1384−1390.

(22) Marcaurelle, L. A., and Bertozzi, C. R. (2001) Chemoselective elaboration of O-linked glycopeptide mimetics by alkylation of 3-thioGalNAc. *J. Am. Chem. Soc. 123*, 1587−1595.

(23) Marcaurelle, L. A., and Bertozzi, C. R. (1998) Direct incorporation of unprotected ketone groups into peptides during solid-phase synthesis: application to the one-step modification of peptides with two different biophysical probes for FRET. *Tetrahedron Lett. 39*, 7279−7282.

(24) Grandjean, C., Rommens, C., Gras-Masse, H., and Melnyk, O. (2000) One-pot synthesis of antigen-bearing, lysine based cluster mannosides using two orthogonal chemoselective ligation reactions. *Angew. Chem., Int. Ed. Engl. 39*, 1068−1072.

(25) For effective targeting of the dendritic cells and their role in immunity, see: Grandjean, C., Angyalosi, G., Loing, E., Adriaenssens, E., Melnyk, O., Pancré, V., Auriault, C., and Gras-Masse, H. (2001) Novel hyperbranched glycomimetics recognized by the human mannose receptor: Quinic and shikimic acid derivatives as mannose bioisosteres. *ChemBioChem 2*, 747−757 and references therein.

(26) Kragol, G., and Otvos, Jr., L. (2001) Orthogonal solid-phase synthesis of tetramannosylated peptide constructs carrying three independent branched epitopes. *Tetrahedron 57*, 957−966.

(27) Kragol, G., Otvos, Jr., L., Feng, J. Q., Gerhard, W., and Wade, J. D. (2001) Synthesis of a disulfide-linked octameric peptide construct carrying three different antigenic determinants. *Bioorg. Med. Chem. Lett. 11*, 1417−1420.

(28) Grandjean, C., Gras-Masse, H., and Melnyk, O. (2001) Synthesis of clustered glycoside-antigen conjugates by two one-pot, orthogonal, chemoselective ligation reactions: Scope and limitations. *Chem. Eur. J. 7*, 230−239.

(29) Grandjean, C., Rommens, C., Gras-Masse, H., and Melnyk, O. (1999) Convergent synthesis of fluorescein-labeled lysine-based cluster glycosides. *Tetrahedron Lett. 40*, 7235−7238.

(30) Fields, G. B., and Noble, R. L. (1990) Solid-phase peptide synthesis utilizing 9-fluorenylmethoxycarbonyl amino acids. *Int. J. Pept. Protein Res.* **1990**, *35*, 161−214.

(31) Melnyk O., Fruchart, J.-S., Grandjean, C., and Gras-Masse, H. (2001) Tartric acid-based linker for the solid-phase synthesis of C-terminal peptide α-oxo aldehydes. *J. Org. Chem. 66*, 4153−4160.

(32) Geoghegan, K. F., and Stroh, J. G. (1992) Site-directed conjugation of nonpeptide groups to peptides and proteins via periodate oxidation of a 2-amino alcohol. Application to modification at N-terminal serine. *Bioconjugate Chem. 3*, 138−146.

(33) Wilson, L. J., Li, M., and Portlock, D. E. (1998) A simple solid-phase synthesis of disubstituted guanidines using Rink amide resin as an amine component. *Tetrahedron Lett. 39*, 5135−5138.

(34) Bourel, L., Carion, O., Gras-Masse, H., and Melnyk, O. (2000) The deprotection of Lys(Mtt) revisited. *J. Pept. Sci. 6*, 264−270.

(35) Bonnet, D., Rommens, C., Gras-Masse, H., and Melnyk, O. (2000) Chemoselective acylation of hydrazinopeptides: a novel and mild method for the derivatization of peptides with sensitive fatty acids. *Tetrahedron Lett. 41*, 45−48.

(36) Bonnet, D., Bourel, L., Gras-Masse, H., and Melnyk, O. (2000) A novel lipophilic glyoxylic acid derivative for the lipidation of peptides using salt-free hydrazone ligation. *Tetrahedron Lett. 41*, 10003−10007.

(37) Bourel-Bonnet, L., Melnyk, O., Malingue, F., Bonnet, D., Gras-Masse, H., Unpublished results.

(38) Hancock, W. S., and Battersby, J. E. (1976) A new micro-test for the detection of incomplete coupling reactions in solid-phase peptide synthesis using 2,4,6-trinitrobenzene-sulphonic acid. *Anal. Biochem. 71*, 260−264.

BC025505O

Improving the Labeling of *S*-Acetyl NHS−MAG_3-Conjugated Morpholino Oligomers

Guozheng Liu,* Surong Zhang, Jiang He, Zhihong Zhu, Mary Rusckowski, and Donald J. Hnatowich*

Division of Nuclear Medicine, Department of Radiology, University of Massachusetts Medical School, Worcester, Massachusetts 01655. Received April 15, 2002

S-Acetyl MAG_3 (S-acetylmercaptoacetyltriglycine) has been used as a chelator for the ^{99m}Tc labeling of a variety of biomolecules. The objective of this study was to improve upon the labeling of morpholino (MORF), a DNA analogue, as a model biomolecule. A 15mer MORF with a primary amine was conjugated with NHS−MAG_3 in the usual manner, and the MORF−MAG_3 was purified over a P4 column as before. The conjugate was radiolabeled using stannous ion as usual, and the impurities were identified using size exclusion high-performance liquid chromatography (SE HPLC). Various methods were then investigated to remove the impurities. With tartrate as the transchelator, two impurities were identified as labeled MAG_3 and labeled tartrate. The labeled MAG_3 could not be removed by simply repurifying the conjugate using the usual pH 5.2 NH_4OAc buffer before labeling. However, this impurity could be completely removed if the conjugate was adjusted to pH 7.6 and heated before repurification. The labeled tartrate impurity was removed by heating during labeling. On the basis of these observations, the following procedure for purification of the conjugation mixture and subsequent labeling was adopted. After MORF was conjugated with NHS−MAG_3 and purified over P4 with pH 5.2 NH_4OAc eluant, the oligomer fractions were combined, adjusted to pH 7.6, and heated in a boiling water bath for 20 min. The conjugated oligomer was then repurified over P4 for storage at refrigerator temperatures. Labeling is achieved simply by adding fresh stannous ion to a solution of the MORF−MAG_3 in pH 7.6 containing tartrate followed by ^{99m}Tc−pertechnetate. After the mixture is heated for 20 min in boiling water, the labeling efficiency is always over 90% as determined by size exclusion HPLC and paper chromatography and the specific activities can exceed 7 mCi/μg. By making several relatively simple changes to the routine procedure used to conjugate and radiolabel biomolecules with ^{99m}Tc via MAG_3, a modified procedure was developed that results in labeling efficiency high enough to avoid postlabeling purification.

INTRODUCTION

Among other bifunctional chelators, this laboratory has used an activated NHS ester of S-acetyl MAG_3 (S-acetylmercaptoacetyltriglycine) for the radiolabeling of a variety of biomolecules (*1*−*15*). An acetyl group protecting the sulfur on MAG_3 was substituted for the benzoyl group to avoid the harsh conditions of alkaline pH and elevated temperatures required for the removal of this group (*14*). Labeling is successful at neutral pH (normal labeling efficiency 50−80%), but separation after labeling is always required to achieve acceptable radiochemical purities (*1*−*15*). Furthermore, because tartrate is used as a transchelator, the labeled biomolecule is often contaminated with labeled tartrate, which may then coelute with the biomolecule during postlabeling purification and subsequently become oxidized to ^{99m}Tc−pertechnetate. Heating can encourage transchelation of the labeled tartrate to the desired product. Heating can also accelerate the oxidation of stannous ion and, in the presence of low concentrations of this reducing agent, can result in oxidation of the labeled tartrate to ^{99m}Tc−pertechnetate. The pertechnetate will then be retained on the size exclusion column during postlabeling purification (*1*, *2*).

* To whom correspondence should be addressed. D.J.H.: Tel: (508)856-4256. Fax: (508)856-4572. E-mail: Donald.hnatowich@umassmed.edu.

Recently, morpholino oligomers (MORF) and their complementary forms (cMORFs) have been under investigation as potentially useful agents for pretargeting applications after radiolabeling via MAG_3 (*1*, *2*). These oligomers were therefore selected as model biomolecules to search for methods leading to efficient labeling with no need for postlabeling purification.

MATERIAL AND METHODS

The 15mer MORF and its complement used herein were identical to those used by us earlier (*1*−*3*). The P4 separation gel (Bio-Gel Medium, Bio-Rad Laboratories, Hercules, CA) was purchased and used as received; S-acetyl NHS−MAG_3 was synthesized in house (*14*), and the structure was confirmed by elemental analysis, proton nuclear magnetic resonance (NMR), and mass spectroscopy. All other chemicals were reagent grade and were used without purification. The ^{99m}Tc−pertechnetate was eluted from a ^{99}Mo−^{99m}Tc generator (Dupont, Billerica, MA).

Size Exclusion High-Performance Liquid Chromatography (HPLC) and Paper Chromatography. Size exclusion HPLC analysis was performed on a Superdex Peptide column (optimal separation range: 1 × 10^2 to 7 × 10^3 Da; Amersham Pharmacia Biotech, Piscataway, NJ) with 0.10 M pH 7.2 phosphate buffer as eluant at a flow rate of 0.60 mL/min. ^{99m}Tc−pertechnetate is retained on this column. The HPLC was equipped with both an inline radioactive detector and an

10.1021/bc0255384 CCC: $22.00 © 2002 American Chemical Society
Published on Web 06/27/2002

inline Waters 2487 dual wavelength absorbance detector. Recovery was routinely measured. The presence of ^{99m}Tc−pertechnetate was confirmed by paper strip chromatography on Whatman No. 1 with acetone as the mobile phase. Only ^{99m}Tc−pertechnetate migrates with the solvent while labeled MORF and other labeled impurities remain at the origin.

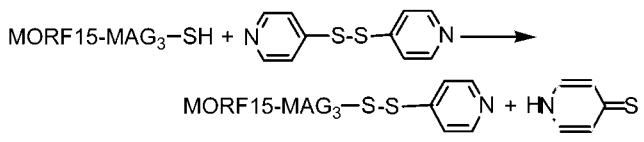
Conjugating MORF with MAG_3 and Radiolabeling. MORF derivitized on the 3′ equivalent end with a primary amine was conjugated with S-acetyl NHS−MAG_3 as previously described (*1*−*3*). A solution of 1000 μg of MORF in 200 μL of 0.2 M, pH 8.0, *N*-(2-hydroxyethyl)piperazine-*N*′-ethanesulfonic acid (HEPES) buffer was added to a vial containing 1700 μg of S-acetyl NHS−MAG_3. The vial was immediately vortexed thoroughly, incubated for 1 h at room temperature, and purified on a 0.7 cm × 20 cm P4 column with 0.25 M, pH 5.2, NH_4OAc buffer as eluant.

MORF−MAG_3 was originally labeled by adding 5 μL (∼300 μCi) of ^{99m}Tc−pertechnetate generator eluate to a solution of 30 μL of MORF−MAG_3 in the pH 5.2 ammonium acetate buffer, 10 μL of 50 μg/μL Na_2·tartrate·$2H_2O$ in a pH 9.2 buffer (0.5 M Na_2HCO_3, 0.25 M NH_4OAc, and 0.175 M NH_3), and 4 μL of 1 μg/μL $SnCl_2$·$2H_2O$ in ascorbate−HCl solution (1 μg/μL sodium ascorbate in 10 mM HCl). The final pH was 7.6.

To better understand the original labeling method, several studies were performed as follows: (i) The pH 7.6 solution of labeled MORF was divided, one-half was stored at room temperature for 10 h while the other was heated in a boiling water bath for 20 min before storage at room temperature for 10 h. (ii) In addition, some of the heated half was purified again over P4. The three samples were then analyzed by HPLC.

As will be shown below, the radioimpurities after labeling by the original method are labeled tartrate and labeled MAG_3. If a 20 min heating step is introduced at the end of the labeling method, the only radioimpurity remaining is labeled MAG_3. Thus, if labeled MAG_3 can be prevented, postlabeling purification will be unnecessary. The labeled MAG_3 may arise from inefficient purification of the free MAG_3 remaining after the conjugation or it may be generated by cleavage during labeling of some relatively unstable MAG_3 conjugate. To better understand the origin of this impurity, (i) the purified MORF−MAG_3 in pH 5.2 was purified again on P4 before labeling and (ii) the purified MORF−MAG_3 in pH 5.2 was adjusted to pH 7.6, heated for 20 min, and then purified over P4 again using the same pH 5.2 NH_4OAc buffer as eluant.

MAG_3 Groups per MORF. After conjugation, the acetyl group on S-acetyl MAG_3 may no longer be necessary to protect the thiol group; nevertheless, its continued presence has been demonstrated following conjugation to one peptide (*10*). By introducing a 20 min heating step at boiling water temperature, especially at pH 7.6, it is possible that most of the acetyl groups are hydrolyzed (*16*, *17*). Because rapid kinetics of labeling may depend on the presence of the unprotected free sulfhydryl on MORF−MAG_3 (*18*, *19*), the number of unprotected MAG_3 groups on MORF−MAG_3 was determined. The assay employed 4,4′-dithiodipyridine (4-DTDP) according to the following reaction (*5*, *20*, *21*):



By measuring on a UV spectrophotometer (U-2000, Hitachi Instruments Inc., Danbury, CT), it was determined that MORF and cysteine show low to nonexistent absorption at the 323 nm absorption maximum of the indicator 4-thiopyridone (4-TP). Only 4-DTDP shows a small but measurable absorbance at this frequency. However, 4-DTDP was present at large excess such that its concentration was effectively unchanged by the reaction. Accordingly, free sulfhydryl groups could be quantitated in the presence of 4-DTDP.

A standard curve of absorbance vs free sulfhydryl concentration was obtained by adding 40 μL of 4-DTDP (80 pmol) in 0.1 M, pH 7.2, phosphate buffer to each of a series of cysteine solutions in the range of 5−45 μM in 100 μL of pH 5.2 acetate buffer and measuring the absorbance against a blank 4-DTDP solution. The concentration of free sulfhydryls in the MORF−MAG_3 sample was then determined by applying its absorbance to the standard curve. In this measurement, the concentration of MORF was obtained by its absorbance at 265 nm using the molar absorbance (1.583×10^5 M^{-1} cm^{-1}) provided by the manufacturer.

Optimization. Optimization of labeling conditions was accomplished by varying the amount of MORF−MAG_3, stannous ion, temperature, and time using a MORF solution with 0.13 unprotected MAG_3 per molecule, determined as described above. Thus, 5 μL (∼300 μCi) of ^{99m}Tc generator eluant was added to a mixture of 35 μL of 0.25 M, pH 5.2, NH_4OAc buffer containing various amounts of MORF−MAG_3, 10 μL of 50 μg/μL tartrate solution in a pH 9.2 buffer (0.5 M $NaHCO_3$, 0.25 M NH_4OAc, and 0.175 M NH_3 buffer), and 5 μL (4 μg/μL) of $SnCl_2$·$2H_2O$ solution in 10 mM HCl containing 1 μg/μL sodium ascorbate followed by heating in boiling water for 20 min. Thereafter, by holding the MORF−MAG_3 concentration constant, the influence of the tin, temperature, and time was evaluated. Finally, the influence of radioactivity levels was established by adding varying volumes of the pertechnetate generator eluant to the labeling solution. All samples were measured by HPLC, and in all cases, the recovery of radioactivity off the column was greater than 90% unless otherwise stated.

RESULTS

Removal of Labeled Tartrate. Figure 1A presents a HPLC radiochromatogram of labeled MORF−MAG_3 prepared from MORF−MAG_3 purified on P4 only once and incubated at room temperature for 1 h before analysis. The peak at 20.8 min is due to labeled MORF, that at 26 min is due to labeled tartrate, and that at 40.6 min is due to labeled MAG_3. Identification was made by comparison to radiochromatograms of labeled tartrate and commercial labeled MAG_3. The high molecular weight shoulder on the labeled MORF peak may be due to the 2:1 complex duplex ^{99m}TcO(MORF−MAG_3)$_2$ (*22*, *23*).

Despite a reasonable separation by HPLC, we were unable to remove labeled tartrate from the radiolabeled MORF using P4. However, increasing the room temperature incubation time from 1 to 5 h resulted in a decrease in labeled tartrate as shown in Figure 1A,B and an increase in HPLC recovery from 85 to 92%. Heating in boiling water for 20 min in place of longer room temperature incubations was more successful in decreasing this radiocontaminant as shown in Figure 1C. Because ^{99m}Tc−pertechnetate is retained on the HPLC column and because the recovery was quantitative, the decrease

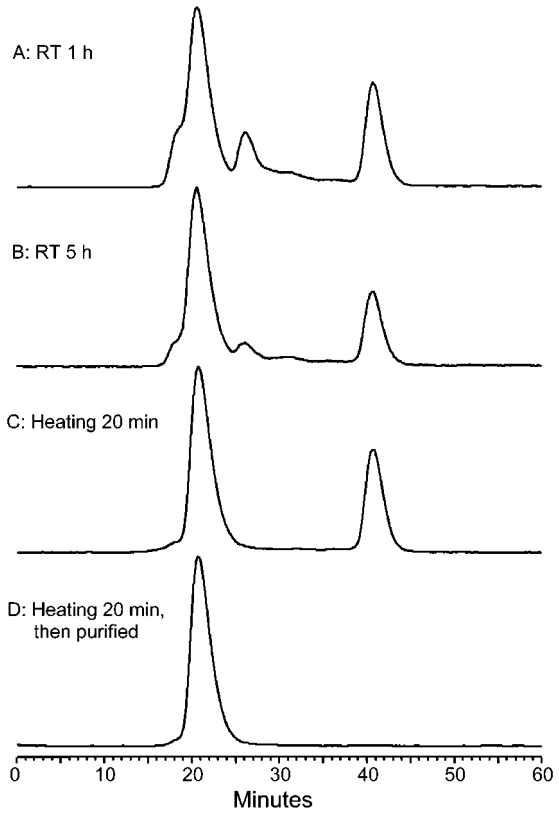


Figure 1. Size exclusion HPLC radiochromatograms of radiolabeled MORF−MAG_3 incubated at room temperature for 1 h (panel A) and 5 h (panel B) and after heating the radiolabeled MORF−MAG_3 for 20 min (panel C) followed by P4 purification (panel D).

in labeled tartrate must have been to the benefit of labeled MORF, presumably by increasing transchelation. Heating also removed the high molecular weight shoulder probably by its transformation from the 2:1 complex to a 1:1 complex (*22*, *23*). Figure 1D was obtained following postlabeling purification on P4 of the labeled MORF after heating for 20 min and shows that labeled MAG_3 can be removed by P4 purification of the heated labeled mixture.

Removal of Labeled MAG_3. Although heating during labeling of MORF−MAG_3 could remove the labeled tartrate radioimpurity, radiolabeled MAG_3 remained. Repurification on P4 before labeling lowered but did not eliminate this radiocontaminant. This indicated that the labeled MAG_3 was not solely due to insufficient purification of the conjugate. However, by adjusting the purified MORF conjugate to pH 7.6 from pH 5.2 and heating for 20 min followed by purification again on P4, the labeled MAG_3 radioimpurity was completely absent after labeling. This suggests that the labeled MAG_3 radioimpurity may be the result of some weak conjugation of MAG_3 to MORF that is susceptible to dissociation during heating in ammonium buffer at pH 7.6.

Therefore, the subsequent investigations were conducted using MORF−MAG_3 conjugates, which after conjugation and purification on P4 were adjusted to pH 7.6 and heated for 20 min before repurification on P4.

Determination of Deprotected MAG_3 Groups per MORF. Figure 2 presents the absorption spectra for cysteine, MORF, 4-DTDP, and the reaction mixture (i.e., 4-TP) in the range of 280−400 nm. Both the free cysteine and the MORF−MAG_3 therefore have no absorption at the 323 nm peak absorbance of the indicator product 4-TP. Only 4-DTDP has measurable absorbance at this

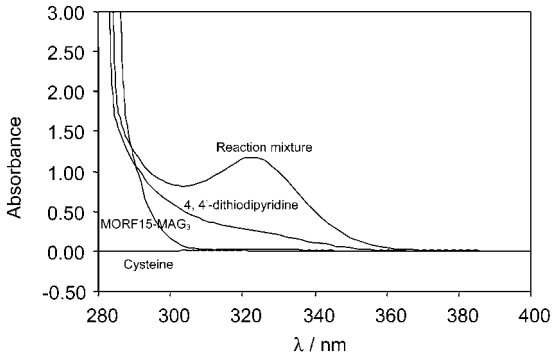


Figure 2. UV spectra of cysteine, MORF−MAG_3, 4,4′-dithiodipyridine, and the reaction mixture (i.e., 4-TP) in the determination of MAG_3 groups per MORF.

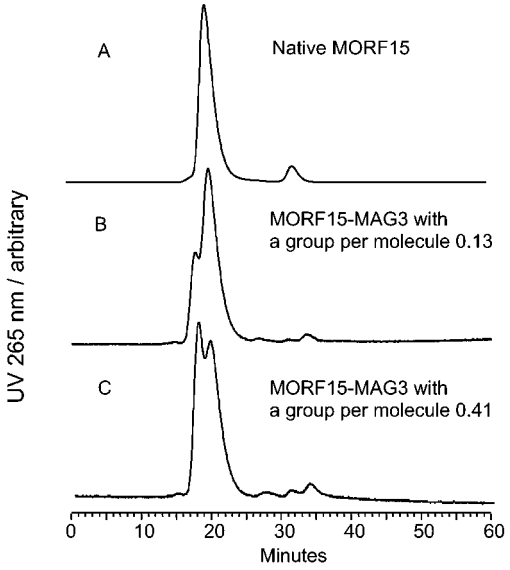


Figure 3. UV HPLC chromatograms of native MORF (panel A) and two MORF−MAG_3 preparations with an average of 0.13 (panel B) and 0.41 (panel C) groups per molecule.

frequency, but its concentration was unchanged during the measurement so that determination against the blank solution of 4-DTDP could eliminate its influence. The standard curve obtained provided a straight line over nine concentrations with a coefficient of regression of 0.998 (data not presented). In this manner, the average number of deprotected MAG_3 groups per MORF was determined for two preparations as 0.13 and 0.41.

These values are in qualitative agreement with the results of HPLC analysis of these samples. As shown in Figure 3, the UV chromatogram of native MORF shows a singlet at the retention time 20.8 min of the oligomer in panel A while those of MORF−MAG_3 conjugated at an average of 0.13 groups per molecule in panel B and MORF−MAG_3 conjugated at an average of 0.41 groups per molecule in panel C show a shoulder at 17.7 min whose intensity increases with increasing conjugation. The closely spaced doublet on HPLC could not be adequately separated for quantitating the relative amount of the new peak.

Optimization. The following studies were performed on the MORF−MAG_3 sample conjugated at an average of 0.13 groups per molecule. The results presented in Table 1 were obtained by HPLC analysis. The weight of MORF−MAG_3 with 300 μCi of ^{99m}Tc is clearly a determinent of labeling efficiency as shown in the table. The poor recovery at low weights of MORF−MAG_3 was

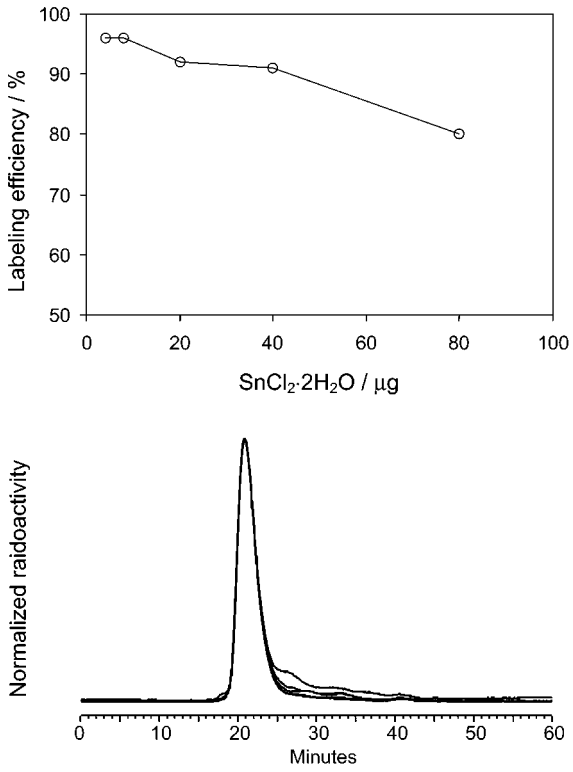


Figure 4. Influence of stannous ion on labeling efficiency.

Table 1. Influence of the Amount of MORF−MAG_3 on the Labeling

MORF−MAG_3 (μg)	0.02	0.04	0.08	0.20	0.78	3.90
recovery (%)	67	90	99	105	100	103
area of labeled MORF (%)	67	75	90	94	96	97
labeling efficiency (%)	45	68	89	94	96	97

assumed to be due to the presence of pertechnetate from oxidation of labeled tartrate, which is retained on the column. After the addition of 300 μCi of ^{99m}Tc to the labeling solution at pH 7.6 containing 0.2 μL of MORF−MAG_3 (i.e., 0.08 μg, 0.28 μM MORF, 0.036 μM MAG_3 as MORF−MAG_3) or more and a fixed amount of tin (20 μg of $SnCl_2{\cdot}2H_2O$), the labeling efficiency was greater than 90%.

Figure 4 presents the influence of stannous ion on labeling efficiency and shows that labeling efficiency drops with increasing tin. For 0.5 μL of MORF−MAG_3 (i.e., 0.20 μg of MORF, 0.026 μg of pure MORF−MAG_3), labeling efficiency drops below 90% when the amount of $SnCl_2{\cdot}2H_2O$ exceeds 40 μg, possibly by increasing the concentration of technetium in oxidation states lower than +5 that cannot be directly transchelated to MORF−MAG_3.

Heating is necessary for efficient labeling as shown in Figure 5. Panel A presents radiochromatograms obtained over time for the labeled MORF−MAG_3 prepared without heating (0.5 μL of 0.20 μg of MORF−MAG_3 and 20 μg of $SnCl_2{\cdot}2H_2O$). As shown, the radiolabeled tartrate peak at 26 min is still prominent even after 10 h postlabeling. In addition, recovery in this sample fell below 80% at 10 h presumably because of oxidation of labeled tartrate to pertechnetate. However, as shown in panel B, by introducing a 20 min heating step, the radiochemical purity is greater than 93% even after 8 h postlabeling.

Thus, at pH 7.6 with tartrate as the transchelator, if the amount of MORF−MAG_3 is greater than 0.08 μg and the amount of $SnCl_2{\cdot}2H_2O$ is between 4 and 20 μg, the

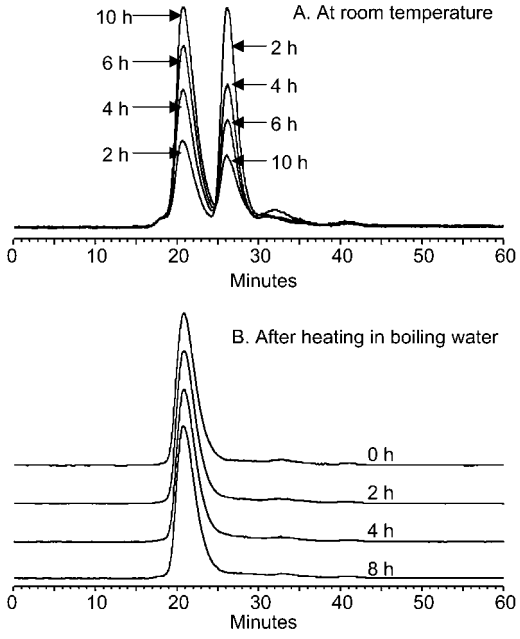


Figure 5. Size exclusion HPLC radiochromatograms of labeled MORF−MAG_3 vs time without heating during labeling (panel A) and with heating for 20 min (panel B).

labeling efficiency of MORF will be greater than 90% after the introduction of 5 μL (300 μCi) of pertechnetate followed by heating for 20 min. With 12 μg of $SnCl_2{\cdot}2H_2O$ and 0.39 μg of MORF−MAG_3, the labeling efficiencies were, respectively, 96, 91, 38, and 17% for 5, 20, 50, and 100 μL of ^{99m}Tc−pertechnetate (145 μCi/μL). The specific activity of at least 7400 μCi/μg (i.e., 38 Ci/μmol) can be achieved without postlabeling purification.

DISCUSSION

The object of this study was to optimize the labeling efficiency with ^{99m}Tc of a model oligomer conjugated with MAG_3. Our goal was to achieve 90% or greater radiochemical purity and thus avoid the need for postlabeling purification. Because in this investigation tartrate was selected as the transchelator, the possible radiochemical impurities are radiolabeled tartrate, radiolabeled MAG_3, and pertechnetate. In fact, using our original MORF−MAG_3 labeling method, both radiolabeled MAG_3 and tartrate were evident as shown in Figure 1A. Furthermore, because any labeled tartrate present will be susceptible to oxidation, it may be continually oxidized during HPLC analysis to explain the poor recoveries of about 85% that we have occasionally observed. If sufficient time is allowed, radiolabeled tartrate can continue its transchelation, in this case to MORF−MAG_3, as shown in Figure 1B. However, the process can be greatly accelerated by heating as shown in Figure 1C.

The removal of labeled MAG_3 is more difficult. All attempts to purify free MAG_3 from MORF−MAG_3 by P4 were unsuccessful in that radiolabeling of the repurified oligomer consistently provided a product contaminated with labeled MAG_3. This radiocontaminant could be removed, however, if the purified conjugated oligomer was placed in the pH 7.6 buffer and heated for 20 min or more before a second P4 purification and the subsequent labeling. We believe that the NHS−MAG_3 used in the conjugation of the amine derivitized MORF is capable of conjugating to the sulfhydryl on the deprotected MAG_3 group. The resulting thio ester bond is relatively unstable

against hydrolysis and aminolysis and may dissociate in neutral pH solution containing a large amount of ammonium (*16*, *17*). Originally (*1*−*3*), the labeled MORF−MAG_3 was placed in neutral pH only during labeling with the results that this dissociation introduced the observed radiolabeled MAG_3 impurity.

On the basis of these observations, the following procedure for purification of the conjugated biomolecule and subsequent labeling was adopted. After conjugation of MORF with NHS−MAG_3 (molar ratio 1:20) in pH 8.0 HEPES buffer and purification over P4 with pH 5.2 NH_4-OAc eluant, the oligomer fractions were combined, adjusted to pH 7.6, and heated for 20 min. The conjugated oligomer was then purified over P4 again for storage at refrigerator temperatures. Labeling is achieved simply by adding fresh stannous ion to a solution of MORF−MAG_3 and tartrate in pH 7.6 buffer followed by ^{99m}Tc−pertechnetate. After the solution is heated for 20 min in boiling water, the labeling efficiency is always over 90% as determined by HPLC and paper chromatography. With the proper selection of MORF−MAG_3, stannous ion, and pertechnetate concentration, specific activities more than 7000 μCi/μg have been achieved.

ACKNOWLEDGMENT

Financial support for this investigation was provided by the National Institutes of Health (CA79507 and CA94994).

LITERATURE CITED

(1) Liu, G., Zhang, S., He, J., Liu, N., Gupta, S., Rusckowski, M., and Hnatowich, D. J. (2002) The influence of chain length and base sequence on the pharmacokinetic behavior of ^{99m}Tc-Morpholinos in mice. *Q. J. Nucl. Med.*, in press.

(2) Liu, G., Mang'era, K., Liu, N., Gupta, S., Rusckowski, M., and Hnatowich, D. J. (2002) Tumor pretargeting in mice using technetium-99m labeled morpholinos, a DNA analogue. *J. Nucl. Med. 43*, 384−391.

(3) Mang'era, O. K., Liu, G., Wang, Y., Zhang, Y., Liu, N., Gupta, S., Rusckowski, M., and Hnatowich, D. J. (2001) Initial investigation of ^{99m}Tc-labeled morpholinos for radiopharmaceutical applications. *Eur. J. Nucl. Med. 28*, 1682−1689.

(4) Wang, Y., Chang, F., Zhang, Y., Liu, N., Liu, G., Gupta, S., Rusckowski, M., and Hnatowich, D. J. (2001) Pretargeting with amplification using polymeric peptide nucleic acid. *Bioconjugate Chem. 12*, 807−816.

(5) Zhu, Z., Wang, Y., Zhang, Y., Liu, G., Liu, N., Rusckowski, M., and Hnatowich, D. J. (2001) A novel and simplified route to the synthesis of N3S chelators for ^{99m}Tc labeling. *Nucl. Med. Biol. 28*, 703−708.

(6) Rusckowski, M., Qu, T., Gupta, S., Ley, A., and Hnatowich, D. J. (2001) A comparison in monkeys of ^{99m}Tc labeled to a peptide by 4 methods. *J. Nucl. Med. 42*, 1870−1877.

(7) Zhang, Y. M., Wang, Y., Liu, N., Zhu, Z. H., Rusckowski, M., and Hnatowich, D. J. (2001) In vitro investigations of tumor targeting with ^{99m}Tc-labeled antisense DNA. *J. Nucl. Med. 42*, 1660−1669.

(8) Qu, T., Wang, Y., Zhu, Z., Rusckowski, M., and Hnatowich, D. J. (2001) Different chelators and different peptides together influence the in vitro and mouse in vivo properties of ^{99}Tc^{m}. *Nucl. Med. Commun. 22*, 203−215.

(9) Zhang, Y. M., Liu, N., Zhu, Z. H., Rusckowski, M., and Hnatowich, D. J. (2001) Influence of different chelators (HYNIC, MAG_3 and DTPA) on tumor cell accumulation and mouse biodistribution of technetium-99m labeled to antisense DNA. *Eur. J. Nucl. Med. 27*, 1700−1707.

(10) Rusckowski, M., Qu, T., Pullman, J., Marcel, R., Ley, A. C., Ladner, R. C., and Hnatowich, D. J. (2000) Inflammation and infection imaging with a ^{99m}Tc-neutrophil elastase inhibitor in monkeys. *J. Nucl. Med. 41*, 363−374.

(11) Hnatowich, D. J., Qu, T., Chang, F., Ley, A. C., Ladner, R. C., Rusckowski, M. (1998) Labeling peptides with technetium-99m using a bifunctional chelator of a N-hydroxysuccinimide ester of mercaptoacetyltriglycine. *J. Nucl. Med. 39*, 56−64.

(12) Rusckowski, M., Qu, T., Chang, F., and Hnatowich, D. J. (1997) Pretargeting using peptide nucleic acid. *Cancer 80*, 2699s−2705s.

(13) Rusckowski, M., Qu, T., Chang, F., and Hnatowich, D. J. (1997) Technetium-99m labeled epidermal growth factor-tumor imaging in mice. *J. Pept. Res. 50*, 393−401.

(14) Winnard, P., Jr., Chang, F., Rusckowski, M., Mardirossian, G., and Hnatowich, D. J. (1997) Preparation and use of NHS-MAG_3 for technetium-99m labeling of DNA. *Nucl. Med. Biol. 24*, 425−432.

(15) Lei, K., Rusckowski, M., Chang, F., Qu, T., Mardirossian, G., and Hnatowich, D. J. (1996) Technetium-99m antibodies labeled with MAG_3 and SHNH: an in vitro and animal in vivo comparison. *Nucl. Med. Biol. 23*, 917−922.

(16) Pratt, L. S., and Reid, E. E. (1915) Studies in esterification. VI. The esterification of benzoic acid by mercaptans. *J. Am. Chem. Soc. 37*, 1934−1948.

(17) Wieland, V. T., and Bokelmann, E. (1952) Das Verhalten einiger S-Acyl-aminomercaptane. *Ann. Chem. 576*, 20−34.

(18) Bormans, G., Cleynhens, B., Adriaens, P., Vanbilloen, H., De Roo, M., and Verbruggen, A. (1995) Investigation of the labeling characteristics of ^{99m}Tc-mercaptoacetyltriglycine. *Nucl. Med. Biol. 22*, 339−349.

(19) Hnatowich, D. J., Chang, F., Lei, K., Qu, T., and Rusckowski, M. (1997) The influence of temperature and alkaline pH on the labeling of free and conjugated MAG_3 with technetium-99m. *Appl. Radiat. Isot. 48*, 587−594.

(20) Grassetti, D. R., Murray, J. F., Jr. (1967) Determination of sulfhydryl groups with 2,2′- or 4,4′- Dithiodipyridine. *Arch. Biochem. Biophys. 119*, 41−49.

(21) Egwim, I. O. C., and Gruber, H. J. (2001) Spectrophotometric measurement of mercaptans with 4,4′-dithiodipyridine. *Anal. Biochem. 288*, 188−194.

(22) Noll, B., Johannsen, B., and Spies, H. (1995) Sources of radiochemical impurities in the ^{99m}Tc/S-unprotected MAG_3 system. *Nucl. Med. Biol. 22*, 1057−1062.

(23) Noll, B., Johannsen, B., May, K., and Spies, H. (1992) Preparation of the renal function and imaging agent ^{99m}Tc-MAG3 starting from S-unprotected mercaptoacetyltriglycine. *Int. J. Radiat. Appl. Instrum. A 43*, 899−901.

BC0255384

Visible Light Induced Biohydrogen Production from Sucrose Using the Photosensitization of Mg Chlorophyll-*a*

Yoshinobu Saiki and Yutaka Amao*

Department of Applied Chemistry, Oita University, Dannoharu 700, Oita 870-1192, Japan.
Received January 17, 2002; Revised Manuscript Received April 21, 2002

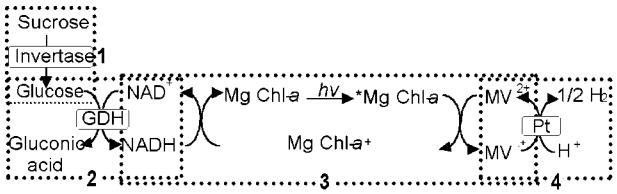
A photoinduced hydrogen production system, coupling sucrose degradation with invertase and glucose dehydrogenase (GDH) and hydrogen production with colloidal platinum as a catalyst using the visible light-induced photosensitization of Mg chlorophyll-*a* (Mg Chl-*a*), has been developed. Continuous hydrogen gas production was observed when the reaction mixture containing sucrose, invertase, GDH, nicotinamide adenine dinucleotide (NAD^+), Mg Chl-*a*, methyl viologen (MV^{2+}, an electron relay reagent), and colloidal platinum was irradiated by visible light.

INTRODUCTION

Hydrogen production from biomass resources is important in the environmental and alternative energy source fields (*1*−*5*). Some renewable biomass resources are starch, cellulose, sucrose, and lactose. These polysaccharides are hydrolyzed to form monosaccharides such as glucose. Thus, the conversion of glucose to hydrogen will be a useful new enzymatic pathway. Some studies on the hydrogen production from glucose using the enzymatic pathway have been reported (*6*−*10*). The hydrogen production from glucose with the combination of glucose dehydrogenase (GDH)[1] and hydrogenase has been reported (*11*, *12*). However, the enzymatic photoinduced hydrogen production from other monosaccharides, oligosaccharides, or polysaccharides has received little attention. Glucose was enzymatically obtained from sucrose by using invertase. Thus, hydrogen production from the oligosaccharide sucrose will be attained using the combination of invertase, GDH, and hydrogenase or some other hydrogen-producing catalyst.

On the other hand, some photoinduced hydrogen production systems consist of electron donor, photosensitizer, electron carrier, and catalyst (*13*−*19*). Regarding hydrogen-producing catalysts, colloidal platinum (*17*−*19*) and hydrogenase from *Desulfovibrio vulgaris* (Miyazaki) (*13*−*16*) are widely used in hydrogen production systems. Especially, colloidal platinum is stable against long-term irradiation. In photoinduced hydrogen production systems with visible light, water-soluble zinc porphyrins have an absorption band in the visible light region (380−600 nm), and these porphyrins have been widely used as effective photosensitizers (*13*, *14*). Especially, zinc tetraphenylporphyrin tetrasulfonate (ZnTPPS) is useful as a photosensitizer (*13*, *14*). However, the molar absorption coefficient of zinc porphyrins in the visible light region (500−600 nm) was lower than that in the near ultravisible light region (380−400 nm). On the other hand, Mg chlorophyll-*a* (Mg Chl-*a*), which acts as an effective photosensitizer in photosynthesis (*20*), has an absorption maximum at 670 nm. Thus, Mg Chl-*a* is attractive as a visible region photosensitizer. Photoinduced hydrogen production systems with chemically modified chlorophyll and hydrogenase (*21*, *22*), and chlorophyll derivatives (*23*−*25*), were reported previously. In photoinduced hydrogen production with a system consisting of an electron donor, photosensitizer, electron relay, and catalyst, the photoexcited photosensitizer reacts with an electron relay to form a reduced electron relay, hydrogen evolves by proton reduction with the catalyst, and then the oxidized photosensitizer is reduced by an electron-donating reagent such as reduced nicotinamide adenine dinucreotide (NADH). Thus, the electron donor, NADH, was a sacrificial reagent, and the oxidized electron donor, NAD^+, was consumed in the reaction system. If NADH is regenerated, the photoinduced hydrogen production system is accomplished without NAD^+ consumption. As GDH uses NAD^+ as a cofactor, photoinduced hydrogen production with GDH, electron donor, photosensitizer, electron relay reagent, and catalyst will be attained.

Scheme 1. Visible Light-Induced Hydrogen Production System Coupling the Sucrose Degradation with Invertase and GDH and Hydrogen Production with Colloidal Platinum Using the Photosensitization of Mg Chl-*a* in the Presence of MV^{2+}



In this work we describe the visible light-induced hydrogen production system that couples sucrose degradation with invertase and GDH, and hydrogen production with colloidal platinum using the photosensitization of Mg Chl-*a* in the presence of methyl viologen (MV^{2+}) as an electron relay reagent as shown in Scheme 1.

* To whom correspondence should be addressed. Phone: +81-97-554-7972. Fax: +81-97-554-7972. E-mail: amao@cc.oita-u.ac.jp.

[1]Abbreviations: GDH, glucose dehydrogenase; NAD^+, nicotinamide adenine dinucreotide; NADH, reduced nicotinamide adenine dinucreotide; MV^{2+}, methyl viologen; $MV^{\bullet+}$, reduced methyl viologen; Mg Chl-*a*, Mg chlorophyll-*a*; ZnTPPS, zinc tetraphenylporphyrin tetrasulfonate; CTAB, cetyltrimethylammonium bromide.

10.1021/bc025506g CCC: $22.00 © 2002 American Chemical Society
Published on Web 06/29/2002

EXPERIMENTAL PROCEDURES

General. Mg Chl-*a* from *Spirulina*, invertase from yeast, and GDH from *Bacillus* sp. were purchased from Wako Pure Chemical Industries Ltd. (Osaka, Japan). NAD^+ and NADH were purchased from Oriental Yeast Co. Ltd. MV^{2+} dichloride and cetyltrimethylammonium bromide (CTAB) were purchased from Tokyo Kasei Co. Lid (Tokyo, Japan). Hydrogen hexachloroplatinate hexahydrate and sodium citrate dihydrate were obtained from Kanto Chemical Co. Ltd (Tokyo, Japan). The other chemicals were analytical grade or the highest grade available. One unit of GDH activity was defined as the amount of enzyme that reduced 1.0 μmol NAD^+ to NADH by glucose per minute. One unit of invertase activity was defined as the amount of enzyme that produced 1.0 μmol glucose by sucrose per minute. Mg Chl-*a* was solubilized with 10 mmol dm^{-3} of CTAB, since Mg Chl-*a* is insoluble in aqueous solution.

Preparation of Colloidal Platinum. Colloidal platinum was prepared by reduction of hexachloroplatinate solution with sodium citrate. The reduction procedure was similar to the previous reported method (*17*). A solution of 400 mL of water containing 30 mg of hydrogen hexachloroplatinate hexahydrate was brought to boiling temperature using a mantle heater with a magnetic stirrer for 1.5 h, and then a solution of 30 mL of water containing 600 mg of sodium citrate dihydrate was added and refluxed with a magnetic stirrer at 100 °C for 4 h. The particle size of colloidal platinum prepared was estimated to be 1.5 nm. In general, the colloidal platinum activity decreased with increase the particle size (more than 2.0 nm) (*17*). The prepared colloidal platinum has the ability to release 0.7 μmol of hydrogen in the reaction system of 10 μL of colloidal platinum, 1.2×10^{-5} mmol of methyl viologen, and 7.7×10^{-5} mmol of sodium dithionite in 4.0 mL of 50 mmol dm^{-3} Tris-HCl buffer (pH 7.4) at 30 °C for 10 min. One unit of colloidal platinum activity was defined as a release of 1.0 μmol of hydrogen per minute.

NADH Formation with Sucrose, Invertase, and GDH. The reaction was started by addition of NAD^+ (0.80 μmol) solution to the sample solution containing sucrose (16 μmol), invertase (4.0 units), and GDH (5.0 units) in 3.0 mL of 10 mmol dm^{-3} potassium phosphate buffer (pH 7.0). The reduction of NAD^+ to NADH by GDH was monitored using UV−vis spectrophotometer at 340 nm, with the molar extinction coefficient of 6.3×10^3 mol dm^3 cm^{-1}.

Photoreduction of MV^{2+}. Photoreduction of MV^{2+} was tested in the reaction mixture containing NAD^+, sucrose, Mg Chl-*a*, MV^{2+}, invertase, and GDH. The reaction system consisted of NAD^+ (15 μmol), sucrose (0.30 mmol), Mg Chl-*a* (3.0 nmol), MV^{2+} (1.2 μmol), invertase (4.0 units), and GDH (5.0 units) in 3.0 mL of 10 mmol dm^{-3} potassium phosphate buffer (pH 7.0). The sample solution was deaerated by repeated freeze−pump−thaw cycles and irradiated with a 200 W tungsten lamp at a distance of 3.0 cm, with a light intensity of 200 J m^{-2} s^{-1}, at 30 °C. The light of the wavelength less than 390 nm was removed by a Toshiba L-39 cutoff filter (Tokyo, Japan). The reduction of MV^{2+} was monitored using UV−vis spectrophotometer at 605 nm, with the molar extinction coefficient of 1.3×10^4 mol dm^3 cm^{-1} (*26*).

Visible Light-Induced Hydrogen Production. The photoinduced hydrogen production from sucrose was carried out as follows. The sample solution containing NAD^+ (15 μmol), sucrose (0.30 mmol), Mg Chl-*a* (3.0 nmol), MV^{2+} (1.2 μmol), colloidal platinum (0.5 unit), invertase (4.0 units), and GDH (5.0 units) in 3.0 mol of 10 mmol dm^{-3} potassium phosphate buffer (pH 7.0) was deaerated by freeze pump thaw cycle for six times and substituted by argon gas. The amount of hydrogen evolved was measured by Schimadzu GC-14B gas chromatography (detector: TCD, column temperature: 40 °C, column: active charcoal with the particle size 60∼80 mesh, carrier gas: nitrogen gas, carrier gas flow rate: 24 mL min^{-1}).

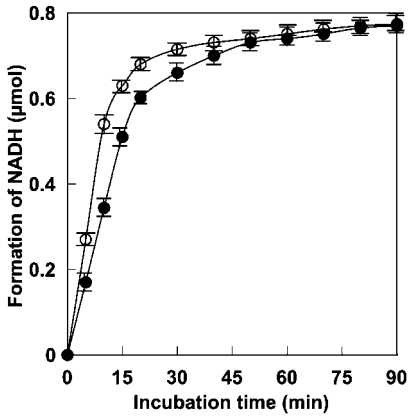


Figure 1. Time dependence of NADH formation with sucrose, invertase, NAD^+, and GDH. (Closed circles): Sucrose (16 μmol), invertase (4.0 units), NAD^+ (0.80 μmol), and GDH (5.0 units) in 3.0 mL of 10 mmol dm^{-3} potassium phosphate buffer (pH = 7.0). (Open circles): Glucose (16 μmol), NAD^+ (0.80 μmol), and GDH (5.0 units) in 3.0 mL of 10 mmol dm^{-3} potassium phosphate buffer (pH = 7.0). Each data point represents the mean of at least three separate experiments; bars are the standard error of the mean (SEM).

RESULTS AND DISCUSSION

NADH Formation with Sucrose, Invertase, and GDH System. When the sample solution containing sucrose, invertase, GDH, and NAD^+ was incubated, the of the NADH was formed in a time-dependent manner (Figure 1, closed circle). The initial rate of NADH formation, which was determined by the amount of NADH with incubation for 15 min, was estimated to be $(3.4 \pm 0.1) \times 10^{-8}$ mol min^{-1}. After 80 min incubation, 0.77 ± 0.03 μmol of NADH was formed. The yield of the conversion of NAD^+ to NADH in this system was ca. 100%. When the sample solution containing glucose (16 μmol), GDH, and NAD^+ (without sucrose and invertase) was incubated, NADH was formed in a time-dependent manner (Figure 1, open circle), and the initial rate of NADH formation was estimated to be $(4.2 \pm 0.1) \times 10^{-8}$ mol min^{-1}. After 80 min incubation, 0.77 ± 0.02 μmol of NADH was formed, and the yield of the conversion of NAD^+ to NADH in this system also was ca. 100%. These results show that glucose formation from sucrose (process 1 in Scheme 1) with invertase proceeded rapidly.

Stability of Mg Chl-*a* against Irradiation. The photostability of Mg Chl-*a* in the reaction mixture was investigated. The photostability was tested by irradiation with visible light using 200 W tungsten lamp (light intensity of 200 J m^{-2} s^{-1}). Figure 2 shows the absorbance change at 670 nm attributed to the absorption maximum of Mg Chl-*a* with irradiation time. CTAB solublized Mg Chl-*a* solution was rapidly bleached by irradiation (curve A). On the other hand, the absorbance decrease of Mg Chl-a in the presence of NAD^+ and NADH was slower as shown in curve B and C, indicating that the degradation of Mg Chl-*a* was suppressed by the addition of NAD^+

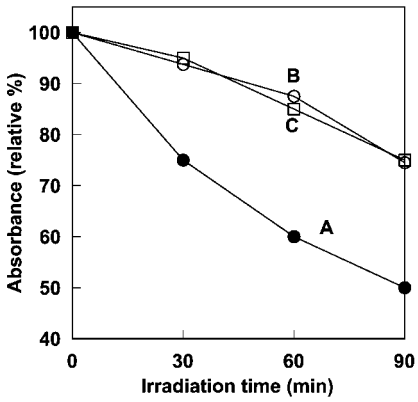


Figure 2. Photostability of Mg Chl-*a* solution under anaerobic condition. Curve A, CTAB solubilized Mg Chl-*a* aqueous solution. Curve B and C, CTAB solubilized Mg Chl-*a* aqueous solution in the presence of NAD^+ and NADH, respectively. Samples were irradiated with visible light using 200 W tungsten lamp at a distance of 3.0 cm (light intensity of 200 J m^{-2} s^{-1}).

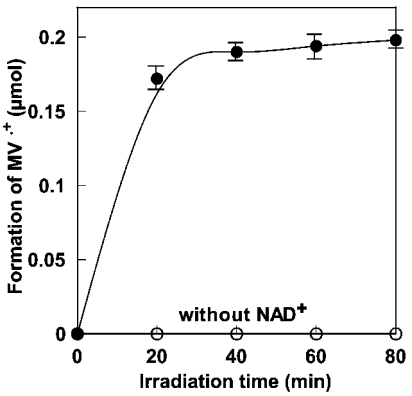


Figure 3. The time dependence of the $MV^{\bullet+}$ concentration under steady-state irradiation with visible light using 200 W tungsten lamp at a distance of 3.0 cm (light intensity of 200 J m^{-2} s^{-1}). The sample solution consisting of invertase (4.0 units), GDH (5.0 units), NAD^+ (15 μmol), sucrose (0.30 mmol), Mg Chl-*a* (3.0 nmol), and MV^{2+} (1.2 μmol) in 3.0 mol of 10 mmol dm^{-3} potassium phosphate buffer (pH = 7.0). (Open circles): In the absence of NAD^+. Each data point represents the mean of at least three separate experiments; bars are the SEM.

and NADH. The photoinduced degradation of Mg Chl-*a* proceeded by the reaction between photoexcited Mg Chl-*a* molecules. In the presence of the electron donor or acceptor reagent such as NAD^+ or NADH, on the other hand, the electron transfer from the photoexcited Mg Chl-*a* to the electron acceptor reagent or from the electron donor reagent to the photoexcited Mg Chl-*a* proceeded. These electron transfer processes rapidly proceeded compared with that of the reaction between photoexcited Mg Chl-*a* molecules. Thus, the reaction between photoexcited Mg Chl-*a* molecules was suppressed by the electron donor or acceptor reagent such as NAD^+ or NADH.

Photoreduction of MV^{2+}. Figure 3 shows the time dependence of the $MV^{\bullet+}$ concentration in the system containing NAD^+, sucrose, Mg Chl-*a*, MV^{2+}, invertase, and GDH with visible light irradiation. The absorbance at 605 nm, absorption band of $MV^{\bullet+}$, increased with irradiation time. After 80 min irradiation, (0.2 ± 0.01) μmol reduced MV^{2+} was produced and the yield of MV^{2+} to $MV^{\bullet+}$ was estimated to be ca. 33%. The photoreduction rate was independent of the concentrations of NAD^+, sucrose, invertase, and GDH. On the other hand, the reduction rate depends on the concentrations of Mg Chl-*a* and MV^{2+}. Thus, the rate-limiting step in the MV^{2+} reduction (processes 1, 2, and 3 in Scheme 1) is the photoinduced electron-transfer process from the photoexcited Mg Chl-*a* (*Mg Chl-*a*) to MV^{2+} (process 3 in Scheme 1). On the other hand, MV^{2+} was not reduced without NAD^+ in the above system (open circle). There is no direct electron transfer between sucrose or glucose formed with invertase and MV^{2+}, and between Mg Chl-*a* and MV^{2+}. Thus, the visible light-induced MV^{2+} reduction proceeded by coupling the sucrose degradation with invertase and GDH (processes 1 and 2 in Scheme 1) and MV^{2+} reduction using the photosensitization of Mg Chl-*a* (process 3 in Scheme 1).

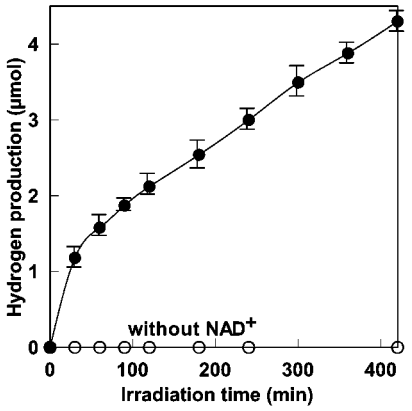


Figure 4. Time dependence of hydrogen production under steady-state irradiation with visible light using 200 W tungsten lamp at a distance of 3.0 cm (light intensity of 200 J m^{-2} s^{-1}). (Closed circles): The sample solution consisting of invertase (4.0 units), GDH (5.0 units) NAD^+ (15 μmol), sucrose (0.30 mmol), Mg Chl-*a* (3.0 nmol), MV^{2+} (1.2 μmol), and colloidal platinum (0.5 unit) in 3.0 mol of 10 mmol dm^{-3} potassium phosphate buffer (pH = 7.0). (Open circles): In the absence of NAD^+. Each data point represents the mean of at least three separate experiments; bars are the SEM.

Visible Light-Induced Hydrogen Production. As the MV^{2+} photoreduction system containing NAD^+, sucrose, Mg Chl-*a*, MV^{2+}, invertase, and GDH was achieved, the photoinduced hydrogen production system was investigated. Figure 4 shows the time dependence of the photoinduced hydrogen production in the system containing NAD^+, sucrose, Mg Chl-*a*, MV^{2+}, colloidal platinum, invertase, and GDH by the visible light. By irradiation, hydrogen evolved continuously for more than 420 min. The amount of hydrogen production was estimated to be 4.3 ± 0.1 μmol after 420 min irradiation. It indicated that 8.6 μmol of proton, that was 2867 times the amount of Mg Chl-*a* (3.0 nmol) in the sample solution, was reduced to hydrogen molecules. Therefore, the Mg Chl-*a* appeared to serve as the system for transferring electrons from NADH, which was formed from sucrose conversion to gluconic acid, to a more reductive molecule. It should be noted that hydrogen was not evolved in the absence of NAD^+ in the above system (open circles, Figure 4). There is no direct electron transfer between sucrose or glucose formed with invertase and colloidal platinum, and among Mg Chl-*a*, MV^{2+}, and colloidal platinum. These results suggest that the visible light-induced hydrogen production proceeded by coupling the sucrose degradation with invertase and GDH (processes 1 and 2 in Scheme 1) and the hydrogen production with colloidal platinum using the photosensitization of Mg Chl-*a* (processes 3 and 4 in Scheme 1).

In conclusion, a hydrogen production system coupling sucrose degradation with invertase and GDH, and hydrogen production with colloidal platinum using the

visible light-induced photosensitization of Mg Chl-*a*, was developed, and continuous generation of hydrogen gas was achieved. Renewable biomass resources are effectively used to produce an environmentally clean energy source, hydrogen gas. In the present system, fructose consumption occurred; glucose and fructose were formed from sucrose by invertase. The system involving fructose dehydrogenation is being studied in detail.

ACKNOWLEDGMENT

This work is partially supported byThe Thermal & Electric Energy Technology (TEET) Foundation.

LITERATURE CITED

(1) Helena, L. C., and Overend, R. P. (2001) Biomass and renewable fuels. *Fuel Process. Technol. 71*, 187−195.
(2) Barbosa, M. J., Rocha, J. M., Tramper, J., and Wijffels, R. H. (2001) Acetate as a carbon source for hydrogen production by photosynthetic bacteria. *J. Biotechnol. 85*, 25−33.
(3) Garcia, L., French, R., Czernik, S., and Chornet, E. (2000) Catalytic steam reforming of bio-oils for the production of hydrogen: effects of catalyst composition. *Appl. Catal. A: Gen. 201*, 225−239.
(4) Wang, D. (1998) Production of hydrogen from biomass by catalytic steam reforming of fast pyrolysis oils. *Fuel. Energy Abstr. 39*, 188.
(5) Minowa, T., and Inoue, S. (1999) Hydrogen production from biomass by catalytic gasification in hot compressed water. *Renew., Energ. 16*, 1114−1117.
(6) Rustamov, V. R., Abdullayev, K. M., Aliyev, F. G., and Kerimov, V. K. (1998) Hydrogen formation from biomass using solar energy. *Int. J. Hydrogen Energy 23*, 649−652.
(7) Woodward, J., Orr, M., Cordray, K., and Greenbaum, E. (2000) Enzymatic biohydrogen production. *Nature 405*, 1014−1015.
(8) Mizuno, O., Dinsdale, R., Hawkes, F. R., Hawkes, D. L., and Noike, T. (2000) Enhancement of hydrogen production from glucose by nitrogen gas sparging. *Bioresour., Technol. 73*, 59−65.
(9) Akashah, M., Yoshida, M., Watanabe, M., Nakamura, M., and Matsumoto, J. (1997) Hydrogen gas production from glucose and its microbial kinetics in anaerobic systems. *Water, Sci., Technol. 36*, 279−286.
(10) Ma, K., and Adams, M. W. (1994) Sulfide dehydrogenase from the hyperthermophilic archaeon Pyrococcus furiosus: a new multifunctional enzyme involved in the reduction of elemental sulfur. *J. Bacteriol. 176*, 6509−6517.
(11) Woodard, J., Mattingly, S. M., Danson, M., Hough, D., Ward, N., and Adams, M. (1996) In vitro hydrogen production by glucose dehydrogenase and hydrogenase. *Nature Biotechnol. 14*, 872−874.
(12) Inoue, T., Kumar, S. N., Kamachi, T., and Okura, I. (1999) Hydrogen evolution from glucose with the combination of glucose dehydrogenase and hydrogenase from *A. eutrophus* H16. *Chem. Lett.* 147−148.
(13) Okura, I. (1985) Hydrogenase and its application for photoinduced hydrogen evolution. *Coord. Chem. Rev. 68*, 53−99.
(14) Okura, I. (1986) Application of hydrogenase for photoinduced hydrogen evolution. *Biochimie 68*, 189−199.
(15) Okura, I., Aono, S., and Kusunoki, S., (1983) Photoreduction of viologens and hydrogen evolution with hydrogenase. *Inorg. Chim. Acta 71*, 77−80.
(16) Okura, I., and Kim-Thuan, N. (1981) Kinetic studies of photoinduced methyl viologen reduction with ruthenium complexes and hydrogen evolution from water by hydrogenase. *J. Chem. Soc., Faraday Trans. 1 77*, 1411−1416.
(17) Darwent, J. R., Douglas, P., Harriman, A., Porter, G., and Richoux, M. C. (1982) Metal phthalocyanines and porphyrins as photosensitizers for reduction of water to hydrogen. *Coord. Chem. Rev. 44*, 93−126.
(18) Brugger, P. A., Cuendet, P., Grätzel, M. (1981) Ultrafine and specific catalysts affording efficient hydrogen evolution from water under visible light illumination. *J. Am. Chem. Soc. 103*, 2923−2927.
(19) Kiwi, J., and Grätzel, M. (1979) Protection size factors, and reaction dynamics of colloidal redox catalysis mediating light induced hydrogen evolution from water. *J. Am. Chem. Soc. 101*, 7214−7217.
(20) Scheer, H. (1991) *Chlorophylls*, CRC Press, London.
(21) Itoh, T., Ishii, A., Kodera, Y., Matsushima, A., Hiroto, M., Nishimura, H., Tsuzuki, T., Kamachi, T., Okura, I., and Inada, Y. (1998) Photostable chlorophyll *a* with poly(vinylpyrrolidone)-smectite catalyzes photoreduction and hydrogen gas evolution by visible light. *Bioconjugate Chem. 9*, 409−412.
(22) Itoh, T., Asada, H., Tobioka, K., Kodera, Y., Matsushima, A., Hiroto, M., Nishimura, H., Kamachi, T., Okura, I., and Inada, Y. (2000) Hydrogen gas evolution and carbon dioxide fixation with visible light by chlorophyllin coupled with poly(ethylene glycol). *Bioconjugate Chem. 11*, 8−13.
(23) Koiso, T., Okuyama, M., Sakata, T., and Kawai, T. (1982) Efficient photoreduction of methyl viologen sensitized by chlorophyll derivatives and hydrogen evolution by visible light. *Bull. Chem. Soc. Jpn. 55*, 2659−2660.
(24) Krasnovski, A. A., Chan-van-Ni; Nikandrov, V. V., and Brin, G. P. (1980) Conditions for effective hydrogen photoevolution by chloroplasts in the presence of bacterial hydrogenase. *Molekuliarnaia Biologiia 14*, 287−298.
(25) Kiwi, J., and Gräetzel, M. (1980) Chlorophyll a sensitized redox processes in microemulsion systems. *J. Phys. Chem. 84*, 1503−1507.
(26) Watanabe, T., and Honda, K. (1982) Measurement of the extinction coefficient of the methyl viologen cation radical and the effeciency of its formation by semiconductor photocatalysis. *J. Phys. Chem. 86*, 2617−2619.

BC025506G

Comparison of Yttrium and Indium Complexes of DOTA-BA and DOTA-MBA: Models for ^{90}Y- and ^{111}In-Labeled DOTA−Biomolecule Conjugates

Shuang Liu,* John Pietryka, Charles E. Ellars, and D. Scott Edwards

Bristol-Myers Squibb Medical Imaging,† 331 Treble Cove Road, North Billerica, Massachusetts 01862.
Received October 8, 2001; Revised Manuscript Received January 18, 2002

Yttrium and indium complexes of 1,4,7,10-tetraaza-4,7,10-tris(carboxymethyl)-1-cyclododecylacetyl-benzylamine (DOTA-BA) and 1,4,7,10-tetraaza-4,7,10-tris(carboxymethyl)-1-cyclododecylacetyl-*R*-(+)-α-methylbenzylamine (DOTA-MBA) were prepared in order to study solution structures of ^{90}Y- and ^{111}In-labeled DOTA−biomolecule conjugates. ^{90}Y and ^{111}In complexes M(L) (M = ^{90}Y and ^{111}In; L = DOTA-BA and DOTA-MBA) were prepared from the reaction of MCl_3 with DOTA-BA and DOTA-MBA, respectively, in ammonium acetate buffer. A reverse phase HPLC method revealed that both ^{90}Y and ^{111}In complexes show only one radiometric peak in their radio-HPLC chromatograms. It was also found that ^{111}In(DOTA-BA) and ^{111}In(DOTA-MBA) are more hydrophilic than their corresponding ^{90}Y analogues, suggesting different coordination spheres in ^{111}In and ^{90}Y complexes of the same DOTA conjugate. Complexes M(L) (M = Y and In; L = DOTA-BA and DOTA-MBA) were prepared and characterized by HPLC, LC-MS, and NMR (^{1}H and ^{13}C) methods. The HPLC concordance experiments for ^{90}Y(DOTA-MBA)/Y(DOTA-MBA) and ^{111}In(DOTA-MBA)/In(DOTA-MBA) show that the same complex is prepared at both tracer and macroscopic levels. The NMR data (^{1}H and ^{13}C) clearly demonstrates that Y(DOTA-BA) and Y(DOTA-MBA) exist in solution as one predominant isomer. VT NMR data (^{1}H and ^{13}C) show that In(DOTA-BA) and In(DOTA-MBA) are fluxional at room temperature while Y(DOTA-BA) and Y(DOTA-MBA) become fluxional only at elevated temperatures. The fluxionality of these complexes is due to rapid rotation of acetate/acetamide chelating arms and inversion of ethylenic groups of the macrocyclic ring.

INTRODUCTION

There is great current interest in the development of target-specific therapeutic radiopharmaceuticals for the treatment of cancers. Several reviews have appeared recently covering a broad range of topics related to radiolabeled small biomolecules (BM) as target-specific therapeutic radiopharmaceuticals (*1*−*7*). Many acyclic and macrocyclic bifunctional chelators (BFCs) have been used for the radiolabeling of biomolecules, including antibodies and small peptides (*2, 6, 8*−*17*). While the ^{90}Y-labeled BFC−BM conjugate is used for tumor therapy, the ^{111}In-labeled BFC−BM conjugate is often used as an imageable surrogate for dosimetry determination and therapy monitoring (*17, 18*−*27*). The advantage of using ^{111}In as the imaging surrogate for ^{90}Y is that $^{111}InCl_3$ is commercially available and its half-life is almost identical to that of ^{90}Y. However, recent studies show biodistribution differences between ^{90}Y- and ^{111}In-labeled antibodies and small peptides (*17, 28*−*30*). The difference in biological properties raises some questions about structural differences between ^{90}Y and ^{111}In DOTA chelates.

To study solution structures of ^{90}Y- and ^{111}In-labeled DOTA−BM conjugates, we prepared yttrium and indium complexes (Figure 1) of two model compounds: 1,4,7,10-tetraaza-4,7,10-tris(carboxymethyl)-1-cyclododecylacetyl-benzylamine (DOTA-BA) and 1,4,7,10-tetraaza-4,7,10-tris(carboxymethyl)-1-cyclododecylacetyl-*R*-(+)-α-methylbenzylamine (DOTA-MBA). In this report, we present the synthesis and characterization of yttrium and indium complexes of DOTA-BA and DOTA-MBA at both tracer and macroscopic levels. The focus of this study is to compare yttrium complexes of DOTA-BA and DOTA-MBS with their corresponding indium analogues with respect to their structures in solution, hydrophilicity, and solution dynamics.

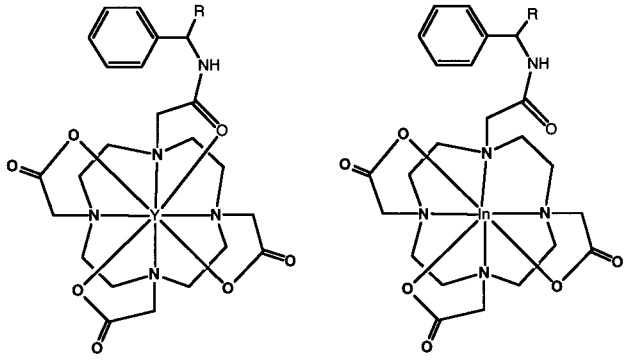


Figure 1. Structures for yttrium and indium complexes of DOTA-BA and DOTA-MBA.

EXPERIMENTAL SECTION

Materials. Acetic acid (ultrapure), ammonium hydroxide (ultrapure), benzylamine, bromoacetyl bromide, chloroacetyl chloride, *R*-(+)-α-methylbenzylamine, and sodium gentisate were purchased from either Aldrich or

* To whom correspondence should be addressed. Tel: 978-671-8696 (S.L.); FAX: 978-436-7500. E-mail: shuang.liu@bms.com.

† Formerly DuPont Pharmaceuticals Company.

10.1021/bc010134h CCC: $22.00 © 2002 American Chemical Society
Published on Web 06/27/2002

Sigma Chemical Co. and were used as received. The tributyl ester of 1,4,7,10-tetraazacyclododecane-1,4,7-triacetic acid (DO3A(OBu-t)$_3$) was purchased from Macrocyclics Inc, Richardson, TX. $^{111}InCl_3$ and $^{90}YCl_3$ (in 0.05 N HCl) was purchased from NEN Life Sciences, N. Billerica, MA.

NMR (^1H, ^{13}C, $^1H-^1H$ COSY, and $^1H-^{13}C$ HMQC) data were obtained using a Bruker DRX 600 MHz FT NMR spectrometer, and chemical shifts as δ are reported in ppm relative to TMS. The LC-MS data were collected using a HP1100 LC/MSD system with an API-electrospray interface. The LC-MS method used a Zorbax C_{18} column (4.6 mm × 150 mm, 3.5 μm particle size) and a mobile phase gradient starting from 100% solvent A (95% water and 5% TFA) to 100% solvent B (95% acetonitrile and 5% water) at 16 min at a flow rate of 1 mL/min.

The HPLC method 1 used a HP-1050 HPLC system with a Rainin Dynamax UV/visible detector (model UV-C, λ = 230 nm) and a Zorbax C_{18} column (4.6 mm × 250 mm, 80 Å pore size). The flow rate was 1 mL/min with the mobile phase starting 10% of solvent A (0.1% TFA in water) and 90% solvent B (0.1% TFA in acetonitrile) to 20% solvent A and 80% of solvent B at 20 min, followed by an isocratic wash using 40% of solvent A and 60% solvent B from 21 to 26 min.

The HPLC method 2 used a HP-1050 HPLC system with a Rainin Dynamax UV/visible detector (model UV-C, λ = 230 nm) and a Zorbax C_{18} column (4.6 mm × 250 mm, 80 Å pore size). The flow rate was 1 mL/min with the mobile phase starting 30% of solvent A (0.1% TFA in water) and 70% solvent B (0.1% TFA in acetonitrile) to 40% solvent A and 60% of solvent B at 20 min, followed by an isocratic wash using 40% of solvent A and 60% solvent B from 21 to 26 min.

The HPLC method 3 used a HP-1100 HPLC system with a UV/visible detector (λ = 230 nm), an IN−US radiodetector, and a Zorbax C_{18} column (4.6 mm × 250 mm, 80 Å pore size). The flow rate was 1 mL/min with a gradient mobile phase starting 95% of solvent A (0.025 M ammonium acetate buffer, pH 6.8) and 5% solvent B (acetonitrile) to 8% solvent A and 92% of solvent B at 18 min, followed by an isocratic wash using 40% of solvent A and 60% solvent B from 19 to 25 min.

Synthesis of *N*-(Chloroacetyl)benzylamine. To solution of benzylamine (2.15 g, 0.02 mol) in chloroform (100 mL) was added chloroacetyl chloride (2.26 g, 0.02 mol) in an ice-bath, followed by slow addition of 3 mL of triethylamine. The resulting mixture was stirred at room-temperature overnight and was then heated to reflux for 2 h. Solvent and excess triethylamine were removed under reduced pressure. The residue was dissolved in 100 mL of chloroform and washed with water (2 × 50 mL). The organic layer was separated and dried over anhydrous sodium sulfate. Removal of chloroform gave a pale yellow waxy solid. Upon addition of a mixture of water and methanol (10:1 = water:methanol), it became a white solid. The solid was collected and dried under vacuum overnight. The yield was 2.5 g (69%). LC-MS: m/z = 184.0 for $[C_9H_{10}ClNO]^+$. ^1H NMR (600 MHz, in $CDCl_3$, chemical shift in ppm relative to TMS): 4.08 (s, 2H, CH_2); 4.54 (d, 2H, CH_2Ph); 6.97 (bs, 1H, NH); and 7.20−7.85 (m, 5H, benzene).

Synthesis of 1,4,7,10-Tetraaza-4,7,10-tris(carboxymethyl)-1-cyclododecyl-acetylbenzylamine (DOTA-BA). To a solution of DO3A(OBu-t)$_3$ (193 mg, 0.375 mmol) in anhydrous acetonitrile (45 mL) was added *N*-(chloroacetyl)benzylamine (195 mg, 1.06 mmol). The resulting mixture was stirred at room temperature for 3 days, and was then heated to reflux for 6 h. Solvents were removed under reduced pressure to give a gummy liquid, which was dissolved in chloroform (50 mL), washed with water, and dried over anhydrous sodium sulfate. Removal of chloroform gave a gummy liquid. To the residue were added dichloromethane (15 mL) and anhydrous TFA (15 mL). The mixture was stirred at room-temperature overnight. Solvents were removed under reduced pressure. The residue was dissolved in concentrated HCl (1.0 mL). Upon addition of acetone (100 mL), a white solid was formed. The solid was collected by filtration, washed with acetone and dried in air. The crude product (150 mg) was dissolved in 1.0 mL of water and was then purified by HPLC (method 1). The fraction at 10−12.5 min was collected. The collected fractions were combined and then lyophilized. The yield was 53 mg. The retention time was 12.5 min with the purity > 98% by HPLC (method 1). LC-MS: m/z = 494.2 for $[C_{23}H_{36}N_5O_7]^+$. ^1H NMR (600 MHz, in D_2O at 40 °C): 3.36−3.46 (m, 16H, CH_2, cyclen); 3.85−3.91 (m, 8H, CH_2Ph); and 7.46−7.56 (m, 5H, benzene).

Synthesis of *N*-(Bromoacetyl)-*R*-(+)-α-Methylbenzylamine. To solution of *R*-(+)-α-methylbenzylamine (2.4 g, 0.02 mol) in chloroform (150 mL) cooled in an ice-bath was added bromoacetyl bromide (4.1 g, 0.02 mol), followed by slow addition of 5 mL of triethylamine. The resulting mixture was stirred at room-temperature overnight. Solvent and excess triethylamine were removed under reduced pressure to give a white solid, which was washed with water and then a mixture of water and methanol (10:1 = water:methanol). The solid was collected and dried under vacuum overnight. The yield was 3.5 g (~73%). LC-MS: m/z = 242.0 for $[C_{10}H_{12}BrNO]^+$. ^1H NMR (600 MHz, in $CDCl_3$): 1.60 (d, 3H, CH_3); 3.85 (q, 2H, CH_2); 5.20 (q, 1H, CH); and 7.20−7.50 (m, 5H, benzene).

Synthesis of 1,4,7,10-Tetraaza-4,7,10-tris(carboxymethyl)-1-cyclododecyl-acetyl-(*R*-(+)-α-methylbenzylamine) (DOTA-MBA). To a solution of DO3A(OBu-t)$_3$ (193 mg, 0.375 mmol) in anhydrous acetonitrile (45 mL) was added *N*-(bromoacetyl)-*R*-(+)-α-methylbenzylamine (103 mg, 0.430 mmol). The resulting mixture was heated to reflux overnight. Solvents were removed under reduced pressure to give a gummy liquid, which was taken up with chloroform (50 mL), washed with water, and dried over anhydrous sodium sulfate. Removal of chloroform gave a liquid residue, to which were added dichloromethane (15 mL) and anhydrous TFA (15 mL). The mixture was stirred at room-temperature overnight. Solvents were removed under reduced pressure. The residue was dissolved in concentrated HCl (1.0 mL). Upon addition of acetone (100 mL), a white solid was formed. The solid was collected by filtration, washed with acetone, and dried in air. The crude product (185 mg) was dissolved in 1.0 mL of water and was then purified by HPLC (method 1). The fraction at 18−20 min was collected. The collected fractions were combined and then lyophilized. The yield was 65 mg. The retention time was 18.5 min with the purity > 98% by HPLC (method 1). LC-MS: m/z = 508.3 for $[C_{24}H_{38}N_5O_7]^+$. ^1H NMR (600 MHz, in D_2O at 40 °C): 1.38 (d, 3H, CH_3); 2.80−3.9 (m, 24H, CH_2, cyclen and acetate); 4.88 (q, H, CHPh); and 7.20−7.35 (m, 5H, benzene).

Synthesis of Y(DOTA-BA). To a 5 mL vial were added DOTA-BA (40 mg, 0.081 mmol) and $Y(NO_3)_3{\cdot}6H_2O$ (60 mg, 0.157 mmol), followed by addition of 0.5 mL of 0.5 N ammonium citrate buffer (pH = 4.8) and 0.5 mL of 0.5 N ammonium acetate buffer (pH = 7.5). The mixture was heated at 100 °C for 20 min. After being cooled to room temperature, the product was separated by HPLC

(method 2). The fraction at 10.0−13.0 min was collected. Lyophilization of collected fractions gave a white powder. The yield was 27 mg. The purity was > 98% by HPLC (method 3). LC-MS: m/z = 580.3 for $[M + H]^+$ ($[C_{23}H_{36}N_5O_7Y]^+$) and 290.7 for $[M + 2H]^{2+}$.

Synthesis of Y(DOTA-MBA). To a 5 mL vial were added DOTA-MBA (56 mg, 0.110 mmol) and $Y(NO_3)_3 \cdot 6H_2O$ (70 mg, 0.183 mmol). To the mixture were added 0.5 mL of 0.5 N ammonium citrate buffer (pH = 4.8) and 0.5 mL of 0.5 N ammonium acetate buffer (pH = 7.5). The resulting solution was heated at 100 °C for 20 min. After being cooled to room temperature, the product was purified by HPLC (method 2). The fraction at 12−15 min was collected, and the collected fractions were evaporated to dryness. The residue was dissolved in water (20 mL), and the resulting solution was lyophilized to give a white powder. The yield was ∼35 mg. The purity was > 98% by HPLC (method 3). LC-MS: m/z = 594.2 for $[M + H]^+$ ($[C_{24}H_{35}N_5O_7Y]^+$) and 297.7 for $[M + 2H]^{2+}$.

Synthesis of In(DOTA-BA). To a 5 mL vial were added DOTA-BA (50 mg, 0.081 mmol) and anhydrous $InCl_3$ (30 mg, 0.157 mmol), followed by addition of 0.5 mL of 0.5 N ammonium citrate buffer (pH = 4.8) and 0.5 mL of 0.5 N ammonium acetate buffer (pH = 7.5). The mixture was heated at 100 °C for 30 min. After being cooled to room temperature, the product was separated by HPLC (Method 2). The fraction at 10.0−13.0 min was collected. Lyophilization of collected fractions gave a white powder. The yield was 37 mg. The purity > 98% by HPLC (method 3). LC-MS: m/z = 606.3 for $[M + H]^+$ ($[C_{23}H_{36}N_5O_7In]^+$) and 303.7 for $[M + 2H]^{2+}$.

Synthesis of In(DOTA-MBA). To a 5 mL vial were added DOTA-MBA (56 mg, 0.110 mmol) and anhydrous $InCl_3$ (50 mg, 0.183 mmol). To the mixture were added 0.5 mL of 0.5 N ammonium citrate buffer (pH = 4.8) and 0.5 mL of 0.5 N ammonium acetate buffer (pH = 7.5). The resulting solution was heated at 100 °C for 30 min. After being cooled to room temperature, the product was purified by HPLC (method 2). The fraction at 12−15 min was collected, and the collected fractions were evaporated to dryness. The residue was dissolved in water (20 mL), and the resulting solution was lyophilized to give a white powder. The yield was ∼40 mg. The purity was > 99% by HPLC (method 3). LC-MS: m/z = 620.2 for $[M + H]^+$ ($[C_{24}H_{35}N_5O_7In]^+$) and 310.6 for $[M + 2H]^{2+}$.

Synthesis of ^{90}Y(DOTA-MBA) and ^{90}Y(DOTA-BA). To a clean sealed 5 mL glass vial were added 1.0 mL of the DOTA-BA or DOTA-MBA solution (50 μg/mL in 0.5 M ammonium acetate buffer, pH 6.0) and 20−30 μL of $^{90}YCl_3$ solution (20 mCi) in 0.05 N HCl. The resulting mixture was heated at 100 °C for 30 min. After being cooled to room temperature, a sample of the resulting solution was first diluted 20−40-fold with 2.0 mM DTPA solution (pH = 5.0) and was then analyzed by radio-HPLC (method 3; injection volume = 5 μL). For the ITLC, a sample of the resulting solution was used without further dilution. The ITLC method used Gelman silica gel paper strips and a 1:1 (v:v) mixture of acetone and saline as eluant. Using this method, both ^{90}Y(DOTA-MBA) and ^{90}Y(DOTA-BA) migrate to the solvent front while ^{90}Y-colloid and unchelated free ^{90}Y remain at the origin.

Synthesis of ^{111}In(DOTA-BA) and ^{111}In(DOTA-MBA). To a sealed 5 mL vial were added 1.0 mL of the DOTA-BA or DOTA-MBA solution (200 μg/mL in 0.5 M ammonium acetate buffer, pH 6.0) and 100 μL of $^{111}InCl_3$ solution (5 mCi) in 0.05 N HCl. The resulting mixture was heated at 100 °C for 30 min. After being cooled to room temperature, a sample of the resulting solution was analyzed by radio-HPLC (method 3) and ITLC. The ITLC method for ^{111}In(DOTA-BA) and ^{111}In(DOTA-MBA) is the same as that for ^{90}Y(DOTA-BA) and ^{90}Y(DOTA-MBA). Using this method, ^{111}In(DOTA-BA) and ^{111}In(DOTA-MBA) migrate to the solvent front while ^{111}In-colloid and unchelated free ^{111}In remain at the origin.

RESULTS

Synthesis of DOTA-BA and DOTA-MBA. The tributyl ester of DOTA-BA was prepared from the reaction of *N*-(2-chloroacetyl)benzylamine with DO3A(OBu-t)$_3$ in the presence of excess triethylamine. Hydrolysis of the tributyl ester of DOTA-BA in a mixture of anhydrous TFA and dichloromethane produced DOTA-BA as its TFA salt. The crude product was purified by HPLC. Lyophilization of collected fractions afforded DOTA-BA in high purity (>98%). DOTA-MBA was prepared in a similar fashion from the reaction of *N*-(bromoacetyl)-α-methylbenzylamine with DO3A(OBu-t)$_3$. Purification by HPLC and lyophilization of collected fractions gave DOTA-MBA with purity > 98%. Both DOTA-BA and DOTA-MBA have been characterized by HPLC, NMR, and LC-MS methods. It is important to note that DOTA-BA and DOTA-MBA have to be extremely pure for the preparation of their ^{90}Y and ^{111}In complexes. Otherwise, it would be very difficult to distinguish radioimpurities from possible isomers of ^{90}Y and ^{111}In complexes of DOTA-BA and DOTA-MBA in their radio-HPLC chromatograms.

Synthesis of M(L) (M = Y and In; L = DOTA-BA and DOTA-MBA). We prepared yttrium and indium complexes M(L) (M = Y and In; L = DOTA-BA and DOTA-MBA) by reacting DOTA-BA and DOTA-MBA, respectively, with excess yttrium(III) nitrate hexahydrate or indium(III) chloride in ammonium acetate buffer (0.5 M, pH ∼ 6) in the presence of ammonium citrate, which was used to prevent metal hydroxide formation. The product was separated from the reaction mixture by HPLC purification. Many attempts were made to grow crystals for these complexes using various solvents or solvent combinations, but were unsuccessful. In(DOTA-MBA) tends to give long needlelike microcrystals, which are unsuitable for X-ray diffraction studies. All four complexes, M(L) (M = Y and In; L = DOTA-BA and DOTA-MBA), have been characterized by HPLC, LC-MS, and NMR (^{1}H and ^{13}C).

Synthesis of M(L) (M = ^{90}Y and ^{111}In; L = DOTA-BA and DOTA-MBA). ^{90}Y and ^{111}In complexes of DOTA-MBA and DOTA-BA were prepared by reacting DOTA-BA and DOTA-MBA, respectively, with MCl_3 (M = ^{90}Y and ^{111}In) and in ammonium acetate buffer (pH = 6.0) at 100 °C for 30 min. We typically used 50 μg of DOTA-BA or DOTA-MBA for 20 mCi of $^{90}YCl_3$ and 100 μg of DOTA-BA or DOTA-MBA for 5.0 mCi of $^{111}InCl_3$. The use of excess DOTA-conjugate is to compensate for the presence of other trace metal contaminants in the reaction mixture and to achieve the high-yield radiolabeling. ^{90}Y(DOTA-BA), ^{90}Y(DOTA-MBA), and ^{111}In(DOTA-MBA) can be prepared in high yield with the radiochemical purity of > 98% while ^{111}In(DOTA-BA) was prepared with the RCP of ∼90% under similar radiolabeling conditions. [^{90}Y]- and [^{111}In]-colloid were usually minimal (<1%).

HPLC Characterization. We used a reverse phase HPLC method to analyze complexes M(L) (M = ^{90}Y/Y and ^{111}In/In; L = DOTA-BA and DOTA-MBA). The HPLC data for M(L) (M = ^{90}Y/Y and ^{111}In/In; L = DOTA-BA and DOTA-MBA) are listed in Table 1. Figures 2 shows typical radio-HPLC chromatograms for ^{90}Y(DOTA-MBA) and ^{111}In(DOTA-MBA). In general, all four complexes,

Table 1. HPLC Data for M(L) (M = ^{90}Y/Y and ^{111}In/Y; L = DOTA-BA and DOTA-MBA)

compound	RCP (%)[a]	retention time (min)
^{90}Y(DOTA-BA)	>99.0	11.2
Y(DOTA-BA)	>99.0	10.5
^{90}Y(DOTA-MBA)	>99.5	17.3
Y(DOTA-MBA)	>99.0	16.5
^{111}In(DOTA-BA)	~90	7.5
In(DOTA-BA)	>99.0	6.7
^{111}In(DOTA-MBA)	>98.5	11.4
In(DOTA-MBA)	>98.5	10.5

[a] Radiochemical purity in percentage.

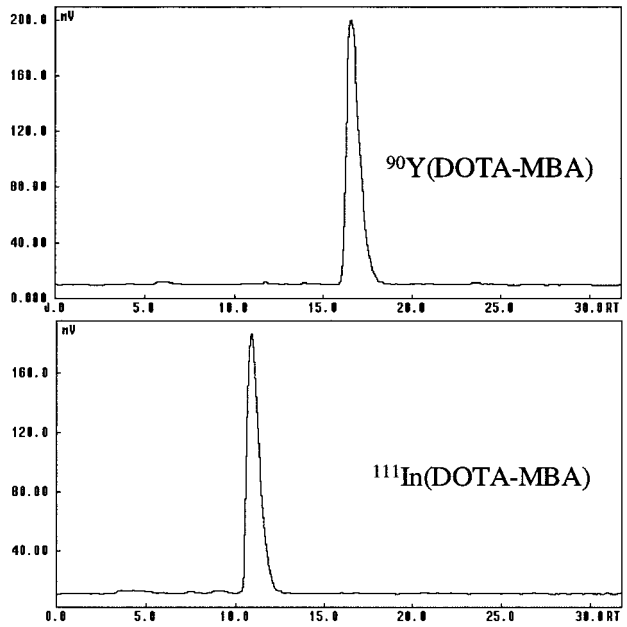


Figure 2. Typical radio-HPLC chromatograms (method 3) of ^{90}Y(DOTA-MBA) (top) and ^{90}Y(DOTA-BA) (bottom).

M(L) (M = ^{90}Y and ^{111}In; L = DOTA-BA and DOTA-MBA), show only one radiometric peak in the region of interest. There are some small peaks due to radioimpurities in their HPLC chromatograms (Figure 2). Since each radioimpurity is less than 0.5%, no further characterization was performed. HPLC retention times of M(DOTA-BA) (M = ^{90}Y and ^{111}In) are ~5 min shorter that those of M(DOTA-MBA) (M = ^{90}Y and ^{111}In) under the same chromatographic conditions, indicating their difference in lipophilicity due to the presence of the extra methyl group. HPLC retention times of M(L) (M = ^{111}In and In; L = DOTA-BA and DOTA-MBA) are 4−6 min shorter than those of M(L) (M = ^{90}Y and Y; L = DOTA-BA and DOTA-MBA). The HPLC concordance experiments for M(DOTA-MBA) (M = ^{90}Y/Y and ^{111}In/In; L = DOTA-BA and DOTA-MBA) showed that the same complex was prepared at both tracer and macroscopic levels.

^{1}H NMR Spectra of M(L) (M = Y and In; L = DOTA-BA and DOTA-MBA). Figure 3 shows the room temperature ^{1}H NMR spectra of Y(DOTA-MBA) (top) and Y(DOTA-BA) (bottom) in a mixture of 90% D_2O and 10% H_2O. In the ^{1}H NMR spectrum of Y(DOTA-MBA), there is only one doublet at ~1.5 ppm from hydrogens of the methyl group and one multiplet at 4.9 ppm from methylene hydrogen of the benzyl group. In the spectrum of Y(DOTA-BA), the two methylene hydrogens of the benzyl group are inequivalent and give an AB quartet at ~4.5 ppm. The hydrogens of the methylene group of each acetate or acetamide chelating arm are also inequivalent and give four sets of AB quartets in the region of 2.0−4.0 ppm. Each hydrogen atom in Y(DOTA-MBA) has its distinctive resonance signal. For both Y(DOTA-MBA) and Y(DOTA-BA), there are several superimposed AA′BB′ resonance signals from ethylenic hydrogens of the macrocyclic ring. NMR signals at ~9.40 ppm are from the amide-hydrogen. The coupling between the amide-hydrogen and methylene hydrogen(s) of the benzyl group is obvious. A close look at the ^{1}H NMR spectrum of Y(DOTA-MBA) shows that there are some small satellite peaks on the right or left side of each resonance, but these peaks are so small that they are barely detectable.

At temperatures <25 °C, all the aliphatic resonance signals from Y(DOTA-BA) become sharper; but no extra signals are seen. For Y(DOTA-MBA), however, the small satellite peaks are more visible, integration of which remains difficult due to partial overlapping. At elevated temperatures (30−85 °C), a general broadening of resonance signals was observed. For Y(DOTA-BA), all the resonance signals in the aliphatic region start to collapse almost simultaneously at temperatures above 35 °C (Figure 4). For Y(DOTA-MBA), however, the AB quartets from methylene hydrogens of the benzyl group and of the acetate or acetamide chelating arm start to collapse at temperatures above 50 °C while resonance signals from hydrogens of the cyclen backbone remain relatively unchanged (Figure 5).

Figures 6 and 7 show variable temperature ^{1}H NMR spectra of In(DOTA-BA) and In(DOTA-MBA), respectively, in a mixture of 90% D_2O and 10% H_2O. At room temperature, all resonance signals from In(DOTA-BA) and In(DOTA-MBA) are broad. As the temperature increases, these resonance signals become sharper until the high-temperature limiting spectrum is reached. At 85 °C, the spectrum of In(DOTA-BA) shows a singlet at 4.47 ppm from the methylene hydrogens of the benzyl group, and two singlets at 3.37 and 3.64 ppm (Figure 6) from methylene hydrogens of the acetamide and those of the acetate chelating arm, respectively. The methylene hydrogens of the remaining two acetate chelating arms, however, are inequivalent and give two doublets at 3.06 and 3.31 ppm, respectively. The ethylenic hydrogens in In(DOTA-BA) show only two pairs of overlapped AA′BB′ NMR patterns (Figure 6). Unlike In(DOTA-BA), In(DOTA-MBA) is not symmetrical due to the presence of the extra methyl group. Each hydrogen in In(DOTA-MBA) has its distinctive signal (Figure 7). For example, there is a doublet at 1.51 ppm due to hydrogens of the methyl group and a quartet at 5.02 ppm from the benzyl group. The methylene hydrogens of the acetamide group and three acetate chelating arms are inequivalent and appear as four distinctive sets of quartets. The coupling between the amide-hydrogen and methylene hydrogen(s) of the benzyl group remains obvious even though the NMR signals at ~9.40 ppm from the amide-hydrogen almost disappear at ~85 °C.

^{13}C NMR Spectra of M(L) (M = Y and In; L = DOTA-BA and DOTA-MBA). Figures 8 and 9 show the room temperature ^{13}C NMR spectra of Y(DOTA-BA) and Y(DOTA-MBA), respectively. For Y(DOTA-BA), ^{13}C NMR signals from benzyl, acetamide, or acetate groups are clearly distinguishable from one another while those from the cyclen backbone are partially superimposed. For Y(DOTA-MBA), however, most aliphatic carbon atoms are distinctive, giving a total of 13 resonance signals from 14 different aliphatic carbons. In all the cases, detailed assignments are difficult for ^{13}C NMR signals from the macrocyclic cyclen backbone. Figures 10 and 11 show VT ^{13}C NMR spectra of In(DOTA-BA) and In(DOTA-MBA), respectively. Most ^{13}C resonance signals from In(DOTA-

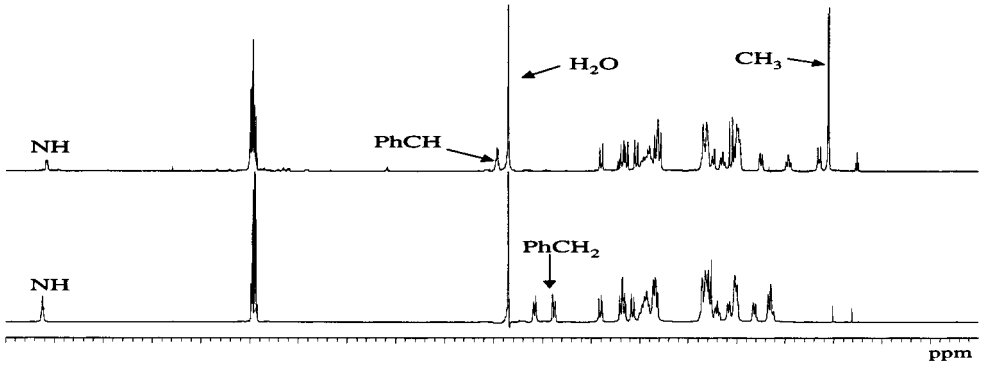


Figure 3. Room temperature ^{1}H NMR (600 MHz) spectra of Y(DOTA-MBA) (top) and Y(DOTA-BA) (bottom) in D_2O/H_2O (90%/10%).

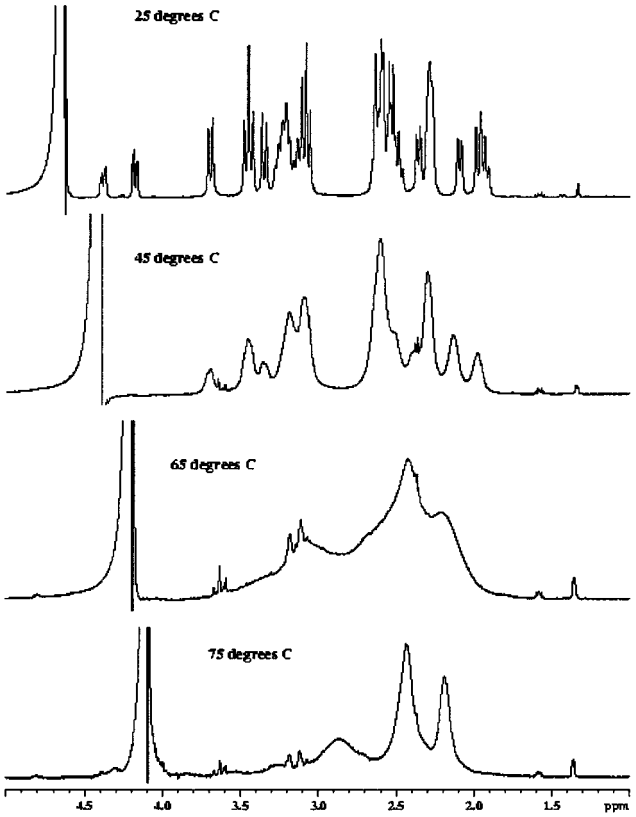


Figure 4. VT ^{1}H NMR (600 MHz) spectrum of Y(DOTA-BA) in the aliphatic region.

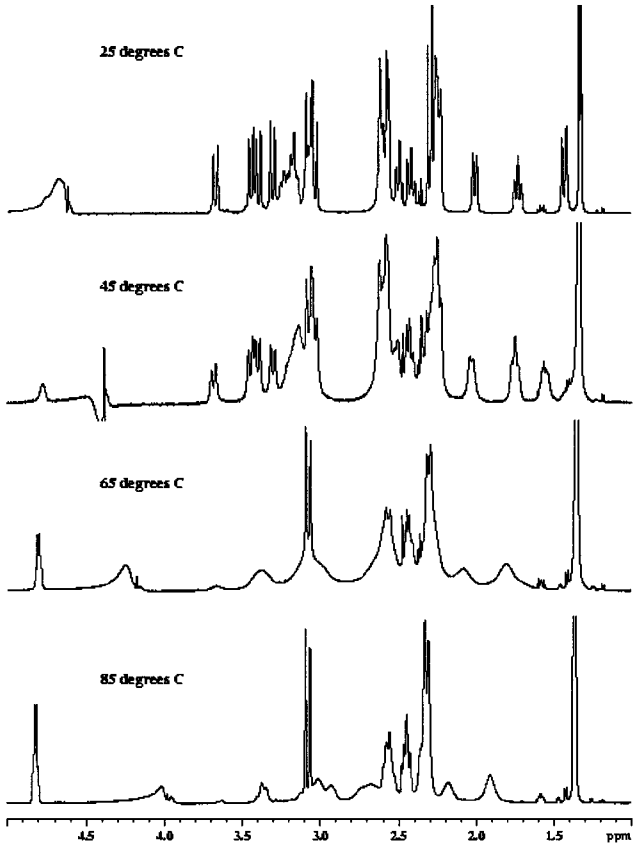


Figure 5. VT ^{1}H NMR (600 MHz) spectrum of Y(DOTA-MBA) in the aliphatic region.

BA) and In(DOTA-MBA) are not seen until the temperature is higher than 65 °C. As the temperature increases, all ^{13}C signals become sharper.

DISCUSSION

We are interested in radiolabeled vitronectin receptor antagonists as potential diagnostic or therapeutic radiopharmaceuticals by targeting tumor angiogenesis (*31*−*35*). Recently, we reported the ^{90}Y-labeling of a DOTA-conjugated vitronectin receptor antagonist. In a separate communication (*36*), we also described the anaerobic ^{90}Y-labeling of a DOTA-conjugated nonpeptide vitronectin receptor antagonist. In both cases, the ^{90}Y-labeled DOTA-conjugates show only one radiometric peak in their radio-HPLC chromatograms (*34, 36*). During these radiolabeling studies, we also noticed that the ^{90}Y-labeled DOTA-conjugates often have different HPLC retention times from those of the corresponding ^{111}In analogues.

Structural Differences between Yttrium and Indium Complexes M(L) (M = Y and In; L = DOTA-BA and DOTA-MBA) in Solution. Yttrium has an ionic radius of 0.87 Å (*37*) and is often treated as a "pseudo-lanthanide" metal due to its similarity to lanthanide metals with respect to the cationic charge, ionic radii, and coordination chemistry. Because of its large size, the coordination number for Y(III) is normally 8 or 9 (*6, 38*). The solution structure of yttrium and lanthanide complexes of DOTA derivatives has been studied by NMR methods (*39*−*50*). Indium is a group 13 element and has an ionic radius of 0.75 Å (*37*). The coordination number of indium is typically 6 or 7 (*51*−*55*). Only a few eight-coordinate indium complexes are known (*56*−*58*).

Recently, Mäcke and co-workers (*17, 58*) described the crystal structures of complexes M(DOTA-D-Phe-NH_2) (M = Y and In) and found that both In and Y in these M(DOTA-D-Phe-NH_2) are eight-coordinated with four

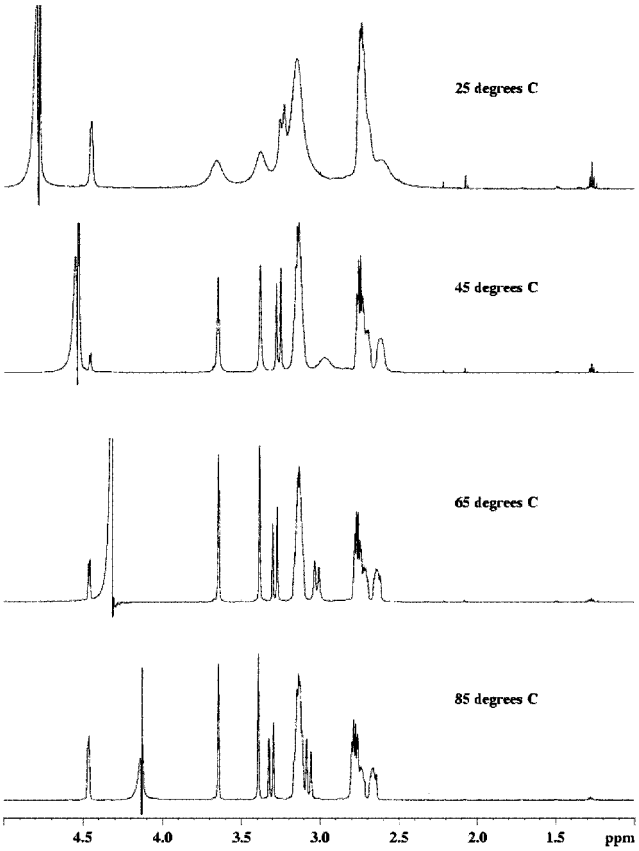


Figure 6. VT ^{1}H NMR (600 MHz) spectrum of In(DOTA-BA) in the aliphatic region.

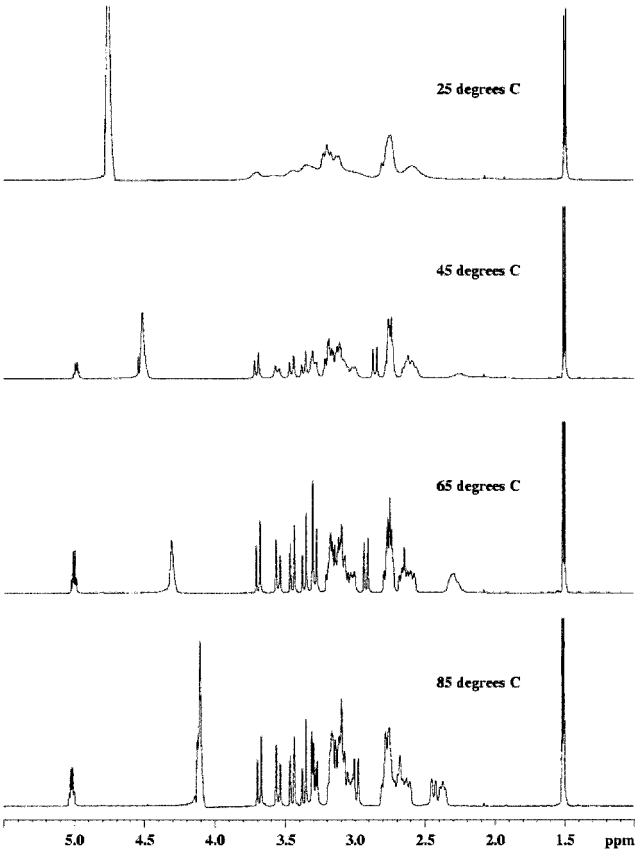


Figure 7. VT ^{1}H NMR (600 MHz) spectrum of In(DOTA-BA) in the aliphatic region.

amine-nitrogen, one carbonyl-oxygen, and three carboxylate-oxygen atoms bonding to the metal center (*17*). The major difference between the two structures arises from a different conformation of the ethylenic bridges and the different orientation of sidearms, leading to two pairs of isomers. The complex Y(DOTA-D-Phe-NH_2) exists in solid state as the m isomer (traditionally designated as the minor isomer) while the complex In(DOTA-D-Phe-NH_2) is observed as the M (major isomer) isomer.

It should be noted that the solution structure of a metal chelate might be different from that in the solid state because of possible dissociation of certain donor atom(s). In some cases, the isomers observed in the solid state may not be seen in solution due to rapid interconversion of different isomers or fluxionality of the ligand framework. On other occasions, only one isomeric form is found in the solid state while more isomers are observed in solution. Thus, it is imperative to study the solution structure of the metal chelate in order to understand the impact of structural differences in metal chelates on biological properties of ^{90}Y- and ^{111}In-labeled DOTA−BM conjugates.

To study the structural differences between ^{90}Y- and ^{111}In-labeled DOTA−BM conjugates in solution, we prepared yttrium and indium complexes of two model compounds: DOTA-BA and DOTA-MBA. We use the same HPLC method to characterize these complexes at both tracer (^{90}Y and ^{111}In) and macroscopic (Y and In) levels. Table 1 list the HPLC retention times of M(L) (M = ^{90}Y/Y and ^{111}In/In; L = DOTA-BA and DOTA-MBA). Since the only difference in In(DOTA-BA) and In(DOTA-MBA) and their yttrium analogues is the metal ion, the difference in HPLC retention times strongly suggests that indium and yttrium do not share the same coordination sphere even though they are coordinated by the same

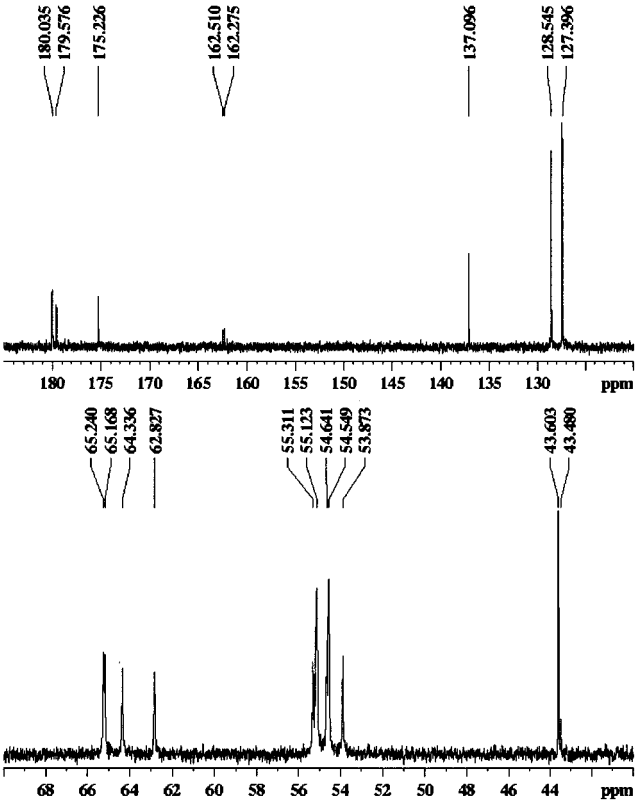


Figure 8. Proton-decoupled ^{13}C NMR spectra of Y(DOTA-BA) in D_2O/H_2O (90%/10%). The signals at 162 ppm are from residual TFA in the sample.

DOTA-conjugate. Since indium is smaller than yttrium, it is possible for the carbonyl-oxygen in complexes M(L)

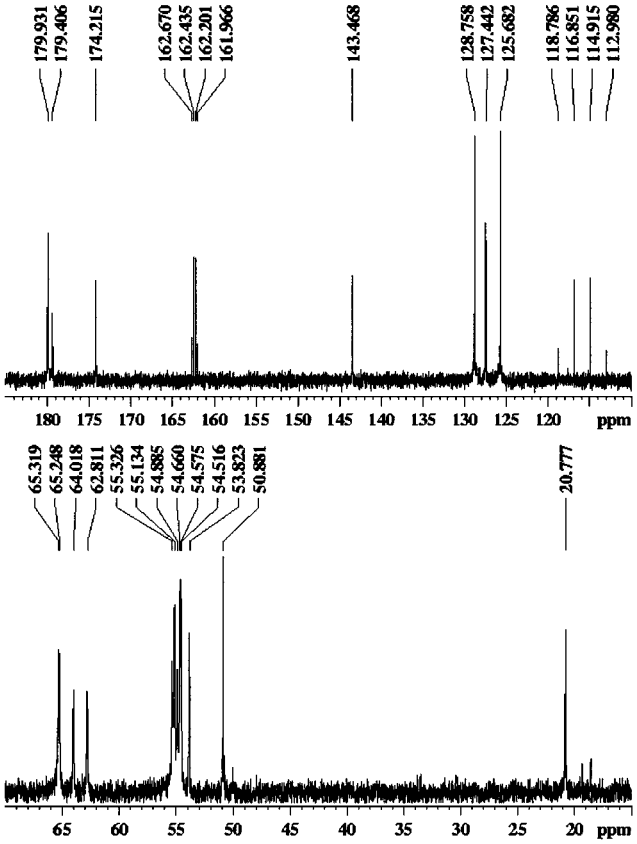


Figure 9. Proton-decoupled ^{13}C NMR spectra of Y(DOTA-MBA) in D_2O/H_2O (90%/10%). The signals at 162 ppm are from residual TFA in the sample.

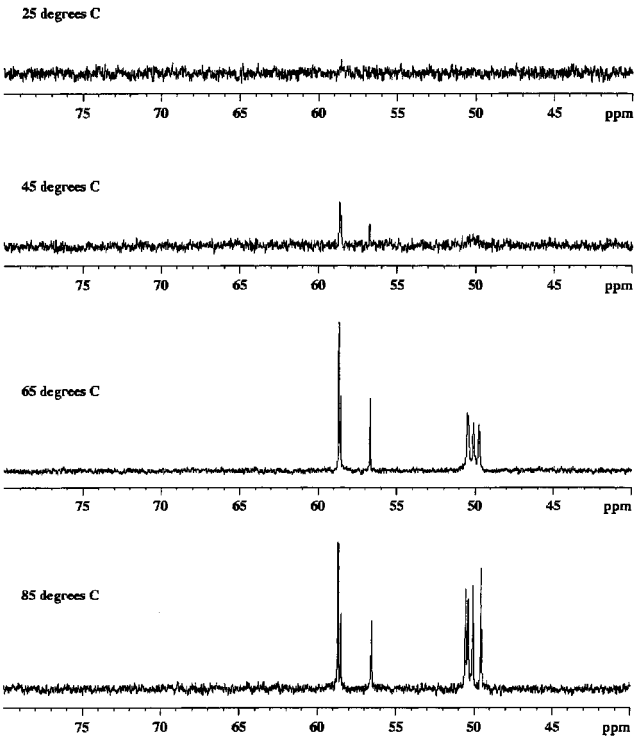


Figure 10. VT ^{13}C NMR spectra of In(DOTA-BA) in D_2O/H_2O (90%/10%). The signals at 116 and 162 ppm are from residual TFA in the sample.

(M = ^{111}In/In; L = DOTA-BA and DOTA-MBA) to become dissociated (Figure 12) due to the poor fit between the chelator cavity and metal ion size, even though both In and Y in M(DOTA-D-Phe-NH_2) are eight-coordinated in

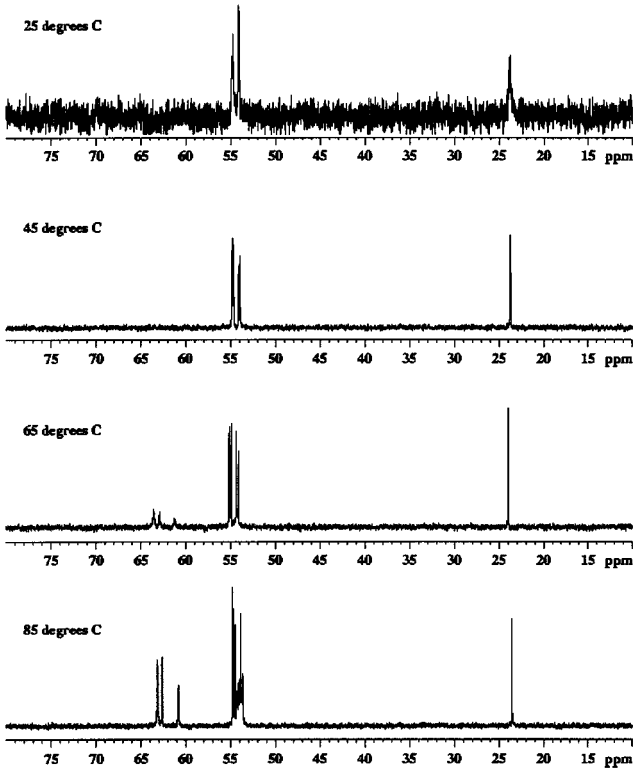


Figure 11. VT ^{13}C NMR spectra of In(DOTA-MBA) in D_2O/H_2O (90%/10%). The signals at 116 and 162 ppm are from residual TFA in the sample.

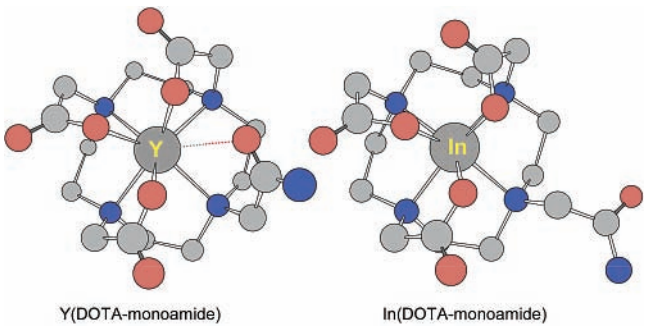


Figure 12. Possible solution structures of Y(DOTA-monoamide) and In(DOTA-monoamide).

the solid state (*58*). The presence of the uncoordinated carbonyl-oxygen in In(DOTA-BA) and In(DOTA-MBA) makes them more hydrophilic with shorter retention times than those of Y(DOTA-BA) and Y(DOTA-MBA). If indium and yttrium were to share the same coordination sphere, In(DOTA-BA) and In(DOTA-MBA) should have had the same retention times as those of Y(DOTA-BA) and Y(DOTA-MBA) under identical chromatographic conditions.

The structural difference between indium and yttrium complexes of DOTA-BA and DOTA-MBA is also reflected by their different solution dynamics. For example, the coordinated DOTA-BA in Y(DOTA-BA) (Figure 12) is rigid at room temperature. The rotation of the acetamide and acetate chelating arms and inversion of ethylenic groups are relatively slow at the NMR time-scale. The ^1H NMR data of Y(DOTA-BA) show four sets of AB quartets in the region of 2.0−4.0 ppm (Figure 3), corresponding to four pairs of hydrogens from the benzyl group, the acetamide group, and three acetate chelating arms. Y(DOTA-BA) becomes fluxional only at elevated temperatures (>45 °C). For In(DOTA-BA) (Figure 12),

however, the presence of the free carbonyl-oxygen makes DOTA-BA much more flexible. Rotation of the acetamide group and acetate chelating arms and inversion of ethylenic groups are relatively fast at the NMR time-scale. Therefore, ^{1}H NMR spectra of both In(DOTA-BA) and In(DOTA-MBA) show broad resonance signals at the room temperature (Figures 6 and 7). This also explains why most ^{13}C resonance signals of In(DOTA-BA) and In(DOTA-MBA) are not seen until the temperature is higher than 65 °C (Figures 10 and 11). If indium and yttrium were to share the same coordination geometry, In(DOTA-BA) and In(DOTA-MBA) should have had a much tighter coordination sphere and should have been more rigid than their yttrium analogues, Y(DOTA-BA) and Y(DOTA-MBA), due to the smaller size of indium.

The rotation of the acetamide and acetate chelating arms and inversion of ethylenic groups make In(DOTA-BA) to become symmetrical. As a result, methylene hydrogens from the acetamide group and those from the opposite acetate chelating arm become equivalent and show two singlets at 3.37 and 3.64 ppm, respectively, in the ^{1}H NMR spectrum of In(DOTA-BA) (Figure 6). However, methylene hydrogens of the remaining two acetate chelating arms remain inequivalent and give two doublets at 3.06 and 3.31 ppm. For In(DOTA-MBA), rotation of the acetamide group and acetate chelating arms and inversion of ethylenic groups do not change the symmetry of the molecule due to the presence of the extra methyl group. All aliphatic hydrogens are distinctive from each other, resulting in four sets of AB quartets for hydrogens from the acetamide group and those from three acetate chelating arms (Figure 6).

Isomerism in M(L) (M = ^{90}Y and Y; L = DOTA-BA and DOTA-MBA). Radio-HPLC is a powerful tool for separation of different diastereomers of radiolabeled compounds. In this study, we used a reverse phase radio-HPLC method to analyze ^{90}Y(DOTA-BA) and ^{90}Y(DOTA-MBA). The advantage of radio-HPLC is its capability to determine the radiochemical purity of the ^{90}Y-labeled DOTA-conjugate and to separate different ^{90}Y species in the reaction mixture. A slow gradient mobile phase was used to maximize the separation of different ^{90}Y-containing species. We also tried several other reverse phase radio-HPLC methods using various reverse phase columns or different solvent combinations. In all the cases, ^{90}Y(DOTA-BA) and ^{90}Y(DOTA-MBA) show only one radiometric peak in their radio-HPLC chromatogram.

DOTA-BA is a DOTA-monoamide with no chiral center. In principle four isomers (**A**−**D** in Figure 13) are possible for Y(DOTA-BA). The interconversion within each enantiomeric pair (**A** ⇔ **B** or **C** ⇔ **D**) occurs through inversion of the ethylenic groups and concerted or stepwise rotation of the acetate arms (*6*, *17*, *38*). On the other hand, the exchange between diastereomers (**A** ⇔ **C** or **B** ⇔ **D**) takes place either by rotation of the acetate/acetamide chelating arms while maintaining the same conformation of the macrocyclic ring or by inversion of the ethylenic groups without changing the orientation of the acetate/acetamide chelating arms. If the interconversion between diastereomers (M and m isomers) is sufficiently slow, they should be readily separable by HPLC, particularly using a slow gradient mobile phase.

There are two possible explanations for the presence of only one radiometric peak in the HPLC chromatogram of ^{90}Y(DOTA-BA). The lipophilicity of two diastereomers is so similar that they could not be separated by the HPLC method used in this study. Alternatively, the interconversion between two diastereomers is so fast at the HPLC time-scale that the observed single peak is an averaged signal from two diastereomers. To eliminate the first possibility, we prepared DOTA-MBA and introduced a chiral center into the DOTA−monoamide conjugate. Unlike those in Y(DOTA-BA), isomers **A** and **B** or **C** and **D** in Y(DOTA-MBA) are no longer enantiomers but diastereomers, if the exchange between isomers is sufficiently slow at room temperature. We hoped that the conjugation of a chiral amine would make these diastereomers more separable by HPLC. To our surprise, ^{90}Y-(DOTA-MBA) shows only one radiometric peak in its radio-HPLC chromatogram, suggesting that it exists in solution as one predominant isomer.

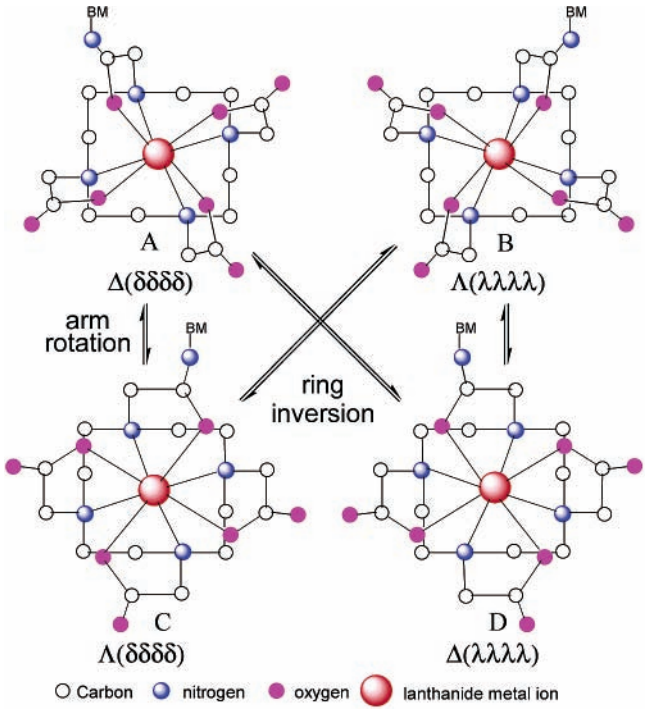


Figure 13. Four possible isomeric forms of the complex Y(DOTA-monoamide).

It should be noted that one radiometric peak in the radio-HPLC-chromatogram does not necessarily mean only one isomer for any radiolabeled small biomolecule. It needs further confirmation using other analytical methods. Therefore, we prepared Y(DOTA-BA) and Y(DOTA-MBA) and used NMR methods (^{1}H and ^{13}C) to study the solution structure of Y(DOTA-BA) and Y(DOTA-MBA). At the NMR time-scale, the rate of exchange between different isomers is relatively slow so that the presence of different isomers in solution is readily detectable.

In the ^{1}H NMR spectrum of Y(DOTA-BA), the two methylene hydrogens of benzyl group are inequivalent and give an AB quartet at ∼4.5 ppm (Figure 3). The methylene hydrogens from each acetate/acetamide chelating arm are also inequivalent, and four sets of AB quartets are seen in the region of 2.0−5.0 ppm. These observations suggest that Y(DOTA-BA) is chiral with DOTA-BA being prochiral and that the coordinated DOTA-BA is rigid and nonfluxional at room temperature. Thus, there should be no *rapid* interconversion within each enantiomeric pair (**A** ⇔ **B** or **C** ⇔ **D**) or between diastereomers (**A** ⇔ **C**, **B** ⇔ **D**, **A** ⇔ **D**, or **B** ⇔ **C**). For Y(DOTA-BA), isomers **A** and **B** or **C** and **D** are enantiomers and indistinguishable by NMR. For Y(DOTA-MBA), however, all isomers (**A**, **B**, **C**, and **D**) are diastereomers and should be distinguishable by NMR. The presence of only one doublet from the methyl group

strongly suggests that Y(DOTA-MBA) exist in solution as one predominant isomer. This conclusion supported by observations of only one ^{1}H NMR signal from the amide group and 13 aliphatic ^{13}C signals from 14 different aliphatic carbon atoms in Y(DOTA-MBA) (Figure 9) and is also consistent with the presence of only m-isomer of Y(DOTA-D-Phe-NH_2) in the solid state (*17*). If all four diastereomers were to exist in solution, a total of 56 aliphatic ^{13}C signals would have been detected in the ^{13}C NMR spectrum of Y(DOTA-MBA).

It should be noted that there are some small satellite peaks on both sides of each main peak of the ^{1}H NMR spectrum of Y(DOTA-MBA). This is particularly true in the ^{1}H NMR spectra of Y(DOTA-MBA) at lower temperatures (<25 °C). These observations suggest that there might be some other isomers in solution for Y(DOTA-MBA). However, the percentage of these minor isomers at the room temperature is so small that they are barely detectable by ^{1}H and ^{13}C NMR methods. For Y(DOTA-BA), there were no extra resonance signals observed except aliphatic resonance signals become sharper at temperatures <25 °C. On the basis of literature data and results from this study, we believe that Y(DOTA-BA) and Y(DOTA-MBA) exist in solution as only one predominant isomer. The exact structure of the predominant isomer observed in Y(DOTA-BA) and Y(DOTA-MBA) is not quite clear. However, it is reasonable to believe that the predominant isomer observed in Y(DOTA-BA) and Y(DOTA-MBA) is the m-isomer as observed in Y(DOTA-D-Phe-NH_2) (*17*).

Similar results have been reported for Na[La(DOTA)-La(HDOTA)]·$10H_2O$ (*59*) and the lanthanum complex of DOTA-pNB, in which the *p*-nitrophenyl group is attached to one of the four acetate chelating arms (*45*). The m-isomer is also present in the X-ray crystal structures of La(DOTPAM) (DOTPAM = 1,4,7,10-tetrakis(2-carbamoylethyl)-1,4,7,10-tetraazacyclododecane) (*60*), Eu(THP) (THP = 1,4,7,10-tetrakis(2-hydroxypropyl)-1,4,7,-10-tetraazacyclododecane) (*61*), Gd(DO3MA) (DO3MA = (1*R*,4*R*,7*R*)-α,α′α″-trimethyl-1,4,7,10-tetraazacyclododecane-1,4,7-triacetic acid) (*40*), and Yb(DOTPBz_4) (DOTPBz_4 = 1,4,7,10-tetraazacyclododecanetetrakis(methylbenzylphosphinic acid)) (*62*) even though the geometries were described as distorted antiprismatic. Apparently, the incorporation of substituents either on the acetate chelating arm or on the macrocyclic ring makes the regular antiprismatic structure (M isomer) much less common than originally expected.

As the temperature increases, all the resonance signals in the aliphatic region start to collapse at temperatures above 35 °C for Y(DOTA-BA) (Figure 4), suggesting that the coordinated DOTA-BA becomes fluxional at higher temperatures. The coalescence of resonance signals in the aliphatic region is most likely caused by the rotation of the acetate/acetamide chelating arms and the inversion of the ethylenic groups. When the sample was cooled to room temperature, the ^{1}H NMR spectrum returned to its original form. Thus, the coalescence process is reversible. The fact that no free DOTA-BA signals were detected over the temperature range (25−85 °C) suggests that the DOTA-BA remains bound to the Y center. For Y(DOTA-MBA), the AB quartets from methylene hydrogens of the acetate or acetamide chelating arm started to collapse at temperatures above 50 °C. It suggests that the presence of the methyl group provide certain steric hindrance for the rotation of acetate/acetamide chelating arms and the inversion of ethylenic groups. Similar inhibition effects on arm rotation have previously been noted for lanthanide complexes of DOTA derivative containing substituents at the acetate chelating arms (*63*) and of the chiral tetraamide (*64*). For Y(DOTA-BA) and Y(DOTA-MBA), the high-temperature limiting spectra could not be reached using D_2O/H_2O as the solvent.

The VT ^{1}H NMR spectra of Y(DOTA-MBA) revealed two interconversion processes: rotation of acetate chelating arms and inversion of ethylenic groups of the macrocyclic ring. At 50 °C, the acetamide and acetate chelating arms undergo rapid rotation, resulting in the coalescence of proton signals from the acetamide and acetate chelating arms. At temperatures higher than 65 °C, the inversion of ethylenic groups occurs and the ^{1}H NMR spectrum gives two overlapped NMR patterns. Similar results were observed for $[Lu(DOTA)(H_2O)]^-$, but the coalescence temperatures for the two process are much lower (*65*). However, the VT ^{1}H NMR spectra of Y(DOTA-BA) shows that both the rotation of acetate chelating arms and the inversion of ethylenic groups of the macrocyclic ring occur almost simultaneously at a lower temperature (35 °C).

CONCLUSIONS

In this study, yttrium and indium complexes of DOTA-BA and DOTA-MBA were prepared in order to study solution structures of ^{90}Y- and ^{111}In-labeled DOTA−BM conjugates. A reverse phase HPLC method revealed that both ^{90}Y and ^{111}In complexes show only one radiometric peak in their radio-HPLC chromatograms. The NMR data (^{1}H and ^{13}C) clearly demonstrates that Y(DOTA-BA) and Y(DOTA-MBA) exist in solution as one predominant isomer, and provide direct evidence for the presence of one radiometric peak in HPLC chromatograms of ^{90}Y-labeled DOTA−BM conjugates, in which the BM is attached to DOTA via one of four acetate chelating arms.

^{111}In(DOTA-BA) and ^{111}In(DOTA-MBA) are more hydrophilic than their corresponding ^{90}Y analogues, ^{90}Y-(DOTA-BA) and ^{90}Y(DOTA-MBA). Similar behavior was also seen for complexes In(DOTA-BA) and In(DOTA-MBA) as compared to their corresponding yttrium analogues, Y(DOTA-BA) and Y(DOTA-MBA). Since the only difference between In(DOTA-BA) and its Y(DOTA-BA) is the metal ion, the difference in their HPLC retention times strongly suggests that indium and yttrium do not share the same coordination sphere even though they are chelated by the same DOTA-conjugate.

The structural difference between indium and yttrium complexes of DOTA-BA and DOTA-MBA is also reflected by their different solution dynamics. Y(DOTA-BA) and Y(DOTA-MBA) are rigid while In(DOTA-BA) and In-(DOTA-MBA) are fluxional at the room temperature. Given the fact that In(DOTA-BA) and In(DOTA-MBA) are more hydrophilic and more fluxional than Y(DOTA-BA) and Y(DOTA-MBA), it is reasonable to believe that the coordinated DOTA-BA and DOTA-MBA are heptadentate with four amine-nitrogen and three carboxylate-oxygen donors binding to the indium center while the carbonyl-oxygen is uncoordinated.

It should be noted that the HPLC retention time is largely depends on the chromatographic conditions, and does not represent the "absolute" value of the hydrophilicity for a specific radiolabeled compound. As a matter of fact, the difference in hydrophilicity between ^{111}In-(DOTA-BA)/^{111}In(DOTA-MBA) and their ^{90}Y analogues is relatively small considering the chromatographic conditions used in this study. The hydrophilicity difference between the ^{111}In- and ^{90}Y-labeled DOTA−BM conjugate also depends on the relative size of the biomolecule. For large biomolecules such as antibodies, a

slight difference in the metal chelate may not cause any significant change in physical and biological properties of the ^{90}Y- and ^{111}In-labeled DOTA-conjugate. For small biomolecules, however, the slight difference in metal chelate may cause significant differences in biological properties of ^{90}Y- and ^{111}In-labeled DOTA−BM conjugates. Therefore, it is critical to prove that the ^{111}In-labeled DOTA−BM conjugate is *biologically* equivalent to the corresponding ^{90}Y analogue in various animal models in order to predict the radiation dosimetry of a specific ^{90}Y-labeled DOTA−BM conjugate more accurately.

LITERATURE CITED

(1) Reubi, J. C. (1997) Regulatory peptide receptors as molecular targets for cancer diagnosis and therapy. *Quart. J. Nucl. Med. 41*, 63−70.

(2) Volkert, W. A., and Hoffman, T. J. (1999) Therapeutic radiopharmaceuticals. *Chem. Rev. 99*, 2269−2292.

(3) Heeg, M. J., and Jurisson, S. (1999) The role of inorganic chemistry in the developmentof radiometal agents for cancer therapy. *Acc. Chem. Res. 32*, 1053−1060.

(4) Kwekkeboom, D., Krenning, E. P., and de Jong, M. (2000) Peptide receptor imaging and therapy. *J. Nucl. Med. 41*, 1704−1713.

(5) Boerman, O. C., Oyen, W. J. G., and Corstens, F. H. M. (2000) Radiol-labeled receptor-binding peptides: A new class of radiopharmaceuticals. *Semin. Nucl. Med. 30*, 195−208.

(6) Liu, S., and Edwards, D. S. (2001) Bifunctional chelators for target specific therapeutic lanthanide radiopharmaceuticals. *Bioconjugate Chem. 12*, 7−34.

(7) Signore, A., Annovazzi, A., Chianelli, M., Coretti, F., Van de Wiele, C., Watherhouse, R. N., and Scopinaro, F. (2001) Peptide radiopharmaceuticals for diagnosis and therapy. *Eur. J. Nucl. Med. 28*, 1555−1565.

(8) Parker, D. (1990) Tumor targeting with radiolabeled macrocycle-antibody conjugates. *Chem. Soc. Rev. 19*, 271−291.

(9) Liu, Y.-F., and Wu, C.-C. (1991) Radiolabeling of monoclonal antibodies with metal chelates. *Pure Appl. Chem. 63*, 427−463.

(10) Moi, M. K., Meares, C. F., McCall, M. J., Cole, W. C., and DeNardo, S. J. (1985) Copper chelates as probes of biological systems: stable copper complexes with macrocyclic bifunctional chelating agent. *Anal. Chem. 148*, 249−253.

(11) Moi, M. K., and Meares, C. F. (1988) The peptide way to macrocyclic bifunctional chelating agents: synthesis of 2-(*p*-nitrobenzyl)-1,4,7,10-tetraazacyclododecane-*N*,*N*′,*N*″,*N*‴-tetraacetic acid and study of its yttrium(III) complex. *J. Am. Chem. Soc. 110*, 6266−6267.

(12) Kline, S. J., Betebenner, D. A., and Johnson, D. K. (1991) Carboxymethyl-substituted bifunctional chelators: preparation of aryl isothionate derivatives of 3-(carboxymethyl)-3-azapentanedioic acid, 3,12-bis(carboxymethyl)-6,9-dioxa-3,12-diazatetradecanedioic acid, and 1,4,7,10-tetraazacyclododecane-*N*,*N*′,*N*″,*N*‴-tetraacetic acid for use as protein labels. *Bioconjugate Chem. 2*, 26−31.

(13) Li, M., and Meares, C. F. (1993) Synthesis, metal chelate stability studies, and enzyme digestion of a peptide-linked DOTA derivative and its corresponding radiolabeled immunoconjugates. *Bioconjugate Chem. 4*, 275−283.

(14) Lewis, M. R., Raubitschek, A., and Shively, J. E. (1994) A facile, water soluble method for modification of proteins with DOTA. Use of elevated temperature and optimized pH to achieve high specific activity and high chelate stability in radiolabeled immunoconjugates. *Bioconjugate Chem. 5*, 565−576.

(15) Kulis, D. L., DeNardo, S. J., DeNardo, G. L., O'Donnell, R. T., and Meares, C. F. (1998) Optimized conditions for chelation of yittrium-90-DOTA immunoconjugates. *J. Nucl. Med. 39*, 2105−2110.

(16) Lewis, M. R., and Shively, J. E. (1998) Maleimidocycteineamido-DOTA derivatives: New reagents for radiometal chelate conjugation to antibody sulfhydryl groups undergo pH-dependent cleavage reactions. *Bioconjugate Chem. 9*, 72−86.

(17) Heppler, A., Froidevaux, S., Mäcke, H. R., Jermann, E., Béhé, M., Powell, P., and Hennig, M. (1999) Radiometal-labeled macrocyclic chelator-derived somatostatin analogue with superb tumor-targeting properties and potential for receptor-mediated internal therapy. *Chem. Eur. J. 5*, 1974−1981.

(18) Smith-Jones, P. M., Stolz, B., Albert, R., Ruser, G., Briner, U., Maecke, H. R., and Bruns, C. (1998) Synthesis and characterization of [^{90}Y]-Bz-DTPA-oct: a yttrium-90-labeled oactreotide analogue for radiotherapy of somatostatin receptor-positive tumors. *Nucl. Med. Biol. 25*, 181−188.

(19) Van Hagen, P. M., Breeman, W. A. P., Bernard, H. F., Schaar, M., Mooij, C. M., Srinivasan, A., Schmidt, M. A., Krenning, E. P., and de Jong, M. (2000) Evaluation of radiolabeled cyclic DTPA-RGD analogue for tumor imaging and radionuclide therapy. *Int. J. Can. (Radiat. Oncol. Invest), 8*, 186−198.

(20) Smith-Jones, P. M., Stolz, B., Albert, R., Ruser, G., Briner, U., Mäcke, H. R., and Bruns, C. (1998) Synthesis and characterization of [^{90}Y]-Bz-DTPA-oct: a yttrium-90-labeled oactreotide analogue for radiotherapy of somatostatin receptor-positive tumors. *Nucl. Med. Biol. 25*, 181−188.

(21) De Jong, M., Bakker, W. H., Breeman, W. A. P., Bernard, B. F., Hofland, L. J., Visser, T. J., Srinivasan, A., Schmidt, M., Béhé, M., Mäcke, H., and Krenning, E. P. (1998) Preclinical comparison of [DTPA^{o}]octreotide, [DTPA^{o}, Tyr^{3}]-octreotide, and [DOTA^{o}, Tyr^{3}]octreotide as carriers for somatostatin receptor-targeted scintigraphy and radionuclide therapy. *Int. J. Cancer 75*, 406−411.

(22) De Jong, M., Bakker, W. H., Bernard, B. F., Valkema, R., Kwekkeboom, D. J., Reubi, J.-C., Srinivasan, A., Schmidt, M., and Krenning, E. P. (1999) Internalization of radiolabeled [DTPA^{o}]octreotide and [DOTA^{o}, Tyr^{3}]octreotide: peptides for somatostatin receptor-targeted scintigraphy and radionuclide therapy. *J. Nucl. Med. 40*, 2081−2087.

(23) De Jong, M., Breeman, W. A. P., Bakker, W. H., Kooij, P. P. M., Bernard, B. F., Hofland, L. J., Visser, T. J., Srinivasan, A., Schmidt, M. A., Erion, J. L., Bugaj, J. E., Mäcke, H., and Krenning, E. P. (1998) Comparison of ^{111}In-labeled somatostatin analogues for tumor scintigraphy and radionuclide therapy. *Anticancer Res. 58*, 437−441.

(24) Reubi, J. C., Waser, B., Schaer, J. C., Laederach, U., Erion, J., Srinivasam, A., Schmidt, M. A., and Bugaj, J. E. (1998) Unsulfated DTPA- and DOTA-CCK analogues as specific high affinity ligands for CCK−B receptor-expressing human and rat tissues in vitro and in vivo. *Eur. J. Nucl. Med. 25*, 481−490.

(25) Behr, T. M., Jenner, N., Béhé, M., Angerstein, C., Gratz, S., Raue, F., and Becker, W. (1999) Radiolabeled peptides for targeting cholecystokinin-B-gastrin receptor-expressing tumors. *J. Nucl. Med. 40*, 1029−1040.

(26) Behr, T. M., Jenner, N., Béhé, M., Angerstein, C., Gratz, S., Raue, F., and Becker, W. (1999) Cholecystokinin-B-gastrin receptor binding peptides: preclinical development and evaluation of their diagnostic and therapeutic potential. *Clin. Cancer Res. 5*, 3124s−3138s.

(27) Kwekkeboom, D. J., Bakker, W. H., Kooj, P. P. M., Erion, J., Srinivasan, A., de Jong, M., Reubi, J.-C., and Krenning, E. P. (2000) Chilecyctokinin receptor imaging using an octapeptide DTPA-CCK analogue in patients with medullary thyroid carcinoma. *Eur. J. Nucl. Med. 27*, 1312−1317.

(28) Carrasquillo, J. A., White, J. D., Paik, C. H., Raubitschek, A., Le N., Rotman, M., Brechbiel, M. W., Gansow, O. A., Top, L. E., Perentesis, P., Reynolds, J. C., Nelson, D. L., and Waldmann, T. A. (1999) Similarities and differences in ^{111}-In- and ^{90}Y-labeled 1B4M-DTPA antiTac monoclonal antibody distribution. *J. Nucl. Med. 40*, 268−276.

(29) Canera, L., Kinuya, S., Garmestani, K., Brechbiel, M. W., Wu, C., Pai, L. H., McMurry, T. J., Gansow, O. A., Pastan, I., Paik, C. H., and Carrasquillo, J. A. (1994) Comparative biodistribution of indium- and yttrium-labeled B3 monoalonal antibody conjugated to either 2-(p-SCN-Bz)-6-methyl-DTPA (1B4M-DTPA) or 2-(p-SCN−Bz-)-1,4,7,10-tetraazacyclododecane tetraacetic acid (2B-DOTA). *Eur. J. Nucl. Med. 21*, 640−646.

(30) Rösch, F., Herzog, H., Stolz, B., Brockmann, J., Köhle, M., Mühlensiepen, H., Marbach, P., and Müller-Gärtner, H.-W. (1999) Uptake kinetics of the somatostatin receptor ligand [^{86}Y]DOTA-$_D$Phe^1-Tyr^3-octreotide ([^{86}Y]SMT487) using positron emission tomography in nonhuman primates and calculation of radiation doses of the ^{90}Y-labeled analogue. *Eur. J. Nucl. Med. 26*, 358−366.

(31) Liu, S., Edwards, D. S., Ziegler, M. C., Harris, A. R., Hemingway, S. J., and Barrett, J. A. (2001) ^{99m}Tc-Labeling of a hydrazinonictotinamide-conjugated vitronectin receptor antagonist. *Bioconjugate Chem. 12*, 624−629.

(32) Liu, S., Cheung, E., Rajopadyhe, M., Williams, N. E., OveroyeK. L., and Edwards, D. S. (2001) Isomerism and solution dynamics of ^{90}Y-labeled DTPA- biomolecule conjugates. *Bioconjugate Chem. 12*, 84−91.

(33) Liu, S., and Edwards, D. S. (2001) Synthesis and characterization of two ^{111}In labeled DTPA-peptide conjugates. *Bioconjugate Chem. 12*, 630−634.

(34) Liu, S., Cheung, E., Rajopadyhe, M., Ziegler, M. C., Edwards, D. S. ^{90}Y- and ^{177}Lu-labeling of a DOTA-conjugated vitronectin receptor antagonist for tumor therapy. *Bioconjugate Chem. 12*, 559−568.

(35) Liu, S., and Edwards, D. S. (2001) Stabilization of ^{90}Y-labeled DOTA-biomolecule conjugates using gentisic and ascorbic acid. *Bioconjugate Chem. 12*, 554−558.

(36) Liu, S., Ellars, C., Singh, S., Williams, N. E., and Edwards, D. S. Anaerobic ^{90}Y- and ^{177}Lu-labeling of a DOTA-conjugated nonpeptide vitronectin receptor antagonist. *Bioconjugate Chem.*, submitted.

(37) Shannon, R. D. (1976) Revised effective ionic radii and systemic studies of interatomic distances in halides and chalogenides. *Acta Crystallogr. A32*, 751−767.

(38) Caravan, P., Ellison, J. J., McMurrym T. J., and Lauffer, R. B. (1999) Gadolinium(III) chelates as MRI contrast agents: structure, dynamics, and applications. *Chem. Rev. 99*, 2293−2352.

(39) Howard, J. A. K., Kenwright, A. M., Moloney, J. M., Parker, D., Port, M., Navet, M., Rousseau, O., and Woods, M. (1998) Structure and dynamics of all of the stereoisomers of europium complexes of tetra(carboxyethyl)derivatives of dota: ring inversion is decoupled from cooperative arm rotation in the *RRRR* and *RRRS* isomers. *Chem. Commun.* 1381−1382.

(40) Kang, S. I., Ranganathan, R. S., Emswiler, J. E., Kumar, K., Gougoutas, J. Z., Malley, M. F., and Tweedle, M. F. (1993) Synthesis, characterization, and crystal structure of gadolinium(III) chelate of (1*R*,4*R*,7*R*)-α,α′,α″-trimethyl-1,4,7,10-tetraazacyclododecane-1,4,7-triacetic acid (DO3MA). *Inorg. Chem. 32*, 2912−2918.

(41) Spirlet, M.-R., Rebizant, J., Desreux, J. F., and Loncin, M.-F. (1984) Crystal and molecular structure of sodium aquo-(1,4,7,10-tetraazacyclododecane-1,4,7,10-tetraacetato)europate-(III) tetrahydrate, $Na^+(EuDOTA{\cdot}H_2O)^-{\cdot}4H_2O$, and its relevance to NMR studies of the conformational behavior of the lanthanide complexes formed by the macrocyclic ligand DOTA. *Inorg. Chem. 23*, 359−363.

(42) Chang, C. A., Francesconi, L. C., Malley, M. F., Kumar, K., Cougoutas, J. Z., and Tweedle, M. F. (1993) Synthesis, characterization, and crystal structures of M(DO3A) (M = Fe, Gd) and Na[(DOTA)] (M = Fe, Y, Gd). *Inorg. Chem. 32*, 3501−3508.

(43) Aime, S., Botta, M., and Ermodi, G. (1992) NMR study of solution structures and dynamics of lanthanide(III) complexes of DOTA. *Inorg. Chem. 31*, 4291−4299.

(44) Aime, S., Anelli, P. L., Botta, M., Fedeli, F., Ermondi, G., Grandi, M., Paoli, P., and Uggeri, F. (1992) Synthesis, characterization, and *1/T*1 NMRD profiles of gadolinium(III) complexes of monoamide derivatives of DOTA-like ligands. X-ray structure of the 10-[2-[[2-hydroxy-1-(hydroxymethyl)-ethyl]amino]-1-(phenylmethoxy)methyl]2-oxoethyl]-1,4,7,10-tetraazacyclododecane-1,4,7-triacetic acid-gadolinium(III) complex. *Inorg. Chem. 31*, 2422−2428.

(45) Aime, S., Botta, M., Ermondi, G., Terreno, E., Anelli, P. L., Dedeli, F., and Uggeri, F. (1996) Relaxometric, structural, and dynamic NMR studies of DOTA-like Ln(III) complexes (ln = La, Gd, Ho, Yb) containing a *p*-nitrophenyl substituent. *Inorg. Chem. 35*, 2726−2736.

(46) Sherry, A. D. (1997) MR imaging and spectroscopy applications of lanthanide complexes with macrocyclic phosphonate and phosphonate ester ligands. *J. Alloys Compd. 249*, 153−157.

(47) Kim, W. D., Kiefer, G. E., Huskens, J., and Sherry, A. D. (1997) NMR studies of the lanthanide(III) complexes of 1,4,7,-10-tetraazacyclododecane-1,4,7,10-tetrakis(methanephosphonic acid mono(2′,2′,2′-trifluoroethyl) ester). *Inorg. Chem. 36*, 4128−4134.

(48) Aime, S., Batsanow, A. S., Botta, M., Dickins, R. S., Faulkner, S., Foster, E. C., Howard, J. A. k., Moloney, J. M., Norman, T. J., Parker, D., Royle, L., and Williams, J. A. G. (1997) Nuclear magnetic resonance, luminescence and structural studies of lanthanide complexes with octadentate macrocyclic ligands bearing benzylphosphinate groups. *J. Chem. Soc., Dalton Trans.* 3623−3636.

(49) Kumar, K., Chang, C. A., Francesconi, L. C., Dischino, D. D., Malley, M. F., Cougoutas, J. Z., and Tweedle, M. F. (1994) Synthesis, stability, and structure of gadolinium(III) and yttrium(III) macrocyclic poly(amino carboxylates). *Inorg. Chem. 33*, 3567−3575.

(50) Keire, D. A., and Kobayashi, M. (1999) NMR studies of the metal loading kinetics and acid−base chemistry of DOTA and butylamide-DOTA. *Bioconjugate Chem. 10*, 454−463.

(51) Yang, L.-W., Liu, S., Wong, E., Rettig, S. J., and Orvig, C. (1995) Lanthanide complexes of potentially heptadentate (N_4O_3) schiff base and aminephenol ligands: influence of rigidity and preorganization of ligands on compound structure. *Inorg. Chem. 34*, 2164−2178.

(52) Liu, S., Wong, E., Rettig, S. J., and Orvig, C. (1993) Hexadentate N_3O_3 amine phenol ligands for group 13 Metal Ions: Evidence for intrastrand and interstrand hrdrogen bonds in polydentate amine phenols. *Inorg. Chem. 32*, 4268−4276.

(53) Liu, S., Wong, E., Karunaratne, V., Rettig, S. J., and Orvig, C. (1993) Highly flexible chelating ligands for group 13 metals. Design, synthesis and characterization of hexadentate (N_3O_3) tripodal amine phenol ligand complexes of aluminum, gallium and indium. *Inorg. Chem. 32*, 1756−1765.

(54) Liu, S., Rettig, S. J., and Orvig, C. (1992) Polydentate ligand chemistry of group 13 metals: Effects of the size and donor-selectivity of metal ions on structures and properties of aluminum, gallium and indium complexes with potentially heptadentate (N_4O_3) amine phenol ligands. *Inorg. Chem. 31*, 5400−5407.

(55) Riesen, A., Kaden, T. A., Ritter, W., and Mäcke, H. R. (1989) Synthesis and X-ray structural characterization of seven coordinate macrocyclic In^{3+} complexes with relavance to radiopharmaceutical applications. *J. Chem. Soc., Chem. Commun.* 460−462.

(56) Mäcke, H. R., Riesen, A., and Ritter, W. (1989) The molecular structure of indium-DTPA. *J. Nucl. Med. 30*, 1235−1239.

(57) Malyrick M. A., Ilyhin, A. B., and Petrosyans, S. P. (1994) Seven- and eight-coordinate complexes of indium(III) with nitrilotriacetic acid. *Main Group Metal Chem. 17*, 707−717.

(58) Maeke, H., Scherer, G., Heppeler, A., and Henig, M. (2001) Is In-111 an ideal surrogate for Y-90? If not, why? *Eur. J. Nucl. Med. 28*, 967 (abstract no. OS-27).

(59) Aime, S., Barge, A., Benetollo, F., Bombieri, G., Botta, M., and Uggeri, F. (1997) A novel compound in lanthanide(III) DOTA series. X-ray crystal and molecular structure of the complex $Na[La(DOTA)La(HDOTA)]{\cdot}10H_2O$. *Inorg. Chem.* 36, 4287−4289.

(60) Morrow, J. R., Amin, S., Lake, C. H., and Churchill, M. R. (1993) Synthesis, structure, and dynamic properties of lanthanum(III) complex of 1,4,7,10-tetrakis(2-carbamoylethyl)1,4,7,10-tetraazacyclododecane. *Inorg. Chem. 32*, 4566−4572.

(61) Aileen Chin, K. O., Morrow, J. R., Lake, C. H., and Churchill, M. R. (1994) Synthesis and solution properties of lanthanum(III), europium(III), and lutetium(III) THP complexes and an X-ray diffraction study of a crystal containing four stereoisomers of a europium(III) THP complex (THP = 1,4,7,10-tetrakis(2-hydroxypropyl)-1,4,7,10-tetraazacyclododе-

cane). Methyl groups impart rigidity to *S*,*S*,*S*,*S*-THP macrocyclic complexes. *Inorg. Chem. 33*, 656−664.

(62) Aime, S., Batsanov, A. S., Botta, M., Howard, J. A. K., Parker, D., Senannavake, K., and Williams, G. (1994) Solution and solid-state characterization of highly rigid, eight-coordinate lanthanide(III) complexes of a macrocyclic tetrabenzylphosphinate. *Inorg. Chem. 33*, 4696−4706.

(63) Woods, M., Aime, S., Botta, M., Howard, J. A. K., Moloney, J. M., Mavet, M., Parker, D., Port, M., and Rousseaux, O. (2000) Correlation of water exchange rate with isomeric composition in diastereoisomeric gadolinium complexes of tetra(carboxyethyl)dota and related macrocyclic ligands. *J. Am. Chem. Soc. 122*, 9781−9792.

(64) Dickins, R. S., Howard, J. A., Maupin, C. L., Moloney, J. M., Parker, D., Siligardi, G., and Williams, J. A. G. (1999) *Chem. Eur. J. 5*, 1095−1105.

(65) Aime, S., Barge, A., Botta, M., Fasano, M, Ayala, J. D., and Bombieri, G. (1996) Crystal structure and solution dynamics of the lutetium(III) chelate of DOTA. *Inorg. Chim. Acta 246*, 423−429.

BC010134H

SEPTEMBER/OCTOBER 2002
Volume 13, Number 5

© *Copyright 2002 by the American Chemical Society*

Bioconjugate Chemistry

ARTICLES

Photoswitching of Ligand Association with a Photoresponsive Polymer−Protein Conjugate

Tsuyoshi Shimoboji, Zhongli L. Ding, Patrick S. Stayton,* and Allan S. Hoffman*

Department of Bioengineering, University of Washington, Seattle, Washington 98195. Received May 10, 2001; Revised Manuscript Received December 18, 2001

Light-regulated molecular switches that reversibly control biomolecular function could provide new opportunities for controlling activity in diagnostics, affinity separations, bioprocessing, therapeutics, and bioelectronics applications. Here we show that site-specific conjugation of light-responsive polymers near the biotin-binding pocket of streptavidin provides control of ligand binding affinity in response to UV and visible light irradiation. Two different light-responsive polymers were utilized that display opposite photoresponsive solubility changes under UV or visible (vis) light irradiation in aqueous solutions. At 40 °C, the *N*,*N*-dimethylacrylamide (DMA)-*co*-4-phenylazophenyl acrylate (AZAA) copolymer (DMAA) was soluble under UV irradiation and precipitated under visible light, while the DMA-*co*-*N*-4-phenylazophenyl acrylamide (AZAAm) copolymer (DMAAm) was soluble under visible irradiation and precipitated under UV light. Both polymers were synthesized with a vinyl sulfone terminus and conjugated to the Glu116Cys (E116C) streptavidin mutant via thiol coupling. The DMAA−streptavidin conjugate bound biotin efficiently when the polymer was in the soluble state under UV irradiation, but under visible irradiation, the polymer collapsed and blocked free biotin association. Furthermore, if biotin was allowed to bind when the polymer was in the soluble state under UV irradiation, then when the polymer was collapsed by visible light, the streptavidin released the bound biotin. The DMAAm−streptavidin conjugate showed the opposite response, with association of biotin allowed under visible light irradiation and blocked under UV irradiation. The photoresponses of the streptavidin conjugates thus correspond to the original photoresponsive phase transition properties of the polymer switches triggered by the cis−trans isomerization of the diazo chromophores.

INTRODUCTION

An important aspect of many technologies that utilize biomolecular components is the control of their recognition properties. For example, changes in solution conditions such as temperature or pH are commonly used to release target antigens from antibodies. These solution changes are often damaging to the biomolecules, and there is thus considerable interest in developing molecular switches that control recognition processes with mild signals. We have been developing molecular switches composed of stimuli-responsive polymers that control protein recognition processes in response to small changes in pH and temperature. Light represents another attrac-

* Correspondence should be addressed to Allan S. Hoffman, Department of Bioengineering, Box 352255, University of Washington, Seattle, WA 98195. Telephone: 206-543-9423, fax: 206-543-6124, e-mail: hoffman@u.washington.edu, and Patrick S. Stayton, Department of Bioengineering, Box 352125, University of Washington, Seattle, WA 98195, Telephone: 206-685-8148, Fax: 206-685-8256, E-mail: stayton@u.washington.edu.

10.1021/bc010057q CCC: $22.00 © 2002 American Chemical Society
Published on Web 07/19/2002

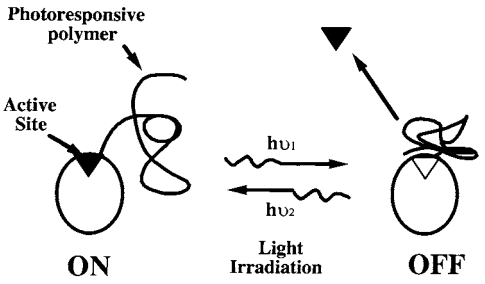


Figure 1. Schematic illustration showing the use of different wavelengths of light to switch the bioactivity of a protein "on" or "off", as provided by switching the conformation of a photoresponsive polymer that has been conjugated at a specific site near the active site of the protein.

tive signal because it would trigger these switches without requiring changes in solution conditions, and it is externally reversible; thus, it is amenable to device design and automation.

The control of enzymatic reactions and ligand affinity with light has been actively investigated by many researchers (*1*−*5*). In previous studies, chemical modification of biomolecules by direct conjugation of photochromomes such as azobenzene (*1*−*3*) or spiropyran (*3*−*5*) have been reported and have provided some photoregulation of catalytic activities and affinity binding processes. Although these bioconjugates of small molecule photochromes have demonstrated the potential of light regulation, their photoresponsiveness has been relatively weak. Intrinsic problems include (a) the thermally activated reversible isomerization of the photochromes that leads to the dyes existing as a mixture of two distinct physical states/conformations, (b) the limited size of the photochromes, and (c) their conjugation to the protein at random, nonideal positions for switching activity.

These results suggested that photoresponsive polymers might be conjugated to proteins at defined sites to control protein function more efficiently than single photochromes (Figure 1). We have described the site-specific conjugation of pH and temperature-sensitive polymers to control ligand association and dissociation in the model streptavidin−biotin system (*6*−*9*). These smart polymers change their size and physical properties reversibly between an extended hydrophilic random coil and a collapsed hydrophobic state over narrow changes of the defined stimulus. Here we report that photoresponsive polymers can serve as light-activated switches to reversibly control biotin-binding by site-specific conjugation to a critical site on streptavidin. The photoresponsive polymers rely on the cis−trans isomerization of diazobenzene chromophores to trigger the change in physical properties. The change in properties is reversible with distinct visible or far UV wavelengths of light, and these bioconjugates can thus be activated and deactivated by external light.

EXPERIMENTAL PROCEDURES

Materials. 4-Aminoazobenzene and 4-hydroxyazobenzene (Aldrich, Milwaukee, WI) were recrystallized from ethanol and water and dried in vacuo. *N*,*N*-Dimethylacrylamide (DMA) (Fluka, Milwaukee, WI), diethyl ether, acryloyl chloride, triethylamine, and 2-mercaptoethanol (MEO) (Aldrich, Milwaukee, WI) were purified by distillation under reduced pressure. 2,2′-Azobisbutyronitrile (AIBN) (J. T. Baker, Phillipsburg, NJ) was recrystallized from methanol. Ethanol, dimethylformamide (DMF), tetrahydrofuran (THF), methylene chloride, potassium ter-butoxide, divinyl sulfone (DVS), ethylenediaminetetraacetic acid (EDTA), 4-phenylazomaleinanil (PAM) (Aldrich, Milwaukee, WI), tris(2-carboxyethyl)phosphine hydrochloride (TCEP-HCl) (Pierce, Rockford, IL), Microcon-30 (Millipore, Bedford, MA), and [^{3}H]Biotin (d-[8,9-^{3}H(N)]-Biotin, Dupont, Wilmington, DE) were used as received. All other reagents were of analytical grade.

Azobenzene Monomer Synthesis. Two azobenzene-containing monomers, *N*-4-phenylazophenylacrylamide (AZAAm) and 4-phenylazophenyl acrylate (AZAA), were synthesized. 4-Aminoazobenzene or 4-hydroxyazobenzene (0.2 mol) and triethylamine (0.26 mol) were dissolved in diethyl ether (200 mL). Acryloyl chloride (0.24 mol) dissolved in 80 mL of diethyl ether was added dropwise at 0 °C under nitrogen atmosphere with stirring. The reaction mixture was allowed to come to room temperature and stirred for 4 h. The reaction solution was filtered to remove triethylammonium chloride, washed with water, and evaporated. The product was recrystallized from ethanol−water mixture and dried in vacuo. The structures were confirmed by ^{1}H NMR (*d*-DMSO).

Photoresponsive Polymer Synthesis. Two photoresponsive polymers with hydroxyl termini, DMAAm (DMA-*co*-AZAAm copolymer) and DMAA (DMA-*co*-AZAA copolymer), were synthesized by chain transfer initiated free-radical polymerization in DMF at 60 °C for 20 h, using MEO as a chain transfer regent and AIBN as an initiator (monomer concentration = 2 mol/L, monomer/MEO/AIBN = 100/1/0.2 molar ratio). The feed ratios of AZAAm and AZAA were 7.0 mol % and 4.0 mol %, respectively. The products were purified by precipitation into diethyl ether three times and dried in vacuo. The contents of AZAAm or AZAA incorporated in the copolymers were determined by ^{1}H NMR (Spectrospin & Bruker, dpx200), comparing the ratio of aromatic and aliphatic hydrogens. The molecular weights (MWs) of the polymers were determined by gel permeation chromatography (GPC, Water, Styragel HR3 and 4) in THF, using polystyrene as standards. The hydroxyl terminus of DMAA or DMAAm was converted to a vinyl sulfone group for conjugation to the protein thiol. DMAA and DMAAm were dissolved in 20 mL of methylene chloride with 0.03 g of potassium *tert*-butoxide and 100 μL of divinyl sulfone (DVS) (DVS/OH = 10/1 molar ratio). The solution was stirred for 12 h at room temperature under nitrogen atmosphere. The polymers were precipitated, washed in diethyl ether, and dried in vacuo.

Conjugation of Polymers to Streptavidin. The streptavidin mutant E116C was constructed by the same method as reported previously (*7*). Conjugation of streptavidin (E116C) and polymers (DMAA-VS, DMAAm−VS) were carried out in 100 mM sodium tetraborate buffer, pH 8.0, containing 50 mM sodium chloride and 5 mM EDTA. Cysteine residues in E116C form disulfide bonds during storage. To reduce disulfide bonds to sulfhydryl groups, TCEP at 50-fold molar excess to the mutants was added into the solution, which was then rotated at room temperature for 20 min. The DMAA-VS or DMAAm−VS was added in 50-fold molar excess to the mutants and reacted for 1 h at room temperature, followed by the reaction for 24 h at 4 °C. The conjugates were separated from the unconjugated mutants by thermally induced precipitation at 60 °C. The unconjugated protein was retained in the supernatant. The thermal-induced precipitation was repeated three times.

Conjugation of Azobenzene to Protein. PAM was reacted with cysteine in E116C in solution at pH 7.0 in phosphate-buffered saline, with TCEP as a disulfide reducing agent, mixing a 50:1 molar excess of 4-phenylazomaleinanil dissolved in DMF (10 vol % of protein

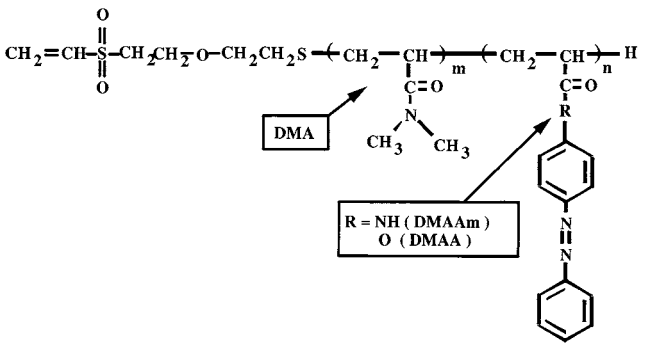


Figure 2. Photoresponsive polymers, DMAAm and DMAA, with vinyl sulfone end groups.

solution). The conjugate was purified from the unreacted PAM by ultrafiltration. The MW of the conjugate was determined as 13523 by electrospray ionization mass spectrometry (ESI-MS), which corresponds to one azobenzene conjugated to one monomer of E116C SA.

Photoirradiation. A UV Cure Lamp (Thorlabs, Newton, NJ) was used with a UG-1 band-pass filter (Edmund Scientific, Barrington, NJ) to select UV light between 300 and 400 nm, and a Fiber-Lite Illuminator (Edmund Scientific, Barrington, NJ) was used with a VG-1 band-pass filter to select for wavelengths greater than 420 nm.

Biotin-Binding Assay. [^{3}H]Biotin (d-[8,9-^{3}H(N)]-Biotin, Dupont, Wilmington, DE) was employed to quantitate biotin binding. A 10 μg amount of the conjugate was suspended in 1200 μL of 100 mM of sodium phosphate buffer, pH 7.4. A mixture of ^{3}H-biotin and unlabeled biotin (100 μL) was added into the conjugate solution (total volume was 1 mL) after incubation at 52 °C for 1 h. The ratio of total biotin/biotin binding sites was 1.5 (molar ratio). The solution temperature was reduced to 4 °C stepwise, incubating for 15 min at each temperature. A 50 μL aliquot was taken at the end of each incubation. The unbound biotin was separated from the bound biotin by ultrafiltration through a Microcon-30 (MW cutoff: 30 kDa) at the incubation temperature of the solution. A 30 μL aliquot of the filtrate, which contained unbound biotin, was measured in a β-counter (LS7000 Liquid scintillation system, Beckman Instruments, Inc. Fullerton, CA), to determine the unbound biotin. The biotin binding could be quantitated by the decrease of free biotin in the solution.

RESULTS AND DISCUSSION

Temperature- and Light-Dependent Polymer Properties. We have prepared two different copolymers that display both temperature- and light-sensitive properties. These copolymers differ mainly in the type of bond (ester vs amide) by which the azobenzene groups are attached to the main backbone chain. (Figure 2) These copolymers are similar to previously described photoresponsive polymers (*10*−*15*). The temperature- and light-responsive properties of copolymers of *N*-isopropylacrylamide (NIPAAm) and *N*-4-phenylazophenylacrylamide (AZAAm) have been characterized by Irie and co-workers (*10, 11*). Kröger et al. (*12, 13*) reported the largest differences in lower critical solution temperature (LCST) detected in aqueous solution using *N*,*N*-dimethylacrylamide (DMA)-*co*-4-phenylazophenyl acrylate (AZAA) copolymer. The photoresponsive properties of the copolymers described here depend on temperature, and conversely, the temperature-responsive properties depend on whether the diazo chromophore is in the cis or trans state. Previous work of Morishima and co-workers (*14, 15*) suggests that hydrophobic interactions of pendant groups such as pyrene and cholesterol will predominantly be intramolecular if the group is attached to the backbone via amide bonds, and intermolecular if it is attached via ester bonds. The trans configuration of azobenzene also permits stacking of the azobenzene moieties, which will enhance such hydrophobic interactions in the trans state. Thus, these very different hydrophobic interactions of the pendant azobenzene groups will depend on whether the groups are attached via ester or amide bonds, and this may explain the opposite visible vs UV photoresponses seen here for the DMAA and DMAAm copolymers. This is demonstrated for the free copolymers in Figure 3, which shows the temperature dependence under visible or UV irradiation of the phase separation. The UV light had a peak at 350 nm and a range from 300 to 400 nm, and the visible light had a peak at 520 nm while light less than 420 nm was filtered. When the LCST of the polymer was determined as the temperature of 10% of maximum biotin-binding, the DMAA and DMAAm exhibited LCST's under visible irradiation of 37 °C and 39 °C, respectively. Upon UV irradiation, the LCST of the DMAA increased to 43 °C, and that of the DMAAm decreased to 34 °C. The LCST transition of these polymers is relatively broad, and the polymers exhibited a maximal difference in the degree of phase separation under UV vs visible irradiation at around 40 °C. A significant feature of these diazo-chromophore-based polymers is that the thermal reconversion of the cis-state to the trans-state is not simultaneously accompanied by a conversion of the polymer from the collapsed state to extended state, or vice versa. This conformational con-

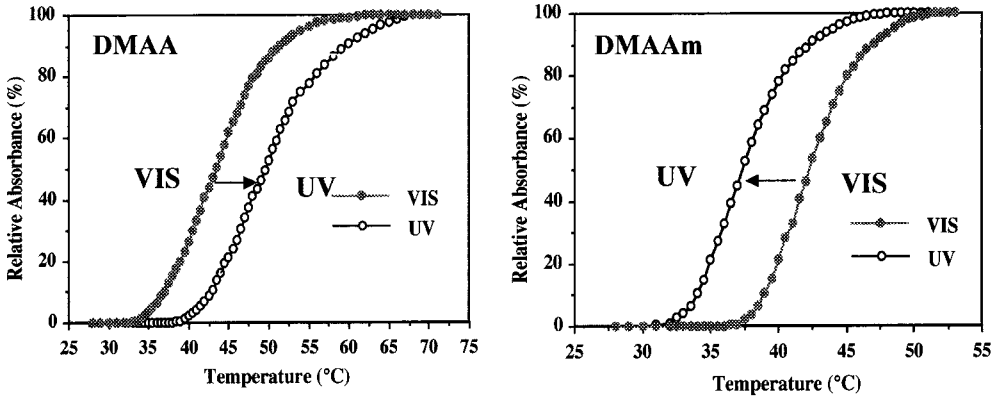


Figure 3. Effect of photoirradiation on the phase transition temperature of DMAA (AZAA: 5.9 mol %) and DMAAm (AZAAm: 9.6 mol %). The absorbance was measured at 600 nm. The polymer concentration was 2 mg/mL in 100 mM PB pH 7.2. The rate of heating was 0.5 °C/min. The UV and visible (vis) light irradiations were for 10 min and 3 h, respectively, before the measurement.

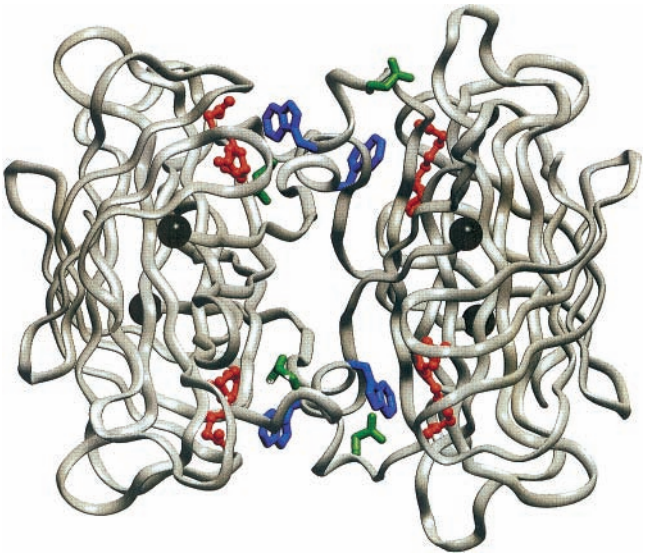


Figure 4. Three-dimensional model of streptavidin with a cysteine at amino acid position 116, showing the spacial relationship between the biotin-binding site and the cysteine-SH polymer conjugation site on E116C SA (*16*).

version of the polymer happens very slowly, on the time scale of days, unlike many diazo compounds where the cis−trans reconversion rate can often be fast, depending on the temperature.

Conjugation of Photoresponsive Polymers to Streptavidin. The general design of the streptavidin−polymer conjugate for light-responsive switching is schematically shown in Figure 1. We have found previously that the E116C SA mutant locates the unique thiol residue in an appropriate position to control both biotin binding and release (*7, 16*). This conjugation site is on the loop close to Trp120, which is critical for biotin-binding (*17*) (Figure 4). The polymers were specifically conjugated to E116C by the reaction of the vinyl sulfone group of the polymer with the thiol group of the protein under conditions that favored the vinyl group addition to the −SH over the $-NH_2$6. The conjugates were separated from the unconjugated E116C by thermally induced precipitation. The conjugation efficiency was estimated by the depletion of the mutant after thermally induced precipitation as 12−20%. For the E116C conjugates reported here, we have utilized two types of photoresponsive polymers (Figure 2) that exhibit phase transitions in aqueous solution in response to UV or visible light irradiation: (1) *N*,*N*-dimethylacrylamide (DMA)-*co*-4-phenylazophenyl acrylate ("AZAA") copolymer ("DMAA") (MW: 18 kDa, AZAA: 5.9 mol %) and (2) DMA-*co*-N-4-phenylazophenyl acrylamide ("AZAAm") copolymer ("DMAAm") (Mw: 10 kDa, AZAAm: 9.6 mol %) (Shimoboji et al., manuscript submitted). These polymers also exhibit thermoresponsive phase transitions in aqueous solutions (*16*). The DMAA polymer becomes soluble upon UV irradiation and insoluble upon visible irradiation, while the DMAAm polymer becomes soluble upon visible light and insoluble upon UV light. Thus, they

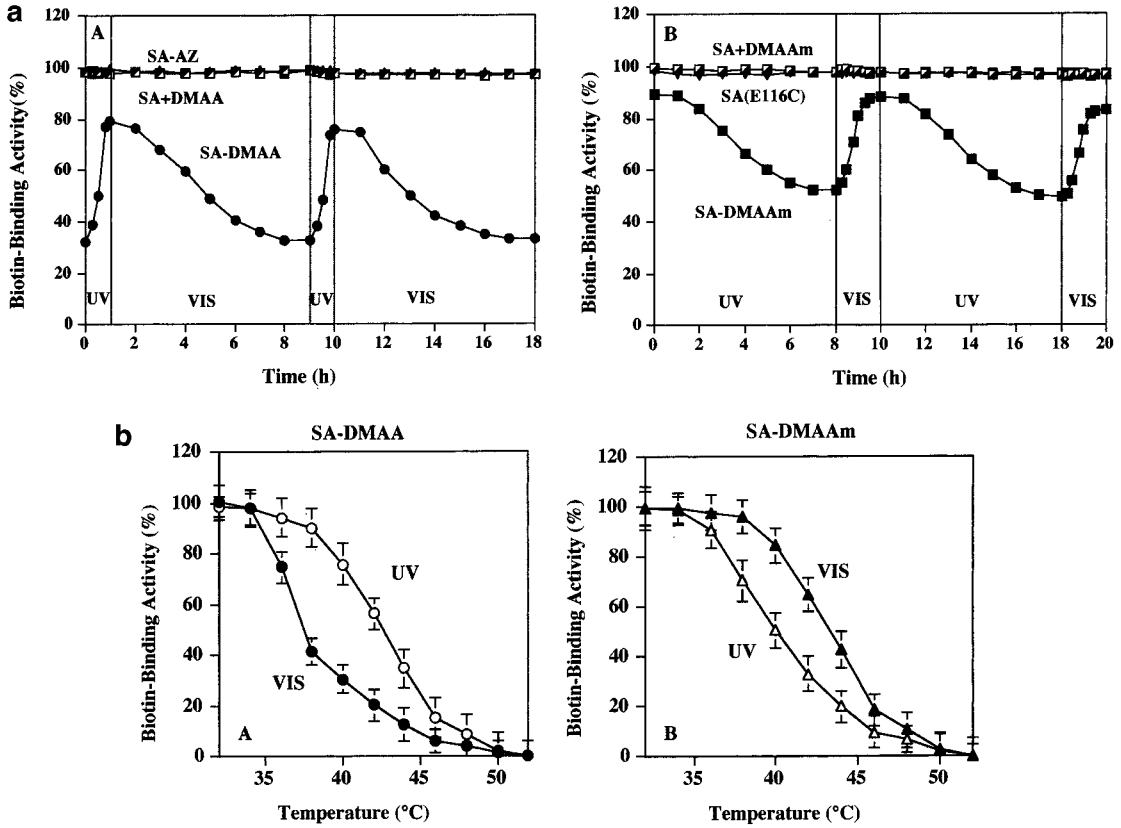


Figure 5. Photoresponsive switching of streptavidin biotin-binding activity. (A) The biotin binding activities for the SA−DMAA and SA−DMAAm conjugates were compared to controls of their physical mixtures, an SA−AZ conjugate, and SA (E116C), in response to UV/VIS cyclic irradiation under isothermal conditions at 40 °C. The biotin-binding activity represents the percentage change in the biotin-binding capacity of the conjugates from 4 °C to 52 °C, assuming 100% binding at 4 °C and 0% binding at 52 °C. (B) The normalized biotin-binding activities for SA−DMAA and SA−DMAAm as a function of temperature, under constant visible (>420 nm) or far-UV (360 nm) light irradiation. The biotin-binding activity represents the percentage change in the biotin-binding capacity of the conjugates with 100% normalized to maximal binding and 0% normalized to the minimal binding activity for each of the conjugates.

exhibited opposite photoresponses, as shown in Figure 3 and discussed above.

Photoresponsive Switching of Biotin Binding Activity. In order to characterize the time dependence of biotin association and release as a function of the photo-dependent polymer transition, biotin binding and release studies were carried out under isothermal conditions at 40 °C where the polymers displayed their maximum photoresponsiveness. As a control, azobenzene (AZ) was also conjugated site-specifically to E116C (SA−AZ conjugate). Figure 5a shows how UV/VIS photocycling alters the biotin binding and release properties of the SA−DMAA and SA−DMAAm conjugates. The unconjugated SA (E116C), a physical mixture of SA and the DMAA or DMAAm, and the SA−AZ conjugate did not exhibit any significant alteration in biotin binding affinity as a function of light irradiation. However, the SA−DMAA conjugate exhibited a 47% greater increase in biotin-blocking or release with VIS light than with UV light. Conversely, the SA−DMAAm conjugate displayed a 38% greater increase in the blocking of biotin association, and the release of bound biotin, with UV irradiation compared to VIS irradiation. These opposite photoresponsive phenomena agree with the photoresponsive phase transitions of the original polymers—i.e., DMAA collapses and becomes insoluble under VIS irradiation, while DMAAm collapses and becomes insoluble under UV irradiation. The temperature dependence of the photoswitch was also characterized and is shown in Figure 5b. The general trends follow the LCST behavior of the free polymers (Figure 3), but are shifted to slightly higher temperatures for the streptavidin conjugates.

Mechanism of Photoresponsive Switches. The time-dependence for the release of the bound biotin was measured, and the dissociation rate was determined to be 1.3×10^{-4} (s^{-1}) at 52 °C. This is within experimental error of the native streptavidin dissociation rate at this temperature. This result implies that biotin dissociates at the normal off-rate when the photoresponsive polymers are in the collapsed state near the binding pocket, but reassociation of biotin with streptavidin is blocked. The collapsed polymer does not interfere with dissociation or induce a faster off-rate through steric interactions at the binding pocket, but it does sterically retard access of free biotin to the binding pocket. The diazo monomers are not capable of modulating the access of biotin to the pocket when conjugated to E116C SA, consistent with the need for the larger polymer to achieve this steric blocking mechanism.

CONCLUSIONS

We have described the use of thermal and photoresponsive diazo-containing polymers that provide photoswitching of ligand-binding properties when conjugated near a protein's recognition binding site. This provides a general approach to the design and development of photoswitchable proteins, where function is controlled by external light signals of distinct wavelengths. In addition to the control of ligand capture and release, this approach should be applicable to a wide-range of technologies, such as photoswitching of enzyme−substrate catalytic reactions, and the optical blocking and de-blocking of recognition sites for light-based patterning of molecules and cells.

ACKNOWLEDGMENT

This work was supported by NIH Grant No. GM53771.

LITERATURE CITED

(1) Willner, I., Rubin, S., and Zor, T. (1991) Photoregulation of α-chymotrypsin by its immobilization in a photochromic azobenzene copolymer. *J. Am. Chem. Soc. 113*, 4013−4014.

(2) Liu, D., Karanicolas, J., Yu, C., Zhang, Z., and Woolley, G. A. (1997) Site-specific incorporation of photoisomerizable azobenzene groups into ribonucleases. *Bioorg. Med. Chem. Lett. 7*, 2677−2680.

(3) Willner, I., and Rubin, S.(1996) Control of the structure and functions of biomaterials by light. *Angew. Chem., Int. Ed. Engl. 35*, 367−385.

(4) Willner, I., Rubin, S., Shatzmiller, R., and Zor, T. (1993) Reversible light-stimulated activation and deactivation of α-chymotrypsin by its immobilization in photoisomerizable copolymers. *J. Am. Chem. Soc. 115*, 8690−8694.

(5) Rathi, R. C., Kopeckova, P., and Kopecek, J. (1997) Biorecognition of sugar containing N−(2-hydroxypropyl)methacrylamide copolymers by immobilized lectin. *Macromol. Chem. Phys. 198*, 1165−1180.

(6) Stayton, P. S., Shimoboji, T., Long, C., Chilkoti, A., Chen, G., Harris, J. M., and Hoffman, A. S. (1995) Control of protein−ligand recognition using a stimuli-responsive polymer. *Nature 378*, 472−474.

(7) Ding, Z. L., Long, C., Hayashi, Y., Bulmus, E. V., Hoffman, A. S., and Stayton, P. S. (1999) Temperature control of biotin binding and release with a streptavidin-poly(*N*-isopropylacrylamide) site-specific conjugate. *Bioconjugate Chem. 10*, 395−400.

(8) Bulmus, E. V., Ding, Z., Long, C. J., Stayton, P. S., and Hoffman, A. S. (2000) A pH- and temperature-sensitive copolymer-streptavidin site-specific conjugate for pH-controlled binding and triggered release of biotin. *Bioconjugate Chem. 11*, 78−83.

(9) Ding, Z., Fong, R. B., Long, C. J., Hoffman, A. S., and Stayton, P. S. (2001) "Size-dependent control of the binding of biotinylated proteins to streptavidin using a polymer shield" *Nature 411*, 59−62.

(10) Kungwatchakun, D., and Irie, M. (1988) *Macromol. Chem. Rapid Commun. 9*, 243.

(11) Irie, M., and Kungwatchakun, D. (1992) *Proc. Jpn. Acad. 68*, 127.

(12) Kröger, R., Menzel, H., and Hallensleben, M. L. (1994) *Macromol. Chem. Phys. 195*, 2291.

(13) Menzel, H., Kröger, R., and Hallensleben, M. L. (1995) *Macromol. Rep. A32*, 779.

(14) Morishima, Y., Seki, M., Nomura, S., and Kamachi, M. (1994) Amphiphilic Polyelectrolytes and their Coulombic Complexes with Surfactants as Novel Photochemical Systems, pp 243−256, ACS Symposium Series 548, American Chemical Society: Washington D.C.

(15) Yusa, S., Kamachi, M., and Morishima, Y. (1998) Hydrophobic self-association of cholesterol moieties covalently linked to polyelectrolytes: Effect of spacer bond. *Langmuir 14*, 6059−6067.

(16) Shimoboji, T., Ding, Z., Stayton, P. S., and Hoffman, A. S. (2001) Mechanistic investigation of smart polymer-protein conjugates. *Bioconjugate Chem. 12*, 314−319.

(17) Chilkoti, A., Tan, P. H., and Stayton, P. S. (1995) Site-directed mutagenesis studies of the high-affinity streptavidin−biotin complex: contributions of tryptophan residues 79, 108, and 120. *Proc. Natl. Acad. Sci. U. S. A. 92*, 1754−1758.

BC010057Q

Local Delivery of Basic Fibroblast Growth Factor (bFGF) Using Adsorbed Silyl-heparin, Benzyl-bis(dimethylsilylmethyl)oxycarbamoyl-heparin

Paul O. Zamora,*,†,‡ Ray Tsang,† Louis A. Peña,‡ Shigemasa Osaki,† and Prantika Som‡

Biosurface Engineering Technologies, Inc., 387 Technology Drive, College Park, Maryland 20742-3371, and Medical Department, Brookhaven National Laboratory, Upton, New York 11973-5000. Received June 27, 2001; Revised Manuscript Received May 3, 2002

A growth factor delivery system was developed that is based on the use of silyl-heparin, a chemically modified analogue of heparin. The silyl-heparin was adsorbed onto surfaces by hydrophobic interaction via the prosthetic unit and can then be used as a solid-phase adsorbent for bFGF. All the coating steps were performed by adsorption, a process that allowed preparation of surfaces by immersion or "dip-coating". In this study a series of silyl-heparins were synthesized and each of the analogues found to function similar to unmodified heparin relative to their binding of antithrombin III and also the binding of bFGF. The silyl-heparins were found to be adsorbed onto a wide variety of substrates including polystyrene and lactide:glycolide copolymer. Enzyme-linked immumosorbant assay (ELISA) was used to establish that bFGF was readily bound to surface adsorbed silyl-heparin, and that the amount bound was directly related to amount offered for binding. Once adsorbed the silyl-heparin/FGF was able to induce capillary tube formation of endothelial cells and to increase the growth of endothelial cells. When coated onto suture material and implanted in muscle, the FGF/silyl-heparin coating caused an increased density of mesenchymal cells in the area of the implant. This coating method could prove to be useful in a number of tissue engineering applications for the local delivery of FGF and other growth factors.

INTRODUCTION

The objective of this research was to develop a growth factor delivery system for use in tissue repair that would provide a localized release of bFGF and related growth factors to enhance the tissue repair process.

Fibroblast growth factors comprise a large family of developmental and physiological signaling molecules (Szebenyi and Fallon, 1999). All FGFs have a high affinity for the glycosaminoglycan heparin and for cell surface heparan sulfate proteoglycans. The affinity of FGF for heparan sulfate limits its diffusion and restricts its release into the extracellular matrix. The binding of FGFs to heparin/HS results in the formation or stabilization of dimers and higher order oliomers along the proteoglycan chain (Herr et al., 1997; Mach et al., 1993; Moy et al., 1997). Heparin/heparan sulfate also play a role in the formation of an active FGF/FGF receptor signaling complex, and heparin/HS increases the affinity and half-life of the FGF/FGFR complex (Flaumenhaft et al., 1990; Szebenyi and Fallon, 1999). bFGF is mitogenic in many cell types including fibroblasts, endothelial cells, smooth muscle cells, and osteoblasts amoung others (Nugent and Iozzo, 2000). It is angiogenic and can protect cells from toxic insult.

Heparin-containing delivery systems for locoregional application of growth factors have been described by several investigators (Edelman et al., 1992; Gosselin et al., 1996; Nimni, 1997; Sakiyama-Elbert and Hubbell, 2000b; Wissink et al., 2000; Zarge et al., 1997). When heparin is covalently bound to a scaffolding, the release of growth factors has been suggested to be influenced by enzymatic factors such as heparinase or plasmin (Sakiyama-Elbert and Hubbell, 2000a), and by diffusion-based release. The current work presents a delivery system that is based on the use of heparin conjugated to silyl-type prosthetic units. The resulting conjugate, benzyl-bis-(dimethylsilylmethyl)oxycarbamoyl-heparin (silyl-heparin), is amphipathic and is readily adsorbed onto hydrophobic surfaces, including biodegradable polymers. The absorbed silyl-heparin can then be used as a solid-phase adsorbent for growth factors such as bFGF. A key advantage of the current method is that all the coating steps are performed by adsorption thereby allowing preparation of surfaces by "dip-coating".

METHODS

A schematic for the synthesis of silyl-heparins is provided in Figure 1, and the various steps are detailed below.

Synthesis of Benzyl(chloromethyl)dimethylsilane, 3 ($n = 1$). Under an atmosphere of nitrogen, chloro-(chloromethyl)dimethylsilane (100 g, 0.685 mol) was added by syringe to THF (500 mL) and solution cooled to 0 °C with an ice/acetone bath. Benzylmagnesium chloride (2.0 M solution, 400 mL, 0.8 mol) was added dropwise over 2 h. Care was taken to maintain the temperature below 10 °C until all the reagent was added. Thereafter, the ice bath was allowed to warm to room temperature and the reaction mixture stirred overnight. Hexane (300 mL) was added and saturated aqueous NH_4-Cl (300 mL) added dropwise. The reaction mixture was transferred to a 2 L separatory funnel with more hexane

* To whom correspondence should be addressed. Tel: (301) 405-8533. Fax: (301) 405-8263. E-mail: pzamora@biosetinc.com.
† Biosurface Engineering Technologies.
‡ Brookhaven National Laboratory.

10.1021/bc0155216 CCC: $22.00 © 2002 American Chemical Society
Published on Web 08/20/2002

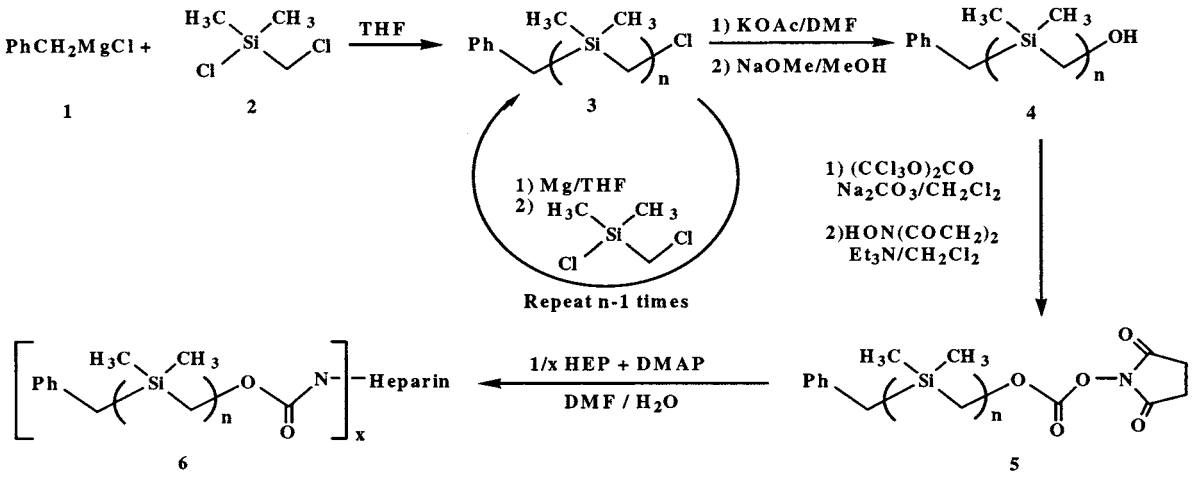


Figure 1. Experimental scheme of preparation of silyl-heparin. Treatment of benzylmagnesium chloride **1** with chloro(chloromethyl)-dimethysilane **2** gave benzyl(chloromethyl)dimethysilane **3** ($n = 1$). **3** then underwent a repetitive reaction resulting in chain elongation. For chain elongation, treatment of $\mathbf{3_n}$ with magnesium gave the Grignard Reagent which was, in turn, treated with chloro-(chloromethyl)dimethylsilane **2** to give the homologous silyl compound $\mathbf{3}_{n+1}$. This Grignard reaction was repeated as needed to obtain the desired chain-length for the silyl compound. At the desired chain length, **3** (or $\mathbf{3_n}$) was treated with potassium acetate, followed by trans-esterification of the corresponding acetate with basified methanol to give the alcohol **4**. The alcohol **4**, when treated with triphosgene, gave the corresponding chloroformate, which on treatment with *N*-hydroxysuccinimide gave the *N*-hydroxysuccinimidyl carbonate **5**. Heparin was conjugated to **5** in 1:1 DMF/H_2O containing 4-(dimethylamino)pyridine to give the silylated heparin **6**. Adjusting the molar ratios of the reactants controlled the number of prosthetic groups per heparin.

(300 mL). After partitioning, the organic layer was washed with saturated aqueous NH_4Cl (200 mL) and saturated aqueous NaCl (200 mL) successively. The combined aqueous layers were backwashed with hexane (2×500 mL), and the combined organic layers were dried over $MgSO_4$, evaporated on a rotory evaporator, and further concentrated under vacuum to give a colorless oil 162.0 g (109.5% yield). A quantitative yield was assumed with a purity of the crude product being 91.3%. The NMR spectrum for this and all other reaction products were recorded on a Varian XL300 300 MHz NMR spectrometer in a ~2% solution in $CDCl_3$ (~0.6 mL) unless otherwise indicated. The residual $CHCl_3$ signal at 7.24 ppm was used as reference line. ^{1}H NMR spectrum for $BnMe_2SiCH_2Cl$: δ 7.0−7.2 (m, 5H, arom Ph), 2.7 (s, 2H, $SiCH_2Cl$), 2.2 (s, 2H, $SiCH_2Ph$), 0.1 (s, 6H, $SiCH_3$). Quantitative organic microcombustion analysis for $BnMe_2SiCH_2Cl$: theoretical C 60.4%, found 60.8%; theoretical H 7.6%, found 7.4%. TLC in hexane, $R_f = 0.4$.

Grignard Reaction of $Bn(SiMe_2CH_2)_nCl$ 3_n and $ClSiMe_2CH_2Cl$ to give $Bn(SiMe_2CH_2)_{n+1}Cl$, 3_{n+1}. Magnesium powder (7.5 g, 0.31 mol), a catalytic amount of iodine, and THF (100 mL) were placed in a 500 mL three-necked flask equipped with a condenser-N_2 inlet, a septum, and a thermometer. The mixture was heated to reflux briefly until the brown color of iodine disappeared. $Bn(SiMe_2CH_2)_nCl$ (0.2 mol) was added by syringe and residual reagent washed into the reaction mixture with THF (2×25 mL). The reaction was initiated with a heat gun: an exothermic reaction was observed, and the reaction flask was placed in a water bath until the exothermic reaction subsided. The resulting gray mixture was heated to reflux for 24 h. The reagent was then cooled to room temperature and cannulated into a pressure filter funnel where it was added directly into another 500 mL round-bottom flask in which was placed a solution of $ClSiMe_2CH_2Cl$ (27.0 mL, 0.2 mol) in THF (50 mL) at room temperature. The magnesium residue was washed into the reaction mixture with THF (2×25 mL). The reaction mixture was heated to reflux overnight. To the resulting gray suspension was added saturated aqueous $NaHCO_3$ (50 mL), and the resulting solution was transferred to a 500 mL separatory funnel with hexane (200 mL). After partition, the organic layer was washed with saturated aqueous $NaHCO_3$ (50 mL) and saturated aqueous NaCl (50 mL). The combined aqueous layers were back-washed with hexane (2×100 mL). The combined organic layers were dried over $MgSO_4$ and extensively evaporated under vacuum to give an amber oil. The amber oil was purified by distillation to give a colorless oil. Yields were over 80%. ^{1}H NMR spectrum for $Bn(Me_2SiCH_2)_2Cl$: δ 7.0−7.2 (m, 5H, arom Ph), 2.7 (s, 2H, $SiCH_2Cl$), 2.0 (s, 2H, $SiCH_2Ph$), 0.0 and 0.1 (2 s, 2×6H, $SiCH_3$), −0.2 (s, 2H, $SiCH_2Si$). Quantitative organic microcombustion analysis for $Bn(Me_2SiCH_2)_2Cl$: theoretical C 57.6%, found 57.8%; theoretical H 8.6%, found 8.6%. TLC in hexane, $R_f = 0.3$.

Conversion of $Bn(SiMe_2CH_2)_nCl$ 3_n to $Bn(SiMe_2CH_2)_nOH$ 4_n. $Bn(SiMe_2CH_2)_nCl$ (0.16 mol) was dissolved in DMF (300 mL) in a 1-L three-necked flask. KOAc (50 g, 0.5 mol) was added followed by $^nBu_4NI$ (4.0 g, 0.01 mol), and the reaction mixture was stirred in a 135 °C oil bath for 24 h. The reaction mixture was worked up by cooling to room temperature and transferring to a 1-L separatory funnel with hexane (500 mL) and washed with saturated aqueous NaCl (3×100 mL). The combined aqueous layers were back-washed with hexane (3×300 mL) and the combined organic layers dried over $MgSO_4$ and vacuum-evaporated to an amber oil, which was dissolved in MeOH (400 mL). A generous amount of freshly prepared NaOMe was added to adjust the pH to >10 and the reaction mixture heated to reflux for 2 h. The reaction mixture was then neutralized with AcOH, evaporated to dryness, and chromatographed with silica gel in a 6.5×100 cm (height of silica 40 cm) flash column and eluted with 0−30% EtOAc/hexane to give the desired product, a slightly yellow oil. Yields were over 80%. ^{1}H NMR spectrum for $Bn(Me_2SiCH_2)_2OH$: δ 7.0−7.2 (multiplet, 5H, aromatic Ph protons); 3.3 (singlet, 2H, $SiCH_2OH$); 2.1 (singlet, 2H, $SiCH_2Ph$); 0.0 & 0.1 (2 singlets, 2×6H, $SiCH_3$); −0.2 (singlet, 2H, $SiCH_2Si$). Quantitative organic microcombustion analysis for $Bn(Me_2SiCH_2)_2OH$: theoretical C 61.8%, found 62.0%; theoretical H 9.6%, found 9.6%. TLC in 20% EtOAc/80%hexane, $R_f = 0.25$.

Conversion of $Bn(SiMe_2CH_2)_nOH$ 4_n to $Bn(SiMe_2CH_2)_nOCO_2N(COCH_2)_2$ 5_n. Triphosgene (60 g, 0.2 mol)

was dissolved in CH_2Cl_2 (200 mL) and stirred at 0 °C under N_2 in a 1-L three-necked flask equipped with thermometer, dropping funnel and N_2 inlet. Na_2CO_3 (65 g, 0.6 mol) was added followed by $Bn(SiMe_2CH_2)nOH$ (0.13 mol dissolved in 200 mL of CH_2Cl_2) dropwise over 30 min. Thereafter, the ice/acetone bath was allowed to come to room temperature. The reaction mixture was stirred overnight and filtered through a sintered glass funnel, and the reaction vessel was rinsed with $PhCH_3$ (200 mL). The solution was concentrated under vacuum to give a colorless oil. The oil was dissolved in CH_2Cl_2 and stirred in an ice bath under N_2. *N*-Hydroxysuccinimide (30 g, 0.26 mol) was added followed by Et_3N (40 mL, 0.28 mol) dropwise over 15 min and the resulting cloudy mixture stirred at room temperature for 1 h. The reaction mixture was diluted with hexane (600 m), washed with saturated aqueous NH_4Cl (3 × 100 mL), and the combined aqueous phases were backwashed with hexane (2 × 200 mL). The combined organic phases were dried over $MgSO_4$ and concentrated under vacuum to give an amber oil. The amber oil was chromatographed with silica gel in a 6.5 × 100 cm (height of silica 40 cm) flash column and eluted with 20−50% EtOAc/hexane to give an amber syrup. Yields are generally greater than 75%. ^{1}H NMR spectrum for $Bn(Me_2SiCH_2)_2OCO_2N(COCH_2)_2$: δ 7.0−7.2 (m, 5H, arom Ph); 4.0 (s, 2H, $SiCH_2OCO$), 2.7 (s, 4H, $N[COCH_2]_2$), 2.1 (s, 2H, $SiCH_2Ph$), 0.0 and 0.1 (2 s, 2 × 6H, $SiCH_3$), −0.2 (s, 2H, $SiCH_2Si$). Quantitative organic microcombustion analysis for $Bn(Me_2SiCH_2)_2$-$OCO_2N(COCH_2)_2$: theoretical C 54.9%, found 54.7%; theoretical H 6.9%, found 7.0%; theoretical N 3.6%, found 3.5%. TLC in 20% EtOAc/80%hexane, $R_f = 0.2$.

Conjugation of Heparin with $Bn(SiMe_2CH_2)_nOCO_2$-$N(COCH_2)_2$ 5_n To Give $6_{n,x}$. Heparin (ammonium ion-free, average molecular weight 10000; 100 g, 10 mmol) was dissolved in H_2O (500 mL) in a 2-L flask with stirring. DMF (400 mL) was added followed by DMAP (1.6× g, 13× mmol). $Bn(SiMe_2CH_2)_nOCO_2N(COCH_2)_2$, $\mathbf{5}_n$ (10× mmol), in DMF (100 mL) was added, and the resulting milky mixture was allowed to stir at room temperature for >24 h. The reaction mixture was concentrated by evaporating most of the water followed by trituration with acetone (1 L). The white suspension was filtered through a sintered glass funnel to give a white solid residue. This crude material was purified by Soxhlet extraction with acetone overnight to give a white powder. The yields were generally greater than 95%.

The average number of prosthetic units per molecule of heparin was estimated based on a comparison of the molar ratios of the hydrolyzed prosthetic unit benzyl-tri-(dimethylsilylmethyl)-OH and heparin as determined by use of dimethyl methylene blue (Groves et al., 1997). Heparin was detected using a commercially available enzyme-linked assay that measures the heparin-induced inhibition of antithrombin/factor Xa as measured with a factor Xa specific chromogenic substrate (Teien and Lie, 1977; Teien et al., 1976).

The silyl-heparin was used as a coating solution at 1% solution (w/v) in 60% aqueous ethanol. Materials were coated with silyl-heparins for 15 min at 37 °C. The coated materials were then rinsed extensively in water, air-dried, and stored until use.

Comparison of Silyl-heparins with Heparin. Comparisons were made using competitive binding to heparin-agarose (end-point attachment, Sigma Chemical Co.) generally following the methods of Ishihara (Ishihara et al., 2000). Heparin agarose was rinsed in phosphate-buffered saline and equilibrated in PBS containing 1% bovine serum albumin (PBS/BSA). Aliquots were added to microfuge tubes and the volume adjusted to 0.5 mL with 0.5 mL of PBS/BSA. An additional 0.5 mL of Dulbecco's modified Eagle's medium containing 10% fetal bovine serum (FBS) containing heparin or silyl-heparin-5135 was added. An aliquot of 5 μL of bFGF (50 ng/mL) was added and the solutions incubated for 30 min with mixing. The unbound bFGF was removed by multiple centrifugations and rinsing in PBS. Rabbit anti-bFGF (1:500) was added in 0.5 mL of PBS/BSA and the solution incubated with mixing for 1 h. After rinsing donkey anti-rabbit (1:500) in PBS/BSA was added and incubated 1 h. After rinsing and transfer to new vials, chromogen (ABTS One-Step, Pierce Chemical Co.) was added and the reaction developed and subsequently read at 595 nm.

Detection of Adsorbed Silyl-heparin. Adsorbed heparin was detected by staining with dimethyl methylene blue (Groves et al., 1997). Stains were filtered through 0.2 μm filters prior to use. The stain associated with the test materials was solublized by addition (1:1) of methanol and an aqueous solution of 0.5 M Tris, pH 6.8, containing 0.4% sodium dodecyl sulfate (SDS). Heparin was also detected by an enzyme-linked assay (Sigma Chemical Co., St. Louis) that measures the heparin-induced inhibition of antithrombin/factor Xa as measured with a factor Xa specific chromogenic substrate (Teien and Lie, 1977; Teien et al., 1976). The assay was performed following the directions of the manufacturer.

ELISA Detection of bFGF Bound to Silyl-heparins. Wells of polystyrene microtiter plates were coated with 30 μL of silyl-heparin for 15 min at 37 °C. The surface area of the well was 0.32 cm^2. The wells were rinsed extensively in water and air-dried. bFGF (Sigma Chemical Co.) in PBS/BSA was added in 150 μl aliquots and in doubling dilutions (final volume 150 μL). The plate was incubated at 37 °C for 1 h and rinsed 5× in PBS. A 150 μL aliquot of PBS/BSA containing 1:500 rabbit anti-FGF antibodies was added, incubated 1 h, and rinsed. In some cases an irrelevant rabbit antibody (rabbit anti-TGF-receptor II, Santa Cruz Biotechnology) was used at a similar concentration. An aliquot of PBS/BSA containing 1:500 HRPO-conjugated donkey anti-rabbit IgG was added, and after incubation and rinsing ABTS-chromogen was added. All antibody solutions were filtered through 0.2 μm filters prior to use. The absorbance was monitored at 405 nm.

Attachment Molecules. The following were used as heparin-complexing materials: murine type IV collagen, human fibrinogen, and bovine fibronectin isolated from plasma. The proteins were used at a concentration of 100 μg/mL in PBS/BSA. The wells were coated adding 100 μL followed by a 1 h incubation at 37 °C. Thereafter, the plates were washed extensively in water. To the wells was added bFGF in PBS/BSA in 150 μl aliquots. The plate was incubated at 37 °C for 1 h and processed as above using dilutions of 1:200 and 1:500 for the primary and secondary antibody, respectively.

Capillary Tube Formation. Bovine aorta endothelial cells were seeded into low-attachment 96-well plates. The wells had been pretreated with saline or silyl-heparin and/or fibrinogen and FGF. The silyl-heparin coating was applied as above, and the fibrinogen was applied as a 0.1% solution in PBS and uncomplexed material washed off with PBS. FGF (100 ng/mL) was allowed to attach for 30 min to the silyl-heparin in PBS containing 1% bovine serum albumin and the unbound material rinsed off with PBS. Endothelial cells (5×10^3 cells) were seeded into the wells in DMEM containing 10% FBS. The cells were allowed to grow for 4 days and the cultures examined by phase contrast microscopy.

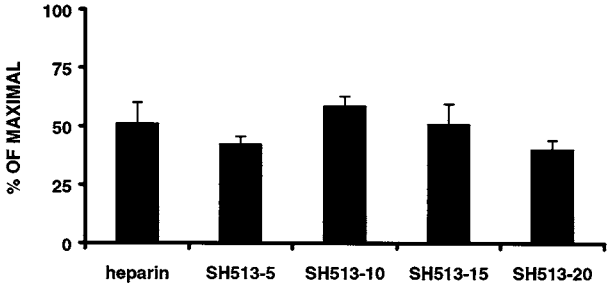


Figure 2. Comparison of the inhibition of bFGF binding to heparin-agarose by either heparin or silyl-heparin analogues as determined by immunochemical methods. The analogues nominally contained 5, 10, 15, and 20 prosthetic groups per heparin. A serial assay was used to establish the EC_{50} for heparin and then the comparison of the silyl-heparins made using identical concentrations. The data represents the average ± SD.

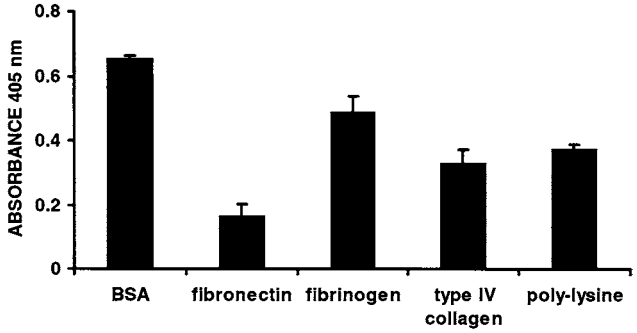


Figure 4. Effect of precomplexing adhesion molecules to silyl-heparin on the subsequent binding of bFGF. All adhesion molecules were complexed to silyl-heparin at a concentration of 100 μg/mL and unbound material rinsed out prior to use in experiments. The data represents the average ± SD. All treatments were statistically significant as indicated by $p < 0.05$ by Student's *t*-test relative to treatment with bovine serum albumin (BSA).

Stimulation of Endothelial Cell Growth. Six-well cluster plates were seeded with 5×10^4 bovine aorta endothelial cells. Cell culture inserts (25 mm diameter) with 3 μm pores in the bottom were placed in each well. Suture material (10 cm) with or without coatings was placed in the well and medium added sufficient to cover the suture (3 mL total). One set of inserts containing an uncoated suture was spiked with 50 ng of FGF by adding the FGF directly to the medium and was used as a positive control. The cells were allowed 4 days to grow, fixed, and stained with crystal violet. Thereafter, the stain was eluted in aqueous methanol and 0.4% SDS and monitored at 595 nm.

Implants. Vicryl suture material was immersed in water, silyl-heparin, or silyl-heparin followed by FGF for 15 min at 37 °C. Vicryl, a synthetic absorbable surgical suture composed of a copolymer made from 90% glycolide and 10% L-lactide. The suture material was then rinsed extensively, air-dried, mounted on 16-guage needles, and stored until use, typically overnight. The batch receiving FGF was immersed in PBS/BSA containing 100 ng/mL FGF (15 min, 37 °C). The sutures were passed through the thigh muscle of adult rats under anesthesia and secured with knots and surgical clips. After two weeks the animals were euthanized and the sutured area removed, fixed in formalin, and processed by standard histological methods.

RESULTS

FGF Binding by Silyl-heparins and Heparin. The inhibition of binding of bFGF to heparin-agarose was used to compare silyl-heparins with heparin. The heparin used in this assay was the same as was used in the synthesis of the silyl-heparins. In this assay silyl-heparin 5135 provided essentially the same EC_{50} as unmodified heparin (Figure 2) when used on equal weight basis. One of the silyl-heparins, SH513−5, was selected for further study, as the EC_{50} was similar for each of the silyl-heparin variants examined.

Adsorption of Silyl-heparin onto Polymeric Substrates. Heparin-specific assays and dimethylene blue dye uptake were used to establish that silyl-heparin could be adsorbed to a variety of materials including polystyrene, hydrogel-coated polystyrene, polycarbonate, polyurethane, polycaprolactone, poly(vinyl chloride), stainless steel, titanium, platinum wire, and glow discharge-deposited siloxane (over stainless steel). The loading efficiency of silyl-heparin was generally in the range of 10 mIU/cm^2, but did vary by type of substrate.

Silyl-heparin Coated onto Polystyrene. Staining with crystal violet and dimethyl methylene blue, stains known to react with heparin verified the presence of silyl-heparin-5135 on the polystyrene. The bound stain could be seen visually as a light coloration on the bottom of the wells. The stains were solubilized in 1:1 methanol/0.1% SDS; this slightly increased the stain intensity. Little if any stain was detected on plates to which 1 mg/mL heparin was added or which were uncoated. Wells coated with silyl-hepain-5135 were positive for bioactive heparin as determined by monitoring the heparin-induced inhibition of antithrombin/factor Xa. Wells simi-

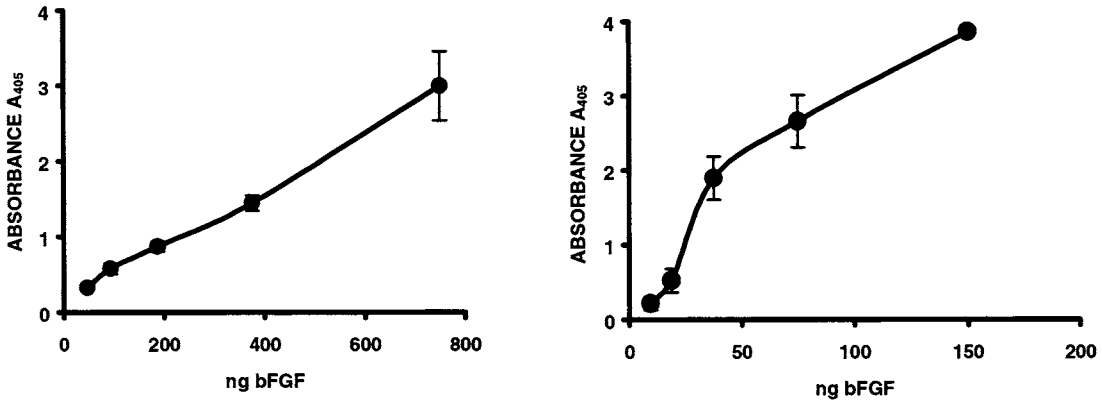


Figure 3. Effect of bFGF loading concentration the amount of bFGF bound to silyl-heparin. Left panel. The primary and secondary antibodies, as described in the Methods section were used at a dilution of 1:500. Right panel. The primary and secondary antibodies were used at a dilution of 1:250. The data represents the average ± SD.

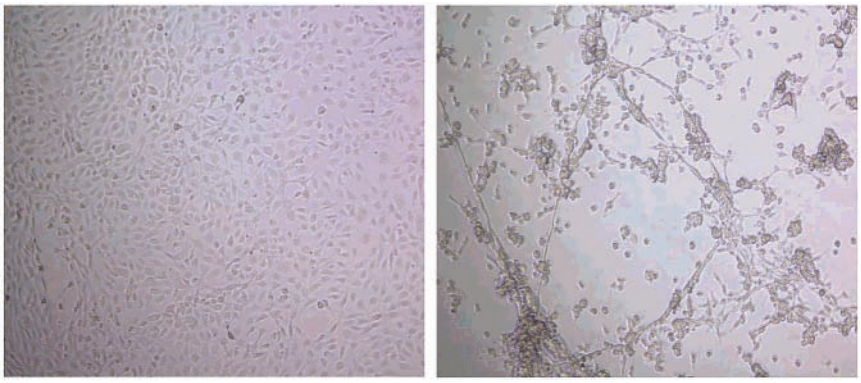


Figure 5. Capillary tube formation induced by growth of bovine aorta endothelial cells on FGF-silyl-heparin. The silyl-heparin was precomplexed to fibrinogen to increase the level of endothelial cell attachment. The panel on the left is a phase contrast micrograph of endothelial cells after 4 days on silyl-heparin/fibrinogen. The panel on the right illustrates endothelial cells grown on FGF-silyl-heparin/fibrinogen. Note the tubelike structures in the right panel and the typical endothelial cell morphology in the left panel.

larly coated with heparin or left untreated did not demonstrate such an inhibition.

bFGF Detection. bFGF was detected over a wide range of concentrations from as much as 750 ng to as low as 20 ng (Figure 3). The color development was linear at high concentrations indicating that under the conditions of the assay the upper saturation limit of the silyl-heparin had not been reached.

As controls, when anti-TGF-betaRII (irrelevant antibody directed against the transforming growth factor receptor) was used instead of FGF and at the same antidilutions, no bFGF was detected. When TGF-beta (40 ng) was used as an alternative to bFGF and with anti-bFGF antibodies, no activity was detected.

Effect of Adhesion Molecules on FGF Binding. Type IV collagen, fibronectin, and fibrinogen are known to complex to heparin, and therefore the effect of precomplexing these extracellular matrix molecules to silyl-heparin was evaluated (Figure 4). Fibronectin was found to considerably decrease the binding of bFGF to silyl-heparin, whereas type IV collagen and fibrinogen decreased the signal less. Immunochemical analysis of fibronectin indicated that it was bound to the silyl-heparin on the plate and had not undergone spurious sloughing.

Capillary Tube Formation. Bovine aorta endothelial cells underwent morphological changes consistent with the formation of capillary tube formation when cultured on a preformed coating of silyl-heparin plus fibrinogen and bFGF (Figure 5). Fibrinogen was used to help the endothelial cells attach to the silyl-heparin. It should be pointed out that the only source of bFGF was that which was bound to the silyl-heparin. Tubes did not form when the cells were cultured in wells coated with silyl-heparin, silyl-heparin and fibrinogen, fibrinogen, fibrinogen and FGF, or FGF. On silyl-heparin plus fibrinogen the cells formed essentially confluent monolayers.

Endothelial Cell Growth. FGF from the FGF/silyl-heparin coating was able to transit a separating membrane and act regionally to stimulate the growth of endothelial cells at the end of 4 days (Figure 6). In these experiments, FGF was complexed via silyl-heparin to suture material and separated from endothelial cells by a permeable membrane. The suture-derived FGF increased cell numbers to a similar extend as that observed in control cultures spiked with soluble FGF. Suture material coated with just silyl-heparin did not result in an increase in cell number.

Suture Implant. Coated sutures implant in rat muscle was selected as a simple model of an implant that could

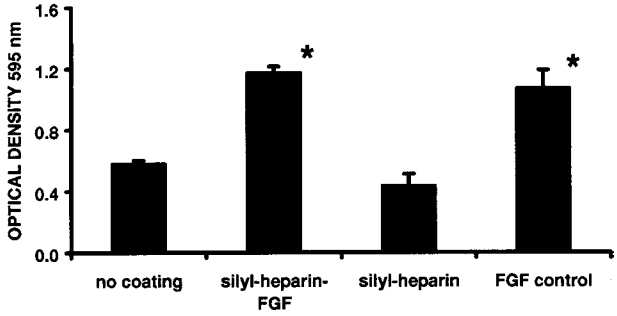


Figure 6. Trans-pore effect of FGF-silyl-heparin from coated sutures on the growth of bovine aorta endothelial cells after 4 days as determined by crystal violet staining. Cells were seeded into cluster plates and with 3 μm pores in the bottom placed in each well. Sutures with or without coatings were placed in the well and medium added sufficient to cover the suture. One set of inserts, containing an uncoated suture, was spiked by adding the FGF directly to the medium (positive control). The cells were allowed 4 days to grow, fixed, and stained with crystal violet. Thereafter, the stain was eluted in aqueous methanol and 0.4% SDS and monitored at 595 nm. The data are presented as the average absorbance ± SD. The asterisk indicates statistical significance greater than 0.05 as determined with Student's *t*-test.

be histologically monitored. At two weeks after implant, sutures coated with FGF/silyl-heparin had a marked increase in cell density in the area surrounding the implant compared to the uncoated suture or the suture coated with silyl-heparin (Figure 7). The diameter of the granulation tissue surrounding the implant coated with FGF/silyl-heparin was approximately 2 -fold larger than that of the uncoated material or silyl-heparin coated material (data not shown). The tissue surrounding the implant coated with FGF/silyl-heparin had numerous blood vessels (Figure 8) suggestive of angiogenesis.

DISCUSSION

FGFs have a well-characterized role in fibroblast and endothelial cell growth and are involved in angiogenesis, wound healing, tissue repair, and tissue regeneration (Powers et al., 2000). One of the defining features of the FGF family is a strong affinity for heparin and heparan sulfate proteoglycans. This affinity for heparin is shared by a number of other growth factors including VEGF, TGF-β, NGF, and PDGF, among others. The broad physiological impacts of growth factors on wound healing has led to efforts to deliver FGF, and other growth factors, from implant material or wound dressings (Nimni, 1997). A variety of approaches have been used for this

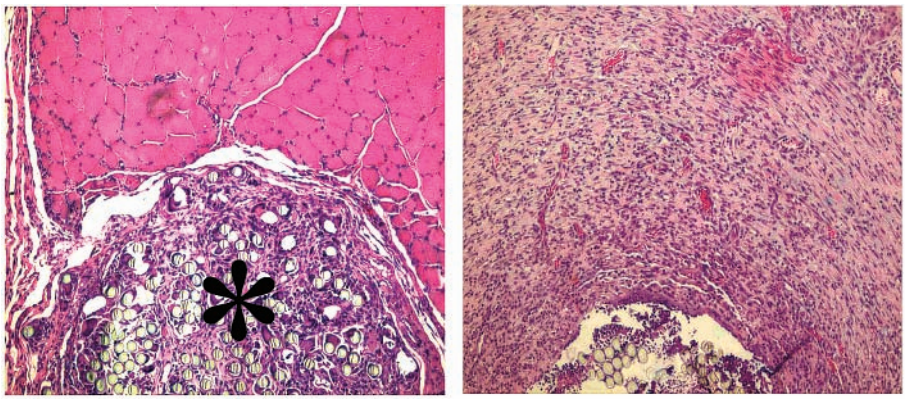


Figure 7. Morphology of tissue surrounding suture material with a silyl-heparin coating (left), and with FGF/silyl-heparin (right). Note the increased cellularity of in the tissue surrounding the suture coated with FGF/silyl-heparin. The suture marked in the panel on the left with an asterisk, and left unmarked (center bottom) in the panel on the right. Original magnification ×100, hematoxylin and eosin stain.

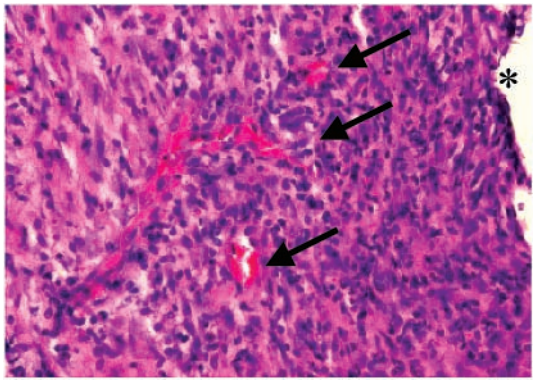


Figure 8. Micrograph of tissue surrounding a suture material coated with FGF/silyl-heparin. Note the presence of blood vessels (arrows) indicative of angiogenisis. The suture is marked with an asterisk. Original magnification ×400, hematoxylin and eosin stain.

purpose including using conjugation of FGF (Sakiyama-Elbert and Hubbell, 2000b), FGF embedded in matrixes (Soparkar et al., 2000; Wang, 1996), FGF complexed to heparin-conjugates (Bos et al., 1999; Wissink et al., 2000), and the use of genetic engineering approaches to producing FGF-secreting cells (Sosnowski et al., 1999).

Because of the potential wide application of FGF to implants ranging from cardiovascular (Post et al., 2001) to osteocartilagenous applications and the variety of matrixes and surfaces that might be involved, our approach was to develop a simple coating approach that could apply FGF to a large number of substrates. To that end, we have synthesized heparins with prosthetic groups that promote heparin adsorption. The bound heparin can then be used to further complex FGF. The overall method is simple and requires a low level of technical skill, as all of the adsorption steps are performed by immersion.

FGF bound to adsorbed silyl-heparin as determined by ELISA, and the amount of FGF bound was directly related to the amount offered for binding. This correlation should allow for predictable loading of FGF on implant surfaces. And while the focus of this report is on FGF, similar approaches have been used for complexing vascular endothelial growth factor (VEGF) and transforming growth factor-beta (TGF-β).

Heparin is known to bind to a variety of extracellular matrix molecules including fibronectin, laminin, and type IV collagen (Kreis, 1993). Additionally, it can bind fibrinogen and fibrin (Mohri et al., 1994; Odrljin et al., 1996). All the aforementioned proteins have been used to support cell attachment on various experimental implants. We evaluated the binding of FGF to silyl-heparin following an initial complexation with silyl-heparin, as this might be a desirable format for certain applications where cell attachment is desired. At the concentration of extracellular matrix protein used, fibronectin was found to substantially reduce the subsequent binding of FGF. Fibrinogen had the least effect.

One interesting observation was that endothelial cells cultured directly on FGF-silyl-heparin that had been precomplexed to fibrinogen underwent capillary tube formation. This appears to be similar to those formed when endothelial cells are cultured on extracellular matrix (Matrigel) in the presence of FGF (Garrido et al., 1995; Zimrin et al., 1995). This clearly indicated that the FGF-silyl-heparin was having a local effect on the endothelial cells. In our studies, capillary tubes rarely developed in cultures grown on silyl-heparin-fibrinogen without FGF. On Matrigel, the formation of capillary tubes is widely used as an in vitro model of angiogenesis.

One prediction of the use of FGF-silyl-heparin was that the complex should elute from an implant surface and effect cells in the general region. The trans-pore studies support that hypothesis as endothelial cell growth was stimulated when implant material was coated with FGF/silyl-heparin and supplied to the cells across a membrane barrier.

The suture model was also used to evaluate the effect of the FGF-silyl-heparin coating on wound repair. Following implant, the granulation tissue surrounding the implant had a larger diameter and a higher cell density than uncoated suture material, clearly suggesting a locoregional effect of the FGF bound to the suture material. A fuller examination of the dose−response characteristics of this response is planned.

Collectively, the results of the current study suggest that silyl-heparin could be a useful vehicle for the local delivery of FGF and other growth factors.

ACKNOWLEDGMENT

BNL is managed by Brookhaven Science Associates for DOE under Contract DE-AC02-98CH10886. This work was supported in part by NIH grant K01CA76483 (L.A.P.).

LITERATURE CITED

(1) Bos, G. W., Scharenborg, N. M., Poot, A. A., Engbers, G. H., Beugeling, T., van Aken, W. G., and Feijen, J. z(1999) Proliferation of endothelial cells on surface-immobilized

albumin-heparin conjugate loaded with basic fibroblast growth factor. *J. Biomed. Mater. Res. 44*, 330−40.
(2) Edelman, E. R., Nugent, M. A., Smith, L. T., and Karnovsky, M. J. (1992) Basic fibroblast growth factor enhances the coupling of intimal hyperplasia and proliferation of vasa vasorum in injured rat arteries. *J. Clin. Invest. 89*, 465−73.
(3) Flaumenhaft, R., Moscatelli, D., and Rifkin, D. B. (1990) Heparin and heparan sulfate increase the radius of diffusion and action of basic fibroblast growth factor. *J. Cell Biol. 111*, 1651−9.
(4) Garrido, T., Riese, H. H., Aracil, M., and Perez-Aranda, A. (1995) Endothelial cell differentiation into capillary-like structures in response to tumour cell conditioned medium: a modified chemotaxis chamber assay. *Br. J. Cancer. 71*, 770−5.
(5) Gosselin, C., Vorp, D. A., Warty, V., Severyn, D. A., Dick, E. K., Borovetz, H. S., and Greisler, H. P. (1996) ePTFE coating with fibrin glue, FGF-1, and heparin: effect on retention of seeded endothelial cells. *J. Surg. Res. 60*, 327−32.
(6) Groves, P. J., Shellis, R. P., and Dieppe, P. A. (1997) Use of poly(vinyl alcohol) to stabilize binding of sulfated glycosaminoglycans to dimethylmethylene blue. *Anal. Biochem. 245*, 247−8.
(7) Herr, A. B., Ornitz, D. M., Sasisekharan, R., Venkataraman, G., and Waksman, G. (1997) Heparin-induced self-association of fibroblast growth factor-2. Evidence for two oligomerization processes. *J. Biol. Chem. 272*, 16382−9.
(8) Ishihara, M., Saito, Y., Yura, H., Ono, K., Ishikawa, K., Hattori, H., Akaike, T., and Kurita, A. (2000) Heparin-carrying polystyrene to mediate cellular attachment and growth via interaction with growth factors. *J. Biomed. Mater. Res. 50*, 144−52.
(9) Kreis, T., Vale, R. (1993) *Guidebook to the Extracellular Matrix and Adhesion Proteins*, Oxford University Press, Oxford.
(10) Mach, H., Volkin, D. B., Burke, C. J., Middaugh, C. R., Linhardt, R. J., Fromm, J. R., Loganathan, D., and Mattsson, L. (1993) Nature of the interaction of heparin with acidic fibroblast growth factor. *Biochemistry 32*, 5480−9.
(11) Mohri, H., Iwamatsu, A., and Ohkubo, T. (1994) Heparin Binding Sites Are Located in a 40-kD gamma-Chain and a 36-kD beta-Chain Fragment Isolated from Human Fibrinogen. *J. Thromb. Thrombolysis 1*, 49−54.
(12) Moy, F. J., Safran, M., Seddon, A. P., Kitchen, D., Bohlen, P., Aviezer, D., Yayon, A., and Powers, R. (1997) Properly oriented heparin-decasaccharide-induced dimers are the biologically active form of basic fibroblast growth factor. *Biochemistry 36*, 4782−91.
(13) Nimni, M. E. (1997) Polypeptide growth factors: targeted delivery systems. *Biomaterials 18*, 1201−25.
(14) Nugent, M. A., and Iozzo, R. V. (2000) Fibroblast growth factor-2. *Int. J. Biochem. Cell Biol. 32*, 115−20.
(15) Odrljin, T. M., Shainoff, J. R., Lawrence, S. O., and Simpson-Haidaris, P. J. (1996) Thrombin cleavage enhances exposure of a heparin binding domain in the N-terminus of the fibrin beta chain. *Blood 88*, 2050−61.
(16) Post, M. J., Laham, R., Sellke, F. W., and Simons, M. (2001) Therapeutic angiogenesis in cardiology using protein formulations. *Cardiovasc. Res. 49*, 522−31.
(17) Powers, C. J., McLeskey, S. W., and Wellstein, A. (2000) Fibroblast growth factors, their receptors and signaling. *Endocr. Relat. Cancer. 7*, 165−97.
(18) Sakiyama-Elbert, S. E., and Hubbell, J. A. (2000a) Controlled release of nerve growth factor from a heparin-containing fibrin-based cell ingrowth matrix. *J. Controlled Release 69*, 149−58.
(19) Sakiyama-Elbert, S. E., and Hubbell, J. A. (2000b) Development of fibrin derivatives for controlled release of heparin-binding growth factors. *J. Controlled Release 65*, 389−402.
(20) Soparkar, C. N., Wong, J. F., Patrinely, J. R., and Appling, D. (2000) Growth factors embedded in an agarose matrix enhance the rate of porous polyethylene implant biointegration. *Ophthal. Plast. Reconstr. Surg. 16*, 341−6.
(21) Sosnowski, B. A., Gu, D. L., D'Andrea, M., Doukas, J., and Pierce, G. F. (1999) FGF2-targeted adenoviral vectors for systemic and local disease. *Curr. Opin. Mol. Ther. 1*, 573−9.
(22) Szebenyi, G., and Fallon, J. F. (1999) Fibroblast growth factors as multifunctional signaling factors. *Int. Rev. Cytol. 185*, 45−106.
(23) Teien, A. N., and Lie, M. (1977) Evaluation of an amidolytic heparin assay method: increased sensitivity by adding purified antithrombin III. *Thromb. Res. 10*, 399−410.
(24) Teien, A. N., Lie, M., and Abildgaard, U. (1976) Assay of heparin in plasma using a chromogenic substrate for activated factor X. *Thromb. Res. 8*, 413−6.
(25) Tsang, R., and Osaki, S. (1998) Nonthrombogenic coating composition and methods for using same, US 5,955,588.
(26) Wang, J. S. (1996) Basic fibroblast growth factor for stimulation of bone formation in osteoinductive or conductive implants. *Acta Orthop. Scand. Suppl. 269*, 1−33.
(27) Wissink, M. J., Beernink, R., Poot, A. A., Engbers, G. H., Beugeling, T., van Aken, W. G., and Feijen, J. (2000) Improved endothelialization of vascular grafts by local release of growth factor from heparinized collagen matrixes. *J. Controlled Release 64*, 103−14.
(28) Zarge, J. I., Husak, V., Huang, P., and Greisler, H. P. (1997) Fibrin glue containing fibroblast growth factor type 1 and heparin decreases platelet deposition. *Am. J. Surg. 174*, 188−92.
(29) Zimrin, A. B., Villeponteau, B., and Maciag, T. (1995) Models of in vitro angiogenesis: endothelial cell differentiation on fibrin but not matrigel is transcriptionally dependent. *Biochem. Biophys. Res. Commun. 213*, 630−8.

BC0155216

NMR Characterization of the DNA Binding Properties of a Novel Hoechst 33258 Analogue Peptide Building Block

Jakob Bunkenborg,[†] Carsten Behrens,[‡,§] and Jens Peter Jacobsen*[,†]

Department of Chemistry, University of Southern Denmark, Odense University, Odense M, DK-5230 Denmark, and Department of Chemistry, University of Copenhagen, Universitetsparken 5, DK-2100 Copenhagen Ø, Denmark. Received January 5, 2002; Revised Manuscript Received May 14, 2002

A novel aryl-bis-benzimidazole amino acid analogue of the DNA-binding compound Hoechst 33258 has recently been designed for incorporation in peptide combinatorial libraries by replacing the *N*-methylpiperazine group with a carboxyl group and the hydroxy group with an amino-methyl group. The DNA-binding properties of the aryl-bis-benzimidazole monomer with the C-terminus derivatized with 3-(dimethylamino)-propylamine has been investigated in this paper by ^{1}H NMR studies of two different complexes with two different DNA sequences: A_5 d(5′-GCCA_5CG-3′):d(5′-CGT_5GGC-3′) and A_3T_3 d(5′-CGA_3T_3CG-3′)$_2$. Chemical shift footprinting shows that the ligand binds at the center of the A_3T_3 sequence but at the 3′-end of A_5. A large number of NOEs show a well-defined complex with the ligand situated at the center of the palindromic A_3T_3 but with the asymmetric A_5 the ligand binds with an orientational preference with the bis-benzimidazole moiety displaced toward the 3′-end from the center of the duplex. Two families of models of the complexes with A_5 and A_3T_3 were derived with restrained molecular dynamics based on a large set of 70 and 61, respectively, intermolecular ligand NOEs. Both models give a picture of a tightly fitting ligand with close van der Waals contacts with the walls of the minor groove and with the two benzimidazole and the amide hydrogens involved in bifurcated cross-strand hydrogen bonds to adenine N3 and thymine O2. The minor groove width of the models correlate well with the binding site of the ligand, and the orientational preference is argued to be a consequence of the minor groove width and hydrogen bonding.

INTRODUCTION

A large number of molecules bind noncovalently to the minor groove of DNA with a preference for AT regions. These minor groove binders, a few of which are illustrated in Figure 1, have some characteristics in common. They are generally aromatic crescent-shaped molecules that are complementary in shape to the minor groove walls giving optimum van der Waals contacts while hiding the hydrophobic surface away from the solvent. They have hydrogen-bonding capabilities and cationic groups suited for the negative electrostatic potential of the AT minor groove. Hoechst 33258 is a prominent member of the minor groove binder family that has been extensively derivatized and studied thoroughly by a number of biophysical methods: calorimetry (Haq et al., 1997), DNase I[1] footprinting (Abu-Daya et al., 1995; Abu-Daya and Fox, 1997), electric linear dichroism (Bailly et al., 1993), X-ray crystallography (Pjura et al., 1987; Teng et al., 1988; Quintana et al., 1991; Spink et al., 1994; Vega et al., 1994; Clark et al., 1996a; Clark et al., 1996b; Clark et al., 1997), and NMR (Searle and Embrey, 1990; Parkinson et al., 1990; Embrey et al., 1991; Fede et al., 1991; Fede et al., 1993; Fede et al., 1993; Embrey et al., 1993; Bostock-Smith et al., 1997; Bostock-Smith et al., 1998; Higgins and Searle, 1999; Gavathiotis et al., 2000).

Hoechst 33258 has been the object of a very large number of investigations (see Lown (Reddy et al., 1999) for a review) because it is a fluorescent DNA stain with easy access across the cell membrane and it has some biological activity (e.g., it has found use as an anthelmintic (Denham et al., 1976)). Hoechst 33258 binds preferentially in the minor groove of DNA sequences that have at least four consecutive AT base pairs and binds strongly with a binding constant of 3×10^8 M^{-1} (Bostock-Smith and Searle, 1999; Haq et al., 1997; Loontiens et al., 1990) but can also bind to GC-rich sequences in an intercalative mode with a smaller affinity constant (Bailly et al., 1993; Rao and Lown, 1991; Moon et al., 1996). NMR and X-ray crystallographic structural studies of Hoechst 33258−DNA complexes have mainly been of palindromic binding sites with four or six AT base pairs (e.g., AATT (Pjura et al., 1987; Teng et al., 1988; Quintana et al., 1991); AAATTT (Vega et al., 1994; Spink et al., 1994) and TAATTA (Embrey et al., 1993)) with the exception of a recent NMR solution structure of the 2:1 complex with d(5′-CTTTTGCAAAAG-3′)$_2$ (Searle and Embrey, 1990; Gavathiotis et al., 2000). These studies unanimously find that Hoechst 33258 penetrates deeply into the minor groove with a binding stoichiometry of only

* To whom correspondence should be addressed (e-mail: jpj@chem.sdu.dk).

[†] University of Southern Denmark.

[‡] University of Copenhagen.

[§] Present address: Novo Nordisk A/S, Novo Nordisk Park 1, DK-2760 Måløv, Denmark.

[1] Abbreviations: CBB = 2′-(4-aminomethylphenyl)-3*H*,3′*H*-[2,5′]bibenzimidazolyl-5-carboxylic acid (3-dimethylaminopropyl)amide; DNA = deoxyribose nucleic acid; DNase I = deoxyribonuclease I; dsDNA = double stranded DNA; DSS = 2,2-dimethyl-2-silapentane-5-sulfonate; EDTA = ethylenediaminetetraacetic acid; HSQC = heteronuclear single quantum coherence; NMR = nuclear magnetic resonance; NOE = nuclear Overhauser effect; NOESY = nuclear Overhauser effect spectroscopy; RMD = restrained molecular dynamics; TOCSY = total correlation spectroscopy; TOPI = topoisomerase I; WATERGATE = water suppression by gradient-tailored excitation.

10.1021/bc020001b CCC: $22.00 © 2002 American Chemical Society
Published on Web 08/14/2002

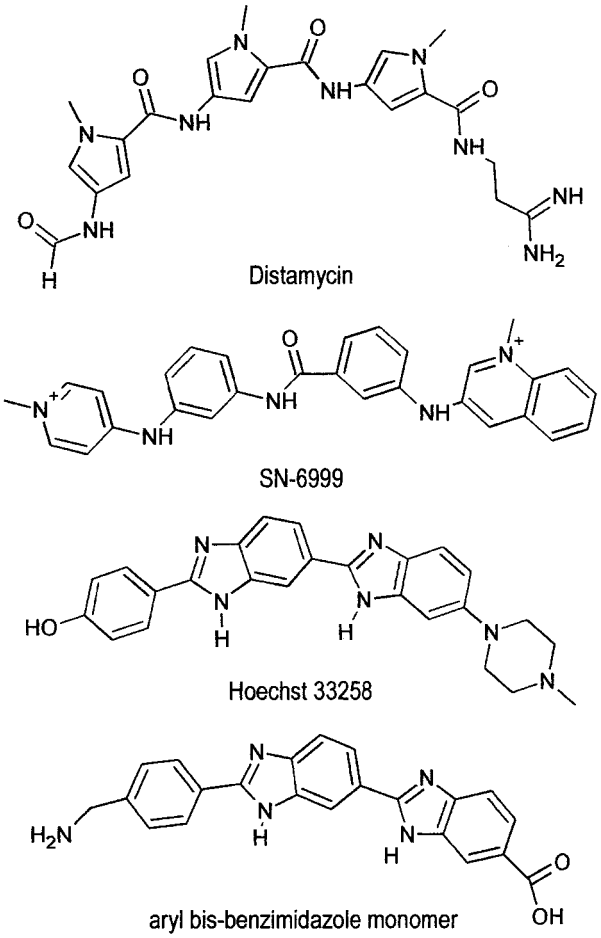
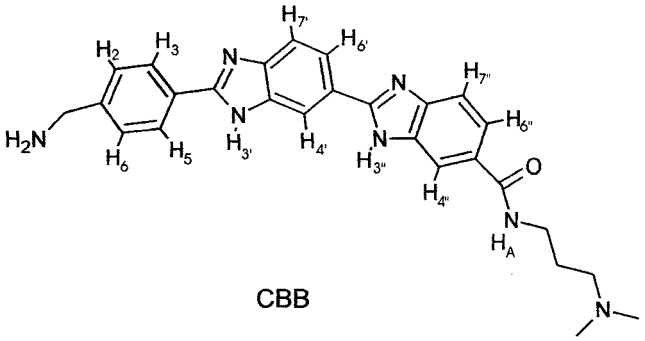


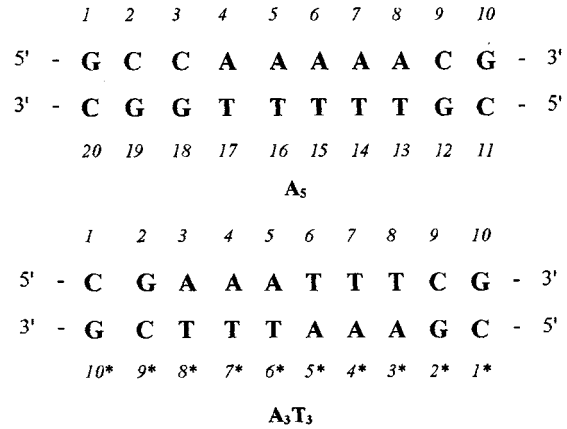
Figure 1. The minor groove binding ligands distamycin, SN-6999, and Hoechst 33258, and the novel Hoechst 33258 analogue bis-benzimidazole amino acid building block. These compounds are characterized by being composed of several planar aromatic moieties, by having a number of hydrogen bond donors, and by having a crescent shape that fits the minor groove.

one molecule bound per site. Each benzimidazole interacts with two A:T base pairs by means of a bifurcated cross strand hydrogen bond and spans approximately one and a half base pairs. The sequence selectivity and high binding affinity for AT regions have been attributed to the negative electrostatic potential within the minor groove of AT sequences (Lavery and Pullmann, 1981) and a narrowing of the walls of the minor groove for A-tracts.

A novel aryl-bis-benzimidazole amino acid analogue of the DNA-binding compound Hoechst 33258 has been designed as described in a preceding paper for incorporation in peptide combinatorial libraries by replacing the *N*-methylpiperazine group with a carboxyl group and the hydroxy group with an amino-methyl group (Behrens and Nielsen, 2001). To investigate the DNA binding properties of the aryl-bis-benzimidazole monomer a short minor groove binder 2′-(4-aminomethylphenyl)-3*H*,3′*H*-[2,5′]-bibenzimidazolyl-5-carboxylic acid (3-dimethylaminopropyl)amide (CBB, Scheme 1) where the C-terminal has been linked to 3-(dimethylamino)-propylamine was synthesized as described (Behrens and Nielsen, 2001). We have used ^{1}H NMR spectroscopy and molecular modeling to characterize the binding of CBB to the synthetic oligonucleotides d(5′-GCCAAAAACG-3′):d(5′-CGTTTTTG-GC-3′) and d(5′-CGAAATTTCG-3′)$_2$ (henceforth A_5 and A_3T_3). A large number of drug−DNA NOE connectivities (70 in all for the A_5−CBB complex and 61 for the A_3T_3−CBB complex) defines the binding site of CBB in the minor groove with some precision. CBB binds to the

Scheme 1. Chemical Structure of CBB and Numbering Scheme for the dsDNA Duplexes Used[a]





[a] Asterisks in the numbering scheme for A_3T_3 become relevant when the asymmetric CBB ligand binds to the DNA duplex and the two strands become distinguishable in the asymmetric complex

asymmetric oligonucleotide with an orientational preference with the NH_2-terminus of CBB situated at the beginning of the A-tract.

EXPERIMENTAL PROCEDURES

Materials. Purified DNA oligonucleotides were purchased from DNA Technology (Aarhus, Denmark) and desalted using a Sephadex G15 column. The non-self-complementary single-stranded DNA oligomers were added to an equivalent amount of the complementary strand, and both duplexes were formed by annealing from 80 °C to room temperature over 2 h. The numbering schemes for the duplexes are shown in Scheme 1 together with a numbering scheme for CBB that follows the conventional Hoechst 33258 naming.

A phosphate buffer containing ethylenediaminetetraacetic acid (EDTA) to complex paramagnetic ions, 2,2-dimethyl-2-silapentane-5-sulfonate (DSS) as a chemical shift reference and NaN_3 as antibacterial agent was added, giving a final concentration in the NMR sample of 10 mM P_i (pD = 7.0), 0.025 mM EDTA, 0.1 mM DSS, and 0.01 mM NaN_3 in 500 μL of 99.96% D_2O (from Cambridge Isotope Laboratories). The concentrations of the single-stranded DNA were determined by UV absorption and the complementary stands were added to yield a concentration of 2 mM. For experiments in H_2O, a mixture of 90% H_2O/10% D_2O (500 μL) were used. A CBB stock solution was prepared in 99.96% D_2O and neutralized with 100 mM NaOD. CBB was titrated into the A_5 duplex DNA sample in approximately 0.4 mol of equiv/addition. The sample was slightly undertitrated (<5% free duplex) because a slight overtitration resulted in line broadening. The sample remained stable for months.

NMR Experiments. All NMR experiments on the DNA−CBB complex were performed on a Varian Unity 500 MHz NMR spectrometer and a Varian INOVA 800 MHz NMR spectrometer. NOESY spectra in D_2O were acquired with a mixing time of 100 and 200 ms using 2048 complex points in t_2 and a spectral width of 5000 Hz for a total of 512 t_1 experiments with 64 scans each at 298 K and at 308 K. An additional NOESY spectrum in D_2O was acquired at 800 MHz with a mixing time of 200 ms using 4096 complex points in t_2 and a spectral width of 8000 Hz for a total of 600 t_1 experiments with 48 scans each at 280 K. NOESY spectra in H_2O were acquired using 2048 complex points and a spectral width of 10000 Hz using a WATERGATE-NOESY (Piotto et al., 1992).

TOCSY experiments in D_2O were acquired with mixing time of 90 ms using 2048 complex points in t_2 and a spectral width of 5000 Hz with total of 512 t_1 experiments with 64 scans each. DQF−COSY experiments in D_2O were acquired using 2048 complex points in t_2 and a spectral width of 5000 Hz with total of 1024 t_1 experiments with 64 scans each. ^{1}H-^{13}C HSQC experiments were collected at natural abundance with 2048 complex points in t_2 using a spectral width of 5000 Hz; 660 t_1 experiments with 48 scans were recorded.

The acquired data were processed using FELIX (Version 97.2, Biosym/MSI, San Diego, CA). The free induction decays were apodized with skewed sine bell squared functions. The B-DNA resonances were assigned in the conventional way as described in the literature (Wijmenga and van Buuren, 1998). Assignment of the CBB resonances with the drug bound to DNA closely resembles the strategy described for Hoechst 33258 and an analogue (Fede et al., 1991; Bostock-Smith et al., 1998) for the aryl-bis-benzimidazole body and the flexible dimethylamino-propylamide linker was assigned nonstereospecifically using a combination of COSY, NOESY, and HSQC spectra.

Molecular Modeling. Molecular modeling was carried out on a Silicon Graphics O_2 with AMBER 6 (Case et al., 1999) software and employing the AMBER 94 force field. The starting canonical Arnott B-DNA models of the A_3T_3 and A_5 duplex were generated with the NUCGEN module. The CBB molecule was built in the XLEAP module, and missing force-field parameters were then estimated from the values of similar fragments and was then energy-minimized. The electrostatic potential was calculated with the HF/6-31G* basis set for the entire molecule using the Gaussian 94 program (Frisch et al., 1995), and the atomic centered charges were fitted to the electrostatic potential using the RESP module. CBB was then docked manually in the B-DNA minor groove using the XLEAP module of AMBER. A total of 70 intermolecular CBB−A_5 distance restraints and 61 CBB−A_3T_3 distance restraints were derived from NOESY data. NOE cross-peaks were classified semiquantitatively into three categories relative to the cytosine H5−H6 cross-peak volume: strong (1.8−2.5 Å), medium (2.5−3.7 Å), and weak (3.7−5.5 Å). A set of 30 structures was generated for each complex with the following protocol: An initial energy minimization was followed by 14 ps restrained molecular dynamics beginning at 400 K for a 4 ps period before cooling to 300 K in two 50 K steps. The outcome of this procedure was then energy minimized to a maximum derivative of 0.01 Å. As a further test, the experimental distance restraints were weighted with a force constant of 20 K cal Å^{-2} mol^{-1} and all of these restraints were fulfilled within 0.1 Å in the final models.

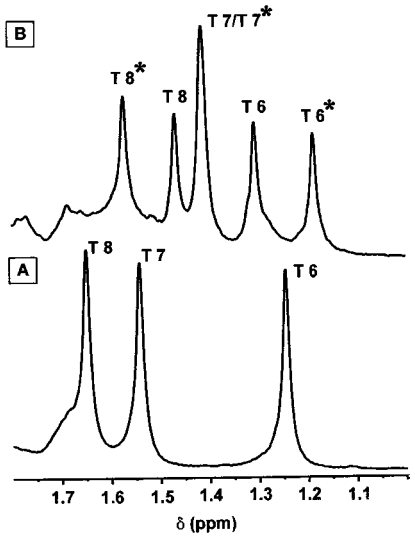


Figure 2. 1D ^{1}H NMR spectra of the thymine methyl region of (A) ligand-free A_3T_3 and (B) of the A_3T_3 complex with CBB. The thymine methyl proton resonances on the two strands are identical in the palindromic A_3T_3 duplex, but the symmetry is broken by the binding of CBB as evidenced by the appearance of a set of thymine methyl resonances for each strand (cf. Scheme 1).

The drug was docked in five different starting positions (∼1 bp apart) to ensure that the binding site was not an artifact of a local minimum energy starting structure and then submitted to the same RMD protocol and energy minimization, and all five ended in the same family of structures as the 30 others.

RESULTS

NMR Titration. One-dimensional ^{1}H NMR spectra were recorded at 298 K during the titration of the two duplexes with CBB, and they showed that the ligand forms a well-defined 1:1 CBB/duplex stoichiometry complex with fairly narrow lines (7 Hz) in both cases. Only a single form of complex was seen during the titration and CBB dissociates slowly on the NMR time scale from the duplex as evidenced by two distinct sets of DNA resonance lines from free and complexed DNA. In both cases, the asymmetric CBB binds to a single site which in the case of A_3T_3 breaks the dyad symmetry of the duplex leading to a doubling of the oligonucleotide resonances. The methyl region, shown in Figure 2, gives a very clear illustration of the symmetry breakage where the three thymine methyl resonances of the symmetric ligand-free A_3T_3 duplex are split into five distinct resonances in the final 1:1 complex. Only one set of resonances from CBB was observed during the titration to A_5 indicating that CBB binds with an orientational preference in the asymmetric AT-tract.

Characterization of the CBB−DNA Complexes. The assignment of resonances for the DNA and ligand followed the conventional approach using a combination of TOCSY and COSY for identifying deoxyribose and CBB spin systems and NOESY for establishing the sequential connectivity (the sequential $H1'_{(n-1)}$ − H6/H8$_{(n)}$ − $H1'_{(n)}$ connectivity pattern is shown in Figure 3). To resolve overlap and to obtain the largest possible number of unambiguous assignments, the spectra were acquired at several temperatures. A ^{1}H-^{13}C HSQC provided valuable information for resolving overlapping H2′/H2″ and dramatically upfield shifted H4′ resonances. The noncovalent binding of CBB to the duplex induces large changes in the DNA resonances and the perturbations

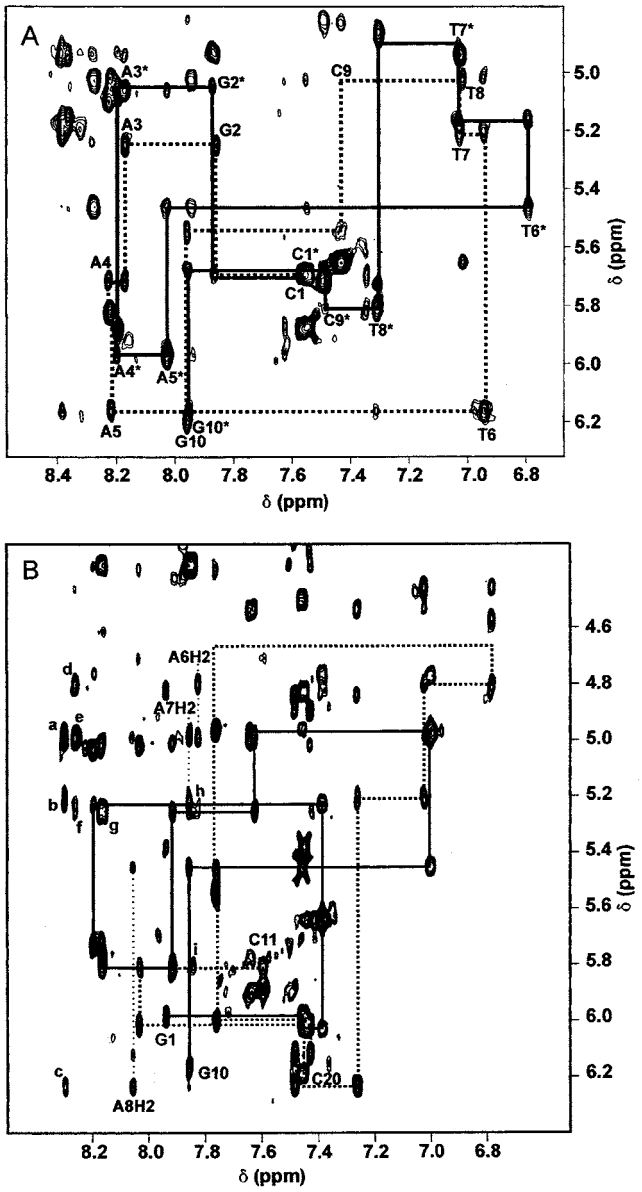


Figure 3. (A) The aromatic to H1′ region of an 800 MHz NOESY spectrum (mixing time of 200 ms) of the CBB−A_3T_3 complex at 280 K. The full sequential $H1'_{(n-1)}$ − $H6/H8_{(n)}$ − $H1'_{(n)}$ connectivity pattern is shown with solid lines for unprimed strand and with dashed lines for the other strand. (B) The aromatic to H1′ region of a 500 MHz NOESY spectrum (mixing time of 200 ms) of the CBB−A_5 complex at 308 K. The sequential $H1'_{(n-1)}$ − $H6/H8_{(n)}$ − $H1'_{(n)}$ connectivity pattern is sketched with solid lines for the A-strand and with dashed lines for the T-strand. The connectivity between T17−G18 is missing due to presaturation of water but is assignable at lower temperatures. A few NOE cross-peaks between CBB and the DNA are highlighted and assigned as follows: (a) H4″-A8H1′, (b) H4″-T15H1′, (c) H4″-T14H1′, (d) H4′−T17H1′, (e) H4′−A7H1′, (f) H4-A6H1′, (g) H3/H5-A6H1′, (f) H2/H6-A6H1′, and (i) H2/H6-A5H1′. Furthermore, NOE connectivities to A6H2, A7H2, and A8H2 are indicated with thin dotted lines.

to the proton chemical shifts ($\Delta\delta = \delta_{DNA-CBB} - \delta_{DNA}$) are shown in Figure 4. The greatest perturbations were observed for the deoxyribose H1′ and H4′, which are located in the minor groove, but significant (> 0.1 ppm) shifts were observed for other DNA protons as well. The chemical shift perturbations are quite similar for the two duplexes, and the pattern indicates that CBB spans 4−5 base pairs. The chemical shift changes for the A_3T_3 H6/H8 and H1′ protons are very much like those of an analogue complex with a Hoechst analogue (Bostock-Smith and Searle, 1999). For the palindromic A_3T_3, the perturbations seem to be particular pronounced for the thymine resonances, and the symmetric pattern suggests that the ligand binds centrally across the dyad axis of the duplex. For A_5, the perturbations are most pronounced for the residues on the A-strand toward the 3′-end of the A-tract, but 2−3 residues earlier the ligand causes the greatest perturbations for the thymines of the T-strand. A very similar chemical shift perturbation pattern is observed for the minor groove binding of SN-6999 to an A_5 binding site (Rydzewski et al., 1996). This strand crossing behavior is seen for a number of minor groove binders and simply reflects that these residues are close in space. The close proximity of the groove walls to CBB causing the dramatic ring current induced upfield shift of H4′ indicates that the ligand penetrates deeply into the minor groove and has close contacts with the walls. The chemical shift changes can be rationalized on the basis of the model where the aromatic rings of CBB are inserted edge-on into the minor groove as illustrated in Figure 8. The H1′ and H4′ resonances (situated at the walls of the minor groove) experience large upfield shifts because they are positioned perpendicular to the ring-plane of the ligand, while the H2 resonances (located at the floor of the minor groove) experience large downfield shifts because they are positioned parallel with the ring plane.

The NOESY data acquired in D_2O and H_2O contain a very large number of intermolecular NOE contacts between ligand protons and DNA sugar and adenine H2 protons, a few of which are shown in Figure 5. These connectivities show that the ligand is bound in the minor groove in agreement with the chemical shift perturbations. NOEs between adenine H2 protons and H1′ protons of the base pairing thymine indicate a narrow minor groove. The orientation of CBB within the A-tract is unambiguously defined by the pattern of NOEs to the floor of the minor groove as indicated in Figure 5: NOEs from the aryl H2/H6 to A4H2 places the NH_2-end of CBB at the 5′-end of the A-tract and the contacts to H2 can be followed along CBB to the A8H2 at the 3′-end of the A-tract. The ligand is situated with the bis-benzimidazole-carbonyl at the 3′-end of the A-tract and the flexible dimethylamino-propylamide extending into the GC region as indicated by a number of NOE connectivities (e.g., *N*-methyl to C9H1′ and G10H1′). No resonances were observed that could be attributed to a complex with the CBB-ligand binding in the opposite direction, and therefore the orientational preference is estimated to be larger than 20:1.

Molecular Modeling. Molecular models of the CBB complexes with the asymmetric A_5 and the symmetric A_3T_3 were generated by restrained molecular dynamics followed by restrained energy minimization using semi-quantitative NOE-derived distance restraints. The models indicate that CBB penetrates deeply into the A-tract with each of the aromatic rings almost parallel to the walls of the groove. Of the 30 models, the 15 with lowest energy were selected for further analysis. The DNA duplex retains an overall right-handed B-DNA conformation in both complexes in accordance with the cross-peak pattern of the DQF−COSY spectra that clearly indicate a B-type DNA-conformation [$J_{1'2'} > J_{1'2''}$] for all residues except the terminal ones.

Intermolecular hydrogen bonds were assigned using the CARNAL module of AMBER for the labile protons on the ligand on the basis of the models (only H3′, H3″, and H_A showed unambiguous bonding partners in all

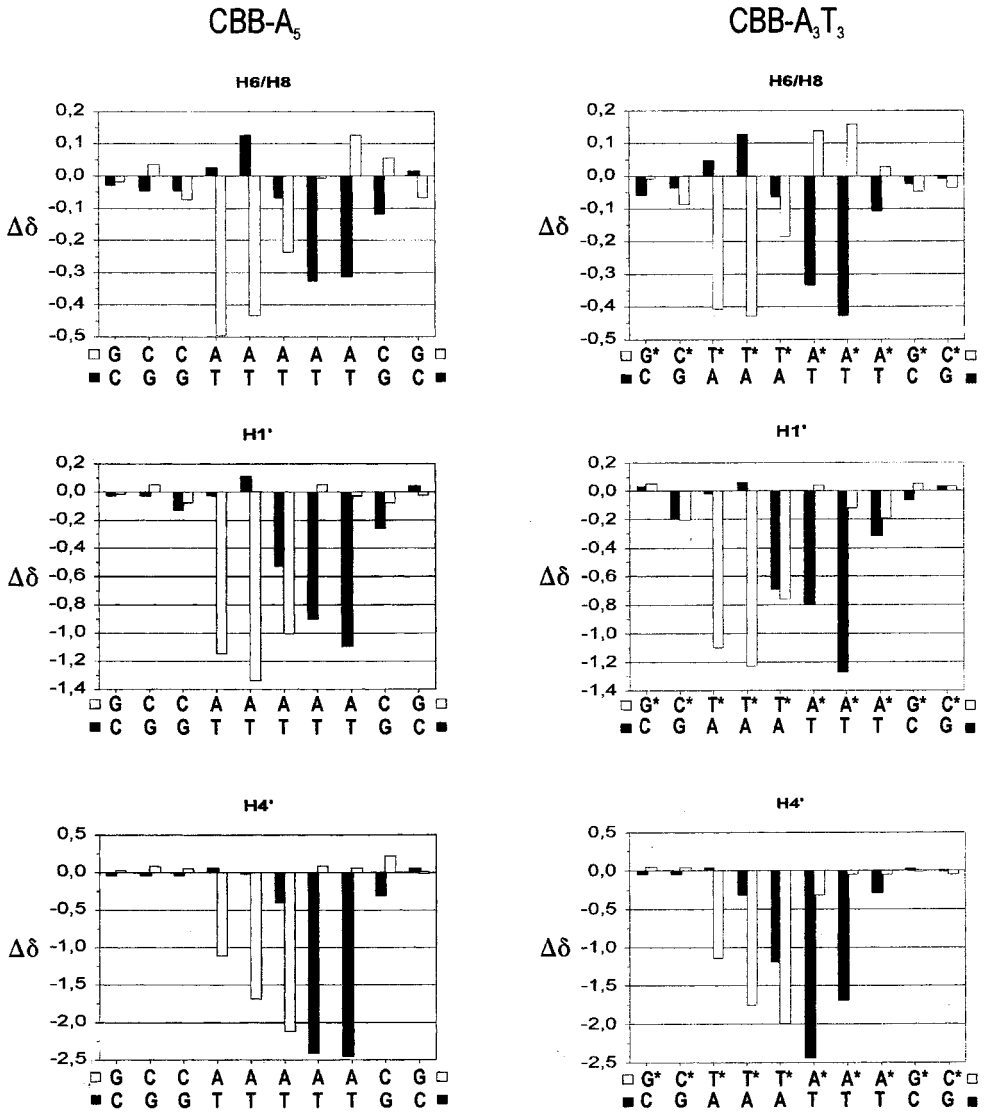


Figure 4. Chemical shift changes in ppm of the H6/H8 aromatic, H1′ and H4′ deoxyribose A_5 (A) and A_3T_3 (B) protons induced by the binding of CBB. The change in proton resonances for each residue is shown with the empty bars corresponding to the first sequence underneath the graph and the black bars to the lowest sequence. The two NOE-based models are consistent with the chemical shift perturbations as illustrated in Figure 8.

models). As indicated in Scheme 2 the protons are engaged in bifurcated cross-stand hydrogen bonds involving the adenine N3 and thymine O2 as hydrogen-bond acceptors.

Both models exhibit a sequence-dependent minor groove width. The average phosphate−phosphate interstrand distance minus the van der Waals radius of phosphorus (5.8 Å) is shown in Figure 7. To assess the resulting models, the minor groove width for a number of related crystallographic structures containing the central 5′-A_3T_3-3′ sequence is shown in Figure 7 with a structure of the native DNA (Edwards et al., 1992), two Hoechst complexes (Spink et al., 1994; Vega et al., 1994) and a distamycin complex (Coll et al., 1987).

DISCUSSION

Extensive studies have made it increasingly clear that the minor groove width is very sequence dependent and that segments of DNA containing four or more consecutive A bases (A-tracts) exhibit a characteristic narrowing of the minor groove. NMR studies have shown that the minor groove becomes increasingly narrow in the 5′−3′ direction of an A-tract reaching a lower plateau after approximately four adenines (Chuprina et al., 1991; Katahira et al., 1990; Nadeau and Crothers, 1989). The minor groove is narrowest at the center of the symmetric sequence A_3T_3, while the A_5 has the smallest minor groove width at the 3′-end of the A-tract. These structural characteristics have been corroborated by a number of observations:

(i) The binding mode of distamycin has been shown to be very sensitive to the width of the minor groove (Pelton and Wemmer, 1989); depending on the sequence of the target duplex DNA distamycin can form either a 1:1 complex or a cooperative side-by-side binding 2:1 complex. For sequences with five or more consecutive AT bases that have narrow minor grooves (e.g., A_5) only 1:1 binding stoichiometry complexes are formed, while sequences with broad minor grooves (e.g., ATATA) only form 2:1 complexes.

(ii) Recent NMR studies by Feigon et al. (Hud et al., 1999) have shown that ammonium ion binding is most favored in the narrowest region of the A-tract minor groove, which turned out to be at the center for d(5′-GCA_4T_4GC-3′)$_2$ and at the 3′ end for the d(5′-GCA_5CG-3′):d(5′-CGT_5CG-3′) sequence.

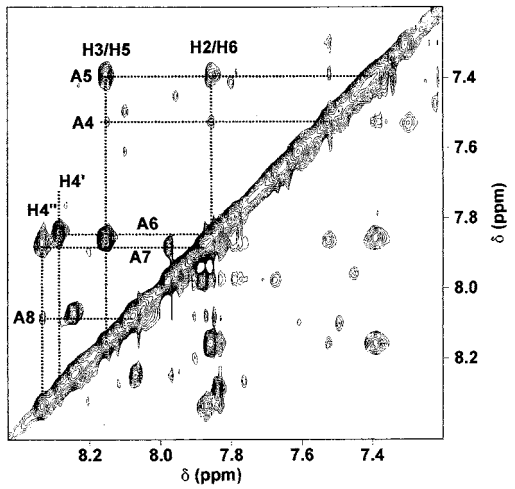


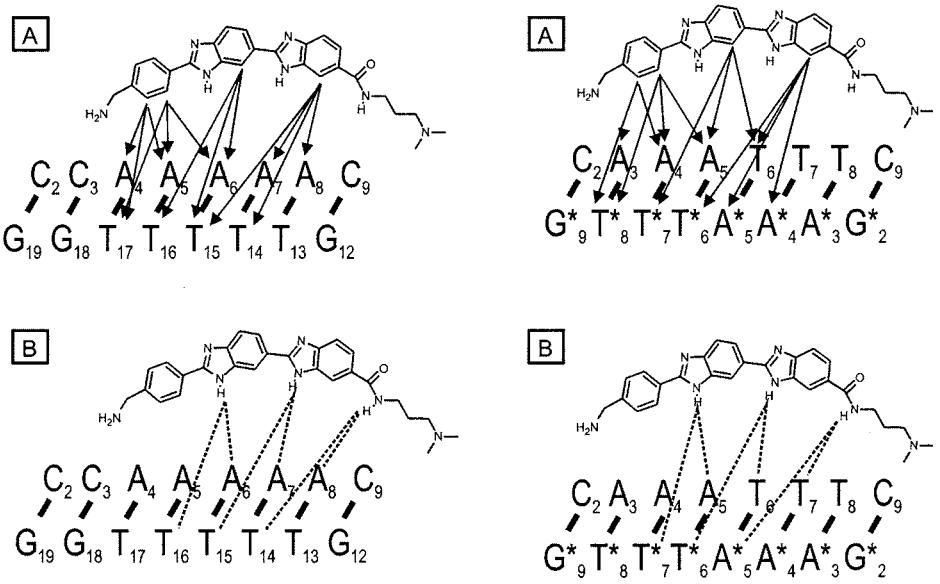
Figure 5. An excerpt of the 200 ms NOESY spectrum at 800 MHz and 280 K showing the aromatic region of the CBB-A_5 complex. The connectivities between the ligand and the adenines H2 protons at the floor of the minor groove can be followed along the A-tract beginning with connectivities between A4H2 and A5H2 to the H2/H6 and H3/H5 aryl protons, A6H2 to H4′ benzimidazole proton and then A7H2/A8H2 to H4″ benzimidazole proton. This unambiguously demonstrates that CBB binds with an orientational preference to the A-tract.

The minor groove width of the models conform very well with the above-mentioned sequence dependence. In the case of A_3T_3, a fairly large number of X-ray structures are available for the related dodecamer d(5′-CGCA_3T_3GCG-3′)$_2$, and there seems to be only fairly small variations in minor groove width from the native dodecamer (Edwards et al., 1992) to the three minor groove binding complexes of Hoechst 33258 (Vega et al., 1994; Spink et al., 1994) and distamycin (Coll et al., 1987). We have not found any obvious structures to compare A_5 with but the two A-tract X-ray structures (DiGabriele et al., 1989; DiGabriele and Steitz, 1993) have minor groove widths that lie within the error bars. Crystal packing forces are always a concern for X-ray structures, but the decrease in minor groove width also follows the pattern for the solution state duplexes found by NMR (Katahira et al., 1990; Nadeau and Crothers, 1989).

The features of the models are in accordance with other observations. Cross-peaks between an adenine H2 and the deoxyribose H1′ of the 3′-neighbor residue on the same strand and the 3′-neighbor of the base pairing residue on the complementary strand are indicative of a narrow minor groove (Chuprina et al., 1991; Katahira et al., 1988). For A_5, these cross-peaks become larger toward the 3′-end (A6H2, A7H2, and A8H2 have fairly large cross-peaks as can be seen in Figure 3) and for A_3T_3 it is especially large for A5H2 and A5*H2 at the center of the duplex. The propeller-twist angles are known to be fairly large at A-tracts and can be estimated from the NOEs between the thymine imino proton and the H2 of the base pairing and 3′-neighboring adenines (Katahira et al., 1988). The relative intensities had a value of around 1:0.4 in the H_2O−Watergate−NOESY spectra for the resolved pairs in CBB−A_5 and CBB−A_3T_3 complexes, which suggests a relatively large propeller-twist angle of about 17° according to Katahira (Katahira et al., 1990).

In the A_3T_3−CBB model, the ligand binds with the bis-benzimidazole moiety at the center of the binding site, which is where the minor groove is at its narrowest. This does not agree particularly well with the two X-ray structures of Hoechst 33258 in a A_3T_3-site: In one, the ligand is displaced somewhat off-center with the piperazine ring moving toward the broader part of the minor groove end of the dodecamer (Vega et al., 1994) and in the other Hoechst is further displaced and binds across the ATTTG sequence (Spink et al., 1994). The position of CBB is altered somewhat from that of Vega et al. (Vega et al., 1994) where the first benzimidazole after the phenyl group makes bifurcated hydrogen bonds to the two thymine O2 across the central ApT step. In the model of CBB, it is the second benzimidazole from the N-terminus that forms hydrogen bonds across the center as indicated in Scheme 2. In the X-ray structure of Spink et al. (Spink et al., 1994), the piperazine group is shifted even further down toward the 5′-end. However, these structures are a bit at variance with two NMR-studies: An analogue of Hoechst 33258 was found to bind at the center of a A_3T_3 binding site (Bostock-Smith and Searle, 1999) and Hoechst 33258 binds at the center of the longer A_4T_4 binding site (Higgins and Searle, 1999). The models

Scheme 2. (A) Schematic Representation of the CBB−A_5 and CBB−A_3T_3 Complexes with a Few of the Observed Intermolecular NOE Connectivities Observed between the Minor Groove Binding Ligand and the Duplexes. (B) On the Basis of the Models, the Bifurcated Hydrogen Bonds between CBB and the Thymine O2 or Adenine N3 at the Floor of the Minor Groove Are Indicated with Dashed Lines



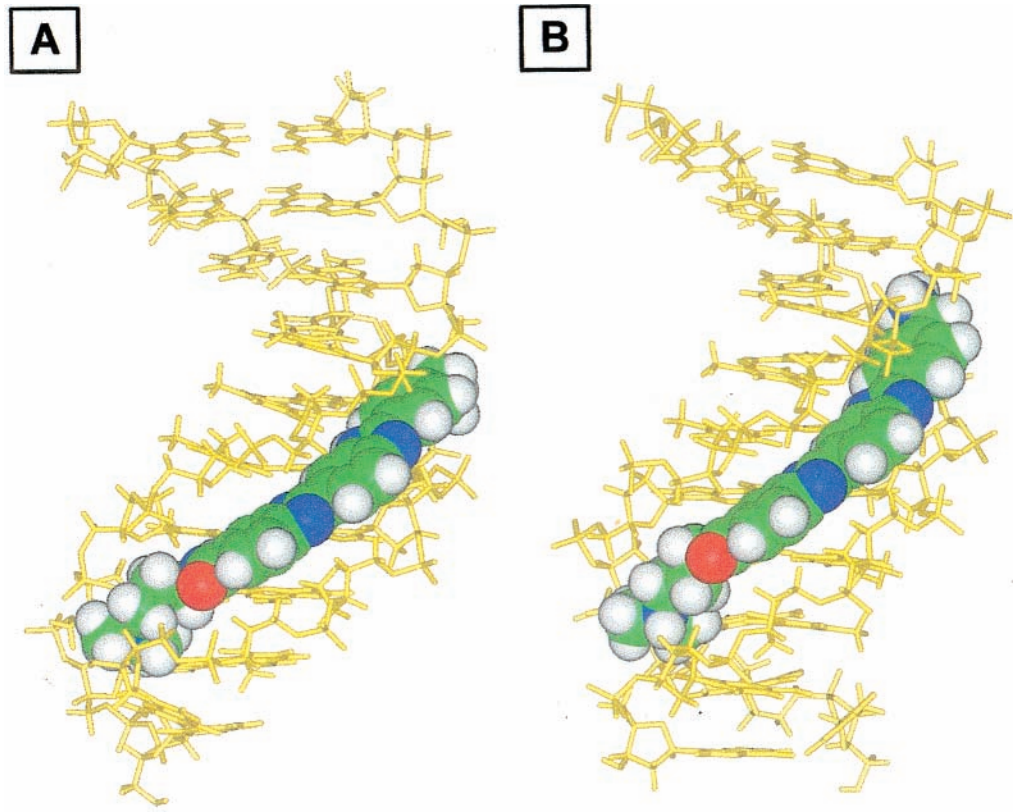


Figure 6. NOE-based models of the (A) CBB−A_5 and (B) CBB−A_3T_3 complexes obtained by restrained molecular modeling viewed into the minor groove. The CBB ligand, shown in a spacefilling CPK mode, fills the minor groove and binds at the center of the A_3T_3 decamer but is displaced toward the 3′-end of the A-tract for the A_5 decamer.

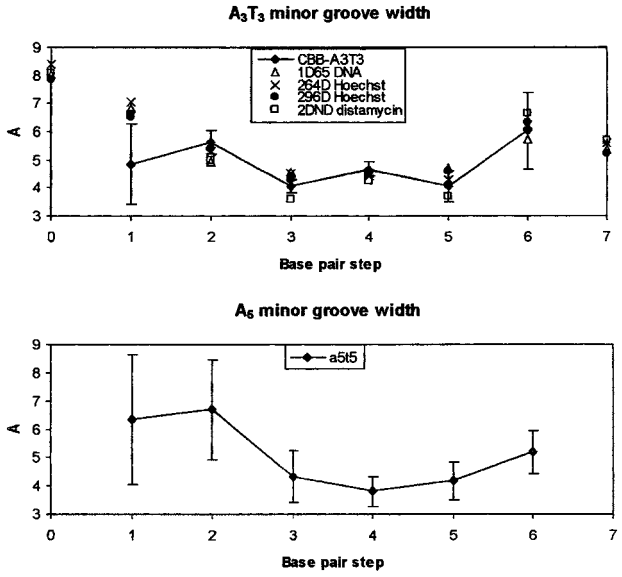


Figure 7. The average minor groove width of the (A) CBB−A_5 and (B) CBB−A_3T_3 complex for the model-ensemble shown together with that of a B-DNA dodecamer $(CGCA_3T_3GCG)_2$ a few analogous minor groove binder complexes (named by the PDB accession code) containing the A_3T_3 binding site. The error bars represent 1 standard deviation for the NOE-RMD derived ensemble.

of the CBB complexes may be sound enough despite this controversy, because the exact position of the Hoechst ligand depends strongly on the DNA conformation and in turn is dependent on the crystal packing as illustrated by a recent set of X-ray diffraction structures of *m*-iodo Hoechst analogue DNA complexes (Squire et al., 2000). On dehydrating the crystals the minor groove becomes increasingly narrow and in response to the changing DNA conformation the Hoechst analogues migrate about 3 Å along the groove—mainly to accommodate the bulky piperazine group in the wider part of the minor groove.

The minor groove width of the crystal structure of ligand free A_3T_3 is very similar to several drug−A_3T_3 complexes, and it seems that the binding of Hoechst 33258 does not perturb the structure greatly. This would suggest that the binding of Hoechst 33258 is more of a "lock-and-key" type of process than an "induced-fit". In both A_3T_3 and A_5, the drug molecule binds to the narrowest part of the AT-region of the ligand free DNA. However, an NMR study by Searle with a recent NMR solution structure has found the binding at the two sites of $d(5'\text{-CTTTTGCAAAAG-}3')_2$ (Searle and Embrey, 1990; Gavathiotis et al., 2000) is highly cooperative with only the 2:1 complex detected in equilibrium with the free duplex. No evidence was found of an intermediate 1:1 complex, and this was taken as conclusive evidence of cooperative binding. This cooperative binding is distinctly different from the side-by-side-binding of distamycin, and it is difficult to envision a mechanism by which the binding of one Hoechst molecule in one end of the DNA strand should facilitate the binding of yet another Hoechst molecule at the other end of the DNA strand.

The binding site placements of CBB seem fairly rationalizable in terms of binding site properties. A calorimetric study has shown that the major driving force for Hoechst 33258 is the hydrophobic transfer of the dye from solution into the binding site with a relatively minor contribution from hydrogen bonding and van der Waals contacts (Haq et al., 1997). How one can distinguish between hydrophobic interactions (dependent on changes in solvent-accessible surface area) and van der Waals interaction (depending on the number of close contacts) is not quite clear because the two contributions seem to be fairly

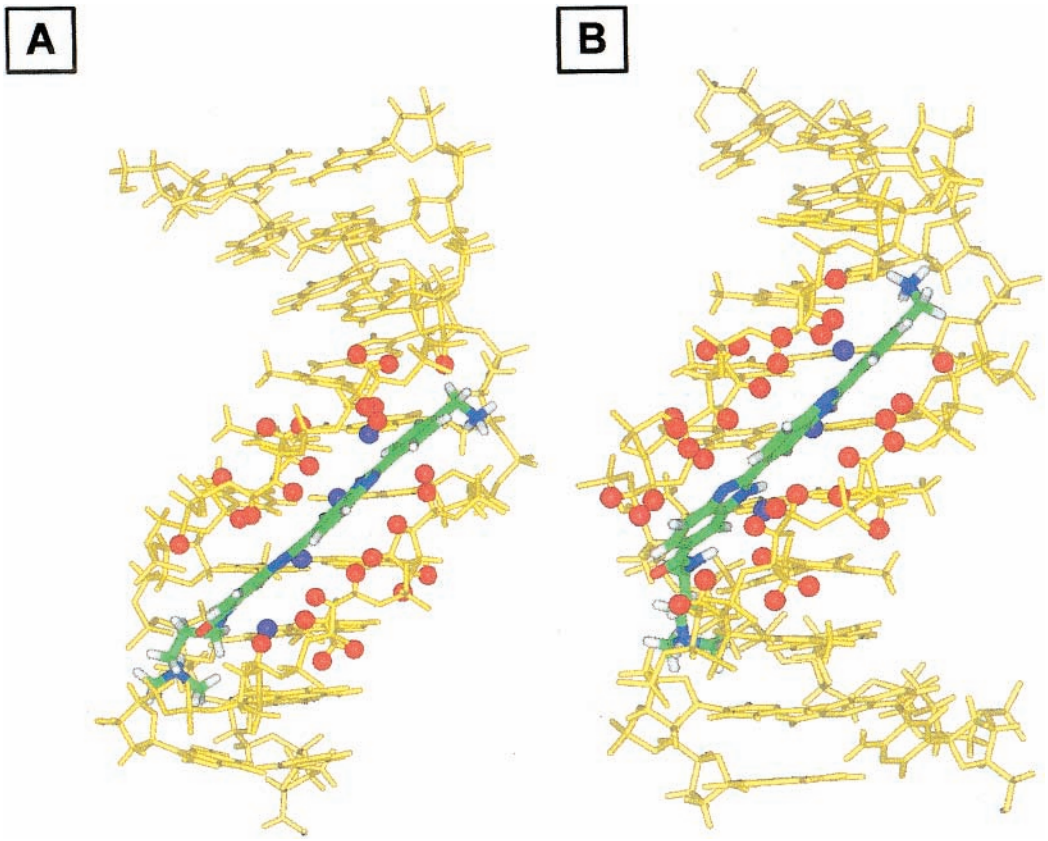


Figure 8. The NOE-based models of the (A) CBB−A_5 and (B) CBB−A_3T_3 complexes highlighting the nonexchangeable protons experiencing an upfield shift greater than −0.5 ppm (in red) or a downfield shift larger than 0.4 ppm (in purple).

correlated. Either way, the snug binding of CBB to the narrowest part of the minor groove can be rationalized either by invoking close van der Waals contacts between CBB and the minor groove walls or by pointing out that the narrower part of the minor groove offers the best possibility of reducing the solvent accessible surface.

The models do the dynamic features inherent in the NMR data less than justice. Resonance averaging is observed for the H2/H6 and H3/H5 aryl protons. A conservative guess on the chemical shift difference between the protons facing the minor groove and the protons facing the solvent would be about 2 ppm; because the chemical shift difference between the free and bound aryl resonances is in excess of 1 ppm for both proton pairs and assuming the solvent exposed protons to be too far away from the aromatic bases to experience significant deshielding means that the inner edge protons should experience a downfield shift of about 2 ppm. This chemical shift difference is averaged by ring rotation even at 280 K at 800 MHz, which suggests that the aryl-ring rotation rate is greater than 1500 s^{-1}. The rate of dissociation of CBB from the complex is estimated to be much slower than the ring-flipping motions. This has also been observed for Hoechst where an estimated ring flipping rate greater than 1000 s^{-1} (Embrey et al., 1993) is much faster than the rate of dissociation estimated to be 2.2 s^{-1} for GAATTC (Fede et al., 1991) and 1.3 s^{-1} for TAATTA (Embrey et al., 1993). It is difficult to reconcile the static model with the aryl-group fitting snugly in the minor groove and the rapid ring-flipping which must happen while CBB is bound to the DNA strand. The averaging of the aryl-group proton resonances suggests that the close van der Waal contacts indicated by the models do not constrain the rotation of the aryl-group, which, in effect, represents a quite bulky moiety.

The CBB binds to the A_5-tract with a larger than 20:1 orientational preference with the aryl-group pointing toward the 5′-end of the A-tract and the dimethylaminopropylamide group at the 3′-end. Hoechst 33258 is also known to bind to A-tracts with a considerable orientational preference with the piperazine group pointing toward the 3′-end (Searle and Embrey, 1990; Hawkins et al., 2000) i.e., with the opposite orientational preference compared to CBB. The orientational preference of Hoechst has been attributed to the sterically bulky *N*-methyl piperazine ring exerting a degree of orientational selectivity by preferring to bind in the wider minor groove of the 5′-end of an A-tract. In CBB, the bulky piperazine group has been replaced with the dimethylaminopropylamide group and still binds with an orientational preference, only that it is opposite that of Hoechst.

Distamycin was found to bind with a strong orientational specificity (>20:1) to an A-tract with the cationic amidine terminus directed toward the 3′-end of the A-tract (Hawkins et al., 2000). Replacement of the charged dimethylaminopropylamide tail group in a side-by-side binding lexitropsin polyamide with an uncharged ethoxyamide group lead to a decrease in orientational specificity (White et al., 1997). Thus, the altered orientational specificity of CBB from Hoechst could to some extent be attributed to the presence of the same cationic tail, but the arylamino group is most likely also protonized so charge cannot be the sole determinant. Another part of the explanation could be that the hydrogen bonding possibilities were better at the 3′-end of the A-tract. Associated with the very narrow minor groove is a high propeller twist for the bases, and a high propeller twist could be favorable for the formation of cross strand bifurcated hydrogen bonds because the

adjacent minor groove hydrogen bond acceptors (either adenine N3 or thymine O2) come into close proximity. Therefore, the hydrogen bond donors of the ligand are situated in the regions where the minor groove width is at its narrowest giving the orientational preference. Placing the cationic end group in the negative electrostatic potential of the A-tract will certainly also be energetically favorable (Gavathiotis et al., 2000).

A DNase I footprinting study (Abu-Daya et al., 1995a) has shown that while planar minor groove binding agents (e.g., distamycin, netropsin, berenil) all prefer AAAA over AATT binding sites, Hoechst 33258 prefers AATT; this could indicate that a broader minor groove is needed to accommodate the bulky piperazine and the narrowest part of the minor groove seems to interact with the benzimidazoles. A_4 offers the narrowest minor groove and thus the best van der Waals contacts but Hoechst 33258 cannot make hydrogen bonds with the bulky piperazine and phenol group at the 3′-end where the bifurcated hydrogen bonding opportunities are best. In AATT, the best bifurcated hydrogen bonding possibilities are at the center where the benzimidazoles have easy access.

The NOE connectivities for CBB-A_5 unambiguously orients the ligand with the aryl NH_2 -terminus at the broader 5′-end of the A-tract and the amide-end at the 3′-end, and it demonstrates the utility of NMR structural information. In the case of nearly symmetrical minor groove binders with narrow cross-sections, it is difficult to get the resolution of the X-ray data high enough to determine the orientation of the ligand from the electron density maps. The two NOE derived models do not have the structural resolution of an X-ray structure, but they do define a solution state binding site, unbiased by crystal packing forces, that seems to correlate well with the minor groove width.

ACKNOWLEDGMENT

We thank The Instrument Centre for NMR-Spectroscopy of Biological Macromolecules at The Carlsberg Laboratory, Copenhagen, granted by The Danish Natural Science Research Council for providing spectrometer time at the 800 MHz spectrometer. Finally, financial support from The Danish Natural Science Research Council and The Technical Research Council is acknowledged.

LITERATURE CITED

(1) Abu-Daya, A., Brown, P. M., and Fox, K. R. (1995) DNA sequence preferences of several AT-selective minor groove binding ligands. *Nucleic Acids Res. 23*, 3385−3392.

(2) Abu-Daya, A., and Fox, K. R. (1997) Interaction of minor groove binding ligands with long AT tracts. *Nucleic Acids Res. 25*, 4962−4969.

(3) Bailly, C., Colson, P., Henichart, J. P., and Houssier, C. (1993) The different binding modes of Hoechst 33258 to DNA studied by electric linear dichroism. *Nucleic Acids Res. 21*, 3705−3709.

(4) Behrens, C., Harrit, N., and Nielsen, P. E. (2001) *Bioconjugate Chem. 12*, 1021−1027.

(5) Bostock-Smith, C. E., Embrey, K. J., and Searle, M. S. (1997) Enhanced binding of a hexacyclic amidine analogue of Hoechst 33258 to the minor groove of DNA: H-1 NMR and UV melting studies with the decamer duplex d(GGTAATTACC)$_2$. *J. Chem. Soc. Chem. Commun.* 121−122.

(6) Bostock-Smith, C. E., Laughton, C. A., and Searle, M. S. (1998) DNA minor groove recognition by a tetrahydropyrimidinium analogue of Hoechst 33258: NMR and molecular dynamics studies of the complex with d(GGTAATTACC)$_2$. *Nucleic Acids Res. 26*, 1660−1667.

(7) Bostock-Smith, C. E., and Searle, M. S. (1999) DNA minor groove recognition by bis-benzimidazole analogues of Hoechst 33258: Insights into structure-DNA affinity relationships assessed by fluorescence titration measurements. *Nucleic Acids Res. 27*, 1619−1624.

(8) Case, D. A., Pearlman, D. A., Caldwell, J. W., Cheatham, T. E., III, Ross, W. S., Simmerling, C. L., Darden, T. A., Merz, K. M., Stanton, R. V., Cheng, A. L., Vincent, J. J., Crowley, M., Tsui, V., Radmer, R. J., Duan, Y., Pitera, J., Massova, I., Seibel, G. L., Singh, U. C., Weiner, P. K., and Kollman, P. A. (1999) *AMBER 6*, University of California, San Francisco.

(9) Chen, A. Y., Yu, C., Gatto, B., and Liu, L. F. (1993) DNA minor groove-binding ligands: A different class of mammalian DNA topoisomerase I inhibitors. *Proc. Natl. Acad. Sci. U.S.A. 90*, 8131−8135.

(10) Chuprina, V. P., Lipanov, A. A., Fedoroff, O. Y., Kim, S. G., Kintanar, A., and Reid, B. R. (1991) Sequence effects on local DNA topology. *Proc. Natl. Acad. Sci. U.S.A. 88*, 9087−9091.

(11) Clark, G. R., Boykin, D. W., Czarny, A., and Neidle, S. (1997) Structure of a bis-amidinium derivative of Hoechst 33258 complexed to dodecanucleotide d(CGCGAATTCGCG)$_2$: the role of hydrogen bonding in minor groove drug−DNA recognition. *Nucleic Acids Res. 25*, 1510−1515.

(12) Clark, G. R., Squire, C. J., Gray, E. J., Leupin, W., and Neidle, S. (1996a) Designer DNA-binding drugs: The crystal structure of a meta-hydroxy analogue of Hoechst 33258 bound to d(CGCGAATTCGCG)$_2$. *Nucleic Acids Res. 24*, 4882−4889.

(13) Clark, G. R., Gray, E. J., Neidle, S., Li, Y. H., and Leupin, W. (1996b) Isohelicity and phasing in drug−DNA sequence recognition: Crystal structure of a tris(benzimidazole)oligonucleotide complex. *Biochemistry 35*, 13745−13752.

(14) Coll, M., Frederick, C. A., Wang, A. H., and Rich, A. (1987) A bifurcated hydrogen-bonded conformation in the d(A.T) base pairs of the DNA dodecamer d(CGCAAATTTGCG) and its complex with distamycin. *Proc. Natl. Acad. Sci. U.S.A. 84*, 8385−8389.

(15) Czarny, A., Boykin, D. W., Wood, A. A., Nunn, C. M., Neidle, S., Zhao, M., and Wilson, W. D. (1995) Analysis of van der Waals and electrostatic contributions in the interactions of minor-groove binding benzimidazoles with DNA. *J. Am. Chem. Soc. 117*, 4716−4717.

(16) Denham, D. A., Suswillo, R. R., Rogers, R., McGreevy, P. B., and Andrews, B. J. (1976) Studies on Brugia pahangi. 13. The anthelmintic effect of compounds F151 (Friedheim), HOE 33258 (Hoechst) and their reaction product. *J. Helminthol. 50*, 243−250.

(17) DiGabriele, A. D., Sanderson, M. R., and Steitz, T. A. (1989) Crystal lattice packing is important in determining the bend of a DNA dodecamer containing an adenine tract. *Proc. Natl. Acad. Sci. U.S.A. 86*, 1816−1820.

(18) DiGabriele, A. D. and Steitz, T. A. (1993) A DNA dodecamer containing an adenine tract crystallizes in a unique lattice and exhibits a new bend. *J. Mol. Biol. 231*, 1024−1039.

(19) Edwards, K. J., Brown, D. G., Spink, N., Skelly, J. V., and Neidle, S. (1992) Molecular structure of the B-DNA dodecamer d(CGCAAATTTGCG)$_2$. An examination of propeller twist and minor-groove water structure at 2.2 Å resolution. *J. Mol. Biol. 226*, 1161−1173.

(20) Embrey, K. J., Searle, M. S., and Craik, D. J. (1991) Probing the Interaction of Hoechst-33258 with an A−T Rich Oligonucleotide Duplex using ^{1}H NMR Spectroscopy. *J. Chem. Soc. Chem. Commun.* 1770−1771.

(21) Embrey, K. J., Searle, M. S., and Craik, D. J. (1993) Interaction of Hoechst 33258 with the minor groove of the A + T-rich DNA duplex d(GGTAATTACC)$_2$ studied in solution by NMR spectroscopy. *Eur. J. Biochem. 211*, 437−447.

(22) Fede, A., Billeter, M., Leupin, W., and Wutrich, K. (1993) Determination of the NMR Solution Structure of the Hoechst 33258-D(GTGGAATTCCAC)(2) Complex and Comparison with the X-ray Crystal-Structure. *Structure 1*, 177−186.

(23) Fede, A., Labhardt, A., Bannwarth, W., and Leupin, W. (1991) Dynamics and binding mode of Hoechst 33258 to d(GTGGAATTCCAC)$_2$ in the 1:1 solution complex as determined by two-dimensional ^{1}H NMR. *Biochemistry 30*, 11377−11388.

(24) Frisch, M. J., Trucks, G. W., Schlegel, H. B., Gill, P. M. W., Johnson, B. G., Robb, M. A., Cheeseman, J. R., Keith, T., Petersson, G. A., Montgomery, J. A., Raghavachari, K., Al-Laham, M. A., Zakrzewski, V. G., Ortiz, J. V., Foresman, J. B., Cioslowski, J., Stefanov, B. B., Nanayakkara, A., Challacombe, M., Peng, C. Y., Ayala, P. Y., Chen, W., Wong, M. W., Andres, J. L., Replogle, E. S., Gomperts, R., Martin, R. L., Fox, D. J., Binkley, J. S., Defrees, D. J., Baker, J., Stewart, J. P., Head-Gordon, M., Gonzalez, C., and Pople, J. A. Gaussian 94, Gaussian, Inc., Pittsburgh, PA.

(25) Gavathiotis, E., Sharman, G. J., and Searle, M. S. (2000) Sequence-dependent variation in DNA minor groove width dictates orientational preference of Hoechst 33258 in A-tract recognition: solution NMR structure of the 2:1 complex with $d(CTTTTGCAAAAG)_2$. *Nucleic Acids Res. 28*, 728−735.

(26) Haq, I., Ladbury, J. E., Chowdhry, B. Z., Jenkins, T. C., and Chaires, J. B. (1997) Specific binding of Hoechst 33258 to the $d(CGCAAATTTGCG)_2$ duplex: Calorimetric and spectroscopic studies. *J. Mol. Biol. 271*, 244−257.

(27) Hawkins, C. A., de Clairac, R. P., Dominey, R. N., Baird, E. E., White, S., Dervan, P. B., and Wemmer, D. E. (2000) Controlling binding orientation in hairpin polyamide DNA complexes. *J. Am. Chem. Soc. 122*, 5235−5243.

(28) Higgins, L. D., and Searle, M. S. (1999) Site-specificity of bis-benzimidazole Hoechst 33258 in A-tract recognition of the DNA dodecamer duplex $d(GCAAAATTTTGC)_2$. *J. Chem. Soc. Chem. Commun.* 1861−1862.

(29) Hud, N. V., Sklenar, V., and Feigon, J. (1999) Localization of ammonium ions in the minor groove of DNA duplexes in solution and the origin of DNA A-tract bending. *J. Mol. Biol. 286*, 651−660.

(30) Katahira, M., Sugeta, H., Kyogoku, Y., Fujii, S., Fujisawa, R., and Tomita, K. (1988) One- and two-dimensional NMR studies on the conformation of DNA containing the oligo(dA)-oligo(dT) tract. *Nucleic Acids Res. 16*, 8619−8632.

(31) Katahira, M., Sugeta, H., and Kyogoku, Y. (1990) A new model for the bending of DNAs containing the oligo(dA) tracts based on NMR observations. *Nucleic Acids Res. 18*, 613−618.

(32) Lavery, R., and Pullmann, B. (1981) Molecular electrostatic potential on the surface envelopes of macromolecules: B-DNA. *Int. J. Quantum Chem. 20*, 259−272.

(33) Loontiens, F. G., Regenfuss, P., Zechel, A., Dumortier, L., and Clegg, R. M. (1990) Binding characteristics of Hoechst 33258 with calf thymus DNA, poly[d(A- T)], and d(CCG-GAATTCCGG): multiple stoichiometries and determination of tight binding with a wide spectrum of site affinities. *Biochemistry 29*, 9029−9039.

(34) Moon, J. H., Kim, S. K., Sehlstedt, U., Rodger, A., and Norden, B. (1996) DNA structural features responsible for sequence-dependent binding geometries of Hoechst 33258. *Biopolymers 38*, 593−606.

(35) Nadeau, J. G., and Crothers, D. M. (1989) Structural basis for DNA bending. *Proc. Natl. Acad. Sci. U.S.A. 86*, 2622−2626.

(36) Parkinson, J. A., Barber, J., Douglas, K. T., Rosamond, J., and Sharples, D. (1990) Minor-groove recognition of the self-complementary duplex $d(CGCGAATTCGCG)_2$ by Hoechst 33258: A high-field NMR study. *Biochemistry 29*, 10181−10190.

(37) Pelton, J. G., and Wemmer, D. E. (1989) Structural characterization of a 2:1 distamycin A.d(CGCAAATTGGC) complex by two-dimensional NMR. *Proc. Natl. Acad. Sci. U.S.A. 86*, 5723−5727.

(38) Piotto, M., Saudek, V., and Sklenar, V. (1992) Gradient-tailored excitation for single-quantum NMR spectroscopy of aqueous solutions. *J. Biomol. NMR 2*, 661−665.

(39) Pjura, P. E., Grzeskowiak, K., and Dickerson, R. E. (1987) Binding of Hoechst 33258 to the minor groove of B-DNA. *J. Mol. Biol. 197*, 257−271.

(40) Quintana, J. R., Lipanov, A. A., and Dickerson, R. E. (1991) Low-temperature crystallographic analyses of the binding of Hoechst 33258 to the double-helical DNA dodecamer C−G−C−G−A−A−T−T−C−G−C−G. *Biochemistry 30*, 10294−10306.

(41) Rao, K. E., and Lown, J. W. (1991) Molecular recognition between ligands and nucleic acids: DNA binding characteristics of analogues of Hoechst 33258 designed to exhibit altered base and sequence recognition. *Chem. Res. Toxicol. 4*, 661−669.

(42) Reddy, B. S., Sondhi, S. M., and Lown, J. W. (1999) Synthetic DNA minor groove-binding drugs. *Pharmacol. Ther. 84*, 1−111.

(43) Rydzewski, J. M., Leupin, W., and Chazin, W. (1996) The width of the minor groove affects the binding of the bisquaternary heterocycle SN-6999 to duplex DNA. *Nucleic Acids Res. 24*, 1287−1293.

(44) Searle, M. S., and Embrey, K. J. (1990) Sequence-specific interaction of Hoechst 33258 with the minor groove of an adenine-tract DNA duplex studied in solution by ^{1}H NMR spectroscopy. *Nucleic Acids Res. 18*, 3753−3762.

(45) Spink, N., Brown, D. G., Skelly, J. V., and Neidle, S. (1994) Sequence-dependent effects in drug−DNA interaction: the crystal structure of Hoechst 33258 bound to the $d(CG-CAAATTTGCG)_2$ duplex. *Nucleic Acids Res. 22*, 1607−1612.

(46) Squire, C. J., Baker, L. J., Clark, G. R., Martin, R. F., and White, J. (2000) Structures of *m*-iodo Hoechst-DNA complexes in crystals with reduced solvent content: Implications for minor groove binder drug design. *Nucleic Acids Res. 28*, 1252−1258.

(47) Teng, M. K., Usman, N., Frederick, C. A., and Wang, A. H. (1988) The molecular structure of the complex of Hoechst 33258 and the DNA dodecamer d(CGCGAATTCGCG). *Nucleic Acids Res. 16*, 2671−2690.

(48) Vega, M. C., Garcia, S., I, Aymami, J., Eritja, R., Van der Marel, G. A., Van Boom, J. H., Rich, A., and Coll, M. (1994) Three-dimensional crystal structure of the A-tract DNA dodecamer d(CGCAAATTTGCG) complexed with the minor-groove-binding drug Hoechst 33258. *Eur. J. Biochem. 222*, 721−726.

(49) White, S., Baird, E. E., and Dervan, P. B. (1997) Orientation preferences of pyrrole-imidazole polyamides in the minor groove of DNA. *J. Am. Chem. Soc. 119*, 8756−8765.

(50) Wijmenga, S. S., and van Buuren, B. N. M. (1998) The use of NMR methods for conformational studies of nucleic acids. *Prog. Nucl. Magn. Reson. Spectrosc. 32*, 287−387.

BC020001B

Design and Formulation of Polyplexes Based on Pluronic-Polyethyleneimine Conjugates for Gene Transfer

Catherine L. Gebhart,*,† Srikanth Sriadibhatla,† Sergey Vinogradov,† Pierre Lemieux,‡ Valery Alakhov,‡ and Alexander V. Kabanov*,†

Department of Pharmaceutical Sciences, College of Pharmacy, 986025 Nebraska Medical Center, Omaha, Nebraska 68198-6025, and Supratek Pharma Inc., c/o Armand-Frappier Institute, Laval, PQ, Canada. Received January 14, 2002; Revised Manuscript Received May 15, 2002

Previously, we reported the evaluation of several polyplex-based gene delivery systems with respect to their effectiveness, toxicity, and cell type dependence in vitro. One system, P123-g-PEI(2K), a cationic graft block copolymer, is of particular interest as it has been demonstrated to successfully deliver genetic material to murine liver following systemic delivery [Nguyen, H. K., Lemieux, P., Vinogradov, S. V., Gebhart, C. L., Guerin, N., Paradis, G., Bronich, T. K., Alakhov, V. Y., and Kabanov, A. V. (2000) Evaluation of Polyether-Polyethyleneimine Graft Copolymers as Gene Transfer Agents. *Gene Ther. 7,* 126−138 (*1*)]. The P123-g-PEI(2K) system requires nonmodified Pluronic P123 as an excipient to stabilize the dispersion. The purpose of the current work was to more closely characterize this system, to assess the role of each component of the system to the overall transfection process. We evaluated particle size, stability, and resistance to nuclease degradation. In addition, cellular uptake and localization of plasmid, as well as transgene expression, were evaluated following in vitro transfection of prostate cancer cells (PC-3) with various individual components of the system. Nonmodified Pluronic alone did not significantly enhance DNA uptake, transgene expression, or DNase protection. Therefore, we conclude that nonmodified Pluronic acted primarily by optimizing the size of the polyplex. Furthermore, though this system displays several characteristics thought desirable of a nonviral gene delivery system, these studies did discriminate a potential limitation of this system for in vivo applications, namely, the insufficient level of protection of plasmid DNA from nuclease degradation. This may limit the effective dose delivered, as well as limiting the effective circulation time. These studies provide vital information that will guide modification of this system to enhance the current in vivo profile.

INTRODUCTION

Nonviral vectors for gene delivery are rapidly gaining increased interest. Researchers are increasingly aware of the potential advantages of these nonviral systems over the currently investigated viral systems, in respect to their safety, production, and versatility (*2*). Complexes of DNA and polycation ('polyplexes') represent one such class of nonviral gene delivery systems that has recently generated significant interest for gene delivery applications (*3*−*5*). The first generation of polyplexes, based on homopolymers, that were developed as gene therapy vectors performed well in vitro, yet suffered from several drawbacks when tested in vivo, primarily due to the fact that they were often poorly soluble, resulting in aggregation in the lung and consequently in pulmonary embolism [reviewed in (*6*)]. Additionally, although a substantial portion of the dose accumulated in the liver, this was primarily the result of uptake by Kupffer cells and did not result in proportionately significant transgene expression. Therefore, several investigators in the area proposed a promising approach to overcome this problem, resulting in the creation of a second generation of polymeric systems. This approach involved the linkage of the polycation to a nonionic water-soluble polymer, resulting in a carrier with a block or graft copolymer architecture, which, upon mixing with DNA, formed soluble DNA delivery vectors. Several such systems have recently been described (*7*−*11*).

One promising type of system reported recently represents graft copolymers that employ Pluronics as the nonionic water-soluble segment, specifically P123-g-PEI(2K), which is a graft copolymer of a 2 kDa polyethyleneimine (PEI) and Pluronic P123 (*1*). Pluronics are poly(ethylene oxide)−poly(propylene oxide) block copolymers that possess the unique ability to incorporate into cell membranes as a result of the presence of the hydrophobic poly(propylene oxide) (PPO) chain (*12*). This is believed to enhance cell interactions, DNA transport, and transgene expression using such polyplexes (*1*). Initial studies determined that this system required the addition of nonmodified Pluronic P123 as an excipient in order to stabilize the dispersion (*1*). Once this was done, the system exhibited improved dispersion stability and improved in vivo biodistribution compared to unmodified PEI. In fact, this system was able to successfully deliver genetic material to the liver of mice following systemic administration (*1*).

The current work represents an expansion upon the initial characterization of the cationic graft copolymer system, P123-g-PEI(2K), with the goal to develop a better understanding of this multicomponent delivery system.

* Correspondence should be addressed to either of these authors at the Department of Pharmaceutical Sciences, College of Pharmacy, 986025 Nebraska Medical Center, Omaha, NE 68198-6025. Telephone: (402)559-9915; FAX: (402)559-9543; E-mail: clgebhar@unmc.edu or akabanov@unmc.edu.

† Nebraska Medical Center.

‡ Armand-Frappier Institute.

10.1021/bc025504w CCC: $22.00 © 2002 American Chemical Society
Published on Web 08/21/2002

The obtained knowledge can then be applied both toward the improvement of the current system and toward the development of additional novel graft copolymer systems. Complete understanding of this P123-g-PEI(2K) system is particularly important in light of the fact that Pluronics are known to exhibit biological activity, including effects on cell membrane properties as well as effects on gene promoters (*13, 14*).

The P123-g-PEI(2K)-based gene delivery system is a self-assembling system, a characteristic that lends a large degree of freedom to the formulation of the polyplexes. This provides for 'built-in' versatility, specifically, the potential to replace or modify individual components of the system to enhance the system for a particular application. For example, there exists a wide array of Pluronic formulations, varying in their hydrophilic/lipophilic characteristics, that could potentially be utilized in place of the originally employed Pluronic P123. For the purposes of this study, we considered reformulation of the system with nonmodified Pluronic F127. This decision was made because: (1) though Pluronic F127 is more hydrophilic than Pluronic P123, the solubilization properties of the two Pluronics are relatively similar (*15*); and (2) Pluronic F127 is approved for use in current pharmaceutical preparations, and therefore the toxicological studies have been completed, a fact that could expedite further in vivo development.

We evaluated particle size and dispersion stability as well as the resistance of incorporated DNA to nuclease digestion in cell-free systems. In the prostate carcinoma cell line PC-3, we examined plasmid DNA (pDNA) uptake and cellular localization, as well as expression of a reporter construct following in vitro transfection with various polyplex formulations as well as with individual components of this delivery system. We determined that nonmodified Pluronic, when combined with naked plasmid DNA, did not significantly enhance the cellular uptake of the DNA, the expression of the encoded reporter gene, or the protection of DNA from nuclease digestion. We conclude that the addition of nonmodified Pluronic to the formulation of the graft copolymer-based polyplexes acted to improve the gene transfer profile of the system primarily by optimizing the size and stability of the polyplex, as well as delivery of the DNA within the cell. These studies provide valuable information regarding the design and formulation of stable and effective gene delivery particles.

EXPERIMENTAL PROCEDURES

Materials. P123-g-PEI(2K) was synthesized by grafting Pluronic P123 to the amino groups of PEI, as described previously (*1*). Briefly, 1,1′-carbonyl-diimidazole-activated Pluronic P123 was reacted with PEI, 2 kDa, to yield a copolymer with a molecular mass of 25 kDa and an average of 3.2 P123 chains per 1 PEI chain. Nonionic block copolymers Pluronic P123 and Pluronic F127 were kindly provided by BASF Corp. (Parispany, NJ). The commercial transfection reagent Exgen 500, a 22 kDa linear PEI, was purchased from MBI Fermentas Inc. (Hanover, MD). Luciferase encoding plasmid gWIZLuciferase was purchased from Gene Therapy Systems, Inc. (San Diego, CA). Green fluorescent protein encoding plasmid pIRES-EGFP was purchased from Clonetech (Palo Alto, CA). Both plasmids were expanded in DH5α *E. coli* and isolated using Qiagen endotoxin-free plasmid Giga-prep kits according to the supplier's protocol. The cyanine dimmer dye YOYO-1 was purchased from Molecular Probes.

Cell Culture. PC-3, a human prostrate carcinoma cell line, was kindly provided by Dr. Pi-Wan Cheng (UNMC). Cells were cultured in RPMI-1640 supplemented with 10% heat-inactivated fetal bovine serum (FBS), 10 mM HEPES, and 100 units/mL penicillin/100 μg/mL streptomycin (complete media). Cells were seeded into 12 well plates at a density of 70 000 cells per well, or at 50 000 cells per well in 24 well plates. For confocal microscopy studies, cells were seeded onto untreated glass coverslips at a density of 50 000 cells per coverslip. Cells were allowed to adhere to plates for 24−48 h prior to transfection.

Labeling of pDNA. YOYO-1 is an ultrasensitive high-affinity DNA labeling dye that exhibits a high fluorescence enhancement upon binding to double-stranded DNA. Therefore, it is a valuable tool to study the early phases of cellular transport during transfection. Briefly, 500 μL of gWIZLuciferase (0.1 mg/mL) was combined with 97.5 μL of 10× TAE buffer and 371 μL of 1.0 μM YOYO-1 dye and incubated at room temperature for 1 h in the dark.

Formation of Complexes and Transfection. The precise mixing order is a critical parameter, and was performed according to the following protocol. To a 1.5 mL eppendorf tube were added the following: (1) 45 μL of pDNA (0.1 mg/mL) or 90 μL of YOYO-1-labeled pDNA (0.05 mg/mL); (2) 9 μL of 50 mg/mL Pluronic P123 or 50 mg/mL Pluronic F127 (only to the appropriate samples); (3) 150 μL of DMEM with 1% Hepes; and, last, (4) 13.6 μL of polycation (10 μmol of NT/mL). The tube was vortexed for 30 s immediately following the addition of polycation. The mixture was incubated for 5 min at room temperature, and then 1270 μL of complete media was added. Immediately prior to transfection, culture medium was aspirated from the cells. Then the transfection mixtures were added to each well (250 μL per well for 24 well plates, 500 μL per well for 12 well plates or coverslips). Cells were exposed to transfection reagents for 2 h at 37 °C (5% CO_2) and then rinsed with PBS to remove polyplexes. For expression studies, cells were incubated an additional 20−22 h in complete media. In the case of luciferase expression, cells were then lysed, and luciferase assays were performed using a Promega Luciferase kit according to the manufacturer's protocol (Promega, Madison WI). Protein assays were also performed on lysates using the BCA Protein Assay (Pierce Scientific) to allow normalization of data. Cells on coverslips were rinsed 2 times with PBS, following the 2 h exposure to complexes, fixed for 10 min with 4% paraformaldehyde, and mounted on slides.

Particle Size Measurements. The effective hydrodynamic diameter was measured by photon correlation spectroscopy using a 'ZetaPlus' Zeta Potential Analyzer (Brookhaven Instrument) equipped with the Multi-Angle Option at 22 °C at an angle of 90°. Prior to particle formation, all reagents were passed through a Whatman 200 nm polysulfone filter. Polyplexes were formed exactly as they were for transfections, unless otherwise indicated. The data presented represent the average of five separate 3 min analyses, which allows for assessment of the stability of the system. Unless otherwise indicated, all systems exhibited stable effective diameters over the time course examined. If effective diameters increased during the 15 min period of measurement, these systems were considered 'unstable'.

Laser Scanning Microscopy. A Zeiss Confocal LSM410 (Goettinger, Germany) was used to obtain both DIC and fluorescent images of cells. When obtaining fluorescent images, all samples were excited at 488 nm,

Table 1. Summary of Results from Various Experiments

formulation	particle size (nm)[a]	DNase protection[b]	pDNA internalization[c]	luciferase (ng/mg)[d]	% EGFP positive[e]
DNA alone	−	0	43.5 ± 6.5*	0	0.08 ± 0.03
Exgen 500	125	2331 ± 156*	357.3 ± 19.7*	1977 ± 86*	9.93 ± 0.55
P123-g-PEI(2K)	658+	1357 ± 68	57.3 ± 2.3*	36 ± 3	0.13 ± 0.05
P123 + P123-g-PEI(2K)[f]	166	986 ± 58	226.3 ± 9.5*	608 ± 59	2.94 ± 0.26
F127 + P123-g-PEI(2K)	341	1126 ± 107	142.6 ± 4.5*	415 ± 44	nd
P123-g-PEI(2K) + P123[g]	560	nd	nd	nd	nd

[a] Prepared as done for transfection (in DMEM-containing serum). [b] Total (o.c.+s.s. fractions) DNA remaining following digestion (volume by densitometry), $N = 3$. Values are represented as mean ± SD. *$p < 0.05$. [c] YOYO-1-labeled plasmid DNA, $N = 4$. Value presented is the mean fluorescent intensity acquired by flow cytometry. Values are represented as mean ± SD. *$p < 0.05$. [d] 24 h following transfection of PC-3 cells with gWIZLuciferase, $N = 4$.Values are represented as mean ± SD. *$p < 0.05$. [e] $N = 4$. Values are represented as mean ± SD. *$p < 0.05$. [f] Complexes formed by addition of reagents in the order of DNA, Pluronic, and, last, P123-g-PEI(2K). [g] Complexes formed by addition of reagents in the order of DNA, P123-g-PEI(2K), and, last, Pluronic.

and images were acquired with a brightness setting of 270 and a contrast setting of 9730. This standardization allowed for the quantitative analysis of uptake of YOYO-1 dye. Data were analyzed to quantitate uptake of pDNA by digital contrast enhancement and area measure using the LSM-PC software provided with the instrument.

Flow Cytometry Analysis. The mean fluorescence intensity of trypsinized, paraformaldehyde-fixed PC-3 cells, following a 2 h exposure plus 2 h additional culture, to polyplexes containing YOYO-1-labeled pDNA was obtained by flow cytometry analysis. In a second set of experiments, the percentage of PC-3 cells expressing green fluorescent protein (GFP) following transfection with pIRES-EGFP-containing polyplexes was also assessed by flow cytometry. The analysis for both sets of experiments was performed using a Becton Dickinson FACStarPlus flow cytometer operating under Lysis II (San Jose, CA), equipped with an argon ion laser (488 nm emission wavelength). The filter used for emission was a 530/30 nm band-pass. Data acquisition was performed in the linear mode, and data were visualized in the logarithmic mode. Dead cells were discriminated by a reduction in forward scatter and were excluded from the analysis.

DNase Protection Assay. Resistance to nuclease digestion was determined using a DNase I protection assay. Unlabeled gWIZLuciferase plasmid DNA (0.625 μg) or polyplexes were prepared in a final volume of 25 μL. Then 10 μL aliquots of each sample were placed into two separate tubes. Then 1 unit of DNase I (2 μL) (Promega, Madison, WI) or 2 μL of PBS was added. The samples were incubated for 15 min at 37 °C. Immediately following incubation, all samples were treated with 5 μL of 100 mM EDTA for 10 min to inactivate the DNase. Finally, 10 μL of 5 mg/mL heparin (Sigma, St. Louis, MO) was added to each tube, and tubes were incubated for 2 h at room temperature to allow complete dissociation of complexes. Samples were visualized using 0.2 μg of DNA/lane on an 0.8% agarose gel, stained with ethidium bromide. Images were acquired using an Alpha Imager (Alpha Innotech, San Leonardo, CA) and analyzed using ImageQuant software to obtain data in the form of volume per area.

RESULTS

Particle Size Analysis. The particle size analysis data presented in Table 1 demonstrate the impact of addition of nonmodified Pluronic P123 and the dependence on the order of mixing of the components of the P123-g-PEI(2K) system on the effective diameter of the resulting polyplex. In the absence of nonmodified Pluronic P123, the mixing of P123-g-PEI(2K) with plasmid DNA results in the formation of large, unstable aggregates (ca. 660+ nm). However, by combining plasmid DNA with 0.03% nonmodified Pluronic P123 prior to addition of the graft copolymer, stable particles with effective diameters of approximately 160 nm can be formed. It is important to note, though, that addition of Pluronic P123 after mixing of DNA and graft copolymer is not sufficient, and results in particles that are only slightly smaller than those formulated without the addition of Pluronic P123.

Table 1 is a summary table presenting the results of various assays performed to characterize this complex transfection system, in relation to the commercial transfection reagent Exgen 500. The particle size data introduced in this table present the effective diameters achieved for polyplexes based on Exgen 500, the graft copolymer alone, and the graft copolymer formulated with either 0.03% Pluronic P123 or 0.03% Pluronic F127. Polyplexes based on Exgen 500 and P123:P123-g-PEI(2K) are both within a relatively similar size range, while F127:P123-g-PEI(2K)-based polyplexes are approximately twice as large. Similar experiments were performed in which the concentration of free Pluronic was gradually increased, to determine the amount of Pluronic necessary to stabilize the dispersion. It was determined that 0.03% Pluronic was sufficient to stabilize the system at the pDNA concentrations used for all studies included in this paper (data not shown). It is noteworthy that by this method of analysis, the contribution of the micelles to the light scattering analysis is negligible as the scattering function is proportional to the sixth power of the particle size. The Pluronic P123 micelles are much smaller than the complex particles (20 nm vs 200 nm), and their volume fraction is low at 0.03%, since this is just slightly above the CMC. In fact, in the absence of polyplexes with Pluronic P123 at 0.03%, the micelles are not detected by the instrument (data not shown). However, particles of this size are clearly seen at copolymer concentration of at least 0.5% and above. Finally, it is important to note, that when preparing polyplexes at higher DNA concentrations, as would be needed for certain in vivo studies, additional free Pluronic must be added to the system to maintain the stability of the dispersion. The exact amount of excess required depends strongly on the exact concentration of the pDNA desired and the particular buffer employed. The maximum DNA solubility when formulated in these multicomponent polyplexes is in the range of 0.1−0.5 mg/mL (data not shown).

Resistance to DNase I Digestion. One primary responsibility of any gene delivery system is to protect DNA from degradation by nucleases. Therefore, the relative quantity remaining, as well as the integrity of the remaining quantity, of plasmid DNA was assessed

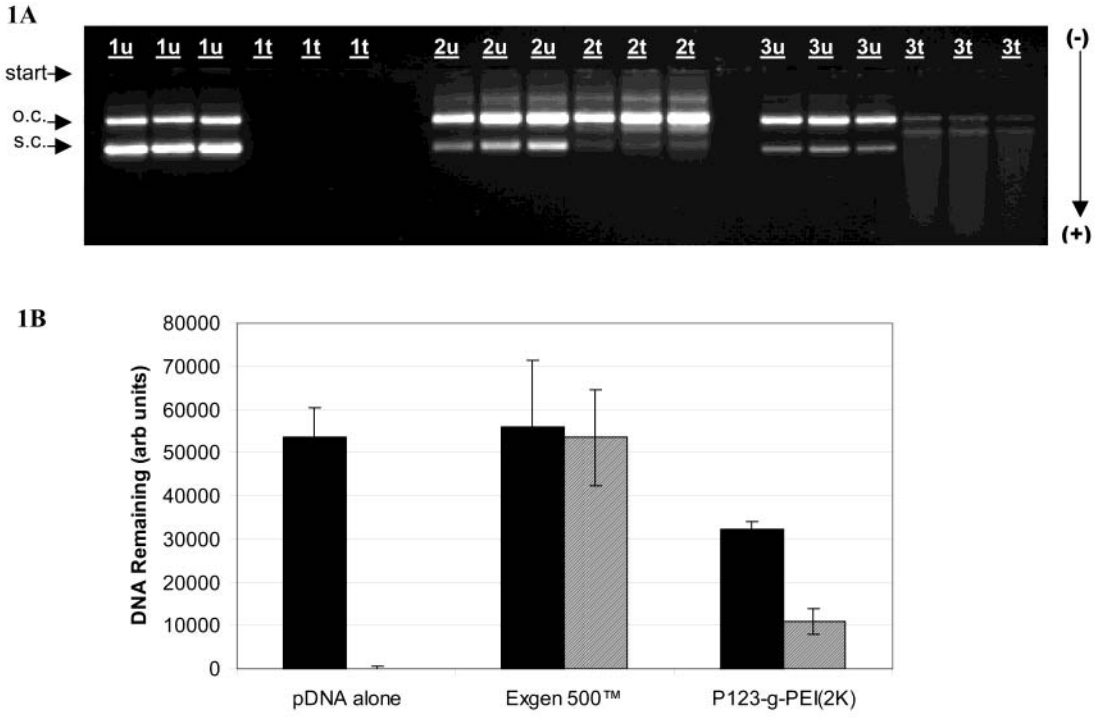


Figure 1. DNase protection assay. (A) Samples, in triplicate, containing (1) pDNA alone, (2) pDNA incorporated into Exgen 500 polyplexes, or (3) pDNA incorporated into P123-g-PEI(2K) complexes were treated with PBS (u) or DNase (t). All samples were subsequently treated with EDTA to inactivate DNase and then heparin to dissociate complexes. Samples were then subjected to agarose gel electrophoresis. (B) Densitometry analysis of the DNase assay presented in panel A. Values are represented as mean ± SD.

following incubation of various polyplexes with DNase I. Figure 1 presents typical results obtained during these experiments. By comparing the relative portions of open circular (o.c.) and supercoiled (s.c.) fractions in the pDNA alone lanes compared to those of the pDNA recovered from both Exgen 500 and P123-g-PEI(2K)-based polyplexes in Figure 1A, it is evident that the process of dissociation of DNA from polycation results in a conversion of a portion of the s.c. pDNA to o.c. pDNA. Furthermore, in the case of P123-g-PEI(2K), there appear to be additional changes in the topology of the pDNA (lanes labeled 3t), resulting in a band that migrates between the indicated o.c. and s.c. bands. The reasons for such changes in pDNA topology are unknown, and this phenomena is currently under investigation in our laboratory. Figure 1B reveals that the dissociation process for P123-g-PEI(2K)-based polyplexes was incomplete, allowing for dissociation of approximately 60% of the pDNA originally incorporated. Such incomplete dissociation was observed in several experiments, and the authors believe it occurs due to hindrance of access of heparin to the DNA as a result of the hydrophobic interactions of Pluronic. Figure 2 presents typical results obtained when comparing various formulations of the P123-g-PEI(2K) polyplex system. This figure shows that, while the positive control (lane 1) was completely degraded, a portion of the polyplex-protected pDNA remains in the case of all polyplexes presented in this figure. It is worthwhile to note the conversion of the supercoiled (s.c.) pDNA to the more relaxed forms, which migrate more slowly through the gel (lanes 3, 5, and 6). The densitometry data in Table 2 were obtained in a separate experiment employing sample replicates utilizing a different batch of pDNA. In this experiment, the pDNA was successfully completely dissociated from the P123-g-PEI(2K)-based polyplexes, allowing for a more accurate assessment of the integrity of the pDNA originally incorporated in the various P123-g-PEI(2K)-based polyplexes following exposure to DNase. These data show that Exgen 500-based polyplexes protected more total DNA than the others, although the integrity of the remaining DNA could be compromised, as demonstrated by the conversion of the majority of the s.c. fraction to a relaxed form. The densitometry data

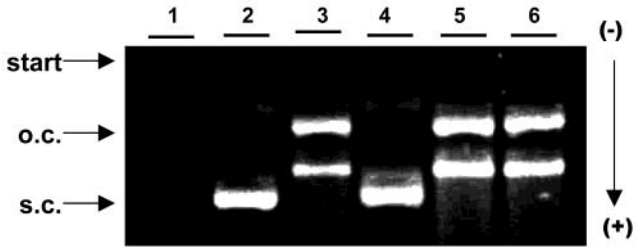


Figure 2. DNase protection assay. Plasmid DNA alone or pDNA incorporated into polyplexes was treated with DNase and subsequently treated with heparin to dissociate complexes; samples were then subjected to agarose gel electrophoresis. The samples were as follows: DNase-treated naked DNA (lane 1); untreated naked DNA (lane 2); DNase-treated P123-g-PEI(2K)-based complexes (lane 3); untreated P123-g-PEI(2K)-based complexes (lane 4); DNase-treated P123:P123-g-PEI(2K)-based complexes (lane 5); DNase-treated F127:P123-g-PEI(2K)-based complexes (lane 6).

Table 2. Plasmid DNA Remaining following DNase I Digestion

formulation	open circular	supercoiled	total (o.c. + s.c.)
Exgen 500	2267 ± 142[a]	64 ± 56[a]	2331 ± 156[a]
P123-g-PEI(2K)	805 ± 30[b]	552 ± 62	1357 ± 68[a]
P123 + P123-g-PEI(2K)	470 ± 46[b]	516 ± 19	986 ± 58
F127 + P123-g-PEI(2K)	649 ± 100	478 ± 8	1126 ± 107

[a] Results statistically different from the other three systems ($p < 0.05$). [b] Results statistically different from each other ($p < 0.05$).

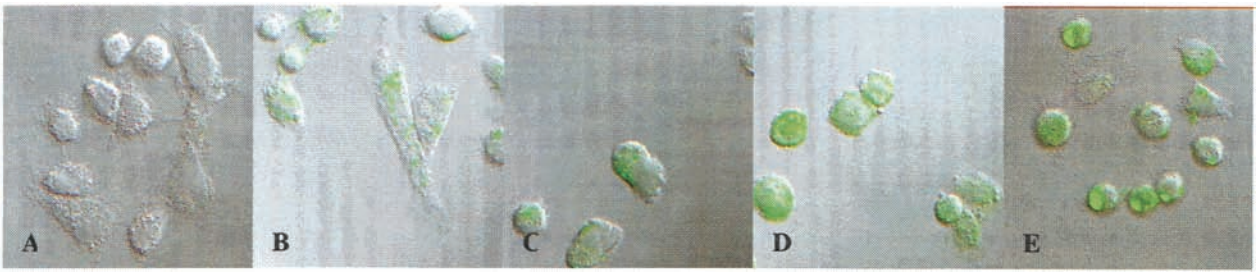


Figure 3. Intracellular distribution of YOYO-1-labeled pDNA. PC-3 cells were exposed for 2 h to YOYO-1-labeled pDNA alone or in combination with polymers: (A) no polymers; (B) Pluronic P123; (C) P123-g-PEI(2K); (D) P123:P123-g-PEI(2K); (E) Exgen 500. The images represent a Z-section through the middle of the cells.

show that the ratio of supercoiled to open circular forms is ca. 0.03. P123-g-PEI(2K) alone (lane 4) and P123-g-PEI(2K) formulated with either Pluronic P123 (lane 5) or Pluronic F127 (lane 6) protected less total DNA. However, it is important to note that the relative fraction of supercoiled versus relaxed DNA is much higher than what was observed with Exgen 500, with ratios ranging from 0.69 to 1.10. All DNase studies were performed in triplicate and are presented as the mean ± SD. Statistically, DNA formulated with P123-g-PEI(2K), without additional Pluronic, was better protected than DNA formulated with the graft copolymer plus either Pluronic, though those differences were small in comparison to the differences seen for Exgen 500 versus P123-g-PEI(2K)-based complexes ($p < 0.05$).

Imaging of Transport of pDNA. To examine internalization and intracellular localization of pDNA, this study conducted a similar set of experiments, transfecting PC-3 cells with YOYO-labeled DNA in polyplexes; in these experiments, the labeled pDNA within the cells was analyzed by confocal microscopy. The confocal microscopy images presented in Figure 3 illustrate the differences in the quantity and the localization of YOYO-1-labeled pDNA in PC-3 cells 2 h after a 2 h exposure to polyplexes. Consistent with the flow cytometry data presented above, both polyplex systems delivered a significant quantity of YOYO-1-labeled pDNA into the cytoplasm of the cells. More importantly, these images depict the apparent differences in the mechanisms of uptake and/or intracellular trafficking between the graft system and Exgen 500. Specifically, in Figure 3E, transfection with Exgen 500-based polyplexes results in localization of the fluorescence in discrete compartments within the cell, while transfection with P123:P123-g-PEI-based polyplexes results in a less localized, more diffuse appearance throughout the cytoplasm (Figure 3D).

Transfection of Complexes. Table 1 also presents the results of transfection of PC-3 cells with various formulations of polyplexes, containing expression plasmids for either luciferase or GFP. The level of transgene expression was examined following transfection with gWIZ-Luciferase, and the percent of cells successfully transfected was evaluated following transfection with pIRES-EGFP. The results quantifying the amount of transgene expressed were consistent with the results quantifying the number of cells successfully transfected. In brief, Exgen 500-based polyplexes were the most effective system, followed by the transfection systems composed of P123:P123-g-PEI(2K) and F127:P123-g-PEI-(2K), while the same graft block copolymer, in the absence of additional nonmodified Pluronic P123, produced little more luciferase than the naked DNA control. Interestingly, although F127:P123-g-PEI(2K)-based polyplexes were approximately twice as large and delivered about half as much pDNA into cells compared to P123:P123-g-PEI(2K)-based polyplexes, the difference in luciferase expression levels was less than 2-fold.

DISCUSSION

This work reports the critical evaluation of the design and formulation of a DNA−polycation polyplex based on a Pluronic-PEI conjugate. This delivery system was chosen for further evaluation because it demonstrated promising results as a systemically administered gene delivery system in vivo (*1*). Furthermore, because the delivery system contains multiple components, it was important to fully understand the function of each component to the overall transfection process.

The first objective of this work was to develop a more clear understanding of the process of particle formation, specifically as it occurs for the P123-g-PEI(2K)-based delivery system. As discussed earlier, when the graft copolymer itself is combined with DNA, it does not form a stable dispersion. In this situation, it is likely that the components are not combining in the appropriate manner to achieve the necessary structure possessing a tight core of DNA bound with PEI segments and a hydrophilic exterior shell stabilizing the system in dispersion. Such structures are, in fact, forming following the reaction of a plasmid DNA with a graft copolymer of PEI(2K) and PEO (*16*). It was demonstrated that PEO(8K) in this graft copolymer is essential for stabilizing the particle dispersion. P123-g-PEI(2K) has a similar structure as the PEO-(8K)-g-PEI that is a graft copolymer of a polycation with uncharged polyether. Furthermore, P123 has comparable length as the PEO(2K), and the architecture of the two graft copolymers is very similar, i.e., containing 1−2 polyether chains per PEI(2K) segment. The difference is that the Pluronic chain is more hydrophobic than the PEO chain since it contains PPO segments flanked by PEO chains (Figure 4). Therefore, the stabilizing ability of Pluronic is less than that of PEO, resulting in the formation of large aggregates. The improved dispersion stability observed following inclusion of nonmodified Pluronic to the formulation is most likely the result of incorporation of Pluronic chains into the polyplexes, driven by the interaction of PPO segments of Pluronic with PPO segments of P123-g-PEI conjugates. This process is very much like the self-assembly of Pluronic micelles, resulting in masking of the hydrophobic PPO sites from the aqueous environment by hydrophilic PEO chains. The final structure of the polyplex particles is complex, and it involves hydrophobic sites from electrostatically neutralized DNA and PEI chains, hydrophobic sites from the PPO chains of Pluronic and the conjugate, and a hydrophilic surface area formed by PEO chains of Pluronic and the conjugate. Therefore, the unconjugated Pluronic plays the role of a cosurfactant that forms mixed micelle-like structures with the complexes of DNA and

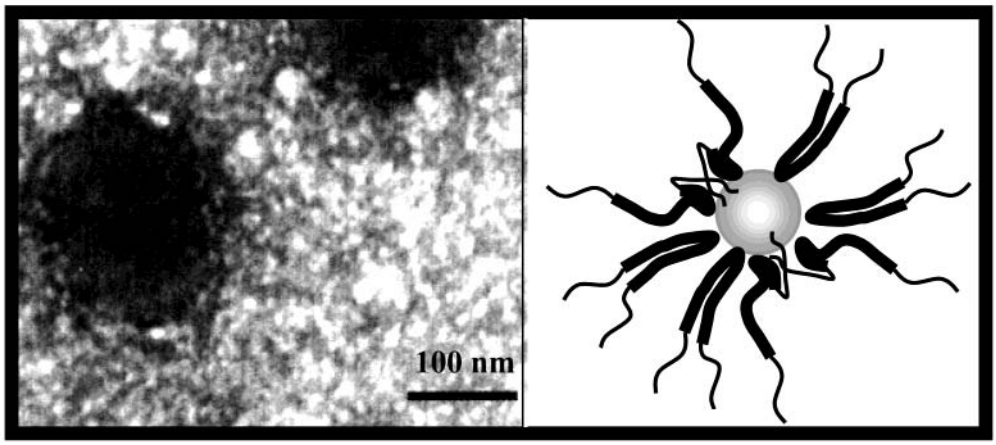


Figure 4. Polyplex structure. (Left) EM photo of complexes [taken from (*1*)] and (right) schematic representation of P123:P123-g-PEI(2K)-based complexes. The sphere represents the core of condensed DNA and polycation. The Pluronic P123 chains that are grafted to the PEI within the core are not incorporated into the core, but form a micelle-like structure around the core, orienting the lipophilic PPO segments (represented by heavy lines in the block copolymer) near the core and the hydrophilic PEO segments forming the exterior corona (represented by the thinner lines in the block copolymer). Additional nonmodified Pluronic P123 chains fill in to optimize the stability of the micelle-like structure.

Table 3. Pluronic Characteristics

copolymer	MW[a]	structure	CMC, M[b]	CMC, %	HLB[c]
P123	5750	$EO_{19}-PO_{69}-EO_{19}$	4.4×10^{-6}	0.0025	8
F127	12600	$EO_{100}-PO_{65}-EO_{100}$	2.8×10^{-6}	0.0035	22

[a] Average molecular weights provided by the manufacturer. [b] The CMC values were determined previously using a pyrene probe. [c] HLB (hydrophilic−lipophilic balances) values of the copolymers were determined by the manufacturer.

P123-g-PEI(2K). Since the stable formulations of polyplexes contained up to 0.03 wt % of Pluronic P123, it was important to determine whether this component can be displaced with another Pluronic capable of fulfilling the same function. There are many Pluronics that could be tested for this role; an overview of their structure and relevant characteristics can be found elsewhere (*17*). This work examined reformulation with Pluronic F127, which was selected for this task for two primary reasons. One, the hydrophobic PPO chains of both Pluronics are nearly identical; therefore, only the size of the hydrophilic PEO chain would be significantly different from the original formulation (Table 3). Two, Pluronic F127 is already approved for use in pharmaceutical preparations; therefore, toxicological dat exists, which can speed the preclinical development of the formulation.

The first step toward understanding the process of particle formation was to establish the relevance of the order of mixing of the components in relation to the size and stability of the resulting polyplexes. By comparing particle size and stability following a variety of mixing protocols, the results of this work demonstrate that, due to the rapidity and nonreversibility of large aggregate formation, the graft copolymer must always be the last component introduced into the system, regardless of the nonmodified Pluronic employed. The next step to understanding the process was to determine the quantity of Pluronic necessary to stabilize the formulation. In the case of both Pluronic P123 and Pluronic F127, concentrations well above the CMC effectively stabilized the system (data not shown). At these concentrations, the dynamic equilibrium between unimers and micelles provides a favorable environment for the displacement of unimers from the solution and incorporation into the polyplexes (Figure 4). It is important to bear in mind that due to the measuring technique employed, the inclusion of Pluronic micelles, which exhibit effective diameters in the range of 20−30 nm, into the mixture could overexaggerate the differences in the effective diameters of polyplexes formulated either with or without the inclusion of nonmodified Pluronic. However, there are two important considerations that argue strongly against that possibility. First, the concentrations of Pluronic micelles used are relatively low when considering the relative concentration of polyplexes present in the solution. Second, although micelles of Pluronic P123 and Pluronic F127 are both within the range of 20−30 nm (data not shown), the effective diameters of P123:P123-g-PEI polyplexes versus F127:P123-g-PEI polyplexes formed with the same concentrations of either Pluronic are significantly higher than the diameters of the Pluronic micelles and significantly different from each other (Table 1). Therefore, the contribution of the small micelles in the overall scattering intensity is marginal compared to that of the large polyplexes.

The second objective of this work was to evaluate the ability of the P123-g-PEI(2K)-based delivery system to protect the incorporated pDNA from degradation by nucleases, specifically degradation by DNase I. This objective included assessment of the impact of each component of the system to the overall protection. The results presented indicate that the inclusion of nonmodified Pluronic had no significant impact on the protective capacity of the polyplexes. Therefore, it can be surmised that the polycationic component of the polyplex, PEI, is solely responsible for imparting the characteristic of nuclease resistance to the delivery system. When considering the total DNA remaining following digestion (open circular plus supercoiled), the 22 kDa linear PEI, Exgen 500, was twice as effective at protecting the DNA compared to the relatively short 2 kDa PEI contained in the graft copolymer. This likely indicates that the PEI segment used in the graft is too small to prevent access of the enzyme to the pDNA. The protective capacity is quite critical, because if even a very small piece of pDNA is accessible to such enzymes, any damage done to that segment of the DNA would likely result in a change in the conformation of the originally supercoiled DNA. A change in DNA conformation could result in changes in the dynamics of the polyplex, perhaps leading to overall destabilization of the polyplex and, further, more rapid degradation of the incorporated therapeutic pDNA. It is

important to realize that the data presented in Table 2 are open to broad interpretation. There are obvious differences in the fractions of open circular and supercoiled DNA recovered following digestion and subsequent dissociation of the complexes. Although Exgen 500 based polyplexes protected the largest quantity of DNA overall, the graft system retained the greatest portion of the supercoiled fraction, which many would argue should be the fraction of DNA retaining the greatest integrity. These questions regarding DNA topology are very important questions to be addressed in light of development of polyplex technology, but they go beyond the scope of this paper (*18*). The significant, undisputable conclusion of this experiment is that the level of protection observed with the current graft copolymer formulation is not nearly as high as the protection observed with Exgen 500 based polyplexes, and is a factor that may represent a significant limiting factor to the effectiveness of this system in vivo by limiting the effective circulatory time of these polyplexes.

The final objective of this work was to take the knowledge regarding the polyplexes obtained in the cell-free systems combined with evaluation of the polyplex systems in in vitro cellular systems in order to identify critical parameters for the successful application of the delivery systems. DNA uptake studies utilized the high affinity of DNA-binding dye YOYO-1, which has proven to be an excellent tool for monitoring this process (*19*−*21*). This dye is well suited for this task for multiple reasons. First, YOYO-1 alone emits negligible levels of fluorescence; however, its binding to DNA results in a persistent, high fluorescence enhancement. Second, the polycations that we have examined do not displace YOYO-1 when binding to labeled DNA, nor do the polycations quench the fluorescence of the DNA-bound dye (data not presented). This makes it possible to monitor the fate of the polyplex as well as the released DNA. Finally, YOYO-1 is membrane impermeable and is transported in the cells only when bound to DNA incorporated within a polyplex. The DNA uptake studies demonstrated that the relative quantity of pDNA taken into a cell by the various polyplex systems correlated inversely with the particle size of the polyplex. However, the differences in size may not be responsible for the differences in cellular uptake, as there are significant differences in the surface characteristics between some of the included polyplex systems. For example, it was previously demonstrated that polyplexes based on the graft copolymer exhibit a nearly neutral charge on their surface by zeta potential analysis (*1*), which is unlikely, due to the strong interactions between the polyplex and the cell surface, compared to the highly positively charged surface of the Exgen 500 based polyplexes, which allows for strong interaction of these complexes with the negatively charged proteoglycans present on cell surfaces (*22*). On the other hand, the data obtained for the graft copolymer based formulations formed with either P123 or F127 support the theory that smaller particle size correlates with higher transfection activity (*23*), as there should be no significant differences in the surface properties between these two systems; however, the smaller system [P123:P123-g-PEI(2K)] consistently transfects cells in vitro more efficiently than its F127 counterpart [F127:P123-g-PEI(2K)].

Finally, both the levels of transgene expression, as determined by luciferase expression, and the percentage of cells transfected, as determined by GFP expression, were as expected based on the particle size and pDNA internalization studies. Formulation of the graft copolymer with either Pluronic resulted in significantly improved pDNA uptake and transgene expression by PC-3 cells relative to the graft system alone; however, none of the formulations were able to perform as well as Exgen 500. There are likely several factors that prevent this graft copolymer based gene delivery system from performing as well, in vitro, as the linear PEI, Exgen 500. First, Exgen 500 protects the DNA from degradation more effectively, allowing more intact DNA to be delivered to the target cell. Second, as mentioned above, there are differences in the polyplex surface properties that likely result in stronger interactions between the Exgen 500 based polyplexes and cell surfaces. Third, there appear to be differences in the mechanism of internalization of the polyplexes formulated with P123-g-PEI(2K) versus complexes formulated with Exgen 500.

In summary, the nonmodified Pluronic component of this gene delivery system enhanced DNA uptake and expression primarily as a result of optimization of the size and morphology of the polyplex. It does not appear that the nonmodified Pluronic contributes significantly, alone, to either enhancement of DNA uptake, transgene expression, or protection from nuclease degradation. Although much of the preliminary work with this nonviral delivery system appears quite promising, the authors acknowledge the potential limitations of this system for in vivo application due to the low level of nuclease protection exhibited in the DNase protection assays. This may limit the effective dose delivered, as well as limiting the effective circulation time, upon systemic delivery of this formulation. The authors suggest that substitution of the relatively small 2K PEI used in this graft copolymer with a larger polycationic segment will enhance the 'tightness' of the polycation binding to the DNA and might significantly improve the nuclease protection characteristics. In addition, attachment of a receptor-specific ligand, such as transferrin, should improve complex cell membrane interactions, and perhaps improve the intracellular trafficking profile.

ACKNOWLEDGMENT

We thank the National Science Foundation (BES-9907281) and the Nebraska Research Initiative Gene Therapy program for supporting this research. We thank Dr. Pi-Wan Cheng of the UNMC Biochemistry Department for providing the PC-3 prostate cancer cell line and for useful discussion of this work, and Janice Taylor of the Confocal Laser Scanning Microscope Core Facility at the UNMC, which is supported by the Nebraska Research Initiative, for providing assistance with confocal microscopy. We also thank Charles Kuszynski, Ph.D., and Linda Wilkie of the UNMC Cell Analysis Core Facility for analyzing the flow cytometry samples. We thank Supratek Pharma Inc. for providing the sample of P123-g-PEI(2K), that was synthesized by Dr. Sergey Vinogradov. M-H-W Laboratories (Phoenix, AZ) did elemental analysis. We thank BASF for the gift of Pluronic P123 and Dr. Albert Descoteaux (Armand Frappier Institute, Montreal, PQ, Canada) for providing the pCMV-Luc plasmid.

LITERATURE CITED

(1) Nguyen, H. K., Lemieux, P., Vinogradov, S. V., Gebhart, C. L., Guerin, N., Paradis, G., Bronich, T. K., Alakhov, V. Y., and Kabanov, A. V. (2000) Evaluation of Polyether-Polyethyleneimine Graft Copolymers as Gene Transfer Agents. *Gene Ther. 7,* 126−138.

(2) Cristiano, R. (1998) Viral and Non-Viral Vectors for Cancer Gene Therapy. *Anticancer Res. 18,* 3241−3245.

(3) Boussif, O., Lezoualc'h, F., Zanta, M. A., Mergny, M. D., Scherman, D., Demeneix, B., and Behr, J. P. (1995) A Versatile Vector for Gene and Oligonucleotide Transfer into Cells in Culture and in Vivo: Polyethylenimine. *Proc. Natl. Acad. Sci. U.S.A. 92,* 7297−7301.
(4) Felgner, P., Barenholz, Y., Behr, J., Cheng, S., Cullis, P., Huang, L., Jessee, f., Seymour, L., Szoka, F., Thierry, A., Wagner, E., and Wu, G. (1997) Nomenclature for Synthetic Gene Delivery Systems. *Hum. Gene Ther. 8,* 511−512.
(5) Kabanov, A. V., and Kabanov, V. A. (1995) DNA Complexes with Polycations for the Delivery of Genetic Material into Cells. *Bioconjugate Chem. 6,* 7−20.
(6) Mahato, R. I., Takakura, Y., and Hashida, M. (1997) Nonviral Vectors for in Vivo Gene Delivery: Physicochemical and Pharmacokinetic Considerations. *Crit. Rev. Ther. Drug Carrier Syst. 14,* 133−172.
(7) Verbaan, F. J., Oussoren, C., van Dam, I. M., Takakura, Y., Hashida, M., Crommelin, D. J., Hennink, W. E., and Storm, G. (2001) The Fate of Poly(2-Dimethyl Amino Ethyl) Methacrylate-Based Polyplexes after Intravenous Administration. *Int. J. Pharm. 214,* 99−101.
(8) Garrett, S. W., Davies, O. R., Milroy, D. A., Wood, P. J., Pouton, C. W., and Threadgill, M. D. (2000) Synthesis and Characterisation of Polyamine-Poly(Ethylene Glycol) Constructs for DNA Binding and Gene Delivery. *Bioorg. Med. Chem. 8,* 1779−1797.
(9) Choi, Y. H., Liu, F., Kim, J.-S., Choi, Y. K., Park, J. S., and Kim, S. W. (1998) Polyethylene Glycol-Grafted Poly-L-Lysine as Polymeric Gene Carrier. *J. Controlled Release 54,* 39−48.
(10) Wolfert, M. A., Schacht, E. H., Toncheva, V., Ulbrich, K., Nazarova, O., and Seymour, L. W. (1996) Characterization of Vectors for Gene Therapy Formed by Self-Assembly of DNA with Synthetic Block Co-Polymers. *Hum. Gene Ther. 7,* 2123−2133.
(11) Ogris, M., Brunner, S., Schuller, S., Kircheis, R., and Wagner, E. (1999) Pegylated DNA/Transferrin-Pei Complexes: Reduced Interaction with Blood Components, Extended Circulation in Blood and Potential for Systemic Gene Delivery. *Gene Ther. 6,* 595−605.
(12) Batrakova, E. V., Miller, D. W., Li, S., Alakhov, V. Y., Kabanov, A. V., and Elmquist, W. F. (2001) Pluronic P85 Enhances the Delivery of Digoxin to the Brain: In Vitro and in Vivo Studies. *J. Pharmacol. Exp. Ther. 296,* 551−557.
(13) Melik-Nubarov, N. S., Pomaz, O. O., Dorodnych, T., Badun, G. A., Ksenofontov, A. L., Schemchukova, O. B., and Arzhakov, S. A. (1999) Interaction of Tumor and Normal Blood Cells with Ethylene Oxide and Propylene Oxide Block Copolymers. *FEBS Lett. 446,* 194−198.
(14) Lemieux, P., Guerin, N., Paradis, G., Proulx, R., Chistyakova, L., Kabanov, A., and Alakhov, V. (2000) A Combination of Poloxamers Increases Gene Expression of Plasmid DNA in Skeletal Muscle. *Gene Ther. 7,* 986−991.
(15) Kozlov, M. Y., Melik-Nubarov, N. S., Batrakova, E. V., and Kabanov, A. V. (2000) Relationship between Pluronic Block Copolymer Structure, Critical Micellization Concentration and Partitioning Coefficients of Low Molecular Mass Solutes. *Macromolecules 33,* 3305−3313.
(16) Bronich, T. K., Kabanov, A. V., and Marky, L. A. (2001) A Thermodynamic Characterization of the Interaction of a Cationic Copolymer with DNA. *J. Phys. Chem. 105,* 6042−6050.
(17) Kabanov, A. V., and Alakhov, V. (2002) Pluronic Block Copolymers in Drug Delivery: From Micellar Nanocontainers to Biological Response Modifiers. *Adv. Drug Deliv. Rev.* (in press).
(18) Bronich, T. K., Nguyen, H.-K., Eisenberg, A., and Kabanov, A. V. (2000) Recognition of DNA Topology in Reactions between Plasmid DNA and Cationic Copolymers. *J. Am. Chem. Soc. 122,* 8339−8343.
(19) Gebhart, C. L., Sriadibhatla, S., Vinogradov, S., and Kabanov, A. (2001) Pluronic-Polyethyleneimine Conjugates for Gene Delivery. *Polym. Prepr. (Am. Chem. Soc., Div. Polym. Chem.) 42,* 119−120.
(20) Wong, M., Kong, S., Dragowska, W. H., and Bally, M. B. (2001) Oxazole Yellow Homodimer Yoyo-1-Labeled DNA: A Fluorescent Complex That Can Be Used to Assess Structural Changes in DNA Following Formation and Cellular Delivery of Cationic Lipid DNA Complexes. *Biochim. Biophys. Acta 1527,* 61−72.
(21) Clamme, J. P., Bernacchi, S., Vuilleumier, C., Duportail, G., and Mely, Y. (2000) Gene Transfer by Cationic Surfactants Is Essentially Limited by the Trapping of the Surfactant/DNA Complexes onto the Cell Membrane: A Fluorescence Investigation. *Biochim. Biophys. Acta 1467,* 347−361.
(22) Chemin, I., Moradpour, D., Wieland, S., Offensperger, W. B., Walter, E., Behr, J. P., and Blum, H. E. (1998) Liver-Directed Gene Transfer: A Linear Polyethlenimine Derivative Mediates Highly Efficient DNA Delivery to Primary Hepatocytes in Vitro and in Vivo. *J. Viral Hepat. 5,* 369−375.
(23) Wagner, E., Cotten, M., Foisner, R., and Birnstiel, M. L. (1991) Transferrin-Polycation−DNA Complexes: The Effect of Polycations on the Structure of the Complex and DNA Delivery to Cells. *Proc. Natl. Acad. Sci. U.S.A. 88,* 4255−4259.

BC025504W

Artificial Ribonucleases: Efficient and Specific in Vitro Cleavage of Human *c-raf-1* RNA

Laurence Canaple,[†] Dieter Hüsken,[‡] Jonathan Hall,[‡] and Robert Häner*[,†]

Universität Bern, Departement für Chemie und Biochemie, Bern, and Novartis Pharma AG, Functional Genomics, Basel. Received January 18, 2002; Revised Manuscript Received April 25, 2002

We report here the first successful sequence-specific cleavage of large RNA using artificial ribonucleases. A series of uniformly 2′-methoxyethoxy-modified oligonucleotides bearing a europium complex were investigated as artificial ribonucleases specific for the human *c-raf-1* mRNA. The efficiency and specificity of these oligonucleotide−metal conjugates to bind and to cleave 571 and 2977 nucleotides long *c-raf-1* RNA transcripts in vitro in a sequence-specific manner is demonstrated. Quantitative analysis reveals a cleavage efficiency of 60−70% within 4 h at 37 °C. Precise mapping of cleavage sites using primer extension analysis shows that cleavage generally occurs at two or three major sites adjacent to the 3′-end of the RNA target region. Cleavage is preferentially observed after purine nucleotides. This study demonstrates the potency of artificial ribonucleases targeting large, biologically relevant RNAs.

INTRODUCTION

Antisense oligonucleotides represent potent agents to modulate the expression of genes (Agrawal and Zhao, 1998; Baker et al., 2001). They act by inhibiting protein expression through the specific binding to complementary RNA targets, followed by the degradation of the targeted RNAs through a RNase H-mediated hydrolysis (Crooke, 1999). Before an antisense molecule can achieve its full potential, several biochemical and biological limitations of the oligonucleotides must be improved, including cellular uptake, nuclease stability, target selectivity, and intracellular localization (Jen and Gewirtz, 2000). The incorporation of chemical modifications at base, sugar or phosphate backbone of oligonucleotides leads to altered nuclease resistance as well as improved hybridization efficiency and pharmacokinetic parameters (Verma and Eckstein, 1998; Henry et al., 2000). Although they are not able to induce RNase H action, 2′-methoxyethoxy-modified oligonucleotides are considered as a promising class of antisense compounds since they combine both a significantly enhanced nuclease stability, an excellent binding affinity for the RNA target, and favorable pharmacokinetics (Geary et al., 2001a,b; Zellweger et al., 2001). The design of oligonucleotide-based artificial ribonucleases, which can selectively cleave targeted RNAs, independently of intracellular ribonuclease activity, could compensate for the loss of RNase H activity observed for almost all types of antisense oligonucleotides. In this approach, a catalytic group promoting the cleavage of the messenger is attached to an antisense oligonucleotide complementary to the targeted mRNA. Covalent attachment of stable macrocyclic lanthanide complexes to oligonucleotides leads to artificial ribonucleases acting without the requirement of cofactors or cellular enzymes for the sequence-specific cleavage of RNA. To date, lanthanide complexes are among the most potent transphosphorylation catalysts known (Magda et al., 1994; Matsumura et al., 1994; Hall et al., 1994, 1996) with a potential for cellular applications (Baker et al., 1999). However, examples of sequence-specific in vitro cleavage using lanthanide conjugates have been limited to short (i.e. < 40 nucleotides) RNA targets (Trawick et al., 1998; Häner and Hall, 1997). Insight into the cleavage of large RNA targets should considerably improve our understanding of the behavior and potency of such artificial ribonucleases.

The serine/threonine kinase Raf-1 functions as a central messenger of the mitogen-activated protein kinase signaling pathway, which is involved in the regulation of cell proliferation, differentiation and apoptosis. Raf-1 largely contributes to the control of the cell proliferation and plays a critical role in the development and the growth of tumors (Hagemann and Rapp, 1999; Robinson and Cobb, 1997). Studies have clearly demonstrated that Raf-1 is the immediate downstream-target of the well-described oncogenic Ras protein (Marshall, 1995), for which gene mutations have been reported in various solid tumors and leukemias (Bos, 1989). Raf-1 itself also presents an oncogenic potential, as *raf* gene mutations have been detected in human tumors and amino-terminal-deleted Raf-1 proteins displayed a transforming activity in a wide variety of cell types (Stanton and Cooper, 1987; Storm and Rapp, 1993). Since activation and aberrant expression of Raf-1 appear to be important mechanisms in malignant transformation, therapies allowing the down-regulation of Raf-1 expression could have a significant impact for the treatment of various human disorders (Cho-Chung, 1999).

In the present study, a series of uniformly 2′-methoxyethoxy-modified oligonucleotides bearing a europium complex were investigated as potential artificial ribonucleases specific for the human *c-raf-1* mRNA. We report the potency of these oligonucleotide-metal conjugates to bind and to cleave RNA transcripts of a length of 571 and 2977 nucleotides in vitro in a sequence-specific way.

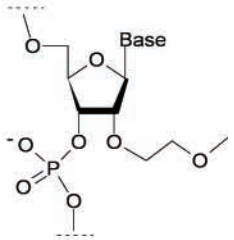
* To whom correspondence should be addressed. Universität Bern, Departement für Chemie und Biochemie, Freiestrasse 3, CH-3012 BERN. Phone: +41 31 631 43 82. Fax: +41 31 631 80 57. E-mail: robert.haener@ioc.unibe.ch.

[†] Universität Bern.

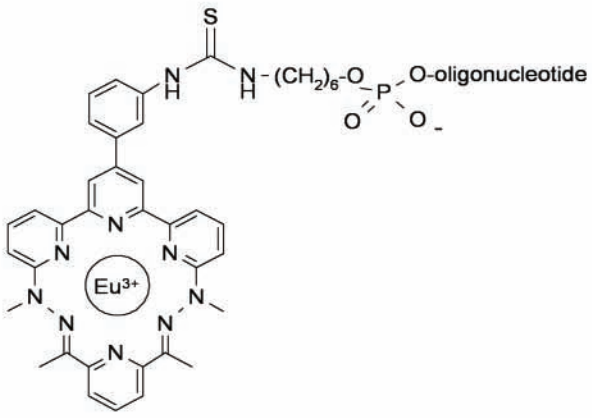
[‡] Novartis Pharma AG.

10.1021/bc0200024 CCC: $22.00 © 2002 American Chemical Society
Published on Web 08/31/2002

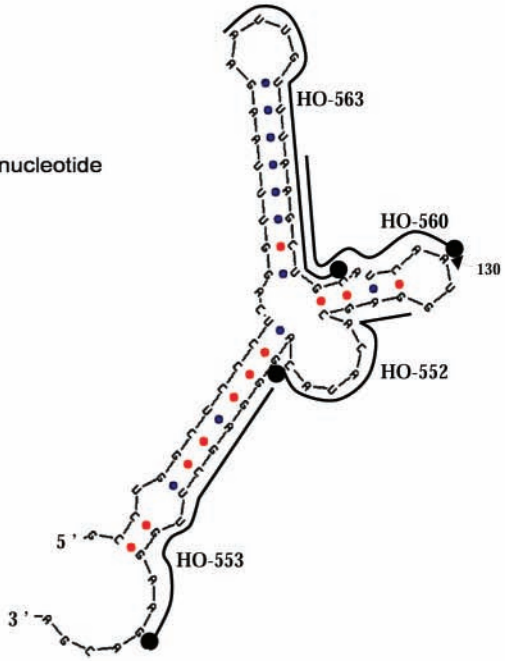
Compound	Sequence	Position	Sugar Modification
HO-554	Eu-(5')-gaagaaagtcc	control	
HO-552	Eu-(5')-ctgtatgtgctc	133 – 144	
HO-553	Eu-(5')-cttccaagctcc	145 – 156	
HO-560	Eu-(5')-ttgatgcagctt	119 – 133	
HO-563	Eu-(5')-gcagcttaaacaat	112 – 125	



Oligonucleotide-Metal Conjugate



Predicted Structure of *c-raf-1* RNA



5' *c-raf-1* RNA

...cagguuuaagaauuguuuaagcugcaucaauggagcacauacagggagcuuggaagacgauc...

101

HO-563 taacaaattcgacg-Eu

HO-560 ttcgacgtagtt-Eu

HO-552 ctcgtgtatgtc-Eu

HO-553 cctcgaaccttc-Eu

Figure 1. Top: sequence of 2′-methoxyethoxy-modified oligonucleotide−metal conjugates used in the present study. Complementary positions of conjugates are indicated as nucleotide number on *c-raf-1*-mRNA. HO-554 is used as a control and is not complementary to *c-raf* messenger. Bottom: structure of the europium complex linked to the 2′-methoxyethoxy-modified oligonucleotides is shown. Possible secondary structure of the target RNA region of interest as predicted by RNA *mfold* (Zuker, 1989, http://bioinfo.math.rpi.edu/~mfold/rna). The AUG start codon used for initiation of translation is located at nucleotide 130. Eu-conjugates are drawn in solid, colored lines at complementary regions. The metal complex is symbolized by a point.

MATERIALS AND METHODS

Synthesis of Europium Complexes Conjugated to 2′-Methoxyethoxy-Modified Oligonucleotides. 2′-Methoxyethoxy-modified oligonucleotides were prepared by automated synthesis on a DNA synthesizer (Applied Biosystems Inc.) using commercially available reagents and following standard procedure. Europium complexes were synthesized in analogy to the previously published procedure (Hall et al., 1996). The europium complexes were covalently attached to the 5′-end of different 2′-methoxyethoxy-modified oligonucleotides via the intermediate isothiocyanate yielding the conjugates shown in Figure 1. All conjugates were purified by RP-HPLC and characterized by mass spectroscopy and UV spectroscopy.

Preparation of Target *c-raf* RNAs by in Vitro Transcription. *c-raf* RNAs were synthesized by in vitro runoff transcription with T7 RNA polymerase (RiboMAX Large Scale Production System, Promega) using Hind III or Pst I linearized plasmid which contains the human c-raf sequence (accession number XØ3484) inserted as a 2977 base pair part at the Eco RI site of pGEM-3Z vector (Promega). The transcription reactions were carried out in 20 μL of 80 mM Hepes-KOH (pH7.5) containing 24 mM magnesium chloride, 2 mM spermidine, 40 mM DTT,

each NTP (7.5 mM), 1−2 μg of linearized DNA template, and T7 RNA polymerase according to the manufacturer's instructions. Reaction mixtures were incubated overnight at 37 °C. The DNA template was removed by digestion with RQ1 RNase-free DNase (1−2 U/μg of DNA) for 30 min at 37 °C. After phenol/chloroform /isoamyl alcohol extraction and ethanol precipitation, the RNAs were washed with ethanol 70%. The dried pellet was resuspended in nuclease-free water and stored at −70 °C. The transcript concentration was estimated by UV-light absorbance and their integrity examined by gel electrophoresis. The labeled *Hind III c-raf* transcripts were made under the same experimental conditions with the four NTPs and in the presence of [α-^{32}P] ATP at a specific activity of 3000 Ci/mmol (Hartmann Analytic GmbH).

RNA Folding Prediction. Secondary structure predictions of *c-raf-1* RNAs were obtained using RNA *mfold* (Zuker, 1989; http://bioinfo.math.rpi.edu/~mfold/rna).

RNA Cleavage Assay. Cleavage of *c-raf* transcripts by europium complex conjugated to modified oligonucleotides were performed in 10 μL cleavage mixture containing at final concentration 20 mM Tris-HCl (pH 7.5), ~0.5 μM RNA, and 1 μM conjugate. The mixture was heated to 80 °C for 1 min and slowly cooled to 37 °C. The standard reaction time is 4 h. For the determination of the sequence-specificity, cleavage reactions were conducted with unlabeled *Hind III c-raf* transcript in the presence of HO-552, HO-553, HO-554, HO-560, or HO-563 conjugates under standard conditions as described above. Reactions were stopped by addition of formamide loading buffer and cleavage products were analyzed on an ethidium bromide-stained 2% agarose gel or on 5% polyacrylamide native gel. Results are representative of three independent experiments. Same protocol was carried out for the cleavage of *full length* transcripts. For the determination of the cleavage efficiency**,** cleavage reactions were performed with radiolabeled *Hind III c-raf* transcript in the presence of HO-552, HO-553, HO-560, or HO-563 conjugates under standard conditions. The cleavage products in formamide buffer were resolved on a 5% polyacrylamide native gel, visualized, and quantified using a Molecular Dynamics PhosphorImager. Results were normalized according to the length of the quantified products. Results are averages of three independent experiments.

Mapping of the Cleavage Site by Primer Extension Analysis. A synthetic oligodeoxynucleotide (5′-atcaaacacggcatc-3′) complementary to nucleotides 184−198 of the *c-raf-1* transcripts and 5′-end labeled with T4 polynucleotide kinase (USB protocol) and [γ-32 P] ATP (5000 Ci/mmol, Hartmann Analytic GmbH) was hybridized in a solution of 0.15 μM of conjugate-RNA (3 μL of cleavage mixture) in 20 μL of 50 mM Tris-HCl pH8.3, 75 mM KCl, 10 mM DTT, 3 mM $MgCl_2$, 1 mM dNTP each and extended with M-MLV reverse transcriptase (10 U/μL of reaction, Gibco BRL) at 37 °C for 90 min. Reverse transcripts were ethanol precipitated, resuspended in formamide loading buffer, and resolved on a 7 M urea/10% polyacrylamide gel. Gels were exposed to the PhosphorImager screen. RNA sequencing was carried out with the same oligonucleotide by a reverse transcription using dideoxy-chain termination. Sequencing reactions were coelectrophoresed with reverse transcripts. Results are representative of three independent experiments.

RESULTS

A series of 2′-methoxyethoxy-modified oligonucleotides targeted against the human *c-raf-1* mRNA were designed.

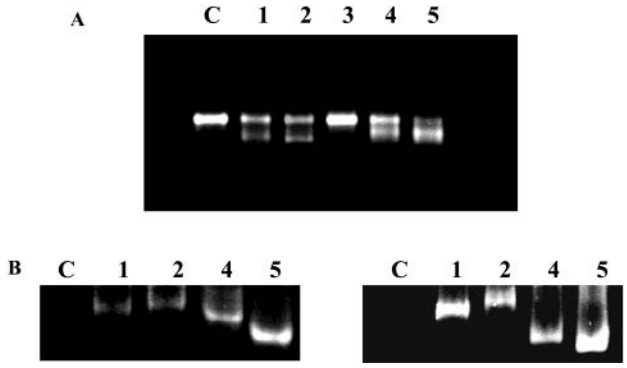


Figure 2. Sequence-specificity of *c-raf* transcript cleavage. A: Cleavage of *Hind III c-raf* transcript (571 nt) by Eu-conjugates as detected by 2% agarose gel stained with ethidium bromide. The upper bands correspond to the uncleaved *Hind III c-raf* transcript and the lower bands to the large cleaved RNA fragment (400−450 nt). B: Detection of the small cleavage products (100−150 nt) by 5% native polyacrylamide gel. Left, for *Hind III c-raf* transcript (571 nt). Right, for full length *c-raf* transcripts (2977 nt). Controls (lanes C) were carried out without addition of conjugate under identical experimental conditions. Cleavage reactions by HO-552, HO-553, HO-554, HO-560, and HO-563 are shown in lanes 1, 2, 3, 4, and 5, respectively.

All oligonucleotides were 12 or 14 bases in length and complementary to the region of nucleotides 112−156 of *c-raf-1* mRNA, which comprises the 5′-AUG translation start codon. The 2′-methoxyethoxy-modified oligonucleotides were covalently linked to a europium complex leading to the formation of the conjugates as detailed in Figure 1. *c-raf-1* RNAs were obtained by in vitro runoff transcription. The use of Hind III for linearization of the plasmid template prior to transcription reaction yielded a small transcript of 571 nucleotides (termed *Hind III c-raf* transcript) whereas Pst I linearization allowed the preparation of the *full length* transcript (2977 nucleotides). In a first series of pilot experiments, the reaction conditions for an in vitro cleavage of *c-raf* transcripts were established. We found that the extent of the RNA cleavage was time and temperature dependent. In addition, an additional step of denaturation of 1 min at 80 °C increased the efficiency of the cleavage, favoring the binding of the conjugate to the RNA target region before cooling to 37 °C. No cleavage was observed during this annealing step (data not shown). Efficient cleavage was obtained within 4 h at 37 °C using a 2-fold excess of the conjugate over the RNA target.

To prove that the action of Eu-conjugates is through an antisense mechanism, i.e., by binding to the complementary RNA sequence, we first tested the sequence requirements for cleaving *c-raf-1* RNAs by comparing the effects of complementary conjugates with a noncomplementary control conjugate (HO-554). As expected for a mechanism based on Watson−Crick recognition, no cleavage was observed when the noncomplementary conjugate HO-554 was incubated with the *Hind III c-raf-1* RNA target. In contrast, all other HO-compounds complementary to *c-raf-1* RNA displayed a potent cleavage, reflecting a high sequence specificity (Figure 2A). Further analyses of the cleavage reaction revealed that two cleavage products were generated over time (for *Hind III c-raf-1* transcript, one cleavage product of an approximate size of 400 nucleotides is shown in Figure 2A, the other small fragment of about 150 nucleotides is seen in Figure 2B, left panel). Treatment of the *full length* transcript with Eu-conjugates yielded the same small cleavage product (Figure 2B, right panel). In a further

Table 1. Cleavage Efficiency of Eu-Conjugates on *Hind III c-raf* Transcript[a]

europium-conjugate	percentage of cleavage
HO-552	68.6 ± 3.1
HO-553	56.3 ± 3.9
HO-560	63.3 ± 2.7
HO-563	70.9 ± 1.2

[a] Yield of the cleavage reaction of radiolabeled *Hind III c-raf* transcript by the different Eu-conjugates as described in Materials and Methods (1 μM conjugate, 0.5 μM RNA and a total reaction time of 4 h). Results are means ± SD of three independent experiments.

control experiment, no cleavage was detected if the conjugates were incubated with *luciferase* RNA instead of *c-raf-1* transcripts, again confirming high sequence specificity (data not shown).

An important aspect for an artificial ribonuclease is the efficiency of the cleavage process. Therefore, the extent of cleavage effected by each europium conjugate was quantified. Experiments were performed with radiolabeled *Hind III c-raf* transcript using a 2-fold excess of the conjugate for 4 h at 37 °C. The results of three independent experiments are given in Table 1. Experimental data showed 60−70% of cleavage of *Hind III c-raf* transcripts. The highest cleavage yield was obtained with the conjugate HO-563 (70,9% ± 1.2).

The precise location of the cleavage sites was mapped using primer extension analysis of the cleavage products. Reactions were carried out using a radiolabeled antisense primer complementary to nucleotides 184−198. As a control, *c-raf* RNAs incubated under the same conditions but without conjugate showed no cleavage bands in the targeted region (Figure 3, top, lanes C1), confirming that no decomposition of the targets occurred during the experiments. Furthermore, primer extension analysis was also performed in the presence of a large excess of a complementary 2′-methoxyethoxy-modified oligonucleotide without a metal complex (Figure 3, top, lanes C2). This control confirmed that the presence of an annealed oligonucleotide on the RNA did not block the reverse-transcriptase activity. As a general observation, several extension products were detected for each conjugate tested, reflecting a relative flexibility of the catalytic part (Figure 3, top). As expected, precise location of the cleavage sites was dependent on the hybridization site of the conjugate on the RNA and generally occurred at or near the 3′ end of the RNA adjacent to the europium complex (illustrated in Figure 3, bottom). Comparison of the cleavage patterns obtained with the *Hind III* (571 nt) and the *full length* (2977 nt) transcripts showed no significant difference (Figure 3, top, units A and B, respectively). Quantification of each cleavage product is shown in Figure 4. Overall, an excellent correlation between the cleavage sites of the two RNA targets differing in size was found. Generally, cleavage occurred at two or three major sites, along with several minor sites of cleavage at the flanking bases. RNA cleavage was predominantly observed after purine bases. An excep-

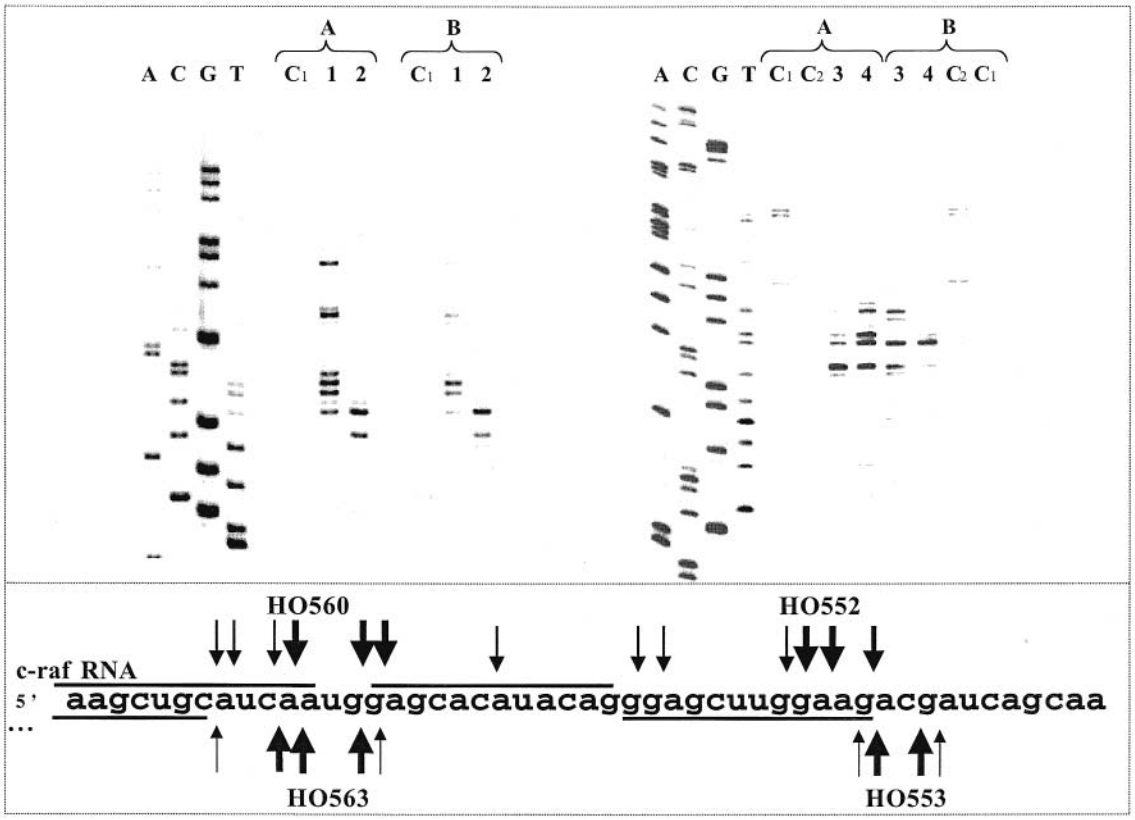


Figure 3. Mapping of the cleavage products. Top: primer extension analysis of cleavage products on a 10% denaturing polyacrylamide gel both for *Hind III* (A) and full length (B) *c-raf* transcripts for HO-552 (lanes 1), HO-553 (lanes 2), HO-560 (lanes 3), and HO-563 (lanes 4). Sequencing reactions (lanes A, C, G, T) of transcripts were coelectrophoresed to locate the cleavage sites. Lanes C1: primer extension products of corresponding RNA incubated in the reaction buffer without Eu-conjugate. Lanes C2: primer extension products of RNA incubated with a large excess of complementary 2′-methoxyethoxy-modified oligonucleotides bearing no metal complex. The data shown are representative of three independent experiments carried out in duplicate. Bottom: cleavage pattern obtained with *c-raf* RNAs and Eu-conjugates showing a preference for cleavage at purine sites. Cleavage sites are indicated by arrows with different size representing approximate cleavage intensities. Hybridization regions of HO-compounds on the *c-raf-1* RNA are displayed by horizontal lines.

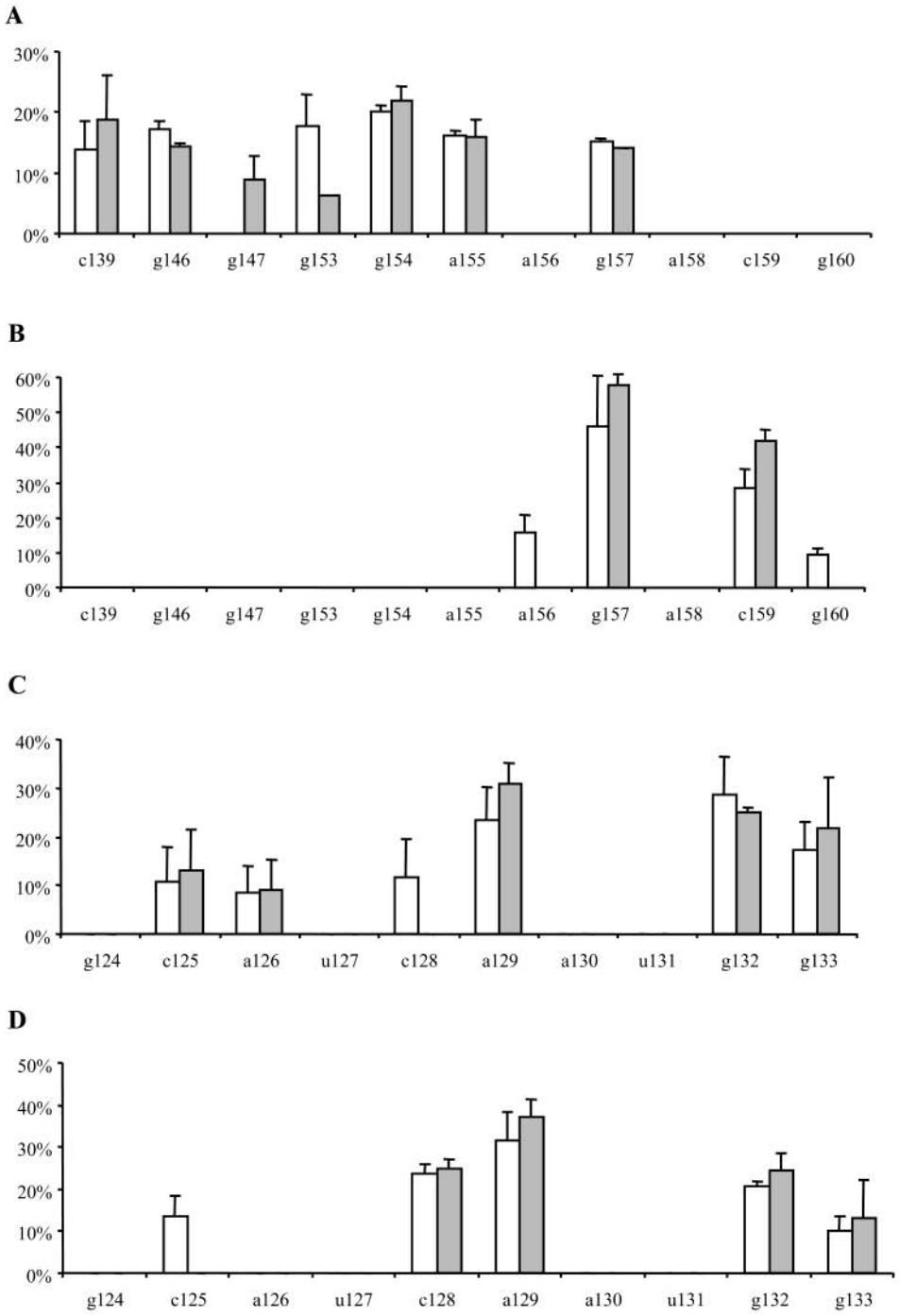


Figure 4. Quantification of cleavage sites for *Hind III* (in white) and full length (in gray) *c-raf-1* transcripts by HO-552 (A), HO-553 (B), HO-560 (C), and HO-563 (D). The values are means ± SD of three independent experiments in duplicate.

tional behavior was found using conjugate HO-552. This compound induced cleavage at sites relatively far downstream (9, 10, and 13 nucleotides) of the metal complex. In addition, one minor cleavage site was also located within the duplex formed by the RNA and this conjugate.

DISCUSSION

A current interest in the antisense field is directed to the development of novel mechanisms of oligonucleotide interference with gene expression. One promising approach in this direction consists of the sequence-specific hydrolytic cleavage of RNA using oligonucleotides bearing chemical moieties inducing phosphodiester transesterification (Trawick et al., 1998; Häner and Hall, 1997). In particular, metals are efficient catalysts for the cleavage of ribonucleic acids acting as *Lewis* acids, thus promoting the nucleophilic attack of the 2′-hydroxyl group on the adjacent phosphodiester group and leading to phosphodiester backbone cleavage. Promising results have been achieved using lanthanide metal complexes linked to oligonucleotides and several groups have reported the sequence-specific cleavage of short model oligoribonucleotides in the presence of at least 10-fold excess of conjugates during 16−24 h (Magda et al., 1994; Matsumura et al., 1994; Hall et al., 1994, 1996). Herein, we have tested the limits of the approach by targeting large RNAs (i.e. up to thousands of nucleotides long). Since the kinase Raf-1 plays an important role in the development of malignant tumors, we chose *c-raf-1* mRNA as a target of biological interest. Runoff transcripts of two different

sizes (571 and 2977 nucleotides) were prepared in vitro. As artificial ribonucleases, several 2′-methoxyethoxy-modified antisense oligonucleotides bearing a europium metal complex at the 5′-end were synthesized and tested against these two targets. 2′-Methoxyethoxy-modified oligonucleotides possess higher stability toward nucleases and exhibit higher hybridization affinity for complementary RNA than unmodified DNA. All oligonucleotides were designed to target the region between nucleotides 119−156 on *c-raf-1* mRNA. While the accessibility of the RNA target region may not be a limiting factor for the present in vitro studies, it will play a crucial role in vivo. Therefore, the choice of the target sites was based on RNA structure predictions obtained using Zuker's RNA folding program *(mfold,* Zuker, 1989). Calculations suggested this region to be folded into a stable structure composed of hairpins and loop structures (Figure 1), which should be ideal sites for hybridization of antisense oligonucleotides. We found that all four complementary conjugates were able to bind and cleave both the small *Hind III* and the *full length c-raf-1* transcripts. RNA cleavage was observed at a single region where the catalytic complex was expected to be located yielding two fragments of different size. No further product could be detected. The high specificity of the cleavage was furthermore confirmed by the absence of cleavage using a nontargeted RNA (luciferase) or a noncomplementary conjugate (HO-554).

We next determined the efficiency of the cleavage process. Quantitative analysis revealed that cleavage of *c-raf-1* transcripts amounts to 60−70% in 4 h at 37 °C using a 2-fold excess of conjugate. Precise location of individual cleavage sites for each conjugate was determined using the primer extension method. The region of cleavage is generally confined to the nucleotides flanking the end of the duplex formed by the target and the conjugate. With few exceptions, cleavage normally takes place after purine bases. The susceptibility of the different nucleotides toward the metal-catalyzed transesterification reaction is likely to be influenced by the particular folding of the targeted region. This may explain why the major cleavage sites induced by HO-552 are relatively distant from the hybridization region. Furthermore, the local RNA structure may also account for the accessibility and the slight but significant reactivity of several nucleotides located in the duplex formed by the RNA and HO-552 or HO-560 (see Figure 3). As previously reported (Hall et al., 1996; Hüsken et al., 1996), the extension of the cleavage into the duplex region can increase the potency of such artificial ribonucleases by facilitating the rapid dissociation of the cleaved RNA fragments from the nucleases and allowing, at the same time, the possibility of a catalytic turnover.

The conjugates tested induced efficient and specific RNA cleavage, which makes them promising reagents for targeting biologically relevant messenger RNAs. This type of conjugates might, therefore, present effective tools to investigate or artificially regulate processes involving RNA. Deregulated genes responsible for various human disorders, such as cancer and viral infectious diseases, represent attractive targets for artificial ribonucleases. The type of conjugates decribed in the present work should be stable and active in biological environment. We previously showed that no loss of metal occurs in the presence of EDTA and that the cleavage is not inhibited by the presence of phosphate or amines (Hall et al., 1994). Oligonucleotide−metal conjugates of this type may also find applications as tools in molecular biology. They can be useful as artificial restriction RNases, which are as yet unknown. Furthermore, they can be of interest to probe particular features of RNA structure. Structural motifs have been reported to affect oligonucleotide hybridization efficiency (Lima et al., 1992) and unpaired or bulged ribonucleotides are more susceptible to the cleavage than ribonucleotides within a duplex (Kolasa et al., 1993; Hüsken et al., 1996).

In conclusion, we have described the specific cleavage of human *c-raf-1* RNA in vitro by 2′-methoxyethoxy-modified oligonucleotides bearing a europium metal complex. The cleavage efficiency was found to be 60−70% within 4 h using 2-fold excess of conjugate. Precise mapping of cleavage sites revealed that cleavage occurred within the expected target region, and a strong preference for purine nucleotides was observed.

ACKNOWLEDGMENT

We thank Luzia Moesch and Andrea Deichert for their excellent technical assistance.

LITERATURE CITED

(1) Agrawal, S., and Zhao, Q. (1998) Antisense therapeutics. *Curr. Opin. Chem. Biol. 2 (4),* 519−528.

(2) Bos, J. L. (1989) ras oncogenes in human cancer, a review. *Cancer Res. 49 (17),* 4682−4689.

(3) Baker, B. F., Lot, S. S., Kringel, J., Cheng-Flournoy, S., Villiet, P., Sasmor, H. M., Siwkowski, A. M., Chappell, L. L., and Morrow, J. R. (1999) Oligonucleotide-europium complex conjugate designed to cleave the 5′ cap structure of the ICAM-1 transcript potentiates antisense activity in cells. *Nucleic Acids Res. 27 (6),* 1547−1551.

(4) Baker, B. F., Condon, T. P., Koller, E., McKay, R. A., Siwkowski, A. M., Vickers, T. A., and Monia, B. P. (2001) Discovery and analysis of antisense oligonucleotide activity in cell culture. *Methods 23 (2),* 191−198.

(5) Cho-Chung, Y. S. (1999) Antisense oligonucleotide inhibition of serine/threonine kinases, an innovative approach to cancer treatment. *Pharmacol. Ther. 82 (2−3),* 437−449.

(6) Crooke, S. T. (1999) Molecular mechanisms of action of antisense drugs. *Biochim. Biophys. Acta 1489 (1),* 31−44.

(7) Geary, R. S., Watanabe, T. A., Truong, L., Freier, S., Lesnik, E. A., Sioufi, N. B., Sasmor, H., Manoharan, M., and Levin, A. A. (2001a) Pharmacokinetic properties of 2′−O−(2-methoxyethyl)-modified oligonucleotide analogues in rats. *J. Pharmacol. Exp. Ther. 296 (3),* 890−897.

(8) Geary, R. S., Khatsenko, O., Bunker, K., Crooke, R., Moore, M., Burckin, T., Truong, L., Sasmor, H., and Levin, A. A. (2001b) Absolute bioavailability of 2′−O−(2-methoxyethyl)-modified antisense oligonucleotides following intraduodenal instillation in rats. *J. Pharmacol. Exp. Ther. 296 (3),* 898−904.

(9) Hagemann, C., and Rapp, U. R. (1999) Isotype-specific functions of Raf kinases. *Exp. Cell. Res. 253 (1),* 34−46.

(10) Hall, J., Hüsken, D., Pieles, U., Moser, H. E., and Häner, R. (1994) Efficient sequence-specific cleavage of RNA using novel europium complexes conjugated to oligonucleotides. *Chem. Biol. 1 (3),* 185−190.

(11) Hall, J., Hüsken, D., and Häner, R. (1996) Towards artificial ribonucleases, the sequence-specific cleavage of RNA in a duplex. *Nucleic Acids Res. 24 (18),* 3522−3526.

(12) Häner, R., and Hall, J. (1997) The sequence-specific cleavage of RNA by artificial chemical ribonucleases. *Antisense Nucleic Acid Drug Dev. 7 (4),* 423−430.

(13) Henry, S., Stecker, K., Brooks, D., Monteith, D., Conklin, B., and Bennett, C. F. (2000) Chemically modified oligonucleotides exhibit decreased immune stimulation in mice. *J. Pharmacol. Exp. Ther. 292 (2),* 468−479.

(14) Hüsken, D., Goodall, G., Blommers, M. J., Jahnke, W., Hall, J., Häner, R., and Moser, H. E. (1996) Creating RNA bulges, cleavage of RNA in RNA/DNA duplexes by metal ion catalysis. *Biochemistry 35 (51),* 16591−16600.

(15) Jen, K. Y., and Gewirtz, A. M. (2000) Suppression of gene expression by targeted disruption of messenger RNA, available options and current strategies. *Stem Cells 18 (5),* 307−319.

(16) Kolasa, K. A., Morrow, J. R., and Sharma, A. P. (1993) Trivalent lanthanide ions do not cleave RNA in DNA-RNA hybrids. *Inorg. Chem. 32,* 3983−3984.

(17) Lima, W. F., Monia, B. P., Ecker, D. J., and Freier, S. M. (1992) Implication of RNA structure on antisense oligonucleotide hybridization kinetics. *Biochemistry 31 (48),* 12055−12061.

(18) Magda, D., Miller, R. A., Wright, M., Rao, J., Sessler, J. L., Iverson, B. L., and Sansom, P. I. (1994) Site-specific hydrolysis of RNA by europium (III) texaphyrin conjugated to a synthetic oligodeoxyribonucleotide. *J. Am. Chem. Soc. 116,* 6439−6440.

(19) Marshall, M. (1995) Interactions between Ras and Raf, key regulatory proteins in cellular transformation. *Mol. Reprod. Dev. 42 (4),* 493−499.

(20) Matsumura, K., Endo, M., and Komiyama, M. (1994) Lanthanide complex-oligo-DNA hybrid for sequence-selective hydrolysis of RNA. *J. Chem. Soc., Chem. Commun.* 2019−2020.

(21) Robinson, M. J., and Cobb, M. H. (1997) Mitogen-activated protein kinase pathways. *Curr. Opin. Cell Biol. 9 (2),* 180−186.

(22) Stanton, V. P. Jr., and Cooper, G. M. (1987) Activation of human raf transforming genes by deletion of normal amino-terminal coding sequences. *Mol. Cell. Biol. 7 (3),* 1171−1179.

(23) Trawick, B. N., Daniher, A. T., and Bashkin, J. K. (1998) Inorganic Mimics of Ribonucleases and Ribozymes, From Random Cleavage to Sequence-Specific Chemistry to Catalytic Antisense Drugs. *Chem. Rev. 98,* 939−960.

(24) Storm, S. M., and Rapp, U. R. (1993) Oncogene activation, c-raf-1 gene mutations in experimental and naturally occurring tumors. *Toxicol. Lett. 67 (1−3),* 201−210.

(25) Verma, S., and Eckstein, F. (1998) Modified oligonucleotides, synthesis and strategy for users. *Annu. Rev. Biochem. 67,* 99−134.

(26) Zellweger, T., Miyake, H., Cooper, S., Chi, K., Conklin, B. S., Monia, B. P., and Gleave, M. E. (2001) Antitumor activity of antisense clusterin oligonucleotides is improved in vitro and in vivo by incorporation of 2′−O−(2-methoxy)ethyl chemistry. *J. Pharmacol. Exp. Ther. 298 (3),* 934−940.

(27) Zuker, M. (1989) Computer prediction of RNA structure. *Methods Enzymol. 180,* 262−288.

BC0200024

Biodegradable, Endosome Disruptive, and Cationic Network-type Polymer as a Highly Efficient and Nontoxic Gene Delivery Carrier

Yong-beom Lim, Seon-mi Kim, Hearan Suh, and Jong-sang Park*

School of Chemistry & Molecular Engineering, Seoul National University, Seoul 151-742, Korea. Received April 22, 2002; Revised Manuscript Received July 10, 2002

The success of gene therapy is largely dependent on the delivery vector system. Efficient transfection and nontoxicity are two of the most important requirements of an ideal gene delivery vector. To generate both an efficient and nontoxic vector, we rationally constructed polymeric vectors to have simultaneous multiple functions, i.e., controlled degradation, an endosome disruptive function, and positive charges. Remarkably, the transfection efficiency of network poly(amino ester) (n-PAE) synthesized in this manner was comparable to that of polyethylenimine (PEI), one of the most efficient polymeric gene delivery vectors reported to date. However, there was a marked difference in cytotoxicity between the polymers. The majority of PEI-transfected cells were granulated and dead, whereas most of the cells transfected with n-PAE were viable and healthy. Successive events of efficient endosome escape of n-PAE/DNA polyplex and n-PAE biodegradation should result in high transfection efficiency and favorable cell viability response. The n-PAE-mediated transfection was also very efficient in the presence of serum. These data show that the approach we applied is a very appropriate way of making an ideal gene delivery carrier.

INTRODUCTION

The vector for the delivery of therapeutic DNA has been considered as a major hurdle in achieving successful gene therapy. A number of delivery systems based on viral (*1*, *2*) or nonviral vectors (*3*−*5*) have been devised until now; however, none of these have proven to be satisfactory. Nonviral vectors have gained a great deal of interest by their advantages over viral vectors, such as low immunogenicity, limitless DNA incorporation capacity, the ease of large-scale production, and the possibility of fine-tuning the physicochemical and biological properties. However, those nonviral vectors efficient in transfection were toxic because of their nondegradable property (*6*). On the contrary, the transfection efficiencies of nontoxic nonviral vectors, e.g., biodegradable cationic polymers, were not satisfactory (*7*−*13*).

Here we demonstrate our approach for generating both a transfection-efficient and nontoxic gene carrier based on a nonviral polymeric vector. To meet these requirements, we rationally designed polymer structure to have simultaneous multiple functions, i.e., biodegradable property, endosome disruptive function, positive charge for DNA condensation, and three-dimensional network-type chain interconnected structure for controlled degradation. n-PAE synthesized in this manner showed very high transfection efficiencies and negligible cytotoxicity in various kinds of mammalian cells. The polymer combined with this type of approach should represent an important step toward the creation of an ideal gene delivery vector.

EXPERIMENTAL PROCEDURES

Materials. PEI (average molecular weight 25 kDa) was obtained from Aldrich. Fmoc-6-aminohexanoic acid (Fmoc-eAhx) was purchased from Novabiochem. pGL3-Control vector was purchase from Promega.

The pCN−LacZ vector encoding β-galactosidase gene was constructed by subcloning *E. coli* β-galactosidase cDNA to pCN, which contains the 600 bp HCMV IE promoter and its entire 5′ untranslated region consisted of 122 bp exon 1, 827 bp intron 1, and 16 bp exon 2 (*14*).

Synthesis of Network Poly(amino ester). Monomer **1**: To a stirred solution of methyl acrylate (150 mL, 1.67 mol) at 45 °C was added a solution of tris(hydroxymethyl)aminomethane (5 g, 41 mmol) in methanol (250 mL). The reaction mixture was stirred for 24 h at 45 °C. Methanol and excess methyl acrylate were evaporated to give 12 g (99%) of monomer **1** as a yellow oil. ^{1}H NMR (300 MHz, DMSO-d_6) δ 2.39 (t, 4H, CH_2CH_2COO), 2.75 (t, 4H, CH_2CH_2COO), 3.28 (s, 6H, $HOCH_2$), 3.57 (s, 6H, CH_3). ^{13}C NMR (75 MHz, DMSO-d_6) δ 35.41 (CH_2CH_2-COO), 36.93 (CH_2CH_2COO), 51.41 (CH_3), 59.98 (quaternary carbon), 61.05 ($HOCH_2$), 173.16 (ester carbonyl carbons). MS (MALDI) Calcd for $C_{12}H_{23}NO_7$ $(M + H)^+$ 294.325; found 294.323.

Polymer **1**: For the polycondensation reaction, monomer **1** (5 g) placed in a glass vial was immersed into a silicon bath. Polymerization was carried out in the bulk at 170 °C under constant argon flow. The temperature of the reaction was increased at a rate of 10 °C/min. After 5 h of reaction, the resulting network-type polymer, which was a solid at room temperature, was pulverized to yield a yellow powder. ^{1}H NMR (300 MHz, DMSO-d_6) δ 1.41−2.77 (br m, CH_2CH_2COO and CH_2CH_2COO), 3.24−3.42 (br m, $HOCH_2$), 3.50−3.57 (br m, CH_3), 4.01−4.10 (br m, $COOCH_2$). ^{13}C NMR (75 MHz, DMSO-d_6) δ 33.63−35.83 (CH_2CH_2COO), 36.61−37.79 (CH_2CH_2COO), 51.60 (*C*H3), 59.32, 62.62 (quaternary carbons), 60.86, 61.44, 64.27 ($HOCH_2$), 165.13−173.53 (ester carbonyl carbons).

n-PAE: A mixture polymer **1** (0.73 g) and Fmoc-eAhx (0.91 g, 2.58 mmol) in DMF (7 mL) at room temperature

* To whom correspondence should be addressed. School of Chemistry & Molecular Engineering, Seoul National University, San 56-1, Shinlim-dong, Kwanak-gu, Seoul 151-742, Korea (South), Phone: +82-2-880-6660. Fax: +82-2-877-5110. E-mail: pfjspark@plaza.snu.ac.kr.

10.1021/bc025541n CCC: $22.00 © 2002 American Chemical Society
Published on Web 08/29/2002

was treated with 1,3-dicyclohexylcarbodiimide (DCC, 1.06 g, 5.15 mmol), 4-(dimethylamino)pyridine (DMAP, 0.16 g, 1.29 mmol), and *p*-toluenesulfonic acid monohydrate (PTSA, 0.23 g, 1.2 mmol). After 15 h at room temperature, the reaction mixture was filtered to remove DCU. The crude polymer was purified first by precipitating it into a large excess of water three times to remove DMAP and PTSA. The precipitates were collected, dissolved in $CHCl_3$, and precipitated into a large excess of EtOAc/ether (1:1) three times to remove residual DCC and Fmoc-eAhx. The resulting polymer obtained (0.6 g) was a viscous semisolid. ^{1}H NMR (300 MHz, DMSO-d_6) δ 1.21−1.47 (br m, $CH_2(CH_2)_3CH_2COO$), 2.26 (br, $CH_2(CH_2)_3CH_2$-COO), 2.93 (br, $CH_2(CH_2)_3CH_2COO$), 3.21−3.44 (br m, $HOCH_2$), 3.50−3.53 (br m, CH_3), 3.91−4.10 (br m, $COOCH_2$), 4.18 (br, CH), 4.26 (br, $CHCH_2$), 7.31−7.94 (br m, aromatic protons). Molecular weight by gel permeation chromatography (GPC): M_n = 3800, M_w = 4500, PDI = 1.18. GPC was carried out using a Waters model 600E Multi Solvent Delivery System, a model 410 refractive index detector, and Autochro-GPC software (Young-In Scientific, Korea) for data acquisition with Styragel 2 and Styragel 4E columns placed in series in order of increasing pore size. THF was used as the eluent at a flow rate of 1 mL/min. The molecular weights were determined relative to narrow molecular weight polystyrene standard.

Fmoc protection groups from the Fmoc-eAhx-coupled polymer **1** (0.5 g) was removed by adding 20% piperidine in DMF (v/v). After 5 min of the deprotection reaction, the mixture was added dropwise into a large excess of EtOAc/ether (1:1) three times to give n-PAE (0.21 g) as a white solid. ^{1}H NMR (300 MHz, DMSO-d_6) δ 1.24−1.47 (br m, $CH_2(CH_2)_3CH_2COO$), 2.27 (br, $CH_2(CH_2)_3CH_2$-COO), 2.66 (br, $CH_2(CH_2)_3CH_2COO$), 3.21−3.40 (br m, $HOCH_2$), 3.51−3.55 (br m, CH_3), 3.85−4.15 (br m, $COOCH_2$).

Quantification of n-PAE Primary Amine Numbers by Using Fluorescamine. A series of known concentrations of *n*-butylamine (2 mL in 0.2 M sodium borate, pH 9.0) were placed in test tubes. While the tube was vigorously agitated on a Vortex mixer, 700 μL of fluorescamine solution (0.28 mg/mL in acetone) was added (*15*). Fluorescence measurements were carried out with an SFM 25 spectrofluorometer (Kontron Instruments). Excitation and emission wavelengths were set at 390 and 475 nm, respectively. A standard curve constructed in this way was used to find the amount of primary amines per mg n-PAE.

Atomic Force Microscopy (AFM). DNA (pGL3-control vector) was dissolved in Hepes-Mg (25 mM Hepes, 10 mM $MgCl_2$, pH 7.6) buffer at a concentration of 1 μg/mL to obtain a DNA image. Two microliters of the solution was deposited onto a freshly cleaved mica substrate. The solution was allowed to adsorb for 2 min, washed with 1 mL of distilled water, and rapidly dried in a stream of N_2 gas. For imaging the polyplex, the polyplex was made by mixing the plasmid solution in water (5 μg/mL) with an equal volume of polymer solution in water. Two microliters of the polyplex solution was deposited onto a freshly cleaved mica substrate. The solution was allowed to dry for 2 min, and then excess fluid was wicked off with filter paper. The solution was dried at room temperature before imaging.

AFM was performed using Nanoscope IIIa instrument equipped with an E scanner (Digital Instruments, Santa Barbara, CA). All AFM imaging was conventional ambient tapping mode AFM with scan speeds of about 5 Hz and data collection at 512 × 512 pixels.

Cytotoxicity Measurement. Cells were seeded at a density of 10000 cells/well in 96-well plate and grown in MEM supplemented with 10% fetal bovine serum (FBS), and 2 mM L-glutamine, 0.1 mM nonessential amino acids, and 1.0 mM sodium pyruvate to reach 60−70% confluence. Following exposure of the cells with polymer or polyplex solution for 4 h, cells were washed with phosphate-buffered saline (PBS), and 100 μL of the culture medium and 25 μL of 5 mg/mL stock solution of 3-[4,5-dimethylthiazol-2-yl]-2,5-diphenyltetrazolium bromide (MTT) were added to each well. After 2 h of incubation at 37 °C, 100 μL of extraction buffer (20% w/v of SDS in a solution of 50% of DMF, pH 4.7) were added. Absorbance was measured at 570 nm after an overnight incubation at 37 °C.

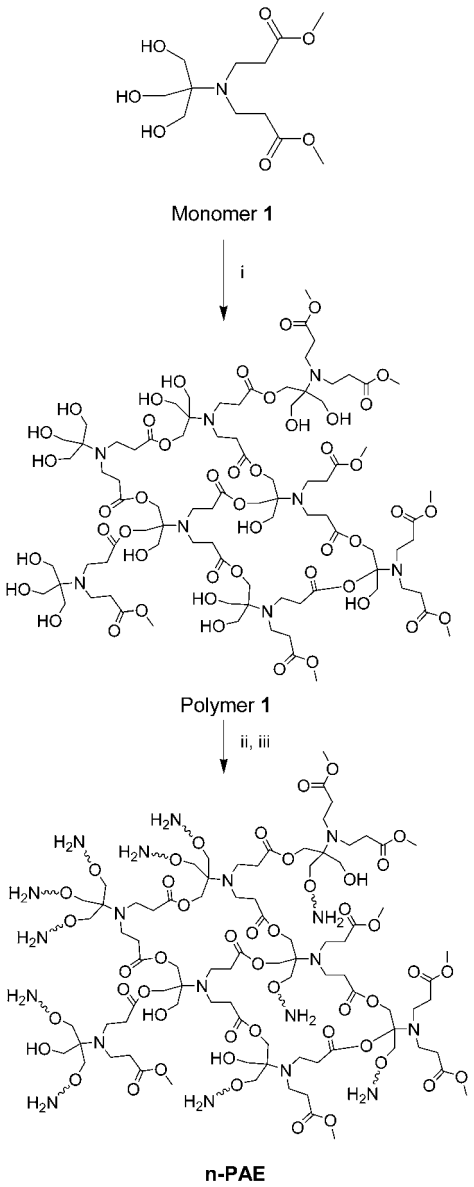
Transfection Protocol. Cells were seeded at a density of 10000 cells/well in 96-well plate and grown in MEM supplemented with 10% fetal bovine serum (FBS), 2 mM L-glutamine, 0.1 mM nonessential amino acids, and 1.0 mM sodium pyruvate to reach 60−70% confluence prior to transfection. Before transfection, cells were rinsed and serum-free or 10% FBS-containing medium was added to each well. The cells were treated with polyplex solution containing 1 μg of plasmid DNA for 4 h at 37 °C. The concentration of polymers varied depending on the polymer/DNA ratios. Then the transfection mixture was replaced with fresh medium. Cells were further incubated for 48 h at 37 °C.

Luciferase gene expression was measured by a luminescence assay. The growth medium was removed, and the cells were rinsed twice with PBS and lysed for 20 min at room temperature in 100 μL of Reporter Lysis Buffer (Promega). The lysate was cleared by centrifugation, and protein content was determined by using Micro BCA Protein Assay Reagent Kit (Pierce). Thirty microliters of the lysate was dispensed into a luminometer tube, and luciferase activity was integrated over 10 s with 2 s measurement delay in a Lumat LB 9507 luminometer (Berthold, Germany) with automatic injection of 100 μL of Luciferase Assay Reagent (Promega). Results were expressed as relative light units per mg of cellular protein.

RESULTS AND DISCUSSION

Synthesis and Characterization of n-PAE. The construction of n-PAE commences with the condensation polymerization of monomer **1**, which has three hydroxyls, two methyl esters, and one tertiary amine, affording polymer **1** (Scheme 1). Coupling of Fmoc-eAhx acid in the remaining hydroxyl groups of polymer **1** and successive deprotection of Fmoc groups yields n-PAE. Quantification of primary amine numbers by fluorescamine method showed that n-PAE had 1.3 μmol primary amines/mg. GPC analysis with linear polystyrene standard showed that M_n and M_w of Fmoc-eAhx-coupled polymer **1** (n-PAE precursor) were 3800 and 4500, respectively. The unusually low polydispersity index (1.18) as a condensation polymer is likely the result of fractionation during precipitation purification. It is well-known that GPC, based on the hydrodynamic radius (R_h) measurement of polymers, underestimate the true molecular weight distribution (MWD) of branched polymers several times (*16*). As a result, it is generally accepted that true MWD of branched polymers should be three to five times higher than the values obtained from GPC. In this respect, the true MWD of n-PAE should be much higher than the values obtained by GPC with linear polymer standard. We are currently investigating the absolute MWD of

Scheme 1. Synthesis of n-PAE[a]



[a] (i) Bulk polycondensation, 170 °C; (ii) Fmoc-6-aminohexanoic acid, DCC, DMAP, PTSA, DMF; (iii) piperidine/DMF (1:4). DCC = 1,3-dicyclohexylcarbodiimide, DMAP = 4-(dimethylamino)pyridine, PTSA = *p*-toluenesulfonic acid monohydrate.

n-PAE by using a multiangle laser light scattering technique in GPC. The structure of n-PAE was designed to be multifunctional by equipping it with biodegradable ester backbone linkages for nontoxicity, multiple primary amines for DNA condensation, multiple tertiary amines for selective protonation according to the pH of surrounding milieu, and network-type chain interconnected structure for controlled degradation.

Formation and Stability of n-PAE/DNA Polyplex. The formation and stability of n-PAE/DNA polyplex at pH 7.4, 37 °C were investigated by agarose gel electrophoresis as a function of time at various n-PAE nitrogen/DNA phosphate ratios (N/P ratios) (Figure 1). Partially formed polyplex was observed at a N/P ratio of 4. When the ratio reached 10, no DNA migrated through the gel, indicating the formation of the polyplex. n-PAE had 1.3 μmol primary amines/mg as describe above. This means that charge neutralization of the polyplex occurs at a N/P ratio of 4.9 on the assumption that only primary amines are protonated at pH 7.4. Therefore, the exact point of charge neutralization should be a N/P ratio of between 4 and 10. As time passed, DNA bands appeared and the polyplex bands at the wells of agarose gel disappeared, indicating that after degradation of n-PAE the condensed DNA was gradually released from the polyplex. The stability of the polyplex increased with increasing N/P ratio where the polyplex remained intact over 3 days at and above a N/P ratio above 20 (Figure 1C and 1D). The appearance of linear DNA, which was not observed in initial plasmid DNA bands, suggests that small parts of nicked circular DNA were cleaved during the incubation period. However, the majority of the released plasmid DNA maintained their initial conformations even after the complete degradation of the polyplex.

It has been reported that the linear polyesters having nucleophilic groups (primary amine, secondary amine, and carboxylic acid) in their structure were degraded very rapidly in aqueous solution through a self-destruction mechanism (*7*, *9*). For this reason, the stability of the polyplexes formed with the linear polyesters could not exceed 8 h at pH 7.4, 37 °C. However, there is a need to extend the degradation to a reasonable rate for the polymeric vector to protect DNA from the harsh extracellular and/or cytosolic environment until it enters the cell nucleus. It can be expected that the MWD of the linear polyesters would be halved by a single cleavage of the polymer chain, which explains the rapid degradation kinetics of the polymers. In a network-type chain interconnected structure, however, the MWD of the polymer is not likely to be changed by a single and/or several chain cleavages. For this reason, the stability of n-PAE/DNA polyplex was much extended over that of linear biodegradable cationic polymers.

AFM observations showed the formation of polyplex between n-PAE and DNA visually. Supercoiled or nicked circular DNA comprised the majority of the plasmid DNA population (Figure 2A). This result is consistent with the

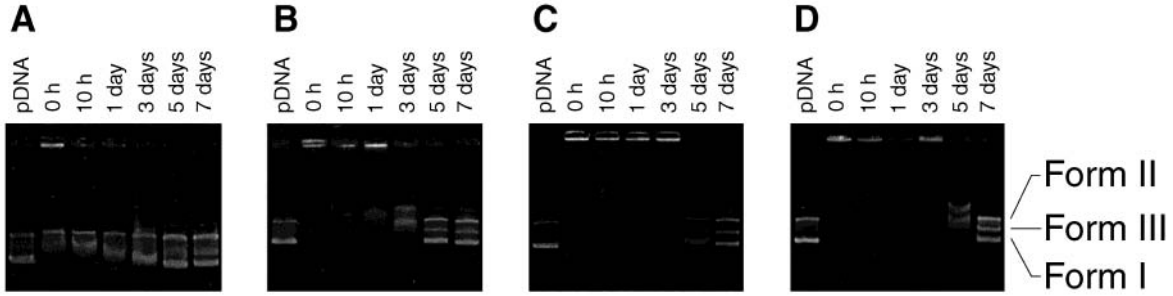


Figure 1. Formation and stability of n-PAE/DNA (pGL3-control) polyplex. The polyplex formed at n-PAE/DNA ratio (N/P) of (A) 4 and (B) 10 and (C) 20 and (D) 40 and incubated at 37 °C. Aliquots taken at the indicated times were electrophoresed through 0.7% agarose gel and stained with ethidium bromide to visualize DNA. Form I = supercoiled, form II = nicked circular, and form III = linear DNA.

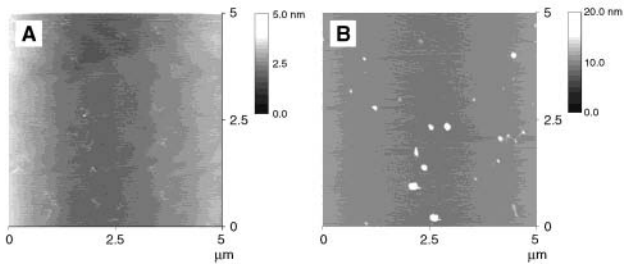


Figure 2. AFM images of (A) plasmid DNA (pGL3-control) and (B) n-PAE/DNA polyplex. The polyplex was formed at a N/P ratio of 10.

electrophoretic observation of the plasmid DNA conformation (vide ante). AFM image of n-PAE/DNA polyplex showed that all of the plasmid DNA was complexed with n-PAE to form a somewhat heterogeneous population of round-shaped particles (Figure 2B).

Cytotoxicity Measurement. The cytotoxicity profiles of n-PAE were investigated by using an MTT assay (Figure 3A and 3B). The results indicated that n-PAE was minimally toxic with 93% and 87% of cells remaining viable even at very high polymer concentration (200 μg/mL) for 293 and HepG2 cells, respectively. The order of cytotoxicity was PEI (branched) > poly[α-(4-aminobutyl)-L-glycolic acid] (PAGA) > n-PAE. PAGA is a biodegradable cationic polymer used for gene transfection as reported previously (*9*, *10*). The polyplexes showed similar cytotoxicity profiles (Figure 3C and 3D). The near nontoxic property of n-PAE should be the result of the biodegradable property of the polymer, which is in line with several biodegradable cationic polymers investigated in the previous reports (*7-13*).

Transfection Efficiency of n-PAE. The transfection efficiency (TE) evaluated by luciferase reporter gene assay revealed that n-PAE was very efficient in transfection (Figure 4A). Transfection was performed in the absence of chloroquine to show the polymers' own effect. Chloroquine is known to accumulate in endosomal compartment, buffer endosome acidification, and induce osmotic swelling of the endosome, which eventually results in endosome destabilization and release of internalized polyplex (*17*). Remarkably, the TE of n-PAE was not less than that of PEI 25 kDa. PEI has been one of the most efficient polymeric gene carriers reported until now. However, the high cytotoxicity of PEI, due to the nondegradable property of the polymer, poses a serious problem for its application in human gene therapy trials (*6*). In 293 cells, the TE of n-PAE was even about 7-fold higher than that of PEI. In comparison, the TE of PAGA was very low, with values 110 and 320-fold lower than those of n-PAE in 293 and HepG2 cells, respectively. PAGA is a linear biodegradable cationic polymer with multiple primary amines. Similarly, the high TE and low cytotoxicity profile of n-PAE were also observed in other mammalian cell lines (data not shown).

In situ X-gal staining of cells transfected with reporter gene expressing β-galactosidase highlighted the differences in cytotoxicity and transfection efficiencies among the polymers more demonstrably (Figure 4B). Far less than 1% of the cells were stained when PAGA was used

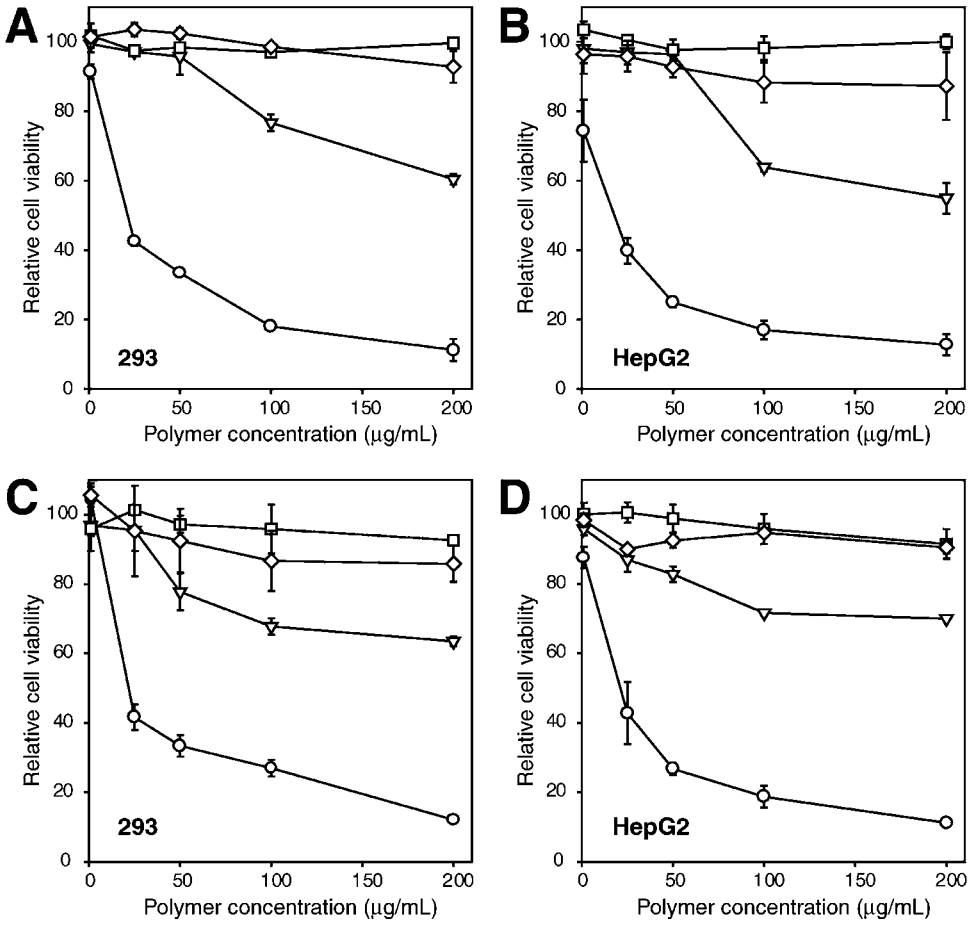


Figure 3. Cytotoxicity in 293 and HepG2 cells by MTT assay. (A, B) Cytotoxicity of polymers. (C, D) Cytotoxicity of polyplexes. All polyplexes were formed at polymer/DNA weight ratios of 5. PEI (○), PAGA (▽), n-PAE (◇), and polymer **1** (□). Relative cell viability was calculated as 100 × [(A_{570} of polymer treated cells − A_{570} of blank)/(A_{570} of control cells − A_{570} of blank)]. Mean ± SEM (n = 5).

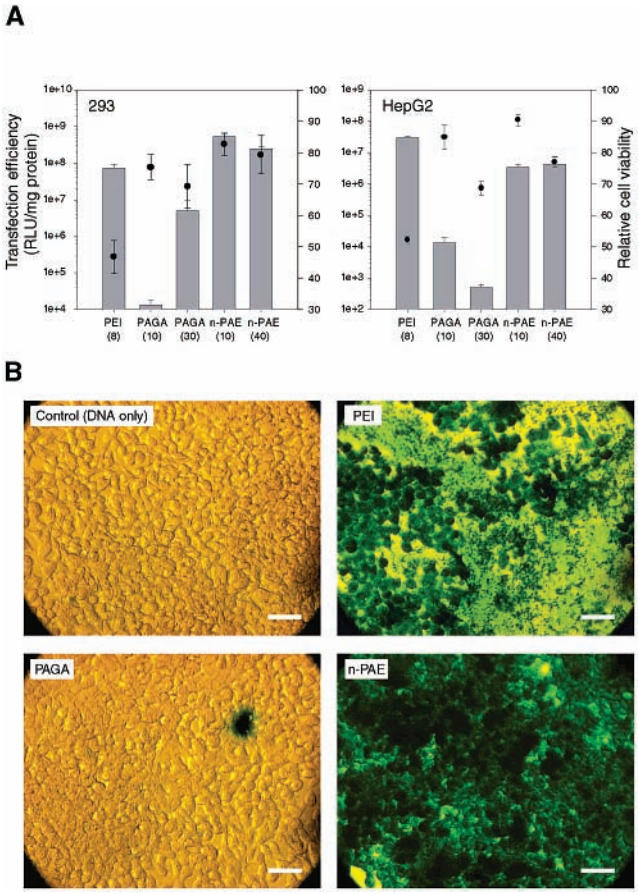


Figure 4. (A) Transfection efficiency (bar graph) and cytotoxicity (filled circle) in 293 and HepG2 cells. The cells were transfected with pGL3 control vector encoding firefly luciferase as a reporter gene. Numbers in parentheses indicate N/P ratios. RLU = relative light unit. Mean ± SEM ($n = 5$) (B) In situ X-gal staining of 293 cells transfected with pCN−LacZ vector encoding β-galactosidase gene. The scale bars represent 50 μm. Transfection experiments were performed without serum, chloroquine, and nigericin.

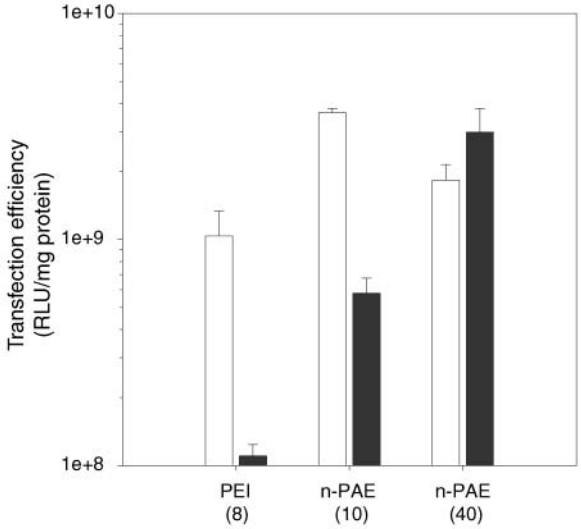


Figure 5. Transfection in the presence of serum. Transfection was performed in 293 cells in the absence (open bars) or the presence (filled bars) of 10% FBS. Numbers in parentheses indicate N/P ratios. Mean ± SEM ($n = 5$). Transfection experiments were performed without chloroquine and nigericin.

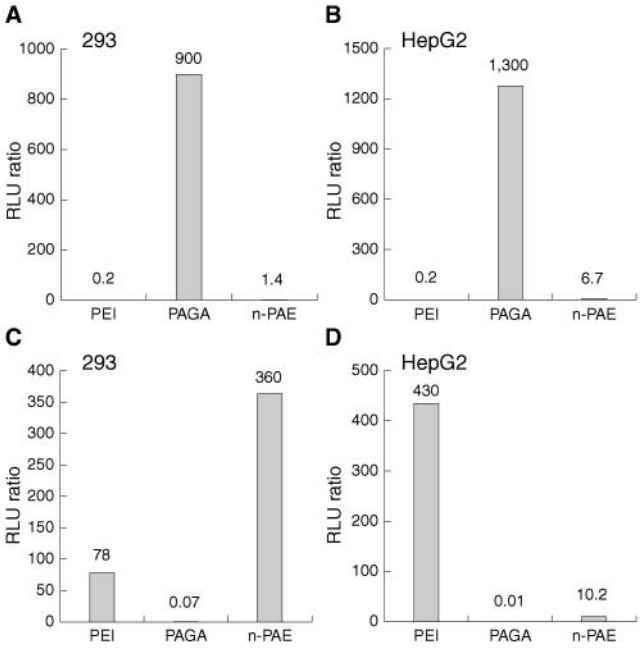


Figure 6. Effect of chloroquine or nigericin treatment on the TEs of PEI, PAGA, and n-PAE. (A, B) RLU in the presence of chloroquine (50 μm)/RLU in the absence of chloroquine. (C, D) RLU in the absence of nigericin/RLU in the presence of nigericin (5 μm). Values are indicated above each bar.

for transfection. In contrast, nearly all of the cells transfected with PEI and n-PAE were stained blue, which indicated the efficient transfection by both the polymers. However, the cells transfected with PEI are in striking contrast to the cells treated with PAGA and n-PAE. The majority of PEI-transfected cells were granulated and dead, whereas most of the cells transfected with PAGA and n-PAE were viable and looked healthy.

If gene delivery carriers are to be used in vivo, the transfection efficiencies of the carriers should be remain relatively unaffected by the presence of serum. As shown in Figure 5, the TE of n-PAE was decrease by 6.3-fold in the presence serum at a N/P ratio of 10. However, n-PAE-mediated transfection was even increased by 1.6-fold by the presence of serum at a N/P ratio of 40. The little or lack of serum inhibition on n-PAE transfection implies that n-PAE will be a promising candidate for in vivo gene therapy.

Transfection Mechanism of n-PAE/DNA Polyplex. The high TEs of n-PAE and PEI are likely to be the result of the "endosome buffering" or "proton sponge" effect of the polymers (*18*). Multiple tertiary amines in the polymers, mostly in the form of free bases at slightly basic physiological pH, become protonated at the acidic pH of endosome, which disrupt the endosomal vesicle either by mechanical swelling or osmotic effects. To verify that the high TE of n-PAE is a result of the endosome buffering effect, transfection experiments were performed in the presence or absence of chloroquine or nigericin (Figure 6). Nigericin is a carboxylic ionophore that mediates exchange of monovalent cations through the membrane and is known to be an inhibitor of endosomal acidification (*19*). Chloroquine treatment resulted in a decrease or a small increase in the TEs of PEI and n-PAE, respectively, but a large increase in the TE of PAGA in both cell lines tested (Figure 6A and 6B). For example, the TE of PAGA increased by 900-fold upon chloroquine treatment in 293 cells. In contrast, the TEs of PEI and n-PAE increased only by 0.2- and 1.4-fold, respectively. These findings suggest that polyplexes formed with PEI or n-PAE do not need chloroquine assistance for endosome escape, as they are already equipped with endosome buffering function

due to the presence of multiple tertiary amines in their structure. The effect of nigericin treatment on TEs further demonstrated the endosome buffering effect of PEI and n-PAE (Figure 6C and 6D). The efficiencies of PEI- and n-PAE-mediated gene delivery were significantly reduced when nigericin was added in the transfection medium, which are attributed to the inhibitory effect of nigericin on endosomal acidification. However, the TE of PAGA was even enhanced by nigericin treatment. Taken together, these results suggest that transfection of PEI and n-PAE is mediated by endosome acidification followed by release of the polyplex into cytosol, which would eventually increase the amount of DNA entering into the nucleus for the transcription.

We have described that through the rational design of polymer structure it was possible to make a nontoxic and efficient gene carrier, which represents a further step in mimicking the cell entry mechanism of viruses, yet maintaining safety profiles. Further elaboration of the structure of n-PAE and/or the analogous polymers based on our approach, such as the attachment of a targeting moiety, a nucleus localization signal, and a stealth function, are expected ultimately to lead to the development of a "safe artificial virus".

ACKNOWLEDGMENT

This work was supported by the Korea Research Foundation (DP-0344) and by the Molecular Therapy Center of KOSEF (R03-2001-00031).

LITERATURE CITED

(1) Kay, M. A., Liu, D., and Hoogerbrugge, P. M. (1997) Gene therapy. *Proc. Natl Acad. Sci. U.S.A. 94*, 12744−12746.

(2) Lee, H. C., Kim, S., Kim, K., Shin, H., and Yoon, J. (2000) Remission in models of type 1 diabetes by gene therapy using a single-chain insulin analogue. *Nature 408*, 483−488.

(3) Nishikawa, M., and Huang, L. (2001) Nonviral vectors in the new millennium: Delivery barriers in gene transfer. *Hum. Gene Ther. 12*, 861−870.

(4) Wagner, E., Plank, C., Zatloukal, K., Cotton, M., and Birnstiel, M. L. (1992) Transferrin-polycation−DNA complexes: The effect of polycations on the structure of the complex and DNA delivery to cells. *Proc. Natl. Acad. Sci. U.S.A. 89*, 7934−7938.

(5) Vigneron, J., Oudrhiri, N., Fauquet, M., Vergely, L., Bradley, J., Basseville, M., Lehn, P., and Lehn, J. (1996) Guanidinium-cholesterol cationic lipids: Efficient vectors for the transfection of eukaryotic cells. *Proc. Natl. Acad. Sci. U.S.A. 93*, 9682−9686.

(6) Godbey, W. T., Wu, K. K., and Mikos, A. G. (1999) Tracking the intracellular path of poly(ethylenimine)/DNA complexes for gene delivery. *Proc. Natl Acad. Sci. U.S.A. 96*, 5177−5181.

(7) Lim, Y., Choi, Y. H., and Park, J. (1999) A self-destroying polycationic polymer: Biodegradable poly(4-hydroxy-L-proline ester). *J. Am. Chem. Soc. 121*, 5633−5639.

(8) Putnam, D., and Langer, R. (1999) Poly(4-hydroxy-L-proline ester): Low-temperature polycondensation and plasmid DNA complexation. *Macromolecules 32*, 3658−3662.

(9) Lim, Y., Kim, C., Kim, K., Kim, S. W., and Park, J. (2000) Development of a safe gene delivery system using biodegradable polymer, poly[α-(4-aminobutyl)-L-glycolic acid]. *J. Am. Chem. Soc. 122*, 6524−6525.

(10) Lim, Y., Han, S., Kong, H., Lee, Y., Park, J., Jeong, B., and Kim, S. W. *Pharm. Res.* (2000) Biodegradable polyester, poly[α-(4-aminobutyl)-L-glycolic acid], as a nontoxic gene carrier. *17*, 811−816.

(11) Lynn, D. M., and Langer, R. (2000) Degradable poly(β-amino esters): Synthesis, characterization, and self-assembly with plasmid DNA. *J. Am. Chem. Soc. 122*, 10761−10786.

(12) Wang, J., Mao, H., and Leong, K. W. (2001) A novel biodegradable gene carrier based on polyphosphoester. *J. Am. Chem. Soc. 123*, 9480−9481.

(13) Lim, Y., Kim, S., Lee, Y., Lee, W., Yang, T., Lee, M., Suh, H., and Park, J. (2001) Cationic hyperbranched poly(amino ester): A novel class of DNA condensing molecule with cationic surface, biodegradable three-dimensional structure, and tertiary amine groups in the interior. *J. Am. Chem. Soc. 123*, 2460−2461.

(14) Lee, Y., Park, E. J., Yu, S. S., Kim, D., and Kim, S. (2000) Improved expression of vascular endothelial growth factor by naked DNA in mouse skeletal muscle: Implication for gene therapy of ischemic disease. *Biochem. Biophys. Res. Commun. 272*, 230−235.

(15) Udenfriend, S., Stein, S., Bohlen, P., Dairman, W., Leimgruber, W., and Weigele, M. (1972) Fluorescamine: A reagent for assay of amino acids, peptides, proteins, and primary amines in the picomole range. *Science 178*, 871−872.

(16) Feast, W. J., and Stainton, N. M. (1995) Synthesis, structure and properties of some hyperbranched polyesters. *J. Mater. Chem. 5*, 405−411.

(17) Plank, C., Zatloukal, K., Cotton, M., Mechtler, K., and Wagner, E. (1992) Gene transfer into hepatocytes using asialoglycoprotein receptor mediated endocytosis of DNA complexed with an artificial tetra-antennary galactose ligand. *Bioconjugate Chem. 3*, 533−539.

(18) Boussif, O., Lezoualc'h, F., Zanta, M. A., Mergny, M. D., Scherman, D., Demeneix, B., and Behr, J. (1995) A versatile vector for gene and oligonucleotide transfer into cells in culture and in vivo: Polyethylenimine. *Proc. Natl Acad. Sci. U.S.A. 92*, 7297−7301.

(19) Uherek, C., Fominaya, J., and Wels, W. (1998) A modular DNA carrier protein based on the structure of diphtheria toxin mediates target cell-specific gene delivery. *J. Biol. Chem. 273*, 8835−8841.

BC025541N

Solid Phase Assembly of Defined Protein Conjugates

John C. Russell,* Tracey L. Colpitts, Shelley R. Holets-McCormack, Thomas G. Spring, Stephen D. Stroupe, Andrew D. Vogt, and Sie-Ting Wong

D09FQ, AP20, Abbott Laboratories, 100 Abbott Park Road, Abbott Park, Illinois 60064-6015.
Received April 26, 2002; Revised Manuscript Received June 25, 2002

We have developed a solid-phase procedure for protein−protein conjugation that gives greater control over product size and composition than previous methods. Conjugates are assembled by sequential addition of activated proteins to the support under conditions suitable for maintaining the activity of the proteins. The total number of conjugate units to be prepared is fixed in the first step by the quantity of the first protein absorbed by the support. In each following step, the added protein links only to previously bound protein. The final conjugate is released to solution by cleaving the linker holding the first protein to the support. This stepwise assembly provides uniformly sized conjugates of the desired size and composition with placement of components at the desired positions within the structure. Using this approach, we have prepared a series of conjugates containing *R*-phycoerythrin as the central protein, with varying quantities of alkaline phosphatase and IgG with expected molecular masses ranging from 1.6 to 11.5 MDa. Size-exclusion chromatography and atomic force microscopy demonstrate homogeneity and control of the conjugate size. In an immunoassay for human thyroid stimulating hormone, the conjugates show signals consistent with their compositions.

INTRODUCTION

There are numerous occasions in life sciences in which it is desirable to link two or more proteins together to obtain a species that combines the properties of each. Most commonly, a protein with specific binding affinity to a target is linked to a second protein with a desired activity. In immunodiagnostic applications, the binding protein is typically an antibody directed against the desired analyte, and the second protein is usually a fluorescent protein or an enzyme that generates a signal detectable by eye or by instrumentation (*1*−*4*). In therapeutic applications, the binding protein may be an antibody or a ligand with specific binding to a cell surface receptor, and the second protein may be a toxin that kills the targeted cell (*5*). A variety of methods have been devised to link proteins together. Most commonly, the two proteins are chemically activated so that groups on one can form stable covalent links to groups on the other. They are then combined in a homogeneous solution and allowed to react under conditions suitable for both linking and maintenance of their activities. When a sufficient proportion of the proteins are linked, the reaction is stopped by adding reagents that deactivate one or both of the reactive groups. These conjugation reactions are difficult to control. The activating agents usually generate numerous active positions on each protein molecule, with the result that many points of attachment are possible. Linkage at one active group on a protein does not prevent linkage at a second or third point, and a broad distribution of aggregates consisting of many units of each of the proteins may result. While it is frequently desirable to produce multimeric conjugates, it is also desirable to control these so that a majority of the species produced contains the number of each protein unit most suitable for the intended purpose of the conjugate. We have developed a method for preparing protein−protein conjugates with highly predictable and controllable composition and size. A first protein, termed the "core", is bound to a solid support via a cleavable linker. Additional proteins are introduced sequentially as "layers" under conditions that allow their stable linkage only to the core or to the immediately previous layer of protein. After completion of the reaction sequence, the protein assembly is released by cleaving the linker holding the core protein to the support. Immobilization of the core protein on the support prevents interaction of the assembly with other immobilized assemblies during the reaction sequence. Therefore, at each step, the assembly can grow only by linking the added free protein. If the added proteins are not self-reactive, the growth at each step is limited to the quantity that can directly link to the previous layer. Excess can be added to saturate all available sites and unreacted material washed from the support before the next step is started. Each successive layer contains more protein than the previous layer, suggesting radial growth of the conjugates. Very large conjugates can be prepared with relatively few steps of protein addition.

This method of protein conjugation has several advantages over solution methods. The narrow distribution of sizes of the released conjugate allows it to be optimized with respect to intended properties. The sequence of addition allows placement of specific components at the most desirable position in the conjugate. Binding agents may be added in the final conjugation step, placing them at the periphery of the conjugate where they can most effectively interact with their target. Other proteins beyond the binding and reporter proteins may be included to confer additional properties. The ability to control the quantities and positions of proteins within the assemblies leads us to term them "defined conjugates".

In the present work, we use the solid-phase technique to prepare a number of defined conjugates containing

* Address correspondence to this author. E-mail: john.c.russell@abbott.com.

10.1021/bc0255438 CCC: $22.00 © 2002 American Chemical Society
Published on Web 08/14/2002

R-phycoerythrin (RPE)[1] as the core, several layers of alkaline phosphatase (AP), and a final layer consisting of antibody specific to the α subunit of thyroid stimulating hormone (Ab). We then compare these with conventionally prepared conjugates using HPLC and atomic force microscopy to compare size and dispersity. The defined conjugates are then tested in an immunoassay format to demonstrate the dependency of enzyme and antibody content on their ability to generate signal. Scheme 1 diagrams the process of controlled conjugation used in this report. An agarose support is oxidized with periodate to give immobilized aldehydes (*6*). The hydrazide function of the heterobifunctional linker *N*-(ϵ-maleimidocaproic acid)hydrazide (EMCH) reacts with the aldehydes to give a maleimide group linked to the support via the hydrazone. Proteins to be conjugated are activated with *N*-succinimidyl *S*-acetylthioacetate (SATA) to give sulfhydryl groups or with γ-maleimidobutyric acid *N*-hydroxysuccinimide ester (GMBS) to give maleimide groups. A sulfhydryl-activated protein reacts with the maleimide of the bound EMCH, forming a stable thioether linkage, still held to the agarose support. Remaining maleimide groups on the support are destroyed by adding mercaptoethanesulfonic acid sodium salt (MESNA). The support is then washed to remove excess MESNA, leaving sulfhydryl groups only on the bound protein. After washing the agarose to remove unbound reactive materials, a second protein, containing maleimide groups, is added. This reacts with remaining sulfhydryl groups on the first protein, again forming a thioether linkage. If an excess of the second protein is added, all the available binding locations on the first protein will be occupied. Remaining sulfhydryl groups on the first protein will be available for reaction only with small molecules. The exposed surface of the growing conjugate consists of the second protein with maleimide groups available for reaction with a third protein (or a repeat of the first) containing sulfhydryl groups. When all the desired layers of protein have been added, the remaining thiol groups are converted to unreactive thioethers with *N*-ethylmaleimide and the remaining maleimide groups likewise capped with MESNA. The conjugate is then released from the support by adding hydroxylamine. This reacts with the linkage holding the conjugate to the support and releases it, presumably as the hydrazide.

EXPERIMENTAL SECTION

Materials. *R*-Phycoerythrin was obtained from Prozyme (San Leandro, CA). Calf intestinal alkaline phosphatase was obtained from Boehringer Mannheim (Indianapolis, IN). AntiTSHalpha IgG (MIT 0414) was obtained from Genzyme (Framingham, MA). Sodium periodate, Sepharose CL2B, *N*-ethylmaleimide, mercaptoethanesulfonic acid sodium salt, 5,5′-dithiobis(2-nitrobenzoic acid), tris-(hydroxymethyl)aminomethane, 3-[(3-cholamidopropyl)-dimethylammonio]-1-propanesulfonate, triethanolamine hydrochloride, and γ-maleimidobutyric acid *N*-hydroxysuccinimide ester were obtained from Sigma (St. Louis, MO). *N*-Succinimidyl *S*-acetylthioacetate, *N*-(ϵ-maleimidocaproic acid)hydrazide, *p*-nitrophenyl phosphate substrate, Superblock blocking agent, and BCA protein assay kit were obtained from Pierce (Rockford, IL). Hydroxylamine 50% solution was obtained from Aldrich (Milwaukee, WI). The monoclonal antibody against the β subunit of human thyroid stimulating hormone (TSH) and standard solutions with known concentrations of TSH were obtained from Abbott Laboratories (North Chicago, IL).

Activation of Proteins. (A) RPE-SH. To 200 μL of *R*-phycoerythrin at 10 mg/mL in 100 mM triethanolamine hydrochloride at pH 7.6 was added 10 μL of 100 mM *N*-succinimidyl *S*-acetylthioacetate (SATA) (*7*) in dimethylformamide. After 1 h incubation at room temperature, 10 μL of 50% hydroxylamine was added. After 40 min at room temperature, the mixture was desalted on Sephadex G25 into PBS with 5 mM EDTA, collecting 550 μL. The concentration was determined by the absorbance at 565 nm to be 10.1 μM (*9*), and the number of SH groups per molecule was determined to be 22.5 using Ellman's reagent.

(B) AP-SH. To 500 μL of alkaline phosphatase at 10 mg/mL in triethanolamine HCl was added 50 μL of 1 M sodium phosphate, pH 7.5, and 25 μL of 100 mM SATA in dimethylformamide. After 1 h incubation at room temperature, 25 μL of 50% hydroxylamine was added. After 40 min at room temperature, the mixture was desalted on Sephadex G25 into PBS with 5 mM EDTA, collecting 1.2 mL. The concentration was determined by the absorbance at 280 nm to be 30.5 μM, and the number of SH groups per molecule was determined to be 15.3 using Ellman's reagent. According to the supplier, calf intestinal alkaline phosphatase contains 18 conjugatable amine groups.

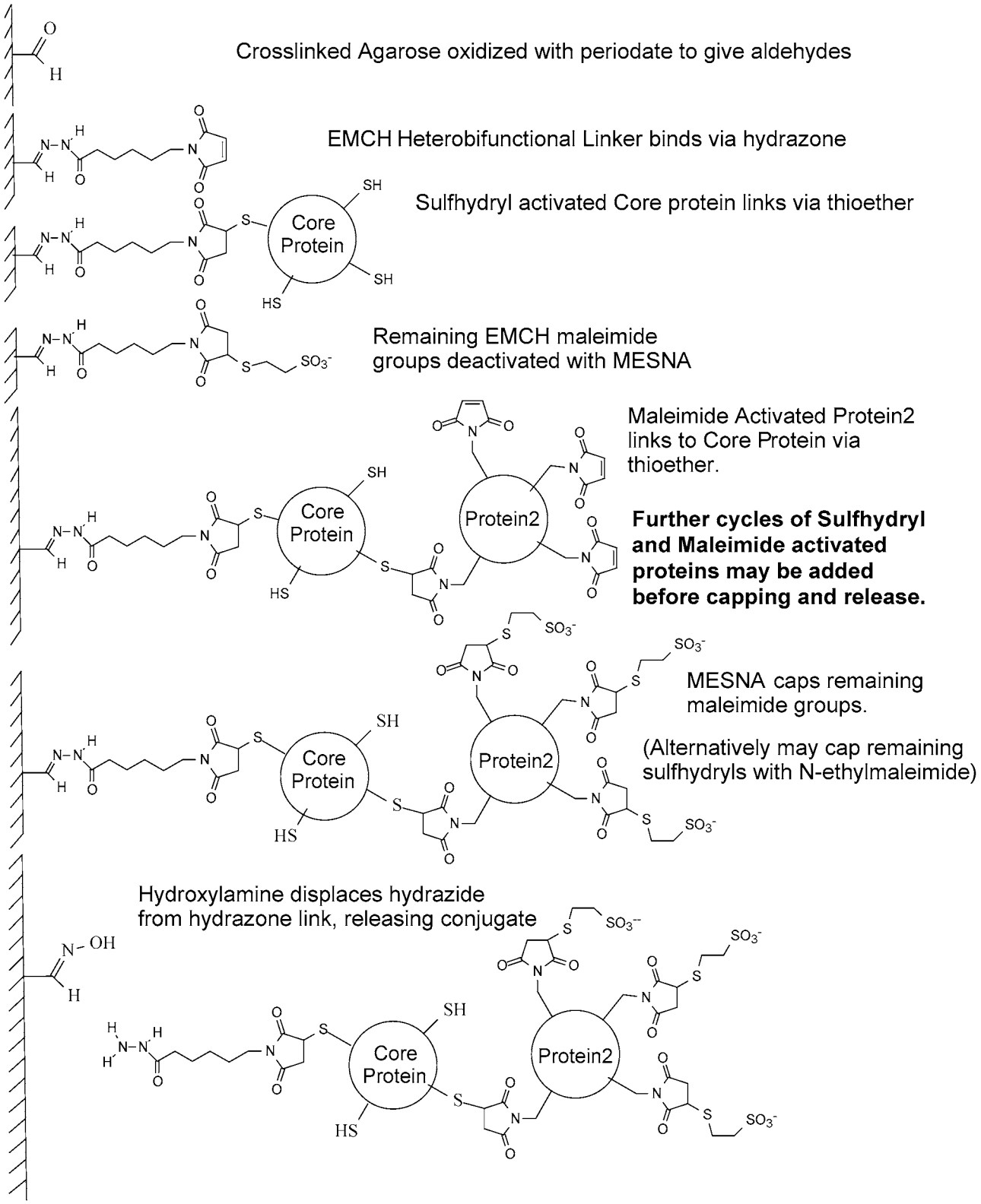
(C) AP-Mal. To 500 μL of alkaline phosphatase at 10 mg/mL in triethanolamine HCl was added 50 μL of 1 M sodium phosphate, pH 7.5, and 25 μL of 100 mM GMBS (*8*) in dimethylformamide. After 100 min at room temperature, the mixture was desalted on Sephadex G25 into PBS with 5 mM EDTA, collecting 1.2 mL. The concentration was determined by the absorbance at 280 nm to be 29.8 μM, and the number of maleimide groups per molecule was determined to be 15.4 by the change in absorbance at 300 nm after addition of MESNA to destroy the maleimide chromophore.

(D) Ab-Mal. To 200 μL of Anti-TSHalpha IgG at 7.03 mg/mL in PBS was added 10 μL of 100 mM GMBS in dimethylformamide and 2 μL of 1 M sodium carbonate to give pH 7.7. After 100 min incubation at room temperature, the mixture was desalted into PBS with 5 mM EDTA, collecting 550 μL. The concentration was determined by the absorbance at 280 nm to be 15.9 μM, and the number of maleimide groups per molecule was determined to be 28.5 by the change in absorbance at 300 nm after addition of MESNA to destroy the maleimide chromophore.

(E) Ab-SH. To 100 μL of Anti-TSHalpha IgG at 7.03 mg/mL in 100 mM sodium phosphate 150 mM sodium chloride, pH 7.2, was added 5 μL of 100 mM SATA in DMF and 1 μL of 1 M sodium carbonate. After 1 h incubation at room temperature, 10 μL of 50% hydroxylamine was added. After 40 min at room temperature, the mixture was desalted into PBS with 5 mM EDTA, collecting 550 μL. The concentration was determined by the absorbance at 280 nm to be 11.7 μM, and the number

[1] Abbreviations: RPE, *R*-phycoerythrin; AP, calf intestinal alkaline phosphatase; Ab, antibody; EMCH, *N*-(ϵ-maleimidocaproic acid)hydrazide; MESNA, mercaptoethanesulfonic acid sodium salt; GMBS, γ-maleimidobutyric acid *N*-hydroxysuccinimide ester; SATA, *N*-succinimidyl *S*-acetylthioacetate; DTNB, 5,5′-dithiobis(2-nitrobenzoic acid); Tris, tris(hydroxymethyl)-aminomethane; CHAPS, 3-[(3-cholamidopropyl)dimethylammonio]-1-propanesulfonate; PBS, 10 mM sodium phosphate, 150 mM sodium chloride, pH 7.2; EDTA, ethylenediaminetetraacetic acid; PCE, PBS containing 2 mg/mL CHAPS and 5 mM EDTA; TC75E, 100 mM Tris with 2 mg/mL CHAPS and 5 mM EDTA, pH 7.5; TC75E, 100 mM Tris with 2 mg/mL CHAPS and 5 mM EDTA, pH 7.5; TC8E, 100 mM Tris with 2 mg/mL CHAPS and 5 mM EDTA, pH 8.0.

Scheme 1. Reaction Sequence in Defined Conjugation



of SH groups per molecule was determined to be 25.4 using Ellman's reagent.

Preparation of Support. (A) Periodate Oxidation of Agarose. Approximately 20 mL of Sepharose CL2B was poured into a column fitted with a fritted disk, washed with water, and suspended in 20 mL of excess water. To this was added 200 μL of 100 mM sodium periodate and the mixture inverted several times to mix. After 75 min at room temperature, 1 mL of glycerol was added and the mixture inverted several times to mix. After 15 min, the column was drained and washed with several column volumes of water and then with PBS.

(B) Activation of Oxidized Agarose with EMCH. To a 20 mL column was added 6.0 mL of oxidized agarose. This was washed with 20 mL of PCE (see list of abbreviations). The washed support was vortexed with 3 mL of PCE and 90 μL of 100 mM EMCH in dimethylformamide. After 30 min incubation at room temperature,

Table 1. Quantities of Activated Proteins Added (italic) and Bound (bold) in Each Step of Conjugation

step:	1	2	3	4	5	6	Ab	*Ab added*	**Ab bound**
reactant:	RPE-SH (nmol)	AP-Mal (nmol)	AP-SH (nmol)	AP-Mal (nmol)	AP-SH (nmol)	AP-Mal (nmol)		(nmol)	(nmol)
added:	*0.200*	*0.800*	*1.80*	*3.00*	*4.50*	*8.00*			
reaction	**bound**								
A	**0.176**	**0.609**					Ab-SH	*1.00*	**0.97**
B	**0.172**	**0.594**	**1.27**				Ab-Mal	*1.00*	**1.00**
C	**0.173**	**0.624**	**1.30**	**2.37**			Ab-SH	*1.00*	**0.99**
D	**0.168**	**0.633**	**1.25**	**2.38**	**3.62**		Ab-Mal	*1.00*	**0.98**
E	**0.174**	**0.633**	**1.26**	**2.36**	**3.65**		Ab-Mal	*0.40*	**0.39**
F	**0.178**	**0.635**	**1.23**	**2.40**	**3.66**		Ab-Mal	*3.00*	**2.85**
G	**0.171**	**0.635**	**1.25**	**2.31**	**3.57**		Ab-Mal	*10.00*	**4.41**
H	**0.176**	**0.636**	**1.27**	**2.37**	**3.63**	**5.15**	Ab-SH	*1.00*	**1.00**

Table 2. Characteristics of Defined Conjugates

					concentration		
	AP/RPE	Ab/RPE	molecular mass (kDa)	% recovery	by RPE (nM)	calculated (μg/mL)	BCA (μg/mL)
A	3.5	5.5	1551	76.0	53.6	83.1	76.8
B	10.8	5.8	2625	70.2	48.3	126.7	117.2
C	24.8	5.7	4566	62.4	43.3	197.7	175.3
D	46.9	5.8	7670	56.1	37.8	289.7	251.1
E	45.4	2.2	6932	58.2	40.5	280.9	255.7
F	44.4	16.0	8866	54.5	38.9	344.5	294.4
G	45.5	25.8	10476	52.5	35.8	375.5	316.6
H	74.1	5.7	11470	50.0	35.2	403.8	376.8

the column was drained, washed with 15 mL of cold TC75E (100 mM Tris, 0.2% CHAPS, 5 mM EDTA, pH 7.5), and placed in ice.

Conjugation on Support. (A) Immobilization of RPE-SH. To each of eight 2 mL columns (reactions A−H of Table 1) was added 600 μL of the EMCH-treated resin, and the mixtures were washed with 2 mL of TC75E. The columns were cooled in ice; then 0.200 nmol (198 μL) of RPE-SH was added to each, and the resins were thoroughly dispersed by vortexing. After 20 min incubation in ice with occasional vortexing, 10 μL of 100 mM MESNA was added to each. After 5 min incubation in ice, the columns were drained and washed with 3.0 mL of cold TC8E. The absorbance of the first 1.5 mL of the effluent was measured at 565 nm to determine the quantity of RPE-SH in the effluent. This was subtracted from that originally added to determine the quantity bound to the support, shown in Table 1.

(B) Addition of AP-Mal and AP-SH to Immobilized RPE-SH. Except for time spent draining and washing, the columns were kept in an ice bath throughout the conjugation procedure. The quantity of activated protein indicated in Table 1 was added to each, along with 100 μL of 1 M magnesium chloride and sufficient TC8E for complete dispersal of the resin on vortexing. The columns were incubated in ice 30 min with occasional vortexing and then drained, and the effluent was recycled through the column for a total of approximately 1 column volume. The columns were then washed with TC8E, and the next addition of activated protein was performed. The absorbance at 280 nm of the effluents was measured to determine the quantity of remaining alkaline phosphatase [$\epsilon(280) = 140\,000$], shown in Table 1.

(C) Addition of Ab-Mal and Ab-SH to Immobilized Conjugate. After the final addition and incubation of activated alkaline phosphatase according to Table 1, the columns were washed with 1.5 mL of TC75E and cooled in ice. The indicated quantity of activated Ab was added, the mixtures were incubated 5 min to allow dispersal of the protein, then 100 μL of 1 M magnesium chloride was added, and the mixture was incubated 30 min in ice. The columns were then drained and washed with 1.5 mL of TC8E. The absorbance at 280 nm of the effluents was measured, and the quantity of Ab remaining in the effluent was calculated using $\epsilon(280) = 210\,000$. From this, the quantity of Ab bound to the resin was calculated, and is shown in Table 1.

(D) Release of Conjugates from Support. After washing off the unbound Ab, the resins were treated with 5 μL of 100 mM *N*-ethylmaleimide to deactivate residual SH groups. The columns were left in ice until protein addition and washing was complete for all of the preparations. To deactivate residual maleimide groups, 10 μL of 100 mM MESNA was added, the mixtures were vortexed, and the columns were returned to the ice bath. After 10 min, 20 μL of 50% hydroxylamine was added, and the mixtures were incubated 60 min at room temperature. The columns were then drained directly into desalting columns equilibrated with PBS and the products washed through with TC8E and PBS collecting 2.5 mL of product. Concentrations of product, shown in Table 2 , were calculated based on the absorbance at 565 nm, and yields were calculated based on recovery of RPE color. Protein concentrations of the conjugates were measured by the BCA protein assay using the enhanced protocol according to the manufacturers' instructions. Alkaline phosphatase was used as the protein standard.

Conjugation of Ab-SH and AP-Mal in Solution. To a solution of PBS with 5 mM EDTA was added 2 nmol of Ab-SH and 4 nmol of AP-Mal prepared as above to give a total 800 μL and the mixture incubated in an ice bath. Aliquots of 200 μL of the reaction mixture were mixed with 4 μL of 100 mM aqueous *N*-ethylmaleimide to stop the conjugations at times of 15, 60, 150, and 300 min.

Characterization of Conjugates. (A) HPLC. To 300 μL of each conjugate was added 30 μL of 10 mg/mL CHAPS in PBS. A sample of 20 μL was passed through a Whatman Macrosphere GPC 1000A 250 × 4.6 mm column with 1 mg/mL CHAPS in PBS as the mobile phase at 0.2 mL/min, monitoring at 280 nm and 566 nm with a diode array detector.

(B) Atomic Force Microscopy. Silicon wafers (International Wafer) were cleaned by immersion in 3% hydrogen peroxide in sulfuric acid at 100 °C for 10 min, then washed with distilled water and blown dry. Samples were prepared by exposing 8 mm squares of the silicon wafers to dilutions of the conjugates at 1:100 in 10 mM sodium phosphate, 150 mM sodium chloride, pH 7.2. After 30 min at room temperature, the wafers were washed with water, blown dry with air, and heated at 45 °C for 2 h. The wafers were imaged using a NanoScope IIIa (Digital Instruments) atomic force microscope. Images were collected in TappingMode at ambient temperature in air using silicon-etched tips with a resonance frequency of 275−395 kHz and a scan rate of 1 μm/s. Tips were changed between samples to eliminate cross-contamination.

(C) Comparison of Conjugates in TSH Assay. Wells of a 96-well microtiter plate were coated with a mAb directed against the β subunit of TSH at 20 μg/mL in PBS for 60 min at 37 °C and blocked with Superblock according to the manufacturers' instructions. To the wells was added 25 μL of TSH standards, and the plate was covered and incubated 3 h at 37 °C. The wells were drained and washed 5× with water, and 100 μL of conjugate in 50 mM bis-tris-propane, 150 mM NaCl, 10 mM $MgCl_2$, 1 mM $ZnCl_2$, pH 7.2, containing 10% Superblock was added. The conjugate concentration was 40 pM RPE for one test and 200 ng/mL protein for another test. After 3 h at 37 °C, the wells were drained and washed 5× with water. One hundred microliters of substrate (PNPP, Pierce) was added, the plate placed at 37 °C, and the absorbance read at 405 nm at 30 s intervals over 30 min. *V*max (mA/min) was reported for each well.

RESULTS

Yields of released conjugate, shown in Table 2, are based on recovery of bound RPE, measured by its absorbance at 565 nm. These range from 76% for conjugate A, with a single layer of AP, to 50% for conjugate H, with five layers. The remainder is visible as pink color remaining in the support. Very little additional conjugate was released from the supports even with prolonged exposure to hydroxylamine.

Table 2 shows the molar ratios of AP to RPE and Ab to RPE absorbed by the support in the defined conjugate preparations. In reactions A, B, C, D, and H, the AP absorbed ranges from 3.5 to 74.1 per RPE, and the Ab is nearly constant at 5.5−5.8. For reactions D, E, F, and G, the AP is nearly constant at 44.4−46.9, and the Ab varies from 2.2 to 25.8. The average molecular mass for each of the assemblies was calculated from the uptake of the activated proteins, assuming a single RPE core in each discrete unit of conjugate and using molecular masses of 240 kDa for RPE, 140 kDa for AP, and 150 kDa for Ab. The molecular masses range from about 1.6 MDa for A to about 11 MDa for H. Molar concentrations of product are used with the molecular masses to calculate the mass concentrations. These compare well with mass concentrations measured by protein assay.

HPLC traces of both defined and solution-phase conjugates on a size-exclusion column are shown in Figure 1. Peaks corresponding to the defined conjugates with more layers of AP elute earlier than those with fewer layers, consistent with the calculated molecular masses. Monitoring at 565 nm shows a decrease in peak intensity with larger conjugate size, reflecting the lower RPE concentrations, while monitoring at 280 nm shows an increase in peak intensity resulting from the higher levels

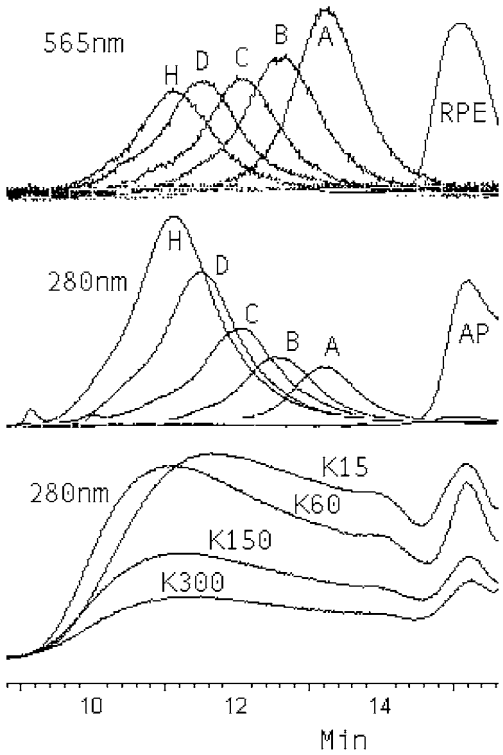


Figure 1. HPLC of conjugates Top: defined conjugates A−H, and native RPE and AP, monitoring at 565 and 280 nm. Bottom: solution-phase conjugates K15, K60, K150, and K300, monitoring at 280 nm.

of AP on the larger conjugates. In contrast, the conjugates prepared by solution-phase reaction (series K) show broad peaks reflecting a heterogeneous size distribution. Traces indicate large average conjugate size with 15 min reaction and some growth to larger size with 60 min reaction. With longer reaction times, the shape of the peak remains the same, but the signal intensity is decreased, suggesting that the conjugate has continued to grow to sizes that do not pass through the column prefilter.

Figure 2 shows representative atomic force microscopy images of defined and solution-phase conjugates. The defined conjugates are uniform in size and shape, with size increasing with the number of layers of AP, consistent with the calculated molecular masses and HPLC results. The solution-phase conjugates show extensive aggregation of the proteins increasing with reaction time, but a broad distribution of sizes for all reaction times.

Figure 3A shows results of an ELISA for TSH using the defined conjugates. When the molar concentration (based on absorbance at 565 nm of the RPE core) is held constant at 40 pM, and the antiTSH Ab is constant at about 5.7 per assembly, V_{max} for the hydrolysis of PNPP increases with AP content at each TSH level. Because the molecular masses of the conjugates vary over nearly an order of magnitude, the same experiment was performed with the weight-based conjugate concentration held constant at 200 ng/mL (results shown in Figure 3B). Here, the molar concentration of conjugate A is higher by a factor of 3 and that of H is lower by a factor of 2 than their respective concentrations in Figure 3A. Most of the conjugates give signals similar to those seen with molarity-based concentrations, supporting the interpretation that the signal depends more on the AP content of each conjugate unit than on the concentration of such units present in incubation. Conjugate H shows significantly less signal in the weight-based experiment. Most likely, the high molecular mass and low molar concentra-

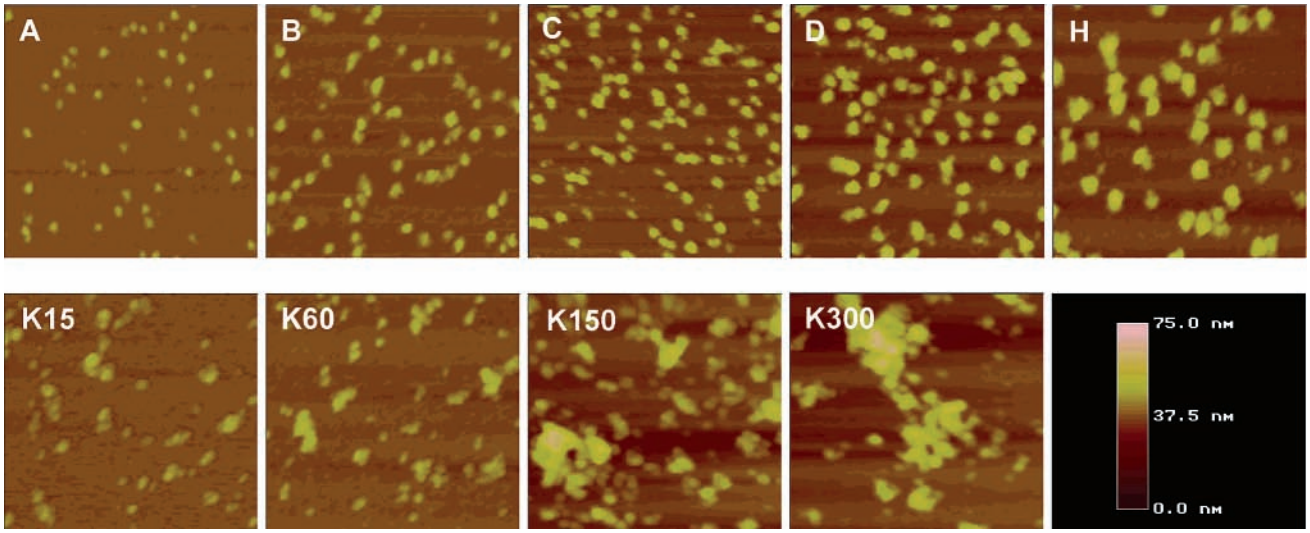


Figure 2. Atomic force microscopy height images of defined conjugates A, B, C, D, and H and solution conjugates K15, K60, K150, and K300 adsorbed to silicon surface. Each image is a 1 μm square. The height of features above the silicon surface is color-coded according to the scale shown.

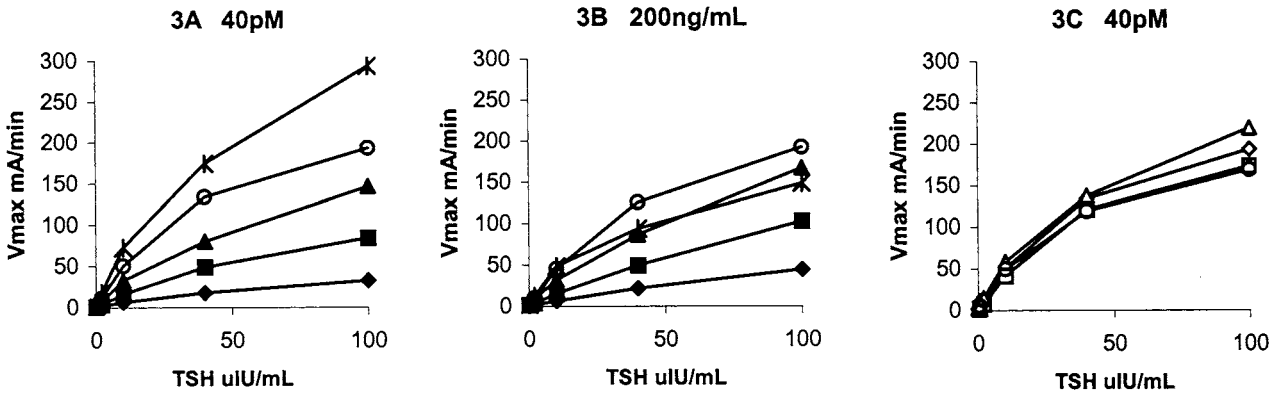


Figure 3. Comparison of defined conjugates varying AP and Ab contents in ELISA for TSH. (A) Conjugate at 40 pM shows that the signal-generating capacity of the conjugate is dependent primarily on its AP content, and (B) conjugate at 200 ng/mL shows that the AP content dependence holds even at constant mass of conjugate (see text for explanation of discrepancy for conjugate H). Conjugates with Ab content held constant at 5.5−5.8 with varying AP: ◆ A (AP = 3.5), ■ B (AP = 10.8), ▲ C (AP = 24.8), ○ D (AP = 46.9), ∗ (AP = 74.1). (C) Conjugate at 40 pM with AP held constant at 44.4−46.9; varying Ab shows that antibody content of conjugate has little effect on signal compared to AP content: □ E (Ab = 2.2), ○ D (Ab = 5.8), △ F (Ab = 16.0), ◇ G (Ab = 25.8).

tion result in slow diffusion of the conjugate to the surface containing the bound TSH.

Figure 3C shows the effect of varying Ab content of the defined conjugate while holding the AP content constant at about 45 per conjugate unit. With Ab content ranging from 2.2 to 26 per conjugate unit, the signal varies only by about 20%, pointing to the AP content of each conjugate unit as the primary determinant of its ability to generate signal.

DISCUSSION

In most applications, protein conjugation has been treated primarily as a combining of the desired functional properties of the proteins, for example, a specific binding property with a specific signaling property. Structural considerations are usually limited to those thought to affect these properties, such as the use of site-specific activation of the antibody to direct coupling away from the binding site. Typically, only two proteins are coupled, since a third protein would complicate the mixture. The intent of the present work is to control the physical construction of protein conjugates, placing arbitrarily chosen proteins in the desired numbers at the desired positions within the assembly.

Other subdisciplines of chemistry have achieved a high level of control of reactions by use of solid supports. Peptides (*10*), nucleic acids (*11*, *12*), and saccharides (*13*) with the desired sequence of subunits can be built up in discrete steps from specific starting points on the solid phase and finally released by chemical treatment. Intermediate reactions in the synthesis are driven to completion by use of excess reagents that are easily washed from the support before starting the next step. In the present work, immobilization of the starting material provides the same benefits, but even more importantly it prevents the uncontrolled polymerization that the plurality of reactive sites per molecule would lead to in a solution-phase reaction.

In peptide, nucleic acid, and saccharide synthesis, the target is a single chemical species, and precise control of the functional groups undergoing reaction is essential. For antibody−enzyme conjugates, linkage may occur at any of many different residues of either protein and still yield a product with the desired properties. Therefore, the target can be defined at a more macroscopic level to be a linkage of the desired protein species in the desired number and location in each independent unit. This relaxed requirement for control allows selection from a

wide range of linking agents, and permits the use of the aqueous reaction media needed to retain binding and enzymatic activity of the proteins.

Many of the same considerations for affinity chromatography hold in solid-phase conjugation. The support must allow free movement of proteins through its pores, but must also provide a high surface area for binding the desired proteins. The support must also be subject to modification to attach the chemical groups intended to interact with the proteins. Cross-linked agarose meets these criteria. The Sepharose CL-2B used in this work has an exclusion limit of 40 MDa, sufficient to allow conjugation and elution of the assemblies prepared here. Periodate oxidation produces aldehyde groups, which can be further modified as needed.

Several chemistries are available for linking proteins to the support and to other proteins. The linkage holding the assembly to the support must be stable throughout the reaction sequence, but must be cleavable by conditions that do not damage the desired properties of the conjugate. The hydrazone linkage we chose for this work is cleaved under mild conditions expected to have minimal effect on the protein. Other possible cleavable linking groups include disulfide (cleavable by reducing agents) and vicinal diol (cleavable by periodate). These would be less generally applicable than the hydrazone link used here, since the reagents used to cleave them would be expected also to react with disulfide and carbohydrate groups, respectively, in the protein conjugates.

The stepwise approach allows assembly of multiple proteins, with assurance that each conjugate unit will contain the desired quantity of each. Here, we have taken advantage of this to include a third protein, RPE, as the core. This adds a third property to the conjugate: a specific optical absorbance allowing accurate quantitation of the product. The high extinction coefficient of RPE at wavelengths at which most proteins have no absorbance makes it easy to measure its concentration even in dilute solutions containing components that would interfere with other protein measurements. Assuming that each conjugate unit contains a single core protein, the absorbance of the conjugate at 565 nm provides a direct measure of the molar concentration of the conjugate independent of the other proteins included.

As a practical note, the intense color of RPE also makes it easy to follow in the manipulations involved in solid-phase conjugation. Its uptake into the support gives visual confirmation that the activation steps to this point have been successful. After cleaving the linkage to the support, the elution of conjugate is easily observed, allowing collection of the product with minimal dilution by wash buffer.

For the purpose of composition and molecular mass calculations, we have assumed that reaction centers remain independent throughout the sequence and that each reaction center absorbs the same number of protein molecules in each step. Both of these assumptions must be considered ideals that are approached but may not be fully achieved in the present work. A small shoulder is present on the left side of the HPLC traces in Figure 1 for all the defined conjugates except the smallest, and is most visible for conjugates B, C, and D. While no molecular mass standards are available for proteins in the desired range, the elution times of these shoulders, each near the peak of the next larger conjugate, suggest the presence of a small proportion of dimeric forms of the conjugates. Most likely, this dimerization occurs during the assembly process when two neighboring reaction centers are bridged by the linking of an added protein to active sites on both. While it may not be possible to completely eliminate the formation of dimers, it may be possible to minimize it by decreasing the density of reaction centers on the support, or by decreasing the number of reactive groups on the proteins.

The assumption that each reaction center absorbs the same number of protein molecules in each step is also an approximation. In the first addition of AP-Mal, the mean uptake is 3.6 AP-Mal per RPE-SH, suggesting that some reaction centers have absorbed 4 enzyme molecules in this step and others only 3. These discrepancies are likely to be propagated through the remaining steps, and can be expected to result in some heterogeneity of size of the final conjugates.

The atomic force microscope was invented in 1986 (*14*) as a microscopic technique to probe surface topography at molecular resolution. Since its invention, AFM has been used to image a variety of materials including polymers (*15*) and biological-modified surfaces (*16*−*18*). In TappingMode AFM, a cantilever holds a tip above the surface of a material, oscillating it at its resonant frequency as it is rastered across the surface. During scanning, the resonant frequency is affected by attractive or repulsive interactions with features on the surface. The motion is measured by reflecting a laser off the back of the cantilever onto a photodiode detector, and the resulting signal is converted into a 3D image by the microscope's electronics. In this work, we imaged a selection of conjugates prepared by both solid-phase and solution methods adsorbed to silicon surfaces. The images are consistent with the HPLC results, showing average size increasing with number of layers of protein addition for the solid-phase preparations and increasing with reaction time for the solution-phase preparations. In solid-phase conjugates A−H, the protein assemblies appear approximately spherical with most at or near a maximum size characteristic of the preparation. A few appear close enough together that they may represent dimeric forms. In contrast, the solution conjugates K15−K300 show much more heterogeneity of size and shape at all reaction times. While the average size increases with reaction time, the size distribution appears largely random, and there is no indication of a preferred shape.

The ability to control the composition and structure of conjugates makes possible detailed studies of the effects of these features on the functional properties of the conjugates. We demonstrated this with a limited study comparing conjugates with different enzyme and antibody contents with regard to the signal generated in an ELISA. Subject to the assumptions discussed above, the RPE chromophore allows direct measurement of the molar concentration of each conjugate independent of the presence of bound AP and antibody. When the molar concentration and Ab content of the conjugates are held constant, the assay signal at each analyte concentration increases with increasing AP content. Over the range tested, the increase in signal was somewhat less than would be expected for full participation of each additional layer of AP: conjugate H with approximately 20 times the AP content of conjugate A shows only about 10 times the signal. This may be due to decreased accessibility of substrate to AP in the interior of the assembly, either from electrostatic repulsion or because of local depletion of the substrate by AP at the surface.

We also showed that, under conditions of the ELISA, the signal shows little change when the AP is held constant and the Ab content is varied over a factor of 10. This suggests that the solid-phase process may be of particular benefit when the binding agent is in limited

supply. It should be noted, however, that these experiments do not address the kinetics of binding. The rate of diffusion of the conjugate and the rate at which it binds to immobilized analyte can be expected to show dependencies on the conjugate size and the content of binding sites. The ability to control these parameters as well as the molar concentration of the conjugate may find application in such investigations.

LITERATURE CITED

(1) Tijssen, P. (1985) *Practice and Theory of Enzyme Immunoassays*, Elsevier, Amsterdam.
(2) Hermanson, G. T. (1996) *Bioconjugate Techniques*, Academic Press, San Diego.
(3) Brinkley, M. (1992) A brief survey of methods for preparing protein conjugates with dyes, haptens, and cross-linking reagents. *Bioconjugate Chem. 3*, 2−13.
(4) Means, G. E., and Feeney, R. E. (1990) Chemical modifications of proteins: history and applications. *Bioconjugate Chem. 1*, 2−12.
(5) Pastan, I., and Kreitman, R. J. (1998) Immunotoxins for targeted cancer therapy. *Adv. Drug Deliv. Rev. 31*, 53−88.
(6) Fisher, E. A. (1985) *Affinity Chromatography: A Practical Approach* (Dean, P. D. G., Johnson, W. S., and Middle, F. A., Eds.) p 46, IRL Press, Oxford.
(7) Duncan, R. J., Weston, P. D., and Wrigglesworth, R. (1983) A new reagent which may be used to introduce sulfhydryl groups into proteins, and its use in the preparation of conjugates for immunoassay. *Anal. Biochem. 132*, 68−73.
(8) Tanimori, H., Kitagawa, T., Tsunoda, T., and Tsuchiya, R. J. (1981) Enzyme immunoassay of neocarzinostatin using beta-galactosidase as label. *Pharmacobiodyn. 4*, 812−819.
(9) Oi, V. T., Glazer, A. N., and Stryer, L. J. (1982) Fluorescent phycobiliprotein conjugates for analyses of cells and molecules. *Cell Biol. 93*, 981−986.
(10) Merrifield, R. B., and Stewart, J. M. (1965) Automated peptide synthesis. *Nature 207*, 522−523.
(11) Powers, G. J., Jones, R. L., Randall, G. A., Caruthers, M. H., van de Sande, J. H., and Khorana, H. G. (1975) Optimal strategies for the chemical and enzymatic synthesis of bihelical deoxyribonucleic acids. *J. Am. Chem. Soc. 97*, 875−884.
(12) Caruthers, M. H. (1985) Gene synthesis machines: DNA chemistry and its uses. *Science 230*, 281−285.
(13) Plante, O. J., Palmacci, E. R., and Seeberger, P. H. (2001) Automated solid-phase synthesis of oligosaccharides. *Science 291*, 1523−1527.
(14) Binnig, G., Quate, C. F., and Gerber, C. (1986) Atomic Force Microscope. *Phys. Rev. Lett. 56*, 930−933.
(15) Godovsky, Y. K., and Magonov, S. N. (2000) Atomic Force Microscopy Visualization of Morphology and Nanostructure of an Ultrathin Layer of Polyethylene during Melting and Crystallization. *Langmuir 16*, 3549−3552.
(16) Morris, V. J., Kirby, A. R., and Gunning, A. P. (1999) *Atomic Force Microscopy for Biologists*, Imperial College Press, London.
(17) Shlyakhtenko, L. S., Gall, A. A., Weimer, J. J., Hawn, D. D., and Lyubchenko, Y. L. (1999) Atomic Force Microscopy Imaging of DNA Covalently Immobilized on a Functionalized Mica Surface. *Biophys. J. 77*, 568−576.
(18) Möller, C., Allen, M., Elings, V., Engel, A., and Müller, D. J. (1999) Tapping-Mode Atomic Force Microscopy Produces Faithful High-Resolution Images of Protein Surfaces. *Biophys. J. 77*, 1150−1158.

BC0255438

Conjugation of Ligands at the 5′-End of CpG DNA Affects Immunostimulatory Activity

Ekambar R. Kandimalla, Lakshmi Bhagat, Dong Yu, Yanping Cong, Jimmy Tang, and Sudhir Agrawal*

Hybridon, Inc., 345 Vassar Street, Cambridge, Massachusetts 02139. Received May 25, 2002; Revised Manuscript Received July 15, 2002

Bacterial DNA and synthetic oligonucleotides containing unmethylated CpG dinucleotides (CpG DNA) activate the vertebrate immune system and promote Th1-like immune responses. Several CpG DNAs are currently being tested in clinical trials as either alone or in combination with vaccines, antibodies, and allergens separately or as conjugates for a number of disease indications including cancers, allergies, and asthma. In this paper, we show that conjugation of an oligonucleotide and a CpG DNA through their 5′-ends (5′-5′-linked DNA) significantly reduces the immunostimulatory activity of the CpG DNA. In addition, we found that the reduction in immunostimulatory activity of 5′-5′-linked CpG DNA depends on the size of the oligonucleotide conjugated to CpG DNA. Conjugation of a smaller group or molecule, such as a phosphorothioate group, at the 5′-end of CpG DNA has an insignificant effect on immunostimulatory activity. However, conjugation of a mononucleotide, tetra- or longer oligonucleotide or a fluorescein molecule to the 5′-end of a CpG DNA (5′-5′-linked DNA) significantly suppresses the immunostimulatory activity of CpG DNA. Surprisingly, conjugation of an oligonucleotide or a ligand through the 3′-end of CpG DNA (3′-3′-linked DNA) has an insignificant effect on immunostimulatory activity. Studies of cellular uptake and activation of transcription factor NF-κB in J774 cells using fluorescein-conjugated CpG DNAs suggest that the differences in the immune stimulation of 5′- and 3′-end-conjugated CpG DNAs is not as a result of differences in their cellular uptake properties. These results suggest that for optimal immunostimulatory activity, ligands should not be attached at the 5′-end of the CpG DNA.

INTRODUCTION

The immune system of vertebrates recognizes unmethylated CpG dinucleotides present in bacterial DNA and synthetic oligonucleotides (CpG DNA) in a sequence-selective manner. As a result of activation by CpG DNA, immune system cells secrete a myriad of cytokines, including IL-12, IL-6, TNF-α, and INF-γ, and up-regulate several costimulatory molecules (*1*−*4*). The cytokines and costimulatory molecules secreted provide nonspecific protection against infectious pathogens and strongly enhance the generation of antigen-specific B-cell responses (*5*−*7*). A number of CpG DNAs are at various stages of preclinical and clinical evaluation as antitumor, antiviral, antibacterial, and antiinflammatory agents and as adjuvants in immunotherapy (*5*−*7*).

A receptor, TLR9, recognizes CpG dinucleotides present in certain specific sequence contexts in CpG DNA and initiates signaling pathways that lead to the activation of NF-κB and the subsequent up-regulation of cytokines and costimulatory molecules (*8*). Alternately, CpG DNA activates DNA protein kinase, which phosphorylates IκB-kinaseB, leading to the activation of NF-κB, which leads to the production of cytokines (*9*). It is not clear whether the two pathways are activated sequentially or in parallel leading to a common function of activating the NF-κB pathway. The growing evidence suggests that TLR9 exhibits considerable sequence selectivity for CpG DNA (*10*, *11*). In addition, the receptor recognizes CpG-dinucleotides with a strict bias for the chemical and conformational nature of the unmethylated d(CpG) dinucleotide. However, it can accommodate a range of flanking sequences (*3*, *12*) that may vary from species to species (*13*, *14*).

Our laboratory has been studying the effects of sequence and structural changes in the flanking sequences that potentiate or neutralize the immunostimulatory activity of CpG DNA in an attempt to understand the molecular recognition events between the receptors and CpG DNA. Our studies suggest that incorporation of certain modified bases in place of C or G in a CpG dinucleotide does not affect immunostimulatory activity (*15*). However, the receptor recognizes only 2′-deoxyribonucleotides with a negatively charged internucleotide linkage between C and G of the CpG-dinucleotide (*16*). Further, a number of different modifications at the 2′-position of the sugar and phosphate backbone are tolerated about three or more nucleotides away from the CpG-dinucleotide in both the 5′- and 3′-flanking sequences (*17*−*19*). In fact, the incorporation of modifications in the 5′-flanking sequence usually potentiates the immunostimulatory activity of CpG DNA, while the incorporation of the same in the 3′-flanking sequence has minimal effect on the immunostimulatory activity. We have also shown that the presence of a nucleobase on nucleosides is not required for the immunostimulatory activity in certain positions in the 5′- or the 3′-flanking sequence to the CpG-dinucleotide (*20*). Although the incorporation of 2′-5′-deoxyribonucleosides within or adjacent to CpG dinucleotide is detrimental for immunostimulatory activity, the incorporation of the same in the flanking sequences is well tolerated and in certain positions they even potentiate the immunostimulatory activity (*21*).

* To whom correspondence should be addressed. Tel: 617-679-5501, Fax: 617-679-5542, email: sagrawal@hybridon.com.

10.1021/bc0200374 CCC: $22.00 © 2002 American Chemical Society
Published on Web 08/28/2002

In recent years, the conjugation of antigens and vaccines to CpG DNA has been reported (*22*−*26*). The use of such CpG DNA conjugates induces more efficient antigen/vaccine-specific immune responses than does CpG DNA and antigen/vaccine combination treatments (*25*, *26*). Our recent studies suggest that an accessible 5′-end of the CpG DNA is critical for the immunostimulatory activity (*27*). To confirm this observation, establish the size of the ligand conjugated at the 5′-end that could block immunostimulatory activity, and examine if cellular uptake is effected by 3′- or 5′-conjugation that could lead to different immunostimulatory activity, we carried out the study described herein. In this study, CpG-DNA was conjugated to different lengths or sizes of nucleotides or ligands through their 5′- or 3′-ends, and the impact on immunostimulatory activity was studied. These studies define the most appropriate site for conjugation on CpG DNA with large molecules such as antigens/vaccines for optimal therapeutic uses.

EXPERIMENTAL PROCEDURES

CpG DNA Synthesis and Purification. CpG DNA and their conjugates were synthesized using β-cyanoethyl phosphoramidite chemistry on a PerSeptive Biosystem's 8909 Expedite DNA synthesizer on 1 to 2 μmol scale as described earlier (*27*−*30*). The phosphoramidites of dA, dG, dC, and T were obtained from PE Biosystems. The 5′-phosphoramidites of dA, dG, dC, and T were obtained from Glen Research Corporation. The DMT-protected fluorescein phosphoramidite and DMT-protected CPG-bound fluorescein were obtained from Glen Research. Beaucage's reagent was used as an oxidant to obtain phosphorothioate backbone modification (*31*). After the synthesis, CpG DNAs were deprotected using standard protocols, purified by HPLC, and dialyzed against USP quality sterile water for irrigation (Braun). The CpG DNA conjugates were lyophilized and dissolved again in distilled water, and the concentrations were determined by measuring the UV absorbance at 260 nm. All the CpG DNAs synthesized were characterized by CGE and MALDI-TOF mass spectrometry (Brucker Proflex III MALDI-TOF mass spectrometer with 337 nm N_2 laser) for purity and molecular mass, respectively. The purity of full-length CpG DNA conjugates ranged from 89 to 95% and the rest being n-1 and n-2 as determined by CGE and/or denaturing PAGE.

Cell Culture Conditions and Reagents. BALB/c mouse (4−8 weeks) spleen cells were cultured in RPMI complete medium as described earlier (*16*, *32*). Murine macrophage-like cells, J774 (American Type Culture Collection, Rockville, MD) were culured in Dulbecco's modified Eagle's medium supplemented with 10% (v/v) FCS and antibiotics (100 IU/mL of penicillin G/streptomycin). All other culture reagents were purchased from Mediatech (Gaithersburg, MD).

ELISAs for IL-12 and IL-6. BALB/c mouse spleen or J774 cells were plated in 24-well dishes at a density of 5×10^6 or 1×10^6 cells/mL, respectively. The CpG DNA dissolved in TE buffer (10 mM Tris-HCl, pH 7.5, 1 mM EDTA) was added to a final concentration of 0.03, 0.1, 0.3, 1.0, 3.0, or 10.0 μg/mL to mouse spleen cell cultures and 1.0, 3.0, or 10.0 μg/mL to J774 cell cultures. The cells were then incubated at 37 °C for 24 h, and the supernatants were collected for ELISA assays. The experiments were performed two or three times for each CpG DNA in triplicate for each concentration.

The secretion of IL-12 and IL-6 was measured by sandwich ELISA. The required reagents, including cytokine antibodies and standards, were purchased from PharMingen. ELISA plates (Costar) were incubated with appropriate antibodies at 5 μg/mL in PBSN buffer (PBS/0.05% sodium azide, pH 9.6) overnight at 4 °C and then blocked with PBS/1% BSA at 37 °C for 30 min. Cell culture supernatants and cytokine standards were appropriately diluted with PBS/1% BSA, added to the plates in triplicate and incubated at 25 °C for 2 h. Plates were washed, 1 μg/mL of appropriate biotinylated antibody was added, and the plates were incubated at 25 °C for 1.5 h. The plates were washed extensively with PBS/0.05% Tween 20 and then further incubated at 25 °C for 1.5 h after the addition of streptavidine-conjugated peroxidase (Sigma). The plates were developed with Sure Blue (Kirkegaard and Perry) chromogenic reagent, and the reaction was terminated by adding Stop Solution (Kirkegaard and Perry). The color change was measured on a Ceres 900 HDI Spectrophotometer (Bio-Tek Instruments) at 450 nm. The levels of IL-12 and IL-6 in the cell culture supernatants were calculated from the standard curve constructed under the same experimental conditions for IL-12 and IL-6, respectively.

Mouse Splenomegaly Assay. Female BALB/c mice (4−6 weeks, 19−21 gm) were divided into different groups with three or four mice in each group. CpG DNAs were dissolved in sterile PBS and administered subcutaneously to mice at a dose of 5 mg/kg. After 72 h, mice were sacrificed, and the spleens were harvested and weighed.

Cellular Uptake. J774 cells were plated at a density of 1×10^5 cells/well in an eight-well chamber slide the day before addition of CpG DNAs. The medium was changed 1 h before the experiment, fluorescein-labeled CpG DNAs were added to a concentration of 10 μg/mL, and the cells were incubated for 1 h at 37 °C. At the end of the incubation period, medium was aspirated. The cells were washed thoroughly with ice-cold phosphate-buffered saline (PBS), fixed with cold 95% ethanol and 5% acetic acid for 10 min, washed, and finally mounted in an antifade medium (Vector Laboratories, Burlingame, CA) with DAPI (for nuclear staining). The slides were then examined, and photomicrographs were taken under a Zeiss Axiophot microscope. The fluorescein and DAPI images were merged using the Spot Imaging software.

Preparation of J774 Cell Nuclear Extracts and EMSA. For NF-κB activation studies, J774 cells were plated at a density of 5×10^6 cells/well in six-well plates, and nuclear extracts were prepared as described earlier (*33*). Briefly, after stimulation of J774 cells for 1 h with CpG DNAs at a concentration of 10 μg/mL, cells were washed three times in ice-cold PBS, harvested, and suspended in 0.24 mL of buffer A (10 mM HEPES, pH 7.9, 10 mM KCl, 0.1 mM EDTA, 0.1 mM EGTA, 1 mM DTT, and protease inhibitor cocktail) (Boehringer-Mannheim) and allowed to swell on ice for 15 min. Then 16 μL of 10% Nonidet-P40 was added, and the tubes were vortexed vigorously for 10 s. Nuclei were separated from cytosol by centrifugation at 500 g for 5 min and were lysed in 60 μL of buffer B (20 mM HEPES, pH 7.9, 0.4 M NaCl, 1 mM EDTA, 1 mM EGTA and protease inhibitor cocktail). After 30 min at 4 °C, lysates were separated by centrifugation (14000*g*, 10 min) and supernatants containing nuclear proteins were transferred to new vials. Protein concentrations were determined (*34*), and the samples were either used immediately or stored frozen at −70 °C.

The oligonucleotide probe (5′-AGTTGAGGGGACTTTC-CCAGGC-3′) containing the κB binding motif was end-labeled with [γ-^{32}P]-ATP using T4 polynucleotide kinase

Chart 1. Sequence of Immunostimulatory CpG DNA 1 and the Chemical Structures of Ligands (b−l) Conjugated at Either the 5′- (R) or the 3′-terminal (R′) of CpG DNA.

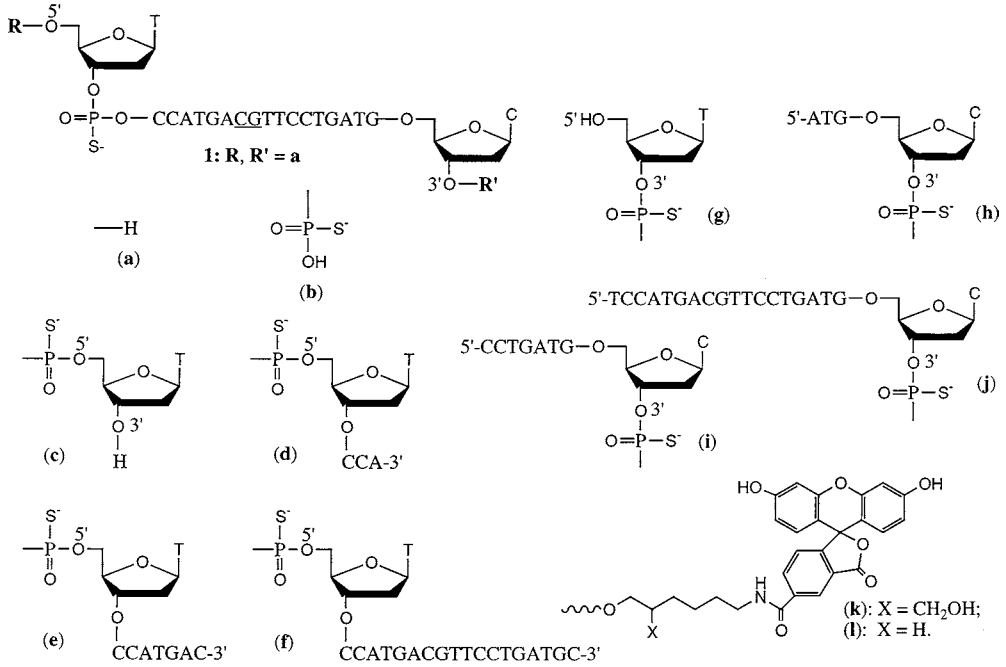


Table 1. Phosphorothioate CpG DNA Sequences and Modifications Used in the Study[a]

CpG DNA no.	sequence	length	5′-end	3′-end
1	5′-TCCATGACGTTCCTGATGC-3′	19-mer	1	1
2	5′-TCCATGACGTTCCTGATGC-3′-**b**	19-mer	1	blocked
3	5′-TCCATGACGTTCCTGATGC-3′-3′-**c**−5′	20-mer	2	blocked
4	5′-TCCATGACGTTCCTGATGC-3′-3′-**d**−5′	23-mer	2	blocked
5	5′-TCCATGACGTTCCTGATGC-3′-3′-**e**−5′	27-mer	2	blocked
6	5′-TCCATGACGTTCCTGATGC-3′-3′-**f**−5′	38-mer	2	blocked
7	**b**−5′-TCCATGACGTTCCTGATGC-3′	19-mer	blocked	1
8	3′-**g**−5′-5′-TCCATGACGTTCCTGATGC-3′	20-mer	blocked	2
9	3′-**h**−5′-5′-TCCATGACGTTCCTGATGC-3′	23-mer	blocked	2
10	3′-**i**−5′-5′-TCCATGACGTTCCTGATGC-3′	27-mer	blocked	2
11	3′-**j**−5′-5′-TCCATGACGTTCCTGATGC-3′	38-mer	blocked	2
12	5′-TCCATGACGTTCCTGATGC-3′-**k**	19-mer	1	blocked
13	**l**−5′-TCCATGACGTTCCTGATGC-3′	19-mer	blocked	1

[a] See Chart 1 for chemical structures **b**−**l**; 5′-CG-3′ dinucleotide is shown underlined.

(Invitrogen) and purified over two successive G-50 mini columns (Amersham Pharmacia Biotech). Reaction mixtures (25 μL) containing 10 μg of nuclear protein, 5 mM Tris (pH 7.5), 100 mM NaCl, 1 mM DTT, 1 mM EDTA, 4% glycerol (v/v), and 0.08 mg/mL salmon sperm DNA were preincubated on ice for 15 min. After preincubation, 1×10^6 cpm of the probe was added and the binding reaction was allowed to proceed for 20 min at room temperature. DNA−protein complexes were then resolved in a 6% native polyacrylamide gel in TBE buffer (22.5 mM Tris, 22.5 mM boric acid and 0.5 mM EDTA, pH 8.3) at 140 V for 2−3 h. Gels were dried and exposed to Kodak Biomax MR film at −70 °C. Films were scanned, and the images were processed using Adobe imaging software.

RESULTS AND DISCUSSION

We chose an oligonucleotide sequence (Chart 1, Table 1) containing a CpG dinucleotide (**1**), which showed immunostimulatory activity in earlier studies (*27*). We synthesized a number of analogues of CpG DNA sequence **1** conjugating a phosphorothioate group (**b**), mono- (**c**, **g**), 4- (**d**, **h**), 8- (**e**, **i**), or 19-mer (**g**, **j**) oligonucleotide, or a fluorescein (**l** or **k**) either at the 5′- (R) or the 3′- end (R′) (see Chart 1 for structures and Table 1 for sequences). CpG DNA conjugates **2**−**6** and **12**, in which a ligand conjugated to CpG DNA **1** through its 3′-hydroxyl group, are shown in Table 1. The 3′-end of these molecules is blocked as a result of conjugation at the 3′-end and CpG DNAs **3**−**6** have two 5′-ends. We also synthesized CpG DNAs **7**−**11** and **13**, in which a ligand conjugated to parent CpG DNA **1** through its 5′-hydroxyl group (Table 1). The 5′-end of these molecules is blocked by conjugation and, therefore, CpG DNAs **8**−**11** have two 3′-ends.

Phosphorothioate and Nucleotide Conjugation at the 3′-End of CpG DNA. In BALB/c mouse spleen cell cultures, all CpG DNAs induced a concentration-dependent IL-12 and IL-6 secretion (Table 2). At a concentration of 1.0 μg/mL, parent CpG DNA **1** induced 2391 ± 175 and 13320 ± 960 pg/mL of IL-12 and IL-6 secretion, respectively (Figure 2A and B). The secretion of IL-12 and IL-6, compared with media (PBS) control, in mouse spleen cell cultures suggest that CpG DNA **1** induced immunostimulatory activity as has been reported earlier (*27*). At the same concentration of 1.0 μg/mL, CpG DNA **2**, which has a phosphorothioate group conjugated to the 3′-end of the parent CpG DNA **1**, induced lower levels of IL-12 and IL-6 (1499 ± 191 and 5420 ± 370 pg/mL, respectively) secretion compared with CpG DNA **1**. CpG DNAs **3**−**6**, which have a mono-, 4-, 8- or 19-mer oligo-

Table 2. Induction of IL-12 and IL-6 Secretion by CpG DNA-conjugates in BALB/c Mice Spleen Cell Cultures

CpG DNA no.[a]	IL-12 (pg/mL) ± SD					IL-6 (pg/mL) ± SD				
	0.1 μg/mL	0.3 μg/mL	1.0 μg/mL	3.0 μg/mL	10.0 μg/mL	0.1 μg/mL	0.3 μg/mL	1.0 μg/mL	3.0 μg/mL	10.0μg/mL
1	991 ± 121	1820 ± 224	2391 ± 175	3507 ± 127	2615 ± 279	652 ± 48	2858 ± 180	13320 ± 960	18625 ± 1504	17229 ± 1750
2	526 ± 32	2100 ± 175	1499 ± 191	3019 ± 35	3489 ± 162	1387 ± 152	1426 ± 124	5420 ± 370	19096 ± 484	19381 ± 2313
3	1030 ± 11	1348 ± 102	2060 ± 130	3330 ± 130	3582 ± 259	923 ± 22	2542 ± 81	9054 ± 120	14114 ± 179	13693 ± 264
4	1119 ± 159	1726 ± 207	2434 ± 100	2966 ± 204	3215 ± 464	870 ± 146	1905 ± 56	7841 ± 350	17146 ± 1246	15713 ± 693
5	1175 ± 68	2246 ± 124	1812 ± 75	2388 ± 320	2545 ± 202	1152 ± 238	3499 ± 116	7142 ± 467	14064 ± 167	13566 ± 477
6	1087 ± 121	1705 ± 163	1797 ± 141	2522 ± 195	3054 ± 103	1039 ± 105	2043 ± 157	4848 ± 288	15527 ± 224	21021 ± 1427
7	1173 ± 107	2170 ± 155	2132 ± 58	2812 ± 203	3689 ± 94	807 ± 0.5	927 ± 0.5	3344 ± 0.5	10233 ± 0.5	9213 ± 0.5
8	866 ± 51	1564 ± 63	1525 ± 63	2666 ± 97	4030 ± 165	750 ± 63	1643 ± 30	5559 ± 415	11549 ± 251	11060 ± 651
9	227 ± 3	495 ± 96	1007 ± 68	897 ± 15	1355 ± 97	302 ± 18	374 ± 22	1000 ± 68	9106 ± 271	13077 ± 381
10	139 ± 18	211 ± 12	452 ± 22	458 ± 29	1178 ± 237	220 ± 23	235 ± 18	383 ± 35	1706 ± 33	11530 ± 254
11	181 ± 85	282 ± 105	846 ± 165	2082 ± 185	3185 ± 63	467 ± 122	437 ± 85	1697 ± 283	9781 ± 13	11213 ± 294
medium	86 ± 6					60 ± 12				

[a] See Table 1 for sequences.

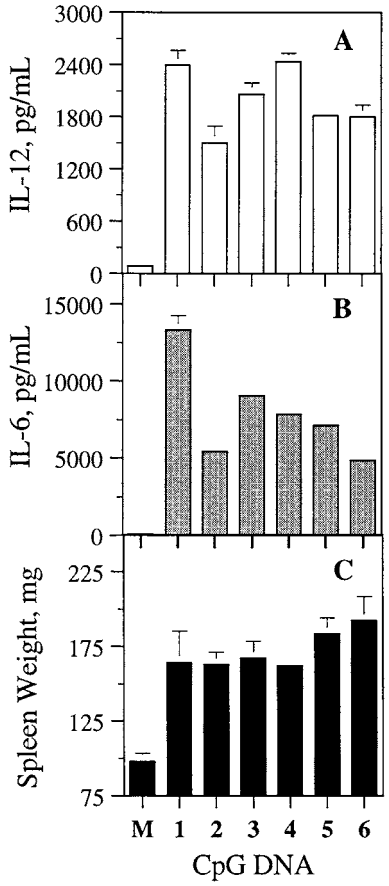


Figure 1. Secretion of IL-12 (A) and IL-6 (B) in BALB/c mouse spleen cell cultures in the presence of CpG DNAs **1**−**6** at a concentration of 1.0 μg/mL. Assays were carried out as described in Experimental Section. M stands for media/vehicle (PBS) control. (C) Spleen enlargement in BALB/c mice following subcutaneous administration of CpG DNAs **1**−**6** at a dose of 5 mg/kg. Control mice received vehicle (PBS). Three or four mice were used for each CpG DNA treatment, and the averages were calculated.

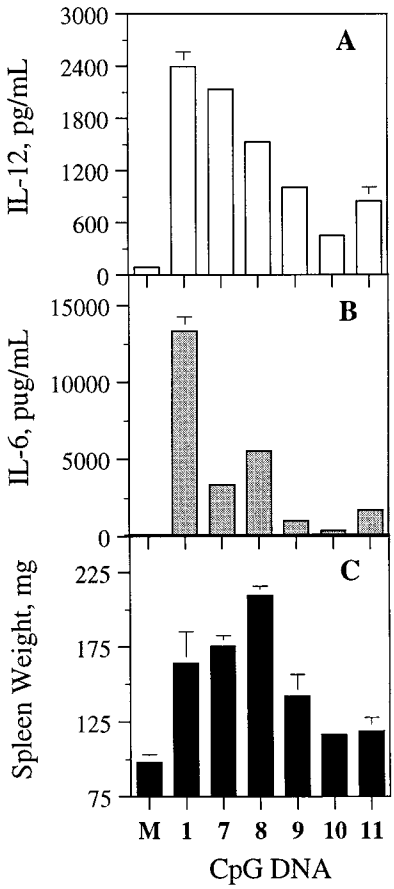


Figure 2. Induction of IL-12 (A) and IL-6 (B) secretion in BALB/c mouse spleen cell cultures in the presence of CpG DNA **1** and **7**−**11** at a concentration of 1.0 μg/mL. Assays were carried out as described in Experimental Section. M stands for media (PBS) control. (C) Spleen enlargement in BALB/c mice following subcutaneous administration of CpG DNA **1** and **8**−**11** at a dose of 5 mg/kg. See Figure 1 legend for other experimental details.

nucleotides conjugated through their 3′-ends to the 3′-end of parent CpG DNA **1**, induced 2060 ± 130, 2434 ± 100, 1812 ± 75, and 1797 ± 141 pg/mL of IL-12 (Figure 2A), and 9054 ± 120, 7841 ± 350, 7142 ± 467, and 4848 ± 288 pg/mL of IL-6 (Figure 2B), respectively, at the same concentration. These in vitro cytokine secretion studies suggest that the conjugation of a ligand at the 3′-end of a CpG DNA, in general, results in a similar or lower levels of IL-12 secretion and lower levels of IL-6 compared with parent CpG DNA. It is important to note that CpG DNA **6** contains two CpG dinucleotides as opposed to one in CpG DNAs **1**−**5**. In addition, the length of CpG DNA **6** is twice that of **1**, and **6** contains two 5′-ends compared with CpG DNA **1**, which has a 3′- and a 5′-end. The results presented here, however, suggest that the number of CpG dinucleotides and the length of CpG DNA do not affect immunostimulatory activity.

CpG DNAs **1** and **3**−**6** were studied for their ability to induce splenomegaly (increase in spleen weight) in BALB/c mice at a single dose of 5 mg/kg administered subcutaneously. The parent CpG DNA **1** caused a 67.5% increase in spleen weight compared with control mice injected with vehicle (PBS) (Figure 1C). At the same dose, CpG DNAs **3**−**6** caused 70.4, 64.3, 86.7, and 96.2% increase in spleen weight, respectively. These results

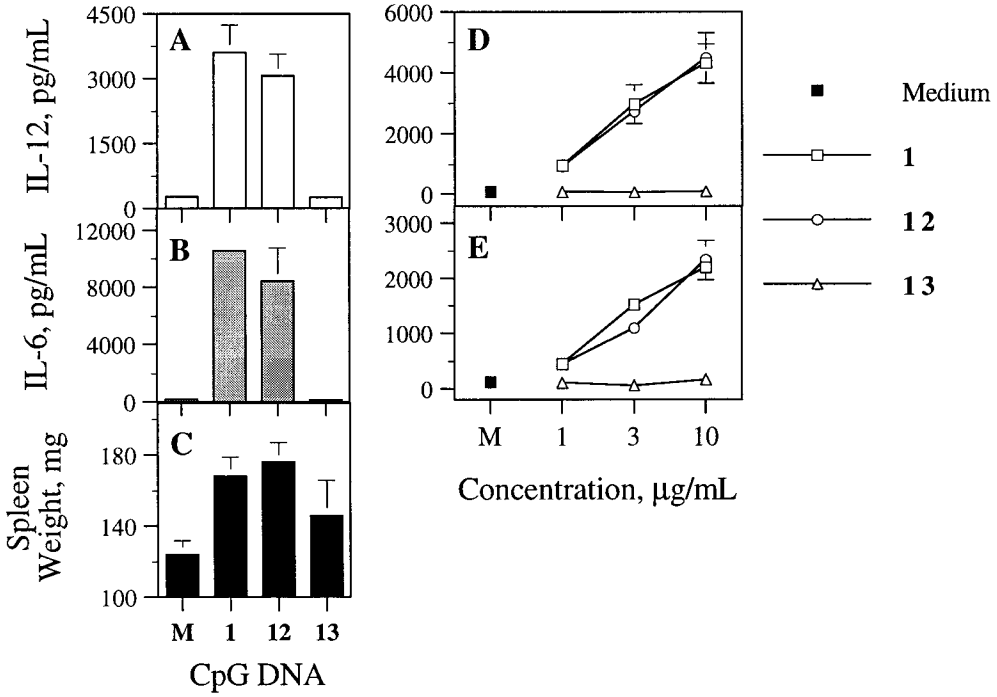


Figure 3. Induction of IL-12 (A) and IL-6 (B) secretion in BALB/c mouse spleen cell cultures in the presence of CpG DNAs **1**, **12**, and **13** at 1.0 μg/mL concentration. Assays were carried out as described in Experimental Section. M stands for media (PBS) control. (C) Spleen enlargement in BALB/c mice following subcutaneous administration of CpG DNAs **1**, **12**, **13** at a dose of 5 mg/kg. Control mice received vehicle (PBS). Three or four mice were used for each CpG DNA treatment, and the averages were calculated. Induction of IL-12 (D) and IL-6 (E) secretion in J774 cell cultures in the presence of CpG DNAs **1**, **12**, and **13** at different concentration. Assays were carried out as described in Experimental Section. M stands for media (PBS) control.

suggest that 3′-conjugation (CpG DNAs **3**−**6**) does not interfere with immunostimulatory activity compared with parent CpG DNA. In fact, CpG DNAs **5** and **6** showed a greater spleen weight increase than did parent CpG DNA **1** (Figure 1C).

Phosphate and Nucleotide Conjugation at the 5′-End of CpG DNA. CpG DNAs, **7**−**11**, which have either phosphate or nucleotide(s) conjugated at the 5′-end of the parent CpG DNA, were also tested for induction of cytokine secretion in BALB/c mouse spleen cell cultures. All CpG DNAs induced concentration-dependent IL-12 and IL-6 secretion (Table 2). The induction of IL-12 and IL-6 secretion by CpG DNAs **7**−**11** at a concentration of 1.0 μg/mL is shown in Figure 2A and 2B, respectively. CpG DNA **7**, which has a phosphorothioate group conjugated at its 5′-end, induced 2132 ± 58 and 3344 ± 0.5 pg/mL of IL-12 and IL-6 secretion, respectively, at 1.0 μg/mL concentration. At the same concentration, CpG DNA **8**, which has a mononucleotide conjugated through its 5′-end to the 5′-end of **1**, induced 1525 ± 45 and 5559 ± 415 pg/mL of IL-12 and IL-6 secretion, respectively. CpG DNAs **9**−**11**, which have a 4-, 8- or 19-mer oligonucleotide conjugated through their 5′-ends to CpG DNA **1**, induced 1007 ± 68, 452 ± 22, and 846 ± 165 pg/mL of IL-12, respectively, at 1.0 μg/mL concentration (Figure 2A). At the same concentration, CpG DNAs **9**−**11** induced 1000 ± 68, 383 ± 35, and 1697 ± 283 pg/mL of IL-6 secretion, respectively (Figure 2B). These in vitro results suggest that a phosphorothioate group conjugated at the 5′-end of CpG DNA has an insignificant effect on IL-12 secretion. However, the conjugation of nucleotides (1−19-mers) to CpG DNA through 5′-end (5′-5′-conjugation) resulted in significantly lower IL-12 and IL-6 secretion.

CpG DNAs **8**−**11** were further examined in vivo for their ability to increase spleen weight at a dose of 5 mg/kg as described above. CpG DNAs **8**−**11** showed 113.3, 44.8, 18.7, and 20.9% increase in spleen weight, respectively, compared with control mice injected with vehicle (PBS). CpG DNAs **9**−**11**, which have 5′-5′-conjugation produced a less spleen enlargement than did parent CpG DNA (67.5%) or the CpG DNA that contained 3′-3′-conjugations (**3**−**6**) (64.3−96.2%). Note that CpG DNA **11** contains two CpG dinucleotides as does CpG DNA **6**. Both CpG DNAs **6** and **11** are of the same length, but **6**, which has two free 5′-ends, caused a greater increase in spleen weight and slightly lower IL-12 secretion compared with that of CpG DNA **1**. In contrast, CpG DNA **11**, which has the 5′-ends blocked, caused a slight increase in spleen weight in BALB/c mice and induced significantly lower levels of IL-12 and IL-6 secretion in spleen cell cultures.

Fluorescein Conjugation at the 3′- or 5′-End of CpG DNA. To examine the effect of conjugation of a nonnucleoside ligand on the immunostimulatory activity of CpG DNA, we conjugated fluorescein (Chart 1, **k**/**l**) either at the 3′- (**12**) or the 5′-end (**13**) of CpG DNA **1**. Both conjugates (**12** and **13**) were studied in BALB/c mouse spleen cell cultures for IL-12 and IL-6 secretion and in BALB/c mice for splenomegaly. In addition, conjugates **12** and **13** were used to study the effect of 3′- and 5′-end conjugation on cellular uptake, activation of transcription factor NF-κB, and subsequent induction of cytokine production in the murine macrophage-like cell line J774 in comparison with parent CpG DNA.

In BALB/c mouse spleen cell cultures, both CpG DNA conjugates **12** and **13** induced a concentration-dependent IL-12 and IL-6 secretion. Figure 3A and B shows the levels of IL-12 and IL-6 secreted at 1.0 μg/mL concentration of **12** and **13** compared with **1**. CpG DNA **12**, which has a fluorescein moiety conjugated at its 3′-end, induced 3059 ± 512 pg/mL of IL-12 and 8422 ± 2327 pg/mL of IL-6 secretion at 1.0 μg/mL concentration. At the same concentration, the parent CpG DNA induced 3610 ± 637

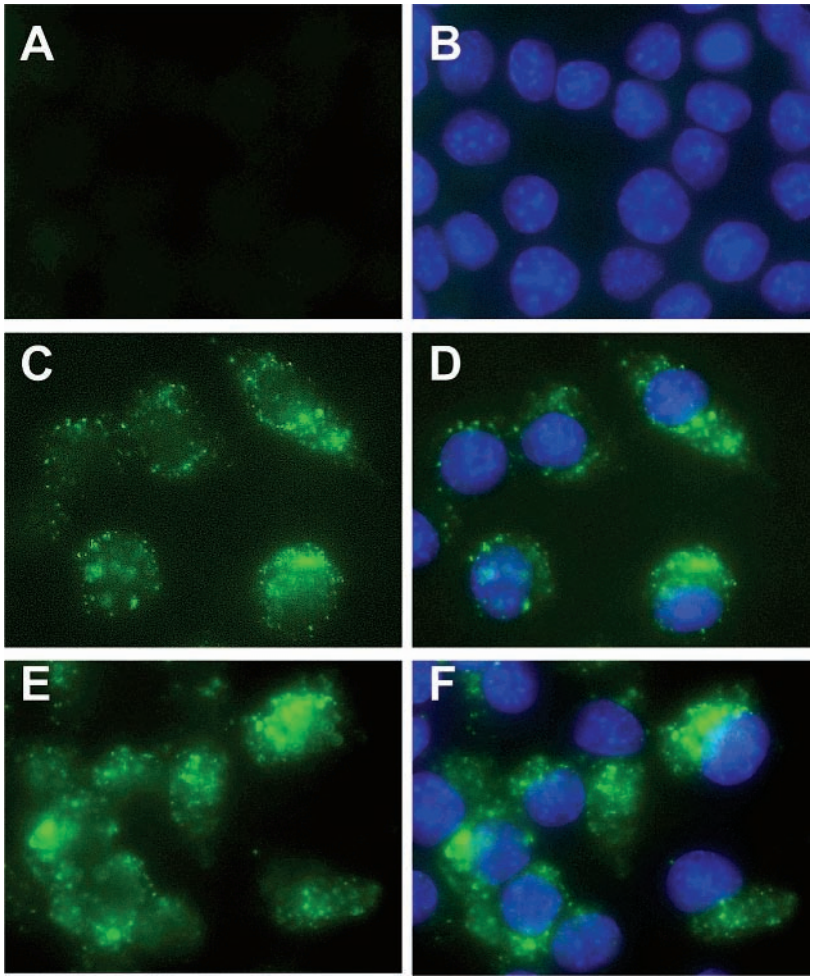


Figure 4. Cellular uptake of fluorescein-conjugated CpG DNAs **12** and **13** by J774 cells. J774 cells were incubated in medium alone (Panels A and B) or with CpG DNAs **12** (Panels C and D) and **13** (Panels E and F) and processed as described in Experimental Section. Panels A, C, and E are images taken in the fluorescein (green) channel. Panels B, D, and F are images A, C, and E superimposed with images taken in DAPI (blue, for nuclear staining) channel. Note the intense green fluorescein cytoplasmic staining in Panels C−F, indicating similar uptake of CpG DNAs **12** and **13**. Cells incubated in medium alone (A and B) are devoid of green color.

and 10540 ± 502 pg/mL of IL-12 and IL-6 secretion, respectively. In in vivo splenomegaly assay in BALB/c mice, CpG DNAs **1** and **12** caused spleen weight increases of 168 and 176 mg, respectively, compared with mice treated with vehicle (124 mg) (Figure 3C). These results suggest that conjugation of a fluorescein moiety at the 3′-end of CpG DNA does not affect (splenomegaly) or slightly reduces (cytokine secretion) immunostimulatory activity compared with the parent CpG DNA. In contrast, CpG DNA **13**, which has a fluorescein group conjugated at its 5′-end, induced 262 ± 20 pg/mL IL-12 secretion in BALB/c mice spleen cell cultures at a concentration of 1.0 μg/mL (Figure 3A). The same CpG DNA induced 168 ± 33 pg/mL of IL-6 secretion at the same concentration (Figure 3B). In BALB/c mice, CpG DNA **13** caused a spleen enlargement of 146 mg (Figure 3C). These results suggest that the conjugation of ligands at the 5′-end of a CpG DNA abrogates immunostimulatory activity significantly compared with the parent CpG DNA.

CpG DNA conjugates **12** and **13** were also examined for their ability to induce cytokine secretion in J774 cell cultures in comparison with parent CpG DNA **1**. Parent CpG DNA and its 3′-fluorescein conjugate **12** induced concentration-dependent IL-12 and IL-6 secretion (Figure 3D and E). The data presented in Figure 3D and 4E obtained from J774 cell cultures complement the results observed in murine spleen cells, which are predominantly B lymphocytes, and confirm the results obtained in BALB/c mouse spleen cell cultures.

Does Conjugation of Ligand at the 3′- or 5′-End of CpG DNA Affect Cellular Uptake? Conjugation of ligands to CpG DNA could also affect the cellular uptake and thereby immunostimulatory activity. Since CpG DNA conjugate **12** induced similar levels of cytokine secretion to that of parent CpG DNA and **13** did not, we examined whether these differences arise from different cellular uptake properties of the two conjugates in J774 cells. Figure 4 shows the uptake of CpG DNAs **12** and **13** after 1 h of incubation in J774 cell cultures. Both CpG DNAs are taken up by J774 cells and show a similar green (FITC) punctate cytoplasmic staining pattern (Figure 4, panels C−F). In some cells at this time, the nuclei also showed positive staining, as was observed with 5′-fluorescein-labeled CpG or antisense DNAs in other studies (*35*, *36*). Control cells that were treated with medium alone showed DAPI (blue) but no fluorescein staining (panels A and B). These results suggest that both 3′- and 5′-fluorescein conjugates are taken up by J774 cells to a similar extent and the differences observed in the immunostimulatory activities of CpG DNAs **12** and **13** are not as a result of differences in their cellular uptake but result from differential recognition of these molecules by receptors in the immunostimulatory pathway.

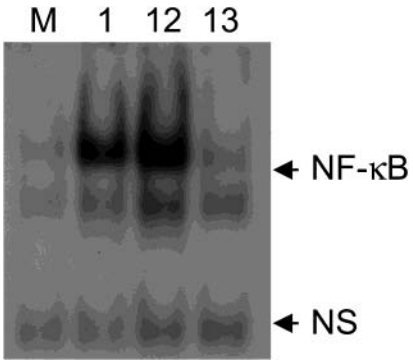


Figure 5. Effect of 3′- or 5′-fluorescein-conjugated CpG DNAs on NF-κB activatation in J774 cells. J774 cells were stimulated with CpG DNAs **1**, **12**, and **13**, nuclear extracts were prepared and analyzed on a native polyacrylamide gel as described in Experimental Section. M and NS stand for medium and nonspecific band, respectively. NF-κB band is shown with an arrow.

Effect of 5′- or 3′-Conjugation on Activation of Transcription Factor NF-κB in J774 Cells. CpG DNA stimulation has been shown to activate a number of signaling pathways, including the NF-κB pathway, which plays a critical role in up-regulation of cytokine gene expression (*37*). To study the effect of 3′- and 5′-conjugation of ligands to CpG DNA on the role of NF-κB activation, J774 cells were stimulated with CpG DNAs **1**, **12**, and **13** and the nuclear extracts were examined for NF-κB activation by EMSA. The results are presented in Figure 5. The presence of complexes that correspond to NF-κB in lanes labeled 1 and 12 suggest that parent CpG DNA **1** and its 3′-fluorescein conjugate, **12** activated transcription factor NF-κB. In contrast, the band intensities in the lane labled 13 were similar to that observed with control cells incubated with medium (lane M), suggesting that 5′-fluorescein-conjugated CpG DNA **13** failed to activate NF-κB. The results of NF-kB activation studies confirm and extend the results observed in cytokine secretion studies in J774 and BALB/c mouse spleen cell cultures.

Degradation of oligonucleotides occurs primarily by 3′-exonucleases present in vivo, which digest the oligonucleotides from their 3′-ends (*38*−*40*). Conjugation of a variety of chemical groups or ligands to the 3′-end of oligonucleotides was known to increase metabolic stability against nucleases (*41*−*44*). In the present study, the conjugation at the 3′-end could contribute to higher nuclease stability and thereby immunostimulatory activity. The splenomegaly data observed with CpG DNAs **3**−**6** and **12** especially support this hypothesis. It is surprising, however, to note that CpG DNAs that have a ligand conjugated at their 5′-ends (**8**−**11** and **13**) show lower immunostimulatory activity despite having equal, if not higher, nuclease stability compared with their parent CpG DNA **1**. In the present study, a phosphorothioate group conjugated at the 5′-end (**7**) failed to block the immunostimulatory activity (except lowering IL-6 secretion). Conjugation of a mononucleotide through 5′-5′-linkage (**8**) did not affect significantly immunostimulatory activity as determined by both in vitro and in vivo studies. Blocking the 5′-end of a CpG DNA with groups such as fluorescein or a tetranucleotide or larger oligonucleotides significantly reduced or blocked immunostimulatory activity compared with the parent CpG DNA. These results obtained with CpG DNAs **8**−**11** and **13** suggest that the differences in immunostimulatory activity of 3′-3′- and 5′-5′-linked DNAs do not arise from differences in nuclease stability or their cellular uptake but from the accessiblity to the 5′-end. In addition, the present results suggest that the size of ligand attached at the 5′-end determines the accessibility of the 5′-end of CpG DNA to the receptors in the immunostimulatory pathway and thereby the immunostimulatory activity. This study is focused on determining the size of ligand that blocks 5′-accessibility of CpG DNA but with insignificant affect on cellular uptake of conjugates. We are currently studying conjugation of other ligands with high lipophillic or cationic nature, including peptide ligands, that could influence physicochemical characteristics of the conjugates to understand the 5′-accessibility of CpG DNA for immunostimulatory activity.

In addition to conjugation of ligands, we also have shown in the past that the addition of guanine-rich sequences at the 5′- or 3′-end of a CpG DNA would effect its biological activity (*45*, *46*). The presence of G-rich sequences (four or more contiguous Gs) in oligonucleotides leads to the formation of secondary structures involving the G-rich sequences. The unusual tetrameric and other higher-order structures formed at the end of the oligonucleotide could also interfere with CpG DNA recognition and thereby pertinent activation of immunostimulatory pathways, as is the case with 5′-conjugated CpG DNAs in the present study. As has been reported earlier, now there is growing evidence that CpG DNAs containing G-rich sequences at their 3′-end are more immunostimulatory than those that contain the same sequences at their 5′-end (*47*). However, the difference in immunostimulatory activity has been presumed in terms of their differential cellular uptake only, the present results strongly suggest that it is not related to differences in cellular uptake but related to their ability to activate immune pathways through an accessible 5′-end of CpG DNA.

CpG DNA evokes host defense mechanisms such as the activation of macrophages/monocytes, B, and NK cells and induction of Th1 cell differentiation. A number of studies have shown improved responsiveness to antigens when the antigens are used together with CpG DNAs compared with antigen alone. Several studies have shown that the direct conjugation of CpG DNA with antigens increased the effectiveness of antigens severalfold compared with the use of antigen and CpG DNA mixtures because of the optimal presentation of antigen to APC by CpG DNA when used as conjugates. In general, ligands are routinely conjugated to oligonucleotides at their 5′-ends because of convenience of attaching required functional groups at the 5′-end in solid-phase synthesis (*48*). However, the present studies suggest that the immunostimulatory activity of CpG DNA conjugates is dependent on whether the ligand conjugated at the 5′-end or the 3′-end and the size of the ligand conjugated.

Taken together, the current results suggest that an accessible 5′-end of CpG DNA is required for its immunostimulatory activity and smaller groups such as a phosphorothioate or a mononucleotide do not effectively block the accessibility of the 5′-end of CpG DNA to receptors or factors involved in the immunostimulatory pathway. However, the conjugation of molecules as large as fluorescein or larger at the 5′-end of CpG DNA could abrogate immunostimulatory activity. These results have a direct impact on the studies of immunostimulatory activity of CpG DNA−antigen/vaccine/monoclonal antibody (mAb) conjugates. The conjugation of large molecules such as vaccines or mAbs at the 5′-end of a CpG DNA could lead to suboptimal immunostimulatory activity of CpG DNA. The conjugation of functional ligands at the 3′-end of CpG DNA not only contributes to

increased nuclease stability but also increased immunostimulatory potency of CpG DNA in vivo.

ACKNOWLEDGMENT

The authors thank Drs. Jin-Yan Tang and Qiuyan Zhao for their helpful suggestions.

LITERATURE CITED

(1) Tokunaga, T., Yamamoto, H., Shimada S., Abe, H., Fukuda, T., Fujisawa, Y., Furutani, Y., Yano, O., Kataoka, T., Sudo, T., Makiguchi, N., and Suganuma, T. (1984) Antitumor activity of deoxyribonucleic acid fraction from *Mycobacterium bovis* BCG. I. Isolation, physicochemical characterization, and antitumor activity. *J. Natl. Cancer Inst. 72*, 955−962.

(2) Messina, J. P., Gilkeson, G. S., and Pisetsky, D. S. (1991) Stimulation of in vitro murine lymphocyte proliferation by bacterial DNA. *J. Immunol. 147*, 1759−1764.

(3) Krieg, A. M., Yi, A. K., Matson, S., Waldschmidt, T. J., Bishop, G. A., Teasdale, R., Koretzky, G. A., and Klinman, D. M. (1995) CpG motifs in bacterial DNA trigger direct B-cell activation. *Nature 374*, 546−549.

(4) Sato, Y., Roman, M., Tighe, H., Lee, D., Corr, M., Nguyen, M. D., Silverman, G. J., Lotz, M., Carson, D. A., and Raz, E. (1996) Immunostimulatory DNA sequences necessary for effective intradermal gene immunization. *Science 273*, 352−354.

(5) Gurunathan, S., Klinman, D. M., and Seder, R. A. (2000) DNA vaccines: immunology, application, and optimization. *Annu. Rev. Immunol. 18*, 927−974.

(6) Krieg, A. M. (2002) CpG motifs in bacterial DNA and their immune effects. *Annu. Rev. Immunol. 20*, 709−760.

(7) Agrawal, S., and Kandimalla, E. R. (2002) Medicinal chemistry and therapeutic potential of CpG DNA. *Trends Mol. Med*. 8, 114−121.

(8) Hemmi, H., Takeuchi, O., Kawai, T., Kaisho, T., Sato, S., Sanjo, H., Matsumoto, M., Hoshino, K., Wagner, H., Takeda, K., and Akira, S. (2000) A Toll-like receptor recognizes bacterial DNA. *Nature 408*, 740−745.

(9) Chu, W., Gong, X., Li, Z., Takabayashi, K., Ouyang, H., Chen, Y., Lois, A., Chen, D. J., Li, G. C., Karin, M., and Raz, E. (2000) DNA-PKcs is required for activation of innate immunity by immunostimulatory DNA. *Cell 103*, 909−918.

(10) Takeshita, F., Leifer, C. A., Gursel, I., Ishii, K. J., Takeshita, S., Gursel, M., and Klinman, D. M. (2001) Role of Toll-Like Receptor 9 in CpG DNA-induced activation of human cells. *J. Immunol. 167*, 3555−3558.

(11) Bauer, S., Kirschning, C. J., Hacker, H., Redecke, V., Hausmann, S., Akira, S., Wagner, H., and Lipford, G. B. (2001) Human TLR9 confers responsiveness to bacterial DNA via species-specific CpG motif recognition. *Proc. Natl. Acad. Sci. U.S.A. 98*, 9237−9242.

(12) Tokunaga, T., Yano, O., Kuramoto, E., Kimura, Y., Yamamoto, T., Kataoka, T., and Yamamoto, S. (1992) Synthetic oligonucleotides with particular base sequences from the cDNA encoding proteins of *Mycobacterium bovis* BCG induce interferons and activate natural killer cells. *Microbiol. Immunol. 36*, 55−66.

(13) Hartmann, G., Weeratna, R. D., Ballas, Z. K., Payette, P., Blackwell, S., Suparto, I., Rasmussen, W. L., Waldschmidt, M., Sajuthi, D., Purcell, R. H., Davis, H. L., and Krieg, A. M. (2000) Delineation of a CpG phosphorothioate oligodeoxynucleotide for activating primate immune responses in vitro and in vivo. *J. Immunol. 164*, 1617−1624.

(14) Verthelyi, D., Ishii, K. J., Gursel, M., Takeshita, F., and Klinman, D. M. (2001) Human peripheral blood cells differentially recognize and respond to two distinct CpG motifs. *J. Immunol. 166*, 2372−2377.

(15) Kandimalla, E. R., Yu, D., Zhao, Q., and Agrawal, S. (2001) Effect of chemical modifications of cytosine and guanine in a CpG-motif of oligonucleotides: structure-immunostimulatory activity relationships. *Bioorg. Med. Chem. 9*, 807−813.

(16) Zhao, Q., Temsamani, J., Iadarola, P. L., Jiang, Z., and Agrawal, S. (1996) Effect of different chemically modified oligodeoxynucleotides on immune stimulation. *Biochem Pharmacol. 51*, 173−182.

(17) Zhao, Q., Yu, D., and Agrawal, S. (1999) Site of chemical modifications in CpG containing phosphorothioate oligodeoxynucleotide modulates its immunostimulatory activity. *Bioorg. Med. Chem. Lett. 9*, 3453−3458.

(18) Zhao, Q., Yu, D., and Agrawal, S. (2000) Immunostimulatory activity of CpG containing phosphorothioate oligodeoxynucleotide is modulated by modification of a single deoxynucleoside. *Bioorg. Med. Chem. Lett. 10*, 1051−1054.

(19) Yu, D., Kandimalla, E. R., Zhao, Q., Cong, Y., and Agrawal, S. (2001) Immunostimulatory activity of CpG oligonucleotides containing nonionic methylphosphonate linkages. *Bioorg. Med. Chem. 9*, 2803−2808.

(20) Yu, D., Kandimalla, E. R., Zhao, Q., Cong, Y., and Agrawal, S. (2001) Modulation of immunostimulatory activity of CpG oligonucleotides by site-Specific deletion of nucleobases. *Bioorg. Med. Chem. Lett. 11*, 2263−2267.

(21) Yu, D., Kandimalla, E. R., Zhao, Q., Cong, Y., and Agrawal, S. (2002) Immunostimulatory properties of phosphorothioate CpG DNA containing both 3′-5′- and 2′-5′-internucleotide linkages. *Nucleic Acids Res. 30*, 1613−1619.

(22) Cho, H. J., Takabayashi, K., Cheng, P. M., Nguyen, M. D., Corr, M., Tuck, S., and Raz, E. (2000) Immunostimulatory DNA-based vaccines induce cytotoxic lymphocyte activity by a T-helper cell-independent mechanism. *Nat. Biotechnol. 18*, 509−514.

(23) Tighe, H., Takabayashi, K., Schwartz, D., Van Nest, G., Tuck, S., Eiden, J. J., Kagey-Sobotka, A., Creticos, P. S., Lichtenstein, L. M., Spiegelberg, H. L., and Raz, E. (2000) Conjugation of immunostimulatory DNA to the short ragweed allergen amb a 1 enhances its immunogenicity and reduces its allergenicity. *J. Allergy Clin. Immunol. 106*, 124−134.

(24) Tighe, H., Takabayashi, K., Schwartz, D., Marsden, R., Beck, L., Corbeil, J., Richman, D. D., Eiden, J. J., Jr., Spiegelberg, H. L., and Raz, E. (2000) Conjugation of protein to immunostimulatory DNA results in a rapid, long-lasting and potent induction of cell-mediated and humoral immunity. *Eur. J. Immunol. 30*, 1939−1947.

(25) Shirota, H., Sano, K., Kikuchi, T., Tamura, G., and Shirato, K. (2000) Regulation of murine airway eosinophilia and Th2 cells by antigen-conjugated CpG oligodeoxynucleotides as a novel antigen-specific immunomodulator. *J. Immunol. 164*, 5575−5582.

(26) Shirota, H., Sano. K., Hirasawa, N., Terui, T., Ohuchi, K., Hattori, T., Shirato, K., and Tamura, G. (2001) Novel roles of CpG oligodeoxynucleotides as a leader for the sampling and presentation of CpG-tagged antigen by dendritic cells. *J. Immunol. 167*, 66−74.

(27) Yu, D., Zhao, Q., Kandimalla, E. R., and Agrawal, S. (2000) Accessible 5′-end of CpG-containing phosphorothioate oligodeoxynucleotides is essential for immunostimulatory activity. *Bioorg. Med. Chem. Lett. 10*, 2585−2588.

(28) Kandimalla, E. R., Agrawal, S., Venkataraman, S., and Sasisekharan, V. (1995) Single strand targeted triplex formation: Parallel-stranded DNA hairpin duplexes for targeting pyrimidine strands. *J. Am. Chem. Soc. 117*, 6416−6417.

(29) Kandimalla, E. R., and Agrawal, S. (1996) Hoogsteen DNA duplexes of 3′-3′- and 5′-5′-linked oligonucleotides and triplex formation with RNA and DNA pyrimidine single strands: Experimental and molecular modeling studies. *Biochemistry 35*, 15332−15339.

(30) Chaix, C., Iyer, R. P., and Agrawal, S. (1996) 3′-3′-Linked oligonucleotides synthesis and stability studies. *Bioorg. Med. Chem. Lett. 6*, 827−832.

(31) Iyer, R. P., Eagan, W., Regan, J. B., and Beaucage, S. L. (1990) 3H-1,2 benzodithiole-3-one 1,1-dioxide as an improved sulfurizing reagent in the solid-phase synthesis of oligodeoxyrionucleoside phosphorothioates. *J. Am. Chem. Soc. 112*, 1253−1254.

(32) Branda, R. F., Moore, A. L., Mathews, L., McCormack, J. J., and Zon, G. (1993) Immune stimulation by an antisense oligomer complementary to the rev gene of HIV-1. *Biochem. Pharmacol. 45*, 2037−2043.

(33) Schreiber, E., Matthias, P., Muller, M. M., and Schaffner, W. (1989) Rapid detection of octamer binding proteins with

'mini-extracts', prepared from a small number of cells. *Nucleic Acids Res. 17*, 6419−6420.
(34) Bradford, M. M. (1976) A rapid and sensitive method for the quantitation of microgram quantities of protein utilizing the principle of protein-dye binding. *Anal. Biochem. 72*, 248−254.
(35) Zhu, F.-G., and Pisetsky, D. S. (2001) Role of the heat shock protein 90 in immune response stimulation by bacterial DNA and synthetic oligonucleotides. *Infect. Immun. 69*, 5546−5552.
(36) Lisziewicz, J., Sun, D., Weichold, F. F., Thierry, A. R., Lusso, P., Tang, J., Gallo, R. C., and Agrawal, S. (1994) Antisense oligodeoxynucleotide phosphorothioate complementary to gag mRNA blocks replication of human immunodeficiency virus type 1 in human peripheral blood cells. *Proc. Natl. Acad. Sci. U.S.A. 91*, 7942−7946.
(37) Hacker, G., Redecke, V., and Hacker, H. (2002) Activation of the immune system by bacterial CpG-DNA. *Immunology 105*, 245−251.
(38) Temsamani, J., Roskey, A., Chaix, C., and Agrawal, S. (1997) In vivo metabolic profile of a phosphorothioate oligodeoxyribonucleotide. *Antisense Nucleic Acid Drug Dev. 7*, 159−165.
(39) Temsamani, J., Kubert, M., and Agrawal, S. (1995) Sequence identity of the n-1 product of a synthetic oligonucleotide. *Nucleic Acids Res. 23*, 1841−1844.
(40) Agrawal, S., Temsamani, J., and Tang, J. Y. (1991) Pharmacokinetics, biodistribution, and stability of oligodeoxynucleotide phosphorothioates in mice. *Proc. Natl. Acad. Sci. U.S.A. 88*, 7595−7599.
(41) Temsamani, J., Tang, J. Y., and Agrawal, S. (1992) Capped oligodeoxynucleotide phosphorothioates. Pharmacokinetics and stability in mice. *Ann. N. Y. Acad. Sci. 660*, 318−320.
(42) Temsamani, J., Tang, J. Y., Padmapriya, A., Kubert, M. and Agrawal, S. (1993) Pharmacokinetics, biodistribution, and stability of capped oligodeoxynucleotide phosphorothioates in mice. *Antisense Res. Dev. 3*, 277−284.
(43) Levis, J. T., and Miller, P. S. (1994) Properties of exonuclease-resistant, psoralen-conjugated oligodeoxyribonucleotides in vitro and in cell culture. *Antisense Res Dev. 4*, 231−241.
(44) Pandolfi, D., Rauzi, F., and Capobianco, M. L. (1999) Evaluation of different types of end-capping modifications on the stability of oligonucleotides toward 3′- and 5′-exonucleases. *Nucleosides Nucleotides 18*, 2051−2069.
(45) Agrawal. S., and Kandimalla, E. R. (2000) Antisense therapeutics: is it as simple as complementary base recognition? *Mol. Med. Today 6*, 72−81.
(46) Agrawal, S., Iadarola, P. L., Temsamani, J., Zhao, Q., and Shaw, D. (1996) Effect of G-rich sequences on the synthesis, purification, binding, cell uptake, and hemolytic activity of oligonucleotides. *Bioorg. Med. Chem. Let. 6*, 2219−2224.
(47) Lee, S. W., Song, M. K., Baek, K. H., Park, Y., Kim, J. K., Lee, C. H., Cheong, H. K., Cheong, C., and Sung, Y. C. (2000) Effects of a hexameric deoxyriboguanosine run conjugation into CpG oligodeoxynucleotides on their immunostimulatory potentials. *J. Immunol. 165*, 3631−3639.
(48) Agrawal, S., Christodoulou, C., and Gait, M. J. (1986) Efficient methods for attaching nonradioactive labels to the 5′ ends of synthetic oligodeoxyribonucleotides. *Nucleic Acids Res. 14*, 6227−6245.

BC0200374

Antisense Oligonucleotides Delivered to the Lysosome Escape and Actively Inhibit the Hepatitis B Virus

Keith D. Jensen,[†] Pavla Kopečková,[†,‡] and Jindřich Kopeček*[,†,‡]

Department of Pharmaceutics and Pharmaceutical Chemistry and Department of Bioengineering, University of Utah, Salt Lake City, Utah 84112. Received June 12, 2002; Revised Manuscript Received July 3, 2002

The subcellular fate and activity in inhibiting the hepatitis B virus of free and *N*-(2-hydroxypropyl)-methacrylamide (HPMA) copolymer-phosphorothioate oligonucleotides were studied. Their internalization and subcellular fate were monitored with confocal microscopy. A fraction of the internalized free oligonucleotides escaped into the cytoplasm and nucleus of Hep G2 cells but were not active antiviral agents. Covalently attaching the oligonucleotides to the HPMA copolymers via nondegradable dipeptide GG spacers resulted in sequestering the oligonucleotides in vesicles after internalization. Conjugation of the oligonucleotides to an HPMA copolymer via a lysosomally cleavable tetrapeptide GFLG spacer resulted in release of the oligonucleotide in the lysosome and subsequent translocation into the cytoplasm and nucleus of the cells. The HPMA copolymer-oligonucleotide conjugate possessed antiviral activity, indicating that phosphorothioate oligonucleotides released from the carrier in the lysosome were able to escape into the cytoplasm and nucleus and remain active. The Hep G2 cells appeared to actively internalize the phosphorothioate oligonucleotides as oligonucleotide-HPMA copolymer conjugates were internalized to a greater extent than unconjugated polymers.

INTRODUCTION

One of the most appealing aspects of antisense oligonucleotides is their inherent specificity. They are designed to inhibit the synthesis of a single unwanted protein (reviewed in ref *1*). Intense research has overcome many of the obstacles facing antisense therapy except delivery of the oligonucleotide to its target. In order for the antisense oligonucleotide to inhibit the synthesis of the target protein, the oligonucleotide must cross at least one cell membrane and hybridize with its target mRNA in the cytoplasm or nucleus of the diseased cell.

Endocytosis appears to be the major pathway by which oligonucleotides enter most cells, although much remains to be learned (*2*). Because phosphorothioate oligonucleotides are inherently large and charged molecules, it has been presumed that they cannot cross cell membranes without some type of help (e.g., permeation enhancers or microinjection), and degradation by lysosomal enzymes is the expected fate of the oligonucleotides. Yet the literature continues to accumulate positive evidence of antisense activity suggesting that at least a fraction of the oligonucleotides escape before being degraded (*3*).

More information on the subcellular fate of free oligonucleotides is needed as free antisense oligonucleotides approved by the FDA or in clinical trials are typically administered by intravenous injection (*4*, *5*). These oligonucleotides are presumed to be internalized by endocytosis and somehow cross the endosomal/lysosomal membrane before being degraded. It is not known at what stage of endocytosis the antisense oligonucleotides escape into the cytoplasm. In this research, we hypothesized that antisense oligonucleotides delivered in the lysosome would be able to escape into the cytoplasm before being degraded and actively inhibit synthesis of the target protein. To test this hypothesis, we conjugated the oligonucleotides to the HPMA copolymers via lysosomally cleavable spacers to ensure delivery of the oligonucleotides in the lysosome. Using confocal microscopy, we monitored the subcellular fate of the oligonucleotides and polymers, and demonstrated antisense activity by a biochemical assay.

EXPERIMENTAL PROCEDURES

Hep G2 (*6*) cells (human hepatocellular carcinoma) were from American Type Culture Collection (Manassas, VA). Minimum essential media alpha modification (MEM-α) and fetal bovine serum (FBS) were from HyClone (Logan, UT). *N*-Benzoyl-Phe-Val-Arg-*p*-nitroanilide was from Sigma (St. Louis, MO). A SlowFade Light Antifade Kit and Lissamine rhodamine B (LR) ethylenediamine were from Molecular Probes (Eugene, OR). Sephadex G-25 (PD-10) columns, a Superose 6 (10/30) column, a Superdex 75 (10/30) column, and a Sephadex LH-20 column were from Pharmacia (Piscataway, NJ). Deionized water was used for the preparation of all buffers. All other chemicals were of reagent grade or better.

The oligonucleotide was synthesized by the Emory Microchemical Facility (Atlanta, GA). The oligonucleotide was a 21-mer phosphorothioate oligonucleotide whose sequence was derived from work by Wu and Wu (*7*), 5′-TTTATAAGGGTCGATGTCCXX-3′. The oligonucleotide had a primary amine on the 5′-end [5′-amino-modifier C6 (Glen Research, Sterling, VA)] and a fluorescein on the 3′-end [6-Fluorescein CPG (Glen Research)]. The oligonucleotide was purified by reverse-phase HPLC [Brownlee ODS-300 (Perkin-Elmer, Wellesley, MA) C18, 250 × 10 mm column with 7 μm, 300 Å silica with a 50

* Correspondence should be addressed to this author at the Department of Pharmaceutics and Pharmaceutical Chemistry, University of Utah, 30 S. 2000 E RM 301, Salt Lake City, UT 84112. Tel: 801-581-4532, Fax: 801-581-3674, E-mail: jindrich.kopecek@m.cc.utah.edu.

† Department of Pharmaceutics and Pharmaceutical Chemistry.

‡ Department of Bioengineering.

10.1021/bc025559y CCC: $22.00 © 2002 American Chemical Society
Published on Web 08/13/2002

mM triethylamine acetate (pH 6.9)/acetonitrile gradient buffer system], and the purity and identity were analyzed by capillary electrophoresis (1 predominate peak) and MALDI-TOF MS [molecular weight measured: 7523.29 (7517.40 calcd)].

Size exclusion chromatography (SEC) was used to estimate the molecular weight of the polymers, detect unbound oligonucleotide, and purify the oligonucleotide-HPMA copolymer conjugates. The molecular weight of the aminolysed (with aminopropanol) polymer precursors was determined on Superose 6 in PBS buffer using laser light scattering detector MiniDawn (Wyatt Inc., Santa Barbara, CA).

Synthesis. *Monomers.* HPMA (*8*), *N*-methacryloylglycylglycylgalactosamine (MA-Gly-Gly-GalN) (*9*), *N*-methacryloylglycylglycine *p*-nitrophenyl ester (MA-GG-ONp) (*10*), and *N*-methacryloylglycylphenylalanylleucylglycyl *p*-nitrophenyl ester (MA-GFLG-ONp) (*11*) were prepared according to previously described procedures.

N-Methacryloylglycylglycyl ethylenediamine Lissamine rhodamine B (MA-GG-LR) was prepared by slowly adding a solution of Lissamine rhodamine B ethylenediamine (20 mg, 33 μmol) in DMF (0.2 mL) to MA-GG-ONp (24 mg, 75 μmol) dissolved in DMF (0.3 mL). To this was added diisopropylethylamine (15 μL, 86 μmol) and allowed to stir for 3 h. The DMF was removed in vacuo, and the product was precipitated with acetone/ether. The product was separated on a Sephadex LH-20 column eluted with MeOH and the purity checked by TLC (methylene chloride/methanol/acetic acid 3:1:0.1, R_f = 0.68). The extinction coefficient of the product was ϵ_{561} = 120 000 M^{-1} cm^{-1} (methanol).

Polymer Conjugate P1 [P-GG-(Oligo-Fl)]. A polymer precursor was prepared by polymerization of the comonomers HPMA and MA-GG-ONp at a molar ratio of 92:8 (acetone, 50 °C, 24 h, AIBN). The polymer (0.47 mmol of ONp/g of polymer, 7.5 mol %, ϵ_{272} = 9500 M^{-1} cm^{-1} in DMSO, M_w = 25 kDa, M_w/M_n = 1.3) was purified by precipitation from methanol into acetone. The polymer precursor (34.3 mg, 16 μmol of ONp) and the oligonucleotide (3.05 mg, 0.41 μmol) were dissolved in anhydrous DMSO (0.2 mL). To this was added diisopropylethylamine (10 μmol) and allowed to stir overnight. The next day, an additional amount of diisopropylethylamine (10 μmol) was added and allowed to stir for 3 h. The reaction mixture was diluted with water, and the product was isolated on a PD-10 column followed by extensive dialysis (cutoff 12−14 kDa). The conjugate was analyzed by SEC (Superose 6 column, PBS, UV and RI detection), which found the oligonucleotide bound to the polymer with no detectable amounts of free oligonucleotide. The amount of bound oligonucleotide was 9.0 μmol/g of polymer [75% efficiency determined from the absorption of fluorescein (ϵ_{494} = 70 000 M^{-1} cm^{-1}, 0.1 M borate buffer, pH 9.1, chemical structure in Figure 1A)].

Polymer Conjugate P2 [P-(GG-LR)-(GFLG-(Oligo-Fl))]. Polymer P2 was similar to P1 except that the polymer backbone was labeled with LR and the oligonucleotide was conjugated via the tetrapeptide spacer, GFLG. Briefly, a precursor polymer was prepared by polymerization of the comonomers HPMA, MA-GFLG-ONp, and MA-GG-LR in the molar ratio 95:5:1 (acetone, 50 °C, 24 h, AIBN). The polymer [0.058 mmol of LR/g of polymer (0.90 mol %, $\epsilon_{563} = 1.2 \times 10^5$ M^{-1} cm^{-1}, methanol), 0.22 mmol of ONp/g of polymer (3.6 mol %, $\epsilon_{400} = 1.8 \times 10^4$ M^{-1} cm^{-1}, 0.1 N NaOH), M_w = 25 kDa, M_w/M_n = 1.4] was purified by reprecipitation from methanol into acetone. To conjugate the oligonucleotide, the precursor polymer (9.5 mg, 2.1 μmol of ONp) and the oligonucleotide (2.8 mg, 0.37 μmol) were dissolved in anhydrous DMSO (70 μL). To this was added diisopropylethylamine (3 μL) and allowed to stir overnight. The next day, an additional amount of diisopropylethylamine (5 μL) was added and allowed to stir for 3 additional hours. The reaction mixture was diluted with water and the product was isolated on a PD-10 column. The product was dialyzed (cutoff 12−14 kDa) extensively, but still contained free oligonucleotide. The conjugate was purified by SEC (Superdex 75 column, PBS), and fractions of the conjugate were collected and dialyzed to remove salts. The purified conjugate (chemical structure in Figure 1B) contained 21 μmol (70% binding efficiency) of fluorescein-labeled oligonucleotide per gram of conjugate and 35 μmol of LR per gram of conjugate.

Cell Culture. Hep G2 cells were cultured in MEM-α media supplemented with 10% FBS in a 37 °C incubator with 5% CO_2 (v/v) with humidified air without antibiotics. For all biological solutions, the pH was adjusted to 7.4 using cell culture grade HCl or NaOH as needed.

Confocal Fluorescent Microscopy. The preparation of the Hep G2 cells for microscopy was described previously (*12*). Briefly, after incubation, the cells were fixed with 3% paraformaldehyde for 20 min at room temperature and mounted with SlowFade Light antifade medium. Cells were analyzed on a Zeiss (Thornwood, NY) LSM 510 confocal imaging system with a Zeiss Axioplan 2 microscope (100 × plan-apo objective, NA = 1.4, oil) and an argon laser (for P1 fluorescein excitation: 488 nm emission, 505 nm long-pass filter; for P2 (LR present), excitation 488 and 543 nm, emission beam splitter 545 nm, green channel emission 500−550 nm, red channel emission 560 nm long-pass). The settings for all the confocal systems were adjusted so that control cells always yielded dark images (i.e., no background fluorescence was visible). To determine if the signals from the two dyes could be separated, two "control" HPMA copolymers labeled with either LR or fluorescein were utilized. Cells were incubated with each of the control polymers, and the microscope settings were adjusted to prevent "bleed-over" of green fluorescence into the red channel. The 8-bit fluorescent images were initially scaled to 256 Gy levels, and colored look-up tables were applied for both dyes.

Oligonucleotide Stability. Rat liver tritosomes (isolated lysosomal enzymes) were harvested as previously described (*13*). The activity of the enzymes was determined by measuring the cleavage of *N*-benzoyl-Phe-Val-Arg-*p*-nitroanilide. The tritosomes (100 μL) and 900 μL of a citrate−phosphate cocktail [citrate−phosphate buffer (pH 5.5), 5 mM glutathione, 0.2% Triton X-100, 0.65 mM EDTA, and 1 mM nitroanilide substrate (final concentrations)] were warmed to 37 °C and mixed, and the absorption at 410 nm (released *p*-nitroaniline) was recorded for 10 min. The change in absorption over 10 min was ΔA = 0.488.

The amount of degradation of the oligonucleotides was measured by HPLC [Dynamax, Varian Inc., Palo Alto, CA, C18 column (Varian), mobile phase: acetonitrile and 50 mM triethylamine acetate buffer (pH 7)] after digestion with the tritosomes. The oligonucleotide and oligonucleotide-HPMA copolymer conjugate, P1 (both at 1 μM final concentration of oligonucleotide), were digested in 250 μL of the citrate−phosphate cocktail (above) with 50 μL of tritosomes at 37 °C. The eluting oligonucleotide was assayed for fluorescence using a fluorescent detector [Waters (Milford, MA), excitation 495 nm, emission 520 nm], and the peak area of the respective peaks was used

to determine the amount of oligonucleotide degradation at various time points in a <15 h period.

Antisense Activity. The activity of the antisense oligonucleotides was determined by Dr. Brent Korba at Georgetown University as previously described (*14*). Briefly, chronically hepatitis B virus-producing human hepatoma cells, 2.2.15, were treated at confluence once daily for 9 days with the test compounds. The cell media were changed daily. HBV DNA levels in the culture medium were assessed by dot blot hybridization 24 h following the last treatment. Toxicity was assessed by uptake of neutral red dye at the time of analysis. As a positive control for the assay, the drug 3-thia-2′,3′-dideoxycytosine (3TC, commonly known as lamivudine) was also tested.

RESULTS

Delivery of the Oligonucleotide to the Lysosome. HPMA copolymers were used to deliver the oligonucleotide to the lysosome. As a small percentage of papers have found evidence of oligonucleotides entering cells by pathways other than endocytosis (reviewed in ref *15*), it was important to ensure lysosomal delivery of the oligonucleotides to test the hypothesis. A large body of evidence over several decades indicates that HPMA copolymers are internalized by endocytosis and are lysosomotropic (*16*−*20*). Conjugating drugs that normally enter cells by diffusion to these polymers result in their internalization by endocytosis (*19*, *20*); therefore, covalent attachment of the oligonucleotides to the HPMA copolymers should ensure that the oligonucleotides reach the lysosome.

Release of the oligonucleotides in the lysosome is accomplished by conjugating the oligonucleotides to HPMA copolymers via a lysosomally degradable spacer. The tetrapeptide spacer, Gly-Phe-Leu-Gly (GFLG), was designed to be stable outside the cell but degraded in the lysosome (reviewed in refs *21* and *22*). Covalent attachment by such a spacer prevents premature release of the oligonucleotide before reaching the lysosome.

To allow independent observation of the oligonucleotide from the polymeric carrier, the oligonucleotide was labeled with fluorescein and the polymer with Lissamine rhodamine B (Figure 1B). As a control, a fluorescein-labeled oligonucleotide was also conjugated to an HPMA copolymer via the nondegradable Gly-Gly spacer (*23*) (Figure 1A).

Subcellular Fate of Phosphorothioate Oligonucleotides. *Free Oligonucleotides.* The subcellular fate of the phosphorothioate oligonucleotides in Hep G2 cells was determined by confocal microscopy. The cellular distribution of the oligonucleotide was followed from 1 to 24 h. Initially the oligonucleotide was restricted to small vesicles distributed throughout the cytoplasm (Figure 2). The nuclei of many cells are visible as dark spheres in the fluorescent image (Figure 2A). From 2 to 4 h (Figure 3), fluorescence began to appear in the cytoplasm followed by nuclear staining and heightened fluorescence of nuclear structures (likely nucleoli). In Figure 3, one nucleus is marked with a ring in both the fluorescent and transmitted images for ease in identification. Dim staining of the nuclei with increased staining of nuclear structures was uniformly observed in all of the cells. In general, the fluorescence increased with longer incubation times, as expected.

A study of the effect of concentration on the distribution of the oligonucleotide did not reveal any qualitative difference between 0.6 and 3 μM (oligonucleotide concentration). The fluorescence was brightest in small vesicles distributed throughout the cytoplasm. In addition, there was considerable staining of the cytoplasm, nucleus, and nuclear structures at the concentrations studied (data not shown as images were similar to that in Figure 3). The fluorescence of the cells increased with a corresponding increase in the concentration.

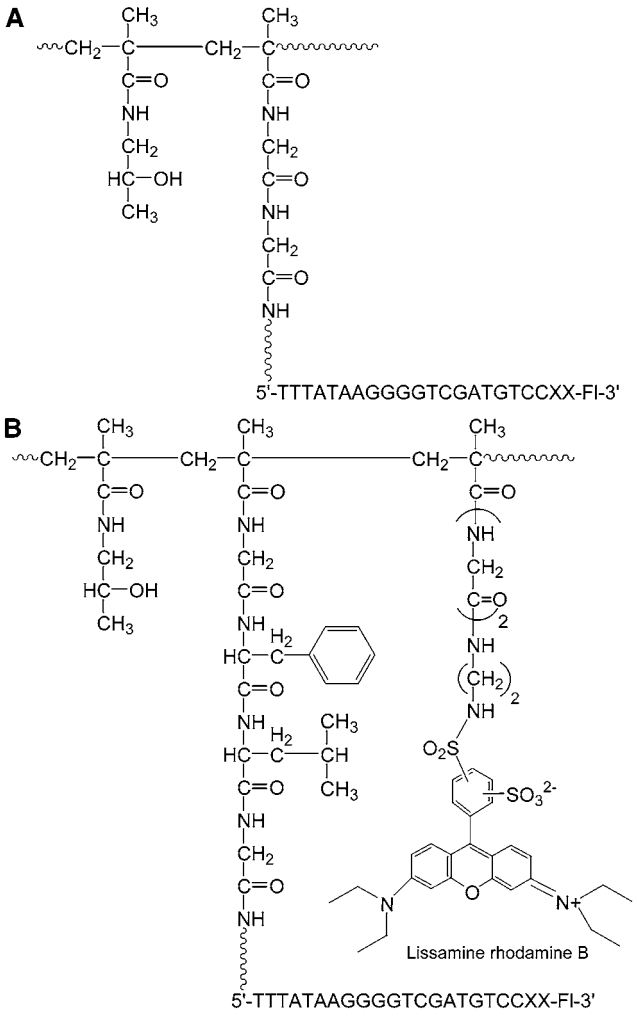


Figure 1. Chemical structures of oligonucleotide-polymer conjugates. (A) Polymer conjugate P1: the phosphorothioate oligonucleotide was covalently linked to the HPMA copolymer via a nondegradable GG linker. The oligonucleotide was labeled with fluorescein on the 3′ end. (B) Polymer conjugate P2: a phosphorothioate oligonucleotide was covalently linked to the HPMA copolymer via the degradable GFLG linker. The oligonucleotide was labeled with fluorescein on the 3′ end. The polymer backbone was labeled with Lissamine rhodamine B to allow independent visualization of the polymer and the oligonucleotide.

Polymer-Bound Oligonucleotides (Nondegradable Spacer). To determine the subcellular fate after conjugating the oligonucleotide to the HPMA copolymer via a nondegradable spacer, the fate of the polymer conjugate P1 was determined in Hep G2 cells from 0.5 to 24 h. For all of the samples, the vast majority of the fluorescence was located in small vesicles distributed throughout the cytoplasm (Figure 4). As expected, increasing the incubation time from 0.5 to 24 h resulted in increasingly bright samples (data not shown). A small amount of fluorescence, just above autofluorescence, was detected in the cytoplasm and nuclei, with less in the nuclei, when higher conjugate concentrations and very high microscope detector gain settings were employed (Supporting Information Figure 1). The amount of fluorescence in the cytoplasm

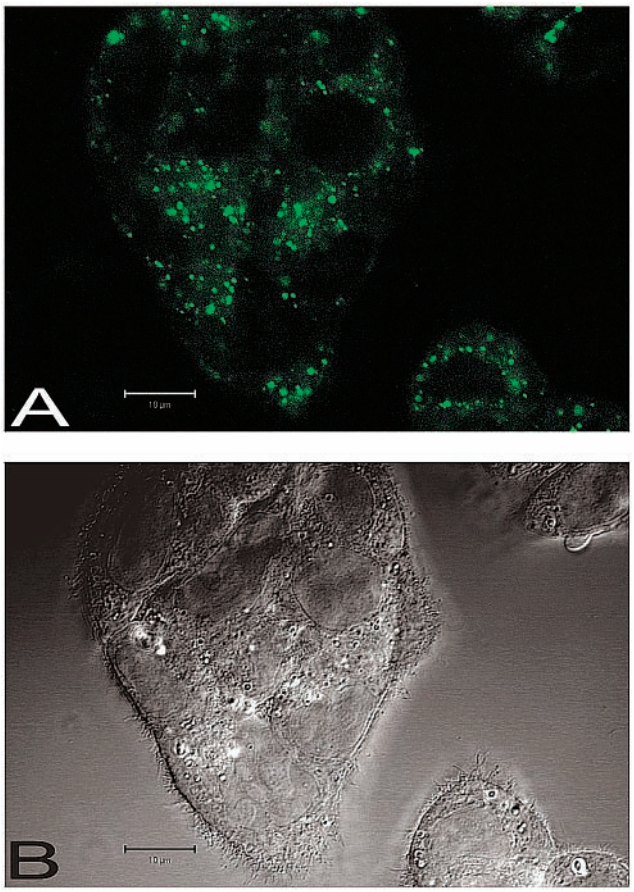


Figure 2. Hep G2 cells incubated with 1.5 μM free oligonucleotide for 2 h. (A) Fluorescent image: the oligonucleotide was predominantly located in small vesicles distributed throughout the cytoplasm. (B) Transmitted image. The scale bars are 10 μm.

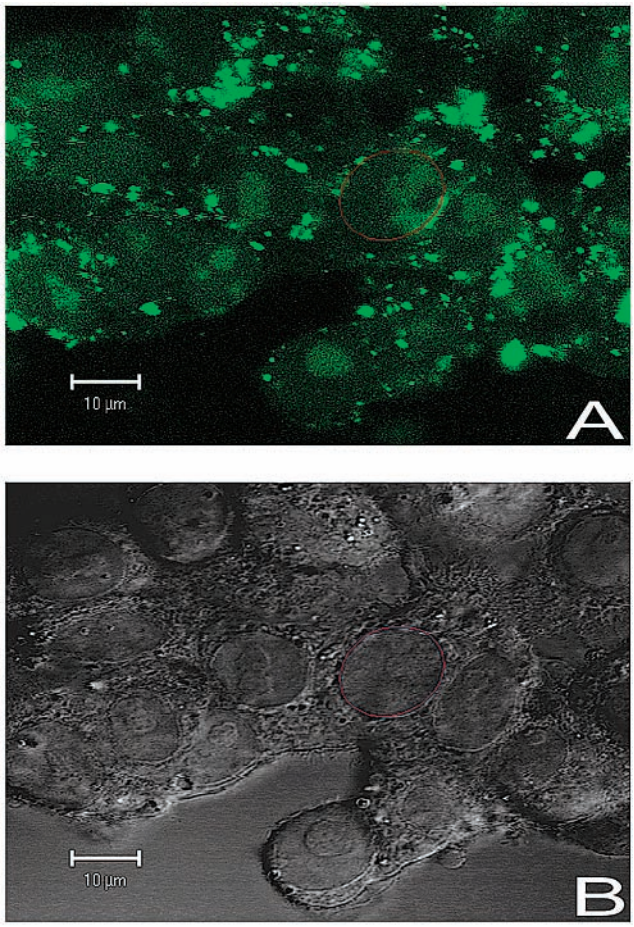


Figure 3. Hep G2 cells incubated with 3 μM free oligonucleotide for 3 h. (A) Fluorescent image: oligonucleotide was found in small vesicles as well as in the cytoplasm and nucleus of the Hep G2 cells. (B) Transmitted image. One nucleus is marked by a ring in both the fluorescent and transmitted images for ease in identification. The scale bars are 10 μm.

and nuclei of the cells was very small and only accounted for a minute fraction of the total fluorescence. Qualitatively, there was no change in the distribution of fluorescence in the cells with increasing incubation time up to 24 h—only an increase in brightness, which was expected (data not shown).

A study of the effect of concentration on the distribution of the conjugate with the nondegradable spacer (polymer conjugate P1) did not yield any unexpected results. Increasing the concentration (18 h incubation) from 0.4 to 3.6 μM (oligonucleotide concentration) resulted in a corresponding increase in the fluorescence of the cells. Qualitative evaluation of the polymer conjugate P1's fate did not reveal any significant difference in the distribution of the oligonucleotide at concentrations between 0.4 and 3.6 μM. The majority of the fluorescence was limited to small vesicles with a small fraction in the cytoplasm (data not shown as images were similar to those in Figure 4 and Supporting Information Figure 1).

Polymer-Bound Oligonucleotides (Degradable Spacer). Conjugating the oligonucleotide to the polymer via a lysosomally degradable bond allows the oligonucleotide to be liberated from the polymer in the lysosome, thus providing an opportunity to determine its ability to escape from the lysosome. To independently monitor the fate of both the polymer and the oligonucleotide, the polymer was labeled with Lissamine rhodamine B, and the oligonucleotide was labeled with fluorescein (Figure 1B).

The subcellular fate of the antisense oligonucleotide conjugated via the degradable spacer (polymer P2) was monitored from 0.5 to 24 h by confocal microscopy. At incubation times less than 2 h, most of the fluorescence was limited to small vesicles in the cytoplasm (Supporting Information Figure 2A,B). Between 2 and 4 h, the green (oligonucleotide) and red fluorescence (polymer) signals began to differ to an appreciable extent (Supporting Information Figure 2C). The green fluorescence increased in the cytoplasm and nucleus and green staining of the nucleolus appeared (Figure 5 and Supporting Information Figure 2C). For Figure 5, the microscope detector gain was increased (autofluorescence still not visible) to view the dim fluorescence in cytoplasm and nuclei—although this resulted in overexposure of the fluorescence in most of the vesicles. The oligonucleotide (green) was dim—but clearly visible—staining the cytoplasm, nucleus, and nuclear structures. The polymer (red) was found almost exclusively in small vesicles distributed throughout the cytosol. After 24 h, there was an increase in the separation of the green and red signals (Figure 6 and Supporting Information Figure 2C versus Figure 2D).

Significant changes in the subcellular distribution of each fluorophore could be observed between the 4 and 24 h time points utilizing higher detector gain settings. The image in Figure 6 contains cells incubated with the polymer conjugate P2 for 24 h. There was significant staining of the cytoplasm, nuclei, and nuclear structures for both sets of cell incubated for 4 (Figure 5) and 24 (Figure 6) h with the oligonucleotide (green), although

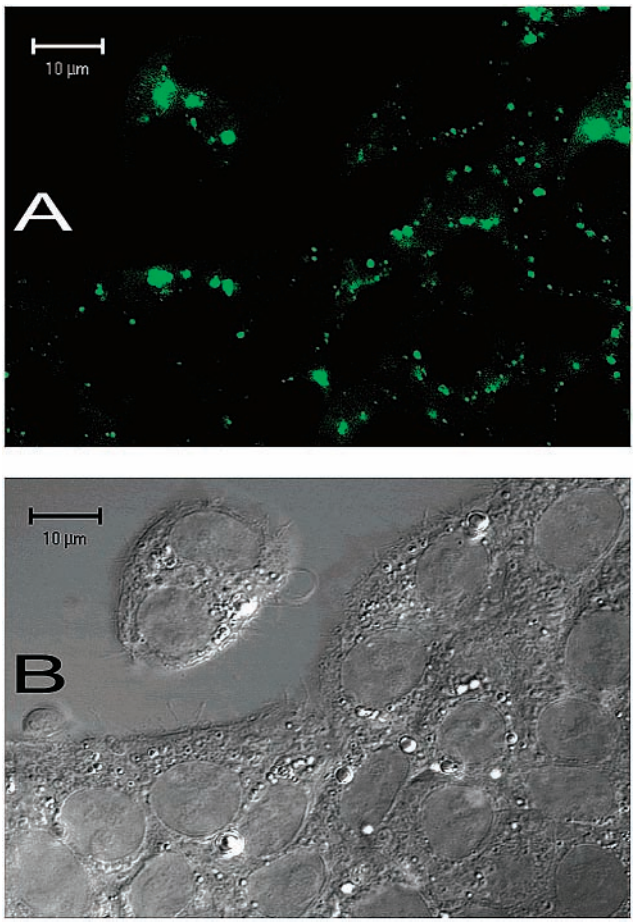


Figure 4. Hep G2 cells incubated with P1 (1.1 μM oligonucleotide) for 24 h. (A) Fluorescent image: the fluorescence was predominantly restricted to small vesicles. (B) Transmitted image. The scale bars are 10 μm.

those at 24 h were noticeably brighter (it should be noted that these two images were not taken at the same settings—the gain was higher for Figure 5 to allow ease in viewing fluorescence in the cytosol and nucleus). In contrast to the high staining by the oligonucleotide (green), the staining of the polymer (red) in the cytoplasm and nucleus was noticeably weaker, although varying the fluorescence of the two dyes only allowed a qualitative comparison. Also for the polymer, the nuclei of the cells were darker than the corresponding cytosol, and no staining of the nucleoli was observed.

Conjugating the oligonucleotide to the polymer resulted in increased uptake of the polymer. Hep G2 cells incubated with LR-labeled polymer were noticeably dimmer than cells incubated with the oligonucleotide-polymer conjugate P2 (Supporting Information Figure 3). The cells were incubated with each of the polymers such that similar amounts of dye were administered to the cells. Identical detector settings allowed a semiquantitative comparison of their respective intensities. The original black and white images acquired were double-checked to ensure that the settings used did not generate any signal in the control cells and to guarantee that the detectors had not been saturated. An equal-sized area inside the cells of each sample was then measured using the histogram feature of Photoshop (Adobe Systems Inc., version 6.0.1) The average pixel intensity was 15 times higher for the cells incubated with polymer conjugate P2 as compared to LR-labeled polymer, although the cells were incubated with about 6% more dye for the LR-labeled polymer compared to the polymer conjugate P2.

Stability. The stability of the phosphorothioate oligonucleotides in isolated rat liver lysosomal enzymes (tritosomes) was measured for +12 h. The stabilities of the free oligonucleotide and the oligonucleotide bound to the polymer via the nondegradable GG spacer (P1) were compared since the assay monitored the amount of oligonucleotide bound to the polymer and would not distinguish between cleavage of the degradable GFLG spacer from oligonucleotide degradation.

The polymer-bound oligonucleotide was approximately 3 times more stable than the free oligonucleotide (Table 1). The degradation of the free oligonucleotide was steady over the course of the experiment, decreasing from 100% to 42% of the intact oligo in 14.2 h. In contrast, for the polymer-bound oligonucleotide, there was an initial decrease to ~90% during the first 4 h; this was followed by a slow, steady decrease to 81% at 12.8 h. The biphasic degradation complicated calculation of the half-life of the polymer-bound oligonucleotide, and to err on the side of caution, we probably underestimated its true value. As such, the half-lives should only be used as relative comparisons to each other.

Activity. Although the free oligonucleotide and the oligonucleotide conjugated to the HPMA copolymer via the degradable spacer were observed in the nucleus using confocal microscopy, it was unknown whether they remained intact and active. The antisense antiviral activities of the free oligonucleotide, oligonucleotide-HPMA copolymer conjugate (P2), unconjugated HPMA copolymer, a physical mixture of free oligonucleotide and unconjugated HPMA copolymer, and 3TC (positive control) were determined (Table 2). The oligonucleotide conjugated to the polymer showed activity inhibiting 50% and 90% of the viral activity at oligonucleotide concentrations of 1.7 and 8.3 μM, respectively. The free oligonucleotide did not show any antiviral activity at the concentrations studied (0.01−10 μM). To ensure that the polymer was not contributing to the antiviral activity of the oligonucleotide-polymer conjugate P2, unconjugated polymer and a physical mixture of free oligonucleotide and unconjugated polymer were also tested and were not found to have any antiviral activity at the studied concentrations. As a positive control, the potent nucleoside analogue reverse transcriptase inhibitor 3TC was also examined to validate the assay.

DISCUSSION

Delivery of antisense oligonucleotides to their targets in the cytoplasm or nucleus is the current greatest challenge in antisense therapy. As most antisense oligonucleotides approved or in clinical trials are administered as free oligonucleotides (*4*, *5*) that are presumably internalized into cells by endocytosis, knowledge of their ability to escape from lysosomes before being degraded is paramount to developing more effective therapies.

Cationic polymers and liposomes are not ideal for determining the ability of the oligonucleotide to escape from the lysosome. Although endocytosis is likely to result using cationic polymers or liposomes to deliver oligonucleotides, such delivery systems present two major challenges for this internalization study: unreliable release of the oligonucleotide and unknown effects of the carrier. With these carriers, it is unclear where the oligonucleotides dissociate from the delivery system. Oligonucleotide release before internalization is even possible (*24*). These types of carriers may also play a role in the entry of the oligonucleotide into the cytoplasm (*25*).

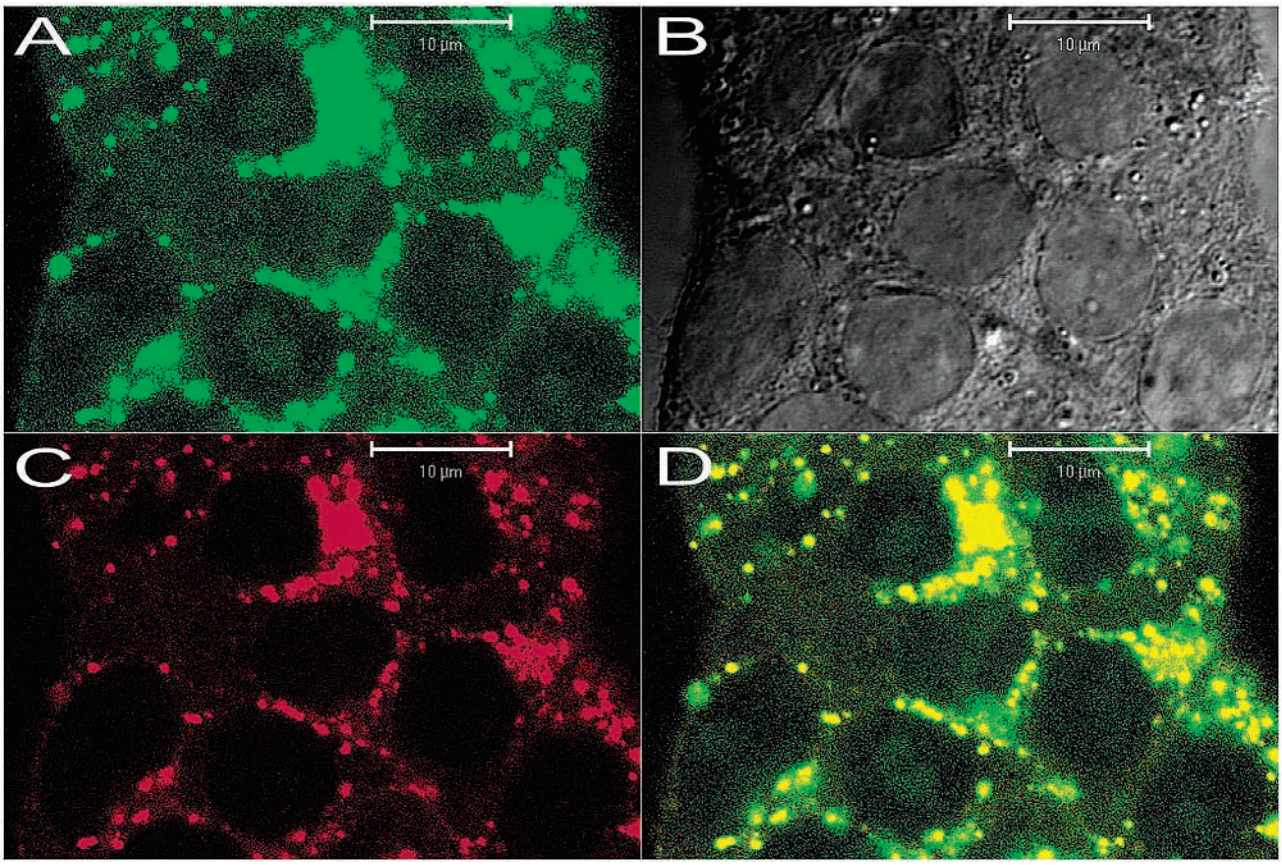


Figure 5. Hep G2 cells incubated with P2 (4.9 μM oligonucleotide, 8.12 μM LR) for 4 h. (A) Green fluorescence from the oligonucleotide was found predominantly in vesicles with minor amounts in the cytoplasm and nucleus. (B) Transmitted image. (C) Red fluorescence from the polymer was found almost exclusively in vesicles. (D) Combined green and red fluorescence; yellow color indicates colocalization. The scale bars are 10 μm.

A much more controlled delivery system was required to test the ability of the oligonucleotide to escape from the lysosome.

HPMA copolymers (reviewed in refs *21* and *26*) are well-suited for delivery of material to the lysosome. They are uncharged, hydrophilic polymers that are easily modified to incorporate various moieties. The polymers have been previously shown to be internalized by endocytosis (*12*, *16*−*20*). Conjugating the oligonucleotide to the polymers ensures their delivery to the lysosome. The covalent attachment of the oligonucleotides to the polymer via the lysosomally degradable GFLG spacer prevents premature release of the oligonucleotides before reaching the lysosome.

The subcellular fate of the free oligonucleotides was determined by confocal microscopy. The free oligonucleotides appeared to enter Hep G2 cells via endocytosis and accumulate in vesicles in the cytoplasm (Figure 2). Beginning at 2 h and continuing up to 24 h, increasing fluorescence was observed in the cytoplasm, nucleus, and nuclear structures of the Hep G2 cells (Figure 3). Fluorescence quenching, pH sensitivity of the fluorescein, and the large difference in fluorescent intensity of the vesicles and the other compartments prevented quantitative analysis. It is even difficult to make an estimate of the fraction of fluorescence which was able to escape from the endosomes/lysosomes. It is also unknown how much of the fluorescence in the cytoplasm and nucleus is due to degraded oligonucleotide. The stability study suggested that only a small fraction would have been degraded at short incubation times, but only a fraction of the fluorescence was found outside of the endosomes/lysosomes.

The subcellular fate of free oligonucleotides we observed in Hep G2 cells is consistent with most studies reported in the literature. Using cell fractionation, researchers have reported both nuclear accumulation and cytoplasmic accumulation of oligonucleotides (*3*, *27*, *28*). The subcellular distribution may be sequence-specific and is likely related to protein binding (*29*−*31*). Although we saw rapid entry of the oligonucleotides into the nucleus once they entered the cytosol, we did not see increased nuclear accumulation often reported after microinjection of phosphorothioate oligonucleotides into the cytoplasm (*32*−*35*).

Conjugating the oligonucleotide to the polymer via the nondegradable spacer (polymer conjugate P1) resulted in significant changes in the distribution of the conjugates. The vast majority of the fluorescence remained in the endosomes/lysosomes (Figure 4). There was a small amount of fluorescence just above the autofluorescence level of the cells found in the cytoplasm and to a lesser extent the nucleus (Supporting Information Figure 1). Contrary to the redistribution of the free oligonucleotide, time did not seem to have a significant effect on the subcellular distribution of the polymer-conjugate P1. Increasing the incubation time from 0.5 to 24 h only increased the intensity of the fluorescence without any distinct change in distribution. Changing the concentration from 0.4 to 3.6 μM (oligonucleotide concentration) did not also noticeably affect the subcellular distribution (data not shown).

There were some points of difference in cytoplasmic and nuclear staining of the oligonucleotide-polymer conjugate P1 from cells incubated or microinjected with

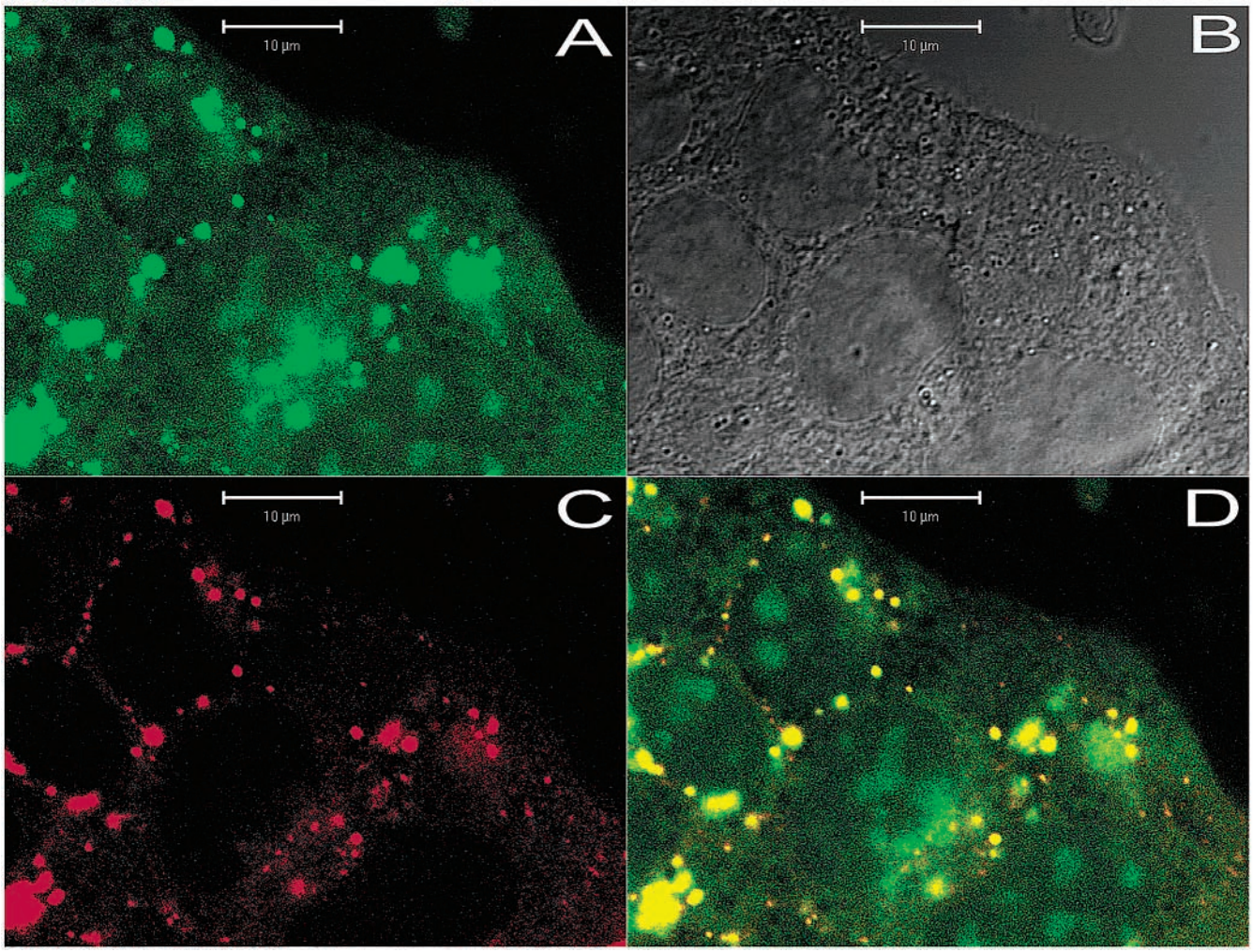


Figure 6. Hep G2 cells incubated with P2 (4.9 μM oligonucleotide, 8.12 μM LR) for 24 h. (A) Green fluorescence from the oligonucleotide. Increased amounts of oligonucleotide were found in the cytoplasm, nucleus, and accumulating in nuclear structures. (B) Transmitted image. (C) Red fluorescence from the polymer was found predominantly in vesicles. (D) Combined green and red fluorescence; yellow color indicates colocalization. The scale bars are 10 μm.

Table 1. Estimated Half-Life of the Free Oligonucleotide and Polymer-Bound Oligonucleotide (P1) after Digestion with Isolated Lysosomal Enzymes (Tritosomes) at 37 °C

compound tested	estimated half-life (h)
free oligonucleotide	14.8
oligonucleotide-polymer conjugate P1	43.3

Table 2. Antiviral Activity of the Antisense Oligonucleotides

compound tested	EC_{50}[a] (μM)	EC_{90}[b] (μM)
oligonucleotide-polymer conjugate P2	1.7	8.3
free oligonucleotide	–[c]	–
polymer without oligonucleotide	–	–
free oligonucleotide + unconjugated polymer	–	–
3TC (positive control)	0.059	0.175

[a] EC_{50}: effective concentration to achieve a 50% viral inhibition. [b] EC_{90}: effective concentration to achieve a 90% viral inhibition. [c] (–): no activity at the concentrations studied (0.01–10 μM for the oligonucleotide and 4.56 mg/mL for the polymer).

fluorescent HPMA copolymers in a previous study (*12*). We previously found (*12*) that HPMA copolymers incubated with Hep G2 cells were able to escape from endosomes/lysosomes, and that the polymer which entered the cytoplasm tended to accumulate in the nucleus. The lack of nuclear accumulation of polymer in this work may be due to a small number of sites with higher affinity for the polymer or oligonucleotide in the cytoplasm. At low polymer concentrations, these sites would be occupied first. More studies would be necessary to test such a hypothesis.

It is interesting to note that there was also a lack of heterogeneous staining previously observed with Hep G2 cells incubated with HPMA copolymers (*12*). In a previous study (*12*), we had found that HPMA copolymers were able to escape from lysosomes into the cytoplasm and nucleus of a fraction of the Hep G2 cells. The fraction of cells with nuclear and cytoplasmic staining increased with time, but it typically took >8 h of incubation to see staining for a majority of the cells. Such variability was not observed in this work as all cells that were incubated with oligonucleotides (free or conjugated) exhibited similar amounts and distribution of staining. The difference is likely due to the presence of the oligonucleotides on the polymers, but more studies are needed to determine the effect of conjugated moieties on the polymer's subcellular fate.

The subcellular distribution of the oligonucleotide conjugated to the polymer by the lysosomally degradable GFLG spacer (P2) differed significantly from that attached by the nondegradable spacer. Labeling the polymer backbone with LR and the oligonucleotide with

fluorescein allowed separate tracking of each component. At incubation times shorter than 2 h, the fluorescence from both dyes was predominantly found together in small vesicles in the cytoplasm (Supporting Information Figure 2). The green (oligonucleotide) and red (polymer) signals began to separate between 2 and 4 h and increase slightly after 24 h of incubation (Supporting Information Figure 2).

The staining of the cytosol, nuclei, and nuclear structures by the oligonucleotide conjugated via the cleavable spacer (polymer P2) appeared to be a combination of the staining of the free oligonucleotide and the oligonucleotide-HPMA copolymer conjugate P1. At incubation times of 4 h or greater, the oligonucleotide of polymer P2 was observed in the cytoplasm and nucleus (Figures 5A and 6A) similar to that of the free oligonucleotide (Figure 3A). There was only minimal staining of the cytoplasm by the polymer (Figures 5C and 6C) similar to that observed for the oligonucleotide-HPMA copolymer P1 with the nondegradable spacer (Figure 4A). There was increased staining of nuclear structures by the oligonucleotide in polymer P2 (Figure 6A) similar to that seen when incubating with the free oligonucleotide (Figure 3A). These results suggest that the oligonucleotide conjugated to the polymer by the degradable spacer was released from the polymer and escaped from lysosomes in a fashion similar to the free oligonucleotide. The oligonucleotide appeared to be able to escape from lysosomes faster than the polymer as more (qualitatively) of the oligonucleotide entered the cytoplasm and nucleus than the polymer (compare Figures 5A vs 5C and 6A vs 6C).

The increased uptake of the oligonucleotide-HPMA copolymer conjugate compared to the LR-labeled polymer (Supporting Information Figure 3) supported previous findings (*36*) that Hep G2 cells actively internalize phosphorothioate oligonucleotides.

The antiviral assay was needed to determine if the antisense oligonucleotide was still active after passing through the lysosome. The confocal microscopy supplied evidence that oligonucleotide delivered to the lysosome escaped into the cytoplasm and nucleus. The positive antiviral activity of the polymer-oligonucleotide conjugate P2 (Table 2) demonstrated that a fraction of the antisense oligonucleotide had not been degraded and was still active.

The relatively high concentration of the oligonucleotide-HPMA copolymer conjugate P2 required for antiviral activity was likely due to a combination of three causes: inefficient delivery of the oligonucleotide to its target, inactivation of the antisense oligonucleotide, and a reduced potency antisense oligonucleotide (fluorescein bound to the oligonucleotide and an unoptimized sequence). A significant amount of the fluorescence from the oligonucleotide appeared to remain in vesicles, indicating that only a fraction of oligonucleotide escaped into the cytoplasm and nucleus of the cells. The inactivity of the free oligonucleotide, at the concentrations studied, suggested that some of the fluorescence observed outside of the lysosomes was due to inactivated oligonucleotide. Degradation was the likely cause—as supported by the stability assay and by the fact that protein binding or modification should have been similar for free and polymer-liberated oligonucleotides.

After observing the free oligonucleotide in the cytoplasm and nuclei of the cells, we expected it to have antiviral activity also. This inactivity was most likely due to degradation of the oligonucleotide in the cell media or endosome/lysosome as some stability was afforded to the oligonucleotide by conjugation to the polymer (Table 1). Using a similar antisense oligonucleotide, Wu and Wu (*7*) also found that the free oligonucleotide had lower activity than the oligonucleotide complexed to a targeted poly-lysine carrier. They attributed the difference in activity to the increased amount of oligonucleotide delivered with the targeted polymeric carrier, increased stability due to the carrier, and potential help from the carrier in escaping the lysosome. In this work, the polymeric carrier likely increased the activity of the oligonucleotide by increasing its stability as the HPMA copolymer was not targeted nor was it likely to help the oligonucleotide escape the lysosome—it was uncharged, had no useful buffering capacity, and was less able to escape the lysosome than the oligonucleotide (Figure 6). The initial rapid degradation of a small fraction of the conjugated oligonucleotide followed by the slow degradation phase suggested that some of the oligonucleotide was easily accessible for degradation, but that the majority of the conjugated oligonucleotide was not. The slow degradation phase of the polymer-conjugated oligonucleotide was probably not due to inactivation of the lysosomal enzymes as the free oligonucleotide was continuously degraded over the course of the experiment. It is unlikely that the uncharged, hydrophilic polymer inactivated the enzymes as it was present from the beginning of the experiment.

Cleavage of the degradable tetrapeptide bond and protection of the oligonucleotide, both on the polymer, may appear an apparent contradiction. Both are likely afforded limited protection from degradation. Cleavage of the tetrapeptide is particularly efficient as its sequence was chosen as a good substrate for lysosomal thiol proteinases, especially cathepsin B (*37*, *38*), whereas the phosphorothioate oligonucleotide is designed to be resistant to nucleases.

CONCLUSIONS

- Phosphorothioate oligonucleotides internalized by endocytosis were able to escape into the cytoplasm and nucleus of Hep G2 cells.
- Binding the oligonucleotides to the HPMA copolymers via nondegradable spacers restricted the oligonucleotides from entering the cytoplasm and nucleus of the cells.
- Conjugation of the oligonucleotides to the HPMA copolymers via degradable spacers afforded them with increased stability and prevented their inactivation before escaping the lysosome and actively inhibiting the hepatitis B virus.

To better deliver antisense oligonucleotides to their targets in the cytoplasm and nucleus, knowledge of their subcellular distribution and ability to escape lysosomes is needed. The many positive examples of antisense oligonucleotides in the literature suggests that despite their large size and multiple negative charges, oligonucleotides are able to escape from lysosomes and actively inhibit synthesis of the target protein (*1*). To study this hypothesis, we delivered phosphorothioate oligonucleotides to the lysosome using HPMA copolymers. Conjugation via lysosomally cleavable spacers assured release of the oligonucleotide only in the lysosome. Confocal microscopy and an antiviral assay provided evidence that the oligonucleotide delivered to the lysosome was able to escape into the cytoplasm and nucleus of Hep G2 cells and actively inhibit its target. The high concentration of antisense oligonucleotides required for antiviral activity, the short half-life of the oligonucleotide, and the high fluorescence of vesicles suggest directions for improving antisense therapies. Increasing the activity and stability of the antisense oligonucleotides, while

maintaining high specificity, will provide potent drugs. Better delivery methods are also needed to ensure interaction of the antisense oligonucleotide with its intended target.

ACKNOWLEDGMENT

The antiviral activities of the antisense oligonucleotides were determined by Dr. Brent Korba (Georgetown University, Rockville, MD) under NIAID Contract N01 AI85349. This research was supported in part by National Institutes of Health Grants CA51578 and CA88047 from the National Cancer Institute. Partial support of K.D.J. was provided by NIH Training Grant GM08537 and by a fellowship from the American Foundation of Pharmaceutical Education.

Supporting Information Available: Three figures showing Hep G2 cells incubated with P1, P2, and polymer P-LR. This material is available free of charge via the Internet at http://pubs.acs.org.

LITERATURE CITED

(1) Chirila, T. V., Rakoczy, P. E., Garrett, K. L., Lou, X., and Constable, I. J. (2002) The use of synthetic polymers for delivery of therapeutic antisense oligodeoxynucleotides. *Biomaterials 23*, 321−342.

(2) Lebedeva, I., Benimetskaya, L., Stein, C. A., and Vilenchik, M. (2000) Cellular delivery of antisense oligonucleotides. *Eur. J. Pharm. Biopharm. 50*, 101−119.

(3) Crooke, S. T. (1998) Basic principles of antisense therapeutics. *Antisense research and application* (Crooke, S. T., Ed.) pp 1−50, Springer, Berlin.

(4) de Smet, M. D., Meenken, C. J., and van den Horn, G. J. (1999) Fomivirsen—a phosphorothioate oligonucleotide for the treatment of CMV retinitis. *Ocul. Immunol. Inflammation 7*, 189−198.

(5) Tamm, I., Dorken, B., and Hartmann, G. (2001) Antisense therapy in oncology: new hope for an old idea? *Lancet 358*, 489−497.

(6) Knowles, B. B., and Aden, D. P. (1983) Human hepatoma derived cell line, process for preparation thereof, and uses therefore. U.S. Patent 4,393,133.

(7) Wu, G. Y., and Wu, C. H. (1992) Specific inhibition of hepatitis B viral gene expression in vitro by targeted antisense oligonucleotides. *J. Biol. Chem. 267*, 12436−12439.

(8) Kopeček, J., and Bažilová, H. (1973) Poly[N-(2-hydroxypropyl)methacrylamide]. 1. Radical polymerization and copolymerization. *Eur. Polym. J. 9*, 7−14.

(9) Rathi, R. C., Kopečková, P., Říhová, B., and Kopeček, J. (1991) N-(2-hydroxypropyl)methacrylamide copolymers containing pendant saccharide moieties. Synthesis and bioadhesive properties. *J. Polym. Sci., Part A: Polym. Chem. 29*, 1895−1902.

(10) Rejmanová, P., Labský, J., and Kopeček, J. (1977) Aminolyses of monomeric and polymeric 4-nitrophenyl esters of methacryloylated amino acids. *Makromol. Chem. 178*, 2159−2168.

(11) Ulbrich, K., Šubr, V., Strohalm, J., Plocová, D., Jelínková, M., and Říhová, B. (2000) Polymeric drugs based on conjugates of synthetic and natural macromolecules. I. Synthesis and physicochemical characterization. *J. Controlled Release 64*, 63−79.

(12) Jensen, K. D., Kopečková, P., Bridge, J. H. B., and Kopeček, J. (2001) The cytoplasmic escape and nuclear accumulation of endocytosed and microinjected HPMA copolymers and a basic kinetic study in Hep G2 cells. *AAPS PharmSci. [serial online] 3*, Article 32.

(13) Trouet, A. (1974) Isolation of modified liver lysosomes. *Methods Enzymol. 31 (Pt. A)*, 323−329.

(14) Schmidt, K., and Korba, B. E. (1999) Hepatitis B virus cell culture assays for antiviral activity. *Methods in molecular medicine: antiviral methods and protocols* (Kinchington, D., and Schinazi, R. F., Eds.) pp 51−67, Humana Press, Totowa, NJ.

(15) Wu-Pong, S. (2000) Alternative interpretations of the oligonucleotide transport literature: insights from nature. *Adv. Drug Delivery Rev. 44*, 59−70.

(16) Duncan, R., Rejmanová, P., Kopeček, J., and Lloyd, J. B. (1981) Pinocytic uptake and intracellular degradation of N-(2-hydroxypropyl)methacrylamide copolymers. A potential drug delivery system. *Biochim. Biophys. Acta 678*, 143−150.

(17) Duncan, R., Seymour, L. C., Scarlett, L., Lloyd, J. B., Rejmanová, P., and Kopeček, J. (1986) Fate of N-(2-hydroxypropyl)methacrylamide copolymers with pendent galactosamine residues after intravenous administration to rats. *Biochim. Biophys. Acta 880*, 62−71.

(18) Wedge, S. R., Duncan, R., and Kopečková, P. (1991) Comparison of the liver subcellular distribution of free daunomycin and that bound to galactosamine targeted N-(2-hydroxypropyl)methacrylamide copolymers, following intravenous administration in the rat. *Br. J. Cancer 63*, 546−549.

(19) Omelyanenko, V., Kopečková, P., Gentry, C., and Kopeček, J. (1998) Targetable HPMA copolymer-adriamycin conjugates. Recognition, internalization, and subcellular fate. *J. Controlled Release 53*, 25−37.

(20) Omelyanenko, V., Gentry, C., Kopečková, P., and Kopeček, J. (1998) HPMA copolymer-anticancer drug-OV-TL16 antibody conjugates. II. Processing in epithelial ovarian carcinoma cells in vitro. *Int. J. Cancer 75*, 600−608.

(21) Kopeček, J., Kopečková, P., Minko, T., and Lu, Z. R. (2000) HPMA copolymer-anticancer drug conjugates: Design, activity, and mechanism of action. *Eur. J. Pharm. Biopharm. 50*, 61−81.

(22) Putnam, D., and Kopeček, J. (1995) Polymer conjugates with anticancer activity. *Adv. Polym. Sci. 122*, 55−123.

(23) Šubr, V., Strohalm, J., Ulbrich, K., Duncan, R., and Hume, I. C. (1992) Polymers containing enzymatically degradable bonds, XII. Effect of spacer structure on the rate of release of daunomycin and adriamycin from poly[N-(2-hydroxypropyl)methacrylamide] copolymer drug carriers in vitro and antitumour activity measured in vivo. *J. Controlled Release 18*, 123−132.

(24) Marcusson, E. G., Bhat, B., Manoharan, M., Bennett, C. F., and Dean, N. M. (1998) Phosphorothioate oligodeoxyribonucleotides dissociate from cationic lipids before entering the nucleus. *Nucleic Acids Res. 26*, 2016−2023.

(25) Merdan, T., Kunath, K., Fischer, D., Kopeček, J., and Kissel, T. (2002) Intracellular processing of poly(ethylene imine)/ribozyme complexes can be observed in living cells by using confocal laser scanning microscopy and inhibitor experiments. *Pharm. Res. 19*, 140−146.

(26) Kopeček, J., Kopečková, P., Minko, T., Lu, Z. R., and Peterson, C. M. (2001) Water soluble polymers in tumor targeted delivery. *J. Controlled Release 74*, 147−158.

(27) Graham, M. J., Crooke, S. T., Monteith, D. K., Cooper, S. R., Lemonidis, K. M., Stecker, K. K., Martin, M. J., and Crooke, R. M. (1998) In vivo distribution and metabolism of a phosphorothioate oligonucleotide within rat liver after intravenous administration. *J. Pharmacol. Exp. Ther. 286*, 447−458.

(28) Graham, M. J., Crooke, S. T., Lemonidis, K. M., Gaus, H. J., Templin, M. V., and Crooke, R. M. (2001) Hepatic distribution of a phosphorothioate oligodeoxynucleotide within rodents following intravenous administration. *Biochem. Pharmacol. 62*, 297−306.

(29) Levin, A. A. (1999) A review of the issues in the pharmacokinetics and toxicology of phosphorothioate antisense oligonucleotides. *Biochim. Biophys. Acta 1489*, 69−84.

(30) Shoeman, R. L., Hartig, R., Huang, Y., Grub, S., and Traub, P. (1997) Fluorescence microscopic comparison of the binding of phosphodiester and phosphorothioate (antisense) oligodeoxyribonucleotides to subcellular structures, including intermediate filaments, the endoplasmic reticulum, and the nuclear interior. *Antisense Nucleic Acid Drug Dev. 7*, 291−308.

(31) Hartig, R., Huang, Y., Janetzko, A., Shoeman, R., Grub, S., and Traub, P. (1997) Binding of fluorescence- and gold-labeled oligodeoxyribonucleotides to cytoplasmic intermediate filaments in epithelial and fibroblast cells. *Exp. Cell Res. 233*, 169−186.

(32) Chin, D. J., Green, G. A., Zon, G., Szoka, F. C., Jr., and Straubinger, R. M. (1990) Rapid nuclear accumulation of injected oligodeoxyribonucleotides. *New Biol. 2*, 1091−1100.

(33) Lorenz, P., Baker, B. F., Bennett, C. F., and Spector, D. L. (1998) Phosphorothioate antisense oligonucleotides induce the formation of nuclear bodies. *Mol. Biol. Cell 9*, 1007−1023.

(34) Fisher, T. L., Terhorst, T., Cao, X., and Wagner, R. W. (1993) Intracellular disposition and metabolism of fluorescently labeled unmodified and modified oligonucleotides microinjected into mammalian cells. *Nucleic Acids Res. 21*, 3857−3865.

(35) Wagner, R. W., Matteucci, M. D., Lewis, J. G., Gutierrez, A. J., Moulds, C., and Froehler, B. C. (1993) Antisense gene inhibition by oligonucleotides containing C-5 propyne pyrimidines. *Science 260*, 1510−1513.

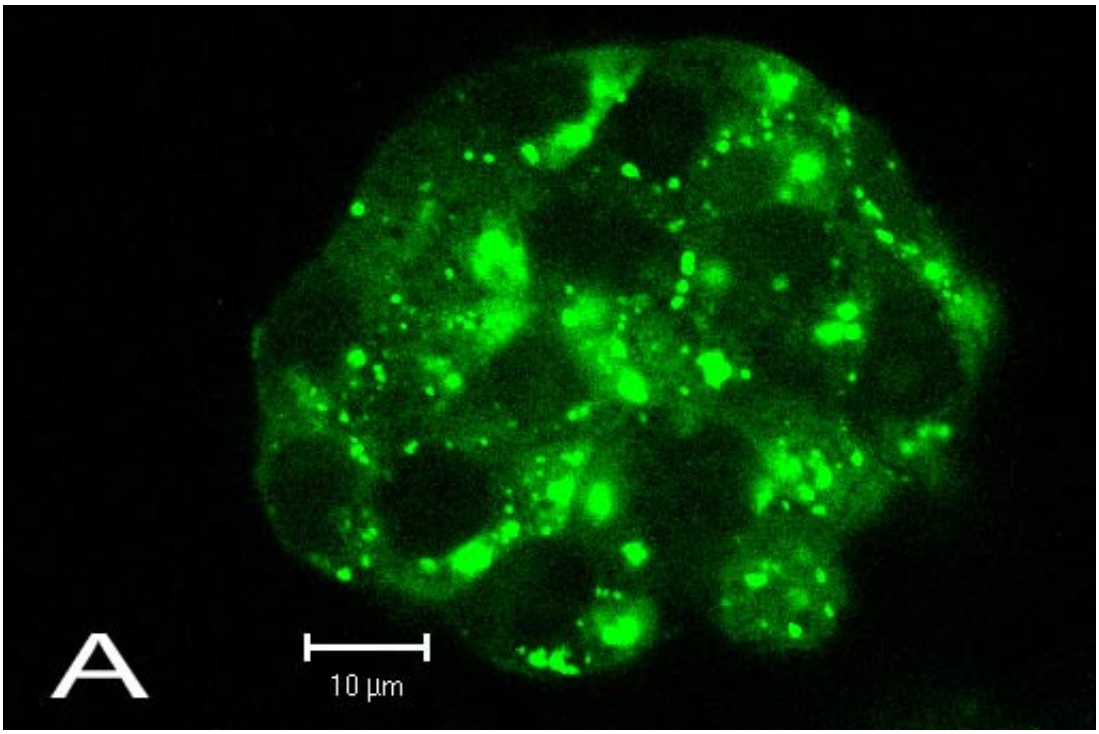
(36) Nakai, D., Seita, T., Terasaki, T., Iwasa, S., Shoji, Y., Mizushima, Y., and Sugiyama, Y. (1996) Cellular uptake mechanism for oligonucleotides: Involvement of endocytosis in the uptake of phosphodiester oligonucleotides by a human colorectal adenocarcinoma cell line, HCT-15. *J. Pharmacol. Exp Ther. 278*, 1362−1372.

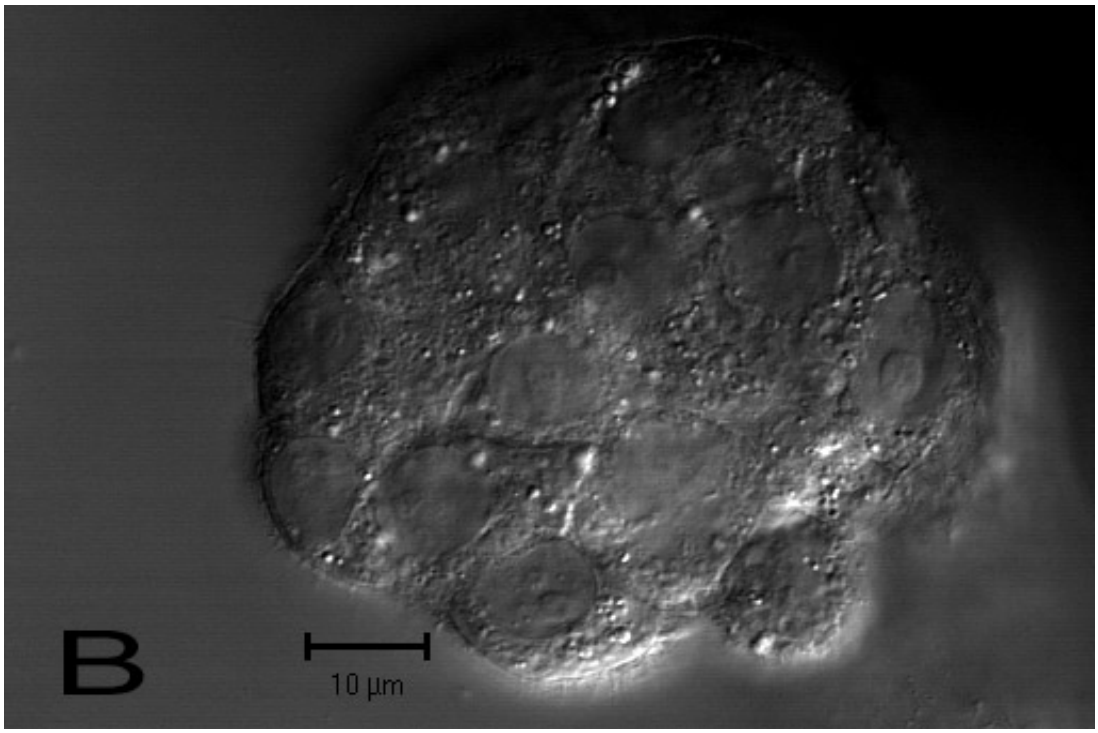
(37) Rejmanová, P., Pohl, J., Baudyš, M., Kostka, V., and Kopeček, J. (1983) Polymers containing enzymatically degradable bonds. 8. Degradation of oligopeptide sequences in N-(2-hydroxypropyl)methacrylamide copolymers by bovine spleen cathepsin B. *Makromol. Chem. 184*, 2009−2020.

(38) Rejmanová, P., Kopeček, J., Duncan, R., and Lloyd, J. B. (1985) Stability in rat plasma and serum of lysosomally degradable oligopeptide sequences in N-(2-hydroxypropyl)-methacrylamide copolymers. *Biomaterials 6*, 45−48.

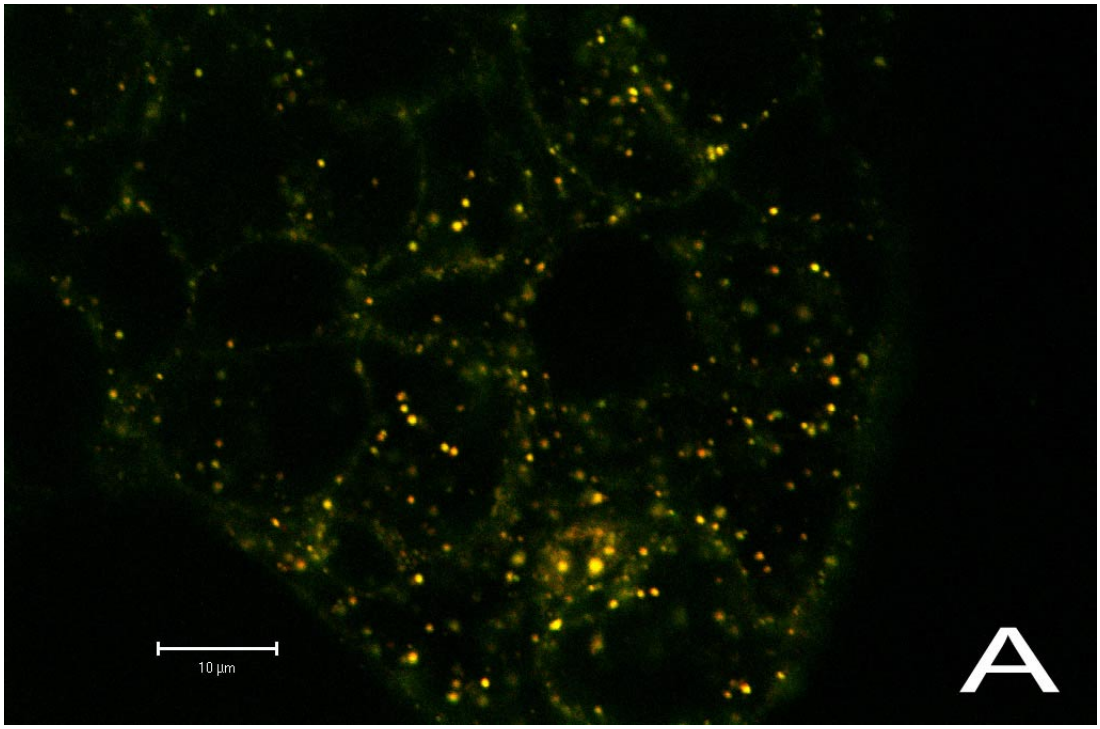
BC025559Y

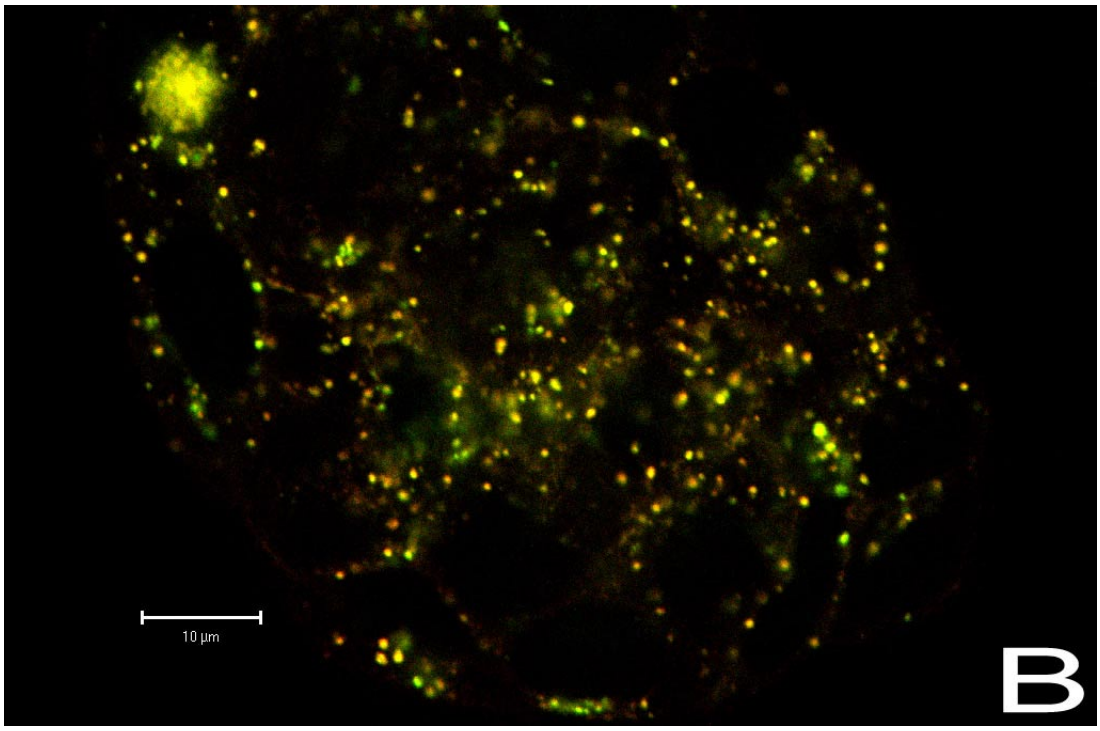
Supplemental material Figure 1. Hep G2 cells incubated with P1 for 24 h (A) green fluorescence (oligonucleotide). At high microscope gain, small amounts of fluorescence were observed in the cytoplasm and to a lesser extent in the nucleus of Hep G2 cells. (B) Transmitted image. Scale bars are 10 µm.



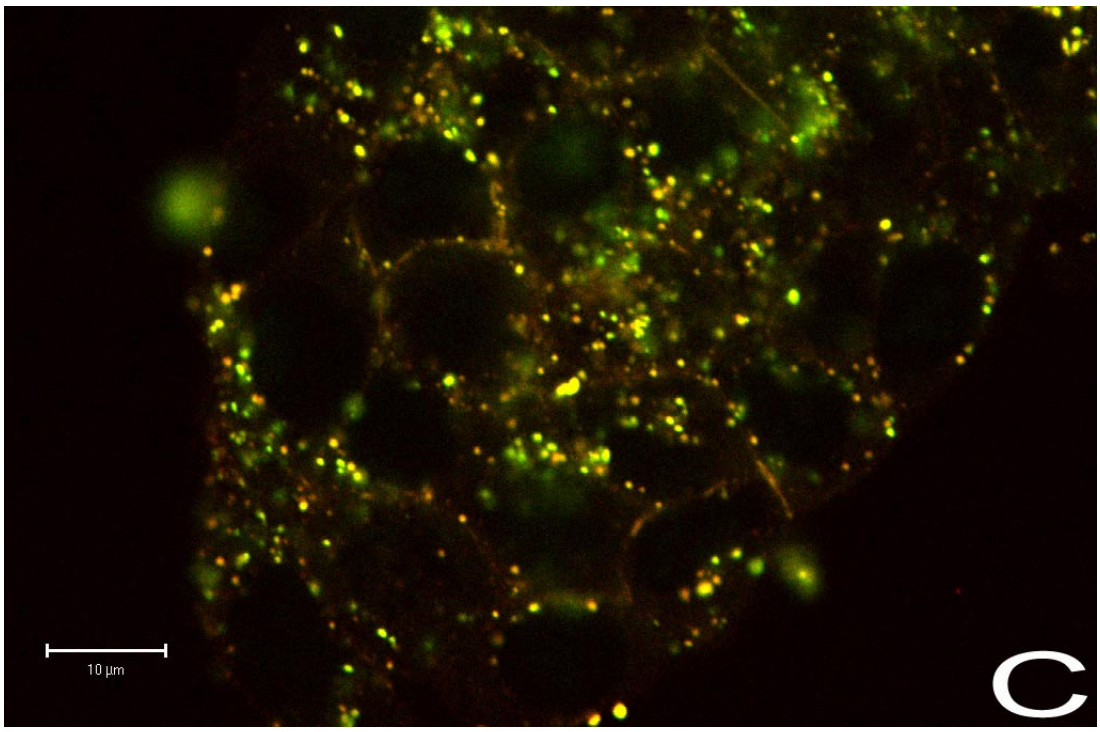


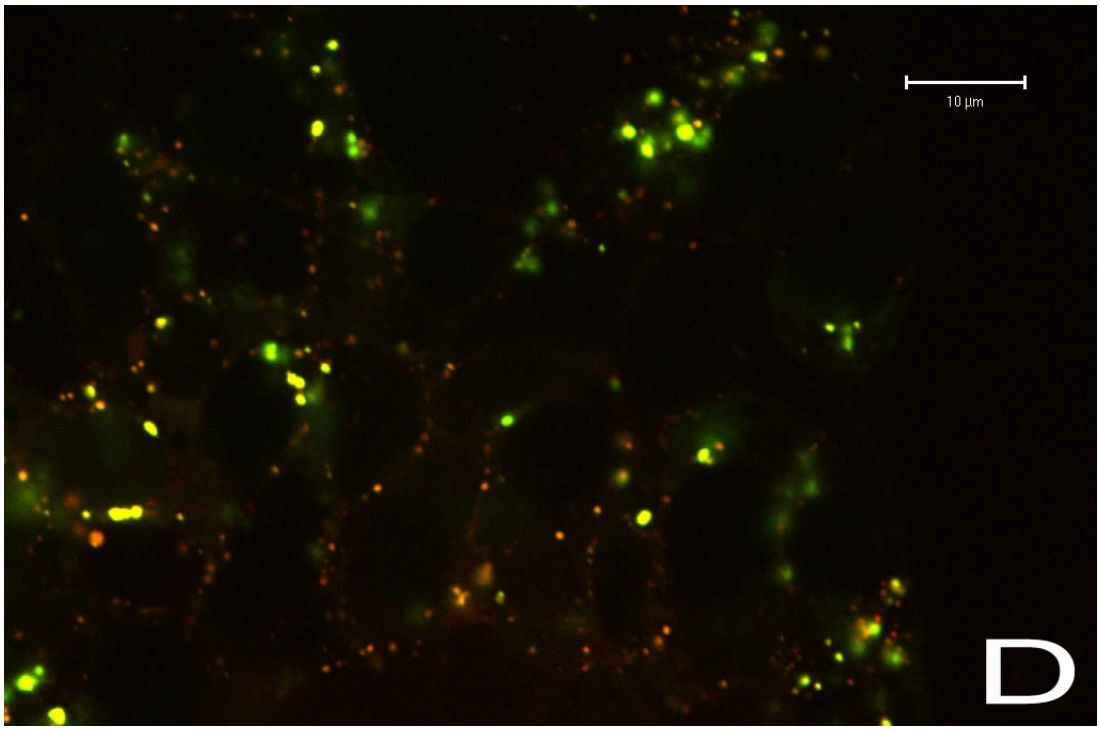
Supplemental material Figure 2. Hep G2 cells incubated with P2 (4.9 μM Fl, 8.1 μM LR) for (A) 0.5 h, (B) 2 h, (C) 4 h, (D) 24 h. All images have the green (oligonucleotide) and red (polymer) fluorescence combined. The images were taken at the same microscope setting to allow comparison of the fluorescent intensity. Scale bars are 10 μm.



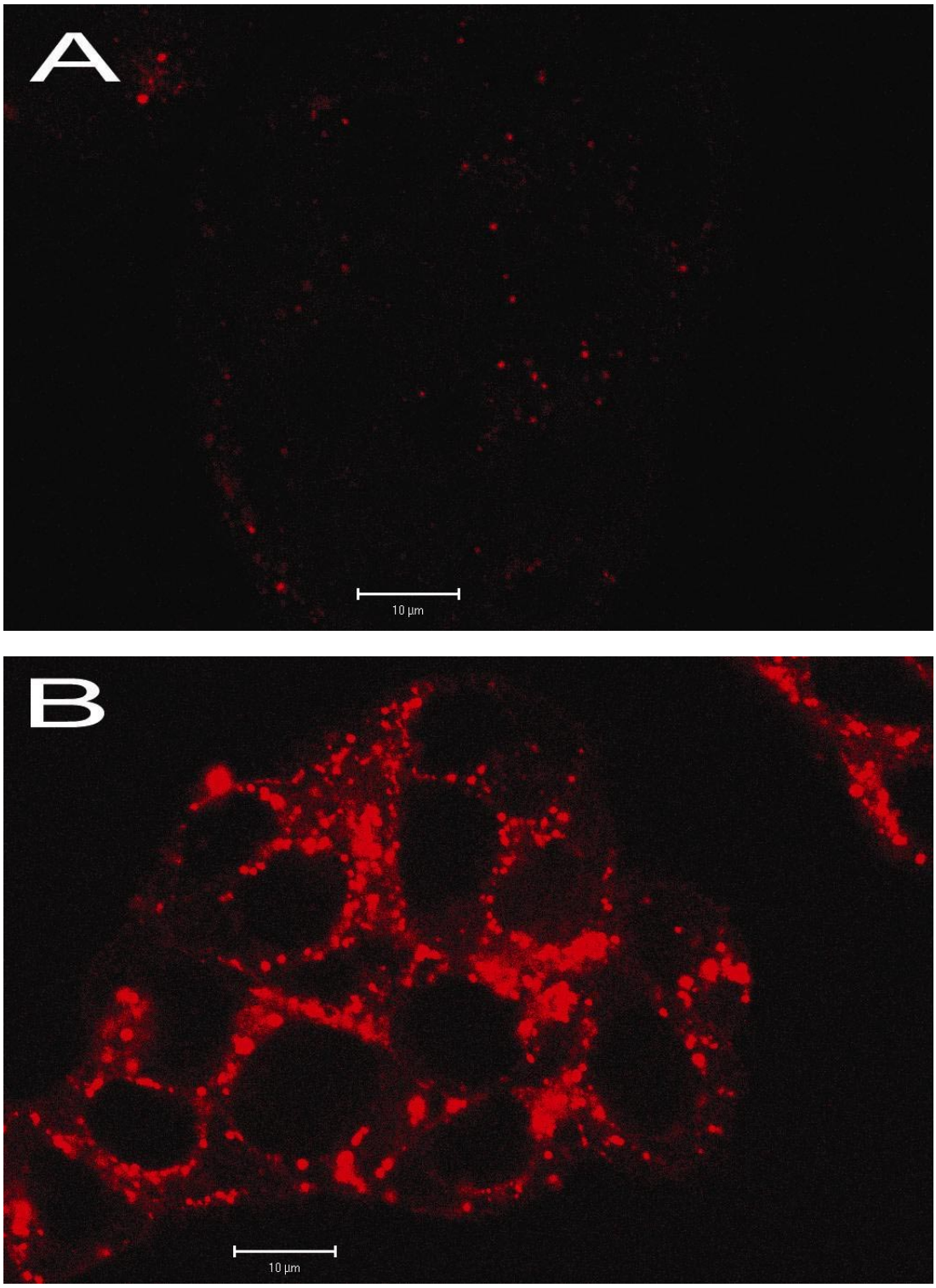


(Supplemental material Figures 2C and 2D cont.)





Supplemental material Figure 3. Hep G2 cells incubated with (A) polymer P-LR (8.6 μM LR) and (B) oligonucleotide conjugate P2 (8.1 μM LR) for 4 h. The same microscope settings were used for both images to allow semi-quantative comparison between the images. Scale bars are 10 μm.



Reduction of Kidney Uptake in Radiometal Labeled Peptide Linkers Conjugated to Recombinant Antibody Fragments. Site-Specific Conjugation of DOTA-Peptides to a Cys-Diabody

Lin Li,[†] Tove Olafsen,[‡] Anne-Line Anderson,[§] Anna Wu,[‡] Andrew A. Raubitschek,[§] and John E. Shively*[,†]

Division of Immunology, Beckman Research Institute of the City of Hope, Duarte, California 91010, Division of Biology, Beckman Research Institute of the City of Hope, Duarte, California 91010, and Department of Radioimmunotherapy, City of Hope Medical Center, Duarte, California 91010. Received June 30, 2002; Revised Manuscript Received July 29, 2002

Arano and co-workers (Arano et al. (1999) *Cancer Res. 59*, 128−134) have synthesized peptides with an N-terminal radioiodinated hippuric acid and a C-terminal lysine linked to antibody fragments via the ϵ-amino group of lysine that show reduced kidney uptake compared to antibody fragments directly radioiodinated. This approach takes advantage of the lysine specific carboxypeptidase activity of the kidney brush border enzymes that cleave off the radiolabeled peptide linker from the antibody fragment prior to uptake by proximal tubule cells. On the basis of their approach, we have synthesized a tetrapeptide with an N-terminal DOTA (1,4,7,10-tetraazacyclododecane-1,4,7,10-tetraacetic acid) and a C-terminal (N^{ϵ}-maleoyl)lysine that was site-specifically conjugated to an anti-CEA diabody (Yazaki et al. (2001) *Bioconjugate Chem. 12*, 220−228) that was engineered to contain a C-terminal cysteine (Cys-diabody). Biodistributions of the In-111-radiolabeled conjugate in nude mice show significantly reduced kidney uptake (a maximum of 82%ID/g at 6 h) compared to In-111 radiolabeled DOTA-diabody (184%ID/g at 6 h) in which DOTA was conjugated to endogenous lysine residues using DOTA-active ester chemistry. To further reduce kidney uptake, a homologous compound with a C-terminal (N^{ϵ}-amino-1,6-hexane-bis-vinyl sulfone)lysine was synthesized and site-specifically conjugated to the Cys-diabody. Biodistributions of this In-111-labeled conjugate reduced kidney uptake to 54%ID/g at 6 h. To explore the effect of the relative positions of the chelate vs the cys-diabody on kidney uptake, we also synthesized a tetrapeptide with an N-terminal bromoacetate for conjugation to Cys-diabody and a C-terminal (N^{ϵ}-amidino-propyl-3-thio-vinylsulfonyl-DO3A)lysine. This peptide essentially reverses the positions of the chelate and Cys-diabody attachment points on the peptide, while retaining the linker length on the ϵ-amino group of the lysine. In this case, biodistributions of the In-111-radiolabeled conjugate in nude mice showed high kidney uptake (189%ID/g at 6 h), comparable to that obtained with the In-111-radiolabeled active ester conjugated DOTA-diabody (184%ID/g at 6 h). We conclude that the peptide linker strategy of Arano and co-workers to reduce kidney uptake can be successfully applied to chelate/radiometal complexes and requires that the chelate/radiometal be located at the N-terminus of the peptide and the antibody fragment attachment site on the ϵ-amino group of the lysine. Furthermore, we demonstrated a role for the attachment chemistry to the ϵ-amino group of the lysine on the magnitude of kidney uptake.

INTRODUCTION

While bifunctional chelating agents (BCAs[1]) are routinely conjugated to recombinant antibodies for radiolabeling with radiometals such as ^{111}In for radioimmunoimaging and ^{90}Y for radioimmunotherapy (*1*−*4*), they suffer from high kidney uptake when conjugated to antibody fragments (*5*−*9*). Although intact antibodies have high clinical utility, their relatively long circulation times and poor tumor penetration (*10*) have prompted many studies on antibody fragments, including proteolytic Fab and F(ab′)$_2$ fragments made from intact antibodies (*6*, *11*−*15*), or recombinant fragments, including scFv (*16*−*18*), diabodies (*9*, *18*, *19*), and novel constructs such as ΔC_H2 (*20*), scFvFc (*21*−*23*), or the minibody scFvC_H3 (*24*). In almost all cases, the antibody fragments have shown unacceptably high kidney uptake when conjugated to chelates and radiometal labeled. Thus, their clinical use has been limited to radioiodinated fragments where the high kidney uptake is offset by rapid dehalogenation (*25*). Unfortunately, dehalogenation also

* Address correspondence to John E. Shively, Division of Immunology, Beckman Research Institute of the City of Hope, Duarte, CA 91010; email: jshively@coh.org.

[†] Division of Immunology, Beckman Research Institute of the City of Hope.

[‡] Division of Biology, Beckman Research Institute of the City of Hope.

[§] Department of Radioimmunotherapy, City of Hope Medical Center.

[1] Abbreviations: BCA, bifunctional chelating agent; CEA, carcinoembryonic antigen; DOTA, 1,4,7,10-tetraazacyclododecane-1,4,7,10-tetraacetic acid; EDC, 1-ethyl-3-[3-(dimethylamino)propyl]carbodiimide; DTPA, diethylenetriaminepentaacetic acid; HSA, human serum albumin; sulfo-NHS, *N*-hydroxysulfosuccinimide; TCEP, tris(carboxyethyl)phosphine; DCM, dichloromethane; DMF, dimethylformamide; HOBT, 1-hydroxybenzotriazole; NMP, 1-methyl-2-pyrrolidinone; TFA, trifluoroacetic acid.

10.1021/bc025565u CCC: $22.00 © 2002 American Chemical Society
Published on Web 08/28/2002

occurs in the tumor, and especially in the cases of internalizing antibodies, tumor dehalogenation further limits the clinical utlility of radiolabeled antibody fragments.

Several groups have studied the metabolism of chelate/radiometal-labeled antibody fragments in the kidney. Rogers et al. (*26*) identified ^{111}In-DTPA-ϵ-amino lysine as the major metabolite of ^{111}In-labeled DTPA-conjugated F(ab′)$_2$ fragments, and Tsai et al. (*27*) identified ^{111}In-DOTA-ϵ-amino lysine as the major metabolite of ^{111}In-labeled DOTA-conjugated Fab fragments. In both studies the BCA was attached to surface lysine residues, suggesting that that uptake of antibody by the kidney leads to complete degradation of the protein leaving the non-metabolizable chelate-lysine derivative as the ultimate product. In similar studies with ^{18}F-labeled disulfide stabilized Fv (dsFv) fragments, Lang et al. (*28*) identified [^{18}F]fluoromethylbenzoyl-ϵ-amino-lysine as the ultimate metabolite in the urine. Kidney uptake depends on both the rate of blood clearance and the molecular size of the fragment. For example, ^{177}Lu-DTPA-sFv (M_r = 27 kDa) of CC49 (anti-B72.3) has a $T_{1/2\beta}$ of 2h and 219% ID/g in the kidney at 6 h (*29*). ^{111}In-DOTA-diabody (M_r = 50 kDa) of T84.66 (anti-CEA) has a $T_{1/2\beta}$ of 3 h and 183% ID/g in kidney at 6 h (*27*). In contrast, ^{111}In-DOTA-scFvC$_H$3 (M_r = 75 kDa) of T84.66 has a $T_{1/2\beta}$ of 4.5h and 12.5% ID/g in kidney at 6 h (*9*). A discussion of the optimum size of antibody fragments as matched to radiolabel half-life is given by Williams et al. (*30*). In general, scFv fragments clear too rapidly and have low antigen binding (monovalent), precluding their use in imaging or therapy, while the larger fragments, such as scFvC$_H$3 (divalent), are attractive due to their rapid clearance and lack of kidney uptake. Although intermediate-sized fragments such as the diabody (also divalent) are highly attractive due to their more rapid blood clearance, their high kidney uptake has limited their clinical utility.

Several possible approaches to the kidney uptake problem have been investigated. The first is the co-administration of L- or D-lysine as originally described by Solling and Morgenson (*31*) and more recently reviewed (*32*, *33*). In one study, the high kidney uptake of ^{99m}Tc-labeled Fab′ (>100%ID/g at 4 h) was reduced to 40%ID/g at 4 h by adminstration of 1 mg/g × 4/h ip of L-lysine in balb/c mice (*34*). In a second study, ^{111}In-DOTA-diabody kidney uptake was reduced from 180%ID/g to 65%ID/g at 6 h by the administration of 100 mg of D-lysine, oral, 30 min prior to injection of antibody (9). In a third study, ^{88}Y-DOTA-Fab′ kidney uptake was reduced from 104%ID/g to 20%ID/g at 4 h by the administration of 4 × 2 mg/g/h ip of D-lysine (*6*). This approach has been applied to human studies in which patients receiving ^{99m}Tc-labeled anti-CEA Fab′ fragments were infused with 2 L of 2.25 g/L of L-lysine-L-glutamate and 2.5 g/L of L-arginine (*35*). The results were minor (11%ID vs 18%ID) compared to the animal studies, perhaps because the amount of lysine administered was less on a per weight basis.

A second approach to the problem is the use of BCAs with organ specific cleavable linkers. Arano and co-workers (*33*, *36*−*38*) have synthesized C-terminal Lys linkers for a radioiodinated hippuric acid−Fab conjugate that lowered kidney uptake by up to 50%. The BCA was hippuric acid-glycyl-N^{ϵ}-maleoyl-lysine which allowed linkage of antibody fragments to the maleimide moiety via thiol-specific Michael addition (*39*). In this study they demonstrated the critical importance of the α-carboxyl group of the C-terminal lysine residue, presumably confirming the role of brush border carboxypeptidase activity in the kidney. They have hypothesized that cleavage of the antibody fragment from the radiolabel prior to uptake by the proximal tubule cells allows excretion of the residualized radiolabel. When the peptide linker-radiolabeled fragment was compared to fragment radioiodinated by standard chemistry in a tumor bearing nude mouse model, no difference was observed in tumor uptake, but kidney uptake was reduced by 25% at 3 h. Thus, the peptide linker played a critical role in reducing kidney uptake while preserving tumor uptake.

In this work, we extend the model of Arano and co-workers to the use of C-terminal lysine peptide linkers with the chelate DOTA at the N-terminus. The Michael addition reagents maleimide (similar to Arano and co-workers) or hexanevinyl sulfone were attached to the ϵ-amino group of the C-terminal lysine residue in order to allow site-specific conjugation to a thiol group in an antibody fragment. We engineered a C-terminal cysteine residue into an anti-CEA diabody to provide the site-specific thiol group. The diabody quantitatively formed covalently linked dimers that had to be reduced prior to conjugation with BCA. We also synthesized a peptide linker in which the positions of DOTA and Cys-Diabody were exchanged, with Cys-diabody at the N-terminus and DOTA attached to the ϵ-amino group of the C-terminal lysine. When the conjugates were radioabeled with ^{111}In and biodistributed in nude mice, kidney uptake was significantly lowered in the first, but not the second conjugate. The results demonstrate that the C-terminal lysine peptide linker approach can be generalized to chelate/radiometal conjugates, and that the relative positions of the chelate and antibody fragment attachment points are critically important.

EXPERIMENTAL PROCEDURES

General. DOTA trisodium salt and the free acid were purchased from Parish Chemical Co. (Orem, UT) and Macrocyclics, Inc. (Richardson, TX), respectively. The tris-*tert*-butyl ester of DO3A was also obtained from Macrocyclics, Inc. DTPA was obtained from Fluka (Milwaukee, WI), 1,6-hexane-bis-vinyl sulfone from Molecular Biosciences (Boulder, CO), 2-iminothiolane HCl from Aldrich (Milwaukee, WI), and Chelex 100 from BioRad (Hercules, CA), Ultrapure water (18 MΩ-cm) was used to make all buffers which were passed over Chelex 100 and pH adjusted if necessary. $^{111}InCl_3$ (1.0 mCi/0.15 mL in 0.04 M HCl) was obtained from Mallinckrodt Medical Inc. (St. Louis, MO). $^{64}CuCl_2$ (2 mCi/0.05 mL in 0.01 M HCl) was obtained from Dr. Michael Welch, Mallinckrodt Radiological Institute, Washington University, St. Louis, MO. The anti-CEA diabody has been previously described (*40*). ITLC were performed as previously described (*41*). Mass spectra were recorded on a Finnigan LCQ ion trap mass spectrometer using a custom nanospray interface or on a Voyager DESTR MALDI-TOF mass spectrometer (Applied Biosystems). NMR spectra were recorded on a Varian Unity Plus 500 MHz spectrometer. Proton chemical shifts are reported relative to HOD (4.80 ppm). Antibody concentrations were calculated at 280 nm (A_{280}, 1 mg/mL = 1.42). UV spectrophometry was performed on a Shimadzu UV160 instrument using a 1 cm cell. Melting points were recorded on a Thomas-Hoover unimelt apparatus and are uncorrected. SDS and IEF gel electrophoresis was performed on a Pharmacia PhastGel apparatus according to the manufacturer's instructions.

Cloning and Expression of Cys-Diabody. The C-terminal sequence of the previously published T84.66/GS8 anti-CEA diabody (...VSS) (*40*) was converted to

(...VSLGGC) by PCR mutagenesis using the QuickChange protocol (Stratagene). Protein was expressed using the pEE12/glutamine synthetase expression system (Lonza Biologics) in NS0 murine myeloma cells. CEA-binding activity was assessed by ELISA using microtiter plates coated with recombinant CEA NA-3 and alkaline phosphatase-conjugated goat anti-mouse Fab as described (Yazaki et al., 2001). Cys-diabody was purified by sequential chromatography using anion exchange (Source 15Q, Amersham Biosciences) followed by ceramic hydroxyapatite chromatography (Bio-Rad Laboratories) using a BioCad 700E perfusion chromatography system (Applied Biosystems) (*42*).

DOTA-glycylleucylglycyl-N^{ϵ}-maleoyllysine, 2a. α-NH_2-GLGK−PS (**1**) was synthesized on α-Fmoc-Lys-(ϵ-Boc)-Wang resin (Bachem). Briefly, 1 g of α-Fmoc(ϵ-Boc)-Lys-resin (0.83 mmol/g) was vortexed 15 min with 5.5 mL of DMF/piperidine (10:1, v/v) at RT, filtered, and washed with ethanol (5 mL × 3), DMF (5 mL × 3), and DCM (5 mL × 3). The procedure was repeated until all traces of cleaved FMOC were removed (A_{300nm}). α-FMOC-Gly (1 mmol) was activated with DCC (2 mL of 1 M DCC in 2 mL of DCM; 2 mmol) and HOBt (2 mL of 0.5 M in NMP, 1 mmol) for 5 min at RT, the precipitate removed, and the filtrate vortexed with the Lys(ϵ-Boc resin) for 30 min at RT. The resin was washed with saturated NaHCO3 12× (or until $A_{300\ nm}$ of the washes were zero), water 3×, and DCM 3×. The α-Fmoc group was removed with DMF/piperidine as described above. The coupling procedure was repeated with α-Fmoc Leu and α-Fmoc Gly. After each step, a small amount of resin was removed, treated with TFA/H_2O (98/2), and analyzed by ESI/MS to determine if the correct mass was obtained. For intermediate **1**, the α-Fmoc group was removed after coupling. The TFA-cleaved peptide, α-Fmoc-GLGK−CO_2H, had the correct mass (MH^+ expected, 596.30, MH^+, observed, 596.47). For intermediate **3**, the Fmoc group was not removed and the TFA-cleaved peptide had the correct mass (MH^+ expected, 374.30, MH^+ observed, 374.34). **1** (129 mg, 110 μmol) was treated with the isobutyl formate ester of DOTA prepared according to Li et al. (*43*). Briefly, the trisodium salt of DOTA (440 μmol) was suspended in 16.8 mL of DMF/TEA (4:1, v/v), stirred overnight until clear, and reacted with isobutyl chloroformate (29 μL, 220 μmol) added dropwise over 15 min at 0 °C. The active ester was added to the resin and vortexed for 6 h at RT. The resin was filtered, washed with ethanol 5 mL ×5 and DCM 5 mL ×5, and cleaved with TFA/H_2O (6 mL, 98/2, v/v). The peptide was purified by RP-HPLC on oligo-R3 (Perseptive Biosciences) using a linear gradient of 100% A (0.1% TFA) to 100% B (0.1/9.9/90, TFA/H_2O/MeCN, v/v/v) at a flow rate of 5 mL/min over 15 min. The purified peptide gave a single peak on analytical RP-HPLC and the correct mass by ESI-MS (MH^+ expected, 760.41, MH^+ observed, 760.74). The yield of lyophilized product was 12.3 mg (14.7% overall). DOTA-GLGK−CO_2H (5.2 mg, 6.9 μmol) was mixed with 3 aliquots of *N*-(methoxycarbonyl)maleimide (18.6 mg, 120 μmol) added over 1 h in 0.5 mL of saturated $NaHCO_3$ at 4 °C. The reaction was stirred for 24 h and neutralized to pH 1 with 10% TFA, and the product was purified by RP-HPLC on an Oligo-R3 column. The approximate yield was 2.8 mg (48.4%) of purified product (MH^+ expected, 840.67, MH^+ observed, 840.41by ESI-MS). The synthesis of *N*-(methoxycarbonyl)maleimide was adapted from that of Arano and co-workers (*39*). Maleimide (2.14 g, 22 mmol) and *N*-methylmorpholine (1.38 mL, 20 mmol) were mixed in 50 mL of ethyl acetate at 4 °C. *N*-Methyl chloroformate (1.41 mL, 20 mmol) was added dropwise and stirred for 2 h. The white precipitate was filtered and washed with ethyl acetate twice (5 mL). The filtrate and washes were combined, concentrated, and redissolved in a minimum volume (3 mL) of ethyl acetate. White crystals were obtained (2.1 g, 67.7% yield).

DOTA-glycylleucylglycyl-(N^{ϵ}-1,6-hexane-bis-vinyl sulfone)lysine, 2b. DOTA-GLGK−CO_2H (2 mg, 2.6 μmol) was mixed with 1,6-hexane-bis-vinyl sulfone (26 μmol) in DMF/H_2O (0.6 mL, 1:1, v/v), the pH was adjusted to 8.5 with 1 M NaOH, and the reaction was run for 24 h at RT. The solution was extracted with ethyl acetate (2 mL, 3×) and the product purified by RP-HPLC as above. The product (**2b**, 2.47 mg, 73.5% yield) had the correct mass by ESI-MS (MH^+ expected, 1292.59, MH^+ observed, 1292.54).

DOTA-glycylleucylglycyllysine-(N^{ϵ}-bromoacetamido), 2c. DOTA-GLGK−CO_2H (2 mg, 2.6 μmol) was reacted with bromoacetyl bromide (4 μL, 45 μmol) in 0.5 mL of 0.1 M $NaHCO_3$ for 1 h at RT. The product was purified by RP-HPLC on an oligo R3 column. The product (1.63 mg, 71.2% yield) eluted as a single peak and had the correct mass (MH^+ expected, 880.46, MH^+ observed, 880.56, first peak of Br isotopic doublet).

N^{α}-Bromoacetamido-glycylleucylglycllysine-(N^{ϵ}-amidino-propyl-3-thio-vinylsulfonyl-DO3A), 4. α-Fmoc-GLGK−CO_2H (**3**, 20 mg, 34 μmol) in 1.0 mL of DMF was mixed with 8.13 mg (59 μmol) of 2-iminothiolane in 2.0 mL of H_2O, and the pH was adjusted to 8.0 with 1 M NaOH and allowed to react for 2 h at RT. The reaction was monitored by ESI-MS for the correct mass of the expected product (MH^+ = 697.4). DO3A-VS (**5**, 17.4 mg, 37 μmol) was then added to the reaction mixture, the pH adjusted to 8.0 and the reaction continued for 2 h at RT. Again the reaction was monitored for the correct mass of the expected product (MH^+ = 1161.5). The product was lyophilized, purified by RP-HPLC, and treated with 0.20 mL of piperidine−DMF (1:10, v/v) for 20 min at RT. The product (MH^+ expected, 939.50, MH^+ observed, 939.60) was repurified by RP-HPLC (yield, 4.1 mg, 12.8% yield). The product (2.8 mg, 3.0 μmol) was dissolved in 0.2 mL of TEA/DMF (1/200, v/v) at 4 °C and reacted with 0.3 μL × 3 additions (3.3 μmol) of bromoacetyl bromide every 2 h for a total of 8 h. The product was lyophilized and purified by RP-HPLC on an oligo R3 column. Two peaks were obtained, a small early eluting peak corresponding to starting material and a large late eluting peak corresponding to the expected product (**4**). The yield was 1.0 mg (31.5%) with the correct mass by ESI-MS (MH^+ expected, 1059.65, MH^+ observed, 1059.70, first peak of Br isotopic doublet).

Vinylsulfonyl-DO3A (5, DO3A-VS). DO3A (1,4,7-tris(carboxymethyl)-1,4,7,10-tetraazacyclododecane was prepared by TFA treatment of the commercially available tris-(*tert*-butyl) ester of DO3A. The tris-(*tert*-butyl) ester of DO3A (100 mg, 190 μmol) was treated with 3.0 mL of 95% TFA for 24h and lyophilized twice from water. DO3A (60 mg, 92% yield) had the correct mass by ESI-MS (MH^+ expected, 347.19, MH^+ observed, 347.21). Vinyl sulfone (55.8 μL, 500 μmol) was dissolved in 0.2 mL of H_2O/DMF (1:1, v/v), the pH was adjusted to 10.0 with 1 M NaOH, and DO3A (18 mg, 50 μmol) was added in 0.2 mL of water and reacted for 1.5h at RT. The reaction mixture was loaded onto a Dowex 1-X8 (formate) column (5 mL), washed with 30 mL of water, and eluted stepwise with 10 mL each of 0.05, 0.1, and 0.2 M formic acid (1 mL fractions). The correct product was found in fractions 7−11 (yield 10.4 mg, 45.0%). Later fractions which contained substantial amounts of the bis product were

discarded. The purified product (**5**) gave the correct mass by ES-MS (MH^+ expected, 465.19, MH^+ observed, 465.30).

Preparation of Cys-Diabody−BCA Conjugates. One example is given. Cys-diabody (FW = 50,000, 2.0 mg, 40 nmole, at 4 mg/mL, 80 μM) was dialyzed vs 20 mM, pH 7.0 PBS (3 changes, × 1L, 4 °C). The sample is treated with 20 μL of 20 mM TCEP (400 nmol) in PBS for 2 h at 37 °C under Ar and centrifuged through a Sephadex G25 spin column (1 mL, 1200 rpm, 2 min). DOTA-glycyl-leucylglycyllysine-(ϵ-amino-bis-1,6-hexanevinyl sulfone) (FW = 1292, 58 μL of 20 mM **2b** in PBS) was added and the solution rotated at 10 rpm for 4h at 25 °C. The conjugate was dialyzed vs 0.25 M NH_4OAc, pH 7.0 (3 changes, × 1L, 4 °C) and concentrated to 0.5 mL (Centricon 10).

Radiolabeling of Conjugates. The conjugates were radiolabeled with $^{111}InCl_3$ as previously described (*44*). For the animal studies, the conjugates (0.1 mL of 5 mg/mL in 250 mM NH_4OAc, pH 5.7) were incubated with 1.0 mCi of ^{111}In (0.15 mL of 0.04 M HCl plus 0.05 mL of 1.0 M NH_4 OAc, pH 7.0) for 60 min at 43 °C. Excess ^{111}In was chelated with 1 mM DTPA and the radiolabeled product purified on a Pharmacia Superdex 75HR column (1.0 × 30 cm in saline, 0.5 mL/min, 0.5 mL fractions). The protein peak was mixed with 1 drop of 25% (w/v) of HSA. In other test labelings, 1.0 mCi of ^{111}In was added to 0.2 mg of conjugate and the specific activity determined by ITLC (kit 151−770, Biodex, Medical, New York). Determination of the number of chelates per conjugate and the immunoreactivity was performed as previously described (*45*).

Stability Studies. Aliquots (0.5 mL) of the radiolabeled conjugates in PBS-1% HSA were incubated at 37 °C and injected at various time points onto tandem Pharmacia Superose 6 columns to determine the amount of radiolabel in the conjugate and any released products. Separate aliquots were mixed with 0.05 mL of 10 mM DTPA and analyzed as above to determine the release of free ^{111}In.

Animal Biodistributions. Groups of five nude mice (Charles River) bearing LS174T human colon tumor xenografts (ave size = 1.5 mg ± 0.5 at t = 0 h) were injected with 2−4 μCi (2 μg) of radiolabeled conjugate via tail vein. Animals were sacrificed at various time points after injection, major organs, tumor, and blood were weighed, radioactivity was measured, and the results were expressed as mean %ID/g ± SD.

RESULTS

Design of Cys-Diabody. The diabody is the smallest bivalent recombinant antibody that retains many of the desirable properties of the scFv, namely fast pharmacokinetics and good tumor penetration, while overcoming many of its deficiencies such as too rapid blood clearance and poor tumor retention. In previous work we showed that an [^{111}In]labeled anti-CEA diabody gave high tumor uptake (12.5%ID/g at 2 h) and an excellent tumor-to-blood ratio of 4.6 at the same time point (*9*). However, this result was offset by high kidney uptake (135%ID/g and 184%ID/g at 2 h and 6 h, respectively), thus reducing the clinical utility of this agent. In that study we used the chelate DOTA which was attached by active ester chemistry to lysine residues in the diabody. In our present work we redesigned both the BCA and the diabody employing site-specific conjugation chemistry using a thiol-directed BCA with a cleavable peptide linker. To introduce a reactive thiol group in the diabody, the C-terminal Ser of the heavy chain was mutated to Leu and extended by three amino acids, Gly-Gly-Cys. Cys-diabody was expressed in high yield from NS/0) cells, purified by conventional chromatography (details to be presented elsewhere), and shown to exist as disulfide bonded dimers (Figure 1). To be used for site specific conjugation to BCAs, it was necessary to reduce the disulfide bond at the C-terminus prior to coupling. As expected, the radiolabeled BCA-Cys-diabody conjugates migrated as noncovalent dimers on gel filtration (data not shown).

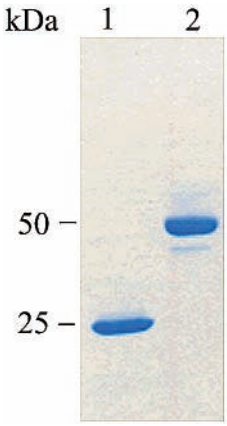
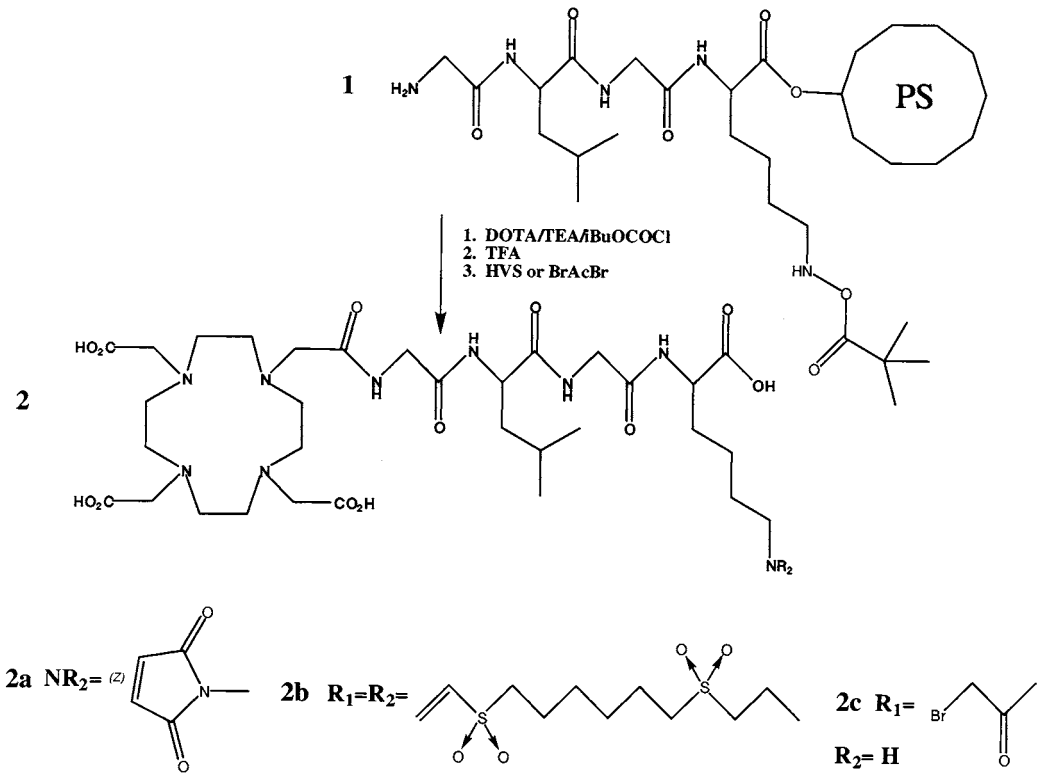


Figure 1. Analysis of Cys-diabody by SDS gel electrophoresis. Cys-diabody was run under either reducing (lane 1) or nonreducing (lane 2) conditions and stained with Coomassie Blue. The molecular weights were determined from the migration of authentic standards.

Synthesis of BCA and Antibody Conjugation. Our goal was to produce a BCA incorporating a peptide linker with DOTA at the N-terminus and lysine at the C-terminus with a thiol-reactive group attached to the ϵ-amino group of lysine. We chose NH_2-GLGK−CO_2H as the peptide because our experience with DOTA attached to Gly_3K peptides indicated that they did not bind to reversed phased resins making purification difficult. Two classes of thiol-reactive compounds were explored. The first was the use of two Michael addition reagents, maleimide and vinyl sulfone. The maleimide moiety, was introduced as N^{ϵ}-maleolyllysine according to Arano and co-workers (*39*). The synthesis of this BCA is shown in Scheme 1 (compound **2a**). The second Michael addition reagent was 1,6-hexane-bis-vinyl sulfone (HVS). The parent compound, vinyl sulfone, reacts with thiol groups specifically at pH 7 and also with amino groups at pH 9 (*46*). Although vinyl sulfone reacted smoothly with the ϵ-amino group of lysine, the product was the six-membered ring sulfone analogue of thiomorpholine, 4-sulfonylmorpholine (confirmed by NMR, data not shown). This product was obtained despite using a large excess of vinyl sulfone in the reaction. To avoid the entropically favorable six-membered ring formation, we used 1,6-hexane-bis-vinyl sulfone. The synthesis of the BCA is shown in Scheme 1 (compound **2b**). In both cases, the isobutyl formate active ester of DOTA was coupled to the free α-amino group of the peptide while still attached to the resin (compound **1**). This facilitated removal of excess DOTA from the reaction mixture and allowed protection of the ϵ-amino group of lysine. The peptide was then cleaved from the resin with TFA and purified by RP-HPLC. In this example, the presence of the leucine residue in the peptide linker promotes easy purification of the desired peptide product by RP-HPLC. The peptide was then reacted with either *N*-methoxycarbonyl-maleimide (compound **2a**) or excess HVS to

Scheme 1



produce the bis-ϵ-amino-HVS derivative (compound **2b**). BFC **2a** was unstable at pH 7 at 37 °C similar to other maleimides (*41*), but was stable indefinitely when stored frozen as a powder. BFC **2b** was shown to be stable in PBS for 7d at 37 °C (data not shown).

The bromoacetamidyl group was the second class of thiol-reactive groups explored. This group was introduced by the reaction of DOTA-GLGK with bromoacetyl bromide in aqueous media to produce the desired product **2c**. In general, this group is thiol-specific if the conjugation conditions are mild (e.g., RT, pH 7, 1−2 h). The BCA **2c** was shown to be stable in PBS for 7d at 37 °C (data not shown).

We also considered reversal of the positions of the DOTA and the thiol-reactive group on the peptide linker. In this case, the starting peptide was α-Fmoc-GLGK (compound **3**). Although we considered the direct coupling of DOTA to the ϵ-amino group of lysine, we were concerned that the close presence of the acidic DOTA derivative would limit the action of the lysine-specific carboxypeptidase in the kidney. Therefore, we devised a strategy to lengthen the distance between the DOTA and the ϵ-amino group while preserving its positive charge (Scheme 2). α-Fmoc-GLGK was reacted with iminothiolane and then with DO3A-VS, which rapidly reacts with the exposed thiol. The peptide was purified by RP-HPLC, deprotected and reacted with bromoacetyl bromide to make the desired product (compound **4**). This synthesis relied on the use of the novel BCA DO3A-VS whose synthesis is shown in Scheme 3. DO3A is the tris-carboxymethyl derivative of cyclen and is readily synthesized from the commercially available tris-*tert*-butyl acetate ester derivative of cyclen. Treatment of DO3A with excess vinyl sulfone produces both the desired product (**5**) and the bis-derivative (DO3A-VS-DO3A). While we made no attempt to optimize the yield of DO3A-VS, sufficient quantities were obtained to proceed with Scheme 2.

All of the BCAs were conjugated to mildly reduced Cys-diabody at a molar ratio of 45 to 1 (BCA/Cys-diabody). The degree of conjugation was determined by IEF gel electrophoresis, wherein conjugation of the acidic BCA to antibody results in a dramatic shift of the Cys-diabody to a more acidic pI. The results of the conjugation reaction at pH 7 are shown in Figure 2. In all four cases there is evidence that the reaction is incomplete. Since all four BCAs react rapidly with thiols, their variable reaction with Cys-diabody may be due to reoxidation of the C-terminal exposed cysteines in the Cys-diabody.

The number of chelates per antibody as determined by trace labeling with ^{111}In in a standard solution of $InCl_3$ is shown in Table 1. Radiolabeling of these four conjugates with $^{111}InCl_3$ gave variable percent radiolabeling efficiencies, specific activities, and immunoreactivities (Table 1). In all cases the percent efficiency for radiolabeling was sufficient to proceed with animal biodistributions. When the radiolabeled conjugates were incubated in PBS-1% HSA plus or minus 1 mM DTPA for 1−4 d, negligible loss of radioactivity was seen for conjugates **2b**, **2c**, and **4**, while **2a** lost 34% of its ^{111}In to

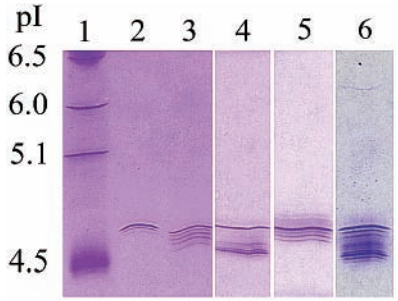
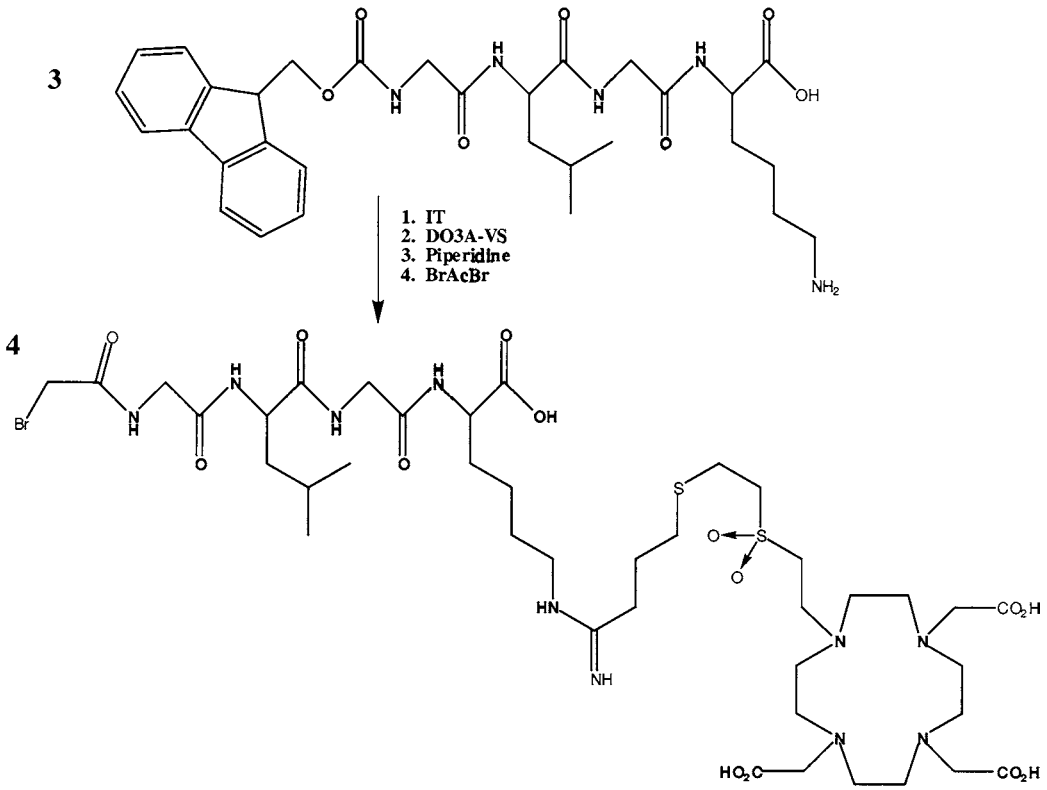


Figure 2. Analysis of BCA−Cys-diabody conjugates by IEF gel electrophoresis. A: Lane 1: IEF standards; Lane 2: Cys-diabody control; Lane 3: BCA = DOTA-GLGK[N^{ϵ}-$(HVS)_2$]; Lane 4: BCA = DOTA-GLGK(N^{ϵ}-AcBr); Lane 5: BCA = (N^{α}-AcBr)-GLGK(N^{ϵ}-IT-VS-DO3A); Lane 6: BCA = DOTA-GLGK(N^{ϵ}-mal).

Scheme 2



Scheme 3

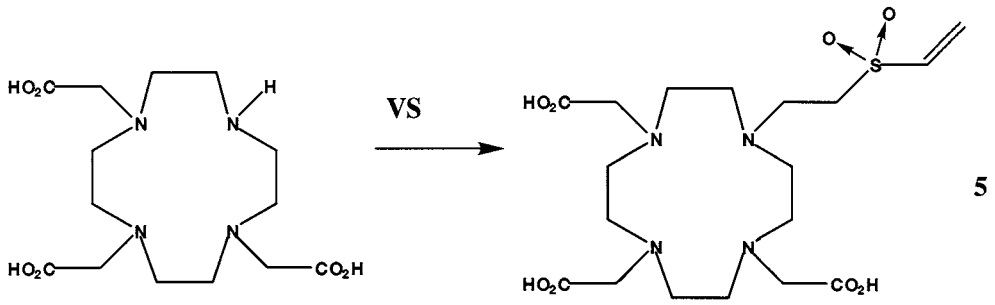


Table 1. Radiometal Labeling Efficiency and Immunoreactivity of BCA−Cys-Diabody Conjugates[a]

sample	chelates/ diab	% incorp	% immun
[^{111}In]DOTA-GLGK(N^{ϵ}-mal)	1.2	27	59
[^{111}In]DOTA-GLGK[N^{ϵ}-(HVS)$_2$]	0.8	8−55[b]	90
[^{64}Cu]DOTA-GLGK[N^{ϵ}-(HVS)$_2$]	0.8	56	24
[^{111}In]DOTA-GLGK(N^{ϵ}-AcBr)	1.3	85	100
(N^{α}-BrAc)-GLGK(N^{ϵ}-IT-VS-[^{111}In]DOTA)	0.6	99	100

[a] BCA was coupled to Cys-diabody as described in the text. The number of chelates per mAb was determined by trace labeling with ^{111}In in a standard solution of $InCl_3$. The labeling ratio was performed with 1.0 mCi of ^{111}In and 0.5 mg of conjugate in 0.3 mL of 0.25 mM ammonium acetate (pH 5.7). Immunoreactivity was performed as described in Methods. [b] This conjugate was test labeled two times at the 0.1 mg level giving labeling efficiencies of 45 and 55%. The labeling for the animal studies gave only 8% efficiency, but the low labeling was due to a rapid drop in pH caused by mixing the sample with the acidic $InCl_3$ and precipitating some of the conjugate. Despite this problem, sufficient sample was available for the HPLC purification of the radiolabeled conjugate and subsequent animal studies.

DTPA over 4 d (Table 1, Figure 3). The loss of radioactivity is found in a new slower migrating peak corresponding to ^{111}In-DOTA-peptide. Addition of DTPA causes no further loss in radioactivity, confirming that the radiolabel is still attached to DOTA. We conclude that the peptide is released due to the hydrolytic instability of the succinimide bonds at pH 7, a finding previously observed by us for other maleimide conjugates (*41*). Despite the instability of the BCA-conjugate, biodistributions were performed because <10% of the radioactivity was lost in 24 h, the critical time period for kidney uptake. In addition, the immunoreactivities of the **2b** and **2c** conjugates were >90% when radiolabled, bound to excess CEA, and analyzed by gel filtration chromatography (Table 1). The **2a** conjugate had lower immunoreactivity, suggesting that the conjugation reaction may have damaged the antibody.

Comparative Animal Biodistributions of BCA−Cys-Diabody Conjugates. [^{111}In]DOTA-GLGK(N^{ϵ}-mal)-Cys-diabody was injected into non-tumor-bearing nude mice, and the biodistribution determined over 24 h (Table 2). The kidney levels reached a maximum of 82%ID/g at 6 h, maintained that level through 15 h, and declined to 71%ID/g by 24 h. This is in contrast to diabody conjugated with the ^{111}In-labeled active ester of DOTA (DOTA-NHS), which reached an uptake in the kidneys of 135%ID/g at 2 h, increased to 184%ID/g at 6 h, and declined to 126%ID/g by 24 h (*9*). Although the reduction in kidney uptake for the **2a** conjugate was an improve-

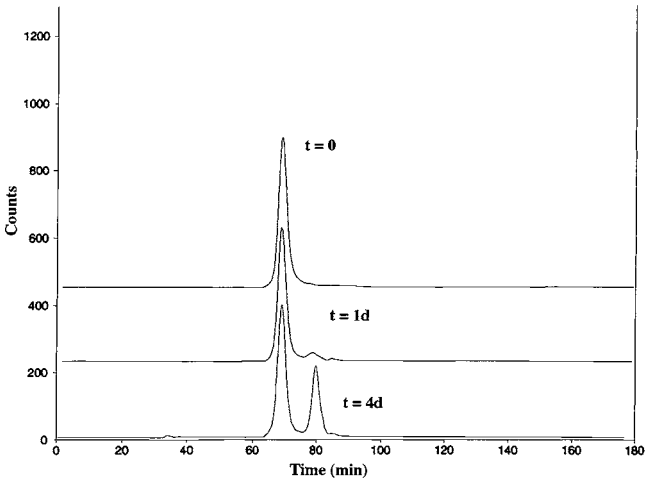


Figure 3. Stability study of [^{111}In] DOTA-GLGK(N^{ϵ}-mal). The sample was incubated at 37 °C in PBS/1% HSA and aliquots analyzed at indicated times by gel filtration on tandem Superose 6 columns as described in Methods. The %area of peak 1 (65 min) was 100% at $t = 0$, 91% at $t = 1$ d, and 66% at $t = 4$ d. The %area of peak 2 (80 min) was 34% at $t = 4$ d.

Table 2. Biodistribution of [^{111}In]DOTA-GLGK(N^{ϵ}-mal)−Cys-Diabody in Non-Tumor-Bearing Nude Mice[a]

	0 h	1 h	2 h	6 h	15 h	24 h
blood	21.00	5.51	3.92	1.45	0.30	0.14
	(0.95)	(0.96)	(0.33)	(0.09)	(0.03)	(0.02)
liver	25.82	23.87	21.42	21.01	13.78	13.78
	(3.55)	(4.25)	(1.66)	(2.03)	(0.92)	(1.64)
spleen	4.14	2.36	2.32	2.01	1.65	2.36
	(0.51)	(0.19)	(0.32)	(0.09)	(0.13)	(0.91)
kidney	17.03	57.72	66.17	81.99	78.85	71.09
	(2.63)	(7.98)	(4.69)	(8.14)	(4.35)	(10.45)
lung	6.45	2.67	2.27	1.27	0.74	0.57
	(0.39)	(0.21)	(0.19)	(0.03)	(0.02)	(0.12)
carcass	1.55	1.93	2.13	1.68	1.36	1.14
	(0.18)	(0.10)	(0.12)	(0.05)	(0.09)	(0.19)

[a] Five animals per group were injected with ^{111}In-labeled conjugate as described in Methods. The results are reported as mean %ID/g (±SD).

ment over the active ester of DOTA conjugated to diabody, **2a** conjugate was not studied further due to its inherent chemical lability at pH 7 and the unexplained reduction in immunoreactivity of its Cys-diabody conjugate (unsuitable for use in tumor bearing animals).

[^{111}In]DOTA-GLGK[N^{ϵ}-$(HVS)_2$]-Cys-diabody was injected into nude mice bearing human colon tumor xenografts and the biodistribution determined over 24 h (Table 3). The kidney levels reached a maximum of 52%ID/g at 2 h, maintained that level through 15 h, and declined to 45%ID/g by 24 h. In contrast to diabody conjugated with the active ester of DOTA (DOTA-NHS) the reduction in kidney uptake at 24 h and 2 h was 64% and 61%, respectively (Table 7). In addition, [^{111}In]DOTA-GLGK[N^{ϵ}-$(HVS)_2$]-cys-diabody showed a tumor uptake of 8%ID/g at 1h and 11%ID/g at 6 h with a slow decline thereafter (Table 3). This is similar to the tumor uptake in [^{111}In]DOTA-NHS-diabody which reached 13%ID/g at 2 h and remained constant through 6 h. The tumor-to-blood ratios for the two BCA-conjugates were very different at all time points: at 2 h (0.8 vs 4.6), 6 h (2.6 vs 39.1), and 24 h (12 vs 193). The higher T/B ratios for [^{111}In]DOTA-NHS-diabody are due to its very high blood clearance rate, probably due to the higher kidney clearance. Although the blood levels are very different for the two BCAs, tumor uptake was comparable in the

Table 3. Biodistribution of [^{111}In]DOTA-GLGK[N^{ϵ}-$(HVS)_2$]-Cys-Diabody in Nude Mice Bearing LS174T Xenografts[a]

	0 h	1 h	2 h	6 h	15 h	24 h
blood	32.68	13.01	9.31	4.35	1.81	0.77
	(2.95)	(2.03)	(1.16)	(0.69)	(0.22)	(0.07)
liver	7.81	9.50	9.48	13.52	9.91	11.80
	(0.25)	(0.87)	(0.35)	(0.65)	(1.99)	(1.12)
spleen	7.79	4.00	3.57	3.50	4.30	3.35
	(1.98)	(0.70)	(0.72)	(0.34)	(1.16)	(0.42)
kidney	16.94	50.04	52.19	53.61	55.35	44.59
	(3.88)	(4.85)	(5.51)	(3.20)	(3.71)	(4.79)
lung	13.59	5.92	4.29	3.10	2.20	1.58
	(3.04)	(0.63)	(0.38)	(0.46)	(0.25)	(0.10)
tumor	2.31	8.14	7.44	11.26	10.78	9.39
	(0.79)	(1.06)	(1.89)	(1.49)	(1.96)	(0.48)
carcass	3.21	3.60	3.48	3.39	2.89	2.63
	(0.18)	(0.27)	(0.32)	(0.29)	(0.16)	(0.33)

[a] Five animals per group were injected with ^{111}In-labeled conjugate as described in Methods. The results are reported as mean %ID/g (±SD).

Table 4. Biodistribution of [^{64}Cu]DOTA-GLGK[N^{ϵ}-$(HVS)_2$]−Cys-Diabody in Nude Mice Bearing LS174T Xenografts[a]

	0 h	1 h	2 h	4 h	16 h	24 h
blood	38.68	15.84	11.91	6.96	1.87	1.39
	(2.68)	(1.42)	(2.81)	(1.12)	(0.56)	(0.29)
liver	7.37	11.43	14.06	19.44	20.00	17.33
	(0.83)	(1.36)	(3.18)	(3.17)	(2.55)	(2.49)
spleen	7.74	3.61	3.97	3.94	5.01	3.61
	(1.91)	(0.33)	(1.07)	(0.56)	(2.54)	(1.08)
kidney	18.03	52.60	51.14	55.11	43.86	29.20
	(2.34)	(6.01)	(8.28)	(4.62)	(11.33)	(6.51)
lung	12.18	5.74	4.74	3.83	3.86	3.27
	(5.63)	(0.48)	(1.07)	(0.39)	(1.05)	(0.27)
tumor	1.51	7.85	10.23	13.98	13.37	11.90
	(0.07)	(2.60)	(4.78)	(2.13)	(1.72	(2.48)
carcass	2.56	3.31	3.33	3.44	2.59	2.40
	(0.11)	(0.25)	(0.33)	(0.38)	(0.30)	(0.23)

[a] Five animals per group were injected with ^{64}Cu-labeled conjugate as described in Methods. The results are reported as mean %ID/g (±SD).

two studies. Possible reasons for these differences are discussed later.

Since we are also interested in PET imaging radionuclides such as ^{64}Cu, we performed biodistribution studies on [^{64}Cu] DOTA-GLGK[N^{ϵ}-$(HVS)_2$]-Cys-diabody (Table 4). This study gave essentially identical results to [^{111}In]DOTA-GLGK[N^{ϵ}-$(HVS)_2$]-Cys-diabody (Table 3). The blood curves are nearly identical; the kidney uptake is identical except at the 24 h time point where the ^{64}Cu-labeled conjugate is lower; the liver uptake is slightly higher for the ^{64}Cu labeled conjugate, tumor uptake is slightly higher for the ^{64}Cu conjugate, and other tissues measured (spleen, lung, and carcass) are identical. Overall, the comparative biodistributions suggest that PET studies with the ^{64}Cu conjugate are feasible. The slightly higher liver levels have been reported for other ^{64}Cu conjugates and may be due to scavenging of ^{64}Cu from the lysosomal compartment in the liver (*1*).

[^{111}In]DOTA-GLGK(N^{ϵ}-AcBr)-Cys-diabody and Cys-diabody-N^{α}-BrAc-GLGK(N^{ϵ}-IT-VS-[^{111}In]DOTA) biodistributions were studied in nontumor bearing nude mice. The biodistributions of these BCA-conjugates (Tables 5 and 6) were similar to [^{111}In]DOTA-NHS-diabody, showing high kidney uptake at 2−6 h (e.g., 137−189%ID/g) and declining by 24h (e.g., 146%ID/g). Curiously, the blood levels of the Cys-diabody-N^{α}-BrAc-GLGK(N^{ϵ}-IT-VS-[^{111}In]DOTA were similar to [^{111}In]DOTA-GLGK[N^{ϵ}-$(HVS)_2$]-Cys-diabody. Thus, the high kidney levels did not

Table 5. Biodistribution of [^{111}In]DOTA-GLGK(N^{ϵ}-AcBr)−Cys-Diabody in Non-Tumor-Bearing Nude Mice[a]

	0 h	1 h	2 h	4 h	6 h	24 h
blood	36.35	9.16	5.96	4.11	2.40	0.18
	(4.30)	(1.09)	(0.98)	(0.33)	(0.26)	(0.04)
liver	6.27	4.27	4.72	4.95	5.66	5.03
	(0.63)	(0.13)	(0.95)	(0.36)	(0.31)	(0.79)
spleen	6.97	2.53	2.14	2.32	1.91	1.55
	(1.75)	(0.20)	(0.35)	(0.30)	(0.24)	(0.46)
kidney	14.56	105.67	122.01	143.83	153.31	134.39
	(2.61)	(21.24)	(13.43)	(16.12)	(12.28)	(15.80)
lung	10.55	4.00	3.53	3.18	2.19	1.13
	(1.30)	(0.27)	(0.46)	(0.85)	(0.13)	(0.34)
carcass	2.30	2.77	2.79	2.51	2.51	1.82
	(0.17)	(0.28)	(0.30)	(0.07)	(0.13)	(0.15)

[a] Five animals per group were injected with ^{111}In-labeled conjugate as described in Methods. The results are reported as mean %ID/g (±SD).

Table 6. Biodistribution of Cys-Diabody−(N^{α}-BrAc)-GLGK(N^{ϵ}-It-vs[^{111}In]DO3A) in Non-Tumor-Bearing Nude Mice[1]

	0 h	1 h	2 h	4 h	6 h	24 h
blood	42.15	13.94	6.77	3.47	2.82	0.25
	(3.09)	(2.78)	(2.31)	(0.48)	(0.38)	(0.03)
liver	7.66	5.70	6.26	6.14	6.93	4.79
	(0.61)	(0.56)	(1.27)	(0.74)	(0.14)	(0.52)
spleen	7.94	3.36	2.53	2.08	2.39	1.59
	(0.74)	(0.15)	(0.73)	(0.30)	(0.76)	(0.27)
kidney	18.10	92.46	137.02	149.98	189.17	145.55
	(2.34)	(7.94)	(46.41)	(18.46)	(34.88)	(13.52)
lung	11.40	5.43	3.63	2.51	2.15	0.96
	(0.73)	(0.78)	(0.42)	(0.18)	(0.24)	(0.11)
carcass	2.90	3.69	3.42	3.14	3.11	2.06
	(0.26)	(0.25)	(0.26)	(0.26)	(0.16)	(0.14)

[a] Five animals per group were injected with ^{111}In labeled conjugate as described in Methods. The results are reported as mean %ID/g (±SD).

Table 7. Comparative Kidney Uptake for [^{111}In]Diabody for Five BCAs[a]

BCA	2 h	24 h
[^{111}In]DOTA-NHS	135 (±19)	126 (±12)
[^{111}In]DOTA-GLGK(N^{ϵ}-mal)	66 (±5)	71 (±11)
[^{111}In]DOTA-GLGK[N^{ϵ}-(HVS)$_2$]	52 (±6)	45 (±5)
[^{64}Cu]DOTA-GLGK[N^{ϵ}-(HVS)$_2$]	51 (±8)	29 (±7)
[^{111}In]DOTA-GLGK(N^{ϵ}-AcBr)	122 (±13)	134 (±16)
BrAc-GLGK(N^{ϵ}-IT-VS-[^{111}In]DO3A)	137 (±46)	146 (±14)

[a] Data for the NHS active ester of diabody taken from Yazaki et al. (*9*). Data for the other four BCAs taken from Tables 2−6, this work. The results are reported as %ID/g (±SD).

necessarily dictate low blood levels as in the case of [^{111}In]DOTA-NHS-diabody. A comparison of the three BCA-conjugates for kidney uptake at 2 and 24h is shown in Table 7. Overall, this comparison demonstrates that the BCA DOTA-GLGK[N^{ϵ}-(HVS)$_2$] has the most substantial impact on reducing kidney uptake of the diabody.

DISCUSSION

Radiometal-labeled antibodies and their fragments exhibit high retention of radiolabel in tumor sites because of their relative inertness to metabolic action and clearance from the lysosomal compartment. Thus, ^{111}In-labeled whole antibodies have superior tumor uptake compared to radioiodine labeled antibodies that are rapidly metabolized in both tumor and normal tissues. In the case of antibody fragments, where rapid blood clearance results in comparatively lower tumor uptake, the use of radiometals is beneficial in that higher tumor retention is obtained. However, this advantage is offset by high kidney uptake due to rapid filtration of the antibody fragment, reabsorption by the kidney tubule, and retention of the metabolic products in the lysosomal compartment (*26*, *27*, *47*). A second approach to increase tumor retention is the use of bivalent antibody fragments, since monovalent fragments such as the scFv have poor tumor retention (*16*, *17*, *19*).

In this study, we have engineered both the antibody fragment and the BCA to maximize tumor retention and minimize kidney uptake. First, we chose the diabody as the lowest molecular size fragment that retains bivalency. Second, we engineered a C-terminal cysteine residue to allow site-specific conjugation at the resultant thiol group. The introduction of a C-terminal cysteine residue into recombinant antibodies has been successfully used by other investigators. For example, Pastan and co-workers (*48*) introduced a C-terminal cysteine into a scFv anti-Tac antibody, but due to its low molecular weight (25 kDa) the antibody had high kidney uptake. In contrast, our Cys-diabody construct was expressed as covalently linked dimers which could be separated into monovalent fragments under reducing, denaturating conditions (Figure 1). Although this result necessitated the reduction of the covalent disulfide bond prior to BCA conjugation, it should be noted that the recombinant fragment is still a dimer held together by noncovalent bonds as shown by its migration at 50 kDa when run on gel filtration prior to injection into animals. Third, we synthesized a BCA that contained both a cleavable peptide linker and a thiol-reactive group for conjugation to the reduced Cys-diabody.

The design of the BCA incorporated the metal binding macrocycle DOTA at the N-terminus of the peptide and a thiol reactive group on the ϵ-amino group of lysine at the C-terminus of the peptide. The overall strategy is similar that of Arano and co-workers (*39*) who showed that carboxypeptidase activity in the kidney tubule brush border was able to cleave the peptide bond of the lysine, thus releasing the antibody fragment attached to the ϵ-amino group of the lysine, from the rest of the peptide which contains the radiolabel (in their case, a radioiodinated hippuric acid residue). In their study they showed that they could reduce kidney uptake by 50−60% and that the α-carboxyl-group of the lysine was essential for the result. Although our radiolabel and antibody fragment differs from that of Arano and co-workers, the result was essentially the same. Compared to the ^{111}In-labeled-DOTA-active ester version of the diabody (*9*), for the ^{111}In-labeled-BCA DOTA-GLGK(N^{ϵ}-mal) conjugated to Cys-diabody there was a 50−60% reduction in kidney uptake (Table 7). This result was further improved by using the BCA DOTA-GLGK[N^{ϵ}-(HVS)$_2$], demonstrating that the nature of the chemical linkage from the antibody to the lysine is important. In comparing the two BCAs, it is also worth noting that the maleimide linkage in DOTA-GLGK(N^{ϵ}-mal) is inherently unstable at pH 7.0 (*41*). In fact, it is possible that some of the reduction in kidney uptake may be due to the hydrolysis of the succinimido bonds between the linker and the antibody. However, in unpublished studies with the bis-maleimidehexane-Cys-DOTA conjugated to Fab′ fragments, we obtained high kidney uptakes, comparable to the NHS active ester conjugates of DOTA to the diabody. Thus, we believe that the C-terminal Lys residue in the linker plays an important role, just as Arano and co-workers suggest.

Overall, DOTA-GLGK[N^{ϵ}-(HVS)$_2$] lowered kidney uptake by up to 73% (Table 7) while retaining equivalent tumor uptake (ca. 12%ID/g at 2−6 h) compared to the

NHS active ester conjugates of DOTA to the diabody. One of the fascinating differences between the two studies is the difference in blood levels, where the blood levels are higher for the BCA DOTA-GLGK[N^{ϵ}-$(HVS)_2$] over the entire 24 h period. This difference is not easily explained, since one would predict the same rate of kidney filtration for both conjugates with the only difference due to the proteolysis of the one, but not the other, prior to reabsorption in the proximal tubule cells. This suggests that blood clearance is not the only factor of kidney clearance in these two studies. Further studies are required to determine the mechanism behind this interesting finding. Since the biodistributions of ^{64}Cu and ^{111}In were almost identical, we conclude that DOTA is a suitable chelate for both radionuclides and that the ^{64}Cu-labeled conjugate can be used in PET studies.

After demonstrating the reduction in kidney uptake with the carboxypeptidase-cleavable linker, we synthesized a related BCA in which the chelator DOTA and the thiol-reactive group positions were exchanged on the peptide. This BCA-Cys-diabody conjugate also labeled well with ^{111}In, but showed high kidney uptake, equivalent to that seen with the ^{111}In-labeled-DOTA-active ester version of the diabody. Thus, it appears that the relative positions of the chelator and antibody attachment site are important. Since this aspect was not tested in the radioiodine labeled compound developed by Arano and co-workers, we cannot compare our result to the literature.

With these results in hand, we decided to explore other conjugation chemistries on the BCA that lowered the kidney uptake the most. In the BCA DOTA-GLGK[N^{ϵ}-$(HVS)_2$], the conjugation chemistry relied on a Michael addition reaction of the free thiol on the mildly reduced Cys-diabody to one of the vinyl groups on the BCA. The conjugation efficiency of the BCA to cys-diabody was rather low as judged by IEF (Figure 2, lane 3), and radiolabeling efficiency (8−50%, Table 1). In the BCA DOTA-GLGK(N^{ϵ}-AcBr), the conjugation chemistry involved alkylation of the free thiol group of the cys-diabody. This conjugation reaction was more efficient as judged by IEF (Figure 2, lane 5) and radiolabeling efficiency (85%, Table 1). Thus, from the chemistry standpoint the alkylation reaction is more efficient, but the biodistribution results show high kidney uptake for the alkylated conjugate. Possible explanations for this biological difference are (a) lysine with an acylated amino group may be a poor substrate for carboxypeptidase in the brush border of the kidney, and (b) the close proximity of the antibody fragment to the lysine may sterically inhibit the carboxypeptidase. The latter explanation does not explain why the N^{ϵ}-maleimide conjugate has reduced kidney uptake, but it would explain why the N^{ϵ}-$(HVS)_2$ conjugate is superior to the N^{ϵ}-maleimide conjugate. Clearly, further derivatives need to be synthesized to further explore the effect of the chemical attachment on the degree of kidney clearance.

CONCLUSION

This study demonstrates that the use of cleavable peptide linkers between the radiolabel and an antibody fragment is a feasible approach to lower kidney uptake while preserving good tumor uptake. This approach incorporates the advantage of using radiometals which have higher tumor uptake compared to radioiodine, and the use of a diabody, that due to its bivalent binding, has higher tumor uptake than scFv fragments. Although the kidney uptake is significantly reduced by the use of an appropriate linker, the chemical linkage between the linker and the antibody fragment plays a large role, and if properly manipulated, has the potential to further reduce kidney uptake. The ultimate goal of this work is to reduce maximal kidney uptake below 10% ID/g, a level shown to be safe in work with radiometal labeled intact antibodies. The incorporation of additional strategies, such as administration of D-lysine or the lowering of the antibody fragment pI, may further lower kidney uptake, allowing the routine use of radiometal labeled antibody fragments in the clinic.

ACKNOWLEDGMENT

The authors thank Stefanie Wright for the animal studies. This research was funded by NCI grant CA43904 (A.A.R. and J.E.S.) and the Department of the Army Grant DAMD 17-98-1-8031 (J.E.S.). T.O. was supported by grant no. 1998/0220 from the Norwegian Foundation for Health and Rehabilitation.

LITERATURE CITED

(1) Anderson, C. J., and Welch, M. J. Radiometal-labeled agents (non-technetium) for diagnostic imaging. (1999) *Chem. Rev. 99*, 2219−2234.

(2) Gansow, O. A. Newer Approaches to the Radiolabeling of Monoclonal Antibodies by Use of Metal Chelates. (1991) *Int. J. Radiat. Appl. Instrum. Part B Nucl. Med. Biol. 18*, 369−381.

(3) Meares, C. F. Chelating Agents for the Binding of Metal Ions to Antibodies. (1986) *Int. J. Radiat. Appl. Instrum. Part B Nucl. Med. Biol. 13*, 311−318.

(4) Liu, S., and Edwards, D. S. Bifunctional chelators for therapeutic lanthanide radiopharmaceuticals. (2001) *Bioconjugate Chem. 12*, 7−34.

(5) Bujis, W. C. A. M., Massuger, L. F. A. G., Claessens, R. A. M. J., Kenemans, P., and Corstens, F. H. M. Dosimetric evaluation of immunoscintigraphy using indium-111-labeled monoclonal antibody fragments in patients with ovarian cancer. (1992) *J. Nucl. Med. 33*, 1113−1120.

(6) Govindan, S. V., Shih, L. B., Goldenberg, D. M., Sharkey, R. M., Karacay, H., Donnelly, J. E., Losman, M. J., Hansen, H. J., and Griffiths, G. L. 90Yttrium-labeled complementarity-determining-region grafted monoclonal antibodies for radioimmunotherpay: radiolabeling and animal biodistribution studies. (1998) *Bioconjugate Chem. 9*, 773−782.

(7) Yemul, S., Leon, J. A., Pozniakoff, T., Esser, P. D., and Estabrook, A. Radioimmunoimaging of human breast carcinoma xenografts in nude mouse model with 111In labeled new monoclonal antibody EBA-1 and F(ab′)2 fragments. (1993) *Nucl. Med. Biol. 20*, 325−335.

(8) Yokota, T., Milenic, D. E., Whitlow, M., and Schlom, J. Rapid tumor penetration of a single-chain Fv and comparison with other immunoglobulin forms. (1992) *Cancer Res. 52*, 3402−3408.

(9) Yazaki, P. J., Wu, A. M., Tsai, S. W., Williams, L. E., Ikler, D. N., Wong, J. Y., Shively, J. E., and Raubitschek, A. A. Tumor targeting of radiometal labeled anti-CEA recombinant T84.66 diabody and T84.66 minibody: comparison to radioiodinated fragments. (2001) *Bioconjugate Chem. 12*, 220−8.

(10) Colcher, D., Goel, A., Pavlinkova, G., Beresford, G., Booth, B., and Batra, S. K. Effects of genetic engineering on the pharmokinetics of antibodies. (1999) *Q. J. Nucl. Med. 43*, 132−139.

(11) Buchegger, F. J., Haskell, C. M., Schreyer, M., Scazziga, B. R., Randin, S., Carrel, S., and Mach, J.-P. Radiolabeled Fragments of Monoclonal Antibodies Against Carcinoembryonic Antigen for Localization of Human Colon Carcinoma Grafted into Nude Mice. (1983) *J. Exp. Med. 158*, 413−427.

(12) Buchegger, F., Pelegrin, A., Delaloye, B., Bischof-Delaloye, A., and Mach, J.-P. Iodine-131-Labeled MAb F(ab′)$_2$ Fragments are More Efficient and Less Toxic than Intact Anti-CEA Antibodies in Radioimmunotherapy of Large Human

Colon Carcinoma Grafted in Nude Mice. (1990) *J. Nucl. Med. 31*, 1035−1044.

(13) Lamki, L. M., Patt, Y. Z., Rosenblum, M. G., Shanken, L. J., Thompson, L. B., Scheighardt, S. A., Frincke, J. M., and Murray, J. L. Metastatic colorectal cancer: radioimmunoscintigraphy with a stabilized In-111-labeled F(ab′)2 fragment on an anti-CEA monoclonal antibody. (1990) *Radiology 174*, 147−151.

(14) Zalutsky, M. R., Gatg, P. D., Friedman, H., and Bigner, D. D. Labeling monoclonal antibodies and $F(ab')_2$ fragments with the α-particle-emitting nuclide astatine-211: Preservation of immunoreactivity and in vivo localizing capacity. (1989) *Proc. Natl. Acad. Sci. U.S.A. 86*, 7149−7153.

(15) Sharkey, R. M., Motta-Hennessy, C., Pawlyk, D., Siegel, J. A., and Goldenberg, D. M. Biodistribution and radiation dose estimates for yttrium and iodine labeled monoclonal antibody IgG and fragments in nude mice bearing humnan colonic tumor xenografts. (1990) *Cancer Res. 50*, 2330−2336.

(16) Milenic, D. E., Yokota, T., Filupa, D. R., Finkelman, M. A. J., Dodd, S. W., Wood, J. F., Whitlow, M., Snoy, P., and Schlom, J. Construction, binding properties, metabolism, and tumor targeting of a single chain Fv derived from the pancarcinoma monoclonal antibody CC49. (1991) *Cancer Res. 51*, 6363−6371.

(17) Huston, J. S., George, A. J. T., Adams, G. P., Stafford, W. F., Jamar, F., Tai, M. S., McCartney, J. E., H., O., Heelan, B. T., Peters, A. M., Houston, L. L., Bookman, M. A., Wolf, E. J., and Weiner, L. M. Single chain Fv radioimmunotargeting. (1996) *Q. J. Nucl. Med. 40*, 320−333.

(18) Adams, G. P., McCartney, J. E., Tai, M.-S., Oppermann, H., Huston, J. S., Stafford, W. F., III., Bookman, M. A., Fand, I., Houston, L. L., and Weiner, L. M. Highly specific in vivo tumor targeting by monovalent and divalent formns of 741F8 anti-c-erbB-2 single chain Fv. (1993) *Cancer Res. 53*, 4026−4034.

(19) Adams, G. P., McCartney, J. E., Wolf, E. J., Eisenberg, J., Tai, M.-S., Huston, J. S., Stafford, W. F., III., Bookmann, M. A., and Weiner, L. M. Optimization of in vivo tumor targeting in SCID mice with divalent forms of 741F8 anti-c-erb-2 single chain Fv: effects of dose escalation and repeated i.v. administration. (1995) *Cancer Immunol. Immunother. 40*, 299−306.

(20) Mueller, B. M., Reisfeld, R. A., and Gillies, S. D. Serum half-life and tumor localization of a chimeric antibody deleted of the CH2 domain and directed against the disialoganglioside GD2. (1990) *Proc. Natl. Acad. Sci. U.S.A. 87*, 5702−5705.

(21) Ray, K., Embleton, M. J., Jailkhani, B. L., Bhan, M. K., and Kumar, R. Selection of single chain variable fragments (scFv) against the glycoprotein antigen of the rabies virus from a human synthetic scFv phage display library and their fusion with the Fc region of human IgG1. (2001) *Clin. Exp. Immunol. 125*, 94−101.

(22) Li, S. L., Liang, S. J., Guo, N., Wu, A. M., and Fujita-Yamaguchi, Y. Single-chain antibodies against human insulin-like growth factor I receptor: expression, purification, and effect on tumor growth. (2000) *Cancer Immunol. Immunother. 49*, 243−52.

(23) Shan, D., Press, O. W., Tsu, T. T., Hayden, M. S., and Ledbetter, J. A. Characterization of scFv-Ig constructs generated from the anti-CD20 mAb 1F5 using linker peptides of varying lengths. (1999) *J. Immunol. 162*, 6589−95.

(24) Hu, S.-Z., Shively, L., Raubitschek, A., Sherman, M., Williams, L. E., Wong, J. Y. C., Shively, J. E., and Wu, A. M. Minibody: a novel engineered anti-carcinoembryonic antigen antibody fragment (single chain Fv-CH3) which exhibits rapid high level targeting of xenografts. (1996) *Cancer Res. 56*, 3055−3061.

(25) Press, O. W., D., S., Howell-Clark, J., Eary, J., Appelbaum, F. R., Matthews, D., King, D. J., Haines, A., M., Hamann, P., Hinman, L., Shochat, D., and Bernstein, I. D. Comparative metabolism and retention of iodine-125, yttrium-90, and indium-111 radioimmunoconjugates by cancer cells. (1996) *Cancer Res. 56*, 2123−2129.

(26) Rogers, B. E., Franano, F. N., Duncan, J. R., Edwards, W. B., Anderson, C. J., Connett, J. M., and Welch, M. J. Identification of metabolites of 111In-diethylenetriaminepentaacetic acid monoclonal antibodies and antibody fragmens in vivo. (1995) *Cancer Res. 55*, 5714s−5720s.

(27) Tsai, S. W., Li, L., Williams, L. E., Anderson, A.-L., Raubitschek, A. A., and Shively, J. E. Metabolism and renal clearance of 111In-labeled DOTA conjugated antibody fragments. (2001) *Bioconjugate Chem. 12*, 264−270.

(28) Lang, L., Jagoda, E., Wu, C., Brechbiel, M. W., Gansow, O. A., Pastan, I., Paik, C. H., Carrasqillo, J. A., and Eckelman, W. C. Factors influencing the in vivo pharmokinetics of peptides and antibody fragments: the pharmokinetics of two PET-labeled low molecular weight proteins. (1997) *Q. J. Nucl. Med. 41*, 53−61.

(29) Schott, M. E., Milenic, D. E., Yokota, T., Whitlow, M., Wood, J. F., Fordyce, W. A., Cheng, R. C., and Schlom, J. Differential metabolic patterns of iodinated versus radiometal chelated anticarcinoma single-chain Fv molecules. (1992) *Cancer Res. 52*, 6413−6417.

(30) Williams, L. E., Wu, A. M., Yazaki, P. J., Liu, A., Raubitschek, A. A., Shively, J. E., and Wong, J. Y. Numerical selection of optimal tumor imaging agents with application to engineered antibodies. (2001) *Cancer Biother. Radiopharm. 16*, 25−35.

(31) Solling, K. and Morgenson, C. E. Studies on the mechanism of renal tubular protein reabsorption. (1977) *Proc. Eur. Dial. Transplant. Assoc. 14*, 543−549.

(32) Behr, T. M., Sharkey, R. M., Sgouros, G., Blumenthal, R. D., Dunn, R. M., Kolbert, K., Friffiths, G. L., Siegel, J. A., Becker, W. S., and Goldenberg, D. M. Overcoming the nephrotoxicity of radiometal labeled immunoconjugates. (1997) *Cancer 80*, 2591−2610.

(33) Arano, Y. Strategies to reduce renal radioactivity levels of antibody fragments. (1998) *Quart. J. Nucl. Med. 42*, 262−270.

(34) Behr, T. M., Sharkey, R. M., Juweid, M. E., Blumenthal, R. D., Dunn, R. M., Griffiths, G. L., Bair, H. J., Wolf, F. G., Becker, W. S., and Goldenberg, D. M. Reduction of the renal uptake of radiolabeled monoclonal antibody fragments by cationic amino acids and their derivatives. (1995) *Cancer Res. 55*, 3825−3834.

(35) Behr, T. M., Becker, W. S., Sharkey, R. M., Juweid, M. E., Dunn, R. M., Bair, H. J., Wolf, F. G., and Goldenberg, D. M. Reduction of renal uptake of monoclonal antibody fragments by amino acid infusion. (1996) *J. Nucl. Med. 37*, 829−833.

(36) Arano, Y., Mukai, T., Uezono, T., Wakisaka, K., Motonari, H., Akizawa, H., Taoka, Y., and Yokoyama, A. A biological method to evaluate bifunctional chelating agents to label antibodies with metallic radionuclides. (1994) *J. Nucl. Med. 35*, 890−898.

(37) Arano, Y., Wakisaka, K., Ohmono, Y., Uezono, T., Akizawa, H., Nakayama, M., Sakahara, H., Tanaka, C., Konishi, J., and Yokoyama, A. Assessment of radiochemical design of antibodies using an ester bond as the metabolizable linkage: evaluation of maleimidoethyl 3-(tri-*n*-butylstannyl)hippurate as a radioiodination reagent of antibodies for diagnostic and therapeutic applications. (1996) *Bioconjugate Chem. 7*, 628−637.

(38) Fujioka, Y., Arano, Y., Ono, M., Uehara, T., Ogawa, K., Namba, S., Saga, T., Nakamoto, Y., Mukai, T., Konishi, J., and Saji, H. Renal metabolism of 3′-iodohippuryl N^{ϵ}-maleoyl-L-lysine (HML)-conjugated Fab fragments. (2001) *Bioconjugate Chem. 12*, 178−185.

(39) Arano, Y., Fujioka, Y., Akizawa, H., Ono, M., Uehara, T., Wakisaka, K., Nakayama, M., Sakahara, H., J., K., and Saji, H. Chemical design of radiolabeled antibody fragments for low renal radioactivity levels. (1999) *Cancer Res. 59*, 128−134.

(40) Wu, A. M., Williams, L. E., Zieran, L., Padma, A., Sherman, M., Bebb, G. G., Odom-Maryon, T., Wong, J. Y. C., Shively, J. E., and Raubitschek, A. A. Anti-carcinoembryonic antigen (CEA) diabody for rapid tumor targeting and imaging. (1999) *Tumor Targeting 4*, 1−12.

(41) Lewis, M. R., and Shively, J. E. Maleimidocysteineamido-DOTA derivatives: new reagents for radiometal chelate conjugation to antibody sulfhydryl groups undergo pH-dependent cleavage reactions. (1998) *Bioconjugate Chem. 9*, 72−86.

(42) Yazaki, P. J., Shively, L., Clark, C., Cheung, C. W., Le, W., Szpikowska, B., Shively, J. E., Raubitschek, A. A., and Wu, A. M. Mammalian expression and hollow fiber bioreactor production of recombinant anti-CEA diabody and minibody for clinical applications. (2001) *J. Immunol. Methods 253*, 195−208.

(43) Li, M., and Meares, C. F. Synthesis, Metal Chelate Stability Studies, and Enzyme Digestion of a Peptide-Linked DOTA Derivative and Its Corresponding Radiolabeled Immunoconjugates. (1993) *Bioconjugate Chem. 4*, 275−283.

(44) Williams, L. E., Lewis, M. R., Bebb, G. G., Clarke, K. G., Odom-Maryon, T. L., Shively, J. E., and Raubitschek, A. A. Biodistribution of ^{111}In- and ^{90}Y-Labeled DOTA and Maleimidocysteineamido-DOTA Conjugated to Chimeric Anti-Carcinoembryonic Antigen Antibody in Xenograft-Bearing Nude Mice: Comparison of Stable and Chemically Labile Linker Systems. (1998) *Bioconjugate Chem. 9*, 87−93.

(45) Meares, C. F., McCall, M. J., Reardan, D. T., Goodwin, D. A., Diamanti, C. I., and McTigue, M. Conjugation of Antibodies with Bifunctional Chelating Agents: Isothiocyanate and Bromoacetamide Reagents, Methods of Analysis, and Subsequent Addition of Metal Ions. (1984) *Anal. Biochem. 142*, 68−78.

(46) Li, L., Tsai, S. W., Anderson, A.-L., Keire, D. A., Raubitschek, A. A., and Shively, J. E. Vinyl sulfone bifunctional derivatives of DOTA allow sulfhydryl or amino directed coupling to antibodies. Conjugates retain immunoreactivity and have similar biodistributions. (2002) *Bioconjugate Chem. 13*, 110−115.

(47) Duncan, J. R., Stephenson, M. T., Wu, H. P., and Anderson, C. J. Indium-111-diethylenetriamine pentaacetic acid octreotide is delivered in vivo to pancreatic, tumor cell, renal, and hepatocyte lysosomes. (1997) *Cancer Res. 57*, 659−671.

(48) Kim, I. S., Yoo, T. M., Kobayashi, H., Kim, M. K., Le, N., Wang, Q. C., Pastan, I., Carrasqillo, J. A., and Paik, C. H. Chemical modification to reduce renal uptake of disulfide bonded variable region fragment of anti-Tac monoclonal antibody labeled with 99mTc. (1999) *Bioconjugate Chem. 10*, 447−453.

BC025565U

A Biomimetic pH-Responsive Polymer Directs Endosomal Release and Intracellular Delivery of an Endocytosed Antibody Complex

Chantal A. Lackey,[†] Oliver W. Press,[§] Allan S. Hoffman,*[,†] and Patrick S. Stayton*[,†]

Department of Bioengineering, University of Washington, Seattle, Washington, and Department of Medicine, University of Washington, Seattle, Washington. Received April 21, 2001;
Revised Manuscript Received March 15, 2002

Poly(propylacrylic acid) (PPAAc) is a synthetic pH-responsive polymer that has been shown to disrupt cell membranes at low pH values typical of the endosome, but not at physiological pH, suggesting its use as an endosomal-releasing agent [Murthy et al. *J. Controlled Release 61*, 137−43]. We have constructed an antibody-targeted biotherapeutic model to investigate whether PPAAc can enhance intracellular trafficking of proteins to the cytoplasm. A ternary complex composed of a biotinylated anti-CD3 antibody, streptavidin, and biotinylated PPAAc was fluorescently labeled, and its intracellular fate was analyzed by confocal microscopy, flow cytometry, and quantitative western blotting of cell fractionates. The 64.1 anti-CD3 antibody was previously shown to direct receptor-mediated endocytosis in the Jurkat T-cell lymphoma cell line and was rapidly trafficked from the endosome to the lysosomal compartment. The antibody−streptavidin complex was also rapidly internalized to the endosomal/lysosomal compartment and retained there, as evidenced by punctate regions of fluorescence observed by confocal fluorescence microscopy. In samples containing the ternary complex of antibody, streptavidin, and PPAAc−biotin, diffuse fluorescence in the cytoplasm was observed, indicating that PPAAc enhanced translocation to the cytoplasm. This was confirmed by western blotting analysis of the isolated cytoplasm. Flow cytometry results demonstrated that neither streptavidin nor PPAAc caused nonspecific uptake of the complex, nor did they inhibit antibody-mediated endocytosis. The striking enhancement of protein delivery to the cytoplasm by complexed PPAAc suggests that this polymer could provide a new delivery agent for theapeutic, vaccine, and diagnostics development.

INTRODUCTION

The delivery of biotherapeutic agents such as DNA or proteins to a cell is often limited by intracellular trafficking barriers (*1*). Internalized biomolecular complexes are generally trafficked rapidly from early endosomes to late endosomes and finally to lysosomes where they are degraded (*2*). The processing of internalized complexes is tied to the increasingly acidic environment as they pass along the endocytic pathway, which is generated by ATP-dependent proton pumps in the membranes of the endocytic vesicles. The lowered pH and accompanying compartmental microenvironment changes are connected to alterations in protease activity, protein unfolding, and receptor−ligand interactions (*3*). Most internalized complexes are not released into the cytoplasm of the cell, including complexes that are readily endocytosed via specific receptor-mediated pathways such as the low-density lipoproteins (LDL) pathway (*2*).

For fragile biomolecular drugs such as DNA, RNA, peptides, and proteins, and particularly for targeted biotherapeutics, this barrier to cytoplasmic entry represents a significant drug delivery challenge. We have been investigating the use of pH-sensitive α-alkyl acrylic acid polymers that are capable of disrupting cell membranes at the lowered pH environment, similar to that in endosomes, while being nondisruptive at a physiologic pH of 7.4. These polymers interact with phospholipid bilayers in a pH-dependent manner (*4*). We have previously shown that poly(propylacrylic acid) (PPAAc), shown in Figure 1A, efficiently induces red blood cell hemolysis at pHs similar to those of the endosome, while being nondisruptive at physiological pH (*5*). We have shown that PPAAc also retains its ability to disrupt red blood cell membranes in a pH- and concentration-dependent manner when it is complexed to a protein (*6*).

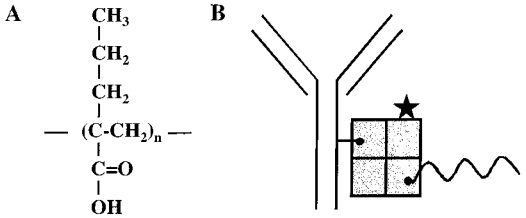


Figure 1. (A) Structure of poly(propylacrylic acid) (PPAAc). (B) Schematic of model biotinylated 64.1 antibody−streptavidin−biotinylated PPAAc complex.

Because red blood cell hemolysis has been correlated with endosomal release (*7*), these synthetic pH-responsive polymers may increase the intracellular efficacy of "fragile" therapeutics internalized via endocytosis. For example, the incorporation of pH-responsive polymers could enhance the endosomal translocation of immunotoxins to the cytosol, increasing access to target ribosomes. In this study, we have characterized the changes in intracellular trafficking elicited by PPAAc of a model antibody-

* Correspondence should be addressed to Allan S. Hoffman or Patrick S. Stayton, Department of Bioengineering, Box 352255, or Box 351721, respectively, University of Washington, Seattle, WA 98195. A.S.H.: Telephone: 206-543-9423. Fax: 206-543-6124. E-mail: hoffman@u.washington.edu. P.S.S.: Telephone: 206-685-8148. Fax: 206-685-8256. E-mail: stayton@u.washington.edu.

[†] Department of Bioengineering, University of Washington.

[§] Department of Medicine, University of Washington.

10.1021/bc010053l CCC: $22.00 © 2002 American Chemical Society
Published on Web 07/25/2002

targeted protein complex. This model is a ternary complex composed of a biotinylated anti-CD3 antibody, streptavidin, and end-biotinylated PPAAc. The monoclonal anti-CD3 antibody 64.1 is a murine IgG2a which is internalized in large numbers by receptor-mediated endocytosis. It is rapidly trafficked to the lysosome for degradation, with minimal translocation from the endosome to the cytoplasm. The 64.1 antibody has been extensively studied for immunotherapy and immunotoxin development (*8*−*11*) and thus serves as an excellent model system for evaluating endosomal release strategies.

EXPERIMENTAL PROCEDURES

Antibody Conjugation. MoAb 64.1 is a murine IgG2a directed against the human CD3 ϵ chain T-cell antigen. MoAb 64.1 was purified from ascitic fluid by affinity chromatography on Sepharose-staphylococcal Protein A (*12*). Protein concentrations were determined using the BCA assay following the recommendations of the manufacturer (Pierce). The antibody was biotinylated using sulfosuccinimidyl 6-(biotinamido)-6-hexanoate (EZ-link Sulfo-NHS-LC−Biotin, Pierce). The NHS-LC-biotin was dissolved in water at a concentration of 20 mg/mL, and 6.4 μL was added to 2.5 mL of the antibody, in 0.1 M sodium phosphate, 0.15 M NaCl, pH 7.4, at a concentration of 2.3 mg/mL. The reaction was allowed to proceed for 30 min at room temperature, followed by purification using a PD-10 desalting column (Pharmacia) to remove unreacted biotin. Fractions containing protein were detected by absorbance at 280 nm and pooled. The protein concentration was determined using the BCA assay (Pierce), and the degree of biotinylation was determined using the avidin−HABA assay, as described previously (*6*). Briefly, avidin was dissolved in 3 mL of 0.1 M sodium phosphate, 0.15 M NaCl, pH 7.4. 4′-Hydroxyazobenzene-2-carboxylic acid (HABA) (Sigma) was dissolved in 10 mM NaOH at a concentration of 2.42 mg/mL (10 mM), and 75 μL was added to the protein. D-Biotin (Sigma) was dissolved in 0.1 M sodium phosphate, 0.15 M NaCl, pH 7.4, at a concentration of 0.5 mM. This solution was added in 10 μL aliquots to the protein−HABA complex, while the absorbance at 500 nm was measured after each addition. By plotting the absorbance at 500 nm versus the amount of biotin added, a calibration curve was constructed. In parallel, incremental amounts of MoAb 64.1-biotin were added to the protein and HABA solution, and the absorbance at 500 nm was measured. The slope of the curve was compared to the calibration curve to determine the biotin concentration, which in conjunction with the protein concentration obtained from the BCA assay yielded the degree of biotinylation.

Streptavidin Labeling. Wild-type streptavidin was expressed and purified as previously described (*13*). It was labeled using Oregon Green (Molecular Probes). The fluorophore was dissolved in DMSO at a concentration of 10 mg/mL, and 40 μL was added to 4 mg of streptavidin in 0.1 M sodium bicarbonate, pH 8.3. The reaction was performed for 1 h at room temperature, followed by purification using a PD-10 desalting column. Fractions containing protein were detected by the absorbance at 280 nm and pooled. Protein concentration and degree of labeling were determined spectrophotometrically. The protein concentration was determined by subtracting 0.12 $\times$ $A_{496\ nm}$ of the fluorophore from $A_{280\ nm}$ of the protein, and using an extinction coefficient of 136000. The degree of labeling was calculated by dividing the $A_{496\ nm}$ of the fluorophore by the molar concentration of the protein, and the extinction coefficient of 70000, according to manufacturer instructions.

Polymer Preparation. Amine-terminated PPAAc (PPAAc-NH_2) was synthesized and end-biotinylated as previously described (*5*, *6*). The propyl acrylic acid monomer (*5*) was mixed with 1 mol % initiator (azobis-(isobutyronitrile)) and 4 mol % chain transfer agent (cysteamine), and polymerized at 60 °C for 24 h to prepare amine-terminated polymers. Polymerization reactions were performed in bulk at 60 °C for 24 h. Polymer purification proceeded by dissolving the polymer in methanol and precipitating in diethyl ether three times.

The weight-averaged molecular weight of PPAA was 61 kD as determined by gel permeation chromatography with PEG standards using Ultrahydrogel 250 and 1000 columns connected in series (Waters Corporation, Milford, MA). A PI of 2.11 was calculated by manual integration of the GPC curve. PPAAc-NH_2 was end-biotinylated using sulfosuccinimidyl 6-(biotinamido)-6-hexanoate (EZ-Link Sulfo-NHS-LC−Biotin, Pierce). PPAAc-NH_2 was dissolved in 0.1 M sodium phosphate, 0.15 M NaC1, pH 7.4. The NHS-LC-biotin was dissolved in water at a concentration of 20 mg/mL and added to the polymer at a 20-fold molar excess. This was reacted for 2 h at room temperature. The biotinylation was repeated using a 15-fold molar excess of biotin to maximize the yield of biotinylated polymer molecules. The samples were purified using a PD-10 desalting column (Pharmacia) in order to ensure that all the free biotin was removed. Absorbance at 220 nm was used to detect fractions containing polymer, and these fractions were subsequently pooled. The quantity of biotinylated polymer was determined using the HABA assay (data not shown).

Preparation of Ternary Ab/SA/PPAAc Complex. The MoAb 64.1-biotin/streptavidin/PPAAc−biotin complex was assembled by mixing together the three components at a 1:1:1 molar ratios. SDS−PAGE was used to characterize the ternary complex, along with controls of the MoAb 64.1-biotin complexed to streptavidin, and physical mixtures of the proteins and PPAAc-NH_2. In addition, controls were run with nonbiotinylated MoAb 64.1, as well as without a targeting antibody.

Uptake of Biomolecule/Polymer Complex. A malignant T-(Jurkat) lymphoma cell line was maintained in log-phase growth in RPMI medium supplemented with 12% fetal calf serum, 2 mM glutamine, and 1 mM pyruvate at 37 °C in a 5% carbon dioxide atmosphere. Jurkat cells were plated at a density of 10^5 cells per well in 0.2 mL RPMI medium in a 96-well microtiter plate. Triplicate samples were prepared in 20 μL 0.1 M sodium phosphate, 0.15 M NaC1, pH 7.4, and incubated with the cells for 4 h at 37 °C in a 5% carbon dioxide atmosphere. The cells were washed twice with 0.2 mL of 0.1 M sodium phosphate, 0.15 M NaCl, pH 7.4, and then resuspended in 0.2 mL of 0.1 M sodium phosphate, 0.15 M NaCl, pH 7.4, with 10 μL of propidium iodide (50 μg/mL in 0.1 M sodium phosphate, 0.15 M NaCl, pH 7.4) for analysis on a Becton Dickinson FACScan analyzer, with excitation at 488 nm. The data collected included forward scatter (FSC), side scatter (SSC), fluorescence-1 (FL-1, Oregon Green), and fluorescence-3 (FL-3, propidium iodide). The instrument settings were E-1, 335V, 452V, and 443V, respectively. In all analyses, viable cells were gated based on their ability to exclude propidium iodide, and FL-1 results are reported for this population. In the first set of samples, the amount of antibody was held constant at 2 μg/10^5 cells, while varying the sample composition to study the effects of polymer incorporation and to compare

physical mixtures with molecular complexes. The number of cells that had taken up the labeled streptavidin was determined by gating cells with FL-1 greater than 9. Control wells with no labeled protein added showed negligible numbers of cells with fluorescence intensity above this level. In the second set of samples, the amount of targeting antibody was varied to verify that the uptake was specifically mediated. Samples containing 1 , 2, and 5 μg of antibody per 10^5 cells were studied both with and without complexed PPAAc−biotin. The mean fluorescence (FL-1) of the total cell population was reported in order to represent the degree of uptake of the labeled biomolecular complex.

Optical Microscopy. Confocal microscopy was used to visualize the intracellular distribution of fluorescently labeled streptavidin. Samples were incubated with Jurkat cells as described for the uptake study. The cells were washed twice and then resuspended in 20 μL of 0.1 M sodium phosphate, 0.15 M NaCl, pH 7.4, mounted on glass slides, and coverslipped for imaging using a BioRad MRC-1024 scanning confocal microscope. Images were acquired using a 63× objective and a 5 μM diameter iris, yielding images with an area of 501.3 μm^2. The fluorescently labeled streptavidin was detected by photomultiplier 2.

Western Blot Analysis of Antibody Compartmentalization. Jurkat cells were incubated with the molecular complexes at a ratio of 20 μg antibody/10^7 cells in 5 mL of RPMI medium. Cells were incubated with duplicate samples of MoAb 64.1-biotin/streptavidin, MoAb 64.1-biotin/streptavidin/PPAAc−biotin, and MoAb 64.1-biotin/streptavidin + PPAAc-NH_2 for 4 h at 37 °C in a 5% carbon dioxide atmosphere. The cells were washed twice with 1 mL 0.1 M sodium phosphate, 0.15 M NaCl, pH 7.4, suspended in 0.5 mL of TES buffer (10 mM triethanolamine, 1 mM EDTA, and 0.25 M sucrose, pH 7.5), homogenized with 30 strokes of a Dounce homogenizer (Kontes Inc.), and centrifuged for 10 min at 250*g* to sediment nuclei and unbroken cells. This crude homogenate was analyzed by western blotting for one set of samples. For the second set of samples, the homogenate was ultracentrifuged at 134000*g* for 1 h to sediment vesicular components. Western blotting was used to quantitate cytoplasmic delivery of the antibody upon incorporation of the polymer into the antibody/streptavidin complex. SDS−PAGE samples were prepared by mixing 20 μL of the homogenized cell samples with 20 μL of 2x SDS−PAGE sample buffer. Precast tris-glycine gels with a gradient of 4−20% (Novex) were run at 130 V for approximately 90 min, until the dye front had reached the end of the gel. The proteins were transferred to a PVDF membrane by running the blotting apparatus for 2 h at 70 V at 4 °C to prevent overheating. The membrane was suspended in blocking buffer (10 mM Tris-HCl pH 7.5, 100 mM NaCl, 0.1% Tween 20, 5% nonfat powdered milk), overnight at 4 °C with agitation. The membrane was stained with goat-anti-mouse horseradish peroxidase (Pierce) at a 1:20000 dilution in the blocking buffer for 1 h at room temperature with rocking. The PVDF was then washed 6 × 10 min with the blocking buffer with no milk. The blot was developed with Super-Signal West Dura Extended Duration Substrate (Pierce) for 5 min.

RESULTS

Characterization of Biomolecular Conjugates. The 64.1 antibody was biotinylated at a biotin/antibody ratio of 3.3, as determined by the avidin−HABA assay in conjunction with the BCA assay. The ability of the biotinylated antibody to bind streptavidin was verified using SDS−PAGE. In all cases, the molecules were mixed at equimolar ratios. This corresponded to 20 μg of antibody (MW 150 kDa), 7 μg of streptavidin (MW 52.8 kDA), and 8 μg of PPAAc (MW 60 kDa) per well. MoAb 64.1-biotin migrated equivalently to the unmodified antibody, yielding a band with a molecular weight of 150 kDa. The unmodified streptavidin and antibody ran at molecular weights of 60 kDa and l50 kDa, respectively. These individual bands disappeared after mixing streptavidin with biotinylated 64.1, and a corresponding band of approximately 200 kDa MW appears. This change in migration is not observed when the unmodified antibody is mixed with streptavidin, demonstrating that complexation is biotin-dependent. When PPAAc−biotin is mixed with streptavidin, the apparent molecular weight of the protein is shifter lower, due to the negative charge introduced by the polymer. The complexation is stoichiometric as the uncomplexed streptavidin band at approximately 60 kDa is no longer visible. There was also a shift to lower apparent molecular weight when the ternary complex consisting of biotinylated antibody, streptavidin, and PPAAc−biotin was electrophoresed. This is consistent with previous results showing that the negatively charged polymer increases migration of the complex toward the cathode, despite its large size.

Uptake of Biomolecule/Polymer Complex. Flow cytometry was used to quantitate the uptake of the antibody conjugates. Test samples included cells incubated with streptavidin alone, MoAb 64.1-biotin/streptavidin, MoAb 64.1-biotin/streptavidin/PPAAc−biotin, MoAb 64.1-biotin/streptavidin + PPAAc-NH_2, MoAb64.1 + streptavidin, MoAb64.1 + streptavidin/PPAAc−biotin, and streptavidin/PPAAc−biotin. These were compared to control samples containing only the cells. All samples contained equimolar amounts of the three components, with 2 μg of antibody per 10^5 cells. To verify that the uptake of the complex was mediated by antibody binding and unaffected by the complexation of streptavidin or PPAAc to the antibody, the fraction of fluorescent cells was measured for all samples. As seen in Figure 2, the percent of fluorescent cells remains constant in all samples in which the labeled streptavidin is targeted by the biotinylated antibody. No uptake of the labeled streptavidin is observed in samples without antibody, or with nonbiotinylated antibody, indicating that the complexation of the antibody is necessary to direct the internalization of the streptavidin moiety. The complexation or physical mixing of PPAAc does not inhibit the receptor-mediated endocytosis. Additionally, neither the streptavidin or the polymer cause any nonspecific uptake, as demonstrated by the fact that cell fluorescence is only seen in samples containing the MoAb 64.1-biotin. The dose dependence of the antibody-targeted internalization was also characterized. In Figure 3, the amount of antibody incubated with the cells was varied, while maintaining a MoAb 64.1-biotin/streptavidin/PPAAc−biotin complexation ratio of 1:1:1. All samples contained MoAb 64.1-biotin and streptavidin with either 1 , 2 , or 5 μg of antibody per 10^5 cells, and some contained PPAAc−biotin, as denoted in the figure legend. As shown by the mean fluorescence of the samples, the total uptake of the complex is controlled by the antibody and is unaffected by the presence of either complexed PPAAc−biotin or free PPAAc-NH_2.

Endosomal Release of Biomolecule/Polymer Complex. Visualization of the intracellular trafficking of the complex was achieved using confocal microscopy and

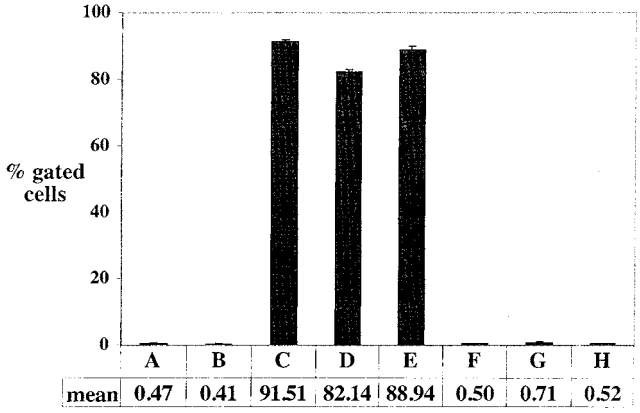


Figure 2. Efficiency of Jurkat cell uptake of antibody/streptavidin/polymer complexes after 4 h incubation in serum-containing medium at 37 °C. Streptavidin was labeled with Oregon Green as described in Materials and Methods. The following samples were characterized to test the specificity of antibody-mediated uptake and the effect of biotin-mediated complexation of streptavidin and PPAAc: (A) Jurkat cell control in culture medium, (B) streptavidin alone control, (C) MoAb 64 1-biotin/streptavidin, (D) MoAb 64.1- biotin/streptavidin/PPAAc−biotin, (E) MoAb 64.1-biotin/streptavidin + PPAAc-NH_2 control, (F) MoAb 64.1 + streptavidin control, (G) MoAb 64.1 + streptavidin/PPAAc−biotin control, and (H) streptavidin/PPAAc−biotin control. The results demonstrate that uptake is mediated by the MoAb 64.1 and not significantly affected by streptavidin or PPAAc complexation.

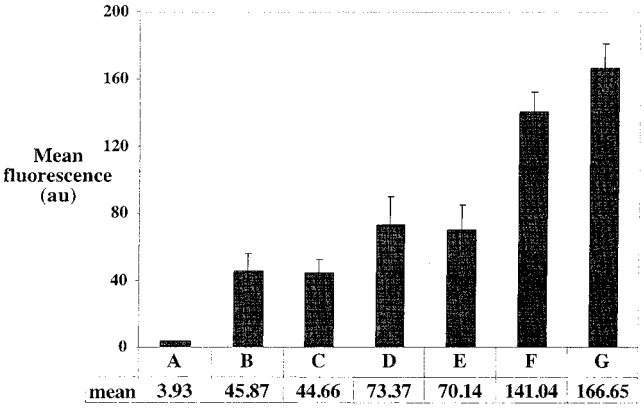


Figure 3. Fluorescence intensity dependence on the amount of antibody targeted to Jurkat cells, after 4 h incubation in serum-containing medium at 37 °C. All samples contained MoAb 64.1-biotin and Oregon Green labeled streptavidin (2.4 fluorophores per protein as determined by the absorbance and extinction coefficients for protein and label at 280 and 496 nm, respectively), with PPAAc−biotin added in the designated samples, all at a 1:1:1 molar ratio. The samples studied were cells incubated with (A) cell culture medium alone, (B) l μg of MoAb 64.1, (C) 1 μg of MoAb 64.1 with PPAAc−biotin, (D) 2 μg of MoAb 64.1, (E) 2 μg of MoAb 64.1 with PPAAc−biotin, (F) 5 μg of MoAb 64.1, and (G) 5 μg of MoAb 64.1 with PPAAc−biotin.

fluorescently labeled streptavidin. Representative images of single cells at roughly their midplane, 4 h after addition of the antibody complexes, are shown in Figure 4. In Figure 4A, the diffuse cytoplasmic staining is achieved upon incorporation of PPAAc−biotin into the biomolecular complex. In contrast, samples with no polymer show punctate fluorescence, indicating confinement of the complex within the endosomal/lysosomal vesicles of the cell, as shown in Figure 4B. Samples incubated with nonbiotinylated PPAAc also displayed punctate fluorescence (data not shown). Equivalent fluorescence localization was reproducibly observed in many fields of view, as well as by fluorescence microscopy on multiple days. In all samples without PPAAc, only punctate fluorescence was observed. In samples containing PPAAc−biotin, roughly half of the cells displayed diffuse cytoplasmic fluorescence after 4 h, comparable to that in Figure 4A. These results indicate that the complexation of PPAAc−biotin with the targeted biomolecule enables its release from the endosome to the cytoplasm.

Quantitation of Cytoplasmic Delivery. The total cell homogenate of the cells was compared to the isolated cytoplasm for the localization of the targeted molecular complexes with and without the polymer. The odd numbered lanes in the western blot of Figure 5 contain the total homogenate, while the even numbered lanes contain the isolated cytoplasmic contents.

In the first two lanes, which contain the MoAb 64.1-biotin/streptavidin complex, there is no detectable band in the isolated cytoplasm, indicating that this molecular complex is not released at significant levels into the cytoplasm at a 4 h timepoint, but is retained in the endosomal/lysosomal pathway as evidenced by the band in whole cell contents. In contrast, lanes 3 and 4 demonstrate that a large fraction of the MoAb 64.1-biotin/streptavidin/ PPAAc−biotin is released into the cytoplasm. The cytoplasmic band has 73% the intensity of the crude homogenate band, as determined by quantitative densitometry. Finally in lanes 5 and 6, the physical mixture of the polymer with the antibody/streptavidin complex does yield some release into the cytoplasm, but significantly less than that evidenced with the biotinylated polymer. The cytoplasmic band intensity is 29% of the whole cell band intensity for this sample.

DISCUSSION

The challenge of delivering proteins to the cytoplasmic compartment represents a significant barrier for the development of protein therapeutics and vaccines. Internalized proteins enter the intracellular trafficking pathway through endosomes and are generally subsequently localized to the lysosomal compartment where they are degraded. Several approaches have been taken to manipulate the intracellular trafficking pathways of biomolecular therapeutics, including the addition of compartment-targeting amino acid sequences (*14*−*16*) and peptides that aid transport either from the endosome (*17*, *18*, *7*) or across the cellular membrane (*19*−*21*).

We have been investigating the use of the polymer PPAAc as a pH-dependent, membrane-disrupting agent that can aid escape of biomolecular therapeutics from the endosome to the cytoplasm. Previous studies have demonstrated that PPAAc can enhance the transfection-efficiency of lipoplex/plasmid delivery systems (*22*). The PPAAc is designed to be inactive at physiological pH, while becoming membrane active in the lower pH environment of developing endosomes, thereby enhancing transport of biomolecules across the endosomal membrane. In this study, we tested whether PPAAc could enhance the cytoplasmic delivery of a model antibody therapeutic. The MoAb 64.1 is an anti-CD3 antibody that has been extensively characterized as a T-cell lymphoma targeting agent. This antibody was chosen because it is rapidly localized to the lysosome after receptor-mediated endocytosis (*8*) and can thus be used to evaluate whether PPAAc promotes cytoplasmic delivery.

Streptavidin has been exploited in this construct as a linker molecule. Because the antibody and the polymer are both easily biotinylated, the formation of the ternary complex is very efficient, as it is driven by biotin/streptavidin affinity. Previous studies have shown that

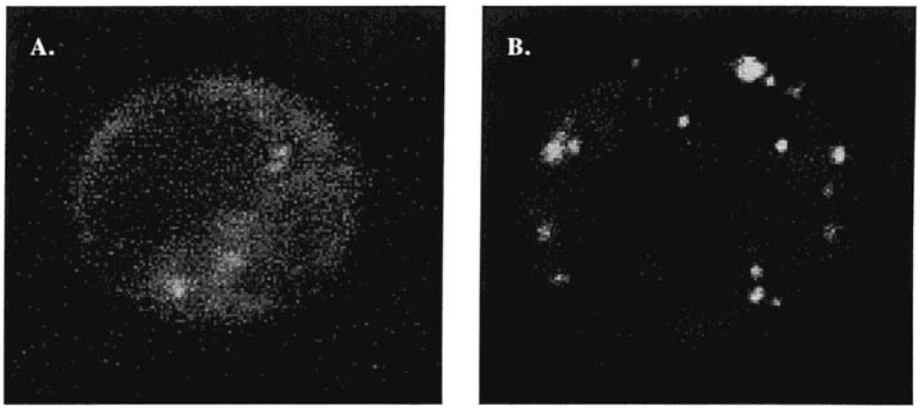


Figure 4. Confocal microscopy analysis of intracellular Oregon-Green-labeled streptavidin after receptor-mediated uptake of ternary antibody−streptavidin−PPAAc complexes. Confocal images of single Jurkat cell midplanes for (A) Jurkat cells incubated with ternary complexes composed of 2 μg MoAb/10^5 cells and equimolar MoAb 64.1-biotin/streptavidin/PPAAc−biotin ratios and (B) Jurkat cells incubated with 2 μg MoAb/10^5 cells and equimolar MoAb 64.1-biotin/streptavidin without PPAAc. Cells were incubated for 4 h in serum-containing medium at 37 °C and subsequently analyzed on a BioRad MRC-1024 scanning confocal microscope using a 63× objective.

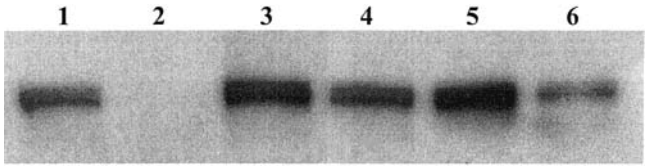


Figure 5. Quantitative western blot analysis of whole cell and isolated cytoplasmic homogenates. Jurkat cells were incubated with 20 μg antibody/10^7 cells and equimolar streptavidin, with and without equimolar biotinylated PPAAc. In addition, the MoAb−streptavidin complexes were physically mixed with PPAAc to quantitate intracellular localization after trans-uptake. The gel lanes were (1) MoAb 64.1-biotin/streptavidin whole cell homogenate, (2) MoAb 64.1-biotin/streptavidin isolated cytoplasmic homogenate, (3) MoAb 64.1-biotin/streptavidin/PPAAc−biotin whole cell homogenate, (4) MoAb 64.1-biotin/streptavidin/PPAAc−biotin isolated cytoplasmic homogenate, (5) MoAb 64.1-biotin/streptavidin + PPAAc-NH_2 whole cell homogenate, and (6) MoAb 64.1-biotin/streptavidin + PPAAc-NH_2 isolated cytoplasmic homogenate.

only one biotinylated macromolecule can bind per binding face of streptavidin (*23*), suggesting that the likely configuration of the complex is that diagrammed in Figure 1.

The trafficking routes of the antibody−streptavidin complexes were initially characterized by laser scanning confocal microscopy. The antibody−streptavidin complex without polymer remained in vesicular compartments, as evidenced by the punctate fluorescence emission that has been shown to be typical of endosomal/lysosomal localization (*24*−*26*). The addition of polymer does not significantly affect targeting and internalization, but the diffuse fluorescence emission within the cells after 4 h demonstrates the release of the complex to the cytoplasm. The nucleus is seen as a darkened region surrounded by the diffuse cytoplasmic fluorescence, indicating that the fluorophore is still attached to streptavidin. The fluorophore can diffuse into the nucleus if it is free to partition out of the vesicular compartment due to degradation of the linkage or of streptavidin.

This finding was confirmed by the western blotting analysis of the isolated cell cytoplasm. No detectable amount of the antibody is released into the cytoplasm in the absence of the polymer, whereas the complexed polymer significantly increases the release of the biomolecular complex into the cytoplasm. The physically mixed polymer also induces endosomal release, but at a much lower level than that of the complexed polymer. This is likely due to uptake of the polymer in trans to the antibody/streptavidin complex, due to their high local concentrations of the free PPAAc-NH_2 in the cell culture medium. The western blotting also verifies that the moiety detected in the cytoplasm has not been degraded, as the molecular weight of the cytoplasmic band is identical to that detected in the crude homogenate.

These results demonstrate that PPAAc can be a potent endosomal releasing agent for targeted antibody conjugates that are internalized through receptor-mediated endocytosis. No toxicity has been observed in samples containing PPAAc at concentrations of up to 2 μM. The MoAb 64.1 has served as a model antibody for immunotoxin therapy, and PPAAc could directly find application as an agent to enhance the cytoplasmic delivery of immunotoxins. The ability of PPAAc to enhance delivery to the cytoplasm could also potentially aid in the delivery of protein antigens for vaccines, where entry into the MHC1 pathway depends on cytoplasmic entry. The generality of PPAAc's ability to deliver a variety of biotherapeutics from the endosomes to the cytoplasm is currently being investigated to determine how broadly this polymer could serve with different cell types and different protein therapeutics.

The authors are grateful to Janet Howell-Clark for excellent technical assistance. This work was supported by NIGMS Grant No. R01-GM53771 (A. S. Hoffman and P. S. Stayton) and Grant No. R01-CA55596 (O. W. Press), the NSF IGERT program DGE-9987620 (graduate fellowship to C.A.L.), the Office of Technology Transfer at UW, the Washington Technology Center, and the Washington Research Foundation.

LITERATURE CITED

(1) Press, O. W., Martin, P. J., Thorpe, P. E., and Vitetta, E. S. (1988) Ricin A-chain containing immunotoxins directed against different epitopes on the CD2 molecule differ in their ability to kill normal and malignant T cells. *J. Immunol. 141*, 4410−7.

(2) Mukherjee, S., Ghosh, R. N., and Maxfield, F. R. (1997) Endocytosis. *Physiol. Rev. 77*, 759−803.

(3) Authier, F., Posner, B. I., and Bergeron, J. J. (1996) Endosomal proteolysis of internalized proteins. *FEBS Lett. 389*, *55*−*60*.

(4) Seki, K. and Tirrell, D. A. (1984) pH-dependent complexation of poly(acrylic acid) derivatives with phospholipid vesicle membranes. *Macromolecules 17*, 1692−8.

(5) Murthy, N., Robichaud, J. R., Tirrell, D. A., Stayton, P. S., and Hoffman, A. S. (1999) The design and synthesis of polymers for eukaryotic membrane disruption. *J Controlled Release 61,* 137−43.
(6) Lackey, C. A., Murthy, N., Press, O. W., Tirrell, D. A., Hoffman, A. S., and Stayton, P. S. (1999) Hemolytic activity of pH-responsive polymer-streptavidin bioconjugates. *Bioconjugate Chem. 10,* 401−5.
(7) Plank, C., Oberhauser, B., Mechtler, K., Koch, C., and Wagner, E. (1994) The influence of endosome-disruptive peptides on gene transfer using synthetic virus-like gene transfer systems. *J. Biol. Chem. 269,* 12918−24.
(8) Press, O. W., Hansen, J. A., Farr, A., and Martin, P. J. (1988) Endocytosis and degradation of murine anti-human CD3 monoclonal antibodies by normal and malignant T-lymphocytes. *Cancer Res. 48,* 2249−57.
(9) Geissler, F., Anderson, S. K., and Press, O. (1991) Intracellular catabolism of radiolabeled anti-CD3 antibodies by leukemic T cells. *Cell Immunol. 137,* 96−110.
(10) Schaffar, L., Dallanegra, A., Breittmayer, J. P., Carrel, S., and Fehlmann, M. (1988) Monoclonal antibody internalization and degradation during modulation of the CD3/*T*-cell receptor complex. *Cell Immunol. 116,* 52−9.
(11) Clinchy, B., and Vitetta, E. S. (1998) The use of an anti-CD3 immunotoxin to prevent the development of lymphoproliferative disease in SCID/PBL mice. *J. Immunol. Methods. 218,* 141−53.
(12) Ey, P. L., Prowse, S. J., and Jenkin, C. R. (1978) Isolation of pure IgGl, IgG2a and IgG2b immunoglobulins from mouse serum using protein A-sepharose. *Immunochemistry 15,* 429−36.
(13) Klumb, L. A., Chu, V., and Stayton, P. S. (1998) Energetic roles of hydrogen bonds at the ureido oxygen binding pocket in the streptavidin−biotin complex. *Biochemistry 37,* 7657−63.
(14) Zhan, J., Stayton, P., and Press, O. W. (1998) Modification of ricin A chain, by addition of endoplasmic reticulum (KDEL) or Golgi (YQRL) retention sequences, enhances its cytotoxicity and translocation. *Cancer Immunol. Immunother. 46,* 55−60.
(15) Deonarain, M. P., and Epenetos, A. A. (1998) Design, characterization and anti-tumour cytotoxicity of a panel of recombinant, mammalian ribonuclease-based immunotoxins. *Br. J. Cancer. 77,* 537−46.
(16) Pichon, C., Arar, K., Stewart, A. J., Dodon, M. D., Gazzolo, L., Courtoy, P. J., Mayer, R., Monsigny, M., and Roche, A. C. (1997) Intracellular routing and inhibitory activity of oligonucleopeptides containing a KDEL motif. *Mol. Pharmacol. 51,* 431−8.
(17) Tolstikov, V. V., Cole, R., Fang, H., and Pincus, S. H. (1997) Influence of endosome- destabilizing peptides on efficacy of anti-HIV immunotoxins. *Bioconjugate Chem. 8,* 38−43.
(18) Wagner, E., Plank, C., Zatloukal, K., Cotten, M., and Birnstiel, M. L. (1992) Influenza virus hemagglutinin HA-2 N-terminal fusogenic peptides augment gene transfer by transferrin-polylysine-DNA complexes: toward a synthetic virus-like gene-transfer vehicle. *Proc. Natl. Acad. Sci. U. S. A. 89,* 7934−8.
(19) Mi, Z., Mai, J., Lu, X. and Robbins, P. D. (2000) Characterization of a class of cationic peptides able to facilitate efficient protein transduction in vitro and in vivo. *Mol. Ther. 2,* 339−47.
(20) Mitchell, D. J., Kim, D. T., Steinman, L., Fathman, C. G., and Rothbard, J. B. (2000) Polyarginine enters cells more efficiently than other polycationic homopolymers. *J, Pept, Res. 56,* 318−25.
(21) Ho, A., Schwarze, S. R., Mermelstein, S. J., Waksman, G., and Dowdy, S. F. (2001) Synthetic protein transduction domains: enhanced transduction potential in vitro and in vivo. *Cancer Res. 61,* 474−7.
(22) Cheung, C. Y., Murthy, N., Stayton, P. S., and Hoffman, A. S. (2001) A pH-Sensitive Polymer That Enhances Cationic Lipid-Mediated Gene Transfer. *Bioconjug Chem.*, submitted.
(23) Ding, Z., Fong, R. B., Long, C. J., Stayton, P. S., and Hoffman, A. S. Size-dependent control of the binding of biotinylated proteins to streptavidin using a polymer shield. *Nature*, in press.
(24) Godbey, W. T., Wu, K. K., and Mikos, A. G. (1999) Tracking the intracellular path of poly(ethylenimine)/DNA complexes for gene delivery. *Proc. Natl. Acad. Sci. U. S. A. 96,* 5177−81.
(25) Van Dyke, R. W. (2000) Effect of cholera toxin and cyclic adenosine monophosphate on fluid- phase endocytosis, distribution, and trafficking of endosomes in rat liver. *Hepatology 32,* 1357−69.
(26) Leopold, P. L., Ferris, B., Grinberg, I., Worgall, S., Hackett, N. R., and Crystal, R. G. (1998) Fluorescent virions: dynamic tracking of the pathway of adenoviral gene transfer vectors in living cells. *Hum. Gene Ther. 9,* 367−78.

BC010053L

Synthesis of Releasable Electrophore Tags for Applications in Mass Spectrometry

Xin Zhang, Linxiao Xu,† Poguan Wang, Zhixian Wang,‡ and Roger W. Giese*

Department of Pharmaceutical Sciences in the Bouve College of Health Sciences, Barnett Institute, and Chemistry Department, Northeastern University, Boston, Massachusetts 02115. Received July 25, 2001; Revised Manuscript Received November 23, 2001

Releasable electrophore mass tags (electrophore tags) are compounds for use as labels in ligand assays such as hybridization assays and immunoassays. In such assays, the electrophore-tagged reagent (e.g., DNA probe or antibody) is quantified at the conclusion of the assay by cleaving a bond in the attached tag so that the electrophore part can be brought into the gas phase (usually thermally) for detection by electron capture mass spectrometry (EC-MS) or a related technique. Interest in these tags is promoted mainly by their potential to provide highly sensitive and multiplexed assays. The high multiplexing arises from the opportunity to measure many such tags simultaneously in the mass spectrometer, where each tag has an electrophore part with a unique mass. In this study five precursors of electrophore mass tags are presented. Each precursor can lead to a large library of electrophore tags in a practical way, since each precursor can be converted to many different electrophore tags by reaction with commonly available phenols that provide a variation in mass. The phenol-reactive part of the tag is either a polyfluorobiphenyl or a benzyl chloride moiety. Representative library compounds are prepared and detected in an inert ester form by gas chromatography electron capture mass spectrometry (GC-EC-MS). Further, one tag is conjugated to DNA, and the resulting product is detected by laser-induced electron capture time-of-flight mass spectrometry on a silver surface. A calculation by the semiempirical method AM1 for an ion formed by one of the electrophores suggests that ring rotation promotes dissociative electron capture. The features of practical synthesis, simple composition, physicochemical stability, high multiplicity, high sensitivity, and potential for high throughput detection make releasable electrophore mass tags attractive for highly multiplexed assays. This includes their use in SNP assays or dideoxy DNA sequencing for detection of mutations in individuals, where the combination of high accuracy and speed is essential.

INTRODUCTION

A variety of substances such as radioisotopes and fluorescent dyes are employed as molecular tags in assays requiring high sensitivity. Examples of such assays are immunoassays, DNA sequencing, and SNP detection. One shortcoming of many current molecular tags is the limited number of them that can be detected simultaneously. For example, it is difficult to quantify more than four fluorescent tags with high sensitivity under ordinary and practical conditions when present as a mixture. This is because of the broadness of the emission bands along with differences, commonly, in their absorbance characteristics. One consequence of this is that automated DNA sequencing by means of capillary electrophoresis with fluorescence detection is done with only one sequence (or less) loaded into each capillary at a time (*1*). This barrier to high throughput is unfortunate since DNA sequencing is regarded as the gold standard for detecting mutations. Screening for DNA mutations in a population of people can be successful when some false positive and negative results are present, because the true positive and negative results are typically present in a larger abundance (*2*). However, as the practice of mutation detection turns to scoring individuals as part of routine diagnostics, high accuracy along with high speed will be essential. Increasing the multiplexing of dideoxy sequencing assays by employing molecular tags with high multiplicity is one way to accomplish this, for example, with releasable electrophore mass tags.

The concept and rationale for using releasable electrophore mass tags (electrophore tags) in chemical analysis is as follows. Each tag contains, effectively, three functional groups: electrophore, release, and reactivity. A tag is attached covalently to an analytical reagent of interest, such as a DNA oligomer or antibody, by means of the reactivity group. Once the assay employing the tagged reagent has reached the detection step, the electrophore part is released by a cleavage reaction at the release group and brought into the gas phase for ionization by electron capture (EC) with subsequent detection based on its mass. Since a mass spectrometer can detect many masses simultaneously, there is a potential for high multiplicity (e.g., 400 electrophore tags) in the assay. While mass spectrometry can detect a moderate number of unlabeled DNA molecules at the same time, large numbers of DNA molecules have never been detected in this way because of complications of fragmentation, adduct ions, isotopic peaks, and loss of signal at higher masses (*3*). Further, electrophores can be detected in general with much higher sensitivity than DNA molecules by mass spectrometry (*4*, *5*).

Previously, we reported the detection of a mixture of four electrophore-labeled DNA oligomers (*6*), and, in a separate study (*7*), of albumin labeled with six different

* To whom correspondence should be addressed. Tel: 617-373-3227; fax: 617-373-8720; e-mail: r.giese@neu.edu.
† Current address: Sigma-RBI, Natick, MA.
‡ Current address: Tropix, Inc., Bedford MA.

10.1021/bc010072v CCC: $22.00 © 2002 American Chemical Society
Published on Web 07/09/2002

electrophores, by electron capture mass spectrometry (EC-MS). While these results were encouraging, the synthetic strategies that we used to prepare the electrophore tags did not open up a practical way to make a large number of them. Here we report our success in overcoming this limitation by designing and preparing five "branchpoint" electrophore tag precursors, each of which is easy to prepare, and reactive toward phenols as the moieties that provide the variation in mass.

EXPERIMENTAL SECTION

Materials and Software. 3-Bromo-2-butanone was purchased from Lancaster Inc, Windham, NH. 2,3,4,5,6-Pentafluorobenzyl alcohol, 2,3,5,6-tetrafluoro-4-(pentafluorophenyl)phenol, piperazine, pyridine, various acid chlorides, 2,3-*O*-isopropylidene-D-erythronolactone, ethyl and methyl isonipecotate, decafluorobiphenyl, phosphomolybdic acid, α-bromoacetic acid, thionyl chloride, dicyclohexylcarbodiimide (DCC), 2,2′-azobisisobutyronitrile, *N*-hydroxysuccinimide (NHS), *N*-bromosuccinimide, and all phenols were purchased from Aldrich Chemical Co. unless indicated otherwise. Acetonitrile was distilled over CaH_2 before use. All solvents were from Fisher Scientific Co. Most reactions were monitored by silica fluorescence-indicator thin-layer chromatography (TLC) with detection by UV (short wavelength) or phosphomolybdic acid. The ^1H, ^{19}F, and ^{13}C spectra were obtained on a Varian 300 MHz spectrometer with tetramethylsilane as internal reference for the proton spectra and $CFCl_3$ for the fluorine spectra. Cation exchange beads in NH_4^+ form (AG 50w−X8, 100−200 mesh 143−5441,) were from Bio-Rad. Hyperchem software was from Hypercube (Waterloo, Ontario). For flash chromatography, the ratio of compound to Si was 1:100 to 1:200.

Mass Spectrometry. GC-EC-MS was performed using a Hewlett-Packard (HP) 5973 mass spectrometer coupled to a HP 6890 gas chromatograph. The instrument was controlled by a HP 5973 MS Chemstation computer for data acquisition in the scan mode. An Ultra-1 HP capillary column (25 m, 0.20 mm i.d., 0.11 μm film thickness) from Hewlett-Packard was used. With helium as carrier gas, the column head pressure was set to 36 psi. The source pressure (methane) was set to 2.0 Torr at 250 °C. Inject (1 μL sample of 100 pg/μL in ethyl acetate) on-column at 50 °C; ramp column oven to 250 C at 30 °C/min after a 4 min solvent delay; then ramp to 300 °C at 50 °C/min and hold for 12 min.

MALDI-TOF-MS experiments were done using a Bruker Daltonics Proflex laser desorption TOF-MS instrument in the linear positive mode. A literature procedure (*8*) was followed with modifications. To 1 μL of oligonucleotide (0.5−1.0 μg/μL water) was added 2 μL of ammonium ion exchange bead suspension. After the suspension was mixed (rocking plate) for 3 min, 3 μL of 70 mg/mL, 3-hydroxypicolinic acid:picolinic acid (9:1 w/w) in 50% acetonitrile was added, and, after brief mixing and settling, 1 μL of the supernatant was placed onto the target and allowed to dry.

LI-EC(Ag)-TOF-MS experiments were carried out as described (*9*).

Synthesis. Ethyl *N*-(4-Hydroxy-2,3-*O*-isopropylidenebutyryl)isonipecotate (2). A 25 mL dry round-bottomed flask equipped with a N_2 inlet and a stir bar was charged with 1.0 g (6.3 mmol) of 2,3-*O*-isopropylidene-D-erythronolactone (**1**), followed by 2.0 mL of ethyl isonipecotate. The resulting mixture was allowed to stir at 70 °C (oil bath) until TLC analysis showed no lactone remained (about 12−16 h). The reaction mixture was then purified on a silica gel column (1:1 ethyl acetate: hexane, followed by 100% ethyl acetate), and 1.5 g (75%) of desired product was obtained. ^{13}C NMR ($CDCl_3$): 13.78, 24.97, 25.07, 26.78, 26.91, 27.18, 27.33, 27.86, 40.45, 40.41, 41.11, 41.21, 44.22, 44.37, 60.20, 61.33, 61.41, 74.31, 74.46, 77.35, 77.47, 109.10, 109.13, 166.11, 165.99, 173.49 ppm. ^1H NMR($CDCl_3$): 1.23−1.29 (m, 3H), 1.40 (s, 3H), 1.55 (s, 3H), 1.6−2.05 (m, 4H), 2.51−2.64 (m, 1H), 2.71−3.31 (m, 2H), 3.56−3.77 (m, 2H), 3.95−4.17 (m, 3H), 4.29−4.45 (m, 2H), 4.91 (dd, J = 3.5 Hz, 1H) ppm. TLC: R_f = 0.40 (100% ethyl acetate).

The methyl derivative (**2a**, 1.2 g, 60%) was prepared in a similar way. ^{13}C NMR ($CDCl_3$): 25.28, 25.36, 27.12, 27.26, 27.54, 27.65, 28.24, 28.31, 40.39, 40.70, 41.56, 41.67, 44.64, 44.79, 51.79, 61.93, 62.01, 75.01, 75.05, 77.98, 77.04, 109.532, 166.47, 166.60, 174.26 ppm. ^1H NMR ($CDCl_3$): 1.34 (s, 3H), 1.48 (s, 3H), 1.54−1.80 (m, 2H), 1.86−1.96 (m, 2H), 2.47−2.60 (m, 1H), 2.71−3.24 (m, 2H), 3.48−3.72 (m, 5H), 3.85−3.95 (m, 1H), 4.20−4.4 (m, 2H), 4.85 (m, 1H) ppm. TLC: R_f = 0.40 (100% ethyl acetate).

Ethyl *N*-[2,3-*O*-Isopropylidene-4-(4′-pentafluorophenyl-2′,3′,5′,6′-tetrafluorophenoxy)butyryl]isonipecotate (I). A 25 mL dry round-bottomed flask equipped with a N_2 inlet and a stir bar was charged with 0.67 g (2 mmol) of **2**, followed by 0.7 g (2.2 mmol) of decafluorobiphenyl, 0.5 g (3 mmol) of CsOH monohydrate, 10 mL of CH_3CN, and 1.5 g of powdered molecular sieves. The resulting mixture was allowed to stir at room temperature until TLC analysis showed no starting material remained (about 16−24 h). The solid was removed by filtration, and the filtrate was concentrated on rotary evaporator and further purified on a silica gel column (1:5 ethyl acetate:hexanes, 300 mL, followed by 1:2 ethyl acetate:hexanes) and 0.62 g (49%) of desired product was obtained. ^{13}C NMR ($CDCl_3$): 14.13, 14.17, 25.41, 25.57, 27.22, 27.45, 27.57, 27.79, 28.29, 40.44, 41.11, 41.49, 41.68, 44.46, 44.61, 60.69, 73.33, 73.40 (m), 73.80 (m), 74.32, 74.53, 75.74, 76.11, 110.46 (m), 136 (m), 139 (m), 143 (m), 146 (m), 165.20, 165.30, 173.84, 173.87 ppm. ^1H NMR ($CDCl_3$): 5.01 (d, J = 5.7 Hz, 1H), 4.60−4.71 (m, 1H), 3.98−4.56 (m, 6H), 2.48−3.32 (m, 3H), 1.60−2.00 (m, 4H), 1.54 (s, 3H), 1.42 (s, 3H), 1.15−1.28 (m, 3H) ppm. ^{19}F NMR ($CDCl_3$): −137.95 (m, 2F), −139.83 (m, 2F), −151.24 (m, 1F), −155.95 (m, 1F), −156.43 (m, 1F), −161.27 (m, 2F) ppm. TLC: R_f = 0.50 (1:1 ethyl acetate: hexanes).

Ethyl *N*-{{4-{4′-[4″-(*p*-Acetophenyl)-2″,3″,5″,6″-tetrafluorophenyl]-2′,3′,5′,6′-tetrafluorophenoxy}-2,3-*O*-isopropylidenebutyryl}}isonipecotate (I-447a). A 25 mL dry round-bottomed flask equipped with a N_2 inlet and a stir bar was charged with 0.40 g (0.64 mmol) of **I**, followed by 0.15 g (1 mmol) of 4-hydroxyacetophenone, 0.7 g K_2CO_3, and 10 mL of CH_3CN. The resulting mixture was allowed to stir at 60 °C oil bath overnight. The solid was removed by filtration and was washed with CH_3CN (3 × 10 mL). The combined organic solution was concentrated and purified on a silica gel column (1:5 ethyl acetate:hexanes, 500 mL, followed by 1:2 ethyl acetate: hexanes) to give 0.25 g (41%) product. ^{13}C NMR ($CDCl_3$): 14.12, 14.15, 25.39, 25.55, 26.50, 27.21, 27.43, 27.54, 27.76, 28.28, 29.67, 40.41, 41.08, 41.46, 41.66, 44.45, 44.60, 60.66, 73.40 (m), 73.84 (m), 74.30, 74.54, 75.74, 76.08, 110.37, 110.43, 115.37, 115.42, 130.68, 133.13, 136 (m), 139 (m), 143 (m), 146 (m), 160.01, 165.20, 165.29, 173.86, 173.81, 196.29 ppm. ^1H NMR ($CDCl_3$): 8.01 (dm, J = 8.9 Hz, 2H), 7.10 (dm, J = 8.8 Hz, 2H), 5.01 (d, J = 6.8 Hz, 1H), 4.68−4.77 (m, 1H), 4.00−4.59 (m, 6H), 2.52−3.32 (m, 3H), 2.60 (s, 3H), 1.60−2.03 (m, 4H), 1.56 (s,

3H), 1.44 (s, 3H), 1.26 (td, $J = 7.1$ Hz, $J = 3.1$ Hz, 3H) ppm. ^{19}F NMR ($CDCl_3$): −137.92 (m, 2F), −139.71 (m, 2F), −153.33 (m, 2F), −155.93 (m, 1F), −156.38 (m, 1F) ppm. TLC: $R_f = 0.45$ (1:1 ethyl acetate:hexanes).

Ethyl *N*-{{2,3-*O*-Isopropylidene-4{4′-[[4″-[*p*-(3‴-oxobutyl)phenoxy]-2″,3″,5″,6″-tetrafluorophenyl]]-2′,3′,5′,6′-tetrafluorophenoxy}butyryl}}isonipecotate (I-475a). Similarly, the reaction of **I** with 4-(hydroxyphenyl)-2-butanone gave 0.35 g (55%) of product. ^{1}H NMR ($CDCl_3$): 7.18 (d, $J = 8.5$ Hz, 2H), 6.97 (d, $J = 8.6$ Hz, 2H), 5.04 (d, $J = 6.1$ Hz, 1H), 4.69−4.77 (m, 1H), 4.02−4.59 (m, 4H), 3.69 (m, 3H), 2.52−3.32 (m, 7H), 2.15 (s, 3H), 1.61−2.14 (m, 4H), 1.56 (s, 3H), 1.40 (s, 3H) ppm. ^{19}F NMR ($CDCl_3$): −138.77 (m, 2F),-139.75 (m, 2F), −153.95 (m, 1F), −156.10 (m, 1F), −156.50 (m, 1F) ppm. TLC: $R_f = 0.25$ (1:1 ethyl acetate:hexanes).

Methyl *N*-(Bromoacetyl)isonipecotate (4). A 25 mL dry round-bottomed flask equipped with a N_2 inlet and a stir bar was charged with 1.30 g (10 mmol) of bromoacetic acid (**3**), followed by 1.38 g (12 mmol) of *N*-hydroxysuccinimide, and the flask was placed in an ice-bath. After 30 min of stirring, 15 mL of acetonitrile containing 3.68 g (12 mmol) of DCC was added dropwise, and the reaction mixture was allowed to stir overnight before addition of 1.43 g (10 mmol) of methyl isonipecotate. After the reaction mixture was stirred another 24 h, it was filtered and the filtrate was concentrated on an evaporator, yielding residue that was redissolved into 200 mL of ethyl acetate. The resulting solution was washed with 3 × 30 mL of H_2O and 30 mL of brine solution and dried over $MgSO_4$. The organic solvent was removed on a rotary evaporator, and the crude product **4** was dried further under vacuum (0.05 mmHg) for 16 h and used without further purification.

Methyl *N*-[α-(4-(Pentafluorophenyl)-2,3,5,6-tetrafluorophenoxy)acetyl]isonipecotate (II). A 25 mL dry round-bottomed flask equipped with a N_2 inlet and a stir bar was charged with 1.1 g of 4-pentafluorophenyl-2,3,5,6-tetrafluorophenol, 2.0 g of crude **4**, 1.5 g of potassium carbonate, and 20 mL of acetonitrile. The resulting mixture was allowed to stir at 60 °C (oil bath) until TLC analysis showed no phenol remained (about 12−16 h). The K_2CO_3 was removed by filtration and washed several times with 3 × 10 mL of acetonitrile. The combined organic solution was concentrated on rotary evaporator, and the residue was purified on a silica gel column (1:5 ethyl acetate:hexanes, followed by 1:2 ethyl acetate:hexanes), to give 1.1 g (65%) of product. ^{13}C NMR ($CDCl_3$): 28.05, 27.48, 40.39, 41.24, 43.85, 51.74, 70.38 (m), 136−146 (m), 164.63, 174.08 ppm. ^{1}H NMR ($CDCl_3$): 1.62−1.78 (m, 2H), 1.91−1.97 (m, 2H), 2.51−2.60 (m, 1H), 2.89 (td, $J = 10.3$ Hz, 1H), 3.16 (tm, $J = 11.3$ Hz, 1H), 3.63 (s, 3H), 3.63−3.71 (m, 1H), 4.25 (dt, $J = 13.5$ Hz, 1H), 5.01 (s, 2H) ppm. ^{19}F NMR ($CDCl_3$): −137.80 (m, 2F), −139.94 (m, 2F), −151.48 (m, 1F), −156.75 (m, 2F), −161.70 (m, 2F) ppm. TLC: $R_f = 0.40$ (1:1 hexanes: ethyl acetate).

Methyl *N*-{{{α-{{4-{4′-[*p*-(3″-Oxobutyl)phenoxy]-2′,3′,5′,6′-tetrafluorophenyl}-2,3,5,6-tetrafluorophenoxy}}acetyl}}}isonipecotate (II-475a). A 25 mL dry round-bottomed flask equipped with a N_2 inlet and a stir bar was charged with 0.12 g (0.23 mmol) of **II**, followed by 0.10 g of 4-(4-hydroxyphenyl)-2-butanone, 0.26 g K_2CO_3, and 3 mL of CH_3CN. The resulting mixture was allowed to stir at 60 °C overnight. The K_2CO_3 was removed by filtration and washed with CH_3CN. The combined organic solution was concentrated and purified on a silica gel column (1:5 ethyl acetate:hexanes, followed by 1:2 ethyl acetate:hexanes) to yield 0.15 g (96%) of desired product. ^{13}C NMR ($CDCl_3$): 27.60, 28.19, 28.83, 30.13, 40.51, 41.39, 44.05, 45.10, 51.96, 70.73 (t, $J = 4.1$ Hz), 115.83, 129.61, 136−146 (m), 155.30, 164.63, 174.15, 207.67 ppm. ^{1}H NMR ($CDCl_3$): 1.69−1.78 (m, 2H), 1.91−2.03 (m, 2H), 2.15 (s, 3H), 2.60 (m, 1H), 2.73−3.01 (m, 5H), 3.17−3.26 (m, 1H), 3.72−3.79 (m, 1H), 3.72 (s, 3H), 4.34 (dt, $J = 13.9$ Hz, 1H), 5.05 (s, 2H), 6.95 (dm, $J = 8.5$ Hz, 2H), 7.17 (dm, $J = 8.7$ Hz, 2H) ppm. ^{19}F NMR ($CDCl_3$): −138.60 (m, 2F), −139.70 (m, 2F), −154.00 (m, 2F), −156.9 (m, 2F) ppm. TLC: $R_f = 0.40$ (1:1 hexanes: ethyl acetate).

Electrophore II-861a was Synthesized in a Similar Way (0.1 g, 51% yield). ^{1}H NMR ($CDCl_3$): 7.55−7.58 (m, 2H), 7.29−7.32 (m, 2H), 7.15−7.18 (m, 2H), 6.93−6.96 (m, 2H), 6.04−6.08 (m, 1H), 4.98 (s, 2H), 4.25−4.30 (m, H), 3.60−3.71 (m, 6H), 3.49 (s, 2H), 3.11−3.18 (m, H), 2.84−2.93 (m, 3H), 2.51−2.58 (m, H), 2.25−2.30 (m, 4H), 1.90−1.98 (m, 2H), 1.61−1.70 (m, 2H), 1.17−1.53 (m, 32H), 0.80 (m, 6H). ^{19}F NMR ($CFCl_3$): −138.4 (m, 2F), −139.7 (m, 2F), −153.9 (m, 2F), −156.7 (m, 2F).

Electrophore II-981a was Synthesized in a Similar Way (0.11 g, 53%). ^{1}H NMR ($CDCl_3$): 7.72 (m, 2H), 7.48 (m, 2H), 7.31 (m, 2H), 7.24 (m, 2H), 7.01 (m, 2H), 6.93 (m, 2H), 6.21 (t, $J = 5.6$ Hz, 1H), 5.12 (s, 2H), 5.05 (s, 2H), 4.34 (m, 1H), 3.73 (m, 6H), 3.21−3.47 (m, 5H), 2.94 (t, $J = 7.0$ Hz, 2H), 2.96−3.00 (m, 1H), 2.59−2.62 (m, 1H), 2.03 (m, 2H), 1.25−1.81 (m, 34H), 0.87 (t, $J = 6.1$ Hz, 6H). ^{19}F NMR ($CFCl_3$): −138.42 (m, 2F), −139.67 (m, 2F), −153.82 (m, 2F), −156.66 (m, 2F).

Acid Form of II-475a. II-475a (145 mg) was dissolved in 3.5 mL of tBuOH/H_2O (2:1), and 35 mg of LiOH was added. The resulting solution was stirred at room temperature until no starting material remained by TLC analysis (usually about 10−20 min). The solution was then quenched in 20 mL of ice H_2O, acidified to pH 4−5 with 5% HCl and extracted with 5 × 10 mL of ethyl acetate. The combined organic solution was washed with 2 × 10 mL of H_2O and 10 mL brine and then dried over $MgSO_4$ or Na_2SO_4. The organic solvent was removed by the rotary evaporator, giving a residue was dried further at 0.05 mmHg for several hours (135 mg, 95%) before storing in a desiccator for further use.

***N*-Hydroxysuccinimide Ester of II-475a.** A 10 mL dry round-bottomed flask equipped with a N_2 inlet and a stir bar was charged with 50 mg of the above acid form of **II-475a**, followed by 15 mg of NHS, 3 mL of dry CH_3CN, and 23 mg of EDC. The resulting mixture was stirred at room-temperature overnight and then was quenched with 40 mL of ice−water. The resulting solution was extracted with 5 × 10 mL of ethyl acetate, and the combined organic solution was washed with 2 × 10 mL of ice-cold water and 10 mL of ice-cold brine and dried over $MgSO_4$. Rotary evaporation gave a residue that was dried at (0.05 mmHg) for several hours, giving 52 mg (95%) of product, $R_f = 0.5$ (100% ethyl acetate), that was stored in a desiccator.

3-(4′-(Pentafluorophenyl)-2′,3′,5′,6′-tetrafluorophenoxy)-2-butanone (III). A 25 mL dry round-bottomed flask equipped with a N_2 inlet and a stir bar was charged with 1.0 g (3 mmol) of 2,3,5,6-tetrafluoro-4-(pentafluorophenyl)phenol, 0.55 g of 3-bromo-2-butanone (**5**), 1.0 g of potassium carbonate, and 20 mL of acetonitrile. The resulting mixture was allowed to stir at 60 °C until TLC showed no phenol remained (about 12−16 h). The K_2CO_3 was moved via filtration and washed with 3 × 10 mL acetonitrile. The organic solvent was removed by rotary evaporation, and the residue was recrystallized from hexanes/diethyl ether to give 1.08 g (90%) of the desired product. ^{1}H NMR ($CDCl_3$): 4.94 (q, $J = 6.9$ Hz, 1H), 2.37

(s, 3H), 1.60 (d, $J = 7.0$ Hz, 3H) ppm. ^{19}F NMR ($CDCl_3$): −137.92 (m, 2F), −139.43 (m, 2F), −151.12 (m, 1F), −155.95 (m, 2F), −161.30 (m, 2F) ppm. $R_f = 0.50$ (ethyl acetate:hexanes, 1:9).

General Procedure for the Preparation of Phenol Derivatives of Compound (III). A 25 mL dry round-bottomed flask equipped with a N_2 inlet and a stir bar was charged with 0.41 g (1 mmol) of 3-[2′,3′,5′,6′-tetrafluoro-4′-(pentafluorophenyl)phenoxy]-2-butanone, 1.1 mmol of a selected phenol (see below), 0.5 g of potassium carbonate, and 20 mL of acetonitrile. The resulting mixture was allowed to stir at 60 °C until TLC analysis showed no starting material remained (about 12−16 h). The K_2CO_3 was removed via filtration and washed with 3 × 10 mL of acetonitrile. The combined organic solution was concentrated on a rotavapor giving a residue that was further purified on a silica gel column to give the product.

3-{4′-[4″-(*p*-Iodophenoxy)-2″,3″,5″,6″-tetrafluorophenyl]-2′,3′,5′,6′-tetrafluorophenoxy}-2-butanone (III-531a). By the above general procedure, the reaction of 4-iodophenol with **III** gave 0.51 g (85%) of product. ^{1}H NMR ($CDCl_3$): 7.66 (dm, $J = 9.2$ Hz, 2H), 6.84 (dm, $J = 9.3$ Hz, 2H), 4.90 (qm, $J = 6.8$ Hz, 1H), 2.37 (s, 3H), 1.60 (d, $J = 7.6$ Hz, 3H) ppm. ^{19}F NMR ($CDCl_3$): −138.19 (m, 2F), −139.25 (m, 2F), −153.5 (m, 2F), −155.9 (m, 2F) ppm.

3-{{4′-{4″-[*o*,*p*-Bis(α,α-dimethylbenzyl)phenoxy]-2″,3″,5″,6″-tetrafluorophenyl}-2′,3′,5′,6-tetrafluorophenoxy}}-2-butanone (III-641a). By the above general procedure, the reaction of 2,4-bis(α,α-dimethylbenzyl)phenol with **III** yielded 0.80 g (87%) product. ^{1}H NMR ($CDCl_3$): 7.03−7.36 (m, 11H), 4.47 (d, $J = 2.3$ Hz, 1H), 6.56 (d, $J = 8.3$ Hz, 1H), 4.88 (q, $J = 6.7$ Hz, 1H), 2.37 (s, 3H), 1.76 (s, 6H), 1.74 (s, 6H), 1.56 (d, $J = 7.0$ Hz, 3H) ppm. ^{19}F NMR ($CDCl_3$): −139.40 (m, 2F), −139.76 (m, 2F), −154.17 (m, 2F), −156.19 (m, 2F) ppm.

***N*,*N*-Didecyl 4-{4′-[4″-(α-Methyl-*β*-oxopropyloxy)-2″,3″,5″,6″-tetrafluorophenyl]-2′,3′,5′,6′-tetrafluorophenoxy}benzamide (III-728a).** By the above general procedure, the reaction of *N*,*N*-didecyl 4-hydroxybenzamide with **III** gave 0.28 g (49%) major product. ^{1}H NMR ($CDCl_3$): 7.39 (dm, $J = 8.4$ Hz, 2H), 7.06 (dm, $J = 8.5$ Hz, 2H), 4.94 (q, $J = 7.4$ Hz, 1H), 3.21−3.47 (m, 4H), 2.37 (s, 3H), 1.61−1.66 (m, 32H), 1.60 (d, $J = 6.9$ Hz, 3H), 0.87 (t, $J = 6.6$ Hz, 6H) ppm. ^{19}F NMR ($CDCl_3$): −138.27 (m, 2F), −139.29 (m, 2F), −153.39 (m, 2F), −156.02 (m, 2F) ppm. Also a minor product (**III-848a**) was obtained. ^{1}H NMR ($CDCl_3$): 8.25 (dm, $J = 9.3$ Hz, 2H), 7.44 (dm, $J = 8.5$ Hz, 2H), 7.25 (dm, $J = 8.8$ Hz, 2H), 7.15 (dm, $J = 8.5$ Hz, 2H), 4.93 (q, $J = 7.2$ Hz, 1H), 3.11−3.48 (m, 4H), 2.38 (s, 3H), 1.61 (d, $J = 6.5$ Hz, 3H), 1.16−1.66 (m, 32H), 0.88 (m, 6H) ppm ^{19}F NMR ($CDCl_3$): −137.68 (m, 2F), −139.15 (m, 2F), −153.10 (m, 2F), −155.82 (m, 2F) ppm.

4′-(Bromomethyl)acetophenone (7). A 50 mL dry round-bottomed flask equipped with a N_2 inlet and a stir bar was charged with 30 mL of CCl_4, 2.0 g of NBS, 1.34 g of 4-methylacetophenone (**6**), and a catalytic amount of 2,2′-azobisisobutyronitrile. The resulting solution was refluxed for 8 h and was monitored by TLC during reflux. After the solvent was removed by rotary evaporation, the residue was quenched with 30 mL of ice−water and extracted with 3 × 30 mL of diethyl ether. The combined organic solution was washed with 2 × 30 mL of water and dried over $MgSO_4$. After removal of solvent by rotary evaporation, the residue was purified further by silica column chromatography (methylene chloride:hexanes, 1:3) to give 1.06 g (50%) of product. ^{1}H NMR ($CDCl_3$): 7.93−7.96 (m, 2H), 7.48−7.5 (m, 2H), 4.51 (s, 2H), 2.61 (s, 3H) ppm.

***p*-(4′-(Pentafluorophenyl)-2′,3′,5′,6′-tetrafluorophenoxy)methylacetophenone (IV).** A 100 mL dry round-bottomed flask equipped with a N_2 inlet and a stir bar was charged with 2.73 g of 2,3,5,6-tetrafluoro-4-(pentafluorophenyl)phenol, 1.75 g of **7**, 2.0 g of potassium carbonate, 30 mL of THF: acetonitrile (1:1), and 0.1 g of potassium iodide. The resulting mixture was allowed to stir at 60 °C until TLC analysis showed no phenol remained (about 12−16 h). The K_2CO_3 was removed by filtration and washed with acetonitrile 3 × 10 mL. The combined organic solution was concentrated on a rotary evaporator, and the residue was recrystallized from hexanes/diethyl ether to give 2.93 g (77%) of product. (Further recrystallization could raise the combined yield to 90%.) ^{13}C NMR ($CDCl_3$): 197.53, 146.27 (m), 142.92 (m), 140.37, 140.36 (m), 138.60 (m), 137.32, 128.75, 127.80, 75.54 (t, $J = 4.0$ Hz), 26.51 ppm. ^{1}H NMR ($CDCl_3$): 8.00−8.03 (m, 2H), 7.56−7.59 (m, 2H), 5.42 (s, 2H), 2.63 (s, 3H) ppm. ^{19}F NMR ($CDCl_3$): −137.99 (m, 2F), −139.55 (m, 2F), −151.01 (m, 1F), −155.77 (m, 2F), −161.18 (m, 2F) ppm.

***p*-[4′-(4″-Piperidinyl-2″,3″,5″,6″-tetrafluorophenyl)-2′,3′,5′6′-tetrafluorophenoxy]methylacetophenone (IV-396a).** A 25 mL dry round-bottomed flask equipped with a N_2 inlet and a stir bar was charged with 0.93 g of **IV**, 0.30 g of piperidine, 1.0 g of potassium carbonate, and 15 mL of acetonitrile. The resulting mixture was allowed to stir at 60 °C until TLC analysis showed no starting material (about 24 to 48 h). The K_2CO_3 was removed filtrated and washed several times with 3 × 10 mL acetonitrile. The combined concentration on a rotary evaporation, and the residue was purified further on a silica gel column to give 0.53 g (50%) of product. ^{1}H NMR ($CDCl_3$): 7.99−8.02 (m, 2H), 7.56−7.59 (m, 2H), 5.39 (s, 2H), 3.27 (m, 4H), 2.63 (s, 3H), 1.68 (m, 6H) ppm. ^{19}F NMR ($CDCl_3$): −139.80 (m, 2F), −141.50 (m, 2F), −151.55 (m, 2F), −156.50 (m, 2F) ppm.

***p*-[4′-(4″-Piperazinyl-2″,3″,5″,6″-tetrafluorophenyl)-2′,3′,5′6′-tetrafluorophenoxy] methyl acetophenone (IV-397a).** A 25 mL dry round-bottomed flask equipped with a N_2 inlet and a stir bar was charged with 0.93 g of **IV**, 0.30 g of anhydrous piperazine,1.0 g of potassium carbonate, and 15 mL of acetonitrile. The resulting mixture was allowed to stir at 60 °C until TLC analysis showed no starting material left (about 24−48 h). After filtration, washing, and concentration, the residue was redissolved in 200 mL of ethyl acetate, and this solution was washed with 3 × 30 mL of water and 30 mL of brine and dried over $MgSO_4$. The solvent was removed by rotary evaporation, and the crude product was further dried under vacuum for several hours prior to the following reaction.

(Note: this key intermediate solution could be stored at 4 °C for 7 days without significant decomposition.)

***p*-{4′-[4″-(4‴-Acetyl-1‴-piperazinyl)-2″,3″,5″,6″-tetrafluorophenyl]-2′,3′,5′,6′-tetrafluorophenoxy}methylacetophenone (IV-439a).** A 25 mL dry round-bottomed flask equipped with a N_2 inlet and a stir bar was charged with 1.0 g of above crude material and 15 mL of dry THF. The solution was cooled to in an ice-bath for 0.5 h prior to addition of 1.0 mL of acetic chloride dropwise, followed by 1.0 mL of pyridine. The resulting mixture with stirring was allowed to warm to room-temperature overnight. The reaction mixture was quenched with 30 mL of ice−water and neutralized with 0.5% HCl. This mixture was extracted with ethyl acetate (5 × 20 mL). The combined organic solution was washed with 3

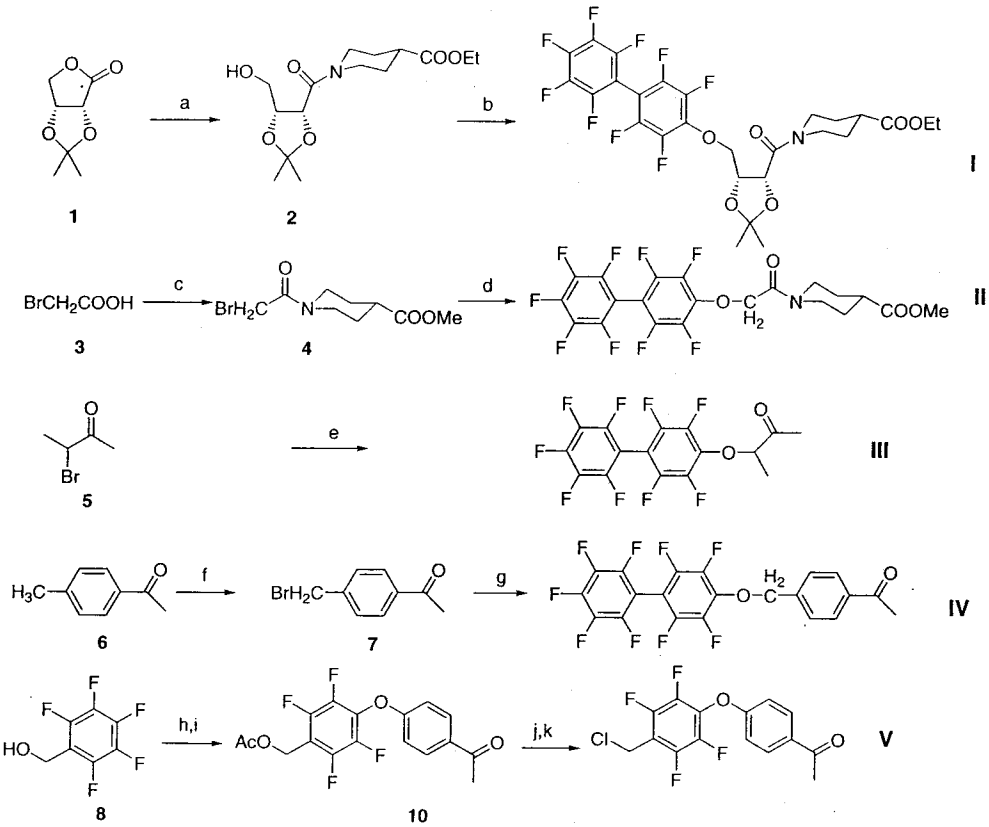


Figure 1. Synthesis of gateway electrophores **I**−**V**. a: Ethyl isonipecotate, 70−80 °C oil bath, 24 h, 80% yield. b: Decafluorobiphenyl, CsOH, molecular sieves, CH_3CN or DMF, room temperature, 48 h, 49% yield. c: *N*-Hydroxysuccinimide, DCC, CH_3CN, room temperature, overnight; then add methyl isonipecotate, 24 h, then evaporate and use crude material in next reaction. d: 2,3,5,6-Tetrafluoro-4-(pentafluorophenyl)phenol, K_2CO_3, CH_3CN, 60 °C, 24 h, 90% yield. e: 2,3,5,6-Tetrafluoro-4-(pentafluorophenyl)phenol, K_2CO_3, CH_3CN 60°, 24 h, 90% yield. f: NBS, CCl_4, reflux for 16 h, 50% yield. g: 2,3,5,6-Tetrafluoro-4-(pentafluorophenyl)phenol, K_2CO_3,CH_3CN, 60 °C, 24 h, 90% yield. h: Ac_2O, pyridine, CH_2Cl_2, reflux for 3 h, 91% yield. i: 4′-Hydroxyacetophenone, K_2CO_3, toluene, 18-crown ether (cat.), reflux for 16 h, 81% yield. j: 20% NaOH (aq), methanol, room-temperature overnight, 95% yield. k: $SOCl_2$, chloroform, reflux for 6 h, 92% yield.

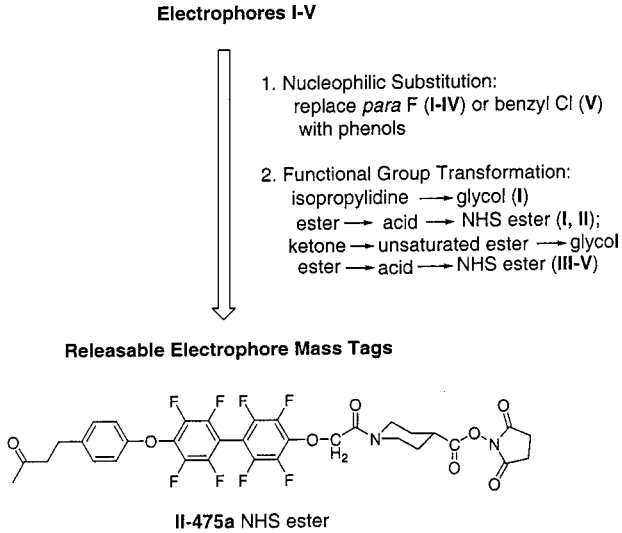


Figure 2. General scheme for conversion of electrophores **I**−**V** to releasable electrophore mass tags.

× 30 mL of water and 30 mL of brine solution and dried over $MgSO_4$. After removal of solvent by rotary evaporation, the residue was further purified on a silica gel chromatography column to give 0.72 g (63%) of product. ^{13}C NMR ($CDCl_3$): 197.86, 169.40, 140.80 (m), 137.49 (m), 128.92 (m), 128.1, 75.75 (m), 50.98 (m), 47.04, 42.13, 26.93, 21.61 ppm. ^1H NMR ($CDCl_3$): 7.99−8.02 (m, 2H), 7.56−7.59 (m, 2H), 5.40 (s, 2H), 3.75−3.79 (m, 2H), 3.60−3.64 (m, 2H), 3.31−3.36 (m, 4H), 2.63 (s, 3H), 2.16 (s, 3H) ppm. ^{19}F NMR ($CDCl_3$): −139.77 (m, 2F), −140.31 (m, 2F), −150.90 (m, 2F), −156.22 (m, 2F) ppm.

***p*-{4′-(4″-(4‴-Benzoyl-1‴-piperazinyl)-2″,3″,5″,6″-tetrafluorophenyl]-2′,3′,5′6′-tetrafluorophenoxy}-methylacetophenone (IV-501a).** Similarly, the crude product from the reaction of 0.5 g of with 0.2 g of piperazine was reacted with 0.6 mL of benzoyl chloride to produce 0.28 g (53%) desired product. ^1H NMR ($CDCl_3$): 7.99−8.02 (m, 2H), 7.56−7.58 (m, 2H), 7.45 (s, 5H), 5.39 (s, 2H), 3.31−3.94 (m, 8H), 2.63 (s, 3H) ppm; ^{19}F NMR ($CDCl_3$): −139.79 (m, 2F), −140.28 (m, 2F), −150.90 (m, 2F), −156.20 (m, 2F) ppm.

***p*-{{4′-{4″-[[4‴-[3⁗,5⁗-Di(trifluoromethyl)benzyl]-1‴-piperazinyl]]-2″,3″,5″,6″-tetrafluorophenyl}-2′,3′,5′6′-tetrafluorophenoxy}}methylacetophenone (IV-623a).** The crude product of the reaction of 0.5 g of **IV** with 0.2 g of piperazine was reacted with 0.2 g of 3,5-ditrifluoromethylbenzyl bromide in the presence of catalytic amount of KI for 24 h to give the product after preparative TLC purification. ^1H NMR ($CDCl_3$): 7.99−8.02 (m, 2H), 7.85 (s, 2H), 7.79 (s, 1H), 7.56−7.59 (m, 2H), 5.39 (s, 2H), 3.68 (s, 2H), 3.40 (m, 4H), 2.60−2.64 (m, 7H) ppm. ^{19}F NMR ($CDCl_3$): −63.27 (s, 6F), −139.81 (m, 2F), −140.86 (m, 2F), −151.28 (m, 2F), −156.35 (m, 2F) ppm.

2,3,4,5,6-Pentafluorobenzyl Acetate (9). To a mixture of 1 g (5 mmol) of 2,3,4,5,6-pentafluorobenzyl alcohol (**8**) and 1 mL of pyridine in 50 mL of anhydrous methylene chloride was added 0.6 g (5.8 mmol) of acetic anhydride. After being refluxed for 3 h, the mixture was cooled to room temperature, and then 10 mL of water

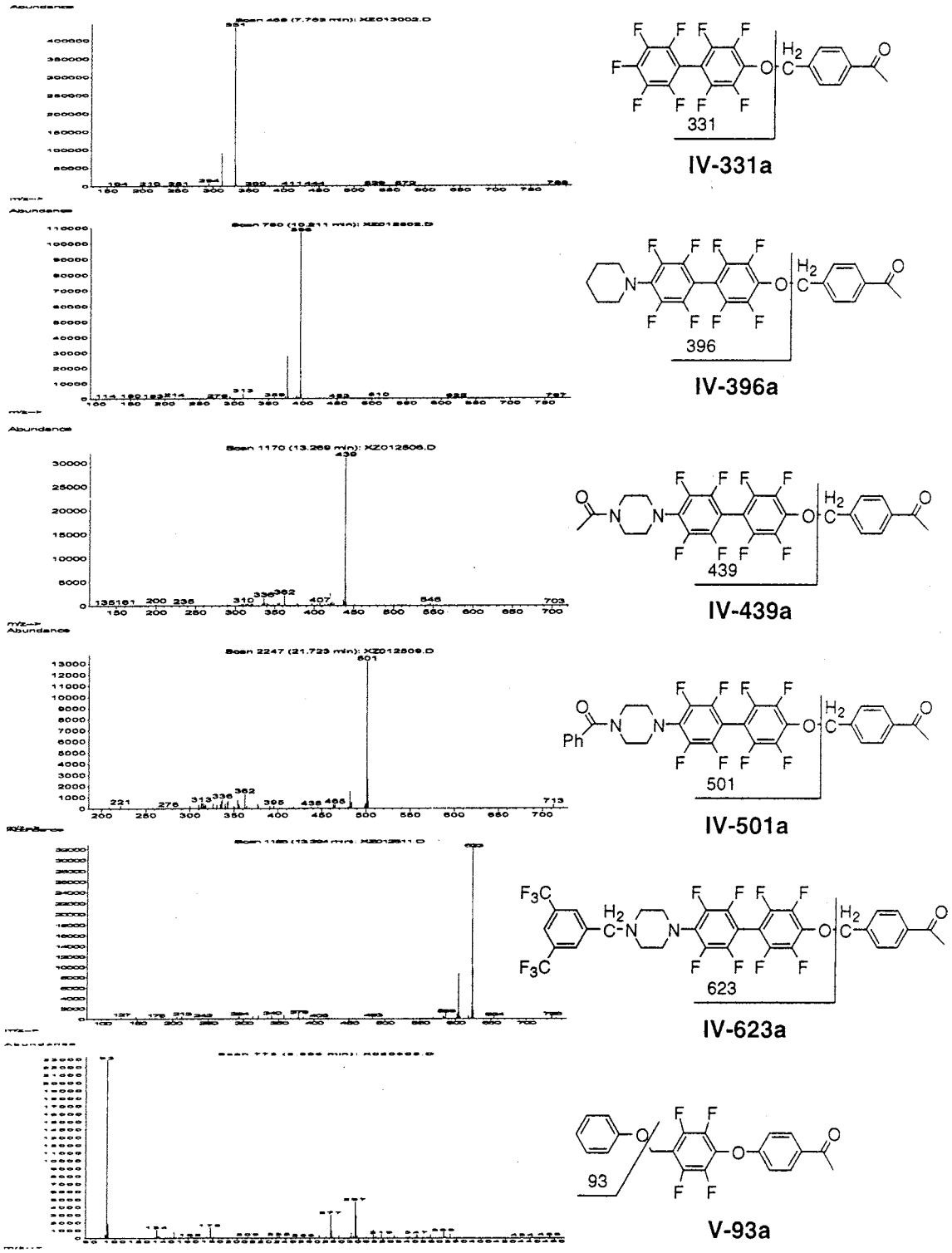


Figure 3. Mass spectra of electrophores by GC-EC-MS. Sample injection: 1 μL injection, 100 pg/μL in ethyl acetate.

was added. The aqueous phase was extracted with methylene chloride three times, and the combined organic solution was washed with 10 mL of brine and then dried over magnesium sulfate. After removal of the solvent on a rotavapor, 1.1 g (91%) of product was obtained as a colorless oil.

4′-(4″-Acetoxymethyl-2″,3″,5″,6″-tetrafluorophenoxy)acetophenone (10). A mixture of 1 g (4.16 mmol) of **9**, 0.57 g (4.18 mmol) of 4′-hydroxyacetophenone, 5 g of potassium carbonate, and 50 mg of 18-crown-ether in 50 mL of anhydrous toluene was refluxed for 16 h. After cooling to room temperature, the reaction mixture was filtered through a Celite bed. The filtrate was concentrated, and the residual solid was loaded on a silica gel column and eluted with 5:1 hexanes/ethyl acetate to afford 1.2 g (81%) of product as a white solid.

4′-(4″-Hydroxymethyl-2″,3″,5″,6″-tetrafluorophenoxy)acetophenone (11). To a solution of 1 g (2.8 mmol) of **10** in 50 mL of methanol was added dropwise 10 mL of 20% aqueous sodium hydroxide. The mixture was then stirred at room-temperature overnight, neutralized to pH 7, and concentrated to about 20 mL to remove most of methanol. The aqueous solution was extracted with ethyl acetate (3 × 50 mL). The combined organic solution was

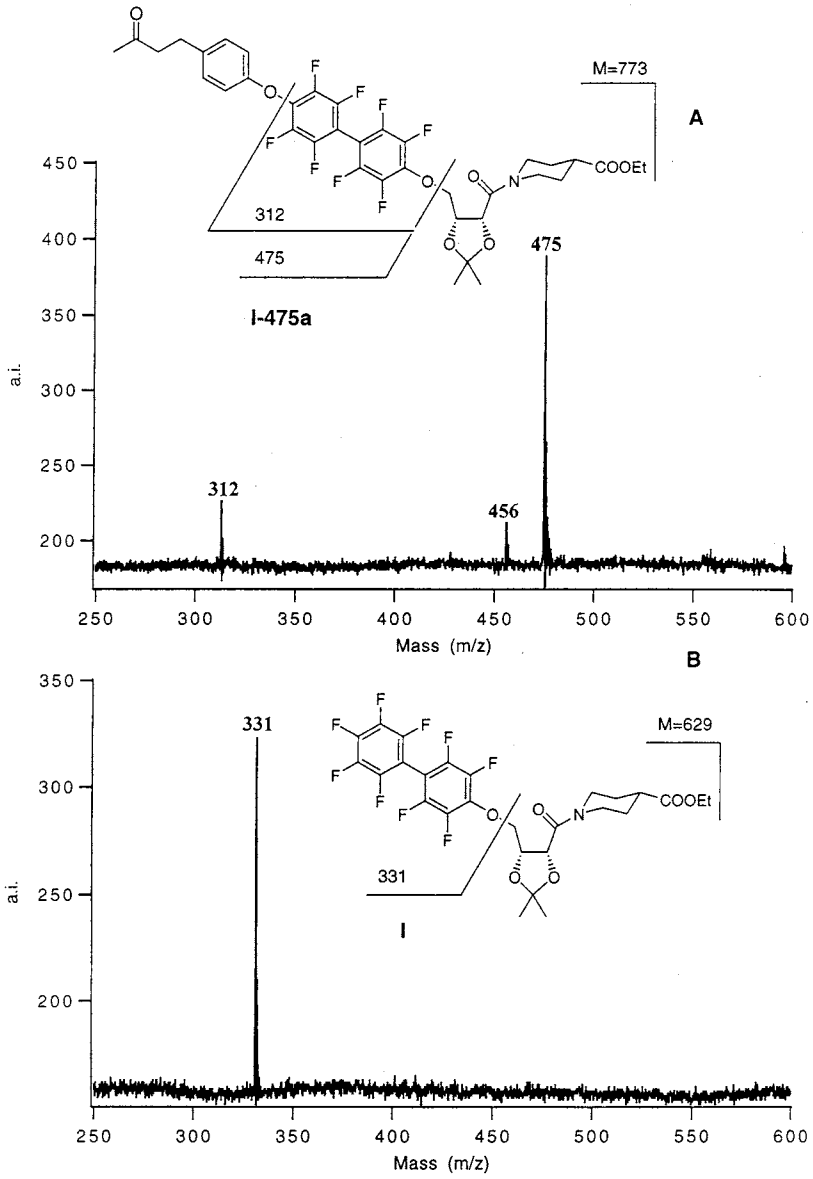


Figure 4. Detection of electrophores by LI-EC(Ag)-TOF-MS: 100 pmol on the target, 10 laser shots.

washed with water and brine and then dried over magnesium sulfate. After removal of the solvent, 0.84 (95%) of product was obtained as a white solid.

4′-(4″-Chloromethyl-2″,3″,5″,6″-tetrafluorophenoxy)acetophenone (V). A mixture of 0.85 g (2.7 mmol) of **11** and 5 mL of thionyl chloride in 30 mL of chloroform was refluxed for 6 h. The solvent was removed on a rotavapor, and the crude product was further purified by chromatography on silica gel to afford 0.83 g (92%) of product.

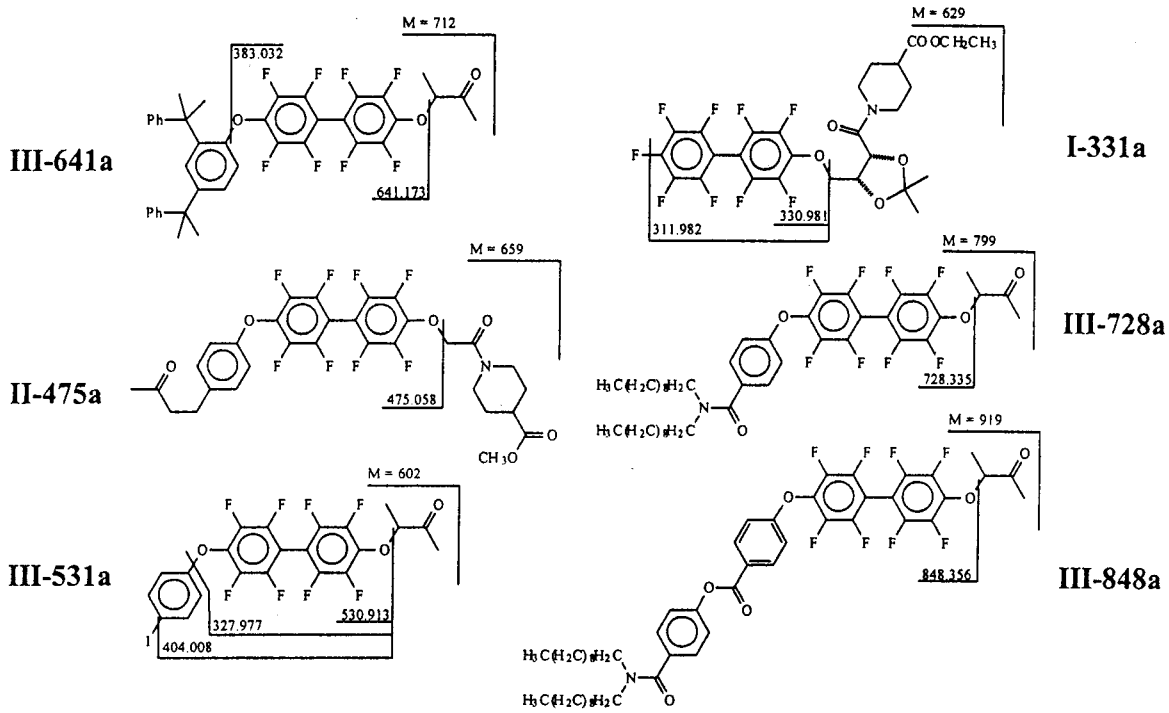
4′-(4″-Phenoxymethyl-2″,3″,5″,6″-tetrafluorophenoxy)acetophenone (V-93a). A mixture of 0.83 g (2.5 mmol) of **V**, 0.3 g (3.2 mmol) of phenol, and 2 g of potassium carbonate in 30 mL of acetone was stirred under reflux for 5 h. After being cooled to room temperature, the mixture was filtered through a Celite bed. The filtrate was concentrated and subjected to chromatography on silica gel with 6:1 hexanes/ethyl acetate to afford 0.95 g (97%) of product as a white solid. ^{1}H NMR ($CDCl_3$): 7.97−8.00 (m, 2H), 7.32−7.37 (m, 2H), 7.00−7.06 (m, 5H), 5.18 (s, 2H), 2.58 (s, 3H) ppm. ^{19}F NMR ($CDCl_3$): −142.66 (m, 2F), −154.10 (m, 2F) ppm.

RESULTS AND DISCUSSION

Shown in Figure 1 are five branchpoint precursors **(I−V)** of electrophore tags, along with their synthetic pathways. Each compound represents a point in a branching synthetic pathway that can lead to many releasable electrophore mass tags. Nucleophilic reactions with phenols can be employed at this branch point in all cases, involving substitution of a *p*-fluorine atom of **I**−**IV**, and of the chlorine atom of **V**, as summarized in Figure 2. Overall this can provide, as explained in more detail later, to two signal libraries, one shared in common by **I**−**IV**, and a second library from **V**.

As seen in Figure 1, precursor tag **I** is established by a synthetic pathway that consists of just two reactions, and all of the reactants are commercially available and inexpensive, including the starting compound, 2,3-O-isopropylidine D-erythronolactone. The isolated yield of **I** from compound **2** (reaction b) is 49%, and the overall yield of **I** from **1** is 37%.

Considerable effort went into the development of reaction conditions b (CsOH monohydrate, molecular sieves, acetonitrile). Many other conditions, involving a variety of bases, solvents, and temperatures, gave a lower



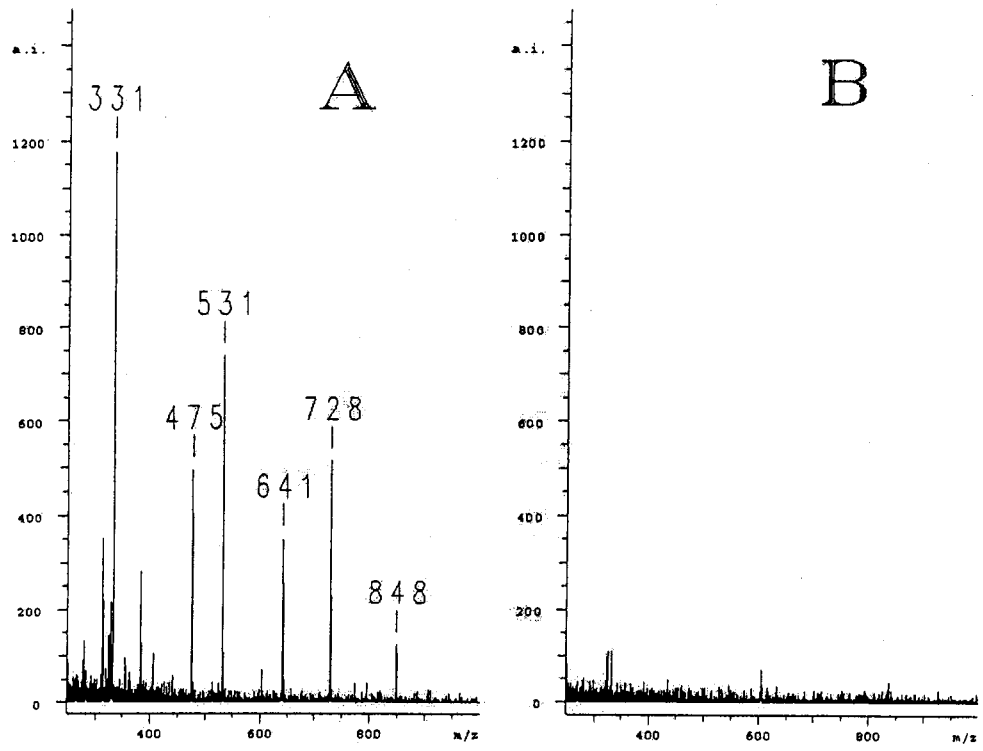


Figure 5. A: Detection of a mixture of six electrophores by LI-EC(Ag)-TOF-MS: 100 fmol of each on the target, 10 laser shots. B: LI-EC(Ag)-TOF-MS of blank silver surface under same condition as in A.

yield of **I**. Since the reactants in this sequence are commercially available and inexpensive, and **I** is easily purified from the side products, the synthetic procedure to form **I** is attractive.

Compound **I** can be converted into electrophore mass tags by a general reaction sequence consisting of the following series of steps: replace the para fluorine with a phenol; acid-hydrolyze the isopropylidine moiety to a corresponding glycol; base-hydrolyze the ester to a corresponding acid; and convert the latter to an *N*-hydroxysucccinimide (NHS) active ester (see Figure 2). Thus, the ensuing reactivity, release, and signal groups in the final release tags derived from **I** are NHS ester, β-hydroxy amide, and a para-substituted octafluorobiphenylate (signal ion form), respectively. The β-hydroxy amide moiety functions as a release group by undergoing a retro thermal-aldol type of reaction at an elevated temperature, as described before (*6*). Relative to our prior work (*6*) this pathway is more practical for the synthesis of many electrophore mass tags.

Analogous reaction pathways are employed to convert branchpoint compounds **II**−**V** into many releasable electrophore mass tags, as also summarized in Figure 2, where an example is shown (**II-475a NHS ester**). The latter tag, upon electron capture, furnishes an ion (RO^-) at *m*/*z* 475, due to dissociative cleavage of the $O-CH_2$ bond.

For the electrophore tags derived from **V**, the mass signals can begin at *m*/*z* 93, since this value corresponds to a phenolate anion, which ultimately forms when the chlorine atom of **V** is replaced by phenol in the synthetic pathway. In contrast, the signal libraries derived from **I**−**IV** begin at about *m*/*z* 343, due to replacing the *p*-fluorine atom of this compound with methoxy. This latter product eventually forms a 4-[(4′-methoxy)tetrafluorophenyl]tetrafluorophenolate ion (*m*/*z* 343). Thus, a main advantage of **V** over **I**−**IV** is that it extends the library of electrophore tags to much lower masses. For all five of the pathways, stable isotope phenols can be employed along with corresponding, ordinary phenols, as needed, to provide additional mass signals or to enhance quantitation by acting as an internal standard. While the use of stable isotopes would be necessary to fill in the mass range immediately above *m*/*z* 93, a large library of mass tags can be prepared without resorting to stable isotopes, because many phenols are readily available, a cost advantage.

In Figure 3 is shown a mass spectrum by GC-EC-MS of **IV** (designated as **IV-331a** in this figure), along with that of four corresponding electrophore mass tags derived from **IV**, and of a ketone electrophore derived from **V**. (Compound **IV** is designated as **IV-331a** here since it gives rise to a major ion at *m*/*z* 331, and is the first compound or "**a**", derived from **IV** that provides a signal at this mass.) It is meaningful to detect these ketones as synthetic intermediates since they are also the very signal compounds that are released for electron capture in the last step of our analytical technique.

Of special interest is the degree to which the compounds of Figure 3 form single ions in the EC-MS, as seen. This important property not only contributes to their sensitivity, but also helps to simplify the overall mass spectrum that a library of such compounds would yield. We consider that all of these derivatives are successful in this respect, since the electron capture mass spectrum of each one is dominated by a single ion (aside from M + 1). A minor, secondary ion arising from loss of a fluorine is seen in some of the spectra. While a 10-fold variation in response is observed for the major ion among these compounds, this result may have no meaning for our purposes. This is because the variation in response may be due to different recoveries of the compounds in the GC injection and separation steps, and these steps will be omitted in our ultimate detection scheme (which will involve laser desorption or laser-induced electron capture desorption).

Precursor tag **I** and the representative, corresponding derivative, **I-474a**, can be measured directly by laser-induced electron capture time-of-flight mass spectrometry on a silver surface (LI-EC[Ag]-TOF-MS), as shown in Figure 4, relying on the conditions that we introduced recently for the latter technique (*9*). We did not comparatively inject these compounds into the GC-EC-MS, because we would expect an irreproducible, low response for compounds of this type (high in mass and containing isopropylidine, amide, and ester groups). Whether the potentially labile isopropylidine moiety of **I** and **I-475a** remains intact throughout the electron capture process that leads to the observed ions is unknown.

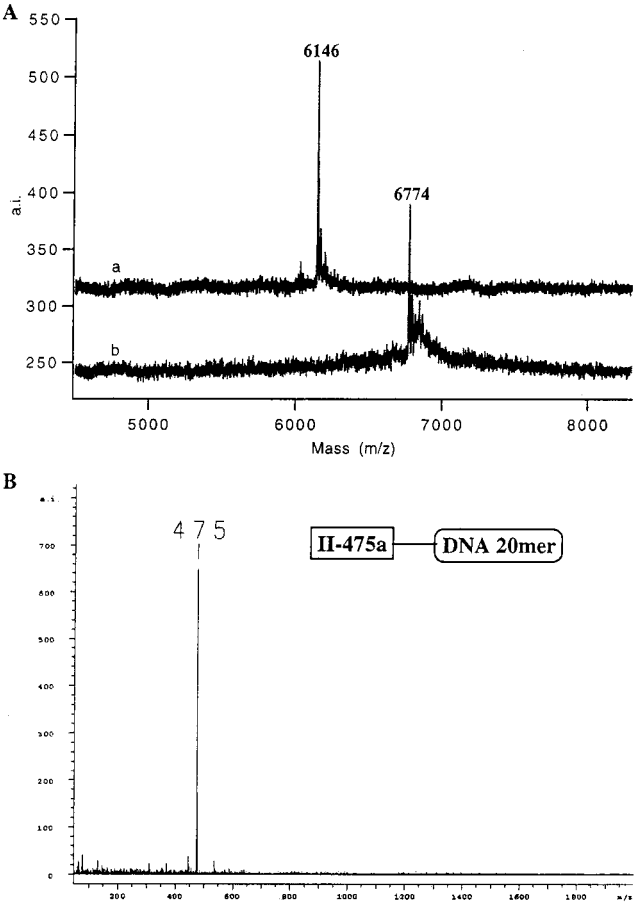


Figure 6. A: Detection by positive ion MALDI-MS of oligonucleotide P107 (5′-[aminoalkyl]-ACCGGCCATGCTCGCGACCA) in trace a; and of P107, after labeling with mass tag **II-475a**, in trace b. The oligomer was labeled with an NHS ester of **II-475a** in aqueous dimethyl sulfoxide containing 5% triethylamine using the conditions described previously (*10*). B: Detection by LI-EC(Ag)-TOF-MS of the latter, electrophore-labeled oligonucleotide, 500 fmol on the target, six laser shots.

Why does compound **I-475a**, but not compound **I**, lose fluorine in the LI-EC(Ag)-TOF-MS experiments of Figure 4? At least part of the reason is the variation in the experimental conditions. Arbitrarily, we used a lower power density for the laser in the detection of **I** (Figure 4B) vs **I-475a** (Figure 4A). Note the noisier baseline in Figure 4B both in terms of thickness and waviness, associated with a less abundant signal. This was confirmed by observing that fluorine loss from **I** could be increased by raising the laser intensity (data not shown).

In Figure 5 are shown the structures, fragmentation, and simultaneous detection by LC-EC(Ag)-TOF-MS, of a mixture of intermediates from the synthetic schemes presented in Figure 1. Importantly, all of the compounds are detected with high sensitivity: the amount of each compound applied to the silver target is 100 fmol, and only about 0.25% of each sample spot is in the laser beam. As seen, a relatively clean baseline is observed for a corresponding blank sample in Figure 5B. Also of note is the success of compound **II-475a** in this experiment. Compound **II-475a** possesses a new release group relative to prior literature. The preparation and testing of this latter compound was motivated by the behavior of **I-475a** (Figure 4A).

Extension of our detection strategy to a DNA oligomer labeled with an electrophore mass tag, for eventual use as a sequencing primer or hybridization probe, is shown in Figure 6. A 5′ amino linked DNA oligomer was labeled

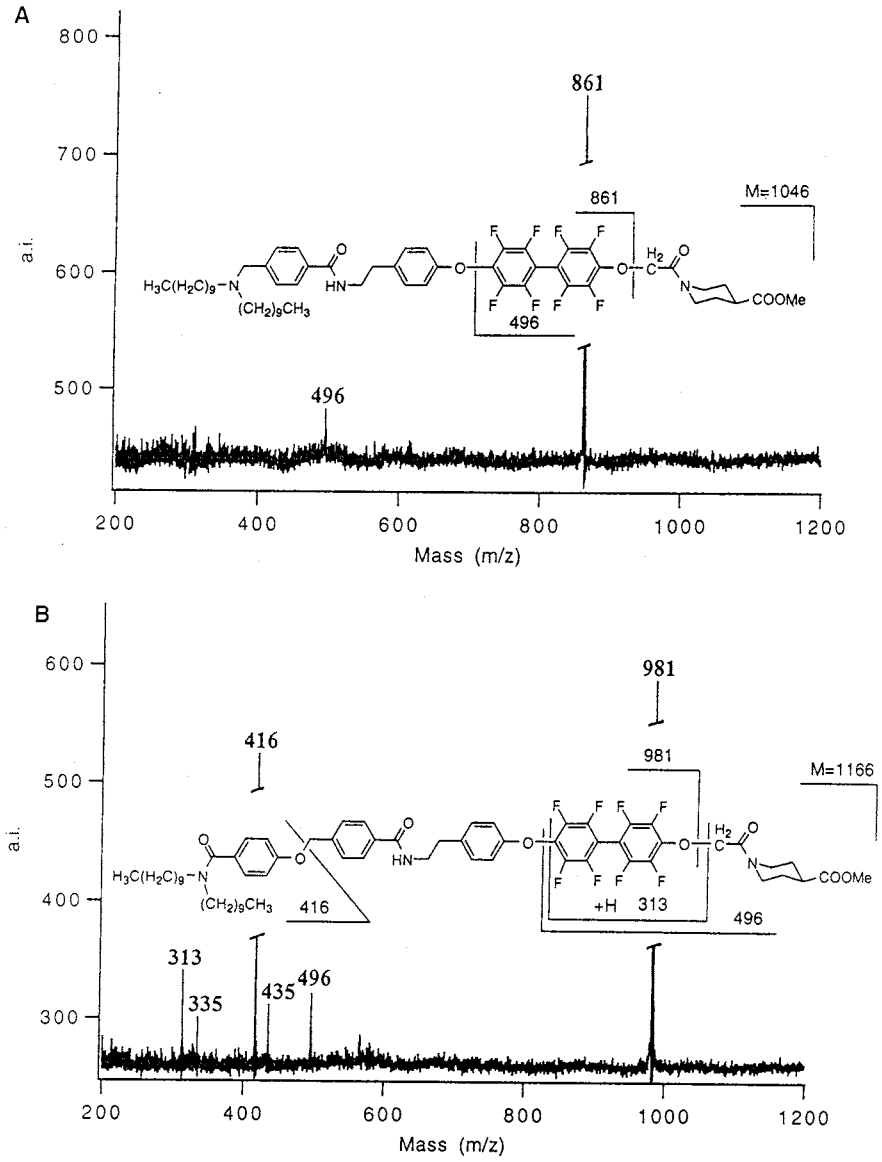


Figure 7. Detection of electrophores by LI-EC(Ag)-TOF-MS: A. 100 pmol of **II-861a** on the target, 17 laser shots. B. 1200 pmol of **II-981a** on the target, nine laser shots.

with a *N*-hydroxysuccinimide (NHS) ester of release tag **II-475a.** Analysis of the starting and electrophore-labeled product oligomers (**a** and **b**, respectively) by conventional MALDI-TOF-MS is shown in Figure 6A, and detection of the product oligomer (actually of the electrophore tag on this oligomer) by LI-EC(Ag)-TOF-MS is shown in Figure 6B. While we did not strive to demonstrate high sensitivity in this experiment, the observation that the simple conditions of LI-EC(Ag)-TOF-MS enable direct oligomer detection with a clean baseline (especially above 450 units of an electrophore-labeled DNA oligomer) is important in this technology.

Toward a goal of expanding the degree of multiplexing available from electrophore release tags, we have begun to explore higher-mass versions of these reagents. Initial success in this endeavor is shown by the data in Figure 7A, where compound **II-861a**, despite its more complicated structure, is detected by LI-EC(Ag)-TOF-MS as nearly a single ion (*m*/*z* 861). In work preceding this experiment, compound **II-981a** was prepared and found to yield six major ions (Figure 7B). The secondary cleavage at the benzyl ether site in **II-981a** is not surprising, since it forms a favorable amidophenolate species (the *m*/*z* 416 ion). The ion at *m*/*z* 496 in both spectra, assuming that we have assigned it correctly, would not be seen if the tag was attached to an oligomer, since the same cleavage would generate an oligomer ion. Our ability to avoid significant secondary cleavages in an ion having a mass as high as 861 units suggests that a considerable mass range can be anticipated for release tag electrophores, creating an opportunity for highly multiplexed assays that utilize them as tags.

Considering our need to design electrophores with favorable fragmentation properties upon electron capture (e.g., compound **II-861a** vs **II-981a** in Figure 7) we explored, in a preliminary way, whether the semiempirical method AM1 (using Hyperchem software) might be useful as a tool to understand some aspects of electron capture for our compounds. Arbitrarily, we selected a simple electrophore, **III**, and considered that the energy of the incoming electron was 0 eV for this calculation. For example, we wanted to find out whether the calculation could rationalize the emergence of ≥50 kcal/mol of excess, internal energy upon electron capture, to account for the observed cleavage of the C−O bond (bond energy 50−67 kcal/mol), aside from kinetic factors.

According to AM1, compound **III** prefers to exist with its two polyfluoro aromatic rings essentially perpendicu-

lar to each other, and this conformation provides a minimum value for the internal energy of −3789 kcal/mol. The corresponding anion radical of **III** in the same conformation is calculated to have an energy which is only 18 kcal/mol lower (−3807 kcal/mol), yielding an insufficient excess of internal energy to break the C−O bond. (What is being assumed is that the difference in energy between these two species is present as excess, internal energy in the incipient anion radical intermediate). Nevertheless, calculating the optimum geometry for the anion radical yields a structure in which the two polyfluoroaromatic rings have rotated to become more planar relative to each other. This furnishes another 35 kcal/mol of additional energy (to −3842 kcal/mol), sufficient in total (53 kcal/mol) to break the C−O bond. Much or most of the added electron density from electron capture, according to AM1, resides on the fluorine atoms of the outer perfluorphenyl ring in both the perpendicular and more planar conformers of the anion radical and then largely shifts to the adjacent polyfluorophenylate moiety that arises when the C−O bond breaks. Perhaps this shift in electron density is easier for the more planar conformer, having more conjugation between the rings.

The calculated energies for the observed anion and radical dissociation products in an optimum geometry from electron capture are −2704 and −1130 kcal/mol, respectively. The sum of these latter values is nearly the same (within 8 kcal/mol) of the energy calculated for the parent anion radical (the calculation assumes no excess internal energy is present) after aromatic ring twisting. From this argument it follows that the excess internal energy from ring rotation may not truly be needed for bond cleavage, since the emerging, extra stability of the favorable fragmentation products, due in part to resonance, could provide the energy necessary to drive (concurrently) the dissociation, assuming that this energy emerges early in the reaction pathway. Some of this resonance is due to the planarity of the polyfluorobiphenylate product, which creates a barrier for the parent, more perpendicular anion radical (−3789 kcal/mol) to access this alternative energy source. Thus, overall the postulated ring rotation may contribute to the observed dissociative electron capture both by increasing the amount of excess internal energy in the starting anion radical reactant and by enabling a shift in electron density from the outer to the inner polyfluorophenyl ring along the reaction pathway as a second source of excess internal energy, thereby breaking the bond.

CONCLUSION

Electrophore mass tags offer the advantages of low cost, physicochemical stability, high multiplicity, high sensitivity, and high throughput detection by mass spectrometry. Some of this promise has been demonstrated in this project. Practical synthetic strategies have been developed to make a large number of these tags which release under both gas phase and surface electron capture conditions, yielding gas phase signal groups that ionize with minimal secondary fragmentation to provide, in turn, nearly mono-ion spectra for high sensitivity. Representative tags with these properties furnishing ions from *m*/*z* 93 to 861 have been prepared, opening up a wide range of multiplicity to enhance multiplexing. This success guides and encourages the further development of these reagents.

ACKNOWLEDGMENT

This work was supported by NIST Award 70NANB5H1038 and, via George Church, DOE Grant DE-FG02-87ER60565 Contribution No. 809 from the Barnett Institute. The authors thank Max Deinzer for reading this manuscript.

LITERATURE CITED

(1) Salas-Solano, O., Carrilho, E., Lotler, L., Miller, A. W., Goetzinger, W., Sosic, Z., and Karger, B. L. (1998) Routine DNA Sequencing of 1000 Bases in Less Than One Hour by Capillary Electrophoresis with Replaceable Linear Plyacrylamide Solutions. *Anal. Chem*. *70*, 3996.

(2) Pennisi, E. (1998) A Closer Look at SNPs Suggests Difficulties. *Science 281*, 1787.

(3) Guo, B. (1999) Mass Spectrometry in DNA Analysis. *Anal. Chem*. *71*, 333R.

(4) Zhang, L.-K., and Gross, M. L. (2000) Matrix-Assisted Laser Desorption/Ionization Mass Spectrometry Methods for Oligodeoxynucleotides: Improvements in Matrix, Detection Limits, Quantification, and Sequencing. *J. Am. Soc. Mass Spectrom*. *11*, 854.

(5) Giese, R. W. (2000) Electron-capture mass spectrometry: recent advances. *J. Chromatogr. 892*, 329.

(6) Xu, L., Bian, N., Wang, Z., Abdel-Baky, S., Pillai, S., Magiera, D., Murugaiah, V., Giese, R. W., Wang, P., O'Keeffe, T., Abushamaa, H., Kutney, L., Church, G., Carson, S., Smith, D., Park, M., Wronka, J., and Laukien, F. (1997) Electrophore Mass Tag Dideoxy DNA Sequencing. *Anal. Chem*. *69*, 3595−3602.

(7) Bian, N., Wang, P., Wang, Z., Xu, L., Church, G., and Giese, R. W. (1997) Detection Via Laser Desorption and Mass Spectrometry of Multiplex Electrophore-labeled Albumin. *Rapid Commun. Mass Spectrom*. *11*, 1781−1784.

(8) Wang, B., and Biemann, K. (1994) Matrix-Assisted Laser Desorption/Ionization Time-of Flight Mass Spectrometry of Chemically Modified Oligonucleotides. *Anal. Chem*. *66*, 1918−1924.

(9) Wang, P., and Giese, R. W. (2000) Laser-Induced Electron Capture Mass Spectrometry. *Anal. Chem*. *72*, 772−776.

(10) Wang, Z., Bian, X., Qian, X., and Giese, R. W. (1998) N-Hydroxysuccinimide Ester Labeling 5′-aminoalkyl DNA Oligomers: Reaction Conditions and Purification, *J. Chromatogr*. *806*, 93−95.

BC010072V

Acridine Conjugates of 3-Clip-Phen: Influence of the Linker on the Synthesis and the DNA Cleavage Activity of Their Copper Complexes

Christophe Boldron, Steven A. Ross, Marguerite Pitié, and Bernard Meunier*

Laboratoire de Chimie de Coordination du CNRS, 205 route de Narbonne, 31077 Toulouse Cedex 4, France.
Received January 15, 2002

To increase the DNA cleavage activity and the cell delivery of the bis(phenanthroline) DNA cleaver "3-Clip-Phen", conjugates between 3-Clip-Phen and the intercalators acridine and 6-chloro-2-methoxyacridine, through amino acid linkers of various length, were prepared. After complexation with $CuCl_2$, the ability of these conjugates to cleave ΦX 174 DNA in the presence of a reductant and air was compared. The results indicated that (i) the coupling of 3-Clip-Phen to an acridine derivative increased the DNA cleavage efficiency of the copper complexes, (ii) the acridine derivatives were more active than 6-chloro-2-methoxyacridine derivatives, (iii) the linker length influenced cleavage efficiency, the highest DNA cleavage activity being obtained for an aminocaproic spacer.

INTRODUCTION

The redox activity of cuprous complexes of 1,10-phenanthroline (Phen) is well-known as an artificial nuclease (*1*, *2*). They are able to realize single-strand cleavages of DNA in the presence of H_2O_2 by oxidative degradation of deoxyribose units from the minor groove of DNA. Active species can also be generated from cupric complexes in the presence of oxygen and reductant. $Cu^I(Phen)_2$ is significantly more active than $Cu^I(Phen)$, but the association constant for the second phenanthroline ligand is only $10^{5.5}$ M^{-1} which is too low for biological use at submicromolar concentrations of these complexes.

We have recently prepared 2- and 3-Clip-Phen derivatives containing two Phen ligands linked at the 2′- or 3′-position by a serinol bridge in order to favor the 2/1 Phen/Cu stoichiometry (*3*, *4*). The oxidative nuclease activity of the copper complexes of these new ligands was found to be higher than with Phen itself, by a factor of 2 for 2-Clip-Phen, but by a factor of 60 for 3-Clip-Phen. The nuclease activity of (3-Clip-Phen)$CuCl_2$ complex has been associated to C1′-, C4′-, and C5′-deoxyribose oxidations resulting from a cleaver interaction within the DNA minor groove (*5*). (3-Clip-Phen)$CuCl_2$ appeared to be poorly sequence selective, but the preparation of a conjugate with an analogue of distamycin (a minor groove binder interacting selectively with five successive AT base pairs) allowed preparation of a sequence-selective DNA cleaver derivative of 3-Clip-Phen (*5*, *6*).

The high DNA cleavage activity of copper complexes of 3-Clip-Phen can be used for the preparation of new tools for molecular biology but also for the preparation of new chemotherapeutic agents based on the model of iron bleomycin (*7*, *8*), a well-known antitumor drug able to cleave the DNA of cancer cells. These new molecules must associate different properties of cell penetration and specificity for DNA associated to the nuclease activity of 3-Clip-Phen. The conjugation of 3-Clip-Phen to acridine derivatives appeared to be a good solution to increase cell penetration and DNA binding (*9*−*12*). These dyes are among the classical intercalators, and they are known to rapidly enter cells and accumulate in the nucleus which is an important consideration with regard to potential in vivo activity. In addition to their synthetic accessibility, derivatives of acridine are colored, stable, usually fluorescent, and exhibit a broad range of chemotherapeutic properties against prokaryotic and eucaryotic cells because of their facile interaction with DNA targets.

We chose to conjugate 3-Clip-Phen with acridine and 6-chloro-2-methoxyacridine, which are the intercalating moieties of the antitumor drug amsacrine and the antimalarial quinacrine, respectively. Previously, DNA minor groove binders, such as netropsine (*13*, *14*), alkylating mustards (*10*), photonucleases such as the nitrobenzamide derivatives (*15*, *16*), or oligonucleotides (*17*−*20*), have been conjugated to these types of acridine derivatives and shown an increased activity due to improved DNA interaction and/or cell delivery; but their activity was highly modulated by the arm of junction with the intercalator (this phenomenon being also described in the case of bis-intercalating agents (*21*, *22*)). To favor the interaction of 3-Clip-Phen with the minor groove (sugar C−H bonds accessible in the minor groove are attacked by copper complexes of Clip-Phen derivatives), the nuclease moiety of the conjugates has been linked through an amino function on the C9 of the acridine derivative which is known to be oriented in the DNA minor groove after intercalation (*10*). The choice of the amino junction has been justified by the good cell penetration capacities of C9-aminoacridine derivatives (*10*). Preliminary results with acridine conjugates of 2-Clip-Phen demonstrated that this strategy increased DNA cleavage activity and that the acridine part of the conjugate conserved DNA intercalation ability (*23*).

In this paper we describe the synthesis of 3-Clip-Phen/acridine conjugates. To obtain the most active compound, the length of spacer connecting the reactive center to the intercalator was modified. The preparation of all the conjugates for $n = 1$ to 7, where n is the number of methylene in the linker, allowed a strict analysis of the influence of the length of the arm of junction on the activity of the conjugates. Two methods of synthesis were

* E-mail: bmeunier@lcc-toulouse.fr.

10.1021/bc020013x CCC: $22.00 © 2002 American Chemical Society
Published on Web 08/31/2002

selected and optimized depending on the length of the tether in the conjugate. After complexation with $CuCl_2$, the DNA cleavage activity of the different conjugates was compared.

MATERIALS AND METHODS

General. Chemical syntheses were monitored by thin-layer chromatography on Merck silica gel 60 F_{254} plates eluted by CH_2Cl_2/CH_3OH (9/1) containing 1% of concentrated NH_4OH, and spots were visualized with UV light. Ligand metalation and DNA reactions were carried out in milli-Q water. DMF was dried over 4 Å molecular sieves. Other commercial reagents were used without purification.

Materials. 3-Clip-Phen (*4*), 9-phenoxyacridine (*23*), and 6-chloro-2-methoxy-9-phenoxyacridine (*23*) were synthesized as previously described in the literature. 2-(*tert*-Butoxycarbonylamino)-1-glycine (**2a**), 3-(*tert*-butoxycarbonylamino)-1-β-alanine (**2b**), 4-(*tert*-butoxycarbonylamino)-1-butyric acid (**2c**), 5-(*tert*-butoxycarbonylamino)-1-valeric acid (**2d**), and 6-(*tert*-butoxycarbonylamino)-1-caproic acid (**2e**) were prepared according to ref 24; see also ref 25 for additional characterizations of these compounds.

General Procedure for the Preparation of Carboxylic Derivatives of 6-Chloro-2-methoxyacridine (1c−g). The synthesis was optimized from ref 26.

6,9-Dichloro-2-methoxyacridine (1 equiv) and phenol (17 equiv) were stirred at 100 °C for 1 h before addition of amino acid (1.06 equiv). The reaction mixture was allowed to react at 100 °C for 3 h and then cooled at room temperature, and a large excess of diethyl ether (>50 volumes) was added. The resulting yellow solid obtained after filtration was dissolved in hot methanol (to about 15 mM of crude product) and precipitated with one volume of diethyl ether at −20 °C overnight. The precipitate was filtrated, washed with diethyl ether, and dried under vacuum.

In all cases, about 10% of 9-amino-6-dichloro-2-methoxyacridine was observed as an impurity. To remove it, the precipitate of compounds **1c** or **1d** was dissolved in a freshly prepared aqueous solution of 1 M NH_4OH/CH_3OH (10/1, v/v) and extracted with CH_2Cl_2 (2 × 50 mL), and then the aqueous layer was evaporated and dried under vacuum. Compounds **1e**, **1f**, and **1g** were purified by column chromatography on silica gel eluted with CH_2Cl_2/CH_3OH (85/15) containing 3% of concentrated NH_4OH.

***N*-[9-(6-Chloro-2-methoxy)acridinyl]-4-aminobutyric acid (1c)** was prepared from 300 mg (1.08 mmol) of 6,9-dichloro-2-methoxyacridine to give **1c** (279 mg, 0.81 mmol, yield = 75%) as a bright yellow powder. ^{1}H NMR (DMSO-d_6): δ 2.05 (m, 2H), 2.44 (t, 2H, J = 9.00 Hz), 3.89 (t, 2H, J = 9.00 Hz), 4.05 (s, 3H), 7.43 (dd, 1H, J = 2.75, 11.75 Hz), 7.53 (dd, 1H, J = 3.00, 11.75 Hz), 7.75 (d, 1H, J = 3.00 Hz), 7.93 (d, 1H, J = 11.75 Hz), 7.97 (d, 1H, J = 2.75 Hz), 8.46 (d, 1H, J = 11.75 Hz). MS m/z (ES > 0): 345 (MH^+, 100%).

***N*-[9-(6-Chloro-2-methoxy)acridinyl]-5-aminovaleric acid (1d)** was prepared from 600 mg (2.16 mmol) of 6,9-dichloro-2-methoxyacridine to give **1d** (619 mg, 1.73 mmol, yield = 80%) as a bright yellow powder. ^{1}H NMR (DMSO-d_6): δ 1.66 (m, 2H), 1.85 (m, 2H), 2.34 (t, 2H, J = 7.00 Hz), 3.87 (t, 2H, J = 7.00 Hz), 4.04 (s, 3H), 7.44 (dd, 1H, J = 2.25, 9.25 Hz), 7.53 (dd,1H, J = 2.50, 9.25 Hz), 7.75 (d, 1H, J = 2.50 Hz), 7.93 (d, 1H, J = 9.25 Hz), 7.97 (d, 1H, J = 2.25 Hz), 8.45 (d, 1H, J = 9.25 Hz). MS m/z (ES < 0): 357 (M−H, 100%).

***N*-[9-(6-Chloro-2-methoxy)acridinyl]-6-aminocaproic acid (1e)** was prepared from 1 g (3.60 mmol) of 6,9-dichloro-2-methoxyacridine to give **1e** (724 mg, 1.94 mmol, yield = 54%) as a bright yellow powder. ^{1}H NMR (DMSO-d_6): δ 1.42 (m, 2H), 1.62 (m, 2H), 1.85 (m, 2H), 2.29 (t, 2H, J = 7.00 Hz), 3.88 (t, 2H, J = 7.00 Hz), 4.04 (s, 3H), 7.45 (dd, 1H, J = 2.00, 9.25 Hz), 7.55 (dd, 1H, J = 2.50, 9.25 Hz), 7.76 (d, 1H, J = 2.50 Hz), 7.93 (d, 1H, J = 9.25 Hz), 7.97 (d, 1H, J = 2.00 Hz), 8.46 (d, 1H, J = 9.25 Hz). MS m/z (ES > 0): 373 (MH^+, 100%).

***N*-[9-(6-Chloro-2-methoxy)acridinyl]-7-aminoheptanoic acid (1f)** was prepared from 300 mg (1.08 mmol) of 6,9-dichloro-2-methoxyacridine to give **1f** (322 mg, 0.83 mmol, yield = 77%) as a bright yellow powder. ^{1}H NMR (DMSO-d_6): δ 1.46 (m, 4H), 1.61 (m, 2H), 2.00 (m, 2H), 2.30 (t, 2H, J = 7.25 Hz), 4.07 (s, 3H), 4.13 (m, 2 H), 7.62 (dd, 1H, J = 2.00, 9.25 Hz), 7.76 (dd, 1H, J = 2.50, 9.25 Hz), 7.98 (d, 1H, J = 9.25 Hz), 8.03 (m, 2H), 8.59 (d, 1H, J = 9.25 Hz). MS m/z (ES < 0): 385 (M − H, 100%).

***N*-[9-(6-Chloro-2-methoxy)acridinyl]-8-aminocaprylic acid (1g)** was prepared from 300 mg (1.08 mmol) of 6,9-dichloro-2-methoxyacridine to give **1g** (307 mg, 0.77 mmol, yield = 71%) as a bright yellow powder. ^{1}H NMR (DMSO-d_6): δ 1.35 (br m, 6H), 1.54 (m, 2H), 1.83 (m, 2H), 2.26 (t, 2H, J = 7.25 Hz), 3.87 (t, 2H, J = 7.00 Hz), 4.04 (s, 3H), 7.45 (dd, 1H, J = 2.00, 9.25 Hz), 7.54 (dd, 1H, J = 2.50, 9.25 Hz), 7.76 (d, 1H, J = 2.50 Hz), 7.93 (d, 1H, J = 9.25 Hz), 7.97 (d, 1H, J = 2.00 Hz), 8.45 (d, 1H, J = 9.25 Hz). MS m/z (ES > 0): 401 (MH^+, 100%).

General Procedure for the Preparation of 3-Clip-Phen-arm-Boc (3a−e). The synthesis was optimized from ref 23.

(Boc-amino)-carboxylic acid (0.28 mmol) was dissolved in 2 mL of CH_2Cl_2 (dried on basic alumina) at 0 °C, and then Et_3N (39 μL, 0.28 mmol) and ethyl chloroformate (26 μL, 0.28 mmol) were added. After the reaction was stirred for 1 h at room temperature, the solvent was evaporated. The residue was dissolved in CH_2Cl_2 (2 mL), Et_3N (39 μL, 0.28 mmol) and 3-Clip-Phen (50 mg, 0.11 mmol) were added, the solution was stirred at room temperature for 20 h, and then the solvent was evaporated. The residue was redissolved in CH_2Cl_2 (50 mL), the solution was washed with 1 M NaOH (2 × 50 mL), the solvent was evaporated, and the crude product was purified by column chromatography on silica gel eluted with CH_2Cl_2/CH_3OH (90/10) containing 1% of concentrated NH_4OH. The purity of products **3a−e** was analyzed by ^{1}H NMR before beginning the coupling reaction with 6-chloro-2-methoxy-9-phenoxyacridine.

3-Clip-Phen-ethyl-Boc (3a). Yield = 76% (51 mg, 84 μmol) as a pale brown powder. ^{1}H NMR (CD_2Cl_2): δ 1.21 (s, 9H), 4.22 (br, 6H), 4.87 (br, 1H), 7.18 (d, 2H, J = 2.75 Hz), 7.32 (t, 1H, J = 5.75 Hz), 7.47 and 7.67 (AB, 4H, J_{AB} = 8.75 Hz), 7.54 (dd, 2H, J = 4.25, 8.00 Hz), 8.17 (dd, 2H, J = 1.50, 8.00 Hz), 8.66 (d, 2H, J = 2.75 Hz), 9.03 (dd, 2H, J = 1.50, 4.25 Hz), 9.10 (d, 1H, J = 7.84 Hz).

3-Clip-Phen-propyl-Boc (3b). Yield = 79% (55 mg, 89 μmol) as a pale brown powder. ^{1}H NMR (CD_2Cl_2): δ 1.35 (s, 9H), 2.75 (t, 2H, J = 6.00 Hz), 3.51 (m, 2H), 4.32 (br, 4H), 4.87 (m, 1H), 5.77 (br, 1H), 7.34 (d, 2H, J = 2.75 Hz), 7.52 and 7.68 (AB, 4H, J_{AB} = 9.00 Hz), 7.53 (dd, 2H, J = 4.25, 8.00 Hz), 8.16 (dd, 2H, J = 1.50, 8.00 Hz), 8.69 (d, 2H, J = 2.75 Hz), 8.93 (d, 1H, J = 6.75 Hz), 9.03 (dd, 2H, J = 1.50, 4.25 Hz).

3-Clip-Phen-butyl-Boc (3c). Yield = 90% (64 mg, 101 μmol) as a pale brown powder. ^{1}H NMR (CD_2Cl_2): δ 1.27 (s, 9H), 1.91 (m, 2H), 2.50 (t, 2H, J = 6.75 Hz), 3.20 (m, 2H), 4.36 (br, 4H), 4.87 (br, 1H), 7.48 (d, 2H, J = 2.50 Hz), 7.55 (dd, 2H, J = 4.25, 8.00 Hz), 7.61 and 7.73 (AB, 4H, J_{AB} = 9.00 Hz), 8.20 (dd, 2H, J = 1.75, 8.00 Hz), 8.39

(d, 1H, $J = 7.50$ Hz), 8.75 (d, 2H, $J = 2.50$ Hz), 9.05 (dd, 2H, $J = 1.75, 4.25$ Hz).

3-Clip-Phen-pentyl-Boc (3d). Yield = 90% (65 mg, 100 μmol) as a pale brown powder. ^{1}H NMR (CD_2Cl_2): δ 1.34 (s, 9H), 1.50 (m, 2H), 1.77 (m, 2H), 2.49 (t, 2H, $J =$ 7.25 Hz), 3.09 (m, 2H), 4.35 (br, 4H), 4.87 (br, 1H), 7.42 (d, 2H, $J = 3.00$ Hz), 7.53 (dd, 2H, $J = 4.25, 8.00$ Hz), 7.57 and 7.70 (AB, 4H, $J_{AB} = 8.75$ Hz), 8.17 (dd, 2H, $J =$ 1.75, 8.00 Hz), 8.36 (d, 1H, $J = 7.25$ Hz), 8.73 (d, 2H, J = 3.00 Hz), 9.04 (dd, 2H, $J = 1.75, 4.25$ Hz).

3-Clip-Phen-hexyl-Boc (3e). Yield = 83% (61 mg, 93 μmol) as a pale brown powder. ^{1}H NMR (CD_2Cl_2): δ 1.36 (s, 9H,), 1.41 (br, 4H), 1.73 (m, 2H), 2.43 (t, 2H, $J = 7.50$ Hz), 3.02 (m, 2H), 4.39 (br, 4H), 4.80 (br, 1H), 4.87 (br, 1H), 7.47 (d, 2H, $J = 3.00$ Hz), 7.55 (dd, 2H, $J = 4.25$, 8.00 Hz), 7.60 and 7.72 (AB, 4H, $J_{AB} = 9.00$ Hz), 8.13 (d, 1H, $J = 7.75$ Hz), 8.19 (dd, 2H, $J = 1.75, 8.00$ Hz), 8.76 (d, 2H, $J = 3.00$ Hz), 9.04 (dd, 2H, $J = 1.75, 4.25$ Hz).

General Procedure for the Preparation of 3-Clip-Phen-acridine Conjugates (4a−h). Method A (for the preparation of 4e, 4f, and 4g). Chloroform was dried on basic alumina. The carboxylic derivative (0.28 mmol) of acridine (**1e**, **1f**, or **1g**) was dissolved in $CHCl_3$ (2 mL) at room temperature, and Et_3N (39 μL, 0.28 mmol) and ethyl chloroformate (26 μL, 0.28 mmol) were then added. After the reaction was stirred for 2 h at 70 °C, the solvent was evaporated. The residue was dissolved in $CHCl_3$ (2 mL), Et_3N (39 μL, 0.28 mmol) and 3-Clip-Phen (50 mg, 0.11 mmol) were added, the solution was stirred overnight at room temperature, and then the solvent was evaporated. The crude product was purified by column chromatography on silica gel eluted with CH_2Cl_2/CH_3OH (7/3). A second column, eluted with CH_2Cl_2/CH_3OH (95/5) containing 0.5% of concentrated NH_4OH, was used to remove the residual unreacted 3-Clip-Phen.

Method B (for the preparation of 4a, 4b, 4c, 4d). The syntheses were optimized from ref 23.

3-Clip-Phen-Boc derivative (1 equiv) was dissolved in 4 mL of CF_3COOH/CH_2Cl_2 (1/3, v/v), the solution was stirred for 1 h at room temperature, and then the solvent was evaporated. The residue was dissolved in acetonitrile (3 mL), 6-chloro-2-methoxy-9-phenoxyacridine (2 equiv) and acetic acid (5 equiv) were added, the solution was heated at reflux for 16 h, and then the solvent was evaporated. Crude product was triturated in diethyl ether, and solvent was evaporated (2×). It was then dissolved in CH_2Cl_2 and precipitated with diethyl ether before purification by chromatography on silica gel as follows: the acridine derivatives were eluted with CH_2Cl_2/CH_3OH (95/5), and then a gradient up to CH_2Cl_2/CH_3OH (80/20) was realized to elute 3-Clip-Phen-acridine conjugate. Concentrated NH_4OH (0.5%) was added to the gradient in the case of conjugates **4c** and **4d**. A supplementary step, consisting of a precipitation with acetone of conjugates **4a** and **4b** (eluted without NH_4OH) dissolved in CH_3OH alkalinized with few drops of concentrated NH_4OH, was necessary to obtain conjugates in nonprotonated form.

3-Clip-Phen-ethyl-chloromethoxyacridine (4a) was prepared from 51 mg (84 μmol) of **3a** to give **4a** (42 mg, 56 μmol, yield = 67%) as a yellow powder. ^{1}H NMR (CD_2Cl_2): δ 3.22 (s, 3H), 4.25 (br, 4H), 4.70 (d, 2H, $J = 4.75$ Hz), 4.95 (br, 1H), 6.76 (dd, 1H, $J = 2.00, 9.25$ Hz), 6.99 (dd, 1H, $J = 2.00, 9.50$ Hz), 7.13 (d, 1H, $J = 2.00$ Hz), 7.19 (d, 2H, $J = 2.50$ Hz), 7.41 and 7.59 (AB, 4H, $J_{AB} =$ 9.00 Hz), 7.45 (dd, 2H, $J = 4.25, 8.00$ Hz), 7.64 (d, 1H, J = 9.50 Hz), 7.73 (d, 1H, $J = 2.00$ Hz), 7.84 (d, 1H, $J =$ 9.25 Hz), 8.09 (dd, 2H, $J = 1.50, 8.00$ Hz), 8.40 (d, 2H, J = 2.50 Hz), 8.90 (dd, 2H, $J = 1.50, 4.25$ Hz), 10.01 (d, 1H, $J = 7.50$ Hz). MS m/z (DCI NH_3): 746 (MH^+, 6%), 550 (68), 259 (100).

3-Clip-Phen-propyl-chloromethoxyacridine (4b) was prepared from 55 mg (89 μmol) of **3b** to give **4b** (34 mg, 45 μmol, yield = 50%) as a yellow powder. ^{1}H NMR (CD_2Cl_2): δ 2.95 (m, 2H), 3.84 (s, 3H), 4.06 (m, 2H), 4.26 (br, 4H), 4.97 (m, 1H), 6.27 (br, 1H), 7.09 (dd, 1H, $J =$ 2.25, 9.50 Hz), 7.23 (d, 2H, $J = 2.75$ Hz), 7.25 (dd, 1H, J = 2.25, 9.50 Hz), 7.43 (d, 1H, $J = 2.25$ Hz), 7.47 and 7.65 (AB, 4H, $J_{AB} = 9.00$ Hz), 7.48 (dd, 2H, $J = 4.25, 8.00$ Hz), 7.82 (d, 1H, $J = 9.50$ Hz), 7.88 (d, 1H, $J = 2.25$ Hz), 8.08 (d, 1H, $J = 9.50$ Hz), 8.13 (dd, 2H, $J = 1.50, 8.00$ Hz), 8.45 (d, 2H, $J = 2.75$ Hz), 8.92 (dd, 2H, $J = 1.50$, 4.25 Hz) 9.68 (d, 1H, $J = 7.25$ Hz). MS m/z (DCI NH_3): 760 (MH^+, 14%), 564 (100).

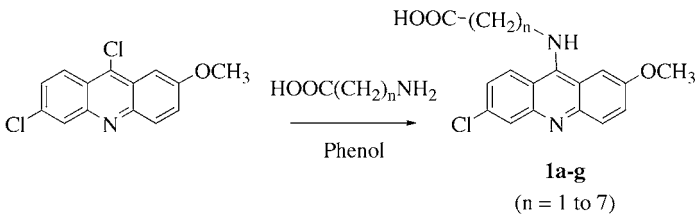
3-Clip-Phen-butyl-chloromethoxyacridine (4c) was prepared from 64 mg (101 μmol) of **3c** to give **4c** (42 mg, 54 μmol, yield = 54%) as a yellow powder. ^{1}H NMR (CD_2Cl_2): δ 2.19 (m, 2H), 2.85 (t, 2H, $J = 6.00$ Hz), 3.85 (m, 5H), 4.22 (m, 4H), 4.90 (m, 1H), 6.97 (dd, 1H, $J = 2.50$, 9.25 Hz), 7.14 (d, 2H, $J = 2.75$ Hz), 7.17 (dd, 1H, $J =$ 2.00, 9.25 Hz), 7.43 and 7.65 (AB, 4H, $J_{AB} = 9.00$ Hz), 7.49 (dd, 2H, $J = 4.25, 8.00$ Hz), 7.75 (d, 1H, $J = 9.25$ Hz), 7.80 (d, 1H, $J = 2.00$ Hz), 8.06 (d, 1H, $J = 9.25$ Hz), 8.14 (dd, 2H, $J = 1.75, 8.00$ Hz), 8.53 (d, 2H, $J = 2.75$ Hz), 8.95 (dd, 2H, $J = 1.75, 4.25$ Hz), 9.46 (d, 1H, $J =$ 7.50 Hz). MS m/z (DCI NH_3): 774 (MH^+, 4%), 578 (100).

3-Clip-Phen-pentyl-chloromethoxyacridine (4d) was prepared from 65 mg (101 μmol) of **3d** to give **4d** (32 mg, 41 μmol, yield = 40%) as a yellow powder. ^{1}H NMR (CD_2Cl_2): δ 1.80 (m, 4H), 2.42 (t, 2H, $J = 6.00$ Hz), 3.68 (t, 2H, $J = 6.00$ Hz), 3.92 (s, 3H), 4.46 (m, 4H), 4.87 (m, 1H), 7.16 (dd, 1H, $J = 2.25, 9.25$ Hz), 7.32 (dd, 1H, $J =$ 2.50, 9.50 Hz), 7.35 (d, 1H, $J = 2.50$ Hz), 7.56 (dd, 2H, J = 4.25, 8.00 Hz), 7.59 (d, 2H, $J = 2.75$ Hz), 7.61 and 7.71 (AB, 4H, $J_{AB} = 9.00$ Hz), 7.82 (d, 1H, $J = 9.50$ Hz), 7.85 (d, 1H, $J = 2.25$ Hz), 8.04 (d, 1H, $J = 9.25$ Hz), 8.20 (dd, 2H, $J = 1.75, 8.00$ Hz), 8.80 (d, 2H, $J = 2.75$ Hz), 8.98 (dd, 2H, $J = 1.75, 4.25$ Hz). MS m/z (DCI NH_3): 788 (MH^+, 0.4%), 592 (100).

3-Clip-Phen-hexylchloromethoxyacridine (4e). Yield = 39% (34 mg, 43 μmol) as a yellow powder. ^{1}H NMR (CD_2Cl_2): δ 1.45 (m, 2H), 1.67 (m, 2H), 1.78 (m, 2H), 2.47 (t, 2H, $J = 7.25$ Hz), 3.54 (t, 2H, $J = 7.00$ Hz), 3.76 (s, 3H), 4.25 (m, 4H), 4.83 (m, 1H), 7.04 (dd, 1H, J = 2.00, 9.50 Hz), 7.14 (d, 1H, $J = 2.50$ Hz), 7.23 (dd, 1H, $J = 2.50, 9.50$ Hz), 7.26 (d, 2H, $J = 2.75$ Hz), 7.43 and 7.61 (AB, 4H, $J_{AB} = 9.00$ Hz), 7.48 (dd, 2H, $J = 4.25$, 8.00 Hz), 7.80 (d, 1H, $J = 9.50$ Hz), 7.85 (d, 1H, $J = 2.00$ Hz), 7.88 (d, 1H, $J = 9.50$ Hz), 8.11 (dd, 2H, $J = 1.50$, 8.00 Hz), 8.47 (d, 1H, $J = 7.25$ Hz), 8.65 (d, 2H, $J = 2.75$ Hz), 8.97 (dd, 2H, $J = 1.50, 4.25$ Hz). MS m/z (DCI NH_3): 802 (MH^+, 5%), 606 (100).

3-Clip-Phen-heptylchloromethoxyacridine (4f). Yield = 36% (33 mg, 40 μmol) as a yellow powder. ^{1}H NMR (CD_2Cl_2): δ 1.35 (br, 4H), 1.65 (br, 4H), 2.30 (t, 2H, $J = 7.25$ Hz), 3.63 (t, 2H, $J = 7.25$ Hz), 3.88 (s, 3H), 4.45 (m, 4H), 4.85 (m, 1H), 7.18 (dd, 1H, $J = 2.25, 9.25$ Hz), 7.31 (d, 1H, $J = 2.50$ Hz), 7.35 (dd, 1H, $J = 2.50, 9.25$ Hz), 7.54 (dd, 2H, $J = 4.50, 8.25$ Hz), 7.66 (d, 2H, $J =$ 3.00 Hz), 7.67 and 7.72 (AB, 4H, $J_{AB} = 8.75$ Hz), 7.80 (d, 1H, $J = 9.25$ Hz), 7.85 (d, 1H, $J = 2.25$ Hz), 7.95 (d, 1H, $J = 8.00$ Hz), 8.01 (d, 1H, $J = 9.25$ Hz), 8.19 (dd, 2H, J = 1.50, 8.25 Hz), 8.80 (d, 2H, $J = 3.00$ Hz), 8.95 (dd, 2H, $J = 1.50, 4.50$ Hz). MS m/z (DCI NH_3): 816 (MH^+, 1%), 620 (53), 197 (100).

3-Clip-Phen-octylchloromethoxyacridine (4g). Yield = 38% (35 mg, 42 μmol) as a yellow powder. ^{1}H NMR (CD_2Cl_2): δ 1.26 (br, 6H), 1.60 (m, 2H), 1.67 (m, 2H), 2.37



Compound	n	yield (%)
1a	1	<40
1b	2	-
1c	3	75
1d	4	80
1e	5	54
1f	6	77
1g	7	71

Figure 1. Synthesis of carboxylic derivatives of 6-chloro-2-methoxyacridine.

(t, 2H, J = 7.25 Hz), 3.50 (t, 2H, J = 7.00 Hz), 3.83 (s, 3H), 4.36 (m, 4H), 4.89 (m, 1H), 7.19 (dd, 1H, J = 2.25, 9.25 Hz), 7.27 (d, 1H, J = 2.75 Hz), 7.34 (dd, 1H, J = 2.75, 9.25 Hz), 7.44 (d, 2H, J = 3.00 Hz), 7.51 (dd, 2H, J = 4.25, 8.00 Hz), 7.58 and 7.68 (AB, 4H, J_{AB} = 9.00 Hz),7.79 (d, 1H, J = 8.00 Hz), 7.89 (d, 1H, J = 9.25 Hz), 7.95 (d, 1H, J = 2.25 Hz), 8.02 (d, 1H, J = 9.25 Hz), 8.15 (dd, 2H, J = 1.75, 8.00 Hz), 8.77 (d, 2H, J = 3.00 Hz), 9.01 (dd, 2H, J = 1.75, 4.25 Hz). MS *m/z* (DCI NH_3): 830 (MH^+, 1%), 634 (63), 197 (100).

3-Clip-Phen-hexylacridine (4h) was prepared according to method A from 40 mg (61 μmol) of **3e** and 33 mg (122 μmol) of 9-phenoxyacridine to give **4h** (32 mg, 43 μmol, yield = 71%) as a yellow powder. ^{1}H NMR (CD_2Cl_2): δ 1.48 (m, 2H), 1.78 (m, 4H), 2.41 (t, 2H, J = 7.25 Hz), 4.38 (m, 4H), 4.87 (m, 1H), 7.24 (m, 2H), 7.46 (br d, 1H, J = 7.50 Hz), 7.51 (d, 2H, J = 2.75 Hz), 7.53 (dd, 2H, J = 8.00, 4.25 Hz), 7.56 (m, 2H), 7.61 and 7.72 (AB, 4H, J_{AB} = 9.00 Hz), 7.92 (br d, 2H, J = 8.25 Hz), 8.11 (br d, 2H, J = 8.75 Hz), 8.18 (dd, 2H, J = 1.75, 8.25 Hz), 8.80 (d, 2H, J = 8.75 Hz), 9.02 (dd, 2H, J = 1.75, 4.25 Hz). MS *m/z* (DCI NH_3): 738 (MH^+, 14%), 542 (100).

Preparation of Cyclic Derivatives (5c and 5d). Chloroform was dried on basic alumina. Carboxylic derivative of acridine **1c** or **1d** (0.28 mmol) was dissolved in $CHCl_3$ (2 mL) at room temperature, and then Et_3N (39 μL, 0.28 mmol) and ethyl chloroformate (26 μL, 0.28 mmol) were added. After the reaction was stirred for 5 h at 70 °C, the solvent was removed under vacuum, and the residue was purified by column chromatography on silica gel eluted with CH_2Cl_2/CH_3OH (95/5) containing 0.5% of concentrated NH_4OH to afford the product.

(Cyclopentyl-9-amido)-6-chloro-2-methoxyacridine (5c). Yield = 73% (68 mg, 0.20 mmol) as a yellow powder, 73%. ^{1}H NMR (CD_2Cl_2): δ 2.51 (m, 2H), 2.82 (t, 2H, J = 8.25 Hz), 3.95−4.06 (m, 2H), 3.98 (s, 3H), 6.97 (d, 1H, J = 2.75 Hz), 7.51 (dd, 1H, J = 2.75, 9.50 Hz), 7.53 (dd,1H, J = 2.00, 9.25 Hz), 7.80 (d, 1H, J = 9.25 Hz), 8.12 (d, 1H, J = 9.50 Hz), 8.22 (d, 1H, J = 2.00 Hz). MS *m/z* (DCI NH_3): 327 (MH^+, 100%).

(Cyclohexyl-9-amido)-6-chloro-2-methoxyacridine (5d). Yield = 33% (31 mg, 0.09 mmol) as a yellow powder. ^{1}H NMR (CD_2Cl_2): δ 2.17 (m, 4H), 2.78 (br, 2H), 3.66 (m, 2H), 3.98 (s, 3H), 6.99 (d, 1H, J = 2.75 Hz), 7.50 (dd, 1H, J = 2.75, 9.50 Hz), 7.52 (dd,1H, J = 2.00, 9.25 Hz), 7.83 (d, 1H, J = 9.25 Hz), 8.10 (d, 1H, J = 9.50 Hz), 8.21 (d, 1H, J = 2.00 Hz). MS *m/z* (DCI NH_3): 341 (MH^+, 100%).

DNA Cleavage Experiments. Metalations by $CuCl_2$ of the different ligands were performed by using 1 equiv of the desired ligand in a DMF/water mixture (2/3, v/v, the final copper concentration being 1 mM) during 2 h at room temperature. These stock solutions of complexes were diluted with water at the desired concentration just before use.

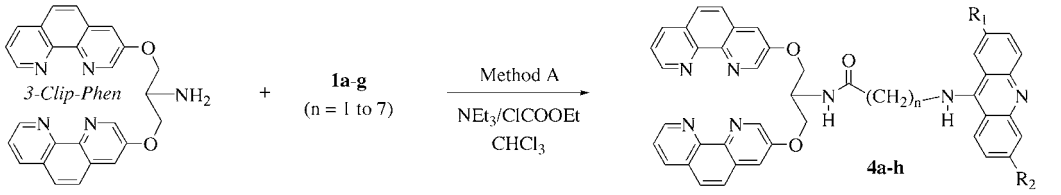
To 10 μL of ΦX174 DNA (7 nM, 40 μM in base pair) in 80 mM Tris-HCl buffer (pH 7.2), 100 mM NaCl, and 20 mM $MgCl_2$ was added 5 μL of the desired complex (0.1, 0.2, 0.3, 0.4, 0.5, 0.6, 0.7, or 0.8 μM). After 30 min at room temperature, DNA cleavage was initiated by addition of a freshly prepared aqueous solution of sodium ascorbate (5 μL, 400 μM), and samples were incubated for 1 h at 37 °C. A 7.5 μL amount of a solution of 50% (v/v) glycerol/40 mM Tris-HCl buffer (pH 8.0) and 0.05% bromophenol blue (w/v) was then added, and samples were immediately loaded on agarose gel (0.8%) containing 1 μg/mL of ethidium bromide. Electrophoresis was run at constant current (25 mA for 15 h) in Tris/borate/EDTA (TBE) buffer. Bands were located by UV light (254 nm), photographed, and quantified by microdensity. The correction coefficient 1.47 was used for the decrease of stainability of form I DNA versus forms II and III (*27*).

RESULTS AND DISCUSSION

Synthesis. To enhance the cell delivery, the DNA affinity, and DNA cleavage activity of 3-Clip-Phen, we have prepared different conjugates with acridine and 6-chloro-2-methoxyacridine intercalators. The acridine derivative was fixed through an amino acid linker of different length on the primary amine of 3-Clip-Phen (*4*) in order to analyze the influence of this linker on the reactivity of the conjugates. We chose an aliphatic linker, and its length was modulated by incorporation of methylene units in order to facilitate the conformational flexibility between the acridine and 3-Clip-Phen entities of the molecule and thus the interaction of the two parts of the conjugate with the DNA target. Two synthetic routes were explored in order to optimize their preparation.

Method A was first used since it involved only two steps. In the first step 6,9-dichloro-2-methoxyacridine was activated as the phenoxyacridine derivative. Then, in a one-pot reaction, an aromatic nucleophilic substitution of the phenoxy group by the primary amine of the amino acid linker produced the acridine derivative **1a**−**g** functionalized by a carboxylic group (Figure 1). The second step consisted of activation of the carboxylic acid by ethyl chloroformate and coupling the resulting activated ester with the primary amine of 3-Clip-Phen through an amide function (Figure 2).

This method appeared to be efficient, with a yield of around 40%, for the preparation of 3-Clip-Phen-acridine conjugates **4e**−**g**, with 5 to 7 methylene groups between the acridine moiety and the 3-Clip-Phen entity of the conjugate. But several problems appeared during the preparation of conjugates with shorter arms of junction: (i) the acridine synthons with a long tether were generally obtained in good yields, but for a short linker (n = 1), the conversion of 6,9-dichloro-2-methoxyacridine into carboxylic derivative **1a** was poor and produced a mixture



Compound	R_1	R_2	n	Method A yield (%)	Method B yield (%)	Overall yield with respect to *3-Clip-Phen* (%)
4a	CH_3O	Cl	1	-[a]	67	51
4b	CH_3O	Cl	2	-	50	40
4c	CH_3O	Cl	3	0[b]	54	49[c]
4d	CH_3O	Cl	4	0[b]	40	36[c]
4e	CH_3O	Cl	5	39	-	39[d]
4f	CH_3O	Cl	6	36	-	36
4g	CH_3O	Cl	7	38	-	38
4h	H	H	5	-	71	59

Figure 2. Two methods for the synthesis of 3-Clip-Phen-acridine conjugates. a: Method A resulted in only a poor overall yield with respect to 3-Clip-Phen since **1a** was obtained in poor yield. b: **1c** and **1b** precursors were quantitatively converted to the corresponding cyclic derivatives. c: From method B. d: **4e** can be obtained in similar overall yield with respect to 3-Clip-Phen from method B.

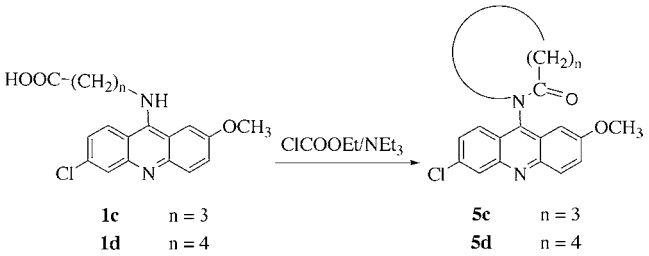


Figure 3. Formation of cyclic derivatives of 6-chloro-2-methoxyacridine.

of acridine derivatives difficult to purify; (ii) the conjugation of the carboxylic derivatives **1c** and **1d** with 3-Clip-Phen was totally inefficient because the acridine derivatives were transformed into new products identified as being the cyclic derivatives **5c** and **5d**, respectively (Figure 3). To confirm this phenomenon, **1c** or **1d** was incubated with ethyl chloroformate: they were converted into cyclic derivatives **5c** and **5d** by intramolecular coupling between the activated carboxylic function and the amine of the acridine derivative. The formation of the five- or six-membered ring was sterically and thermodynamically favored in comparison to the intermolecular reaction with the primary amine of 3-Clip-Phen. Consequently the synthesis of **4c** or **4d** with the method A was totally inefficient. This last interpretation was confirmed by attempts to activate **1c** or **1d** by (benzotriazol-1-yloxy)tris(dimethylamino)phosphonium (BOP) directly in the presence of 3-Clip-Phen: **5c** or **5d** were again the major reaction products, and the conjugation was inefficient.

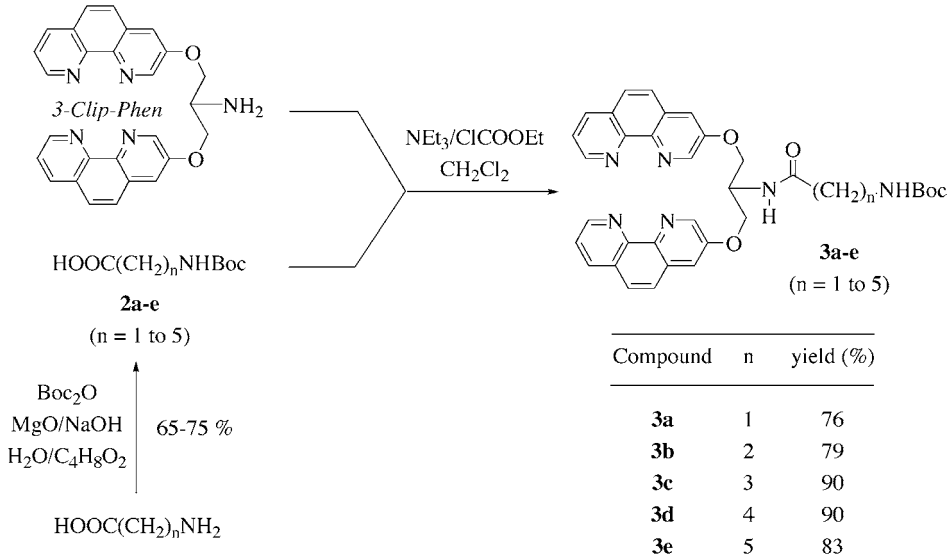
To overcome these difficulties, we considered another way of synthesis for the conjugates. Thus compounds **4a**−**e** were prepared with the more step-demanding method B (Figure 2). The primary amine function of the amino acid linker was first protected as a Boc-derivative to prevent the possibility of intramolecular amidification or its polymerization during the activation of the carboxylic acid. Then the amino acid linker was conjugated on 3-Clip-Phen to generate the protected 3-Clip-Phen derivatives **3a**−**e** in good yields (Figure 4). The Boc-protecting group was removed through acid hydrolysis. Then the free primary amine produced the aromatic nucleophilic substitution of the phenoxy group of 9-phenoxy-6-chloro-2-methoxyacridine derivative to generate the 3-Clip-Phen−acridine conjugates (Figure 2).

We compared the overall yield with respect to the starting 3-Clip-Phen in the preparation of conjugates **4a**−**g** (table of Figure 2). In all cases 50 mg of 3-Clip-Phen was used to facilitate this comparison. It appeared that methods A and B had roughly the same efficiency (around 40% overall yield). This result was confirmed in the case of conjugate **4e** which has been obtained by the two methods in similar yields. However, method B is more general and can be used for all arms of junction, but is more expensive and time-consuming than method A since this method requires five steps of synthesis. The 3-Clip-Phen-6-chloro-2-methoxyacridine conjugates were obtained from method A in only two steps.

The 3-Clip-Phen-acridine conjugate **4h** was also prepared in similar yield by method B (Figure 2) in order to study the influence of chloro and methoxy substituents on the DNA cleavage efficiency. An aminocaproic linker was used in **4h** since DNA cleavage experiments indicated that this tether led to higher DNA cleavage efficiency (see below).

DNA Cleavage. Ligands **4a**−**h** and 3-Clip-Phen have been metalated with 1 equiv of $CuCl_2$, and the DNA cleavage activity of the copper complexes obtained was evaluated. DNA cleavage was monitored by relaxation of supercoiled circular ΦX 174 DNA (form I) into nicked circular (form II) and linear (form III) conformations in 1 h at 37 °C. The redox activity of the Cu^{II} centers was initiated by addition of 100 μM ascorbate in the presence of air. Different concentrations of copper complexes have been tested.

Figure 5 shows a representative gel illustrating the relative reactivities of the different copper complexes at 100 nM concentration. In these experiments, the comparison of cleavage patterns of copper complexes of 6-chloro-2-methoxyacridine-3-Clip-Phen conjugates (compounds **4a**−**g**, lanes 6−12) allowed analysis of the influence of the length of the linker on the DNA cleavage efficiency. Since all the conjugates of this series were at the same concentration and differed only by the number *n* of methylene groups in the linker and since all values between $n = 1$ to 7 have been tested, a strict comparison



Compound	n	yield (%)
3a	1	76
3b	2	79
3c	3	90
3d	4	90
3e	5	83

Figure 4. Synthesis of "3-Clip-Phen-arm-Boc" derivatives.

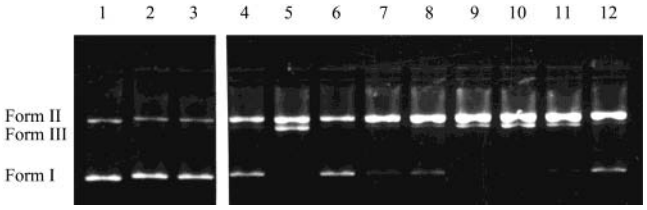


Figure 5. Comparison of DNA cleavage efficiency on ΦX 174 DNA (3.5 nM, 20 μM in bp) between copper complexes of 3-Clip-Phen and 3-Clip-Phen-acridine conjugates (**4a**−**h**) 100 nM. Reactions were done in the presence of ascorbate and air for 1 h in 40 mM Tris-HCl buffer (pH 7.2), 50 mM NaCl, 10 mM $MgCl_2$. Lane 1: Control $CuCl_2$. Lane 2: **4h** without ascorbate. Lane 3: **4e** without ascorbate. Lane 4: 3-Clip-Phen. Lane 5: **4h**. Lane 6: **4a**. Lane 7: **4b**. Lane 8: **4c**. Lane 9: **4d**. Lane 10: **4e**. Lane 11: **4f**. Lane 12: **4g**.

could be performed. Figure 5 shows that the residual percentage of DNA form I decreased (and thus that the quantity of cleaved DNA increased) when the length of the linker increased from $n = 1$ (**4a**−$CuCl_2$, lane 6) to $n = 5$ (**4e**−$CuCl_2$, lane 10). For the more active compounds, DNA form III could be also observed, its quantity being again higher in the case of DNA cleavage by **4e**−$CuCl_2$ ($n = 5$). It is reasonable to propose that conjugates with shortest linker ($n < 5$) are sterically constrained and therefore less efficient. But it is remarkable that copper complexes of conjugates with a larger arm of junction ($n > 5$) are also less efficient than **4e**−$CuCl_2$ since the residual percentage of form I increased again for $n = 6$ then 7 (conjugates **4f**−$CuCl_2$ and **4g**−$CuCl_2$, lanes 11 and 12, respectively), showing that the optimal linker was obtained for $n = 5$.

The influence of the chloro and methoxy substituents on the acridine part of the conjugates, with the same optimal linker with $n = 5$ and in the same cleavage conditions, was accessible (Figure 5) in comparing **4e**−$CuCl_2$ and **4h**−$CuCl_2$ (lanes 10 and 5, respectively). Both copper complexes cleaved all DNA form I which was transformed into form II and form III. However, the conjugate with the unsubstituted acridine was the more active since it produced more form III.

The cleavage pattern obtained for the same concentration of 3-Clip-Phen-$CuCl_2$ (lane 4, Figure 5) showed a residual form I, indicating that this parent ligand was less efficient than both **4e**−$CuCl_2$ and **4h**−$CuCl_2$ (Figure 5, lanes 10 and 5, respectively) and that the conjugation

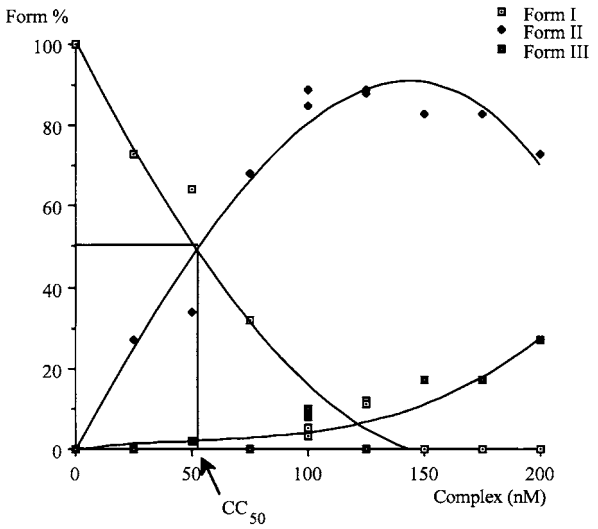


Figure 6. Example of determination of CC_{50} values: case of **4f**−$CuCl_2$.

of 3-Clip-Phen to an intercalator such as acridine had a positive effect on its DNA cleavage efficiency.

To quantify the nuclease activity of the different conjugates, DNA cleavage was also studied for different concentrations of all copper complexes. In all cases, the percentage of residual DNA form I decreased when the copper complex concentration increased, and form III appeared only when most of form I was transformed into form II. This result is in accordance to complexes producing single strand breaks on double stranded DNA, form III resulting from the accumulation of neighboring multi-single-strand breaks on form II. Figure 6 shows a typical example obtained for conjugate **4f**−$CuCl_2$.

Since the 3-Clip-Phen parent ligand has poor sequence selectivity (*5*), we tried to quantify the single-strand cleavage according to a random cleavage of the ΦX 174 DNA as in reference 28, but no linear relationship between the number of breaks and the concentration of copper complexes was observed in the case of the acridine conjugates. Other observations were also not in accordance to the fact that not all of these copper complexes cleaved DNA in a random fashion. For example, although low concentrations of copper complexes of **4a** and 3-Clip-Phen seemed to have roughly the same ability to cleave

Table 1. Comparative Efficiency of Copper Complexes of 3-Clip-Phen and 3-Clip-Phen−Acridine Conjugates (4a−f) on ΦX 174 DNA Cleavage. CC_{50} Values and Percentage of ΦX 174 DNA Forms I, II, and III Obtained after 1 h of Reaction of 45 nM of the Different Copper Complexes in the Presence of 100 μM Ascorbate

					comparison at 45 nM of copper conjugate		
conjugate $CuCl_2$	R_1	R_2	n	CC_{50} (nM)	form I (%)	form II (%)	form III (%)
4a	CH_3O	Cl	1	100	80	20	0
4b	CH_3O	Cl	2	80	75	25	0
4c	CH_3O	Cl	3	60	68	32	0
4d	CH_3O	Cl	4	55	60	40	0
4e	CH_3O	Cl	5	45	50	50	0
4f	CH_3O	Cl	6	55	60	40	0
4g	CH_3O	Cl	7	75	75	25	0
4h	H	H	5	35	27	68	5
3-Clip-Phen	−	−	−	100	85	15	0
2-Clip-Phen conjugate	CH_3O	Cl	5	195	95	5	0

DNA form I, a higher percentage of form III was observed in the case of 3-Clip-Phen-$CuCl_2$ than in the case of **4a**-$CuCl_2$ at higher concentration (data not shown). This last result could reflect differences in the ability of the complexes to cleave supercoiled or relaxed DNA conformations, 3-Clip-Phen being perhaps more active than the acridine conjugates to cleave relaxed form II. Although there is little sequence selectivity for the intercalation of acridine derivatives (*24*), the presence and the position of the amide junction with 3-Clip-Phen could influence the interaction of the conjugates with DNA and consequently the cleavage pattern (*29*, *30*).

For these reasons, we chose to quantify the relative DNA cleavage efficiency of the different copper complexes through the classical determination of the concentration of chemical nuclease cleaving 50% of form I of ΦX174 DNA in 1 h at 37 °C (CC_{50} values, Table 1) (see references 31−35 for typical examples). Figure 6 illustrates the method of determination of the CC_{50} in the case of compound **4f**−$CuCl_2$. The advantage of using CC_{50} values is that they concern the same cleavage event and thus the comparison of the different copper complexes seemed easier. Data of Table 1 confirmed that (i) the conjugation of 3-Clip-phen-$CuCl_2$ (CC_{50} = 100 nM) to an acridine derivative generally increased the DNA cleavage efficiency, (ii) the optimized conjugate linker was obtained for $n = 5$ (CC_{50} = 45 nM for compound **4e**−$CuCl_2$ with five methylene groups in the arm of junction of the conjugate), (iii) conjugate with unsubtituted acridine **4h**−$CuCl_2$ (CC_{50} = 35 nM) was the more active DNA cleaver.

The determination of the CC_{50} has been also performed for the same acridine derivative and the same linker in the case of conjugates including 2-Clip-Phen, the less efficient isomer of 3-Clip-Phen (*23*). Table 1 shows that the conjugation to 3-Clip-Phen (compound **4e**−$CuCl_2$, CC_{50} = 45 nM) was more efficient than one with 2-Clip-phen (CC_{50} = 195 nM). This last result showed that the DNA cleavage efficiency of the copper complex was not only due to a better DNA affinity due to the presence of an acridine functionality in the conjugate but also to a higher nuclease activity of the 3-Clip-phen derivatives in comparison to 2-Clip-Phen derivatives.

However, it is remarkable to note that if the determination of CC_{50} values allowed easy comparison of the DNA cleavage efficiency between the different copper complexes, it cannot be used to quantify it. This problem is probably due to the fact that the overcleavage of DNA molecules is underestimated. This phenomenon appeared clearly in the comparison of the percentages of DNA form I, II, and III observed in the case of 45 nM of copper complexes (Table 1). This concentration was chosen since it is the CC_{50} of **4e**−$CuCl_2$, the more active 3-Clip-Phen-6-chloro-2-methoxyacridine conjugate observed in the optimization of the linker. Sometimes minor variation of the cleavage pattern, reflecting minor variation in the DNA cleavage activity, was observed for a small variation (10 nM) of the CC_{50} value, as is the case for the comparison of cleavage patterns of **4e**−$CuCl_2$ (CC_{50} = 45 nM) and **4d**−$CuCl_2$ or **4f**−$CuCl_2$ (CC_{50} = 55 nM). However, higher variations of the cleavage pattern, in particular the formation of DNA form III resulting from recleavage events, reflecting higher variation in the DNA cleavage activity, were observed during the comparison of the cleavage pattern of **4e**−$CuCl_2$ (CC_{50} = 45 nM) and **4h**−$CuCl_2$ (CC_{50} = 35 nM) although the difference of the CC_{50} values between these two compounds was again 10 nM.

CONCLUSION

Two methods of preparation of Clip-Phen−acridine conjugates have been described in the present report. These molecules incorporate in their structure different entities designed for specific functions: (i) an intercalator (acridine or 6-chloro-2-methoxyacridine) for cell penetration and DNA binding, (ii) a 2- or 3-Clip-Phen entity endowed with both binding and DNA cleavage functions, (iii) a flexible linker with an optimal length. The constitutive entities were modulated in these conjugates to get an insight to their mode of action and to prepare more active compounds. It appeared that the copper complex including 3-Clip-Phen, an aminocaproic linker, and acridine produced the most DNA cleavage. The next goal is to analyze the influence of acridine derivatives of the more active conjugates on the selective drug delivery of these potentially cytotoxic compounds within cells.

LITERATURE CITED

(1) Sigman, D. S., Mazumder, A., and Perrin, D. M. (1993) Chemical nucleases. *Chem. Rev. 93*, 2295−2316.

(2) Meunier, B., Ed. (1996) *DNA and RNA Cleavers and Chemotherapy of Cancer and Viral Diseases*, Kluwer, Dordrecht.

(3) Pitié, M., Donnadieu, B., and Meunier, B. (1998) Preparation of the new bis(phenanthroline)ligand "Clip-Phen" and evaluation of the nuclease activity of the corresponding copper complex. *Inorg. Chem. 37*, 3486−3489.

(4) Pitié, M., Sudres, B., and Meunier, B. (1998) Dramatic increase of the DNA cleavage activity of Cu(Clip-phen) by fixing the bridging linker on the C^3 position of the phenanthroline units. *Chem. Commun.* 2597−2598.

(5) Pitié, M., Burrows, C. J., and Meunier, B. (2000) Mechanism of DNA cleavage by copper complexes of 3-Clip-phen and of its conjugates with a distamycin analogue. *Nucleic Acids Res. 28*, 4856−4864.

(6) Pitié, M., Van Horn, J. D., Brion, D., Burrows, C. J., and Meunier, B. (2000) Targeting the DNA cleavage activity of copper phenanthroline and Clip-Phen to A. T tracts via linkage to a poly-*N*-methylpyrrole. *Bioconjugate Chem. 11*, 892−900.

(7) Claussen, C. A., and Long, E. C. (1999) Nucleic acid recognition by metal complexes of bleomycin. *Chem. Rev. 99*, 2797−2816.
(8) Burger, R. M. (1998) Cleavage of nucleic acids by bleomycin. *Chem. Rev. 98*, 1153−1169.
(9) Albert, A. (1966) *The Acridines*, 2nd ed.; E. Arnold, London.
(10) Baguley, B. C. (1991) DNA intercalating anti-tumour agents. *Anti-Cancer Drug Design 6*, 1−35.
(11) Denny, W. A. (1989) DNA-intercalating ligands as anti-cancer drugs: prospects for future design. *Anti-Cancer Drug Design 4*, 241−263.
(12) Neidle, S., and Abraham, Z. (1985) Structural and sequence-dependent aspects of drug intercalation into nucleic acids. *Crit. Rev. Biochem. 17*, 73−120.
(13) Bailly, C., and Hénichart, J.-P. (1991) DNA recognition by intercalator-minor- groove binder hybrid molecules. *Bioconjugate Chem. 2*, 379−397.
(14) Bailly, C., and Chaires, C. B. (1998) Sequence specific DNA minor groove binders. Design and synthesis of netropsin and distamycin analogues. *Bioconjugate Chem. 9*, 513−538.
(15) Buchart, O., Egholm, M., Karup, G., and Nielsen, P. E. (1987) 9-(4- Nitrobenzamidopolymethylene)aminoacridines and their photochemical cleavage of DNA. *J. Chem. Soc., Chem. Commun.* 1696−1697.
(16) Nielsen, P. E., Egholm, M., Koch, T., Christensen, J. B., and Buchart, O. (1991) Photolytic cleavage of DNA by nitrobenzamido ligands linked to 9-aminoacridines gives DNA polymerase substrates in a wavelength-dependent reaction. *Bioconjugate Chem. 2*, 57−66.
(17) Asseline, U., Delarue, M., Lancelot, G., Toulmé, F., Thuong, N. T., Montenay- Garestier, T., and Hélène, C. (1984) Nucleic acid-binding molecules with high affinity and base sequence specificity: intercalating agents covalently linked to oligodeoxynucleotides. *Proc. Natl. Acad. Sci. U.S.A. 81*, 3297−3301.
(18) Asseline, U., Thuong, N. T., and Hélène, C. (1986) Oligothymidylates substitués en position 3′ par un dérivé de l′acridine. *Nucleosides Nucleotides 5*, 45−63.
(19) Nelson, P. S., Kent, M., and Muthini, S. (1992) Oligonucleotide labeling methods 3. Direct labeling of oligonucleotides employing a novel, nonnucleosidic, 2-aminobutyl-1,3-propanediol backbone. *Nucleic Acids Res. 20*, 6253−6259.
(20) Fukui, K., Iwane, K., Shimidzu, T., and Tanaka, K. (1996) Oligonucleotides covalently linked to an acridine at artificial abasic site: influence of linker length and the base-sequence *Tetrahedron Lett. 37*, 4983−4986.
(21) Girault, S., Grellier, P., Berecibar, A., Maes, L., Mouray, E., Lemière, P., Debreu, M.-A., Davioud-Charvet, E., and Sergheraert, C. (2000) Antimalarial, antitrypanosomal, and antileishmanial activities and cytotoxicity of bis(9-amino-6-chloro-2-methoxyacridines): influence of the linker. *J. Med. Chem. 43*, 2646−2654.
(22) Le Pecq, J.-B., Le Bret, M., Barbet, J., and Roques, B. (1975) DNA polyintercalating drugs: DNA binding of diacridine derivatives. *Proc. Natl. Acad. Sci. U.S.A. 72*, 2915−2919.
(23) Ross, S. A., Pitié, M., and Meunier, B. (1999) Synthesis of two acridine conjugates of the bis(phenanthroline) ligand "Clip-Phen" and evaluation of the nuclease activity of the corresponding copper complexes. *Eur. J. Inorg. Chem.* 557−563.
(24) Natasi, M., Morris, J. M., Rayner, D. M., Seligy, V. L., Szabo, A. G., Williams, D. F., Williams, R. E., and Yip, R. W. (1976) Structural implications of the electronic spectra of quinacrine-deoxyribonucleic acid complexes in the ultraviolet region (250−300 nm). *J. Am. Chem. Soc. 98*, 3979−3986.
(25) Branik, M., and Kessler, H. (1975) NMR− und IR−Untersuchungen von Boc-ω-Aminosäuren. *Chem. Ber. 108*, 2722−2727.
(26) Fukui, K., Morimoto, M., Segawa, H., Tanaka, K., and Shimidzu, T. (1996) Synthesis and properties of an oligonucleotide modified with an acridine derivative at the artificial abasic site. *Bioconjugate Chem. 7*, 349−355.
(27) Bernadou, J., Pratviel, G., Bennis, F., Girardet, M., and Meunier, B. (1989) Potassium monopersulfate and a water soluble manganese porphyrin, $(Mn(TMPyP))(OAc)_5$, as an efficient reagent for the oxidative cleavage of DNA. *Biochemistry 28*, 7268−7275.
(28) Hertzberg, R. P., and Dervan, P. B. (1984) Cleavage of DNA with methidiumpropyl-EDTA-iron(II): reaction conditions and products analyses. *Biochemistry 23*, 3934−3945.
(29) Gaugain, B., Markovits, J., Le Pecq, J.-B., and Roques, B. P. (1981) Hydrogen bonding in deoxyribonucleic acid base recognition. 1. Proton nuclear magnetic resonance studies of dinucleotide-acridine alkylamide complexes. *Biochemistry 20*, 3035−3042.
(30) Markovits, J., Gaugain, B., Barbet, J., Roques, B. P., and Le Pecq, J.-B. (1981) Hydrogen bonding in deoxyribonucleic acid base recognition. 2. Deoxyribonucleic acid binding studies of acridine alkylamides. *Biochemistry 20*, 3042−3048.
(31) Ding, L., Etemad-Moghadam, G., and Meunier, B. (1990) Oxidative cleavage of DNA mediated by hybrid metalloporphyrin-ellipticine molecules and functionalized metalloporphyrin precursors. *Biochemistry 29*, 7868−7875.
(32) Yu, H., Kwok, Y., Hurley, L. H., and Kervin, S. M. (2000) Efficient, Mg^{2+}-dependent pohotochemical DNA cleavage by the antitumor quinobenzoxazine (S)-A-62176. *Biochemistry 39*, 10236−10246.
(33) Silver, G. C., and Trogler, W. C. (1995) Efficient cleavage of DNA by Iron(III) triazacyclononane derivatives. *J. Am. Chem. Soc. 117*, 3983−3993.
(34) Hiort, C., Goodisman, J., and Dabrowiak, J. C. (1996) Cleavage of DNA by the insulin-mimetic compound, $NH_4[VO(O_2)_2(phen)]$. *Biochemistry 35*, 12354−12362.
(35) Nielsen, P. E., Jeppesen, C., Egholm, M., and Buchardt, O. (1988) Photochemical Cleavage of DNA by nitrobenzamides linked to 9-aminoacridine. *Biochemistry 27*, 6338−6343.

BC020013X

Improvement of Pharmacokinetics of Radioiodinated Tyr^3-Octreotide by Conjugation with Carbohydrates

Margret Schottelius,[†] Hans-Jürgen Wester,*[,†] Jean Claude Reubi,[‡] Reingard Senekowitsch-Schmidtke,[†] and Markus Schwaiger[†]

Nuklearmedizinische Klinik und Poliklinik, Klinikum rechts der Isar, Technische Universität München, 81675 München, Germany, and Institute of Pathology, University of Berne, 3010 Berne, Switzerland .
Received January 16, 2002; Revised Manuscript Received May 10, 2002

Among a variety of other factors, the clearance kinetics and routes of excretion of radiopharmaceuticals are of crucial importance for early and high tumor/background ratios and thus signal intensity in diagnostic imaging by single photon emission tomography (SPECT) or positron emission tomography (PET). To overcome the unfavorable pharmacokinetics of radiohalogenated octreotide analogues, we evaluated three carbohydrated conjugates of Tyr^3-octreotide (TOC). Glucose ([^{125}I]Gluc-TOC), maltose ([^{125}I]Malt-TOC), and maltotriose ([^{125}I]Mtr-TOC) derivatives of [^{125}I]TOC were synthesized via Maillard reaction and subsequent radioiodination. In cells transfected with sst1-sst5, I-Malt-TOC, and I-Mtr-TOC show sst-subtype binding profiles similar to I-TOC with high affinity for sst2. Comparative biodistribution studies 10, 30, and 60 min pi in nude mice bearing rat pancreatic tumor xenografts showed fast blood clearance for all glycosylated derivatives. Due to their markedly increased hydrophilicity, [^{125}I]Gluc-TOC and [^{125}I]Malt-TOC were mainly cleared via the kidneys, which led to a significant decrease in activity accumulation in liver and intestine (5.3 and 1.4 versus 10.6%ID/g for [^{125}I]TOC in the liver, 1.7 and 1.0 versus 3.8%ID/g for [^{125}I]TOC in the intestine 60 min pi). For all compounds, hydrophilicity and uptake in liver and intestines correlate. Uptake of the carbohydrate conjugates in the kidney was comparable. Compared to the parent compound, the accumulation of the carbohydrated compounds in sst-rich tissues (pancreas, adrenals) was increased by a factor of 1.5−3.5. While tumor uptake of [^{125}I]TOC (6.7 ± 2.6%ID/g), [^{125}I]Malt-TOC (5.3 ± 1.9%ID/g), and [^{125}I]-Mtr-TOC (4.9 ± 2.2%ID/g) at 30 min postinjection was comparable, accumulation of [^{125}I]Gluc-TOC was significantly increased (10.1 ± 2.8%ID/g at 30 min pi). Somatostatin receptor specificity of tumor uptake was confirmed by pretreatment, competition, and displacement experiments in vivo using 0.8 mg TOC/kg and γ-camera imaging. Glycosylation proved to be a powerful tool for the development of high affinity sst ligands with excellent excretion profiles and improved tumor accumulation.

INTRODUCTION

On the basis of the findings that many human tumors overexpress a variety of receptors for regulatory peptides and peptide hormones (*1*−*6*), neuropeptide receptor targeted diagnostic imaging and radiotherapy has become a major concept for the detection, localization, and therapeutic intervention of malignant neoplasms in Nuclear Medicine (*7*−*11*). For this purpose, a number of radiolabeled analogues of endogenous peptides are presently investigated and under preclinical evaluation: e.g., analogues of somatostatin (SS) (*9*, *12*, *13*), substance P (*14*), gastrin (*15*), bombesin (BB) (*16*), α-melanocyte stumulation hormone (α-MSH) (*17*, *18*), neurotensin (NT) (*19*), or vasoactive intestinal peptide (VIP) (*20*). The clinical potential of these tracers will rely, among a variety of other factors, such as high receptor affinity and selectivity, high metabolic stability, low nonspecific uptake, and high specific accumulation, upon two main factors with crucial importance for early and high tumor/background ratios, namely favorable blood clearance and excretion kinetics. New radiolabeling strategies mainly focus on improved in vivo stability against dehalogenation (e.g., *21*, *22*, *23*) or transchelation (e.g., *24*, *25*, *26*), fast and high yield radiolabeling, or basic aspects such as radiolabeling without affecting biological integrity (*27*, *28*) of the peptide investigated. However, peptide radiotracers often only suffer from disadvantages of less than optimal blood clearance, excretion pathways and nonspecific uptake (*29*, *30*).

Thus, to generate more adequate radioligands, the use and evaluation of suitable chemical tools with broad utility is recommended.

What are the demands for such a tool? To increase target-to-nontarget tissue ratio (tumor-to-nontumor ratio), the tracer should be rapidly cleared from the circulation. Furthermore, to reduce the whole body radiation exposure, the modification used should reduce hepatobiliary excretion. The tracer should be cleared via the kidneys. However, to avoid nephrotoxicity after application of therapeutic dosages, renal uptake should be minimized ([^{90}Y]DOTATOC) (*31*, *32*). Receptor affinity and selectivity should remain unchanged, and the modification used has to be compatible with the radiolabeling strategy, thus not affecting radiolabeling yield.

To influence receptor binding and enhance peptide delivery to the brain or spinal cord, attachment of carbohydrate groups to enkephalin peptides has been

* To whom correspondence should be addressed. Hans-J.Wester, Ph.D., Nuklearmedizinische Klinik und Poliklinik, Klinikum rechts der Isar, Technische Universität München, Ismaninger Strasse 22, D − 81675 München, Germany. Tel: 49 89 4140 4586. Fax: 49 89 4140 4841. E-mail: H.J.Wester@lrz.tum.de.

[†] Technische Universität München.

[‡] University of Berne.

10.1021/bc0200069 CCC: $22.00 © 2002 American Chemical Society
Published on Web 08/31/2002

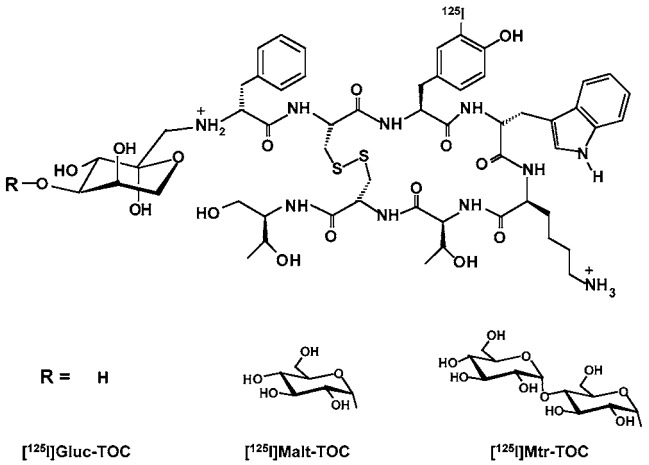


Figure 1. Structures of [125I]Gluc-TOC, [125I]Malt-TOC, and [125I]Mtr-TOC.

studied (*33*−*36*). It has been shown, that glycosyl groups, if properly placed, will preserve previously determined structure−activity relations (SAR) of the native peptides (*34*, *35*, *37*, *38*). Enkephalin analogues glycosylated in the near or at the C-terminus were shown to elicit prolonged and profound analgesia in mice (*34*, *35*). Furthermore it has been demonstrated, that the in vivo stability of an (N-linked) glycopeptide renin inhibitor is enhanced (*39*). Glucosyl, mannosyl, galactosyl, and 2-deoxy-glucosyl derivatives of Arg^8-vasopressin exhibited a sugar dependent renal uptake and intrarenal distribution (*40*). Glycosylated vasopressin analogues displayed an increased bioavailability resulting from absorption from the small intestine and most likely from an increased stability toward enzymatic degradation (*41*). Studies on the uptake of a glycosylated derivative of the tetrapeptide Gly-Gly-Tyr-Arg into brush border membrane vesicles and transport though the intestinal membrane has indicated increased resistance to aminopeptidases. Furthermore, the Na^+-dependent glucose transporter SGLT-1 played an important role in the intestinal absorption of both the α- and β-glucopyranoside derivative (*42*).

Recently, sugar-conjugated integrin antagonists have been investigated in our laboratory (*27*, *30*, *43*). It was shown that coupling of sugar amino acids significantly improves the pharmacokinetics of $\alpha_V\beta_3$-integrin antagonists (*27*, *43*). Furthermore we introduced radiolabeled carbohydrated octreotide analogues as a new series of somatostatin receptor (sst) binding radiotracers with excellent physicochemical characteristics (*44*−*48*).

The goal of the current study was to directly compare three carbohydrated conjugates of Tyr^3-octreotide (TOC), an agent previously evaluated for targeted imaging and radiotherapy of somatostatin receptor (sst) expressing tumors. The glucose ([125I]Gluc-TOC), maltose ([125I]Malt-TOC), and maltotriose ([125I]Mtr-TOC) derivatives of [125I]-TOC were synthesized via formation of an N-terminal N_α-glycosylamine with the respective aldose followed by Amadori rearrangement (*48*) and subsequent radioiodination (Figure 1).

The affinity profiles of I-Malt-TOC, I-Mtr-TOC and I-TOC were assessed in cells stably expressing sst1-sst5. We compared the effects of carbohydration on biodistribution in rat pancreatic tumor (AR42J) xenografted mice, particularly on hepatic uptake, biliary excretion, renal uptake, and tumor accumulation and demonstrate the suitablity of carbohydration to modify the physicochemical tracer characteristics in vivo by γ-camera imaging of tumor bearing mice. Specificity of tumor uptake was demonstrated in vivo by pretreatment, competition, and displacement experiments.

MATERIALS AND METHODS

Instrumentation. Analytic reversed phase high performance liquid chromatography (RP-HPLC) was performed using a Sykam gradient HPLC System (Sykam GmbH, Gilching, Germany) and a Nucleosil 100 C18 (5 mm, 250 × 4.0 mm) column. The peptides were eluted (if not stated otherwise in the text) applying a gradient of 10−60% B (solvent A: 0.1% TFA (trifluoro acetic acid) in H_2O, solvent B: 0.1% TFA in acetonitrile) in 30 min at a constant flow of 1 mL/min. UV-Detection was performed at 220 nm in a 206 PHD UV−Vis detector (Linear Instruments Corporation, Reno, NV).

Preparative RP-HPLC of all peptides was performed on the Sykam HPLC system using a Multospher 100 RP 18−5 (250 × 10 mm) column at a constant flow of 5 mL/min.

Mass spectra were recorded on the LC-MS system LCQ from Finnigan (Bremen, Germany) using the Hewlett-Packard series 1100 HPLC system.

Sample preparation for peptide sequence analysis was performed according to the following protocol:

For reduction of the disulfide bridge, 1 nmol of the synthetic peptide was dissolved in 5 μL of 10 mM NH_4HCO_3 containing 10 mM dithiothreitol and incubated at 56 °C for 30 min. The reduced peptide (10 pmol) was desalted over a POROS R2 microcolumn (Perseptive, Framingham, MA), packed in a GELoader Tip (Eppendorf, Hamburg, Germany), and eluted with 1 μL of 5% formic acid/60% methanol directly into the nanoelectrospray needle (MDS Proteomics, Odense, Denmark).

All experiments were performed on a QSTAR Pulsar quadrupole time-of-flight tandem mass spectrometer (AB/MDS Sciex, Toronto, Canada) equipped with a nanoelectrospray ion source (MDS Proteomics). The MS experiments were performed in the positive ion mode. Nitrogen was used as the collision gas at a pressure of 5.3×10^{-5} Torr. Peptide fragmentation data are listed according to the Roepstorff−Fohlmann−Biemann nomenclature (Figure 2).

Purification of all radioiodinated peptides was carried out on a J'Sphere R&D ODS−H80 (4 mm, 150 × 4.6 mm, 80A) column using a Sykam HPLC system connected to a UVIS 200 Photometer (Linear Instruments Corporation, Reno, NV) using a gradient of 10−60% B in 15 min. For radioactivity measurement, the outlet of the UV-photometer was connected to a NaI(Tl) well-type scintillation counter from EG&G (München, Germany).

Radioactivity measurements for the determination of lipophilicity and biodistribution assays were performed on a 1480 Wizard 3 gamma counter from Wallac (Turku, Finland).

Reagents. Fmoc-(9-fluorenylmethoxycarbonyl) amino acids as well as the DHP−HM (3,4-Dihydro-2*H*-pyran-2-ylmethoxymethylpolystyrene) resin were purchased from novabiochem (Bad Soden, Germany). IodoGen (1,3,4,6-tetrachloro-3α,6α-diphenylglycoluril) came from Pierce (Rockford, IL). N.c.a. [125I]NaI and [123I]NaI were supplied by Amersham (Buckinghamshire, UK). All other organic reagents were purchased from Merck Eurolab (Darmstadt, Germany), Alexis (Grünberg, Germany), Aldrich, or Fluka (Neu-Ulm, Germany).

Synthesis of the Glycosylated Derivatives of Tyr^3-Octreotide. *Reduction of Fmoc-Thr(tBu)-OH to the Corresponding Amino Alcohol (49).* A solution of Fmoc-Thr(tBu)-OH (1.391 g, 3.5 mmol) in 30 mL of THF

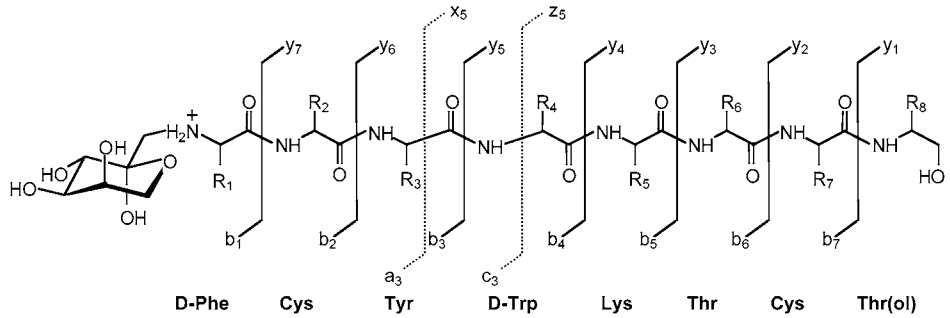


Figure 2. Fragmentation scheme and fragment nomenclature for Tyr³-octreotide and Gluc-Tyr³-octreotide in MS/MS-sequence analysis. Data are given in Tables 1 and 2.

(tetrahydrofuran) was cooled to −10 °C. *N*-Methylmorpholine (386 μL, 3.5 mmol) and ethyl chloroformate (333 μL, 3,5 mmol) were added successively. The reaction mixture was stirred at −10 °C for 30 min. Then $NaBH_4$ (396 mg,10.5 mmol) was added. Over a period of 30 min, 60 mL of MeOH (methanol) were slowly added to the reaction mixture, which was then stirred at 0 °C for 3 h.

After adding 50−70 mL of 1 N HCl (the cloudy reaction mixture has to become transparent), the organic solvents were evaporated and the remaining aequous phase was extracted twice with DCM (dichloromethane). The combined organic layers were dried over $MgSO_4$ and evaporated to dryness. The crude product, a yellowish oil, was purified by flash chromatography (ethyl acetate). Yield: 94%.

Calculated monoisotopic mass for $C_{23}H_{29}NO_4 = 383.21$; found: $m/z = 406.1$ $[M + Na]^+$ ^1H NMR ($CDCl_3$): δ(ppm) 1.16 (3H, d, $J = 6.2$ Hz, CH*CH₃*), 1.20 (9H, s, ^{t}Bu), 2.88 (1H, broad, OH), 3.61 (1H, broad, C*H*CH₂OH), 3.66 (2H, broad, CHC*H₂*OH), 3.94 (1H, m, C*H*CH₃), 4.22 (1H, t, $J = 6.8$ Hz, C*H*CH₂CO), 4.40 (2H, m, CHC*H₂*CO), 5.28 (1H, d, $J = 7.5$ Hz, N*H*), 7.30 (2H, d, $J = 7.4$ Hz, aromatics), 7.38 (2H, t, $J = 7.2$ Hz, aromatics), 7.59 (2H, d, $J = 7.4$ Hz, aromatics), 7.74 (2H, d, $J = 7.4$ Hz, aromatics).

SPPS of Tyr³-Octreotide (TOC) (50). DHP−HM-resin (1.000 g, load: 0.94 mmol linker/g) was allowed to preswell in 10 mL of dry DCE (1,2-dichloroethane) for 1 h. Then a solution of Fmoc-Thr(tBu)-ol (1.266 g, 3.3 mmol) and of pyridinium-*p*-toluenesulfonate (414 mg, 1.75 mmol) in 7 mL of abs. DCE was added, and the reaction mixture was stirred overnight at 80 °C under argon. To cap free functional groups on the resin, 5 mL of pyridine was added, and the suspension was stirred for another 15 min at RT. The loaded resin was then filtered off, washed twice with DMF (*N*,*N*-dimethylformamide) and DCM, respectively, and dried in vacuo. Synthesis of the peptide sequence Cys(Trt)−Thr(tBu)−Lys(Boc)−DTrp−Tyr−Cys(Trt)−DPhe−NH_2 on the resin-bound amino alcohol was performed according to Standard Fmoc-protocol using 1.5 equiv of HOBt (1-hydroxybenzotriazole) and TBTU (*O*-(1*H*-benzotriazol-1-yl)-*N*,*N*,*N*′,*N*′-tetramethyluronium tetrafluoroborate) as coupling reagents.

After removal of the N-terminal Fmoc protection-group with 20% piperidine in DMF, the peptide was cleaved from the resin using a mixture of 95% TFA/2.5% TIBS (triisobutylsilane)/2.5% H_2O and DCM (1:1). After 90 min, the resin was filtered and washed twice with DCM. The combined filtrates were concentrated in vacuo, and the crude product was precipitated with Et_2O (diethyl ether).

Cyclization of TOC. The crude peptide was resuspended in 50 mL of THF (per 300 mg of peptide), and 5 mM NH_4OAc was added, until a clear solution was obtained. The pH was adjusted to 7 by dropwise addition of saturated $NaHCO_3$ solution. Then 100 μL (per 300 mg of peptide) of H_2O_2 (30%) were added. After 30 min of stirring at room temperature cyclization was complete (gradient HPLC control: 30→80% B in 30 min). The solvents were evaporated, and the cyclized product was lyophilized. Purification was performed using preparative gradient RP-HPLC.

Table 1. Fragmentation of Tyr³-Octreotide in MS/MS-sequence Analysis. Fragment Nomenclature and Fragmentation Schemes Are Given in Figure 2

fragment	sum formula	calculated mass [*m*/*z*]	found [*m*/*z*]
y_1	$[C_4H_{12}NO_2]^+$	106.09	106.08
y_2	$[C_7H_{17}N_2O_3S]^+$	209.10	209.09
y_3	$[C_{11}H_{24}N_3O_5S]^+$	310.14	310.14
y_4	$[C_{17}H_{36}N_5O_6S]^+$	438.24	438.24
y_5	$[C_{28}H_{46}N_7O_7S]^+$	624.32	624.31
y_6	$[C_{37}H_{55}N_8O_9S]^+$	787.38	787.38
y_7	$[C_{40}H_{60}N_9O_{10}S_2]^+$	890.39	890.39
b_2	$[C_{12}H_{15}N_2O_2S]^+$	251.09	251.08
b_3	$[C_{21}H_{24}N_3O_4S]^+$	414.15	414.14
b_4	$[C_{32}H_{34}N_5O_5S]^+$	600.23	600.21
b_5	$[C_{38}H_{46}N_7O_6S]^+$	728.32	728.30
b_6	$[C_{42}H_{53}N_8O_8S]^+$	829.37	829.36
b_7	$[C_{45}H_{58}N_9O_9S_2]^+$	932.38	932.36
$[M + 2H]^{2+}$	$[C_{49}H_{70}N_{10}O_{11}S_2]^+$	519.23	519.22

HPLC (10→60% in 30 min): t_R (linear peptide) = 14.1 min; $K' = 4.96$; t_R (cyclic peptide) = 12.9 min; $K' = 4.48$; Calculated monoisotopic mass for TOC ($C_{49}H_{66}N_{10}O_{11}S_2$) = 1034.49; found: $m/z = 1035.2$ $[M + H]^+$; the fragmentation of Tyr³-octreotide (linear) in MS/MS-sequence analysis is shown in Table 1.

Boc Protection of the Lys⁵-Side Chain. The peptide was redissolved in DMF (1 mL/100 mg). After the addition of 1.1 equiv (with respect to free Lys-N_ϵ-amino groups in the peptide) of Boc_2O (di-*tert*-butyl dicarbonate) in DMF, the solution was stirred at RT for 30 min. The protected peptide was precipitated by the addition of Et_2O, washed with Et_2O, and dried in vacuo.

HPLC (30→80% in 30 min): $t_R = 10.94$ min; $K' = 3.63$; calculated monoisotopic mass for $C_{54}H_{74}N_{10}O_{13}S_2$ = 1134.49; found: $m/z = 1135.3$ $[M + H]^+$.

Conjugation with Carbohydrates. On the basis of a method reported previously (*51*), 1 equiv of Lys⁵(Boc)-TOC and 10 equiv of the respective aldose (glucose, maltose, maltotriose) were dissolved in methanol/acetic acid (95/5 (v/v)), and the reaction mixture was stirred at 60°C for 24−48 h. The solvents were then evaporated, and the crude product was precipitated by the addition of Et_2O.

Boc Deprotection. A solution of protected peptide in TFA/H_2O/TIBS (95:2,5:2,5 (v/v/v); 1 mL/100 mg) was stirred at RT for 15−60 min. The deprotected peptide was precipitated by the addition of Et_2O, washed with Et_2O,

Table 2. Fragmentation of Gluc-Tyr³-octreotide in MS/MS Sequence Analysis. Fragment Nomenclature and Fragmentation Schemes Are Given in Figure 2

fragment	sum formula	calculated mass [*m*/*z*]	found [*m*/*z*]
y_1	$[C_4H_{12}NO_2]^+$	106.09	106.08
y_2	$[C_7H_{17}N_2O_3S]^+$	209.10	209.09
y_3	$[C_{11}H_{24}N_3O_5S]^+$	310.14	310.14
y_4	$[C_{17}H_{36}N_5O_6S]^+$	438.24	438.24
y_5	$[C_{28}H_{46}N_7O_7S]^+$	624.32	624.32
y_6	$[C_{37}H_{55}N_8O_9S]^+$	787.38	787.38
y_7	$[C_{40}H_{60}N_9O_{10}S_2]^+$	890.39	890.37
a_1	$[C_{14}H_{20}NO_5]^+$	282.13	282.14
$a_1 - H_2O$	$[C_{14}H_{18}NO_4]^+$	264.12	264.12
b_1	$[C_{15}H_{20}NO_6]^+$	310.13	310.14
$b_1 - H_2O$	$[C_{15}H_{18}NO_5]^+$	292.12	292.13
$b_2 - H_2O$	$[C_{18}H_{23}N_2O_6S]^+$	395.13	395.12
$b_4 - 3\ H_2O$	$[C_{38}H_{38}N_5O_7S]^+$	708.25	708.28
$b_5 - 3\ H_2O$	$[C_{44}H_{50}N_7O_8S]^+$	836.34	836.34
$b_6 - 3\ H_2O$	$[C_{48}H_{57}N_8O_{19}S]^+$	937.39	937.39
$b_7 - 3\ H_2O$	$[C_{51}H_{62}N_9O_{10}S_2]^+$	1040.40	1040.41
$[M + 2H]^{2+}$	$[C_{55}H_{80}N_{10}O_{16}S_2]^+$	600.26	600.26

and dried in vacuo. Purification was carried out using preparative gradient RP-HPLC.

Gluc-TOC: HPLC (10→60% in 30 min): $t_R = 13.1$ min; $K' = 4.13$; calculated monoisotopic mass for $C_{55}H_{76}N_{10}O_{16}S_2 = 1196.5$, found: $m/z = 1197.1\ [M + H]^+$, 1219.7 $[M + Na]^+$.

Fragmentation of Gluc-TOC (linear) in MS/MS-sequence analysis is shown in Table 2.

Malt-TOC: HPLC (10→60% in 30 min): $t_R = 12.56$ min; $K' = 3.85$; calculated monoisotopic mass for $C_{61}H_{86}N_{10}O_{21}S_2 = 1358.54$, found: $m/z = 1359.1\ [M + H]^+$.

Mtr-TOC: HPLC (10→60% in 30 min): $t_R = 13.07$ min; $K' = 3.78$; calculated monoisotopic mass for $C_{67}H_{96}N_{10}O_{26}S_2 = 1520.59$, found: $m/z = 1521.1\ [M + H]^+$.

Radioiodination. TOC, Gluc-TOC, Malt-TOC, and Mtr-TOC were labeled with ^{125}I (or ^{123}I for γ-camera imaging) using the IodoGen method. A solution of 100−500 μg of peptide in 200 μL of PBS (phosphate-buffered saline, pH 7.4) was transferred to an Eppendorf cap coated with 150 μg of IodoGen. A 5−10 μL (18−37 MBq) amount of n.c.a. [^{125}I]NaI (specific activity > 2000 Ci/mmol) or c.a. [^{123}I]NaI (specific activity ∼5000 Ci/mmol) was added. The labeling reaction was allowed to proceed for 20 min at RT. The peptide solution was then removed from the insoluble oxidizing agent. Separation of the labeled products was achieved using gradient RP-HPLC. For biodistribution experiments, the collected fraction was evaporated to dryness, and the residue was redissolved in PBS to yield a solution of radiolabeled peptide with an activity concentration of about 370 kBq/100 μL.

Determination of Lipophilicity. To a solution of approximately 2 kBq of radiolabeled peptide in 500 μL of PBS (pH 7.4) was added 500 μL of octanol ($n = 6$). Vials were vortexed vigorously for 3 min. To achieve quantitative phase separation, the vials were centrifuged at 14600*g* for 6 min in a Biofuge 15 (Heraeus Sepatech, Osterode, Germany). The activity concentrations in 100 μL samples of both the aequous and the organic phase were measured in a γ-counter. Both the partition coefficient P_{ow}, which is defined as the molar concentration ratio of a single species A between octanol and water at equilibrium, and log P_{ow}, which is an important parameter used to characterize lipophilicity of a compound (*52*), were calculated.

Determination of the Affinity Profiles to hsst. Cells stably expressing human sst_1, sst_2, sst_3, sst_4, and sst_5 were grown as described previously (*53*). All culture reagents were supplied by GIBCO/BRL and Life Technologies (Grand Island, NY). Cell membrane pellets were prepared, and receptor autoradiography was performed on pellet sections (mounted on microscope slides), as described in detail previously (*53*). For each of the tested compounds, complete displacement experiments were performed with the universal somatostatin radioligand ^{125}I-[Leu^8,D-Trp^{22},Tyr^{25}]-somatostatin 28 using increasing concentrations of the unlabeled peptide ranging from 0.1 to 1000 nM. Somatostatin 28 was run in parallel as control using the same increasing concentrations. IC_{50} values were calculated after quantification of the data using a computer-assisted image processing system. Tissue standards (autoradiographic [^{125}I]microscales Amersham), containing known amounts of isotopes, cross-calibrated to tissue equivalent ligand concentrations, were used for quantification (*53*).

Tumor Xenografts. AR42J is a rat pancreatic acinar tumor cell line with high somatostatin receptor (sst_2) expression (*54*) and was obtained from ECACC (European Collection of Cell Cultures, Salisbury, UK). Cells were maintained in RPMI 1640 medium supplemented with 10% FCS (Biochrom Seromed (Berlin, Germany)) and 2 mM L-glutamine (Gibco BRL Life Technologies (Karlsruhe, Germany)) at 37 °C and 5% CO_2.

Animal Model. For all in vivo experiments, nude mice (CD1 nu/nu, male and female, 6−8 weeks) were used. To establish tumor growth, subconfluent monolayer cells were treated with 1 mM EDTA in PBS, suspended, centrifuged, and resuspended in serum free RPMI 1640. Mice were inoculated subcutaneously in the flank with 2.5−3 × 10E6 cells. Ten days postinoculation all mice showed solid palpable tumor masses (tumor weight 150−500 mg) and were used for the experiments.

Biodistribution Studies. About 370 kBq (10 μCi) of the ^{125}I-labeled peptides in 100 μL of PBS (pH 7.4) were injected intravenously (iv) into the tail vein of nude mice bearing an AR42J tumor. The animals were sacrificed 10, 30, and 60 min postinjection (pi) ($n = 5$), and the organs of interest were dissected. The radioactivity was measured in weighted tissue samples using a γ-counter. Data are expressed in %ID/g tissue (mean ± SD).

Pretreatment, Coinjection, and Displacement Studies. For pretreatment studies, 0.8 mg/kg Tyr³-octreotide (20 μg/mouse) was injected iv into the tail vein as a 100 μL bolus 10 min prior to the injection of 370 kBq (10 μCi) of radioligand in 100 μL of PBS. Coinjection was performed injecting a solution of radioligand and 0.8 mg/kg Tyr³-octreotide (20 μg/mouse) in 100 mL of PBS. For displacement studies, 0.8 mg/kg Tyr³-octreotide (20 μg/mouse) were administered 10 min after the injection of the radioiodinated tracer. All animals were sacrificed 30 min pi of the radioligand. Subsequent determination of the activity accumulation in all organs of interest was performed as described above (biodistribution studies).

γ-Camera Imaging. The ^{123}I-labeled peptides (3.7 MBq (100 μCi) in 100 mL of PBS (pH 7.4)) were injected iv into the tail vein of nude mice bearing an AR42J tumor. Mice were euthanized at 120 min pi of the radioligand. Acquisition of γ-camera images was performed on a Siemens Diacam γ-camera (20 min, medium energy general purpose collimator) by positioning the mice directly on the collimator. Region-of-interest (ROI) analysis was performed using the IconTM software, version 5.2.1 (1994), from Siemens Medical Systems, applying the RegionRatio protocol.

RESULTS

Peptide Synthesis. Solid-phase peptide synthesis yielded TOC in 82−86% yield, based on the amount of

Table 3. Lipophilicity of [^{125}I]TOC and Its Glycosylated Derivatives (n = 6, values are mean ± SD))

	[^{125}I]TOC	[^{125}I]Gluc-TOC	[^{125}I]Malt-TOC	[^{125}I]Mtr-TOC
P_{OW}	1.50 ± 0.09	0.26 ± 0.01	0.06 ± 0.01	0.10 ± 0.01
log P_{OW}	0.18 ± 0.03	−0.59 ± 0.02	−1.21 ± 0.03	−0.99 ± 0.03

Fmoc-Thr(tBu)ol initially coupled to the resin, and in UV-purities > 90%. Subsequent synthesis steps were performed without further purification of the peptide. Boc-protection of the Lys5-side chain usually led to quantitative transformation of the precursor. Final yields of the glycosylated octreotide derivatives generally ranged from 14 to 33% with respect to Boc-protected starting peptide. The glycosylation reaction itself usually proceeded smoothly within 16 h and yielded ratios of glycosylated product to precursor of 60/40 up to 90/10 (values are based on the results of the integration of RP-HPLC chromatograms (UV absorption at 220 nm); impurities were excluded from integration). Product-to-precursor ratios were higher for the maltose and maltotriose derivatives than for the glucose derivative.

The moderate overall yields of the sugar−octreotide conjugates can mainly be attributed to the preparative HPLC conditions. On the RP-18 column generally used, baseline-separation of the carbohydrate conjugate and the nonglycosylated precursor could hardly be achieved, even when a very slow gradient was used.

The structure of radioiodinated Gluc-TOC is shown in Figure 1. For the sugar moiety, only one of four possible conformations is shown. Beside the β-pyranoid structure (Figure 1), the α- and β-furanoid and the open-chain conformations of the deoxy-ketoses are possible and may be present in equilibrium mixtures (*55*).

Radiolabeling. Radioiodination efficiency generally exceeded 99%. Radiochemical yields ranged from 45 to 85% and were limited both by formation of radioiodinated sideproducts and by restrictions during [^{125}I]glycopeptide product-fractioning caused by tailing of the unreacted precursor.

After RP-HPLC isolation, all radioiodinated compounds were obtained in high radiochemical purity (>99.8%). Specific activities of all ^{123}I- and ^{125}I-labeled compounds were >1800 Ci/mmol.

Lipophilicity. The lipophilicity of the radioiodinated compounds is shown in Table 3. While log P_{ow} for the parent compound [^{125}I]TOC is > 0, all glycosylated derivatives exhibited log P_{ow} values below zero in the following order: log P_{ow} [^{125}I]Gluc-TOC > log P_{ow} [^{125}I]-Mtr-TOC > log P_{ow} [^{125}I]Malt-TOC.

Affinity Profiles to hsst. In vitro binding properties of the three compounds were evaluated in cells stably expressing sst1−sst5 in displacement experiments using [^{125}I]-]Leu^{8},D-Trp^{22},Trp^{25}]-somatostatin 28 as radioligand. Table 4 shows the IC_{50} of somatostatin-28, I-TOC, I-Malt-TOC, and I-Mtr-TOC to the five somatostatin receptor subtypes sst1−5.

Natural somatostatin 28, which binds with high affinity to all five subtypes, was used as control peptide. Both sugar conjugates of octreotide showed a binding profile to sst similar to I-TOC: no affinity to sst1, high affinity to sst2, and moderate or low affinity to sst3−5.

In Vivo Biodistribution. The tissue distributions of all radioiodonated tracers in AR42J tumor bearing nude mice 10, 30, and 60 min postinjection are shown in Table 5.

Table 4. Affinity Profiles (IC_{50}) of Somatostatin 28 and the Compounds Investigated for Human sst1−sst5 Receptors (values are IC_{50} ± SD [nM], Number of Experiments in Parentheses)

peptide	sst1	sst2	sst3	sst4	sst5
SS-28	3.6 ± 0.3 (5)	2.1 ± 0.3 (5)	3.2 ± 0.2 (5)	3 ± 0.3 (5)	2.5 ± 0.2 (5)
I-TOC[a]	>10000 (3)	1.3 ± 0.3 (3)	128 ± 22 (3)	867 ± 33 (3)	50 ± 12 (3)
I-Malt-TOC[b]	>10000 (3)	1.2 ± 0.2 (3)	243 ± 47 (3)	>1,000 (2)	75 ± 19 (3)
I-Mtr-TOC[c]	>10000 (3)	1.1 ± 0.2 (3)	210 ± 15 (3)	>1,000 (3)	110 ± 35 (3)
values are mean ± SD					

[a] (3-iodo-Tyr³)-octreotide. [b] N^{α}-(α-D-glucopyranosyl-(1−4)-1-deoxy-D-fructosyl)-(3-iodo-Tyr³)-octreotide. [c] N^{α}-(*O*-α-D-glucopyranosyl-(1−4)-(*O*-α-D-glucopyranosyl-(1−4)-1-deoxy-D-fructosyl)-(3-iodo-Tyr)³-octreotide.

Table 5. Tissue Biodistribution [%ID/G] of [^{125}I]TOC and Its Glycosylated Derivatives[a]

organ	time pi [min]	[^{125}I]TOC	[^{125}I]Gluc-TOC	[^{125}I]Malt-TOC	[^{125}I]Mtr-TOC
blood	10	1.69 ± 0.54	2.60 ± 0.45	3.42 ± 1.09	
	30	1.06 ± 0.24	1.58 ± 0.48	1.38 ± 0.20	2.66 ± 0.19
	60	1.23 ± 0.30	0.88 ± 0.38	0.74 ± 0.13	
liver	10	7.36 ± 0.92	3.51 ± 0.77	2.43 ± 0.78	
	30	5.95 ± 1.19	2.44 ± 0.16	1.33 ± 0.32	2.66 ± 0.17
	60	3.76 ± 1.28	1.73 ± 0.59	0.96 ± 0.17	
intestine	10	3.58 ± 1.20	2.80 ± 0.72	1.46 ± 0.47	
	30	7.02 ± 1.32	3.99 ± 1.19	1.25 ± 0.55	3.31 ± 0.58
	60	10.60 ± 2.81	5.28 ± 1.27	1.48 ± 0.18	
kidney	10	5.55 ± 0.71	7.44 ± 1.77	9.63 ± 3.24	
	30	6.70 ± 1.59	6.35 ± 0.66	7.23 ± 1.39	9.61 ± 1.69
	60	6.95 ± 1.44	6.25 ± 1.94	6.78 ± 1.52	
tumor	10	4.95 ± 1.53	4.42 ± 1.15	6.79 ± 2.58	
	30	6.72 ± 2.60	10.12 ± 2.81	5.30 ± 1.87	4.87 ± 2.15
	60	5.53 ± 1.06	8.73 ± 1.45	5.24 ± 0.61	
pancreas	10	1.65 ± 0.55	4.10 ± 0.82	3.61 ± 1.71	
	30	1.22 ± 0.37	4.48 ± 0.67	2.21 ± 0.59	2.12 ± 0.44
	60	1.17 ± 0.32	3.36 ± 1.20	1.92 ± 0.26	
adrenals	10	1.63 ± 0.76	2.08 ± 0.40	3.08 ± 0.92	
	30	1.63 ± 0.74	2.40 ± 0.73	2.07 ± 0.21	2.98 ± 0.82
	60	1.25 ± 0.21	2.05 ± 0.97	1.93 ± 0.68	
muscle	10	0.39 ± 0.14	0.60 ± 0.13	0.94 ± 0.79	
	30	0.18 ± 0.03	0.39 ± 0.37	0.33 ± 0.14	0.51 ± 0.08
values are mean ± SD	60	0.26 ± 0.08	0.17 ± 0.05	0.20 ± 0.08	

[a] Groups of five nude mice bearing AR42J tumors. Values are mean ± SD. %ID/g = percentage of injected dose per gram tissue

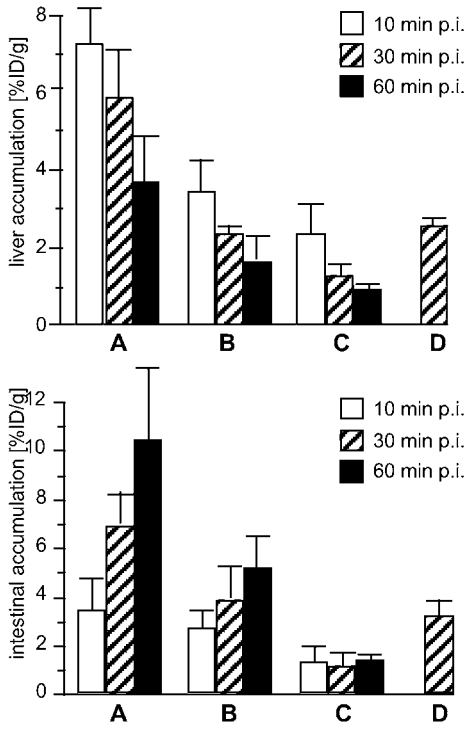


Figure 3. Activity accumulation of [^{125}I]TOC (**A**), [^{125}I]Gluc-TOC (**B**), [^{125}I]Malt-TOC (**C**) and [^{125}I]Mtr-TOC (**D**) in liver and intestine of AR42J tumor bearing nude mice 10, 30, and 60 min pi ($n = 5$, mean ± SD).

While [^{125}I]TOC was rapidly cleared from the blood via hepatobiliary excretion, resulting in high initial liver uptake (7.36 ± 0.92%ID/g 10 min pi), the glycosylated derivatives exhibited delayed initial blood clearance. Activity accumulation in the liver was decreased for all glycosylated analogues, in particular for [^{125}I]Malt-TOC. The maltose derivative exhibited only 25% of the liver uptake of the parent compound 60 min pi, while for [^{125}I]-TOC activity accumulation in the intestine reached 10.6 ± 2.8%ID/g at 60 min pi, intestinal uptake was reduced to 5.28 ± 1.27%ID/g for [^{125}I]Gluc-TOC and to 1.48 ± 0.18%ID/g for [^{125}I]Malt-TOC (Figure 3). Renal activity accumulation for [^{125}I]TOC, [^{125}I]Gluc-TOC, and [^{125}I]-Malt-TOC remained almost unchanged (6.95 ± 1.44%ID/g for [^{125}I]TOC, 6.25 ± 1.94 for [^{125}I]Gluc-TOC and 6.78 ± 1.52%ID/g for [^{125}I]Malt-TOC 60 min pi).

While for sst-rich tissues such as pancreas and adrenals activity accumulation was increased by a factor of 1.5−3.5 for all glycosylated derivatives compared to [^{125}I]TOC, tumor uptakes of [^{125}I]TOC and [^{125}I]Malt-TOC were comparable at all time points. In contrast, [^{125}I]Gluc-TOC exhibited an increase in tumor uptake of up to 160% compared to [^{125}I]TOC.

For [^{125}I]Mtr-TOC, highest activity concentrations 30 min pi could be detected in the kidneys (9.61 ± 1.69%ID/g), the tumor (4.87 ± 2.15%ID/g) and in the intestine (3.31 ± 0.58%ID/g).

Pretreatment, Competition, and Displacement Experiments. Both for [^{125}I]Gluc-TOC and for [^{125}I]Malt-TOC binding to sst-rich tissues in vivo was demonstrated to be specific. While tumor accumulation was significantly reduced in the pretreatment and co-injection experiments compared to the control experiment, resulting in tumor/sst-negative tissue ratios < 1 (Figure 4), displacement of the radioiodinated tracers by injection of 20 μg of Tyr^3-octreotide/mouse 10 min pi of the labeled compound was less effective, demonstrating fast internalization of the radiotracer.

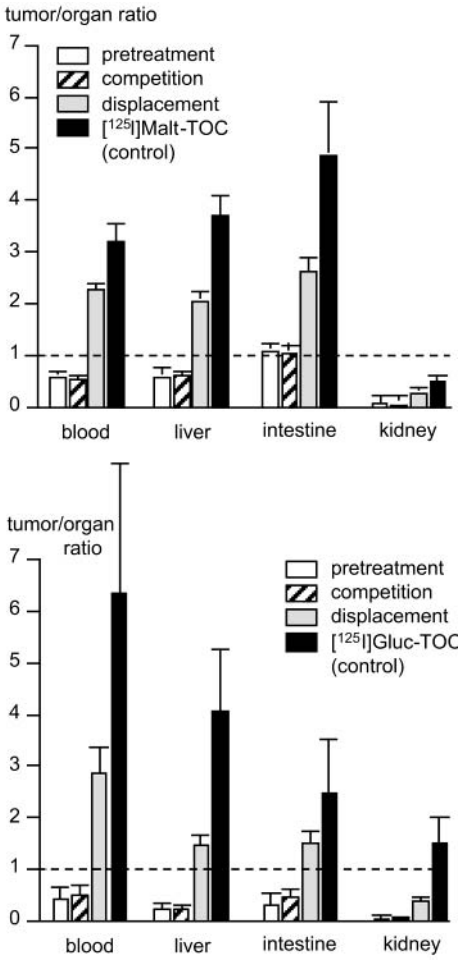


Figure 4. Tumor/organ ratios for [^{125}I]Malt-TOC and [^{125}I]Gluc-TOC under different experimental conditions in AR42J tumor bearing nude mice 30 min pi ($n = 3$, mean ± SD) *pretreatment*: injection of 0.8 mg/kg TOC (20 μg/mouse) 10 min prior to injection of the respective radioiodinated tracer, *competition*: injection of 0.8 mg/kg TOC (20 μg/mouse) with the respective radioiodinated tracer, *displacement*: injection of 0.8 mg/kg TOC (20 mg/mouse) 10 min after injection of the respective radioiodinated tracer.

γ-Camera Imaging. Images acquired 120 min pi of [^{123}I]TOC, [^{123}I]Gluc-TOC, and [^{123}I]Malt-TOC in AR42J tumor-bearing nude mice are shown in Figure 5. In the case of [^{123}I]TOC, the tumor is barely discernible from the high intestinal background. ROI analysis revealed a low tumor/intestine ratio of 0.62 (0.52 ± 0.17 in the biodistribution study 60 min pi). As expected from the biodistribution data, [^{123}I]Gluc-TOC still shows considerable nonspecific accumulation in the intestine, but also an increased tumor/intestine ratio due to its higher tumor accumulation (ROI analysis: 1.48; biodistribution study (60 min pi): 1.65 ± 0.48). This results in an improved contrast of the scintigraphic image. When [^{123}I]Malt-TOC was administered, only the kidneys and the tumor showed significant uptake of the radioligand, while abdominal activity accumulation was negligible. The tumor/kidney ratio determined via ROI analysis (0.81) is in accordance with the value found in the biodistribution study (0.77 ± 0.19 at 60 min pi). In all three scintigraphic images, the stomach is also visible. The intensity of activity accumulation in stomach shows some correlation with the tumor uptake of the respective radioligand. This observation is in accordance with the detection of somatostatin receptors in stomach in rats (*56*).

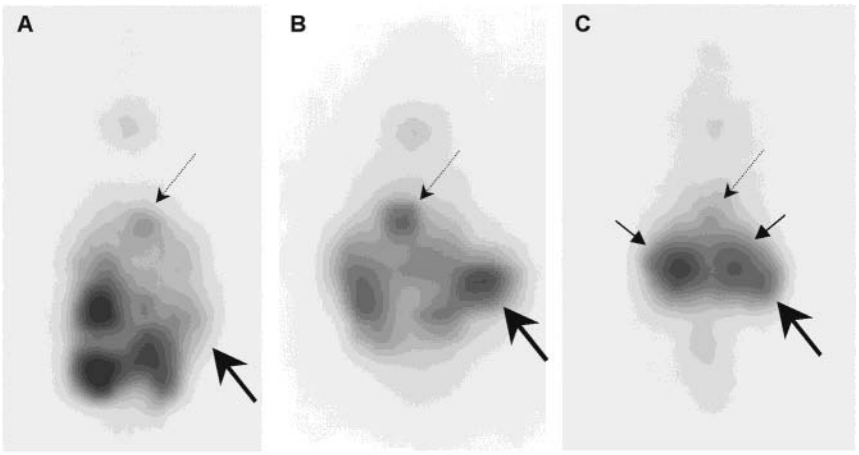


Figure 5. γ-Camera images of AR42J tumor-bearing nude mice 120 min pi of 100 μCi of [^{125}I]TOC (**A**), [^{125}I]Gluc-TOC (**B**), and [^{125}I]Malt-TOC (**C**). Large arrows indicate the tumor, small arrows indicate the kidneys, dashed arrows indicate the stomach.

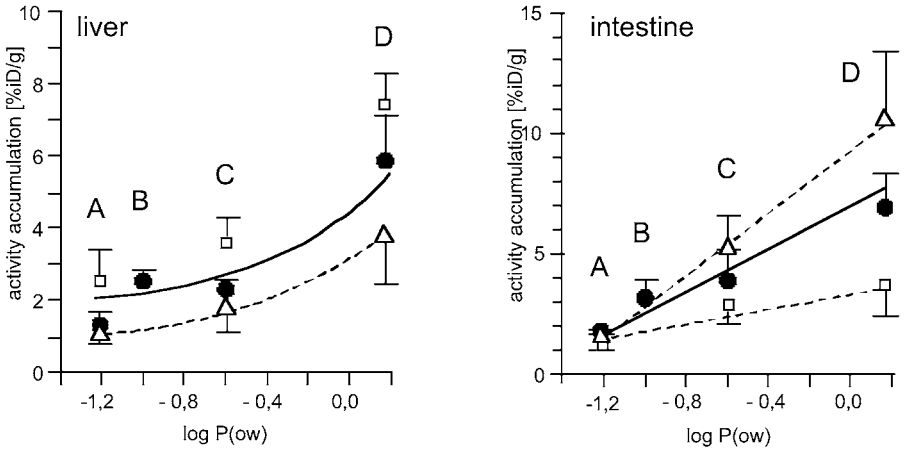


Figure 6. Correlation between the activity accumulation of [^{125}I]Malt-TOC (**A**), [^{125}I]Mtr-TOC (**B**), [^{125}I]Gluc-TOC (**C**), and [^{125}I]-TOC (**D**) in liver and intestine of AR42J tumor bearing nude mice ($n = 5$, mean $\pm$ SD) 10 (□) min, 30 (●) min, and 60 (△) min pi and the lipophilicity (log P_{OW}) of the respective compound.

DISCUSSION

[^{123}I]Tyr³-octreotide (TOC) (*57*) was the first radiolabeled SRIF analogue that was applied for scintigraphic in vivo localization of sst_2-expressing primary tumors and metastases. However, already in the first studies it was shown, that two major drawbacks restricted the applicability of this new tracer: its predominant hepatobiliary excretion and low tumor retention (*58*, *59*). Due to these disadvantages interpretation of planar as well as SPET images of the abdominal region are complicated considerably. In a pharmacokinetic study with patients with neuroendocrine tumors 55% of the administered activity was found in the feces 40 h pi (*29*). While average tumor doses were approximately 0.9−5 rad/mCi ([^{131}I]-TOC), doses calculated for the gallbladder wall and the lower colon were 2.37 rad/mCi and 16.4 rad/mCi, respectively. Therefore [^{131}I]TOC is not suited for PRRT, and there are certainly restrictions with respect to its suitability for tumor scintigraphy.

To make radioiodinated derivatives of TOC accessible for these applications, we evaluated the suitability of radiolabeled, carbohydrate-conjugated octreotide analogues and optimized the biokinetics in vivo (*44*−*47*). In previous studies we successfully applied sugar amino acid conjugation to improve the biokinetics of $\alpha v\beta 3$-antagonists (*27*, *43*). Furthermore, carbohydration was applied to increase peptide solubility (*60*), to enhance in vivo stability (*51*), to improve blood−brain barrier penetration (*33*, *34*) or intestinal absorption (*42*). In previous studies it has been demonstrated that derivatization of SMS 201−995 at D-Phe¹ with different aldoses via Maillard reaction yielded potent sst agonists with high receptor affinity (*51*). These compounds failed to misuse the transport system in hepatocyte sinusoidal plasma membranes (*61*) and thus showed significantly reduced hepatobiliary clearance and intestinal excretion. In a rat model, the maltose derivative of Phe³-octreotide ((*N*-α-(α-D-Glucosyl(1−4)-1-deoxy-D-fructosyl))Phe³-octreotide), SDZ CO-611, showed a cumulated biliary excretion of only 5% of the injected activity over a period of 120 min, while 65% were found for SMS 201−995.

The biodistribution studies in rat pancreatic tumor bearing mice demonstrate that carbohydrate conjugation of [^{125}I]TOC leads to significant changes in the pharmacokinetics of this tracer, too. The most lipophilic compound in our series, the reference [^{125}I]TOC, is mainly excreted via the liver and the intestine. The glucose derivative [^{125}I]Gluc-TOC already shows a 50% decrease in liver and intestinal uptake, while for the most hydrophilic derivative, [^{125}I]Malt-TOC, the activity accumulation in the liver and intestine is only 25% and 14%, respectively, of that of [^{125}I]TOC. These data indicate that the hydrophilicity of the tracers in this series has a major influence on the favored excretion pathway. For the mono- and disaccharide derivatives log P_{OW} decreased gradually with the size of the carbohydrate moiety, which correlated with decreasing hepatobiliary excretion (Figure 6).

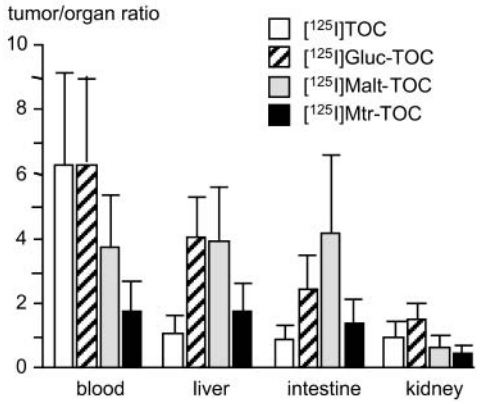


Figure 7. Tumor/organ ratios found for [^{125}I]TOC, [^{125}I]Gluc-TOC, [^{125}I]Malt-TOC, and [^{125}I]Mtr-TOC in AR42J tumor bearing nude mice 30 min pi ($n = 5$, mean ± SD).

Conjugation of [^{125}I]TOC with maltotriose (a trisaccharide) yielded a tracer with a log P_{OW} similar to that of [^{125}I]Gluc-TOC and therefore with a comparable degree of accumulation in liver and intestine. As previously suggested for non-carbohydrated radiometal labeled octreotide derivatives (*62*) and demonstrated in Figure 6 for the carbohydrated compounds, the correlation between the log P_{OW}'s of [^{125}I]TOC and its glycosylated derivatives and their accumulation in liver and intestine may be applied for predictions concerning the degree of hepatobiliary clearance of radiolabeled TOC-derivatives with N-terminal modifications.

Almost identical renal uptake was found for all compounds investigated. Whether these peptides are subject to renal tubular peptide-reabsorption by transport-mediated processes or charge dependent endocytosis (*31*) needs further investigations. In some studies, coadministration of lysine was reported to reduced renal accumulation of radiometalated octreotide derivatives (*63*, *64*). This effect was explained by competition of lysine at the charge dependent endocytosis of octreotide in the kidneys. Since the net charge of the four derivatives investigated are assumed to be nearly identical under physiological conditions (+1.7 to +2.0) no major differences in renal uptake were expected.

Concerning activity accumulation in tumor and other SSTR-positive tissues (pancreas, adrenals), we observed significant differences between [^{125}I]Gluc-TOC and the other derivatives. Tumor uptake of [^{125}I]Gluc-TOC ≫ [^{125}I]-TOC, [^{125}I]Malt-TOC, and [^{125}I]Mtr-TOC. However, due to the improved excretion profile of the carbohydrated compounds, improved tumor/nontumor ratios were found for [^{125}I]Gluc-TOC, [^{125}I]Malt-TOC, and [^{125}I]Mtr-TOC (Figure 7), especially for liver, kidney and intestine, well-known to be critical organs in [^{123}I]TOC-scintigraphy with tumor/nontumor ratios of about 1 or less. Interestingly, although the carbohydrated compounds are mainly cleared via the kidneys, tumor/kidney ratios of [^{125}I]TOC and its glycosylated analogues were comparable.

In cells transfected with sst1-sst5, I-Malt-TOC, and I-Mtr-TOC show high affinity for sst2- and sst-subtype binding profiles similar to I-TOC. Knowing that human tumors preferably express sst2 (*1*, *4*), a radiotracer with high selectivity and high binding affinity for sst2 such as the carbohydrated octreotide derivatives may be extremely valuable for clinical use.

As demonstrated by pretreatment, competition, and displacement experiments in tumor-bearing mice, activity uptake in AR42J tumors was sst_2 receptor specific. As expected, tumor/nontumor ratios decreased to 1 or less when 8 mg unlabeled TOC per kg was given prior to the tracer administration or when the cold compound was coadministered. Less effective displacement already 10 min postinjection of the tracer indicates fast internalization of the radioligand, a prerequisite for activity retention in the tumor.

CONCLUSION

Carbohydration fulfils the demands for a chemical tool suitable to modify the physicochemical behavior of TOC. Carbohydration leads to significantly improved general pharmacokinetics. The carbohydrated tracers were rapidly cleared from the circulation via the kidneys without increased renal uptake. Additionally, the reduced hepatic uptake and biliary excretion, the improved tumor uptake, and thus increased tumor-to-nontumor ratios minimize the effective whole body dose. Especially the glucose and the maltose analogue of Tyr^3-octreotide will be the basis for a new series of carbohydrated peptide receptor ligands with high potential for targeted imaging and radiotherapy of somatostatin receptor postive tumors. We assume that the concept of carbohydration is also a promising strategy for the development of tracers for other peptide receptor systems.

ACKNOWLEDGMENT

The authors are indebted to Jutta Grahneis for her excellent technical assistance. We also thank Dr. Hanno Steen from Odense University (Denmark) for carrying out the peptide sequence analyses. Furthermore, we appreciate the editorial help of Jodi Neverve in the preparation of the manuscript.

LITERATURE CITED

(1) Reubi, J. C., Krenning, E., Lamberts, S. W., and Kvols, L. (1990) Somatostatin receptors in malignant tissues. *J. Steroid Biochem. Mol. Biol. 37* (6), 1073−1077.

(2) Reubi, J. C., Laderach, U., Waser, B., Gebbers, J. O., Robberecht, P., and Laissue, J. A. (2000) Vasoactive intestinal peptide/pituary adenylate cyclase-activating peptide receptor subtypes in human tumors and their tissues of origin. *Cancer Res. 60* (11), 3105−3112.

(3) Reubi, J. C., Waser, B., Friess, H., Buchler, M., and Laissue, J. A. (1998) Neurotensin receptors: a new marker for human ductal pancreatic adenocarcinoma. *Gut 42* (2), 546−550.

(4) Reubi, J. C., Zimmermann, A., Jonas, S., Waser, B., Neuhaus, P., Laderach, U., and Wiedenmann, B. (1999) Regulatory peptide receptors in human hepatocellular carcinomas. *Gut 45* (5), 766−774.

(5) Hennig, I. M., Laissue, J. A., Horisberger, U., and Reubi, J. C. (1995) Substance-P receptors in human primary neoplasms: tumoral and vascular localization. *Int. J. Cancer 61* (6), 786−792.

(6) Schaer, J. C., and Reubi, J. C. (1999) High gastrin and cholecystokinin (CCK) gene expression in human neuronal, renal, and myogenic stem cell tumors: comparison with CCK-A and CCK−B receptor contents. *J. Clin. Endocrinol. Metab. 84* (1), 233−239.

(7) Otte, A., Jermann, E., Behe, M., Goetze, M., Bucher, H. C., Roser, H. W., Heppeler, A., Mueller-Brand, J., and Mäcke, H. R. (1997) DOTATOC: a powerful new tool for receptor-mediated radionuclide therapy. *Eur. J. Nucl. Med. 24* (7), 792−795.

(8) Cremonesi, M., Ferrari, M., Zoboli, S., Chinol, M., Stabin, M. G., Orsi, F., Maecke, H. R., Jermann, E., Robertson, C., Fiorenza, M., Tosi, G., and Paganelli, G. (1999) Biokinetics and dosimetry in patients administered with [^{111}In]DOTA-Tyr^3-octreotide: implications for internal radiotherapy with [^{90}Y]DOTATOC. *Eur. J. Nucl. Med. 26* (8), 877−886.

(9) Otte, A., Herrmann, R., Heppeler, A., Behe, M., Jermann, E., Powell, P., Maecke, H. R., and Muller, J. (1999) Yttrium-

90 DOTATOC: first clinical results. *Eur. J. Nucl. Med. 26 (11),* 792−795.
(10) Kwekkeboom, D., Krenning, E. P., and de Jong, M. (2000) Peptide receptor imaging and therapy. *J. Nucl. Med. 41* (10), 1704−1713.
(11) Slooter, G. D., Mearadji, A., Breeman, W. A., Marquet, R. L. de Jong, M., Krenning, E. P., and van Eijck, C. H. (2001) Somatostatin receptor imaging, therapy and new strategies in patients with neuroendocrine tumours. *Br. J. Surg. 88* (1), 31−40.
(12) Krenning, E. P., Bakker, W. H., Breeman, W. A., Koper, J. W., Kooij, P. P., Ausema, L., Lameris, J. S., Reubi, J. C., and Lamberts, S. W. (1989) Localisation of endocrine-related tumours with radioiodinated analogue of somatostatin. *Lancet 1,* 242−244.
(13) Bruns, C., Stolz, B., Albert, R., Marbach, P., and Pless, J. (1993) OctreoScan 111 for imaging of a somatostatin receptor-positive islet cell tumor in rat. *Horm. Metab. Res. Suppl. 27,* 5−11.
(14) Breeman, W. A., Van Hagen, M. P., Visser-Wisselaar, H. A., van der Pluijm, M. E., Koper, J. W., Setyono-Han., B., Bakker, W. H., Kwekkeboom, D. J., Hazenberg, M. P., Lamberts, S. W., Visser, T. J., and Krenning, E. P. (1996) In vitro and in vivo studies of substance P receptor expression in rats with the new analogue [indium[111]-DTPA-Arg[1]]substance P. *J. Nucl. Med. 37* (1), 108−117.
(15) Behr, T. M., Jenner, N., Béhé, M., Angerstein, C., Gratz, S., Raue, F., and Becker, W. (1999) Radiolabeled peptides for targeting cholecystokinin-B/gastrin receptor-expressing tumors. *J. Nucl. Med. 40* (6), 1029−1044.
(16) Baidoo, K. E., Lin, K. S., Zhan, Y., Finley, P., Scheffel, U., and Wagner, H. N., Jr. (1998) Design, synthesis and initial evaluation off high-affinity technetium bombesin analogues. *Bioconjugate Chem. 9* (2), 218−225.
(17) Bagutti, C., Stolz, B., Albert, R., Bruns, C., Pless, J., and Eberle, A. N. (1994) [[111]In]DTPA-labeled analogues of alpha-melanocyte-stimulating hormone for melanoma targeting: receptor binding in vitro and in vivo. *Int. J. Cancer 58* (5), 749−755.
(18) Vaidyanathan, G., and Zalutsky, M. (1997) Fluorine-18-labeled [Nle[4], dPhe[7]]-alpha-MSH, an alpha-melanocyte-stimulating hormone analogue. *Nucl. Med. Biol. 24* (2), 171−178.
(19) Egli, A., Alberto, R., Tanahill, L., Schibli, R., Abram, U., Schaffland, A., Waibel, R., Tourwé, D., Jeannin, L., Iterbeke, K., and Schubiger, P. A. (1999) Organometallic [99m]Tc-aquaion labels peptide to an unprecedented high specific activity. *J. Nucl. Med. 40,* 1913−1917.
(20) Virgolini, I., Raderer, M., Kurtaran, A., Angelberger, P., Banyai, S., Yang, Q., Li, S., Banyai, M., Pidlich, J., Niederle, B. et al. (1994) Vasoactive intestinal peptide-receptor imaging for the localization of intestinal adenocarcinomas and endocrine tumors. *N. Engl. J. Med. 331* (17), 1116−1121.
(21) Wester, H. J., Hamacher, K., and Stöcklin, G. (1996) A comparative study of nca fluorine-18 labeling of proteins via acylation and photochemical conjugation. *Nucl. Med. Biol. 23* (3), 365−372.
(22) Foulon, C. F., Alston. K. L., and Zalutsky, M. R. (1997) Synthesis and preliminary biological evaluation of (3-iodobenzoyl)norbiotinamide and ((5-iodo-3-pyridinyl)carbonyl)-norbiotin-amide: two radioiodinated biotin conjugates with improved stability. *Bioconjugate Chem. 8* (2), 179−186.
(23) Vaidyanathan, G., Affleck, D., Welsh, P., Srinivasan, A., Schmidt, M., Zalutsky, M. R. (2000) Radioiodination and astatination of octreotide by conjugation labeling *Nucl. Med. Biol. 27* (4), 329−337.
(24) Rogers, B. E., Anderson C. J., Connett, J. M., Guo, L. W., Edwards, W. B., Sherman, E. L., Zinn, K. R., and Welch, M. J. (1996) Comparison of four bifunctional chelates for radiolabeling monoclonal antibodies with copper radioisotopes: biodistribution and metabolism. *Bioconjugate Chem. 7* (4), 511−522.
(25) Bass, L. A., Wang, M., Welch, M. J., and Anderson, C. J. (2000) In vivo transchelation of copper-64 from TETA-octreotide to superoxide dismutase in rat liver. *Bioconjugate Chem. 11* (4), 527−532.
(26) Iznaga-Escobar, N. (2001) Direct radiolabeling of monoclonal antibodies with rhenium-188 for radioimmunotherapy of solid tumors − a review of radiolabeling characteristics, quality control and in vitro stability studies. *Appl. Radiat. Isot. 54* (3), 399−406.
(27) Haubner, R., Wester, H. J., and Burkhart, F., Senekowitsch-Schmidtke, R., Weber, W., Goodman, S., Kessler, H., Schwaiger, M. (2001) Glycosylated RGD-containing peptides: tracer for tumor targeting and angiogenesis imaging with improved biokinetics. *J. Nucl. Med. 42* (2), 326−336.
(28) Garayoa, E. G., Allemann-Tannahill, L., Blauenstein, P., Willmann, M., Carrel-Remy, N., Tourwé, D., Iterbeke, K., Conrath, P., and Schubiger, P. A. (2001) In vitro and in vivo evaluation of new radiolabeled neurotensin(8−13) analogues with high affinity for NT1 receptors. *Nucl. Med. Biol. 28* (1), 75−84.
(29) O′Connor, M. K., Kvols, L. K., Brown, M. L., Hung, J. C., Hayostek, R. J., Cho, D. S., and Vetter, R. J. (1992) Dosimetry and Biodistribution of a Iodine-123 labeled somatostatin analogue in patients with neuroendocrine tumors. *J. Nucl. Med. 33,* 1613−1619.
(30) Haubner, R., Wester, H. J., Reuning, U., Senekowitsch-Schmidtke, R., Diefenbach, B., Kessler, H., Stöcklin, G., and Schwaiger, M. (1999) Radiolabeled alpha(v)beta(3) integrin antagonists: a new class of tracers for tumor targeting. *J. Nucl. Med. 40* (6), 1061−1071.
(31) Behr, T. M., Sharkey, R. M., Sgouros, G., Blumenthal, R. D., Dunn, R. M., Kolbert, K., Griffiths, G. L., Siegel, J. A., Becker, W. S., and Goldenberg, D. M. (1997) Overcoming the nephrotoxicity of radiometal-labeled immunoconjugates: improved cancer therapy administered to a nude mouse model in relation to the internal radiation dosimetry. *Cancer 80* (12 Suppl), 2591−2610.
(32) Rösch, F., Herzog, H., Stolz, B., Brockmann, J., Kohle, M., Muhlensiepen, H., Marbach, P., and Müller-Gärtner, H. W. (1999) Uptake kinetics of the somatostatin receptor ligand [[86]Y]DOTA-dPhe[1]-Tyr[3]-octreotide ([[86]Y]SMT487) using positron emission tomography in nonhuman primates and calculation of radiation doses of the [90]Y-labeled analogue. *Eur. J. Nucl. Med. 26* (4), 358−366.
(33) Bilsky, E. J., Egleton, R. D., Mitchell, S. A., Palian, M. M., Davis, P., Huber, J. D., Jones, H., Yamamura, H. I., Janders, J., Davis, T. P., Porreca, F., Hruby, V. J., and Polt, R. (2000) Enkephalin glyopeptide analogues produce analgesia with reduced dependence liability. *J. Med. Chem. 43,* 2586−2590.
(34) Polt, R., Porreca, F., Szabo L. Z., Bilsky, E. J., Davis, P., Abbruscato, T. J., Davis, T. P., Horcath, R., Yamamura, H. I., and Hruby, V. (1994) Glycopeptide enkephalin analogues produce analgesia in mice: Evidence for penetration of the blood-brain barrier. *Proc. Natl., Acad. Sci. U.S.A. 91,* 7114−7118.
(35) Mitchell, S. A., Pratt M. R., Hruby, V. J., and Polt, R. (2001) Solid-Phase Synthesis of O−Linked Glycopeptide Analogues of Enkephalin, *J. Org. Chem. 66,* 2327−2342.
(36) Filippi, B., Biondi, A., Filiara, F., Rocchi, R., Bellini, C., and Giamietro, S. (1983) Synthesis and biological activity of (D)Ala[2], Leu[5]-enkephalins containing hydrophilic or Hydrophobic moieties. *Bioploymers* 22, 575−578.
(37) Renzetti, A. R., Catalioto, R.-M., Criscuoli, M., Cucchi, P., Lippi A., Guelfi, M., Quartara, L., and Maggi, C. A. (1998) Characterization of [[3]H]MEM 11420, a Novel Glycosylated Peptide Antagonist Radioligand of the Tachykinin NK_2 Receptor. *Biochem. Biophys. Res. Commun. 248,* 78−82.
(38) Kriss, C. T., Lou, B.-S., Szabo, L. Z., Mitchell, S. A., Hruby, V. J., and Polt, R. (2000) Enkephalin-based drug design: conformational analysis of O-linked glycopeptides by NMR and molecular modelling. *Tetrahedron Asymm. 11,* 9−25.
(39) Fisher, J. F., Harrison, A. W., Bundy, G. L., Wilkinson, K. F., Rush B. D., and Ruwart, M. J. (1991) Peptide to glycopeptide: glycosylated oligopeptide renin inhibitors with attenuated in vivo clearance properties. *J. Med. Chem. 34,* 3140−3143.
(40) Suzuki, K., Susaki, H., Okuno, S., Yamada, H., Watanabe, H. K., and Sugiyama, Y. (1999) Specific renal delivery of sugar-modified low-molecular-weight peptides. *J. Pharmacol. Exp. Ther. 288* (2), 888−897.

(41) Kihlberg, J., Ahman, J., Walse, B., Drakenberg, T., Nilsson, A., Soderberg-ahlm, C., Begntsson, B., and Olsson, H. (1995) Glycosylated peptide hormones: pharmacological properties and conformational studies of analogues of [1-desamino, 8-D-arginine]vasopressin. *J. Med. Chem. 38*, 161−169.

(42) Nomoto, M., Yamada, K., Haga, M., and Hayashi, M. (1998) Improvement of Intestinal Absorption of Peptide Drugs by Glycosylation: Transport and Tetrapeptide by the Sodium Ion-Dependent D-Glucose Transporter. *J. Pharm. Sci. 87*, 326−332.

(43) Haubner, R., Wester, H.-J., Weber, W., Mang, C., Ziegler, S. I., Senekowitsch-Schmidtke, R., Kessler, H., and Schwaiger, M. (2001) Non invasive imaging of $\alpha_v\beta_3$-integrin expression using a F-18-labeled RGD-containing glycopeptide and positron emission tomography. *Cancer Res. 61*, 1781−1785.

(44) Leisner, M., Kessler, H., Schwaiger, M., and Wester, H.-J. (1999) Synthesis of N^a-d-Phe^1-Amadori derivatives of Tyr^3-octreotide: Precursors for ^{123}I-/^{18}F-labeled sstr-binding SPECT/PET tracers with improved biodistribution. *J. Labeled Cpd. Radiopharm. 42*, S549 (abstract).

(45) Wester, H.-J., Schottelius, M., Scheidhauer, K., Reubi, J. C., Wolf, I., and Schwaiger, M. (2002) Comparison of radioiodinated TOC, TOCA and Mtr-TOCA: the effect of carbohydration on the pharmacokinetics. *Eur. J. Nucl. Med. Mol. Imaging 29*, 28−38.

(46) Wester, H. J., Schottelius, M., and Schwaiger, M. (2001) $[^{99m}Tc](CO)_3$-labeled carbohydrated SSTR-ligands: synthesis, internalisation kinetics and biodistribution on a rat pancreatic tumor model. *J. Nucl. Med. 42* (Suppl.), 115 P (abstract).

(47) Schottelius, M., Wester, H.-J., and Schwaiger, M. (2001) Carbohydration: a new approach to F-18-octreotide analogues. *J. Nucl. Med. 42* (Suppl.), 148 P (abstract).

(48) Paulsen, H., and Pflughaupt, K.-W. (1980) *The Carbohydrates, Chemistry and Biochemistry* (W. Pigman, D. Horton, Eds.) Academic Press, New York, pp 899−907.

(49) Kokotos, G. (1990) A convenient one-pot conversion of *N*-protected amino acids and peptides into alcohols. *Synthesis* 299−301.

(50) Lohof, E. (1999) dissertation TU München.

(51) Albert, R., Marbach, P., Bauer, W., Briner, U., Fricker, G., Bruns, C., and Pless, J. (1993) SDZ CO 611: A highly potent glycosylated analogue of somatostatin with improved oral acitivity. *Life Sci. 53*, 517−525.

(52) Buchwald, P., and Bodor, N. (1998) Octanol−water partition of nonzwitterionic peptides: predictive power of a molecular size-based model. *Proteins: Structure, Function and Genetics*, *30*, 86−99.

(53) Reubi, J. C., Schär, J. C., Waser, B., Wenger, S., Heppeler, A., Schmitt, J. S., and Mäcke, H. R. (2000) Affinity profiles for human somatostatin receptor subtypes SST1-SST5 of somatostatin radiotracers selected for scintigraphic and radiotherapeutic use. *Eur. J. Nucl. Med. 27*, 273−282.

(54) Viguerie, N., Tahiri-Jouti, N., Esteve, J. P., Clerc, P., Logsdon, C., Svoboda, M., Susini, C., Vaysse N., and Ribet, A. (1988) Functional somatostatin receptors on a rat pancreatic acinar cell line *Am. J. Physiol. 255*, G113−G120.

(55) Funcke, W. (1978) ^{13}C NMR-Untersuchungen an Mutarotationsgemischen C-6- und C-4- sowie C-6-modifizierter Amadoriverbindungen *Liebigs Ann. Chem*. 2099−2104.

(56) Bruno, J. F., Xu, Y., Song, J., and Berelowitz, M. (1993) Tissue distribution of somatostatin receptor subtype messenger ribonucleic acid in the rat. *Endocrinology 133*, 2561−2567.

(57) Lamberts, S. W. J., Bakker, W. H., Reubi, J. C., and Krenning, E. P. (1990) Somatostatin receptor imaging in the localization of endocrine tumors *N. Engl. J. Med. 323*, 1246−1249.

(58) Krenning, E. P., Kwekkeboom, D. J., Bakker, W. H., Breemann, W. A. P., Kooji, P. P. M., Oei, H. Y., vanHagen, M., Postema, P. T. E., deJong, M., Reubi, J. C., Visser, T. J., Reijs, A. E. M., Hofland, L. J., Koper, J. W., and Lamberts, S. W. J. (1993) Somatostatin receptor scintigraphy with [^{111}-In-DTPA-D-Phe^1]- and [^{123}I]-Tyr^3-octreotide: the Rotterdam experience with more than 1000 Patients. *Eur. J. Nucl. Med. 20*, 716−731.

(59) Bakker, W. H., Breemann, W. A. P., deJong, M., Visser, T. J., and Krenning, E. P. (1996) Iodine-131 labeled octreotide: not an option for somatostatin receptor therapy. *Eur. J. Nucl. Med. 23*, 775−781.

(60) Prammer, K. V., and Otvos, L. Jr. (1995) Structural effects of glycosylation on the C-terminal pentapeptide of peptide T. *Biomed. Pept. Proteins Nucleic Acids 1*, 221−226.

(61) Fricker, G., Dubost, V., Schwab, D., Bruns, C., and Thiele, C. (1994) Heterogeneity in hepatic transport of Somatostatin analogue octapeptides. *Hepatology 20*, 191−200.

(62) Wester, H. J., Brockmann, J., Rösch, F., Wutz, W., Herzog, H., Smith-Jones, P., Stolz, B., Bruns, C., and Stöcklin, G. (1997) PET-pharmacokinetics of ^{18}F-octreotide: a comparison with ^{67}Ga-DFO- and ^{86}Y-DTPA-octreotide. *Nucl. Med. Biol. 24* (4), 275−286.

(63) de Jong, M., Rolleman, E. J., Bernard, B. F., Visser, T. J., Bakker, W. H., Breeman, W. A., and Krenning, E. P. (1996) Inhibition of renal uptake of indium-111-DTPA-octreotide in vivo. *J. Nucl. Med. 37* (8), 1388−1392.

(64) Bernard, B. F., Krenning, E. P., Breeman, W. A., Rolleman, E. J., Bakker, W. H., Visser, T. J., Maecke, H. R., and de Jong, M. (1997) d-lysine reduction of indium-111 octreotide and yttrium-90 octreotide renal uptake. *J. Nucl. Med. 38* (12), 1929−1933.

BC0200069

Pegylated Zinc Protoporphyrin: A Water-Soluble Heme Oxygenase Inhibitor with Tumor-Targeting Capacity

S. K. Sahoo, T. Sawa, J. Fang, S. Tanaka, Y. Miyamoto, T. Akaike, and H. Maeda*

Department of Microbiology, Kumamoto University School of Medicine, 2-2-1 Honjo, Kumamoto 860-0811, Japan. Received January 21, 2002; Revised Manuscript Received March 25, 2002

Heme oxygenase (HO) is a key enzyme in heme metabolism; it oxidatively degrades heme to biliverdin, accompanied by formation of free iron and carbon monoxide. Biliverdin is subsequently reduced by cytosolic biliverdin reductase to form bilirubin, a potent antioxidant. We recently found that tumor cells utilize HO to protect themselves from oxidative stress by producing the antioxidant bilirubin. This result suggested an important potential therapeutic strategy: suppression of bilirubin production with the use of HO inhibitors; hence, cancer cells become vulnerable to oxidative stress induced by anticancer drugs or leukocytes of the host. This concept was validated by using the intraarterial administration of an HO inhibitor, zinc protoporphyrin, in nonphysiological solution. In the present study, zinc protoporphyrin (ZnPP) was conjugated with poly(ethylene glycol) (PEG) with molecular weight of 5000, to make ZnPP, a water-soluble compound (PEG-ZnPP), and to improve its tumor-targeting efficiency. PEG was conjugated to ZnPP through newly introduced amino groups, where ethylenediamine residues were added at C6 and C7 of protoporphyrin. The divalent zinc cation was chelated into the protoporphyrin ring to obtain PEG-ZnPP. PEG-ZnPP did become highly water-soluble, and it formed multimolecular associations with molecules larger than 70 kDa in aqueous media. PEG-ZnPP inhibited splenic microsomal HO activity in vitro in a competitive manner in the presence of hemin, with an apparent inhibitory constant of 0.12 μM. Most important, PEG-ZnPP injected intravenously significantly suppressed intratumor HO activity in a murine solid tumor model, which suggests that tumor-targeted inhibition of HO is possible with the use of PEG-ZnPP.

INTRODUCTION

Heme oxygenase (HO)[1] is an enzyme of significant clinical importance because of its key role in heme degradation. HO oxidatively degrades the closed tetrapyrrole heme molecule to produce biliverdin; this process is accompanied by the release of free iron (Fe^{2+}) and carbon monoxide (CO) (*1*, *2*). To date, two isoforms of HO have been found: an inducible type HO-1, and a constitutive type HO-2. HO-1, a well-known heme oxygenase, is induced by a wide variety of oxidative stimuli including heme (*3*), ultraviolet irradiation (*4*), hydrogen peroxide (*4*), heavy metals (*4*, *5*), heat shock (*3*), hypoxia (*6*), and nitric oxide (NO) (*7*, *8*).

Biliverdin, one of the products of heme degradation, is immediately reduced by the cytosolic enzyme biliverdin reductase to form bilirubin (*1*, *2*). Although excessive increases in serum bilirubin concentrations cause hyperbilirubinemia or jaundice (*9*), recent findings suggest that adequate levels of bilirubin play an important role in protecting cells from oxidative stress because of bilirubin's potent antioxidant activity. It was reported that bilirubin can scavenge free radicals, especially peroxyl radicals (*10*); prevent protein oxidation by the potent reactive nitrogen species peroxynitrite (*11*); and protect neuronal cells from oxidative stress injury (*12*). We recently found that HO-1 production was enhanced in an experimental solid tumor model (*8*) and, more important, that HO-1 played a vital role in tumor growth by providing, at least in part, antioxidant bilirubin to protect tumor cells from host-derived oxidative stress. The evidence for this role was the marked antitumor effect of a specific HO inhibitor, zinc protoporphyrin (ZnPP) (*8*). These findings suggest a therapeutic potential of this HO inhibitor, which would act as a novel antitumor agent via disruption of the antioxidant defense system of cancer cells.

Metalloporphyrins represent a class of compounds in which the central iron of heme is replaced by various other metals such as cobalt, zinc, manganese, chromium, or tin (*13*). These metalloporphyrins function as competitive inhibitors of the HO reaction because of their inefficient binding to molecular oxygen, thus preventing HO from degrading metalloporphyrins (*1*, *13*). Inhibitory actions of these metalloporphyrins have been studied extensively, especially with respect to therapy for hyperbilirubinemia (*14*−*16*). As mentioned above, we also demonstrated antitumor activity of ZnPP in a solid tumor model (*8* and our unpublished data, S. Tanaka et al.). However, the very low solubility of these metalloporphyrins in aqueous media limits the use of these compounds in injectable formulations. In addition to the issue of solubility, targeted delivery of the HO inhibitor to tumor tissue is indispensable for antitumor treatment because nonspecific inhibition of HO may cause oxidative stress-related side effects by reducing the favorable antioxidant capacity of bilirubin in normal organs.

* To whom correspondence should be addressed: Professor Hiroshi Maeda, Department of Microbiology, Kumamoto University School of Medicine, 2-2-1 Honjo, Kumamoto 860-0811, Japan. Tel: 81-96-373-5098. Fax: 81-96-362-8362. E-mail: msmaedah@gpo.kumamoto-u.ac.jp.

[1] Abbreviations: HO, heme oxygenase; ZnPP, zinc protoporphyrin; PEG-ZnPP, pegylated ZnPP; EPR effect, enhanced permeability and retention effect.

10.1021/bc020010k CCC: $22.00 © 2002 American Chemical Society
Published on Web 07/16/2002

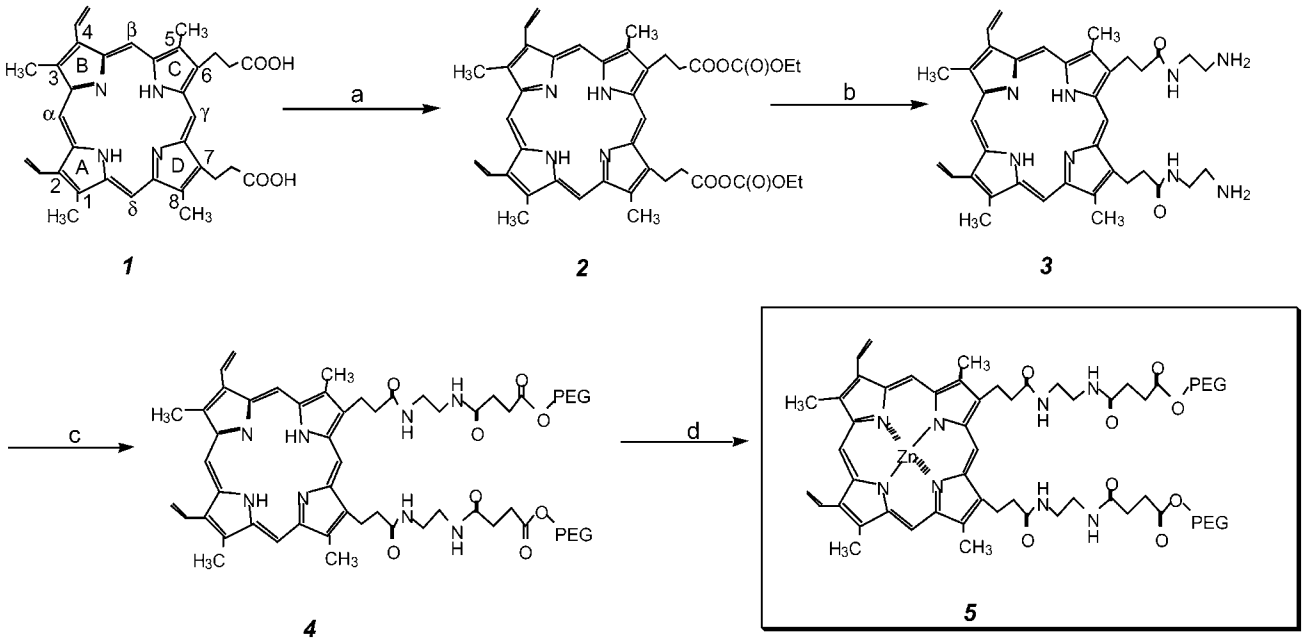


Figure 1. Synthesis of pegylated zinc protoporphyrin (PEG-ZnPP). Reagents and conditions: (a) ethylchloroformate, triethylamine, tetrahydrofuran, 0 °C, 2 h; (b) ethylenediamine, room temperature, 24 h; (c) succinimidyl PEG (M_r 5000), chloroform, room temperature, 24 h; (d) zinc acetate, room temperature, 1 h (See text for details).

Tumor-specific accumulation of biocompatible macromolecules and lipids, after intravenous and intraarterial administration, has been observed in many types of solid tumors of mice, rats, rabbits, and human patients. We called this phenomenon the "enhanced permeability and retention (EPR) effect" of macromolecules and lipids in solid tumor (*17*). The EPR effect is mainly mediated by four major factors: (i) hypervasculature of tumor tissues due to active angiogenesis, (ii) defective anatomical structure of tumor blood vessels (thus leaky), (iii) enhanced production of vascular mediators such as nitric oxide and bradykinin, and (iv) incomplete lymphatic drainage system (*17*−*20*). We hypothesized that if we could increase the molecular size as well as the water-solubility of an HO inhibitor such as ZnPP by conjugating it with water-soluble polymers, we will be able to achieve, based on the EPR effect, more effective and selective delivery of the HO inhibitor to tumor sites.

The present study describes the synthesis and characterization of a water-soluble derivative of ZnPP obtained by conjugation with PEG (PEG-ZnPP). The inhibitory constant (K_i) of PEG-ZnPP against HO was determined in vitro and compared with that of native ZnPP. The biological significance of PEG-ZnPP is further discussed in view of antitumor effect in vivo.

EXPERIMENTAL PROCEDURES

Materials. Protoporphyrin IX was purchased from Sigma Chemical Co. (St. Louis, MO). ZnPP was from Wako Pure Chemical Industries Ltd., Osaka, Japan. The succinimidyl derivative of PEG (MEC-50HS), with an average molecular weight of 5000, was kindly provided by NOF Co., Tokyo, Japan. PEGs used in this experiment have a molecular weight dispersity (Mw/Mn) of 1.025. Other reagents, of reagent grade, were from Wako Pure Chemical Industries and were used without further purification.

General Methods. Absorption spectra were determined by using a spectrophotometer (U-2000, Hitachi Ltd., Tokyo, Japan). Fluorescence spectra were recorded by a fluorescence spectrophotometer (F-4500, Hitachi). Mass spectra were obtained via a liquid chromatography spectrometer (LCMS QP8000α, Shimadzu Corp., Kyoto, Japan), with the electron spray ionization probe operating in the positive mode. Methanol was used as a solvent. Infrared spectra were recorded with a JIR-6500w spectrometer (JEOL, Tokyo, Japan). Thin-layer chromatography (TLC) was performed on 60 A silica with F254 aluminum-backed plates (Merck); UV−visualization was at 254 nm.

Animals and Tumor Implantation. Male ddY mice, 6 weeks of age and weighing 30−35 g (from SLC, Inc., Sizuoka, Japan), were used in this study. S-180 tumor cells (2×10^6 cells) were implanted subcutaneously in the dorsal skin of the ddY mice. The inhibitory activity of PEG-ZnPP in vivo was examined on days 10−14 after tumor inoculation, when the tumors were approximately 10 mm in diameter but contained no necrotic region. All experiments were carried out according to the guidelines of the Laboratory Protocol of Animal Handling, Kumamoto University School of Medicine.

Synthesis of PEG-ZnPP. The overall scheme of synthesis of PEG-ZnPP is shown in Figure 1. PEG-ZnPP synthesis proceeded by three major steps: (i) the introduction of amino groups into the protoporphyrin ring by reacting ethylenediamine with the intrinsic carboxyl groups of the ring; (ii) PEG conjugation to the amino groups; and (iii) chelation of Zn^{2+} into the PEG-porphyrin ring. Detailed procedures for each step are described in the following text.

Synthesis of the Aminated Derivative of Protoporphyrin IX (Compound 1; cf. Compound 3). Triethylamine (2.45 mL, 17.6 mmol) was added to a suspension of protoporphyrin IX (100 mg, 178 mmol) (**1**) in dry tetrahydrofuran (20 mL) to remove the hydrochloric acid formed. The suspension was then cooled to 0 °C; 1.7 mL (17.9 mmol) of ethylchloroformate was added in dropwise fashion, with stirring, and the reaction was continued at 0 °C for 2 h. The resultant suspension was then filtered to remove the triethylamine hydrochloride salt. By TLC (chloroform/methanol, 9:1 v/v), R_f was 0.9. To the solution obtained (**2**) was added an excess of

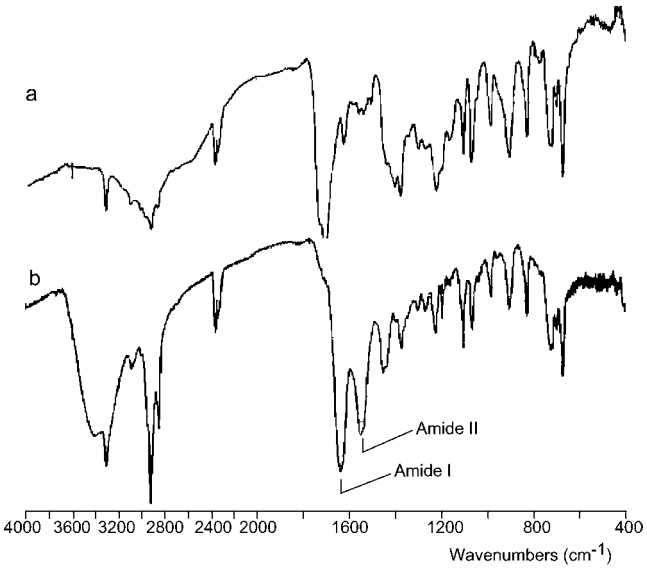


Figure 2. IR spectra of **1** (a) and **3** (b). Clear appearance of amide I (1641 cm^{-1}) and amide II (1552 cm^{-1}) was observed in **3** suggesting the conjugation of diaminoethylene to propionic acid residues of **1** through amide bond.

ethylenediamine (1.2 mL, 17.9 mmol) against mixed anhydride to introduce amino groups into the porphyrin ring (Figure 1). The reaction proceeded at room temperature for 24 h. The solvent was removed by evaporation in vacuo, and the solid material obtained (**3**) was washed several times with chilled distilled water. Finally, **3** was suspended in a small aliquot of distilled water and was then lyophilized, yielding 60 mg of product. By TLC (chloroform/methanol 9:1 v/v), $R_f = 0.3$. IR (KBr): 1641 cm^{-1} (amide I) and 1552 cm^{-1} (amide II) were distinct (Figure 2). The mass analysis (electron spray ionization, polarity positive) result, calculated for M+H, was 647.

Conjugation of PEG with Bis(ethylenediamino)-protoporphyrin. Bis(ethylenediamino)protoporphyrin (5 mg, 7.7 μmol, **3**) was dissolved in 20 mL of chloroform. To this solution, 860 mg (172 μmol) of succinimidyl PEG was added in stepwise fashion (five times, about 170 mg each time) at 30-min intervals, and the reaction proceeded at room temperature for 24 h with stirring. Pegylated protoporphyrin (PEG-PP) (**4**) thus obtained was subjected to dialysis (cutoff size of 50 000) against distilled water for 2 days with several changes of water to remove unreacted PEG. The resultant solution was then lyophilized to obtain a powder of **4**. The yield was 120 mg. The content of porphyrin moiety was determined spectroscopically, and the yield of **4** based on porphyrin moiety was 4 μmol (52%).

Chelation of Zinc into the Porphyrin Ring of PEG-PP. PEG-PP (100 mg, 0.16 mM porphyrin equivalent) was dissolved in 20 mL of chloroform, to which was added 20 mg (27 mM) of zinc acetate. The solution was stirred at room temperature for 1 h to complete chelation of Zn^{2+} into the porphyrin ring. After the reaction, chloroform was removed by evaporation, to yield the crude PEG-ZnPP (**5**). PEG-ZnPP was then purified by overnight dialysis against 1 L of distilled water, with a membrane filter having a cutoff size of 8000; the water was changed three times. The yield of PEG-ZnPP after lyophilization was 77 mg.

Size Exclusion Chromatography. The apparent molecular sizes of PEG-PP (**4**) and PEG-ZnPP were studied by means of size exclusion chromatography with the use of both polar (buffer) and nonpolar (chloroform) mobile phases. As molecular size standards for PEG, conjugates of nitrotyrosine and PEG were prepared in a manner similar to the procedure used for PEG-PP. Succinimidyl PEG, with a molecular size of 5 or 12 kDa, was incubated overnight with nitrotyrosine in 100 mM phosphate buffer (pH 7) at room temperature. During this incubation, the amino group of nitrotyrosine reacted with succinimidyl PEG, which was confirmed from the loss of free amino groups determined by fluorescamine assay (see below). The solution was then dialyzed to remove unreacted nitrotyrosine. PEG-nitrotyrosine thus obtained was easily detected by absorption at 390 nm during chromatographic separation.

Size exclusion chromatography was performed by using a Sephadex LH-60 column (13 mm inner diameter, 400 mm long), with chloroform as the mobile phase, at a flow rate of 60 mL/h. Absorption of each fraction (2 mL) was measured at 415 nm for porphyrin derivatives and at 390 nm for PEG-nitrotyrosine.

Also, a high-performance liquid chromatography (HPLC) system (LC-10DA and SPD-10A, Shimadzu) equipped with a YMC Diol-60 column was used for size exclusion chromatography of PEG-ZnPP in buffer. The mobile phase consisted of 20 mM sodium phosphate buffer (pH 7) containing 0.2 M sodium chloride. In this experiment, bovine serum albumin (M_r 67 000) was used as the molecular size standard.

Quantification of Free Amino Groups. To determine whether PEG reacted with the amino groups of **3**, loss of the primary amino group after the reaction was quantified by means of an amino group-reactive fluorescence agent, fluorescamine, according to the literature (*21*). In brief, 2 μM (protoporphyrin equivalent) PEG-PP was dissolved in distilled water and was then reacted with fluorescamine. The intensity of fluorescence at 475 nm (under excitation at 390 nm) was determined. The concentration of free amino groups in PEG-PP was estimated by using glycine as a standard.

Inhibitory Activity of PEG-ZnPP against HO in Vitro. A rat splenic microsomal fraction was prepared for measurement of splenic HO activity according to the literature (*15*). A liver cytosolic fraction was used as the source of bilirubin reductase (*15*). The HO reaction mixture was composed of the splenic microsomal fraction (1.0 mg of protein), the liver cytosolic fraction (3.0 mg of protein), and 333 μM nicotinamide adenine dinucleotide phosphate (NADPH), without or with inhibitors at a given concentration, in 1.0 mL of 90 mM potassium phosphate buffer (pH 7.4). The reaction was initiated by adding hemin (33 μM) to the mixture. In some experiments, the HO fraction and the inhibitors were incubated for 30 min before starting the reaction to permit interaction of the inhibitor to bind to HO before substrate ligand (hemin) binds to HO. The mixture was incubated for 15 min at 37 °C, and then the reaction was terminated by addition of 33 μL of 0.01 M HCl. The bilirubin formed in the reaction was extracted with 1.0 mL of chloroform, and the bilirubin concentration was determined spectroscopically by the difference in absorbance at 465 and 530 nm with a molar extinction coefficient of 40 mM^{-1} cm^{-1} as described previously (*15*). The K_i of PEG-ZnPP was determined by using double reciprocal Lineweaver−Burk plots and the slope of the plotted lines with added inhibitor (*15*).

Inhibitory Activity of PEG-ZnPP against HO in an in Vivo Solid Tumor Model. To examine whether PEG-ZnPP can be targeted to tumor tissue and can inhibit intratumor HO activity, PEG-ZnPP was administered intravenously to ddY mice bearing S-180 solid

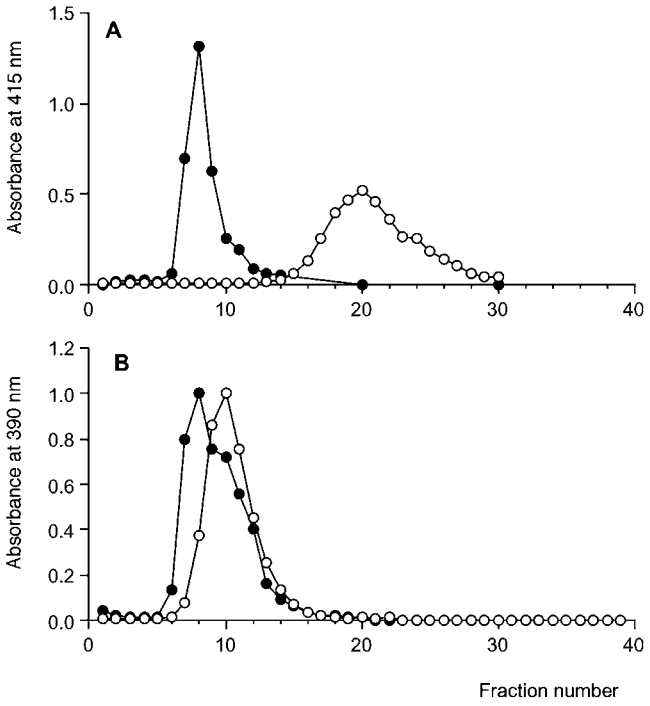


Figure 3. Size exclusion chromatography with chloroform. (A) bis(ethylenediamino)protoporphyrin before and after PEG conjugation. Symbols: open circle, aminated protoporphyrin; closed circle, pegylated protoporphyrin. (B) molecular weight standards of PEG-nitrotyrosine conjugates. Symbols: open circle, pegylated (5 kDa) nitrotyrosine; closed circle, pegylated (12 kDa) nitrotyrosine. Detection wavelengths were 415 and 390 nm for porphyrin derivatives and nitrotyrosine derivatives, respectively.

tumor. In this study, 300 or 600 μM PEG-ZnPP dissolved in distilled water (0.1 mL) was injected via the tail vein (0.5 or 1 mg of ZnPP equiv/kg). At 24 h after injection, tumor tissue was collected, and intratumor HO activity was measured as described previously. Control animals received distilled water without PEG-ZnPP.

RESULTS

Synthesis of PEG-ZnPP. In the present study, amino groups were first introduced to protoporphyrin IX (**1**) as reactive nucleophils (*22*), because a variety of polymer conjugates can be targets for nucleophilic amino groups. PEG with a succinimidyl ester group at one end was utilized to introduce water-soluble moieties to the porphyrin structure (Figure 1).

LC-MS analysis indicated that **3** shows a single peak at a molecular weight of 647, which is identical to that of calculated mass (data not shown). Formation of an amide bond was demonstrated by infrared spectroscopy; **3** shows characteristic absorption at 1641 cm^{-1} (amide I) and 1552 cm^{-1} (amide II) (Figure 2).

Size exclusion chromatography with chloroform (Figure 3) clearly indicated that, under the present conditions, the reaction between **3** and succinimidyl PEG proceeded completely as that no **3** remained (Figure 3A). Comparison of the chromatographic profile of **4** with those of the molecular size markers nitrotyrosine conjugated with PEG, either 5 or 12 kDa (Figure 3B), indicated that **4** has an apparent molecular size similar to PEG 12 kDa-nitrotyrosine, and larger than PEG 5 kDa-nitrotyrosine. Thus, PEG conjugation might occur at both two amino groups of compound **3**. This notion was supported by the fact that **4** has no reactive free amino groups as determined by a fluorescamine-assisted amino group assay (data not shown).

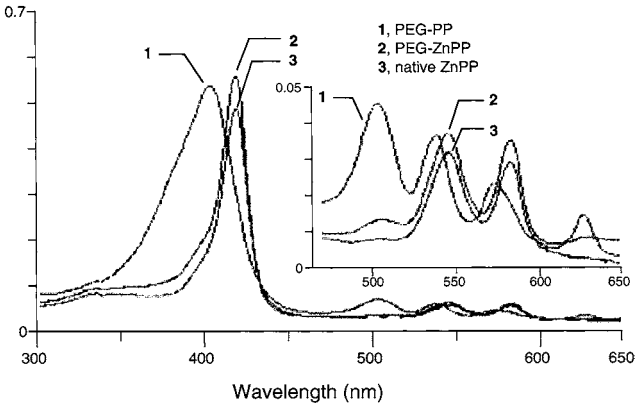


Figure 4. UV spectra of PEG−protoporphyrin conjugate (PEG-PP, 3.3 μM), PEG-ZnPP (4.0 μM), and native ZnPP (3.3 μM) in dimethyl sulfoxide. Inset shows the amplified spectra from 475 to 650 nm.

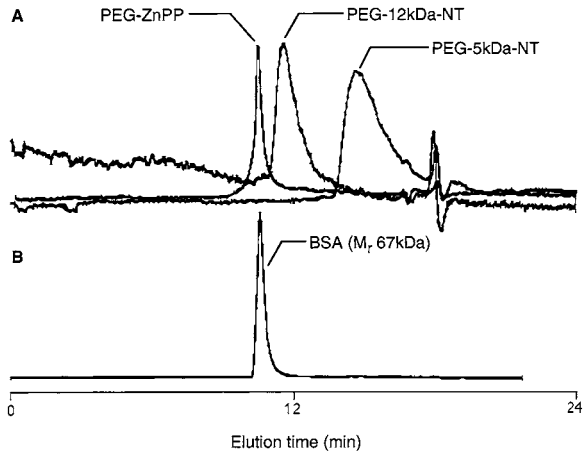


Figure 5. HPLC profiles of PEG in various conjugates (A) and the molecular size marker bovine serum albumin (BSA) (B) with the use of size exclusion column (Diol-60) eluted by sodium phosphate buffer (pH 7.0). Detection wavelengths of compounds were 415 nm (PEG-ZnPP), 390 nm (pegylated nitrotyrosine, PEG-12 kDa-NT and PEG-5 kDa-NT), and 280 nm (BSA), respectively.

Compound **4** shows intense absorption at 406 nm corresponding to the Soret band of protoporphyrin moiety (Figure 4). In addition, there are four bands, 505, 540, 575, 627 nm in the visible region, which correspond to the bands numbered I (627 nm), II (575 nm), III (540 nm), and IV (505 nm) for the porphyrin ring as reported previously (*23*). After the reaction with zinc acetate, the Soret band of **5** was found to red shift (422 nm) compared to that of **4**. A marked difference was also observed in the visible region, i.e., **5** shows two major bands at 548 and 584 nm, respectively (Figure 4). These observations are well consistent with the finding that divalent metal insertion into porphyrin ring induces a red shift of the Soret band and the formation of two major bands, alpha (584 nm) and beta (548 nm) (*23*). Furthermore, the spectrum of native ZnPP showed good agreement with that of **5**. Taken together, it was suggested that zinc was chelated into the porphyrin ring of **4**, and hence, the formation of **5** (PEG-ZnPP) as depicted in Figure 1.

Molecular Association of PEG-ZnPP in Aqueous Media. The PEG-ZnPP obtained here was highly water-soluble. The saturated concentration of PEG-ZnPP in water was determined to be 3.15 mM; in contrast, native ZnPP shows virtually no dissolution in water.

The apparent molecular size of PEG-ZnPP in an aqueous system was studied by using size exclusion

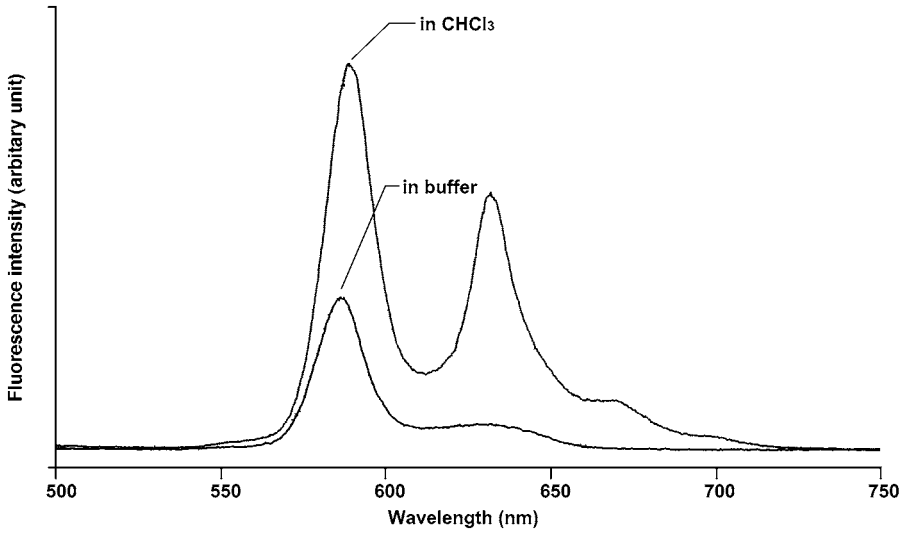


Figure 6. Fluorescence spectra of PEG-ZnPP in chloroform and in 200 mM phosphate buffer (pH 7.4). Excitation was at 370 nm.

chromatography. Interestingly, PEG-ZnPP was eluted much faster than PEG 12 kDa-nitrotyrosine (Figure 5). This result is different from the chromatographic data obtained by using chloroform as a mobile phase (Figure 3). These observations suggest that PEG-ZnPP behaves differently in solution as the tertiary and quaternary structure of macromolecules may differ depending on the type of solvents; PEG-ZnPP might form multimolecular association in aqueous media, resulting in increased apparent molecular size; whereas, it behaves as free monomolecular dispersion in chloroform.

It has been known that molecular size is an important factor for preferred tumor accumulation due to the EPR effect (*17*−*20*). Compounds smaller than 40 kDa will rapidly be cleared from circulation by urinary excretion mechanism, and hence, show no tumor accumulation. Elution time of PEG-ZnPP was comparable to that of bovine serum albumin (67 kDa), suggesting that PEG-ZnPP behaves as large as BSA in aqueous system. This increased molecular size of PEG-ZnPP would facilitate its tumor accumulation based on the EPR effect.

Fluorescence Spectroscopy of PEG-ZnPP. Porphyrins have intense fluorescence when they are well dispersed (monomeric form) in solution, whereas upon aggregation the fluorescence is strongly quenched (*24*). This different fluorescent property has been utilized to study the monomer−aggregate transition of porphyrins in solutions. As shown in Figure 6, we observed intense fluorescence of PEG-ZnPP dissolved in chloroform solution. The fluorescence of PEG-ZnPP was, however, strongly quenched when aqueous buffer is used as a solvent. These observations suggest that the porphyrin moiety of PEG-ZnPP may aggregate, but not disperse homogeneously, in buffer solution. Considering the size exclusion chromatographic data together, PEG-ZnPP might form multimolecular association facilitated in aqueous solution similar to the micelle system.

Inhibitory Activity of PEG-ZnPP against HO in Vitro. The inhibitory activity of PEG-ZnPP against HO was examined by using a rat splenic microsomal fraction as described earlier (*8*, *14*−*16*). The addition of PEG-ZnPP (1.0 μM) to a splenic HO incubation mixture drastically decreased the formation of bilirubin in a manner that depended on preincubation time (Figure 7A). This requirement for such a preincubation period was not observed for native ZnPP (Figure 7A). This result suggests a number of possibilities: (i) binding of PEG-ZnPP is a very weak and slow process, and it needs time to access or fit to the catalytic site; (ii) dissociation of monomeric PEG-ZnPP from associated molecules is required for inhibitory action, and/or (iii) hydrolytic cleavage between the PEG chain and the porphyrin ring results in the ZnPP moiety being more accessible to the catalytic site of HO, or a combination of these. Further investigation is needed to clarify this point. Neither PEG-

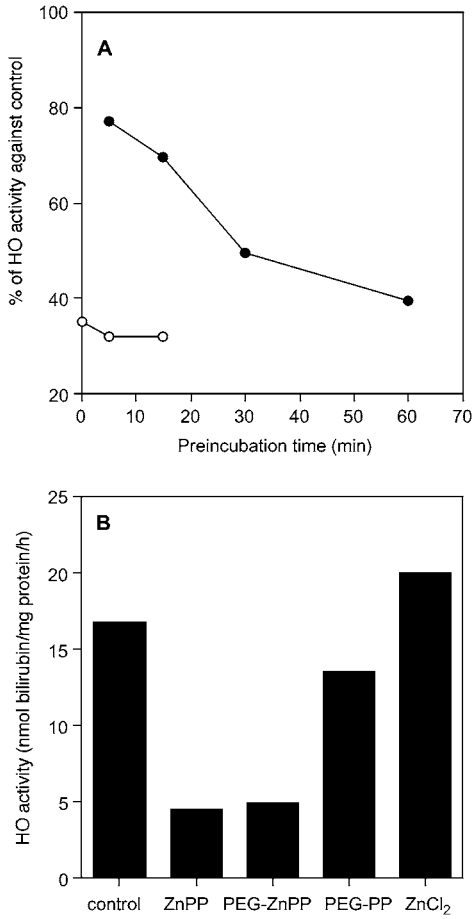


Figure 7. Inhibitory activity of PEG-ZnPP on splenic microsomal heme oxygenase (HO). (A) Effect of preincubation period. Symbols: open circle, native ZnPP (1 μM); closed circle, PEG-ZnPP (1 μM). (B) Effect of various compounds on HO activity. The concentration of each compound was 1.0 μM. Preincubation period was 30 min. Data were averages of two measurements.

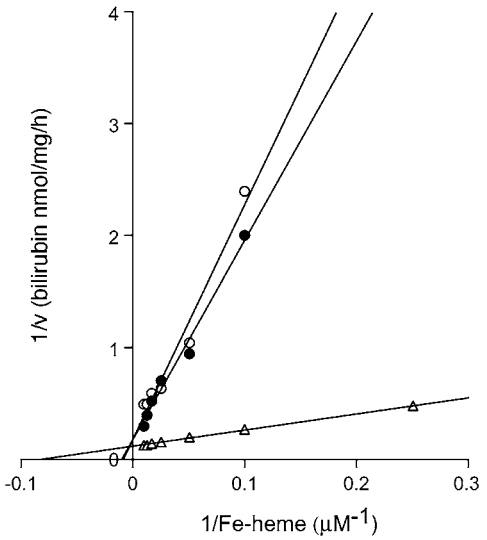


Figure 8. Lineweaver−Burk plot analysis of the effects of PEG-ZnPP and native ZnPP on the oxidation of Fe-heme in vitro by microsomal splenic HO. The concentration of both native ZnPP and PEG-ZnPP was 1.0 μM. Symbols: triangle (control without inhibitor), closed circle (native ZnPP), open circle (PEG-ZnPP). Data were averages of two measurements.

PP nor zinc alone showed any inhibitory activity against the splenic HO system, whereas PEG-ZnPP and ZnPP showed similar inhibitory activity (Figure 7B). This finding suggests that PEG-ZnPP inhibits HO activity in a manner similar to that of native ZnPP.

The apparent Michaelis−Menten constant (K_m) for heme in the splenic HO system was determined to be 12.2 μM (Figure 8), which is consistent with the previously reported value (*15*). Native ZnPP inhibited splenic HO activity in a competitive manner (Figure 8). The K_i of native ZnPP was determined to be 0.11 μM, which is also within the range of previously reported values (*15*). We found that PEG-ZnPP inhibited splenic HO activity in a competitive manner, similar to native ZnPP (Figure 8): the K_i of PEG-ZnPP was determined to be 0.12 μM, which is comparable to that of native ZnPP.

Inhibition of Intratumor HO Activity by PEG-ZnPP. As mentioned above, we recently found a high level of HO expression in the rat AH136B solid tumor model in vivo (*8*). This high level of HO expression in the solid tumor could be mediated by, at least in part, a high level of NO produced by monocyte-derived macrophages that infiltrated the tumor (*8*, *25*). In the murine S-180 solid tumor model, the model used in this study, we also previously demonstrated extensive production of NO in tumor tissue (*26*). We thus expected upregulation of HO-1 in the S-180 tumor in this study.

Here, at 15 days after tumor inoculation, S-180 tumor tissue excised from mice that had received no treatment was determined to contain HO activity of 4.17 ± 1.07 nmol of bilirubin (mg protein)$^{-1}$ h^{-1} (Table 1). This activity is comparable to that found in AH136B tumors reported previously (*8*) and is 3-fold higher than that in normal liver tissue (Table 1). Most important, PEG-ZnPP (30 or 60 nmol/mouse) administered intravenously significantly reduced HO activity in tumor tissue to almost 50% of the control level, i.e., tumor without treatment (Table 1). No acute lethal effect of PEG-ZnPP was observed at this dosage (n = 6, data not shown). These findings clearly demonstrate the potential of PEG-ZnPP to inhibit intratumor HO activity.

Table 1. Heme Oxygenase (HO) Activity in Tumor and Liver Tissues with or without PEG-ZnPP Administration[a]

tissue sample	dose of PEG-ZnPP (mg of ZnPP equiv/kg)	HO activity (nmol of bilirubin /mg of protein/h)
liver	0	1.32 ± 0.26
tumor	0	4.17 ± 1.07
	0.5	2.23 ± 0.54*
	1.0	2.46 ± 0.33*

[a] n = 6. *P < 0.05. ddY mice bearing S-180 solid tumor received 0.1 mL of distilled water (control) or an aqueous solution of PEG-ZnPP via the tail vein. After 24 h, tumor tissue was collected, and HO activity in the tissue was measured as described in Experimental Procedures.

DISCUSSION

The present study provides evidence that polymer-conjugated ZnPP possesses potent inhibitory activity against HO. PEG-ZnPP became highly water-soluble and showed potent inhibition of the splenic HO activity in vitro, inhibition that was equivalent to that of the well-known HO inhibitor ZnPP as its native form (Figure 8). Most important, PEG-ZnPP injected intravenously markedly suppressed intratumor HO activity (Table 1).

Chemical modifications of porphyrin structure have been found to affect the inhibitory potential of metalloporphyrin analogues. For example, reduction of vinyl groups at the C2 and C4 positions, to form mesoporphyrin, slightly increased the inhibitory potential of zinc porphyrin (*16*). Zinc deuterioporphyrin (ZnDP), which has no vinyl groups on C2 and C4, showed activity similar to that of ZnPP (*14*). Introduction of glycol moieties at positions C2 and C4 of ZnDP significantly increased the inhibitory potential, compared with the most potent HO inhibitor tin protoporphyrin, whereas introduction of sulfonic acid at these positions completely nullified the activity (*14*). In our study here with a zinc-modified porphyrin, although mechanisms of action of PEG-ZnPP remain unclear, the results obtained indicate a similarity to native ZnPP, in that PEG-ZnPP inhibited HO in a competitive manner to the substrate (hemin) concentration (Figure 8), with the zinc metal center playing an essential role (Figure 7B).

Crystal structure analysis of HO indicates that the heme substrate binds to the catalytic site of HO, called a heme pocket, by an α-methene bridge as a head, opposite a σ-methene bridge with both propionic acid residues exposed to the outer surface (*27*). This analysis may help understanding of the effect of PEG conjugation into the porphyrin ring. In this study, PEG chains were conjugated to propionic acid residues through an ethylenediamine linkage, which may not have a great effect on the binding affinity of the porphyrin portion of PEG-ZnPP to the heme pocket. The outer surface of the heme pocket is thought to play an important role in electron transfer from NADPH-cytochrome P450 reductase to the catalytic domain (*27*). Thus, binding of PEG-ZnPP to the heme pocket may disturb the interaction between HO and NADPH-cytochrome P450 reductase through steric hindrance caused by the PEG chains. Further investigation is needed to clarify these mechanistic points.

Several recent studies have demonstrated a high level of HO expression in tumor tissues: a human prostate malignant tumor (*28*), a human renal adenocarcinoma (*29*), and the AH136B rat hepatocyte solid tumor model (*8*). The remarkable inhibition of tumor growth after administration of ZnPP to AH136B-bearing rats supports a vital role for HO in tumor growth (*8*). Very recently,

we found that bilirubin could function as an antiapoptotic factor against oxidative stress-induced tumor cell apoptosis which is induced by caspase activation, and the caspase is induced by oxidative stress (S. Tanaka et al., unpublished data). In addition, expression of HO is reportedly involved in the resistance of tumor cells to oxygen radical-generating agents such as Adriamycin (*30*). Therefore, antitumor activity of PEG-ZnPP may exist as a function of decreasing the antioxidant defense capacity of tumor cells, which results in sensitizing tumor cells against host-derived oxidative stress as well as oxygen radicals generated by administration of antitumor agents.

Size exclusion chromatography analyses suggested that PEG-ZnPP spontaneously formed multimolecular associations in aqueous media, resulting in an increase in apparent molecular size, to that of bovine serum albumin (67 kDa) (Figure 5). Fluorescence spectroscopic analyses demonstrated a clear decrease in fluorescence intensity of PEG-ZnPP in buffer compared with that in chloroform (Figure 6). This phenomenon is explained by the different status of molecular associations of porphyrins in different media: porphyrin is well dispersed (monomeric dispersion) in chloroform and shows a high fluorescence intensity, whereas porphyrin has diminished fluorescence intensity in buffer because of molecular association, probably through $\pi-\pi$ stacking and hydrophobic interaction (*24*). These findings, together with size exclusion chromatography data, indicate that PEG-ZnPP forms a molecular association in neutral buffer in this way: a hydrophobic inner core consisting of porphyrin moieties covered with hydrophilic PEG chains.

Self-assembly association has been observed in a block copolymer system consisting of hydrophilic and hydrophobic polymeric chains, termed a "polymer micelle" (*31*). Core segregation in an aqueous milieu is the direct driving force for micellization and proceeds through hydrophobic interaction. Yokoyama and Kataoka and colleagues have extensively studied the physicochemical and biological importance of these polymer micellar systems and the application of these systems as anticancer drug carriers (*31*−*33*). These researchers found that polymer micelles with hydrophilic surfaces (i.e., polymers such as PEG) show an extremely prolonged circulation time in vivo because of the low excretion efficiency (renal clearance). Furthermore, these polymer conjugates and micelles preferentially accumulate in solid tumor after intravenous injection because of the unique vessel biology, the EPR effect, that operates in tumors (see recent reviews, refs *17*−*20*). Interestingly, both monoclonal antibody and normal immunoglobulin G accumulated similarly to solid tumor, indicating the EPR effect is the prime importance for tumor targeting of macromolecular drugs (*34*). In this context, the EPR effect is also relevant for PEG-ZnPP, with enhanced delivery of PEG-ZnPP to the tumor. Further studies of PEG-ZnPP targeting to tumors as well as its tissue distribution are now under way. A preliminary result shows almost complete suppression of S-180 tumor growth with PEG-ZnPP alone, by three times of iv injection (30 nmol/mouse for each time) (unpublished data).

In conclusion, we demonstrate here, for the first time, that a polymer conjugate of ZnPP effectively inhibits HO activity both in vitro and in vivo. The strategy of the synthesis described here (Figure 1) may allow us to produce functional water-soluble polymers as well as a series of metalloporphyrin analogues by alternating metal center (e.g., tin, manganese). The rational design of polymer chains may provide better organ-specific targeting capacity of HO inhibitors.

ACKNOWLEDGMENT

The authors thank Ms. Judith Gandy for editing and Ms. Chie Honda for typing the manuscript. This work was supported in part by a Grant-in-Aid for Research on Cancer from Ministry of Education, Culture, Sports and Science of Japan. S.K.S. would like to thank the Japan Society for the Promotion of Science (JSPS) for financial support through a postdoctoral fellowship.

LITERATURE CITED

(1) Schacter, B. A. (1988) Heme catabolism by heme oxygenase: Physiology, regulation, and mechanism of action. *Semin. Hematol. 25*, 349−369.

(2) Maines, M. D. (1988) Heme oxygenase: function, multiplicity, regulatory mechanisms, and clinical applications. *FASEB J. 2*, 2557−2568.

(3) Shibahara, S. (1988) Regulation of heme oxygenase gene expression. *Semin. Hematol. 25*, 370−376.

(4) Keyse, S. M., and Tyrrell, R. M. (1989) Heme oxygenase is the major 32-kDa stress protein induced in human skin fibroblasts by UVA radiation, hydrogen peroxide, and sodium arsenite. *Proc. Natl. Acad. Sci. U.S.A. 86*, 99−103.

(5) Mitani, K., Fujita, H., Fukuda, Y., Kappas, A., and Sassa, S. (1993) The role of inorganic metals and metalloporphyrins in the induction of haem oxygenase and heat-shock protein 70 in human hepatoma cells. *Biochem. J. 290*, 819−825.

(6) Motterlini, R., Foresti, R., Bassi, R., Calabrese, V., Clark, J. E., and Green, C. J. (2000) Endothelial heme oxygenase-1 induction by hypoxia. Modulation by inducible nitric oxide synthase and S-nitrosothiols. *J. Biol. Chem. 275*, 13613−13620.

(7) Foresti, R., Clark, J. E., Green, C. J., and Motterlini, R. (1997) Thiol compounds interact with nitric oxide in regulating heme oxygenase-1 induction in endothelial cells. Involvement of superoxide and peroxynitrite anions. *J. Biol. Chem. 272*, 18411−18417.

(8) Doi, K., Akaike, T., Fujii, S., Tanaka, S., Ikebe, N., Beppu, T., Shibahara, S., Ogawa, M., and Maeda, H. (1999) Induction of haem oxygenase-1 by nitric oxide and ischaemia in experimental solid tumours and implications for tumour growth. *Br. J. Cancer 80*, 1945−1954.

(9) Valaes, T., Petmezaki, S., Henschke, C., Drummond, G. S., and Kappas, A. (1994) Control of jaundice in preterm newborns by an inhibitor of bilirubin production: Studies with tinmesoporphyrin. *Pediatrics 93*, 1−11.

(10) Farrera, J. A., Jauma, A., Ribo, J. M., Peire, M. A., Parellada, P. P., Roques-Choua, S., Bienvenue, E., and Seta, P. (1994) The antioxidant role of bile pigments evaluated by chemical tests. *Bioorg. Med. Chem. 2*, 181−185.

(11) Minetti, M., Mallozzi, C., Di Stasi, A. M., and Pietraforte, D. (1998) Bilirubin is an effective antioxidant of peroxynitrite-mediated protein oxidation in human blood plasma. *Arch. Biochem. Biophys. 352*, 165−174.

(12) Dore, S., Takahashi, M., Ferris, C. D., Zakhary, R., Hester, L. D., Guastella, D., and Snyder, S. H. (1999) Bilirubin, formed by activation of heme oxygenase-2, protects neurons against oxidative stress injury. *Proc. Natl. Acad. Sci. U.S.A. 96*, 2445−2450.

(13) Drummond, G. S. (1987) Control of heme metabolism by synthetic metalloporphyrins. *Ann. N. Y. Acad. Sci. 514*, 87−95.

(14) Chernick, R. J., Martasek, P., Levere, R. D., Margreiter, R., and Abraham, N. G. (1989) Sensitivity of human tissue heme oxygenase to a new synthetic metalloporphyrin. *Hepatology 10*, 365−369.

(15) Drummond, G. S., and Kappas, A. (1981) Prevention of neonatal hyperbilirubinemia by tin protoporphyrin IX, a potent competitive inhibitor of heme oxygenase. *Proc. Natl. Acad. Sci. U.S.A. 78*, 6466−6470.

(16) Vreman, H. J., Ekstrand, B. C., and Stevenson, D. K. (1993) Selection of metalloporphyrin heme oxygenase inhibitors based on potency and photoreactivity. *Pediatric Res. 33*, 195−200.

(17) Matsumura, Y., and Maeda, H. (1986) A new concept for macromolecular therapeutics in cancer chemotherapy: mechanism of tumoritropic accumulation of proteins and the antitumor agent smancs. *Cancer Res. 46*, 6387−6392.

(18) Maeda, H. (2001) SMANCS and polymer-conjugated macromolecular drugs: advantages in cancer chemotherapy. *Adv. Drug Deliv. Rev. 46*, 169−185.

(19) Maeda, H. (2001) The enhanced permeability and retention (EPR) effect in tumor vasculature: the key role of tumor-selective macromolecular drug targeting. *Adv. Enzyme Regul. 41*, 189−207.

(20) Maeda, H., Sawa, T., and Konno, T. (2001) Mechanism of tumor-targeted delivery of macromolecular drugs, including the EPR effect in solid tumor and clinical overview of the prototype polymeric drug SMANCS. *J. Controlled Release 74*, 47−61.

(21) Stocks, S. J., Jones, A. J., Ramey, C. W., and Brooks, D. E. (1986) A fluorometric assay of the degree of modification of protein primary amines with poly(ethylene glycol). *Anal. Biochem. 154*, 232−244.

(22) Kimura, M., Matsumura, Y., Miyauchi, Y., and Maeda, H. (1988) A new tactic for the treatment of jaundice: An injectable polymer-conjugated bilirubin oxidase. *Proc. Soc. Exp. Biol. Med. 188*, 364−369.

(23) Falk, J. E. (1964) Spectra. *Porphyrins and Metalloporphyrins, Their General, Physical and Coordination Chemistry, and Laboratory Methods*, pp 72−84, Elsevier Publishing Company, Amsterdam.

(24) Nishide, H., Mihayashi, K., and Tsuchida, E. (1977) Dissociation of aggregated ferroheme complexes and protoporphyrin IX by water-soluble polymers. *Biochim. Biophys. Acta 498*, 208−214.

(25) Doi, K., Akaike, T., Horie, H., Noguchi, Y., Fujii, S., Beppu, T., Ogawa, M., and Maeda, H. (1996) Excessive production of nitric oxide in rat solid tumor and its implication in rapid tumor growth. *Cancer 77*, 1598−1604.

(26) Wu, J., Akaike, T., and Maeda, H. (1998) Modulation of enhanced vascular permeability in tumors by a bradykinin antagonist, a cyclooxygenase inhibitor, and a nitric oxide scavenger. *Cancer Res. 58*, 159−165.

(27) Schuller, D. J., Wilks, A., Ortiz de Montellano, P. R., and Poulos, T. L. (1999) Crystal structure of human heme oxygenase-1. *Nat. Struct. Biol. 6*, 860−867.

(28) Maines, M. D., and Abrahamsson, P. A. (1996) Expression of heme oxygenase-1 (HSP32) in human prostate: normal, hyperplastic, and tumor tissue distribution. *Urology 47*, 727−733.

(29) Goodman, A. I., Choudhury, M., da Silva, J. L., Schwartzman, M. L., and Abraham, N. G. (1997) Overexpression of the heme oxygenase gene in renal cell carcinoma. *Proc. Soc. Exp. Biol. Med. 214*, 54−61.

(30) Lee, T. C., and Ho, I. C. (1994) Expression of heme oxygenase in arsenic-resistant human lung adenocarcinoma cells. *Cancer Res. 54*, 1660−1664.

(31) Kwon, G. S., and Kataoka, K. (1995) Block copolymer micelles as long-circulating drug vehicles. *Adv. Drug Delivery Rev. 16*, 295−309.

(32) Kataoka, K., Matsumoto, T., Yokoyama, M., Okano, T., Sakurai, Y., Fukushima, S., Okamoto, K., and Kwon, G. S. (2000) Doxorubicin-loaded poly(ethylene glycol)-poly(β-benzyl-L-aspartate) copolymer micelles: their pharmaceutical characteristics and biological significance. *J. Controlled Release 64*, 143−153.

(33) Yokoyama, M., Fukushima, S., Uehara, R., Okamoto, K., Kataoka, K., Sakurai, Y., and Okano, T. (1998) Characterization of physical entrapment and chemical conjugation of adriamycin in polymeric micelles and their design for in vivo delivery to a solid tumor. *J. Controlled Release 50*, 79−92.

(34) Marecos E., Weissleder R., and Bogdanov A., Jr. (1998) Antibody-mediated versus nontargeted delivery in a human small cell lung carcinoma model. *Bioconjugate Chem. 9*, 184−191.

BC020010K

Specific Labeling of Polypeptides at Amino-Terminal Cysteine Residues Using Cy5-benzyl Thioester

Benjamin Schuler*,† and Lewis K. Pannell‡

Laboratory of Chemical Physics, National Institute of Diabetes and Digestive and Kidney Diseases, National Institutes of Health, Bethesda, Maryland 20892-0520 and Structural Mass Spectrometry Facility, Laboratory of Bioorganic Chemistry, National Institute of Diabetes and Digestive and Kidney Diseases, National Institutes of Health, Bethesda, Maryland 20892-0805. Received January 29, 2002; Revised Manuscript Received May 25, 2002

Even for moderately sized proteins, the multiple occurrence of cysteine and lysine residues often prevents the specific labeling of polypeptides with a single probe. To increase specificity, a method was developed to convert the commonly available succinimidyl esters of fluorescent dyes into benzyl thioesters via trimethyl aluminum-activated benzyl mercaptan. The thioester can then be reacted very specifically with polypeptides containing an N-terminal cysteine residue, forming a stable amide bond, analogous to the native chemical ligation of peptide fragments. Both reaction steps are easy to perform and proceed to high yields. The practicability of the approach was demonstrated using the popular cyanine dye Cy5 and a soluble peptide, and it is expected to be applicable to a wide range of succinimidyl esters and both chemically and recombinantly synthesized proteins. The method should dramatically facilitate the preparation of proteins for experiments requiring exact positioning of labels, for instance, Förster resonance energy transfer studies.

INTRODUCTION

A general problem in the specific conjugation of chromophores or other molecules to polypeptides is the limitation to sulfhydryls and amines as suitable reactive groups. Therefore, most commercially available fluorophores can be obtained with functionalities that allow specific labeling of cysteine or lysine residues and the free amine at the N-terminus (Haugland, 2001). However, except for small peptides, the statistical and therefore often multiple occurrence of cysteine and lysine residues in one polypeptide prevents the specific attachment of just one label to a protein. For some applications, like in vivo imaging, the degree of labeling is only of secondary importance, although it is well-known for several fluorophores that severe fluorescence quenching can occur if multiple sites on one protein are modified (Hermanson, 1996; Gruber et al., 2000). For an increasing number of experimental approaches, specificity is strictly required, for instance the use of fluorophores for FRET[1] or polarization studies both in ensemble and single molecule experiments (Weiss, 1999). So far, the only solution to this problem has been solid-phase peptide synthesis followed by labeling of the polypeptide before side chain deprotection, sometimes in combination with native chemical ligation of peptide fragments (Deniz et al., 2000). A general approach for the specific attachment of single labels to recombinantly expressed proteins has not been available, which sometimes makes extensive sequence changes necessary to eliminate cysteine and lysine residues, thus potentially interfering with the stability and function of the protein. Here we present a simple protocol for the synthesis of thioester derivatives starting from succinimidyl esters, the function most commonly employed for the specific labeling of amino groups. These thioester derivatives can then be used to label polypeptides with an aminoterminal cysteine residue in a highly specific reaction analogous to the native chemical ligation of peptides (Dawson and Kent, 2000). In this case, the necessary sequence changes are limited to the introduction of a cysteine residue at the amino terminus.

EXPERIMENTAL PROCEDURES

Materials. The peptide Cys-(Ala-Gly-Gln)$_5$-Trp-CONH$_2$ (calculated average mass 1587.6 Da, ESI-MS, positive mode, observed average mass 1587.3 ± 0.3 Da) was obtained from California Peptide Research (Napa, CA). The carboxy terminal Trp residues was included to provide an intrinsic chromophore for accurate peptide concentration determination. The control peptide Ala-Gly-Gln-Lys-Cys-Lys-Ala-Gly-Gln-Trp was synthesized using standard FastMoc chemistry with a Model 433A peptide synthesizer (Applied Biosystems) on Fmoc-Trp-resin (Biosearch Research Chemicals). After cleavage, the raw material was purified by preparative reversed phase HPLC. Fractions containing the pure peptide as confirmed by electrospray ionization mass spectroscopy (calculated mass 1075.5 Da, ESI-MS, positive mode, observed mass 1075.5 ± 0.3 Da) were lyophilized and stored at −20 °C. Cy5-succinimidyl ester was obtained from Amersham Pharmacia Biotech, hydroxylamine from Pierce. All other chemicals and solvents were from Aldrich (Milwaukee, WI). All reactions were performed at room temperature. Exposure of dye solutions to bright light was avoided. A VirTis Benchtop 3.3 freeze-dryer with a condenser temperature of −105 °C was used for

* To whom correspondence should be addressed. Laboratory of Chemical Physics. Phone: 301-402-1198. Fax: 301-496-0825. E-mail: ben.schuler@gmx.de.

† Laboratory of Chemical Physics.

‡ Structural Mass Spectrometry Facility, Laboratory of Bioorganic Chemistry.

[1] Abbreviations: DMF, dimethylformamide; ESI-MS, electrospray ionization mass spectroscopy; FRET, Förster resonance energy transfer; FABMS, fast atom bombardment mass spectroscopy, TFA, trifluoroacetic acid; NHS, *N*-hydroxysuccinimide.

10.1021/bc025509t Not subject to U.S. Copyright. Published 2002 by American Chemical Society
Published on Web 07/18/2002

lyophilization in order to minimize damage to the vacuum pump from uncondensed acetonitrile and other organic solvents.

Synthesis of Cy5-thioester. The following reactions were performed under a dry nitrogen atmosphere. It is advisable to use Hamilton syringes, ensure good ventilation, and avoid contact of the reaction mixture with water or oxygen. Benzyl mercaptan (117 μL, 1.0 mmol) was slowly added to a mixture of 0.5 mL of 2.0 M trimethylaluminum (1.0 mmol) in hexane and 2 mL of anhydrous dichloromethane cooled to 0 °C in a 4 mL glass reaction vessel while stirring. The reaction was allowed to warm to room temperature over a 20 to 30 min period. A 100 μL volume of this solution was added to 1 mg of Cy5-succinimidyl ester thoroughly dissolved in 50 μL of anhydrous DMF, yielding a clear colorless solution, and stirred for about 60 min. Solubilization of the dye in DMF at high concentration was slightly batch-dependent. Incomplete dissociation of the dye can be detected by a characteristic increase of the absorbance band at 600 nm. In this case, sonication should be continued until the absorbance spectrum of the monomeric dye is observed.

To avoid precipitation of the product under purification conditions, 20 μL portions of the reaction mixture were diluted 5-fold with DMF and added to 1 mL of a 10% acetonitrile/90% water mixture plus 0.1% TFA while stirring vigorously, centrifuged for 5 min at 10000*g* in a regular 1.5 mL polypropylene reaction vessel to clear the solution completely, and applied to a preparative reversed phase HPLC column. Fractions containing Cy5-thioester as detected by absorbance at 648 nm were combined, and the dye concentration was determined using the same molar extinction coefficient (ϵ = 250000 M^{-1} cm^{-1}) as published for the Cy5-monofunctional dye (Mujumdar et al., 1993). Portions corresponding to 10 to 100 nmol of Cy5-thioester were frozen in liquid nitrogen, lyophilized, and stored at −20 °C.

Reversed Phase HPLC. Analytical and preparative gradient HPLC were performed on a Waters 600E multisolvent delivery system equipped with a Waters 996 photodiode array absorbance detector. Preparative HPLC was run on a Vydac C4 column (214TP1022, 5 μm particle diameter, 22 × 250 mm) at a flow rate of 5 mL/min over 45 min. Analytical HPLC was performed on a Vydac C4 column (214TP54, 5 μm particle diameter, 4.6 × 250 mm) at a flow rate of 1 mL/min over 30 min. All runs used linear gradients of 0.1% TFA in 10% acetonitrile/90% water vs 0.1% TFA in 90% acetonitrile/10% water.

Peptide Labeling. The peptides were dissolved in buffer containing 6 M GdmCl, 100 mM sodium phosphate, pH 7.6, to a concentration of 1 to 2 mM, and 4% thiophenol was added. Peptide concentrations were determined using the absorbance of the single tryptophan residue present in the sequence (ϵ = 5690 M^{-1} cm^{-1} at 280 nm; Gill and von Hippel, 1989). Cy5-thioester was dissolved in DMF to a concentration of 20 mM, sonicated, and vortexed to completely dissolve the dye and then added to the peptide solution to give a final dye concentration equimolar with the peptide. The solution was vortexed to dissolve the thiol additive and then incubated at room temperature in the dark. The reactions were monitored by analytical reversed phase HPLC.

RESULTS AND DISCUSSION

The family of cyanine dyes (Mujumdar et al., 1993) has become one of the most frequently used groups of fluorophores in high sensitivity fluorescence detection and optical single molecule experiments due to their high extinction coefficients, high fluorescence quantum yields, and resistance to photobleaching. Especially Cy5 has attracted much attention due to its extremely long-wavelength fluorescence emission maximum at 667 nm, allowing excellent spectral separation in studies requiring multiccolor detection, e.g., single molecule fluorescence resonance energy transfer experiments (Ha, 2001). Currently, it is commercially available as a succinimidyl ester, which can be used for the modification of amines, and as a maleimide, which reacts with the sulfhydryl groups of cysteine residues. To increase the selectivity of protein labeling even further, we decided to devise a method that allows modification of a single position in a polypeptide chain. To this end, the succinimidyl ester of Cy5 was first converted to a benzyl thioester, which can then undergo a highly specific conjugation reaction with an N-terminal cysteine residue in a polypeptide chain.

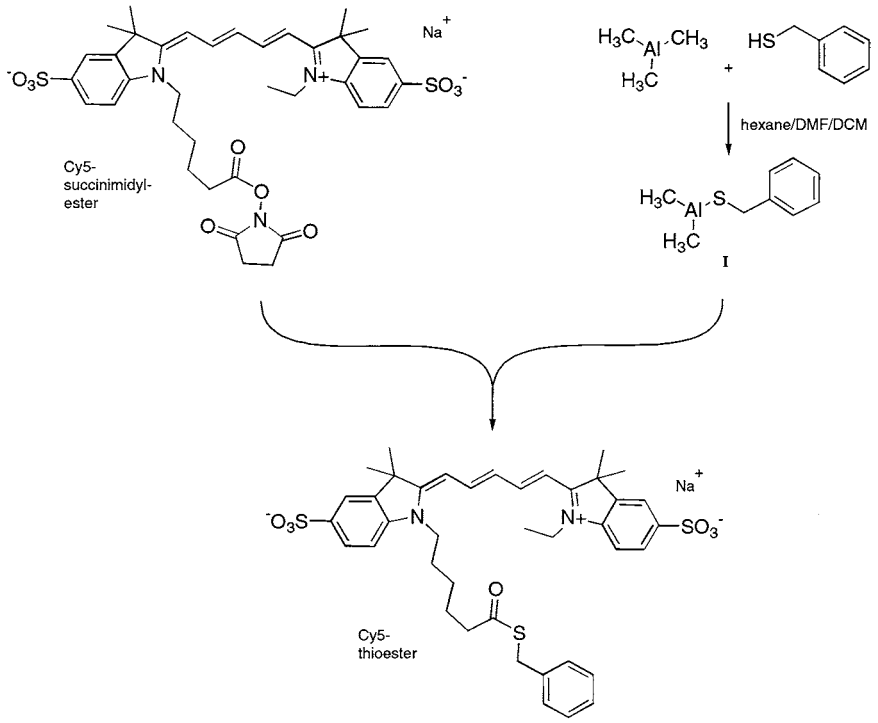
Synthesis of Cy5-thioester. The direct formation of Cy5-thioester from the succinimidyl ester and an aromatic thiol like benzyl mercaptan proceeds to only very low yields (unpublished observation) and can thus not be used for an efficient synthesis. Therefore, a two-step reaction was used to synthesize Cy5-thioester starting from the Cy5-succinimidyl ester (or N-hydroxy succinimide/NHS ester) (Scheme 1). Initially, the aluminum reagent **I** was prepared from an equimolar mixture of trimethylaluminum and benzyl mercaptan in a protocol similar to the one described by Hatch and Weinreb in 1977. These aluminum compounds are known to react with a variety of esters at room temperature to produce the respective thioesters in good yield (Corey and Beames, 1973; Cohen and Gapinski, 1978) and can be used without further purification. It was therefore attempted to use this very simple procedure to generate the benzyl thioester of Cy5.

Surprisingly, incubation of Cy5-succinimidyl ester with the reaction mixture containing compound **I** resulted in a colorless solution, possibly via interaction of the chromophore with the aluminum compounds. It regained its deep blue color after dilution in aqueous solutions or acetonitrile/water mixtures, indicating a reversible association with some component of the reaction mixture. Analytical reversed phase HPLC indicated quantitative conversion of the succinimidyl ester after 60 min. The product eluted as a single peak with a clear shift to larger elution volume (Cy5-succinimidyl ester: 14.5 mL, Cy5-thioester: 16.5 mL), as would be expected from the presence of the more hydrophobic benzyl group instead of the *N*-hydroxysuccinimidyl group. The yield of thioester as calculated from the integrated absorbance signal at 648 nm was 95 ± 5%. The calculated molecular mass of the Cy5-benzyl thioester of 762.2 Da was confirmed by ESI-MS (positive mode, $[M - H]^+$ 763.3 ± 0.2 Da) and FABMS (negative mode, $[M - H]^-$ 761.2 ± 0.2 Da). Lyophilized product retained its reactivity for months if stored at −20 °C.

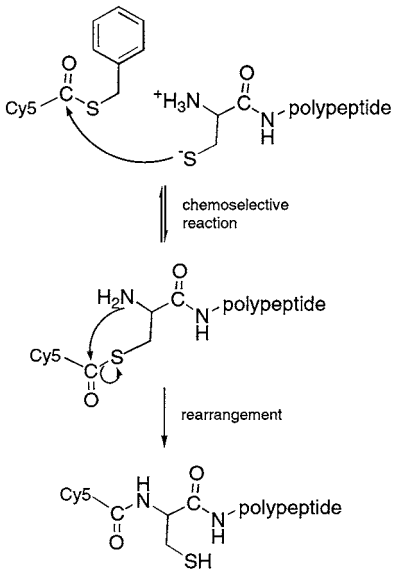
Spectroscopically, no significant differences of Cy5-thioester compared to the succinimidyl ester were detected. The absorbance maximum was at 648 nm for both derivatives, and the fluorescence quantum yield was unaltered in the thioester.

Peptide Labeling. The labeling approach described here makes use of the same chemistry as the method known as native chemical ligation (Scheme 2; Dawson et al., 1994; Dawson and Kent, 2000), which was developed for the synthesis of proteins from smaller, in particular chemically synthesized peptides. Exchange of a thioester with the thiol moiety of the N-terminal cysteine side chain gives a thioester-linked intermediate

Scheme 1. Conversion of Cy5-succinimidyl Ester to Cy5-thioester via Activation of Benzyl Mercaptan with Trimethylaluminum



Scheme 2. Probable Mechanism of the Peptide Labeling Reaction in Analogy to Native Chemical Ligation[a]



[a] Adapted from Dawson and Kent, 2000.

as the initial covalent product in a reversible reaction. Without change in the reaction conditions, a rapid intramolecular reaction occurs, forming the thermodynamically favored amide bond at the ligation site. This second step is irreversible under the conditions used, leading to the formation of the ligation product in high yield. Assuming that the mechanism of this reaction is not influenced significantly by the structure of the component containing the thioester, the reaction was adapted for the "ligation" of a polypeptide with the benzyl thioester of Cy5.

To test the reactivity of the Cy5-thioester in this type of reaction, a chemically synthesized model peptide with an N-terminal cysteine residue was used (see Experimental Procedures), and the reaction was carried out under essentially the same conditions as described for the native chemical ligation of peptides. The reaction is usually performed in 6 M GdmCl, under strongly denaturing conditions, which causes the reactivity of the N-terminal cysteine residue to be independent of the three-dimensional structures of the polypeptides in their native state. Additionally, 4% thiophenol were included in the reaction mixture. This has been shown to accelerate the reaction and increase reaction yields due to the formation of the more reactive phenyl thioester through in situ transesterification (Dawson et al., 1997). Additionally, excess thiol keeps cysteine side chains reduced and catalyzes the reversal of unproductive thioester formation. The advantage of using the less activated benzyl thioester as the primary component in the reaction mixture is its lower susceptibility to hydrolysis during storage and handling.

Analytical HPLC showed the emergence of two new components during the course of the labeling reaction eluting at volumes of 13.8 and 15.8 mL, which were identified by mass spectrometry as the labeled peptide (calculated average mass: 2226.5 Da, ESI-MS positive mode: observed average mass 2226.2 ± 0.3 Da) and Cy5-phenyl thioester (calculated mass: 748.2 Da, ESI-MS positive mode: $[M - H]^+$ 749.2 ± 0.2 Da), respectively. Figure 1 shows the kinetics of their formation at a peptide and Cy5-thioester concentration of 1.4 mM. The appearance of the signal corresponding to the labeled peptide exhibits a slight lag phase, during which a steady-state level of phenyl thioester builds up. This supports the concept of in situ transesterification of Cy5-benzyl thioester to the more reactive Cy5-phenyl thioester preceding the ligation reaction as described above. Under these conditions, a final Cy5-peptide yield of about 37% was reached after 24 h (Figure 1). At peptide and Cy5-thioester concentrations of about 2 mM, final yields of up to 68% labeled peptide were achieved. It would obviously be expected that the equilibrium can be shifted

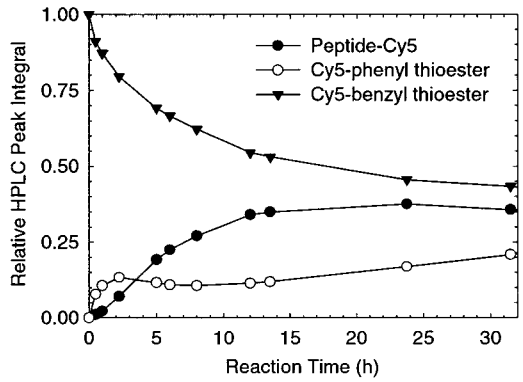


Figure 1. Kinetics of peptide labeling with Cy5-benzyl thioester at 20 °C in 6 M GdmCl, 100 mM sodium phosphate, pH 7.6, 4% thiophenol. Both peptide and Cy5-thioester concentration were 1.4 mM. Analytical HPLC runs were monitored by absorbance at 648 nm, all eluting peaks were integrated, and the relative fraction of the individual species was calculated, assuming equal extinction coefficients.

toward the products even further by increasing the concentrations of the reactants. Concentrated solutions of GdmCl (6 M) are very good solvents for unfolded proteins, allowing concentrations of up to 100 mg/mL (Rudolph et al., 1997). The solubility of the Cy5-thioester is more limited under these conditions. Even at 1 mM, it needs to be thoroughly predissolved in DMF, and a concentration of about 10% DMF must be present in the reaction mixture to avoid precipitation of the dye. At higher DMF concentrations, analytical HPLC indicated the accumulation of an unidentified side product heterogeneous in molecular mass at an elution volume of about 14.4 mL in analytical HPLC, which limits the concentration of DMF that can be used. Depending on the availability of the individual reaction components, increasing the protein concentration may thus be the more practicable approach.

After purification of the Cy5-peptide conjugate by preparative reversed phase HPLC, the lyophilized powder was redissolved in 6 M GdmCl, 100 mM sodium phosphate buffer, pH 7. The spectroscopic properties of the labeled peptide were very similar to those of the unreacted succinimidyl ester and the benzyl thioester of Cy5. The absorbance maximum was at 648 nm in 6 M GdmCl, and at 649 nm after dilution to 100 mM GdmCl. Cy5 fluorescence was quenched by 10 to 20% after attachment to the peptide (depending on GdmCl concentration), possibly due to the proximity of the tryptophan residue in the peptide. Similar effects are well-known for a variety of fluorescent dyes upon attachment to proteins and are apparently due to charge-transfer interactions with aromatic amino acid residues (Watt and Voss, 1977). Altogether, the peptide labeled by the protocol described here has the same spectroscopic properties expected from Cy5 conjugates using other commonly available chemistries such as maleimides or succinimidyl esters.

To determine the degree of specificity of the reaction for aminoterminal Cys residues, we used the peptide Ala-Gly-Gln-Lys-Cys-Lys-Ala-Gly-Gln as a control, which contains a central Cys flanked by two Lysine residues. In this case, the Cys would also be expected to form a thioester derivative with Cy5, which could then possibly be attacked by the ϵ-amino groups of the neighboring lysines, which have a p*K* value very similar to that of the α-amino group of cysteine. In a control reaction of this peptide with Cy5-benzyl thioester set up analogous to the one described above, 49% of the control peptide were found to be derivatized by the dye after 24 h, as determined by analytical HPLC and mass spectrometry (ESI-MS positive mode: observed average mass 1714.3 $\pm$ 0.3 Da). However, the mass of the thioester and a potential amide derivative are indistinguishable (calculated average mass:1714.0 Da), necessitating further characterization of the linkage. After incubation of samples of the reaction diluted 10-fold with 50 mM hydroxylamine in 6 M GdmCl, 100 mM sodium phosphate, pH 7.6 for 5 h, no labeled peptide was detectable by HPLC or mass spectrometry. This shows that no amide bonds had been formed between the ϵ-amino group of the lysine residues and Cy5. Instead, only Cy5-hydroxylamine was found as a product (calculated mass: 671.0 Da, ESI-MS positive mode: $[M - H]^+$ 671.1 $\pm$ 0.2 Da), resulting from the reaction of both the peptide-Cy5 thioester and unreacted Cy5-benzyl or Cy5-phenyl thioester with hydroxylamine. In the case of the peptide labeled at the aminoterminal Cys, on the other hand, hydroxylamine did not cause removal of the dye, as expected for an amide linkage. All the Cy5-hydroxylamine formed in this reaction originated from unreacted Cy5-benzyl and Cy5-phenyl thioester. This result demonstrates the extremely high specificity of the labeling reaction for aminoterminal Cys residues and illustrates the important role of the geometric arrangement of the α-NH_2 moiety with respect to the thioester formed in the first reaction step (Dawson et al., 1994). Additionally, it shows that dye molecules bound to internal Cys residues via thioester bonds can be removed efficiently by incubation with hydroxylamine, a step that should always be performed after labeling of proteins with the method presented here.

Applications and Limitations. In the case of native chemical ligation, the success of the reaction is largely independent of the amino acid residues neighboring the thioester moiety (Dawson and Kent, 2000). The preparation of thioesters using the activation of thiols with trimethylaluminum has been shown to work very efficiently with a wide variety of starting esters (Hatch and Weinreb, 1977). This indicates that the protocol described here will be applicable to succinimidyl esters of other fluorescent dyes and labels without major modifications. Here we focused on Cy5 because of its widespread use and its outstanding fluorescence properties.

The most important feature of the chemistry of native chemical ligation is that conjugation occurs at a unique N-terminal Cys residue. As shown above, it does not matter how many additional internal Cys residues are present in the polypeptide, and no protecting groups are necessary for any of the side-chain functional groups normally found in proteins, similar to what has been found for peptide−peptide ligation (Hackeng et al., 1997). This makes it an ideal approach for attaching a single label even to a large, recombinantly expressed protein containing many cysteine and lysine residues, a situation in which the usual labeling methods do not provide sufficient specificity.

The recombinant expression of proteins with an N-terminal cysteine residue is easily possible either by proteolytic cleavage next to a cysteine residue (Erlanson et al., 1996) or using an intein-based approach (Perler et al., 1997). The more straightforward method is usually the former. It involves constructing an expression vector in which a DNA sequence encoding a recognition site for a highly specific protease like FactorXa followed by cysteine is inserted between an upstream affinity-purification handle (e.g., maltose binding protein MBP, glutathione-S-transferase GST, or a polyhistidine tag) and the appropriate gene fragment of interest. Following

expression and affinity purification, the fusion protein is treated with the protease to give the desired Cys-polypeptide, which can be used directly in the labeling reaction described here and then purified, for instance by HPLC or size-exclusion chromatography.

One potentially limiting property of the method is that it requires refolding of the labeled protein to its native three-dimensional structure, because the reaction does not proceed efficiently in the absence of GdmCl, even for a highly soluble and unstructured peptide like the one used in this study (unpublished observation). The same requirement applies to proteins synthesized by native chemical ligation (Dawson and Kent, 2000) and to many recombinant proteins that aggregate and form inclusion bodies when expressed to high concentrations. For single domain proteins, refolding in vitro is usually simple and proceeds to very high yields, but even most larger multidomain proteins can be refolded very efficiently (Rudolph et al., 1997). Assuming that the N-terminus of the protein is surface-exposed, a serious effect of the additional cysteine or the attached dye on the folding of the protein is improbable, such that the refoldability of the protein under investigation can be investigated before any changes to the sequence are made.

An additional advantage of the dye conjugation to N-terminal cysteins using thioester derivatives is the high stability of the resulting chemical bond compared to many other labeling chemistries. As for the reaction of the commonly used succinimidyl esters with amines, an amide bond is formed, which allows storage and repeated use over an extended period of time. This is an important factor in many of the applications using bioconjugates. The conjugates are also stable in the presence of reducing agents such as dithiothreitol (unpublished observation), which can be important in the investigation of proteins or peptides with reduced cysteine residues.

In summary, the reaction of Cy5-benzyl thioester with N-terminal cysteine residues provides a reliable and uniquely specific method to label polypeptides. The synthesis of thioesters from the respective succinimidyl esters, which are available for most commonly used probes, is a simple and quantitative reaction. The protocol presented here is expected to be applicable to a wide range of labels and polypeptides, including large recombinantly expressed proteins. This will be an important tool for studies requiring the exact positioning of a label in a polypeptide containing multiple sulfhydryl or amino groups.

ACKNOWLEDGMENT

We thank John Inman and Paul Wingfield for discussion and William Eaton for his support. B.S. is supported by an Emmy Noether Fellowship from the Deutsche Forschungsgemeinschaft.

LITERATURE CITED

(1) Cohen, T., and Gapinski, R. E. (1978) The conversion of esters to phenyl thioesters by boron thiophenoxide and aluminum thiophenoxide. *Tetrahedron Lett. 45*, 4319−4322.

(2) Corey, E. J., and Beames, D. J. (1973) A method for the protection of lactones and esters against nucleophilic attack. *J. Am. Chem. Soc. 95*, 5829−5831.

(3) Dawson, P. E., Churchill, M. J., Ghadiri, M. R., and Kent, S. B. H. (1997) Modulation of reactivity in native chemical ligation through the use of thiol additives. *J. Am. Chem. Soc. 119*, 4325−4329.

(4) Dawson, P. E., and Kent, S. B. (2000) Synthesis of native proteins by chemical ligation. *Annu. Rev. Biochem. 69*, 923−960.

(5) Dawson, P. E., Muir, T. W., Clark-Lewis, I., and Kent, S. B. (1994) Synthesis of proteins by native chemical ligation. *Science 266*, 776−779.

(6) Deniz, A. A., Laurence, T. A., Beligere, G. S., Dahan, M., Martin, A. B., Chemla, D. S., Dawson, P. E., Schultz, P. G., and Weiss, S. (2000) Single-molecule protein folding: Diffusion fluorescence resonance energy transfer studies of the denaturation of chymotrypsin inhibitor 2. *Proc. Natl. Acad. Sci. U.S.A. 97*, 5179−5184.

(7) Erlanson, D. A., Chytil, M., and Verdine, G. L. (1996) The leucine zipper domain controls the orientation of AP-1 in the NFAT.AP-1.DNA complex. *Chem. Biol. 3*, 981−991.

(8) Gill, S. C., and von Hippel, P. H. (1989) Calculation of protein extinction coefficients from amino acid sequence data. *Anal. Biochem. 182*, 319−326.

(9) Gruber, H. J., Hahn, C. D., Kada, G., Riener, C. K., Harms, G. S., Ahrer, W., Dax, T. G., and Knaus, H. G. (2000) Anomalous fluorescence enhancement of Cy3 and Cy3.5 versus anomalous fluorescence loss of Cy5 and Cy7 upon covalent linking to IgG and noncovalent binding to avidin. *Bioconjugate Chem. 11*, 696−704.

(10) Ha, T. (2001) Single-molecule fluorescence resonance energy transfer. *Methods 25*, 78−86.

(11) Hackeng, T. M., Dawson, P. E., Griffin, J. H., Kent, S. B. H. (1997) Total chemical synthesis of enzymatically active human type II secretory phospholipase A2. *Proc. Natl. Acad. Sci. U.S.A.* 94, 7845−7850.

(12) Hatch, P. H., and Weinreb, S. M. (1977) Preparation of *tert*-Butyl Thioesters. *J. Org. Chem. 42*, 3960−3961.

(13) Haugland, R. (2001) *Handbook of fluorescent probes and research chemicals*, Molecular Probes, Inc., Eugene, OR

(14) Hermanson, G. T. (1996) *Bioconjugate Techniques*, Academic Press, London.

(15) Mujumdar, R. B., Ernst, L. A., Mujumdar, S. R., Lewis, C. J., and Waggoner, A. S. (1993) Cyanine dye labeling reagents: sulfoindocyanine succinimidyl esters. *Bioconjugate Chem. 4*, 105−111.

(16) Perler, F. B., Xu, M. Q., and Paulus, H. (1997) Protein splicing and autoproteolysis mechanisms. *Curr. Opin. Chem. Biol. 1*, 292−299.

(17) Rudolph, R., Böhm, G., Lilie, H., and Jaenicke, R. (1997) Folding proteins. In: *Protein Function. A Practical Approach* (T. E. Creighton, Ed.) pp 57−99, Oxford University Press, Oxford.

(18) Watt, R. M., and Voss, E. W., Jr. (1977) Mechanism of quenching of fluorescein by anti-fluorescein IgG antibodies. *Immunochemistry 14*, 533−551.

(19) Weiss, S. (1999) Fluorescence spectroscopy of single biomolecules. *Science 283*, 1676−1683.

BC025509T

Incorporation of Reversibly Cross-Linked Polyplexes into LPDII Vectors for Gene Delivery

Michael A. Gosselin, Wenjin Guo, and Robert J. Lee*

Division of Pharmaceutics and Pharmaceutical Chemistry, College of Pharmacy, The Ohio State University, Columbus, Ohio 43210. Received February 5, 2002; Revised Manuscript Received June 12, 2002

LPDII vectors are synthetic vehicles for gene delivery composed of polycation-condensed DNA complexed with anionic liposomes. In this study, we evaluated the stability and transfection properties of polyethylenimine (PEI, 25 kDa)/DNA polyplexes before and after covalent cross-linking with dithiobis(succinimidylpropionate) (DSP) or dimethyl·3,3′-dithiobispropionimidate·2HCl (DTBP), either alone or as a component of LPDII vectors. We found that cross-linking PEI/DNA polyplexes at molar ratios ≥10:1 (DSP or DTBP:PEI) stabilized these complexes against polyanion disruption, and that this effect was reversible by reduction with 20 mM dithioerythritol (DTE). Transfection studies with polyplexes cross-linked at molar ratios of 10:1−100:1 in KB cells, a folate receptor-positive oral carcinoma cell line, showed decreasing luciferase gene expression with increasing cross-linking ratio. Subsequently, polyplexes, cross-linked with DSP at a molar ratio of 10:1, were combined with anionic liposomes composed of diolein/cholesteryl hemisuccinate (CHEMS) (6:4 mol/mol), diolein/CHEMS/poly(ethylene glycol)-distearoylphosphatidylethanolamine (PEG-DSPE) (6:4:0.05 mol/mol), or diolein/CHEMS/folate-PEG-cholesterol (folate-PEG-Chol) (6:4:0.05 mol/mol) for LPDII formation. Transfection studies in KB cells showed that LPDII vectors containing cross-linked polyplexes mediated ∼2−15-fold lower gene expression than LPDII prepared with un-cross-linked polyplexes, depending on the lipid:DNA ratio. Inclusion of PEG-DSPE at 0.5 mol % appeared to further decrease transfection levels ∼2−5-fold. Compared with LPDII formulated with PEG-DSPE, LPDII incorporating 0.5 mol % folate-PEG-Chol exibited higher luciferase activities at all lipid:DNA ratios tested, achieving an ∼10-fold increase at a lipid:DNA ratio of 5. Compared with cross-linked LPDII vectors without PEG-DSPE, inclusion of folate-PEG-Chol increased luciferase acitivities 3−4-fold between lipid:DNA ratios of 1 and 5. Interestingly, inclusion of 1 mM free folate in the growth media during transfection increased transfection activity ∼3−4-fold for cross-linked LPDII vectors and LPDII containing folate-PEG-Chol, but had no effect on the transfection activity of LPDII formulated with PEG-DSPE. However, in the presence of 5 mM free folate, the luciferase activity mediated by LPDII vectors containing folate-PEG-Chol was reduced ∼6-fold. Transmission electron micrographs were also obtained to provide evidence of LPDII complex formation. Results showed that cross-linked LPDII vectors appear as roughly spherical aggregated complexes with a rather broad size distribution ranging between 300 and 800 nm.

INTRODUCTION

Nonviral delivery of gene therapy is an emerging strategy for the treatment of genetic disease, but progress is currently limited by inadequacies in the vectors available for gene transfer (*1*). The main deficiency of nonviral vectors is their relatively low in vivo gene transfer efficiency, compared with viral vectors. Therefore, research efforts have been focused on the design of nonviral vectors capable of achieving high tissue-specific gene expression with low immunogenicity and minimal toxicity. One particular strategy being evaluated to achieve these goals involves the use of LPD (liposome-entrapped polycation-condensed DNA) vectors containing covalently cross-linked polyplexes for gene delivery.

LPD vectors are synthetic vehicles for gene delivery composed of polycation-condensed DNA (polyplex) complexed with cationic or anionic liposomes via electrostatic interactions. Early LPD formulations, coined LPDI, utilized poly-L-lysine (PLL)-condensed DNA in association with cationic liposomes composed of dioleoylphosphatidylethanolamine/1-*β*-[*N*-(*N*′,*N*′-dimethylaminoethane)carbamoyl]cholesterol (DOPE/DC-Chol; 6:4 mol/mol) (*2*). Subsequent alteration of the lipid component led to the development of LPDII transfection vectors. In contrast to LPDI, LPDII vectors are prepared with anionic pH-sensitive liposomes, such as dioleoylphosphatidylethanolamine/cholesteryl hemisuccinate (DOPE/CHEMS; 6:4 mol/mol) (*3*, *4*). Since LPDII can be prepared with a net negative charge, these vectors have greater potential for receptor targeting, due to reduced nonspecific electrostatic interactions with nontarget cells. Moreover, neutral or negatively charged transfection vectors should be more compatible with the physiological environment of the systemic circulation, due to reduced interactions with components of the blood and decreased activation of the complement system (*5*).

First-generation LPDII vectors, those formulated with DOPE/CHEMS liposomes, exhibit nearly a complete loss of transfection activity in the presence of serum. Recently, our lab has developed a method to circumvent this limitation through incorporation of a novel anionic pH-sensitive liposome formulation composed of diolein/

* Address correspondence to this author at the Division of Pharmaceutics and Pharmaceutical Chemistry, College of Pharmacy, The Ohio State University, 500 W. 12th Ave., L. M. Parks Hall, Columbus, OH 43210. Phone: (614) 292-4172. FAX: (614) 292-7766. E-mail: lee.1339@osu.edu.

10.1021/bc025512c CCC: $22.00 © 2002 American Chemical Society
Published on Web 08/20/2002

CHEMS (6:4 mol/mol) (*28*). Transfection studies with LPDII vectors containing diolein/CHEMS liposomes showed that transfection activity was sustained even when transfection was carried out in the presence of 50% fetal bovine serum (*28*). In addition, it has been shown that the DNA condensing agent can consist of polycations other than PLL, such as polyethylenimine (PEI) (*6*) or cationic dendrimers (*7*), without negatively affecting gene expression.

Recent efforts in our lab have been directed toward assessing the utility of homobifunctional cross-linking reagents for the development of reducibly cross-linked polyplexes for gene delivery (*8*). Two cross-linking reagents, dithiobis(succinimidylpropionate) (DSP) and dimethyl·3,3′-dithiobispropionimidate·2HCl (DTBP) (*9*), were utilized to create relatively high molecular weight polymers, composed of cross-linked low molecular weight PEI, for polyplex assembly. DSP is a homobifunctional *N*-hydroxysuccinimide (NHS) ester-based electrophilic cross-linking reagent containing an 8-atom spacer 12 Å in length. DTBP is similar to DSP in structure and length, but contains an imidoester reactive group for amidine bond formation. The significance of the amidine bond is that net molecular charge is retained after conjugation with DTBP, whereas amide bond formation mediated by DSP results in the elimination of two positive charges. Both cross-linking reagents react with primary amines to form stable covalent bonds, and are constructed around a centrally located disulfide linkage that is cleavable with common reducing agents after conjugation (Figure 1).

In the present study, we describe a novel LPDII transfection vector containing a covalently stabilized PEI-based polyplex core complexed with anionic pH-sensitive liposomes composed of diolein/CHEMS. We hypothesized that since LPDII formation is predicated on electrostatic interactions between a cationic polymer and plasmid DNA initially, and subsequently between cationic polyplexes and anionic liposomes, that covalent cross-linking of the polyplex core, after DNA condensation, would stabilize the polyplex against dissociation due to charge competition from the anionic lipid component. Therefore, studies were performed to assess the effects of cross-linking PEI/DNA polyplexes with DSP or DTBP on polyplex stability and transfection potential, and subsequently the transfection performance of LPDII vectors containing covalently cross-linked polyplexes in folate receptor-positive KB oral cancer cells in vitro. Furthermore, additional studies were perfomed to evaluate the effect of introducing a lipid-anchored folate receptor-targeting ligand or hydrophilic poly(ethylene glycol) (PEG) coating into the LPDII formulation. Covalent attachment of folate for receptor targeting has proven to be effective in vitro for targeting liposomes (*10*−*12*) and LPDII vectors (*3*) to cancer cells which overexpress the high-affinity folate receptor. In addition, incorporation of PEG into liposome formulations has been shown to enhance tumor accumulation in vivo by reducing clearance by the reticuloendothelial system (RES), thus extending the circulation half-life (*13, 14*).

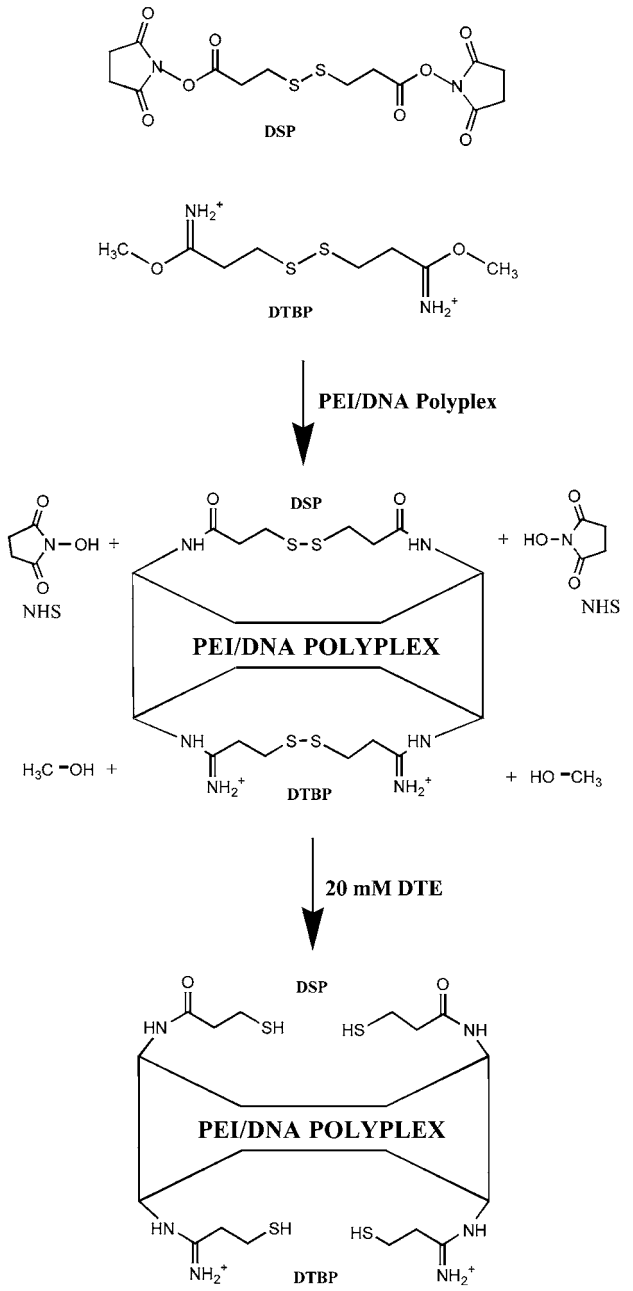


Figure 1. Proposed reaction scheme for covalent cross-linking of PEI/DNA polyplexes with cross-linking reagents DSP and DTBP. DSP cross-linking is illustrated above the schematic polyplex, while DTBP cross-linking is shown below. Also shown is the effect of disulfide bond reduction from 20 mM dithioerythritol (DTE).

MATERIALS AND METHODS

Materials. Cholesteryl hemisuccinate (CHEMS), di-9-octadecenoylglycerol (diolein, ∼85% 1,3- and 15% 1,2-isomer), dithioerythritol (DTE), bovine serum albumin (BSA) protein standards, ethidium bromide (EtBr), and other general use chemicals were purchased from Sigma Chemical Co. (St. Louis, MO). Dithiobis(succinimidylpropionate) (DSP), dimethyl·3,3′-dithiobispropionimidate·2HCl (DTBP), and bicinchoninic acid (BCA) protein assay reagents were purchased from Pierce (Rockford, IL). Anhydrous dimethyl sulfoxide (DMSO), polyethylenimine (PEI, branched, M_r ∼25 000), and poly(methacrylic acid) (PMAA, M_w ∼6500) were purchased from Aldrich Chemical Co. (Milwaukee, WI). Luciferase assay reagents and recombinant luciferase were obtained from Promega (Madison, WI). All tissue culture media and supplies were purchased from Gibco BRL (Rockville, MD).

Plasmid Preparation. pcDNA3-CMV-Luc (pLuc, 7.1 kb) plasmid DNA encoding the firefly luciferase gene under control of the cytomegalovirus enhancer/promoter was obtained as a gift from Dr. Leaf Huang at the University of Pittsburgh School of Pharmacy. Cloning and preparation of plasmid DNA were performed by propagating transformed DH5-α *E. coli* in LB media containing 50 μg/mL ampicillin, followed by isolation and

purification with a commercially available plasmid purification kit (Qiagen, Valencia, CA). Concentration and purity of DNA were assessed spectrophotometrically by measuring absorbance at 260 and 280 nm ($OD_{260}/OD_{280} \sim 1.7$). Plasmid size and integrity were confirmed using agarose gel electrophoresis (0.9% agarose gel containing 0.5 μg/mL ethidium bromide) and cleavage with the restriction endonuclease *Hin*dIII (Gibco BRL).

Cell Culture. KB cells, a folate receptor-positive human oral squamous cell carcinoma, were obtained as a gift from Dr. Philip Low at Purdue University. The cells were cultured in folate-free RPMI 1640 media supplemented with 10% fetal bovine serum (FBS), 100 units/mL penicillin, 100 μg/mL streptomycin, and 300 μg/mL L-glutamine at 37 °C in a 5% CO_2 humidified atmosphere. FBS provided the only source of folate in the growth media, which achieved physiologically relevant folate concentrations.

Liposome Preparation. Three pH-sensitive anionic liposome formulations were prepared: diolein/CHEMS (6:4 mol/mol); diolein/CHEMS/PEG ($M_r \sim 2000$)-distearoylphosphatidylethanolamine (DSPE) (6:4:0.05 mol/mol); and diolein/CHEMS/folate-PEG ($M_r \sim 3350$)-cholesterol (Chol) (6:4:0.05 mol/mol). PEG-DSPE was purchased from Avanti Polar Lipids, Inc., and folate-PEG-Chol was synthesized as described previously (*15*). Liposomes were prepared by mixing ~8−15 mg of total lipid (dissolved in chloroform as 20 mg/mL solutions) at the appropriate ratios in 13 × 100 mm glass test tubes. The chloroform was evaporated under a stream of nitrogen, and the lipids were further dried in a desiccator under vacuum for 30 min. The resulting lipid film was rehydrated with 20 mM HEPES buffer to a concentration of 3.33 mg/mL, and adjusted to pH 8.0−8.5. The suspensions were then vortexed and sonicated in a bath sonicator until the mean particle diameter was between 100 and 150 nm, as determined by dynamic light scattering using a NICOMP submicron particle sizer model 370. Lipid suspensions were stored at 4 °C until use.

Preparation of PEI/DNA Polyplexes and Stabilization by Cross-Linking. For polyplex preparation, 10 μg of pLuc DNA and the amount of PEI required to achieve the desired N/P (PEI nitrogen:DNA phosphate) ratios were each diluted in 250 μL of HEPES buffer (20 mM, pH 8.0). The PEI solution was quickly added to the DNA, and the resulting solution was then mixed and allowed to stand at room temperature (RT) for 15 min. For covalent cross-linking of polyplexes, DSP or DTBP, dissolved in anhydrous DMSO as a concentrated stock solution (1−10 mg/mL), was added to polyplexes at various concentrations depending on the desired cross-linking ratio. Cross-linking ratios are expressed as DSP:PEI molar ratios, and DMSO was kept below 5% of the total volume of polyplex solutions. After addition of the appropriate cross-linking reagent, samples were incubated at RT for 1 and 3 h for DSP and DTBP, respectively. Preparation of cross-linked and un-cross-linked polyplexes for transfection studies was performed similarly, with exceptions noted below.

Stability of Cross-Linked Polyplexes against Polyanion Disruption with PMAA. Polyplex stability against polyanion disruption was examined by measuring the ability of PMAA to restore DNA access to EtBr binding. Polyplexes with various N/P ratios containing 10 μg of pLuc DNA in 500 μL of HEPES buffer (20 mM, pH 8.0), either with or without DSP cross-linking, were diluted into 1.9 mL of 0.1× phosphate-buffered saline (PBS: 136.9 mM NaCl, 2.68 mM KCl, 8.1 mM Na_2HPO_4, 1.47 mM KH_2PO_4, pH 7.4). PMAA was added at various concentrations and incubated with polyplexes for 30 min at RT. To evaluate the reducibility of the disulfide bond present in the cross-linking reagent, 20 mM dithioerythritol (DTE) was added to some samples prior to the PMAA incubation. EtBr was present in the solution at a final concentration of 0.4 μg/mL, and EtBr fluorescence was measured on a Perkin-Elmer LS-50-B spectrometer, operated with a FTWinlab computer program (Morena Valley, CA). The excitation and emission wavelengths were set at 523 nm, with a 5 nm slit width, and 602 nm, with a 10 nm slit width, respectively.

Polyplex stability was further evaluated by agarose gel electrophoresis with EtBr staining. Polyplexes containing 1 μg of pLuc DNA prepared at a N/P ratio of 6, either with or without DSP cross-linking, were incubated with 100 μM PMAA for 30 min at RT. The reducibility of cross-linking was analyzed by including 20 mM DTE during the incubation. Half of each sample (0.5 μg of DNA) was then loaded on a 0.9% agarose gel containing 0.5 μg/mL EtBr, and run at 120 V for ~90 min.

Transfection of KB Cells with Cross-Linked Polyplexes or LPDII Vectors. For transfections, 10^5 KB cells/well were seeded in 24-well plates (Falcon) and allowed to incubate in folate-free RPMI 1640 growth media containing 10% FBS for approximately 20 h at 37 °C in a 5% CO_2 humidified atmosphere (~70−80% confluence). Immediately prior to transfection, cells were rinsed with warm PBS, and 0.5 mL of folate-free RPMI 1640 growth media was added to each well. LPDII transfections were carried out in the presence of 10% FBS, whereas polyplex transfections were performed under serum-free conditions. Transfection complexes were added to each well and incubated with KB cells for 2 or 4 h for LPDII vectors or polyplexes, respectively. After rinsing the cells with 300 μL of warm PBS, the transfection medium was replaced with 0.5 mL of fresh RPMI containing 10% FBS. A further 24 h incubation was imposed, followed by cell lysis and analysis of luciferase gene expression (see below).

PEI/pLuc polyplexes (N/P = 10) utilized for transfection were prepared as described above for EtBr fluorescence analysis, but with 1 μg of DNA and the desired amount of PEI, each dissolved in 30 μL of 20 mM HEPES buffer prior to mixing. Various concentrations of DSP or DTBP, dissolved in DMSO, were then added to polyplex solutions to achieve different cross-linking ratios, and incubated at RT for 1 or 3 h, respectively. DMSO comprised less than 5% of the solution volume.

LPDII vectors, containing PEI/pLuc polyplexes (N/P = 4) and diolein/CHEMS liposomes, were prepared as described above by diluting 3 μg of DNA and the desired amount of PEI, each in 50 μL of HEPES buffer (20 mM, pH 8.0) prior to mixing. For cross-linking, 2.5 μL of DSP in DMSO (0.1 mg/mL) was added to each sample, lightly vortexed, and incubated at RT for 1 h. Various concentratons of diolein/CHEMS liposomes in 50 μL of HEPES buffer were then added to each sample, depending on the desired lipid:DNA ratio, and allowed to stand at RT for 15 min. Finally, 50 μL (1 μg of DNA/well) of the resulting solution was added to each well of a 24-well plate to evaluate transfection potential.

To analyze luciferase expression, the growth medium was removed from each well, and the cells were rinsed twice with cold PBS. Next, 200 μL of ice-cold lysis buffer (0.5% Triton X-100, 100 mM Tris-HCl, 2 mM EDTA, pH 7.8) was added to each well, followed by incubation on ice for 30 min. The lysate was then removed and centrifuged for 1 min at 13 000 rpm. Finally, 10 μL of cellular lysate was mixed with 50 μL of luciferase substrate (Promega), and the luminescence was measured for 10 s on a Mini-Lum luminometer (Bioscan, Inc.,

Washington, DC). Relative light units were standardized for protein concentration as determined by the BCA protein determination assay using bovine serum albumin standards. Luciferase activity is also expressed as femtomoles of luciferase per milligram of protein, determined from a standard curve of luciferase activity using recombinant luciferase.

Negative Stain Transmission Electron Microscopy (TEM). DSP cross-linked polyplexes (10:1) and LPDII particles were prepared as described above at an N/P ratio of 6 and a lipid:DNA ratio of 5 (w/w), respectively, with each sample containing 10 μg of plasmid DNA. An aqueous solution of bacitracin was prepared at a concentration of 200 mg/mL, and diluted to a working strength of 10 mg/mL. An aqueous 1% uranyl acetate solution was also prepared, and was filtered and centrifuged to remove any particulate matter before use. Samples were prepared by placing a 200 mesh size Formvar-coated copper grid on a drop of bacitracin solution (10 mg/mL) for 1 min, before wicking away excess solution from the grid with filter paper. Next, each grid was placed in contact with the appropriate sample for 3 min, and the excess liquid was again wicked away with filter paper. The grid was then subjected to two brief sequential rinses by placing the grid on a drop of water and wicking away excess fluid. Finally, the grid was incubated in 1% uranyl acetate solution for 2.5 min, excess liquid was removed, and the grid was allowed to dry at RT for 5 min. Electron micrographs were obtained at 60 kV at 100000× magnification for polyplexes and diolein/CHEMS liposomes or 45000× magnification for LPDII particles.

RESULTS

To evaluate the effect of cross-linking on polyplex-mediated transfection of KB cells in vitro, 25 kDa PEI/pLuc DNA polyplexes were prepared at an N/P (PEI nitrogen:DNA phosphate) ratio of 10, followed by cross-linking with DSP or DTBP at various cross-linker:PEI molar ratios, as described under Materials and Methods. Specifically, cross-linking ratios of 0, 10, 20, 50, and 100:1 were evaluated. An N/P ratio of 10 was chosen based on previous studies showing efficient gene expression at this ratio (*16*). Figure 2 shows that as the cross-linking ratio with DSP or DTBP increases from 0 (control) to 100:1, luciferase gene expression decreases by approximately 3−4 orders of magnitude. The data further show that transfection is relatively independent of the reagent used for cross-linking, with nearly identical luciferase activity at a cross-linking ratio of 10. However, at higher cross-linking ratios (≥20), slightly better gene expression was observed with polyplexes cross-linked with DTBP.

Our next goal was to evaluate the stability of polyplexes, either with or without covalent stabilization by cross-linking, in the presence of a competing polyanion. Our initial stability analysis was performed on conventional PEI/DNA polyplexes prepared at a variety of N/P ratios, namely, 0 (DNA only), 2, 3, 5, and 10. These polyplexes were exposed to various concentrations of poly(methacrylic acid) (PMAA), an organic polyanion, ranging from 0 to 100 μM, followed by addition of ethidium bromide (EtBr) and quantitative fluorescence measurements. Detection of EtBr fluorescence is an indication of DNA being accessible for EtBr binding due to polyplex dissociation, or at least local decondensation of DNA. The EtBr fluorescence observed upon incubation with free plasmid DNA, in the absence of PEI and PMAA, was used as a reference control (i.e., 100% relative fluorescence). As seen in Figure 3, the addition of PMAA to free plasmid DNA, at concentrations up to 100 μM, had virtually no effect on fluorescence (N/P = 0). The results also show that in the absence of PMAA, EtBr fluorescence for all polyplexes decreases to ~10% of control, with the exception of polyplexes prepared at an N/P ratio of 2. Polyplexes prepared at this ratio are known to cause incomplete condensation of DNA due to inadequate charge neutralization, which led to an EtBr fluorescence reading of ~30%. As the concentration of PMAA was increased, progressively higher fluorescence readings were observed for all polyplexes, with values eventually approaching 100% of control at a PMAA concentration of 100 μM. Furthermore, polyplexes prepared at higher N/P ratios appeared more resistant to polyanion disruption, which can be seen in Figure 3 from the lower fluorescence readings obtained at high N/P ratios and low PMAA concentrations.

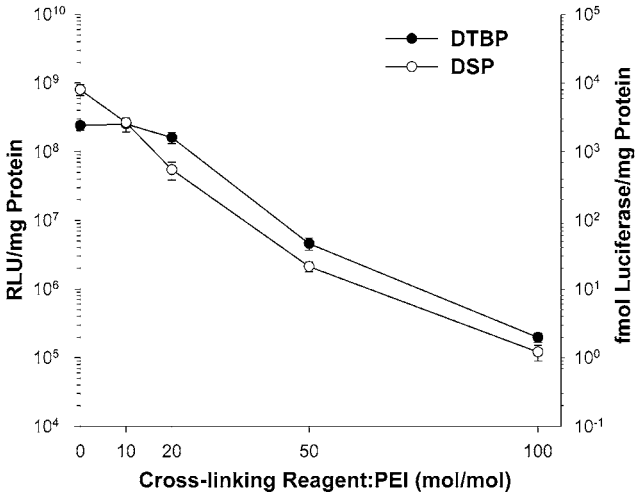


Figure 2. Effect of reducible cross-linking on the transfection activities of PEI/DNA polyplexes. Polyplexes were prepared at an N/P ratio of 10. Polyplexes were then cross-linked with DSP or DTBP at cross-linker:PEI molar ratios of 0, 10, 20, 50, and 100:1. The transfection activity of the covalently cross-linked polyplexes was then evaluated in KB cells in vitro. Cells were exposed to transfection vectors for 4 h in serum-free media, and luciferase activity was assayed 24 h later.

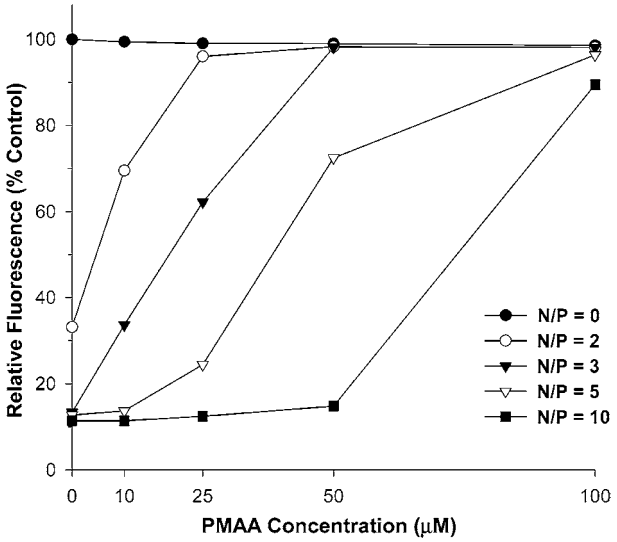


Figure 3. EtBr fluorescence from interactions with PEI/DNA polyplexes in the presence of a competing polyanion (PMAA). Polyplexes were prepared at N/P ratios of 0, 2, 3, 5, and 10, and exposed to various concentrations of PMAA up to 100 μM. EtBr was added to each sample at a concentration of 0.4 μg/mL, and fluorescence was measured at excitation and emission wavelengths of 523 and 602 nm, respectively.

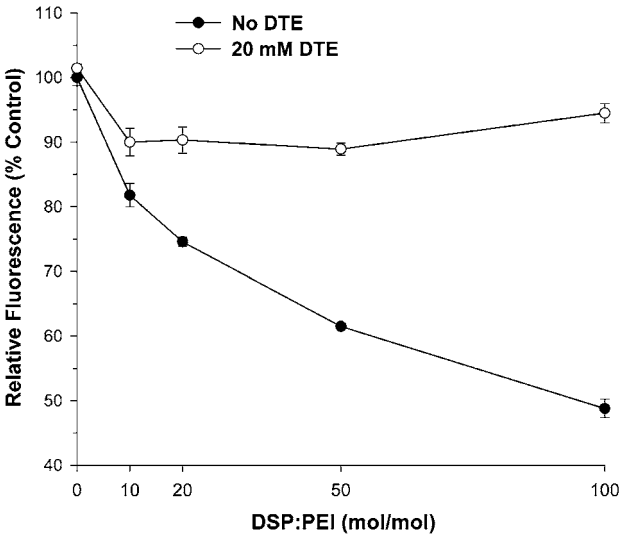


Figure 4. EtBr fluorescence from interactions with DSP cross-linked PEI/DNA polyplexes in the presence of 100 μM PMAA, with or without disulfide bond reduction with DTE. Polyplexes were prepared at a N/P ratio of 6, and cross-linked with DSP at DSP:PEI molar ratios of 0, 10, 20, 50, and 100:1. Cross-linked polyplexes were then exposed to 100 μM PMAA for 30 min, with or without 20 mM DTE. EtBr was added to each sample at a concentration of 0.4 μg/mL, and fluorescence was measured at excitation and emission wavelengths of 523 and 602 nm, respectively.

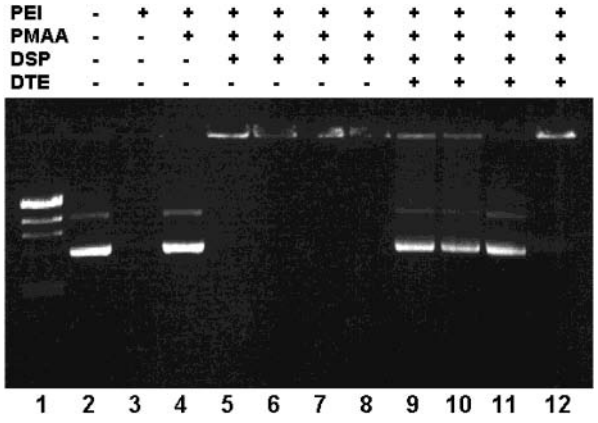


Figure 5. Stability of covalently cross-linked polyplexes analyzed by agarose gel electrophoresis. Polyplexes were prepared at a N/P ratio of 6, and cross-linked with DSP at DSP:PEI molar ratios of 10, 20, 50, and 100:1. Cross-linked polyplexes were then exposed to 100 μM PMAA for 30 min, with or without 20 mM DTE, and analyzed by agarose gel electrophoresis (0.5 μg of DNA/lane). Lane 1 is *Hin*dIII-digested phage λ DNA, used as a size marker; lane 2 is pLuc DNA only; lane 3 is PEI/pLuc polyplex (N/P = 6); lane 4 is PEI/pLuc polyplex with 100 μM PMAA; lanes 5−8 are PEI/pLuc polyplexes cross-linked with DSP at 10:1, 20:1, 50:1, and 100:1, respectively, with 100 μM PMAA; lanes 9−12 are identical to lanes 5−8, except for the addition of 20 mM DTE.

Since polyplex stability is apparently compromised by the presence of a competing polyanion, experiments were then performed to evaluate the consequence of cross-linking PEI/DNA polyplexes with DSP, at various DSP:PEI molar ratios, before exposure to PMAA. Polyplexes were prepared at an N/P ratio of 6, and were then cross-linked with DSP at molar ratios of 10, 20, 50, and 100:1. PMAA was included in all samples at a concentration of 100 μM, since that concentration restored nearly 100% EtBr fluorescence when incubated with un-cross-linked polyplexes. As seen in Figure 4, the results show that as the DSP:PEI cross-linking ratio is increased, PEI/DNA polyplexes become increasingly resistant to polyanion challenge, exhibited by the decrease in EtBr fluorescence. In fact, fluorescence readings for polyplexes cross-linked at a ratio of 100:1 decreased by more than 50%. However, when 20 mM dithioerythritol (DTE) was introduced to promote reduction of the intramolecular disulfide bond present in DSP, effectively reversing stabilization, EtBr fluorescence was restored to ~90% of control for all samples.

To obtain visual evidence, to supplement the quantitative fluorescence readings in Figure 4, agarose gel electrophoresis was performed. The underlying principle was the same as for fluorometric analysis (i.e., EtBr fluorescence is restored upon polyplex dissociation or local decondensation of DNA); however, visualization by electrophoresis provides a basis to discern between dissociation or local DNA decondensation. As seen in lane 4 of Figure 5, incubation of un-cross-linked polyplexes (N/P = 6) with 100 μM PMAA results in polyplex dissociation, as evidenced by the DNA migration through the gel. The results also show (lanes 5−8) that despite DSP cross-linking, some EtBr fluorescence can be seen in the loading wells, with the intensity slightly decreasing as the cross-linking ratio is increased. Lanes 9−12 illustrate the effect of DTE reduction of disulfide bonds on DNA migration and EtBr fluorescence. At cross-linking ratios of 10, 20, and 50:1 (lanes 9−11), pLuc DNA regained its fluorescence and was free to migrate through the gel. However, at 100:1 (lane 12), fluorescence was mainly visible in the loading well, with a faint band appearing where plasmid DNA would be expected, despite DTE reduction.

Transfection studies were performed to compare the transfection performance between LPDII vectors either with or without covalent cross-linking of polyplexes in KB cells in vitro. Polyplexes were prepared at an N/P ratio of 4, yielding condensed particles with a slight positive charge. Where DSP cross-linking was employed, polyplexes were cross-linked at a molar ratio of 10:1 (DSP:PEI). Figure 6 displays the transfection results from a series of four different LPDII formulations, along with results from a 1 mM free folate competition study for the folate receptor-targeted formulation. Specifically, the formulations tested included conventional diolein/CHEMS LPDII particles without DSP cross-linking, LPDII including covalently cross-linked polyplexes, LPDII prepared with PEG containing liposomes, and receptor-targeted LPDII particles containing a lipid-anchored folate moiety. As indicated, all polyplexes were PEI/DNA complexes, and the anionic liposome component was composed of diolein/CHEMS prepared at a molar ratio of 6:4. Inclusion of PEG-DSPE, for steric stabilization, or folate-PEG-Chol, for receptor targeting, was achieved by adding 0.5 mol % of the appropriate lipid-anchored molecule during preparation of the diolein/CHEMS liposomes.

Figure 6A,B depicts the luciferase gene expression achieved with each LPDII formulation as a function of lipid:DNA (w/w) ratio. Transfection levels mediated by all formulations increased initially, before achieving peak luciferase activities at a lipid:DNA ratio of 2.5. All formulations then exhibited a subsequent decrease in luciferase activity at a lipid:DNA ratio of 5. At ratios beyond 5, luciferase activities appeared to level off, with the exception of LPDII prepared without DSP cross-linking, which displayed steadily decreasing luciferase activities with increasing lipid:DNA ratio. From a comparison of conventional diolein/CHEMS LPDII vectors and LPDII that include DSP cross-linked polyplexes, it can be seen that cross-linking at a ratio of 10:1 led to an ~2−16-fold decrease in gene expression at lipid:DNA

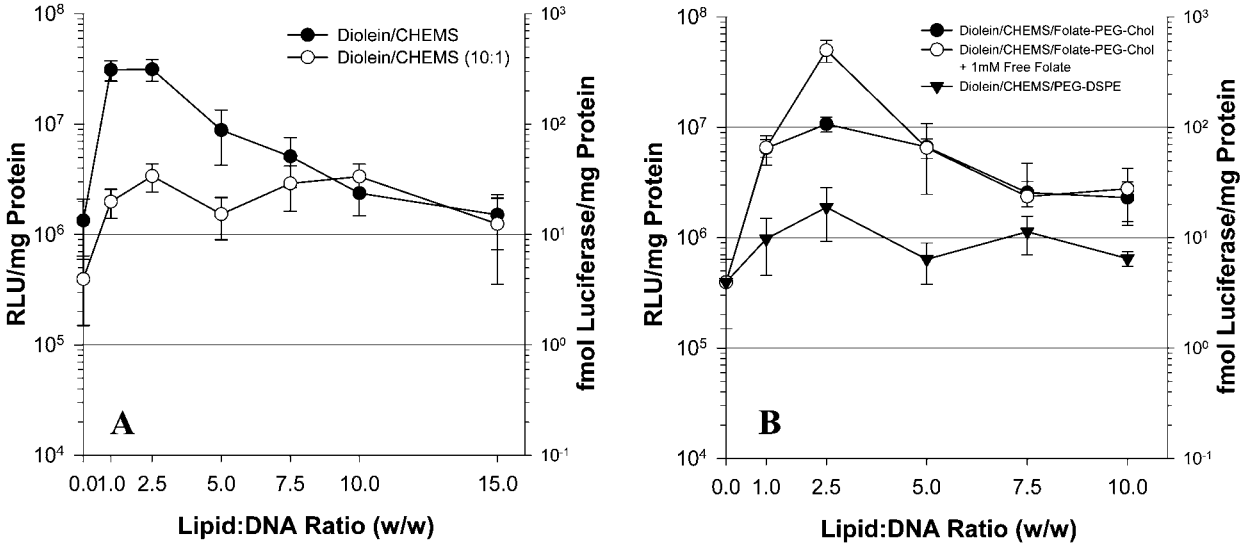


Figure 6. Transfection of KB cells with various LPDII formulations as a function of lipid:DNA ratio. The lipid:DNA ratios tested were 0 (cross-linked or un-cross-linked polyplex alone), 2.5, 5, 7.5, 10, and 15. All formulations contain PEI/pLuc DNA polyplexes prepared at a N/P ratio of 4. Except where noted in the figure, all polyplexes were cross-linked with DSP at a DSP:PEI molar ratio of 10:1. Diolein/CHEMS liposomes were prepared at a molar ratio of 6:4, and where indicated, 0.5 mol % PEG-DSPE or folate-PEG-Chol was included.

ratios ≤7.5, but that similar luciferase activities were achieved at ratios beyond 10. Inclusion of PEG-DSPE at 0.5 mol % appeared to consistently hinder transfection levels, reducing luciferase activities ∼2−5-fold, compared to LPDII containing cross-linked polyplexes prepared without PEG-DSPE. In contrast, LPDII containing folate-PEG-Chol exibited higher gene expression at all lipid:DNA ratios tested, compared with LPDII vectors containing PEG-DSPE. In fact, luciferase activities for LPDII containing folate-PEG-Chol were ∼5−10 times greater than the PEG-DSPE formulation at lipid:DNA ratios between 1 and 5, with decreasing differences at higher ratios. Compared with cross-linked LPDII without PEG-DSPE, inclusion of 0.5 mol % folate-PEG-Chol increased luciferase acitivities 3−4-fold between lipid:DNA ratios of 1 and 5, and, again, led to decreasing differences at high lipid:DNA ratios. Inclusion of 1 mM free folate in the growth media during transfection with LPDII vectors containing folate-PEG-Chol led to luciferase activities nearly identical to those achieved in the absence of free folate, with the exception of an ∼4.5-fold increase in activity at a lipid:DNA ratio of 2.5.

In contrast to the observed results, luciferase activities were expected to decrease for LPDII containing folate-PEG-Chol in the presence of 1 mM free folate, due to competition for the folate receptor. However, it has been shown previously that addition of free folate to the growth media during transfection increases transfection levels mediated by PEI/DNA polyplexes (*17*). Therefore, transfection studies to compare the effect of free folate on gene expression were repeated with conventional diolein/CHEMS LPDII vectors, LPDII formulated with PEG-DSPE, and LPDII containing folate-PEG-Chol, all containing DSP cross-linked polyplexes at a ratio of 10:1 (DSP:PEI). Free folate was included in the growth media at a concentration of 1 mM, as in earlier transfection studies, with additional concentrations of 2 and 5 mM included for the folate receptor-targeted formulation. Figure 7 shows that inclusion of 1 mM free folate in the growth media increased luciferase activities 3−4-fold for diolein/CHEMS LPDII and LPDII containing folate-PEG-Chol, but had little effect on LPDII containing PEG-DSPE. Furthermore, increasing the free folate concentration to 2 mM during transfection with folate receptor-targeted LPDII vectors decreased luciferase activity, in comparison to 1 mM free folate, and achieved similar transfection levels to those observed in the absence of free folate. Increasing the free folate concentration to 5 mM led to a further decrease in luciferase activity, which was ∼6-fold lower than transfection levels obtained without free folate present in the growth media.

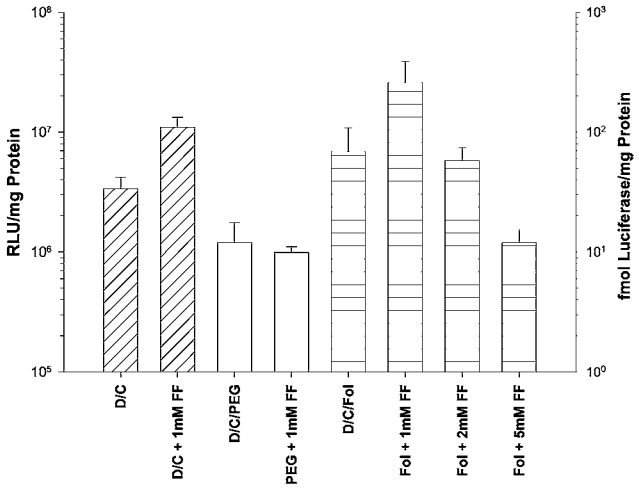


Figure 7. Effect of free folate on the transfection activity of the LPDII formulations containing DSP cross-linked polyplexes. Free folate (FF) was included at 1, 2, or 5 mM in the growth media during transfection. All polyplexes used in LPDII preparation were cross-linked with DSP at a DSP:PEI molar ratio of 10:1. The three LPDII formulations tested include diolein/CHEMS (D/C), diolein/CHEMS/PEG-DSPE (D/C/PEG or PEG), and diolein/CHEMS/folate-PEG-Chol (D/C/Fol or Fol). Diolein/CHEMS liposomes were prepared at a molar ratio of 6:4, and where indicated, 0.5 mol % PEG-DSPE or folate-PEG-Chol was included.

Finally, negative stain transmission electron microscopy was performed in order to obtain evidence confirming the association between diolein/CHEMS liposomes and cross-linked polyplexes. Samples were prepared as described under Materials and Methods, and the results are illustrated in Figure 8. Panel A shows PEI/DNA polyplexes cross-linked with DSP at a molar ratio of 10:1. Polyplexes appeared as small dark spherical particles

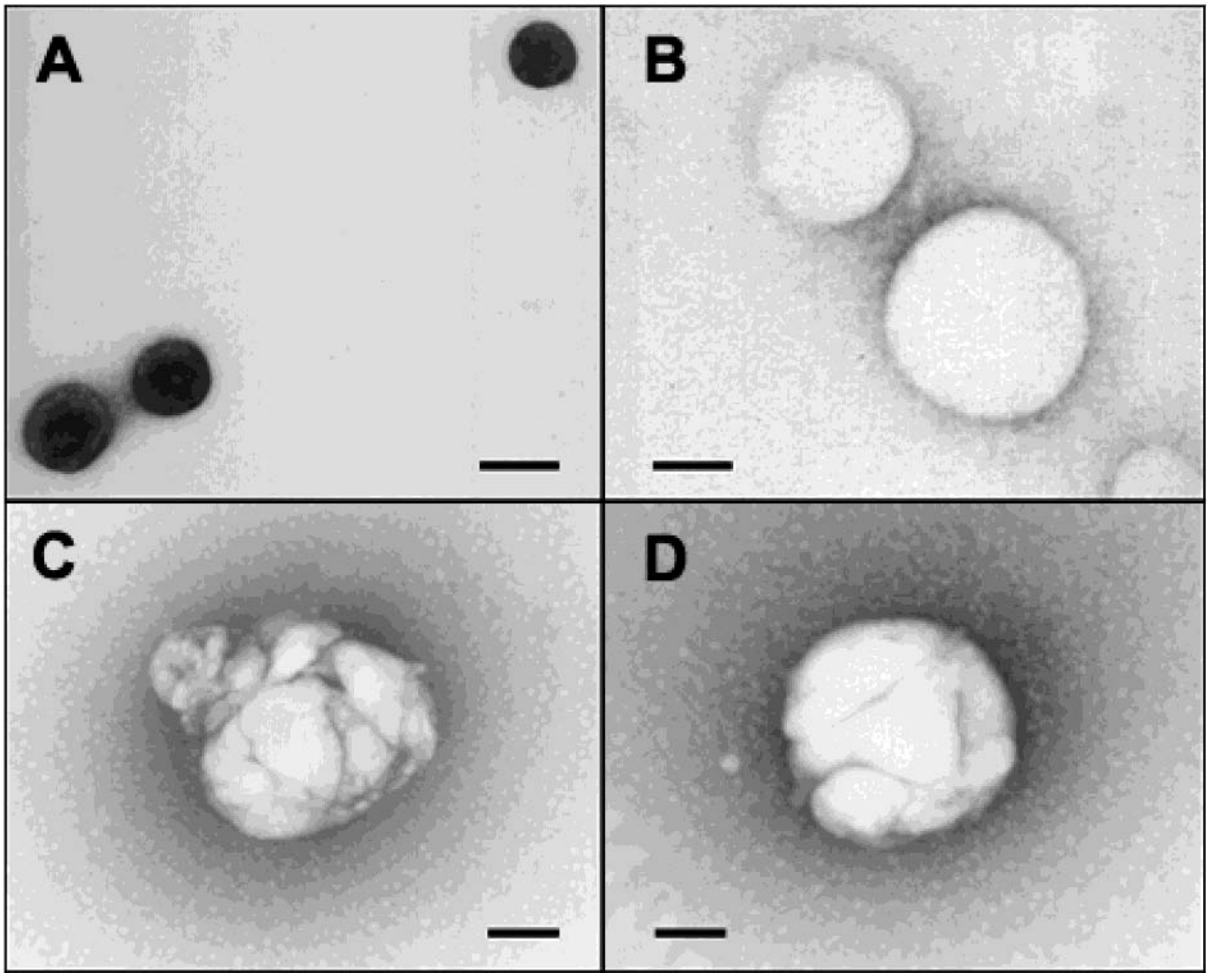


Figure 8. Negative stain transmission electron microscopy. DSP cross-linked polyplexes (10:1) and LPDII particles were prepared at an N/P ratio of 6 and a lipid:DNA ratio of 5 (w/w), respectively, with each sample containing 10 μg of plasmid DNA. Electron micrographs were obtained at 60 kV. (Panel A) DSP cross-linked PEI/DNA polyplexes at 100000× magnification. (Panel B) Diolein/CHEMS liposomes (6:4, mol/mol) at 100000× magnification. (Panels C and D) DSP cross-linked LPDII vectors at 45000× magnification. In panels A and B, the bar = 100 nm; in panels C and D, the bar = 200 nm.

ranging in diameter from ~70 to 100 nm. Panel B shows diolein/CHEMS liposomes prepared at a molar ratio of 6:4, which appeared as white spherical particles having a diameter between 100 and 250 nm. Finally, panels C and D depict LPDII particles formed at a lipid:DNA ratio of 5. These complexes were manifested as aggregated structures, roughly spherical in shape, with diameters ranging between 300 and 800 nm.

DISCUSSION

Currently, the primary limitation in the development of clinically useful nonviral gene therapy protocols is the lack of safe and efficient nonviral vectors for in vivo gene delivery. Here, we evaluate a novel approach to improve the stability and transfection potential of polyplex- and LPDII-mediated gene transfer. We have shown that cross-linking PEI/DNA polyplexes stabilizes these complexes against polyanion disruption, and that cross-linking is reversible upon reduction by DTE. We further demonstrated that LPDII transfection vectors mediate variable levels of transfection, depending on the presence of DSP cross-linking and the incorporation of PEG-DSPE or folate-PEG-Chol as a component of the diolein/CHEMS liposomes used for LPDII formation. It was also observed that the presence of 1 mM free folate in the transfection media has a surprisingly beneficial effect on transfection, but that this effect was dose-dependent for LPDII vectors containing folate-PEG-Chol. Finally, we provide evidence, by way of electron micrographs, that diolein/CHEMS liposomes and DSP cross-linked polyplexes form aggregated complexes under our experimental conditions.

Initial transfection studies with cross-linked polyplexes were performed to assess the effects of DSP or DTBP cross-linking of PEI/DNA polyplexes on luciferase reporter gene expression. Branched, 25 kDa PEI was used as the condensing agent because previous studies indicate that PEI is an effective transfection agent both in vitro (*16, 18*) and in vivo (*19*−*21*). Transfection results indicated that cross-linking polyplexes with DSP or DTBP, after DNA condensation, leads to a reduction in gene expression in KB cells, with significantly lower luciferase activities (3−4 orders of magnitude) observed at higher cross-linking ratios. These results were not surprising, since increasing the cross-linking ratio would be expected to increase polyplex stability. While increased stability may be beneficial prior to cellular uptake, ultimately the DNA has to be accessible by the nuclear transcription machinery, thus mandating polyplex dissociation and DNA decondensation preceding gene expression. High cross-linking ratios would require more extensive intracellular reduction of disulfide bonds present in the cross-linking reagents in order to reverse stabilization, which may ultimately limit gene expression.

Comparing the two cross-linking reagents, we found transfection activity to be slightly higher with DTBP cross-linked polyplexes, at cross-linking ratios ≥20.

However, in our experience, DTBP is less reactive toward PEI, compared with DSP, under the chosen reaction conditions. The slightly greater transfection levels mediated by DTBP cross-linked polyplexes at higher cross-linking ratios may be a reflection of less extensive cross-linking, and consequently a lower reduction in gene expression. Alternatively, the retention of positive charge after DTBP cross-linking may promote more efficient gene transfer. In the end, DSP was used to cross-link polyplexes for inclusion in LPDII vectors because cross-linking with DSP can be accomplished with a shorter reaction time, and it is possible to monitor the appearance of NHS from DSP spectrophotometrically to gauge reaction progress. In addition, there were relatively insignificant differences in transfection levels between DSP and DTBP cross-linked polyplexes, especially at a cross-linking ratio of 10:1.

While it was important to understand the effect of cross-linking on transfection levels, it was equally important to investigate the stability of cross-linked polyplexes, to justify covalent stabilization. Therefore, polyplex stability was evaluated in the presence of a competing polyanion, namely, PMAA, which should mimic the effect of polyanionic liposomes on polyplex integrity during LPDII formation. Anionic liposomes themselves were not used as the competing polyanion because lipid concentrations utilized for LPDII formulation interfered with EtBr fluorescence detection. Initially, we were interested in determining whether un-cross-linked polyplexes were susceptible to dissociation from polyanion disruption as a function of N/P ratio. Therefore, polyplexes were prepared at several N/P ratios, and incubated with various PMAA concentrations, followed by EtBr fluorescence analysis. This analysis is based on the concept that a large increase in fluorescence is observed upon intercalation of DNA by the phenanthridium moiety of EtBr (*22*). Condensed DNA, like the DNA present in polyplexes prepared with a net positive charge, will exclude EtBr from intercalating between base pairs, thus providing minimal fluorescence. In contrast, uncondensed DNA, resulting from local decondensation of DNA or polyplex dissociation, will permit EtBr intercalation to yield a sharp increase in EtBr fluorescence. The increase in fluorescence should be proportional to the amount of DNA available for intercalation. Our results showed that polyplexes exposed to PMAA exhibit an increase in EtBr fluorescence, and that fluorescence was directly related to PMAA concentration and inversely related to the N/P ratio. This result suggests that conventional polyplexes are susceptible to polyanion disruption, and that polyplexes prepared with large N/P ratios are more stable than those prepared with low ratios.

We anticipated that reversible cross-linking would stabilize polyplexes, and that reduction of the intramolecular disulfide bond present in DSP would restore polyplex susceptibility to polyanion disruption. Therefore, we cross-linked PEI/DNA polyplexes at various DSP:PEI molar ratios and evaluated EtBr fluorescence in the presence of 100 μM PMAA, either with or without 20 mM DTE. The results showed that increasing the cross-linking ratio leads to a decrease in EtBr fluorescence, suggesting more stable polyplexes at higher cross-linking ratios. Reduction with 20 mM DTE was found to restore fluorescence levels to ~90% of control. While these results are useful in demonstrating covalent stabilization with DSP, and we believe it is reasonable to infer that polyanionic liposomes would have a similar effect on polyplex integrity, we recognize that polymers such as PMAA may interact somewhat differently with polyplexes, and, therefore, these results do not provide actual evidence regarding the interaction between polyplexes and diolein/CHEMS liposomes. Nevertheless, although these results were considered positive in terms of demonstrating stabilization and cross-linking reversibility, they also introduced a dilemma in choosing the appropriate cross-linking ratio of polyplexes for incorporation into LPDII transfection particles. On one hand, earlier transfection results with cross-linked polyplexes showed a minimal reduction in gene expression if the cross-linking ratio was relatively low. However, the stability results showed that EtBr fluorescence was still ~75−80% of control for complexes cross-linked to the same extent. Therefore, the degree by which DSP might have contributed to cross-linking stability was unclear.

Consequently, polyanion disruption of cross-linked polyplexes was repeated as described above, but the samples were instead visualized by agarose gel electrophoresis. This assay provided a basis to distinguish between polyplex dissociation and local decondensation of DNA. With polyplex dissociation, free plasmid DNA would be expected to migrate through the gel at a rate proportional to its size, but with local decondensation of DNA, fluorescence would likely be observed in the loading well. This stems from the fact that DNA migration through the agarose gel is based on electrostatic attraction between polyanionic DNA and a positively charged anode. However, when DNA is present in the form of a polyplex, the negative charge is neutralized by the cationic polymer, consequently precluding its migration through the gel. In addition, the size increase resulting from the presence of the high molecular weight PEI in the polyplex would further hinder DNA migration. Ultimately, the electrophoresis results suggested that low cross-linking ratios are adequate to prevent dissociation, but will not completely prevent local DNA decondensation. This was shown in Figure 5 by DNA migration with un-cross-linked polyplexes in the presence of 100 μM PMAA (lane 4), but after cross-linking with DSP, fluorescence was only visible in the loading wells (lanes 5−9). These results provided a logical basis for cross-linking polyplexes at a DSP:PEI molar ratio of 10:1 for incorporation into LPDII vectors. Specifically, this ratio was chosen because preliminary transfection results using polyplexes cross-linked at 10:1 showed a minimal reduction in gene expression, compared with un-cross-linked polyplexes, and agarose gel analysis further showed that these complexes remained associated even with relatively strong polyanion challenge (100 μM PMAA).

To delineate the effects on gene expression, the transfection potential of four related LPDII vectors was evaluated in KB cells in vitro. PEI/DNA polyplexes were formed at an N/P ratio of 4, and, where indicated, cross-linked with DSP at a DSP:PEI molar ratio of 10:1. An N/P ratio of 4 was utilized because this ratio mediates complete condensation of plasmid DNA to form positively charged complexes, yet minimizes free PEI in solution not participating in polyplex formation (*19, 23*). If free PEI were present in the solution after polyplex formation, DSP could react preferentially with free PEI and reduce polyplex stabilization by consuming DSP. The anionic liposomes used for LPDII formation were composed of a novel serum-resistant formulation consisting of diolein/CHEMS (6:4 mol/mol). The four LPDII formulations tested for luciferase reporter gene expression included conventional LPDII vectors without DSP cross-linking, LPDII including covalently cross-linked polyplexes, LPDII prepared with PEG-containing liposomes, and receptor-targeted LPDII vectors containing a lipid-anchored folate moiety.

From the transfection results shown in Figure 6A, the first comparison can be made between LPDII vectors containing DSP cross-linked polyplexes and those without cross-linking. The transfection results show that LPDII vectors with covalent cross-linking mediated lower luciferase activities at lipid:DNA ratios ≤7.5, yet similar transfection levels at lipid:DNA ratios ≥10. Results from the transfection studies using cross-linked polyplexes for gene transfer, illustrated in Figure 2, showed that DSP cross-linking inhibited gene expression, and this effect may contribute to the observed decrease in transfection activity mediated by LPDII vectors containing cross-linked polyplexes. Alternatively, LPDII particle formation may be deleteriously altered by the presence of DSP, or more likely by the elimination of positive charges on PEI after reaction with DSP, since LPDII particles largely depend on electrostatic attraction for complex formation. LPDII vectors prepared in the absence of cross-linking achieve a peak luciferase activity at a lipid:DNA ratio of 2.5, and then display steadily decreasing transfection levels. In contrast, LPDII containing cross-linked polyplexes display a more level luciferase activity profile over the entire range of lipid:DNA ratios. This observation suggests that particle assembly may be saturable at low lipid:DNA ratios, again possibly due to the elimination of positive charge after DSP cross-linking. Despite the disparity in transfection activity between these two formulations, LPDII particles containing cross-linked polyplexes did mediate significant levels of transfection, and, therefore, may prove useful under in vivo conditions where complex stability could be a more dominant factor.

Inclusion of PEG-DSPE at 0.5 mol % into the LPDII formulation containing DSP cross-linking resulted in a further reduction in gene expression at all lipid:DNA ratios tested, compared with the cross-linked formulation in the absence of PEG-DSPE. This effect may be the result of reduced interaction between polyplexes and liposomes, or a reduction in cellular uptake. Since particle size is an important determinant for in vitro transfection, with smaller particles achieving lower transfection, it could also be postulated that incorporation of PEG-DSPE reduces any interactions between transfection complexes in solution that might cause an increase in particle size, thus reducing gene expression.

The contribution of folate receptor targeting, through incorporation of 0.5 mol % folate-PEG-Chol, can be seen in Figure 6B by comparing the transfection activity of folate receptor-targeted LPDII vectors with LPDII formulated with PEG-DSPE. Based on that comparison, the data suggest that attachment of folate to the distal end of a PEG linker does mediate an increase in luciferase activity at all lipid:DNA ratios, but especially at ratios ≤5. However, to confirm that folate receptor-mediated endocytosis contributes to increased gene expression, a folate receptor competition study was performed by introducing 1 mM free folate in the growth media during transfection. The results, also shown in Figure 6B, were inconsistent with our expectations that luciferase activity would decrease in the presence of competition by free folate. However, as indicated earlier, previous studies in our lab have shown that inclusion of free folate in the growth media during transfection increases the transfection activity of PEI-based polyplexes. In effect, transfection studies were performed to determine if free folate had a similar effect on LPDII particles prepared at a lipid:DNA ratio of 2.5. We found that inclusion of 1 mM free folate in the growth media during transfection increased the transfection activity of LPDII containing cross-linked polyplexes and LPDII containing folate-PEG-Chol, but had little effect on the transfection activity of LPDII formulated with PEG-DSPE. To determine if higher concentrations of free folate could inhibit the transfection activity of folate receptor-targeted LPDII vectors, similar transfection studies were performed in the presence of 2 and 5 mM free folate. The results showed that luciferase activity was inversely related to the concentration of free folate in the growth media. The mechanism responsible for the increased gene expression in the presence of 1 mM free folate has not been determined, and it is curious that LPDII containing PEG-DSPE were relatively unaffected. Regardless, we conclude that inclusion of folate-PEG-Chol in LPDII vectors mediates greater luciferase activities compared with LPDII formulated with PEG-DSPE. Furthermore, the presence of 1 mM free folate in the growth media during transfection apparently has a beneficial effect on transfection activity, and, therefore, does not offer conclusive evidence that increased gene expression from inclusion of folate-PEG-Chol is truly receptor-mediated. The fact that higher concentrations of folate do reduce observed transfection levels is consistent with expectations, but 5 mM free folate is orders of magnitude greater than the K_d for folic acid, $10^{-9}-10^{-10}$ M. Although the concentrations cited below are ∼10-times lower, similar observations have been reported previously that show the IC_{50} for folate receptor-targeted liposomes is 0.2−0.4 mM (*10*, *15*). The high binding strength of these liposomes has been attributed, in part, to the high binding affinity achieved by multivalent attachment of multiple targeting ligands.

Finally, negative stain transmission electron micrographs of DSP cross-linked polyplexes, diolein/CHEMS liposomes, and LPDII vectors containing covalently cross-linked polyplexes were obtained to gather size and structural information, and to provide evidence of LPDII complex assembly. The images shown in Figure 8A display cross-linked polyplexes that appear as dark spherical particles having a diameter between 70 and 100 nm. This micrograph is consistent with previously published observations of PEI-based polyplexes (*24*, *25*). Figure 8B displays images of diolein/CHEMS liposomes, which appear as white spherical particles smaller than 250 nm. To our knowledge, these are the first published images of diolein/CHEMS liposomes. Figure 8C,D portrays LPDII particles composed of diolein/CHEMS liposomes and cross-linked polyplexes. The diameter of these particles was somewhat variable, but was generally larger than either the polyplexes or the liposomes. The LPDII particles displayed in Figure 8 had diameters between 500 and 700 nm. This size information suggests that the increased transfection performance of LPDII particles may in part be a result of increased particle size, which would promote sedimentation of transfection particles in vitro. In addition, these images appear consistent with the hypothesis that LPDII complexes are composed of aggregated complexes of polyplex and anionic liposomes. However, since the polyplex would theoretically be located inside this complex, and the LPDII particles were not visualized in cross section, it cannot be ruled out that the particles observed in Figure 8C,D are simply aggregates of liposomes. The fact that these types of particles were not observed when viewing diolein/CHEMS liposomes, however, does provide some support to the notion that the complexes observed in Figure 8 are LPDII particles.

To our knowledge, this is the first report describing covalent stabilization of PEI/DNA polyplexes for subsequent inclusion in LPDII vectors. The concept of reversible cross-linking via reducible disulfide bonds has been investigated by other groups, but only in the context of

polyplex-mediated gene transfer (*26*, *27*). The underlying theory behind this approach is that reversible disulfide cross-linking will confer stability to transfection complexes until intracellular reduction of the disulfide bonds takes place. If the transfection vectors are in fact able to gain access to the reducing environment of the cytoplasm, it is plausible that reduction of these bonds will occur, possibly through interaction with reduced glutathione. Accordingly, the data presented here indicate that the effects of cross-linking are reversible upon disulfide bond reduction with DTE in vitro. Furthermore, our results show that polyplexes are more stable in terms of dissociation in the presence of a competing polyanion after DSP cross-linking, and that inclusion of cross-linked polyplexes into LPDII vectors mediates variable transfection, depending on the lipid:DNA ratio and the presence of PEG-DSPE or folate-PEG-Chol. The combination of serum resistance conferred by the diolein/CHEMS liposomes and the increased stability owed to cross-linking may make LPDII vectors incorporating these features more stable in the systemic circulation after intravenous delivery. This improved stability may ultimately translate into higher gene expression and improved therapeutic effects. Based on these results, further evaluation of the transfection properties of covalently cross-linked LPDII vectors in an animal model is warranted.

ACKNOWLEDGMENT

In addition to a grant (RPG-99-097-01-MGO) from the American Cancer Society National Division, this work was partly supported by a development grant from the Parenteral Drug Association (PDA).

LITERATURE CITED

(1) Pouton, C. W., and Seymore, L. W. (2001) Key issues in nonviral gene delivery. *Adv. Drug Deliv. Rev. 46*, 187−203.
(2) Gao, X., and Huang, L. (1996) Potentiation of Cationic Liposome-Mediated Gene Delivery by Polycations. *Biochemistry 35*, 1027−1036.
(3) Lee, R. J., and Huang, L. (1996) Folate-targeted, Anionic Liposome-entrapped Polylysine-condensed DNA for Tumor Cell-specific Gene Transfer. *J. Biol. Chem. 271* (14), 8481−8487.
(4) Li, S., and Huang, L. (1997) Targeted Delivery of Antisense Oligodeoxynucleotides by LPDII. *J. Liposome Res. 7* (1), 63−75.
(5) Plank, C., Mechtler, K., Szoka, F. C., and Wagner, E. (1996) Activation of the Complement System by Synthetic DNA Complexes: A Potential Barrier for Intravenous Gene Delivery. *Hum. Gene Ther. 7*, 1437−1446.
(6) Guo, W., and Lee, R. J. (2000) Efficient Gene Delivery Using Anionic Liposome-Complexed Polyplexes (LPDII). *Biosci. Rep. 20* (5), 419−431.
(7) Reddy, J. A., Dean, D., Kennedy, M. D., and Low, P. S. (1999) Optimization of Folate-Conjugated Liposomal Vectors for Folate Receptor-Mediated Gene Therapy. *J. Pharm. Sci. 88* (11), 1112−1118.
(8) Gosselin, M. A., Guo, W., and Lee, R. J. (2001) Efficient Gene Transfer Using Reversibly Cross-Linked Low Molecular Weight Polyethylenimine. *Bioconjugate Chem. 12*, 989−994.
(9) Hermanson, G. T. (1996) Homobifunctional Cross-linkers. *Bioconjuagate Techniques*, pp 187−227, Academic Press, Inc., San Diego.
(10) Lee, R. J., and Low, P. S. (1994) Delivery of Liposomes into Cultured KB Cells via Folate Receptor-mediated Endocytosis. *J. Biol. Chem. 269* (5), 3198−3204.
(11) Gabizon, A., Horowitz, A. T., Goren, D., Tzemach, D., Mandelbaum-Shavit, F., Qazen, M. M., and Zalipsky, S. (1999) Targeting Folate Receptor with Folate Linked to Extremities of Poly(ethylene glycol)-Grafted Liposomes: In Vitro Studies. *Bioconjugate Chem. 10*, 289−298.
(12) Gosselin, M. A., and Lee, R. J. (2002) Folate receptor-targeted liposomes as vectors for therapeutic agnets. *Biotechnology Annual Review* (El-Gewely, M. R., Ed.) Vol. 8, pp 103−131, Elsevier, Amsterdam.
(13) Drummond, D. C., Meyer, O., Hong, K., Kirpotin, D. B., and Papahadjopoulos, D. (1999) Optimizing Liposomes for Delivery of Chemotherapeutic Agents to Solid Tumors. *Pharmacol. Rev. 51* (4), 691−743.
(14) Gabizon, A., and Papahadjopoulos, D. (1988) Liposome formulations with prolonged circulation time in blood and enhanced uptake by tumors. *Proc. Natl. Acad. Sci. U.S.A. 85*, 6949−6953.
(15) Guo, W., Lee, T., Sudimack, J., and Lee, R. J. (2000) Receptor-specific Delivery of Liposomes via Folate-PEG-Chol. *J. Liposome Res. 10* (2,3), 179−195.
(16) Boussif, O., Lezoualc'h, F., Zanta, M. A., Mergny, M. D., Scherman, D., Demeneix, B., and Behr, J. P. (1995) A versatile vector for gene and oligonucleotide transfer into cells in culture and in vivo: Polyethylenimine. *Proc. Natl. Acad. Sci. U.S.A. 92*, 7297−7301.
(17) Guo, W., and Lee, R. J. (2001) Efficient gene delivery via noncovalent complexes of folic acid and polyethylenimine. *J. Controlled Release 77*, 131−138.
(18) Godbey, W. T., Wu, K. K., and Mikos, A. G. (1999) Poly(ethylenimine) and its role in gene delivery. *J. Controlled Release 60*, 149−160.
(19) Zou, S. M., Erbacher, P., Remy, J. S., and Behr, J. P. (2000) Systemic linear polyethylenimine (L-PEI)-mediated gene delivery in the mouse. *J. Gene Med. 2*, 128−134.
(20) Coll, J. L., Chollet, P., Brambilla, E., Desplanques, D., Behr, J. P., and Favrot, M. (1999) In Vivo Delivery to Tumors of DNA Complexed with Linear Polyethylenimine. *Hum. Gene Ther. 10*, 1659−1666.
(21) Abdallah, B., Hassan, A., Benoist, C., Goula, D., Behr, J. P., and Demeneix, B. A. (1996) A Powerful Nonviral Vector for In Vivo Gene Transfer into the Adult Mammalian Brain: Polyethylenimine. *Hum. Gene Ther. 7*, 1947−1954.
(22) Geall, A. J., and Blagbrough, I. S. (2000) Rapid and sensitive ethidium bromide fluorescence quenching assay of polyamine conjugate−DNA interactions for the analysis of lipoplex formation in gene therapy. *J. Pharm. Biomed. Anal. 22*, 849−859.
(23) Erbacher, P., Bettinger, T., Belguise-Valladier, P., Zou, S., Coll, J.-L., Behr, J.-P., and Remy, J.-S. (1999) Transfection and Physical Properties of Various Saccharide, Poly(ethylene glycol), and Antibody-Derivatized Polyethylenimines (PEI). *J. Gene Med. 1*, 210−222.
(24) Remy, J.-S., Abdallah, B., Zanta, M. A., Boussif, O., Behr, J.-P., and Demeneix, B. (1998) Gene transfer with lipospermines and polyethylenimines. *Adv. Drug Deliv. Rev. 30*, 85−95.
(25) Pollard, H., Remy, J.-S., Loussouarn, G., Demolombe, S., Behr, J.-P., and Escande, D. (1998) Polyethylenimine but Not Cationic Lipids Promotes Transgene Delivery to the Nucleus in Mammalian Cells. *J. Biol. Chem. 273*, 7507−7511.
(26) Trubetskoy, V. S., Loomis, A., Slattum, P. M., Hagstrom, J. E., Budker, V. G., and Wolff, J. A. (1999) Caged DNA Does Not Aggregate in High Ionic Strength Solutions. *Bioconjugate Chem. 10*, 624−628.
(27) McKenzie, D. L., Smiley, E., Kwok, K. Y., and Rice, K. G. (2000) Low Molecular Weight Disulfide Cross-Linking Peptides as Nonviral Gene Delivery Carriers. *Bioconjugate Chem. 11*, 901−909.
(28) Shi, G., Guo, W., Stephenson, S. M., and Lee, R. J. (2002) Efficient intracellular drug and gene delivery using folate receptor-targeted pH-sensitive liposomes composed of cationic/anionic lipid combinations. *J. Controlled Release 80*, 309−319.

BC025512C

Pretargeting for Cancer Radioimmunotherapy with Bispecific Antibodies: Role of the Bispecific Antibody's Valency for the Tumor Target Antigen

H. Karacay,[†] R. M. Sharkey,*[,†] W. J. McBride,[‡] G. L. Griffiths,[‡] Z. Qu,[‡] K. Chang,[§] H. J. Hansen,[‡] and D. M. Goldenberg[†]

Center for Molecular Medicine and Immunology, Belleville, New Jersey 07109, Immunomedics, Inc., Morris Plains, New Jersey 07950, and IBC Pharmaceuticals, Inc. Morris Plains, New Jersey 07950.
Received February 28, 2002; Revised Manuscript Received June 3, 2002

The use of a divalent effector molecule improves bispecific antibody (bsMAb) pretargeting by enabling the cross-linking of monovalently bound bsMAb on the cell surface, thereby increasing the functional affinity of a bsMAb. In this work, it was determined if a bsMAb with divalency for the primary target antigen would improve bsMAb pretargeting of a divalent hapten. The pretargeting of a ^{99m}Tc-labeled divalent DTPA-peptide, IMP-192, using a bsMAb prepared by chemically coupling two Fab′ fragments, one with monovalent specificity to the primary target antigen, carcinoembryonic antigen (CEA), and to indium-loaded DTPA [DTPA(In)], was compared to two other bsMAbs, both with divalency to CEA. One conjugate used the whole anti-CEA IgG, while the other used the anti-CEA F(ab′)$_2$ fragment to make bsMAbs that had divalency to CEA, but with different molecular weights to affect their pharmacokinetic behavior. The rate of bsMAb blood clearance was a function of molecular weight (IgG × Fab′ < F(ab′)$_2$ × Fab′ < Fab′ × Fab′ conjugate). The IgG × Fab′ bsMAb conjugate had the highest uptake and longest retention in the tumor. However, when used for pretargeting, the F(ab′)$_2$ × Fab′ conjugate allowed for superior tumor accretion of the ^{99m}Tc-IMP-192 peptide, because its more rapid clearance from the blood enabled early intervention with the radiolabeled peptide when tumor uptake of the bsMAb was at its peak. Excellent peptide targeting was also seen with the Fab′ × Fab′ conjugate, albeit tumor uptake was lower than with the F(ab′)$_2$ × Fab′ conjugate. Because the IgG × Fab′ bsMAb cleared from the blood so slowly, when the peptide was given at the time of its maximum tumor accretion, the peptide was captured predominantly by the bsMAb in the blood. Several strategies were explored to reduce the IgG × Fab′ bsMAb remaining in the blood to take advantage of its 3−4-fold higher tumor accretion than the other bsMAb conjugates. A number of agents were tested, including those that could clear the bsMAb from the blood (e.g., galactosylated or nongalactosylated anti-id antibody) and those that could block the anti-DTPA(In) binding arm [e.g., DTPA(In), divalent-DTPA(In) peptide, and DTPA coupled to bovine serum albumin (BSA) or IgG]. When clearing agents were given 65 h after the IgG × Fab′ conjugate (time of maximum tumor accretion for this bsMAb), ^{99m}Tc-IMP-192 levels in the blood were significantly reduced, but a majority of the peptide localized in the liver. Increasing the interval between the clearing agent and the time the peptide was given to allow for further processing of the bsMAb-clearing agent complex did not improve targeting. At the dose and level of substitution tested, galacosylated BSA-DTPA(In) was cleared too quickly to be an effective blocking agent, but BSA- and IgG-DTPA(In) conjugates were able to reduce the uptake of the ^{99m}Tc-IMP-192 in the blood and liver. Tumor/nontumor ratios compared favorably for the radiolabeled peptide using the IgG × Fab′/blocking agent combination and the F(ab′)$_2$ × Fab′ (no clearing/blocking agent), and peptide uptake 3 h after the blocking agent even exceeded that of the F(ab′)$_2$ × Fab′. However, this higher level of peptide in the tumor was not sustained over 24 h, and actually decreased to levels lower than that seen with the F(ab′)$_2$ × Fab′ by this time. These results demonstrate that divalency of a bsMAb to its primary target antigen can lead to higher tumor accretion by a pretargeted divalent peptide, but that the pharmacokinetic behavior of the bsMAb also needs to be optimized to allow for its clearance from the blood. Otherwise, blocking agents will need to be developed to reduce unwanted peptide uptake in normal tissues.

INTRODUCTION

Pretargeting methods have become an important strategy for conveying targeting specificity to isotopes and drugs for a variety of applications, including tumor imaging and therapy (Chang et al., 2002; Goldenberg, 2002). Unlike direct targeting methods that rely on the association of the effector molecule directly with the antibody, a pretargeting method separates the effector molecule (e.g., isotope or drug) from the primary targeting agent (Goodwin and Meares, 1999). The primary targeting agent in a pretargeting method must have binding specificity for the target and bear a receptor capable of binding to the effector molecule. The vast majority of primary targeting agents used in pretargeting

* To whom correspondence should be addressed. Phone: (973) 844-7121. Fax: (973) 844-7020.
[†] Center for Molecular Medicine and Immunology.
[‡] Immunomedics, Inc..
[§] IBC Pharmaceuticals, Inc..

10.1021/bc0200172 CCC: $22.00 © 2002 American Chemical Society
Published on Web 08/31/2002

have been antibodies directed to different tumor antigens. Many effector-binding systems employed by pretargeting methods have used the avidin/streptavidin−biotin recognition system, while others have used bispecific antibodies (bsMAbs)[1] and even oligonuclide binding systems (Bos et al., 1994; Cremonesi et al., 1999; Goodwin et al., 1992; Hnatowich et al., 1987; Paganelli et al., 1988; Rusckowski et al., 1997a; Stickney et al., 1991).

As initially evaluated by Hnatowich et al. (1987), the avidin−biotin pretargeting method can be configured according to several strategies, but two approaches have prevailed. One approach uses a streptavidin-conjugated antibody as the primary targeting agent, which is then followed by a derivatized biotin as the effector carrier. A third step is used to facilitate the clearance of the primary streptavidin-antibody conjugate from the blood prior to administering the biotin-effector molecule (Axworthy et al., 1994, 2000). The other strategy uses a biotin-conjugated antibody as the primary targeting agent (Cremonesi et al., 1999; Paganelli et al., 1988). After allowing sufficient time for the antibody-biotin conjugate to localize the tumor, avidin is given. Because it is highly glycosylated, avidin acts primarily as a clearing agent, binding to the biotin-antibody in the blood and removing it to the liver. Although some avidin could also localize to the tumor-bound biotin-conjugated antibody, streptavidin is also given. Streptavidin is not glycosylated, and therefore it has a longer residence time in the blood, which allows more time for it to localize to the biotin-conjugated antibody. Finally, the biotin-effector molecule is given, which then localizes to the biotin-conjugated antibody containing the streptavidin/avidin bridge. Both of these approaches have been used clinically and shown to produce high tumor/background ratios (Breitz et al., 2000; Magnani et al., 2000), and have even been used therapeutically (Breitz et al., 1999, 2000; Knox et al., 2000; Paganelli et al., 2001).

Another pretargeting approach relies on the use of bsMAb. The principal behind pretargeting was initially described by Reardon et al. (1985), who suggested that antibodies could be composed of dual binding specificity, one to a particular target and the other capable of binding a chelate. This group subsequently showed that the passive accumulation of an anti-chelate antibody in mice bearing the transplantable KHJJ tumor (Goodwin et al., 1988) could be used to target a radiolabeled chelate. A "chase" step using transferrin-conjugated chelate was introduced prior to administering the radiolabeled chelate as a means of reducing the anti-chelate antibody in the blood. More recently, this same passive targeting model was used to show the feasibility of pretargeting ^{90}Y-labeled chelate for therapy (Lubic et al., 2001). Subsequently, tumor-targeting specificity has been achieved with bispecific antibodies directed against tumor markers and, for the most part for the targeting of radionuclides by means of antibodies to metal chelators. Bispecific antibodies can be conveniently produced by chemically combining Fab′ fragments of one antibody with specificity to a tumor antigen with another antibody specific for the effector molecule. Effector molecules initially were monovalent metal-binding chelates (Goodwin et al., 1988), but then it was shown that a divalent effector molecule greatly enhances the residence time of the effector molecule at the site (Le Doussal et al., 1989). This method was called an affinity enhancement system (AES), since the bivalent effector molecule bridges two bispecific antibodies on the tumor cell surface, thereby increasing their functionally affinity [reviewed by Chang et al. (2002)]. Others have subsequently verified the advantage of a divalent effector molecule over a monovalent form (Goodwin et al., 1992; Boerman et al., 1999).

The bsMAb and avidin−biotin pretargeting approaches have their advantages and disadvantages. For example, the avidin−biotin system is subject to potential blockade by endogenous biotin. This is especially problematic when testing in mouse models, since mice have nearly 10 times the amount of biotin in their serum as humans (Rosebrough and Hartley, 1995; Rusckowski et al., 1997b). Using a biotin-deficient diet, the stores of biotin in their bodies can be minimized. Another potential problem with the avidin−biotin strategy is the immunogenic nature of avidin and streptavidin. Antibodies to avidin and streptavidin can develop, which could affect the subsequent use of these agents after an initial exposure. The greatest advantage of the avidin−biotin approach is the strength of the binding between avidin or streptavidin and biotin, such that once biotin is bound to avidin or streptavidin, these complexes are highly stable (Hnatowich et al., 1987). In contrast, the bispecific antibody approach combined with a monovalent effector molecule has a higher dissociation rate. Using a divalent effector molecule greatly enhances the cell binding but, still, antibody dissociation rates are typically several log units higher than that of the avidin−biotin complex (e.g., $K_D = 10^{-15}$ M for biotin with streptavidin/avidin vs 10^{-9} M most typically found for antigen−antibody complexes). In this regard, it is important to emphasize that the residence time in the tumor for both bsMAb and avidin/biotin pretargeting approaches is limited by the agent bound to the cell target, i.e., the affinity of an antibody.

Since many of the bispecific antibody-pretargeting studies have used bsMAbs with monovalent binding arms (i.e., chemically cross-linked Fab′ × Fab′ or hybrid IgG produced from a quadroma), the bridging of two bsMAbs by a divalent effector molecule was an important binding enhancement for these complexes at the primary target site. However, would a bispecific antibody with divalent binding to the primary target antigen increase tumor uptake of a radiolabeled peptide while maintaining excellent tumor/nontumor ratios typically associated with pretargeting methods? Increasing the amount of the peptide targeting to a tumor would be highly advantageous for use in radioimmunotherapy (RAIT). To test this hypothesis, a pretargeting system involving bispecific antibodies to carcinoembryonic antigen (CEA) and diethylenetriaminepentaacetic acid (DTPA), together with a divalent indium-loaded DTPA [(In)DTPA] peptide capable of binding ^{99m}Tc, was used (Karacay et al., 2000). Bispecific antibodies were prepared by chemically conjugating the IgG, F(ab′)$_2$, and Fab′ component of a humanized antibody to CEA to the Fab′ fragment of a chimeric anti-(In)DTPA antibody (c734). A ^{99m}Tc-labeled divalent (In)DTPA peptide (IMP-192) was used as the

[1] Abbreviations: AES, affinity enhancement system; BSA, bovine serum albumin; bsMAb, bispecific antibody; c734, chimeric 734 anti-(In)DTPA antibody; CEA, carcinoembryonic antigen; DTPA, diethylenetriaminepentaacetic acid; gal rWI2, galactosylated rWI2; hMN-14, humanized MN-14 anti-CEA antibody; HPLC, high-pressure liquid chromatography; HSA, human serum albumin; IACUC, Institutional Animal Care and Use Committee; ID, injected dose; (In)DTPA, indium-loaded DTPA; RAIT, radioimmunotherapy; RF, reverse phase; rWI2, a rat anti-idiotype monoclonal antibody to MN-14; s.c., subcutaneously; SDS−PAGE, sodium dodecyl sulfate−polyacrylamide gel electrophoresis; SE, size-exclusion; SMCC, sulfosuccinimidyl 4-(*N*-maleimidomethyl)-cyclohexane-1-carboxylate; T/NT, tumor/nontumor ratio; TscGc, thiosemicarbazonylglyoxylcysteinyl group.

effector molecule to assess each bsMAb conjugate's utility for pretargeting.

MATERIALS AND METHODS

Antibodies. hMN-14 IgG was prepared as described (Sharkey et al., 1995). The $F(ab')_2$ of hMN-14 was prepared by pepsin digestion, and purified using protein A and ion-exchange chromatography. A chimeric version of the murine 734 anti-(In)DTPA antibody originally described by Le Doussal et al. (1990) was prepared using the VH and Vλ sequences of murine 734, which were linked to human γ1 and κ constant domain sequences, respectively, using methods that have been described previously (Leung et al., 1994, 1995). The antigen-binding activity of c734 was determined with ELISA using (In)-DTPA-BSA-coated wells, and was found to be identical to murine 734.

The $F(ab')_2$ fragment of c734 was prepared by pepsin digestion. The fragment was purified by ammonium sulfate precipitation and then by size exclusion chromatography on a Superdex 200 (Amersham, Pharmacia Bio, Piscataway, NJ) column.

Bispecific Antibodies and Other Conjugates. The hMN-14 IgG × c734 Fab′ bsMAb was chemically prepared by cross-linking the Fab′-SH fragment of c734 to maleimide-derivatized hMN-14 IgG. The maleimide group was introduced by modification of the hMN-14 IgG lysine residues with 3×-molar excess of sulfosuccinimidyl 4-(*N*-maleimidomethyl)-cyclohexane-1-carboxylate (sulfo-SMCC, Molecular Biosciences, Boulder, CO) at pH 7.2 for 55 min at room temperature. The excess sulfo-SMCC was removed by centrifuged size exclusion chromatography (Penefsky, 1979; Meares et al., 1984) using Sephadex G-50−80 in 50 mM sodium acetate, 0.5 mM EDTA, pH 5.3. c734 Fab′-SH was produced by reduction of the $F(ab')_2$ fragment in 10 mM mercaptoethylamine, 20 mM HEPES, 150 mM NaCl, 10 mM EDTA, pH 7.2, at 37 °C for 1 h. Centrifuged size exclusion chromatography was used to isolate the Fab′-SH (c734) and IgG-mal (hMN-14) intermediates. The IgG × Fab′ conjugate was produced by reaction of a 1:1 mixture of the IgG-mal and Fab′-SH components at pH 5.3 for 1 h at room temperature. Sodium tetrathionate was added to the conjugation mixture to a final concentration of 6 mM. After 5 min at room temperature, excess sodium tetrathionate was removed by centrifuged size exclusion chromatography. The product was isolated following purification by affinity chromatography (Affigel-DTPA column) to isolate antibodies capable of binding DTPA, and then by size exclusion chromatography (Superdex 200, Amersham, Pharmacia Bio, Piscataway, NJ) to separate the anti-CEA × anti-DTPA bsMAb from anti-DTPA Fab′ or possibly $F(ab')_2$ that might have formed.

The hMN-14 $F(ab')_2$ × c734 Fab′ bsMAb preparation was similar to IgG × Fab′. $F(ab')_2$ fragment of hMN-14 was treated with 3.5-molar excess of sulfo-SMCC at pH 7.3 for 55 min to modify lysine residue(s) to introduce maleimide groups. Fab′-SH fragment of c734 was prepared as described above. The $F(ab')_2$-mal and Fab′-SH intermediates were purified on centrifuged size exclusion columns. The $F(ab')_2$ × Fab′ conjugate was formed by reaction of a 1:1 mixture of the two fragments at room temperature for 1.5 h at pH 5.3. The conjugation mixture was treated with 5 mM sodium tetrathionate, and the excess sodium tetrathionate was removed by centrifuged size exclusion chromatography. The reaction mixture was applied to Affigel-DTPA column to remove impurities containing hMN-14 only. To isolate the pure conjugate, the c734-containing portion from the Affigel-DTPA column was purified by size-exclusion chromatography (Superdex 200).

The hMN-14 Fab′ × c734 Fab′ bsMAb was prepared by the chemical coupling of the two reduced Fab′-SH fragments using *N*,*N*′-*o*-phenylenedimaleimide (PDM) by a standard literature method (Glennie et al., 1987). Briefly, MAbs were separately reduced to their Fab′-SH fragments by incubation with 10 mM 2-mercaptoethylamine at 37 °C for 1 h. The c734-Fab′-SH was converted to c734-Fab′-maleimide by reaction with 4 mM PDM at room temperature for 1 h. Centrifuged size exclusion chromatography was used to isolate the Fab′-SH (hMN-14) and Fab′-maleimide (c734) intermediates. Cross-linking of hMN-14-Fab′-SH to c734-Fab′-maleimide proceeded for 95 min at room temperature at a 1:1 molar ratio. The bsMAb was isolated after purification by DTPA affinity chromatography and by size exclusion chromatography (Superdex-200).

The purity and specificity of the bsMAbs were analyzed by SDS−PAGE (reducing and nonreducing conditions), as well as by SE-HPLC. SE-HPLC was used to examine the chromatographic properties of the bsMAbs alone and when mixed with an excess of CEA and after mixing with ^{111}In-labeled IMP-156, another divalent DTPA peptide (Karacay et al., 2000), or both CEA and the radiolabeled peptide. In both assays, the percentage of product failing to shift to a higher MW on SE-HPLC (shown by in-line monitoring of either UV or radioactivity) indicated the level of monospecific MAbs present in the preparations.

DTPA-conjugated bovine serum albumin (BSA) and DTPA-IgG, used as blocking/clearing agents, were prepared according to published procedures (Hnatowich et al., 1982). BSA and diethylenetriaminepentaacetic acid anhydride were obtained from Sigma (St. Louis, MO). The IgG was humanized LL2 anti-CD22 (Leung et al., 1995). MALDI-mass spectral analysis determined there were four DTPA conjugated to the BSA, and eight DTPA per IgG. The BSA- and IgG-DTPA conjugates were preloaded with indium on the day of their use by adding 20-times mole excess of indium to a prescribed amount of each conjugate.

Rat WI2 (rWI2) is an anti-idiotype antibody that is reactive with the hMN-14 IgG (Losman et al., 1994). It, along with a galactosylated conjugate of this antibody, has been used as a clearing agent to remove MN-14 IgG or MN-14 IgG-streptavidin conjugates from the blood (Karacay et al., 1997; Sharkey et al., 1997). BSA-DTPA and rWI2 were conjugated with galactose (43:1 and 49:1 mole substitution, respectively) using the methodology reported by others (Lee et al., 1976; Mattes, 1987). The ability of rWI2 and gal-rWI2 and BSA- and IgG-DTPA-(In) conjugates to bind to hMN-14 × 734 bsMAb was tested by SE-HPLC. A molar excess of each agent was mixed with ^{125}I-labeled bsMAb and after a brief incubation period the mixture was loaded on a Bio-Sil SE 250 size-exclusion HPLC column (BioRad, Richmond, CA). In each instance, the resulting product was shifted to a higher molecular weight than that of the ^{125}I-bsMAb alone.

Radiolabeling. IMP-192, a divalent DTPA peptide containing a thiosemicarbonylglyoxyl-cysteinyl group (TscGc) for radiolabeling with ^{99m}Tc, was prepared as previously reported by Karacay et al. (2000). For ^{99m}Tc-radiolabeling, IMP-192 was formulated in individually lyophilized vials that contained 50 μg of the peptide with Sn(II) for pertechnetate reduction and a 6-fold excess of nonradioactive indium to peptide for binding to DTPA. These vials were reconstituted with up to 77 mCi of

^{99m}Tc-pertechnetate (Mallinckrodt, Pine Brook, NJ) in 1.5 mL of saline. After 10 min at room temperature, the vials were heated in a water bath for 15 min. Quality assurance checks of the ^{99m}Tc-labeled IMP-192 included instant thin-layer chromatography (ITLC), which showed >95% of the radioactivity bound to the peptide, as well as an incubation with a mole excess of the bsMAb, which always showed >95% of the radioactivity shifted to a higher molecular weight peak by size-exclusion, high-pressure liquid chromatography (SE-HPLC).

The bsMAb was radiolabeled with Na^{125}I (Perkin-Elmer, Boston, MA) by the chloramine-T method (Greenwood and Hunter, 1963) to a specific activity of 10−14 mCi/mg. Quality assurance of the radiolabeled bsMAb included ITLC, SE-HPLC, and immunoreactive fraction. All radiolabeled bsMAb preparations had to have ≤ 5% unbound radioiodine by ITLC, ≥85% of the product migrating at the expected SE-HPLC elution volume for the bsMAb (i.e., no appreciable aggregation or other products), and an immunoreactive fraction when mixed with CEA >85%. The immunoreactive fraction of the bsMAb was tested against CEA by mixing 0.5 μCi of the radiolabeled bsMAb with 5 × the moles of CEA (Scripps Laboratories, San Diego, CA) for 5 min at room temperature. The dual specificity of the bsMAbs for CEA and DTPA was also spot-checked by incubating the ^{125}I-bsMAb with both CEA and another divalent DTPA-peptide, IMP-156, radiolabeled with ^{111}In (Karacay et al., 2000).

In Vitro Stability and Binding Studies. The in vitro stability of the bsMAbs in human serum was tested by incubating the ^{125}I-labeled bsMAb at 37 °C in fresh, sterile-filtered serum taken from a healthy donor. Samples were analyzed by SE-HPLC before and after mixing with CEA. The ability of the bsMAbs to retain binding ability to the peptide and CEA was analyzed using size-exclusion HPLC and radiolabeled bsMAbs and peptides. ^{99m}Tc-labeled peptide was diluted in 1.0% HSA and injected onto HPLC alone, and immediately after mixing with variable amounts of bsMAb. To demonstrate binding of the radiolabeled peptide to the antigen−bsMAb complex, bsMAb was mixed with CEA before addition of the radiolabeled peptide.

Animal Model. All animal studies were carried out with IACUC approved protocols. Female nude mice (Taconic, Germantown, NY) approximately 6−8 weeks old were inoculated subcutaneously (s.c.) with a 10% suspension of the serially transplanted GW-39 human colonic cancer cell line (Goldenberg et al., 1966; Goldenberg and Hansen, 1972). After allowing 2−3 weeks for tumor growth, the animals were given an intravenous injection of the bsMAb conjugate that contained a trace amount of ^{125}I-bsMAb so that its distribution properties could be evaluated. In all studies, a constant amount, 1.5 × 10^{-10} mol, of the bsMAb was administered (15, 22.5, and 30 μg of the Fab′ × Fab′, F(ab′)$_2$ × Fab′, and IgG × Fab′ conjugates, respectively). After waiting a defined period of time based on the conjugate used, the ^{99m}Tc-IMP-192 peptide was given at a constant bsMAb:peptide mole ratio of 10:1 based on the moles of bsMAb administered. Animals were then scheduled for necropsy at 3 and/or 24 h after the peptide was given. A number of studies were performed with the IgG × Fab′ bsMAb conjugate using a variety of clearing or blocking agents at a prescribed time after the bsMAb's injection. The timing of the administration of these agents after the bsMAb, the dose administered, and the time allotted before the ^{99m}Tc-IMP-192 peptide was given are provided for each study under Results. The dosage of these agents was based on a prescribed molar ratio in relation to the average amount of bsMAb in the blood as determined from samples taken by retroorbital bleeding of a minimum of three anesthetized animals, using the specific activity of the ^{125}I-bsMAb to estimate its concentration.

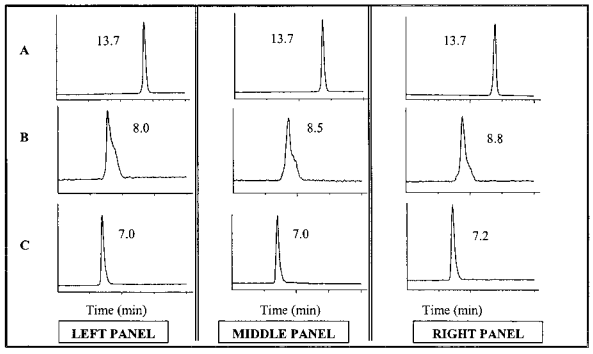


Figure 1. Size-exclusion HPLC chromatograms of the hMN-14 × c734 bsMAbs (IgG × Fab′ bsMAb, left panel; F(ab′)$_2$ × Fab′ bsMAb, middle panel; Fab′ × Fab′ bsMAb, right panel) showing the radioactivity traces for ^{111}In-IMP-156 alone (A), when mixed with the bsMAb (B), and mixed with the bsMAb after addition of CEA (C). The bsMAb was added in a 20-fold mole excess to the ^{111}In-IMP-156 (row B). A 5-fold mole excess of CEA was added to the bsMAb followed by the addition of the peptide (20:1, bsMAb/peptide ratio).

At the scheduled time of necropsy, groups of animals (n = 4−5) were anesthetized, approximately 0.2 mL of blood was removed by cardiac puncture, and then they were euthanized prior to dissection. Organs were removed, weighed, and placed in glass vials for counting ^{125}I- and ^{99m}Tc-activity. Windows were set to exclude ^{125}I from the ^{99m}Tc-window, and samples were first counted for their ^{99m}Tc content and then after allowing 2 days for decay, recounted for ^{125}I. For each counting session, standards were placed along with the tissues to calculate the total injected radioactivity. The amount of radioactivity in each tissue was first divided by the weight of the tissue and then by the total radioactivity injected to derive the percent injected dose per gram of tissue (% ID/g). Tumor to nontumor tissue ratios (T/NT) were derived by dividing the percent injected dose per gram of the tumor by the percentage in the respective tissue. A ratio of the % ID/g of ^{99m}Tc-IMP-192 peptide in each tissue compared to the % ID/g of ^{125}I-bsMAb (peptide/bsMAb ratio) was also calculated in a similar manner. Statistical analysis of these data was performed using an ANOVA with a two-tailed F-test.

RESULTS

In Vitro and in Vivo Properties of Chemically-Stabilized bsMAb Constructs. BsMAb composed of hMN-14 IgG, F(ab′)$_2$, or Fab′ chemically cross-linked to the Fab′ fragment of c734 were prepared, and according to SE-HPLC and SDS−PAGE, each conjugate contained the anti-CEA and anti-DTPA antibody at a 1:1 mole ratio. Figure 1 shows the SE-HPLC chromatograms of the bsMAb preparations when mixed in a molar excess with ^{111}In-IMP-156 divalent-DTPA peptide alone or with CEA and then the peptide. All of the peptide shifted to a higher molecular weight consistent primarily with the formation of complexes composed of 2 mol of bsMAb/peptide, and with a smaller fraction of bsMAb with 1 mol of peptide (Figure 1, row B). When added to the bsMAb after CEA addition, the complexes uniformly migrated as a higher molecular weight (Figure 1, row C). This shows that all of the antibody in each bsMAb preparation that is capable of binding the DTPA-peptide is also able to bind to CEA.

Table 1. Biodistribution of ^{125}I-Labeled hMN-14 × c734 bsMAb Constructs Alone[a]

	% ID/g				
	4 h	day 1	day 2	day 3	day 7
			IgG × Fab′		
tumor	2.71 ± 1.33	7.42 ± 2.04	12.8 ± 2.7	11.8 ± 1.6	5.92 ± 1.50
liver	2.81 ± 0.42	1.31 ± 0.15	1.01 ± 0.09	0.80 ± 0.06	0.23 ± 0.07
kidney	2.93 ± 0.45	1.62 ± 0.23	1.42 ± 0.29	0.95 ± 0.12	0.32 ± 0.11
blood	10.2 ± 1.2	5.67 ± 0.74	3.89 ± 0.44	3.01 ± 0.17	0.77 ± 0.32
tumor wt (g)	0.18 ± 0.112	0.20 ± 0.128	0.32 ± 0.029	0.34 ± 0.054	0.80 ± 0.318
			F(ab′)$_2$ × Fab		
tumor	2.61 ± 0.60	2.59 ± 0.81	2.52 ± 0.71	1.37 ± 0.24	ND
liver	2.20 ± 0.35	0.40 ± 0.04	0.20 ± 0.02	0.12 ± 0.02	
kidney	2.86 ± 0.47	0.44 ± 0.03	0.31 ± 0.08	0.18 ± 0.03	
blood	7.00 ± 0.94	0.74 ± 0.10	0.19 ± 0.03	0.06 ± 0.01	
tumor wt (g)	0.31 ± 0.288	0.31 ± 0.097	0.44 ± 0.304	0.44 ± 0.146	
			Fab′ × Fab′		
tumor	2.86 ± 0.53	1.46 ± 0.33	0.58 ± 0.19	0.37 ± 0.11	ND
liver	1.43 ± 0.50	0.15 ± 0.01	0.07 ± 0.01	0.06 ± 0.01	
kidney	3.98 ± 0.59	0.28 ± 0.08	0.12 ± 0.03	0.12 ± 0.03	
blood	3.31 ± 0.44	0.12 ± 0.01	0.04 ± 0.01	0.02 ± 0.01	
tumor wt (g)	0.24 ± 0.115	0.42 ± 0.08	0.30 ± 0.103	0.47 ± 0.128	

[a] Nude mice bearing GW-39 human colon cancer xenografts were injected i.v., with 1.5×10^{-10} mol of each bsMAb that contained a tracer amount (10 μCi) of the ^{125}I-bsMAb. Animals were necropsied at the times indicated, and the percentage of ^{125}I-bsMAb in the tissues shown was determined. Values represent the means ± SD ($n = 5$ per group).

Bispecific antibody conjugates placed in sterile-filtered mouse serum for 3 days were examined for stability by size-exclusion HPLC. After 3 days, 93%, 86%, and 76% of the IgG, F(ab′)$_2$, and Fab′ bsMAb conjugates shifted to a higher molecular weight fraction when mixed with CEA.

The distribution and clearance properties of the bsMAbs in tumor-bearing nude mice followed a predictable behavior based on the molecular size of the conjugates; e.g., the larger the construct, the slower it cleared from the blood (Table 1). Tumor uptake was highest for the IgG × Fab′ construct, but it took 2 days before it reached its maximum accretion level of 12.8 ± 2.7% ID/g. The maximum accretion in the tumor of the F(ab′)$_2$ × Fab′ and the Fab′ × Fab′ conjugates was observed at the earliest sampling time (4 h after the bsMAb injection). The F(ab′)$_2$ × Fab′ construct maintained this level for a period of 2 days, whereas the Fab′ × Fab′ conjugate steadily declined over the next 3 days, sustaining a loss of about 50% each day. The IgG × Fab′ conjugate stayed at its highest level for at least 2 days (days 2 and 3 after bsMAb injection), but by day 7 had decreased to 50% of its maximum level. The Fab′ × Fab′ fragment had somewhat higher renal uptake at 4 h than the other bsMAb constructs, but none of the constructs had sustained renal retention. This is most likely explained by the fact that all of these conjugates are a molecular size too large to be cleared directly by renal excretion, and because these were all radioiodinated by conventional means, any iodinated catabolic product would be rapidly filtered though the kidneys rather than retained in any major organ (e.g., liver).

Pretargeting ^{99m}Tc-IMP-192 with Each of the bsMAb Conjugates. Our earlier experience (Karacay et al., 2000) indicated that optimal pretargeting occurred when sufficient time was given for the bsMAb conjugate to clear from the blood prior to giving the radiolabeled peptide. Based on the data in Figure 1, a clearance time of 6 days, 49 h, and 19 h was selected for the initial testing of the IgG ×, F(ab′)$_2$ ×, and Fab′ × Fab′ conjugates, respectively. The protein dosage of the bsMAb was adjusted so that each conjugate was administered in equal mole amounts [1.5×10^{-10} mol; the molecular weights were assumed to be 200 000 for the IgG × Fab′, 150 000 for the F(ab′)$_2$ × Fab′, and 100 000 for the Fab′ × Fab′]. After allowing the allotted time for bsMAb clearance, ^{99m}Tc-IMP-192 was administered (1.5×10^{-11} mol; i.e., a bsMAb/peptide ratio of 10:1). Animals were then necropsied at 3 and 24 h after the peptide injection. As shown in Table 2, the ^{125}I-IgG × Fab′ bsMAb had the highest concentration in the tumor at 21.2 ± 9.7% ID/g 3 h after the peptide was injected, compared to the F(ab′)$_2$ × Fab′ conjugate, which was only 3.88 ± 0.66% ID/g, and the Fab′ × Fab′ at 1.45 ± 0.35% ID/g. At the time intervals selected, blood concentrations of the F(ab′)$_2$ × Fab′ and Fab′ × Fab′ conjugates were similar, but the blood concentration of the IgG × Fab′ was nearly 10-fold higher. Thus, despite having a higher concentration of bsMAb in the tumor, the peptide uptake was higher for the F(ab′)$_2$ × Fab′ and Fab′ × Fab′ conjugates than the IgG × Fab′. These results suggest that the peptide was more likely to bind to the IgG × Fab′ bsMAb in the blood, which could have reduced its availability for binding to the tumor. The ratio of the amount of peptide to the amount of bsMAb localized in the tumor (peptide/bsMAb ratio) was determined to illustrate the peptide's ability to localize with the bsMAb (see Table 2). For example, the peptide/bsMAb ratio was only 0.34 ± 0.15 for the IgG × Fab′ conjugate, which was 7 times lower than the peptide/bsMAb ratio for the F(ab′)$_2$ × Fab conjugate (2.38 ± 0.56) and 11 times lower than that observed for the Fab′ × Fab′ conjugate (3.79 ± 0.16). The IgG × Fab′ conjugate only had 1 mol of peptide for every 37 mol of bsMAb, whereas the F(ab′)$_2$ × Fab′ and Fab′ × Fab′ conjugate in the tumor had 1 mol of peptide for every 3−4 mol of bsMAb. Thus, the mole substitution level for the F(ab′)$_2$ × Fab′ and Fab′ × Fab′ conjugates was close to the theoretically ideal ratio for an affinity enhancement model, i.e., 1 mol of peptide for every 2 mol of bsMAb.

Although there were significant differences in the peptide/bsMAb ratios in the blood among the three groups, unlike the ratios seen in the tumor, the magnitude separating them was no greater than a factor of 2.0. It was estimated, using the radiotracers to determine the number of bsMAb for each mole of peptide in the blood at 3 h, that there was 4.4, 6.3, and 2.6 mol of the IgG ×, F(ab′)$_2$ ×, and Fab′ × Fab′ conjugates, respectively. The comparison of the peptide/bsMAb in the blood for these three conjugates may provide some insight into the

Table 2. Pretargeting Using Various Forms of hMN-14 × c734 bsMAb Conjugates and ^{99m}Tc-IMP-192 Peptide[a]

	3 h[b]				24 h[b]			
	% bsMAb/g	% peptide/g	T/NT pep	pep/bsMAb	% bsMAb/g	% peptide/g	T/NT pep	pep/bsMAb
				IgG × Fab′ (6 Day Interval)				
tumor	21.2 ± 9.7	6.04 ± 0.86	–	0.34 ± 0.15	26.0 ± 10.4	10.0 ± 2.5	–	0.46 ± 0.26
liver	0.93 ± 0.29	8.15 ± 2.31	0.81 ± 0.34	8.97 ± 0.98	0.74 ± 0.09	3.85 ± 0.66	2.68 ± 0.85	4.61 ± 1.60
kidney	0.89 ± 0.32	3.57 ± 0.98	1.84 ± 0.71	ND	0.82 ± 0.19	2.59 ± 0.46	4.07 ± 1.57	ND
blood	2.71 ± 0.59	6.24 ± 1.96	1.07 ± 0.45	2.28 ± 0.32	2.51 ± 0.34	3.19 ± 0.50	3.21 ± 0.93	1.68 ± 0.96
tumor wt (g)		0.38 ± 0.112				0.32 ± 0.108		
				F(ab′)$_2$ × Fab′ (49 h Interval)				
tumor	3.88 ± 0.66	9.00 ± 1.40	–	2.38 ± 0.56	2.12 ± 0.58	6.39 ± 1.86	–	3.24 ± 1.19
liver	0.23 ± 0.03	0.34 ± 0.05	27.3 ± 7.3	1.50 ± 0.11	0.11 ± 0.01	0.21 ± 0.03	30.3 ± 9.5	1.94 ± 0.12
kidney	0.23 ± 0.04	1.90 ± 0.28	4.88 ± 1.24	ND	0.16 ± 0.02	0.74 ± 0.12	8.75 ± 2.65	ND
blood	0.33 ± 0.05	0.52 ± 0.10	18.1 ± 5.3	1.59 ± 0.21	0.12 ± 0.03	0.15 ± 0.04	46.2 ± 19.3	1.21 ± 0.19
tumor wt (g)		0.15 ± 0.023				0.25 ± 0.183		
				Fab′ × Fab′ (19 h Interval)				
tumor	1.45 ± 0.35	5.47 ± 1.23	–	3.79 ± 0.16	1.58 ± 0.24	3.75 ± 0.52	–	2.39 ± 0.10
liver	0.19 ± 0.03	0.36 ± 0.04	15.1 ± 2.7	2.26 ± 0.71	0.10 ± 0.01	0.18 ± 0.02	21.6 ± 3.6	1.75 ± 0.07
kidney	0.31 ± 0.04	2.40 ± 0.31	2.30 ± 0.52	ND	0.17 ± 0.03	0.64 ± 0.10	5.94 ± 1.12	ND
blood	0.29 ± 0.03	1.11 ± 0.11	4.90 ± 0.99	3.60 ± 1.22	0.08 ± 0.01	0.34 ± 0.02	10.9 ± 1.5	4.22 ± 0.51
tumor wt (g)		0.11 ± 0.028				0.19 ± 0.058		

[a] Data include the percent injected dose per gram for ^{125}I-bsMAb and ^{99m}Tc-peptide, the tumor/nontumor ratio for ^{99m}Tc-peptide (T/NT pep), and the ratio of the % bsMAb and % peptide in the tissues (pep/bsMAb). 1.5×10^{-10} mol of bsMAb and 1.5×10^{-11} mol of ^{99m}Tc-IMP-192 were given for each conjugate. Values represent mean ± SD; $n = 5$ for each observation. The interval is the amount of time between the bsMAb and peptide injections. [b] Time after ^{99m}Tc-IMP-192 given.

relative efficiency of each conjugate for binding the peptide in vivo. For example, in the case of the F(ab′)$_2$ × Fab′ and the Fab′ × Fab conjugates, the concentration of bsMAb in the blood, as measured by the ^{125}I-bsMAb, was not significantly different ($p = 0.105$), yet the amount of peptide found in the blood at 3 h was significantly higher with the Fab′ ($p = 0.023$), and the difference between the peptide/bsMAb ratios for these two groups was significantly different at a level of $p = 0.007$. This assessment suggests that the Fab′ × Fab′ bsMAb conjugate was able to bind more avidly to the peptide than the F(ab′)$_2$ × Fab′ conjugate. This is not unexpected since the chemical coupling process of the hMN-14 Fab′ and the c734 Fab′ more effectively orients the twp molecules by binding each molecule at its hinge region. Because the Fab′ is coupled to lysine groups on the IgG and F(ab′)$_2$, it can be randomly positioned on the molecule, which could affect its ability to bind to the peptide. Although the IgG × Fab′ conjugate had higher peptide/bsMAb ratio in the blood compared to the F(ab′)$_2$ × Fab′, it is more likely that this occurred because the IgG × Fab′ conjugate had nearly 10 times the amount of bsMAb in the blood at the time the peptide was given, rather than an indication of it being more capable of avidly binding the peptide than the F(ab′)$_2$ × Fab′. Thus, this assessment can only apply to the F(ab′)$_2$ × Fab′ and Fab′ × Fab′ conjugates, since the blood concentration at the time of the injection was the same. It is also important to point out that Karacay et al. (2000) had previously shown ^{99m}Tc-IMP-192 was rapidly cleared from the blood, and since there is no detectable binding of the peptide to other serum proteins, such as albumin, as determined by SE-HPLC of ^{99m}Tc-IMP-192 incubated in plasma (not shown), it is reasonable to assume that any peptide remaining in the blood is most likely bound to the bsMAb.

There was also a substantial amount of ^{99m}Tc-IMP-192 in the liver with the IgG × Fab′ conjugate. This could have been a consequence of peptide binding directly to the bsMAb in the liver, but it is also possible that a portion of the liver uptake was a consequence of either mono- or dimeric complexes of the bsMAb formed with the peptide in the blood, which were then transported to the liver. Renal uptake of the ^{99m}Tc=IMP-192 alone (i.e., without pretargeting) was previously shown to be about 2.0% ID/g (Karacay et al., 2000). In a pretargeting setting, renal uptake is not much higher unless there is a substantial level of bsMAb in the blood. This suggests that a substantial portion of the bsMAb is not itself sequestered in the kidneys, leading to peptide localization.

Twenty-four hours after the peptide injection, the tumor uptake of the ^{99m}Tc-IMP-192 increased from 6.0 ± 0.9 to 10.0 ± 2.4% ID/g for the IgG × Fab′ conjugate, while it decreased for the other conjugates. Some of this increase could have been due to the subsequent tumor localization of the IgG × Fab′–^{99m}Tc-IMP-192 complexes that were formed in the blood. Indeed, the bsMAb–^{99m}Tc-IMP-192 complexes in the blood at 3 h after the peptide injection were more highly laden with peptide, having 1 mol of peptide for every 4.3 mol of bsMAb, than the bsMAb in the tumor, which had only 1 mol of peptide for every 37 ± 22 mol of bsMAb.

As a consequence of higher tumor accretion of the peptide with lower amounts in the blood, the ^{99m}Tc-IMP-192 tumor/blood ratios for the F(ab′)$_2$ × Fab′ and Fab′ × Fab′ bsMAb were higher than the IgG × Fab′ conjugate (Table 2). Although there was some improvement in the IgG × Fab′ conjugate by 24 h, the tumor/blood ratios never exceeded that seen with the other 2 conjugates. Thus, despite having the highest level of bsMAb uptake in the tumor, the higher concentration of IgG × Fab′ in the blood at the time of the peptide injection inhibited tumor accretion. Since the peptide was given to animals when the amount of the F(ab′)$_2$ × Fab′ and Fab′ × Fab′ conjugate in the blood were the same, the higher tumor uptake of the F(ab′)$_2$ × Fab′ resulted in this conjugate having the highest tumor/nontumor ratios for the peptide under these targeting conditions.

Examination of Clearing and Blocking Agents. Although the targeting results described above favored the F(ab′)$_2$ × Fab′ conjugate, the fact that the IgG × Fab′ conjugate had nearly 5 times the concentration of bsMAb in the tumor as the F(ab′)$_2$ × Fab′ conjugate meant that it might be possible to enhance peptide accretion in the tumor further if the blood concentration of the IgG × Fab′ could be reduced to a lower level at the time the peptide was given. A number of strategies were examined to determine a means of maintaining a high amount of IgG

× Fab′ bsMAb in the tumor while removing or blocking it in the blood.

Clearing Agents. We previously used galactosylated and nongalactosylated rat WI2 anti-MN-14 idiotype antibody as a clearing agent for an avidin−biotin pretargeting procedure (Karacay et al., 1997; Sharkey et al., 1997). Thus, these clearing agents were examined in combination with the hMN-14 IgG × c734 Fab′ in an attempt to improve pretargeting with the ^{99m}Tc-IMP-192 peptide. In the first studies, galactosylated rWI2 (gal-rWI2) was given 48 h after the bsMAb at a 5:1 mole ratio based on the concentration of bsMAb in the blood immediately prior to its administration. After waiting 3 h to allow for bsMAb clearance, ^{99m}Tc-IMP-192 was given, and then 3 h later, animals were necropsied to determine the distribution of the bsMAb and peptide. As shown in Table 3, gal-rWI2 was effective in clearing the bsMAb from the blood, reducing it from 9.5 ± 1.4% ID/g seen in the group that did not receive any clearing agent to 1.8 ± 0.50% ID/g in the group given gal-rWI2 clearing agent. With a lower amount of bsMAb in the blood, animals given the gal-rWI2 had only 0.9 ± 0.28% ID/g of the peptide in the blood, whereas the group that was not given the clearing agent had 11.3 ± 2.9% ID/g of the injected peptide in the blood. Despite the significant reduction of peptide binding in the blood, tumor uptake of the peptide for the animals given the gal-rWI2 was not any higher than that of the control animals. Liver accretion of the peptide, however, increased significantly in the animals given the gal-rWI2 (14.3 ± 2.1 vs 5.8 ± 0.6% ID/g for the control; $p < 0.001$), suggesting that bsMAb had been transported to the liver by the clearing agent, but had not been sufficiently processed to prevent its binding to the peptide, which in turn reduced the availability of the peptide for tumor localization. Therefore, despite improving tumor/blood ratios as compared to the control group (1.84 ± 0.87 vs 0.19 ± 0.05), the tumor/nontumor ratios and amount of peptide targeted to the tumor were not higher than those seen with the F(ab′)$_2$ × Fab′ or Fab′ × Fab′ bsMAbs.

It was also noted that the peptide/bsMAb ratio in the blood for the control group was 1.18 ± 0.15 (representing 1 peptide for every 8.4 mol of bsMAb). In contrast, the animals given the gal-rWI2 had a peptide/bsMAb ratio of 0.49 ± 0.08 (1 mol of peptide for every 20 mol of bsMAb in the blood). This substantially lower peptide/bsMAb ratio could be a result of less favorable kinetics for peptide binding to the lower amount of bsMAb in the blood of the gal-rWI2 group, or steric hindrance created by the binding of the gal-rWI2 to the bsMAb.

In the next study, galactosylated and nongalactosylated rWI2 were independently evaluated as clearing agents, and additional modifications were made in an attempt to reduce the amount of bsMAb that would be present at the time the ^{99m}Tc-IMP-192 was given. In this regard, the IgG × Fab′ bsMAb was allowed to clear for 65 h (rather than 48 h) before giving the clearing agents, and the radiolabeled peptide was not given until either 5 or 24 h after the clearing agents (rather than 3 h). Increasing the interval between the clearing agent and the peptide injection was intended to allow more time for the bsMAb−anti-id antibody complexes diverted to the liver to be processed, and therefore inaccessible at the time the peptide is given. Immune complexes cleared by the gal-rWI2 and nongalactosylated rWI2 would also be expected to localize to different cell types in the liver, which could also influence the processing of the bsMAb and peptide. The same amount of bsMAb and peptide were given as before (1.5 × 10^{-10} and 1.5 × 10^{-11} mol,

Table 3. Assessment of Pretargeting Using the hMN-14 IgG × c734 Fab′ bsMAb with or without Clearing/Blocking Agents Prior to the Administration of ^{99m}Tc-IMP-192[a]

	gal-rat WI2 (clearing)[b]				In-DTPA (Blocking)[b]				no clearing/blocking agent[b]			
	% ID/g bsMAb	% ID/g peptide	T/NT peptide	pep/bsMAb	% ID/g bsMAb	% ID/g peptide	T/NT peptide	pep/bsMAb	% ID/g bsMAb	% ID/g peptide	T/NT peptide	pep/bsMAb
tumor	16.0 ± 3.5	1.5 ± 0.43	–	0.09 ± 0.03	14.1 ± 3.3	2.6 ± 0.53	–	0.19 ± 0.03	16.5 ± 7.9	2.1 ± 0.39	–	0.14 ± 0.03
liver	9.3 ± 1.01	14.3 ± 2.1	0.10 ± 0.03	1.54 ± 0.19	3.1 ± 0.33	6.9 ± 1.18	0.39 ± 0.14	2.20 ± 0.19	2.7 ± 0.35	5.8 ± 0.63	0.36 ± 0.05	2.19 ± 0.18
kidney	1.4 ± 0.35	1.2 ± 0.18	1.24 ± 0.32	ND	3.5 ± 0.50	3.7 ± 0.31	0.71 ± 0.11	ND	3.1 ± 0.59	3.2 ± 0.63	0.64 ± 0.13	ND
blood	1.8 ± 0.50	0.9 ± 0.28	1.84 ± 0.87	0.49 ± 0.08	10.1 ± 1.0	11.1 ± 1.5	0.23 ± 0.02	1.12 ± 0.20	9.5 ± 1.40	11.3 ± 2.9	0.19 ± 0.05	1.18 ± 0.15
tumor wt (g)		0.37 ± 0.12				0.80 ± 0.22				0.53 ± 0.09		

[a] hMN-14 IgG × c734 Fab′ (1.5 × 10^{-10} mol; 10 μCi) was given intravenously. Forty-eight hours later, the clearing/blocking agent was given, and after 3 h, the ^{99m}Tc-IMP-192 (1.5 × 10^{-11} mol) was given. Three hours later, the animals were necropsied, and the ^{125}I-bsMAb and ^{99m}Tc-IMP-192 radioactivity levels were determined. [b] gal-rWI2 was given at a 5:1 mole ratio, and In-DTPA was given at a 1:1 mole ratio based on the amount of bsMAb in blood at the time of their administration. The group that was not given a clearing/blocking agent received the ^{99m}Tc-IMP-192 51 h after the bsMAb and necropsied 3 h later. Values represent the means ± SD with 5 animals per group.

Table 4. Evaluation of Galactosylated and Nongalactosylated Rat Anti-MN-14 Idiotype Antibody, rWI2, as a Clearing Agent for Improving Pretargeting Using hMN-14 IgG × c734 Fab′ bsMAb[a]

	rWI2, 5 h clearance				rWI2, 24 h clearance			
	% bsMAb/g	% peptide/g	T/NT pep	pep/bsMAb	% bsMAb/g	% peptide/g	T/NT pep	pep/bsMAb
tumor	13.7 ± 4.1	3.12 ± 0.74	–	0.25 ± 0.09	7.25 ± 2.14	7.16 ± 1.68	–	1.08 ± 0.47
liver	5.20 ± 1.77	17.9 ± 4.2	0.19 ± 0.09	3.59 ± 0.72	0.98 ± 0.57	6.97 ± 3.83	1.66 ± 1.70	7.90 ± 4.55
kidney	1.26 ± 0.33	2.88 ± 0.52	1.11 ± 0.31	ND	0.28 ± 0.12	2.19 ± 0.43	3.41 ± 1.25	ND
blood	2.31 ± 0.71	1.41 ± 1.05	3.07 ± 2.02	0.65 ± 0.59	0.61 ± 0.30	1.50 ± 1.09	9.25 ± 9.92	2.87 ± 2.86
tumor wt (g)	0.44 ± 0.396				0.49 ± 0.185			
	gal-rWI2, 5 h clearance				gal-rWI2, 24 h			
	% bsMAb/g	% peptide/g	T/NT pep	pep/bsMAb	% bsMAb/g	% peptide/g	T/NT pep	pep/bsMAb
tumor	10.9 ± 2.77	2.84 ± 0.66	–	0.27 ± 0.09	7.64 ± 1.54	7.27 ± 1.49	–	0.97 ± 0.23
liver	9.72 ± 1.78	23.0 ± 4.9	0.13 ± 0.06	2.38 ± 0.40	2.66 ± 0.47	17.3 ± 2.4	0.43 ± 0.14	6.66 ± 1.47
kidney	0.62 ± 0.11	1.19 ± 0.14	2.42 ± 0.57	ND	0.37 ± 0.15	1.91 ± 0.58	3.95 ± 0.67	ND
blood	0.88 ± 0.46	0.47 ± 0.29	10.4 ± 11.2	0.57 ± 0.39	0.55 ± 0.39	1.00 ± 1.13	19.0 ± 18.8	1.48 ± 0.80
tumor wt (g)	0.44 ± 0.077				0.82 ± 0.293			
	no clearing agent, 70 h ($n = 4$)				no clearing agent, 90 h			
	% bsMAb/g	% peptide/g	T/NT pep	pep/bsMAb	% bsMAb/g	% peptide/g	T/NT pep	pep/bsMAb
tumor	11.7 ± 2.7	3.60 ± 1.20	–	0.31 ± 0.06	14.8 ± 6.5	3.45 ± 1.3	–	0.27 ± 0.14
liver	2.63 ± 0.73	13.1 ± 4.9	0.29 ± 0.18	4.87 ± 0.86	1.67 ± 0.68	10.4 ± 5.3	0.45 ± 0.32	5.97 ± 0.97
kidney	2.43 ± 0.18	5.49 ± 0.89	0.57 ± 0.04	ND	1.35 ± 0.46	3.41 ± 0.65	1.07 ± 0.55	ND
blood	7.21 ± 1.68	15.5 ± 6.0	0.18 ± 0.04	2.11 ± 0.63	4.71 ± 1.82	12.4 ± 7.2	0.40 ± 0.33	2.60 ± 1.2
tumor wt (g)	0.86 ± 0.281				0.61 ± 0.550			

[a] Nude mice bearing GW-39 tumors were given an intravenous injection of hMN-14 IgG × c734 Fab′ bsMAb (1.5×10^{-10} mol) that contained a trace amount of ^{125}I-bsMAb. Sixty-five hours later, the clearing agent was given intravenously, and then after waiting either 5 or 24 h, ^{99m}Tc-IMP-192 (1.5×10^{-11} mol) was administered. Animals ($n = 5$, except where indicated) were necropsied 3 h later, and the amount of ^{125}I-bsMAb and ^{99m}Tc-IMP-192 was determined. Control animals not given any clearing agent received the ^{99m}Tc-IMP-192 at either 70 or 90 h after the bsMAb injection.

respectively), and animals were all necropsied 3 h after the peptide injection. The peptide was also given to animals that did not receive a clearing agent at either 70 or 90 h after the bsMAb injection so the time of necropsy would coincide closely with the animals given the clearing agents for comparison. Table 4 shows the % ID/g for the bsMAb and peptide, tumor/nontumor ratios for the peptide, and the peptide/bsMAb ratios obtained in these groups.

Delaying the ^{99m}Tc-IMP-192 injection until 70 and 90 h after the bsMAb was given reduced the blood concentration of the bsMAb to 7.21 ± 1.68 and 4.71 ± 1.82% ID/g, respectively, compared to 9.5 ± 1.40% ID/g seen in the previous study. However, the ^{99m}Tc-IMP-192 continued to show higher concentrations of the peptide in the blood and liver than the tumor. Both the rWI2 and gal-rWI2 effectively reduced the blood concentration of the IgG × Fab′ bsMAb, with the gal-rWI2 showing a greater ability to reduce the bsMAb level in the blood more quickly than the rWI2. For example, the bsMAb in blood was 2.31 ± 0.71% ID/g for the rWI2 group, which was about 4-fold lower than the group that was given no clearing agent (7.11 ± 1.68 at 70 h), but the blood concentration of the bsMAb in animals gal-WI2 was reduced to 0.88 ± 0.46% ID/g. When the period between the time the clearing agent and the peptide was extended to 24 h, then the level of bsMAb in the blood of galactosylated and nongalactosylated rWI2 was the same (0.55 ± 0.39 and 0.61 ± 0.30% ID/g, respectively), which was about 8-fold lower than if no clearing agent was given (4.71 ± 1.82% ID/g). It was also interesting to note that in the groups receiving the clearing agents, the ratio of peptide/bsMAb in the blood for the 5 h clearance group was 0.57 to 0.65, but with a 24 h clearance interval, this ratio increased to 1.48 to 2.87. This indicates that the bsMAb in the blood at the earlier time was not as receptive to binding the peptide as the bsMAb in the blood after 24 h, supporting the possibility of steric hindrance.

Tumor uptake of the bsMAb in the treated groups with a 5 h clearance time and control group (70 h) was the same, but despite having lower blood concentrations of the bsMAb, the animals given the clearing agents had the same amount of ^{99m}Tc-IMP-192 in the tumor as the control animals. In each of the treated groups, there was considerable peptide uptake in the liver with highly unfavorable tumor/liver ratios. Increasing the interval between the clearing agent and the time the peptide was given to 24 h reduced the bsMAb concentration in the blood to levels that were comparable to those seen with the F(ab′)$_2$ × Fab′ conjugate (0.61 ± 0.30, 0.55 ± 0.39, and 0.33 ± 0.15% ID/g for rWI2 and gal rWI2, and F(ab′)$_2$ × Fab′, respectively). Under these conditions, tumor uptake of the ^{99m}Tc-IMP-192 was 7.16 ± 1.68 and 7.27 ± 1.49% ID/g for the rWI2 and gal-rWI2, respectively, which was not significantly different ($p = 0.156$) to the peptide uptake seen with the F(ab′)$_2$ × Fab′ (9.0 ± 1.4% ID/g). Although tumor/blood ratios in animals given the clearing agents with a 24 h interval before administering the peptide were highly variable, the individual animal data revealed that when the blood concentration of the bsMAb was reduced to about 0.2−0.4% ID/g, tumor/blood ratios were between 13 and 26, thus being comparable to that achieved with the F(ab′)$_2$ × Fab′ conjugate. However, there continued to be considerable liver accretion of the peptide, most noticeably with the gal-WI2 clearing agent. In conclusion, tumor/liver ratios for the ^{99m}Tc-IMP-192 using IgG × Fab′ bsMAb with either clearing agent and a 24 h interval were much lower than that seen with the F(ab′)$_2$ × Fab′ bsMAb (i.e., <0.5 for the clearing agents compared to 27.3 ± 7.35 for the F(ab′)$_2$ × Fab′).

To see whether additional delays in the interval between the time the clearing agent and ^{99m}Tc-IMP-192 was given would yield any improvements, animals were again given 1.5×10^{-10} mol of the hMN-14 IgG × c734 Fab′ bsMAb, and after 65 h, rWI2 was given at a 5:1 mole ratio (anti-antibody to bsMAb) based on the blood con-

Table 5. Evaluation of Pretargeting Using hMN-14 IgG × c734 Fab′ bsMAb with ^{99m}Tc-IMP-192 Peptide with and without a Clearing Agent: Extending the Interval between bsMAb and Peptide Injection without a Clearing Agent and Extending the Interval between the rWI2 Clearing Agent and Peptide Injection[a]

	11 days bsMAb clearance			rWI2, 24 h clearance		
	% bsMAb/g	% peptide/g	T/NT peptide	% bsMAb/g	% peptide/g	T/NT peptide
tumor	3.01 ± 0.49	6.16 ± 1.03	–	4.54 ± 1.03	10.3 ± 1.59	–
liver	0.29 ± 0.13	4.62 ± 1.99	1.66 ± 1.03	0.64 ± 0.26	5.04 ± 1.86	2.27 ± 0.79
kidney	0.22 ± 0.08	2.23 ± 0.50	2.85 ± 0.70	0.21 ± 0.03	2.88 ± 0.48	3.67 ± 0.87
blood	0.84 ± 0.36	3.01 ± 1.53	2.47 ± 1.21	0.29 ± 0.07	0.66 ± 0.13	15.79 ± 1.87
tumor wt (g)		1.04 ± 0.166			0.56 ± 0.066	
	rWI2, 48 h clearance			rWI2, 72 h clearance		
	% bsMAb/g	% peptide/g	T/NT peptide	% bsMAb/g	% peptide/g	T/NT peptide
tumor	6.55 ± 3.50	8.73 ± 2.94	–	3.71 ± 2.00	6.12 ± 1.35	–
liver	0.31 ± 0.12	3.48 ± 1.98	4.0 ± 3.8	0.46 ± 0.22	5.85 ± 2.14	1.09 ± 0.21
kidney	0.14 ± 0.03	2.62 ± 0.58	3.4 ± 1.1	0.23 ± 0.11	2.55 ± 0.53	2.45 ± 0.65
blood	0.25 ± 0.13	0.75 ± 0.14	12.8 ± 8.0	0.64 ± 0.34	2.37 ± 1.88	3.38 ± 1.38
tumor wt (g)		0.31 ± 0.255			0.43 ± 0.148	

[a] Nude mice bearing GW-39 tumors were injected i.v. with 1.5×10^{-10} mol of the bsMAb that included a trace amount of ^{125}I-bsMAb. In one group, bsMAb blood concentration was monitored, and the peptide was given when it was <1.0% ID/g. The other groups of animals were given rWI2 65 h after the bsMAb injection (rWI2 given at a 5:1 mole ratio based on bsMAb concentration at 65 h). Following a delay of 24, 48, or 72 h, the peptide was given. In all groups, animals were necropsied 3 h after the peptide injection. Values represent means ± SD with 5 animals in each group.

centration of the ^{125}I-bsMAb at this time. The nongalactosylated rWI2 was selected because of the lower bsMAb and peptide accretion in the liver compared to the gal-WI2. After waiting 24, 48, or 72 h, ^{99m}Tc-IMP-192 was given (1.5×10^{-11} mol). In addition, another group of animals, without the aid of a clearing agent, was monitored until the concentration of ^{125}I-bsMAb in the blood was ≤1.0%/g, at which time the ^{99m}Tc-IMP-192 was given. In all instances, animals were then necropsied 3 h later.

In order for the IgG × Fab′ conjugate to be cleared from the blood to ≤1.0% ID/g, a period of 11 days was required. Three hours after the peptide was injected, the tumor contained 3.01 ± 0.49% ID/g of the bsMAb, which was able to capture 6.16 ± 1.03% ID/g of the ^{99m}Tc-IMP-192 (Table 5). However, the ^{99m}Tc-IMP-192 concentration in the blood was 3.01 ± 1.53% ID/g, which resulted in tumor/blood ratios of only 2.47 ± 1.21. Even though the concentration of the IgG × Fab′ bsMAb in the blood and liver was low, there was a high concentration of ^{99m}Tc-IMP-192 in the liver. Indeed, the concentration of the bsMAb in the liver was only 0.29 ± 0.13% ID/g, which was similar to that seen with the F(ab′)$_2$ × Fab′ conjugate (Table 2). This suggests that the IgG × Fab′ conjugate is more highly susceptible to forming complexes with the divalent IMP-192, which then subsequently localize in the liver.

Similar targeting results with the rWI2 clearing agent and a 24 h clearance period were obtained as seen previously (refer to data in Tables 4 and 5). Waiting for 48 h before administering the ^{99m}Tc-IMP-192 did not provide any significant improvements in the peptide targeting data (Table 5). By waiting 72 h, the amount of bsMAb in the tumor decreased while its concentration in the blood did not change significantly, which resulted in decreased tumor/blood ratios. Liver uptake of the peptide also remained a considerable obstacle, regardless of the interval. Thus, a 24 h clearance period for the rWI2 was considered to be the optimal clearing agent and condition for use with the IgG × Fab′ bsMAb, but even these conditions failed to meet the targeting results seen with the F(ab′)$_2$ × Fab′.

Blocking and Blocking/Clearing Agents. These data indicated that the primary problem with an agent that only clears the bsMAb from the blood is that a portion of the bsMAb remains in the system and is able to bind to the peptide, potentially redirecting it to the liver. Thus, additional agents were examined that had the ability to block the anti-DTPA-binding arm of the bsMAb to prevent it from subsequently binding the peptide.

Indium-loaded DTPA and indium-loaded IMP-156 (a divalent DTPA peptide; Karacay et al., 2000) represent agents that should only be able to block the bsMAb's anti-DTPA binding arm without necessarily altering its biodistribution (i.e., acting as a clearing agent). Because these compounds are similar to the peptide, and therefore could quickly penetrate into the tumor and block the subsequent binding to the radiolabeled peptide, the dosage of these agents was kept low. Indium-loaded DTPA was given to animals 48 h after the injection of the IgG × Fab′ clearance at a molar ratio of only 1:1, based on the amount of bsMAb in the blood at the time of the peptide injection. After waiting 3 h, ^{99m}Tc-IMP-192 was given. The data shown in Table 3 indicate that the indium-loaded DTPA had no impact on either the distribution of the bsMAb or the peptide, since the data for this group and the group that only received the ^{99m}Tc-IMP-192 were identical, with an identical peptide/bsMAb ratio in the blood. Indium-loaded IMP-156 was given at a slightly higher mole ratio of 1.5:1 and at 65 h after the bsMAb was given with the ^{99m}Tc-IMP-192, injected 30 min after the indium-loaded IMP-156. As shown in Table 6, a substantial portion of the ^{99m}Tc-IMP-192 was bound to the bsMAb in the blood. Although the percentage of the ^{99m}Tc-IMP-192 was significantly lower in the blood of the animals given the indium-loaded IMP-156 ($p = 0.019$), the peptide/bsMAb ratio for these 2 groups did not achieve statistical significance ($p = 0.087$). The data using the indium-loaded IMP-156 also indicated that the % ID/g of ^{99m}Tc-IMP-192 in the tumor was higher than in the control group [4.44 ± 2.0 and 8.45 ± 1.83% ID/g, control vs (In)IMP-156, respectively]. However, because the peptide/bsMAb ratio for the tumor in both groups was the same (0.47 ± 0.31 and 0.49 ± 0.17, control vs (In)IMP-156, respectively), this higher amount was likely a reflection of this group's higher concentration of bsMAb in the tumor than the control (e.g., 11.0 ± 4.1 vs 17.8 ± 3.8) as compared to a specific enhancement of peptide uptake. Thus, this dosing scheme did not produce the desired blocking effect. Since there was a concern that these small molecular weight blocking agents could also

Table 6. Examination of Pretargeting Using hMN-14 IgG × c734 Fab′ with Blocking Agents[a]

	no blocking agent				1.5:1 BSA-(4.4)DTPA(In)			
	% bsMAb/g	% peptide/g	T/NT pep	pep/bsMAb	% bsMAb/g	% peptide/g	T/NT pep	pep/bsMAb
tumor	11.0 ± 4.1	4.43 ± 2.00	–	0.47 ± 0.31	11.5 ± 8.63	6.94 ± 3.45	–	0.67 ± 0.20
liver	1.39 ± 0.58	7.52 ± 3.55	0.85 ± 0.91	5.92 ± 2.85	1.39 ± 0.48	1.52 ± 0.66	5.53 ± 3.70	1.08 ± 0.18
kidney	1.77 ± 0.81	5.40 ± 0.96	0.90 ± 0.65	ND	1.48 ± 0.34	2.47 ± 0.31	2.86 ± 1.41	ND
blood	6.13 ± 2.41	20.8 ± 2.9	0.22 ± 0.13	4.07 ± 2.27	5.79 ± 2.42	5.79 ± 3.19	1.61 ± 1.26	0.96 ± 0.23
tumor wt (g)	0.48 ± 0.256				0.46 ± 0.251			
	5:1 BSA-(4.4)DTPA(In)				5:1 BSA-(8.3)DTPA(In)			
	% bsMAb/g	% peptide/g	T/NT pep	pep/bsMAb	% bsMAb/g	% peptide/g	T/NT pep	pep/bsMAb
tumor	12.8 ± 4.6	9.25 ± 2.74	–	0.75 ± 0.18	14.7 ± 6.2	8.62 ± 4.57	–	0.64 ± 0.32
liver	1.93 ± 1.59	0.50 ± 0.20	19.7 ± 5.3	0.38 ± 0.23	2.15 ± 1.66	0.46 ± 0.18	18.3 ± 4.5	0.25 ± 0.10
kidney	1.51 ± 0.85	2.23 ± 0.27	4.11 ± 0.88	ND	1.96 ± 0.71	2.30 ± 0.72	3.64 ± 1.08	ND
blood	5.58 ± 3.90	0.90 ± 0.53	12.3 ± 5.2	0.19 ± 0.08	5.89 ± 2.32	0.61 ± 0.16	13.4 ± 3.9	0.11 ± 0.04
tumor wt (g)	0.86 ± 0.447 ($n = 4$)				0.50 ± 0.273			

	1.5:1 In-IMP-156			
	% bsMAb/g	% peptide/g	T/NT pep	pep/bsMAb
tumor	17.8 ± 3.8	8.45 ± 1.83	–	0.49 ± 0.17
liver	2.03 ± 0.77	7.12 ± 3.60	1.77 ± 1.72	3.36 ± 0.66
kidney	2.17 ± 0.52	4.79 ± 0.37	1.79 ± 0.51	ND
blood	8.16 ± 2.36	15.7 ± 2.6	0.56 ± 0.19	2.04 ± 0.53
tumor wt (g)	0.42 ± 0.245			

[a] Animals were given 1.5×10^{-10} mol of the bsMAb (hMN-14 IgG × c734 Fab′), and then 65 h later, BSA-DTPA or indium-loaded IMP-156 was given. Two hours after the BSA-DTPA or 30 min after the IMP-156, the ^{99m}Tc-IMP-192 was given (1.5×10^{-11} mol), and then 3 h afterward, the animals were necropsied and tissues counted for ^{125}I-bsMAb and ^{99m}Tc-IMP-192. Groups A, B, C, and E used ^{125}I-bsMAb data from re-run groups as these were counted after decay of ^{99m}Tc. Values represent the means and SD of the percent injected dose per gram for the bsMAb and peptide, the tumor/nontumor ratio for the peptide, and the mole ratio of the concentration of the peptide and bsMAb in the tissues. $N = 5$ for each group, except where indicated.

quickly bind to bsMAb in the tumor, and therefore block the uptake of the radiolabeled peptide, additional escalation studies were not performed.

Efforts were then directed to an examination of indium-loaded DTPA bound to BSA. BSA-DTPA(In) conjugates could act as both a blocking agent and a clearing agent, since depending on the number of DTPA per BSA molecule, more than one bsMAb could be bound with the resulting complex being potentially cleared from the blood. To evaluate the role of DTPA substitution on the blocking and clearing ability of these agents, two BSA-DTPA conjugates were examined, one with an average of 4.4 mol of DTPA/BSA and another with 8.3 mol of DTPA/BSA. These 2 agents were given 65 h after the IgG × Fab′ bsMAb was injected, and 2 h later, the ^{99m}Tc-IMP-192 was given. The dosage of the blocking agent was also evaluated, with one group of animals receiving a 1.5:1 BSA-(4.4)DTPA(In):bsMAb ratio, while another was given a higher dose of the blocking agent, i.e., 5:1 BSA-(4.4)-DTPA(In):bsMAb ratio. BSA-(8.3)DTPA(In) was tested only at the 5:1 level. All animals were necropsied 3 h after the ^{99m}Tc-IMP-192 injection. A control group of animals were given the ^{99m}Tc-IMP-192 67 h after the bsMAb to coincide with the time the radiolabeled peptide was given to the animals receiving the BSA-DTPA conjugates.

Since the amount of ^{125}I-bsMAb in the blood of all animals given the BSA-DTPA(In) was the same as the control group, this indicates that they were not effective in removing the bsMAb from the blood under the conditions tested (Table 6). However, the BSA-DTPA(In) conjugates were effective in preventing the ^{99m}Tc-IMP-192 from binding to the bsMAb in the blood, reducing the amount from 20.8% ID/g seen in the control group to 5.8 ± 3.2% ID/g and 1.0 ± 0.5% ID/g in the animals given the 1.5:1 to 5:1 BSA-DTPA(In) dose, respectively. Increasing the mole substitution to 8.3 mol of DTPA did not significantly decrease the amount of ^{99m}Tc-IMP-192 bound to the bsMAb in the blood (0.90 ± 0.53 vs 0.61 ± 0.16% ID/g), but the variability among the various animals was considerably less with the higher level of DTPA substitution, suggesting that this conjugate may provide more reliable results. Regardless of the dose level given, the BSA-DTPA(In) conjugates significantly improved the tumor/nontumor ratios compared to the control group, with the 5:1 dose of BSA-(4.4)DTPA(In) and BSA-(8.3)DTPA(In) providing similar, but significantly higher ratios compared to the 1.5:1 dose of the BSA-(4.4)DTPA(In) ($p = 0.001$). In comparison to the peptide localization seen with the F(ab′)$_2$ × Fab′ bsMAb, tumor uptake was similar, regardless of the dose or DTPA substitution. However, peptide/bsMAb ratios were all substantially lower than that seen with the F(ab′)$_2$ × Fab′, indicating a diminished capacity of the bsMAb to bind the peptide. Tumor/blood ratios for the 1.5:1 dose of BSA-(4.4)DTPA(In) were lower than those achieved with the F(ab′)$_2$ × Fab′ conjugate, but by increasing the dose of the blocking agent to 5:1, the tumor/blood ratios were not significantly different from the F(ab′)$_2$ × Fab′ conjugate ($p = 0.197$). Tumor/liver ratios for the 5:1 dose of BSA-DTPA blocking agents were also not significantly different from the ratios for the F(ab′)$_2$ × Fab′ group ($p = 0.073$).

Peptide uptake in the kidneys of animals given the BSA-DTPA(In) conjugate was consistently about 2-fold lower than that seen in the control group or even in animals given the IMP-156 or (In)DTPA. This was most likely a consequence of the lower amount of peptide in the blood in these animals than a specific blockade of peptide uptake in the kidney, since this finding also was seen in the animals given the anti-id antibody as a clearing agent (i.e., no ability to block peptide binding).

Additional studies were performed with the BSA-(4.4)-DTPA(In) blocking agent to examine whether increasing the interval between the blocking agent from 2 to 24 h would improve the results, and a new conjugate, a galactosylated-BSA-(4.4)DTPA(In), was prepared and

Table 7. Examination of Galactosylated and Nongalactosylated BSA-DTPA (In) Blocking Agents with the hMN-14 IgG × c734 Fab′ bsMAb Using 2 and 24 h Intervals between the Blocking Agent and ^{99m}Tc-IMP-192 Peptide Injections[a]

	BSA-(4.4)DTPA(In), 2 h clearance				BSA-(4.4)DTPA(In), 24 h clearance			
	bsMAb	peptide	T/NT pep	pep/bsMAb	bsMAb	peptide	T/NT pep	pep/bsMAb
tumor	13.4 ± 5.6	13.6 ± 6.1	–	1.00 ± 0.06	8.33 ± 4.47	2.51 ± 1.15	–	0.34 ± 0.17
liver	3.07 ± 2.21	0.63 ± 0.22	21.9 ± 7.3	0.40 ± 0.42	1.52 ± 1.00	1.20 ± 0.49	2.18 ± 0.98	1.05 ± 0.63
kidney	1.36 ± 0.64	2.04 ± 0.32	6.74 ± 2.96	ND	0.87 ± 0.39	2.91 ± 1.58	2.12 ± 3.04	ND
blood	6.23 ± 2.97	1.00 ± 0.41	14.2 ± 4.9	0.18 ± 0.06	3.09 ± 1.83	1.17 ± 0.54	2.20 ± 0.74	0.46 ± 0.23
tumor wt (g)		0.20 ± 0.044 (n = 4)				0.43 ± 0.288		
	gal-BSA-(4.4)DTPA(In), 2 h clearance				gal-BSA-(4.4)DTPA(In), 24 h clearance			
	bsMAb	peptide	T/NT pep	pep/bsMAb	bsMAb	peptide	T/NT pep	pep/bsMAb
tumor	16.6 ± 7.4	5.42 ± 0.98	–	0.36 ± 0.11	13.1 ± 4.4	6.71 ± 1.94	–	0.60 ± 0.37
liver	2.99 ± 0.90	10.9 ± 2.7	0.53 ± 0.19	3.71 ± 0.56	1.31 ± 0.57	11.4 ± 4.2	0.70 ± 0.40	9.17 ± 2.11
kidney	1.86 ± 0.31	4.58 ± 0.13	1.18 ± 0.22	ND	1.17 ± 0.42	5.11 ± 1.08	1.35 ± 0.50	ND
blood	7.09 ± 1.62	16.2 ± 2.7	0.35 ± 0.12	2.33 ± 0.34	4.03 ± 1.81	14.7 ± 7.7	1.11 ± 1.69	3.69 ± 2.20
tumor wt (g)		0.33 ± 0.212				0.20 ± 0.071		

	bsMAb → 67 h → ^{99m}Tc-IMP-192			
	bsMAb	peptide	T/NT pep	pep/bsMAb
tumor	14.7 ± 5.2	5.68 ± 1.51	–	
liver	1.52 ± 0.58	10.2 ± 6.5	0.85 ± 0.68	
kidney	1.52 ± 0.38	5.27 ± 0.75	1.11 ± 0.39	
blood	6.28 ± 2.25	18.8 ± 2.5	0.31 ± 0.09	
tumor wt (g)		0.363 ± 0.159 (n = 4)		

[a] Animals were given an intravenous injection of hMN-14 IgG × Fab′ bsMAb (1.5×10^{-10} mol with a trace of ^{125}I-bsMAb), and 65 h later, BSA- or gal-BSA-(4.4)DTPA(In) was given using a 5:1 ratio of the blocking agent to blood concentration of the bsMAb at 65 h. After waiting the allotted time (2 or 24 h), ^{99m}Tc-IMP-192 was given (1.5×10^{-11} mol), and the animals were necropsied 3 h later. Values represent the means ± SD with 5 animals studied per group except where indicated.

tested using both a 2 and a 24 h clearance time prior to administering the ^{99m}Tc-IMP-192 (Table 7). In agreement with the previous study, nongalactosylated BSA-DTPA-(In) failed to clear the bsMAb from the blood, but it was effective in reducing the amount of peptide found in the blood at the time of necropsy (1.00 ± 0.41 and 1.17 ± 0.54% ID/g of the ^{99m}Tc-IMP-192 in the blood for the 2 and 24 h clearance groups, respectively, compared to 15.81 ± 2.48% ID/g seen in the control group at the 70 h necropsy time). However, not only did the gal-BSA-(4.4)-DTPA(In) fail to clear the bsMAb from the blood (7.09 ± 1.6% bsMAb/g blood for the gal-BSA(4.4)DTPA(In) group and 6.28 ± 2.25% bsMAb/g blood for the control), it also failed to block the peptide binding to the bsMAb in the blood (16.24 ± 2.67% ^{99m}Tc-IMP-192/g blood for the gal-BSA-DTPA blocking agent and 18.81 ± 2.48 for the control group). Regardless of the interval between the peptide and the time the gal-BSA-(4)DTPA(In) was given, peptide uptake in the blood as well as the other tissues was similar to that of control group. This suggests that the gal-BSA-DTPA was most likely cleared too quickly from the blood to allow for significant interaction with the bsMAb.

The 2 h clearance time for the BSA-(4.4)DTPA(In) yielded very good targeting results for the peptide, with 13.60 ± 6.09% ID/g in the tumor, and only 0.63 ± 0.22% ID/g in the liver and 1.0 ± 0.4% ID/g in the blood. Extending the clearance interval between the BSA-(4.4)-DTPA(In) and the peptide injection to 24 h showed a significant reduction in the amount of peptide in the tumor, reducing the uptake to 2.51 ± 1.15% ID/g, even though the percentage of bsMAb in the tumor had not decreased significantly (13.42 ± 5.56 vs 8.33 ± 4.47% ID/g for the 2 and 24 h clearance intervals, respectively). Extending the interval between the time the blocking agent was given to 24 h could have conceptually allowed the blocking agent time to bind to the bsMAb in the tumor, which could explain the lower peptide binding under this condition. Despite the fact that there was no statistical significance between the percentages of bsMAb in the tumor, the number of moles of bsMAb in the tumor was significantly 16.2 times more at the time the peptide was given with only a 2 h clearance compared to the 24 h clearance (p = 0.001). Another factor that could have contributed to the lower tumor uptake was the higher bsMAb in the blood capable of binding to the peptide (i.e., unblocked) at the 24 h interval. This can be seen by the peptide/bsMAb ratio in the blood at 24 h was higher than that observed with a 2 h spacing (0.46 ± 0.23 vs 0.18 ± 0.06). Thus, the lower percentage of peptide targeting to the tumor in the 24 h clearance group could have been due to a combination of both a higher proportion of unblocked bsMAb in the blood and a lower amount of bsMAb in the tumor, but a blockade effect cannot be ruled out.

Thus, the most promising of the agents tested for use with the IgG × Fab′ fragment was the nongalactosylated BSA-(4.4 or 8.3)DTPA(In), since the targeting results obtained in this study compared favorably with the F(ab′)$_2$ × Fab′. Overall, however, even this procedure failed to take full advantage of the higher amount of IgG × Fab′ bsMAb in the tumor and allow for even higher amounts of peptide targeting. For example, in this study, 13.4 ± 5.56% of the bsMAb was in the tumor of the BSA-(4.4)DTPA(In) group, but only 13.6 ± 6.09% ID/g of the peptide subsequently targeted to the tumor. In contrast with the F(ab′)$_2$ × Fab′, there was only 3.88 ± 0.66% of the bsMAb in the tumor, but 2.3-fold more peptide was able to localize to the tumor (i.e., 9.0 ± 1.40% ID/g). There could be 2 explanations for this finding. First, the amount of bsMAb in the blood had to be lowered to a level more comparable to that seen with the F(ab′)$_2$ × Fab′, which then might allow a higher portion of the ^{99m}Tc-IMP-192 peptide to gain access to the tumor. This could potentially be achieved by further adjusting the dose of the BSA-DTPA conjugate. Second, it was possible that even with a 2 h interval between the time the BSA-DTPA conjugate and the ^{99m}Tc-IMP-192 was given, this conjugate was able to also bind to the bsMAb in the tumor, thereby preventing the subsequent binding of the radiolabeled peptide.

Table 8. Testing of BSA-DTPA(In) Blocking Agent Using a Shorter Interval before the ^{99m}Tc-IMP-192 Is Given and Testing of an IgG-DTPA(In) Blocking Agent[a]

	BSA-(4.4)DTPA(In), 0.5 h clearance				BSA-(4.4)DTPA(In), 1.0 h clearance			
	% bsMAb/g	% peptide/g	T/NT pep	Pep/bsMAb	% bsMAb/g	% peptide/g	T/NT pep	Pep/bsMAb
tumor	6.05 ± 1.82	4.13 ± 0.55	–	0.71 ± 0.13	5.26 ± 2.77	4.90 ± 2.49	–	1.80 ± 1.05
liver	0.85 ± 0.54	1.01 ± 0.65	6.90 ± 6.29	1.15 ± 0.10	0.87 ± 0.22	0.87 ± 0.48	6.73 ± 3.40	0.54 ± 0.17
kidney	0.39 ± 0.26	0.82 ± 0.37	5.83 ± 2.45	ND	0.33 ± 0.13	0.83 ± 0.32	6.33 ± 2.90	ND
blood	2.66 ± 1.42	1.43 ± 0.63	3.55 ± 1.99	0.58 ± 0.13	2.71 ± 0.82	1.10 ± 0.60	4.79 ± 1.54	1.02 ± 0.27
tumor wt (g)	0.78 ± 0.188 (n = 4)				1.17 ± 0.583			
	IgG-(4)DTPA(In), 0.5 h clearance				IgG-(4)DTPA(In), 4 h clearance			
	% bsMAb/g	% peptide/g	T/NT pep	Pep/bsMAb	% bsMAb/g	% peptide/g	T/NT pep	Pep/bsMAb
tumor	4.62 ± 2.32	6.69 ± 1.02	–	1.00 ± 0.43	5.39 ± 1.99	8.19 ± 3.36	–	1.73 ± 0.88
liver	0.68 ± 0.40	0.67 ± 0.47	15.5 ± 13.8	0.94 ± 0.34	0.64 ± 0.33	0.47 ± 0.14	18.0 ± 6.3	1.04 ± 0.86
kidney	0.69 ± 0.34	1.93 ± 0.47	3.59 ± 0.78	ND	0.62 ± 0.25	2.35 ± 0.33	3.54 ± 1.42	ND
blood	1.99 ± 1.03	1.05 ± 0.72	9.66 ± 8.34	0.39 ± 0.13	1.85 ± 0.97	0.57 ± 0.15	15.3 ± 6.90	0.38 ± 0.20
tumor wt (g)	1.35 ± 0.138				0.569 ± 0.301			

	no blocking agent			
	% bsMAb/g	% peptide/g	T/NT pep	Pep/bsMAb
tumor	5.95 ± 1.50	2.89 ± 1.36	–	0.49 ± 0.16
liver	0.68 ± 0.14	9.22 ± 2.32	0.32 ± 0.13	13.8 ± 3.7
kidney	0.85 ± 0.27	4.54 ± 0.95	0.66 ± 0.32	ND
blood	2.59 ± 0.90	12.0 ± 4.6	0.29 ± 0.23	4.81 ± 1.61
tumor wt (g)	1.573 ± 0.863 (n = 4)			

[a] Animals were given an intravenous injection of hMN-14 IgG × Fab′ bsMAb (1.5×10^{-10} mol with a trace of ^{125}I-bsMAb), and 65 h later, a blocking agent was given using a 5:1 ratio of blocking agent to blood concentration of the bsMAb at 65 h. After waiting the allotted time, ^{99m}Tc-IMP-192 was given (1.5×10^{-11} mol), and the animals were necropsied 3 h later. Values represent the means ± SD with 5 animals studied per group, except where indicated.

To evaluate this second possibility, another study was performed where the length of time between the BSA-DTPA conjugate was shortened to 0.5 and 1.0 h. In addition, a larger molecular weight conjugate, namely, an IgG-(4)DTPA(In) conjugate, was prepared to determine if its larger size might delay its uptake in the tumor longer than that of the BSA-DTPA conjugate, and therefore further reduce the potential for blocking tumor uptake. With this latter conjugate, a period of 0.5 and 4.0 h was tested between the time the conjugate and peptide was given. This study showed that both the BSA- and the IgG-DTPA(In) conjugates effectively blocked peptide uptake in the blood, with 12.0 ± 4.6% ID/g of the ^{99m}Tc-IMP-192 in the blood for the control where the peptide was given without prior administration of a blocking agent, whereas the blocking groups averaged 0.6−1.4% ID/g (Table 8). There was no significant difference between the percentage of peptide bound in the blood in the group of animals where a 0.5 h or a 1.0 h interval was given, and this percentage was similar to that seen in the previous study with a 2 h interval between the time the BSA-DTPA(In) and ^{99m}Tc-IMP-192 was given. Thus, the BSA-DTPA(In) conjugate appeared to effectively block the bsMAb in the blood within 30 min. However, the peptide/bsMAb ratio in the tumor remained unchanged regardless of the interval given between the 2 injections. There were no significant differences between the % ID/g of peptide in the blood or tumor, nor were there significant differences in peptide/bsMAb ratios for the IgG-DTPA(In) at 0.5 or 4.0 h, and these targeting results were not significantly different from those obtained with the BSA-DTPA(In) blocking agent.

With the preliminary testing suggesting that the BSA- and IgG-DTPA(In) conjugates might provide the best ability to enhance the targeting results of the IgG × Fab′ bsMAb, a final study was performed where the biodistribution was monitored at 3 and 24 h after the peptide was injected, so that the results of these time periods could be compared to that of the F(ab′)$_2$ × Fab′. Animals were given the IgG × Fab′ bsMAb, and then 65 h later they received the BSA-(4.4)DTPA(In) or another IgG-DPTA(In) conjugate that had 8 mol of DTPA per IgG (IgG-(8)DTPA(In)). After waiting 2 h for clearance with the BSA-(4.4)DTPA(In) or 4 h for the IgG-(8)DTPA(In), the ^{99m}Tc-IMP-192 was given. Another control group received the IgG × Fab′ bsMAb and then the peptide 65 h later, without the intervention of a blocking agent.

The control group in which no blocking agent was given had the typical high concentration of peptide bound in the blood at 3 h, with only 50% of the bsMAb in the tumor having peptide bound (Table 9). Twenty-four hours after the peptide was given, tumor uptake had increased from 6.0 to 14.0% ID/g, which was most likely a consequence of the tumor localization of the bsMAb present in the blood that was radiolabeled in vivo with the ^{99m}Tc-IMP-192. Despite the higher tumor uptake, blood concentrations of the peptide remained elevated (9.5 ± 2.0% ID/g). Both the BSA- and IgG-DTPA(In) conjugates effectively blocked the uptake of the peptide by the bsMAb in the blood, reducing levels at 3 h from 19.5% ID/g in the control group to 0.7−1.2% in the animals receiving the blocking agents. Excellent uptake of the peptide was achieved at 3 h in both groups receiving the blocking agents, with the peptide uptake in the animals given the BSA-(4.4)DTPA(In) reaching an average of 19.8 ± 6.3% ID/g, significantly higher (p = 0.006) than the peptide uptake with the F(ab′)$_2$ × Fab′ (9.0 ± 1.4% ID/g). This result was directly related to a significantly higher tumor accretion of the IgG × Fab′ bsMAb in comparison to other studies reported herein. Tumor uptake of the ^{99m}Tc-IMP-192 for the group given the IgG-(8)DTPA(In) was not significantly higher than that seen with the F(ab′)$_2$ × Fab′ conjugate, but tumor to nontumor ratios were comparable to those obtained with the F(ab′)$_2$ × Fab′. However, the average peptide/bsMAb ratio did not exceed 1.0 (0.78 ± 0.25 and 0.83 ± 0.65, for the BSA- and IgG-DTPA(In) blocking agents, respectively), whereas a ratio 2.38 ± 0.56 was observed with the F(ab′)$_2$ × Fab′ at 3 h. Thus, the peptide targeting efficiency was not equal to that of the F(ab′)$_2$ × Fab′ conjugate. Of more concern was

Table 9. Extended Biodistribution after the Administration of ^{99m}Tc-IMP-192[a]

No Blocking Agent

	3 h after ^{99m}Tc-IMP-192				24 h after ^{99m}Tc-IMP-192			
	% bsMAb/g	% peptide/g	T/NT pep	Pep/bsMAb	% bsMAb/g	% peptide/g	T/NT pep	Pep/bsMAb
tumor	12.8 ± 3.9	6.04 ± 2.21	–	0.47 ± 0.15	16.1 ± 5.20	14.0 ± 1.2	–	0.98 ± 0.45
liver	0.97 ± 0.45	6.65 ± 2.71	1.11 ± 0.63	ND	0.89 ± 0.43	4.55 ± 2.16	19.4 ± 5.1	ND
kidney	1.08 ± 0.45	5.44 ± 0.84	1.15 ± 0.49	ND	1.02 ± 0.49	2.80 ± 0.76	17.4 ± 6.4	ND
blood	3.69 ± 1.87	19.5 ± 3.6	0.33 ± 0.15	5.90 ± 1.48	3.61 ± 1.97	9.50 ± 2.03	6.02 ± 4.0	3.13 ± 1.30
tumor wt (g)		0.22 ± 0.023				0.276 ± 0.045		

5 × BSA-(4.4)DTPA(In), 2 h Clearance

	3 h after ^{99m}Tc-IMP-192				24 h after ^{99m}Tc-IMP-192			
	% bsMAb/g	% peptide/g	T/NT pep	Pep/bsMAb	% bsMAb/g	% peptide/g	T/NT pep	Pep/bsMAb
tumor	25.6 ± 6.3	19.8 ± 6.3	–	0.78 ± 0.25	14.6 ± 7.6	4.84 ± 3.40	–	0.30 ± 0.12
liver	2.19 ± 0.96	0.63 ± 0.23	33.8 ± 9.6	ND	0.94 ± 0.39	0.17 ± 0.06	26.4 ± 13.7	ND
kidney	1.72 ± 0.53	2.42 ± 0.63	8.19 ± 1.7	ND	0.80 ± 0.35	0.59 ± 0.20	7.68 ± 4.3	ND
blood	6.12 ± 1.50	1.14 ± 0.50	20.2 ± 8.7	0.18 ± 0.08	1.98 ± 1.33	0.07 ± 0.03	62.4 ± 36.5	0.05 ± 0.03
tumor wt (g)		0.20 ± 0.040				0.23 ± 0.070		

5 × IgG-(8)DTPA(In), 4 h Clearance

	3 h after ^{99m}Tc-IMP-192				24 h after ^{99m}Tc-IMP-192			
	% bsMAb/g	% peptide/g	T/NT pep	Pep/bsMAb	% bsMAb/g	% peptide/g	T/NT pep	Pep/bsMAb
tumor	16.9 ± 6.5	11.9 ± 8.6	–	0.83 ± 0.65	16.8 ± 4.3	3.80 ± 0.64	–	0.23 ± 0.04
liver	2.23 ± 1.04	0.64 ± 0.34	18.3 ± 9.2	ND	0.93 ± 0.30	0.17 ± 0.03	22.8 ± 4.3	ND
kidney	1.16 ± 0.44	2.37 ± 0.40	4.73 ± 2.7	ND	0.83 ± 0.15	0.60 ± 0.18	6.87 ± 2.5	ND
blood	3.72 ± 1.42	0.69 ± 0.14	16.7 ± 10.0	0.21 ± 0.10	2.74 ± 1.04	0.11 ± 0.03	36.6 ± 6.2	0.04 ± 0.01
tumor wt (g)		0.28 ± 0.164				0.28 ± 0.131		

[a] Sixty-five hours after the intravenous injection of 1.5×10^{-10} mol of IgG × Fab′ bsMAb, BSA-DTPA(In) or IgG-DTPA(In) was given. Two or four hours later (respectively), ^{99m}Tc-IMP192 (1.5×10^{-11} mol) was injected, and animals were then necropsied 3 and 24 h later. Control animals were given ^{99m}Tc-IMP-192 67 h after the bsMAb without the aid of a blocking agent, being necropsied 3 and 24 h thereafter.

the finding that 24 h after the peptide was given, the % ID/g of the peptide in the tumor decreased significantly in both groups of animals receiving the blocking agents. There was a concomitant significant decrease in the amount of bsMAb in the tumor at 24 h, but the loss in bsMAb from the tumor was not proportional to that of the peptide, with the peptide/bsMAb ratio decreasing about 3−4-fold. In contrast, the peptide/bsMAb ratio using the F(ab′)$_2$ × Fab′ bsMAb remained relatively constant over this same period (3.24 ± 1.19 at 24 h), and the percentage of peptide in the tumor decreased only 1.4-fold during this time.

DISCUSSION

Pretargeting methods are attractive alternatives to directly radiolabeled antibodies because the radioactivity is not associated with an antibody that has a long half-life in the blood. When the radioactivity is associated with a small, rapidly clearing compound, such as a peptide or biotin in a pretargeting approach, the residence time in the blood is greatly reduced and vastly improved tumor/blood ratios are possible very early after the peptide's injection. Excellent for imaging, but for therapy, rapid blood clearance decreases the proportion of the injected product that is available for tumor binding. Thus, the challenge for pretargeting is to provide sufficient surrogate targets within the tumor to facilitate the capture and retention of enough radioactivity for sufficient time so that the cumulative radiation exposure will result in tumor cell death.

In the early work with bsMAb pretargeting, bsMAbs were composed of F(ab′)$_2$ × Fab′ fragments (Le Doussal et al., 1989, 1990), but the major breakthrough in achieving optimum tumor loading came with the observation that divalent haptens greatly enhance the delivery and stability of the hapten in the tumor according to a mechanism termed "affinity enhancement". Using the AES concept, Le Doussal et al. (1990) ultimately selected the Fab′ × Fab′ bsMAb configuration for pretargeting because of its faster blood clearance provided higher tumor/nontumor ratios. Animal and clinical studies have shown the utility of this method for providing high-contrast images, and there have even been some investigations of this procedure for positron-emitters and PET imaging (Klivenyi et al., 1998; Schuhmacher et al., 2001). Excellent therapeutic responses in animal xenograft models and some promising clinical results have also been reported with a bsMAb pretargeting approach using a Fab′ × Fab′ bsMAb and an ^{131}I-labeled divalent hapten (Gautherot et al., 1998, 2000; Kraeber-Bodere et al., 1999;Vuillez et al., 1999). Although these studies clearly support the ability of the bsMAb pretargeting approach to have utility for both imaging and therapy, further optimization of the amount of radioactivity that can be delivered to a tumor without significant sacrifice of normal tissue exposure would be important. To this end, we hypothesized that one way to further optimize the amount of bsMAb delivered to the tumor with greater stability was to have a bsMAb constructed with more than one binding arm directed to the primary tumor antigen. To examine this, three bsMAb conjugates were prepared by chemically combining anti-CEA and anti-DTPA(In) antibodies so that they have different valencies to the primary target antigen, CEA. The conjugates were prepared using methods designed to produce stable thioether bonds between the two antibody molecules. The IgG × Fab′ and F(ab′)$_2$ × Fab′ conjugates are divalent to CEA, and therefore should have had similar dissociation rates, which is expected to be lower than that of the monovalent Fab′ × Fab′ conjugate. However, because the IgG and F(ab′)$_2$ bsMAb conjugates differ in their molecular weight, their clearance rate from the blood is slower than the Fab′ × Fab′ conjugates, with the IgG × Fab′ conjugate having the slowest rate of clearance. The pharmacokinetic behavior of the agent is also an important delivery property. The slower clearance rate may explain why, although both the F(ab′)$_2$ × Fab′ and the IgG × Fab′ conjugates are divalent to CEA, the IgG ×

Fab′ conjugate had the highest uptake in the tumor along with the longest retention time. The IgG × Fab′ conjugate's extended retention in the blood required an evaluation of agents capable of reducing the accessibility of the conjugate remaining in the blood for the radiolabeled peptide in order to optimize pretargeting. From this perspective, the $F(ab')_2$ × Fab′ conjugate's faster blood clearance was an advantage, and because it had a higher level in the tumor than the Fab′ × Fab′ conjugate, the peptide uptake was higher. Furthermore, the in vivo tumor targeting data for the ^{125}I-$F(ab')_2$ × Fab′ alone and together with the pretargeting data for the ^{99m}Tc-IMP-192 indicated that the $F(ab')_2$ × Fab′ had a longer retention in the tumor than the Fab′ × Fab′. This suggests that the avidity of this divalent construct to CEA might be higher than that of the monovalent conjugate. These data support the main concept explored by this work, namely, that increasing the valency of a bsMAb to the tumor antigen could improve pretargeting. However, the pharmacokinetic behavior of the bsMAb is also a critical factor. Overall, with tumor uptake of the radiolabeled peptide for the $F(ab')_2$ × Fab′ conjugate was significantly higher than that found for the Fab′ × Fab′ conjugate, and with tumor/nontumor ratios significantly better than that achieved with the IgG × Fab′ conjugate, the $F(ab')_2$ × Fab′ conjugate was considered to be the best of the 3 conjugates for pretargeting.

It is also noteworthy that the peptide/bsMAb ratio for the $F(ab')_2$ × Fab′ conjugate in the blood was significantly lower than that of the Fab′ × Fab′ conjugate, which suggested the possibility that a portion of the $F(ab')_2$ × Fab′ conjugate was not able to bind the peptide as avidly as rest of the preparation. This is not unexpected, since the chemical conjugation method used for the hMN-14 IgG or $F(ab')_2$ permits random placement of the c734 Fab′ on lysine residues, but the c734 Fab′ binding orientation to the lysine is directed toward its hinge region sulfhydryl groups. With Fab′ × Fab′ conjugates, the methodology is more site-selective, with each Fab′ coupling to their respective partner's hinge region to form conjugates with similar orientation as a $F(ab')_2$. The immunoreactivity testing of these conjugates showed that all of the bsMAbs were reactive with CEA, and when the peptide was mixed with a molar excess of the bsMAb, all of the peptide was associated with the bsMAb. However, this testing would be unable to detect subtle differences in bsMAb binding affinity to the peptide that might be more likely to occur with the IgG and $F(ab')_2$ bsMAb products. Thus, given the data supporting the concept that increasing the valency to the tumor antigen can improve bsMAb pretargeting and the need to develop a more uniform product with predictable orientation, efforts are already underway to construct a number of engineered bsMAbs with divalent specificity to the tumor target. Preliminary data with a recombinant bsMAb composed of single chain to CEA and a single chain to another effector molecule (monovalent × monovalent binding specificity) suggest that the engineered protein has an advantage over the chemically conjugated Fab′ × Fab′ fragment (Sharkey et al., 2001).

The IgG × Fab′ conjugate maximized the amount of bsMAb delivered to the tumor, but its slow clearance from the blood inhibited its use for pretargeting. Extending the amount of time between the bsMAb and the peptide injection only resulted in a decrease in the concentration of the IgG × Fab′ conjugate in the tumor to levels equal to that seen with the $F(ab')_2$ × Fab′ conjugate, with subsequently no ^{99m}Tc-IMP-192 pretargeting advantage. A number of strategies were examined to determine if the benefits of the higher tumor uptake of the IgG × Fab′ at an earlier time point could be realized if the bsMAb in the blood was either cleared or blocked prior to peptide administration. An agent capable of only clearing the bsMAb from the blood, namely, an anti-idiotype antibody, might not be suitable primarily because the bsMAb was only shifted to another compartment, the liver, and the peptide subsequently became sequestered there. Unexpectedly, neither extending the interval between when the clearing agent and peptide was given, nor did galacosylating the clearing agent so that it would be more rapidly cleared to the liver hepatocytes (Mattes, 1987) provide sufficient improvements in peptide targeting. This suggested that in this model system the bsMAb was not catabolized; and, therefore, it was accessible at the time the peptide was administered. Another important factor to consider when using a clearing agent is that once the antibody is cleared from the blood, its concentration in the tumor could decrease. Since it is not important whether the bsMAb is in the blood, but the fact that its peptide-binding arm is active, agents with an ability to block the bsMAb's peptide-recognition arm with or without the ability to clear the bsMAb from the blood would be expected to perform more successfully. The pretargeting results confirmed this, with BSA- or IgG-DTPA-(In) conjugates producing the most promising results.

Developing an appropriate blocking agent must also be approached carefully, since such an agent could also block the peptide-binding arm of the bsMAb in the tumor. At the doses tested, neither the prospective blocking agents DTPA(In) nor the divalent DTPA(In) peptide, IMP-156, inhibited the binding of the peptide to the bsMAb in the blood. We elected not to aggressively pursue further dose escalation of these agents, because their small size could allow them to easily penetrate the tumor vasculature and block tumor sites if the dose was not adjusted very carefully. In a similar bsMAb targeting system as used here, Gautherot et al. (1998) tested the use of monovalent peptide in conjunction with the targeting of preformed bsMAb × peptide complexes. Tumor uptake was decreased nearly 2-fold even with a 1:1 mole excess of peptide. Over time, tumor uptake of the preformed bsMAb × peptide complex in animals given the peptide chase decreased significantly compared to animals not receiving a chase. Again, this shows that once the concentration of the targeting agent is lowered, the level in the tumor will also decrease. The extent of this decrease will be dependent on the affinity of the agents, as well as other factors, such as the shedding of the targeting antigen or the potential for the processing of the agents in the tumor.

Coupling DTPA(In) to BSA or IgG provides a larger substrate that would decrease the rate of vascular leak, which in turn could limit the accessibility of the blocking component to the prelocalized bsMAb in the tumor. Both of these agents showed significant abilities to reduce the peptide binding to the bsMAb in the blood, even when the interval between the blocking agent and the peptide injection was just 0.5 h. Although increasing the interval between the blocking agent and peptide injections could allow the blocking agent more time to block sites in the tumor, there was not conclusive evidence of this occurring. Nevertheless, limiting the time the blocking agent is in the blood and potentially accessible to block the bsMAb in the tumor is important. Galactosylating a blocking agent's carrier has been the most widely used means of accomplishing this (Mattes, 1987; Karacay et al., 1997; Axworthy et al., 2000). In our studies, coupling galactose to BSA-DTPA(In) to encourage the clearance

of the BSA-DTPA(In) from the blood made this blocking agent completely ineffective, probably because it simply cleared too quickly to have sufficient time to interact with the bsMAb. In contrast, galactosylated rWI2 was very effective in clearing the bsMAb from the blood. We have previously shown that the rate of clearance of a galactosylated IgG was dependent on the galactose substitution level (Karacay et al., 1997), and both the BSA and IgG galactose conjugates were highly substituted to encourage rapid blood clearance. Thus, possible affinity differences between the rWI2 for hMN-14 and the c734 for BSA-DTPA(In) might explain the differences in the performance of these agents. Perhaps modifying the substitution level would have improved the performance of the gal-BSA-DTPA(In) and even the gal-rWI2 conjugate. Another parameter to consider is the level of DTPA substitution and even the spacer between the DTPA and the carrier molecule. Substituting either 4 or 8 DTPA's per BSA did not appear to have any significant impact on the utility of this blocking agent. With 4−8 DTPAs per BSA or IgG, these blocking agents could have bound several bsMAb molecules, which could have facilitated their clearance from the blood. However, based on the ^{125}I-bsMAb levels in the blood, there was no evidence of its enhanced clearance by any of the blocking agents. Studies to further elaborate the reason for this were not performed, because these agents were able to sufficiently block the bsMAb to enable peptide targeting to be equal, and in the case of the percent uptake of the peptide in the BSA-(4.4)DTPA(In) group, exceed that seen with the $F(ab')_2 \times Fab'$ bsMAb. This encouraging result was tempered by the finding that the tumor uptake of the radiolabeled peptide for animals given the IgG × Fab′ bsMAb and the blocking agents dropped 3− 4-fold by 24 h after the peptide injection. In contrast, the peptide concentration in the tumor of animals given the $F(ab')_2 \times Fab'$ conjugate only dropped 1.4-fold. These findings suggest that there may be an advantage for using the IgG × Fab′ conjugate combined with a blocking agent, especially when isotopes with a short physical half-life are considered. Indeed, it should be reemphasized that an exhaustive examination of each clearing and blocking agent was not performed, and therefore the possibility exists that further examination of any one of these methods could reveal significant targeting improvements. Significant improvements in pretargeting using clearing/blocking agents have been reported (Axworthy et al., 2000), but as the results described herein illustrate, these methods are not entirely trivial. Thus, if a primary targeting agent could be constructed that had sufficient tumor loading and retention time, along with adequate natural clearance from the blood, a clearing/blocking step would not be required. With the advances in molecular engineering, this might be realized.

In conclusion, these data support the view that increasing the valency of the primary targeting agent is one way to increase the stability of the bsMAb on the tumor. However, the molecular size of the bsMAb is also an important factor to consider, as this will have an impact on whether a clearing/blocking agent will be required. The results presented herein also demonstrate that should a clearing/blocking agent be required, a blocking agent has an advantage over a clearing agent. Given some of the inherent difficulties with preparing materials by chemical conjugation methods, our group is examining constructs prepared by recombinant technologies to determine if a bsMAb with ideal targeting properties can be made.

ACKNOWLEDGMENT

We thank Ms. L. Reed, H. Richel, and Mr. T. Jackson, P. Andrews, and G. Newsome for their technical support. Supported in part by USPHS Grants CA-81760 (W.J.M.), CA-37895 (R.M.S.), and CA-84379 (R.M.S.).

LITERATURE CITED

(1) Axworthy, D. B., Fritzberg, A. R., Hylarides, M. D., Mallett, R. W., Theodore, L. J., Gustavson, L. M., Su, F.-M., Beaumier, P. L., and Reno, J. M. (1994) Preclinical evaluation of an antitumor monoclonal antibody/streptavidin conjugate for pretargeted ^{90}Y radioimmunotherapy in a mouse xenograft model. *J. Immunother. 16*, 158.

(2) Axworthy, D. B., Reno, J. M., Hylarides, M. D., Mallett, R. W., Theodore, L. J., Gustavson, L. M., Su, F., Hobson, L. J., Beaumier, P. L., and Fritzberg, A. R. (2000) Cure of human carcinoma xenografts by a single dose of pretargeted yttrium-90 with negligible toxicity. *Proc. Natl. Acad. Sci. U.S.A. 97*, 1802−1807.

(3) Barbet, J., Peltier, P., Bardet, S., Vuillez, J. P., Bachelot, I., Denet, S., Olivier, P., Leccia, F., Corcuff, B., Huglo, D., Proye, C., Rouvier, E., Meyer, P., and Chatal, J.-F. (1998) Radioimunodetection of medullary thyroid carcinoma using indium-111 bivalent hapten and anti-CEA × anti-DTPA-indium bispecific antibody. *J. Nucl. Med. 39*, 1172−1178.

(4) Boerman, O. C., Kranenborg, M. H. G. C., Oosterwijk, E., Griffiths, G. L., McBride, W. J., Oyen, W. J., de Weijert, M., Oosterwijk, J., Hansen, H. J., and Corstens, F. H. M. (1999) Pretargeting of renal cell carcinoma: Improved tumor targeting with a bivalent chelate. *Cancer Res. 59*, 4400−4405.

(5) Bos, E. S., Kuijpers, W. H., Meesters-Winters, M., Pharm, D. T., de Haan, A. S., van Doornmalen, A. M., Kaspersen, F. M., van Boeckel, C. A., and Gougeon-Betrand, F. (1994) In vitro evaluation of DNA-DNA hybridization as a two-step approach in radioimmunotherapy of cancer. *Cancer Res. 54*, 3479−3486.

(6) Breitz, H. B., Fisher, D. R., Goris, M. L., Knox, S., Ratliff, B., Murtha, A. D., and Weiden, P. L. (1999) Radiation absorbed dose estimation for ^{90}Y-DOTA-biotin with pertargeted NR-LU-10/streptavidin. *Cancer Biother. Radiopharm. 14*, 381−395.

(7) Breitz, H. B., Weiden, P. L., Beaumier, P. L., Axworthy, D. B., Seiler, C., Su, F. M., Graves, S., Bryan, K., and Reno, J. M. (2000) Clinical optimization of pretargeted radioimmunotherapy with antibody-streptavidin conjugate and 90Y-DOTA-biotin. *J. Nucl. Med. 41*, 131−140.

(8) Chang, C.-H., Sharkey, R. M., Rossi, E. A., Karacay, H., McBride, W., Hansen, H. J., Chatal, J.-F., Barbet, J., and Goldenberg, D. M. (2002) Molecular advances in pretargeting radioimmunotherapy with bispecific antibodies. *Mol. Cancer Ther. 1*, 553−563.

(9) Cremonesi, M., Ferrari, M., Chinol, M., Stabin, M. G., Grana, C., Prisco, G., Robertson, C., Tosi, G., and Paganelli, G. (1999) Three-step radioimmunotherapy with yttrium-90 biotin: dosimetry and pharmacokinetics in cancer patients. *Eur. J. Nucl. Med. 26*, 110−120.

(10) Gautherot, E., Le Doussal, J.-M., Bouhou, J., Manetti, C., Martin, M., Rouvier, E., and Barbet, J. (1998) Delivery of therapeutic doses of radioiodine using bispecific antibody-targeted bivalent haptens. *J. Nucl. Med. 39*, 1937−1943.

(11) Gautherot, E., Rouvier, E., Daniel, L., Loucif, E., Bouhou, J., Manetti, C., Martin, M., Le Doussal, J.-M., and Barbet, J. (2000) Pretargeted radioimmunotherapy of human colorectal xenografts with bispecific antibody and ^{131}I-labeled bivalent hapten. *J. Nucl. Med. 41*, 480−487.

(12) Goldenberg, D. M. (2002) Targeted therapy of cancer with radiolabeled antibodies. *J. Nucl. Med. 43*, 693−713.

(13) Goldenberg, D. M., and Hansen, H. J. (1972) Carcinoembryonic antigen present in human colonic neopasms serially propagated in hamsters. *Science 175*, 1117−1118.

(14) Goldenberg, D. M., Witte, S., and Elster, K. (1966) GW-39: A new human tumor serially transplantable in the golden hamster. *Transplantation 4*, 760−763.

(15) Goodwin, D. A., and Meares, C. F. (1999) Pretargeted peptide imaging and therapy. *Cancer Biother. Radiopharm. 14*, 145−152.
(16) Goodwin, D. A., Meares, C. F., McCall, M. J., McTigue, M., and Chaovapong, W. (1988) Pre-targeted immunoscintigraphy of murine tumor with indium-111-labeled bifunctional haptens. *J. Nucl. Med. 29*, 226−234.
(17) Goodwin, D. A., Meares, C. F., McTigue, M., Chaovapong, W., Diamanti, C. I., Ransone, C. H., and McCall, M. J. (1992) Pretargeted immunoscintigraphy: Effect of hapten valency on murine tumor uptake. *J. Nucl. Med. 33*, 2006−2013.
(18) Greenwood, F. C., and Hunter, W. M. (1963) The preparation of I-131 labeled human growth hormone of high specific radioactivity. *Biochem. J. 89*, 114−123.
(19) Hnatowich, D. J., Layne, W. W., and Childs, R. L. (1982) The preparation and labeling of DTPA-coupled albumin. *Int. J. Appl. Radiat. Isot. 33*, 327−332.
(20) Hnatowich, D. J., Virzi, F., and Rusckowski, M. (1987) Investigations of avidin and biotin for imaging applications. *J. Nucl. Med. 28*, 1294−1302.
(21) Karacay, H., Sharkey, R. M., Griffiths, G. L., Govindan, S. V., McBride, W. J., Goldenberg, D. M., and Hansen, H. J. (1997) Development of a streptavidin-anti-carcinoembryonic antigen antibody, radiolabeled biotin pretargeting method for radioimmunotherapy of colorectal cancer: Reagent development. *Bioconjugate Chem. 8*, 585−594.
(22) Karacay, H., McBride, W. J., Griffiths, G. L., Sharkey, R. M., Barbet, J., Hansen, H. J., and Goldenberg, D. M. (2000) Experimental pretargeting studies of cancer with a humanized anti-CEA × murine anti-[In-DTPA] bispecific antibody construct and a ^{99m}Tc-/^{188}Re-labeled peptide. *Bioconjugate Chem. 11*, 842−854.
(23) Klivényi, G., Schuhmacher, J., Patzelt, E., Hauser, H., Matys, R., Moock, M., Regiert, T., and Maier-Borst, W. (1998) Gallium-68 chelate imaging of human colon carcinoma xenografts pretargeted with bispecific anti-CD44$_{v6}$/anti-gallium chelate antibodies. *J. Nucl. Med. 39*, 1769−1776.
(24) Knox, S. J., Goris, M. L., Tempero, M., Weiden, P. L., Gentner, L., Breitz, H., Adams, G. P., Axworthy, D., Gaffigan, S., Bryan, K., Fisher, D. R., Colcher, D., Horak, I. D., and Weiner, L. M. (2000) Phase II trial of yttrium-90-DOTA-biotin pretargeted by NR-LU-10 antibody/streptavidin in patients with metastatic colon cancer. *Clin. Cancer Res. 6*, 406−414.
(25) Kraeber-Bodéré, F., Faivre-Chauvet, A., Saï-Maurel, C., Gautherot, E., Fiche, M., Campion, L., Le Boterff, J., Barbet, J., Chatal, J.-F., and Thédrez, P. (1999) Bispecific antibody and bivalent hapten radioimmunotherapy in CEA-producing medullary thyroid cancer xenograft. *J. Nucl. Med. 40*, 198−204.
(26) Le Doussal, J.-M., Martin, M., Gautherot, E., Delaage, M., and Barbet, J. (1989) In vitro and in vivo targeting of radiolabeled monovalent and divalent haptens with dual specificity monoclonal antibody conjugates: Enhanced divalent hapten affinity for cell bound antibody conjugates. *J. Nucl. Med. 30*, 1358−1366.
(27) Le Doussal, J.-M., Gruaz-Guyon, A., Martin, M., Gautherot, E., Delaage, M., and Barbet, J. (1990) Targeting of indium 111-labeled bivalent hapten to human melanoma mediated by bispecific monoclonal antibody conjugates: Imaging of tumors hosted in nude mice. *Cancer Res. 50*, 3445−3452.
(28) Le Doussal, J.-M., Chetanneau, A., Gruaz-Guyon, A., Martin, M., Gautherot, E., Lehur, P.-A., Chatal, J.-F., Delaage, M., and Barbet, J. (1993) Bispecific monoclonal antibody-mediated targeting of an indium-111-labeled DTPA dimer to primary colorectal tumors: Pharmacokinetics, biodistribution, scintigraphy and immune response. *J. Nucl. Med. 34*, 1662−1671.
(29) Lee, Y.-C., Atowell, C. P., and Krantz, M. J. (1976) 2-Imino-2-methoxyethyl-1-thioglycosides: New reagents for attaching sugars to proteins. *Biochemistry 15*, 3956−3963.
(30) Leung, S. O., Shevitz, J., Pellegrini, M. C., Dion, A. S., Shih, L. B., Goldenberg, D. M., and Hansen, H. J. (1994) Chimerization of LL2, a rapidly internalizing antibody specific for B cell lymphoma. *Hybridoma 13*, 469−476.
(31) Leung, S. O., Goldenberg, D. M., Dion, A. S., Pellegrini, M. C., Shevitz, J., Shih, L. B., and Hansen, H. J. (1995) Construction and characterization of a humanized, internalizing, B-cell (CD22)-specific, leukemia/lymphoma antibody, LL2. *Mol. Immunol. 32*, 1413−1427.
(32) Losman, M. J., Novick, K. E., Goldenberg, D. M., and Monestier, M. (1994) Mimicry of a carcinoembryonic antigen epitope by a rat monoclonal anti-idiotype antibody. *Int. J. Cancer 56*, 580−584.
(33) Lubic, S. P., Goodwin, D. A., Meares, C. F., Song, C., Osen, M., and Hays, M. (2001) Biodistribution and dosimetry of pretargeted monoclonal antibody 2D12.5 and Y-Janus-DOTA in BALB/c mice with KHJJ mouse adenocarcinoma. *J. Nucl. Med. 42*, 670−678.
(34) Magnani, P., Fazio, F., Grana, C., Songini, C., Frigerio, L., Pecorelli, S., Mangili, G., Colombo, N., Mariani, C. D., and Paganelli, G. (2000) Diagnosis of persistent ovarian carcinoma with three-step immunoscintigraphy. *Br. J. Cancer 82*, 616−620.
(35) Mattes, M. J. (1987) Biodistribution of antibodies after intraperitoneal or intravenous injection and the effect of carbohydrate modification. *J. Natl. Cancer Inst. 79*, 855−863.
(36) Meares, C. F., McCall, M. J., Reardon, D. T., Goodwin, D. A., Diamanti, C. I., and McTigue, M. (1984) Conjugation of antibodies with bifunctional chelating agents: Isothiocyanate and bromoacetamide reagents, methods of analysis, and subsequent addition of metal ions. *Anal. Biochem. 142*, 68−78.
(37) Paganelli, G., Riva, P., Deleide, G., Clivio, A., Chiolerio, F., Scassellati, G. A., Malcovati, M., and Siccardi, A. G. (1988) In vivo labeling of biotinylated monoclonal antibodies by radioactive avidin: a strategy to increase tumor radiolocalization. *Int. J. Cancer Suppl. 2*, 121−125.
(38) Paganelli, G., Bartolomei, M., Ferrari, M., Cremonesi, M., Broggi, G., Maira, G., Sturiale, C., Grana, C., Prisco, G., Gatti, M., Caliceti, P., and Chinol, M. (2001) Pre-targeted locoregional radioimmunotherapy with ^{90}Y-biotin in glioma patients: phase I study and preliminary therapeutic results. *Cancer Biother. Radiopharm. 16*, 227−235.
(39) Penefsky, H. S. (1979) A centrifuged column procedure for the measurement of ligand binding by beef heart F1. Part G. *Methods Enzymol. 56*, 527−530.
(40) Reardan, D. T., Meares, C. F., Goodwin, D. A., McTigue, M., David, G. S., Stone, M. R., Leung, J. P., Bartholomew, R. M., and Frincke, J. M. (1985) Antibodies to metal chelates. *Nature 316*, 265−268.
(41) Rosebrough, S. F., and Hartley, D. F. (1995) Quantification and lowering of serum biotin. *Lab Anim. Sci. 45*, 554−557.
(42) Rusckowski, M., Qu, T., Chang, F., and Hnatowich, D. J. (1997a) Pretargeting using peptide nucleic acid. *Cancer (Suppl.) 80*, 2699−2705.
(43) Rusckowski, M., Fogarasi, M., Fritz, B., and Hnatowich D. J. (1997b) Effect of endogenous biotin on the application of streptavidin and biotin in mice. *Nucl. Med. Biol. 24*, 263−268.
(44) Schuhmacher, J., Kaul, S., Klivenyi, G., Junkermann, H., Magener, A., Henze, M., Doll, J., Haberkorn, U., Amelung, F., and Bastert, G. (2001) Immunoscintigraphy with positron emission tomography: gallium-68 chelate imaging of breast cancer pretargeted with bispecific anti-MUC1/anti-Ga chelate antibodies. *Cancer Res. 61*, 3712−3717.
(45) Sharkey, R. M., Juweid, M., Shevitz, J., Behr, T., Dunn, R., Swayne, L. C., Wong, G. Y., Blumenthal, R. D., Griffiths, G. L., Siegel, J. A., Leung, S., Hansen, H. J., and Goldenberg, D. M. (1995) Evaluation of a complementarity-determining region-grafted (humanized) anti-carcinoembryonic antigen monoclonal antibody in preclinical and clinical studies. *Cancer Res. 55*, 5935s−5945s.
(46) Sharkey, R. M., Karacay, H., Griffiths, G. L., Behr, T. M., Blumenthal, R. D., Mattes, M. J., Hansen, H. J., and Goldenberg, D. M. (1997) Development of a streptavidin-anti-carcinoembryonic antigen antibody, radiolabeled biotin pretargeting method for radioimmunotherapy of colorectal cancer. Studies in a human colon cancer xenograft model. *Bioconjugate Chem. 8*, 595−604.
(47) Sharkey, R. M., Rossi, E., Karacay, H., McBride, W., Chang, K., Zang, L., Qu, T., Griffiths, G. L., Hansen, H. J., and Goldenberg, D. M. (2001) A novel, recombinant, bispecific

antibody pretargeting system for cancer radioimmunotherapy. *Clin. Cancer Res. (Suppl.) 7*, 3786s.
(48) Stickney, D. R., Anderson, L. D., Slater, J. B., Ahlem, C. N., Kirk, G. A., Schweighardt, S. A., and Frincke, J. M. (1991) Bifunctional antibody: A binary radiopharmaceutical delivery system for imaging colorectal carcinoma. *Cancer Res. 51*, 6650−6655.
(49) Vuillez, J.-P., Kraeber-Bodéré, F., Moro, D., Bardiès, M., Douillard, J.-Y., Gautherot, E., Rouvier, E., Barbet, J., Garban, F., Moreau, P., and Chatal, J.-F. (1999) Radioimmunotherapy of small cell lung carcinoma with the two-step method using a bispecific anti-carcinoembryonic antigen/anti-diethylenetriaminepentacetic acid (DTPA) antibody and iodine-131 di-DTPA hapten: Results of a phase I/II trial. *Clin. Cancer Res. (Suppl.) 5*, 3259s−3267s.

BC0200172

Synthesis of *N*-Acetyl-D-galactosamine and Folic Acid Conjugated Ribozymes

Jasenka Matulic-Adamic,* Vladimir Serebryany, Peter Haeberli, Victor R. Mokler, and Leonid Beigelman*

Department of Chemistry & Biochemistry, Ribozyme Pharmaceuticals, Inc., 2950 Wilderness Place, Boulder, Colorado 80301. Received March 7, 2002; Revised Manuscript Received April 8, 2002

To evaluate potential improvement in tissue specific targeting and cellular uptake of therapeutic ribozymes, we have developed three new phosphoramidite reagents. These reagents can be used in automated solid-phase synthesis to produce oligonucleotide conjugates containing *N*-acetyl-D-galactosamine (targeting hepatocytes) and folic acid (targeting tumor). *N*-Acetyl-D-galactosamine was attached through a linker to both 2′-amino-2′-deoxyuridine and D-threoninol scaffolds, and these conjugates were converted to phosphoramidite building blocks. Incorporation of a D-threoninol-based monomer into ribozymes provided multiply labeled ribozyme conjugates. Attachment of the fully protected pteroic acid to the D-threoninol-6-aminocaproyl-L-glutamic acid construct afforded the folic acid conjugate, which was converted into the phosphoramidite and incorporated onto the 5′-end of the ribozyme.

INTRODUCTION

The ability of catalytic RNA (*1*, *2*) to specifically bind and cleave other RNAs has been recognized as a method of controlling gene expression (*3*). The hammerhead ribozyme, being the smallest natural phosphodiesterase, has been chemically modified to function in a therapeutic setting (*4*, *5*). Several stabilized hammerhead ribozymes are currently being evaluated in human clinical trials.

To exert their activity, ribozymes (Rzs) must cross the cellular membrane(s), thereby gaining access to the cellular compartments containing their intended target. It is reasonable to expect that the potency of therapeutic Rzs will be directly dependent on the efficiency and specificity of cellular uptake. Therefore, improving tissue specific targeting and cellular uptake can potentially increase the efficacy and therapeutic index of intravenously or subcutaneously administered ribozymes.

A variety of methods to improve cellular uptake of oligonucleotides (ONs) have been described (*6*). Liposomes have been most extensively used to aid the cellular uptake of ONs in vivo. Most liposomes used for this purpose are cationic liposomes that can form stable complexes with the polyanionic ONs. Conjugation of ONs with lipophilic molecules such as cholesterol and phospholipids increases the cellular uptake by severalfold, and these ON conjugates are more potent antisense agents than their unmodified counterparts (*7*). Polymeric nanoparticles bind oligonucleotides and can protect them from degradation. Polylysine (PL) is another agent that has been shown to increase the uptake efficiency of ONs by nonspecific adsorptive endocytosis (*7*). Unfortunately, in the absence of targeting ligand, these approaches have limited promise for in vivo application.

Another approach explores receptor-mediated endocytosis to achieve drug targeting, as well as drug uptake enhancement.

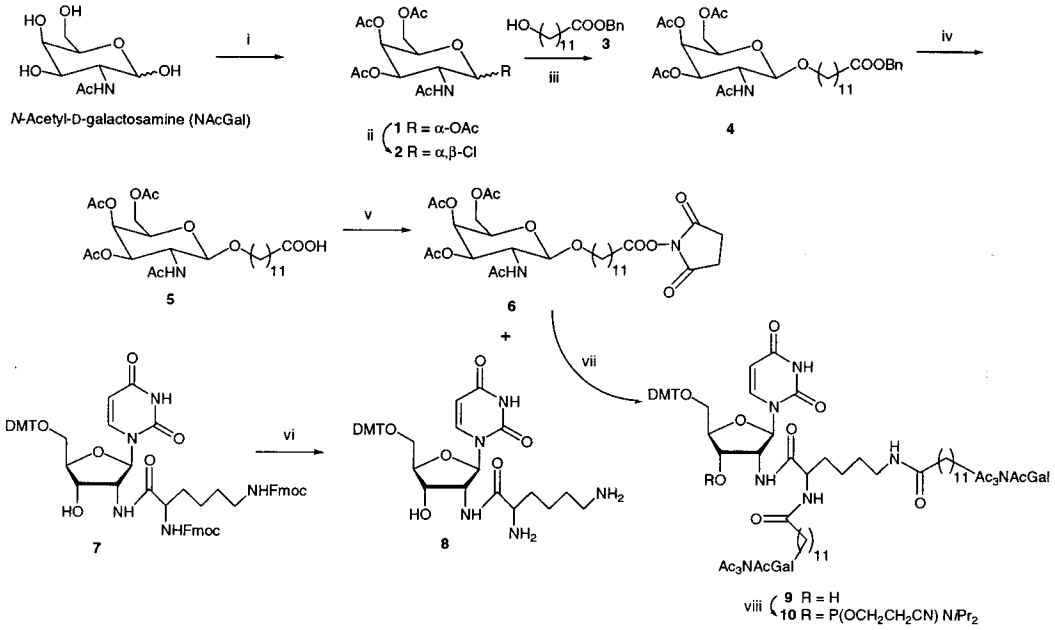
One of the best characterized endocytic receptor systems is the asialoglycoprotein receptor (ASGPr) which is unique to hepatocytes. This receptor binds branched galactose-terminal glycoproteins, such as asialoorosomucoid (ASOR). Binding of such glycoproteins or synthetic glycoconjugates to the receptor takes place with an affinity that strongly depends on the degree of branching of the oligosaccharide chain: triatennary structures are bound with greater affinity than biatenarry or monoatennary chains (*9*, *10*). Lee and Lee (*11*) obtained this high specificity through the use of *N*-acetyl-D-galactosamine (NAcGal) as the carbohydrate moiety, which has higher affinity for the receptor, compared to galactose. The above "clustering effect" has also been described for the binding and uptake of mannose-terminated glycoproteins and other glycoconjugates (*12*, *13*).

Further practical advancements in this field resulted in development of synthetic ligand-based conjugates for targeted delivery of DNA to hepatocytes. It was shown that galactose-containing ligands smaller than proteins can achieve specific and potent ASGPr binding and internalization. In addition, association of these ligands with "cargo" in the form of condensed DNA resulted in targeted delivery of DNA to hepatocytes (*14*, *15*). In one such constructs the triatennary *N*-acetyl-D-galactosamine neoglycopeptide, YEE(ah-GalNAc)$_3$ (*11*), conjugated to human serum albumin which was in turn linked to poly-L-lysine, promoted efficient delivery of DNA into Hep G2 cells (*16*). Finally, it was demonstrated that a directly linked conjugate of the above-mentioned ligand and a model oligodeoxynucleoside methylphosphonate is efficiently taken up by mouse liver (*17*).

We decided to explore the ASGPr system to facilitate uptake of therapeutic ribozymes into hepatocytes with potential application for the treatment of hepatitis C, hepatitis B, and liver cancer. We designed both nucleoside− and nonnucleoside−*N*-acetyl-D-galactosamine conjugates **10** and **13**, respectively (Schemes 1 and 2). These monomers are suitable for incorporation at any desired position of the ribozyme using solid-phase phosphoramidite chemistry. Multiple incorporations of these monomers into the ribozyme construct (Figure 1) could result in the highly desired "glycoside cluster effect".

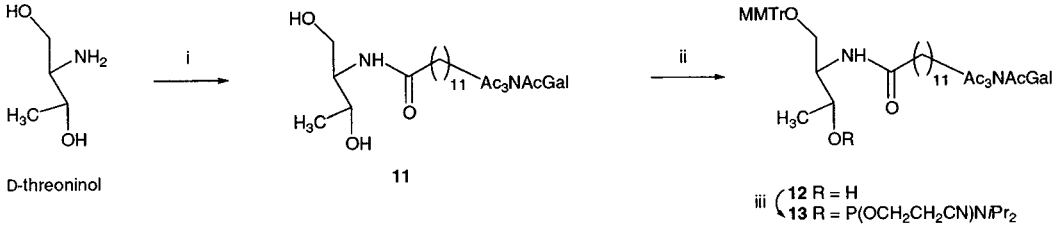
10.1021/bc025525q CCC: $22.00 © 2002 American Chemical Society
Published on Web 07/10/2002

Scheme 1. Synthesis of *N*-Acetyl-D-galactosamine−2′-Deoxy-2′-aminouridine Conjugate[a]

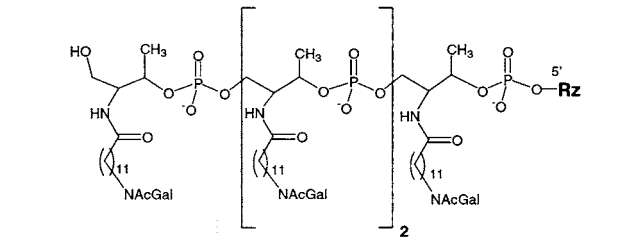


[a] Reagents and conditions: (i) Ac_2O, TEA, CH_3CN, (ii) HCl, Ac_2O, (iii) $HgCN_2$, mol sieves 4 Å, CH_3CN, CH_3NO_2−toluene 1:1, (iv) H_2, 5% Pd−C, ethanol, (v) *N*-hydroxysuccinimide, DCC, THF, (vi) diethylamine, DMF, (vii) **6**, diisopropylethylamine, DMF, (viii) 2-cyanoethyl *N*,*N*-diisopropylchlorophosphoramidite, 1-methylimidazole, DIPEA, CH_2Cl_2.

Scheme 2. Synthesis of *N*-Acetyl-D-galactosamine-D-Threoninol Conjugate[a]



[a] Reagents and conditions: (i), **6**, DCC, *N*-hydroxysuccinimide, (ii) MMTr-Cl, pyridine, (iii) 2-cyanoethyl *N*,*N*-diisopropylchlorophosphoramidite, 1-methylimidazole, DIPEA, CH_2Cl_2.



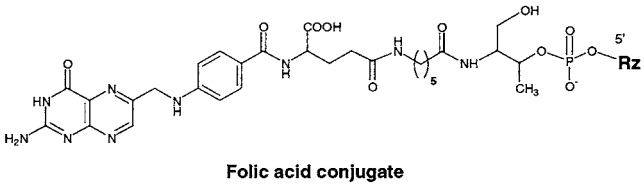


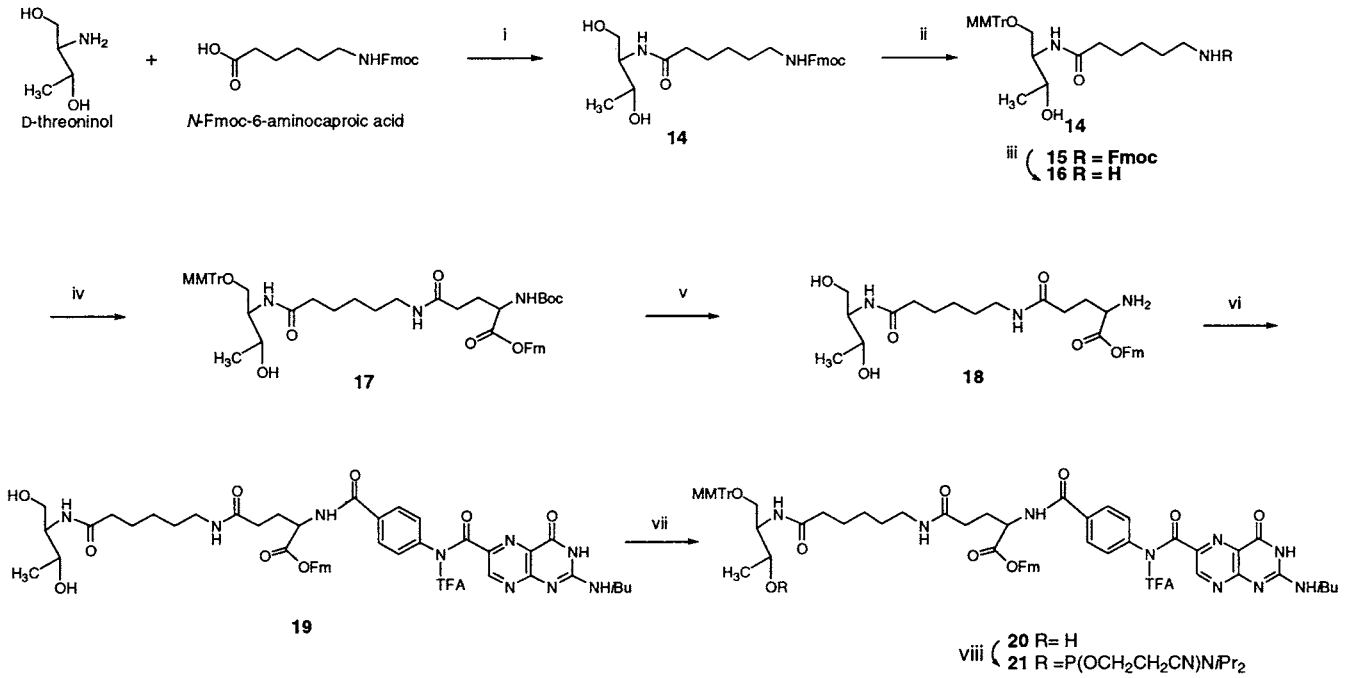
Figure 1. Conjugation of targeting ligands to the 5′-end of the ribozyme.

Among receptor-mediated endocytic systems with potential anticancer applications, the folate receptor attracted widespread attention. Indeed, several papers have described the facilitated intracellular delivery of proteins (*18*) and other macromolecules (*19*) as well as liposomes containing entrapped drugs (*20*) by folate complexation. Presumably, folic acid-receptor-mediated endocytosis is operative in these cases. Recently, a conceptually similar idea was explored in which antisense ONs were complexed with folic acid−polylysine conjugate (*21*). Importantly, it is claimed that macromolecular folate conjugates are internalized into cells by a nondestructive nonlysosomal pathway (*19*).

Several groups have recently conjugated folic acid to oligonucleotides, but most methods are difficult to scale up and lack regioselectivity. Conjugations are generally performed in a "postsynthetic" fashion. Habus et al. (*22*) coupled EDC-activated folic acid with the amino-linked antisense ON attached to the solid support, while Harrison and Balasubramanian (*23*) described a solution-phase coupling of 3′-thiol- or 3′-maleimide-derivatized oligonucleotides with cysteinyl folate to afford disulfide- and thioether-linked conjugates, respectively.

Recently, Bhat et al. (*24*) reported the synthesis of nucleoside−folic acid conjugate building blocks and their incorporation into oligonucleotides using solid-supported phosphoramidite chemistry. Their synthetic approach allowed for regioselective coupling of folic acid through the α- or γ-carboxylic group. It has been demonstrated that only those conjugates containing the adduct attached at the γ-carboxyl of folic acid retain the ability to bind to cell surface folate receptors with the same affinity as free folic acid (*25*).

Scheme 3. Synthesis of Folic Acid−D-Threoninol Conjugate[a]



[a] Reagents and conditions: (i) *N*-hydroxysuccinimide, DCC, DMF, (ii) MMTr-Cl, pyridine (iii) piperidine, DMF, (iv) *N*-Boc-α-OFm-glutamic acid, *N*-hydroxysuccinimide, DCC, DMF, (v) HCl, anisole, dioxane, (vi) N^2-*i*Bu-N^{10}-TFA-pteroic acid, 1-hydroxybenzotriazole, EDC, DMF, (vii) MMTr-Cl, pyridine, (viii) 2-cyanoethyl tetraisopropylphosphordiamidite, pyridinium trifluoroacetate, CH_2Cl_2.

In analogy with these studies, we hoped to achieve tissue-specific targeting and facilitated intracellular delivery of the ribozyme−folate conjugate (Figure 1) by a receptor-mediated endocytosis mechanism, since the receptors for certain growth factors, hormones, and vitamins (incliding folic acid) are overexpressed in rapidly dividing tumor cells (*26*−*29*).

Folic acid monomer **19** was assembled by stepwise peptide coupling of D-threoninol and 6-aminocaproic acid, followed by α-protected L-glutamic acid and N^2,N^{10}-bis-protected pteroic acid (Scheme 3). As in the case of NAcGal phosphoramidites **10** and **13**, folic acid phosphoramidite **21** can be incorporated at any desired position within the oligonucleotide.

EXPERIMENTAL PROCEDURES

All reactions were carried out under a positive pressure of argon in anhydrous solvents. Commercially available reagents and anhydrous solvents were used without further purification. ^{1}H (400.035 MHz) and ^{31}P (161.947 MHz) NMR spectra were recorded in $CDCl_3$, unless stated otherwise, and chemical shifts in ppm refer to TMS and H_3PO_4, respectively. Analytical thin-layer chromatography (TLC) was performed with Merck Art. 5554 Kieselgel 60 F_{254} plates and flash column chromatography using Merck 0.040−0.063 mm silica gel 60. The general procedures for RNA synthesis, deprotection, and purification have been described previously (*30*). MALDI-TOF mass spectra were determined on PerSeptive Biosystems Voyager spectrometer. Electrospray mass spectrometry was run on the PE/Sciex API365 instrument.

***N*-Acetyl-1,4,6-tri-*O*-acetyl-2-amino-2-deoxy-*β*-D-galactopyranose (1).** *N*-Acetyl-D-galactosamine (6.77 g, 30.60 mmol) was suspended in acetonitrile (200 mL), and triethylamine (50 mL, 359 mmol) was added. The mixture was cooled in an ice-bath, and acetic anhydride (50 mL, 530 mmol)) was added dropwise under cooling. The suspension slowly cleared and was then stirred at room temperature for 2 h. It was then cooled in an ice-bath, and methanol (60 mL) was added and the stirring continued for 15 min. The mixture was concentrated under reduced pressure and the residue partitioned between dichloromethane and 1 N HCl. Organic layer was washed twice with 5% $NaHC_3O_3$, followed by brine, dried (Na_2SO_4), and evaporated to dryness to afford 10 g (84%) of **1** as a colorless foam. ^{1}H NMR was in agreement with published data (*32*).

2-Acetamido-3,4,6-tetra-*O*-acetyl-1-chloro-D-galactopyranose (2). This compound was prepared from **1** as described by Findeis (*32*).

Benzyl 12-Hydroxydodecanoate (3). To a cooled (0 °C) and stirred solution of 12-hydroxydodecanoic acid (10.65 g, 49.2 mmol) in DMF (70 mL) was added DBU (8.2 mL, 54.1 mmol), followed by benzyl bromide (6.44 mL, 54.1 mmol). The mixture was left overnight at room temperature and then concentrated under reduced pressure and partitioned between 1 N HCl and ether. The organic phase was washed with saturated $NaHCO_3$, dried over Na_2SO_4, and evaporated. Flash chromatography using 20−30% gradient of ethyl acetate in hexanes afforded the benzyl ester as a white powder (14.1 g, 93.4%). ^{1}H NMR spectral data were in accordance with the published values (*33*).

1-(12-Benzyloxydodecanoyl)-2-acetamido-3,4,6-tri-*O*-acetyl-2-deoxy-*β*-D-galactopyranose (4). 1-Chloro sugar **2** (4.26 g, 11.67 mmol) and benzyl 12-hydroxydodecanoate (**3**) (4.3 g, 13.03 mmol) were dissolved in nitromethane−toluene 1:1 (122 mL) under argon, and $Hg(CN)_2$ (3.51 g, 13.89 mmol) and powdered molecular sieves 4 Å (1.26 g) were added. The mixture was stirred at room temperature for 24 h and then filtered and the filtrate concentrated under reduced pressure. The residue was partitioned between dichloromethane and brine, and the organic layer was washed with brine, followed by 0.5 M KBr, dried (Na_2SO_4), and evaporated to a syrup. Flash silica gel column chromatography using 15−30% gradient of acetone in hexanes yielded product **4** as a colorless foam (6 g, 81%). ^{1}H NMR δ 7.43 (m, 5H, phenyl), 5.60 (d,

1H, $J_{NH,2}$ = 8.8, NH), 5.44 (d, $J_{4,3}$ = 3.2, 1H, H4), 5.40 (dd, $J_{3,4}$ = 3.2, $J_{3,2}$ = 10.8, 1H, H3), 5.19 (s, 2H, CH_2Ph), 4.80 (d, $J_{1,2}$ = 8.0, 1H, H1), 4.23 (m, 2H, CH_2), 3.99 (m, 3H, H2, H6), 3.56 (m, 1H, H5), 2.43 (t, J = 7.2, 2H,CH_2), 2.22 (s, 3H, Ac), 2.12 (s, 3H, Ac), 2.08 (s, 3H, Ac), 2.03 (s, 3H, Ac), 1.64 (m, 4H, 2 × CH_2), 1.33 (br m, 14H, 7 × CH_2). MS/ESI$^-$ m/z 634.5 $(M - H)^-$.

1-(12-Hydroxydodecanoyl)-2-acetamido-3,4,6-tri-*O*-acetyl-2-deoxy-*β*-D-galactopyranose (5). Conjugate **4** (2 g, 3.14 mmol)) was dissolved in ethanol (50 mL), and 5% Pd−C (0.3 g) was added. The reaction mixture was hydrogenated overnight at 45 psi H_2, the catalyst was filtered off, and the filtrate was evaporated to dryness to afford pure **5** (1.7 g, quantitative) as a white foam. ^{1}H NMR δ 5.73 (d, 1H, $J_{NH,2}$ = 8.4, NH), 5.44 (d, $J_{4,3}$ = 3.0, 1H, H4), 5.40 (dd, $J_{3,4}$ = 3.0, $J_{3,2}$ = 11.2,1H, H3), 4.78 (d, $J_{1,2}$ = 8.8, 1H, H1), 4.21(m, 2H, CH_2), 4.02 (m, 3H, H2, H6), 3.55 (m, 1H, H5), 2.42 (m, 2H, CH_2), 2.23(s, 3H, Ac), 2.13 (s, 3H, Ac), 2.09 (s, 3H, Ac), 2.04 (s, 3H, Ac), 1.69 (m, 4H, 2 × CH_2), 1.36 (br m, 14H, 7 × CH_2). MS/ESI$^-$ m/z 544.0 $(M - H)^-$.

2′-(*N*-L-Lysylamino)-5′-*O*-4,4′-dimethoxytrityl-2′-deoxyuridine (8). 2′-(*N*-α,ϵ-bis-Fmoc-L-lysyl)amino-5′-*O*-4,4′-dimethoxytrityl-2′-deoxyuridine (**7**) (*31*) (4 g, 3.58 mmol) was dissolved in anhydrous DMF (30 mL), and diethylamine (4 mL) was added. The reaction mixture was stirred at room temperature for 5 h and then concentrated (oil pump) to a syrup. The residue was dissolved in ethanol, and ether was added to precipitate the product (1.8 g, 75%). ^{1}H NMR (DMSO-d_6-D_2O) δ 7.70 (d, $J_{6,5}$ = 8.4, 1H, H6), 7.48−6.95 (m, 13H, aromatic), 5.93 (d, $J_{1',2'}$ = 8.4, 1H, H1′), 5.41 (d, $J_{5,6}$ = 8.4, 1H, H5), 4,62 (m, 1H, H2′), 4.19 (d, 1H, $J_{3',2'}$ = 6.0, H3′), 3.81 (s, 6H, 2 × OMe), 3.30 (m, 4H, 2H5′, CH_2), 1.60−1.20 (m, 6H, 3 × CH_2). MS/ESI$^+$ m/z 674.0 $(M + H)^+$.

2′-(*N*-α,ϵ-Bis(12′-hydroxydodecanoyl-2-acetamido-3,4,6-tri-*O*-acetyl-2-deoxy-*β*-D-galac-topyranose)-L-lysyl)amino-2′-deoxy-5′-*O*-4,4′-dimethoxytrityl uridine (9). 5 (1.05 g, 1.92 mmol) was dissolved in anhydrous THF and *N*-hydroxysuccinimide (0.27 g, 2.35 mmol), and 1,3-dicyclohexylcarbodiimide (0.55 g, 2.67 mmol) were added. The reaction mixture was stirred at room temperature overnight and then filtered through Celite pad and the filtrate concentrated under reduced pressure. The crude NHSu ester **6** was dissolved in dry DMF (13 mL) containing diisopropylethylamine (0.67 mL, 3.85 mmol) and to this solution was added nucleoside **2** (0.64 g, 0.95 mmol). The reaction mixture was stirred at room temperature overnight and then concentrated under reduced pressure. The residue was partitioned between water and dichloromethane, the aqueous layer was extracted with dichloromethane, and the organic layers were combined, dried (Na_2SO_4), and evaporated to a syrup. Flash silica gel column chromatography using 2−3% gradient of methanol in ethyl acetate yielded **9** as a colorless foam (1.04 g, 63%). ^{1}H NMR δ 7.42 (d, $J_{6,5}$ = 8.4, 1H, H6 Urd), 7.53−6.97 (m, 13H, aromatic), 6.12 (d, $J_{1',2'}$ = 8.0, 1H, H-1′), 5.41 (m, 3H, H5 Urd, H4 NAcGal), 5.15 (dd, $J_{3,4}$ = 3.6, $J_{3,2}$ = 11.2, 2H, H3 NAcGal), 4.87 (dd, $J_{2',3'}$ = 5.6, $J_{2',1'}$ = 8.0, 1H, H2′), 4.63 (d, $J_{1,2}$ = 8.0, 2H, H1 NAcGal), 4.42 (d, $J_{3',2'}$ = 5.6, 1H, H3′), 4.29−4.04 (m, 9H, H4′, H2 NAcGal, H5 NacGal, CH_2), 3.95−3.82 (m, 8H, H6 NAcGal, 2 × OMe), 3.62−3.42 (m, 4H, H5′, H6 NAcGal), 3.26 (m, 2H, CH_2), 2.40−1.97 (m, 28H, CH_2, Ac), 1.95−1.30 (m, 50H, CH_2). MS/ESI$^-$ m/z 1727.0 $(M - H)^-$.

2′-(*N*-α,ϵ-Bis(12′-hydroxydodecanoyl-2-acetamido-3,4,6-tri-*O*-acetyl-2-deoxy-*β*-D-galactopyranose)-L-lysyl)amino-2′-deoxy-5′-*O*-4,4′-dimethoxytrityl uridine 3′-*O*-(2-Cyanoethyl *N,N*-Diisopropylphosphoramidite) (10). Conjugate **9** (0.87 g, 0.50 mmol) was dissolved in dry dichloromethane (10 mL) under argon, and diisopropylethylamine (0.36 mL, 2.07 mmol) and 1-methylimidazole (21 μL, 0.26 mmol) were added. The solution was cooled to 0 °C, and 2-cyanoethyl diisopropylchlorophosphoramidite (0.19 mL, 0.85 mmol) was added. The reaction mixture was stirred at room temperature for 1 h and then cooled to 0 °C and quenched with anhydrous ethanol (0.5 mL). After stirring for 10 min, the solution was concentrated under reduced pressure (40 °C) and the residue dissolved in dichloromethane and chromatographed on the column of silica gel using hexanes−ethyl acetate 1:1, followed by ethyl acetate and finally ethyl acetate−acetone 1:1 (1% triethylamine was added to solvents) to afford the phosphoramidite **10** (680 mg, 69%). ^{31}P NMR δ 152.0 (s), 149.3 (s). MS/ESI$^-$ m/z 1928.0 $(M - H)^-$.

***N*-(12′-Hydroxydodecanoyl-2-acetamido-3,4,6-tri-*O*-acetyl-2-deoxy-*β*-D-galactopyranose)-D-threoninol (11).** 12′-Hydroxydodecanoyl-2-acetamido-3,4,6-tri-*O*-acetyl-2-deoxy-*β*-D-galactopyranose **5** (850 mg, 1.56 mmol) was dissolved in DMF (5 mL), and to the solution were added *N*-hydroxysuccinimide (215 mg, 1.87 mmol) and 1,3-dicyclohexylcarbodimide (386 mg, 1.87 mmol). The reaction mixture was stirred at room temperature overnight, the precipitate was filtered off, and to the filtrate was added D-threoninol (197 mg, 1.87 mmol). The mixture was stirred at room temperature overnight and concentrated in vacuo. The residue was partitioned between dichloromethane and 5% $NaHCO_3$, and the organic layer was washed with brine, dried (Na_2SO_4), and evaporated to a syrup. Silica gel column chromatography using 1−10% gradient of methanol in dichloromethane afforded **11** as a colorless oil (0.7 g, 71%). ^{1}H NMR δ 6.35 (d, J = 7.6, 1H, NH), 5.77 (d, J = 8.0, 1H, NH), 5.44 (d, $J_{4,3}$ = 3.6, 1H, H4), 5.37 (dd, $J_{3,4}$ = 3.6, $J_{3,2}$ = 11.2, 1H, H3), 4.77 (d, $J_{1,2}$ = 8.0, 1H, H1), 4.28−4.18 (m, 3H, CH_2, CH), 4.07−3.87 (m, 6H), 3.55 (m, 1H, H5), 3.09 (d, J = 3.2, 1H, OH), 3.02 (t, J = 4.6, 1H, OH), 2.34 (t, J = 7.4, 2H, CH_2), 2.23 (s, 3H, Ac), 2.10 (s, 3H, Ac), 2.04 (s, 3H, Ac), 1.76−1.61 (m, 2 × CH_2), 1.35 (m, 14H, 7 × CH_2), 1.29 (d, J = 6.4, 3H, CH_3). MS/ESI$^-$ m/z 631.5 $(M - H)^-$.

1-*O*-(4-Monomethoxytrityl)-*N*-(12′-hydroxydodecanoyl-2-acetamido-3,4,6-tri-*O*-acetyl-2-deoxy-*β*-D-galactopyranose)-D-threoninol (12). To the solution of **11** (680 mg, 1.1 mmol) in dry pyridine (10 mL) was added *p*-anisylchlorodiphenylmethane (430 mg, 1.39 mmol), and the rection mixture was stirred and protected from moisture overnight. Methanol (3 mL) was added and the solution stirred for 15 min and evaporated in vacuo. The residue was partitioned between dichloromethane and 5% $NaHCO_3$, and the organic layer was washed with brine, dried (Na_2SO_4), and evaporated to a syrup. Silica gel column chromatography using 1−3% gradient of methanol in dichloromethane afforded **12** as a white foam (0.75 g, 77%). ^{1}H NMR δ 7.48−6.92 (m, 14 H, aromatic), 6.15 (d, J = 8.8, 1H, NH), 5.56 (d, J = 8.0, 1H, NH), 5.45 (d, $J_{4,3}$ = 3.2, 1H, H4), 5.40 (dd, $J_{3,4}$ = 3.2, $J_{3,2}$ = 11.2, 1H, H3), 4.80 (d, $J_{1,2}$ = 8.0, 1H, H1), 4.3−4.13 (m, 3H, CH_2, CH), 4.25−3.92 (m, 4H, H6, H2, CH), 3.89 (s, 3H, OMe), 3.54 (m, 2H, H5, CH), 3.36 (dd, J = 3.4, J = 9.8, 1H, CH), 3.12 (d, J = 2.8, 1H, OH), 2.31 (t, J = 7.6, 2H, CH_2), 2.22 (s, 3H, Ac), 2.13 (s, 3H, Ac), 2.03 (s, 3H, Ac), 1.80−1.55 (m, 2 × CH_2), 1.37 (m, 14H, 7 × CH_2), 1.21 (d, J = 6.4, 3H, CH_3). MS/ESI$^-$ m/z 903.5 $(M - H)^-$.

1-*O*-(4-Monomethoxytrityl)-*N*-(12′-hydroxydodecanoyl-2-acetamido-3,4,6-tri-*O*-acetyl-2-deoxy-*β*-D-galactopyranose)-D-threoninol 3-*O*-(2-Cyanoethyl *N,N*-Diisopropylphosphoramidite) (13). Conjugate **12**

(1.2 g, 1.33 mmol) was dissolved in dry dichloromethane (15 mL) under argon, and diisopropylethylamine (0.94 mL, 5.40 mmol) and 1-methylimidazole (55 μL, 0.69 mmol) were added. The solution was cooled to 0 °C, and 2-cyanoethyl *N*,*N*-diisopropylchlorophosphoramidite (0.51 mL, 2.29 mmol) was added. The reaction mixture was stirred at room temperature for 2 h and then cooled to 0 °C and quenched with anhydrous ethanol (0.5 mL). After stirring for 10 min, the solution was concentrated under reduced pressure (40 °C), and the residue dissolved in dichloromethane and chromatographed on the column of silica gel using 50−80% gradient of ethyl acetate in hexanes (1% triethylamine) to afford the phosphoramidite **13** (1.2 g, 82%). ^{31}P NMR δ 149.41 (s), 149.23 (s).

***N*-(6-(*N*-Fmoc-6-Aminocaproyl)-D-threoninol (14).** *N*-Fmoc-6-Aminocaproic acid (10 g, 28.30 mmol) was dissolved in DMF (50 mL), and *N*-hydroxysuccinimide (3.26 g, 28.30 mmol) and 1,3-dicyclohexylcarbodiimide (5.84 g, 28.3 mmol) were added to the solution. The reaction mixture was stirred at room temperature overnight and the precipitated 1,3-dicyclohexylurea filtered off. To the filtrate D-threoninol (2.98 g, 28.30 mmol) was added and the reaction mixture stirred at room temperature overnight. The solution was reduced to ca. half the volume in vacuo and the residue diluted with ethyl acetate and extracted with 5% $NaHCO_3$, followed by brine. The organic layer was dried (Na_2SO_4), evaporated to a syrup, and chromatographed by silica gel column chromatography using 1−10% gradient of methanol in ethyl acetate. Fractions containing the product were pooled and evaporated to a white solid (9.94 g, 80%). ^{1}H NMR (DMSO-d_6−D_2O) δ 7.97−7.30 (m, 8H, aromatic), 4.34 (d, J = 6.80, 2H, Fm), 4.26 (t, J = 6.80, 1H, Fm), 3.9 (m, 1H, H3 Thr), 3.69 (m, 1H, H2 Thr), 3.49 (dd, J = 10.6, J = 7.0, 1H, H1 Thr), 3.35 (dd, J = 10.6, J = 6.2, 1H, H1′ Thr), 3.01 (m, 2H, CH_2CO Acp), 2.17 (m, 2H, CH_2-NH Acp), 1.54 (m, 2H, CH_2 Acp), 1.45 (m, 2H, CH_2 Acp), 1.27 (m, 2H, CH_2 Acp), 1.04 (d, J = 6.4, 3H, CH_3). MS/ESI$^+$ m/z 441.0 $(M + H)^+$.

1-*O*-(4-Monomethoxytrityl)-*N*-(*N*-Fmoc-6-aminocaproyl)-D-threoninol (15). To the solution of **14** (6 g, 13.62 mmol) in dry pyridine (80 mL) was added *p*-anisylchlorodiphenylmethane (6 g, 19.43 mmol), and the reaction mixture was stirred at room temperature overnight. Methanol was added (20 mL) and the solution concentrated in vacuo. The residual syrup was partitioned between dichloromethane and 5% $NaHCO_3$, and the organic layer was washed with brine, dried (Na_2SO_4), and evaporated to dryness. Flash column chromatography using 1−3% gradient of methanol in dichloromethane afforded **15** as a white foam (6 g, 62%). ^{1}H NMR (DMSO-d_6) δ 7.97−6.94 (m, 22H, aromatic), 4.58 (d, 1H, J = 5.2, OH), 4.35 (d, J = 6.8, 2H, Fm), 4.27 (t, J = 6.8, 1H, Fm), 3.97 (m, 2H, H2,H3 Thr), 3.80 (s, 3H, OCH_3), 3.13 (dd, J = 8.4, J = 5.6, 1H, H1 Thr), 3.01 (m, 2H, CH_2CO Acp), 2.92 (m, dd, J = 8.4, J = 6.4, 1H, H1′ Thr), 2.21 (m, 2H, CH_2NH Acp), 1.57 (m, 2H, CH_2 Acp), 1.46 (m, 2H, CH_2 Acp), 1.30 (m, 2H, CH_2 Acp), 1.02 (d, J = 5.6, 3H, CH_3). MS/ESI$^+$ m/z 735.5 $(M + Na)^+$.

1-*O*-(4-Monomethoxytrityl)-*N*-(6-aminocaproyl)-D-threoninol (16). 15 (9.1 g, 12.77 mmol) was dissolved in DMF (100 mL) containing piperidine (10 mL), and the reaction mixture was kept at room temperature for 1 h. The solvents were removed in vacuo, and the residue was purified by silica gel column chromatography using 1−10% gradient of methanol in dichloromethane to afford **16** as a syrup (4.46 g, 71%). ^{1}H NMR δ 7.48−6.92 (m, 14H, aromatic), 6.16 (d, J = 8.8, 1H, NH), 4.17 (m, 1H, H3 Thr), 4.02 (m, 1H, H2 Thr), 3.86 (s, 3H, OCH_3), 3.50 (dd, J = 9.7, J = 4.4, 1H, H1 Thr), 3.37 (dd, J = 9.7, J = 3.4, 1H, H1′ Thr), 2.78 (t, J = 6.8, 2H, CH_2CO Acp), 2.33 (t, J = 7.6, 2H, CH_2NH Acp), 1.76 (m, 2H, CH_2 Acp), 1.56 (m, 2H, CH_2 Acp), 1.50 (m, 2H, CH_2 Acp), 1.21 (d, J = 6.4, 3H, CH_3). MS/ESI$^+$ m/z 491.5 $(M + H)^+$.

1-*O*-(4-Monomethoxytrityl)-*N*-(6-(*N*-(*N*-Boc-α-OFm-L-glutamyl)aminocaproyl))-D-threoninol (17). To the solution of *N*-Boc-α-L-OFm-glutamic acid (1.91 g, 4.48 mmol) in DMF (10 mL) were added *N*-hydroxysuccinimide (518 mg, 4.50 mmol) and 1,3-dicyclohexylcarbodiimide (928 mg, 4.50 mmol), and the reaction mixture was stirred at room temperature overnight. 1,3-Dicyclohexylurea was filtered off, and to the filtrate were added **16** (2 g, 4.08 mmol) and pyridine (2 mL). The reaction mixture was stirred at room temperature for 3 h and then concentrated in vacuo. The residue was partitioned between ethyl acetate and 5% $NaHCO_3$, and the organic layer extracted with brine, dried (Na_2SO_4), and evaporated to a syrup. Column chromatography using 2−10% gradient of methanol in dichloromethane afforded **17** as a white foam (3.4 g, 93%). ^{1}H NMR δ 7.86−6.91 (m, 22H, aromatic), 6.13 (d, J = 8.8, 1H, NH), 5.93 (br s, 1H, NH), 5.43 (d, J = 8.4, 1H, NH), 4.63 (dd, J = 10.6, J = 6.4, 1H, Fm), 4.54 (dd, J = 10.6, J = 6.4, 1H, Fm), 4.38 (m, 1H, Glu), 4.30 (t, J = 6.4, 1H, Fm), 4.18 (m, 1H, H3 Thr), 4.01 (m, 1H, H2 Thr), 3.88 (s, 3H, OCH_3), 3.49 (dd, J = 9.5, J = 4.4, 1H, H1 Thr), 3.37 (dd, J = 9.5, J = 3.8, 1H, H1′ Thr), 3.32 (m, 2H, CH_2CO Acp), 3.09 (br s, 1H, OH), 2.32 (m, 2H, CH_2NH Acp), 2.17 (m, 3H, Glu), 1.97 (m, 1H, Glu), 1.77 (m, 2H, CH_2 Acp), 1.61 (m, 2H, CH_2 Acp), 1.52 (s, 9H, *t*Bu), 1.21 (d, J = 6.4, 3H, CH_3). MS/ESI$^+$ m/z 920.5 $(M + Na)^+$.

***N*-(6-(*N*-α-OFm-L-Glutamyl)aminocaproyl))-D-threoninol Hydrochloride (18). 17** (2 g, 2.23 mmol) was dissolved in methanol (30 mL) containing anisole (10 mL), and to this solution was added 4 M HCl in dioxane. The reaction mixture was stirred for 3 h at room temperature and then concentrated in vacuo. The residue was dissolved in ethanol and the product precipitated by addition of ether. The precipitate was washed with ether and dried to give **18** as a colorless foam (1 g, 80%). ^{1}H NMR (DMSO-d_6−D_2O) δ 7.97−7.40 (m, 8H, aromatic), 4.70 (m, 1H, Fm), 4.55 (m, 1H, Fm), 4.40 (t, J = 6.4, 1H, Fm), 4.14 (t, J = 6.6, 1H, Glu), 3.90 (dd, J = 2.8, J = 6.4, 1H, H3 Thr), 3.68 (m, 1H, H2 Thr), 3.49 (dd, J = 10.6, J = 7.0, 1H, H1 Thr), 3.36 (dd, J = 10.6, J = 6.2, 1H, H1′ Thr), 3.07 (m, 2H, CH_2CO Acp), 2.17 (m, 3H), 1.93 (m, 2H), 1.45 (m, 2H), 1.27 (m, 2H), 1.04 (d, J = 6.4, 3H, CH_3). MS/ESI$^+$ m/z 526.5 $(M + H)^+$.

***N*-(6-(*N*-α-OFm-L-Glutamyl)aminocaproyl))-D-threoninol-N^2-*i*Bu-N^{10}-TFA-pteroic Acid Conjugate (19).** To the solution of N^2-*i*Bu-N^{10}-TFA-pteroic acid (*34*) (480 mg, 1 mmol) in DMF (5 mL) were added 1-hydroxybenzotriazole (203 mg, 1.50 mmol), EDC (288 mg, 1.50 mmol) and **18** (free base, 631 mg, 1.2 mmol, obtained by stirring methanolic solution of **18** with silver carbonate for 5 min). The reaction mixture was stirred at room temperature for 2 h and then concentrated to ca. 3 mL and loaded on the column of silica gel. Elution with dichloromethane, followed by 1−20% gradient of methanol in dichloromethane, afforded **19** (0.5 g, 51%). ^{1}H NMR (DMSO-d_6−D_2O) δ 9.09 (d, J = 6.8, 1H, NH) 8.96 (s, 1H, H7 pteroic acid), 8.02−7.19 (m, 13H, aromatic, NH), 5.30 (s, 2H, pteroic acid), 4.50 (m, 1H, Glu), 4.41 (d, J = 6.8, 2H, Fm), 4.29 (t, J = 6.8, 1H, Fm), 3.89 (dd, J = 6.2, J = 2.8, 1H, H3 Thr), 3.68 (m, 1H, H2 Thr), 3.48 (dd, J = 10.4, J = 7.0, 1H, H1 Thr), 3.36 (dd, J = 10.4, J = 6.2, 1H, H1′ Thr), 3.06 (m, 2H, CH_2CO Acp), 2.84 (m, 1H, *i*Bu), 2.25 (m, 2H, CH_2NH Acp), 2.16 (m, 3H, Glu), 1.99 (m, 1H,

Glu), 1.52 (m, 2H, Acp), 1.42 (m, 2H, Acp), 1.27 (m, 2H, Acp), 1.20 (s, 3H, *i*Bu), 1.19 (s, 3H, *i*Bu), 1.03 (d, $J = 6.2$, 3H, CH_3). MS/ESI$^-$ *m*/*z* 984.5 $(M - H)^-$.

1-*O*-(4-Monomethoxytrityl)-*N*-(6-(*N*-(α-OFm-L-glutamyl)aminocaproyl))-D-threoninol-N^2-*i*Bu-N^{10}-TFA-pteroic Acid Conjugate (20). To the solution of conjugate **19** (1 g, 1.01 mmol) in dry pyridine (15 mL) was added *p*-anisylchlorodiphenylmethane (405 mg, 1.31 mmol), and the reaction mixture was stirred and protected from moisture at room temperature overnight. Methanol (3 mL) was added and the reaction mixture concentrated to a syrup in vacuo. The residue was partitioned between dichloromethane and 5% $NaHCO_3$, and the organic layer washed with brine, dried (Na_2SO_4), and evaporated to dryness. Column chromatography using 0.5−10% gradient of methanol in dichloromethane afforded **20** as a colorless foam (0.5 g, 39%). ^{1}H NMR (DMSO-d_6−D_2O) δ 9.09 (d, $J = 6.8$, 1H, NH) 8.94 (s, 1H, H7 pteroic acid), 8.00−6.93 (m, 27H, aromatic, NH), 5.30 (s, 2H, pteroic acid), 4.50 (m, 1H, Glu), 4.40 (d, $J = 6.8$, 2H, Fm), 4.29 (t, $J = 6.8$, 1H, Fm), 3.94 (m, 2H, H3,H2 Thr), 3.79 (s, 3H, OCH_3) 3.11 (dd, $J = 8.6$, $J = 5.8$, 1H, H1 Thr), 3.04 (m, 2H, CH_2CO Acp), 2.91 (dd, $J = 8.6$, $J = 6.4$, 1H, H1′ Thr), 2.85 (m, 1H, *i*Bu), 2.25 (m, 2H, CH_2-NH Acp), 2.19 (m, 2H, Glu), 2.13 (m, 1H, Glu), 1.98 (m, 1H, Glu), 1.55 (m, 2H, Acp), 1.42 (m, 2H, Acp), 1.29(m, 2H, Acp), 1.20 (s, 3H, *i*Bu), 1.18 (s, 3H, *i*Bu), 1.00 (d, $J = 6.4$, 3H, CH_3). MS/ESI$^-$ *m*/*z* 1257.0 $(M - H)^-$.

1-*O*-(4-Monomethoxytrityl)-*N*-(6-(*N*-(α-OFm-L-glutamyl)aminocaproyl))-D-threoninol-N^2-*i*Bu-N^{10}-TFA-pteroic Acid Conjugate 3′-*O*-(2-Cyanoethyl *N*,*N*-Diisopropylphosphoramidite) (21). To a solution of **20** (500 mg, 0.40 mmol) in dichloromethane (2 mL) was added 2-cyanoethyl tetraisopropylphosphordiamidite (152 μL, 0.48 mmol), followed by pyridinium trifluoroacetate (93 mg, 0.48 mmol). The reaction mixture was stirred at room temperature for 1 h and then loaded on the column of silica gel in hexanes. Elution using ethyl acetate−hexanes 1:1, followed by ethyl acetate and ethyl acetate−acetone 1:1 in the presence of 1% pyridine, afforded **21** as a colorless foam (480 mg, 83%). ^{31}P NMR δ 149.4 (s), 149.0 (s).

Oligonucleotide Synthesis. Phosphoramidites **10**, **13**, and **21** were used along with standard 2′-*O*-TBDMS and 2′-*O*-methyl nucleoside phosphoramidites as previously described (*30*). Synthesis was conducted on a 394 (ABI) synthesizer using modified 2.5 μmol scale protocol with 2.5 min coupling step for monomers **13**, **21**, and 2′-*O*-methyl nucleotides. The coupling time was extended to 5 min for 2′-*O*-TBDMS protected nucleotides. Coupling efficiency for the phosphoramidite **10** (coupling time 15 min) was lower than 50%, while coupling efficiencies for phosphoramidites **13** and **21** were typically greater than 95% based on the measurement of released trityl cations. Removal of monomethoxytrityl groups was conducted using 3% trichloroacetic acid in four 30 s intervals. Once the synthesis was completed, the conjugated oligonucleotides in Tr-on form were deprotected as previously described (*30*) with the exception of using 20% piperidine in DMF for 15 min for the removal of Fm protection from the folic acid conjugated ribozyme, prior methylamine treatment. The 5′-tritylated oligomers were separated from shorter (trityl-off) failure sequences using a short column of SEP−PAK C-18 adsorbent. The bound, tritylated oligomers were detritylated on the column by treatment with 1% trifluoroacetic acid, neutralized with triethylammonium acetate buffer, and then eluted using 30% acetonitrile in water. Further purification was achieved by reverse-phase HPLC (column − C18 Trans-genomic, temp. 80 °C, buffer A: 100 mM TEAA, buffer B: 100 mM TEAA/50% ACN, gradient: 22% B to 40% B in 35 min).

Structures of the ribozyme conjugates were confirmed by MALDI-TOF MS. Conjugate A: calcd 13823.19, found 13822.05; conjugate B: calcd 12078.56, found 12077.56.

RESULTS AND DISCUSSION

***N*-Acetyl-D-galactosamine Conjugates.** We have designed, synthesized, and characterized a low molecular weight conjugates useful for targeting ribozymes to galactose receptor (Figure 1). The design of these conjugates was motivated by recent reports demonstrating viability of using synthetic galactose containing ligands smaller than proteins to achieve receptor binding and internalization of the ligand bound DNA (*14*−*17*). The triattenary cluster glycoside YEE(ah-GalNAc)$_3$ is the highest affinity synthetic ligand of the ASGPr reported to date. In binding assays using rat hepatocytes, this compound was reported to affect a 50% inhibition at a concentration of 0.2 nM of ASOR binding (*11*).

We reasoned that the attachment of two *N*-acetylgalactosamine residues through a linker to 2′-(*N*-lysylamino)-2′-deoxyuridine **8** (Scheme 1) will yield the monomer which can generate high density of carbohydrate ligands upon multiple incorporations into ribozyme. On the basis of the extensive ribozyme structure−activity studies (*4*, *35*), one can expect that incorporation of this conjugate into U4 and /or U7 positions of the catalytic core, as well as into the stem II loop, will not impair ribozyme catalytic activity.

Synthesis of desired amidite **10** consisted of the preparation of two key intermediates: *N*-Ac-galactosamine synthon **6** and 2′(*N*-lysylamino)-2′-deoxyuridine **8** to produce, following condensation, conjugate **9**. Synthesis of 2-acetamido-3,4,6-tetra-*O*-acetyl-1-chloro-D-galactopyranose **2** was accomplished according to the reported procedure (*31*) with minor modifications. Mercury salt-catalyzed glycosylation of 1-chloro sugar **2** with the benzyl ester of 12-hydroxydodecanoic acid **3** afforded β-glycoside **4** in 81% yield. An attempt to glycosylate **2** using the unprotected 12-hydroxydodecanoic acid resulted in a complex mixture, and no attempt was made to isolate the desired product. Hydrogenolysis of benzyl protecting group of **4** yielded carboxylate **5** which was activated as NHSu ester **6**.

On the other side, the bis-Fmoc protected lysine linker was attached to the 2′-amino group of 2′-amino-2′-deoxyuridine using the EEDQ-catalyzed peptide coupling as described by us earlier (*32*). The 5′-OH was protected with 4,4′-dimethoxytrityl group to give **7**, followed by the cleavage of *N*-Fmoc groups with diethylamine, to afford synthon **8** in the high overall yield.

Coupling of the sugar derivative **6** with the nucleoside synthon **8** yielded the final conjugate **9** which was phosphitylated under standard conditions to afford phosphoramidite **10** in 69% yield.

Unfortunately, phosphoramidite **10** coupled to the growing oligonucleotide chain with low efficiency and incorporation of only one monomer was possible. Utilization of "double coupling" technique, increasing coupling time, or extensive drying of the acetonitrile solution of amidite **10** over molecular sieves did not improve the coupling of **10**. The low efficiency of incorporation of **10** into the stem loop region or at the 5′-end of the stabilized ribozyme can be explained by steric crowding due to the bulky 2′-aminoacyl substituent.

To solve this problem, we redesigned the monomer by attaching *N*-acetyl-D-galactose to nonnucleosidic thre-

oninol moiety through the same $(CH_2)_{11}$ spacer as used for the nucleoside-based conjugate (Scheme 2). The three-carbon threoninol molecule, once incorporated into oligomer, closely mimics the spacing of a traditional ribose moiety. Using similar strategy as described for nucleoside-based conjugate, D-threoninol was coupled to NHSu ester **6** to afford conjugate **11** in a good yield. Monomethoxytritylation, followed by phosphitylation, yielded the desired phosphoramidite **13**.

Phosphoramidite **13** was incorporated into ribozymes with the efficiency comparable to unmodified phosphoramidites. Five consecutive couplings at the 5′-end of an anti-HCV ribozyme produced the desired conjugate in a good yield.

Folate Conjugate. We also designed, synthesized, and characterized phosphoramidite monomer **21** to target folate receptor. By incorporating this monomer into synthetic ribozymes, we hope to achieve tumor specific targeting and facilitated intracellular delivery of ribozyme−folate conjugates (Figure 1) by receptor-mediated endocytosis mechanism.

It is desirable to attach the targeting ligands to drug molecules through spacers in order to facilitate receptor−ligand recognition. Capitalizing on our experience in incorporation of *N*-Ac-galactosamine monomers **10** and **13** into oligonucleotides, we decided to pursue the synthesis of a nonnucleosidic folic acid monomer **21** (Scheme 3). 6-Aminocaproic acid was chosen as a spacer between folate and threoninol linker.

The choice of the protecting group for glutamic acid α-carboxylate is crucial for the successful phosphoramidite-based synthesis of the folate−ribozyme conjugate: it has to be stable to reagents used to assemble the oligonucleotide chain on the solid support and also has to generate carboxylic functionality under mild deprotection conditions. The fluorenylmethyl ester, which is cleaved by β-elimination with amine bases, fulfills these requirements.

D-Threoninol was condensed with NHSu ester of *N*-Fmoc-6-aminocaproic acid to yield conjugate **14** in 80% yield. Selective monomethoxytritylation, followed by Fmoc cleavage resulted in formation of 1-*O*-(4-monomethoxytrityl)-*N*-(6-aminocaproyl)-D-threoninol **16**. Coupling of **16** with *N*-Boc-α-OFm-L-glutamic acid NHSu ester afforded conjugate **17** in a high yield. Cleavage of both the monomethoxytrityl and *N*-Boc protecting groups with HCl in dioxane yielded the Fm-protected conjugate **18**. After conversion to the free base, this compound was conjugated to N^2-*i*Bu-N^{10}-TFA protected pteroic acid (*34*) in the presence of EDC and 1-hydroxybenzotriazole to afford conjugate **19** in a moderate yield. Primary hydroxyl of **19** was selectively protected with monomethoxytrityl group, and the resulting **20** was phosphitylated using 2-cyanoethyl tetraisopropylphosphordiamidite and pyridinium trifluoroacetate as a catalyst (*36*). It is worth noting that pyridine was successfully used during the chromatographic purification of the phosphoramidite **21**, instead of the commonly used triethylamine which is not compatible with the base-sensitive Fm protection.

The fully protected phosphoramidite **21** was attached to the 5′-end of the ribozyme using standard oligonucleotide synthesis protocol. The glutamic α-carboxylic acid function is unmasked using piperidine-catalyzed cleavage of the Fm-ester prior to methylamine removal of base protecting groups and cleavage from the solid support.

In conclusion, the new *N*-acetyl-D-galactosamine and folate monomers are synthesized and successfully incorporated into ribozymes using solid-phase phosphoramidite chemistry. Tissue localization studies using these ribozyme conjugates are under way and will be reported in due course.

ACKNOWLEDGMENT

We thank Kevin Johnson and Mark Sanseverino for recording mass spectra and David Eidenmueller for the oligonucleotide synthesis.

LITERATURE CITED

(1) Kruger, K., Grabowski, P. J., Zaug, A. J., Sands, J.; Gottschling, D. E., and Cech, T. R. (1982) Self-splicing RNA: Autoexcision and autocyclization of the ribosomal RNA intervening sequence. *Cell 31*, 147−157.

(2) Guerrier-Takada, C., Gardiner, K., Marsh, T., Pace, N., and Altman, S. (1983) The RNA moiety of ribonuclease P is the catalytic subunit of the enzyme. *Cell* 35, 849−857.

(3) Christoffersen, R. E., and Marr, J. J. (1955) Ribozymes as human therapeutic agents. *J. Med. Chem. 38*, 2024−2037.

(4) Beigelman, L., McSwiggen, J. A., Draper, K. G., Gonzalez, C., Jensen, K., Karpeisky, A. M., Modak, A. S., Matulic-Adamic, J., DiRenzo, A. B., Haeberli, P., Sweedler, D., Tracz, D., Grimm, S., Wincott, F. E., Thackray, V. G., and Usman, N. (1995) Chemical modification of hammerhead ribozymes. *J. Biol. Chem. 43*, 25702−25708.

(5) Paolella, G., Sproat, B. S., and Lamond, A. I. (1992) Nuclease-resistant ribozyme with high catalytic activity. *EMBO J. 11*, 1913−1919.

(6) Akhtar, S., Hughes, M. D., Khan, A., Bibby, M., Hussain, M., Nawaz, Q., Double, J., and Sayyed, P. (2000) The delivery of antisense therapeutics. *Adv. Drug Deliv. Rev. 44*, 3−21 and references therein.

(7) Dokka, S., and Rojanasakul, Y. (2000) Novel nonendocytic delivery of antisense oligonucleotides. *Adv. Drug Deliv. Rev. 44*, 35−49 and references therein.

(8) Wu, G. Y., and Wu, C. H. (1987) Receptor-mediated in vitro gene transformation by a soluble DNA carrier system. *J. Biol. Chem. 262*, 4429−4432.

(9) Baenziger, J., and Fiete, D. (1980) Galactose and *N*-acetylgalactosamine-specific endocytosis of glycopeptides by isolated rat hepatocytes. *Cell 22*, 611−620.

(10) Connolly, D. T., Townsend, R. R., Kawakuchi, K., Bell, W. R., and Lee, Y. C. (1982) Binding and endocytosis of cluster glycosides by rabbit hepatocytes. *J. Biol. Chem.* 257, 939−945.

(11) Lee, R. T., and Lee, Y. C. (1987) Preparation of cluster glycosides of *N*-acetylgalactosamine that have subnanomolar binding constants toward the mammalian hepatic Gal/GalNac-specific receptor. *Glycoconjugate J. 4*, 317−328.

(12) Kornfeld, R., and Kornfeld, S. (1976) Comparative aspects of glycoprotein structure. *Annu. Rev. Biochem. 45*, 217−237.

(13) Ponpipom, M., Bugianesi, R. L., Robbius, J. C., Doebber, T. W., and Shen, T. Y. (1981) Cell specific ligands for selective drug delivery to tissue and organs. *J. Med. Chem. 24*, 1388−1395.

(14) Plank, C., Zatloukal, K., Cotton, M., Mechtler, K., and Wagner, E. (1992) Gene transfer into hepatocytes using asialoglycoprotein receptor mediated endocytosis of DNA complexed with an artificial tetra-antennary galactose ligand. *Bioconjugate Chem. 4*, 85−93.

(15) Haensler, J., and Szoka, F. C., Jr. (1993) Synthesis and characterization of a trigalactosylated bisacridine compound to target DNA to hepatocytes. *Bioconjugate Chem.* 4, 85−93.

(16) Merwin, J. R., Noell, G. S., Thomas, W. L., Chiou, H. C., DeRome, M. E., McKee, T. D., Spitalny, G. L., and Findeis, M. A. (1994) Targeted delivery of DNA using YEE(GalNAcAH)$_3$, a synthetic glycopeptide ligand for the asialoglycoprotein receptor. *Bioconjugate Chem. 5*, 612−620.

(17) Hangeland, J. J., Flesher, J. E., Scott, F. D., Lee, Y. C., Ts'o, P. O. P., and Frost, J. J. (1997) Tissue distribution and Metabolism of the [^{32}P]-labeled oligodeoxynucleoside methylphosphonate-neoglycopeptide conjugate, [YEE(ah-GalNAc)$_3$]-SMCC-AET-pUmpT_7, in the mouse. *Antisense Nucleic Acid Drug Dev. 7*, 141−149.

(18) Leamon, C. P., and Low, P. S. (1993) Membrane folate-binding proteins are responsible for folate-protein conjugate endocytosis into cultured cells. *Biochem. J. 291*, 855−860.
(19) Leamon, C. P., and Low, P. S. (1991) Delivery of macromolecules into living cells: A method that exploits folate receptor endocytosis. *Proc. Natl. Acad. Sci. U.S.A. 88*, 5572−5576.
(20) Lee, R. J., and Low, P. S. (1994) Delivery of liposomes into cultured KB cells via folate receptor-mediated endocytosis. *J. Biol. Chem. 269*, 3198−3204.
(21) Citro, G., Szczylik, C., Ginobbi, P., Zupi, G., and Calabretta, B. (1994) Inhibition of leukemia cell proliferation by folic acid−polylysine-mediated introduction of c-myb antisense oligodeoxynucleotides into HL-60 cells. *Br. J. Cancer 69*, 463−467.
(22) Habus, I., Xie, J., Iyer, R. P., Zhou, W.-Q., Shen, L. X., and Agarwal, S. (1998) A mild and efficient solid-support synthesis of novel oligonucleotide conjugates. *Bioconjugate Chem. 9*, 283−291.
(23) Harrison, J. G., and Balasubramanian, S. (1997) A convenient synthetic route to oligonucleotide conjugates. *Bioorg. Med. Chem. Lett. 7*, 1041−1046.
(24) Bhat, B., Balow, G., Guzaev, A., Cook, D. P., and Manoharan, M. (1999) Synthesis of fully protected nucleoside-folic acid conjugated phosphoramidites and their incorporation into antisense oligonucleotides. *Nucleosides Nucleotides 18*, 1471−1472.
(25) Wang, S., Mathias, C. J., Green, M. A., and Low, P. S. (1996) Synthesis, purification, and tumor cell uptake of 67Ga-deferoxamine-folate, a potential radiopharmaceutical for tumor imaging. *Bioconjugate Chem. 8*, 673−679.
(26) Lacey, S. W., Sanders, J. M., Rothberg, K. G., Anderson, R. G. W., and Kamen, B. A. (1989) Complementary DNA for the folate binding protein correctly predicts anchoring to the membrane by glycosyl-phosphatidylinositol. *J. Clin. Invest. 84*, 715−720.
(27) Selhub, J., and Franklin, W. A. (1984) The folate-binding protein of rat kidney. Purification, properties and cellular distribution. *J. Biol. Chem. 259*, 6601−6606.
(28) Asok, A. C., Utley, C., Van Horne, K. C., and Kolhouse, J. F. (1981) Isolation and characterisation of a folate receptor from human placenta. *J. Biol. Chem. 256*, 9684−9692.
(29) Rothenberg, S. P., and Da Costa, M. (1971) Further observations on the folate binding factor in some leukemic cells. *J. Clin. Invest. 50*, 719−726.
(30) Wincott, F. E., DiRenzo, A., Shaffer, C., Grimm, S., Tracz, D., Workman, C., Sweedler, D., Gonzalez, C., Scaringe, S., and Usman, N. (1995) Synthesis, deprotection, analysys and purification of RNA and ribozymes. *Nucleic Acids Res. 23*, 2677−2684.
(31) Findeis, M. A. (1994) Stepwise synthesis of a GalNAc-containing cluster glycoside ligand of the asialoglycoprotein receptor. *Int. J. Pept. Protein Res. 43*, 477−485.
(32) Matulic-Adamic, J., Beigelman, L., Dudycz, L. W., Gonzalez, C., and Usman, N. (1995) Synthesis and incorporation of 2′-amino acid conjugated nucleotides into ribozymes. *Bioorg. Med. Chem. Lett. 5*, 2721−2724.
(33) Holt, D. A., Luengo, J. I., Yamashita, D. S., Oh, H.-J., Konialian, A. L., Yen, H.-K., Rozamus, L. W., Brandt, M., Bossard, M. J., Levy, M. A., Eggleston, D. S., Liang, J., Schultz, L. W., Stout, T. J., and Clardy, J. (1993) Design, synthesis, and kinetic evaluation of high-affinity FKBP ligands and the X-ray crystal structures of their complexes with FKBP12. *J. Am. Chem. Soc. 115*, 9925−9938.
(34) Guzaev, A. P., Cook, P. D., Manoharan, M., and Bhat, B. (2002) Nucleosidic and nonnucleosidic folate conjugates, US Patent 6335434 B1.
(35) Kuimelis, R. G., and McLaughlin, L. W. (1997) Probing the cleavage activity of the hammerhead ribozyme using analogue complexes, in *Nucleic Acids and Molecular Biology. Catalytic RNA* (F. Eckstein, and D. M. Lilley, Eds.) vol. 10, pp 197−215, Springer-Verlag, New York.
(36) Sanghvi, Y., Guo, Z., Pfundheller, H. M., and Converso, A. (2000) Improved process for the preparation of nucleosidic phosphoramidites using a safer and cheaper activator. *Org. Process Res. Dev. 4*, 175−181.

BC025525Q

Trifunctional Conjugation Reagents. Reagents That Contain a Biotin and a Radiometal Chelation Moiety for Application to Extracorporeal Affinity Adsorption of Radiolabeled Antibodies

D. Scott Wilbur,*,† Ming-Kuan Chyan,† Donald K. Hamlin,† Brian B. Kegley,† Rune Nilsson,‡ Bengt E. B. Sandberg,‡ and Martin Brechbiel§

Department of Radiation Oncology, University of Washington, Seattle, Washington 98195, Mitra Medical Technology, Lund, Sweden, and National Cancer Institute, Bethesda, Maryland. Received April 1, 2002; Revised Manuscript Received May 21, 2002

A method of removing radiolabeled monoclonal antibodies (mAbs) from blood using a device external to the body, termed extracorporeal affinity-adsorption (EAA), is being evaluated as a means of decreasing irradiation of noncancerous tissues in therapy protocols. The EAA device uses an avidin column to capture biotinylated-radiolabeled mAbs from circulated blood. In this investigation, three trifunctional reagents have been developed to minimize the potential deleterious effect on antigen binding brought about by the combination of radiolabeling and biotinylation of mAbs required in the EAA approach. The studies focused on radiolabeling with ^{111}In and ^{90}Y, so the chelates CHX-A″-DTPA and DOTA, which form stable attachments to these radionuclides, were incorporated in the trifunctional reagents. The first trifunctional reagent prepared did not incorporate a group to block the biotin cleaving enzyme biotinidase, but the two subsequent reagents coupled aspartic acid to the biotin carboxylate for that purpose. All three reagents used 4,7,10-trioxa-1,13-tridecanediamine as water-soluble spacers between an aminoisophthalate core and the biotin or chelation group. The mAb conjugates were radioiodinated to evaluate cell binding as a function of substitution. Radioiodination was used so that a direct comparison with unmodified mAb could be made. Evaluation of the number of conjugates per antibody versus cell binding immunoreactivities indicated that minimizing the number of conjugates was best. Interestingly, a decrease of radioiodination yield as a function of the number of isothiocyanate containing conjugates per mAb was noted. The decreased yields were presumably due to the presence of thiourea functionality formed in the conjugation reaction. Radiolabeling with ^{111}In and ^{90}Y was facile at room temperature for conjugates containing the CHX-A″, but elevated temperature (e.g., 45 °C) was required to obtain good yields with the DOTA chelate. Stability of ^{90}Y labeled mAb in serum, and when challenged with 10 mM EDTA, was high. However, challenging the ^{90}Y labeled mAb with 10 mM DTPA demonstrated high stability for the DOTA containing conjugate, but low stability for the CHX-A″ containing conjugate. Thus, the choice between these two chelating moieties might be made on requirements for facile and gentle labeling versus very high in vivo stability. Application of the trifunctional biotinylation reagents to the blood clearance of labeled antibodies in EAA is under investigation. The new reagents may also be useful for other applications.

INTRODUCTION

The high-affinity binding pairs biotin/avidin (Av[1]) and biotin/streptavidin (SAv) have become important chemical tools in capture processes for a large number of diverse applications, both in vitro and in vivo. The most widely used in vitro detection systems employ biotinylated receptor binding biomolecules, particularly monoclonal antibodies (mAbs), in capture processes with avidin or streptavidin (*2*−*5*). An in vivo application of this capture process uses the biotin/streptavidin binding pair as conjugates of mAbs in an approach, termed "pretargeting", to selectively localize radionuclides on cancer cells for therapy (*6*−*8*). The pretargeting approach to "endoradiotherapy"[2] is being investigated due to the inherent problems associated with using directly radio-

* Corresponding author. Address: Department of Radiation Oncology, University of Washington, 2121 N. 35th Street, Seattle, WA 98103-9103. Phone: 206-685-3085. FAX: 206-685-9630. E-mail: dswilbur@u.washington.edu.

† University of Washington.

‡ Mitra Medical Technology.

§ National Cancer Institute.

[1] Abbreviations: Av, avidin; FAB$^+$, fast atom bombardment; BCA, bicinchoninic acid; BSA, bovine serum albumin; DOTA, 1,4,7,10-tetraazacyclododecane-N,N′,N″,N‴-tetraacetic acid; DTPA, diethylenetriaminepentaacetic acid; EAA, extracorporeal affinity adsorption; EDC, 1-(3-dimethylaminopropyl)-3-ethylcarbodiimide; ES$^+$, electrospray; HABA, 4′-hydroxyazobenene-2-carboxylic acid; HRMS, high-resolution mass spectrometry; LRMS, low-resolution mass spectrometry; mAb, monoclonal antibody; IEF, isoelectric focusing electrophoresis; NHS-LC-biotin, N-hydroxysuccinimidyl biotinyl-6-aminocaproic acid; rt, room temperature; SAv, streptavidin; (strept)avidin, signifies either avidin or streptavidin; t-Boc, *tert*-butoxycarbonyl; TCDI, thiocarbonyldiimidazole; TFA, trifluoroacetic acid; TFP, tetrafluorophenyl; TFP−OH, tetrafluorophenol; TFP−OTFA, tetrafluorophenyl trifluoroacetate.

[2] "Endoradiotherapy" is a term used to describe an approach to radiotherapy in which a radiopharmaceutical, composed of a radionuclide coupled with a cancer cell targeting carrier molecule, is injected into a patient for cancer therapy. This approach is also termed "targeted radiotherapy".

10.1021/bc025535r CCC: $22.00 © 2002 American Chemical Society
Published on Web 07/13/2002

labeled mAbs in this application (*9*). Those problems include long blood residence times, low concentrations of radioactivity in the tumor, and heterogeneous deposition of radioactivity in tumors. While encouraging results have been obtained using pretargeting protocols (*10*, *11*), that approach has problems as well, including complexity of protocols, immunogenicity of SAv, and interference by endogenous biotin (*12*, *13*). The difficulty of circumventing the problems associated with pretargeting protocols has led investigators to consider other approaches to improve the in vivo characteristics of directly radiolabeled mAbs. One approach being investigated, termed "extracorporeal affinity-adsorption" (EAA[3]), uses a device external to the body to remove radiolabeled mAbs from the patient's blood (*14*). If efficient removal of radiolabeled mAbs from blood is obtained, use of such a device may permit administration of higher doses of radiolabeled mAbs. This is important, as higher doses could increase the total amount of radioactivity in the tumor and decrease the heterogeneity of radiolabeled mAb deposition in the tumor.

The biotin/avidin capture system can be used in the EAA approach to remove directly labeled mAbs from blood (*15*−*17*). To achieve its removal in the EAA approach, the radiolabeled mAb must be biotinylated. Thus, the procedure involves administration of a biotinylated and radiolabeled mAb, which after sufficient time for tumor localization is removed from a patient's blood by passing it through a device that contains a high flow rate, high capacity avidin column. Using the EAA approach, complete removal of the radiolabeled antibodies will not be obtained unless every antibody has at least one biotin moiety conjugated. Unfortunately, biotinylation in combination with radiolabeling of mAbs can result in a heterogeneous mixture of products. This is particularly true when radionuclides other than radioiodine are used because radionuclide chelation moieties must also be conjugated to the mAb. While multiple conjugates of radiometal chelates and biotin can improve radiolabeling efficiency and capture by avidin columns, they can also result in a dramatic decrease in mAb binding to the target antigen. As a means of circumventing this problem and the issue of high conjugation heterogeneity, we have investigated the design and synthesis of trifunctional reagents that contain a biotin moiety, a radiometal chelation moiety, and a functional group for protein conjugation. By combining the biotin moiety and the radiolabeling moiety into a single molecule, every mAb that is radiolabeled will also have a biotin on it. Further, heterogeneity of radiolabeled mAb is diminished, as the same number of biotin molecules as chelates is always present, and a minimum number of conjugation reagents or moieties can be used. In the studies, three trifunctional reagents were synthesized, conjugated with mAbs, tested for radiolabeling with ^{111}In and ^{90}Y, and evaluated for efficiency for capture by an avidin column. The results of the investigation are described herein.

EXPERIMENTAL PROCEDURES

General. Solvents and chemicals obtained from commercial sources were analytical grade or better and were used without further purification. Solvents for HPLC analysis were obtained as HPLC grade and were filtered (0.2 μm) prior to use. *d*-Biotin, 4,7,10-trioxa-1,13-tridecanediamine, 2,3,5,6-tetrafluorophenol, aminoisophthalate, di-*tert*-butyl dicarbonate, thiophosgene, 1,1′-thiocarbonyl-diimidazole, and most other chemicals were purchased from Aldrich Chemical Co. (Milwaukee, WI). L-Aspartic acid α-*tert*-butyl ester was obtained from Calbiochem-Novabiochem Corp. (San Diego, CA) or BACHEM California, Inc. (Torrance, CA). *p*-Isothiocyanatobenzyl-DOTA, **18**, was purchased from Macrocyclics (www.macrocyclics.com, Dallas, TX). N-Hydroxysuccinimidyl biotinyl-6-aminocaproic acid (NHS-LC-biotin) and immobilized Avidin were purchased from Pierce (Rockford, IL). 2,3,5,6-Tetrafluorophenyl trifluoroacetate was prepared as previously described (*18*). High-purity, low-metal HCl (Ultrex II) was obtained from J.T. Baker (Phillipsburg, NJ). High-purity NaOAc was obtained from Alfa Aesar (Ward Hill, MA). High-purity water was obtained from a Barnstead Easypure-Ultrapure water system. Microcon centrifugal filter devices, Microcon YM-30, were obtained from Amicon/Millipore Corporation (Bedford, MA). Size exclusion columns, PD-10, were obtained from Amersham Pharmacia Biotech AB (Lund, Sweden). Silica gel chromatography was conducted with 70−230 mesh 60 Å silica gel (Aldrich Chemical Co.). Melting points were obtained in open capillary tubes on a Mel-Temp II apparatus with a Fluke 51 K/J electronic thermometer and are uncorrected. ^{1}H NMR data, MS data, and HPLC chromatography were used to assess compound identity and purity (Data provided in the Supporting Information).

Radioactive Materials. All reactions involving radioactive materials were conducted in a charcoal filtered-Plexiglas enclosure within a fume hood. All radioactive materials were opened, handled, and stored in the Plexiglas enclosure until used in studies or removed as radiation waste. Standard radiation safety procedures were used. Radiation monitoring followed approved procedures.

^{111}In and ^{90}Y were obtained in 0.05 M HCl from NEN/Dupont (now-Perkin-Elmer Life Sciences, Inc, Billerica, MA) in high specific activity. Na[^{125}I]I was purchased from NEN/Dupont (Billerica, MA) as high-concentration/high-specific-activity radioiodide in 0.1 N NaOH. Measurement of radioactivity was accomplished in a Capintec CRC-15R or a Logic Model 111B gamma counter (Abbott Labs, Chicago, IL).

Spectral Analyses. All ^{1}H NMR were obtained on either a Bruker AC-200 (200 MHz) or Bruker AF-301 (300 MHz) instrument. Proton chemical shifts are expressed as ppm using tetramethylsilane or 3-(trimethylsilyl)propionic-2,2,3,3-d_4 acid, sodium salt as an internal standard (δ = 0.0 ppm). Mass spectral data were obtained on either (1) a VG Analytical (Manchester, England) VG-70SEQ mass spectrometer with associated 11250J Data System using fast atom bombardment (FAB$^+$) at 8 keV in a matrix of MeOH/DMIX (Thioglycerol/DMSO/TFAA: 90/9/1) or 3NBA (3-nitrobenzyl alcohol) or (2) a PerSeptive Biosystems Mariner Electrospray Time of Flight Mass Spectrometer (ESI-TOF). For ES$^+$ analysis, the samples were dissolved in 50/50 MeOH/H_2O and were introduced by an integral syringe infusion pump.

Analytical Chromatography. *Small Molecules.* Reaction progress and purity of compounds were evaluated by reversed-phase HPLC analysis. HPLC separations were obtained on Hewlett-Packard quaternary 1050 gradient pumping system with a variable-wavelength UV detector (254 nm) and a Varex ELSD MKIII evaporative light-scattering detector. Analyses of the HPLC data were conducted on Hewlett-Packard HPLC ChemStation soft-

[3] The terms extracorporeal immunoadsorption (ECIA) and whole blood immunoadsorption (WBIA) have also been used for this approach.

ware. Reversed-phase HPLC chromatography was carried out using an Alltech Altima C-18 column (5 μm, 250 mm × 4.6 mm) with a gradient solvent system at a flow rate of 1 mL/min. The gradient mixture was composed of MeOH (solvent A) and 0.1% aqueous HOAc (solvent B). Starting with 40% MeOH, the initial solvent mixture was held for 2 min, increased to 100% MeOH over the next 10 min, and then held at 100% MeOH for 8 min. Retention times (t_R) are provided with the compound experimental.

Proteins. All antibody conjugates were analyzed by size exclusion HPLC analysis. Size exclusion HPLC analyses were conducted on a system consisting of a Hewlett-Packard 1050 Multiple Wavelength Detector (280 nm), isocratic pump, and a Protein-Pak glass 300SW column (7.5 mm × 300 mm, 10 μm; Waters Corp., Milford, MA). The mobile phase was an aqueous solution containing 50 mM potassium phosphate (pH 6.8), 300 mM NaCl, 1 mM EDTA, and 1 mM NaN_3. A flow rate of 1.0 mL/min was used. Retention time for intact mAb is 8.4−8.6 min using this system.

Radio-HPLC. Radiolabeled antibodies were analyzed by size exclusion HPLC. HPLC separations of radiolabeled conjugated antibodies were conducted on a system consisting of a Waters 510 pump, a Waters Lambda Max model 481 UV detector (280 nm), and a Beckman model 170 radioisotope detector. The radiolabeled mAbs were separated by size exclusion chromatography on a Bioselect 250-5 column (8 mm × 300 mm; 10 μm; Bio-Rad, Hercules, CA). The mobile phase was an aqueous solution containing 50 mM potassium phosphate (pH 6.8), 300 mM NaCl, 1 mM EDTA, and 1 mM NaN_3. A flow rate of 1.0 mL/min was used. The retention time for the radiolabeled proteins (gamma trace) was approximately 10.8 min using this system.

5-N-*tert*-Boc-3-((15′-Biotinyl)-4′,7′,10′-Trioxapentadecanylamino)Isophthalamic Acid 2,3,5,6-Tetrafluorophenyl Ester, 5. N-(13-Amino-4,7,10-trioxatridecanyl)-biotinamide (*19*), **4**, (54 mg, 0.12 mmol) in anhydrous DMF (2.0 mL) was added over 20 min to a solution of N-*tert*-Boc-5-aminoisophthalate bis-tetrafluorophenyl ester (*20*), **3** (100 mg, 0.17 mmol), and Et_3N (0.048 mL, 0.34 mmol) in anhydrous DMF (8 mL) at room temperature. After the mixture was stirred at room temperature for 1 h, volatile materials were removed under vacuum. The residue was purified by silica gel column (60 g) eluting with 10% MeOH/EtOAc to afford 51 mg (49%) of **5** as a colorless solid, mp 180−183 °C. ^{1}H NMR (CD_3OD, 200 MHz): δ 1.43 (m, 1H), 1.54 (s, 9 H), 1.67 (m, 3H), 1.90 (m, 2H), 2.18 (m, 2H), 2.69 (d, 2H), 2.92 (m, 1H), 4.28 (dd, 1H), 4.47 (dd, 1H), 7.49 (m, 1H), 7.83 (t, 1H), 7.97 (s, 2H); LRMS (ES^+; M + H) 858.3. HRMS calcd for $C_{39}H_{52}F_4N_5O_{10}S$ $(M + H)^+$: 858.3371. Found: 858.3374. HPLC: t_R = 14.0 min.

13-(Benzylthiourea-CHX-A″)-4,7,10-Trioxatridecane-Diamine, 6. A quantity (10.4 mg, 0.018 mmol) of isothiocyanatobenzyl-CHX-A″ DTPA (*21*), **17**, in 2 mL of anhydrous DMF was added over 10 min to a solution of 4,7,10-trioxa-1,13-tridecanediamine (39 mg, 0.18 mmol) in 2 mL of anhydrous DMF at room temperature. After the addition was completed, the reaction mixture was stirred at room temperature for 30 min and then triturated with 40 mL of EtOAc. The product was filtered and washed with EtOAc/$CHCl_3$ to afford 9.6 mg (67%) of **6** as a tacky material. ^{1}H NMR (D_2O, 200 MHz): δ 1.26 (t, J = 7.3 Hz, 4H), 1.92 (m, 8H), 2.17 (m, 2H), 3.03 (t, 8H), 3.40 (m, 4H), 3.65 (m, 9H), 3.69 (s, 10H), 7.24 (d, J = 8.0 Hz, 2H), 7.39 (d, J = 8.0 Hz, 2H); LRMS (FAB^+; M + H) 815. HRMS calcd for $C_{36}H_{59}N_6O_{13}S$ $(M + H)^+$: 815.3861. Found: 815.3853. HPLC: t_R = 2.6 min.

5-N-*tert*-Boc-3-((15′-Biotinyl)-4′,7′,10′-Trioxapentadecanylamino)-1-((13-(Benzylthiourea-CHX-A″)-4,7,-10-Trioxatridecanediamino)Aminoisophthalic Acid, 7. A 15.3 mg quantity of **5** (0.018 mmol) in 1.0 mL of anhydrous DMF was added to a solution of **6** (9.6 mg, 0.012 mmol) and Et_3N (5.0 μL, 0.036 mmol) in 1.5 mL of anhydrous DMF at room temperature. The solution was stirred at room temperature for 4 h and then triturated with 40 mL of EtOAc/$CHCl_3$ to give 11.0 mg (62%) of **7** as an oil, which was used in the subsequent reaction without purification. ^{1}H NMR (CD_3OD, 200 MHz): δ 1.43 (s, 9H), 1.58 (m, 8H), 1.79 (m, 6H), 2.08 (t, 4H), 2.83 (m, 4H), 3.15 (t, 4H), 3.21 (m, 8H), 3.25 (m, 6H), 3.41 (m, 20H), 3.53 (m, 16H), 4.18 (dd, 1H), 4.38 (dd, 1H), 4.65 (m, 1H), 7.11 (m, 4H), 7.83 (m, 1H), 7.89 (m, 1H), 7.99 (m, 1H). LRMS (ES^+) mass calcd for $C_{69}H_{107}N_{11}O_{22}S_2$ $(M + Na)^+$: 1528. Found: 1528. HPLC: t_R = 10.9 min.

5-Isothiocyanato-3-((15′-Biotinyl)-4′,7′,10′-Trioxapentadecanylamino)-1-((13-(Benzylthiourea-CHX-A″)-4,7,10-Trioxatridecanediamino)Aminoisophthalic Acid, 8. A solution containing 11.0 mg, (0.0073 mmol) of **7** in 0.5 mL TFA was stirred at room temperature for 30 min; then the volatile materials were removed under vacuum. The residue was redissolved in 2.0 mL of H_2O; then thiophosgene (1.7 μL, 0.022 mmol) in 2.0 mL of $CHCl_3$ was added, and that mixture was stirred at room temperature for 1 h. The excess thiophosgene and $CHCl_3$ were evaporated in fume hood under a stream of argon. The remaining aqueous phase was evaporated to dryness under vacuum to afford the 9.2 mg (87%) of **8** as a colorless tacky material. ^{1}H NMR (DMSO-d_6, 200 MHz): δ 1.69 (m, 8H), 1.93 (m, 6H), 2.20 (m, 4H), 2.73 (t, 4H), 3.15 (t, 4H), 3.25 (m, 8H), 3.35 (m, 6H), 3.54 (m, 20H), 3.65 (m, 16H), 4.33 (m, 1H), 4.51 (m, 1H), 4.70 (m, 1H), 7.36 (m, 4H), 7.93 (m, 1H), 7.96 (m, 1H), 8.02 (m, 1H). LRMS (FAB^+) mass calcd for $C_{65}H_{98}N_{11}O_{20}S_3K$ $(M + K)^+$: 1487. Found: 1487. HPLC: t_R = 11.5 min.

1-((*N*-Biotinyl)-L-Aspartyl)-4,7,10-Trioxatridecane-1,13-Diamine TFA Salt, 9. This compound was synthesized as previously reported (*22*). In the final synthetic step, a 396 mg quantity (0.55 mmol) of 13-N-*tert*-Boc-1-((*N*-biotinyl)-L-aspartyl-α-*tert*-butyl ester)-4,7,10-trioxatridecane-1,13-diamine in 2 mL TFA was stirred at room temperature for 30 min, and then the volatile materials were removed under vacuum. The isolated **9** was used directly in the next reaction.

5-N-*tert*-Boc-3-((15′-((*N*-Biotinyl)-β-L-Aspartyl)-4′,7′,-10′-Trioxapentadecanylamino)-Isophthalamic Acid 2,3,5,6-Tetrafluorophenyl Ester, 10. A solution of **9** (310 mg, 0.55 mmol), Et_3N (0.23 mL, 1.65 mmol), and anhydrous DMF (5 mL) was dripped slowly into a solution of **3** (320 mg, 0.55 mmol) in anhydrous DMF (3 mL) at room temperature. The reaction mixture was stirred at room temperature for 30 min, and then volatile materials were removed under vacuum. The residue was purified by silica gel column (50 g) eluting with 10% MeOH/EtOAc to afford 190 mg (31%) of **10** as a colorless tacky material. ^{1}HNMR (CD_3OD, 200 MHz): δ 1.45 (m, 2H), 1.54 (s, 9 H), 1.70 (m, 8H), 1.91 (m, 2H), 2.25 (m, 2H), 2.59−3.01 (m, 2H), 3.11−3.33 (m, 6H), 3.45−3.70 (m, 11H), 4.32 (dd, J = 4.4, 7.7 Hz, 1H), 4.50 (dd, J = 4.4, 7.7 Hz, 1H), 4.65 (t, J = 6.2 Hz, 1H), 7.51 (m, 1H), 8.25 (m, 2H), 8.48 (t, J = 1.8 Hz, 1H); LRMS (ES^+; M + Na) 995.4. HRMS calcd for $C_{43}H_{56}F_4N_6O_{13}SNa$ $(M + Na)^+$: 995.3460. Found: 995.3393. HPLC: t_R = 13.8 min.

3-((15′-(*N*-Biotinyl)-β-L-Aspartyl)-4′,7′,10′-Trioxapentadecanylamino)-1-((13-(Benzylthiourea-CHX-A″)-4,7,10-Trioxatridecanediamine)-Aminoisophthalic Acid, 11. *Preparation A (Scheme 2*). A solution of **6** (64 mg, 78.7 μmol) and Et_3N (19 μL, 137 μmol) in anhydrous DMF (3 mL) was added dropwise to a solution of **10** (76 mg, 78.7 μmol) in anhydrous DMF (2 mL) at room temperature. The reaction mixture was stirred at room temperature for 1h; then DMF was removed under vacuum. The residue was redissolved in 2 mL of neat TFA and stirred at room temperature for 10 min. After that time, TFA was removed under vacuum, and the crude product was purified on a Sephadex G-15 column eluting with water. This provided 100 mg (83%) of **11** as a colorless tacky material. ^{1}H NMR (D_2O, 200 MHz): δ 0.86 (t, J = 6.6 Hz, 4H), 1.25 (m, 8H), 1.41−1.83 (m, 16H), 2.08 (m, 4H), 2.56 (m, 4H), 2.80 (m, 1H), 3.07 (m, 6H), 3.17−3.93 (m, 34H), 4.14 (m, 2H), 4.28 (m, 1H), 6.38 (m, 2H), 6.52 (m, 2H), 7.13 (s, 2H), 7.40 (m, 1H), 8.40 (m, 2H). LRMS (FAB^+) mass calcd for $C_{68}H_{105}N_{12}O_{23}S_2$ $(M + H)^+$: 1521. Found: 1521. HPLC: t_R = 7.9 min.

Preparation B (Scheme 3). A quantity (200 mg, 0.18 mmol) of **15** was dissolved in 2 mL of neat TFA, and the solution was stirred for 10 min at room temperature. The TFA was removed under vacuum, and the residue was dissolved in H_2O (4 mL). To that solution was added Na_2CO_3 (140 mg, 1.30 mmol), **17** (80 mg, 0.13 mmol), H_2O (4 mL), and DMF (4 mL). The reaction mixture was stirred at room temperature for 4 h and then neutralized with HOAc. The neutralized solution was placed on a gel filtration column (Sephadex G-15, 2.5 × 50 cm) and eluted with H_2O to provide 157 mg (77%) of **11** with physical and spectral properties identical to those reported above.

1-Isothiocyanato-3-((15′-(*N*-Biotinyl)-β-L-Aspartyl)-4′,7′,10′-Trioxapenta-Decanylamino)-1-((13-(Benzylthiourea-CHX-A″)-4,7,10-Trioxatridecanediamine)-Aminoisophthalic Acid, 12. Thiophosgene (25 μL, 0.33 mmol) in 3 mL of $CHCl_3$ was added to a 3 mL aqueous solution of **11** (100 mg, 66 μmol) at room temperature. The mixture was stirred at room temperature for 1 h; then excess thiophosgene and $CHCl_3$ were evaporated in fume hood under a stream of argon. The aqueous phase was evaporated to dryness under vacuum to afford the 84 mg (82%) of **12** as a light yellow tacky material. ^{1}H NMR (D_2O, 200 MHz): δ 0.86 (t, J = 6.6 Hz, 4H), 1.25 (m, 8H), 1.44−1.82 (m, 16H), 2.09 (m, 4H), 2.54 (m, 4H), 2.81 (2d, J = 5.1 Hz, 1H), 3.09 (m, 6H), 3.27−3.83 (m, 34H), 4.12 (m, 1H), 4.30 (m, 1H), 4.49 (m, 1H), 7.31 (d, 2H), 7.44 (d, 2H), 7.87 (t, 1H), 7.97 (s, 2H), 8.03 (d, J = 7.0 Hz, 1H), 8.30 (s, 1H), 8.72 (t, J = 5.5 Hz, 2H). LRMS (FAB^+) mass calcd for $C_{69}H_{103}N_{12}O_{23}S_3$ $(M + H)^+$: 1563. Found: 1563. HPLC: t_R = 11.7 min.

3-(13′-*N*-*tert*-Boc)-Trioxatridecanediamine-5-*N*-*tert*-Boc-Aminoisophthalate TFP Ester, 14. *N*-*tert*-Boc-trioxadiamine (*23*), **13** (0.44 g, 1.39 mmol), and Et_3N (0.29 mL, 2.08 mmol) in anhydrous DMF (5 mL) were added dropwise over 3 h to a solution of *N*-*tert*-Boc-aminoisophthalate di-TFP ester, **3** (0.80 g, 1.39 mmol), in anhydrous DMF (5 mL) at room temperature. After the addition was completed, the mixture was stirred at room temperature for another 30 min, and then the volatile materials were evaporated under vacuum. The product was purified by silica gel column (40 g) eluting with 50% EtOAc/Hexane to afford 0.74 g (73%) of **14** as a colorless oil. ^{1}H NMR ($CDCl_3$, 200 MHz): δ 1.42 (s, 9H), 1.54 (s, 9H), 1.69 (m, 2H), 1.77 (s, 1H), 1.91 (m, 2H), 2.92 (d, J = 14.7 Hz, 1H), 3.17 (m, 2H), 3.42−3.51 (m, 4H), 3.56−3.72 (m, 8H), 4.89 (t, J = 5.1 Hz, 1H), 6.97−7.14 (m, 1H), 7.51 (s, 1H), 7.57 (s, 1H), 8.01 (s, 1H), 8.28 (t, J = 1.5 Hz, 1H), 8.63 (s, 1H); LRMS (ES^+; M + Na) 754.3. HRMS calcd for $C_{34}H_{45}F_4N_3O_{10}Na$ $(M + Na)^+$: 754.2939. Found: 754.2941. HPLC: t_R = 14.8 min.

3-(13′-*N*-*tert*-Boc)Trioxatridecanediamine-1-(13″-Biotin-Asp-OH)Trioxadiamine-5-*N*-*tert*-Boc-Aminoisophthalate, 15. Biotin-Asp-OH-trioxadiamine TFA salt, **9** (0.32 g, 0.48 mmol), was added to a solution containing **14** (0.35 g, 0.48 mmol) and Et_3N (0.15 mL, 1.05 mmol) in anhydrous DMF (5 mL). The resultant mixture was stirred at room temperature for 1 h. Volatile materials were removed under vacuum and the residue was purified by silica gel column (40 g, 50% MeOH/EtOAc) to yield 0.45 g (83%) of **15** as a tacky oil. ^{1}H NMR (CD_3OD, 200 MHz): δ 1.41 (s, 9H), 1.53 (s, 9H), 1.63−1.74 (m, 6H), 1.86−1.92 (m, 4H), 2.18−2.29 (m, 2H), 2.58 (dd, J = 8.0, 14.8 Hz, 1H), 2.68 (d, J = 12.4 Hz, 1H), 2.74 (dd, J = 4.9, 14.8 Hz, 1H), 2.91 (dd, J = 4.9, 13.0 Hz, 1H), 3.09 (t, J = 6.8 Hz, 2H), 3.16−3.20 (m, 1H), 3.22 (t, J = 6.8 Hz, 2H), 3.30−3.31 (m, 4H), 3.44−3.54 (m, 12H), 3.59−3.66 (m, 16H), 4.30 (dd, J = 4.3, 8.0 Hz, 1H), 4.48 (dd, J = 4.3, 8.0 Hz, 1H), 4.55 (dd, J = 4.9, 7.4 Hz, 1H), 7.84 (t, J = 1.2 Hz, 1H), 7.99 (t, J = 1.9 Hz, 1H), 8.02 (t, J = 1.9 Hz, 1H). LRMS (ES^+) calcd for $C_{52}H_{87}N_8O_{17}S$ $(M + H)^+$: 1128. Found: 1128. HPLC: t_R = 11.4 min.

3-(13′-ThioureabenzylDOTA)Trioxadiamine-1-(13″-Biotin-Asp-OH)Trioxadiamine-5-Aminoisophthalate, 19. A 34 mg quantity (0.03 mmol) of **15** was dissolved in 1 mL of neat TFA and stirred at room temperature for 10 min. The TFA was removed under a stream of Ar, and the residue was redissolved in H_2O (1 mL). To that solution was added sodium carbonate (31.8 mg, 0.3 mmol) and DOTA-benzyl-NCS, **18** (20 mg, 0.036 mmol) in DMF (1 mL). The reaction mixture was stirred at room temperature for 4 h, neutralized with HOAc, and purified by gel filtration (Sephadex G-15) eluting with water to give 33 mg (74%) of **19**. ^{1}H NMR (D_2O): δ 1.24−1.45 (m, 3H), 1.47−1.99 (m, 14H), 2.26 (t, J = 7.1 Hz, 3H), 2.52 (dd, J = 10.0, 14.9 Hz, 1H), 2.69−2.82 (m, 1H), 2.95 (dd, J = 4.4, 13.2 Hz, 1H), 3.11−3.30 (m, 17H), 3.42−3.71 (m, 38H), 4.37 (dd, J = 4.0, 7.7 Hz, 1H), 4.48−4.60 (m, 2H), 7.18−7.31 (m, 5H), 7.38 (s, 1H), 7.45 (t, J = 1.5 Hz, 1H). LRMS (ES^+) calcd for $C_{66}H_{104}N_{13}O_{21}S_2$ $(M + H)^+$: 1479. Found: 1479. LRMS calcd for $C_{66}H_{103}N_{13}NaO_{21}S_2$ $(M + Na)^+$: 1501. Found: 1501. HPLC: t_R = 8.2 min.

3-(13′-ThioureabenzylDOTA)Trioxadiamine-1-(13″-Biotin-Asp-OH)Trioxadiamine-5-Isothiocyanato-Aminoisophthalate, 20. 1,1′-Thiocarbonyldiimidazole (3.6 mg, 0.02 mmol) was added to a solution of **19** (25 mg, 0.017 mmol) in anhydrous DMF (1 mL). The reaction mixture was stirred at room temperature for 1 h; then 30 mL of ether was added and stirred for another 20 min. Solvents were carefully decanted, and the residue was washed with ether (2 × 20 mL) to afford the 21 mg (82%) of **20** as light-yellow tacky solid. ^{1}H NMR (D_2O): δ 1.25−1.44 (m, 3H), 1.50−1.99 (m, 14H), 2.20−2.31 (m, 3H), 2.53 (dd, J = 9.9, 14.7 Hz, 1H), 2.66−2.83 (m, 1H), 2.91−3.00 (m, 4H), 3.13−3.34 (m, 14H), 3.46−3.71 (m, 38H), 4.39 (dd, J = 4.7, 8.1 Hz, 1H), 4.48−4.61 (m, 2H), 7.18−7.38 (m, 4H), 7.47 (s, 1H), 7.80 (s, 1H), 8.02 (s, 1H). LRMS calcd for $C_{67}H_{102}N_{13}O_{21}S_3$ $(M + H)^+$: 1521. Found: 1521. LRMS calcd for $C_{67}H_{101}N_{13}NaO_{21}S_3$ $(M + Na)^+$: 1543. Found: 1543. HPLC: t_R = 11.0 min.

Antibody Demetalation and Conjugation. The following procedure is an example; other quantities of the two antibodies (the antirenal cell antibody A6H (*24*) and the anti-PSMA antibody 107-1A4 (*25*)) and conjugation

reagents were also used in the studies. *(a) Reagent Preparation*. Preparation of low-metal reagents and buffers used was as previously described (*26*).

(b) Demetalation. A 5 mg quantity of a monoclonal antibody was placed in a Slide-A-Lyzer 10K dialysis cassette (Pierce) and dialyzed against 1L metal free HEPES with a minimum of 5 buffer changes over 3 days at 4 °C. To each buffer change solution was added 5 g of Chelex-100 resin. The antibody was then removed from the dialysis cassette and placed in an acid washed microcentrifuge tube. Care was taken to avoid the introduction of metals to the final solution. The demetalated mAb was stored at 4−8 °C until used in conjugation reactions.

(c) Conjugation with A6H. (1) A stock solution of **8** was prepared by dissolving 2 mg in 150 μL of 10% aqueous DMSO[4]. Aliquots of that solution were diluted with additional 10% aqueous DMSO to obtain 5, 10, 25, or 50 equiv in 15 μL. Then, 15 μL aliquot of the solutions containing the varying quantities of **8** were added to vials containing 150 μL of a 0.67 mg/mL (100 μg) of A6H in HEPES buffer at pH 8.5 for 16−18 h. After the reaction period, the A6H conjugates were purified by elution over a size exclusion column (Sephadex G-25, PD-10). The quantity of **8** conjugated with A6H was determined from the HABA and UV/BCA analyses as described in the following section. The analyses indicated that 0.4−11.5 conjugates of **8** were obtained per A6H molecule, depending on the amount reacted.

(2) A stock solution of **8** was prepared by dissolving 1.3 mg in 58 μL of DMSO. Then 30 μL of the DMSO solution of **8** (15 equiv) was added to a vial containing 1.2 mL of a 3.87 mg/mL solution of A6H in HEPES buffer at pH 8.5. The reaction mixture was stirred at room temperature overnight. After conjugation, the reaction mixture was placed in a dialysis cassette and was dialyzed against 3 × 1L of metal free citrate buffer (50 mM Na citrate, 150 mM NaCl, 0.05% NaN_3, pH 5.5) containing 5 g Chelex-100, followed by 2 × 1L metal free saline. The A6H conjugate had 2.9 conjugates of **8** per mAb.

107-1A4. Stock solutions of the trifunctional biotinylation reagents **12** and **20** were made in water. Aliquots of the stock solutions were diluted with additional water to obtain reagent solutions that contained 10, 25, or 50 equiv in 100 μL. Stock solutions of NHS-LC-biotin (1.15 mg in 38 μL), isothiocyanatobenzyl-CHX-A″, **17** (1.15 mg in 29 μL), and isothiocyanatobenzyl-DOTA, **18** (1.15 mg in 34 μL), were prepared in DMSO. The conjugation reactions were conducted as follows: To 303 μL of a 6.6 mg/mL solution of demetalated 107-1A4 (2 mg, 13.3 nmol) was added the appropriate volume (2 μL/10 equiv; 5 μL/25 equiv; 10 μL/50 equiv) of a DMSO solution containing NHS-LC-biotin, **12**, **17**, **18**, or **20**. After conjugation, the reaction mixtures were placed in dialysis cassettes and were dialyzed against 3 × 1L of metal free citrate buffer containing 5 g Chelex-100, followed by 2 × 1L metal free saline. The demetalated conjugated antibody (in saline) was stored at 4−8 °C until used in radiolabeling experiments.

[4] Due to their low water solubility, some of the reagents (i.e., **17**, **18**, and NHS-LC-biotin) were dissolved in DMSO prior to addition to the aqueous solutions. It should be noted that the trifunctional reagent **8** is soluble in water so the 10% aqueous DMSO does not have to be used. Addition of **8** in 10% aqueous DMSO solution for conjugation with A6H, and additions of **17**, **18** and NHS-LC-biotin in neat DMSO for conjugation with 107-1A4, resulted in conjugation solutions that had <3% DMSO by volume.

Antibody Conjugate Characterization. The conjugated antibodies were characterized by HPLC analysis, IEF, and SDS−PAGE electrophoresis, and the number of conjugates per antibody was determined. The methods used are described below.

Protein Concentration. Protein concentrations were estimated via UV absorption using the Beer's law equation, wherein the measured absorbance in water at 280 nm was divided by 1.5 L/g and by the BCA analysis method (*27*). The BCA analysis was conducted with a BCA Protein Assay Kit (Pierce, www.piercenet.com, Rockford, IL) following the procedure provided in the kit. The standard method was employed, but twice the concentration of copper in the working reagent was used to ensure that chelation of copper to the CHX-A″ or DOTA moieties did not give erroneous results.

Biotin Moieties per mAb. The spectrophotometric method of 4′-hydroxyazobenzene-2-carboxylic acid (HABA) displacement by biotin was used to evaluate the number of biotin moieties conjugated with the antibody (*28*). A modification of the original procedure by Green that was provided by Pierce (Rockford, IL) was used. A description of that procedure follows.

A HABA-avidin solution was prepared by adding 10 mg avidin and 600 μL of a 10 mM solution of HABA in 10 mM NaOH into 19.4 mL of PBS. A 900 μL aliquot of the HABA-avidin solution was placed in a cuvette, and the UV absorbance was measured at 500 nm. This measurement provides the A_{500} HABA and should be between 0.9 and 1.3. Following that measurement, 100 μL of the conjugated antibody is added to the cuvette and mixed well. The UV absorbance is again measured at 500 nm, and the value is taken after it stabilizes for at least 15 s. This value is the A_{500} biotin and should be 0.3 or higher. To determine the number of mmoles of biotin/mmole antibody, the following calculations were performed. First, the change in absorbance is calculated from $\Delta A_{500} = (0.9)(A_{500}{}^{HABA}) - (A_{500}{}^{biotin})$. Second, the mmol quantity of biotin/mL of the mixture is obtained from the equation $(\Delta A_{500}/34{,}000) \times 10$. Because the biotinylated antibody is diluted by a factor of 10 when it is put in the cuvette, the amount of biotin must be multiplied by that factor. Then, the calculated millimoles of biotin per milliliter are divided by the millimoles of antibody per milliliter obtained from the BCA or UV analysis to give the number of conjugates per antibody.

Electrophoresis. IEF analyses were conducted on a Novex PowerEase 500 instrument with the XCell II chamber using Invitrogen (Novex) precast gels, pH 3−10 or 3−7 (1.0 mm × 12 well) running under the standard IEF Program. The protein was stained with GelCode Blue Stain (Pierce). IEF standards were from Serva Electrophoresis GmbH: pH 10.7, cytochrome C; 9.5, ribonuclease A; 8.3, 8.0, and 7.8, lectin; 7.4 and 6.9, myoglobin; 6.0, carbonic anhydrase; 5.3 and 5.2, β-lactoglobulin; 4.5, trypsin inhibitor; 4.2, glucose oxidase; 3.5, amyloglucosidase. Examples of IEF gels are shown as Figure 1.

SDS−PAGE analyses were conducted on the Novex instrument described above using 8−16% Tris-Glycine precast gels (1.0 mm × 12 well) running under the tris−glycine gel program. The samples were prepared by addition of 5 μL of a 10% aqueous sodium dodecyl sulfate (SDS) solution to 20 μL of an aqueous 1 mg/mL solution of sample. For reducing gels, 1 μL of β-mercaptoethanol was added to each sample. After mixing, the samples were boiled for 5 min, and then a 10 μL aliquot of the sample to be run was added the gel. Molecular weight standards, MultiMark Multi-Colored Standard (5 μL, Novex), were used for reference. Those standards include

myosin (250 kDa), phosphorylase B (148 kDa), glutamic dehydrogenase (60 kDa), carbonic anhydrase (42 kDa), myoglobin (30 kDa; 22 kDa), lysozyme (17 kDa), Aprotinin (6 kDa), and insulin (4 kDa).

Radioiodination. Radioiodination of antibodies and their conjugates was conducted using the Chloramine-T method as previously described (*19*). For example, radioiodination of 107-1A4 and its conjugates was accomplished as follows. To 25 μL 0.5M sodium phosphate, pH 7.4, was added 1 μL (200 μCi) of $Na^{125}I$ in 0.1N NaOH. To that solution was added 133 μL of a 1.5 mg/mL solution of 107-1A4 derivative (200 μg) in PBS, followed by 22 μL of a 1 mg/mL solution of Chloramine-T in water. The reaction was allowed to proceed for 1 min at room temperature before quenching with 2.2 μL of a 10 mg/mL solution of sodium metabisulfite in water. The mixture was then passed over a G-25 Sephadex column (NAP-10, Pharmacia) eluting with 0.9% saline. Fractions were collected, and those containing protein were combined. Radiochemical yields ranged from 19% to 85% (Table 1).

^{111}In and ^{90}Y Labeling. *Labeling of A6H-**8**.* To a vial containing 100 μL of 50 mM NaOAc (high purity) was added 1−3 μL of [^{111}In]$InCl_3$ or [^{90}Y]YCl_3 in 0.05 M HCl. To that solution was added either 100 μL or 200 μL of a 1.47 mg/mL solution of the demetalated A6H (150 or 300 μg of mAb or mAb conjugate) in PBS. The radiolabeling was conducted at room temperature for 5 min; then the reaction was quenched by the addition of 10−20 μL of 10 mM DTPA. The radiolabeled antibody was eluted on a size exclusion column (either NAP-10 or PD-10) for purification. Labeling yields ranged from 74% to 97% (Table 1).

*Labeling of 107-1A4 Conjugated with **12**, **17**, **18**, or **20**.* To 200 μL of 0.05M NaOAc, pH 5.0, was added 200 μL of a 1.5 mg/mL solution of demetalated, conjugated 107-1A4 (300 μg) in PBS followed by 1 μL (160 μCi) of [^{111}In]-$InCl_3$ in 0.05N HCl or 0.5 μL (380 μCi) of [^{90}Y]YCl_3 in 0.05N HCl. The reaction solution was then heated to 45 °C for 1h. Following that, the radiolabeled antibody was passed over a G-25 Sephadex column (NAP-10, Pharmacia) eluting with 0.9% saline. Those fractions containing protein were combined. Radiochemical yields ranged from 36% to 100% (Table 1).

Stability of Y-90 Labeled Antibody. To 200 μL of either human serum, 10 mM EDTA, or 10 mM DTPA was added 2 μL of the radiolabeled mAb. The samples were vortexed lightly and incubated for 1h at room temperature, except for the serum sample, which was incubated at 37 °C. The stability was analyzed by placing a 100 μL aliquot in a centrifugal filter device (Microcon-30) and centrifuged at 4000 rpm for 5 min. The material remaining in the top portion of the Microcon-30 was rinsed with 3 × 100 μL PBS. The percent protein bound activity was determined by dividing the cpm remaining in the top portion of the Microcon by the total cpm in the Microcon device (top and bottom).

Avidin Column Binding. A series of 1 mL pipet tips were filled with approximately 750 μL of immobilized avidin (Pierce) to be used as columns. Half of the columns were washed with 3 mL of PBS/1% BSA (specific binding) and the other half with 3 mL of PBS/1% BSA/0.5 mg/mL biotin (nonspecific binding). Approximately 100,000 cpm (10 μL) of the labeled biotinylated mAb was placed on each column (duplicate), and they were eluted with either 2 × 1.5 mL PBS/1% BSA or PBS/1% BSA/0.5 mg/mL biotin as appropriate. The activity on the column and in the eluate was counted to determine % bound to the column.

Antibody Cell Binding Assay. The assay was conducted by addition of approximately 200,000 counts per min (cpm) of radiolabeled 107-1A4 or a conjugate in 0.1 mL PBS to 2 million trypsinized LNCaP prostate carcinoma cells suspended in 1.0 mL PBS containing 1% BSA. The actual cpm added to each tube was determined by quantification in a gamma counter. Cells were incubated at room temperature for 1 h with constant rotary inversion mixing, pelleted by centrifugation at 5000*g* for 3 min, decanted to remove supernatant, and resuspended in 1 mL PBS. The cell binding immunoreactivity estimation was taken as the counts remaining divided by initial total counts times 100. The cell binding values (average of 2) obtained are listed in Table 1.

RESULTS

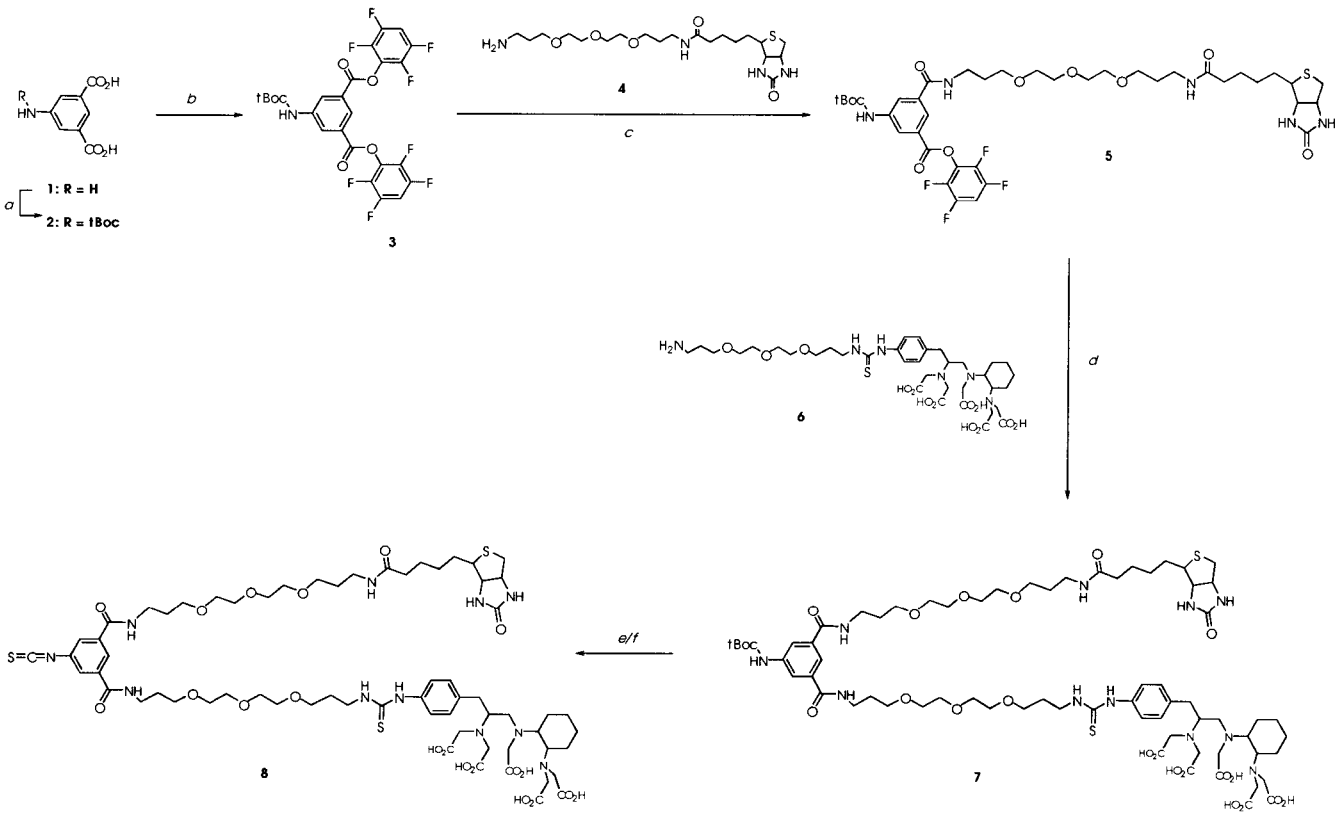
Trifunctional Reagent Syntheses. Three trifunctional reagents, **8**, **12**, and **20**, were synthesized as shown in Schemes 1−3. All three syntheses used aminoisophthalic acid, **1**, as the core of the trifunctional reagent. In the first synthetic step, the amine in **1** was converted to the *tert*-butoxycarbonyl (t-Boc) derivative, **2**, using di-*tert*-butyl dicarbonate in a basic solution of H_2O and DMF. Subsequently, **2** was converted to the bis-tetrafluorophenyl (TFP) ester, **3**, using tetrafluorophenol (TFP−OH) and 1-(3-dimethylaminopropyl)-3-ethylcarbodiimide (EDC) in DMF. The trifunctional reagent **3** has also been used to prepare radiolabeled bis-biotin compounds (*20*).

The trifunctional reagent **8** was synthesized as shown in Scheme 1. The bis-TFP ester, **3**, was reacted with 0.7 equiv of N-(13-amino-4,7,10-trioxatridecanyl)biotinamide, **4** (*19*), to provide the biotinyl-monoadduct **5**. Reaction of **5** with the adduct of 4,7,10-trioxatridecane-1,13-diamine and isothiocyanato-benzyl-CHX-A″, **17** (*21*), in the presence of triethylamine provided the N-*tert*-Boc-protected **7**. Conversion of **7** to the free amine was facile using trifluoroacetic acid (TFA), and the isolated amine was directly converted to the targeted isothiocyanate containing trifunctional reagent **8** by employing an aqueous biphasic reaction with thiophosgene in chloroform. Using this synthetic route, **8** was prepared in 13% overall chemical yield.

The synthetic route for preparing a second trifunctional reagent, **12**, is shown in Scheme 2. This synthesis is the same as that for reagent **8**, with the exception that 2-(N-biotinoyl)-4-(*N*′-(13′-*tert*-butoxycarbonylamino)-4′,7′,10′-trioxatridecaneamino)-L-aspartic acid, **9**, was reacted in the place of N-(13-amino-4,7,10-trioxatridecanyl)biotinamide, **4** (*22*). The incorporation of aspartic acid between the biotin carboxylate and the trioxadiamine linker introduces a carboxylate alpha to the biotinamide bond, which blocks the cleavage of that bond by the enzyme biotinidase (*29*,*30*). The overall chemical yield of **12** using this synthetic approach was 10%.

The synthetic steps for preparation of a third trifunctional reagent, **20**, is shown in Scheme 3. Due to difficulties encountered in purifying the trioxatridecanediamine adducts of the isothiocyanatobenzyl-CHX-A″, **6**, and the isothiocyanatobenzyl-DOTA (not reported), an alternate approach to that in Schemes 1 and 2 was taken. Reaction of one equivalent of the mono-*tert*-Boc protected trioxatridecanediamine, **13** with the aminoisophthalate bis-TFP ester, **3**, yielded the monoadduct, **14** in 73% yield. After conjugation of the biotin-aspartate derivative **9**, removal of two *tert*-Boc groups with TFA yielded a compound, **16**, which has a primary aliphatic amine and an aromatic amine. Preferential reaction of the aliphatic

Scheme 1. Synthesis of a Trifunctional Reagent Containing a Biotin Moiety, a Benzyl-CHX-A″ (DTPA) Chelation Moiety, and an Isothiocyanate for Protein Conjugation[a–f]



[a] $(tBuO)_2CO$, NaOH, H_2O, DMF, rt, 30 h, 73%. [b] TFP−OH, EDC, DMF, rt, 16 h, 67%. [c] Et_3N, DMF, rt, 1 h, 49%. [d] Et_3N, DMF, rt, 4 h, 62%. [e] TFA, rt, 30 min. [f] H_2O, $CHCl_3$, Cl_2CS, rt, 1 h, 87%.

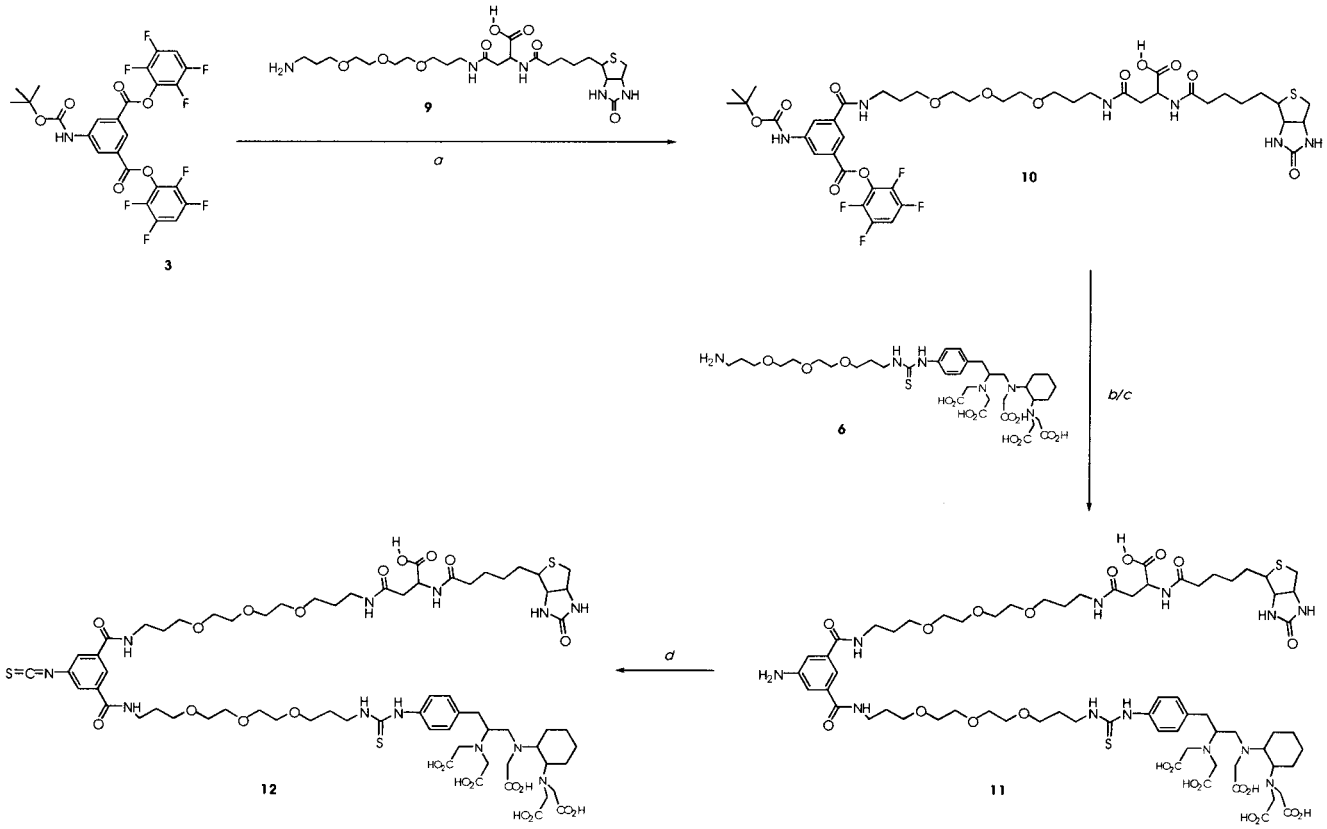
amine in Na_2CO_3/H_2O with the isothiocyanatobenzyl-DOTA, **18**, yielded the anilino-derivative **19**, which was converted to the desired trifunctional reagent, **20**, by reaction with 1,1′-thiocarbonyldiimidazole. The overall yield of **20** was 23%. This route provided a convenient synthesis of **20**, but importantly, the diamino intermediate, **16**, can be used in the preparation of other trifunctional biotinylation reagents as well. Although trifunctional reagent **12** was prepared as shown in Scheme 2, the overall yield was nearly doubled (19%) when it was prepared from the reaction of **16** with **17** as depicted in Scheme 3.

Antibody Conjugation. Antibody conjugations were conducted with the trifunctional reagents **8**, **12**, and **20**. Two monoclonal antibodies, A6H and 107-1A4, were used in the studies. In the initial conjugation studies, the trifunctional reagent **8**, was conjugated with A6H. A6H is an murine IgG_1 monoclonal antibody that reacts with a 206 kDa cell surface antigen, which is present on renal cells, and is overexpressed on renal cell carcinoma cells (*24*, *31*). In later studies, the biotinidase-stabilized trifunctional reagents, containing the metal chelates CHX-A″ (**12**), and DOTA (**20**) were conjugated with 107-1A4 (*25*). 107-1A4 is a murine IgG_1 monoclonal antibody that reacts with the cell surface antigen, prostate-specific membrane antigen (PSMA), which is present on prostate cells and is overexpressed on prostate carcinoma cells (*32*, *33*). Due to a concern that metals associated with the antibodies could decrease radiolabeling yields, the antibodies were subjected to exhaustive demetalation prior to conjugation of the trifunctional reagents.

Conjugations with A6H and 107-1A4 were conducted with varying quantities of **8**, **12**, or **20** to determine the number of conjugates per mAb obtained per equivalent offered. Initial conjugations reacted 100 μg quantities of A6H with 5, 10, 25, and 50 M equiv of **8** in HEPES buffer at pH 8.5 for 16−18 h. The A6H conjugates were purified from the nonreacted/hydrolyzed **8** by passing them over small size exclusion columns (Pharmacia PD-10). The quantity of **8** conjugated per A6H molecule was obtained by determining the number of biotin moieties and amount of protein present in a known volume of the antibody conjugate. The number of biotin moieties present (in an aliquot) was determined by conducting a HABA assay, and the protein concentration was determined by conducting both UV and BCA protein concentration analyses. Both analyses were conducted as the protein concentrations obtained from the UV analyses when higher conjugation ratios were employed appeared to be erroneous (i.e., analyses indicated that there was more protein at the end of the conjugation than was used at the initiation). The analyses indicated that 0.4−11.5 conjugates of **8** were obtained per A6H molecule, depending on the amount reacted. The results are listed in columns 2 and 3 of Table 1. A larger quantity of A6H conjugated with **8** was prepared for radiolabeling studies. In that conjugation, 15 equiv of **8** was offered and 2.9 biotin conjugates per mAb was obtained. Due to concerns for introducing metals to the A6H-**8** conjugate, dialysis was used rather than size exclusion columns to rid it of unconjugated chelate and change the solvent to saline.

Conjugations of varying quantities (10, 25, and 50 equiv) of the trifunctional reagents **12** and **20** with 107-1A4 were conducted under conditions similar to those for A6H, except that **12** and **20** were dissolved in water rather than DMSO. In the conjugations, 2 mg quantities of mAb were used so that ample conjugate was available

Scheme 2: Synthesis of a Trifunctional Reagent Containing a Biotin Moiety, a Biotinidase Stabilizing Moiety, a Benzyl-CHX-A″ (DTPA) Chelation Moiety, and an Isothiocyanate Moiety for Protein Conjugation[a—d]



[a] Et_3N, DMF, 30 min, 31%. [b] Et_3N, DMF, rt, 1 h. [c] TFA, rt, 10 min, 83%. [d] $CHCl_3$, H_2O, Cl_2CS, rt, 1 h, 82%.

Table 1. Conjugation, Radiolabeling, and Cell Binding Yields as a Function of the Number of Conjugates/MAb[a]

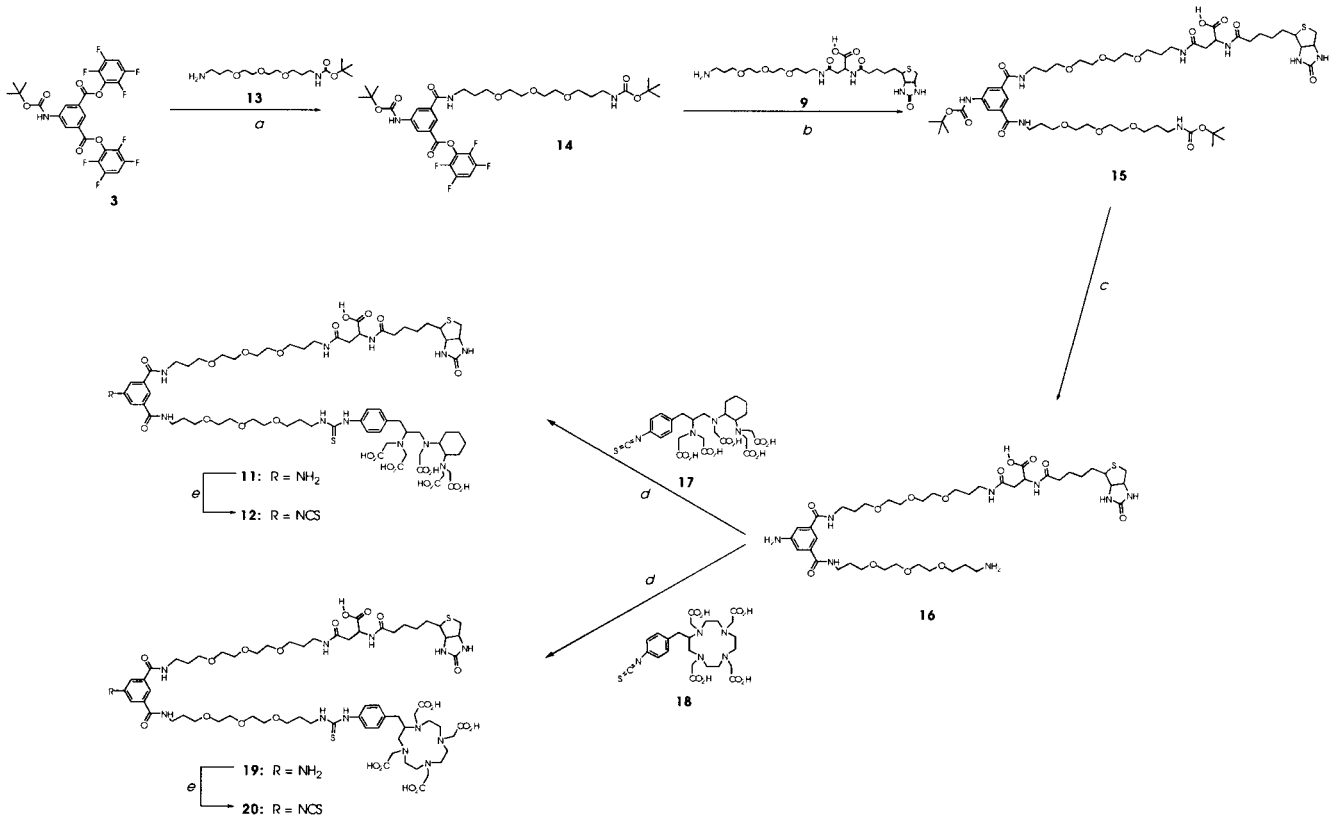
mAb conjugate	# equiv offered	# biotin per mAb	1−125 labeling yields (%)	In-111 labeling yields (%)	Y-90 labeling yields (%)	% cell binding I-125	% cell binding In-111	% cell binding Y-90
A6H								
—								
no chelate	—	—	85	<2	8			
8	5	0.4						
8	10	1.7						
8	15	2.9	67	85, 74, 90	84, 87			
8	25	5.1						
8	50	11.5						
107-1A4	—	—	—	—	—	—	—	—
—								
no chelate	—	—	75	2	3	81	71	84
LC−biotin	10	6	78	—	—	49	—	—
LC−biotin	25	9.2	83	—	—	20	—	—
LC−biotin	50	10.2	79	—	—	3	—	—
17	10	0.13	85	91	100	84	63	86
17	25	0.12	83	—	—	75	—	—
17	50	0.15	73	—	—	73	—	—
12	10	2.1	70	91	100	49	29	53
12	25	3.6	45	93	—	30	—	—
12	50	3.8	51	—	—	21	—	—
18	10	0.05	76	36	79	79	35	89
18	25	0.01	65	—	—	50	—	—
18	50	0.01	32	—	—	66	—	—
20	10	2.6	57	53	78	47	23	48
20	25	4	37	77	—	25	—	—
20	50	5.1	19	—	—	16	—	—

[a] Dash signifies that it was not determined.

for radiolabeling, cell binding, and stability experiments. After reaction was complete, the conjugated 107-1A4 was dialyzed in a cassette against metal-free buffer. The number of conjugates per mAb was determined to be 2.1−5.1 by conducting HABA and BCA analyses. The quantities of **12** and **20** offered and the number of conjugates per mAb obtained are listed in columns 2 and 3 of Table 1.

Additional conjugations of 107-1A4 were conducted with the commercially available biotinylation reagent

Scheme 3: Synthesis of a Trifunctional Reagent Containing a Biotin Moiety, a Biotinidase Stabilizing Moiety, a Benzyl-DOTA Chelation Moiety, and an Isothiocyanate Moiety for Protein Conjugation[a–g]



[a] Et_3N, DMF, rt, 3 h, 73%. [b] Et_3N, DMF, rt, 1 h, 83%. [c] TFA, rt, 10 min. [d] H_2O, Na_2CO_3, DMF, rt, 4 h, 74%. [e] DMF, TCDI, rt, 1 h, 82%. [f] H_2O, Na_2CO_3, DMF, rt, 4 h, 77%. [g] $CHCl_3$, H_2O, Cl_2CS, rt, 1 h, 82%.

N-hydroxysuccinimidyl biotinyl-6-aminocaproic acid (NHS-LC-biotin) and the bifunctional conjugation reagents, isothiocyantobenzyl-CHX-A″ (**17**) and isothiocyanatobenzyl-DOTA (**18**). These mAb conjugates were prepared to provide comparisons of radiolabeling and cell binding when only one functionality is present on the conjugate. The conjugations were conducted with the same number of equivalents offered (e.g., 10, 25, and 50) under the same reaction conditions as those described for **12** and **20**, except that the reagents were dissolved in DMSO due to their low solubility in water. The quantities of these reagents offered and the number of conjugates per mAb obtained, are also listed in columns 2 and 3 of Table 1. Conjugations with NHS-LC-biotin were efficient, resulting in 6−10 biotin moieties per mAb. Conjugations with the isothiocyanates were not as efficient, resulting in 2−5 conjugates of **12** and **20** per mAb. Since there were no biotins present when **17** and **18** were conjugated alone, the number of biotin moieties per antibody observed represent the error found in these analyses. The number of conjugated **17** or **18** per mAb was not assessed,[5] but IEF data comparing all the 107-1A4 conjugates (Figure 1) confirmed that the antibody was conjugated with these chelation moieties.

Analyses of Conjugates. The conjugates were analyzed by size exclusion HPLC, SDS−PAGE, and IEF. HPLC chromatograms for conjugates were essentially the same as those for the unmodified antibodies. This indicated that the conjugation process did not alter their structure significantly and did not cause aggregation. The SDS−PAGE analyses confirmed what was observed by HPLC. Interestingly, shifts to (an apparent) higher molecular weight could be seen on the SDS−PAGE gels (both reducing and nonreducing), but quantification was not possible (see Figures in Supporting Information). Analysis by IEF was most useful in that it provided evidence of the degree of substitution that occurred. Because the conjugations, with the exception of the NHS-LC-biotin, resulted in the elimination of a positive lysine amine and addition of four or five carboxylate functionalities, significant changes from the pI of the unmodified mAb was noted. When a broad pI gel was used (i.e., pH 3.0−10), only small differences in the pI of substituted mAbs was noted because they were all in the 4.5−6 range. Use of a short-range gel (i.e., pH 3.0−7) provided much better delineation of the changes in the protein pI. Digitized scans of short-range IEF gels for the conjugates **12**, **17**, **18**, and **20** are provided in Figure 1. Consistent with the HABA/BCA analyses (Table 1), the IEF indicate that about the same amount of substitution was obtained when 10 or 25 equiv of **12** or **20** was reacted with the mAb. In contrast with the HABA/BCA analyses, the IEF did not provide a measurable difference for reaction of 50 equiv **12** and **20** with the mAb. Conjugation of varying quantities of the isothiocyanatobenzyl-CHX-A″, **17**, and isothiocyanatobenzyl-DOTA, **18**, appears to have resulted in less substitution than for **12** or **20**. The reason for this is not certain but may be due to the fact that these reagents were stored for a length of time prior to their reaction, whereas freshly prepared **12** and **20** were used

[5] The spectrophotometric method of determining the number of chelates per antibody using Arsenzo III (*1*) was not employed to conserve the antibody conjugate for radiolabeling studies. Although the average number of chelates per mAb was not determined, IEF showed the extent of substitution from the conjugation reactions.

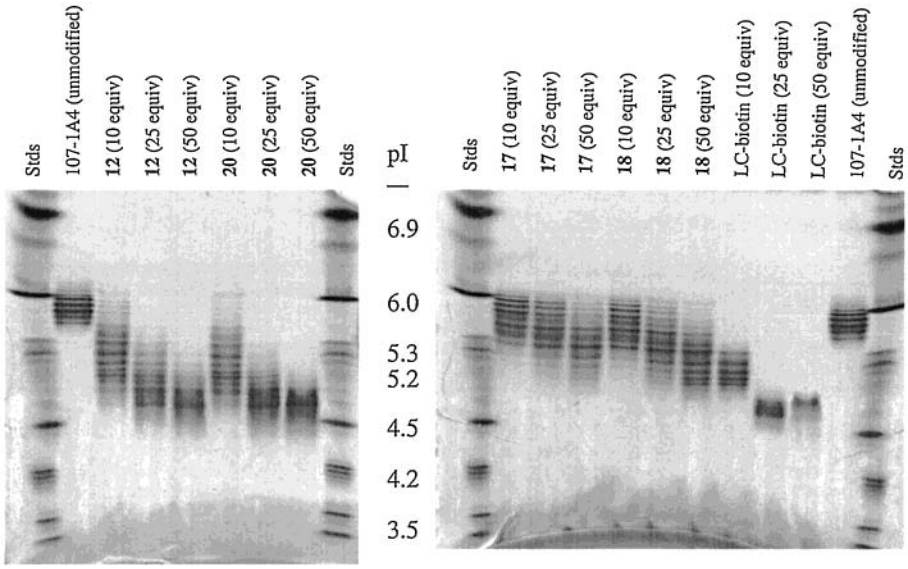


Figure 1. Digitized scans of to IEF gels that compare the pI of the anti-PSMA mAb and conjugates formed from reaction with 10, 25, or 50 equiv of (a) the trifunctional reagents **12** (CHX-A″) and **20** (DOTA), (b) the bifunctional chelating reagents **17** (CHX-A″) and **18** (DOTA), and (c) NHS-LC-biotin. The samples are identified above the lanes in the gel. IEF standards (stds) are identified in the Materials and Methods section.

in the conjugation reactions. Conjugation of the NHS-LC-biotin resulted in much higher substitution than that observed for the other reagents studied, presumably due to the higher reactivity of the N-hydroxysuccinimide ester.

Radiolabeling. The mAb conjugates were radiolabeled with ^{125}I, ^{111}In, and ^{90}Y. The purpose of radioiodination was to permit evaluation of the effect conjugation and radiolabeling had on the cell binding (immunoreactivity). In addition, the radioiodination yields were of interest in conjugates that are prepared from isothiocyanates. We have observed that radioiodination yields of compounds, including proteins, are dramatically decreased in compounds containing thiourea bonds (*34*). The standard Chloramine-T radioiodination method was used in the radioiodinations. The yields obtained for radioiodination reactions are shown in column 4 of Table 1. Radioiodination yields of 75−85% were obtained for unmodified A6H and 107-1A4. Radioiodination of the 107-1A4 that has up to 10 biotin per mAb were within the range of yields for unmodified mAb. However, there is a significant decrease in the radioiodination yields with increasing numbers of the conjugates **12**, **18**, and **20**. The decrease in radioiodination yield for conjugates prepared from reaction of 50 equiv of **18** is considerably larger than that observed for the conjugate formed from reaction of 50 equiv of **17** (32% vs 73%). Careful inspection of the IEF gel for these conjugates (Figure 1) shows that there is a higher degree of conjugation with **18** than with **17**, making the difference in radioiodination yields consistent with the other results. Importantly, the striking difference in radioiodination yields between those obtained with an active ester reaction and those obtained from an isothiocyanate reaction appear to further support the observation that thiourea bonds interfere with radioiodination reactions.

Several ^{111}In and ^{90}Y radiolabeling experiments were conducted using A6H conjugated with 2.9 conjugates of **8** per mAb. The labeling reactions were complete within 5 min at room temperature. Isolated purified radiolabeling yields of 74−90% were obtained with ^{111}In, and 84% and 97% were obtained with ^{90}Y. To ensure that the radiolabel was in the chelate and not associated with other functional groups on the protein, we added 10 mM DTPA to the reaction mixtures prior to purification by size exclusion chromatography. Additionally, labeling experiments with A6H that was not modified were conducted with ^{111}In and ^{90}Y, and only 2−8% of the radioactivity came out in the protein fraction when purified by size exclusion chromatography, indicating that the chelation groups were required for radiolabeling.

All ^{111}In and ^{90}Y labeling reactions of 107-1A4 conjugates were conducted at 45 °C rather than room temperature, as the higher temperature is required for efficient ^{90}Y labeling with the DOTA chelate. Although conjugates containing CHX-A″ will label at room temperature, the elevated temperature was used so that the mAb conjugates were treated in the same manner for comparison of immunoreactivities. The CHX-A″ conjugates (**12** and **17**) provided very good (91−100%) radiolabeling yields; however, the yields were significantly lower (36−79%) for the DOTA conjugates (**18** and **20**) under the reaction conditions employed. Importantly, attempts to radiolabel demetalated unmodified 107-1A4 with ^{111}In and ^{90}Y under the same reaction conditions proved that the labeling occurred specifically on the chelates as <3% of counts were found in fractions from size exclusion chromatography containing protein when no chelate was present. More recently, studies involving another mAb conjugated with **20** have provided radiochemical yields of >80% for both ^{111}In and ^{90}Y using 500 mM ammonium acetate as the radiolabeling buffer [unreported results].

Cell Binding Assessment. The effect of the number of conjugates per mAb on antigen binding was assessed in a radiolabeled mAb cell binding assay. In the assay, radiolabeled 107-1A4, or one of its conjugates, was incubated at room temperature with LNCaP human prostate carcinoma cells for 1h, and then the cells were separated from supernatant by centrifugation. The assay was run with excess antigen so that all antibody could bind. The percent cell binding for the radiolabeled conjugates is provided in columns 7−9 of Table 1. The data for radioiodinated 107-1A4 conjugates (column 7) clearly show that immunoreactivity decreases with increasing number of conjugates. As might be expected, the

highest level of substitution resulted in complete loss of cell binding. It is interesting to note that the mAb with six LC-biotin moieties had essentially the same cell binding properties as those that had 2−3 conjugates of **12** or **18**. Due to the differences observed in sensitivities of mAbs to radiolabeling and substitution, it should be emphasized that the results obtained with 107-1A4 shown in Table 1 may not be predictive of other antibodies. However, the trend of higher substitution causing diminished binding is consistent with all antibodies.

Stability of ^{90}Y label. An experiment was conducted to determine if ^{90}Y remained stably bound when 107-1A4 conjugated with **12** or **20** was incubated in serum or in the presence of chelates. In the experiment, the ^{90}Y-labeled 107-1A4 conjugates in 0.9% saline were incubated with serum (37 °C), 10 mM EDTA (rt), or 10 mM DTPA (rt) for 1 h. Approximately 10% of the activity dissociated from the labeled mAb when challenged with DTPA or EDTA. This is not surprising, as the concentration of these chelates was in large excess, and one might expect a transchelation process to occur to some extent. No dissociation was noted in normal saline, and only 3−5% dissociated in serum (at 37 °C) in the same time period. These data indicate that the label is very stably attached.

Avidin Column Binding. Specific binding of ^{111}In- or ^{90}Y-labeled A6H and 107-1A4 conjugates was determined by passing a solution of the radiolabeled antibody over a small avidin column. Nonspecific binding to the avidin column was determined in the same manner, except that the radiolabeled mAb solution contained a large excess of biotin. To diminish nonspecific binding to the column, BSA was added to the radiolabeled mAb solution. In an initial evaluation, avidin column binding of ^{111}In- and ^{90}Y-labeled A6H was assessed. Both labeled mAb preparations achieved 88−89% column binding. The nonspecific binding was high (9−10%), but that was attributed to the fact that only 0.1% BSA was used. The low BSA quantity was used, as there was a concern for the presence of biotin in the BSA. Higher percentages of avidin column binding was obtained for ^{111}In and ^{90}Y-labeled 107-1A4 conjugated with either **12** or **20.** In the later experiments, 1% BSA was used to diminish nonspecific binding. Although it may not have been the only influencing factor, the increased BSA concentration resulted in a much lower nonspecific binding (e.g., 1% or less). It is important to note that the avidin column binding experiments for the two different radiolabeled mAbs were conducted some time apart and agarose from different sources were used. We believe that this may have contributed to the differences observed in specific column binding.

DISCUSSION

Radiolabeled mAbs have not proven to be the "magic bullets" that they were once hoped to be. Although many clinical studies have been conducted with radiolabeled mAbs, problems associated with low tumor concentrations, heterogeneous deposition in tumors, and unacceptably high bone marrow and normal organ toxicity, have kept radiolabeled mAbs from being an effective treatment for cancer (*35*−*38*). A significant contributor to these problems is the long residence time of the radiolabeled antibody in blood. This fact has led investigators to evaluate other approaches for systemic delivery of radionuclides to cancer cells, such as those termed "pretargeting". Alternatively, development of a clinical method that can remove radiolabeled mAbs from blood after a period of sufficient time for tumor deposition could potentially result in an effective therapy for some types of cancers. This approach would allow administration of much higher quantities of radiolabeled antibodies, which in turn could result in higher tumor concentrations and a more homogeneous distribution of the radionuclide. Of course, it is important that the approach used to remove the radiolabeled mAbs from blood does not result in their deposition in organs or tissues of the body. Such an approach, termed extracorporeal affinity-adsorption (EAA), which removes radiolabeled mAbs from blood by passing it through a device external to the body, is under investigation (*14*, *39*, *40*).

As the EAA name implies, removal of the radiolabeled mAb from blood is achieved by conjugation of the antibody with a moiety that has an affinity for (binds with) a component in the device. While a number of affinity adsorbents could be used in such a device, the biotin/avidin binding pair was chosen because of their very high binding affinity and specificity (*41*). Thus, the EAA approach under investigation uses a high-capacity, high-flow-rate avidin column to capture biotinylated-radiolabeled mAbs as the blood is circulated through it. Although endogenous biotin can bind with the column, the amount present in blood of patients (e.g., 215−750 pg/mL; *42*), or released from liver stores during the procedure, can be offset by having a large excess of avidin on the column. The large quantity of avidin also helps to compensate for the requisite high flow rate. Preclinical studies have been conducted to determine the efficacy and safety of the EAA approach. In animal models, 80−95% of radioactivity in blood, and around about 50% of the radioactivity in the whole body, was removed from athymic rats bearing murine and human tumor xenografts (*15*, *39*, *43*, *44*). The removal of radiolabeled antibody from blood was accomplished with little effect on the radioactivity in the tumor, and no observable toxicity. Ex vivo studies have also shown good biocompatibility of avidin columns with perfused human whole blood (*45*).

The EAA approach requires that the radiolabeled mAb be biotinylated so that it can be captured on the avidin column. Unfortunately, the chemistry of radiolabeling and conjugation can result in decreased binding of the radiolabeled mAbs with cancer cells. Thus, to generalize and improve the applicability of EAA to a wide variety of radiolabeled mAbs, a standardized method for biotinylation and radiolabeling that minimizes the deleterious effects needs to be developed. This is particularly important as mAbs can vary greatly in sensitivity to conjugation and radiolabeling. Early EAA studies were conducted with the biotinylated and radioiodinated mAbs, L6 and chimeric BR96 (chBR96) (*15*, *16*, *40*, *43*). Generally, direct radioiodination on tyrosine phenols, and conjugation of a biotin on lysine amines, of mAbs is well tolerated. The combination of these two protein modifications might also be expected to be well tolerated when minimal derivatization is done. However, some mAbs are quite sensitive to the oxidizing conditions used in direct radioiodinations, and other mAbs are internalized, which can result in the rapid release of radioiodine. Therefore, the combination of direct radioiodination and biotinylation can lead to undesirable results. In studies comparing direct radioiodination, and radioiodination using an iodobenzoate, of the internalizing mAb chBR96, it was found that the conjugate radioiodination method provided higher tumor concentration (*46*, *47*). Additionally, previous studies with the internalizing mAb chimeric BR96 demonstrated that ^{111}In labeling gave better results than those obtained with direct radioiodination (48). Other metal radionuclides,

including Re-188 (*49*), have been studied, but our choice of radionuclides for this investigation, ^{111}In and ^{90}Y, was based on their favorable emission properties and on the fact that they are widely used in diagnostic and therapeutic procedures.

The studies described herein were undertaken to develop reagents that minimized the effect of conjugating both radionuclide chelation groups and biotin moieties to mAbs. It was envisioned that combining the two functionalities (metal chelation moiety and biotin) on a single molecule for conjugation would minimize the effect of conjugation, as fewer conjugates could be coupled to the mAb. Such a combined functionality molecule could also provide other benefits. Importantly, every mAb that was radiolabeled would also have a biotin moiety present so that it could be removed via the avidin column. Also, minimal derivatization could be undertaken as the mAbs that did not contain at least one conjugate would not radiolabel, and thus would not need to be removed by the avidin column. The design of a combined functionality conjugation molecule requires that it be trifunctional in nature, also incorporating a protein conjugation moiety. Thus, the trifunctional reagent design had to contain a biotin moiety, a chelation moiety that binds In and Y, and a protein reactive moiety for application to radiolabeled monoclonal antibodies for EAA.

Several studies have demonstrated that linkers between biotin and the protein conjugation functionality are sometimes required to obtain maximal binding with avidin or streptavidin (*50*−*53*). Thus, as in our previous studies, 4,7,10-trioxatridecane-1,13-diamine was incorporated as a 19 Å spacer between biotin and the other portion of the conjugation molecule. Additionally, this linker moiety provides increased water solubility of the reagents. Two metal chelation groups were chosen for incorporated into the trifunctional reagents based on previously determined labeling characteristics and in vivo stability with ^{111}In and ^{90}Y. A cyclohexyl modified DTPA derivative, termed CHX-A″ was chosen, as previous studies had shown that it labels under mild conditions and has high stability in vivo (*54*, *55*). The macrocyclic chelate DOTA, was chosen as an alternate to the CHX-A″ because it forms radiometal complexes that are very stable to in vivo demetalation (*56*, *57*). While the highest in vivo stability is sought, radiolabeling DOTA conjugates requires elevated temperatures which may be deleterious to some mAbs. Fortunately, both the isothiocyanatobenzyl-CHX-A″ and isothiocyanatobenzyl-DOTA derivatives were available from either synthesis (*21*) or commercial sources. Although it was not clear that a linker molecule was required between the DTPA or DOTA moiety and the rest of the molecule, it was decided that incorporation of another trioxatridecanediamine moiety might improve their aqueous solubility at physiological pH. To conjugate the metal chelate and biotin to the mAbs, a reactive functionality was required. The isothiocyanate was an obvious choice, as it is readily prepared in the presence of the carboxylates of the DTPA and DOTA moieties. The only other consideration in the design of the trifunctional reagent was that of blocking in vivo degradation by the serum enzyme, biotinidase (*58*, *59*). Because studies in our laboratory with a few biotinylated mAbs demonstrated that biotin was not cleaved by biotinidase when conjugated to mAbs (*60*), the initial trifunctional reagent, **8**, did not incorporate a biotinidase blocking functionality. However, in the two other trifunctional reagents, **12** and **20**, aspartic acid was incorporated adjacent to the biotin moiety to block the action of biotinidase (*61*). The biotinidase blocking group was incorporated, as insufficient data was available to state definitively that it would not be required with some mAbs. Additionally, we wanted to make the reagents generally applicable for other radionuclide carriers, so we felt that it was necessary to incorporate the biotinidase blocking moiety.

Table 2. Stability of Y-90 Labeled mAb When Challenged[a]

mAb conjugate	serum (37 °C)	10 mM EDTA (rt)	10 mM DTPA (rt)
free Y-90	4	2	2
17	92	85	2
12	94	85	2
18	97	93	96
20	91	91	92

[a] Values are percent remaining in Microcon top (e.g., protein bound).

Table 3. Specific and Nonspecific Binding of Conjugates with an Avidin Column

mAb conjugate	specific In-111	nonspecific In-111	specific Y-90	nonspecific Y-90
A6H[a]				
8 (15 equiv)	88	10	89	9
107-1A4	−	−	−	−
12 (10 equiv)	93	1	94	0.3
12 (25 equiv)	98	1	98	1
20 (10 equiv)	98	0.1	98	−
20 (25 equiv)	99	0.1	96	0.2

[a] The radiolabeled antibody was mixed with 0.1% BSA.

The synthesis of the three trifunctional reagents following the routes outlined in Schemes 1−3 was straightforward. The synthetic route outlined in Scheme 3 proved to be the best, as it utilizes a common intermediate, **16**, for addition of either chelation group and resulted in good overall chemical yields. Although not conducted, a similar intermediate can be prepared without the biotinidase blocking aspartate moiety. More importantly, the biotinyl-trifunctional intermediate **16**, and the corresponding reagent without the aspartate, could be used to incorporate other radionuclide binding moieties or other (reporter) functionalities such as chromophores or fluorophores (*62*) into new trifunctional reagents.

The three trifunctional reagents, **8**, **12**, and **20**, were readily conjugated with mAbs. In the studies, varying quantities of reagents were used in the conjugations to determine the ratio of trifunctional reagent to mAb to obtain a desired level of conjugation. While it is expected that both radiolabeling and capture by the avidin column would be improved with higher numbers of conjugates per mAb molecule, the cell binding studies demonstrate that even with the trifunctional reagents, minimal derivatization is best. On the basis of the results, it seems that 2−3 conjugates per mAb would be the maximum that one might want to have, but this should be evaluated for each mAb. Although based on high concentrations of challenging chelate (i.e., 10 mM), the stability difference between the CHX-A″ and DOTA chelates was clearly demonstrated (Table 2). It seems prudent to use the trifuntional reagent containing the DOTA chelate, **20**, unless the mAb is sensitive to the radiolabeling conditions required for that chelate. Most importantly, it was demonstrated that a high percentage of the radiolabeled mAb conjugated with the trifunctional reagents could be bound to an avidin column in one pass.

In Summary. Three trifunctional reagents that contain a metal chelation moiety and a biotin moiety have been prepared for modification of mAbs used in blood

clearance by extracorporeal affinity adsorption. Conjugation of a low number of trifunctional reagents (fewer than three) results in retention of the mAb's cell binding properties. Good radiolabeling yields and high avidin column binding were achieved with the minimally derivatized mAbs. On the basis of the results obtained, testing of mAbs modified with a trifunctional reagent in combination with a device containing an avidin column is planned. The trifunctional reagents may also be useful when conjugated with other cancer-targeting agents.

ACKNOWLEDGMENT

We thank Dr. Robert Vessella (Department of Urology, University of Washington) for supplying the mAbs, A6H, and 107-1A4, used in the studies. Financial support for the majority of the studies was provided by Mitra Medical Technology AB of Lund, Sweden. Funding for portions of the studies was provided by the Department of Energy, Medical Applications and Biophysical Research Division, Office of Health and Environmental Research under Grant Number DE-FG03-98ER62572. We are grateful for the funding from both of these sources.

Supporting Information Available: HPLC chromatograms, NMR spectra, and mass spectra of all new compounds (**5**−**8**, **10**−**12**, **14**, **15**, **19**, and **20**) (33 pages) and scanned SDS−PAGE gels (reducing and nonreducing) of 107-1A4 conjugates (3 pages). This material is available free of charge via the Internet at http://pubs.acs.org.

LITERATURE CITED

(1) Pippin, C. G., Parker, T. A., McMurry, T. J., and Brechbiel, M. W. (1992) Spectrophotometric Method for the Determination of a Bifunctional DTPA Ligand in DTPA-Monoclonal Antibody Conjugates. *Bioconjugate Chem. 3*, 342−345.

(2) Wilchek, M., and Bayer, E. A. (1990) Introduction to Avidin−Biotin Technology. *Methods Enzymol. 184*, 5−45.

(3) Bayer, E. A., and Wilchek, M. (1996) The Avidin-Biotin System. In *Immunoassay* (E. P. Diamandis and T. K. Christopoulos, Eds.) pp 237−267, Academic Press, San Diego.

(4) Diamandis, E. P., and Christopoulos, T. K. (1991) The Biotin-(Strept)Avidin System: Principles and Applications in Biotechnology. *Clin. Chem. 37*, 625−636.

(5) Schetters, H. (1999) Avidin and Streptavidin in Clinical Diagnostics. *Biomol. Eng. Dec 16*, 73−78.

(6) Goodwin, D. A., and Meares, C. F. (1997) Pretargeting: General Principles. *Cancer (Suppl.) 80*, 2675−2680.

(7) Chinol, M., Grana, C., Gennari, R., Cremonesi, M., Geraghty, J. G., and Paganelli, G. (2000) Pretargeted Radioimmunotherapy of Cancer. In *Radioimmunotherapy of Cancer* (P. G. Abrams and A. R. Fritzberg, Eds.) pp 169−193, Marcel Dekker, New York.

(8) Stoldt, H. S., Aftab, F., Chinol, M., Paganelli, G., Luca, F., Testori, A., and Geraghty, J. G. (1997) Pretargeting Strategies for Radio-immunoguided Tumour Localisation and Therapy. *Eur. J. Cancer 33*, 186−192.

(9) Theodore, L. J., Fritzberg, A. R., Schultz, J. E., and Axworthy, D. B. (2000) Evolution of a Pretarget Radioimmunotherapeutic Regimen. In *Radioimmunotherapy of Cancer* (P. G. Abrams, P. G. and A. R. Fritzberg, Eds.) pp 195−221, Marcel Dekker, New York.

(10) Press, O. W., Corcoran, M., Subbiah, K., Hamlin, D. K., Wilbur, D. S., Johnson, T., Theodore, L., Yau, E., Mallett, R., Meyer, D. L., and Axworthy, D. (2001) A Comparative Evaluation of Conventional and Pretargeted Radioimmunotherapy of CD20-Expressing Lymphoma Xenografts. *Blood 98*, 2535−2543.

(11) Axworthy, D. B., Reno, J. M., Hylarides, M. D., Mallett, R. W., Theodore, L. J., Gustavson, L. M., Su, F., Hobson, L. J., Beaumier, P. L., and Fritzberg, A. R. (2000) Cure of Human Carcinoma Xenografts by a Single Dose of Pretargeted Yttrium-90 with Negligible Toxicity. *Proc. Natl. Acad. Sci. U.S.A. 97*, 1802−1807.

(12) Rusckowski, M., Fogarasi, M., Fritz, B., and Hnatowich, D. J. (1997) Effect of Endogenous Biotin on the Applications of Streptavidin and Biotin in Mice. *Nucl. Med. Biol. 24*, 263−268.

(13) Rosebrough, S. F., and Hartley, D. F. (1995) Quantification and Lowering of Serum Biotin. *Lab. Anim. Sci. 45*, 554−557.

(14) Strand, S.-E., Sjogren, H.-O., Chen, J., Hindrof, C., Tennvall, J. G., Garkavij, M., Nilsson, R., and Sandberg, B. E. B. (2000) Extracorporeal Techniques in Radioimmunotherapy. In *Radioimmunotherapy of Cancer* (P. G. Abrams and A. R. Fritzberg, Eds.), pp 223−243, Marcel Dekker, Inc., New York.

(15) Garkavij, M., Tennvall, J., Strand, S.-E., Nilsson, R., Lindgren, L., Chen, J., Isaksson, M., Eriksson, H., and Sjögren, H.-O. (1996) Extracorporeal Immunoadsorption from Whole Blood Based on the Avidin−Biotin Concept. Evaluation of a New Methodology. *Acta Oncol. 35*, 309−312.

(16) Garkavij, M. (1996) Improving Radioimmunotargeting of Tumors. The Impact of Extracorporeal Immunoadsorption and Preload in Rats. Doctoral Dissertation, Lund University, Lund, Sweden.

(17) Garkavij, M., Tennvall, J., Strand, S.-E., Sjögren, H.-O., JianQing, C., Nilsson, R., and Isaksson, M. (1997) Extracorporeal Whole-Blood Immunoadsorption Enhances Radioimmunotargeting of Iodine-125-Labeled BR96-Biotin Monoclonal Antibody. *J. Nucl. Med. 38*, 895−901.

(18) Gamper, H. B., Reed, M. W., Cox, T., Virosco, J. S., Adams, A. D., Gall, A. A., Scholler, J. K., and Meyer, R. B. (1993) Facile Preparation of Nuclease Resistant 3′ Modified Oligodeoxynucleotides. *Nucleic Acids Res. 21*, 145−150.

(19) Wilbur, D. S., Hamlin, D. K., Vessella, R. L., Stray, J. E., Buhler, K. R., Stayton, P. S., Klumb, L. A., Pathare, P. M., and Weerawarna, S. A. (1996) Antibody fragments in tumor pretargeting. Evaluation of Biotinylated Fab′ Colocalization with Recombinant Streptavidin and Avidin. *Bioconjugate Chem. 7*, 689−702.

(20) Hamblett, K. J., Kegley, B. B., Hamlin, D. K., Chyan, M. K., Hyre, D. E., Press, O. W., Wilbur, D. S., and Stayton, P. S. (2002) A Streptavidin-Binding System that Minimizes Blocking by Endogenous Biotin. *Bioconjugate Chem. 13*, 588−598.

(21) Brechbiel, M. W., and Gansow, O. A. (1992) Synthesis of C-Functionalized trans-Cyclohexyldiethylenetriaminepentaacetic Acids for Labeling of Monoclonal Antibodies with the Bismuth-212 α-Particle Emitter. *J. Chem. Soc., Perkin Trans. 1*, 1173−1178.

(22) Wilbur, D. S., Hamlin, D. K., Chyan, M. K., Kegley, B. B., and Pathare, P. M. (2001) Biotin Reagents for Antibody Pretargeting. 5. Additional Studies of Biotin Conjugate Design to Provide Biotinidase Stability. *Bioconjugate Chem. 12*, 616−623.

(23) Wilbur, D. S., Hamlin, D. K., Buhler, K. R., Pathare, P. M., Vessella, R. L., Stayton, P. S., and To, R. (1998) Streptavidin in Antibody Pretargeting. 2. Evaluation of Methods for Decreasing Localization of Streptavidin to Kidney while Retaining its Tumor Binding Capacity. *Bioconjugate Chem. 9*, 322−330.

(24) Vessella, R. L., Moon, T. D., Chious, R.-K., Nowak, J. A., Arfman, E. W., Palme, D. F., Peterson, G. A., and Lange, P. H. (1985) Monoclonal Antibodies to Human Renal Cell Carcinoma: Recognition of Shared and Restricted Tissue Antigens. *Cancer Res. 45*, 6131−6139.

(25) Brown, L., Wegner, S., Wang, H., Buhler, K., Arfman, E., Lange, P., and Vessella, R. (1998) A Novel Monoclonal Antibody 107-1A4 with High Prostate Specificity: Generation Characterization of Antigen Expression, and Targeting of Human Prostate Cancer Xenografts. *Prostate Cancer Prostatic Dis. 1*, 208−215.

(26) Mirzadeh, S. (1990) Radiometal Labeling of Immunoproteins: Covalent Linkage of 2-(4-Isothiocyanatobenzyl)diethylenetriaminepentaacetic Acid Ligands to Immunoglobulin. *Bioconjugate Chem. 1*, 59−65.

(27) Walker, J. M. (1994) The Bicinchoninic Acid (BCA) Assay for Protein Quantification. In *Basic Protein and Peptide Protocols* (J. M. Walker, Ed.) pp 5−8, Humana Press, Totowa, NJ.

(28) Green, N. M. (1965) A Spectrophotometric Assay for Avidin and Biotin Based on Binding of Dyes by Avidin. *Biochem. J. 94*, 23−24.

(29) Pispa, J. (1965) Animal Biotinidase. *Ann. Med. Exptl. Bio. Fenniae 43*, 3−40.

(30) Hymes, J., Fleischhauer, K., and Wolf, B. (1997) Biotinidase in Serum and Tissues. *Methods Enzymol. 279*, 422−434.

(31) Vessella, R. L., Alvarez, V., Chious, R.-K., Rodwell, J., Elson, M., Palme, D., Shafer, R., and Lange, P. (1987) Radioimmunoscintigraphy and Radioimmunotherapy of Renal Cell Carcinoma Xenografts. *NCI Monogr. 3*, 159−167.

(32) Silver, D. A., Pellicer, I., Fair, W. R., Heston, W. D. and Cordon-Cardo, C. (1997) Prostate-specific Membrane Antigen Expression in Normal and Malignant Human Tissues. *Clin. Cancer Res. 3*, 81−85.

(33) Zhang, S., Zhang, H. S., Reuter, V. E., Slovin, S. F., Scher, H. I., and Livingston, P. O. (1998) Expression of Potential Target Antigens for Immunotherapy on Primary and Metastatic Prostate Cancers. *Clin. Cancer Res. 4*, 295−302.

(34) Wilbur, D. S., Hamlin, D. K., Kegley, B. B., Chyan, M. K., Pathare, P. M., and Wan, F. (2001) Studies Which Indicate That Thiourea Bonds Interfere With Radioiodination Reactions. *J. Labeled Cpd. Radiopharm. 44*, S973−S975.

(35) White, C. A., Weaver, R. L., and Grillo-Lopez, A. J. (2001) Antibody-targeted Immunotherapy for Treatment of Malignancy. *Annu. Rev. Med. 52*, 125−145.

(36) Larson, S. M., Sgouros, G., and Cheung, N.-K. (1997) Radiolabeled Antibodies: General Issues. In *Encyclopedia of Cancer* (J. R. Bertino, Ed.) pp 1420−1431, Academic Press, New York.

(37) Stigbrand, T., Ullén, A., Sandström, P., Mirzaie-Joniani, H., Sundström, B., Nilsson, B., Ärlestig, L., Norrlund, R. R., Ahlström, K. R., and Hietala, S.-O. (1996) Twenty Years With Monoclonal Antibodies. State of the Art? Where Do We Go? *Acta Oncol. 35*, 259−265.

(38) Kairemo, K. J. A. (1996) Radioimmunotherapy of Solid Cancers. *Acta Oncol. 35*, 343−355.

(39) Tennvall, J., Garkavij, M., Chen, J., Sjogren, H. O., and Strand, S. E. (1997) Improving Tumor-to-Normal-Tissue Ratios of Antibodies by Extracorporeal Immunoadsorption Based on the Avidin-Biotin Concept: Development of a New Treatment Strategy Applied to Monoclonal Antibodies Murine L6 and Chimeric BR96. *Cancer 80*, 2411−2418.

(40) Garkavij, M., Tennvall, J., Strand, S. E., Nilsson, R., Lindgren, L., Chen, J., Isaksson, M., Eriksson, H., and Sjogren, H. (1996) Extracorporeal Immunoadsorption from Whole Blood Based on the Avidin-Biotin Concept. Evaluation of a New Method. *Acta Oncol. 35*, 309−312.

(41) Green, N. M. (1975) Avidin. *Adv. Prot. Chem. 29*, 85−133.

(42) Baker, H. (1985) Assessment of Biotin Status: Clinical Implications. *Ann. N. Y. Acad. Sci. 447*, 129−132.

(43) Garkavij, M., Tennvall, J., Strand, S.-E., Norrgren, K., Lindgren, L., Nilsson, R., and Sjoegren, H.-O. (1995) Enhanced Radioimmunotargeting of ^{125}I-Labeled L6-Biotin Monoclonal Antibody (MAb) by Combining Preload of Cold L6 MAb and Subsequent Immunoadsorption in Rats. *Cancer Res. 55*, 5874S-5880S.

(44) Garkavij, M., Tennvall, J., Strand, S. E., Sjogren, H. O., JianQing, C., Nilsson, R., and Isaksson, M. (1997) Extracorporeal Whole-Blood Immunoadsorption Enhances Radioimmunotargeting of Iodine-125-Labeled BR96-Biotin Monoclonal Antibody. *J. Nucl. Med. 38*, 895−901.

(45) Bosch, T., Lennertz, A., Duhr, C., Fink, E., and Samtleben, W. (2000) Ex vivo Biocompatibility of Avidin-Agarose: A New Device for Direct Adsorption of Biotinylated Antibodies from Human Whole Blood. *Artif. Organs 24*, 696−704.

(46) Chen, J., Strand, S.-E., and Sjoegren, H.-O. (1996) Optimization of Radioiodination and Biotinylation of Monoclonal Antibody Chimeric BR96: An Indirect Labeling Using N-succinimidyl-3-(tri-n-butylstannyl)benzoate Conjugate. *Cancer Biother. Radiopharm. 11*, 217−226.

(47) Chen, J., Strand, S. E., Isaksson, M., Ljunggren, K., Sjoegreen, K., Garkavij, M., Tennvall, J., and Sjoegren, H. O. (1996) Biodistribution and Pharmacokinetics of ^{125}I/^{131}I Pair-Labeled Biotinylated Chimeric BR96 in Colon Carcinoma Isografted Rats. *Tumor Targeting 2*, 204−214.

(48) Garkavij, M., Tennvall, J., Ohlsson, T., Lindgren, L., Hindorf, C., Sjogren, H.-O., and Strand, S.-E. (1999) Comparison of ^{125}I- and ^{111}In-Labeled Monoclonal Antibody BR96 for Tumor Targeting in Combination with Extracorporeal Immunoadsorption. *Clin. Cancer Res. 5*, 3059s−3064s.

(49) Chen, J., Strand, S.-E., Tennvall, J., Lindgren, L., Hindorf, C., and Sjogren, H.-O. (1997) Extracorporeal Immunoadsorption Compared to Avidin Chase: Enhancement of Tumor-to-Normal Tissue Ratio for Biotinylated Rhenium-188-Chimeric BR96. *J. Nucl. Med. 38*, 1934−1939.

(50) Bernstein, K. E., Welsh, S. L., and Inman, J. K. (1990) A Deeply Recessed Active Site in Angiotensin-Converting Enzyme is Indicated From The Binding Characteristics of Biotin-Spacer-Inhibitor Reagents. *Biochem Biophys. Res. Commun. 167*, 310−316.

(51) Polli, J. W., and Billingsley, M. L. (1991) Preparation, Characterization and Biological Properties of Biotinylated Derivatives of Calmodulin. *Biochem. J. 275*, 733−743.

(52) Deguchi, Y., Kurihara, A., and Pardridge, W. M. (1999) Retention of Biologic Activity of Human Epidermal Growth Factor Following Conjugation to a Blood-Brain Barrier Drug Delivery Vector via an Extended Poly(ethylene glycol) Linker. *Bioconjugate Chem. 10*, 32−37.

(53) Hashimoto, M., Yang, J., and Holman, G. D. (2001) Cell-Surface Recognition of Biotinylated Membrane Proteins Requires Very Long Spacer Arms: An Example from Glucose-Transporter Probes. *ChemBioChem 2*, 52−59.

(54) Roselli, M., Milenic, D. E., Brechbiel, M. W., Mirzadeh, S., Pippin, C. G., Gansow, O. A., Colcher, D., and Schlom, J. (1999) In Vivo Comparison of CHX-DTPA Ligand Isomers in Athymic Mice Bearing Carcinoma Xenografts. *Cancer Biother. Radiopharm. 14*, 209−220.

(55) Kobayashi, H., Wu, C. C., Yoo, T. M., Sun, B. F., Drumm, D., Pastan, I., Paik, C. H., Gansow, O. A., Carrasquillo, J. A., and Brechbiel, M. W. (1998) Evaluation of the in vivo Biodistribution of Yttrium-Labeled Isomers of CHX-DTPA-Conjugated Monoclonal Antibodies. *J. Nucl. Med. 39*, 829−836.

(56) Li, M., and Meares, C. F. (1993) Synthesis, Metal Chelate Stability Studies and Enzyme Digestion of a Peptide-Linked DOTA Derivative and Its Corresponding Radiolabeled Immunoconjugates. *Bioconjugate Chem. 4*, 275−283.

(57) Lewis, M. R., Raubitschek, A., and Shively, J. E. (1994) A Facile, Water-Soluble Method for Modification of Proteins with DOTA. Use of Elevated Temperature and Optimized pH to Achieve High Specific Activity and High Chelate Stability in Radiolabeled Immunoconjugates. *Bioconjugate Chem. 5*, 565−576.

(58) Chauhan, J., Ebrahim, H., Bhullar, R. P., and Dakshinamurti, K. (1985) Human Serum Biotinidase. *Ann. N. Y. Acad. Sci. 447*, 386-388.

(59) Wolf, B., Hymes, J., and Heard, G. S. (1990) Biotinidase. *Methods Enzymol. 184*, 103−111.

(60) Hamlin, D. K., Wilbur, D. S., Pathare, P. M., Subramaniam, D. S., Corcoran, M., and Press, O. W. (2000) Evaluation fo Antibody Biotinylation Reagents for Application to Targeted Radiotherapy. In *Isotope Production and Applications in the 21st Century.* (N. Stevenson, Ed.) pp 353−355, World Scientific Publishing Co., Inc., River Edge, NJ.

(61) Wilbur, D. S., Hamlin, D. K., Chyan, M.-K., Kegley, B. B., and Pathare, P. M. (2001) Biotin reagents for antibody pretargeting. 5. Additional Studies of Biotin Conjugate Design to Provide Biotinidase Stability. *Bioconjugate Chem. 12*, 616−623.

(62) Wilbur, D. S., Chyan, M.-K., Hamlin, D. K., and Sandberg, B. E. B. (2001) Synthesis and Evaluation of Protein Biotinylation Reagents that also Contain UV and/or Fluorescence Absorbing Moieties. *Abstr. Pap.—Am. Chem. Soc. 221*, MEDI-031.

BC025535R

A Novel 2′-(*N*-Methylpyridinium Acetate) Prodrug of Paclitaxel Induces Superior Antitumor Responses in Preclinical Cancer Models

Wolfgang Wrasidlo,[†] Gerhard Gaedicke,[†] Rodney Kiplin Guy,[‡] Johanne Renaud,[‡] Emmanuel Pitsinos,[‡] Kyriaco C. Nicolaou,[‡] Ralph A. Reisfeld,[§] and Holger N. Lode*[,†]

Charité Children's Hospital, Humboldt University, Berlin, Germany, and The Scripps Research Institute, Departments of Chemistry and Immunology, La Jolla, California 92037. Received April 1, 2002; Revised Manuscript Received July 30, 2002

The development of novel strategies for the treatment of malignancies by successful intervention in advanced stage disease is a major challenge in oncology. We tested the hypothesis that this can be achieved by the rational design of taxoid onium salts modified at C-7 and C-2′ positions. The characterization of these molecules revealed a dramatically improved water solubility and prodrug behavior in plasma. Specifically, all compounds released parental paclitaxel with half-lives ranging from 0.9 to 180 min. In the absence of plasma, only the 2′-(*N*-methylpyridinium acetate) derivative of paclitaxel (2′-MPA-paclitaxel) revealed a complete abrogation of paclitaxel specific microtubule assembly disassembly dynamics and a 3 log reduction in cellular binding, indicating that reversible blockage of the C-2′ position by methylpyridinium acetate yields a true paclitaxel prodrug. Structure/activity profiles of all compounds in tissue culture revealed cytotoxicity effective at picomolar concentrations with a panel of 16 cancer cell lines in contrast to 4 nonmalignant cell lines. Importantly, the decisive cytotoxic potential observed in vitro for all compounds correlated only with in vivo findings for 2′-MPA-paclitaxel. Specifically, the 2′-MPA-paclitaxel prodrug induced regression of primary tumors in three xenograft models of nonsmall cell lung carcinoma, ovarian carcinoma and prostate cancer, in contrast to ineffective C-7 derivatives and parental paclitaxel. At the same time, a reduced systemic toxicity of 2′-MPA-paclitaxel was observed in contrast to a far more toxic parental paclitaxel. Taken together, these findings demonstrate that the 2′-MPA-paclitaxel prodrug is a promising new candidate for cancer therapy.

INTRODUCTION

Paclitaxel is an anticancer agent with established value for clinical application (*1*) including prostate, lung, breast, and ovarian cancer (*2*−*11*). However, limited response rates, significant side effects, and low solubility remain as major obstacles for more effective cancer therapy.

Paclitaxel is a natural product gained from the bark of the pacific yew tree (*Taxus brevifolia*). Its chemical structure was first described by Wani at al. in 1971 (*9*). Unlike other anti-microtubule drugs, such as vinca alkaloids, colchicine, or podophyllotoxin, paclitaxel promotes the irreversible polymerization of tubulin (*12*−*15*). The presence of stable and dysfunctional microtubules causes disruption of the cell division and thus cell death or reversible cell cycle arrest. This arrest in the premitotic G2 and the mitotic phases, the so-called G2M-arrest, enhances the effect of irradiation and possibly the activity of other cytotoxic drugs (*16*). Paclitaxel also enhances the expression of tumor necrosis factor (TNF) α and IL-1 and downregulates TNF receptors, activities which are shared by bacterial lipopolysaccharides. This cytokine stimulatory activity may also contribute to its antitumor properties and seems not to be related to the effect on microtubule assembly (*17*). Paclitaxel also induced internucleosomal DNA fragmentation associated with bcl-2 expression in leukemic cells, suggesting that its action triggers a gene-directed mechanism of programmed cell death (*18*). Toxicity consists mainly of hypersensitivity reactions, hematologic toxicity, and neurotoxicity. Hypersensitivity, despite proper premedication with dexametasone and/or histamine H2 antagonist diphenhydramine, is reported in 1−3% of patients (*19*−*21*).

The clinical application of paclitaxel, which has a limited solubility in water (<0.004 mg/mL), requires formulations as emulsions between alcohol and oils such as Cremophor EL, accounting for vehicle specific hypersensitivity reactions observed following paclitaxel therapy (*22*). It appears that the most critical issue in producing effective water soluble paclitaxel prodrugs involves the pharmacokinetics of prodrug reversion to the natural compound, which requires a balance between in vivo hydrolytic stability, bioavailability, and rate of elimination. We have evaluated paclitaxel analogues containing structural modifications at different locations of the parent molecule, which influence both their chemical and pharmacological properties. Here, we report results with analogues based on oxonium salts of paclitaxel with different structure/activity profiles depending on the nature and position of these substitutions.

* To whom reprint requests should be addressed at Charité Children's Hospital, Augustenburger Platz 1, 13353 Berlin, Germany. Phone: +49 30 450 559217; FAX: +49 30 450 559917; E-mail: holger.lode@charite.de.

[†] Humboldt University.

[‡] Scripps Research Institute, Department of Chemistry.

[§] Scripps Research Institute, Department of Immunology.

10.1021/bc0200226 CCC: $22.00 © 2002 American Chemical Society
Published on Web 08/20/2002

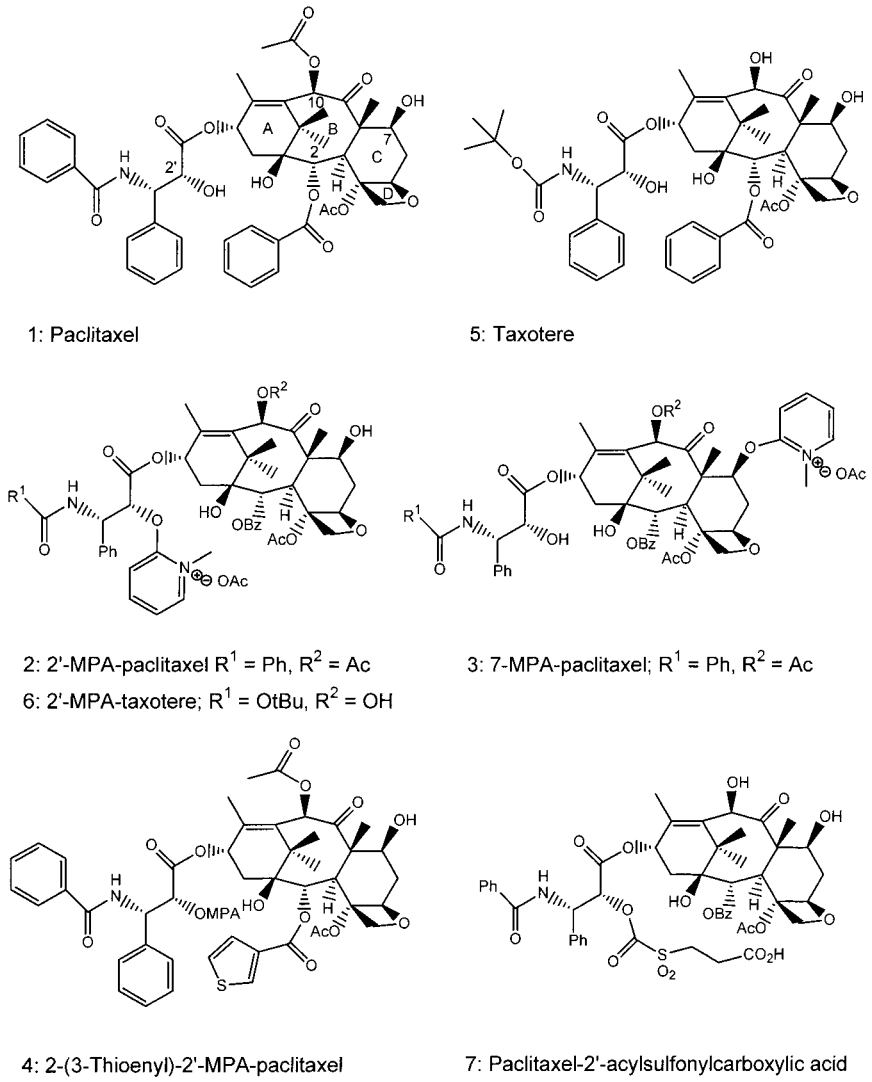


Figure 1. Chemical structures of paclitaxel, taxotere, and C-2′, C-7, and C-2 substituted derivatives.

MATERIALS AND METHODS

Synthesis of Taxoid-Onium Salts. Structures of compounds used in this study are shown in Figure 1. Paclitaxel (**1**) was purchased from the Napro Co. (Boulder, CO). Taxotere (**5**) was synthesized in house from deacetylbacatin III. The C-2′-methyl pyridinium acetate salts (MPA[1]) of paclitaxel (**2**), and taxotere (**6**) and the 2-(3-thienyl)-2′-MPA-paclitaxel analogue (**4**), were synthesized as described previously (*23*, *24*). The synthesis of the 7-MPA-paclitaxel (**3**) was previously described (*25*). Tritiated paclitaxel was obtained from Perkin-Elmer (former New England Nuclear, Boston MA).

Cells. Tumor cell lines (A549, PC-3, Ovcar 3, Molt-4) were obtained from ATCC, Rockville, MD, grown in RPMI, 10% FCS in the presence of 100 IU/mL penicillin/streptomycin (P/S) and propagated under standard tissue culture conditions of 5% CO_2 and 37 °C. Human dermal fibroblasts, peripheral blood lymphoblasts, and mammary epithelial cells were obtained from Clonogenic Corp. (San Diego, CA) and maintained in media provided by the supplier.

Mice. Athymic nude mice were obtained at 8 weeks of age from Harlan−Sprague−Dawley. They were housed in the pathogen-free mouse colony at our institution in groups of eight mice per cage. Mice were fed ad libitum on standard mouse laboratory chow. Animal experiments were performed according to the German guide for the care and use of laboratory animals, i.e., "Tierschutzgesetz".

Cytotoxicity Assays. Cytotoxicity was determined by the XTT tetrazolium/formazan assay as previously described (*26*). Briefly, cells were seeded in 96 flat bottom well plates at a density of 10^4/well in 100 μL of media and exposed to drug concentrations ranging from 10^{-4} to 10^{-12} M. At the indicated time points (72 h), cell viability was assessed by adding 50 μL of XTT-reagent (1 mg/mL in serum free RPMI) activated with 0.2% v/v PMS (1.53 mg/mL in PBS) and incubated at 37 °C for 4 h. Plates were analyzed in a Thermomax (Molecular Devices) micro plate reader at 450 nm. OD values were plotted as a function of drug concentration and the curves were integrated using the softmax software to obtain the IC_{50} concentration values.

Cell Uptake and Competition Assays. Tritiated paclitaxel was reacted with 2-fluoropyridinium tosylate as previously described for the nontritiated analogues (*23*) to yield the 2′-MPA-^{3}H-paclitaxel. Six well plates were incubated with 10^6 Molt-4 cells in 50 mM PBS to which 10^{-9} M of the radiolabeled paclitaxel or paclitaxel onium salt were added together with increasing concentrations of nonradiolabeled compound. After 30 min, the cells were centrifuged and washed with PBS, and 1% SDS

[1] Abbreviations: MPA, *N*-methylpyridinium acetate; IL, interleukin; TNF, tumor necrosis factor.

Table 1. Summary of Preclinical Results with Paclitaxel- and Taxotere-Derivatives

compound	no.[c]	$t^1/_2$ [min] plasma	EtAc extractable from plasma [%]	inhibition of tubulin depolymerization	antitumor effect in vivo	toxicity in vivo	survival [%][b]
paclitaxel	1	stable	95	+	+	high	0−20
2′-MPA-paclitaxel	2	2.4	21	−	+	low	100
7-MPA-paclitaxel	3	180	20	+	−	low	100
2-(3-thienyl)−2′-MPA-paclitaxel	4	14	23	−	−	low	100
paclitaxel-2′-acylsulfonylcarboxylic acid	7	100	34	−	−	low	75
taxotere	5	stable	95	+	ND[a]	ND	ND
2′-MPA-taxotere	6	0.9	18	−	ND	ND	ND

[a] Not performed. [b] At end of the experiment. [c] Structures are depicted in Figure 1.

was added. The radioactivity of lysed cells was then determined by means of a LKB Model 1219 scintillation counter.

Microtubule Assembly−Disassembly Assay. Tubulin was isolated from calf brain according to a procedure previously described (*27*). It was stored at a concentration of 5.5 mg/mL in liquid nitrogen. The analysis of tubulin polymerization−depolymerization was accomplished as follows: 96-well microtiter plates were charged with 30 μL of PEM buffer (100 mM PIPES, 1 mM EGTA, 1 mM $MgSO_4$, pH 6.9) and 10 μL of DMSO containing drug. Then 35 μL of tubulin solution (2 mg/mL) and 8 μL of GTP (1 mM) in water were added to initiate tubulin polymerization. The plates were shaken on a titer plate shaker for 10 s and placed into the microplate reader and absorbance determined at 1 min intervals at 340 nm and a plate temperature of 37 °C. After 15 min, 10 μL of calcium chloride (10 mM) was added to initiate tubulin depolymerization, and the determination of the absorbance at 340 nm was continued for another 5 min.

Antitumor Effect in Xenograft Models. Primary tumors were induced by sc injection of 1×10^6 A549 lung adenocarcinoma, Ovcar-3 ovarian carcinoma or PC-3 prostate carcinoma cells in 100 μL of RPMI (pH 7.4) into the skin of the left lateral flank of each nude mouse. Primary tumors in mice ($n = 8$) were treated by intraperitoneal injection of solvent (0.9% saline), paclitaxel (Cremophor EL/ 5% Dextrose in water (D5W), 5/95, v/v), or taxoid-onium salts (0.9% saline) in a total volume of 400 μL. Each mouse received a total of six injections on days 1, 3, 5, 7, 9, and 11 after tumor cell inoculation. Primary tumor size was determined over time by microcaliper measurements, and volumes were calculated according to $^1/_2 \times$ width $\times$ width $\times$ length. Body weight was determined on a standard digital scale.

Statistics. The statistical significance of differential findings between experimental groups of animals was determined by two-tailed Student's t test. Findings were regarded as significant if two-tailed p values were <0.01.

RESULTS

Prodrug Activation. To establish that onium salts of paclitaxel are prodrugs, we determined the release of free paclitaxel in human plasma at 37 °C by ethyl acetate extraction of free compounds, followed by HPLC analysis of concentrates. Due to differences in the retention times under the HPLC conditions used and differing ultraviolet absorption maxima between the prodrug and the drug, the activation could easily be assayed by UV detection. The only products detected were the free taxoids and the pyridinones released by hydrolysis of the taxoid-onium salts. In water, these compounds show stability for up to four weeks at 4 °C (data not shown). The plasma half-lives and fraction of free drug present are listed in Table 1. All three C-2′ substituted MPA derivatives (**2**, **4**, **6**) exhibited relatively short half-lives of less than 14 min while the C-2′ substituted paclitaxel-2′-acylsulfonylcarboxylic acid analogue (**7**) and the C-7 substituted 7-MPA-paclitaxel (**3**) had a half-life of 100 and 180 min, respectively. The fraction of ethyl acetate-extractable material was between 18 and 23% for all onium salts and 95% for the parent compounds. Since the partition coefficients for the organic/water phases for these compounds are greater than 50, the relatively low ethyl acetate extractable values shown in Table 1 are most likely due to a strong affinity of the onium salts for plasma proteins.

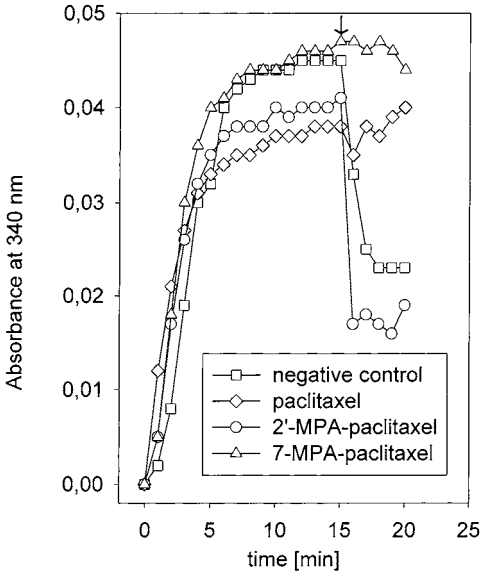


Figure 2. Effect of onium salt derivatives of paclitaxel on tubulin polymerization−depolymerization. GTP-induced tubulin polymerization ($t = 0$ min) and $CaCl_2$-promoted depolymerization (arrow, $t = 15$ min) were determined in the absence (square = negative control) and presence of paclitaxel (diamond), 7-MPA-paclitaxel (triangle), and 2′-MPA-paclitaxel (circle). Each drug was used at 10^{-6} M concentration. Turbidity was determined in a microplate reader at 340 nm. Graphs represent a typical result of three experiments.

Effect of Paclitaxel Derivatives on Microtubule Assembly−Disassembly. In order to determine which derivatives are true prodrugs, abrogation of paclitaxel specific cytotoxic effects, GTP-induced polymerization, and calcium chloride-induced depolymerization of tubulin were evaluated. Results obtained with paclitaxel and the 2′- (**2**) and 7-MPA (**3**) substituted derivatives are shown in Figure 2. The 2′-MPA-paclitaxel (**2**) behaved in this assay similar to the negative control, demonstrating that blockage of the C-2′ hydroxyl group with ′ *N*-methylpyridinium acetate (MPA) is effective in abrogating paclitaxel-specific effects. The GTP controls and 2′-MPA-paclitaxel (**2**) revealed the characteristics of calcium-induced depolymerization profiles, with about 70% reversal to tubulin. This finding was in contrast to those

Table 2. Cytotoxicity of Paclitaxel Prodrugs against a Panel of Transformed and Nontransformed Mammalian Cells

cell line	type	paclitaxel (**1**)[a] IC_{50} [nM]	2′-MPA-paclitaxel (**2**)[a] IC_{50} [nM]	7-MPA-paclitaxel (**3**)[a] IC_{50} [nM]	2-(3-thienyl)-2′-MPA-paclitaxel (**4**)[a] IC_{50} [nM]	taxotere (**5**)[a] IC_{50} [nM]	2′-MPA-taxotere (**6**)[a] IC_{50} [nM]
M-24	metastatic melanoma	0.018	0.35	0.62	0.54	0.017	-
SK-Mel-28	melanoma	524	87.9	702	110	614	68.2
A-549	lung carcinoma	5.79	152	42.5	2.35	0.8	0.72
UCLA-P3	lung carcinoma	0.66	2.44	12.8	1.88	0.12	19.9
BT-549	breast carcinoma	0.066	5.72	140	0.11	0.01	0.065
U-2511	CNS cancer	15.6	860	170	31.7	21.0	0.61
Capan 1	pancreas cancer	0.967	5.70	34.5	0.35	0.011	0.59
HAT-29	colon carcinoma	1.16	1.94	35.3	0.99	0.84	3.08
OVCAR-3	ovarian carcinoma	0.74	7.49	84.2	0.86	0.11	81.8
SIHA	squameous cell carcinoma	8.89	3.78	8.79	7.55	1.56	4.12
SK−N−SH	neuroblastoma	2.38	3.19	19.6	4.18	0.65	7.34
786−0	renal cell carcinoma	10.8	27.4	454	11.5	41.5	0.56
PC-3	prostate carcinoma	1.01	6.47	70.7	1.15	0.46	ND[b]
Molt-4	t-cell leukemia	0.096	7.07	9.94	0.066	0.01	ND[b]
HL-60	promyelocytic leukemia	0.061	0.25	5.85	0.12	0.035	0.89
L1210	mouse leukemia	3.24	12.8	178	1.2	0.59	0.019
CHO	chinese hamster ovary	615	214	612	815	80	292
HMEC	mammary epithelial cells	62	127	81	219	32.9	56
NHDF	dermal fibroblast	765	377	85.5	655	65	1.59
RPMI-7666	blood lymphoblast	584	131	123	408	71.2	596

[a] Structures are depicted in Figure 1. [b] Not performed.

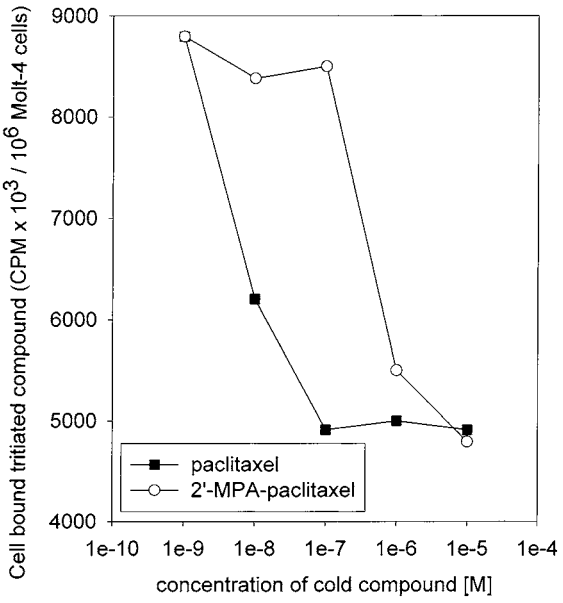


Figure 3. Competition binding of paclitaxel and 2′-MPA-paclitaxel to Molt-3 cells. Binding of tritiated paclitaxel (1×10^{-9}M) (closed square) and 2′-MPA-paclitaxel (1×10^{-9}M) (open circle) to 10^6 Molt-4 cells was determined in the presence of increasing concentrations of the respective cold analogue as described in Materials and Methods. Cell lysates were subjected to scintillation counting in an LKB 1219 counter, and results were plotted as a function of the concentration of added nonradioactive analogue. Graphs represent a typical result of three experiments.

obtained with both paclitaxel and its 7-MPA salts, which induced essentially complete inhibition of depolymerization of microtubules to tubulin. The C-2-substituted 2-(3-thienyl)-2′-MPA-paclitaxel derivative (**4**) inhibited depolymerization similar to paclitaxel (data not shown).

Specific Binding to Intact Cells. Binding to intact cells in PBS was demonstrated using a competition assay comparing 2′-MPA-paclitaxel (**2**) with parental paclitaxel on the suspension cell line Molt-4 (Figure 3). The binding constants were obtained from Scatchard plots and were 5×10^{-9} and 3×10^{-6} for paclitaxel (**1**) and 2′-MPA-paclitaxel (**2**), respectively. Addition of increasing concentrations of cold competitor resulted in saturation kinetics reaching a plateau, which constitutes nonspecific background binding. The kinetics determined with 2′-MPA-paclitaxel were similar to those obtained for paclitaxel; however, the specific binding affinity was 1000-fold lower. These results are consistent with data obtained from the microtubule assay and demonstrate that cellular binding is also reduced by blocking the C-2′ position of paclitaxel.

In summary, the 2′-MPA-paclitaxel derivative shows no paclitaxel specific activity in the absence of plasma but reverts to free paclitaxel in human plasma, clearly documenting its prodrug characteristics.

Cytotoxic Evaluations. The cytotoxic potencies of the six paclitaxel derivatives were determined against a panel of human and murine tumor cell lines and results compared to several nonmalignant cell lines (Table 2). In general, the cytotoxic potencies of these analogues were comparable to their parent compounds generally within 1.5 logs of molar concentrations with median values for tumor cell lines in the nanomolar range.

Cell lines with high resistance against paclitaxel and paclitaxel prodrugs were derived from melanoma (SK-Mel-28), CNS cancer (U2511), and renal cell adenocarcinoma (786−0) with IC_{50} values > 10.0 nM. The cytotoxicity obtained against these cell lines was within the range for nonmalignant cells (CHO, HMEC, NHDF, and RPMI-7666).

For most cell lines, Taxotere (**5**) and 2′-MPA-taxotere (**6**) were about 10-fold more cytotoxic than paclitaxel or its onium salts. Furthermore, 2′-MPA-paclitaxel (**2**) resulted for most cell lines used in about 10-fold higher IC_{50} values than the C-7-isomer 7-MPA-paclitaxel (**3**).

Antitumor Activity and Drug Elimination. The antitumor activity of the onium salts of paclitaxel was assessed in nude mice bearing tumors of human nonsmall cell lung carcinoma (A-549), ovarian carcinoma (Ovcar-3), and prostate carcinoma (PC-3) cells (Figures 4−6). Interestingly, in contrast to cytotoxicity assays in vitro, large differences in antiproliferative activity between the two 2′-substituted pro-paclitaxels were demonstrated in xenograft models. In a nonsmall cell lung carcinoma model (Figure 4), the 2′-MPA-paclitaxel derivative (**2**) completely inhibited tumor growth in contrast to paclitaxel-2′-acylsulfonylcarboxylic acid (**7**) which resulted in

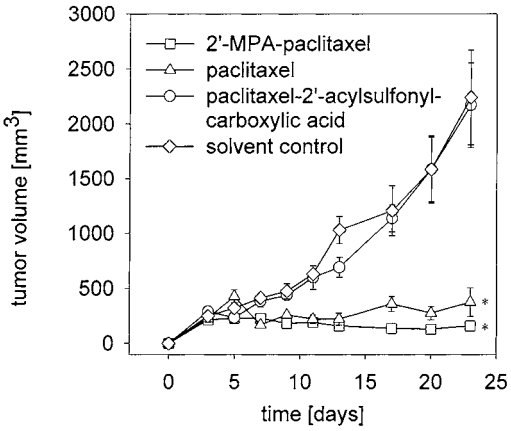


Figure 4. Effect of paclitaxel derivatives in a human lung xenograft model. The antitumor effects of paclitaxel-2′-acylsulfonylcarboxylic acid (circle), paclitaxel (triangle), and 2′-MPA-paclitaxel (square) were determined in a non-small-cell lung carcinoma model and compared to a solvent control (diamond). For this purpose, 10^6 A549 cells were injected sc, and mice were treated by intraperitoneal injections on days 1, 3, 5, 7, 9, and 11. Drugs were provided in a total volume of 0.4 mL of diluted in Cremophor EL/D5W (5/95; v/v) and administered to four experimental groups of mice ($n = 6$). One of each group was treated with Paclitaxel (18 mg/kg) and an equivalent amount of 2′-MPA-paclitaxel (24 mg/kg) and paclitaxel-2′-acylsulfonylcarboxylic acid (26 mg/kg) based on molecular weight. Tumor size was determined by microcaliper measurements as described in Materials and Methods. Graphs represent mean values ± standard error. Differences between paclitaxel/2′-MPA-paclitaxel and solvent/paclitaxel-2′-acylsulfonylcarboxylic acid were statistically significant starting on day 9 (* $p < 0.01$).

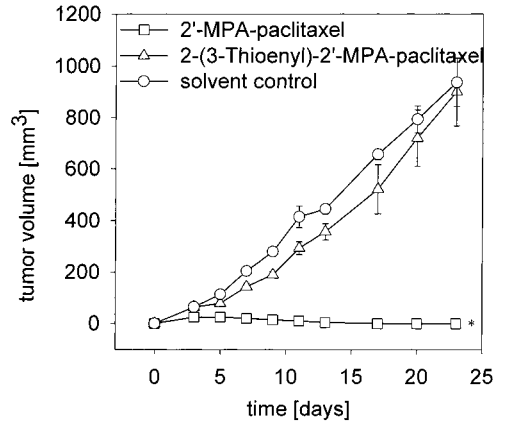


Figure 5. Effect of paclitaxel derivatives on tumor growth in a human ovarian carcinoma xenograft model. The antitumor effects of 2-(3-thienyl)-2′-MPA-paclitaxel (triangle) and 2′-MPA-paclitaxel (square) were determined in an ovarian carcinoma model and compared to a solvent control (circle). Ovcar-3 cells (10^6) were injected sc and mice treated by intraperitoneal injections on days 1, 3, 5, 7, 9, and 11. Drugs were provided in a total volume of 0.4 mL diluted in Cremophor EL/D5W (5/95; v/v) and administered to three experimental groups of mice ($n = 6$). One of each group was treated with 2′-MPA-paclitaxel (24 mg/kg) and an equivalent amount of 2-(3-thienyl)-2′-MPA-paclitaxel (26 mg/kg) based on molecular weight. Tumor size was determined by microcaliper measurements as described. Graphs represent mean values ± standard error. Differences between 2′-MPA-paclitaxel and solvent/2-(3-thienyl)-2′-MPA-paclitaxel were statistically significant starting on day 7 (* $p < 0.01$).

continuous tumor growth similar to that observed with the solvent control. Antiproliferative activities for 2-(3-thienyl)-2′-MPA-paclitaxel (**4**) and 2′-MPA-paclitaxel (**2**) were investigated in the ovarian carcinoma model (Figure 5). Results demonstrated complete inhibition of tumor growth in 100% of animals by the 2′-MPA-paclitaxel (**2**).

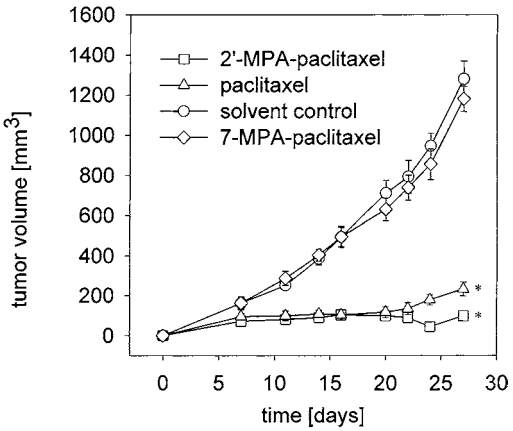


Figure 6. Effect of paclitaxel derivatives on tumor growth in a human prostate cancer xenograft model. The antitumor effects of 7-MPA paclitaxel (diamond), paclitaxel (triangle), and 2′-MPA-paclitaxel (square) were determined in a prostate carcinoma model and compared to a solvent control (circle). For this purpose, 10^6 PC-3 cells were injected sc, and mice were treated by intraperitoneal injections on days 1, 3, 5, 7, 9, and 11. Drugs were provided in a total volume of 0.4 mL diluted in Cremophor EL/D5W (5/95; v/v) and administered to four experimental groups of mice ($n = 6$). One of each group was treated with paclitaxel (18 mg/kg) and an equivalent amount of 2′-MPA-paclitaxel (24 mg/kg) and 7-MPA-paclitaxel (24 mg/kg) based on molecular weight. Tumor size was determined by microcaliper measurements as described in Materials and Methods. Graphs represent mean values ± standard error. Differences between paclitaxel/2′-MPA-paclitaxel and solvent/7-MPA-paclitaxel were statistically significant starting on day 11 (* $p < 0.01$).

In the prostate carcinoma model, paclitaxel was compared with both, the 2′- and 7-substituted oxonium salts (Figure 6). Therapy with the paclitaxel control (**1**) and the 2′-MPA-paclitaxel (**2**) resulted in regression of primary tumors. Significantly, five of eight animals treated with compound **2** remained tumor free for a total of 4 weeks. The 7-MPA isomer (**3**) showed essentially no antitumor activity as indicated by the lack of a significant difference with the solvent controls. Importantly, only three of eight mice survived the paclitaxel treatment, whereas all eight mice survived when treated with either the 2′-MPA-paclitaxel or 7-MPA-paclitaxel.

DISCUSSION

Paclitaxel continues to be extensively investigated because of its well documented clinical utility as an anticancer agent (*28*−*32*). Several distinct cellular response mechanisms induced by paclitaxel were described thus far. For example it has been reported that paclitaxel aids in inducing TNF-α and IL-1 involved in inflammatory responses as well as LPS-like activity by inducing genes such as D3, D7, and IP-10 in macrophages (*33*, *34*). This drug is also capable of inducing hematopoetic growth factor G-CSF, an activity that occurs in B-cells where it is regulated by the cytokine IL-4 (*35*). At very low concentrations, in the nanomolar range, paclitaxel was shown to inhibit mitotic spindle progression without affecting the function of preformed spindles or causing mitotic arrest in tumor cells (*36*), suggesting a mechanism of cytotoxic action other than the general inhibition of microtubule depolymerization.

A generally recognized shortcoming of paclitaxel is its extremely low solubility in the aqueous media normally employed in administering drugs, thus requiring formulation of this compound in mineral oil suspensions which exacerbate undesirable side effects in patients. The main

objective of the current study was to assess the potential of water soluble pyridinium salts of paclitaxel as antitumor leads. In this regard, it was of interest to evaluate the effects of chemical modifications of the parent compounds on in vitro and in vivo activities. The 2′- and 7-hydroxyl groups of paclitaxel and taxotere are most readily amenable to modifications and have been exploited for modification in previous reports (*37* −*40*). All paclitaxel derivatives reported including the prodrugs of this study showed relatively high cytotoxicity profiles for tumor cell lines with IC_{50} values in the nanomolar range, results which did not uniformly correlate with antiproliferative effects observed in various nude mouse tumor models. In fact, the nature of the substituents for a given position as well as the location of a given substituent at different positions in the molecule had profound effects on the antitumor activity of these compounds, which could not be predicted from the in vitro results. For example, the 7-substituted pyridinium salt of paclitaxel 7-MPA-paclitaxel (**3**) was as effective as paclitaxel in inhibiting calcium induced microtubule disassembly and showed cytotoxicities in human tumor cell lines comparable to paclitaxel; however, it completely failed to inhibit the growth of these tumors in nude mice. In contrast, the 2′- substituted paclitaxel-2′-acylsulfonylcarboxylic acid derivative (**7**), which in our previous study exhibited a high cytotoxicity profile in vitro and behaved as a prodrug (*37*), completely failed to demonstrate any antitumor effects in vivo.

Here we report for the first time that 2′-MPA-paclitaxel (**2**) is a prodrug with excellent efficacy in human xenograft models and improved antitumor activity over parental paclitaxel. In fact, in the absence of human plasma, 2′-MPA-paclitaxel showed no tubulin binding and in competition assays with intact cells revealed affinity profiles 3 orders of magnitudes below that of the parent paclitaxel. When tested in vivo, this compound produced tumor regressions with a high percentage of animals remaining tumor free at the end of the experiment. At the same time, this compound was tolerated better than paclitaxel, without detectable toxic side effects and no significant weight loss in tumor bearing nude mice. In contrast, paclitaxel administered on an equimolar basis induced significant weight losses in all animals with a death rate increased to over 50%. However, when paclitaxel was administered at lower doses to avoid toxicity, its efficacy declined dramatically (data not shown), indicating that this drug has a relatively narrow therapeutic window. The higher plasma affinity of the onium salts may be one reason for their improved tolerance in animals.

In summary, we could demonstrate that a C-2′ methylpyridinium acetate derivative of paclitaxel shows prodrug characteristics in vitro and excellent cytotoxic efficacy in the nanomolar range against a panel of cancer cell lines. It also demonstrated superior efficacy in human tumor xenograft models in contrast to parental paclitaxel. At the same time the 2′-MPA-paclitaxel revealed a lower systemic toxicity when applied in doses equimolar with parental paclitaxel. Taken together, these data suggest that 2′-MPA-paclitaxel is a promising new candidate to further improve the success rate of cancer chemotherapy.

ACKNOWLEDGMENT

This work was supported by the Deutsche Forschungsgemeinschaft (DFG), Emmy-Noether Program, Lo 635/2-1 (to H.N.L) and "klinische Forschergruppe pädiatrische Molekularbiologie", Ga 167/6-2 (to G.G.) as well as by the "Stiftung zur Erforschung der Leukämieerkrankung".

LITERATURE CITED

(1) Rowinsky, E. K., and Donehower, R. C. (1995) Paclitaxel (taxol). *N. Engl. J. Med. 332,* 1004−1014.

(2) Chang, A. Y., Kim, K., Glick, J., Anderson, T., Karp, D., and Johnson, D. (1993) Phase II study of taxol, merbarone, and piroxantrone in stage IV non-small-cell lung cancer: The Eastern Cooperative Oncology Group Results. *J. Natl. Cancer Inst. 85,* 388−394.

(3) Einzig, A. I., Gorowski, E., Sasloff, J., and Wiernik, P. H. (1991) Phase II trial of taxol in patients with metastatic renal cell carcinoma. *Cancer Invest 9,* 133−136.

(4) Eisenhauer, E. A., Bokkel Huinink, W. W., Swenerton, K. D., Gianni, L., Myles, J., van der Burg, M. E., Kerr, I., Vermorken, J. B., Buser, K., Colombo, N., and (1994) European-Canadian randomized trial of paclitaxel in relapsed ovarian cancer: high-dose versus low-dose and long versus short infusion. *J. Clin. Oncol. 12,* 2654−2666.

(5) Nabholtz, J. M., Gelmon, K., Bontenbal, M., Spielmann, M., Catimel, G., Conte, P., Klaassen, U., Namer, M., Bonneterre, J., Fumoleau, P., and Winograd, B. (1996) Multicenter, randomized comparative study of two doses of paclitaxel in patients with metastatic breast cancer. *J. Clin. Oncol. 14,* 1858−1867.

(6) Bonomi, P., Kim, K., Kusler, J., and Johnson, D. (1997) Cisplatin/etoposide vs paclitaxel/cisplatin/G-CSF vs paclitaxel/cisplatin in nonsmall-cell lung cancer. *Oncology (Huntingt) 11,* 9−10.

(7) Johnson, D., Arriagada, R., Barthelemy, N., Bonner, J., Bonomi, P., Enami, B., Minatel, E., Park, K., Quoix, E., and Van Houtte, P. (1997) Post-operative adjuvant therapy for non-small-cell lung cancer. *Lung Cancer 17 Suppl 1,* S23−S25.

(8) Bookman, M. A., McGuire, W. P., III, Kilpatrick, D., Keenan, E., Hogan, W. M., Johnson, S. W., O'Dwyer, P., Rowinsky, E., Gallion, H. H., and Ozols, R. F. (1996) Carboplatin and paclitaxel in ovarian carcinoma: a phase I study of the Gynecologic Oncology Group. *J. Clin. Oncol. 14,* 1895−1902.

(9) Wani, M. C., Taylor, H. L., Wall, M. E., Coggon, P., and McPhail, A. T. (1971) Plant antitumor agents. VI. The isolation and structure of taxol, a novel antileukemic and antitumor agent from Taxus brevifolia. *J. Am. Chem. Soc. 93,* 2325−2327.

(10) Horwitz, S. B., Lothstein, L., Manfredi, J. J., Mellado, W., Parness, J., Roy, S. N., Schiff, P. B., Sorbara, L., and Zeheb, R. (1986) Taxol: mechanisms of action and resistance. *Ann. N. Y. Acad. Sci. 466,* 733−744.

(11) Schiff, P. B., Fant, J., and Horwitz, S. B. (1979) Promotion of microtubule assembly in vitro by taxol. *Nature 277,* 665−667.

(12) Manfredi, J. J., Fant, J., and Horwitz, S. B. (1986) Taxol induces the formation of unusual arrays of cellular microtubules in colchicine-pretreated J774.2 cells. *Eur. J. Cell Biol. 42,* 126−134.

(13) Manfredi, J. J., Parness, J., and Horwitz, S. B. (1982) Taxol binds to cellular microtubules. *J. Cell Biol. 94,* 688−696.

(14) Kumar, N. (1981) Taxol-induced polymerization of purified tubulin. Mechanism of action. *J. Biol. Chem. 256,* 10435−10441.

(15) Jordan, M. A., Toso, R. J., Thrower, D., and Wilson, L. (1993) Mechanism of mitotic block and inhibition of cell proliferation by taxol at low concentrations. *Proc. Natl. Acad. Sci. U.S.A 90,* 9552−9556.

(16) Tishler, R. B., Schiff, P. B., Geard, C. R., and Hall, E. J. (1992) Taxol: a novel radiation sensitizer. *Int. J. Radiat. Oncol. Biol. Phys. 22,* 613−617.

(17) Burkhart, C. A., Berman, J. W., Swindell, C. S., and Horwitz, S. B. (1994) Relationship between the structure of taxol and other taxanes on induction of tumor necrosis factor-alpha gene expression and cytotoxicity. *Cancer Res. 54,* 5779−5782.

(18) Bhalla, K., Ibrado, A. M., Tourkina, E., Tang, C., Mahoney, M. E., and Huang, Y. (1993) Taxol induces internucleosomal

DNA fragmentation associated with programmed cell death in human myeloid leukemia cells. *Leukemia 7,* 563−568.
(19) Weiss, R. B., Donehower, R. C., Wiernik, P. H., Ohnuma, T., Gralla, R. J., Trump, D. L., Baker, J. R., Jr., Van Echo, D. A., Von Hoff, D. D., and Leyland-Jones, B. (1990) Hypersensitivity reactions from taxol. *J. Clin. Oncol. 8,* 1263−1268.
(20) Rowinsky, E. K., Eisenhauer, E. A., Chaudhry, V., Arbuck, S. G., and Donehower, R. C. (1993) Clinical toxicities encountered with paclitaxel (Taxol). *Semin. Oncol. 20,* 1−15.
(21) Kintzel, P. E. (2001) Prophylaxis for paclitaxel hypersensitivity reactions. *Ann. Pharmacother. 35,* 1114−1117.
(22) Gelderblom, H., Verweij, J., Nooter, K., and Sparreboom, A. (2001) Cremophor EL: the drawbacks and advantages of vehicle selection for drug formulation. *Eur. J Cancer 37,* 1590−1598.
(23) Nicolaou, K. C., Guy, R. K., Pitsinos, E. N., and Wrasidlo, W. (1994) A water soluble prodrug of taxol with self-assembling properties. *Angew. Chem., Int. Ed. Engl 34,* 1583−1587.
(24) Nicolaou, K. C., Renaud, J., Nantermet, P. G., Couladouros, E. A., Guy, R. K., and Wrasidlo, W. (1995) Chemical synthesis and biological evaluation of C-2 taxoids. *J. Am. Chem. Soc. 117,* 2409−2420.
(25) Gomez, P. L., Guy, R. K., Wrasidlo, W., and Nicolaou, K. C. (1994) Conformation of a water-soluble derivative of taxol in water by 2D-NMR spectroscopy. *Chem Biol. 1,* 107−112.
(26) Scudiero, D. A., Shoemaker, R. H., Paull, K. D., Monks, A., Tierney, S., Nofziger, T. H., Currens, M. J., Seniff, D., and Boyd, M. R. (1988) Evaluation of a soluble tetrazolium/formazan assay for cell growth and drug sensitivity in culture using human and other tumor cell lines. *Cancer Res. 48,* 4827−4833.
(27) Williams, R. C., Jr., and Lee, J. C. (1982) Preparation of tubulin from brain. *Methods Enzymol. 85 Pt B,* 376−385.
(28) Wadler, S. (2001) New developments in the treatment of ovarian cancer. *Expert. Opin. Investig. Drugs 10,* 1167−1172.
(29) Plosker, G. L., and Hurst, M. (2001) Paclitaxel: a pharmacoeconomic review of its use in nonsmall cell lung cancer. *Pharmacoeconomics 19,* 1111−1134.
(30) Senzer, N. N. (2001) Prostate cancer: multimodality approaches with docetaxel. *Semin. Oncol. 28,* 77−85.
(31) Razis, E. D., and Fountzilas, G. (2001) Paclitaxel: epirubicin in metastatic breast cancer−a review. *Ann. Oncol. 12,* 593−598.
(32) Mukherjee, A. K., Basu, S., Sarkar, N., and Ghosh, A. C. (2001) Advances in cancer therapy with plant based natural products. *Curr. Med. Chem. 8,* 1467−1486.
(33) Manthey, C. L., Perera, P. Y., Salkowski, C. A., and Vogel, S. N. (1994) Taxol provides a second signal for murine macrophage tumoricidal activity. *J. Immunol. 152,* 825−831.
(34) Manthey, C. L., Brandes, M. E., Perera, P. Y., and Vogel, S. N. (1992) Taxol increases steady-state levels of lipopolysaccharide-inducible genes and protein-tyrosine phosphorylation in murine macrophages. *J. Immunol. 149,* 2459−2465.
(35) Pluznik, D. H., Lee, N. S., and Sawada, T. (1994) Taxol induces the hematopoietic growth factor granulocyte-macrophage colony-stimulating factor in murine B-cells by stabilization of granulocyte-macrophage colony-stimulating factor nuclear RNA. *Cancer Res. 54,* 4150−4154.
(36) Long, B. H., and Fairchild, C. R. (1994) Paclitaxel inhibits progression of mitotic cells to G1 phase by interference with spindle formation without affecting other microtubule functions during anaphase and telephase. *Cancer Res. 54,* 4355−4361.
(37) Nicolaou, K. C., Riemer, C., Kerr, M. A., Rideout, D., and Wrasidlo, W. (1993) Design, synthesis and biological activity of protaxols. *Nature 364,* 464−466.
(38) Nicolaou, K. C., Dai, W. M., and Guy, R. K. (1994) Chemistry and biology of taxol. *Angew. Chem., Int. Ed. Engl. 33,* 15−44.
(39) Mathew, A. E., Mejillano, M. R., Nath, J. P., Himes, R. H., and Stella, V. J. (1992) Synthesis and evaluation of some water-soluble prodrugs and derivatives of taxol with antitumor activity. *J. Med. Chem. 35,* 145−151.
(40) Deutsch, H. M., Gelbaum, L. T., McLaughlin, M., Fleischmann, T. J., Earnhart, L. L., Haugwitz, R. D., and Zalkow, L. H. (1986) Synthesis of congeners and prodrugs of the benzene maleimide photoadduct mitindomide as potential antitumor agents. 2. *J. Med. Chem. 29,* 2164−2170.

BC0200226

Functionalized Congeners of Tyrosine-Based $P2X_7$ Receptor Antagonists: Probing Multiple Sites for Linking and Dimerization

Wangzhong Chen,[†] R. Gnana Ravi,[†] Sylvia B. Kertesy,[‡] George R. Dubyak,[‡] and Kenneth A. Jacobson*,[†]

Molecular Recognition Section, Laboratory of Bioorganic Chemistry, National Institute of Diabetes, Digestive and Kidney Diseases, National Institutes of Health, Bethesda, Maryland 20892-0810, and Department of Physiology and Biophysics, Case Western Reserve University School of Medicine, Cleveland, Ohio 44106. Received April 6, 2002; Revised Manuscript Received July 17, 2002

Chemically funtionalized analogues of antagonists of the $P2X_7$ receptor, an ATP-gated cation channel, were synthesized as tools for biophysical studies of the receptor. These functionalized congeners were intended for use in chemical conjugation with retention of biological potency. The antagonists were L-tyrosine derivatives, related to [*N*-benzyloxycarbonyl-*O*-(4-arylsulfonyl)-L-tyrosyl]benzoylpiperazine (such as MRS2409, **2**). The analogues were demonstrated to be antagonists in an assay of human $P2X_7$ receptor function, consisting of inhibition of ATP-induced K^+ efflux in HEK293 cells expressing the recombinant receptor. The analogues were of the general structure R_1-Tyr(OR_2)-piperazinyl-R_3, in which three positions (R_1-R_3) were systematically varied in structure through introduction of chemically reactive groups. Each of the three positions was designed to incorporate a 3- or 4-nitrophenyl group. The nitro groups were reduced using $NaBH_4$−copper(II) acetylacetonate to amines, which were either converted to the isothiocyanate groups, as potential affinity labels for the receptor, or acylated, as models for conjugation. An alternate route to N^{α}-3-aminobenzyloxycarbonyl functionalization was devised. The various positions of functionalization were compared for effects on biological potency, and the R_2 and R_3 positions were found to be most amenable to derivatization with retention of high potency. Four dimeric permutations of the antagonists were synthesized by coupling each of the isothiocyanate derivatives to either the precursor amine or to other amine congeners. Only dimers linked at the R_2-position were potent antagonists. In concentration−response studies, two derivatives, a 3-nitrobenzyloxycarbonyl derivative **18** and a 4-nitrotoluenesulfonate **26b**, displayed IC_{50} values of roughly 100 nM as antagonists of $P2X_7$ receptor-mediated K^+ flux.

INTRODUCTION

P2X receptors are ligand-gated cation channels activated by ATP (adenosine 5′-triphosphate) and other purine nucleotides. Seven mammalian subtypes of P2X receptors (termed $P2X_1$ through $P2X_7$) have been cloned (*1*, *2*). Each functional ion channel consists of an oligomeric assembly, probably a trimer. Both homo- and heterooligomerization seem to occur commonly; however the $P2X_7$ subtype exists exclusively as a homomer, and the $P2X_6$ subtype always occurs as a homomer. The cationic selectivity of the P2X receptors is Na^+, $K^+ > Ca^{2+}$ (*3*).

* Correspondence to: Dr. Kenneth A. Jacobson, Chief, Molecular Recognition Section, Bldg. 8A, Rm. B1A-19, NIH, NIDDK, LBC, Bethesda, MD 20892-0810, tel.: (301) 496-9024; fax: (301) 480-8422; e-mail: kajacobs@helix.nih.gov.

[†] National Institutes of Health.

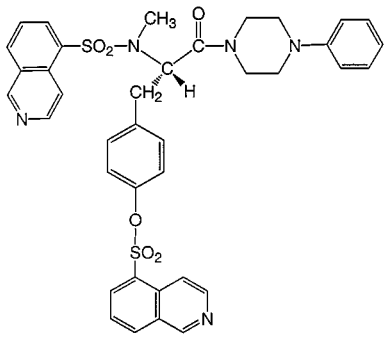
[‡] Case Western Reserve University School of Medicine.

[1] Abbreviations: Bop-Cl, bis(2-oxo-3-oxazolidinyl)phosphinic chloride; Boc, *tert*-butyloxycarbonyl; BSA, bovine serum albumin; Cbz, benzyloxycarbonyl; DMAP, 4-(dimethylamino)pyridine; DMF, dimethylformamide; DMSO, dimethyl sulfoxide; EtOAc, ethyl acetate; FAB, fast atom bombardment; Fmoc, 9-fluorenylmethyloxycarbonyl; HEK, human embryonic kidney; HEPES, *N*-(2-hydroxyethyl)piperazine-*N*′-(2-ethanesulfonic acid); HRMS, high-resolution mass spectrometry; KN-62, 1-[*N*,*O*-bis-(5-isoquinolinesulfonyl)-*N*-methyl-L-tyrosyl]-4-phenylpiperazine; MRS 2409, [*N*-benzyloxycarbonyl-*O*-[4-(isoquinolinylsulfonyl)]-L-tyrosyl]benzoylpiperazine; TFA, trifluoroacetic acid; THF, tetrahydrofuran; TLC, thin-layer chromatography.

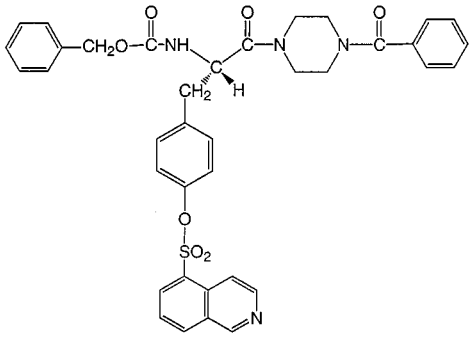
The $P2X_7$ receptor (formerly known as the P_{2Z} receptor) is expressed primarily in the immune/inflammatory system (*4*−*9*), i.e., in blood cells (monocytes, macrophages, and lymphocytes) and in the brain on microglial cells, and in the salivary gland (*10*). Its activation is associated with apoptosis in the immune system and release of inflammatory cytokines, such as IL-1β (*8*, *9*, *11*). The $P2X_7$ receptor is distinct from the other P2X subunits in that at high μM concentrations of agonists, it forms or activates a large pore in addition to a cation channel (*12*, *13*). This pore increases permeability indiscriminately to molecules having MW ≤ 900, such as ethidium bromide, which is used as a marker for pore activity. The $P2X_7$ receptor also has a long C-terminal segment which contributes to pore formation (*13*). 2′- and 3′-*O*-(4-benzoylbenzoyl)-ATP (BzATP) is among the most potent agonists at $P2X_7$ receptors, but also has nanomolar potency at $P2X_1$ receptors (*14*). Affinity labeling of the $P2X_7$ receptor in mast cells has been carried out using [^{3}H]-BzATP (*15*).

An objective of the present study was to design antagonist ligand probes based on tyrosine derivatives, to be used for biophysical characterization of the $P2X_7$ receptor. The isoquinoline derivative of tyrosine 1-(*N*,*O*-bis[5-isoquinolinesulfonyl]-*N*-methyl-L-tyrosyl)-4-phenylpiperazine (**1**, KN-62), is a potent noncompetitive antagonist at $P2X_7$ receptors in the submicromolar range (*6*,*7*,*12*). It is also an antagonist of Ca^{2+}/calmodulin-dependent protein kinase II (CaMKII) in the micromolar range (*16*). We recently reported a series of potent $P2X_7$ receptor

10.1021/bc020025i Not subject to U.S. Copyright. Published 2002 by American Chemical Society
Published on Web 08/30/2002



1, KN-62



2, MRS 2409

antagonists derived from KN-62, of the general structure R_1-Tyr(OR_2)-piperazinyl-R_3, in which three positions (R_1, R_2, and R_3) were systematically varied (*17*). The derivative MRS 2409 ([N-benzyloxycarbonyl-O-[4-(isoquinolinylsulfonyl)]-L-tyrosyl]benzoylpiperazine), **2**, in which R_1 and R_3 differed from the structure of KN-62, was among the most potent analogues prepared (IC_{50} of 200 nM, for release of K^+ stimulated by 3 mM ATP in HEK293 cells expressing the human P2X$_7$ receptor). We now extend the SAR (structure activity relationship) analysis in this series to include more varied functionalization of congeners (*18*−*20*) of MRS 2409, directed toward probing multiple sites on the antagonist molecules for sites of chain attachment that preserve the biological properties. This functionalization is intended for the purpose of cross-linking, either with the receptor and/or with reporter moieties such as fluorescent dyes or radioisotopes. Dimerization of the antagonists through various linkage points has also been carried out in order to explore the spatial relationship between possible multiple binding sites on the large extracellular loop (*13*, *21*) of P2X$_7$ receptor homomers.

MATERIALS AND METHODS

Chemical Synthesis. Protected tyrosine compounds are from Novabiochem (San Diego, CA). Other chemicals are from Aldrich (Milwaukee, WI). ^{1}H NMR spectra were recorded using a Varian Gemini-300 spectrometer. High-resolution FAB (fast atom bombardment) mass spectra were taken with a JEOL SX102 spectrometer using nitrobenzoic acid as matrix. Elemental analysis was performed by Atlantic Microlab Inc. (Norcross, GA).

General Procedure for the Synthesis of 46, 51, 62. A mixture of Fmoc-Tyr-OH or Cbz-Tyr-OH (3.0 mmol), Boc-piperazine, or benzoyl-piperazine (3.0 mmol), Bis(2-oxo-3-oxoazolidinyl)phosphinic chloride (Bop-Cl) (0.77 g, 3.0 mmol), and CH_2Cl_2 (15 mL) was treated with Et_3N (0.96 mL, 6.8 mmol) and stirred at room temperature for 1 h. The solvent was removed in vacuo, and the crude product was purified with silica gel chromatography eluting with methanol−chloroform (5:95) to furnish a white solid foam (yield 75−85%).

*[N-Fmoc-L-tyrosyl]benzoylpiperazine (**46**).* ^{1}H NMR ($CDCl_3$): δ 7.77 (d, J = 7.4 Hz, 2H), 7.59 (d, J = 7.4 Hz, 2H), 7.50−7.28 (m, 5H), 7.05 (d, J = 8.0 Hz, 2H), 6.75 (d, J = 8.0 Hz, 2H), 5.70 (d, J = 8.5 Hz, 1H), 4.84(b, 1H), 4.50−4.25 (m, 2H), 4.25−4.10 (t, J = 7.0 Hz, 1H), 3.80−2.80 (m, 10H).

*[N-Fmoc-L-tyrosyl]-Boc-piperazine (**51**).* ^{1}H NMR ($CDCl_3$): δ 7.77 (d, J = 7.3 Hz, 2H), 7.59 (d, J = 7.3 Hz, 2H), 7.40 (t, J = 7.3 Hz, 2H), 7.31 (t, J = 7.3 Hz, 2H), 7.04 (d, J = 7.7 Hz, 2H), 6.74 (d, J = 7.7 Hz, 2H), 5.88 (s, 1H), 5.72 (d, J = 8.4 Hz, 1H), 4.90−4.78 (m, 1H), 4.44−4.28 (m, 2H), 4.24−4.16 (t, J = 7.0 Hz, 1H), 3.60−2.80 (m, 10 H), 1.45 (s, 9H).

*[N-Benzyloxycarbonyl-O-toluenesulfonyl-L-tyrosyl]piperazine (**62**).* ^{1}H NMR ($CDCl_3$): δ 7.30−7.40 (m, 5H), 7.02 (d, J = 8.2 Hz, 2H), 6.72 (d, J = 8.2 Hz, 2H), 5.65 (d, J = 8.5 Hz, 1H), 5.45 (br s, 1H), 5.14−5.00 (ABq, J = 12.4 Hz, 2H), 4.90−4.75 (m, 1H), 3.60−2.80 (m, 10H), 1.45 (s, 9H).

General Procedure for the Synthesis of 23a, 23b, 47, 52a, 52b, 55. N-Substituted tyrosine (**46**, **51**, or **62**; 2.0 mmol) was dissolved in 10 mL of anhydrous CH_2Cl_2 and cooled to 0 °C. A solution of benzenesulfonyl chloride or related sulfonyl chloride (4.0 mmol), Et_3N (0.3 mL, 2.2 mmol), DMAP (214 mg, 1.7 mmol), and CH_2Cl_2 (5.0 mL) was added dropwise and stirring continued for 30 min at 0 °C. TLC showed the completion of the reaction. The solvent was removed under reduced pressure. Column chromatography (silica gel, CH_3OH:$CHCl_3$ = 5:95) yielded a white solid foam (70−75% yield).

*[N-Benzyloxycarbonyl-O-(3-nitrobenzenesulfonyl)-L-tyrosyl]-Boc-piperazine (**23a**).* ^{1}H NMR ($CDCl_3$): δ 8.71 (t, J = 1.9 Hz, 1H), 8.52 (ddd, J = 1.1, 2.2, 8.2 Hz, 1H), 8.12 (m, 1H), 7.78 (t, J = 8.0 Hz, 1H), 7.40−7.30 (m, 5H), 7.14 (d, J = 8.5 Hz, 1H), 6.93 (m. 1H), 5.58 (d, J = 8.8 Hz, 1H), 5.14−5.00(ABq, J = 12.4 Hz, 2H), 4.88−4.77 (m, 1H), 3.60−2.84 (m, 10H), 1.44 (s, 9H). FAB−HRMS for $C_{32}H_{37}N_4O_{10}S$ (MH^+): calcd 669.2230, found 669.2231. Anal. ($C_{32}H_{36}N_4O_{10}S\cdot0.1H_2O$).

*[N-Benzyloxycarbonyl-O-(4-nitrobenzenesulfonyl)-L-tyrosyl]-Boc-piperazine (**23b**).* ^{1}H NMR ($CDCl_3$): δ 8.39 (d, J = 9.0 Hz, 2H), 8.02 (d, J = 9.1 Hz, 2H), 7.42−7.28 (m, 5H), 7.13 (d, J = 8.5 Hz, 2H), 6.90 (d, J = 8.5 Hz, 2H), 5.60 (d, J = 8.5 Hz, 1H), 5.14−5.00 (ABq, J = 13.7 Hz, 2H), 4.90−4.77 (m, 1H), 3.60−2.78 (m, 10H), 1.45 (s, 9H). FAB-MS: *m*/*z* (relative intensity) 669.1 (M + 1, 6), 613.1 (16), 91 (100). Anal. ($C_{32}H_{36}N_4O_{10}S\cdot0.1H_2O$).

*[N-Fmoc-O-toluenesulfonyl-L-tyrosyl]benzoylpiperazine (**47**).* ^{1}H NMR ($CDCl_3$): δ 7.86−7.64 (m, 4H), 7.60 (d, J = 7.7 Hz, 2H), 7.50−7.28 (m, 11H), 7.13 (d, J = 8.2 Hz, 2H), 6.84−6.88 (d, J = 8.2 Hz, 2H), 5.66 (d, J = 8.2 Hz, 1H), 4.82 (b, 1H), 4.50−4.25 (m, 2H), 4.25−4.10 (m, 1H), 3.8−2.7 (m, 10H), 2.45 (s, 3H).

*[N-Fmoc-O-benzenesulfonyl-L-tyrosyl]-Boc-piperazine (**52a**).* ^{1}H NMR ($CDCl_3$): δ 7.88−7.72 (m, 4H), 7.70−7.60 (m, 2H), 7.46−7.27 (m, 7H), 7.10 (d, J = 8.5 Hz, 2H), 6.90 (d, J = 8.5 Hz, 2H), 5.66 (d, J = 8.2 Hz, 1H), 4.90−4.70 (m, 1H), 4.50−4.30 (m, 2H), 4.25−4.10 (m, 1H), 3.8−2.7 (m, 10H), 1.45 (s, 9H).

*[N-Fmoc-O-(4-nitrobenzenesulfonyl)-L-tyrosyl]-Boc-piperazine (**52b**).* ^{1}H NMR ($CDCl_3$): δ 8.38 (d, J = 8.8 Hz, 2H), 8.02 (d, J = 8.8 Hz, 2H), 7.77 (d, J = 7.7 Hz, 2H), 7.56 (d, J = 7.4 Hz, 2H), 7.47−7.27 (m, 4H), 7.14 (d, J = 7.4 Hz, 2H), 6.91 (d, J = 8.5 Hz, 2H), 5.61 (d, J = 8.5 Hz, 1H), 4.90−4.70 (m, 1H), 4.50−4.28 (m, 2H), 4.26−4.10 (m, 1H), 3.58−2.70 (m. 10H), 1.45 (s, 9H).

*[N-Fmoc-O-toluenesulfonyl-L-tyrosyl]-Boc-piperazine (**55**).* ^{1}H NMR ($CDCl_3$): δ 7.76 (d, J = 7.1 Hz, 2H), 7.70 (d, J = 8.0 Hz, 2H), 7.57 (d, J = 6.9 Hz, 2H), 7.46−7.27 (m, 6H), 7.10 (d, J = 7.9 Hz, 2H), 6.90 (d, J = 7.8 Hz, 2H), 5.65 (d, J = 8.2 Hz, 1H), 4.85−4.70 (m, 1H), 4.50−4.25 (m, 2H), 4.24−4.15 (m, 1H), 3.80−2.70 (m, 10H), 2.43 (s, 3H), 1.45 (s, 9H).

General Procedure for the Synthesis of 17, 19, 20b, 25, 26a, 26b, 28, 31a, 31b, 33, 53a, 53b, 53c, 53d, 57a, 57b. A tyrosine derivative containing a free amine (**20a**, **24**, **27**, **32**, **52a**, **52b**, **56**, **58a**, **58b**, or **63**; 3.0 mmol) was dissolved in CH_2Cl_2 (8.0 mL). DMAP (300 mg) was added, and the solution was cooled to 0 °C. A solution of a benzoyl chloride (4.2 mmol) (alternatively a benzyl chloroformate or acetyl chloride), Et_3N (0.45 mL), and CH_2Cl_2 (5.0 mL) was added dropwise and stirring continued at 0 °C for 40 min. The solvent was removed, and the residue was washed with petroleum ether three times. The resulting crude product was purified by column chromatography (silica gel, CH_3OH:$CHCl_3$ = 5:95) to yield a white solid foam (80−90% yield).

*[N-(4-Nitrobenzyloxycarbonyl)-O-toluenesulfonyl-L-tyrosyl]benzoylpiperazine (**17**).* ^{1}H NMR ($CDCl_3$): δ 8.22 (d, J = 8.8 Hz, 2H), 7.73 (d, J = 8.2 Hz, 2H), 7.60−7.30 (m, 9H), 7.13 (d, J = 8.2 Hz, 2H), 6.93 (d, J = 8.5 Hz, 2H), 5.70 (d, J = 8.5 Hz, 1H), 5.26−5.10 (b, 2H), 4.92−4.70 (b, 1H), 3.90−2.70 (m, 10H), 2.46 (s, 3H). FAB-MS: *m/z* (relative intensity) 687.2 (M + 1, 35), 391.3 (70), 149.1 (100). Anal. ($C_{35}H_{34}N_4O_9S$·0.4EtOAc).

*[N-(3-Nitrobenzyloxycarbonyl)-O-toluenesulfonyl-L-tyrosyl]benzoylpiperazine (**19**).* ^{1}H NMR ($CDCl_3$): δ 8.22−8.16 (m, 2H), 7.72 (d, J = 8.5 Hz, 2H), 7.68−7.62 (m, 1H), 7.54 (t, J = 8.0 Hz, 1H), 7.46−7.30 (m, 7H), 7.13 (d, J = 8.5 Hz, 2H), 6.92 (d, J = 8.5 Hz, 2H), 5.70 (d, J = 8.5 Hz, 1H), 5.22−5.12 (m, 2H), 4.92−4.70 (b, 1H), 4.00−2.70 (m, 10H), 2.43 (s, 3H). FAB−HRMS for $C_{35}H_{35}N_4O_9S$ (MH^+): calcd 687.2125, found 687.2136.

*[N-(3-Acetylaminobenzyloxycarbonyl)-O-toluenesulfonyl-L-tyrosyl]benzoylpiperazine (**20b**).* ^{1}H NMR ($CDCl_3$): δ 7.71 (d, J = 8.5 Hz, 2H), 7.52−7.28 (m, 10H), 7.16−6.98 (m, 3H), 6.91 (d, J = 8.5 Hz, 2H), 5.88−5.52 (b, 1H), 5.05 (br s, 2H), 4.88−4.68 (b, 1H), 3.80−2.70 (m, 10H), 2.46 (s, 3H), 2.18 (s, 3H). FAB−HRMS for $C_{37}H_{39}N_4O_8S$ (MH^+): calcd 699.2489, found 699.2507.

*[N-Benzyloxycarbonyl-O-(4-acetylamino)benzenesulfonyl-L-tyrosyl]-Boc-piperazine (**25**).* ^{1}H NMR ($CDCl_3$): δ 7.72 (d, J = 8.8 Hz, 2H), 7.63 (d, J = 8.6 Hz, 2H), 7.40−7.28 (m, 5H), 7.10 (d, J = 8.2 Hz, 2H), 6.94 (d, J = 8.6 Hz, 2H), 5.64 (d, J = 8.5 Hz, 1H), 5.20−5.00 (ABq, J = 12.3 Hz, 2H), 4.90−4.70 (m, 1H), 4.00−2.70 (m, 10H), 2.23 (s, 3H), 1.47 (s, 9H). FAB−HRMS for $C_{34}H_{41}N_4O_9S$ (MH^+): calcd 681.2594, found 681.2610. Anal. ($C_{34}H_{40}N_4O_9S$).

*[N-Benzyloxycarbonyl-O-(3-nitrobenzenesulfonyl)-L-tyrosyl]benzoylpiperazine (**26a**).* ^{1}H NMR ($CDCl_3$): δ 8.76−8.64 (b, 1H), 8.58−8.30 (dq, J = 8.3, 1.1 Hz, 1H), 8.20−8.14 (m, 1H), 7.80 (t, J = 8.0 Hz, 1H), 7.48−7.28 (m, 10H), 7.16 (d, J = 8.5 Hz, 2H), 7.00−6.92 (m, 2H), 5.57 (d, J = 8.5 Hz, 1H), 5.14−5.02 (m, 2H), 4.92−4.70 (b, 1H), 3.80−2.70 (m, 10H). FAB−HRMS for $C_{34}H_{33}N_4O_9S$ (MH^+): calcd 673.1968, found 673.1981. Anal. ($C_{34}H_{32}N_4O_9S$).

*[N-Benzyloxycarbonyl-O-(4-nitrobenzenesulfonyl)-L-tyrosyl]benzoylpiperazine (**26b**).* ^{1}H NMR ($CDCl_3$): δ 8.40 (d, J = 8.8 Hz, 2H), 8.05 (d, J = 8.5 Hz, 2H), 7.48−7.28 (m, 10H), 7.16 (d, J = 8.2 Hz, 2H), 6.92 (d, J = 8.5 Hz, 2H), 5.76 (d, J = 8.5 Hz, 1H), 5.18−5.00 (m, 2H), 4.94−4.72 (b, 1H), 3.70−2.80 (m, 10H). Compound 26b (R_f = 0.85, CH_3OH/$CHCl_3$ = 1: 9) was shown to be pure by TLC.

*[N-Benzyloxycarbonyl-O-(4-acetylamino)benzenesulfonyl-L-tyrosyl]benzoylpiperazine (**28**).* ^{1}H NMR ($CDCl_3$): δ 7.72 (q, J = 9.1, 14.8 Hz, 4H), 7.50−7.30 (m, 10H), 7.10 (d, J = 7.7 Hz, 2H), 7.04−6.90 (b, 2H), 5.68−5.52 (b, 1H), 5.16−5.00 (ABq, J = 12.1, 16.2 Hz, 2H), 4.88−4.68 (b, 1H), 3.90−2.70 (m, 10H), 2.17 (s, 3H). FAB-MS: *m/z* (relative intensity) 685.4 (M + 1, 100), 641.4 (5), 91.1 (70).

*[N-Benzyloxycarbonyl-O-toluenesulfonyl-L-tyrosyl]-(3-nitrobenzoyl) piperazine (**31a**).* ^{1}H NMR ($CDCl_3$): δ 8.34−8.22 (m, 2H), 7.80−7.70 (m, 3H), 7.68−7.36 (m, 1H), 7.42−7.30 (m, 7H), 7.16 (d, J = 8.5 Hz, 2H), 6.96 (d, J = 8.8 Hz, 2H), 5.58 (d, J = 8.8 Hz, 1H), 5.26−5.00 (m, 2H), 4.90−4.70 (b, 1H), 4.00−2.70 (m, 10H), 2.45 (s, 3H). FAB-MS: *m/z* (relative intensity) 687.2 (M + 1, 40), 643.3 (10), 91.0 (90). FAB−HRMS (NOBA/CsI) for $C_{35}H_{34}N_4O_9SCs$ $[M + Cs]^+$: calcd 819.1101, found 819.1096.

*[N-Benzyloxycarbonyl-O-toluenesulfonyl-L-tyrosyl]-(4-nitrobenzoyl)piperazine (**31b**).* ^{1}H NMR ($CDCl_3$): δ 8.36−8.18 (m, 3H), 7.76 (d, J = 8.2 Hz, 2H), 7.56 (d, J = 8.5 Hz, 2H), 7.42−7.28 (m, 6H), 7.16 (d, J = 8.2 Hz, 2H), 6.96 (d, J = 8.0 Hz, 2H), 5.70−5.56 (m, 1H), 5.18−5.00 (m, 2H), 4.92−4.70 (b, 1H), 4.00−2.70 (m, 10H), 2.48 (s, 3H). FAB-MS: *m/z* (relative intensity) 687.2 (M + 1, 20), 643.3 (2), 91.0 (50). FAB−HRMS for $C_{35}H_{35}N_4O_9S$ $[MH]^+$: calcd 687.2125, found 687.2139. Anal. ($C_{35}H_{34}N_4O_9S$·0.2EtOAc).

*[N-Benzyloxycarbonyl-O-toluenesulfonyl-L-tyrosyl]-(4-acetylaminobenzoyl) piperazine (**33**).* ^{1}H NMR ($CDCl_3$): δ 7.72 (d, J = 8.2 Hz, 2H), 7.53 (d, J = 8.5 Hz, 2H), 7.45 (s, 1H), 7.40−7.28 (m, 9H), 7.13 (d, J = 8.2 Hz, 2H), 6.91 (d, J = 7.7 Hz, 2H), 5.80−5.56 (b, 1H), 5.20−5.00 (m, 2H), 4.90−4.72 (b, 1H), 3.90−2.70 (m, 10H), 2.45 (s, 3H), 2.19 (s, 3H). FAB−HRMS for $C_{37}H_{39}N_4O_8S$ $[MH]^+$: calcd 699.2489, found 699.2505. Compound **33** (R_f = 0.35, CH_3OH/$CHCl_3$ = 5: 95) was shown to be pure by TLC. Anal. ($C_{37}H_{38}N_4O_8S$·0.5EtOAc).

*[N-Fmoc-O-benzenesulfonyl)-L-tyrosyl]benzoylpiperazine (**53a**).* ^{1}H NMR ($CDCl_3$). δ 7.80−7.28 (m, 18H), 7.16 (d, J = 8.2 Hz, 2H), 6.93 (d, J = 8.2 Hz, 2H), 5.64 (d, J = 8.5 Hz, 1H), 4.83 (br s, 1H), 4.50−4.28 (m, 2H), 4.20 (m, 1H), 3.85−2.70 (m, 10H).

*[N-Fmoc-O-(4-nitrobenzene)sulfonyl-L-tyrosyl]-(4-nitrobenzoyl)piperazine (**53b**).* ^{1}H NMR ($CDCl_3$): δ 8.42 (d, J = 8.3 Hz, 2H), 8.27 (d, J = 7.7 Hz, 2H), 8.10 (d, J = 8.8 Hz, 2H), 7.78 (d, J = 7.7 Hz, 2H), 7.56 (m, 4H), 7.41 (t, J = 7.4 Hz, 2H), 7.36−7.27(m, 2H), 7.19 (d, J = 8.2 Hz, 2H), 6.98 (d, J = 7.4 Hz, 2H), 5.58 (d, J = 8.8 Hz, 1H), 4.83 (b, 1H), 4.50−4.26 (m, 2H), 4.19(m, 1H), 3.80−2.55 (m, 10H).

*[N-Fmoc-O-benzenesulfonyl-L-tyrosyl]-(4-nitrobenzoyl)-piperazine (**53c**).* ^{1}H NMR ($CDCl_3$): δ 8.40−8.16 (b, 2H), 7.90 (d, J = 7.7 Hz, 2H), 7.78 (d, J = 7.4 Hz, 2H), 7.70 (d, J = 7.1 Hz, 1H), 7.64−7.48 (m, 6H), 7.46−7.28 (m, 4H), 7.17 (d, J = 8.2 Hz, 2H), 7.06−6.90 (m, 2H), 5.75−5.50 (b, 1H), 4.90−4.70 (b, 1H), 4.50−4.30 (m, 2H), 4.25−4.10 (m, 1H), 4.00−2.70 (m, 10H).

*[N-Fmoc-O-(4-nitrobenzene)sulfonyl-L-tyrosyl]benzoylpiperazine (**53d**).* ^{1}H NMR ($CDCl_3$): δ 8.38 (d, J = 8.5 Hz, 2H), 8.05 (d, J = 8.2 Hz, 2H), 7.77 (d, J = 7.4 Hz, 2H), 7.56 (d, J = 7.4 Hz, 2H), 7.50−7.28 (m, 9H), 7.16 (d, J = 8.2 Hz, 2H), 6.94 (d, J = 8.2 Hz, 2H), 5.63 (d, J = 8.5 Hz, 1H), 4.90−4.47 (b, 1H), 4.50−4.25 (m, 2H), 4.25−4.10 (m, 1H), 3.80−2.70 (m, 10H).

*[N-(4-Nitrobenzyloxycarbonyl)-O-toluenesulfonyl-L-tyrosyl]Boc-piperazine (**57a**).* ^{1}H NMR ($CDCl_3$): δ 8.21 (d, J = 8.5 Hz, 2H), 7.76 (d, J = 8.2 Hz, 2H), 7.48 (d, J = 8.5 Hz, 2H), 7.36 (d, J = 8.2 Hz, 2H), 7.18 (d, J = 8.4 Hz, 2H), 7.02 (d, J = 8.5 Hz, 2H), 5.62(d, J = 8.5 Hz, 1H),

5.20 (ABq, J = 12.3, 15.6 Hz, 2H), 4.60−4.40 (m, 1H), 4.00−2.80 (m, 10H), 2.46 (s, 3H), 1.45 (s, 9H).

*[N-Benzyloxycarbonyl-O-toluenesulfonyl-*L*-tyrosyl]Boc-piperazine (**57b**).* ^{1}H NMR ($CDCl_3$): δ 7.69 (d, J = 7.9 Hz, 2H), 7.42−7.28 (m, 7H), 7.09 (d, J = 7.9 Hz, 2H), 6.88 (d, J = 7.9 Hz, 2H), 5.65 (d, J = 8.5 Hz, 1H), 5.07 (ABq, J = 12.6, 15.4 Hz, 2H), 4.90−4.76 (m, 1H), 3.60−2.70 (m, 10H), 2.45 (s, 3H), 1.44 (s, 9H).

General Procedure for the Synthesis of 3−16. The appropriate tyrosine derivative (**48**, **54a**, **54b**, **54c**, or **54d**; 1.0 mmol), Bop-Cl (1.0 mmol) and appropriate cinnamic acid derivative (1.0 mmol) were dissolved in CH_2Cl_2 (5.0 mL). The solution was treated with Et_3N (2.0 mmol) and stirred at room temperature for 5 h. The solvent was removed, and the residue was purified using silica gel chromatography eluting with methanol−chloroform (5:95) to get a solid foam (40−60% yield).

*[N-(trans-Cinnamoyl)-O-benzenesulfonyl-*L*-tyrosyl]benzoylpiperazine (**3**).* ^{1}H NMR ($CDCl_3$): δ 7.85 (d, J = 7.7 Hz, 2H), 7.74−7.60 (m, 2H), 7.60−7.30 (m, 11H), 7.17 (d, J = 8.5 Hz, 2H), 6.94 (d, J = 8.5 Hz, 2H), 6.58−6.46 (m, 1H), 6.40 (d, J = 15.7 Hz, 1H), 5.40−5.10 (b, 1H), 3.90−2.90 (m, 10H). FAB-MS: *m/z* (relative intensity) 624.3 (M + 1, 40), 434.2 (20), 191.2 (100), 131.1 (100), 105.0 (100). Compound **3** (R_f = 0.60, $CH_3OH/CHCl_3$ = 5: 95) was shown to be pure by TLC.

*[N-(trans-2-Methoxycinnamoyl)-O-toluenesulfonyl-*L*-tyrosyl]benzoylpiperazine (**4**).* ^{1}H NMR ($CDCl_3$): δ 7.72 (d, J = 8.1 Hz, 2H), 7.52−7.32 (m, 10H), 7.16−6.80 (m, 5H), 6.34 (d, J = 8.4 Hz, 1H), 6.00 (d, J = 15.7 Hz, 1H), 5.20−5.00 (m, 1H), 4.00−2.70 (m, 13H), 2.45 (s, 3H).

*[N-(cis-2-Methoxycinnamoyl)-O-toluenesulfonyl-*L*-tyrosyl]-benzoylpiperazine (**5**).* ^{1}H NMR ($CDCl_3$): δ 7.70 (d, J = 7.7 Hz, 2H), 7.50−7.30 (m, 10H), 7.14−6.82 (m, 5H), 6.34 (d, J = 8.5 Hz, 1H), 5.96 (d, J = 12.4 Hz, 1H), 5.20−5.00 (m, 1H), 4.00−2.60 (m, 13H), 2.46 (s, 3H).

*[N-(trans-3-Chlorocinnamoyl)-O-toluenesulfonyl-*L*-tyrosyl]benzoylpiperazine (**6**).* ^{1}H NMR ($CDCl_3$): δ 7.72 (d, J = 8.0 Hz, 2H), 7.61−7.29 (m, 11H), 7.16 (d, J = 8.5 Hz, 2H), 6.94 (d, J = 8.2 Hz, 2H), 6.57 (d, J = 8.3 Hz, 1H), 6.45−6.37 (d, J = 15.7 Hz, 1H), 5.37−5.07 (b, 1H), 4.00−2.70 (m, 10H), 2.46 (s, 3H).

*[N-(trans-2,4,5-Trimethoxycinnamoyl)-O-toluenesulfonyl-*L*-tyrosyl]benzoylpiperazine (**7**).* ^{1}H NMR ($CDCl_3$): δ 7.88 (s, 1H), 7.82 (s, 1H), 7.71 (d, J = 7.7 Hz, 2H), 7.56−7.30 (m, 5H), 7.17 (d, J = 8.2 Hz, 2H), 7.02−6.86 (m, 4H), 6.56 (d, J = 15.9 Hz, 1H), 6.43 (d, J = 8.3 Hz, 1H), 5.40−5.05 (b, 1H), 4.00−2.70 (m, 19H), 2.45 (s, 3H).

*[N-(trans-4-Nitrocinnamoyl)-O-benzenesulfonyl-*L*-tyrosyl]-benzoylpiperazine (**8**).* ^{1}H NMR ($CDCl_3$): δ 8.24 (d, J = 8.5 Hz, 2H), 7.86 (d, J = 8.0 Hz, 2H), 7.76−7.50 (m, 6H), 7.48−7.30 (m, 4H), 7.17 (d, J = 8.2 Hz, 2H), 6.96 (d, J = 8.5 Hz, 2H), 6.64 (d, J = 8.2 Hz, 1H), 6.52 (d, J = 15.9 Hz, 1H), 5.40−5.32 (b, 1H), 3.90−2.60 (m, 10H). FAB-MS: *m/z* (relative intensity) 669.2 (M + 1, 25), 251.1 (40), 119.0 (100). Compound **8** (R_f = 0.47, $CH_3OH/CHCl_3$ = 5: 95) was shown to be pure by TLC.

*[N-(trans-Cinnamoyl)-O-(4-nitrobenzenesulfonyl)-*L*-tyrosyl]-benzoylpiperazine (**9**).* ^{1}H NMR ($CDCl_3$): δ 8.40 (d, J = 8.5 Hz, 2H), 8.06 (d, J = 8.3 Hz, 2H), 7.70−7.30 (m, 10H), 7.20 (d, J = 8.2 Hz, 2H), 6.95 (d, J = 8.5 Hz, 2H), 6.52 (d, J = 8.2 Hz, 1H), 6.40 (d, J = 15.7 Hz, 1H), 5.40−5.34 (b, 1H), 3.90−2.80 (m, 10H). FAB-MS: *m/z* (relative intensity) 669.2 (M + 1, 20), 191.2 (85), 131.1 (100), 119.0 (75). Compound **9** (R_f = 0.59, $CH_3OH/CHCl_3$ = 5: 95) was shown to be pure by TLC.

*[N-(trans-Cinnamoyl)-O-benzenesulfonyl-*L*-tyrosyl]-(4-nitrobenzoyl)piperazine (**10**).* ^{1}H NMR ($CDCl_3$): δ 8.26 (d, J = 7.7 Hz, 2H), 7.89 (d, J = 7.7 Hz, 2H), 7.78−7.30 (m, 10H), 7.21 (d, J = 8.5 Hz, 2H), 7.00 (d, J = 7.4 Hz, 2H), 6.60−6.46 (m, 1H), 6.44−6.34 d, J = 15.7 Hz, 1H), 5.40−5.06 (b, 1H), 4.00−2.80 (m, 10H). FAB-MS: *m/z* (relative intensity) 669.2 (M + 1, 20), 434.2 (35), 131.1 (100). Compound **10** (R_f = 0.56, $CH_3OH/CHCl_3$ = 5: 95) was shown to be pure by TLC.

*[N-(trans-4-Nitrocinnamoyl)-O-(4-nitrobenzenesulfonyl)-*L*-tyrosyl]-benzoylpiperazine (**11**).* ^{1}H NMR ($CDCl_3$): δ 8.41 (d, J = 8.5 Hz, 2H), 8.24 (d, J = 8.5 Hz, 2H), 8.07 (d, J = 8.5 Hz, 2H), 7.74−7.58 (m, 3H), 7.50−7.34 (m, 4H), 7.20 (d, J = 8.5 Hz, 2H), 6.97 (d, J = 8.5 Hz, 2H), 6.64 (d, J = 8.0 Hz, 1H), 6.52 (d, J = 15.7 Hz, 1H), 5.40−5.16 (b, 1H), 3.84−2.80 (m, 10H). FAB-MS: *m/z* (relative intensity) 714.2 (M + 1, 2), 119.0 (100), 91.0 (50). Compound **11** (R_f = 0.50, $CH_3OH/CHCl_3$ = 5: 95) was shown to be pure by TLC.

*[N-(trans-4-Nitrocinnamoyl)-O-benzenesulfonyl-*L*-tyrosyl]-(4-nitrobenzoyl)piperazine (**12**).* ^{1}H NMR ($CDCl_3$): δ 8.36−8.14 (m, 4H), 7.90 (d, J = 7.4 Hz, 2H), 7.80−7.50 (m, 7H), 7.22 (d, J = 8.5 Hz, 2H), 7.10−6.92 (m, 2H), 6.72−6.40 (m, 2H), 5.40−5.08 (b, 1H), 4.00−2.80 (m, 10H). FAB-MS: *m/z* (relative intensity) 714.2 (M + 1, 10), 119.0 (100). Compound **12** (R_f = 0.47, $CH_3OH/CHCl_3$ = 5: 95) was shown to be pure by TLC.

*[N-(trans-Cinnamoyl)-O-(4-nitrobenzenesulfonyl)-*L*-tyrosyl]-(4-nitrobenzoyl)piperazine (**13**).* ^{1}H NMR ($CDCl_3$): δ 8.43 (d, J = 8.8 Hz, 2H), 8.28 (d, J = 8.2 Hz, 2H), 8.10 (d, J = 8.8 Hz, 2H), 7.70−7.46 (m, 4H), 7.44−7.34 (m, 3H), 7.23 (d, J = 8.5 Hz, 2H), 7.00 (d, J = 8.0 Hz, 2H), 6.49 (d, J = 8.2 Hz, 1H), 6.40 (d, J = 15.7 Hz, 1H), 5.40−5.16 (b, 1H), 3.90−2.80 (m, 10H). FAB-MS: *m/z* (relative intensity) 714.2 (M + 1, 5.5), 119.0 (100). Compound **13** (R_f = 0.56, $CH_3OH/CHCl_3$ = 5: 95) was shown to be pure by TLC.

*[N-(trans-4-Nitrocinnamoyl)-O-(4-nitrobenzenesulfonyl)-*L*-tyrosyl]-(4-nitrobenzoyl)piperazine (**14**).* ^{1}H NMR ($CDCl_3$): δ 8.43 (d, J = 8.8 Hz, 2H), 8.34−8.20(m, 4H), 8.10 (d, J = 8.8 Hz, 2H), 7.78−7.50 (m, 4H), 7.24 (d, J = 8.5 Hz, 2H), 7.01 (d, J = 7.7 Hz, 2H), 6.64 (d, J = 8.2 Hz, 1H), 6.54 (d, J = 15.6 Hz, 1H), 5.40−5.10 (b, 1H), 3.90−2.90 (m, 10H). FAB-MS: *m/z* (relative intensity) 759.2 (M + 1, 1.5), 119.0 (100). Compound **14** (R_f = 0.45, $CH_3OH/CHCl_3$ = 5: 95) was shown to be pure by TLC.

*[N-Benzyloxycarbonyl-O-toluenesulfonyl-*L*-tyrosyl]-benzoylpiperazine (**15**).* ^{1}H NMR ($CDCl_3$): δ 7.72 (d, J = 8.2 Hz, 2H), 7.48−7.28 (m, 12H), 7.12 (d, J = 8.2 Hz, 2H), 6.90 (d, J = 8.2 Hz, 2H), 5.61 (d, J = 8.5 Hz, 1H), 5.16−4.96 (m, 2H), 4.92−4.74 (m, 1H), 3.80−2.60 (m, 10H), 2.45 (s, 3H). Anal. ($C_{35}H_{35}N_3O_7S\cdot 0.1\ H_2O$).

*[N-(2-Chlorobenzyloxycarbonyl)-O-toluenesulfonyl-*L*-tyrosyl]-benzoylpiperazine (**16**).* ^{1}H NMR ($CDCl_3$): δ 7.72 (d, J = 7.7 Hz, 2H), 7.48−7.30 (m, 11H), 7.13 (d, J = 8.2 Hz, 2H), 6.92 (d, J = 8.2 Hz, 2H), 5.56 (d, J = 8.2 Hz, 1H), 5.28−5.10 (ABq, J = 13.1 Hz, 2H), 4.94−4.74 (m, 1H), 3.90−2.70 (m, 10H), 2.46 (s, 3H). Compound **16** (R_f = 0.64, $CH_3OH/CHCl_3$ = 5: 95) was shown to be pure by TLC.

General Procedure for the Synthesis of 20a, 24, 27, 32. To a solution of an aromatic nitro compound (**19**, **23b**, **26b**, or **31b**; 2.0 mmol) in methanol (10 mL), sodium borohydride (10.0 mmol) was added and the solution stirred at room temperature for 5 min. Then copper(II) acetylacetonate was added and stirring continued for 1 h. TLC showed the completion of the reaction. The solvent was removed, and the residue was washed with petroleum ether two times. Then, the crude product was purified using silica gel chromatography eluting with methanol−chloroform (5:95) to provide a white solid foam (80−85% yield).

*[N-(3-Aminobenzyloxycarbonyl)-O-toluenesulfonyl-*L*-tyrosyl]benzoylpiperazine (**20a**).* ^{1}H NMR ($CDCl_3$): δ 7.72 (d, J = 8.5 Hz, 2H), 7.46−7.28 (m, 7H), 7.18−7.06 (m, 3H), 6.92 (d, J = 8.8 Hz, 2H), 6.74−6.58 (m, 3H), 5.57 (d, J = 9.3 Hz, 1H), 5.04−4.92 (m, 2H), 4.88−4.74 (b, 1H), 3.95−2.70 (m, 10H), 2.45 (s, 3H). FAB-MS: *m/z* (relative intensity) 657.3 (M + 1, 45), 658.3 (M + 2, 15), 85 (100). FAB−HRMS for $C_{35}H_{37}N_4O_7S$ [M + H]$^+$: calcd 657.2383, found 657.2385.

*[N-Benzyloxycarbonyl-O-(4-aminobenzenesulfonyl)-*L*-tyrosyl]Boc-piperazine (**24**).* ^{1}H NMR ($CDCl_3$): δ 7.53 (d, J = 8.5 Hz, 2H), 7.40−7.28 (m, 5H), 7.08 (d, J = 8.5 Hz, 2H), 6.92 (d, J = 8.4 Hz, 2H), 6.61 (d, J = 8.8 Hz, 2H), 5.61 (d, J = 8.5 Hz, 1H), 5.02−4.96 (ABq, J = 12.3, 16.0 Hz, 2H), 4.81 (b, 1H), 4.38 (br s, 2H), 3.80−2.60 (m, 10H), 1.45 (s, 9H). FAB-MS (NOBA): *m/z* (relative intensity) 639.3 (M + 1, 1), 661.3 (M + Na, 7), 583.2 (8), 539.3 (10). 91.0 (100). FAB-MS (NOBA/LiCl): *m/z* (relative intensity) 645.3 (M + Li, 15), 687.3 (M + Li$^+_2$Cl, 5).

*[N-Benzyloxycarbonyl-O-(4-aminobenzenesulfonyl)-*L*-tyrosyl]benzoylpiperazine (27).* ^{1}H NMR ($CDCl_3$): δ 7.55 (d, J = 8.5 Hz, 2H), 7.48−7.28 (m, 10H), 7.10 (d, J = 8.0 Hz, 2H), 6.94 (d, J = 8.0 Hz, 2H), 6.64 (d, J = 8.5 Hz, 2H), 5.63 (d, J = 8.8 Hz, 1H), 5.16−5.00 (ABq, J = 12.4, 15.9 Hz, 2H), 4.92−4.70 (b, 1H), 4.50−4.20 (b, 2H), 4.00−2.80 (m, 10H). FAB-MS: *m/z* (relative intensity) 643.4 (M + 1, 24), 391.4 (20), 251.2 (60), 91.1 (100). FAB−HRMS for $C_{34}H_{35}N_4O_7S$ [M + H]$^+$: calcd 643.2226, found 643.2244.

*[N-Benzyloxycarbonyl-O-toluenesulfonyl-*L*-tyrosyl]-(4-aminobenzoyl)piperazine (**32**).* ^{1}H NMR ($CDCl_3$): δ 7.70 (d, J = 8.2 Hz, 2H), 7.40−7.30 (m, 7H), 7.23 (d, J = 8.2 Hz, 2H), 7.12 (d, J = 8.5 Hz, 2H), 6.90 (d, J = 8.5 Hz, 2H), 6.70 (d, J = 8.4 Hz, 2H), 5.61 (d, J = 8.5 Hz, 1H), 5.12−5.02 (ABq, J = 12.3, 15.1 Hz, 2H), 4.88−4.76 (m, 1H), 3.89 (s, 2H), 3.90−2.80 (m, 10H), 2.45 (s, 3H). FAB-MS: *m/z* (relative intensity) 657.2 (M + 1, 95), 679.2 (M+ Na, 25), 120.1 (100), 91.0 (85). FAB−HRMS for $C_{35}H_{37}N_4O_7S$ [M + H]$^+$: calcd 657.2383, found 657.2396. Anal. ($C_{35}H_{36}N_4O_9S\cdot 0.1H_2O$).

General Procedure for the Synthesis of 21, 29, 34. An amine compound (**20a**, **27**, or **32**; 0.08 mmol) was mixed with chloroform (2.0 mL), water (1.0 mL), and sodium bicarbonate (20 mg. 0.24 mmol) and stirred vigorously for 10 min. Thiophosgene (2.0 mmol) was added and stirring continued for 1 h. The solvent was removed, and the residue was washed two times with petroleum ether. The crude product was purified with a preparative TLC plate to provide a white solid foam (70−85% yield).

*[N-(3-Isothiocyanato)benzyloxycarbonyl-O-toluenesulfonyl-*L*-tyrosyl]benzoylpiperazine (**21**).* ^{1}H NMR ($CDCl_3$): δ 7.72 (d, J = 8.8 Hz, 2H), 7.46−7.30 (m, 8H), 7.24−7.08 (m, 5H), 6.92 (d, J = 8.8 Hz, 2H), 5.64 (d, J = 8.5 Hz, 1H), 5.05 (s, 2H), 4.90−4.72 (b, 1H), 4.00−2.70 (m, 10H), 2.45 (s, 3H). FAB−HRMS for $C_{36}H_{35}N_4O_7S_2$ [M + H]$^+$: calcd 699.1947, found 699.1948. Anal. ($C_{36}H_{34}N_4O_7S_2$).

*[N-Benzyloxycarbonyl-O-(4-isothiocyanato)benzenesulfonyl-*L*-tyrosyl]benzoylpiperazine (**29**).* ^{1}H NMR ($CDCl_3$): δ 7.82 (d, J = 8.5 Hz, 2H), 7.48−7.28 (m, 12H), 7.14 (d, J = 8.5 Hz, 2H), 6.92 (d, J = 8.5 Hz, 2H), 5.59 (d, J = 8.5 Hz, 1H), 5.16−5.00 (ABq, J = 12.1, 14.8 Hz, 2H), 4.92−4.72 (b, 1H), 3.80−2.70 (m, 10H). FAB−HRMS for $C_{35}H_{33}N_4O_7S_2$ [M + H]$^+$: calcd 685.1791, found 685.1810.

*[N-Benzyloxycarbonyl-O-toluenesulfonyl-*L*-tyrosyl]-(4-isothiocyanatobenzoyl)piperazine (**34**).* ^{1}H NMR ($CDCl_3$): δ 7.42 (d, J = 8.5 Hz, 2H), 7.40−7.30 (m, 9H), 7.24 (d, J = 8.2 Hz, 2H), 7.14 (d, J = 8.5 Hz, 2H), 6.93 (d, J = 8.5 Hz, 2H), 5.60 (d, J = 8.5 Hz, 1H), 5.16−5.00 (ABq, J = 12.4, 15.4 Hz, 2H), 4.90−4.72 (b, 1H), 3.80−2.60 (m, 10H), 2.47 (s, 3H). FAB-MS (NOBA): *m/z* (relative intensity) 699.2 (M + 1, 22), 721.2 (M+ Na, 14), 91.1 (100). FAB−HRMS (CsI) for $C_{36}H_{34}N_4O_7S_2Cs$ [M + Cs]$^+$: calcd 831.0923, found 831.0895. Anal. ($C_{36}H_{34}N_4O_7S_2\cdot$ 0.4EtOAc).

General Procedure for the Synthesis of 22, 30, 35a, 35b. 1,4-Diaminobutane (100 mg, 1.1 mmol) or 1,2-diaminoethane (100 mg, 1.7 mmol) was added in the flask. Then, a solution of isothiocyanate compound (**21** or **29** or **34**) (0.01 mmol) and CH_2Cl_2 (0.1 mL) was added dropwise and stirring continued at room temperature for 1 h. The solvent was removed and the residue was washed two times with petroleum ether. The crude product was purified on a preparative TLC plate using methanol−chloroform (1:9) as mobile phase to afford a white solid foam (40−45% yield).

*[N-3-{3-(4-Aminobutyl)thioureido}benzyloxycarbonyl-O-toluenesulfonyl-*L*-tyrosyl]benzoylpiperazine (**22a**).* ^{1}H NMR ($CDCl_3$): δ 7.71 (d, J = 8.2 Hz, 2H), 7.48−7.30 (m, 10H), 7.18−7.10 (m, 2H), 7.08−7.00 (m, 1H), 6.90 (d, J = 8.2 Hz, 2H), 5.40−4.60 (m, 4H), 3.80−2.80 (m, 14H), 2.45 (s, 3H), 1.30−1.20 (m,4H). FAB−HRMS for $C_{40}H_{47}N_6O_7S_2$ [M + H]$^+$: calcd 787.2948, found 787.2957.

*[N-Benzyloxycarbonyl-O-4-{3-(4-aminobutyl)thioureido} benzenesulfonyl-*L*-tyrosyl]benzoylpiperazine (**30**).* ^{1}H NMR ($CDCl_3$): δ 7.80−7.56 (m, 4H), 7.54−7.30 (m, 10H), 7.20−6.90 (m, 4H), 5.64 (d, J = 8.5 Hz, 1H), 5.18−5.00 (ABq, J = 12.4, 15.0 Hz, 2H), 4.88−4.72 (b, 1H), 3.80−2.25 (m, 14H), 1.30−1.20 (m, 4H). FAB−HRMS (CsI) for $C_{39}H_{44}N_6O_7S_2Cs$ [M + Cs]$^+$: calcd 905.1767, found 905.1771.

*[N-Benzyloxycarbonyl-O-toluenesulfonyl-*L*-tyrosyl](4-{3-[(2-aminoethyl)thioureido})benzoylpiperazine (**35a**).* ^{1}H NMR ($CDCl_3$): δ 7.71 (d, J = 8.0 Hz, 2H), 7.52−7.28 (m, 11H), 7.13 (d, J = 8.0 Hz, 2H), 6.91 (d, J = 8.0 Hz, 2H), 5.70 (d, J = 7.7 Hz, 1H), 5.16−4.86 (ABq, J = 12.4, 17.0 Hz, 2H), 4.90−4.72 (b, 1H), 3.84−2.56 (m, 14H), 2.45 (s, 3H). FAB−HRMS (CsI) for $C_{38}H_{42}N_6O_7S_2Cs$ [M + Cs]$^+$: calcd 891.1611, found 891.1641.

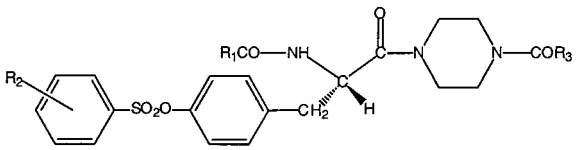
*[N-Benzyloxycarbonyl-O-toluenesulfonyl-*L*-tyrosyl](4-{3-[(4-aminobutyl)thioureido})benzoylpiperazine (**35b**).* ^{1}H NMR ($CDCl_3$): δ 7.73 (d, J = 8.5 Hz, 2H), 7.48−7.28 (m, 11H), 7.15 (d, J = 8.2 Hz, 2H), 6.93 (d, J = 8.5 Hz, 2H), 5.61 (d, J = 9.1 Hz, 1H), 5.14−5.02 (ABq, J = 12.4, 15.9 Hz, 2H), 4.92−4.74 (b, 1H), 3.80−2.60 (m, 14H), 2.43 (s, 3H), 1.40−1.20 (m, 4H). FAB−HRMS (CsI) for $C_{40}H_{47}N_6O_7S_2$ [M + H]$^+$: calcd 787.2948, found 787.2919.

General Procedure for the Synthesis of 64. A solution of isothiocyanate compound **21** (20 mg, 0.029 mmol) in dry DMF (0.5 mL) was stirred under nitrogen for 4 days at 80 °C. The solvent was removed with nitrogen stream, and the residue was purified with preparative TLC (methanol: chloroform = 3:97) to afford a white solid (4.5 mg, 10% yield).

*1,3-Bis{[3-N-benzyloxycarbonyl-O-toluenesulfonyl-*L*-tyrosyl]benzoylpiperazinethiourea (**64**).* ^{1}H NMR ($CDCl_3$): δ 8.02 (b, 2H), 7.70 (d, J = 8.0 Hz, 4H), 7.50−7.30 (m, 20H), 7.22−7.02 (m, 6H), 6.90 (d, J = 8.2 Hz, 4H), 5.88 (b, 2H), 5.18−4.94 (m, 4H), 4.81 (b, 2H), 3.80−2.80 (m, 20H), 2.45 (s, 6H).). FAB-MS: *m/z* (relative intensity) 1377.3 (M + Na, 15), 1355.3 (M + H, 5), 261.2 (100). FAB−HRMS (CsI) for $C_{71}H_{70}N_8O_{14}S_3Cs$ [M + Cs]$^+$: calcd 1487.3228, found 1487.3258. FAB−HRMS (CsI) for $C_{71}H_{69}N_8O_{14}S_3Cs_2$ {[(M − H)Cs]Cs}$^+$: calcd 1619.2204, found 1619.2222.

General Procedure for the Synthesis of 65, 66, 67. Mixing equimolar amounts of isothiocyanate and amine

Table 1. Antagonistic Effects of Tyrosine Derivatives on Function of Human P2X$_7$ Receptors Expressed in HEK293 Cells[a]



compound	R_1	R_2	R_3	% inhibition	*n*
		Monomeric			
3	Ph-CH=CH (trans)	H	Ph	62 ± 4	2
4	2-OCH_3-Ph-CH=CH (trans)	4-CH_3	Ph	27 ± 2	2
5	2-OCH_3-Ph-CH=CH (cis)	4-CH_3	Ph	17 ± 1	2
6	3-Cl-Ph-CH=CH (trans)	4-CH_3	Ph	57 ± 5	2
7	2,4,5-$(OCH_3)_3$-Ph-CH=CH (trans)	4-CH_3	Ph	−2 ± 6	2
8	4-NO_2-Ph-CH=CH (trans)	H	Ph	43 ± 20	2
9	Ph-CH=CH (trans)	4-NO_2	Ph	72 ± 4	3
10	Ph-CH=CH (trans)	H	Ph-4-NO_2	41 ± 1	2
11	4-NO_2-Ph-CH=CH (trans)	4-NO_2	Ph	58 ± 1	2
12	4-NO_2-Ph-CH=CH (trans)	H	Ph-4-NO_2	30 ± 2	2
13	Ph-CH=CH (trans)	4-NO_2	Ph-4-NO_2	43 ± 14	3
14	4-NO_2-Ph-CH=CH (trans)	4-NO_2	Ph-4-NO_2	4 ± 9	2
15	Ph-CH_2O	4-CH_3	Ph	71 ± 21	2
16	2-Cl-Ph-CH_2O	4-CH_3	Ph	43 ± 17	3
17	4-NO_2-Ph-CH_2O	4-CH_3	Ph	69 ± 25	3
18	3-NO_2-Ph-CH_2O	4-CH_3	O-$C(CH_3)_3$	94 ± 28	3
19	3-NO_2-Ph-CH_2O	4-CH_3	Ph	72 ± 6	2
20a	3-NH_2-Ph-CH_2O	4-CH_3	Ph	50 ± 6	2
20b	3-CH_3CONH−Ph-CH_2O	4-CH_3	Ph	9 ± 13	2
21	3-SCN-Ph-CH_2O	4-CH_3	Ph	−4 ± 5	2
22	3-[$H_2N(CH_2)_4NH$-CSNH]-Ph-CH_2O	4-CH_3	Ph	17 ± 4	2
23a	Ph-CH_2O	3-NO_2	O-$C(CH_3)_3$	74 ± 2	2
23b	Ph-CH_2O	4-NO_2	O-$C(CH_3)_3$	30 ± 28	2
24	Ph-CH_2O	4-NH_2	O-$C(CH_3)_3$	64 ± 17	2
25	Ph-CH_2O	4-$NHCOCH_3$	O-$C(CH_3)_3$	64 ± 27	2
26a	Ph-CH_2O	3-NO_2	Ph	75 ± 10	2
26b	Ph-CH_2O	4-NO_2	Ph	78 ± 18	3
27	Ph-CH_2O	4-NH_2	Ph	56 ± 9	2
28	Ph-CH_2O	4-$NHCOCH_3$	Ph	31 ± 41	2
29	Ph-CH_2O	4-NCS	Ph	72 ± 1	2
30	Ph-CH_2O	4-[$H_2N(CH_2)_4NH$-CSNH]-	Ph	80 ± 11	3
31a	Ph-CH_2O	4-CH_3	Ph-3-NO_2	60 ± 16	2
31b	Ph-CH_2O	4-CH_3	Ph-4-NO_2	61 ± 6	2
32	Ph-CH_2O	4-CH_3	Ph-4-NH_2	93 ± 3	2
33	Ph-CH_2O	4-CH_3	Ph-4-$NHCOCH_3$	45 ± 21	2
34	Ph-CH_2O	4-CH_3	Ph-4-NCS	30 ± 16	2
35a	Ph-CH_2O	4-CH_3	Ph-4-NHCS-$NH(CH_2)_2NH_2$	14 + 19	2
35b	Ph-CH_2O	4-CH_3	Ph-4-NHCS-$NH(CH_2)_4NH_2$	63 ± 16	2
		Dimeric			
	linkage				
64	R_1−R_1			−5 ± 4	2
65	R_3−R_3			26	1
66	R_2−R_3			61 ± 29	2
67	R_2−R_2			72 ± 41	2

[a] All experiments were performed using adherent HEK293 cells stably transfected with cDNA encoding the human P2X$_7$ receptor. Cells were preincubated with antagonists (3 μM final concentration) for 15 min prior to stimulation for 10 min with 3 mM ATP (final concentration). Antagonist function was measured by the percent inhibition of the K^+ release triggered by 3 mM ATP in paired wells in the absence of antagonist. Data points represent the mean ± SD of values obtained. **15**, MRS 2427; **18**, MRS 2464; **26b**, MRS 2447; **30**, MRS 2483; **32**, MRS 2452; **35b**, MRS 2484; **66**, MRS 2454; **67**, MRS 2455.

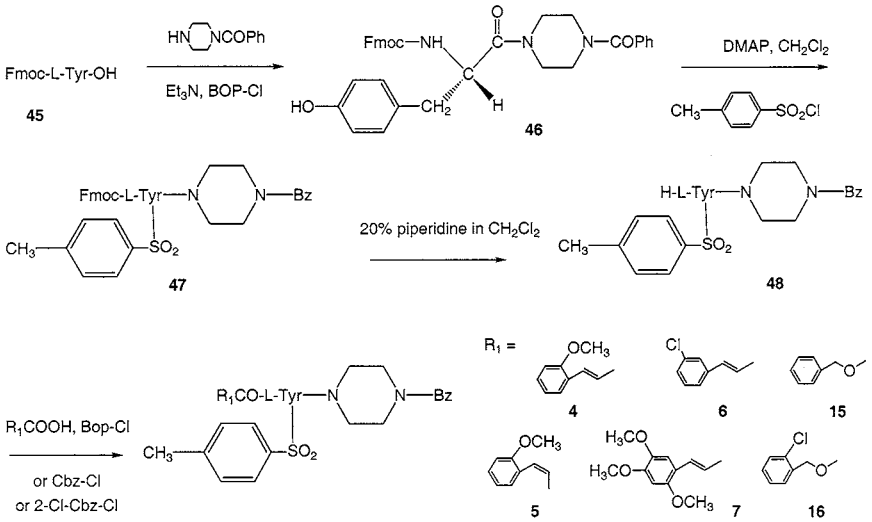
component (Scheme 7) in dry DMF, and following the same synthetic procedure as for compound **64**, the correspondence dimer was obtained in 5−10% yield.

*1,3-Bis{[N-benzyloxycarbonyl-O-toluenesulfonyl-*L*-tyrosyl]-(benzo-4-yl)piperazine}thiourea (**65**).* ^{1}H NMR ($CDCl_3$): δ 8.38 (b, 2H), 7.72 (d, J = 8.0 Hz, 4H), 7.50−7.28 (m, 20H), 7.24−7.06 (m, 6H), 6.94 (d, J = 8.2 Hz, 4H), 5.68−5.58 (m, 2H), 5.14−5.00 (m, 4H), 4.90−4.74 (b, 2H), 3.80−2.80 (m, 20H), 2.45 (s, 6H). FAB-MS: *m*/*z* (relative intensity) 1355.41 (M + H, 7), 1356.41 (M + 2H, 5.5), 1377.38 (M + Na, 1), 1393.35 (M + K, 2.5), 119.0 (100). FAB−HRMS (CsI) for $C_{71}H_{70}O_{14}N_8S_3Cs$ [M + Cs]$^+$, calcd; 1487.3228; found, 1487.3210.

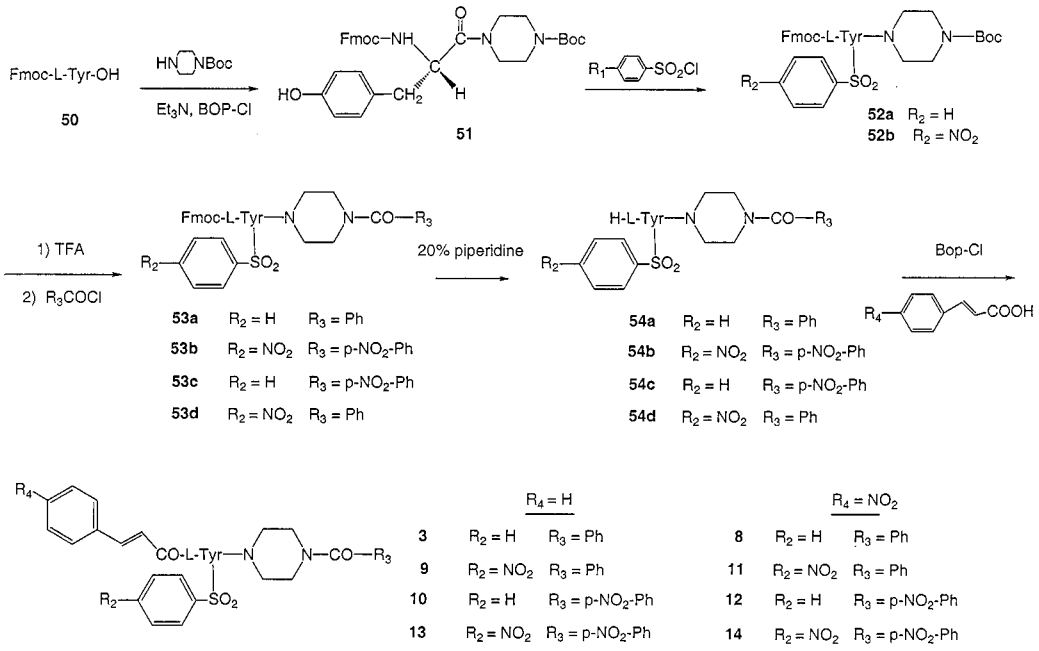
*1-[(N-Benzyloxycarbonyl-O-(benzenesulfon-4-yl)-*L*-tyrosyl)benzoylpiperazine]-3-[(N-benzyloxycarbonyl-O-toluenesulfonyl-*L*-tyrosyl)(benzo-4-yl)piperazine]thiourea (**66**).* ^{1}H NMR ($CDCl_3$): δ 7.80 (b, 2H), 7.72 (d, J = 8.2 Hz, 4H), 7.50−7.28 (m, 10H), 7.22−7.28 (m, 6H), 6.93 (d, J = 8.0 Hz, 4H), 5.60 (b, 2H), 5.16−4.98 (m, 4H), 4.80 (b, 2H), 3.80−2.80 (m, 20H), 2.45 (s, 3H). FAB-MS: *m*/*z* (relative intensity) 1341.4 (M + H, 5), 119.0 (100). FAB−HRMS (CsI) for $C_{70}H_{68}O_{14}N_8S_3Cs$ [M + Cs]$^+$, calcd; 1473.3071; found, 1473.3105.

*1,3-Bis{[N-benzyloxycarbonyl-O-(benzenesulfon-4-yl)-*L*-tyrosyl]benzoylpiperazine}thiourea (**67**).* ^{1}H NMR ($CDCl_3$): δ 9.30 (b, 2H), 7.90−7.55 (m, 8H), 7.50−7.30 (m, 20H), 7.20−6.80 (m, 8H), 5.65 (d, J = 8.5 Hz, 2H), 5.25−4.90 (m, 4H), 4.80 (b, 2H), 3.80−2.50 (m, 20H). FAB−HRMS (CsI) for $C_{69}H_{66}N_8O_{14}S_3Cs$ [M + Cs]$^+$: calcd 1459.2915, found 1459.2919.

Scheme 1. Synthesis of P2X$_7$ Receptor Antagonists Consisting of L-Tyrosine Derivatives Differing in the Cinnamoyl or Urethane Substituent Present at the Nα Position



Scheme 2. Synthesis of P2X$_7$ Receptor Antagonists Consisting of L-Tyrosine Derivatives Containing a Nitro Substitution at Either the *N*α-Cinnamoyl Substituent, the Aryl Sulfonate Group Present on the Tyrosyl Side Chain, or the *C*α-Benzoylpiperazine Substituent

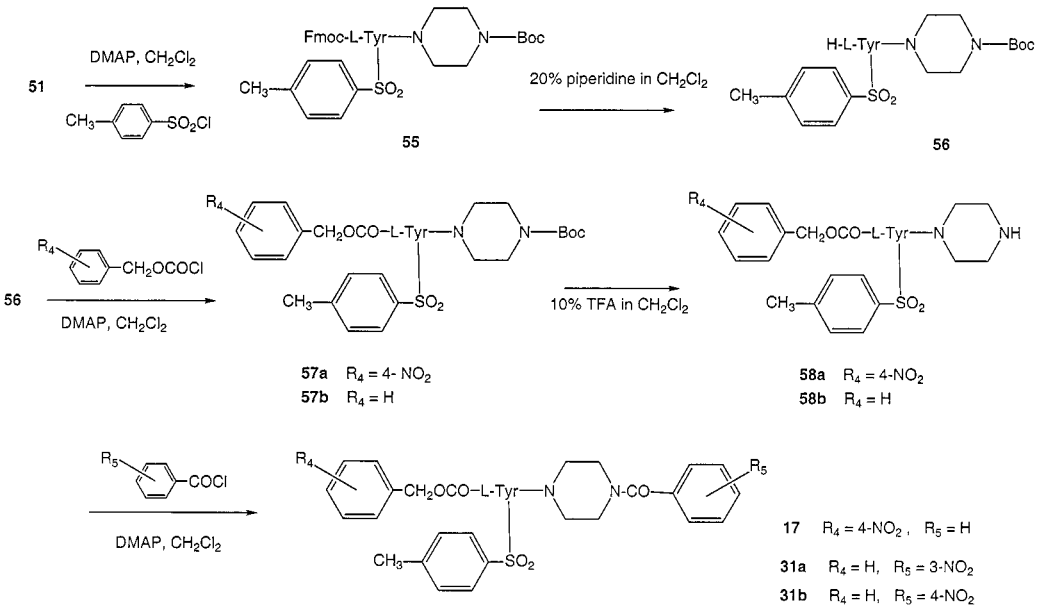


Pharmacological Analysis. P2X$_7$ Receptor Channel Activation. All experiments were performed using adherent HEK293 cells stably transfected with cDNA encoding the human P2X$_7$ receptor. Adherent cells on 12-well polylysine-coated plates were incubated at 37 °C in 1 mL of physiological salt solution (125 mM NaCl, 5 mM KCl, 1 mM $MgCl_2$, 1.5 mM $CaCl_2$, 25 mM NaHEPES (pH 7.5), 10 mM D-glucose, 1 mg/mL BSA). Antagonists were added from 1000× stock solutions dissolved in DMSO. Cells were preincubated with antagonists for 15 min prior to stimulation for 10 min with 3 mM ATP (final concentration). Reactions were terminated by rapid aspiration of the extracellular medium in each well. The adherent cells in each well were then extracted overnight with 1 mL 10% HNO_3. K^+ content in these nitric acid extracts was assayed by atomic absorbance spectrophotometry. Duplicate or triplicate wells were run for all test conditions in each separate experiment, and the measured K^+ contents were averaged. Antagonist function was measured by the percent inhibition of the K^+ release triggered by 3 mM ATP in paired wells in the absence of antagonist.

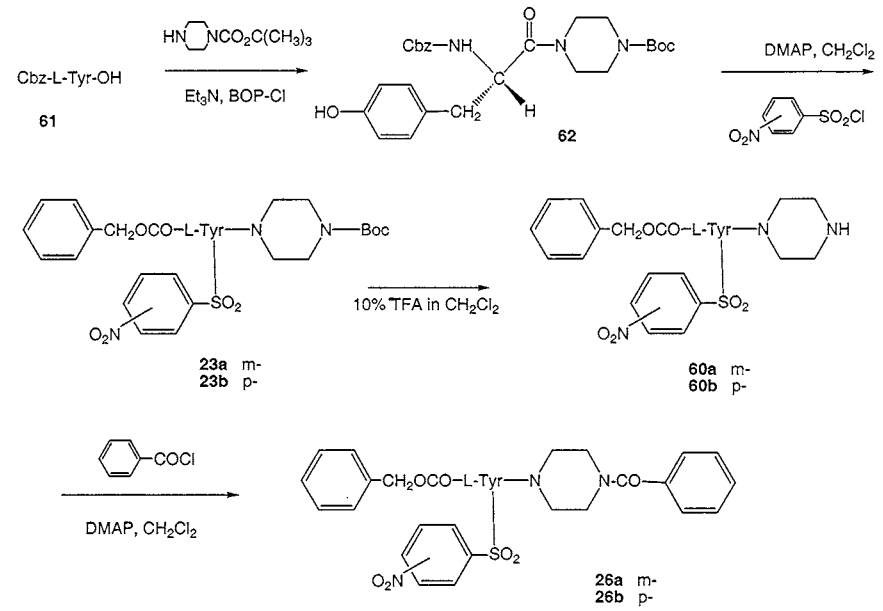
RESULTS

Chemical Synthesis. The analogues consisted of L-tyrosine derivatives, of the general structure R_1-Tyr-(OR_2)-piperazinyl-R_3 (Table 1), in which three variable regions were systematically varied in structure (compounds **3**−**35**) through facile acylation reactions and other procedures. The lead compound MRS 2409 (*17*), **2**, contained an isoquinolinyl sulfonate at the tyrosyl hydroxyl group. For the present study, this group was first substituted with a phenyl sulfonate ester, a structural simplification known to preserve affinity for the receptor (*17*). Each of the three regions (R_1−R_3) was probed systematically for possbile attachment sites, through synthesis alternating with biological evaluation, which consisted of screening at a single concentration (initially

Scheme 3. Synthesis of P2X$_7$ Receptor Antagonists Consisting of L-Tyrosine Derivatives Containing a Nitro Substitution at the *N*α-Benzyloxycarbonyl Substituent or of the *C*α-Benzoylpiperazine Substituent



Scheme 4. Synthesis of P2X$_7$ Receptor Antagonists Consisting of L-Tyrosine Derivatives Containing a Nitro Substitution at the Aryl Sulfonate Group Present on the Tyrosyl Side Chain



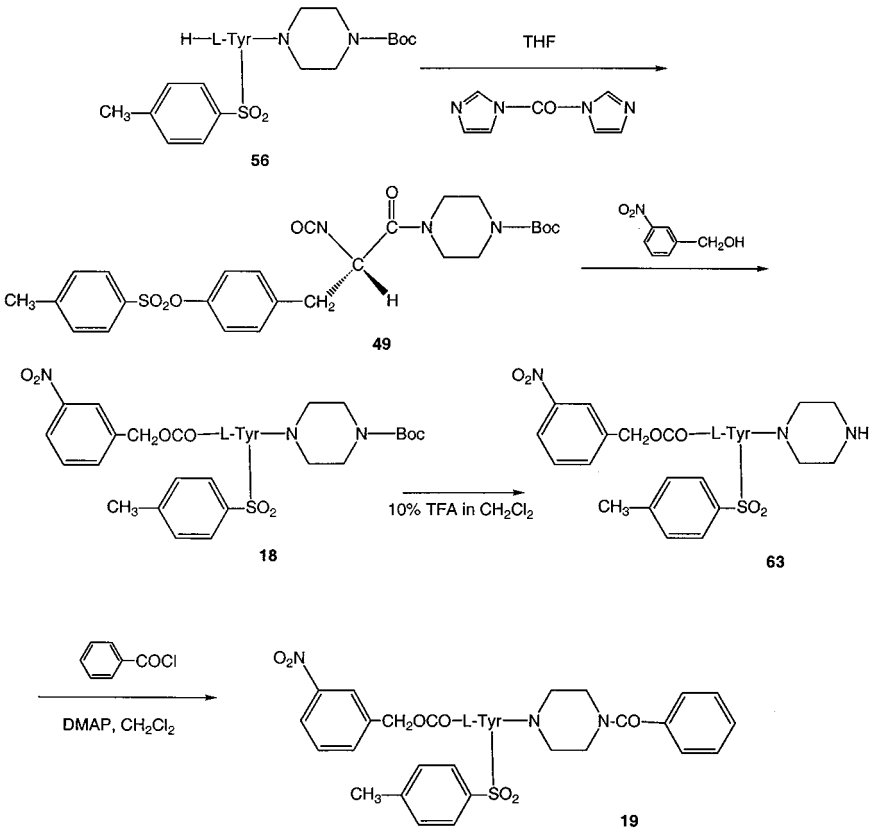
3 μM). This process led to the identification and partial optimization of potent, functionalized P2X$_7$ antagonists.

The synthetic routes for systematic substitution at three positions on the molecule are shown in Schemes 1−5. Subsequent functional group replacement beginning with nitro groups is shown in Scheme 6. Synthetic yields are listed in Materials and Methods. General probing of the SAR at each position was carried out. Scheme 1 indicates substitutions made at the R_1 position, including both *N*-cinnamoyl (**4**−**7**) and *N*-benzyloxycarbonyl (**15** and **16**) derivatives. Each of the three ring-substitution positions shown in Table 1 (R_1−R_3) was designed for the initial incorporation of a nitro group (at the meta-position for R_1, meta- or para-positions for R_2 and R_3). For a series of *N*-cinnamoyl derivatives (Scheme 2), multiple nitro groups (**11**−**14**) were also included. At R_2 and R_3 the nitro groups were introduced as shown in Schemes 3 and 4.

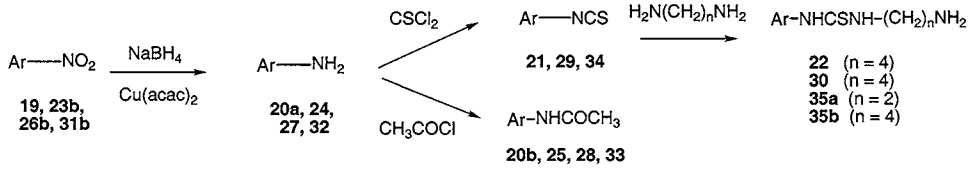
The synthesis of *N*-(nitrobenzyloxycarbonyl)-L-tyrosine derivatives (Scheme 5) required a modification of the original route based on simple reduction of 4-nitro groups. Since the *N*-(4-aminobenzyloxycarbonyl)tyrosine derivative of **17** proved to be unstable, we sought to develop an alternate synthetic method, aimed instead at the 3-nitro derivative, **18**. Usually, benzyl chloroformates are synthesized through the reaction of benzyl alcohol with phosgene (*22*). Here, an interesting alternative for the incorporation of *N*-(3-nitrobenzyloxycarbonyl) into tyrosine was the transformation of the α-amine of the tyrosyl moiety into an isocyanate group first with the aid of 1,1′-carbonyldiimidazole (*23*) to yield **49**, and subsequent addition of the alcohol to yield **18**.

The nitro groups at R_1, R_2, and R_3 were directly reduced to amines (Scheme 6), which were either converted to the isothiocyanate groups, in **21**, **29**, and **34**, as potential affinity labels for the receptor, or acylated, as models for conjugation. The isothiocyanate groups also reacted with alkyl diamines to produce the primary amine congeners **22**, **30**, and **35**. Several methods were compared for

Scheme 5. Synthesis of P2X$_7$ Receptor Antagonists Consisting of L-Tyrosine Derivatives Containing 3-Nitro Substitution at the *N*α-Benzyloxycarbonyl Substituent



Scheme 6. Functional Group Replacement in P2X$_7$ Receptor Antagonists



reduction of the aromatic nitro compounds. Many reducing reagents have been used to reduce aromatic nitro compounds (*24*) with the most classic being zinc, tin, or iron in the presence of an acid. Other reagents include hydrazine, $TiCl_4$−dialkyl telluride and sulfide (*25*). However, most of them lack the desired chemoselectivity over the functional groups that are present in our compounds such as amide, *tert*-butoxycarbonyl (Boc), 9-fluorenylmethoxycarbonyl (Fmoc), and benzyloxycarbonyl (Cbz). Though aromatic nitro compounds are seldom reduced by sodium borohydride in alcoholic solution, we found $NaBH_4$−copper(II) acetylacetonate (*26*) to be the most effective and a mild catalyst for the reduction of nitro groups on these tyrosine derivatives. This reaction occurred nearly quantitatively as judged using TLC.

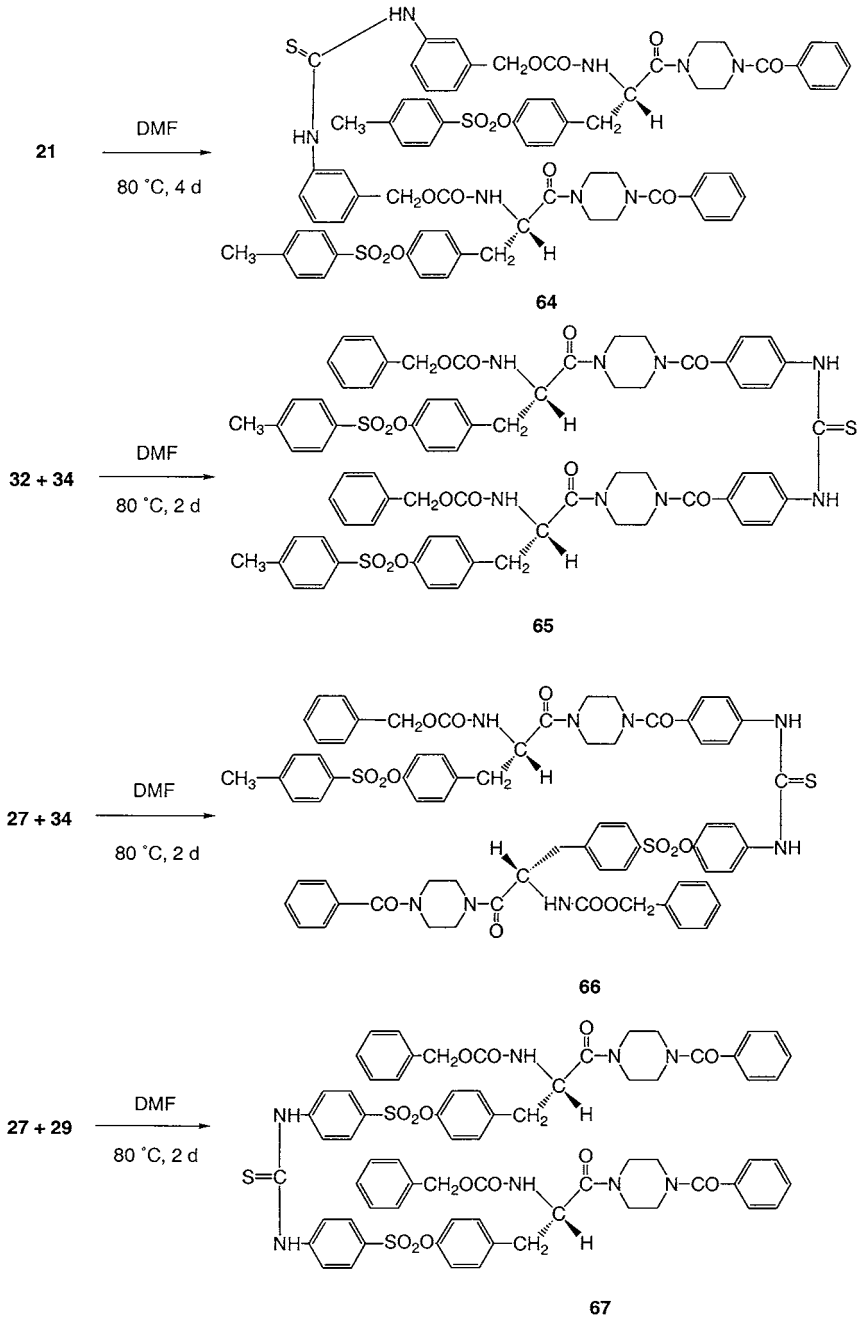
Four dimer permutations (**64**−**67**) were created by coupling each of the isothiocyanate derivatives to either the precursor amine or to other amine congeners (Scheme 7). These coupling reactions required elevated temperature and were carried out in moderate yield.

Biological Activity. The effects of substitution at R_1, R_2, and R_3 on inhibition of P2X$_7$ receptor-mediated ion flux (Table 1) were compared. Experiments were performed using adherent HEK293 cells stably transfected with cDNA encoding the human P2X$_7$ receptor. Cells were preincubated with each antagonist at a fixed concentration (3 μM) prior to stimulation for 10 min with 3 mM ATP. The percent inhibition of the K^+ release was the parameter used to indicate antagonist function.

The three structural regions for conjugation were compared in their effects on biological potency. Among *N*-cinnamoyl derivatives, more favorable potency was associated with the unsubstituted derivative **9** than with methoxy substitution. Multiple methoxy substitution, e.g., **7**, eliminated the antagonistic effect at the P2X$_7$ receptor. The 4-nitro substitution of the cinnamoyl group also reduced potency (cf. **14** vs **13**). The Cbz derivative **15** was a potent antagonist of the human P2X$_7$ receptor, and 4- or 3-nitro substitution preserved that property, as in **18** and **19**. However, reduction and acetylation of the 3-nitro group, **20a** and **20b**, reduced potency. The corresponding isothiocyanate **21** and amine congener **22** were inactive or weakly potent, respectively.

Nitro subsitution of the tyrosyl side chain (R_2 substituent), at the 3- or 4-position, as in benzoylpiperazine (at R_3) derivatives **26a** and **26b**, respectively, maintained potency at the human P2X$_7$ receptor. There was no difference in biological potency between 3- and 4-nitro derivatives. The corresponding t-Boc derivatives (at the R_3 position, e.g., **23a** and **23b**) similarly antagonized the human P2X$_7$ receptor. This antagonism was preserved when the 4-nitro group was reduced and acetylated (e.g. **24** and **25**; **27** and **28**). A primary amine congener linked at the R_2 4-position, **30**, was a potent antagonist of the

Scheme 7. Dimerization of P2X$_7$ Receptor Antagonists through Formation of Thiourea Linkages



human P2X$_7$ receptor. The corresponding isothiocyanate **29** displayed considerable potency as a P2X$_7$ receptor antagonist and warranted examination as an irreversible receptor inhibitor.

For the R_3 substituent, 3- or 4-nitrobenzoyl subsitution, **31a** and **31b**, respectively, preserved antagonistic properties at the human P2X$_7$ receptor. As for the R_2 substituent, there was no difference in biological potency between 3- and 4-nitro derivatives. The P2X$_7$ receptor antagonism was increased when the 4-nitro group was reduced but diminished upon acetylation (e.g., **32** and **33**). An isothiocyanate **34** only weakly antagonized the effects of ATP at the P2X$_7$ receptor. A primary amine congener containing four methylenes linked at the R_2 4-position, **35b**, was a potent antagonist of the human P2X$_7$ receptor, while a shorter homologue **35a** (two methylenes) antagonized weakly.

Full concentration−response curves provided a more precise means of comparison among some selected, potent compounds, including the 3-nitro-Cbz derivative **18**, a 4-nitrotoluenesulfonate **26b**, a primary amine congener **30**, and 4-aminobenzoyl derivative **32** (Figure 1). Compounds **18** and **26b**, were roughly as potent as **1** as P2X$_7$ receptor antagonists, and appeared to have IC_{50} values in the 0.1 μM range. The other compounds appeared to have IC_{50} values in the 0.3 μM range (**30**) or > 0.3 μM (**32**).

Among antagonist dimers, only the R_2-R_3- and R_2-R_2-linked dimers, **66** and **67**, respectively, displayed significant antagonistic properties at the P2X$_7$ receptor.

DISCUSSION

The binding site for KN-62, **1**, resides within the first 335 residues of the human P2X$_7$ receptor, likely within the large extracellular loop (*13, 21*). While it is not feasible to model this binding interaction, due to lack of a high-resolution template for this ion channel and

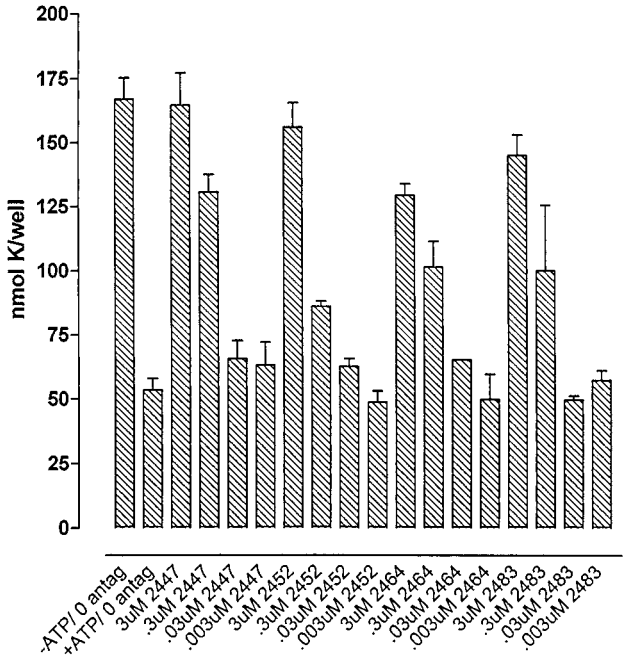


Figure 1. Effects of tyrosyl derivatives on $P2X_7$ receptor-activation in $hP2X_7$−HEK cells. Cells were preincubated with or without the indicated concentrations of selected antagonists (**26b** MRS2447; **32** MRS2452; **18** MRS2464; and **30** MRS2483) prior to stimulation with 3 mM ATP. Data points represent the mean (± SD) K^+ contents from triplicate wells in a single experiment. IC_{50} values mentioned in the text are rough estimates from visual inspection of the concentration−response relationships. Hill coefficients were not determined, since previous studies have shown that the lead compound (KN-62) represses $P2X_7$ receptor function via complex mechanisms that are not readily amenable to standard ligand-binding analyses.

uncertainty about the oligomeric nature of the channel (*27*), chemical probes of the receptor may be very useful in studying the structure. The stoichiometry of association of subunits in P2X receptors has been studied suggesting a trimeric organization (*2*, *27*, *28*), but little is known about the correspondence of antagonist binding sites to the overall oligomeric ion channel structure. By functionalizing derivatives (*17*) of the widely used $P2X_7$ antagonist KN-62 it may be possible to locate the binding site (in conjunction with mutagenesis studies). Mutagenesis studies of the $P2X_7$ receptor aimed at structural and functional elucidation have already been carried out (*29*, *32*). Peptide mapping of receptor digests (*30*) using electrophoretic or mass spectroscopic methods following affinity labeling of the receptor would also be useful in this regard.

Since there may be multiple binding sites on the $P2X_7$ receptor homomer, it may be possible to detect the preferred orientation of covalently linked antagonist dimers that may occupy two distinct binding sites, based on divergent biological potencies for a variety of linkage combinations. Since the dimerization of the antagonists in the present study through the tyrosyl side chain, alone, provided retention of antagonist properties, it is likely that this region of the antagonist occurs in a portion of the binding site that is somewhat relaxed in its steric requirements. Whether the dimers **66** and/or **67** are able to bridge two putative binding sites on the $P2X_7$ homomer will be the object of further studies. The species selectivity of the new functionalized congeners also should be investigated, since differences have been noted for KN-62 (*33*).

Receptor ligands that bridge two subunits of a multimeric receptor may also potentially be of use for tissue selectivity, if there are differences between tissues in the organization of subunits. Such differences have been demonstrated for native $P2X_7$ receptors (*34*), which in peritoneal macrophage and bone marrow cells exist as a strongly bound multimeric complex, and in brain glia and/or astrocytes appear to form only as monomeric subunits.

In conclusion, we have systematically varied substituent groups in a series of tyrosyl analogues, resulting in analogues, among which are antagonists that are equipotent to the lead structure **1** and also contain chemical functional groups for linking purposes. Such functionalized congeners have been used effectively for the structural investigations of other purine receptors (*18*, *19*, *31*), including adenosine A_1, A_{2A}, and A_3 receptors. Suitable sites and chemical approaches to cross-linking these antagonists have been found on the tyrosyl side chain (R_2) and on the Cα-substituent (R_3). The more versatile region for functionalization appears to be the R_2 substituent, since even dimerization through this substituent preserves the receptor binding property. We have prepared several amine functionalized congeners, that may potentially be conjugated to fluorescent probes for receptor characterization, or immobilized on a solid support for isolation of the receptor by affinity chromatography. Among P2X receptors, only the $P2X_1$ subtype has so far been isolated in this manner (*35*).

ACKNOWLEDGMENT

We thank Gilead Sciences (Foster City, CA) for financial support to W. Z. Chen. This work was supported by NIH grant GM36387 to G.D. We thank Mr. Noel Whittaker and Mr. Victor Livengood for determination of mass spectra.

LITERATURE CITED

(1) Fredholm, B. B., Abbracchio, M. P., Burnstock, G., Dubyak, G. R., Harden, T. K., Jacobson, K. A., Schwabe, U., and Williams, M. (1997) Toward a revised nomenclature for P1 and P2 receptors. *Trends. Pharm. Sci. 18*, 79−82.

(2) Khakh, B. S., Burnstock, G., Kennedy, C., King, B. F., North, R. A., Seguela, P., Voigt, M., and Humphrey, P. P. (2001) International union of pharmacology. XXIV. Current status of the nomenclature and properties of P2X receptors and their subunits. *Pharmacol. Rev. 53*, 107−118.

(3) King, B. F. (1998) *Cardiovascular Biology of Purines*, Ch. 10, pp 159−186, Kluwer Academic Publishers, Norwell, MA.

(4) Collo, G., Neidhart, S., Kawashima, E., Kosco-Vilbois, M., North, R. A., and Buell, G. (1997) Tissue distribution of the P2 × 7 receptor. *Neuropharmacology 36*, 1277−1283.

(5) Ferrari, D., Stroh, C., and Schulze-Osthoff K. (1999) $P2X_7$/P_{2Z} purinoreceptor-mediated activation of transcription factor NFAT in microglial cells. *J. Biol. Chem. 274*, 13205−13210.

(6) Humphreys, B. D., Rice, J., Kertesy, S. B., and Dubyak, G. R. (2000) Stress-activated protein kinase/JNK activation and apoptotic induction by the macrophage $P2X_7$ nucleotide receptor. *J. Biol. Chem 275*, 26792−26798.

(7) Gargett, C. E., and Wiley, J. S. (1997) The isoquinoline derivative KN-62 a potent antagonist of the P2Z-receptor of human lymphocytes. *Br. J. Pharmacol. 120*, 1483−1490.

(8) Ferrari, D., La Sala, A., Chiozzi, P., Morelli, A., Falzoni, S., Girolomoni, G., Idzko, M., Dichmann, S., Norgauer, J., and Di Virgilio, F. (2000) The P2 purinergic receptors of human dendritic cells: identification and coupling to cytokine release. *FASEB J. 14*, 2466−2476.

(9) Solle, M., Labasi, J., Perregaux, D. G., Stam, E., Petrushova, N., Koller, B. H., Griffiths, R. J., and Gabel, C. A. (2001) Altered Cytokine Production in Mice Lacking $P2X_7$ Receptors. *J. Biol. Chem 276*, 125−132.

(10) Turner, J. T., Landon, L. A., Gibbons, S. J., and Talamo, B. R. (1999) Salivary gland P2 nucleotide receptors. *Crit. Rev. Oral. Biol. Med. 10,* 210−224.
(11) Hu, Y., Fisette, P. L., Denlinger, L. C., Guadarrama, A. G., Sommer, J. A., Proctor, R. A., and Bertics, P. J. (1998) Purinergic receptor modulation of lipopolysaccharide signaling and inducible nitric-oxide synthase expression in RAW 264.7 macrophages. *J. Biol. Chem. 273,* 27170−27175.
(12) Wiley, S., Gargett, C. E., Zhang, W., Snook, M. B., and Jamieson, G. P. (1998) Partial agonists and antagonists reveal a second permeability state of human lymphocyte P_{2Z}/$P2X_7$ channel. *Am. J. Physiol. 275,* C1224−C1231.
(13) Rassendren, F., Buell, G. N., Virginio, C., Collo, G., North, R. A., and Surprenant, A. (1997) The permeabilizing ATP receptor, $P2X_7$. Cloning and expression of a human cDNA. *J. Biol. Chem. 272,* 5482−5486.
(14) Bianchi, B. R., Lynch, K. J., Touma, E., Niforatos, W., Burgard, E. C., Alexander K. M., Park, H. S., Yu, H., Metzger, R., Kowaluk, E., Jarvis, M. F., and van Biesen, T. (1999) Pharmacological characterization of recombinant human and rat P2X receptor subtypes. *Eur. J. Pharmacol. 376,* 127−138.
(15) Erb, L., Lustig, K. D., Ahmed, A. H., Gonzalez, F. A., and Weisman, G. A. (1990) Covalent incorporation of 3′-O-(4-benzoyl)benzoyl-ATP into a P2 purinoceptor in transformed mouse fibroblasts. *J. Biol. Chem. 265,* 7424−7431.
(16) Tokumitsu, H., Chijiwa, T., Hagiwara, M., Mizutani, A., Terasawa, M., and Hidaka, H. (1990) KN-62, 1-[N,O-bis(5-isoquinolinesulfonyl)-N-methyl-L-tyrosyl]-4-phenylpiperazine, a specific inhibitor of Ca2+/calmodulin-dependent protein kinase II. *J. Biol. Chem. 265,* 4315−4320.
(17) Ravi, R. G., Kertesy, S. B., Dubyak, G. R., and Jacobson, K. A. (2001) Potent $P2X_7$ receptor antagonists: Tyrosyl derivatives synthesized using a sequential parallel synthetic approach. *Drug Devel. Res. 54,* 75−87.
(18) Jacobson, K. A., Ukena, D., Padgett, W., Kirk, K. L., and Daly, J. W. (1987) Molecular probes for extracellular adenosine receptors. *Biochem. Pharmacol. 36,* 1697−1707.
(19) Boring, D. L., Ji, X. D., Zimmet, J., Taylor, K. E., Stiles, G. L., and Jacobson, K. A. (1991) Trifunctional agents as a design strategy for tailoring ligand properties: Irreversible inhibitors of A_1 adenosine receptors. *Bioconjugate Chem. 2,* 77−88.
(20) Karton, Y., Baumgold, J., Handen, J. S., and Jacobson, K. A., (1992) Molecular probes for muscarinic receptors: Derivatives of the M_1-antagonist telenzepine, *Bioconjugate Chem. 3,* 234−240.
(21) Chessell, I. P., Simon, J., Hibell, A. D., Michel, A. D., Barnard, E. A., and Humphrey, P. P. A. (1998) Cloning and functional characterization of the mouse $P2X_7$ receptor. *FEBS Lett. 439,* 26−30.
(22) Carter, H. E., Frank, R. L., and Johnston, H. W. (1955) *Organic Synthesis* (E. D. Horning, Ed.), New York: Wiley Press, Coll. Vol. III, p 167.
(23) Staab, H. A., and Benz, W. (1961) Darstellung von isocyanaten. *Angew. Chem. 73,* 66.
(24) Yu, C., Liu, B., and Hu, L. (2001) Samarium (0) and 1, 1′-dioctyl-4, 4′-bipyridinium dibromide: a novel electron-transfer system for the chemoselective reduction of aromatic nitro groups. *J. Org. Chem. 66,* 919−924.
(25) Suzuki, H., and Hanazaki, Y. (1986) Titanium-mediated reduction of nitrobenzenes and benzil with dialkyl telluride. *Chem. Lett. 4,* 549−550.
(26) Hanaya, K., Muramatsu, T., and Kudo, K. (1979) Reduction of aromatic nitro-compounds to amines with sodium borohydride-copper (II) acetylacetonate. *J. Chem. Soc., Perkin Trans. 1 10,* 2409−2410.
(27) Torres, G. E., Egan, T. M., and Voigt, M. M. (1999) Hetero-oligomeric assembly of P2X receptor subunits. Specificities exist with regard to possible partners. *J. Biol. Chem. 274,* 6653−6659.
(28) Nicke, A., Baumert, H. G., Rettinger, J., Eichele, A., Lambrecht, G., Mutschler, E., and Schmalzing, G. (1998) $P2X_1$ and $P2X_3$ receptors form stable trimers: a novel structural motif of ligand-gated ion channels. *EMBO J. 17,* 3016−3028.
(29) Kim, M., Jiang, L. H., Wilson, H. L., North, R. A., and Surprenant, A. (2001) Proteomic and functional evidence for a $P2X_7$ receptor receptor signaling complex. *EMBO J. 20,* 6347−6358.
(30) Kennedy, A. P., Mangum, K. C., Linden, J., and Wells, J. N. (1996) Covalent modification of transmembrane span III of the A_1 adenosine receptor with an antagonist photoaffinity probe. *Mol Pharmacol. 50,* 789−798.
(31) Barrington, W. W., Jacobson, K. A., Hutchison, A. J., Williams, M., and Stiles, G. L. (1989) Identification of the A_2 adenosine receptor binding subunit by photoaffinity cross-linking. *Proc. Natl. Acad. Sci. U.S.A. 86,* 6572−6576.
(32) Klapperstuck, M., Buttner, C., Schmalzing, G., and Markwardt, F. (2001) Functional evidence of distinct ATP activation sites at the human $P2X_7$ receptor. *J. Physiol. 534,* 25−35.
(33) Humphreys, B. D., Virginio, C., Surprenant, A., Rice, J., and Dubyak, G. R. (1998) Isoquinolines as antagonists of the $P2X_7$ nucleotide receptor: high selectivity for the human versus rat receptor homologues. *Mol. Pharmacol. 54,* 22−32.
(34) Kim, M., Spelta, V., Sim, J., North, RA., and Surprenant A. (2001) Differential assembly of rat purinergic $P2X_7$ receptor in immune cells of the brain and periphery. *J. Biol. Chem. 276,* 23262−23267.
(35) Chen, L., Hardwick, J. P., McPhie, P., Sitkovsky, M., and Jacobson, K. A. (2001) Purification and recognition of recombinant mouse $P2X_1$ receptors expressed in a baculovirus system, *Drug Devel. Res. 51,* 7−19.

BC020025I

Chemical Synthesis and Characterization of Conjugates of a Novel Catechol-*O*-methyltransferase Inhibitor

David A. Learmonth* and Ana P. Freitas

Laboratory of Chemistry, Department of Research and Development, BIAL, 4745-457 S. Mamede do Coronado, Portugal. Received April 19, 2002; Revised Manuscript Received July 1, 2002

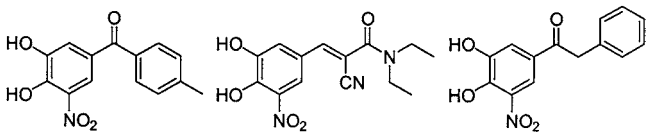
BIA 3-202, 1-(3,4-dihydroxy-5-nitrophenyl)-2-phenylethanone **3**, is a novel, reversible, and tight-binding peripheral inhibitor of the enzyme catechol-*O*-methyltransferase (COMT), which is currently under clinical evaluation for the treatment of Parkinson's disease as an adjunct to current L-Dopa/peripheral decarboxylase inhibitor therapy. Chemically pure, well-characterized reference standards of conjugates of **3** were required for investigation of the routes of metabolism in several animal species (including humans) and for pharmacokinetic studies. The lack of suitable literature precedents for efficient, regioselective synthesis of nitrocatechol conjugate metabolites prompted us to develop efficient and highly selective chemical preparations of *O*-glucuronide and *O*-sulfate conjugates of **3** such that multigram quantities of excellent purity can now be conveniently synthesized. It is anticipated that these procedures could be applied to the synthesis of conjugates of other COMT inhibitors, also based on the 3-nitrocatechol pharmacophore.

INTRODUCTION

Catechol-*O*-methyltransferase is a magnesium-dependent enzyme, widely distributed in mammalian tissues, which is now known to play a fundamental role in the inactivation of endogenous catechols (*1*) and detoxification of xenobiotic catechol-based structures (*2*), namely, by catalyzing the transfer of a methyl group from *S*-adenosyl-L-methionine to a hydroxyl group of the catechol (*3*). Potential inhibitors of COMT have aroused great interest from medicinal chemists, based on the premise that COMT inhibition could enhance the bioavailability and thus prolong the therapeutic effect of L-Dopa (3,4-dihydroxy-L-phenylalanine) in patients suffering from Parkinson's disease (*4*), by preventing O-methylation to 3-*O*-methyldopa (3-OMD).

Of the so-called second-generation COMT inhibitors, structures containing the 3-nitrocatechol motif were discovered to be highly potent. Two of these in particular, tolcapone **1** and entacapone **2** (Figure 1), were found to have inhibition constants (K_i) in the low nanomolar range and which were additionally poor substrates for the enzyme (*5*, *6*). **1** is characterized as an equipotent inhibitor of both central and peripheral COMT, while **2** is a purely peripheral inhibitor. Both have entered into clinical practice, although due to liver toxicity concerns **1** was recently withdrawn. It is thought that peripheral COMT inhibitors may be more effective in the treatment of Parkinson's disease, since L-Dopa undergoes its most extensive metabolic breakdown in the periphery. Due, however, to the very short in vivo half-life of **2**, we were encouraged to investigate the possibility of developing a potent and long-acting inhibitor of peripheral COMT, which eventually led to the discovery of BIA 3-202, **3** (*7*).

The metabolic profile and excretion of **1** have been reported (*8*), but no synthetic details of metabolites were given. Conversely, enzyme-assisted synthesis of 3-*O*-glucuronide conjugates of **2** has been described (*9*), this procedure allowing the production of only small milligram quantities of generally average purity. The lack of literature precedent on nitrocatechol metabolism in general and the synthesis of COMT inhibitor metabolites in particular prompted us to develop efficient chemical methodologies for the regioselective synthesis of highly pure, multigram quantities of conjugates of **3** as standards for identification of metabolic products.



1 **2** **3**

Figure 1. Chemical structures of tolcapone (**1**), entacapone (**2**), and BIA 3-202 (**3**).

EXPERIMENTAL PROCEDURES

Chemistry. Melting points were measured in open capillary tubes on an Electrothermal model 9100 hot stage apparatus and are uncorrected. NMR spectra were recorded on a Bruker Avance DPX (400 MHz) spectrometer with solvent used as an internal standard, and data are reported in the following order: chemical shift (parts per million), multiplicity (s, singlet; d, doublet; t, triplet; m, multiplet; and br, broad), number of protons, approximate coupling constant in hertz, and assignment of a signal. IR spectra were recorded with a Bomem Hartmann & Braun MB Series FTIR spectrometer using KBr tablets. Analytical HPLC was performed on a Gilson system equipped with a model 305 pump, a model 117 UV detector, and LiChrospher 100 RP-18 EcoCART 125-3 Cartridges (Merck) in combination with acetonitrile/water mixtures. Reverse-phase preparative HPLC was carried out on an automated Gilson system equipped with

* To whom correspondence should be addressed: Department of Research and Development, BIAL, 4745-457 S. Mamede do Coronado, Portugal. Telephone: 351-22-9866100. Fax: 351-22-9866192. E-mail: david.learmonth@bial.com.

10.1021/bc0200327 CCC: $22.00 © 2002 American Chemical Society
Published on Web 08/29/2002

a model 321 pump, a model 155 UV−vis detector, a model 215 liquid handler, and a Waters SymmetryPrep (RP-18, 7 μm) preparative column (19 mm × 150 mm) in combination with acetonitrile/water mixtures. Analytical TLC was performed on precoated silica gel plates (either Merck 60 Kieselgel F_{254} or Merck RP-18 F_{254s}) and visualized with UV light. Preparative chromatography was carried out on Merck 60 Kieselgel (0.063−0.2 mm). Elemental analyses were performed on a Fisons EA 1110 CHNS instrument, and all analyses are consistent with theoretical values to within ±0.4% unless otherwise indicated. Solvents and reagents were purchased from Aldrich, E. Merck, and Fluka.

1-(3-Hydroxy-4-methoxy-5-nitrophenyl)-2-phenylethanone (5). A red suspension of **3** (1.0 g, 3.66 mmol), potassium carbonate (1.77 g, 12.82 mmol), and dimethyl sulfate (1.38 g, 10.98 mmol) in dimethylformamide (DMF, 10 mL) was stirred at 80 °C for 1 h and then allowed to cool to room temperature. The inorganic material was removed by filtration, and the filter cake was washed with DMF (2 mL). The combined filtrate was poured onto water (50 mL) and extracted with ethyl acetate (3 × 30 mL). The combined organic extracts were washed with water (20 mL) and brine (20 mL), then dried over anhydrous sodium sulfate, and filtered. Evaporation (50 °C, water aspirator pressure) afforded a red oil which was chromatographed on silica gel (2:1 petroleum ether/ethyl acetate) to give the major product as an off-white solid. Recrystallization (dichloromethane/heptane) gave the title product as white crystals (0.26 g, 25%): mp 121−123 °C; IR (KBr) 3361 (OH), 1681 (C═O), 1539 cm^{-1} (NO2); ^{1}H NMR (DMSO-d_6) δ 8.10 (d, 1H, J = 2.1 Hz, H-6), 7.82 (d, 1H, J = 2.1 Hz, H-2), 7.4−7.2 (m, 5H, Ph), 6.26 (br, 1H, 3-OH), 4.25 (s, 2H, CH_2), 4.01 (s, 3H, 4-OCH_3); ^{13}C NMR (DMSO-d_6) δ 195.3, 151.3, 145.4, 142.9, 134.0, 132.7, 129.9, 129.5, 127.9, 120.4, 118.1, 63.2, 46.0. Anal. ($C_{15}H_{13}NO_5$) C, H, N.

1-(3,4-Dimethoxy-5-nitrophenyl)-2-phenylethanone (6). A stirred suspension of **3** (0.50 g, 1.83 mmol), potassium carbonate (0.89 g, 6.41 mmol), and dimethyl sulfate (0.69 g, 5.48 mmol) in acetone (10 mL) was heated at reflux for 2 h and then cooled to room temperature. The inorganic material was removed by filtration and, the filter cake was washed with acetone (3 mL). The combined filtrate was evaporated (40 °C, water aspirator pressure) to leave a yellow oil that solidified on standing. Recrystallization (96% ethanol) afforded pale yellow crystals (0.47 g, 86%): mp 81−82 °C; IR (KBr) 1697 (C═O), 1533 cm^{-1} (NO_2); ^{1}H NMR (DMSO-d_6) δ 8.01 (d, 1H, J = 2.1 Hz, H-6), 7.75 (d, 1H, J = 2.1 Hz, H-2), 7.4−7.25 (m, 5H, Ph), 4.28 (s, 2H, CH_2), 4.05 (s, 3H, 4-OCH_3), 3.96 (s, 3H, 3-OCH_3); ^{13}C NMR (DMSO-d_6) δ 195.3, 154.8, 147.4, 144.8, 134.3, 132.1, 129.9, 129.5, 127.8, 117.8, 115.5, 62.7, 57.2, 45.9. Anal. ($C_{16}H_{15}NO_5$) C, H, N.

1-[3-Hydroxy-5-nitro(4-*O*-2,3,4-triacetyl-β-D-glucuronopyranosidophenyl)]-2-phenylethanone Methyl Ester (8). To a stirred suspension of **3** (1.50 g, 5.49 mmol) and 1α-bromo sugar **7** (1.76 g, 4.63 mmol) in acetonitrile (20 mL) at room temperature was added silver(I) oxide (1.53 g, 6.62 mmol) in one portion. The resulting suspension was stirred in the dark for 1 h, and then filtered through a short Celite pad. The filter cake was washed with ethyl acetate (50 mL), and the combined filtrate was washed with water (3 × 50 mL) and brine (50 mL) and then filtered through Celite again. The organic phase was dried over anhydrous sodium sulfate, filtered, and evaporated (40 °C, water aspirator pressure) to leave a dark brown oil. Chromatography over silica gel (1:1 petroleum ether/ethyl acetate) afforded the major product as a pale orange solid that was recrystallized (MeOH) to give beige crystals (1.44 g, 53%): mp 153−155 °C; IR (KBr) 3400 (OH), 1755 (C═O, ester), 1690 (C═O, ketone), 1544 cm^{-1} (NO_2); ^{1}H NMR (DMSO-d_6) δ 11.1 (vbr, 1H, 3-OH), 7.97 (d, 1H, J = 2.1 Hz, H-6), 7.73 (d, 1H, J = 2.1 Hz, H-2), 7.4−7.2 (m, 5H, Ph), 5.54 (d, 1H, J = 7.9 Hz, H-1′), 5.45 (t, 1H, J = 9.6 Hz, H-3′), 5.03 (dd, 1H, J = 7.9 and 9.6 Hz, H-2′), 5.00 (t, 1H, J = 9.7 Hz, H-4′), 4.48 (d, 1H, J = 9.9 Hz, H-5′), 4.38 (s, 2H, CH_2), 3.60 (s, 3H, OCH_3), 2.03 (s, 3H, $COCH_3$), 1.99 (s, 3H, $COCH_3$), 1.97 (s, 3H, $COCH_3$); ^{13}C NMR (DMSO-d_6) δ 196.4, 170.6, 170.3, 170.0, 167.7, 152.1, 146.6, 139.8, 135.6, 134.2, 130.8, 129.4, 127.7, 120.3, 115.6, 100.8, 71.9, 71.8, 71.8, 69.8, 53.5, 45.5, 21.4, 21.3, 21.2. Anal. ($C_{27}H_{27}NO_{14}$·0.5H_2O) C, H, N.

1-(4-*O*-β-D-Glucuronopyranosido-3-hydroxy-5-nitrophenyl)-2-phenylethanone (9). To a cooled (ice bath) and stirred suspension of the glucuronate **8** (1.40 g, 2.38 mmol) in methanol (30 mL) was added dropwise an aqueous 1 N sodium hydroxide solution (24 mL, 24 mmol). The resulting red mixture was stirred in the cold for 30 min and then left at room temperature for 30 min. A small amount of undissolved material was removed by filtration, and the filtrate was added to cold water containing Amberlyst 15 ion-exchange resin so that the pH reached 2. The mixture was filtered and the resin washed with methanol and water (10 mL, 1:1). The filtrate was evaporated (50 °C, water aspirator pressure) and the residue dried over phosphorus pentoxide at high vacuum to give the title product as an amorphous yellow solid (0.99 g, 93%): mp 84−88 °C; IR (KBr) 3386 (broad, OH), 1733 (C═O, acid), 1693 (C═O, ketone), 1541 cm^{-1} (NO_2); ^{1}H NMR (DMSO-d_6) δ 7.94 (d, 1H, J = 2.1 Hz, H-6), 7.73 (d, 1H, J = 2.1 Hz, H-2), 7.4−7.2 (m, 5H, Ph), 5.2 (vbr, 1H, 3-OH), 5.13 (d, 1H, J = 7.5 Hz, H-1′), 4.38 (s, 2H, CH_2), 3.6 (d, 1H, J = 9.7 Hz, H-5′), 3.5−3.15 (m, 3H, H-2′, H-3′, H-4′); ^{13}C NMR (DMSO-d_6) δ 196.3, 170.7, 152.0, 146.7, 140.7, 135.7, 133.4, 130.8, 129.3, 127.6, 120.4, 115.6, 103.8, 77.0, 76.6, 74.5, 72.2, 45.4. Anal. ($C_{20}H_{19}NO_{11}$·1.5H_2O) C, H, N.

1-[4-Hydroxy-5-nitro(3-*O*-2,3,4-triacetyl-β-D-glucuronopyranosidophenyl)]-2-phenylethanone Methyl Ester (11). To a stirred solution of **3** (3.74 g, 13.7 mmol) and trichloroacetimidate **10** (6.9 g, 14.38 mmol) in dichloromethane (130 mL) at room temperature was added dropwise boron trifluoride diethyl etherate (2.91 g, 20.55 mmol). The resulting mixture was stirred for 2 h and then poured onto water (100 mL). A small amount of unreacted **3** precipitated and was removed by filtration. The organic phase was separated and washed with a cold saturated aqueous sodium bicarbonate solution (3 × 100 mL), water (100 mL), and brine (100 mL), then dried over anhydrous sodium sulfate, filtered, and evaporated (40 °C, water aspirator pressure), leaving a yellow foam. Recrystallization (ethyl acetate/petroleum ether) afforded pale yellow crystals (4.50 g, 56%): mp 181−182 °C; IR (KBr) 3437 (OH), 1752 (C═O, ester), 1678 (C═O, ketone), 1549 cm^{-1} (NO_2); ^{1}H NMR (DMSO-d_6) δ 8.34 (d, 1H, J = 2.1 Hz, H-6), 7.82 (d, 1H, J = 2.1 Hz, H-2), 7.35−7.2 (m, 5H, Ph), 5.78 (d, 1H, J = 7.5 Hz, H-1′), 5.45 (t, 1H, J = 9.6 Hz, H-3′), 5.17 (dd, 1H, J = 7.7 and 9.4 Hz, H-2′), 5.11 (t, 1H, J = 9.7 Hz, H-4′), 4.70 (d, 1H, J = 9.9 Hz, H-5′), 4.36 (d, 1H, J = 15.9 Hz, CH_2), 4.28 (d, 1H, J = 15.9 Hz, CH_2), 3.61 (s, 3H, OCH_3), 1.99 (s, 3H, $COCH_3$), 1.98 (s, 3H, $COCH_3$), 1.96 (s, 3H, $COCH_3$); ^{13}C NMR (DMSO-d_6) δ 195.4, 170.6, 170.4, 170.1, 168.2, 151.5, 148.2, 138.5, 136.1, 130.6, 129.4, 127.6, 124.9, 122.5, 120.5, 99.0, 72.1, 72.1, 71.6, 69.7, 53.6, 45.1, 21.5, 21.3, 21.2. Anal. ($C_{27}H_{27}NO_{14}$·H_2O) C, H, N.

1-(3-*O*-*β*-D-Glucuronopyranosido-4-hydroxy-5-nitrophenyl)-2-phenylethanone (12). Hydrolysis of glucuronate **11** (1.40 g, 2.38 mmol) was carried out as described for preparation of **9** above; the product was obtained as an amorphous yellow solid (1.02 g, 96%): mp 118−122 °C; IR (KBr) 3393 (broad, OH), 1734 (C=O, acid), 1686 (C=O, ketone), 1546 cm^{-1} (NO_2); ^1H NMR (DMSO-d_6) δ 11.1 (vbr, 1H, 4-OH), 8.25 (d, 1H, J = 1.9 Hz, H-6), 7.93 (d, 1H, J = 1.9 Hz, H-2), 7.4−7.1 (m, 5H, Ph), 5.20 (d, 1H, J = 7.3 Hz, H-1′), 4.44 (d, 1H, J = 16.0 Hz, CH_2), 4.29 (d, 1H, J = 16.0 Hz, CH_2), 4.04 (d, 1H, J = 9.7 Hz, H-5′), 3.5−3.3 (m, 3H, H-2′, H-3′, H-4′); ^{13}C NMR (DMSO-d_6) δ 195.8, 171.0, 147.7, 147.3, 138.6, 135.8, 130.7, 129.4, 127.6, 127.6, 120.3, 119.5, 102.5, 76.5, 76.0, 73.8, 72.3, 45.3. Anal. ($C_{20}H_{19}NO_{11}$·1.5H_2O) C, H, N.

1,2-Dioxo-1-[3-hydroxy-5-nitro(4-*O*-2,3,4-triacetyl-*β*-D-glucuronopyranosidophenyl)]-2-phenylethane Methyl Ester (14). A stirred suspension of dione **13** (3.43 g, 11.9 mmol) and 1α-bromo sugar **7** (4.73 g, 11.9 mmol) in acetonitrile (70 mL) at room temperature was treated with silver(I) oxide (2.76 g, 11.9 mmol). The resulting suspension was stirred in the dark, and workup as described for the preparation of **8** above afforded the crude product as a brown foam. Chromatography over silica gel (2:1 to 1:1 petroleum ether/ethyl acetate) gave the major product as a yellow oil that was crystallized from dichloromethane/petroleum ether to give yellowish crystals (3.91 g, 54%): mp 117−119 °C; IR (KBr) 3384 (OH), 1756 (C=O, ester), 1678 (C=O, ketone), 1546 cm^{-1} (NO_2); ^1H NMR (DMSO-d_6) δ 11.39 (br, 1H, 3-OH), 7.96 (d, 2H, *o*-Ph), 7.81 (d, 1H, J = 2.1 Hz, H-6), 7.8 (t, 1H, *p*-Ph), 7.71 (d, 1H, J = 2.1 Hz, H-2), 7.64 (t, 2H, *m*-Ph), 5.64 (d, 1H, J = 8.0 Hz, H-1′), 5.46 (t, 1H, J = 9.7 Hz, H-3′), 5.04 (dd, 1H, J = 7.9 and 9.7 Hz, H-2′), 5.00 (t, 1H, J = 9.9 Hz, H-4′), 4.50 (d, 1H, J = 10.1 Hz, H-5′), 3.60 (s, 3H, OCH_3), 2.02 (s, 3H, $COCH_3$), 1.99 (s, 3H, $COCH_3$), 1.98 (s, 3H, $COCH_3$); ^{13}C NMR (DMSO-d_6) δ 194.1, 192.5, 170.6, 170.3, 170.0, 167.7, 152.6, 146.8, 141.3, 136.7, 132.9, 131.0, 130.4, 129.8, 121.3, 116.8, 100.6, 72.0, 71.8, 71.8, 69.8, 53.5, 21.4, 21.3, 21.2. Anal. ($C_{27}H_{25}NO_{15}$) C, H, N.

1,2-Dioxo-1-[4-hydroxy-5-nitro(3-*O*-2,3,4-triacetyl-*β*-D-glucuronopyranosidophenyl)]-2-phenylethane Methyl Ester (15). To a stirred solution of dione **13** (0.50 g, 1.74 mmol) and trichloroacetimidate **10** (1.25 g, 2.61 mmol) in dichloromethane (20 mL) at room temperature was added dropwise boron trifluoride diethyl etherate (0.37 g, 2.61 mmol). The resulting mixture was stirred for 2 h followed by workup as described for **11** above; recrystallization of the crude product from diethyl ether afforded orange crystals (0.56 g, 53%): mp 181−183 °C; IR (KBr) 3437 (OH), 1756 (C=O, ester), 1675 (C=O, ketone), 1555 cm^{-1} (NO_2); ^1H NMR (DMSO-d_6) δ 7.97 (d, 1H, J = 2.1 Hz, H-6), 7.90 (d, 2H, *o*-Ph), 7.77 (t, 1H, *p*-Ph), 7.61 (t, 2H, *m*-Ph), 7.47 (d, 1H, J = 2.1 Hz, H-2), 5.65 (d, 1H, J = 7.9 Hz, H-1′), 5.45 (t, 1H, J = 9.6 Hz, H-3′), 5.09 (dd, 1H, J = 7.7 and 9.6 Hz, H-2′), 5.06 (t, 1H, J = 9.7 Hz, H-4′), 4.62 (d, 1H, J = 9.7 Hz, H-5′), 3.62 (s, 3H, OCH_3), 2.01 (s, 3H, $COCH_3$), 2.00 (s, 3H, $COCH_3$), 1.99 (s, 3H, $COCH_3$); ^{13}C NMR (DMSO-d_6) δ 196.0, 191.3, 170.5, 170.4, 170.2, 168.3, 138.6, 136.1, 133.9, 130.5, 130.4, 127.9, 118.4, 99.0, 72.1, 72.0, 71.8, 69.9, 53.6, 21.5, 21.4, 21.3. Anal. ($C_{27}H_{25}NO_{15}$·3H_2O) C, H, N.

1-(5-Amino-3,4-dihydroxyphenyl)-2-phenylethanone (16). To a stirred, yellow suspension of **3** (5.0 g, 18.3 mmol) in methanol (100 mL) at room temperature was added 10% palladium on charcoal (0.30 g). Hydrogen gas was bubbled through the mixture for 2 h, leading to formation of a new, gray precipitate. Dimethylformamide (40 mL) was added, and the catalyst was removed by filtration through Celite. The filtrate was evaporated (50 °C, water aspirator pressure) and the residue crystallized from dichloromethane/diethyl ether to give beige crystals (4.07 g, 91%): mp 234−237 °C; IR (KBr) 3364 (OH), 3290 (NH_2), 1669 (C=O, ketone), 1540 cm^{-1} (NO_2); ^1H NMR (DMSO-d_6) δ 9.2 (vbr, 2H, 3-OH, 4-OH), 7.4−7.1 (m, 5H, Ph), 6.94 (d, 1H, J = 2.1 Hz, H-2), 6.84 (d, 1H, J = 2.1 Hz, H-6), 4.8 (vbr, 2H, NH_2), 4.12 (s, 2H, CH_2); ^{13}C NMR (DMSO-d_6) δ 197.2, 145.5, 138.2, 137.9, 136.9, 130.5, 129.2, 128.7, 127.3, 108.4, 106.4, 45.2. Anal. ($C_{14}H_{13}NO_3$) C, H, N.

1-[5-(*N*-Acetylamino)-3,4-dihydroxyphenyl]-2-phenylethanone (17). A stirred suspension of **16** (1.95 g, 8 mmol) in dichloromethane (20 mL) was treated with pyridine (1.90 g, 24 mmol), acetic anhydride (2.44 g, 24 mmol), and 4-(dimethylamino)pyridine (DMAP, 0.01 g). The mildly exothermic reaction subsided after 15 min, and the reaction mixture was washed with cold 2 N HCl (100 mL) and brine (50 mL), then dried over anhydrous sodium sulfate, filtered, and evaporated (40 °C, water aspirator pressure), leaving a beige solid which was recrystallized from dichloromethane/petroleum ether to give off-white crystals (2.40 g, 81%).

This product (2.35 g, 6.36 mmol) was suspended in methanol (35 mL) and cooled in an ice−water bath. An aqueous 1 N sodium hydroxide solution (13 mL, 13 mmol) was added dropwise, and the resulting brown solution was stirred for 30 min and then poured onto ice and 2 N HCl (150 mL). The mixture was extracted with dichloromethane (2 × 150 mL), and the extracts were washed with brine (100 mL), dried over anhydrous sodium sulfate, filtered, and evaporated (40 °C, water aspirator pressure), leaving a beige solid which was recrystallized from petroleum ether/ethyl acetate to give off-white crystals (1.20 g, 66%): mp 150−153 °C; IR (KBr) 3445 (OH), 3322 (NH), 1690 (C=O, acetyl), 1640 (C=O, ketone), 1542 cm^{-1} (NO_2); ^1H NMR ($CDCl_3$) δ 10.95 (br, 1H, 4-OH), 9.16 (br, 1H, NH), 7.55 (d, 1H, J = 2.1 Hz, H-6), 7.49 (d, 1H, J = 2.1 Hz, H-2), 7.4−7.1 (m, 5H, Ph), 6.36 (br, 1H, 3-OH), 4.24 (s, 2H, CH_2), 1.95 (s, 3H, $COCH_3$); ^{13}C NMR ($CDCl_3$) δ 198.8, 172.8, 147.8, 142.1, 134.9, 130.2, 129.3, 129.0, 127.7, 126.7, 115.0, 113.0, 45.8, 23.5. Anal. ($C_{16}H_{15}NO_4$·0.3H_2O) C, H, N.

1-[5-Amino-3-hydroxy(4-*O*-2,3,4-triacetyl-*β*-D-glucuronopyranosidophenyl)]-2-phenylethanone Methyl Ester (20). A stirred semisolution of **8** (0.81 g, 1.38 mmol) in methanol (50 mL) at room temperature was treated with 10% palladium on charcoal (0.25 g), and hydrogen gas was bubbled through the mixture for 1 h. The catalyst was removed by filtration through Celite, and the filtrate was concentrated (40 °C, water aspirator pressure). Chromatography of the residue on silica gel allowed separation of two products. The faster-running component was obtained after recrystallization from dichloromethane/diisopropyl ether as beige crystals (0.5 g, 65%), subsequently identified as the title product: mp 155−157 °C; IR (KBr) 3450 (OH), 3384 (NH_2), 1755 (C=O, ester), 1673 cm^{-1} (C=O, ketone); ^1H NMR (DMSO-d_6) δ 9.63 (br, 1H, 3-OH), 7.35−7.15 (m, 5H, Ph), 6.92 (d, 1H, J = 2.1 Hz, H-6), 6.78 (d, 1H, J = 2.1 Hz, H-2), 5.47 (t, 1H, J = 9.7 Hz, H-3′), 5.26 (d, 1H, J = 7.9 Hz, H-1′), 5.12 (dd, 1H, J = 7.9 and 9.7 Hz, H-2′), 5.02 (m, 1H, H-4′), 4.55 (d, 1H, J = 9.9 Hz, H-5′), 4.17 (s, 2H, CH_2), 3.62 (s, 3H, OCH_3), 2.02 (s, 3H, $COCH_3$), 2.00 (s, 3H, $COCH_3$), 1.99 (s, 3H, $COCH_3$); ^{13}C NMR (DMSO-d_6) δ 197.9, 170.5, 170.4, 170.2, 168.3, 151.0, 144.0, 136.3, 135.6, 134.3,

130.6, 129.3, 127.4, 108.2, 105.5, 102.1, 72.0, 71.8, 71.6, 70.0, 53.6, 45.5, 21.6, 21.4, 21.3. Anal. ($C_{27}H_{29}NO_{12}$) C, H, N.

The slower-running component obtained from the column was recrystallized from dichloromethane/petroleum ether to give white crystals (0.15 g, 19%), subsequently identified as 1-[5-amino-3-hydroxy(4-*O*-2,3,4-triacetyl-*β*-D-glucuronopyranosidophenyl)]-1-hydroxy-2-phenylethane methyl ester (**21**): mp 172−174 °C; IR (KBr) 3450 (OH), 3411 (NH_2), 1754 cm^{-1} (C═O, ester); ^1H NMR ($CDCl_3$) δ 7.4−7.15 (m, 5H, Ph), 6.6 (vbr, 1H, 3-OH), 6.43, 6.40 (d, 1H, J = 2.1 Hz, H-2), 6.34, 6.32 (d, 1H, J = 2.1 Hz, H-2), 5.3 (m, 3H, H-2′, H-3′, H-4′), 4.88 (m, 1H, H-1′), 4.69 (m, 1H, C*H*OH), 4.07 (m, 1H, H-5′), 3.9 (vbr, 2H, NH_2), 3.78 (s, 3H, OCH_3), 2.99 (dd, 1H, J = 4.1 and 13.8 Hz, CH_2), 2.90 (dd, 1H, J = 8.9 and 13.8 Hz, CH_2), 2.14 (s, 3H, $COCH_3$), 2.11 (s, 3H, $COCH_3$), 2.06 (s, 3H, $COCH_3$); ^{13}C NMR ($CDCl_3$) δ 170.7, 170.0, 169.7, 167.1, 150.2, 150.1, 143.6, 140.7, 140.6, 138.8, 138.7, 131.4, 131.4, 130.0, 129.1, 127.2, 106.0, 105.9, 105.1, 105.0, 102.7, 75.5, 75.4, 72.7, 72.5, 72.0, 69.3, 53.8, 46.3, 21.3, 21.2, 21.0. Anal. ($C_{27}H_{31}NO_{12}$·1.5H_2O) C, H, N.

1-(5-Amino-4-*O*-*β*-d-glucuronopyranosido-4-hydroxyphenyl)-2-phenylethanone (18). A stirred semisolution of **20** (0.34 g, 0.6 mmol) in methanol (5 mL) was treated dropwise with an aqueous 1 N sodium hydroxide solution (6 mL, 6 mmol) at room temperature. The resulting orange solution was stirred for 2 h and then cooled in an ice−water bath. Acetic acid was added until the pH reached 4, and the solvents were evaporated (60 °C, water aspirator pressure). The residue was purified by reverse-phase preparative HPLC as described above using acetonitrile/water (2:8) as the eluent. Inorganic salt-rich initial fractions were discarded. Homogeneous fractions were combined and evaporated (60 °C, water aspirator pressure) and then dried over phosphorus pentoxide at high vacuum to give the title product as a beige solid (0.2 g, 79%): mp 120−121 °C; IR (KBr) 3431 (broad, OH), 3290 (NH_2), 1682 (C═O, acid), 1640 cm^{-1} (C═O, ketone); ^1H NMR (DMSO-d_6) δ 7.4−7.15 (m, 5H, Ph), 6.88 (d, 1H, J = 2.1 Hz, H-6), 6.78 (d, 1H, J = 2.1 Hz, H-2), 4.52 (d, 1H, J = 8.0 Hz, H-1′), 4.19 (s, 2H, CH_2), 3.64 (d, 1H, J = 9.4 Hz, H-5′), 3.5−3.2 (m, 3H, H-2′, H-3′, H-4′); ^{13}C NMR (DMSO-d_6) δ 198.1, 173.1, 150.9, 143.6, 136.7, 136.5, 134.6, 130.6, 129.3, 127.4, 107.5, 106.6, 106.0, 76.6, 75.9, 74.4, 72.6, 45.5. Anal. ($C_{20}H_{21}NO_9$·1.6H_2O) C, H, N.

1-[5-Amino-4-hydroxy(3-*O*-2,3,4-triacetyl-*β*-D-glucuronopyranosidophenyl)]-2-phenylethanone Methyl Ester (22). To a stirred suspension of **11** (1.10 g, 1.87 mmol) in methanol (50 mL) at room temperature was added 10% palladium on charcoal (0.28 g). Hydrogen gas was bubbled through the reaction mixture for 30 min, and then the catalyst was removed by filtration through Celite. The filtrate was concentrated (40 °C, water aspirator pressure) to leave a foam which was recrystallized from diisopropyl ether to give white crystals (1.01 g, 97%): mp 93−94 °C; IR (KBr) 3445 (broad, OH), 3290 (NH_2), 1755 (C═O, ester), 1670 cm^{-1} (C═O, ketone); ^1H NMR (DMSO-d_6) δ 7.35−7.15 (m, 5H, Ph), 7.14 (d, 1H, J = 2.1 Hz, H-6), 7.11 (d, 1H, J = 2.1 Hz, H-2), 5.70 (d, 1H, J = 7.9 Hz, H-1′), 5.47 (t, 1H, J = 9.6 Hz, H-3′), 5.15 (dd, 1H, J = 7.6 and 9.6 Hz, H-2′), 5.08 (t, 1H, J = 9.6 Hz, H-4′), 4.71 (d, 1H, J = 9.9 Hz, H-5′), 4.20 (d, 1H, J = 14.9 Hz, CH_2), 4.12 (d, 1H, J = 14.9 Hz, CH_2), 3.63 (s, 3H, OCH_3), 2.02 (s, 3H, $COCH_3$), 1.99 (s, 3H, $COCH_3$), 1.95 (s, 3H, $COCH_3$); ^{13}C NMR (DMSO-d_6) δ 197.0, 170.6, 170.4, 170.0, 168.2, 145.0, 139.9, 139.2, 136.7, 130.5, 129.3, 128.6, 127.4, 110.9, 107.0, 99.0, 72.5, 72.0, 71.9, 69.9, 53.6, 45.2, 21.5, 21.4, 21.2. Anal. ($C_{27}H_{29}NO_{12}$) C, H, N.

1-(5-Amino-3-*O*-<bold>d</bold>>*β*-D-glucuronopyranosido-3-hydroxyphenyl)-2-phenylethanone (19). A cooled (ice−water bath) and stirred solution of **22** (0.78 g, 1.39 mmol) in methanol (14 mL) at room temperature was treated dropwise with an aqueous 1 N sodium hydroxide solution (14 mL, 14 mmol). After the mixture had been stirred in the cold for 30 min, acidification, workup, and purification as described for **18** above afforded light brown crystals (0.5 g, 86%): mp 158−163 °C; IR (KBr) 3445 (broad, OH), 3290 (NH_2), 1706 (C═O, acid), 1640 cm^{-1} (C═O, ketone); ^1H NMR (DMSO-d_6) δ 7.3−7.1 (m, 6H, Ph, H-2), 7.04 (d, 1H, J = 2.1 Hz, H-6), 4.49 (d, 1H, J = 7.2 Hz, H-1′), 4.10 (d, 1H, J = 14.9 Hz, CH_2), 4.08 (d, 1H, J = 14.9 Hz, CH_2), 3.38 (d, 1H, J = 9.2 Hz, H-5′), 3.3−3.1 (m, 3H, H-2′, H-3′, H-4′); ^{13}C NMR (DMSO-d_6) δ 196.3, 173.8, 146.5, 145.8, 139.3, 137.2, 130.5, 129.9, 129.2, 127.2, 111.9, 110.3, 105.8, 77.0, 75.0, 74.2, 73.0, 45.1. Anal. ($C_{20}H_{21}NO_9$·1.5H_2O) C, H, N.

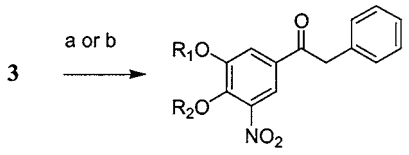
1-(3,4-Dihydroxy-5-nitrophenyl)-2-phenylethanone, 3-*O*-Pyridinium Sulfate (23). A stirred solution of **3** (3.0 g, 10.99 mmol) in pyridine (50 mL) at room temperature was treated with the sulfur trioxide−pyridine complex (5.24 g, 32.96 mmol) in portions. The resulting mixture was left stirring for 4 h and then poured slowly onto ice and 2 N HCl (300 mL). After the mixture had been stirred for 30 min, the pale yellow precipitate was filtered off and washed with water (50 mL). Recrystallization (methanol) afforded pale yellow crystals (4.32 g, 91%): mp 143−146 °C; IR (KBr) 3423 (OH), 1688 (C═O), 1550 cm^{-1} (NO_2); ^1H NMR (DMSO-d_6) δ 8.92 (d, 2H, *o*-Pyr), 8.58 (t, 1H, *p*-Pyr), 8.31 (d, 1H, J = 2.2 Hz, H-6), 8.25 (d, 1H, J = 2.2 Hz, H-2), 8.05 (t, 2H, *m*-Pyr), 7.35−7.15 (m, 5H, Ph), 4.35 (s, 2H, CH_2); ^{13}C NMR (DMSO-d_6) δ 195.9, 149.1, 146.8, 144.4, 143.7, 139.0, 135.9, 130.8, 129.3, 128.1, 127.6, 127.3, 125.5, 121.4, 45.2. Anal. ($C_{14}H_{10}NO_8S$·C_5H_6N) C, H, N, S.

1-(5-Amino-3,4-dihydroxyphenyl)-2-phenylethanone, 3-*O*-Pyridinium Sulfate (24). A stirred semisolution of **23** (2.0 g, 4.63 mmol) in methanol (100 mL) at room temperature was treated with 5% palladium on charcoal (0.2 g). Hydrogen gas was passed through the mixture for 3 h, and then the catalyst was removed by filtration through Celite. The filtrate was concentrated (40 °C, water aspirator pressure) to leave a slightly hygroscopic brownish solid (1.78 g, 79%): mp 68−71 °C; IR (KBr) 3423 (OH), 3230 (NH_2), 1671 (C═O), 1550 cm^{-1} (NO_2); ^1H NMR (DMSO-d_6) δ 8.82 (d, 2H, *o*-Pyr), 8.34 (t, 1H, *p*-Pyr), 7.85 (t, 2H, *m*-Pyr), 7.67 (d, 1H, J = 2.1 Hz, H-6), 7.50 (d, 1H, J = 2.1 Hz, H-2), 7.35−7.15 (m, 5H, Ph), 4.21 (s, 2H, CH_2); ^{13}C NMR (DMSO-d_6) δ 196.5, 145.6, 145.5, 144.0, 142.0, 136.3, 130.7, 129.4, 129.3, 128.5, 127.5, 127.2, 118.8, 116.3, 45.3. Anal. ($C_{14}H_{12}NO_6S$·C_5H_6N·H_2O) C, H, N, S.

RESULTS AND DISCUSSION

The major metabolic pathways after oral administration of **3** in several animal species were expected to give rise to three main classes of products: O-methylated catechols and several glucuronide and sulfate conjugates (this work will be published elsewhere). We recently disclosed an efficient synthesis of **3** from commercially available vanillin (*7*) and have developed an improved method (*10*) for the demethylation of the 3-O-methylated derivative **4** (the precursor of **3**). The corresponding 4-*O*-methyl isomer **5** was obtained by regioselective monom-

Scheme 1. Synthesis of Putative O-Methylated Metabolites of 3[a]



4, R_1=CH_3, R_2=H[a]

5, R_1=H, R_2=CH_3

6, R_1=R_2=CH_3

[a] Reagents: (a) $(CH_3O)_2SO_2$, K_2CO_3, DMF, 80 °C (25%); (b) $(CH_3O)_2SO_2$, K_2CO_3, $(CH_3)_2CO$, Δ (86%). [b]See ref *10*.

ethylation of **3** using potassium carbonate and dimethyl sulfate in warm DMF. Dimethylation to give **6** proceeded without incident in acetone (Scheme 1).

A variety of methods exist for the preparation of glucuronide conjugates of phenolic compounds and have been reviewed (*11*). Often, traditional methods are low-yielding, giving rise to byproducts and/or mixtures of α- and *β*-anomers. Furthermore, regiospecific glucuronidation of substituted catechols has not thus far been reported. In agreement with the 4-O-regioselectivity of methylation above, we found that Koenigs−Knorr coupling of the 1α-bromo sugar **7** with **3** using silver oxide in acetonitrile gave the protected 4-*O*-*β*-glucuronate **8** in acceptable yield (53%, Scheme 2). The ^{1}H NMR spectrum confirmed that only the *β*-anomer was formed, as seen from the coupling constant (J = 7.5 Hz) of the anomeric proton. Hydrolysis of the acetyl protecting groups was achieved using aqueous 1 N sodium hydroxide in methanol. Acidic workup (Amberlyst 15 ion-exchange resin) and evaporation of the solvents afforded the 4-*O*-*β*-glucuronide **9** in good yield (93%) and purity (HPLC, >99%).

An alternative method for enzymatic glucuronidation for direct preparation of the regioisomeric 3-*O*-*β*-glucuronide **10** from **3** was required. This could not be achieved using **7** with heavy metal catalysts (Ag, Cd, and Hg salts). Model studies showed, however, that acetylation of **3**, rather than alkylation, led to exclusive formation of the 3-O-acylated derivative. Further encouraged by a report that the trichloroacetimidate **10** reacts with 4-nitrophenol to afford the corresponding *β*-conjugate in high yield (*12*), we were delighted to discover that reaction of **3** with **10** in the presence of excess boron trifluoride (*13*) afforded exclusively the protected methyl 3-*O*-glucuronate **11** (*β*-anomer only) in reasonable (56%) yield (Scheme 3). The unusually large excess of boron trifluoride (1.5 equiv) was necessary as the reaction proceeded poorly with only catalytic quantities normally utilized in glucuronide synthesis by this procedure, although a similar observation with an unrelated steroidal aglycone has been reported (*14*). The subsequent basic hydrolysis of **11** gave the free glucuronide **12**, again in good yield and excellent chemical purity (HPLC analysis).

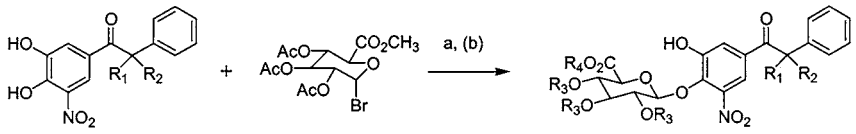
Table 1. ^{1}H NMR Chemical Shifts (*δ*, ppm) of 9 and 12[a]

proton	9	12
2	7.7, d (J = 2.1)	7.9, d (J = 2.1)
6	7.9, d (J = 2.1)	8.2, d (J = 2.1)
8	4.4, s	4.4, d (J = 16.0)
		4.3, d (J = 16.0)
10	7.2[b]	7.25[b]
11	7.3[b]	7.3[b]
12	7.2[b]	7.25[b]
1′	5.1, d (J = 7.5)	5.2, d (J = 7.3)
2′	3.2[b]	3.4[b]
3′	3.2[b]	3.35[b]
4′	3.4, m	3.45[b]
5′	3.6, d (J = 9.7)	4.0, d (J = 9.7)

[a] All these assignments are in agreement with HMQC, HMBC, COSY, and NOESY spectra. [b] Overlapped signals; *δ* values were measured from the HMQC spectra.

The ^{1}H and ^{13}C NMR resonances (Tables 1 and 2) of compounds **9** and **12** were completely and unequivocally assigned by the concerted application of homonuclear (COSY and NOESY) and ^{1}H-detected heteronuclear one-

Scheme 2. Regioselective 4-O-*β*-D-Glucurodination of 3 and 13[a]



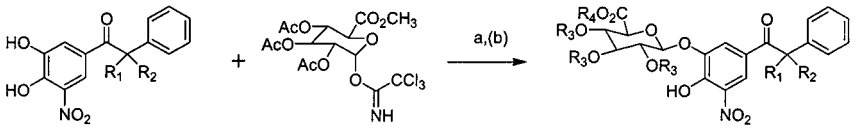
3, R_1=R_2=H **7** **8**, R_1=R_2=H, R_3=Ac, R_4=CH_3

13, R_1+R_2=O **9**, R_1=R_2=R_3=R_4=H

14, R_1+R_2=O, R_3=Ac, R_4=CH_3

[a] Reagents: (a) Ag_2O, CH_3CN; (b) (i) 1 N NaOH (aq), CH_3OH, 0 °C, (ii) Amberlyst 15 ion-exchange resin.

Scheme 3. Regioselective 3-O-*β*-D-Glucurodination of 3 and 13[a]



3, R_1=R_2=H **10** **11**, R_1=R_2=H, R_3=Ac, R_4=CH_3

13, R_1+R_2=O **12**, R_1=R_2=R_3=R_4=H

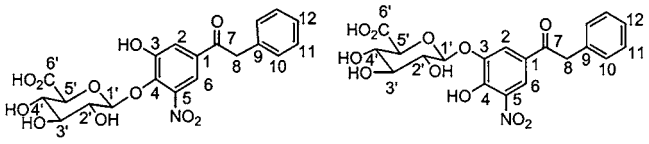
15, R_1+R_2=O, R_3=Ac, R_4=CH_3

[a] Reagents: (a) BF_3·OEt_2, CH_2Cl_2; (b) (i) 1 N NaOH (aq), CH_3OH, 0 °C, (ii) Amberlyst 15 ion-exchange resin.

Table 2. ^{13}C NMR Chemical Shifts (δ, ppm) of 9 and 12[a]

carbon	9	12	carbon	9	12	carbon	9	12
1	133.4	127.6	7	196.3	195.8	1′	103.8	102.5
2	120.4	119.5	8	45.4	45.3	2′	74.5	73.8
3	152.0	147.7	9	135.7	135.8	3′	76.6	76.0
4	140.7	147.3	10	130.8	130.7	4′	72.2	72.3
5	146.7	138.6	11	129.3	129.4	5′	77.0	76.5
6	115.6	120.3	12	127.6	127.6	6′	170.7	171.0

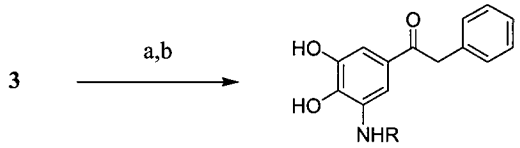
[a] All these assignments are in agreement with HMQC and HMBC spectra.



9 **12**

Figure 2. Chemical structures and numbering of glucuronides **9** and **12**.

Scheme 4. Synthesis of Amino Metabolites of 3[a]



16, R=H

17, R=Ac

[a] Reagents: (a) 10% Pd/C, CH_3OH, H_2 (91%); (b) (i) Ac_2O, pyridine, DMAP, CH_2Cl_2, (ii) 1 N NaOH, CH_3OH (66%).

bond (HMQC) and long-range (HMBC) gradient-selected correlation experiments. The HMQC sequence was first employed to determine the direct H−C correlations and to assign the proton-containing carbons. The HMBC technique was then performed to establish the long-range H−C correlations of the quaternary aromatic carbons. COSY and NOESY experiments were also performed and confirmed these assignments.

The strategy for the ^{1}H and ^{13}C signal assignment of these compounds was as follows. For **9** and **12** (Figure 2), both H-2 and H-6 exhibited HMBC three-bond connectivities with the quaternary carbon C-4 and also with C-6 and C-2, respectively. H-2 exhibited for both compounds an HMBC two-bond correlation with C-3 and H-6 an HMBC two-bond correlation with C-5. These results allowed complete ring assignments, which were strictly required to establish the position (3- or 4-*O*-) of the glucuronide substituent.

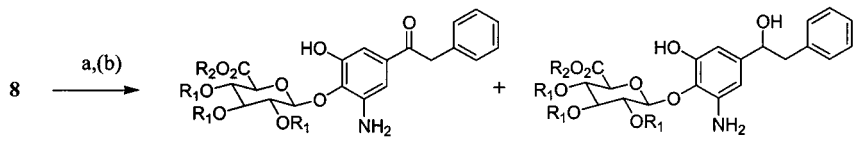
For compound **12**, H-1′ (δ 5.2) exhibited an HMBC connectivity with C-3 (δ 147.7), confirming the glucuronide substituent on the 3-O-position. For regioisomer **9**, the corresponding connectivity is also seen and there is a further HMBC correlation between the 3-hydroxyl (δ 10.8) and C-4 (δ 140.7) that confirms the glucuronide substituent at the 4-O-position.

The Koenigs−Knorr and Schmidt trichloroacetimidate methods are therefore complementary in that either the 3- or 4-*O*-β-glucuronides of **3** may be preferentially prepared. That this chemistry can be applied to other 3-nitrocatechols can be seen from the same reactions applied to the dione **13**, which gave either the 4-O-β-glucuronide precursor **14** (Koenigs−Knorr) or 3-*O*-β-glucuronide precursor **15** (Schmidt) (Schemes 2 and 3).

Reduction of the nitro moiety is a common metabolic pathway for aromatic nitro compounds (and for **1**), and several potential amino conjugates of **3** were envisaged. **3** was subjected to catalytic hydrogenation at room temperature and atmospheric pressure (Pd/C, H_2, MeOH), undergoing rapid reduction to amino analogue **16** (Scheme 4). Exhaustive acetylation of **16** followed by careful alkaline hydrolysis of the *O*-acetyl residues gave *N*-acetyl derivative **17**. Catalytic hydrogenation (Pd/C, H_2, MeOH) of nitro 4-*O*-β- and 3-*O*-β-glucuronides **9** and **12**, respectively, afforded the corresponding amino 4-*O*-β- and 3-*O*-β-glucuronides **18** and **19**, respectively, as rather impure (80−90%) amorphous solids. Reverse-phase chromatography failed to considerably improve the purity of each. Surprisingly, catalytic hydrogen transfer using cyclohexene, formic acid, or ammonium formate as a hydrogen donor failed to return any **18** or **19**. The suspicion that the major impurity arose from concomitant reduction of the carbonyl group was confirmed on hydrogenation of **8** under the same conditions, which gave on first attempt a separable 2:1 mixture of ketone **20** and alcohol **21**. Careful monitoring of the reaction and a significant reduction in the reaction time (from 6 to 1 h), however, allowed isolation of **20** in 65% yield (Scheme 5). Basic hydrolysis and acidification with acetic acid to pH 4 followed by preparative reverse-phase HPLC to remove inorganic salts gave **18** in good yield and purity (>99%, HPLC). Nitroglucuronate **11** easily underwent hydrogenation to give **22** exclusively (97%), and subsequent basic hydrolysis gave origin to amino-3-*O*-β-glucuronide **19** (>99% purity) under the same conditions previously mentioned (Scheme 6).

Sulfate conjugation catalyzed by sulfotransferase is also a metabolic pathway for phenolic and catecholic substrates in mammals; unsurprisingly, therefore, two sulfate conjugates, of both **3** and amine **16**, were detected. Synthesis of these sulfates proved to be somewhat more complicated than glucuronidation, due to the high lability of the sulfate moiety. Sulfation of **3** with the sulfur trioxide−DMF complex occurred rapidly in a DMF solution, giving a single product (as monitored by HPLC) which, on attempted isolation, reverted back to **3**. The product was, however, stable in solution at room tem-

Scheme 5. Synthesis of Amino 4-*O*-β-D-Glucuronide Conjugate 18[a]

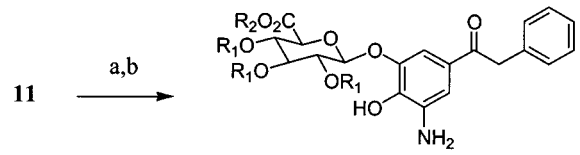


20, R_1=Ac, R_2=CH_3 **21**, R_1=Ac, R_2=CH_3

18, R_1=R_2=H

[a] Reagents: (a) 10% Pd/C, CH_3OH, H_2 (65% for **20** and 19% for **21**); (b) (i) 1 N NaOH, CH_3OH, (ii) AcOH (pH 4), reverse-phase preparative HPLC (79%).

Scheme 6. Synthesis of Amino 3-*O*-*β*-D-Glucuronide Conjugate 19[a]

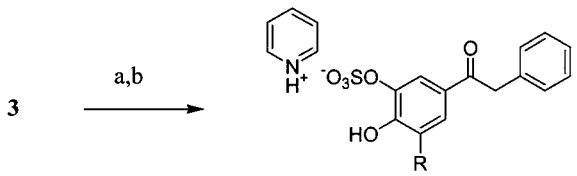


22, R_1=Ac, R_2=CH_3

19, R_1=R_2=H

[a] Reagents: (a) 10% Pd/C, CH_3OH, H_2 (97%); (b) (i) 1 N NaOH, CH_3OH, (ii) AcOH (pH 4), reverse-phase preparative HPLC (86%).

Scheme 7. Synthesis of 3-*O*-Sulfate Conjugates of 3 and 16[a]



23, R=NO_2

24, R=NH_2

[a] Reagents: (a) SO_3−pyridine complex, pyridine (91%); (b) 5% Pd/C, CH_3OH, H_2 (79%).

perature. Reaction of **3** with the pyridine−sulfur trioxide complex also gave a single product, which precipitated during the workup (Scheme 7). This was perfectly stable and could be readily isolated and recrystallized (>99% purity). ^1H and ^{13}C NMR showed that the product was exclusively the 3-*O*-pyridinium sulfate **23**; compared to that of **3**, the aromatic proton on C-2 (δ 8.25) of **23** was deshielded by the 3-sulfate ester ($\Delta\delta$ = 0.55 ppm). The ^{13}C spectrum also exhibits a significant deshielding effect on the ortho and para carbon atoms. C-2 has a carbon shift $\Delta\delta$ of 7.3 ppm, C-6 4.0 ppm, and C-4 2.5 ppm. Similar behavior has been reported with dopamine and its 3-*O*- and 4-*O*-sulfates (*15*).

Reduction of the nitro group under catalytic hydrogenation conditions afforded the corresponding hygroscopic amino-3-*O*-sulfate **24** in reasonable yield (78%) and good purity (>98%).

CONCLUSIONS

Efficient chemical methods suitable for the regioselective gram-scale synthesis of highly pure putative *O*-methyl, *O*-glucuronide, and *O*-sulfate metabolic conjugates of BIA 3-202, 1-(3,4-dihydroxy-5-nitrophenyl)-2-phenylethanone **3**, have been developed. These compounds are currently used as standards for the determination of the metabolic profile of **3** in various species, including humans. It is foreseen that these procedures will be useful for the synthesis of conjugates of other COMT inhibitors based on the nitrocatechol pharmacophore.

ACKNOWLEDGMENT

We thank Paula C. Alves for valuable technical assistance.

LITERATURE CITED

(1) Guldberg, H., and Marsden, C. (1975) Catechol-*O*-methyltransferase: pharmacological aspects and physiological role. *Pharmacol. Rev. 27*, 135−206.

(2) Zhu, B. T., Ezell, E. L., and Liehr, J. G. (1994) Catechol-*O*-methyltransferase-catalysed rapid *O*-methylation of mutagenic flavanoids. Metabolic inactivation as a possible reason for their lack of carcinogenicity in vitro. *J. Biol. Chem. 269*, 292−299.

(3) Axelrod, J., and Tomchick, R. (1958) Enzymatic *O*-methylation of epinephrine and other catechols. *J. Biol. Chem. 233*, 702−705.

(4) Mannisto, P. T., and Kaakkola, S. (1990) Rationale for selective COMT inhibitors as adjuncts in the drug treatment of Parkinson's disease. *Pharmacol. Toxicol. 66*, 317−323.

(5) Borgulya, J., Da Prada, M., Dingemanse, J., Scherschlicht, R., Schlappi, B., and Zurcher, G. (1991) Ro 40-7592. Catechol-*O*-methyltransferase (COMT) inhibitor. *Drugs Future 16*, 719−721.

(6) Nissinen, E., Lindén, I.-B., Schultz, E., and Pohto, P. (1992) Biochemical and pharmacological properties of a peripherally acting catechol-*O*-methyltransferase inhibitor Entacapone. *Naunyn-Schmiedebergs Arch. Pharmacol. 346*, 262−266.

(7) Learmonth, D. A., Vieira-Coelho, M. A., Benes, J., Alves, P. C., Borges, N., Freitas, A. P., and Soares-da-Silva, P. (2002) Synthesis of 1-(3,4-dihydroxy-5-nitrophenyl)-2-phenyl-ethanone and derivatives as potent and long-acting peripheral inhibitors of catechol-*O*-methyltransferase. *J. Med. Chem. 45* (3), 685−695.

(8) Jorga, K., Fotteler, B., Heizmann, P., and Gasser, R. (1999) Metabolism and excretion of tolcapone, a novel inhibitor of catechol-*O*-methyltransferase. *Br. J. Clin. Pharmacol. 48*, 513−520.

(9) Luukkanen, L., Kilpelainen, I., Kangas, H., Ottoila, P., Elovaara, E., and Taskinen, J. (1999) Enzyme-assisted synthesis and structural characterization of nitrocatechol glucuronides. *Bioconjugate Chem. 10*, 150−154.

(10) Learmonth, D. A., and Alves, P. C. (2002) Improved method for demethylation of nitro-catechol methyl ethers. *Synth. Commun. 32* (4), 641−649.

(11) Stachulski, A. V., and Jenkins, G. N. (1998) The synthesis of *O*-glucuronides. *Nat. Prod. Rep.*, 173−186.

(12) Fischer, B., Nudelman, A., Ruse, M., Herzig, J., Gottlieb, H. E., and Keinan, E. (1984) A novel method for stereoselective glucuronidation. *J. Org. Chem. 49*, 4988−4993.

(13) Schmidt, R. R., and Grundler, G. (1981) Simple synthesis of *β*-D-glucopyranosyluronates. *Synthesis*, 885−887.

(14) Ferguson, J. R., Harding, J. R., Lumbard, K. W., Scheinmann, F., and Stachulski, A. V. (2000) Glucuronide and sulfate conjugates of ICI 182,780, a pure anti-estrogenic steroid. Order of addition, catalysis and substitution effects in glucuronidation. *Tetrahedron Lett. 41*, 389−392.

(15) Jain, T., Kaiser, C., Ackerman, D. M., Ladd, D. L., Fong, K. L., Roberts, G. D., Staiger, D. B., Davis, L. L., and Webb, R. L. (1986) Sulfoconjugation of dopamine. A critical examination of the reaction between dopamine and concentrated sulphuric acid. *Can. J. Chem. 64*, 2418−2422.

BC0200327

Development of Annexin V Mutants Suitable for Labeling with Tc(I)-Carbonyl Complex

Jonathan F. Tait,*[,†,‡] Christina Smith,[†] and Donald F. Gibson[†]

Departments of Laboratory Medicine, Medicine (Medical Genetics), and Pathology, University of Washington, Seattle, Washington 98195-7110 . Received May 1, 2002; Revised Manuscript Received July 16, 2002

^{99m}Tc-annexin V can be used to image organs undergoing cell death during cancer chemotherapy and organ transplant rejection. We investigated whether the novel Tc-carbonyl labeling method would be suitable for annexin V. Two mutant molecules of annexin V, called annexin V-122 and annexin V-123, were constructed with N-terminal extensions containing either three or six histidine residues. These molecules were expressed cytoplasmically in *E. coli* and purified with a final yield of 33 mg of protein/L of culture. Analysis by SDS−PAGE, isoelectric focusing, gel filtration chromatography, and mass spectrometry confirmed the purity and homogeneity of the protein preparations. Both mutant proteins retained full binding affinity for cell membranes with exposed phosphatidylserine. Using the Tc-carbonyl reagent, both proteins could be labeled with ^{99m}Tc to specific activities of at least 10−20 μCi/μg with full retention of bioactivity. The radiolabeled proteins were stable when incubated with phosphate-buffered saline or serum in vitro, and there was no transchelation of label to serum proteins during in vitro incubation. In conclusion, annexin V can be modified near its N-terminus to incorporate sequences that form specific chelation sites for ^{99m}Tc-carbonyl without altering its high affinity for cell membranes.

INTRODUCTION

The phospholipid binding protein annexin V can be used to detect the exposure of PS[1] at the extracellular face of the plasma membrane (*1*). Alterations in PS exposure occur in both blood coagulation and apoptosis (*2*, *3*). We have developed annexin V as a means to detect PS exposure in vivo. Annexin V labeled with radioiodine and ^{99m}Tc was used to detect thrombus formation in experimental animals (*4*, *5*). ^{99m}Tc-annexin V was used to detect cell death in vivo in animal models (*6*−*10*). Because of the clinical applicability of this work in monitoring cancer chemotherapy, rejection of transplanted organs (*11*), and mycoardial infarction (*12*), there is interest in developing new annexin V derivatives with improved imaging properties or greater ease of use in the clinical setting.

There have been several methods developed so far for labeling annexin V with technetium. The N_2S_2 preformed chelate method (*13*) was used in the earliest studies (*5*). More recently, annexin V was chemically derivatized with HYNIC (*6*, *7*) or iminomercaptobutylate (*12*). Most recently, we developed novel forms of annexin V that contain genetically engineered sequences that can directly chelate technetium in the +V oxidation state without need for any chemical derivatization with exogenous chelation groups (*14*). Although all these technetium-labeled forms of annexin have certain benefits and uses, none is ideal, and there is still a need to explore additional ways of radiolabeling the protein to provide derivatives with high specific activity and radiostability.

A novel reagent was recently developed for Tc labeling of biomolecules. Alberto et al. (*15*) developed a convenient aqueous synthesis of $[^{99m}Tc(OH_2)_3(CO)_3]^+$ (abbreviated TcCO). Egli et al. (*16*) used this reagent to label peptides to high specific activities, and they showed that among the amino acids histidine formed complexes of highest stability with TcCO. Waibel et al. (*17*) used TcCO to label a recombinant single-chain Fv antibody containing five histidine residues at the C-terminus; this derivative showed high radiochemical stability in vitro and in vivo. Other groups have recently applied this method to label the peptides somatostatin (*18*) and bitistatin (*19*).

In view of the potential advantages of this radiolabeling method, we investigated whether it would be suitable for labeling annexin V. Since histidine is the amino acid likely to form complexes of highest stability with TcCO, and trivalent complexes are the most stable (*20*), we added peptide sequences containing either three or six histidines to annexin V. Although the C-terminal carboxyl group may help to stabilize histidine−TcCO complexes (*17*), we chose to add the histidine residues to the N-terminus of annexin V because alterations in this region are much less likely to affect either membrane binding affinity or protein folding in *E. coli* (*14, 21, 22*). We show that these novel derivatives can be produced in high yield and purity by expression in *E. coli*, and they can be readily labeled with TcCO.

MATERIALS AND METHODS

Materials. Recombinant annexin V was produced in *E. coli* as described (*23*). Fluorescein-annexin V was

* Address correspondence to this author at the Department of Laboratory Medicine, University of Washington, Room NW-120, Box 357110, Seattle, WA 98195-7110. Telephone: (206)-598-6131; Fax: (206)598-6189; Email: tait@u.washington.edu.

† Department of Laboratory Medicine.

‡ Departments of Medicine (Medical Genetics) and Pathology.

[1] Abbreviations: HEPES, 4-(2-hydroxyethyl)-1-piperazine-ethanesulfonic acid; HYNIC, 6-hydrazinopyridine-3-carboxylate; IC_{50}, 50% inhibitory concentration; ITLC, instant thin-layer chromatography; PBS, phosphate-buffered saline; PS, phosphatidylserine; TcCO, $[^{99m}Tc(OH_2)_3(CO)_3]^+$; SDS−PAGE, sodium dodecyl sulfate−polyacrylamide gel electrophoresis; wt, wild-type.

10.1021/bc025545s CCC: $22.00 © 2002 American Chemical Society
Published on Web 08/16/2002

prepared as described (*24*). Lyophilized carbonyl reaction mixture was a gift from Mallinckrodt (St. Louis, MO). Erythrocytes with exposed PS (4CPlus Normal Control, part number 7546923) were from Beckman-Coulter (Miami, FL).

Construction and Verification of Plasmids. Two plasmids were constructed to express mutant forms of human annexin V in *E. coli* under control of the phage T7 promoter. Plasmid pJ122 was constructed with oligonucleotides JT-319 (5′-ATGGCCCATCATCATGCACAGGTTCTCAGA-3′) and JT-321 (5′-TTAGTCATCTTCTCCACAGAGCAGCAG-3′); plasmid pJ123 with JT-320 (5′-ATGGCCCATCATCATCATCATCACGCACAGGTTCTCAGA-3′) and JT-321. These oligonucleotides were designed to amplify the entire protein-coding region of wild-type annexin V and add the desired coding sequences to the 5′ end of the gene. PCR of the template pET9a-PAP1, which encodes wild-type annexin V (*25*), was performed with proofreading *Pfu* DNA polymerase (Stratagene) and with annealing steps first at 45 °C for 15 cycles and next at 65 °C for 15 cycles. PCR products were purified by phenol/chloroform extraction and ethanol precipitation; the purified PCR products were amplified again for three cycles with the same primer sets with annealing steps at 65 °C using *Taq* DNA polymerase to add the 3′-dA nucleotide overhangs necessary for ligation. The PCR product was ligated into pETBlue-1 Acceptor Vector (Novagen, Madison, WI), and the ligation mixture was transformed into *E. coli* strain Nova Blue (Novagen) and plated on LB agar containing 50 μg/mL carbenicillin, 70 μg/mL X-gal, and 80 μM IPTG. Plasmid DNA was prepared from white, carbenicillin-resistant colonies and screened by restriction mapping for the presence of the desired insert. Positive clones were subjected to DNA sequence analysis with the Big-Dye kit (Perkin-Elmer) to verify the presence of the desired insertion and the absence of other adventitious mutations.

Expression and Purification of Proteins. Plasmids pJ122 and pJ123 were each transformed into *E. coli* strain Tuner(DE3)pLac I (Novagen) for cytoplasmic expression. Each clone was grown overnight to saturation at 37 °C with shaking in Terrific Broth containing carbenicillin (50 μg/mL). The cells were separated from culture medium by centrifugation for 10 min at 2560*g* and washed in ice-cold buffer (50 mmol/L Tris-HCl, 150 mmol/L NaCl, pH 8.0). Bacteria were disrupted by sonication in ice-cold 50 mmol/L Tris-HCl, pH 7.2, 10 mmol/L $CaCl_2$ and then centrifuged for 20 min at 22530*g* in a Sorvall SS-34 rotor. The supernatant was discarded, and the annexin V bound to bacterial membranes was released by resuspending the pellet in 50 mmol/L Tris-HCl, pH 7.2, 20 mmol/L EDTA. Bacterial membranes were removed by centrifugation for 20 min at 22530*g*; the supernatant containing the annexin V was treated with 10 units/mL Benzonase (Novagen) plus 25 mM $MgCl_2$ for 1 h on ice, to digest DNA and RNA. After centrifugation for 20 min at 4800*g*, the supernatant was filtered with a 0.45 μm filter and then dialyzed against 20 mmol/L Tris-HCl, pH 8.0, at 4 °C.

The dialysand of annexin V-122 was further dialyzed against 20 mmol/L sodium acetate, pH 5.2, filtered through a 0.2 μm filter, applied to a Mono S HR 10/10 column (Pharmacia, Piscataway, NJ), and eluted with a gradient of 0−1 mol/L NaCl in the same buffer. The annexin V-122 eluted at approximately 0.170 mol/L NaCl. The dialysand of annexin V-123 was dialyzed against 20 mmol/L HEPES-Na, pH 7.0, filtered with a 0.2 μm filter, loaded onto a Mono Q HR 10/10 column (Pharmacia), and eluted with 0−1 mol/L NaCl in the same buffer. Annexin V-123 eluted at 0.170 mol/L NaCl. Each purified protein was dialyzed against 20 mmol/L HEPES, pH 7.4, 100 mmol/L NaCl, and stored in aliquots at −70 °C. The final yield of each protein was approximately 33 mg/L of bacterial culture (or 3.3 mg/g wet weight of cell paste), with a purity of ∼98% as judged by SDS−PAGE. Electrophoresis using 10−15% gradient SDS−PAGE and IEF 4−6.5 gels was performed on a PHAST System (Amersham-Pharmacia). Electrospray mass spectrometry was performed on a Micromass Quattro II tandem quadrupole mass spectrometer (Micromass Ltd., Manchester, U.K.) in the Mass Spectrometry Center (Department of Medicinal Chemistry, University of Washington).

Labeling of Proteins with ^{99m}Tc. The ^{99m}TcCO was made by adding 1 mL of TcO_4 (usually 1−10 mCi) in 0.9% deoxygenated NaCl to a 10 mL vial of lyophilized carbonyl reaction mixture (13 mg of L-tartaric acid; 7.6 mg of KBH_4; 20 mg of lactose; borate buffer, pH 11.6; carbon monoxide in headspace). The vial was incubated for 15 min in a boiling water bath, cooled to room temperature, vented with a syringe needle, and neutralized with 0.25 mL of 1 N HCl. Except where noted otherwise, labeling reactions were set up with 100 μL (100 μg) of annexin V-122 or annexin V-123 in 20 mM HEPES-Na, pH 7.4, 100 mM NaCl; 25 μL of 0.5 M HEPES-Na, pH 7.4; 125 μL of ^{99m}TcCO in 0.9% saline and incubated at 37 °C for 1 h. Percent incorporation of ^{99m}Tc was determined by ITLC on oven-dried silica gel plates with PBS as solvent. Radiolabeled proteins were purified by applying the reaction mixture (diluted to 400 μL with PBS) to a Sephadex G-25 column (0.9 × 2.8 cm) previously equilibrated with PBS and eluting the column with 1000 μL of PBS; radiolabeled protein eluted in the last 600 μL. Percent protein-bound radioactivity after gel filtration was determined by ITLC as above. For studies of radiolabel stability in serum, percent protein-bound radioactivity was determined by centrifugal ultrafiltration (3 min at 1860*g*) through a membrane with a 10 000 dalton cutoff (Centricon-10 filter, Amicon, Danvers, MA). Radiolabel stability was also assessed by gel filtration on a Superose-12 column (1 × 30 cm). The column was equilibrated with PBS and eluted at a flow rate of 0.5 mL/min at room temperature; 0.5 mL fractions were collected.

Cell Binding Assays. The affinity of nonradioactive proteins for cell membranes was determined by their ability to compete with fluorescein-annexin V for binding to erythrocytes with exposed phosphatidylserine (*21*). Mutant proteins were added at various concentrations to 1 mL of a solution containing 5 nmol/L fluorescein-annexin V and 8.3×10^6 erythrocytes in a buffer consisting of 10 mmol/L HEPES-Na, pH 7.4, 136 mmol/L NaCl, 2.7 mmol/L KCl, 5 mmol/L glucose, 1 mg/mL BSA (buffer HNKGB) plus 2.5 mmol/L $CaCl_2$. The sample was incubated for 15 min at room temperature. The cells were centrifuged for 3 min at 8300*g*, the supernatant was removed, and the fluorescein-annexin V bound to the pelleted cells was released by resuspension in 980 μL of HNKGB buffer containing 5 mmol/L EDTA. The sample was centrifuged again, the supernatant removed, and the concentration of fluorescein-annexin V in the supernatant determined by fluorometry. The results of this assay are summarized as the concentration of competitor protein that inhibits 50% of the binding of fluorescein-annexin V, abbreviated IC_{50}.

The ability of radiolabeled proteins to bind to cell membranes was determined by incubating them with a large excess of cells in a similar procedure. Radiolabeled protein at 10 nmol/L final concentration was added to

Protein	*N-terminal Sequence*	M_r	*pI*
Annexin V-wt	NH_2-Ala-Gln-Val...	35,805	4.94
Annexin V-122	NH_2-Ala-His-His-His-Ala-Gln-Val...	36,288	5.09
Annexin V-123	NH_2-Ala-His-His-His-His-His-His-Ala-Gln-Val...	36,699	5.26

Figure 1. Primary structures of annexin V mutants. Each mutant protein contains the indicated N-terminal extension (underlined) followed by amino acids 2−320 of human annexin V (*25*). The initiator methionine is not shown because it is removed posttranslationally. The calculated molecular mass (M_r) and calculated isoelectric point (p*I*) are listed to the right. For convenience, the mutant molecules are given arbitrary numerical designations.

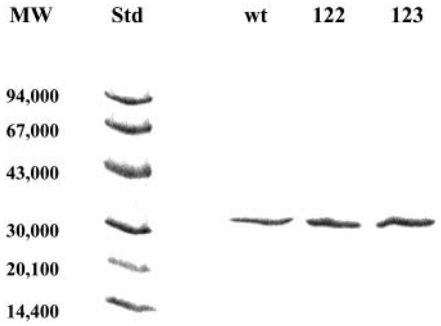


Figure 2. SDS−PAGE analysis of mutant proteins. Recombinant wild-type annexin V (wt) and the two mutant annexin V molecules (122 and 123) were analyzed on a nonreducing 10−15% gradient gel and stained with Coomassie Brilliant Blue. Molecular mass standards (with M_r in parentheses) were phosphorylase *b* (94 000), albumin (67 000), ovalbumin (43 000), carbonic anhydrase (30 000), trypsin inhibitor (20 100), and α-lactalbumin (14 400).

Table 1. Membrane Binding Activity of Mutant Proteins[a]

protein	IC_{50} (nmol/L)
annexin V-wt	9 ± 4
annexin V-122	7 ± 1
annexin V-123	6 ± 2

[a] Results are given as mean ± SD (n = 3).

duplicate tubes containing a final volume of 1 mL of buffer HNKGB plus 2.5 mmol/L $CaCl_2$. One tube then received 4.2×10^8 erythrocytes in 100 μL; the other tube received an equal volume of buffer. After a 15 min incubation at room temperature, both tubes were centrifuged for 3 min at 8320*g*. Radioactivity was measured in 800 μL of the supernatants. The percentage of radioactivity bound to the cells was calculated from 100 × [1 − (supernatant counts in the presence of cells)/(supernatant counts in absence of cells)].

RESULTS

Protein Production and Characterization. Two mutant proteins were designed to have N-terminal sequences potentially suitable for labeling with TcCO (Figure 1). Annexin V-122 has three adjacent His residues, and annexin V-123 has six. The structures of the expression constructs were verified by DNA sequencing. Both proteins could be expressed cytoplasmically in *E. coli* and purified in reasonable yield (33 mg of pure protein per liter of bacterial culture) under conditions similar to those used to produce wild-type and mutant annexin V (*14*, *23*, *26*). SDS−PAGE analysis (Figure 2) showed that both mutants could be produced in highly pure form. As expected, both mutant proteins (323 and 326 amino acids in length) also migrated with the same apparent molecular weight as wild-type annexin V (319 amino acids). Isoelectric focusing showed that the isoelectric points of the mutant proteins were consistent within 0.1 pH unit with the calculated values given in Figure 1. Gel filtration analysis (described further below) indicated that both proteins were pure and migrated as monomers. Mass spectrometry showed a single major peak at 36 287 (calculated MW 36 288) for annexin V-122, and a single major peak at 36 696 (calculated MW 36 700) for annexin V-123. These results indicate that the initiator methionine was removed from both proteins, and that there were no posttranslational modifications such as N-terminal acetylation. The bioactivity of the mutant proteins was verified by measuring their ability to compete with wild-type annexin V for binding to erythrocyte membranes with exposed PS (Table 1). Both proteins displaced fluorescein-annexin V with the same relative affinity as wild-type annexin V, indicating that attachment of the N-terminal peptide did not interfere with membrane binding.

Table 2. Radiochemical Purity and Bioactivity of Labeled Proteins[a]

protein	labeling yield (%)	radiochemical purity (%)	radioactivity bound to erythrocytes (%)
annexin V-wt	43.0 ± 3.9	91.2 ± 1.7	78.3
annexin V-122	60.6 ± 6.4	96.7 ± 0.9	80.7 ± 0.9
annexin V-123	80.6 ± 0.6	98.4 ± 0.5	85.0 ± 2.8

[a] Labeling was performed with 100 μg of protein and 1 mCi of TcCO for 60 min. Results are given as mean ± SD for two experiments.

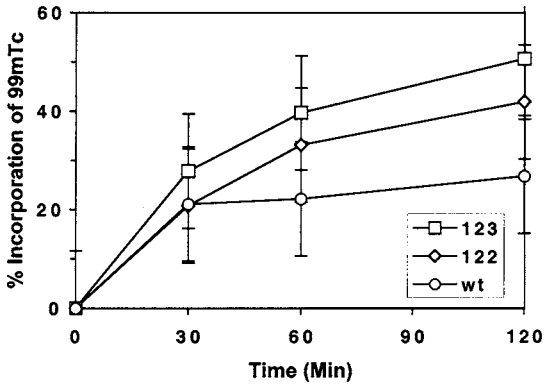


Figure 3. Time course of radiolabeling. Protein (100 μg) was reacted with ^{99m}TcCO (1 mCi) at 37 °C, and ITLC was performed on aliquots taken at the indicated times. Results are mean ± SD for two experiments.

Radiolabeling with ^{99m}Tc. Wild-type and mutant proteins were radiolabeled with TcCO (Table 2). There was some labeling of the wild-type protein, presumably due to its three endogenous histidine residues, but the two mutant proteins incorporated substantially more radioactivity. The radiolabel remained attached to protein after separation from labeling reagents, as indicated by the high radiochemical purity of gel-filtered proteins. To verify that the radiolabeled proteins retained bioactivity, radiolabeled proteins were incubated with erythrocytes in the presence of calcium, and the percentage of radioactivity bound to cells was measured. All proteins showed comparable levels of binding, and this level was comparable to the binding of ^{99m}Tc-HYNIC-annexin V and ^{99m}Tc-annexin V-117 previously tested under the same conditions (*14*). (Even with fully bioactive protein, binding never exceeds about 85% under these assay conditions because of the finite amounts of cells and protein that can be added to the assay.) The time course of labeling was fairly rapid, with most of the Tc being incorporated

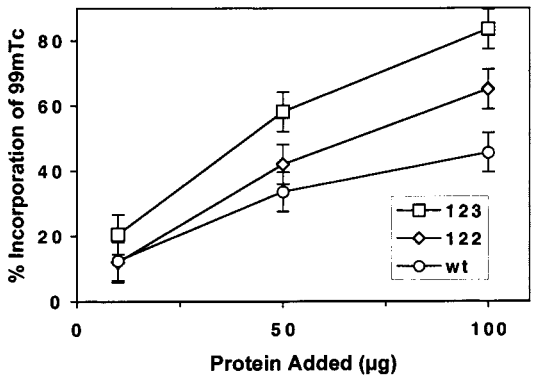


Figure 4. Radiolabeling as a function of technetium/protein ratio. Protein (10−100 μg) was added to TcCO (1 mCi). After 60 min at 37 °C, ITLC was performed on the reaction mixture to determine percent incorporation of technetium into protein. Results are mean ± SD for two experiments.

Table 3. Stability of Radiolabeled Proteins in Vitro[a]

protein	% protein-bound ^{99m}Tc in PBS[b]	% protein-bound ^{99m}Tc in serum[c]
annexin V-122 at 1 h	93.9 ± 0.8	98.4 ± 0.1
annexin V-122 at 4 h	90.1 ± 1.5	98.3 ± 0.6
annexin V-123 at 1 h	96.8 ± 1.4	99.1 ± 0.6
annexin V-123 at 4 h	95.3 ± 2.5	98.8 ± 0.4

[a] Results are given as mean ± SD for two experiments. [b] Determined by ITLC. [c] Determined by centrifugal ultrafiltration.

by 60 min (Figure 3). To determine if proteins could be labeled to higher specific activity, the technetium/protein ratio was varied. As shown in Figure 4, the specific activity could be increased by increasing the ^{99m}TcCO/protein ratio, although at a cost of lower percent incorporation; specific activities of ∼10−20 μCi/μg were readily obtainable for both mutant proteins.

Stability of Radiolabeled Proteins in Vitro. The stability of the radiolabeled protein in vitro was determined after challenge with phosphate-buffered saline and serum. ITLC or ultrafiltration analysis showed that the mutant proteins retained the radiolabel over a period of several hours, indicating that the Tc-protein chelate was of high affinity (Table 3). These results were confirmed by gel filtration chromatography (Figure 5). After incubation of ^{99m}Tc-annexin V-122 or -123 with PBS for 2 h, almost all of the radioactivity eluted in the same position as monomeric annexin V (M_r 36 000); there was no evidence for either multimeric protein aggregates or large-scale release of free Tc. Similarly, gel filtration chromatography of ^{99m}Tc-annexin V-122 or -123 after a 2 h incubation with human serum showed that the radioactivity still eluted in the same position as monomeric annexin V (Figure 5). Thus, there was no evidence for either degradation or transchelation of ^{99m}Tc to other serum proteins over a time period consistent with the normal blood clearance time of annexin V.

DISCUSSION

We have developed and evaluated two mutant forms of annexin V that contain clusters of histidine residues suitable for labeling with TcCO reagent. Both proteins can be produced in good yield and high purity by recombinant-DNA methods. These mutant molecules retain bioactivity both before and after labeling with ^{99m}Tc, as measured by their ability to bind with high affinity to cell membranes with exposed PS. Labeling of these molecules with ^{99m}TcCO is simple, and high specific

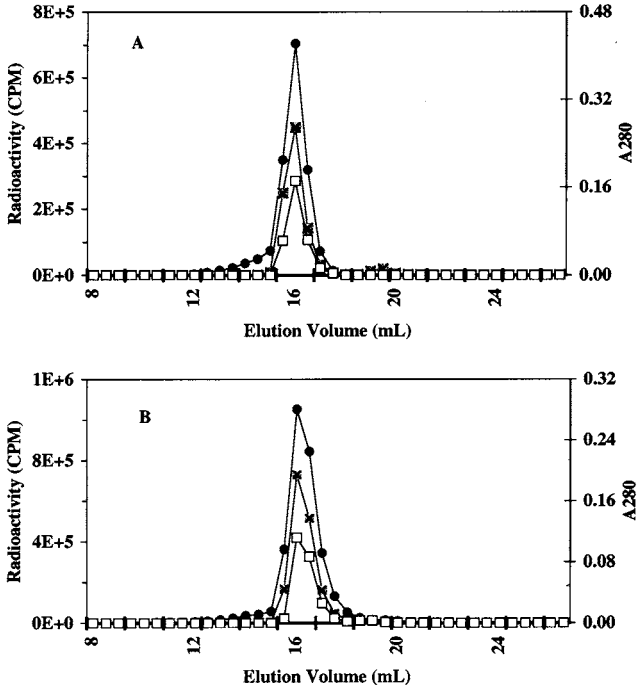


Figure 5. Gel filtration analysis. Labeled protein (50 μg in 300 μL) was mixed with either 300 μL of human serum (circles) or 300 μL of PBS (squares with x), incubated for 2 h at room temperature, and then analyzed on a Superose-12 column as described under Materials and Methods. An aliquot of unlabeled protein (500 μg; open squares) was chromatographed separately to determine the purity and elution position of unlabeled protein. Panel A: ^{99m}Tc-annexin V-122. Panel B: ^{99m}Tc-annexin V-123.

activities can be achieved. The mutant annexins show good radiolabel stability in vitro in PBS and serum, and there is no evidence for transchelation of ^{99m}Tc to other serum proteins during in vitro incubation (Figure 5). Since annexin V does not bind to normal erythrocytes, leukocytes, or platelets in whole blood (*27*), these results imply that TcCO-labeled annexin V will be confined to the plasma fraction of blood in vivo, and it will be stable in this compartment until cleared into other body compartments. Although both proteins are suitable for further development as potential in vivo imaging agents, annexin V-123 may be better than annexin V-122 since it labels to higher specific activity and has slightly higher in vitro radiostability. Presumably, the annexin V-123 mutant labels better than the V-122 mutant because it has six rather than three adjacent histidine residues. Wild-type annexin V labeled less well than either mutant protein, and would thus be the least desirable molecule for further development.

As mentioned in the introduction, there are now several methods available for technetium labeling of annexin V. Each of these methods has certain advantages and disadvantages. Recombinant proteins with endogenous labeling sites are much simpler to produce, since they can be used directly for ^{99m}Tc labeling without the need for attachment of organic Tc chelation groups either during production or at the point of use. The annexin V mutants are also chemically homogeneous, in contrast to the heterogeneous labeling that usually occurs with amine-directed bifunctional organic labeling reagents used on proteins with multiple lysine residues. On the other hand, methods involving derivatization with chemical groups such as N_2S_2 or HYNIC have longer track records to date, which may simplify clinical testing and regulatory approval. The possible immunogenicity of both

chemically modified proteins and recombinant proteins is unknown. The HYNIC-annexin V and annexin V-117 derivatives are the simplest to use in the clinical setting, since both can be labeled with short one-step reactions performed at room temperature or 37 °C; in contrast, the TcCO labeling is a two-step procedure in which the TcCO compound must be first formed in a separate reaction at high temperature, while the N_2S_2 method is a rather complex multistep procedure.

In conclusion, we have shown the feasibility of labeling annexin V with the TcCO reagent, and the novel mutant molecules reported here are promising for future imaging studies of apoptosis, cancer chemotherapy, and myocardial infarction.

ACKNOWLEDGMENT

We thank Alex Pagon for excellent assistance in initial efforts to construct expression vectors; Ross Lawrence of the Department of Medicinal Chemistry for performing mass spectrometry measurements; and Dr. J.-L. Vanderheyden for helpful advice on preparation of the TcCO reagent. This work was supported by a grant from Theseus Medical Imaging, Inc., and by NIH Grant HL-61717.

LITERATURE CITED

(1) Thiagarajan, P., and Tait, J. F. (1990) Binding of annexin V/placental anticoagulant protein I to platelets. Evidence for phosphatidylserine exposure in the procoagulant response of activated platelets. *J. Biol. Chem. 265*, 17420−17423.

(2) Zwaal, R. F., and Schroit, A. J. (1997) Pathophysiologic implications of membrane phospholipid asymmetry in blood cells. *Blood 89*, 1121−1132.

(3) Bevers, E. M., Comfurius, P., Dekkers, D. W., and Zwaal, R. F. (1999) Lipid translocation across the plasma membrane of mammalian cells. *Biochim. Biophys. Acta 1439*, 317−330.

(4) Tait, J. F., Cerqueira, M. D., Dewhurst, T. A., Fujikawa, K., Ritchie, J. L., and Stratton, J. R. (1994) Evaluation of annexin V as a platelet-directed thrombus targeting agent. *Thromb. Res. 75*, 491−501.

(5) Stratton, J. R., Dewhurst, T. A., Kasina, S., Reno, J. M., Cerqueira, M. D., Baskin, D. G., and Tait, J. F. (1995) Selective uptake of radiolabeled annexin V on acute porcine left atrial thrombi. *Circulation 92*, 3113−3121.

(6) Blankenberg, F. G., Katsikis, P. D., Tait, J. F., Davis, R. E., Naumovski, L., Ohtsuki, K., Kopiwoda, S., Abrams, M. J., Darkes, M., Robbins, R. C., Maecker, H. T., and Strauss, H. W. (1998) In vivo detection and imaging of phosphatidylserine expression during programmed cell death. *Proc. Natl. Acad. Sci. U.S.A. 95*, 6349−6354.

(7) Blankenberg, F. G., Katsikis, P. D., Tait, J. F., Davis, R. E., Naumovski, L., Ohtsuki, K., Kopiwoda, S., Abrams, M. J., and Strauss, H. W. (1999) Imaging of apoptosis (programmed cell death) with 99mTc annexin V. *J. Nucl. Med. 40*, 184−191.

(8) Vriens, P. W., Blankenberg, F. G., Stoot, J. H., Ohtsuki, K., Berry, G. J., Tait, J. F., Strauss, H. W., and Robbins, R. C. (1998) The use of technetium Tc 99m annexin V for in vivo imaging of apoptosis during cardiac allograft rejection. *J. Thorac. Cardiovasc. Surg. 116*, 844−853.

(9) Blankenberg, F. G., Robbins, R. C., Stoot, J. H., Vriens, P. W., Berry, G. J., Tait, J. F., and Strauss, H. W. (2000) Radionuclide imaging of acute lung transplant rejection with annexin V. *Chest 117*, 834−840.

(10) Ogura, Y., Krams, S. M., Martinez, O. M., Kopiwoda, S., Higgins, J. P., Esquivel, C. O., Strauss, H. W., Tait, J. F., and Blankenberg, F. G. (2000) Radiolabeled annexin V imaging: diagnosis of allograft rejection in an experimental rodent model of liver transplantation. *Radiology 214*, 795−800.

(11) Narula, J., Acio, E. R., Narula, N., Samuels, L. E., Fyfe, B., Wood, D., Fitzpatrick, J. M., Raghunath, P. N., Tomaszewski, J. E., Kelly, C., Steinmetz, N., Green, A., Tait, J. F., Leppo, J., Blankenberg, F. G., Jain, D., and Strauss H. W. (2001) Annexin-V imaging for noninvasive detection of cardiac allograft rejection. *Nat. Med. 7*, 1347−1352.

(12) Hofstra, L., Liem, I. H., Dumont, E. A., Boersma, H. H., van Heerde, W. L., Doevendans, P. A., De Muinck, E., Wellens, H. J., Kemerink, G. J., Reutelingsperger, C. P., and Heidendal, G. A. (2000) Visualization of cell death in vivo in patients with acute myocardial infarction. *Lancet 356*, 209−212.

(13) Fritzberg, A. R., Abrams, P. G., Beaumier, P. L., Kasina, S., Morgan, A. C., Rao, T. N., Reno, J. M., Sanderson, J. A., Srinivasan, A., Wilbur, D. S., et al. (1988) Specific and stable labeling of antibodies with technetium-99m with a diamide dithiolate chelating agent. *Proc. Natl. Acad. Sci. U.S.A. 85*, 4025−4029.

(14) Tait, J. F., Brown, D. S., Gibson, D. F., Blankenberg, F. G., and Strauss, H. W. (2000) Development and characterization of annexin V mutants with endogenous chelation sites for (99m)Tc. *Bioconjugate Chem. 11*, 918−925.

(15) Alberto, R., Schibli, R., Egli, A., and Schubiger, A. P. (1998) A novel organometallic aqua complex of technetium for labeling of biomolecules. *J. Am. Chem. Soc. 120*, 7987−7988.

(16) Egli, A., Alberto, R., Tannahill, L., Schibli, R., Abram, U., Schaffland, A., Waibel, R., Tourwe, D., Jeannin, L., Iterbeke, K., and Schubiger, P. A. (1999) Organometallic 99mTc-aquaion labels peptide to an unprecedented high specific activity. *J. Nucl. Med. 40*, 1913−1917.

(17) Waibel, R., Alberto, R., Willuda, J., Finnern, R., Schibli, R., Stichelberger, A., Egli, A., Abram, U., Mach, J. P., Pluckthun, A., and Schubiger, P. A. (1999) Stable one-step technetium-99m labeling of his-tagged recombinant proteins with a novel Tc(I)-carbonyl complex. *Nat. Biotechnol. 17*, 897−901.

(18) Du, J., Hiltunen, J., Marquez, M., Nilsson, S., and Holmberg, A. R. (2001) Technetium-99m labeling of glycosylated somatostatin-14. *Appl. Radiat. Isot. 55*, 181−187.

(19) Knight, L. C., Baidoo, K. E., Marmion, M. E., and Romano, J. E. (2000) Tc-99m tricarbonyl labeling of DTPA-bitistatin for imaging thrombi and emboli. *Nucl. Med. Commun. 21*, 589.

(20) Schibli, R., La Bella, R., Alberto, R., Garcia-Garayoa, E., Ortner, K., Abram, U., and Schubiger, P. A. (2000) Influence of the denticity of ligand systems on the in vitro and in vivo behavior of (99m)Tc(I)-tricarbonyl complexes: a hint for the future functionalization of biomolecules. *Bioconjugate Chem. 11*, 345−351.

(21) Tait, J. F., Engelhardt, S., Smith, C., and Fujikawa, K. (1995) Prourokinase-annexin V chimeras. Construction, expression, and characterization of recombinant proteins. *J. Biol. Chem. 270*, 21594−21599.

(22) Tanaka, K., Einaga, K., Tsuchiyama, H., Tait, J. F., and Fujikawa, K. (1996) Preparation and characterization of a disulfide-linked bioconjugate of annexin V with the B-chain of urokinase: an improved fibrinolytic agent targeted to phospholipid-containing thrombi. *Biochemistry 35*, 922−929.

(23) Wood, B. L., Gibson, D. F., and Tait, J. F. (1996) Increased erythrocyte phosphatidylserine exposure in sickle cell disease: flow-cytometric measurement and clinical associations. *Blood 88*, 1873−1880.

(24) Tait, J. F., Gibson, D., and Fujikawa, K. (1989) Phospholipid binding properties of human placental anticoagulant protein-I, a member of the lipocortin family. *J. Biol. Chem. 264*, 7944−7949.

(25) Funakoshi, T., Hendrickson, L. E., McMullen, B. A., and Fujikawa, K. (1987) Primary structure of human placental anticoagulant protein. *Biochemistry 26*, 8087−8092.

(26) Tait, J. F., and Smith, C. (1991) Site-specific mutagenesis of annexin V: role of residues from Arg-200 to Lys-207 in phospholipid binding. *Arch. Biochem. Biophys. 288*, 141−144.

(27) Tait, J. F., Smith, C., and Wood, B. L. (1999) Measurement of phosphatidylserine exposure in leukocytes and platelets by whole-blood flow cytometry with annexin V. *Blood Cells Mol. Dis. 25*, 271−278.

BC025545S

Copolymers of Ethylene Imine and *N*-(2-Hydroxyethyl)-ethylene Imine as Tools To Study Effects of Polymer Structure on Physicochemical and Biological Properties of DNA Complexes

Dagmar Fischer,[†,‡] Anke von Harpe,[‡,§] Klaus Kunath,[†] Holger Petersen,[†] Youxin Li,[||] and Thomas Kissel*[,†]

Department of Pharmaceutics and Biopharmacy, University of Marburg, Ketzerbach 63, 35032 Marburg, Germany, Procter & Gamble Pharmaceuticals, Dr. Otto Röhm-Strasse 2-4, 64331 Weiterstadt, Germany, and Schwarz Pharma AG, Alfred-Nobel-Strasse 10, 40789 Monheim, Germany.
Received May 14, 2002; Revised Manuscript Received June 27, 2002

A series of five poly[(ethylene imine)-*co*-*N*-(2-hydroxyethyl-ethylene imine)] copolymers with similar molecular weights and different degrees of branching was established to study structure−function relationship with regard to physicochemical and biological properties as gene delivery systems. Copolymers were synthesized by acid-catalyzed ring-opening copolymerization of aziridine and *N*-(2-hydroxyethyl)-aziridine in aqueous solution and characterized by GPC-MALLS, ^{1}H- and ^{13}C NMR, IR, potentiometric titration, and ion exchange chromatography. Complexation of DNA was determined by agarose gel electrophoresis, and complex sizes were quantitated by PCS. Cytotoxicity of the copolymers in fibroblasts was assessed by MTT-assay, LDH-assay, and hemolysis. The transfection efficiency was determined using the reporter plasmid pGL3 in 3T3 mouse fibroblasts. The copolymers obtained by solution polymerization had relatively low molecular weights of about 2000 Da, and the degree of branching increased with increasing ethylene imine ratio. The pK_a as well as the buffer capacity increased proportional to the number of primary and secondary amines. Higher branched polymers showed stronger complexation and condensation of DNA, formed smaller polymer/DNA complexes, and induced the expression of plasmids to a higher extent than less branched polymers. In vitro cytotoxic effects and the hemolysis of erythrocytes decreased with decreased branching. Our results indicate that the basicity and degree of protonation of the polymers depending on their amount of primary and secondary amines seem to be important factors both for their transfection efficiency and for their cytotoxicity in gene transfer.

INTRODUCTION

The polycation polyethylene imine (PEI)[1] is generally regarded as a useful reagent for nonviral delivery of DNA and RNA under both in vitro and in vivo conditions (Remy et al., 1998). PEI, compared to other nonviral vectors, is assumed to affect endosomal escape and the enzymatic protection of DNA and RNA (Behr, 1997). PEI is commercially available with different average molecular weights and degrees of branching. The transfection efficiencies, cytotoxicity, and DNA binding characteristics of PEI have been discussed somewhat controversially in the literature (Fischer et al., 2000; Gebhart and Kabanov, 2001). Systematic studies probing the relationship between the structure of PEI, especially the molecular weight, the degree of branching, the relative ratio of amino functions, and physicochemical and biological effects, are rare.

DNA delivery using PEI was found to depend on the molecular weight of the polymer. Often highly branched PEIs with molecular weights in the range from 25 to 800 kDa were reported to be useful for gene delivery. These PEI/DNA complexes yield high levels of transgene expression in many cell lines and primary cells under in vitro conditions (Boussif et al., 1996; Erbacher et al., 1999), as well as in vivo, e.g., in kidney, lung, and brain (Abdallah et al., 1997; Boletta et al., 1997; Lecocq et al., 2000). Cytotoxic effects, however, limit their utility. Comparing the potential for transgene expression of highly branched PEI with molecular weights in the range from 0.6 to 70 kDa, Godbey et al. (1999) observed an increase in gene expression with increasing molecular weight of the polymers. The transfection efficiency for 1.8 kDa PEI was essentially zero. The inability of PEIs <2 kDa to yield gene expression was also described by others (Baker et al., 1997; Remy et al., 1998). We synthesized a PEI of low molecular weight and a low degree of branching compared to the commercially available PEIs. Despite its relatively low molecular weight, LMW-PEI was efficient and less cytotoxic than 800 kDa

* Address correspondence to this author at the Department of Pharmaceutics and Biopharmacy, Philipps-University, Ketzerbach 63, D-35032 Marburg/Lahn, Germany. Tel: (0049)-6421-282-5881; Fax: (0049)-6421-282-7016; E-mail: kissel@mailer.uni-marburg.de.

† University of Marburg.

‡ These authors contributed equally to this work.

§ Procter & Gamble Pharmaceuticals.

|| Schwarz Pharma AG.

[1] Abbreviations: DNA deoxyribonucleic acid, EI ethylene imine, HEEI N−(2-hydroxyethyl) ethylene imine, HMW high molecular weight, IR infrared, LDH lactate dehydrogenase, LMW low molecular weight, MALLS multiple angle laser light scattering, MTT 3-(4,5-dimethylthiazol-2-yl)-2,5-diphenyl tetrazolium bromide, MW molecular weight, NMR nuclear magnetic resonance, PCS photon correlation spectroscopy, PEI poly(ethylene imine), PEIHEEI poly[(ethylene imine)-*co*-N−(2-hydroxyethyl-ethylene imine)], SEC size exclusion chromatography.

10.1021/bc025550w CCC: $22.00 © 2002 American Chemical Society
Published on Web 08/29/2002

PEI (Fischer et al., 1999). In addition to branched PEI, also linear polymers (22 kDa) have become commercially available (ExGen 500). Linear PEI efficiently transfected lung epithelial cells as well as the central nervous system of mice in vivo without any signs of acute toxicity (Ferrari et al., 1997; Goula et al., 1998).

Both the structure of branched PEI and its buffer capacity were thought to be relevant for the escape mechanism from endosomes, also known as the proton sponge mechanism (Behr, 1997), postulating that endo/lysosomal release of the DNA/PEI-polyplexes occurs after protonation of PEI and subsequent swelling of the polymer. Boletta et al. (1997) reported that branched PEI 25 kDa was superior to linear PEI 22 kDa under in vivo conditions in kidney cells. Also branched PEI appeared to be more effective in condensing DNA at low N/P ratios as compared to the 22 kDa product (Dunlap et al., 1997). However, in other studies linear PEI was found to be superior to the branched form (Ferrari et al., 1997). A dependency of cytotoxicity and transfection of cells on molecular weight and charge density of the linear form was also reported (Jeong et al., 2001). Consequently, we hypothesized that the efficiency and cytotoxicity of PEI as a nonviral vector system may depend not only on the molecular weight, but also on the structure of PEI. The optimal structure of PEI for gene delivery is not yet known with certainty.

We synthesized a series of five PEI derivatives by copolymerization of aziridine and *N*-(2-hydroxyethyl)-aziridine, a reagent which allowed a systematic manipulation of the degree of branching. Homo- and copolymers of comparable molecular weights were then used to determine the influence of polymer structure on in vitro cytotoxicity, DNA-binding characteristics, polyplex formation, and transfection efficiency.

EXPERIMENTAL PROCEDURES

Synthesis of Poly[(ethylene imine)-*co*-*N*-(2-hydroxyethyl-ethylene imine)] Copolymers. Aziridine was prepared from mono-ethanolamine (Fluka, Deisenhofen, Germany) as described by Wenker (1935). Aziridine and *N*-(2-hydroxyethyl)-aziridine (Sigma, Deisenhofen, Germany) monomers were copolymerized in different molar ratios by cationic ring-opening polymerization according to the procedure described earlier (von Harpe et al., 2000). For purification, the reaction mixtures were cooled to room temperature and neutralized with sodium hydroxide, and water was removed under reduced pressure (50 °C, 10 mbar). The crude polymers were redissolved in ethanol and precipitated in diethyl ether. After recovery, the polymers were dried at 50 °C in a vacuum for 3 weeks.

Physicochemical Characterization of the Copolymers. *Molecular weight and distribution* of the copolymers were determined using SEC in combination with multiple angle laser light scattering (MALLS). Formic acid (1%) was used as eluent with a flow rate of 1 mL/min. The column, Novema 100, was purchased from Polymer Standard Service (PSS, Mainz, Germany). The refractive index detector from Merck-Hitachi (RI-71), equipped with an 18 angle light scattering detector, DAWN EOS (Enhanced Optical System) from Wyatt Technology Corp. (Santa Barbara, CA) and in line with the RI detector, allowed the determination of the absolute MW. The weight average MW was determined using a Zimm plot (ASTRA software version 4.73). Refractive index increments, d*n*/d*c*, for the copolymers were calculated with the same software using the data from the RI detector and the polymer concentration.

Infrared spectroscopy was conducted with a Nicolet 510 FT-IR spectrometer and PC/IR v. 3.20 software using potassium bromide disks (Merck, Darmstadt, Germany).

^{1}H NMR and ^{13}C NMR spectra were recorded in deuterium oxide (D_2O, Merck, Darmstadt, Germany) with a LA 500 Eclipse+ Delta FT spectrometer (JEOL, USA) at 500 MHz for ^{1}H and 125 MHz for ^{13}C spectra. To suppress the nuclear Overhauser effect (NOE), all ^{13}C spectra used for quantitative analysis were recorded using inverse gated decoupling pulse sequences. Spectra were evaluated with the NMR data processing program WinNuts 2D (Acorn NMR). Signal intensities of ^{13}C NMR spectra were determined relative to signal 3 (Figure 2).

Buffer capacities of 0.1 mol/L PEI solutions were measured in bidistilled water by potentiometric titration with a Schott CG820 pH meter using 0.1 N HCl (Titrisol, Merck) as the titrant. Each determination was carried out in triplicate at 25 ± 0.1 °C according to Suh et al. (1994). The buffer capacity was calculated as described in Seel (1970).

A CM-Sephadex C50 cation exchanger column (bed volume 6.5 mL, Pharmacia Biotech, Freiburg, Germany), equilibrated with 0.1 M sodium borate, pH 10.0, was used for ion exchange chromatography. Two milligrams of copolymer in 300 μL of distilled water was loaded onto the column and eluted with a gradient of 0.1 M sodium borate, pH 10−13. Fractions were collected and analyzed for polymer content after Cu(II) chelation at 635 nm using UV spectrophotometry as described previously (von Harpe et al., 2000).

DNA-Binding Characteristics and Complex Size. DNA from herring testes (Sigma) was purified by ultrafiltration to remove low molecular weight impurities (cutoff: 300 kDa; Millipore, Eschborn, Germany) and adjusted to a final concentration of 1.0 mg/mL (determined by UV 260/280 nm ratio). Ten micrograms of herring testes DNA and the appropriate amounts of the polymer stock solutions (0.9 mg/mL, pH 7.4) were complexed as described earlier (Fischer et al., 1999). The complex composition was calculated on the basis of PEI nitrogen (N) per DNA phosphate (P) and expressed as the N/P ratio.

Electrophoresis was carried out in 1% agarose gels containing ethidium bromide with a current of 80 V. The DNA localization was visualized by UV transillumination at 254 nm (Fischer et al., 1999). The intensity of the gel bands was determined using Scion Image Beta 4.02 software (Scion Corp., Frederick, MD). An intensity profile of the area at the origin was examined by measuring the size of the peaks corresponding to the individual bands.

Polymer/DNA complexes were prepared as described above using 40 μg of purified DNA from herring testes in a final volume of 500 μL of 50 mM NaCl/3.3% glucose for size measurements. The complexes were measured by photon correlation spectroscopy (PCS) at 25 °C with a Zetasizer 4 (Malvern Instruments, Herrsching, Germany) equipped with a nominal 5 mW helium neon laser and Malvern software version 1.26. Samples were measured in the AZ 110 cell at 633 nm and a scattering angle of 90 °C. The viscosity and refractive index of pure water at 25 °C were used for data analysis.

Cytotoxicity Assays. The MTT assay was performed as described previously (Fischer et al., 1999) using the L929 mouse fibroblast cell line (DSMZ, Braunschweig, Germany).

LDH release was studied in L929 cells (25 000/well) seeded in 6-well multidishes (Gibco, Eggenstein, Germany) and incubated for 48 h. Cell culture medium was

Table 1. Relative Ratio of Primary, Secondary, and Tertiary Amino Groups in the Polymers and Degree of Branching[a]

EI/HEEI molar ratio	primary amino groups (%)	secondary amino groups (%)	tertiary amino groups (%)	branches (%)	Mn (kDa)	Mw (kDa)	Mw/Mn	d*n*/d*c* (mL/g)	yield (%)
PEI 100/0	26.4	50.5	23.1	23.1	2.000	2.660	1.34	0.333	54
PEIHEEI 76/24	19.3	46.1	34.6	18.5	1.490	2.070	1.39	0.291	64
PEIHEEI 61/39	13.2	42.2	44.6	17.7	1.650	2.290	1.39	0.268	75
PEIHEEI 44/56	8.5	33.7	57.8	14.0	1.540	2.120	1.38	0.248	75
PEIHEEI 27/73	4.6	26.5	68.9	10.7	1.470	2.160	1.47	0.234	84
PEIHEEI 7/93	2.3	14.0	83.7	6.0	1.290	1.930	1.49	0.226	61
LMW-HEEI 0/100	0	8.9	91.1	0	1.800	2.530	1.40	0.213	75
HMW-HEEI 0/100	0	2.0	98.0	0	6.980	8.700	1.25	0.182	15

[a] Calculated from ^{13}C NMR analysis. The molecular weight was determined by GPC as described under Experimental Procedures. An increase in the HEEI content of the copolymers resulted in a decrease of the primary amino groups and reduced the degree of branching. The molecular weights of the copolymers were in a comparable range from Mw 1.925 to 2.291 kDa.

replaced by 2 mL of the polymer solutions, and 100 μL samples were withdrawn after 1, 3, 6, and 11 h of exposure. The LDH content of the samples was measured using a commercial test kit (DG 1340-K, Sigma). Control experiments were performed with 0.1% (w/v) Triton X-100, and the resulting values were set to 100% cytotoxicity.

The hemolytic activity of the polymers was tested according to Parnham and Wetzig (1993). Blood, collected in heparinized tubes from Wistar rats, was centrifuged at 700*g* for 10 min, washed 3 times with cold PBS, pH 7.4, and resuspended in the same buffer. The erythrocyte suspension was freshly prepared for every experiment and used within 24 h. The polymer solutions of different concentrations were mixed with the red blood cell suspension and were incubated at 37 °C for 60 min in a shaking water bath. The release of hemoglobin was investigated after centrifugation (700*g* for 10 min) by spectrophotometric measurement of the absorbance of the supernatant at 540 nm. Complete hemolysis of a control aliquot was achieved with 0.2% (w/v) Triton X-100 and the effect of the polymers expressed as relative percentage of hemoglobin.

Transfection Experiments under in Vitro Conditions. pGL3-control plasmid from Promega (Mannheim, Germany) was amplified in JM109 competent cells (Promega) and purified using QIAfilter kits (Qiagen, Hilden, Germany) according to the manufacturer's protocol. Transfection experiments were carried out in triplicate in NIH 3T3 cells (Fischer et al., 1999). Luciferase expression was evaluated using a commercial kit (Luciferase Assay System, Promega) and a Berthold Sirius luminometer (Berthold, Pforzheim, Germany). Cells were washed twice with PBS, lysed in cell culture lysis reagent (200 μL/well), transferred into Eppendorf vials, and centrifuged at 18000*g* for 5 min. Then 20 μL of the supernatant was mixed with 100 μL of luciferase assay reagent, and luminescence was determined immediately in relative light units per second as the mean of a 10 s measurement time. RLUs were converted into nanograms of luciferase by creating a calibration curve with recombinant luciferase (Promega). Protein concentrations in the samples were analyzed using a modified BCA assay (Pierce, Rockford, IL) (*25*). Undesired DTT was inactivated with iodoacetamide before the addition of the BCA assay reagent (Hill et al., 1988). Absorption was measured on a Dynatech MR5000 plate reader (Dynatech, Denkendorf, Germany) at 570 nm and compared to a standard curve calibrated with BSA samples of known concentrations.

RESULTS AND DISCUSSION

Synthesis and Structural Characterization of the Copolymers. Homo- and copolymers with a composition of 0, 7, 27, 44, 61, 76, and 100% (w/w) aziridine, respectively, were synthesized by acid-catalyzed polymerization of aziridine with *N*-(2-hydroxyethyl) aziridine in aqueous solutions. The polymerization of aziridine resulted in a branched polymer, in which approximately one-fourth of all nitrogen atoms formed branches (Dick and Ham, 1970). In contrast, the polymerization of PEI and HEEI led to copolymers with a lower degree of branching, since branches originate only from aziridine monomers, due to substitution of HEEI. The synthesis was reproducible with respect to composition and structure (data not shown). All polymers were obtained as free bases and had a colorless, clear, highly viscous appearance. Product yields varied between 54 and 84% (Table 1). The homo- and copolymers were characterized with regard to molecular weight, monomer composition, distribution of the different amino groups, and degree of branching. Table 1 summarizes the characteristics of the polymers used in this investigation.

All polymers showed similar molecular weights (Mn 1500 Da and Mw 2500 Da). Polydispersities were relatively narrow with a polydispersity index (Mw/Mn) of approximately 1.4. Significant differences were only observed for the refractive index increment (d*n*/d*c*), which is a function of the copolymer composition. An increasing amount of ethylene imine repeating units in the copolymer was shown to increase the d*n*/d*c* (Table 1).

As determined by IR and ^1H NMR spectroscopy, the polymer composition corresponded exactly to the monomer composition in the feed. In IR spectra, the C−O stretching absorption at 1050 cm^{-1} increased with increasing content of hydroxyethyl groups, whereas the N−H bending absorption band at 1590 cm^{-1} decreased, due to the increasing number of tertiary amino groups in the molecule. O−H bending absorption at 1400−1200 cm^{-1} was covered by C−N streching (1300−1200 cm^{-1}) and C−H rocking absorption bands at 1450 cm^{-1} (Figure 1). In ^1H NMR spectra, two signals were observed, one at 2.6 ppm for CH_2−N and one at 3.6 ppm for CH_2−O.

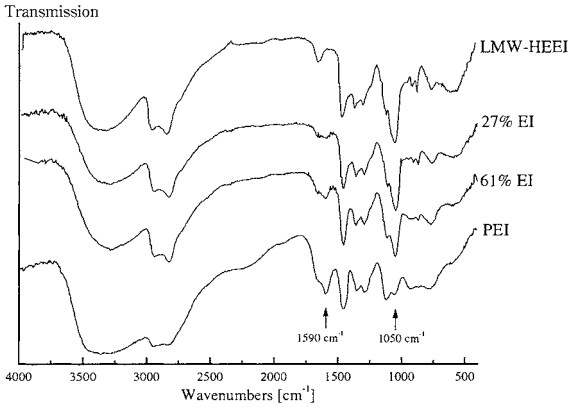
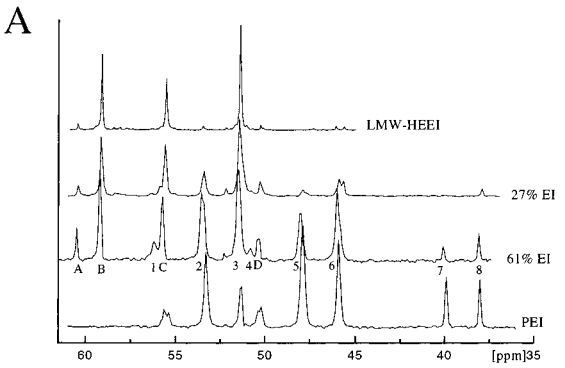


Figure 1. Infrared spectra of selected co- and homopolymers. Absorption bands at 1590 cm^{-1} (N−H, only in EI-containing polymers) and 1050 cm^{-1} (C−O, only in HEEI-containing polymers) are highlighted to show the main differences between the polymers. The polymer composition was found to correspond to the monomer feed.

The ratio of HEEI to EI monomer units in each polymer was calculated from the ratio of these two signals, and again, the results showed that the polymer composition exactly corresponded to monomer feed. Additional signals from residual monomer traces could not be detected in any of the spectra recorded. Since methylene groups adjacent to primary, secondary, or tertiary amino groups could not be distinguished in the ^{1}H NMR spectra, ^{13}C NMR spectroscopy was employed for further structural information. The signals in the ^{13}C NMR spectra appeared between 38 and 61 ppm. Whereas some of the same signals and corresponding structures originated from pure PEI (von Harpe et al., 2000), additional signals appeared for the carbon atoms of the hydroxyethyl side chain and those directly next to a hydroxyethyl-substituted nitrogen. Typical ^{13}C NMR spectra of PEI, PEIHEEI containing 61 and 27 mol % EI, and pure LMW-HEEI are shown in Figure 2A. The signals of the corresponding methylene groups were assigned as indicated (Figure 2B). Results of 2D-INADEQUATE ^{13}C NMR experiments verified the signal assignment proposed here (Figure 3).

The ratio of the different amino groups in the polymers (Table 1) was calculated from signal intensities in ^{13}C NMR spectra as described in von Harpe et al. (2000). The degree of branching increased with increasing ethylene imine content. In pure LMW-HEEI, no branching was observed. The secondary amino groups found in this polymer resulted from the initialization step of the polymerization, during which the addition of a proton formed a secondary amine function. All tertiary amino groups in this polymer were formed by a hydroxyethyl-substituted nitrogen atom and, therefore, did not contribute to branching. In the homopolymer, PEI, on the other hand, all tertiary amino groups can be potential branching points. For the copolymers, signals C and 3 allowed not only the determination of tertiary amino groups, but also the calculation of branching points formed by EI monomer units. Even at values as low as 7 mol % EI branching (6%) occurred, and with increasing EI content, the branching increased up to 23.1% in pure PEI. The content of primary amino groups in the copolymers could be directly correlated to the content of EI monomer ($R = 0.987$). The ratio of the different amino groups and the degree of branching are shown in Table 1.

The commercially available N-substituted aziridine was used to manipulate the three-dimensional structure of PEI since it polymerizes via the same acid-catalyzed



B

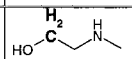
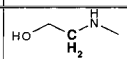
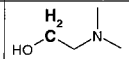
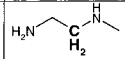
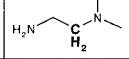
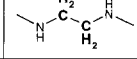
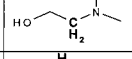
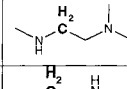
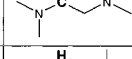
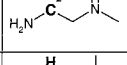
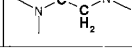
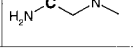
Label	Corresponding Structure	Label	Corresponding Structure
A		D	
B		4	
1		5	
C		6	
2		7	
3		8	

Figure 2. (A) ^{13}C NMR spectra of selected co- and homopolymers. From ^{13}C NMR, the distribution of the different amino groups has been calculated. With increasing EI content, the degree of branching increased up to 23.1% in pure PEI. (B) Labels and corresponding structural elements for ^{13}C NMR spectra.

ring-opening polymerization mechanism as ethylene imine and contains a "protective" group generating linear structures. Furthermore, hydroxyethyl groups do not compromise the hydrophilicity of the copolymers. The polymerization of HEEI in various organic solvents has been described earlier (Rivas et al., 1991). The copolymerization of aziridine with HEEI allowed the manipulation of the degrees of branching at similar molecular weights.

Characterization of Basicity and Protonation Behavior. Polymer solutions of equivalent nitrogen concentrations were examined to determine the influence of polymer structure on the protonation behavior. Potentiometric titration with 0.1 N HCl yielded titration curves as shown in Figure 4A. As found in homo-PEI (von Harpe et al., 2000), an area of high buffer capacity is situated above the physiological pH range, namely, between 8 and 10, an area characteristic for polyamines. With an increase of EI monomer, an increase of pK_a and buffer capacity was observed which is mainly due to a lower basicity of the hydroxyethyl-substituted nitrogens. Second, the higher degree of branching with increasing EI content is another important factor due to the higher basicity of the primary and secondary groups compared to the tertiary ones. Between pH 4.5 and 6, a second area of buffer capacity was detected, which was not as distinct as the first one. In this range, our polymers showed comparable basicity.

Analysis of the copolymers by ion exchange chromatography revealed a similar behavior as found in the titration study. The polymers were bound to the ex-

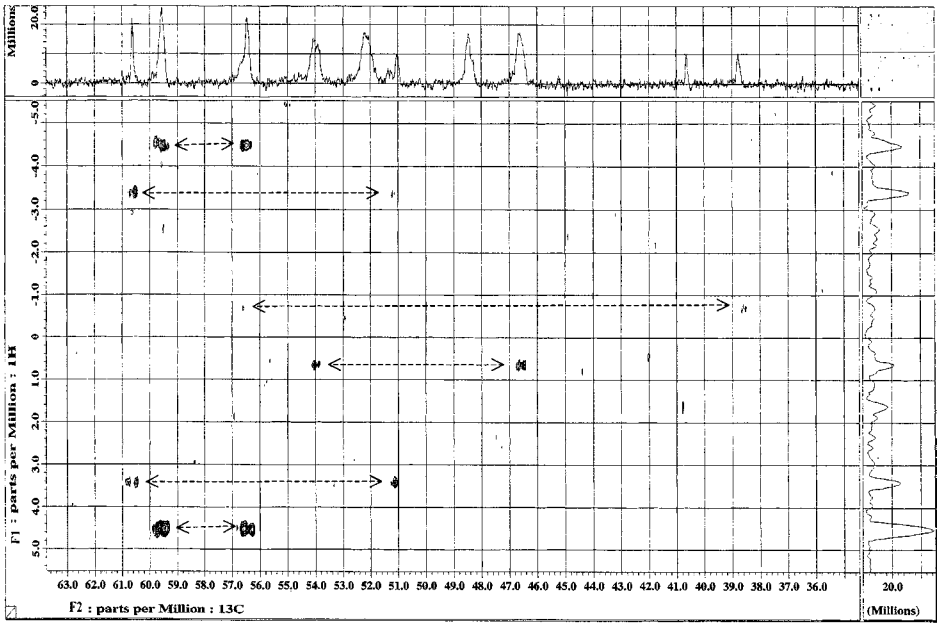


Figure 3. 2D-^{13}C INADEQUATE-NMR spectrum of PEIHEEI copolymer containing 61 mol % EI.

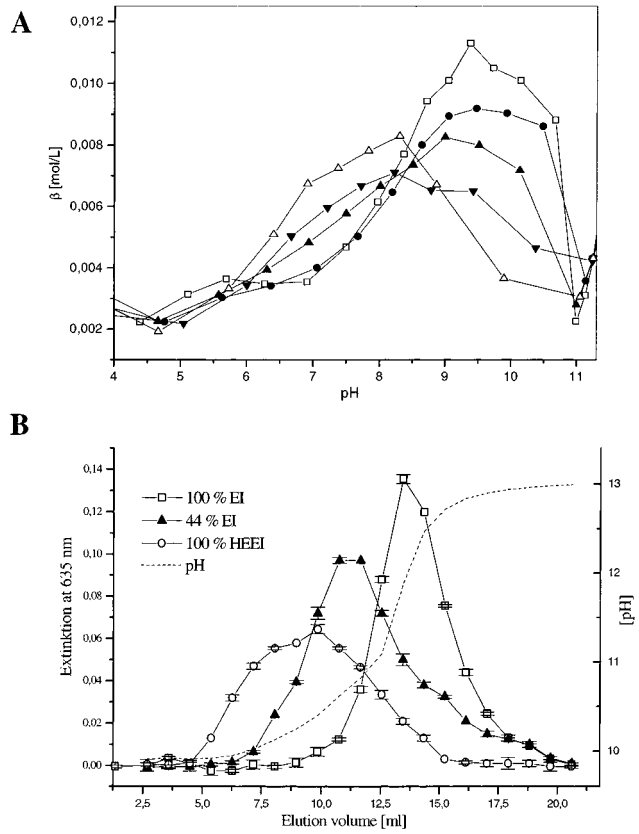


Figure 4. (A) Buffer capacities (β) of PEI and PEIHEEI copolymers in solution as a function of pH (△, LMW-HEEI 0/100; ▼, PEIHEEI 7/93; ▲, PEIHEEI 44/56; ●, PEIHEEI 76/24; - □ -, PEI 100/0). Buffer capacities were calculated from potentiometric titration curves according to Perrine and Landis (1967). The titration analysis showed an increase of pK_a value and buffer capacity with increasing ethylene imine content. (B) Ion exchange chromatography of the polymers on CM-Sephadex G50 cation exchanger. Polymers with high EI content required a higher pH for elution from the column than those with low EI content.

changer resin under loading conditions (pH 10.0). Increasing buffer pH during elution reduced polymer protonation, and the polymer was released from the column. Polymers with high EI content required a higher pH for elution from the column than those with low EI content (Figure 4B), which is consistent with the different pK_a values found by titrations and results in a higher proton affinity with increasing EI content and branching. In accordance to the structural results described above, the fact that all copolymers eluted as one single peak at a pH between the elution pHs of the two homopolymers again demonstrates that copolymers were obtained and not mixtures of homopolymers. Furthermore, the interactions between the ion-exchange resin and the polymers can be used as model for the binding of DNA, which is also driven by electrostatic interactions. Therefore, one would expect stronger interpolyelectrolyte interactions with increasing ethylene imine content of the copolymers. Consequently, the binding of the negatively charged DNA with the cationic polymers was determined by agarose gel electrophoresis.

DNA Binding and Complex Formation. Complexes of all polymers were formed with DNA from herring testes (3−4 kbp) as model DNA at an N/P ratio of 66 (Figure 5A). This ratio was chosen due to the preliminary experiments with LMW-PEI (Fischer et al., 1999). Free DNA (lane 1) gave a broad fluorescent band corresponding to its broad molecular weight distribution. The five PEIHEEI copolymers (lanes 2−6) showed complete retardation of the DNA at the origin, indicating complete complexation of the DNA at this N/P ratio. However, we observed that the fluorescence of the complexes at the origin increased with increasing HEEI content of the copolymers. We interpret the extent of ethidium bromide exclusion from DNA as a reflection of DNA condensation. Higher extents of dye displacement are compatible with a higher fraction of DNA compacted by the polycations. LMW-HEEI completely retained the DNA in the starting position, but showed the highest fluorescence, i.e., the lowest DNA condensation. For HMW-HEEI, we found comparable results indicating a negligible effect of molecular weight. A clear correlation was observed between the integrated intensity of the bands' fluorescence and the HEEI content of the polymers (Figure 5B).

Since condensation of DNA is known to be an important prerequisite for the formation of small polyplexes, the size range of the complexes made with the copolymers

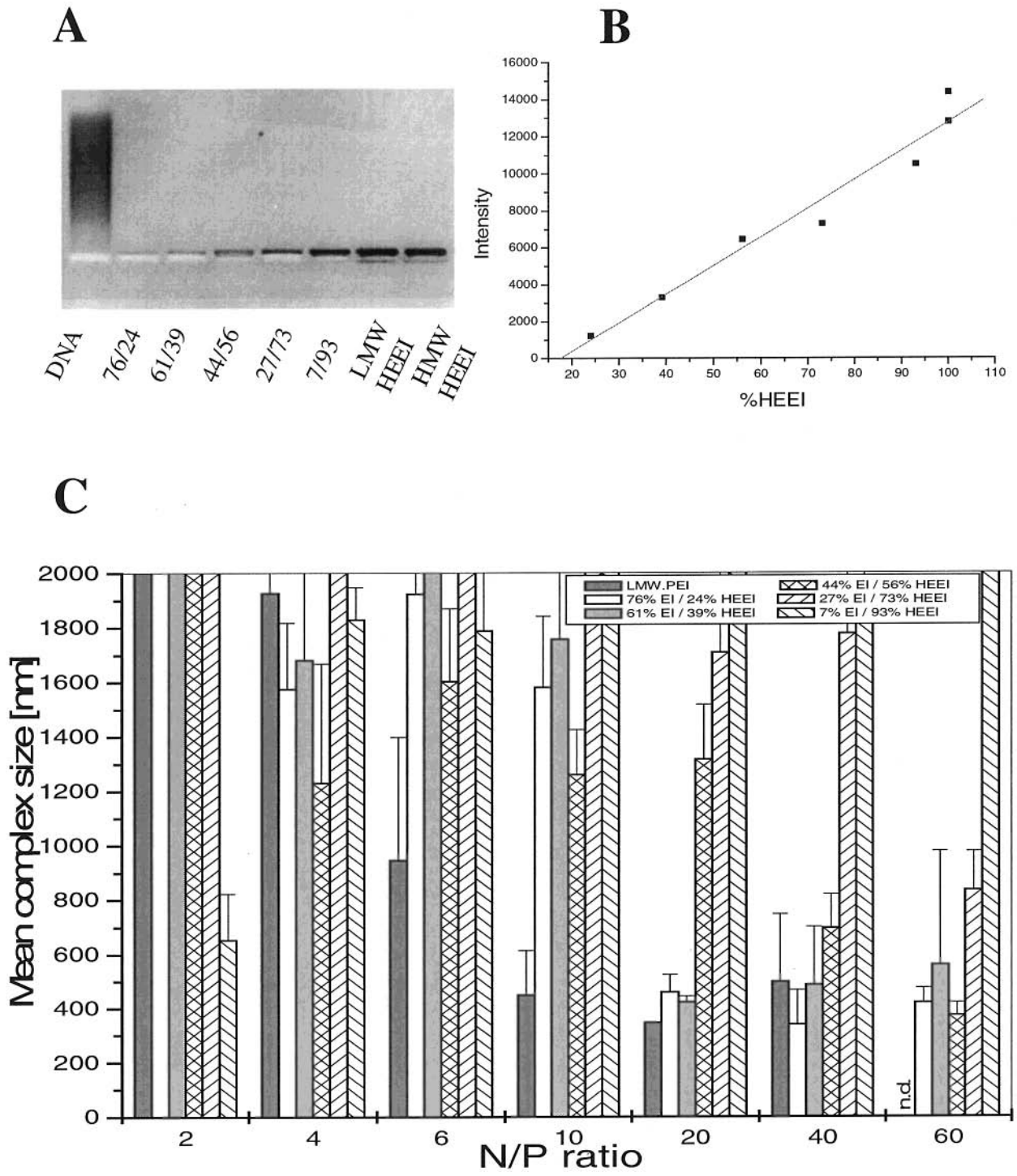


Figure 5. (A) Agarose gel electrophoresis of polymer/herring testes DNA complexes at an N/P ratio of 66. Free DNA (lane 1) was compared with the polymer/DNA complexes of the five copolymers (lanes 2−6), LMW-HEEI (lane 7), and HMW-HEEI (lane 8). All polymers showed complete DNA retardation, but with increasing HEEI content of the polymers the exclusion of the intercalant dye ethidium bromide decreased. (B) The degree of DNA complexation expressed as intensity of the gel bands showed a clear relationship to the HEEI content of the polymers. (C) Mean complex size ± SD of polymer/herring testes DNA complexes at different N/P ratios were measured by photon correlation spectroscopy in 50 mM NaCl/3.3% glucose ($n = 3$).

and herring testes DNA as dependent on the N/P ratio was determined by photon correlation spectroscopy (Figure 5C). At an N/P ratio of 2, all copolymers and PEI formed large aggregates >1 μm with a broad size distribution. One exception was the 7/93 copolymer with only little branching (6%) and a high content of hydroxyethyl substituents, forming complexes of about 650 nm. Increasing the N/P ratio of the complexes, particle sizes were reduced according to the polymer composition. LMW-PEI formed complexes <1 μm at a ratio of 6 and smaller, <500 nm complexes at a ratio of 10 and above. With the PEIHEEIs 76/24 and 6/39, complex sizes <500 nm could be reached at N/P ratios of 20 and higher; with copolymer 44/56, the required ratio was between 40 and 60. Copolymer 27/73 formed larger particles under the chosen conditions, but the size reduction to about 800 nm at N/P 60 indicates that smaller complexes may be formed when higher ratios are used. PEIHEEI 7/93 did not show any tendency to form smaller particles by increasing the N/P ratio. In accordance to the observa-

tions of electrophoresis, LMW-HEEI and HMW-HEEI were not able to form small condensed, measurable particles (data not shown).

The ability of the copolymers to neutralize the charges of DNA sufficiently to form an adequately compacted structure increased with higher N/P ratios and higher EI content of the polymers. The influence of the N/P ratio on complex size has been already described by others (Ogris et al., 1998). Complexation and condensation are expected to occur mainly by electrostatic interactions. According to our observation of a higher pK_a and the stronger binding of the polymers to the exchanger resin with increasing EI content, the interactions with the negatively charged DNA should also increase with a higher content of EI. Since all complexes were formed at pH 7.4, the different basicity of the polymers may result in different numbers and densities of the cationic charges influencing the interaction with DNA. Branched oligocationic peptides bind DNA with affinities that increase with the number of cationic groups (Plank et al., 1999). DNA binding was found to be related to the content of primary amino groups, but for this study polymers of completely different compositions (poly-L-lysine, dendrimers, PEI) were used (Tang and Szoka, 1997). If the content of primary amino groups of our copolymers is reduced to 50%, twice the N/P ratio is needed to form small particles with DNA. Branched 25 kDa PEI condensed DNA to a greater degree compared to a linear 22 kDa PEI (Dunlap et al., 1997). For branched copolymers of histidine and lysine, a reduced particle size of complexes by enhanced condensation compared to linear ones was reported (Chen et al., 2001). Basicity and protonation behavior seem to have a more profound effect than molecular weight, since HMW-HEEI gave results comparable to LMW-HEEI. According to Tang and Szoka (1997), electrostatic interactions dominate over steric and chemical contributions in the primary interactions of the polycations with DNA, resulting in stronger DNA binding with higher proton affinity. Our results are in agreement with these observations.

In Vitro Cytotoxicity Assays. The in vitro cytotoxicity was quantitated by the release of cytosolic enzyme lactate dehydrogenase into cell culture medium, hemolysis of rat red blood cells as markers for membrane activity, and the MTT assay representing the metabolic and mitochondrial activity of the polymer-treated cells. The assays were carried out using cationic polymers not complexed with DNA and at higher concentrations than used for transfection experiments, presenting a worst-case scenario for the interaction of polyplexes with cells. All three assays gave similar results.

LMW-HEEI and PEIHEEI 7/93 did not induce any damage effect in all three assays compared to control cells. For all other polymers, the cytotoxicity was found to increase with longer incubation times, higher polymer concentrations, and higher EI content of the copolymers.

Using concentrations ≤0.1 mg/mL, independent from incubation time, no significant decrease of the mitochondrial activity (80−100%) could be observed for all copolymers (Figure 6A), except for PEIHEEI 76/24 which reduced the cell viability to about 60%. At a 10-fold higher concentration (1 mg/mL) after 3 h again, about 90% viable cells in all cases could be observed (Figure 6B). However, after 12 and 24 h, the viability decreased with increasing EI content of the polymers. This effect was intensified with longer incubation periods from 12 to 24 h. Using 10 mg/mL, generally, the viability decreased about 10%, but the trend of the curves was unchanged

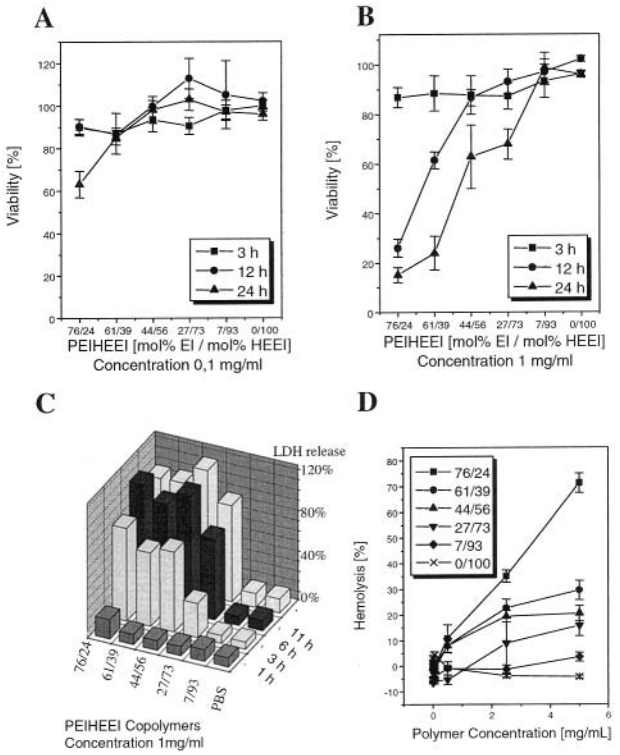


Figure 6. In vitro cytotoxicity testing of the copolymers. The cytotoxic effects as well as hemolysis were reduced with increasing HEEI content in the copolymers. L929 mouse fibroblasts were incubated for 3, 12, and 24 h with (A) 0.1 mg/mL and (B) 1 mg/mL PEIHEEI copolymers of different composition. Cytotoxic effects were quantitated by MTT assay. Each value represents the mean ± SD of seven determinations. (C) The membrane damaging effects were characterized by LDH-release incubating L929 cells with 1 mg/mL polymer solution for 1, 3, 6, and 11 h ($n = 3$). (D) After 1 h incubation, the hemolytic activity of different concentrations of the polymers was determined by UV spectrophotometric measurement of released hemoglobin at 540 nm ($n = 3$).

(data not shown). The homo-PEI showed a cytotoxicity profile comparable to copolymer 76/24 (Fischer et al., 1999).

The LDH assay gave corresponding results. Whereas with the exception of PEIHEEI 76/24 (10.61%), none of the copolymers (1 mg/mL) caused any release of LDH after 1 h, with longer incubation times up to 11 h the level of released enzyme increased with increasing amount of EI of the copolymers. The results of the LDH assay correlated with the changes in cell morphology as observed by phase contrast microscopy. With increasing PEI content in the copolymers, cytotoxic effects could be microscopically detected by the loss of spindle shape and detachment from the dish bottom of the usually adherent, spindle-shaped fibroblasts (data not shown).

Hemolysis of rat red blood cells increased as a function of polymer concentration and composition of the polymers. The hemolytic activity of the PEIHEEI 76/24 increased in a linear manner with higher concentrations up to 70%. Using the polymers with 61, 44, and 27% EI, the relative extent of hemolysis increased significantly from 15% (27/73) to 30% (61/39).

As also discussed for DNA binding, electrostatic interactions between the positive polymer and the negatively charged cell membrane were identified to induce membrane damage and cell death (Choksakulnimitr et al., 1995). The number and density of charges due to the degree of protonation and their arrangement in the three-dimensional polymeric structure were assumed to be

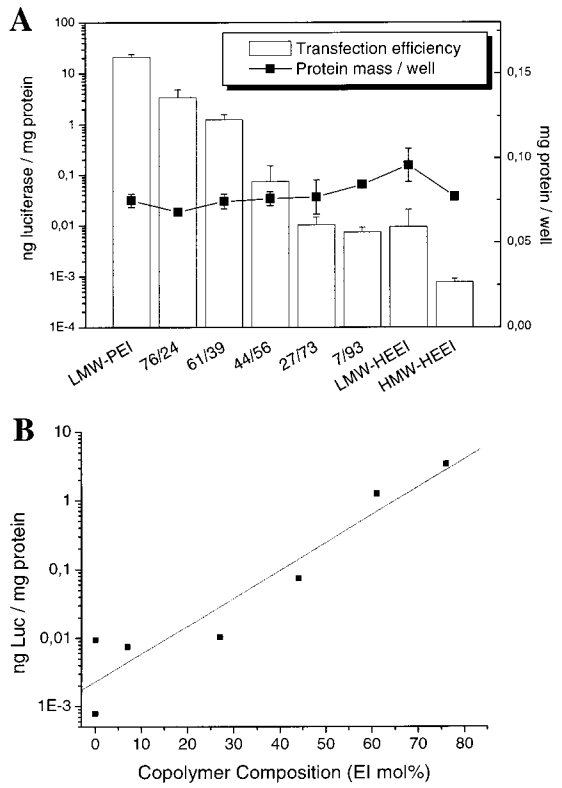


Figure 7. (A) Transfection efficiency in nanograms of luciferase per milligram of protein (black bars) and protein concentration in cell lysates (white bars). Gene expression decreased with increasing HEEI content of the polymers. Protein concentration in cell lysates was very similar for all polymers tested and was not responsible for the differences between the quotients nanograms of luciferase per milligram of protein. (B) Linear regression of log transfection efficiency (in nanograms of luciferase per milligram of protein) versus molar ethylene imine content gave a correlation coefficient of 0.95.

responsible for the different degree of cytotoxicity of polycations. We observed a similar trend: Higher ratios of EI in the copolymers correlated with increasing proton affinity and higher number of primary and secondary amines. This results in a higher degree of protonation, allowing more efficient electrostatic interactions with cell membranes.

The degree of protonation exhibited a greater influence on cytotoxicity than the molecular weight of the polymers. Using HMW-HEEI, only a slightly increased cytotoxicity could be detected compared to LMW-HEEI. Up to 10 mg/mL for LMW-HEEI, no significant cytotoxic effect could be observed over up to 24 h. HMW-HEEI (data not shown) was also nontoxic over 3 and 12 h under the chosen conditions. After 24 h at concentrations $\geq$1 mg/mL, cell viability was reduced (70%) compared to LMW-HEEI, but was still higher compared to all other copolymers.

Transfection Efficiency. If DNA condensation and small complex sizes are essential for transfection, one would predict that at a given N/P ratio the copolymers with high EI contents should perform better than the polymers with high HEEI content in gene delivery experiments. For comparison of the transfection efficiency of our copolymers, a N/P ratio of 66 was chosen because all complexes showed complete DNA complexation at this ratio. In 3T3 cells, the EI content of the copolymers had a clear effect on transfection efficiency in the sense that higher EI content led to higher transfection efficiencies (Figure 7A). While PEIHEEI 76/24 showed a transfection efficiency of 3440 pg of luciferase/mg of protein, PEIHEEI 7/93 showed a transfection efficiency of as low as 7.5 pg of luciferase/mg of protein. Values for the other copolymers lied between those two with decreasing transfection efficiency with decreasing EI content. The two HEEIs showed transfection efficiencies of 0.78 pg of luciferase/mg of protein (HMW-HEEI) and 9.5 pg of luciferase/mg of protein (LMW-HEEI), respectively. Transfection experiments at a N/P ratio of 6.7 showed similar relative results but with much lower values for luciferase expression per protein mass and high standard deviations (data not shown).

We found a strong correlation between the results of the transfection studies and the structure of our polymers. Linear regression of log transfection efficiency (in nanograms of luciferase per milligram of protein) versus molar ethylene imine content gave a satisfactory correlation coefficient (Figure 7B). The observed trends are in line with the physicochemical experiments: As uptake of complexes into cells imposes certain size and stability requirements on the endocytosed material, it is necessary for successful gene transfer that the cation in polyplexes not only bind DNA but also compact it. According to observations reported by Plank et al. (1999) for branched oligocationic peptides, Chen et al. observed that branched histidine/lysine polymers enhanced the transfection efficiency more effectively than the linear derivative and efficiency was positively correlated with the degree of branching (Chen et al., 2001). The linear polymer had little effect on transfection. Dendrimers showed a correlation between transfection efficiency and the degree of polymeric flexibility due to a different degree of branching after heat treatment (Tang et al., 1996). Uptake of particles into cells as well as the diffusion of complexes in the cytoplasm has been described to increase with reduced sizes of the polymer/DNA complexes (Mahato et al., 2000). Since the condensation of DNA is also known to protect the genetic material from enzymatic degradation (Godbey et al., 2000), the decrease of transfection ability of the complexes formed by copolymers with low EI content could therefore be due to instabilities in physiological medium, dissociation, enzymatic degradation, or aggregation. The issue of complex stability requires further studies. Since we used complexes with N/P 66 and therefore an excess of polymer presumably not associated with the DNA, also the cytotoxicity of the polycations should be taken into consideration. However, cytotoxicity-related effects as the reason for the declining transfection efficiencies are unlikely, since the protein concentrations in cell lysates, an indicator for cell growth, treated with the different polymers were very similar (Figure 7A). The role of the excessive polymer in transfection needs further investigation.

According to the "proton sponge" hypothesis, enhanced buffering of endosomal pH by the polymer should be associated with a high transgene expression. Chen et al. (2001, 2002) reported a significant role of the buffering capacity of histidine/lysine-based polymers in augmenting the transfection efficiency. Gene expression was more effectively reduced by the lysosomotropic buffering agent bafilomycin A1 with higher buffering capacity of the polymers. However, in our experiments, the copolymers showed comparable basicity at the pH of the endosomal/lysosomal compartment, suggesting that the ability of the PEIHEEIs to bind the protons should not be a sufficient factor to ensure a high transfection. This was also suggested by Gebhart and Kabanov (2001) comparing the efficiency of polycations of different monomeric struc-

tures. This point needs further investigation. In contrast, Chen et al. (2002) reported that the optimal transfection depends not only on the structure of the polymer but also on the pH of the endocytic vesicles varying in different cell lines and primary cells.

Although we observed a positive correlation between transfection efficiency and branching of our polycations, the high activity of the linear 22 kDa PEI compared to the 25 kDa branched PEI cannot be explained by this effect. Some authors (Wightman et al., 2001) suggested that this could be due to an aggregation and sedimentation behavior of the polyplexes of the linear form different from that of the branched polymer.

CONCLUSION

In this study, we described five new PEI-related copolymers and their chemical and physicochemical characterization and biological effects. By copolymerization with HEEI, we obtained a family of poly[(ethylene imine)-*co*-*N*-(2-hydroxyethyl-ethylene imine)] copolymers with similar molecular weights and different degree of branching. Polymers with a higher EI content and hence higher branching yielded higher reporter gene expression than polymers with more HEEI. The increase in transfection efficiency could be correlated with a higher ability of DNA binding and condensation and the formation of small sized complexes. Since complexation and condensation are mainly based on electrostatic interactions, the degree of protonation of the polymer is an important factor. The binding efficiency correlated with the higher content of primary and secondary amines as well as the higher pK_a values of the polymers.

Many reports suggested that the molecular weight of the polycation is the most critical factor for successful gene delivery. This study with a series of poly[(ethylene imine)-*co*-*N*-(2-hydroxyethyl-ethylene imine)] copolymers suggests that the polymer structure influences basicity and protonation of the copolymers and leads to different DNA binding, complex size, cytotoxicity, and transfection efficiency. Therefore, the structure seems to be of greater importance than the molecular weight of the polymers. Insight into the structure−function relationship may form the basis for rationalization of the development of improved gene delivery systems.

ACKNOWLEDGMENT

We thank the Department of Pharmacology and Toxicology, University of Marburg, for the supply of rat blood. We thank C. Selignow for technical assistance. Support of this work in part by the Deutsche Forschungsgemeinschaft (DFG) is gratefully acknowledged.

LITERATURE CITED

(1) Abdallah, B., Hassan, A., Benoist, C., Goula, D., Behr, J. P., and Demeneix, B. A. (1997) A powerful nonviral vector for in vivo gene transfer into the adult mammalian brain: polyethylenimine. *Hum. Gene Ther. 7*, 1947−1954.

(2) Baker, A., Salik, M., Lehmann, H., Killisch, I., Mautner, V., Lamm, G., and Christofori, C. (1997) Polyethylenimine (PEI) is a simple, inexpensive and effective reagent for condensing and linking plasmid DNA to adenovirus for gene delivery. *Gene Therapy 4*, 773−782.

(3) Behr, J. P. (1997) The proton sponge: a trick to enter cells the viruses did not exploit. *Chimia 51*, 34−36.

(4) Boletta, A., Benigni, A., Lutz, J., Remuzzi, G., Soria, M. S., and Monaco, L. (1997) Nonviral gene delivery to the rat kidney with polyethylenimine. *Hum. Gene Ther. 8*, 1243−1251.

(5) Boussif, O., Zanta, M. A., and Behr, J. P. (1996) Optimized galenics improve *in vitro* gene transfer with cationic molecules up to 1000-fold. *Gene Ther. 3*, 1074−1080.

(6) Chen, Q. R., Zhang, L., Stass, S. A., and Mixson, A. J. (2001) Branched copolymers of histidine and lysine are efficient carriers of plasmids. *Nucleic Acids Res. 29*, 1334−1340.

(7) Chen, Q. R., Zhang, L., Luther, P. W., and Mixson, A. J. (2002) Optimal transfection with the HK polymer depends on its degree of branching and the pH of endocytic vesicles. *Nucleic Acids Res. 30*, 1338−1345.

(8) Choksakulnimitr, S., Masuda, S., Tokuda, H., Takakura, Y., and Hashida, M. (1995) In vitro cytotoxicity of macromolecules in different cell culture systems. *J. Controlled Release 34*, 233−241.

(9) Dick, C. R., and Ham, G. E. (1970) Characterization of poly(ethylenimine). *J. Macromol. Sci. A 4*, 1301.

(10) Dunlap, D., Maggi, A., Soria, M. R., and Monaco, L. (1997) Nanoscopic structure of DNA condensed for gene delivery. *Nucleic Acids Res. 25*, 3095−3101.

(11) Erbacher, P., Remy, J. S., and Behr, J. P. (1999) Gene transfer with synthetic virus-like particles via the integrin-mediated endocytosis pathway. *Gene Ther. 6*, 138−145.

(12) Ferrari, S., Moro, E., Pettenazzo, A., Behr, J. P., Zacchello, F., and Scarpa, M. (1997) ExGen 500 is an efficient vector for gene delivery to lung epithelial cells in vitro and in vivo. *Gene Ther. 4*, 1100−1106.

(13) Fischer, D., Bieber, T., Li, Y. X., Elsässer, H. P., and Kissel, T. (1999) A novel nonviral vector for DNA delivery based on low molecular weight, branched polyethylenimine: Effect of molecular weight on transfection efficiency and cytotoxicity. *Pharm. Res. 16*, 1273−1279.

(14) Fischer, D., von Harpe, A., and Kissel, T. (2000) Polyethylenimine: Polymer structure influences the physicochemical and biological effects of plasmid/PEI complexes. *Biomaterials and drug delivery toward new millenium* (Park, K. D., Kwon, I. C., Yui, N., Jeong, S. Y., and Park, K., Eds.) Han Rim Wan Publishing Co., Seoul, Korea.

(15) Gebhart, C. L., and Kabanov, A. V. (2001) Evaluation of polyplexes as gene transfer agents. *J. Controlled Release 73*, 401−416.

(16) Godbey, W. T., Wu, K. K., and Mikos, A. G. (1999) Size matters: Molecular weight affects the efficiency of poly(ethylenimine) as a gene delivery vehicle. *J. Biomed. Mater. Res. 45*, 268−275.

(17) Godbey, W. T., Barry, M. A., Saggau, P., Wu, K. K., and Mikos, A. G. (2000) Poly(ethylenimine)-mediated transfection: A new paradigm for gene delivery. *J. Biomed. Mater. Res. 51*, 321−328.

(18) Goula, D., Remy, J. S., Erbacher, P., Wasowicz, M., Levi, G., Abdallah, B., and Demeneix, B. A. (1998) Size, diffusibility and transfection performance of linear PEI/DNA complexes in the mouse central nervous system. *Gene Ther. 5*, 712.

(19) Hill, H. D., and Straka, J. G. (1988) Protein determination using bichinchonic acid in the presence of sulfhydryl reagents. *Anal. Biochem. 170*, 203−208.

(20) Jeong, H., Song, S. H., Lim, D. W., Lee H., and Park, T. G. (2001) DNA transfection using linear poly(ethylenimine) prepared by controlled acid hydrolysis of poly(2-ethyl-2-oxazoline). *J. Controlled Release 73*, 391−399.

(21) Lecocq, M., Wattiaux-De Coninck, S., Laurent, N., Wattiaux, R., and Jadot, M. (2000) Uptake and intracellular fate of polyethylenimine in vivo. *Biochem. Biophys. Res. Commun. 278*, 414−418.

(22) Mahato, R. I., Furgeson, D. Y., Maheshwari, A., Han, S., and Kim, S. W. (2000) Polymeric delivery for cancer treatment. *Biomaterials and drug delivery toward new millenium* (Park, K. D., Kwon, I. C., Yui, N., Jeong, S. Y., and Park, K., Eds.) Han Rim Wan Publishing Co., Seoul, Korea.

(23) Ogris, M., Steinlein, P., Kursa, M., Mechtler, K., Kircheis, R., and Wagner, E. (1998) The size of DNA/transferrin-PEI complexes is an important factor for gene expression in cultured cells. *Gene Ther.*, 1425−1433.

(24) Parnham, M. J., and Wetzig, H. (1993) Toxicity screening of liposomes. *Chem. Phys. Lipids 64*, 263−274.

(25) Perrine T. D., and Landis, W. R. (1967) Analysis of polyethylenimine by spectrophotometry of its copper chelate. *J. Polym. Sci., Polym. Chem. Ed. 5*, 1993−2003.
(26) Plank, C., Tang, M. X., Wolfe, A. R., and Szoka, F. C. (1999) Branched cationic peptides for gene delivery: Role of type and number of cationic residues in formation and in vitro activity of DNA polyplexes. *Hum. Gene Ther. 10*, 319−332.
(27) Remy, J. S., Abdallah, B., and Zanta, M. A., Boussif, O., Behr, J. P., and Demeneix, B. (1998) Gene transfer with lipospermines and polyethylenimines. *Adv. Drug Delivery Rev. 30*, 85−95.
(28) Rivas, B. L., Geckeler, K. E., and Bayer, E. (1991) Synthesis and characterization of poly[1-(2-hydroxyethyl)aziridine]. *Eur. Polym. J. 27*, 1165−1169.
(29) Seel, F. (1970) *Grundlagen der analytischen Chemie*, Verlag Chemie, Weinheim.
(30) Suh, J., Paik, H. J., and Hwang, B. K. (1994) Ionization of poly(ethylenimine) and poly(allylamine) at various pHs. *Bioorg. Chem. 22*, 318−327.
(31) Tang, M. X., and Szoka, F. C. (1997) The influence of polymer structure on the interactions of cationic polymers with DNA and morphology of the resulting complexes. *Gene Ther. 4*, 823−832.
(32) Tang, M. X., Redemann C. T., and Szoka, F. C., Jr. (1996) In vitro gene delivery by degraded polyamidoamine dendrimers. *Bioconjugate Chem. 7*, 703−714.
(33) von Harpe, A., Petersen, H., Li, Y. X., and Kissel, T. (2000) Characterization of commercially available and synthesized polyethylenimines for gene therapy. *J. Controlled Release 69*, 309−322.
(34) Wenker, H. (1935) The preparation of ethylene imine from monoethanolamine. *J. Am. Chem. Soc. 57*, 2328.
(35) Wightman, L., Kircheis, R., Rossler, V., Carotta, S., Ruzicka, R., Kursa, M., and Wagner, E. (2001) Different behaviour of branched and linear polyethylenimine for gene delivery in vitro and in vivo. *J. Gene Med. 3*, 362−372.

BC025550W

Coupling of a Targeting Peptide to Plasmid DNA Using a New Type of Padlock Oligonucleotide

Thibaut Roulon,† Claude Hélène, and Christophe Escudé*

Laboratoire de Biophysique, Muséum National d'Histoire Naturelle, INSERM U201, CNRS UMR8646, 43, rue Cuvier, 75231 Paris Cedex 05, France. Received May 17, 2002; Revised Manuscript Received June 28, 2002

We have recently described a new method for attaching padlock oligonucleotides to supercoiled plasmid DNA at specific sequences. A variant of this method has been developed in order to allow the coupling of targeting moieties to plasmids using a convenient strategy. After sequence-specific winding around the double-stranded target DNA sequence by ligand-induced triple helix formation, the extremities of a triplex-forming oligonucleotide hybridize to each other, leaving a dangling single-stranded sequence, which is then ligated to a hairpin oligonucleotide using T4 DNA ligase. Any targeting moiety may be attached to the hairpin oligonucleotide. This strategy was used to attach an NLS peptide to a luciferase-expressing plasmid. Despite the presence of the padlock oligonucleotide, the reporter gene was efficiently expressed after transfection of the plasmid in HeLa or T24 cells, using either cationic lipids or cationic polymers as transfecting agents. However, no increase in gene expression could be observed as a result of peptide attachment. Nevertheless, the coupling strategy described in this paper may find applications as a tool for plasmid functionalization in other targeting experiments, and may lead to the development of improved vectors for gene therapy.

INTRODUCTION

Plasmids are commonly used as expression vectors for gene transfer into eukaryotic cells in vitro and in vivo. They are generally delivered as a complex with chemical and/or biochemical vectors such as cationic lipids or polymers. Such complexes offer several advantages compared to viral vectors, such as a better safety profile, a lower immunogenicity, the possibility of incorporating a larger expression cassette, and an easier large scale production. However, they suffer from a relatively low efficiency of transfection. Although the mechanism of nonviral gene transfer is not perfectly understood, several obstacles to a good efficiency have been reported, including the passage of DNA accross the cellular membrane, the escape from endosomal compartments, the low metabolic stability of plasmids in the cytoplasm, and the inefficient trafficking of genes to the nucleus (*1*). Therefore, the design of new delivery methods has been the focus of intense research efforts in the past years to overcome these limitations.

Exploiting naturally existing biological pathways is a tempting option for improving plasmid targeting and trafficking. Interactions between a ligand on the plasmid/vector complex and an extracellular receptor may enhance cell-specific targeting, whereas the use of signal sequences that are recognized by the intracellular transport machinery may improve intracellular trafficking. The targeting ligand may be coupled to the DNA condensing agent, for example polylysine (*2*) or PEI (*3*). These condensing agents dissociate from the plasmid once inside the cells. Therefore, there is a need for methods that allow for conjugation of functional domains directly to plasmid DNA, especially when the goal is to improve the nuclear localization of the plasmid. These conjugation methods must maintain the activity of the plasmid, i.e., the expression cassette must remain fully functional. This can be achieved using sequence-specific targeting methods. Two different strategies have been reported to date. The first one involves the formation of a covalent triple helix (*4*); the other one is based on the very strong affinity of PNA for locally denatured double-stranded DNA (*5*−*7*). These methods have been used to link NLS (nuclear localization signal) peptides to plasmids in order to increase plasmid uptake into the nucleus, however with limited success (*4*, *5*).

We have developed a new methodology to conjugate a targeting ligand to plasmid DNA without any covalent modification of the DNA backbone. We report here the synthesis and characterization of plasmid-peptide conjugates. The ability of an NLS peptide to enhance gene delivery has been tested in cellular models.

EXPERIMENTAL PROCEDURES

Oligonucleotide and Peptide Synthesis. The following oligonucleotides were synthesized by Eurogentec (Herstal, Belgium): the 63-mer triplex-forming oligonucleotide (TFO) 5′CATCGACCTAGTTCGACGCTAGCTTTTTGTTGGGTTGGTTTGTTTTCACGTGGAGCTACTAGG3′, the nonmodified 32-mer hairpin 5′TCGATGTCCGGATTGGCTTTTGCCAATCCGGA3′, the amino-modified hairpin 5′TCGATGTCCGGATTGGCTTXTGCCAATCCGGA3′ where X is an amino-modifier C6 dT (Glen Research, USA), and the TRAP oligonucleotide 5′CTTTCCTTCTCTCCTTTTTGGAGAGAAGGAAAGTTTTTGTTTGGTTGTGTGG3′. The 32-mers were 5′-phosphorylated during synthesis. All oligonucleotides were ethanol-precipitated, and their concentration was calculated using a nearest-neighbor model for extinction coefficients (*8*). Synthesis of the triplex stabilizing agent BQQ (6-[3-(dimethylamino)propyl]amino-11-methoxybenzo[*f*]quino-[3,4-*b*]quinoxaline) has been described elsewhere (*9*). Peptides containing the wild-type SV40 large T NLS sequence (NLS) (PKKKRKVEDPYC) or a mutated

* To whom correspondence should be addressed. Phone: (44) 1 40793774. Fax: (44) 1 40793705. E-mail: escude@mnhn.fr.

† Present address: ANOSYS Inc., 1014 Hamilton Court, Menlo Park, CA 94025.

10.1021/bc025551o CCC: $22.00 © 2002 American Chemical Society
Published on Web 08/24/2002

SV40 large T NLS sequence (mNLS) (PKTKRKVEDPYC) were obtained from Sigma-Genosys (U.K.).

Synthesis of the Oligonucleotide-Peptide Conjugate. SMCC [*N*-succinimidyl 4-(*N*-maleimidomethyl)-cyclohexane-1-carboxylate ester] was obtained from Sigma. The NLS peptide was linked to the hairpin oligonucleotide using a previously described method (*10*, *11*). Briefly, 10 nmol of oligonucleotide was resuspended in 150 μL of 0.1 M Tris−borate, pH 7.0. Then 150 μL of SMCC (0.3 M in DMF) was added, and the mixture was incubated at room temperature for 2 h with gentle agitation. The sample was purified on a nick-spin column (Amersham Pharmacia Biotech) preequilibrated with PBS, to remove the excess SMCC. An equal volume of peptide (2 mg/mL) was then added, and the mixture was left overnight at room temperature with gentle agitation. The conjugate was purified by PAGE.

Formation of Plasmid−Oligonucleotide Complexes. For experiments with radiolabeled molecules, 10 pmol of TFO was incubated in 20 μL of T4 Polynucleotide Kinase (PNK) buffer (New England Biolabs, NEB) with 10 μCi of [γ-^{32}P]ATP (Amersham, >5000 Ci/mmol) and 5 units of T4 PNK (NEB) for 1 h at 37 °C. Unincorporated [γ-^{32}P]ATP was removed using Micro Bio-Spin columns (BIO-RAD). The 5′-labeled TFO (20 nM) was mixed with 50 nM plasmid, 100 nM 32-mer hairpin oligonucleotide, and 20 μM BQQ in T4 DNA ligase buffer. This mixture was heated to 80 °C and slowly cooled to 37 °C. Then, 40 units of T4 DNA ligase (NEB) was added, and the samples were incubated at 37 °C for 1 h. For probing the circular structure of some of the products of the reaction, 0.5 μL (50 units) of Exonuclease III (NEB) was added after heat inactivation of the ligase, and the sample was further incubated for 30 min at 37 °C. Reaction products were analyzed on denaturing 8% polyacrylamide gels. The gels were dried and exposed on phosphorimager screens.

For nonradiolabeled plasmid preparations, 300 pmol of TFO was 5′-phosphorylated using the same protocol as above except that the solution contained 1 mM cold ATP instead of the radioactive label. For attaching the oligonucleotide to the plasmid, the same process as above was also adopted, except that 200 nM plasmid, 400 nM TFO, 600 nM hairpin oligonucleotide, and 133 units of DNA ligase were used. To remove BQQ from the triplex, the sample (10 μL) was first diluted to 50 μL so that the final buffer concentration was 40 mM Tris-HCl, pH 8.0, 80 mM NaCl, 16 mM $MgCl_2$, and the solution contained 5 μM TRAP oligonucleotide. The samples were heated to 80 °C and then slowly cooled to 37 °C. Then, 50 μL of 40 mM spermidine was added, and the samples were left for 30 min at room temperature with frequent vortex-mixing, to allow for plasmid compaction. After centrifugation, the pellet was washed with 200 μL of a solution containing 50% 2-propanol, 10 mM $MgCl_2$, 300 mM NaCl, and 25 mM EDTA as previously described (*12*). Plasmid was resuspended in 20 μL of Tris−EDTA buffer (10 mM Tris, pH 8.0, 0.1 mM EDTA). For larger scale preparations, all these volumes and quantities were increased up to 10-fold.

Gel-Shift Experiments. One microgram of plasmid was diluted in 18 μL of restriction enzyme (RE) buffer containing 10 mM BisTris-propane-HCl, 10 mM $MgCl_2$, 1 mM dithiothreitol (pH 7.0 at 25 °C), and 2 μM BQQ. The samples were heated to 80 °C and slowly cooled to 37 °C. Then, 2 μL of a solution containing 5 units of *Xmn*I, 5 units of *Dra*III, and 1 μg/μL BSA was added to the sample. Digestion was carried out for 2 h at 37 °C. Then, samples were mixed with 5 μL of 50% glycerol and loaded on nondenaturing polyacrylamide gels. The 6% polyacrylamide gel was prepared with a 29:1 acrylamide-to-bisacrylamide ratio. The gel and buffer contained TBM (100 mM Tris/90 mM boric acid, 1 mM EDTA, pH 8.3, 10 mM $MgCl_2$). They were run at 4 °C, then stained for 15 min with SybrGreen (Molecular Probes), washed for an additional 15 min in water, and then imaged by UV transillumination.

Cell Transfection. HeLa cells (ATCC) were grown in modified Eagle's medium (MEM) containing 2.5 mM glucose, supplemented with 2 mM L-glutamine, 10% fetal bovine serum, 100 units/mL penicillin, and 100 μg/mL streptomycin. The T24 cell line was grown in DMEM containing the same supplements. Cells were grown at 37 °C in a 5% CO_2/air incubator. One day before the transfection assay, 24-well culture plates were seeded with 50 000 cells/well.

For transfections using PEI, 75 μL of a solution containing 150 mM NaCl and PEI 25 kDa (Sigma) at a concentration of 1 mM amino groups was prepared from a 10 mM stock solution. The amount of DNA for 3 wells (3 μg) was diluted into 75 μL (final volume) of 150 mM NaCl. Both solutions were left at room temperature for 10 min, vortexing every 5 min. Then, they were mixed together, and incubated at room temperature for 10 min, again vortexing every 5 min. The concentrations that were used correspond to a N/P ratio of 8:1, which was shown to give the best transfection efficiencies. One milliliter of culture medium without serum was then added. Cells were washed with PBS (Gibco BRL), and then transfected with 350 μL of the PEI/DNA mixture. Cells were incubated for 3 h at 37 °C; then the transfection medium was changed to the serum-containing culture medium.

For transfection with Superfect (Qiagen), 3 μg of DNA was diluted to 165 μL in the cell culture medium devoid of serum and of antibiotics, then vortexed briefly. Superfect was then added at a lipid:DNA mass ratio of 5:1. Volume was adjusted to 180 μL with the same medium, and the solution was vortexed. After 10 min incubation at room temperature, 1.05 mL of medium containing serum and antibiotics was added to the lipid−DNA mixture. Cells were washed with PBS, and 390 μL of the DNA solution was added. After 2 h, cells were washed with PBS, and 1 mL of cell culture medium was added.

Luciferase gene expression was measured by a luminescence assay. The cells were washed twice with PBS and lysed with 100 μL of cell culture lysis reagent (Promega) at room temperature for 30 min, with gentle agitation. Samples were then transferred to 96-well plates. Luciferase expression was measured using the Luciferase Assay Reagent (Promega). Light emission was measured by integration over 10 s using a multilabel counter Victor^2 (EG&G Wallac, Evry, France). Light emission was normalized to the protein concentration determined using the Biorad Protein Assay (Biorad). Briefly, 250 μl of a 5 times dilution of the supplied dye reagent concentrate was added to 5 μL of cell lysate or of serial dilutions of a BSA reference solution, and the absorbance at 595 nm was measured in 96-well microtiter plates using the same multilabel counter as above.

RESULTS

Oligonucleotide Design. We designed a new strategy for plasmid modification employing two self-complementary oligonucleotides: a 63-mer TFO with a stem−loop structure, and a 32-mer hairpin oligonucleotide. A sequence made of G and T located in the loop of the TFO

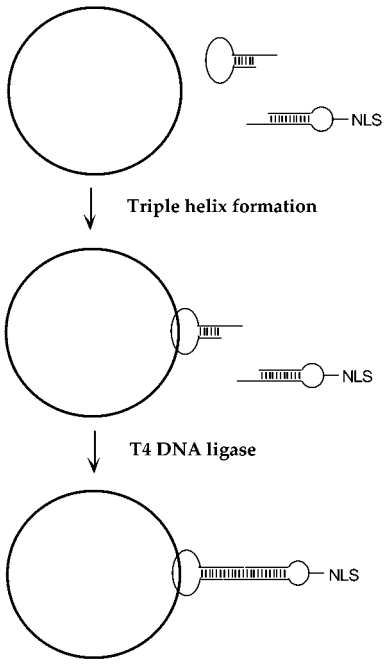


Figure 1. Strategy for the coupling of an NLS peptide to a plasmid. The triplex-forming oligonucleotide binds to an oligopurine·oligopyrimidine sequence in the phage f1 replication origin. This requires a heating step where the oligonucleotide opens and winds around the double-stranded DNA. Then this TFO is ligated to a hairpin oligonucleotide which has previsouly been conjugated to a peptide.

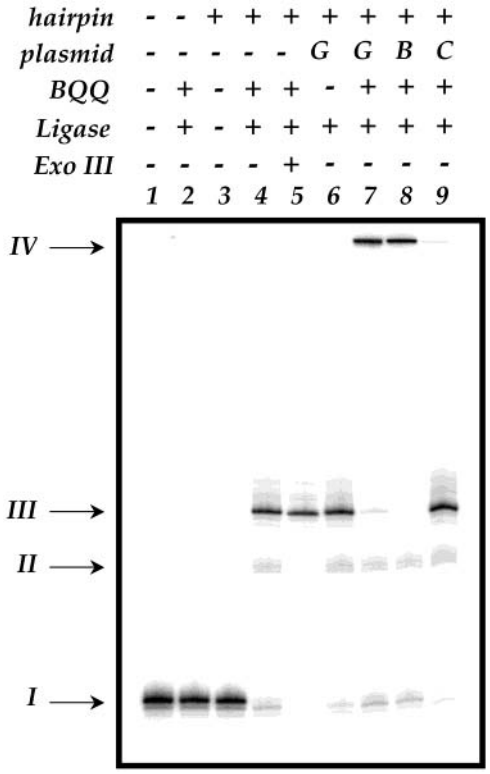


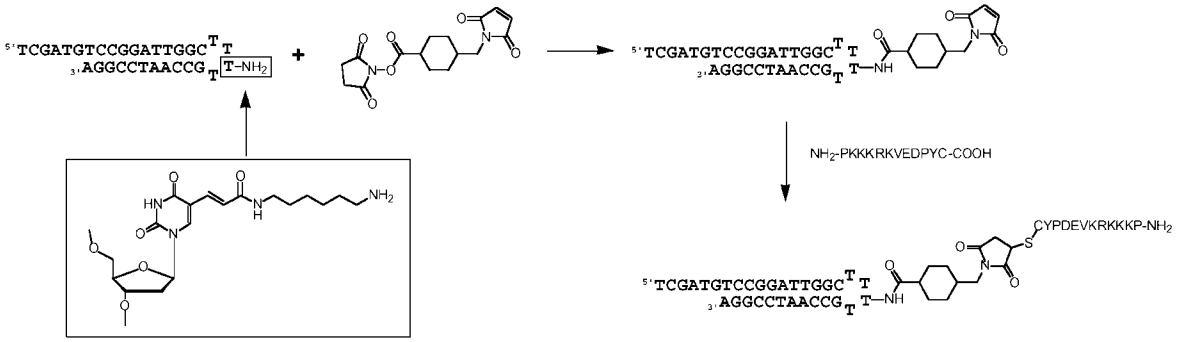
Figure 2. Autoradiogram of a denaturing polyacrylamide gel, showing the attachment of the padlock oligonucleotide to a plasmid. The radiolabeled 63-mer TFO was incubated in the absence or presence of plasmid and treated as described at the top of the gel (see also Experimental Procedures). The different plasmids that have been used are as follows: G, pGL3; B, pBl; C, pBR322. The presence of BQQ, as well as the various enzymatic reactions (ligation and digestion) that were carried out, is also indicated. Band I corresponds to a linear 63-mer oligonucleotide, band II to a linear 95-mer, band III to a circular 95-mer, and band IV to a circular 95-mer catenated to a plasmid.

can form a triple helix in the presence of a triplex-stabilizing agent by binding to a sequence in the phage f1 replication origin, as already described in a previous paper (*13*). This sequence was present on both the pBl (pBluescript SK+, Stratagene) and the pGL3 (pGL3 control, Promega) plasmids. The 3′- and 5′-regions of the TFO can hybridize to each other, thereby forming a short double-stranded stem and leaving a single-stranded dangling 5′-end, which can hybridize to a complementary sequence at the 5′-end of the hairpin oligonucleotide. A length of 6 bp was chosen for the stem so that it can dissociate upon heating, thereby allowing during the cooling step the formation of a triple helix between the loop of the TFO and the target double-stranded sequence on the plasmid, followed by the rehybridization of the complementary sequences of the stem. The length of the complementary single-stranded ends should ensure proper hybridization of the oligonucleotides for the ligation to occur. In the hybridized dumbbell-like structure, ligation of the 5′-end of each oligonucleotide to the 3′-end of the other should result in the formation of a circular 95-mer oligonucleotide (see Figure 1).

Sequence-Specific Formation of a Catenated Plasmid−Oligonucleotide Complex. The radiolabeled 63-mer TFO and the 32-mer hairpin oligonucleotide were incubated in T4 DNA ligase buffer, heated to 80 °C, and slowly cooled to allow for hybridization of the single-stranded ends. T4 DNA ligase was then added, and the sample was incubated at 37 °C for 1 h. This led to the formation of two radiolabeled species with a slower migration rate, the slowest one being the most abundant (Figure 2 , lane 4). To identify these bands, the sample was treated with exonuclease III, which led to the disappearance of the fastest band and of the shorter nonreacted oligonucleotides (lane 5). The fastest band should therefore correspond to a linear 95-mer, whereas the slowest band is a circular 95-mer, as circular oligonucleotides are resistant to digestion by exonuclease III. When the same process was performed in the presence of pGL3 (lane 7) or pBl (lane 8) plasmid and 20 μM BQQ, a band with a very slow migration rate was observed, and the band corresponding to the circular 95-mer almost disappeared. This suggests that the complex formed in this reaction was made of the circular oligonucleotide catenated to the plasmid, as already described in our previous studies (*13, 14*). The catenation was not observed in the absence of the triplex-stabilizing ligand (lane 6), or if plasmid pBR322 was used, which does not contain the phage f1 replication origin recognized by the triplex-forming region of the 63-mer hairpin oligonucleotide (lane 9). Neither was it observed if the ligation reaction was carried out without heating or if the sample was treated with a restriction enzyme which linearizes the plasmid after removal of the triplex-stabilizing agent (data not shown). These results clearly show that the 63-mer and 32-mer oligonucleotides can be assembled into a circular 95-mer oligonucleotide with a dumbbell-like structure catenated to a supercoiled plasmid. Analysis of the sample by agarose gel electrophoresis confirmed that the supercoiled conformation was not affected (data not shown).

Construction and Characterization of Peptide-Plasmid Conjugates. The hairpin oligonucleotide can be modified in order to allow the coupling of a targeting moiety, such as an NLS peptide, for example. A peptide containing the NLS sequence of the wild-type SV40 large T antigen was synthesized and covalently linked to a 32-

Scheme 1. Reaction Scheme for the Synthesis of the Oligonucleotide-NLS Peptide Conjugate



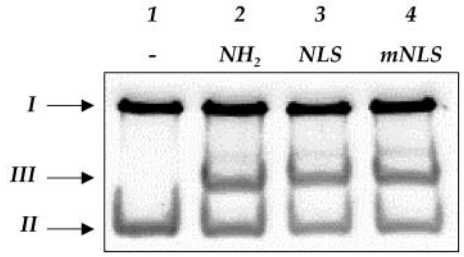


Figure 3. Yield determination by a gel-shift assay. Modified pGL3 plasmids were prepared as indicated under Experimental Procedures, using an excess of 5′-phosphorylated 63-mer TFO and the various 32-mer hairpin oligonucleotides (NH2, carrying an amino group; NLS, carrying an NLS peptide; mNLS, carrying the mutated NLS peptide). After purification by spermidine precipitation, samples were digested by *Xmn*I and *Dra*III to produce a short restriction fragment containing the ORI sequence. Samples were then loaded on a 6% native polyacrylamide gel containing 10 mM $MgCl_2$, stained with Sybr Green I, and imaged with a camera. I and II refer to the restriction fragments of 4704 and 552 bp, respectively. III corresponds to fragment II shifted by the presence of a catenated padlock oligonucleotide.

mer hairpin oligonucleotide containing a thymine with a C(5) amino group in the loop region, using a previously described method (*10, 11*) (see Experimental Procedures). Scheme 1 illustrates the reaction scheme used to prepare the peptide-oligonucleotide conjugates. The yield of conjugate formation was about 50%, which led to an overall yield of 10% after purification, which is in agreement with previous reports.

The pGL3 plasmid, which expresses the firefly luciferase reporter gene, was chosen as a substrate for the reaction, as further experiments were planned to investigate the effects of plasmid modification on transgene expression. Plasmid pGL3 was mixed with the 63-mer TFO, the peptide-oligonucleotide conjugate, and the triplex-stabilizing agent, and the circularization reaction was allowed to proceed as described above. After elimination of both the free oligonucleotides and the triplex-stabilizing agent (see Experimental Procedures and ref *12*), the yield of plasmid modification was measured using the previously described band shift assay (*13*). Briefly, the plasmid was digested in the presence of BQQ by *Xmn*I and *Dra*III to give a 552 bp fragment containing the target sequence, and the samples were analyzed using nondenaturing polyacrylamide gel electrophoresis. When the plasmid was catenated to the circular oligonucleotide, the 552 bp band migrates less far in the gel (Figure 3 , lane 2). Approximately 60% of the fragment was shifted, showing that at least 60% of the plasmids were carrying the circular oligonucleotide at the expected site. In fact, when experiments carried out with radiolabeled oligonucleotides in the presence of an excess of plasmid, only 60% of the labeled oligonucleotide comigrated with the plasmid (see Figure 2). Some truncated oligonucleotides are not circularized, and some are circularized outside of the plasmid. As explained in our previous study (*13*), the yields varied between different oligonucleotide synthesis batches, and were therefore highly influenced by oligonucleotide quality. This parameter is even more important in the present construct as the oligonucleotides have to be ligated to each other at both ends. Importantly, the yield was not affected by the presence of a conjugated peptide on the 32-mer hairpin oligonucleotide (Figure 3, lanes 3 and 4).

Transfection Studies. HeLa and T24 cells can be transfected with the pGL3 plasmid by using a cationic lipid formulation (Superfect) or a polycation, polyethyleneimine (PEI). A series of experiments was undertaken with both cell types and both transfection methods in order to observe the effect of padlock oligonucleotide attachment and peptide grafting on transfection efficiency. Luciferase activity was measured 24 h after transfection. As shown in Figure 4 (A and B), both cell types were efficiently transfected with cationic PEI/DNA complexes (N/P ratio of 8). To check that the protocol used for plasmid modification did not influence transfection efficiency, cells were also transfected using complexes formed with DNA which had been subjected to the treatment used for plasmid modification, but in the absence of oligonucleotides (i.e., the treatment included addition of ligand, heating, addition of ligase, and purification). No significant change in the level of luciferase expression was observed. This was true also for plasmids carrying the amino-substituted oligonucleotide, but no change in transfection efficiency could be observed when the NLS peptide was linked to the plasmid, or when a mutated NLS was used. To check whether using a Lipoplex would lead to different results, T24 cells were also transfected with Superfect as a transfecting agent. Again, no significant change in transfection efficiency could be observed when the plasmids had been submitted to the same treatments and/or modifications as above (Figure 4C).

DISCUSSION

Our goal was to develop a versatile method for attaching a peptide to a plasmid in an irreversible way without affecting the chemical structure of the plasmid. This could have been achieved using the previously described method for padlock oligonucleotide formation, which involves the use of a long TFO (>50 nt) and a short template oligonucleotide for juxtaposition of the 3′- and 5′-ends followed by enzymatic ligation. The peptide may have been linked to the TFO or to the template. However, the synthesis and purification of a peptide-oligonucleotide conjugate is much more difficult with a long oligonucle-

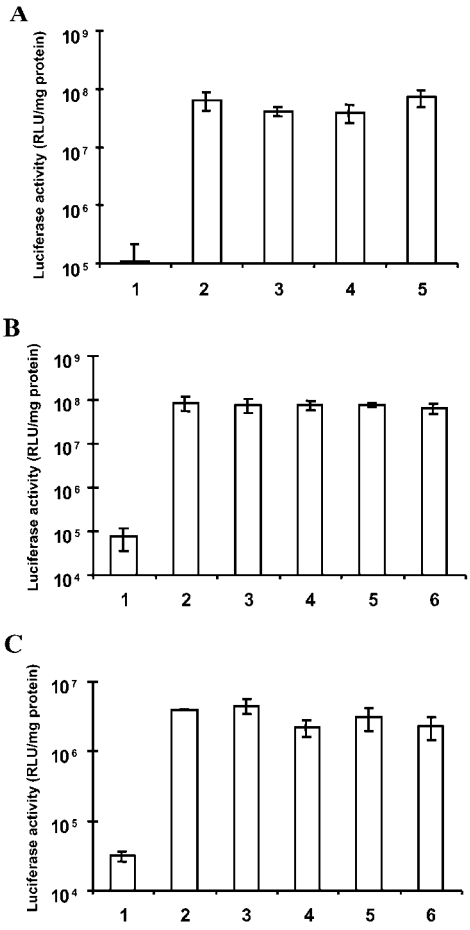


Figure 4. Transgene expression after transfection of plasmid-NLS conjugates. HeLa cells (A and B) and T24 cells (C) were transfected with the nonmodified plasmid and the plasmid which has been submitted to various procedures, using either PEI (A) or Superfect (B and C). Luciferase expression was measured after 24 h and normalized for protein content ($n = 3$ in all cases). (1) No plasmid; (2) nonmodified plasmid; (3) plasmid was treated and purified as for modification, except that the oligonucleotides and the ligase were not added; (4) plasmid carrying an amino-oligonucleotide; (5) plasmid carrying one wild-type NLS peptide; (6) plasmid carrying one mutant NLS peptide.

otide than with a short one, and the template oligonucleotide was linked to the catenated plasmid by Watson−Crick hydrogen bonds, which may be disrupted within cells. Moreover, linking a peptide may have interfered with triplex formation or template hybridization. Therefore, we chose to devise a new approach in which a short oligonucleotide could be used to introduce a chemical modification in an irreversible manner. This method involves the use of two hairpin oligonucleotides which have complementary single-stranded ends and therefore can be ligated to each other using T4 DNA ligase (see Figure 1). One of them can form a triple helix by binding to an oligopurine•oligopyrimidine sequence which is present in the replication origin of phage f1, and therefore in the pGL3 plasmid that we use in gene expression studies. After triple helix formation, the 3′- and 5′-ends of the oligonucleotide reassociate and are ligated to the shorter oligonucleotide. In the resulting complex, the plasmid is catenated to a dumbbell-like circular oligonucleotide. If the short hairpin oligonucleotide has been conjugated to a targeting moiety, this moiety becomes irreversibly linked to the plasmid, although the covalent structure of the plasmid has not been changed. The same conjugated oligonucleotide can be adressed to different double-stranded DNA targets by changing the TFO sequence.

We have used this strategy to construct plasmids carrying a cationic peptide, the NLS from SV40 large T antigen. The synthesis of the oligonucleotide-peptide conjugate was relatively simple. This conjugate was linked to the plasmid with a good efficiency, the yield being solely limited by the quality of the olignucleotides. The use of a peptide-oligonucleotide conjugate did not decrease the yield of plasmid modification when compared to a nonmodified oligonucleotide. This reaction did not alter the supercoiled conformation of the plasmid nor its biological properties as shown by identical transgene expression levels. However, plasmids modified with one single NLS peptide did not display higher transgene expression levels than nonmodified plasmids.

Other groups have attempted to link NLS peptides to DNA. When a single NLS was linked to a plasmid by covalent triple helix formation, no enhancement was observed (*4*). An improvement was observed when the NLS was linked at the end of a linear DNA fragment (*11*), when several peptides were linked using PNAs (*5*), or when the plasmid was condensed with positively charged peptides containing NLS (*15*). The structural context and the mode of attachment that were used in our study were exactly the same as the ones used for the linear DNA study (*11*). Therefore, a single NLS peptide may be sufficient only when the linear DNA can creep inside the nucleus through the nuclear pore. Supercoiled DNA has a modest size which may be compatible with the passage through the nuclear pore. However, the forces, the process, and the folding pathway may be different than with linear DNA. It may be possible that supercoiled DNA requires the presence of several peptides, or even NLS peptides that would differ in the sequence or in the conjugation scheme. The lack of effect of the grafting of a single NLS peptide in our experimental system may also be explained by the fact that luciferase expression was observed after 24 h, and therefore the breakage of the nuclear envelope during cell division may hide the potential benefits that nuclear targeting moieties would provide on nondividing cells.

Other targeting moieties have been linked to plasmids. When a dexamethasone-psoralen conjugate was photocross-linked to a plasmid, an increase of plasmid nuclear uptake was observed (*16*). Binding occurred randomly on the plasmid, and the authors chose conditions that resulted in a mean of one psoralen conjugate per DNA molecule, as more would have resulted in plasmid inactivation. In another study, the protein transferrin was linked to a plasmid using PNA, and these complexes were shown to improve slightly the efficiency of gene delivery into muscle cells (*6*). In this last study, the presence of a conjugated protein in the PNA was shown to decrease its binding efficiency. Both of these approaches may be accommodated with our plasmid modification method, which gives a well-defined product and ensures that gene expression will not be perturbed and that the targeting moiety will not dissociate from the plasmid unless the oligonucleotide or the plasmid is cleaved by a cellular endonuclease or the two molecules are decatenated by an enzymatic process. This is not likely to occur before the plasmid has reached the nucleus.

In conclusion, we have designed a novel versatile method for coupling peptides to plasmid DNA. This technology allows an efficient and well-characterized modification and maintains plasmid integrity and tran-

scriptional activity. The present strategy may be used for coupling other ligands to plasmid DNA, such as cell-targeting antibodies, internalized molecules, or fluorescent reporters. In previously described methods for site-specific incorporation of peptides, for example, using PNA or psoralen-conjugated TFOs, the label is bound to a fixed site on the DNA. Here, the peptide may slide along the plasmid, thereby increasing its accessibility and facilitating interaction with its target. Despite the absence of improvement by attaching one NLS peptide, our strategy may be extended to the use of other targeting agents or the coupling of several peptides. Therefore, the full potential of this strategy still remains to be explored.

ACKNOWLEDGMENT

We thank Dr. Daniel Sherman for helpful discussions, Hélène Walbott for participating in some experimental work, Dr. Jean-Christophe François for advice in cell culture experiments, and Evelyne Charlier for plasmid preparation. T.R. was supported by a Bourse de Docteur Ingénieur from CNRS and a grant from the Association Française contre les Myopathies (AFM). This work was supported by the French Ministery of Research (ACI jeunes chercheurs 2000).

LITERATURE CITED

(1) Brown, M. D., Schatzlein, A. G., and Uchegbu, I. F. (2001) Gene delivery with synthetic (non viral) carriers. *Int. J. Pharm. 229*, 1−21.

(2) Wagner, E., Zenke, M., Cotten, M., Beug, H., and Birnstiel, M. L. (1990) Transferrin-polycation conjugates as carriers for DNA uptake into cells. *Proc. Natl. Acad. Sci. U.S.A. 87*, 3410−3414.

(3) Kircheis, R., Kichler, A., Wallner, G., Kursa, M., Ogris, M., Felzmann, T., Buchberger, M., and Wagner, E. (1997) Coupling of cell-binding ligands to polyethylenimine for targeted gene delivery. *Gene Ther. 4*, 409−418.

(4) Neves, C., Byk, G., Scherman, D., and Wils, P. (1999) Coupling of a targeting peptide to plasmid DNA by covalent triple helix formation. *FEBS Lett. 453*, 41−45.

(5) Branden, L. J., Mohamed, A. J., and Smith, C. I. (1999) A peptide nucleic acid-nuclear localization signal fusion that mediates nuclear transport of DNA. *Nat. Biotechnol. 17*, 784−787.

(6) Liang, K. W., Hoffman, E. P., and Huang, L. (2000) Targeted delivery of plasmid DNA to myogenic cells via transferrin-conjugated peptide nucleic acid. *Mol. Ther. 1*, 236−243.

(7) Zelphati, O., Liang, X., Nguyen, C., Barlow, S., Sheng, S., Shao, Z., and Felgner, P. L. (2000) PNA-dependent gene chemistry: stable coupling of peptides and oligonucleotides to plasmid DNA. *BioTechniques 28*, 304−316.

(8) Cantor, C. R., and Warshaw, M. M. (1970) Oligonucleotide interactions. III. Circular dichroïsm studies of the conformation of deoxyoligonucleotides. *Biopolymers 9*, 1059−1077.

(9) Zain, R., Marchand, C., Sun, J.-S., Nguyen, C. H., Bisagni, E., Garestier, T., and Hélène, C. (1999) Design of a triple-helix-specific cleaving reagent. *Chem. Biol. 6*, 771−777.

(10) Seibel, P., Trappe, J., Villani, G., Klopstock, T., Papa, S., and Reichmann, H. (1995) Transfection of mitochondria: strategy towards a gene therapy of mitochondrial DNA diseases. *Nucleic Acids Res. 23*, 10−17.

(11) Zanta, M. A., Belguise-Valladier, P., and Behr, J. P. (1999) Gene delivery: a single nuclear localization signal peptide is sufficient to carry DNA to the cell nucleus. *Proc. Natl. Acad. Sci. U.S.A. 96*, 91−96.

(12) Roulon, T., Hélène, C., and Escudé, C. (2001) A Ligand-Modulated Padlock Oligonucleotide for Supercoiled Plasmids. *Angew. Chem., Int. Ed. Engl. 40*, 1523−1526.

(13) Roulon, T., Coulaud, D., Delain, E., Lecam, E., Hélène, C., and Escudé, C. (2002) Padlock Oligonucleotides as a Tool for Labeling Superhelical DNA. *Nucleic Acids Res. 30*, e12.

(14) Escudé, C., Garestier, T., and Hélène, C. (1999) Padlock oligonucleotides for duplex DNA based on sequence-specific triple helix formation. *Proc. Natl. Acad. Sci. U.S.A. 96*, 10603−10607.

(15) Subramanian, A., Ranganathan, P., and Diamond, S. L. (1999) Nuclear targeting peptide scaffolds for lipofection of nondividing mammalian cells. *Nat. Biotechnol. 17*, 873−877.

(16) Rebuffat, A., Bernasconi, A., Ceppi, M., Wehrli, H., Verca, S. B., Ibrahim, M., Frey, B. M., Frey, F. J., and Rusconi, S. (2001) Selective enhancement of gene transfer by steroid-mediated gene delivery. *Nat. Biotechnol. 19*, 1155−1161.

BC025551O

A Trithiolate Tripodal Bifunctional Ligand for the Radiolabeling of Peptides with Gallium(III)

Leonard G. Luyt and John A. Katzenellenbogen*

Department of Chemistry, University of Illinois, Urbana, Illinois 61801. Received May 20, 2002; Revised Manuscript Received July 2, 2002

A tripodal bifunctional chelator for gallium has been prepared with a chelation core consisting of three thiols and a tertiary amine. The synthesis proceeds in 13 steps with an overall yield of 22%. An aromatic amine is available for conjugation to peptides through carbodiimide coupling. Gallium(III) complexes were readily prepared from both the bifunctional chelator and a phenylalanine-conjugated system. These complexes underwent stability evaluation and were found to be stable to ligand exchange and enzymatic hydrolysis. This bifunctional chelator appears to be suitable for conjugation to peptides for the preparation of gallium radiopharmaceuticals.

INTRODUCTION

Gallium-68 ($t_{1/2}$ = 68 min) is considered to be a promising radionuclide for use in positron emission tomography (PET) and has been used in a number of clinical studies. A particular convenience associated with the use of ^{68}Ga is that it can be obtained from a ^{68}Ge/^{68}Ga generator system; thus, PET imaging can be done with this isotope without the need for an on-site cyclotron (*1*). Gallium-67 ($t_{1/2}$ = 3.3 days) is a gallium isotope that has been used for single-photon emission computed tomography (SPECT) for many years, even though its long half-life limits its usefulness as an imaging radionuclide.

Current gallium-based radiopharmaceuticals are, for the most part, simple metal−ligand complexes, such as Ga-citrate.(*2*) Recently, however, a number of gallium radiopharmaceuticals have been successfully developed by the conjugation of a gallium chelation unit to a large biomolecule (*3*−*6*). We are interested in developing methods for radiolabeling large biomolecules, such as peptides and proteins, with gallium for use in receptor-based imaging. Ideally, a chelation unit for labeling biomolecules with gallium for in vivo use should have the following characteristics: (a) it should bind the metal with high kinetic stability, (b) it should have a single site for chelation to facilitate complete spectroscopic characterization of a single product, and (c) and it should have bifunctional character that will allow its conjugation to a variety of biomolecules through a single linking site.

A 4-coordinate tripodal S_3N ligand for gallium(III) was previously described by Koch and co-workers and was found to be stable, neutral, and uniquely, for a gallium(III) complex, able to pass through the blood−brain barrier (*7*−*10*). In contrast to indium and iron complexes with the same chelate system, the gallium(III) complex retains its tetrahedral geometry in the presence of water and DMF. This tripodal ligand appeared to be a suitable candidate for the radiolabeling of peptides with gallium, through a pendant approach as depicted in Figure 1.

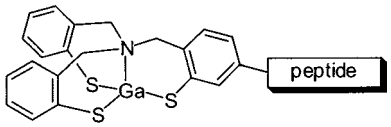


Figure 1. A tripodal gallium(III) bioconjugate.

Herein is a description of the synthesis of this bifunctional chelator, its conjugation to a biomolecule model, and a discussion of the stability of the resultant gallium(III) complexes.

EXPERIMENTAL SECTION

Reagents and solvents were purchased from Acros, Aldrich, Fisher, Strem, or TCI. $[GaCl_4][PPh_4]$ was prepared as previously reported (*11*). Diethyl ether, methylene chloride, and tetrahydrofuran were dried by a solvent delivery system (using activated neutral alumina columns) designed by J. C. Meyer. All air-sensitive reactions were carried out under a nitrogen or argon atmosphere, using flame- or oven-dried glassware. Reaction progress was monitored by analytical thin-layer chromatography (silica). Flash chromatography was performed using Woelm silica gel (0.040−0.063 mm) packing. Hexane for chromatography was distilled prior to use.

^{1}H and ^{13}C NMR spectra were obtained using a Unity 400, Unity 500, or Unity INOVA 500NB Varian FT-NMR spectrometer. Chemical shifts (δ) are reported in parts per million downfield from internal tetramethylsilane and referenced from solvent resonances. NMR coupling constants are reported as absolute values in Hertz. Low-resolution electron impact (EI) mass spectra and high-resolution EI mass spectra (HRMS) were obtained on Micromass 70-VSE, or Micromass 70-SE−4F spectrometers. Both low- and high-resolution fast atom bombardment (FAB) mass spectra were obtained on Micromass ZAB−SE and 70-SE−4F spectrometers, respectively. Melting points were determined on a Thomas-Hoover melting point apparatus and are uncorrected.

HPLC analysis was performed with a ThermoQuest Spectrasystem P4000/AS4000/UV1000, with the UV detector set to 254 nm. A Microsorb-MV C_{18} reversed-phase column (5 μm, 100 Å) was used, with an isocratic eluent of 80% MeOH/20% water at 1.0 mL/min.

* Corresponding author: Department of Chemistry, University of Illinois, 600 S. Mathews Ave., Urbana, IL 61801. Telephone 217-333-6310. Fax 217-333-7325. E-mail jkatzene@uiuc.edu.

10.1021/bc025552g CCC: $22.00 © 2002 American Chemical Society
Published on Web 08/24/2002

(*S*-Benzylthio)salicylic Acid. Thiosalicylic acid (6.33 g, 41.1 mmol) was dissolved in 100 mL of ethanol and 100 mL of 1 M NaOH solution. The solution was cooled to 0 °C; then benzyl bromide (5.13 mL, 43.1 mmol) was added, and the solution was warmed to room temperature and stirred for three h. A 1 M HCl solution was added to acidify the reaction, and the crude product was collected by filtration and then recrystallized from benzene to yield 9.95 g (99%) of off-white needles: mp 186−187 °C. ^{1}H NMR (d_6-acetone): δ 4.21 (s, 2H), 7.20 to 7.53 (m, 8H), 8.01 (m, 1H), 11.33 (br s, 1H). ^{13}C NMR (d_6-acetone): δ 37.24, 124.66, 126.68, 127.98, 128.21, 129.29, 130.00, 132.11, 133.24, 137.64, 143.26, 167.55. MS (EI, 70 eV): *m*/*z* 244 (15.9%, M^+), 91 (100%, SBn).

2-(Benzylthio)benzyl Alcohol (1). A three-necked, flame-dried flask was filled with 30 mL of THF and 16 mL of 1.0 M BH_3·THF and then cooled on an ice-bath (0 °C). To the flask was added (benzylthio)salicylic acid (2.53 g, 7.85 mmol) dissolved in 30 mL of THF, and the reaction was stirred at 0 °C for 1 h and then at RT for 3 h. To this was carefully added 40 mL water, and stirring was continued for 1 h. Solid K_2CO_3 was added until the solution was saturated, and the layers were separated. The organic layer was evaporated to dryness, partioned between ether and water, and extracted into ether (×2). The original aqueous layer was extracted with ether (×2), and all organics were combined, washed with 1 M NaOH, water, and brine, dried over $MgSO_4$, evaporated, and dried under vacuum. The solid product was recrystallized from diethyl ether/petroleum ether (37−54 °C) to give colorless needles (1.77 g, 97%): mp 50 °C (lit. 48.5−49.5 °C) (*10*). ^{1}H NMR ($CDCl_3$): δ 1.97 (br s, 1H, OH), 4.05 (s, 2H, CH_2S), 4.61 (s, 2H, CH_2O), 7.17 to 7.40 (m, 9H). ^{13}C NMR ($CDCl_3$): δ 39.88, 63.58, 127.29, 127.34, 128.27, 128.41, 128.50, 128.75, 131.84, 134.05, 137.36, 141.76. MS (EI, 70 eV): *m*/*z* 230 (7.6%, M^+), 139 (61.9%, M-SBn), 91 (100%, SBn).

2-(Benzylthio)benzyl Bromide (2). A flame-dried flask was charged with benzylic alcohol **1** (1.71 g, 7.43 mmol) dissolved in 100 mL of diethyl ether. After cooling to 0 °C, 0.78 mL of freshly distilled PBr_3 (8.18 mmol) was added, and the reaction was stirred at 0 °C for 15 min. then at RT for 1 h. The reaction was quenched with methanol; then water was added, and the organic layer was washed with sat. $NaHCO_3$, water, brine, dried over $MgSO_4$, evaporated and dried under vacuum yielding 2.12 g (97%) of a clear, colorless oil. ^{1}H NMR ($CDCl_3$): δ 4.14 (s, 2H, CH_2S), 4.61 (s, 2H, CH_2Br), 7.20 to 7.39 (m, 9H). ^{13}C NMR ($CDCl_3$): δ 32.08, 39.65, 127.29, 127.39, 128.48, 128.92, 129.14, 130.58, 132.11, 135.95, 137.09, 138.66. MS (EI, 70 eV): *m*/*z* 294 (5.1%, M^+), 292 (5.0%, M^+), 213 (21.9%, M-Br), 91 (100%, SBn); HRMS calcd $C_{14}H_{13}BrS$, 291.9921, found, 291.9924.

4-Nitro-2-thiocyanatobenzoic Acid (3). This material was prepared from 2-amino-4-nitrobenzoic acid by diazotization followed by treatment with copper thiocyanate, as previously described (yield 86%) (*12*). ^{1}H NMR (CD_3OD): δ 8.29 (dd, 1H, J = 8.4, 1.9 Hz), 8.36 (d, 1H, J = 8.4 Hz), 8.68 (d, 1H, J = 1.9 Hz). ^{13}C NMR (CD_3OD): δ 112.11, 123.13, 123.54, 133.36, 134.26, 134.77, 151.99, 167.95. MS (EI, 70 eV): *m*/*z* 224 (17.9%, M^+), 197 (100%, M − CN); HRMS calcd $C_8H_4N_2O_4S$, 223.9892, found, 223.9888.

2,2′-Dithiobis(4-nitrosalicylic Acid) (4). This material was prepared from **3** as previously described in 86% yield (*12*). ^{1}H NMR (d_6-DMSO): δ 8.14 (dd, 2H, J = 2.4, 8.8 Hz), 8.26 (d, 2H, J = 8.8 Hz), 8.38 (d, 2H, J = 2.4 Hz). ^{13}C NMR (d_6-DMSO): δ 119.94, 121.33, 133.31, 133.61, 140.69, 150.25, 166.56.

4-Nitrothiosalicylic Acid. Disulfide **4** (2.05 g, 5.16 mmol) was dissolved in 150 mL of abs ethanol and heated to 70 °C. Sodium borohydride (0.78 g, 20.6 mmol) was added portionwise. The reaction was heated at reflux for 90 min (TLC, 40% MeOH/60% $CHCl_3$), cooled, poured into 300 mL of water, and acidified with concentrated HCl. The product was extracted into diethyl ether (×3), washed with water, dried over Na_2SO_4, and filtered, the solvent was evaporated, and the product was dried under vacuum to yield 1.91 g (93%) of yellow crystals: mp 267−268 °C. ^{1}H NMR (CD_3OD): δ 7.95 (dd, 1H, J = 2.1, 8.6 Hz), 8.20 (d, 1H, J = 8.6 Hz), 8.33 (d, 1H, J = 2.1 Hz). ^{13}C NMR (CD_3OD): δ 119.74, 126.14, 132.55, 134.00, 142.64, 150.81, 168.20. MS (EI, 70 eV): *m*/*z* 199 (9.1%, M^+), 181 (100%, M-OH_2); HRMS calcd $C_7H_5NO_4S$, 198.9939, found, 198.9937.

2-(Benzylthio)-4-nitrobenzoic Acid (5). To a solution of 4-nitrothiosalicylic acid, prepared above, (1.81 g, 9.08 mmol) in 60 mL of abs ethanol were added 30 mL of 1 M NaOH and 1.1 mL (9.25 mmol) of benzyl bromide. The solution was stirred at 0 °C for 1 h and then at RT for 2 h (TLC, 30% MeOH/70% $CHCl_3$). Water (30 mL) was added, followed by 32 mL of 1 M HCl. The mixture was cooled to 0 °C, and the product, which precipitated, was collected by filtration to yield, after drying, 2.12 g (81%) of a yellow crystalline solid: mp 194−196 °C. ^{1}H NMR (CD_3OD): δ 4.30 (s, 2H), 7.25 (m, 1H), 7.32 (m, 2H), 7.47 (m, 2H), 7.97 (dd, 1H, J = 2.2, 8.5 Hz), 8.12 (d, 1H, J = 8.5 Hz), 8.25 (d, 1H, J = 2.2 Hz). ^{13}C NMR (CD_3OD): δ 37.88, 119.43, 121.66, 128.56, 129.68, 130.26, 133.38, 134.30, 137.17, 145.61, 151.05, 168.03. MS (EI, 70 eV): *m*/*z* 289 (6.3%, M^+), 91 (100%, Bn); HRMS calcd $C_{14}H_{11}NO_4S$, 289.0409, found, 289.0408.

2-(Benzylthio)-4-nitrobenzamide (6). In a flame-dried, N_2-purged flask, a slurry of the nitrobenzoic acid **5** (1.92 g, 6.64 mmol) in 150 mL of CH_2Cl_2 and 2 drops DMF, was cooled to 0 °C. Oxalyl chloride (1.2 mL, 13.3 mmol) was added, the solution was warmed to RT and stirred for 2 h (gas evolution had ceased). The solvent was evaporated, and the resultant yellow solid was dissolved in 100 mL of CH_2Cl_2. Ammonium hydroxide solution (10 mL) was added, and the reaction mixture was stirred at RT for 40 min. The mixture was diluted with water, and the organic layer was separated and washed with sodium bicarbonate, water, and brine. The organic phase was dried over magnesium sulfate and filtered, and the solvent was evaporated to leave 1.81 g (94%) of a yellow solid: mp 171−173 °C. ^{1}H NMR (CD_3OD): δ 4.28 (s, 2H), 7.22 (m, 1H), 7.28 (m, 2H), 7.38 (m, 2H), 7.62 (m, 1H), 8.02 (m, 1H), 8.17 (m, 1H). ^{13}C NMR (CD_3OD): δ 38.12, 120.58, 123.23, 128.19, 129.35, 129.58, 129.96, 137.33, 140.01, 142.46, 149.33, 168.70. MS (EI, 70 eV): *m*/*z* 288 (134%, M^+), 197 (22.3%, M − SBn), 91 (100%, Bn); HRMS calcd $C_{14}H_{12}N_2O_3S$, 288.0569, found, 288.0574.

2-(Benzylthio)-4-nitrobenzylamine (7). A flame-dried flask with attached condenser was charged with 40 mL of THF and 30 mL of 1.0 M BH_3·THF. To this was slowly added nitro amide **6** (1.76 g, 6.11 mmol) dissolved in 60 mL of THF, and the solution was heated at reflux overnight. After cooling to room temperature, 40 mL of 6.0 M HCl was carefully added, the mixture was heated at 50 °C for 90 min and then cooled, and the THF was removed using a rotary evaporator. HCl (1 M) was added to the aqueous solution, followed by ether extraction (×2), with the combined organics being washed with additional 1 M HCl. The combined aqueous layers were basified with solid NaOH, extracted with ether (×3), washed with brine, dried over $MgSO_4$, evaporated, and

dried under vacuum to give a yellow solid (0.96 g, 57%). ^{1}H NMR ($CDCl_3$): δ 3.90 (s, 2H), 4.21 (s, 2H), 7.24 to 7.34 (m, 5H), 7.53 (d, 1H, J = 8.4 Hz), 8.00 (dd, 1H, J = 8.4, 2.3 Hz), 8.16 (d, 1H, J = 2.1 Hz). ^{13}C NMR ($CDCl_3$): δ 38.06, 43.98, 120.85, 122.69, 127.73, 128.01, 128.72, 128.87, 135.73, 137.39, 147.01, 148.86. MS (EI, 70 eV): m/z 274 (1.3%, M^+), 183 (100%, M − SBn); HRMS calcd $C_{14}H_{14}N_2O_2S$, 274.0776, found, 274.0775.

Bis((2-(benzylthio)benzyl)(2-(benzylthio)-4-nitrobenzyl)amine (8). 2 (1.92 g, 6.55 mmol) and the nitrobenzylamine **7** (0.90 g, 3.28 mmol) were dissolved in 100 mL of acetonitrile and then stirred at RT overnight. The solids were removed by filtration, and the solvent was removed using a rotary evaporator to give 2.40 g of crude material. Flash column purification (silica, 1:1/CH_2Cl_2:hexane) yielded the product **8** as a yellow oil (1.73 g, 75%). ^{1}H NMR ($CDCl_3$): δ 3.53 (s, 2H, NCH_2), 3.56 (s, 4H, $N(CH_2)_2$), 4.01 (s, 4H, $S(CH_2)_2$), 4.11 (s, 2H, SCH_2), 7.10 to 7.30 (m, 21H), 7.48 (m, 2H), 7.71 (d, 1H, J = 7.5 Hz), 7.81 (dd, 1H, J = 8.5, 2.2 Hz), 8.04 (d, 1H, J = 2.2 Hz). ^{13}C NMR ($CDCl_3$): δ 38.19, 39.09, 55.34, 56.34, 120.18, 122.04, 126.16, 127.21, 127.49, 127.62, 128.42, 128.66, 128.82, 128.96, 129.53, 129.56, 129.88, 135.81, 136.25, 137.13, 138.20, 138.60, 145.95, 146.78. MS (FAB, +): m/z 699 (100%, $M^+ + H$); HRMS calcd $C_{42}H_{38}N_{22}O_2S_3$, 699.2174, found, 699.2169.

Bis(2-(benzylthio)benzyl)(2-(benzylthio)-4-aminobenzyl)amine (9). The benzylamine **8** (1.72 g, 2.46 mmol) was dissolved in 50 mL of abs ethanol and 50 mL of 1,2-dichloroethane. To this solution was added 0.5 mL of hydrazine hydrate followed by 0.1 mL of 50% Raney nickel slurry. These additions were repeated twice until the reaction was complete by TLC (1 h). The slurry was filtered through Celite, evaporated, and dried under vacuum to yield 1.57 g (95%) of clear, pale yellow viscous oil. ^{1}H NMR ($CDCl_3$): δ 3.53 (s, 2H), 3.61 (s, 4H), 4.02 (s, 2H), 4.05 (s, 4H), 6.49 (dd, 1H, J = 8.1, 2.4 Hz), 6.64 (d, 1H, J = 2.4 Hz), 7.13 to 7.31 (m, 21 H), 7.38 (d, 1H, J = 8.1 Hz), 7.65 (m, 2H). ^{13}C NMR ($CDCl_3$): δ 39.05, 39.09, 55.20, 55.50, 113.48, 115.91, 126.19, 126.94, 127.08 (2 peaks), 128.39 (2 peaks), 128.89, 128.91, 129.25, 129.38, 129.52, 130.62, 135.70, 136.82, 137.31, 137.33, 139.74, 145.28. MS (FAB, +): m/z 669 (100%, $M^+ + H$); HRMS calcd $C_{42}H_{40}N_2S_3$, 669.2432, found, 669.2431.

Bis(2-thio)benzyl-(2-thio-4-aminobenzyl)amine gallium(III) (11). A flame-dried three-necked flask with attached dry ice condenser was cooled to −78 °C and filled with 15 mL of anhydrous ammonia. To this was added the chelate system **9** (143 mg, 0.214 mmol) dissolved in 2 mL of THF, followed by small pieces of sodium. The mixture was warmed to −33 °C to improve solubility and allowed to gently reflux for 45 min. The reaction was quenched with solid NH_4Cl, and the ammonia was evaporated under argon flow, followed by vacuum-drying. The crude trithiol was dissolved in 8 mL of degassed methanol, and $[PPh_4][GaCl_4]$ (118 mg, 0.214 mmol) dissolved in 2 mL of degassed acetonitrile was then added. The pH was adjusted to basic with 0.8 mL of 1 M KOH solution (degassed); the mixture was stirred at room temperature for 30 min, and the solvents were evaporated and dried under vacuum. The crude product was triturated with chloroform, and the solvent was removed by rotary evaporation and dried under vacuum to yield a yellow solid (40 mg, 40%). ^{1}H NMR ($CDCl_3$): δ 3.27 (d, 1H, J = 12.5 Hz to 4.54), 3.32 (d, 1H, J = 12.5 Hz to 4.70), 3.36 (d, 1H, J = 12.5 Hz to 4.59), 3.76 (br s, 2H, NH_2), 4.54 (d, 1H, J = 12.2 Hz), 4.59 (d, 1H, J = 12.2 Hz), 4.70 (d, 1H, J = 12.2 Hz), 6.44 (dd, 1H, J = 2.0, 8.1 Hz), 6.86 (d, 1H, J = 2.2 Hz), 6.94 (d, 1H, J = 8.1 Hz), 7.16 (m, 4H), 7.24 (m, 2H), 7.52 (m, 2H). MS (FAB, +): m/z 467 (11%, ^{71}Ga), 465 (13%, ^{69}Ga); HRMS calcd $C_{21}H_{19}N_2S_3{}^{69}Ga$, 465.0044, found, 465.0043.

Bis(2-(benzylthio)benzyl)(2-(benzylthio)-4-aminobenzyl)amido(*tert*-butoxycarbonyl)phenylalanine (10). The chelate system **9** (213 mg, 0.318 mmol) was combined with *N*-(*tert*-butoxycarbonyloxy)phenylalanine (89 mg, 0.334 mmol), 1,3-dicyclohexylcarbodiimide (66 mg, 0.334 mmol), 1-hydroxybenzotriazole (43 mg, 0.334 mmol), and 111 μL of *N*,*N*-diisopropylethylamine (0.637 mmol) in a flask with 20 mL of methylene chloride. The mixture was stirred at RT for 24 h and then filtered and washed with 0.1 M NaOH, water, and brine. The organic layer was filtered through cotton wool and then evaporated and dried under vacuum. Purification was carried out by flash chromatography (silica, 30% ethyl acetate/70% hexanes) to yield **10** (259 mg, 89%). ^{1}H NMR ($CDCl_3$): δ 1.43 (s, 9H), 3.15 (m, 2H), 3.48 (s, 2H), 3.55 (s, 4H), 4.01 (s, 4H), 4.03 (s, 2H), 4.45 (br, 1H), 5.16 (br, 1H), 7.01 (m, 1H), 7.10 to 7.33 (m, 27H), 7.49 (m, 1H), 7.57 (m, 2H). ^{13}C NMR ($CDCl_3$): δ 28.21, 38.35, 38.67, 39.05, 55.20, 55.62, 56.62, 80.55, 117.45, 119.80, 126.23, 127.06, 127.09, 127.17, 128.38, 128.40, 128.44, 128.81, 128.85, 129.01, 129.26, 129.29, 129.56, 129.67, 134.99, 135.72, 136.16, 136.58, 136.83, 136.94, 137.24, 139.42, 155.77, 169.40. MS (FAB, +): m/z 916 (100%); HRMS calcd $C_{56}H_{57}N_3O_3S_3$, 916.3640, found, 916.3643.

Bis(2-thio)benzyl-(2-thio-4-aminobenzyl)amido-(*tert*-butoxycarbonyl)phenylalanine gallium(III) (12). A flame-dried three-necked flask with attached dry ice condenser was cooled to −78 °C and filled with 15 mL of anhydrous ammonia. To this was added the chelate system **10** (57 mg, 0.062 mmol) dissolved in 1.5 mL of THF, followed by small pieces of sodium until a blue color persisted, and the reaction was stirred at −78 °C for 1 h. The reaction was quenched with solid NH_4Cl, and then the ammonia was evaporated under nitrogen flow, followed by vacuum-drying. The crude trithiol was dissolved in 10 mL of degassed methanol, and then $[GaCl_4][PPh_4]$ (34 mg, 0.062 mmol) was added dissolved in 2 mL of degassed acetonitrile. The pH was adjusted to basic with 0.2 mL of 1 M KOH solution (degassed) and then stirred at room temperature for 35 min, after which the solvents were evaporated and the product was dried under vacuum. The crude material was purified by flash chromatography (silica, 50% ethyl acetate/50% hexanes) to yield 25 mg (57%) of **12** as a colorless solid. ^{1}H NMR ($CDCl_3$): δ 1.41 (s, 9H), 3.12 (m, 2H, CH_2 of Phe), 3.37 (m, 3H, N−CH(H) × 3), 4.42 (m, 1H, CH), 4.55 (d, 1H, J = 12.2 Hz coupled to 3.37 ppm, N−CH(H)), 4.60 (d, 1H, J = 12.4 Hz coupled to 3.37 ppm, N−CH(H)), 4.63 (d, 1H, J = 12.4 Hz coupled to 3.37 ppm, N−CH(H)), 5.08 (m, 1H, NH(BOC)), 7.11 to 7.83 (12H, ar and NH). MS (FAB, +): m/z 714 (3%), 713 (6%), 712 (4%), 711 (6%); HRMS calcd $C_{35}H_{35}N_3O_3S_3{}^{69}Ga$, 711.1175, found, 711.1174.

Histidine and Cysteine Challenge. A conical vial containing a stir bar was charged with 900 μL of test solution (10 mM histidine or cysteine in a buffered saline solution) and 100 μL of substrate (1 mM of **11** or **12** dissolved in methanol). The vial was sealed with a Teflon lined cap and maintained with stirring at 37 °C, with periodic analysis by HPLC.

Enzymatic Hydrolysis. A conical vial containing a stir bar was charged with 800 μL buffered saline solution, 100 μL of substrate solution (1 mM **12** in DMF), 20 μL of Tween solution (1% in water), and 100 μL of α-chymotrypsin solution (approximately 0.7 units in a buffered saline solution). The vial was sealed with a Teflon-lined

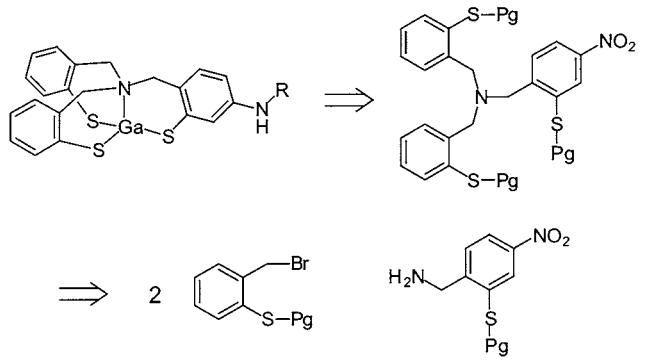
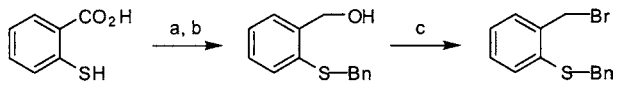


Figure 2. Retrosynthetic analysis.

Scheme 1 [a]



1 **2**

[a] Reagents and conditions (yield): (a) BnBr, NaOH, EtOH (76%); (b) BH_3·THF, THF (97%); (c) PBr_3, ether (97%).

cap and maintained with stirring at 37 °C, with periodic analysis by HPLC (retention time for **11** = 4.4 min, retention time for **12** = 15.5 min). The activity of the α-chymotrypsin was confirmed by the hydrolysis of *N*-benzoyl-L-tyrosine ethyl ester.

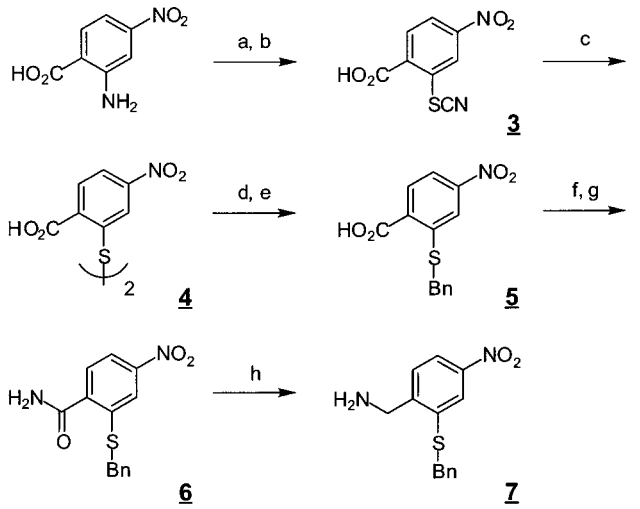
RESULTS AND DISCUSSION

The conjugation of the S_3N tripodal chelate system to a peptide (Figure 2, R = peptide) requires a point of attachment on one of the mercaptobenzene groups of the ligand. Since the other two mercaptobenzenes will be identical, this design permits the bifunctional tertiary amine tripodal chelate system to be prepared by a 2 + 1 approach, as depicted in Figure 2. Scheme 1 outlines the preparation of the benzyl bromide derivative **2** starting from thiosalicylic acid, an approach modified from that described earlier for the preparation of the chloride analogue of **2** (*13*). Thiol protection with a benzyl group proceeds in 76% yield, and reduction to the alcohol **1** in 97% yield using borane−THF complex. The benzyl bromide **2** was obtained through reaction with PBr_3 in 97% yield.

The preparation of the benzylamine portion of the tripodal ligand is described in Scheme 2. Prior to developing this route, a more direct approach was taken whereby 4-nitroanthranilic acid was diazotized and then reacted with benzyl mercaptan under basic conditions. Although this produced (benzylthio)nitrobenzoic acid **5** in two steps, the yield was poor (20%) and the chromatographic purification difficult. The improved route proceeds in five steps also starting with 4-nitroanthranilic acid, with the first three steps following a literature precedent (*12*).

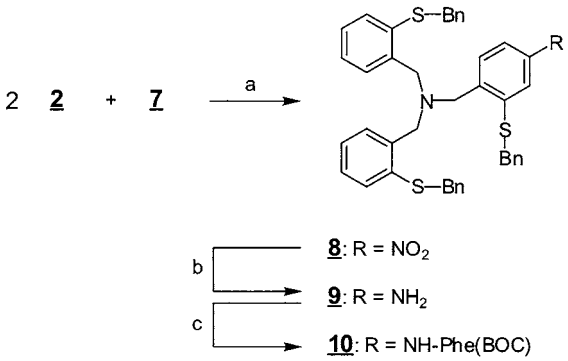
Formation of the diazonium salt followed by Sandmeyer-type reaction with copper thiocyanate produced the aryl thiocyanate **3** in 86% yield. Disulfide **4**, prepared by ammonolysis followed by spontaneous oxidation of the thiolate, was rereduced with sodium borohydride, and the resultant thiol was protected with a benzyl group. This five-step transformation to the acid **5** was carried out in 53% yield, a significant improvement over the initial direct approach, with only simple crystallizations required for product recovery. The remaining three steps to the desired benzylamine derivative involve formation

Scheme 2 [a]



[a] Reagents and conditions (yield): (a) $NaNO_2$, HCl; (b) CuSCN, KSCN (86%, two steps); (c) NH_4OH (86%); (d) $NaBH_4$, EtOH (94%); (e) BnBr, NaOH, EtOH (76%); (f) oxalyl chloride, DMF, CH_2Cl_2; (g) NH_4OH, CH_2Cl_2 (94% two steps); (h) BH_3·THF, THF (88%).

Scheme 3 [a]



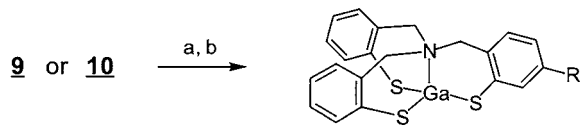
[a] Reagents and conditions (yield): (a) K_2CO_3, acetone (75%); (b) Raney Ni, hydrazine, EtOH, 1,2-dichloroethane (95%); (c) Phe(BOC), DCC, 1-HOBT, DiPEA, CH_2Cl_2 (89%).

of the acid chloride with oxalyl chloride and subsequent reaction with ammonia to generate benzamide **6** in 94% yield. Reduction with borane−THF complex proceeds in 88% yield giving the benzylamine **7**.

Construction of the tripodal ligand is illustrated in Scheme 3. Initial attempts were carried out using the chloride equivalent of the benzylic bromide **2**, but reaction ceased after formation of the secondary amine and could not be driven further to the tertiary amine. The addition of sodium iodide produced byproducts due to sulfonium salt formation. The benzyl bromide **2** provided the correct reactivity, and with it the tertiary amine **8** could be formed at room temperature in 75% yield. The aromatic nitro substituent was readily reduced with hydrazine/Raney nickel to give the aniline **9** in excellent yield. This amino group is available for attachment of peptides. To model the attachment to peptides, BOC-protected phenylalanine was conjugated via carbodiimide amide formation, to give 89% of **10**.

Deprotection of the thiol groups was carried out using sodium in liquid ammonia, as indicated in Scheme 4. It also proved possible to proceed directly from **8** to the deprotected trithiol, using sodium in liquid ammonia, thus carrying out both the nitro reduction and the thiol deprotection in one step. Due to the air sensitivity of the trithiol compounds, complexation with $[PPh_4][GaCl_4]$ was

Scheme 4 [a]



11: R = NH_2
12: R = NH-Phe(BOC)

[a] Reagents and conditions: (a) NH_3, THF, −78 °C; (b) $[PPh_4][GaCl_4]$, KOH, MeOH, CH_3CN.

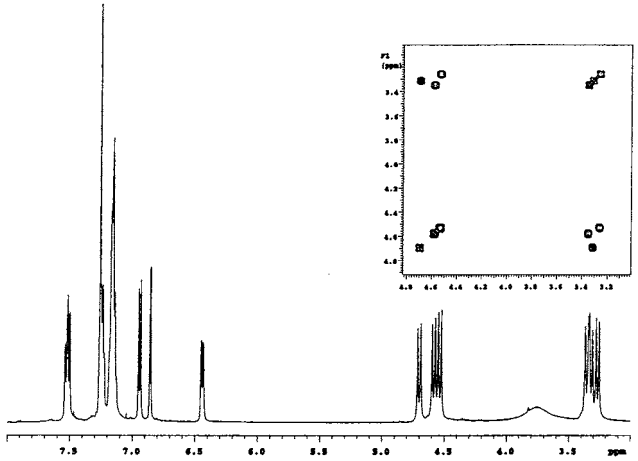


Figure 3. ^1H NMR ($CDCl_3$, 500 MHz) of **11** from δ 8.0 to 3.0 with inset $^1H-^1H$ COSY.

Table 1. [a] **Stability of Complexes 11 and 12 against Ligand Exchange and Enzymatic Hydrolysis**

	11			12		
conditions	1 h	4 h	24 h	1 h	4 h	24 h
aqueous	>99	>99	>99	>99	>99	>99
histidine	>99	98	>99	99	94	55
cysteine	97	94	91	98	92	44
α-chymotrypsin				97	98	93

[a] Percent of complex remaining at the indicated time. Conditions tested: aqueous medium at room temperature; ligand exchange with histidine; ligand exchange with cysteine; enzymatic hydrolysis with α-chymotrypsin. See Experimental Section for details.

carried out immediately, without purification of the trithiol intermediates. This two-step procedure for the aniline derivative **9** resulted in a 40% yield of the gallium complex **11**. For the phenylalanine conjugate **10**, a 57% yield was achieved in forming the complex **12**.

These four-coordinate gallium complexes have a propeller-type conformation, suggesting that the six benzylic protons (all diastereotopic pairs) would exist as four distinct doublets in the ^1H NMR spectrum. Figure 3 shows the ^1H NMR spectrum of **11**, with an inset COSY ($^1H-^1H$ correlation) for the relevant aliphatic region. The six benzylic protons appear as six distinct doublets, suggesting that in solution complex **11** exists as a twisted propeller, resulting in all six protons being nonequivalent.

To test the applicability of this system for use as an in vivo imaging agent, we analyzed the stability of the gallium complexes **11** and **12** to ligand exchange, as presented in Table 1. In the presence of histidine and cysteine, both complexes appear relatively stable over 24 h. Thus, even with the increased electron density from the free amino group in **11**, there is no significant loss in complex stability at a neutral pH. The decreased stability of the phenylalanine conjugate may be due to the BOC protecting group. However, complex **11** was found to be much less stable under strongly alkaline conditions, as compared to complex **12**. Under neutral conditions, both complexes are stable for long time periods in an aqueous medium.

We were also interested in determining the stability of conjugates with an amide attachment to this gallium core, such as represented by **12**. Thus, the susceptibility of **12** to enzymatic hydrolysis was studied (which would produce **11** as the product), following the hydrolysis by HPLC analysis. With both the phenylalanine substrate specific hydrolase chymotrypsin, and the more general amide hydrolyzing enzyme subtilisin, there was an insignificant level enzymatic hydrolysis of **12**. Thus, the bulky chelate must hinder access of the complex to the active site of these enzymes. This suggests that conjugation of a biomolecule at this location through an amide linkage will provide a complex that will be stable in vivo.

CONCLUSIONS

A tripodal S_3N chelate system has been developed for the radiolabeling of large biomolecules with gallium radioisotopes. The conjugation of this chelator to phenylalanine demonstrates the appropriateness for utilizing this system in the production of gallium-labeled peptides. The bioconjugate complex was found to be stable to ligand exchange and enzymatic hydrolysis, providing initial evidence of its suitability for in vivo use.

ACKNOWLEDGMENT

This research has been supported through a grant from the Department of Energy (DE FG02 86ER60401). NMR spectra were obtained in the Varian Oxford Instrument Center for Excellence in NMR Laboratory. Funding for this instrumentation was provided in part from the W.M. Keck Foundation and the National Science Foundation (NSF CHE 96-10502). Mass spectra were obtained on instruments supported by grants from the National Institute of General Medical Sciences (GM 27029), the National Institute of Health (RR 01575), and the National Science Foundation (PCM 8121494).

LITERATURE CITED

(1) Green, M. A. (1990) The Potential for Generator-Based PET Perfusion Tracers. *J. Nucl. Med. 31*, 1641−1645.

(2) Green, M. A., and Welch, M. J. (1989) Gallium Radiopharmaceutical Chemistry. *Nucl. Med. Biol. 16*, 435−448.

(3) Wang, S., Lee, R. J., Mathias, Green, M. A., and Low, P. S. (1996) Synthesis, Purification, and Tumor Cell Uptake of ^{67}-Ga-Deferoxamine-Folate, a Potential Radiopharmaceutical for Tumor Imaging. *Bioconjugate Chem. 7*, 56−62.

(4) Wu, C., Jagoda, E., Brechbiel, M., Webber, K. O., Pastan, I., Gansow, O., and Eckelman, W. C. (1997) Biodistribution and Catabolism of Ga-67-Labeled Anit-Tac dsFv Fragment. *Bioconjugate Chem. 8*, 365−369.

(5) Sun, Y. S., Martell, A. E., Motekaitis, R. J., and Welch, M. J. (1998) Synthesis and Stabilities of the Ga(III) and In(III) Chelates of a New Diaminodithiol Bifunctional Liagnd. *Tetrahedron 54*, 4203−4210.

(6) Heppeler, A., Froidevaux, S., Mäcke, H. R., Jermann, E., Béhé, M., Powell, P., and Hennig, M. (1999) Radiometal-Labeled Macrocyclic Chelator-Derivatised Somatostatin Analogue with Superb Tumour-Targeting Properties and Potential for Receptor-Mediated Internal Radiotherapy. *Chem. Eur. J. 5*, 1974−1981.

(7) Govindaswamy, N., Quarless, Jr., D. A., and Koch, D. A. (1995) New Amine Trithiolate Tripod Ligand and Its Iron-(II) and Iron(III) Complexes. *J. Am. Chem. Soc. 117*, 8468−8469.

(8) Motekaitis, R. J., Martell, A. E., Koch, S. A., Hwang, J., Quarless, Jr., D. A., and Welch, M. J. (1998) The Gallium-(III) and Indium(III) Complexes of Tris(2-mercaptobenzyl)-amine and Tris(2-hydroxybenzyl)amine. *Inorg. Chem. 37*, 5902−5911.

(9) Cutler, C. S., Giron, M. C., Reichert, D. E., Snyder, A. Z., Herrero, P., Anderson, C. J., Quarless, D. A., Koch, S. A., and Welch, M. J. (1999) Evaluation of Gallium-68 Tris(2-mercaptobenzyl)amine: A Complex with Brain and Myocardial Uptake. *Nucl. Med. Biol. 26*, 305−316.

(10) Sun, Y., Cutler, C. S., Martell, A. E., and Welch, M. J. (1999) New Multidentate Ligands Containing Mercaptobenzyl Functional Groups, and Biodistribution of Gallium-67-TACN−HSB. *Tetrahedron 55*, 5733−5740.

(11) Maelia, L., and Koch, S. A. (1986) Gallium Analogues of Iron-Sulfide-Thiolate Compounds. Analysis of the Structural Parameters in Gallium(III) and Iron(III) Chalcogenide Compounds. *Inorg. Chem. 25*, 1896−1904.

(12) van der Stelt, C., van der Lugt, W., and Nauta, W. T. (1951) The Synthesis of 2-Mercapto-4-aminobenzoic Acid. *Recueil. Trav. Chim. 70*, 285−288.

(13) Stacy, G. W., Villaescusa, F. W., and Wollner, T. E. (1965) 2-Aminobenzo[*b*]thiophene. An Aromatic Ring Tautomer. *J. Org. Chem. 30*, 4074−4078.

BC025552G

New Reagents and Methods for the Synthesis of Internal and 3′-Labeled DNA

Matthew H. Lyttle,* Troy A. Walton, Daren J. Dick, Timothy G. Carter, Jacob H. Beckman, and Ronald M. Cook

Biosearch Technologies, Inc., 81 Digital Drive, Novato, California 94949. Received January 22, 2002

The syntheses of two new nucleoside phosphoramidites containing a hydroxyl functionality masked by a levulinate protecting group are presented; N^4-(2-(ethylene glycol-2-levulinate)ethyl)-5-methyl-5′-(4,4′-dimethoxytrityl)-3′-*O*-(2-cyanoethyldiisopropylphosphoramidite)-2′-deoxycytidine **1** and 5-(*N*-(6-*O*-levulinoyl-1-aminohexyl)-3(*E*)-acrylamido)-5′-(4,4′-dimethoxytrityl)-3′-(2-cyanoethyldiisopropylphosphoramidite)-2′-deoxyuridine **3**. Optimization of solid-phase-supported synthetic parameters for incorporation of these into DNA, removal of the levulinate group by exposure to dilute hydrazine, and subsequent attachment of dye labels is described. Synthesis of the known compound 5-(*N*-(6-trifluoroacetylaminohexyl)-3(*E*)-acrylamido)-5′-(4,4′-dimethoxytrityl)-3′-(2-cyanoethyldiisopropylphosphoramidite)-2′-deoxyuridine **2** (*1*), containing a masked amine at the end of an alkyl chain attached at the 5 position, was also revisited using new techniques developed for **3**.

INTRODUCTION

Modern, high-speed synthesis of labeled DNA requires the fewest amount of steps conducted in the shortest possible time. Synthetic methodology (*2*−*4*) has been continuously evolving to meet these challenges. These current trends utilize direct attachment of rapidly reacting reagents to solid-phase-immobilized nascent oligonucleotides, followed by cleavage from the support and purification of the product in precisely the form desired.

While a variety of efficient strategies for solid-phase synthesis of 3′ and 5′ terminal labeled structures are available, there are not many choices for solid-phase-supported internal labeling of DNA. Useful information about the preparation of the needed reagents as well as the performance of the structures produced is limited. Internal labels are usually attached by solution-phase active ester coupling to alkylamines pendant on pyrimadine bases (*5*). These procedures involve multiple purifications and other cumbersome methods not amenable to high throughput synthesis. Label derivatized nucleoside phosphoramidites for internally modified DNA synthesis are commercially available (*6*), but at considerable expense. Furthermore, coupling efficiencies of these have been low in our hands, perhaps due to the high molecular weight and polar nature of some of these compounds. Recently, palladium-assisted coupling of acetylenic compounds to iodinated pyrimidine nucleosides immobilized on solid supports has been reported (*7*). Other current work details solid-phase photolytic deprotection of 2′ amine oligonucleotides and subsequent *on support* attachment of various useful moieties (*8*). Hopefully these methods will achieve widespread application in this area.

We have developed solid-phase-supported methods in which phosphoramidites normally used to functionalize only the 5′ terminus of DNA can also be used to effect labeling internally or at the 3′ terminus of the sequence. Removal of masking groups and the incorporation of labels are done while the DNA is attached to the solid-phase support, which facilitates the separation of tagged DNA products from excess label and deprotection reagents.

Chang, Urdea and Horn (*9*) developed a synthesis of novel branching nucleotide structures in which a hydroxyl functionality, attached via a hydrocarbon chain at N-4 of cytidine, was masked by a levulinate group and then deprotected with a hydrazine cocktail after synthesis of the primary strand. Branching sequences were then added to the oxygen with standard phosphoramidite chemistry. Another phosphoramidite **4** based on 1,2,3-propanetriol containing a similarly masked oxygen is commercially available (*10*). Neither of these structures is desirable for internally labeled DNA which is expected to anneal to a complementary strand at energies (T_ms) close to that of the unmodified DNA sequences. To address this issue we have developed the uridine derivative **3** which has a hydroxyl at the end of a hydrocarbon chain, pendant at C-5, masked by a levulinate group. Groups attached at the C-5 position of uridine would be expected to be less disruptive of double helix formation than at the N-4 of cytidine (*11*). A companion paper (*12*) compares the performance of oligonucleotides made with **1**, **2**, and **3** in practical applications involving annelation to complementary DNA structures.

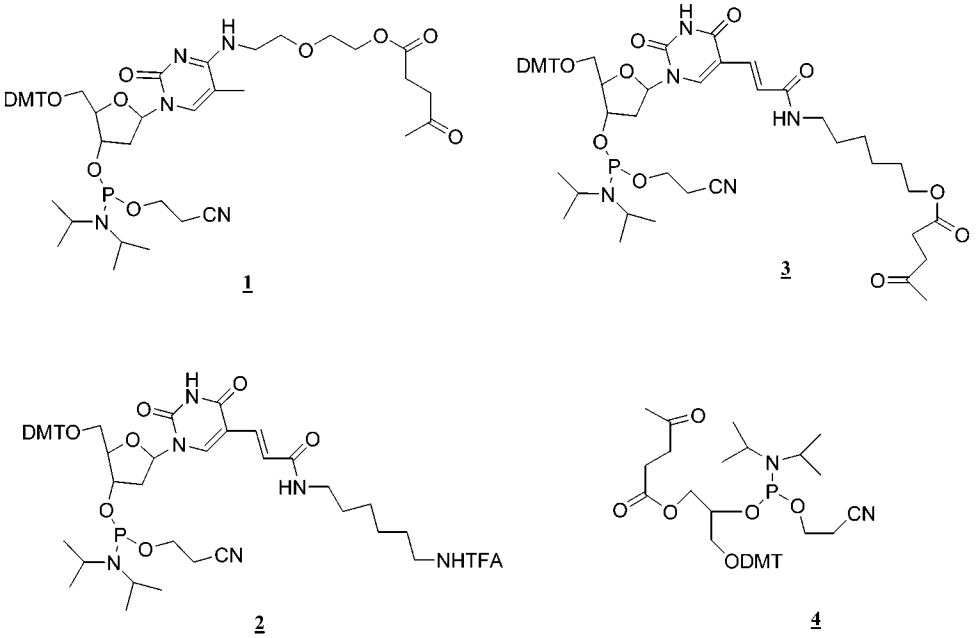
MATERIALS AND METHODS

Aqueous ammonia, lithium chloride, and concentrated HCl were reagent grade from J. T. Baker. Dichloromethane (DCM), tetrahydrofuran (THF), ethyl acetate (EtOAc), acetonitrile, ethanol, methanol (MeOH), and petroleum ether were Omnisolve grade from VWR. Sodium hydroxide, mercuric acetate, sodium bicarbonate, magnesium sulfate, 6-amino-1-hexanol, 1,6-hexanediamine, acryloyl chloride, methyl trifluoroacetate, levulinic acid, 2-(2-aminoethoxy)ethanol, phosphorus oxychloride, triethylamine, 1,2,4-triazole, iron sulfide, triethylamine, and tetrabutlyammonium fluoride were from Aldrich. Chromatographic silica was from Grace Chemical Co. Deoxyuridine was obtained from Crystal Chem. Co. DMT T, TET and HEX amidites were obtained from

* To whom correspondence should be addressed. Phone 415-883-8400; fax 415-883-8488. E-mail matt@biosearchtech.com.

10.1021/bc020011c CCC: $22.00 © 2002 American Chemical Society
Published on Web 07/19/2002

Chart 1. Phosphoramidite Synthons for Internal Labeling



Annovis Corp. Potassium tetrachloropalladate was obtained from Alfa (J. M. Corp.). Controlled pore glass DNA synthesis supports, 6-carboxyfluorescein amidite (6-FAM) and Tamra amidite (*3*), were obtained in house. All other DNA synthesis reagents were as previously described (*13*). Elemental analyses were performed by Desert Analytics (Tucson, AZ), and NMR work was performed by Acorn NMR (Livermore, CA). MALDI Mass spectra were performed in house on a Bruker Biflex MALDI-TOF.

EXPERIMENTAL PROCEDURES

***N*⁴-(2-(Ethylene glycol-2-levulinate)ethyl)-5-methyl-5′-(4,4′-dimethoxytrityl)-3′-*O*-*tert*-butyldimethylsilyl-2′-deoxycytidine, 7.** A solution of 12 mL (20 g, 130 mmol) of phosphorus oxychloride and 40 g (580 mmol) of 1,2,4-triazole in 400 mL of dry CH_3CN was chilled on ice to 0 °C under argon. Triethylamine (90 mL, 90 g, 900 mmol) was added slowly dropwise with stirring over 0.5 h. Next, 31 g (47 mmol) of 5′-(4,4′-dimethoxytrityl)-3′-*O*-*tert*-butyldimethysilylthymidine **5** (*14*) was dissolved in 200 mL of dry CH_3CN and added slowly dropwise over 0.5 h. The solution was stirred and allowed to warm to room temperature overnight. The solution was concentrated to a gum under reduced pressure and dissolved in 500 mL of EtOAc. Saturated aqueous $NaHCO_3$ (300 mL) was added, and the mixture was shaken and separated. The organic phase was washed with another 300 mL portion of satd aqueous $NaHCO_3$ and then dried over $MgSO_4$, filtered, and evaporated to give the N^4-triazolide as a brown foam. This material was dissolved in 150 mL of CH_3CN and added dropwise with stirring to a solution of 30 mL (31.4 g, 300 mmol) of 2-(2-aminoethoxy)ethanol in 300 mL of CH_3CN which had been chilled to 0 °C on ice. The mixture was stirred overnight and allowed to warm to room temperature. The solution was reduced to a tar by rotary evaporation and then redissolved in 300 mL of EtOAc. The solution was washed with 300 mL of satd $NaHCO_3$ and dried over $MgSO_4$. Filtration, followed by reduction to a tar by rotary evaporation and high vacuum overnight, gave 24.3 g of the N^4-(2-(ethylene glycol)ethyl) adduct **6** as a foam. All of this material was dissolved in 300 mL of dry pyridine and 12 mL of *N*-methylimidazole, 12 mL (13.6 g, 117 mmol) levulinic acid was added, and the solution was reduced to an oil by rotary evaporation. Dry CH_3CN, 200 mL, was added along with 12 mL (9.7 g, 77 mmol) diisopropylcarbodiimide. The solution was allowed to stand overnight after thorough mixing. Crystals of *N*,*N*′-diisopropylurea were removed by filtration, and the solution was concentrated to a tar by rotary evaporation. The residue was dissolved in 300 mL of EtOAc, and the organic phase was washed with 150 mL of 1 M citric acid followed by 150 mL of satd $NaHCO_3$ and then dried over $MgSO_4$ and filtered. The product was purified by column chromatography on a 5 × 20 cm bed of activated silica gel eluted with 1% MeOH and 1% pyridine in DCM. Fractions were inspected by TLC in 5% MeOH, 1% pyridine in DCM, and visualized with 10% H_2SO_4 and heat. Once the product (R_f 0.5) began to elute from the column, the MeOH in the column mobile phase was increased to 2%. Fractions containing pure product were pooled and concentrated by rotary evaporation and high vacuum to yield 28 g (70%) of **7** as a white foam. ^{1}H NMR (δ, $CDCl_3$): 7.8 (s, 1H), 7.5−7.2 (m, 11H), 6.8 (d, 4H), 6.4 (t, 1H), 5.4 (t, 1H), 4.5 (q, 1H), 4.2 (dd, 2H), 3.8 (s, 6H), 3.75 (m, 2H), 3.7 (m, 4H), 3.5 (dd, 1H), 3.2 (dd, 1H), 2.8 (t, 2H), 2.6 (t, 2H), 2.4 (m, 1H), 2.2 (m, 1H), 2.1 (s, 3H), 1.5 (s, 3H), 0.8 (s, 9H), 0.0 (d, 6H). Anal. Calcd for $C_{46}H_{61}N_3O_{10}Si\cdot{}^1/_2MeOH$: C, 64.94; H, 7.38. Found: C, 64.59; H, 7.34.

***N*⁴-(2-(Ethylene glycol-2-levulinate)ethyl)-5-methyl-5′-(4,4′-dimethoxytrityl)-2′-deoxycytidine, 8. 7** (24 g, 28 mmol) was dissolved in a solution of 200 mL of THF, 60 mL of 1 N TBAF (in THF), and 10 mL of HOAc. The solution was allowed to stand for 24 h. An aliquot of the solution for TLC was prepared by mixing a few drops of the mixture with 1 mL of EtOAc and 1 mL of satd $NaHCO_3$ in a test tube and spotting the upper phase. The TLC (same mobile phase and visualization as above) showed complete conversion to a new lower spot (R_f 0.15). The reaction mixture was quenched with 20 mL of satd $NaHCO_3$ and most of the THF was removed by rotary evaporation. The residue was dissolved in 300 mL of EtOAc and the organic phase washed with 300 mL of satd $NaHCO_3$ followed by drying with $MgSO_4$ and filtration. The solution was concentrated to a foam by rotary

evaporation, and the product was purified by column chromatography on a 5 × 20 cm bed of activated silica gel eluted with a gradient of 1−6% MeOH over 8 L of mobile phase and 1% pyridine in DCM. Fractions were inspected by TLC as above, and those with pure product were pooled and evaporated to yield 19 g (93%) of **8** as a white foam. ^{1}H NMR (δ, $CDCl_3$): 7.8 (s, 1H), 7.5−7.2 (m, 11H), 6.8 (d, 4H), 6.4 (t, 1H), 5.4 (t, 1H), 4.5 (s, 1H), 4.2 (dd, 2H), 4.1 (s,1H), 3.8 (s, 6H), 3.75 (m, 2H), 3.7 (m, 4H), 3.5 (dd, 1H), 3.4 (m, 2H), 2.7 (t, 2H), 2.6 (m, 3H), 2.25 (m, 1H), 2.2 (s, 3H), 1.5 (s, 3H). Anal. Calcd for $C_{40}H_{47}N_3O_{10}$: C, 65.83; H, 6.49; N, 5.76. Found: C, 65.74; H, 6.68; N, 6.41.

***N*^{4}-(2-(Ethylene glycol-2-levulinate)ethyl)-5-methyl-5′-(4,4′-dimethoxytrityl)-3′-*O*-(2-cyanoethyldiisopropylphosphoramidite)-2′-deoxycytidine, 1. 8** (19 g, 26 mmol) was dried by rotary evaporation from pyridine followed by high vacuum in a 500 mL round-bottom flask. A mixture of 8 g (27 mmol) of 2-cyanoethyl tetraisopropylphosphorodiamidite and 480 mg of tetrazole in 250 mL of CH_3CN was prepared and added to the flask containing the nucleoside **8**. The flask was stoppered and allowed to stand for 2 h after thorough mixing. Inspection of the reaction mixture by TLC as above showed complete conversion to a new product, R_f 0.4. The reaction mixture was concentrated to a tar by rotary evaporation and redissolved in 300 mL of EtOAc. The solution was washed with 200 mL of satd $NaHCO_3$ followed by drying with $MgSO_4$ and filtration. The solution was concentrated to a tar by rotary evaporation and the product purified by column chromatography as above for **8**. Fractions containing pure **1** were pooled and concentrated by rotary evaporation and high vacuum to yield 13.3 g (55%) of **1** as a white foam. ^{31}P NMR (ppm, $CDCl_3$): 149.756, 149.211. Anal. Calcd for $C_{49}H_{64}N_5O_{11}P$: C, 63.28; H, 6.94; N, 7.53. Found: C, 62.99; H, 6.61; N, 7.82.

***N*-Acrylolyl-*N*′-*tert*-butyloxycarbonyl-1,6-hexanediamine, 9.** 1,6-Hexanediamine (100 g, 0.86 mol) was dissolved in 800 mL of THF and chilled in an ice bath. Di-*tert*-butyl dicarbonate, 60 g (0.28 mol) was dissolved in 400 mL of THF and added slowly over 1 h by a dropping funnel. The solution was stirred for 2 h and then filtered. The solid was washed with 200 mL of THF, and the combined filtrates were concentrated by rotary evaporation to 70 g of an oil. The oil was redissolved in 700 mL of $CHCl_3$ and washed three times with 400 mL of water. The solution was concentrated by rotary evaporation and redissolved in 300 mL of THF, and 200 mL of satd Na_2CO_3 was added. The mixture was chilled in an ice bath, and 30 mL (33.4 g, 0.37 mol) of acryloyl chloride was added in 10 mL portions over 2 h. Solid Na_2CO_3 was added, as needed, to keep the pH of the aqueous layer above 8. The mixture was stirred overnight and poured into a separatory funnel. EtOAc, 500 mL, was added, and the lower aqueous layer was removed after the mixture was shaken and allowed to separate. The organic phase was washed with 500 mL of 0.5 M KH_2PO_4 followed by 500 mL of satd $NaHCO_3$ and dried over $MgSO_4$. The solution was filtered and concentrated by rotary evaporation. The material was purified by column chromatography on a 15 × 50 cm bed of activated silica gel eluted with a gradient of 0−4% MeOH over 18 L of mobile phase and 1% pyridine in DCM. Fractions were inspected by TLC (R_f desired product 0.6, UV active, in 2% MeOH, 2% pyridine in DCM), and those with pure product were pooled and evaporated to yield 39 g (52%) of **9** as a white solid. ^{1}H NMR (δ, $CDCl_3$): 6.5−6.0 (m, 3H), 5.9 (d, 1H), 5.8 (d, 1H), 3.3 (m, 2H), 3.0 (m, 2H), 1.5−1.3 (m, 17H). Anal. Calcd for $C_{14}H_{26}N_2O_3$: C, 62.19; H, 9.69; N, 10.36. Found: C, 62.43; H, 9.83; N, 10.42.

5-(*N*-(6-Trifluoroacetylaminohexyl)-3(*E*)-acrylamido-5′-(4,4′dimethoxytrityl)-2′-deoxyuridine, 11. (This reaction must be done in a fume hood because H_2S, which is a toxic and malodorous gas, is used to precipitate metals during workup). Potassium tetrachloropalladate-(II), K_2PdCl_4 (40 g 122 mmol), was added over 1 h in 10 g portions to a gently refluxing solution of LiCl (24 g, 0.6 mol) in 1200 mL of THF. A solution of **9** (33 g, 122 mmol) in 200 mL of THF was added slowly over 10 min. The reaction mixture became dark brown. The solution was stirred and refluxed for 20 min, and then 57 g (123 mmol) of finely powdered 5-chloromercurate-2′-deoxyuridine (*1*) was added in small portions over 15 min. The solution became black and a silver mirror was deposited on the sides of the reaction vessel. Stirring and gentle reflux was continued overnight. The solution was allowed to cool, and H_2S gas was bubbled into the solution. A trap containing Clorox was used to control the odor of the gas. Once the brown precipitate was no longer generated, H_2S delivery was stopped and the solution was filtered to produce a clear yellow solution. The solvent was removed by rotary evaporation and high vacuum overnight to give 75 g of alkylated nucleoside **10** as a beige foam. A small amount of the foam was purified by dissolution in MeOH, addition of water to a cloud point, and chilling. Crystals were obtained, TLC R_f 0.4 (20% MeOH, 2% pyridine in DCM) which was UV (254 nm) active; the spot also fluoresced blue when irradiated with 312 nm UV. The bulk, unpurified material was dissolved in a mixture of 900 mL of DCM and 100 mL of MeOH, and 100 mL of trifluoroacetic acid was added. The solution was refluxed overnight during which a milky precipitate appeared. The suspension was concentrated to a gum by rotary evaporation, and high vacuum was applied to the material for 24 h. The resulting solid was dissolved in 700 mL of MeOH, and 60 mL of TEA was added, followed by 40 mL of methyl trifluroacetate. The solution was mixed and allowed to stand for 6 h and was concentrated to a solid by rotary evaporation. The solid was dried by rotary evaporation with 500 mL of dry pyridine and was then redissolved in 500 mL of dry pyridine. 4,4′-Dimethoxytrityl chloride (25 g, 75 mmol) was added, and the mixture was stirred for 4 h. A drop of the reaction mixture was dissolved in 1 mL of EtOAc and washed with 1 mL of satd $NaHCO_3$. TLC showed the appearance of product (R_f 0.2, 10% MeOH, 2% pyridine in DCM) which had the same UV characteristics as above and also became orange when the plate was sprayed with 10% H_2SO_4 and heated. MeOH (20 mL) was added to quench the reaction, and the brown solution was concentrated to a gum by rotary evaporation. The material was dissolved in 700 mL of DCM and washed with 500 mL of 0.5 KH_2PO_4 solution followed by 500 mL of satd aq $NaHCO_3$. The solution was dried over $MgSO_4$, filtered, concentrated by rotary evaporation, and then purified by column chromatography on a 15 × 150 cm bed of activated silica gel eluted with a gradient of 1−8% MeOH over 18 L of mobile phase and 1% pyridine in DCM. Fractions were inspected by TLC (R_f desired product 0.2, UV active as above, in 10% MeOH, 2% pyridine in DCM), and those with pure product were pooled and evaporated to yield 16.5 g (17%) of **11** as a white foam. ^{1}H NMR (δ, $CDCl_3$): 7.9 (s, 1H), 7.7 (t, 1H), 7.4 (d, 1H), 7.3 (m, 5H), 7.1 (m, 1H), 6.8 (d, 4H), 6.6 (d, 1H), 6.4 (t, 1H), 5.4 (broad s, 1H), 4.5 (s, 1H), 4.1 (s, 1H), 3.75 (s, 6H), 3.5 (dd, 1H), 3.3 (m, 3H), 3.2−3.0 (m, 2H), 2.5 (m, 1H), 2.3 (m, 1H), 1.5 (m, 2H), 1.4−1.2 (m, 6H). Anal.

Calcd for $C_{41}H_{45}F_3N_4O_9 \cdot C_5H_5N$: C, 63.27; H, 5.77; N, 8.02. Found: C, 63.47; H, 5.92; N, 8.13.

5-(*N*-(6-Trifluoroacetylaminohexyl)-3(*E*)-acrylamido-5′-(4,4′-dimethoxytrityl)-3′-(2-cyanoethyldiisopropylphosphoramidite)-2′-deoxyuridine, 2. 11 (16.5 g, 21 mmol) was dried by rotary evaporation from 200 mL of dry pyridine followed by high vacuum in a 1000 mL round-bottom flask. A mixture of 8.3 g (27 mmol) of 2-cyanoethyl tetraisopropylphosphorodiamidite and 500 mg of tetrazole (7.2 mmol) in 300 mL of dry CH_3CN was prepared and added to the flask containing the nucleoside **11**. The flask was stoppered and allowed to stand for 2 h after thorough mixing. Inspection of the reaction mixture by TLC (2% pyridine/EtOAc) showed complete conversion to a new product, R_f 0.5. The reaction mixture was concentrated to a tar by rotary evaporation and redissolved in 300 mL of EtOAc. The solution was washed with 200 mL of satd $NaHCO_3$ followed by drying with $MgSO_4$ and filtration. The solution was concentrated to a tar by rotary evaporation and the product purified by column chromatography on a 5 × 20 cm bed of activated silica gel eluted with 2% pyridine in EtOAc. Fractions were inspected by TLC (2% pyridine in EtOAc) and visualized with 10% H_2SO_4 and heat. Fractions containing pure **2** were pooled and concentrated by rotary evaporation and high vacuum to yield 13.5 g (65%) of **2** as a white foam. ^{31}P NMR (ppm, $CDCl_3$): 149.462, 149.363. Anal. Calcd for $C_{50}H_{62}F_3N_6O_{10}P$: C, 60.35; H, 6.28; N, 8.45. Found: C, 60.32; H, 6.32; N, 8.57.

***N*-Acryloyl-*O*-levulinoyl-6-amino-1-hexanol, 12.** 6-Amino-1-hexanol (50 g, 427 mmol) was dissolved in 400 mL of THF, and 200 mL of satd $NaHCO_3$ was added. Acryloyl chloride (caution: lachrymator) (35 mL, 39 g, 430 mmol) was added dropwise over 1 h. Solid $NaHCO_3$ was added, as needed, to maintain a basic pH. The mixture was stirred overnight. EtOAc (600 mL) was added, and the mixture was partitioned. The organic phase was washed with 300 mL of 1 N HCl, and then 300 mL of water followed by 300 mL of satd $NaHCO_3$. The solution was dried over $MgSO_4$, filtered, and evaporated to 53 g of a beige solid. The solid was dissolved in 400 mL of EtOAc with heating and applied to a 15 × 50 cm bed of activated silica gel packed and eluted with EtOAc. Fractions were inspected by TLC (R_f 0.25, 2% pyridine in EtOAc) and visualized with iodine vapor. Fractions containing pure material were pooled and concentrated by rotary evaporation and high vacuum to yield 25.2 g of *N*-acryloyl-6-amino-1-hexanol as a white solid. A portion of this material (10 g, 58 mmol) was dissolved in a mixture of levulinic acid (7 mL, 8 g, 68 mmol), 5 mL of *N*-methylimidazole, and 200 mL of dry pyridine. The solution was concentrated to a tar by rotary evaporation and redissolved in 300 mL of dry CH_3CN. Diisopropylcarbodiimide (10 mL, 8 g, 64 mmol) was added, and the mixture was allowed to stand overnight after mixing. Solids were filtered off, and the solution was concentrated to a tar by rotary evaporation. The material was dissolved in 300 mL of DCM and washed with 200 mL of 1 N citric acid followed by 200 mL of satd $NaHCO_3$ followed by drying with $MgSO_4$ and filtration. The solution was concentrated to a tar by rotary evaporation and the product purified by column chromatography on a 5 × 20 cm bed of activated silica gel eluted with 1:1 petroleum ether: EtOAc. Fractions were inspected by TLC (1:1 petroleum ether: EtOAc) and visualized with iodine vapor. Fractions containing pure **13** (R_f 0.35) were pooled and concentrated by rotary evaporation and high vacuum to yield 6 g (38%) of **12** as a white solid. ^1H NMR (δ, $CDCl_3$): 6.3−6.25 (dd, 1H), 6.2 (broad s, 1H), 6.15−6.05 (dd, 1H), 5.6 (dd, 1H), 4.0 (t, 2H), 3.3 (q, 2H), 2.75 (t, 2H), 2.55 (t, 2H), 2.2 (s, 3H), 1.7−1.5 (m, 4H), 1.4−1.3 (m, 4H). Anal. Calcd for $C_{14}H_{23}NO_4$: C, 62.43; H, 8.61; N, 5.20. Found: C, 61.91; H, 8.94; N, 5.74.

5-(*N*-(6-*O*-Levulinoyl-1-aminohexyl)-3(*E*)-acrylamido-5′-(4,4′dimethoxytrityl)-2′-deoxyuridine, 14. (This reaction must be done in a fume hood because H_2S, which is a toxic and malodorous gas, is used to precipitate metals during workup). Potassium tetrachloropalladate-(II), K_2PdCl_4 (12 g, 36 mmol), was added over 20 min in three 4 g portions to a gently refluxing solution of LiCl (8 g, 194 mol) in 800 mL of THF. A solution of **12** (10 g, 37 mmol) in 200 mL of THF was added slowly over 10 min. The reaction mixture became dark brown. The solution was stirred and refluxed for 20 min, and then 17 g (37 mmol) of finely powdered 5-chloromercurate-2′-deoxyuridine (*1*) was added in small portions over 15 min. The solution became black, and a silver mirror was deposited on the sides of the reaction vessel. Stirring and gentle reflux was continued overnight. The solution was allowed to cool, and H_2S gas was bubbled into the solution. A trap containing Clorox was used to control the odor of the gas. Once the brown precipitate was no longer generated, H_2S delivery was stopped and the solution was filtered to produce a clear yellow solution. The solvent was removed by rotary evaporation and high vacuum overnight to give 28 g of alkylated nucleoside **13** as a beige solid. A small amount of the foam was purified by dissolution in MeOH, addition of water to a cloud point, and chilling. Crystals were obtained, TLC R_f 0.3 (20% MeOH, 2% pyridine in DCM), which was UV (254 nm) active; the spot also fluoresced blue when irradiated with 312 nm UV. The bulk, unpurified material was dried by rotary evaporation with 300 mL of dry pyridine and was then redissolved in 300 mL of dry pyridine. 4,4′-Dimethoxytrityl chloride (10 g, 29 mmol) was added, and the mixture was stirred overnight. A drop of the reaction mixture was dissolved in 1 mL of EtOAc and washed with 1 mL of satd $NaHCO_3$. TLC showed the appearance of product (R_f 0.5, 6% MeOH, 2% pyridine in DCM) which had the same UV characteristics as **11** and also became orange when the plate was sprayed with 10% H_2SO_4 and heated. MeOH (10 mL) was added to quench the reaction, and the brown solution was concentrated to a gum by rotary evaporation. The material was dissolved in 500 mL of DCM and washed with 400 mL of 0.5 M KH_2PO_4 solution followed by 400 mL of satd $NaHCO_3$. The solution was dried over $MgSO_4$, filtered, concentrated by rotary evaporation, and then purified by column chromatography on a 7 × 50 cm bed of activated silica gel eluted with a gradient of 1−5% MeOH over 10 L of mobile phase and 1% pyridine in DCM. Fractions were inspected by TLC (R_f desired product 0.5, UV active as above, in 6% MeOH, 2% pyridine in DCM), and those with pure product were pooled and evaporated to yield 6.8 g (24%) of **14** as a white foam. ^1H NMR (δ, $CDCl_3$): 7.9 (s, 1H), 7.7 (t, 1H), 7.4 (d, 1H), 7.3 (m, 5H), 7.1 (m, 1H), 6.8 (d, 4H), 6.6 (d, 1H), 6.4 (t, 1H), 5.4 (broad s, 1H), 4.5 (s, 1H), 4.1 (s, 1H), 4.0 (t, 2H), 3.75 (s, 6H), 3.4 (m, 1H), 3.3 (m, 1H), 3.1 (m, 2H), 2.7 (t,2H), 2.5 (m, 3H), 2.2 (m, 1H), 2.1 (s, 3H), 1.5 (m, 2H), 1.4−1.2 (m, 6H). Anal. Calcd for $C_{44}H_{51}N_3O_{11} \cdot {}^1/_2C_5H_5N$: C, 66.76; H, 6.44; N, 5.86. Found: C, 66.52; H, 6.37; N, 5.91.

5-(*N*-(6-*O*-Levulinoyl-1-aminohexyl)-3(*E*)-acrylamido-5′-(4,4′dimethoxytrityl)-3′-(2-cyanoethyldiisopropylphosphoramidite)-2′-deoxyuridine, 3. 14 (6.8 g, 8.5 mmol) was dried by rotary evaporation from 100 mL of dry pyridine followed by high vacuum in a 500 mL round-bottom flask. A mixture of 3.0 g (10 mmol) of

2-cyanoethyl tetraisopropylphosphorodiamidite and 180 mg of tetrazole (2.6 mmol) in 100 mL of dry CH_3CN was prepared and added to the flask containing the nucleoside **14**. The flask was stoppered and allowed to stand for 2 h after thorough mixing. Inspection of the reaction mixture by TLC (2% pyridine/EtOAc) showed complete conversion to a new product, R_f 0.6. The reaction mixture was concentrated to a tar by rotary evaporation and redissolved in 200 mL of EtOAc. The solution was washed with 100 mL of satd $NaHCO_3$ followed by drying with $MgSO_4$ and filtration. The solution was concentrated to a tar by rotary evaporation and the product purified by column chromatography on a 3 × 20 cm bed of activated silica gel eluted with 2% pyridine in EtOAc. Fractions were inspected by TLC (2% pyridine in EtOAc) and visualized with 10% H_2SO_4 and heat. Fractions containing pure **3** were pooled and concentrated by rotary evaporation and high vacuum to yield 5.5 g (81%) of **3** as a white foam. ^{31}P NMR (ppm, $CDCl_3$): 149.677, 149.329. Anal. Calcd for $C_{53}H_{68}N_5O_{12}P$: C, 63.78; H, 6.87; N, 7.02. Found: C, 63.75; H, 6.91; N, 7.13.

DNA Synthesis. DNA was made on Biosearch 8750 DNA synthesizers with standard conditions as previously described (*13*). Test sequences 5′-CGATCTGA**X**TAGCT**Y**-3′, 5′-TTTT**X**TTTTT-3′ and 5′-TTTTTTTTT**X**-3′where **X** was the nucleotide residue resulting from the use of **1** or **3** and **Y** were different natural bases were made at 1.0 μm and 200 nm synthesis scales. For internal labeling, first a hydrazine solution of 160 μL of hydrazine hydrate (Aldrich, 50 wt % water) in 8 mL of pyridine and 2 mL of HOAc was prepared and well mixed. The DNA sequencer was halted after the base (before **X**) added and the DMT was removed. After thorough washing with CH_3CN, a solution of 200 μL of 100 mg/mL of **1** or **3** in dry acetonitrile and 200 μL of 0.4 M *S*-ethyltetrazole in dry acetonitrile were introduced onto the column by the DNA synthesizer. After 2−3 min, the coupling solution was washed off the column with acetonitrile, and oxidation, followed by capping, was performed. Manual coupling with syringes was also successfully performed (*15*). The hydrazine cocktail above was introduced into the columns; we did this with 200 μL of solution in 1 mL syringes but it can also be done on the instrument. After the support was well wetted with the solution, it was allowed to stand 12−15 min and then was thoroughly washed with CH_3CN. Either TAMRA amidite or 6-FAM was coupled next; the same procedures as above were used. A 10 min coupling time was used for the TAMRA amidite. Oxidation and capping were performed after the coupling solution was washed off the column with acetonitrile. The TAMRA coupling sample was exposed to the capping solution for 5 min. Next, automated DNA synthesis was continued to the 5′ terminus, and the final DMT was removed. The CPG was placed into screw cap eppendorf tubes, and 1 mL of ammonia for the fluorescein DNA and 1 mL of the TAMRA deprotection cocktail for the TAMRA DNA was added to each. The tubes were heated at 55 °C for 18 h and cooled and the solutions evaporated. Yields of labeled DNA at all synthesis scales were close to those without hydrazine treatment, indicating negligible loss of material due to premature cleavage by the hydrazine reagent.

3′-HEX and TET CPG. DMT-*O*-ethylsulfonyl CPG (*16*) (15 g) was placed in a 300 mL coarse frit sintered glass funnel atop a 2 L sidearm flask. 3% Dichloroacetic acid in CH_2Cl_2 (200 mL) was poured in, and the support was agitated briefly with a spatula. The solution became brightly orange. After 2 min, the solution was drained and the step was repeated twice with 200 mL of fresh 3% dichloroacetic acid in CH_2Cl_2. The support was then washed three times with 200 mL of CH_2Cl_2, twice with 100 mL of CH_3CN, and once with 100 mL of pyridine. The support was transferred into a 250 mL round-bottom flask, and 1 g of **1** was added. 40 mL of dry pyridine was added, and the solvent was removed by rotary evaporation. A plug of glass wool was used to keep the CPG from leaving the flask. Once dry, high vacuum was applied to the flask for 18 h. A solution of 150 mL of 0.4 M *S*-ethyltetrazole in dry acetonitrile was prepared, and enough of this was added to the flask containing the CPG to make a slurry. The slurry was allowed to stand for 15 min and was poured into a sintered glass funnel. The support was washed three times with 100 mL of CH_3CN, and then 100 mL of amidite oxidizer solution (*13*) was added. After 5 min, the support was washed twice with 100 mL of CH_3CN. Next, 100 mL of a mixture of acetic anhydride, *N*-methyl imidazole, and THF (1:1:8) was added to the support. After 15 min exposure, the acetylation solution was removed and the support was washed three times with 100 mL of CH_3CN, and a small amount of this was dried. The DMT loading was 18 μm/g (*17*). The hydrazine cocktail above (100 mL) was mixed and added to the support. After 15 min, the support was washed three times with 100 mL of CH_3CN and was divided into two roughly equal portions. HEX and TET Amidite, 0.5 g respectively, were added to each portion, and coupling, oxidation, and capping steps using these amidites proceeded as above. Test sequences 5′-TTTTTTTTTdC(N4-(2-(ethylene glycol)ethyl)-HEX)-3′ and the analogous TET sequence were made; the HEX sample was deprotected with concentrated ammonia for 18 h at room temperature while standard conditions were used for the TET sample.

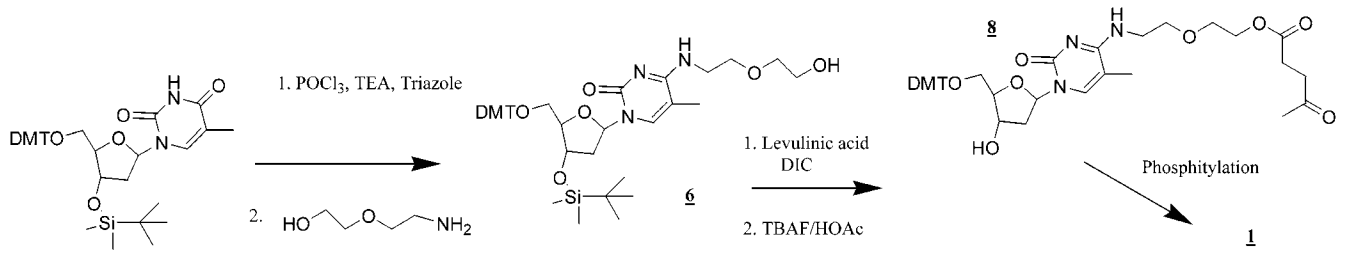
Anion exchange HPLC analyses were performed as follows: 2−20 μL of the aqueous samples, depending on the concentration, was injected onto a Dionex anion exchange column (4.6 × 250 mm); samples were eluted at 2 mL/min with aqueous buffers of (A) 0.025 M Tris HCl and 0.01 M TRIS, and (B) 0.025 M Tris HCl, 0.01 M TRIS, and 1.0 M NaCl, using a linear gradient of 1:0 to 0:1 over 20 min, with UV detection at 260 nm. Reverse phase HPLC as follows: 20 μL of the aqueous sample was injected onto a HAISIL HL C18 5 μm particle size column (4.6 × 150 mm); samples were eluted at 1 mL/min with buffers of (A) 0.1M TEAA, 5% acetonitrile, (B) acetonitrile, with a linear gradient of 1:0 to 0:1 A:B over 15 min. UV detection at 260 nm. Samples were prepared for MALDI mass spectral analysis as per Bruker.

RESULTS AND DISCUSSION

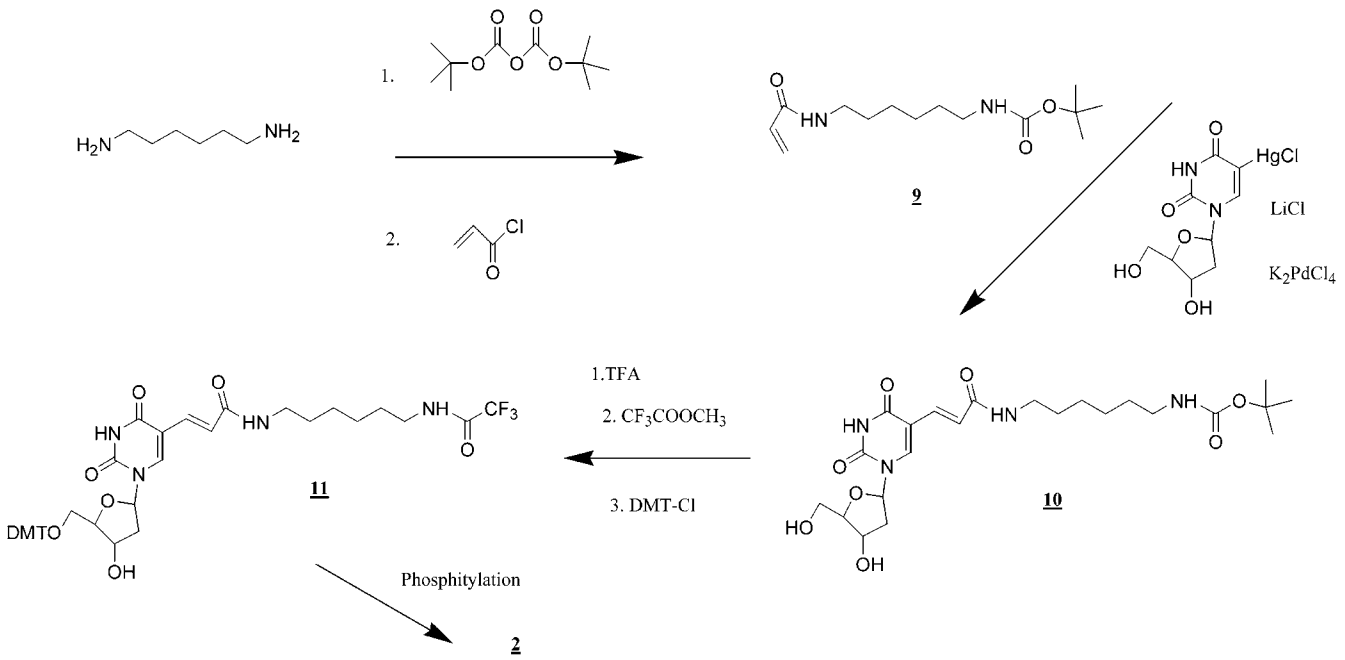
To develop this technology in an efficient manner, several endeavors had to be successfully completed: (1) Reliable and cost-effective processes for the synthesis of **1** and **3** had to be developed. (2) Easy and efficient solid-phase synthesis methods for incorporation of these compounds into DNA as well as subsequent label attachment had to be established. (3) Finally analytical techniques had to be devised to establish the purity and efficacy of the product DNA in practical applications.

Synthesis of Compounds 1−3. For **1**, commercially available DMT-T was treated with TBDMS-Cl to give **5** (*14*) in 84% yield. **5** was treated with 2-(2-aminoethoxy)-ethanol after activation as per Chang (*9*) to give **6**, which was converted into levulinate ester **7**, obtained as a white foam. The use of the TBDMS group instead of the trimethylsilyl transient protection used in (*9*) afforded certain advantages: the 3′-OTBDMS triazolide was a

Scheme 1. Synthesis of 1



Scheme 2. Synthesis of 2



stable compound which could be prepared in large quantities and stored cold, allowing many different derivatives to be prepared from one preparation of triazolide. Also, the 3′-OTBDMS group lent greater solubility in organic solvents which facilitated extraction and isolation of more polar conjugates containing pendant moieties such as biotin. Removal of the 3′-hydroxyl masking TBDMS group with TBAF gave alcohol **8**, followed by phosphitylation with 2-cyanoethyl tetraisopropylphosphorodiamidite and catalytic tetrazole gave **1**. See Scheme 1. The principal advantage of the use of **1** is cost; a similar derivative without the 5-methyl group can be made starting with more expensive deoxyuridine. This compound should also be accessible from $DMTdC^{(Bz)}$, but more steps would be required (*18*). The primary disadvantage to the use of **1** are anticipated lower T_ms of DNA made with this residue internally than with a natural deoxycytidine in binding to a complimentary DNA strand. A companion paper compares structures made with **1** with those made with **2** and **3** and bears this out. For this reason **1** is primarily used by us as a 3′ labeling tool.

Synthesis of 2. The Heck palladium-assisted coupling of organomercurials to olefins was first applied to nucleoside modification by Bergstrom (*19*). There is a recent paper about palladium-mediated reactions applied to nucleosides also coauthored by Bergstrom (*20*). We attempted first the literature synthesis (*1*) of **2**. Formation of *N*-acryloyl-*N*′-trifluoroacetyl-1,6-hexanediamine by a one-pot mixing of 1,6-hexanediamine, acryloyl chloride, and trifluoroacetic anhydride gave a mixture of products which gave the desired product in low yield. Purification was difficult with the conditions described, owing to close R_f values of products and contaminants. A palladium(II)-mediated coupling reaction with the material and 5-chloromercurated deoxyuridine also gave a mixture of products, which afforded only a few percent overall yield of the desired DMT nucleoside **11** when treated with DMT chloride followed by chromatography. Upon consideration of the low overall yield and high cost of the lithium tetrachloropalladate(II) used, we decided that this was not a cost-effective way to prepare **2**. An alternative scheme was developed, see Scheme 2. 1,6-Hexanediamine was treated with di-*tert*-butyl dicarbonate, and the resulting 6-*tert*-butyloxycarbonamidyl-1-aminohexane was partially purified by extraction. Acryloyl chloride was added to the compound under basic conditions to give 6-acrylolyl-*N*′-*tert*-butyloxycarbonyl-1,6-hexanediamine, **9**, which was obtained in high purity after chromatography. 5-Chloromurcurated deoxyuridine was prepared as per Ruth (*1*), and a palladium(II)-mediated coupling reaction with **9** gave, after several steps, the DMT nucleoside **11** in 24% yield (see Scheme 2). Significant savings in the cost of the palladium reagent was achieved by refluxing a THF solution of potassium tetrachloropalladate with lithium chloride prior to the addition of **9** and the chloromurcurated nucleoside. Recent literature reports that the needed palladium reagent can also be prepared by mixing $PdCl_2$ and LiCl in MeOH for 24 h (*20*) and this also works well, as long as all of the methanol is removed prior to dissolution in THF. **11** was converted into **2** by phosphitylation with

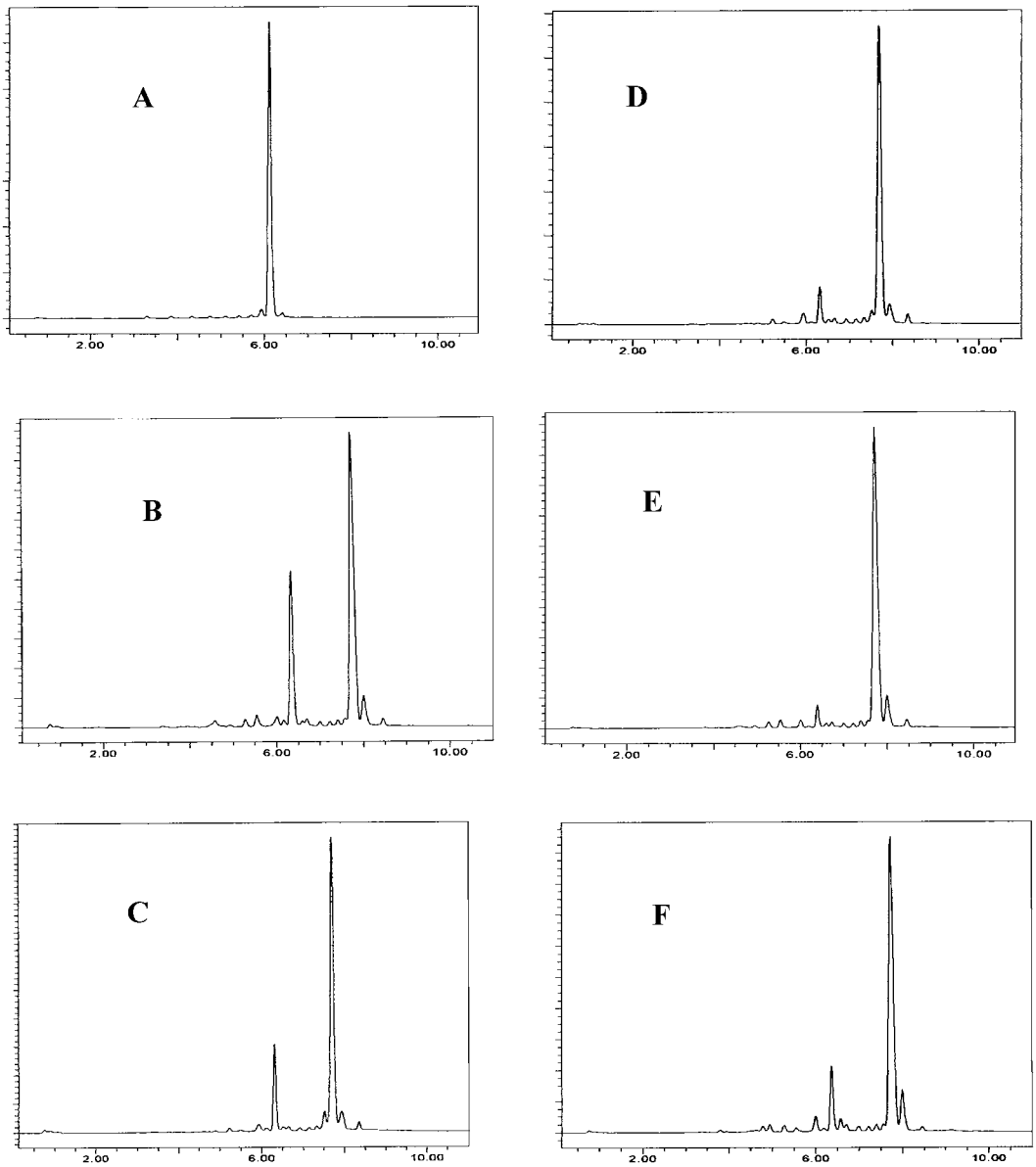


Figure 1. Time course for levulinoyl protecting group removal; A = 5′T_9C(N^4linker-O-lev)-3′ only; B = 2 min hydrazine exposure, then FAM, then T_9 addition; C = 4 min hydrazine, same other conditions; D = 8 min hydrazine, same other conditions; E = 12 min hydrazine, same other conditions; F = FAM after chain assembly with 12 min hydrazine exposure.

2-cyanoethyltetraisopropylphosphorodiamidite and catalytic tetrazole.

Synthesis of 3. A similar strategy to that used for **2** was employed. 6-amino-1-hexanol was first reacted with acryloyl chloride to give 6-acryloylamido-1-hexanol, followed by esterification with levulinic acid to give 6-acryloylamido-1-hexane levulinate **12**, obtained as a white solid after chromatography. **12** was coupled to chloromurcurated deoxyuridine by those methods used for **2** to give **13**, which gave **14** after treatment with DMT chloride. Conversion of **14** into phosphoramidite **3** was accomplished by the same method as for **2**.

Labeled DNA Synthesis. Incorporation of **1** and **3** into DNA was accomplished with standard methods and coupling times (*13*) and removal of levulinate protection was carefully optimized; previously reported conditions (*9*) were too harsh (0.5 M hydrazine in 1:1 pyridine:HOAc for 60 min), resulting in unwanted DMT loss and poor products, in our hands. We found that 0.25 M hydrazine in 4:1 pyridine:HOAc for 12−15 min gave the best results. This mixture and time is closer to the levulinate removal conditions originally described by Van Boom, et al. (*21*) for 5′ deprotection during a phosphate triester DNA oligomerization scheme. For us, the optimum exposure time was determined by an experimental system wherein **1** was first coupled onto sulfonylethyl CPG (*16*) and then subjected to various times of hydrazine exposure (2−12 min). 6-FAM was then coupled onto the deprotected hydroxyl, followed by oxidation and capping, and then extension of the DNA fragment by nine more addition cycles of T amidite. The product 3′-nucleoside fluoresceinated 10 mers were then cleaved with ammonia, and AX HPLC showed that the best results were obtained with 12 min of hydrazine exposure. The composition was confirmed by MALDI mass spectroscopy, calcd 3682, found 3687 amu. Longer exposure times gave more extraneous products. The same conditions using **4** in lieu of **1** did not produce good results (data not shown).

Another question to be addressed was the order of addition. Was it best to build the whole DNA fragment with the internal levulinated base and then deprotect and add the tag? This would be easier than the converse,

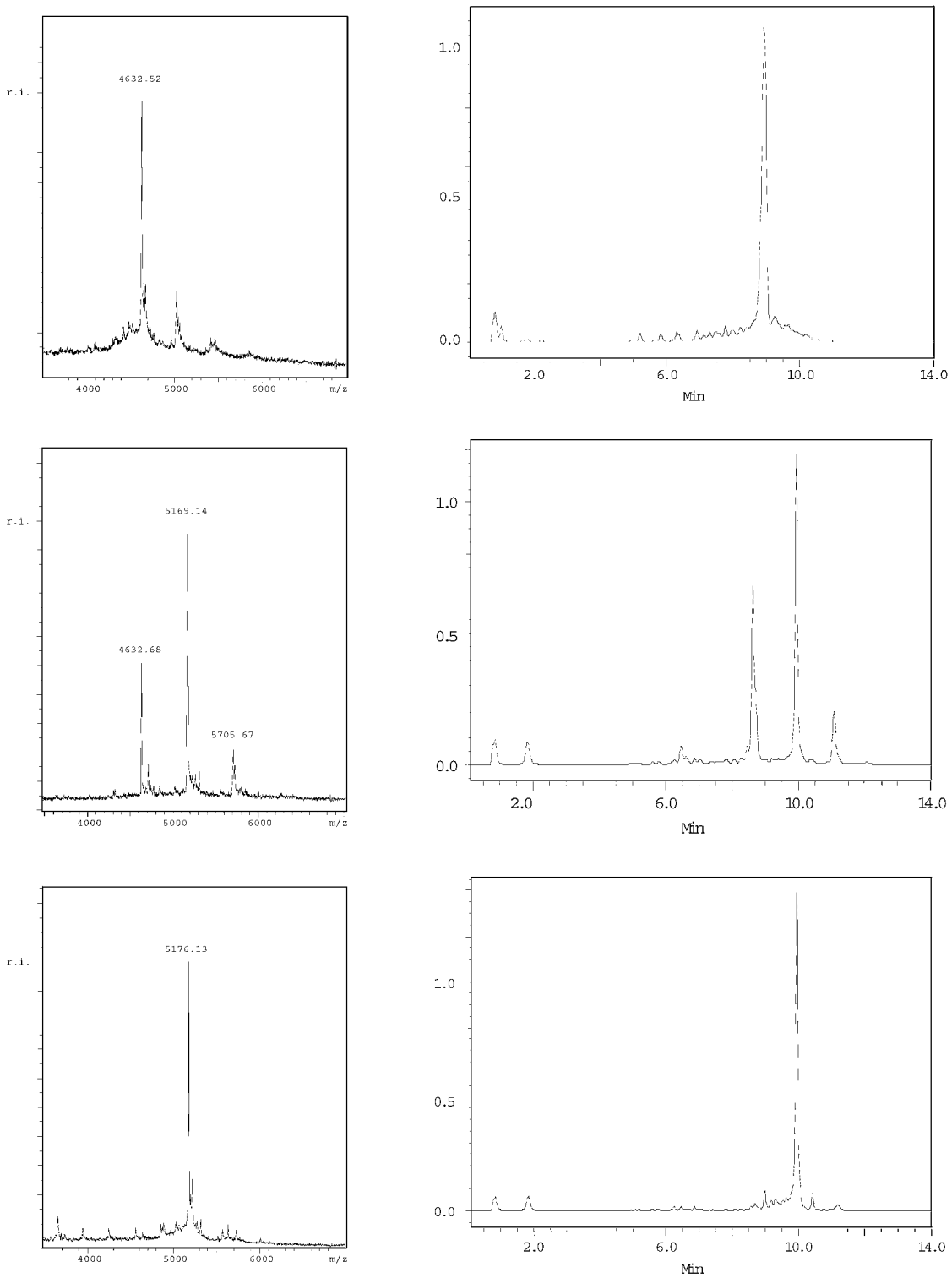


Figure 2. Order of label addition comparison with the synthesis of 5′-CGATCTGAC(N^{4}linker-O−FAM)TAGCTT-3′ by (left) MALDI mass spectra and (right) AX HPLC. Top: No FAM coupling control. Middle: whole fragment synthesis, then OLev removal and FAM addition at the end. Bottom: OLev removal and FAM addition after addition of base 7, then chain completion.

which was to deprotect the levulinated hydroxyl at the position where it was added, add the tag, and then continue the synthesis out to the 5′ terminus. An additional experiment was done with the time course study above, which removed the OLev group with the 12 min (best) conditions after all 10 bases were added and added 6-FAM as the last step. Figure 1 panel F shows clearly a result inferior to addition of fluorescein amidite prior to building the DNA fragment. 3′-HEX and TET CPGs were made with these techniques and gave good results in the synthesis of the analogous 10 mers. See Figures S1 and S2. Another comparison of the order of addition was done with 5′-CGATCTGA**X**TAGCTT-3′ where **X** resulted from the incorporation of **1**; good product purity was seen when addition of FAM occurred after addition of **1** and before chain extension (MALDI *m/e* calcd 5182, found 5176). Addition of fluorescein after the completion of the sequence gave other products in addition to that desired; incomplete FAM addition as well as double FAM addition were seen by mass spectroscopy (see Figure 2) Similar

results were obtained with **3** and FAM. The analogous internally labeled DNA fragment was made with **3** and a TAMRA amidite (*3*) and also gave good results when the TAMRA amidite was added before the rest of the chain, *m*/*e* calcd 5288, found 5275 amu (see Figure S3). Finally, the question of potential base modification by the conditions employed had to be addressed. CPG samples containing DMT-A^{Bz}, -C^{Bz}, -C^{Ac}, -G^{iBu}, -G^{DMF} and -T were subjected to the conditions employed for TAMRA amidite incorporation which includes the hydrazine treatment and a 5 min acetylation step before DMT removal and cleavage with *tert*-butylamine cocktail (18 h, 55 °C). The cleaved nucleosides were analyzed by RP-HPLC, and no extraneous peaks were seen compared to controls (data not shown).

CONCLUSION

Oligonucleotide protecting group chemistry first developed by Van Boom for 5′-hydroxyl protection (*21*) and later applied to side chain branching structures (*9*) has now been extended by us to allow the synthesis of internally dye-labeled DNA. New techniques and novel nucleoside phosphoramidite synthons have been developed which should allow the rapid synthesis of internally labeled structures. Utility of the new methods has been demonstrated with a variety of currently used fluorophores. Significant advantages in speed and simplicity over widely used solution-phase coupling methods, usually of an internally amine-labeled oligonucleotide with an active ester in aqueous solution, should be realized.

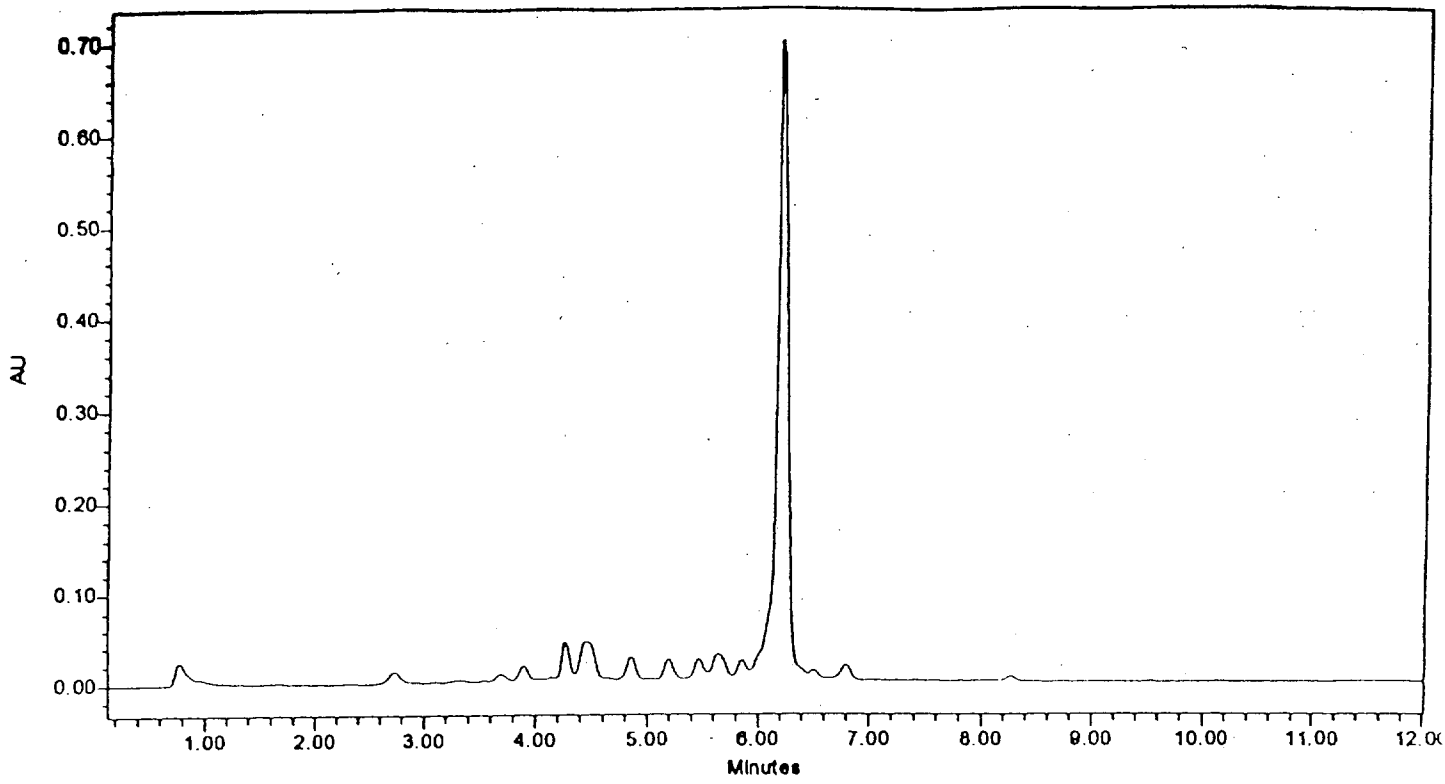
Supporting Information Available: Spectra and combustion analyses data. This material is available free of charge via the Internet at http://pubs.acs.org.

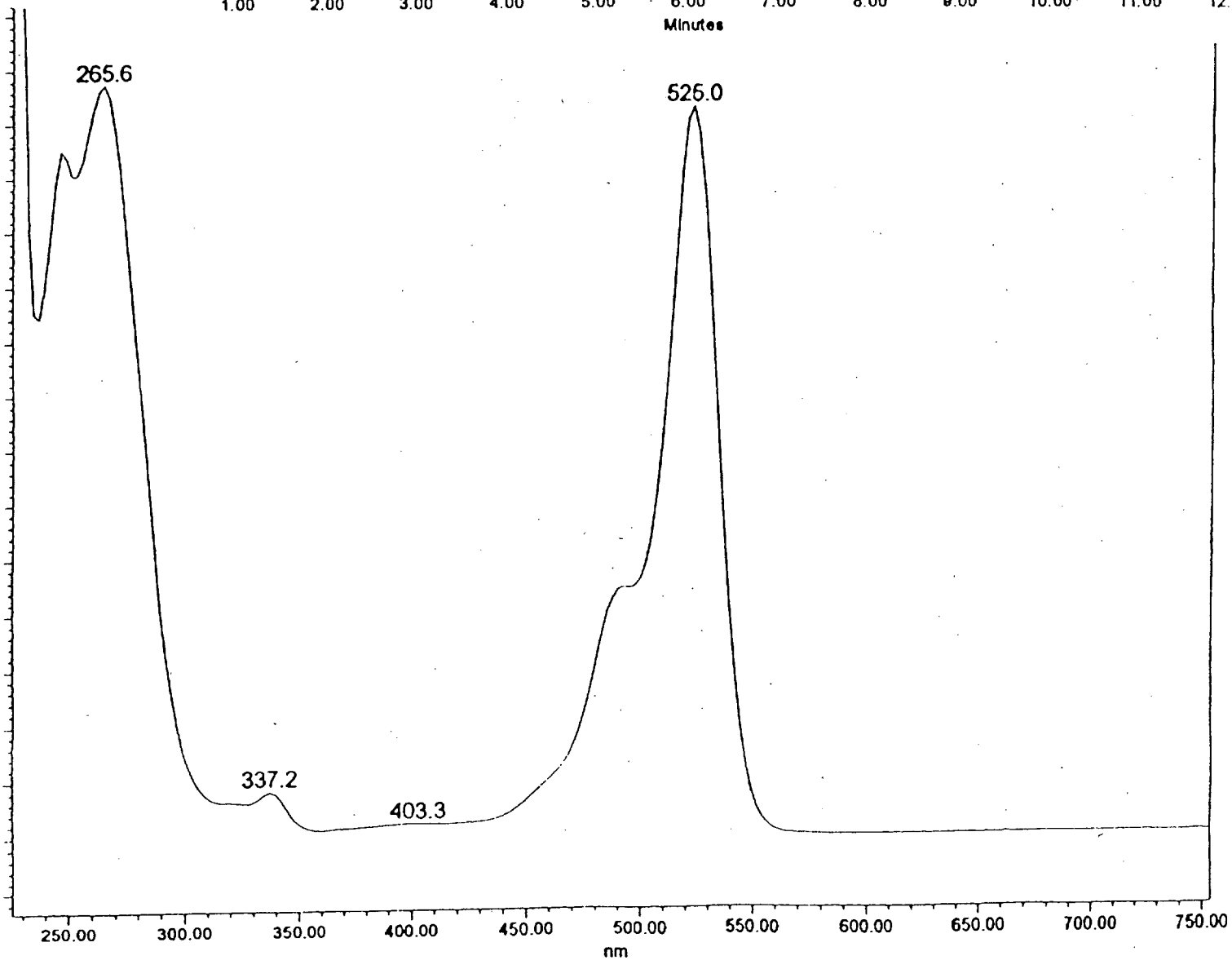
LITERATURE CITED

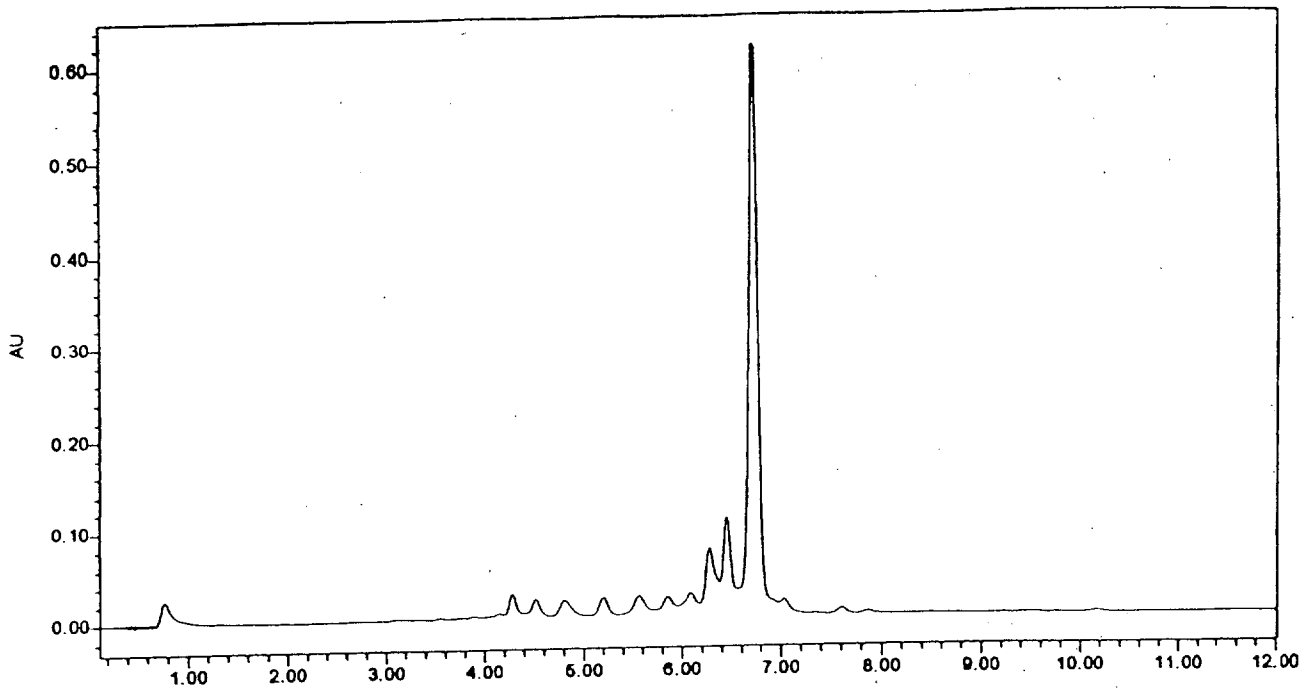
(1) Ruth, J. (1991) Oligodeoxynucleotides with reporter groups attached to the base. *Oligonucleotides and Analogues* (Eckstein, F., Ed.) pp 255−282, IRL Press, Oxford.
(2) Vinayak, R. (1999) A convenient, solid-phase coupling of rhodamine dye acids to 5′ amino-oligonucleotides. *Tetrahedron Lett. 40*, 7611−7613.
(3) Lyttle, M. H., Carter, T. C., Dick, D. J., and Cook, R. M. (2000) A tetramethyl rhodamine (Tamra) phosphoramidite facilitates solid-phase-supported synthesis of 5′-Tamra DNA. *J. Org. Chem. 65*, 9033−9038.
(4) Mullah, B., and Andrus, A. (1997) Automated Synthesis of Double Dye-Labeled Oligonucleotides using Tetramethylrhodamine (TAMRA) Solid Supports *Tetrahedron Lett. 38*, 5751−5754.
(5) Rudert, W. A., Braun, E. R., Faas, S. J., Menon, R., Jaquins-Gerstl, A., and Trucco, M. (1997) Double Labeled Fluorescent Probes for 5′ Nuclease Assays: Purification and Performance Evaluation. *Biotechniques 22*, 1140−1145.
(6) Glen Research has biotin, fluorescein, and TAMRA functionalized dU amidites.
(7) Kahn, S. I., and Grinstaff, M. W. (1999) Palladium(0)-Catalyzed Modificatons of Oligonucleotides during Automated Solid-Phase Synthesis *J. Am. Chem. Soc. 121*, 4704−4705.
(8) Hwang, J., and Greenberg, M. (2001) Synthesis of 2′-Modified Oligonucleotides via On-Column Conjugation. *J. Org. Chem. 66*, 363−369.
(9) Chang, C., Urdea, M. S., and Horn, T. (1996) N-4 Modified Pyrimadine Deoxynucleotides and Oligonucleonucleotide Probes Synthesized Therewith. US Patent 5580731.
(10) Clontech, Inc., cat. no. 5251.
(11) Otvos, L., Sagi, J., Sagi, G., and Szemzo, A. (1999) Base Modified Oligonucleotides. II. Increase of Stability to Nucleases by 5-Alkyl, 5(1-alkenyl)- and 5(1-alkynyl) pyrimadines. *Nucleosides Nucleotides 18*, 1929−1933.
(12) Walton, T., Lyttle, M., Dick, D., and Cook, R. (2002) Evaluation of New Linkers and Synthetic Methods for Internal Labeled Oligonucleotides *Bioconjugate Chem. 13*, 1155−1158.
(13) Wang, W. W., Lyttle, M. H., and Borer, P. N. (1990) Enzymatic and NMR Analysis of Oligoribonucleotides Synthesized with 2′-*tert*-butyldimethylsilyl Protected Cyanoethylphosphoramidite Monomers. *Nucleic Acids Res. 18*, 3347−3355.
(14) Lyttle, M. H., Napolitano, E. W., Calio, B. L., and Kauvar, L. M. (1995) Mutagenesis Using Trinucleotide *β*-Cyanoethyl Phosphor-amidites. *Biotechniques 19*, 274−280.
(15) Lyttle, M. H., Adams, H., Hudson, D., and Cook, R. M. (1997) Versatile Linker Chemistry for Synthesis of 3′-Modified DNA. *Bioconjugate Chem. 8*, 193−198.
(16) Biosearch Technologies, Inc.
(17) Extinction coefficient of DMT cation 70000 @ 498 nm; 3% DCA in DCM.
(18) Hovinen, J. (1998) A simple synthesis of N-4 (6-aminohexyl)-2-deoxy-5′-*O*-(4,4′dimethoxytrityl) cytidine *Nucleosides Nucleotides 17*, 1209−1213.
(19) Bergstrom, D. E., and Ogawa, M. K. (1978) C-5 Substituted pyrimidine nucleosides. 2. Synthesis via olefin coupling to organopalladium intermediates derived from uridine and 2′-deoxyuridine. *J. Am. Chem. Soc. 100*, 8106−8112.
(20) Ahmadian, M., Klewer, D. A., and Bergstrom, D. E. (2000) Palladium-mediated C-5 substitution of Pyrimidine Nucleosides. *Current Protocols in Nucleic Acid Chemistry* (Beaucage, S., and Jones, R., Eds.) 1.1.1−1.1.18.
(21) Van Boom, J. H., and Burgers, P. M. (1976) Synthesis of complementary DNA fragments via phosphotriester intermediates. *Tetrahedron Lett. 17*, 4875−4882.

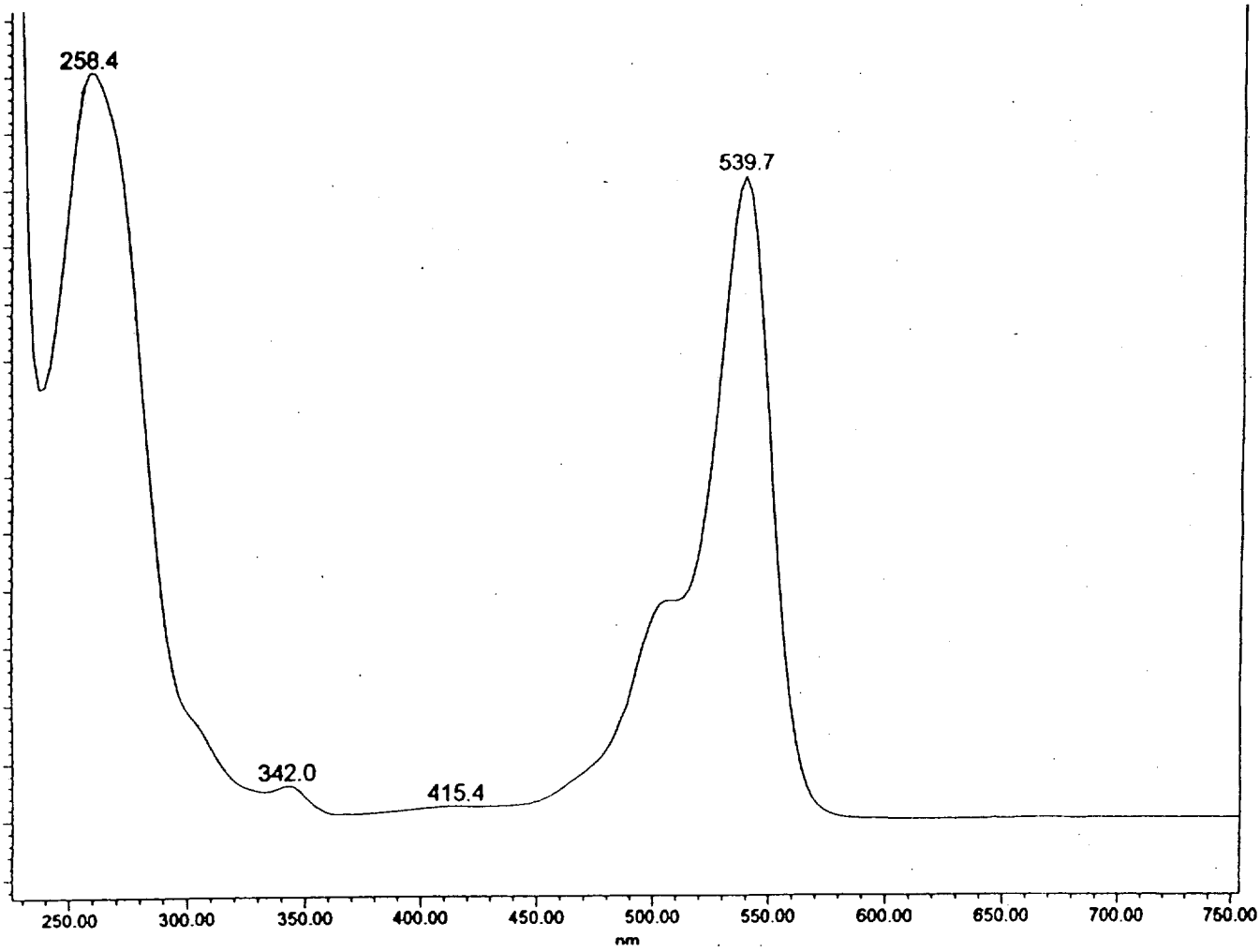
BC020011C

© 2002 American Chemical Society, Bioconjugate Chem., Lyttle bc020011c Supporting Info Page 1

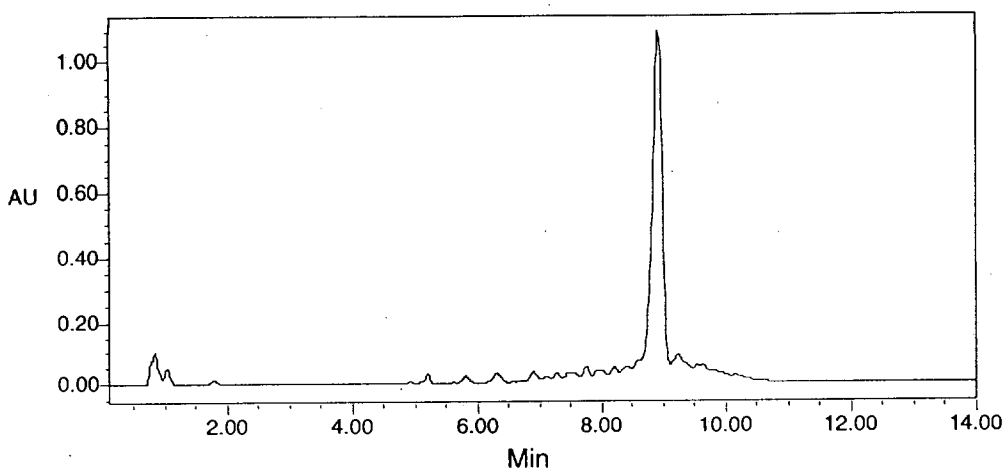


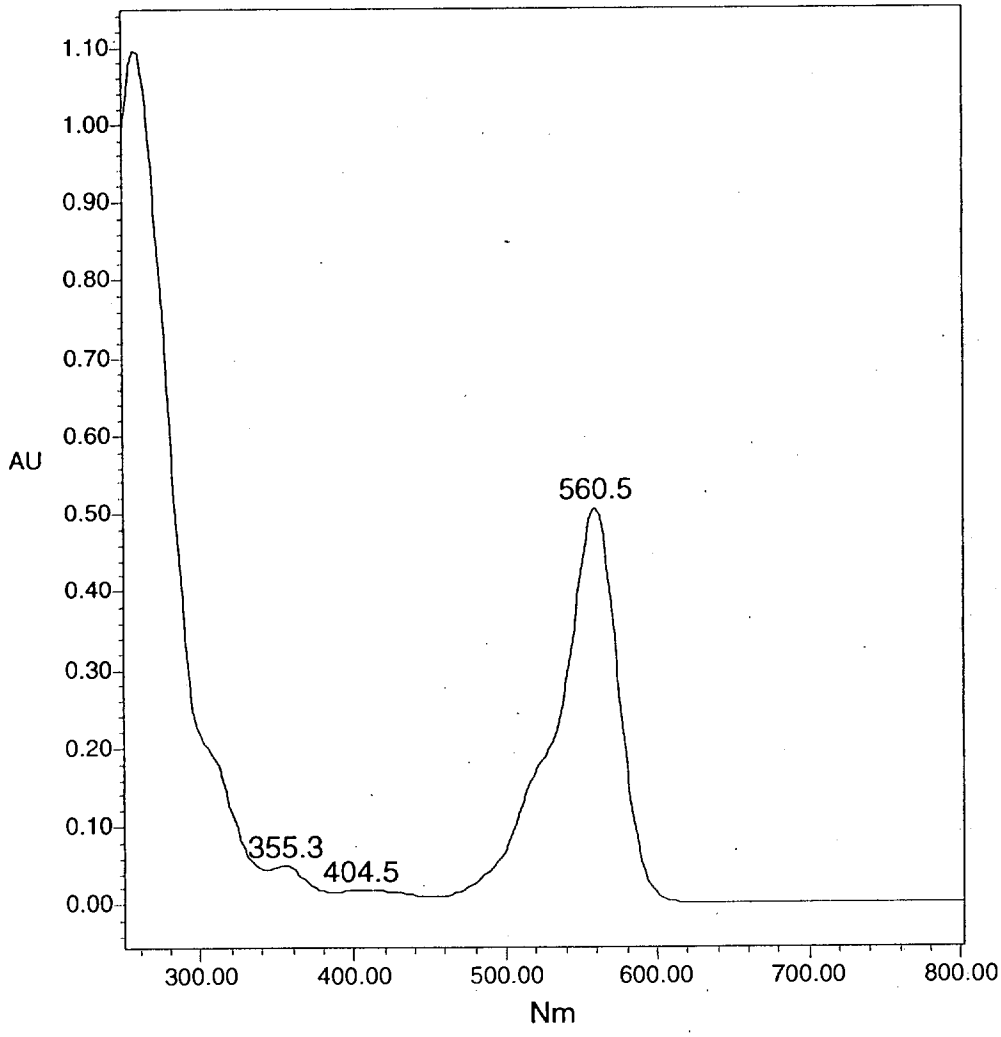



AU
0.60
0.50
0.40
0.30
0.20
0.10
0.00
1.00
2.00
3.00
4.00
5.00
6.00
7.00
8.00
9.00
10.00
11.00
12.00


258.4
539.7
342.0
415.4
250.00
300.00
350.00
400.00
450.00
500.00
550.00
600.00
650.00
700.00
750.00
nm

© 2002 American Chemical Society, Bioconjugate Chem., Lyttle bc020011c Supporting Info Page 3





Compound Elemental Analysis Data

N^4-(2-(ethyleneglycol-2-levulinate)ethyl)-5-methyl-5'-(4,4'-dimethoxytrityl)-3'-O-tertbutyldimethylsilyl-2'deoxycytidine, **7**

Anal Calc'd for $C_{46}H_{61}N_3O_{10}Si \cdot 1/2MeOH$: C, 64.94; H, 7.38.

Found: C, 64.59; H, 7.34.

N^4-(2-(ethyleneglycol-2-levulinate)ethyl)-5-methyl-5'-(4,4'-dimethoxytrityl)-2'-deoxycytidine, **8**

Anal Calc'd for $C_{40}H_{47}N_3O_{10}$: C, 65.83; H, 6.49; N, 5.76.

Found: C, 65.74; H, 6.68; N, 6.41.

N^4-(2-(ethyleneglycol-2-levulinate)ethyl)-5-methyl-5'-(4,4'-dimethoxytrityl)-3'-O-(2-cyanoethyldiisopropylphosphorodiamidite) 2'-deoxycytidine, **1**

Anal Calc'd for $C_{49}H_{64}N_5O_{11}P$: C, 63.28; H, 6.94; N, 7.53.

Found: C, 62.99; H, 6.61; N, 7.82.

N-acrylolyl-N'-tertbutyloxycarbonyl-1,6-hexanediamine, **9**

Anal Calc'd for $C_{14}H_{26}N_2O_3$: C, 62.19; H, 9.69; N, 10.36.

Found: C, 62.43; H, 9.83; N, 10.42.

5(N-(6-trifluoroacetylaminohexyl)-3-(E)acrylamido-5′(4,4′dimethoxy-trityl)-2′-deoxyuridine, **11**

Anal Calc'd for $C_{41}H_{45}F_3N_4O_9 \cdot C_5H_5N$: C, 63.27; H, 5.77; N, 8.02.

Found: C, 63.47; H, 5.92; N, 8.13.

5(N-(6-trifluoroacetylaminohexyl)-3-(E)acrylamido-5′(4,4′dimethoxy-trityl)-3′-(2-cyanoethyldiisopropylphosphoramidite)-2′-deoxyuridine, **2**

Anal Calc'd for $C_{50}H_{62}F_3N_6O_{10}P$: C, 60.35; H, 6.28; N, 8.45.

Found: C, 60.32; H, 6.32; N, 8.57.

N-acryloyl-O-levulinoyl –6-amino-1-hexanol, **12**

Anal Calc'd for $C_{14}H_{23}NO_4$: C, 62.43; H, 8.61; N, 5.20

Found: C, 61.91; H, 8.94; N, 5.74.

5(N-(6-O-levulinoyl-1-aminohexyl)-3-(E)acrylamido-5′(4,4′dimeth-oxytrityl)- 2′-deoxyuridine, **14**

Anal Calc'd for $C_{44}H_{51}N_3O_{11} \cdot 1/2C_5H_5N$: C, 66.76; H, 6.44; N, 5.86.

Found: C, 66.52; H, 6.37; N, 5.91.

5(N-(6-O-levulinoyl-1-aminohexyl)-3-(E)acrylamido-5′(4,4′dimeth-oxytrityl)-3′-(2-cyanoethyldiisopropylphosphoramidite)-2′-deoxy-uridine, **3**

Anal Calc'd for $C_{53}H_{68}N_5O_{12}P$: C, 63.78; H, 6.87; N, 7.02.

Found: C, 63.75; H, 6.91; N, 7.13.

TECHNICAL NOTES

Evaluation of New Linkers and Synthetic Methods for Internal Modified Oligonucleotides

Troy A. Walton,* Matthew H. Lyttle, Daren J. Dick, and Ronald M. Cook

Biosearch Technologies, Inc., 81 Digital Drive, Novato, California 94949. Received January 21, 2002; Revised Manuscript Received May 15, 2002

Several fluorescence resonance energy transfer (FRET) oligonucleotide probes were made with different internal linkages between the DNA and the quencher dye. In one example, a 5′-fluorescein β-actin-based 26-mer DNA sequence was synthesized bearing an internal Tamra quencher. Two different versions were prepared using either conventional C5 [*N*-(6-aminohexyl)-3-acrylamido]pyrimidine-modified uridine and solution-phase Tamra active ester coupling or solid-phase addition of a Tamra amidite to a C5 [*N*-(6-hydroxyhexyl)-3-acrylamido]pyrimidine-modified uridine. The products were compared in functional assays. They performed very similarly both in a fluorescence-based melting point assay as well as in quantitative PCR. Another set of β-actin probes were synthesized utilizing N4 [*N*-2-(ethylene glycol ethyl)-5-methyl]cytidine and solid-phase Tamra amidite addition at positions flanking those of the uridine. These versions gave lower T_ms than either uridine-labeled probe and did not work as well in quantitative PCR. A control experiment using oligonucleotides with the same modified residues but without fluorophores attached revealed the same trend as the T_m study of internal Tamra-labeled probes. Experimental details for the synthesis, purification, and testing are presented.

INTRODUCTION

A variety of different FRET oligonucleotide probes require internal modifications, including sunrise (*1*), scorpion (*2*), tandem dye reporters or FRET reporters (*3*), and the invader fluorescent assay (*4*). The maximum FRET effect has been reported with 4−5 nucleotide bases separating reporter and quencher dyes (*5*, *6*), which suggests that the use of internally linked fluorophores (or quenchers) would provide the best performance for longer sequences. Methods for generating internally labeled synthetic oligonucleotides are limited, with solution-phase coupling of active esters to alkylamine internal modifications being prevalent (*3*). Traditionally, solid-phase fluorescent-tagged DNA synthesis is restricted to fluorophore incorporation at the 3′ or 5′ terminus. In recent work, we developed a method using an internal uridine nucleotide modified at C5 with a protected alkyl hydroxyl group to synthesize internally labeled probes on a solid-phase support (*7*). We report here application of this technique to the synthesis of dual-labeled FRET probes and compare the performance of these structures to those synthesized using conventional uridine C5 alkylamine and solution-phase *N*-hydroxysuccinimide (NHS) active ester coupling methods. Probes were also made with a cheaper internal linkage system, utilizing N4-protected alkylhydroxyl functionalized cytidine. Figure 1 shows the structure of the three internal linkages to Tamra. The different probes were compared by a quantitative PCR (qPCR, *3*) assay and melting temperature assays (*8*, *10*). Probes were synthesized with fluorescein on the 5′ end and Tamra internally or with no fluorophore modifications.

MATERIALS AND METHODS

Oligo Synthesis. The probes with sequence 5′-ATGC-C**CTC**CCCCATGCCATCCTGCGT-3′ were targeted for the human β-actin gene (*3*). All oligos were synthesized on Biosearch 8700 DNA synthesizers, using 3′-phosphate controlled pore glass (CPG) (p/n BG5-5000). Modified nucleotide amidites (*7*) and Tamra and fluorescein amidite (FAM) (*9*) were synthesized in-house along with the Tamra NHS ester used for solution-phase coupling. The modified bases were incorporated at the boldface underlined positions shown above. Syntheses were done at a 1 μmol scale. For structure **I** (see Figure 1), also T7-NH-Tamra in Table 1, 5-[*N*-(6-trifluoroacetylaminohexyl)-3-(*E*)-acrylamido]-5′-(4,4′-dimethoxytrityl)-3′-(2-cyanoethyldiisopropylphosphoramidite)-2′-deoxyuridine (*7*) was used in lieu of the T, 7 bases from the 5′ end, and the rest of the bases were added followed by FAM addition (*7*). Workup and Tamra incorporation were done with solution-phase methods as previously reported (*3*). Figure 2A shows an anion exchange (AX) HPLC trace and photodiode array (PDA) spectrum of the purified probe. For the probe containing internal modification **II**, also T7-O-Tamra, automated synthesis was halted after the addition of 5-[*N*-(6-*O*-levulinoyl-1-aminohexyl)-3-(*E*)-acrylamido]-5′-(4,4′-dimethoxytrityl)-3′-(2-cyanoethyldiisopropylphosphoramidite)-2′-deoxyuridine (*7*) at T7, and the CPG was treated with the dilute hydrazine/pyridine/acetic acid (HOAc) cocktail outlined in (*7*). Tamra amidite (*9*) was coupled onto the now unmasked hydroxyl group, followed by oxidation and capping. The rest of the bases were then added by automated synthesis, followed by

* Address correspondence to this author. Phone: 415-883-8400; fax: 415-883-8488; e-mail: Troy.Walton@colorado.edu.

10.1021/bc0200125 CCC: $22.00 © 2002 American Chemical Society
Published on Web 08/16/2002

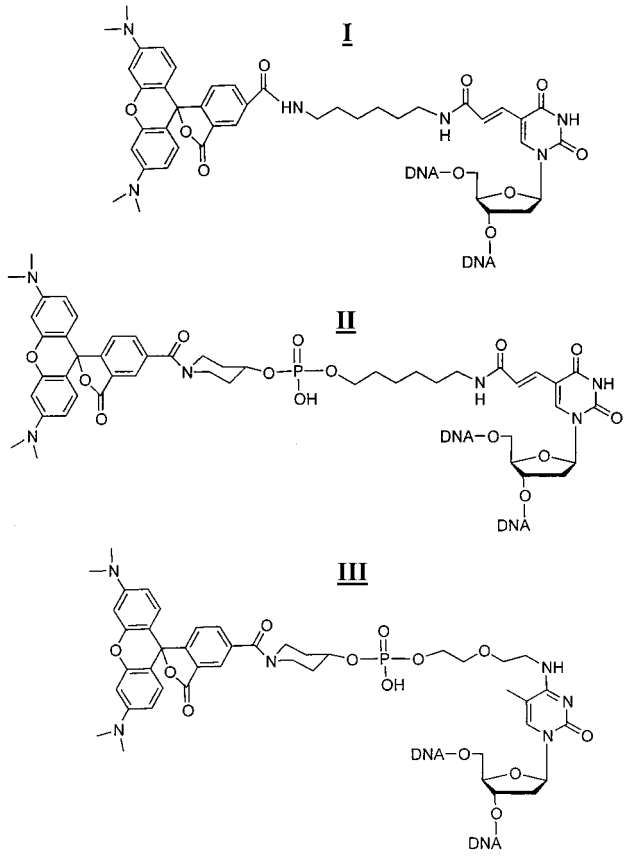


Figure 1. Structures of internal Tamra linkages. I = conventional amine and Tamra NHS coupling; II = Tamra amidite functionalized T C5 alkylhydroxyl; III = Tamra amidite functionalized C N4 alkylhydroxyl.

Table 1. Oligonucleotide Sequences of Probes Used in This Study[a]

atgccc**t**cccccatgccatcctgcgt	T7-NH-Tamra
atgccc**t**cccccatgccatcctgcgt	T7-O-Tamra
atgcc**c**tcccccatgccatcctgcgt	C6-O-Tamra
atgccct**c**cccccatgccatcctgcgt	C8-O-Tamra
atgccctcccccatgccatcctgcgt	unmodified
atgccc**t**cccccatgccatcctgcgt	T7-OH
atgcc**c**tcccccatgccatcctgcgt	C6-OH
atgccct**c**cccccatgccatcctgcgt	C8-OH

[a] Modified residues are indicated in boldface type. Oligos with internal Tamra modifications were 5′-FAM-modified as well.

FAM addition. Figure 2B shows an AX HPLC trace and PDA spectrum of this purified probe. For the other probes containing modification **III** at the C positions flanking T7, N^4-[2-(ethylene glycol-2-levulinate)ethyl]-5-methyl-5′-(4,4′-dimethoxytrityl)-3′-*O*-(2-cyanoethyldiisopropylphosphoramidite)-2′-deoxycytidine (*7*) was used at the appropriate position to generate either C6-O-Tamra or C8-O-Tamra (Table 1), and the other manipulations were the same as those used to generate **II**. Figure 2C,D has the comparative analysis of these probes. A similar set of probes was synthesized without fluorescent dyes for use as nonlabeled controls in a Sybr Green I melting temperature assay (*10*). These are referred to as T7-OH, C6-OH, C8-OH, and unmodified. After synthesis, Tamra deprotection cocktail (*9*) and 16 h of heating at 60 °C were used to deprotect and remove the probes from the CPG. Volatile components were removed under vacuum, and the crude sample was dissolved in 1 mL of water. Probes were purified using a double-preparative HPLC method consisting of an anion exchange (AX) purification followed by a reversed phase (RP) purification. A Dionex DNA Pac

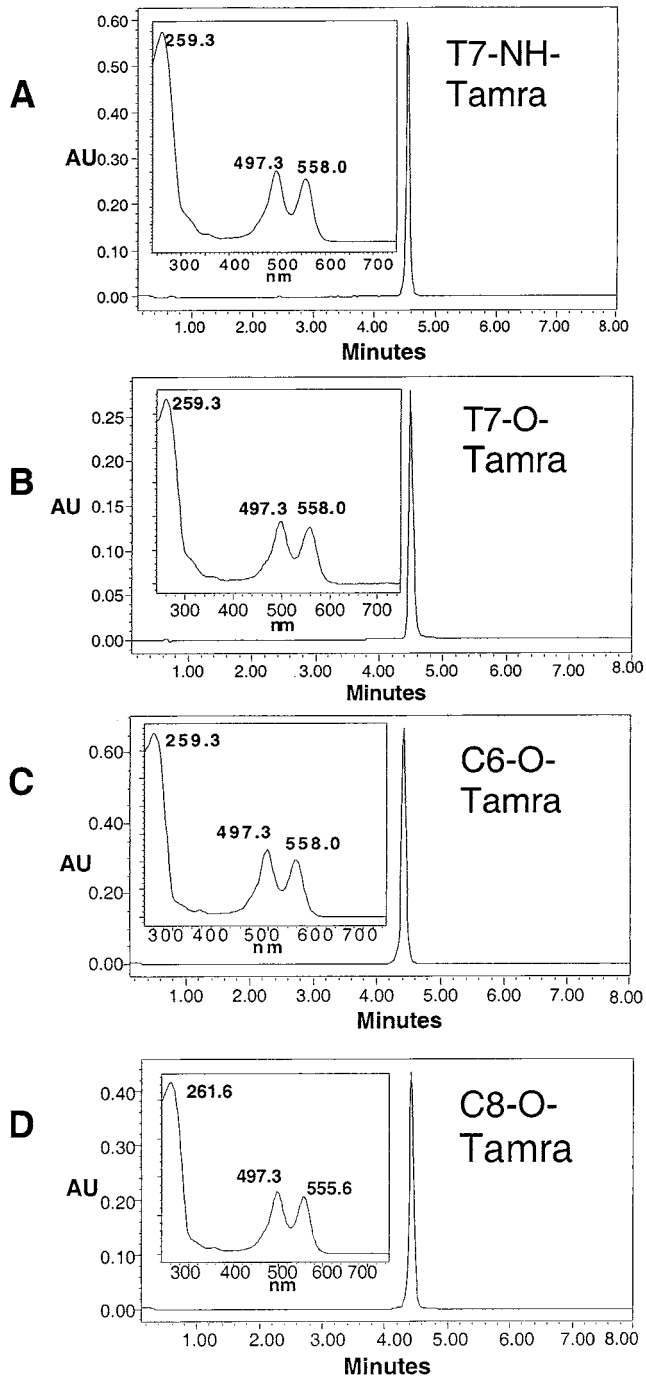


Figure 2. Analytical AX HPLC of internally Tamra-labeled FRET probes. The inset shows the PDA spectrum of each sample. Sequences shown in Table 1.

PA100 9 × 250 mm column was used for AX, and a Hamilton PRP-1 10 × 250 mm 7 μm particle size column was used for RP. A 5 mL injection loop with a 10 mL/min flow rate for AX and a 6 mL/min flow rate for RP were used. The buffers for the AX preparation consisted of 0.038 M Tris at pH 8.0 plus 15% acetonitrile (ACN) for buffer A, and buffer B was buffer A plus 1 M NaBr. The purification gradient was 10−70% B over 12 min. The buffers for the RP purification consisted of 0.1 M TEAA (triethylamine acetate) + 5% ACN for A, and B was ACN. The gradient was 0−75% B over 15 min. A Waters 600 controller and pump with a Waters 490 multiple wavelength detector were used for purification. Intensely colored fractions were inspected by analytical HPLC, and those containing pure material with the

proper spectrum were pooled and evaporated. The yield of purified probes made at this scale was 60−120 nmol.

PCR and Melting Temperature Conditions. The PCR reactions were carried out on an ABI 7700 using 50 μL reaction volumes in Taqman Buffer A (Applied Biosystems). The reactions contained 200 nM primers (Applied Biosystems), 400 nM FRET probe, 100 or 1 ng of sheared human genomic DNA (Clontech), with 4 mM MgCl (Applied Biosystems), 200 μM each dNTP (Sigma), 0.3 unit of *Bst*Xl (Boehringer Mannheim), and 2.5 units of Platinum Taq (Gibco). Thermal cycling conditions were 48 °C for 30 min, then 95 °C for 10 min followed by 40 cycles of 95 °C (25 s) and 60 °C (60 s). The ABI 7700 was set for a single dye (FAM) with Tamra as the quencher. The melting curves were also generated on the 7700 in PCR buffer consisting of 10 mM Tris, pH 8.3, 50 mM KCl, and 3.5 mM $MgCl_2$. The temperature was decreased in 1 °C steps from 90 to 50 °C using the auto increment function with each step lasting 1 min. Probes were suspended at 200 nm, and compliment was suspended at 1 μM. For nonlabeled DNA reactions, Sybr Green I was used at a final 1:40 000 dilution from the stock solution provided by the manufacturer.

RESULTS AND DISCUSSION

Melting Temperature (T_m) Experiments. Instead of conventional T_m measurements using UV absorbance, we chose a system more relevant to the evaluation of FRET probes. Similar buffers and the same instrument were used to generate the T_m data as for qPCR. When the probe hybridizes to exact complement and forms duplex DNA, the fluorescence increases relative to the single-stranded probe free in solution (*3*). Because of this, the T_m can be determined by measuring the fluorescence over a temperature range the same way one would use absorbance measurements at 260 nm (*8*). In the nonlabeled DNA reactions, the intercalating dye Sybr Green I was added to the reaction mix. Sybr Green I increases in fluorescence when it binds to double-stranded DNA. In this melting temperature assay, the change in fluorescence of the Sybr Green I with respect to increasing double-stranded DNA concentration vs temperature reveals melting curves similar to those obtained for the dual dye-labeled oligos (*10*). The data for the dual-labeled probes show that probes containing internal structures **I** and **II** anneal to complement at similar T_ms. In contrast, both of the modified cytidine compounds (structure **III**) give lower T_ms than those given by the modified thymine compounds. They also have a much broader T_m range than the thymine-based probes, suggesting less specificity during the hybridization event (see Figure 3). This same trend is apparent in Figure 4, which shows a similar melting temperature experiment. In this experiment, the same probe structures were synthesized without fluorescent dyes, and the amine modified probe was replaced by a totally unmodified oligo. The conditions for the nonlabeled DNA experiment were the same except that SYBR Green I was used as the reporter. In the Sybr Green I experiment, the melting curves for the unmodified DNA and the hydroxyl-modified thymine oligo (T7-OH in Figure 4) overlap, while the hydroxyl-modified cytidine compounds show a significantly lower melting temperature.

When using either amine- or hydroxyl-modified thymine chemistries, the performance of the dual-labeled probe is virtually unaffected. This same trend has been observed when comparing N4-modified cytidine compounds with hydroxyl functionality and amine functionality (data not shown). We can attribute the difference between the T- and C-labeled probes to the modifications that were used for internal labeling, although other factors might be at play. One plausible explanation is that the thymine residue used has a modification on the methyl group at position C5, while the cytidine residue is modified at N4, and N4 in unmodified cytosine participates in an energetically important G−C base pair. The appendage at position C5 of thymine protrudes out into the major groove of B-DNA and should not affect base pairing. Realistically, we have empirically compared several easily accessible linkages in an important application. Different spacer length and geometry, as well as the presence of a phosphate moiety in some of the linkers, may also be having an effect. Although the linkage differences are more directly compared in the nonlabeled DNA experiment using SYBR Green I, the intercalation itself appears to have some effect on the T_m of these oligos (Figure 4).

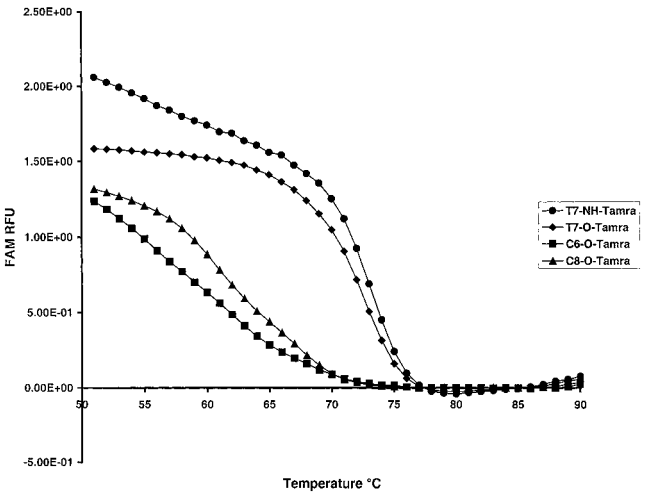


Figure 3. Melting temperature curves of Tamra-quenched probes generated as a function of increasing fluorescein fluorescence on an ABI 7700. RFU = relative fluorescence units.

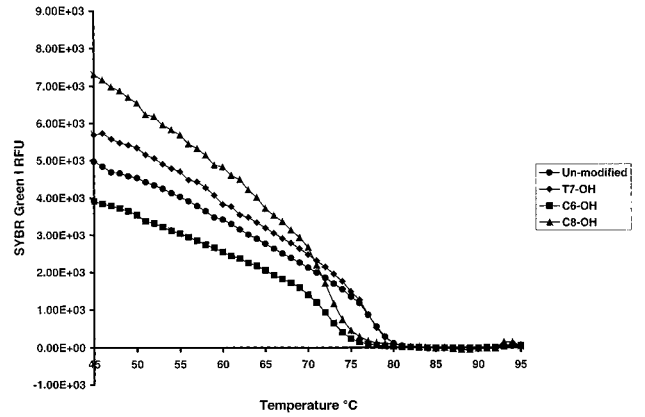


Figure 4. Melting temperature curves of unlabeled probes generated as a function of increasing Sybr Green I fluorescence on an ABI 7700. RFU = relative fluorescence units.

Quantitative PCR Experiments. There are several different chemistries available for qPCR (*11*), including the 5′→3′ exonuclease assay, which was used for this comparison (*12*). In this assay, a dual-labeled fluorescent oligonucleotide is hybridized to the amplicon between the primers and is cleaved by the 5′→3′ nucleolytic activity of Taq polymerase. This cleavage event generates fluorescence because the reporter fluorophore is no longer in close enough proximity to the quencher for efficient

Table 2. Data from qPCR Experiments[a]

	1 ng target		100 ng target	
probe	C_T	std dev	C_T	std dev
T7-NH-TMR	28.85	0.14	21.88	0.13
T7-O-TMR	29.13	0.06	22.2	0.02
C6-O-TMR	31.89	0.13	24.7	0.04
C8-O-TMR	31.09	0.08	24.0	0.02

[a] All reactions were run in triplicate. The average C_T is shown with the standard deviation for each triplicate reaction. Reactions were done for two different input amounts of target human genomic DNA (1 and 100 ng).

energy transfer via the FRET mechanism (*13*). By monitoring the increase in fluoresence produced by this cleavage event over several cycles of PCR, the amount of original target DNA in the reaction mix can be measured (*13*). The cycle in which the fluorescence rises above a certain background level is referred to as threshold cycle (C_T) and is used to calculate the amount of target DNA. Comparison of the oligos from Table 1 in a quantitative PCR assay is summarized in Table 2. While the performance difference, as expressed with the C_T value, is small between the two thymine compounds ($dC_T = 0.28$ for 1 ng target), the difference between the thymine and cytidine compounds is quite dramatic ($dC_T = 2.76$ for 1 ng target, T7-O-Tamra compared with C6-O-Tamra). This same trend is also seen in the 100 ng target samples. The difference in the melting temperature between these probes quite possibly accounts for the difference in performance seen here. The modified cytidine probes have a lower T_m (~62 °C) compared to the modified thymine probes (~73 °C) and therefore would not hybridize as well at the 60 °C extension temperature of the PCR reaction. This difference in hybridization would lead to fewer of the modified cytidine probes being cleaved by the nucleolytic activity of Taq polymerase, thus requiring more cycles of PCR to generate the same fluorescence as the thymine probes. Reprogramming the thermal cycler used for this qPCR experiment with a lower extension temperature would perhaps give improved or equivalent performance, with respect to C_T.

CONCLUSION

Several different ways of attaching Tamra to internal positions of a FRET probe targeting the human β-actin gene have been compared in practical applications. We have supplied useful data, which should be helpful in the design of more effective internally labeled FRET probes. A logical extension of this work would be the preparation of analogous C5-modified cytidine derivatives with a free amine at position N4; this work is in progress.

Our experiments show that when designing an oligonucleotide with an internal label on a modified nucleotide, N4-modified cytidine compounds do not perform the same as C5-modified thymine compounds. The synthetic toolbox for providing these modifications has been expanded, and both C and T are now available with added amine or hydroxyl functions for additional elaboration. The resulting different linker structures do not significantly change the performance of the modified T probes we tested. The solution-phase amine to active ester coupling method requires more synthetic manipulations. Therefore, we prefer the ease and faster throughput of solid-phase synthesis method made possible with the hydroxyl compounds.

LITERATURE CITED

(1) Nazarenko, I. A., Bhatnagar, S. K., and Hohman, R. J. (1997) A closed tube format for amplification and detection on DNA based on energy transfer. *Nucleic Acids Res. 25*, 2516−2521.

(2) Whitcombe, D., Theaker, J., Guy, S., Brown, T., and Little, S. (1999) Detection of PCR products using self-probing amplicons and fluorescence. *Nat. Biotechnol. 17*, 804−807.

(3) Livak, K., Flood, S., Marmaro, J., Giusti, W., and Deetz, K. (1995) Oligonucleotides with fluorescent dyes at opposite ends provide a quenched probe system useful for detecting PCR product and nucleic acid hybridization. *PCR Methods Appl. 4*, 1−6.

(4) Hall, J., Eis, P., Law, S., Reynaldo, J., Prudent, D., Marshall, H., Allawi, A., and Mast, A. (2000) Sensitive detection of DNA polymorphisms by the serial invasive signal amplification reaction. *Proc. Natl. Acad. Sci. U.S.A. 97*, 8272−8277.

(5) Cardullo, R. A., Agarwal, S., Flores, C., Zamecnik, P. C., and Wolf, D. E. (1988) Detection of Nucleic acid hybridization by nonradiative fluorescence resonance energy transfer. *Proc. Natl. Acad. Sci. U.S.A. 85*, 8790−8794.

(6) Morrison, L. (1992) Detection of energy transfer and fluorescence quenching. *Nonisotopic DNA Probe Techniques* (Kricka, L. J., Ed.) pp 311−352, Academic Press, San Diego.

(7) Lyttle, M., Walton, T., Dick, D., Carter, T., Beckman, J., and Cook, R. (2002) New Reagents and Methods for the Synthesis of Internal and 3′-Labeled DNA. *Bioconjugate Chem. 13*, 1146−1154.

(8) Tyagi, S., Bratu, D., and Kramer, F. R. (1998) Multicolor molecular beacons for allele discrimination. *Nat. Biotechnol. 16*, 49−53.

(9) Lyttle, M., Carter, T., Dick, D., and Cook, R. (2000) A tetramethyl rhodamine (Tamra) phosphoramidite facilitates solid-phase-supported synthesis of 5′-Tamra DNA. *J. Org. Chem. 65*, 9033−9038.

(10) Ririe, K. M., Rasmussen, R. P., and Wittwer, C. T. (1997) Product Differentiation by Analysis of DNA Melting Curves during the Polymerase Chain Reaction. *Anal. Biochem. 245*, 154−160.

(11) Bustin, S. A. (2000) Absolute quantification of mRNA using real-time reverse transcription polymerase chain reaction assays. *J. Mol. Endocrinol. 25*, 169−193.

(12) Holland, P. M., Abramson, R. D., Watson, R., and Gelfand, D. H. (1991) Detection of specific polymerase chain reaction product by utilizing the 5′→3′ exonuclease activity of *Thermus aquaticus* DNA polymerase. *Proc. Natl. Acad. Sci. 88*, 7276−7280.

(13) Heid, C. A., Stevens, J., Livak, K. J., and Williams, P. M. (1996) Real Time Quantitative PCR. *Genome Res. 6*, 986−994.

BC0200125

A Convenient Method for the Synthesis of Amine-Terminated Poly(ethylene oxide) and Poly(ϵ-caprolactone)

Feng-Zhu Lu,[†] Xiang-Yuan Xiong,[‡] Zi-Chen Li,*[,‡] Fu-Sheng Du,[‡] Bao-Yan Zhang,[†] and Fu-Mian Li[‡]

Department of Polymer Science & Engineering, College of Chemistry, Peking University, Beijing 100871, China, and Department of Chemistry, Northeastern University, Shenyang 110004, China. Received March 19, 2002; Revised Manuscript Received June 25, 2002

A convenient synthetic route to prepare amine-terminated poly(ethylene oxide) (PEO) and poly(ϵ-caprolactone) (PCL) was described. The strategy involved two-step reactions, the condensation of hydroxyl-terminated PEO and PCL with *N*-benzyloxycarbonyl amino acid followed by the catalytic hydrogenation under mild conditions. NMR and GPC measurements indicated that the reactions proceeded nearly quantitatively. Amine-terminated PEO thus prepared was used to initiate the polymerization of α-(*N*$^{\epsilon}$-benzyloxycarbonyl-L-lysine) *N*-carboxy anhydride [lys(Z)-NCA], and the results confirmed that the reactivity of the amino group was high.

INTRODUCTION

Poly(ethylene oxide) (PEO) and poly(ϵ-caprolactone) (PCL) have found many applications as biomedical materials (*1, 2*). Chemical modification, especially end-functionalization, is an important way to expand the applications of these polymers. Amine-terminated polymers are important intermediates for the synthesis of novel polymeric materials. They can react with molecules containing reactive groups such as acid chlorides, sulfonyl chlorides, acid anhydrides, and activated esters to conjugate other bioactive molecules at the end of the polymer chains (*3*). Furthermore, they can also be used as macroinitiators for the ring-opening polymerization of amino acid *N*-carboxy anhydrides (NCAs) to prepare block copolymers containing polypeptide segments (*4*).

The first paper for the synthesis of amine-end capped polyester was reported by Teyssie et al. (*5*). In their report, diethylaluminum 12-bromododecyloxide was used as an initiator of CL, yielding a bromo-terminated PCL, which was then converted into an azide-terminated PCL by the treatment with an excess of sodium azide. An amine-terminated PCL was finally obtained after catalytic hydrogenation. Star-like PCLs with amino end groups have also been reported by this group by using the same approach (*6*). But the synthesis of amine-terminated PLA by this method was demonstrated to be with side reactions (*7*). A similar approach has been reported by Kricheldorf et al. for the synthesis of amine-terminated aliphatic polycarbonates (*8*). The difference is that a nitrophenyl group was introduced to the aluminum alkoxide as an active initiator of trimethylene carbonate (TMC), aminophenyl end-capped poly(TMC), was obtained after catalytic reduction. Other approaches to prepare amine-terminated polyesters are the chain end modification of the polymer precursor under mild conditions. This can be achieved by the in situ reaction of 4-nitrobenzoyl chloride with a macrocyclic PCL, resulting in the formation of a α,ω-diamine-terminated telechelic PCL after reduction (*9*). Recently, Yuan et al. (*10*) prepared an amine-terminated MPEO−PCL diblock polymer from the hydroxyl-terminated polymer through a three-step reaction based on the chemistry as in the case of Teyssie's work.

There have been many reports on the preparation of amine-terminated PEO from hydroxyl-terminated PEO in the literature. The chemistry involved in this synthesis is to convert the hydroxyl groups into bromo, chloro, sulfonic, and aldehyde groups, followed by other chemical reactions leading to the formation of amino groups. For example, Buckmann and Johansson reduced the bromized PEO in alcohol using ammonia and hexadiamine, respectively (*11*). Sulfonic group end-capped PEO was transferred into amine-terminated PEO via a classical Gabriel process (*12*). The aldehyde group precursor of PEO was treated with $NaCNBH_3$ and converted into an amino group (*13*). Besides the above strategies, an approach similar to that for the preparation of amine-terminated PCL was carried out by treating the chloro precursor with NaN_3- and Pd/C-catalyzed hydrogenation successively (*14*). Though amine-terminated PEO can now be commercially available, these methods are still being used for the preparation of amine-terminated PEO of different chain lengths.

We tried another general procedure to obtain amine-terminated PCL and PEO from the hydroxyl-terminated precursors. It involved the condensation of hydroxyl-terminated PEO and PCL with *N*-benzyloxycarbonyl amino acid and subsequent catalytic hydrogenation under mild conditions to liberate the amino groups. The purification procedure was easy. Yet, to the best of our knowledge, only one publication has appeared so far dealing with the synthesis of an amine-terminated PLA by a similar procedure (*4b*). Although the structure of the amino acid used is not the same as the polymer, the short chain length compared with PEO and PCL would not influence the properties of the main chain, but alternate their reactivities. This approach may be a universal synthetic route with a high potential utility for the preparation of amine-end capped polymers from hydroxyl-terminated polymer precursors.

EXPERIMENTAL PROCEDURES

Materials. ϵ-Caprolactone (ϵ-CL) was purchased from Acros, dried over calcium hydride for 48 h at room

* Corresponding author. Tel: +86-10-6275-7155. Fax: +86-10-6275-1708. E-mail: zcli@pku.edu.cn.

[†] Northeastern University.

[‡] Peking University.

10.1021/bc025531m CCC: $22.00 © 2002 American Chemical Society
Published on Web 08/14/2002

temperature, and then distilled under reduced pressure. $Al(OiPr)_3$ and 10% Pd/C were also from Acros; 10% Pd/C was used as received, and $Al(OiPr)_3$ was distilled under reduced pressure prior to use. Methoxy PEO (MPEO, M_n = 2000) was obtained from Aldrich, and was treated by azeotropic distillation with toluene to get rid of the small amount of water prior to use. *N*-Benzyloxycarbonyl glycine and 6-[(*N*-benzyloxycarbonyl)amino]hexanoic acid were synthesized according to the published procedure (*15*). α-(*N*$^{\epsilon}$-Benzyloxycarbonyl-L-lysine) *N*-carboxy anhydride [lys(Z)-NCA] was synthesized according to the literature method (*16*). (Dimethylamino)pyridine toluenesulfonate (DPTS) was prepared as described previously (*17*). Other regents were commercially available and used as received unless otherwise noted. All solvents were thoroughly dried and distilled before use.

Measurements. ^{1}H NMR spectra were recorded with a Bruker AXR-400 spectrometer operated at 400 MHz, $CDCl_3$ was used as solvent, and tetramethylsilane was used as an internal standard. The average molecular weights and molecular weight distributions were measured on a Waters 410 gel permeation chromatography (GPC) equipped with three Ultrastyragel columns (10^4, 10^3, and 500 Å pore size) at room temperature. The eluent was THF, and polystyrene standards were used as calibrations.

Synthesis of Poly(ϵ-caprolactone) (PCL-OH) (*18*). Dried toluene (40 mL) and 10 mL of ϵ-CL solution in toluene (0.1 mol) were injected through a syringe into a flask which had been dried, purged with nitrogen, and vacuumized several times. Then a solution (0.11 g/mL, 9.27 mL) of $Al(OiPr)_3$ in toluene was introduced at 0 °C to the reactor under nitrogen. The reaction mixture was incubated for 2 h at 0 °C and then diluted with 80 mL of toluene. Afterward, the solution was washed with 0.3 N HCl aqueous solution (3 × 20 mL) and water (3 × 30 mL). The organic phase was obtained and dried over $MgSO_4$. The solution was concentrated to about 10 mL by a rotary evaporator and poured into 100 mL of hexane. The precipitated polymer was obtained by filtration and was redissolved in 10 mL of $CHCl_3$, precipitated again in hexane. The purified product was dried under vacuum at room temperature, yielding 9 g of a white powder. Yield: 90%, M_w/M_n = 1.33, M_n = 4900.

Synthesis of PCL-Cn-NH-Z and MPEO-Cn-NH-Z (*16*). *(1) PCL-Cn-NH-Z.* A 250 mL round-bottomed flask, fitted with a magnetic stir bar, was charged with 4 g of PCL-OH (1.67 mmol), 0.52 g of DCC (4.7 mmol), 0.29 g of DPTS (0.98 mmol), and 100 mL of CH_2Cl_2. To this mixture was added 0.53 g (2 mmol) of 6-[(*N*-benzyloxycarbonyl)amino]hexanoic acid or 0.42 g (2 mmol) of *N*-benzyloxycarbonyl glycine. The reaction mixture was stirred at room temperature for 48 h. After filtration, the solution was reduced in volume to 20 mL by a rotary evaporator, and the polymer was precipitated into cold methanol (400 mL), dissolved in chloroform (30 mL), reprecipitated out by cold methanol (200 mL), and dried under vacuum. PCL-C_6-NH-Z: 65%; PCL-C_2-NH-Z: 53%.

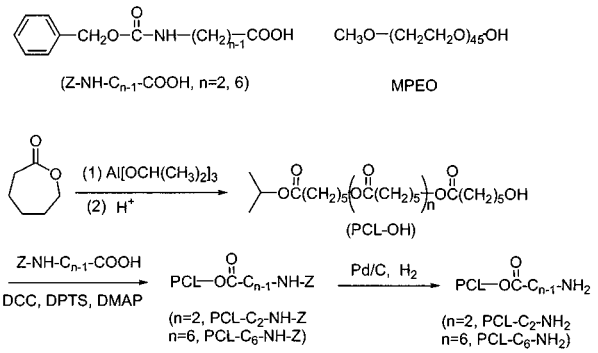
(2) MPEO-Cn-NH-Z. These polymers were prepared from MPEO under the same conditions as in the case of PCL. But the purification procedure is different. The resulting reaction mixture was first precipitated into cold diethyl ether (400 mL), and the products obtained were dissolved in 40 mL of THF. After filtration, the solution was concentrated and precipitated into cold diethyl ether and dried in a vacuum oven. MPEO-C_6-NH-Z: 79%; MPEO-C_2-NH-Z: 85%.

Synthesis of PCL-Cn-NH_2 and MPEO-Cn-NH_2. *(1) PCL-Cn-NH_2.* A suspension of PCL-Cn-NH-Z (2.0 g) in EtOAc/MeOH (v/v, 2:1) (40 mL) and 1.0 g of 10% Pd supported on activated carbon was subjected to hydrogenation under a H_2 blanket at room temperature for 24 h. After filtration over Celite, the solution was concentrated and precipitated into cold methanol. The obtained polymer was reprecipitated from cold methanol by dissolving in chloroform. PCL-C_6-NH_2: 70%, M_n = 4800, M_w/M_n = 1.21; PCL-C_2-NH_2: 60%, M_n = 4200, M_w/M_n = 1.34.

(2) MPEO-Cn-NH_2. The polymers were prepared by using a similar procedure as for PCL-Cn-NH_2, except that the precipitator was cold diethyl ether. MPEO-C_6-NH_2: 87%, M_n = 2100, M_w/M_n = 1.06; MPEO-C_2-NH_2: 80%, M_w/M_n = 2100, M_n = 1.10.

Synthesis of Poly[ethylene oxide-β-(*N*$^{\epsilon}$-benzyloxycarbonyl-L-lysine)] [MPEO-β-P(lys(Z))] (*4e*). A 4.5 g aliquot of α-(*N*$^{\epsilon}$-benzyloxycarbonyl-L-lysine) *N*-carboxy anhydride (15 mmol) was dissolved in 45 mL of DMF. The resultant solution was added to a solution of MPEO-C_2-NH_2 (2 g, 1 mmol) in DMF (70 mL). The reaction mixture was stirred under an inert atmosphere for 72 h at 40 °C and was precipitated into cold diethyl ether, followed by filtration and drying under reduced pressure to give 5.8 g of white powder. Yield: 89%, M_w/M_n = 1.19, M_n = 6000. Elemental analysis was conducted. Assume the average degree of polymerization is 15, Calcd for $C_{303}H_{457}N_{31}O_{92}$ (%): C, 60.61; H, 7.62; N, 7.23. Found: C, 60.51; H, 7.83; N, 7.28.

Scheme 1



RESULTS AND DISCUSSION

The amine-terminated MPEO and PCL were accomplished via a two-step process from hydroxyl-terminated MPEO and PCL as shown in Scheme 1. The hydroxyl-terminated PCL was prepared by the well-known coordination-insertion ring-opening polymerization of ϵ-caprolactone (ϵ-CL) in toluene using $Al(OiPr)_3$ as an initiator (*18*). In our experiment, the reaction temperature was 0 °C, and the polymerization time was 2 h. ^{1}H NMR spectrum of the resulting PCL is shown in Figure 1A. It can be seen that typical signals due to -$\underline{CH_2}$-OH, $(\underline{CH_3})_2$-CHO-, and $(CH_3)_2\underline{CH}$O- are observed at 3.62, 1.22−1.24, and 4.97−5.04 ppm, respectively, and their molar ratio was 2:6:1, confirming the α-hydroxyl ω-isopropyl structure. Based on the integral ratio of -OOC-$\underline{CH_2}$-CH_2- at 2.27−2.36 ppm to $(\underline{CH_3})_2$CHO- at 1.22−1.24 ppm, the average molecular weight of the product was calculated to be 2400. The average molecular weight obtained by GPC measurements shown in Figure 2A is 4900. This value is larger than that derived from ^{1}H NMR, which is normal when PS standards are used for GPC measurements (*9, 20*). The molecular weight distribution is 1.33.

The condensation of hydroxyl-terminated PCL and MPEO with an excess of *N*-benzyloxycarbonyl amino acid was easily done at room temperature according to the literature approach (*19*). To confirm whether the reaction

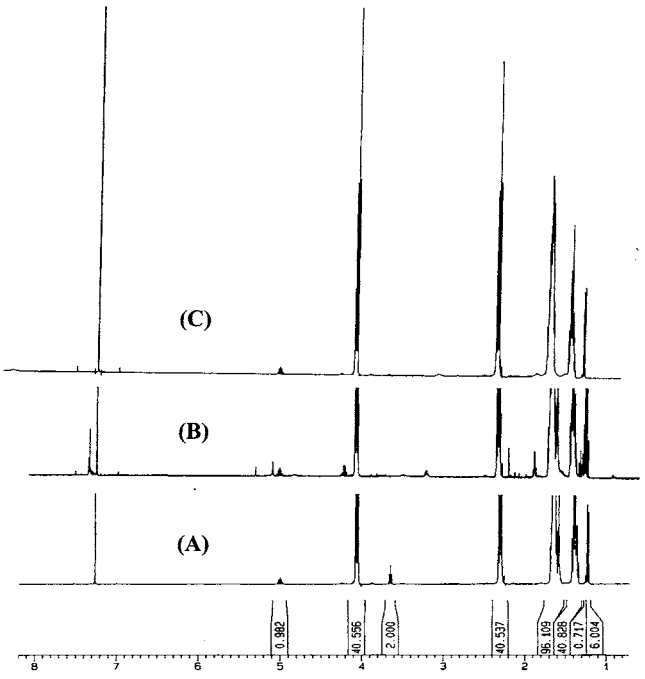


Figure 1. ^{1}H NMR spectra of (A) PCL-OH, (B) PCL-C_6-NH-Z, and (C) PCL-C_6-NH_2.

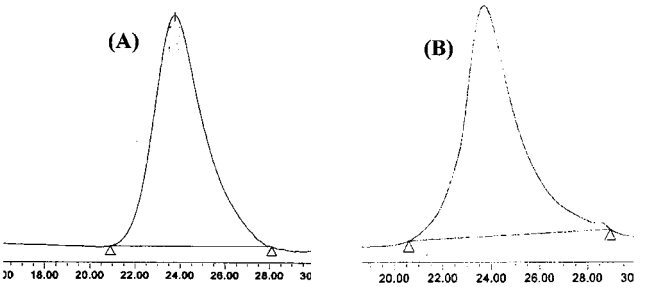


Figure 2. GPC trace of PCL (A) hydroxyl-terminated and (B) amine-terminated.

is applicable for both α-amino acids and α,*ω*-amino acids, two different amino acids, *N*-benzyloxycarbonyl glycine and 6-[(*N*-benzyloxycarbonyl)amino]hexanoic acid, were tested. The reaction conditions were the same. The purification procedure was different for PCL and MPEO. In the case of PCL, purification was easily done by precipitation into cold methanol. Due to the good solubility of DPTS and DCC and the excess of amino acid in methanol, they were easily removed to give pure polymer. But in the case of MPEO-Cn-NH-Z, the solubility of DPTS in cold diethyl ether was not high enough, and the product may contain little DPTS if the final solution was precipitated out directly from diethyl ether. However, DPTS could be eliminated by filtrating the concentrated mixture of DPTS and MPEO-Cn-NH-Z in THF before precipitation into diethyl ether. The ^{1}H NMR spectrum of PCL-C_6-NH-Z is shown in Figure 1B. The emergence of the peaks at 5.10, 7.36 ppm assignable to the benzyloxycarbonyl protons and the disappearance of the peaks at 3.62 ppm belonging to the methylene group near the hydroxyl terminal indicate condensation is taking place. Figure 3 A is the ^{1}H NMR spectrum of MPEO-C_2-NH-Z. The triple peaks at 4.30−4.32 ppm are from the methylene groups adjacent to the newly formed ester bonds (-OCH_2CH_2OOC-). Again, the peaks belonging to protective groups appear at 5.1 and 7.30−7.36 ppm, respectively. Based on the intensity ratio of benzyl or methylene groups adjacent to the ester bond to unchangeable

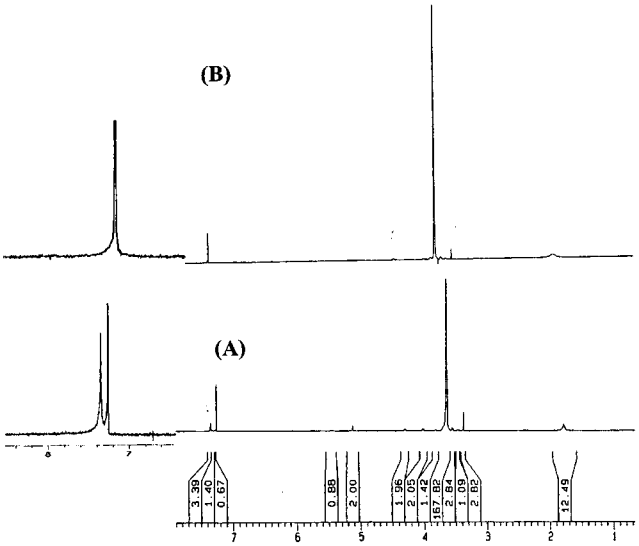


Figure 3. ^{1}H NMR spectra of MPEO. (A) MPEO-C_2-NH-Z. (B) MPEO-C_2-NH_2.

terminal groups [($\underline{CH_3}$)$_2$CH- for PCL-C_6-NH-Z, $\underline{CH_3}$O- for MPEO-C_2-NH-Z], the efficiencies of the end-group functionalization are close to 100%. PCL-C_2-NH-Z and MPEO-C_6-NH-Z gave similar results. The relatively lower yields of the resulting polymers were due to the solubility of polymers in methanol or diethyl ether.

Catalytic hydrogenation is one of the most important methods to liberate the *N*-benzyloxycarbonyl-protected amino group. The catalyst is 10% Pd supported on activated carbon. The reaction condition is mild and is not sensitive to environmental factors such as water moieties. The reaction is known to proceed at the surface of Pd; therefore, once the stirring is gentle enough and H_2 is sufficient, the reaction could proceed smoothly and completely. However, due to the adsorption of the polymer on Celite, the filtration over Celite to remove Pd/C decreases the yields. It can be seen from the ^{1}H NMR spectrum of PCL-C_6-NH_2 as shown in Figure 2C that the signals at 5.10, 7.36 ppm disappear, while the signals at 3.21 ppm assignable to the methylene groups adjacent to amino groups shift to higher field, indicating complete deprotection. In the ^{1}H NMR spectrum of MPEO-C_2-NH_2 (Figure 3B), the disappearance of the peaks belonging to the protective groups at 5.31, 7.30−7.36 ppm indicates that the benzyloxy carbonyl groups have been removed. At the same time, the signals assignable to -$CH_2\underline{CH_2}$-OOC- at 4.3 ppm remain, and the ratio of this peak to the methyl end group is 2:3, so the ester bond of the main chain does not change during the reaction. The structure of PCL-C_6-NH_2 was also confirmed by the ^{13}C NMR spectrum as shown in Figure 4. The signal at 64.08 ppm is the characteristic peak assignable to the methylene close to the amino group, and the peaks due to (CH_3)$_2\underline{C}$H-O- and -$\underline{C}H_2$-OCO- are overlapped with the signals of $CDCl_3$.

The GPC trace of PCL-C_6-NH_2 displays a single and sharp peak as shown in Figure 2B. Compared with the hydroxyl precursor, no obvious change of average molecular weight and molecular weight distributions is observed. It reveals that PCL was stable under the present conditions and little or no transesterification occurred. By increasing of the reaction time to 4 days, a decrease of molecular weight and an increase of molecular weight distributions were found, which might be caused by hydrolysis and transesterification. This phenomenon was reported by Langer et al. in other similar reactions (*21*),

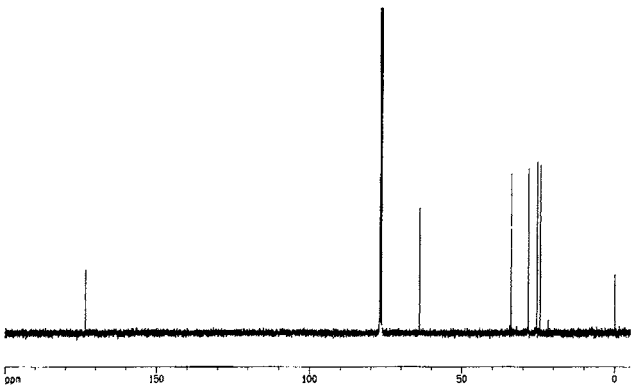


Figure 4. ^{13}C NMR spectrum of PCL-C_6-NH_2.

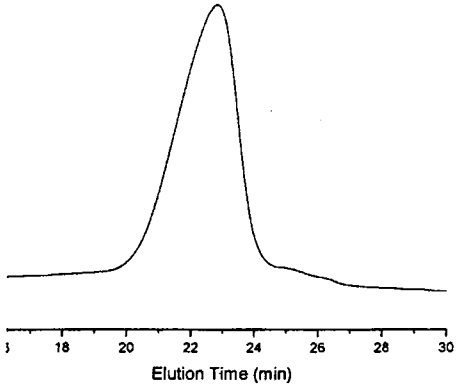


Figure 5. GPC trace of MPEO-β-P[Lys(Z)].

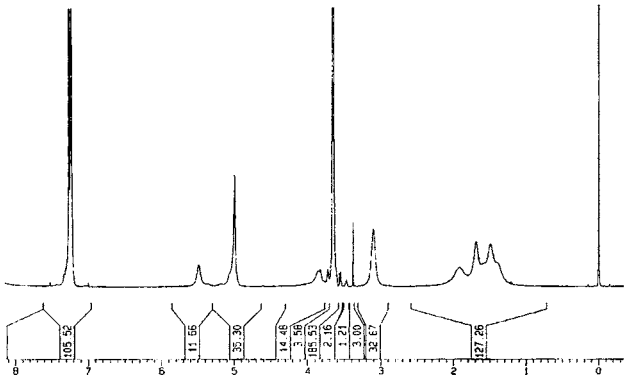
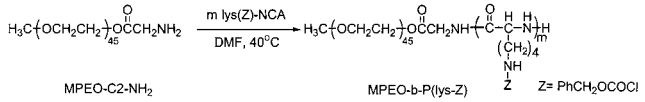


Figure 6. ^1H NMR spectrum of MPEO-β-P[Lys(Z)].

while in the case of MPEO such a side reaction is less possible.

To test the reactivity of the amine-terminated polymers prepared above, MPEO-C_2-NH_2 was used as a macroinitiator to initiate the ring-opening polymerization of a cyclic monomer of lysine, α-(N^ϵ-benzyloxycarbonyl-L-lysine) *N*-carboxy anhydride [lys(Z)-NCA] (Scheme 2). The targeted degree of polymerization of lys(Z)-NCA is designed to be 15. The GPC trace of the resulting copolymer (Figure 5) is a single peak, and the molecular weight distribution of the product is 1.19, showing that the reactivity of MPEO-C_2-NH_2 is high enough and the final product does not contain unreacted MPEO-C_2-NH_2. The ^1H NMR spectrum of MPEO-β-P[lys(Z)] is shown in Figure 6. Besides the signals of the PEO block, new peaks at about 7.26, 1.20−1.90, 5.10, and 5.55 ppm corresponding to the N-protected polypeptide block appeared. From the integral ratio of $\underline{CH_3}$-O- (3.38 ppm) to -$\underline{CH_2}$-NH-Z (3.12 ppm), the average degree of polymerization (DP) of the cyclic monomer is calculated to be 16. Based on the elemental analysis of the final copolymer, the DP is

Scheme 2



15, which confirmed that the initiation reactivity of MPEO-C_2-NH_2 was high.

In conclusion, amine-terminated PCL and MPEO can be prepared conveniently from their hydroxyl-terminated precursors under mild conditions. This method may also be used for the preparation of other kinds of amine-containing polymers from the hydroxyl precursors, and may even be used for α,ω-diamine-terminated polymers.

ACKNOWLEDGMENT

This work was partially supported by the NSFC (Grant 20074002) and the Ministry of Education, China.

LITERATURE CITED

(1) Harris, J. M., Ed. (1992) in *Poly(ethylene oxide) Chemistry, Biotechnical, and Biomedical Applications*, Plenum Press, New York.
(2) Albertsson, A.-C., and Karlson, S., Eds. (1998) in *Degradable Polymers*, Huthig & Wepl Verlag, Heidelberg and Oxford.
(3) Ashton, P. R., Boyd, S. E., Brown, C. I., Nepogodiev, S. A., et al. (1997) *Chem.—Eur. J. 6*, 974.
(4) (a) Hrkach, J. S., Ou, J., Lotan, N., and Langer, R. (1995) *Macromolecules 28*, 4736. (b) Gotsche, M., Keul, H., and Hocker, H. (1995) *Macromol. Chem. Phys. 196*, 3891. (c) Kricheldorf, H. R., and Hauser, K. (2001) *Biomacromolecules 2*, 1110. (d) Degee, Ph., Dubios, R., Jerome, R., and Teyssie, P. (1993) *J. Polym. Sci., Part A: Polym. Chem. 31*, 275. (e) Harada, A., and Kataoka, K. (1995) *Macromolecules 28*, 5294.
(5) Dubois, Ph., Degee, Ph., Jerome, R., and Teyssie, Ph. (1992) *Macromolecules 25*, 2614.
(6) (a) Degee, Ph., Dubios, R., Jerome, R., and Teyssie, Ph. (1992) *Macromolecules 25*, 4242. (b) Tian, D., Dubios, Ph., Jerome, R., and Teyssie, Ph. (1994) *Macromolecules 27*, 4134.
(7) Degee, Ph., Dubios, R., Jerome, R., and Teyssie, Ph. (1994) *J. Polym. Sci., Part A: Polym. Chem. 32*, 2443.
(8) Carter, K. R., Richter, R., Kricheldorf, H. R., and Hedrick, J. L. (1997) *Macromolecules 30*, 6074.
(9) Kricheldorf, H. R., and Hauser, K. (1998) *Macromolecules 31*, 614.
(10) Yuan, M. L., Wang, Y. H., Li, X. H., Xiong, C. D., and Deng, X. M. (2000) *Macromolecules 33*, 1613.
(11) (a) Buckmann, A. F., Morr, M., and Johansson, G. (1981) *Makromol. Chem. 182*, 1379. (b) Johansson, G., Gysoin, R., and Flanagan, S. D. (1981) *J. Biol. Chem. 256*, 9126.
(12) (a) Mutter, M. (1978) *Tetrahedron Lett.*, 2839. (b) Ciuffarin, E., Isola, M., and Leoni, P. (1981) *J. Org. Chem. 46*, 3064.
(13) Harris, J. M., Yalpani, M., Van Alstine, J. M., Struck, E. C., Case, M. G., Parley, M. S., and Brooks, D. E. (1984) *J. Polym. Sci., Polym. Chem. Ed. 22*, 341.
(14) Zalibsky, S., Gilon, C., and Zilkha, A. (1983) *Eur. Polym. J. 19*, 1177.
(15) Mecerreyes, D., Atthoff, B., Boduch, K. A., Trollsas, M., and Hedrick, J. L. (1999) *Macromolecules 32*, 5175.
(16) Van De-Wetering, P., and Van Steenbergen, M. J. (1997) *Macromol. Chem. Phys. 198*, 3893.
(17) Moore, J., and Stupp, S. I. (1990) *Macromolecules 23*, 65.
(18) (a) Duda, Z., Penczek, S., Dubois, P., Mecerreyes, D., and Jerome, R. (1996) *Macromol. Chem. Phys. 197*, 1273. (b) Ropson, N., Dubois, Ph., Jerome, R., and Tessie, Ph. (1995) *Macromolecules 28*, 7589.
(19) Carrot, G., Hilborn, J. G., Trollsas, M., and Hedrick, J. L. (1999) *Macromolecules 32*, 5264.
(20) Schindler, A., Hibionada, Y. M., and Pitt, C. G. (1982) *J. Polym. Sci., Polym. Chem. Ed. 20*, 319.
(21) Barrera, D. A., Zylstra, E., Lansbury, P. T., and Langer, R. (1993) *J. Am. Chem. Soc. 115*, 11010.

BC025531M

A General Strategy for Site-Specific Double Labeling of Globular Proteins for Kinetic FRET Studies

V. Ratner, E. Kahana, M. Eichler, and E. Haas*

Faculty of Life Sciences, Bar-Ilan University, Ramat Gan 52900, Israel. Received April 6, 2002; Revised Manuscript Received June 5, 2002

Site-directed mutagenesis provides a straightforward means of creating specific targets for chemical modifications of proteins. This capability enhanced the applications of spectroscopic methods adapted for addressing specific structural questions such as the characterization of partially folded and transient intermediate structures of globular proteins. Some applications such as the steady state or time-resolved fluorescence resonance energy transfer (FRET) detection of the kinetics of protein folding require relatively large quantities (∼10−100 mg) of site-specific doubly labeled protein samples. Engineered cysteine residues are common targets for labeling of proteins. The challenge here is to develop methods for selective modification of one of two reactive sulfhydryl groups in a protein molecule. A general systematic procedure for selective labeling of each of two cysteine residues in a protein molecule was developed, using *Escherichia coli* adenylate kinase (AKe) as a model protein. Potential sites for insertion of cysteine residues were selected by examination of the crystal structure of the protein. A series of single-cysteine mutants was prepared, and the rates of the reaction of each engineered cysteine residue with a reference reagent [5,5′-dithiobis(2-nitrobenzoic acid) (DTNB)] were determined. Two-cysteine mutants were prepared by selection of pairs of sites for which the ratio of this reaction rate constant was high (>80). The conditions for the selective labeling reaction were optimized. In a first cycle of labeling, the more reactive cysteine residue was labeled with a fluorescent probe (donor). The second probe was attached to the less reactive site under unfolding conditions in the second cycle of labeling. The doubly and singly labeled mutants retained full enzymatic activity and the capacity for a reversible folding−unfolding transition. High yields (70−90%) of the preparation of the pure, site-specific doubly labeled AK mutant were obtained. The procedure described herein is a general outline of procedures, which can meet the double challenge of both site specificity and large-scale preparation of doubly labeled proteins.

INTRODUCTION

The folding transition of many globular proteins involves transient intermediate states (Kuwajima, 1989; Ptitsyn, 1995; Miranker and Dobson, 1996; Fersht, 1997). This finding raises the following two research questions: what are the early intermediate steps of the folding process, and what is the order of the events leading to the final native structure? To directly respond to these questions, we propose to characterize transient intermediate structures during fast refolding transitions. The characterization of these structures presents an intricate experimental challenge, and available knowledge of such structures is limited. The main difficulties in characterizing these structures are due to their very short lifetime and the need for new methods of detection.

The determination of intramolecular distances and rates of the fast changes of such distances by time-resolved fluorescence resonance energy transfer (FRET)[1] measurements is a powerful method for the characterization of the structures of partially folded proteins and their transitions. Steady state fluorescence detection of FRET is also a powerful method for monitoring fast changes of the conformations of proteins even with fairly simple instrumentation (Stryer, 1978; Van Der Meer et al., 1994; Haas, 1997). The application of this method is most effective when the dependence of distances between pairs of sites on changes of global or subdomain conformations is maximal. Such cases rarely occur naturally, and therefore, application of this method depends on the development of biochemical methods for site-specific attachment of fluorescent probes by chemical modification of proteins. The most effective design of FRET applications in the present context is achieved when pairs of fluorescent probes are attached at pairs of sites associated with secondary or tertiary structural elements. A major obstacle that hinders a wide range application of this method is the difficulty of preparing suitable protein samples.

Three labeled protein species should be prepared for each well-controlled, time-resolved FRET experiment. These are two singly labeled mutants (one labeled by the donor and the other labeled by the acceptor) and the doubly labeled (by both the donor and acceptor) sample of the protein. The most general and versatile solution to the problem of site-directed labeling is based on site-directed mutagenesis and insertion of cysteine residues at the target sites (Haran et al., 1992; Pennington, 1994; Sinev et al., 1996, 2000; DeSantis et al., 1998; Navon et al., 2001; Ortiz, 2001). Reagents for selective alkylation

* To whom correspondence should be addressed. E-mail: haas@mail.biu.ac.il.

[1]Abbreviations: Cl-Bi, monochlorobimane; DMSO, dimethyl sulfoxide; DTNB, 5,5′-dithiobis(2-nitrobenzoic acid); DTT, dithiothreitol; EDTA, ethylenediaminetetraacetate; ET, energy transfer; FRET, fluorescence (Förster) resonance energy transfer; I-Py, *N*-(1-pyrenylmethyl)iodoacetamide; TCEP, tris(2-carboxyethyl)phosphine; Tris, tris(hydroxymethyl)aminomethane; wt, wild type.

10.1021/bc025537b CCC: $22.00 © 2002 American Chemical Society
Published on Web 08/20/2002

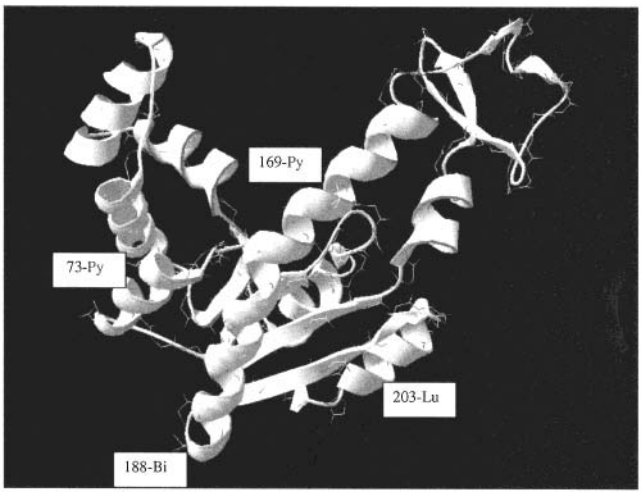


Figure 1. Backbone structure of wt *E. coli* adenylate kinase (AKe) (Schultz et al., 1991). The residues which serve as targets for chemical modifications are marked.

of sulfhydryl residues are available. The challenge here is to develop methods for selective modification of one of the two reactive sulfhydryl groups in the same protein molecule.

Sub-milligram amounts of labeled proteins can suffice for a full set of FRET experiments under equilibrium conditions. Such minute amounts of site-specific doubly labeled protein samples can be prepared, based on high-resolution chromatographic separations. Hundred-fold larger preparations of labeled proteins are needed for flow experiments. In this case, it is desirable to develop methods in which the selectivity is achieved by differential reactivity of selected sites on the protein molecule. The development of a new general systematic procedure for selective labeling of each one of two cysteine residues in a protein molecule is reported here, using *Escherichia coli* adenylate kinase (AKe) as a model protein.

AKe is a ubiquitous enzyme, which catalyzes the phosphoryl transfer reaction ATP + AMP ↔ 2ADP (Noda, 1973). The *E. coli* AKe molecule (Figure 1) consists of a single chain of 214 residues folded in three domains: the large CORE domain (~154 residues) and two smaller domains (~30 residues each) (Schultz, 1990; Müller and Schultz, 1992; Schultz et al., 1997). Residues 161−188 of AKe form a long stretch of helical structure.

Ratner et al. (2000) studied the refolding of fluorescently labeled mutants of AKe by means of fast mixing and time-resolved FRET detection. The starting mutant of AKe used by Ratner et al. (2000) (AK) contained the C77S mutation. The protein was labeled at residue 73 with *N*-(1-pyrenylmethyl)iodoacetamide (I-Py) and residue 203 with lucifer yellow, with a yield of 80%. This experiment showed at least two steps in the refolding kinetics of AK (Ratner et al., 2000). A transient intermediate, formed within 2 ms from the initiation of refolding, was found. The characterization of this intermediate, and the search for possible additional transient intermediate states of the refolding of this protein using FRET detection, requires labeling of additional pairs of sites in 50−100 mg quantities. Residues 169 and 188 were labeled with a donor and an acceptor of excitation energy, respectively. Tens of milligrams of each specifically labeled (>95%) mutant were prepared and characterized.

THEORETICAL BACKGROUND

Calculation of the Maximal Yield of Site-Specific Labeling of Two-Cysteine Mutants. Let [X] be the concentration of the SH groups at the first site, [Y] the concentration of SH groups at the second site, and [D] the concentration of the modifying reagent. All three concentrations decrease during a reaction that modifies cysteine residues in accordance with eqs 1a−c.

$$d[X]/dt = -k_x[X][D] - \sum k_{ix}[A_i][X] \quad (1a)$$

$$d[Y]/dt = -k_y[Y][D] - \sum k_{iy}[A_i][Y] \quad (1b)$$

$$d[D]/dt = -k_x[X][D] - k_y[Y][D] - k_{iD}[D] \quad (1c)$$

where k_{iX} and k_{iY} are the miscellaneous reaction rate constants for various competing reactions of the SH groups, which make the SH groups nonreactive with the modifying reagent. A_i terms represent various solvent additives that can be involved in such reactions. These reactions can be eliminated by the addition of the reducing agent such as tris(2-carboxyethyl)phosphine (TCEP) to the reaction mixture. This reagent maintains the reduced state of the cysteine side chains, and it does not react with alkylating reagents. Thus, the last term in eqs 1a and 1b can be neglected. k_{iD} is the rate constant for reaction of D with solvent components resulting in the deactivation of the reagent.

The division of eq 1a by eq 1b (the last terms are ignored) yields

$$d[X]/d[Y] = (1/R)([X]/[Y]) \quad (2)$$

where $R = k_y/k_x$.

The division of [X] and [Y] by [P], the protein concentration, gives the corresponding fractions of the reactive SH groups, at sites 1 and 2, respectively; $x = [X]/[P]$, and $y = [X]/[P]$. Integration of eq 2 then yields $x = y^R$. The following four species are found in a reaction mixture of any modifying reagent with a protein that carries two reactive cysteine groups at sites 1 and 2: C_1-C_2, D_1-C_2, C_1-D_2, and D_1-D_2 (where C_i and D_i represent the unmodified and modified sites, respectively, in each species). The corresponding fractions are xy, $(1 - x)y$, $x(1 - y)$, and $(1 - x)(1 - y)$. In a case where k_y, the rate constant for the reaction of the sulfhydryl group at site 2, is greater than the rate of reaction of the first site, k_x, i.e., $R > 1$, the goal is to maximize the fraction of the species (C_1-D_2) in the product mixture.

Combining the expressions $x = y^R$ and the fraction of that species, $x(1 - y)$, one obtains

$$[C_1,D_2] = y^R(1-y) \quad (3)$$

This goal can be achieved when y corresponds to the condition $d[C_1-D_2]/dy = 0$. The solution yields

$$y_{opt} = R/(1 + R) \quad (4)$$

At this magnitude of y, the concentration of the desired product is maximal and is provided by eq 5.

$$[C_1-D_2]_{max} = R^R/[(1 + R)^{R+1}] \quad (5)$$

For a given value of R, the control of the yield of the desired product depends on the initial concentrations of the mutant protein ([P]) and the reagent ($[D_o]$) and the ratio k_y/k_{iD}. Practically, two modes of control of the extent

of the reaction are available: either the limitation of the initial concentration of the modifying reagent, $[D_o]$, or the limitation of the time course of the reaction.

In a case where $k_{iD} \ll k_y$, the composition of the product mixture can be controlled by the duration of the reaction. In this case, the link between $[D_o]$ and y is as expected when the calculated extent of labeling of site 2, $(1 - y)$, reaches the optimal value (eq 5). The expected optimal duration of the modification reaction can be determined using the standard kinetics rate law for bimolecular reactions and the rate constants for the reactions of the pairs of single-cysteine mutants and their ratios (R). It was found that for the reaction of iodoacetamidofluorescein, monochlorobimane (Cl-Bi), I-Py, and 4-iodoacetamidosalicylic acid with AK mutants, the competing deactivation reactions can be ignored; i.e., $k_{iD} \ll k_y$.

In the case where $k_{iD} \geq k_y$, i.e., the rate of deactivation of the modifying reagent is greater than the rate of the modification reaction, both modes of control can be used. When the extent of the reaction is controlled by the initial concentration of D ($[D_o]$), the reaction is allowed to proceed to completion, without any time limitation. Under these conditions, the link between $[D_o]$ and y is given by

$$[D_o] = [P](y + y^{1/R}) - (k_{iD}/k_y) \ln(1 - y) \qquad (6)$$

The rate constants (k_x, k_y, and k_{iD}) can be determined for each modification reagent in preliminary experiments using minute amounts of the single-cysteine mutants. Given these rate constants, eq 6 can be applied to calculate the optimal $[D_o]$, which corresponds to the optimal final concentration of the product (C_1−D_2). The commonly used ratio $[D_o]/[P]$ is not valid in this case. A typical example of the fluorescent reagent for which $k_{iD} \gg k_y$ dye is the iodoacetamido derivative of lucifer yellow (Molecular Probes). In an aqueous solution at pH 7.2 and room temperature, this reagent is hydrolyzed in the dark within 15 min.

EXPERIMENTAL PROCEDURES

Procedure for the Systematic Search for Potential Sites for Mutagenesis and Labeling. The task is to prepare a mutant protein with two different organic groups attached to two different sites. These sites were selected according to the needs of a biophysical experiment with minimal perturbation of the native structure and function of the protein. A general procedure for the selection of suitable pairs of sites includes several steps in which the set of residues considered for chemical modification is reduced. (1) Screening for all the residues that could be labeled. The available three-dimensional native structure of the target protein is screened in-search for all the solvent-exposed residues, i.e., those with ≥30% solvent accessibility (algorithms such as the Swiss PDB viewer can be used). The product of this search is a set of residues expected to be accessible to soluble reagents in solution and whose chemical modification is expected to cause minimal perturbation of the global and local structure of the protein. Exposed charged residues are not considered for modification and are eliminated from this set. (2) Producing single-cysteine mutants. Residues included in the reduced set are mutated, one at a time, and single-cysteine mutants are produced and purified. (3) Determining the rate constants for the reaction of the single-cysteine mutants with a reference reagent. A systematic search will be conducted for reaction conditions. These conditions should enhance differences in the reactivity of the selected and purified cysteine mutants with sulfhydryl modification reagents. (4) On the basis of the results of this search, it is possible to select pairs of sites, which show large differences in the reaction rates with the reference reagent, reducing the set by the selection of pairs whose modification is of interest for specific biophysical experiments. These can be pairs of sites where probes can detect changes of conformation according to the goals of the experiment, e.g., secondary or tertiary structural elements, loops, etc. (5) Measurement of the spectroscopic properties (fluorescence lifetimes, spectral shifts, and parameters affecting the Förster critical distance R_o) of the potential probes in situ (at the selected sites) is performed to select the most appropriate probes for each experiment. (6) Optimizing the methods for separation of the protein mutants labeled by a single probe at different sites. (7) Measuring of the kinetics of the reaction of the two single-cysteine mutants with the modification reagents under the optimized conditions. (8) Preparing two-cysteine mutants (cysteine residues inserted at the two sites selected in step 5). (9) Carrying out the reaction of the two-cysteine protein with a chemical modification reagent under the optimized conditions. This reaction produces a mixture of the unlabeled protein and three products: two singly labeled species and the doubly labeled species. Enrichment of the fraction of a selected singly labeled species in the reaction mixture is possible on the basis of knowledge of the ratio of the reaction rate constants of these sites with a modifying reagent.

Expression and Purification of AKe. The expression of cysteine-mutated *E. coli* adenylate kinase and protein purification were performed as described previously (Sinev et al., 1996). The protein was stored in 50% glycerol in 40 mM sodium phosphate buffer (pH 6.5) containing 0.1 M NaCl, 2 mM EDTA, and 2 mM DTT at −18 °C. The starting mutant of *E. coli* adenylate kinase used in this study (AK) contained the C77S mutation.

Small-Scale Labeling of AK Mutants. *Reactivation of Stored Protein Samples.* Samples of the stored protein (3 mg in 0.2 mL) were diluted 5-fold with 100 mM Tris-HCl buffer (pH 8.0) containing 10 mM DTT and 2 mM EDTA (the reactivation buffer). After 30 min, the protein solution was applied to a Sephadex G15 column (1.5 cm × 5 cm for 1 mL protein samples) equilibrated and eluted with 20 mM HEPES buffer (pH 7.2) containing 2 mM EDTA.

Labeling of Single-Cysteine Mutants. The single-cysteine mutants, AK(V169C) and AK(A188C), were labeled with the fluorescent reagent *N*-(1-pyrenylmethyl)iodoacetamide (I-Py) (Molecular Probes). The labeling was performed in 20 mM HEPES (pH 7.2) which contained 2 mM EDTA and 30 μM reducing agent tris(2-carboxyethyl)phosphine (TCEP) (Molecular Probes) (folding buffer). The reaction mixture contained 20 μM protein in this buffer and 75 μM I-Py, which was added in DMSO [the final concentration of DMSO was 10% (v/v)]. The reaction was allowed to proceed at room temperature. Aliquots of the reaction mixture were taken at several time points between 4 and 24 h and analyzed. Excess insoluble pyrene was filtered using a 0.2 μm sterile filter, and the soluble excess of the reagent was removed by gel filtration on a Sephadex G15 column equilibrated with 20 mM Tris-HCl (pH 8). The separation of the labeled protein was performed by anion exchange chromatography. Samples of ∼0.5 mg were applied to a MonoQ column (0.5 cm × 5 cm) (Pharmacia) equilibrated with 20 mM Tris-HCl (pH 8). Proteins were eluted with a linear gradient of NaCl (from 0 to 0.5 M) for 120 min at a flow

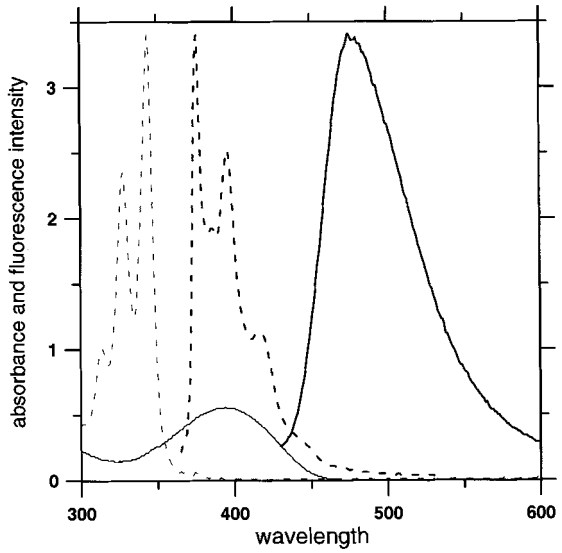


Figure 2. Absorbance and fluorescence spectra of AK(V189C-Py) (donor) (- - -) and AK(A188C-Bi) (acceptor) (—). Emission spectra were recorded by excitation at 345 and 390 nm for Py and Bi, respectively (bandwidth of 3 nm).

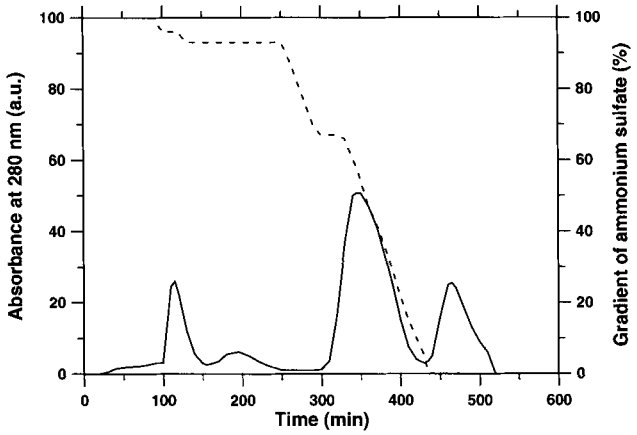


Figure 3. Elution profile (—) of the preparative reaction mixture applied to a Phenyl Sepharose 6 Fast Flow column. Four peaks were resolved. The fractions were as follows: I, unlabeled AK; II, AK(V169C/A188C-Py); III, AK(V169C-Py/A188C); and IV, AK(V169C-Py/A188C-Py) The salt gradient is shown (- - -). The reference preparations for identification of these fractions were the base mutant, AK(V169C-Py), AK-(A188C-Py), and AK(V169C-Py/A188C-Py) labeled in unfolding buffer with excess I-Py.

rate of 0.5 mL/min. The free protein eluted first, at 100−111 mM NaCl; AK(V169C-Py) eluted at 112−119 mM NaCl, and AK(A188C-Py) eluted at 180−190 mM NaCl. The extent of protein labeling was evaluated by determining the area under the peaks, divided by molar extinction coefficients of the unlabeled protein at 280 nm (11 800 M^{-1} cm^{-1}) or the labeled protein at 280 nm (49 200 M^{-1} cm^{-1}).

AK(A188C) (14 μM) was also labeled with monochlorobimane (Molecular Probes) (final concentration of 530 μM), 20 mM HEPES (pH 7.8), 1.8 M GuHCl, 30 μM TCEP, and 2 mM EDTA (unfolding buffer). The concentration of the soluble reagent in the reaction was determined by the absorbance at 390 nm, using a molar extinction coefficients of bimane of 5560 M^{-1} cm^{-1} in HEPES buffer (pH 7.2).

Large-Scale Double Labeling. A quantity of 65 mg of reactivated AK(V169C/A188C) was dialyzed in 20 mM HEPES (pH 7.2) and 2 mM EDTA. Both TCEP (from a 10 mM stock solution in water) and NaCl (from a 4 M stock solution in water) were added to final concentrations of 30 μM and 100 mM, respectively. A solution of 4.6 mg of I-Py in 3.85 mL of DMSO was added in two portions (2.2 and 1.65 mL) at the initiation of the reaction and after 8 h, respectively. The reaction was allowed to proceed for 24 h under slow stirring at room temperature (24 °C) protected from light. The reaction was stopped by the addition of DTT to a final concentration of 50 mM. The excess Py derivatives were removed by filtration through a 0.2 mm filter (acrodisc 32, Gelman Science, Ann Arbor, MI) and by gel filtration on a G15 Sephadex column in Tris buffer (pH 8.0).

The product mixture was resolved by hydrophobic interaction chromatography. NH_4SO_4 was added to a final concentration of 0.8 M, and after 10 min, the solution was applied to a Phenyl Sepharose 6 Fast Flow (low sub) (Pharmacia Biotech) column (2.5 cm × 16 cm), pre-equilibrated with 0.6 M NH_4SO_4 in 20 mM HEPES (pH 7.2). The labeled species were eluted in a linear gradient from 0.6 to 0 NH_4SO_4 in 350 mL at a flow rate of 3 mL/min (Figure 3). The third eluted peak (0.0 M NH_4SO_4, ∼100 mL) was concentrated to ∼10 mL in an ultrafiltration cell with a YM membrane with a 10K cutoff (Amicon) and dialyzed in 20 mM HEPES (pH 7.2) and 2 mM EDTA.

Acceptor Labeling. AK(V169C-Py/A188C) was reactivated and dialyzed against 20 mM HEPES and 2 mM EDTA. GuHCl (8.2 M stock solution in water) and TCEP were added to final concentrations of 1.8 M and 30 μM, respectively. The addition of GuHCl shifted the pH to 7.8. Solid Cl-Bi (Molecular Probes) was added to a final concentration of 500 μM in excess of the protein concentration. The reaction was allowed to proceed for 24 h at room temperature (gently stirring, protected from light) and then terminated by the addition of DTT to a final concentration of 20 mM. The unbound reagent was removed by gel filtration on a Sephadex G15 column (2.5 cm × 24 cm) equilibrated with 1.8 M GndHCl in 20 mM Tris (pH 8.0). Refolding was performed by dialysis in 20 mM Tris-HCl (pH 8). After concentration in a Centriprep-10 ultrafiltration concentrator (Amicon) and being dialyzed in 50 mM imidazole buffer (pH 7.2), all the labeled protein samples were stored in 50 mM imidazole buffer (pH 7.2) containing 50% glycerol at −18 °C.

Large-Scale Preparation of Singly Labeled Mutants. Singly labeled AK(V169C-Py) and AK(A188C-Bi) were prepared from the respective single-cysteine AK mutants. Reactivated AK(V169C) was dialyzed in 20 mM HEPES (pH 7.2) and 2 mM EDTA and labeled in unfolding buffer. The final reaction mixture contained equivalent amounts of protein and dye with an additional portion of 50 μM I-Py in excess of the protein concentration. The total amount of the reagent dissolved in DMSO was added in two equal portions (at the initiation of the reaction and 4 h later). The final DMSO concentration was 15% (v/v), and the reaction was allowed to proceed for 24 h under slow stirring at room temperature (24 °C) protected from light. The reaction was terminated by the addition of DTT to a final concentration of 20 mM. The excess Py derivatives were removed by filtration (0.2 μm) followed by gel filtration on a Sephadex G15 column in 50 mM Tris-HCl (pH 8) containing 1.8 M GuHCl. The unfolded protein was refolded by dialysis in 50 mM Tris-HCl (pH 8.0). The protein was then concentrated and stored in 50 mM imidazole buffer (pH 7.2) containing 50% glycerol at −18 °C.

Table 1. Rate Constants for the Reaction of SH Groups in a Series of AK Mutants with DTNB at pH 7.2 in 20 mM HEPES at Two Temperatures, with and without Salt

	k (mM^{-1} s^{-1})			
	without salt		with 100 mM NaCl	
mutant[a]	22.5 °C	40 °C	22.5 °C	40 °C
AK(V203C)	5.3 ± 0.2	0.84 ± 0.04	10.9 ± 0.3	1.78 ± 0.05
AK(V169C)	1.81 ± 0.09	0.48 ± 0.02	3.58 ± 0.04	0.89 ± 0.05
AK(A55C)	1.13 ± 0.08	0.154 ± 0.013	1.11 ± 0.02	0.16 ± 0.01
AK(V142C)	0.186 ± 0.009	0.059 ± 0.004	0.383 ± 0.008	0.133 ± 0.005
AK(A73C)	0.027 ± 0.002	ND	0.115 ± 0.005	0.050 ± 0.003
AK(A188C)	0.017 ± 0.001	ND	0.077 ± 0.004	0.039 ± 0.004

[a] *E. coli* adenylate kinase in which cysteine 77 was replaced with serine and one surface-exposed residue was replaced with cysteine.

Reactivated, dialyzed AK(A188C) was labeled with Cl-Bi using the same procedure described for AK(V169C-Py/A188C); it was then concentrated and stored in 50 mM imidazole buffer (pH 7.2) containing 50% glycerol at −18 °C.

The degree of homogeneity of the products AK(V169C-Py/A188C-Bi) and AK(V169C-Py) was analyzed using analytical FPLC ion exchange chromatography.

Spectroscopic Instrumentation. Rate constants for the reaction of AK mutants with DTNB were determined using a homemade stopped-flow device based on a DX17MV mixing unit (Applied Photophysics, Leatherhead, U.K.) (Ratner and Haas, 1998). Reactions were initiated by mixing equal volumes of 12 μM protein and of 0.5−2.0 mM DTNB in 20 mM HEPES and 5 mM EDTA (pH 7.2). The kinetics of the reactions were monitored by recording the absorbance at 440 nm (selected by an interference filter). Rate constants were extracted by curve fitting of the kinetics data using a fitting module prepared by A. Goldin and implemented in MatLab (Ratner and Haas, 1998).

Fluorescence spectra were recorded using an Aviv F105 spectrofluorimeter. Absorbance spectra were recorded using an Aviv 17DS spectrophotometer.

RESULTS

Preparation of Cysteine Mutants of AKe. The single native cysteine residue of Ake(Cys77) was replaced with a serine residue without any perturbation of the folding and activity of the enzyme (Sinev et al., 1996). Ake(C77S) (AK) was the base mutant for all further modifications in this project. Single-cysteine mutants, prepared by the replacement of residues 55, 73, 142, 169, 188, and 203, were produced, expressed, and purified in ∼200 mg quantities (Sinev et al., 1996).

Determination of Reaction Rate Constants with a Reference Reagent. Elman reagent [5,5′-dithiobis-(2-nitrobenzoic acid) (DTNB)] was used as the reference reagent. The rate constants for the reaction of DTNB and each of the single-cysteine mutants were determined in 20 mM HEPES (pH 7.2) and in the same buffer with the addition of 100 mM NaCl at two temperatures. The rate of light absorption change at 440 nm was measured in a stopped-flow device. Table 1 shows that the rate constants for the DTNB−AK reaction varied over a wide range. Pairs of sites for which the ratio of rate constants was nearly 100 were selected for labeling. The first example was the pair AK(V203C) and AK(A73C), which were labeled with lucifer yellow and I-Py, respectively (Ratner et al., 2000). The pair AK(A169C) and AK-(A188C), which had a ratio of rate constants as high as 106, was used in the experiment presented here.

Fluorescent Probes for Labeling Cysteine 169 and 188. The two fluorescent alkylating reagents used in this study were the donor I-Py and Cl-Bi, the acceptor of excitation energy. The alkylation with the pyrene reagent creates a very hydrophobic product, which is a possible source of perturbation of the protein structure or folding. Yet this reagent was used for its favorable spectroscopic properties (very long fluorescence lifetime and high extinction coefficient). The bimane reagent is a comparatively small, uncharged probe.

Preparation of Singly Labeled Mutants. The two single-cysteine mutants, AK(V169C) and AK(A188C) (∼40 μM), were labeled with I-Py (∼100 μM) under reducing−unfolding conditions where every protein sulfhydryl group was accessible to the dye. The solubility of I-Py in folding buffer did not exceed ∼10 μM at 10% DMSO. Therefore, a heterogenic (pseudo-first-order) reaction was used. The insoluble excess of the reagent formed microaggregates, which served as a stock. This stock provided a saturated concentration of the reagent, and was gradually depleted during the reaction.

The reaction was complete (100% labeling) within 4 h at room temperature. The quantum yields of pyrene fluorescence were 0.33 and 0.06 for AK(V169C-Py) and AK(A188C-Py), respectively. Cysteine 169 was chosen as the target for Py conjugation for the planned FRET experiments since it was difficult to find an acceptor probe that has a suitable R_o value when paired with the low-quantum yield pyrene attached to residue 188. Singly labeled AK(A188C-Bi) was obtained by the reaction of 40 μM protein in the unfolding buffer with 550 μM Cl-Bi for 24 h at room temperature. Figure 2 presents the fluorescence spectrum of AK(V169C-Py) and the absorbance spectrum of AK(A188C-Bi). The Förster critical distance, R_o, of the pair *N*-(1-pyrenylmethyl)acetamide (Py) and bimane (Bi) attached to residues 169 and 188, respectively (calculated assuming an orientation factor κ^2 of $^2/_3$), is 26 Å. This length is close to the separation of these two residues in the crystal structure (28.9 Å). The wild-type level of specific enzymatic activity was measured for both singly labeled mutants. This activity is an indication that the above-referenced genetic and chemical modifications did not significantly perturb the native conformation of the protein.

Chromatographic Purification. The search for a method of separating the reaction products was conducted using the singly labeled mutants. Nonlabeled protein and the two singly Py-labeled mutants (at residues 169 and 188) were separated on an analytical MonoQ ion exchange column. Larger-scale preparative separations were performed by hydrophobic chromatography using a Phenyl Sepharose 6 Fast Flow column. The two species of singly Py-labeled AK [AK(V169C-Py) and AK(A188C-Py)], which differed only in the attachment sites of the probe, were resolved with this column. Figure 3 presents the results of the separation of the alkylation reaction products.

Preparation of the Doubly Labeled Mutant. The rate constants for the reaction of the two single-cysteine mutants with I-Py were measured under reducing−folding conditions at room temperature. The following values were obtained: 0.002 and 0.08 h^{-1} for I-Py and cysteine 188 and 169, respectively. These rate constants were used for optimization of the site-directed labeling of the two cysteine residues in AK(V169C/A188C) as outlined above. An ∼40 μM solution of AK(V169C/A188C) was first reacted with I-Py (∼100 μM) in folding buffer at room temperature. Under these conditions, the rate constants obtained for AK(V169C/A188C) matched the rates obtained for single-cysteine mutants AK(V169C) and AK(A188C). The reaction mixture was resolved by ion exchange chromatography on a Mono-Q column.

Large-Scale (∼100 mg) Production of the Doubly Labeled Mutant. With a 10-fold increase in the concentration of the protein in the reaction mixture, the amount of I-Py in this mixture was increased accordingly. Under these conditions, the insoluble excess of I-Py formed large flakes. In addition, the ratio of the reaction rates was reduced due to a cooperative effect, which increased the fraction of AK(V169C-Py/A188C-Py) and reduced the yield of the desired product. Adsorption of protein molecules on the surface of the reagent flakes possibly enhanced the reactivity of the slow-reacting side chain and caused the cooperativity. This undesired cooperative effect was reduced to some extent by the stepwise addition of the reagent (two steps).

The reaction proceeded for 24 h and was terminated by the addition of excess DTT. The resulting product mixture contained ∼70% AK(V169C-Py/A188C) along with smaller fractions of AK(V169C/A188C), AK(V169C/A188C-Py), and AK(V169C-Py/A188C-Py). This mixture was separated by hydrophobic interaction chromatography on a Phenyl Sepharose 6 Fast Flow column (Figure 3).

Second-Site Labeling. The pure AK(V169C-Py/A188C) was reacted with excess Cl-Bi in unfolding buffer. Here, the low reactivity of the side chain of Cys188 was enhanced. After 24 h, the reaction was terminated by the addition of DTT (final concentration of 20 mM). The excess reagent and its products were removed by gel filtration [Sephadex G15 column in 50 mM Tris buffer (pH 8.0) and 1.8 M GndHCl], followed by dialysis against 50 mM Tris buffer. The homogeneity of the final doubly labeled product, AK(V169C-Ph/A188C-Bi), was analyzed by analytical chromatography on a Mono-Q FPLC column. In a control experiment, the base mutant AK (which contains the C77S mutation) was subjected to the same labeling procedure. No trace of fluorescence was detected in the final protein fraction. This finding indicates that only the specific covalent attachment of the probes to the cysteine residues was involved. The chromatography and dialysis steps efficiently removed nonspecifically adsorbed reagents.

Observation of FRET. The bimane fluorescence that was directly excited in AK(A188C-Bi) in the native state was very close to the value obtained for that probe in AK(V169C-Py/A188C-Bi) under those conditions. Under denaturing conditions (in 1.8 M GuHCl), the fluorescence of bimane decreased by ∼10 and ∼70% for AK(A188C-Bi) and AK(V169C-Py/A188C-Bi), respectively, relative to the corresponding values obtained in the native state. The decrease in the fluorescence of bimane in the doubly labeled mutant occurred at the same concentration of GuHCl as the change of the pyrene fluorescence. Figure 4 shows the denaturant concentration dependence of the fluorescence emission intensities of the Py probe in the singly and doubly labeled mutants AK(V169C-Py) and AK(V169C-Py/A188C-Bi). A sharp drop in the emission intensity at ∼0.7−0.8 M GuHCl appears for both mutants. The drop in Py fluorescence intensity in the singly labeled mutant reflects the change in the local environment of the probe. This change affects the Förster critical distance, R_o, which is recalculated for each state of the protein (Table 1). The relative amplitude of the decrease of the donor emission intensity observed for the doubly labeled mutant is greater than that of the singly labeled mutant, due to the enhanced efficiency of the FRET effect upon denaturation. The ratio of the emission intensity of the donor in the doubly and singly labeled mutants (absence and presence of FRET) is used as a measure of the extent of FRET efficiency. The increased ratio found at high GuHCl concentrations indicates enhanced transfer efficiency. Upon unfolding, the extended α-helical conformation (residues 161−188) (Schultz et al., 1991) collapsed to an apparent unordered state, where the apparent mean inter-residue distance between residues 169 and 188 was considerably shorter than in the native state.

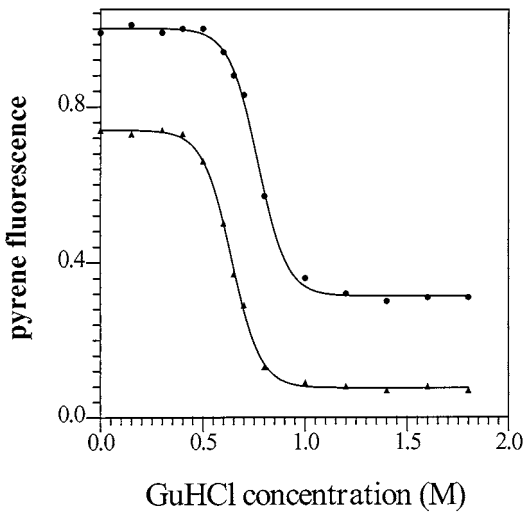


Figure 4. Dependence of pyrene fluorescence in singly (asterisks) and doubly (triangles) labeled AK on GuHCl concentration. The lines show the fits to a two-state model with an m of 8.5 kcal/M and midtransitions at 0.77 and 0.64 M for the singly and doubly labeled mutants, respectively. The FRET parameters for the attached Py-Bi pair were as follows: $R_o = 22$ Å and R_{mean} (apparent mean distance) = 20 Å for the unfolded state and R_o = 25.5 Å and R_{mean} = 32 Å for the folded state of the protein.

The mean FRET efficiencies were calculated for the two equilibrium states (native and denatured). An apparent mean distance between the two probes was calculated for each state. This distance is a rough approximation, because it is obtained by ignoring the effect of the width of the intramolecular distance distributions and the possible contributions to the FRET efficiencies by the fast segmental fluctuations. The distances were calculated under the assumption that distributions of distances were narrow. This is a reasonable approximation for the native state. However, for the denatured states, this approximation is probably somewhat biased toward lower values. Thus, the apparent change in the mean distance from the denatured to the native states may indeed be partially due to a reduction of the distributions.

DISCUSSION

Site-directed mutagenesis provides a straightforward means of creating specific targets for chemical modifica-

tions of proteins. This capability enhanced the applications of spectroscopic methods adapted for addressing specific structural questions. The procedure described herein is a general outline of procedures, which can meet the double challenge of both site specificity and large-scale preparation of doubly labeled proteins.

The selectivity of the labeling reaction can be further enhanced by a local increase or reduction in the reactivity of selected side chains by means of conformational effects. Solvent composition (organic solvents, salt components, and pH) and temperature are the most common variables that can differentially affect the reaction rate constants of selected side chains. Drastic effects can be obtained by ligand binding (substrates, inhibitors, and protein−protein interactions). In this work, the ratio of the reaction rate constants was examined only under a range of temperatures and salt concentrations which yielded satisfactory results for two pairs of sites (residues 73 and 203 and residues 169 and 188).

The level of homogeneity required for spectroscopic measurements makes the chromatographic separation steps indispensable. Separation of the reaction products can be enhanced when one of the reagents is either charged or very hydrophobic. Yet either hydrophobicity or extra electrostatic charges can affect the folding pathway of proteins and can be a disadvantage when the modifications are made for structural studies. Affinity chromatography was also used to separate multiply labeled protein derivatives (Amir et al., 1986; Amir and Haas, 1987). It is also possible to use a mixed disulfide resin for separation of fractions with free cysteine residues in the process of labeling two-cysteine mutants. The excellent separation that was achieved between unlabeled AK and AK labeled with I-Py at either residue 169 or 188 was based on the hydrophobicity of the pyrene moiety.

The procedure described here is based on the preparation of three mutants: two single-cysteine mutants and one two-cysteine mutant. In principle, it is possible to accomplish the FRET experiments without the preparation of the two single-cysteine mutants. The need to prepare two single-cysteine mutants depends on the required quantities of labeled proteins and the availability of analytical procedures for the identification of the labeling sites.

Large-scale preparations can be done either by increasing the volume of the reaction mixture (thus maintaining low protein concentrations) or by increasing the protein concentration. The second procedure was applied in the study presented here since it has two practical advantages: (1) reduction of the waste of precious fluorescent reagents and (2) the prevention of the losses of the labeled protein in the extra concentration step required after a reaction in a large volume. The precipitation of the hydrophobic fluorescent reagent, the ensuing changes of the reaction conditions, and the reduced maximal yield of the labeled protein are the disadvantages of this approach. The optimization of the reaction volume and of the reagent's concentrations in a large-scale labeling reaction depends on the solubility of the protein and the reagents.

FRET Measurements. The reduced quantum yield of the pyrene florescence in the denatured state of the singly labeled mutant AK(V169C-Py) was not due to solvent quenching by the denaturant. This conclusion is evident from the observation that the same probe attached to cysteine 73 exhibited only a minimal reduction of the fluorescence quantum yield under the same conditions (Ratner et al., 2000). A possible source for a specific quenching of pyrene fluorescence in AK(V169C-Py) might be the side chain of one of the neighboring residues. Collision quenching by an adjacent neighbor side chain was restricted by its orientation in the native state helical structure. When this well-defined structure was collapsed by denaturation, the stereochemical restriction was relaxed and collision quenching was made more efficient. Charged side chains, either positive or negative, are possible quenchers found in the vicinity of both residue 73 and residue 169. The phenol side chain of tyrosine is found only near residue 169. Therefore, it is reasonable to speculate that the likely near-neighbor quencher side chain is Tyr171. Incidentally, the donor's specific non-FRET quenching helped to improve the resolution of the distance determination in the experiment described here, since it caused a decrease in the Förster critical distance, R_o, from 26 Å (in the native state) to 21.8 Å. This R_o value is closer to the apparent mean distance between the two residues in the denatured state (Table 2). The mean length of the 20-residue labeled helical segment in the native state (31.7 Å) is close to the theoretically expected value (Cα−Cα separation of 29.3 Å) and the Cγ−Cβ separation in the crystal structure (30.5 Å).

CONCLUSIONS

The preparation of large-scale amounts of site-specific, doubly chemically modified mutant proteins for spectroscopic studies of protein folding and dynamics can be improved. Such improvement can be achieved by following a systematic procedure, which is based on structural and chemical kinetics data. The native three-dimensional structure should be used for the preliminary selection of a set of residues, which can be mutated with minimal structural perturbation, and with a large variation of reactivity of inserted cysteine residues. The determination of individual reaction rate constants of the engineered SH groups and the optimization of reaction conditions allowed high yields (70−90%) of the preparation of the pure, site-specific doubly labeled AK mutant. These high yields make some otherwise difficult experiments, such as the double kinetics time-resolved FRET measurements (Ratner and Haas, 1998; Ratner et al., 2000), feasible. Preliminary FRET measurements show the effectiveness of this experimental approach.

ACKNOWLEDGMENT

This work was supported by research and equipment grants from the Israel Science Foundation, by NIH Grant GM39372, and by the Demedian Center for Magnetic Resonance Research at Bar-Ilan University.

LITERATURE CITED

(1) Amir, D., and Haas, E. (1987) Estimation of Intramolecular Distance Distributions in Bovine Pancreatic Trypsin Inhibitor by Site-Specific Labeling and Nonradiative Excitation Energy Transfer Measurements. *Biochemistry 26*, 2162−2175.

(2) Amir, D., Levy, D. P., Levin, J., and Haas, E. (1986) Selective Fluorescent Labeling of Amino Groups of Bovine Pancreatic Trypsin Inhibitor by Reductive Alkylation. *Biopolymers 25*, 1645−1658.

(3) DeSantis, G., Berglund, P., Stabile, M. R., Gold, M., and Jones, J. B. (1998) Site-directed mutagenesis combined with chemical modification as a strategy for altering the specificity of the S1 and S1′ pockets of subtilisin *Bacillus lentus*. *Biochemistry 37* (17), 5968−5973.

(4) Fersht, A. R. (1998) Nucleation mechanisms in protein folding. *Curr. Opin. Struct. Biol. 7* (1), 3−9.

(5) Forster, Th. (1948) Zwischen Molekulare Energie Wanderung und Fluoreszenz. *Ann. Phys. (Berlin) 2*, 55−75.

(6) Foucaud, B., Perret, P., Grutter, T., and Goeldner, M. (2001) Cysteine mutants as chemical sensors for ligand−receptor interactions. *Trends Pharmacol. Sci. 22* (4), 170−173.
(7) Guiso, N., Michelson, S., and Barzu, O. (1984) Inactivation and proteolysis of heat-sensitive adenylate kinase of *Escherichia coli* CR341 T28. *J. Biol. Chem. 259*, 8713−8717.
(8) Haas, E. (1996) The problem of protein folding and dynamics: time-resolved dynamic non-radiative excitation energy transfer measurements. *IEEE-JSTC 2*, 1088.
(9) Haas, E., Katchalski-Katzir, E., and Steinberg, I. Z. (1978) Brownian motion of the ends of oligopeptide chains in solution as estimated by energy transfer between the chain ends. *Biopolymers 17*, 11−31.
(10) Kuwajima, K. (1989) The molten globule state as a clue for understanding the folding and cooperativity of globular-protein structure. *Proteins: Struct., Funct., Genet. 6*, 87−103.
(11) Miranker, A. D., and Dobson, C. M. (1996) Collapse and cooperativity in protein folding. *Curr. Opin. Struct. Biol. 6*, 31−42.
(12) Müller, C. W., and Schulz, G. E. (1992) Structure of the complex between adenylate kinase from *Escherichia coli* and the inhibitor AP_5A refined at 1.9 Å resolution. A model for a catalytic transition state. *J. Mol. Biol. 224*, 159−177.
(13) Navon, A., Ittah, V., Scheraga, H. A., and Haas, E. (2001) Distributions of intramolecular distances in the reduced and denatured states of bovine pancreatic ribonuclease A. Folding initiation structures in the C-terminal portions of the reduced protein. *Biochemistry 40*, 105−118.
(14) Noda, L. (1973) Adenylate kinase. In *The Enzymes* (Boyer, P. D., Ed.) Vol. 8, pp 279−305, Academic Press, New York.
(15) Ortiz, J. O., and Bubis, J. (2001) Effects of differential sulfhydryl group-specific labeling on the rhodopsin and guanine nucleotide binding activities of transducin. *Arch. Biochem. Biophys. 387* (2), 233−234.
(16) Pennington, M. W. (1994) Site-specific chemical modification procedures. *Methods Mol. Biol. 35*, 171−185.
(17) Ptitsyn, O. B. (1995) Molten globule and protein folding. *Adv. Protein Chem. 47*, 83−229.
(18) Ratner, V., and Haas, E. (1998) An instrument for time-resolved monitoring of fast chemical transitions: application to the kinetics of refolding of a globular protein. *Rev. Sci. Instrum. 69*, 2147−2154.
(19) Ratner, V., Sinev, M., and Haas, E. (2000) Determination of intramolecular distance distributions during protein folding on the millisecond time scale. *J. Mol. Biol. 299*, 1363−1371.
(20) Schultz, G. E. (1991) Domain motions in proteins. *Curr. Opin. Struct. Biol. 1*, 883−888.
(21) Schultz, G. E., Muller, C. W., and Diederichs, K. (1990) Induced-fit movements in adenylate kinases. *J. Mol. Biol. 213*, 627−630.
(22) Sinev, M. A., Sineva, E. V., Ittah, V., and Haas, E. (1996) Domain closure in adenylate kinase. *Biochemistry 35*, 6425−6437.
(23) Sinev, M., Landsmann, P., Sineva, E., Ittah, V., and Haas, E. (2000) *Bioconjugate Chem. 11*, 352−362.
(24) Stryer, L. (1978) Fluorescence energy transfer as a spectroscopic ruler. *Annu. Rev. Biochem. 47*, 819−846.
(25) Van der Meer, B. W., Raymer, M. A., Wagoner, S. L., Hackney, R. L., Beechem, J. M., and Gratton, E. (1993) Designing matrix models for fluorescence energy transfer between moving donors and acceptors. *Biophys. J. 64*, 1243−1263.
(26) Van Der Meer, B. W., Coker, G., III, and Chen, S.-Y. (1994) *Resonance energy transfer: Theory and data*, VCH Publishers, New York.

BC025537B

NOVEMBER/DECEMBER 2002
Volume 13, Number 6

© *Copyright 2002 by the American Chemical Society*

Bioconjugate Chemistry

COMMUNICATIONS

A New Class of RNA-Binding Oligomers: Peptoid Amide and Ester Analogues

Venkitasamy Kesavan,† Natarajan Tamilarasu,† Hong Cao, and Tariq M. Rana*

Chemical Biology Program, Department of Biochemistry and Molecular Pharmacology, University of Massachusetts Medical School, 364 Plantation Street, Worcester, Massachusetts 01605-2324. Received June 28, 2002

Replication of human immunodeficiency virus type 1 (HIV-1) requires specific interactions of Tat protein with the *trans*-activation responsive region (TAR) RNA, a 59-base stem-loop structure located at the 5′-end of all HIV mRNAs. Here we report the design, synthesis and in vitro activities of oligopeptoid amide and ester analogues which bind TAR RNA with high affinities. These results show that we have identified a new class of unnatural oligomers for RNA targeting.

RNA−protein interactions are involved in many cellular functions such as transcription, RNA splicing, and translation. Small peptides with unnatural backbones that can bind with high affinity to a specific sequence or structure of nucleic acids and interfere with protein−nucleic acid interactions would provide useful tools in molecular biology and medicine. Successful approaches used thus far include duplex-forming (antisense) (*1*) and triplex-forming (anti-gene) oligonucleotides (*2*−*4*), peptide nucleic acids (PNA) (*5*), and pyrrole-imidazole polyamide oligomers (*6*, *7*). Each class of compounds employs a readout system based on simple rules for recognizing the primary or secondary structure of a linear nucleic acid sequence. Another approach employs carbohydrate-based ligands, calicheamicin oligosaccharides, which interfere with the sequence-specific binding of transcription factors to DNA and inhibit transcription in vivo (*8*, *9*). While antisense oligonucleotides and PNA employ the familiar Watson−Crick base-pairing rules, two others, the triplex-forming oligonucleotides and the pyrrole-imidazole polyamides, take advantage of straightforward rules to read the major and minor grooves, respectively, of the double helix itself.

In addition to its primary structure, RNA has the ability to fold into complex tertiary structures consisting of such local motifs as loops, bulges, pseudoknots, and turns (*10*, *11*). It is not surprising that, when they occur in RNAs that interact with proteins, these local structures are found to play important roles in protein−RNA interactions (*12*). This diversity of local and tertiary structure, however, makes it impossible to design synthetic agents with general, simple-to-use recognition rules analogous to those for the formation of double- and triple-helical nucleic acids. Since RNA−RNA and protein−RNA interactions can be important in viral and microbial disease progression, it would be advantageous to have a general method for rapidly identifying synthetic compounds for targeting specific RNA structures. A particu-

* To whom correspondence should be addressed. Phone: (508) 856-6216. Fax: (508) 856-8015. E-mail: tariq.rana@umassmed.edu.

† These authors contributed equally to this work.

10.1021/bc0255642 CCC: $22.00 © 2002 American Chemical Society
Published on Web 10/31/2002

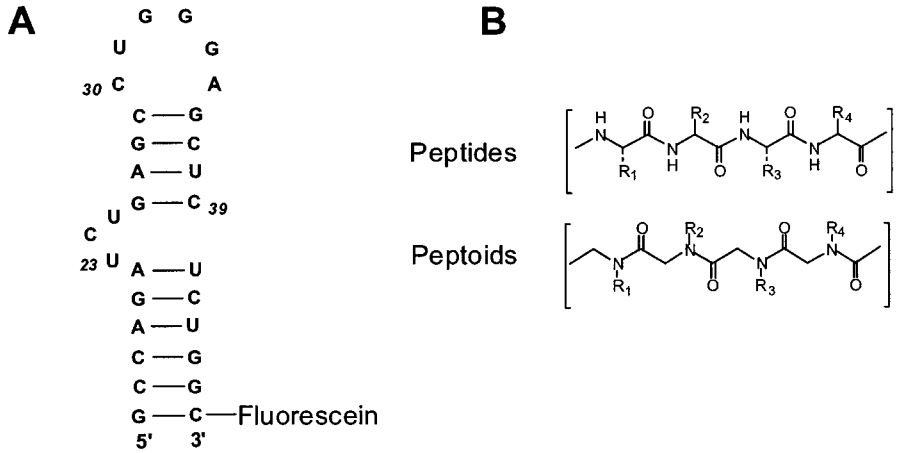


Figure 1. (A) Secondary structure of TAR RNA used in this study. TAR RNA spans the minimal sequences that are required for Tat responsiveness in vivo (*27*) and for in vitro binding of Tat-derived peptides (*28*). Chemical syntheses were performed on ABI synthesizer Model 392 using standard protocols. TAR RNA was chemically synthesized on a fluorescein-containing CPG 500 support. Synthesis of RNA, deprotection, characterization, and purification were performed as described earlier (*20*, *22*). **(B)** Schematic comparison of peptides and peptoids.

lar protein-binding RNA structure can be considered as a molecular receptor not only for the protein with which it interacts but also for synthetic compounds, which may prove to be antagonists of the protein−RNA interaction.

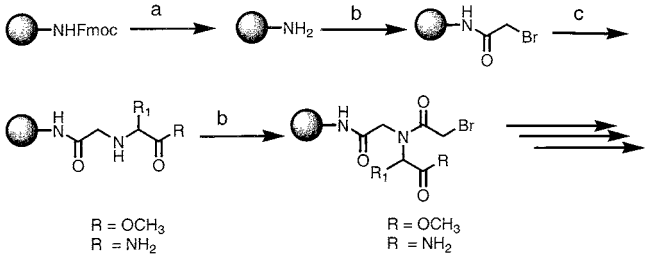
The mechanism of transactivation of human immunodeficiency virus type 1 (HIV-1) gene expression requires the interaction of Tat protein with the transactivation responsive region (TAR) RNA, a 59-base stem-loop structure located at the 5′-end of all nascent HIV-1 transcripts (*13*). Inhibition of Tat-TAR interactions is a potential approach for anti-HIV therapeutics. Here we report that two oligopeptoids bind TAR RNA with high affinities in vitro.

We have recently begun to examine TAR RNA recognition by unnatural biopolymers containing urea and carbamate backbone structures (*14*, *15*). Small Tat-derived oligocarbamate and oligourea bind TAR RNA specifically with high affinities in vitro (*14*, *15*). TAR RNA-binding oligocarbamate and oligourea are also resistant to protease degradation in vitro (*14*, *15*). While devising oligomers alternative to the natural polymers, the following points should be taken into consideration: (i) Monomers should be straightforward to synthesize in large amounts, (ii) the monomers should have wide variety of functional groups presented as the side chains of the oligomeric backbone, and (iii) the linkage should be resistant to hydrolytic enzymes. To effect the above attributes, we planned to synthesize peptoid analogue oligomers (*16*−*18*).

The schematic comparison of peptides and peptoids (Figure 1B) shows the similarities in the spacing of the side chains and carbonyl groups and the differences in the chirality of two monomers. Similarities between peptides and peptoids should not obscure the important differences in stereochemical and conformational characteristics of the two oligomers. In addition, peptoids are stable to hydrolysis by proteases (*19*). We envisioned that modification of oligopeptoids with ester or amide moieties would change the physical and chemical properties of the oligomers that could result in enhanced bioavailability and in vivo stability.

We synthesized oligopeptoids containing basic arginine-rich region of Tat through solid-phase synthesis (Scheme 1). Rink-amide MBHA resin was treated with piperidine and then coupled with bromoacetic acid in the presence of diisopropylcarbodiimide. Bromide was displaced with ester or amide of the corresponding amino

Scheme 1. The Synthesis of Oligopeptoid Ester and Amide Analogs[a]



[a] (a) 20% piperidine/DMF; (b) bromoacetic acid/diisopropylcarbodiimide, DMF; (c) methyl ester or amide of amino acid, diisopropylethylamine, DMF.

acid in the presence of diisopropylethylamine. These cycles were repeated to synthesize Tat-derived oligopeptoids containing amide or ester groups (Figure 2). For the oligopeptoid ester synthesis, rink amide resin (0.1 mmol) was swelled in dimethylformamide (2 mL) for 15 min. After filtration, 1 M bromoacetic acid in DMF (2 mL) and diisopropylcarbodiimide (400 μL) were added. The resin was filtered after 2 h and washed with DMF (5 × 3 mL). Bromide displacement was effected in the presence of side chain protected amino ester (1 mmol) and triethylamine (1 mmol) in DMF for 12 h. The above procedure was repeated with bromoacetic acid followed by respective amino ester to obtain Tat-derived peptoid ester oligomer. After the completion of synthesis, the resin was cleaved with a mixture of TFA (95%), triisopropylsilane (2.5%), and water (2.5%) and purified by HPLC. The peptoid ester oligomer was characterized by MALDI mass spectrometry (calculated mass for M + H = 2352.5; observed = 2353.8). Similar procedures were used to synthesize the amide analogues of the Tat-derived peptoids.

For dye labeling, MBHA resin containing oligopeptoid amide (14.4 μmol) was treated with 5-(and-6)-carboxytetramethylrhodamine (150 μmol) and diisopropylcarbodiimide (150 μmol) for 3 h. The resin was washed repeatedly with DMF and dichloromethane. Rhodamine-labeled Tat-peptoid was cleaved from the resin by treating with trifluoroacetic acid, water, and phenol (95:2.5:2.5). The product was purified by reverse phase HPLC and characterized by MALDI mass spectrometry (calculated mass = 2378.2; observed = 2376.26).

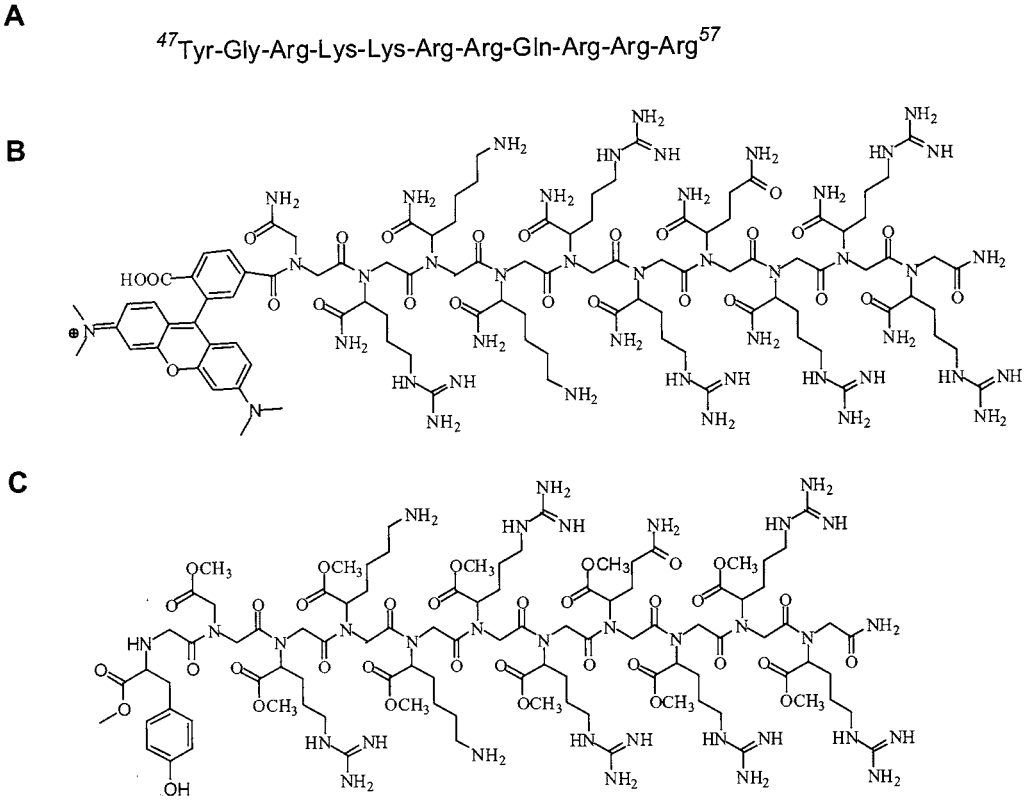


Figure 2. (A) Amino acid sequence of a Tat derived peptide (47−57) that contains RNA-binding region of HIV-1 Tat protein. Structures of the carboxytetramethylrhodamine-labeled oligopeptoid amide **(B)** and the tyrosine containing oligopeptoid ester **(C).** Side chains corresponding to the Tat peptide are shown in **(**A**)**.

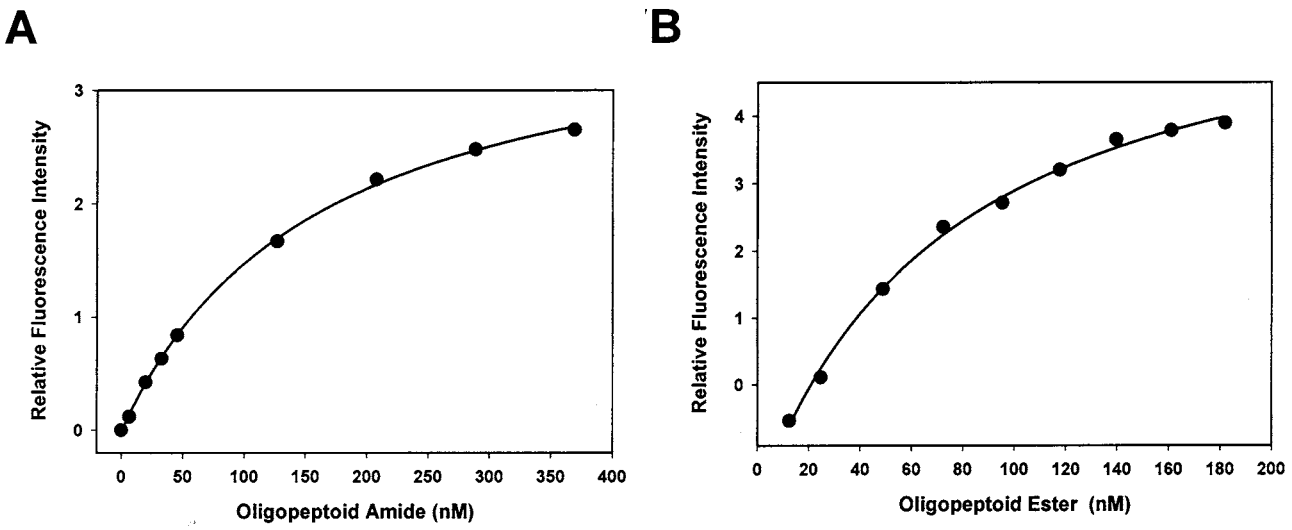


Figure 3. TAR RNA-binding affinities of oligopeptoid amide by FRET **(**A**)** and by fluorescence quenching **(**B**)**. The fluorescence resonance energy transfer (FRET) from fluorescein to rhodamine was measured on PTI (Photon Technology International) fluorescence spectrophotometer. The fluorescein-labeled TAR RNA (Fl-TAR) was excited at 490 nm. The emission spectrum was recorded from 500 to 650 nm for each scan. The slits were set to 4 nm for both excitation and emission lights. All experiments were carried out at room temperature. The initial concentration of Fl-TAR (3′-end fluorescein labeled TAR RNA) was 5.2 nM for all experiments. Each addition of rhodamine-labeled oligopeptoid amide to the Fl-TAR solutions was followed by a 2-min equilibration before the fluorescence spectrum was recorded. For fluorescence quenching experiments, unlabeled oligopeptoid ester was added, the spectra were recorded as described above for the oliogpeptoid amide, and K_D values were determined by fitting data to quadratic eq 3.

To determine the TAR RNA binding activities of Tat-derived oligopeptoids, we employed fluorescence spectroscopy techniques. Modified TAR RNA was synthesized on an Applied Biosystems Model 392 DNA/RNA synthesizer using 2-cyanoethylphosphoramidite chemistry (Figure 1A). All the monomers of (2-cyanoethyl)phosphoramidites were obtained from Glen Research (Sterling, VA). TAR RNA was chemically synthesized on a fluorescein-containing CPG 500 support. RNA (1 μmol) containing fluorescein was deprotected by treatment with NH_3 saturated methanol (2 mL) at 25 °C for 17 h. Product was filtered and dried in SpeedVac. To deprotect 2′-OH silyl groups, the pellet was dissolved in 50% triethylamine trihydrofluoride in dimethyl sulfoxide (0.5 mL) and left at room temperature for 16 h. Deprotected RNA was precipitated by the addition of 2 mL of isopropyl alcohol.

After deprotection, RNA was purified and characterized as described previously (*20*−*22*). This fluorescein-labeled TAR RNA was used to perform fluorescence resonance energy transfer (FRET) and fluorescence quenching experiments.

We carried out FRET experiments to determine the dissociation constant of TAR RNA and peptoid−amide complex. FRET, in which a fluorescent donor molecule transfers energy via a nonradiative dipole−dipole interaction to an acceptor molecule (which is usually also a fluorescent molecule) is a standard spectroscopic technique for measuring distances in the 10−70 Å range (*23*, *24*). The donor's lifetime and intensity are reduced upon energy transfer, and the acceptor fluorescence is increased, or sensitized. Quantification of the efficiency of energy transfer allows determination of the distance between the two fluorophores. We used a well-characterized donor−acceptor dye-pair, fluorescein−rhodamine, for FRET experiments. Rhodamine was incorporated at the terminal amino groups of the oligopeptoid amide during solid-phase synthesis.

The fluorescence resonance energy transfer (FRET) from fluorescein to Rhodamine was measured on PTI (Photon Technology International) fluorescence spectrophotometer. The fluorescein-labeled TAR RNA (Fl-TAR) was excited at 490 nm. The emission spectrum was recorded from 500 to 650 nm for each scan. The slits were set 4 nm for both excitation and emission lights. All experiments were carried out at room temperature. Samples were placed in a plastic microcuvette with a starting volume of 300 μL. The initial concentration of Fl-Tar was around 5.2 nM for all experiments. Each addition of rhodamine-labeled Tat peptoid amide to the Fl-TAR solutions was followed by a 2-min equilibration before the fluorescence spectrum was recorded. The fluorescence intensities were calibrated for the background of buffer (TKT buffer: 50 mM Tris-HCl, pH = 7.4, 20 mM KCl, and 0.02% (w/w) Tween20).

The energy transfer efficiency (E) from the donor to the acceptor was calculated from the decrease of the donor fluorescence intensity at 516 nm according to eq 1:

$$E = (1 - I_{DA}/I_D) \quad (1)$$

where I_{DA} and I_D are the donor fluorescence intensities in the presence and absence of the acceptor, respectively. The distance between the donor and acceptor (R) was calculated according to eq 2:

$$R = R_0(E^{-1} - 1)^{1/6} \quad (2)$$

where $R_0 = 47.6$ Å for fluorescein−rhodamine pair in our system (*25*).

The dissociation constant (K_D) of oligopeptoid amide bound to TAR RNA was obtained by fitting data to quadratic eq 3:

$$F = F_{min} - \{(F_{max} - F_{min})[(e_0 + x + K_D) - ((e_0 + x + K_D)^2 - 4e_0x)^{1/2}]\}/2e_0 \quad (3)$$

where F is the relative fluorescence intensity of the donor (Fl-TAR). F_{min} is the fluorescence intensity at the start of the titration. F_{max} is the fluorescence intensity at saturating concentration of oligopeptoid amide, x. e_0 is the initial concentration of Fl-TAR, 5.2 nM. Results of these experiments are shown in Figure 3A indicating that a high affinity complex between the Tat-derived peptoid amide analogue and TAR RNA was formed ($K_D \approx 155$ nM). The energy transfer efficiency was 47.6%, and a distance of 48.4 Å was calculated between two dyes.

We were unable to incorporate rhodamine at the amino terminal position during the synthesis of Tat-derived oligopeptoid ester analogue due to the formation of a terminal diketopiperazine under basic conditions (diisopropylamine) during rhodamine dye labeling reactions. Therefore, we used fluorescence quenching of fluorescein-TAR RNA by the addition of oligopeptoid ester and determined the binding affinities of Tat-oligopeptoid ester to TAR RNA. As shown in Figure 3B, the oligopeptoid ester was able to bind TAR RNA with high affinity ($K_D \approx 68$ nM). It is interesting that the ester analogue of the Tat-derived oligopeptoid displays a higher affinity to TAR as compared to the amide analogue which contains more functional groups for nucleic acid backbone interactions. Future structural studies may elucidate the differences in RNA recognition by these two oligopeptoids.

Wender et al. recently demonstrated the use of peptoids as molecular transporters (*26*). Peptoid transporters proved to be substantially better than Tat (49−57) peptide. In addition to better uptake performance, these peptoids offer several advantages over Tat peptides including ease of synthesis of analogues and protease stability. These features along with their significant water solubility (>100 mg/mL) indicate that the peptoids could serve as drug candidates, effective transporters for the molecular delivery of drugs and other agents into cells. Our findings reported here show that two analogues of oligopeptoids (ester and amide) derived from Tat sequence binds TAR RNA with high affinities. RNA recognition by an oligopeptoid provides a new tool for the design of drugs and cellular probes which could modulate RNA−protein interactions in vivo. Studies to analyze cellular uptake and in vivo activities of these oligopeptoids are in progress.

ACKNOWLEDGMENT

We thank Drs. C. U. Dinesh, Satish Awasthi, Akbar Ali, and Lei Zhang for critical reading of the manuscript. This work was supported by an NIH grant AI 45466 (T.M.R).

LITERATURE CITED

(1) Miller, P. S. (1996) Development of antisense and antigene oligonucleotide analogues. *Progr. Nucl. Acid Res. Mol. Biol. 52*, 261−291.

(2) Beal, P. A.; P. B. Dervan (1991) Second structural motif for recognition of DNA by oligonucleotide-directed tripl-helix formation. *Science 251*, 1360−1363.

(3) Maher, L. J. d., B. Wold, and P. B. Dervan (1991) Oligonucleotide-directed DNA triple-helix formation: an approach to artificial repressors? *Antisense Res. Dev. 1*, 277−281.

(4) Helene, C., N. T. Thuong, and A. Harel-Bellan (1992) Control of gene expression by triple helix-forming oligonucleotides. The antigene strategy. *Ann. N. Y. Acad. Sci. 660*, 27−36.

(5) Nielsen, P. E. (1999) Applications of peptide nucleic acids. *Curr. Opin. Biotechnol. 10*, 71−75.

(6) Gottesfeld, J. M., L. Neely, J. W. Trauger, E. E. Baird, and P. B. Dervan (1997) Regulation of gene expression by small molecules. *Nature 387*, 202−205.

(7) White, S., J. W. Szewczyk, J. M. Turner, E. E. Baird, and P. B. Dervan (1998) Recognition of the four Watson−Crick base pairs in the DNA minor groove by synthetic ligands. *Nature 391*, 468−471.

(8) Ho, S. N., S. H. Boyer, S. L. Schreiber, S. J. Danishefsky, and G. R. Crabtree (1994) Specific inhibition of formation of transcription complexes by a calicheamicin oligosaccharide:

a paradigm for the development of transcriptional antagonists. *Proc. Natl. Acad. Sci. U.S.A. 91*, 9203−9207.
(9) Liu, C., B. M. Smith, K. Ajito, H. Komatsu, L. Gomez-Paloma, T. Li, E. A. Theodorakis, K. C. Nicolaou, and P. K. Vogt (1996) Sequence-selective carbohydrate-DNA interaction: dimeric and monomeric forms of the calicheamicin oligosaccharide interfere with transcription factor function. *Proc. Natl. Acad. Sci. U.S.A. 93*, 940−944.
(10) Chastain, M.; I. Tinoco, Jr. (1991) Structural elements in RNA. *Progr. Nucleic Acid Res. Mol. Biol. 41*, 131−177.
(11) Chow, C. S.; F. M. Bogdan (1997) A structural basis for RNA-ligand interactions. *Chem. Rev. 97*, 1489−1514.
(12) Weeks, K. M.; D. M. Crothers (1993) Major Groove Accessibility of RNA. *Science 261*, 1574−1577.
(13) Rana, T. M.; K.-T. Jeang (1999) Biochemical and functional interactions between HIV-1 Tat protein and TAR RNA. *Arch. Biochem. Biophys. 365*, 175−185.
(14) Wang, X., I. Huq, and T. M. Rana (1997) HIV-1 TAR RNA recognition by an unnatural biopolymer. *J. Am. Chem. Soc. 119*, 6444−6445.
(15) Tamilarasu, N., I. Huq, and T. M. Rana (1999) High affinity and specific binding of HIV-1 TAR RNA by a Tat-derived oligourea. *J. Am. Chem. Soc. 121*, 1597−1598.
(16) Zuckermann, R., J. Kerr, S. Kent, and W. Moos (1992) Efficient method for the preparation of peptoids [oligo(N-substituted glycines)] by submonomer solid-phase synthesis. *J. Am. Chem. Soc. 114*, 10646−10647.
(17) Simon, R., R. Kania, R. Zuckermann, V. Huebner, D. Jewell, S. Banville, S. Ng, L. Wang, S. Rosenberg, and C. Marlowe (1992) Peptoids: a modular approach to drug discovery. *Proc. Natl. Acad. Sci. U.S.A. 89*, 9367−9371.
(18) Zuckermann, R. N., E. J. Martin, D. C. Spellmeyer, G. B. Stauber, K. R. Shoemaker, J. M. Kerr, G. M. Figliozzi, D. A. Goff, M. A. Siani, and R. J. Simon (1994) Discovery of nanomolar ligands for 7-transmembrane G-protein-coupled receptors from a diverse N-(substituted)glycine peptoid library. *J. Med. Chem. 37*, 2678−2685.
(19) Miller, T. R., S. C. Alley, A. W. Reese, M. S. Solomon, W. V. McCallister, C. Mailer, B. H. Robinson, and P. B. Hopkins (1995) A probe for sequence-dependent nucleic acid dynamics. *J. Am. Chem. Soc. 117*, 9377−78.
(20) Shah, K., H. Wu, and T. M. Rana (1994) Synthesis of uridine phosphoramidite analogues: Reagents for site-specific incorporation of photoreactive sites into RNA sequences. *Bioconjugate Chem. 5*, 508−512.
(21) Shah, K., H. Neenhold, Z. Wang, and T. M. Rana (1996) Incorporation of an artificial protease and nuclease at the HIV-1 tat binding site of trans-activation response RNA. *Bioconjugate Chem. 7*, 283−289.
(22) Ping, Y.-H., Y. Liu, X. Wang, H. R. Neenhold, and T. M. Rana (1997) Dynamics of RNA-protein interactions in the HIV-1 Rev-RRE complex visualized by 6-thioguanosine-mediated photo-cross-linking. *RNA 3*, 850−860.
(23) Clegg, R. M. (1992) Fluorescence resonance energy transfer and nucleic acids. *Methods Enzymol. 211*, 353−88.
(24) Yang, M.; D. P. Millar (1997) Fluorescence resonance energy transfer as a probe of DNA structure and function. *Methods Enzymol. 278*, 417−444.
(25) Zhang, J., N. Tamilarasu, S. Hwang, M. E. Garber, I. Huq, K. A. Jones, and T. M. Rana (2000) HIV-1 TAR RNA enhances the interaction between tat and cyclin T1. *J. Biol. Chem. 275*, 34314−34319.
(26) Wender, P. A., D. J. Mitchell, K. Pattabiraman, E. T. Pelkey, L. Steinman, and J. B. Rothbard (2000) The design, synthesis, and evaluation of molecules that enable or enhance cellular uptake: peptoid molecular transporters. *Proc. Natl. Acad. Sci. U.S.A. 97*, 13003−13008.
(27) Jakobovits, A., D. H. Smith, E. B. Jakobovits, and D. J. Capon (1988) A Discrete Element 3′ of Human Immunodeficiency Virus 1 (HIV-1) and HIV-2 mRNA Initiation Sites Mediates Transcriptional Activation by an HIV Trans Activator. *Mol. Cell. Biol. 8*, 2555−2561.
(28) Cordingley, M. G., R. L. La Femina, P. L. Callahan, J. H. Condra, V. V. Sardana, D. J. Graham, T. M. Nguyen, K. Le Grow, L. Gotlib, A. J. Schlabach, and R. J. Colonno (1990) Sequence-specific Interaction of Tat protein and Tat peptides with the Transactivation-responsive Sequence Element of Human Immunodeficiency Virus Type 1 in vitro. *Proc. Natl. Acad. Sci. 87*, 8985−8989.

BC0255642

Radiometal-Labeled Peptide−PNA Conjugates for Targeting *bcl-2* Expression: Preparation, Characterization, and in Vitro mRNA Binding

Michael R. Lewis,*[,†,‡] Fang Jia,[†] Fabio Gallazzi,[§] Yi Wang,[†] Jiuli Zhang,[†] Nalini Shenoy,[§] Susan Z. Lever,[§,#] and Mark Hannink[||]

Department of Veterinary Medicine and Surgery, Department of Radiology, Department of Chemistry, University of Missouri Research Reactor, and Department of Biochemistry, University of Missouri−Columbia, Columbia, Missouri 65211 . Received August 6, 2002

A new antisense peptide−peptide nucleic acid (peptide−PNA) conjugate, designed for targeting *bcl-2* expression, has been radiolabeled, characterized, and evaluated for *bcl-2* mRNA binding in a cell-free system. A PNA complementary to the first six codons of the *bcl-2* gene was synthesized by standard solid-phase Fmoc chemistry and conjugated to a new derivative of 1,4,7,10-tetraazacyclododecane-*N*,*N*′,*N*″,*N*‴-tetraacetic acid (DOTA) that allows macrocyclic radiometal chelates to be incorporated into any sequence position of a peptide−PNA conjugate. The DOTA−PNA conjugate was then coupled to a membrane-permeating transduction peptide, PTD-4, designed for intracellular delivery of the radiolabeled PNA. The conjugate was characterized by HPLC and ESI-MS and labeled with ^{111}In and ^{90}Y to high specific activities (>1000 Ci/mmol) with high radiochemical purity. Northern blot analysis showed that ^{90}Y-PTD-4−K(DOTA)−anti-*bcl-2*-PNA bound specifically to as little as 50 fmol of *bcl-2* mRNA, a result equivalent to that obtained with the analogous ^{32}P-labeled DNA antisense oligonucleotide. Thus, the mRNA targeting properties of ^{111}In- and ^{90}Y-PTD-4−K(DOTA)−anti-*bcl-2*-PNA demonstrate potential for diagnostic imaging and targeted radiotherapy applications in *bcl-2*-positive cancers.

The processes of carcinogenesis and cancer progression often involve deregulation of proto-oncogenes that confer malignant or aggressive phenotypes to tumor cells. For example, the *B-cell lymphoma/leukemia-2* (*bcl-2*) proto-oncogene (*1*) produces an inhibitor of apoptosis (*2*) that is thought to provide a survival advantage to tumor cells and has been implicated in the development of radiation (*3*−*5*) and chemoresistance (*6*−*8*). *Bcl-2* is overexpressed in non-Hodgkin's lymphoma (NHL) (*9*−*13*) and many other cancers, including breast (*14*), lung (*15, 16*), colon (*17, 18*), prostate (*19, 20*), and neuroendocrine cancers (*21*), malignant melanoma (*22*), acute myeloid leukemia (*23*), and multiple myeloma (*24*).

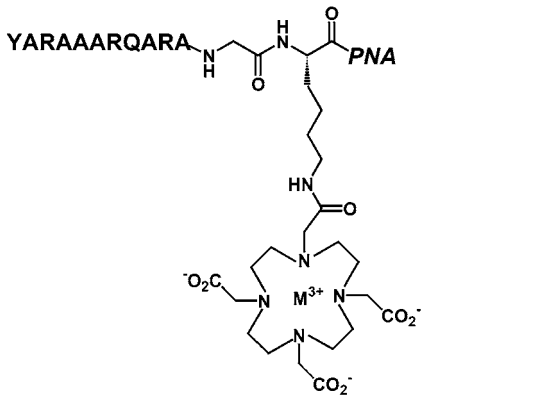
Response of NHL patients to conventional combination chemotherapy is initially good, with 30−35% achieving long-term survival at 10−15 years follow-up (*25*). Unfortunately, in most cases relapse is inevitable, with transformation to a more aggressive histologic phenotype and development of resistance to radiation and/or chemotherapy. In two large cohort studies of patients with aggressive NHL receiving combination chemotherapy (*26, 27*), multivariate analyses revealed that *bcl-2* overexpression was the only clinical feature that correlated strongly with high relapse rate, reduced disease-free survival, and poor overall survival. Thus *bcl-2* overexpression might be considered a new independent prognostic parameter in NHL, aiding in the identification of patient risk groups. Such patients might respond better to alternative treatments, such as targeted immunotherapy, radioimmunotherapy, or antisense therapy, all of which act through mechanisms that down-regulate *bcl-2*. Therefore, development of new *bcl-2*-targeted diagnostic and therapeutic agents may provide a better understanding of the role this proto-oncogene plays in disease progression and treatment response or failure.

The objective of the present research was to develop *bcl-2* antisense agents labeled with diagnostic and therapeutic radiometals and coupled to a peptide vector for intracellular delivery. Peptide nucleic acid (PNA), developed by Nielsen et al. (*28*), has great potential for antisense applications. PNA is resistant to biological degradation and binds complementary mRNA with affinity, specificity, and stability exceeding those of corresponding DNA:RNA duplexes (*29*). However, studies of antisense properties of PNAs have been limited by their poor cellular uptake. Recent work demonstrated that PNA uptake can be increased substantially (*30, 31*) by conjugation to membrane-permeating peptides such as *Drosophila* antennapedia(43−58) (pAntp) (*32*) or the HIV Tat peptide (*33*). More recently, a synthetic protein transduction domain, PTD-4, was shown to exhibit a 33-fold increase in cellular uptake, compared to the Tat sequence (*34*).

* To whom correspondence should be addressed: Michael R. Lewis, Ph.D., Department of Veterinary Medicine and Surgery, College of Veterinary Medicine, 379 E. Campus Drive, University of Missouri-Columbia, Columbia, MO 65211. Phone: (573) 814-6000, ext. 3703. FAX: (573) 814−6551. E-mail: LewisMic@missouri.edu.

† Department of Veterinary Medicine and Surgery.
‡ Department of Radiology.
§ Department of Chemistry.
# University of Missouri Research Reactor.
|| Department of Biochemistry.

10.1021/bc025591s CCC: $22.00 © 2002 American Chemical Society
Published on Web 11/05/2002



PNA = 1 TCTCCCAGCGTGCGCCAT (anti-*bcl-2*)
2 TGTGTTGCGACCCTCTTG (nonsense)

M^{3+} = a ^{111}In
b ^{90}Y

Figure 1. Structures of radiometal-labeled PTD-4−K(DOTA)−anti-*bcl-2*-PNA (**1a**, **1b**) and PTD-4−K(DOTA)−nonsense-PNA (**2a**, **2b**).

We report here the preparation, characterization, and target binding of a PTD-4-antisense PNA conjugate, complementary to the first six codons of *bcl-2* mRNA, and an analogous nonsense PNA conjugate, for which a BLAST database search revealed no homology with any known mammalian gene or DNA sequence. The conjugates were labeled with the diagnostic imaging radiometal ^{111}In ($T_{1/2}$ = 67.4 h; EC 849 keV (100%); γ 173 keV (89%), 247 keV (94%)) and the therapeutic radiometal ^{90}Y ($T_{1/2}$ = 64.0 h; β^- 2.27 MeV (100%)). To provide maximum flexibility in the preparation of radiometal-labeled peptide−PNA conjugates, a bifunctional derivative of 1,4,7,10-tetraazacyclododecane-*N*,*N*′,*N*″,*N*‴-tetraacetic acid (DOTA), which can be incorporated into any sequence position of a PNA or peptide by standard solid-phase coupling techniques, was synthesized. DOTA chelates a large number of radiometals, including ^{111}In and ^{90}Y, with extremely high in vivo stability. *N*-α-(9-Fluorenylmethoxycarbonyl)-*N*-ϵ-[tris(*tert*-butyl)DOTA]-L-lysine (Fmoc-K(DOTA)), was synthesized by activation of DOTA-tris(*tert*-butyl ester) (Macrocyclics, Dallas, TX) with 2-(1*H*-7-azabenzotriazol-1-yl)-1,1,3,3-tetramethyl uronium hexafluorophosphate (HATU, Applied Biosystems, Foster City, CA) and 1-hydroxy-7-azabenzotriazole (HOAt, Applied Biosystems) in 1-methyl-2-pyrrolidinone and reaction of the resulting active ester with *N*-α-Fmoc-L-lysine (Advanced ChemTech, Louisville, KY). The compound was purified by solvent extraction using ethyl acetate and water, followed by concentration of the organic phase in vacuo and precipitation of the product with cold diethyl ether. Alternatively, Fmoc-K(DOTA) could be purified by semipreparative reversed-phase HPLC. Analytical reversed-phase HPLC, electrospray ionization mass spectrometry (ESI-MS), high-resolution ^1H NMR, and elemental analysis of Fmoc-K(DOTA) were consistent with the structure of the desired product.

Bcl-2 antisense and nonsense PNAs (Figure 1) were synthesized manually on XAL PEG PS resin (Applied Biosystems), using Fmoc-protected PNA monomers (B = T-OH, A(Bhoc)-OH, C(Bhoc)-OH, and G(Bhoc)-OH, Applied Biosystems) and standard solid-phase coupling techniques, followed by manual coupling of Fmoc-K(DOTA) and Fmoc-glycine as a small spacer between the PNA conjugate and PTD-4. Then the fully protected PTD-4 sequence was added to Fmoc-G-K(DOTA)−anti-*bcl-2*-PNA using an automated peptide synthesizer. The PTD-4−K(DOTA)−anti-*bcl-2*-PNA conjugate (**1**) was cleaved and deprotected with trifluoroacetic acid (TFA) containing 2.5% each of triisopropylsilane, *m*-cresol, thioanisole, ethanedithiol, phenol, and H_2O for 4 h at room temperature. Unfortunately, the fully deprotected conjugate coeluted with unmodified PNA at the solvent front when reversed-phase HPLC purification was attempted. Therefore, slightly deprotected PTD-4−K(DOTA)−anti-*bcl-2*-PNA was cleaved from the resin with 25% TFA, 5% triisopropylsilane, 5% *m*-cresol, and 5% H_2O in dichloromethane for two cycles of 15 min at room temperature. Two major slightly deprotected intermediates were purified by semipreparative reversed-phase HPLC. These intermediates were collected separately and fully deprotected as described above, after which **1** was isolated by precipitation with cold diethyl ether and characterized by ESI-MS. Observed molecular ions at *m*/*z* = 2190.0 ($(M + 3H)^{3+}$), 1642.5 ($(M + 4H)^{4+}$), 1314.2 ($(M + 5H)^{5+}$), 1095.1 ($(M + 6H)^{6+}$), and 938.9 ($(M + 7H)^{7+}$) were consistent with the mass of the desired product, 6568 Da. PTD-4−K(DOTA)-nonsense-PNA (**2**) was synthesized and purified using the same procedure, followed by ESI-MS analysis. Molecular ions observed at *m*/*z* = 2211.5 ($(M + 3H)^{3+}$), 1659.1 ($(M + 4H)^{4+}$), 1327.2 ($(M + 5H)^{5+}$), 1106.4 ($(M + 6H)^{6+}$), 948.5 ($(M + 7H)^{7+}$), 830.2 ($(M + 8H)^{8+}$), and 737.8 ($(M + 9H)^{9+}$) were consistent the mass of the desired product, 6629 Da. Synthesis of PTD-4−K(DOTA)-PNA conjugates has been described in brief (*35a*) and will be reported in detail subsequently (*35b*).

Conjugates **1** and **2** were labeled with ^{111}In (**1a**, **2a**) and ^{90}Y (**1b**, **2b**) in 0.2 M ammonium acetate, pH 5.0, containing approximately 1 mg/mL of gentisic acid, for 30 min at 90 °C. The antisense conjugate lacking PTD-4, K(DOTA)−anti-*bcl-2*-PNA (**3**) was labeled with ^{111}In (**3a**) using the same conditions. Diethylenetriaminepentaacetic acid (DTPA) was added to a final concentration of 1 mM, and after 5 min at room temperature the

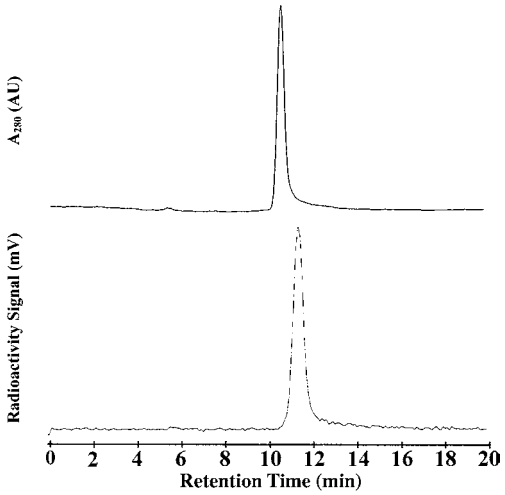


Figure 2. Size exclusion HPLC of **1** (top) and **1a** (bottom). The peak eluting at 10.6 min retention time corresponds to an apparent molecular weight of 5.94 kDa.

Table 1. ^{111}In and ^{90}Y Labeling of Conjugates 1 and 3.

conjugate	radiometal	labeling ratio (μCi/μg)	incorporation (%)[a]	specific activity (Ci/mmol)
3	^{111}In	199	98.77 ± 1.41	1068
1	^{111}In	201	96.62 ± 0.29	1300
1	^{90}Y	820	98.61 ± 2.25	5397

[a] n = 3.

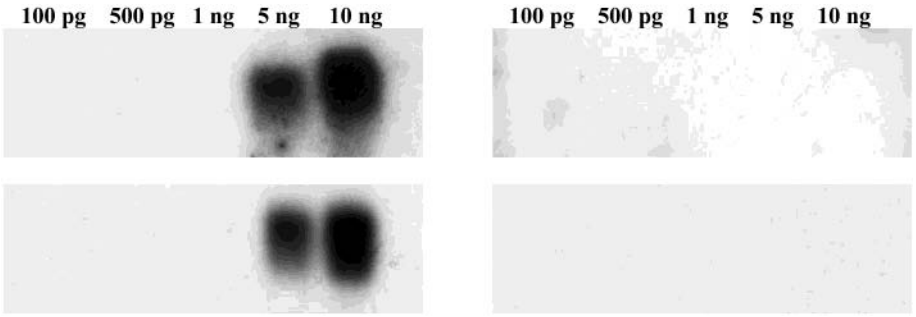


Figure 3. (Top) Northern blot analysis of *bcl-2* mRNA (left) and *luciferase* mRNA (right), using **1b**. (Bottom) Northern blot analysis of *bcl-2* mRNA (left) and *luciferase* mRNA (right), using ^{32}P-anti-*bcl-2*-DNA.

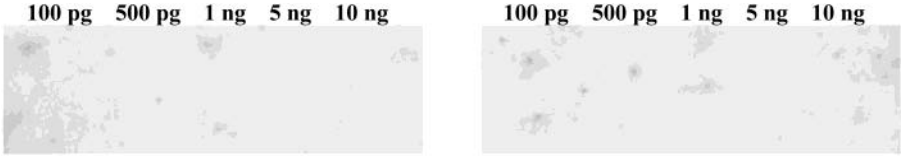


Figure 4. Northern blot analysis of *bcl-2* mRNA (left) and *luciferase* mRNA (right), using **2b**.

reaction mixtures were analyzed by normal-phase TLC and size exclusion HPLC. Both methods showed that ^{111}In and ^{90}Y incorporation into **1** was nearly quantitative at specific activities >1000 Ci/mmol (Table 1), as was ^{111}In labeling of **3**. These specific activities are considerably higher than those employed previously for in vivo imaging of *c-myc* mRNA with ^{111}In-labeled DNA oligonucleotides (*36*) and are also in the range proposed to image mRNA concentrations as low as 1 pM (*37*). Conjugate **2** was also labeled efficiently with ^{111}In and ^{90}Y by the same procedure. Analysis of **1** by size exclusion HPLC (Figure 2) showed that the conjugate had an apparent molecular weight of 5.94 kDa, determined from a calibration curve generated using a Bio-Rad (Hercules, CA) molecular weight standard. This value, lower than the calculated molecular weight, is consistent with the size of an α helix-random coil peptide−PNA conjugate (*38, 39*). Size exclusion HPLC of **1a** (Figure 2) revealed that the radiochemical purity of the compound was 100%.

The kinetic stability of **1a** was evaluated by size exclusion HPLC during incubation in mouse plasma at 37 °C for 168 h (data not shown). No evidence of instability of the ^{111}In-K(DOTA) chelate was seen, and no changes in the chromatographic profile of **1a** were observed for 24 h. At later time points, a reproducible increase of approximately 0.1 min in the retention time of the ^{111}In-labeled conjugate and peak tailing suggested that some proteolytic degradation of PTD-4 may have occurred. However, the *retro-inverso* counterpart of pAntp displays equivalent transduction activity and is much more stable to proteolysis (*30*). Therefore, we intend to synthesize the *retro-inverso*-PTD-4−K(DOTA)−anti-*bcl-2*-PNA analogue and evaluate it in future in vitro and in vivo studies.

A pcDNA3-hygro vector (Invitrogen, Carlsbad, CA) containing the open reading frame of human *bcl-2* was constructed for mRNA synthesis. *Bcl-2* and *luciferase* mRNAs were prepared by in vitro transcription, subjected to electrophoresis through a 1% agarose gel containing 2.2 M formaldehyde (*40*), and immobilized on nylon membranes by capillary transfer (*41*). RNA transfer was determined qualitatively to be complete by ethidium bromide staining of the gel before and after transfer and by methylene blue staining of the membrane. Then 50-μCi aliquots of **1b** and **2b** (5458 Ci/mmol) were incubated with membranes in hybridization solution (CLONTECH, Palo Alto, CA), containing 5% nonfat dry milk, for 1 h at 63.2 °C, after which the membranes were washed according to the manufacturer's instructions. Autoradiography of membranes for 1 h (Figure 3, top) showed that **1b** bound specifically to as little as 5 ng (50 fmol) of the *bcl-2* transcript, while no binding to *luciferase* mRNA was observed. The analogous anti-*bcl-2* DNA oligonucleotide was end-labeled to a specific activity of 6000 Ci/mmol, using γ-[^{32}P]ATP and T4 polynucleotide kinase, and 50 μCi of ^{32}P-anti-*bcl-2*-DNA was hybridized with the immobilized mRNAs under the same conditions, except that nonfat dry milk was not added. Autoradiography with ^{32}P-labeled DNA was carried out for 5.25 h, such that the film was exposed to the same number of radioactive decays as for ^{90}Y-labeled PNA. As shown in Figure 3 (bottom), ^{32}P-anti-*bcl-2*-DNA gave equivalent results to those obtained with **1b**. Analogous control experiments using **2b** showed no binding to either transcript (Figure 4). Thus, the ^{90}Y-labeled antisense peptide−PNA conjugate was qualitatively equal to ^{32}P-labeled antisense DNA in terms of *bcl-2* mRNA detection sensitivity and specificity. However, Northern blot analysis at elevated temperatures demonstrated that **1b** bound to *bcl-2* mRNA with greater thermodynamic stability than ^{32}P-anti-*bcl-2*-DNA (see Supporting Information). Synthetic *bcl-2* and *luciferase* mRNAs were also spiked into a total RNA preparation from 293 human embryonic kidney cells, and the resulting mixtures were analyzed by Northern blotting with **1b** after agarose gel electrophoresis. While some nonspecific binding to cellular RNA was seen (Figure 5), 10 ng (100 fmol) of *bcl-2* mRNA was detected clearly in the presence of a large excess of cellular RNA, and no binding to *luciferase* mRNA was observed.

In conclusion, a new *bcl-2* antisense PNA conjugate, coupled to a membrane-permeating peptide for intracellular delivery, was prepared and labeled to high specific activities with the diagnostic imaging radiometal ^{111}In and the therapeutic radiometal ^{90}Y. Hybridization experiments demonstrated that **1b** was able to bind to immobilized *bcl-2* mRNA with high sensitivity and specificity equivalent to ^{32}P-labeled antisense DNA, yet with greater thermodynamic stability. We are currently evaluating the *bcl-2* targeting properties of **1a** and **1b** in cultured NHL cells and tumor-bearing animal models.

In preliminary studies, uptake of **1a** in Raji cells, which express high levels of *bcl-2* mRNA (*42*), increased significantly ($p < 0.05$) from 6.53% of the total radioactivity added after 30 min at 37 °C to 8.04% at 4 h, while initial

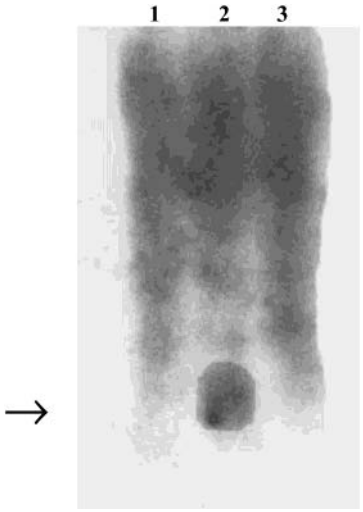


Figure 5. Northern blot analysis of total cellular RNA from 293 cells, using **1b**. Lane 1: total RNA (10 μg); lane 2: total RNA (10 μg), spiked with 10 ng of synthetic *bcl-2* mRNA; lane 3: total RNA (10 μg), spiked with 10 ng of *luciferase* mRNA. The arrow indicates the *bcl-2* transcript, determined to be equal to the theoretical molecular size of 0.754 kb by ethidium bromide staining and comparison with a DNA molecular weight standard (1kb DNA Ladder, Promega, Madison, WI).

uptake of **3a** was approximately 13-fold lower. In U937 cells, which express low levels of *bcl-2* mRNA (*43*), uptake of **1a** decreased significantly ($p < 0.05$) from 4.05% at 30 min to 2.07% at 4 h. At all time points, uptake of **1a** was significantly greater ($p < 0.05$) in Raji cells than in U937 cells. We are currently developing Raji- and U937-bearing mouse models of NHL to evaluate the tumor targeting properties of ^{111}In- and ^{90}Y-*retro-inverso*-PTD-4−K(DOTA)−anti-*bcl-2*-PNA.

ACKNOWLEDGMENT

This work was supported by NIH Grant CA86290 (W. A. Volkert, PI) and a grant from the University of Missouri Research Reactor Research Partnerships Initiative (to M.R.L.). The authors would like to acknowledge the support of the Department of Veterans Affairs and the University of Missouri Research Reactor for purchasing an Advanced ChemTech ACT Model 396 Omega Multiple Biomolecular Synthesizer used in this research.

Supporting Information Available: Experimental details on purification, radiometal labeling, and analytical characterization of PTD-4-PNA conjugates, subcloning of *bcl-2*, and mRNA binding assays. This material is available free of charge via the Internet at http://pubs.acs.org.

LITERATURE CITED

(1) Tsujimoto, Y., Finger, L. R., Yunis, J., Nowell, P. C., and Croce, C. M. (1984) Cloning of the Chromosome Breakpoint of Neoplastic B Cells with the t(14; 18) Chromosome Translocation. *Science 226*, 1097−1099.

(2) Hockenbery, D., Nuñez, G., Milliman, C., Schreiber, R. D., and Korsmeyer, S. J. (1990) Bcl-2 is an inner mitochondrial membrane protein that blocks programmed cell death. *Nature 348*, 334−336.

(3) Sentman, C. L., Shutter, J. R., Hockenbery, D., Kanagawa, O., and Korsmeyer, S. J. (1991) bcl-2 Inhibits Multiple Forms of Apoptosis but Not Negative Selection in Thymocytes. *Cell 67*, 879−888.

(4) Strasser, A., Harris, A. W., and Cory, S. (1991) *bcl-2* Transgene Inhibits T Cell Death and Perturbs Thymic Self-Censorship. *Cell 67*, 889−899.

(5) Mirkovic, N., Voehringer, D. W., Story, M. D., McConkey, D. J., McDonnell, T. J., and Meyn, R. E. (1997) Resistance to radiation-induced apoptosis in Bcl-2-expressing cells is reversed by depleting cellular thiols. *Oncogene 15*, 1461−1470.

(6) Miyashita, T., and Reed, J. C. (1992) *bcl-2* Gene Transfer Increases Relative Resistance of S49.1 and WEHI7.2 Lymphoid Cells to Cell Death and DNA Fragmentation Induced by Glucocorticoids and Multiple Chemotherapeutic Drugs. *Cancer Res. 52*, 5407−5411.

(7) Miyashita, T., and Reed, J. C. (1993) Bcl-2 Oncoprotein Blocks Chemotherapy-Induced Apoptosis in a Human Leukemia Cell Line. *Blood 81*, 151−157.

(8) Reed, J. C., Kitada, S., Takayama, S., and Miyashita, T. (1994) Regulation of chemoresistance by the *bcl-2* oncoprotein in non-Hodgkin's lymphoma and lymphocytic leukemia cell lines. *Ann. Oncol. 5*, S61−S65.

(9) Yunis, J. J., Oken, M. M., Kaplan, M. E., Ensrud, K. M., Howe, R. R., and Theologides, A. (1982) Distinctive Chromosomal Abnormalities in Histologic Subtypes of Non-Hodgkin's Lymphoma. *N. Engl. J. Med. 307*, 1231−1236.

(10) Tsujimoto, Y., Cossman, J., Jaffe, E., and Croce, C. M. (1985) Involvement of the *bcl-2* Gene in Human Follicular Lymphoma. *Science 228*, 1440−1443.

(11) Levine, E. G., Arthur, D. C., Frizzera, G., Peterson, B. A., Hurd, D. D., and Bloomfield, C. D. (1985) There Are Differences in Cytogenetic Abnormalities Among Histologic Subtypes of the Non-Hodgkin's Lymphomas. *Blood 66*, 1414−1422.

(12) Pezzella, F., Tse, A. G. D., Cordell, J. L., Pulford, K. A. F., Gatter, K. C., and Mason, D. Y. (1990) Expression of the *bcl-2* Oncogene Protein Is Not Specific for the 14; 18 Chromosomal Translocation. *Am. J. Pathol. 137*, 225−232.

(13) Zutter, M., Hockenbery, D., Silverman, G. A., and Korsmeyer, S. J. (1991) Immunolocalization of the Bcl-2 Protein Within Hematopoietic Neoplasms. *Blood 78*, 1062−1068.

(14) Lanzafame, S., Emmanuele, C., Torrisi, A., and Magro, G. (1998) Correlated Expression of BCL-2 Protein, Estrogen Receptor, Cathepsin D and Low Growth Fraction (PCNA) in Intracystic Papillary Breast Carcinoma. *Pathol. Res. Pract. 194*, 541−547.

(15) Pezzella, F., Turley, H., Kuzu, I., Tungekar, M. F., Dunnill, M. S., Pierce, C. B., Harris, A., Gatter, K. C., and Mason, D. Y. (1993) *bcl-2* Protein in Non-Small-Cell Lung Carcinoma. *N. Engl. J. Med. 329*, 690−694.

(16) Jiang, S.-X., Sato, Y., Kuwao, S., and Kameya, T. (1995) Expression of *bcl-2* Oncogene Protein is Prevalent in Small Cell Lung Carcinomas. *J. Pathol. 177*, 135−138.

(17) Sinicrope, F. A., Ruan, S. B., Cleary, K. R., Stephens, L. C., Lee, J. J., and Levin, B. (1995) *bcl-2* and p53 Oncoprotein Expression during Colorectal Tumorigenesis. *Cancer Res. 55*, 237−241.

(18) Yang, H.-B., Chow, N.-H., Sheu, B.-S., Chan, S.-H., Chien, C.-H., and Su, I.-J. (1999) The Role of bcl-2 in the Progression of the Colorectal Adenoma-Carcinoma Sequence. *Anticancer Res. 19*, 727−730.

(19) Colombel, M., Symmans, F., Gil, S., O'Toole, K. M., Chopin, D., Benson, M., Olsson, C. A., Korsmeyer, S., and Buttyan, R. (1993) Detection of the Apoptosis-Suppressing Oncoprotein *bcl-2* in Hormone-Refractory Human Prostate Cancers. *Am. J. Pathol. 143*, 390−400.

(20) Sullivan, G. F., Amenta, P. S., Villanueva, J. D., Alvarez, C. J., Yang, J.-M., and Hait, W. N. (1998) The Expression of Drug Resistance Gene Products during the Progression of Human Prostate Cancer. *Clin. Cancer Res. 4*, 1393−1403.

(21) Wang, D.-G., Johnston, C. F., and Buchanan, K. D. (1997) Oncogene Expression in Gastroenteropancreatic Neuroendocrine Tumors. Implications for Pathogenesis. *Cancer 80*, 668−675.

(22) Cerroni, L., Soyer, H. P., and Kerl, H. (1995) *bcl-2* Protein Expression in Cutaneous Malignant Melanoma and Benign Melanocytic Nevi. *Am. J. Dermatopathol. 17*, 7−11.

(23) Karakas, T., Maurer, U., Weidmann, E., Miething, C. C., Hoelzer, D., and Bergmann, L. (1998) High expression of *bcl-2* mRNA as a determinant of poor prognosis in acute myeloid leukemia. *Ann. Oncol. 9*, 159−165.

(24) Puthier, D., Pellat-Deceunynck, C., Barillé, S., Robillard, N., Rapp, M.-J., Juge-Morineau, N., Harousseau, J.-L., Bataille, R., and Amiot, M. (1999) Differential expression of Bcl-2 in human plasma cell disorders according to proliferation status and malignancy. *Leukemia 13*, 289−294.

(25) Fisher, R. I. (1997) Cyclophosphamide, doxorubicin, vincristine, and prednisone versus intensive chemotherapy in non-Hodgkin's lymphoma. *Caner Chemother. Pharmacol. 40 (Suppl),* S42−S46.

(26) Hermine, O., Haioun, C., Lepage, E., d′Agay, M.-F., Briere, J., Lavignac, C., Fillet, G., Salles, G., Marolleau, J.-P., Diebold, J., Reyes, F., and Gaulard, P. (1996) Prognostic Significance of bcl-2 Protein Expression in Aggressive Non-Hodgkin's Lymphoma. *Blood 87*, 265−272.

(27) Hill, M. E., MacLennan, K. A., Cunningham, D. C., Vaughan Hudson, B., Burke, M., Clarke, P., Di Stefano, F., Anderson, L., Vaughan Hudson, G., Mason, D., Selby, P., and Linch, D. C. (1996) Prognostic Significance of BCL-2 Expression and *bcl-2* Major Breakpoint Region Rearrangement in Diffuse Large Cell Non-Hodgkin's Lymphoma: A British National Lymphoma Investigation Study. *Blood 88*, 1046−1051.

(28) Nielsen, P. E., Egholm, M., Berg, R. H., and Buchardt, O. (1991) Sequence Selective Recognition of DNA by Strand Displacement with a Thymine-substituted Polyamide. *Science 254*, 1497−1500.

(29) Larsen, H. J., Bentin, T., and Nielsen, P. E. (1999) Antisense properties of peptide nucleic acid. *Biochim. Biophys. Acta 1489*, 159−166.

(30) Aldrian-Herrada, G., Desarménien, M. G., Orcel, H., Boissin-Agasse, L., Méry, J., Brugidou, J., and Rabié, A. (1998) A peptide nucleic acid (PNA) is more rapidly internalized in cultured neurons when coupled to a *retro-inverso* delivery peptide. The antisense activity depresses the target mRNA and protein in magnocellular oxytocin neurons. *Nucleic Acids Res. 26*, 4910−4916.

(31) Pooga, M., Soomets, U., Hällbrink, M., Valkna, A., Saar, K., Rezaei, K., Kahl, U., Hao, J.-X., Xu, X.-J., Wiesenfeld-Hallin, Z., Hökfelt, T., Bartfai, T., and Langel, U. (1998) Cell penetrating PNA constructs regulate galanin receptor levels and modify pain transmission in vivo. *Nat. Biotechnol. 16*, 857−861.

(32) Derossi, D., Joliot, A. H., Chassaing, G., and Prochiantz, A. (1994) The Third Helix of the Antennapedia Homeodomain Translocates through Biological Membranes. *J. Biol. Chem. 269*, 10444−10450.

(33) Fawell, S., Seery, J., Daikh, Y., Moore, C., Chen, L. L., Pepinsky, B., and Barsoum, J. (1994) Tat-mediated delivery of heterologous proteins into cells. *Proc. Natl. Acad. Sci. U.S.A. 91*, 664−668.

(34) Ho, A., Schwarze, S. R., Mermelstein, S. J., Waksman, G., and Dowdy, S. F. (2001) Synthetic Protein Transduction Domains: Enhanced Transduction Potential in Vitro and in Vivo. *Cancer Res. 61*, 474−477.

(35) (a) Gallazzi, F., Wang, Y., Jia, F., Shenoy, N., Lever, S. Z., and Lewis, M. R. (2002) Preparation of a radiolabeled peptide−PNA conjugate for imaging oncogene expression. 27th European Peptide Symposium, Sorrento, Italy, Abstract P E21. (b) Gallazzi, F., Wang, Y., Shenoy, N., Lever, S. Z., and Lewis, M. R., manuscript in preparation.

(36) Dewanjee, M. K., Ghafouripour, A. K., Kapadvanjwala, M., Dewanjee, S., Serafini, A. N., Lopez, D. M., and Sfakianakis, G. N. (1994) Noninvasive Imaging of c-*myc* Oncogene Messenger RNA with Indium-111-Antisense Probes in a Mammary Tumor-Bearing Mouse Model. *J. Nucl. Med. 35*, 1054−1063.

(37) Dewanjee, M. K., Haider, N., and Narula, J. (1999) Imaging with radiolabeled antisense oligonucleotides for the detection of intracellular messenger RNA and cardiovascular disease. *J. Nucl. Cardiol. 6*, 345−356.

(38) Snyder, L. R., and Kirkland, J. J. (1979) Size-Exclusion Chromatography. *Introduction to Modern Liquid Chromatography*, First Edition, pp 483−540, John Wiley & Sons, Inc., New York.

(39) Atkins, P. W. (1982) The structures and properties of macromolecules. *Physical Chemistry*, Second Edition, p 825, W. H. Freeman and Company, San Francisco.

(40) Sambrook, J., and Russell, D. W. (2001) Separation of RNA According to Size: Electrophoresis of RNA through Agarose Gels Containing Formaldehyde. *Molecular Cloning: A Laboratory Manual*, 3rd ed., Vol. 2, pp 7.31−7.34, Cold Spring Harbor, New York.

(41) Sambrook, J., and Russell, D. W. (2001) Transfer and Fixation of Denatured RNA to Membranes. *Molecular Cloning: A Laboratory Manual*, 3rd ed., Vol. 2, pp 7.35−7.41, Cold Spring Harbor, New York.

(42) Graninger, W. B., Seto, M., Boutain, B., Goldman, P., and Korsmeyer, S. J. (1987) Expression of Bcl-2 and Bcl-2-Ig Fusion Transcripts in Normal and Neoplastic Cells. *J. Clin. Invest. 80*, 1512−1515.

(43) Seto, M., Jaeger, U., Hockett, R. D., Graninger, W., Bennett, S., Goldman, P., and Korsmeyer, S. J. (1988) Alternative promoters and exons, somatic mutation and deregulation of the *Bcl-2-Ig* fusion gene in lymphoma. *EMBO J. 7*, 123−131.

BC025591S

Self-Assembled Ternary Complex of Cationic Dendrimer, Cucurbituril, and DNA: Noncovalent Strategy in Developing a Gene Delivery Carrier

Yong-beom Lim,[†] Taeil Kim,[†] Jae Wook Lee,[‡] Seon-mi Kim,[†] Hee-Joon Kim,[‡] Kimoon Kim,*[,‡] and Jong-sang Park*[,†]

School of Chemistry & Molecular Engineering, Seoul National University, Seoul 151-742, Korea, and Department of Chemistry, Pohang University of Science and Technology (POSTECH), Pohang 790-784, Korea.
Received July 22, 2002

A ternary complex of PPI-DAB dendrimer [(1,4-diaminobutane); Gen = *N*; *dendri*-poly(propyleneimine); -[NHC(=O)$CH_2NH_2^+(CH_2)_4NH_3^+$]$_z$], DNA, and cucurbituril (CB) was evaluated as an example of a totally self-assembled gene delivery carrier. The complex was formed in a noncovalent way in which DNA interacts with PPI-DAB electrostatistically and CB with PPI-DAB through multiple noncovalent interactions. Dynamic light scattering data indicated that the diameter and size distributions of the complexes were dependent upon the sequence of mixing of each component with unimodal distribution ranging from 150.8 to 210.2 nm under favorable conditions. Fluorescence studies showed the quantitative binding of CB to PPI-DAB after ternary complex formation. The complex was able to transfect mammalian cells with high efficiency and the cytotoxicity of the PPI-DAB/CB complex was relatively low.

Spontaneously assembled supramacromolecular complexes have been the subject of considerable interest, with the noncovalent self-assembly process between biological macromolecules being mimicked in a chemical approach (*1*−*8*). The study of nonviral gene delivery vectors is one such approach in which virus corelike particles are assembled through electrostatic interactions, e.g., between cationic polymer and negatively charged DNA (*9*). A number of cationic polymers, such as poly-L-lysine (*10*), poly(ethylenimine) (PEI) (*11*), PAMAM dendrimer (*12*), and hyperbranched poly(amino ester) (*13*), were able to compact DNA into submicron-sized water-soluble particles (polyplexes) and carry DNA into the cell nucleus. The polyplexes were made to have specialized functional moieties such as targeting ligands, endosome disruptive functions, and nucleus localization signals by directly (covalently) attaching them to the cationic polymer (*14*−*17*). This covalent strategy has worked well; however, it would be more interesting if we were able to produce similar or even more advanced systems by the use of a noncovalent approach.

The packaging of viruses is also an elaborate multistep noncovalent self-assembly process between the viral genome (DNA or RNA) and a number of proteins (*18*). In this regard, a synthetic functional module that recognizes a specific moiety in the cationic polymer in a noncovalent manner would be useful in the realization of synthetic viruslike particles.

In this paper we report on the development of a noncovalently assembled ternary gene delivery complex based on cationic dendrimer, DNA, and CB reminiscent of virus particles (Scheme 1). CB was regarded as a functional module. CB itself has no biological activity; however, this system can be applied to other noncovalent molecular recognitions, and it would be possible to create a really functional polyplex if the functionalized-CB were synthesized, which we are currently investigating. For example, peptide ligand−CB conjugate could easily be made if amine (NH_2)-, alcohol (OH)-, or sulfhydryl (SH)-functionalized CB was synthesized. The purpose of this work is to evaluate the possibility of generating a three-component gene delivery system consisting of cationic polymer, DNA, and noncovalent ligand equivalent. CB is a large-cage compound composed of glycoluril units interconnected with methylene bridges and is able to form stable pseudorotaxanes with strings derived from diaminoalkanes through multiple noncovalent interactions (*19*, *20*).

The ternary complex was prepared by the sequential treatment of PPI-DAB (G4) with CB and DNA (PPI-DAB/CB/DNA), or DNA and CB (PPI-DAB/DNA/CB). Synthetic details for the preparation of PPI-DAB have been described previously (*21*). The hydrodynamic radii (R_h) of the two preparations were investigated by dynamic light scattering (DLS)[1] as shown in Figure 1. The measured average R_h of PPI-DAB/CB/DNA was 150.8

* Corresponding authors: Jong-sang Park. Phone: +82-2-880-6641. Fax: +82-2-877-5110. E-mail: pfjspark@plaza.snu.ac.kr. Kimoon Kim. Phone: +82-54-279-2113. Fax: +82-54-279-8129. E-mail: kkim@postech.ac.kr.

[†] Seoul National University.

[‡] Pohang University of Science and Technology (POSTECH).

[1] Light scattering experiments were performed at 25 °C with BI-200SM Goniometer (Brookhaven Instruments Corporation) using a Lexel laser model 95 argon laser (100 mW output power at a wavelength of 514.5 nm). Correlator was PD2000 (Precision Detectors), and the scattering angle was 90°. Data were analyzed using the CONTIN algorithm. The sample was prepared by directly mixing each solution of polymer and DNA in water. The final DNA concentration was adjusted to 5 μg/mL.

[2] pEGFPLuc (Clontech) encodes a luciferase from the firefly *Photinus pyralis* under the control of the immediate early promoter of CMV.

10.1021/bc025581r CCC: $22.00 © 2002 American Chemical Society
Published on Web 10/18/2002

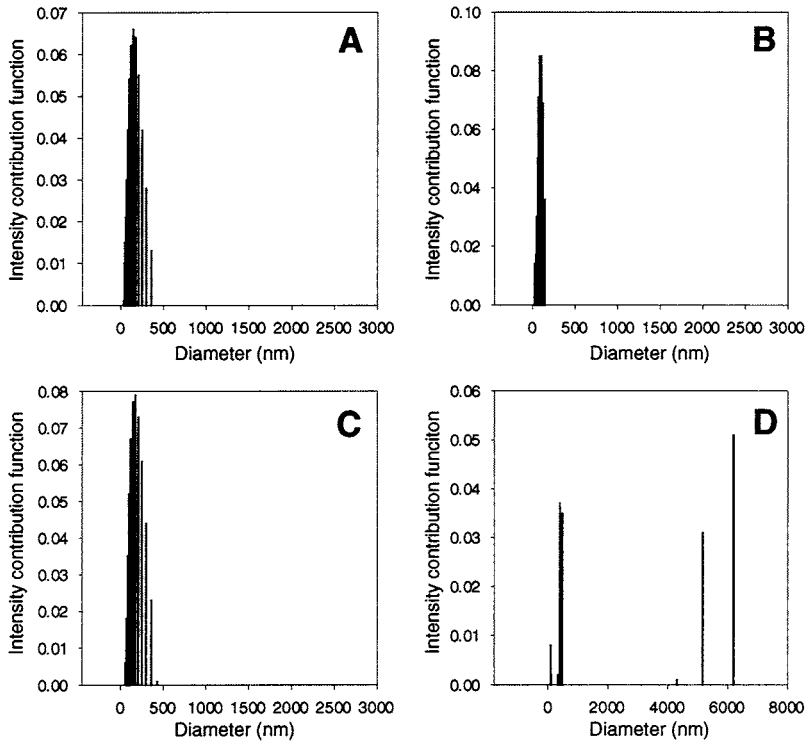
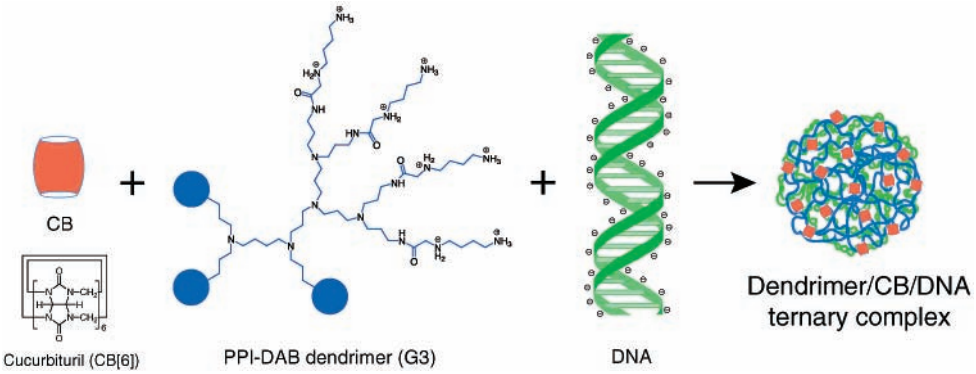


Figure 1. Size distribution of (A) PPI-DAB/CB/DNA (with 100% CB relative to DAB), (B) PPI-DAB/DNA, (C) PPI-DAB/DNA/CB (10% CB), and (D) PPI-DAB/DNA/CB (30% CB) complexes by dynamic light scattering.[1] DNA was pEGFPLuc plasmid DNA.[2] All complexes were formed at a charge ratio (+/−) of 3. Charge ratios were calculated based on the assumption that only primary and secondary amines in DAB are protonated.

Scheme 1. Ternary Complex of PPI-DAB Dendrimer, CB, and DNA



nm. PPI-DAB/CB/DNA was prepared with all the DAB moieties being occupied by CB. The average R_h of PPI-DAB/DNA (83.5 nm) was smaller than that of PPI-DAB/CB/DNA; however, the complex grew larger as CB was added. At 10% and 20% CB concentrations (relative to DAB moieties), the average R_h became 176.2 and 506.1 nm, respectively. Two intensity populations existed above 30% CB concentration, with the smaller sizes presumably due to that of well-defined ternary complexes and the larger sizes probably attributed to aggregates. These results imply differences in tertiary structures between the two preparations. Therefore, further characterization of the ternary complex was conducted with PPI-DAB/CB/DNA for simplification.

The formation of the ternary complex was investigated by observing the shift of DNA electrophoretic migration in agarose gel (Figure 2). All third-generation (G3) polymers and G4 of PPI formed polymer/DNA complexes (polyplexes) at charge ratios (polymer to DNA, +/−) above unity. However, G5 of PPI, G4 and G5 of PPI-DAB, and G4 and G5 of PPI-DAB/CB formed polyplexes at charge ratios above 2. These results indicate that the DNA binding capacity of the three polymers is decreased as the generation number is increased. In addition, the DNA binding capacities were increased in the order, PPI > PPI-DAB ≥ PPI-DAB/CB. Examination of the structural conformations of PPI-DAB and PPI-DAB/CB by molecular dynamic simulation revealed that PPI-DAB/CB adopts a more rigid shell at the exterior than PPI-DAB (*21*). The decreased binding capacity of the higher generation dendrimers and of PPI-DAB/CB and PPI-DAB relative to that of PPI may be related to the formation of a more rigid and compact shell at the exterior where DNA binding amine groups are located, and to the effect of the polymers' different molecular structure and CB on pK_a of amino groups.

To verify the formation of the ternary complex, it was necessary to prove that CB remained associated with PPI-DAB and was not expelled from the polymer in the process of DNA binding. To demonstrate the validity of this assumption, each of CB, PPI-DAB (G4)/CB, and PPI-DAB (G4)/CB/DNA were dialyzed using 3500 M_r cutoff tubing against 0.2 m Na_2SO_4, in which CB dissolves very

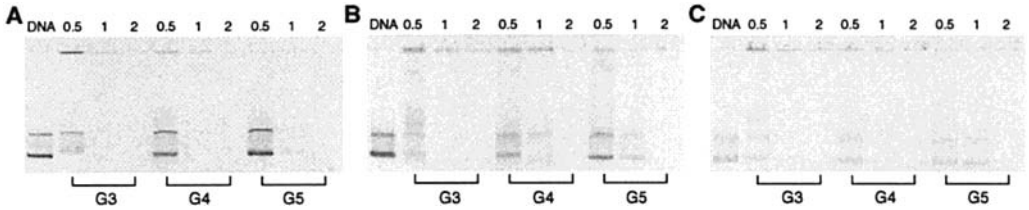


Figure 2. Investigation of polyplex formation by agarose gel band shift assay. Numbers indicate charge ratios (+/−). (A) PPI/DNA polyplex. (B) PPI-DAB/DNA polyplex. (C) PPI-DAB/CB/DNA polyplex. In PPI-DAB/CB/DNA polyplex, all of the DAB moieties are occupied by CB. The original positive image was inverted to make it negative for ease of band discrimination.

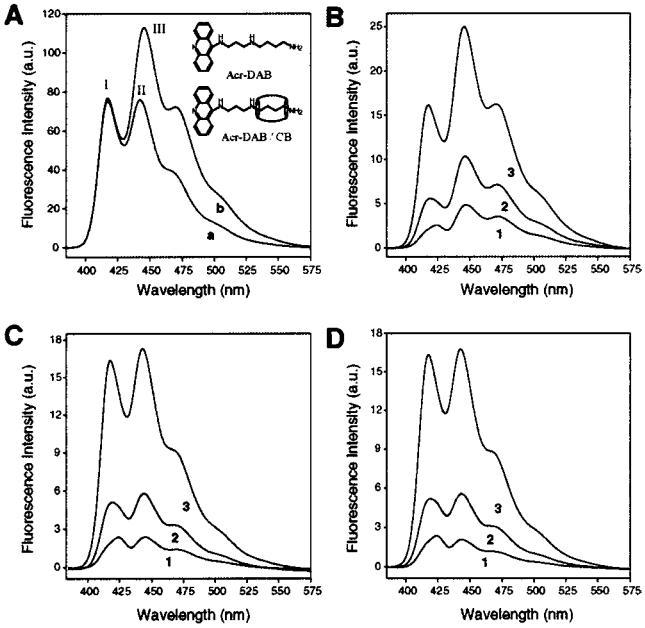


Figure 3. Fluorescence emission spectra of (A) **a**: Acr-DAB; **b**: Acr-DAB/CB and the solution outside the dialysis membrane of (B) CB, (C) PPI-DAB/CB, and (D) PPI-DAB/CB/DNA dialysates after addition of Acr-DAB. **1**: 0.1 μg (1/40 molar equivalent of total CB); **2**: 0.3 μg (3/40); **3**: 1.0 μg (10/40) of Acr-DAB were added to the solution.

well (*20*). In this system, only CB is expected to be freely permeable to the membrane.

The presence of CB in the solution outside the membrane could easily be detected by using DAB-tethered acridine (Acr-DAB) with high sensitivity (Figure 3).[3] The spectrum of Acr-DAB exhibited acridine emission with peaks at 418 (band I) and 442 nm (band II). However, there was a red shift (4 nm) of band II after binding of CB to Acr-DAB with a strong increase in the fluorescence intensity (band III), due to the interaction of CB with the acridine moiety. The shapes of the emission spectra, which were recorded after addition of Acr-DAB to the outside solution of CB dialysate, were identical to that of Acr-DAB/CB (Figure 3B). Varying the amount of added Acr-DAB (1/40, 3/40, and 10/40 molar equivalent of CB) did not influence the shape of the spectrum except in relation to the emission intensity. Identical spectra were obtained in the case where the same amount of Acr-DAB as indicated above was added to an estimated amount of CB, on the assumption that the membrane is freely permeable to CB (data not shown).[4] These results indicate that equilibrium of CB across the membrane had been reached. In contrast, the shape of the emission spectra recorded after addition of varying amounts of Acr-DAB to the outside solution of PPI-DAB/CB or PPI-DAB/CB/DNA dialysate are almost identical to that of Acr-DAB (Figure 3, parts C and D). However, there were slight increases in the fluorescence intensity of band II, indicating that a small amount of CB exists outside the membrane. It has been well established that CB binds tightly to the diaminobutane moiety with high affinity (*19*−*21*). Therefore, the amount of CB present outside the membrane would be minute, and the nearly identically shaped spectra in parts C and D of Figure 3 indicate that there was no change in the CB "beads" threaded on PPI-DAB after the addition of DNA to the PPI-DAB/CB binary complex.

To evaluate the ternary complex as a potential gene delivery vector, the cytotoxicity of the polymers and gene transfer mediated by the complexes were investigated (Figure 4). The results indicated that PPI-DAB/CB polymer had relatively low toxicity with about 50% cells remaining viable even at high concentrations of 100 μg/mL (Figure 4A). Transfection efficiencies (TE) were dependent on the cell type, usually 300−500 times higher in 293 cells than in Vero 76 cells for all polyplexes (PEI, PPI, PPI-DAB, and PPI-DAB/CB polyplexes) tested (Figure 4B). It is well-known that 293 cells are very susceptible to transfection. However, the relative TEs among the polyplexes were similar between the two cell lines. Transfection mediated by PPI-DAB/CB polyplexes was relatively high and was only about 10 times lower than that of PEI, which is one of the most efficient gene carriers hitherto reported (*9*). Szoka and colleagues have shown that fractured PAMAM dendrimers are more efficient in transfection than intact PAMAMs due to the increased flexibility of the fractured dendrimers that enables them to be compact when complexed with DNA and swell when released from DNA (*22*). The lower TEs of PPI, PPI-DAB, and PPI-DAB/CB polyplexes than that of PEI polyplexes may be related to the same mechanism. The TEs of PPI, PPI-DAB, and PPI-DAB/CB polyplexes were increased as the generation number of dendrimers became higher (Figure 4C). Taken together, these results indicated that CB had no negative influence on the TE of polymer/DNA binary complex and the ternary complex is a highly active form of gene delivery vector. This prototype of supramacromolecular ternary complex can

[3] PPI-DAB (G4)/CB or PPI-DAB (G4)/CB/DNA (+/−, 2) each containing 60.4 μg of CB was dissolved in 2 mL of 0.2 M Na_2SO_4. Each of the two solutions and 2 mL of 0.2 M Na_2SO_4 solution containing 60.4 μg of CB were dialyzed against 8 mL of 0.2 M Na_2SO_4 using 3500 molecular weight cutoff tubing (Spectrum Laboratories). After extensive dialysis, 1 mL of the solution outside the tubing was taken. Varying amounts of Acr-DAB (0.1 to 1.0 μg) were added to the solution, and then fluorescence measurements were taken. Fluorescence emission spectra were recorded at room temperature on a Jasco FP-750 spectrofluorometer. The emission bandwidth was set at 5 nm. The excitation wavelength was 370 nm.

[4] For the spectra measurements in Figure 2B, 60.4 μg of CB in 2 mL of 0.2 M Na_2SO_4 was dialyzed against 8 mL of the same solution and 1 mL of the solution outside the membrane was taken for the measurement (final 10-fold dilution). Therefore, 6.04 μg of CB was used for this control.

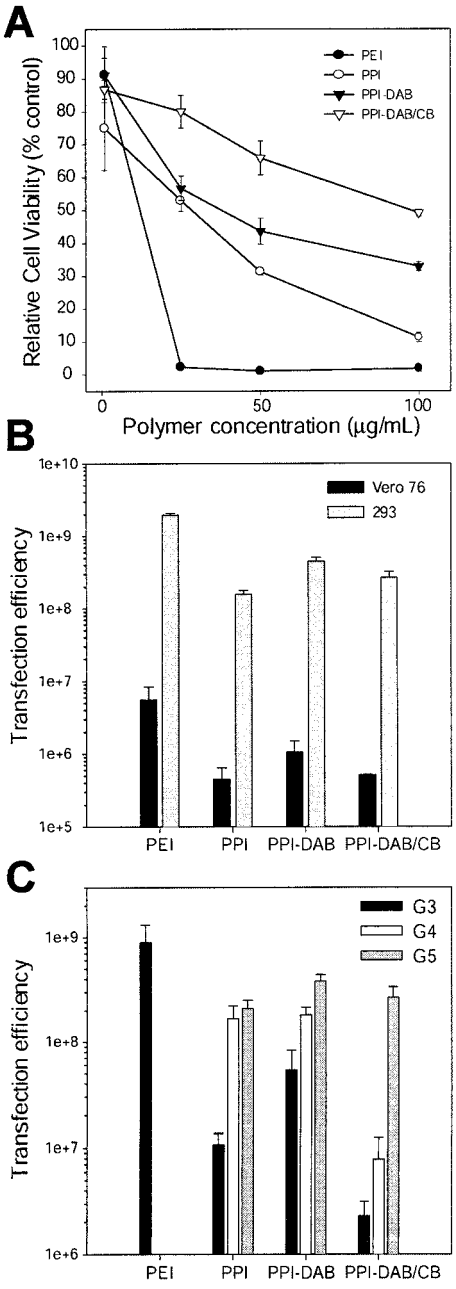


Figure 4. (A) Cytotoxicity in Vero 76 cells by MTT assay. (B) Transfection of Vero 76 and 293 cells with PEI (25 kDa, branched), PPI (G5), PPI-DAB (G5), PPI-DAB (G5)/CB polyplexes. (C) Effects of dendrimer generation on transfection in 293 cells. All polyplexes were formed at charge ratios (+/−) of 2 except PEI polyplex, which was prepared at a weight ratio (polymer/DNA) of 1. TE was expressed as relative light units per mg of cellular protein.

be applied to any type of polymer bearing suitable alkyl diaminobutane moieties and will assist in the further development of artificial viruslike particles.

ACKNOWLEDGMENT

This work was supported by the Korea Research Foundation (DP-0344) and by the Korea Science and Engineering Foundation (R02-2001-000-00031-0 and R11-2000-080-01002-0) for J.-s Park, and the Creative Research Initiative Program of the Korean Ministry of Science and Technology and Brain Korea 21 Program of the Korean Ministry of Education for K. Kim.

LITERATURE CITED

(1) Jenekhe, S. A., and Chen, X. L. (1998) Self-assembled aggregates of rod-coil block copolymers and their solubilization and encapsulation of fullerenes. *Science 279*, 1903−1907.

(2) Ohkita, M., Lehn, J.-M., Baum, G.., and Fenske, D. (1999) Helicity coding: programmed molecular self-organization of achiral nonbiological strands into multiturn helical superstructures: synthesis and characterization of alternating pyridine-pyrimidine oligomers. *Chem. Eur. J. 5*, 3471−3481.

(3) Archut, A., Azzellini, G. C., Balzani, V., De Cola, L., and Vögtle, F. (1998) Toward photoswitchable dendritic hosts. Interaction between azobenzene-functionalized dendrimers and eosin. *J. Am. Chem. Soc. 120*, 12187−12191.

(4) Harada, A., and Kataoka, K. (1999) On−off control of enzymatic activity synchronizing with reversible formation of supramolecular assembly from enzyme and charged block copolymers. *J. Am. Chem. Soc. 121*, 9241−9242.

(5) Prins, L. J., Huskens, J., de Jong, F., Timmerman, P., Reinhoudt, D. N. (1999) Complete asymmetric induction of supramolecular chirality in a hydrogen-bonded assembly. *Nature 398*, 498−502.

(6) Haycock, R. A., Yartsev, A., Michelsen, U., Sundström, V., and Hunter, C. A. (2000) Self-assembly of pentameric porphyrin light-harvesting antennae complexes. *Angew. Chem., Int. Ed. 39*, 3616−3619.

(7) Isobe, H., Tomita, N., Lee, J. W., Kim, H.-J., Kim, K., and Nakamura, E. (2000) Ternary complexes between DNA, polyamine, and cucurbituril: A modular approach to DNA-binding molecules. *Angew. Chem., Int. Ed. 39*, 4257−4260.

(8) Gibson, H. W., Yamaguchi, N., Hamilton, L., and Jones, J. W. (2002) Cooperative self-assembly of dendrimers via pseudorotaxane formation from a homotritopic guest molecule and complementary monotopic host dendrons. *J. Am. Chem. Soc. 124*, 4653−4665.

(9) Nishikawa, M., and Huang, L. (2001) Nonviral vectors in the new millennium: Delivery barriers in gene transfer. *Hum. Gene Ther. 12*, 861−870.

(10) Wu, G. Y., Wilson, J. M., Shalaby, F., Grossman, M., Shafritz, D. A., and Wu, C. H. (1991) Receptor-mediated gene delivery in vivo. Partial correction of genetic analbuminemia in Nagase rats. *J. Biol. Chem. 266*, 14338−14342.

(11) Boussif, O., Lezoualc'h, F., Zanta, M. A., Mergny, M. D., Scherman, D., Demeneix, B., and Behr, J. (1995) A versatile vector for gene and oligonucleotide transfer into cells in culture and in vivo: Polyethylenimine. *Proc. Natl. Acad. Sci. U.S.A. 92*, 7297−7301.

(12) Kukowska-Latallo, J. F., Bielinska, A. U., Johnson, J., Spindler, R., Tomalia, D. A., and Baker, J. R., Jr. (1996) Efficient transfer of genetic material into mammalian cells using Starburst polyamidoamine dendrimers. *Proc. Natl. Acad. Sci. U.S.A. 93*, 4897−4902.

(13) Lim, Y.-B., Kim, S.-M., Lee, Y., Lee, W.-K., Yang, T.-G., Lee, M.-J., Suh, H., and Park, J.-S. (2001) Cationic hyperbranched poly(amino ester): A novel class of DNA condensing molecule with cationic surface, biodegradable three-dimensional structure, and tertiary amine groups in the interior. *J. Am. Chem. Soc. 123*, 2460−2461.

(14) Eaton, M. A. W., Baker, T. S., Catterall, C. F., Crook, K., Macaulay, G. S., Mason, B., Norman, T. J., Parker, D., Perry, J. J. B., Taylor, R. J., Turner, A., and Weir, A. N. (2000) A new self-assembling system for targeted gene delivery. *Angew. Chem., Int. Ed. 39*, 4063−4067.

(15) Cartier, R.; Reszka, R. (2002) Utilization of synthetic peptides containing nuclear localization signals for nonviral gene transfer systems. *Gene Ther. 9*, 157−167.

(16) Wagner, E., Plank, C., Zatloukal, K., Cotton, M., and Birnstiel, M. L. (1992) Influenza virus hemagglutinin HA-2 N-terminal fusogenic peptides augment gene transfer by transferrin-polylysine-DNA complexes: Toward a synthetic virus-like gene-transfer vehicle. *Proc. Natl. Acad. Sci. U.S.A. 89*, 7934−7938.

(17) Wu, G. Y.; Wu, C. H. (1988) Evidence for targeted gene delivery to Hep G2 hepatoma cells in vitro. *Biochemistry 27*, 887−892.
(18) Frankel, A. D., and Young, J. A. (1998) HIV-1: Fifteen proteins and an RNA. *Annu. Rev. Biochem. 67*, 1−25.
(19) Whang, D., Jeon, Y.-M., Heo, J., and Kim, K. (1996) Self-assembly of a polyrotaxane containing a cyclic "bead" in every structural unit in the solid state: Cucurbituril molecules threaded on a one-dimensional coordination polymer. *J. Am. Chem. Soc. 118*, 11333−11334.
(20) Jeon, Y.-M., Kim, J., Whang, D., and Kim, K. (1996) Molecular container assembly capable of controlling binding and release of its guest molecules: Reversible encapsulation of organic molecules in sodium ion complexed cucurbituril. *J. Am. Chem. Soc. 118*, 9790−9791.
(21) Lee, J. W., Ko, Y. H., Park, S.-H., Yamaguchi, K., and Kim, K. (2001) Novel pseudorotaxane-terminated dendrimers: Supramolecular modification of dendrimer periphery. *Angew. Chem., Int. Ed. 40*, 746−749.
(22) Tang, M. X., Redemann, C. T., and Szoka, F. C., Jr. (1996) In vitro gene delivery by degraded polyamidoamine dendrimers. *Bioconjugate Chem. 7*, 703−714.

BC025581R

ARTICLES

Class-Selective Drug Detection: Fluorescently-Labeled Calmodulin as the Biorecognition Element for Phenothiazines and Tricyclic Antidepressants

Phillip M. Douglass, Lyndon L. E. Salins, Emre Dikici, and Sylvia Daunert*

Departments of Chemistry and Pharmaceutical Sciences, University of Kentucky, Lexington, Kentucky 40506-0055. Received September 3, 2001; Revised Manuscript Received May 17, 2002

A small-scale, homogeneous, rapid sensing system for phenothiazines and tricyclic antidepressants (TCAs) has been developed by employing fluorescently labeled mutant calmodulin (CaM) as the recognition element. A calmodulin mutant containing a unique cysteine residue at position 109 on the protein was expressed in *Escherichia coli*. Following purification, the environment-sensitive, thiol-specific fluorophores *N*-[2-(1-maleimidyl)ethyl]-7-(diethylamino)coumarin-3-carboxamide (MDCC), 6-acryloyl-2-dimethylaminonaphthalene (acrylodan), and 4-[*N*-(2-(iodoacetoxy)ethyl)-*N*-methylamino]-7-nitrobenz-2-oxa-1,3-diazole (IANBD ester) were coupled to the C109 site of the mutant protein. The response of labeled CaM in the presence of calcium to increasing concentrations of chlorpromazine hydrochloride (CPZ), as well as other phenothiazines and structurally related antipsychotics and antidepressants, was investigated. Fluorescence measurements were performed on benchtop and microtiter plate fluorometers. The responses were characterized as a change in the signal intensity of the labeled protein upon ligand binding, and the stability of the system was monitored over a nine-month period. The assay showed specificity for the phenothiazine and TCA classes of drugs, with limits of detection in the micromolar range. Selectivity studies indicated negligible response of the biosensing system to structurally unrelated compounds. This work represents a proof-of-concept assay for rapid, homogeneous detection of drugs employing binding proteins as the biorecognition element.

INTRODUCTION

The use of fluorescently labeled proteins has recently resulted in a number of biosensing systems for a variety of biomolecules (*1*−*4*). With proteins, one can capitalize on a highly evolved natural sensing system that provides selective and sensitive detection of target ligands and analytes. Such systems have not only been indicated for detection of drugs in a homogeneous-based format as reported herein, but also as a means of studying drug activity in cell-based screens (*2*, *5*).

In high-throughput screening (HTPS) applications, assays are not necessarily required to be highly specific. Screens that are designed to detect classes of drugs versus assays that detect single compounds are more practical and cost-effective in the analysis of combinatorial chemistry products (*6*). "Hits" identified from these preliminary screens need further analysis, and conventional analytical methods are then employed to characterize the nature and level of drug response. Ideal HTPS systems should be homogeneous, facile, and rapid. In addition, they should be amenable for miniaturization and small volume detection of a large number of compounds.

Calmodulin is a 148 amino acid, 17-kDa calcium binding protein. Ubiquitous in nature, CaM plays an important role in intracellular signaling pathways (*7*, *8*). In the presence of calcium, the protein undergoes a conformational change resulting in the exposure of two hydrophobic pockets, one each in the N- and C-termini of the protein. These hydrophobic pockets have a high affinity for enzymes such as phosphodiesterase and myosin light chain kinase, which are activated upon binding to CaM (*9*). The phenothiazines, a family of antipsychotic drugs, bind to the C-terminal hydrophobic pocket of CaM, acting as antagonists of such enzymes (*8*, *10*). In addition, CaM also has affinity for the structurally related tricyclic antidepressants (TCAs). Controversy exists in the literature as to whether the phenothiazines and TCAs also bind to the N-terminal hydrophobic pocket as one might expect, given that the two domains share a 44% residue homology (*9*). Most, however, tend to support the idea of the drugs only binding to the C-terminal with significant affinity (K_d's in the micromolar range). Upon binding to the drug, CaM undergoes a hinge-motion conformational change about its central, 8-turn α-helix, resulting in a collapse of the protein as evident in Figure 1. The crystal structure of CaM bound to trifluoperazine (TFP) has been determined (see Figure 1, at right). Cook et al found that 13 residues form contacts with TFP. Ten of these are hydrophobic; the others are glutamates and interact via van der Waals forces. Only one (Glu11) is in the N-terminal domain of the protein (*11*). The tricyclic ring lies between the side chains of Met124 and Met144; these residues interact directly with the ligand's aromatic rings (*9*, *11*, *12*).

* To whom correspondence should be addressed. Phone: (859) 257-7060. Fax: (859) 323-1069. E-mail: daunert@pop.uky.edu.

10.1021/bc010080b CCC: $22.00 © 2002 American Chemical Society
Published on Web 10/19/2002

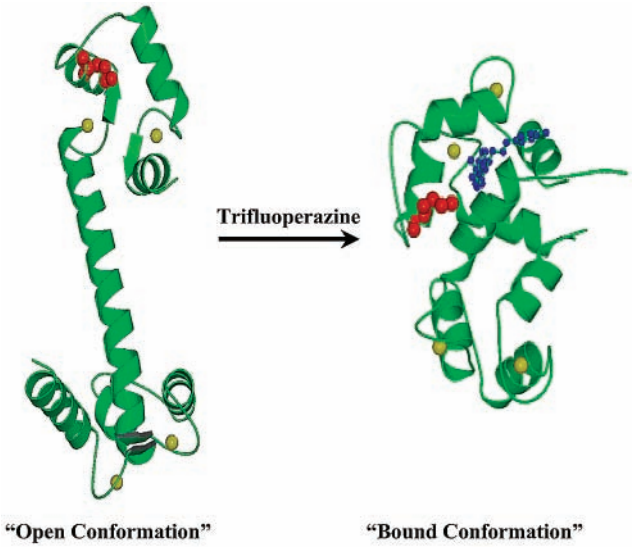


Figure 1. Ribbon diagram of calcium-bound calmodulin in the absence (left) and presence (right) of the phenothiazine trifluoperazine. Calcium is represented by yellow spheres, trifluoperazine is colored blue, and the site of fluorophore conjugation, Cys109, is colored red. Crystal structures were obtained from the Brookhaven Protein Data Bank (files 1CLL and 1CTR) and displayed using Molscript 1.4 (*31*) and Raster3D (*32*) software.

In this work, we report a proof-of-concept approach to drug detection utilizing the changes in conformation that binding proteins undergo upon binding to their ligand. Specifically, the study of fluorescently labeled CaM as a sensing element for the phenothiazine class of drugs and the related TCAs is described. The affinity of CaM for phenothiazines has previously been used in our laboratory as the basis of developing an affinity purification method for the protein and other recombinant proteins fused to CaM (*13*−*15*). Most recently, site-selective fluorescently labeled CaM has been employed in our group as a biosensing system for the detection of calcium (*16*). Given that CaM binds not only to calcium but also to phenothiazines, it is hypothesized that the change in conformation and environment that calcium-bound CaM undergoes upon binding to these drugs will allow the protein to act as a highly sensitive sensing element in their detection (*16*). It has been demonstrated that the location of the fluorophore on the protein highly influences the change in signal observed and thereby the sensitivity and detection limits of the sensing system (*16*). The CaM employed in our studies lacks any native cysteine residues (*17*). A mutant of this CaM has been rationally designed to contain a unique cysteine at a position on the protein that appeared to undergo significant environmental and conformational change upon drug binding (*16*). Utilizing the cysteine's thiol group, mutant CaM was coupled to three different sulfhydro-specific environment-sensitive fluorophores, namely, MDCC, acrylodan, and IANBD ester. The resulting CaM conjugates were then evaluated as biosensing elements for the detection of phenothiazines and related TCAs. Steady-state fluorescence experiments were conducted to verify a difference in fluorescence signal emitted by the fluorescently labeled protein in the presence or absence of analyte. The class-selectivity of the biosensing system toward compounds both structurally related and unrelated to the phenothiazines and TCAs was also evaluated.

EXPERIMENTAL PROCEDURES

Reagents. Luria-Bertani (LB) medium was purchased from GibcoBRL (Gaithersburg, MD). Ethylenebis(oxyethylenenitrilo)tetraacetic acid (EGTA), dithiothreitol (DTT), chlorpromazine hydrochloride (CPZ), trifluoperazine dihydrochloride (TFP), thioridazine hydrochloride, amitryptiline hydrochloride, α-D-glucose, and acetylsalicylic acid were obtained from Aldrich (Milwaukee, WI). Ampicillin, chlorprothixene hydrochloride, and imipramine hydrochloride were obtained from Sigma (St. Louis, MO). Tris(hydroxymethyl)aminomethane (Tris) and 4-(2-hydroxyethyl)-1-piperazineethanesulfonic acid (HEPES) were purchased from Research Organics (Cleveland, OH). The fluorophores *N*-[2-(1-maleimidyl)ethyl]-7-(diethylamino)coumarin-3-carboxamide (MDCC), 6-acryloyl-2-dimethylaminonaphthalene (acrylodan), and 4-[*N*-(2-(iodoacetoxy)ethyl)-*N*-methylamino]-7-nitrobenz-2-oxa-1,3-diazole (IANBD ester) were obtained from Molecular Probes (Eugene, OR). Isopropyl β-D-thiogalactopyranoside (IPTG) was purchased from GibcoBRL (Gaithersburg, MD). Fluoronunc white C96 Maxisorp microtiter plates were purchased from VWR (South Plainfield, NJ). The expression plasmid pVUC-1 was kindly provided by Dr. D. M. Watterson (*17*). The phenothiazine 2-(trifluoromethyl)-10*H*-(3′-aminopropyl) phenothiazine hydrochloride (TAPP) was synthesized in our group as previously described (*13*, *15*, *18*). The bicinchoninic acid (BCA) protein microassay reagent kit from Pierce (Rockford, IL) was used to determine the concentration of the purified CaM. Deionized distilled water (Milli-Q water purification system, Millipore, Bedford, MA) was used to prepare all solutions and mobile phases. All chemicals employed were reagent grade or better.

Apparatus. Bacterial colonies were grown on agar plates at 37°C in a Fisher Scientific Incubator (Fair Lawn, NJ). Cell cultures were grown in an Orbital Shaker from Forma Scientific (Marietta, OH) and pelleted using a Beckman J2-MI Centrifuge (Palo Alto, CA). Unpurified protein fractions were filtered with a 0.2 μm filter from Nalgene (Rochester, NY). A BIOCAD SPRINT Perfusion Chromatography System by PE Biosystems (Foster City, CA) was used for protein purification. Protein purity was verified by sodium dodecyl sulfate polyacrylamide gel electrophoresis (SDS−PAGE) using a PhastSystem from Pharmacia Biotech (Uppsala, Sweden). Purified protein was concentrated via lyophilization using a VirTis Bench Top 3 Freeze-Dryer (Gardiner, NY). Protein was dialyzed against the correct buffer using 10000 MWCO Snakeskin pleated dialysis tubing by Pierce (Rockford, IL). Initial fluorescence studies were performed on a Fluorolog-2 fluorometer, Spex Industries (Edison, NJ) equipped with a 450-W xenon lamp and excitation and emission monochromators. Assay development was carried out on a Cytofluor 4000 fluorescence microtiter plate reader by PE Biosystems (Foster City, CA) equipped with the following filters: 420/50-nm excitation and 490/40-nm emission (for MDCC), 380/20-nm excitation, 490/40-nm emission (for acrylodan), 485/20-nm excitation, 530/25-nm emission (for IANBD ester), 313/55-nm excitation, 460/40-nm emission (for chlorpromazine).

Expression of Calmodulin. The plasmid pVUC-1 (*17*), containing the gene for mutant CaM with a methionine−cysteine mutation at residue 109 (*16*) was transformed into *Escherichia coli* JM109 competent cells and then plated on LB plates containing ampicillin (100 μg/mL). After growing overnight at 37 °C, a colony of transformed cells was picked and incubated overnight in 5 mL of LB media containing 75 μg/mL ampicillin. The culture was transferred into 500 mL of LB and incubated for an additional 7−8 h, until an optical density at 600 nm of 0.6 was obtained. Protein expression was induced

by the addition of 1 mM IPTG. Following 5 h of incubation with IPTG, the cells were harvested by centrifugation, washed in 10 mM HEPES buffer containing 0.5 mM $CaCl_2$, pH 7.5 (Buffer A), and lysed via sonication. The crude extract was boiled for 5 min to precipitate out additional undesired proteins.

Purification of CaM109. A TAPP affinity column was used to purify the mutant CaM following the method of Hentz et al. (*13*). Purified protein was concentrated overnight by lyophilization, and the purity of the protein was confirmed by SDS−PAGE employing silver staining development.

The lyophilized protein was resuspended in 500 μL of deionized water and dialyzed in Buffer A for 24 h to remove any remaining EGTA present from the purification process. Protein concentration was determined by using the BCA protein assay.

Preparation of Fluorescently-Labeled CaM109. A volume of 1 mL of purified CaM109 was dialyzed against Buffer A, containing DTT to eliminate any disulfide linkage formation in preparation for fluorophore conjugation. The protein was then dialyzed to remove any excess DTT. Immediately following DTT removal, a 5-fold molar excess of fluorophore (MDCC, IANBD ester, or acrylodan) was added in the dark. The coupling reactions were allowed to proceed for 4 h with stirring, at which time the samples were loaded onto a Sephadex G-25 size-exclusion column to separate conjugated protein from excess fluorophore. The conjugates were eluted with Buffer A. A SDS−PAGE was run to verify which elution fractions contained the protein conjugate. The fractions containing the conjugate were pooled together, and the final protein concentration was calculated. The purified CaM109 conjugate was stored at 4 °C in the dark until use.

Fluorescence Studies of CaM109-MDCC with CPZ. With the exception of initial optimization studies (where noted), all experiments were performed on the microtiter plate fluorometer with an assay volume of 300 μL, utilizing the CaM109-MDCC conjugate, and CPZ as the analyte. All results reported are the average of a minimum of three replicates, corrected for background, with the blank consisting of Buffer A. Detection limits reported were calculated with S/N = 3.

Chlorpromazine Fluorescence. Solutions of increasing concentrations of CPZ, 1×10^{-7} to 0.1 M, were prepared in Buffer A. Fluorescence measurements were taken on the microtiter plate fluorometer, using the filters previously noted.

MDCC/CPZ Interaction. Aliquots of 25 μL of CPZ solutions ranging in concentration from 1×10^{-7} to 0.1 M were added to 1.5 mL samples of MDCC in Buffer A. Response of the biosensing system to MDCC was measured in the fluorescence microtiter plate reader employing the parameters described above.

Dilution Curve. To determine the optimum concentration of labeled CaM109 to be used in subsequent experiments, the fluorescence emitted by increasing concentrations of each conjugate was measured on the benchtop fluorometer (CaM109-MDCC) or on the fluorescence microtiter plate reader (CaM109-MDCC, CaM109-acrylodan, CaM109-IANBD). Dilutions of labeled CaM109 were prepared ranging from 1×10^{-10} to 1×10^{-5} M. The protein concentration at which an increase in fluorescence signal was considerably larger than that of the background while still being relatively low was chosen as the concentration to be employed in all subsequent experiments.

Time Study of CaM109-MDCC/CPZ Interaction. An experiment was conducted on the benchtop fluorometer to observe the change in fluorescence response of the conjugated CaM109-MDCC to the binding of CPZ at various incubation times. A volume of 1.5 mL of CaM109-MDCC was incubated with 25 μL of 1×10^{-2} M CPZ in Buffer A at RT on a 400 rpm shaker for various periods of time. Average fluorescence quenching values were plotted against the incubation times in minutes. The minimum incubation time allowing for maximal fluorescence response was chosen for all subsequent assays.

Calibration Curves for CaM109-MDCC with Analyte. Aliquots of 25 μL of various concentrations of analytes (phenothiazines, TCAs, structurally related chlorprothixene, and other analytes) were added to a 1.5 mL volume of the labeled protein. The mixture was then incubated on a 400 rpm shaker at RT for 2 min and analyzed in the benchtop fluorometer (CPZ only) or fluorescence microtiter plate reader as previously described. Average fluorescence quenching was plotted against the log of the analyte concentration in the sample. Experiments were also conducted with the additional fluorophores, acrylodan, and IANBD ester following the same procedure.

Stability Studies. The fluorescent response of the CaM109-MDCC conjugate to 1.6×10^{-5} M CPZ was measured on days 3, 14, 21, 99, 151, and 269 of postconjugation in the fluorescence microtiter plate reader following the procedure outlined above.

RESULTS AND DISCUSSION

The detection of phenothiazines and TCAs by the fluorescently labeled mutant CaM described here is based on the calcium-dependent change in conformation of the protein. Calmodulin belongs to a family of binding proteins that contain helix-loop-helix motifs referred to as EF hands. Calmodulin has four such motifs; two are located in both the N- and C-terminal regions of the protein (*8*). Upon binding calcium, CaM undergoes a conformational change about the central α-helix, exposing a hydrophobic region in each domain (*11, 12*). By capitalizing on this change, we have reported herein the development of a class-selective means of drug detection. In addition, employing a biological recognition element, namely the binding protein CaM, takes advantage of nature's highly evolved means of detection and demonstrates the potential application of these binding proteins to current needs of the chemical, pharmaceutical, and biotechnology industries. In particular, our approach provides an alternative solution in the demand for rapid, reliable, and reproducible screening methods in drug discovery programs.

The synthetic CaM employed in our studies (*17*) resembles higher plant CaM with the exception of threonine-26, glycine-96, valine-136, and glutamine-143, which are common to vertebrate CaM. As such, it does not contain any cysteine residues in its structure (*17*). Site-directed mutagenesis on this gene has been performed previously in our group (*16*) to study the structure−activity of certain specific mutations on the protein and to develop a biosensing system for the detection of calcium. On the basis of crystallographic analyses of calcium-bound CaM in both the presence and absence of the phenothiazine trifluoperazine (Figure 1) (*11, 12*), CaM containing a mutation at residue 109 (Met109Cys; CaM109) was chosen as the biosensing element to be employed in the development of the assay for the phenothiazines and TCAs. Located on the surface of the hydrophobic pocket of CaM's C-terminal domain, residue

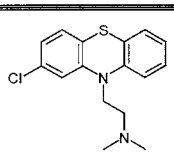
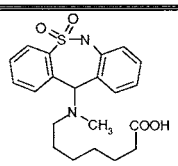
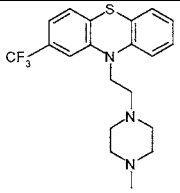
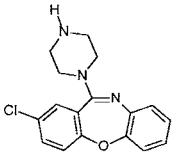
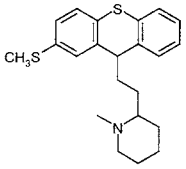
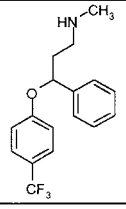
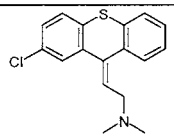
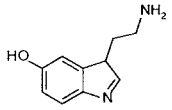
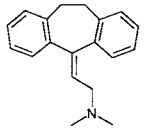
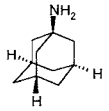
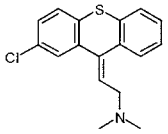
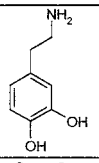
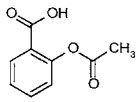
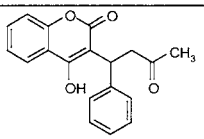
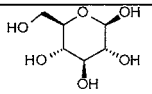
Compound	Structure	Compound	Structure
Chlorpromazine		Tianeptine	
Trifluoperazine		Amoxapine	
Thioridazine		Fluoxetine	
Chloprothixene		Serotonin	
Amitriptyline		Amantadine	
Imipramine		Dopamine	
Acetylsalicylic acid		Warfarin	
Glucose			

Figure 2. General structure of the substances employed in this study.

109's location should allow for efficient conjugation of the fluorophore to the protein (*16*). Studies of these crystal structures have shown that the microenvironment surrounding residue 109 undergoes changes upon the addition of drug, as residue 109 is one of 10 involved in hydrophobic interactions with the phenothiazine class of drugs (*11*, *12*). From the results reported in these studies in addition to previous mutational studies performed with fluorescently labeled CaM (*16*), it was hypothesized that a fluorophore attached at this position would be sensitive to drug binding.

It is important to note, as one can observe from Figure 2, that the phenothiazines and related compounds are naturally fluorescent. Thus, it should be possible to detect them based on their intrinsic fluorescence alone. Having a λ_{ex} of 340 nm and a λ_{em} of 460 nm, CPZ fluorescence could also potentially interfere with the emission wavelength of MDCC, the fluorophore employed in the majority of the studies reported herein. Therefore, detection of a change in CPZ fluorescence as a result of increasing concentrations was evaluated. Figure 3 demonstrates that although CPZ fluorescence can be used in the direct detection of the drug in a sample solution, the detection limit, 6.3×10^{-4} M, may not be sensitive enough for the HTPS of this class of drugs.

The detection of CPZ using CaM109 coupled to three different fluorophores, MDCC, acrylodan, and IANBD ester, was then investigated. The unique cysteine of CaM109 was conjugated with these sulfhydro-specific fluorophores; the concentration of the fluorophore in the reaction mixture was five times that of the protein. Following conjugation, excess fluorophore was separated from the conjugated protein by using size-exclusion chromatography. Fractions of eluant corresponding to CaM109-fluorophore, as determined by SDS−PAGE, were pooled together and employed as the sensing element used in all studies. Initial assay development was performed on a standard benchtop fluorometer, with

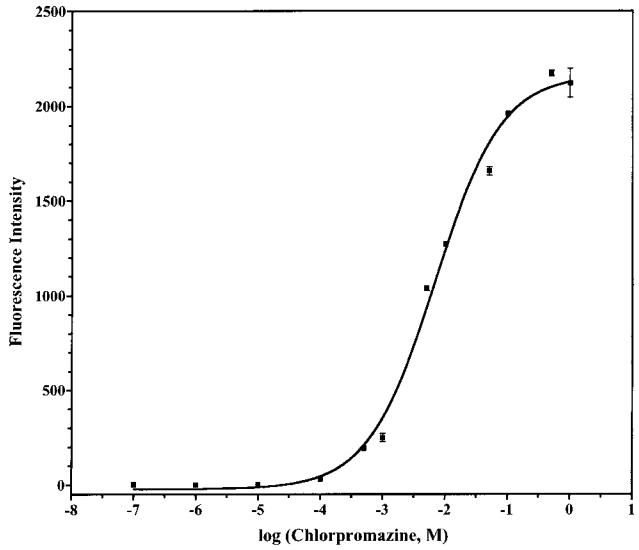


Figure 3. Chlorpromazine fluorescence in the absence of CaM109-MDCC. Error bars not visible are concealed by the points on the graph.

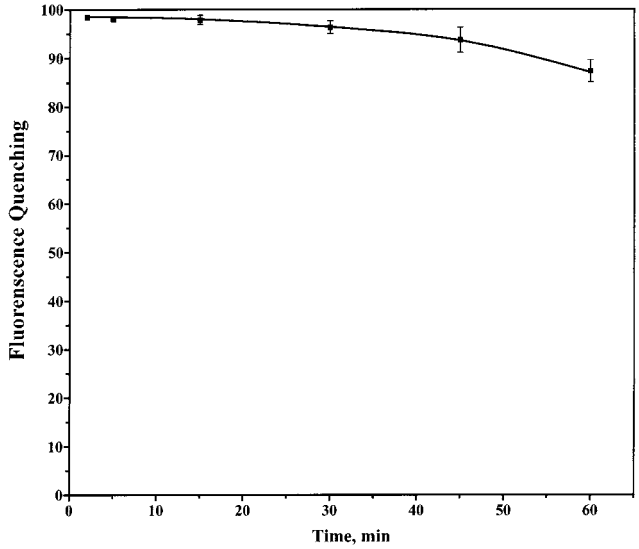


Figure 4. Effect of incubation time between CaM109-MDCC and 1×10^{-4} M CPZ. Error bars not visible are concealed by the points on the graph.

assay volumes of 1.5 mL. To determine the CaM109 concentration that would be used in subsequent experiments, dilution curves were constructed. In these experiments, fluorescence measurements were made employing increasing concentrations of the conjugated protein. For CaM109-MDCC, a concentration of 5×10^{-8} M was chosen. This concentration provided a large enough signal for development of the assay while not consuming a significant amount of reagent.

To determine how long the biosensing element needed to be incubated with the analyte, a time study was performed. From this study, it was determined that an incubation time of 2 min resulted in the generation of maximal sensitivity of the reagent (CaM) to analyte (CPZ) (Figure 4). Such rapid reaction kinetics can provide an advantage for this type of sensing scheme; rapid detection is one of the desired properties of assays employed in the HTPS of drugs and allows for a greater number of compounds to be screened per time.

CaM109 coupled to MDCC has previously been reported by our group as a sensitive biorecognition element

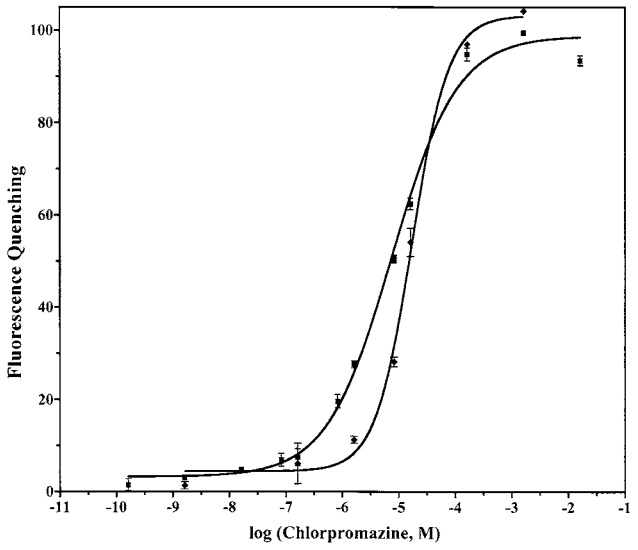


Figure 5. Calibration curve for CPZ employing CaM-MDCC and performed in a benchtop fluorometer (●), with a total assay volume of 1.5 mL, and on a microtiter plate fluorometer (◆), with a total assay volume of 300 μL.

for calcium detection (*16, 19*). As such, we decided to initially focus on this conjugate when designing a sensing scheme for phenothiazines due to their calcium-dependent binding to CaM. MDCC is composed of a reactive maleimide connected to a fluorescent coumarin moiety by a flexible aliphatic spacer arm; MDCC is excited at 425 nm and emits fluorescence at 474 nm. Upon coupling CaM109 with MDCC, a blue shift to 460 nm occurs in the fluorescence emission spectra of the fluorophore (data not shown). We postulate that MDCC is residing in the hydrophobic pocket in the C-terminal domain of the protein in the absence of CPZ. Residues 92, 100, 105, 109, 124, 125, 127, 128, 136, 141, and 144 have been shown to compose this hydrophobic pocket (*11*). As seen in Figure 5, a decrease in the fluorescence quantum yield (quenching) is observed upon binding of the phenothiazine chlorpromazine (CPZ) to the CaM109-MDCC, with a detection limit of 5×10^{-7} M (on the benchtop fluorometer). This quenching could be explained by the change in environment that MDCC experiences upon binding of CPZ to this hydrophobic region. To allow for binding, the flexible spacer arm and the coumarin of the MDCC may be displaced from this region, exposing the fluorophore to a more polar environment. A subsequent red shift in the fluorescence spectra observed upon the addition of increasing concentrations of CPZ supports this idea (data not shown). Red shifts are often, but not always, associated with a decrease in quantum yield (*20*). Also, it is possible that the diethylamino group of the fluorophore is less constrained in the presence of CPZ. Previous work from other groups has shown that coumarins having the lone pair of the amino substituent constrained and not able to interact optimally with the π electrons of the aromatic ring are highly fluorescent (*21*). Studies performed by us and others on the mechanism of response of fluorescently labeled proteins support this theory (*21*−*23*). Although the CPZ native fluorescence spectrum (λ_{ex} and λ_{em} of 340 and 460 nm, respectively) interferes with that of CaM109-MDCC, it does not significantly hinder the sensitivity of our biosensing system. In addition, a steady-state study conducted with MDCC and CPZ indicated that in the absence of CaM the fluorescence signal generated by MDCC is not significantly quenched by the analyte. This observation indicates that the

quenching observed in the CaM-based assays is a result of the changes occurring in the dynamics of the protein−analyte interactions, and not simply due to an interaction between the analyte and the fluorophore itself. An alternative explanation, related to the fact that CaM is being employed as a molecular handle, would be that the fluorophore and analyte are brought into close proximity causing a change in fluorescence as a result of the interaction between the two. To elucidate the exact mechanism by which changes in fluorescently labeled CaM conformation affects the fluorescence emission of the fluorophore, studies involving time-resolved anisotropy measurements need to be performed.

It is important to note that the detection limit of 1.6×10^{-6} M observed for CPZ when measured on the fluorescence microtiter plate reader was higher than that observed in the larger volume format. A shift in the detection limit to higher concentrations when measuring the CPZ levels on the fluorescence microtiter plate reader can in part be explained to a lower collection efficiency of the instrument, and the total amount of reagent present in the 300 μL samples vs the 1 mL samples. Since this assay has been scaled down 10-fold in volume, for optimal sensitivity the concentration of reagent may need to be increased to compensate for this reduction in sample volume. It should be noted that concentrations in primary high-throughput screens can be as high as 10^{-5} M, allowing for the identification of compounds with moderate interaction. There is a need, however, for small volume assays, especially when the supply of new compounds from combinatorial libraries may be limited (*24*−*27*). Reduced consumption as a result of small volume assays allows for synthetic or biological samples to be subjected to a greater number of analyses at these higher concentrations (*28*).

The other two fluorophores, acrylodan and IANBD ester, were similarly evaluated. These CaM109 conjugates were also able to sense increasing levels of CPZ, although with worse detection limits. The acrylodan- and IANBD-labeled CaM each had a shift in detection limits 1 order of magnitude higher (1.6×10^{-5} M), and a reduced maximal fluorescence quenching of 80% at 1×10^{-3} M of CPZ as opposed to 100% for CaM109-MDCC. Nonetheless, CPZ detection using these additional CaM conjugates demonstrates the adaptability of the CaM-based sensing system to fluorophores of differing fluorescence emission profiles.

As previously mentioned, this assay was intended to detect the structurally related TCAs as well, which also are used in the treatment of psychoses and depression. These compounds are also CaM inhibitors (*29*); thus, it was expected the system would elicit a similar response to these drugs. Table 1 includes the response of CaM109-MDCC to the TCAs imipramine and amitriptyline and the structurally related chlorprothixene and compares their response to representative phenothiazines. All phenothiazines and related tricyclic drugs tested had detection limits of 7.4×10^{-6} M or lower, with the phenothiazine trifluoperazine having the lowest detection limit of 1.6×10^{-7} M. Also shown in Table 1 is the response to nine unrelated compounds: acetylsalicylic acid, α-D-glucose, and several nontricyclic antidepressants. Acetylsalicylic acid, dopamine, serotonin, and warfarin were selected as models of structurally unrelated drugs that contain an aromatic ring, and serotonin and dopamine act on the central nervous system. Amantadine and glucose were chosen due to their polarity as compared to TCAs. Tianeptine, amoxapine, and fluoxetine were tested, because they are structurally similar to tricyclic antidepressants but have different activity and mechanism of action. The results showed minimal fluorescence change for all of these compounds, except for fluoxetine. Tianeptine and amoxapine, selective serotonin reuptake inhibitors (SSRI), are structurally similar to tricyclic antidepressants. Their mechanism of action is different, and they do not inhibit calmodulin (*30*). We postulate that tianeptine's long hydrophilic chain and amoxapine's piperazine ring with truncated spacer, prevents them from binding to calmodulin. Fluoxetine, although not a tricyclic antidepressant, showed some response in the assay. This drug has two aromatic rings and contains a hydrophilic side chain with the proper length. We hypothesize that due to its flexibility, fluoxetine can fit into the hydrophobic pocket of calmodulin and the hydrophilic side chain can further stabilize the binding. However, to achieve 30% quenching, as with the TCAs, the concentration required for this was substantially greater. The detection limit for fluoxetine was found to be 5.9×10^{-4} M. This value is above the usual concentration range of drug detection required in high-throughput screening applications. Therefore, CaM provides class-selective detection, more specifically for those drugs belonging to the phenothiazines and TCA families of compounds.

Table 1. Comparison of CaM109-MDCC Response to Phenothiazines, Related Tricyclics, and Other Structurally Unrelated Compounds[c]

compound	max. fluorescence quenching (%)	detection limit (M)
chlorpromazine[a]	97.2	1.6×10^{-6}
trifluoperazine[a]	99.8	1.6×10^{-7}
thioridazine[a]	100.0	1.6×10^{-6}
chlorprothixene[b]	100.0	7.4×10^{-6}
amitriptyline[b]	91.3	1.5×10^{-6}
imipramine[b]	100.0	7.4×10^{-6}
amoxapine[b]	0.5	−
tianeptine[b]	13.7	−
fluoxetine[c]	30.1	5.9×10^{-4}
acetylsalicylic acid[c]	8.7	−
glucose[c]	8.3	−
warfarin[c]	8.3	−
dopamine[c]	13.7	−
amantadine[c]	1.4	−
serotonin[c]	6.9	−

[a] Note: all studies were performed on fluorescence microtiter plate reader. [b] Phenothiazines. [c] Related tricyclics. [d] Structurally unrelated compounds.

A stability study was conducted over a nine-month period to observe the change in fluorescence signal of CaM109-MDCC since initial conjugation (data not shown). The reagent was stored in solution at 4 °C in the dark. These studies were performed to evaluate the long-term storage of the CaM109-MDCC biosensing reagent. Typical calibration curves for CPZ were obtained each time as shown in Figure 5. Results indicated a shift in the detection limit toward higher concentrations; after nine months, the detection limit for CPZ was an order of magnitude higher (1×10^{-5} M) than that observed when fresh CaM109-MDCC was employed.

In conclusion, it has been demonstrated that site-specific fluorescently labeled CaM can be employed as a biosensing reagent in the preliminary screening of certain pharmaceuticals. The CaM-based assay showed to be class-selective toward drugs used in the treatment of psychoses and depression, which contain a phenothiazine/phenothiazine-like structural moiety. The assay developed is reproducible over long periods of time and analyses volumes in the microliter range have shown adequate sensitivity for HTPS. The work presented

herein illustrates a proof-of-concept, model system employing a binding protein (CaM) as the detection element. Given that the assay is homogeneous in nature, this technology is envisioned to offer a valid alternative approach to rapid initial screening of potential new drug candidates in HTPS formats. In addition, not requiring the addition of reagents to generate a signal (i.e., reagentless) provides potential advantages over more conventional means of pharmaceutical analyses. Specifically, this assay offers minimal sample preparation, minimal analyte consumption, and rapid detection kinetics. It is believed that the strategy employed herein could be easily adapted to other binding proteins specific to other classes of ligand/analytes and/or drugs.

ACKNOWLEDGMENT

The authors would like to thank the National Aeronautics and Space Administration for support of this work. P. M. Douglass acknowledges the National Science Foundation IGERT program and the American Foundation for Pharmaceutical Education for predoctoral fellowships. S. Daunert is a Cottrell Scholar and a Lilly Faculty Awardee.

LITERATURE CITED

(1) D'Auria, S., Gryczynski, Z., Gryczynski, I., Rossi, M., and Lakowicz, J. R. (2000) A protein biosensor for lactate. *Anal. Biochem. 283*, 83−88.

(2) Giuliano, K. A. and Taylor, D. L. (1998) Fluorescent-Protein Biosensors: New Tools for Drug Discovery. *Trends Biotechnol. 16*, 135−140.

(3) D′Auria, S., Herman, P., Rossi, M., and Lakowicz, J. R. (1999) The fluorescence emission of the apo-glucose oxidase from *Aspergillus niger* as probe to estimate glucose concentrations. *Biochem. Biophys. Res. Commun. 263*, 550−553.

(4) Doi, N., and Yanagawa, H. (1999) Design of generic biosensors based on green fluorescent proteins with allosteric sites by directed evolution. *FEBS Lett. 453*, 305−307.

(5) Giuliano, K. A. and Post, P. L. (1995) Fluorescent Protein Biosensors: Measurement of Molecular Dynamics in Living Cells. *Annu. Rev. Biophys. Biomol. Struct. 24*, 405−434.

(6) Giuliano, K. A., DeBiasio, R. L., Dunlay, T., Gough, A., Volosky, J. M., Zock, J., Pavlakis, G. N., and Taylor, D. L. (1997) High-content screening: a new approack to easing key bottlenecks in the drug discovery process. *J. Biomol. Screen. 2*, 249−259.

(7) Hidaka, H. and Hartshorne, D. J., Eds. (1985) *Calmodulin Antagonists and Cellular Physiology,* Academic Press, Inc., Orlando.

(8) VanEldik, L. and Watterson, D. M., Eds. (1998) *Calmodulin and Signal Transduction*, Academic Press, Inc., New York.

(9) Osawa, M., Swindells, M. B., Tanikawa, J., Tanaka, T., Mase, T., Furuya, T., and Ikura, M. (1998) Solution Structure of Calmodulin-W-7 Complex: The Basis of Diversity in Molecular Recognition. *J. Mol. Biol. 276*, 165−176.

(10) Prozialeck, W. C. and Weiss, B. (1982) Inhibition of Calmodulin by Phenothiazines and Related Drugs: Structure−Activity Relationships. *J. Pharmacol. Exp. Ther. 222*, 509−516.

(11) Cook, W. J., Walter, L. J., and Walter, M. R. (1994) Drug Binding by Calmodulin: Crystal Structure of a Calmodulin−Trifluoperazine Complex. *Biochemistry 33*, 15259−15265.

(12) Chattopadhyaya, R., Meador, W. E., Means, A. R., and Quiocho, F. A. (1992) Calmodulin structure refined at 1.7 A resolution. *J. Mol. Biol. 228*, 1177−1192.

(13) Hentz, N. G., Vukasinovic, V., and Daunert, S. (1996) Affinity Chromatography of Recombinant Peptides/Proteins Based on a Calmodulin Fusion Tail. *Anal. Chem. 68*, 1550−1555.

(14) Schauer-Vukasinovic, V. and Daunert, S. (1999) Purification of recombinant proteins based on the interaction between a phenothiazine-derivatized column and a calmodulin fusion tail. *Biotechnol. Prog. 15*, 513−516.

(15) Patel, J., Daunert, S., Bachas, L. G., and Bhattacharyya, D. Unpublished data.

(16) Schauer-Vukasinovic, V., Cullen, L., and Daunert, S. (1997) Rational Design of a Calcium Sensing System Based on Induced Conformational Changes of Calmodulin. *J. Am. Chem. Soc. 119*, 11102−11103.

(17) Roberts, D. M., Crea, R., Malecha, M., Alvarado-Urbina, G., Chiarello, R. H., and Watterson, D. M. (1985) Chemical synthesis and expression of a calmodulin gene designed for site-specific mutagenesis. *Biochemistry 24*, 5090−5098.

(18) Hart, R. C., Bates, M. D., Cormier, M. J., Rosen, G. M., and Conn, P. M. (1983) Synthesis and characterization of calmodulin antagonistic drugs. *Methods Enzymol. 102*, 195−204.

(19) Salins, L. L. E., Schauer-Vukasinovic, V., and Daunert, S. (1998) Optical Sensing Systems Based on Biomolecular Recognition of Recombinant Proteins. *Proc. SPIE- Int. Soc. Opt. Eng. 3115*, 16−24.

(20) Lakowicz, J. R. (1983) *Principles of Fluorescence Spectroscopy*, Plenum Press, New York.

(21) Hirshberg, M., Henrick, K., Haire, L. L., Vasisht, N., Brune, M., Corrie, J. E., and Webb, M. R. (1998) Crystal structure of phosphate binding protein labeled with a coumarin fluorophore, a probe for inorganic phosphate. *Biochemistry 37*, 10381−10385.

(22) Lundgren, J. S., Salins, L. L., Kaneva, I., and Daunert, S. (1999) A dynamical investigation of acrylodan-labeled mutant phosphate binding protein. *Anal. Chem. 71*, 589−595.

(23) Watkins, A. N. and Bright, F. V. (1998) Effects of Fluorescent Reporter Group Structure on the Dynamics Surrounding Cysteine-26 in Spinach Calmodulin: A Model Biorecognition Element. *Appl. Spectrosc. 52*, 1447−1456.

(24) Wolcke, J. and Ullmann, D. (2001) Miniaturized HTS technologies − μHTS. *Drug Discov. Today 6*, 637−646.

(25) Masimirembwa, C. M., Thompson, R., and Andersson, T. B. (2001) In vitro high throughput screening of compounds for favorable metabolic properties in drug discovery. *Comb. Chem. High Throughput Screen. 4*, 245−263.

(26) Schullek, J. R., Butler, J. H., Ni, Z. J., Chen, D., and Yuan, Z. (1997) A high-density screening format for encoded combinatorial libraries: assay miniaturization and its application to enzymatic reactions. *Anal. Biochem. 246*, 20−29.

(27) Kenny, B. A., Bushfield, M., Parry-Smith, D. J., Fogarty, S., and Treherne, J. M. (1998) The application of high-throughput screening to novel lead discovery, in *Progress in Drug Research* (E. Jucker, Ed.) pp 245−269, Birkhauser Verlag, Basel.

(28) Ramsey, J. M., Jacobson, S. C., and Knapp, M. R. (1995) Microfabricated chemical measurement systems. *Nat. Med. 1*, 1093−1096.

(29) Roufogalis, B. D., Minocherhomjee, A.-E.-V. M., and Al-Jobore, A. (1983) Pharmacological Antagonism of Calmodulin. *Can. J. Biochem. Cell Biol. 61*, 927−933.

(30) Montgomery, S. A., 1995. Selective serotonin reuptake inhibitors in the acute treatment of depression, in *Psychopharmacology, The Fourth Generation of Progress* (F. E. Bloom, and D. J. Kupfer, Eds.) pp 451−461, Raven Press, New York.

(31) Kraulis, P. J. (1991) MOLSCRIPT: a program to produce both detailed and schematic plots of protein structures. *J. Appl. Crystallogr. 24*, 946−949.

(32) Merrit, E. A. and Murphy, M. E. P. (1994) *Acta Crystallogr. D50*, 869−873.

BC010080B

Ferrocenylnaphthalene Diimide-Based Electrochemical Hybridization Assay for a Heterozygous Deficiency of the Lipoprotein Lipase Gene

Kenichi Yamashita,[†] Atsuko Takagi,[§] Makoto Takagi,[†] Hiroki Kondo,[||] Yasuyuki Ikeda,[‡] and Shigeori Takenaka[†,*]

Department of Applied Chemistry, Faculty of Engineering, Kyushu University, Fukuoka 812-8581, Japan; Department of Biochemical Engineering and Science, Kyushu Institute of Technology, Iizuka 820-8502, Japan; Departments of Etiology and Pathophysiology, and Pharmacology, National Cardiovascular Center Research Institute, Fujishirodai, Suita, Osaka 565-8565, Japan. Received February 25, 2002; Revised Manuscript Received July 5, 2002

An electrochemical hybridization assay has been devised that enables the rapid analysis of a heterozygous deficiency of the human lipoprotein lipase (LPL) gene. PCR products of 350 base pairs (bp) containing the wild-type sequence, a mutated $G^{818} \rightarrow A$ transition or a G^{916} deletion of the LPL gene were subjected to hybridization with a probe DNA of 13 or 15 bases that represented either the wild-type or the mutated sequence immobilized on a gold electrode. The differential pulse voltammetry of the electrode before and after hybridization was determined in the presence of ferrocenylnaphthalene diimide (FND) at 460 mV. The measured change in peak current, Δi, was defined by $(i - i_o)/i_o \times 100\%$, where i_o and i represent the current before and after hybridization, respectively. Matched combinations of sample and probe gave Δi values of 40−90%, whereas mismatched combinations gave values of 20−35%, enabling the discrimination of matched hybrids from mismatched ones across a slim margin. Because the heterozygote contains both the wild-type and mutated sequences, however, it alone gives large Δi values with both the wild- and mutant-type probes. This system was validated on 10 unknown samples of each of the two types of LPL mutation, which were correctly identified in every case.

INTRODUCTION

The analysis of single nucleotide polymorphisms (SNPs) in genes is important both for diagnosing the risk of common diseases such as hypertension and diabetes and for determining the optimum tailor-made medications (*1, 2*). Each human gene is classified by two identical alleles in homozygotes or two different alleles in heterozygotes. Because the differences in SNPs are so subtle, it is essential that any analytical method for detecting SNPs is sensitive and efficient in order to be practical. Currently, SNP analysis is carried out by one of two techniques that are based on enzymatic reactions (*3, 4*) and mismatch detection on the DNA duplex (*5, 6*). The latter technique is especially useful, as it is an extension of a routine DNA probe method.

Recently, mismatch detection by means of an electrochemical DNA sensor has been reported (*7*−*12*). The advantages of this technique lie in its high analytical sensitivity, speed, and low cost. Two notable variations of this technique have been reported: Willner and co-workers (*9*) carried out heterozygote detection using enzyme amplification, and Marrazza and co-workers (*12*) carried out heterozygote detection using the chronopotentiometric stripping analysis (PSA) developed by Wang (*7*). We have also succeeded in highly sensitive detection of DNA using an electrochemical hybridization assay (*11, 13, 14*). Our breakthrough was the design and synthesis of ferrocenylnaphthalene diimide (FND) as an effective indicator of hybridization. In this paper, we have assessed our electrochemical hybridization assay using two electrodes with different immobilized-DNA probes for the analysis of human lipoprotein lipase (LPL) gene.

Human LPL protein is expressed mainly in adipose tissue and hydrolyzes triglycerides in chylomicrons and in very low-density lipoprotein (VLDL) particles in order to supply the resulting fatty acids and triglycerols to adipose tissue, where they are stored effectively (*15, 16*). A malfunctional form of LPL expressed by homozygotes carrying a mutated LPL gene is known to lead to hypertriglyceridemia with a high probability of pancreatitis (*17*). People with heterozygous LPL deficiency usually manifest with a normolipidemic state, but they can develop type IV hyperlipoproteinemia through the superposition of factors that stimulate triglyceride synthesis, such as high alcohol intake and/or a hyperinsulinemic state (*18*−*22*), which is thought to be a risk for cardiovascular heart disease (*23*). The identification of heterozygous mutations in the LPL gene as an early determination of the etiology underlying type IV hyperlipoproteinemia is therefore important for preventing the progress of hypertriglyceridemia and the subsequent

* To whom correspondence should be addressed. Tel and Fax: +81-92-642-3603, e-mail: staketcm@mbox.nc.kyushu-u.ac.jp.

[†] Department of Applied Chemistry, Faculty of Engineering, Kyushu University.

[‡] Department of Etiology and Pathophysiology, National Cardiovascular Center Research Institute.

[§] Department of Pharmacology, National Cardiovascular Center Research Institute.

[||] Department of Biochemical Engineering and Science, Kyushu Institute of Technology, Iizuka 820-8502, Japan.

10.1021/bc025519u CCC: $22.00 © 2002 American Chemical Society
Published on Web 11/05/2002

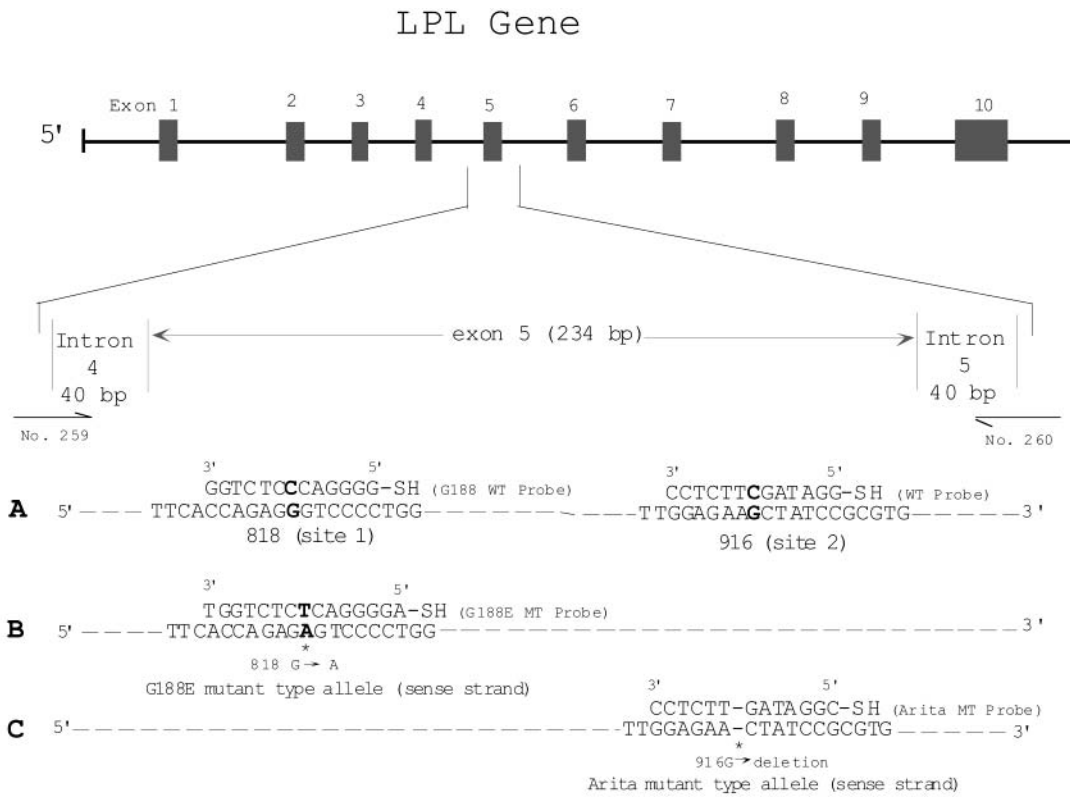


Figure 1. Organization of the human LPL gene with the focus on exon 5, where the two types of mutations studied here are located (sites 1 and 2) (*19*,*24*). The partial nucleotide sequences of the WT for sites 1 and 2 are depicted in (A), together with their complementary probe sequences (13 bases each). The asterisk in (B) indicates the G to A transition at base 818 ($GG^{818}G \rightarrow GAG$), which results in the amino acid substitution $Gly^{188} \rightarrow Glu$ (G188E), together with the G188E mutant type (MT) probe (15 bases). The asterisk in (C) indicates the deletion of G at base 916 ($G^{916}CT$; first position of Ala^{221}), which is designated the Arita mutation, which results in premature termination by a frameshift, together with the Arita MT probe (13 bases).

outbreak of cardiovascular disease (*23*), as the patient can be advised to change to a more healthy life style.

The heterozygous LPL deficiencies studied here are a missense mutation carried on the G188E ($GG^{818}G \rightarrow GAG/Gly^{188} \rightarrow Glu$, site 1) allele (*24*) and a one-base deletion carried on the LPL arita allele ($G^{916} \rightarrow$ deletion, site 2) (*19*), which are both found on exon 5 (Figure 1). We subjected 350-bp PCR products comprising these mutated sites to our electrochemical assay. Because these two mutations are the major forms of mutation in the LPL gene, their successful analysis should lead to the analogous analysis of most other LPL mutations.

RESULTS

Principle of the Electrochemical Hybridization Assay for Heterozygotes. The principles underlying the electrochemical hybridization assay using FND on a gold electrode with a wild-type (WT) probe immobilized for discriminating the WT allele from a mutant-type (MT) allele are illustrated in Figure 2. Before hybridization, the differential pulse voltammetry (DPV) of this electrode is measured at 460 mV, and the current obtained is designated as i_o. The same gold electrode is then allowed to hybridize with the PCR products prepared from a WT/WT homozygote, a WT/MT heterozygote, and an MT/MT homozygote under conditions that have been optimized (e.g., the salt concentration of the hybridization buffer and the temperature) for hybridization of the WT probe with the WT allele. The electrode gives rise to a larger signal, designated as *i*, for PCR products from the WT/WT homozygote and the WT/MT heterozygote, owing to the intercalation of FND into the DNA duplex that forms on it; however, the signal increase is much smaller with PCR products from the MT/MT homozygote because of the one-base mismatch. This signal change is converted into the net increase in current, Δi, which is defined by the equation: $(i - i_o)/i_o \times 100$.

In this assay system, a significant increase in current is observed for a combination of the WT probe and the WT allele from the WT/WT homozygote and the WT/MT heterozygote, but a marginal increase is observed for the WT probe and the MT allele from the MT/MT homozygote. Conversely, a gold electrode with an MT probe immobilized produces a significant increase in current for the MT allele from a WT/MT heterozygote and an MT/MT homozygote, but a marginal increase for the WT allele from a WT/WT homozygote. Thus, only the heterozyote produces a large Δi with both electrodes which allows its identification. If the differences observed are large enough, the WT allele can be discriminated from the MT allele with certainty by this assay system. In other words, a heterozygous genotype can be identified correctly by a significant value of Δi obtained with two electrodes carrying either a WT probe or an MT probe.

Experimentally, a gold electrode carrying a DNA probe was prepared by immobilizing 0.1 pmol of oligonucleotide on a 2 mm^2 gold surface. This electrode gave rise to a current of 1 μA at 460 mV in the presence of 0.05 mM FND (100 pmol), 80% of which seemed to derive from nonspecific binding and/or diffusion of the ligand (unpublished observation). The current increased by 0.3−0.9 μA upon hybridization of 0.2 pmol of a denatured PCR product. An increase in current above 0.3 μA was ascribed to the FND bound to the duplex formed on the electrode, whereas that below 0.3 μA was ascribed to nonspecific binding to the electrode of sample DNA and FND in

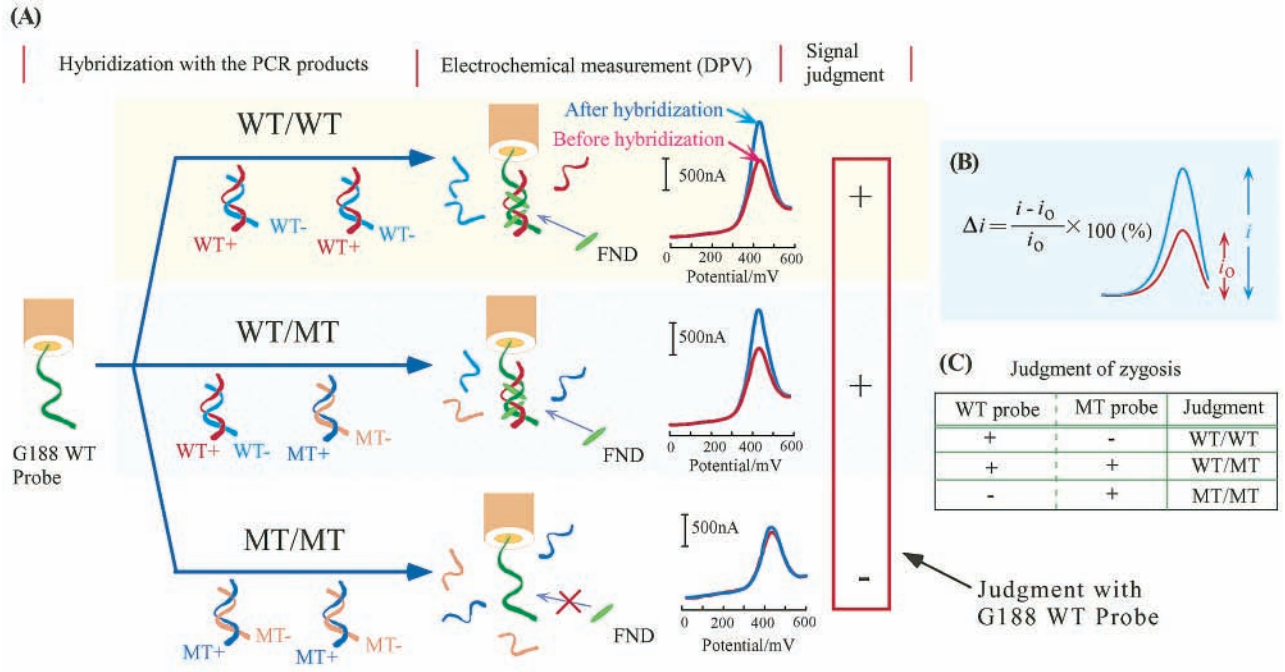


Figure 2. Principles underlying the electrochemical hybridization assay with FND for heterozygotes. (A) An electrode with an immobilized wild-type (WT) probe is allowed to hybridize with PCR products from WT/WT, WT/MT (mutant), or MT/MT genotypes. Differential pulse voltammetry (DPV) of the electrode is measured in the presence of FND at 460 mV before and after hybridization. Samples containing the WT allele (WT/WT and WT/MT) give rise to a large signal increase after hybridization. (B) The peak current due to FND before (i_o) and after hybridization (i) is converted to Δi, which represents a net increase in the current on duplex formation. (C) Identification of the state of zygosis. The same experiment as in (A) is carried out with an electrode carrying an MT probe, which gives a large signal increase with samples containing the MT allele (WT/MT and MT/MT). In other words, only heterozyogous samples give a large Δi with both types of electrode, thereby allowing their identification.

succession (unpublished observation). It thus follows that 3.7 pmol of FND binds to the electrode in a desired fashion, that is, one FND molecule binds to the DNA duplex every five base pairs. Given a large difference in these systems, this estimate is roughly consistent with previous data showing that FND binds to duplex DNA at every other base pair in solution (*14*).

Evaluation of the Electrochemical Hybridization Assay System. To establish optimal conditions for hybridization between the PCR product of exon 5 (350 bp) in the human LPL gene and an allele-specific DNA probe (Figure 1) immobilized on a gold electrode, both the salt concentration of the buffer and the temperature were surveyed for the following four combinations: a site 1 G188 WT probe (13 bases) and a WT allele of exon 5; a G188E MT probe (15 bases) and a G188E allele; a site 2 WT probe (13 bases) and a WT allele; and an Arita MT probe (13 bases) and an Arita allele. The best conditions were found to be 0.25 x SSC (0.3 M sodium citrate and 3 M NaCl) and 35 °C for the G188 WT probe and the WT allele; 0 x SSC and 35 °C for the G188E MT probe and the G188E allele; 0.25 x SSC and 40 °C for the site 2 WT probe and the WT allele; 0 x SSC and 40 °C for the Arita MT probe and the Arita allele after several experiments under the varied salt conditions (0−0.5 × SSC) and temperature (15−60 °C).

Under the best conditions, the PCR products for site 1 of exon 5 (350 bp), prepared from a WT/WT homozygote, a WT/G188E heterozygote and a G188E/G188E homozygote were examined by the electrochemical hybridization assay in the presence of FND on a gold electrode with either the G188 WT probe or the G188E MT probe immobilized. As shown in Figure 3A, the assay with the G188 WT probe gave a Δi (%) of 52 ± 19 (mean ± standard deviation) for WT/WT homozygotes (n = 17), 47 ± 15 for WT/G188E heterozygotes (n = 17), and 17 ± 10 for G188E/G188E homozygotes (n = 17) in 0.25 x SSC at 35 °C. The difference between the G188E/G188E and the WT/WT homozygotes was statistically significant as was the difference between the G188E/G188E homozygote and the WT/G188E heterozygote ($p < 0.0001$ in both cases). These findings demonstrate that the G188 WT probe hybridizes with the G188E allele only weakly because of the one-base mismatch, and that the G188E allele can be identified with certainty under the assay conditions employed. The threshold value that distinguishes the WT allele from the G188E allele was estimated from the Δi values (mean ± SD) of the above three groups as follows: [(52 − 19) + (47 − 15) + (17 + 10)]/3 = 31%.

The electrochemical hybridization assay with the G188E MT probe gave a Δi (%) of 20 ± 13 (mean ± SD) for WT/WT homozygotes (n = 20), 60 ± 15 for WT/G188E heterozygotes (n = 20) and 67 ± 31 for G188E/G188E homozygotes (n = 20) in 0 x SSC at 35 °C (Figure 3B). The differences between the WT/WT homozygote and the G188E/G188E homozygote and those between the WT/WT homozygote and the WT/G188E heterozygote were statistically significant, indicating that the WT allele can also be discriminated by using the G188E MT probe. The threshold value that distinguishes the WT allele from the G188E allele was estimated from the Δi values (mean ± SD) of the above three groups as follows: [(20 + 13) + (60 − 15) + (67 − 31)]/3 = 38%.

Likewise, the electrochemical hybridization assay with the site 2 WT probe gave a Δi (%) of 44 ± 17 (mean ± SD) for WT/WT homozygotes (n = 20), 41 ± 11 for WT/Arita heterozygotes (n = 20), and 16 ± 11 for Arita/Arita homozygotes (n = 20) in 0.25 x SSC at 40 °C, as shown in Figure 3C. The differences between the Arita/Arita homozygote and the WT/WT homozygote and those between the Arita/Arita homozygote and the WT/Arita

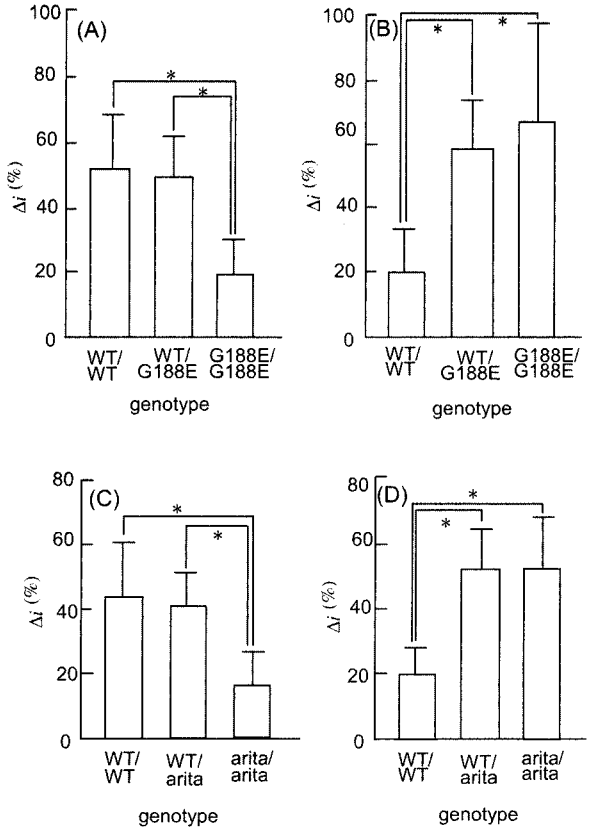


Figure 3. Discrimination between wild-type (WT) and mutant-type (MT) alleles of the human LPL gene by the electrochemical hybridization assay. In A and B, 350-bp PCR products, prepared from a WT/WT homozygote, a WT/G188E heterozygote, and a G188E/G188E homozygote, were analyzed with a gold electrode carrying a G188 WT probe (A) or a G188E MT probe (B) in the presence of 0.05 mM FND. In C and D, 350-bp PCR products, prepared from a WT/WT homozygote, a WT/Arita heterozygote, and an Arita/Arita homozygote, were analyzed with a gold electrode carrying a site 2 WT probe (C) or an Arita MT probe (D) in the presence of 0.05 mM FND. The currents obtained are shown as mean ± standard deviation (SD). The difference between the two combinations marked by the asterisk is statistically significant at $p < 0.0001$.

heterozygote were significant statistically ($p < 0.0001$). The threshold value that distinguishes the WT allele from the Arita MT allele was estimated from the Δi values (mean ± SD) of the above three groups as follows: $[(44 - 17) + (41 - 11) + (16 + 11)]/3 = 28\%$.

The electrochemical hybridization assay with the Arita MT probe gave a Δi (%) of 20 ± 8 (mean ± SD) for WT/WT homozygotes ($n = 20$), 53 ± 13 for WT/Arita heterozygotes ($n = 20$), and 53 ± 16 for Arita /Arita homozygotes ($n = 20$) in 0 x SSC at 40 °C (Figure 3D). Again, the differences between the WT/WT homozygote and the Arita/Arita homozygote and those between the WT/WT homozygote and the WT/Arita heterozygote were significant statistically. These findings indicate that the Arita MT probe hybridizes with the WT allele only weakly because of the one-base mismatch, and that it can discriminate the WT allele with certainty under the conditions employed. The threshold value that distinguishes the WT allele from the Arita allele was estimated from the Δi values (mean ± SD) of the above three groups as follows: $[(20 + 8) + (53 - 13) + (53 - 16)]/3 = 35\%$.

Blind Test of the Electrochemical Hybridization Assay System. The validity of the electrochemical hybridization assay for discriminating between a WT allele and an MT allele was examined in a blind test.

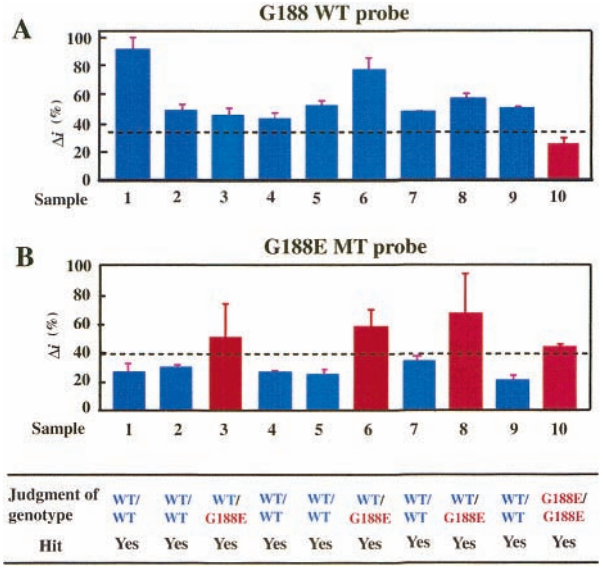


Figure 4. Verification of the electrochemical hybridization assay with FND by testing unknown samples for their LPL genotypes. The 350-bp PCR products, prepared from 10 unknown blood samples, were analyzed with a gold electrode carrying a site 1 G188 WT probe (A) or a G188E MT probe (B) in the presence of 0.05 mM FND. Analysis was carried out for four distinct samples per sample number ($n = 4$), and the currents shown are the mean ± standard error of the mean (SEM). The genotype of each sample was judged on the basis of the threshold values at which the WT allele can be discriminated from the MT allele taken from the data shown in Figures 3A and 3B; that is, 31% for the site 1 G188 WT probe (A) and 38% for the G188E MT probe (B). The threshold values are represented by the dotted horizontal lines in A and B.

PCR products amplified from site 1 of exon 5 (350 bp) in the human LPL gene were prepared from 10 unknown samples and examined by the electrochemical hybridization assay in the presence of FND on a gold electrode with an immobilized G188 WT probe or a G188E MT probe. The data obtained were judged on the basis of the threshold values (31 and 38%) derived from the data shown in Figures 3A and 3B. The genotypes of these samples determined by the hybridization assay were found to be completely consistent with the results from DNA sequencing, as shown in Figure 4. In other words, it appears that this assay system is effective for analyzing unknown or practical samples.

Another blind test was carried out for site 2 of exon 5 of the human LPL gene. PCR products amplified from this site (350 bp) were prepared from 10 unknown samples and analyzed by the electrochemical hybridization assay in the presence of FND on a gold electrode with an immobilized site 2 WT probe or an Arita MT probe. The data obtained were judged on the basis of the threshold values (28 and 35%) derived from the data shown in Figures 3C and 3D. The genotypes of these samples determined by the hybridization assay were completely consistent with results from DNA sequencing, as shown in Figure 5. Again, the usefulness of this assay system was proved by these site 2 samples. In future studies it would be worth investigating this utility of this electrochemical method for the practical analysis of a wider range of genes with known mutations.

DISCUSSION

The analysis of SNPs has become more important since it has been closely associated with the prediction and prevention of various syndromes. Currently, SNPs are analyzed by direct DNA sequencing or new techniques

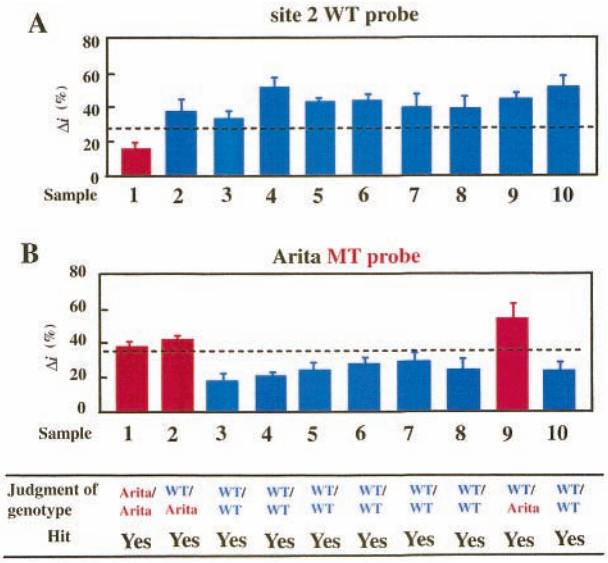


Figure 5. Further verification of the electrochemical hybridization assay with FND by testing unknown samples for their LPL genotypes. The 350-bp PCR products, prepared from 10 unknown blood samples, were analyzed with a gold electrode carrying a site 2 WT probe (A) or an Arita MT probe (B) in the presence of 0.05 mM FND. Analysis was carried out as in Figure 4. The genotype of each sample was judged on the basis of the threshold values at which the WT allele can be distinguished from the MT allele taken from the data shown in Figures 3C and 3D; that is, 28% for the WT probe (A) and 35% for the Arita MT probe (B). The threshol values are represented by the dotted horizontal lines in A and B.

such as dynamic allele-specific hybridization (DASH) (*5*) and template-directed dye-terminator incorporation (TDI) (*3*). The demand for simpler methods never ceases, however, as normally several samples need to be processed at any one time during SNP analysis. An electrochemical method seems to be a promising alternative to the existing fluorescence methods owing to its speed, low operational costs, and amenability to automation. In fact, the highly sensitive detection of gene mutations has been achieved electrochemically by using $Co(phen)_3^{3+}$ or daunomycin as a redox active marker (*9, 12*).

As described above, we have been able to analyze two types of mutations present on exon 5 of the human LPL gene electrochemically with FND. The key to this success lies in the use of two different DNA probes, comprising WT and mutant DNA, immobilized on an electrode. Only heterozygous samples produce a large increase in current with both electrodes, thereby allowing identification of the sample as heterozygous.

Samples containing as little as 0.2 pmol of PCR product can be analyzed by this method, which corresponds to a sensitivity that is 1000-fold higher than that of existing methods. Once the electrodes with the immobilized probes have been prepared, the analysis is straightforward. First, chromosomal DNA is extracted from blood donated by individuals and subjected to PCR. Second, after denaturation, the PCR products are subjected to the electrochemical analysis. This method is based on the fact that the DNA duplex does not form with DNA sequences containing a mismatch(es). Currently, there is only a modest 3−4-fold difference in the value of Δi between the WT and MT alleles. If this difference can be magnified, however, the analysis will become more sensitive, and efforts toward this goal are being made in our laboratories.

Another area that needs future investigation concerns the data values, which fluctuate rather significantly even among given genotypes (ca. 50% of the mean). At present, the exact reason for this fluctuation is not known, but it is possible that material affecting the electrochemical reaction may not have been removed completely by the methods used to isolate the chromosomal DNA. In regard to the background current, its magnitude tends to increase with increasing sizes of DNA; that is, nonspecific adsorption to the electrode becomes marked with DNA larger than 40 bases. Nonspecific binding can be eliminated by warming, but this process can also partially detach the probe DNA from the electrode. A solution to this problem may be the use of other masking agents such as mercaptohexanol instead of 2-mercaptoethanol (unpublished observation).

Despite these limitations, the SNPs of the human LPL gene could be analyzed successfully and practically by our electrochemical hybridization assay with FND. Although only the two types of known mutations were examined in this study, other types of mutations may be analyzed easily if electrodes carrying suitable probes are prepared. Moreover, an electrochemical DNA microarray system based on this technique may be even more useful. Studies are now under way to attain this goal in our laboratories.

EXPERIMENTAL SECTION

Extraction of Chromosomal DNA. Human chromosomal DNA was isolated from whole cells taken from the peripheral blood of a healthy male YI, patient MN (*24*) carrying a heterozygous LPL G188E allele ($GG^{818}G \rightarrow GAG/Gly^{188} \rightarrow Glu$; corresponding to a G-to-A transition at position 818 of exon 5 of the LPL gene), patient EN (*19*) carrying a heterozygous LPLarita allele ($G^{916} \rightarrow$ deletion; corresponding to deletion of G at position 916 on exon 5), and patient TN (*19*) who was homozygous for the LPLarita allele, using a QIAamp DNA Blood kit (QIAGEN GmbH, Germany). With respect to the LPL gene, the genotypes of these individuals were WT/WT, WT/G188E, WT/arita and arita/arita, respectively.

PCR Amplification and Purification of PCR Products. Exon 5 (base numbers 730−963, 234 bp) and its flanking regions (40 bp each side) of the LPL gene were amplified from chromosomal DNA by PCR using the following primer pair: forward (5′-TGT AAA ACG ACG GCC AGT AAA TTT ACA AAT CTG TGT TCC TGC TTT TT-3′, No. 259) and reverse (5′-CAG GAA ACA GCT ATG ACC GAT AAG AGT CAC ATT TAA TTC GCT TCT A-3′, No. 260). Note that each primer contains an extra sequence of 18 bases at their 5′-terminus for direct sequencing, making the size of the PCR product 350 bp. PCR was performed in a 100 μL volume consisting of 1 x PCR buffer containing 1.5 mM $MgCl_2$, 10 pmol of each of the forward and reverse primers, 50 ng of chromosomal DNA, 200 μM dNTPs, and 2.5 U of AmpliTaq Gold (Perkin-Elmer). The PCR reaction protocol was 95 °C for 10 min, 40 cycles of 94 °C for 0.5 min, 55 °C for 1 min, 72 °C for 2 min, and finally an incubation at 72 °C for 7 min in a GeneAmp PCR System 9600 (Perkin-Elmer). Each PCR product was purified by a QIAquick spin column in a QIAquick PCR Purification Kit (QIAGEN), and its integrity was assessed by agarose gel electrophoresis.

In Vitro Preparation of the Homozygote of LPL G188E. Exon 5 and its flanking regions of the LPL gene were amplified from the chromosomal DNA of patient MN carrying a heterozygous LPL G188E allele by PCR using the primer pair described above, and the PCR product (350 bp) was purified with a QIAquick spin

column. After ligation into a pCR2.1 vector, the recombinant was transformed into transfection-competent *E. coli* cells using an Original TA Cloning Kit (Invitrogen, Carlsbad, CA). After verifying the presence of the G188E mutation by Ava II digestion and DNA sequencing, the 350-bp DNA fragment containing the G188E mutation was amplified from this subclone by PCR using the primer pair described above, purified with a QIAquick Spin column, and used for hybridization experiments as a genotype of G188E/G188E.

DNA Probes. DNA probes for site 1 G188 WT and G188E MT, site 2 WT and arita MT with a 5′-thiol moiety (Figure 1) were custom synthesized by Hokkaido System Science Co. Ltd. (Sapporo, Japan), and their concentrations were estimated from their molar absorptivities at 260 nm (*25*): 119 200 cm^{-1} M^{-1}, 142 100 cm^{-1} M^{-1}, 119 000 cm^{-1} M^{-1}, and 120100 cm^{-1} M^{-1}, respectively.

Preparation of Probe DNA-Immobilized Electrodes. *Hybridization of the PCR Product with Immobilized Probe DNA.* A solution of the PCR product in 10 mM Tris HCl buffer (pH 8.5) was mixed with a small volume of 20 x SSC (0.3 M sodium citrate and 3 M NaCl) to bring the final concentration to 0 x SSC or 0.25 x SSC for hybridization. Before hybridization, DNA was denatured in boiling water for 10 min and then cooled quickly on liquid nitrogen. The denatured PCR product was kept at 0 °C until use. One microliter of the denatured PCR product (ca. 0.2 pmol) was placed on the electrode and hybridization with the DNA probe was allowed to proceed for 1 h at 20 °C.

Electrochemical Measurements. Differential pulse voltammetry (DPV) was measured with an ALS model 900 electrochemical analyzer (CH Instruments Inc., Austin, TX), using a normal three-electrode configuration consisting of an Ag/AgCl reference electrode, a Pt counter electrode, and the electrode with the immobilized DNA probe, before and after the hybridization reaction in 2 mL of 0.1 M AcOH−AcOK buffer (pH 5.6) containing 0.1 M KCl and 0.05 mM FND. Measurement temperatures were optimized at 40 °C for the site 1 DNA probes and at 35 °C for site 2 DNA probes. The conditions for DPV measurements were as follows: initial potential, 0 V; final potential, 0.6 V; scan rate, 100 mV/s; pulse amplitude, 0.05 V; sample width, 16.7 ms; pulse period, 0.2 s; pulse width, 0.05 s; quiet time, 2 s; sensitivity, 10^{-6} A/V. Peak currents due to FND were measured at 460 mV before and after hybridization with the sample DNA.

Data Treatment. Data were converted into Δi values, which were defined as $(i - i_o)/i_o \times 100\%$, where i_o and i refer to the current before and after hybridization, respectively. Δi represents a net increase in the current of FND bound to the duplex DNA formed per immobilized DNA probe on the electrode. Nearly 30% of the observed current could be accounted for by the background as noted previously (*26*). The statistical significance of the differences in Δi among three groups was evaluated by Scheffe's *F*-test in a one-factor factorial ANOVA (*27*).

ACKNOWLEDGMENT

The authors thank Ms. N. Fujino, M. Yokoyama, and N. Katakura for expert technical assistance. This work was supported in part by a Grant-in-Aid for Scientific Research on Priority Areas (A) (No. 13031063) from the Ministry of Education, Culture, Sports, Science and Technology and Grants-in-Aid for Scientific Research (A) (No. 12305054), (B)(No. 12555236), (C)(Nos. 13680672, 11670402, 12670384, and 14570376), a Grant-in-Aid for Research (H13-Tiryo-001) on Advanced Medical Technology from the Ministry of Health Labor and Welfare of Japan, and a Grant-in-Aid for JSPS Fellows (No. 200000715) from the Japan Society for the Promotion of Science. The authors are also grateful for financial support from the New Energy and Industrial Technology Development Organization (NEDO).

LITERATURE CITED

(1) Brookes, J. (1999). The essence of SNPs. *Gene 234*, 177−186.

(2) McCarthy, J. J., and Hilfiker R. (2000). The use of single-nucleotide polymorphism maps in pharmacogenomics. *Nature Biotechnol. 18*, 505−508.

(3) Chan, X., Zehnbauer, B., Gnirke, A., and Kwok, P.-Y. (1997). Fluorescence energy transfer detection as a homogeneous DNA diagnostic method. *Proc. Natl. Acad. Sci. U.S.A. 94*, 10756−10761.

(4) Dubiley, S., Kirillov, E., Lysov, Y., and Mizabekov, A. (1997). Fractionation, phosphorylation and ligation on oligonucleotide microchips to enhance sequencing by hybridization. *Nucleic Acids Res. 25*, 2259−2265.

(5) Howell, W. M., Jobs, M., Gyllensten, U., and Brookes, A. J. (1999). Dynamic allele-specific hybridization. *Nature Biotechnol. 17*, 87−88.

(6) Pease, A. C., Solas, D., Sullivan, E. J., Cronin, M. T., Holmes, C. P., and Fodor, A. P. A. (1994). Light-generated oligonucleotide arrays for rapid DNA sequence analysis. *Proc. Natl. Acad. Sci. U.S.A. 91*, 5022−5026.

(7) Wang, J., Palecek, E., Nielsen, P. E., Rivas, G., Cai, X., Shiraishi, H., Dontha, N., Luo, D., and Farias, A. M. (1996). Peptide nucleic acid Probes for sequence-specific DNA biosensors. *J. Am. Chem. Soc. 118*, 7667−7670.

(8) Wang, J., Rivas. G., Cai, A., Chicharro, M., Parrado, C., Dontha, N., Bergleiter, A., Mowat, M., Palecek, E., and Nielsen, P. E. (1997). Detection of point mutation in the p53 gene using a peptide nucleic acid biosensor. *Anal. Chim. Acta 344*, 111−118.

(9) Patolsky, F., Lichtenstein, A., and Willner, I. (2001). Detection of single-base DNA mutations by enzyme-amplified electronic transduction. *Nature Biotechnol. 19*, 253−257.

(10) Boon, E. M., Ceres, D. M., Drummond, T. G., Hill, M. G., and Barton, J. K. (2000) Mutation detection by electrocatalysis at DNA-modified electrodes. *Nature Biotechnol. 18*, 1096−1100.

(11) Yamashita, K., Takagi, M., Kondo, H., and Takenaka, S. (2000) Electrochemical detection of base pair mutation. *Chem. Lett.* 1038−1039.

(12) Marrazza, G., Chiti, G., Maschini, M., and Anichini, M. (2000). Detection of human apolipoprotein E genotypes by DNA electrochemical biosensor coupled with PCR. *Clin. Chem. 46*, 31−37.

(13) Takenaka, S., Uto, Y., Saita, H., Yokoyama, M., Kondo, H., and Wilson, W. D. (1998). Electrochemically active threading intercalator with high double stranded DNA selectivity. *J. Chem. Soc., Chem. Commun.* 1111−1112.

(14) Takenaka, S., Yamashita, K., Takagi, M., Uto, Y., and Kondo, H. (2000). DNA sensing on a DNA probe-modified electrode using ferrocenylnaphthalene diimide as the electrochemically active ligand. *Anal. Chem. 72*, 1334−1341.

(15) Havel, R. J., Goldstein, J. L., and Brown, M. S. (1980). *Lipoproteins and lipid transport, in Metabolic Control and Disease*, Saunders, Philadelphia.

(16) Krauss, R. M., Levy, R. I., and Fredrickson, D. S. (1974). Selective measurement of two lipase activities in postheparin plasma from normal subjects and patients with hyperlipoproteinemia. *J. Clin. Invest. 54*, 1107−1124.

(17) Brunzell, J. D. (1995). Familial lipoprotein lipase deficiency and other causes of the chylomicronemia syndrome. *The metabolic and molecular bases of inherited disease*, 7th ed, Vol. II, McGraw-Hill, New York.

(18) Takagi, A., Ikeda, Y., Mori, A., Tsutsumi, Z., Oida, K., Nakai, T., and Yamamoto, A. (1994). A newly identified heterozygous lipoprotein lipase gene mutation (Cys239 → stop/TGC972 → TGA.; LPL obama) in a patient with primary type IV hyperlipoproteinemia. *J. Lipid Res. 35*, 2008−2018.

(19) Takagi, A., Ikeda, Y., Tsutsumi, Z., Shoji, T., and Yamamoto, A. (1992). Molecular studies on primary lipoprotein lipase (LPL) deficiency. One base deletion (G916) in exon 5 of LPL gene causes no detectable LPL protein due to the absence of LPL mRNA transcript. *J. Clin. Invest. 89*, 581−591.

(20) Syvanne, M., Antikainen, M., Ehnholm, S., Tenkanen, H., Lahdenpera, S., Ehnholm, C., and Taskinen, M. R. (1996). Heterozygosity for Asn291 → Ser mutation in the lipoprotein lipase gene in two Finnish pedigrees: effect of hyperinsulinemia on the expression of hypertriglyceridemia. *J. Lipid Res. 37*, 727−738.

(21) Takagi, A., Ikeda, Y., Takeda, E., and Yamamoto, A. (2000). A newly identified lipoprotein lipase (LPL) gene mutation (F270L) in a Japanese patient with familial LPL deficiency. *Biochim. Biophys. Acta 1502*, 433−446.

(22) Emi, M., Wilson, D. E., Iverius, P. H., Wu, L., Hata, A., Hegele, R., Williams, R. R., and Lalouel, J. M. (1990). Missense mutation (Gly → Glu188) of human lipoprotein lipase imparting functional deficiency. *J. Biol. Chem. 265*, 5910−5916.

(23) Austin, M. A., Hokanson, J. E., and Edwards, K. L. (1998). Hypertriglyceridemia as a cardiovascular risk factor. *Am. J. Cardiol. 81*, 7B−12B.

(24) Takagi, A., Ikeda, Y., Tachi, K., Shinozuka, T., and Yamamoto, A. (1999). Identification of compound heterozygous mutations (G188E/W382X) of lipoprotein lipase gene in a Japanese infant with hyperchylomicronemia: the G188E mutation was newly identified in Japanese. *Clin. Chim. Acta 285*, 143−154.

(25) Cantor, R., and Warshaw, M. M. (1970). Oligonucleotide interactions. 3. Circular dichroism studies of the conformation of deoxyoligonucleotides. *Biopolymers 9*, 1059−1077.

(26) Miyahara, H., Yamashita, K., Kanai, M., Uchida, K., Takagi, M., Kondo, H., and Takenaka, S. Electrochemical analysis of single nucleotide polymorphisms of p53 gene. *Talanta*, in press.

(27) Wonnacott, T. H., and Wonnacott, R. J. (1990). *Introductory statistics*, 5th ed., John Wiley & Sons, New York.

BC025519U

Synthesis and Biological Evaluation of EC20: A New Folate-Derived, ^{99m}Tc-Based Radiopharmaceutical

Christopher P. Leamon,* Matthew A. Parker, Iontcho R. Vlahov, Le-Cun Xu, Joseph A. Reddy, Marilynn Vetzel, and Nikki Douglas

Endocyte, Inc., 1205 Kent Avenue, West Lafayette, Indiana 47906. Received June 5, 2002; Revised Manuscript Received August 3, 2002

A new peptide derivative of folic acid was designed to efficiently coordinate ^{99m}Tc. This new chelate, referred to as EC20, was found to bind cultured folate receptor (FR)-positive tumor cells in both a time- and concentration-dependent manner with very high affinity ($K_D \sim 3$ nM). Using an in vitro relative affinity assay, EC20 was also found to effectively compete with ^{3}H-folic acid for cell binding when presented either alone or as a formulated metal chelate. Following intravenous injection into Balb/c mice, ^{99m}Tc-EC20 was rapidly removed from circulation (plasma $t_{1/2} \sim 4$ min) and excreted into the urine in a nonmetabolized form. Data from γ scintigraphic and quantitative biodistribution studies performed in M109 tumor-bearing Balb/c mice confirmed that ^{99m}Tc-EC20 predominantly accumulates in FR-positive tumor and kidney tissues. These results suggest that ^{99m}Tc-EC20 may be clinically useful as a noninvasive radiodiagnostic imaging agent for the detection of FR-positive human cancers.

INTRODUCTION

The field of nuclear medicine has been revitalized with the arrival of tissue-specific radiopharmaceutical targeting technologies. Ligands capable of concentrating at pathological sites have been derivatized with chelator−radionuclide complexes and then used as noninvasive probes for diagnostic imaging purposes. For example, vasoactive intestinal peptide, somatostatin analogues, monoclonal antibodies, vitamin B12, and even folic acid have all been used as ligands to localize radionuclides to tumors (*1*−*10*). Applications with monoclonal antibodies and various fragments thereof initially received the most attention because it was believed that precise, or perhaps superior, tumor-specific targeting might easily be achieved. Unfortunately, this approach was found to be technically challenging and inferior to other methods since (i) antibodies have prolonged circulation times due to their rather large molecular size (an unfavorable trait for imaging purposes), (ii) antibodies are expensive to produce, (iii) antibodies can be immunogenic, forcing their laborious humanization whenever multiple doses would be anticipated, and (iv) tumor to nontarget tissue ratios (T/NT) of antibody-linked radionuclides were essentially sub-optimal (*11*−*13*). Thus, more focus has recently been directed toward the use of smaller tumor-specific ligands that do not suffer from such limitations.

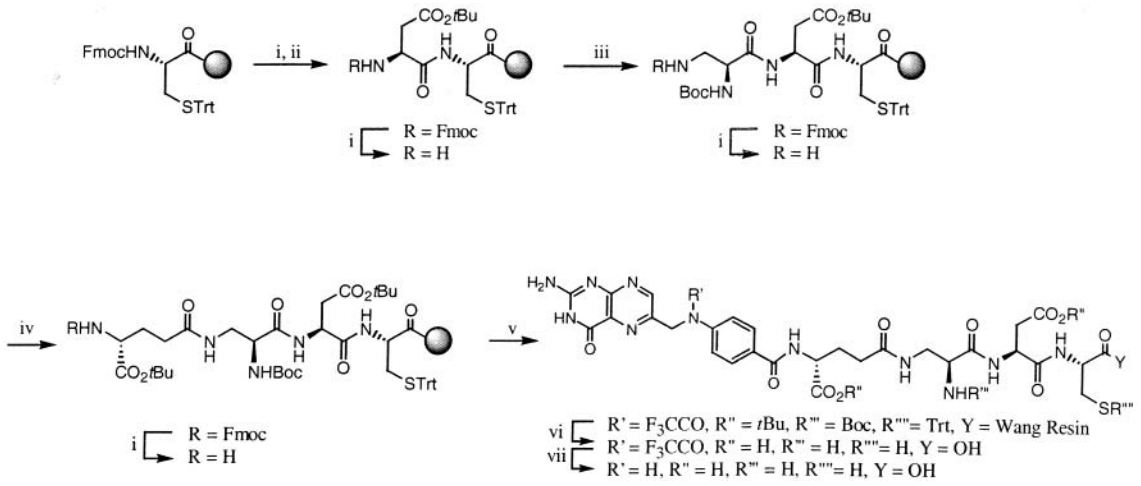
Use of the vitamin folic acid for the targeting of bioactive agents to tumors has been effectively exemplified over the past eleven years (*14*). In fact, folate conjugates of radiopharmaceutical agents (*1*−*6*), MRI contrast agents (*15*), low molecular weight chemotherapeutic agents (*16*), antisense oligonucleotides and ribozymes (*17*−*21*), proteins and protein toxins (*22*−*27*), immunotherapeutic agents (*28*−*31*), liposomes with entrapped drugs (*32*−*36*), and plasmids (*37*−*43*) have all been successfully delivered to FR-expressing cancer cells. Chronologically, the first folic acid "conjugate" described for in vivo tumor imaging was a histamine derivative containing 125-iodine (*44*). Although impressive tumor images were obtained with this conjugate, it was not considered a relevant clinical candidate owing to the long-lived ^{125}I radionuclide component. Subsequent reports described the synthesis and use of a deferoxamine−folate conjugate for tumor targeting (*1*, *2*). Deferoxamine chelates ^{67}Ga, a γ-emitting radionuclide that has a 78 h half-life. Favorable pharmacokinetic biodistribution profiles and high T/NT ratios were obtained with this agent in a tumor-bearing nude mouse model, however partial hepatobiliary clearance was also noted. Thus, further preclinical development was stopped due to anticipated problems in accurately imaging regio-abdominal locations in humans. This obstacle was easily overcome, however, by simply replacing the deferoxamine chelator with diethylenetriamine pentaacetic acid (DTPA), an efficient chelator of ^{111}In (68 h half-life). ^{111}In-DTPA-folate displayed similar tumor-accumulating properties to its deferoxamine predecessor, but its primary route of elimination was confirmed to be through the kidneys (*3*). Thus, ^{111}In-DTPA-folate was selected for development, and phase I/II clinical trials were conducted at several US sites in 1999 and 2000 (*14*).

There were no plans to commercialize ^{111}In-DTPA-folate, mostly because the field of radiodiagnostic imaging had been transitioning toward using ^{99m}Tc-based probes. Nonetheless, clinical evaluation of ^{111}In-DTPA-folate was continued for the purpose of obtaining valuable human biodistribution data while the development of a newer ^{99m}Tc-based folate conjugate was concurrently underway. ^{99m}Tc has been adopted as the preferred radionuclide for diagnostic imaging because (i) the radionuclide is easily obtained in a clinical laboratory from commercially available ^{99}Mo−^{99m}Tc generators, (ii) the cost of producing large amounts of ^{99m}Tc is insignificant compared to the cost of ^{111}In, and (iii) ^{99m}Tc has a much shorter (6 h) half-life, which allows higher radionuclide doses (~25 mCi) to be administered, yielding higher resolution images

* To whom correspondence should be addressed. Phone: (765) 463-7175. Fax: (765) 463-9271. E-mail: Leamon@Endocyte.com.

10.1021/bc0200430 CCC: $22.00 © 2002 American Chemical Society
Published on Web 11/01/2002

Scheme 1[a]



[a] Reagents and conditions: (i) 20% Piperdine, DMF; (ii) Fmoc-Asp(O*t*Bu)-OH, PyBop, DIPEA, DMF; (iii) Boc-Dap(Fmoc)-OH, PyBop, DIPEA, DMF; (iv) Fmoc-D-Glu-O*t*Bu, PyBop, DIPEA, DMF; (v) N^{10}-TFA-Pte-OH, DIPEA, DMSO; (vi) TFAA, $HSCH_2CH_2SH$, iPr_3SiH; (vii) H_4NOH, pH 10.3.

without the risk of hazardous radiation exposure to vital organs.

Several folate-based ^{99m}Tc conjugates have already been described in the literature. For example, folate conjugates of ^{99m}Tc-6-hydrazinonicotinamido-hydrazido (HYNIC) (*5*), ^{99m}Tc-12-amino-3,3,9,9-tetramethyl-5-oxa-4,8 diaza-2,10-dodecanedinoe dioxime (OXA) [6], ^{99m}Tc-ethylenedicysteine (*4*), and even ^{99m}Tc-DTPA-folate (*45*), have all shown promising in vivo tumor uptake qualities. The objective of this study, however, was to develop an alternative, proprietary ^{99m}Tc−folate conjugate that would be suitable for clinical development. Thus a new agent, herein referred to as EC20, was prepared and characterized. Detailed analytical and preclinical biological data were collected, and much of the data used to support an Investigational New Drug application is reported below.

EXPERIMENTAL PROCEDURES

Materials. N^{10}-Trifluoroacetylpteroic acid was purchased from Eprova AG, Schaffhausen, Switzerland. Peptide synthesis reagents were purchased from Nova-Biochem and Bachem. ^{99m}Tc Sodium Pertechnetate was supplied by Syncor. $[ReO_2(en)_2]Cl$ was prepared according to Rouschias (*46*). Cellulose plates and DEAE ion exchange plates were purchased from J. T. Baker.

Synthesis, Purification, and Analytical Characterization of EC20. EC20 is a folate-containing peptide consisting in sequence of pteroic acid (Pte), D-Glu, β-L-diaminopropionic acid (βDpr), Asp, and Cys. EC20 was synthesized on an acid-sensitive Wang resin loaded with Fmoc-L-Cys (Trt)-OH, as detailed in Scheme 1. Benzotriazole-1-yl-oxy-tris-pyrrolidino-phosphoniumhexafluorophosphate (PyBOP) was applied as the activating reagent to ensure efficient coupling using low equivalents of amino acids. Fmoc protecting groups were removed after every coupling step under standard conditions (20% piperidine in DMF). After the last assembly step, the peptide was cleaved from the polymeric support by treatment with 92.5% trifluoroacetic acid containing 2.5% ethanedithiol, 2.5% triisopropylsilane, and 2.5% deionized water. This reaction also resulted in simultaneous removal of the t-Bu, Boc and trityl protecting groups. Finally, the trifluoroacetyl moiety was removed in aqueous ammonium hydroxide to give EC20.

The crude EC20 product was purified by HPLC using an Xterra RP18 30 × 300 mm 7 μm column (Waters), mobile phase 32 mM HCl (A) and MeOH (B), and gradient conditions starting with 99% A and 1% B and reaching 89% A and 11% B in 37 min at a flow rate of 20 mL/min. Under these conditions, EC20 monomer typically eluted at 14.4 min, whereas EC20 disulfide dimer (minor contaminant) eluted at 16.8 min.

A 2 mg sample of HPLC-purified EC20 was dissolved in 0.62 mL of D_2O, and a 500 MHz ^{1}H NMR spectrum was collected. Table 1 lists the chemical shifts, signal shapes, and *J* values for all nonexchangeable protons of the EC20 molecule.

EC20 was also analyzed by electrospray-mass spectrometry. Major positive ion peaks (*m*/*z*, relative intensity): 746.1 $(M+H)^+$, 100; 747.1, 44; 556.8, 32; 570.8, 16. Importantly, the calculated molecular weight for the formula $C_{29}H_{35}N_{11}O_{11}S$ is 745.2.

Preparation of the Nonradioactive Reagent Vial. EC20 kits are used for preparation of the ^{99m}Tc-EC20 radioactive drug substance. Each kit contains a sterile, nonpyrogenic lyophilized mixture of 0.1 mg of EC20, 80 mg of sodium α-D-glucoheptonate, 80 mg of tin (II) chloride dihydrate, and sufficient sodium hydroxide or hydrochloric acid to adjust the pH to 6.8 ± 0.2 prior to lyophilization. The lyophilized powder is sealed in a 5 mL vial under an argon atmosphere. The kits are then stored frozen at −20 °C until use or expiration (current shelf life is >2 years). Importantly, the tin (II) component is required to reduce the added ^{99m}Tc-pertechnetate, while the sodium α-D-glucoheptonate component is necessary to stabilize the newly reduced ^{99m}Tc prior to its final chelation to the EC20 compound.

Preparation of ^{99m}Tc-EC20. The procedure for chelating ^{99m}Tc to EC20 consists of the following steps. First, a boiling water bath containing a partially submerged lead vial shield is prepared. The top of an EC20 vial is swabbed with 70% ethanol to sanitize the surface, and it is placed in a suitable shielding container. Using a shielded syringe with 27-gauge needle, 1 mL of Sodium Pertechnetate ^{99m}Tc Injection (<50 mCi) is injected into the shielded vial. Before removal of the syringe from the vial, a volume of gas from the vial equal to the volume of pertechnetate added is withdrawn in order to normalize the pressure inside the vial. The vial is gently swirled for 30 s to ensure complete dissolution of the lyophilized powder. The vial is then placed into the lead shield that is standing in the boiling water bath, heated for ∼18 min,

Table 1. ^{1}H NMR Data for EC20[a]

residue	protons observed	chemical shift (δ)	signals	J values
	H-7	8.76	s	
Pte	2 x H-9	4.64	s	
	H-12 a. H-16	7.68	d	$^3J12,13 = {}^3J15,16 = 8.8$ Hz
	H-13 a. H-15	6.8	d	
	H-2	4.41	dd	$^3J2,3a = 9.1$ Hz; $^3J2,3b = 4.5$ Hz
D-Glu	H-3a	2.08	m	$^2J3a,3b = 14.2$ Hz
	H-3b	2.27	m	
	2 x H-4	2.44	dd	$^3J3a,4 = {}^3J3b,4 = 5.6$ Hz
	H-2	4.1	dd; X of ABX system	$^3J2,3A = 6.6$ Hz; $^3J2,3B = 4.7$ Hz
Dpr	H-3A	3.52	dd; A of ABX system	$^2JA,B = 14.7$ Hz
	H-3B	3.72	dd; B of ABX system	
	H-2	4.71	dd; X of ABX system	$^3J2,3A = 9.5$ Hz; $^3J2,3B = 4.3$ Hz
Asp	H-3A	2.62	dd; A of ABX system	$^2JA,B = 16.1$ Hz
	H-3B	2.81	dd; B of ABX system	
	H-2	4.3	dd; X of ABX system	$^3J2,3A = 5.5$ Hz; $^3J2,3B = 4.4$ Hz
Cys	H-3A	2.85	dd; A of ABX system	$^2JA,B = 14.1$ Hz
	H-3B	2.89	dd; B of ABX system	

[a] EC20 was dissolved in D_2O, and a 500 MHz spectrum was collected. Chemical shifts (δ) are in ppm. The signal for HOD at $\delta = 4.80$ ppm was used as the reference. pD = 4.78; s = singlet; d = doublet; m = multiplet.

and then cooled to room temperature for a minimum of 15 min. This solution can be stored at room temperature (15−25 °C) protected from light, but it should be used within 6 h of preparation.

The radiochemical stability of the radioactive drug substance was determined by HPLC after storing at room temperature in a lead-shielded container for up to 24 h. Samples of ^{99m}Tc-EC20 solution (20 μL) were analyzed using an HPLC system consisting of a Waters 600E Multisolvent Delivery System and 490 UV detector, a Bioscan FC-3200 radiodetector, Laura v1.5 radiochromatogram software, and a Waters Nova-Pak C18 (3.9 × 150 mm) column. Injected samples were eluted isocratically using an aqueous mobile phase containing 20% methanol and 0.1% trifluoroacetic acid at a flow rate of 1 mL/min. The HPLC analysis was monitored with both the UV detector (280 nm) and the γ radiodetector. Notably, the radiochemical purity of ^{99m}Tc-EC20 remained greater than 90% for at least 24 h in all cases.

Determination of Radiochemical Purity of ^{99m}Tc-EC20 by TLC. The major radiochemical impurities in the preparation of ^{99m}Tc-EC20 are (1) ^{99m}Tc pertechnetate, (2)^{99m}Tc-glucoheptonate (ligand exchange precursor), (3) nonspecific binding ^{99m}Tc (^{99m}Tc bound at a site other than the expected Dap-Asp-Cys chelating moiety of the EC20 molecule), and (4) hydrolyzed ^{99m}Tc. Since ^{99m}Tc-EC20 was being tested for possible clinical use, a three-TLC-based method had been developed to determine the amounts of each impurity and to estimate the overall radiochemical purity of ^{99m}Tc-EC20.

In the first system a cellulose plate is developed with deionized water. ^{99m}Tc-EC20, ^{99m}Tc-glucoheptonate, nonspecific binding ^{99m}Tc, and ^{99m}Tc pertechnetate move to the solvent front (R_f = 1.0), while hydrolyzed ^{99m}Tc remains at the origin (R_f = 0.0). The cellulose plate is cut into two pieces at $R_f = 0.3$, and each piece is counted using a dose calibrator. The percent of hydrolyzed ^{99m}Tc is calculated as follows: A = % hydrolyzed ^{99m}Tc = (μCi in bottom piece/μCi in both pieces) × 100.

In the second system, a cellulose plate is developed with acetone and 0.9% NaCl (7:3,v/v). ^{99m}Tc-pertechnetate moves with $R_f = 0.9$, while ^{99m}Tc-EC20, ^{99m}Tc-glucoheptonate, nonspecific binding ^{99m}Tc, and hydrolyzed ^{99m}Tc remain at the origin (R_f = 0.0). The cellulose/acetone−saline plate is cut into two pieces at $R_f = 0.6$, and each piece is counted using a dose calibrator. The percent of ^{99m}Tc-pertechnetate is calculated as follows: B = % ^{99m}Tc-pertechnetate = (μCi in top piece/μCi in both pieces) × 100.

Finally, in the third system a DEAE ion exchange plate is developed with 0.3 M Na_2SO_4. ^{99m}Tc-glucoheptonate moves to the solvent front ($R_f = 1.0$), nonspecific binding ^{99m}Tc moves with $R_f = 0.6$, and ^{99m}Tc-EC20, hydrolyzed ^{99m}Tc and ^{99m}Tc-pertechnetate remain near the origin (^{99m}Tc-EC20: $R_f = 0.1$; hydrolyzed ^{99m}Tc: $R_f = 0.0$; ^{99m}Tc pertechnetate: $R_f = 0.3$). The cellulose/Na_2SO_4 plate is cut into two pieces at $R_f = 0.5$, and each piece is counted using a dose calibrator. The percent of ^{99m}Tc-glucoheptonate and nonspecific binding ^{99m}Tc are calculated as follows: C = % (^{99m}Tc-Glucoheptonate + nonspecific binding ^{99m}Tc) = (μCi in top piece/μCi in both pieces) × 100. The overall radiochemical purity of ^{99m}Tc-EC20 is then calculated as follows: radiochemical purity = 100 − (A + B + C).

Synthesis of Re-EC20. A 52 mg (0.070 mmol) sample of EC20 and 52 mg (0.14 mmol) of [ReO_2 (en)$_2$]Cl (*46*) was dissolved in 6 mL and 1 mL of argon-purged phosphate buffer (0.05 M, pH 5.8), respectively. The two solutions were combined and heated under an argon atmosphere in a boiling water-bath for 2 h. The reaction mixture was frozen and lyophilized overnight. The crude product was purified by HPLC (Xterra RP18 column, 19 × 150 mm, 10 mM NH_4OAc/CH_3CN, flow rate 10 mL/min; gradient 1−8%). The fractions were collected, lyophilized, and stored at −20 °C until use.

Cell Culture. Cells were grown continuously as a monolayer using folate-free RPMI medium (FFRPMI) containing 10% heat-inactivated fetal calf serum (HIFCS) at 37 °C in a 5% CO_2/95% air-humidified atmosphere with no antibiotics. The HIFCS contained its normal complement of endogenous folates which enabled the cells to sustain growth in this more physiologically relevant medium (*22*). All cell experiments were performed using FFRPMI containing 10% HIFCS (FFRPMI/HIFCS) as the growth medium, except where indicated.

Relative Affinity Assay. The relative affinity of various folate derivatives was determined according to the method described by Westerhoff et al. (*47*) with slight modification. In short, FR-positive KB cells were gently trypsinized in 0.25% trypsin in phosphate-buffered saline (PBS) at room temperature for 3 min and then diluted in FFRPMI/HIFCS. Following a 5 min 800*g* spin and one PBS wash, the final cell pellet was suspended in FFRPMI 1640 (no serum). Cells were incubated for 15 min on ice with 100 nM of ^{3}H-folic acid in the absence and presence of increasing concentrations of folate-containing test articles. Samples were centrifuged at 10 000*g* for 5 min, and cell pellets were suspended in buffer, transferred to

individual vials containing 5 mL of scintillation cocktail, and then counted for radioactivity. Negative control tubes contained only the ^{3}H-folic acid in FFRPMI (no competitor). Positive control tubes contained a final concentration of 1 mM folic acid, and CPMs measured in these samples (representing nonspecific binding of label) were subtracted from all samples. Notably, relative affinities were defined as the inverse molar ratio of compound required to displace 50% of ^{3}H-folic acid bound to FR on KB cells, and the relative affinity of folic acid for the FR was set to 1.

Time-Dependent Cell Uptake. KB cells were seeded in 12-well Falcon plates and allowed to form subconfluent monolayers overnight. Following one rinse with 1 mL of fresh FFRPMI/HIFCS, each well received 1 mL of FFRPMI/HIFCS containing 10 nM ^{99m}Tc-EC20. Cells were incubated for the indicated times at 37 °C and then rinsed four times with 1 mL of ice-cold PBS, pH 7.4. The monolayers were dissolved in 0.5 mL of PBS, pH 7.4, containing 1% sodium dodecyl sulfate for 15 min at room temperature, and then counted for radioactivity using a Packard γ counter. The protein in each sample was next quantitated using a BioRad DC Protein Assay kit, and cellular protein values were converted to cell number using the conversion factor of 2.23×10^{-7} mg protein per cell (*48*). Final tabulated values were expressed in terms of molecules EC20 per cell.

Concentration-Dependent Cell Uptake. KB cells were seeded in 12-well Falcon plates and allowed to form sub-confluent monolayers overnight. Following one rinse with 1 mL of fresh FFRPMI/HIFCS, each well received 1 mL of FFRPMI/HIFCS containing increasing concentrations of ^{99m}Tc-EC20. Cells were incubated for 2 h at 37 °C and then rinsed four times with 1 mL of ice-cold PBS, pH 7.4. The monolayers were dissolved in 0.5 mL of PBS, pH 7.4, containing 1% sodium dodecyl sulfate for 15 min at room temperature and then counted for radioactivity using a Packard γ counter. Protein content was determined as described above, and final tabulated values were expressed in terms of molecules EC20 per cell.

Blood Clearance. Animals used for this study were maintained on a folate-free diet (Harlan #TD-90261) for approximately 3 weeks prior to dose administration. Acclimation to this special diet is essential because regular rodent diets contain large amounts of folic acid (6 mg/kg chow) and promote high serum folate levels in mice (*2*). Furthermore, previous studies have shown that mice placed on a folate-free diet for 3 weeks had maintained a safe serum folate level of 25 ± 7 nM, which is slightly higher than the 9−14 nM concentration measurable in human serum (*5*).

The ^{99m}Tc-EC20 solution was prepared on the day of use and had initially contained 100 μg of EC20 per milliliter. It was further diluted with sterile saline to prepare working stock solutions. The radiochemical purity of the product was estimated to be ≥94% by TLC. Each animal received a dose of 50 μg/kg EC20 (67 nmol/kg) in approximately 0.1 mL volume i.v. via the tail vein during brief diethyl ether anesthesia. At the designated times postinjection, each animal was euthanized by CO_2 asphyxiation, and blood was immediately collected by cardiac puncture.

Tissue Distribution Studies. Four- to five-week-old mice (Balb/c strain) were purchased from Harlan Sprague Dawley, Inc. (Indianapolis, IN) and were maintained on a folate-free diet for a total of 3 weeks prior to the experiment. Syngeneic, FR-positive M109 tumor cells (1×10^{6} per animal) were inoculated in the subcutis of the right axilla two weeks prior to the experiment. All mice were females, and the tumor weights were 54.2 ± 29.8 mg on the day of this experiment. A stock ^{99m}Tc-EC20 solution containing 100 μg of agent per mL was prepared on the day of use, and its radiochemical purity was >96%. Two additional ^{99m}Tc-chelating agents, ^{99m}Tc-EC14 (an EC20 analogue containing 1 additional Glu residue: Pte-D-Glu-D-Glu-βDpr-Asp-Cys) and ^{99m}Tc-EC28 (a non pteridine-containing control: benzoyl-D-Glu-D-Glu-βDpr-Asp-Cys), as well as ^{111}In-DTPA-folate (*3*) were also prepared to >90% radiochemical purity and were coevaluated in this study. All solutions were diluted with either saline alone or a saline solution containing 100 equivalents of folic acid (for competition) such that the final radiopharmaceutical concentration was 10 μmol/mL.

Animals received an approximate 40 μmol/kg i.v. dose of test article in 100 μL volume via a lateral tail vein during brief diethyl ether anesthesia. Four hours after injection, animals were sacrificed by CO_2 asphyxiation and dissected. Selected tissues were removed, weighed, and counted to determine ^{99m}Tc distribution. CPM values were decay-corrected, and results were tabulated as % injected dose per gram of wet weight tissue.

Gamma Scintigraphy. M109 tumor cells (1×10^{6} per animal) were inoculated in the subcutis of the right axilla of Balb/c mice two weeks prior to the experiment. Animals received an approximate 50 μmol/kg i.v. dose of test article in 100 μL volume via a lateral tail vein during brief diethyl ether anesthesia. Four hours after injection, animals were sacrificed by CO_2 asphyxiation and then placed on top of an image acquisition surface. Whole-body image acquisition was performed for 1 min at a count rate of 50−75 000 counts per min using a Technicare Omega 500 Sigma 410 Radioisotope Gamma Camera. All data were analyzed using a Medasys MS-DOS-based computer equipped with Medasys Pinnacle software.

Urinary Excretion and Metabolism. The urinary HPLC speciation profile of ^{99m}Tc-EC20 was obtained using Balb/c mice. Mice (~20 g each) were injected with 1 mCi (6.7 nmol) of ^{99m}Tc-EC20 via a lateral tail vein. Following a 1, 4, or 6 h time period, groups of two mice were euthanized by CO_2 asphyxiation, and urine was collected. After filtration through a GV13 Millex filter, the radiochemical speciation was assessed using an HPLC system equipped with a Nova-Pak C18 3.9 × 150 mm column and a radiochemical detector. The system was isocratically eluted with 20% methanol containing 0.1% TFA at a flow rate of 1 mL/min.

Serum Protein Binding. Fresh rat serum and commercial male human serum (type AB donors, Sigma Chemical Co.) were used to evaluate in vitro binding of ^{99m}Tc-EC20 to serum proteins. One minute after ^{99m}Tc-EC20 was mixed with 1 mL of serum at room temperature, 0.3 mL of the serum solution was transferred to a clean Amicon Centrifree ultrafiltration device (30 000 NMWL) in triplicate. Within one minute of loading the centrifuge with the serum solution, the device was spun at 1000*g* for 20 min at 20 °C. Fifty microliter samples of the original solution, and of the filtrate from each device, were transferred to a clean tube and counted in an automatic γ counter. A control solution of ^{99m}Tc-EC20 mixed with 1 mL of normal saline was ultrafiltered in an identical fashion. The percentage of free ^{99m}Tc was calculated for each of the three samples.

RESULTS

EC20 and Related Structures. The structure of the EC20 molecule is depicted in Figure 1. The folic acid

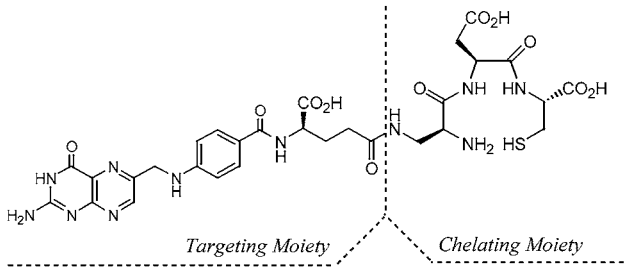


Figure 1. Structure of EC20.

moiety in the EC20 molecule is present to allow its high-affinity binding to cellular FRs. The other part of the molecule consists of a bifunctional peptide-based chelator, which provides the site of ^{99m}Tc coordination. Interestingly, the most successful class of bifunctional technetium chelators to date is represented by similar amine/amide thiolate compounds that coordinate TcO^{3+} via an $(N_{amine/amide})_{4-x}$ $(S_{thiolate})_x$ donor atom set (*49*−*56*).

Radiochemical Characterization. EC20 kits are used for preparation of the ^{99m}Tc-EC20 radioactive drug substance. Each kit contains a sterile, nonpyrogenic lyophilized mixture of EC20, sodium α-D-glucoheptonate, and tin (II) chloride that is sealed under an argon atmosphere. The final ^{99m}Tc-EC20 drug product formulation is then formed by the simple reconstitution of the lyophilized powder with ^{99m}Tc pertechnetate in saline followed by a brief heating step.

As shown in Figure 2, HPLC analysis of the ^{99m}Tc-EC20 formulation shows four radiochemical components, designated as peaks A−D. Peak A was confirmed to be free ^{99m}Tc, and this byproduct is typically present at <1%. Peak B, which was different from that of ^{99m}Tc-glucoheptonate (data not shown), eluted with a retention time of 2.8 min. This component represented about 3% of the mixture and was thought to result from ^{99m}Tc chelating at some other site on the EC20 molecule besides the expected Dap−Asp−Cys moiety (vide infra). Peaks C and D (retention times of 4.8 min and 13.2 min, respectively) account for the majority of the formulated radiochemical activity.

Since no mass spectral facilities were available for analysis of radioactive materials, a nonradioactive rhenium analogue, Re-EC20, was synthesized. Both rhenium and technetium are Group VIIA metals that have significant similarity in physical and chemical properties. They also form similar complexes with organic ligands. This analogous chemical behavior has been frequently used in structure elucidation of new classes of technetium radiopharmaceuticals based on nonradioactive rhenium analogues (*57*−*59*). Interestingly, HPLC analysis of Re-EC20 also showed two major peaks eluting at 5 and 14.2 min, respectively, similar to Peaks C and D for ^{99m}Tc-EC20 (chromatogram not shown). Mass spectral analysis confirmed that these two components were isomers corresponding to the Re-EC20 complex (m/z = 945). In fact, these species were likely diastereomers possessing either a syn or anti configuration of the technetium−oxygen bond in the Dap−Asp−Cys chelating ring, as depicted in Figure 3. Since (i) the two peaks in the Re-EC20 chromatogram represent isomeric complexes and (ii) reports of similar isomerism in technetium complexes exists in the literature, we concluded that components C and D in the ^{99m}Tc-EC20 radiochromatogram are also isomers.

Relative Affinity Assay. EC20 was first evaluated biologically using an in vitro relative affinity assay that measures a ligand's ability to directly compete with folic acid for binding to cell surface FRs. Importantly, a relative affinity value of 1.0 implies that the test article ligand has an affinity equal to that of folic acid for the FR. Likewise, values lower than unity reflect weaker affinity, and values higher than unity reflect stronger affinity.

Cultured KB cells were incubated with 100 nM ^{3}H-folic acid in the presence of increasing concentrations of nonradioactive folic acid, EC20, Rhenium-EC20 (isomer 1; peak C), Rhenium-EC20 (isomer 2; peak D), or a related folate-based radiopharmaceutical, DTPA-folate (*3*). Following a 15 min incubation at 4 °C, cells were rinsed free of unbound material and counted for residual cell-associated radioactivity. The quantity of bound radioactivity was plotted against the concentration of unlabeled ligand, and IC_{50} values (concentration of ligand required to block 50% of ^{3}H-folic acid binding) were estimated. As shown in Figure 4 and Table 2, EC20 was experimentally determined to have an affinity of 0.92 relative to that of folic acid for human FRs. Consequently, both isomers of Rhenium-EC20 displayed relative affinity values that were very similar to, if not better then, the parent EC20 molecule (1.42 and 1.37 for Re-EC20 isomer 1 and isomer 2, respectively). Furthermore, DTPA-folate, an ^{111}In-chelating folate radiopharmaceutical agent, displayed a relative affinity of 0.87 for the folate receptor. Thus, chemical modification of folate with various metal chelating motifs did not disturb the vitamin's intrinsic affinity for the FR.

Time-Dependent Cell Uptake. The kinetics of ^{99m}Tc-EC20 uptake into FR-positive KB cells was quantitatively measured. As shown in Figure 5, steady-state uptake was reached within 2 h at 37 °C, where approximately 3.2 million molecules of EC20 were cell associated. Half-maximal cell association occurred 9 min after mixing 10 nM of this radiopharmaceutical with the cells. Interestingly, the half-maximal saturation point was reached in only 37 s when cells were incubated with a 10-fold higher concentration of ^{99m}Tc-EC20 (100 nM; data not shown).

Concentration-Dependent Cell Uptake. Ligands of the high-affinity FR, including folate conjugates of radiopharmaceuticals and proteins etc., all display dose-dependent cell association (*1, 22, 40, 48, 60*). As shown in Figure 6, the cell uptake of ^{99m}Tc-EC20 was also found to be dependent on the extra-cellular concentration. The particular KB cells maintained in our laboratory were determined to bind a maximum of four million molecules of the folate radiopharmaceutical per cell. Scatchard analysis of the data estimated the dissociation constant (K_D) to be 3.2 nM, a value comparable with the K_D observed for the binding of unmodified folate to these same cells (*61*).

Concentration-Dependent Cell Uptake of Peak B. Although the full identity of the peak B component was not established, UV absorption analysis indicated that it contained a folate moiety (e.g., the absorption spectrum contained folate's signature secondary absorption peak at 363 nm). This HPLC-purified radio-labeled material was collected and then added to cultured KB cells. As shown in Figure 7, the cell uptake of ^{99m}Tc-labeled Peak B component was also found to be dependent on the extra-cellular concentration. Scatchard analysis of the data estimated the K_D of binding to be 1.1 nM. Importantly, the cell association of Peak B was completely blocked when in the presence of excess folic acid, indicating that this minor formulation byproduct is also capable of targeting FR-positive cells for radiodiagnostic purposes.

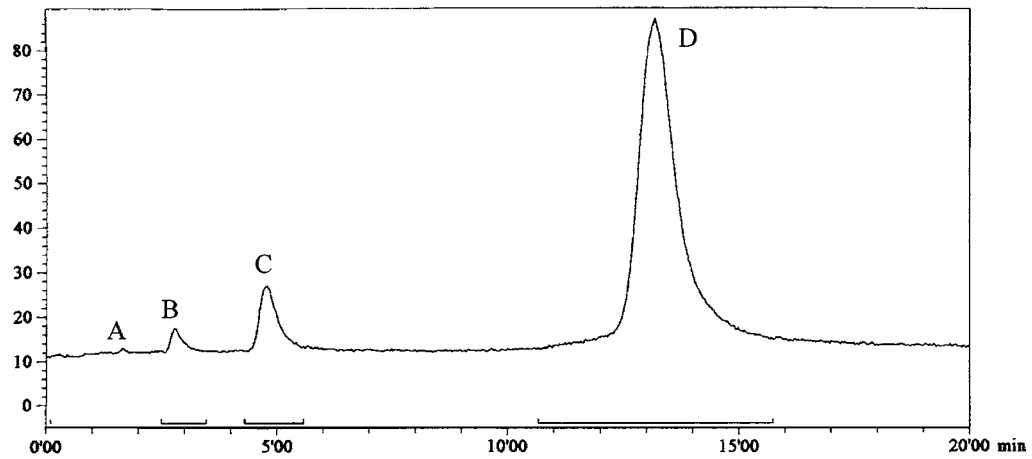


Figure 2. HPLC radiochromatogram of ^{99m}Tc-EC20. Samples of ^{99m}Tc-EC20 were eluted isocratically on a Waters Nova-Pak C18 (3.9 × 150 mm) column using an aqueous mobile phase containing 20% methanol and 0.1% trifluoroacetic acid at a flow rate of 1 mL/min. The HPLC analysis was monitored with both the UV detector (280 nm) and a Bioscan FC-3200 radiodetector. Peak A, free ^{99m}Tc; peak B, a folate-containing chelate of unknown structure; peaks C and D, diastereomers possessing either a syn or anti configuration of the technetium−oxygen bond in the Dap−Asp−Cys chelating ring of EC20.

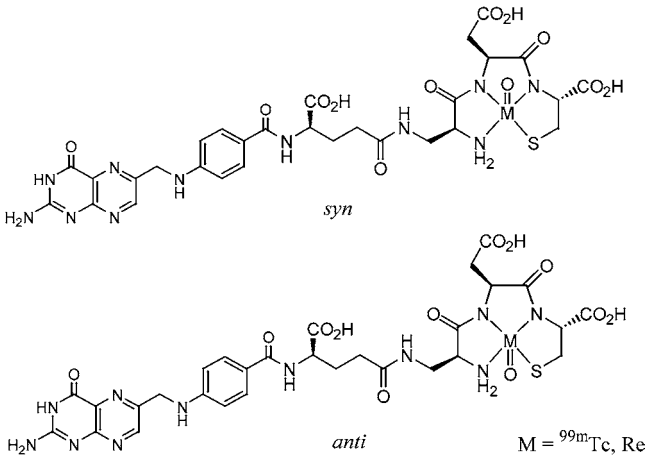


Figure 3. Structures of Re-EC20 and ^{99m}Tc-EC20 isomers (syn or anti position of metal-oxo bond).

Protein Binding. Prior to the onset of tissue distribution studies, we examined the ability of ^{99m}Tc-EC20 to bind proteins in both rat and human sera. Following a 1 min mix of ^{99m}Tc-EC20 with 1 mL of serum at room temperature, samples were ultrafiltered, and the quantity of radioactivity detected in the filtrate was measured to reveal the amount of unbound radiopharmaceutical. While ^{99m}Tc-EC20 exhibited only a minor level of nonspecific binding to the ultra-filtration device (~5%), approximately 70% of it was found to predominantly associate with the >30kDa serum protein fraction in solutions of rat or human serum (69% and 72%, respectively). Importantly, since ^{99m}Tc-EC20 does preferentially accumulate within FR-positive tissues (vide infra), its apparent affinity for serum proteins appears to be inconsequential.

Blood Clearance. We next evaluated the pharmacokinetic blood clearance of the ^{99m}Tc-EC20 formulation. Thus, Balb/c mice received an intravenous dose of 50 μg/kg ^{99m}Tc-EC20, and blood samples were collected at various time intervals thereafter. As shown in Figure 8, ^{99m}Tc-EC20 was rapidly removed from circulation in the Balb/c mouse. The plasma half-life of this radiopharmaceutical was estimated to be ~4 min, and less than 0.2% of the injected ^{99m}Tc-EC20 dose remained in circulation after 4 h (assuming that blood represents 5.5% of the total body mass). These data indicates that folate conjugates are rapidly removed from circulation following intravenous administration and that valuable tissue biodistribution data can be obtained after only a few hours postinjection without the concern for nonspecific tissue uptake due to blood-borne radioactivity.

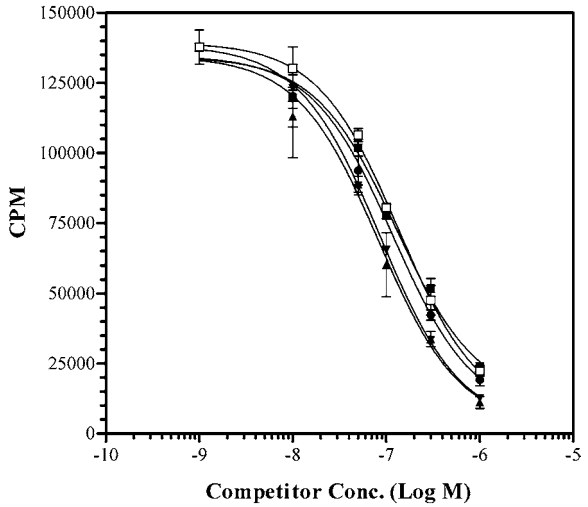


Figure 4. Blocking of ^{3}H-folic acid binding to KB cells with various folate-containing competitors. KB cells were incubated for 15 min on ice with 100 nM ^{3}H-folic acid in the presence and absence of increasing competitor concentrations. (•) Folic acid; (■) EC20; (▲) EC20:Re isomer 1; (▼) EC20:Re isomer 2; (□) DTPA−folate. Error bars represent 1 standard deviation (n = 3).

Table 2. Relative Affinity Estimations[a]

test article	IC_{50} (nM)	S.D.	RA	S.D.
folic acid	118	± 19	1.00	
EC20	128	± 25	0.92	± 0.23
EC20:Re isomer 1	83	± 16	1.42	± 0.36
EC20:Re isomer 2	86	± 3	1.37	± 0.23
DTPA-folate	136	± 12	0.87	± 0.16

[a] Relative affinities (RA) were defined as the inverse molar ratio of compound required to displace 50% of ^{3}H-folic acid bound to FR-positive KB cells. The relative affinity of folic acid was set to 1. Each test article was evaluated in triplicate.

Tissue Biodistribution. The ability of ^{99m}Tc-EC20 to target tumors in vivo was assessed using a FR-positive M109 model (*36*). These tumor cells are syngeneic for the

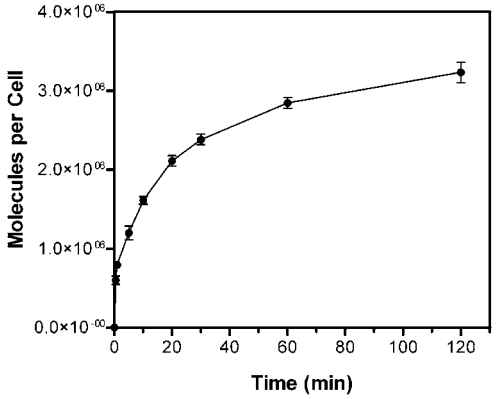


Figure 5. Time-dependent association of ^{99m}Tc-EC20. KB cells were incubated with 10 nM ^{99m}Tc-EC20 for increasing periods of time at 37 °C. Following multiple washes, cells were harvested and counted for associated radioactivity. Error bars represent 1 standard deviation ($n = 3$).

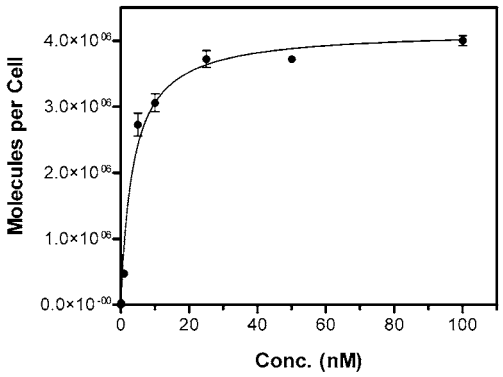


Figure 6. Concentration-dependent association of ^{99m}Tc-EC20. KB cells were incubated for 2 h at 37 °C in the presence of increasing concentrations of ^{99m}Tc-EC20. Following multiple washes, cells were harvested and counted for associated radioactivity. Error bars represent 1 standard deviation ($n = 3$).

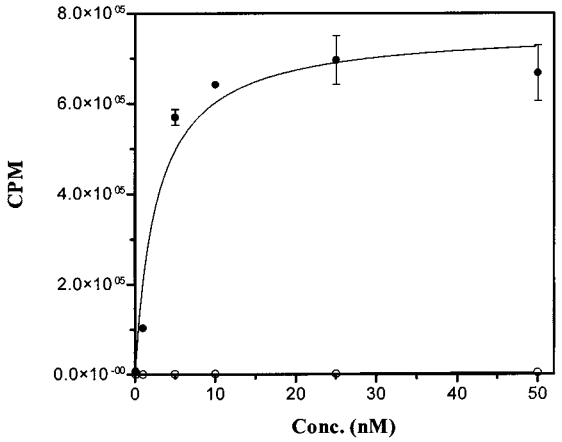


Figure 7. Concentration-dependent association of ^{99m}Tc-EC20 "peak B". KB cells were incubated for 2 h at 37 °C in the presence of increasing concentrations of "peak B" that was chromatographically isolated from the ^{99m}Tc-EC20 formulation. Following multiple washes, cells were harvested and counted for associated radioactivity. Error bars represent 1 standard deviation ($n = 3$). (●) peak B; (○) peak B plus 1 mM folic acid.

Balb/c mouse, and they reproducibly form subcutaneous solid tumors within two weeks post inoculation. ^{99m}Tc-EC14, which is structurally similar to ^{99m}Tc-EC20 except it contains one additional D-Glu residue (i.e., Pte-D-Glu-D-Glu-βDpr-Asp-Cys), ^{99m}Tc-EC28 (a nonpteroate containing control consisting of benzoyl-D-Glu-D-Glu-βDpr-Asp-Cys), and the previously reported ^{111}In-DTPA-folate radiopharmaceutical (*3*) were also evaluated in this bioassay. Importantly, the ^{99m}Tc-EC28 control agent should not bind to cell surface FRs because it lacks an essential pteridine ring moiety.

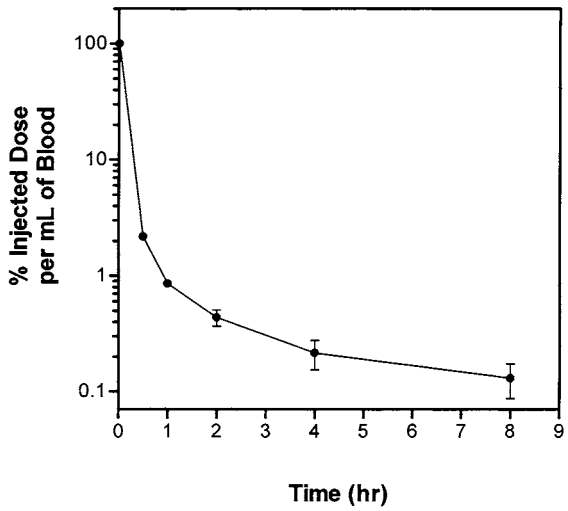


Figure 8. Blood clearance of ^{99m}Tc-EC20 in Balb/c mice. Each animal received an intravenous dose of 50 μg/kg EC20 (67 nmol/kg) in approximately 0.1 mL PBS during brief diethyl ether anesthesia. At the designated times postinjection, each animal was euthanized by CO_2 asphyxiation, and blood was collected and counted for associated radioactivity. Error bars represent 1 standard deviation ($n = 3$ animals).

Four hours after receiving an approximate 40 μmol/kg i.v. dose, animals were euthanized, and selected tissues were removed, weighed, and counted to determine ^{99m}Tc distribution. As shown in Table 3, the three "folate" containing radiopharmaceuticals, ^{99m}Tc-EC14, ^{99m}Tc-EC20, and ^{111}In-DTPA-folate, predominantly accumulated in the FR-positive tumor and kidneys; however, the kidneys concentrated a higher percent injected dose per gram of tissue (%ID/g) than did the tumor. Interestingly, the net tumor accumulation of ^{111}In-DTPA-folate and ^{99m}Tc-EC20 was nearly the same (19% and 17% ID/g, respectively), whereas the tumor uptake of ^{99m}Tc-EC14 was somewhat less at ~10% ID/g. Regardless, all three agents displayed high tumor-to-blood ratios (>30:1).

Folate-specific targeting was further demonstrated by two distinct methods. First, the accumulation of ^{99m}Tc-EC14, ^{99m}Tc-EC20, and ^{111}In-DTPA-folate in the FR-positive tumor and kidneys was effectively blocked (>94%) when these agents were co-administered with a 100-fold excess of folic acid. Second, the ^{99m}Tc-EC28 control agent failed to appreciably accumulate in the kidneys and tumor. Both observations provide evidence that an intact "folate-like" (or pteroate) moiety is required to afford targeted uptake and retention of these radiopharmaceutical agents into FR-positive tissues.

Scintigraphic Imaging. The predominant uptake of ^{99m}Tc-EC20 by the FR-positive M109 tumors and kidneys was further demonstrated using γ scintigraphy. As shown in Figure 9, a ventral image taken of a mouse 4 h after receiving a 50 μmol/kg i.v. dose of ^{99m}Tc-EC20 distinctively localizes the γ radiation to the two kidneys and the M109 tumor mass (shoulder region). No appreciable radiotracer was observed in other body tissues. Importantly, a similar image profile has been reported for the ^{111}In-DTPA-folate radiopharmaceutical (*3*).

Urinary Excretion and Metabolism. It was previously determined that the primary elimination route for ^{111}In-DTPA-folate was via the urine (*3*). Because

Table 3. Biodistribution of Folate Radiopharmaceuticals in Balb/c Mice Bearing Subcutaneous M109 Tumors.

	% injected dose per gram tissue (4 hr post intravenous injection)[a]						
	^{99m}Tc-EC14	^{99m}Tc-EC14 + folic acid	^{99m}Tc-EC20	^{99m}Tc-EC20 + folic acid	^{111}In-DTPA-folate	^{111}In-DTPA-folate + folic acid	^{99m}Tc-EC28
blood	0.31 ± 0.14	0.19 ± 0.07	0.34 ± 0.03	0.09 ± 0.02	0.21 ± 0.10	0.09 ± 0.04	0.06 ± 0.04
heart	2.39 ± 0.64	0.08 ± 0.01	1.57 ± 0.26	0.08 ± 0.01	2.57 ± 0.82	0.06 ± 0.02	0.03 ± 0.01
lung	2.08 ± 0.40	0.15 ± 0.04	2.22 ± 0.63	0.31 ± 0.26	1.72 ± 0.61	0.09 ± 0.02	0.05 ± 0.01
liver	3.44 ± 2.19	1.37 ± 0.98	3.56 ± 0.25	1.15 ± 0.22	5.21 ± 2.63	0.81 ± 0.03	0.50 ± 0.26
spleen	2.68 ± 2.49	2.99 ± 1.43	0.95 ± 0.15	0.38 ± 0.33	3.30 ± 2.33	1.46 ± 0.73	0.60 ± 0.38
intestine	1.70 ± 0.55	0.32 ± 0.11	2.56 ± 0.61	2.93 ± 1.49	1.87 ± 0.69	0.82 ± 0.14	0.47 ± 0.19
kidney	98.0 ± 40.7	5.94 ± 0.52	138 ± 12.4	5.64 ± 2.13	191 ± 79.2	3.14 ± 1.96	0.62 ± 0.14
muscle	0.99 ± 0.28	0.09 ± 0.11	0.67 ± 0.20	0.06 ± 0.02	1.19 ± 0.48	0.05 ± 0.04	0.02 ± 0.01
stomach	1.47 ± 0.58	0.10 ± 0.03	1.45 ± 0.55	3.35 ± 5.19	1.62 ± 0.65	0.25 ± 0.20	0.21 ± 0.19
tumor	**9.83 ± 2.77**	**0.43 ± 0.52**	**17.2 ± 1.02**	**0.45 ± 0.18**	**19.3 ± 5.86**	**0.46 ± 0.42**	**0.11 ± 0.06**
tumor/blood	34.1 ± 7.41	2.00 ± 2.00	51.0 ± 8.20	4.70 ± 1.30	102 ± 43.4	5.00 ± 4.60	2.00 ± 0.50

[a] Values shown represent the mean ± s.d. of data from three animals per cohort.

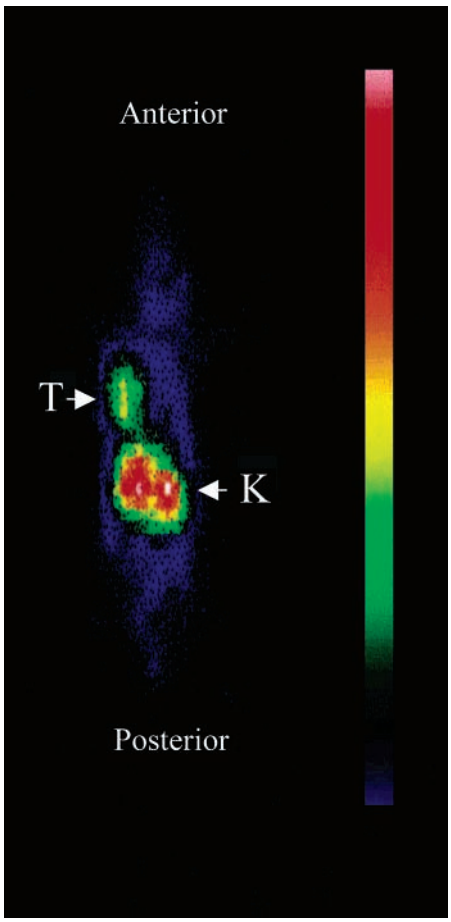


Figure 9. Whole-body γ images (ventral view). Images were obtained 4 h following intravenous administration of ^{99m}Tc-EC20 to a Balb/c mouse bearing a subcutaneous folate receptor-positive M109 tumor. Only the kidneys (K) and tumor (T) exhibit significant accumulation of this radiotracer.

^{99m}Tc-EC20 is a related folate-based radiopharmaceutical, we elected to evaluate its urinary excretion and metabolic profile using a radiochemical HPLC method. Thus, following a 1 mCi injection (6.7 nmol per mouse) of ^{99m}Tc-EC20, mice were euthanized at various time intervals, and urine samples were collected for HPLC analysis.

Similar to the HPLC profile shown in Figure 2, both the ^{99m}Tc-EC20 standard and the urine samples exhibited four radioactive peaks. As shown in Table 4, the radiochemical purity of the standard (sum of peaks C and D presumably corresponding to the syn and anti ^{99m}Tc-EC20) remained constant at ~93% over the 6 h duration of this experiment. The amount of free ^{99m}Tc in the standard (peak A) was ~2%. Importantly, peak B within this radiochemical profile is believed to be EC20 chelated to ^{99m}Tc at an unconventional, less stable position. However, the radioactivity measured in this fraction was not included in the overall radiochemical purity estimation for ^{99m}Tc-EC20. Collectively, these data indicate that the ^{99m}Tc-EC20 formulation remained stable in saline solution throughout this 6 h investigation.

After 1 and 4 h postinjection into Balb/C mice, the radiochemical speciation profile of ^{99m}Tc-EC20 in the mouse urine did not change. The radioactivity present in the urine at 6 h postinjection, however, was too low to accurately assay by HPLC. The proportion of parent drug among radioactive species recovered in urine remained relatively constant at approximately 90% throughout the 4 h during which it could be quantitated. This value is very similar to the ~93% purity of the standard, indicating that ^{99m}Tc-EC20 is predominately excreted into the urine in an un-modified form.

DISCUSSION

The primary goal of this investigation was to identify a folate-based ^{99m}Tc chelator candidate for clinical development. This project required the design, synthesis, analytical, and radiochemical characterization of a new chemical entity, as well as in vitro and in vivo biological evaluations.

We adopted an efficient solid-phase synthetic procedure to produce EC20, a small molecular weight peptide derivative of folate that contains a D-γ-Glu peptide linkage (Figure 1). In its natural form, folate (or pteroylglutamate) has a single glutamyl residue present in an L configuration. However, a D-Glu enantiomer residue was incorporated into the EC20 molecule for the purpose of providing additional metabolic protection against tissue-resident γ-glutamyl hydrolases (*62*). Importantly, similar to EC20, we have found that substitution of the L-Glu residue with a D-Glu residue does not alter folic acid's ability to bind to the high affinity FR (unpublished data).

EC20 was found to efficiently chelate ^{99m}Tc when in the presence of α-D-glucoheptonate and tin (II) chloride. When analyzed by radiochemical HPLC, >95% of the resulting ^{99m}Tc-EC20 formulation consisted of a mixture of syn and anti stereoisomers, each equally capable of binding to FR with high affinity (Figure 3). Approximately 3% of the ^{99m}Tc in the formulation was chelated to EC20 at some other site on the EC20 molecule besides the expected Dap−Asp−Cys moiety. Although this component was not isolated in sufficient quantity for optimal

Table 4. Excretion and Metabolism of ^{99m}Tc-EC20 from the Balb/c Mouse[a]

		area percent						
		^{99m}Tc-EC20 Standard			urine samples (two mice/timepoint)			
peak	rt (min)	0 hr	1 hr	6 hr	1 hr		4 hr	
A (pertechnetate)	1.4	2	2.1	1.8	8.3	6.3	9.4	10.2
B (unknown)	3.4	4.5	4.5	4.8	2.5	2.6	5.4	0
C (isomer 1)	5.5	15.5	15.7	15.9	20.4	18.1	7.3	11.1
D (isomer 2)	18.5	78	77.7	77.5	68.8	73	77.9	78.7
sum C and D		93.5	93.4	93.4	89.2	91.1	85.2	89.8

[a] Mice were injected with 1 mCi (6.7 nmol) of ^{99m}Tc-EC20 via a lateral tail vein. At the indicated times, groups of two mice were euthanized, and urine was collected. The radiochemical speciation was then determined by HPLC. The area percent sum of peaks C and D (syn and anti isomers) is used to calculate the overall purity of intact ^{99m}Tc-EC20.

characterization, it was determined to bind to FR with high affinity (Figure 6). Finally, the remaining ~ 2% of the radioactivity in the ^{99m}Tc-EC20 formulation was attributed to free ^{99m}Tc.

This radiopharmaceutical demonstrated both time- and concentration-dependent association with FR-positive cells, as expected (*22*, *48*). ^{99m}Tc-EC20 was rapidly cleared from the blood ($t_{1/2}$ ~ 4 min), which is a great quality for diagnostic imaging agents, and it preferentially accumulated within FR-positive tumors in large amounts.

The performance of ^{99m}Tc-EC20 was directly compared to that of a similar FR targeting agent, ^{111}In-DTPA-folate, using two different methods. First, both folate-based radiopharmaceuticals were found to equally compete with folic acid for binding to FRs on KB cells (Figure 3 and Table 1). Second, the biodistribution of each agent in tumor-bearing mice was nearly identical (Table 2). High tumor uptake and tumor-to-blood ratios were measured for ^{99m}Tc-EC20 and ^{111}In-DTPA-folate. Taken together, these results suggest that, like ^{111}In-DTPA-folate (*63*), ^{99m}Tc-EC20 has the potential to effectively localize in FR-positive tumors when clinically administered to patients.

Several folate-based ^{99m}Tc conjugates have previously been described in the literature. Limited biodistribution data are available on a ^{99m}Tc-12-amino-3,3,9,9-tetramethyl-5-oxa-4,8 diaza-2,10-dodecanedinoe dioxime (OXA) folate conjugate; however, moderate levels (~7% ID/g) of tracer uptake in a KB tumor was reported (*6*). Studies involving the biodistribution of a ^{99m}Tc-ethylenedicysteine-folate conjugate in mammary tumor-bearing rats were also reported. Unfortunately, the rats in that study were fed a folate-rich diet. Thus, low tumor uptake and low tumor-to-blood ratios were obtained presumably because of competition with endogenous folate ligands (*4*). Last, a ^{99m}Tc-6-hydrazinonicotinamido-hydrazido (HYNIC) folate derivative (HYNIC-folate) was shown to accumulate in large amounts within 24JK-FBP tumors (*5*). Interestingly, ^{99m}Tc-EC20 accumulated within M109 tumors to nearly identical levels as that of HYNIC-folate in 24JK−FBP tumors (~17% ID/g) (*5*; Table 2). These two agents also displayed a roughly 50:1 tumor-to-blood ratio at 4 h post intravenous injection. Thus, folate clearly has the ability to deliver many different types of ^{99m}Tc chelates to FR-positive tumors, and EC20 has proven to be among the best.

The high-affinity FR is expressed at high levels mainly on cancer cells. For example, epithelial cancers of the ovary, mammary gland, colon, lung, nose, throat, and brain have all been reported to express elevated levels of the FR (*64*−*72*). In fact, >90% of all human ovarian tumors are known to express large amounts of this receptor (*66*, *70*, *73*). Overexpression of FR by cancer cells may well be selected for to provide the cells with a growth advantage relative to neighboring normal tissue. Indeed, highly de-differentiated metastatic cancers express considerably more FR than their localized, low-grade counterparts (*71*).

Each year ~26 000 women in the United States are diagnosed with ovarian cancer, and less than 50% of those women survive more than five years. One reason for the low survival rate is the difficulty in diagnosing this form of cancer. Because of the fear of rupturing an unidentified abdominal mass and the potential for spreading cancer throughout the abdominal cavity, fine needle biopsy is not often performed. Rather, the diagnoses and staging of suspicious ovarian masses is typically done through surgical laparotomy, which is an invasive and expensive procedure. Since ^{99m}Tc-EC20 binds tightly to FR which is present in large amounts on ovarian and other cancers, this radiopharmaceutical may provide an inexpensive, noninvasive, but reliable method for the early diagnosis of cancer. Importantly, ^{99m}Tc-EC20 may also help guide the clinical decision process with these patients by making more definitive and earlier diagnoses of recurrent or residual disease.

In summary, a new peptide derivative of folate was created to efficiently chelate ^{99m}Tc. This new compound, referred to as ^{99m}Tc-EC20, avidly binds to FR-positive tumor cells in vitro and in vivo despite its moderately high propensity to bind to serum protein. ^{99m}Tc-EC20 displayed rapid pharmacokinetic distribution out of the blood and into FR-positive tumors and kidney, and it was eliminated via the urine in a nonmetabolized form. These results indicate that ^{99m}Tc-EC20 should be clinically investigated as a noninvasive radiodiagnostic imaging agent for the detection of FR-positive cancers.

ACKNOWLEDGMENT

This work was supported in part by a Phase I and II SBIR grant from the National Institutes of Health. The authors also wish to thank Dr. Mark Green and Carla Mathias for conducting the serum protein binding study and Dr. Philip S. Low for his valuable comments.

LITERATURE CITED

(1) Wang, S., et al. (1996) Synthesis, purification, and tumor cell uptake of ^{67}Ga-deferoxamine-folate, a potential radiopharmaceutical for tumor imaging. *Bioconjugate Chem*. *7*, 56−62.

(2) Mathias, C. J., et al. (1996) Tumor-selective radiopharmaceutical targeting via receptor-mediated endocytosis of Gallium-67-deferoxamine-folate. *J. Nuc. Med.*, *37* (6), 1003−1008.

(3) Mathias, C. J., et al. (1998) Indium-111-DTPA-folate as a potential folate-receptor-targeted radiopharmaceutical. *J. Nucl. Med.*, *39*, 1579−1585.

(4) Ilgan, S., et al. (1998) ^{99m}Tc-Ethylenedicysteine-folate: A new tumor imaging agent. Synthesis, labeling and evaluation in animals. *Cancer Biother. Radiopharm*. *13* (6), 427−435.

(5) Guo, W., G. H. Hinkle, and Lee, R. J. (1999) ^{99m}Tc−HYNIC-folate: A novel receptor-based targeted radiopharmaceutical for tumor imaging. *J. Nucl. Med*. *40* (9), 1563−1569.

(6) Linder, K. E., et al. (2000) In vitro & in vivo studies with α- and γ-isomers of ^{99m}Tc-OXA-Folate show uptake of both isomers in folate-receptor (+) KB cell lines. *Soc. Nucl. Med. Proc. 47th Annual Meeting 41* (5), 119P.

(7) Olsen, J. O., et al. (1995) Somatostatin receptor imaging of neuroendocrine tumors with indium-111 pentetreotide (Octreoscan). *Semin. Nucl. Med. 25* (3), 251−61.

(8) Virgolini, I., et al. (1994) Vasoactive intestinal peptide-receptor imaging for the localization of intestinal adenocarcinomas and endocrine tumors. *N. Engl. J. Med. 331* (17), 1116−1121.

(9) van Zanten-Przybysz, I., et al. (1999) ^{131}I-labeled chimeric monoclonal antibody MOv18 in ovarian cancer patients: a pilot study. *Tumor Targeting 4*, 179−188.

(10) Collins, D. A., Hogenkamp, H. P. , and Gebhard, M. W. (1999) Tumor imaging via indium 111-labeled DTPA-adenosylcobalamin. *Mayo Clin. Proc. 74* (7), 687−91.

(11) Modorati, G., et al. (1994) Immunoscintigraphy with three step monoclonal pretargeting technique in diagnosis of uveal melanoma: preliminary results. *Br. J. Ophthalmol. 78* (1), 19−23.

(12) Seccamani, E., et al. (1989) A simple qualitative determination of human antibodies to murine immunoglobulins (HAMA) in serum samples. *Int. J. Radiat. Appl. Instrum. B, 16* (2), 167−170.

(13) Colcher, D., et al. (1990) In vivo tumor targeting of a recombinant single-chain antigen-binding protein. *J. Natl. Cancer Inst. 82* (14), 1191−1197.

(14) Leamon, C. P., Low, P. S. (2001) Folate-mediated targeting: from diagnostics to drug and gene delivery. *Drug Discov. Today, 6* (1), 44−51.

(15) Konda, S. D., et al. (2000) Development of a tumor-targeting MR contrast agent using the high-affinity folate receptor. *Invest. Radiol. 35* (1), 50−57.

(16) Ladino, C. A., et al. (1997) Folate-maytansinoids: Target-selective drugs of low molecular weight. *Int. J. Cancer 73*, 859−864.

(17) Citro, G., et al. (1994) Inhibition of leukaemia cell proliferation by folic acid-polylysine-mediated introduction of c-myb antisense oligodeoxynucleotides into HL-60 cells. *Br. J. Cancer 69*, 463−467.

(18) Li, S., Huang, L. (1997) Targeted delivery of antisense oligodeoxynucleotides by LPDII. *J. Liposome Res. 7* (1), 63−75.

(19) Li, S., Huang, L. (1998) Targeted delivery of antisense oligodeoxynucleotides formulated in a novel lipidic vector. *J. Liposome Res. 8* (2), 239−250.

(20) Li, S., Deshmukh, H. M. , and Huang, L. (1998) Folate-mediated targeting of antisense oligonucleotides to ovarian cancer cells. *Pharm. Res. 15* (10), 1540−1545.

(21) Leopold, L. H., et al. (1995) Multi-unit ribozyme-mediated cleavage of bcr-abl mRNA in myeloid leukemias. *Blood 85* (8), 2162−2170.

(22) Leamon, C. P., Low, P. S. (1991) Delivery of Macromolecules into Living Cells: A Method that Exploits Folate Receptor Endocytosis. *Proc. Natl. Acad. Sci. U.S.A. 88*, 5572−5576.

(23) Ward, C. M., Acheson, N. , and Seymour, L. M. (2000) Folic acid targeting of protein conjugates into ascites tumor cells from ovarian cancer patients. *J. Drug Targeting 8* (2), 119−123.

(24) Lu, J. Y., et al. (1999) Folate-targeted enzyme prodrug cancer therapy utilizing penicillin-V amidase and a doxorubicin prodrug. *J. Drug Targeting 7* (1), 43−53.

(25) Leamon, C. P.; Low, P. S. (1992) Cytotoxicity of Momordin-Folate Conjugates in Cultured Human Cells. *J. Biol. Chem. 267*, 24966−24971.

(26) Leamon, C. P., Pastan, I., and Low, P. S. (1993) Cytotoxicity of Folate-Pseudomonas Exotoxin Conjugates Toward Tumor Cells. *J. Biol. Chem. 268*, 24847−24854.

(27) Leamon, C. P., Low, P. S. (1994) Selective Targeting of Malignant Cells with Cytotoxin-Folate Conjugates. *J. Drug Targeting 2*, 101−112.

(28) Kranz, D. M., et al. (1995) Conjugates of folate and anti-T-cell-receptor antibodies specifically target folate-receptor-positive tumor cells for lysis. *Proc. Natl. Acad. Sci. U.S.A. 92*, 9057−9061.

(29) Cho, B. K., et al. (1997) Single-chain Fv/folate conjugates mediate efficient lysis of folate-receptor-positive tumor cells. *Bioconjugate Chem. 8*, 338−346.

(30) Kranz, D. M., et al. (1998) Targeting tumor cells with bispecific antibodies and T cells. *J. Controlled Release 53*, 77−84.

(31) Rund, L. A., et al. (1999) Bispecific agents target endogenous murine T cells against human tumor xenografts. *Int. J. Cancer 83*, 141−149.

(32) Lee, R. J., Low, P. S. (1994) Delivery of Liposomes into Cultured KB Cells via Folate Receptor- mediated Endocytosis. *J. Biol. Chem. 269*, 3198−3204.

(33) Lee, R. J., Low, P. S. (1995) Folate-mediated tumor cell targeting of liposome-entrapped doxorubicin in vitro. *Biochim. Biophys. Acta 1233*, 134−144.

(34) Vogel, K., et al. (1996) Peptide-mediated release of folate-targeted liposome contents from endosomal compartments. *J. Am. Chem. Soc. 118* (7), 1581−1586.

(35) Rui, Y., et al. (1998) Diplasmenylcholine-folate liposomes: An efficient vehicle for intracellular drug delivery. *J. Am. Chem. Soc. 120* (44), 11213−11218.

(36) Gabizon, A., et al. (1999) Targeting folate receptor with folate linked to extremities of poly (ethylene glycol)-grafted liposomes: in vitro studies. *Bioconjugate Chem. 10* (2), 289−98.

(37) Gottschalk, S., et al. (1994) Folate receptor mediated DNA delivery into tumor cells: potosomal disruption results in enhanced gene expression. *Gene Ther. 1*, 185−191.

(38) Mislick, K. A., et al. (1995) Transfection of folate-polylysine DNA complexes: Evidence for lysosomal delivery. *Bioconjugate Chem. 6*, 512−515.

(39) Douglas, J. T., et al. (1996) Targeted gene delivery by tropism-modified adenoviral vectors. *Nat. Biotech. 14*, 1574−1578.

(40) Leamon, C. P., Weigl, D., and Hendren, R. W. (1999) Folate copolymer-mediated transfection of cultured cells. *Bioconjugate Chem. 10*, 947−957.

(41) Guo, W., Lee, R. J. (1999) Receptor-targeted gene delivery via folate-conjugated polyethylenimine. *PharmSci 1* (4), 19.

(42) Reddy, J. A., et al. (1999) Optimization of folate-conjugated liposomal vectors for folate receptor-mediated gene therapy. *J. Pharm. Sci. 88* (11), 1112−1118.

(43) Reddy, J. A., Low, P. S. (2000) Enhanced folate receptor mediated gene therapy using a novel pH-senistive lipid formulation. *J. Controlled Release 64*, 27−37.

(44) Antich, P., et al. (1994) Imaging of folate receptors with I-125 labeled folate using small animal imaging system built with plastic scintillating optical fibers. *J. Nucl. Med. 35*, 222 (abstract).

(45) Mathias, C. J., et al. (2000) Synthesis of [(99m)Tc]DTPA-folate and its evaluation as a folate-receptor-targeted radiopharmaceutical. *Bioconjugate Chem. 11* (2), 253−7.

(46) Rouschias, G. (1974) *Chem. Rev. 74*, 531.

(47) Westerhof, G. R., et al. (1995) Carrier- and receptor-mediated transport of folate antagonists targeting folate-dependent enzymes: Correlates of molecular structure and biological activity. *Mol. Pharm. 48*, 459−471.

(48) Leamon, C. P., Low, P. S. (1993) Membrane Folate-binding Proteins are Responsible for Folate- protein Conjugate Endocytosis into Cultured Cells. *Biochem. J. 291*, 855−860.

(49) Eisenhut, M., et al. (1991) *J. Labeled Compd. Radiopharm. 29*, 1283.

(50) Liu, S., et al. (1996) Labeling cyclic glycoprotein IIb/IIIa receptor antagonists with 99mTc by the preformed chelate approach: effects of chelators on properties of [99mTc]-chelator-peptide conjugates. *Bioconjugate Chem. 7* (2), 196−202.

(51) Liu, S., et al. (1996) Labeling a hydrazino nicotinamide-modified cyclic IIb/IIIa receptor antagonist with 99mTc using aminocarboxylates as coligands. *Bioconjugate Chem. 7* (1), 63−71.

(52) Fritzberg, A. R., et al. (1988) Approaches to radiolabeling of antibodies for diagnosis and therapy of cancer. *Pharm. Res. 5* (6), 325−334.

(53) Liang, F. H., Virzi, F., and Hnatowich, D. J. (1987) The use of diaminodithiol for labeling small molecules with technetium-99m. *Int. J. Radiat. Appl. Instrum. B 14* (1), 63−67.
(54) Chianelli, M., et al. (1992) *Eur. J. Nucl. Med. 19*, 625.
(55) Baidoo, K. E., Lever, S. Z., and Scheffel, U., (1994) Bifunctional chelator for facile preparation of neutral technetium complexes. *Bioconjugate Chem. 5* (2), 114−118.
(56) Eisenhut, M., et al. (1996) Bifunctional NHS-BAT ester for antibody conjugation and stable technetium-99m labeling: conjugation chemistry, immunoreactivity and kit formulation. *J. Nucl. Med. 37* (2), 362−70.
(57) Wong, E., et al. (1997) Rhenium (V) and Technetium (V) Oxo Complexes of an N (2)N′S Peptidic Chelator: Evidence of Interconversion between the Syn and Anti Conformations. *Inorg. Chem. 36* (25), 5799−5808.
(58) Francesconi, L. C., et al. (1993) Synthesis and characterization of neutral MVO (M = technetium, rhenium) aminethiol complexes containing a pendant phenylpiperidine group. *Inorg. Chem. 32* (14), 3114−3124.
(59) Marzilli, L. G., et al. (1994) Linking Deprotonation and Denticity of Chelate Ligands. Rhenium (V) Oxo Analogues of 99mTechnetium Radiopharmaceuticals Containing N2S2 Chelate Ligands. *Inorg. Chem. 33* (22), 4850−4860.
(60) Leamon, C. P., DePrince, R. B., and Hendren, R. W. (1999) Folate-mediated drug delivery: Effect of alternative conjugation chemistry. *J. Drug Targeting 7* (3), 157−169.
(61) Antony, A. C. (1992) The Biological Chemistry of Folate Receptors. *Blood 79* (11), 2807−2820.
(62) Jodrell, D. I., et al. (1993) The in vivo metabolic stability of dipeptide analogues of the quinazoline antifolate, ICI 198583, in mice. *Biochem. Pharm. 46* (12), 2229−2234.
(63) Mathias, C. J., Green, M. A. (1998) A kit formulation for preparation of [^{111}In]In-DTPA-Folate, a folate-receptor-targeted radiopharmaceutical. *Nuc. Med. Biol. 25*, 585−587.
(64) Coney, L. R., et al. (1991) Cloning of a Tumor-associated Antigen: MOv18 and MOv19 Antibodies Recognize a Folate-binding Protein. *Cancer Res. 51*, 6125−6132.
(65) Weitman, S. D., et al. (1992) Distribution of the folate receptor GP38 in Normal and Malignant Cell Lines and Tissues. *Cancer Res. 52*, 3396−3401.
(66) Ross, J. F., Chaudhuri, P. K., and Ratnam, M. (1994) Differential regulation of folate receptor isoforms in normal and malignant tissues in vivo and in established cell lines. *Cancer 73*, 2432−2443.
(67) Weitman, S. D., et al. (1992) Cellular Localization of the Folate Receptor: Potential Role in Drug Toxicity and Folate Homeostasis. *Cancer Research 52*, 6708−6711.
(68) Weitman, S. D., Frazier, K. M., and Kamen, B. A. (1994) The folate receptor in central nervous system malignancies of childhood. *J. Neurol. Oncol. 21*, 107.
(69) Mattes, M. J., et al. (1990) Patterns of antigen distribution in human carcinomas. *Cancer Res. Suppl. 50*, 880S.
(70) Garin-Chesa, P., et al. (1993) Trophoblast and Ovarian Cancer Antigen LK26. *Am. J. Pathol. 142* (2), 557−567.
(71) Toffoli, G., et al. (1997) Overexpression of folate binding protein in ovarian cancers. *Int. J. Cancer 74*, 193−198.
(72) Holm, J., et al. (1991) High-affinity folate binding in human choroid plexus. *Biochem. J. 280*, 267−271.
(73) Campbell, I. G., et al. (1991) *Cancer Res. 51*, 5329−5338.

BC0200430

Effects of Structure of Polyamidoamine Dendrimer on Gene Transfer Efficiency of the Dendrimer Conjugate with α-Cyclodextrin

Fumihiro Kihara, Hidetoshi Arima, Toshihito Tsutsumi, Fumitoshi Hirayama, and Kaneto Uekama*

Faculty of Pharmaceutical Sciences, Kumamoto University, 5-1 Oe-honmachi, Kumamoto 862-0973, Japan.
Received June 9, 2002; Revised Manuscript Received September 3, 2002

To improve gene transfer activity of a new nonviral vector, a polyamidoamine dendrimer (G2) conjugate with α-cyclodextrin (α-CDE conjugate (G2)), we prepared α-CDE conjugates with dendrimer having different generations (G3 and G4), and their gene transfer activities were compared with those of α-CDE conjugate (G2) and TransFast, a novel transfection reagent. α-CDE conjugates (G2, G3, and G4) formed the complexes with pDNA, changing the ζ-potential and particle size of pDNA complexes and the protection of pDNA from DNase I in a charge ratio-dependent manner, although their differences at higher charge ratios (vector/pDNA) were small. The gene transfer activity of α-CDE conjugates (G2, G3, and G4) was higher than that of the corresponding dendrimer alone in NIH3T3 and RAW264.7 cells. Of these CDE conjugates, α-CDE conjugate (G3) had a superior gene transfer activity which was comparable to that of TransFast in NIH3T3 cells. The intracellular distribution of pDNA after application of the pDNA complex with α-CDE conjugate (G3) to NIH3T3 cells was different from that with dendrimer alone (G3), although the cellular association of pDNA was almost comparable among all vectors. α-CDE conjugate (G3) strongly interacted with a fluorescence probe, 2-(*p*-toluidinyl)-naphthalene-6-sulfonate (TNS), suggesting that the conjugate possesses the inclusion ability with biomembrane constituents such as phospholipids after transfection. These results suggest that α-CDE conjugates, particularly the G3 conjugate, could be novel nonviral gene transfer agents.

INTRODUCTION

The promising concept of gene therapy has encouraged the improvement of gene transfer techniques (*1*). At present, the following four methods may be available for gene transfer, i.e., viral vector, nonviral vector and physical (electroporation and gene gun, etc.) methods as well as naked plasmid DNA (pDNA[1]) method without vectors (*2, 3*). Nonvirus vectors have been noticed due to easy preparation of vector/pDNA complexes, low cytotoxicity, and lack of immunogeneity of vectors, but the insufficient gene transfer ability should be improved (*4, 5*). Starburst polyamidoamine (PAMAM) dendrimer (dendrimer) employed in this study is a spherical, highly ordered, dendritic polymer with positively charged primary amino groups on the surface at physiological pH (*6*) and is reported to be useful as nonviral vectors (*7*−*11*). Although the dendrimers with generations higher than 5 (G5) have sufficient gene transfer activity, cytotoxicity increases concomitantly as the generation increases due to higher positive charges (*12*).

Cyclodextrins (CyDs) are cyclic (α-1,4)-linked oligosaccharides of α-D-glucopyranose containing a hydrophobic central cavity and hydrophilic outer surface (*13*−*15*). The most common CyDs are α-, *β*-, and *γ*-CyDs, which consist of six, seven, and eight D-glucopyranose units, respectively. CyDs are known to form inclusion complexes with a variety of guest molecules in solution and in a solid state (*16, 17*). The solubilization of lipophilic compounds by CyDs has many uses in the pharmaceutical field (*18, 19*), while CyDs at higher concentrations induce hemolysis and decrease the integrity of the nasal and intestinal epithelial cells, leading to an increase in the permeability of water-soluble drugs through the membranes (*20*−*22*).

Recently, CyDs have been applied to gene transfer (*23*−*25*) and oligonucleotides delivery (*26*−*29*). Notably, Davis and his colleagues (*30, 31*) reported that of cationic *β*-CyD polymers, a water soluble *β*-CyD polymer with 6^A,6^D-dideoxy-6^A,6^D-di-(2-aminoethanethio)-*β*-CyD and dimethylsuberimidate (*β*CDP6) gave gene transfer activity much higher than Superfect and poly-L-lysine in BHK-21 and CHO-K1 with less cytotoxicity. In addition, most recently they reported that the combination of *β*CDP6 and poly(ethylene glycol) conjugate with adamantane (PEG-AD) forms stable complexes with pDNA through *β*-CyD/adamantane host/guest interactions and the ternary complex of *β*CDP6, galactosylated PEG-AD, and pDNA possesses higher transfection efficiency in hepatoma cells through receptor-mediated endocytosis (*32*).

We reported previously that gene transfer activity was significantly improved when the dendrimer (G2) conjugates with α-CyD, *β*-CyD, and *γ*-CyD were employed as vectors, where the activity was most enhanced by the α-CyD conjugate (α-CDE conjugate) almost 100 times, compared with that of dendrimer (G2) (*30*). Thus, the attachment of a molecule of α-CyD to a terminal amino group of dendrimer (G2) provoked the marked improvement of gene transfer activity, so we expected that the conjugation of α-CyD with dendrimer of higher generation would provide much more gene transfer activity. Therefore, we prepared α-CDE conjugates with dendrimers having different generations (G2, G3, and G4) and

* To whom correspondence should be addressed.. Telephone: (81)-96-371-4160. Fax: (81)-96-371-4420. E-mail: uekama@gpo.kumamoto-u.ac.jp.

[1] Abbreviation: CyDs, cyclodextrins; CDE conjugate, cyclodextrin−dendrimer conjugate; pDNA, plasmid DNA; dendrimer, Starburst polyamidoamine dendrimer; TNS, 2-(*p*-toluidinyl)-naphthalene-6-sulfonate potassium salt; [^{32}P]pDNA, [^{32}P]-labeled plasmid DNA; FITC-pDNA, fluorescein isothiocianate-labeled pDNA.

10.1021/bc025557d CCC: $22.00 © 2002 American Chemical Society
Published on Web 11/01/2002

investigated the effects of generation on physicochemical properties such as net charge, ζ-potential, particle size, pDNA degradation by DNase I, gene transfer activity, and cytotoxicity of pDNA complexes with dendrimers (pDNA/dendrimers) and α-CDE conjugates (pDNA/α-CDE conjugates). In addition, the enhancing mechanism of gene transfer activity of α-CDE conjugate (G3) was examined.

MATERIALS AND METHODS

Materials. α-CyD was donated by Nihon Shokuhin Kako (Tokyo) and recrystallized from water. Starburst PAMAM dendrimers (ethylenediamine core, G2, G3, and G4) were purchased from Aldrich Chemical (Tokyo). *p*-Toluenesulfonyl chloride was purchased from Nakarai Tesque (Kyoto, Japan). Fetal calf serum (FCS) was purchased from Nichirei (Tokyo). Dulbecco's modified Eagle's medium and RPMI1640 medium were purchased from Nissui Pharmaceuticals (Tokyo). TransFast transfection reagent, the plasmid pGL3 control vector, which contains the firefly luciferase gene under the control of the SV40 promoter (pDNA) and DNase I were obtained from Promega (Tokyo). 2-(*p*-Toluidinyl)naphthalene-6-sulfonate potassium salt (TNS) was obtained from Research Organics (Cleveland, OH). [α-^{32}P]CTP was obtained from Amersham Pharmacia Biotech (Tokyo). The purification of pDNA amplified in bacteria was carried out using QIAGEN EndoFree plasmid maxi kit (<0.1 EU/μg endotoxin). Other chemicals and solvents were of analytical reagent grade.

Preparation of α-CDE Conjugates. α-CyD was attached to a primary amino residue of dendrimers (G2, G3, and G4) according to the method of Suh et al. (*34*). Monotosyl-α-CyD was prepared according to the method of Melton et al. (*35*). The methanol solution containing dendrimer (2.6×10^{-5} mol) was added to a flask and evaporated under reduced pressure. Monotosyl-α-CyD (25 mg, 2.6×10^{-5} mol) and dimethyl sulfoxide (DMSO, 0.5 mL) were added into the flask. Under nitrogen atmosphere, the mixture was stirred at 60 °C for 24 h. α-CDE conjugates were purified by gel-filtration (TOSOH TSK-Gel HW-40S, Tokyo) and then precipitated with methanol to remove the free dendrimer. ^{1}H NMR spectra of the α-CDE conjugates were measured, and the molar ratio of dendrimer and α-CyD was calculated from the peak areas of anomeric proton of α-CyD and ethylene protons of the dendrimer. These measurements indicated that α-CyD covalently binds to the dendrimer in a molar ratio of 1:1 in α-CDE conjugates (G2, G3, and G4), as shown in Figure 1. The yields of α-CDE conjugate (G2, G3, and G4) were 18%, 15%, and 12%, respectively. α-CDE (G2) conjugate: ^{1}H NMR (500 MHz, D_2O) δ (from TMS) 5.29 and 4.96 (H1, α-CyD), 3.94−3.61 (H3, H5, H6, α-CyD), 3.60−3.33 (H2, H4, α-CyD), 3.33−3.08 (dendrimer methylene), 3.08−2.94 (dendrimer methylene), 2.94−2.60 (dendrimer methylene), 2.60−2.43 (dendrimer methylene), 2.43−2.15 (dendrimer methylene). α-CDE (G3) conjugate: ^{1}H NMR (500 MHz, D_2O) δ (from TMS) 4.93 (H1, α-CyD), 3.85−3.74 (H3, H5, H6, α-CyD), 3.53−3.38 (H2, H4, α-CyD), 3.38−3.13 (dendrimer methylene), 3.10−2.80 (dendrimer methylene), 2.80−2.54 (dendrimer methylene), 2.54−2.38 (dendrimer methylene), 2.38−2.30 (dendrimer methylene). α-CDE (G4) conjugate: ^{1}H NMR (500 MHz, D_2O) δ (from TMS) 4.92 (H1, α-CyD), 3.86−3.72 (H3, H5, H6, α-CyD), 3.52−3.36 (H2, H4, α-CyD), 3.36−3.12 (dendrimer methylene), 3.08−3.02 (dendrimer methylene), 2.95−2.49 (dendrimer methylene), 2.33−2.15 (dendrimer methylene).

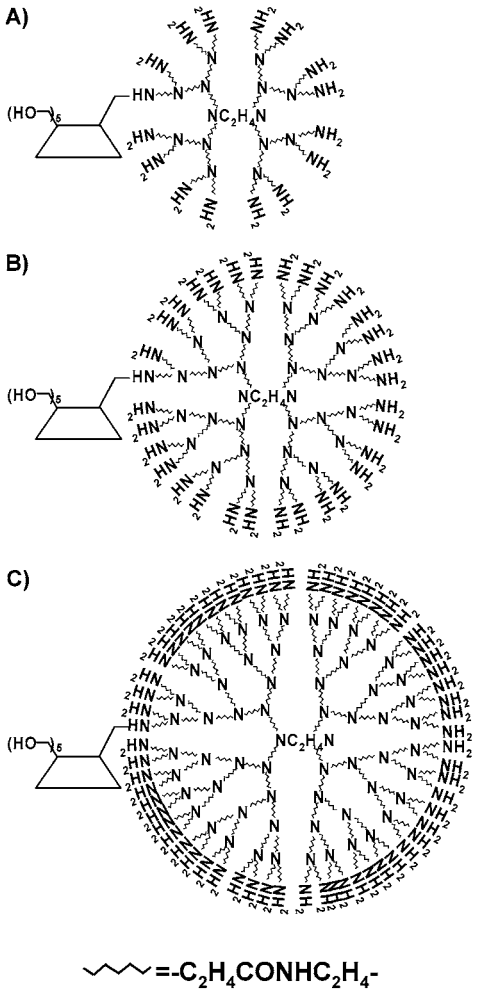


Figure 1. Chemical structures of α-CDE conjugates (G2, G3, and G4). A, α-CDE conjugates (G2); B, α-CDE conjugates (G3); C, α-CDE conjugates (G4).

Gel Electrophoresis. Electrophoretic mobility of the complexes of pDNA/dendrimers or pDNA/α-CDE conjugates was measured using a gel electrophoresis system. Various amounts of dendrimers or α-CDE conjugates were mixed with 0.2 μg of pDNA in Hanks's balanced salt solution (HBSS, pH 7.4). Gel electrophoresis was carried out at room temperature in TBE (45 mM Tris-borate, 1 mM EDTA) buffer (pH 8.0) in 1% (w/v) agarose gel (include 0.1 μg/mL ethidium bromide) using Mupid system (Cosmo Bio, Tokyo) at 100 V for 50 min. pDNA bands were visualized by an UV illuminator.

Measurements of ζ-Potential. To estimate the ζ-potential, the electrophoretic mobility of the complexes of pDNA/dendrimers or pDNA/α-CDE conjugates in HBSS (pH 7.4) was determined by an electrophoretic light scattering spectrophotometer (ELS-800, Otsuka Electronics, Osaka, Japan) at 25 °C. The dendrimers or α-CDE conjugates were added to the pDNA solution (2.5 μg/mL of pDNA) at various charge ratios.

Measurements of Particle Size. Dendrimer- or α-CDE conjugate (G2, G3, or G4)-containing solutions (0.1 mL in HBSS) at various charge ratios were added to pDNA solution (4 μg/1.5 mL in HBSS) and incubated for 15 min. Particle sizes of the complexes of pDNA/dendrimer and pDNA/α-CDE conjugates were determined by quasi-elastic (dynamic) light scattering using a Beckman Coulter N4 Plus machine (Fullerton, CA). The wavelength of the He−Ne laser used was 632.8 nm. The

measurement was carried out at a fixed angle of 62.6°, and the measuring time was 102 s at 25 °C. The measurements were carried out at least in triplicates.

DNase I Protection Assay. The complexes of pDNA (0.2 μg) with dendrimers or α-CDE conjugates were prepared as described above and then incubated for 30 min at 37 °C in the reaction buffer (pH 7.4, 10 mM Tris-HCl, 10 mM NaCl, 10 mM $CaCl_2$, 6 mM $MgCl_2$, and 2 mM DTT, 0.2 μg/mL bovine serum albumin) containing 0.1 unit/μL of DNase I. After the incubation, DNase I was inactivated by heating the solution at 70 °C for 10 min, 1 μL of EDTA (0.5 M), and 10 μL of SDS (10% w/v) were added to each sample and incubated at 37 °C for 60 min to dissociate pDNA from the complexes. After the incubation, gel electrophoresis was carried out in the same manner as described above in the gel electrophoresis section.

Cell Culture. NIH3T3 cells, a mouse fibroblast cell line, and RAW264.7 cells, a mouse macrophage-like cell line, were obtained from the Japan Health Sciences Foundation (Osaka, Japan) and the Riken Cell Bank (Tsukuba, Japan), respectively. NIH3T3 and RAW264.7 cells were grown in Dulbecco's modified Eagle's medium (include 1×10^5 mU/mL of penicillin, 0.1 mg/mL of streptomycin) and RPMI1640 medium (include 4×10^5 mU/mL of penicillin, 0.2 mg/mL of streptomycin), respectively, supplemented with 10% (v/v) FCS at 37 °C in a humidified 5% CO_2 and 95% air atmosphere.

Cytotoxicity. The cell viability was assayed by using a Cell Counting Kit (WST-1 method) from Wako Pure Chemical Industries (Osaka, Japan) (36). This method is a colorimetric assay based on the cleavage of the tetrazolium salt WST-1 by mitochondrial dehydrogenase of viable cells to a water-soluble formazan dye and is similar to MTT assay. In brief, NIH3T3 and RAW264.7 cells were seeded at 2×10^5 cells onto 35-mm dishes (Iwaki, Tokyo) and incubated for 18 h in a humidified atmosphere containing 5% CO_2 and 95% air at 37 °C. Cells were washed twice with serum free medium and then incubated for 1 h with 800 μL of serum-free medium containing pDNA or the complexes with various vectors. The culture medium (1.5 mL) supplemented with 10% (v/v) FCS was added to each well, and the cells were incubated for 24 h in a humidified atmosphere containing 5% CO_2 and 95% air at 37 °C. After washing twice with HBSS (pH 7.4) to remove pDNA and/or various vectors, 0.5 mL of fresh HBSS and 50 μL of WST-1 reagent were added to the plates and incubated for 4 h at 37 °C. The absorbance of aliquot (100 μL) of the solution was measured at 405 nm, with referring the absorbance at 630 nm, with a microplate reader (Bio-Rad Model 550, Tokyo).

Transfection. Transfection of the complexes of pDNA/dendrimers, pDNA/α-CDE conjugates, or pDNA/TransFast was performed utilizing the expression of pDNA encoding firefly luciferase gene under control of SV40 enhancer/promoters. The pDNA (2.0 μg) was mixed with dendrimers at various charge ratios. The pDNA complexes with dendrimers or α-CDE conjugates were then allowed to stand for 15 min at room temperature. The cells (2×10^5 per 35 mm culture dish) were seeded 18 h before transfection and then washed twice with serum-free medium. Eight hundred microliters of serum-free medium containing pDNA or the complexes with various vectors was added to each dish and then incubated for 1 h at 37 °C. The culture medium (1.5 mL) supplemented with 10% (v/v) FCS was added to each dish and then incubated for 24 h (total 25 h) before being harvested for analysis of the expression of the transfected pDNA. Control transfection was performed with TransFast in the same manner as described above. The charge ratio of the complex of pDNA/TransFast was 1/1, at which an optimal transfection activity was obtained under the present experimental conditions.

Measurements of Gene Expression. When pDNA encoding luciferase gene was used, after transfection for 25 h, firefly luciferase content in the cell lysate was quantified using the Promega luciferase assay reagent (Tokyo) and a luminometer (Lumat LB9506, EG&G Berthold Japan, Tokyo). Absolute light emission generated from the luciferase enzyme reaction was determined. It was confirmed that α-CyD and α-CDE conjugates have no influence on the luciferase assay under the experimental conditions. Total protein content of the supernatant was determined by BCA protein assay kit (Pierce, Rockford, IL).

Cellular Association. pDNA was labeled with [α-^{32}P]-CTP using nick translation kit II (Nippon Gene, Toyama, Japan) according to the manufacturer's protocols. [^{32}P]-labeled pDNA ([^{32}P]pDNA) was purified using QIAquick PCR purification Kit (Qiagen, Tokyo). NIH3T3 and RAW264.7 cells were cultured in 35-mm culture dish. The cells were washed twice with 1 mL of culture medium, and [^{32}P]pDNA (1 μg/mL, 5.0×10^4 cpm/μL) with or without dendrimers and α-CDE conjugates were added. After incubation at 37 °C for the indicated time, the cells were washed twice with 0.5 mL of ice-cold PBS and then solubilized with 0.5 mL of 1 N NaOH followed by incubation for 2 h. One-half milliliter of the total solution was added to Hionic-Flour (Packard Japan, Tokyo) and taken for the determination of ^{32}P radioactivity using a liquid scintillation counter (Aloka LSC-5100, Tokyo). Nonspecific binding of labeled pDNA was defined as the binding to the dishes in the absence of cells, and the extent of nonspecific binding was subtracted from that of total binding to calculate the specific binding.

Confocal Microscopic Study. Fluorescein isothiocianate (FITC)-labeled pDNA (FITC-pDNA) was prepared using Mirus label IT fluorescein labeling kit (Madison, WI). FITC-pDNA complexes with dendrimer (G3) or α-CDE conjugate (G3) at a charge ratio of 200/1 (vector/pDNA) were then allowed to stand for 15 min at room temperature. The transfection was performed as described above. After 25 h incubation, the cells were rinsed twice with 2 mL of PBS (pH 7.4) and fixed with 3.7% (v/v) formaldehyde in PBS for 40 min. Then, the cells were washed twice with 2 mL of PBS. The cells were scanned with a confocal fluorescence microscopic system (Olympus FV300−BX, Tokyo) with an argon ion laser (excitation wavelength, 488 nm).

Complexation of α-CDE Conjugates. The fluorescence spectra of TNS were measured by a Hitachi F-4500 spectrofluorometer at 25 °C. The concentration of TNS in 10 mM acetate buffer (pH 5.0) was 0.1 mM and that of dendrimer (G3), α-CyD and α-CDE conjugate (G3) was 1 mM. The excitation wavelength was 333 nm, and the fluorescence spectra were measured in the range of 350−550 nm.

Data Analysis. Data are given as means ± SEM. Statistical significance of mean coefficients was performed by analysis of variance followed by Student's *t*-test. *P* values for significance were set at 0.05.

RESULTS

Physicochemical Properties of pDNA Complexes with α-CDE Conjugates. We first studied the complex-

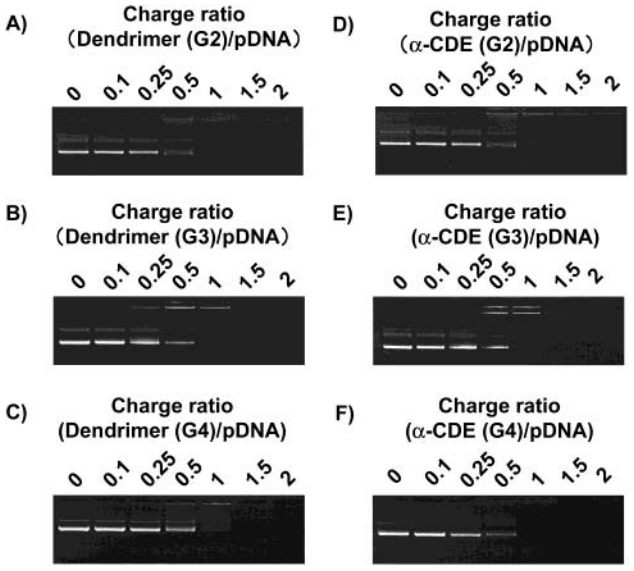


Figure 2. Agarose gel electrophoretic analysis of the complexes of pDNA/dendrimers (G2, G3, and G4) and pDNA/α-CDE conjugates (G2, G3, and G4) using TBE buffer (pH 8.0). The solutions containing the complexes of pDNA/dendrimers or pDNA/α-CDE conjugates were incubated for 15 min at room temperature after slight agitation. The electrophoresis was performed at 100 V for about 50 min. A, dendrimer (G2); B, dendrimer (G3); C, dendrimer (G4); D, α-CDE conjugate (G2); E, α-CDE conjugate (G3); F, α-CDE conjugate (G4).

ation of pDNA with dendrimers or α-CDE conjugates (G2, G3, and G4) using agarose electrophoresis. In the case of the dendrimer (G2) or α-CDE conjugate (G2), the intensity of the band corresponding to pDNA decreased as the charge ratio (vector/pDNA) increased, and the bands disappeared at the charge ratio of 1/1, as shown in Figure 2A and 2D. Similar patterns were observed in the dendrimers (G3 and G4) and α-CDE conjugates (G3 and G4) (Figure 2B, C, E, and F). The addition of parent α-CyD to pDNA solution did not change the electrophoretic band pattern of pDNA (data not shown), suggesting much less interaction of pDNA with α-CyD. These results suggest that α-CDE conjugates (G2, G3, and G4) form the complexes with pDNA in a manner similar to dendrimers (G2, G3, and G4).

ζ-potentials of pDNA complexes with dendrimers and α-CDE conjugates were measured to examine their electric property. The ζ-potential of the pDNA complexes used here increased as the charge ratio (vector/pDNA) increased, and the values were in the range of 14 to 25 mV (Figure 3A). The difference in ζ-potential value between dendrimers and α-CDE conjugates was rather small in each generation. Next, the particle sizes of the complexes of pDNA/dendrimes or pDNA/α-CDE conjugates were measured using quasi-elastic (dynamic) light scattering. As shown in Figure 3B, the particle sizes of the complex of pDNA/dendrimer (G2) or pDNA/α-CDE conjugate (G2) were not significantly affected by the charge ratio, although they decreased slightly at the charge of 1/1. In the G3 and G4 systems, the particle sizes were smallest at the charge ratio of 1/1, which was consistent with the ratio that the band disappeared (Figure 2). These results suggest that α-CDE conjugates (G3 and G4) form the most compact complexes at the charge ratio of 1/1, and at the higher charge ratios the particle sizes of these pDNA/vectors complexes were almost comparable. These results indicate that physicochemical properties of the pDNA complexes were de-

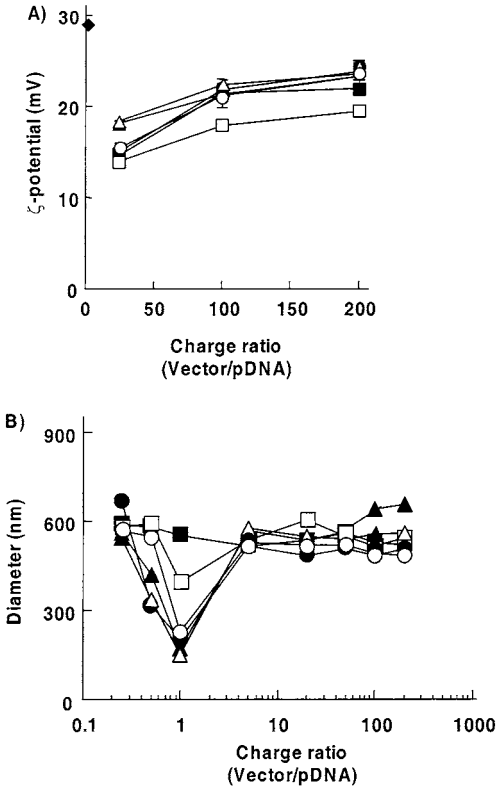


Figure 3. (A) ζ-Potential of the complexes of pDNA/dendrimers (G2, G3, and G4) and pDNA/α-CDE conjugates (G2, G3, and G4). The electrophoretic mobility of the complexes of pDNA/dendrimer or pDNA/α-CDE conjugates in HBSS (pH 7.4) was determined by electrophoretic light scattering spectrophotometer at 25 °C. The dendrimers or α-CDE conjugates were added to the pDNA solution (2.5 μg/mL of pDNA) at various charge ratios. Square, dendrimer (G2) or α-CDE conjugate (G2); circle, dendrimer (G3) or α-CDE conjugate (G3); triangle, dendrimer (G4) or α-CDE conjugate (G4); diamond, TransFast. Open and closed symbols represent dendrimers and α-CDE conjugates, respectively. (B) Particle sizes of the complexes with pDNA/dendrimers (G2, G3, and G4) or pDNA/α-CDE conjugates (G2, G3, and G4). Dendrimer- or α-CDE conjugate (G2, G3 or G4)-containing solutions (0.1 mL in HBSS) at various charge ratios were added to pDNA solution (4 μg/1.5 mL in HBSS) and incubated for 15 min. Particle sizes of the pDNA complexes with dendrimer and α-CDE conjugates were determined by quasi-elastic (dynamic) light scattering. The wavelength of the He−Ne laser used was 632.8 nm. The measurement was carried out at a fixed angle of 62.6°, and the measuring time was 102 s at 25 °C. Square, dendrimer (G2) or α-CDE conjugate (G2); circle, dendrimer (G3) or α-CDE conjugate (G3); triangle, dendrimer (G4) or α-CDE conjugate (G4). Open and closed symbols represent dendrimers and α-CDE conjugates, respectively.

pendent on the generation and the charge ratio, but there is insignificant difference in the property between the complexes of pDNA/dendrimers and pDNA/α-CDE conjugates at higher charge ratios (vector/pDNA).

DNase I Protection Assay. We tested the stabilizing effect of α-CDE conjugates (G2, G3, and G4) on pDNA degradation. The concentration of DNase I was set to 0.1 unit/μL, because the activity in human serum is 2×10^{-4}-8.2×10^{-2} unit/μL (*37*). When pDNA alone was treated with DNase I for 30 min, it degraded into smaller size fractions (data not shown). The addition of dendrimer (G2, G3, and G4) or α-CDE conjugates (G2, G3, and G4) increased the band intensity of pDNA as the charge ratio (vector/pDNA) increased in the region of higher charge ratios (Figure 4A−F). No obvious difference was observed in the protective effect between dendrimers and α-CDE conjugates. Since parent α-CyD alone possessed no protective ability against the DNase I-catalyzed degrada-

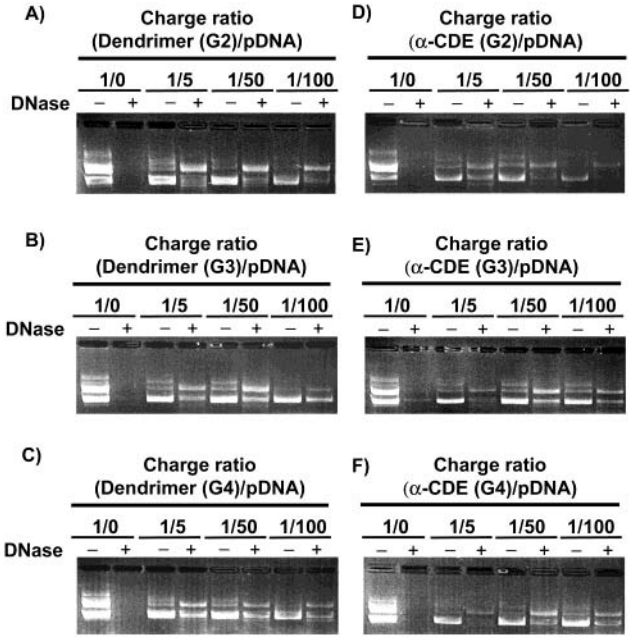


Figure 4. Effects of dendrimers (G2, G3, and G4) and α-CDE conjugates (G2, G3, and G4) on electrophoretic mobility of pDNA treated with DNase I. The complexes of pDNA/dendrimers or pDNA/CDE conjugates were incubated with 0.1 unit/mL of DNase I for 30 min. After DNase I was inactivated at 70 °C for 10 min, 1 mL each of EDTA (0.5 M) and SDS (10% w/v) were added to each sample and incubated at 37 °C for 1 h to dissociate pDNA from the complexes. After incubation, gel electrophoresis was carried out at room temperature in TBE (45 mM Tris-borate and 1 mM EDTA) buffer (pH 8.0) in 1% (w/v) agarose gel (include 0.1 mg/mL of ethidium bromide) using Mupid system at 100 V for 50 min. A, dendrimer (G2); B, dendrimer (G3); C, dendrimer (G4); D, α-CDE conjugate (G2); E, α-CDE conjugate (G3); F, α-CDE conjugate (G4).

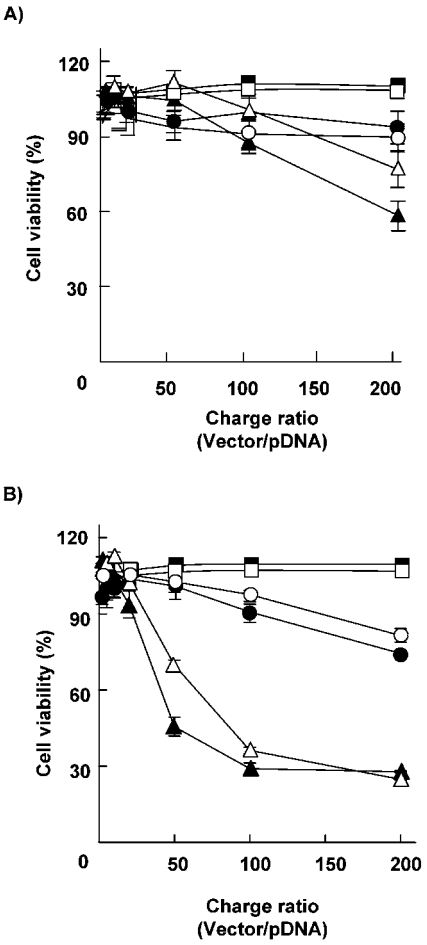


Figure 5. Cytotoxicity of the complexes of pDNA/dendrimers (G2, G3, and G4) or pDNA/α-CDE conjugates (G2, G3, and G4) at various charge ratios in NIH3T3 cells (A) and RAW264.7 cells (B). The cell viability was assayed by WST-1 method. In brief, NIH3T3 and RAW264.7 cells (2×10^5 cells) onto 35-mm dishes were incubated for 1 h after adding 800 μL of serum-free medium containing pDNA or the complexes with various vectors. The culture medium (1.5 mL) supplemented with 10% (v/v) FCS was added to each well, and the cells were incubated for 24 h at 37 °C. After washing, 0.5 mL of fresh HBSS and 50 μL of WST-1 reagent were added to the plates and incubated for 4 h at 37 °C. The absorbance of the solution at 405 nm was measured by referring the absorbance at 630 nm. Square, dendrimer (G2) or α-CDE conjugate (G2); circle, dendrimer (G3) or α-CDE conjugate (G3); triangle, dendrimer (G4) or α-CDE conjugate (G4); diamond, TransFast. Open and closed symbols represent dendrimers and α-CDE conjugates, respectively. Each value represents the mean ± SEM of 4−6 (A) or 4 (B).

tion of pDNA (data not shown), these results suggest that both dendrimers (G2, G3, and G4) and α-CDE conjugates (G2, G3, and G4) are able to protect pDNA against DNase I through the complexation at higher charge ratios (vector/pDNA).

Cytotoxicity. From the safe and potency points of view, cytotoxicity of virus and nonvirus vectors would be evaluated. Cytotoxicity of dendrimers or α-CDE conjugates (G2, G3, and G4) to NIH3T3 and RAW264.7 cells was studied using the WST-1 method (36). As shown in Figure 5A, the cytotoxicity of these vectors in NIH3T3 cells was negligible up to the charge ratio of 100/1 (vector/pDNA), but it increased as the generation increased. Likewise, an increase in the generation resulted in higher cytotoxicity in RAW264.7 cells, especially the complex of pDNA/dendrimer (G4) or pDNA/α-CDE conjugate (G4), provoked significant cytotoxicity in higher charge ratios (vector/pDNA, Figure 5B). These results indicate that the cytotoxicity of α-CDE conjugates (G2 and G3) was moderate in these cells, although α-CDE conjugate (G4) was severe at higher charge ratios (vector/pDNA), presuming that a decrease in the gene transfer activity of α-CDE conjugate (G4) in the cells, especially RAW264.7 cells (Figure 5B).

Transfection. Gene transfer activity of dendrimers (G2, G3, and G4) and α-CDE conjugates (G2, G3, and G4) was examined and compared with that of TransFast, which was employed as a positive control. Figure 6A and 6B show gene transfer activity of dendrimers and α-CDE conjugates at the charge ratio of 200/1 (vector/pDNA) in NIH3T3 cells and RAW264.7 cells, respectively. When pDNA alone was transfected in the absence and presence of α-CyD, no luciferase activity was observed (data not shown). In NIH3T3 cells, the gene transfer activity of the pDNA complexes with α-CDE conjugate (G3) was highest, followed by the activities of the complex with α-CDE conjugate (G4) > dendrimer (G3) > dendrimer (G4) > α-CDE conjugate (G2) ≫ dendrimer (G2) in a deceasing order. In addition, the gene transfer activity of α-CDE conjugate (G3) was higher than approximately 20 and 2 times than that of α-CDE conjugate (G2) and α-CDE conjugate (G4), respectively, and was comparable with that of TransFast in NIH3T3 cells. On the other hand, in RAW264 cells, the greatest gene transfer activity was elicited by the pDNA complexes with α-CDE conjugate (G3), followed in a decreasing order by the complex with α-CDE conjugate (G2) > dendrimer (G3) > dendrimer (G2) > dendrimer (G4) ≥ α-CDE conjugate (G4). These results indicate that of the vectors used here, α-CDE conjugate (G3) possesses highest gene transfer activity

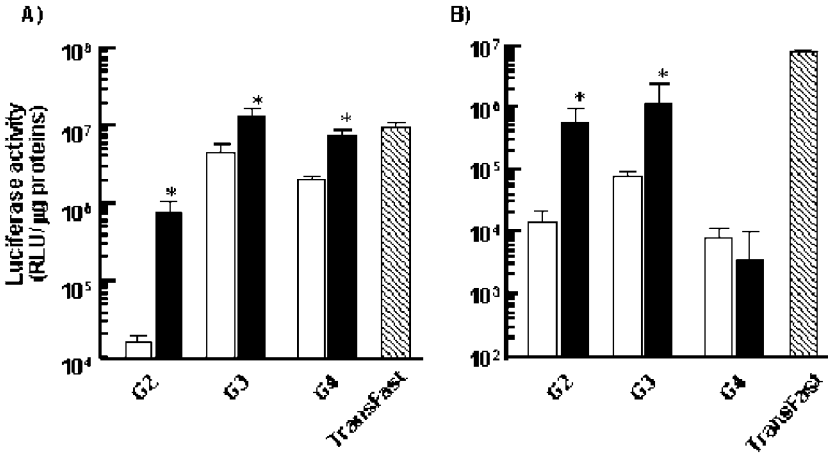


Figure 6. Transfection efficiency of the complexes of pDNA/dendrimers (G2, G3, and G4) or pDNA/α-CDE conjugates (G2, G3, and G4) at the charge ratio of 200/1 (vector/pDNA) in NIH3T3 cells (A) and RAW264.7 cells (B). The luciferase activity in cell lysates was determined 25 h after incubation with pDNA alone or various complexes. The charge ratio of pDNA and TransFast is 1/1. Open, closed and hatched columns represent the complexes of pDNA/dendrimer, pDNA/α-CDE conjugate and pDNA/TransFast. Each value represents the mean ± SEM of 4−6 (A) or 4 (B). *$p < 0.05$, compared with dendrimer alone.

in NIH3T3 and RAW264.7 cells. Figure 7A and 7B show the charge ratios of the complexes on gene transfer activity of dendrimers and α-CDE conjugates in NIH3T3 cells and RAW264.7 cells, respectively. In NIH3T3 cells, the transfection efficiency of all dendrimers and α-CDE conjugates employed increased as the charge ratio (vector/pDNA) increased in the region of lower ratios, and especially α-CDE conjugates possessed higher gene transfer activity than the corresponding dendrimer alone. Thus, α-CDE conjugate (G3) conferred the greatest transfection activity in the charge ratios of 5/1−200/1 (vector/pDNA). As shown in Figure 7B, the transfection efficiency of the complexes of pDNA/α-CDE conjugates (G2 and G3) gradually increased as the charge ratio (vector/pDNA) increased in RAW264.7 cells. The transfection efficiency of the complexes of pDNA/dendrimer (G4) and pDNA/α-CDE conjugate (G4) significantly decreased as the charge ratio increased more than 50/1 (vector/pDNA), although the efficiency of the complex of pDNA/α-CDE conjugate (G4) was higher than that of pDNA/α-CDE conjugates (G2 and G3) at lower charge ratios (vector/pDNA). Thus, low gene transfer activity of the pDNA complexes with dendrimers or α-CDE conjugates may be due to the cytotoxicity to NIH3T3 cells (Figure 5). These results clearly indicate that α-CDE conjugate (G3) possesses preferable gene transfer activity among the dendrimers and α-CDE conjugates used here.

CyDs are known to induce hemolysis and enhance the permeation of water-soluble drugs through biological membranes via the release of membrane components such as phospholipids and cholesterol as described above (*21, 22*). This fact allows us to deduce that α-CyD enhances gene transfer activity through membrane-permeability of pDNA/α-CDE conjugates. To confirm this possibility, we examined the effects of physical mixture of α-CyD and the pDNA complexes with dendrimers (G3 and G4) at various charge ratios in the gene transfer. As a result, there is no difference in the gene transfer activity in NIH3T3 and RAW264.7 cells between the pDNA complex with dendrimer (G3 or G4) and the simple physical mixture of the pDNA/dendrimer complex and α-CyD (data not shown). The same results were conferred in dendrimer (G2) and α-CDE conjugate (G2) (*33*). Therefore, the conjugation of dendrimers with α-CyD is crucial for the gene transfer activity.

Cellular Association of pDNA. We previously reported that the enhancing effect of α-CDE conjugate (G2) relative to dendrimer (G2) could not be attributed to the increased cellular association of pDNA. To test whether α-CDE conjugates (G3 and G4) increase the association of pDNA, we measured the extent of pDNA associating to cells using [^{32}P]pDNA. The association of pDNA to the NIH3T3 (Figure 8A) and RAW264.7 (Figure 8B) cells increased as the charge ratio increased up to 5/1 (vector/pDNA), and above the ratio the association showed a plateau in all of the complexes of pDNA/dendrimers and pDNA/α-CDE conjugates. Here α-CyD showed no influence on the cellular association of pDNA under the present experimental conditions (data not shown), suggesting that α-CyD perturbs the integrity of plasma membrane of cells only very slightly. These results suggest that α-CDE conjugate (G3) may decrease the physical barrier function such as endosomal and nuclear membranes more efficiently than α-CDE conjugate (G2).

Intracellular Distribution of pDNA. Cellular uptake of pDNA and its release from endosomes are necessary for gene expression of pDNA (*38*). Thus, the intracellular distribution of pDNA was observed using FITC-pDNA under confocal laser microscopy. Figure 9A and 9B show the results 25 h after transfection of the complexes of pDNA/dendrimer (G3) and pDNA/α-CDE conjugate (G3) in NIH3T3 cells. The complex of pDNA/α-CDE conjugate (G3) provided higher fluorescence intensity in cytoplasm than that of pDNA/dendrimer (G3), whereas there was no fluorescence in the cells when pDNA alone was applied (data not shown). These results suggest that α-CDE conjugate (G3) changes the distribution of pDNA in the cells, possibly in terms of increase in the release of pDNA from the endosomes into cytoplasm after endocytosis.

Inclusion Ability of α-CDE Conjugate (G3). It is possible that α-CDE conjugate (G3) may interact with membrane constituents. However, the ability of inclusion complexation of α-CDE conjugates still remains unclear. Thus, we examined the ability of inclusion complexation of α-CDE conjugate (G3) spectrophotometrically. Here we used a fluorescent guest molecule, TNS, because the inclusion of TNS into hydrophobic environment such as the α-CyD's cavity is known to induce prominent fluorescence. As shown in Figure 10, the addition of dendrimer (G3) to TNS solution induced fluorescence corresponding to TNS, and the fluorescence intensity was increased by the addition of α-CyD. Importantly, α-CDE conjugate (G3) increased the fluorescent intensity re-

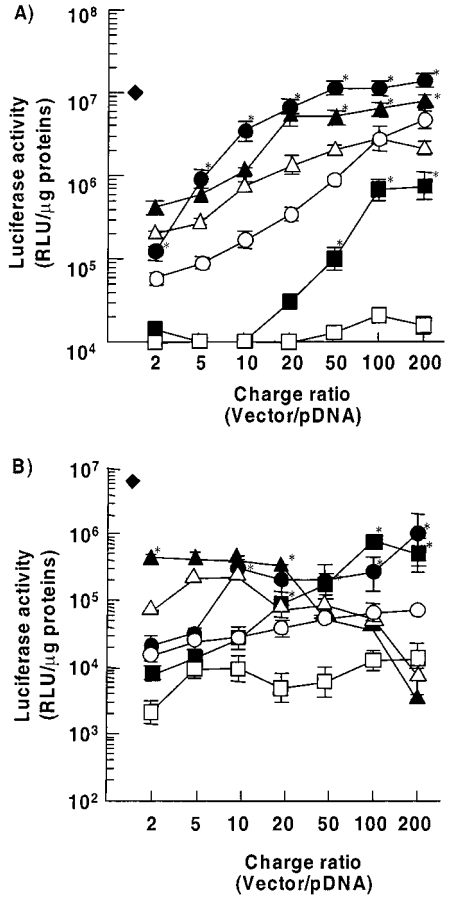


Figure 7. Transfection efficiency of the complexes of pDNA/dendrimers (G2, G3, and G4) or pDNA/α-CDE conjugates (G2, G3, and G4) at the charge ratios of 200/1 (vector/pDNA) in NIH3T3 cells (A) and RAW264.7 cells (B). The luciferase activity in cell lysates was determined 25 h after incubation with pDNA alone or various complexes. The charge ratio of pDNA and TransFast is 1/1. Square, dendrimer (G2) or α-CDE conjugate (G2); circle, dendrimer (G3) or α-CDE conjugate (G3); triangle, dendrimer (G4) or α-CDE conjugate (G4). Open and closed symbols represent the complex of pDNA/dendrimer and the complex of pDNA/α-CDE conjugate, respectively. Each value represents the mean ± SEM of 4−6 (A) or 4 (B). $*p < 0.05$, compared with dendrimer alone.

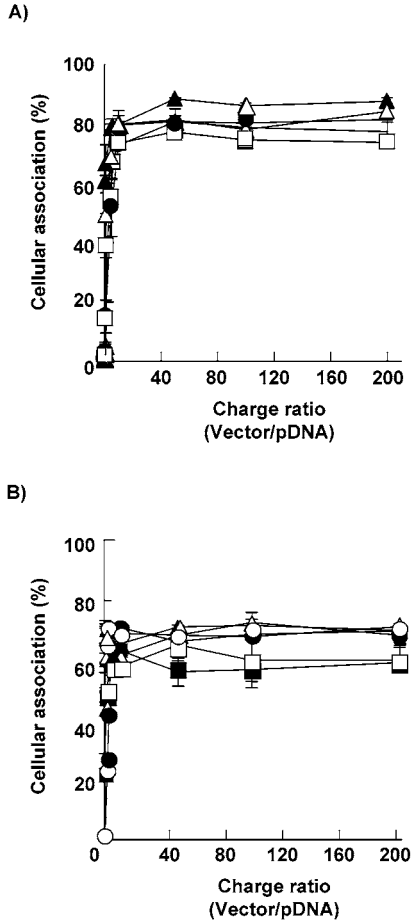


Figure 8. Cellular associations of [α-^{32}P] labeled pDNA at various charge ratios in NIH3T3 cells (A) and RAW264.7 cells (B). Square, dendrimer (G2) or α-CDE conjugate (G2); circle, dendrimer (G3) or α-CDE conjugate (G3); triangle, dendrimer (G4) or α-CDE conjugate (G4). Open and closed symbols represent dendrimer and α-CDE conjugate, respectively. Each value represents the mean ± SEM of 4. $*p < 0.05$, compared with dendrimer alone.

markably, compared with that of the dendrimer (G3) system. These results suggest that α-CDE conjugate (G3) possesses the inclusion ability of guest molecules into the cavity of α-CyD and thus it may interact with constituents of endosomal membranes such as phospholipids after endocytosis.

DISCUSSION

We previously reported that of three CDE conjugates in which α-, β-, and γ-CyD covalently bound to dendrimer (G2) at a molar ratio of 1:1, α-CDE conjugate (G2) possesses the highest transfection activity (33). To improve the efficacy, we prepared three α-CDE conjugates (G2, G3, and G4) with different generation of dendrimers, and their interaction with pDNA, the protective effect of pDNA against DNase I, the gene transfer activity, and the cytotoxicity were examined. Consequently, we clarified that α-CDE conjugate (G3) possesses the greatest gene transfer activity with lower cytotoxicity.

Cationic polymer-mediated transfection should overcome three major barriers for transfection: (1) binding of pDNA to cell surface, (2) endosomal release, and (3) entry of pDNA into the nucleus (*39*). Likewise, the physicochemical properties of polyplex such as net charge and particle size markedly affect these barriers, eventually changing transfection efficiency (*36*). In the present study, the complexes of pDNA/α-CDE conjugates (G2, G3, and G4) showed gel mobility rates (Figure 2) and ζ-potentials (Figure 3A) similar to those of pDNA/dendrimers (G2, G3, and G4) at the higher charge ratios (vector/pDNA). This similarity could be attributed to the two reasons: (1) the structure of α-CDE conjugate and (2) a lack of interaction between α-CyD and pDNA, and α-CyD and the pDNA complexes with dendrimers. The first reason may be explained by the fact that only a molecule of α-CyD binds to an amino group of dendrimers, thereby many intact positively charged amino groups still remains on the surface of these molecules. Second reason may be showed the following data: the addition of α-CyD to the solution containing pDNA or the complex of pDNA/dendrimer (G2, G3, or G4) did not affect their gel mobility rates (data not shown), indicating that α-CyD interacts with pDNA and their complexes only very slightly. Furthermore, a parallel of physicochemical properties between the pDNA complexes with dendrimers and α-CDE conjugate at higher charge ratio may be due to the relatively larger and complicated structure of the complexes because the calculated molar ratio (vector and pDNA) of the pDNA complexes with α-CDE conjugates (G2, G3, and G4) are 701, 339, and 167 in the complexes with α-CDE conjugates (G2, G3, and G4), respectively, even at the charge ratio of 1/1. Therefore, α-CyD changed

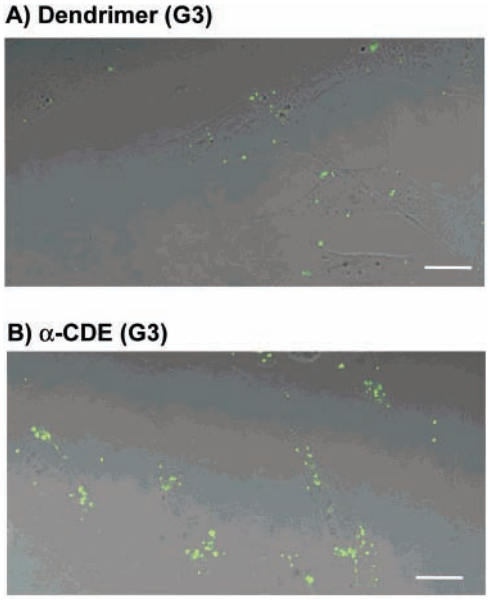


Figure 9. Confocal laser microscopic images for the distribution of FITC-pDNA in NIH3T3 cells after transfection of the complexes of pDNA/dendrimer (G3) (A) and pDNA/α-CDE conjugate (G3) (B). The cells were incubated with the pDNA complexes for 25 h at 37 °C. The charge ratio (vector/pDNA) of the complexes of pDNA/dendrimer (G3) and of pDNA/α-CDE conjugate (G3) was 200/1. Scale bars represent 20 μm. The images shown are typical among similar ones in the several visual fields.

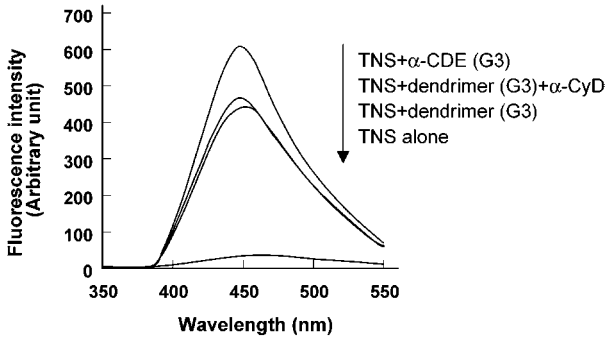


Figure 10. Fluorescence spectra of TNS in the absence and presence of dendrimer (G3) or α-CDE conjugate (G3). The fluorescent spectra of TNS were measured at 25 °C. The concentrations of TNS, dendrimer, α-CyD and α-CDE conjugate (G3) in 10 mM acetate buffer (pH 5.0) were 0.1 mM, 1 mM, 1 mM, and 1 mM, respectively. The excitation wavelength was 333 nm and the fluorescence spectra were measured in the range of 350−550 nm.

the intricate structure of the pDNA complex only very slightly. Thus, physicochemical properties of the pDNA complexes with α-CDE conjugates were changed in the generation-dependent manner, because the number of primary amino groups increases as the generation increases (Figures 2 and 3).

It is evident that the stability against enzymatic degradation of pDNA influences gene transfer activity. The DNase I protection assay demonstrated that pDNA is protected from DNase I by the complexation with dendrimers and α-CDE conjugates, and the protective effects were almost identical between dendrimers and α-CDE conjugates regardless of their generation, up to the charge ratio of 100/1 (vector/pDNA, Figure 4). The stabilizing effect of dendrimers and α-CDE conjugates on pDNA degradation could be concerned with gene transfer into the cells under the experimental conditions. However, the stabilizing effect of dendrimer (G2) and α-CDE conjugate (G2) on the degradation of pDNA in our previous paper (*33*) seems to be somewhat different from the present data: dendrimer (G2) and α-CDE conjugate (G2) prevented the disappearance of the bands by the charge ratio of 20/1 (vector/pDNA), but above the ratios the bands vanished. This inconsistency may be due to difference in the experimental conditions, i.e., the concentration of SDS used for dissociation of pDNA from the vectors in the complexes were 3.8% (w/v) and 4.8% (w/v) in the previous and present studies, respectively. Taken together, the physicochemical properties such as gel mobility shift, ζ-potential, particle size, and enzymatic stability of the complexes of pDNA/dendrimers and pDNA/α-CDE conjugates (G2, G3, and G4) were almost comparable, at least, at the higher charge ratios (vector/pDNA).

Gene transfer activity of dendrimers augmented in the order of G2 < G3 < G4 at the lower charge ratios (Figure 7), probably due to an increase in the proton sponge effect in endosomes (*8*). However, the transfection efficiency of dendrimer (G4) significantly attenuated at the higher charge ratios (vector/pDNA, Figures 6 and 7). This attenuation is certainly due to cytotoxicity (Figure 5), consistent with the results reported by Roberts et al., i.e., the cytotoxicity of dendrimers (G3, G5, and G7) to Chinese hamster lung fibroblasts increased as the generation increased (*40*). The similar patterns of gene transfer activity and cytotoxicity were also observed in the α-CDE conjugate system. The severe cytotoxicity of the pDNA complexes with dendrimer (G4) and α-CDE conjugate (G4) observed in RAW264.7 cells may be due to the distinction in the cellular sensitivity to positively charged amino groups.

It is of importance that of the three α-CDE conjugates used in this study, gene transfer activity of α-CDE conjugate (G3) was the highest. The superior enhancing effect of α-CDE conjugate (G3) to dendrimer (G3) on gene transfer was observed at various times (4, 6, 12, and 25 h) after transfection in NIH3T3 cells. This greatest gene transfer activity could be attributed to the synergistic effects of the proton sponge effect of dendrimer (G3) and the tentative membrane-disrupting effect of α-CyD on endosomal membranes (Figures 9 and 10) because α-CDE conjugate (G3) possesses inclusion ability with a guest molecule, TNS (Figure 10). In addition, the inclusion ability of α-CDE conjugate (G3) with lipids was confirmed by our preliminary experiments: α-CDE conjugate (G3) is able to disrupt liposomal membranes consisting of phospholipids in vitro (data not shown). Thus, it is noteworthy that the introduction of an α-CyD molecule to dendrimer augmented the gene transfer activity of dendrimer (G2 and G3) than the parent dendrimers, showing no increase in cytotoxicity. Moreover, it should be noted that α-CDE conjugate (G3) possessed the comparable gene transfer activity to TransFast in NIH3T3 cells (Figure 6A).

In conclusion, gene transfer activity of α-CDE conjugate (G3) was higher than that of dendrimers (G2, G3, and G4) and α-CDE conjugate (G2), and cytotoxicity of α-CDE conjugate (G3) was lower than that of α-CDE conjugate (G4). Therefore α-CDE conjugate (G3) may be a potent candidate for nonviral vectors. The present data may be useful for design of α-CyD conjugates with other nonviral vectors.

ACKNOWLEDGMENT

We thank Dr. Makoto Uemura for assistance with the light scattering experiments Coulter N4 Plus machine at the Kumamoto Industrial Research Institute. We are

grateful to Dr. Yoko Yamashita for assistance with measurements of ζ potential ELS-800 machine at the Fukuoka Industrial Technology Center. This work was supported by a Grant-in-Aid from Tokyo Biochemical Research Foundation, a Grant-in-Aid from the Research Foundation for Pharmaceutical Sciences and a Grant-in-Aid for Encouragement of Young Scientists from the Ministry of Education, Science and Culture of Japan (12771464).

Supporting Information Available: ^{1}H NMR spectra of the α-CDE conjugates. This material is available free of charge via the Internet at http://pubs.acs.org.

LITERATURE CITED

(1) Luo, D., and Saltsmn, W. M. (2000) Synthetic DNA delivery systems. *Nature Biotech. 18*, 33−37.

(2) Rolland, A. P. (1998) From genes to gene medicines: recent advances in nonviral gene delivery. *Crit. Rev. Ther. Drug Carrier Syst. 15*, 143−198.

(3) Nishikawa, M., and Huang, L. (2001) Nonviral vectors in the new millennium: delivery barriers in gene transfer. *Human Gene Ther. 12*, 861−870.

(4) Subramanian, A., Ranganathan, P., and Diamond, S. L. (2000) Nuclear targeting peptide scaffolds for lipofection of nondividing mammalian cells. *Nature Biotech. 17*, 873−877.

(5) Ledly, F. D. (1995) Nonviral gene therapy: the promise of genes as pharmaceutical products. *Human Gene Ther. 6*, 1129−1144.

(6) Tomalia, D. A., Naylor, A. M., and Goddard, W. A., III. (1990) Starburst dendrimers: Molecular-level control of size, shape, surface chemistry, topology, and flexibility from atoms to macroscopic matter. *Angew. Chem., Int. Ed. Engl. 29*, 138−175.

(7) Eichman, J. D., Bielinska, A. U., Kukowska-Latallo, J. F., and Baker, J. R., Jr. (2000) The use of PAMAM dendrimers in the efficient transfer of genetic material into cells. *Pharm. Sci. Technol. Today. 3*, 32−245.

(8) Haensler, J., and Szoka, F. C., Jr. (1993) Polyamidoamine cascade polymers mediate efficient transfection of cells in culture. *Bioconjugate Chem. 4*, 372−379.

(9) Bielinska, A., Kukowska-Latallo, J. F., Johnson, J., Tomalia. D. A., and Baker, J. R., Jr. (1996) Regulation of in vitro gene expression using antisense oligonucleotides or antisense expression plasmids transfected using starburst PAMAM dendrimers. *Nucleic Acid Res. 24*, 2176−2182.

(10) Qin, L., Pahud, D. R., Ding, Y., Bielinska, A. U., Kukowska-Latallo, J. F., Baker, J. R., Jr., and Bromberg, J. S. (1998) Efficient transfer of genes into murine cardiac grafts by starburst polyamidoamine dendrimers. *Human Gene Ther. 9*, 553−560.

(11) Tang, M. X., Redemann, C. T., and Szoka, F. C., Jr. (1996) In vitro gene delivery by degraded polyamidoamine dendrimers. *Bioconjugate Chem. 7*, 703−714.

(12) Kukowska-Latallo, J. F., Bielinska, A. U., Johnson, J., Spindler, R., Tomalia, D. A., and Baker, J. R., Jr. (1996) Efficient transfer of genetic material into mammalian cells using Starburst polyamidoamine dendrimers. *Proc. Natl. Acad. Sci. U.S.A. 93*, 4897−4902.

(13) Bender. M., and Komiyama, M. (1978) in *Cyclodextrin Chemistry*, Springer-Verlag, Berlin.

(14) Saenger, W. (1980) Cyclodextrin inclusion compound as research and industry. *Angew. Chem., Int. Ed. Engl. 19*, 344−362.

(15) Szejtli, J. (1982) in *Cyclodextrins and their inclusion complexes*, Akadémiai Kiadó: Bupapest.

(16) Szejtli, J. (1988) in *Cyclodextrin technology*, Kluwer: Dordrecht, The Netherlands.

(17) Uekama, K., Hirayama, F., and Irie, T. (1998) Cyclodextrin drug carrier systems. *Chem. Rev. 5*, 2045−2076.

(18) Thompson, D. O. (1997) Cyclodextrins-enabling excipients: their present and future use in pharmaceuticals. *Crit. Rev. Ther. Drug Carrier Syst. 14*, 1−104.

(19) Albers, E., and Muller, B. W. (1995) Cyclodextrin derivatives in pharmaceutics. *Crit. Rev. Ther. Drug Carrier Syst. 12*, 311−337

(20) Irie, T., and Uekama, K. (1999) Cyclodextrins in peptide and protein delivery, *Adv. Drug Deliv. Rev. 36*, 101−123.

(21) Irie, T., and Uekama, K. (1997) Pharmaceutical application of cyclodextrin. III. Toxicological issues and safety evaluation. *J. Pharm. Sci. 86*, 147−162.

(22) Marttin, E., Verhoef, J. C., and Merkus, F. W. (1998) Efficacy, safety and mechanism of cyclodextrins as absorption enhancers in nasal delivery of peptide and protein drugs. *J. Drug Target. 6*, 17−36.

(23) Roessler, B. J., Bielinska, A. U., Janczak, K., Lee, I., and Baker, J. R., Jr. (2001) Substituted *β*-cyclodextrins interact with PAMAM dendrimer-DNA complexes and modify transfection efficiency. *Biochem. Biophys. Res. Commun. 283*, 124−129.

(24) Croyle, M. A., Rosseler, B. J., Hsu, C. P., Sun, R., and Amidon, G. L. (1998) *β*-cyclodextrins enhance adenoviral-mediated gene delivery to the intestine. *Pharm. Res. 15*, 1348−1355.

(25) Freean, D. J., and Niven, R. W. (1996) The influence of sodium glycholate and other additives on the in vivo transfection of plasmid DNA in the lungs. *Pharm. Res. 13*, 202−209.

(26) Dass, C. R. (2002) Vehicles for oligonucleotide delivery to tumours. *J. Pharm. Pharmacol. 54*, 3−27.

(27) Redenti, E., Pietra, C., Gerloczy, A., and Szente, L. (2001) Cyclodextrins in oligonucleotide delivery. *Adv. Drug Deliv. Rev. 53*, 235−244.

(28) Zhao, Q., Temsamani, J., and Agrawal, S. (1995) Use of cyclodextrin and its derivatives as carriers for oligonucleotide delivery. *Antisense Res. Dev. 5*, 185−192.

(29) Abdou, S., Collomb, J., Sallas, F., Marsura, A., and Finance, C. (1997) *β*-cyclodextrin derivatives as carriers to enhance the antiviral activity of an antisense oligonucleotide directed toward a coronavirus intergenetic consensus sequence. *Arch. Virol. 142*, 1585−1602.

(30) Gonzalez, H., Hwang, S. J., and Davis, M. E. (1999) New class of polymers for the delivery of macromolecular therapeutics. *Bioconjugate Chem. 10*, 1068−1074.

(31) Hwang, S. J., Bellocq, N. C., and Davis, M. E. (2001) Effects of structure of *β*-cyclodextrin-containing polymers on gene delivery. *Bioconjugate Chem. 12*, 280−290.

(32) Pun, S. H., and Davis M. E. (2002) Development of a nonviral gene delivery vehicle for systemic application. *Bioconjugate Chem. 13*, 630−639.

(33) Arima, H., Kihara, F., Hirayama, F., and Uekama, K. (2001) Enhancement of gene expression by polyamidoamine dendrimer conjugates with α-, *β*-, and *γ*-cyclodextrins. *Bioconjugate Chem. 12*, 476−484.

(34) Suh, J., Lee, S. H., and Zoh, K. D. (1992) A novel host containing both binding site and nucleophilic prepared by attachment of *β*-cyclodextrin to poly(ethylenimine). *J. Am. Chem. Soc. 114*, 7916−7917.

(35) Melton, L. D., and Slessor, K. N. (1971) Synthesis of monosubstituted cyclohexaamyloses. *Carbohydrate Res. 18*, 29−37.

(36) Ishiyama, M., Tominaga, H., Shiga, M., Sasamoto, K., Ohkura, Y., and Ueno, K. (1996) A combined assay of cell viability and in vitro cytotoxicity with a highly water-soluble tetrazolium salt, neutral red and crystal violet. *Biol. Pharm. Bull. 19*, 1518−1520.

(37) Avall-Lundqvist, E., Economidou-Karaoglou, A., Sjovall, K., Lans, M., Taper, H. S., Roberfroid, M., and Eneroth, P. (1989) Serum alkaline DNase activity in normal or nonhospitalised individuals. *Clin. Chim. Acta 185*, 35−43.

(38) Ma, H., and Diamond, S. L. (2001) Nonviral gene therapy and its delivery systems. *Curr. Pharm. Biotechnol. 2*, 1−17.

(39) De, Smedt, S. C., Demeester, J., and Hennink, W. E. (2000) Cationic polymer based gene delivery systems. *Pharm. Res. 17*, 113−126.

(40) Roberts, J. C., Bhalgat, M. K., and Zera, R. T. (1996) Preliminary biological evaluation of polyamidoamine (PAMAM) Starburst dendrimers. *J. Biomed. Mater. Res. 30*, 53−65.

BC025557D

Efficient Intracellular Delivery of Oligonucleotides Formulated in Folate Receptor-Targeted Lipid Vesicles

Wen Zhou,[†,‡] Xing Yuan,[†,‡] Annette Wilson,[§] Lijuan Yang,[†,‡] Michael Mokotoff,[‡] Bruce Pitt,[§] and Song Li*[,†,‡]

Center for Pharmacogenetics and Department of Pharmaceutical Sciences, School of Pharmacy; and Department of Environmental and Occupational Health, Graduate School of Public Health, University of Pittsburgh, Pittsburgh, Pennsylvania 15213. Received July 8, 2002; Revised Manuscript Received August 7, 2002

In this study, a novel lipid vector has been developed for targeted delivery of oligodeoxynucleotides (ODN) to tumors that overexpress folate receptor. This is based on a method developed by Semple et al. (*1*), which utilizes an ionizable aminolipid (1,2-dioleoyl-3-(dimethylammonio)propane, DODAP) and an ethanol-containing buffer system for encapsulating large quantities of polyanionic ODN in lipid vesicles. Folate is incorporated into the lipid vesicles via a distearoylphosphatidylethanolamine−poly(ethylene glycol) (DSPE−PEG) spacer. These vesicles are around 100−200 nm in diameter with an ODN entrapment efficiency of 60−80%. Folate mediated efficient delivery of ODN to KB cells that overexpress folate receptor. Uptake of folate-targeted lipidic ODN by KB cells is about 8−10-fold more efficient than that of lipidic ODN without a ligand or free ODN. This formulation is resistant to serum. Thus, targeted delivery of ODN via this novel lipid vector may have potential in treating tumors that overexpress folate receptors.

INTRODUCTION

Functional oligodeoxynucleotides (ODN) such as antisense ODN and DNA enzymes hold promise as new therapeutics for the treatment of various types of diseases such as cancers (*2*, *3*). A number of studies have suggested the existence of ODN receptors on the cell surface (*4*, *5*). However, intracellular delivery of ODN without a delivery vehicle is generally inefficient. Successful application of therapeutic ODN is largely dependent on the development of a vehicle that selectively delivers the ODN into target cells with minimal toxicity. A number of vectors have been developed to improve the intracellular delivery of ODN such as neutral liposomes (*6*) and cationic liposomes (*7*, *8*). ODN can be entrapped inside neutral liposomes. The liposomes can also be designed such that they are long-circulating in the blood and target cell-specific. However, the size of liposomes required for achieving long circulation in the blood and efficient localization is too small for efficient entrapment of ODN. Cationic liposomes readily form complexes with ODN through electrostatic interactions. Almost 100% of ODN can be recovered in complex form. The resulting complexes usually contain slight excess amount of positive charges that allows efficient interaction with the negatively charged cell membrane. A number of cationic liposomes have been developed that significantly enhance the intracellular delivery of ODN. ODN complexed with cationic liposomes exhibit biological activity up to 1000-fold higher than ODN alone (*7*, *8*). However, targeted delivery of ODN to solid tumors via systemic administration remains problematic, although we have shown that cationic liposomes mediate efficient delivery of ODN to pulmonary endothelium (*9*). Recently, a novel lipid formulation has been developed (*1*) that appears to avoid the problems that are associated with each of the formulations discussed above. This formulation is composed of distearoylphosphatidylcholine (DSPC), cholesterol, DODAP, and *N*-palmitoylsphingosine-1-[succinyl(methoxypoly(ethylene glycol))2000] (PEG-CerC_{16}). DODAP is an ionizable cationic lipid that has a p*K* of 6.6 in lipid bilayer systems. At acidic pH values (i.e. pH 4.0), this lipid is positively charged and helps to improve the ODN entrapment via electrostatic interactions. DODAP/ODN complexes can interact with other lipids in an ethanol-containing buffer, and ODN-containing lipid vesicles are formed upon the removal of the ethanol by dialysis. Subsequent adjustment of the external pH to neutral pH values results in a neutral surface charge on the resulting particles. This method led to a significant increase in ODN entrapment efficiency (60−80%) with a final lipid/ODN ratio of 0.15−0.25 (w/w) (*1*). This formulation has also been shown to be long circulating in the blood following systemic administration (*1*). In this study, we have shown that this formulation can be further improved via the incorporation of a targeting ligand, folate. Folate-targeted vesicles are much more efficient than the nontargeted vectors in delivering ODN to KB cells. This improved formulation may have potential for the targeted delivery of therapeutic oligonucleotides to tumors that overexpress folate receptors.

EXPERIMENTAL PROCEDURES

Lipids and Chemicals. Distearoylphosphatidylcholine (DSPC), *N*-palmitoylsphingosine-1-[succinyl(methoxypoly(ethylene glycol))2000] (PEG-CerC_{16}), and 1,2-dioleoyl-3-(dimethylammonio)propane (DODAP) were obtained from Avanti Polar Lipids, Inc. (Alabaster, AL). Folic acid

* Address correspondence to Dr. Song Li, Center for Pharmacogenetics, University of Pittsburgh School of Pharmacy, 639 Salk Hall, Pittsburgh, PA 15213, Tel: 412-383-7976, Fax: 412-648-1664, E-mail: sol4@pitt.edu.

[†] Center for Pharmacogenetics, School of Pharmacy.

[‡] Department of Pharmaceutical Sciences, School of Pharmacy.

[§] Department of Environmental and Occupational Health, Graduate School of Public Health.

10.1021/bc025569z CCC: $22.00 © 2002 American Chemical Society
Published on Web 10/23/2002

Table 1. The Sequences of ODN Used in This Study

no.	sequence (5′-3′)
1	tat gat ctg tca cag ctt ga (*19*)
2	cgg agg gtc gca tcg ctg (*20*)
3	cac gcc ctt acc ttt ctt ttc ct (*20*)
4	ccg tgg tca tgc tcc (*6*)
5	ccc cag cag ctc cca ttg gg (*21*)
6	gct gac gca ctg act (*6*)

and cholesterol (CH) were purchased from Sigma-Aldrich. All lipids were >99% pure. Folate-free RPMI 1640 medium, F12 medium, and other tissue culture reagents were purchased from Gibco-BRL (Grand Island, NY). Folate−poly(ethylene glycol) (MW ∼ 3350 or 2000 Da)−distearoyl phosphatidylethanolamine (folate−PEG−DSPE) was synthesized as described previously (10). The final folate−PEG−DSPE product was purified on a column of silica gel (70−200 mesh) using a solvent gradient of 15 to 80% methanol in CH_2Cl_2. Product purity was confirmed by thin-layer chromatography analysis on silica gel GF.

Antisense ODN. All ODN were synthesized with phosphorothioate (PS) backbone chemistry (the Midland Certified Reagent Company, Midland, TX). The sequences of ODN used in this study are shown in Table 1.

Preparation of ODN-Containing Lipid Vesicles. ODN-containing lipid vesicles were prepared according to the method described by Semple et al. (*1*) except that folate−PEG−DSPE was added when preparing the folate-targeted lipid vesicles. Briefly, a lipid solution composed of DSPC, cholesterol, DODAP, and PEG-CerC_{16} in 100% ethanol at indicated molar ratios (Figures 1−7) was prepared. For preparation of folate-targeted lipid vesicles, various amounts of folate−PEG−DSPE were added. To the lipid solution was then added 300 mM citric acid, pH 4.0 to a final ethanol concentration of 40% (v/v). Similarly, ODN were prepared in separate tubes in 300 mM citric acid, pH 4.0, with 40% ethanol. The solutions were prewarmed to 65 °C, and then the lipid solution was slowly added to the ODN with gentle vortexing. The input ratio was 150 μg ODN/μmol lipid. The mixture was passed 10 times through three stacked 100 nm polycarbonate filters. The preparation was dialyzed (12−14 kDa cutoff) against 300 mM citrate buffer, pH 4.0, for approximately 1 h to remove excess ethanol and further dialyzed against HBS (20 mM HEPES, 145 mM NaCl, pH 7.6) for 12−18 h to remove the citrate buffer, neutralize the DODAP, and release any ODN that was associated with the surface of the vesicles. ODN-containing lipid vesicles were finally separated from free ODN via gel filtration on a Sepharose CL-4B column (1 cm × 25 cm).

Cells and Medium. KB human cancer cells, derived from an epidermal carcinoma of the oral cavity, were obtained from American Type Culture Collection (ATCC). The cells were maintained in folate-free RPMI 1640 medium supplemented with 100 units/mL penicillin, 100 g/mL streptomycin, and 10% fetal bovine serum, which provides the only source of folate (the final folate concentration in the serum-supplemented medium was approximately physiological). The cells were cultured as a monolayer in a humidified atmosphere containing 5% CO_2 at 37 °C. CHO cells were obtained from ATCC and cultured in F12 medium supplemented with 10% fetal calf serum.

Uptake of ODN by KB and CHO Cells. Cells were seeded to a 24-well plate at a cell density of 2.5×10^4/well and allowed to grow overnight. ODN, free or encapsulated in lipid vesicles, were added to the cells in various concentrations [determined according to a carbocyanine dye (Cy3)-labeled ODN]. Following incubation at 37 °C for 1 h, cells were washed with PBS (3 × 3 min). Cells were lysed using a lysis buffer (0.1% Triton X in 100 mM Tris, 2 mM EDTA, pH 7.6). The lysed cells were centrifuged at 14000 rpm for 10 min at 4 °C. The amount of Cy3-labeled ODN in the supernatant was determined by examining its fluorescence intensity on a LS50B Perkin-Elmer Luminescence Spectrometer. The protein content of the supernatant was measured with Bio-Rad protein assay system (Bio-Rad, Hercules, CA). The result of ODN uptake was expressed as the pg Cy3-labeled ODN/μg protein.

Fluorescence Microscopic Examination of Cellular Uptake of Folate-Targeted Lipidic ODN. KB cells were seeded at a density of 1×10^5 cells/well in a 4-well Nalge Nunc Lab-Tek chamber slide (Naperville, IL) and kept overnight at 37 °C. ODN, free or formulated in lipid vesicles with or without a folate ligand, were added at a Cy3-ODN concentration of 100 ng/mL. In one well, free folate was added to the folate-targeted lipidic ODN at a final concentration of 1 mM. One hour following the incubation at 37 °C cells were washed three times with PBS. Cells were then fixed with 2% paraformaldehyde at 37 °C for 20 min and further washed three times with PBS. Cellular uptake of Cy3-labeled ODN was examined under a Nikon Eclipse TE 300 fluorescence microscope with a blue filter at 200× magnification.

RESULTS

Preparation and Characterization of Folate-Targeted, ODN-Containing Lipid Vesicles. Cy3-labeled ODN were used as a label for quantification of ODN encapsulation efficiency and for following the cellular uptake of ODN-containing lipid vesicles. Cy3-labeled ODN were mixed with unlabeled ODN at a 1:9 ratio (w/w). ODN were first mixed with a lipid solution composed of DSPC, cholesterol, DODAP, PEG-CerC_{16}, and folate−PEG−DSPE under an acidic condition in the presence of 40% ethanol. DODAP/ODN complexes and other lipids were then self-assembled to form ODN-containing lipid vesicles during the dialysis against 300 mM citrate buffer, pH 4.0, and then against HBS (20 mM HEPES, 145 mM NaCl, pH 7.6). Figure 1 shows the profile of separation of the mixture on Sepharose CL-4B. The lipid-associated ODN were well separated from free ODN. The size of the ODN-containing vesicles ranges from 100 to 200 nm with 60−80% of input ODN being associated with the lipid vectors. These vesicles carry a negative charge surface as confirmed by Zeta potential analysis (data not shown). The ODN that were associated with lipid vesicles were fully protected from degradation by nuclease, suggesting that ODN were encapsulated inside the lipid vesicles (data not shown). These studies were performed with six different ODN ranging from 15 to 23 mer in length (Table 1), and similar results were obtained.

Effect of the Amount of Folate−PEG−DSPE on the Cellular Uptake of Folate-Targeted Lipidic ODN. Figure 2 shows the cellular uptake of lipidic ODN by KB cells with increasing amount of input folate−PEG−DSPE. The total amount of lipid-derivatized PEG (folate−PEG−DSPE plus PEG-CerC_{16}) added is 2 mol %. Increasing the amount of folate from 0.1 to 0.5 mol % resulted in a significant increase in the cellular uptake of ODN. Increasing the input folate beyond 0.5 mol % was not associated with a further increase in the cellular uptake of ODN.

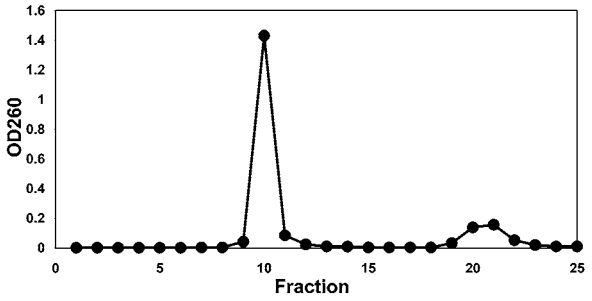


Figure 1. Size-exclusion chromatographic fractionation of ODN-containing lipid vesicles on a Sepharose CL-4B column. DSPC, cholesterol, DODAP, PEG-CerC_{16}, and folate−PEG−DSPE were individually dissolved in ethanol and mixed in a molar ratio of 25/45/25/4/1. To the lipid solution was added 300 mM citric acid, pH 4.0, to a final ethanol concentration of 40% (v/v). Similarly ODN were prepared in separate tubes in 300 mM citric acid, pH 4.0, with 40% ethanol. The solutions were prewarmed to 65 °C, and the lipids were slowly added to the ODN with gentle vortexing. The mixture was passed 10 times through three stacked 100 nm polycarbonate filters. The preparation was dialyzed (12−14 kDa cutoff) against 300 mM citrate buffer, pH 4.0, for approximately 1 h to remove excess ethanol and further dialyzed against HBS (20 mM HEPES, 145 mM NaCl, pH 7.6) for 12−18 h. The dialyzed solution (0.5 mL) was loaded on to a Sepharose CL-4B column (1 cm × 25 cm), which had been equilibrated with HEPES (pH7.6). Lipidic ODN and free ODN were collected with 1 mL in each fraction and examined for their absorbance at 260 nm.

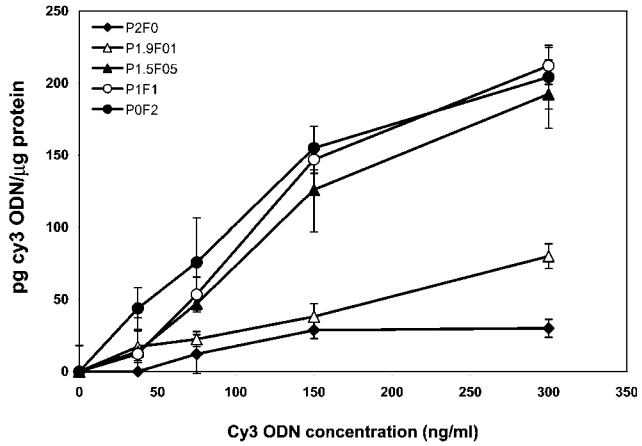


Figure 2. Effect of the amount of folate-PEG-DSPE on the cellular uptake of folate-targeted lipidic ODN. ODN-containing lipid vesicles were prepared as described in the legend to Figure 1 with various amounts of input folate−PEG−DSPE. The total amount of PEG added in the lipid mixture is 2 mol %. KB cells were seeded to a 24-well plate at a cell density of 2.5×10^4/well and allowed to grow overnight. Lipidic ODN were added to the cells in various concentrations (determined according to the Cy3-labeled ODN). Following incubation at 37 °C for 1 h, cells were washed with PBS and then lysed using a lysis buffer. The lysed cells were centrifuged at 14000*g* for 10 min at 4 °C. The amount of Cy3-labeled ODN in the supernatant was determined by examining its fluorescence intensity on a fluorometer. The protein content of the supernatant was measured with Bio-Rad protein assay system. The result of ODN uptake was expressed as the pg Cy3-labeled ODN/μg protein. The *x* and *y* in PxFy (Figures 2, 3, and 5) represent the mol % of PEG-Cer16 and folate−PEG−DSPE in the lipid vesicles, respectively. $n = 3$.

Effect of the Amount of Ceramide-Derivatized PEG on the Cellular Uptake of Folate-Targeted Lipidic ODN. Figure 3 shows the effect of the amount of input ceramide-derivatized PEG on the cellular uptake of folate-targeted lipidic ODN. The amount of input folate−PEG−DSPE is 0.1 (Panel A) or 1 mol % (Panel B). Increasing the amount of ceramide-derivatized PEG from 0 to 10 mol % resulted in a significant decrease in the cellular uptake of ODN when 0.1 mol % of folate−PEG−DSPE was used (Panel A). However, such an inhibitory effect was diminished when the amount of input folate−PEG−DSPE was increased to 1 mol % (Panel B).

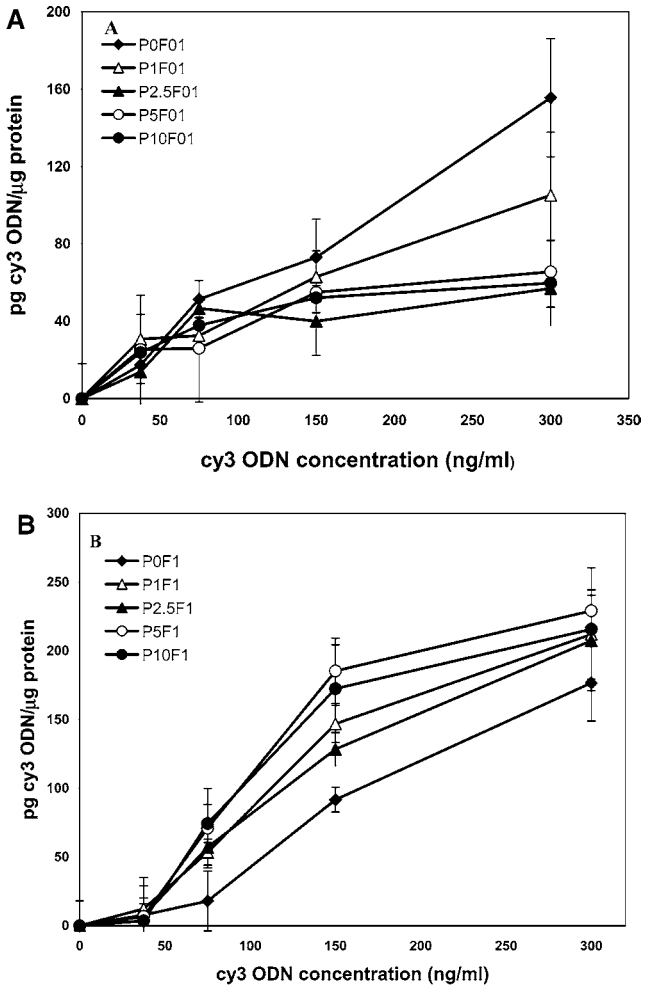


Figure 3. Effect of the amount of ceramide-PEG on the cellular uptake of folate-targeted lipidic ODN. ODN-containing lipid vesicles were prepared as described in the legend to Figure 1 with various amounts of input ceramide-PEG. The amount of input folate−PEG−DSPE was 0.1 mol % (Panel A) or 1 mol % (Panel B). Various amounts of ODN were added to KB cells and the cellular uptake of ODN was evaluated as described in the legend to Figure 2. $n = 3$.

Effect of PEG Length on the Cellular Uptake of Lipidic ODN. Previous studies have shown that folate-mediated targeting of liposomes is affected by the length of PEG spacer between folate and the lipid anchor (such as DSPE in this study) (*10*, *11*). Similar results were observed in this study with ODN targeting using our new lipidic vector (Figure 4). Folate with a PEG of 3500 Da appeared to be more efficient than that with a PEG of 2000 Da in mediating the targeting of ODN to KB cells. This difference became more dramatic with increasing amounts of ceramide−PEG (data not shown).

Cellular Uptake of Folate-Conjugated, Lipidic ODN is Mediated by Folate Receptors. To demonstrate whether the cellular uptake of folate-conjugated, lipidic ODN is mediated by folate receptor, their uptake was also examined on CHO cells, which have a low level of folate receptors (Figure 5). As shown in Panel A, coupling of folate to lipidic ODN led to a significant increase in the cellular uptake by KB cells. The level of ODN uptake was about 8−10-fold higher for folate-

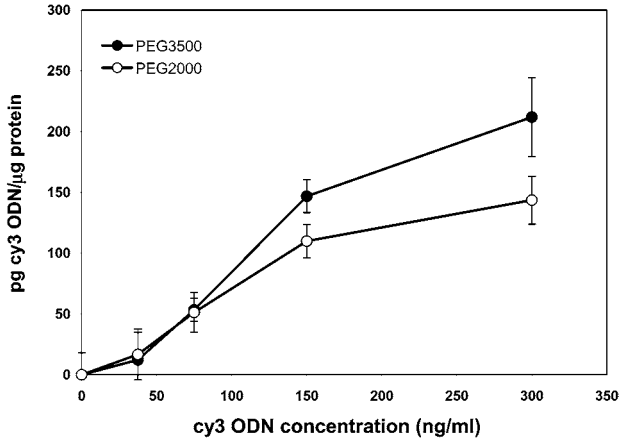


Figure 4. Effect of PEG length on the cellular uptake of lipidic ODN. Lipidic ODN were prepared as described in the legend to Figure 1. The molecular weight of PEG in folate−PEG−DSPE was 2000 or 3500 Da. Various amounts of ODN were added to KB cells and the cellular uptake of ODN was evaluated as described in the legend to Figure 2. $n = 3$.

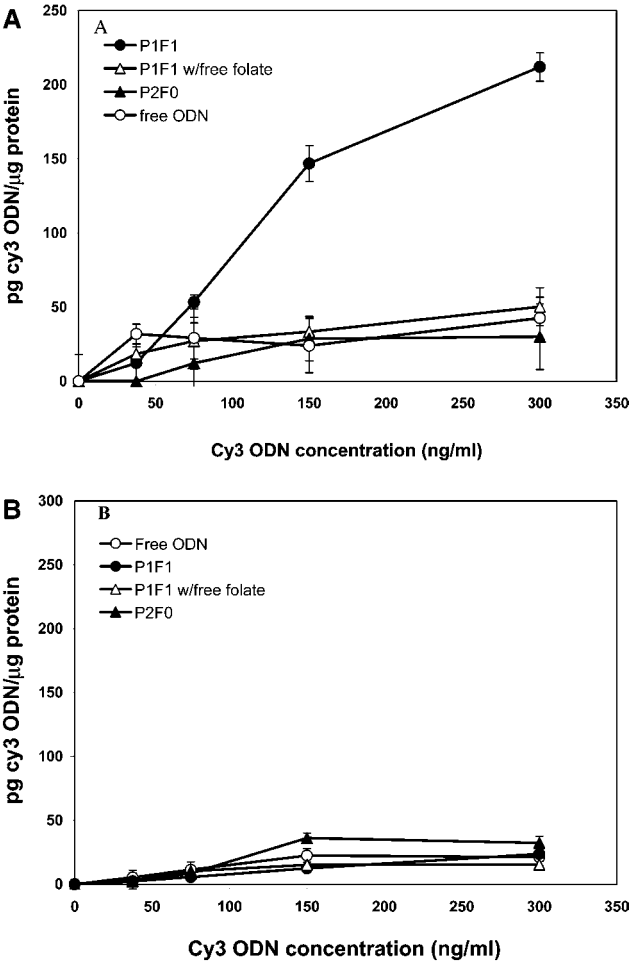


Figure 5. Cell type-specific uptake of folate-targeted lipidic ODN. KB (Panel A) or CHO (Panel B) cells were plated in a 24-well plate. ODN, free or formulated in lipid vesicles with or without a folate ligand, were added to cells in various concentrations. In a separate experiment, free folate was added to folate-targeted lipidic ODN at a final concentration of 1 mM. Cellular uptake of ODN was then evaluated as described in the legend to Figure 2. $n = 3$.

targeted lipidic ODN than that of free ODN or lipidic ODN without a ligand. The improvement in ODN uptake was almost completely blocked by adding excess amount of free folate. There was essentially no difference in the ODN uptake by CHO cells whether ODN were free or formulated in ligand-free lipid vesicles or folate-targeted lipid vesicles (Panel B).

Fluorescence Microscopic Examination of the Cellular Uptake of Folate-Targeted Lipidic ODN. Figure 6 shows the fluorescence images of ODN uptake by KB cells. At 1 h following incubation at 37 °C, folate-targeted ODN were found to be associated with the cell membrane as well as inside the cells (Panel B). In agreement with the quantitative analysis (Figure 5), the level of cell-associated fluorescence intensity is substantially higher with folate-targeted ODN (Panel B) than that with either free ODN (Panel D) or ODN formulated in nontargeted lipid vesicles (Panel A). However, the fluorescence intensity with folate-targeted ODN was decreased to background level by adding excess amounts of free folate (Panel C). These results suggest that the binding and the subsequent internalization of the folate-targeted ODN are mediated by the folate receptors.

Effect of Serum on ODN Uptake by KB Cells. Figure 7 shows the uptake of folate-targeted ODN by KB cells in the presence or absence of 10% FBS. Serum appears to have only a slight effect on the cellular uptake of folate-targeted ODN. Similar phenomenon was observed for free ODN or ODN formulated in nontargeted lipid vesicles (data not shown).

DISCUSSION

An ideal ODN vector should have a large ODN loading capacity and deliver the ODN to target cells in a cell-type-specific manner. Neutral liposomes are suitable for active targeting but suffer from low encapsulation efficiencies and drug-to-lipid ratios. This problem can be resolved via incorporation of cationic lipids into the formulation, but the resulting lipid/nucleic acid complexes are generally unstable and short-lived in blood circulation. Furthermore, substantial amounts of ODN are associated with the positively charged surface of the particles. These ODN may be released from the particles by the highly negatively charged molecules in the blood following systemic administration (*12*). Recently, Stuart and Allen (*13*) described a method by which 80−100% of input ODN were entrapped in a lipid vector that was stable in human plasma. This involves the formation in and extraction of cationic lipid/ODN complex from an organic solvent. The cationic lipid/ODN complex was then mixed with other neutral lipids and ODN-containing lipid vesicles were obtained by a reverse phase evaporation method (*13*). More recently, a much simpler method was developed by Semple and colleagues (*1*), which utilizes an ionizable aminolipid (DODAP) and an ethanol-containing buffer system. A similar level of encapsulation efficiency was achieved (*1*). These ODN-containing lipid vesicles, however, are inefficient in interacting with cells. Furthermore, they lack cell type specificity. In this study we investigated whether a targeting ligand can be incorporated into these vesicles to further improve their efficiency in intracellular delivery of ODN. Folate was chosen as a targeting ligand since folate receptors have been shown to be overexpressed in a number of cancer cells. Folate has been used successfully in targeting to tumors various types of agents including chemotherapeutic drugs (*10*), radionucleotides (*14*, *15*), ODN (*6*, *16*), DNA (*17*, *18*), etc. The advantages of a folate-targeting system include its excellent safety profile and the low immunogenicity. Folate receptors have also been shown to mediate efficient internalization of free folate or the

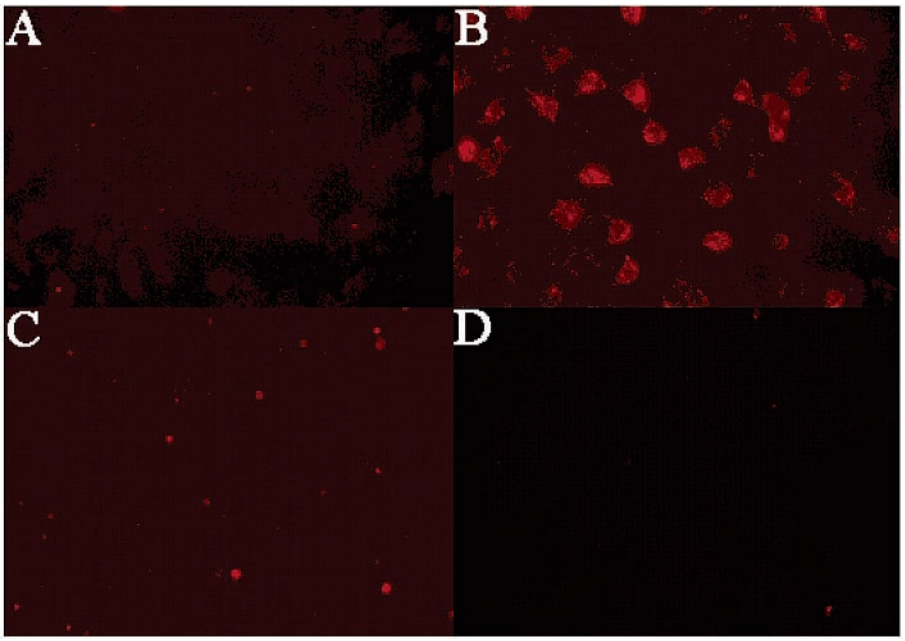


Figure 6. Fluorescence microscopic examination of cellular uptake of folate-targeted lipidic ODN. KB cells were seeded at a density of 1×10^5 cells/well in a 4-well Nalge Nunc Lab-Tek chamber slide (Naperville, IL) and kept overnight at 37 °C. ODN, free or formulated in lipid vesicles with or without a folate ligand, were added at a Cy3-ODN concentration of 100 ng/mL. In one well, free folate was added to the folate-targeted lipidic ODN at a final concentration of 1 mM. One hour following the incubation at 37 °C cells were washed three times with PBS. Cells were then fixed with 2% paraformaldehyde at 37 °C for 20 min and further washed with PBS three times. Cellular uptake of Cy3-labeled ODN was examined under a Nikon fluorescence microscope with a blue filter at 200X magnification. A: Lipidic ODN without a ligand; B: folate-targeted lipidic ODN; C: folate-targeted lipidic ODN + 1 mM free folate; D: free ODN.

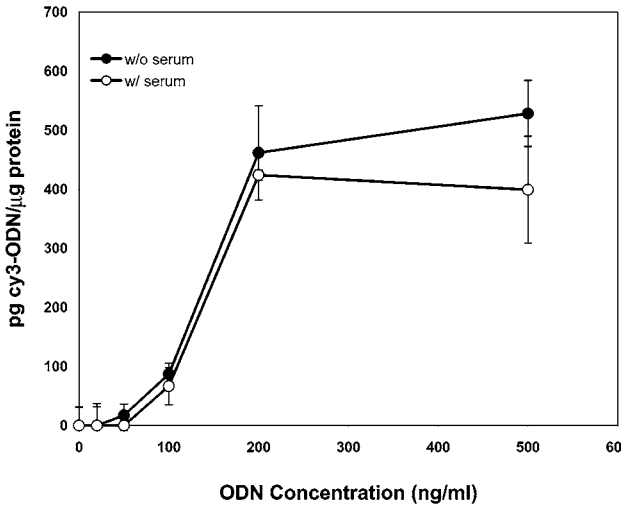


Figure 7. Effect of serum on ODN uptake by KB cells. KB cells were seeded to a 24-well plate at a cell density of 2.5×10^4/well and allowed to grow overnight. Various concentrations of folate-targeted ODN were added to cells in the presence or absence of 10% FBS. Cellular uptake of ODN was then evaluated as described in the legend to Figure 2. $n = 3$.

conjugates, which should facilitate intracellular delivery of the therapeutic agent. Results from this study clearly show that incorporation of folate into the ODN-containing vesicles leads to a significant improvement in delivery of ODN to KB cells that overexpress folate receptors (Figures 5 and 6). The increase in the ODN uptake was almost completely blocked by excess amount of free folate (Figures 5 and 6). Conjugation of folate led to little change in ODN uptake by CHO cells that are negative for folate receptor expression (Figure 5). These studies clearly indicate that targeted delivery of ODN to KB cells via this novel lipid vector is mediated by the folate receptors.

The targeting efficiency of folate-conjugated vesicles is affected by the amount of input folate−PEG−DSPE. Increasing the amount of folate from 0 to 0.5 mol % was associated with a significant increase in ODN uptake. However, increasing the input folate beyond 0.5 mol % was not associated with a further increase in the cellular uptake of ODN (Figure 2). Interestingly, the targeting efficiency of folate-conjugated vesicles is also affected by the amount of input ceramide−PEG (Figure 3). Ceramide−PEG was included for two purposes: (a) to render the resulting particles long-circulating in the blood, and (b) to prevent aggregation during the preparation of ODN-containing lipid vesicles, particularly when the vectors were prepared at high lipid concentrations. However, at a high concentration of ceramide-PEG, substantial amounts of PEG have been shown to be excluded from the lipid vesicles (*1*). Similarly, some of the input folate might be excluded from the vesicles, which may lead to incoporation of less than sufficient amounts of folate needed to achieve efficient targeting when a small amount of input folate−PEG−DSPE is used. This may explain the fact that, at a folate concentration of 0.1 mol %, the efficiency of ODN delivery was decreased dramatically when the ceramide−PEG was increased to above 2.5 mol % (Figure 3A). This problem, however, can be resolved by increasing the amount of input folate−PEG−DSPE. As shown in Figure 3B, increasing the amount of input folate from 0.1 to 1 mol % resulted in a full recovery of targeting efficiency at high concentrations of ceramide−PEG (above 5 mol %). No purification is required to remove the free folate−PEG−DSPE from the folate-conjugated, ODN-containing lipid vesicles.

Similar to liposomal targeting (*10*, *11*), the efficiency of ODN delivery via the new lipid vector is affected by the length of the PEG spacer. This might be due to the fact that the PEG coating imposes steric hindrance for

the folate to interact efficiently with the folate receptors on the cell surface when a short PEG spacer (such as 2000 Da) is used. This interference becomes more pronounced with increasing amounts of ceramide−PEG (data not shown). This problem, however, can be resolved via the use of a longer PEG spacer between the folate and the lipid anchor. As shown in Figure 4, increasing the length of PEG spacer from 2000 to 3500 Da results in a significant improvement in the targeting efficiency. Furthermore, the targeting efficiency of the resulting lipid vectors is not significantly affected by the amount of the input ceramide−PEG (Figure 3B).

In summary, we have developed a novel lipid vector that is highly efficient in delivering ODN to tumor cells that overexpress folate receptor. We have also shown recently that this vector mediates efficient delivery of ODN to mouse lung endothelial cells using an endothelial cell-specific antibody as a ligand (Wilson et al., unpublished data). Currently we are examining the targeting efficiency of this vector in vivo.

ACKNOWLEDGMENT

This work was supported by DOD grant PC001525 and NIH grant HL RO1 63080 (to S Li). We would like to thank Dr. Takuro Niidome for his helpful discussion in this study.

LITERATURE CITED

(1) Semple, S. C., Klimuk, S. K., Harasym, T. O., Dos Santos, N., Ansell, S. M., Wong, K. F., Maurer, N., Stark, H., Cullis, P. R., Hope, M. J., and Scherrer, P. (2001) Efficient encapsulation of antisense oligonucleotides in lipid vesicles using ionizable aminolipids: formation of novel small multilamellar vesicle structures. *Biochim. Biophys. Acta 1510* (1−2), 152−66.

(2) Agrawal, S., and Zhao, Q. (1998) Antisense therapeutics. *Curr. Opin. Chem. Biol. 2* (4), 519−528.

(3) Crooke, S. T. (1998) An overview of progress in antisense therapeutics. *Antisense Nucleic Acid Drug Dev. 8* (2), 115−122.

(4) Yakubov, L. A., Deeva, E. A., Zarytova, V. F., Ivanova, E. M., Ryte, A. S., Yurchenko, L. V., and Vlassov, V. V. (1989) Mechanism of oligonucleotide uptake by cells: involvement of specific receptors? *Proc. Natl. Acad. Sci. U.S.A. 86* (17), 6454−6458.

(5) Loke, S. L., Stein, C. A., Zhang, X. H., Mori, K., Nakanishi, M., Subasinghe, C., Cohen, J. S., and Neckers LM. (1989) Characterization of oligonucleotide transport into living cells. *Proc. Natl. Acad. Sci. U.S.A. 86* (10), 3474−3478.

(6) Wang, S., Lee, R. J., Cauchon, G., Gorenstein, D. G., and Low, P. S. (1995) Delivery of antisense oligodeoxyribonucleotides against the human epidermal growth factor receptor into cultured KB cells with liposomes conjugated to folate via poly(ethylene glycol). *Proc. Natl. Acad. Sci. U.S.A. 92* (8), 3318−3322.

(7) Bennett, C. F., Chiang, M. Y., Chan, H., Shoemaker, J. E., and Mirabelli, C. K. (1992) Cationic lipids enhance cellular uptake and activity of phosphorothioate antisense oligonucleotides. *Mol. Pharmacol. 41*(6), 1023−1033.

(8) Cumin, F., Asselbergs, F., Lartigot, M., and Felder, E. (1993) Modulation of human prorenin gene expression by antisense oligonucleotides in transfected CHO cells. *Eur. J. Biochem. 212* (2), 347−354.

(9) Ma, Z., Zhang, J., Alber, S., Dileo, J., Negishi, Y., Stolz, D., Watkins, S. C., Huang, L., Pitt, B., and Li S. (2002) Lipid-mediated delivery of oligonucleotide to pulmonary endothelium. *Am. J. Respir. Cell Mol. Biol. 27* (2), 151−159.

(10) Lee, R. J., and Low, P. S. (1995) Folate-mediated tumor cell targeting of liposome-entrapped doxorubicin in vitro. *Biochim. Biophys. Acta 1233* (2), 134−44.

(11) Gabizon, A., Horowitz, A. T., Goren, D., Tzemach, D., Mandelbaum-Shavit, F., Qazen, M. M., and Zalipsky S. (1999) Targeting folate receptor with folate linked to extremities of poly(ethylene glycol)-grafted liposomes: in vitro studies. *Bioconjugate Chem. 10* (2), 289−298.

(12) Zelphati, O., and Szoka, F. C., Jr. (1996) Mechanism of oligonucleotide release from cationic liposomes. *Proc. Natl. Acad. Sci. U.S.A. 93* (21), 11493−11498.

(13) Stuart, D. D., and Allen, T. M. (2000) A new liposomal formulation for antisense oligodeoxynucleotides with small size, high incorporation efficiency and good stability. *Biochim. Biophys. Acta 463* (2), 219−29.

(14) Mathias, C. J., Wang, S., Lee, R. J., Waters, D. J., Low, P. S., and Green, M. A. (1996) Tumor-selective radiopharmaceutical targeting via receptor-mediated endocytosis of gallium-67-deferoxamine-folate. *J. Nucl. Med. 37*(6), 1003−1008.

(15) Guo, W., Hinkle, G. H., and Lee, R. J. (1999) 99mTc−HYNIC-folate: a novel receptor-based targeted radiopharmaceutical for tumor imaging. *J. Nucl. Med. 40* (9), 1563−1569.

(16) Li, S., Deshmukh, H. M., and Huang, L. (1998) Folate-mediated targeting of antisense oligodeoxynucleotides to ovarian cancer cells. *Pharm. Res. 15* (10), 1540−1545.

(17) Lee, R. J., and Huang, L. (1996) Folate-targeted, anionic liposome-entrapped polylysine-condensed DNA for tumor cell-specific gene transfer. *J. Biol. Chem. 271* (14), 8481−8487.

(18) Xu, L., Pirollo, K. F., and Chang, E. H. (2001) Tumor-targeted p53-gene therapy enhances the efficacy of conventional chemo/radiotherapy. *J. Controlled Release 74* (1−3), 115−128.

(19) Ciardiello F., Caputo, R., Troiani, T., Borriello, G., Kandimalla, E. R., Agrawal, S., Mendelsohn, J., Bianco, A. R., and Tortora, G. (2001) Antisense oligonucleotides targeting the epidermal growth factor receptor inhibit proliferation, induce apoptosis, and cooperate with cytotoxic drugs in human cancer cell lines. *Int. J.* Cancer *93* (2), 172−178.

(20) Grandis, J. R., Chakraborty, A., Melhem, M. F., Zeng, Q., and Tweardy, D. J. (1997) Inhibition of epidermal growth factor receptor gene expression and function decreases proliferation of head and neck squamous carcinoma but not normal mucosal epithelial cells. *Oncogene 15*, 409−416.

(21) Witters, L., Kumar, R., Mandal, M., Bennett, C. F., Miraglia, L., and Lipton, A. (1999) Antisense oligonucleotides to the epidermal growth factor receptor. *Breast Cancer Res. Treat. 53*, 41−50.

BC025569Z

Characterization of Novel Histidine-Tagged Tat-Peptide Complexes Dual-Labeled with ^{99m}Tc-Tricarbonyl and Fluorescein for Scintigraphy and Fluorescence Microscopy

Kristin E. Bullok, Mary Dyszlewski, Julie L. Prior, Christina M. Pica, Vijay Sharma, and David Piwnica-Worms*

Molecular Imaging Center, Mallinckrodt Institute of Radiology, Department of Molecular Biology and Pharmacology, Washington University Medical School, St. Louis, Missouri 63110. Received July 12, 2002; Revised Manuscript Received August 15, 2002

To enable concurrent whole body scintigraphy and direct imaging of subcellular localization of permeation peptides, dual-labeled Tat-peptides useful for both radiometric analysis and fluorescence microscopy are desired for molecular imaging applications. Thus, novel dual-labeled D-Tat-peptides comprising Tat-basic domain (hgrkkrrqrrrgc), C-terminus conjugated with fluorescein-5-maleimide (FM) and N-terminus chelated with [^{99m}Tc(CO)$_3$] via histidine coordination, were synthesized and characterized. In human Jurkat cells, radiotracer uptake and washout studies revealed concentration-dependent accumulation of the dual-labeled Tat-peptide within cells. Subcellular localization of Tat-peptide was confirmed by fluorescence microscopy using an analogous [Re(CO)$_3$] dual-labeled Tat-peptide. As seen with C-terminus single-labeled Tat-peptides, localization to the nucleoli was observed with the dual-labeled Tat-peptide, suggesting that the mechanism of Tat-peptide uptake and localization was not dependent on free peptide termini at either end. In Balb/c mice, biodistribution studies performed with the dual-labeled Tat-peptide showed fluorescence intensity by microscopic analysis that visually confirmed and correlated directly with scintigraphic and radiometric data. Of note, following intravenous administration, little brain penetration of these permeation sequences was observed in vivo. His[^{99m}Tc(CO)$_3$]-, DTPA[^{99m}Tc(CO)$_3$]-, and ϵ-lys-gly-cys[^{99m}Tc(O)]-labeled Tat-peptides showed significant pharmacokinetic differences in liver and kidney depending on labeling strategy, indicating that Tat-peptide biodistribution can be impacted by the chelation moiety coordinated with ^{99m}Tc. Thus, we have shown that dual-labeled ^{99m}Tc-tricarbonyl Tat-peptide−FM conjugates can be conveniently synthesized and enable direct comparison of quantitative radiometric and qualitative fluorescence data both in vitro as well as in vivo.

INTRODUCTION

Permeation peptides, including the Tat-peptide basic domain, have been intensely studied recently after early observations demonstrated rapid translocation properties, seemingly independent of receptor-mediated endocytosis, into various cell types. The ability of permeation peptides to cross cell membranes is especially promising for drug delivery, since one major barrier to successful therapies and bioimaging is the need for membrane translocation (*1, 2*). Initial studies of the HIV Tat protein in the late 1980s (*3, 4*) showed the feasibility of utilizing Tat-derived polypeptides for rapid transport of various cargo into cells. Subsequent work with Tat-basic domain and related sequences has shown transport and delivery of polypeptides, immunoreactive epitopes, fluorescent probes, oligonucleotides, and derivatized superparamagnetic iron oxide nanoparticles (*5*−*12*) into various cell types. Tat-peptide has also been pursued as a possible molecular imaging and radiotherapeutic agent via chelation to various radioisotopes, such as ^{99m}Tc (*13*).

^{99m}Tc is a widely used radioisotope in medical imaging because it is readily available through ^{99}Mo/^{99m}Tc generator systems, has an ideal photon energy for imaging applications, and possesses a short half-life (6.02 h) (*14*−*16*). In addition, chelation chemistry for ^{99m}Tc has received much attention because donor cores also enable radiation therapy using chemically analogous ^{186}Re/^{188}Re species (*17*). ^{99m}Tc can be coordinated by a variety of chelators including various tetradentate N or S ligands (N_2S_2, N_3S, etc. donor cores) and diethylenetriaminepentaacetic acid (DTPA) (*1*). Recently, $[M(CO)_3(OH_2)_3]^+$ where (M = ^{99m}Tc or Re) has been incorporated into peptides via facial replacement of water molecules using chelators such as phosphines (*18*) and α-amino moieties of N-terminal histidine (*19*). These ^{99m}Tc triaquo-tricarbonyl species have been shown to be highly stable (*20*−*22*), thereby providing another promising candidate chelation strategy for coordination of [^{99m}Tc(CO)$_3$] to Tat-peptides. We report here the novel use of [^{99m}Tc(CO)$_3$] to radiolabel his-tagged Tat-peptide sequences to yield single-labeled Tat-peptides or in combination with fluorescein-5-maleimide (FM) conjugated to the C-terminus thiol to yield dual-labeled Tat-peptides. Both his[^{99m}Tc(CO)$_3$] and the analogous his[Re(CO)$_3$]-coordinated Tat-peptides were characterized and analyzed in vitro and in vivo. Dual-labeled Tat-peptides were employed to quantitatively measure cellular uptake and tissue biodistribution as well as to qualitatively confirm subcellular localization by fluorescent microscopy.

* Correspondence to David Piwnica-Worms, M.D., Ph.D., Molecular Imaging Center, Mallinckrodt Institute of Radiology, Washington University Medical School, 510 S. Kingshighway Blvd., Box 8225, St. Louis, MO 63110. Tel: 314-362-9356, Fax: 314-362-0152, E-mail: piwnica-wormsd@mir.wustl.edu.

10.1021/bc025573a CCC: $22.00 © 2002 American Chemical Society
Published on Web 10/18/2002

METHODS

Peptide Synthesis. Peptides **1** (H-his-gly arg-lys-lys-arg-arg-gln-arg-arg-arg-gly cys-NH_2), **2** (H-his-gly arg-lys-lys-arg-arg-gln-arg-arg-arg-NH_2), and **3** (H-gly arg-lys-lys-arg-arg-gln-arg-arg-arg-gly cys-Resin) were prepared by solid-phase peptide synthesis (Tufts University Peptide Synthesis Core Facility, Boston, MA) using all D N-α-Fmoc-protected amino acids and standard BOP/HOBt coupling chemistry. Peptides **1** and **2** were C-terminus amidated and purified (>95%) by C_{18} reversed-phase HPLC at a flow rate of 1 mL/min using as eluent 0.1% trifluoroacetic acid in 5% acetonitrile/95%water [0.1% TFA/(5% CH_3CN/H_2O)] modified with 0.1% trifluoroacetic acid in 90% acetonitrile/10% water [0.1% TFA/(90% CH_3CN/H_2O)] by a linear gradient of 5% to 40% acetonitrile over 40 min. A single HPLC peak was observed (t_R (**1**) = 14.6 min; t_R (**2**) = 13.5 min) and identity of each was confirmed by amino acid analysis (**1**, 13 amino acids: gln 1; his 1; gly 2; cys 1; lys 2, arg 6; **2**, 11 amino acids: gln 1; his 1; gly 1; lys 2, arg 6; **3**, 12 amino acids: gln 1; gly 2; cys 1; lys 2, arg 6; on resin) and electrospray mass spectrometry (EMS) (**1**, *m*/*z*: 1694.0, calcd: $C_{66}H_{125}N_{37}O_{14}S_1$, 1693.0; **2**, *m*/*z*: 1533.9, calcd: $C_{61}H_{117}N_{35}O_{12}$, 1532.8; **3** cleaved from resin, *m*/*z*: 1556.3, calcd: $C_{60}H_{118}N_{34}O_{13}S_1$, 1555.9).

Synthesis of DTPA−Tat-Peptide. To dry tri-*tert*-butyl DTPA (39 mg; 69 μmol) (Mallinckrodt, Inc., St. Louis, MO (*23*)) was added dicyclohexylcarbodiimide (DCC, 17 mg, 1.2 equiv) in anhyd DMF (1.0 mL). Tri-*tert*-butyl DTPA was activated with stirring in DCC for 30−60 min. To 100 mg of dried peptide resin **3**, suspended in 30−35 μL of anhydrous triethylamine, was added the activated tri-*tert*-butyl DTPA solution, and N-terminal coupling was allowed to proceed with stirring overnight. DMF was removed, and resin was washed twice each with DMF followed by acetonitrile and then dried under argon. The peptide was cleaved from resin, and the protecting groups were removed by stirring in TFA stock solution [(TFA (10 mL), phenol (0.75 g), thioanisole (0.5 mL), deionized water (0.5 mL), and ethanedithiol (0.25 mL)] (*24*) at room temp for 3 h. The cleaved and deprotected peptide was then filtered through glass wool to separate from the resin, precipitated in cold ether, pelleted by centrifugation, and the supernatant removed. Finally, pelleted peptide was dissolved in water and lyophilized to obtain dried crude product. Purification was carried out as described above (t_R = 11.6 min; yield ~40%). Purity was assessed by RP-HPLC (>95% pure) and identity by EMS (DTPA-gly-arg-lys-lys-arg-arg-gln-arg-arg-arg-gly-cys-NH_2 (**4**), *m*/*z*: 1932.2, calcd: $C_{74}H_{141}N_{37}O_{23}S_1$, 1932.3).

Synthesis of Tat-Peptide−FM. To **1** or **4** (5 mg) dissolved in PBS (200 μL) was added FM (1.2 mol equiv; Molecular Probes, Eugene, OR) dissolved in DMF (200 μL). The reaction was stirred at ambient temp for 2 h in the dark. Resulting FM-labeled Tat-peptide conjugates were purified by RP-HPLC (>98%; single doublet peak, t_R (**5**) = 25.6, 26.0 min and t_R (**6**) = 24.1, 24.6 min) using the eluent mixture described above and each product was identified by EMS (H-his-gly-arg-lys-lys-arg-arg-gln-arg-arg-arg-gly-cys-FM (**5**), *m*/*z*: 2120.0, calcd: $C_{90}H_{138}N_{38}O_{21}S_1$, 2120.4; DTPA-gly-arg-lys-lys-arg-arg-gln-arg-arg-arg-gly-cys-FM (**6**), *m*/*z*: 2358.0, calcd: $C_{98}H_{154}N_{38}O_{30}S_1$, 2358.6). To further characterize the two closely eluting peaks observed on HPLC chromatograms, the peaks for **5** were separated and analyzed by EMS. Both peaks revealed the same mass, thus confirming that these species were isomers. Because the isomers did not show interconversion for 1 h after purification, the two species were considered as the desired product.

Synthesis of [Re(CO)$_3$]Tat-Peptide−FM. To **5** or **6** (2 mg) in RO water (100 μL) was added $[Re(CO)_3Br_3][NEt_4]_2$ (1 equiv) (*25*) (gift from Roger Schibli, Paul Scherrer Institute, Switzerland) dissolved in water (100 μL). The reaction mixture was stirred at 85 °C − 90 °C for 30 min. For $Re(CO)_3$ coordinated with **5**, RP-HPLC analysis revealed three major doublet peaks (t_R = 27.8, 28.1 min; 28.7, 29.0 min; 30.1, 30.4 min) and two unidentified minor peaks, and for $Re(CO)_3$ coordinated with **6**, a complex spectra, probably due to structural isomers arising from the presence of multiple NO coordination combinations (*26*, *27*). From the $Re(CO)_3$ coordinated with **6**, the main doublet peak was isolated (t_R (**8**) = 26.4, 26.8 min). All product peaks were collected from the $Re(CO)_3$ coordinated with **5**. Purification was performed using the solvent gradient system described above with collection of appropriate fractions. Identity of isolated [Re(CO)$_3$]Tat-peptide complexes was confirmed by EMS ([Re(CO)$_3$]his-gly-arg-lys-lys-arg-arg-gln-arg-arg-arg-gly-cys-FM (**7**), *m*/*z*: 2390.0, calcd: $C_{93}H_{138}N_{38}O_{24}Re_1S_1$, 2390.6; [Re(CO)$_3$]DTPA-gly-arg-lys-lys-arg-arg-gln-arg-arg-arg-gly-cys-FM (**8**), *m*/*z*: 2628.0, calcd: $C_{101}H_{154}N_{38}O_{33}S_1$, 2628.8).

Synthesis of [^{99m}Tc(CO)$_3$]Tat-Peptides. Tat-peptide conjugates were labeled with $[^{99m}Tc(CO)_3]$ using a commercially available tricarbonyl radiopharmaceutical kit ($K_2BO_3CO_2$ (4 mg), $K_2B_4O_7{\cdot}H_2O$ (10 mg), NaK tartrate (10 mg), pH 10; Mallinckrodt, Inc., St. Louis, MO). Kits were reconstituted with Na[$^{99m}TcO_4$] (20−40 mCi) in isotonic saline (1.0 mL), obtained by eluting a commercial radionuclide $^{99}Mo/^{99m}Tc$ generator, and reacted in a 100 °C oil bath for 10−15 min. Following neutralization by 1 N HCl (80 μL), 90 μL of the $[^{99m}Tc(CO)_3(OH_2)_3]^+$ solution was added to 100 μg of **1**, **2**, **4**, **5**, or **6** (10 μL of a 10 mg/mL peptide solution) and reacted for 20−30 min at 85−90 °C. Radiochemical yields (>94%) of $[^{99m}Tc(CO)_3]$-Tat-peptide complexes were determined by TLC using silica gel plates developed with eluent, either methanol:saline:TFA (68:30:2) or H_2O, as indicated, and scanning radiometric detection (Bioscan, Inc., Washington, D.C.). In methanol:saline:TFA, $[^{99m}Tc(CO)_3]$ complexes of **1, 2, 4**, **5**, and **6**, with R_f values between 0.85 and 0.95, were readily distinguished from reduced species such as $[^{99m}Tc]TcO_2$ at the origin. In H_2O, $[^{99m}Tc(CO)_3]$Tat-complexes remained at the origin while $[^{99m}TcO_4]$ moved with the solvent front. Radiochemical purity of aliquots was determined by radiometric RP-HPLC using the solvent gradient system described above. Radiochemical purity of labeled complexes **1**, **2**, and **5** was >94%. Therefore, for complexes **1**, **2**, and **5**, no purification was carried out, and compounds were directly utilized for both in vitro and animal studies. Following radiolabeling, complexes of **4** and **6** were either directly utilized or further purified by RP-HPLC as described to obtain >86% purity with no difference in results. When purified, collected fractions utilized for biodistribution studies were diluted to 35 μCi/mL with phosphate-buffered saline (PBS) to obtain a final pH slightly less than neutral. In contrast, collected fractions utilized for transport assays were spiked with either cold compound **4** or **6** (to simulate the specific activity of nonpurified radiolabeled peptides) for a final peptide concentration of 75 μM. Transport assays were then carried out as described below.

Stability Studies. In vitro and in vivo studies were carried out as previously described (*13*) with slight modifications. Briefly, stability in vitro of $[^{99m}Tc(CO)_3]$-

Tat-peptide complex **5** in aqueous buffers between pH 4 and 9 was evaluated by incubation of the radiolabeled peptide (10 mg/mL) for 1 h at 37 °C in HEPES (10 mM) or Tris base (50 mM) buffer pH adjusted with HCl or NaOH, followed by TLC and scanning radiometric analysis as well as RP-HPLC with UV-radiometric detection. Additional effects of reduced histidine (2.5 mM), cysteine (2.5 mM), or EDTA (2.5 mM) on radiolabeled Tat-peptide stability were evaluated by addition of competing chelator to buffers at each pH. Stability in vitro was further assessed by radio-TLC after incubation of [^{99m}Tc(CO)$_3$]-Tat-peptide of **5** for 1 and 24 h at 37 °C in fetal bovine serum or PBS. Stability in vivo of radiolabeled [^{99m}Tc(CO)$_3$]-Tat-peptide of **5** was characterized by radio-TLC analysis of serum and urine samples 30 min after intravenous administration of 850 μCi of the radiolabeled peptide to FVB mice.

Cell Culture. Monolayers of human epidermoid carcinoma KB 3-1 cells were grown at 37 °C in an atmosphere of 5% CO_2 as previously described (*28, 29*). To attain 60% confluent cell monolayers for experiments, cells were plated 1 day prior to experimentation in 10-cm Petri dishes containing seven 25-mm coverslips and maintained in DMEM (GIBCO, Grand Island, NY) supplemented with L-glutamine (1%), penicillin/streptomycin (0.1%), and heat-inactivated fetal bovine serum (10%). Suspensions of human Jurkat leukemia cells were maintained in RPMI also supplemented with L-glutamine, penicillin/streptomycin, and heat-inactivated fetal bovine serum at 37 °C in an atmosphere of 5% CO_2 (*13*).

Transport Assays. Assays were performed with a minor modification to a previously described procedure (*13*). Briefly, tracer transport assays were carried out with Jurkat cells incubated in modified Earl's balanced salt solution (MEBSS) containing (mM): 145 Na^+, 5.4 K^+, 1.2 Ca^{2+}, 0.8 Mg^{2+}, 152 Cl^-, 0.8 $H_2PO_4^-$, 0.8 SO_4^{2-}, 5.6 dextrose, 4.0 HEPES, and 1% fetal bovine serum (vol/vol), pH 7.4 ± 0.05. Experiments were performed in siliconized microfuge tubes each containing 10 μL of [^{99m}Tc(CO)$_3$]Tat-peptides (with or without purification) and 740 μL of a MEBSS suspension of 10^7 cells. Unless stated otherwise, [^{99m}Tc(CO)$_3$]Tat-peptide complex was added to MEBSS without purifying from the molar excess of unlabeled Tat-peptide as obtained directly from the labeling procedure; final total peptide concentration was typically 1 μM (20−50 nmol/mCi; ∼25 μCi/ml). Tubes were incubated at 37 °C for 20 min with occasional mixing, and the reaction was terminated by spinning two separate 250 μL aliquots from the reaction tubes for 10 s through 800 μL of a mixture (75:25) of silicone oil (density = 1.050; Aldrich) and mineral oil (density = 0.875; Acros). A 50 μL amount of the aqueous phase was obtained to normalize extracellular concentration of the [^{99m}Tc(CO)$_3$]Tat-peptide to cell-associated activity. Remaining aqueous and oil layers were then aspirated, and the cell pellet was extracted in 0.5 mL of 1% SDS, 10 mM sodium borate. For peptide washout experiments, immediately after a 20 min uptake period, cell pellets were collected by rapid spinning and resuspended in 750 μL of peptide-free 4 °C MEBSS buffer. Immediately, another rapid spin was performed and the collected pellet was suspended in 750 μL of fresh 37 °C MEBSS buffer for a 30 min washout period. The experiment was terminated as above, and all cell extracts were assayed for protein by BCA analysis (Pierce Chemical Co.) using bovine serum albumin as the protein standard. Cell extracts, stock solutions, and extracellular buffer samples were assayed for gamma activity in a well-type sodium iodide gamma counter (Cobra II, Beckman; 130−165 keV window). Absolute concentration of total [Tc(CO)$_3$]Tat-peptide complex in solution was determined from the specific activity of ^{99m}Tc, based on equations of ^{99}Mo/^{99m}Tc generator equilibrium (*30*). Transport data are reported as fmol of peptide$_i$ (mg protein)$^{-1}$ (nM$_o$)$^{-1}$, wherein peptide$_i$ represents total peptide (labeled and unlabeled) within the cells and (nM$_o$)$^{-1}$ represents concentration of total peptide in the extracellular buffer (*13, 31*). Data are reported as mean ± SEM.

Fluorescence Microscopy. Just prior to the study, 1 mM peptide solutions (freshly made or from stock solutions stored at −20 °C) were diluted in MEBSS buffer (pH = 7.4; 37 °C) to obtain 1 μM peptide solutions, for incubation with KB 3-1 cells, and 10 μM peptide solutions, for incubation with Jurkat cells. For uptake experiments with KB 3-1 cells, coverslips of 60% confluent KB 3-1 cells were removed from incubation and washed briefly in a 37 °C MEBSS buffer bath. After placing a single coverslip in a 35 mm dish, 200 μL of the respective 1 μM peptide conjugates **5**, **6**, **7**, or **8** were added on top of the coverslip. Following a 20 min uptake at 37 °C, the cells were fixed in the presence of peptide solution with 200 μL of 8% paraformaldehyde (4% final PFA) for 10−15 min and washed three times with PBS. For uptake experiments with Jurkat cells, cells were pelleted at 1000 rpm for 5 min. Cells were then resuspended in MEBSS buffer (pH = 7.4; 37 °C) at a concentration of 10^5 cells/90 μL. A 90 μL amount of the cell suspension was directly added to 10 μL of 10 μM peptide solutions of **5** or **7** for a final peptide concentration of 1 μM. Following a 20 min incubation at 37 °C, cells were cytospun onto slides, fixed for 10 min with PFA (4%), and washed three times with PBS. All cells were then mounted with antifading mounting medium according to recommended procedures of the manufacturer (Vector) and analyzed by epifluorescence microscopy on a Zeiss microscope coupled to a Nikon camera equipped with a CCD interfaced to a PC (*32, 33*).

Biodistribution and Imaging Studies. Vertebral animal procedures were approved by the appropriate institutional review committee. Balb/c mice (Taconic, Germantown, NY) were anesthetized by metofane inhalation and injected with [^{99m}Tc(CO)$_3$]Tat-peptide complexes (2 μCi in 50−100 μL of saline) via bolus injection through a tail vein. Animals were sacrificed by cervical dislocation at 5, 30, 60, and 120 min postinjection (n = 2−4). Blood samples were obtained by cardiac puncture and tissues harvested rapidly and weighed. Gamma activity in organ samples was counted for 1 min or until two standard deviations of sampling were below 0.5%. Data are expressed as percent of injected dose (% ID) per organ [(organ μCi) (injected μCi)$^{-1}$ × 100] or % ID per gram of tissue [(tissue μCi) (injected μCi)$^{-1}$ (g tissue)$^{-1}$ × 100].

Fluorescent biodistribution was carried out by injecting mice with conjugate **7** (700 μg/50 μL saline) spiked with [^{99m}Tc(CO)$_3$]Tat-peptide complex of **5** (2 μCi) via bolus injection through a tail vein. Mice were sacrificed 30 min postinjection. Organs were harvested, and half of each organ was weighed and gamma counted as described above. The remaining portions of organs were frozen in O.C.T. (Sakura Finetek, Torrence, CA). Cryosections of frozen tissues were fixed with PFA (4%) and washed three times with PBS. Sections were mounted with antifading mounting media (Vector) and analyzed by epifluorescence microscopy.

For imaging studies, Balb/c mice also were lightly anesthetized with metofane inhalation. [^{99m}Tc(CO)$_3$]Tat-peptide complex of **5** (∼500 μCi in 100 μL of saline) was injected via a tail vein into mice positioned under a

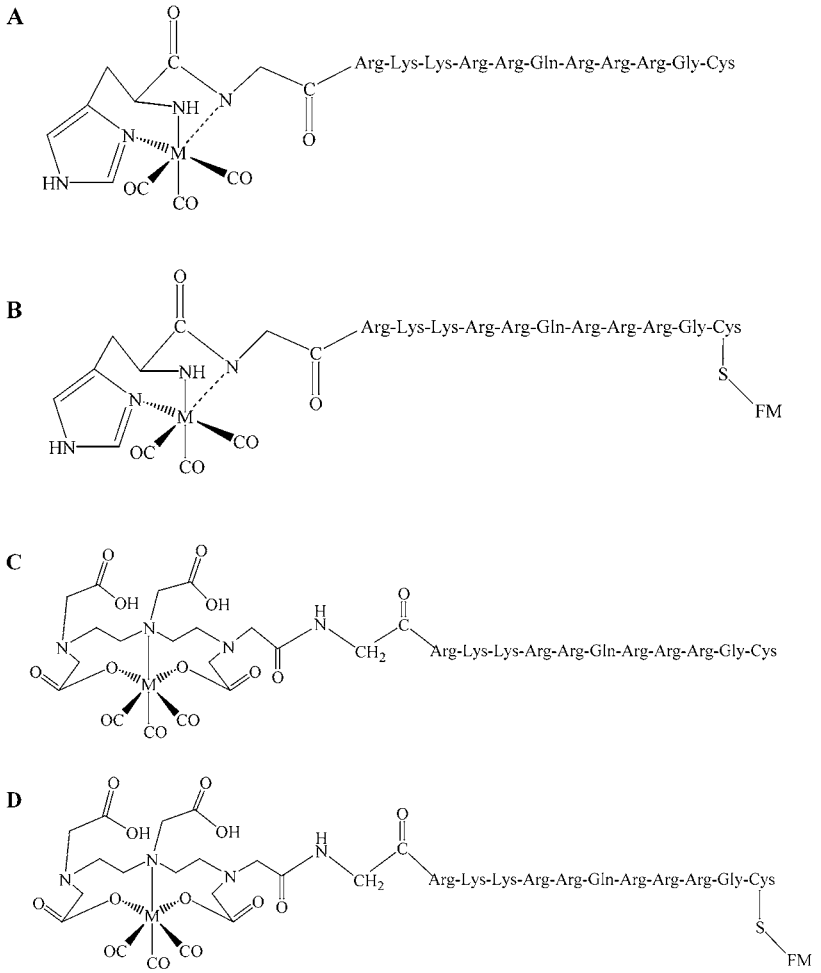


Figure 1. Structure of $[M(CO)_3]$Tat-peptide complex where M represents either ^{99m}Tc or Re and FM represents fluorescein-5-maleimide. (A) Complex of Tat-peptide **1**. (B) Complex of Tat-peptides **5** and **7**. (C) Complex of Tat-peptide **4**. (D) Complex of Tat-peptides **6** and **8**. Note that many isomers are possible with coordination to DTPA (*26*). Only one isomer is presented.

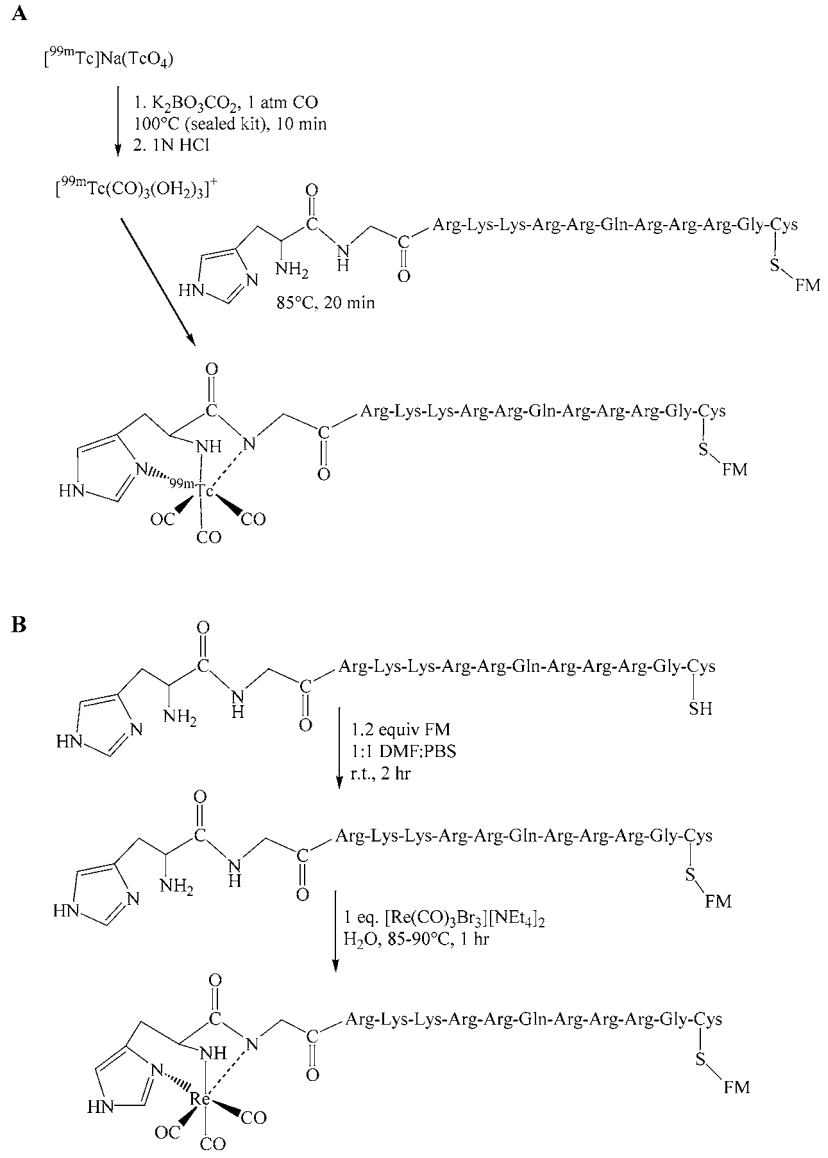
gamma scintillation camera (Siemens Basicam, Siemens Medical Systems, Iselin, NJ; 5 mm pinhole collimator; 20% energy window centered over 140 keV photopeak of Tc-99m). Sequential posterior images of mice were collected for 5 min each at 3 and 30 min postinjection of the radiotracer with the mouse recovering and being reanesthetized just prior to the 30 min timepoint. A 256 × 256 image matrix with correction for radioactive decay was used on a PC platform and standard image analysis software (ImageJ; National Cancer Institute). No corrections were made for scatter or attenuation. Whole body distribution of the complexes is presented with gray scale images.

RESULTS

Chemistry. Tat-peptides **1**−**4** were synthesized by standard solid-phase methods. Fluorescein-5-maleimide was initially coupled to **1** and **4**, and final synthesis of dual-labeled peptides was accomplished by treating with precursors $[^{99m}Tc(CO)_3(OH_2)_3]^+$ and $[Re(CO)_3Br_3][NEt_4]_2$. Incorporation of the $[M(CO)_3]$ into tridentate ligand systems has been shown to result in facial-type coordination with the tricarbonyl ligands covering one face of the metal and the final three ligands coordinating on the opposite face (*20*, *34*). Aromatic amines have been shown to be the most stable chelation source for tricarbonyl species. One major example is utilization of histidine-type molecules for displacement of water and total coordination of $[Tc/Re(CO)_3]$ (*19*, *21*, *35*). In such systems, metal coordination results in formation of 1 or 2 *fac*-five-membered rings depending on availability of the α-amino group adjacent to histidine for coordination with $[M(CO)_3]$ (referred to as filling the 6th coordination site). With respect to $[^{99m}Tc/Re(CO)_3]$Tat-peptides synthesized and presented here, two putative ligands filling the 4th and 5th coordination sites, were donated from histidine itself, whereas the third putative ligand, filling the 6th coordination site, was donated by the α-amine of the adjacent glycine residue (Figure 1). $[^{99m}Tc(CO)_3]$Tat-peptide complexes were synthesized (Scheme 1A) with radiochemical yields and purity (>94% for histidine coordination; >86% for DTPA coordination) determined by radio-TLC and by radiometric RP-HPLC. Two solvent systems were utilized for TLC development. By developing TLC plates in water, $[^{99m}TcO_4]$ was readily distinguished from $[^{99m}Tc(CO)_3]$Tat-complexes, since pertechnetate moved at or near the solvent front (Figure 2A). A methanol:saline:TFA (68:30:2) solvent system was developed to mobilize $[^{99m}Tc(CO)_3]$-Tat-peptides to near the solvent front for revelation of any reduced $[^{99m}Tc]$ species that may be present at the origin (Figure 2B). By combining these two systems, a more accurate TLC analysis of radiochemical yield of products was obtained.

Coordination of $[Re(CO)_3]$ to Tat-peptides was then carried out (Scheme 1B). RP-HPLC analysis and UV detection of $[Re(CO)_3]$Tat-peptide complex **8** produced a complex chromatogram, while $[Re(CO)_3]$Tat-peptide com-

Scheme 1. Coordination of Tat-Peptides to $^{99m}Tc(CO)_3$ (A) and to $Re(CO)_3$ (B)



plex **7** revealed three major peaks (a, b, and c) each comprising doublets (Figure 3A). Retention times between each doublet were resolved by ~0.5 min, while retention times between peaks a and b and between peaks b and c were 1 and 1.5 min, respectively. Peaks a and b were isolated and kept at 4 °C for 1−2 h until reanalysis for interconversion of isomers by RP-HPLC. Peaks a and b each comprised a majority of the species in their respective vials (~70%) with minor amounts of the other peaks appearing within this time interval (data not shown). When kept at −20 °C for multiple days, purified peaks retained these ratios, suggesting slow interconversion of structural isomers at that temperature. The identity of a and b were confirmed by EMS with both peaks having identical mass (*m*/*z*: 2390). We concluded that each peak represented an isomer of facial coordination of the anticipated metal-tricarbonyl complex **7**. This conclusion is consistent with studies of another planar coordination environment, [^{99m}TcO], that previously established the presence of two isomeric species (*13*). Peak c was not readily isolated but interconverted, mainly into peak b. A series of studies was carried out wherein a mixture of peaks b and c was dissolved in water and acetonitrile/water (0, 10, 30, and 50% acetonitrile) at 40 °C for 15 min. Results indicated peak c gradually increased relative to peak b as acetonitrile percentage increased, suggesting peak c is solvent related and perhaps exchanging into the 6th coordination site. Additionally, when the $Re(CO)_3$ labeling reaction was carried out in a potassium phosphate/sodium hydroxide buffer solution (pH = 6.8), peak c was significantly reduced (data not shown).

The presence of doublets was explained by analyzing compound **5**, synthesized by reacting **1** with fluorescein-5-maleimide. RP-HPLC analysis of **5** revealed a single doublet peak (d and e) resolved by 0.4−0.5 min (Figure 3B). Isolation of each peak and subsequent analysis by mass spectrometry revealed doublets d and e had identical mass (*m*/*z*, 2120; calcd, 2120.03) consistent with two isomeric species. Overall, this suggested d and e were isomers resulting from fluorescein labeling and that these isomers were present in [$Re(CO)_3$] coordination complexes as doublets within peaks.

To study stability of his-tagged Tat-peptide chelate conjugates in vitro, a representative [$^{99m}Tc(CO)_3$] complex of **5** was examined by radio-TLC analysis after incubation in buffered solutions ranging from pH 4−9 (Figure 4). As shown, the [$^{99m}Tc(CO)_3$] complex of **5** was stable to transchelation between pH 4 and pH 7, a physiologically relevant range of pH values encountered in vivo. Percent

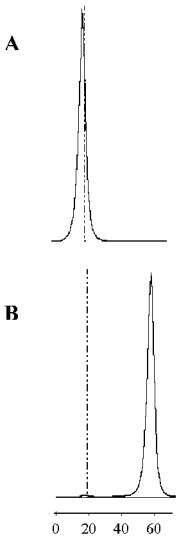


Figure 2. Representative radio-TLC chromatogram of the [^{99m}Tc(CO)$_3$]Tat-peptide complex of **5** in water (A), for identification of remaining pertechnetate, and in methanol:saline:TFA (B), for identification of reduced ^{99m}Tc species. Scale represents millimeters.

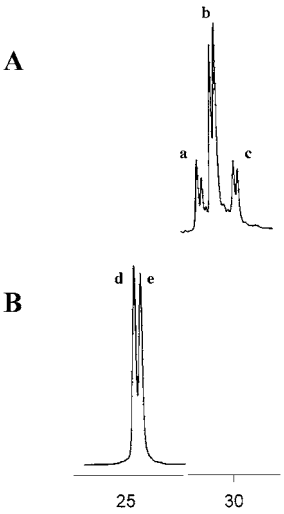


Figure 3. (A) RP-HPLC chromatogram (UV) of [Re(CO)$_3$]Tat-peptide conjugate **7** demonstrating the three major doublet peaks. Peak isolation and mass spectrometry revealed identical masses consistent with the formation of isomers. (B) RP-HPLC chromatogram (UV) of Tat-peptide conjugate **5** demonstrating the single doublet peak. Isolation and mass spectrometry of each peak revealed identical masses consistent with the formation of isomers. Scale represents retention time in min.

intact complex remained >80% over 1 h. The presence of histidine (2.5 mM), a competing physiologic chelator with modest binding affinity, showed only a slight affect below pH 9. Furthermore, the [^{99m}Tc(CO)$_3$] complex of **5** remained >80% intact in the presence of high concentrations of the strong chelator cysteine (2.5 mM), even under alkaline conditions. However, under extreme conditions of alkaline pH (≥9) and highly concentrated EDTA (2.5 mM), only 60% intact complex was observed. Additionally, incubation of the [^{99m}Tc(CO)$_3$] complex of **5** in PBS for 1 and 24 h at 37 °C showed little evidence of transchelation by TLC (data not shown). With incubation for 1 h in fetal bovine serum (FBS), evidence of interaction with serum components began to appear. After a 24 h incubation with FBS, TLC revealed 60% original intact complex present. Overall, these data were generally consistent with published stability studies of aromatic amines coordinated to [^{99m}Tc(CO)$_3$] (*20, 35*).

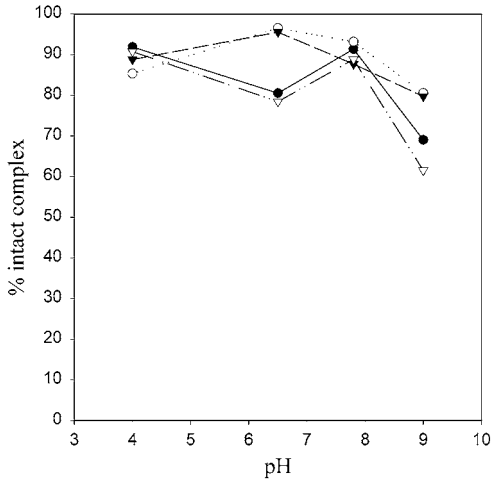


Figure 4. Effect of pH and competing chelation agents on stability of [^{99m}Tc(CO)$_3$]Tat-peptide. Following incubation of [^{99m}Tc(CO)$_3$]Tat-peptide complex **5** for 1 h at 37 °C in HEPES or Tris buffer adjusted to the indicated pH in the absence (●) or presence of cysteine (2.5 mM; ○), histidine (2.5 mM; ▼) or EDTA (2.5 mM; ▽), radiochemical purity (% intact complex) was determined by radio-TLC.

Table 1. Cell Tracer Kinetics of [^{99m}Tc(CO)$_3$]Tat-Peptides with and without Conjugation to FM[a]

peptide	uptake (fmol peptide$_i$ (mg protein)$^{-1}$ (nM$_o$)$^{-1}$)	washout (fmol peptide$_i$ (mg protein)$^{-1}$ (nM$_o$)$^{-1}$)
[Tc(CO)$_3$]**1**	628.0 ± 48.7 (n = 9)	116.0 ± 18.0 (n = 10)
[Tc(CO)$_3$]**5**	93.5 ± 6.8 (n = 14)	35.6 ± 13.8 (n = 11)
[Tc(CO)$_3$]**4**	145.9 ± 14.8 (n = 18)	87.7 ± 7.1 (n = 16)
[Tc(CO)$_3$]**6**	97.7 ± 10.8 (n = 13)	47.7 ± 12.0 (n = 11)

[a] In vitro tracer content following 20 min incubation of Jurkat cells with respective [^{99m}Tc(CO)$_3$]Tat-peptide complexes at 37 °C (uptake) or following 20 min incubation and subsequent 30 min washout in isotope-free MEBSS buffer at 37 °C (washout). Values represent mean ± SEM; n indicates number of determinations.

Additionally, an in vivo stability study was carried out as described. Urine and blood samples at 30 min post-injection indicated that the [^{99m}Tc(CO)$_3$] complex of **5** was >80% intact. However, it was not clear with this analysis whether partial losses of the original complex were a result of conjugate metabolism or coordination of serum components into the 6th coordination site of the [^{99m}Tc(CO)$_3$] complex.

Transport Assay. Using human Jurkat cells, tracer transport studies were performed with [^{99m}Tc(CO)$_3$]Tat-peptide complexes. Both [^{99m}Tc(CO)$_3$]Tat-peptides with fluorescein-5-maleimide conjugated to the C-terminal cysteine (**5**, **6**) and [^{99m}Tc(CO)$_3$]Tat-peptide complexes lacking fluorescein-5-maleimide (**1**, **4**) were compared. All peptides rapidly accumulated into cells over the 20 min uptake period, with Tat-peptides **1** and **4** achieving uptake levels of 628.1 ± 48.7 and 145.9 ± 14.8 fmol (mg protein)$^{-1}$ (nM$_o$)$^{-1}$, respectively, and Tat-peptides **5** and **6** achieving uptake levels of 93.5 ± 6.8 and 97.7 ± 10.8 fmol (mg protein)$^{-1}$ (nM$_o$)$^{-1}$, respectively (Table 1). These levels were compatible with concentration-dependent accumulation of Tat-peptides into cells (*13*). Modest differences were observed between uptake values of single-labeled versus dual-labeled Tat-peptide conjugates in some experiments, while larger differences were observed in others. The cause for uptake variability between experiments was not clearly understood. Nonetheless, these data provided quantitative evidence that

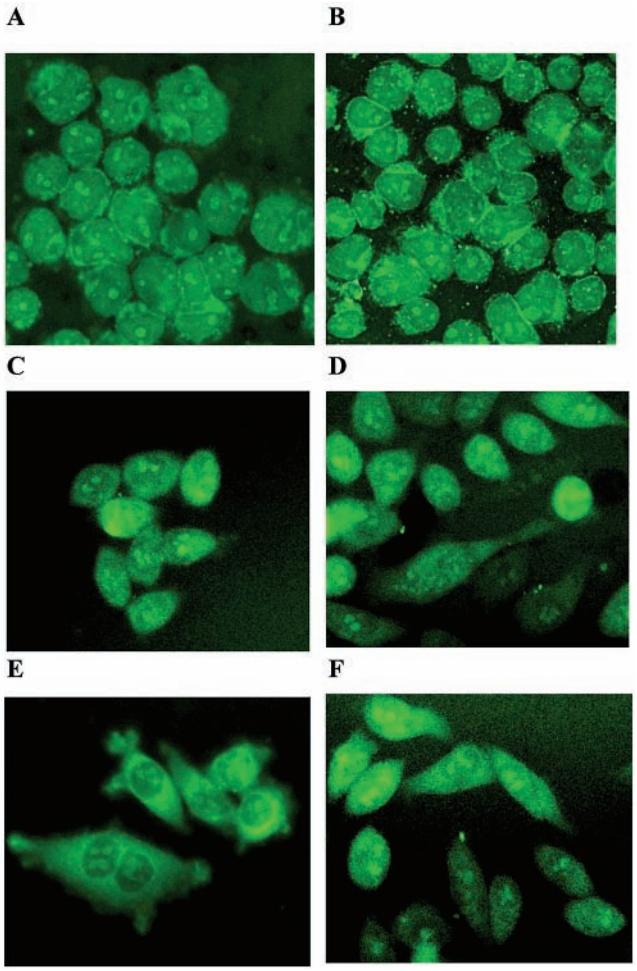


Figure 5. Intracellular localization of Tat-peptide conjugates **5** (A) and **7** (B) in Jurkat cells and conjugates **5**−**8** (C−F, respectively) in KB 3-1 cells. Incubation of cells with Tat-peptide conjugates at 37 °C was carried out for 20 min followed by fixation. Subcellular localization of both single- (A, C, and D) and dual-labeled (B, E, and F) Tat-peptide conjugates was identical both in Jurkat and in KB 3-1 cells.

both single and dual-labeled peptides became similarly cell-associated.

Fluorescence Microscopy. While cell-associated radioactivity was determined in a quantitative manner using radio-tracer experiments, the exact subcellular location of [^{99m}Tc(CO)$_3$]Tat-peptides could not be evaluated by population-based γ-counting techniques. Thus, fluorescein labeled Tat-peptides (**5** and **6**) were used in cell fluorescent uptake experiments to directly determine subcellular localization and thereby prove intracellular translocation of Tat-peptide conjugates. Analogous [Re(CO)$_3$]Tat-peptide chelates (**7** and **8**, respectively) were utilized as isostructural analogues for [^{99m}Tc(CO)$_3$]Tat-peptides to determine the effect of metal coordination on Tat-peptide uptake and subcellular localization. Thus, we hypothesized that these peptides would map the behavior of tracer [^{99m}Tc(CO)$_3$] labeled Tat-peptides inside cells while providing sufficient molar mass to enable direct visualization by fluorescence microscopy. Previous fluorescent cell studies from our laboratory revealed similar translocation efficiency of single-labeled Tat-peptide basic domain into both Jurkat and KB 3−1 cells, resulting in diffuse cytoplasmic fluorescence and focal nucleolar localization (*13*). Thus, both suspension Jurkat and adherent KB 3−1 cells were utilized in the present cell fluorescent study to not only confirm Tat-peptide uptake and localization, but also to determine if qualitative differences could be seen between single-labeled (fluorescein) and dual-labeled (rhenium and fluorescein) Tat-peptide conjugates. No significant differences were observed as both single and dual-labeled peptides exhibited diffuse cytoplasmic and focal nucleolar fluorescence over the entire cell population (Figure 5), similar to analogous Tat-peptides (*13, 36*−*38*). However, perinuclear type staining could also be identified in a subpopulation of KB 3−1 cells that appeared more prominent with dual-labeled Tat-peptide **7** than with single-labeled Tat-peptide **5** (data not shown). It was interesting to note that labeling both ends of Tat-peptide seemed to have little effect on overall peptide uptake and intracellular localization compared to C-terminus labeling with FM alone. Whether single or dual-labeled, Tat-peptide conjugates **1** and **4** localized within cells in a qualitatively similar manner when viewed on the same day and under the same conditions. Overall, fluorescence-staining patterns provided direct evidence for intracellular localization of novel dual-labeled [Re(CO)$_3$]Tat-FM peptide complexes **7** and **8**.

Table 2. Biodistribution of [^{99m}Tc]Tat-Peptide Complex of 5 in Balb/c Mice

	5 min[a]	30 min[b]	60 min[b]	120 min[a]
		% ID/organ		
blood	7.95 ± 0.68	1.92 ± 0.24	0.95 ± 0.07	0.73 ± 0.02
lung	2.61 ± 0.22	1.20 ± 0.10	0.59 ± 0.13	0.54 ± 0.02
liver	42.32 ± 3.56	65.66 ± 3.11	62.02 ± 7.51	72.37 ± 3.06
spleen	1.25 ± 0.06	1.19 ± 0.05	0.98 ± 0.09	1.06 ± 0.10
kidney	14.05 ± 0.86	23.16 ± 0.91	19.38 ± 2.81	28.85 ± 1.74
muscle	17.94 ± 1.99	6.74 ± 0.20	3.55 ± 0.13	2.39 ± 0.07
fat	1.55 ± 0.20	0.51 ± 0.05	0.41 ± 0.06	0.31 ± 0.01
heart	0.62 ± 0.08	0.13 ± 0.01	0.09 ± 0.01	0.07 ± 0.01
brain	0.10 ± 0.01	0.02 ± 0.00	0.02 ± 0.01	0.01 ± 0.00
bone	17.52 ± 0.68	14.33 ± 1.26	11.71 ± 0.49	11.33 ± 1.10
small intestine	6.21 ± 0.39	1.55 ± 0.03	1.20 ± 0.04	1.01 ± 0.07
large intestine	2.18 ± 0.25	0.57 ± 0.02	0.39 ± 0.01	0.46 ± 0.05
skin	7.15 ± 0.18	6.25 ± 0.08	3.20 ± 0.61	1.96 ± 0.17
		% ID/gram		
blood	5.73 ± 0.27	1.40 ± 0.13	0.75 ± 0.07	0.53 ± 0.03
lung	19.93 ± 0.98	9.07 ± 1.47	5.01 ± 1.12	4.71 ± 0.34
liver	32.11 ± 3.70	51.62 ± 0.04	55.32 ± 4.28	56.85 ± 1.80
spleen	13.98 ± 0.22	12.90 ± 0.35	12.04 ± 0.36	12.00 ± 1.14
kidney	41.67 ± 4.49	70.55 ± 2.09	66.67 ± 6.43	84.45 ± 0.67
muscle	2.58 ± 0.19	0.99 ± 0.06	0.56 ± 0.01	0.35 ± 0.02
fat	1.36 ± 0.23	0.45 ± 0.03	0.38 ± 0.05	0.27 ± 0.01
heart	5.79 ± 0.36	1.25 ± 0.03	0.98 ± 0.06	0.72 ± 0.06
brain	0.27 ± 0.02	0.06 ± 0.01	0.06 ± 0.01	0.04 ± 0.01
bone	5.07 ± 0.10	4.19 ± 0.23	3.67 ± 0.10	3.29 ± 0.24
small intestine	4.91 ± 0.22	1.29 ± 0.13	1.15 ± 0.01	0.83 ± 0.09
large intestine	3.06 ± 0.11	0.84 ± 0.08	0.57 ± 0.01	0.69 ± 0.07
skin	3.11 ± 0.05	2.75 ± 0.06	1.50 ± 0.26	0.85 ± 0.05

[a] Mean ± SEM of three determinations. [b] Mean ± range of two determinations. Error values of 0.00 indicate <0.005.

Biodistribution and Imaging. Biodistribution studies were performed to monitor the amount of radioactivity associated with organs or tissues at 5, 30, 60, and 120 min postinjection ($n = 2$−4 each). Results are presented as % ID/organ and % ID/gm (Tables 2−5). For the [^{99m}Tc(CO)$_3$]Tat-peptide-FM complex of **5**, initial uptake was high in liver and kidneys and even continued to accumulate over the 120 min observation period (Figure 6A; Table 2). To confirm that the C-terminal FM was not cleaved, thereby exposing a reduced cysteine and causing prolonged retention through nonspecific binding or conjugation reactions, biodistribution studies were also carried out utilizing [^{99m}Tc(CO)$_3$]Tat-peptide complex of **2**, a conjugate devoid of the C-terminal glycine-cysteine

Table 3. Biodistribution of [^{99m}Tc]Tat-Peptide Complex of 2 in Balb/c Mice

	5 min	30 min	60 min	120 min[a]
		% ID/organ		
blood	10.47 ± 0.17	3.65 ± 0.22	2.67 ± 0.15	2.53 ± 0.14
lung	2.09 ± 0.37	0.71 ± 0.01	0.51 ± 0.02	0.33 ± 0.01
liver	41.73 ± 1.84	57.45 ± 1.75	60.17 ± 1.44	59.71 ± 2.72
spleen	1.02 ± 0.01	0.82 ± 0.01	0.75 ± 0.06	0.77 ± 0.02
kidney	13.15 ± 1.22	21.92 ± 1.23	23.67 ± 0.98	25.47 ± 1.02
muscle	17.83 ± 0.19	8.58 ± 0.71	5.66 ± 0.25	3.64 ± 0.21
fat	1.93 ± 0.13	0.91 ± 0.07	0.47 ± 0.04	0.41 ± 0.02
heart	0.55 ± 0.04	0.17 ± 0.01	0.12 ± 0.01	0.08 ± 0.00
brain	0.14 ± 0.02	0.05 ± 0.00	0.04 ± 0.00	0.03 ± 0.00
bone	19.75 ± 0.55	18.38 ± 0.44	18.14 ± 0.47	16.10 ± 0.57
small intestine	6.54 ± 0.09	2.35 ± 0.08	2.30 ± 0.13	2.35 ± 0.08
large intestine	2.70 ± 0.13	1.71 ± 0.05	1.98 ± 0.12	2.79 ± 0.20
skin	8.48 ± 0.48	7.83 ± 0.06	5.41 ± 0.35	2.92 ± 0.03
		% ID/gram		
blood	8.08 ± 0.54	2.98 ± 0.13	2.15 ± 0.06	2.00 ± 0.15
lung	17.65 ± 3.65	6.11 ± 0.33	4.30 ± 0.16	2.75 ± 0.10
liver	33.95 ± 2.59	51.56 ± 4.05	54.15 ± 2.85	56.56 ± 2.16
spleen	14.81 ± 0.66	11.05 ± 0.39	10.52 ± 0.93	11.43 ± 0.91
kidney	43.67 ± 4.89	73.36 ± 3.55	83.03 ± 3.01	83.76 ± 2.94
muscle	2.75 ± 0.11	1.42 ± 0.20	0.91 ± 0.05	0.58 ± 0.05
fat	1.78 ± 0.11	0.89 ± 0.05	0.45 ± 0.05	0.39 ± 0.03
heart	6.13 ± 0.77	1.80 ± 0.11	1.27 ± 0.06	0.87 ± 0.06
brain	0.38 ± 0.07	0.12 ± 0.02	0.10 ± 0.02	0.07 ± 0.00
bone	6.09 ± 0.34	6.03 ± 0.31	5.86 ± 0.28	5.07 ± 0.18
small intestine	4.92 ± 0.36	1.97 ± 0.19	2.03 ± 0.09	2.06 ± 0.10
large intestine	3.44 ± 0.38	2.14 ± 0.05	2.55 ± 0.17	3.97 ± 0.22
skin	3.90 ± 0.08	3.86 ± 0.22	2.62 ± 0.17	1.39 ± 0.06

[a] Mean ± SEM of four determinations. Mean ± SEM of three determinations at all other time points. Error values of 0.00 indicate <0.005.

Table 4. Biodistribution of [^{99m}Tc]Tat-Peptide Complex of 4 in Balb/c Mice[a]

	5 min	30 min	60 min	120 min
		% ID/organ		
blood	13.08 ± 0.22	7.03 ± 0.14	5.53 ± 0.20	4.56 ± 0.01
lung	2.50 ± 0.27	1.54 ± 0.03	1.01 ± 0.08	0.98 ± 0.03
liver	38.02 ± 3.52	38.82 ± 0.55	42.90 ± 3.21	44.67 ± 2.30
spleen	1.39 ± 0.11	1.62 ± 0.02	1.60 ± 0.05	1.40 ± 0.12
kidney	18.18 ± 0.16	24.77 ± 1.16	27.25 ± 1.03	29.99 ± 1.17
muscle	13.77 ± 0.40	12.33 ± 0.44	9.12 ± 0.23	8.06 ± 0.37
fat	1.82 ± 0.37	1.52 ± 0.18	0.96 ± 0.13	0.97 ± 0.23
heart	0.75 ± 0.02	0.37 ± 0.03	0.29 ± 0.00	0.24 ± 0.01
brain	0.14 ± 0.04	0.08 ± 0.01	0.06 ± 0.00	0.05 ± 0.01
bone	8.56 ± 8.71	18.74 ± 1.18	19.19 ± 3.26	17.46 ± 1.12
small intestine	7.30 ± 0.16	5.37 ± 0.02	4.93 ± 0.11	3.22 ± 1.40
large intestine	2.17 ± 0.13	1.64 ± 0.18	1.18 ± 0.14	3.44 ± 1.43
skin	7.11 ± 0.20	8.22 ± 0.03	6.41 ± 0.60	4.63 ± 0.09
		% ID/gram		
blood	9.84 ± 0.31	5.38 ± 0.10	4.19 ± 0.08	3.63 ± 0.00
lung	21.06 ± 1.92	13.77 ± 1.37	8.57 ± 0.07	8.14 ± 0.29
liver	31.26 ± 0.18	35.23 ± 0.29	36.22 ± 0.95	41.35 ± 4.5
spleen	17.19 ± 0.56	21.66 ± 2.14	19.80 ± 1.81	19.97 ± 0.67
kidney	53.78 ± 1.46	74.70 ± 5.83	86.72 ± 4.38	103.04 ± 5.47
muscle	2.07 ± 0.04	1.89 ± 0.07	1.38 ± 0.01	1.28 ± 0.05
fat	1.66 ± 0.41	1.40 ± 0.17	0.87 ± 0.10	0.92 ± 0.21
heart	6.73 ± 0.15	4.09 ± 0.15	3.00 ± 0.05	2.70 ± 0.01
brain	0.35 ± 0.09	0.22 ± 0.02	0.14 ± 0.00	0.15 ± 0.03
bone	2.45 ± 2.50	5.74 ± 0.37	5.80 ± 0.89	5.55 ± 0.33
small intestine	5.71 ± 0.13	4.77 ± 0.04	4.25 ± 0.27	3.50 ± 0.40
large intestine	2.92 ± 0.14	1.96 ± 0.18	1.73 ± 0.19	3.68 ± 0.70
skin	3.21 ± 0.07	3.78 ± 0.01	2.91 ± 0.22	2.21 ± 0.05

[a] Mean ± range of two determinations at each time point. Error values of 0.00 indicate <0.005.

dipeptide. Similar kidney and liver accumulation was observed (Figure 6B; Table 3). To determine if histidine

Table 5. Biodistribution of [^{99m}Tc]Tat-Peptide Complex of 6 in Balb/c Mice

	5 min[a]	30 min	60 min	120 min
		% ID/organ		
blood	15.96 ± 0.06	9.70 ± 0.34	7.72 ± 0.08	5.51 ± 0.22
lung	1.65 ± 0.12	1.12 ± 0.04	0.79 ± 0.03	0.52 ± 0.06
liver	16.85 ± 0.49	17.58 ± 0.68	22.29 ± 0.27	23.53 ± 0.99
spleen	0.64 ± 0.01	0.36 ± 0.01	0.35 ± 0.00	0.32 ± 0.01
kidney	20.20 ± 0.76	32.37 ± 0.06	37.50 ± 1.05	47.00 ± 2.62
muscle	17.04 ± 1.29	13.25 ± 0.39	8.76 ± 0.30	4.93 ± 0.23
fat	2.26 ± 0.24	1.05 ± 0.05	0.72 ± 0.02	0.68 ± 0.00
heart	0.72 ± 0.01	0.37 ± 0.02	0.27 ± 0.01	0.19 ± 0.01
brain	0.16 ± 0.00	0.10 ± 0.01	0.06 ± 0.01	0.06 ± 0.01
bone	14.58 ± 0.90	12.05 ± 0.03	10.86 ± 0.44	8.94 ± 0.66
small intestine	6.47 ± 0.05	3.48 ± 0.15	3.14 ± 0.03	2.27 ± 0.08
large intestine	2.40 ± 0.00	1.23 ± 0.02	0.96 ± 0.03	0.99 ± 0.03
skin	7.53 ± 0.52	9.18 ± 0.08	7.55 ± 0.42	5.02 ± 0.16
		% ID/gram		
blood	11.29 ± 0.54	6.90 ± 0.11	5.17 ± 0.28	3.72 ± 0.03
lung	13.32 ± 1.82	9.48 ± 0.42	6.01 ± 0.02	2.28 ± 1.76
liver	14.51 ± 1.42	16.21 ± 0.15	18.78 ± 2.29	19.45 ± 0.30
spleen	8.86 ± 0.84	5.01 ± 0.18	4.34 ± 0.26	4.16 ± 0.30
kidney	54.49 ± 2.87	90.51 ± 5.58	103.23 ± 13.89	124.65 ± 0.17
muscle	2.40 ± 0.10	1.89 ± 0.09	1.18 ± 0.12	0.67 ± 0.01
fat	1.94 ± 0.30	0.90 ± 0.03	0.58 ± 0.02	0.55 ± 0.02
heart	7.16 ± 0.31	3.50 ± 0.22	2.41 ± 0.13	1.71 ± 0.05
brain	0.43 ± 0.04	0.25 ± 0.04	0.16 ± 0.01	0.15 ± 0.00
bone	4.11 ± 0.19	3.43 ± 0.08	2.92 ± 0.31	2.42 ± 0.10
small intestine	5.41 ± 0.56	3.02 ± 0.01	2.73 ± 0.31	1.86 ± 0.05
large intestine	3.15 ± 0.12	1.76 ± 0.13	1.36 ± 0.08	1.48 ± 0.07
skin	3.18 ± 0.16	3.92 ± 0.04	3.04 ± 0.37	2.04 ± 0.00

[a] Mean ± SEM of three determinations. Mean ± range of two determinations at all other time points. Error values of 0.00 indicate <0.005.

coordination affected retention, a separate and classical chelation core, DTPA, was N-conjugated in place of the N-terminal histidine to **4**, which contained a free C-terminal thiol, or to **6**, which contained an FM-conjugated C-terminal thiol. After radiolabeling, biodistribution analysis of the [^{99m}Tc(CO)$_3$]Tat-peptide complexes of both **4** and **6** revealed a decrease in liver retention relative to complex of **5**, but persistent accumulation of radioactivity in the kidneys (Figures 6C and 6D; Tables 4 and 5). Brain uptake of all peptide conjugates was consistently low (Tables 2−5). Of note, muscle and bone uptakes of each complex were modestly high. In general, bone clearance of complexes of **2** and **4** (single-labeled Tat-peptides) was minimal whereas clearance of complexes of **5** and **6** (dual-labeled Tat-peptides) was greater. Scintigraphic images, obtained 3 and 30 min post-intravenous injection of [^{99m}Tc(CO)$_3$]Tat-peptide-FM complex of **5** into Balb/c mice, visually confirmed these results (Figure 7).

To further analyze biodistribution results, fluorescent microscopy was used to assess intracellular localization in vivo 30 min after intravenous coinjection of dual-labeled [Re(CO)$_3$]Tat-peptide-FM conjugate **7** spiked with the [^{99m}Tc(CO)$_3$]Tat-peptide−FM complex of **5**. [^{99m}Tc(CO)$_3$]Tat-peptide−FM was coinjected as an internal control to correlate results with radiometric biodistribution data. Fluorescence intensity, as observed by fluorescence microscopy (Figure 8), correlated with γ-counts from the biodistribution studies revealing high intracellular fluorescence in kidneys and liver and no significant fluorescence in brain tissue.

DISCUSSION

Design of Novel Dual-Labeled Tat-Peptides. The ability of permeation sequences such as HIV-1 Tat basic domain peptides to transport various cargo into many

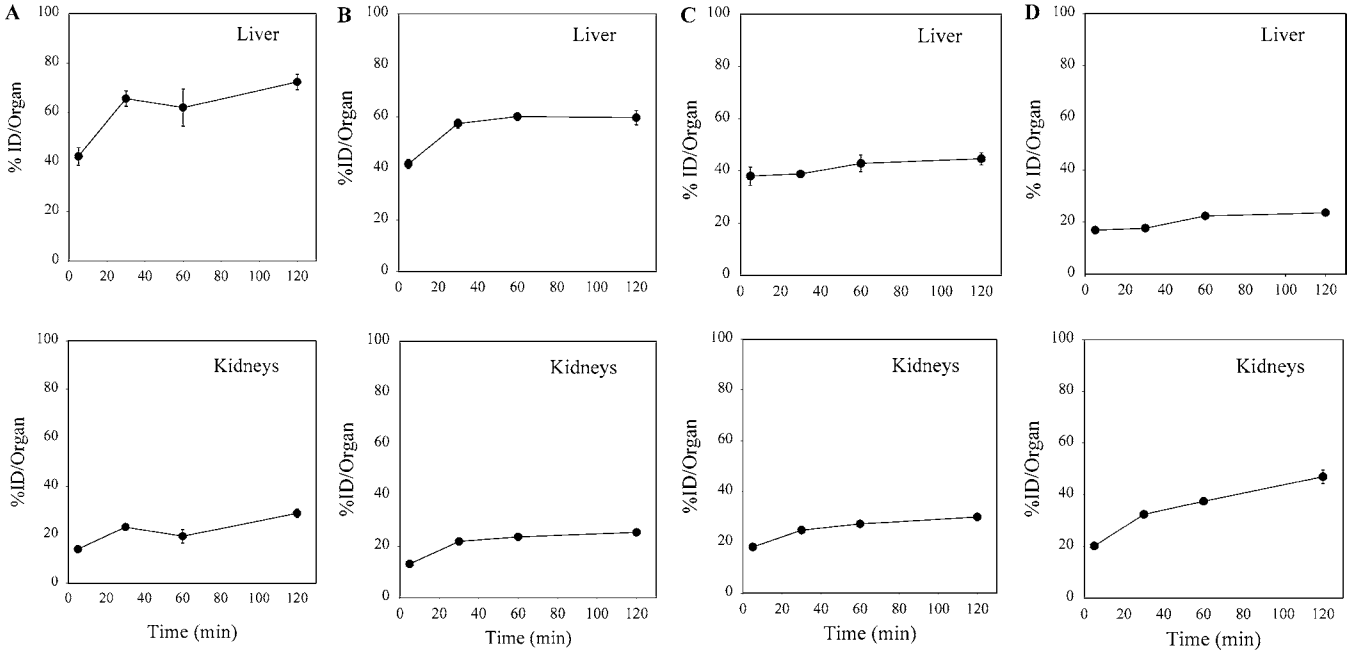


Figure 6. Biodistribution time-activity curves of liver and kidneys showing in vivo uptake of [^{99m}Tc(CO)$_3$]Tat-peptides complexes of **5**, **2**, **4**, and **6** (A−D, respectively). Following bolus intravenous injection, tissues were harvested and counted at 5, 30, 60, and 120 min. Error bars smaller than symbol when not shown.

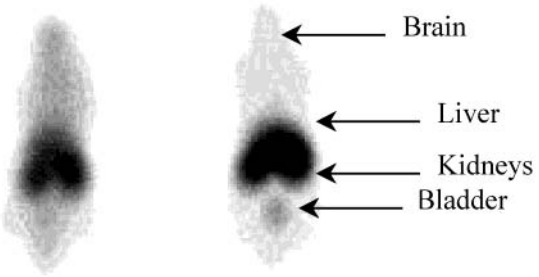


Figure 7. Scintigraphic gray scale images of [^{99m}Tc]Tat-peptide complex of **5** in a Balb/c mouse. Following bolus intravenous injection, posterior images of the mouse were obtained with a gamma scintillation camera. Representative planar images obtained 3 min (left) and 30 min (right) postinjection are shown. Rapid whole body distribution is followed by predominantly hepatic and renal retention of the [^{99m}Tc]Tat-peptide complex and appearance in the urinary bladder.

types of cells has led to wide utilization of permeation peptides in various fields of research (*11, 39, 40*), including exploration of their potential as molecular imaging reagents (*7, 13*). Using [^{99m}Tc/Re(CO)$_3$]-labeled Tat-peptides along with fluorescein-5-maleimide, we have synthesized novel dual-labeled Tat-peptides to quantitatively and qualitatively study cell tracer kinetics, intracellular localization and murine biodistribution. Such a strategy could be applied generally to various N-terminal his-tagged permeation peptide sequences.

[^{99m}Tc(CO)$_3$(OH$_2$)$_3$]$^+$ is an ideal complex for chelation of peptides because simple and relatively facile coordination can be achieved with an N-terminal histidine—an amino acid which is readily added to any peptide during solid-phase synthesis or tagged to polypeptides in common cloning vectors (*19*). Coordination was carried out at atmospheric pressures and reasonable temperatures, a necessity for practical and wide use of radiolabeling (*20, 34*). Additionally, [^{99m}Tc(CO)$_3$(OH$_2$)$_3$]$^+$ has a stable and small donor core (*21*) that is less likely to disrupt secondary structure of the peptide compared to conventional macrocyclic chelators. Further, by utilizing N-terminal histidine-glycine dipeptides for labeling, a less

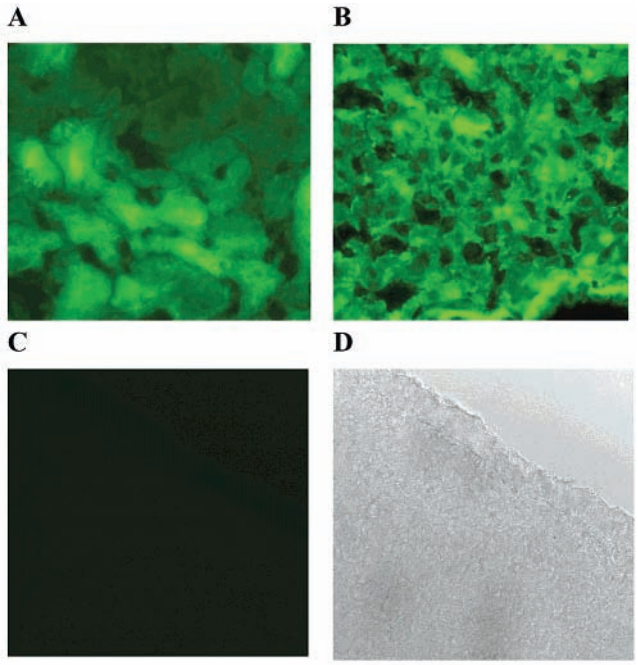


Figure 8. Fluorescence distribution in vivo of [Re(CO)$_3$]Tat-peptide-FM complex **7** spiked with [^{99m}Tc(CO)$_3$]Tat-peptide−FM complex of **5**. Organs were harvested and assayed both by gamma counting and by epifluorescence microscopy. Panels compare fluorescent signal in kidney (A) and liver (B) to brain (C). Panel D represents phase contrast microscopy of the identical brain tissue section as in panel C. Liver and brain fluorescent pictures were obtained at identical magnification and exposure times. The kidney fluorescent picture was taken at an identical magnification as liver and brain, but at a lower exposure time due to intense intracellular fluorescent signal within the tissue.

restricted metal coordination site was established compared to macrocyclic chelators. Thus, Re, a slightly larger metal than ^{99m}Tc, could easily be accommodated by the dipeptide tag and enable a more direct comparison between technetium and rhenium complexes. By examining overall trends, the dual-labeled [^{99m}Tc(CO)$_3$]Tat-

peptide−FM complex of **5** resulted in somewhat lower uptake values than its corresponding single-labeled [^{99m}Tc(CO)$_3$]Tat-peptide; but both complexes retained about the same percentage of radioactivity after a 30 min washout. Reasons for the observed quantitative variations in uptake were not clearly understood, but point to details in cellular mechanisms of translocation requiring further study. However, subcellular localization of the dual-labeled peptides was unaffected by labeling both termini of the peptide. Both Tat-peptides **5** and **7** localized to the nucleus and showed diffuse cytoplasmic fluorescence (Figure 5) as seen previously with single-labeled Tat-peptides. Transport assays and fluorescent cell uptake studies collectively suggested that the mechanism of Tat-peptide translocation is not wholly dependent on the C- or N-termini, although quantitative uptake of dual-labeled [^{99m}Tc(CO)$_3$]Tat-peptide−FM complex of **5** was lower than single-labeled [^{99m}Tc(CO)$_3$]Tat-peptide−FM complex of **1**. Tat-peptide translocation has been suggested to occur via a facial-type interaction wherein the arginine residues associate with the membrane and cause cellular internalization of the entire peptide (*41*). Florescein-5-maleimide, a slightly bulky and hydrophobic moiety, could effect a change in conformation or membrane−peptide interaction that would decrease the efficiency of Tat-peptide basic domain translocation. However, further analysis would be necessary to determine if the reduced quantity of internalized peptide resulted from such an induced conformational change or interaction.

In Vivo Distribution of Dual-Labeled Tat-Peptide. As presented (Figures 6A and 6B), biodistribution utilizing [^{99m}Tc(CO)$_3$]Tat-peptide complexes of **5** and **2** resulted in accumulation of radioactivity in the liver and kidneys. Since the only difference between Tat-peptide complexes of **5** and **2** was the presence of a masked C-terminal cysteine (**5**), retention was not likely due to FM degradation, a reaction that would reveal a free thiol for interaction with other proteins or redox enzymes. Previous [^{99m}Tc(CO)$_3$] studies have indicated that accumulation in liver and kidneys can occur with bidentate coordinated ligands (*34*). Because accumulation of [^{99m}Tc(CO)$_3$]Tat-peptide complexes of **5** and **2** occurred, we hypothesized that the α amine of glycine was coordinated in a weaker fashion to the [^{99m}Tc(CO)$_3$] than the histidine ligands, allowing for exchange with stronger competing ligands. With such a coordination site, biological competitors could potentially compete and coordinate to [^{99m}Tc(CO)$_3$], thus effectively trapping the [^{99m}Tc(CO)$_3$]Tat-peptide in tissues. To test this hypothesis, we coupled DTPA, a chelator with four strong chelating ligands for [^{99m}Tc(CO)$_3$] coordination, to form single-labeled [^{99m}Tc(CO)$_3$]Tat-peptide complexes of **4** and dual-labeled [^{99m}Tc(CO)$_3$]Tat-peptide complexes of **6** for comparative biodistribution with two different chelating groups. Biodistribution of [^{99m}Tc(CO)$_3$]Tat-peptide of **4** revealed a slightly lower initial uptake in the liver that remained constant over time. Initial kidney uptake and accumulation remained similar to complex of **5**. Biodistribution of [^{99m}Tc(CO)$_3$]Tat-peptide of **6** revealed an even more significant reduction (greater than 50%) in initial uptake and retention in the liver compared to [^{99m}Tc(CO)$_3$]Tat-peptide complex of **5**. Instead of accumulation being 72% ID/organ at 120 min, liver radioactivity remained ∼20%. Unexpectedly, radioactivity in the kidney continued to increase throughout the biodistribution time period even though radioactivity in the liver remained consistently lower. These data suggested that Tat-peptide uptake and clearance were strongly influenced by the chelation core, as well as by the coordination of the terminal thiol, rather than being dominated by the permeation peptide itself. Previously published experiments (*13*) utilizing an ϵ-Lys-Gly-Cys [^{99m}TcO]-labeled Tat-peptide lend support to the effect of chelation cores on biodistribution. In those experiments, liver uptake occurred over the first 30 min, similar to the present complexes, with a peak accumulation around 30%. However, in contrast to his[^{99m}Tc(CO)$_3$] coordination, significant clearance from the liver followed peak accumulation, continuing throughout the duration of the experiment for a final % ID/organ of ∼18% at 120 min (*13*). These results are in accord with other observations showing that chelation cores influence pharmacokinetics for a variety of peptide imaging agents (*34, 42−44*). Additionally, these and other studies (*13, 39, 45*) are consistent with our observation that Tat-peptide is characterized by high blood clearance rates, indicating the need for strategies, such as introduction of binding moieties or cleavable domains, that would slow blood clearance rates and increase targeted delivery.

To further determine the utility in vivo of dual-labeled Tat-peptides, fluorescence biodistribution studies were assessed utilizing dual-tagged [Re(CO)$_3$]Tat-peptide−FM complexes. As with radiometric biodistribution and imaging data, the highest fluorescence intensity was observed in liver and kidney tissue with no significant fluorescence intensity in brain tissue. The present results contrast with a previous report suggesting high brain uptake and blood−brain barrier penetration of a similar Tat basic domain fused to β-galactosidase (*9*). In those experiments, β-galactosidase substrate (X-gal) was incubated on brain slices for 16 h and interpreted to indicate high penetration of the blood−brain barrier by the functional fusion protein containing the peptide transduction domain. However, the amount of protein that actually entered the brain parenchyma was not directly measured, and it remains possible that the enzymatically amplified β-galactosidase signal overestimated the quantity of polypeptide penetrating the brain. Other studies (*46, 47*) also have suggested enhanced brain uptake of a biologically active molecule, doxorubicin, when conjugated to permeation peptides. However, these data were obtained mainly utilizing in situ brain perfusion techniques, not intravenous injection as presented here. When intravenous injection was utilized (*46*), the concentration of doxorubicin in the heart and plasma remained significantly greater than in the brain. Additionally, doxorubicin clearance from the brain was slightly greater upon conjugation with the permeation peptide than without. Thus, for delivery of biologically active molecules to the brain utilizing permeation peptides, these and our data suggest that intravenous injection of conjugated permeation peptides may not be an effective method of administration.

CONCLUSION

In summary, we have synthesized and characterized novel dual-labeled Tat-peptides. Evaluation of fluorescein-5-maleimide-labeled [^{99m}Tc(CO)$_3$]Tat-peptide complexes has provided a tool for studying the same peptide both qualitatively by fluorescence microscopy and quantitatively by radiometric analysis in vitro as well as in vivo. As suggested by the radiotracer transport assays indicating concentrative cellular accumulation, a dual-labeled peptide allowed easy confirmation that measured activity was largely due to peptide translocation into the cell interior both in vitro and in vivo. Of significance, following intravenous administration, little brain penetration

of these permeation peptides was observed in mice either by radiometric or fluorescence analyses. These data will assist the design and characterization of permeation sequences, such as the choice of chelation moiety and incorporation of cleavable domains for targeted intracellular drug delivery. The dual-labeled permeation-peptide design also will provide rigor to the study of novel permeation-peptide modifications by the potential to confirm qualitatively and quantitatively the impact of effector moieties on uptake at the target site.

ACKNOWLEDGMENT

We thank Delynn Silvestros and Tracy Nelson for technical assistance. This work was supported by grants from the National Institutes of Health (RO1 CA82841 and P50 CA94056).

LITERATURE CITED

(1) Liu, S., and Edwards, D. (1999) ^{99m}Tc-labeled small peptides as diagnostic radiopharmaceuticals. *Chem Rev. 99*, 2235−2268.

(2) Schwarze, S., Hruska, K., and Dowdy, S. (2000) Protein transduction: unrestricted delivery into all cells? *Trends Cell Biol. 10*, 290−295.

(3) Frankel, A., and Pabo, C. (1988) Cellular uptake of the tat protein from human immunodeficiency virus. *Cell 55*, 1189−1193.

(4) Green, M., and Loewenstein, P. (1988) Autonomous functional domains of chemically synthesized human immunodeficiency virus tat trans-activator protein. *Cell 55*, 1179−1188.

(5) Schluesener, H. (1996) Protection against experimental nervous system autoimmune diseases by a human immunodeficeincy virus-1 Tat peptide-based polyvalent vaccine. *J. Neurosci. Res. 46*, 258−262.

(6) Vives, E., Brodin, P., and Lebleu, B. (1997) A truncated HIV-1 Tat protein basic domain rapidly translocates through the plasma membrane and accumulates in the cell nucleus. *J. Biol. Chem. 272*, 16010−16017.

(7) Josephson, L., Tung, C.-H., Moore, A., and Weissleder, R. (1999) High-efficiency intracellular magnetic labeling with novel superparamagnetic-Tat peptide conjugates. *Bioconjugate Chem. 10*, 186−191.

(8) Vocero-Akbani, A., Heyden, N., Lissy, N., Ratner, L., and Dowdy, S. (1999) Killing HIV-infected cells by transduction with an HIV protease-activated caspase-3 protein. *Nat. Med. 5*, 29−33.

(9) Schwarze, S., Ho, A., Vocero-Akbani, A., and Dowdy, S. (1999) In vivo protein transduction: delivery of a biologically active protein into the mouse. *Science 285*, 1569−1572.

(10) Bhorade, R., Weissleder, R., Nakakoshi, T., Moore, A., and Tung, C. (2000) Macrocyclic chelators with paramagnetic cations are internalized in to mammalian cells via a HIV−Tat derived membrane translocation peptide. *Bioconjugate Chem. 11*, 301−305.

(11) Fischer, P. M., Krausz, E., and Lane, D. P. (2001) Cellular delivery of impermeable effector molecules in the form of conjugates with peptides capable of mediating membrane translocation. *Bioconjugate Chem. 12*, 825−841.

(12) Wunderbaldinger, P., Josephson, L., and Weissleder, R. (2002) Tat peptide directs enhanced clearance and hepatic permeability of magnetic nanoparticles. *Bioconjugate Chem. 13*, 264−268.

(13) Polyakov, V., Sharma, V., Dahlheimer, J., Pica, C., Luker, G., and Piwnica-Worms, D. (2000) Novel Tat-peptide chelates for direct transduction of technetium-99m and rhenium into human cells for imaging and radiotherapy. *Bioconjugate Chem. 11*, 762−771.

(14) Schwochau, K. (1994) Technetium radiopharmaceuticals − fundamentals, synthesis, structure and development. *Angew. Chem., Int. Ed. Engl. 33*, 2258−2267.

(15) Hom, R., and Katzenellenbogen, J. (1997) Technetium-99m-labeled receptor-specific small-molecule radiopharmaceuticals: recent developments and encouraging results. *Nucl. Med. Biol. 24*, 485−498.

(16) Jurisson, S., and Lydon, J. (1999) Potential technetium small molecule radipharmaceuticals. *Chem. Rev. 99*, 2205−2218.

(17) Volkert, W., and Hoffman, T. (1999) Therapeutic radiopharmaceuticals. *Chem. Rev. 99*, 2269−2292.

(18) Schibli, R., Katti, K. V., Volkert, W. A., and Rarnes, C. L. (2001) Development of novel water-soluble, organometallic compunds for potential use in nuclear medicine: synthesis, characterization, and ^{1}H and ^{31}P NMR investigations of the complexes *fac*-[ReBr(CO)$_3$L] (L = Bis(bis(hydroxymethyl)-phosphino)ethane, Bis(bis(hydroxymethyl)phosphino)benzene). *Inorg. Chem. 40*, 2358−2362.

(19) Waibel, R., Alberto, R., Willuda, J., Finnern, R., Schibli, R., Stichelberger, A., Egli, A., Abram, U., Mach, J.-P., Pluckthun, A. et al. (1999) Stable one-step technetium-99m labeling of His-tagged recombinant proteins with a novel Tc(I)-carbonyl complex. *Nat. Biotech. 17*, 897−901.

(20) Alberto, R., Schibli, R., Egli, A., and Schubiger, A. (1998) A novel organometallic aqua complex of technetium for the labeling of biomolecules: synthesis of [^{99m}Tc(OH$_2$)$_3$(CO)$_3$]$^+$ from [^{99m}TcO$_4$]$^-$ in aqueous solution and its reaction with a bifunctional ligand. *J. Am. Chem. Soc. 120*, 7987−7988.

(21) Pietzsch, H.-J., Gupta, A., Reisgys, M., Drews, A., Seifert, S., Syhre, R., Spies, H., Alberto, R., Abram, U., Schubiger, P. A. et al. (2000) Chemical and biological characterization of technetium(I) and rhenium(I) tricarbonyl complexes with dithioether ligands serving as linkers for coupling the Tc(CO)$_3$ and Re(CO)$_3$ moieties to biologically active molecules. *Bioconjugate Chem. 11*, 414−424.

(22) Alberto, R., Ortner, K., Wheatley, N., Schibli, R., and Schubiger, A. P. (2001) Synthesis and properties of boranocarbonate: a convenient in situ CO source for the aqueous preparation of [^{99m}Tc(OH$_2$)$_3$(CO)$_3$]$^+$. *J Am Chem Soc. 123*, 3135−3136.

(23) Achilefu, S., Wilhelm, R. R., Jimenez, H. N., Schmidt, M. A., and Srinivasan, A. (2000) A new method for the synthesis of tri-*tert*-butyl diethylenetriaminepentaacetic acid and its derivatives. *J. Org. Chem. 65*, 1562−1565.

(24) Feng, Y., Wang, Z., Jin, S., and Burgess, K. (1998) SNAr cyclization to form cyclic peptidomimetics of beta-turns. *J. Am. Chem. Soc. 120*, 10768−10769.

(25) Alberto, R., Schibli, R., and Schgiger, A. (1996) Reactions with the technetium and rhenium carbonyl complexes (NEt$_4$)$_2$-[MX$_3$(CO)$_3$]. Synthesis and structure of [Tc(CN−But)$_3$(CO)$_3$](NO)$_3$ and (NEt$_4$)[Tc$_2$(M-SCH$_2$CH$_2$OH)$_3$(CO)$_6$]. *Polyhedron 15*, 1079−1080.

(26) Liu, S., and Edwards, D. S. (2001) Synthesis and characterization of two ^{111}In-labeled DTPA-peptide cojugates. *Bioconjugate Chem. 12*, 630−634.

(27) Dewanjee, M. (1990) The chemistry of ^{99m}Tc-labeled radiopharmaceuticals. *Semin. Nucl. Med. 20*, 5−27.

(28) Akiyama, S. I., Fojo, A., Hanover, J. A., Pastan, I., and Gottesman, M. M. (1985) Isolation and genetic characterization of human KB cell lines resistant to multiple drugs. *Somatic Cell Mol. Genet. 11*, 117−126.

(29) Piwnica-Worms, D., Chiu, M., Budding, M., Kronauge, J., Kramer, R., and Croop, J. (1993) Functional imaging of multidrug-resistant P-glycoprotein with an organotechnetium complex. *Cancer Res. 53*, 977−984.

(30) Lamson, M., Kirscher, A., Hotte, C., Lipsitz, E., and Ice, R. (1975) Generator-produced ^{99m}Tc-TcO$_4^-$: carrier free? *J. Nucl. Med. 16*, 639−641.

(31) Piwnica-Worms, D., Kronauge, J., and Chiu, M. (1990) Uptake and retention of hexakis (2-methoxy isobutyl isonitrile) technetium(I) in cultured chick myocardial cells: mitochondrial and plasma membrane potential dependence. *Circulation 82*, 1826−1838.

(32) Rao, V., Dahlheimer, J., Bardgett, M., Snyder, A., Finch, R., Sartorelli, A., and Piwnica-Worms, D. (1999) Choroid plexus epithelial expression of MDR1 P-glycoprotein and multidrug resistance-associated protein contribute to the blood-cerebrospinal fluid drug-permeability barrier. *Proc. Natl. Acad. Sci. U.S.A. 96*, 3900−3905.

(33) Luker, G., Sharma, V., Pica, C., Dahlheimer, J., Li, W., Ochesky, J., Ryan, C., Piwnica-Worms, H., and Piwnica-Worms, D. (2002) Noninvasive imaging of protein−protein interactions in living animals. *Proc. Natl. Acad. Sci. U.S.A. 99*, 6961−6966.

(34) Schibli, R., La Bella, R., Alberto, R., Garcia-Garayoa, E., Ortner, K., Abram, U., and Schubiger, P. A. (2000) Influence of the denticity of ligand systems on the in vitro and in vivo behavior of ^{99m}Tc(I)-tricarbonyl complexes: A hint for the future functionalization of biomolecules. *Bioconjugate Chem. 11*, 345−351.

(35) Alberto, R., Schibli, R., and Schubiger, A. P. (1999) First application of *fac*-$[^{99m}Tc(OH_2)_3(CO)_3]^+$ in bioorganometalic chemistry: design, structure, and in vitro affinity of a 5-HT_{1A} receptor ligand labeled with ^{99m}Tc. *J Am Chem Soc. 121*, 6076−6077.

(36) Mann, D., and Frankel, A. (1991) Endocytosis and targeting of exogenous HIV-1 Tat protein. *EMBO J. 10*, 1733−1739.

(37) Fawell, S., Seery, J., Daikh, Y., Moore, C., Chen, L., Pepinsky, B., and Barsoum, J. (1994) Tat-mediated delivery of heterologous proteins into cells. *Proc. Natl. Acad. Sci. U.S.A. 91*, 664−668.

(38) Wender, P., Mitchell, D., Pattabiraman, K., Pelkey, E., Steinman, L., and Rothbard, J. (2000) The design, synthesis, and evaluation of molecules that enable or enhance cellular uptake: peptoid molecular transporters. *Proc. Natl. Acad. Sci. U.S.A. 97*, 13003−13008.

(39) Lee, H. J., and Pardridge, W. M. (2001) Pharmacokinetics and delivery of Tat and Tat-protein conjugates to tissues in vivo. *Bioconjugate Chem. 12*, 995−999.

(40) Eguchi, A., Akuta, T., Okuyama, H., Senda, T., Yokoi, H., Inokuchi, H., Fujita, S., Hayakawa, T., Takeda, K., Hasegawa, M. et al. (2001) Protein transduction domain of HIV-1 Tat protein promotes efficient delivery of DNA into mammalian cells. *J. Biol. Chem. 276*, 26204−26210.

(41) Ho, A., Schwarze, S. R., Mermelstein, S. J., Waksman, G., and Dowdy, S. (2001) Synthetic protein transduction domains: enhanced transduction potential in vitro and in vivo. *Cancer Res. 61*, 474−477.

(42) Decristoforo, C., and Mather, S. (1999) Technetium-99m somatostatin analogues: effect of labeling methods and peptide sequence. *Eur. J. Nucl. Med. 26*, 869−876.

(43) Liu, Y., Jones, M., Hingtgen, C., Bu, G., Laribee, N., Tanzi, R., Moir, R., Nath, A., and He, J. (2000) Uptake of HIV-1 tat protein mediated by low-density lipoprotein receptor-related protein disrupts the neuronal metabolic balance of the receptor ligands. *Nat. Med. 6*, 1380−1387.

(44) Qu, T., Wang, Y., Zhu, Z., Rusckowski, M., and Hnatowich, D. (2001) Different chelators and different peptides together influence the in vitro and mouse in vivo properties of 99Tcm. *Nucl. Med. Commun. 22*, 203-215.

(45) Niesner, U., Halin, C., Lozzi, L., Günthert, M., Neri, P., Wunderli-Allenspach, H., Zardi, L., and Neri, D. (2002) Quantitation of the tumor-targeting properties of antibody fragments conjugated to cell-permeating HIV-1 Tat peptides. *Bioconjugate Chem. 13*, 729−736.

(46) Rousselle, C., Clair, P., Lefauconnier, J.-M., Kaczorek, M., Scherrmann, J.-M., and Temsamani, J. (2000) New advances in the transport of doxorubicin through the blood-brain barrier by a peptide vector-mediated strategy. *Mol. Pharmacol. 57*, 679−686.

(47) Rousselle, C., Smirnova, M., Clair, P., Lefauconnier, J.-M., Chavanieu, A., Calas, B., Scherrmann, J.-M., and Temsamani, J. (2001) Enhanced delivery of doxorubicin into the brain via a peptide-vector- mediated strategy: saturation kinetics and specificity. *J. Pharmacol. Exp. Ther. 296*, 124−131.

BC025573A

Selective Alkylation and Acylation of α and ϵ Amino Groups with PEG in a Somatostatin Analogue: Tailored Chemistry for Optimized Bioconjugates

Margherita Morpurgo,[†] Cristina Monfardini,[†] Leo J. Hofland,[‡] Mauro Sergi,[†] Paolo Orsolini,[§] Jean M. Dumont,[§] and Francesco M. Veronese*[,‡]

Universitá degli Studi di Padova, Dipartimento Scienze Farmaceutiche, via Marzolo, 5, 35131 Padova, Italy, Department of Internal Medicine, Academic Hospital Dijkzigt, Rotterdam, The Netherlands, and Debio R.P., Martigny, Switzerland. Received April 16, 2001; Revised Manuscript Received November 3, 2001

The effects of the type and location of polymer grafting on the biological activity of different mono-PEG derivatives of the somatostatin analogue RC160 were evaluated. A chemical strategy to obtain mono-PEG alkylation or acylation of the peptide's α-terminal or lysil-ϵ primary amines was devised. Selective BOC protection of the two available primary amines, followed by reaction with two different PEG reagents and removal of the protecting group, was carried out. Chemical characterization, structural studies, and the evaluation of the biological activity of the bioconjugates synthesized allowed the identification of the one having characteristics more suitable for therapeutic application. This corresponds to the mono-ϵ-lysil-pegylated form, obtained by reductive alkylation, where the amine's positive charge is preserved. The results obtained suggest the importance of preliminary studies in the development of new polymer−peptide conjugates with improved pharmacological properties.

INTRODUCTION

Bioconjugation and protein derivatization are fundamental for many biotechnological applications such as, for example, the development of affinity chromatography media, immunoassays, or biosensors (Self and Cook,1996; Yoo, 1976; Wilchek, 1975; Chaiken, 1979). In pharmaceutical sciences, chemical derivatization of bioactive proteins with biocompatible polymers is often used to improve their pharmacokinetic, immunogenic, and antigenic profiles. Polymer-conjugated proteins normally also exhibit higher stability toward harsh environments (high temperature, wide pH range, organic solvents, proteolytic digestion) and are less immunoreactive than their non-modified counterparts (Inada et al., 1986; Nucci et al., 1991; Delgado et al., 1992; Monfardini and Veronese, 1998; Morpurgo and Veronese, 2000; Greenwald et al., 2000; Veronese, 2001).

In bioconjugation, both the choice of the target amino acid in the protein or the type of chemical bond can influence the bioactivity of the final product, and nowadays, several alternative chemical strategies for ligand-to-protein coupling are available to researchers. The most frequent chemical strategy relies on the modification of lysil and/or α-terminal (Kinstler, 1996) primary amines because their acylation often leads to conjugates with desired properties and good residual biological activity. Nevertheless, different approaches may sometimes be necessary, such as, for example, when the integrity of certain lysines is important for the biological activity. Possible alternative targets are the carboxyl functions of aspartic and glutamic acid or the cysteine thiols. The chemistry for the modification of each of these residues has been developed (Zalipsky, 1995; Herman et al., 1995). Nevertheless, loss of biological activity is a complex issue in protein modification and sometimes, as in the case of proteins or peptides with weak structural conformation, it cannot be solved simply by changing the target amino acid. For example, when high molecular weight polymers are used, the polymeric environment can cause protein destabilization with partial to total unfolding, or it may prevent the interaction with the substrate or receptor. In these cases, a tailored chemistry can be of help in minimizing the activity loss: reversible site protection can be carried out to preserve relevant residues during chemical coupling (Caliceti et al., 1993), or alternatively, selective modification of sites that are known to be less important for biorecognition can be tried (Ehrat and Luisi, 1983; Uchio et al., 1999). Besides, the size of the polymer (Veronese et al., 1996 and 1997; Sherman, 1997) and the chemistry for its grafting can be optimized for minimal negative effects. Unfortunately, data about specific residue integrity or steric requirements in biologically active peptides are not always available, and often their importance has to be assessed randomly by using a trial and error approach.

In this work, the principle of tailored chemistry has been applied for the monomethoxypoly(ethylene glycol) (PEG) derivatization of the somatostatin analogue RC-160, (Vapreotide) an octapeptide with potential application as a therapeutic agent (Hofland et al., 1994). Analogues of somatostatin are primarily used for the treatment of patients with growth hormone (GH) secreting adenomas and for the treatment of symptoms related to the hormonal hypersecretion induced by various neuroendocrine tumors. Moreover, the efficacy of vapreotide in the treatment of acute variceal bleeding in cirrhotic patients was recently demonstrated (Calès et al., 2001). However, the administration of this class of molecules is sometimes difficult to optimize. For example, in the case of somatostatin, a continuous intravenous infusion is

* Corresponding author. E-mail: francesco.veronese@.unipd.it. Phone: ++39-049-8275694. Fax: ++39-049-8275366.
[†] Universita' degli Studi di Padova.
[‡] Academic Hospital Dijkzigt.
[§] Debio R.P.

10.1021/bc0100511 CCC: $22.00 © 2002 American Chemical Society
Published on Web 10/29/2002

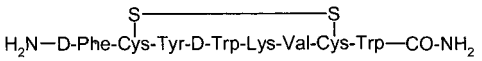


Figure 1. Schematic representation of Vapreotide (RC160).

required to reach a suitable blood concentration because single parenteral boosts are not very effective: a large administration dose is responsible for a re-bound effect and several side effects, while low doses are ineffective. New controlled release systems—based on matrixes suitable for polypeptide release (Rothen-Weinhold et al., 1998) or on the conjugation with soluble polymers—that prolong the circulation time without the risk of immunogenicity may therefore offer valuable alternatives in the administration profile of this class of compounds.

From a chemical point of view, RC160 (Figure 1) is an eight-amino acid peptide, and it carries two primary amino groups that offer potential sites for polymer coupling. The first one comes from the peptide's α-amino function (phenylanine), and the other one is the lysine's ϵ-amino residue in position 3. In this work, four mono-PEG derivative of RC160 were synthesized where the α or ϵ amino functions were modified either through an acyl or an alkyl bond. Circular dichroism studies were carried out in order to evaluate the structural conformation of the PEG derivatives, and their biological activity was assessed by measuring their capability to inhibit GH release from rat anterior pituitary cells. On the basis of the results obtained, it has been possible to select the best conjugate for further therapeutic developments.

METHODS

General. RC160 was gently provided by Debiopharm (Lausanne, Switzerland). The native hormone somatostatin (SS-14) was purchased from Sigma (St. Louis, MO); Monomethoxy poly(ethylene glycol)norleucine-N-hydroxysuccinimide (MW 5000) (PEG-Nle-NHS) (Sartore et al., 1991) and PEG-aldehyde (PEG-ALD) (Chamow et al., 1994) were purchased by Shearwater Polymers (Huntsville, AL). High-performance liquid chromatography (HPLC) eluants were of HPLC grade or Microselect (Fluka-Chemie, Amersham, Germany). All other chemicals were of analytical or reagent grade. UV−vis determinations were performed on Perkin-Elmer λ2 and λ5 spectrophotometers; circular dichroism spectra were recorded with a Jasco J-500 spectropolarimeter.

The value of ϵ 280 nm of 12 050 ($A^{1\%}{}_{1\ cm} = 100$) for RC160 was calculated by spectroscopic analysis of weighted samples, and it was used for the determination of protein concentration in all experiments.

All of the RC160 derivatives were characterized by RP-HPLC. Analyses were performed on a Vydac-C4 column, using either CH_3CN/H_2O/0.05%TFA or MeOH/10 mM amonium acetate, pH 6.6, as elution systems. Peaks were detected at 220 or 280 nm. In the CH_3CN/H_2O/TFA elution system, CH_3CN/TFA was linearly increased from 25% to 55% in 15 min; then a 5 min isocratic step at 55% CH_3CN/TFA was applied, followed by a washing step with 95% of the acetonitrile eluant. In the methanol/amonium acetate system, a linear gradient of methanol from 60 to 100% in 15 min was used, followed by a 10 min isocratic step with 100% methanol.

The degree of amino group substitution in the modified RC160 samples was measured by fluorescamine assay (Udenfriend et al., 1972; Stocks et al. 1986): 1 mL of fluorescamine solution (0.3 mg/mL in acetone) was added, while mixing vigorously, to 3 mL of the RC160 sample (10−15 μg) dissolved in 0.1 M phosphate, pH 8.0. After 10 min, the fluorescence (λ exc. 290 nm, λ em.475 nm) was measured.

Matrix-Assisted Laser Desorption Ionization Mass Spectrometry (MALDI-MS) was carried out on the derivatives to confirm the degree of modification on the basis of the increase in molecular weight of the conjugates. Analyses were carried out on a TOF-reflex mass spectrometer (Bruker-Franz Analytik, Brema, Germany). Equal volumes of analyte (100 pmol/mL in milliQ water) and matrix (saturated sinapinic acid in 50% CH_3CN, 50% H_2O) solutions were mixed prior to the analysis, and 2 mL of the final solution was applied on the stainless steel target. Final spectra are the sum of ∼30−60 laser shots, calibrated externally using human insulin.

RC160,α,ϵ-bi-BOC. Di-*tert*-butyl dicarbonate (BOC_2) (0.25 M in THF) was added in a 20-fold excess to RC160, dissolved in ethanol/0.2M borate buffer, pH 8.5, 1/1 (2 mg/mL). The reaction mixture was stirred overnight at room temperature, and the product was analyzed and purified by RP-HPLC and dried by Speed-Vac evaporation

RC160,α-mono-BOC. Di-*tert*-butyl dicarbonate (BOC_2) (0.25 M in THF) was added in 5-fold excess to RC160 dissolved in ethanol/0.1M phosphate buffer, pH 6.0, 1/1 (2 mg/mL), and the mixture was stirred overnight at room temperature. The product was analyzed and purified from the bi-BOC derivative by RP-HPLC and dried by Speed-Vac evaporation.

RC160,ϵ-mono-BOC. Di-*tert*-butyl dicarbonate (BOC_2) (0.25 M in THF) was added in equimolar amounts to RC160 dissolved in ethanol/0.2M borate buffer, pH 8.5, 1/1 (2 mg/mL), and the reaction was stirred overnight at room temperature. The product was analyzed and purified from the bi-BOC-ylated derivative by RP-HPLC and dried by Speed-Vac evaporation.

RC160,α-mono-BOC,ϵ-PEG-Nle (acyl). α-MonoBOC-RC160 was dissolved in ethanol/0.2M borate buffer, pH 8.5, 1/1 (final concentration 2 mg/mL), and a 5-fold excess of PEG-Nle-NHS (M. W. 5000) (Sartore et al., 1991) was added while stirring. The reaction was over after 1 h at room temperature, as confirmed by analytical RP-HPLC. The product was purified by semipreparative HPLC and lyophilized. Total amine substitution was confirmed by fluorescamine assay.

RC160,α-mono-BOC,ϵ-PEG (alkyl). α-MonoBOC-RC160 was dissolved in ethanol/50mM sodium phosphate pH 6.0, 1/1, to a final concentration of 2 mg/mL. Five equivalents of PEG-ALD (M. W.5.000) (Shearwater Pol., Huntsville, AL) and 2 equiv of $NaCNBH_3$ were added to the solution, and the pH was adjusted to 8.0. The reaction, followed by RP-HPLC, was completed in 20 h. The product was purified by RP-HPLC and freeze-dried.

RC160,α-NH_2,ϵ-PEG-Nle (acyl) and RC160,α-NH_2,ϵ-PEG (alkyl). The BOC protective group was removed by acidic treatment (95%TFA, 30 min, room temperature). The acid was neutralized by adding an equimolar amount of triethylamine (TEA) while cooling the solution with an ice bath. After ultrafiltration (Amicon membrane YM1, cutoff 1000), the product was purified by RP-HPLC and freeze-dried.

RC160,α-PEG-Nle (acyl),ϵ-NH_2 and RC160,α-PEG (alkyl),ϵ-NH_2. The same procedures as for the syntheses of RC160-α-NH_2,ϵ-PEG-Nle and RC160-α-NH_2,ϵ-PEG were used. Instead of RC160,α-mono-BOC, RC160,ϵ-mono-BOC was used as the starting compound.

RC160-$TNBS_2$. RC160 (0.5 mg) was dissolved in 400 μL of ethanol/0.2M borate buffer, pH 9.5, 1/1, and trinitrobenzenesulfonic acid (TNBS) (15 mg, 100 equiv.) was added while stirring. After 45 min., 10 mL of

deionized water was added, the product was purified by extensive ultrafiltration (membrane YM1) and freeze-dried. Purity was assessed by RP-HPLC.

RC160,α-TNBS,ϵ-PEG-Nle (acyl). RC160,α-NH_2,ϵ-PEG-Nle was dissolved in 0.1 M borate buffer, pH 9.5 (0.18 mg/100 μL), and TNBS (6.22 mg) was added while stirring. After 1 h., the product was purified by extensive ultrafiltration and freeze-dried. Analysis was carried out by RP-HPLC.

Amino Acid Analysis of unmodified RC160, RC160-$TNBS_2$, RC160,α-TNBS,ϵ-PEG-Nle, and RC160,α-NH_2,ϵ-PEG-Nle was carried out after acidic hydrolysis (24 h, at 110 °C in 6 N HCl, 0.1% phenol). Analysis was carried out by HPLC according to standard protocols (Bidlingmeyer et al., 1984).

Circular Dichroism analyses on unmodified RC160 and its four PEGylated derivatives were carried out in PBS buffer with sample concentration of 0.1 mg/mL.

Biological Activity. The biological activity of RC160, its PEGylated derivatives and of natural somatostatin was measured as previously described (Hofland et al., 1994, Breeman et al., 1994) by assaying their ability to inhibit GH release from anterior pituitary cells obtained from adult male rats. In short, anterior pituitary cells, obtained from rat pituitary glands (Hofland et al., 1994, Breeman et al. 1994) were seeded in 24-well cluster plates (10^5 cells/well) in MEM medium with Earle's salts at pH 7.4, supplemented with nonessential amino acids, sodium pyruvate, 10% fetal calf serum, penicillin, fungizone, L-glutamine, and sodium bicarbonate and incubated in 95% air/ 5% $C0_2$ humidified at 37 °C. After 4−5 days, the medium was refreshed and incubated for 4 h in the presence or absence of several logarithmic dilutions of the RC160 derivatives (10^{-6} to 10^{-14} M), dissolved in the medium above. The native hormone, somatostatin, was tested as positive control. Assays were carried out in quadruplicates.

The amount of GH released in the medium was measured by a commercial radioimmunoassay kit, purchased from Amersham Pharmacia Biotech (Uppsala, Sweden). IC_{50} values for inhibition of growth hormone were calculated from the plots expressing the amount of released GH versus somatostatine analogue concentration, using the computer fitting program of Graphpad (ISI software, Philadelphia, PA). These values reflect the concentration of peptide that allows a level of GH release equal to 50% of the maximal inhibition observed.

RESULTS AND DISCUSSION

In recent years, the use of biocompatible, low molecular weight (5−20 000 Da) polymers to modify peptides or proteins devised for therapy enabled overcoming many of the problems associated with the use of these therapeutically useful molecules. Monomethoxypoly(ethylene glycol) (PEG) is the polymer most commonly used for this purpose because of its high biocompatibilty and its amphiphilic properties. Besides, the monofunctionality of this polymer, which has one single hydroxyl group per molecule, allows a clean chemistry without the risk of cross-linking. In this work, we describe the synthesis and characterization of four mono-PEG derivatives of RC160, a peptide hormone with two reactive amino groups, the α-amino function, and the ϵ function of its unique lysine (Figure 1). Specific modification of each one of its two primary amines with PEG was achieved by selective pH-driven BOC protection of each of them, followed by reaction of the second one with PEG. Two PEG reagents were used, the active succinimidyl ester (NHS) of PEG-norleucine (16) that leads to the formation of an acyl-bond or PEG-ALD, followed by $NaCNBH_3$ treatment, that leads to an alkyl bond where the amine positive charge is maintained (Chamow et al., 1994).

Selective pH-driven BOC protection of each of the two primary amines was carried out by taking advantage of their different acidic and nucleophilic properties that allow modulation of their reactivity according to the reaction pH. In fact, complete primary amine deprotonation occurs at pH above pH 8.0, and in this environment, the reactivity of different amines depends on their nucleophilic properties. Under these conditions, the more nucleophilic lysine ϵ-NH_2 is generally more reactive toward electrophiles than α-amino groups. On the contrary, at a lower pH (6.0), the more acidic α-amino functions are generally more deprotonated than the ϵ-ones, and the order of reactivity is generally inverted.

Selective Reversible Amine Protection with BOC. Figure 2 shows HPLC analysis of the products of BOC reaction carried out at pH 6.0 or 8.5. In both cases, a binary mixture of products was obtained. RP-HPLC (Figure 2), fluorescamine assay and MALDI-MS analysis of each isolated peak (data not shown) confirmed that a mixture of mono- and bi-BOC-ylated RC160 is produced in both cases. However, HPLC co-injection (Figure 2.c) of the two reaction mixtures clearly shows that the mono-BOC adducts obtained at the two pHs are two different products, thus suggesting a different selectivity of the BOC reaction. The α- or ϵ-amino-protected RC160 was then PEGylated at the residual free amino group.

Even though the rationale of the chemical approach could have been enough to allow identification of each one of the mono-BOC-ylated RC160 forms (the α-modified one being obtained at pH 6.0 and the one at the ϵ-lysine obtained at pH 8.5), the identity of the two mono-PEG adducts was confirmed by the following procedure: (1) hypothetical RC160,α-NH_2,ϵ-PEG-Nle was synthesized by coupling PEG-Nle-NHS to the purified mono-BOC-RC160 obtained at pH 6.0, followed by removal of the BOC group by acidic treatment; (2) the free primary amine of this product was derivatized with a trinitrophenyl residue using the TNBS reagent, and similarly, native RC160 was totally modified with TNBS; (3) acidic hydrolysis and amino acid analysis of the four individual products, native RC160, RC160-$TNBS_2$, and the hypothetical RC160,α-NH_2,ϵ-PEG-Nle and RC160,α-TNBS,ϵ-PEG-Nle, was carried out, and the recovery of each amino acid in the samples (Table 1) was evaluated.

It is known from literature (Schiavon et al., 1990) that when a protein is fully trinitrophenylated with TNBS, its lysines cannot be quantified by acidic treatment and amino acid analysis because of the stability of the trinitrophenyl-(TNP)-ϵ amino−lysil bond. On the contrary, the α-amino−TNP bond is less stable to the 6 M HCl treatment, and the α-amino acid of a TNP−protein is almost fully recovered in the amino acid analysis. Furthermore, the PEGϵ−acyl linkage is completely hydrolyzed under the same conditions. This was confirmed when amino acid analysis after acidic treatment was carried out on the RC160−$TNBS_2$ derivative since almost total phenylalanine recovery (80%) was obtained, whereas the amount of lysine was negligible (Table 1). Moreover, when the same analysis was performed on the hypothetical RC160,α-TNBS,ϵ-PEG-Nle and RC160,α-NH_2,ϵ-PEG-Nle, total recovery of both lysine and phenylalanine was obtained in the two samples. These data, added to the fact that 50% of the primary amines in the RC160-NH_2,PEG-Nle could be titrated by the fluorescamine assay, can lead to the conclusion that the lysine in the

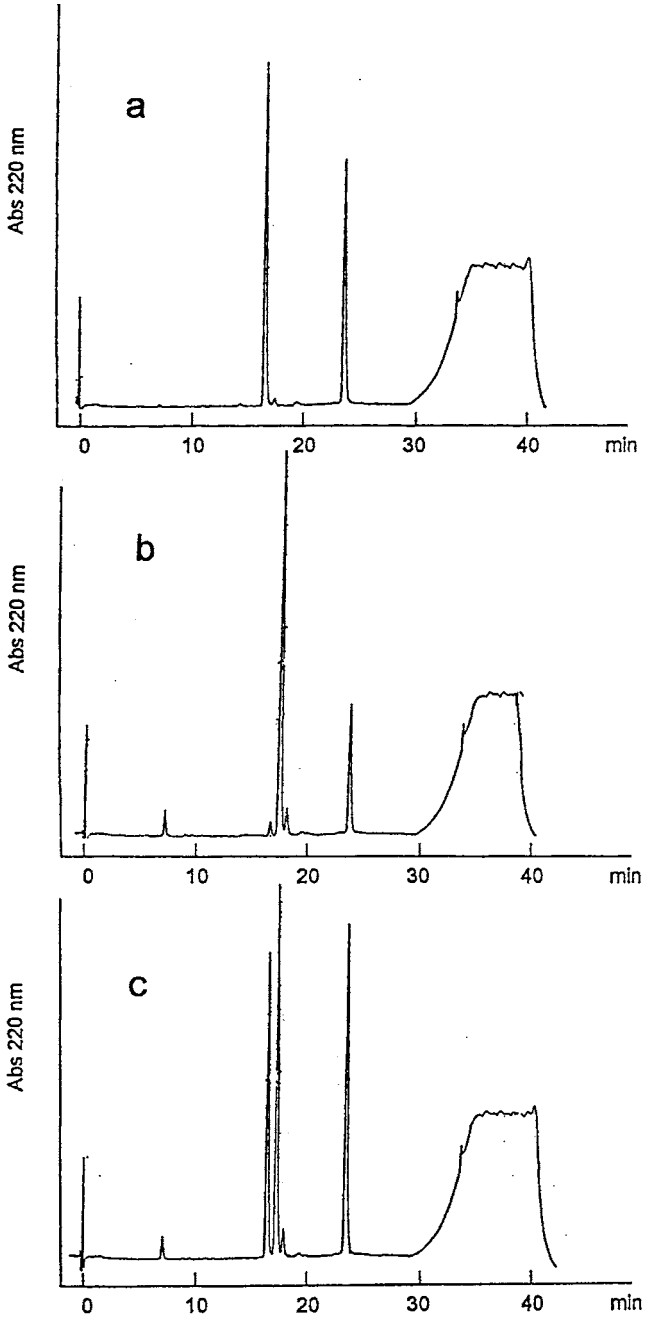


Figure 2. RP-HPLC analysis of the reaction mixtures obtained by reaction RC160 with di-*tert*-butyl dicarbonate at pH 6.0 (a) and 8.5 (b). The reaction mixtures were co-injected (c) to prove the different identity of the mono-modified products (r.t. = 17 and 17.8 min). Analysis was performed on a Vydac C-4 column with water/acetonitrile/ TFA as eluants and a flow of 1 mL/min. Peaks were detected at 220 nm. The compound eluted at 23 min was identified as the bi-BOC-ylated derivative. Unmodified RC160 has a retention time of 7 min, and it is noticeable only as a small peak in the pH 8.5 reaction mixture.

RC160-TNBS,PEG-Nle was linked to PEG and not to the TNBS moiety, thus confirming that the mono-BOC adduct obtained at pH 6.0 is the α-modified one. As a consequence, the product obtained at pH 8.5 was assumed to be the one protected at the ϵ-amino group.

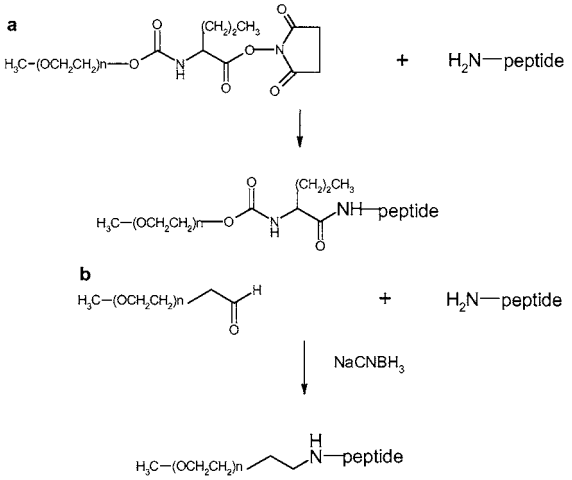
PEGylation of RC160 by Acylation or Alkylation Reaction. Two different chemical approaches were used to "PEGylate" the free amino function of the two mono-BOC-derivatives (Scheme 1). In one approach, the NHS ester of PEG-norleucine (PEG-Nle) was used, this reagent leading to an amide bond. In the second approach, reductive alkylation was carried out by using PEG-aldehyde, followed by $NaCNBH_3$. The advantage of this second approach is that the positive charge in the site of coupling is maintained.

Table 1. Recovery of Phenylalanine (α-NH2) and Lysine (ϵ-NH2) and Nle in the Amino Acid Analysis of Different RC160 Derivatives[a]

	Phe (%)	Lys (%)	Nle (%)
unmodified RC160	100	100	–
RC160-$TNBS_2$	80	9	–
RC160,α-NH_2,ϵ-PEG-Nle	100	100	100
RC160,α-TNBS,ϵ-PEG-Nle	75	100	100

[a] Numbers are reported as percentages and are referred to the recovery of the stable valine in the peptide

Scheme 1. Schematic Representation of Peptide NH_2 Modification: Acylation with PEG-Nle-NHS (a) and Alkylation with PEG-ALD (b)



After PEG coupling, the protective BOC group was removed by acidic treatment to obtain the desired final product. Preparative HPLC was needed for the purification of the final product that was obtained with overall yield of about 65% and 50% for the acyl and alkyl derivatives, respectively. The purity and the identity of the final compounds were then confirmed by RP-HPLC and MALDI-MS spectrometry (Table 2).

Structural Studies by CD Evaluation. The effect of the location of polymer grafting on the peptide's was assayed by circular dichroism. The four mono-PEGylated derivatives were analyzed and compared to the unmodified peptide. The results obtained (Figure 3) demonstrated that modification of the α position causes a stronger perturbation than the one in ϵ: the ϵ-PEGylate alkyl and acyl derivatives maintained about 70% and 50% of the original secondary structure, respectively. On the other hand, the α-modified ones showed more significant loss in their conformation.

On the basis of this result, only the two ϵ-modified peptides were selected for the evaluation of the biological activity.

Biological Activity of RC160 Conjugates on Cell Culture. The biological activity of the unmodified RC160 and the acyl and alkyl ϵ-PEGylated derivatives was assayed in vitro on cultured normal rat anterior pituitary cells measuring the inhibition on GH release. Levels of GH released were normalized against those obtained from cells treated with GRF in the absence of the RC160 derivative. IC_{50} values express the concentration of RC160 derivative that leads to a level of GH release equal to 50% of the maximal inhibitory effect by the compound.

Table 2. MALDI-MS Spectrometry Data on Different RC160 Samples

compound	expected M/Z value	measured M/Z value
RC160	1147	1134,1153
PEG-aldehyde	poly-dispersed peak, ca. 5000	poly-dispersed peak, ca. 5390
PEG-Nle-OH	5150 ca	nd
RC160,α-mono-BOC	1247	1255
RC160,ϵ-mono-BOC	1247	nd
RC160ϵ-PEG (acyl)	poly-dispersed peak, ca. 6300[a]	poly-dispersed peak, ca. 6300
RC160,α-PEG (acyl)	poly-dispersed peak, ca. 6300[a]	poly-dispersed peak, ca. 6310
RC160,ϵ-PEG (alkyl)	poly-dispersed peak, ca. 6540[b]	poly-dispersed peak, ca. 6550
RC160,α-PEG (alkyl)	poly-dispersed peak, ca. 6540[b]	poly-dispersed peak, ca. 6560

[a] Calculated on the basis of the MW reported by the supplier. [b] Calculated on the basis of the MW determined by MALDI-MS (see table).

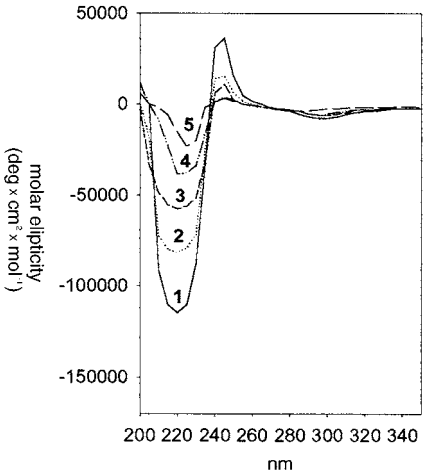


Figure 3. Circular dichroism spectra of unmodified RC160 (**1**) and its four PEG conjugates: RC160,α-NH_2,ϵ-PEG (alkyl) (**2**), RC160,α-NH_2,ϵ-PEGNle (acyl) (**3**), RC160,α-PEG,ϵ-NH_2 (alkyl) (**4**), and RC160,α-PEG-Nle,ϵ-NH_2 (acyl) (**5**). Spectra were recorded in PBS buffer with sample concentration of 0.1 mg/mL.

Table 3. IC50 Values of Inhibition of GH Release by Cultured Rat Anterior Pituitary cells by RC160 Derivatives and Somatostatin (See Methods Section for Experimental Details)

derivative	$IC_{50} \pm SD$
RC160	$(3.15 \pm 4) \times 10^{-13}$ M
RC160,α-NH_2,ϵ-PEG-Nle (acyl)	not active
RC160,α-NH_2,ϵ-PEG (alkyl)	$(4.3 \pm 4.9) \times 10^{-10}$ M
somatostatin	$(1.4 \pm 0.85) \times 10^{-10}$ M

Table 3 shows the mean values of IC50 obtained from two separated sets of experiments, each one carried out in quadruplicates. Only the alkylated derivative showed significant biological activity in the system studied, whereas the acylated compound did not show any effect, thus demonstrating the importance of the lysine's positive charge for the peptide's biological activity.

The ϵ-alkyl PEG derivative is 3 orders of magnitude less active than unmodified RC160. Nevertheless, this bioconjugate is still quite active (for example, its potency is comparable to the one of natural somatostatin in our in vitro test) and might still be useful in therapy. Biological activity of somatostatin analogues depends on both their affinity for the cellular receptor and stability toward enzymatic degradation. For example, natural somatostatin is highly susceptible to degradation, whereas RC160 is more resistant, this property being correlated to the latter's higher potency. In the case of PEGylated RC160, loss of activity might be related to a steric impediment that affects its affinity for the cellular receptor. On the other hand, PEGylation may improve the peptide's bioavailability in vivo thanks to a higher stability and a longer body permanence, as already demonstrated with several PEGylated proteins. Therefore, the real efficacy of this new conjugate as a potential drug will have to be evaluated by further in vivo pharmacological studies.

CONCLUSIONS

In this work, the possibility of using a tailored chemistry for the modification of small peptides with monomethoxy poly(ethylene glycol) has been exploited to prevent total loss of conformation and biological activity.

The problem of preserving the biological potentials of biomolecules after coupling bulky polymers to their surface is particularly important when small peptides are considered. The results here reported confirm this thinking. Four mono-PEGylated derivatives of RC160, an eight-amino acid amino acid analogue of somatostatin, were synthesized by using a tailored chemistry where both the site of polymer grafting and the type of chemical bond were defined. By a combination of chemical, structural, and biological analysis, we could verify that only one of the four synthesized products may be suitable for further therapeutic development. More precisely, circular dichroism analyses demonstrated the importance of the integrity of α-amino function in the peptide, while in vitro biological tests proved that the preservation of lysine's charge is fundamental for the activity.

These result confirm the importance of using a tailored chemistry in the development of polymer-peptide conjugates and, in this specific case, the usefulness of reversible amino acid protection to direct the modification only to the desired residues for the synthesis of bioconjugates with the most favorable properties.

ACKNOWLEDGMENT

This work was partially funded by the Italian CNR "Targeted Project in Biotechnology" and by MURST (40%).

LITERATURE CITED

Bidlingmeyer, B. A., Cohen, S. A., and Tarvin, T. L. (1984) Rapid analysis of amino acids using precolumn derivatization. *J. Chromatogr. 336*, 93−104.

Breeman, V. A. P., Hofland, I. J., Van der Pluijm, M., Koetsveld, P. M., de Jong, M., Setyono-Han, B., Bakker, W. H., Kwekkeboom, C. K., Visser, T. J., Lamberts, S. W. J., and Krenning, E. P. (1994) A new radiolabelled somatostatin analogue [^{111}In-DTPA-D-Phe^1]RC-160: preparation, biological activity, receptor scintigraphy in rats and comparison with [^{111}In-DTPA-D-Phe^1]octreotide. *Eur. J. Nucl. Med. 21*, 328−335.

Cales, P., Masliah, C., Bernard, B., Garnier, P. P., Silvain, C., Szostak-Talbodec, N., Bronowicki, J. P., Ribard, D., Botta-Fridlund, D., Hillon, P., Besseghir, K., and Lebrec, D. (2001) Early administration of vapreotide for variceal bleeding in patients with cirrhosis. French Club for the Study of Portal Hypertension. *N. Engl. J. Med. 344*, 23−28.

Caliceti, P., Schiavon, O., Sartore, L., Monfardini, C., and Veronese, F. M. (1993) Active site protection of proteolytic enzymes by polyethylene glycol surface modification. *J. Bioact. comp. Pol.* 841−850.

Chaiken, I. M. (1979) Quantitative uses of affinity chromatography. *Anal. Biochem. 97*, 1−10.

Chamow, S. M., Kogan, T. P., Venuti, M., Gadek, T., Harris, R. J., Peers, D. H., Mordenti, J., Shak, S., Ashkenazi, A. (1994) Modification of CD4 immunoadhesin with monomethoxypoly-(ethylene glycol) aldehyde via reductive alkylation. *Bioconjugate Chem. 5*, 133−140.

Delgado, C., Francis, G. E., and Fisher, D. (1992) The uses and properties of PEG-linked proteins. *Crit. Rev. Drug Carrier Syst. 9*, 249−304.

Ehrat, M., and Luisi, P. L. (1983), Synthesis and Spectroscopic Charcaterization of Insulin Derivatives Containing One or Two Poly(ethylene oxide) Chains at Specific Positions. *Biopolymers 22*, 569−573.

Greenwald, R. B., Conover, C. D., and Choe, Y. H. Poly(ethylene glycol) conjugated drugs and prodrugs: a comprehensive review. (2000) *Crit. Rev. Ther. Drug Carrier Syst. 17*, 101−161.

Herman, S., Hooftman, G., and Schacht, E. (1995) Poly(ethylene glycol) with reactive end groups: I Modification of proteins. *J. Bioact. Biocomp. Polymer 10*, 145−187.

Hofland, L. J., Van Koetsveld, P. M., Waaijers, M., Hofland, L. J., Zuydermy, K. J., and Lamberts, S. W. J. (1994) Relative potenties of the somatostatin analog octreotide, BIM-23014 and RC160 on the inhibition of hormone release by cultured human endocrine tumor cells and rat anteriory pituitary cells. *Endocrinology 134*, 301−306.

Inada, Y., Yoshimoto, T., Matsushima, A., and Saiti, Y. (1986) Engineering physicochemical and biological properties of proteins by chemical modification. *Trends Biotechnol. 4*, 68−73.

Kinstler, O. B., Brems, D. N., Lauren, S. L., Paige, A. G., Hamburger, J. B., and Treuheit, M. J. (1996) Characterization and stability of N-terminally PEGylated rhG-CSF. *Pharm. Res. 13*, 996−1002.

Monfardini, C., and Veronese, F. M. (1998) Stabilization of substances in circulation. *Bioconjugate Chem. 9*, 418−50.

Murphy, W. A., Taylor, J. E., Moreau, J. P., and Coy, D. H. (1989) Novel heptapeptide somatostatin analog displays antitumor activity independent of effects on growth hormone secretion. *Peptide Res. 2*, 128−132.

Nucci, M. L., Shorr, R., and Abuchowsky, A. (1991) The therapeutic value of poly(ethylene glycol) modified proteins. *Adv. Drug Delivery Rev. 6*, 133−151.

Rothen-Weinhold, A., Besseghir, K., De Zalicant, Y., and Gurny, R. (1998) Development and evaluation in vivo of a long-term delivery system for Vapreotide, a somatostatin analogue. *J. Controlled Release 52*, 205−213.

Sartore, L., Caliceti, P., Schiavon, O., Monfardini, C., and Veronese, F. M. (1991) Accurate evaluation method of the polymer content in monomethoxypoly(ethylene glycol) modified proteins based on amino acid analysis. *Appl. Biochem. Biotechnol. 31*, 213−222.

Schiavon, O., Sartore, L., Caliceti, P., Veronese, F. M. (1990) A direct assay for evaluation of polyethylene glycol in enzyme adducts used as drugs or biocatalysts. *Farmaco 45*, 791−795.

Self, C. H. and Cook, D. B. (1996) Advances in immunoassay technologies. *Curr. Opin. Biotechnol. 7*, 60−65.

Sherman, M. R., Williams, L. D., Saifer, M. G. P., French, J. A., Kwak, L. W., and Oppenheim, J. J. (1997) Conjugation of High Molecular Weight Poly(ethylene glycol) to Cytokines: Granulocytes-Macrophage Colony Stimulating Factors as Model Substrates. In *Poly(Ethylene Glycol): Chemistry and Biological Applications* (J. M. Harris and S. Zalipsky, Eds.) p 155, American Chemical Society, Washington, DC.

Stocks, S. J., Jones, A. J., Ramey, C. W., and Brooks, D. E. (1986) A Fluorimetric assay of the degree of modification of proteins with polyethylene glycol. *Anal. Biochem. 154*, 232−236.

Uchio, T., Baudys, M., Liu, F., Song, S. C. and Kim, S. W. (1999) Site-specific insulin conjugates with enhanced stability and extended action profile. *Adv. Drug Delivery Rev. 35*, 289−306.

Udenfriend, S., Stein, S., Bohlen, P., Bairman, W., Lwimgruber, W., and Weigele, M. (1972) Fluorescamine: a reagent for assay of amino acid, peptides, proteins and primary amines in the picomole range. *Science 178*, 871−872.

Veronese, F. M. (2001) Peptide and protein PEGylation: a review of problems and solutions. *Biomaterials 22*, 405−417.

Veronese, F. M., Caliceti, P., and Schiavon, O.(1997) Branched and linear polyethylene glycol. Influence of the polymer structure on enzymological pharmacokinetic and immunological properties of protein conjugates. *J. Bioact. Compat. Pol. 12*, 196−207.

Veronese, F. M., Monfardini, C., Caliceti, P., Schiavon, O., Scrawen, M. D., and Beer, D. (1996) Improvement of pharmacokinetic, immunological and stability properties of asparaginase by conjugation to linear and branched monomethoxy polyethylene glycol. *J. Controlled Release 40*, 199−209.

Wilchek, M., Oka, T. and Topper, Y. J. (1975) Structure of a soluble super-active insulin is revealed by the nature of the complex between cyanogen-bromide-activated sepharose and amines. *Proc. Natl. Acad. Sci. U.S.A. 72*, 1055−1058.

Yoo, T. J. (1976) Fluorescent probes for antibody active sites. In *Biochemical Fluorescence: Concepts* (R. F. Chen and H. Edelhoch, Eds.) Vol. 2, pp 879−899.

Zalipsky, S. (1995) Functionalized poly(ethylene glycol) for preparation of biologically relevant conjugates. *Bioconjugate Chem. 6*, 150−165.

BC0100511

Asymmetrical, Water-Soluble Phthalocyanine Dyes for Covalent Labeling of Oligonucleotides

Robert P. Hammer,* Clyde V. Owens, Seok-Hwan Hwang, Christie M. Sayes, and Steven A. Soper*

Department of Chemistry, Louisiana State University,
Baton Rouge, Louisiana 70803-1804. Received November 30, 2001; Revised Manuscript Received July 31, 2002

Two new water-soluble, porphyrazine (Pz) dyes containing an isothiocyanate function for covalent linking have each been prepared by cross condensation of two different aromatic dinitriles, one containing carboxylates for solubilizing purposes and the other containing a nitro group for conversion into the labeling function. The initial mononitrotricarboxylato Pzs have been purified to homogeneity from the mixture of Pz congeners formed in the condensation reaction by anion exchange chromatography. The phthalocyanine dye **1** has an absorption maxima at 683 nm while the trinaphthoporphyrazine dye **2** has an absorption maxima at 755 nm, due to the increased size of the aromatic system. Both dyes were successfully conjugated to oligonucleotide primers, showing their potential for use in near-infrared-based DNA diagnostic applications.

INTRODUCTION

Most bioanalytical applications using fluorescence as the readout mode for detection typically use labeling reagents that fluoresce in the visible region (400−650 nm) of the electromagnetic spectrum (*1*, *2*). Unfortunately, the spectroscopic range utilized by these fluorophores is susceptible to biological interferences from the sample matrix, which inevitably limits the sensitivity of the measurement. An attractive alternative is the use of near-IR fluorescence (650−1000 nm), which has recently been demonstrated to be a viable detection strategy in many bioanalytical assays, such as liquid chromatography (*3*−*5*), free solution capillary electrophoresis (*6*−*10*), and capillary gel electrophoresis for DNA sequencing and fragment analysis (*11*, *12*). Near-IR fluorescence offers reduced background matrix interferences compared to UV or visible fluorescence resulting primarily from the fact that a limited number of components show intrinsic fluorescence in this region of the electromagnetic spectrum. In addition, lower scattering levels are also observed in the near-IR because of the λ^{-4} dependence of the Raman cross section on the excitation wavelength. Indeed, we have demonstrated improved limits of detection in the near-IR compared to visible excitation for oligonucleotides separated using capillary gel electrophoresis (*11*). Also, near-IR fluorescence allows the use of inexpensive semiconductor devices, such as diode lasers and detectors, significantly simplifying the readout hardware (*13*).

Recently, reports on near-IR water-soluble dyes that can covalently and noncovalently label biomolecules such as amino acids, proteins and oligonucleotides, have been discussed (*14*−*23*). The dyes typically used are the tricarbocyanines, which consist of heteroaromatic structures linked by a polymethine chain containing conjugated carbon/carbon double bonds. These dyes possess large molar absorptivities ($>10^5$ cm^{-1} M^{-1}) and display favorable solubility in aqueous solvents provided by the negatively charged sulfopropyl groups attached to the heteroaromatic rings (*24*). The major limitations associated with these dyes are their poor chemical and photochemical stabilities and low quantum yields in aqueous media, therefore limiting their utility in ultrasensitive applications (*25*, *26*).

An attractive alternative to the cyanine-based near-IR fluorophores is the phthalocyanine [Pc; also know as tetraazaporphyrins or porphyrazines (Pz)] family of compounds. The Pc dyes are chemically and photochemically robust and have large extinction coefficients ($>10^5$ cm^{-1} M^{-1}) as well as favorable quantum yields (*27*). Additionally, absorbance and fluorescence maxima can easily be altered by varying the substituents around the ring or by changing the metal center (Zn, Sn Al, Si, etc.). For example, annulation of benzene rings onto the Pc core will produce the naphthalocyanine (Npc) dyes, which have λ_{max} red-shifted by 50−100 nm compared to the Pc dyes (*28*, *29*). Unfortunately, the Pc and Npc dyes are very hydrophobic and essentially insoluble in water. Functionalization of the periphery of the dye with charged groups (SO_3^-, CO_2^-, PO_3^{2-}, etc.) or attachment of a polar functionality to the metal center (PEG-OSi) does provide water-soluble Pc dyes (*30*). General routes to water-soluble Pc dyes that also contain a labeling function have not been reported to-date because of the need for preparing asymmetrical analogues, which can be very difficult to purify due to statistical formation of isomers during ring assembly.

One way to approach the preparation of labeling water-soluble Pc is to put the reactive group (**L**) in one "quadrant" of the macrocycle (see Figure 1) and then use one or more of the remaining quadrants to incorporate water-solubilizing groups (**S**). Pc and Npc dyes are generally prepared by cyclo-tetramerization of aromatic 1,2-dinitriles (phthalonitriles or naphthalonitriles) using either Lewis base or acid conditions (*31*, *32*). The simplest route to prepare nonsymmetrically substituted Pc dyes as discussed above would use one phthalonitrile that contains the (latent) labeling group **L** and another containing the solubilizing group **S** in a molar ratio of 1:3. This mixed "condensation" route is commonly used to prepare asymmetric Pc and Npc dyes, but as yet has not been applied to dyes containing a mixture of labeling

* To whom correspondence should be addressed. E-mail: rphammer@lsu.edu; chsope@lsu.edu.

10.1021/bc0155869 CCC: $22.00 © 2002 American Chemical Society
Published on Web 11/01/2002

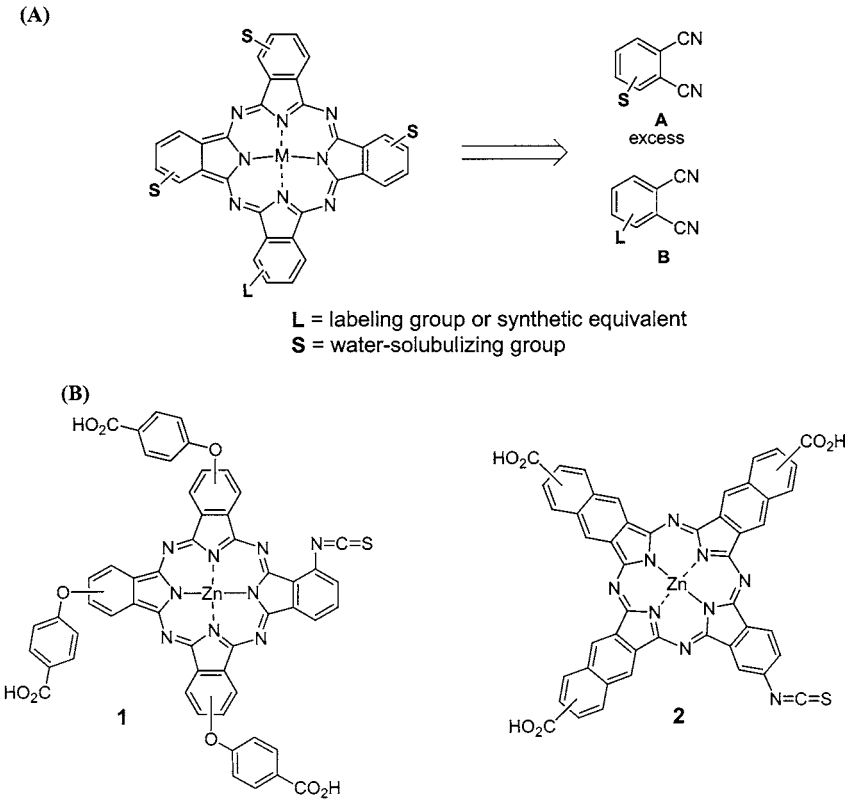


Figure 1. (A) Preparation of labeling, water-soluble Pc dye placing the reactive group (**L**) in one "quadrant" of the macrocycle with one or more of the remaining quadrants used to incorporate water-solubilizing groups (**S**). (B) Structure of water-soluble Pc (**1**) and pseudo-Npc (**2**) dyes containing reactive isothiocyanates for labeling.

and water-solubilizing groups we desire. Herein, we report the synthesis, spectroscopic properties, and labeling reactions of two new water-soluble near-IR dyes, Pc **1** and pseudo-Npc benzotrinaphthoporphyrazine (Tnpz) **2** (Figure 1), both of which contain a reactive isothiocyanate functional group used for covalent labeling of targets containing primary amines.

EXPERIMENTAL SECTION

Reagents. 2,3-Naphthalenedicarbonitrile, 3-nitropthalonitrile, 4-nitropthalonitrile, 1,1′-thiocarbonyldi-2(1*H*)-pyridone, palladium 10% on activated carbon, sodium thiosulfate, fumaronitrile, sodium iodide, carbon tetrachloride, 3,4-dimethylbenzoic acid, and zinc acetate dihydrate were obtained from Aldrich Chemical Co. (Milwaukee, WI). Hydrochloric acid and sulfuric acid were obtained from Fisher Scientific (Houston, TX). Potassium nitrate, sodium carbonate, sodium hydroxide, and urea were obtained from Sigma Chemical Co (St. Louis, MO). All chemicals were used as received. The dinitrile derivatives **3** and **4** used for final ring assembly were synthesized according to Kliesch et al. (*33*).

Chromatographic Purification and Spectroscopic Characterization. The crude reaction mixtures containing the water-soluble macrocycles were assayed by a Rainin HPLC system using a Hamilton PRP-1 analytical column (0.46 × 15 cm; Hamilton, Reno, NV) using a flow rate of 2.0 mL/min and a gradient consisting of 0.1 M triethylammonium acetate/20 mM sodium phosphate buffer (pH = 10.1) and tetrahydrofuran (THF). The absorbance detector (Shimadzu, Columbia, MD) was set at either 680 or 780 nm to monitor elution of the near-IR dyes. For typical analytical analyses, 1 mg of the crude dye mixture was dissolved in 2 mL of 20 mM sodium phosphate buffer. A 20 μL aliquot was injected into the column, which had been equilibrated with 100% 20 mM sodium phosphate buffer. Elution was carried out by a stepwise gradient from 0 to 100% THF over a period of 25 min.

Large-scale separations were carried out on a 2.15 × 25 cm Hamilton PRP-1 preparatory column (Hamilton, Reno, NV) packed with a polymeric reverse phase (C_{18}) that was equilibrated for 10 min with 20 mM sodium phosphate buffer (pH = 10.1). The water-soluble dye mixture (less than 1 g) was dissolved in 10 mL of buffer and injected into the preparatory column. The HPLC stepwise gradient used for analytical separations was slightly modified for preparatory work by extending the gradient step times to compensate for the increased flow rate (5 mL min^{-1}). Dyes were recovered from collected fractions by removing the solvent (HPLC mobile phase) using a rotary evaporator.

The absorption spectra were acquired on a Perkin-Elmer Lambda 3B UV/Vis spectrophotometer. The fluorescence spectra were obtained using a SPEX Fluorolog spectrofluorometer (SPEX, Edison, NJ) equipped with a 75 W xenon lamp. The emission gratings were blazed for 750 nm and the photomultiplier tube was a Hammamatsu R636 red-sensitive tube (Hammamatsu Corporation, Bridgewater, NJ).

Synthesis of Dyes. *[1-Nitro-9(10),16(17),23(24)-tris-(4-carboxyphenoxy)phthalocyanato]zinc(II) (**5**).* 4-(3,4-Dicyanophenoxy)benzoic acid (**3**; 0.425 g, 1.60 mmol) and 3-nitropthalonitrile (0.135 g; 0.81 mmol) were combined with 0.100 g of zinc acetate dihydrate. The reaction mixture was ground together into a fine homogeneous powder and heated at 200 °C for 20 min.

Reactions with the metal salts at 200−210 °C proceeded rapidly. Further heating decreased the yield of the desired metal complex as determined by the loss in

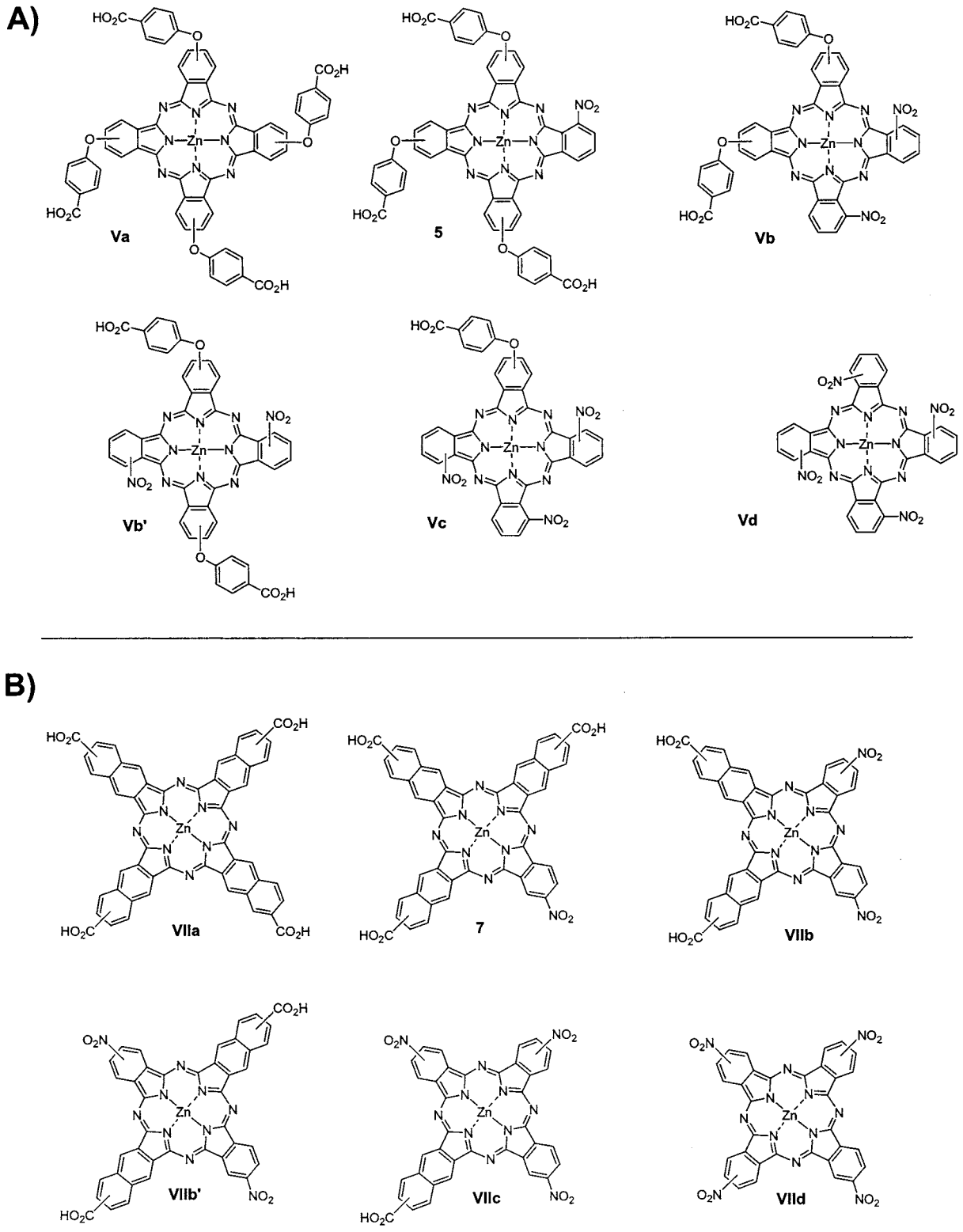


Figure 2. (A) Structures of nitro-Pc congeners (**Va**, **5**, **Vb**, **Vb′**, **Vc**, **Vd**) obtained from the reaction of 3-nitrophthalonitrile with 4-(3,4-dicyanophenoxy)benzoic acid (**3**). (B) Structures of the nitro-Tnpz congeners (**VIIa**, **7**, **VIIb**, **VIIb′**, **VIIc**, **VIId**) obtained from the reaction of 4-nitrophthalonitrile with 6,7-dicyanonaphthalenecarboxylic acid (**4**).

absorption in the near-IR. Lowering the temperature slowed the reaction, but did not increase product yield. The dark green precipitate containing desired Pc **5** and the other Pc congeners **Va-d** was dispersed in boiling 1 M HCl, cooled to room temperature, and collected. The precipitate was dissolved in 1 M NaOH and filtered to remove any insoluble impurities (e.g., tetranitrocongener **Vd**). The filtrate was neutralized with 1 M HCl and rotary-evaporated under vacuum to yield a green solid. This product was a mixture of at least four components, which varied in the number of water soluble groups (**S**) or functional labeling components (**L**) present in the dye (Figures 1 and 2A).

The chromatographic purification/isolation involved injecting 1.0 mg of the water-soluble Pc dye into a polymeric C_{18} column equilibrated with 0.1 M TEAA/20

mM sodium phosphate buffer (pH = 10.1). The components eluted in the following order: tetracarboxylate, tricarboxylate, dicarboxylate, and monocarboxylate, compounds **Va**, **5**, **Vb/b′**, **Vc**, respectively. They were characterized by their electronic absorbance spectra and mass spectra (data not shown). Tetracarboxylate ($4CO_2^-$) Pc **Va**: HPLC t_r = 9.22 min; λ_{max} (DMSO) = 677 nm. Tricarboxylate/mononitro (3 CO_2^-/1 NO_2) Pc **5**: HPLC t_r = 11.11 min; λ_{max} (DMSO) = 672 nm; MALDI (*m*/*z*) 1028 $(M - H)^-$. Dinitro/dicarboxylate (2 CO_2^-/2 NO_2) Pc (**Vb/b′**): HPLC t_r = 12.13 min; MALDI (*m*/*z*) 938 $(M - H)^-$. Trinitro/monocarboxylate (1 CO_2^-/3 NO_2) Pc (**Vc**): HPLC t_r = 17.07 min; MALDI (*m*/*z*) 847 $(M - H)^-$.

The tricarboxylate/mononitro compound **5** is the preferred compound for labeling because of its greater water solubility (3 CO_2^-) and its single nitro group. Crude yield is typically 20% of theory as expected for the isomeric mixture obtained from the reaction. Elemental analysis shows correct C/N ratio for this product: calculated 4.99; found 5.15. MALDI-MS calculated for $C_{53}H_{27}N_9O_{11}Zn$ = 1029, found *m*/*z* 1028 $(M - H)^-$. (λ_{max} (DMSO) = 672 nm).

[1-Amino-9(10),16(17),23(24)-tris(4-carboxyphenoxy)-phthalocyanato]zinc(II) (**6**) A large pressure flask containing mononitro-Pc **5** (500 mg; 0.48 mmol) in water (20 mL) and 30 mg of 10% palladium on charcoal was pressurized to 40 psi of hydrogen and was shaken for 3 h at room temperature. The reaction product was filtered to remove the catalyst. The filtrate was concentrated in vacuo and the dark green precipitate dried under vacuum. Crude yield 275 mg (54%). Elemental analysis shows correct C/N ratio for this product: calculated 5.71; found 5.75. MALDI-MS calculated for $C_{53}H_{29}N_9O_9Zn$ = 999, found *m*/*z* 1000 (M + H). (λ_{max} (DMSO) = 702 nm).

[1-(Isothiocyanato)-9(10),16(17),23(24)-tris(4-carboxyphenoxy)phthalocyanato]zinc(II) (**1**). Amino-Pc **6** (350 mg; 0.35 mmol) was added to a solution of 1,1′-thiocarbonyldi-2(1H)-pyridone (250 mg, 1.08 mmol) in DMF (3 mL) and stirred for 2 h. The DMF was removed in vacuo and the dark green product was taken up in HPLC grade H_2O and filtered through a 0.45 μM filter to remove insoluble 1,1′-thiocarbonyldi-2(1*H*)-pyridone products. The filtrate was dried under vacuum to yield 86 mg (27%). Elemental analysis for $C_{54}H_{27}N_9O_9SZn{\cdot}3H_2O$, Calculated (Found): C, 59.33 (59.58); H 3.35 (2.99); N, 11.32 (11.18). MALDI-MS calculated for $C_{54}H_{27}N_9O_9SZn$ = 1041, found *m*/*z* 1040 $(M - H)^-$. (λ_{max} (DMSO) = 686 nm).

[2-Nitro-10(11),19(20),28(29)-tricarboxybenzo[b]trinaphtho[2,3-g:2′,3′−l:2″,3″-q]porphyrazinato]zinc(II) (**7**). In a condensation reaction, 6,7-dicyano-2-naphthalenecarboxylic acid (**4**) (0.474 g; 1.69 mmol) and 4-nitrophthalonitrile (0.135 g; 0.78 mmol) were combined with 0.100 g of zinc acetate dihydrate (see Scheme 2). The reaction mixture was ground together into a fine homogeneous powder and heated to 200 °C for 20 min. The resulting solid black cake (Compound **7**, plus other congeners, **VIIa**, **VIIb**, **VIIb′**, **VIIc**, **VIId;** Figure 2B) was monitored by UV absorbance for the appearance of a near-IR peak.

The dark green precipitate was dispersed in boiling 1 M HCl, cooled to room temperature and collected. The precipitate was dissolved in 1 M NaOH and filtered to remove any insoluble impurities (e.g., tetranitrocongener **VIId**). The filtrate was then neutralized with 1 M HCl and rotary-evaporated under vacuum to yield a green solid. This product was a mixture of at least four components, which varied in the number of water soluble groups (**S**) or functional labeling components (**L**) present in the dye (Figure 1 and Figure 2B).

The chromatographic purification/isolation involved injecting 1.0 mg of the water-soluble dye into a polymeric C_{18} column equilibrated with 0.1 M TEAA/20 mM sodium phosphate buffer (pH = 10.1). The components eluted in the following order: tetracarboxylate, tricarboxylate, dicarboxylate, and monocarboxylate, compounds **VIIa**, **7**, **VIIb/b′**, **VIIc**, respectively **(**see Figure 2B) and were characterized by their electronic absorbance spectra and mass spectra. Tetracarboxylate (4 CO_2^-) Npc **VIIa**: HPLC t_r = 5.68 min; λ_{max} (DMSO) = 768 nm; MALDI (*m*/*z*) 952 $(M - H)^-$. Tricarboxylate/mononitro (3 CO_2^-/1 NO_2) Npc (**7**): HPLC t_r = 7.08 min; λ_{max} (DMSO) = 765 nm, 727 nm; MALDI (*m*/*z*) 905 $(M - H)^-$. Dinitro/dicarboxylate (2 CO_2^-/2 NO_2), Npc **VIIb/b′**: HPLC t_r = 16.03 min; λ_{max} (DMSO) = 720 nm, 689 nm; MALDI (*m*/*z*) 856 $(M - H)^-$. Trinitro/monocarboxylate (1 CO_2^-/3 NO_2), Npc **VIIc**: HPLC t_r = 18.82 min; λ_{max} (DMSO) = 684 nm; MALDI (*m*/*z*) 806 $(M - H)^-$.

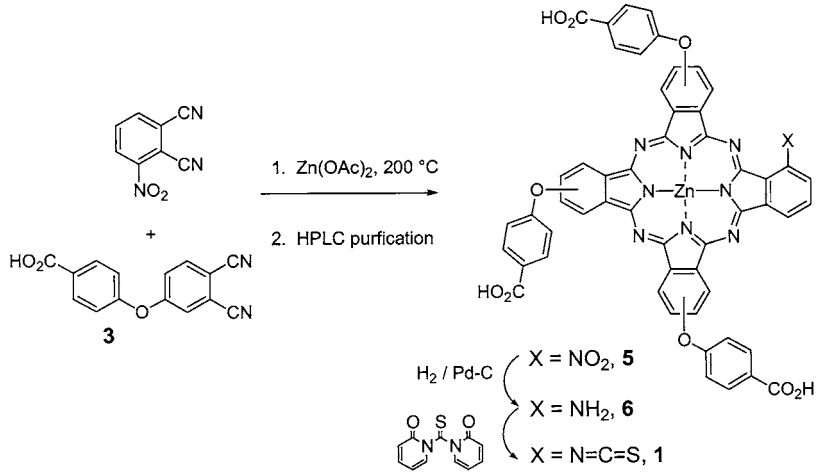
The tricarboxylate/mononitro compound, **7**, is a preferred compound for labeling because of its high number of water soluble groups (3 CO_2^-) and its single nitro group, which can be converted to a labeling function. The yield of **7** is typically ∼25% of theory as is expected for the mixture of compounds obtained in the initial condensation. IR (KBr) ν = 1645 cm^{-1} (C═O), 1525 cm^{-1} (NO_2), 1350 cm^{-1}(NO_2); MALDI-MS calculated for $C_{47}H_{21}N_9O_8Zn$ = 904, found *m*/*z* 905 $(M + H)^+$. (λ_{max} (DMSO) = 765 nm, 727 nm).

[2-Amino-10(11),19(20),28(29)-tricarboxybenzo[b]trinaphtho[2,3-g:2′,3′−l:2“,3”-q]porphyrazinato]zinc(II) (**8**). In a large pressure flask, the nitro-Tnpz **7 (**0.40 g; 0.44 mmol) was dissolved in water (20 mL) and reduced as described for amino-Pc **6.** Crude yield 210 mg (54%). Elemental analysis shows correct C/N ratio for this product: calculated 4.56; found 4.47. MALDI-MS calculated for $C_{47}H_{23}N_9O_6Zn$ = 873, found *m*/*z* 874 $(M + H)^+$. (λ_{max} (DMSO) = 750 nm).

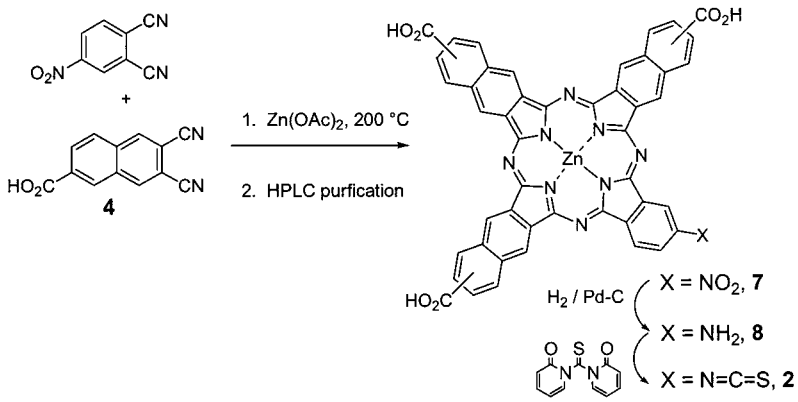
[2-Isothiocyanato-10(11),19(20),28(29)-tricarboxy-benzo[b]trinaphtho[2,3-g:2′,3′−l:2“,3”-q]porphyrazinato]zinc-(II) (**2**). Amino-Tnpz **8** (300 mg; 0.34 mmol) was added to a solution of 1,1′-thiocarbonyldi-2(1*H*)-pyridone (250 mg, 1.08 mmol) in DMF (3 mL) and stirred for 2 h (Scheme 2). The DMF was removed in vacuo and the dark green product was taken up in HPLC grade H_2O and filtered through a 0.45 μM filter to remove insoluble 1,1′-thiocarbonyldi-2(1*H*)-pyridone products. The yield 60 mg (28%). Elemental analysis for $C_{48}H_{21}N_9SO_6Zn{\cdot}7H_2O$, Calculated (Found): C, 51.8, (51.76); H, 3.2 (2.86); N, 11.3 (11.29). MALDI-MS calculated for $C_{48}H_{21}N_9SO_6Zn$ = 916, found *m*/*z* 917 $(M + H)^+$, (λ_{max} (DMSO) = 756 nm, 723 nm).

Labeling and Purification of DNA Oligonucleotides with Pc and Tnpz Functionalized Dyes. An M13 universal sequencing primer (17mer) containing a 6-carbon alkyl linker terminated with an amino group on the 5′-end was derivatized with the dyes according to procedures outlined by Li−COR (*34*). Briefly, 50 nmol of DNA was added to 25 μL of 40 mM carbonate buffer (pH = 9.1), 25 μL of 2 mM EDTA, and 100 μL of the appropriate dye (2.5 mM) dissolved in DMF. After the reaction was allowed to proceed at room temperature for approximately 4 h, 10 μL of 3 M sodium carbonate and 480 μL of cold EtOH were added to the reaction mixture. The solution was centrifuged for 20 min at 4 °C. The supernatant was discarded and the cold ethanol precipitation step repeated again. The DNA/dye conjugate was then dried and 200 μL of water added to the pellet. The DNA/dye conjugate was finally purified using preparatory HPLC under the following conditions: Column, C_{18}; flow rate, 1.7 mL/min; mobile phase A, 0.1 M triethylammonium acetate, 4% acetonitrile, 96% water; mobile

Scheme 1. Synthesis of [1-(Isothiocyanato)-9(10),16(17),23(24)-tris(4-carboxyphenoxy)phthalocyanato]zinc(II) (1)



Scheme 2. Synthesis of [2-Isothiocyanato-10(11),19(20),28(29)-tricarboxy-benzo[*b*]trinaphtho[2,3-*g*:2′,3′−l:2“,3”-*q*]-porphyrazinato]zinc(II) (2)



phase B, 0.1 M triethylammonium acetate, 80% acetonitrile, 20% water. The gradient conditions were 90/10 to 55/45 A/B over 5 min, 55/45 to 0/100 A/B over 20 min, hold 0/100 A/B for 5 min. The collected fractions were pooled and taken to dryness using a centrifugal evaporator and stored in the dark at 0 °C until required for use.

RESULTS AND DISCUSSION

Several different strategies were considered for preparing the water-soluble Pc or Npc dyes containing a labeling moiety. One issue that predicated the selected scheme was the identity of the labeling group on the chromophore. In our case, we selected a labeling group to target primary amines, either an isothiocyanate or succinimide ester. Neither of these reactive groups [Figure 1A, L = NCS, or L = CO(OSu)] would be expected to survive Pc or Npc ring assembly even under the mildest basic or acidic conditions. Therefore, it was decided that the reactive group “L” (Figure 1A) would have to be incorporated following ring assembly from a precursor that was stable to these reaction conditions. We selected isothiocyanates as the final amine-labeling group, since they can be quantitatively prepared from amines using thiophosgene (or synthetic equivalents). However, in our hands the condensation of aminophthalonitriles (L = NH_2) to form the final ring structure was not successful (data not shown). Thus, we chose the *nitro*phthalonitriles (L = NO_2) as masked forms of *amino*phthalonitriles as these were found to be stable under our ring assembly conditions (vide infra, Schemes 1 and 2). Sulfonates are the most commonly used water-solubilizing groups and can be incorporated into the phthalonitrile precursor or added postsynthetically by aromatic sulfonation. In our hands, postassembly sulfonation of nitro-substituted Pc or Npc analogues was unsuccessful due to decomposition of the macrocycle from harsh acidic conditions (*14*). Coassembly of nitrophthalonitriles and sulfonaphthalonitriles did produce near-IR products, but separation of the congeners of these reactions proved impossible either before or after the reduction of the nitro group (data not shown).

We chose to use Zn as the metal center for the Pc and pseudo-Npc dyes as this was both synthetically convenient and provided highly fluorescent dyes (*28*). Metals such as Cu or Co incorporated into the ring center yielded chromophores with only weak fluorescence. Coassembly of the nitrophthalonitrile with the carboxynaphthalonitrile in the presence of zinc acetate provided the most successful synthetic route for preparing our asymmetrical macrocycles (Schemes 1 and 2).

In general, the condensation of two different phthalonitriles, **A** and **B**, with an appropriate metal should produce a mixture of Pcs containing a statistical mixture of products: four **A** or **B** units (**AAAA** or **BBBB**), three **A** units and one **B** unit (**AAAB**), three **B** units and one **A** unit (**BBBA**), or two **A** units and two **B** units (two isomers: **ABAB** and **AABB**). To skew the product mixture toward the desired product having three water-solubilizing groups and one conjugatable group, we used a 3:1 stoichiometric ratio of the two phthalonitrile coupling partners. However, solventless condensation of 3 equiv of 4-(3,4-dicyanophenoxy)benzoic acid (**3**) and

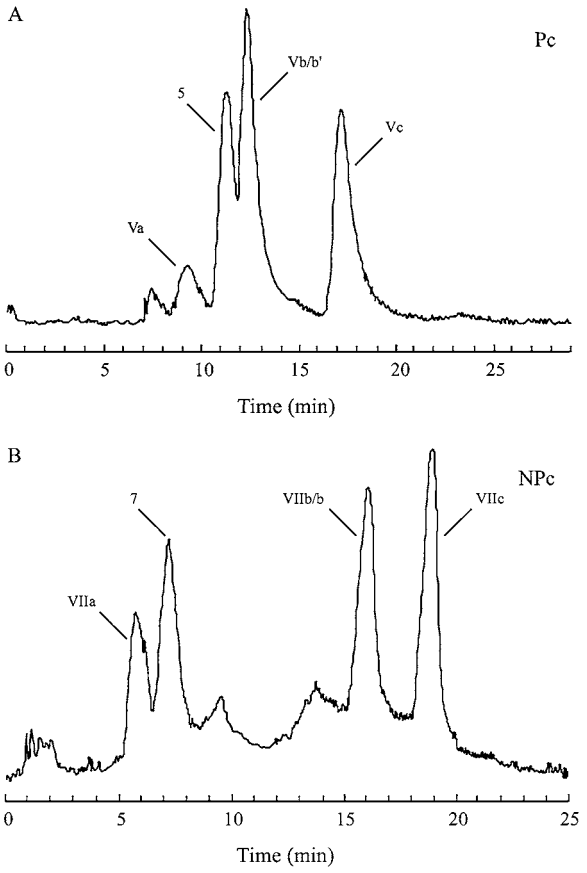


Figure 3. (A) HPLC chromatogram of the crude mixture of Pc congers **Va**, **5**, **Vb**, **Vb′** and **Vc**. Note the uncharged tetranitro-Pz congener **Vd** is removed during the workup of the crude reaction as it is not at all soluble in water. HPLC conditions: Hamilton PRP-1 analytical column (4.6 × 15 cm; flow rate 2 mL/min) and a gradient of 0.1 M triethylammonium acetate/20 mM sodium phosphate buffer (pH = 10.1) and THF (0−100% THF) over 25 min, detection 680 nm. (B) HPLC chromatogram of the crude mixture of Tnpz congeners (**VIIa**, **7**, **VIIb/b′**, **VIIc**). Note the uncharged tetranitro-Tnpz congener **VIId** is removed during the workup of the crude reaction as it is not at all soluble in water. HPLC conditions: same as above except detection at 700 nm.

with 1 equiv of 3-nitrophthalonitrile in the presence of zinc acetate still produced a mixture of at least four congeners (as mixtures of constitutional/positional isomers) as shown by HPLC and MS analysis (see Figure 3A). The organic soluble self-condensation product of 3-nitrophthalocyanine was likely removed during extraction of the product. Similar condensation of 3 equiv of 6,7-dicyano-2-naphthalenecarboxylic with 1 equiv of 4-nitrophthalonitrile again produced four major congeners as seen in the chromatograms shown in Figure 3B.

To aid in characterization of the mixtures, the individual precursors, 6,7-dicyano-2-naphthalenecarboxylic acid precursor and nitrophthalonitrile, were reacted separately with zinc acetate and monitored by UV absorbance (see Figure 4). The water-soluble tetracarboxylate zinc Npc **VIIa** was determined to have an absorption maximum at 768 nm, which corresponded to the absorption maximum of the first fraction eluting from the HPLC (t_r = 5.68 min, Figure 3B). The more hydrophobic trinitro zinc Pc **VIIc** was determined to have an absorbance maximum at 684 nm, which also corresponded to the fourth eluting component (t_r = 18.82 min) shown in the chromatogram of Figure 3B.

Following HPLC purification, the isolated product was brought to dryness under reduced pressure and the

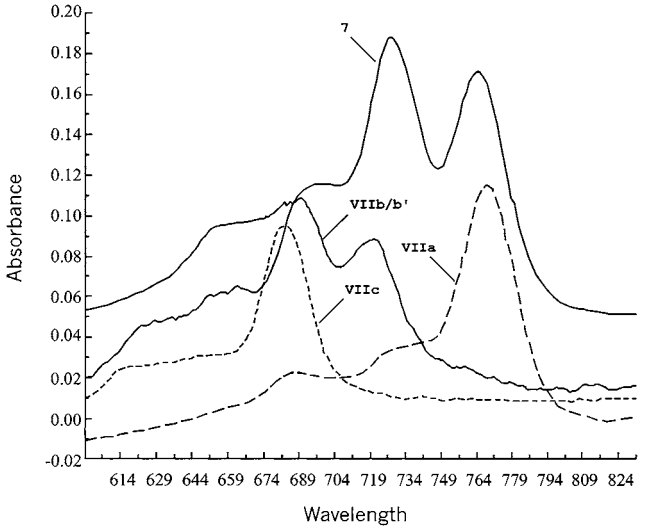


Figure 4. UV absorbance profiles of crude HPLC fractions containing Tnpz congeners (**VIIa**, **7**, **VIIb/b′**, **VIIc**; see Figure 2A) were evaluated after collection from the HPLC (concentrations are unknown).

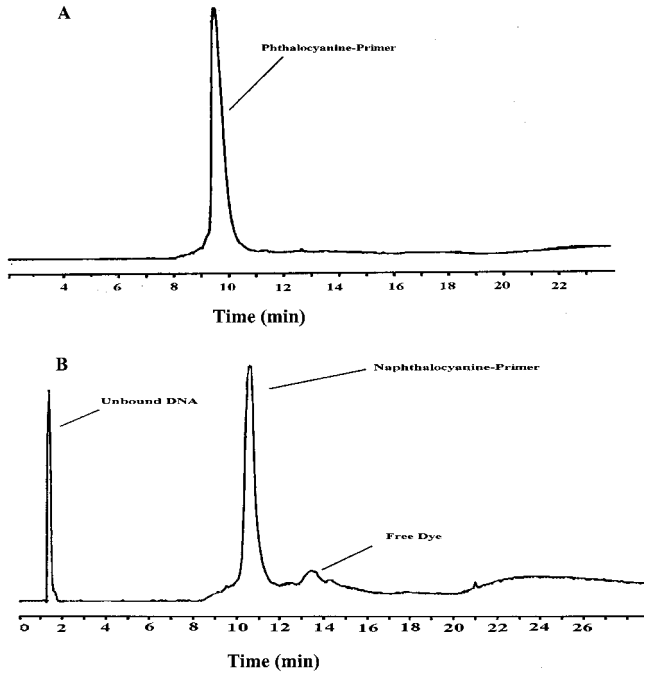
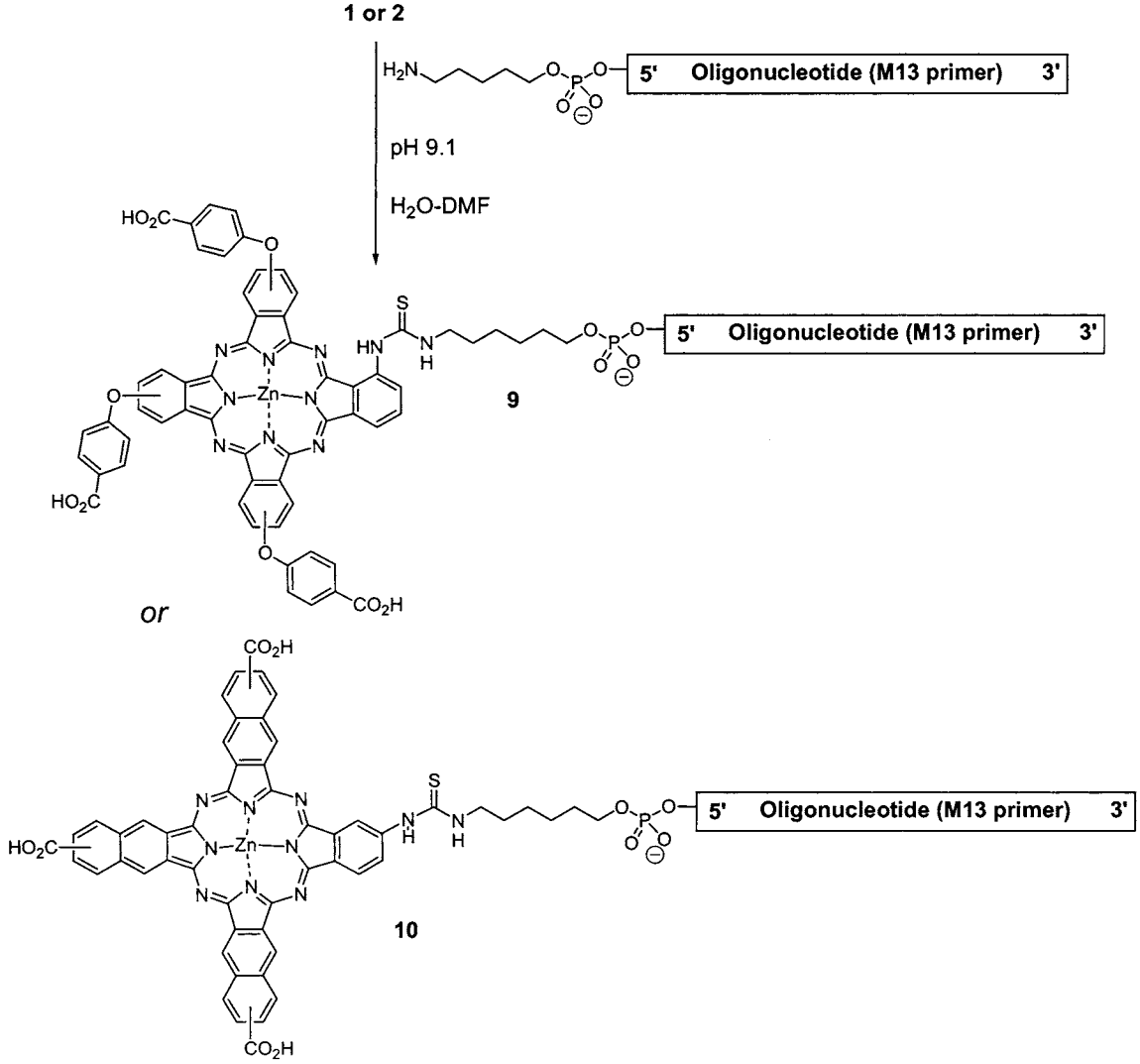


Figure 5. Reverse-phase HPLC chromatograms of (A) Pc-labeled M13 primer (**9**) and (B) Tnpz-labeled M13 primer (**10**). Column: Reverse Phase-C_{18} 50 × 4.6 mm i.d.; mobile phase: 0.1 M TEAA, pH = 7.0 linear gradient 4 to 80% acetonitrile in 20 min; flow rate: 1.7 mL/min. UV absorbance detection at 254 nm. See Experimental Section for gradient conditions.

water-soluble nitro compound (**5** or **7**) was reduced to the amino group (**6** or **8**) by hydrogenation over palladium/charcoal (Schemes 1 and 2). We originally attempted to reduce the nitro group using Sn(II) chloride in hydrochloric acid. However, the reaction was unsuccessful due to decomposition of the macrocycle and possible exchange of the zinc metal with tin. For conversion of the amino group to the reactive isothiocyanate (**1** or **2**), 1,1′-thiocarbonyldi-2(1*H*)-pyridone was preferred over thiophosgene because of its ease of handling and higher stability, which resulted in higher product yields.

After purification by reverse-phase chromatography, the analysis and structural characterization by mass

Scheme 3. Conjugation of Pc Dyes to an Oligonucleotide



spectrometry (MALDI-MS, negative mode) of the substituted derivatives exhibited the characteristic pseudomolecular ion for Pc **1** and **Tnpz 2**. The infrared spectra demonstrated very strong lines at 1645 cm^{-1} (C═O), 1525 cm^{1} (NO_2), 1350 cm^{-1} (NO_2) for compounds **5** and **7**. Unfortunately, the infrared spectra of the amino (**6**, **8**) and isothiocyanate (**1**, **2**) groups in the target dyes were obscured by other absorbances. The H^1 NMR spectrum provided little information due to substantial aggregation of the samples in the solvents required for NMR, which produced significant broadening in the signal peaks.

The HPLC chromatograms shown in Figure 5 depict the conjugates formed following reaction of an amine-modified DNA 17mer oligonucleotide with the water-soluble Pc (**1**) or Tnpz (**2**) dyes containing the reactive isothiocyanate functional group (Scheme 3) to make DNA−dye conjugates **9** (Figure 5A) and **10** (Figure 5B), respectively. Both dyes demonstrated reasonable conjugation efficiency toward the amine-containing oligonucleotide. In the chromatogram of the Pc **1** conjugation mixture, it is apparent that the conjugation efficiency was slightly better compared to the Tnpz **2** because of the disappearance of unbound DNA in the conjugation reaction. The extinction coefficients for both dyes at 260 nm were found to be small, thereby producing little or no detectable absorbance signal in the chromatogram from free dye. We are not sure of the reason for the slightly poorer conjugation of the Tnpz dye, but it may be due to greater aggregation of the more hydrophobic Tnpz in the conjugation solvent, which lowered its availability for conjugation to the amine of the DNA.

In Figure 6A is shown the absorbance spectrum of the Tnpz dye **2** in methanol/DMF, which displayed two absorption bands at 755 and 725 nm, while the spectrum for this dye in an aqueous buffer solution showed significant broadening, indicative of extensive ground-state aggregation. In the case of the dye−oligonucleotide conjugate, the absorption maximum was found to be 735 nm, with the peak at ~755 nm appearing as only a weak shoulder on the band at 735 nm. The fluorescence emission profile (see Figure 6B) for the Tnpz dye **2** displayed a maximum at ~ 765 nm, while the oligonucleotide conjugate **10** showed a 15 nm red shift (λ_{em} = 780 nm). Using procedures outlined in our previous work for determining the quantum yields of near-IR dyes (*35*), the quantum yield of the conjugate was found to be 0.20 with an extinction coefficient of 1.82×10^5 cm^{-1} M^{-1}.

The dual absorbance bands observed in the electronic spectra of pseudo-Npc **2** most likely resulted from the asymmetrical character of this type of compound. When one of the four naphtho groups along the macrocycle is replaced by a benzo group, it would be expected that only one major absorption band be observed. The presence of a symmetric, single absorption band would suggest that both the molecular asymmetry and the substituents exert a synergistic effect on the electronic properties of the

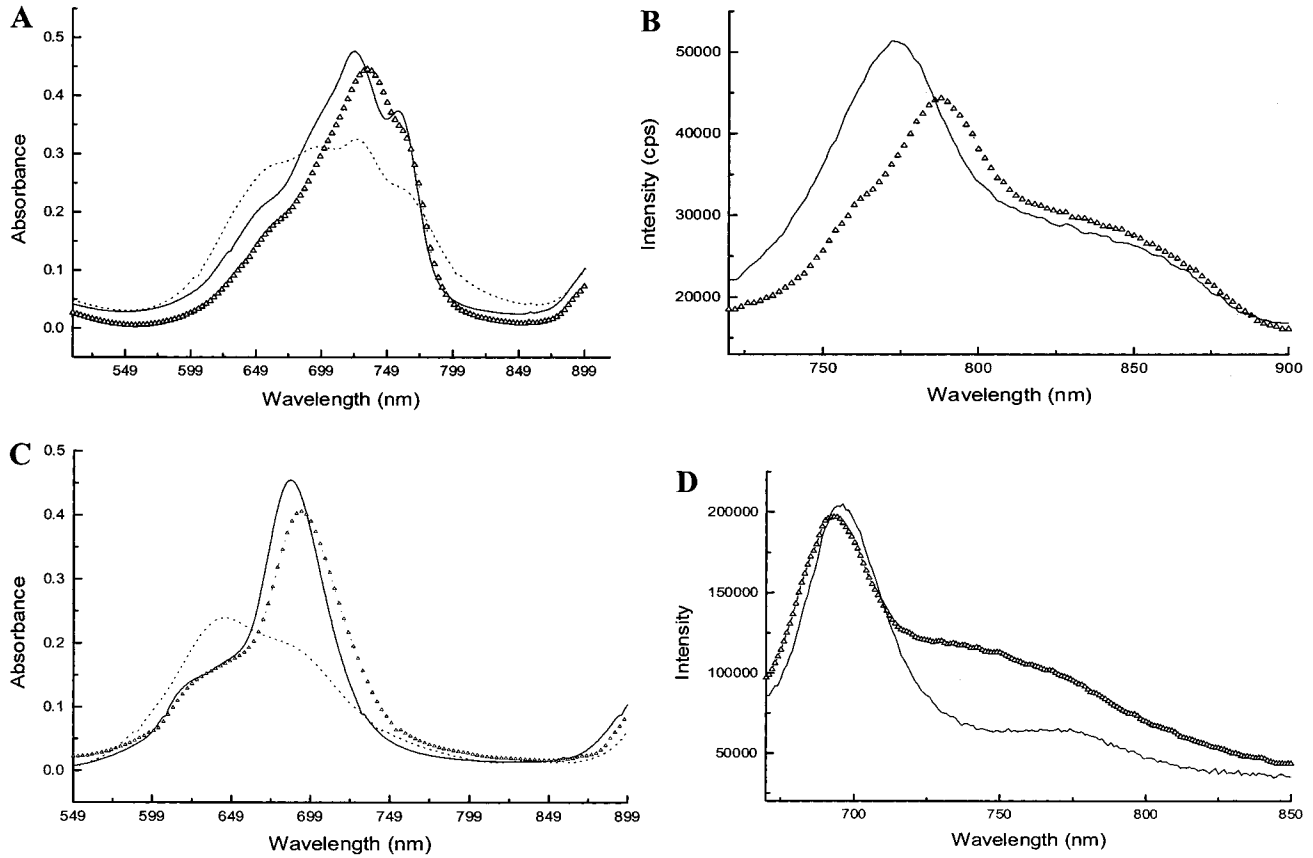


Figure 6. Absorbance (A) and emission (B) spectra of: Tnpz dye **2** in 40 mM borate buffer (- - -); Tnpz dye **2** in 70:30 methanol/DMF (—), and Tnpz-oligonucleotide conjugate **10** in 40 mM borate buffer/30% DMF (△). Absorbance (C) and emission (D) spectra of: Pc dye **1** in 40 mM borate buffer (- - -); Pc dye **1** in 70:30 methanol/DMF (—); and Pc-oligonucleotide conjugate **9** in 40 mM borate buffer/30% DMF (△). The dye concentration for all the experiments was ~2.5×10^{-6} M.

macrocycle derivatives. Instead, we observed two bands in the naphthalocyanine absorption region in organic solvent, which would be expected to be relatively free of aggregation. This observation is in agreement with the 2-fold orbital degeneracy of the excited electronic state of the metallomacrocycle when the group symmetry changes from pseudo-D_{4h} (as in Zn−Pc **1**) to pseudo-C_{2v} (as in Tnpz **2**) (*36*).

The extensive broadening of the absorption spectrum of the free dye in the aqueous buffer solution resulted from extensive ground-state aggregation; however, the dye−oligonucleotide conjugate in this same solvent system displayed predominately the monomeric form, as was evident from the similarity of the electronic spectra for the conjugate in water and free dye in CH_3OH/DMF, where only the monomeric form is expected to be the major component.

The absorption maximum for the Pc **1** dye was found to be 683 nm (see Figure 7C) and the maximum for the **1**−oligonucleotide conjugate was determined to be 694 nm, an 11 nm red shift with respect to the free dye. As with the Tnpz dye in aqueous solvents, Pc dye **1** demonstrated extensive ground state aggregation as is evident from the broad electronic spectrum. However, this aggregation effect was reduced to a large degree when the free dye was conjugated to the highly anionic DNA oligonucleotide. The fluorescence emission profile (see Figure 6D) for the free dye and dye/oligonucleotide conjugate were determined to be 700 and 692 nm, respectively. The extinction coefficient for the conjugate was found to be 1.9×10^5 cm^{-1} M^{-1} with a quantum yield of 0.26.

CONCLUSIONS

We have prepared two near-IR labeling dyes, **1** and **2** (see Figure 1), which are asymmetric Pc and Npc dyes that contain water-solubilizing groups and a labile functional group appropriate for tagging compounds containing primary amines. While most Pc and Npc dyes show poor water solubility, the excellent water solubility demonstrated by these dyes was achieved by insertion of the negatively charged carboxylate groups into the metallomacrocycle. The labeling dyes demonstrated facile conjugation to nucleic acids containing a primary amine group and yielded DNA conjugates that fluoresced strongly in the near-IR. Due to the favorable photophysical properties of these labeling dyes and their superior water solubility, they will make excellent fluorescent tags for genetic assays requiring ultrasensitive fluorescence analysis.

ACKNOWLEDGMENT

The authors would like to thank the NIH (R01-HG01499 and R24-CA84625) for financial support of this work. The authors would also like to express their appreciation to Dr. Tracy McCarley for assistance on obtaining the mass spectrometric measurements and Dr. Frank Zhou for his assistance with the NMR spectrometry.

LITERATURE CITED

(1) Wehr, E. L. (1976) *Modern Fluorescence Spectroscopy*, Plenum Press, New York.
(2) Bright, F. V. (1988) Bioanalytical Applications of Fluorescence Spectroscopy. *Anal. Chem. 60*, A1031-A1039.

(3) Sauda, K., Imasaka, T., and Ishibashi, N. (1986) High-Performance Liquid-Chromatographic Detector Based on Near-Infrared Semiconductor-Laser Fluorometry. *Anal. Chim. Acta 187*, 353−356.
(4) Sauda, K., Imasaka, T., and Ishibashi, N. (1986) Determination of Protein in Human-Serum by High-Performance Liquid-Chromatography with Semiconductor-Laser Fluorometric Detection. *Anal. Chem. 58*, 2649−2653.
(5) Williams, R. J., Lipowska, M., Patonay, G., and Strekowski, L. (1993) Comparison of Covalent and Noncovalent Labeling with near- Infrared Dyes for the High-Performance Liquid-Chromatographic Determination of Human Serum-Albumin. *Anal. Chem. 65*, 601−605.
(6) Bachteler, G., Drexhage, K. H., Ardenjacob, J., Han, K. T., and Kollner, M. et al. (1994) Sensitive Fluorescence Detection in Capillary Electrophoresis Using Laser-Diodes and Multiplex Dyes. *J. Luminesc. 62*, 101−108.
(7) Fuchigami, T., and Imasaka, T. (1994) Capillary Micellar Electrokinetic Chromatography Based on Indirect Semiconductor-Laser Fluorescence Detection. *Anal. Chim. Acta 291*, 183−188.
(8) Fuchigami, T., Imasaka, T., and Shiga, M. (1993) Subatomole Detection of Amino-Acids by Capillary Electrophoresis Based on Semiconductor-Laser Fluorescence Detection. *Anal. Chim. Acta 282*, 209−213.
(9) Flanagan, J. H., Legendre, B. L., Hammer, R. P., and Soper, S. A. (1995) Binary Solvent Effects in Capillary Zone Electrophoresis with Ultrasensitive near-IR Fluorescence Detection of Related Tricarbocyanine Dyes and Dye-Labeled Amino-Acids. *Anal. Chem. 67*, 341−347.
(10) Higashijima, T., Fuchigami, T., Imasaka, T., and Ishibashi, N. (1992) Determination of Amino-Acids by Capillary Zone Electrophoresis Based on Semiconductor-Laser Fluorescence Detection. *Anal. Chem. 64*, 711−714.
(11) Williams, D. C., and Soper, S. A. (1995) Ultrasensitive near-IR Fluorescence Detection for Capillary Gel-Electrophoresis and DNA-Sequencing Applications. *Anal. Chem. 67*, 3427−3432.
(12) Flanagan, J. H., Owens, C. V., Romero, S. E., Waddell, E., Kahn, S. H., Hammer, R. P., and Soper, S. A. (1998) Near-infrared heavy-atom-modified fluorescent dyes for base- calling in DNA-sequencing applications using temporal discrimination. *Anal. Chem. 70*, 2676−2684.
(13) Mank, A. J. G., Lingeman, H., and Gooijer, C. (1992) Diode Laser-Induced Fluorescence Detection in Chromatography. *Trac-Trends in Anal. Chem. 11*, 210−217.
(14) Shealy, D. B., Lipowska, M., Lipowski, J., Narayanan, N., Sutter, S., Strekowski, L., and Patonay, G. (1995) Synthesis, Chromatographic-Separation, and Characterization of near-Infrared-Labeled DNA Oligomers for Use in DNA-Sequencing. *Anal. Chem. 67*, 247−251.
(15) Shealy, D. B., Lohrmann, R., Ruth, J. R., Narayanan, N., Sutter, S. L., Casay, G., Evans, L., and Patonay, G. (1995) Spectral characterization and evaluation of modified near-infrared laser dyes for DNA sequencing. *Appl. Spectrosc. 49*, 1815−1820.
(16) Ernst, L. A., Gupta, R. K., Mujumdar, R. B., and Waggoner, A. S. (1989) Cyanine Dye Labeling Reagents for Sulfhydryl-Groups. *Cytometry 10*, 3−10.
(17) Mujumdar, R. B., Ernst, L. A., Mujumdar, S. R., and Waggoner, A. S. (1989) Cyanine Dye Labeling Reagents Containing Isothiocyanate Groups. *Cytometry* **1989**, *10*, 11−19.
(18) Strekowski, L., Lipowska, M., and Patonay, G. (1992) Facile Derivatizations of Heptamethine Cyanine Dyes. *Synth. Commun. 22*, 2593−2598.
(19) Strekowski, L., Lipowska, M., Gorecki, T., Mason, J. C., and Patonay, G. (1996) Functionalization of near-infrared cyanine dyes. *J. Heterocycl. Chem. 33*, 1685−1688.
(20) Strekowski, L., Gorecki, T., Mason, J. C., Lee, H., and Patonay, G. (2001) New heptamethine cyanine reagents for labeling of biomolecules with a near-infrared chromophore. *Heterocycl. Commun. 7*, 117−122.
(21) Strekowski, L., Lipowska, M., and Patonay, G. (1992) Substitution-Reactions of a Nucleofugal Group in Heptamethine Cyanine Dyes − Synthesis of an Isothiocyanato Derivative for Labeling of Proteins with a near-Infrared Chromophore. *J. Org. Chem. 57*, 4578−4580.
(22) Lipowska, M., Patonay, G., and Strekowski, L. (1991) Synthesis of Novel near-Infrared (NIR) Dyes with Improved Properties for Bioanalytical Applications. *Abstracts of Papers*, 201st National Meeting of the American Chemical Society, 68-ORGN.
(23) Lipowska, M., Patonay, G., and Strekowski, L. (1993) New near-Infrared Cyanine Dyes for Labeling of Proteins. *Synth. Commun. 23*, 3087−3094.
(24) Ambroz, M., Beeby, A., Macrobert, A. J., Simpson, M. S. C., Svensen, R. K., and Phillips, D. (1991) Preparative, Analytical and Fluorescence Spectroscopic Studies of Sulfonated Aluminum Phthalocyanine Photosensitizers. *J. Photochem. Photobiol. B-Biol. 9*, 87−95.
(25) Soper, S. A., and Legendre, B. L. (1998) Single-molecule detection in the near-IR using continuous-wave diode laser excitation with an avalanche photon detector. *Appl. Spectrosc. 52*, 1−6.
(26) Soper, S. A., Mattingly, Q. L., and Vegunta, P. (1993) Photon Burst Detection of Single near-Infrared Fluorescent Molecules. *Anal. Chem. 65*, 740−747.
(27) Wheeler, B. L., Nagasubramanian, G., Bard, A. J., Schechtman, L. A., Dininny, D. R., and Kenney, M. E. (1984) A Silicon Phthalocyanine and a Silicon Naphthalocyanine − Synthesis, Electrochemistry, and Electrogenerated Chemi-Luminescence. *J. Am. Chem. Soc. 106*, 7404−7410.
(28) Bradbrook, E. F., and Linstead, R. P. (1936) Preparation of 10 dicyanonaphthalenes and the related naphthalenedicarboxylic acids. *J. Chem. Soc.* 1739−1744.
(29) Kovshev, E. I., Pichnova, V. A., and Lik′yanets, E. A. (1971) Phthalocyanines and related compounds. VI. Synthesis of dinitriles of substituted naphthalene-2,3-dicarboxylic acids. *Zh. Org. Khim.* 369−371.
(30) Sharman, W. M., Kudrevich, S. V., and van Lier, J. E. (1996) Novel water-soluble phthalocyanines substituted with phosphonate moieties on the benzorings. *Tetrahedron Lett. 37*, 5831−5834.
(31) Leznoff, C. C., Svirskaya, P. I., Khouw, B., Cerny, R. L., Seymour, P., and Lever, A. B. P. (1991) Syntheses of Monometallated and Unsymmetrically Substituted Binuclear Phthalocyanines and a Pentanuclear Phthalocyanine by Solution and Polymer Support Methods. *J. Org. Chem. 56*, 82−90.
(32) Weitemeyer, A., Kliesch, H., and Wohrle, D. (1995) Unsymmetrically Substituted Phthalocyanine Derivatives Via a Modified Ring Enlargement Reaction of Unsubstituted Subphthalocyanine. *J. Org. Chem. 60*, 4900−4904.
(33) Kliesch, H., Weitemeyer, A., Muller, S., and Wohrle, D. (1995) Synthesis of Phthalocyanines with One Sulfonic-Acid, Carboxylic-Acid, or Amino Group. *Liebigs Ann.* 1269−1273.
(34) Li-COR, Lincoln, NE private communication.
(35) Soper, S. A., and Mattingly, Q. L. (1994) Steady-State and Picosecond Laser Fluorescence Studies of Nonradiative Pathways in Tricarbocyanine Dyes − Implications to the Design of near-IR Fluorochromes with High Fluorescence Efficiencies. *J. Am. Chem. Soc. 116*, 3744−3752.
(36) Solov′ev, K. N., Mashenkov, V. A., and Kachura, T. F. (1969) Effect of aza substitution on the spectral-luminescent properties of benzoporphyrins. *Opt. Spectrosk. 27*, 50−60.

BC0155869

Fractionation and Characterization of a Conjugate between a Polymeric Drug-Carrier and the Antitumor Drug Camptothecin

R. Mendichi,*,† V. Rizzo,‡ M. Gigli,‡ and A. Giacometti Schieroni†

Istituto per lo Studio delle Macromolecole (CNR), Via E. Bassini 15, 20133 Milan, Italy, and Pharmacia, Viale Pasteur 10, 20014 Nerviano (MI), Italy Received February 26, 2002; Revised Manuscript Received July 12, 2002

A conjugate between the antitumor drug camptothecin and the polymeric drug-carrier poly[*N*-(2-hydroxypropyl)methacrylamide] was synthesized and fractionated. The conjugate samples, both fractionated and unfractionated, were characterized with a multi-detector SEC system using three on-line detectors: a multi-angle light scattering photometer, a viscometer, and a refractometer. The used mobile phase (DMF + 0.01 M LiBr + 0.05 M CH_3COOH) derives from previous experience with similar conjugates. Narrow molar mass distribution fractions of the conjugate obtained by means of a semipreparative LC system were used to derive the coefficients of the Mark−Houwink−Sakurada relationship and to check the universal calibration of the SEC system. This study has demonstrated that the conjugate elutes according to the hydrodynamic volume. Thus, a conventional SEC method that uses only an on-line refractometer detector, commercially available narrow standards, and the universal calibration is adequate for the characterization of the molar mass distribution. Also the size and the conformation of the conjugate were studied by means of the gyration radius−molar mass power law.

INTRODUCTION

The use of synthetic polymers in controlled drug delivery attracts more and more interest (*1*−*5*). It is generally accepted that the success of a polymeric drug delivery system mainly depends on the properties of the used macromolecular carrier (*6*−*8*). Consequently, extensive characterization of the polymeric drug-carrier (both physicochemical and toxicologic) is of paramount relevance. Specifically, in the past few years we have characterized two different conjugates between the polymer poly[*N*-(2-hydroxypropyl)methacrylamide] (PHPMA) and two antitumor drugs. In 1996, we presented the characterization of the conjugate between PHPMA and doxorubicin (DOX) (*9*). In 1998, we presented the characterization of the conjugate between PHPMA and paclitaxel (TAX) (*10*, *11*). Both conjugates underwent phase I clinical studies, and the corresponding results were published (*12*, *13*). Continuing the project, this article presents the characterization of a new conjugate between PHPMA and the antitumor drug camptothecin (CPT). This conjugate and other related analogues have shown very promising results in preclinical models (*14*, *15*). Figure 1 shows a schematic structure of this new PHPMA-CPT conjugate that recently underwent a phase I clinical study.

PHPMA-CPT is water-soluble, and, as with the previous two conjugates, the drug is covalently bound to the carrier via an appropriate spacer. PHPMA is a synthetic polymeric drug-carrier suitable for cancer chemotherapy. PHPMA is biocompatible, water-soluble, nontoxic, and nonimmunogenic, but unfortunately is not biodegradable.

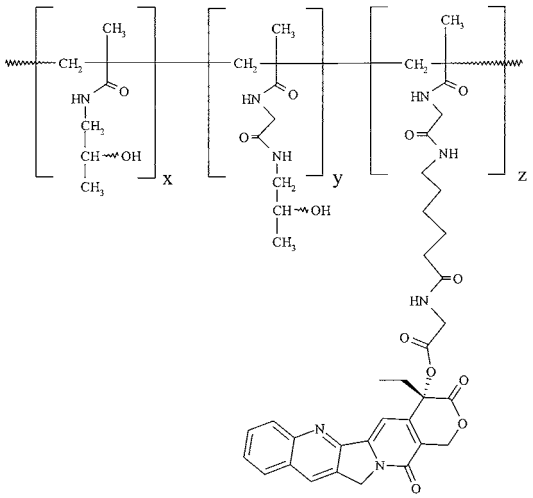


Figure 1. Structure of the PHPMA-CPT conjugate.

Thus, accumulation of the polymer in the body of patients has to be carefully avoided by keeping the whole molar mass distribution (MMD) below the renal excretion threshold (*16*). Moreover, the properties of the whole conjugate have to be studied in detail. Great importance in the biodistribution and excretion patterns of a macromolecular conjugate is attributed to its molecular properties, including MMD and molecular size (*7*, *17*, *18*). However, the conformational properties and the affinity of the macromolecule with the biochemical environment may influence its biodistribution into the organism (*19*).

This study presents the fractionation and the molecular characterization of the PHPMA-CPT conjugate by means of a size exclusion chromatography (SEC) system using three on-line detectors: a multi-angle laser light scattering (MALS) photometer, a single capillary viscometer (SCV), and a differential refractometer as concentration detector. We also report on the determination of the

* Correspondence should be addressed to this author at the Istituto per lo Studio delle Macromolecole (CNR), Via Bassini 15, 20133 Milan, Italy. Phone: +39 02 23699375, Fax: +39 02 2362946, E-mail: carmol@icm.mi.cnr.it.

† Istituto per lo Studio delle Macromolecole (CNR).

‡ Pharmacia.

10.1021/bc025522d CCC: $22.00 © 2002 American Chemical Society
Published on Web 09/11/2002

Table 1. Origin of the 11 PHPMA-CPT Narrow MMD Fractions

lot[a]	fractions	M_w (kg/mol)	D
1	1−5	128.2	2.8
2	6−9	19.9	1.4
3	10	3.7	1.4
4	11	2.7	1.3

[a] For the synthesis of the four lots, see Materials.

bound drug content with an appropriate combination of selective hydrolysis and HPLC separation.

MATERIALS AND METHODS

MATERIALS

PHPMA-CPT samples were Pharmacia (Nerviano, Milan, Italy) products. The study was performed using both fractionated and unfractionated PHPMA-CPT samples. Table 1 summarizes the starting broad MMD lots and the narrow MMD fractions of the PHPMA-CPT conjugate. Two laboratory scale lots of PHPMA-CPT, with sizeably different molar mass values, have been used as starting material for the preparation of nine narrow MMD fractions. Lot 1 was obtained by copolymerization of methacryloyl-glycyl-6-NH_2-hexanoyl-glycyl-20-*O*-camptothecin and methacryloyl-2-propanolamide in the presence of α,α′-azo-isobutyro-nitrile in dimethyl sulfoxide at 50 °C for 48 h under stirring. Lot 2 was obtained by coupling a polymeric precursor bearing an activated ester with H_2N-$(CH_2)_5$-CO-Gly camptothecin as described in detail elsewhere (*15*). Two other low molar mass copolymers, lots 3 and 4, were obtained as described for lot 1, with the following changes: solvent was acetonylacetone (80 °C) for fraction 10 and *N*,*N*-dimethylformamide (DMF, 80 °C) for fraction 11, respectively. Lot 5 is a typical laboratory scale preparation as used during the preclinical investigation phase on PHPMA-CPT.

METHODS

Hydrolysis of Bound Camptothecin. A sample of the polymeric conjugate is weighed (about 6 mg), transferred into a screw cap tube, and dissolved under tube shaking with 7.5 mL of methanol and 7.5 mL of borate buffer (50 mM, pH 9.4). The solution is sonicated for 2 min and placed in a thermostat at 30 °C. After 20 h, the reaction is stopped with the addition of 0.1 mL of 42.5% phosphoric acid ($pH_{app} = 3$). After 1 h at room temperature (to allow reestablishment of the camptothecin lactone ring), this solution can be used for HPLC analysis within the next 20 h. A similar procedure has been applied to the bioassay of polymer-bound camptothecin in plasma samples (*20*).

A stock solution of standard camptothecin in methanol is prepared by dissolving a weighed amount (about 5 mg) of camptothecin in 50 mL of methanol. As a reference for total camptothecin assay, 5 mL of the above stock solution is transferred into a screw cap tube and diluted with 2.5 mL of methanol, 0.1 mL of 42.5% phosphoric acid, and 7.5 mL of borate buffer.

Chromatographic Method for the Determination of Bound Camptothecin. The HPLC system was a Hewlett & Packard 1090 equipped with diode array detector. After sample injection (50 μL), separation was obtained on a Waters Symmetry C18 150 × 3.9 mm 100 Å, 5 μm at 1 mL/min flow and 40 °C using 25 mM KH_2PO_4, pH 2.5, and methanol as mobile phase and the gradient program as indicated below. After 4 min of isocratic run at 45% methanol, this was linearly increased to 55% in 1 min and maintained for the next 3 min. A second linear gradient up to 90% methanol was then applied within 1 min, and this methanol content was maintained for the next 5 min. Finally, the methanol content was restored to 45% and the system allowed to reequilibrate for 8 min. Data were collected at 370 nm with a bandwidth of 4 nm (reference wavelength 550 nm, bandwidth 100 nm).

This method was applied to a solution of PHPMA-CPT for the determination of free camptothecin, and subsequently to the hydrolysate for the determination of total (free + bound) camptothecin. The amount of bound drug was obtained from the difference of the two determinations. However, in all cases reported in this paper, the contribution of the free drug was negligible.

SEC Chromatographic System. SEC fractionation and characterization was performed by means of a multidetector system. The SEC system consisted of an Alliance 2690 LC separation module (degasser, pump, and autoinjector), a single-capillary viscometer (SCV), a differential refractometer (DRI) from Waters (Milford, MA), and an additional MALS on-line detector from Wyatt (Santa Barbara, CA). This multi-detector SEC system has been described in detail previously (*21*). The used ternary mobile phase (DMF + 0.01 M LiBr + 0.05 M CH_3COOH) proved already suitable for similar conjugates (*9*−*11*). In general, the column set was composed of two Styragel columns (HR4 and HR3) from Waters. In the characterization of the higher molar mass fractions, we have used also a third Styragel HR5 column. The experimental conditions were the following: 50 °C temperature, 0.8 mL/min flow rate, and 200 μL injection volume.

Light Scattering. The MALS photometer uses a vertically polarized He−Ne laser and simultaneously measures the intensity of the scattered light at 16 angular locations ranging in the mobile phase from 16.5° to 156.9°. The calibration constant was calculated using toluene as standard and assuming a Rayleigh factor of 1.406×10^{-5} cm^{-1}. The normalization of the photodiodes was performed by measuring the scattering intensity of a narrow low molar mass polystyrene standard ($M = 10.9$ kg/mol, $D < 1.03$) in the mobile phase assumed as an isotropic scatterer. Details of the MALS detector have been described elsewhere (*22*) and are not reported herein.

Viscometers. The on-line viscometer was a custom-assembly. Details of this on-line SCV detector have been described elsewhere (*21*). The on-line SCV detector uses the universal calibration (*23*). The universal calibration curve was generated by means of 14 narrow MMD PEO/PEG standards with the molar mass ranging from 106 to 8.5×10^5 g/mol. The off-line viscometer was a classical Ubbelohde capillary viscometer.

d*n*/d*c*. The specific refractive index increment, d*n*/d*c*, with respect to the mobile phase was measured by a Chromatix KMX-16 differential refractometer from LDC Milton Roy (Riviera Beach, FL). The d*n*/d*c* value of the PHPMA-CPT conjugate was 0.128 mL/g.

PHPMA-CPT Fractionation. Fractionation of PHPMA-CPT was performed by semipreparative chromatography on the same type of columns used for SEC analysis, according to molar mass. In particular, lot 1 was loaded at 40 mg/mL on the Styragel HR4 column, whereas lot 2 was chromatographed on a Styragel HR3 column, at the same initial concentration. Fractionation was obtained by diverting the eluate by means of a programmable multi-position valve. The valve switch times had been previously established by injecting a 20 mg/mL sample and by dividing the integrated surface of the peak

Table 2. Summary of the Results for 11 PHPMA-CPT Narrow MMD Fractions

	SEC-MALS		SEC-SCV				SEC-CU			
no.	M_w (kg/mol)	D	M_w (kg/mol)	M_p (kg/mol)	D	$[\eta]$ (dL/g)	M_w (kg/mol)	D	$[\eta]$ (dL/g)	CPT (%, w/w)
1	253.8	1.13	249.7	221.8	1.14	0.555	252.7	1.15	0.547	10.1
2	164.3	1.11	169.8	148.1	1.11	0.383	159.6	1.13	0.409	10.2
3	111.3	1.10	115.5	99.90	1.11	0.305	109.6	1.13	0.321	10.4
4	75.35	1.15	69.06	66.41	1.19	0.249	76.28	1.18	0.254	10.4
5	35.04	1.12	33.60	30.69	1.15	0.138	35.36	1.14	0.156	10.3
6	24.12	1.10	23.18	21.11	1.10	0.111	24.79	1.11	0.124	10.5
7	17.62	1.09	17.22	15.67	1.10	0.094	18.53	1.11	0.103	10.6
8	13.07	1.11	12.90	11.61	1.10	0.083	13.59	1.11	0.085	10.7
9	8.96	1.10	7.99	7.90	1.11	0.069	9.02	1.13	0.065	10.6
10			5.71	3.78	1.39	0.057	6.24	1.37	0.050	9.4
11			3.42	2.71	1.30	0.044	3.53	1.31	0.035	9.8

(obtained from the refractive index detector) into 4−5 fractions. Fractions 1−5 were obtained from lot 1, fractions 6−9 from lot 2. Fractions 10 and 11 were obtained from the two low molar mass copolymers (lots 3 and 4) without any processing.

For each fraction, the eluate volume (DMF, 0.01 M $LiNO_3$, 0.3% v/v acetic acid) was diluted with 5 volumes of ethyl acetate. The precipitate was isolated either by centrifugation and subsequent filtration on sintered glass, or by direct filtration on Whatman 1.0 μm PTFE membranes. Typically, fractions were redissolved in 5 mL of ethyl alcohol and reprecipitated with 10 volumes of ethyl acetate. Finally, products were dried under vacuum at 30 °C overnight.

RESULTS AND DISCUSSION

The practical goal of this study was a simple, accurate, and reproducible SEC method for the MMD characterization of the production batches of the PHPMA-CPT conjugates. Investigation of the molar mass, size, and intrinsic viscosity distributions is necessary to this scope, but it is also beneficial to understanding the conformational properties of the conjugate. Substantially, we have used the same approach applied to the molecular characterization of the previous PHPMA-DOX and PHPMA-TAX conjugates (*9*−*11*). The true, nonrelative MMD of the polymers can be obtained using suitable SEC methods. For this goal, an on-line light scattering detector is the primary choice because it provides directly the molar mass of the polymer eluting from the SEC columns without calibration of the system. Accordingly, in this study we have used a MALS on-line detector for an accurate characterization of the conjugates. However, the light scattering detector is complex and expensive and is not ideal for the quick quality control of the production batches of the conjugates. As an alternative, the MMD of the polymers can be obtained using a calibrated SEC system. In our case, a direct calibration of the SEC system was not convenient because of the continuous need of well-characterized narrow MMD fractions of the PHPMA-CPT conjugate. Consequently, we have chosen the universal calibration (SEC-UC) method performed with commercially available PEO/PEG standards on a conventional SEC system using only an on-line differential refractometer detector. It is well-known that SEC-UC works if the fractionation of the macromolecules is exclusively steric, i.e., based on the size. Other LC enthalpic interactions (adsorption, partition, ionic inclusion or exclusion, etc.) have to be accurately avoided or at least minimized. Specifically, SEC-UC fractionation is based on the hydrodynamic volume of the macromolecules (*23*). The hydrodynamic volume of a macromolecule is proportional to the product of its molar mass times the intrinsic viscosity ($M\cdot[\eta]$). Hence, in a SEC-UC method, the calibration function is: $\log(M\cdot[\eta]) = f(V)$ where V denotes the elution volume. Usually the universal calibration of the SEC system is approximated with a third-order polynomial function. A convenient method to calculate $[\eta]$ from the molar mass, without the use of an on-line viscometer, is the Mark−Houwink−Sakurada (MHS) relationship. The MHS relationship, $[\eta] = k\cdot M^a$, correlates the intrinsic viscosity to the molar mass. The slope a and the intercept k are valid only for the specific combination of polymer, solvent, and temperature. The SEC-UC method requires the MHS coefficients both for the calibrants and for the PHPMA-CPT conjugate. The MHS constants for PEO and PEG in the mobile phase at 50 °C were determined in previous studies (*9*−*11*): PEO: $k = 2.538 \times 10^{-4}$ ($[\eta]$ in dL/g), $a = 0.709$; PEG: $k = 7.895 \times 10^{-4}$, $a = 0.594$. The MHS constants of the PHPMA-CPT conjugate were determined in this study using the 11 narrow MMD fractions.

Characterization of the PHPMA-CPT Fractions. The 11 narrow MMD fractions of the PHPMA-CPT conjugate were carefully characterized using MALS and SCV detectors on-line to the SEC system. Table 2 reports the most important results obtained with three on-line SEC methods. In short, SEC-MALS denotes the dual-detector system MALS and DRI, SEC-SCV denotes the dual-detector system SCV and DRI, and finally SEC-UC denotes the conventional SEC and universal calibration method using narrow MMD PEO/PEG standards as calibrants. SEC-UC data are reported only for comparison. Table 2 shows the weight-average molar mass, M_w, the dispersity index, $D = M_w/M_n$ (where M_n is the numeric-average molar mass), and the molar mass of the apex of the chromatographic peak, M_p, used in the SEC calibration. In addition, by means of SEC-MALS, we have obtained the z-average of the root-mean square radius, $\langle s^2\rangle_z^{1/2}$ (in short hereafter denoted as gyration radius R_g), and by means of SEC-SCV the intrinsic viscosity, $[\eta]$. There is a very good agreement between SEC-MALS and SEC-SCV molar mass values for fractions 1−9 (Table 2) whereas the molar mass of fractions 10 and 11 as obtained by SEC-MALS was substantially higher than the SEC-SCV values. The low molar mass and the comparatively higher polydispersity of these two fractions may well explain this discrepancy. The lower camptothecin content of fractions 10 and 11 with respect to the other nine fractions may also contribute. At variance with the case of the previous two conjugates, PHPMA-DOX and PHPMA-TAX, the influence of the drug on the dn/dc value for PHPMA-CPT was not negligible. The dn/dc value for a reference PHPMA-CPT conjugate, in the mobile phase at 50 °C, was 0.128 mL/g, and the dn/dc value for PHPMA homopolymer was significantly lower:

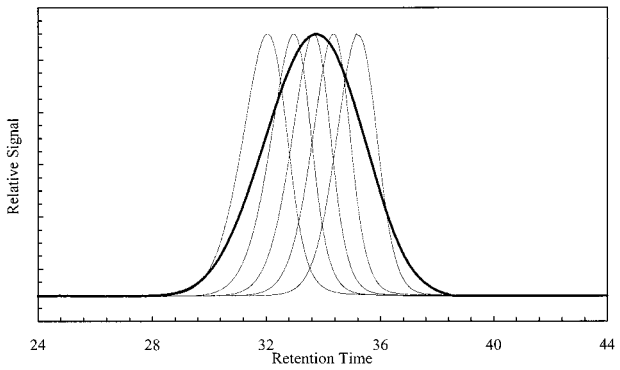


Figure 2. Comparison of the refractometer signals of five narrow MMD fractions (5−9) and of a broad MMD PHPMA-CPT sample (lot 5, boldface line).

0.106 mL/g. This difference is due to the higher drug content of the PHPMA-CPT conjugate, with regard to the former conjugates, and to the relatively high refractive contribution of the camptothecin drug. In view of the problems with the MALS characterization of the two lower molar mass fractions, we have assumed that the molar mass for these two fractions as obtained with the SEC-SCV method was more accurate.

The molar mass range of the 11 PHPMA-CPT fractions is quite large and the MMD very narrow. Figure 2 shows the comparison of the refractometer normalized signals of five narrow MMD fractions (*5*−*9*) and of a broad MMD PHPMA-CPT sample (lot 5). With the exception of the two lower molar mass fractions, the dispersity index D ranges from 1.1 to 1.2, which is adequate for SEC calibration. However, we have to remind ourselves that our final goal was the use of commercially available SEC standards.

For comparison, a selection of the four higher molar mass PHPMA-CPT fractions was characterized also by off-line methods. M_w, the second virial coefficient A_2, and R_g were determined by off-line MALS, that is, using the classical elaboration of a MALS experiment (Zimm-Plot). For each fraction, the use of four concentrations and double extrapolation to infinite dilution and zero-angle led to the three molecular parameters. Furthermore, with a classical Ubbelohde capillary viscometer, we obtained $[\eta]$ of the PHPMA-CPT fractions. The agreement between off-line and on-line M_w and $[\eta]$ results was very good. Finally, M_w, D, and $[\eta]$ values recovered with the conventional SEC-UC method were very close to the corresponding SEC-MALS and SEC-SCV values.

$[\eta] = f(M)$ and $R_g = f(M)$ Power Laws for the PHPMA-CPT Conjugate. The MHS power law for the PHPMA-CPT conjugate is shown in Figure 3. Values of $[\eta]$ and M_w of the 11 narrow MMD PHPMA-CPT fractions, reported in Table 2, were used for the numerical evaluation of "*k*" and "*a*" coefficients of the MHS equation in the SEC mobile phase at 50 °C. The MHS plot is substantially linear with a small discrepancy in the lower molar mass range: approximately $M < 10$ kg/mol. The MHS coefficients as calculated by using nine higher molar mass PHPMA-CPT fractions were $a = 0.64$ and $k = 1.94 \times 10^{-4}$. This result is congruent with the MHS coefficients for the PHPMA homopolymer (*11*).

The MHS coefficients for the PHPMA-CPT conjugate were also estimated using on-line SEC-MALS and SEC-SCV data. The method has been previously described (*11*). The MHS plot is obtained by gathering M and $[\eta]$ data of each slice of the six higher molar mass PHPMA-CPT fractions. Figure 4 shows the MHS plot estimated with on-line M data, from SEC-MALS, and $[\eta]$ data, from

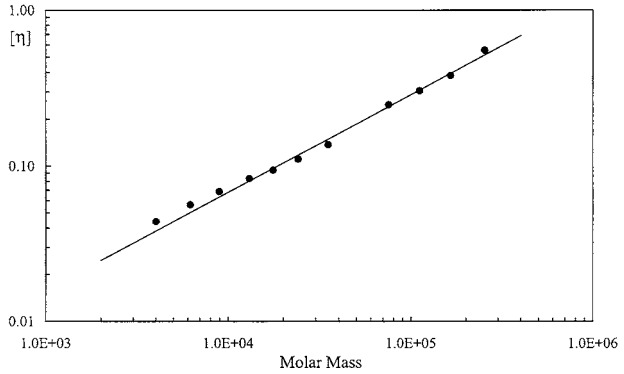


Figure 3. MHS plot for the PHPMA-CPT conjugate from 11 narrow MMD fractions.

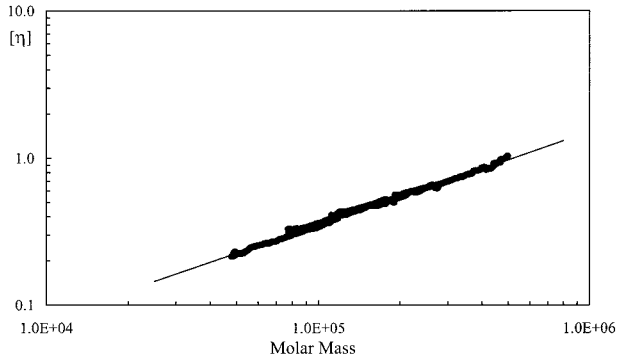


Figure 4. MHS plot for the PHPMA-CPT conjugate from on-line MALS and SCV data.

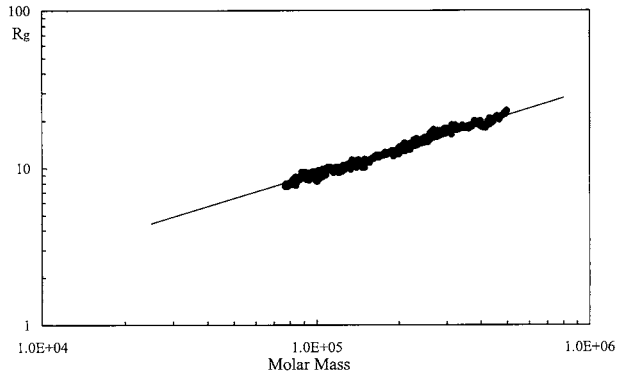


Figure 5. $R_g = f(M)$ power law for the PHPMA-CPT conjugate from on-line MALS data.

SEC-SCV. This approach presents two main advantages: it overcomes the problem of a residual polydispersity of the fractions, and it leads to a derivation of the MHS coefficients from a wide molar mass range. The MHS coefficients derived from on-line measurements were $a = 0.65$ and $k = 1.88 \times 10^{-4}$, with very good agreement between off-line and on-line results. In conclusion, the MHS coefficients obtained with the off-line method have been used in the universal calibration method.

Unfortunately, with the exception of the two higher molar PHPMA-CPT fractions, R_g was too small for an accurate estimation by the MALS detector that uses a He−Ne laser ($\lambda = 633$ nm). However, as for the previously described MHS plot, the $R_g = f(M)$ power law is obtained by gathering M and R_g data for each slice of the four higher molar mass PHPMA-CPT fractions. Figure 5 shows the $R_g = f(M)$ power law evaluated with the SEC-MALS data. The coefficients of the $R_g = K \cdot M^{\alpha}$ power law for the PHPMA-CPT conjugate were intercept $K = 1.7 \times$

Table 3. Comparison of the More Important Results for a Broad MMD PHPMA-CPT Conjugate (Lot 5)

	units	MALS	VISC	SEC-MALS	SEC-SCV	SEC-UC
M_w	g/mol	20000	–	20060	19360	19570
D		–	–	1.46	1.65	1.60
$[\eta]$	dL/g	–	0.100	–	0.100	0.102
A_2	mol·mL·g^{-2}	7.5×10^{-4}	–	–	–	–

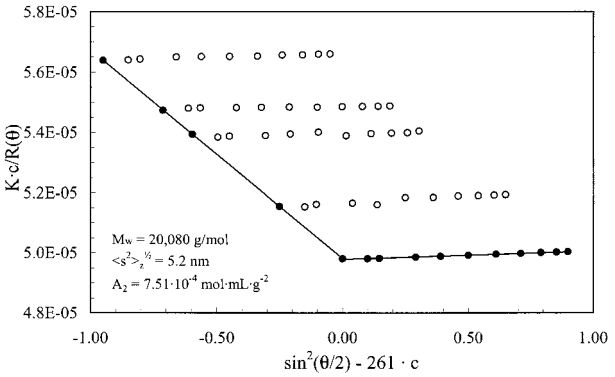


Figure 6. Zimm plot of a broad MMD PHPMA-CPT conjugate sample (lot 5).

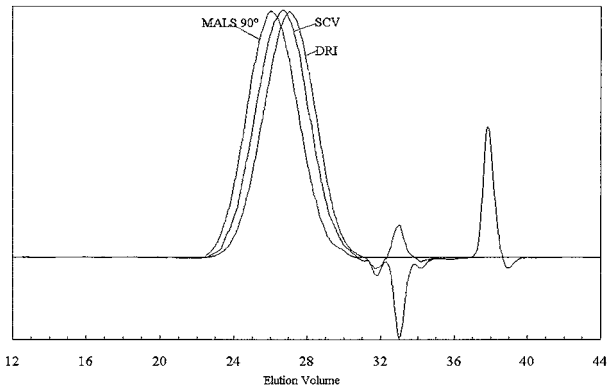


Figure 7. Comparison of the raw signals (MALS 90°, SCV, and DRI) of typical lab-scale batch of PHPMA-CPT conjugate (lot 5).

10^{-2} (R_g in nm) and slope $\alpha = 0.54$. Also these coefficients are congruent with the results obtained for the PHPMA homopolymer (*11*).

Characterization of a Broad MMD PHPMA-CPT Sample. A summary of the more important results for an unfractionated broad MMD PHPMA-CPT conjugate (lot 5) as obtained by five off-line and on-line characterization methods is listed in Table 3. In addition to the on-line SEC methods, Table 3 reports results from two off-line methods denoted in short as MALS and VISC. MALS is the classical static off-line light scattering and VISC the off-line capillary viscometer. Figure 6 shows the Zimm plot of the broad MMD PHPMA-CPT conjugate sample. The M_w of the sample was 20.08 kg/mol, R_g = 5.2 nm, and $A_2 = 7.51 \times 10^{-4}$ mol·mL·g^{-2}. The R_g result is the less accurate, because 5.2 nm is at the lower limit of the MALS measuring range. The large positive A_2 value proves that the used mobile phase was a good solvent for PHPMA-CPT.

A comparison of the raw signals of the three on-line detectors (MALS 90° photodiode, SCV, and DRI), as obtained using the experimental conditions described under Materials and Methods, is shown in Figure 7. As for the previous two PHPMA-DOX and PHPMA-TAX conjugates under identical experimental conditions, the signal-to-noise ratio for all the on-line detectors is quite high, and the polymer is well separated from the low molar mass components with only two SEC columns in series. Also for the broad MMD PHPMA-CPT conjugate sample, the agreement between the different methods was quite good. For the M_w average, the difference between MALS and SEC-MALS results was only 0.3%, between MALS and SEC-SCV 3.2%, between MALS and SEC-UC 2.2%. $[\eta]$ values obtained by off-line and on-line viscometers were identical, and the difference with the SEC-UC value was not significant. Finally, the dispersity index D was 1.50 by the SEC-MALS method, 1.65 by SEC-SCV, and 1.60 by SEC-UC. Because of the low molar mass of the PHPMA-CPT sample, the recovered values from SEC-SCV and SEC-UC are more accurate than the SEC-MALS value.

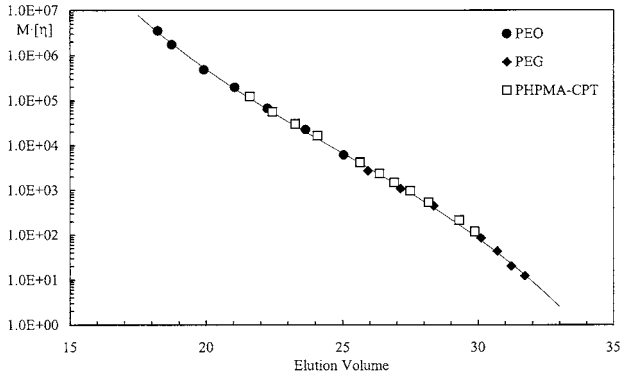


Figure 8. Fitting of the narrow MMD PHPMA-CPT fractions on the universal calibration constructed with PEO and PEG narrow standards.

Use of a Conventional SEC and Universal Calibration Method. In a previous section, we have seen that the recovered M_w, D, and $[\eta]$ values from the SEC-UC method were very close to the absolute values obtained using light scattering and viscometry on-line methods. Obviously, these results are an important confirmation that the SEC-UC method provides a congruent and accurate set of results. However, the fractionation and the accurate characterization of the narrow MMD PHPMA-CPT fractions provide a better test of the universal calibration. The universal calibration holds if the experimental function log (M·[η]) = $f(V)$ is common for calibrants (in our case PEO and PEG) and for the PHPMA-CPT conjugate. Figure 8 shows the experimental data of the above cited narrow MMD standards and the narrow MMD fractions of the PHPMA-CPT conjugate together with a third-order polynomial data fitting. The figure clearly shows that the PHPMA-CPT conjugate fractions follow the universal calibration function and confirms that this polymeric system elutes according to the hydrodynamic volume and therefore can be characterized by a conventional SEC-UC method.

CONCLUSIONS

The PHPMA-CPT conjugate has been fractionated and characterized. Combining multi-angle light scattering and viscometry, the molecular properties of 11 narrow MMD fractions and a typical broad MMD laboratory scale batch have been studied. A complete molecular characterization by means of molar mass, intrinsic viscosity, size, dispersity index, MHS relationship, and gyration radius−molar mass power law has been obtained. Notably, the SEC method used for the previous PHPMA-DOX and PHPMA-TAX conjugates proved suitable also for the new PHPMA-CPT conjugate. It is thus possible to characterize the new conjugate through a conventional SEC and universal calibration method. In essence, the

chromatographic separation of the new PHPMA-CPT conjugate is based on the hydrodynamic volume. This interesting result makes the conventional SEC-UC method suitable for the quality-control of the PHPMA-CPT conjugate samples.

Finally, we can observe that the average molar mass of the typical PHPMA-CPT conjugate sample, $M_w = 20$ kg/mol, is lower than those of the previous two conjugates, PHPMA-DOX and PHPMA-TAX (*9*−*11*). The MMD of this sample is relatively narrow, approximately $D = 1.6$, and compares very well with the results obtained for the conjugates of doxorubicin or paclitaxel. On the basis of the existing clinical experience with the above two conjugates, we can conclude that PHPMA-CPT is suitable for parenteral administration.

LITERATURE CITED

(1) Gebelein, C. G. (1987) *Advances in Biomedical Polymers*, p 405, Plenum Press, New York.
(2) Konno, T., and Maeda, H. (1987) *Neoplasma of the liver* (Okada, K., and Ishak, K. G., Eds.) pp 343−352, Springer-Verlag, New York.
(3) Duncan, R. (1992) Drug-polymer conjugates: potential for improved chemotherapy. *Anti-Cancer Drugs 3*, 175−210.
(4) Dumitriu, S., and Dumitriu, M. (1994) *Polymeric Drug Carriers in Polymeric Biomaterials* (Dumitriu, S., Ed.) Marcel Dekker Inc., New York.
(5) Duncan, R., Dimitrijevic, S., and Evagorou, E. G. (1996) The role of polymer conjugates in the diagnosis and treatment of cancer. *Pharma Sci. 6*, 237−263.
(6) Domb, A. J. (1994) *Polymeric Site-Specific Pharmacotherapy*, John Wiley & Sons, New York.
(7) Takakura, Y., Mahato, R. I., Vishikawa, M., and Hashida, M. (1996) Control of pharmacokinetic profiles of drug-macromolecule conjugates. *Adv. Drug Delivery Rev. 19*, 377−399.
(8) Ottembrite, R. M. (1998) *Frontiers in Biomedical Polymer Applications* (Ottembrite, R. M., Ed.) Technomic Publishing Co., Lancaster, PA.
(9) Mendichi, R., Rizzo, V., Gigli, M., and Schieroni, A. G. (1996) Molecular characterization of polymeric antitumor drug carrier by SEC and universal calibration. *J. Liq. Chrom., & Relat. Techn. 19*, 1591−1605.
(10) Mendichi, R., Rizzo, V., Gigli, M., Razzano, G., Angelucci, F., and Schieroni, A. G. (1998) Molar mass distribution of a polymer-drug conjugate containing the antitumor drug Paclitaxel by size exclusion chromatography and universal calibration. *J. Liq. Chromatogr. Relat. Technol. 21*, 1295−1309.
(11) Mendichi, R., Rizzo, V., Gigli, M., and Schieroni, A. G. (1998) Dilute solution properties of a polymer antitumor drug carrier by size exclusion chromatography, viscometry, and light scattering. *J. Appl. Polym. Sci. 70*, 329−338.
(12) Vasey, P. A., Kaye, S. B., Morrison, R., Twelves, C., Wilson, P., Duncan, R., Thomson, A. H., Murray, L. S., Hilditch, T. E., Murray, T., Burtles, S., Fraier, D., Frigerio, E., and Cassidy, J. (1999) Phase I clinical and pharmacokinetic study of PK1 [*N*-(2-hydroxypropyl)methacrylamide copolymer doxorubicin]: first member of a new class of chemotherapeutic agents—Drug-polymer conjugates. *Clin. Cancer Res. 5*, 83−94.
(13) Terwogt, J. M. M., Huinink, W. W. t. B., Schellens, J. H. M., Schot, M., Mandjes, I. A. M., Zurlo, M. G., Rocchetti, M., Rosing, H., Koopman, F. J., and Beijnen, J. H. (2001) Phase I clinical and pharmacokinetic study of PNU166945, a novel water-soluble polymer-conjugated prodrug of paclitaxel. *Anti-Cancer Drugs 12*, 315−323.
(14) Caiolfa, V. R., Zamai, M., Fiorino, A., Frigerio, E., Pellizzoni, C., D'Argy, R., Ghiglieri, A., Castelli, M. G., Farao, M., Pesenti, E., Gigli, M., Angelucci, F., and Suarato, A. (2000) Polymer-bound camptothecin: initial biodistribution and antitumour activity. *J. Controlled Release 65*, 105−119.
(15) Angelucci, F., Orzi, F., Fachin, G., Caiolfa, V., Zamai, M., and Suarato, A. Preparation of polymeric derivatives of camptothecins having antitumor activity. *PCT Int. Appl. WO 9917804*.
(16) Seymour, L. W., Duncan, R., Strohalm, J., and Kopacek, J. (1987) Effect of molecular weight (Mw) of *N*-(2-hydroxypropyl)methacrylamide copolymers on body distribution and rate of excretion after subcutaneous, intraperitoneal, and intravenous administration to rats. *J. Biomed. Mater. Res. 21*, 1341−1358.
(17) Matthews, S. E., Pouton, C. W., and Threadgill, M. D. (1996) Macromolecular systems for chemotherapy and magnetic resonance imaging. *Adv. Drug Delivery Rev. 18*, 219−267.
(18) Krinick, N. L., and Kopecek, J. (1991) Soluble Polymers as Targetable Drug Carriers. *Handb. Exp. Pharmacol. 100*, 105.
(19) Kataoka, K. (1997) Targetable Polymeric Drugs. *Controlled Drug Delivery: Challenges and Strategies* (Park, K., Ed.) p 49, ACS, Washington, DC.
(20) Fraier, D., Frigerio, E., Brianceschi, G., Casati, M., Benecchi, A., and James, C. (2000) Determination of MAG-camptothecin, a new polymer-bound camptothecin derivative, and free camptothecin in dog plasma by HPLC with fluorimetric detection. *J. Pharm. Biomed. Anal. 22*, 505−514.
(21) Mendichi, R., and Schieroni, A. G. (1999) Hyphenated and Multidimensional Techniques. Use of the single-capillary viscometer detector, on-line to a size exclusion chromatography system with a new pulse-free pump. *ACS Symp. Ser. 731*, 66−83.
(22) Wyatt, P. J. (1993) Light Scattering and absolute characterization of macromolecules. *Anal. Chim. Acta 272*, 1−40.
(23) Grubisic, Z., Rempp, P., and Benoit, H. (1967) A universal calibration for gel permeation chromatography. *J. Polym. Sci., Part B 5*, 753−759.

BC025522D

Cellular Internalization of Poly(ethylene oxide)-*b*-poly(ϵ-caprolactone) Diblock Copolymer Micelles

Laibin Luo,[†] Joseph Tam,[‡] Dusica Maysinger,*[,‡] and Adi Eisenberg*[,†]

Department of Chemistry, McGill University, 801 Sherbrooke Street West, Montreal, Quebec, H3A 2K6, Canada, and Department of Pharmacology and Therapeutics, McGill University, 3655 Drummond Street, Montreal, Quebec, H3G 1Y6, Canada. Received March 6, 2002; Revised Manuscript Received May 22, 2002

Poly(ethylene oxide)-*b*-poly(ϵ-caprolactone) (PEO-*b*-PCL) block copolymers self-assemble into micelles in aqueous solution. We have examined whether these micelles can internalize into P19 cells in vitro. Fluorescently labeled PEO_{45}-*b*-PCL_{23} block copolymer was prepared by conjugating a tetramethylrhodamine molecule to the end of the hydrophobic PCL block. Dynamic light scattering (DLS) and transmission electron microscopy (TEM) studies yielded 24 ± 2 and 25 ± 2 nm, respectively, for the diameters of the micelles. The studies also showed that chemical labeling did not effect the morphology or size. When the rhodamine-labeled PEO_{45}-*b*-PCL_{23} block copolymer micelles were tested in vitro, time-, concentration-, and pH-dependence of the internalization process suggested that internalization proceeded by endocytosis. The results from these studies provide the first direct evidence for the internalization of PEO_{45}-*b*-PCL_{23} micelles. Future studies will utilize multiple labeling of these micelles, allowing questions to be addressed related to the fate of internalized micelles as drug carriers, the destination of the incorporated drugs or fluorescent probes released from micelles, and the identification of the subcellular localization of the whole drug−carrier system within cells, both in vitro and in vivo.

INTRODUCTION

Recently, the use of block copolymer micelle based delivery systems to improve the therapeutic efficiency of many drugs has received considerable attention (*1*−*3*). Polymeric drug-carrying micelles were first prepared by the group of Ringsdorf (*4*). The drug molecules were attached to the hydrophobic side chains of amphiphilic graft copolymers or to the hydrophobic block of amphiphilic diblock copolymers. Such polymers, in solution, formed nanosized polymeric micelles with hydrophilic shells and drug-modified hydrophobic cores. One system consisted of cyclophosphamide, an alkylating antitumor agent in the core of poly(ethylene oxide)-*b*-poly(L-lysine) (PEO−PLL) micelles. In those studies, cyclophosphamide was conjugated to the poly(L-lysine) block as the sulfido derivative. It was reported that the rate of hydrolysis of cyclophosphamide derivatives in the micellar system varied from minutes to several hours. Recently, the field of polymeric micelles as drug carriers has advanced greatly by the work of the groups of Kabanov and Kataoka, among others (*5*−*21*). Many studies from the group of Kabanov utilized Pluronic copolymers with the poly(ethylene oxide)-poly(propylene oxide)-poly(ethylene oxide) (PEO−PPO−PEO) structure, which can self-assemble into micelles with PPO in the core and PEO in the corona. Such micelles, for expample, enhance the delivery of haloperidol to the brain, resulting in a significant increase in neuroleptic activity of the drug (*5*, *9*). Similarly, Kataoka's group found, for example, that polymeric micelles carrying adriamycin are more effective in vivo than free adriamycin. Micelle-incorporated adriamycin accumulates selectively in a solid tumor, very likely due to the enhanced permeability and retention effect (EPR effect) of the vascular endothelia at the tumor site (*6*, *7*, *10*, *13*, *20*).

Drugs and other agents can be incorporated into the inner core of polymeric micelles both by chemical conjugation and physical entrapment. In fact, many hydrophobic low molecular weight drugs were successfully incorporated into hydrophobic cores (*1*−*21*). Also, cisplatin and poly(ethylene oxide)-poly(α,β-aspartic acid) (PEO−PAA) block copolymers in an aqueous medium can form polymer−metal complex micelles (*22*). The concept has also been extended to polyion complex micelles, in which the block or graft polymers contain ionic and nonionic blocks, and in which a polyion or surfactant with opposite charge interacts with the ionic block to form the core of the complex micelles. Such micelles have been developed to deliver biological macromolecules such as DNA (*23*−*25*).

Polymeric micelles with poly(ethylene oxide) (PEO) as the hydrophilic block forming the corona of the micelles can avoid uptake by the reticuloendothelial system (RES) and thus stay in blood circulation for prolonged times (*1*−*3*). A wide range of polymeric materials has been utilized as the hydrophobic block or the charged block in complexes to form the core of the micelles, the choice depending on the compatibility between the polymers and the incorporated drugs (*2*). In this group, poly(ethylene oxide)-*b*-poly(ϵ-caprolactone) (PEO-*b*-PCL) diblock copolymer micelles have been explored as a drug delivery system (*16*, *17*). PCL is a well-known biodegradable polymer which has been utilized in various biomedical applications because of its excellent biocompatibility and degradability. It has been found that PEO-*b*-PCL micelles

* To whom correspondence should be addressed. Dr. Dusica Maysinger: E-mail: dmaysing@pharma.mcgill.ca. Tel: (514) 398-1264. Fax: (514) 398-6690. Dr. Adi Eisenberg: E-mail: adi.eisenberg@mcgill.ca. Tel: (514) 398-6934. Fax: (514) 398-3797.

[†] Department of Chemistry.

[‡] Department of Pharmacology and Therapeutics.

10.1021/bc025524y CCC: $22.00 © 2002 American Chemical Society
Published on Web 11/02/2002

are an effective carrier for lipophilic drugs, such as FK506, L-685,818, and dihydrotestosterone (*16*, *17*).

An understanding of micelle internalization is needed to develop drug delivery systems, especially carriers for subcellular targeting (*26*−*37*). At present, little is known about cellular internalization of polymeric micelles (*31*−*37*). Kabanov's group reported that Pluronic copolymer micelles can be internalized by an endocytotic pathway, and Pluronic copolymers can increase drug absorption by inhibition of the P-glycoprotein (P-gp) drug efflux system in cells (*31*−*34*). Our previous studies suggested cellular internalization of PEO-*b*-PCL into PC12 cells via endocytosis (*36*, *37*). However, since the probes used in these studies were only physically incorporated into micelles, no direct evidence has been provided for the internalization of the polymer micelles themselves. Therefore, we have chemically conjugated a rhodamine molecule to the end of the PCL block, prepared micelles containing these labeled chains, and investigated the internalization of such micelles into P19 cells, a pluripotent embryonic carcinoma cell line (*38*−*40*).

EXPERIMENTAL PROCEDURES

Materials. Poly(ethylene oxide) (number average molecule weight, M_n ca. 2000, Aldrich), tetramethylrhodamine-5-carbonyl azide (T6219) (Molecular Probes), and stannous(II) octoate (SnOct) (Sigma) were used without further purification. ϵ-Caprolactone (Aldrich) was twice dried over CaH_2 at room temperature and distilled under reduced pressure. Tetrahydrofuran (THF) and toluene were distilled just before use.

Synthesis and Characterization of PEO_{45}-*b*-PCL_{23} Block Copolymers and Rhodamine-Conjugated Copolymers. PEO_{45}-*b*-PCL_{23} block copolymers were synthesized as described elsewhere (*41*). A predetermined volume (6.6 mL) of ϵ-caprolactone monomer was placed in a flask containing a preweighed amount (5 g) of PEO under a nitrogen atmosphere. Then a drop of SnOct was added. After cooling to liquid-nitrogen temperature, the flask was evacuated, sealed off, and kept at 130 °C for 24 h. The synthesized polymers were then dissolved in THF, recovered by precipitation into cold hexane, and dried under vacuum at room temperature.

The degree of the polymerization of the PCL and the polydispersity of the polymers were determined by GPC. The degree of polymerization of the PCL was also measured by ^{1}H NMR relative to the degree of polymerization of the PEO.

The rhodamine-conjugated PEO_{45}-*b*-PCL_{23} block copolymers (PEO_{45}-*b*-PCL_{23}-Rh) were synthesized by employing a modified version of an existing procedure (*42*): 20 mg of the dried PEO_{45}-*b*-PCL_{23} block copolymers and 10 mg of tetramethylrhodamine-5-carbonyl azide were dissolved in 10 mL of freshly distilled toluene under a nitrogen atmosphere. After heating at 80 °C for 5 h, the reaction mixture was placed in a dialysis bag (MW = 1000) and dialyzed against DMF for one week to remove unconjugated rhodamine. Both the dialysis bag and the DMF were changed several times. Then the solution was dialyzed against MilliQ water for 3 days to remove any organic solvents. Again, both the dialysis bag and the MilliQ water were changed until no trace of rhodamine in either the external solvent or the dialysis bag in the absence of the internal solution could be detected. The aqueous solution was freeze-dried. The rhodamine-conjugated block copolymers were obtained in 60% yield. ^{1}H NMR was used to determine the amount of rhodamine in the conjugated block copolymers.

Preparation of Unlabeled Micelles (PM). A 20 mg amount of PEO_{45}-*b*-PCL_{23} block copolymers was dissolved in 0.38 g of DMF to yield 0.4 g of solution; the solution was stirred for 4 h. A 1.6 g amount of water was added at a rate of 10 μL every 30 s to induce micellization. The aqueous solution was placed in a dialysis bag (MW 50000) and dialyzed against MilliQ water for 1 day. After dialysis, the solution was diluted to 0.67 wt % of polymer.

Preparation of Labeled Micelles (RhPM). A block copolymer mixture consisting of PEO_{45}-*b*-PCL_{23}/PEO_{45}-*b*-PCL_{23}-Rh (molar ratio: 19/1) was used to prepare the rhodamine-labeled micelles. The polymer mixture was then handled as described above. The polymer and rhodamine concentrations in the solution were 0.67 wt % and 67 μM, respectively.

Preparation of Tetramethylrhodamine-5-carbonyl Azide (T6219) Aqueous Solution. One hundred microliters of 2 mM tetramethylrhodamine-5-carbonyl azide acetone solution was placed in a vial. After acetone was removed under vacuum, 3 mL of MilliQ water was added to dissolve the tetramethylrhodamine-5-carbonyl azide. The concentration of rhodamine in the resulting solution was 67 μM.

Preparation of Nonconjugated Tetramethylrhodamine-5-carbonyl Azide Containing Polymer Micelle Solution (NconRhPM). One hundred microliters of 2 mM tetramethylrhodamine-5-carbonyl azide acetone solution was placed in a vial. After the acetone was removed under vacuum, 3 mL of 0.67 wt % PEO_{45}-*b*-PCL_{23} block copolymers micelle solution was added to dissolve the tetramethylrhodamine-5-carbonyl azide. The total concentration of rhodamine in the micelle solution was 67 μM.

Dynamic Light Scattering (DLS). A Brookhaven laser light scattering instrument with an Uniphase μBlue laser at wavelength of 532 nm was used to determine the size distributions of the micelles at 25 °C. Labeled and unlabeled PEO_{45}-*b*-PCL_{23} block copolymers micelle solutions were filtered through 200 nm filter and used at a concentration of 0.05%.

Electron Microscopy. Transmission electron microscopy (TEM) was carried out on a JEOL microscope with a CCD camera operating at an acceleration voltage of 80 kV. Copper EM grids were precoated with a thin film of Formvar and then coated with carbon. Drops of 0.05 wt % solution of the labeled or unlabeled micelles were deposited on the resulting grids. After being dried in air overnight, the samples were shadowed with palladium/platinum alloy and carbon.

Cell Cultures. P19 mouse embryonal carcinoma cells (European Collection of Cell Cultures), as described by McBurney (*38*−*40*), were cultured in bacteriological Petri dishes (Falcon) for spectrofluorometric analyses or in 16-well chamber glass slides (Nunc) for fluorescent microscopy studies. Cells were grown in RPMI 1640 medium (Gibco-BRL) supplemented with 10% fetal bovine serum (FBS, Gibco-BRL), and serum-free medium was used in all internalization experiments.

Fluorescence Microscopy. Fluorescence microscopy studies were performed to assess the concentration and time dependent internalization of rhodamine-labeled micelles. In the concentration dependent studies, 10, 5, 2.5, or 1 μL PM, RhPM, T6219, or NconRhPM were added to well chambers containing 90 ul RPMI 1640 medium. After a 12 h incubation period, the media were removed and the P19 cells were washed with cold phosphate-buffered saline (PBS), acid solution (0.2 M acetic acid and 0.5 M NaCl aqueous solution), and PBS. In the time course studies, 10 μL of PM, RhPM, T6219, or NconRhPM

were added to chambers containing 90 μL of RMPI 1640 medium. The incubation times were 1, 4, 12, 18, and 24 h. Fluorescent images were captured using an Olympus BX60 system microscope equipped with an Olympus BX-FLA reflected light fluorescence attachment and a Dage-MTI DC-330 color camera coupled to a Compaq Pentium II computer with 128 MB RAM. Magnification was obtained using 20X or 40X objectives. Images were stored in uncompressed tagged image file format (TIFF) at a resolution of 1200 dpi using Image Pro Plus 3.0 image analysis software.

Fluorescence Spectroscopy. To obtain more quantitative data, similar studies were performed using regular fluorescence spectroscopy. For the studies of concentration dependent internalization, cells were grown in 900 μL of RPMI 1640 medium in the Petri dishes and 100, 25, 10, or 5 μL of PM, RhPM, T6219, or NconRhPM solution was added to each dish. After a 12 h incubation period, the media were removed and P19 cells were washed with cold PBS, acid solution, and PBS. Cells were lysed in 300 μL of DMSO. The DMSO solutions were then diluted with 3.7 mL of water. The resulting solutions were used for the determination of the amount of rhodamine using a FluoroMax-2 fluorescence spectrometer: $\lambda_{ex} = 545$ nm, $\lambda_{em} = 578$ nm.

For the studies of time dependent internalization, 100 μL of PM, RhPM, T6219, or NconRhPM solution was added to each dish containing 900 μL of RMPI 1640 medium. After a specific incubation period (30, 24,18, 12, 8, 4, and 1 h, respectively), the P19 cells were treated as described in the experiments of concentration dependent internalization.

Factors Affecting Internalization: Temperature, pH, Ca^{2+}, Drugs. Cells were grown in Petri dishes in the RPM1 1640 medium containing 10% serum. Four hours prior to the start of the experiments, the cells were placed in the serum free RMPI 1640 medium (900 uL) and different agents were added in the following concentrations: calcium (3mM), chlorpromazine (5 μM), FK506 (5 μM), and EGTA (5 mM) (*43*−*48*). The effects of temperature were assessed by incubating the cells at 4 °C and 37 °C (*49*). The pH effect was investigated on cells in a serum-free medium (pH 7.4) and in an acidified medium (pH 5.5) (*50*−*54*). Incubation periods varied, and the details are indicated in the legend to Figure 6.

RESULTS AND DISCUSSION

Synthesis of PEO_{45}-*b*-PCL_{23} Block Copolymers and Rhodamine-Conjugated Copolymers. PEO_{45}-*b*-PCL_{23} block copolymers and rhodamine-conjugated copolymers were synthesized as shown in Scheme 1. The number average molecular weight (M_n) and polydispersity of PEO_{45}-*b*-PCL_{23} block copolymer determined by GPC are 4500 and 1.41, respectively. The block copolymer was also characterized by ^{1}H NMR. An NMR spectrum of the labeled polymer is shown in Figure 1. The methylene protons of ethylene oxide units of the PEO correspond to the singlet at 3.7 ppm (labeled b). The methylene peaks of the caprolactone appear at 4.1, 2.3, 1.63, and 1.37 ppm (e, c, d, and d, respectively) (*41*). The molar ratio of ethylene oxide units to caprolactone units can be calculated based on the ratios of their peak areas. Therefore, the degree of polymerization of caprolactone can be obtained relative to the degree of polymerization of ethylene oxide. In our case, the calculated degree of polymerization of caprolactone is 23. The molecular weight based on the degree of polymerization of caprolactone and ethylene oxide from NMR is 4600 g/mol, which is consistent with the GPC result (4500 g/mol).

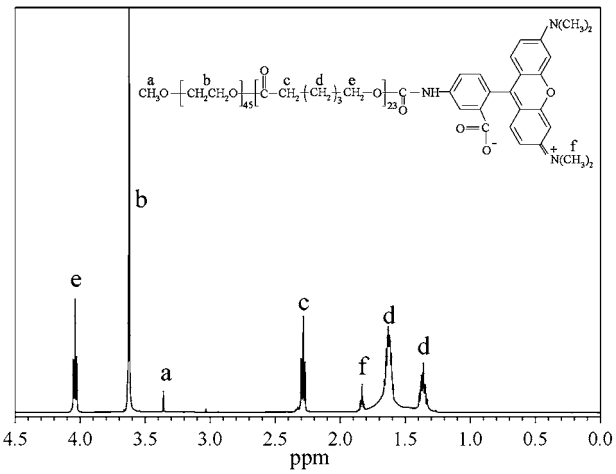
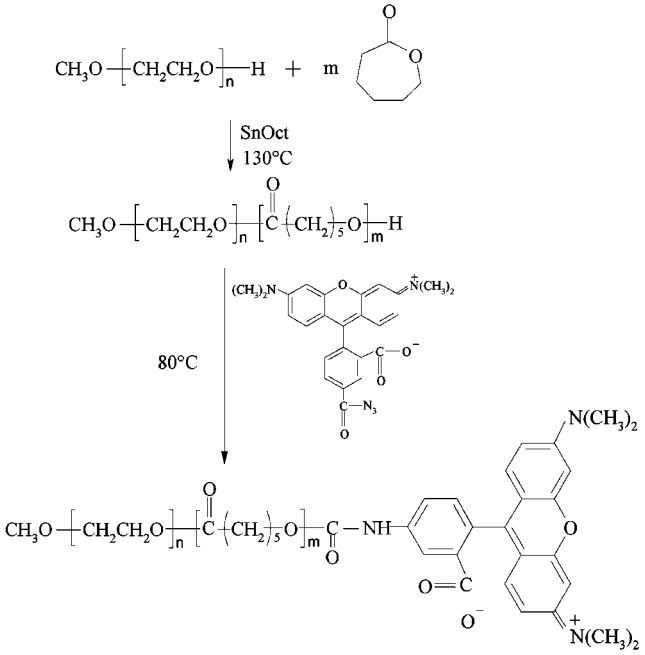


Figure 1. ^{1}H NMR spectrum of PEO45-*b*-PCL23-Rh in CDCl3.

Scheme 1. Synthesis of Poly(ethylene glycol)-*b*-poly(ϵ-caprolactone) Diblock Copolymer and Rhodamine-Conjugated Poly(ethylene glycol)-*b*-poly(ϵ-caprolactone) Diblock Copolymer



As shown in Scheme 1, the acyl azide group in tetremethylrhodamine-5-carbonyl azide is rearranged to an isocyanate on heating at 80 °C (*42*). In our PEO_{45}-*b*-PCL_{23} block copolymers, the functional group at the end of PEO chain is methoxy, while the functional group at the end of PCL chain is hydroxy. The hydroxy group can react with the freshly formed isocyanate. Therefore, tetramethylrhodamine can be attached to the end of the PCL chain. The success of the conjugation of tetramethylrhodamine to the block copolymer can be proven by ^{1}H NMR. The signal of methyl protons of tetramethylrhodamine is found at 1.84 ppm (f in Figure 1). The ratios of peak areas of the methyl group in tetramethylrhodamine to those of the methylene groups in PEO or poly(caprolactone) were used to calculate the molar ratio of tetramethylrhodamine to block copolymer chains. The average molar ratio is 0.94, suggesting that 95% of the polymer chains may be functionalized. Despite all the efforts, there may still be an undetectable trace of unconjugated rhodamine. This should lead to only a small

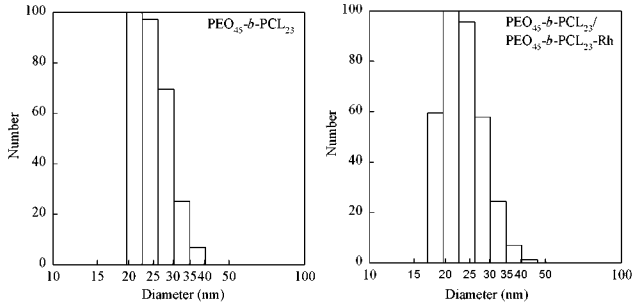


Figure 2. Size distribution of PEO_{45}-*b*-PCL_{23} and PEO_{45}-*b*-PCL_{23}/PEO_{45}-*b*-PCL_{23}-Rh (molar ratio: 19/1) micelles analyzed by DLS.

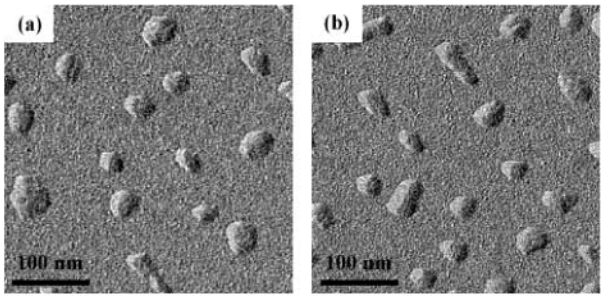


Figure 3. Transmission electron micrograph (TEM) of micelles of (a) PEO_{45}-*b*-PCL_{23} and (b) PEO_{45}-*b*-PCL_{23}/PEO_{45}-*b*-PCL_{23}-Rh (molar ratio: 19/1).

increase of size of error bar of our results, but should not affect the general conclusions.

Characterization of Labeled and Unlabeled Micelles. Rhodamine-conjugated block copolymer (5%) was mixed with the of the unlabeled block copolymer (95%) to prepare the rhodamine-labeled micelles. Both the labeled and unlabeled micelles were studied by DLS. As shown in Figure 2, the average diameters of unlabeled and labeled micelles are 25 ± 2 and 24 ± 1 nm, respectively. The results suggest that the size distributions of both labeled and unlabeled micelles are narrow, and that there is no significant change on the sizes of micelles after incorporation of rhodamine-conjugated PEO_{45}-*b*-PCL_{23} block copolymer chains.

The sizes and morphologies of labeled and unlabeled micelles were also studied by TEM. As shown in Figure 3, both labeled and unlabeled micelles are generally spheroidal. The sizes (from TEM) for both labeled and unlabeled micelles are identical (25 ± 2 nm and 25 ± 2 nm, respectively) and consistent with the DLS results. It should be noted that in the calculation of average sizes from TEM micrographs, only the spherical units are counted, since some of the elongated aggregates are probably the results of the attachment of two or more micelles during deposition.

Internalization of Micelles into P19 Cells. P19 cells are pluripotent cells, commonly used for in vitro studies, particularly those related to cell differentiation. Some drugs and also DMSO can transform P19 cells into neurons or muscle cells (*38*−*40*). We have grown the cells in the media without drug manipulations to retain them in the nondifferentiated pluripotent state.

We have investigated the rate and the extent of the internalization of rhodamine-labeled micelles, taking unlabeled block copolymer micelles (PM) as a negative control, as well as tetramethylrhodamine-5-carbonyl azide (T6219) and tetramethylrhodamine-5-carbonyl azide incorporated into block copolymer micelles (NconRhPM) as positive controls. Internalization of block copolymer

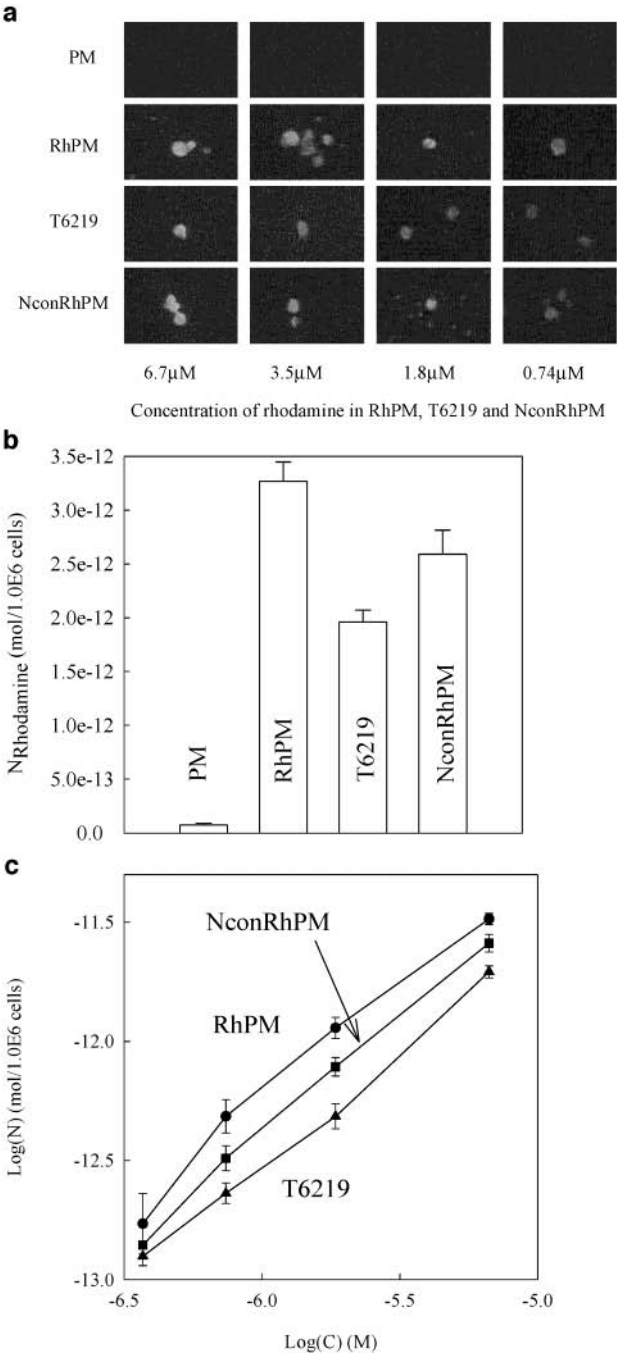


Figure 4. (a) Photographs of fluorescence intensity for rhodamine concentration-dependent internalization with P19 cells in 12 h. The polymer concentrations in RhPM, PM, and NconRhPM are 0.067%, 0.035%, 0.018%, and 0.0074%, respectively. (b) Internalization of PEO_{45}-*b*-PCL_{23} block copolymer micelles and of rhodamine T6219 into P19 cells in 12 h. The concentrations of the polymer in incubation solutions of PM, RhPM and NconRhPM are 0.067 wt %. The rhodamine concentrations of solutions of RhPM, T6219, and NconRhPM are 6.7 μM. (c) Rhodamine concentration-dependent internalization of PEO_{45}-*b*-PCL_{23} block copolymer micelles into P19 cells in 12 h. The polymer concentrations in RhPM and NconRhPM are 0.0037 wt %, 0.0074 wt %, 0.018 and 0.067 wt %, respectively.

micelles into P19 cells is dependent on both polymer concentration (Figure 4−c) and internalization time (Figure 5a,b). The fluorescence intensity of the rhodamine-labeled micelles was very low in low micromolar concentrations and at early time points (between 30 min and 6 h). Therefore, we conducted polymer concentration de-

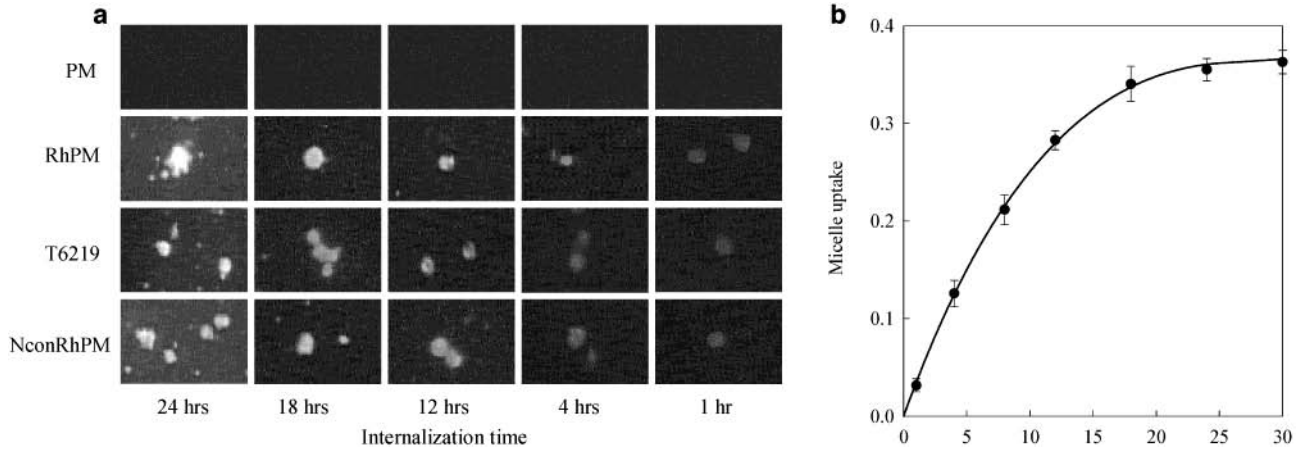


Figure 5. (a) Photographs of time-dependent internalization with P19 cells in 24 h. The polymer concentrations of PM and NconRhPM are 0.067%. The rhodamine concentrations of RhPM and T6219 are 6.7 μM. (b) Time-dependent internalization of RhPM with P19 cells as determined by spectrofluorometry. The polymer concentrations are 0.067%. The rhodamine concentrations are 6.7 μM.

pendent studies employing different concentrations of micelles at fixed 12 h incubation with P19 cells. Fluorescent microscopy studies suggest that fluorescence intensities increase in proportion to the increasing concentrations of rhodamine, and signals in RhPM-treated cells are stronger than those treated with T6219 or NconRhPM. Specrofluorometric measurements corroborate the findings from fluorescent microscopy (Figure 4b). Since the rhodamine molecules in RhPM are chemically linked to the PEO_{45}-*b*-PCL_{23} block copolymers, the results provide direct evidence for internalization of the block copolymer micelles. In addition, the amounts of rhodamine taken up by P19 cells are in the order RhPM > NconRhPM > T6219, suggesting that the block copolymer micelles enhance the accumulation of rhodamine T6219 molecules in the cells.

In most block copolymer solutions, both free unimers and micelles generally coexist. Results from studies with Pluronic P85 block copolymers suggest two different mechanisms of internalization involving free unimers and micelles, respectively (*31*−*35*). In the present case, we can show that it is the micelles which are responsible for the observed internalization. The considerations are as follows:

The polymer concentrations in the experiments described here are 0.067 wt % (150 μM), 0.035 wt % (78 μM), 0.018 wt % (40 μM), and 0.0074 wt % (16 μM), 0.0037% (8 μM), respectively. The CMC of PEO_{44}-*b*-PCL_{21} block copolymers micelles is 1.2 mg/L (unpublished observations); it is reasonable to take the CMC of PEO_{45}-*b*-PCL_{23} block copolymers micelles as also being around 1.2 mg/L, i.e., 0.00012 wt % (0.27 μM). Therefore, the PEO_{45}-*b*-PCL_{23} block copolymers in the solutions of our studies are mainly in the form of micelles, since the concentrations of polymer exceed the CMC by factors of ca. 30 to 600. Therefore, micelles are the primary form in the investigated solutions. Most importantly, free unimer concentrations of the PEO_{45}-*b*-PCL_{23} block copolymer are practically unchanged with changing polymer concentration. If the free unimers were responsible for the internalization, the internalization of RhPM should not be dependent on the total polymer concentration above the CMC. Since the internalization does depend on polymer concentration, we conclude that it is the micelles and not the free unimers of PEO_{45}-*b*-PCL_{23} that are responsible for the transport of PEO_{45}-*b*-PCL_{23} block copolymers into P19 cells.

Time dependent internalization of the block copolymers into P19 cells was confirmed by fluorescence microscopy

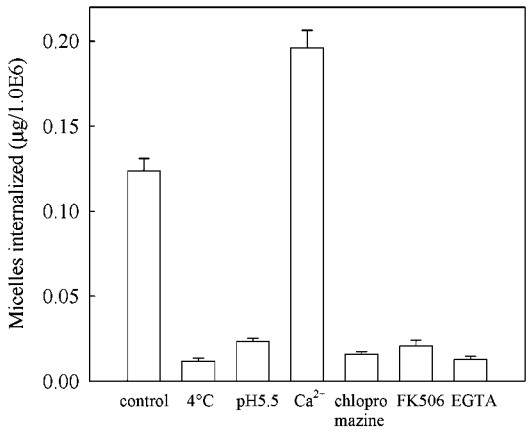


Figure 6. The effect of various pharmacological manipulations on the internalization of P19 cells with RhPM. The polymer concentration of RhPM is 0.067%. The rhodamine concentration is 6.7 μM.

(Figure 5a). As expected, there was no fluorescence in samples with empty PEO_{45}-*b*-PCL_{23} block copolymer micelles. The fluorescence intensities of P19 cells incubated with RhPM, T6219, and NconRhPM increased within 24 h. The amount of internalized PEO_{45}-*b*-PCL_{23} block copolymer micelles increased relatively rapidly initially, and the equilibrium was reached within ca. 24 h (Figure 5b).

If the micelles are internalized by endocytosis, then several basic criteria must be fulfilled (*43*−*54*). For instance, the process is time and energy dependent. Extent of internalization is reduced at low temperature (*49*) and low pH of the medium (*50*−*54*). Moreover, calcium and a number of drugs can significantly alter the extent of the internalization (*43*−*48*). In the present studies, various conditions in the medium significantly alter the extent of internalization of micelles as shown in Figure 6. For example, P19 cells treated with rhodamine-conjugated micelles and incubated at 4 °C, or in an acidified medium (pH 5.5), internalize a significantly smaller amount of micelles than the cells incubated at 37 °C or in the cell culture medium at pH 7.4 (control). Similarly, drug treatment with chlorpromazine or FK506 significantly reduces the amount of internalized micelles. These drugs are often used in internalization studies (*46*−*47*). Endocytosis is a calcium-dependent process. The ion concentrations were manipulated by EGTA (*48*). The internalization of rhodamine-labeled micelles is maximal in the presence of high (3 mM)

calcium concentration. By contrast, chelation of calcium by EGTA, significantly reduces the amount of internalized micelles.

In summary, results from the present studies show that the internalization of PEO_{45}-*b*-PCL_{23} micelles into P19 cells occurs by endocytosis. The influx of the rhodamine derivative used for labeling of the PCL chain appears to be increased when incorporated into PEO_{45}-*b*-PCL_{23} micelles. The studies also show changes in the extent of micelle internalization by pH, temperature, calcium, chlorpromazine, FK506, and ethylene glycol-bis-(*β*-aminoethyl ether)-*N*,*N*′-tetraacetic acid (EGTA) providing additional evidence for endocytosis (Figure 6).

Our earlier studies suggested that PEO-*b*-PCL micelles are internalized into PC12 cells and primary neuron-glia cultures via an endocytotic mechanism. However, in those early studies we did not have available fluorescent block copolymers, and the conclusions were based on studies involving noncovalently incorporated fluorescent or radiolabeled probes within the micelles (*36*, *37*). In agreement with the present findings and those by others (*31*−*37*), we now provide direct evidence for this mode of micelle internalization by employing covalently labeled block copolymers. The availability of these micelles provides a new tool for future studies in other cellular contexts in which the fate of the polymer carrier and incorporated agent can be followed at the subcellular level. Studies employing dual (micelle and probe) and multiple labels (micelle, probe, subcellular compartment) are currently underway in our laboratories to answer questions about the detailed subcellular distributions and in order to devise specific carriers to target different subcellular compartments.

CONCLUSIONS

The tetramethylrhodamine molecule was successfully conjugated to the end of the hydrophobic PCL block of PEO_{45}-*b*-PCL_{23} block copolymers. These fluorescently labeled block copolymers were used to prepare fluorescently labeled PEO_{45}-*b*-PCL_{23} block copolymer micelles. Chemical fluorescent labeling does not affect the spherical morphology or size of such micelles. Utilizing the rhodamine-labeled PEO_{45}-*b*-PCL_{23} block copolymer micelles, we have demonstrated that these micelles can be internalized into P19 cells by endocytosis. The internalization is time and concentration dependent. The results from these studies provide the first direct evidence for internalization of PCL-*b*-PEO micelles. The availability of rhodamine-labeled micelles will allow future studies involving multiple labels (drugs, drug−carrier, and subcellular compartment) to address the questions related to the fate of internalized micelles and the incorporated drugs or fluorescent probes.

ACKNOWLEDGMENT

This work was supported by the Natural Science and Engineering Research Council of Canada (NSERC).

LITERATURE CITED

(1) Kabanov, A. V., and Alakhov, V. Y. (1997) Micelles of amphiphilic block copolymers as vehicles for drug delivery. *Amphiphilic Block Copolymers: Self-Assembly and Applications* (P. Alexamdris, and B. Lindman, Eds.) Elsevier, Netherlands.

(2) Allen, C., Eisenberg, A., and Maysinger, D. (1999) Copolymer Drug Carriers: Conjugates, Micelles and Microspheres. *S. T. P. Pharma Sci. 9*, 139−151.

(3) Kataoka, K., Harada, A., and Nagasaki, Y. (2001) Block copolymer micelles for drug delivery: design, characterization and biological significance. *Adv. Drug Delivery Rev. 47*, 113−131.

(4) Bader, H., Ringsdorf, H., and Schmidt, B. (1984) Water soluble polymers in medicine. *Angew. Makromol. Chem. 123*−*124*, 457−485.

(5) Kabanov, A. V., Chekhonin, V. P., Alakhov, V. Y., Batrakova, E. V., Lebedev, A. S., Melik-Nubarov, N. S., Arzhakov, S. A., Levashov, A. V., Morozov, G. V., Severin, E. S., and Kabanov, V. A. (1989) The neuroleptic activity of haloperidol increases after its solubilization in surfactant micelles. Micelles as microcontainers for drug targeting. *FEBS Lett. 258*, 343−345.

(6) Yokoyama, M., Miyauchi, M., Yamada, N., Okano, T., Sakurai, Y., Kataoka, K., and Inoue, S. (1990) Characterization and anticancer activity of the micelle-forming polymeric anticancer drug adriamycin-conjugated poly(ethylene glycol)-poly(aspartic acid) block copolymer. *Cancer Res. 50*, 1693−1700.

(7) Yokoyama, M., Okano, T., Sakurai, Y., Ekimoto, H., Shibazaki, C., and Kataoka, K. (1991) Toxicity and antitumor activity against solid tumors of micelle-forming polymeric anticancer drug and its extremely long circulation in blood. *Cancer Res. 51*, 3229−3336.

(8) Muller, R. H. (1991) *Colloidal Carriers for Controlled Drug Delivery and Targeting: Modification, Characterization and In Vivo Distribution*, CRC Press Inc., Boca Raton, FL.

(9) Kabanov, A. V., Batrakova, E. V., Melik-Nubarov, N. S., Fedoseev, N. A., Dorodnich, T. Y., Alakhov, V. Y., Chekhonin, V. P., Nazarova, I. R., and Kabanov, V. A. (1992) A new class of drug carriers: micelles of poly(oxyethylene)-poly(oxypropylene) block copolymers as microcontainers for drug targeting from blood in brain. *J. Controlled Release 22*, 141−158.

(10) Kwon, G., Suwa, S., Yokoyama, M., Okano, T., Sakurai, Y., and Kataoka, K. (1994) Enhanced tumor accumulation and prolonged circulation times of micelle-forming poly(ethylene oxide-aspartate) block copolymer-adriamycin conjugate. *J. Controlled Release 29*, 17−23.

(11) Hagan, S. A., Coombes, A. G. A., Garnett, M. C., Dunn, S. E., Davies, M. C., Illum, L., Davis, S. S., Harding, S. E., Purkiss, S., and Gellert, P. R. (1996) Polylactide-poly(ethylene glycol) copolymers as drug delivery systems. 1. characterization of water dispersible micelle-forming system. *Langmuir 7*, 2153−2161.

(12) Ramaswamy, M., Zhang, X., Burt, H. M., and Wasan, K. M. (1997) Human plasma distribution of free paclitaxel and paclitaxel associated with diblock copolymers. *J. Pharm. Sci. 86*, 460−464.

(13) Yokoyama, M., Fukushima, S., Uehara, R., Okamoto, K., Kataoka, K., Sakurai, Y., and Okano, T. (1998) Characterization of physical entrapment and chemical conjugation of adriamycin in polymeric micelles and their design for in vivo delivery to a solid tumor. *J. Controlled Release 50*, 79−92.

(14) Shin, IL G., Kim, S. Y., Lee, Y. M., Cho, C. S., and Sung, Y. K. (1998) Methoxy poly(ethylene glycol)/*ϵ*-caprolactone amphiphilic block copolymeric micelle containing indomethacin. I. Preparation and characterization. *J. Controlled Release 51*, 1−11.

(15) Inoue, T., Chen, G., Nakamae, K., and Hoffman, A. S. (1998) An AB block copolymer of oligo(methyl methacrylate) and poly(acrylic acid) for micellar delivery of hydrophobic drugs. *J. Controlled Release 51*, 221−229.

(16) Allen, C., Yu, Y., Maysinger, D., and Eisenberg, A. (1998) Polycaprolactone-*b*-poly(ethylene Oxide) Block Copolymer Micelles as a Novel Drug Delivery Vehicle for Neurotrophic Agents FK506 and L-685, 818. *Bioconjugate Chem. 9*, 564−572.

(17) Allen, C., Han, J., Yu, Y., Maysinger, D., and Eisenberg, A. (2000) Polycaprolactone-*b*-poly(ethylene oxide) copolymer micelles as a delivery vehicle for dihydrotestosterone. *J. Controlled Release 63*, 275−286.

(18) Walter, E., Dreher, D., Kok, M., Thiele, L., Kiama, S. G., Gehr, P., and Merkle, H. P. (2001) Hydrophilic poly(D, L-lactide-*co*-glycolide) microspheres for the delivery of DNA to human-derived macrophages and dendritic cells. *J. Controlled Release 76*, 149−168.

(19) Yoo, H. S., and Park, T. G. (2001)Biodegradable polymeric micelles composed of doxorubicin conjugated PLGA-PEG block copolymer. *J. Controlled Release 70*, 63−70.
(20) Yamamoto, Y., Nagasaki, Y., Kato, Y., Sugiyama, Y., and Kataoka, K. (2001) Long-circulating poly(ethylene glycol)-poly(D,L-lactide) block copolymer micelles with modulated surface charge. *J. Controlled Release 77*, 27−38.
(21) Benahmed, A., Ranger, M. and Leroux, J.-C. (2001) Novel polymeric micelles based on the amphiphilic diblock copolymer poly(*N*-vinyl-2-pyrrolidone)-*block*-poly(D,L-lactide). *Pharm. Res. 18*, 323−328.
(22) Nishiyama, N., Yokoyama, M., Aoyagi, T., Okano, T., Sakurai, Y., and Kataoka, K. (1999) Preparation and characterization of self-assembled polymer-metal complex micelles from *cis*-dichlorodiammineplatinum(II) and poly(ethylene glycol)-poly($\alpha\beta$-aspartic acid) block copolymer in an aqueous medium. *Langmuir 15*, 377−383.
(23) Kabanov, A. V., Vinogradov, S. V., Suzdaltseva, Yu. G., and Alakhov, V. Yu. (1995) Water-soluble block polycations for oligonucleotide delivery. *Bioconjugate Chem. 6*, 639−643.
(24) Katayose, S., and Kataoka, K. (1997) Water-Soluble Polyion Complex Associates of DNA and Poly(ethylene glycol)-Poly(L-lysine) Block Copolymer. *Bioconjugate Chem. 8*, 702−707.
(25) Harada, A. and Kataoka, K. (1999) Chain length recognition: core−shell supramolecular assembly from oppositely charged block copolymers. *Science 283*, 65−67.
(26) Higashi, N., and Sunamoto, J. (1995) Endocytosis of poly(ethylene oxide)-modified liposome by human lymphoblastoid cells. *Biochim Biophys. Acta 1243*, 386−92.
(27) Vittaz, M., Bazile, D., Spenlehauer, G., Verrecchia, T., Veillard, M., Puisieux, F., and Labarre, D. (1996) Effect of PEO surface density on long-circulating PLA-PEO nanoparticles which are very low complement activators. *Biomaterials 17*, 1575−81.
(28) Higashi, N., Yamauchi, M., Okumura, Y., Nakanishi, M., and Sunamoto, J. (1996) Fusion between Jurkat cell and PEO-lipid modified liposome. *Biochim. Biophys. Acta 1285*, 183−91.
(29) Liaw, J., Aoyagi, T., Kataoka, K., Sakurai, Y., and Okano, T. (1999) Permeation of PEO−PBLA-FITC polymeric micelles in aortic endothelial cells. *Pharm. Res. 16*, 213−20.
(30) De Jaeghere, F., Allemann, E., Leroux, J. C., Stevels, W., Feijen, J, Doelker, E., and Gurny, R. (1999) Formulation and lyoprotection of poly(lactic acid-*co*-ethylene oxide) nanoparticles: influence on physical stability and in vitro cell uptake. *Pharm. Res. 16*, 859−66.
(31) Kabanov, A. V., Slepnev, V. I., Kuznetsova, L. E., Batrakova, E. V., Alakhov, V. Y., Melik-Nubarov, N. S., Sveshnikov, P. G., and Kabanov, V. A. (1992) Pluronic micelles as a tool for low-molecular compound vector delivery into a cell: effect of *Staphylococcus aureus* enterotoxin B on cell loading with micelle incorporated fluorescent dye. *Biochem. Int. 26*, 1035−1042.
(32) Venne, A., Li, S., Mandeville, R., Kabanov, A. V., and Alakhov, V. Yu. (1996) Hypersensitizing effects of Pluronic L61 on cytotoxic activity, transport, and subcellular distribution of doxorubicin in multiple drug-resistant cells. *Cancer Res. 56*, 3626−3629.
(33) Alakhov, V. Y., Moskaleva, E. Y., Batrakova, E. V., and Kabanov, A. V. (1996) Hypersensitization of multidrug resistant human ovarian carcinoma cells by Pluronic P85 block copolymer. *Bioconjugate Chem. 7*, 209−216.
(34) Miller, D. W., Batrakova, E. V., Waltner, T. O., Alakhov, V. Y., and Kabanov, A. V. (1997)Interactions of Pluronic Block Copolymers with Brain Microvessel Endothelial Cells: Evidence of Two Potential Pathways for Drug Absorption. *Bioconjugate Chem. 8*, 649−657.
(35) Batrakova, E. V., Li, S., Elmquist, W. F., Miller, D. W., Alakhov, V. Y.; Kabanov. A. V. (2001) Mechanism of sensitization of MDR cancer cells by Pluronic block copolymers: Selective energy depletion. *Br. J. Cancer 85*, 1987−1997.
(36) Allen, C., Yu, Y., Eisenber, A., and Maysinger, D. (1999) *Biochim. Biophys. Acta 1421*, 32−38.
(37) Maysinger, D., Berezovska, O., Savic, R., Lim Soo, P., and Eisenberg, A. (2001) Block copolymers modified the internalization of micelle-incorporated probes into neural cells. *Biochim. Biophys. Acta 1539*, 205−217.
(38) Mcburney, M. W., Jones-Villeneuve, E. M. V., Edwards, M. K. S., and Anderson, P. J. (1982) Control of muscle and neuronal differentiation in a cultured embryonal carcinoma cell line. *Nature 299*, 165−167.
(39) Is, S. (1999) Cardiac and skeletal muscle development in P19 embryonal carcinoma cells. *Trends Cardiovasc. Med. 9*, 139−143.
(40) Ventura, C., and Maioli, M. (2000) Opioid peptide gene expression primes cardiogenesis in embryonal pluripotent stem cells. *Circ. Res. 87*, 189−194.
(41) Bogdanov, B., Vidts, A., Bulcke, A. V. D., Verbeeck, R., and Schacht, E. (1998) Synthesis and thermal properties of poly(ethylene glycol)-poly(ϵ-caprolactone) copolymers. *Polymer 39*, 1631−1636.
(42) Balestrieri, C., Camussi, G., Giovane, A., Iorio, E. L., Quagliuolo, L., and Servillo, L (1996) Measurement of platelet-activating factors acetylhydrolase activity by quantitative high-performance liquid chromatography determination of coumarin-derivatized 1-*O*-alkyl-2-*sn*-lysoglyceryl-3-phosphorylcholine. *Anal. Biochem. 233*, 145−150.
(43) Beutner, D., Voets, T., Neher, E., and Moser, T. (2001) Calcium dependence of exocytosis and endocytosis at the cochlear inner hair cell afferent synapse. *Neuron 29*, 681−90.
(44) Sankaranarayanan, S., and Ryan, T. A. (2001) Calcium accelerates endocytosis of vSNAREs at hippocampal synapse. *Nat. Neurosci. 4*, 129−36.
(45) Lai, M. M., Hong, J. J., Ruggiero, A. M., Burnett, P. E., Slepnev, V. I., De Camilli, P., and Snyder, S. H. (1999) The calcineurin-dynamin 1 complex as a calcium sensor for synaptic vesicle endocytosis. *J. Biol. Chem. 274*, 25963−6.
(46) Gonda, K., Komatsu, M., and Numata, O. (2000) Calmodulin and Ca^{2+}/calmodulin-binding proteins are involved in *Tetrahymena thermophila*. *Cell Struct. Funct. 25*, 243−51.
(47) Lai, M. M., Luo, H. R., Burnett P. E., Hong, J. J., and Snyder, S. H. (2000) The calcineurin-binding protein cain is a negative regulator of synaptic vesicle endocytosis. *J. Biol. Chem. 275*, 34017−20.
(48) Yuan, A, Siu, C. H, and Chia, C. P. (2001) Calcium requirement for efficient phagocytosis by Dictyostelium discoideum. *Cell Calcium 29*, 229−38.
(49) Steinman, R. M., Mellman, I. S., Muller, W. A., and Cohn, Z. A. (1983) Endocytosis and the recycling of plasma membrane. *J. Cell Biol. 96*, 1−27.
(50) Davoust, J., Gruenberg, J., and Howell, J. E. (1987) Two threshold values of low pH block endocytosis at different stages. *EMBO J. 6*, 3601−3609.
(51) Sandvig, K., Olsnes, S., Petersen, O. W., and Van Deurs, B. (1987) Acidification of the cytosol inhibits endocytosis form coated pits. *J. Cell Biol. 105*, 679−689.
(52) Heuser, J. E., and Anderson, R. G. W. (1989) Hypertonic media inhibit receptor-mediated endocytosis by blocking clathrin coated pit formation. *J. Cell Biol. 108*, 389−400.
(53) Heuser, J. E. (1989) Effects of cytoplasmic acidification on clathrin lattice morphology. *J. Cell Biol. 108*, 401−411.
(54) Hansen, S. H., Sandvig, K., and Van Deurs, B. (1993) Clathrin and HA2 adaptors: effects of potassium depletion, hypertonic medium and cytosol acidification. *J. Cell Biol. 121*, 61−72.

BC025524Y

Bis-Pyrene-Labeled Oligonucleotides: Sequence Specificity of Excimer and Monomer Fluorescence Changes upon Hybridization with DNA

Kazushige Yamana,* Tatsuya Iwai, Yusuke Ohtani, Sayaka Sato, Mitsunobu Nakamura,† and Hidehiko Nakano

Departments of Applied Chemistry and Engineering Science, Himeji Institute of Technology, 2167 Shosha, Himeji, Hyogo 671-2201, Japan. Received March 18, 2002; Revised Manuscript Received July 23, 2002

The design, synthesis, and properties of a new pyrene excimer-forming probe of DNA have been described. 2,2-(Aminomethyl)propanediol was converted by the reaction with 1-pyrenebutylic acid to bis-pyrene-modified propanediol as a fluorescent non-nucleosidic linker. The bis-pyrene-modified linker can be incorporated via phosphoramidite chemistry into the 5′-terminal or internal positions of oligonucleotides (ODNs). The terminally modified ODNs showed almost similar affinity for complementary DNA when compared with the corresponding unmodified ODNs. The duplexes containing the bis-pyrene in the main chain exhibited higher melting temperatures relative to the corresponding duplexes containing propanediol linker at the same position. The UV and CD spectral studies indicate that the stacking interactions between the pyrene and DNA bases occur in the internally modified duplex and do not in the terminally modified duplex. The bis-pyrene modified linker itself displays excimer (E at 480 nm) and monomer (M at 380 nm) emission in a quantum yield (QY) of 0.17 and the E/M intensity ratio of 15. Incorporation of this linker into the terminal or internal positions of ODNs reduced the QY (0.003−0.009) and the E/M ratio (0.3−0.8). While small changes in the QY and E/M ratio was obtained in binding of the internally labeled ODNs to DNA, up to 27-fold increase in the QY and 17-fold increase in the E/M ratio was observed upon hybridization of the terminally labeled ODNs with DNA. The excimer and monomer fluorescence changes were found to be sensitive to a mismatch base present in the target DNA. The bis-pyrene-modified ODNs thus provide a sequence-sepcific fluorescent probe of DNA.

INTRODUCTION

There is current interest in the design and synthesis of fluorescence-labeled oligonucleotides that display a strongly enhanced signal upon hybrid formation. These types of oligonucleotide probes are attractive, since they can be used for solution-based assays of DNA and RNA. The homogeneous assays have some advantages over heterogeneous ones because of favorable hybridization kinetics and no requirement of washing steps. There have been several approaches to the synthesis of oligonucleotides labeled by fluorophores with useful properties (*1*−*4*). Notable approach has been reported on hairpin-forming oligonucleotides attached to a fluorescent dye at one end and a fluorescence quencher at the other (*5*−*8*). The fluorescence increase upon hybridization to a target DNA has facilitated real-time analysis of DNA sequences being amplified in polymerase chain reaction (PCR) and detection of mutant DNA. The use of fluorescence energy transfer (FRET) between donor and acceptor dyes is another example for solution-based detection of DNA (*9*−*15*). In this approach, changes in fluorescence emission wavelength as well as fluorescence intensity can be used to define a specific sequence in target DNA.

The other example of solution-based assays is the use of pyrene fluorescence (*16*−*29*). Both pyrene monomer and excimer fluorescence has been used as indicator for monitoring hybridization. We have recently disclosed RNA oligonucleotides possessing a pyrenylmethyl group at 2′-position that exhibit significantly enhanced monomer emission upon binding to an RNA segment (*23*). The fluorescence enhancement has been found to be very sensitive to the presence of a base-mismatch in RNA. However, these probes do not emit well upon hybridization with DNA. For detection of DNA in solution, several works have focused on the use of excimer emission (*24*−*29*). Kool et al. have showed that specific DNA sequences can be detected by utilizing oligonucleotides containing pyrene modified C-nucleoside (*28*). Masuko et al. have described a similar strategy that hybridization of two oligonucleotides labeled by a single pyrene group at the terminal ends with complementary DNA results in the excimer formation (*29*). Lewis et al. have indicated that oligonucleotide probes labeled by a bis-pyrenyl group at the 5′-terminus can be used to monitor hybridization with a target DNA (*27*).

Several years ago, we developed a method for single or multiple incorporation of a pyrene-derivatized glycerol linker into the main chain of oligonucleotides (*26*). The oligonucleotide containing two pyrene linkers displayed a strong excimer emission upon duplex formation with a DNA segment. To yield excimer, however, this approach inevitably needs repetitive incorporation of more than two linkers into oligonucleotide chain. We have designed a new excimer forming non-nucleosidic linker that possesses two pyrenyl groups at one backbone. It was expected that the bispyrenyl backbone may be easily

* Corresponding author: e-mail: yamana@chem.eng.himeji-tech.ac.jp, telephone: +81−792−67−4895, FAX: +81−792−67−4895.

† Department of Engineering Science, Himeji Institute of Technology.

10.1021/bc025530u CCC: $22.00 © 2002 American Chemical Society
Published on Web 10/19/2002

prepared from 2,2-substituted-1,3-propanediol and versatile in labeling at any position of oligonucleotides. In this report, we describe the synthesis, hybridization, and fluorescence of bis-pyrene-labeled olignucleotides. Pyrene excimer and monomer fluorescence was largely altered upon hybridization with a specific sequence of DNA.

EXPERIMENTAL PROCEDURES

General Methods. ^{1}H NMR spectra were measured on a JEOL EX-270 or Bruker DRX-500 spectrometer, in which chemical shifts (δ, ppm) were determined on the basis of a residual peak of solvent (2.49 for DNSO-d_6). High-performance liquid chromatography (HPLC) was performed on Waters 600 E equipped with UV detector at 260 nm, using a reversed phase Mightysil RP-18 column (4.6 × 150 mm). Column chromatography and thin-layer chromatography (TLC) were carried out Merck silica gel 60 and Merck 60 PF_{254}, respectively. Ultraviolet spectra (UV) spectra were recorded with a Hitachi U-3000 spectrophotometer equipped with a Hitachi SPR-10 thermoelectrically controlled cell holder. Circular dichroism (CD) spectra were obtained on a JASCO CD J-805 spectrophotometer. Steady-state fluorescence emission spectra were measured on a Hitachi F-2500 spectrophotometer using excitaion and emission slits of 5 nm.

Materials and Solvents. 5′-Dimethoxytrityl deoxynucleoside 3′-(2-cyanoethyl)-*N,N′*-diisopropylphosphoramidites, protected propanediol 2-cyanoethyl-*N,N′*-diisopropylphosphoramidite, and nucleoside-loaded controlled pore glass (CPG) supports were purchased from Cruachem. 2-Cyanoethyl-*N,N,N′,N′*-tetraisopropyl phosphorodiamidite was obtained from Aldrich. Oligonucleotides were prepared by phosphoramidite chemistry on ABI 394 DNA/RNA synthesizer. Dichroromethane (CH_2Cl_2) and pyridine were refluxed over CaH_2 for 5 h under nitrogen atmosphere, distilled, and stored over molecular sieves or CaH_2. Dimethylformamide (DMF) was distilled under reduced pressure over ninhydrin and then stored over molecular sieves. All other reagents and solvents were used as received.

Synthesis of 2,2-Bis(aminomethyl)-1,3-(*O*-isopropyridene)-1,3-propanediol (1). The title compound was obtained in two steps from 2,2-bis(bromomethyl)-1,3-propanediol. The starting diol (5 g, 19 mmol) was allowed to react with acetone (50 mL) at reflux conditions in the presence of *p*-toluenesulfonic acid (1.3 g, 7 mmol) as a catalyst to give a protected diol (4 g, 70%). The resulting diol (2.5 g, 5.8 mmol) was treated with potassium phthalimide (3 g, 12 mmol) in DMF (15 mL) and then with excess amount of hydrazine-monohydrate, giving the compound **1** (2 g, 80%). TLC (9:1, CH_2Cl_2-MeOH, v/v) R_f 0.26; ^{1}H NMR (DMSO-d_6): δ = 1.25 (s, 6H, CH_3), 2.65 (s, 4H, CH_2O), 3.55 (s, 4H, CH_2).

Synthesis of 2,2-Bis[(4-pyrenylbutylamide)methyl]-1,3-propanediol (2). Compound **1** (0.75 g, 4.3 mmol) was allowed to react with 1-pyrenebutyric acid (2.5 g, 8.7 mmol) in the presence of DCC (1.9 g, 9.2 mmol) and 1-hydrohybenzotriazole (HOBT)(1.2 g, 8.9 mmol) for 1 day at rt in dry DMF (33 mL). The material was purified with a silica gel column by using CH_2Cl_2 and methanol mixture (20:1, v/v) for elution. The deprotection was done in 0.1 M HCl (16 mL) and THF (140 mL) at reflux conditions for 30 min. The organic solvent was removed in vacuo, and then water (150 mL) was added. The insoluble material was filtered and then dried. Recrystalization from CH_2Cl_2 gave a pale yellow solid (1.2 g, 40%). TLC (9:1, CH_2Cl_2−MeOH, v/v) R_f 0.53; ^{1}H NMR (DMSO-d_6): δ = 1.98−2.03 (m, 4H, CH_2), 2.32 (t, 4H, CH_2-aromatic), 3.04 (d, 4H, CH_2OH), 3.20 (d, 4H, CH_2-NH), 3.30 (t, 4H, CH_2CO), 4.57 (t, 2H, OH), 7.90−8.35 (m, total 20 H, amide and aromatic); EIMS (positive) *m/z* 674.

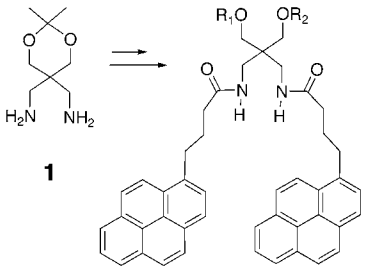
Synthesis of 2,2-Bis[(4-pyrenylbutylamide)methyl]-1-*O*-mono(dimethoxytrityl)-1,3-propanediol (3). The compound **2** (0.6 g, 0.9 mmol) was dried by coevaporation with dry pyridine three times and then reacted in dry pyridine (18 mL) with 4,4′-dimethoxytrityl chloride (DMT-Cl) (0.27 g, 0.8 mmol) in the presence of 4-(dimethylamino)pyridine (DMAP) (0.022 g, 0.18 mmol) at rt for 1 h. After methanol (1 mL) was added to the mixture, the solvent was removed in vacuo. The resulting material was dissolved in ethyl acetate (150 mL) and then washed with water. The organic layer was dried with Na_2SO_4 and then evaporated to near dryness. The residual material was purified with a silica gel column that was eluted with CH_2Cl_2 containing methanol (15:1, v/v). The appropriate fractions were pooled and then evaporated to near dryness. The residual solution was poured into cold hexane to give a pale yellow powder (0.6 g, 78%). TLC (9:1, CH_2Cl_2−MeOH, v/v) R_f 0.82; ^{1}H NMR (DMSO-d_6): δ = 1.91−1.97 (m, 4H, CH_2), 2.19 (t, 4H, CH_2-pyrene), 2.97 (s, 2H, CH_2-ODMT), 3.05−3.15 (m, total 6H, CH_2-NH and CH_2OH), 3.22 (t, 4H, CH_2CO), 3.60 (s, 6H, CH_3O), 4.62 (t, 1H, OH), 6.73−7.53 (m, total 13 H, DMT), 7.86−8.32 (m, total 20 H, amide and aromatic of pyrene); EIMS (positive) *m/z* 976.

Synthesis of Bis-Pyrene Modified Oligonucleotides. The conversion of **3** to phosphoramidite derivative **4** was carried out in a standard phosphitilation procedure described earlier (*30*). Bispyrene-labeled oligonucleotides were synthesized by phosphoramidite chemistry beginning with 5′-DMT-T (1 μmol) bound to a CPG support. All the coupling of normal nucleoside phosphoramidites (0.1 M in acetonitrile) and the bispyrene amidite **4** (0.15 M in CH_2Cl_2) were performed by a standard protocol of the DNA synthesizer used. With these conditions, all the coupling efficiencies including the modified amidite were 98% based on the dimethoxytrityl cation assay. The CPG-bound oligonucleotides were treated with concentrated ammonium hydroxide in a usual manner. Oligonucleotides modified at the 5′-terminus were purified with reversed phase HPLC. A linear gradient of CH_3CH (0.5%/min) from 10% CH_3CN in 0.05 M triethylammonium acetate (pH 7.0) was used at a flow rate of 1.0 mL/min. Purification of oligonucleotides modified in the main chain was performed by 20% denaturing polyacrylamide gel electrophoresis (DPAGE) as described (*30*). The integrity of oligonucleotide structure was verified with ion-spray MS analysis.

Oligonucleotide Solutions for Physical Measurements. All solutions were prepared using a buffer containing 10 mM sodium phosphate and 100 mM NaCl, adjusted to pH 7.0. Oligonucleotide concentrations were determined by absorbance at 260 nm and the calculated single-strand extinction coefficients based on a nearest neighbor model (*31*).

UV-monitored melting curves of the duplexes were obtained for solutions containing 1:1 strand ratio (2.15×10^{-5} M each) of oligonucleotides with increase in temperature from 0 to 80 °C at a rate of 0.5 °C/min. The solutions were heated at 80 °C, kept there for 5 min, and then gradually cooled before melting experiments. CD spectra were measured for the same solutions used for the UV melting studies at 23 °C. Steady-state fluorescence emission spectra were measured for the same solutions at 23 °C using excitation wavelength of 350 nm. Fluorescence quantum yields were determined by using

Scheme 1. Synthesis of Bis-Pyrene-Modified Propanediol Linker



1

2 (BP) : $R_1 = R_2 =$ -OH
3 : $R_1 =$ 4,4'-dimethoxytrityl
$R_2 =$ -OH
4 : $R_1 =$ 4,4'-dimethoxytrityl
$R_2 =$ -P(N-iPr$_2$)OCH$_2$CH$_2$CN

quinine sulfate in 0.5 M H_2SO_4 as a standard ($f = 0.55$). Excimer vs monomer fluorescence ratio (E/M ratio) was measured at 23 °C by using the intensity at the wavelength of 480 nm for the excimer (E) and 380 nm for the monomer (M) fluorescence. No attempts were made for eliminating dissolved oxygen in the fluorescence measurements.

RESULTS

Design of Bis-Pyrene Probe. The design of our bispyrene derivative was based on the researches that are concerned with non-nucleoside phosphoramidites derived from 1,3-propanediol for labeling of oligonucleotides at internal position as well as 5′-terminus (*32, 33*). Lewis and Letsinger et al. have shown that bispyrenyl alcohol can be used for 5′-terminal labeling of oligonucleotides and the bis-pyrene probes exhibit significant enhancement of excimer intensity upon hybrid formation with a specific DNA sequence (*27*). To explore the potential of bis-pyrene strategy, we have chosen 2,2-bis-susituted-1,3-propanediol as a building unit that enabled us to incorporate the bis-byrene at any position of oligodeoxynucleotides (ODNs).

Synthesis of Bis-Pyrene-Modified Oligonucleotides. As shown in Scheme 1, the synthesis of bispyrenyl backbone began with conversion of 2,2-bis(bromomethyl)-1,3-propanediol into the protected bisamino derivative **1**. The reaction of **1** with 1-pyrenebutyric acid using DCC/HOBT afforded the desired bis-pyrene derivative **2**. The compound **2** was then converted to the monoprotected diol **3**. The use of small amount of DMT-Cl and DMAP as a catalyst was found to be essential to obtain the desired compound in good yield. The phosphoramidite **4** being obtained in a standard phopshitilating method was used for incorporation of the bispyrenyl group into 5′-terminal (**I**−**IV**) or internal position (**V**−**VII**) of ODNs. The oligomers having the lipophilic residue at the terminus were purified with reversed-phase HPLC. Purification of the internally modified oligomers was carried out with conventional DPAGE. The integrity of each oligomer was verified with ion-spray MS.

The sequences of bis-pyrene labeled ODNs in the present study are shown in Table 1. With covalent attachment of pyrene and bis-pyrene residues into ODNs, both excimer and monomer emission are known to be considerably affected by the nucleobase adjacent to the site of attachment (*23, 29*). The bis-pyrene was therefore placed at the next position of pyrimide (**I**−**III**) or purine (**IV**) in the terminally labeled ODNs. The internally labeled ODNs have the bispyrenyl backbone at the position between purine nucleosides (**V**), pyrimidines (**VI**) and pyrimidine-purine (**VII**).

Table 1. Sequences, Binding, and Fluorescence Properties of Bis-Pyrene-Modified ODNs

	T_m (°C)[a]	QY[b]	E/M ratio[c]
I: 5′-(BP)TCCTCGCCCTTGCTCACCAT		0.005	0.5
duplex I:	68.9	0.130	4.4
I +3′-AGGAGCGGGAACGAGTGGTA			
unmodified duplex I:	67.5		
5′-TCCTCGCCCTTGCTCACCAT			
+ 3′-AGGAGCGGGAACGAGTGGTA			
II: 5′-(BP)CGGTTCATGCCGCC		0.009	0.8
duplex II:	65.1	0.050	13.7
II + 3′-GCCAAGTACGGCGG			
unmodified duplex II:	65.0		
5′-CGGTTCATGCCGCC			
+ 3′-GCCAAGTACGGCGG			
III: 5′-(BP)CATGCAGTGTTGAT		0.003	0.5
duplex III:	53.6	0.018	3.2
III + 3′-GTACGTCACAACTA			
unmodified duplex III:	52.5		
5′-CATGCAGTGTTGAT			
+ 3′-GTACGTCACAACTA			
IV: 5′-(BP)ACATGCAGTGTTGAT		0.003	0.4
duplex IV:	53.7	0.028	2.1
IV + 3′-TGTACGTCACAACTA			
unmodified duplex IV:	54.7		
5′-ACATGCAGTGTTGAT			
+ 3′-TGTACGTCACAACTA			
V: 5′-ACA(BP)GCAGTGTTGAT		0.005	0.3
duplex V:	52.0	0.006	1.0
V + 3′-TGTACGTCACAACTA			
C3-modified duplex V:	44.9		
5′-ACA(C3)GCAGTGTTGAT			
+ 3′-TGTACGTCACAACTA			
VI: 5′-ACATGCAGT(BP)TTGAT		0.006	0.7
duplex VI:	42.3	0.009	2.2
VI +3′-TGTACGTCACAACTA			
C3-modified duplex VI:	35.1		
5′-ACATGCAGT(C3)TTGAT			
+ 3′-TGTACGTCACAACTA			
VII: 5′-GGGCCTC(BP)GGTTCAT		0.004	0.5
duplex VII:	60.4	0.003	0.8
VII + 3′-TACCCGGAGGCCAAGTACGGAGG			
unmodified duplex VII:	60.5		
5′-GGGCCTCCGGTTCAT			
+ 3′-TACCCGGAGGCCAAGTACGGAGG			
C3-modified duplex VII:	48.4		
5′-GGGCCTC(C3)GGTTCAT			
+ 3′-TACCCGGAGGCCAAGTACGGAGG			

[a] Duplex melting measurements were carried out at 260 nm for 1:1 mixture of ODNs (2.15×10^{-5} M each) in a buffer containing 10 mM sodium phosphate and 100 mM NaCl, adjusted to pH 7.0. [b] Fluorescence quantum yields (QY) were determined by using quinine sulfate in 0.5 M H_2SO_4 as a standard (QY = 0.55). [c] Excimer vs monomer fluorescence ratio (E/M ratio) was measured at 23 °C by using the intensity at the wavelength of 480 nm for the excimer and 380 nm for the monomer fluorescence. BP and C3 indicate bis-pyrene **2** and propanediol linker, respectively.

Duplexes of Bis-Pyrene Modified Oligonucleotides with DNA. The binding of bis-pyrene modified ODNs to DNA was investigated by UV monitored melting study. Some examples of duplex melting profiles are shown in Figure 1. The melting profiles exhibited sigmoidal curves whose shapes are similar to those of the corresponding unmodified DNA/DNA duplex. All the duplex studied here showed biphasic helix-coil transition. Table 1 summarizes the duplex melting temperatures (T_m) monitored at 260 nm. The terminally modified ODNs **I**−**IV** showed almost similar affinity for complementary DNA when compared with the corresponding unmodified ODN. The duplexes containing the bis-pyrene in the main

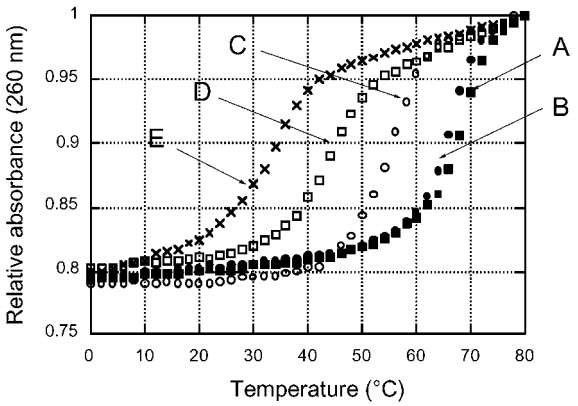


Figure 1. UV melting curves for duplex **I** (curve A), unmodified duplex **I** (curve B), unmodified duplex **IV** (curve C), duplex **VI** (curve D), and C3-modified duplex **VI** (curve E). The measurements were carried out at 260 nm for 1:1 mixture of oligonucleotide (2.15×10^{-5} M each) in a buffer containing 10 mM sodium phosphate and 100 mM NaCl, adjusted to pH 7.0. The sequences of oligomers used in these studies are shown in Table 1.

chain **V**−**VII** had higher melting temperatures when compared with the corresponding duplexes containing propanediol linker at the same position (C3-modifed duplex **V**−**VII**). While the duplex **V** or **VII** showed almost similar T_m to that of the unmodified duplex **IV** or **VII**, the duplex of **VI** had the lower T_m relative to the unmodified duplex **IV**.

The UV spectral changes for the pyrene residues during the duplex melting were shown in Figure 2. At the higher temperature where the duplexes are dissociated to single-stranded oligomers, the absorption maxima at 315, 320, and 345 nm were observed for both the terminally modified duplex **II** and the internally modified duplex **VII**. With decrease in the temperature or upon duplex formation, the red-shift (3−5 nm) of the absorption maxima and the absorption band hypochromism occurs in the internally modified duplex. In contrast, little shifts of the absorption maxima and small increase in the absorption were observed for the terminally modified duplex. Figure 3 indicates the CD spectra for the duplexes **II** and **VII** at ambient temperature. The CD profiles for the terminally modified duplex **II** and the internally modified duplex **VII** exhibit almost the same shapes as those of the corresponding unmodified duplexes, showing that the global conformation of these duplexes is similar to a B-form helix. While little induced CD at around 350 nm was observed in the terminally modified duplex **II**, the positive induced CD bands at this region appear in the internally modified duplex **VII**. These UV and CD spectral observations indicate that the stacking interactions between the pyrene and DNA bases occur in the internally modified duplex and do not in the terminally modified duplex.

Excimer and Monomer Fluorescence Changes upon Binding of Bis-Pyrene Modified Oligonucleotides to DNA. The fluorescence properties of bis-pyrene

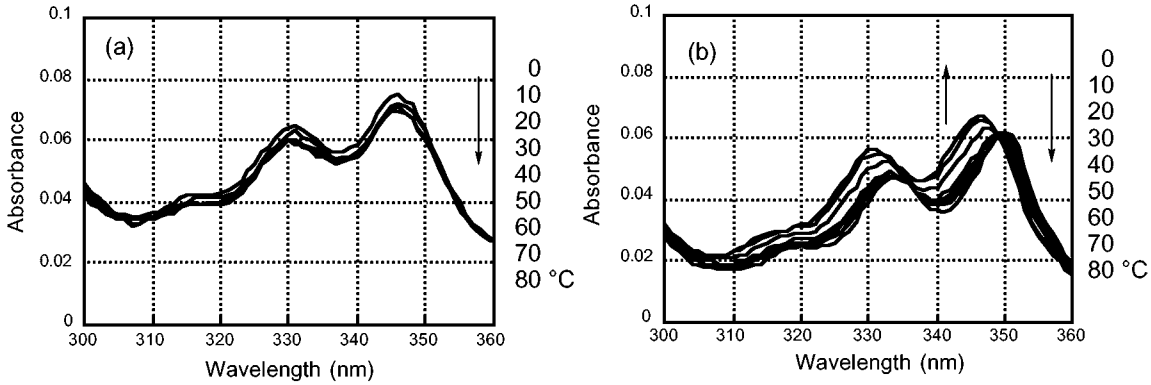


Figure 2. Panel a: UV−vis spectra for duplex **II** at different temperatures (0, 10, 20, 30, 40, 50, 60, 70, 80 °C). Panel b: UV−vis spectra for duplex **VII** at different temperatures (0, 10, 20, 30, 40, 50, 60, 70, 80 °C). UV−vis spectra were recorded under the same conditions described in Figure 1.

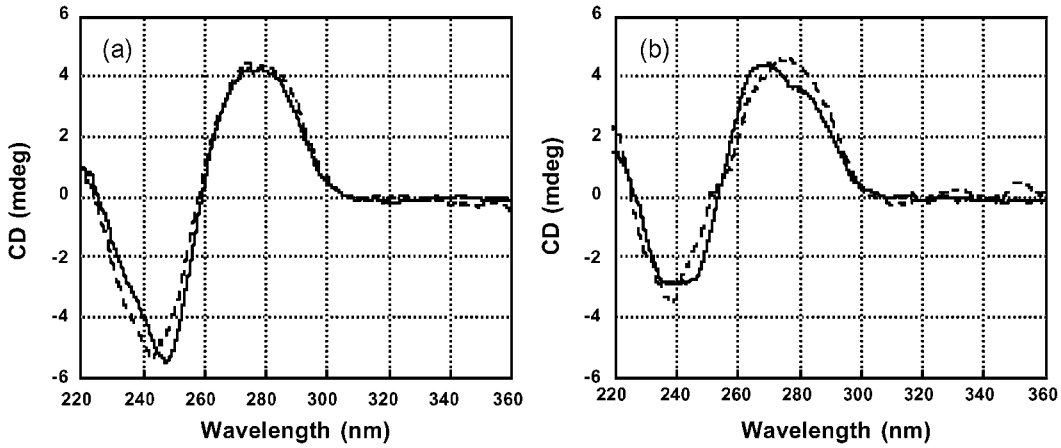


Figure 3. Panel a: CD spectra for duplex **II** (broken line) and unmodified duplex **II** (solid line). Panel b: CD spectra for duplex **VII** (broken line) and unmodified duplex (solid line). The measurements were carried out at 23 °C for the duplexes at total strand concentration of 4.3×10^{-5} M in a buffer containing 10 mM sodium phosphate and 100 mM NaCl, adjusted to pH 7.0. The sequences of oligomers used in these studies are shown in Table 1.

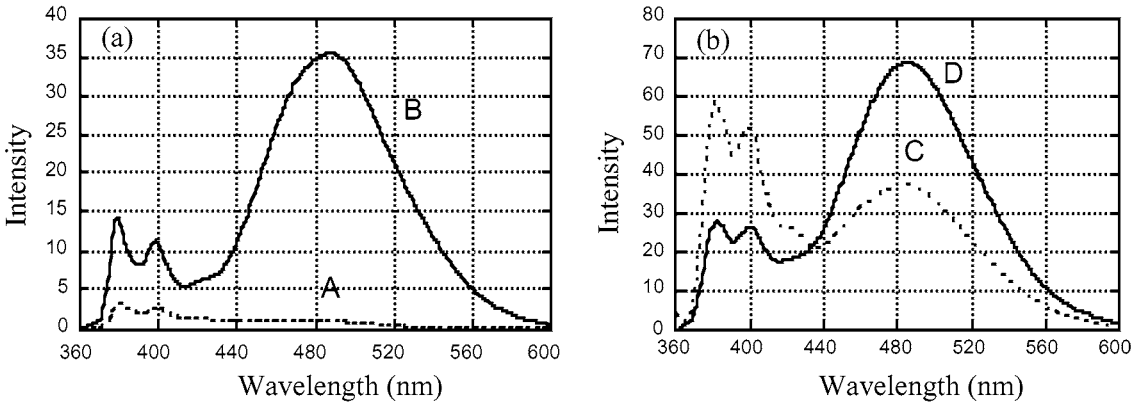


Figure 4. Panel a: Fluorescence spectra for bis-pyrene modified ODN **I** (curve A) and duplex **I** (curve B). Panel b: Fluorescence spectra for bis-pyrene modified ODN **VI** (curve C) and duplex **VI** (curve D). Fluorescence spectra were recorded at 23 °C with an excitation wavelength of 350 nm. The sequences of oligomers used in these studies are shown in Table 1.

Table 2. Relative Fluorescence Quantum Yields, Excimer/Monomer Fluorescence Ratio, and T_m Values for the Duplexes of Bis-Pyrene-Modified ODNs II or III with DNA Containing a Base Mismatch or Extra Bases

bispyrene-modified ODN	DNA[a]	relative QY[b]	E/M ratio	T_m (°C)
II	3′-GCCAAGTACGGCGG	5.5	13.7	65.1
	3′-**A**CCAAGTACGGCGG	1.2	2.6	63.6
	3′-**C**CCAAGTACGGCGG	0.5	2.0	62.5
	3′-**T**CCAAGTACGGCGG	0.3	0.9	61.7
	3′-*TACCCGG*AGGCCAAGTACGGCGG	0.6	0.8	65.1
III	3′-GTACGTCACAACTA	5.9	3.2	53.6
	3′-**A**TACGTCACAACTA	1.6	0.3	49.6
	3′-**C**TACGTCACAACTA	2.0	0.9	48.9
	3′-**T**TACGTCACAACTA	0.8	0.5	49.9
	3′-*TTT*GTACGTCACAACTA	0.6	0.7	54.4

[a] The mismatch base and extra bases in DNA are indicated by the bold font and italic, respectively. [b]Relative flourescence quantum yields were determined at 23 °C based on the single-stranded bis-pyrene-modified ODN II or III. The other conditions were described in Table 1.

modified ODNs (**I**−**VII)** and their duplexes with fully matched DNA are indicated in Table 1. In aqueous solution, compound **2** exhibits excimer emission as major fluorescence in a fluorescence quantum yield of 0.17. The intensity ratio (15) of excimer (E at 480 nm) versus monomer fluorescence (M at 380 nm) was unchanged with dilution, indicating that the intramolecular excimer formation is favorable in aqueous media. Introduction of the bis-pyrene into the terminal or internal positions of oligonucleotides resulted in large decrease in fluorescence quantum yields (0.003−0.009) and switched the E/M ratio to be small (0.3−0.8). The fluorescence spectra for terminal labeled ODNs **I** in the presence or absence of DNA are shown in Figure 4a. Upon binding to fully complementary DNA, the oligomer showed significant enhancement of excimer fluorescence with higher E/M ratio relative to the corresponding single-stranded ODN. All the terminally labeled ODNs **I**−**III** possessing the pyrimidine and **IV** having the purine nucleoside adjacent to the bis-pyrene exhibited strong excimer fluorescence upon hybridization to fully matched DNA. These results indicate that the kind of the adjacent nucleobase appears to have little effect on the excimer formation for the terminally labeled ODNs. Figure 4b shows the fluorescence spectra for oligomer **VI** as an example for internally modified ODNs. Binding of **IV** to DNA with a base facing to the bis-pyrene residue gave higher E/M ratio relative to the single-stranded form that was resulted from increase in the excimer fluorescence and decrease in the monomer emission. The excimer and monomer fluorescence changes for **V** and **VII** were also observed in hybrid formation with DNA, although these changes were smaller relative to **VI**. In hybridization of the internally labeled ODNs, the extent of the fluorescence changes was dependent on the adjacent bases at the bis-pyrene modification.

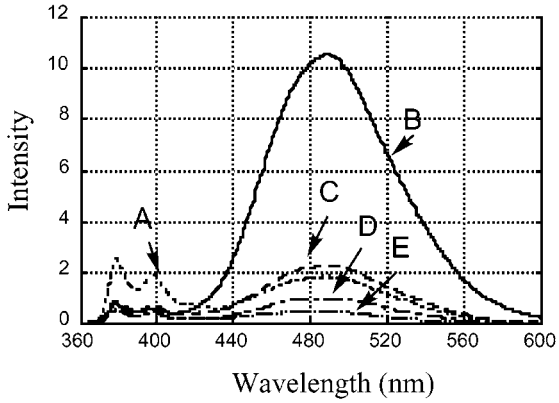
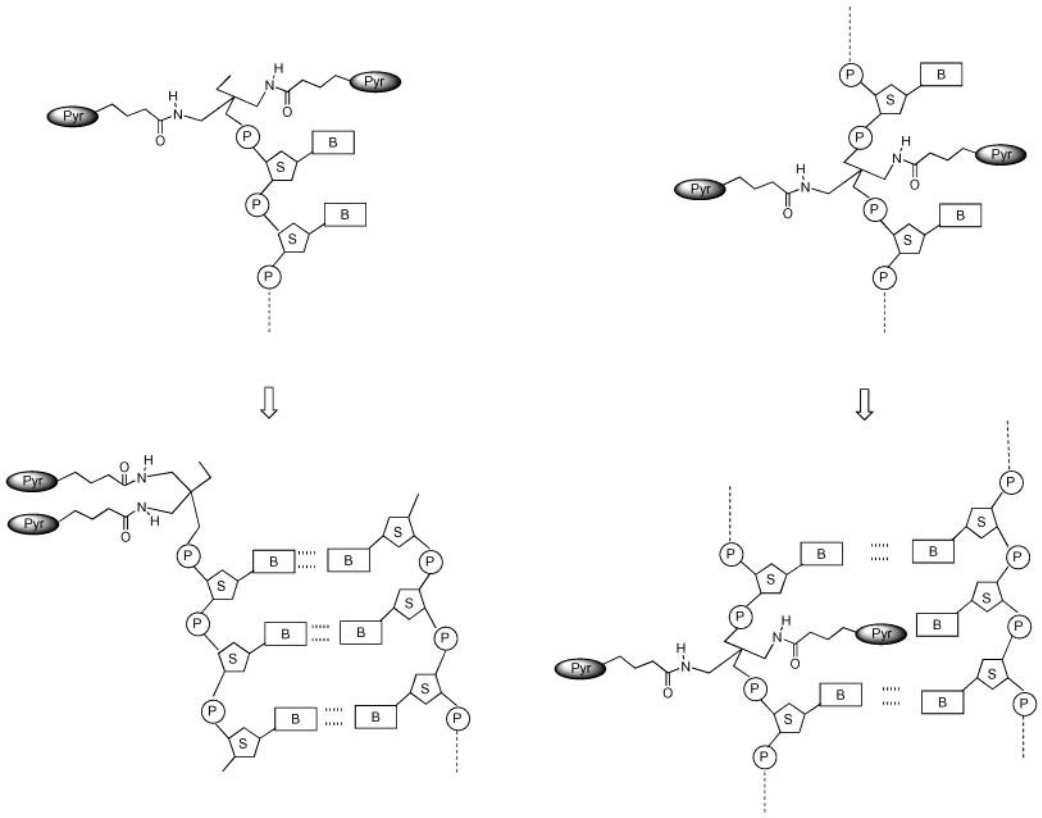


Figure 5. Fluorescence spectra for bis-pyrene modified ODN **II** (curve A), duplex **II** (curve B), and duplexes with DNA containing G−A mismatch (curve C), G−C mismatch (curve D), and G−T mismatch (curve E). Fluorescence spectra were recorded at 23 °C with an excitation wavelength of 350 nm. The sequences of oligomers used in these studies are shown in Tables 1 and 2. (a) The mismatch base and extra bases in DNA are indicated by the bold font and underlined, respectively. (b) Relative fluorescence quantum yields were determined at 23 °C based on the single-stranded bis-pyrene modified ODN **II** or **III**. The other conditions were described in Table 1.

Sequence Specificity of Excimer Fluorescence upon Hybridization. The fluorescence spectra for the duplexes of the bis-pyrene modified ODN **II** with DNA possessing a single base-mismatch are shown Figure 5. The fluorescence and melting data from the mismatch study for ODN **II** and **III** are summarized in Table 2. In hybridization of **II** or **III** with DNA containing a single

Scheme 2. Schematic Representation of Interaction between Bis-Pyrene-Modified ODN and DNA



base-mismatch, much smaller changes of the fluorescence, especially in the G to T mismatch, were observed relative to the hybrids with fully matched DNA. The quenching of the excimer and monomer fluorescence was observed upon binding to DNA possessing fully matched bases to **II** or **III** but extra bases at the 3′-terminus.

DISCUSSION

We have designed and synthesized a new non-nucleosidic backbone containing a bispyrenyl group for labeling of ODNs. Since the propanediol backbone has two pyrenyl residues at 2,2-positions, it can be used for introduction a bis-pyrene group into the terminal or internal position of ODNs by a single synthetic cycle in an automated DNA synthesis. Our approach, therefore, provides an easy and simple method for preparation of a pyrene excimer-forming probe (*24*, *27*, *28*, *29*).

2,2-Bispyrenyl propanediol exhibited strong excimer emission together with small monomer fluorescence in aqueous solution. Excimer versus monomer ratio was not altered with dilution of the solution, indicating that intramolecular excimer formation favorably occurs as expected for bis-pyrene with a 13-atoms linker. Covalent attachment of this backbone into the terminal position of ODNs resulted in large decrease in fluorescence quantum yield and afforded emission spectra of monomer fluorescence as a major component. Similarly, a 7-atoms linker containing bis-pyrene attached at the terminal end of ODNs displays excimer and monomer (almost equal intensity) fluorescence in a lowered quantum yield relative to a free bispyrene alcohol (*27*). Incorporation of our bis-pyrene into the internal position of ODNs also reduced the quantum efficiency of pyrene fluorescence and exhibited emission spectra of monomer fluorescence as a major component.

When the terminal labeled ODNs **I**−**IV** bind to fully complementary DNA sequences, the duplexes formed show almost comparable thermal stability to unmodified duplexes. These results suggest that the interaction of the bis-pyrene group with neighboring nucleobases may not occur with little or no stabilizing energy providing to the duplexes. This is evident from the observations that little shifts of the apsorption maxima and small increase in the absorption occur upon hybridization of the terminally modified duplex. In addition, no induced CD at around the pyrene absorption supports the mode of the pyrene interactions discussed for the terminally modified duplex. Binding of the internally labeled ODNs **V**−**VII** to DNA possessing a base facing at the bis-pyrene provides the duplexes whose stability is considerably higher relative to the duplexes containing the propanediol linker in place of the bis-pyrene (C3-modified duplex **V**−**VII**). The stabilizing energy for the internally labeled duplexes should be originated from the interaction of the pyrenyl residue with the neighboring bases. The stacking interactions occurred between the pyrene and DNA bases in the internally modified duplex were consistent with the spectral observations in the red-shift and hypochromism of the pyrene absorption, and the induced CD appeared at around the pyrene apsorption band.

Based on the bis-pyrene interaction with the nucleobases in the duplexes, the excimer and monomer fluorescence changes upon hybridization may be accounted according to the models as shown in Scheme 2. The model shown at the left is consistent well to the terminally labeled ODNs (**I**−**IV**). In the single stranded form, one (or both) pyrene ring(s) in the bis-pyrene probes has some interaction with neighboring bases, resulting in the low fluorescence quantum yield and disrupting intramolecular excimer formation. As a result of duplex formation, both two pyrene chromophores become relatively free

from the interaction leading to increase in the fluorescence efficiency and formation of the pyrene excimer. This interaction model is likey to explain the observations that the kind of the adjacent base to the bis-pyrene showed little effect on the excimer formation (compare **I**−**III** with **IV**). From the mismatch study, the base-pairing at the terminus adjacent to the bis-pyrene in the labeled duplexes is essential for the observed strong excimer fluorescence. Extra nucleobases present in the target DNA nearby the bis-pyrene in the ODNs disrupt the excimer formation. It is therefore concluded that ODNs modified by the bis-pyrene at the 5′-terminus provide a highly sensitive probe for DNA in a distinctive manner of sequence specificity.

The other model shown at the right is most likely to explain the fluorescence properties of the internally labeled ODNs (**V**−**VII**). In this case, the bis-pyrene backbone serves as an analogue for abasic nucleoside (*34*). The excimer and monomer fluorescence changes were observed upon hybrid formation with DNA containing one base facing to the bis-pyrene and remaining bases fully matched. However, these changes were relatively small when compared with the terminally labeled ODNs (**I**−**IV**) and the extent of the fluorescence changes appeared to be dependent on the probe sequences. The small fluorescence changes dependent on the probe sequences are consistent with the observations that the duplexes of **V**−**VII** are more stable than those for the corresponding C3-modified duplexes. It is therefore strongly suggested that the interaction of the bis-pyrene residue with the neighboring bases occurs in the duplex form as well as in the single-stranded form and is not a favorable factor to form the pyrene excimer. The fluorescence changes of ODN **VI** upon hybridization is larger than those for the ODNs **V** or **VII**, being consistent with the relative stability of the duplex or the extent of the pyrene interaction.

CONCLUSION

In summary, we have demonstrated that oligonucleotides possessing bis-pyrene backbone at the designated position can be easily synthesized by phosphoramidite chemistry. Terminally labeled bis-pyrene probes exhibit strongly enhanced excimer fluorescence upon binding to DNA. The attractive features of our probes are that excimer and monomer fluorescence is sensitive to local base sequences of probe−DNA duplex around the pyrene modification. The pyrene excimer-forming probe would thus be useful in sequence-specific detection of DNA.

ACKNOWLEDGMENT

We are very grateful to Professor Isao Saito for use of his CD spectrometer. We thank Professors Hiroshi Sugiyama, and Kazuhiko Nakatani for mass spectral analysis. This research is supported by Sumitomo Foundation (K.Y.).

LITERATURE CITED

(1) Murakami, A., Nakamura, M., Nakatsuji, Y., Nagahara, S., Tran-Cong, Q., and Makino, K. (1991) Fluorescent-labeled oligonucleotide probes: detection of hybrid formation in solution by fluorescence polarization spectroscopy. *Nucleic Acids Res. 19*, 4097−4102.

(2) Jenkins, Y., and Barton, J. (1992) Sequence specific molecular light switch: tethering of an oligonucleotide to a dipyridophenazine complex of ruthenium(II). *J. Am. Chem. Soc. 114*, 8736−8738.

(3) Ishigro, T., Saitoh, J., Yawata, H., Ohtsuka, M., Inoue, T., and Sugiura, Y. (1996) Fluorescence detection of specific sequence of nucleic acids by oxazole yellow-linked oligonucleotides. Homogeneous quantitative monitoring of in vitro transcription. *Nucleic Acids Res. 24*, 4992−4997.

(4) Yamana, K., Ohashi, Y., Nunota, K., and Nakano, H. (1997) Synthesis, binding, and fluorescence properties of oligonucleotide derivatives having a dansyl fluorescence label attached to the 2′-position of a ribonucleoside. *Tetrahedron 53*, 4265−4270.

(5) Tyagi, S., Marras, S. A. E., and Kramer, F. (2000) Wavelength-shifting molecular beacons. *Nature Biotechnol. 18*, 1191−1196.

(6) Kostriks, L. G., Tyagi, S., Mhlanda, M. M., Ho, D. D., and Kramer,F. (1998) Molecular beacons: spectral genotyping human alleles. *Science 279*, 1228−1229.

(7) Tyagi, S., and Kramer, F. (1996) Molecular beacons: Probes that fluorescence upon hybridization. *Nature Biotechnol. 14*, 303−307.

(8) Zang, P., Beck, T., Tan, W. (2001) Design of a molecular beacon DNA probe with two fluorophores. *Angew. Chem., Int. Ed. Engl. 40*, 402−405.

(9) Oser, A., and Valet, G. (1990) Nonradioactive assay of DNA hybridization by DNA-template-mediated formation of a ternary Tb^{III} complex in pure liquid phase. *Angew. Chem., Int. Ed. Engl. 29*, 1167−1169.

(10) Mergny, J. L., Grrestier, T., Rougee, M., Alexandre, A. V., Chassignol, M., Thoung, N. T., and Helene, C. (1994) Fluorescence energy transfer between two triple helix-forming oligonucleotides bound to duplex DNA. *Biochemistry 33*, 15321−15328.

(11) Chen, X., and Kwok, P. Y. (1997) Template-directed dye-terminator incorporation (TDI) assay: a homogeneous DNA diagnostic method based on fluorescence resonance energy transfer. *Nucleic Acids. Res. 25*, 347−353.

(12) Ota, N., Hirano, K., Warashina, N., Andrus, A., Mullah, B., Hatanaka, K., and Taira, K. (1998) Determination of interactions between structured nucleic acids by fluorescence resonance energy transfer (FRET): selection of target sites for functional nucleic acids. *Nucleic Acids Res. 26*, 735−743.

(13) Okamura, Y., Kondo, S., Sase, I., Suga, T., Mise, K., Furusawa, I., Kawakami, S., and Watanabe, Y (2000) Double-labeled donor probe can enhance the signal of fluorescence resonance energy transfer (FRET) in detection of nucleic acid hybridization. *Nucleic Acids. Res. 28*, e107.

(14) Sei-Iida, Y., Koshimoto, H., Kondo, S and Tsuji, A. (2000) Real-time monitoring of in vitro transcriptional RNA synthesis using fluorescence resonance energy transfer. *Nucleic Acids. Res. 28*, e59.

(15) Masuko, M., Ohuchi, O., Sode, K., Ohtani, H., and Shimadzu, A. (2000) Fluorescence resonance energy transfer from pyrene to perylene labels for nucleic acid hybridization assays under homogeneous solution conditions. *Nucleic Acids. Res. 28*, e34.

(16) Yamana, K., and Letsinger, R. L. (1985) Synthesis and properties of oligonucleotides bearing a pendant pyrene group. *Nucleic Acids Res. Symp. Ser. 16*, 169−172.

(17) Telser, J., Cruickshank, K. A., Morrison, L. E., Netzel, T. L., and Chan, C. (1989) DNA duplexes covalently labeled at two sites: synthesis and characterization by steady-state and time-resolved optical spectroscopies. *J. Am. Chem. Soc. 111*, 7226−7231.

(18) Yamana, K., Ohashi, Y., Nunota, K., Kitamura, M., Nakano, H., Sangen, O., and Shimidzu, T. (1991) Synthesis of oligonucleotide derivatives with pyrene group at sugar fragment. *Tetrahedron Lett. 32*, 6347−6351.

(19) Yamana, K., Gokota, T., Ozaki, H., Nakno, H., Sangen, O., and Shimidzu, T. (1992) Enhanced fluorescence in the binding of oligonucleotides with a pyrene group in the sugar fragment to complementary polynucleotides. *Nucleosides Nucleotides 11*, 386−390.

(20) Kierzek, R., Li, Y., Turner, D., and Bevilacqua, P. C. (1993) 5′-Amino pyrene provides a sensitive, nonperturbing fluorescent probe of RNA secondary and tertiary structure formation. *J. Am. Chem. Soc. 115*, 4985−4992.

(21) Yamana, K., Kumamoto, S., and Nakano, H. (1997) Homopyrimidine oligonucleotides modified by a pyrenylmthyl

group at the terminal position: Enhanced fluorescence upon binding to double helical DNA. *Chem. Lett.* 1173−1174.
(22) Yamana, K., Iwase, R., Frutani, S., Tsuchida, H., Zako, H., Yamaoka, T., and Murakami, A. (1999) 2′-Pyrene modified oligonucleotide provides a highly sensitive fluorescent probe of RNA. *Nucleic Acids Res.*, *27*, 2387−2392.
(23) Yamana, K., Zako, H., Asazuma, K., Iwase, R., Nakano, H., and Murakami, A. (2001) Fluorescence detection of specific RNA sequences using 2′-pyrene modified oligoribonucleotides. *Angew. Chem., Int. Ed. Engl. 40*, 1104−1107.
(24) Kitamura, M., Nimura, A., Yamana, K., and Shimidzu, T. (1991) Oligonucleotides with bis-pyrene adduct in the backbone: synthesis and properties of intramolecular excimer forming probe. *Nucleic Acids Res. Symp. Ser. 25*, 67−71.
(25) Yamana, K., Nunota, K., Nakano, H., and Sangen, O. (1994) A new method for introduction of a pyrene group into a terminal position of an oligonucleotide. *Tetrahedron Lett. 35*, 2555−2559.
(26) Yamana, K., Takei, M., and Nakano, H. (1997) Synthesis of oligonucleotide derivatives containing pyrene labeled glycerol linkers: Enhanced excimer fluorescence on binding to a complementary DNA sequence. *Tetrahedron Lett. 38*, 6051−6055.
(27) Lews, F. D., Zhang, Y., and Letsinger, R. L. (1997) Bispyrenyl Excimer Fluorescence: A Sensitive Oligonucleotide Probe. *J. Am. Chem. Soc. 119*, 5451−5452.
(28) Paris, P. L., Langenhan, J. M., and Kool, E. T. (1998) Probing DNA sequences in solution with a monomer−excimer fluorescence color change. *Nucleic Acids Res. 26*, 3789−3793.
(29) Masuko, M., Ohtani, H., Ebata, K., and Shimadzu, A. (1998) Optimization of excimer-forming two-probe nucleic acid hybridization method with pyrene as a fluorophore. *Nucleic Acids Res. 26*, 5409−5416.
(30) Yamana, K., Mitsui, T., Yoshioka, J., Isuno, T., and Nakano, H. (1996) Incorporation of two anthraquinonylmethyl groups into the 2′-O-positions of oligonucleotides: increased affinity and sequence specificity of anthraquinone-modified oligonucleotides in hybrid formation with DNA and RNA. *Bioconjugate Chem. 7*, 715−720.
(31) Fasman, G. D., Ed. (1985) *Handbook of biochemistry and molecular biology: Nucleic Acids*, 2nd ed., Vol. 1, p 589, CRC Press, Boca Raton, FL.
(32) Misiura, K., Durrant, I., Evans, M. R., and Gait, M. J. (1990) Biotinyl and phosphotyrosinyl phosphoramidite derivatives useful in the incorporation of multiple reporter groups on synthetic oligonucleotides. *Nucleic Acids. Res. 18*, 4345−4354.
(33) Nelson, P. S., Kent, M., and Muthini, S. (1992) Oligonucleotide labeling methods. 3. Direct labeling of oligonucleotides employing a novel, non-nucleosidic, 2-aminobutyl-1, 3- propanediol backbone. *Nucleic Acids Res. 20*, 6253−6259.
(34) Pompizi, I., Herli, A., and Leumann, C. J. (2000) Oligodeoxynucleotides containing conformationally constrained abasic sites: a UV and fluorescence spectroscopic investigation on duplex stability and structure. *Nucleic Acids Res. 28*, 2702−2708.

BC025530U

Oligonucleotides Incorporating 7-(Aminoalkynyl)-7-deaza-2′-deoxyguanosines: Duplex Stability and Phosphodiester Hydrolysis by Exonucleases†

Helmut Rosemeyer, Natalya Ramzaeva, Eva-Maria Becker, Elisabeth Feiling, and Frank Seela*

Laboratorium für Organische und Bioorganische Chemie, Institut für Chemie, Fachbereich Biologie/Chemie, Universität Osnabrück, Barbarastrasse 7, D-49069 Osnabrück, Germany. Received March 28, 2002; Revised Manuscript Received July 3, 2002

Oligonucleotides containing 7-(ω-aminoalkyn-1-yl)-7-deaza-2′-deoxyguanosines (**1a**−**c**) were investigated regarding their thermal stability (T_m values) as well as their phosphodiester hydrolysis catalyzed by exonucleases. Those derivatives are suitable for the labeling of nucleic acid constituents as well as for the postlabeling of DNA. For this, the phosphoramidites **7a**,**c** (obtained from the nucleoside **1a**,**b**), protected by an isobutyryl group at the 2-amino group and a phthaloyl residue at the side-chain amino function, were synthesized. Using compounds **7a**,**c** together with the phosphoramidite of **1c** in solid-phase synthesis, a series of self-complementary and non-self-complementary oligonucleotides were prepared and characterized by MALDI-TOF mass spectrometry. A comparison of the T_m values of the modified oligomers shows that the thermal stability of the duplexes decreases with the length of the nucleobase 7-(ω-aminoalkyn-1-yl) side chain. Exonucleolytic cleavage of oligonucleotide single strands incorporating either the 7-(3-aminopropyn-1-yl)- or the 7-(4-aminobutyn-1-yl)-substituted nucleosides **1a** or **1b**, respectively, reveals that 3′ → 5′ specific snake venom phosphodiesterase liberates **1a** 5′-monophosphate but not the methylene-extended **1b** 5′-monophosphate. On the contrary, the 5′ → 3′ specific bovine spleen exonuclease is able to cleave off single **1a** and **1b** 3′-monophosphate residues; its action is, however, terminated in the case of oligonucleotides containing two consecutive **1a** or **1b** nucleotide units.

INTRODUCTION

The introduction of aminoalkynyl, aminoalkenyl, and aminoalkyl groups to pyrimidine and purine constituents of DNA has a major impact on its structure and stability. These groups can be used in particular for the conjugation of a DNA with reporter groups (Randolph and Waggoner, 1997; Ramzaeva et al., 2000; Cook et al., 1988; Ramasamy et al., 1994; Takeda et al., 1987; Ono et al., 1994; Haginoya et al., 1997). The incorporation of such cationic groups into a DNA or RNA leads to a partial neutralization of the phosphate negative charge (Hashimoto et al., 1993; Ramzaeva et al., 1997; Seela and Zulauf, 1999; Seela et al., 2001b; Bijapur et al., 1999; Soto et al., 2001). Interestingly, nature has implemented a design of this general type in bacteriophage DNA where half of the thymidine residues are replaced by positively charged α-putrescinylthymidine (= 5-{[(4-aminobutyl)-amino]methyl}thymidine), resulting in one positively charged base for every eight nucleotides on average (Miller Black et al., 1985; Kropinski et al., 1973). On the basis of the proposition of a *neutralization-collaps* model by Manning and Rich (Manning, 1978; Manning et al., 1989), Maher and co-workers showed that the introduction of tethered cationic groups into a DNA in phase with the helical turn leads inevitably to an intrinsic curvature of the nucleic acid (Strauss et al. 1996; Williams and Maher, 2000; Hardwidge, 2001 and literature cited therein). This is due to the partial neutralization of the negatively charged sugar−phosphate backbone leading to an asymmetric decrease in phosphate−phosphate charge repulsions. The latter causes a bias of the opposing but normaly balanced forces of compression (e.g. base stacking, van der Waals contacts) and stretching (e.g. interphosphate Coulombic repulsion) rendering an oligonucleotide to a stiff rod with elastic resilience.

A further impact concerns the incorporation of charge tags into nucleic acids (DNA and RNA) in order to enhance their detectability in MALDI-TOF mass spectrometry. It has been shown that the incorporation of already one charge into a DNA molecule enhances the sensitivity by which it can be detected by a factor of 100 (Wenzel et al., 2001; Gut and Beck, 1995). This result has recently found application in the development of a novel procedure for efficient genotyping of single nucleotide polymorphism ('GOOD' assay) (Sauer et al. 2000).

Apart from that, D. M. Williams and co-workers (Lee et al., 2001, Gorlain et al., 2001) used C(7)-modified 7-deaza-dATP derivatives with pendant 3-aminopropyl, (*Z*)-3-aminopropenyl, and 3-aminopropynyl side chains together with a C(5)-imidazolyl-modified dUTP as substrates for *Taq* polymerase during PCR and demonstrated the simultaneous incorporation of both functionalities into a DNA molecule. Cleavage of the modified oligonucleotide by restriction endonucleases, however, failed.

In this manuscript the synthesis of phosphoramidite building blocks of functionalized 7-deaza-2′-deoxyguanosine derivatives carrying either 7-(3-aminopropyn-1-yl)- or 7-(4-aminobutyn-1-yl) side chains is described. These building blocks are used for the preparation of ami-

* To whom correspondence should be addressed. Phone +49-541-9692791. Fax: +49-541-9692370. E-mail: Frank.Seela@uni-osnabrueck.de.

† Dedicated to Prof. Dr. Dr. h. c. Wolfgang Pfleiderer, Konstanz, Germany, on the occasion of his 75th birthday.

10.1021/bc020024q CCC: $22.00 © 2002 American Chemical Society
Published on Web 11/01/2002

noalkynyl-functionalized oligodeoxyribonucleotides. The latters are studied with respect to their thermal stability as well as toward their resistance against phosphodiester hydrolysis by two single strand-specific exonucleases.

EXPERIMENTAL PROCEDURES

General Remarks. All chemicals were purchased from Aldrich, Sigma, or Fluka (Sigma-Aldrich Chemie GmbH, Deisenhofen, Germany). Snake venom phosphodiesterase (from *Crotallus adamanteus*) was purchased from USB Amersham Life Science (Cleveland, OH), bovine spleen phosphodiesterase from Sigma (Sigma-Aldrich Chemie GmbH, Deisenhofen, Germany) and alkaline phosphatase from Roche Diagnostics (Penzberg, Germany). Solvents were of laboratory grade and were distilled before use. Dimethylformamide (DMF) was purified by codistillation with H_2O and benzene before use. Compounds **4a**, **5a**, **6a**, and **7a**,**b** were prepared as described (Ramzaeva et al., 1999; Seela et al. 2001b). Thin-layer chromatography (TLC): aluminum sheets, silica gel 60 F_{254}, 0.2 mm layer (Merck, Germany). Column flash chromatography (FC): silica gel *60* (Merck, Germany) at 0.5 bar (4×10^4 Pa); sample collection with an UltroRac II fractions collector (LKB Instruments, Bromma, Sweden). UV spectra: U-3200 spectrometer (Hitachi, Japan). Elemental analyses were performed by Mikroanalytisches Laboratorium Beller (Göttingen, Germany). NMR Spectra were measured on an AMX-500 spectrometer (Bruker, Germany) operating at a proton resonance frequency of 500.14 MHz (125.1 MHz for ^{13}C and 101.3 MHz for ^{31}P nuclei). Chemical shifts are in ppm relative to tetramethylsilane (TMS) as internal standard or external 85% H_3PO_4. *J* values are given in hertz.

Solid-Phase Synthesis of Oligodeoxyribonucleotides. The synthesis of the oligonucleotides was accomplished on a 1-μmol scale using the 3′-phosphoramidites **7a** and **7c**, respectively, as well as those of the regular 2′-deoxyribonucleosides being commercially available (Sigma, St. Louis, MO). The synthesis followed the regular protocol of the DNA synthesizer (Model 392 B, Applied Biosystems, Weiterstadt, Germany). The oligonucleotides were recovered from the synthesizer as the 5′-dimethoxytritylated derivatives. After treatment with 25% aq NH_3 (12 h, 60 °C) and then with 10% aq methylamine (24 h, room temp) to cleave off the nucleobase protecting groups, the 5′-dimethoxytritylated oligomers were purified by reverse-phase HPLC (see below; RP-18 column, 250 × 4 mm, 7 μm, solvent system I). Detritylation was performed by using 80% HOAc/H_2O for 2 min at room temperature. Detritylated oligomers were again purified by RP-18 HPLC (solvent system II). Oligonucleotides were desalted on a 4 × 25 mm HPLC cartridge (RP-18 silica gel). Inorganic material was eluted with H_2O (10 mL) while the oligomers were eluted with MeOH/H_2O (3:2, v/v). The oligomers were lyophilized on a Speed-Vac evaporator and stored frozen at −23 °C.

The enzymatic hydrolysis of the unmodified oligomers using snake-venom phosphodiesterase (EC 3.1.15.1, *Crotallus adamanteus*) and alkaline phosphatase (EC 3.1.3.1, *E. coli*) was carried out as described (Seela and Lampe, 1991). The reaction mixture was analyzed on reversed-phase HPLC (RP-18, solvent system III). Quantification of the resulting nucleosides was made on the basis of the peak areas which were divided by the extinction coefficients of the nucleoside constituents at $\lambda = 260$ nm: dA 15400, dC 7300, dG 11700, dT 8800 M^{-1} cm^{-1}.

HPLC Separation. HPLC was carried out on a 250 × 4 mm RP-18 column (Merck, Germany) on a Merck-Hitachi HPLC apparatus with one pump (model 655-A-12) connected with a proportioning valve, a variable wavelength monitor (model 655 A), a controller (model L-5000), and an integrator (model D-2000). The solvent gradients, consisting of 0.1 M (Et_3HN)OAc (pH 7.0)/MeCN 95:5 (A) and MeCN (B), were used in the following order: gradient I, 3 min 15% B in A, 7 min 15−40% B in A, flow rate 1 mL/min; gradient II, 20 min 0−20% B in A, flow rate 1 mL/min; solvent system III 20 min 100% A, flow rate 0.6 mL/min.

Melting Experiments. The thermal dissociation/association of the oligomers was measured by temperature-dependent UV melting profiles using a Cary 1E UV/VIS spectrophotometer (Varian, Australia) equipped with a Cary thermoelectrical controller; the actual temperature was measured in the reference cell with a Pt-100 resistor. The thermodynamic data of duplex formation were calculated by curve fitting to a two-state-model using the program *MeltWin* (McDowell and Turner, 1996) or by concentration-dependent T_m measurements.

Mass Spectrometry. MALDI-TOF mass spectra were run on a BIFLEX III instrument (Bruker Saxonia Analytik GmbH, Leipzig, Germany) in the reflector mode. The average power of the nitrogen laser (337.1 nm) at 20 Hz was 3−4 mW (150−200 μJ/pulse) with a delay time of 600 ns. All measurements were performed using the positive detection mode with the following parameters: dwell time: 1.00 ns, delay: 40000 ns, Uis1: 19.00 kV, Uis2: 15.80 kV, Urefl 20.00 kV, Ulens: 9.35 kV. The spectra were obtained by overlaying 500−1000 single pulses with a cutoff mass of 1000 Da. The spectrometer was calibrated using an oligonucleotide calibration standard (Bruker, Part No. 206200) containing a 12-mer (3645.44 Da), a 20-mer (6117.04 Da) and a 30-mer (9191.03 Da).

The sample preparation was performed on Scout MTP MALDI targets (Bruker) as follows: 1 μL of the supernatant of a saturated solution of recrystallized 3-hydroxypicolinic acid in doubly distilled H_2O containing BioRad microbeads AG 50W-X8 (100−200 mesh, NH_4^+-form) was spotted on a target well. A suspension (1 μL) containing 15−20 microbeads in H_2O was added followed by 1 μL of an aq oligonucleotide solution (concentration: 0.1 A_{260} units/10 μL H_2O). The mixture was carefully dried on the target, and the microbeads were removed mechanically with a tip.

Sequencing of Oligonucleotides. The sequencing of oligonucleotides was carried out by time-dependent enzymatic degradation reactions. All reactions were run in H_2O without the addition of salts or buffer. Oligonucleotides were degraded from both ends in separate reactions.

5′ → 3′ Degradation. Two A_{260} units of the oligonucleotide, dissolved in H_2O, was mixed with 1 μL (0.1 U) of an aq solution of bovine spleen phosphodiesterase (BSPDE, EC 3.1.16.1). The mixture was diluted to a total volume of 30 μL with H_2O and then incubated at 37 °C. Aliquots of 1 μL were taken at different time intervals and analyzed as described above.

3′ → 5′ Degradation. As described for the 5′ → 3′ degradation but using 1 μL (0.1 U) of snake venom phosphodiesterase (SVPDE, EC 3.1.15.1).

3-Phthalimido-1-propyne (3a). Compound **3a** was prepared according to Gibson and Benkovic (Gibson and Benkovic, 1987) from 3-amino-1-propyne (20 mL, 0.29 mol) and *N*-ethoxycarbonylphthalimide (64 g, 0.29 mol). Colorless crystals (45 g, 83%); mp 151−153 °C. ^1H NMR (d_6-DMSO): 7.84 (4H, m, phthaloyl); 4.36 (2H, d, ^4J = 2.4, CH_2); 3.25 (1H, t, ^4J = 2.4, CH).

4-Phthalimido-1-butyne (3b) (Meyer, 1994). To an ice-cold solution of triphenylphosphine (6.5 g, 25 mmol)

in dioxane (50 mL) was added dropwise diisopropylazidodicarboxylate (5 mL, 22.5 mmol) over a period of 30 min. After the addition has been completed, a solid precipitated. Subsequently, a mixture of phthalimide (3.7 g, 25 mmol) and 3-butyn-1-ol (1.75 g, 25 mmol), dissolved in dioxane (12.5 mL), was added in one portion. After stirring overnight at ambient temperature, the reaction mixture was evaporated and the residue crystallized from CH_2Cl_2 to afford 2.1 g (42%) of **3b** as colorless crystals; mp 134−138 °C. ^{1}H NMR (d_6-DMSO): 7.80 and 7.70 (2 m, 2 × 2H, phthaloyl); 3.84 (t, 2H, CH_2N); 2.55 ('sextett', 2H, CH_2); 1.93 (t, 1H, ^4J = 2.6, CH).

2-Amino-7-(2-deoxy-β-D-erythro-pentofuranosyl)-3,7-dihydro-5-(phthalimido-1-propynyl)-4*H*-pyrrolo-[2,3-*d*]pyrimidin-4-one (4a). Compound **4a** was prepared from **2b** (1.2 g, 3.0 mmol) and 3-phthalimido-1-propyne (**3a**, 1.2 g, 6.5 mmol) as described for compound **4b**. Yield: 1.1 g (80%) of **4a** as a yellowish solid. The crude product was used without additional purification. For elemental analysis the compound was purified by FC (CH_2Cl_2/MeOH, 9:1) R_f 0.44. ^{1}H NMR (d_6-DMSO): 2.07 (1H, m, 2′-H$_\alpha$), 2.29 (1H, m, 2′-H$_\beta$), 3.49 (2H, m, 5′-H), 3.75 (1H, m, 4′-H), 4.27 (1H, m, 3′-H), 4.59 (2H, s, CH_2), 4.87 (1H, t, ^3J = 5.4, 5′-OH), 5.18 (1H, d, ^3J = 3.7, 3′-OH), 6.26 (1H, t, ^3J = 6.0, 1′-H), 6.31 (2H, s, NH_2), 7.26 (1H, s, 6-H), 7.87−7.94 (4H, m, Pht), 10.45 (1H, s, NH). Anal. Calcd for $C_{22}H_{19}N_5O_6$ (449.42): C 58.80, H 4.26, N 15.58. Found: C 58.49, H 4.08, N 15.38.

7-(2-Deoxy-β-D-erythro-pentofuranosyl)-3,7-dihydro-2-(isobutyrylamino)-5- (3-phthalimido-1-propynyl)-4*H*-pyrrolo[2,3-*d*]pyrimidin-4-one (5a). Compound **5a** was prepared from **4a** (1.0 g, 2.2 mmol) as described for **5b**. Chromatographic workup (silica gel, 5−10% MeOH/CH_2Cl_2) gave 765 mg (67%) of **5a** as a colorless solid. TLC (silica gel, CH_2Cl_2/MeOH, 9:1): R_f 0.48. ^{1}H NMR (d_6-DMSO): 1.11 (6H, m, 2 Me), 2.12 (1H, m, 2′-H$_\alpha$), 2.34 (1H, m, 2′-H$_\beta$), 2.73 (1H, m, CH), 3.49 (2H, m, 5′-H), 3.77 (1H, m, 4′-H), 4.29 (1H, m, 3′-H), 4.60 (2H, s, CH_2), 4.88 (1H, t, ^3J = 5.3, 5′-OH), 5.20 (1H, d, ^3J = 3.2, 3′-OH), 6.35 (1H, t, ^3J = 6.2, 1′-H), 7.56 (1H, s, 6-H), 7.86−7.93 (4H, m, Pht), 11.52 (1H, s, NH), 11.78 (1H, s, NH). Anal. Calcd for $C_{26}H_{25}N_5O_7$ (519.15): C 60.11, H 4.85, N 13.48. Found: C 59.82, H 4.95, N 13.31.

7-[2-Deoxy-5-*O*-(4,4′-dimethoxytrityl)-β-D-erythro-pentofuranosyl]-3,7-dihydro-2-(isobutyrylamino)-5-(3-phthalimido-1-propynyl)-4*H*-pyrrolo[2,3-*d*]pyrimidin-4-one (6a). Compound **6a** was prepared from **5a** (519 mg, 1.0 mmol) as described for **6b**. FC (silica gel, 10−20% acetone/CH_2Cl_2) afforded 710 mg (86%) of **6a** as a colorless foam. TLC (silica gel, CH_2Cl_2/acetone, 85:15) R_f 0.30. ^{1}H NMR (d_6-DMSO): 1.12 (6H, m, 2 Me), 2.21 (1H, m, 2′-H$_\alpha$), 2.49 (1H, m, 2′-H$_\beta$), 2.77 (1H, m, CH), 3.12 (2H, m, 5′-H), 3.72 (6H, d, ^3J = 3.0, 2 OMe), 3.91 (1H, m, 4′-H), 4.32 (1H, m, 3′-H), 4.62 (2H, s, CH_2), 5.28 (1H, d, ^3J = 3.7, 3′-OH), 6.37 (1H, t, ^3J = 6.5, 1′-H), 6.82−7.35 (13H, m, arom H), 7.88−7.95 (4H, m, Pht), 11.56 (1H, s, NH), 11.83 (1H, s, NH). Anal. Calcd for $C_{47}H_{43}N_5O_9$ (821.88): C 68.69, H 5.27, N 8.52. Found: C 68.58, H 4.98, N 8.54.

7-[2-Deoxy-5-*O*-(4,4′-dimethoxytrityl)-β-D-erythro-pentofuranosyl]-3,7-dihydro-2-(isobutyrylamino)-5-(3-phthalimido-1-propynyl)-4*H*-pyrrolo[2,3-*d*]pyrimidin-4-one 3′-[(2-Cyanoethyl)-*N*,*N*-(diisopropyl)]-phosphoramidite (7a). Compound **7a** was prepared from **6a** (500 mg, 0.6 mmol) as described for **7b**. FC (silica gel, CH_2Cl_2/EtOAc/Et_3N, 69:30:1) gave a mixture of diastereoisomers **7a** (520 mg, 84%). TLC (silica gel, CH_2Cl_2/acetone, 85:15) R_f 0.8. ^{31}P NMR ($CDCl_3$): 148.17, 148.62.

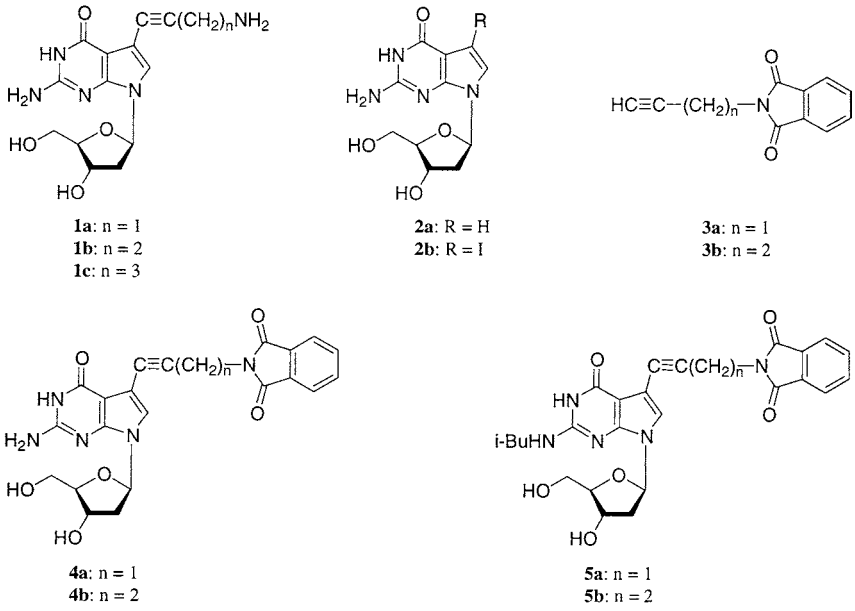
7-[2-Deoxy-5-*O*-(4,4′-dimethoxytrityl)-β-D-erythro-pentofuranosyl]-3,7-dihydro-2-(isobutyrylamino)-5-(3-phthalimido-1-propynyl)-4*H*-pyrrolo[2,3-*d*]pyrimidin-4-one 3′-(Triethylammonium Phosphonate) (7b). To a solution of PCl_3 (180 μl, 2.0 mmol) and *N*-methylmorpholine (2.2 mL, 20 mmol) in CH_2Cl_2 (15 mL) was added 1*H*-1,2,4-triazole (480 mg, 6.8 mmol). The solution was cooled to 0 °C, **6a** (340 mg, 0.4 mmol) in CH_2Cl_2 (15 mL) was added slowly, and stirring was continued for 30 min at 0 °C. The mixture was poured into 1 M $(Et_3NH)HCO_3$ (TBK, pH 8.5, 30 mL). The aq layer was extracted with CH_2Cl_2 (3 × 40 mL) and the combined organic extract dried (Na_2SO_4) and evaporated. FC (silica gel, CH_2Cl_2/Et_3N, 98:2, then CH_2Cl_2/MeOH/Et_3N, 88:10:2) furnished a main zone which was evaporated. The residue was dissolved in CH_2Cl_2, extracted with aq 0.1 M TBK (6 × 25 mL), dried (Na_2SO_4) and evaporated to give **7b** (270 mg, 69%) as a colorless foam. ^{1}H NMR (d_6-DMSO): δ, 1.14 (15H, m, 5 Me), 2.32 (1H, m, 2′-H$_\alpha$), 2.74 (1H, m, 2′-H$_\beta$), 2.99 (7H, m, 3 CH_2 + CH), 3.20 (2H, m, 5′-H), 3.72 (6H, s, 2 OMe), 4.09 (1H, m, 4′-H), 4.69 (2H, m, CH_2), 4.74 (1H, m, 3′-H), 6.07 (0.5H, s, PH), 6.42 (1H, t, 1′-H), 6.83−7.34 (14.5H, m, arom H + H-6 + PH), 7.89−7.93 (4H, m, Pht), 11.79 (2H, bs, 2 NH). ^{31}P NMR (d_6-DMSO): 0.91 (^1J(P,H) = 581.8; ^3J (P,H) = 8.6). Anal. Calcd for $C_{52}H_{59}N_6O_{11}P$ (975.04): C 64.06, H 6.10, N 8.62. Found: C 63.96, H 6.34, N 8.50.

2-Amino-7-(2-deoxy-β-D-erythro-pentofuranosyl)-3,7-dihydro-5-(4-phthalimido-1-butynyl)-4*H*-pyrrolo-[2,3-*d*]pyrimidine-4-one (4b). A suspension of compound **2b** (1.2 g, 3.1 mmol), [Pd(0)(PPh_3)$_4$] (690 mg, 0.6 mmol), CuI (228 mg, 1.20 mmol), Et_3N (0.6 mL, 4.3 mmol), and 4-phthalimido-1-butyne (**3b**,1.2 g, 6.0 mmol) in anhydrous amine-free DMF (30 mL) was stirred under Ar for 24 h at room temperature. After the reaction was complete, the solvent was evaporated, and the residue precipitated from CH_2Cl_2, filtered, suspended in CH_2Cl_2/MeOH (9:1, v/v), filtered again, and dried. Yield: 1.1 g (78%) of **4b** as a brownish foam. TLC (silica gel, CH_2Cl_2/MeOH, 9:1): R_f 0.45. ^{1}H NMR (d_6-DMSO): 2.10 (1H, m, 2′-H$_\alpha$), 2.26 (1H, m, 2′-H$_\beta$), 2.76 (2H, t, CH_2), 3.52 (2H, m, 5′-H), 3.80 (3H, m, 4′-H + CH_2), 4.30 (1H, m, 3′-H), 4.70 (1H, t, 5′-OH), 5.04 (1H, d, ^3J = 3.0, 3′-OH), 6.14 (2H, s, NH_2), 6.26 (1H, t, ^3J = 6.4, 1′-H), 7.01 (1H, s, 6-H), 7.86−7.88 (4H, m, Pht), 10.25 (1H, s, NH). Anal. Calcd for $C_{23}H_{21}N_5O_6$ (463.44): C, 59.61; H, 4.57; N 15.11. Found: C, 59.88; H, 4.37; N, 14.85.

2-Amino-7-(2-deoxy-β-D-erythro-pentofuranosyl)-3,7-dihydro-5-(1-aminobut-3-ynyl)-4*H*-pyrrolo[2,3-*d*]-pyrimidin-4-one (1b). Compound **4b** (5 mg) was dissolved in concentrated aq ammonia and stirred at 60 °C for 20 h. The reaction mixture was filtered and the filtrate evaporated to dryness yielding a colorless solid. ^{1}H NMR (d_6-DMSO): 2.00 (1H, m, 2′-H$_\alpha$), 2.14 (1H, m, 2′-H$_\beta$), 3.00 (2H, m, CH_2), 3.54 (2H, m, 5′-H), 3.81 (1H, m, 4′-H), 3.88 (2H, m, CH_2), 4.33 (1H, m, 3′-H), 4.98 (1H, br, 5′-OH), 5.23 (1H, br., 3′-OH), 6.20 (2H, br., NH_2), 6.37 (1H, pt, ^3J = 6.7, 1′-H), 7.62 (1H, s, 6-H). RP-18 HPLC (solvent system III): t_R = 12.8 min.

7-(2-Deoxy-β-D-erythro-pentofuranosyl)-3,7-dihydro-2-(isobutyrylamino)-5-(4-phthalimido-1-butynyl)-4*H*-pyrrolo[2,3-*d*]pyrimidine-4-one (5b). Compound **4b** (380 mg, 0.82 mmol) was dried by coevaporation from anhydrous pyridine. The residue was suspended in pyridine (5 mL), and Me_3SiCl (0.53 mL, 4.2 mmol) was added at room temperature. After 15 min of stirring, the solution was treated with isobutyric anhydride (0.67 mL, 4.0 mmol) and maintained at room temperature for 3 h. The mixture was cooled in an ice bath; then H_2O (1 mL)

Chart 1



1a: n = 1
1b: n = 2
1c: n = 3

2a: R = H
2b: R = I

3a: n = 1
3b: n = 2

4a: n = 1
4b: n = 2

5a: n = 1
5b: n = 2

and 5 min later a 25% aq NH_3 solution (1 mL) were added, and stirring was continued for 15 min. The solution was evaporated nearly to dryness and the residue precipitated from H_2O. The solid was filtered, washed with Et_2O, dried in vacuo, and subjected to flash column chromatography (column: 6 × 10 cm, 5 → 10% of MeOH in CH_2Cl_2). Yield: 320 mg (73%) of a colorless solid. TLC (silica gel, CH_2Cl_2/MeOH, 9:1): R_f 0.5. ^{1}H NMR (d_6-DMSO): 1.10 (6H, m, 2 Me), 2.13 (1H, m, 2′-H$_\alpha$), 2.32 (1H, m, 2′-H$_\beta$), 2.74 (3H, m, CH_2 + CH), 3.49 (2H, m, 5′-H), 3.77 (3H, m, CH_2 + 4′-H), 4.29 (1H, m, 3′-H), 4.93 (1H, t, 5′-OH), 5.25 (1H, d, 3′-OH), 6.34 (1H, t, 1′-H), 7.38 (1H, s, 6-H), 7.85 (4H, m, Pht), 11.54 (1H, s, NH), 11.74 (1H, s, NH). Anal. Calcd for $C_{27}H_{27}N_5O_7$ (533.53): C, 60.78; H, 5.10; N, 13.13. Found: C, 60.35; H, 5.12; N 12.98.

7-[2-Deoxy-5-*O*-(4,4′-dimethoxytrityl)-*β*-D-erythro-pentofuranosyl]-3,7-dihydro-2-(isobutyrylamino)-5-(4-phthalimido-1-butynyl)-4*H*-pyrrolo[2,3-*d*]pyrimidin-4-one (6b). Compound **5b** (510 mg, 0.96 mmol) was dried by repeated coevaporation from anhydrous pyridine and then dissolved in pyridine (20 mL). After addition of 4.4′-dimethoxytrityl chloride (360 mg, 1.06 mmol), the solution was stirred for 4 h at room temperature. Then, MeOH (3 mL) was added, and stirring was continued for 10 min; subsequently, a 5% aq $NaHCO_3$ solution (30 mL) was added, and the aqueous layer was extracted with CH_2Cl_2 (3 × 60 mL) affording, after evaporation of the solvent, 520 mg (65%) of a colorless solid. TLC (silica gel, CH_2Cl_2/acetone, 85:15): R_f 0.3. ^{1}H NMR (d_6-DMSO): 1.13 (6H, d, 2 Me), 2.23 (1H, m, 2′-H$_\alpha$), 2.47 (1H, m, 2′-H$_\beta$), 2.76 (3H, m, CH + CH_2), 3.18 (2H, m, 5′-H), 3.75 (6H, s, 2 OMe), 3.79 (2H, m, CH_2), 3.93 (1H, m, 4′-H), 4.33 (1H, m, 3′-H), 5.32 (1H, d, ^3J = 2.4, 3′-OH), 6.38 (1H, pt, ^3J = 6.2, 1′-H), 6.86−7.39 (14H, m, 6-H + arom H), 7.82−7.85 (4H, m, Pht), 11.54 (1H, s, NH), 11.79 (1H, s, NH). Anal. Calcd for $C_{48}H_{45}N_5O_9$ (835.90): C, 68.97; H, 5.43; N, 8.38. Found: C, 68.67; H, 5.32; N. 8.16.

7-[2-Deoxy-5-*O*-(4,4′-dimethoxytrityl)-*β*-D-erythro-pentofuranosyl]-3,7-dihydro-2-(isobutyrylamino)-5-(4-phthalimido-1-butynyl)-4*H*-pyrrolo[2,3-*d*]pyrimidin-4-one 3′-[(2-Cyanoethyl)-*N*,*N*-(diisopropyl)]-phosphoramidite (7c). To a solution of **6b** (400 mg, 0.48 mmol) in anhydrous CH_2Cl_2 (15 mL) were added (i-Pr)$_2$-EtN (162 μL, 0.93 mmol) and chloro-(2-cyanoethoxy)-(diisopropylamino)phosphine (160 μL, 0.72 mmol). After stirring for 40 min at room temperature, a 5% aq $NaHCO_3$ solution (6 mL) was added, and the mixture was extracted with CH_2Cl_2 (2 × 15 mL). The organic layer was dried (Na_2SO_4), filtered, and evaporated. Flash chromatography (column: 6 × 10 cm, CH_2Cl_2/acetone, 85:15) gave a mixture of diastereoisomers of **7c** (300 mg, 61%). TLC (silica gel, CH_2Cl_2/acetone, 85:15): R_f 0.6. ^{31}P NMR ($CDCl_3$): 148.79, 149.2.

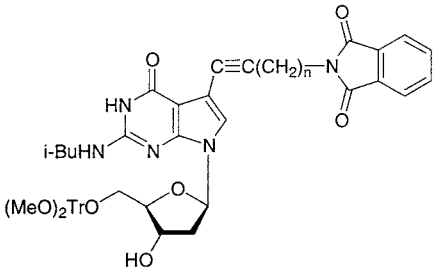
RESULTS AND DISCUSSION

Synthesis of Monomers. The key intermediate for the synthesis of the title compounds is the 7-iodo nucleoside **2b** (Chart 1)which has been described earlier (Ramzaeva and Seela, 1995). Pd(0)-catalyzed cross coupling reaction of compound **2b** with 3-phthalimido-1-propyne (**3a**) (Gibson and Benkovic, 1987) gave **4a** in 80% yield (Ramzaeva et al., 1999; Seela et al., 2001). Analogously, compound **2b** was now reacted with 4-phthalimido-1-butyne (**3b**) (Meyer, 1994) to give **4b** in about the same yield. Cleavage of the phthalimido group is unproblematic in concentrated aqueous ammonia at elevated temperature (60 °C) and leads to compound **1b** (see Experimental Procedures).

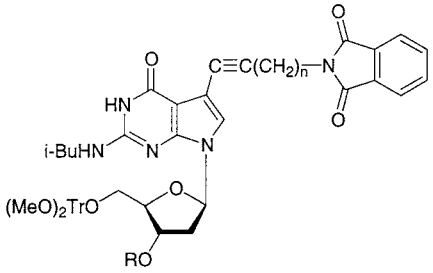
Upon the basis of our work on 7-alkynylated 7-deaza-2′-deoxyguanosine derivatives (Ramzaeva et al., 1997), we have chosen the isobutyryl group for the protection of the 2-amino function of compounds **4a** and **4b (**Ti et al., 1982). For comparison, the isobutyryl group of 2-(isobutyrylamino)-7-(hexyn-1-yl)-7-deaza-2′-deoxyguanosine exhibits a half-life value of 80 min (25% aq NH_3, 40 °C) (Ramzaeva et al., 1997). Isobutyrylation of compounds **4a** and **4b** was performed using the protocol of transient protection and furnished compound **5a** (67%) and **5b** (73%).

Subsequently, both compounds were treated with 4,4′-dimethoxytriphenyl-methyl chloride (Schaller et al., 1963) in pyridine to give the 5′-protected derivatives **6a** (86%) and **6b** (65%), respectively (Chart 2). The dimethoxytrityl derivative **6a** was phosphitylated with 2-cyanoethyl diisopropylphosphoramidochloridite (Beaucage and Caruthers, 1981) following a standard protocol to yield the phosphoramidite **7a** (Ramzaeva et al., 1999; Seela et al., 2001 b). Additionally, from compound **6a** the phosphonate **7b** was prepared using PCl_3/*N*-methylmorpholine/1*H*-1,2,4-triazole (Ramzaeva et al., 1999; Seela et al., 2001;

Chart 2



6a: n = 1
6b: n = 2



7a: n = 1, R = $NCCH_2CH_2OPN(i\text{-}Pr)_2$
7b: n = 1, R = $HP(O)O^{\ominus}\ {}^{\oplus}NHEt_3$
7c: n = 2, R = $NCCH_2CH_2OPN(i\text{-}Pr)_2$

Froehler et al., 1986). The 7-(4-aminobutyn-1-yl) derivative **6b** was phosphitylated as described for **6a** to give the phosphoramidite **7c**. It should be mentioned that the 5′-triphosphates of compounds **1b** and **1c** as well as of the phthaloyl-protected **4b** have been prepared earlier and used for dye labeling (Seela et al. 2001a).

Characterization of the Monomers. The newly synthesized derivatives (Charts 1 and 2) were characterized by elemental analysis as well as by ^1H, ^{13}C, and ^{31}P NMR spectroscopy (Tables 1, 2, and Experimental Procedures). Unambiguous assignment of the ^{13}C NMR resonances was made on the basis of gated-decoupled ^{13}C NMR, DEPT-135, and 2D [^1H,^{13}C] HETCORR spectra. As can be seen from Table 1, substitution of the iodo atom of **2b** by an *ω*-aminoalkynyl side chain shifts the *ipso* carbon [C-7] to lower field by about 43 ppm demonstrating the electron-withdrawing effect of the C≡C triple bond. Isobutyrylation of the amino function of **4a** and **4b** results in typical high-field shifts of C-2 ($\Delta\delta = 5.5$ ppm), C-4 ($\Delta\delta = 3$ ppm), and C-6 ($\Delta\delta = 2$ ppm) and in a low-field shift of C-5 ($\Delta\delta = 4$ ppm). Moreover, isobutyrylation affects the chemical shift of the pyrrole carbon C-8: a low-field shift ($\Delta\delta = 2$ ppm) proves an electronic long-range coupling between the exocyclic amino group and the pyrrole ring.

Table 2 summarizes vicinal $^3J(H,H)$ coupling constants of compounds **4a** and **4b** as well as of the parent nucleosides 2′-deoxyguanosine (G_d) and 7-deaza-2′-deoxyguanosine (c^7G_d , **2a**). The data were taken from well-resolved ^1H NMR spectra measured in D_2O. The sugar conformation in solution ($^{3'}T_{2'} \rightleftarrows {}_{3'}T^{2'} \equiv N \rightleftarrows S$) was deduced from the pseudorotational parameters *P* and Ψ_m by application of the PSEUROT program (van Wijk and Altona, 1993). The rotational equilibrium about the C-4′−C5′ bond was calculated according to E. Westhof (Westhof et al., 1975) using the vicinal couplings between H-4′ and H-5′ as well as H-5″. From these data a slight trend can be deduced: The sugar puckering of the 7-(3-aminopropyn-1-yl) derivative **4a** is very similar to that of c^7G_d (28 and 27%, respectively) (Rosemeyer and Seela, 1998). Simultaneously, the three-state equilibrium about the C-4′−C-5′ bond of compounds **4a** and of c^7G_d ($\gamma^{(+)g} \rightleftarrows \gamma^t \rightleftarrows \gamma^{(-)g}$) exhibits very similar populations. On the other hand, the 7-(4-aminobutyn-1-yl) derivative **4b** shows slightly different conformational features: The sugar puckering is shifted toward a higher *N*-type conformer population, and the equilibrium at the C-4′−C-5′ bond is biased away from the $\gamma^{(+)g}$ conformation.

Synthesis and Characterization of Oligonucleotides. Automated solid-phase synthesis of the oligonucleotides **15**−**20** was performed with the phosphoramidites **7a** and **7c** (Froehler, 1993). The oligomer **15** has been also prepared using the phosphonate **7b**. The synthesis followed the standard protocols, and the coupling yields were always higher than 92% for the phosphoramidites and ca. 90% for the phosphonate. Deprotection was performed with 25% aq ammonia (60 °C, overnight) followed by a 24 h-treatment with 10% aq methylamine at room temperature (Seela et al., 2001a) to complete the removal of the phthaloyl residues. The oligonucleotides were detritylated and purified by reversed-phase HPLC (RP-18, see Experimental Procedures). The homogenity of the compounds was established by HPLC (RP-18) as well as by ion-exchange chromatography (NucleoPac-PA-100 column, 4 × 50 mm; Dionex, P/N 043018). The modified oligonucleotides were characterized by MALDI-TOF mass spectra. The detected masses were in good agreement with the calculated values (Table 3).

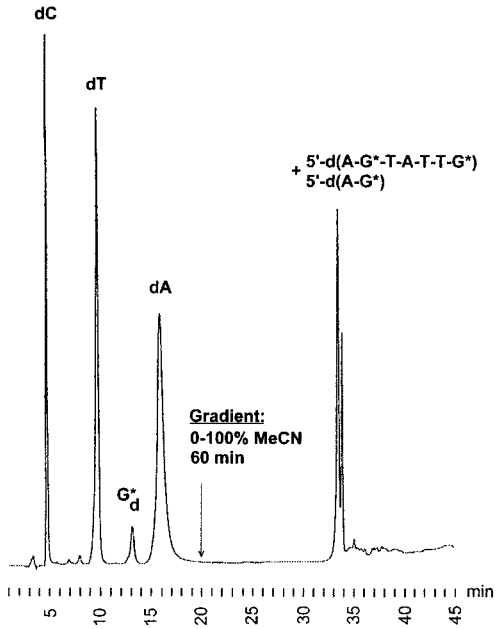


Figure 1. RP-18 HPLC profile of an enzymatic hydrolysis reaction mixture of the oligomer 5′-d(A-G*-T-A-T-T-G*-A-C-C-T-A) after treatment with snake venom phosphodiesterase and alkaline phosphatase (37 °C, 16 h). G^*_d = 7-(4-Aminobutyn-1-yl)-7-deaza-2′-deoxyguanosine. For details see Experimental Procedures.

Attempts to determine the composition of the oligonucleotides **19** and **20** by enzymatic tandem hydrolysis with snake venom phosphodiesterase (SVPDE) and alkaline phosphatase (AP) followed by reversed phase HPLC (RP-18) (Seela and Lampe, 1991) turned out to be problematic. After 16 h of treatment with the above-mentioned enzymes, RP-18 HPLC indicated incomplete cleavage of the modified oligonucleotides (Figure 1).

Table 1. ^{13}C NMR Chemical Shifts of 2′-Deoxy-β-D-ribonucleoside Derivatives[a]

compd	C(2) C(2)	C(4) C(7a)	C(5) C(4a)	C(6) C(4)	– C(5)	C(8) C(6)
2	152.7	150.5	99.8	158.0	54.9	121.6
4a	153.1	150.2	99.3	157.7	97.6	122.6
5a	147.6	147.1	103.3	155.7	98.3	124.8
6a	147.6	147.3	103.6	155.7	98.4	126.6
7b	147.7	147.4	103.5	155.7	98.5	126.5
4b	153.0	150.0	99.3	157.7	98.7	121.3
5b	147.6	147.1	103.4	155.9	99.5	123.8
6b	147.5	147.1	103.6	155.7	99.5	123.6

	C(1″)	C(2″)	CH_2	CH	CH_3	C=O (^{i}Bu)
4a	83.5	76.7	27.7			
5a	84.3	75.8	27.7	34.7	18.8	180.0
6a	84.3	75.6	27.6	34.7	18.8	180.0
7b	84.4	75.5	27.6	34.8	18.7	180.0
4b	85.8	76.1	18.7; 36.4			
5b	85.4	75.3	19.0; 36.5	34.8	18.9	180.1
6b	85.5	75.1	18.8; 36.4	34.7	18.7; 18.8	180.0

	C(1′)	C(2′)	C(3′)	C(4′)	C(5′)	C_{quart}
2	82.2	DMSO	70.9	87.1	61.8	
4a	82.1	DMSO	70.9	87.1	61.8	
5a	82.6	DMSO	70.8	87.8	61.7	
6a	82.6	DMSO	70.5	85.5	64.1	113.0
7b	82.9	37.9	72.5	85.4	63.9	113.0
4b	82.1	DMSO	70.8	87.0	61.9	
5b	82.7	DMSO	70.9	87.0	61.9	
6b	82.6	DMSO	70.5	86.9	64.1	113.1

	OCH_3	phthaloyl (C1‴)	phthaloyl (C2‴)	phthaloyl (C3‴)	C=O (Pht)
4a		131.4	123.3	134.7	166.8
5a		131.4	123.3	134.7	166.7
6a	54.9	131.4	123.3	134.7	166.7
7b	54.8; 54.9	131.4	123.3	134.6	166.7
4b		131.5	123.0	134.3	167.5
5b		131.7	123.2	134.5	167.8
6b	54.9	131.6	123.0	134.3	167.5

[a] Measured in d_6-DMSO.

Table 2. $^3J_{H,H}$ Coupling Constants of the Sugar Moieties and Conformer Population of 2′-Deoxy-β-D-ribonucleosides (303 K) as well as Polarizabilities and log*P* Values of the Corresponding Nucleobases[a]

	$^3J_{H,H}$ [Hz]						
compd	1′,2′	1′,2″	2′,3′	2″,3′	3′,4′	4′,5′	4′,5″
dG	7.30	6.50	6.30	3.60	3.20	3.60	4.70
c^7G_d	7.25	6.50	6.25	3.00	3.35	4.20	5.00
4a	6.85	6.35	6.00	2.80	2.85	4.30	4.70
4b	6.90	6.60	6.25	3.35	3.50	4.50	5.00

	conformation						
compd	% N	% S	% $\gamma^{(+)g}$	% γ^t	% $\gamma^{(-)g}$	α_m [10^{-24} cm^3]	log*P*[b]
dG	29	71	53	30	17	14.1 ± 0.5	−1.28 ± 0.62
c^7G_d	28	72	43	33	24	14.7 ± 0.5	−1.26 ± 0.89
4a	27	73	45	30	25	20.9 ± 0.5	−1.10 ± 1.38
4b	32	68	39	33	28	22.7 ± 0.5	−0.93 ± 1.37

[a] Measurements were performed in D_2O at a concentration of 5 mg of nucleoside per 0.5 mL; RMS ≤ 0.4 for all calculations; | Δ | ⩽ 0.5 Hz. [b] log*P* data refer to uncharged molecules as (1)NH tautomers.

Table 3. Molecular Masses (Da) of Selected Oligodeoxynucleotides

oligomer		MH^+ calcd	MH^+ found
5′-d(TA**1a** **1a**TC AAT ACT)	**16**	3749	3751
5′-d(A**1a**T ATT **1a**AC CTA)	**17**	3749	3745
5′-d(**1a**-C)$_4$	**15**	2618	2620
5′-d(TA**1b** **1b**TC AAT ACT)	**19**	3780	3772
5′-d(A**1b**T ATT **1b**AC CTA)	**20**	3780	3776
5′-d(**1b**-C)$_4$	**18**	2674	2675

Only after extension of the total reaction time to 6 d were the oligomers hydrolyzed completely. As it is known that oligonucleotides carrying unsubstituted 7-deaza-2′-deoxyguanosine residues are enzymatically cleaved without problems, it was concluded that the ω-aminoalkynyl side chain of the modified bases causes termination of the phosphodiesterase hydrolysis. In this context it is worth mentioning that it has been reported previously (Seela et al., 1995) that alternating oligonucleotides of the type [5′-d(G*-C)$_4$]$_2$ with G*$_d$ being 7-methylated or iodinated 7-deaza-2′-deoxyguanosine are hydrolyzed at a significantly slower rate by both calf spleen PDE as well as SVPDE. This topic will be taken up below.

Thermal Stability of Oligonucleotides. For all duplexes shown in Table 4, T_m values were measured (10

Table 4. T_m Values and Thermodynamic Data of Duplex Formation of Oligonucleotides Containing 7-(ω-Aminoalk-1-ynyl)-Functionalized 7-Deazaguanine Bases[a]

oligonucleotide		T_m [°C]	$\Delta H°$ [b] [kcal/mol]	$\Delta S°$ [b] [cal/K mol]	$\Delta G°_{310}$ [kcal/mol]
[5′-d(G-C)$_4$]$_2$	**8 · 8**	59	−67.0	−179.0	−11.5
5′-d(TAG GTC AAT ACT)	**9**	47	−86.8	−243.7	−11.3
3′-d(ATC CAG TTA TGA)	**10**				
5′-d(TAG GTC AAT ACT)	**9**	45	−92.1	−264.0	−10.2
3′-r(AUC CAG UUA UGA)	**11**				
[5′-d(**2a**-C)$_4$]$_2$	**12 · 12**	53	−53.0	−162.0	−11.5
5′-d(TA**2a 2a**TC AAT ACT)	**13**	46	−98.3	−283.0	−10.6
3′-d(AT C C AG TTA TGA)	**10**				
5′-d(TAG GT C AAT ACT)	**9**	46	−84.2	−239.0	−10.1
3′-d(ATC CA**2a** TTA T**2a**A)	**14**				
5′-d(TA**2a 2a**TC AAT A C T)	**13**	43	−85.6	−245.3	−9.6
3′-d(AT C C A**2a** TTA T**2a**A)	**14**				
5′-d(TA**2a 2a**TC AAT ACT)	**13**	43	−94.9	−275.0	−9.7
3′-r(AU C C AG UUA UGA)	**11**				
[5′-d(**1a**-C)$_4$]$_2$	**15 · 15**	72	−73.8	−192.4	−14.2
5′-d(TA**1a 1a**TC AAT ACT)	**16**	52	−96.9	−272.2	−12.5
3′-d(AT C C AG TTA TGA)	**10**				
5′-d(TA**1a 1a**TC AAT ACT)	**16**	48	−80.7	−226.2	−10.5
3′-r(AU C C AG UUA UGA)	**11**				
5′-d(TAG GT C AAT ACT)	**9**	52	−95.5	−268.4	−12.2
3′-d(ATC CA**1a** TTA T**1a**A)	**17**				
5′-d(TA**1a 1a**TC AAT ACT)	**16**	55	−97.5	−271.8	−13.2
3′-d(AT C CA**1a** TTA T**1a**A)	**17**				
[5′-d(**1b**-C)$_4$]$_2$	**18 · 18**	63	−62.7	−165.5	−11.4
5′-d(TA**1b 1b**TC AAT ACT)	**19**	50	−89.1	−250.1	−11.5
3′-d(AT C C AG TTA TGA)	**10**				
5′-d(TA**1b 1b**TC AAT ACT)	**19**	49	−84.7	−237.6	−11.0
3′-r(AU C C AG UUA UGA)	**11**				
5′-d(TAG GT C AAT A CT)	**9**	51	−89.9	−251.9	−11.8
3′-d(ATC CA**1b** TTA T**1b**A)	**20**				
5′-d(TA**1b 1b**TC AAT ACT)	**19**	52	−83.9	−232.9	−11.6
3′-d(AT C CA**1b** TTA T**1b**A)	**20**				
[5′-d(**1c**-C)$_4$]$_2$	**21 · 21**	ncm	-	-	-
5′-d(TA**1c 1c**TC AAT ACT)	**22**	47	−59.2	−158.9	−9.9
3′-d(AT C C AG TTA TGA)	**10**				
5′-d(TA**1c 1c**TC AAT ACT)	**22**	45	−82.7	−233.7	−10.2
3′-r(AU C C AG UUA UGA)	**11**				
5′-d(TAG GT C AAT AC T)	**9**	51	−80.0	−221.8	−11.2
3′-d(ATC CA**1c** TTA T**1c**A)	**23**				
5′-d(TA**1c 1c**T C AAT AC T)	**22**	49	−79.4	−220.9	−10.9
3′-d(AT C C A**1c** TTA T**1c**A)	**23**				

[a] Measured at 260 nm in 10 mM Na-cacodylate, 10 mM $MgCl_2$, 100 mM NaCl, pH 7, at 5 μM + 5 μM of single strand concentration; ncm: no cooperative melting. [b] Data are within 15% of error.

mM Na-cacodylate, 10 mM $MgCl_2$, 100 mM NaCl, pH 7), and the thermodynamic data of duplex formation were calculated from each individual melting profile according to a two-state model (duplex ⇄ random coil) model with the program *Meltwin* (release version 3.0) (McDowell and Turner, 1996) (Table 4). Replacement of all c^7G_d residues within the alternating oligomer [5′-d(c^7G−C)$_4$]$_2$ (**12·12**) (Ramzaeva et al., 1997) by the (3-aminopropyn-1-yl) − derivative **1a** (→ **15·15**) leads to a significant duplex stabilization compared to the parent **12·12** (ΔT_m = 19 °C; ≅ 5 °C/base pair). This increase of thermal stability is, however, reduced to 2.5 °C/base pair when the ω-aminoalkynyl side chain is extended by one methylene group (**18·18**, T_m = 63°).

Further extension of the side chain to a (5-aminopentyn-1-yl) substituent abolishes duplex formation of the alternating oligomer **21** (Ramzaeva et al., 1999; Seela et al., 2001b).

These surprising results, summarized in Table 5, are apparently related to the positioning of the protonated amino group within the major groove of the B-DNA helix because the corresponding oligomer carrying four uncharged 7-(hexyn-1-yl)-7-deaza-2′-deoxyguanosines (Ramzaeva et al., 1997) shows a T_m value of 59 °C under analogous conditions. It has been demonstrated earlier

Table 5. T_m Values of [5′-d(G*-C)$_4$]$_2$ as a Function of the Number of Methylene Groups in the 7-(ω-Aminoalk-1-ynyl) Side Chain of G*$_d$[a]

number of methylene groups in the ω-aminoalk-1-ynyl side chain	$d_{C(7),N}$ [Å]	T_m [°C]
1	4.9	72
2	6.3	63
3	7.3	<15
3[b]	7.3	59

[a] Measured at 260 nm in 10 mM Na-cacodylate, 10 mM $MgCl_2$, 100 mM NaCl, pH 7, 10 μM of single strand concentration. [b] CH_3 instead of terminal NH_2 group. G*$_d$ = 7-(ω-aminoalkyn-1-yl)-7-deaza-2′-deoxyguanosine (**1a**−**c**). Distances *d* were calculated using the *Alchemy III* force field (Tripos Co., St. Louis, MO).

that 7-substituents of 7-deazapurine are well accommodated in the major groove of a B-DNA (Seela and Zulauf, 1999; Pullman and Pullman, 1981), the depth of which amounts to 8.5 Å and the width at the periphery to 11.7 Å (Conner et al., 1982). Table 5 shows how the distance between C-7 and the amino group increases with the extension of the ω-aminoalkynyl side chain. A simple reflection reveals that the distance between the protonated amino group of the aminoalkynyl chain and the negatively charged phosphate−sugar backbone of the double helix is minimal for the (5-aminopentyn-1-yl)

Table 6. Positive Ion MALDI TOF Mass Spectrometric Data Resulting from Partial Digestion of Modified Oligonucleotides Incorporating 2a by Snake Venom or Bovine Spleen Phosphodiesterase; for Details See Experimental Procedures

oligomer	exonuclease	sequence	MH^+ (Da) calcd	MH^+ (Da) found
24	SVPDE (3′ → 5′)	5′-d(C**2a**AACT**2a2a**C**2a**TC)-3′	3643.4	3642.2
		5′-d(C**2a**AACT**2a2a**C**2a**T)-3′	3354.2	3353.4
		5′-d(C**2a**AACT**2a2a**C**2a**)-3′	3050.0	3049.6
		5′-d(C**2a**AACT**2a2a**C)-3′	2720.8	2721.7
		5′-d(C**2a**AACT**2a2a**)-3′	2431.6	2431.8
		5′-d(C**2a**AACT**2a**)-3′	2102.4	2103.9
		5′-d(C**2a**AACT)-3′	1773.2	1775.9
		5′-d(C**2a**AAC)-3′	1469.0	1472.0
		5′-d(C**2a**AA)-3′	1179.8	1183.3
24	BSPDE (5′ → 3′)	5′-d(C**2a**AACT**2a2a**C**2a**TC)-3′	3643.4	3642.2
		5′-d(**2a**AACT**2a2a**C**2a**TC)-3′	3354.2	3352.5
		5′-d(AACT**2a2a**C**2a**TC)-3′	3025.0	3024.9
		5′-d(ACT**2a2a**C**2a**TC)-3′	2711.8	2714.2
		5′-d(CT**2a2a**C**2a**TC)-3′	2398.6	2401.8
		5′-d(T**2a2a**C**2a**TC)-3′	2109.4	2113.5
		5′-d(**2a2a**C**2a**TC)-3′	1805.2	1809.7
		5′-d(**2a**C**2a**TC)-3′	1476.2	1482.3
		5′-d(C**2a**TC)-3′	1148.6	1154.4

Table 7. Positive Ion MALDI TOF Mass Spectrometric Data Resulting from Partial Digestion of Modified Oligonucleotides Incorporating 1a by Snake Venom or Bovine Spleen Phosphodiesterase; for Details See Experimental Procedures

oligomer	exonuclease	sequence	MH^+ (Da) calcd.	MH^+ (Da) found
16	BSPDE (5′ → 3′)	5′-d(TA**1a1a**TCAATACT)-3′	3747.6	3746.0
		5′-d(A**1a1a**TCAATACT)-3′	3444.4	3444.3
		⇒ 5′-d(**1a1a**TCAATACT)-3′	3131.2	3131.4
		5′-d(**1a1a**TCAATAC)-3′	2827.0	2827.6
		5′-d(**1a1a**TCAATA)-3′	2537.8	2538.7
		5′-d(**1a1a**TCAAT)-3′	2224.6	2225.8
		5′-d(**1a1a**TCAA)-3′	1920.4	1921.8
		5′-d(**1a1a**TCA)-3′	1607.2	1607.9
17	SVPDE (3′ → 5′)	5′-d(A**1a**TATT**1a**ACCTA)-3′	3747.6	3747.3
		5′-d(A**1a**TATT**1a**ACCT)-3′	3436.4	3434.6
		5′-d(A**1a**TATT**1a**ACC)-3′	3132.2	3131.4
		5′-d(A**1a**TATT**1a**AC)-3′	2843.0	2842.5
		5′-d(A**1a**TATT**1a**A)-3′	2553.8	2553.7
		5′-d(A**1a**TATT**1a**)-3′	2240.6	2240.7
		5′-d(A**1a**TATT)-3′	1859.4	1858.7
		5′-d(A**1a**TAT)-3′	1555.2	1554.9
		5′-d(A**1a**TA)-3′	1251.0	1250.9
17	BSPDE (5′ → 3′)	5′-d(A**1a**TATT**1a**ACCTA)-3′	3747.6	3748.0
		5′-d(**1a**TATT**1a**ACCTA)-3′	3434.4	3435.7
		5′-d(TATT**1a**ACCTA)-3′	3053.2	n.d.
		5′-d(ATT**1a**ACCTA)-3′	2749.0	2747.5
		5′-d(TT**1a**ACCTA)-3′	2436.0	2439.3
		5′-d(T**1a**ACCTA)-3′	2131.8	2135.8
		5′-d(**1a**ACCTA)-3′	1827.4	1832.1
		5′-d(ACCTA)-3′	1446.2	1451.6[a]
		5′-d(CCTA)-3′	1133.0	1138.6

[a] Signal intensity is small compared to the preceding and the subsequent ones; ⇒/⇐ termination of the reaction; n.d.: not detected.

residue. Therefore, the Coulomb attraction, being proportional to $1/r^2$, should be maximal in the latter case. Nevertheless, the thermal stability of **21·21** is the lowest one within the series of alternating oligonucleotides. Possibly, the spatial approximation of positively charged nucleobase side chains and the negatively charged backbone leads to a shrinkage or bending of the double helix structure with an obvious penalty in stability as described in the Introduction. In case of the oligonucleotides containing protonated (4-aminobutyn-1-yl) or (3-aminopropyn-1-yl) side chains within the major groove the Coulomb interaction between the ammonium group, and the phosphate backbone is gradually reduced. In these latter cases enhanced stacking interactions of the alkynylated c^7G_d residues compared to unsubstituted c^7G_d are more and more taking effect and overcompensate the Coulomb interaction.

These apparently improved stacking interactions are due to the alkynyl side chain confering (i) a higher molecular polarizability α_m (Rosemeyer and Seela, 2002)[1] and (ii) a higher lipophilicity (expressed in terms of log*P*[1]) to the 7-substituted nucleobase (Table 2) with the consequence of a stabilization of the duplex structure.

Next, compounds **1a** and **1b** were incorporated into non-self-complementary oligonucleotides (Table 4). The oligomers containing the (5-aminopentyn-1-yl) derivative **1c** had already been described earlier (Ramzaeva et al., 1997), but the thermodynamic data of duplex formation are now reevaluated.

[1] Molecular polarizability values (α_m) were calculated from polarizability increments (central atom and neighboring sphere considering the order and aromaticity of bonds) using the program ChemSketch (version 4.55, provided as freeware by Advanced Chemistry Developments Inc., Toronto, Canada; http: www.acdlabs.com). log*P* values were calculated using the program "log*P*" (version 1.0) delivered by the same company; for the log*P* value of G_d see also: Viswanadhan and co-workers (Viswanadhan et al., 1993).

Table 8. Positive Ion MALDI TOF Mass Spectrometric Data Resulting from Partial Digestion of Modified Oligonucleotides Incorporating 1b by Snake Venom or Bovine Spleen Phosphodiesterase; for Details See Experimental Procedures

oligomer	exonuclease	sequence	MH^+ (Da) calcd.	MH^+ (Da) found
19	BSPDE (5′→3′)	5′-d(TA**1b1b**TCAATACT)-3′	3777.6	3781.9
		5′-d(A**1b1b**TCAATACT)-3′	3473.4	3466.5
		⟹ 5′-d(**1b1b**TCAATACT)-3′	3160.2	3159.6
		5′-d(**1b1b**TCAATAC)-3′	2856.0	2855.8
		5′-d(**1b1b**TCAATA)-3′	2566.8	2565.8
		5′-d(**1b1b**TCAAT)-3′	2253.6	2253.9
20	SVPDE (3′ → 5′)	5′-d(A**1b**TATT**1b**ACCTA)-3′	3777.6	3777.3
		5′-d(A**1b**TATT**1b**ACCT)-3′	3464.4	3466.9
		5′-d(A**1b**TATT**1b**ACC)-3′	3160.2	3160.1
		5′-d(A**1b**TATT**1b**AC)-3′	2871.0	2871.2
		5′-d(A**1b**TATT**1b**A)-3′	2581.8	2582.1
		5′-d(A**1b**TATT**1b**)-3′ ⟸	2268.6	2269.0
20	BSPDE (5′ → 3′)	5′-d(A**1b**TATT**1b**ACCTA)-3′	3777.6	3776.2
		5′-d(**1b**TATT**1b**ACCTA)-3′	3464.4	3463.7
		5′-d(TATT**1b**ACCTA)-3′	3069.2	3068.9[a]
		5′-d(ATT**1b**ACCTA)-3′	2765.0	2765.9
		5′-d(TT**1b**ACCTA)-3′	2451.8	2453.4
		5′-d(T**1b**ACCTA)-3′	2147.6	2149.9
		5′-d(**1b**ACCTA)-3′	1843.4	1846.1
		5′-d(ACCTA)-3′	1448.2	1451.7[a]
		5′-d(CCTA)-3′	1135.0	1138.7
		5′-d(CTA)-3′	846.0	850.0

[a] Signal intensity is small compared to the preceding and the subsequent ones; ⟹/⟸ termination of the reaction.

The results of the melting experiments are summarized in Table 4. As can be seen from a comparison of the T_m data of corresponding oligonucleotide duplexes among the different series such as **13·14** (containing **2a**), **16·17** (containing **1a**), **19·20** (containing **1b**), and **22·23** (containing **1c**), the above-described results are confirmed; a clear tendency is followed: the shorter the ω-aminoalkynyl side chain, the higher the duplex stabilization compared with the parent sequence containing unsubstituted 7-deaza-2′-deoxyguanosine. Replacement of c^7G_d–C_d base pairs by **1a**–C_d pairs leads to a T_m enhancement of 12 °C (3 °C/base pair). The same trend holds also for the other corresponding duplexes (e.g., **13·10**, **16·10**, **19·10**, **22·10** etc.). The reason for this behavior is probably the same as described for the alternating, self-complementary oligonucleotides.

Sensitivity of the Base-Modified Oligonucleotides against Exonucleases. As described above the enzymatic hydrolysis of the oligomers **19** and **20** catalyzed by SVPDE was strongly retarded. Therefore, the hydrolysis of the oligomers **16** and **19** by the 5′ → 3′ exonuclease from bovine spleen (BSPDE) and the hydrolysis of **17** and **20** by the 3′ → 5′ exonuclease from snake venom (*Crotallus adamanteus*) was investigated by matrix-assisted laser desorption and ionization mass spectrometry (MALDI-TOF MS) (Karas and Hillenkamp, 1988). From the reaction mixtures aliquots were taken after different time intervals over a total period of up to 7d and analyzed.

For comparison, the hydrolysis of the oligomer 5′-d(C**2a**AACT**2a2a**C**2a**TC) (**24**) containing four 7-deaza-2′-deoxyguanosine residues as well as of the unmodified oligonucleotides **9** and **10** was also studied. MALDI TOF mass spectra showed complete cleavage of the unmodified oligomers by both exonucleases within at least 24 h (data not shown).

Figure 2 displays the mass spectrum of an SVPDE digest of the oligomer **24** after 2d allowing the sequencing of the first eight nucleotide 5′-monophosphates of the oligomer (Pieles et al., 1993; Nordhoff et al., 1995; Schneider and Chait, 1995). Treatment of **24** with BSPDE for 45 min at 37 °C and MALDI-TOF analysis after different time intervals results in a similar MALDI-TOF pattern from which the sequence of the first eight

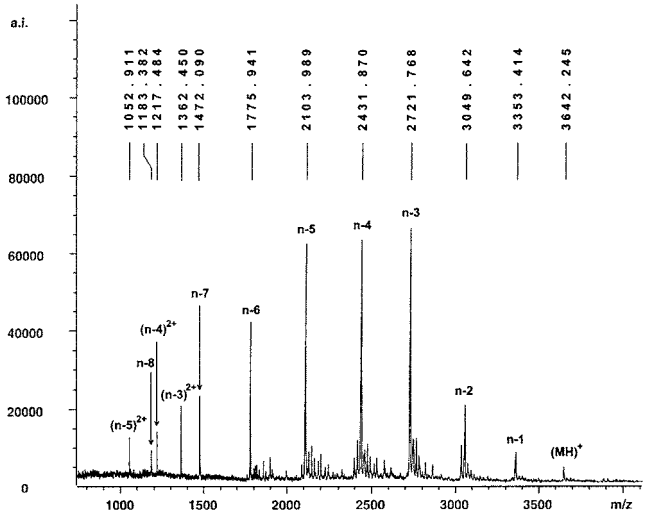


Figure 2. MALDI-TOF mass spectrum of an enzymatic hydrolysis reaction mixture of the oligomer 5′-d(C-G*-A-A-C-T-G*-G*-C-G*-T-C) after treatment with snake venom phosphodiesterase (0.02 units of enzyme/1 μmol of oligomer) in H_2O. G^*_d = 7-Deaza-2′-deoxyguanosine. For details see Experimental Procedures.

nucleoside 3′-monophosphates starting from the 5′-terminus can be read (Table 6).

MALDI-TOF mass spectra of the digestion of the oligomer **17** by SVPDE and of the oligomer **16** by BSPDE (Table 7) imply that the 3′→5′ exonuclease (SVPDE) is able to cleave off the 7-(3-aminopropyn-1-yl)-7-deaza-2′-deoxyguanosine 5′-monophosphate residue (**1a**-MP) being incorporated at position 6 from the 3′-end of **17** (n-6). Even the further signals for the (n-7) and the (n-8) residual oligomers can be detected (Figure 3).

On the other hand, the action of BSPDE on **16** carrying two consecutive **1a** residues is terminated by the modified base: after a reaction time of 24 h, the mass spectrum shows that the 5′ → 3′ exonuclease has cleaved off only the first two nucleotides (dTMP, dAMP) from the 5′-end (Table 7) but not the subsequent **1a**-MP residues. Instead, a digestion from the 3′-terminus occurs, generating the indicated mass peaks. This might be either due to a

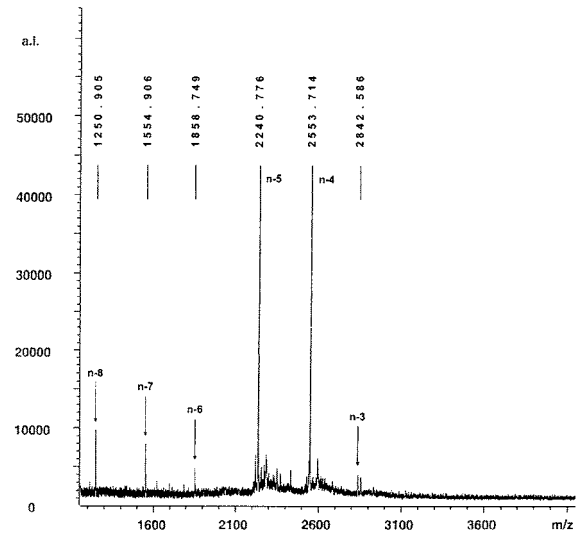


Figure 3. MALDI-TOF mass spectrum of an enzymatic hydrolysis reaction mixture of the oligomer 5′-d(A-G*-T-A-T-T-G*-A-C-C-T-A) after treatment with snake venom phosphodiesterase (0.02 units of enzyme/1 μmol of oligomer) in H_2O. G^*_d = 7-(3-Aminopropyn-1-yl)-7-deaza-2′-deoxyguanosine. For details see Experimental Procedures.

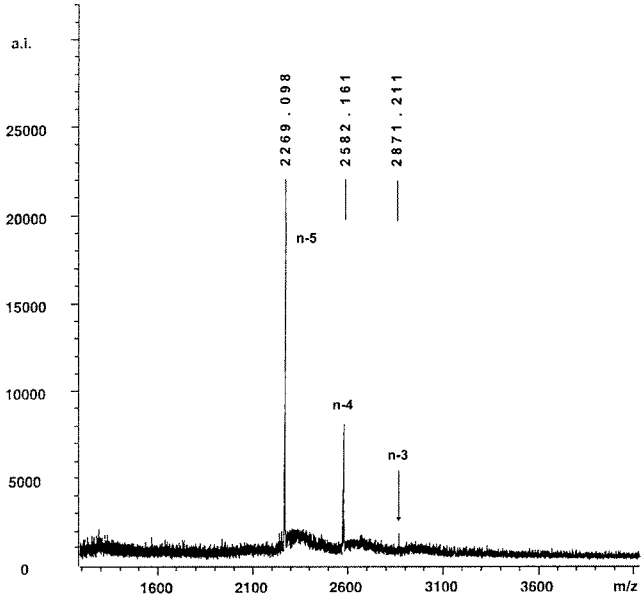


Figure 4. MALDI-TOF mass spectrum of an enzymatic hydrolysis reaction mixture of the oligomer 5′-d(A-G*-T-A-T-T-G*-A-C-C-T-A) after treatment with snake venom phosphodiesterase (0.02 units of enzyme/1 μmol of oligomer) in H_2O. G^*_d = 7-(4-Aminobutyn-1-yl)-7-deaza-2′-deoxyguanosine. For details see Experimental Procedures.

≤1% impurity of the 5′ → 3′ exonuclease by a 3′ → 5′ exonuclease or to a unspecificity of the enzyme with respect to its cleavage direction. The last result is similar to that obtained for the digestion of the oligomer **19**, containing two consecutive (4-aminobutyn-1-yl) derivatives **1b**, by BSPDE (Table 8): also here the mass spectrum, measured after 72 h, indicates a termination of the 5′ → 3′ exonucleolytic activity, but a further digestion of the oligomer from its 3′-end. Interestingly, the SVPDE-digestion of the oligomer **20** with a **1b** residue at position 6 from the 3′-end is completely terminated by **1b**; a further digestion from the 5′-end of **20** cannot be observed (Figure 4, Table 8).

Next, we investigated the BSPDE-mediated cleavage of the oligomers **17** and **20**, both containing isolated **1a** or **1b** residue in positions 2 and 7 from the 5′-terminus. The MALDI-TOF mass spectra (Tables 7, 8) indicate that in both cases the base-modified nucleotides are cleaved off. However, the signals of the residual oligomers from which **1a** or **1b** have just been split off are small compared to the preceding and subsequent peaks; this points to the fact that preferentially dinucleotides (**17**: 5′-d(**1a**-T)p-3′ and 5′-d(**1a**-A)p-3′; **20**: 5′-d(**1b**-T)p-3′ and 5′-d(**1b**-A)p-3′) are released.

CONCLUSION AND PERSPECTIVES

The experiments clearly demonstrate that the incorporation of 7-(ω-aminoalkyn-1-yl)-7-deaza-2′-deoxyguanosine building blocks which differ just in one methylene group within the side chain (**1a** vs **1b**) changes both the rate of hydrolysis of oligonucleotides by exonucleases as well as their propensity of duplex formation. In particular, the results on oligonucleotides carrying the 7-(ω-aminobutyn-1-yl) derivative **1b** opens the possibility to protect an oligonucleotide core against exonucleolytic cleavage. These results are in line with findings reported recently by Matsuda and co-workers (Ueno et al., 2000).

On the other hand, oligonucleotides carrying nucleotide units with primary amino groups can be labeled with various nonradioactive reporter groups such as fluorophores, dyes, biotin, or others by postsynthetic conjugation. With the provision of reactive derivatives (e.g., *N*-hydroxysuccinimide esters) of such reporter molecules this postlabeling technique has almost replaced the former common technique of radioisotope (e.g., ^{32}P) labeling (Agrawal, 1994; Hermanson, 1996). However, care has to be taken concerning (i) the accessibility of the primary amino groups located in the major groove of the functionalized oligonucleotide for the postlabeling reaction, and (ii) the thermal duplex stability of the resulting labeled nucleic acid.

Furthermore, the incorporation of compounds such as **1a**−**c**, mimicing the side chain of basic amino acids, into oligonucleotides may enhance their catalytic repertoire beyond that of ribozymes and aptamers (Burgstaller and Famulok, 1995; Sakhtivel and Barbas, 1998; Santoro et al., 2000; Breaker and Joyce, 1995; Santoro and Joyce, 1997; Carmi et al., 1996; Carmi et al., 1998; Tarasow et al., 1997; Thum et al., 2001).

ACKNOWLEDGMENT

The authors thank the ChemBioTech, Germany, for financial support.

LITERATURE CITED

(1) Agrawal, S. (1994) Functionalization of Oligonucleotides with Amino Groups and Attachment of Amino Specific Reporter Groups. *Methods in Molecular Biology, Vol. 26: Protocols for Oligonucleotide Conjugates* (S. Agrawal, Ed.) pp 93−120, Humana Press Inc., Totowa, NJ.

(2) Beaucage, S. L., and Caruthers, M. (1981) Deoxynucleoside Phosphoramidites − A New Class of Key Intermediates for Deoxypolynucleotide Synthesis. *Tetrahedron Lett. 22*, 1859−1862.

(3) Bijapur, J., Keppler, M. D., Bergqvist, S., Brown, T., and Fox, K. R. (1999) 5-(1-Propargylamino)-2′-deoxyuridine (U^P): a novel thymidine analogue for generating DNA triplexes with increased stability. *Nucleic Acids Res. 27*, 1802−1809.

(4) Breaker, R. R., and Joyce, G. F. (1995) A DNA enzyme with Mg^{2+}-dependent RNA phosphoesterase activity. *Chem. Biol. 2*, 655−660.

(5) Burgstaller, P., and Famulok, M. (1995) Synthetische Ribozyme und das erste Desoxyribozyme. *Angew. Chem. 107*, 1303−1307.

(6) Carmi, N., Balkhi, S. R., and Breaker, R. R. (1998) Cleaving DNA with DNA. *Proc. Natl. Acad. Sci. U.S.A.* 95, 2233−2237.
(7) Carmi, N., Shultz, L. A., and Breaker, R. R. (1996) In vitro selection of self-cleaving DNAs. *Chem. Biol. 3*, 1039−1046.
(8) Conner, B. N., Takano, T., Tanaka, S., Itakura, K., and Dickerson, R. E. (1982) The Molecular Structure of d(^{1}-CpCpGpG), a fragment of right-handed double-helical A-DNA. *Nature 295*, 294−299.
(9) Cook, A. F., Vuocolo, E., and Brakel, C. L. (1988) Synthesis and hybridization of a series of biotinylated oligonucleotides. *Nucleic Acids Res. 16*, 4077−4095.
(10) Froehler, B. C., Ng, P. G., and Matteucci, M. D. (1986) Synthesis of DNA via deoxynucleoside H-phosphonate intermediates. *Nucleic Acids Res. 14*, 5399−5407.
(11) Froehler, B. C. (1993) Protocols of Oligonucleotides and Analogues. *Methods in Molecular Biology* (S. Agrawal, Ed.) Vol. 20, p 63, Humana Press, Totowa, NJ.
(12) Gibson, K. J., and Benkovic, S. J. (1987) Synthesis and application of derivatizable oligonucleotides. *Nucleic Acids Res. 15*, 6455−6467.
(13) Gorlain, T., Sidorov, A., Miguet, N., Thorpe, S. J., Lee, S. E., Grasby, J. A., and Williams, D. M. (2001) Enhancing the catalytic repertoire of nucleic acids. II Simultaneous incorporation of amino and imidazolyl functionalities by two modified triphosphates during PCR. *Nucleic Acids Res. 29*, 1898−1905.
(14) Gut, I. G., and Beck, S. (1995) A procedure for selective DNA alkylation and detection by mass spectrometry. *Nucleic Acids Res. 23*, 1367−1373.
(15) Haginoya, N., Ono, A., Nomura, Y., Ueno, Y., and Matsuda, A. (1997) Nucleosides and Nucleotides. 160. Synthesis of Oligodeoxyribonucleotides Containing 5-(*N*-Aminoalkyl)carbamoyl-2′-deoxyuridines by a New Postsynthetic Modification Method and Their Thermal Stability and Nuclease-Resistance Properties. *Bioconjugate Chem. 8*, 271−280.
(16) Hardwidge, P. R., Lee, D.-K., Prakash, T. P., Iglesias, B., Den, R. B., Switzer, C., and Maher, L. J., III (2001) DNA bending by asymmetrically tethered cations: influence of tether flexibility. *Chem. Biol. 8*, 967−980 and literature cited therein.
(17) Hashimoto, H., Nelson, M. G., and Switzer, C. (1993) Zwitterionic DNA. *J. Am. Chem. Soc. 115*, 7128−7134.
(18) Hermanson, G. T. (1996) *Bioconjugate Techniques*, Academic Press, New York.
(19) Karas, M., and Hillenkamp, F. (1988) Laser Desorption Ionization of Proteins with Molecular Masses Exceeding 10000 Daltons. *Anal. Chem. 60*, 2299−2301.
(20) Kropinski, A. M. B., Bose, R. J., and Warren, R. A. J. (1973) 5-(4-Aminobutylaminomethyl)uracil, an Unusual Pyrimidine from the Deoxyribonucleic Acid of Bacteriophage ϕW-14. *Biochemistry 12*, 151−157.
(21) Lee, S. E., Sidorov, A., Gourlain, T., Miguet, N., Thorpe, S. J., Brazier, J. A., Diekman, M. J., Hornby, D. P., Grasby, J. A., and Williams, D. M. (2001) Enhancing the catalytic repertoire of nucleic acids: a systematic study of linker length and rigidity. *Nucleic Acids Res. 29*, 1565−1573.
(22) Manning, G. S. (1978) The molecular theory of polyelectrolyte solutions with applications to the electrostatic properties of polynucleotides. *Quart. Rev. Biophys. 11*, 179−246.
(23) Manning, G. S., Ebralidse, K. K., Mirzabekov, A. D., and Rich, A. (1989) An Estimate of the Extent of Folding of Nucleosomal DNA by Laterally Asymmetric Neutralization of Phosphate Groups. *J. Biomol. Struct. Dyn. 6*, 877−889.
(24) Manoharan, M. (1993) Designer Antisense Oligonucleotides: Conjugation Chemistry and Functionality Placement. *Antisense Research and Applications* (S. T. Crooke, and B. Lebleu, Eds.) pp 303−349, CRC Press, Inc.
(25) McDowell, J. A., and Turner, D. H. (1996) Investigation of the Structural Basis for Thermodynamic Stabilities of Tandem GU Mismatches: Solution Structure of (rGAGGUCUC)$_2$ by Two-Dimensional NMR and Simulated Annealing. *Biochemistry 35*, 14077−14089.
(26) Meyer Jr., R. B. (1994) Incorporation of Modified Bases into Oligonucleotides. Protocols for Oligonucleotide Conjugates. *Methods Mol. Biol. (Totowa, N.J.) 26*, 73−91.
(27) Miller Black, P., Wakarchuk, W. W., and Warren, R. A. J. (1985) α-Putrescinylthymine and its sensitivity of bacteriophage ϕW-14 DNA to restriction endonucleases. *Nucleic Acids Res. 13*, 2559−2568.
(28) Nordhoff, E., Karas, M., Cramer, R., Hahner, S., Hillenkamp, F., Kirpekar, F, Lezius, A., Muth, J., Meier, C., and Engels, J. W. (1995) Direct Mass Spectrometric Sequencing of Low-picomole Amounts of Oligodeoxynucleotides with up to 21 Bases by Matrix-Assisted Laser Desorption/Ionization Mass Spectrometry. *J. Mass Spectrom. 30*, 99−112.
(29) Ono, A., Haginoya, N., Kiyokawa, M., Minakawa, N., and Matsuda, A. (1994) Nucleosides and Nucleotides. 127. A Novel and Convenient Postsynthetic Modification Method for the Synthesis of Oligodeoxyribonucleotides Carrying Amino Linkers at the 5-Position of 2′-Deoxyuridine. *Bioorg. Med. Chem. Lett. 4*, 361−366.
(30) Pieles, U., Zürcher, W., Schär, M., and Moser, H. E. (1993) Matrix-assisted laser desorption ionization time-of-flight mass spectrometry: a powerful tool for the mass and sequence analysis of natural and modified oligonucleotides. *Nucleic Acids Res. 21*, 3191−3196.
(31) Pullman, A., and Pullman, B. (1981) Molecular electrostatic potential of the nucleic acids. *Quart. Rev. Biophys. 14*, 289−380.
(32) Ramasamy, K. S., Zounes, M., Gonzales, C., Freier, S. M., Lesnik, E. A., Cummins, L. L., Griffey, R. H., Monia, B. P., and Cook, P. D. (1994) Remarkable Enhancement of Binding Affinity of Heterocycle-Modified DNA to DNA and RNA. Synthesis, Characterization and Biophysical Evaluation of N^2-Imidazolylpropylguanine and N^2-Imidazolylpropyl-1-aminoadenine Modified Oligonucleotides. *Tetrahedron Lett. 35*, 215−218.
(33) Ramzaeva, N., and Seela, F. (1995) 7-Substituted 7-Deaza-2′-deoxyguanosines: Regioselective Halogenation of Pyrrolo-[2,3-d]pyrimidine Nucleosides. *Helv. Chim. Acta 78*, 1083−1090.
(34) Ramzaeva, N., Mittelbach, C., and Seela, F. (1997) 7-Deazaguanine DNA: Oligonucleotides with Hydrophobic or Cationic Side Chains. *Helv. Chim. Acta 80*, 1809−1822.
(35) Ramzaeva, N., Mittelbach, C., and Seela, F. (1999) 7-Deaza-2′-deoxyguanosines Functionalized with 7-(ω-Aminoalk-1-ynyl) Residues. *Nucleosides, Nucleotides 18*, 1439−1440.
(36) Ramzaeva, N., Rosemeyer, H., Leonard, P., Mühlegger, K., Bergmann, F., von der Eltz, H., and Seela, F. (2000) Oligonucleotides Functionalized by Fluorescein and Rhodamine Dyes: Michael Addition of Methyl Acrylate to 2′-Deoxypseudouridine. *Helv. Chim. Acta 83*, 1108−1126.
(37) Randolph, J. B., and Waggoner, A. S. (1997) Stability, specificity and fluorescence brightness of multiply labeled fluorescent DNA probes. *Nucleic Acids Res. 25*, 2923−2929.
(38) Rosemeyer, H., and Seela, F. (1998) Stereoelectronic effects of modified purine bases on the sugar conformation of nucleosides: pyrrolo[2,3-d[pyrimidines. *J. Chem. Soc., Perkin Trans. 2* 2341−2345.
(39) Rosemeyer, H., and Seela, F. (2002) Modified purine bases as dangling ends of DNA duplexes: The effect of the polarizability on stacking interactions. *J. Chem. Soc., Perkin Trans. 2*, 746−750.
(40) Sakhtivel, K., and Barbas, C. F., III (1989) Erweiterung der Bindungs- und Katalyseeigenschaften von DNA.; hochfunktionalisierte dUTP-Derivate als Substrate für thermostabile DNA-Polymerasen. *Angew. Chem. 110*, 2998−3002.
(41) Santoro, S. W., Joyce, G. F., Sakthivel, K., Gramatikova, S., and Barbas, C. F., III (2000) RNA Cleavage by a DNA Enzyme with Extended Chemical Functionality. *J. Am. Chem. Soc. 122*, 2433−2439.
(42) Santoro, S. W., and Joyce, G. F. (1997) A general purpose RNA-cleaving DNA enzyme. *Proc. Natl. Acad. Sci. U.S.A. 94*, 4262−4266.
(43) Sauer, S., Lechner, D., Berlin, K., Lehrach, H., Escary, J.-L., Fox, N., and Gut, I. G. (2000) A novel procedure for efficient genotyping of single nucleotide polymorphisms. *Nucleic Acids Res. 28*, e13.
(44) Schaller, H., Weimann, G., Lerch, B., and Khorana, H. G. (1963) Studies on Polynucleotides. XXIV. The Stepwise Synthesis of Specific Deoxyribopolynucleotides (4). Protected

Derivatives of Deoxyribonucleosides and New Syntheses of Deoxyribonucleoside-3′ Phosphates. *J. Am. Chem. Soc. 85*, 3821−3827.

(45) Schneider, K., and Chait, B. T. (1995) Increased stability of nucleic acids containing 7-deaza-adenosine and 7-deazaadenosine may enable rapid DNA sequencing by matrix-assisted laser desorption mass spectrometry. *Nucleic Acids Res. 23*, 1570−1575.

(46) Seela, F., and Lampe, S. (1991) 3-Deazaguanine N^7- and N^9-(2′-Deoxy-β-D-ribofuranosides): Building Blocks for Solid-Phase Synthesis and Incorporation into Oligodeoxyribonucleotides. *Helv. Chim. Acta 74*, 1790−1800.

(47) Seela, F., Ramzaeva, N., and Chen, Y. (1995) Oligonucleotide Duplex Stability Controlled by the 7-Substituents of 7-Deazaguanine Bases. *Bioorg. Med. Chem. Lett. 5*, 3049−3052.

(48) Seela, F., and Zulauf, M. (1999) Oligonucleotides Containing 7-Deazaadenines: The Influence of the 7-Substituent Chain Length and Charge on the Duplex Stability. *Helv. Chim. Acta 82*, 1878−1898.

(49) a) Seela, F., Feiling, E., Gross, J., Hillenkamp, F., Ramzaeva, N., Rosemeyer, H., and Zulauf, M. (2001) Fluorescent DNA: the development of 7-deazapurine nucleoside triphosphates applicable for sequencing at the single molecule level. *J. Biotechnol. 86*, 269−279.

(50) b) Seela, F., Ramzaeva, N., Leonard, P., Chen, Y., Debelak, H., Feiling, E., Kröschel, R., Zulauf, M., Wenzel, T., Fröhlich, T., and Kostrzewa, M. (2001) Phosphoramidites and Oligonucleotides Containing 7-Deazapurines and Pyrimidines Carrying Aminopropargyl Side Chains. *Nucleosides, Nucleotides, Nucleic Acids 20*, 1421−1424.

(51) Soto, A. M., Kankia, B. I., Dande, P., Gold, B., and Marky, L. A. (2001) Incorporation of a cationic aminopropyl chain in DNA hairpins: thermodynamics and hydration. *Nucleic Acids Res. 29*, 3638−3645.

(52) Strauss, J. K., Roberts, C., Nelson, M. G., Switzer, C., and Maher, L. J., III (1996) DNA bending by hexamethylene-tethered ammonium ions. *Proc. Natl. Acad. Sci. U.S.A. 93*, 9515−9520.

(53) Takeda, T., Ikeda, K., Mizuno, Y., and Ueda, T. (1987) Synthesis and Properties of Deoxyoligonucleotides Containing Putrescinylthymine (Nucleosides and Nucleotides. LXXVI). *Chem. Pharm. Bull. 35*, 3558−3567.

(54) Ti, G. S., Gaffney, B. L., and Jones, R. A. (1982) Transient Protection: Efficient One-Flask Syntheses of Protected Deoxynucleosides. *J. Am. Chem. Soc. 104*, 1316−1319.

(55) Ueno, Y., Karino, N., and Matsuda, A. (2000) Nucleosides and Nucleotides. 204. Synthesis of Oligodeoxynucleotides Containing 6′α-[*N*-(Aminoalkyl)carbamoyloxy]-carbocyclic-thymidines and the Thermal Stability of the Duplexes and Their Nuclease-Resistance Properties. *Bioconjugate Chem. 11*, 933−940.

(56) van Wijk, J., and Altona, C. (July 1993) PSEUROT 6.2 − A Program for the Conformational Analysis of the Five-Membered Ring, University of Leiden.

(57) Viswanadhan, V. N., Reddy, M. R., Bacquet, R. J., and Erion, M. D. (1993) Assessment of methods used for predicting lipophilicity: application to nucleosides and nucleoside bases. *J. Comput. Chem. 14*, 1019−1026.

(58) Wenzel, T., Fröhlich, T., Strassburger, K., Richter, S., Bimmler, J., Franke, C., Thomas, I., and Kostrzewa, M. (2001) Novel Propargylamine-Linked Nucleosides for High Throughput SNP Genotyping by MALTI-TOF MS. *Nucleosides, Nucleotides, Nucleic Acids 20,* 883−887

(59) Westhof, E., Röder, O., Croneiss, I., and Lüdemann, H.-D. (1975) Ribose Conformations in the Common Purine(beta)-ribosides, in some Antibiotic Nucleosides, and in some isopropylidene Derivatives: a Comparison. *Z. Naturforsch. C 30*, 131−140.

(60) Williams, L. D., and Maher, L. J., III (2000) Electrostatic Mechanisms of DNA Deformation. *Annu. Rev. Biophys. Biomol. Struct. 29*, 497−521.

(61) Tarasow, T. M., Tarasow, S. L., and Eaton, B. E. (1997) RNA-catalyzed carbon−carbon bond formation. *Nature 389*, 54−57.

(62) Thum, O., Jäger, S., and Famulok, M. (2001) Funktionalisierte DNA: ein neues replizierbares Biopolymer. *Angew. Chem. 113*, 4112−4115.

BC020024Q

Synthesis and Photochemical Properties of Nitro-Naphthyl Chromophore and the Corresponding Immunoglobulin Bioconjugate

Anil K. Singh* and Prashant K. Khade

Department of Chemistry, Indian Institute of Technology, Bombay, Powai, Mumbai − 400 076, India Received March 28, 2002

Synthesis, photochemistry, and biomolecular caging properties of a new chromophore namely 3-nitro-2-naphthalenemethanol are described. This chromophore is photoexcitable with photons in 350−400 nm range and in several solvents including aqueous medium. On irradiation, it gives the expected nitroso-aldehyde photoproduct with high quantum yield (0.6−0.8). Further, it can be conveniently coupled to the amino residues of immunoglobulin (IgG) using diphosgene. Irradiation of the resulting IgG−nitronaphthyl chromophore bioconjugate at 380 nm causes photorelease of IgG as evidenced by Protein-A affinity binding studies. The bioconjugate showed low level of binding to Protein-A. However, the binding increases after irradiation and, thus, modifies the Fc site of the IgG. Electrophoresis studies of the irradiated bioconjugate show that IgG does not undergo fragmentation or molecular weight change under the irradiation conditions. Thus, 3-nitro-2-naphthalenemethanol can be used as a photocaging agent under physiological conditions at wavelengths, which does not cause significant damage to the biomolecule. The work provides new directions for the development of organic chromophores for biomolecular caging applications.

INTRODUCTION

Photochemical release of biologically active component from "caged biomolecule" is an important strategy in the study of numerous aspects of structure and dynamics of biochemical and medical significance (*1*−*5*). This is because of the ability of light to control the site, time, and concentration of the released molecule. A caged biomolecule is defined as a biomolecule whose activity or function is lost or altered upon its chemical modification with a photolabile group (i.e., masking of the functional group(s) of the biomolecule by a photocleavable protecting reagent), and irradiation of the caged biomolecule with light results in removal of the protecting group with simultaneous rapid generation of the active or functional biomolecule. Such photochemical deprotection of masked functional groups of biomolecules presents a simple, noninvasive technology to investigate a wide range of cellular activities and gives rise to many practical applications including site directed drug delivery.

Several photocleavable nitroaryl groups have been employed as protecting groups in organic synthesis (*6*). Further, nitroaryl chromophore-based photoactivable caged nucleotides (*7*−*12*) and proteins and peptides (*13*−*23*) have been developed to study intracellular dynamics, metabolism, and enzymatic activities. More recently, applications of photocleavable chromophores have been made in site-directed photocleavage for mapping protein architecture (*24*), synthesis of difficult cyclic peptides by inclusion of photolabile nitrobenzyl auxiliary in a ring contraction strategy (*25*), and selective inhibition, separation, and purification of serine proteases (*26*).

In most cases, caging of the biomolecules has been done with *ortho*-nitrobenzyl chromophoric group, which absorbs mainly in the ultraviolet region, a wavelength that may not be very suitable for biomolecular applications. For practical purposes, it is important to have photocleavable systems, which are useful under physiological conditions and can be photoexcited at a number of wavelength and more importantly at wavelengths which are less damaging to the biological systems.

In this paper are described synthesis, photochemistry, and biomolecular caging properties of a new chromophore, namely, 3-nitro-2-naphthalenemethanol (**7**). It is photoexcitable in 350−400 nm range, and it shows expected photochemical reaction of *ortho*-nitroaryl group giving the nitroso-aldehyde photoproduct. Further, **7** can be conveniently coupled to the amino residues of immunoglobulin (IgG) using diphosgene method via chloroformate **8**. Irradiation of the resulting IgG−**7** biconjugate **9** at 380 nm causes photorelease of IgG, as evidenced by Protein-A affinity binding studies. It has been demonstrated that chromophore **7** can be employed to cage proteins and the conjugated proteins can be photochemically released at wavelengths which are less damaging to the biological matrix in aqueous medium.

EXPERIMENTAL PROCEDURES

Chemicals, Apparatus, and General Methods. Starting materials for synthesis were obtained from M/s. Lancaster and M/s. SRL, India Ltd. Mumbai. Human immunoglobulin (IgG), gel electrophoresis chemicals, and buffers were purchased from M/s. Bangalore Genie, India Ltd. Bangalore. Diphosgene was obtained from the Indian Institute of Chemical Technology, Hyderabad. Protein-A sepharose CL-4B was purchased from Pharmacia Biotech. Synthetic compounds were purified by column chromatography using 60−120 mesh silica gel. Deionized and double distilled water was used for buffer preparation, electrophoresis, and affinity experiments.

Melting points were recorded on Veego melting point apparatus and are uncorrected. UV−vis spectra were

* To whom correspondence should be addressed. Phone: (091-22) 576 7167. Fax: (091-22) 576 7152. E-mail: Retinal@chem.iitb.ac.in.

10.1021/bc020021d CCC: $22.00 © 2002 American Chemical Society
Published on Web 11/05/2002

recorded on Shimadzu Uv-260 spectrophotometer. FTIR spectra were measured on Impact Nicolet-400 spectrophotometer. ^{1}H NMR spectra were recorded on Varian 300 MHz NMR spectrometer using TMS as the internal standard. Mass spectra were recorded on GCD 1800A Hewlett-Packard GC-MS spectrometer. Elemental analysis was performed on Theroquest CE instrument-1112 series CHN auto-analyzer. Protein samples were centrifuged at 4 °C in L8M55 Beckman ultracentrifuge equipped with Ti-45 rotor. Electrophoresis experiments were performed on a vertical gel electrophoresis instrument (mini model) from M/s. Bangalore Genie.

Irradiations were done using a 400 W medium pressure mercury lamp (Applied Photophysics Ltd., London, Model R-607), fitted either with a f/3.4 monochromator or with a glass filter to isolate the desired wavelength for irradiation. The organic solvents used for various electronic measurements or photochemical purposes were freshly distilled and thoroughly deoxygenated by bubbling dry nitrogen. The irradiated solutions were analyzed by UV−vis, FTIR, and ^{1}H NMR methods. The relative quantum yield (Φ_{PR}) was determined against potassium ferrioxalate actinometer (*27*).

Synthesis of 3-Nitro-2-naphthalenemethanol (7). Compound **7** was synthesized by reacting phthalaldehyde (**5**) with 3-nitropropionic ethyl ester (**4**) in the presence of sodium ethoxide in absolute ethanol as previously described (*28*). Reduction of the resulting 3-nitro-2-naphthoic acid (**6**) with $NaBH_4-BF_3-Et_2O$ in 1,2-dimethoxyethane followed by usual workup and column chromatographic purification yielded the desired alcohol **7**: yield, 40%; mp, 118−19 °C [lit. (*28*) mp 118−19 °C]. UV−vis: λ_{max}, nm (ϵ, mol^{-1} cm^{-1} L) in CH_3CN, 350 (2285). FTIR (KBr): ν_{max} (cm^{-1}) 3458−3372 (OH), 1513, 1331 (NO_2). ^{1}H NMR (DMSO): δ 4.91 (2H, d, J = 5.12 Hz, $-CH_2$), 5.90 (1H, t, −OH), 7.75−7.59 (2H, m, H−C_6 and H−C_7), 8.06 (1H, d, J = 8.24, H−C_8), 8.17 (1H, d, J = 8.05 Hz, H−C_5), 8.24 (1H, s, H−C_1), 8.75 (1H, s, H−C_4). MS *m*/*z* (%): 205 ($M^+ + 2$), 171 (74), 143 (100), 126 (55), 115 (58). Anal. Calcd for $C_{11}H_9NO_3$: C, 65.05; H, 4.47; N, 6.90. Found: C, 65.49; H, 4.33; N, 6.72.

Preparation of 3-Nitro-2-naphthyloxycarbonyl chloride (8). In a typical procedure, 3-nitro-2-naphthalenemethanol (**7**, 0.005 g, 0.25 mmol) was treated with diphosgene (20 μL) and dry pyridine (8 μL) as a catalyst in dried and freshly distilled 1,4-dioxane (150 μL). A yellow precipitate was immediately formed. The reaction mixture was magnetically stirred at ambient temperature for 24 h. The reaction was monitored by TLC using 20% ethyl acetate in petroleum ether (60−80 °C fraction). 1,4-Dioxane, pyridine, and excess of diphosgene were evaporated by using a stream of dry nitrogen. The residue was taken-up in dry 1,4-dioxane (125 μL), and the resulting solution was used for protein conjugation. The chloroformate **8** showed expected IR peaks at 1738 (−OCO) and 1535 and 1377 ($-NO_2$) cm^{-1}.

Coupling of Chloroformate 8 with IgG−Preparation of Bioconjugate 9. In a typical experiment, human immunoglobulin (IgG, 0.004 g) was taken in sodium bicarbonate (4 mL, 0.1 M; pH, 8.3) in a 10 mL round-bottom flask. To this was added 80 μL of chloroformate **8**. The reaction mixture was left overnight for coupling at 4 °C. Subsequently, the mixture was dialyzed twice against 200 mL each of 0.153 M sodium chloride (pH, 6.7). The white insoluble complexes were removed by centrifugation at 15 000*g* for 15 min at 4 °C to obtain bioconjugate **9** as clear solution. To this was added a solution of **9** 4 mL of 0.153 M aq. sodium chloride (pH 6.7), and the resulting solution was used for further study. The bioconjugate thus prepared showed UV−vis band extending up to 410 nm.

To determine the maximum number of chromophores that bind to IgG, the coupling of IgG to chloroformate **8** was done by using different amounts of **8** (0 μL as the control, and 5,10, and 20 μL aliquots of chloroformates) in 0.001 g of IgG solution in 1 mL of sodium bicarbonate buffer (0.1 M, pH, 8.3). It has been found that 20 μL of 1,4-dioxane solution of chloroformate **8** is sufficient to maximally modify the IgG.

The number of chromophores coupled to the protein was determined as follows. The concentration of chromopohre in bioconjugate was obtained from the absorbance value at the absorption maximum at 350 nm due to the chromophore. The concentration of protein in the bioconjugate was determined by considering its absorbance at 280 nm. However, in bioconjugate there is present absorption contribution by the chromophore also. Therefore, first the absorption contribution of the chromophore at 280 nm was determined from its absorbance at 280 nm in the bioconjugate, followed by subtracting it from the total absorbance of the bioconjugate at 280 nm. In calculating the concentration of chromophore from the absorbances obtained from bioconjugates, the extinction coefficients of chromophore at 280 and 350 nm in ethanol were used. From the concentrations, the number of molecules of IgG and the chromophore were calculated. Thus, the relative number of chromophores attached to the protein was obtained.

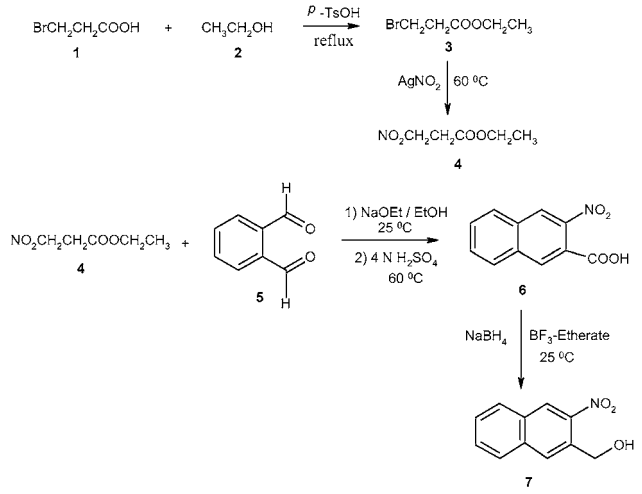
Irradiation of Compound 7 and Bioconjugate 9. A solution of **7** in acetonitrile (3 mL of 1.0×10^{-4} M) taken in a quartz cuvette and degassed by passing dry nitrogen was irradiated at 380 nm at ambient temperature. The distance between the sample and the lamp was kept 35 cm. The progress of the photochemical reaction was monitored spectrophotometrically by observing the changes at 350 nm. The photomixture was subsequently analyzed by FTIR and ^{1}H NMR analysis.

The dialyzed solution of bioconjugate **9** (3 mL, 0.153 M NaCl, pH, 6.7) was irradiated at 380 nm under the same conditions as described above. The bioconjugate was also irradiated with light filtered with a glass filter having 47% and 96% transmittance at 370 and 420 nm, respectively. Under this irradiation condition, the distance between the sample and the 400 W medium-pressure mercury lamp was kept 2 cm. The progress of the photolysis was monitored spectrophotometrically.

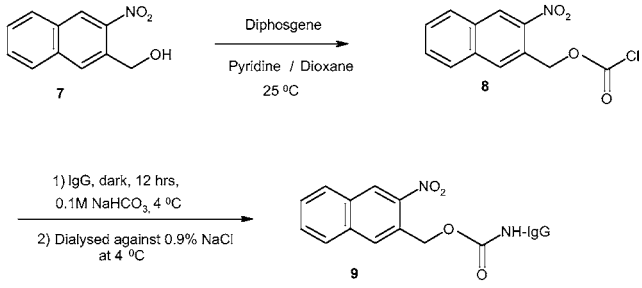
One aliquot of bioconjugate sample being irradiated was removed time to time and eluted from Protein-A affinity column. In a control experiment, the native IgG solution (3 mL, 0.153 M NaCl, pH 6.7) was subjected to irradiation under conditions identical to the irradiation conditions of conjugate **9**, and its binding affinity to protein-A was also studied.

Affinity Chromatography Studies of Bioconjugate Samples. A 3 cm long and 0.5 cm wide column was packed with Protein-A and equilibrated with 0.05 M Tris-buffer (pH, 7.4). One aliquot (0.5 mL) of irradiated bioconjugate sample was removed time to time and loaded on the affinity column, which was washed with the binding buffer until the absorbance of the eluted solution at 280 nm approached background level. The column was then eluted with 0.05 M glycine buffer (pH, 3.0) to remove the bound IgG protein and washed until the absorbance of elute at 280 nm approached the background level. The fractions collected were neutralized by addition of 100 μL of 1.0 M glycine buffer (pH, 9) in each test tube. Subsequently, the column was washed with 25 mL of binding buffer (0.05 M Tris-buffer, pH 7.4)

Scheme 1



Scheme 2



and equilibrated with it. From the absorbance at 280 nm, the concentration of IgG protein was calculated.

Protein-A binding affinity studies showed that unirradiated protein conjugate **9** binds to Protein-A to the extent of 18%.

Electrophoresis Studies of IgG, Bioconjugate, and Photoreleased IgG. The sample buffer (50 μL, 1.0×10^{-7} M) containing 10% glycerol and SDS, 0.5% bromophenol blue, and 0.5 M Tris-HCl (pH, 6.8) was added separately to irradiated bioconjugate, unirradiated bioconjugate, and unconjugated, native IgG. The mixture was heated to 85 °C for 10 min. The various protein samples, including 50 μL each of irradiated bioconjugate, unirradiated bioconjugate, unconjugated, native IgG, and the marker proteins in 14−200 kD MW range, which contain 5 μL of denaturing buffer were loaded on 10% SDS-polyacrylamide discontinuous gel. The electrophoresis was done in nonreducing conditions by applying 90−120 V and 10 A current. The electrophoresis was stopped when bromophenol blue reached to the bottom of the gel and the gels were stained (brilliant blue G stain, 0.1% w/v brilliant blue G, 25% methanol, 7% acetic acid). The destaining was done by 40% methanol, 10% acetic acid and 50% deionized water.

RESULTS AND DISCUSSION

Synthesis of 3-Nitro-2-naphthalenemethanol (7) and IgG-7 Bioconjugate (9). Synthesis of compound **7** and its IgG-bioconjugate **9** was done by following the steps outlined in Schemes 1 and 2. Esterification of 3-bromopropanoic acid (**1**) with ethanol gave ester **3**, which on reaction with silver nitrate yielded the nitroester **4**. The reaction of nitroester **4** with phthaldehyde **5** in the presence of sodium ethoxide, followed by acidic hydrolysis (of the ester group), resulted in the formation of nitro-naphthoic acid **6**, which on subsequent reduction with sodium borohydride gave the desired compound **7** in an overall yield of 40%. Compound **7** showed a mp identical to the mp reported in the literature (*28*). However, compound **7** was satisfactorily characterized additionally by other physicochemical methods, including electronic absorption, FTIR, ^{1}H NMR, mass, and elemental analysis as described in the Experimental Section.

Table 1. UV−Vis Absorption Spectral[a] and Quantum Yield (Φ_{PR}) Data of 7

solvent	λ/nm	ϵ/M L^{-1} cm^{-1}	Φ_{PR} at 380 nm
1,4-dioxane	217	70 000	
	258	28 000	
	265	26 667	0.82
	302	8 466	
	345	3 333	
acetonitrile	215	32 000	
	256	24 000	
	263	24 000	0.796
	301	5 547	
	350	2 285	
ethanol	222	25 000	
	256	30 000	
	263	26 667	0.75
	303	6 655	
	346	3 000	
0.153 NaCl	217	12 323	
	259	7 298	
	306	2 435	0.63
	350	1 289	

[a] Absorption coefficient at 280 nm: 6 826 (1,4-dioxane), 5 124 (acetonitrile), 6 200 (ethanol) ,and 2 124 (0.153 M NaCl). At 380 nm: 1 415 (1,4-dioxane), 1 264 (acetonitrile), 1 350 (ethanol), and 809 (0.153 M NaCl).

Bioconjugate **9** could conveniently be prepared via chloroformate **8**. As outlined in Scheme 2, reaction of compound **7** with diphosgene yielded chloroformate **8**, which reacted with the amino residues of IgG to give the desired bioconjugate **9** in about 40% yield. Under the present preparative conditions, about 22 (±2) molecules of **8** coupled to a molecule of IgG. The IgG has a total of 50 lysine units and it is possible that 22 (±2) ϵ-amino groups of lysine in IgG underwent coupling with **8** in the present experimental conditions.

Electronic Absorption and Photochemical Properties of 3-Nitro-2-naphthalenemethanol (7). The UV−vis absorption spectral data and the Φ_{PR} of **7** are summarized in the Table 1. This compound exhibits major absorption bands in 220−250 and 300−350 nm range with tail end absorption extending up to 410 nm for a 1.0×10^{-4} M solution. The longer wavelength absorptions of **7** can be due to the ^1L_a (vertically polarized) transition of the naphthyl group. The molar absorption coefficient of the band in 220−250 range is larger than the band in 300−350 nm range. The UV−vis absorption of **7** remains similar in a variety of solvents including acetonitrile, ethanol, 1,4-dioxane, and 0.153 M aq. NaCl (pH, 6.7). However, the molar absorption coefficient varies with the solvent. An ethanolic solution of **7** shows absorption at 346 nm with molar absorptivity of about 3000 mol^{-1} cm^{-1} L. However, for the same solution, the molar absorptivity is 1350 mol^{-1} cm^{-1} L for absorption at 380 nm. Compound **7** in aq. NaCl medium shows absorption at 350 nm with a molar absorptivity of about 1 289 mol^{-1} cm^{-1} L. Its molar absorptivity at 380 nm is found to be about 809 mol^{-1} cm^{-1} L.

Typical UV−vis absorption changes during 380 nm irradiation of a 1.0×10^{-4} M acetonitrile solution of **7** are shown in Figure 1. The FTIR spectrum of the photomixture is characterized by the presence of bands at 1 532 and 1 341 cm^{-1} due to nitroso group and 1 703

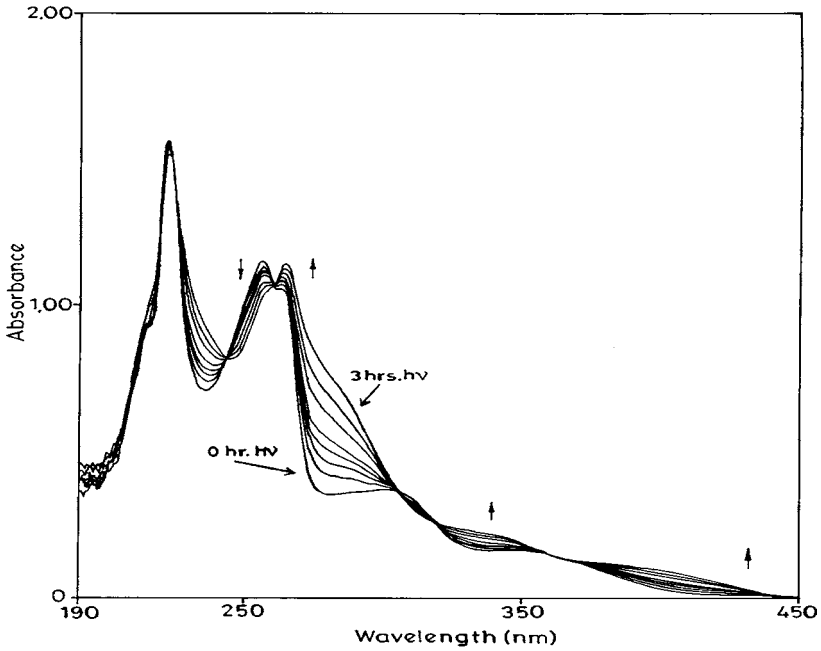


Figure 1. UV−vis absorption spectral changes during 380 nm photolysis of a 1.0×10^{-4} M acetonitrile solution of **7**.

cm^{-1} due to aldehyde group. The alcohol group peak (3 372−3 458 cm^{-1}) that was present in the starting chromophore disappeared after irradiation. The ^{1}H-NMR spectrum of the photomixture showed peak at δ 10.50 due to an aldehyde proton.

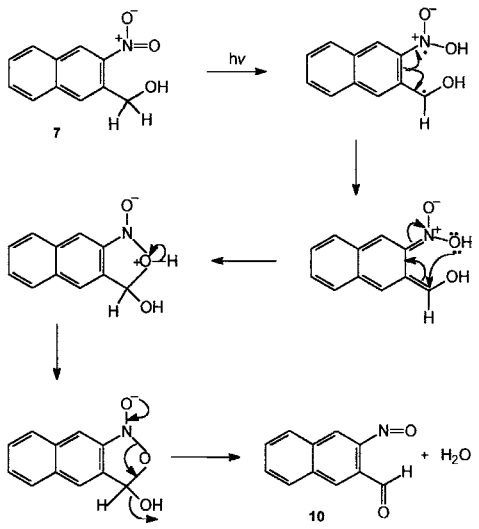
Similar photobehavior was observed when **7** was irradiated in protic ethanol, nonpolar 1,4-dioxane, and 0.153 M aq. NaCl solutions, indicating the absence of any solvent effect on the photochemical properties of **7**. Irradiation of **7** at 300, 350, and 400 nm also showed photochemical product profile similar to its irradiation at 380 nm.

The above photochemical and spectroscopic results suggest that compound **7**, on irradiation with photons in 300 to 400 nm range, undergoes the expected light-induced internal oxidation−reduction reaction of aromatic nitro compounds containing a carbon−hydrogen bond ortho to the nitro group (*6*). The primary photochemical process in this reaction is an intramolecular hydrogen abstraction by the nitro group generating free radical species; this is then followed by electron redistribution to the *aci*-nitro form, which subsequently rearranges to the nitroso-aldehyde photoproduct (**10**) (Scheme 3). Thus, it has been possible to develop a chromophore that can be photoexcited with desired photochemistry at wavelengths greater than 350 nm.

Electronic Absorption and Photochemical Properties of Bioconjugate 9. The UV−vis absorption spectrum of bioconjugate **9** in 0.1 M aq. NaCl solution is characterized by absorption bands at 198 and 266 nm, with extended absorption up to 410 nm. The IgG protein peak at 278 nm is masked due to the absorption by chromophoric group of **7** having absorption in 250−300 nm range. The bioconjugate can, however, be photoexcited by taking the advantage of absorption in 350−410 nm, where unconjugated protein has insignificant absorption.

Thus, a 1.0×10^{-5} M solution of bioconjugates **9** in 0.9% (0.153 M) aq. NaCl was irradiated at 380 nm. The irradiation resulted in changes in the absorption at 266 nm (Figure 2). The irradiated bioconjugate samples were analyzed by affinity chromatography on a Protein-A

Scheme 3



sepharose CL4B column, and the extent of binding of photoreleased IgG was determined (Figure 3). The bioconjugate sample irradiated for 3 h showed 70% binding affinity to Protein-A. However, bioconjugate samples irradiated for 5 and 7 h showed binding affinity of only 50% and 40%, respectively, to Protein-A. Thus, the binding affinity was increased from 18% (the extent to which unirradiated IgG binds to Protein-A) to 70% after 3 h of irradiation. However, the binding affinity decreased to 40% after 7 h of irradiation. As control experiments, uncoupled and unirradiated native IgG was irradiated for 0 (control), 3, 5, and 7 h at 380 nm, and the binding affinity for such samples was found to be 100%, 85%, 83%, and 73% respectively.

Further, a sample of bioconjugate **9** irradiated for 40 min using a glass filter having 47% and 96% transmittance at 370 and 420 nm, respectively, showed binding affinity to Protein-A to the extent of 74%. Continued irradiation up to 60 min caused further decrease in binding affinity to 51%. This shows that as the intensity of the photons is increased, the rate of the photoreaction was increased. Thus, photorelease of IgG from the

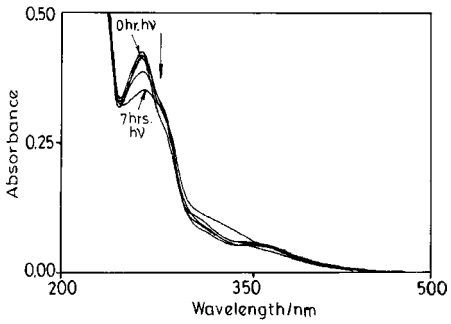


Figure 2. UV−vis absorption spectral changes during 380 nm photolysis of a 1.0×10^{-5} M aq. NaCl (0.153 M) solution of bioconjugate **9**.

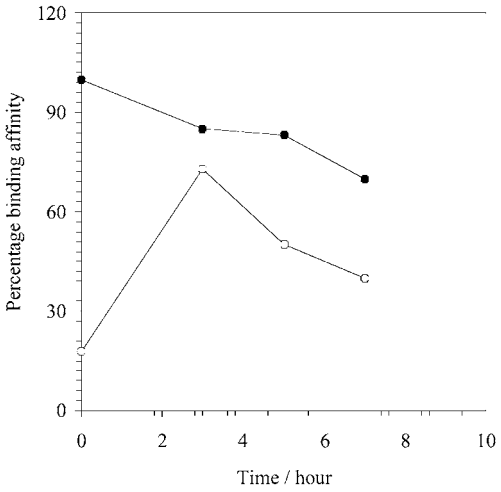


Figure 3. A plot of irradiation time vs percent Protein-A binding affinity. (○) Photo-released IgG (upon irradiation of bioconjugate **9**), and (●) native IgG (which was subjected to irradiation under conditions identical to the irradiation of bioconjugate **9**).

bioconjugate can be effected in much shorter time by use of appropriate light source (e.g. lasers).

It is believed that irradiation of bioconjugate **9** results into the photoconversion of its nitronaphthyl chromophore to nitroso-aldehyde and subsequent release of IgG, as outlined in Scheme 4. The primary photochemical process of bioconjugate **9** is similar to the photochemical process of *ortho*-nitroaryl chromophores having abstractable hydrogen atoms in the vicinity (*6*). Overall, the photochemical reaction of bioconjugate **9** results into release of IgG via the formation of nitroso-aldehyde **10** and carbon dioxide.

The decrease in binding can be due to the artificial irradiation in case of control protein and in case of coupled protein it may be due to the artificial irradiation as well as due to reaction or association of the nitroso-aldehyde photoproduct (**10**) with the photoreleased free protein.

These results further show that the nitro-naphthyl chromophore modifies the F_C site of IgG molecule. The modified protein showed low level of binding, and after irradiation, binding of released protein to Protein-A was increased. This can be due to the fact that irradiation of the conjugate leads to photorelease of the nitro-naphthyl chromophore from the Fc site of IgG, which then becomes available for binding to Protein-A.

Electrophoresis studies of unconjugated native IgG (as control), unirradiated bioconjugate (**9** as the control), and irradiated bioconjugate in discontinuous gel and nonreducing conditions showed that irradiation does not cause

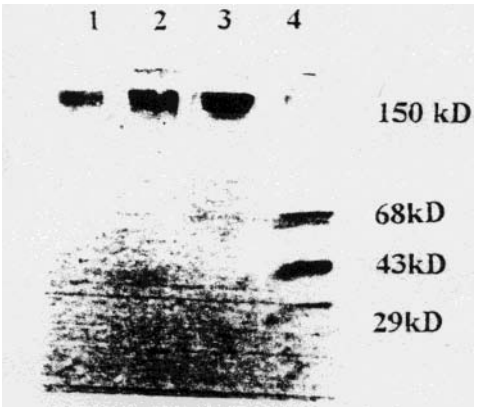
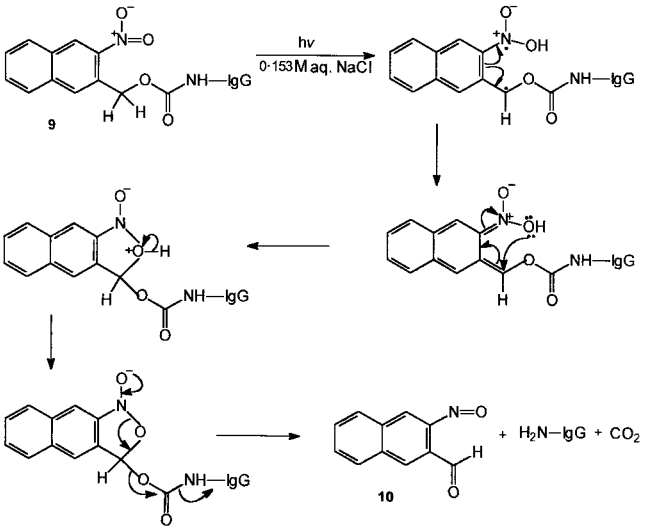


Figure 4. Electrophoresis of various protein samples. (1) Irradiated bioconjugate. (2) Unirradiated bioconjugate. (3) Native IgG. (4) Marker proteins.

Scheme 4



any fragmentation or molecular weight changes in IgG (Figure 4). UV−vis absorption and electrophoresis studies thus indicate IgG protein molecules are not fragmented under the present irradiation conditions.

In conclusion, it can be said that 3-nitro-2-naphthalenemethanol **7** can be used for caging of biomolecules. It can be photoexcited in aqueous solution and at wavelengths that do not cause significant damage to the biomolecules. Further, this chromophore is photoexcitable at many wavelengths in 300−400 nm range. This work provides new directions for the development of organic chromophores for biomolecular caging applications.

ACKNOWLEDGMENT

A research grant [01/1509/98-EMR-II] for this work from the Council of Scientific and Industrial Research, New Delhi, Government of India, is gratefully acknowledged.

LITERATURE CITED

(1) McCray, J. A., and Trentham, D. R. (1989) Properties and uses of photoactive caged compounds. *Annu. Rev. Biophys. 18*, 239−270.
(2) Kaplan, J. H. (1990) Photochemical manipulation of divalent cation levels. *Annu. Rev. Physiol. 52*, 897−914.
(3) Adams, S. R., and Tsien, R. Y. (1993) Controlling cell chemistry with caged compounds. *Annu. Rev. Physiol. 55*, 755−784.

(4) Corrie, J. E. T., and Trentham, D. R. (1993) Caged nucleotides and neurotransmitters. In *Bioorganic Photochemistry* (H. Morrison, Ed.), Vol. 2, pp 243−305, John Wiley, New York.
(5) Marriot, G. (1998) Caged compounds. *Methods Enzymol. 291*, 1−515.
(6) Pillai, V. N. R. (1980) Photoremovable protecting groups in organic synthesis. *Synthesis 9*, 1−26.
(7) Tjoeng, F. S., Staines, W., St-Pierre, S., and Hodges, R. S. (1977) Liquide-phase method for peptide synthesis utilizing photolytic cleavage from a new *o*-nitrobenzoyl polyethylene glycol support. *Biochim. Biophys. Acta 490*, 489−496.
(8) Nargeot, J., Nerbonne, J. M., Engels, J., and Lester, H. A. (1983) Time course of the increase in the myocardial slow inward current after a photochemically generated concentration jump of intracellular cAMP. *Proc. Natl. Acad. Sci. U.S.A. 80*, 2395−2399.
(9) Nerbonne, J. M., Richard, S., Nargeot, J., and Lester, H. A. (1984) New photoactivatable cyclic nucleotides produce intracellular jumps in cyclic AMP and cyclic GMP concentrations. *Nature 310*, 74−76.
(10) Walker, J. W., Somlyo, A. V., Goldman, Y. E., Somlyo, A. P., and Trentham, D. R. (1987) Kinetics of smooth and skeletal muscle activation by laser pulse photolysis of caged inositol-1,4,5-triphospate. *Nature 327*, 249−252.
(11) Walker, J. W., Reid, G. P., and Trentham, D. R. (1989) Synthesis and properties of caged nucleotides. *Methods Enzymol. 172*, 288−301.
(12) Dantzig, J. A., Hibberd, M. G., Trentham, D. R., and Goldman, Y. E. (1991) Cross bridge kinetics in the presence of MgADP investigated by photolysis of caged ATP in rabit proas muscle fibers. *J. Physiol. 432*, 639−680.
(13) Senter, P. D., Tansey, M. J., Lambert, J. M., and Blattler, W. A. (1985) Novelphotocleavable cross-linking reagents and their use in the preparation of antibody-toxin conjugates. *Photochem. Photobiol. 42*, 231−237.
(14) Theriot, J. A., and Mitchison, T. J. (1991) Acting microfilament dynamics in locomoting cells. *Nature 352*, 126−131.
(15) Mendal, D., Ellamanand, J. A., and Schultz, P. G. (1991) Constuction of a light-activated protein by unnatural amino acid mutagenesis. *J. Am. Chem. Soc. 113*, 2758−2760.
(16) Goldmacher, V. S., Senter, P. D., Lambert, J. M., and Blattler. W. A. (1992)Photoactivation of toxin conjugates. *Bioconjugate Chem. 3*, 104−107.
(17) Marriott, G., Miyata, H., and Kinosita, K. (1992) Photomodulation of the nucleating activity of a photocleavable cross-linked actin dimer. *Biochem. Int. 26*, 9943−9951.
(18) Mariott, G. (1994) Caged protein conjugates and light directed generation of protein activity preparation, photoactivation, and spectroscopic characterization of caged G- Actin conjugates. *Biochemistry 33*, 9092−9097.
(19) Thompson, S., Spoor, J. A., Fawcett, M. C., and Self, C. H. (1994) Photoclevable nitrobenzyl-protein coonjugates. *Biochem. Biophys. Res. Commun. 201*, 1213−1219.
(20) Thompson, S., Fawcett, M. C., Spoors, J. A., and Self, C. H. (1995) The modulation of protein A-IgG(Fc) binding by the reversible addition of 2-nitrobenzyl groups. *Biochem. Soc. Trans. 23*, 155S.
(21) Self, C. H., Fawcett, M. C., Spoors, J. A., Pulman, I. B., and Thompson, S. (1995)Studies on photolabile nitrobenzyl-bovine serum albumin conjugates. *Biochem. Soc. Trans. 23*, 156S.
(22) Self, C. H., and Thompson, S. (1996) Light activatable antibodies: Modles for remotely activatable proteins. *Nature (Medicine) 2*, 817−820.
(23) Odaka, M., Furata, T., Kobayashi, Y., and Iwamura, M. (1996) Synthesis,photoreactivity and cytotoxic activity of caged compounds of L-leucyl-L-lucine methyl ester, an apoptosis inducer. *Photochem. Photobiol. 63*, 800−806.
(24) Miyake, R., Owens, J. T., Xu, D., Jakson, W. M., and Meares. C. F. (1999) Site- directed photocleavage for mapping of protein architecture. *J. Am. Chem. Soc. 121*, 7453−7454.
(25) Meutermans, W. D. F., Golding, S. W., Bourne, G. T., Miranda, L. P., Dooley, M. J., Alewood, P. F., and Smythe, M. L. (1999) Synthesis of difficult cyclic peptides by inclusion of a novel photolabile auxiliary in a ring contraction strategy. *J. Am. Chem. Soc. 121*, 9790−9796.
(26) Porter, N. A., Thuring, J. W., and Li, H. (1999) Selective inhibition, separation, and purification of serine proteases: A strategy based on a photoremovable inhibitor. *J. Am. Chem. Soc. 121*, 7716−7717.
(27) Rabek, J. F. (1982) Radiometry and actinometry. In *Experimental Methods In Photochemistry and Photophysics*, Vol. 2, pp 944−946, Wiley, New York.
(28) Kienzle, F. (1980) The reaction of phthalaldehydes with 3-nitropropionates. A simple route to 3-nitro-2-naphthoic acids. *Helv. Chim. Acta 63*, 2364−2369.
(29) Sjodahl, J. (1977) Structural studies on the four repetitive Fc-binding regions in Protein-A from *Staphylococcus aureus*. *Eur. J. Bochem. 78*, 471−490.

BC020021D

Polycationic Diblock and Random Polyethylene Glycol- or Tris(hydroxymethyl)methyl-Grafted (Co)telomers for Gene Transfer: Synthesis and Evaluation of Their in Vitro Transfection Efficiency

Bertrand Le Bon,[†] Nathalie Van Craynest,[†] Otmane Boussif,[‡,§] and Pierre Vierling*[,†]

Laboratoire de Chimie Bioorganique, UMR 6001 CNRS, Université de Nice Sophia-Antipolis, Faculté des Sciences, 06108 Nice Cédex 2, France, and Transgène SA, 11 rue de Molsheim, 67082 Strasbourg Cédex, France. Received May 1, 2002; Revised Manuscript Received July 1, 2002

We report on the synthesis of a series of polycationic telomers, polycationic diblock and random polyethylene glycol (PEG)-grafted (co)telomers, and polycationic random tris(hydroxymethyl)methyl (THM) cotelomers, and on their in vitro gene transfer capability. These compounds were obtained by a telomerization process of various amino-, tetraethylene glycol-, or THM-acrylamide taxogens with thiols which might derive from PEG2000. For *N*/*P* ratios [*N* is the number of (co)telomer amine equivalents; *P* is the number of DNA phosphate equivalents] from 0.8 to 10, these (co)telomers condensed DNA, forming (co)teloplexes with mean sizes in the 85−330 nm range, even for an *N*/*P* ratio of 0.8 or 1.25. Some structure−transfection efficiency relationships were established. Among the new polycationic derivatives that were synthesized and investigated for their transfection efficiency, the ^{i}Bu-[NH]$_{75}$ telomers and the diblock polyethylene glycol-conjugated **PEG2000-[NH]$_n$** telomers are very promising candidates for gene transfer purposes.

INTRODUCTION

Introducing a gene into cells with synthetic (nonviral) vectors is a promising alternative for gene therapy. Although viral vectors are useful clinical tools for delivering genes and infect cells, they suffer from several serious drawbacks (*1*−*3*, and references therein). To circumvent these drawbacks, a large number of nonviral vectors, including (poly)cationic lipid- (liposome-) and polymer-based DNA complexes (lipoplexes and polyplexes, respectively) have been evaluated (*3*−*8*, and references therein). Unlike viral vectors, nonviral vectors have advantages in their large scale and easy production, simplicity of use, safety (fewer immunogenic and inflammatory responses, an inability to replicate or to recombine to form an infectious agent, and low integration frequency), and ability to transfer expression cassettes of unlimited size. Although they demonstrated in vitro a real capacity for transfecting culture cells, lipoplexes and polyplexes are not as efficient as viral vectors in achieving successful gene transfer. In addition, nonviral (and viral) gene delivery systems are currently fraught with a number of serious problems when their in vivo use, i.e., after systemic administration for example, is contemplated (*3*, *9*−*12*). To successfully transfect its target cells at a remote site, the gene delivery system must, at least, reach this site while in blood circulation. Unfortunately, clearance of "conventional" DNA carriers from the bloodstream is rapid (*12*). Furthermore, it is very difficult to control their biodistribution and transgene expression in vivo which are not necessarily correlated (*13*, *14*). Gene delivery to a specific target tissue is more challenging and requires strategies that limit nonspecific interactions with the biological environment. For intravenous administrations, formation of large aggregates and interactions with the blood components (e.g., opsonization with plasma proteins) and nontarget cells such as the mononuclear phagocytic system (MPS) are most important obstacles for targeting genes in vivo. Attempts have been made to avoid aggregation of the lipoplexes and polyplexes, to reduce the level of protein binding to the DNA complexes, and to divert them from the MPS by coupling of (i) hydrophilic nonimmunogenic polymers, such as polyethylene glycol (PEG) which provides a "stealth"-like coating, and/or (ii) specific cell-binding ligands (*12*, *15*−*23*).

Recently, as a contribution to this field, some of us have reported on lipoteloplexes and lipo(co)teloplexes, e.g., DNA complexes formulated with lipopolyamine telomers and random cotelomers, respectively, as alternative efficient gene transfer agents (*24*, *25*). These lipopolyamine (co)telomers were obtained from telomerizing one polymerizable acrylamide M monomer or a mixture of polymerizable acrylamide M and M′ monomers comprising a (poly)amine precursor, in the presence of a hydrophobic long chain thiol (L-SH). The lipopolyamine (co)telomers thus obtained, of formula L-S-(M)$_n$-H or random L-S-(M)-*n*-(M′)*n*′-H, exhibited controllable degrees of (co)polymerization (*24*, *25*).

We report herein on the synthesis of new diblock PEG-grafted polycationic telomers and of new random tetraethylene glycol (TEG)- or polyol tris(hydroxymethyl)-methyl (THM)-grafted polycationic cotelomers (Figure 1), on their capabilities of compacting and transferring, in vitro, DNA into a cell, and on their effect on cell viability. These PEG-, TEG-, or THM-grafted polycationic derivatives show a modular structure aimed at modulating the physicochemical and biological properties (e.g., stability with respect to aggregation, biodegradability, cell viability, biodisponibility, and transfection efficacy) of the

* To whom correspondence should be addressed. E-mail: vierling@unice.fr. Phone: 33 4 92 07 61 43. Fax: 33 4 92 07 61 51.

[†] Université de Nice Sophia-Antipolis.

[‡] Transgène SA.

[§] Present address: Aventis Pharma, 13, quai Jules Guesde, 94403 Vitry-sur-Seine Cédex, France.

10.1021/bc0255440 CCC: $22.00 © 2002 American Chemical Society
Published on Web 09/14/2002

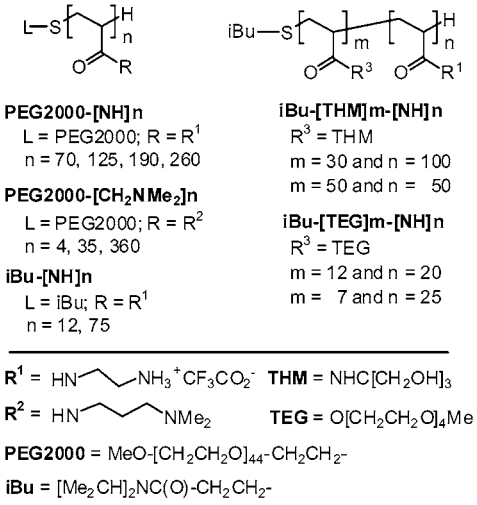


Figure 1. Molecular structure of the polycationic diblock telomers and random cotelomers and of the pcTG90−DOPE reference gene transfer lipids used in this study.

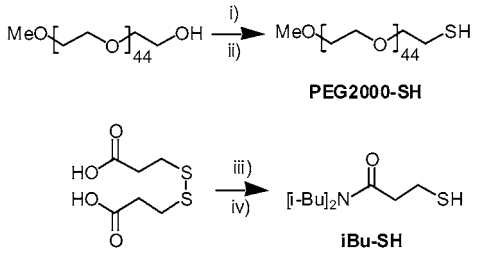
teloplexes and coteloplexes they form with DNA. The diblock PEG-grafted polycationic telomers include a long PEG chain (PEG2000) and a variable number (from 4 to 360) of primary or tertiary amine functions. The random cotelomers contain a random combination of primary amine functions and TEG or THM units. The neutral, hydrophilic PEG, TEG, and THM units were selected for improving cell viability (*26*, *27*) and/or reducing the the number of interactions with plasma constituents and opsonization of the DNA complexes (*12*, *15*−*23*). For comparison, we developed and evaluated also the polycationic ^{i}Bu-[NH]$_n$ telomers that were obtained from telogen ^{i}Bu-SH (Figure 1). This telogen was also selected for its diisobutyl group with the aim of facilitating the determination of the average degree of polymerization of the (co)telomers by ^{1}H NMR (*24*, *25*).

EXPERIMENTAL SECTION

General Experimental and Analytical Conditions. All the reactions were performed in anhydrous solvents under dry and oxygen-free nitrogen. The purifications by column chromatography were carried out using silica gel 60 (Merck, 70−230 mesh) and chloroform ($CHCl_3$), dichloromethane (CH_2Cl_2), methanol (MeOH), or mixtures thereof as indicated. The progress of the polymerization reaction was followed by thin-layer chromatography (TLC) on silica plates (SDS 60F254, 60/15 μm). The following developing systems were used: UV light (254 nm), Draggendorff reagents, DTNB [5,5′-dithiobis(2-nitrobenzoic acid)] (Sigma), and ninhydrin reagent (Sigma). The synthesis of taxogen **A**, *N*-{2-[(BOC)aminoethyl]}acrylamide, was performed as reported elsewhere (*24*). Taxogens *N*-[3-(dimethylamino)-propyl]acrylamide (**B**) and *N*-[tris(hydroxymethyl)methyl]-acrylamide (**D**) were purchased from Aldrich and used without further purification.

^{1}H, ^{13}C, and ^{19}F NMR spectra were recorded on a Bruker AC-200 instrument at 200, 50.3, and 188.3 MHz, respectively. Chemical shifts were measured relative to that of $CHCl_3$ (δ 7.27) or CH_3OD (δ 3.35) for ^{1}H, to that of $CDCl_3$ (δ 76.9) for ^{13}C and expressed indirectly in relation to TMS, and to that of CCl_3F as an internal reference for ^{19}F. The following abbreviations are used to describe the signal multiplicities: s (singlet), d (doublet), t (triplet), q (quadruplet), and m (multiplet). Chemical shifts are expressed in parts per million and listed as follows: shift in parts per million (multiplicity, integration, coupling, and attribution). Melting points were measured on an Electrothermal Digital Series 9100 and were not corrected. Mass spectra (MS) were recorded on a Finnigan MAT TSQ 7000 apparatus equipped with an atmospheric-pressure ionization (API) source. Electrospray ionization mass spectrometry (ESI-MS) was used depending on the polar moiety of the molecules to be studied. This method used in the positive mode can give either a M + H$^+$ or a M + Na$^+$ signal.

Scheme 1. Synthesis of Telogen ^{i}Bu-SH and PEG2000-SH[a]



[a] Reagents and conditions: (i) TsCl, NEt_3, DMAP, CH_2Cl_2, 0 °C; (ii) Amberlite IR400 (SH^- form), NaSH in CH_3CN, 50 °C; (iii) EDC, HOBt, THF, CH_2Cl_2, 0 °C, then (^{i}Bu)$_2$NH, NEt_3, THF, 0 °C; (iv) Zn, AcOH.

Synthesis of Taxogen C (2-{2-[2-(2-Methoxyethoxy)ethoxy]ethoxy}ethyl Ester Acrylate). To a solution of 0.6 mL (7.2 mmol) acryloyl chloride (Aldrich) in 10 mL of anhydrous CH_2Cl_2 was added dropwise during 1 h at 0 °C a solution of 0.7 mL (4.8 mmol) of triethylamine and 0.96 mL (4.8 mmol) of 2,5,8,11-tetraoxatridecan-13-ol (tetraethylene glycol monomethyl ether, MeO-TEG, Acros) in 10 mL of anhydrous CH_2Cl_2. After being stirred for 4 h at room temperature, the reaction mixture was concentrated under vacuum, and the residue was chromatographed over a silica column [$CHCl_3$/MeOH eluent, from 100 to 97/3 (v/v)]; 540 mg (2.06 mmol, 43%) of taxogen **C** was obtained as a colorless oil: TLC (98/2 $CHCl_3$/MeOH, UV and Draggendorf) R_f = 0.71; ^{1}H NMR ($CDCl_3$) δ 3.30 (s, 3H, OCH_3), 3.47 (m, 2H, CH_2OCH$_3$), 3.55 (m, 10H, CH_2OCH_2), 3.68 (m, 2H, CH_2CH$_2$OCO), 4.25 (m, 2H, CH_2OCO), 5.78 (dd, 1H, ^3J = 1.7 Hz, ^3J = 10.4 Hz, CH_2CH), 6.08 (dd, 1H, ^3J = 10.4 Hz, ^3J = 17.2 Hz, CH$_2$CH), 6.36 (dd, 1H, ^2J = 1.7 Hz, ^3J = 10.4 Hz, CH_2CH); ^{13}C NMR ($CDCl_3$) δ 59.0 (CH_3O), 63.7 (CH_2-OCO), 69.2 (CH_2CH_2OCO), 70.6 and 70.7 (CH_2OCH_2), 72.0 ($CH_2CH_2OCH_3$), 128.4 (CH_2=CH), 130.9 (CH_2=CH), 166.2 (CO).

Synthesis of the Telogen *N*,*N*-Diisobutyl-3-mercaptopropionamide (^{i}Bu-SH). The synthesis of the telogen ^{i}Bu-SH was carried out in two steps as shown in Scheme 1.

Synthesis of 3-(2-Diisobutylcarbamoylethyldisulfanyl)-*N*,*N*-diisobutylpropionamide. A solution of 250 mg (1.2 mmol) of 3,3′-dithiodipropionic acid (Aldrich) and 480 mg (3.6 mmol) of HOBt (1-hydroxybenzotriazole, Aldrich) in 30 mL of anhydrous THF was added to 680 mg (3.6 mmol) of EDC [1-(3-*N*,*N*-dimethylaminopropyl)-3-ethylcarbodiimide chlorohydrate, Aldrich] in 25 mL of anhydrous CH_2Cl_2 at 0 °C. Then, a solution of 0.5 mL (3.6 mmol) of triethylamine and 0.42 mL (2.4 mmol) of diisobutylamine (Aldrich) in 10 mL of THF was added dropwise at 0 °C, and the resulting reaction mixture was stirred at room temperature for 12 h. The reaction mixture was then concentrated and $CHCl_3$ added. The organic solution was washed with aqueous $NaHCO_3$ (8%) and H_2O until the solution reached neutrality, dried over Na_2SO_4, and filtered. The solution was then concentrated

under vacuum, and the residue was chromatographed over a silica column [hexane/ethyl acetate eluent, from 9/1 to 85/15 (v/v)]; 403 mg (0.93 mmol, 78%) of the title disulfide were obtained as an oil: TLC (9/1 CH_2Cl_2/ethyl acetate, UV) $R_f = 0.61$; ^{1}H NMR ($CDCl_3$) δ 0.79 and 0.85 (d, d, 12H, 12H, $^3J = 6.7$ Hz, CH_3), 1.76−2.02 (m, 4H, CH), 2.69 (m, 4H, CH_2CO), 2.89 (m, 4H, CH_2S), 3.04 and 3.12 (d, d, 4H, 4H, $^3J = 7.5$ Hz, CH_2NCO); ^{13}C NMR ($CDCl_3$) δ 20.0 and 20.1 (CH_3), 26.4 and 27.8 (CH), 33.0 (CH_2S), 33.8 (CH_2CO), 54.3 and 55.5 (CH_2N), 171.0 (CO). The doubling of some signals is due to restricted rotation of the amide bond.

Synthesis of ^{i}Bu-SH. To a solution of 403 mg (0.93 mmol) of the above disulfide in 8 mL of acetic acid was added 600 mg (9.31 mmol) of zinc powder (Aldrich). The solution was stirred under reflux. After completion of the reaction [followed by TLC (UV/DTNB)], the mixture was filtered over Celite 521 (Aldrich). The excess of acetic acid was removed by evaporation in the presence of $CHCl_3$ and cyclohexane. The residue was dissolved in $CHCl_3$ and washed with H_2O until the solution reached neutrality, and the organic phase was then dried over Na_2SO_4, filtered, and concentrated under vacuum; 380 mg (1.75 mmol, 94%) of ^{i}Bu-SH was obtained as a colored oil: TLC (8/2 hexane/ethyl acetate, DTNB) $R_f = 0.56$; ^{1}H NMR ($CDCl_3$) δ 0.89 and 0.87 (d, d, 6H, 6H, $^3J = 6.7$ Hz, CH_3), 1.69 (t, 1H, $^3J = 8.1$ Hz, SH), 1.93 (m, 2H, CH), 2.63 (m, 2H, CH_2CO), 2.77 (m, 2H, CH_2S), 3.05 and 3.16 (d, d, 2H, 2H, $^3J = 7.6$ Hz, CH_2N); ^{13}C NMR ($CDCl_3$) δ 20.0 and 20.1 (CH_3), 20.4 (CH_2SH), 26.4 and 27.8 (CH), 37.7 (CH_2CO), 53.3 and 55.4 (CH_2N), 171.0 (CO); ESI-MS *m*/*z* 218.4 (in agreement with the mass calculated for $C_{11}H_{23}NOS + H^+$).

Synthesis of the Telogen PEG2000-SH. The synthesis of **PEG2000-SH** was carried out in two steps as shown in Scheme 1.

PEG2000-OTs. To a solution of 1.0 g (0.5 mmol) of PEG2000-OH (polyethylene glycol monomethyl ether 2000, Aldrich), 0.21 mL (1.5 mmol) of triethylamine, and 24.5 mg (0.2 mmol) of (dimethylamino)pyridine (DMAP, Aldrich) in 5 mL of anhydrous CH_2Cl_2 was added dropwise 143 mg (0.75 mmol) of tosyl chloride (Fluka) in 2 mL of anhydrous CH_2Cl_2 at 0 °C. The reaction mixture was stirred at room temperature for 1 day and then washed with H_2O. The organic phase was dried over Na_2SO_4, filtered, and concentrated under vacuum. The residue was chromatographed on a silica column [$CHCl_3$/MeOH eluent, from 95/5 to 85/15 (v/v)]; 815 mg (0.37 mmol, 85%) of **PEG2000-OTs** was obtained as a white solid: TLC (8/2 $CHCl_3$/MeOH, Draggendorf) $R_f = 0.77$; mp 50−51 °C; ^{1}H NMR ($CDCl_3$) δ 2.43 (s, 3H, CH_3, Ts), 3.36 (s, 3H, CH_3O), 3.50−3.75 (sl, 178H, CH_2OCH_2), 4.14 (dd, 2H, $^3J = 5.0$ Hz, CH_2OTs), 7.33 (d, 2H, $^3J = 8.3$ Hz, C*H*CH, Ts), 7.78 (d, 2H, $^3J = 8.3$ Hz, CHC*H*, Ts); ^{13}C NMR ($CDCl_3$) δ 21.2 (CH_3, Ts), 59.0 (OCH_3), 68.7 (CH_2OTs), 69.3 (CH_2CH_2OTs), 70.6 (CH_2OCH_2), 128.0 (*C*HC-S, Ts), 129.8 (*C*HC-CH_3, Ts), 134.4 (CH*C*-S, Ts), 144.8 (CH*C*-CH_3, Ts). ESI-MS shows the presence of MeO-$(CH_2CH_2$-$O)_n$-CH_2CH_2OTs compounds with an *n* of 30−56 (*m*/*z* 230.1 + 44*n* + 23), in agreement with the masses calculated for $[C_{10}H_{14}O_4S + n(C_2H_4O) + Na^+]$.

PEG2000-SH. To a solution of 0.5 g (0.23 mmol) of **PEG2000-OTs** in 5 mL of anhydrous acetonitrile (CH_3CN) was added 5 g of anion-exchange resin Amberlite IRA400 (SH^- form) and 130 mg (2.3 mmol) of NaSH (Aldrich). The reaction mixture was stirred at 50 °C. After completion of the reaction (followed by TLC UV, Draggendorf, DTNB), the resin was filtered and washed with CH_2Cl_2. The organic phase was evaporated and concentrated under vacuum. The residue was purified by gel permeation chromatography on a Sephadex LH 20 column (Fluka) ($CHCl_3$/MeOH eluent, 9/1); 367 mg (0.18 mmol, 78%) of **PEG2000-SH** was obtained as a white solid: TLC (9/1 CH_2Cl_2/MeOH, UV, DTNB) $R_f = 0.51$; mp 53−54 °C; ^{1}H NMR (DMSO-d_6) δ 1.82 (m, 1H, SH), 2.60 (m, 2H, CH_2S), 3.22 (s, 3H, OCH_3), 3.40−3.60 (m, 178H, CH_2O); ^{13}C NMR (DMSO-d_6) δ 58.0 (OCH_3), 69.7 (CH_2O) (the CH_2CH_2S resonances could not be detected).

Synthesis of (co)Telomers. *General Procedure for the (Co)telomerization Reactions.* An acetonitrile solution of telogen **PEG2000-SH**, or ^{i}Bu-SH, and taxogen **A**, or **B**, or a mixture of **A** and **C**, or **A** and **D**, at a fixed taxogen/telogen molar ratio, was heated to 50 °C before AIBN was added (0.4 equiv with respect to telogen). The reaction medium was stirred under reflux until the telogen had disappeared (followed by TLC/DTNB) (∼24 h). The solution was concentrated and purified by gel permeation chromatography on a Sephadex LH 20 or LH-60 column (Fluka) with $CHCl_3$ as the eluent. The aDP*n* (=*n*) values were determined by ^{1}H NMR on each collected fraction.

General Procedure for the TFA Deprotection of the BOC-(Co)telomers. The deprotection of telomers **^{i}Bu-[NHBOC]$_n$** and **PEG2000-[NHBOC]$_n$** and cotelomers **^{i}Bu-[TEG]$_m$-[NHBOC]$_n$** and **^{i}Bu-[THM]$_m$-[NHBOC]$_n$** was quantitatively achieved by dissolving and keeping these (co)telomers in a large excess of TFA at room temperature for 2 h. The excess of TFA was removed by evaporation in the presence of CH_2Cl_2 and cyclohexane and by gel permeation on a Sephadex LH-20 or LH-60 column. The respective telomers **^{i}Bu-[NH]$_n$** and **PEG2000-[NH]$_n$** and cotelomers **^{i}Bu-[THM]$_m$-[NH]$_n$**, as their TFA salts, were obtained in the form of white solids, except **^{i}Bu-[TEG]$_m$-[NH]$_n$** which was obtained in the form of resin. The presence of the TFA anions is confirmed by ^{19}F NMR (δ −75.7 in CD_3OD).

Synthesis of Telomers ^{i}Bu-[NH]$_n$. The telomerization protocol applied to (i) 10 mg (46 μmol) or (ii) 1.3 mg (5.8 μmol) of telogen **^{i}Bu-SH** and (i) 197 mg (0.92 mmol) or (ii) 250 mg (1.2 mmol) of taxogen **A** [taxogen/telogen molar ratio of (i) 20 or (ii) 200, respectively] led after gel permeation chromatography to (i) 150 mg of telomers **^{i}Bu-[NHBOC]$_{12}$** or (ii) 276 mg of telomers **^{i}Bu-[NHBOC]$_{75}$**, respectively. The aDP*n* (=*n*) values were determined by ^{1}H NMR: aDP$n = 12H_x/9H_z$ or $12H_y/4H_z$, H_x and H_z being the integration of the signals corresponding to the CH_3 protons of BOC and diisobutyl, respectively, and H_y being the integration of the signal corresponding to the NCH_2 protons. Telomers **^{i}Bu-[NH]$_{12}$** and **^{i}Bu-[NH]$_{75}$** were obtained quantitatively after BOC deprotection of their respective **^{i}Bu-[NHBOC]$_n$** telomers.

***^{i}Bu-[NHBOC]$_{12}$*:** TLC (9/1 CH_2Cl_2/MeOH, UV, ninhydrin) $R_f = 0.56$; ^{1}H NMR ($CDCl_3$) δ 0.80−0.90 (m, 12H, C*H*$_3$CH), 1.00−2.50 [m, (12*n* + 1)H, CH_3 (BOC), C*H*$_2$C*H*, CH_2CO, C*H*CH_3], 2.50−3.50 [m, (4*n* + 10)H, C*H*$_2$C*H*$_2$N, C*H*$_2$SC*H*$_2$, CH_2CO, CH_2N], 5.50−6.50 (m, nH, NHCOO), 6.90−7.90 (m, nH, NHCO), with $n = 12$; ^{13}C NMR ($CDCl_3$) δ 20.1 and 20.2 (*C*H$_3$CH), 26.7 and 27.9 (CHN), 28.5−30.5 (sl, CH_3, BOC, CH*C*H$_2$), 33.8 (CH_2S), 34.9 (*C*H$_2$CO), 40.2−40.4 (m, CH_2CH and *C*H$_2$*C*H$_2$), 53.3 and 55.3 (CH_2N), 79.2−79.4 [*C*(CH$_3$)$_3$], 156.6 (CO, BOC), 177.0 (NHCO) (the NCO resonance could not be detected).

***^{i}Bu-[NH]$_{12}$*:** ^{1}H NMR (CD_3OD) δ 0.85−0.95 (m, 12H, C*H*$_3$CH), 1.00−2.80 [m, (3*n* + 7)H, C*H*$_2$C*H*, C*H*$_2$SC*H*$_2$, C*H*CH$_3$, CH_2CO], 2.80−4.00 [m, (4*n* + 4)H, C*H*$_2$C*H*$_2$N, CH_2N], 6.50−7.40 (m, nH, NHCO) with $n = 12$; ^{13}C NMR (CD_3OD) δ 20.2 and 20.3 (*C*H$_3$CH), 27.7 and 29.1 (CHN), 28.0−30.0 (m, *C*H$_2$CH), 33.8 (CH_2S), 34.9 (CH_2CO), 38.2−

39.0 (m, CH_2NH_3), 40.3−40.5 (m, $NHCH_2$), 43.2−44.5 (m, CH_2CH), 54.7 and 56.8 (CH_2N) (the CO resonances could not be detected).

***^{i}Bu-[NHBOC]$_{75}$*:** TLC (9/1 CH_2Cl_2/MeOH, UV, ninhydrin) R_f = 0.43. The ^{1}H NMR ($CDCl_3$) and ^{13}C NMR ($CDCl_3$) spectra are identical to those of **^{i}Bu-[NHBOC]$_{12}$** but with n = 75.

***^{i}Bu-[NH]$_{75}$*.** The ^{1}H NMR (CD_3OD) and ^{13}C NMR (CD_3OD) spectra are identical to those of **^{i}Bu-[NH]$_{12}$** but with n = 75.

Synthesis of Diblock Telomers PEG2000-[NH]$_n$. The telomerization protocol applied to telogen **PEG2000-SH** [(i) 30 mg or 0.015 mmol, (ii) 30 mg or 0.015 mmol, (iii) 10 mg or 0.005 mmol, and (iv) 10 mg or 0.005 mmol] and taxogen **A** [(i) 160 mg or 0.75 mmol, (ii) 126 mg or 0.6 mmol, (iii) 106 mg or 0.05 mmol, and (iv) 212 mg or 0.09 mmol] at taxogen/telogen molar ratios of (i) 50, (ii) 40, (iii) 100, and (iv) 200 led, after gel permeation chromatography, to telomer (i) **PEG2000-[NHBOC]$_{70}$** (16 mg), (ii) **PEG2000-[NHBOC]$_{125}$** (150 mg), (iii) **PEG2000-[NHBOC]$_{190}$** (87 mg), and (iv) **PEG2000-[NHBOC]$_{260}$** (174 mg), respectively. The aDPn (=n) values were determined by ^{1}H NMR: aDPn = 178H_x/9H_z or 178H_y/4H_z, H_x, H_y, and H_z being the integration of the signals corresponding to the BOC methyl, NCH_2, and OCH_2 groups, respectively. The diblock **PEG2000-[NH]$_n$** telomers were obtained quantitatively after BOC deprotection of their respective **PEG2000-[NHBOC]$_n$** telomers.

PEG2000-[NHBOC]$_{70}$: TLC (7/3/0.4 $CHCl_3$/MeOH/NH_3, UV, ninhydrin) R_f = 0.50; ^{1}H NMR ($CDCl_3$) δ 1.05−2.50 [m, (12n − 1)H, CH_3 (BOC), C*H*CH_2CH, CH_2CO], 2.50−3.50 [m, (4n + 7)H, CH_2CH_2NHBOC, CH_2SCH_2, OCH_3], 3.55−3.65 (m, 178H, CH_2O), 5.40−6.30 (m, nH, NHCOO), 6.80−7.80 (m, nH, NHCO) with n = 70; ^{13}C NMR ($CDCl_3$) δ 27−30 (CH*C*H$_2$CH), 28.6 (CH_3, BOC), 38.0−45.0 (m, NCH_2, CH_2CH), 58.4 (OCH_3), 70.6 (CH_2O), 77.5−81.0 (m, *C*CH$_3$), 155.0−157.0 (m, CO, BOC) (the CH_2S and CONH resonances could not be detected).

***PEG2000-[NHBOC]$_n$** with n = 125, 190, or 260*: TLC (7/3/0.4 $CHCl_3$/MeOH/NH_3, UV, ninhydrin) R_f = 0.83 for n = 125; TLC (85/15 CH_2Cl_2/MeOH, UV, ninhydrin) R_f = 0.4 and 0.63 for n = 190 and 260, respectively. The ^{1}H and ^{13}C NMR ($CDCl_3$) spectra are identical to those of telomer **PEG2000-[NHBOC]$_{70}$** but with n = 125, 190, or 260.

PEG2000-[NH]$_{70}$: ^{1}H NMR (CD_3OD) δ 1.05−3.05 [m, (3n + 3)H, CH_2SCH_2, CH_2C*H*, CH_2CO], 3.05−3.60 [m, (4n + 3)H, CH_2NH$_3$, OCH_3], 3.60−3.70 (m, 178H, CH_2O), 6.80−7.80 (m, nH, N*H*CO) with n = 70; ^{13}C NMR (CD_3OD) δ 26.6−28.2 (m, *C*H$_2$CH), 38.2−39.2 (m, CH_2NH_3), 40.5−40.9 (m, $NHCH_2$), 43.5−44.1 (m, CH_2CH), 59.3 (OCH_3), 71.5 (CH_2O), 178.2−178.6 (m, NHCO) (the CH_2S resonances could not be detected).

***PEG2000-[NH]$_n$** with n = 125, 190, or 260*. The ^{1}H NMR (CD_3OD) and ^{13}C NMR (CD_3OD) spectra are identical to those of **PEG2000-[NH]$_{70}$** but with n = 125, 190, or 260.

Synthesis of Diblock Telomers PEG2000-[CH$_2$-NMe$_2$]$_n$. The telomerization protocol applied to telogen **PEG2000-SH** [(i) 30 mg or 15 μmol and (ii) 50 mg or 25 μmol] and taxogen **B** [(i) 92 mg or 0.6 mmol and (ii) 190 mg or 1.23 mmol] at a taxogen/telogen molar ratio of (i) 40 or (ii) 50 led, after gel permeation chromatography, to diblock telomers (i) **PEG2000-[CH$_2$NMe$_2$]$_4$** (19 mg) and **PEG2000-[CH$_2$NMe$_2$]$_{35}$** (134 mg) and (ii) **PEG2000-[CH$_2$NMe$_2$]$_{360}$** (50 mg), respectively. The aDPn values (=n) were determined by ^{1}H NMR: aDPn = 178H_w/2H_z, 178H_x/2H_z, or 178H_y/8H_z, with H_w, H_x, and H_z being the integration of the signals corresponding to CONHCH$_2$, CH_2NMe_2, and CH_2O methylenes, respectively, and H_y being the integration of the signal corresponding to the CONHCH$_2$CH_2 methylenes and NMe_2 groups.

***PEG2000-[CH$_2$NMe$_2$]$_n$** with n = 4, 35, or 360*: ^{1}H NMR (D_2O) δ 1.05−2.80 [m, (13n + 3)H, $CH_2CH_2CH_2N$, CH_2C*H*, N(CH_3)$_2$, CH_2CO, CH_2SCH_2], 2.80−3.50 [m, (2n + 3)H, CH_3O, NHCH_2], 3.63 (s, 178H, CH_2O), 7.20−8.10 (m, nH, NHCO) with n = 4, 35, or 360; ^{13}C NMR ($CDCl_3$) δ 24.7−24.9 (m, $CH_2CH_2CH_2N$), 40.4−40.5 (m, CH*C*H$_2$), 41.7−41.8 (m, $NHCH_2$), 43.3−43.6 (m, NCH_3, CH_2CH), 55.6−55.8 (m, CH_2N), 69.9 (CH_2O) (the CH_2S, OCH_3, and NHCO resonances could not be detected).

Synthesis of Random Cotelomers ^{i}Bu-[TEG]$_m$-[NH]$_n$. *^{i}Bu-[TEG]$_m$-[NHBOC]$_n$ with m = 12 and n = 20*. The telomerization protocol applied to 20 mg (0.09 mmol) of telogen **^{i}Bu-SH** and a mixture of 241 mg (0.9 mmol) of taxogen **A** and 197 mg (0.9 mmol) **of** taxogen **C** led, after gel permeation chromatography, to 214 mg of random cotelomer **^{i}Bu-[TEG]$_{12}$-[NHBOC]$_{20}$**. The aDP-m,n values of TEG and NHBOC units were determined by ^{1}H NMR. The average number of NHBOC units (n) is equal to 12H_x/9H_z or to 12H_y/4H_z, H_x, H_y, and H_z being the integration of the signals corresponding to the BOC, NCH_2, and CH_3 (diisobutyl group) protons, respectively. The average number of TEG units (n) is equal to 12H_x'/14H_z, H_x' being the integration of the signal corresponding to the OCH_2 group.

^{i}Bu-[TEG]$_{12}$-[NHBOC]$_{20}$: TLC (9/1 CH_2Cl_2/MeOH, UV, ninhydrin) R_f = 0.54; ^{1}H NMR ($CDCl_3$) δ 0.85−0.90 (m, 12H, CH_3CH), 1.00−2.90 [m, (12n + 3m + 7)H, CH_3 (BOC), CH_2C*H*, CH_2SCH_2, CH_3C*H*, CH_2CO], 2.90−4.00 [m, (3n + 19m + 4)H, CH_2N, OCH_3, OCH_2], 5.50−6.20 (m, nH, NHCOO), 6.40−7.30 (m, nH, NHCO) with m = 12 and n = 20; ^{13}C NMR ($CDCl_3$) δ 28.6−29.5 [m, CH_3 (BOC), *C*H$_2$CH], 40.2−40.5 (m, NCH_2CH_2, CH_2CH), 59.1 (CH_3O), 68.5−68.8 (CH_2OCO), 70.1−70.6 [m, $(CH_2O)_4$, $COOCH_2CH_2$], 71.8−72.1 (CH_2OCH_3), 75.6−79.1 [*C*(CH$_3$)$_3$], 156.5−156.7 (m, NHCOO), 173.2 (COO), 175.5−175.8 (NHCO) (the $CHCH_3$, CH_2N, CH_2CO, CH_2S, and CO resonances could not be detected).

***^{i}Bu-[TEG]$_m$-[NHBOC]$_n$** with m = 7 and n = 25*. The telomerization protocol applied to 10.2 mg (47 μmol) of telogen **^{i}Bu-SH** and a mixture of 300 mg (1.4 mmol) of taxogen **A** and 123 mg (0.47 mmol) of taxogen **C** led, after gel permeation chromatography, to 256 mg of random cotelomer **^{i}Bu-[TEG]$_m$-[NHBOC]$_n$** with m = 7 and n = 25. The aDPm,n values of TEG and NHBOC units were determined as described for **^{i}Bu-[TEG]$_{12}$-[NHBOC]$_{20}$**.

^{i}Bu-[TEG]$_7$-[NHBOC]$_{25}$: TLC (85/15 CH_2Cl_2/MeOH, UV, ninhydrin) R_f = 0.6. The ^{1}H NMR ($CDCl_3$) and ^{13}C NMR ($CDCl_3$) spectra are identical to those of cotelomer **^{i}Bu-[TEG]$_{12}$-[NHBOC]$_{20}$** but with m = 7 and n = 25.

***^{i}Bu-[TEG]$_m$-[NH]$_n$** with m = 12 and n = 20, and m = 7 and n = 25*. Cotelomers **^{i}Bu-[TEG]$_m$-[NH]$_n$** were obtained quantitatively after BOC deprotection of their respective cotelomers **^{i}Bu-[TEG]$_m$-[NHBOC]$_n$**.

^{i}Bu-[TEG]$_{12}$-[NH]$_{20}$: ^{1}H NMR (CD_3OD) δ 0.85−0.90 (m, 12H, CH_3CH), 1.00−2.80 [m, (3n + 3m + 7)H, CH_2C*H*, CH_2SCH_2, CH_2CO, CH_3C*H*], 2.80−4.00 [m, (4n + 17m + 4)H, CH_2N, OCH_2, OCH_3], 4.00−4.50 (m, 2nH, CH_2OCO), 6.40−7.30 (m, nH, NHCO) with m = 12 and n = 20; ^{13}C NMR (CD_3OD) δ 38.1−38.4 (m, CH_2NH_3), 40.6−40.8 (m, CH_2NH), 43.1−43.7 (m, CH_2CH), 59.1 (CH_3O), 70.0−70.2 (m, $COOCH_2$), 70.4−70.7 [m, $(CH_2O)_4$, $COOCH_2CH_2$], 71.1−71.4 (CH_2OCH_3), 177.3−177.5 (NHCO) (the CH_2S, CH_2N, CH_2CO, $CHCH_3$, and CO resonances could not be detected).

^{i}Bu-[TEG]$_7$-[NH]$_{25}$. The ^{1}H NMR (CD_3OD) and ^{13}C NMR (CD_3OD) spectra are identical to those of cotelomer **^{i}Bu-[TEG]$_{12}$-[NH]$_{20}$** but with $m = 7$ and $n = 25$.

Synthesis of Random Cotelomers ^{i}Bu-[THM]$_m$-[NH]$_n$. Telogen **^{i}Bu-SH** (20 mg, 0.09 mmol), taxogen **A** (236 mg, 1 mmol), and taxogen **D** (192 mg, 1 mmol) led after gel permeation chromatography to random cotelomers **^{i}Bu-[THM]$_{50}$-[NHBOC]$_{50}$** (224 mg) and **^{i}Bu-[THM]$_{30}$-[NHBOC]$_{100}$** (69 mg). The aDPn ($=n$) corresponding to the number of NHBOC units, determined by ^{1}H NMR, is equal to $12H_x/9H_z$ or to $12H_y/4H_z$, H_x, H_y, and H_z being the integration of the signals corresponding to the BOC methyl, NCH_2, and isobutyl methyl groups, respectively. The aDPm ($=m$) corresponding to the number of THM functions, determined by ^{1}H NMR, is equal to $12H_x'/6H_z$, H_x' being the integration of the signal corresponding to the $HOCH_2$ methylenes. Cotelomers **^{i}Bu-[THM]$_{50}$-[NH]$_{50}$** and **^{i}Bu-[THM]$_{30}$-[NHB]$_{100}$** were obtained quantitatively after BOC deprotection of cotelomers **^{i}Bu-[THM]$_{50}$-[NHBOC]$_{50}$** and **^{i}Bu-[THM]$_{30}$-[NHBOC]$_{100}$**, respectively.

^{i}Bu-[THM]$_{50}$-[NHBOC]$_{50}$: TLC (9/1 CH_2Cl_2/MeOH, UV, ninhydrin) $R_f = 0.25$; ^{1}H NMR ($CDCl_3$) δ 0.85−0.90 (m, 12H, C*H*$_3$CH), 1.00−2.80 [m, (12n + 3m + 7)H, CH_3 (BOC), C*H*$_2$C*H*, NCH, C*H*$_2$SC*H*$_2$, CH_2CO], 2.90−3.50 [m, (4n + 4)H, $NHCH_2$, CH_2N], 3.50−4.00 (m, 6mH, C*H*$_2$OH), 6.50−7.20 (m, nH, NHCOO), 7.80−8.20 (m, nH, NHCO) with $m = 50$ and $n = 50$; ^{13}C NMR ($CDCl_3$) δ 28.4−28.9 [m, CH_3 (BOC), *C*H$_2$CH], 40.1−40.8 (m, NCH_2, *C*HCH$_2$), 59.2−59.8 (m, CH_2OH) (the CH_2S, CH_2CO, NCH_2, CH_3-CH, NHCO, and CO resonances could not be detected).

^{i}Bu-[THM]$_{30}$-[NHBOC]$_{100}$: TLC (8/2 $CHCl_3$/MeOH, UV, ninhydrin) $R_f = 0.4$. The ^{1}H and ^{13}C NMR spectra are identical to those of **^{i}Bu-[THM]$_{50}$-[NHBOC]$_{50}$** but with $m = 30$ and $n = 100$.

^{i}Bu-[THM]$_{50}$-[NH]$_{50}$: ^{1}H NMR (CD_3OD) δ 0.85−0.90 (m, 12H, C*H*$_3$CH), 1.00−2.80 {m, [3(n + m) + 7], C*H*$_2$C*H*, CH, C*H*$_2$SC*H*$_2$, CH_2CO}, 2.90−4.00 [m, (4n + 6m + 4)H, NHC*H*$_2$, C*H*$_2$OH, CH_2N], 7.50−8.10 (m, nH, NHCO) with $m = 50$ and $n = 50$; ^{13}C NMR (CD_3OD) δ 38.0−38.5 (m, $CH_2NH_3^+$), 40.3−40.6 (m, NCH_2), 42.9−43.5 (m, CH_2CH), 59.6 (CH_2OH) (the CH_2S, CH_2CO, NCH_2, CH_3CH, NHCO, and CO resonances could not be detected).

^{i}Bu-[THM]$_{30}$-[NH]$_{100}$. The ^{1}H and ^{13}C NMR spectra are identical to those of **^{i}Bu-[THM]$_{50}$-[NH]$_{50}$** but with $m = 30$ and $n = 100$.

Preparation of Complexes Composed of the Polyamine Telomer Compounds and Plasmid pTG11236. The plasmid pTG11236 was produced by Transgène SA. The endotoxin content of the plasmid preparation was checked using a Limulus Amebocyte Lysat kit (Biogenic, Maurin, France). This value was <1 endotoxin unit/mg of plasmid, hence below the 5 eu/mg of DNA recommended for in vivo protocols. The quantities of compound used were calculated according to the desired DNA concentration of 0.1 mg/mL, the *N*/*P* ratio, the molar weight, and the number of potential positive charges in the selected (co)telomer. The polyamine (co)telomer−DNA complex is formulated by adding a desired volume of (co)telomer preparation at a concentration of 10 mg/mL (in 5% glucose) to the desired volume of a DNA solution to reach the desired DNA concentration (for example, 0.1 mg/mL), as described in refs *8*, *24*, and *25*. This preparation was vortexed for 10 s and was used within 24 h for the particle size measurements and the in vitro transfection experiments.

Measurement of the Size of the (Co)teloplexes. The average sizes were measured by photon correlation spectroscopy using a Coulter N4Plus particle size analyzer. The analyses were performed at 25 °C, after equilibrating the sample at 25 °C for 20 min. The sample was diluted with 5% glucose in the measurement tube and homogenized. These analyses were carried out on complexes having a DNA concentration of 10 μg/mL. The formulations and analyses were reproduced twice.

Agarose Gel Electrophoresis. Each sample (0.5 μg of plasmid) was analyzed by electrophoresis for ∼30 min under 75 V/cm, through a 0.8% agarose gel in 1× TAE (Tris-acetate-EDTA) buffer. The DNA was visualized in 400 mL of TAE buffer containing 40 μL of ethidium bromide (10 mg/mL, Sigma, Saint Quentin Fallavier, France). The plasmid integrity in each sample (0.25 μg) was confirmed by electrophoresis after decomplexing the lipoplexes (10 μL of a plasmid, 0.05 mg/mL) with sodium dodecyl sulfate (10 μL, 80 g/L).

In Vitro Transfection of A549 Cells. Twenty-four hours before transfection, A549 cells (epithelial cells derived from human pulmonary carcinoma) were grown in Dulbecco's modified Eagle's medium (DMEM) (Invitrogen, Life Technologies, Cergy Pontoise, France), containing 1% glutamine (200 mM, Sigma), 0.4% gentamicine (10 μg/mL, Sigma), and 10% fetal calf serum (Sigma), in 96-well plates (2×10^4 cells per well), in a wet (37 °C) and 5% CO_2/95% air atmosphere. The volume of the DNA−polyamine telomer complex (10 μL of DNA and 5 μL of telomer, respectively) was diluted to 100 μL in DMEM supplemented with 10% FCS to obtain various amounts of DNA (1 and 0.5 μg per well, respectively) in the preparation. The culture medium was removed and replaced with 100 μL of DMEM supplemented with 10% FCS and containing the desired amount of DNA. After 4 and 24 h, 50 and 100 μL of DMEM supplemented with 30 and 10% FCS, respectively, were added, respectively.

Forty-eight hours after transfection, the culture medium was discarded and the cells were washed with 100 μL of PBS and then lysed with 50 μL of lysis buffer (Promega, Charbonnières, France). The lysates were frozen at −32 °C, awaiting analysis of luciferase activity. This measurement was taken for 10 s on 10 μL of the lysis mixture in a Berthold LB96P luminometer in dynamic mode, using the "Luciferase" determination system (Promega) in 96-well plates. The total protein concentration per well was determined using conventional techniques (BCA test, Pierce, Montluçon, France). For cells grown in the absence of DNA complexes, a well contains ∼30−50 μg of proteins. Each (co)telomer−DNA complex was formulated twice, and each formulation was tested in triplicate.

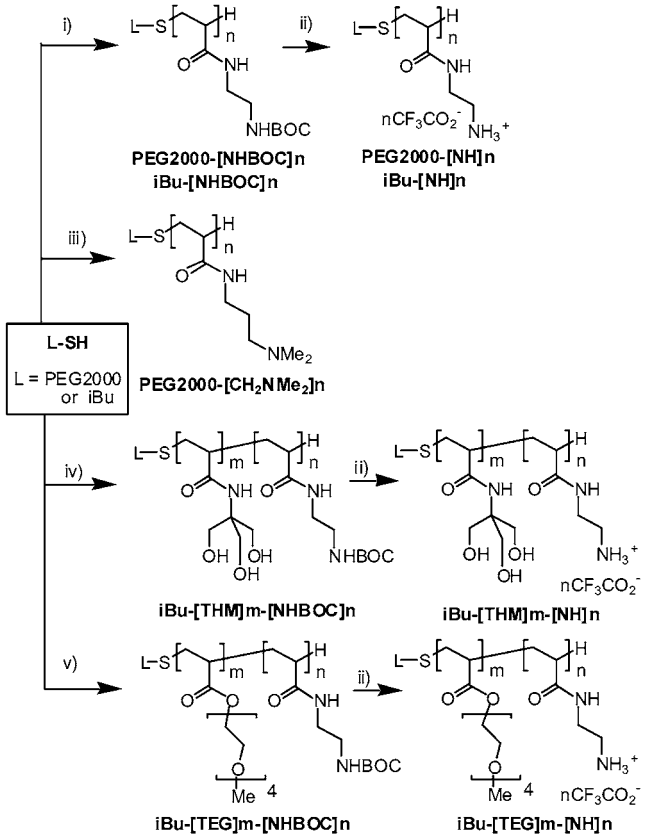
Statistical Analyses. Statistical tests were performed with STATGRAPHICS Plus5.0 software. Analysis of variance (Anova) was run on the logarithmic transformation of luciferase expression levels [log(femtograms of luciferase per milligram of protein)] to fit normal distributions of the data.

Three factors, i.e., the chemical nature of the product, the amount of DNA per well (0.5 and 1 μg/well), and the *N*/*P* ratio (10, 5, and 2.5), were analyzed as sources of the variation of the logarithmic transformation of the transfection levels, using a multiple-comparison procedure. Tukey's honestly significant difference (HSD) method was used to discriminate among the means of the logarithmic transformation of luciferase expression levels.

RESULTS AND DISCUSSION

Telogen and Taxogen Synthesis. Telomerization and cotelomerization reactions were performed with telogen **PEG2000-SH** or **^{i}Bu-SH** (the syntheses of which are outlined in Scheme 1).

Scheme 2. Synthesis of ^{i}Bu-[NH]$_n$ Telomers, PEG2000-[NH]$_n$ and PEG2000-[CH$_2$NMe$_2$]$_n$ Diblock Telomers, and of ^{i}Bu-[THM]$_m$-[NH]$_n$ and ^{i}Bu-[TEG]$_m$-[NH]$_n$ Random Cotelomers[a]



[a] Reagents and conditions: (i) CH_2=CHC(O)NH$(CH_2)_2$NHBOC (**A**), AIBN, Δ in CH_3CN; (ii) TFA; (iii) CH_2=CHC(O)NH$(CH_2)_3$-NMe_2 (**B**), AIBN, Δ in CH_3CN; (iv) **A**, CH_2=CHC(O)NH-[$C(CH_2OH)_3$] (**D**), AIBN, Δ in CH_3CN with a 1/1 **A**/**D** molar ratio; (v) **A**, CH_2=CHC(O)O[$(CH_2CH_2O)_4$]Me (**C**), AIBN, Δ in CH_3CN with a 1/1 **A**/**C** molar ratio for $m = 12$ and $n = 20$ or with a 3/1 **A**/**C** molar ratio for $m = 7$ and $n = 25$.

Thiol **PEG2000-SH** was obtained in two steps from commercially available **PEG2000-OH.** The free hydroxyl was first replaced with a tosyl group by the action of tosyl chloride (85%). The resulting tosylate was then converted into the corresponding thiol using an anion-exchange resin (SH^- form) (78%). Thiol **^{i}Bu-SH** was obtained in two steps by coupling 3,3′-dithiodipropionic acid with diisobutylamine using HOBt and EDC as coupling reagents, followed by reduction of the disulfide bond with Zn and AcOH (75% overall yields).

The synthesis of taxogen **C** was performed from acryloyl chloride and tetraethylene glycol monomethyl ether, using the procedure described for that of the NHBOC-containing taxogen **A** (*24*). The NMe_2- and THM-containing taxogens **B** and **D** are commercially available.

Telomer and Cotelomer Synthesis. All (co)telomerization reactions (Scheme 2) were performed under nitrogen by refluxing in acetonitrile and (i) taxogen **A** or **B**, or a mixture of taxogens **A** and **C**, or **A** and **D**, (ii) the thiols **PEG2000-SH**, or **^{i}Bu-SH** in a fixed taxogen/telogen concentration ratio, and (iii) AIBN. At the end of the reaction, the solvent was evaporated under reduced pressure. The random cotelomers were purified and fractionated by gel permeation chromatography on a Sephadex LH20 or LH60 column. This allows separation of the (co)telomers from AIBN and residual disulfide which has formed during telomerization. The diblock PEG2000-grafted BOC-protected telomers were purified after BOC deprotection. The *N*-BOC-telomers and cotelomers obtained from taxogen **A** were deprotected in excess TFA at room temperature. The (poly)cationic telomers and random cotelomers thus obtained were isolated as TFA salts by evaporation of excess reagent in the presence of cyclohexane followed by lyophilization. The diblock PEG-grafted telomers were further purified from residual PEG disulfide by washing with CH_2Cl_2 in which they are not soluble. Quantitative deprotection was confirmed by ^{1}H NMR (the absence of the signal corresponding to the BOC protons). For each telogen and taxogen(s), the different (co)telomers that were isolated and their code names are reported in Table 1. Oxygen- and peroxide-free solvents were used throughout these experimental procedures to avoid oxidation of sulfur into sulfoxide in the (co)telomers (*24*, *25*).

Table 1. Mean Sizes, Determined by Light Scattering Spectroscopy, of the (Co)teloplexes Formed by the Dilution Method Applied to Plasmid pTG11236 and the ^{i}Bu-[NH]$_{75}$, PEG2000-[NH]$_n$, PEG2000-[CH$_2$NMe$_2$]$_n$, ^{i}Bu-[TEG]$_{12}$-[NH]$_{20}$, or ^{i}Bu-[THM]$_m$-[NH]$_n$ (Co)telomers

	(co)teloplexes	
(co)telomer	*N*/*P* ratio[a]	mean diameter (nm) (SD)
^{i}Bu-[NH]$_{75}$	10	75 (30)
	5	115 (55)
	2.5	135 (55)
	1.25	p[b]
	0.8	135 (50)
PEG2000-[NH]$_{125}$	10	120 (40)
	5	130 (45)
	2.5	180 (70)
	1.25	p[b]
	0.8	200 (70)
PEG2000-[NH]$_{190}$	10	120 (45)
	5	120 (35)
	2.5	170 (60)
	1.25	p[b]
	0.8	195[c]
PEG2000-[NH]$_{260}$	10	140 (50)
	5	120 (45)
	2.5	180 (60)
	1.25	175[c]
	0.8	175[c]
PEG2000-[CH$_2$NMe$_2$]$_4$	10	120 (40)
	5	100 (30)
	2.5	125 (35)
	1.25	260 (70)
	0.8	145 (50)
PEG2000-[CH$_2$NMe$_2$]$_{35}$	10	135 (50)
	5	140 (50)
	2.5	220 (70)
	1.25	155 (45)
	0.8	150 (50)
^{i}Bu-[TEG]$_{12}$-[NH]$_{20}$	10	125 (40)
	5	105 (40)
	2.5	155 (55)
	1.25	330[c]
	0.8	295[c]
^{i}Bu-[THM]$_{50}$-[NH]$_{50}$	10	100 (35)
	5	140 (50)
	2.5	140 (50)
	1.25	p[b]
	0.8	165 (60)
^{i}Bu-[THM]$_{30}$-[NH]$_{100}$	10	85 (25)
	5	100 (35)
	2.5	260 (70)
	1.25	p[b]
	0.8	175 (60)

[a] *N* equals the number of (co)telomer amine equivalents; *P* equals the number of plasmid phosphate equivalents. [b] Precipitate. [c] Large.

The average degrees of polymerization, aDP*n* (=*n*), of the PEG-grafted diblock telomers resulting from taxogen **A** or **B** were determined by ^{1}H NMR on the protected **PEG2000-[NHBOC]$_n$** or **PEG2000-[CH$_2$NMe$_2$]$_n$** telomers, respectively. These aDP*n* values were calculated by comparing the integration of the BOC and NCH_2 or NMe signals, respectively, with that of the PEG2000 OCH_2 protons. For the telomers resulting from taxogen **A** and telogen **^{i}Bu-SH** and for all random cotelomers resulting from a mixture of taxogens **A** and **C**, or **A** and **D**, the average degrees of (co)polymerization corresponding to the number of NHBOC, TEG, and THM units were also determined by ^{1}H NMR on the BOC-protected (co)telomers. The number of NHBOC units was calculated by comparing the integration of the NCH_2CH_2NHBOC signals with that of the isobutyl methyl protons. The number of TEG and THM units was calculated by comparing the integration of the TEG (OCH_2 and OCH_3) or THM ($C\underline{H}_2OH$) signals with that of the isobutyl methyl and $NCH_2\underline{C}H_2NHBOC$ resonances.

Formation and Characterization of the DNA Complexes. The capability of the polycationic (co)telomers to condense DNA and to form (co)teloplexes was analyzed with plasmid pTG11236, which was also used for the in vitro transfection assays described in the next section. The sizes of the DNA complexes [size being an important parameter to control when in vivo uses are contemplated or when their in vitro transfection efficiency is evaluated (*28*)] were analyzed by light scattering spectroscopy. The preparation of the (co)teloplexes was performed by mixing a (co)telomer solution with the plasmid in 5% glucose using *N*/*P* ratios of 10, 5, 2.5, 1.25, and 0.8 [*N* equals the number of amine functions of the (co)telomer; *P* equals the number of DNA phosphates]. Table 1 collects the mean particle diameters measured for the different (co)teloplexes. These measurements were performed after 24−48 h of aging at 25 °C.

These formulations were also analyzed by gel electrophoresis which showed the presence of a fully complexed plasmid (not accessible to ethidium bromide) for all *N*/*P* = 10−2.5 formulations and for most *N*/*P* = 1.25 ones. DNA that is complexed, but accessible to ethidium bromide, was however detected for the **PEG2000-[NH]$_{260}$** and **^{i}Bu-[THM]$_{30}$-[NH]$_{100}$** *N*/*P* = 1.25 formulations, and for all the *N*/*P* = 0.8 formulations that were investigated (data not shown). When gel electrophoresis of the (co)teloplexes was performed in the presence of detergent (sodium dodecyl sulfate), dissociation of the complexes was observed in all cases.

In terms of telomer impact on teloplex size and stability (with respect to aggregation), the behavior of the diblock PEG-grafted and random TEG or THM (co)telomers is worth noting. Indeed, these polycationic derivatives led often to stable formulations with a polydispersed population of small-sized teloplexes (85−330 nm), even for *N*/*P* ratios of 1.25 and 0.8, while precipitates were most frequently detected for complexes with *N*/*P* ratios close to 1 (*24*, *25*, *29*).

In Vitro Transfection. The transfection potency of the (co)teloplexes formulated with the luciferase reporter plasmid pTG11236 was assayed in vitro on lung epithelial A549 cells. Although transfection efficiencies with DNA complexes are generally impaired by the presence of serum components, these experiments were nevertheless run in a culture medium containing 10% fetal calf serum. The transfection efficiency of the (co)teloplexes (expressed in femtograms of luciferase per milligram of protein) was evaluated for a DNA dose of 0.5 and 1 μg per well, as compared to naked DNA and to control lipoplexes based on a pcTG90−DOPE *N*/*P* = 5 complex (1/1 molar ratio). These lipoplexes proved to be among the most efficient nonviral formulations for transfecting A549 cells (*8*, *24*). Cells treated with naked DNA under equivalent conditions exhibited expression levels of $\sim 10^2-10^3$ fg of luciferase/mg of protein. The effect on cell viability of the (co)teloplexes was also checked by determining the total amount of protein per well of the transfected cells relative to that measured for untreated cells (for which the total protein amount per well is in a 30−50 μg/well range).

The transfection and cell viability results are illustrated in Figure 2. These data indicate that the (co)teloplexes formulated with telomer **^{i}Bu-[NH]$_{75}$**, diblock **PEG2000-[NH]$_n$** (*n* = 70, 125, 190, or 260), random **^{i}Bu-[THM]$_m$-[NH]$_n$** (*m* = *n* = 50, or *m* = 30 and *n* = 100), and **^{i}Bu-[TEG]$_7$-[NH]$_{25}$** cotelomers do allow transfection of the plasmid into the A549 cells with a much higher efficiency than with naked DNA; luciferase expression levels in the 10^5-10^8 fg of luciferase/mg of protein range were indeed measured for most of these formulations and for *N*/*P* ratios of 5. In contrast, for *N*/*P* ratios of 0.8 and 1.25 (data not shown) and for the NMe_2 diblock **PEG2000-[CH$_2$NMe$_2$]$_n$** and random **^{i}Bu-[TEG]$_{12}$-[NH]$_{20}$** teloplexes, whatever the value of their *N*/*P* ratios, much lower transgene expression levels (10^3-10^4 fg of luciferase/mg of protein) were detected.

As most frequently observed for lipoplexes and polyplexes, the level of luciferase expression of the (co)teloplexes increased when the DNA dose was increased from 0.5 to 1 μg/well and when their *N*/*P* ratios were progressively increased from 0.8−1.25 to 10 (statistical analysis data not shown). These results are likely related to an increase in their level of binding, through electrostatic interactions, to the anionic proteoglycans expressed at the cellular surface and, consequently, of their cellular uptake by endocytosis (*30*−*32*). Concomitantly, a small decrease in their cell tolerance (Figure 2) was seen. It remained, however, very high even for a DNA dose of 1 μg/well for which 80% of the 39 formulations that were investigated displayed a percentage of cell viability within a range of 80−120%. It is therefore noticeable that high transfection levels were attained that were further compatible with high levels of cell survival.

When compared with the control pcTG90−DOPE lipids which display a high transfection efficiency (10^7-10^9 fg of luciferase/mg of protein), none of the new polycationic (co)telomers was found to be as efficient in mediating DNA transfer and expression. This is illustrated in Figure 3 which compares, irrespective of the *N*/*P* ratio and of the amount of DNA per well, the means of luciferase expression obtained with the control pcTG90−DOPE lipoplexes and with the (co)teloplexes. A more detailed analysis (Figure 4) shows that, for *N*/*P* ratios of 2.5 and 5, significantly higher luciferase levels (1−2 orders of magnitude) were obtained with the pcTG90−DOPE lipoplexes than with the most efficient **^{i}Bu-[NH]$_{75}$** or **PEG2000-[NH]$_{190}$** formulations found in this study (see the next section). However, for an *N*/*P* ratio of 10, these latter formulations displayed luciferase levels comparable to those of the control. One should further underline that the **^{i}Bu-[NH]$_{75}$** or **PEG2000-[NH]$_{190}$** formulations displayed a higher cell viability than the control lipoplexes, e.g., 60−120% of cell survival for the **^{i}Bu-[NH]$_{75}$** or **PEG2000-[NH]$_{190}$** formulations versus 40 to ~70% of cell survival for the controls for a DNA dose of 0.5 μg/well (Figure 2B).

Structure−Transfection Efficiency Relationships. One of the objectives of this study was aimed at deter-

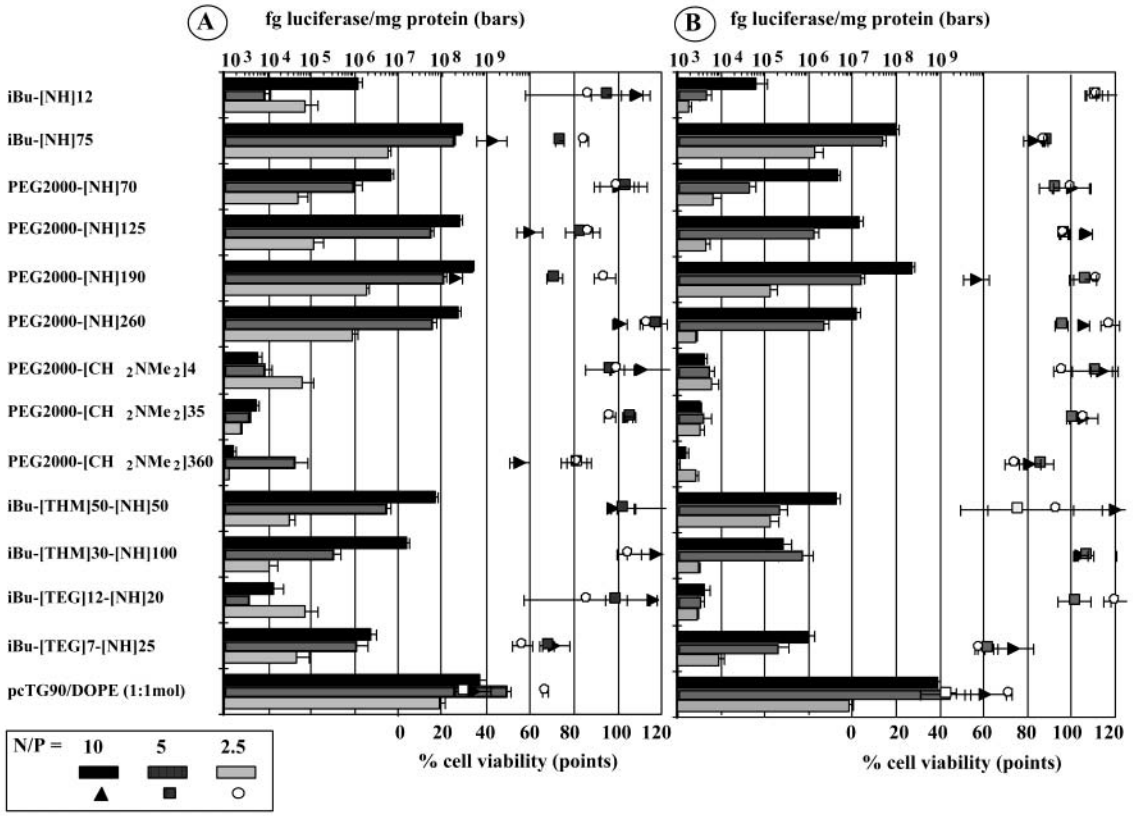


Figure 2. Luciferase expression (bars) and cell viability (points) of the pTG11236 complexes made with **^{i}Bu-[NH]$_n$** telomers, **PEG2000-[NH]$_n$** and **PEG2000-[CH$_2$NMe$_2$]$_n$** diblock telomers, and **^{i}Bu-[TEG]$_m$-[NH]$_n$** and **^{i}Bu-[THM]$_m$-[NH]$_n$** random cotelomers as compared to control pcTG90−DOPE (1/1 molar ratio) lipoplexes in A549 cells. Transfection was performed in the presence of 10% fetal calf serum. Data represent means ± SEM (standard error of the mean) from two independent experiments, each performed in triplicate (for more details, see Experimental Section): DNA doses of 1 (A) and 0.5 μg/well (B).

mining the effects of structural elements of the polyamine (co)telomers on their transfection potential and on cell survival. The structural modifications that were investigated here concern (i) the number of amine functions, (ii) the nature of the polyamine polar head [aminoethyl vs (*N*,*N*-dimethylamino)propyl], (iii) the presence of a block PEG2000 moiety connected to a block polyamine unit of variable length, and (iv) a random combination of primary amines with short tetraethylene glycol (TEG) or THM residues.

One can observe, irrespective of the *N*/*P* value and of the DNA dose, that increasing the average number of primary amine functions from 12 to 75 in the **^{i}Bu-[NH]$_n$** telomer series (hence, its degree of polymerization) induced a substantial (2- to 4-orders of magnitude) transgene expression increase (see Figure 3) and, concomitantly, a slight cell toxicity increase (Figure 2). In the di-block **PEG2000-[NH]n** series, transgene expression rose also but to a much lesser extent when the average number of amine functions was increased from 70 to 125 then to 190. Figure 3 demonstrates further that, in this series, the dependence of the luciferase expression means with the polyamine unit length (n) had a bell-shaped character, an optimum of transfection being attained for $n = 190$. The multiple comparison procedure using the Tukey's HSD method indicated that five of the six different **PEG2000-[NH]n/PEG2000-[NH]n′** pairs of means show statistically significant differences at the 95.0% confidence level, the exception being the **PEG2000-[NH]125/PEG2000-[NH]260** pair. In the di-block **PEG2000-[NH]n** series, increasing the average degree of polymerization did not impair cell survival (Figure 2).

Where the impact on transfection of replacement of the ethyl-NH_3^+ functions (as in **PEG2000-[NH]$_n$**) with propyl-$NHMe_2^+$ ones (as in **PEG2000-[CH$_2$NMe$_2$]$_n$**) is concerned, the level of transgene expression was drastically decreased (see Figures 2 and 3). This result differs substantially from a previous study from this laboratory where it was found that the random replacement of part of NH_3^+ with $NHMe_2^+$ units had no effect on transfection (*25*). However, this result concerned aminoethyl acrylate-deriving cotelomers. The low transfection efficiency of the diblock aminopropyl acrylate **PEG2000-[CH$_2$NMe$_2$]$_n$** cotelomers as compared to that of their aminoethyl acrylate analogues is more likely attributable to the ethyl−propyl backbone replacement rather than to the NH_3^+−$NHMe_2^+$ substitution. Indeed, it was shown that polymers derived from 2-(dimethylamino)propyl methacrylate were less effective gene transfer agents than polymers derived from 2-(dimethylamino)ethyl methacrylate (*33*). This was attributed to the higher pK_a values of the propyl polymers and, consequently, to their lower capacity of buffering endosomes and of their DNA complexes to escape from these endosomes (*33*).

With regard to the impact of the block PEG2000 moiety on transfection, its presence was found to decrease the level of transgene expression. As illustrated in Figure 3, the DNA complexes made with the diblock **PEG2000-[NH]$_{70}$** telomers led to much lower transgene expression levels than those formulated with **^{i}Bu-[NH]$_{75}$** which possesses a polyamine backbone with a comparable degree of polymerization. To compensate in part this transfection efficiency decrease, the length of the polyamine block in **PEG2000-[NH]$_n$** must be increased to up

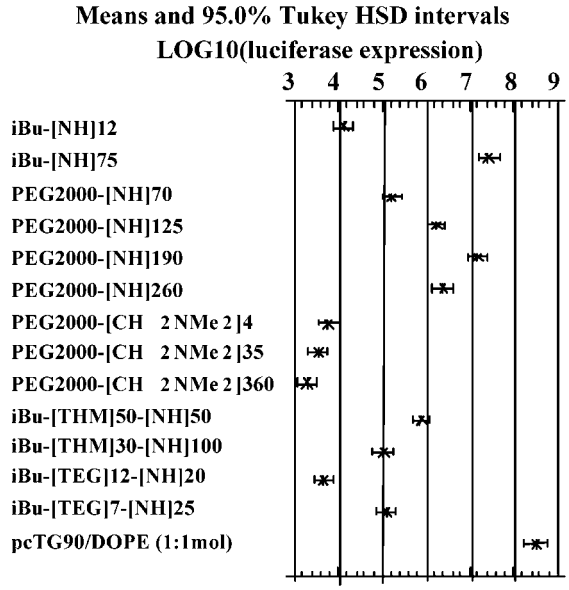


Figure 3. Means and 95.0% Tukey HSD intervals of the logarithmic transformation of luciferase expression levels [log-(femtograms of luciferase per milligram of protein)] for the pTG11236 complexes made with ^{i}**Bu-[NH]**$_n$ telomers, **PEG2000-[NH]**$_n$ and **PEG2000-[CH$_2$NMe$_2$]**$_n$ diblock telomers, or ^{i}**Bu-[TEG]**$_m$**-[NH]**$_n$ and ^{i}**Bu-[THM]**$_m$**-[NH]**$_n$ random cotelomers or with control pcTG90−DOPE (1/1 molar ratio) lipids, irrespective of the DNA dose and of the *N*/*P* ratio. Statistical tests were performed with STATGRAPHICS Plus5.0 software. This comparison was performed using the multiple-sample comparison procedure, and the method used to discriminate among the means of the logarithmic transformation of luciferase expression levels was Tukey's honestly significant difference (HSD) procedure.

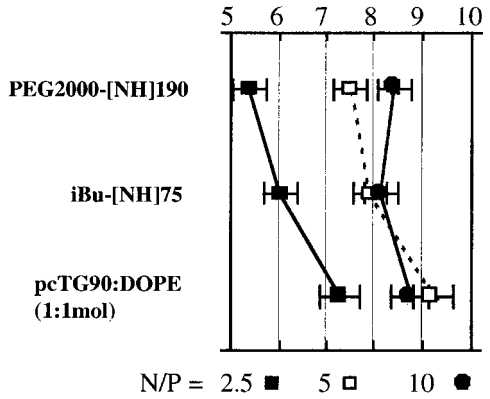


Figure 4. Means and 95.0% Tukey HSD intervals of the logarithmic transformation of luciferase expression levels [log-(femtograms of luciferase per milligram of protein)] for the pTG11236 complexes made with ^{i}**Bu-[NH]**$_{75}$ telomers, **PEG2000-[NH]**$_{190}$ diblock telomers, or control pcTG90−DOPE (1/1 molar ratio) lipids, as a function of the *N*/*P* ratios of the complexes.

to an average number of amine units of 190, as in **PEG2000-[NH]**$_{190}$.

A decrease in the level of transgene expression was also observed upon random replacement of part of primary amine functions with tetraethylene glycol (TEG) residues. Among the coteloplexes formulated with random ^{i}**Bu-[TEG]**$_{12}$**-[NH]**$_{20}$ or ^{i}**Bu-[TEG]**$_7$**-[NH]**$_{25}$, it appears that the most efficient ones were those formulated with the random cotelomers which contain the smallest number of TEG units (see Figure 3). Comparable results were also noticed in the literature for random copolymers derived from 2-(dimethylamino)ethyl methacrylate and ethoxytriethylene glycol methacrylate (*26*).

In a previous study from this laboratory concerning the effect on transfection of replacing randomly part of the primary amine functions by polyol THM residues in lipotelomers, transgene expression was shown to be unaffected while cell viability was seen to be improved to some extent (*25*). Similar results were also noticed in the literature for polylysines and polyallylamines after partial glycosylation (*27*). In contrast, we found here, as illustrated in Figure 3, that the random replacement of part of primary amine functions in ^{i}**Bu-[NH]**$_{75}$ with THM residues, as in ^{i}**Bu-[THM]**$_{30}$**-[NH]**$_{100}$ or ^{i}**Bu-[THM]**$_{50}$**-[NH]**$_{50}$, induced a substantial (10−500-fold) decrease in the transfection efficiency of their corresponding DNA complexes.

Altogether, these results showing a transfection potential decrease induced by the presence either of a block long polyethylene glycol residue (PEG2000) or of a random combination of primary amines with tetraethylene glycol (TEG) or THM residues were in fact to be expected. These residues provide a shielding effect, reducing the strength of electrostatic interactions between the cationic DNA complexes and the anionic cell proteoglycans, and consequently reducing their level of cellular uptake.

CONCLUSION

This work suggests that, among the new polycationic derivatives synthesized and investigated for their transfection efficiency, the ^{i}**Bu-[NH]**$_{75}$ telomers and the diblock polyethylene glycol-conjugated **PEG2000-[NH]**$_n$ telomers are very promising candidates for gene transfer purposes. The variation of structure parameters allowed the establishment of some structure−activity relationships, and the optimization of (co)teloplex formulations, where both high transfection levels and cell viability were achieved. Moreover, these in vitro findings do not prejudge all of their in vitro and in vivo behaviors which remain worthy of investigation.

ACKNOWLEDGMENT

We thank Transgène SA for financial support and Dr. B. Cavallini (Transgène SA) for supplying with plasmid. We also thank Drs. D. Heissler and A. Nazih (ULP Strasbourg) for supplying pcTG90. Thanks to Drs. H. V. J. Kolbe, S. Braun, and O. Meyer (Transgène SA) for their interest in this project and for helpful discussions.

LITERATURE CITED

(1) Marshall, E. (1999) Gene therapy death prompts review of adenovirus vector. *Science 286*, 2244−2245.
(2) Wivel, N. A., and Wilson, J. M. (1998) Methods of gene delivery. *Hematol. Oncol. Clin. North Am. 12*, 483−501.
(3) Schätzlein, A. G. (2001) Non-viral vectors in cancer therapy: principles and progress. *Anti-Cancer Drugs 12*, 275−304.
(4) Luo, D., and Saltzman, W. M. (2000) Synthetic DNA delivery systems. *Nat. Biotechnol. 18*, 33−37.
(5) Brown, M. D., Schätzlein, A. G., and Uchegbu, I. F. (2001) Gene delivery with synthetic (non viral) carriers. *Int. J. Pharm. 229*, 1−21.
(6) Zuber, G., Dauty, E., Nothisen, M., Belguise, P., and Behr, J. P. (2001) Towards synthetic viruses. *Adv. Drug Delivery Rev. 52*, 245−253.
(7) Mahato, R. I., Smith, L. C., and Rolland, A. (1999) Pharmaceutical perspectives of non-viral gene therapy. *Adv. Genet. 41*, 95−156.
(8) Gaucheron, J., Santaella, C., and Vierling, P. (2001) Highly fluorinated lipospermines for gene transfer: synthesis and evaluation of their in vitro transfection efficiency. *Bioconjugate Chem 12*, 114−128.

(9) Liu, F., Qi, H., Huang, L., and Liu, D. (1997) Factors controlling the efficiency of cationic lipid-mediated transfection *in vivo* via intravenous administration. *Gene Ther. 4*, 517−523.
(10) Ishiwata, H., Suzuki, N., Ando, S., Kikuchi, H., and Kitagawa, T. (2000) Characteristics and biodistribution of cationic liposomes and their DNA complexes. *J. Controlled Release 69*, 139−148.
(11) Anwer, K., Kao, G., Proctor, B., Rolland, A., and Sullivan, S. (2000) Optimization of cationic lipid/DNA complexes for systemic gene transfer to tumour lesions. *J. Drug Targeting 8*, 125−135.
(12) Dash, P. R., Read, M. L., Barrett, L. B., Wolfert, M. A., and Seymour, L. W. (1999) Factors affecting blood clearance and in vivo distribution of polyelectrolyte complexes for gene delivery. *Gene Ther. 6*, 643−650.
(13) Li, S., Tseng, W. C., Stolz, D. B., Wu, S. P., Watkins, S. C., and Huang, L. (1999) Dynamic changes in the characteristics of cationic lipidic vectors after exposure to mouse serum; implications for intravenous lipofection. *Gene Ther. 6*, 585−594.
(14) Ferrari, F. E., Rusalov, D., Enas, J., and Wheeler, C. J. (2001) Trends in lipoplex physical properties dependent on cationic lipid structure, vehicle and complexation procedure do not correlate with biological activity. *Nucleic Acids Res. 29*, 1539−1548.
(15) Lemieux, P., Vinogradov, S. V., Gebhart, C. L., Guérin, N., Paradis, G., Nguyen, H.-K., Ochietti, B., Suzdaltseva, Y. G., Bartakova, E. V., Bronich, T. K., St-Pierre, Y., Alakhov, V. Y., and Kabanov, A. V. (2000) Block and graft copolymers and Nanogel copolymer networks for DNA delivery into cell. *J. Drug Targeting 8*, 91−105.
(16) Harvie, P., Wong, F. M. P., and Bally, M. B. (2000) Use of poly(ethylene glycol)-lipid conjugates to regulate the surface attributes and transfection activity of lipid-DNA particles. *J. Pharm. Sci. 89*, 652−663.
(17) Oupicky, D., Carlisle, R. C., and Seymour, L. W. (2001) Triggered intracellular activation of disulfide crosslinked polyelectrolyte gene delivery complexes with extended systemic circulation in vivo. *Gene Ther. 8*, 713−724.
(18) Ogris, M., Brunner, S., Schuller, S., Kircheis, R., and Wagner, E. (1999) PEGylated DNA/transferrin-PEI complexes: reduced interaction with blood components, extended circulation in blood and potential for systemic gene delivery. *Gene Ther. 6*, 595−605.
(19) Lee, H., Jeong, J. H., and Park, T. G. (2002) PEG grafted polylysine with fusogenic peptide for gene delivery: high transfection efficiency with low cytotoxicity. *J. Controlled Release 79*, 283−291.
(20) Dash, P. R., Read, M. L., Fisher, K. D., Howard, K. A., Wolfert, M., Oupicky, D., Subr, V., Strohalm, J., Ulbrich, K., and Seymour, L. W. (2000) Decreased binding to proteins and cells of polymeric gene delivery vectors surface modified with a multivalent hydrophilic polymer and retargeting through attachment of transferrin. *J. Biol. Chem. 275*, 3793−3802.
(21) Garrett, S. W., Davis, O. R., Milroy, D. A., Wood, P. J., Pouton, C. W., and Threadgill, M. D. (2001) Synthesis and characterisation of polyamine-poly(ethylene glycol) constructs for DNA binding and gene delivery. *Bioorg. Med. Chem. 8*, 1779−1797.
(22) Sagara, K., and Kim, S. W. (2002) A new synthesis of galactose-poly(ethylene glycol)-polyethylenimine for gene delivery to hepatocytes. *J. Controlled Release 79*, 271−281.
(23) Oupicky, D., Konak, C., Ulbrich, K., Wolfert, M. A., and Seymour, L. W. (2000) DNA delivey systems based on complexes of DNA with synthetic polycations and their copolymers. *J. Controlled Release 65*, 149−171.
(24) Verderone, G., Van Craynest, N., Boussif, O., Santaella, C., Bischoff, R., Kolbe, H. V. J., and Vierling, P. (2000) Lipopolycationic telomers for gene transfer: synthesis and evaluation of their in vitro transfection efficiency. *J. Med. Chem. 43*, 1367−1379.
(25) Craynest, N. V., Santaella, C., Boussif, O., and Vierling, P. (2002) Polycationic telomers and cotelomers for gene transfer: synthesis and evaluation of their in vitro transfection efficiency. *Bioconjugate Chem. 13*, 59−75.
(26) Van de Wetering, P., Moret, E. E., Schuurmans-Nieuwenbroek, N. M. E., Van Steenbergen, M. J., Crommelin, D. J. A., and Hennink, W. E. (2000) Copolymers of 2-(dimethylamino)ethyl methacrylate with ethoxytriethylene glycol methacrylate or *N*-vinylpyrrolidone as gene transfer agents. *J. Controlled Release 64*, 193−203.
(27) Boussif, O., Delair, T., Brua, C., Veron, L., Pavirani, A., and Kolbe, H. V. J. (1999) Synthesis of polyallylamine derivatives and their use as gene transfer vectors in vitro. *Bioconjugate Chem. 10*, 877−883.
(28) Boussif, O., Zanta, M. A., and Behr, J. P. (1996) Optimized galenics improve in vitro gene transfer with cationic molecules up to 1000-fold. *Gene Ther. 3*, 1074−1080.
(29) Pitard, B., Aguerre, O., Airiau, M., Lachagès, A.-M., Boukhnikachvili, T., Byk, G., Dubertret, C., Herviou, C., Scherman, D., Mayaux, J.-F., and Crouzet, J. (1997) Virus-sized self-assembling lamellar complexes between plasmid DNA and cationic micelles promote gene transfer. *Proc. Natl. Acad. Sci. U.S.A. 94*, 14412−14417.
(30) Girao da Cruz, M. T., Simoes, S., Pires, P. P. C., Nir, S., and De Lima, M. C. P. (2001) Kinetic analysis of the initial steps involved in lipoplex-cell interactions: effect of various factors that influence transfection activity. *Biochim. Biophys. Acta 1510*, 136−151.
(31) Mislick, K. A., and Baldeschwielr, J. D. (1996) Evidence for the role of proteoglycans in cation-mediated gene transfer. *Proc. Natl. Acad. Sci. U.S.A. 93*, 12349−12154.
(32) Mounkes, L. C., Zhong, W., Cipres-Paladin, G., Heath, T. D., and Debs, R. J. (1998) Proteoglycans mediate cationic liposome-DNA complex-based gene delivery in vitro and in vivo. *J. Biol. Chem. 273*, 26164−26170.
(33) Van de Wetering, P., Moret, E. E., Schuurmans-Nieuwenbroek, N. M. E., Van Steenbergen, M. J., and Hennink, W. E. (1999) Structure/activity relationship of water-soluble cationic methacrylate/methacrylamide polymers for nonviral gene delivery. *Bioconjugate Chem. 10*, 589−597.

BC0255440

Effect of Hb-Encapsulation with Vesicles on H_2O_2 Reaction and Lipid Peroxidation

Shinji Takeoka, Yuji Teramura, Tomoyasu Atoji, and Eishun Tsuchida*

Advanced Research Institute for Science and Engineering, Waseda University, Tokyo 169-8555, Japan. Received May 1, 2002; Revised Manuscript Received September 26, 2002

We encapsulated a purified and concentrated hemoglobin (Hb) solution with a phospholipid bilayer membrane to form Hb vesicles (particle diameter, ca. 250 nm) for the development of artificial oxygen carriers. Reaction of Hb inside the vesicle with hydrogen peroxide (H_2O_2) is one of the important safety issues to be clarified and compared with a free Hb solution. During the reaction of the Hb solution with H_2O_2, metHb (Fe^{III}) and ferrylHb (Fe^{IV}=O) are produced, and H_2O_2 is decomposed by the catalase-like reaction of Hb. The aggregation of discolored Hb products due to heme degradation is accompanied by the release of iron (ferric ion). On the other hand, the concentrated Hb within the Hb vesicle reacts with H_2O_2 that permeated through the bilayer membrane, and the same products as the Hb solution are formed inside the vesicle. However, there is no turbidity change, no particle diameter change of the Hb vesicles, and no peroxidation of lipids comprising the vesicles after the reaction with H_2O_2. Furthermore, no free iron is detected outside the vesicle, though ferric ion is released from the denatured Hb inside the vesicle, indicating the barrier effect of the bilayer membrane against the permeation of ferric ion. When vesicles composed of egg york lecithin (EYL) as unsaturated lipids are added to the mixture of Hb and H_2O_2, the lipid peroxidation is caused by ferrylHb and hydroxyl radical generated from reaction of the ferric iron with H_2O_2, whereas no lipid peroxidation is observed in the case of the Hb vesicle dispersion because the saturated lipid membrane of the Hb vesicle should prevent the interaction of the ferrylHb or ferric iron with the EYL.

INTRODUCTION

Enormous efforts have been made to develop red blood cell substitutes for clinical applications in recent years (*1*−*3*). Potential benefits of red blood cell substitutes are their infusion in emergency situations without concern for blood type, virus infections, and long-term storage. Hemoglobin (Hb)-based oxygen carriers (HBOCs), which have been developed so far, are generally classified into two types: one is the acellular-type modified Hb molecules such as intramolecularly cross-linked Hb (*4*), recombinant cross-linked Hb (*5*), polymerized Hb (*6*), and intramolecularly polymer-conjugated Hb (*7*). Some of these Hb modifications are currently in the final stage of clinical trials. However, clinical trials have revealed some side effects such as hypertension relating to vasoconstriction, which have been extensively reported in vivo and in vitro (*8*, *9*). Another is the cellular-type Hb such as Hb vesicles which are being developed by our group (*10*) or liposome-encapsulating Hb (*11*). They have a vesicular structure in which concentrated Hb molecules are encapsulated, like red blood cells. Though the Hb vesicles have not yet been clinically studied, their safety and efficacy have been confirmed in comparison with Hb modifications in order to insist on the benefits of the cellular structure (*12*−*17*). From safety tests involving microvascular responses (*12*, *13*) and heme detoxification in liver (*17*), we have clarified the sufficient oxygen-transporting ability comparable with red blood cells in 40% hemorrhage shock (*14*) and 90% exchange transfusion (*16*).

Recently, after the administration of the Hb modifications, it has been noted that heme-mediated reactions such as ligand coordinations and redox reactions could cause organ dysfunction and/or tissue damage (*18*, *19*). Especially, redox reactions may affect the physiological protection against reactive oxygen species (*20*). The oxidation of oxyHb by H_2O_2 is known to generate ferrylHb and metHb accompanied by heme degradation and the release of free iron (*21*). Furthermore, during the autoxidation of oxyHb to metHb, reactive oxygen species such as superoxide, hydrogen peroxide, and the hydroxyl radical are generated to damage not only the remaining oxyHb but also living cells and organs (*22*−*24*). Especially, ferrylHb is known to be a potent oxidant which catalyzes the peroxidation of lipids comprising the biomembrane and other biomaterials (*25*, *26*). In normal human plasma, the concentration of H_2O_2 is 4−5 μM (*27*) and elevates to 100−600 μM under inflammatory (*28*) or ischemia/reperfusion conditions (*29*), in fact, ferrylHb can be found both in the red blood cells (*30*) and in the endothelial cells model after hypoxia reoxygenation (*31*, *32*). Several in vitro studies suggest that free radicals or degradation products catalyzed by ferrylHb could damage the endothelial cells in the presence of acellular-type Hb modifications. Hb-mediated cytotoxicity via ferrylHb is one of the important safety issues of HBOCs (*20*, *33*−*36*). On the other hand, in the cellular-type Hb vesicles (*37*), reactive oxygen species generated within the Hb vesicles during metHb formation were completely consumed by Hb (unpublished data). Though such a reaction leads to Hb oxidation, no reactive oxygen species have been detected outside the vesicles.

* To whom correspondence should be addressed. E-mail: eishun@mn.waseda.ac.jp.

10.1021/bc025546k CCC: $22.00 © 2002 American Chemical Society
Published on Web 10/19/2002

Here, we describe the chemical reactions between H_2O_2 and Hb (acellular type), or H_2O_2 and Hb vesicle (cellular type) and demonstrate the influence of the resulting ferrylHb on the peroxidation of unsaturated lipids, which were added to the system as egg york lecithin vesicles to clarify the advantage of Hb vesicle over acellular-type Hb concerning heme-mediated cytotoxicity via ferrylHb.

MATERIALS AND METHODS

(1) Purification of an Hb Solution from Red Blood Cells (*38*). Hb was purified from outdated human red blood cells provided by Japanese Red Cross. The red blood cells were washed three times with saline by centrifugation (2000*g*, 10 min) and concentrated by the removal of the supernatant. They were hemolyzed by the addition of the equal volume of the water for injection, and stromata were removed by ultrafiltration (cutoff M_w 1000 kDa, Biomax-1000V, Millipore Co., Ltd., Bedford). The ligand exchange from O_2 to CO was carried out for the stroma-free Hb solution by CO gas flowing. The proteins other than HbCO were denatured by heat treatment at 60 °C for 12 h and removed as precipitates. The HbCO solution was fractionated using ultrafiltration filters of which cutoff molecular weight were between 1000 kDa and 8 kDa (Biomax-8V, Millipore) followed by concentration with the same 8 kDa ultrafilter.

(2) Preparation of an Hb Vesicle Dispersion (*37*). Pyridoxal 5′-phosphate (PLP, Merck, Whitehouse Station) as an allosteric effector was added to the HbCO solution (40 g/dL) at a 3/1 molar ratio of PLP to Hb. Presome PPG-I [1,2-dipalmitoyl-*sn*-glycero-3-phosphatidylchorine (DPPC)/cholesterol/1,2-dipalmitoyl-*sn*-glycero-3-phosphatidylglycerol (DPPG), Nippon Fine Chemical, Osaka] powder was mixed with the HbCO solution, and the mixture was stirred at 4 °C for 12 h. The resulting dispersion of multilamellar vesicles was extruded through membrane filters (Fuji Film Co., Tokyo) with a Remolino (Millipore). The Hb vesicles with an average diameter of 250 ± 20 nm were obtained after extrusion through the membrane filter with 0.22 μm pore size. After the separation of unencapsulated Hb by ultracentrifugation (10000*g*, 60 min), the precipitate of the Hb vesicles was redispersed into saline. 1,2-Distearoyl-*sn*-glycero-3-phosphatidylethanolamine-*N*-PEG (PEG molecular weight was 5000, Sunbright DSPE−50H, H-form, NOF Co., Tokyo) was added to the dispersion of the Hb vesicles until its concentration to the membrane components became 0.3 mol %. The mixture was incubated at 37 °C for 2 h for the surface modification with PEG-DSPE. Finally, unincorporated DSPE−50H was removed by ultracentrifugation (10000*g*, 60 min) as a supernatant.

(3) Analyses of Hb Samples (Hb Solution or Hb Vesicle Dispersion). After the decarbonylation of HbCO (HbCO→HbO_2) by the irradiation of visible light to the liquid film, the oxyHb solution and the oxyHb vesicle dispersion containing 1.6 mM deferoxamine mesylate (DFO, Sigma, St. Louis, MO) were used as Hb samples. Reaction of the Hb samples ([heme] = 20 μM) with H_2O_2 at various ratios in phosphate buffer (pH7.4, at 37 °C) was assessed by repetitive scanning of a visible region from 450 to 700 nm at 2 min intervals by using an UV−vis spectrophotometer (V-570, Jasco, Tokyo). Under a nitrogen atmosphere, deoxyHb or metHb was rapidly mixed with the H_2O_2 solution using a rapid scan apparatus (model TSP-601, UNISOKU, Osaka), and the repetitive scanned spectra were recorded to calculate the reaction rate.

After the reaction of the Hb samples with H_2O_2, the bottom of the vials was carefully observed to confirm whether precipitates formed. The turbidity change was measured as ΔOD at 700 nm. The particle size of the Hb vesicles was measured by a dynamic light-scattering method (Coulter particle analyzer N4SD, Coulter Co., FL).

(4) Quantitative Analyses of H_2O_2 and Ferric Ion. The concentration of H_2O_2 was measured spectrofluorometrically by the formation of 6,6′-dihydroxy-[1,1′-biphenyl]-3,3′-diacetic acid (DBDA, E_x: 317 nm, E_m: 405 nm) during horseradish peroxidase (HRP)-catalyzed reaction of *p*-hydroxyphenylacetic acid (HPA) with H_2O_2 (*39*). To the reaction mixtures of H_2O_2 and the Hb samples were added HRP and HPA to be 4 μM and 6mM, respectively, to determine the remaining amount of H_2O_2 during the reaction of H_2O_2 with the Hb samples. The amount of produced DBDA was calculated after separating the Hb samples by centrifugal filtration (cutoff 10 kDa, Ultrafree-MC, Millipore) and measured with a fluorescence spectrophotometer (F-4500. Hitachi, Tokyo).

After the reaction of the Hb samples with H_2O_2 in different periods at 37 °C, the aqueous phase was separated by centrifugal filtration. Ferric ion in the filtrate was measured by an ICP emission spectroscopy (SPS-7000, Seiko Instruments Inc., Chiba).

(5) Lipid Analysis of Hb Vesicle by Liquid Chromatography−Mass Spectroscopy. The Hb vesicles were lyophilized after reaction with H_2O_2 and dissolved in chloroform and filtered through PTFE membrane filters with the pore size of 0.22 μm. The mixed lipid components were analyzed with a liquid chromatography−mass spectrometry system (LCQ-DECA, Thermo Quest, Tokyo), equipped with an apparatus of atmospheric pressure chemical ionization (ACPI) and a gel permeation chromatographic column (TSK gel Silica 60, 7.6 mm o.d. × 300 mm h, TOSOH, Tokyo). Two micro liter of the sample solutions was injected and developed with a mixed solvent (chloroform/acetone/methanol/acetic acid/water = 10/4/2/2/1, by vol ratio). The flow rate was 1.0 mL/min, and the temperature was maintained at 40 °C with a column oven. In the mass spectroscopic system, the gas flow rate, the applied voltage, and the CDL temperature were 0.5 mL/min, 2.5 kV, and 250 °C, respectively.

(6) Lipid Peroxidation of Egg York Lecithin Vesicles. The powder of egg york lecithin (EYL) was dispersed into pure water (40 mM) and hydrated at 4 °C for 2 h under an argon atmosphere. The resulting multilamellar vesicles were extruded through the membrane filters with the final pore size of 0.22 μm to prepare the vesicles of which average diameter is 270 ± 50 nm. The Hb samples were mixed with the EYL vesicles (37 mM) and reacted with H_2O_2 at 37 °C for 30 min, and trichloroacetic acid (42 mM) was added to precipitate the Hb samples. The supernatant separated from the Hb samples by centrifugation (12000*g*, 30 min) was mixed with thiobarbituric acid (TBA, 28 mM) and heated for 30 min at 100 °C. Resulting thiobarbituric acid-reacted substance in the solution was measured with a fluorescence spectrophotometer (E_x: 532 nm, E_m: 553 nm).

RESULTS AND DISCUSSION

Figure 1 shows the spectral change in the Hb solution (A) and the Hb vesicle dispersion (B), both of which have a heme concentration of 20 μM, after the addition of H_2O_2 of three different concentrations: (a) 20 μM, (b) 200 μM, and (c) 2 mM. In Figure 1A (a), the two peaks (540 and 575 nm) in the Q-band region of oxyHb gradually decreased after the addition of 20 μM H_2O_2 accompanied

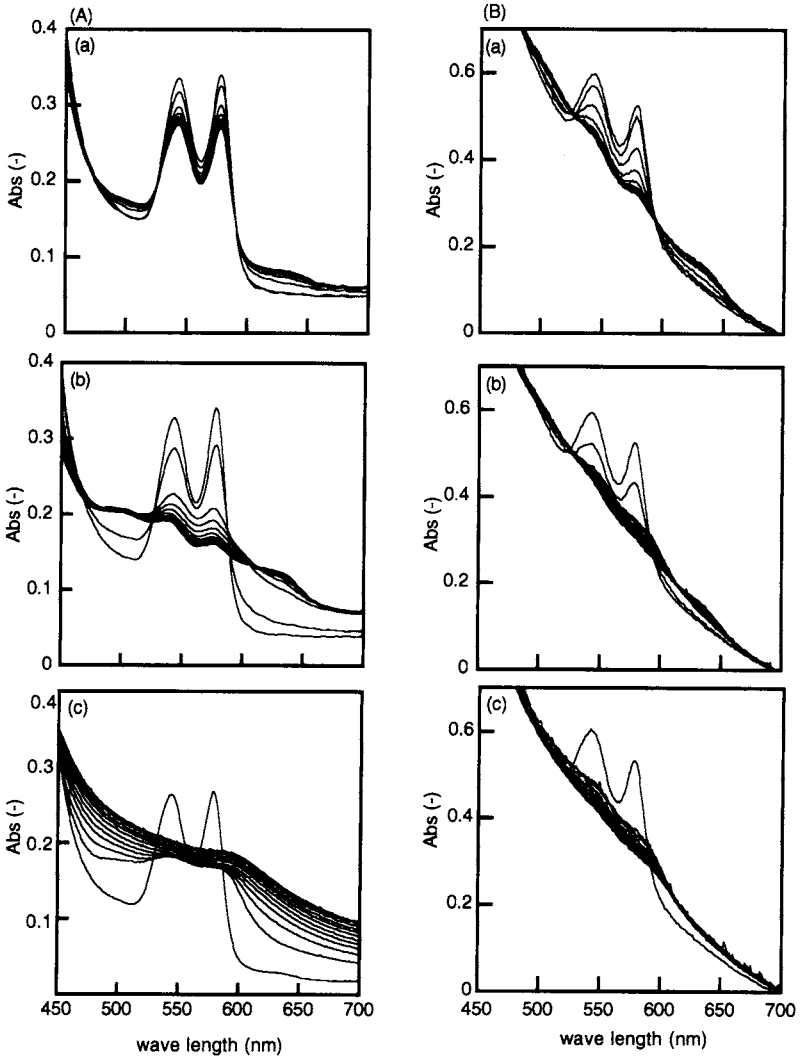


Figure 1. Spectral changes of (A) the Hb solution and (B) the Hb vesicle dispersion ([heme] = 20 μM) during the reaction with H_2O_2 at 37 °C ((a) 20 μM, (b) 200 μM, and (c) 2 mM). The repeatative sacanning was started at a 2 min interval, immediately after the addition of a solution of H_2O_2 to Hb sample solutions.

by the appearance of a small peak at 630 nm showing an isosbestic point at 586 nm. It is considered that oxyHb was gradually oxidized to metHb by H_2O_2 and stopped when H_2O_2 was consumed before the completion of the metHb formation. In the dispersion of Hb vesicles in which a purified Hb solution was encapsulated with a phospholipid bilayer membrane (particle diameter, 250 nm, Figure 1B (a)), the large decline in the baseline from the lower wavelength typically shows the turbidity of the vesicles. The oxyHb in the Hb vesicle was converted to metHb after reaction with 20 μM H_2O_2, and the degree of metHb conversion was greater than that of the oxyHb solution.

When the added amount of H_2O_2 was increased to 200 μM, a completely different feature in the spectral change was observed as shown in Figure 1AB (b). Namely, in the Hb solution, the decrease in the two peaks attributed to oxyHb was accompanied by the total increase in the absorbance from 478 nm to over 700 nm, which can be identified as ferrylHb. The following growth of the peak at 630 nm then had an isosbestic point at 612 nm, indicating the conversion of ferrylHb to metHb. A similar trend was observed for the Hb vesicles except for the baseline change as shown in Figure 1B(b). It is noted that the ratio of metHb in both Hb samples was significantly small after the reaction with 200 μM H_2O_2, in comparison with the metHb spectra of the Hb samples ([heme] = 20 μM) completely converted by the reaction with excess $NaNO_2$, suggesting the existence of discolored Hb products (degraded heme) (*21*).

When 2 mM of H_2O_2 was added to the Hb solution, the transient formation of ferrylHb with the subsequent conversion to the discolored products was confirmed from the baseline increase with no isosbestic points as shown in Figure 1A (c). We also confirmed the white aggregates at the bottom of the flask. A similar trend was also seen in the Hb vesicles but with no aggregation (Figure 1B (c)).

The composition changes of oxyHb, metHb, ferrylHb, and discolored products after the addition of H_2O_2 are summarized in Figure 2. These curves were obtained by a curve fitting technique using computer-simulated spectra from those Hb elements measured one by one.

Figure 2A (a) shows the conversion of the oxyHb solution, of which the heme concentration was 20 μM, to the other Hb products after the reaction with 20 μM H_2O_2. The oxyHb was reduced to 66% within 8 min accompanied by the formation of 29% metHb. The release of ferric ion and the generation of discolored products were slightly detected. The amount of H_2O_2 was below the detectable level (ca. 1 μM) within 7 min, thus showing the catalytic decomposition of H_2O_2 in this system. The direct conversion of oxyHb to metHb induced by a stoichiometric amount of H_2O_2 was also reported in

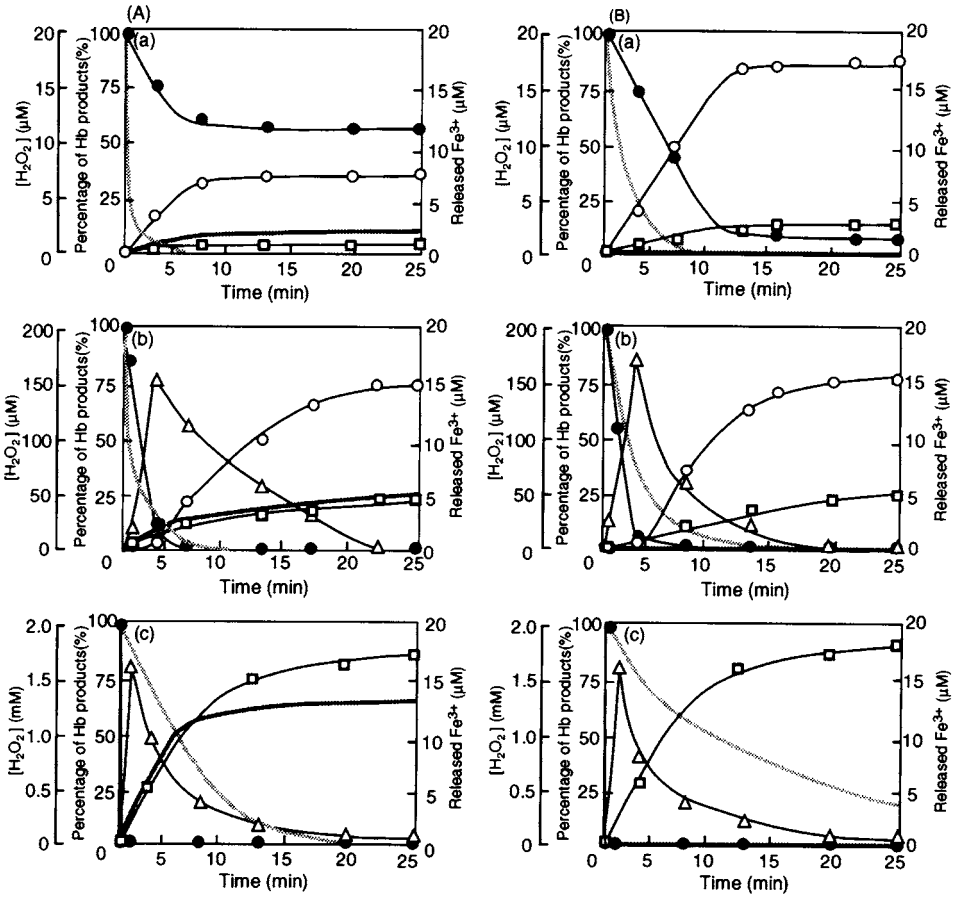


Figure 2. Changes of Hb components and the concentrations of H_2O_2 and Fe^{3+} in (A) the Hb solution and (B) the Hb vesicle dispersion during the reaction with H_2O_2 at 37 °C. Hb or Hb vesicle ([heme] = 20 μM) were reacted with H_2O_2 ((a) 20 μM, (b) 200 μM and (c) 2 mM, respectively). Each Hb component in the vesicle ratio was calculated from the repetative UV−vis spectral changes. ●: oxyHb, ○: metHb, △: ferrylHb, □: discolorated products. black line: Released Fe^{3+} measured by an ICP emission spectroscopy, grey line: H_2O_2 concentration determined with HRP and HPA.

some papers (*40*, *41*) and explained in terms of "comproportionation" between ferrylHb and oxyHb to two metHbs by Giulivi and Davies (*41*). On the other hand, to the dispersion of oxyHb vesicles having the heme concentration of 20 μM, the same concentration of H_2O_2 was added as shown in Figure 2A (b). The oxyHb was reduced to 5% within 13 min accompanied by the formation of 85% metHb and 10% discolored products. No ferric ion was detected during our observation period (30 min). The main difference between these two samples is that the conversion of metHb from the oxyHb solution remained at 29%, whereas that from the oxyHb vesicle dispersion was over 85%. This can be explained as follows. Initially, oxyHb would react with H_2O_2 to convert metHb via comproportionation of ferrylHb with a large amount of oxyHb. The resulting metHb would show more effective catalase-like reactivity than oxyHb (*21*, *30*). In the Hb solution, 20 μM H_2O_2 was completely decomposed by only 6 μM heme. In the case of the Hb vesicle dispersion, the rate-determining stage would be the reaction between oxyHb molecules that are located the vicinity of the bilayer membrane inside the vesicle and H_2O_2 that had just permeated through the bilayer membrane. The resulting metHb would diffuse toward the core of the vesicle and exchange with unreacted oxyHb, and then the oxyHb would react with H_2O_2 to convert metHb. This would result in the higher metHb conversion and ristriction of the catalase-like reaction of metHb. In fact, as shown in Figure 2 AB (a), the half-lives of the H_2O_2 decomposition in the Hb solution and in the Hb vesicle dispersion were 12 s and 115 s, respectively.

The reaction between 10-fold (200 μM) H_2O_2 and oxyHb (20 μM) in the solution state or within a vesicle as a dispersion is shown in Figure 2AB (b) as the conversion of each Hb product. The concentrations of H_2O_2 and ferric ion are also included in these figures. OxyHb completely disappeared within 7 min after the addition of H_2O_2. It was transiently converted to ferrylHb with a maximum at 4 min, followed by the conversion of metHb from the ferrylHb. Furthermore, discolored products were gradually generated from the beginning of the reaction. It is noted that the release of ferric ion was accompanied by the generation of the discolored products in the oxyHb solution. However, no ferric ion was observed in the outer aqueous phase of the oxyHb vesicle dispersion. The half-lives of 200 μM H_2O_2 in the 20 μM oxyHb solution and the vesicle dispersion were 21 s and 200 s, respectively. When compared with those in Figure 2AB (a), only twice the time was needed to decompose the 10-fold H_2O_2. It is indicated that the catalase-like activity that cycles between metHb and ferrylHb (globin) radical, which is one oxidizing equivalent above ferrylHb, remained during the reaction. As described above, once metHb formed by the reaction of oxyHb with H_2O_2 via ferrylHb, the resulting metHb should be rapidly oxidized by H_2O_2 to the ferrylHb radical. The ferryl Hb radical is considered to act like the so-called compound I of catalase, which converts H_2O_2 to H_2O and O_2, and back to metHb (*30*). Since the latter reaction would be slow in comparison with the ferrylHb formation, the ferrylHb from oxyHb and ferrylHb radical from metHb are apparently the main products during the reaction with H_2O_2. These

ferrylHbs gradually returned to metHb after the extinction of H_2O_2 because of its instability.

The discolored products should be degraded to heme fragments and apo-protein during the redox cylcle between oxyHb and ferrylHb, because we confirmed that metHb showed a more stable equilibrium state between metHb and the ferrylHb radical during reaction with H_2O_2 (data not shown). A recent report described that heme degradation was caused by superoxide generated from the reaction of ferrylHb with H_2O_2 (*21*). It is easy to understand that heme degradation triggered the release of ferric ion, and the resulting apo-proteins were so unstable that they aggregated as white precipitates. The generation of such discolored products indicates the nonperfect catalase-like activity of Hb against H_2O_2.

When 1000-fold H_2O_2 was added to the Hb sample solutions, oxyHb in both cases instantly disappeared to convert ferrylHb as an intermediate, and interestingly, the final product was not metHb but discolored products. This indicates that the comproportionation of ferrylHb with oxyHb did not occur because almost all of the oxyHb was instantly converted to ferrylHb, and heme degradation should occur due to the reaction of ferrylHb with the large amount of H_2O_2.

The decomposition of H_2O_2 could also be recognized even if no ferrylHb and metHb existed. The half-lives of H_2O_2 in the oxyHb solution and the oxyHb vesicle dispersion were 390 s and 760 s, respectively. H_2O_2 was hardly decomposed if H_2O_2 was added to the discolored Hb products in the presence of DFO, indicating that the discolored products should have no catalase activity, but H_2O_2 should be decomposed by a Fenton reaction caused by ferric ion released from the degraded heme. For the Hb vesicles, we did not observe the ferric ion in the outer aqueous phase; therefore, H_2O_2 should be decomposed by ferric ion in the inner aqueous phase of the Hb vesicle.

Figure 3 shows the turbidity changes monitored at 700 nm for the six samples depicted in Figure 2 and two samples, i.e., the Hb solution and the Hb vesicle dispersion without the addition of H_2O_2, as references. The turbidity of the Hb solution gradually increases during the reaction with H_2O_2 (Figure 3a). The slope of the turbidity change increases with the increasing amount of H_2O_2. This clearly indicates that the turbidity increase is caused by the reaction of Hb with H_2O_2. We observed the white precipitates at the bottom of the vial soon after finishing the experiments, suggesting the formation of apo-protein, from which degraded heme molecules are lost. On the other hand, there were no changes in the turbidity and the diameter for all the Hb vesicle samples after the reaction with H_2O_2 as shown in Figure 3b. Of course, no white precipitate was observed. We could confirm the encapsulation of all the Hb products such as ferrylHb, metHb, and discolored products within the vesicle after the separation of the vesicles by ultracentrifugation.

Next, the free iron (ferric ion) was determined by ICP emission spectroscopy in the reaction system between H_2O_2 and the Hb samples after 24 h (Figure 4). With the addition of 20 μM, 200 μM, and 2 mM H_2O_2 to the Hb solution, 5.1 μM, 7.2 μM, and 19.8 μM ferric ion were released, respectively. These values respectively correspond to 26, 36, and 99 mol % Hb denaturation. On the other hand, for the Hb vesicle despersion, even with the addition of 2 mM H_2O_2, only 2.0 μM ferric ion was detected in the outer aqueous phase of the vesicles after 24 h. However, when the Hb vesicles after the reaction with H_2O_2 for 24 h was solubilized by 5 mM polyoxyethylene 10 lauryl ether ($C_{12}E_{10}$), which is a good surfactant

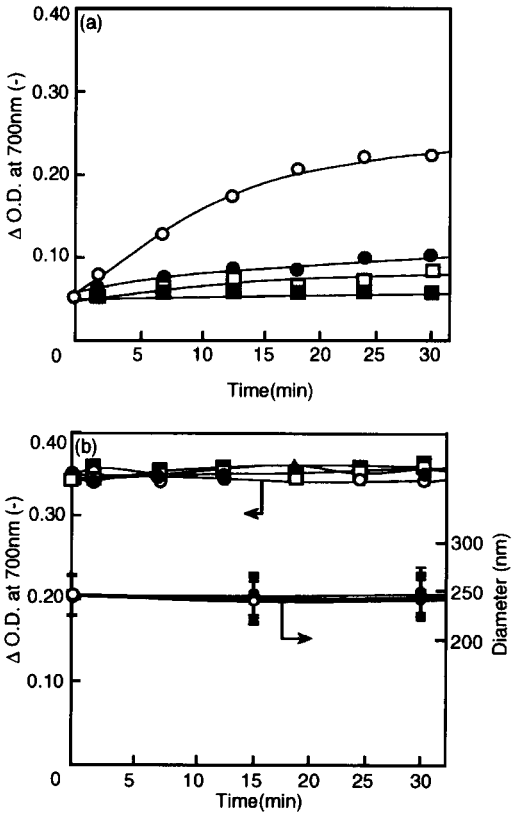


Figure 3. Changes in (a) the solution state of Hb and in (b) the dispersion state of Hb vesicles during the reaction with H_2O_2 at 37 °C. Hb or Hb vesicle ([heme] = 20 μM) were reacted with H_2O_2 (20 μM (□), 200 μM (●), and 2 mM (○), respectively). (■): the Hb solution or the Hb vesicle dispersion without the addition of H_2O_2. The turbidities of the Hb solution and the Hb vesicle dispersion were monitored as ΔOD at 700 nm. The particle diameter was determined by a dynamic light scattering method.

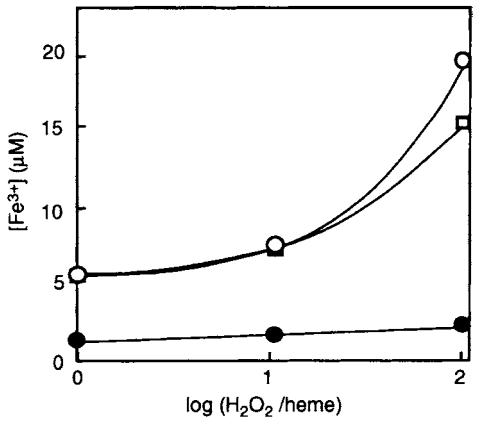


Figure 4. Released Fe^{3+} from Hb (○), Hb vesicle (●), or Hb vesicle solubilized with lauryl ether (□) after the reaction with H_2O_2 and incubation at 37 °C for 24 h. All samples have the same heme concentration of 20 μM.

for the solubilization of the vesicles and does not cause Hb denaturation, the amount of ferric ion similar to that in the Hb solution system was detected. The amount of ferric ion increased corresponding to the added amount of H_2O_2 as shown in Figure 4. Therefore, it was confirmed that ferric ion was also released from the denatured Hb inside the vesicle, but the ferric ion was hard to permeate through the bilayer membrane because of the high resistance of the membrane to ferric ion and the high integrity of the membrane.

Besides the physical integrity of the Hb vesicles, we analyzed the chemical stability of the bilayer membrane

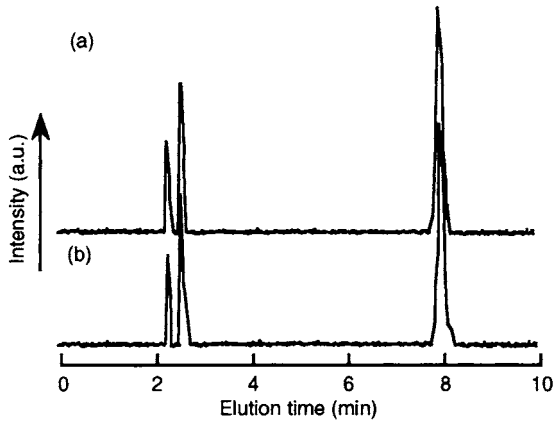


Figure 5. The LC-MS elution profiles of the lipid components of Hb vesicles ([heme] = 20 μM) (a) before and (b) after the reaction with 2 mM H_2O_2. The peaks at around 2.2, 2.5, and 7.9 min correspond to DPPG, cholesterol, and DPPC, respectively.

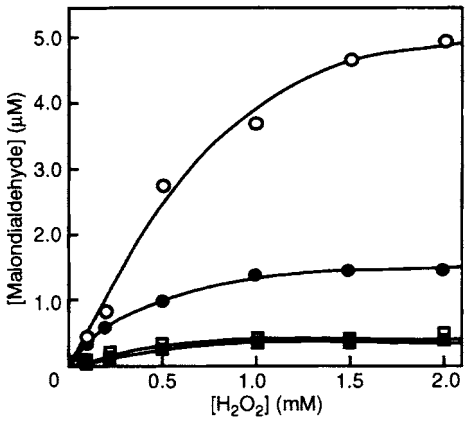


Figure 6. Lipid peroxidation of the EYL vesicles catalyzed by the Hb samples during the reaction with H_2O_2 in the presence or absence of DFO. The 37 mM EYL vesicle was dispersed in the Hb solution or the Hb vesicle dispersion ([heme] = 20 μM) and reacted with H_2O_2 at 37 °C for 30 min. ○: Hb, ●: Hb + DFO, □: Hb vesicle, ■: Hb vesicle + DFO

by liquid chromatography−mass spectroscopy (LC-MS). The membrane components were extracted from the freeze-dried powder of the Hb vesicles after reaction with 2 mM H_2O_2. In the elution profiles, the three peaks were detected at 2.2, 2.5, and 7.9 min, corresponding to DPPG, cholesterol, and DPPC, respectively, as shown in Figure 5. From the mass spectrum of each elution peak and the peak position, we could not confirm any new products and degraded fragments of the lipids after the reaction with even 100-fold H_2O_2 to Hb in the vesicles. Therefore, it was clarified that the saturated phospholipids and cholesterol were stable against H_2O_2, the active products from the reaction of H_2O_2 with Hb, such as ferrylHb and reactive oxygen species.

In the reaction with egg york lecithin (EYL), we could not confirm that either Hb or H_2O_2 had peroxidized the EYL comprising vesicles. However, EYL was surely peroxidized when H_2O_2 was added to the EYL vesicle dispersion in the presence of 20 μM ferric ion, indicating that the hydroxyl radical produced from the Fenton reaction between ferric ion and H_2O_2 should cause lipid peroxidation. Such lipid peroxidation was inhibited by the addition of 1.6 mM DFO as a chelator of ferric ion. To the mixture of 37 mM EYL vesicles, 20 μM Hb, and 1.6 mM DFO were added various concentrations of H_2O_2, and the lipid peroxidation value was measured by a TBA method after incubation for 30 min at 37 °C. The closed circle plots in Figure 6 show evidence of the lipid peroxidation in the triadic reaction system of EYL, Hb, and H_2O_2. No concentration dependence of H_2O_2 was seen above the H_2O_2 concentration of more than 1.0 mM. This suggests that the rate-determining process would be the reaction of Hb with EYL because both concentrations were constant. Therefore, we looked at the relationship between the concentration of ferrylHb and the concentration of malondialdehyde. The linear relationship proves that the ferrylHb converts EYL to the peroxidized lipid (data not shown here).

To study the influence of the ferric ion released from denatured Hb, the same experiment was carried out in the absence of DFO. The open circle plots in Figure 6 clearly demonstrate that the ferric ion significantly contributes to the lipid peroxidation through the Fenton reaction. The proportional relationship between the ferric ion concentration from $FeCl_3$ artificially added to the solution instead of Hb and the concentration of the resulting malondialdehyde suggests that the reaction of H_2O_2 and ferric ion released from the Hb denatured by H_2O_2 should produce the hydroxyl radical which results in the lipid peroxidation. On the other hand, in the Hb vesicle dispersion, the small increase in malondialdehyde despite the absence of DFO is due to the encapsulation

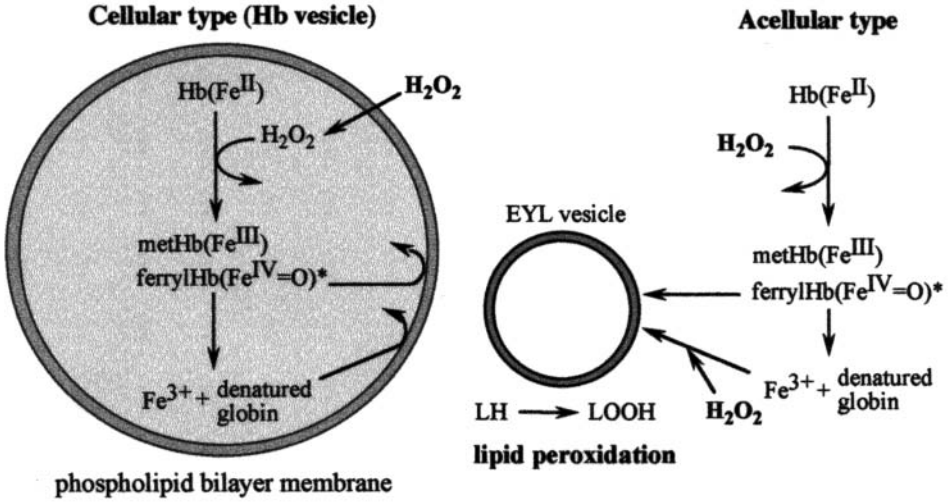


Figure 7. Interaction of acellular-type Hb and cellular-type Hb vesicle with H_2O_2, and their effects on lipid peroxidation of EYL.

effect of Hb and ferric ion with the saturated phospholipid bilayer membrane. This suggests the low cytotoxicity of the endotherial cells in the Hb vesicles in comparison with Hb modifications under oxidative stress (*33*). We are now studying the effect of the Hb samples reacted with H_2O_2 on the endotherial cells.

Figure 7 concludes our experimental results. H_2O_2 reacts with the acellular-type Hb solution to produce metHb and ferrylHb. The ferrylHb and ferric ion from those unstable Hb products facilitates the lipid peroxidation of the EYL vesicles, which represents the cytotoxicity of the reaction series. On the other hand, for the celullar Hb vesicle dispersion, those products are also generated by the reaction of Hb with H_2O_2 permeated through the bilayer membrane of the vesicle. However, they are stably encapsulated within the vesicle and do not cause the lipid peroxidation due to the separation from the EYL vesicles. These results indicate the high safety of the Hb vesicles which enclose the reactive Hb products in the reaction with H_2O_2.

ACKNOWLEDGMENT

The authors thank Prof. Takashi Yonetani and Dr. Antonio Tsuneshige (Medical Center, Univerisity of Pennsylvania) and Dr. Hiromi Sakai and Dr. Keitaro Sou (ARISE, Waseda University) for their advice and useful discussions. This work was supported in part by Health and Labor Sciences Research Grants (Research on Pharmaceutical and Medical Safety, Artificial Blood Project) of the Ministry of Health, Labor and Welfare, Japan, and Grants in Aid for Scientific Research (B) from the Ministry of Education, Science, Sports, and Culture, Japan (12558112). One of the authors (Y.T.) thanks Research Fellowships of the Japan Society for the Promotion of Science for Young Scientists grant.

LITERATURE CITED

(1) Tsuchida, E. (1995) *Artificial Red Cells*, John Wiley and Sons, New York.
(2) Winslow, R. M. (1995) *Nature Med. 1*, 1212−1215.
(3) Chang, T. M. S. (1991) *Biomater. Artif. Cell Immobil. Biotechnol. 20*, 159−182.
(4) Przybelski, R. J., Daily, E. K., and Birnbaum, M. L. (1997) *Advances in Blood Sbstitutes: Industrial Opportunities and Medical Challenges*, Birkhauser, Boston.
(5) Murray, J. A., Ledlow, A., Launspach, J., Evans, D., Loveday, M., and Conklin, J. L. (1995) *Gastroenterology 109*, 1241−1248.
(6) Gould, S. A., Moore, E. E., Hoyt, D. B., Burch, J. M., Haenel, J. B., Garcia, J., DeWoskin, R., and Moss, G. S. (1998) *J. Am. Coll. Surg. 187*, 113−122.
(7) Caron, A., Menu, P., Labrude, P., and Vigneron, C. (1998) *Artif. Cells, Blood Substitutes, Immobilization Biotechnol. 26*, 293−308.
(8) Doherty, D. H., Doyle, M. P., Curry, S. R., Vali, R. J., Fattor, T. J., Olsen, J. S., and Lemon, D. D. (1998) *Nat. Biotechnol. 1*, 672−676.
(9) Saxena, R., Wijnhoud, A. D., Carton, H., Hacke, W., Kaste, M., Przybelski, R. J., Stern, K. N., and Koudstaal, P. J. (1999) *Stroke 30*, 993−996.
(10) Tsuchida, E., Ed. (1998) *Blood substitutes: present and future perspectives*, Elsevier Science, Amsterdam.
(11) Rudolph, A. S., Sulpizio, A., Hieble, P., MacDonald, V., Chavez, M., and Feuerstein, G. (1997) *J. Appl. Physiol. 82*, 1826−1835.
(12) Sakai, H., Yuasa, M., Onuma, H., Takeoka, S., and Tsuchida, E. (2000) *Bioconjugate Chem. 11*, 56−64.
(13) Sakai, H., Hara, H., Yuasa, M., Tsai, A. G., Takeoka, S., Tsuchida, E., and Intaglietta, M. (2000) *Am. J. Physiol. Heart Circ. Physiol. 279*, H908−H915.
(14) Izumi, Y., Sakai, H., Hamada, K., Takeoka, S., Yamahata, T., Kato, R., Nishide, H., Tsuchida, E., and Kobayashi, K. (1996) *Circ. Care Med. 24*, 1869−1873.
(15) Sakai, H., Tomiyama, K., Sou, K., Takeoka, S., and Tsuchida, E. (2000) *Bioconjugate Chem. 11*, 425−432.
(16) Sakai, H., Takeoka, S., Park, S.-I., Kose, T., Izumi, Y., Yoshizu, A., Nishide, H., Kobayashi, K., and Tsuchida, E. (1997) *Bioconjugate Chem. 8*, 15−22.
(17) Kyokane T., Norizumi, S., Taniai, H., Yamaguchi, T., Takeoka, S., Tsuchida, E., Naito, M., Ishimura, Y., and Suematsu, M. (2001) *Gastroenterology 120*, 1227−1240.
(18) Alayash, A. I., and Cashon, R. E. (1995) *Mol. Med. Today 1* 122−127.
(19) Sharma, V., Traylor, T., and Gardiner R. (1987) *Biochemistry 26*, 3837−3843.
(20) Alayash, A. I. (1999) *Nat. Biotechnol. 17*, 545−549.
(21) Giulivi, C., and Cadenas, E. (1998) *Free Radic. Biol. Med. 24*, 269−279.
(22) Gutteridge, J. M. C. (1986) *FEBS Lett. 201*, 291−295.23. Macdonald, V. W. (1994) *Methods Enzymol. 231*, 480−490.
(23) , Everse, J., Johnson, M. C., and Marini, M. A. (1994) *Methods Enzymol. 231*, 547−561.
(24) Grisham, M. B., and Everse, J. (1991) *Peroxidases in Chemistry and Biology*, pp 335−344, CRC Press, Boca Raton, FL.
(25) Yamamoto, Y., Brodsky, M. H., Baker, J. C., and Ames, B. N. (1987) *Anal. Biochem. 160*, 7−13.
(26) Grisham, M. B., Gaginell, T. S., Von Ritter, C., Tamai, H., Be, R. M., and Granger, D. N. (1990) *Inflammation 14*, 531−542.
(27) Nagababu, E., and Rifkind, J. M. (2000) *Biochemistry 39*, 12503−12511.
(28) Gunther, M. R., Sampath, V., and Caughey, W. S. (1999) *Free Radic. Biol. Med. 26*, 1388−1395.
(29) Svistunenko, D. A., Patel, R. P., Voloshchenko, S. V., and Wilson, M. T. (1997) *J. Biol. Chem. 272*, 7114−7121.
(30) Clark, M. R. (1988) *Physiol. Rev. 68*, 503−554.
(31) Mcleod, L. L., and Alayash, A. I. (1999) *Am. J. Physiol. Heart Circ. Physiol. 277*, H92−H99.
(32) Goldman, D. W., Breyer, R. J., III, Yeh, D., Brockner-Ryan, B. A., and Alayash, A. I. (1998) *Am. J. Physiol. Heart Circ. Physiol. 275*, H1046−H1053.
(33) D'Agnillo, F., and Alayash, A. I. (2000) *Am. J. Physiol. Heart Circ. Physiol. 279*, H1880−H1889.
(34) Darley-Usmar, V., and White, R. (1997) *Exp. Physiol. 82*, 305−316.
(35) Natarajan, V. (1995) *J. Lab. Clin. Med. 123*, 461−463.
(36) Takeoka, S., Ohgushi, T., Terase, K., Ohmori, T., and Tsuchida, E. (1996) *Langmuir 12*, 1755−1759.
(37) Sakai, H., Hamada, K., Takeoka, S., Nishide, H., and Tsuchida, E. (1996) *Biotechnol. Prog. 12*, 119−125.
(38) Hinsberg, W. D., III, Milby, K. H., and Zare, R. N. (1981) *Anal. Chem. 53*, 1509−1512.
(39) Yusa, K., and Shikama, K. (1987) *Biochemistry 26*, 6684−6688.
(40) Giulivi, C., and Davies, K. J. (1990) *J. Biol. Chem. 265*, 19453−19460.

BC025546K

Glycosaminoglycan-Mimetic Biomaterials. 3. Glycopolymers Prepared from Alkene-Derivatized Mono- and Disaccharide-Based Glycomonomers

Subramanian Baskaran,[‡] Daniel Grande,[‡] Xue-Long Sun,[‡] Avner Yayon,[§] and Elliot L. Chaikof*[,†,‡]

Laboratory for Biomolecular Materials Research, Department of Surgery and Biomedical Engineering, Emory University, Atlanta, Georgia 30322, School of Chemical Engineering, Georgia Institute of Technology, Atlanta, Georgia 30332, and Weizmann Institute of Science, Rehovot, Israel. Received May 3, 2002; Revised Manuscript Received August 11, 2002

Mono- and disaccharide-containing glycopolymers were synthesized by two different free-radical processes, and their ability to act as heparan sulfate glycomimetics in promoting the binding of Fibroblast Growth Factor-2 (FGF-2) to its receptor (FGFR-1) was evaluated using an in vitro cell-based assay. Cyanoxyl (•OC≡N)-mediated polymerization of acrylamide with alkene-derivatized mono- and disaccharides including sulfated or nonsulfated *N*-acetyl-D-glucosamine is described. The results of this approach are compared to those obtained via the classical ammonium peroxodisulfate (APS)/*N*,*N*,*N*′,*N*′-tetramethylethylenediamine (TMEDA) initiating system and confirm the capacity of cyanoxyl-mediated polymerization to generate a variety of glycopolymers with high saccharide contents and low polydispersity indexes. In vitro assays demonstrate that specific glycopolymers can potentiate FGF-2/FGFR-1 binding interactions.

INTRODUCTION

Heparan sulfates (HS) are a large family of polydisperse anionic polysaccharides encountered both in the extracellular matrix and on cell surfaces that bind numerous proteins of biological interest. For example, fibroblast growth factor-2 (FGF-2) binds to heparan sulfate, which stabilizes and protects it against inactivation and facilitates its binding to the FGF receptor-1 (FGFR-1) (*1*). Moreover, heparan sulfates are required for the oligomerization of the FGF-2/FGFR-1 complex that is necessary for effective transmembrane signaling and a biological response (*2*). As a consequence of modulating the FGF-2/FGFR-1 signaling pathway, heparan sulfates have a significant functional role in a wide array of physiological processes, including cell proliferation and migration, as well as angiogenesis, wound healing, and inflammatory responses (*3*−*5*). Thus, the development of synthetic biopolymers that incorporate some of the biological functionality of heparan sulfate, particularly with respect to FGF-2, carries potential significance in a variety of areas, including drug delivery and tissue engineering (*6*).

Heparan sulfates are structurally complex and consist on average of 20 or more repeating disaccharides units composed of a hexauronic acid (D-glucuronic or L-iduronic acid) attached in 1→4 fashion to *N*-acetyl-D-glucosamine with varying patterns of sulfation (*7*). While smaller oligosaccharide sequences have been identified that are responsible for some of the unique biological activities of heparan sulfate (*8*, *9*), optimal binding of FGF-2 to FGFR-1 requires heparan sulfate-derived oligosaccharides containing eight or more sugar residues (*10*). Thus, the generation of heparan sulfate-mimetic compounds that modulate FGF-2-dependent responses remains a challenging endeavor, despite reported advances in solution- and solid-phase methods of carbohydrate synthesis. As an alternative approach, efforts in our group have been recently directed at the investigation of 'glycopolymer'-based strategies in which pendant saccharides are incorporated into a polymer backbone. The observation of enhanced protein binding affinity derived from multivalent oligosaccharide ligands suggested that monomers carrying this or other related saccharides as pendant groups could be used to generate glycopolymers with FGF-2-related bioactivity.

Optimization of glycopolymer properties requires the generation of biomolecular architectures that exhibit low fluctuations both in polymer size and in composition. As a consequence, we are currently examining the applicability of cyanoxyl (•OC≡N)-mediated free-radical polymerization in the synthesis of model glycopolymers from unprotected glycomonomers. Notably, this polymerization technique can be conducted in aqueous solution, is tolerant of a broad range of functional groups (OH, NH_2, COOH, etc.), and can be applied to the synthesis of block and graft copolymers with reported polydispersities below 1.5 (*11*, *12*). In this report, we describe the preparation of alkene-derivatized mono- and disaccharide glycomonomers. Cyanoxyl-mediated and classical free-radical polymerization techniques were then exploited to create a wide variety of water-soluble glycopolymers with high monosaccharide contents and low polydispersity indexes. Finally, the ability of test glycopolymers to potentiate the binding of FGF-2 to FGFR-1 is examined in preliminary bioactivity studies.

* Address correspondence to Elliot L. Chaikof, M.D., Ph.D., 1639 Pierce Drive − 5105 WMB, Emory University, Atlanta, GA 30322. Phone: (404) 727-8413. Fax: (404) 727-3660. E-mail: echaiko@emory.edu.

† Georgia Institute of Technology.

‡ Emory University School of Medicine.

§ Weizmann Institute of Science.

10.1021/bc0255485 CCC: $22.00 © 2002 American Chemical Society
Published on Web 11/05/2002

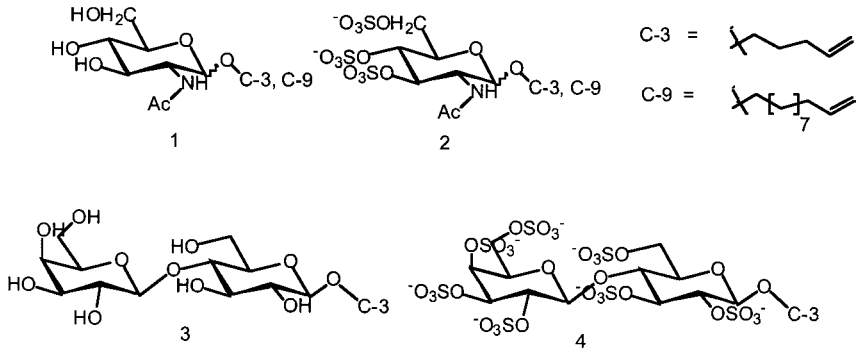


Figure 1. Alkenyl mono- and disaccharide-based glycomonomers used for the synthesis of corresponding glycopolymers.

EXPERIMENTAL SECTION

Materials. All solvents and reagents were purchased from commercial sources and were used as received, unless otherwise noted. Heparin was obtained from Hepar Industries and is polydisperse with a range of molecular weight between 5 and 30 kD (Franklin, OH). Deionized water with a resistivity of 18 MΩ·cm was used as solvent in all polymerization reactions.

Methods. All reactions were performed in flame-dried glassware under an atmosphere of dry argon. The reaction medium solutions were evaporated under reduced pressure with a rotary evaporator, and the residue was chromatographed on a silica gel (230−400 mesh) column. Analytical thin-layer chromatography (TLC) was performed on Whatman silica gel aluminum-backed plates of 250 μm thickness on which spots were visualized with UV light or charring the plate before and/or after dipping in a H_2SO_4−EtOH mixture. Melting point (mp) measurements were performed with a Thomas-Hoover melting point apparatus in open capillary tubes and were uncorrected. Mass spectra (MS/FAB) were obtained at an ionizing voltage of 70 eV. Optical rotations were determined with a Perkin-Elmer-2 GIMC polarimeter. ^{1}H and ^{13}C NMR spectra were recorded at room temperature with a Varian INOVA 400 spectrometer (magnetic field strengths of 400 and 100 MHz for ^{1}H and ^{13}C NMR analyses, respectively). In all cases, the sample concentration was 10 mg/mL, and the appropriate deuterated solvent was used as the internal standard.

Size-exclusion chromatography (SEC) equipment was comprised of a Waters model 510 HPLC pump, a Waters Ultrahydrogel 250 column, and a Wyatt Technology Optilab 903 refractometer. The eluent consisted of a 0.1 mol/L $NaNO_3$ deionized water solution containing 0.05 wt % sodium azide at a flow rate of 0.7 mL/min. The actual molar masses of the glycopolymer samples were determined from the response of the DAWN F (Wyatt Technology) multiangle laser light-scattering (LLS) detector that was connected to the outlet of the SEC apparatus.

Synthesis of Alkene-Derivatized Glycomonomers with Pendant Monosaccharides. Synthesis and detailed characterization of *n*-pentenyl 2-acetamido-2-deoxy-α-D-glucopyranoside (**1**(C-3)), *ω*-undecenyl 2-acetamido-2-deoxy-α-D-glucopyranoside (**1**(C-9)), and sulfated derivatives thereof (**2**(C-3) and **2**(C-9), respectively) have been reported in detail elsewhere (Figure 1).[13]

Synthesis of Alkene-Derivatized Glycomonomers Bearing Lactose. *n*-Pentenyl *O*-(*β*-D-galactopyranosyl)-(1→4)-*β*-D-glucopyranoside, 3. To a mixture of D-lactose (10 g) and 4-penten-1-ol (large excess, ∼125−175 mL) was added a catalytic amount of 10-camphorsulfonic acid (CSA) (∼400 mg), and the mixture was refluxed at 110 °C for 7 h. The reaction mixture was then cooled and neutralized with triethylamine (E_3N), and the excess of alcohol was removed under vacuum. The solid mass was subsequently rinsed with hot petroleum ether to remove the remaining alkenyl alcohol. The residue was purified by column chromatography using a chloroform/methanol (97/3) mixture to afford the expected product, **3**. Yield: 45%; $[\alpha]^{20}_D = +20.6°$ (*c* 1.8, CH_3OH). ^{1}H NMR (CD_3OD), δ_{ppm}: 1.69 (m, 2H, C−CH_2−C), 2.12 (m, 2H, CH_2−C═), 3.38−3.88 (m, all other H), 5.07 (m, 2H, CH_2═), 5.78 (m, 1H, C*H*═). ^{13}C NMR (CD_3OD), δ_{ppm}: 28.6, 30.2, 67.6, 69.7, 71.5, 71.8, 74.1, 98.6, 115.1, 137.9. MS/FAB, *m*/*z*: 411 (M + 1) (*14*, *15*).

***n*-Pentenyl *O*-(2,3,4,6-Tetra-*O*-sulfo-*β*-D-galactopyranosyl)-(1→4)-2,3,6-tri-*O*-sulfo-*β*-D-glucopyranoside Heptasodium Salt, 4.** Under argon atmosphere, sulfur trioxide−trimethylamine (SO_3−NMe_3) complex (4 equiv for each hydroxyl group) was added to the nonsulfated glycomonomer (**3**) in DMF, and the mixture was stirred at 60 °C for 12 h. The reaction medium was then cooled to 0 °C, and a saturated $NaHCO_3$ aqueous solution was added. The crude mixture was stirred for 1 h and concentrated to a smaller volume that was passed through a diethylaminoethyl (DEAE)-sephacel anion-exchange resin column. It was first eluted with a 10 mmol/L sodium phosphate buffer (pH ∼ 7.0), thereby removing the unreacted nonsulfated compound. The sulfated homologue was then eluted with a 1 mol/L NaCl buffer (pH ∼ 7.0) and recovered as a mixture of its heptasodium salt with a NaCl excess. The latter eluate was concentrated, redissolved in a minimum amount of water, and passed through a Trisacryl (Gf05 M grade, Sigma-Aldrich) size-exclusion resin column for isolation of the sulfated compound free of NaCl. Yield: 45%; $[\alpha]^{20}_D = +64.7°$ (*c* 1.7, H_2O). ^{1}H NMR (D_2O), δ_{ppm}: 1.72 (m, 2H, C−CH_2−C), 2.21 (m, 2H, CH_2−C═), 3.42−3.92 (m, all other H), 5.09 (m, 2H, CH_2═), 5.81 (m, 1H, C*H*═). MS/FAB, *m*/*z*: 986 ($M^+ + 1Na^+$).

Statistical Copolymerization of Alkene-Derivatized Glycomonomers and Acrylamide Initiated by $ClC_6H_4N{\equiv}N^+BF_4^-$/NaOCN. In a three-neck flask, 6.03×10^{-5} mol (0.008 g) of *p*-chloroaniline was reacted with 9.04×10^{-5} mol of HBF_4 (actually 0.017 g of 48 wt % aqueous solution), at 0 °C, in 2 mL of water and under argon atmosphere. The diazonium salt $ClC_6H_4N{\equiv}N^+BF_4^-$ was then generated by adding 7.2×10^{-5} mol (0.005 g) of sodium nitrite ($NaNO_2$) to the reaction medium. After 30 min, a degassed mixture of 6.03×10^{-4} mol (0.225 g) of glycomonomer **1**(C-9), 2.41×10^{-3} mol (0.171 g) of acrylamide, and 6.03×10^{-5} mol (0.004 g) of sodium cyanate (NaOCN), dissolved in 1 mL of water/tetrahydrofuran (1/1), was introduced into the flask containing the diazonium salt. The polymerization medium was then

heated to 50 °C. The statistical copolymers formed after 1.5 and 16 h of reaction were isolated by precipitation in a 10-fold excess of cold methanol, dried, and weighed so as to determine the conversion.

Binding of FGF-2 to FGF Receptor-1 (FGFR-1). High-affinity binding of FGF-2 to CHO cells was performed as described in detail elsewhere (*10*, *16*). Briefly, confluent CHO-*pgs*A-745-*flg* cells, which are deficient in heparan sulfates and genetically engineered to express the FGF receptor-1, were incubated with 125 I-FGF-2 and increasing concentrations of test gycopolymer for 90 min at 40 °C. Low-affinity-bound FGF-2 was released from the cell surface by a 5 min incubation with a cold solution containing 1.6 M NaCl and 20 mM HEPES, pH 7.4. High-affinity-bound FGF-2 was determined by a 2 M NaCl and 20 mM acetate buffer, pH 4.0, extraction.

RESULTS AND DISCUSSION

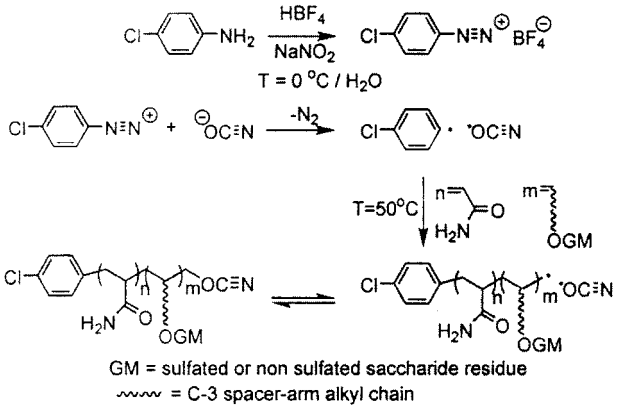
1. Synthesis of Glycomonomers Bearing Nonsulfated and Sulfated *N*-Acetyl-D-glucosamine and Lactose. Three different glycosidation methods have been previously reported for the synthesis of monosaccharides containing spacer side chains. Specifically, $FeCl_3$ has been used as a catalyst for generating monosaccharides derivatized in positions C-1 (*17*). Similarly, trifluoromethanesulfonic acid (*18*), as well as 10-camphorsulfonic acid (CSA) (*19*, *20*), has been utilized for the synthesis of spacer-armed glycosides either from glucose or an oxazoline derivative. For our purpose, we resorted to the CSA/reflux method that provided a facile means of yielding nonsulfated and sulfated alkene-derivatized monosaccharides from *N*-acetyl-D-glucosamine (Figure 1) (*15*). The reflux of *N*-acetyl-D-glucosamine with a catalytic amount of CSA and a large excess of either *n*-pentenyl or *ω*-undecenyl alcohol provided a mixture of α- and *β*-anomers (**1**(C-3) or **1**(C-9)), with an average crude yield of 60−70%. The α- and *β*-anomeric configurations of the separated products were determined on the basis of unique $J_{1,2}$ coupling constants of 3.6 and 8.0 Hz, respectively. Compounds were separated by column chromatography with a ratio α/*β* of 3/1 for both C-3 and C-9 glycosides.

The preparation of compound **3** has been reported previously by two groups (*14*, *15*). Matsuoka et al. (*14*) synthesized **3** from bromolactose using HgCN during the glycosidation step with a 40% yield for the *n*-pentenyl lactose. Likewise, Allen and Danishefsky (*15*) reported that glycosidation proceeds smoothly using $AgCO_3$ with a 75% yield of the pentenyl glycoside and an overall yield from octaacetyl lactose of ∼65% in three to four steps. We elected to synthesize the *n*-pentenyl glycosides via CSA reflux methodology, which afforded the *n*-pentenyl lactoside **3** in a single step with moderate yield (∼45%) from inexpensive and commercially available D-lactose (Figure 1).

Chemoselective sulfation of all hydroxyl groups on α-anomers, namely compounds **1**(C-3), **1**(C-9), and **3**, was achieved by reaction with SO_3−NMe_3 at 60 °C in DMF. Preparative chromatography through successive columns containing diethylaminoethyl (DEAE)-sephacel anion-exchange resin and trisacryl size-exclusion resin was required for isolation of the pure sulfated product (Figure 1, compounds **2**(C-3), **2**(C-9), and **4**).

2. Synthesis of *ω*-Alkenyl Mono- and Disaccharide-Based Glycopolymers. Druliner (*11*) in the early 1990s and more recently Grande and Gnanou (*12*) have observed that a certain degree of control can be achieved when polymerizing a broad range of (meth)acrylic monomers, and particularly acrylamide, in the presence of

Scheme 1. Cyanoxyl-Mediated Free-Radical Copolymerization of AM with Alkene-Derivatized Unprotected Glycomonomers



cyanoxyl (•OC≡N) persistent radicals, as moderators of the polymerization reaction. Significantly, these persistent radicals function under milder conditions (25−70 °C) than those required for nitroxide-controlled free-radical polymerization or ATRP processes. Given the potential advantages of cyanoxyl-mediated free-radical polymerization, we investigated the copolymerization of acrylamide with a variety of unprotected alkene-derivatized saccharides (compounds **1**−**4**).

Cyanoxyl radicals were readily generated by an electron-transfer reaction between cyanate anions ($^-$OC≡N) from a NaOCN aqueous solution, and *p*-chlorobenzene-diazonium salts ($ClC_6H_4N{\equiv}N^+BF_4^-$) that were previously prepared in situ through a diazotization reaction of *p*-chloroaniline in water. In addition to cyanoxyl persistent radicals, aryl-type active radicals were simultaneously produced, and only the latter species were able to initiate chain growth (Scheme 1). A series of water-soluble glycopolymers were prepared by varying the nature of the *ω*-alkenyl glycomonomer (nonsulfated/sulfated, mono-/disaccharide-based), as well as the initial molar ratio of glycomonomer (GM) to AM in the statistical copolymerization of both comonomers performed at 50 °C (Table 1). These statistical copolymers were isolated by precipitation in a 10-fold excess of methanol and characterized by ^{1}H NMR spectroscopy, as well as by SEC coupled with both refractive index and laser light-scattering detectors (*13*). The absence of residual comonomers, including glycomonomer, was assessed by ^{1}H NMR. The ratio of the resonance signal intensity from the methyl protons of *N*-acetyl groups from sugar moieties (2.0 ppm) to that of methine protons from the hydrocarbon skeleton (2.1−2.4 ppm) enabled the determination of saccharide content, for those glycopolymers containing *N*-acetyl-D-glucosamine residues. As for lactose-based samples, elemental analysis was used to assess carbohydrate composition. Notably, saccharide contents as well as molar masses increased with monomer conversion while polydispersity indexes remained below 1.5. Regardless of the glycomonomer used (mono/disaccharide-based, nonsulfated/sulfated), an initial ratio GM/AM of 1/4, associated with a copolymerization time of 16 h, permitted the access to a copolymer that displayed a saccharide content in close agreement with that expected. Samples exhibiting sugar compositions as high as 69 wt % were thus obtained. Nonetheless, copolymers with higher carbohydrate contents were associated with an increase in the polydispersity index. This may be attributable to some loss of control over the copolymerization process in the presence of increasing concentrations of *ω*-alkenyl

Table 1. Statistical Free-Radical Copolymerization of AM with ω-Alkenyl Mono- or Disaccharide-Based Unprotected Glycomonomers Using $ClC_6H_4N{\equiv}N^+BF_4^-$/NaOCN as the Initiating System[a]

glycomonomer (GM)	monomer ratio GM/AM (mol)	time (h)	yield[b] (%)	polymer composition GM/AM (mol)	saccharide content (wt %)	M_n (g/mol)	M_w/M_n SEC
1(C-3)	1/4	1.5	10	1/7	38	24100	1.46
		16	30	1/5	50	43000	1.47
	1/20	1.5	23	1/90	4	94000	1.17
		16	30	1/70	5	112100	1.20
1(C-9)	1/4	1.5	15	1/16	25	43400	1.25
		16	20	1/6	46	99300	1.45
	1/20	1.5	21	1/166	3	25800	1.14
		16	29	1/100	5	28200	1.24
2(C-3)	1/4	1.5	21	1/10	44	16100	1.13
		16	35	1/6	55	57300	1.37
	1/20	1.5	35	1/93	07	25400	1.10
		16	51	1/58	11	47200	1.29
2(C-9)	1/4	16	26	1/10	45	57200	1.20
	1/20	16	11	1/42	17	16300	1.17
3	1/20	16	15	1/30	16	28800	1.31
4	1/4	16	30	1/6	69	38000	1.50

[a] $T = 50$ °C, $[GM]_0 + [AM]_0 = 1$ mol/L, $[I]_0 = [ClC_6H_4N{\equiv}N^+BF_4^-]_0 = [NaOCN]_0 = 0.02$ mol/L. [b] Total conversion of comonomers as determined by gravimetry.

Table 2. Statistical Free-Radical Copolymerization of AM with ω-Alkenyl Mono- or Disaccharide-Based Unprotected Glycomonomers Using APS/TMEDA as the Initiating System[a]

glycomonomer (GM)	monomer ratio GM/AM (mol)	time (h)	yield[b] (%)	polymer composition GM/AM (mol)	saccharide content (wt %)	M_n (g/mol)	M_w/M_n SEC
1(C-3)	1/4	1.5	67	1/14	22	133000	1.63
		16	73	1/11	28	146000	1.73
3	1/4	16	83	1/10	38	140000	1.78
	1/20	16	80	1/48	11	156000	2.08
4	1/4	16	50	1/18	43	70500	1.59
	1/20	16	70	1/60	18	80000	1.89

[a] $T = 25$ °C, $[M]_0 = [GM]_0 + [AM]_0 = 1$ mol/L, $[I]_0 = [APS]_0 = [TMEDA]_0 = 0.02$mol/L. [b] Total conversion of comonomers as determined by gravimetry.

glycomonomers, considering the innate low chemical reactivity of the vinyl group in these saccharide monomers. The limited reactivity of the vinyl group, particularly in association with disaccharide bearing monomers, may also be a contributory factor in reducing monomer conversion. Despite a 16-h reaction period, overall yields for polymers derived from glycomonomers **3** and **4** ranged from 15 to 30%.

In a comparative study, classical free-radical copolymerization of glycomonomers and AM were performed using APS/TMEDA as the initiating system. TMEDA accelerates the homolytic scission of APS yielding sulfate ($SO_4^{\bullet-}$), hemiTMEDA ($(CH_3)_2NCH_2CH_2(CH_3)$-$NCH_2^{\bullet}$), and hydroxyl ($^{\bullet}OH$) radical species. The reaction medium was homogeneous and the polymerization proceeded smoothly at room temperature (Table 2). Utilizing otherwise identical experimental conditions as those used for cyanoxyl-mediated processes ($[M]_0 = 1$ mol/L, $[I]_0 = 2 \times 10^{-2}$ mol/L), the resulting glycopolymers exhibited lower saccharide contents (maximum: 43 wt %) with higher molar masses and polydispersity indexes (1.6−2.0). Moreover, increasing the polymerization time from 1.5 to 16 h increased the polydispersity index, but otherwise had little influence on either saccharide content or molar mass. The observed increase in polydispersity, however, was offset by significantly higher polymer yields, ranging up to 80% for monomers **3** and **4**. In summary, these investigations illustrate the anticipated absence of control over the copolymerization process by employing the classical APS/TMEDA initiating system, while confirming the significant role of cyanoxyl radicals in moderating the polymerization process.

3. Binding of FGF-2 to FGF Receptor-1 (FGFR-1). The capacity of selected glycopolymers to promote the binding of FGF-2 to FGFR-1 was defined using CHO-*pgs*A-745-*flg* cells, which are deficient in heparan sulfates and genetically engineered to express a single FGF receptor subtype, FGFR-1. FGFR-1 is normally expressed on a wide variety of cell types and when activated can initiate cell proliferation and migration and other cell type-specific responses. Given the preliminary nature of these bioactivity studies, limited yields for glycomonomers, and low conversions associated with cyanoxyl-mediated polymerization for vinyl monomers bearing pendant disaccharides, both classical and cyanoxyl-mediated polymerization strategies were used to synthesize the glycopolymers available for receptor binding experiments (Table 3). Results of these investigations for polymers bearing mono- and disaccharides are summarized in Figures 2 and 3, respectively. As anticipated, heparin is a strong promotor of FGF-2 binding to FGFR-1. Monosaccharide bearing glycopolymers were all of similar saccharide content, nominal molecular weight, and polydispersity (Figure 2). Sulfation-enhanced receptor binding of FGF-2 with a biphasic response observed for polymers (**GP2**) composed of monomer **2**(C-3). The reduction in receptor binding at high glycopolymer concentrations is also characteristic of heparin and is likely related to a sequestration effect, which limits FGF-2 availability. Notably, the use of a longer (C-9) spacer arm (**GP3**) did not enhance receptor binding.

Table 3. Structure-bFGF Binding Activity Relationships Studies: Summary of Molecular Characteristics Associated with Glycopolymers

glyco-monomer (GM)	polymer composition GM/AM (mol)	saccharide content (wt %)	M_n (g/mol)	M_w/M_n SEC	code
1(C-3)	1/5	50	43000	1.47	GP1
2(C-3)	1/6	55	57300	1.37	GP2
2(C-9)	1/10	45	57200	1.20	GP3
3	1/10	38	140000	1.78	GP4
4	1/18	43	70500	1.59	GP5

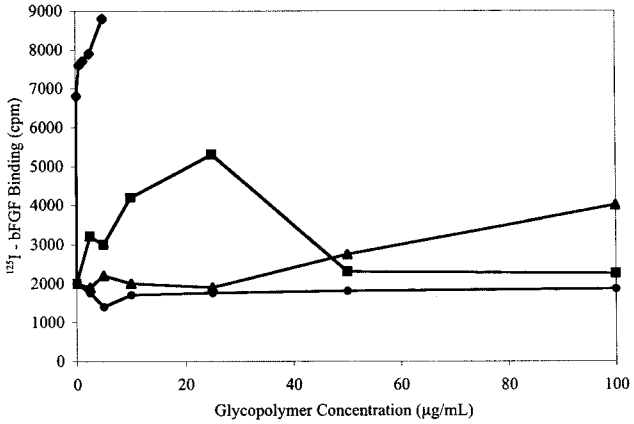


Figure 2. bFGF-binding assays for monosaccharide-based glycopolymers (◆ heparin, ● GP1, ■ GP2, ▲ GP3). The data are representative of binding assays performed in duplicate. Free sulfated monomer did not potentiate FGF-2 binding to heparan sulfate-deficient CHO cells.

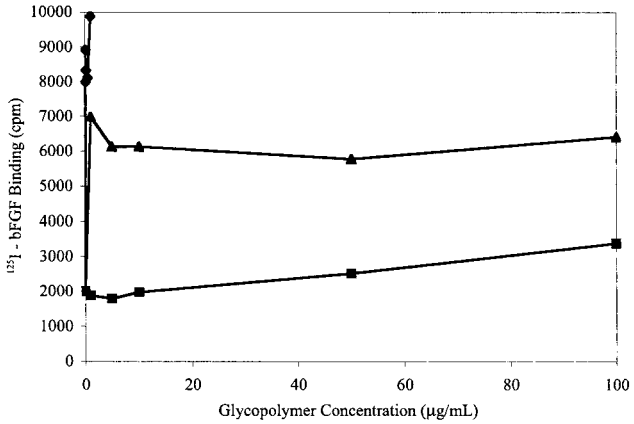


Figure 3. bFGF-binding assays for disaccharide-based glycopolymers (◆ heparin, ■ GP4, ▲ GP5). The data are representative of binding assays performed in duplicate. Free sulfated monomer did not potentiate FGF-2 binding to heparan sulfate-deficient CHO cells.

Disaccharide-bearing glycopolymers were all of similar saccharide content and polydispersity (Figure 3). Polymers bearing pendant lactose units (**GP4**) had little effect on receptor binding. A pronounced effect, however, was observed for polymers that contain sulfated lactose groups (**GP5**), even at very low polymer concentrations ($\sim$1 μg/mL). Of interest, an inhibitory effect on receptor binding was not observed as polymer concentration was increased.

CONCLUSIONS

We have synthesized a series of model mono- and disaccharide-carrying unprotected glycomonomers for the design of heparan sulfate glycomimetics. The present study broadens the family of vinyl monomers that are polymerizable with some degree of control by cyanoxyl-mediated free-radical polymerization. Both nonsulfated and sulfated alkene-derivatized monosaccharides and disaccharides were polymerized using this approach. While high carbohydrate contents and low polydispersity indexes ($1.1 < M_w/M_n < 1.6$) can be achieved further optimization of this strategy is required to enhance polymer yield, particularly for monomers bearing disaccharide units. Preliminary bioactivity studies reveal that glycopolymers containing pendant sulfated lactose groups significantly enhance FGF-2 binding to its receptor, FGFR-1, even at low polymer concentrations. We believe that tailored glycopolymers will contribute to the progress of glycotechnology, including the design of biomaterials for tissue regeneration and wound-healing applications.

ACKNOWLEDGMENT

This work was supported by grants from the NIH. The authors acknowledge the Emory University NMR and Mass Spectrometry Centers for their facilities. They are also indebted to Dr. Suri Iyer for kind technical assistance.

LITERATURE CITED

(1) Saksela, O.; Moscatelli, D.; Sommer, A.; Rifkin, D. B. (1988) *J. Cell. Biol. 107*, 743.
(2) Schlessinger, J.; Lax, I.; Lemmon, M. (1995) *Cell 83*, 357.
(3) Clowes, A. W.; Karnovsky, M. J. (1977) *Nature 265*, 625.
(4) Jackson, R. L.; Busch, S. J.; Cardin, A. L. (1991) *Physiol. Rev. 71*, 481.
(5) Linhardt, R. J.; Kerns, R. J.; Vlahov, I. R. (1996) In *Biomedical Functions and Biotechnology of Natural and Artificial Polymers*, p 45, ATL Press,
(6) (a) Jozefowicz, M.; Jozefonvicz, J. (1997) *Biomaterials 18*, 1633. (b) de Raucourt, E.; Mauray, S.; Chaubet, F.; Maiga-Revel O.; Jozefowicz, M.; Fischer, A. M. (1998) *J. Biomed. Mater. Res. 41*, 49. (c) Blanquaert, F.; Barritault, D.; Caruelle, J. P. (1999) *J. Biomed. Mater. Res. 44*, 63. (d) Logeart-Avramoglou, D.; Jozefonvicz, J. (1999) *J. Biomed. Mater. Res. 48*, 578. (e) Tardieu, M.; Gamby, C.; Avramoglou, T.; Jozefonvicz, J.; Barritault, D. (1992) *J. Cell. Physiol. 150*, 194. (f) Desgranges, P.; Caruelle, J. P.; Carpentier, G.; Barritault, D.; Tardieu, M. (2001) *J. Biomed. Mater. Res. 58*, 1.
(7) Gallagher, J. T. (1995) In *Glycoimmunology*, p 125, Plenum Press, New York.
(8) (a) van Boeckel, C. A. A.; Petitou, M. (1993) *Angew. Chem., Int. Ed. Engl. 32*, 2, 1671. (b) Westerduin, P.; Basten, J. E. M.; Broekhoven, M. A.; De Kimpe, V.; Kuijpers, W. H. A.; Van Boeckel, C. A. A. (1996) *Angew. Chem., Int. Ed. Engl. 35*, 331. (c) Petitou, M.; Duchaussoy, P.; Driguez, P.-A.; Jaurand, G.; Hérault, J.-P.; Lormeau, J.-C.; van Boeckel, C. A. A.; Herbert, J.-M. (1998) *Angew. Chem., Int. Ed. Engl. 37*, 3009. (d) Petitou, M.; Hérault, J.-P.; Bernat, A.; Driguez, P.-A.; Duchaussoy, P.; Lormeau, J.-C.; Herbert, J.-M. (1999) *Nature 398*, 417.
(9) (a) Westman, J.; Nilsson, M.; Ornitz, D. M.; Svahn, C.-M. (1995) *J. Carbohydr. Chem. 14*, 95. (b) Ornitz, D. M.; Herr, A. B.; Nilsson, M.; Westman, J.; Svahn, C.-M.; Waksman, G. (1995) *Science, 268*, 432.
(10) (a) Ornitz, D. M.; Yayon, A.; Flanagan, J. G.; Svahn, C. M.; Levi, E.; Leder, P. (1992) *Mol. Cell. Biol., 12*, 240. (b) Aviezer, D.; Levy, E.; Safran, M.; Svahn, C.; Buddecke, E.; Schmidt, A.; David, G.; Vlodavsky, I.; Yayon, A. (1994) *J. Biol. Chem. 269*, 114.
(11) Druliner, J. D. (1991) *Macromolecules 24*, 6079.
(12) Gnanou, Y.; Grande, D.; Guerrero, R. (1999) *Polym. Prepr. (Am. Chem. Soc., Div. Polym. Chem.) 40* (2), 99.
(13) (a) Grande, D.; Baskaran, S.; Baskaran, C.; Gnanou, Y.; Chaikof, E. L. (2000) *Macromolecules 33*, 1123. (b) Grande, D.; Baskaran, S.; Chaikof, E. L. (2001) *Macromolecules 34*, 1640.
(14) Matsuoka, K.; Nishimura, S.-I. (1995) *Macromolecules 28*, 2961.
(15) Allen, J. R.; Danishefsky, S. J. (1999) *J. Am. Chem. Soc. 121*, 10875 (and further references therein).
(16) Yayon, A.; Klagsbrun, M.; Esko, J. D.; Leder, P.; Ornitz, D. M. (1991) *Cell 64*, 841.
(17) Peter, M. G.; Boldt, P. C.; Peterson, S. (1992) *Liebigs Ann. Chem*. 1275.
(18) Udodong, U. E.; Rao, C. S.; Fraser-Reid, B. (1992) *Tetrahedron 48*, 4713.
(19) (a) Nishimura, S.-I.; Matsuoka, K.; Kurita, K. (1990) *Macromolecules 23*, 4182. (b) Nishimura, S.-I.; Matsuoka, K.; Furuike, T.; Ishii, S.; Kurita, K. (1991) *Macromolecules 24*, 4236.
(20) Konradsson, P.; Roberts, C.; Fraser-Reid, B. (1991) *Recl. Trav. Chim. Pays-Bas 110*, 23.

BC0255485

Ion Conductors Derived from Biogenic Amines, Bile Acids, and Amino Acids

Punam Bandyopadhyay, Prasun Bandyopadhyay, and Steven L. Regen*

Department of Chemistry, Lehigh University, Bethlehem, Pennsylvania 18015. Received May 24, 2002; Revised Manuscript Received August 20, 2002

A family of conjugates has been synthesized from spermine, putrescine, lysine, γ-aminobutyric acid, sarcosine, cholic acid, glycocholic acid, 3α,7α-dihydroxycholic acid, and 3α,12α-dihydroxycholic acid, based on a design principle previously reported (Bandyopadhyay, P., Janout, V., Zhang, L., Regen, S. L. (2001) *J. Am. Chem. Soc. 123,* 7691). Each of these conjugates was found to exhibit significant activity in promoting the transport of Na^+ across liposomal membranes derived from 1,2-dimyristoleoyl-*sn*-glycero-3-phosphocholine, and also from 1,2-dipalmitoleoyl-*sn*-glycero-3-phosphocholine. In all cases, plots of pseudo first-order rate constants, k_{obsd} vs (mol % of ion conductor)^2 were found to be linear, indicating that transport-active dimers are involved and that only a small fraction of the conjugates are in an aggregated form. An operational comparison that has been made within this series of conjugates indicates that Na^+ transport activity and membrane selectivity have a moderate dependency on the composition and the structure of the ion conductor.

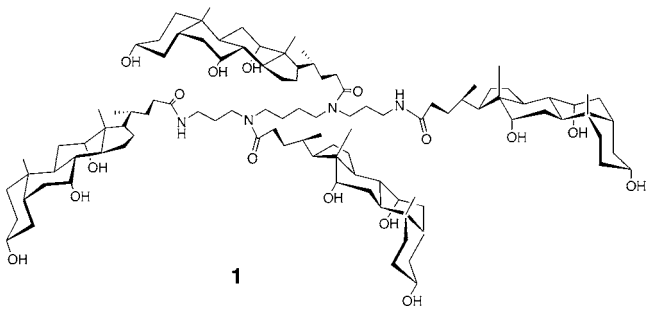
INTRODUCTION

We have been involved in the synthesis of new classes of ion conductors (i.e., molecules that transport ions across phospholipid bilayers) over the past several years (*1*). Our motivation for such work stems from belief that those ion conductors, which exhibit high activity and high membrane selectivity, have potential as antibiotics. In particular, ion conductors that are capable of selectively killing microorganisms in the presence of mammalian cells, by destroying their membrane integrity, would circumvent two of the major mechanisms of drug resistance; that is, enzymatic degradation within the cell and export pathways (*2*, *3*).

Recently, we introduced a new design principle for the construction of ion conductors in which two or more facial amphiphiles are covalently attached to a linear backbone (Scheme 1) (*1k*,*l*). When incorporated into a lipid bilayer, such conjugates are expected to favor conformation **B** where each hydrophobic face (darkened rectangle) is in intimate contact with the alkyl chains of neighboring phospholipids, and each hydrophilic face (lightly shaded rectangle) points toward a hydrophilic face of a nearest-neighbor.

Conformation **A**, on the other hand, is expected to be favored when the conjugate is adsorbed to the membrane surface. In principle, dimerization of **B** across a lipid bilayer should produce a contiguous pathway that permits a flow of ions. One prototype that was recently reported (i.e., **1**) exhibited ion conducting and monolayer properties that were consistent with this model. As noted previously, **1** is unique in the sense that it is derived from the direct conjugation of two underivatized biogenic precursors—spermine and cholic acid.

In the work that is reported herein, we sought to expand this class of ion conductors by preparing a series

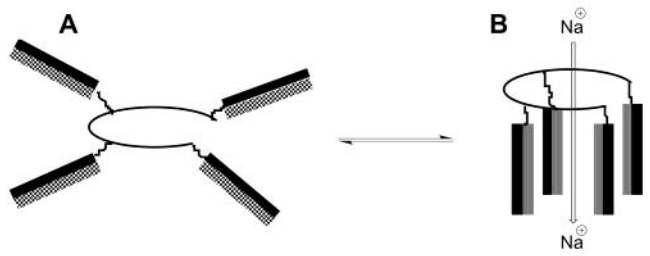


1

of analogues; that is, *a variety of ion conductors from naturally occurring facial amphiphiles and biogenic amines or amino acids*. Our primary interest in this study was to determine the sensitivity of ion transport activity and membrane selectivity toward modest changes in the structure and composition of the ion conductor.

With this aim in mind, we focused on the synthesis of a series of conjugates derived from spermine, putrescine, lysine, γ-aminobutyric acid, sarcosine, cholic acid, glycocholic acid, 3α,7α-dihydroxycholic acid, and 3α,12α-dihydroxycholic acid, and a determination of their ability to promote Na^+ transport across liposomal bilayers made from 1,2-dimyristoleoyl-*sn*-glycero-3-phosphocholine [(C14:1)PC], and also from 1,2-dipalmitoleoyl-*sn*-glycero-3-phosphocholine [(C16:1)PC]. As discussed previously, the

Scheme 1

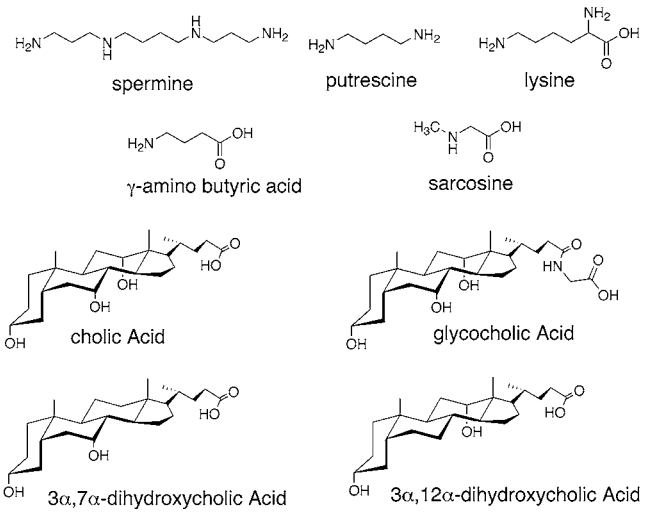


* To whom correspondence should be addressed. E-mail: slr0@lehigh.edu.

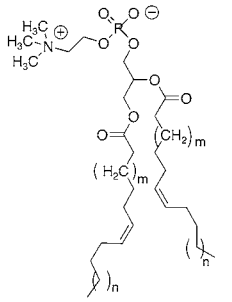
10.1021/bc0255539 CCC: $22.00 © 2002 American Chemical Society
Published on Web 10/19/2002

ability of an ion conductor to respond to differences in membrane thickness raises the possibility of being able to exploit subtle differences between the membranes of mammals and of microorganisms from a therapeutic standpoint (*1j*). In particular, fungal and bacterial membranes are expected to have regions that are thinner and more susceptible toward ion transport than mammalian membranes, since the cholesterol that is present in the latter is known to condense and thicken bilayers.

Natural Building Blocks for Ion Conductors



Liposome-Forming Lipids



MATERIALS AND METHODS

General Methods. Unless stated otherwise, all reagents were obtained from commercial sources and used without further purification. Phospholipids that were used for preparing liposomes were obtained from Avanti Polar Lipids (Alabaster, AL). Specific procedures for preparing a paramagnetic shift reagent, for forming vesicles, and for measuring rates of Na^+ transport by NMR spectroscopy have previously been described in detail (*1l*). House-deionized water was purified using a Millipore Milli-Q-filtering system containing one carbon and two ion-exchange stages. Vesicle extrusions were carried out using a Lipex Biomembrane apparatus (Vancouver, BC). All ^1H NMR and $^{23}Na^+$ NMR spectra were recorded on 500 and 360 MHz instruments, respectively; chemical shifts are reported in ppm relative to residual solvent. The pH of the NaCl solution that was used in these transport experiments was typically ca. 6.

Conjugate 2. To a solution of glycocholic acid (0.200 g, 0.43 mmol) in 1 mL of DMF was added 0.10 mL of diisopropylethylamine (DIPEA) plus *O*-(3,4-dihydro-4-oxo-1,2,3-benzotriazin-3-yl)-*N*,*N*,*N*′*N*′-tetramethyluronium tetrafluoroborate (0.163 g, 0.47 mmol). After stirring this mixture for 2 h at room temperature, a solution of spermine (18.2 mg, 0.090 mmol) and DIPEA (0.3 mL) in 1 mL DMF was added, dropwise, followed by additional stirring for 16 h at 55 °C. Removal of solvent under reduced pressure at 50 °C afforded a residue, which was then dissolved in 1 mL of methanol. This solution was then added to 15 mL of a 10% aqueous $NaHCO_3$ solution, and the solid collected via filtration and purified by column chromatography (SiO_2, $CHCl_3$/MeOH/H_2O, 120/60/2, v/v/v) affording 80 mg (47%) of **2** having R_f 0.45 (SiO_2, $CHCl_3$/MeOH/H_2O, 120/60/2, v/v/v) and ^1H NMR (CD_3OD, 500 MHz) δ (ppm): 4.07 (m, 4 H), 3.95 (bs, 4 H) 3.79 (m, 8 H), 3.35 (m, 4 H), 3.30−3.10 (m, 12 H), 2.21−0.91 (m, 128 H), 0.71 (s, 12 H). HRMS for $C_{114}H_{190}N_8O_{20}(MNa^+)$: Calcd: 2014.3989. Found: 2014.4086.

Conjugate 3. A solution was prepared from cholic acid succinimide ester (2.0 g, 4 mmol), 10 mL of DMF, 2 mL of DIPEA, and 4-aminobutyric acid (0.404 g, 4 mmol) and stirred at 40 °C for 24 h. Removal of solvent under reduced pressure afforded a residue that was dissolved in 1.5 mL of methanol and then precipitated via the addition of 15 mL of a 10% aqueous $NaHCO_3$ solution. The resulting solid was filtered and purified via column chromatography (SiO_2, $CHCl_3$/MeOH/H_2O, 120/60/1, v/v/v) yielding 1.0 g (55%) of the corresponding 4-aminobutyric acid conjugate of cholic acid having R_f 0.50 (SiO_2, $CHCl_3$/MeOH/H_2O, 120/60/1, v/v/v) and ^1H NMR (CD_3OD 500 MHz) δ (ppm): 3.95 (s, 1 H), 3.78 (s, 1 H), 3.35 (m, 1 H) 3.21 (t, 2 H), 2.30−0.91 (m, 34 H), 0.70 (s, 3 H).

A solution was then made from 0.200 g (0.40 mmol) of the above conjugate, along with 1 mL of DMF, 0.2 mL of DIPEA, and *O*-(3,4-dihydro-4-oxo-1,2,3-benzotriazin-3-yl)-*N*,*N*,*N*′*N*′-tetramethyluronium tetrafluoroborate (0.152 g, 0.44 mmol), which was then stirred at room temperature for 2 h. To this solution was added, dropwise, a solution made from spermine (17.0 mg, 0.084 mmol) and 0.3 mL of DIPEA in 1 mL of DMF, and the resulting solution was stirred at 55 °C for 16 h. Removal of solvent under reduced pressure (50 °C) afforded a residue that was dissolved in 1 mL of methanol. Subsequent precipitation via the addition of 15 mL of a 10% aqueous $NaHCO_3$ solution, followed by filtration and purification via preparative thin-layer chromatography (SiO_2, $CHCl_3$/MeOH/H_2O, 120/73/2, v/v/v), afforded 60 mg (35%) of **3** having R_f 0.50 (SiO_2, $CHCl_3$/MeOH/H_2O, 120/73/2, v/v/v) and ^1H NMR (CD_3OD, 500 MHz) δ (ppm): 3.95 (br s, 4 H), 3.79 (m, 4 H), 3.35 (m, 4 H), 3.30−3.20 (m, 8 H), 3.18 (m, 12 H), 2.21−0.91(m, 144 H), 0.71 (s, 12 H). HRMS for $C_{122}H_{206}N_8O_{20}$ (Na^+) Calcd: 2126.5241. Found: 2126.5343.

Conjugate 4. A solution was prepared from cholic acid succinimide ester (1.015 g, 2 mmol), 7 mL of DMF, 1 mL of DIPEA, and sarcosine (0.178 g, 2 mmol) and allowed to stir at 50 °C for 48 h. The solvent was then removed under reduced pressure, and the residue purified by column chromatography (SiO_2, $CHCl_3$/MeOH/H_2O, 120/100/5, v/v/v) to give 0.450 g (45%) of the corresponding sarcosine conjugate of cholic acid having R_f 0.54 (SiO_2, $CHCl_3$/CH_3OH/H_2O, 120/100/5, v/v/v) and ^1H NMR (D_2O, 500 MHz): δ (ppm): 4.0−3.94 (m, 3 H); 3.79 (s, 1 H), 3.41 (m, 1 H), 2.90 (d, 3 H), 2.31−0.91 (m, 30 H), 0.64 (s, 3 H).

The above conjugate (0.100 g, 0.22 mmol) was dissolved in 0.2 mL of DIPEA plus 1 mL of DMF, followed by addition of *O*-(3,4-dihydro-4-oxo-1,2,3-benzotriazin-3-yl)-*N*,*N*,*N*′*N*′-tetramethyluronium tetrafluoroborate, (0.079 g, 0.23 mmol). This solution was then stirred at room temperature for 2 h, followed by the dropwise addition of a solution made from spermine (8.6 mg, 0.042 mmol)

and 0.2 mL of DIPEA in 0.5 mL of DMF; stirring was continued for an additional 16 h. Removal of solvent under reduced pressure (50 °C) afforded a residue that was dissolved in a minimum volume of methanol and added, dropwise, to a stirred 10% aqueous $NaHCO_3$ solution (20 mL). The resulting solid was purified by column chromatography (SiO_2, $CHCl_3$/MeOH/H_2O, 120/80/3, v/v/v) to give 36 mg (45%) of **4** having R_f 0.65 (SiO_2, $CHCl_3$/MeOH/H_2O, 120/80/3, v/v/v) and ^{1}H NMR [$(CD_3)_2$SO, 500 MHz] δ ppm 4.15 (s, 4 H), 3.94 (s, 4 H); 3.83 (s, 4 H), 3.69 (s, 4 H), 3.32−3.13 (m, 16 H), 2.95 (br s, 12 H), 2.41−0.91 (m, 128 H), 0.70 (s, 12 H). HRMS: $C_{118}H_{198}N_8O_{20}$-(Na^+) Calcd: 2070.4615. Found: 2070.4578.

Conjugate 5. A suspension was prepared from cholic acid succinimide ester (0.566 g, 1.12 mmol), 1 mL of DIPEA, lysine (0.078 g, 0.5 mmol), and Na_2CO_3 (0.056 g, 0.5 mmol) in DMF and stirred for 16 h at 50 °C. Removal of solvent under reduced pressure (50 °C) afforded a residue that was dissolved in 1 mL of methanol. This methanolic solution was then added, dropwise, to a saturated aqueous Na_2CO_3 solution with stirring. The precipitate was removed by filtration and purified by column chromatography (SiO_2,$CHCl_3$/MeOH/H_2O, 65/25/4, v/v/v) to give 0.356 g (72%) of the corresponding lysine conjugate of cholic acid having R_f 0.30 (SiO_2,$CHCl_3$/MeOH/H_2O, 65/25/4, v/v/v) and ^{1}H NMR (CD_3OD, 360 MHz) δ ppm 4.25 (m, 1 H), 3.94 (m, 2 H), 3.79 (s, 2 H), 3.35 (m, 2 H); 3.16 (t, 2 H), 2.21−0.91 (m, 66 H), 0.70 (s, 6 H).

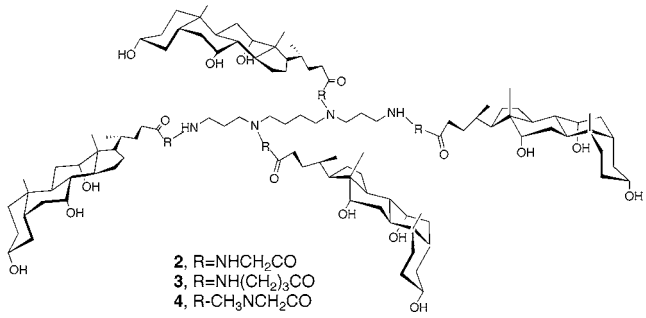
The above conjugate (0.100 g, 0.107 mmol) was dissolved in 0.2 mL of DIPEA plus 1 mL of DMF, followed by the addition of *N*,*N*,*N*′,*N*′-tetramethyl-*O*-(*N*-succinimidyl)uronium terafluoroborate (0.039 g, 0.129 mmmol). The resulting solution was then allowed to stir for 2 h at 50 °C. To this solution was added a solution that was made from putrescine (0.3 mL), 0.2 mL of DIPEA, and 0.5 mL of DMF. After stirring for 16 h at 50 °C, the solvent was then removed under reduced pressure (50 °C) and the residue dissolved in 1 mL of methanol. This solution was then added, dropwise, to an 10% aqueous Na_2CO_3 solution. The resulting solid was collected by filtration and purified by column chromatography (SiO_2, $CHCl_3$/MeOH/H_2O, 120/50/2, v/v/v) to give 30 mg (47%) of **5** having R_f 0.55 (SiO_2, $CHCl_3$/MeOH/H_2O, 120/50/2, v/v/v), and ^{1}H NMR [(CD_3OD), 360 MHz]: δ (ppm): 4.25 (m, 2 H), 3.94 (m, 4 H), 3.79 (s, 4 H), 3.35 (m, 4 H), 3.16 (t, 8 H), 2.21−0.91 (m, 136 H), 0.70 (s, 12 H). HRMS for $C_{122}H_{188}N_6O_{18}$(Na^+) Calcd: 1928.3872. Found: 1928.3809.

Conjugate 6. To a solution of 5β-cholanic acid-3α,7α-diol (0.106 g, 0.26 mmol) in 0.2 mL of DIPEA plus 1 mL of DMF was added *O*-(3,4-dihydro-4-oxo-1,2,3-benzotriazin-3-yl)-*N*,*N*,*N*′*N*′-tetramethyluronium tetrafluoroborate, (0.096 g, 0.28 mmol). After stirring for 2 h at room temperature, a solution of spermine (12.0 mg, 0.060 mmol) in 0.2 mL of DIPEA plus 0.5 mL of DMF was then added, dropwise, and the mixture was allowed to stir for an additional 16 h at room temperature. Removal of solvent under reduced pressure (50 °C) afforded a residue that was dissolved in 1 mL of methanol. Subsequent precipitation via addition to a saturated aqueous $NaHCO_3$ solution, followed by filtration and purification by preparative thin-layer chromatography (SiO_2, $CHCl_3$/MeOH/H_2O, 100/20/1, v/v/v), afforded 50 mg (50%) of **6** having R_f 0.45 (SiO_2, $CHCl_3$/MeOH/H_2O, 100/20/1, v/v/v) and ^{1}H NMR (CD_3OD 360 MHz) δ (ppm): 3.79 (bs, 4 H), 3.35 (m, 4 H), 3.22−3.36 (m, 8 H), 3.16 (m, 4 H), 2.21−0.91 (m, 136 H), 0.70 (s, 12 H). HRMS for $C_{106}H_{178}N_4O_{12}$-(Na^+) Calcd: 1722.3334. Found: 1722.3235.

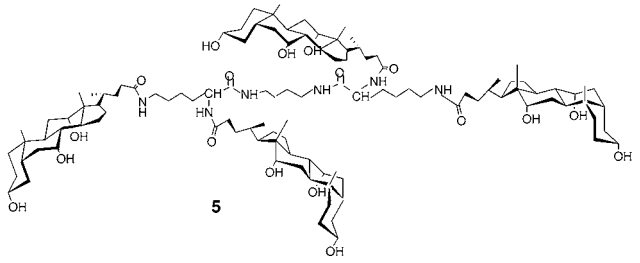
Conjugate 7. To a solution of 5β-cholanic acid-3α,12α-diol (0.106 g, 0.27 mmol) in 0.2 mL of DIPEA plus 1 mL DMF was added *O*-(3,4-dihydro-4-oxo-1,2,3-benzotriazin-3-yl)-*N*,*N*,*N*′*N*′-tetramethyluronium tetrafluoroborate, (0.096 g, 0.28 mmol). After stirring the mixture at room temperature for 2 h, a solution of spermine (12.0 mg, 0.060 mmol) and 0.2 mL of DIPEA plus 0.5 mL of DMF was added, dropwise, and the mixture was allowed to stir for an additional 16 h at room temperature. Removal of solvent under reduced pressure (50 °C) afforded a residue that was dissolved in 1 mL of methanol. Subsequent precipitation via addition to an aqueous solution that was saturated with $NaHCO_3$, and purification by preparative thin-layer chromatography (SiO_2, $CHCl_3$/MeOH/H_2O, 100/20/1, v/v/v), afforded 55 mg (55%) of **7** having R_f 0.50 (SiO_2, $CHCl_3$/MeOH/H_2O, 100/20/1, v/v/v) and ^{1}H NMR (CD_3OD, 360 MHz) δ (ppm): 3.90 (bs, 4 H), 3.35 (m, 4 H), 3.22−3.36 (m, 8 H), 3.16 (m, 4 H), 2.21−0.91 (m, 136 H), 0.70 (s, 12 H). HRMS for $C_{106}H_{178}N_4O_{12}$(Na^+) Calcd: 1722.3334. Found: 1722.3298.

RESULTS AND DISCUSSION

Ion Conductors from Biogenic Precursors. The specific molecules that were chosen as synthetic targets for this work were **2**, **3**, **4**, **5**, **6**, and **7**. Conjugates **2** and **3**, bearing sterols derived from glycocholic acid and a

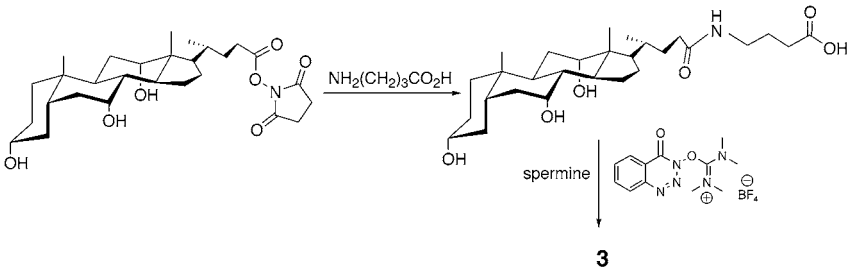


conjugate of cholic acid plus γ-amino butyric acid, respectively, extend the distance between each facial amphiphile and the spermine backbone, relative to **1**; at the same time, they add four secondary amide groups, each of which may act as a hydrogen bond donor or acceptor—a feature that could promote aggregation of the ion conductor, leading to increased activity. Ion conductor **4**, which bears facial amphiphiles made from a conjugate of sarcosine and cholic acid, is an analogue of **2**. In this case, each of the four additional amide groups can only function as hydrogen bond acceptors. Conjugate **5**, de-

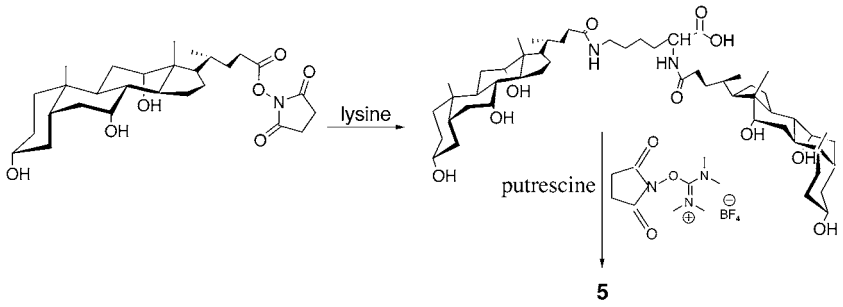


rived from four molecules of cholic acid, two lysine molecules, and one putrescine unit, may be viewed as an "expanded" analogue of **1**, which also has additional space between each of the sterol units. In addition, this conjugate contains a total of six secondary amide groups.

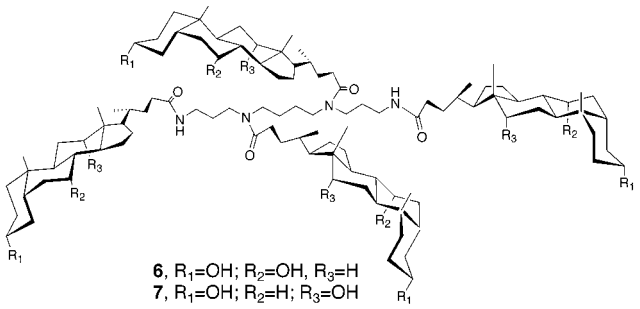
Scheme 2



Scheme 3



Finally, conjugates **6** and **7** are close analogues of **1**



having increased hydrophobicity; in this case, the hydroxyl group at the C12 and C7 carbons have been replaced by hydrogen atoms, respectively.

Conjugate **2** was synthesized by direct condensation of glycocholic acid with spermine (not shown). Conjugate **3** was prepared by first coupling γ-amino butryic acid to the cholic acid framework (Scheme 2); conjugate **4** was prepared similarly, using sarcosine in place of γ-amino butryic acid. Acylation of both amino groups of lysine with an activated form of cholic acid, followed by condensation of the resulting carboxylic acid with putrescine afforded **5** (Scheme 3). Finally, conjugates **6** and **7** were obtained by direct condensation of spermine with 3α,7α-dihydroxycholic acid and 3α,12α-dihydroxycholic acid, respectively (not shown).

Ion Conducting Properties. Liposomes that were used as model membranes in this work were in the form of 200 nm diameter unilamellar vesicles. Under the conditions used (i.e., 35 °C), liposomes derived from **C***14*, as well as from **C***16*, were maintained in the physiologically relevant fluid phase.

Using procedures similar to those that have been described in detail elsewhere, the rate at which Na^+ crosses these liposomal membranes was measured via $^{23}Na^+$ NMR spectroscopy (*1l, 4*). In all cases, varying percentages of ion conductor were introduced into the liposomes at the time of their preparation (i.e., "double-sided addition"). For these experiments, a membrane-impermeable paramagnetic shift reagent was added to the external aqueous phase so that liposomal-entrapped and external Na^+ could be distinguished. In all cases, pseudo-first-order rate constants (k_{obsd}) exhibited a second-order dependency on the mol % of the conjugate that was present. For one such experiment, where vesicles were made from **C***16*, and **2** was used as an ion conductor, both the rate of $^{23}Na^+$ influx and the rate of $^{7}Li^+$ efflux were monitored, simultaneously. Within experimental error, the rate constants for both transport processes were identical. This finding lends support for an antiport mechanism of transport. Figure 1 shows typical plots for k_{obsd} versus (mol % of **2**) (*2*) for the two different membranes investigated (**C***14* and **C***16*). As discussed previously, the linearity of such plots indicates that transport-active dimers are involved (*1g*). Here, it is assumed that only a small fraction of the conjugate is aggregated, where it can be shown that:

$$k_{obsd} = k_2[\text{monomer}]^2/K$$

where K is the equilibrium constant for dissociation of the dimer, k_2 is the rate constant for ion transport, and

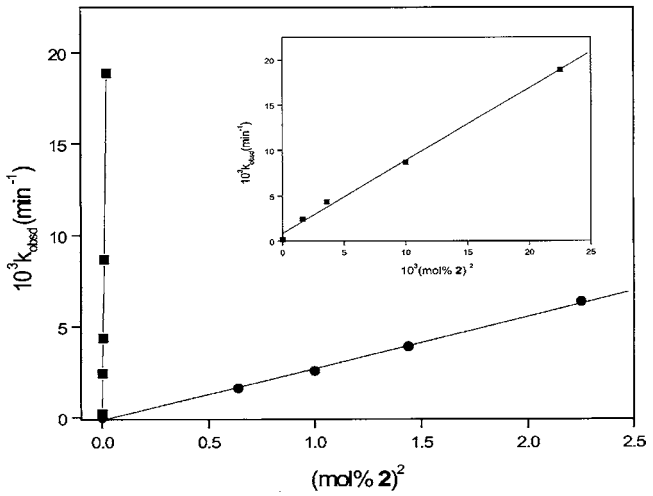


Figure 1. Plot of k_{obsd} versus (mol % **2**)^2 for vesicles made from (■) **C***14* and (●) **C***16* at 35 °C; inset shows data for **C***14* with an expanded *x*-axis.

Table 1. Ion Conducting Activities and Membrane Selectivities[a]

ion conductor	lipid	$10^4\ k_2/K$ (min^{-1} mol $\%^{-2}$)	S (**C***14*/**C***16*)
1	**C***14*	190000	1500
	C*16*	130	
2	**C***14*	8000	290
	C*16*	28	
3	**C***14*	54000	965
	C*16*	56	
4	**C***14*	29200	750
	C*16*	39	
5	**C***14*	35000	2258
	C*16*	15.5	
6	**C***14*	10560	297
	C*16*	35.6	
7	**C***14*	6028	262
	C16	23	

[a] All kinetic experiments were carried out at 35 °C; the error in k_{obsd} is estimated to be ±10%.

[monomer] is the analytical concentration of the ion conductor that is present in the dispersion.

Specific values of k_2/K that have been determined for **2**, **3**, **4**, **5**, **6**, and **7** are shown in Table 1. Since k_2 and K cannot be separated by such analysis, we are limited to operational comparisons among the conjugates. Also listed in Table 1 are membrane-selectivity factors, S, which represent the ratio of $(k_2/K)_{14}/(k_2/K)_{16}$, where *14* and *16* refer to liposomes derived from **C***14* and **C***16*, respectively.

In all cases, significant ion conductivity was observed. When the thicker **C***16* membranes were used as model systems, the differences in ion conducting activity were modest. Thus, the conjugate having the highest activity (**3**) and the one having the lowest activity (**5**), within the series **2**−**7**, differed by a factor of ca. 4. In addition, conjugate **1** was only ca. two times more active than **3**. In the thinner **C***14* membranes, however, the differences in activity were more pronounced. In this case, **3**, having the greatest activity, was ca. nine times more active than **7**. A greater difference in activity within the thinner membrane was also apparent when **1** was compared to analogues **6** and **7**. Here, removal of a single hydroxyl group from each of the sterols resulted in a reduction in Na^+ transport activity by factors of 18 and 32, respectively. An examination of the S factors in Table 1 further reveals that membrane selectivities range from 262 for **7** to 2258 for **5**. Thus, both the activity and membrane selectivity show a significant dependency on the structure and the composition of the ion conductor.

In a broader context, the present findings demonstrate the generality of our design principle. Thus, all members within this family of conjugates derived from spermine, putrescine, lysine, γ-aminobutyric acid, sarcosine, cholic acid, glycocholic acid, 3α,7α-dihydroxycholic acid, and 3α,12α-dihydroxycholic acid showed significant activity in promoting the transport of Na^+ across phospholipid membranes. Whether the observed variations in activity and membrane selectivity are due to differences in intrinsic activities (i.e., k_2) or to the extent of aggregation (K) remains to be established. In addition, the extent to which each of these conjugates is drawn into the membrane via conformation **B** (Scheme 1) is uncertain. Thus, one can rationalize the greater activity of **1**, relative to **6** and **7** in terms of a greater percentage of **1** being drawn into the bilayer through a larger number of intramolecular hydrogen bonds in conformation **B**. Alternatively, the larger number of hydroxyl groups of **1** could increase the extent of hydration of the pathway for diffusion, which, in turn, could facilitate the flow of ions; that is, its intrinsic activity could be higher. Depsite these uncertainties, the results reported herein demonstrate the feasibility of constructing an entire family of ion conductors that span a moderate range of ion transport properties, based on biogenic precursors. Efforts aimed at extending this approach with a view toward drug design are continuing in our laboratories.

ACKNOWLEDGMENT

We are grateful to the National Science Foundation (Grant CHE-9612702) for support of this research.

LITERATURE CITED

(1) (a) Stadler, E., Dedek, P., Yamashita, K., and Regen, S. L. (1994) *J. Am. Chem. Soc. 116*, 6677. (b) Sadownik, A., Deng, G., Janout, V., Bernard, E. M., Kikuchi, K., Armstrong, D., and Regen, S. L. (1995) *J. Am. Chem. Soc. 117*, 6138. (c) Yamashita, K., Janout, V., Bernard, E. M., Armstrong, D., and Regen, S. L. (1995) *J. Am. Chem. Soc. 117*, 6249. (d) Deng, G., Merritt, M., Yamashita, K., Janout, V., Sadownik, A., and Regen, S. L. (1996) *J. Am. Chem. Soc. 118*, 3307. (e) Deng, G., Dewa, T., and Regen, S. L. (1996) *J. Am. Chem. Soc. 118*, 8975. (f) Kikuchi, K., Bernard, E. M., Sadownik, A., Regen, S. L., and Armstrong, D. (1997) *Antimicrob. Agents Chemother. 41*, 1433. (g) Merritt, M., Lanier, M., Deng, G., and Regen, S. (1998) L. *J. Am. Chem. Soc. 120*, 8494. (h) Otto, S., Osifchin, M., and Regen, S. L. (1999) *J. Am. Chem. Soc. 121*, 7276. (i) Otto, S., Osifchin, M., and Regen, S. L. (1999) *J. Am. Chem. Soc. 121*, 10440. (j) DiGiorgio, A. F., Otto, S., Bandyopadhyay, P., and Regen, S. L. (2000) *J. Am. Chem. Soc. 122*, 11029. (k) Bandyopadhyay, P., Janout, V., Zhang, L., Sawko, J. A., and Regen, S. L. (2000) *J. Am. Chem. Soc. 122*, 12888. (l) Bandyopadhyay, P., Janout, V., Zhang, L., and Regen, S. L. (2001) *J. Am. Chem. Soc. 123*, 7691.

(2) For general reviews on nonpeptide ion channels and channel models, see: (a) Kobuke, Y. (1997) in *Advances in Supramolecular Chemistry* (G. W. Gokel, Ed.) Vol. 4, p 163, JAI, Greenwich, London. (b) Koert, U. (1997) *Chem. Unserer Z. 31*, 20. (c) Gokel, G. W., and Murillo, O. (1996) *Acc. Chem. Res. 29*, 425.

(3) For selected examples of other ion conductors from the recent literature, see: (a) Sakai, N., Gerard, D., and Matile, S. (2001) *J. Am. Chem. Soc. 123*, 2517. (b) Renkes, T., Schafer, H. J., Siemens, P. M., and Neumann, E. (2000) *Angew. Chem., Int. Ed. 39*, 25112. (c) Forman, S. L., Fettinger, J. C., Pieraccini, S., Gottarelli, G., and Davis, J. T. (2000) *J. Am. Chem. Soc. 122*, 4060. (d) Perez, C., Espinola, C. G., Foces-Foces, C., Nunez-Coello, P., Carrasco, H., and Martin, J. D. (2000) *Org. Lett. 2*, 1185. (e) Das, S., Kurok, P., Jedlinski, Z., and Reusch, R. N. (1999) *Macromolecules 32*, 8781. (f) Abel, E., Maguire, G. E. M., Murillo, O., Suzuki, I., De Wall, S. L., and Gokel, G. W. (1999) *J. Am. Chem. Soc. 121*, 9043. (g) Qi, Z., Sokabe, M., Donowaki, K., and Ishida, H. (1999) *Biophys. J. 76*, 631. (h) Hall, C. D., Kirkovits, G. J., and Hall, A. C. (1999) *Chem. Commun.* 1897. (i) Fritz, M. G., Walde, P., and Seebach, D. (1999) *Macromolecules 32*, 574. (j) Fyles, T. M., Hu, C., and Knoy, R. (2001) *Org. Lett. 3*, 1335.

(4) (a) Degani, H., and Elgavish, G. A. (1978) *FEBS Lett. 90*, 357. (b) Gupta, R. K., and Gupta, P. (1982) *J. Magn. Reson. 47*, 344. (c) Pike, M. M., Simon, S. R., Balschi, J. A., and Springer, C. S., Jr. (1982) *Proc. Natl Acad. Sci. U.S.A. 79*, 810. (d) Pregel, M. J., Jullien, L., and Lehn, J. M. (1992) *Angew. Chem., Int. Ed. Engl. 31*, 1637.

BC0255539

Plasmid DNA-Entrapped Nanoparticles Engineered from Microemulsion Precursors: In Vitro and in Vivo Evaluation

Zhengrong Cui and Russell J. Mumper*

Division of Pharmaceutical Sciences, College of Pharmacy, University of Kentucky, Lexington, Kentucky 40536-0082. Received June 10, 2002; Revised Manuscript Received July 29, 2002

Nonviral gene therapy has been a rapidly growing field. However, delivery systems that can provide protection for pDNA and potential targeting are still desired. A novel pDNA−nanoparticle delivery system was developed by entrapping hydrophobized pDNA inside nanoparticles engineered from oil-in-water (O/W) microemulsion precursors. Plasmid DNA was hydrophobized by complexing with cationic surfactants DOTAP and DDAB. Warm O/W microemulsions were prepared at 50−55 °C with emulsifying wax, Brij 78, Tween 20, and Tween 80. Nanoparticles were engineered by simply cooling the O/W microemulsions containing the hydrophobized pDNA in the oil phase to room temperature while stirring. The nanoparticles were characterized by particle sizing, zeta-potential, and TEM. Nanoparticles were challenged with serum nucleases to assess pDNA stability. In addition, the nanoparticles were coincubated with simulated biological media to assess their stability. In vitro hepatocyte transfection studies were completed with uncoated nanoparticles or nanoparticles coated with pullulan, a hepatocyte targeting ligand. In vivo biodistribution of the nanoparticles containing I-125 labeled pDNA was monitored 30 min after tail-vein injection to Balb/C mice. Depending on the hydrophobizing lipid agent employed, uniform pDNA-entrapped nanoparticles (100−160 nm in diameter) were engineered within minutes from warm O/W microemulsion precursors. The nanoparticles were negatively charged (−6 to −15 mV) and spherical. An anionic exchange column was used to separate unentrapped pDNA from nanoparticles. Gel permeation chromatography of pDNA-entrapped and serum-digested nanoparticles showed that the incorporation efficiency was ∼30%. Free 'naked' pDNA was completely digested by serum nucleases while the entrapped pDNA remained intact. Moreover, in vitro transfection studies in Hep G2 cells showed that pullulan-coated nanoparticles resulted in enhanced luciferase expression, compared to both pDNA alone and uncoated nanoparticles. Preincubation of the cells with free pullulan inhibited the transfection. Finally, 30 min after tail vein injection to mice, only 16% of the 'naked' pDNA remained in the circulating blood compared to over 40% of the entrapped pDNA. Due to the apparent stability of these pDNA-entrapped nanoparticles in the blood, they may have potential for systemic gene therapy applications requiring cell and/or tissue-specific delivery.

INTRODUCTION

Gene therapy has attracted a great deal of attention in recent years. The current gene delivery systems can be divided into two categories: (1) viral-based systems, and (2) non-viral-based systems. Delivery of interesting genes with viral vectors has proven to the most efficient method. However, potential toxicity, including mutagenesis and carcinogenesis, from the viral vectors presents a major limitation. In contrast, delivery of genes with plasmid DNA (pDNA) may be much safer, and perhaps more pharmaceutically acceptable. However, the efficiency of current non-viral-based systems is very poor (Rolland and Felgner, 1998; Liu and Huang, 2002). Moreover, due to the presence of serum nucleases in the blood and the rapid clearance rate of pDNA, improved formulations and delivery systems for pDNA are needed for successful systemic gene therapy (Kawabata et al., 1995; Mahato et al., 1995a; Yoshida et al., 1997; Houk et al., 2001).

* Corresponding author: Russell J. Mumper, Ph.D., Assistant Professor of Pharmaceutical Sciences, Assistant Director, Center for Pharmaceutical Science and Technology, College of Pharmacy, University of Kentucky, Lexington, KY 40536-0082. Tel: (859) 257-2300 ext. 258, Fax: (859) 323-5985, e-mail: rjmump2@uky.edu.

To date, many pDNA delivery systems, including lipoplexes (Clark and Hersh, 1999; Ishiwata et al., 2000), polyplexes (Nishikawa et al., 2000a and 2000b; Oh et al., 2001; Verbaan et al., 2001), and lipopolyplexes (Liu and Huang, 2002), have been developed. However, in general, these systems remain very sensitive to serum challenge. Moreover, these systems tend to aggregate due to extensive interaction with serum proteins and/or self-association in the blood (Chesnoy and Huang, 2000). Therefore, when administered by intravenous injection, these systems tend to accumulate into the lung. Significant work has been done to improve these systems and overcome the stated limitations. For example, for lipoplexes, complexes of cationic lipids or liposomes with pDNA, careful balance of the hydrophilicity/lipophilicity of the surface of the lipoplex particle, modification of the surface charge, and/or deposition of "shielding" agents such as poly(ethylene glycol) (PEG) on the surface of the lipoplexes, has proven to be able to extend the circulation of the complexes and therefore lead to increased distribution of pDNA to distal sites of interest (Ishiwata et al., 2000; Patel, 1992; Hong et al., 2002).

Despite some promising leads using the complexes described above, delivery systems that protect pDNA from serum nuclease digestion, provide stability for

10.1021/bc0255586 CCC: $22.00 © 2002 American Chemical Society
Published on Web 10/12/2002

prolonged circulation in blood, and that can be easily modified for potential cell or tissue targeting are still needed. Recently, researchers have attempted to encapsulate or entrap pDNA inside stable lipid-based particles for potential systemic administration. Wheeler et al. described a method to prepare stabilized plasmid−lipid particles (SPLP) (around 70 nm in diameter) using a detergent dialysis procedure (Wheeler et al., 1999). The particles allowed for the encapsulation of pDNA within a lipid envelope, which in turn protected the plasmid from digestion by serum nucleases. The particles were further stabilized in aqueous media by PEG coating. The particles demonstrated extended circulation with approximately 10% of the intravenously injected dose accumulating in a distal tumor. Further, Bailey and Sullivan have described the encapsulation of pDNA in neutral liposomes (Bailey and Sullivan, 2000). Lipoproteins, or emulsion particles that consist of lipids and apolipoproteins, have also been described by Hara et al. (1997b). This group took advantage of the hydrophobic interior of these natural emulsions to solubilize DNA. Negatively charged DNA was first complexed with cationic lipids containing a quaternary amine headgroup. The resulting hydrophobized complex was extracted by chloroform and then incorporated into reconstituted chylomicron remnant particles (∼100 nm in diameter) with an efficiency of ∼65%. When injected into the portal vein of mice, the level of transgene expression in the liver was ∼100-fold greater than that of mice injected with 'naked' pDNA. Histochemical examination revealed that a large number of parenchymal cells and other types of cells in the liver expressed the transgene. Unfortunately, very poor expression was found in the liver after tail vein injection. In addition, other pDNA encapsulated cationic emulsions have been reported (Hara et al., 1997a). For example, Hara et al. formed a hydrophobic complex of pDNA with DC-Chol (3β[*N*-(*N*′,*N*′-dimethylaminoethane)carbamoyl]-cholesterol) and then encapsulated the complex into the oil core of emulsion prepared with castor oil, Tween 80, phosphatidylcholine, and DOPE (dioleoylphosphatidylethanolamine). More recently, Chesnoy et al. described stabilization of pDNA encapsulated cationic emulsions by coating with PEG (Chesnoy et al., 2001). Compared to the unmodified emulsions, stabilization with PEG (9−10%, w/w) significantly decreased the plasma clearance and liver uptake of the emulsion.

Our laboratories have likewise been interested in the development of improved nanoparticle-based pDNA delivery systems. Previously, we reported on a novel method to engineer stable cationic nanoparticles (∼100 nm) from oil-in-water (O/W) microemulsion precursors, comprised of emulsifying wax as the oil phase and CATB (cetyltrimethylammonium bromide) as the cationic surfactant (Cui and Mumper, 2002a and 2002b). Using this method, uniform nanoparticles were engineered within minutes in a single vessel without the use of organic solvents or the application of high torque mechanical mixing. Plasmid DNA was then coated on the surface of these preformed cationic nanoparticles and administered to mice resulting in significant enhancements in humoral, Th1-type, and proliferative immune responses over 'naked' pDNA after both topical and subcutaneous administration to mice.

In these present studies, we sought to further explore this novel nanoparticle engineering method by entrapping pDNA inside the nanoparticles. These pDNA-entrapped nanoparticles were characterized and evaluated both in vitro and in vivo.

EXPERIMENTAL PROCEDURES

Reagents. Plasmid containing a CMV promoter luciferase gene (pCMV-luc, 4.7 kp) was a gift from Valentis, Inc. (The Woodlands, TX). I-125 labeled plasmid pBR332 was purchased from the Lofstrand Labs, Ltd. (Gaithersburg, MD). Emulsifying wax, Tween 20, and Tween 80 were from Spectrum Chemical (New Brunswick, NJ). Brij 78 was a free sample from Uniqema (Wilmington, DE). Dimethyldioctadecylammonium bromide (DDAB), diethylaminoethyl (DEAE) Sepharose CL-6B anion exchanger, and mouse serum were purchased from Sigma-Aldrich Corporation (St. Louis, MO). 1.2-Dioleoyl-3-trimethylammoniopropane (DOTAP) and dioleoyl phosphotidylethanolamine (DOPE) were purchased from Avanti Polar Lipids, Inc. (Alabaster, AL). Sepharose CL-4B was purchased from Amersham Pharmacia Biotech, Inc. (Piscataway, NJ). Luciferase assay kits were purchased from Promega Corporation (Madison, WI). {*N*-[2-(Cholesterylcarboxyamino)ethyl]carbamorylmethyl}-pullulan (Chol-pullulan) was purchased from Dojindo Molecular Technologies, Inc. (Gaithersburg, MD). Lipofectin reagent was from Gibco BRL, Life Technologies (Gaithersburg, MD).

Bligh and Dyer Extraction. Bligh and Dyer extraction was performed as described by Reimer et al. with slight modification (Reimer et al., 1995). Briefly, DDAB or DOTAP and pDNA were solubilized in the monophase of chloroform/methanol/water (1:2.1:1 v/v/v). The pDNA concentration was fixed at 10 μg/mL while the concentrations of the lipids were varied so that the charge ratios of the cationic lipid to the pDNA were ranged from 0:1 to 2:1 (±). The mixtures were incubated at room temperature for 30 min in a total volume of 1 mL and then were partitioned into two phases by the addition of water and chloroform (250 μL each). The two phases were briefly mixed by vortexing. After a further incubation of 15 min, the lower organic phase and the upper aqueous phase were separated by centrifugation at 14000 rpm at room temperature for 5 min. The aqueous phase was removed and diluted with water, if necessary, for determination of the pDNA concentration using a F-2000 Fluorescence Spectrophotometer (Hitachi Instruments, Danbury, CT) after staining with PicoGreen (Molecular Probes, Eugene, OR).

DDAB/pDNA and DOTAP/pDNA complexes with charge ratio of 1:1 (±) were used to investigate the dissociation of these complexes by NaCl. Briefly, cationic lipid/pDNA complexes (1:1 ±) were prepared in Bligh and Dyer monophases. The required amount of NaCl (2 M in water) was then added into the monophase system. After 15 min of incubation at room temperature, Bligh and Dyer extractions and pDNA concentration determination were performed as described above.

Engineering of pDNA-Entrapped Nanoparticles. Nanoparticles were cured from warm microemulsion precursors engineered as previously described with modifications (Cui and Mumper, 2002a and 2002b). Cationic lipid/pDNA complexes (1:1 ±; pDNA concentration of 10 or 30 μg) were prepared in the monophase as described above. After Bligh and Dyer extraction, the lower organic phase was collected. Consequently, depending on the amount of pDNA formulated, either 2 or 6 mg of emulsifying wax was dissolved into this organic phase. The organic phase was then evaporated at room temperature to obtain a dried mixture of emulsifying wax and cationic lipid/pDNA complexes in glass scintillation vials. After melting of the mixture at 50−55 °C, a required volume of deionized and filtered (0.22 μm) water was

added to the vial. The suspension was vigorously stirred at 50−55 °C until a homogeneous milky slurry was formed. Then, required volumes of Brij 78 (100 mM in water), Tween 20 (1/4, w/w in water), and/or Tween 80 (1/4, w/w in water) were added while stirring. Stirring was maintained until a clear transparent microemulsion system was formed (within 3−5 min). The microemulsions, if formed, were then cooled to room temperature while stirring to cure nanoparticles. DOPE (5% w/w) was incorporated in the nanoparticles as previously described (Cui and Mumper, 2002a and 2002b).

For comparison and as a control, empty cationic nanoparticles with no pDNA were also prepared as previously described while maintaining the identical concentrations of all components. Plasmid DNA was then added to the preformed suspension for adsorption on the surface of the nanoparticles.

Physical Characterization of Nanoparticles. The nanoparticle size was measured by photon correlation spectroscopy (PCS) using a Coulter N4 Plus Submicron Particle Sizer (Coulter, Miami, FL) by scattering light at 90° at 25 °C for 120 s for each 1 mL sample. The zeta potentials of the nanoparticles were measured using a Zeta Sizer 2000 from Malvern Instruments (Southborough, MA).

Gel Permeation Chromatography. Nanoparticle purification and confirmation of pDNA entrapment were completed using gel permeation chromatography (GPC). For all GPC, 100 μL samples were applied to either Sepharose CL-4B or DEAE Sepharose CL-6B columns (10 × 55 mm). The samples were eluted with 5 mM HEPES in 150 mM NaCl pH 7.4 (HBS), and the fractions (0.5 mL) were assessed for pDNA concentration using either a gamma counter (for I-125 labeled pDNA) or PicoGreen fluorescence assay (for unlabeled pDNA). If the samples applied were nanoparticle suspension, the counts per second (CPS, an indication of nanoparticle concentration) of all eluted fractions were also measured with Coulter N4 Plus Submicron Particle Sizer.

Serum Stability Assays. The in vitro stability of the pDNA in the presence of mouse serum nucleases was investigated by mixing 50 μL of either pCMV-luc or nanoparticle suspensions (prepared with pCMV-luc and trace amount of I-125 labeled pBR332) with 150 μL of mouse serum (Sigma-Aldrich). The mixture was then allowed to remain at room temperature for 8 h for enzymatic digestion of the plasmid. One hundred microliters (100 μL) of the samples, before and after serum digestion, were applied to Sepharose CL-4B column as mentioned above to confirm the protection of pDNA from serum nucleases after entrapment in the nanoparticles. Intact pDNA eluded out in the void volume while digested pDNA was fractionated.

Stability of the Entrapped pDNA Extracted from the Nanoparticles. To investigate the stability of the pDNA after entrapment, pDNA was extracted from purified nanoparticles and was applied on a 1% Seakem Gold Agarose Ready-to-use Gel from BioWhittaker Molecular Applications (Rockland, ME) for electrophoresis. Specifically, nanoparticles containing DOTAP complexed pDNA (30 μg/mL) were prepared (see nanoparticle Composition **II**). The nanoparticles were purified with DEAE Sepharose CL-6B column and reconcentrated using ultrafiltration (100 kDa molecular weight cutoff, Brinkmann Instruments, Inc., Westbury, NY). The purified and concentrated nanoparticle suspensions were air-dried in a 37 °C incubator to form a dry nanoparticle powder. A combination of 200 μL of chloroform, 200 μL of NaCl solution (150 mM), and 420 μL of methanol were added to the nanoparticle dry powder. This mixed Bligh & Dyer system was then gently stirred for 30 min on hot plate maintained at 50−55 °C. Plasmid DNA was finally partitioned with water and chloroform (100 μL each) into the upper aqueous phase as mentioned above. The pDNA in the aqueous phase was then used for gel electrophoresis analysis. For comparison, pDNA was also extracted from a physical mixture of emulsifying wax with pDNA/DOTAP complexes. The extraction procedure was the same as that used for the pDNA-entrapped nanoparticles.

Chol-Pullulan Coated Nanoparticles. Chol-pullulan was deposited on the surface of the nanoparticles using a previously described method (Cui and Mumper, 2002a and 2002b). Briefly, 250 μg of chol-pullulan (suspension in water, 5 mg/mL) was added into the preformed warm microemulsions. After being stirred at 50−55 °C for 5 min, the microemulsions were cooled to room temperature while stirring to form nanoparticles. Overnight stirring at room temperature was continued for complete deposition of pullulan on the surface of the nanoparticles. Free surfactants and chol-pullulan were removed by GPC using a DEAE Sepharose CL-6B column.

Stability of the Nanoparticles in Simulated Biological Media. The stability of the nanoparticles, coated or uncoated with pullulan, in either normal saline (0.9% w/v NaCl) or 10% (v/v) fetal bovine serum (FBS) in normal saline was monitored as previously described by diluting the nanoparticle suspensions in these media and measuring the particle size over 30 min at 37 °C.

In Vitro Hep G2 Cell Transfection. In vitro cell transfection studies were completed as previously described (Cui and Mumper, 2002a and 2002b). Hep G2 cells were obtained from American Type Culture Collection (ATCC, Rockville, MD) and were maintained in Eagle's Minimum Essential Medium (EMEM) (Gibco, BRL) containing 10% fetal bovine serum (Gibco, BRL) and 1% penicillin−streptomycin (Gibco, BRL). Transfections were performed on cells that were approximately 80% confluent. Cells were plated in 48 well plates at a density of 5×10^5 cells/well and incubated overnight. The cells were coincubated with the formulations to provide a final plasmid (pCMV-luc) concentration of 2 μg/well. After 4 h of coincubation, the medium was replaced with fresh EMEM medium. Cells were harvested 48 h later by removing the medium, washing with 1X PBS buffer (three times), and then adding 200 μL 1 × lysis buffer (Promega), leaving for 5−10 min and freeze−thawing three times. A 20 μL sample was assayed for luciferase activity by injecting 100 μL reconstituted luciferase assay solution (Promega) and measuring the light produced for a period of 10 s using a ML2250 Dynatech Luminometer (Dynatech Laboratories, Chantilly, CA). The protein content of a 20 μL sample of the supernatant was determined using the Coomassie Plus Protein Assay Reagent (Pierce). In one treatment, the Hep G2 cells were preincubated with 100 μg of chol-pullulan for 5 min before the addition of the pullulan-coated pDNA-entrapped nanoparticles. As recommended by Dynatech, luciferase expression data were reported as the ratio of the full integral of the samples to that of the negative control, divided by the total amount of protein in the 20 μL of samples assayed.

Biodistribution of Nanoparticles after Tail-Vein Injection to Mice. Ten to twelve week old female Balb/C mice (average weight, 18 g) from Harlan Sprague−Dawley Laboratories were used for the animal studies. NIH guidelines for the care and use of laboratory animal were observed. The mice were anesthetized and then

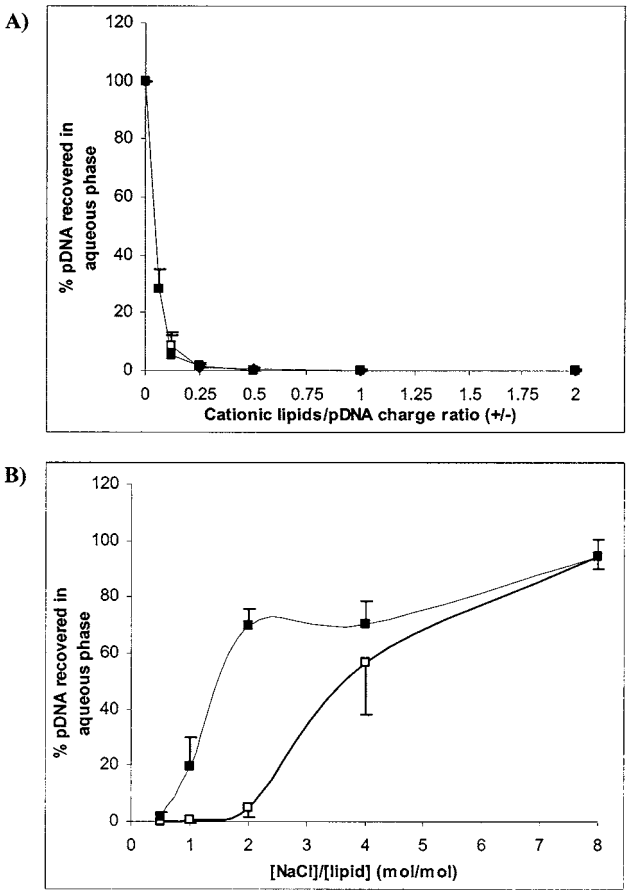


Figure 1. (A) The effect of increasing amounts of either DDAB (■) or DOTAP (□) on the recovery of pDNA in the upper aqueous phase following Bligh and Dyer extraction of the lipid/pDNA complexes (see Materials and Methods). (B) The effect of increasing amounts of NaCl on the recovery of pDNA from the aqueous phase following Bligh and Dyer extraction. The pDNA used was 10 μg. The charge ratio for the lipid vs pDNA was 1:1 (±). All data points are shown as the mean ± SD (n = 3).

injected via the tail vein with 200 μL (2 μg pDNA) of either pDNA alone in normal saline (n = 5), pDNA-entrapped nanoparticles (n = 5), and pullulan-coated pDNA-entrapped nanoparticles coated with pullulan (n = 7). The nanoparticles were purified using normal saline as the mobile phase before injection. In all formulations, a trace amount of I-125 labeled pDNA was included. Thirty minutes after tail-vein injection, blood (400 μL) was collected by cardiac puncture. The liver, lungs, heart, spleen, kidneys, and tail of the mice were also collected. Radioactivity in each sample was determined using a Cobra II Auto Gamma Counter from Packard BioScience Company (Meriden, CT). The total blood volume of a mouse was assumed to be 7.5% (v/w) of the total mouse weight (Mosqueira et al., 2001).

RESULTS AND DISCUSSION

Hydrophobizing Plasmid DNA. Cationic lipids have previously been used to complex pDNA by electrostatic interaction and thereby increase the lipophilicity of pDNA (Reimer et al., 1995). As expected, if pDNA alone was added into the Bligh and Dyer monophase system, almost all of the pDNA was recovered in the aqueous phase (Figure 1A). However, by complexing the pDNA with an increasing amount of either DDAB or DOTAP, a correspondingly decreasing amount of pDNA was recovered in the aqueous phase. In fact, starting from a charge ratio of 0.5:1 (±), no detectable pDNA was

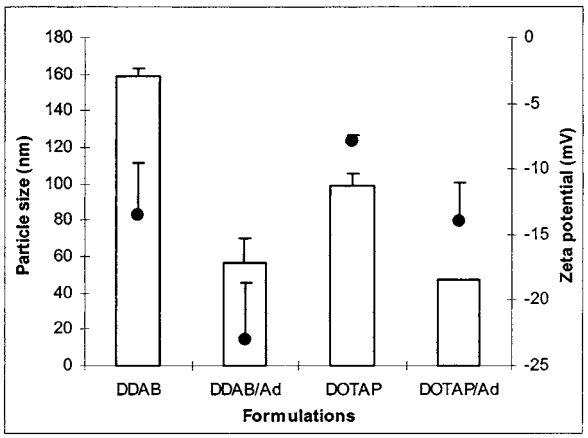


Figure 2. Particle size and zeta potential nanoparticles engineered from microemulsion precursors. DDAB = Composition **I** (pDNA-entrapped nanoparticles); DDAB/Ad = pDNA added to preformed nanoparticles having Composition **I**; DOTAP = Composition **II** (pDNA-entrapped nanoparticles); DOTAP/Ad = pDNA added to preformed nanoparticles having Composition **II**. (●) represents zeta potential measurements. All data points are shown as the mean ± SD (n = 3).

recovered from the aqueous phase as determined using the PicoGreen fluorescence DNA quantification assay. These results demonstrated that both DDAB and DOTAP can be used to hydrophobize pDNA.

To confirm that the complex formation was due to electrostatic interaction, and to determine the concentration of NaCl required to disrupt the formation of cationic lipids/pDNA complexes in Bligh and Dyer monophase system, an increasing amount of NaCl was added into the monophase system formed with either DDAB or DOTAP at a charge ratio of 1:1 (±) before extraction. As shown in Figure 1B, the addition of NaCl disrupted the cationic lipids/pDNA complexes and prevented the partition of pDNA into the lower organic phase. At a molar ratio of NaCl to cationic lipid of 8:1, binding of pDNA to both cationic lipids, was completely prevented, leading to almost no pDNA partitioning into the organic phase. This effective NaCl concentration was estimated to be only ~8 mM.

Preparation and Characterization of pDNA-Entrapped Nanoparticles. In formulation optimization studies, a matrix of various excipient combinations were tested to identify those systems that formed a clear and transparent microemulsion at 50−55 °C. After varying the concentrations of surfactants including Brij 78, Tween 20, and Tween 80, two different nanoparticle compositions were selected for further studies by monitoring the clarity of the microemulsions and measuring the size and uniformity of the cured nanoparticles. The two nanoparticle compositions were Composition **I**: 1:1 charge ratio (±) of either DDAB or DOTAP with pDNA (final pDNA concentration: 10 μg/mL), emulsifying wax (2 mg/mL), Brij 78 (5 mM), and Tween 20 (15 mM); and Composition **II**: 1:1 charge (±) ratio of either DDAB or DOTAP with pDNA (final pDNA concentration: 30 μg/mL), emulsifying wax (6 mg/mL), Brij 78 (14 mM), and Tween 20 (22 mM), and Tween 80 (2 mM).

Shown in Figure 2 are the particle sizes and zeta potentials of two representative nanoparticles. The DDAB containing nanoparticles (Composition **I**) had particle size and zeta potential of 159 ± 4 nm and −13.5 ± 4 mV, respectively. The DOTAP-containing nanoparticles (Composition **II**) had particle size and zeta potential of 99 ± 7 nm and −7.9 ± 0.5 mV, respectively. Figure 3 shows the distribution of the nanoparticles obtained from the

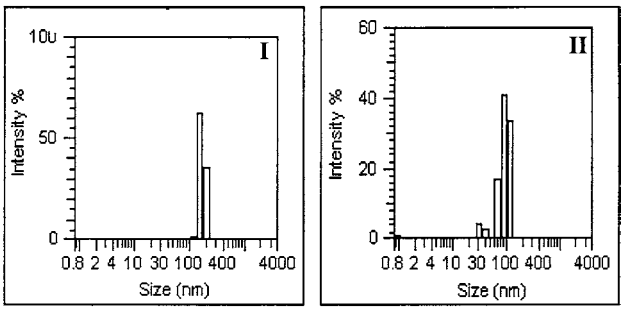


Figure 3. The particle size distribution of pDNA-entrapped nanoparticles (Composition **I** and **II**).

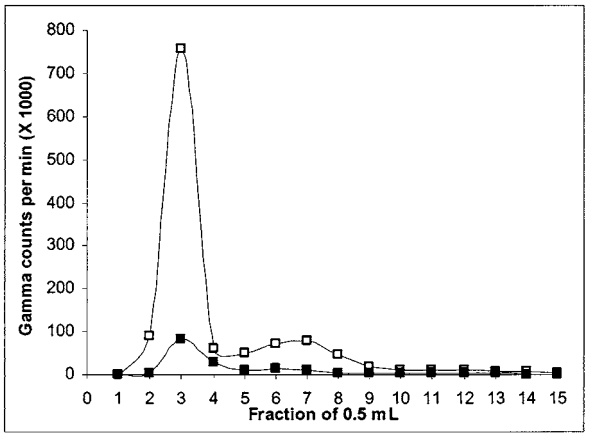


Figure 4. Gel permeation chromatograph (GPC) of pDNA with Sepharose CL-4B (□) or DEAE Sepharose CL-6B (■). A trace amount of I-125 labeled pDNA was included in the formulations. Columns were equilibrated and eluted with 5 mM HEPES in 150 mM NaCl pH 7.4 (HBS).

particle sizer. The very narrow distribution demonstrated that the nanoparticles were uniform. Moreover, the nanoparticles were spherical as demonstrated by TEM (data not shown).

Also shown in Figure 2 are nanoparticles (Composition **I** and **II**) as mentioned above except that the pDNA was added into preformed cationic nanoparticle suspensions for adsorption ("Ad"). Both particle size and zeta potential of these pDNA-coated nanoparticles were significantly different from that of the pDNA-entrapped nanoparticles. The particle size data showed that the entrapment of pDNA in nanoparticles resulted in larger nanoparticles, perhaps due to issues relating to packing of the lipid/pDNA complexes in the nanoparticles.

Confirmation of Plasmid DNA Entrapment in the Nanoparticles. The following studies were carried out to further confirm the entrapment of pDNA in the nanoparticles and to estimate the entrapment efficiency.

Using a Sepharose CL-4B column, pDNA eluted out mostly in fraction number 3 (void volume) demonstrated by the highest CPM in this fraction (Figure 4). However, as expected, the positively charged DEAE Sepharose CL-6B column efficiently bound most of the pDNA (>90%) (Figure 4). In contrast, after entrapment of the same pDNA into the nanoparticles, DEAE Sepharose CL-6B column was no long able to retard most of the pDNA from eluting out for both the Composition **I** nanoparticles (Figure 5A) and the Composition **II** nanoparticles (Figure 5B). Moreover, the nanoparticle eluent profiles, estimated by the counts per second (CPS), overlapped with the CPM strongly suggesting the association of pDNA with the nanoparticles.

The presence of pDNA inside the nanoparticles was further confirmed by an in vitro mouse serum digestion

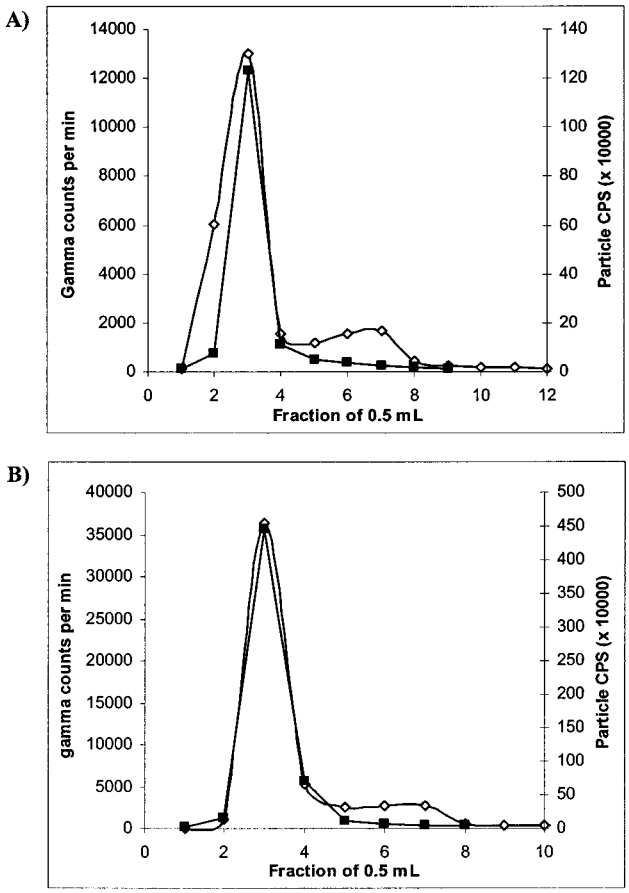


Figure 5. Gel permeation chromatograph of pDNA-entrapped nanoparticles. A trace amount of I-125 labeled pDNA was included in the formulations. One hundred microliters of nanoparticle suspensions was passed through the DEAE Sepharose CL-6B column. Eluent fractions (0.5 mL) were collected and measured in a gamma counter and particle sizer to determine radioactivity (counts per minute, CPM, ◊) and particle intensity (counts per sec, CPS, ■), respectively. (A) pDNA-entrapped nanoparticles (Composition **I**). (B) pDNA-entrapped nanoparticles (Composition **II**).

assay. As shown in Figure 6A, after 8 h of coincubation of the pDNA alone with mouse serum, all 'naked' pDNA was digested into small oligo- or mononucleotides as demonstrated by the shifted eluent profiles when applied to Sepharose CL-4B column. The same pDNA, when entrapped in the nanoparticles (Composition **I** and **II**), was not completely digested by the mouse serum nucleases (Figure 6B and 6C) demonstrating that the nanoparticles provided some protection against degradation. Serum digested plasmids were likely located in the bulk aqueous phase of the suspension or loosely associated on the surface of the nanoparticles. It was reported that cationic lipids, such as DDAB, may complex pDNA without condensing it. Therefore, it is likely that pDNA in these complexes were still susceptible to enzymatic degradation (Reimer et al., 1995). The entrapment efficiencies of pDNA in the nanoparticles were determined by area under curve (AUC) analysis using the Linear Trapezoidal Method. The entrapment efficiencies for the DDAB/DNA-entrapped nanoparticles (Composition **I**; Figure 6B) and the DOTAP/DNA-entrapped nanoparticles (Composition **II**; Figure 6C) were estimated to be 24.5 ± 3.4% and 29.4 ± 2.1%, respectively. As shown in Figure 7, entrapped pDNA remained stable after extraction from the nanoparticles. The entrapment efficiencies in nanoparticles were lower than expected based on the Bligh and Dyer extraction experiments wherein all

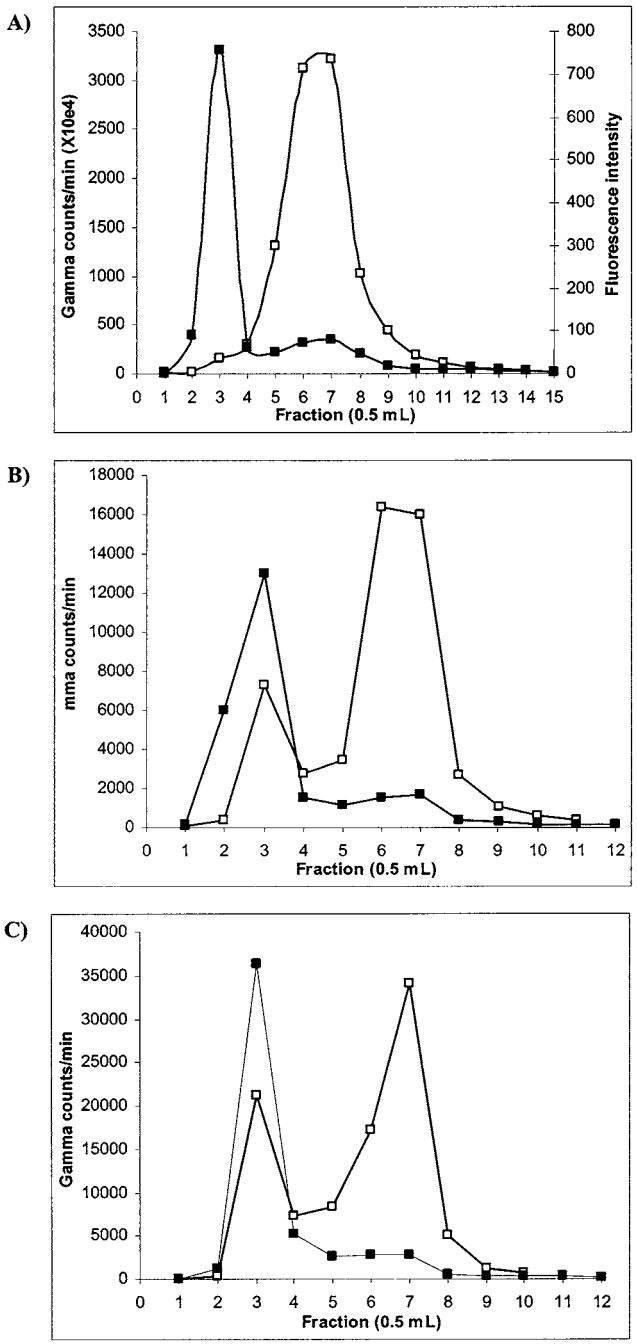


Figure 6. Gel permeation chromatograph of pDNA-entrapped nanoparticles with Sepharose CL-4B column for 'naked' pDNA alone (A) and pDNA-entrapped nanoparticles (B, C). A trace amount of I-125 labeled pDNA was included in the plasmids. One hundred microliters of nanoparticle suspensions, before (■) or after (□) mouse serum digestion, was passed through the column. Eluent fractions (0.5 mL) were collected and measured in a gamma counter to determine plasmid concentration (counts per min, CPM). (B) pDNA-entrapped nanoparticles (Composition **I**). (C) pDNA-entrapped nanoparticles (Composition **II**). In the case of 'naked' pDNA alone after digestion, the pDNA concentration was determined using PicoGreen and was reported as fluorescence intensity (A).

plasmid DNA was extracted into the organic (chloroform) phase when complexed with cationic lipid at a charge ratio of at least 0.5:1 (±). It is likely that the cationic lipid/pDNA complexes had lower affinity for the melted emulsifying wax oil phase in the microemulsion precursor as compared to the Bligh and Dyer organic (chloroform) phase. The reduced affinity of the complex in the melted

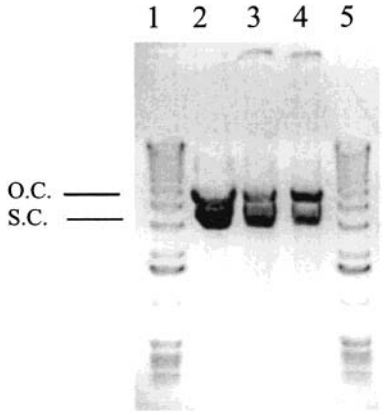


Figure 7. Agarose gel electrophoresis of pDNA extracted from pDNA-entrapped nanoparticles (see Materials and Methods for the extraction procedure). Lane 1 and 5, Gibco BRL 1kb DNA ladder; lane 2, plasmid CMV-luc as a positive control; lane 3, CMV-luc extracted from the mixture of pDNA/DOTAP complexes and emulsifying wax; lane 4, CMV-luc extracted from pDNA-entrapped nanoparticles. O.C. indicates open circular plasmid; S.C. indicates supercoiled plasmid.

oil phase could therefore explain the lower than expected entrapment efficiencies of pDNA in the cured nanoparticles.

In Vitro Hep G2 Cell Transfection. Pullulan has been successfully used as a ligand for liver hepatocyte targeting (Cui and Mumper, 2002a; Tabata et al., 1999; Xi et al., 1996; Kaneo et al., 2001). In vitro cell transfections studies were completed to further assess the integrity and functionality of the entrapped pDNA and to investigate whether pullulan, coated on the nanoparticle surface, could enhance nanoparticle uptake and transgene expression. After coating with pullulan, the size of the nanoparticles (DDAB, composition **I**) was significantly increased to 254 ± 72 nm ($p = 0.01$, two-sample *t*-test). The zeta potential of the pullulan-coated nanoparticles, (−12.4 ± 5 mV) was comparable to that of uncoated nanoparticles (−13.5 ± 4 mV) uncoated nanoparticles. As shown in Figure 8, pDNA alone or pDNA entrapped into nanoparticles did not result in measurable transfection. Incorporation of DOPE as an endosomolytic lipid enhanced the transfection by about 4-fold. Moreover, after deposition of pullulan on the surface of these pDNA-entrapped nanoparticles (DOPE-free), significantly enhanced transfection was observed. Preincubation of the Hep G2 cells with free chol-pullulan significantly reduced the transfection enhancement (Figure 8), suggesting that the uptake of the pullulan-coated pDNA-entrapped nanoparticles may be via a receptor mediated endocytic process. These results were comparable to our previously reported in vitro transfection results using pDNA-coated cationic nanoparticles with pullulan (Cui and Mumper, 2002a and 2002b). In these previous studies, coating of pDNA on the surface of the cationic nanoparticles significantly enhanced in vitro cell transfection, compared to that of 'naked' pDNA. Further, the incorporation of DOPE in the pDNA-coated nanoparticles enhanced the transfection efficiency by over 5-fold. The coating of nanoparticles with pullulan increased the transfection ability of the pDNA-coated nanoparticles by over 40-fold to levels that were comparable to that of the Lipofectin. A similar trend was observed in these present studies; however, the overall magnitude of expression compared to Lipofectin using pDNA-entrapped nanoparticles was significantly lower. The lower relative levels of expression with pDNA-entrapped nanoparticles in these studies may have been

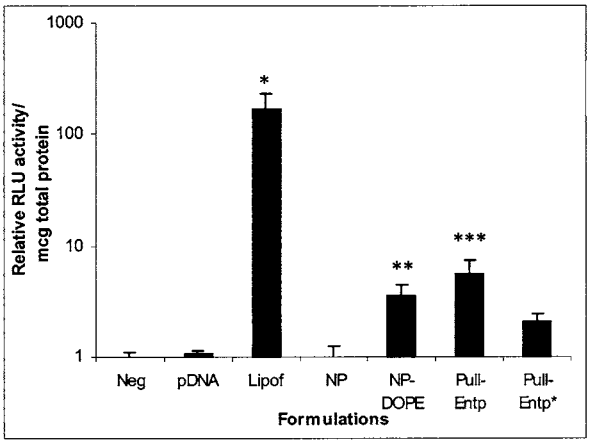


Figure 8. In vitro transfection of liver Hep G2 cells (500000 cells) ($n = 3$) in the presence of 10% FBS after 48 h with pDNA alone (pDNA), pDNA-Lipofectin (Lipof), uncoated pDNA-entrapped nanoparticles (NP), uncoated pDNA-entrapped nanoparticles with DOPE (NP-DOPE), or pullulan-coated pDNA-entrapped nanoparticles (Pull-Entp). For the group of Pull-Entp*, Hep G2 cells were preincubated with free chol-pull 5 min before the addition of the Pull-NPs. The pDNA dose was 2 μg for all samples. A one-way ANOVA followed by pairwise comparison with Fisher's protected least significant difference procedure (PLSD) was completed to analyze the data. *Indicates that the result of the Lipofectin was significantly different ($p < 0.05$) from that of the others. **Indicates that the result for NP-DOPE was significantly different ($p < 0.05$) from that of NP and pDNA alone. ***Indicates that the result for Pull-NP was significantly different ($p < 0.05$) from that of all other groups, except for NP-DOPE. NP = Composition **II**.

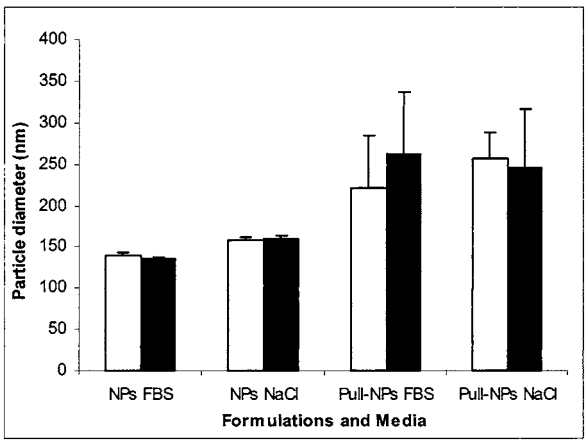


Figure 9. The particle size of the uncoated nanoparticles (NPs) and pullulan-coated nanoparticles (Pull-NPs) in various media at 37 °C for 30 min. For particle size measurement, the nanoparticle preparations were diluted with either 0.9% (w/v) of NaCl (normal saline) or 10% (v/v) of FBS in normal saline. Statistical analyses (two-sample *t*-test assuming equal variances) demonstrated no difference between the particle size at 0 and 30 min for all groups.

due to (1) the nanoparticles used in the present studies were net negatively charged while those in our previous studies were net positively charged even after pDNA coating, (2) the use of different nanoparticle compositions, and/or (3) issues relating to the kinetics of release of the entrapped pDNA from the nanoparticles. These factors are currently being assessed in ongoing experiments in our laboratories.

Biodistribution of the pDNA-Entrapped Nanoparticles in Mice. A short-term stability study of the nanoparticles in stimulated biological media was completed prior to the in vivo biodistribution studies to predict the nanoparticle stability. As shown in Figure 9, the size of pullulan-coated or uncoated nanoparticles did not change after 30 min of incubation at 37 °C in either normal saline (0.9% NaCl w/v) or 10% (v/v) of fetal bovine serum (FBS) in normal saline. Thirty minutes after tail vein injection, 47.6 ± 7.5%, 77.3 ± 10.4%, and 69.3 ± 3.8% of the total radioactivity administered was recovered from the mice injected with 'naked' pDNA alone, pDNA-entrapped nanoparticles, and pullulan-coated pDNA-entrapped nanoparticles, respectively. The majority of the recovered radioactivity was located in the blood and liver (Figure 10). Compared to only 16% for the 'naked' pDNA, 35−40% of the nanoparticle-entrapped pDNA were still circulating in the blood 30 min after tail-vein administration. The retention of pDNA in the blood at 30 min using both nanoparticle formulations was statistically significant over 'naked' pDNA alone. This suggests that the nanoparticles may have the potential for prolonged circulation and avoidance of the RES, problems commonly observed with other plasmid DNA delivery systems. Plasmid DNA, both free and entrapped, was also found in lung, heart, spleen, and kidney of the mice although in relatively low levels. The absence of a high level of radioactivity in the lung with both types of pDNA-entrapped nanoparticles strongly suggested that

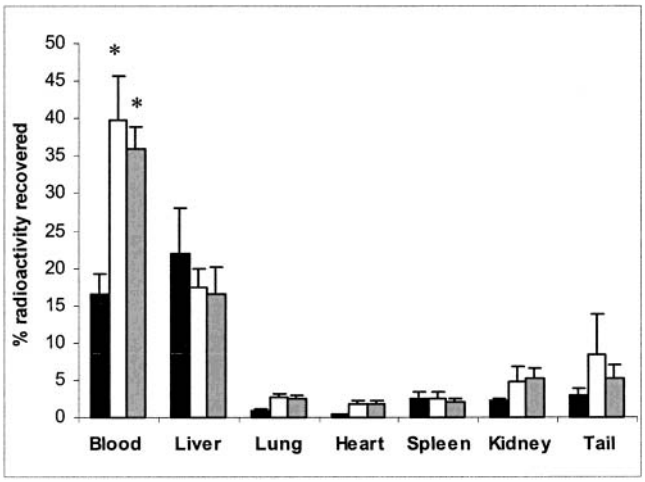


Figure 10. In vivo biodistribution of 'naked' pDNA alone (black bars, $n = 5$), pDNA-entrapped nanoparticles (white bars, $n = 5$), and pullulan-coated pDNA-entrapped nanoparticles (gray bars, $n = 7$) 30 min after tail vein injection to Balb/C mice. Statistical analyses were completed using a one-way ANOVA followed by pairwise comparison with Fisher's protected least significant difference procedure (PLSD). *Indicates that, in blood, the results for nanoparticles are significantly different from that for the free 'naked' pDNA alone.

these nanoparticles did not aggregate in blood resulting in rapid lung accumulation, an event that is common for cationic lipid complexes with pDNA (Mahato et al., 1995a and 1995b; Bailey and Sullivan, 2000; Takakura et al., 2001). The biodistribution results for both free 'naked' pDNA and pDNA-entrapped nanoparticles agreed both qualitatively and quantitatively to those of Bailey and Sullivan (2000). Bailey and Sullivan (2000) entrapped pDNA in neutral liposomes (~200 nm) with the aid of ethanol and calcium. Biodistribution studies with these pDNA-entrapped liposomes showed about 32−37% of the total dose remaining in the blood 1 h following tail vein injection to mice, with about 15−20% remaining in the liver. Interestingly, the total radioactivity recovered with the pDNA-entrapped liposomes (~60%) agreed well with that for pDNA-entrapped nanoparticles in our studies. Other organs/tissues that were not collected in either study that may account for unrecovered radioactivity include thyroid, brain, urine, extravascular tissue, and/

or intestines. Blood retention after tail-vein injection using these pDNA-entrapped nanoparticles compare very favorably to published reports of other systems. For example, Chesonyl et al. (2001) showed that 30 min after iv injection, 14−22% of the injected pDNA/emulsion complexes stabilized by 9−10% of PEG remained in mouse plasma. Further, Minchin et al. (2001) reported that 20 min after intraarterial injection, about 30% of the injected pDNA complexed with polyinosinic acid and polycationic liposomes was found in the circulation. Finally, Tam et al. (2000) showed that 4 h after iv injection, 55% of the injected plasmid−lipid particles (SPLP) were remained in the plasma.

It was also found in these present studies that the pullulan coating did not statistically enhance liver accumulation of pDNA entrapped in nanoparticles. The pullulan-coated nanoparticles were larger than the uncoated nanoparticles, thus it is possible that the larger pullulan-coated nanoparticles had reduced penetration through the sinusoidal endothelial barrier of the liver. Other possible reasons include (1) relatively low binding affinity of the pullulan ligand, (2) suboptimal concentration of the pullulan ligand on the nanoparticles. To this end, we are currently assessing the application of alternative hepatocyte-specific ligands and the optimization of the pullulan-coating on the nanoparticle surface.

Nonviral gene therapy involving the delivery of plasmid DNA has gained considerable attention over the past decade. However, to administer pDNA by intravenous injection, improved delivery systems are needed that can (1) protect DNA from serum nuclease digestion, (2) circulate in the blood long enough to reach distal organs and tissues, and (3) be readily modified for cell- and tissue-specific targeting. In addition to delivery strategies employing microparticles, liposomes, or cationic condensing agents such as lipids, polymer, and peptides/proteins, researchers have attempted to hydrophobize DNA and then incorporate the hydrophobized DNA into micron or nanometer sized particles. Examples include the stabilized plasmid-lipid particles (SPLP) prepared using a detergent dialysis procedure by Wheeler et al. (1999), reconstituted chylomicron remnant particles reported by Hara et al. (1997a), and more recently the poly(ethylene glycol)-stabilized DNA/emulsion systems based on the reconstituted chylomicron remnant particles described by Chesnoy et al. (2001).

The pDNA-entrapped nanoparticles reported in these present studies demonstrated prolonged circulation in blood (Figure 10). Although the mechanism(s) need further investigation, several possible explanations may be mentioned. The pDNA-entrapped nanoparticles were slightly net negatively charged. Therefore, possible association of negatively charged lipoproteins present in the blood with the nanoparticle surface may have been reduced and/or prevented (Nishikawa et al., 1998). Second, surfactants such as Brij 78, Tween 20, and Tween 80 may provide a more hydrophilic ('stealth'-like) surface on the nanoparticles, thereby precluding the aggregation of the nanoparticles by self-association or the rapid elimination by the RES (Lundberg et al., 1996). Similarly, the particle size of the nanoparticles was relatively small, perhaps reducing elimination of the nanoparticles by the mononuclear phagocytes in the liver (Kupfer cells) (Sakadea and Hirano, 1998).

It was demonstrated in this current study that pDNA-entrapped nanoparticles having diameters from 100 to 160 nm could be engineered from oil-in-water (O/W) microemulsion precursors formed at increased temperatures (i.e., 40−55 °C) and then simply cooled to form nanoparticles. The engineering process used in the present studies for pDNA-entrapped nanoparticle preparation has the following advantages: (i) the nanoparticle engineering process is rapid and spontaneous and completed in a single vessel, (ii) stable pDNA-entrapped nanoparticles (∼150 nm) can be engineered within minutes, and (iii) cell-specific ligands can be incorporated into the nanoparticles during the engineering process.

Nonionic emulsifying wax (comprised of cetyl alcohol and polysorbate 60 in a molar ratio of about 20:1) was selected as the oil phase since it is generally regarded as safe (GRAS) and has a melting point of ∼50−55 °C. The wax is typically used in cosmetics and topical pharmaceutical formulations and is generally regarded as a nontoxic and nonirritant material. For example, cetyl alcohol is currently used as an excipient in the marketed product Exosurf Neonatal. In addition, polysorbate 60 is used in many pharmaceutical products including parenteral products. In these present and previous studies using nanoparticles with similar compositions, no gross inflammatory, allergic, or toxic affects have been observed in mice after administration of these nanoparticles by the intravenous, subcutaneous, intramuscular, and topical routes (Cui and Mumper, 2002a and 2002b).

ACKNOWLEDGMENT

This work was supported, in part, by NSF grant BES-9986441, and from the AFPE and the Burroughs Wellcome Fund through the AACP New Investigators Program for Pharmacy Faculty.

LITERATURE CITED

(1) Bailey, A. L., and Sullivan, S. M. (2000) Efficient encapsulation of DNA plasmids in small neutral liposomes induced by ethanol and calcium. *Biochim. Biophys. Acta 1468*, 239−252.

(2) Chesnoy, S., Durand, D., Doucet, J., Stolz, D. B., and Huang, L. (2001) Improved DNA/emulsion complex stabilized by poly(ethylene glycol) conjugated phospholipids. *Pharm. Res. 18*, 1480−1484.

(3) Chesnoy, S., and Huang, L. (2000) Structure and function of lipid-DNA complexes for gene delivery. *Annu. Rev. Biophys. Biomol. Struct. 29*, 27−47.

(4) Clark, M., and Hersh, E. M. (1999) Cationic lipid-mediated gene transfer: current concepts. *Curr. Opin. Mol. Ther. 1*, 158−76.

(5) Cui, Z. R., and Mumper, R. J. (2002a) Genetic immunization using nanoparticles engineered from microemulsion precursors. *Pharm. Res. 19*, 939−946.

(6) Cui, Z. R., and Mumper, R. J. (2002b) Topical immunization using nanoengineered genetic vaccines. *J. Controlled Release 81*, 173−184.

(7) Hara, T., Tan, Y., and Huang, L. (1997a) In vivo gene delivery to the liver using reconstituted chylomicron remnants as a novel nonviral vector. *Proc. Natl. Acad. Sci. U.S.A. 94*, 14547−14552.

(8) Hara, T., Liu, F., Liu, D., and Huang, L. (1997b) Emulsion formulation as a vector for gene delivery in vitro and in vivo. *Adv. Drug Del. Rev. 24*, 265−271.

(9) Hong, M. S., Lim, S. J., Oh, Y. K., and Kim, C. K. (2002) pH-sensitive, serum-stable and long-circulating liposomes as a new drug delivery system. *J. Pharm. Pharmocol. 54*, 51−58.

(10) Houk, B. E., Martin, R., Hochhaus, C., and Hughes, J. A. (2001) Pharmacokinetics of plasmid DNA in the rat. *Pharm. Res. 18*, 67−74 (2001).

(11) Ishiwata, H., Suzuki, N., Ando, S., Kikuchi, H., and Kitagawa, T. (2000) Characteristics and biodistribution of cationic liposome and their DNA complexes. *J. Controlled Release 69*, 139−148.

(12) Kaneo, Y., Tanaka, T., Nakano, T., and Yamaguchi, Y. (2001). Evidence for receptor-mediated hepatic uptake of pullulan in rats. *J. Controlled Release 70*, 365−373.

(13) Kawabata, K., Takakura, Y., and Hashida, M. (1995) The fate of plasmid DNA after intravenous injection in mice: involvement of scavenger receptors in its hepatic uptake. *Pharm. Res. 12*, 825−830.

(14) Liu, F., and Huang, L. (2002) Development of nonviral vectors for systemic gene delivery. *J. Controlled Release 78*, 259−266.

(15) Lundberg, B. B., Mortimer, B. C., and Redgrave, T. G. (1996) Submicron lipid emulsions containing amphipathic poly(ethylene glycol) for use as drug-carriers with prolonged circulation time. *Int. J. Pharm. 134*, 119−127.

(16) Mahato, R. I., Kawabata, K., Nomura, T., Takakura, Y., and Hashida, M. (1995a) Physicochemical and pharmacokinetics characteristics of plasmid DNA/cationic liposome complexes. *J. Pharm. Sci. 84*, 1267−1271.

(17) Mahato, R. I., Kawabata, K., Takakura, Y., and Hashida, M. (1995b) In vivo disposition characteristics of plasmid DNA complexed with cationic liposomes. *J. Drug Target. 3*, 149−157.

(18) Minchin, R. F., Carpenter, D., Orr, R. J., (2001) Polyinosinic acid and polycationic liposomes attenuate the hepatic clearance of circulating plasmid DNA. *J. Pharmacol. Exp. Ther. 296*, 1006−1012.

(19) Mosqueira, V. C. F., Legrand, P., Morgat, J., Vert, M., Mysiakine, E., Gref, R., Devissaguet, J., and Barratt, G. (2001) Biodistribution of long-circulating PEG-grafted nanocapsules in mice: effects of PEG chain length and density. *Pharm. Res. 18*, 1411−4119.

(20) Nishikawa, M., Takakura, Y., and Hashida, M. (1998) Biofate of fat emulsions, in *Submicron emulsions in drug targeting and delivery* (S. Benita, Ed.) pp 99−118, Harwood Academic Publishers, Amsterdam.

(21) Nishikawa, M., Takemura, S., Yamashita, F., Takakura, Y., Meijer, D. K., Hashida, M., and Swart, P. J. (2000a) Pharmacokinetics and in vivo gene transfer of plasmid DNA complexed with mannosylated poly(L-lysine) in mice. *J. Drug Target. 8*, 29−38.

(22) Nishikawa, M., Yamauchi, M., Morimoto, K., Ishida, E., Takakura, Y., and Hashida, M. (2000b) Hepatocyte-targeted in vivo gene expression by intravenous injection of plasmid DNA complexed with synthetic multi-functional gene delivery system. *Gene Ther. 7*, 548−555.

(23) Oh, Y. K., Kim, J. P., Yoon, H., Kim, J. M., Yang, J. S., and Kim, C. K. (2001) Prolonged organ retention and safety of plasmid DNA administered in polyethylenimie complexes. *Gene Ther. 8*, 1587−1592.

(24) Pam, P., Monck, M., Lee, D., Ludkovski, O., Leng, E. C., Clow, K., Stark, H., and Scherrer, P. (2000) Stabilized plasmid-lipid particles for systemic gene therapy. *Gene Ther. 7*, 1867−1874.

(25) Patel, H. M. (1992) Serum opsonins and liposomes: their interaction and opsonophagocytosis. *Crit Rev. Ther. Drug Carrier Syst. 9*, 1437−1446.

(26) Reimer, D. L., Zhang, Y. P., Kong, S., Wheeler, J. J., Graham, R. W., and Bally, M. B. (1995) Formation of novel hydrophobic complexes between cationic lipids and plasmid DNA. *Biochemistry 34*, 12877−12883.

(27) Rolland, A., and Felgner, P., Eds. (1998) Nonviral gene delivery systems. *Adv. Drug Deliv. Rev. 30*, 1−227.

(28) Sakaeda, T., and Hirano, K. (1998) Effect of composition on biological fate of oil particles after intravenous injection of O/W lipid emulsion. *J. Drug Target. 6*, 273−284.

(29) Tabata, Y., Matsui, Y., Uno, K., Sokawa, Y., and Ikada, Y. (1999) Simple mixing of IFN with a polysaccharide having high liver affinity enables IFN to target to the liver. *J. Interferon Cytokine Res. 19*, 287−292.

(30) Takakura, Y., Nishikawa, F., Yamashita, F., and Hashida, M. (2001) Development of gene drug delivery systems based on pharmacokinetic studies. *Eur. J. Pharm. Sci. 13*, 71−76.

(31) Verbaan, F. J., Oussoren, C., van Dam, I. M., Takakura, Y., Hashida, M., Crommelin, D. A. J., Hennink, W. E., and Storm, G. (2001) The fate of poly(2-dimethyl amino ethyl)-methacrylate-based polyplexes after intravenous administration. *Int. J. Pharm. 214*, 99−101.

(32) Wheeler, J. J., Palmer, L., Ossanlou, M., MacLachlan, I., Graham, R. W., Zhang, Y. P., Hope, M. J., Scherrer, P., and Cullis, P. R. (1999) Stabilized plasmid-lipid particles: construction and characterization. *Gene Ther. 6*, 271−281.

(33) Xi, K., Tabata, Y., Uno, K., Yoshimoto, M., Kishida, T., Sokawa, Y., Ikada, Y. (1996) Liver targeting of interferon through pullulan conjugation. *Pharm. Res. 13*, 1846−1850.

(34) Yoshida, M., Mahato, R. I., Kawabata, K., Takakura, T., and Hashida, M. (1997) Disposition characteristics of plasmid DNA in the single-pass rat liver perfusion. *Pharm. Res. 12*, 597−603.

BC0255586

Engineering Tumor-Targeted Gadolinium Hexanedione Nanoparticles for Potential Application in Neutron Capture Therapy

Moses O. Oyewumi and Russell J. Mumper*

Division of Pharmaceutical Sciences, College of Pharmacy, University of Kentucky, Lexington, Kentucky 40536-0082. Received June 20, 2002; Revised Manuscript Received September 17, 2002

Microemulsions (oil-in-water) have been employed as templates to engineer nanoparticles containing high concentrations of gadolinium for potential application in neutron capture therapy of tumors. Gadolinium hexanedione (GdH), synthesized by complexation of Gd^{3+} with 2,4-hexanedione, was used as the nanoparticle matrix alone or in combination with either emulsifying wax or PEG-400 monostearate. Solid nanoparticles (<125 nm size) were obtained by simple cooling of the microemulsions prepared at 60 °C to room temperature in one vessel. The feasibility of tumor targeting via folate receptors was studied. A folate ligand was synthesized by chemically linking folic acid to distearoylphosphatidylethanolamine (DSPE) via a poly(ethylene glycol) (PEG; MW 3350) spacer. To obtain folate-coated nanoparticles, the folate ligand (0.75% w/w to 15% w/w) was added to either the microemulsion templates at 60 °C or nanoparticle suspensions at 25 °C. Efficiencies of folate ligand attachment/adsorption to nanoparticle formulations were monitored by gel permeation chromatography. Cell uptake studies were carried out in KB cells (human nasopharyngeal epidermal carcinoma cell line), known to overexpress folate receptors. The uptake of folate-coated nanoparticles was about 10-fold higher than uncoated nanoparticles after 30 min at 37 °C. The uptake of folate-coated nanoparticles at 4 °C was 20-fold lower than the uptake at 37 °C and comparable to the uptake of uncoated nanoparticles at 37 °C. Folate-mediated endocytosis was further verified by the inhibition of folate-coated nanoparticles uptake by free folic acid. It was observed that folate-coated nanoparticles uptake decreased to ~2% of its initial value with the coincubation of 0.001 mM of free folic acid. The results suggested that these tumor-targeted nanoparticles containing high concentrations of Gd may have potential for neutron capture therapy.

INTRODUCTION

Neutron capture therapy (NCT) is a potential cancer therapy that utilizes a stable, nonradioactive nuclide delivered to tumor cells, which upon irradiation by thermal or epithermal neutrons, produces localized cytotoxic radiations (Bath and Soloway, 1994; Bernard, 1995). Using several nuclides, the effectiveness of NCT in treating cases of malignant melanoma and glioblastoma have been reported (Matsumoto, 1992; Akine et al., 1993). Boron-10 was applied in most of the earlier clinical trial studies (Chen et al., 1997). A general requirement of a suitable NCT agent after accumulation in the target tumor is that upon exposure to external neutrons, it should emit radiation of sufficient energy and tissue penetration depth, so that the majority of cancer cells are killed with limited exposure to healthy tissues. Gadolinium has been proposed as an alternative to boron for neutron capture therapy of tumors (Martin et al., 1988; Tokumitsu et al., 2000). The tumor killing effect of Gd-neutron capture therapy (Gd-NCT) is attributed to the emission of γ rays and Auger electrons by the ^{157}Gd $(n,\gamma)^{158}$Gd reaction (Shih and Brugger, 1992; Shikata et al., 2002). The thermal neutron cross section of Gd-157 is 66-times greater than that of boron-10. Thus, compared to boron-10, Gd-157 has the ability to absorb neutrons much more efficiently, and as such, requires shorter neutron irradiation times. In addition, the emission of photons with long flight ranges in Gd-NCT will increase the probability of extensively hitting the target tumors thereby enhancing the overall therapeutic effect of NCT. Another factor that contributes to the attractiveness of Gd-NCT is the fact that many Gd-based compounds are already being used as contrast agents in magnetic resonance imaging (MRI). Therefore, the application of Gd in NCT may afford the opportunity of coordinating and achieving both diagnostic and therapeutic effects simultaneously.

In general, Gd-NCT may be described as a two-step radiotherapy in which a selective therapeutic effect on tumor cells is achieved by first targeting the tumor with nonradioactive Gd-157 and then exposing the target site to an external neutron source. Therefore, the success of Gd-NCT is dependent on localization and retention of high concentrations of Gd-157 within the target tumor site prior to neutron irradiation. In response to the challenge, Gd has been delivered previously through magnetic resonance imaging (MRI) contrast agents such as Gd-DTPA, Gd-DOTA, and Gd-EDTA (Shih and Brugger, 1992; Morel et al., 1998). However, the water solubility of these agents will likely make it difficult to achieve satisfactory tumor retention. New delivery systems are continually being sought that will achieve and retain high overall tumor concentrations of Gd.

* Corresponding author: Russell J. Mumper, Ph.D. Assistant Professor of Pharmaceutical Sciences Assistant Director, Center for Pharmaceutical Science and Technology, College of Pharmacy, 907 Rose St., University of Kentucky, Lexington, KY 40536-0082. Tel: (859) 257-2300 ext. 258. Fax: (859) 323-5985. E-mail: rjmump2@uky.edu.

10.1021/bc025560x CCC: $22.00 © 2002 American Chemical Society
Published on Web 10/12/2002

Recently, the direct intratumoral injection of gadopentetic acid/chitosan complexes, gadolinium emulsions, and microspheres were reported (Jono et al., 1999; Tokumitsu et al., 1999; Miyamoto et al., 1999; Shikata et al., 2002). Most of the delivery systems applied in these earlier studies were untargeted and/or biologically unstable. Several groups using liposomes and other macromolecules have shown that particles less than 400 nm, and ideally less than 150 nm, are much more efficient in targeting tumors as compared to systems with larger particle sizes (Wu et al., 1993; Jain 1997; Desai et al., 1997; Hobbs et al., 1998; Bally et al., 1994). Thus, based on these previous studies, the goal of this work was to engineer stable nanoparticles (<100 nm) that could selectively deliver high concentrations of Gd to solid tumors.

It is known that, due to their small size, nanoparticles meeting specific criteria may be able to deliver molecules to specific tissues of interest and/or enhance the direct entry of entrapped drug molecules into cells (Kreuter, 1995). We recently demonstrated that oil-in-water microemulsions can serve as templates for engineering stable nanoparticles having diameters below 100 nm and entrap gadolinium acetylacetonate (GdAcAc; mp 143 °C). Apart from achieving high entrapment efficiencies of up to 1 mg of GdAcAc per 2 mg emulsifying wax or polyoxyl 2 stearyl ether (Brij 72) nanoparticles, it was also observed that the nanoparticle engineering process increased the apparent water solubility of GdAcAc by 2000-fold (Oyewumi and Mumper, 2001; Oyewumi and Mumper, 2002). The microemulsion templates were made at increased temperature (40−60 °C) and upon simple cooling in one vessel resulted in solid nanoparticles. Since the concentration of Gd is critical to the success of Gd-NCT, engineered nanoparticles containing higher concentrations of gadolinium in the form of gadolinium hexanedione were sought. The suitability of GdH over GdAcAc is due to the lower melting point of GdH (55 °C) and increased hydrophobicity that make it more amenable for incorporation into the oil phase of oil-in-water microemulsions. The therapeutic performance of GdH in NCT may also be enhanced since previous studies have shown that hydrophobic Gd-compounds were accumulated and retained in tumor cells longer than water soluble compounds (Jono et al., 1999; Shikata et al., 2002).

In these present studies, folate was used in targeting Gd to tumors, since it is known that many human cancer cells overexpress folate receptors (Weitman et al., 1992; Wang and Low, 1998). Folic acid binds to the folate receptors at cell surfaces with very high affinity and is internalized by receptor-mediated endocytosis (Kamen et al., 1986; Lee and Low, 1994). As a low molecular weight ligand, folic acid has the advantages of being stable and nonimmunogenic when compared to monoclonal antibodies. It has been shown that folate-conjugated macromolecules can be specifically taken up by cultured receptor-bearing tumor cells (Lee and Hang, 1996; Lee and Low, 1995; Atkinson et al., 2001). Folate-coated nanoparticles (<100 nm) containing high concentrations of GdH were engineered. Uptake studies in tumor-cultured cells were investigated. It is expected that achieving tumor-targeted delivery of nanoparticles containing high concentrations of Gd may enhance the overall success of Gd-NCT.

EXPERIMENTAL PROCEDURES

Materials. Emulsifying Wax and PEG-400 monostearate were obtained from Spectrum Chemicals (New Brunswick, NJ). Polyoxyl 20 stearyl ether (Brij 78) was purchased from Uniqema (Wilmington, DE). Gadolinium chloride and 2,4-hexanedione were purchased from Aldrich Chemicals (Milwaukee, WI). Sephadex G-75, Sepharose CL-4B, distearoylphosphatidylethanolamine (DSPE), folic acid, polyoxyethylene-bis-amine (PEG-bis-amine, Mw 3350), L-glutamine fetal bovine serum (heat inactivated), trypsin−EDTA, and penicillin−streptomycin solution were purchased from Sigma Chemicals (St. Louis, MO). Fluorescein−DOPE was purchased from Avanti Polar-Lipids (Alabaster, AL). KB cells (human nasopharyngeal epidermal carcinoma cell line) were obtained from ATCC (Manassas, VA).

Synthesis of Gadolinium Hexanedione. Gadolinium hexanedione (GdH) was synthesized using the modified method previously described by Mumper and Jay (1992). Briefly, 40 mL of an aqueous solution (pH 2.5) containing approximately 5 g of Gd chloride and approximately 6 mL of the complexing agent (2,4-hexanedione) was titrated with a standard solution of sodium hydroxide (1.038 N) to raise the pH to 7.0. All titrations were performed with continuous stirring at 25 °C, and the pH of the reaction mixture after each addition of NaOH was recorded. At pH 7.4, precipitated GdH was collected on a preweighed filter paper, washed with distilled/deionized water, and further purified as described by Mumper and Jay (1992), to remove excess complexing agent.

Preparation of Oil-in-Water Microemulsion Templates. GdH was used alone as the matrix material or in combination with either emulsifying wax or PEG-400 monostearate to prepare oil-in-water microemulsion templates at 60 °C. To prepare the microemulsions, matrix material (0.5−2.5 mg) and/or GdH (0−2.5 mg) were accurately weighed into a glass vial and melted using a hotplate. To the melted matrix materials and/or GdH at 60 °C, various concentrations (0−100 mM) of polyoxyl 20 stearyl ether (Brij 78) were added under magnetic stirring with subsequent addition of water (0.22 μm filtered) to make a final volume of 1 mL. The formation of oil-in-water microemulsions was verified by the clarity of the mixture and by photon correlation spectroscopy (PCS) using a Coulter N4 Plus Submicron Particle Sizer (Beckman Coulter Corporation, Miami, FL) at 60 °C by scattering light at 90° for 180 s. To prevent the warm microemulsions from cooling during the droplet size measurement, both the cuvette and the particle sizer sample holder were maintained at 60 °C.

Preparation and Characterization of GdH Nanoparticles. Using appropriate microemulsion templates, nanoparticles were prepared by various methods of curing the warm oil-in-water microemulsion templates including simple cooling to room temperature, dilution with cold water, and cooling of the entire template in a freezer. The particle sizes of the diluted solid nanoparticles (1:10 v/v with water) were determined using PCS at 20 °C by scattering light at 90° for 180 s. The retention of nanoparticles integrity was evaluated based on gel permeation chromatography (GPC) elution profiles. In brief, 80 μL of nanoparticle suspension was passed down the Sephadex G-75 column (1.5 cm × 8 cm), using water (0.22 μm filtered) as the mobile phase. The elution of nanoparticles in each fraction was detected by laser light scattering counts per second (CPS).

Stability of Nanoparticles in Biological Media. To assess the potential stability of nanoparticles in biological media, nanoparticles were diluted 1:10 v/v with 10% fetal bovine serum (FBS) in water or with 10 mM phosphate

buffered saline (pH 7.4). The particle size of nanoparticles in each media was monitored for 60 min at 37 °C.

Synthesis of Folate Ligand. A folate ligand was synthesized by chemically linking folic acid to distearoylethanolamine (DSPE) via a PEG spacer (MW 3350) using the modified method of Lee and Low (1995). Briefly, the procedure involved the synthesis of the two main components of the ligand: folate-PEG-NH_2 and *N*-succinyl-DSPE. Folate-PEG-NH_2 was synthesized by reacting overnight in the dark at room temperature, 450 mg of polyoxyethylene-bis-amine with equimolar amount of folic acid in 5 mL of dimethyl sulfoxide (DMSO) with dicyclohexylcarbodiimide (DCC), and 10 μL of pyridine. Folate-PEG-NH_2 was purified by (i) centrifugation (to remove the insoluble byproduct dicyclohexylurea), (ii) dialysis (to remove DMSO and unreacted folic acid), and (iii) by gel permeation chromatography using cellulose cation-exchange resin (to remove unreacted polyoxyethylene-bis amine). To synthesize *N*-succinyl-DSPE, 100 mg of DSPE was reacted overnight with a 1.2 mol equiv of succinic anhydride in chloroform. The product was precipitated with cold acetone. *N*-Succinyl-DSPE, whose carboxyl group had been previously activated with DCC, was reacted with folate-PEG-NH_2 overnight at room temperature in chloroform to obtain the final product (folate-PEG-DSPE). The solvent was removed, and the precipitate of folate-PEG-DSPE was washed three times with cold acetone and stored at −20 °C. To obtain fluorescence-labeled folate ligand, the procedure was modified appropriately by reacting 7-nitrobenzoxadiolzol-4-amine (NBD) and DSPE with succinic anhydride. The presence of NBD in the final folate ligand was detected by fluorescence spectroscopy (460 nm excitation and 534 nm emission). Characterization of folate−PEG−DSPE was carried out using the method of Lee and Low (1995) as well as by mass spectroscopy, GPC thin-layer chromatography, and infrared spectroscopy.

Addition of Folate Ligand to Engineered Gd Nanoparticles. Using a stock aqueous solution of folate ligand (0.5 mg/mL), two methods were used to add the ligand to nanoparticle formulations. First, various amounts were added to microemulsions templates at 60 °C, and the mixture was stirred for 15 min at 60 °C. The microemulsions were then cooled to room temperature under gentle stirring. The preparation was further stirred gently for 4 h at 25 °C to obtain folate-coated nanoparticles. In the second method, various amounts of folate ligand were added to nanoparticle suspension at 25 °C (after cooling the warm microemulsions). The mixture was then gently stirred for 4 h at 25 °C. The efficiency of folate ligand attachment/adsorption was assessed by gel permeation chromatography (GPC) elution profiles using both Sephadex G-75 and Sepharose CL-4B columns. In a separate study, the GPC elution profiles of control nanoparticles (without folate ligand) and free folate ligand were obtained using laser light scattering counts per second and fluorescence spectroscopy, respectively, to serve as references for folate-coated nanoparticles.

Cell Culture. Cell uptake studies were performed in KB cells, a human nasopharyngeal epidermal carcinoma cell line (ATCC, Manassas, VA). The cells were cultured in T-75 flasks at 37 °C in a humidified atmosphere containing 5% CO_2 using folate-free Dulbecco's Modified Eagle's Medium (DMEM) supplemented with 10% heat-inactivated fetal bovine serum. The media contained final folate concentration similar to that of human plasma.

Nanoparticle Cell Uptake Studies. The growth medium was aspirated from each T-75 flask and KB cells monolayer was washed with sterile phosphate-buffered saline (154 mM PBS; pH 7.4). After aspirating the PBS, 1.5 mL of trypsin−EDTA was added to the flask to detach the cells. The suspended cells in growth medium were centrifuged at 1500 rpm (4 °C) for 5 min. After discarding the supernatant, the cells were dispersed in a known volume of growth medium, and the cells were counted using a hemocytometer. To study the cell uptake of nanoparticles, KB cells were seeded in 48-well plates at a density of 10^5 cells/well in complete growth medium and allowed to grow for 4 days, with the medium changed once on the second day. To determine the effect of nanoparticle concentration on uptake, various dilutions of folate-coated nanoparticles or control nanoparticles without folate ligand in complete growth medium were made in the concentration range of 20 to 600 μg/mL. The medium in each well was replaced with nanoparticles suspended in growth medium and incubated for 30 min. The experiment was carried out at 37 °C or 4 °C. In a separate experiment, nanoparticle suspensions (360 μg/mL) were incubated in the presence of various concentrations of free folic acid ranging from 0.001 mM to 100 mM. The effect of incubation time on nanoparticles uptake was also studied. At the end of the incubation period, nanoparticle suspensions were removed from the wells, and the cell monolayers were rinsed three times with cold PBS and lysed using 1% Triton X-100. Cell associated fluorescence was measured by a fluorometer (Hitachi, Model F-2000). The concentration of cell internalized Gd was measured by the fluorescence intensity of Gd at 270 nm (excitation) and 550 nm (emission) using a predetermined standard curve. In a separate study, Gd nanoparticle formulation (Formulation B) was prepared to contain fluorescein−DOPE, as an alternative fluorescence marker. Up to 0.25% w/w fluorescein−DOPE was entrapped in nanoparticles prior to folate ligand coating. The amount of nanoparticles taken up by KB cells was measured by the intensity of internalized fluorescence at 521 nm (emission) with excitation at 497 nm. In addition, 50 μL of the cell lysate from each well was used to determine the total cell protein content using the Coomassie Plus assay protocol (Pierce, Rockford, IL).

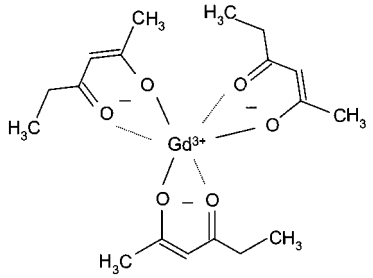


Figure 1. Structure of gadolinium hexanedione (GdH), synthesized by complexation of Gd^{3+} with 2,4-hexanedione.

RESULTS AND DISCUSSION

Synthesis of Gadolinium Hexanedione (GdH). GdH was synthesized by the complexation of Gd^{3+} with 2,4-hexanedione. GdH (94% yield) was subsequently characterized by mass spectroscopy, infrared spectroscopy, and differential scanning calorimetry. The basic steps involved in the synthesis of GdH are the loss of the acidic proton in 2,4-hexanedione at neutral pH and the subsequent complexation with Gd^{3+} in solution. The chemical structure of GdH is shown in Figure 1. Since the overall goal of the study was to engineer nanoparticles that can be employed in delivering high concentrations of Gd into tumors for Gd-NCT, GdH makes a very

Table 1. Components of Three Different Gadolinium Hexanedione (GdH) Nanoparticle Formulations. Each Formulation Was Made with Brij 78 (2 mM to 10 mM) and Water (0.22 μm filtered) To Make the Final Volume of 1 mL

	nanoparticle formulation (per 1 mL)		
components (mg)	A	B	C
GdH	2.5	2.5	2.5
emulsifying wax	0	0.5	0
PEG-400 monostearate	0	0	0.5

suitable choice. Compared to other complexes of Gd (such as Gd-DTPA, Gd-DOTA, and Gd-EDTA), GdH has a relatively high weight percentage of Gd. Previous studies have also shown that lanthanides complexed with dicarbonyl chelating agents have favorable physical and thermal stability (Mumper and Jay, 1992). In particular, the high hydrophobicity and lower melting point of GdH were employed in this study to increase Gd concentration in the final nanoparticle formulations. We have reported earlier that oil-in-water microemulsions can be used as templates to engineer stable nanoparticles using matrix materials such as emulsifying wax and polyoxyl 2 stearyl ether (Brij 72). The nanoparticle matrix materials (mp 50−55 °C) served as the oil phase of the microemulsions that are produced at elevated temperatures (Oyewumi and Mumper, 2002). Therefore, since GdH possesses properties that are comparable to the matrix materials studied earlier, it was therefore thought that GdH could be used alone or in combination with other matrix materials to engineer stable nanoparticles having even higher concentrations of GdH in the final formulations.

GdH Nanoparticles Engineered from Microemulsion Templates. The feasibility of using GdH alone as a nanoparticle matrix material was initially investigated. It was observed that melted GdH was miscible with other melted matrix materials (emulsifying wax, Brij 72, PEG-400 monosterate) in weight ratios ranging from 1:1 to 1:6 (GdH/matrix materials). The final formulations were made using GdH alone or in a 1:5 (w/w) combination with other matrix materials. The components of the three GdH nanoparticle formulations are shown in Table 1 using GdH alone (Formulation A) or in combination with emulsifying wax (Formulation B) or PEG-400 monostearate (Formulation C). The oil-in-water microemulsions were prepared at 60 °C with polyoxyl 20 stearyl ether (Brij 78) as the surfactant. The microemulsion windows for the three nanoparticle formulations are shown in Figure 2 using Brij 78 concentrations ranging from 2 mM to 10 mM. The formation of the microemulsion was verified by both the visual clarity of the mixture and by the droplet sizes measured at 60 °C using PCS. As expected, microemulsions were not formed in systems without Brij 78 as the mixture remained turbid. As shown in Figure 2, microemulsions with large droplet sizes were obtained with a final Brij 78 concentration of 2.0 mM; however, the inclusion of either emulsifying wax or PEG-400 monostearate caused a reduction in microemulsion droplet sizes. The droplet sizes of microemulsions in Formulations A, B, and C were: 484 ± 35 nm, 171 ± 19 nm, and 144 ± 26 nm, respectively (Figure 2). Emulsifying wax is composed of cetyl alcohol and polysorbate 60 in a molar ratio of about 20:1. Thus, the presence of surfactants, polysorbate 60 and PEG-400 monostearate, most likely contributed to the formation of microemulsions even at the lower Brij 78 concentrations for these formulations.

Microemulsions that had small oil droplet sizes using lower Brij 78 concentrations were selected for subsequent

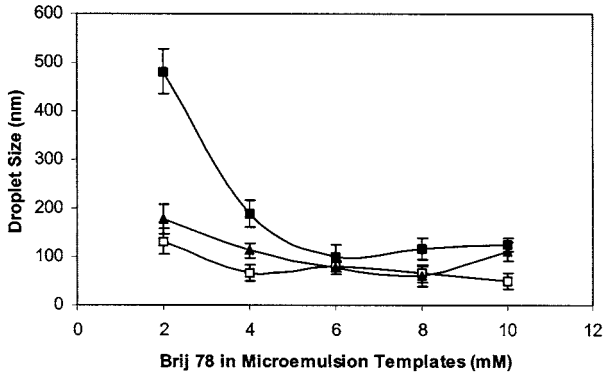


Figure 2. Microemulsion droplet sizes for three GdH Formulations: A (■), B (□), and C (▲). The microemulsions were prepared at 60 °C using Brij 78 at concentrations ranging from 2 mM to 10 mM. The final volume of 1 mL was obtained with water (0.22 μm filtered). The droplet sizes in each microemulsion were measured using laser light scattering at 60 °C. Each value represents the mean ± SD (n = 3).

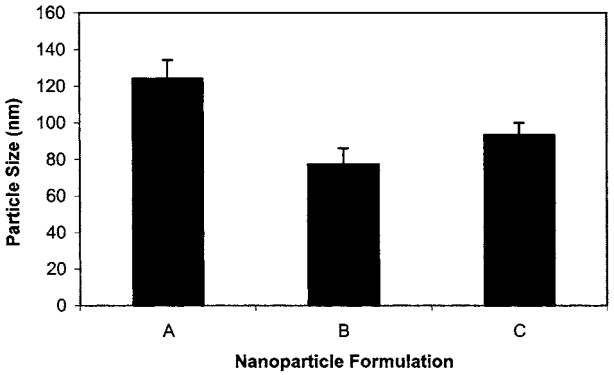


Figure 3. Particle size of GdH nanoparticle Formulations A, B, and C (3 mg/mL) made with 6.0 mM, 4.0 mM and 6.0 mM of Brij 78, respectively, and 0.2 μm filtered water. The nanoparticles were engineered by cooling warm microemulsions prepared at 60 °C to room temperature. The particle size of each sample (diluted 1:10 v/v in water) was determined by laser light scattering at 25 °C. Each value represents the mean ± SD (n = 3).

nanoparticle formulations. This was based on our earlier findings that demonstrated a direct correlation between the microemulsion droplet sizes and resulting cured nanoparticle size (Oyewumi and Mumper, 2001; Oyewumi and Mumper, 2002). In addition, previous studies showed that nanoparticles were unstable over time when higher concentrations of surfactant (about 10 mM) were used to prepare the microemulsion templates (Oyewumi and Mumper, 2002). Therefore, using the microemulsion window as a guide (Figure 2), the final formulation were made with 6 mM, 4 mM, and 6 mM Brij 78 in Formulations A, B, and C, respectively. Solid nanoparticles were cured from the selected microemulsions by simple cooling of the warm microemulsion prepared at 60 °C to room temperature (25 °C) in one vessel. The average particle size of cured nanoparticle Formulations A, B, and C measured at 20 °C are shown in Figure 3 demonstrating that solid nanoparticles were obtained directly from microemulsion templates. The nanoparticles sizes ranged from 77.2 to 124.1 nm. In addition, the polydispersity index of the three formulations ranged from 0.1 to 0.3, suggesting the uniformity of the particle size distribution. Compared to earlier studies, all of the nanoparticle formulations contained higher concentrations of GdH (2.5 mg/mL). The variations in particles sizes among Formulations A, B, C were directly attributed to the initial

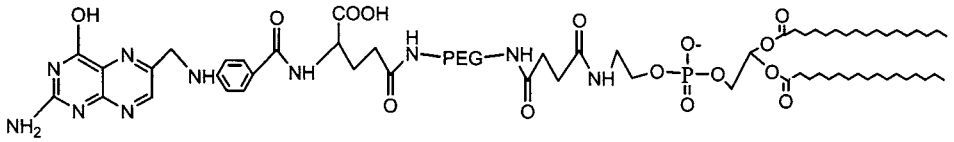


Figure 4. Chemical structure of folate−PEG−DSPE synthesized by linking folic acid to DSPE via a PEG spacer (MW 3350).

microemulsion droplet sizes. For example, Formulation A which had the largest droplet microemulsion droplet size using 6.0 mM Brij 78 (Figure 2) resulted in nanoparticles with the largest size (Figure 3). Additional studies were carried out to determine the effects of modifying the component ratios of nanoparticle matrix in the microemulsion pseudo-phase diagrams. It was observed that cured nanoparticle sizes increased with an increase in the GdH concentration in all formulations (data not shown). For instance, for Formulation C, increasing the GdH concentration from 0.5 mg/mL to 2.5 mg/mL, using a constant concentration of PEG-400 monostearate (0.5 mg/mL), resulted in a corresponding increase in nanoparticle size from 48.7 ± 7.8 nm to 93.4 ± 8.7 nm. Further, nanoparticles engineered with a concentration of GdH greater than 2.5 mg/mL had polydispersity indices ranging from 0.8 to 1.4, indicating that the formulations were not monodispersed. All formulations were purified and characterized by GPC using Sephadex G-75 and water as the mobile phase. Up to 10 fractions (1 mL each) were collected from the column. The GPC elution profiles were obtained using laser light scattering counts per second as well as fluorescence intensity of each fraction. It was observed that nanoparticles eluted primarily in fraction number 3 corresponding to the void volume of the column (data not shown).

Addition of Folate Ligand to Nanoparticles. The chemical structure of the synthesized folate ligand is shown in Figure 4. The basis of the synthesis of folate ligand was to link folic acid to DSPE via a PEG spacer. Previous studies have shown that folate retains its affinity to the receptor when derivatized via its γ-carboxyl group (Lee and Low, 1995; Wang et al., 1996; Atkinson et al., 2001). Since the folate ligand was added to nanoparticle formulations by physical mixing rather than by covalent attachment, adsorption of the ligand onto the nanoparticles was likely facilitated by the hydrophobic groups on DSPE. In addition, previous studies on folate-targeted delivery systems showed that the length and flexibility of PEG spacer influenced recognition by folate receptors and with little or no cell uptake occurring with systems that contained short PEG spacers (Lee and Low, 1994). The PEG used in the study (MW 3350) had earlier been proven to be a sufficient spacer (Lee and Low, 1994; Goren et al., 2000). Therefore, it is expected that the presence of DSPE and PEG spacer on the synthesized folate ligand will ensure both the attachment to nanoparticles as well as cell recognition. It was thought that addition of the folate ligand to microemulsion templates (before curing nanoparticles) may result in improved folate insertion, incorporation, and/or adsorption onto nanoparticles thereby enhancing the coating efficiency in the final nanoparticle formulations. Various concentrations of the folate ligand were added to either microemulsion templates at 60 °C (before cooling to room temperature) or nanoparticle suspensions at 25 °C. In the two cases, sufficient time was allowed to stir the mixture to ensure complete adsorption/insertion of folate ligand within the oil-in-water microemulsions or nanoparticles. Gel permeation chromatography (GPC) was used to determine the extent of folate ligand attachment on nanoparticles which was expressed as the coating

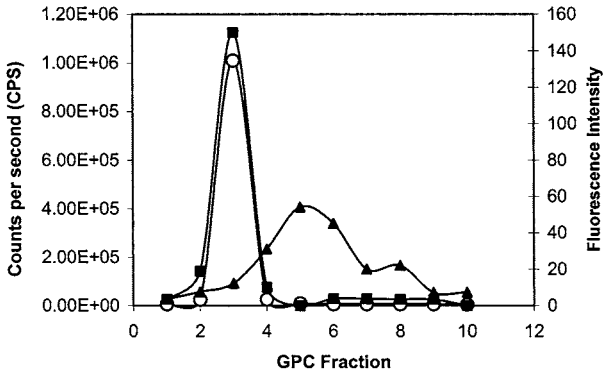


Figure 5. Gel permeation chromatography elution profiles demonstrating that the elution of free folate ligand (▲) was separated from folate-coated nanoparticles (○). Folate elution was detected by fluorescence intensity at 460 nm (excitation) and 534 nm (emission). The elution of folate-coated GdH nanoparticles (■) in the void volume was monitored by PCS as a control. Folate-coated nanoparticles (Formulation B) were obtained by adding the folate ligand (3% w/w) to the microemulsion template at 60 °C and then cooling the template to room temperature.

efficiency of the folate ligand. Particular attention was placed on the elution of free folate ligand and folate-coated nanoparticles. GPC elution profiles of folate were monitored by UV absorption at 363 nm as well as by fluorescence intensity at 460 nm (excitation) and 534 nm (emission) using fluorescent-labeled folate ligand that was synthesized using the procedure described earlier. The elution of nanoparticles after coating with 0.75% w/w folate ligand is shown in Figure 5. The results showed that folate-coated nanoparticles were engineered by the addition of folate ligand to microemulsion templates either at 60 °C (before curing nanoparticles) or to nanoparticle suspensions at 25 °C. To calculate the coating efficiency, both the elution of control nanoparticles (without folate ligand) and free folate ligand were obtained. Nanoparticle elution was monitored by laser light scattering counts per second which showed that the nanoparticles eluted in fraction 3 (void volume) while the elution of free folate ligand as detected by fluorescence intensity occurred later (Figure 5). Since it was possible to separate the elution of folate ligand as free ligand and folate-coated nanoparticles, the coating efficiency was calculated from folate elution profiles as follows:

$$\text{folate coating efficiency (\%)} = \frac{\text{area under nanoparticle elution profile}}{\text{area under the total elution profile}} \times 100\%$$

Using the equation above, the efficiency of coating nanoparticle Formulation A, B, and C with various amounts of folate ligand was calculated. Figure 6A demonstrates that folate ligand could be attached to all nanoparticle formulations. Up to 15% w/w folate ligand was added to all formulations, and the coating efficiency obtained was comparable in all the cases. However, the difference between folate addition to the microemulsion templates and onto cured nanoparticles was statistically significant for Formulation C ($P < 0.05$; two-sample t-test)

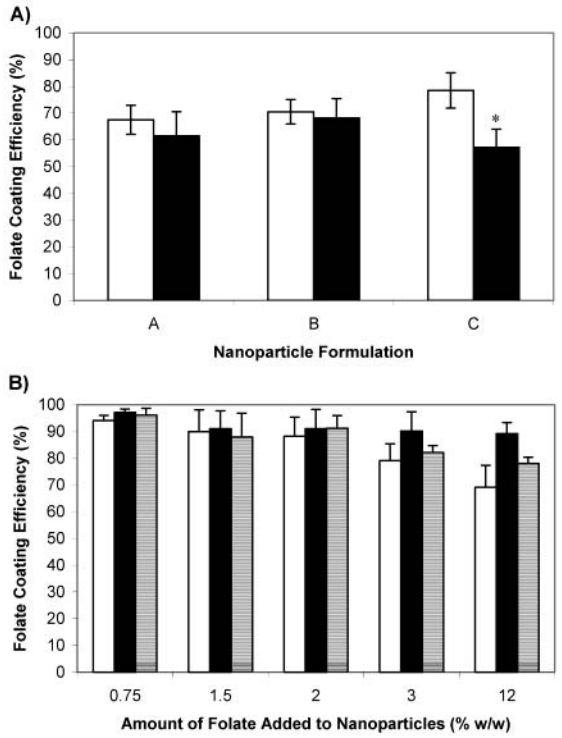


Figure 6. (A) Coating efficiencies of folate ligand (15% w/w) when added to nanoparticle Formulations A, B, and C either to the microemulsion template at 60 °C (□) or to nanoparticle suspensions at 25 °C (■). The coating efficiencies were obtained from GPC elution profiles of free folate ligand and folate-coated nanoparticles. Values represent mean ± SD ($n = 4$). (B) The effect of folate ligand concentration on the coating efficiency on nanoparticles. Folate ligand (0.75% w/w to 12% w/w) was added to microemulsion templates at 60 °C. Folate-coated nanoparticles Formulation A (□), Formulation B (■), and Formulation C (striped bars) were obtained after cooling to room temperature. Each data point represents mean ± SD ($n = 3$). *$P < 0.05$ as determined by a two-sample *t*-test assuming unequal variances.

where lower coating efficiency was obtained when the folate ligand was added to cured nanoparticles at 25 °C. Figure 6B shows the effects of the addition of various concentrations of folate ligand to the three nanoparticle formulations. For all formulations, high coating efficiencies (~96%) were obtained at low concentrations of folate ligand (0.75% w/w) added to microemulsion templates before curing nanoparticles. However, the coating efficiency decreased to below 90% when the final folate ligand concentration added to Formulations A, B, and C were above 2% w/w, 3% w/w, and 2% w/w, respectively. Since folate ligand attachment to cured nanoparticles was expected to be through the hydrophobic anchors (DSPE), the decrease in coating efficiency with increase in folate ligand concentration may be due to saturation of the nanoparticle surface with the folate ligand. For example, for Formulation A, increasing the folate ligand concentration from 0.75% w/w to 12% w/w resulted in a reduction in the coating efficiency from 96% to 55.6%. A slightly different trend was observed with Formulation B, wherein the addition of 25% w/w folate ligand to Formulation B resulted in a coating efficiency of 51.9% (data not shown), suggesting that higher amounts of folate ligand may be coated on these nanoparticles for reasons not yet known.

Cell Uptake of Folate-Coated Nanoparticles. Cell uptake studies were carried out in KB cells (human nasopharyngeal carcinoma cell lines), since it has been shown that they overexpress folate receptors (Lee et al., 1996). The cells were cultured in medium that contained no folic acid to facilitate the expression of folate receptors. Nanoparticle Formulation B coated with 3% w/w folate ligand was used in cell uptake studies based on their small size (below 100 nm) and high folate ligand coating efficiency. Since the addition of folate ligand (3% w/w) resulted in >92% coating efficiency, the final formulation was used without further purification by GPC. GdH cell uptake was monitored by fluorescence spectroscopy. The dependence of fluorescence intensity of Gd on concentrations had been previously published (Reisfeld and Biron, 1970). Preliminary studies showed that GdH fluorescence intensity was concentration dependent. The standard curve of concentration versus fluorescence was linear in the concentration range of 0−50 μg/mL, and the sensitivity of detection was as low as 0.1 μg/mL. Prior to the uptake studies, the stability of folate ligand coating on nanoparticles was investigated to account for any form of detachment or leakage of folate ligand from nanoparticles. The folate-coated nanoparticles were stable when incubated at 37 °C for 150 min in PBS (pH 7.4), 10% fetal bovine serum, and in the cell growth medium. The uptake of nanoparticles by KB cells was dependent on the concentration of the nanoparticles in the medium. The cell uptake of Gd nanoparticles increased with increasing nanoparticle dose exhibiting nearly a linear correlation (Figure 7). The reduction of cell uptake efficiency at higher concentrations of nanoparticles may suggest saturation. In contrast to the results obtained at 37 °C, uptake studies at 4 °C resulted in lower Gd uptake with an apparent plateau as from 90 μg/mL to 180 μg/mL nanoparticle concentrations (Figure 7). For instance, Gd uptake efficiency at nanoparticles concentration of 360 μg/mL was about 82% at 37 °C and only 4.5% at 4 °C. Since ligand binding and uptake is dependent on temperature (Holm et al., 1981; Holm et al., 1983), the uptake of Gd nanoparticles by KB cells was likely an energy dependent process. The enhanced cellular uptake at 37 °C was attributed to endocytosis that was active at 37 °C but suppressed at 4 °C. Suppression of uptake at 4 °C was perhaps due to geometrical changes in the receptor as reported by others (Hassan et al., 1992; Davda and Labhasetwar, 2002; Shikata et al., 2002). Thus, the results demonstrated that cultured KB cells could selectively take up folate-coated nanoparticles. The uptake of folate-coated nanoparticles was about 10-fold higher than uncoated nanoparticles after 30 min at 37 °C. The uptake of folate-coated nanoparticles at 4 °C was 20-fold lower than the uptake at 37 °C and comparable

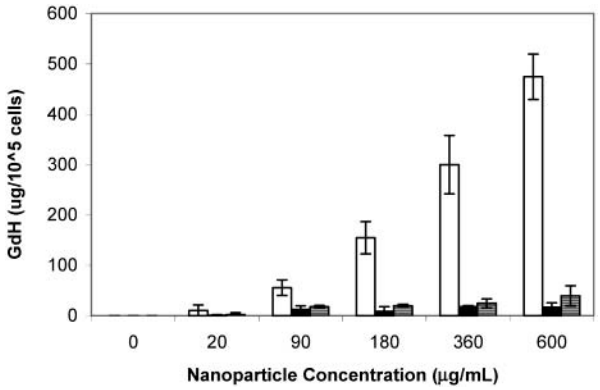


Figure 7. The effect of nanoparticle concentration on KB cells uptake for folate-coated nanoparticles after incubation for 30 min at 37 °C (□) and at 4 °C (■). In the control experiments, various concentrations of control nanoparticles (without folate) were also incubated with KB cells at 37 °C for 30 min (stripped bars). Each data point represents the mean ± SD ($n = 3$).

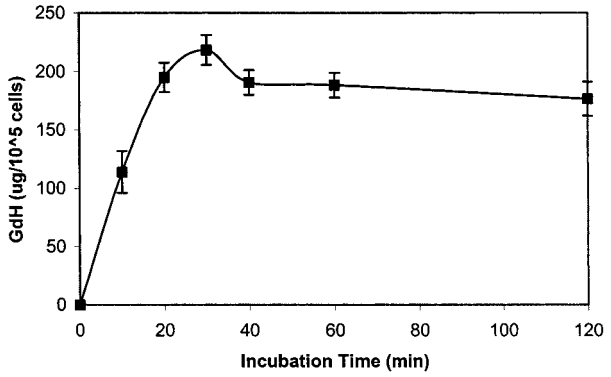


Figure 8. The effect of incubation time on the uptake of folate-coated nanoparticles (300 μg/mL) by KB cells. Nanoparticle Formulation B coated with 3% w/w folate ligand was used. Cell internalized fluorescence was measured at 497 nm (excitation) and 521 nm (emission) using fluorescein−DOPE as the marker. Entrapment of fluorescein−DOPE 0.25% w/w in nanoparticles as confirmed by gel permeation chromatography was ~100%. Values represent mean ± SD (n = 3).

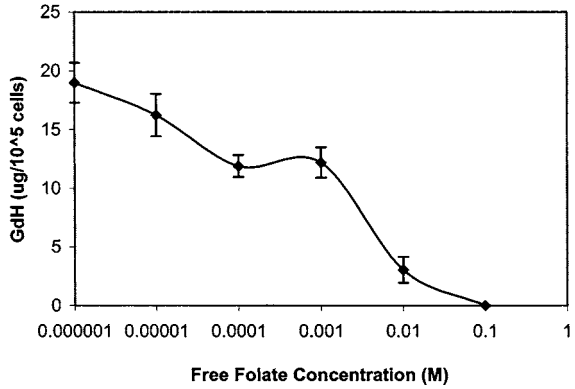


Figure 9. Inhibition of folate-coated nanoparticle uptake by free folic acid. KB cells were incubated at 37 °C for 30 min with folate-coated nanoparticles (360 μg/mL) in the presence of various concentrations of free folic acid. Each value represents the mean ± SD (n = 3).

to the uptake of uncoated nanoparticles at 37 °C. Similar levels of enhanced uptake of folate-targeted over non-targeted delivery systems have been published previously (Pan et al., 2002). Incubation time also played a role in the uptake of folate-coated nanoparticles as shown in Figure 8. Within 30 min of incubation, up to 290 μg GdH per 10^5 cells was internalized as indicated by the fluorescence intensity of fluorescein−DOPE entrapped in nanoparticles. The results showed a rapid cell uptake of GdH nanoparticles reaching an apparent maximum at 30 min (Figure 8). To verify the involvement of folate receptors on KB cell uptake of GdH nanoparticles, competition between folate-coated nanoparticles and free folic acid was carried out (Figure 9). Coincubation of free folic acid inhibited folate-coated nanoparticles uptake (Figure 9). At very high concentration of free folic acid of about 100 mM, little or no uptake of folate-coated nanoparticles was observed. In addition, reducing the concentration of free folic acid (as a competitive inhibitor) from 100 mM to 0.001 mM resulted in up to 18-fold increase in the uptake of folate-coated nanoparticles (Figure 9), demonstrating that free folic acid served as a competitive inhibitor. It was observed that the uptake of folate-coated nanoparticles decreased to only ~2% of its initial value with the coincubation of about 0.001 mM free folic acid (the lowest free folic acid concentration studied). The inhibition studies by coincubation with free folic acid indicated that the uptake of folate-coated nanoparticles occurred in much the same manner as free folic acid.

In general, these studies have indicated that folate-coated Gd nanoparticles may have potential of selectively delivering high concentrations of Gd to tumors thereby enhancing the success of NCT. Previous reports have suggested that targeted Gd-NCT strategies may be of therapeutic interest (Akine et al., 1990; Tokuuye et al., 2000). Folate-coated nanoparticles may therefore serve as effective carrier systems for Gd-NCT since (i) nanoparticle size of ~100 nm could facilitate internalization by tumor cells, (ii) the formulations contain high concentrations of Gd, (iii) nanoparticles may potentially enhance the therapeutic potential Gd-NCT via selective uptake by folate receptors, and (iv) previous studies have shown that presence of Gd in the intracellular space can enhance the therapeutic effectiveness of Gd-NCT (Akine et al., 1990). Current studies are evaluating the in vivo biodistribution of folate-coated nanoparticles in a KB cell tumor model in nude (nu/nu) mice.

LITERATURE CITED

(1) Akine, Y., Tokita, T., Matsumoto, H., Oyama, S., Egawa, O., and Aizawa, O. (1990) Radiation effect of gadolinium-neutron capture reactions on survival of Chinese hamster cells. *Strahlenther. Onkol. 166*, 831−833.

(2) Atkinson, S. F., Bettinger, T., Seymour, L. W., Behr, J., and Ward, C. (2001) Conjugation of folate via gelonin carbohydrate residues retains ribososmal-inactivating properties of the toxin and permits targeting to folate receptor positive cells. *J. Biol. Chem. 276*, 27930−27935.

(3) Bally, M. B., Masin, D., Nayar, R., Cullis, P. R., and Mayer, L. D. (1994) Transfer of liposomal drug carriers from blood to the peritoneal cavity of normal and ascitic tumor-bearing mice. *Cancer Chemother. Pharmacol. 34*, 137−146.

(4) Barth, R. F., and Soloway, A. H. (1994) Boron neutron capture therapy of primary and metastatic brain tumors. *Mol. Chem. Neuropathol. 21*, 139−154.

(5) Bernard, J. A. (1995) Procedures for Implementation of MIT program on Neutron capture therapy. *Trans Am. Nucl. Soc. 72*, 114.

(6) Chen, W., Mehta, S. C., and Lu, R. D. (1997) Selective boron drug delivery to brain tumors for neutron capture therapy. *Adv. Drug Deliv. Rev. 26*, 231−247.

(7) Davda, J., Labhasetwar, V., (2001) Characterization of nanoparticles uptake by endothelial cells. *Int. J. Pharm. 233*, 51−59.

(8) Desai, M. P., Labhasetwar, V., Amidon, G. L., and Levy, R. J. (1996) Gastrointestinal uptake of biodegradable microparticles in Caco-2 cells is size dependent. *Pharm. Res. 14*, 1568−1573.

(9) Goren, D., Horowitz, A. T., Tzemach, D., Tarshish, M. M., Zalipsky, S., and Gabizon, A. (2000) Nuclear delivery of doxorubicin via folate-targeted liposomes with bypass of multidrug-resistance efflux pump. *Clin. Cancer Res. 6*, 1949−1957.

(10) Hassan, E. E., Parish, C. R., and Gallo, M. J. (1992) Optimized formulation of magnetic chitosan microparticles containing anticancer agent, oxantrazole. *Pharm. Res. 9*, 390−397.

(11) Hobbs, S. K., Monsky, W. L., Yuan, F., Roberts, W. G., Griffith, L., Torchilin, V. P., and Jain, R. K. (1998) Regulation of transport pathways in tumor vessels: role of tumor type and microenvironment. *Proc. Natl. Acad. Sci. 95*, 4607−1612.

(12) Holm, J., Hansen, S., and Lyngbye, J. (1981) High-affinity binding of folate to a serum protein in chronic myelogenous leukemia: effect of binder concentration, pH and temperature. *Clin. Chem.* 27, 316−318.

(13) Holm, J., Hansen, S., and Lyngbye, J. (1983) High-affinity folate binding in leukocyte lysate from normal subjects: effect of concentration of binding protein, temperature and pH. *Acta Heamatol. 70*, 269−272.

(14) Jain, R. K. (1997) Delivery of molecular and cellular medicine to solid tumors. *Adv. Drug Deliv. Rev. 26*, 71−90.
(15) Jono, K., Ichikawa, H., Fujioka, K., Fukumori, Y., Akine, Y., and Tokuuye, K. (1999) Preparation of lecithin microcapsules by a dilution method using the wuster process for intraaterial administration in gadolinium neutron capture therapy. *Chem. Pharm. Bull. 47*, 54−63.
(16) Kamen, B. A., and Caston, J. D. (1986) Properties of a folate binding protein (FBP) isolated from porcine kidney. *Biochem. Pharmacol. 35*, 2323−2329.
(17) Kreuter, J. (1995) Nanoparticles as adjuvants for vaccines. *Pharm. Biotechnol. 6*, 463−472.
(18) Lee, R. J., and Low, P. S. (1994) Delivery of liposomes into cultured KB cells via folate receptor-mediated endocytosis. *J. Biol. Chem. 269*, 3198−3204.
(19) Lee, R. J., and Low P. S. (1995) Folate-mediated tumor cell targeting of liposome-entrapped doxorubicin in-vitro. *Biochim. Biophys. Acta. 1233*, 134−144.
(20) Lee, R. J., and Huang, L. (1996) Folate-targeted, anionic liposome-entrapped polylysine-condensed DNA for tumor cell-specific gene transfer. *J. Biol. Chem. 271*, 8481−8487.
(21) Martin, R. F., D'Cunha, G., Pardee, M., and Allen, B. J. (1988) Induction of double-strand breaks following neutron capture by DNA-bound 157Gd. *Int. J. Radiat. Biol. 54*, 205−208.
(22) Matsumoto, T. (1992) Transport calculations of depth-dose distributions for gadolinium neutron capture therapy. *Phys. Med. Biol. 37*, 155−162.
(23) Mehta, S. C., and Lu, R. D. (1996) Targeted drug delivery for boron neutron capture therapy. *Pharm. Res. 13*, 345−351.
(24) Miyamoto, M., Hirano, K., Ichikawa, H., Fukumori, Y., Akine, Y., and Tokuuye, K. (1999) Biodistribution of gadolinium incorporated in lipid emulsions intraperitoneally administered for neutron capture therapy with tumor-bearing hamsters. *Biol. Pharm. Bull. 12*, 1331−1340.
(25) Morel, S., Terreno, E., Ugazio, E., Aime, S., and Gasco, M. R. (1998) NMR relaxometric investigations of solid lipid nanoparticles (SLN) containing gadolinium (III) complexes. *Eur. J. Pharm. Biopharm. 45*, 157−163.
(26) Mumper, R. J., and Jay, M. (1992) The formation and stability of lanthanide complexes and their encapsulation into polymeric microspheres. *J. Physical Chem. 33*, 398−402.
(27) Oyewumi, M. O., and Mumper, R. J. (2001) Microemulsions as templates to engineer cell specific nanoparticles. *Proc. Int. Symp. Controlled Release Bioact. Mater. 28*, 7179.
(28) Oyewumi, M. O., and Mumper, R. J. (2002) Gadolinium-loaded nanoparticles engineered from microemulsions templates. *Drug. Dev. Ind. Pharm. 28*, 317−328.
(29) Pan, X. Q., Wang, H., Shukla, S., Sekido, M., Adams, D., Tjarks, W., Barth, R. F., and Lee, R. J. (2002) Boron-containing folate receptor-targeted liposomes as potential delivery agents for neutron capture therapy. *Bioconjugate Chem. 13*, 435−442.
(30) Reisfeld, R., and Biron, E. (1970) Determination of gadolinium in sodium borate glasses. *Talanta 17*, 105−108.
(31) Shih, J., and Brugger, R. M. (1992) Gadolinium as a neutron capture agent. *Med. Phys. 3*, 733−744.
(32) Shikata, F., Tokumitsu, H., Ichikawa, H., and Fukumori, Y. (2002) In vitro cellular accumulation of gadolinium incorporated into chitosan nanoparticles designed for neutron-capture therapy of cancer. *Eur. J. Pharm. Biopharm. 53*, 57−63.
(33) Tokumitsu, H., Ichikawa, H., and Fukumori, Y. (1999) Chitosan-gadopentetic acid complex nanoparticles for gadolinium neutron capture therapy of cancer: preparation by novel emulsion droplet coalescence technique and characterization. *Pharm. Res. 16*, 1830−1835.
(34) Tokumitsu, H., Hiratsuka, J., Sakurai, Y., Kobayashi, T., Ichikawa, H., and Fukumori, Y. (2000) Gadolinium neutron-capture therapy using novel gadopentetic acid-chitosan complex nanoparticles: in vivo growth suppression of experimental melanoma solid tumor. *Cancer Lett. 150*, 177−182.
(35) Tokuuye, N., Tokita, Y., Akine, H., Nakayama, Y., Sakurai, T., Kobayashi, K. K. (2000) Comparison of radiation effects of gadolinium and boron neutron capture reactions. *Strachlenther. Onkol. 176*, 81−83.
(36) Wang, S., and Low, P. S. (1998) Folate-mediated targeting of antineoplastic drugs, imaging agents and nucleic acids to cancer cells. *J. Controlled Release 53*, 39−48.
(37) Weitman, S. D., Lark, R. H., Coney, L. R., Fort, D. W., Frasca, V., Zurawski, V. R., and Kamen, B. A. (1992) Distribution of the folate receptor GP38 in normal and malignant cell lines and tissues. *Cancer Res. 52*, 3396−3401.
(38) Wu, N. Z., Da, D., Rudoll, T. L., Needham, D., Whorton, A. R., and Dewhisrt, M. W. (1993) Increased microvascular permeability contributes to preferentially accumulation of shealth liposomes in tumor tissue. *Cancer Res. 53*, 3765−3770.

BC025560X

High Temperature Biocatalysis by Chemically Modified Cytochrome *c*

Humberto García-Arellano, Brenda Valderrama, Gloria Saab-Rincón, and Rafael Vazquez-Duhalt*

Instituto de Biotecnología, UNAM, Apartado Postal 510-3, Cuernavaca, Morelos, CP 62250 México
Received June 20, 2002; Revised Manuscript Received August 19, 2002

Chemically modified cytochrome *c* with poly(ethylene glycol) (PEG) showed activity at temperatures higher than 100 °C and to be highly thermostable. The molecular size of PEG moieties and the coupling site affected the thermal stabilization. An optimal PEG/protein mass ratio of 2.8 was found, producing a fully thermostable biocatalyst at 80 °C. Site-directed mutagenesis on yeast cytochrome *c* showed an increased thermostabilization when lysine 79 residue, localized at the edge of the active site, was replaced by a nonreactive residue. Tertiary, secondary, and active-site structures were analyzed by fluorescence, CD, and UV/visible spectroscopies. Besides its disordered structure, the pegylated protein showed a lower unfolding rate at the active-site than the unmodified ones. A shell-like structure seems to protect the heme environment, in which PEG is coiled on the protein surface with a primary shield of rigid water molecules solvating the hydrophilic region of bound-PEG, and the PEG hydrophobic regions interacting with the hydrophobic clusters on protein surface.

INTRODUCTION

Enzymatic catalysis is increasingly used as an alternative to traditional chemical synthesis. The driving force behind this change is the necessity to innovate products and to establish new ecoefficient processes (*1*). However, in many cases the industrial application of enzymes is hampered by the instability of the biocatalyst under process conditions, which may involve extreme pH, high temperature, the presence of organic solvents, and other denaturing agents. The generation of robust biocatalysts can be accomplished by genetic and biochemical approaches, and progress will continue after the systematic identification of novel sources of enzymes with unusual properties, e.g., from extremophile microorganisms.

Any enhancement of the thermal stability of an enzyme would confer significant operational advantages such as higher reaction rates, increased substrate solubility in lower viscosity media, productive shifts in thermodynamic equilibrium, and reduced risks of microbial contamination. Genetic approaches have yielded significant results in obtaining more thermostable enzymes, with higher temperature optima through directed evolution (*2*−*4*). A combination of rational and random mutagenesis has been used to obtain a fungal peroxidase 174-times more thermostable than the wild-type protein (*5*). However, although directed evolution seems to be a powerful tool to enhance biocatalytic performance, its main drawback is that the knowledge of the properties gained during site-directed mutagenesis or evolution processes cannot be used as a general method to be applied to other proteins. On the other hand, chemical modification seems to be a more general method to improve intrinsic properties of proteins such as stability and activity without a deeper knowledge of the gene or protein structure. Several chemical methods have been employed to obtain more stable protein derivatives, including plastic conjugates (*6*, *7*), cross-linked enzyme crystals (CLECs) (*8*−*10*), attachment to polysaccharides (*11*−*12*), and chemical modification with amphiphilic polymers (*13*−*15*).

It is well-known that the modification with PEG or polysaccharides may confer certain thermostability to the enzymes at a temperature range from 50 to 70 °C (*15*, *16*). Stabilization of proteins was explained by the solvation of PEG-bound molecules, which restricted the molecular mobility, thus decreasing the unfolding rate of the protein.

Catalytically active and stable enzymes at temperatures higher than 80 °C are considered hyperthermophilic enzymes. Only two enzymatic preparations have been shown to be active and stable at temperatures higher than 100 °C in aqueous systems, both hydrolytic enzymes: a pegylated trypsin (*13*) and a dextran-glycosylated amylase (*12*). The thermal protective effect of PEG on trypsin was attributable to the presence of the polymer, which may change the microenvironment through the formation of a hydrogen-bond network around the protein (*13*). The higher the molecular mass of PEG, the higher the thermostability of trypsin. The effect of the size of the polymer on the thermostability of amylolytic enzymes has also been reported by Lenders et al. (*11*). The increased thermal stability of the dextran−protein conjugate was mainly due to the formation of multiple covalent links between the enzyme and the polymer leading to the formation of a more rigid conformation of the protein. It was also shown that the stability decreased when the number of linkages between the enzyme and the carbohydrate was lower. Only two peroxidases have been shown to be stable at temperatures higher than 80 °C in their native form: soybean (*17*) and palm oil (*18*) peroxidases, and this stability does not necessarily mean activity at high temperatures. However, no information is available on chemically modified peroxidases showing activity and stability at hyperthermophilic conditions (80 to ≥ 100 °C) in aqueous systems.

As a novel source of biocatalysts, we are exploring the peroxidase activity of nonenzymatic hemoproteins, such

* Corresponding author. Fax: (52) 777-317-2388. E-mail: vazqduh@ibt.unam.mx.

10.1021/bc025561p CCC: $22.00 © 2002 American Chemical Society
Published on Web 10/15/2002

as cytochrome *c* (*19*−*23*) and hemoglobin (*24*, *25*), with emphasis on the oxidation of polycyclic aromatic hydrocarbons (PAHs). The catalytic properties of these hemoproteins have been significantly improved by site-directed mutagenesis (*21*, *22*) and chemical modification (*22*, *23*). In addition, rational design methods have been used to obtain cytochrome *c* variants with higher stability against inactivation by hydrogen peroxide (*26*). In this work, we present the enhanced peroxidase catalytic performance of a chemically modified cytochrome *c* at temperatures above 80 °C, and we discuss the possible mechanism of thermoprotection.

EXPERIMENTAL PROCEDURES

Chemicals. Horse heart cytochrome *c*, *Saccharomyces cerevisiae* cytochrome *c*, methoxypoly(ethylene glycol) (MW 350, 750, and 2000 Da), cyanuric chloride-activated monomethoxypoly(ethylene glycol) (MW 5000 Da), hydrogen peroxide (30%), and cyanuric chloride (2,4,6 trichloro-1,3,5-triazine) were obtained from Sigma Chemical Company (St. Louis, MO). Pyrene, anthracene, benzo[*a*]pyrene, thianthrene, dibenzothiophene, and phenyl disulfide were obtained from Aldrich (Milwaukee, WI). Organic solvents (HPLC grade) were purchased from Fisher Scientific (Fairlawn, NJ). Ultrapure guanidine hydrochloride (GuHCl) was from Gibco BRL (Rockville, MD). All DNA restriction and modification reagents were from New England Biolabs (Beverly, MA). All other reagents were analytical grade.

Methoxypoly(ethylene glycol) (PEG) Activation. Activation of PEG species of different molecular sizes (350, 750, or 2000 Da) was carried out by a modification of the method reported by Abuchowski et al. (*27*). PEG aliquots (10 mmol) were dissolved in 40 mL of dry toluene containing 1 g of sodium carbonate. Cyanuric chloride (30 mmol) was added, and the resulting mixture was stirred overnight at room temperature. The solution was filtered, and the activated PEG fraction was recovered by adding the filtrate to 80 mL of cold petroleum ether followed by a 10 min centrifugation at 12100*g*. The resulting precipitate was separated and washed with cold petroleum ether until it was free of residual cyanuric chloride as detected by UV spectrometry. The chlorine content in activated PEGs was determined by titration with silver nitrate (0.02 N) after overnight hydrolysis in 50 mM sodium carbonate buffer, pH 10.0.

Chemical Modification of Cytochrome *c*. Poly(ethylene glycol)-modified horse heart cytochrome *c* (Cyt−PEG) was produced according to the method reported by Gaertner and Puigserver (*13*). Cytochrome *c* (9 mg) was dissolved in 5 mL of 40 mM borate buffer pH 10.0, and then a five molar excess in a free amino group basis of cyanuric chloride-activated monomethoxypoly(ethylene glycol) (MW 5000 Da) was added. The mixture was stirred for 1 h at room temperature and then diluted to 100 mL with 60 mM sodium phosphate buffer pH 6.1 and dialyzed extensively against the same buffer. The Cyt−PEG conjugate solution was concentrated using an Amicon ultrafiltration cell (Millipore, Bedford, MA) using a 10 kDa cutoff membrane. Yeast cytochrome *c* conjugates were obtained by the same procedure. The degree of protein modification was estimated by titration of the residual free amino groups with trinitrobenzenesulfonic acid (*28*).

Site-Directed Mutagenesis of *S. cerevisiae cyc1*. Single and double mutants of *cyc1* (Table 3) were obtained by megaprimer-extension (*29*) upon the pBTR1 plasmid (*30*) using the following primers: pf1 5′-cggtacccggggatccataactaac-3′, pr4 5′-aaaaagctagcctgtttactcagtgctttttcaagaaggtaattaagtc-3′, K79A 5′-cccaccaaaggccatcgcggtaccaggaatat-3′, K27A 5′-gtttggaccaaaccgcatgtgggccacc-3′.

All amplifications were performed using the high-fidelity DNA-polymerase Expand from Roche (Mannheim, Germany) following the manufacturer instructions. Megaprimers were obtained by amplification of plasmid pBTR1 with the primer sets pf1-K27A or K79A and purified from the gel. Extension of the megaprimers was performed upon plasmid pBTR1 using primer pr4. The extension products were purified from the gel, restricted with BamHI and NheI and ligated onto pBTR1 restricted with the same enzymes and harboring *cyc3* coding for the cytochrome *c*-heme lyase (*30*). The nucleotide sequence of all clones was confirmed twice using the Big dye Terminator kit (Applied Biosystems, Foster City, CA) in an ABI Prism 377 System (Applied Biosystems).

Overexpression and Purification of Mutant Cytochrome *c* Proteins. Transcription of cyc1 and cyc3 is driven from a low-constitutive *tet* promoter located upstream from the BamHI restriction site in plasmid pBTR1 and in all the derivatives here described. All plasmids were transformed into the *E. coli* strain JM101 and maintained in Luria-Bertani (LB) rich medium (*31*) supplemented with ampicillin (100 μg/mL). Accumulated expression of cytochrome *c* was achieved by growing each recombinant *E. coli* strain in a 2 L New Brunswick (Edison, NJ) fermenter in 1.5 L LB rich medium supplemented with ampicillin for 30 h. Typical cell yield was 2.5 g wet weight per fermenter. Cell pellets (5 g per strain) were resuspended in 50 mL of cold breaking buffer (20 mM sodium phosphate, pH 6.1, 25% sucrose, 10 mM EDTA, 0.2 mM DTT, 50 μg/mL lysozyme) and incubated in ice for 10 min. The cell suspension was then supplemented with 5 mg/mL Brij 35, 0.01 mM $MgCl_2$, 20 μg/mL RNAse, 100 μg/mL DNAse, 1 mM PMSF, and incubated at 37 °C for 10 min. Cells were disrupted by two 1 min pulses in a Sonicator (Sonics and Materials Inc., Danbury, CT). Cell debris was removed by centrifugation. Cell extracts were precipitated with one volume of saturated ammonium sulfate, and the supernatants were recovered and dialyzed overnight against 80 volumes of cold 20 mM sodium phosphate buffer, pH 6.1. Enriched extracts were subjected to cation-exchange chromatography using a Macro-Prep High S support (BioRad, Hercules, CA) packed column and the Econo System purification system from BioRad using a linear NaCl gradient. The chromatography was followed by absorbance at 280 and 410 nm. The cytochrome *c*-enriched peak was collected, concentrated by ultrafiltration in an Amicon system (Millipore, Bedford, MA) fitted with a 10 kDa cutoff membrane, and dialyzed overnight against 4 L of cold 20 mM sodium phosphate buffer, pH 6.1. All proteins were purified to homogeneity as assessed by SDS-PAGE and silver staining of the gel. Typical R_z values ranged from 4.8 to 5.4.

Protein Concentration. Cytochrome preparations were dissolved in 60 mM sodium phosphate buffer, pH 6.1. Unmodified cytochrome concentration was estimated in the reduced state using an extinction coefficient $\epsilon = 29.5\ mM^{-1}\ cm^{-1}$ at 550 nm (*32*). The absorption spectrum of Cyt−PEG was altered as a result of the chemical modification, the typical 550 nm band observed in the reduced state was lost, and the Soret band maximum was UV-shifted. Ahmad, et al. (*33*) reported a ϵ value of $1.061 \times 10^5\ M^{-1}\ cm^{-1}$ at 410 nm for the oxidized state of cytochrome *c*. We applied the same value to estimate the concentration of Cyt−PEG in the oxidized state using the

absorbance of the 402 nm Soret band. To confirm the concentration, Cyt−PEG samples were digested and iron was estimated by atomic absorption. The predicted Cyt−PEG concentration, obtained with each of the methods described above, gave a correlation of 0.994.

Activity Assays. Cytochrome *c* reaction mixtures contained 15% acetonitrile, 20 μM polycyclic aromatic hydrocarbons (PAHs) or organosulfur compounds as substrate and 0.5−3.5 μM of unmodified or chemically modified cytochrome in 1 mL of 60 mM sodium phosphate buffer, pH 6.1. Reactions were carried out in individual sealed vessels and started by the addition of 5 μL of 200 mM H_2O_2 (1 mM final concentration) and stopped by adding 1 mL of acetonitrile. The extent of the reaction was followed by substrate consumption on a HPLC (Perkin-Elmer, Norwalk, CT) equipped with a reverse phase C_{18} 5 μm column (15 × 3.9 mm). Specific activity was determined by measuring the moles of substrate oxidized per mole of cytochrome preparation in 1 min and expressed as min^{-1}. All reactions were performed in triplicate.

Activity vs Temperature Profile. Cytochrome *c* reactions were assayed from 20 °C to 120 °C in 4 mL glass vials sealed with Teflon septa. Reaction mixtures contained 15% acetonitrile, 20 μM pyrene, and 0.5−4.6 μM cytochrome preparation in 1 mL 60 mM sodium phosphate buffer, pH 6.1. Complete mixtures were kept at the desired temperature for 5 min before starting the reactions by the addition of H_2O_2 (1 μmol). Reaction extent was followed by the decrease in absorbance at 335 nm. Residual pyrene was estimated using the extinction coefficient $\epsilon = 32.6\ mM^{-1}\ cm^{-1}$ at 336 nm (*34*). Specific activity is expressed as min^{-1}.

Stability Assays. The horse-heart cytochrome *c* thermal stability was determined by estimating the specific activity after different incubation times at 80 °C in the absence or presence of substrate. Inactivation constants were determined by fitting the experimental data to the first-order equation ($A = A_0e^{-kt}$). Yeast cytochrome *c* thermal stability was assayed after 5 h at 70 °C using pyrene as substrate.

Circular Dichroism Measurements. CD measurements were performed on an AVIV 62Ds spectropolarimeter (Lakewood, NJ). Unmodified or modified cytochrome *c* samples (20 μM) were dissolved in 10 mM phosphate buffer, pH 6.1. Blank tests with buffer and controls containing 5 mM PEG (MW 5000 Da) in the same buffer were conducted, and the reference signals were subtracted from the sample signals. CD scans were performed from 180 to 260 nm and from 350 to 450 nm under the following conditions: bandwidth 1 nm, scan step 1 nm, and average time 1 s. For each sample, an average of three repetitions is given. For the assays at 7 or 24 h, incubations were carried out in a water bath previously equilibrated at 80 °C. Samples were contained in sealed vials to avoid evaporation. At the specified times, samples were removed from the water bath and placed in the quartz cell. Samples were equilibrated at the scan temperature for at least 10 min. Temperature in the cell compartment was controlled by a Peltier module. Protein concentration was determined before and after each assay.

Fluorescence Measurements. Fluorescence spectra were performed on a Perkin-Elmer LS-50B luminiscence spectrometer (Norwalk, CT). Samples containing 2 μM cytochrome *c* preparations were incubated at different GuHCl concentrations until reaching equilibrium. Afterward, each sample was excited at 295 nm, and three emission spectra from 300 to 500 nm were recorded and averaged. Data analyses were carried out using the center of mass obtained from each recorded spectrum.

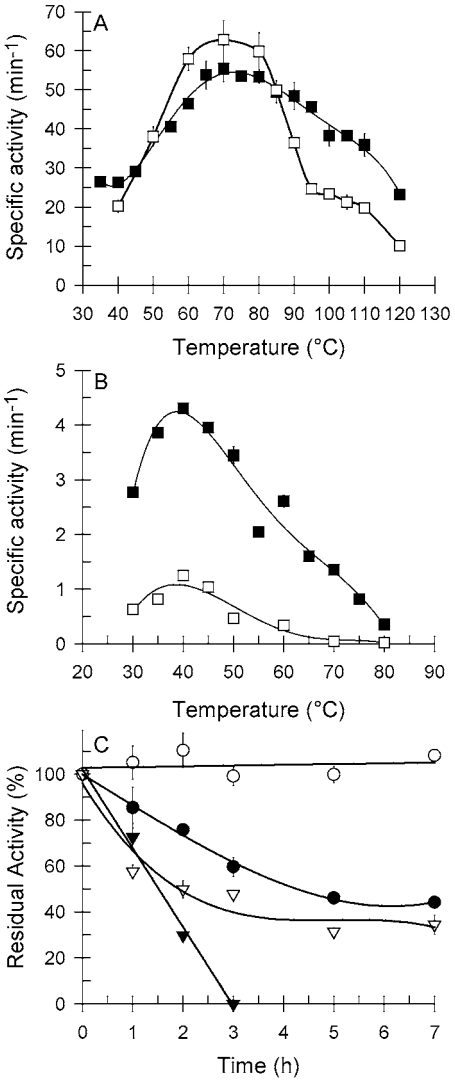


Figure 1. Biocatalytic oxidation of (A) pinacyanol chloride and (B) pyrene by unmodified (□) and chemically modified (■) cytochrome *c* at different temperatures. (C) Thermal stability of unmodified and chemically modified cytochrome *c* incubated at 80 °C with or without the presence of substrate (pinacyanol chloride). The reaction was started by the addition of hydrogen peroxide, and the residual activity was measured at 80 °C. (○) Cyt−PEG_{5000} incubated with substrate, (●) Cyt−PEG_{5000} incubated without substrate, (▽) Cyt incubated with substrate, (▼) Cyt incubated without substrate.

Data Analysis. Unfolding profiles were simultaneously fit by global analysis of the data obtained by fluorescence and CD. The thermodynamic and spectroscopic features were optimized in global fits by nonlinear least-squares analysis using an in-house version of Savuka 5.0 software package (*35*).

RESULTS AND DISCUSSION

Cytochrome *c* (Cyt) is a compact globular protein with an unusual intrinsic stability provided by a complex hydrogen-bond network (*36*, *37*). This stability leads Cyt to a remarkable catalytic performance as a peroxidase at temperatures as high as 120 °C (hyperthermophilic conditions), with maximal activity between 70 °C and 80 °C (Figure 1a). Horse heart cytochrome *c* was modified with PEG of 5000 Da MW (Cyt−PEG_{5000}). Chemical modification did not alter the specific activity nor the

Table 1. Specific Activities of Unmodified and Chemically Modified Horse Heart Cytochrome *c* on PAHs and Organosulfur Compounds in 15% Acetonitrile

	specific activity (min^{-1})			
	30 °C		80 °C	
substrate	Cyt	Cyt−PEG_{5000}	Cyt	Cyt−PEG_{5000}
pyrene	0.63 (± 0.02)	2.78 (± 0.08)	0.01 (± 0.001)	0.35 (± 0.01)
anthracene	0.96 (± 0.1)	3.34 (± 0.1)	0.12 (± 0.002)	0.54 (± 0.01)
benzo[*a*]pyrene	0.75 (± 0.1)	2.6 (± 0.4)	0.49 (± 0.05)	1.2 (± 0.03)
thianthrene	5.83 (± 0.2)	11.6 (± 0.6)	0.63 (± 0.04)	2.6 (± 0.3)
dibenzothiophene	1.91 (± 0.03)	5.12 (± 0.8)	0.13 (± 0.003)	1.0 (± 0.01)
phenyl disulfide	1.24 (± 0.1)	3.9 (± 0.2)	0.08 (± 0.002)	0.7 (± 0.01)

temperature profile of cytochrome *c* when hydrophilic substrates are used, as in the case of pinacyanol chloride (Figure 1a). However, when the hydrophobic substrate pyrene is used, the Cyt−PEG_{5000} preparation showed higher specific activity than the unmodified Cyt (Figure 1b). Surprisingly, the maximal activity temperature was displaced from 70 °C with pinacyanol to 40 °C with pyrene for both preparations. Chemical modification with PEG produces an increase of the overall hydrophobicity of the protein (*38*, *39*) and an increased enzyme solubility in organic solvents with little loss of activity (*40*), facilitating homogeneous catalysis. Pinacyanol chloride is a relatively hydrophilic substrate; thus the activity toward this molecule was expected to be independent of the biocatalyst modification. On the other hand, the activity toward more hydrophobic molecules, such as polycyclic aromatic hydrocarbons and organosulfur compounds, would be especially increased by PEG modification of the enzyme, following a more favorable partition of the substrate from the solvent toward the active site (*22*, *41*).

Chemical modification dramatically increased the thermostability of the protein (Figure 1c). While Cyt lost all detectable activity after 3 h of incubation at 80 °C, Cyt−PEG_{5000} retained 45% of the initial activity after 7 h of incubation. In the presence of substrate (pinacyanol chloride), the intrinsic stability of both preparations was improved. In the case of Cyt−PEG_{5000}, the presence of substrate resulted in a stable catalyst, retaining 100% of the initial activity after 7 h of incubation at 80 °C. Poly(ethylene glycol) (PEG) is an amphiphilic polymer with the capability of binding water molecules (*42*) which might form an intricate hydrogen-bond lattice between the protein and the polymer. Chemical modification with PEG has been used to enhance the stability of several enzymes such as trypsin (*13*), horseradish peroxidase (*14*), chymotrypsin (*16*), and *C. rugosa* lipase (*15*, *16*). In this work, 80% of the surface lysine residues of the Cyt−PEG_{5000} were modified by PEG after the reaction, resulting in a biocatalyst with a predicted molecular weight of 94.7 kDa in which only 13% of the mass is protein. SDS−PAGE electrophoresis and gel filtration chromatography failed to confirm the average molecular weight of this preparation possibly due to the low motility of the polymer in gels (*43*) or to an increase in the hydrodynamic volume of the protein (*38*). The modified preparation was analyzed by electrospray mass spectrometry. The mass spectrum showed the presence of a variety of species; however, by deconvolution treatment the main species showed 94367 Da. Beside the complexity of the protein preparation and the limitations of the technique, the mass spectrum data showed that the chemical modification was extensive. The assumption of the complex hydrogen lattice as a stabilizing element suggests that it might contribute not only to enhance the tolerance of Cyt−PEG_{5000} to high temperatures, but also to stabilize the protein, which is in fact the case, as can be seen in Figure 1c.

Polycyclic aromatic compounds and organosulfur compounds were tested with cytochrome preparations at high temperature (Table 1). As expected, Cyt−PEG_{5000} showed higher activity against all substrates tested than the unmodified protein. This effect might be caused by the higher surface hydrophobicity of Cyt−PEG_{5000} active site, which in turn may be reflected in a more favorable partition of the hydrophobic substrate to the active site. The increased surface hydrophobicity has been reported to result in up to 9-fold increase in the overall catalytic efficiency of the biocatalyst (*22*).

The thermal stability of PEG-modified trypsin has been directly correlated to the molecular mass of the PEG moiety (*13*). To evaluate the effect of PEG sizes upon Cyt stability, we modified the protein with different methoxypoly(ethylene glycol)s previously activated with cyanuric chloride. Activation of low molecular weight PEG (350 Da) resulted in two batch preparations: PEG_{350} in which only one molecule of polymer was coupled to one molecule of 2,4,6 trichloro-1,3,5-triazine, and other, bisPEG_{350}, with two coupled molecules of polymer per molecule of activating reagent. The cyanuric chloride coupling with higher molecular weight polymers yielded mainly the mono derivatives. Incorporation of PEG_{350} and bisPEG_{350} into Cyt resulted in preparations with low degree of modification (20% to 30%), while modification with polymers of higher molecular masses produced biocatalysts with more than 70% modification (Table 2). A threshold value of the size of the polymer for the activity of the modified protein was found, independent of the temperature tested (Table 2). The specific activity increased as the polymer size and PEG/protein mass ratio increased up to values of 750 Da and 1.03, respectively. Then, the specific activity decreased as the polymer size and PEG/protein ratio increased. This effect might be the result of the steric hindrance of the active site by the polymer. In particular, PEG_{2000} and PEG_{5000} are molecules with a large exclusion volume that might prevent the interaction of substrates and the active site.

The thermal inactivation process for the Cyt−PEG preparations at 80 °C in all cases followed a first order kinetics. Surprisingly no loss in activity was found for Cyt−PEG_{2000} after 7 h at 80 °C in the absence of substrate, whereas the calculated half-lives for Cyt−PEG_{750} and Cyt−PEG_{5000} were 27 and 14 h, respectively (Table 2). The assumption of the protective effect of PEG upon the protein thermal stability through a shell-like structure suggested that the larger the PEG/Cyt ratio, the more stable would be the protein. This assumption was shown to be correct up to a threshold mass ratio of 2.8, while the preparation with larger value (PEG_{5000}) presented reduced stability. Thus, our results show that there is an optimal polymer/protein ratio for thermal stability of cytochrome *c*. The lower stability obtained at

Table 2. Modification Degree and Specific Activity of Modified Horse Heart Cytochrome *c* with PEG of Different Molecular Weights

preparation	modification g PEG/g Cyt	specific activity (min^{-1})[a] 30 °C	specific activity (min^{-1})[a] 80 °C	residual activity after 7 h at 80 °C (%)
unmodified	------	0.63 (± 0.2)	0.015 (± 0.001)	nd[b]
Cyt−PEG_{350}	0.25	0.88 (± 0.01)	0.05 (± 0.001)	nd
Cyt-bisPEG_{350}	0.30	1.45 (± 0.1)	0.03 (± 0.001)	nd
Cyt−PEG_{750}	1.03	4.58 (± 0.1)	1.54 (± 0.03)	80
Cyt−PEG_{2000}	2.79	3.65 (± 0.02)	1.44 (± 0.03)	102.3
Cyt−PEG_{5000}	6.76	2.77 (± 0.1)	0.35 (± 0.002)	66.2

[a] Specific activity was estimated using 20 μM pyrene as substrate in 15% acetonitrile. [b] nd: not determined due to the low activity found at 80 °C.

Table 3. Activity and Stability in the Absence of Substrate of Chemically Modified Mutant Yeast Cytochromes *c*

cytochrome	g PEG/g Cyt	specific activity (min^{-1}) 30 °C	specific activity (min^{-1}) 70 °C	residual activity after 5 h at 70 °C (%)[b]
parental Cyt−PEG_{5000}[a]	4.05	2.17 (± 0.02)	0.73 (± 0.01)	69 (± 1.5)
(K27A)−PEG_{5000}	4.54	2.12 (± 0.13)	0.66 (± 0.01)	54 (± 0.3)
(K79A)−PEG_{5000}	4.11	2.15 (± 0.04)	0.47 (± 0.01)	113 (± 2.4)
(K27A, K79A)−PEG_{5000}	3.84	2.06 (± 0.05)	0.56 (± 0.01)	113 (± 10.3)

[a] Parental y-cytochrome *c* contains the following mutations: T-5A, Y97F, C102T. [b] Residual activity was measured against pyrene and expressed as relative to initial activity values at 70 °C.

both sides of the optimal ratio may be attributable at two different factors: (a) in the case of low ratios, a less structured hydrogen-bonded network caused by few polymer molecules on the protein surface, and (b) in the case of high ratios, an steric effect may occur with molecules having high exclusion volumes, which could distort the protein conformation.

The crystal structure of yeast cytochrome *c* (y-Cyt) (*36*) shows only two lysine residues close to the active site, Lys 27 and Lys 79. One of them, Lys79, is located at the edge of the active site and it is H-bonded with Ser 47 in yeast or Thr 47 in horse heart cytochrome *c*. Under reducing conditions, this H-bond results in the closure of the active site. The other lysine, Lys27, is part of a reversed γ-turn. This unusual structure is maintained by three main-chain H-bonds between Lys27, Gly29, and Cys17 and by one H-bond involving side-chain and main-chain atoms (Lys27 to Leu15). Substitution at this position with other residues makes the protein unable to form the last interaction, yielding a less stable protein (*36*). Despite the high homology between yeast and horse heart cytochromes, thermal and chemical denaturation studies had shown that yeast cytochrome *c* is less stable than those from mammalian sources (*44*). With the aim of clearing the polymer from the active site surface of cytochrome, Lys27 and Lys79 residues in y-Cyt were substituted by alanine, which has a nonreactive side-chain. Yeast cytochrome *c* has only 16 lysine residues, while horse heart cytochrome *c* has 19 lysine residues. Thus, it was expected a lower PEG/protein mass ratio for pegylated y-Cyt than that of horse heart cytochrome *c* preparations. We were unable to detect any activity in the yeast unmodified protein at temperatures above 70 °C (data not shown). Nevertheless, chemical modification with PEG_{5000} significantly increased the activity and stability of these preparations (Table 3). Our results indicate that (K27A)−PEG_{5000} retained only 54% of initial activity, while (K79A)−PEG_{5000} showed activity above 100% of the initial activity at 70 °C, both in the absence of substrate. On the other hand, the presence of the K27A substitution did not suppress the effect of K79A, as could be seen in the double mutant (K27A, K79A)−PEG_{5000} which showed the same residual activity as the single mutant. Our results suggest that in order to obtain higher stability, chemical modification of Lys27 is required and, at the same time, PEG must be excluded from Lys79. Four structural units have been described in horse heart cytochrome *c* (*37*). The fourth unit, reported as the less stable (*37*), is formed by the loop joining the 60−70 helix to the C-terminal helix and comprises the heme group axial coordinating side-chain Met80. It is reasonable to consider that the introduction of a very large molecule on the amino acid 79 would cause loop distortion and disruption of the Met80-heme ligation, which in turn would yield a less stable protein. On the other hand, the second unit contains the other proximal heme ligand, His18, being the second more stable unit within Cyt (*37*). Lys27 is located in this unit, leading its amino reactive group exposed to the solvent; thus it was expected that modification of Lys 27 would have no effect on the structural features of this unit.

To get a deeper understanding of the structural basis underlying PEG-induced thermal stabilization, we focused on the spectroscopic properties of horse heart Cyt−PEG_{5000} preparations. CD ellipticities at 222 nm have been widely used as an estimate of the α-helical content in proteins (*45*−*47*). Cytochrome *c* is a compact single domain protein of 104 amino acids with an α-helical content of about 30% (*33*). The changes in helical content of both Cyt and Cyt−PEG_{5000} after incubation at 80 °C are shown in Figure 2. A sharp decrease in ellipticity at 222 nm was observed for Cyt, when it was incubated at 80 °C for 24 h, indicating a complete loss of the protein secondary structure. Its noteworthy the increased noise in the Cyt−PEG_{5000} spectra. Control experiments in the presence of 5 mM of free PEG_{5000} did not show a significant signal in the wavelength range where the spectra were collected, discarding a contribution of the polymer to the signal. Thus, the increase in the noise is only attributable to the scattering produced by the chemical modification of cytochrome with PEG. Interestingly the signal minimum observed in Cyt−PEG_{5000} was displaced from 222 to 210 nm, suggesting that the chemical modification was enough to disturb the secondary structure. This fact is also confirmed by the lower mean residual ellipticity at 222 nm of the native Cyt−PEG as compared to Cyt (Figure 2). However, even if the initial structure of Cyt−PEG_{5000} was probably altered, with respect to the unmodified Cyt, its overall CD spectral features suffer a small decrement in CD signal at 222 nm during the first 10 min of incubation at 80 °C, after which remain unchanged even after extensive

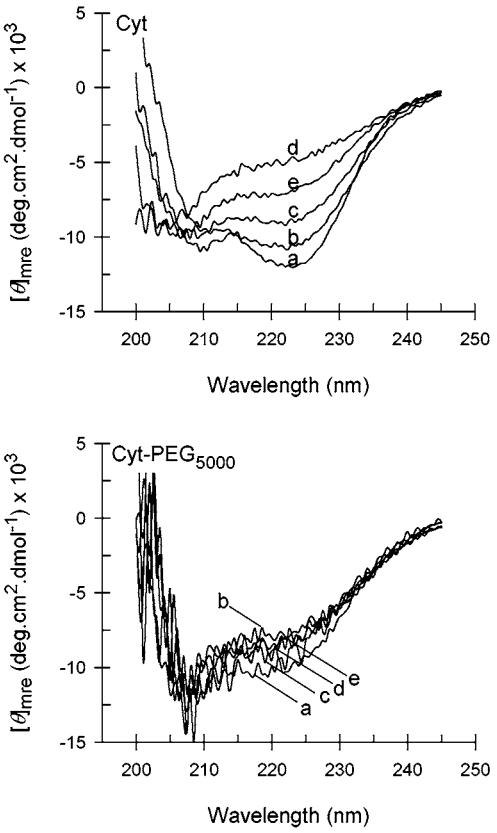


Figure 2. Mean residual ellipticity of cytochrome *c* preparations. Scans were obtained after samples were incubated under following conditions: (a) 30 °C, 10 min; (b) 80 °C, 10 min; (c) 80 °C, 7 h; (d) 80 °C, 24 h; (e) 80 °C, 24 h followed by cooling to 30 °C.

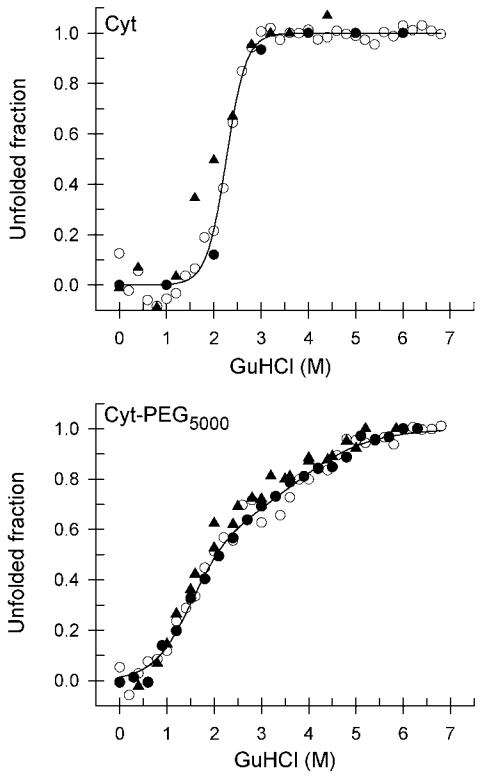


Figure 3. Equilibrium unfolding of Cyt and Cyt−PEG_{5000} after chemical denaturation by guanidine hydrochloride. Experimental data were fitted to a two-state model for Cyt and to a three-state model for Cyt−PEG_{5000}. Unfolding was followed by (○) fluorescence, (●) circular dichroism, and (▲) specific activity; (—) fit to a two-state model for Cyt and to a three-state model for Cyt−PEG_{5000}.

incubation at 80 °C (Figure 2). This result suggested a more conserved residual structure in Cyt−PEG_{5000}, which in turn could be the responsible for the thermotolerant activity found.

Urea denaturation studies of Cyt have shown that the unfolding proceeds through at least two intermediate states (*48*) while guanidine hydrochloride (GuHCl) denaturation has been considered as a two-state transition (*49*). Additionally, at least three intermediate states have been reported on unfolding of horse heart cytochrome *c*, which result from the cooperative unfolding of one or more of four known structural units (*37*). In this work we carried out the chemical denaturation of unmodified and modified cytochrome *c* with GuHCl and monitored the unfolding process through fluorescence and CD (Figure 3). For both preparations unfolding was found to be fully reversible. Denaturation data of Cyt fit into a two-state model, showing a highly cooperative transition between 1.6 and 2.8 M GuHCl. On the other hand, Cyt−PEG denaturation fit into a three-state model and the unfolding was less cooperative, showing a first transition between 0.6 and 2.2 M GuHCl and a second one between 3.4 and 4.8 M GuHCl. It is important to note that the loss of activity precede the loss of structure in the unmodified cytochrome and is less cooperative, while in the PEG-modified protein the activity is strongly associated to the loss of structure. The appearance of the intermediate state may explain the activity found at high temperature in the case of Cyt−PEG_{5000}.

The thermodynamic parameters for the unfolding of Cyt and Cyt−PEG_{5000} presented in Table 4 were calculated by fitting experimental data to the corresponding unfolding models (see Figure 3). The global unfolding free-energy for Cyt was estimated to be 6.4 kcal/mol which is close to the reported value of 7.27 kcal/mol (*50*, *51*). The calculated $\Delta(\Delta G)_{25°C}$ between the unmodified and the chemically modified preparations was 1.36 kcal/mol, indicating a reduced thermodynamic stability for Cyt−PEG_{5000}, which is contradictory to the higher stability conferred by the chemical modification on cytochrome activity. A striking difference between the denaturation profiles of Cyt and Cyt−PEG_{5000} is the absence of a well-

Table 4. Thermodynamic Unfolding Parameters of Cyt and Cyt−PEG_{5000} at 25 °C

parameter	Cyt[a]	parameter	Cyt−PEG[b]
ΔG_{nu} (kcal/mol)	6.4 (± 0.8)	ΔG_{ni} (kcal/mol)	2.19 (± 0.15)
m_{nu} (kcal/mol/M)	2.83 (± 0.34)	m_{ni} (kcal/mol/M)	1.45 (± 0.14)
$[GuHCl]_{1/2nu}$ (M)	2.27	ΔG_{iu} (kcal/mol)	2.85 (± 0.55)
		m_{iu} (kcal/mol/M)	0.76 (± 0.09)
		Z parameter	0.58 (± 0.08)
		global $\Delta G_{25°C}$ (kcal/mol)	5.04 (± 0.6)
		$[GuHCl]_{1/2ni}$ (M)	1.51
		$[GuHCl]_{1/2iu}$ (M)	3.75

[a] Data were calculated using a two-state model. [b] Data were calculated using a three-state model.

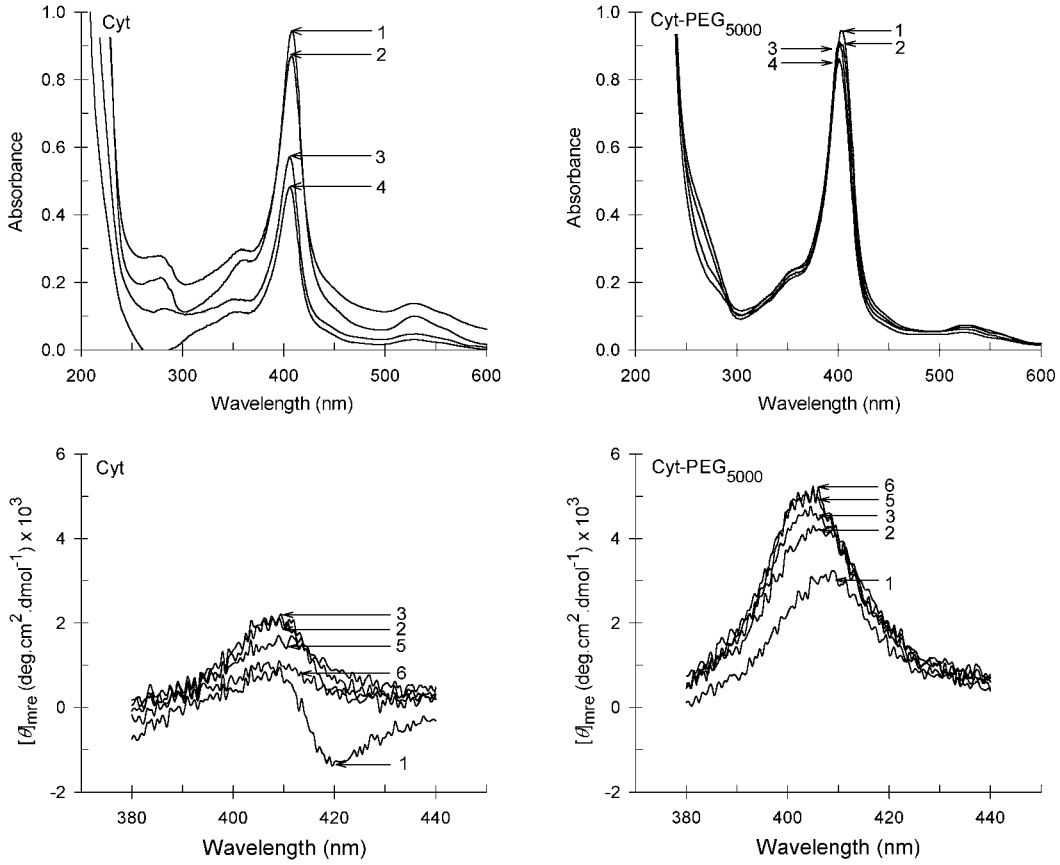


Figure 4. UV-visible (top panels) and CD (bottom panels) spectra of cytochrome *c* and Cyt−PEG_{5000} preparations. Scans were obtained after samples were incubated under following conditions: (1) 10 min at 30 °C; (2) 10 min at 80 °C; (3) 7 h at 80 °C; (4) 7 h at 80 °C and cooling to 30 °C; (5) 24 h at 80 °C; (6) 24 h at 80 °C and cooling to 30 °C.

defined native baseline in the latter. This feature can be interpreted as an altered initial structure, attributable to the chemical modification, and in agreement with the lower mean residual ellipticity observed at 222 nm.

To investigate the structural implications of the chemical modification upon Cyt activity, we performed the spectrometric study of the tertiary structure around the active site. The absorption signal at 695 nm has been associated to the heme-iron coordination state and can be used to follow coupled reactions, such as Met80-heme coordination, opening of the heme crevice, and global unfolding (*52*). As reported previously (*53*), none of our Cyt−PEG_{5000} preparations presented the 695 nm band, which may be the result of the loss of the Met80-heme sixth ligand. The spectrometric analysis of Cyt at the Soret region (350−450 nm) provides a mean to probe the active site conformation (*52*) in a nondisruptive manner. This analysis yielded additional evidence of the intrinsic active site distortion due to the chemical modification: (a) the analysis of the active site through CD showed that the negative signal at 420 nm is lost upon Cyt chemical modification (Figure 4, bottom panels); this band reflects the heme−polypeptide interactions and can be used to measure the integrity of heme crevice (*45*). On the other hand, this band is irreversibly lost during heating of the unmodified cytochrome, (b) the CD spectra of Cyt−PEG_{5000} showed an enhancement of the 410 nm signal during the first 10 min at 80 °C, after which the spectra remain unchanged, suggesting a more conserved secondary structure around the heme pocket, and (c) the Soret band of the Cyt−PEG_{5000} shifted from the 410 nm maximum to 402 nm, indicating a more hydrophobic heme microenvironment. As expected, our results showed that the Soret band of Cyt disappeared irreversibly after incubation at 80 °C, indicating the total disruption of the active site (Figure 4, top panels). On the other hand, the Soret band of Cyt−PEG_{5000} remained basically unaltered after the same treatment, reflecting the stable conformation of the active site (Figure 4). This more conserved structure around the heme could be responsible for the thermostable activity. The kinetics of unfolding of the active site was also evaluated by following the loss of the Soret band of cytochrome preparations. The results obtained indicated a half-life of 167 h for Cyt−PEG_{5000} at 80 °C, while for Cyt it was only 42 h under the same conditions. Thus, our results suggest that PEG acts as a cage in which the destabilized structure of Cyt−PEG_{5000} is trapped. In other words, the polymer works as a kinetic trap stabilizing an intermediate state upon unfolding of the modified protein. This catalytically active intermediate state may arise from a more conserved structure around the active site and seems to be responsible for the activity found after long periods of incubation at high temperature.

The conformation of PEG in aqueous solutions ranges from a random coil to a helix in which oxygen acts as an anchor for hydrogen bond formation. In fact, it has been demonstrated that each residue of ethylene in PEG is able to hydrogen-bond from two to three water molecules (*42*, *54*). It has also been found that PEG is flexible in nonpolar solvents and rigid in aqueous solutions. This entropy loss is explained by an increase in the water structure around the hydrophilic region of PEG and to a lesser extent in the hydrophobic region (*55*). Thus, the mechanism of stabilization of poly(ethylene glycol) seems to be due to the adduct amphiphilicity (*16*). A primary shield of rigid water molecules solvate the hydrophilic region of bound PEG, helping to maintain the structure

of the protein, whereas the hydrophobic regions in PEG interact with the hydrophobic clusters on protein surface. Those sets of interactions would produce a shell-like structure in which PEG is coiled on the protein surface avoiding direct contact with water molecules in the solvent and producing a more conserved structure around heme. The global effect of those interactions is a decreased unfolding rate of the active site as confirmed by UV−visible spectroscopy and CD.

CONCLUSIONS

Chemical modification with PEG has shown to be an interesting tool to enhance the kinetic stabilization of proteins and to obtain catalytic activity at very high temperatures. The polymer/protein ratio and the modification sites seem to be determinant factors on the protein stabilization. The absence of polymer near the active site is desirable in order to achieve higher stability. Contrary to what we expected, the overall effect of chemical modification was a thermodynamic destabilization of the protein conformation. However, the polymer also works as a cage in which the destabilized structure is trapped. This cage increases the activation barrier, and thus the resulting structure can stand longer times under destabilizing conditions. Our results suggest that the peroxidasic activity found for Cyt−PEG_{5000} at hyperthermophilic conditions might be the result of two factors, a more conserved structure of the heme pocket and a decreased unfolding rate of the active site. A thermostable biocatalyst obtained by chemical modification of cytochrome *c* and with enhanced activity on hydrophobic substrates may have potential industrial applications.

ACKNOWLEDGMENT

We thank Prof. Michael A. Pickard for the critical reading and discussion on protein thermostabilization, and Dr. Cesar Ferreira for the mass spectroscopy analysis. This work was supported by a grant from the Mexican Oil Institute (FIES 98-110-VI) and by the National Council for Science and Technology of México (grant 33611-U). We acknowledge Eugenio López Bustos and Paul Gaytán for their assistance in oligonucleotide synthesis.

LITERATURE CITED

(1) DeSimone, L. D., and Popoff, F. (1997) *Eco-eficiency: The Business Link to Sustainable Development*, MIT Press, Cambridge, MA.

(2) Akanuma, S., Yamagishi, A., Tanaka, N., and Oshima, T. (1998) Serial increase in the thermal stability of 3-isopropylmalate dehydrogenase from *Bacillus subtilis* by experimental evolution. *Protein Sci. 7*, 698−705.

(3) Giver, L., Gershenson, A., Freskgard, P. O., and Arnold, F. H. (1998) Laboratory evolution of a thermostable enzyme. *Proc. Natl. Acad. Sci. U.S.A. 95*, 12809−12813.

(4) Zhao, H., and Arnlod, F. H. (1999) Directed evolution converts subtilisin E into a functional equivalent of thermitase. *Protein Eng. 12*, 47−52.

(5) Cherry, J. R., Lamsa, M. H., Schneider, P., Vind, J., Sevendsen, A., Jones, A., and Pedersen, A. H. (1999) Directed evolution of a fungal peroxidase. *Nature Biotechnol. 17*, 379−384.

(6) Aksoy, S., Tumturk, H., and Hasirci, N. (1998) Stability of α-amylase immobilized on poly(methyl methacrylate-acrylic acid) microspheres. *J. Biotechnol. 60*, 37−46.

(7) Wang, P., Sergeeva, M. V., Lim, L., and Dordick, J. S. (1997) Biocatalytic plastics as active and stable materials for biotransformations. *Nature Biotechnol. 15*, 789−793.

(8) Govardhan, C. P. (1999) Cross-linking of enzymes for improved stability and performance. *Curr. Opin. Biotechnol. 10*, 331−335.

(9) St Clair, N. L., and Navia, M. A. (1992) Cross-linked enzyme crystals as robust biocatalysts. *J. Am. Chem. Soc. 114*, 7314−7316.

(10) Wong, S. S., and Wong, C. L. J. (1992) Chemical crosslinking and the stabilization of protein and enzymes.*Enzyme Microb. Technol. 14*, 866−874.

(11) Lenders, J. P., and Crichton, R. R. (1984) Thermal stabilization of amylolitic enzymes by covalent coupling to soluble polysaccharides. *Biotechnol. Bioeng. 26*, 1343−1351.

(12) Srivastava, R. A. K. (1991) Studies on stabilization of amylase by covalent coupling to soluble polysaccharides. *Enzyme Microb. Technol. 13*, 164−170.

(13) Gaertner, H. F., and Puigserver, A. J. (1992) Increased activity and stability of poly(ethylene glycol)-modified trypsin. *Enzyme Microb. Technol. 14*, 150−155.

(14) Garcia, D., Ortéga, F., and Marty, J. L. (1998) Kinetics of thermal inactivation of horseradish peroxidase: stabilizing effects of methoxypoly(ethylene glycol). *Biotechnol. Appl. Biochem. 27*, 49−54.

(15) Hernáiz, M. J., Sánchez-Montero, J. M., and Sinisterra, J. V. (1999) Modification of purified lipases from *Candida rugosa* with poly(ethylene glycol): a systematic study. *Enzyme Microb. Technol. 24*, 181−190.

(16) Longo, M. A., and Combes, D. (1999) Thermostability of modified enzymes: a detailed study. *J. Chem. Technol. Biotechnol. 74*, 25−32.

(17) McEldoon, J. P., and Dordick, J. S. (1996) Unusual themal stability of soybean peroxidase. *Biotechnol. Prog. 12*, 555−558.

(18) Sakharov, I. Y., Vesga, M. K., Galaev, I. Y., Sakharova I. V., and Pletjushkina O. Y. (2001) Peroxidase from leaves of royal palm tree *Roystonea regia*: purification and some properties. *Plant Sci. 161*, 853−860.

(19) Vazquez-Duhalt, R., Westlake, D. W. S., and Fedorak, P. M. (1993) Cytochrome *c* as biocatalyst for the oxidation of thiophenes and organosulfides. *Enzyme Microb. Technol. 15*, 494−499.

(20) Vazquez-Duhalt, R., Semple, K. M., Westlake, D. W. S., and Fedorak, P. M. (1993) Effect of water-miscible organic solvents on the catalytic activity of cytochrome *c*. *Enzyme Microb. Technol. 15*, 936−943.

(21) Torres, E., Sandoval, J. V., Rosell, F. I., Mauk, G., and Vazquez-Duhalt, R. (1995) Site-directed mutagenesis improves biocatalytic activity of iso-1-cytochrome *c* in polycyclic hydrocarbon oxidation. *Enzyme Microb. Technol. 17*, 1014−1020.

(22) Tinoco, R., and Vazquez-Duhalt, R. (1998) Chemical modification of cytochrome *c* improves their catalytic properties in oxidation of polycyclic aromatic hydrocarbons. *Enzyme Microb. Technol. 22*, 8−12.

(23) Vazquez-Duhalt, R. (1999) Cytochrome *c* as biocatalyst. *J. Mol. Catal. B: Enzymatic 7*, 241−249.

(24) Ortiz-Leon, M., Velasco, L., and Vazquez-Duhalt, R. (1995) Biocatalytic oxidation of polycyclic aromatic hydrocarbons by hemoglobin and hydrogen peroxide. *Biochem. Biophys. Res. Commun. 215*, 968−973.

(25) Torres, E. and Vazquez-Duhalt, R. (2000) Chemical modification of hemoglobin improves biocatalytic oxidation of PAHs. *Biochem. Biophys. Res. Commun. 273*, 820−823.

(26) Villegas, A., Mauk, G., and Vazquez-Duhalt, R. (2000) A cytochrome *c* variant resistant to heme degradation by hydrogen peroxide. *Chem. Biol. 7*, 237−244.

(27) Abuchowski, A., van Es, T., Palczuk, N. C., and Davis, F. F. (1977) Alteration of immunological properties of bovine serum albumin by covalent attachment of poly(ethylene glycol). *J. Biol. Chem. 252*, 3578−3581.

(28) Habeeb, A. F. S. A. (1966) Determination of free amino groups in proteins by trinitrobenzenesulfonic acid. *Anal. Biochem. 14*, 328−336.

(29) Horton, R. M., and Pease, L. R. (1991) Recombination and mutagenesis of DNA secuences using PCR. *Directed mutagenesis. A practical approach*; McPherson, M. J., Ed.; pp 217−247. IRL Press, Oxford, UK.

(30) Pollock, W. B., Rosell, F. I., Twitchett, M., Dumont, M., and Mauk, A. G. (1998) Bacterial expression of a mitochondrial cytochrome *c*. Trimethylation of Lys72 in yeast iso-cytochrome *c* and the alkaline transition. *Biochemistry 37*, 6124−6131.
(31) Ausubel, F. M., Brent, R., Kingston, R. E., Moore, D. D., Seidman, J. G., Smith, J. A., and Struhl, K. (1999) *Short protocols in molecular biology*, Wiley & Sons, Inc., New York.
(32) Margoliash, E., and Schejter, A. (1966) Cytochrome *c*. *Adv. Protein. Chem. 21*, 113−286.
(33) Ahmad, A., Madhusudanan, K. P., and Bhakuni, V. (2000) Trichloroacetic acid and trifluoroacetic acid-induced unfolding of cytochrome *c*: stabilization of a nativelike folded intermediate. *Biochim. Biophys. Acta 1480*, 201−210.
(34) Vazquez-Duhalt, R., Westlake, D. W. S., and Fedorak, P. M. (1994) Lignin peroxidase oxidation of aromatic compounds in systems containing organic solvents. *Appl. Environ. Microbiol. 60*, 459−466.
(35) Ionescu, R., Smith, V. F., O'Neill, J. C., Jr., and Mathews, R. (2000) Multistate equilibrium unfolding of *Escherichia coli* dihydrofolate reductase: thermodynamic and spectroscopic description of the native, intermediate, and unfolded ensembles. *Biochemistry 39*, 9540−9550.
(36) Louie, G. V., and Brayer, G. D. (1990) High-resolution refinement of yeast iso-1-cytochrome *c* and comparisons with other eukaryotic cytochromes *c*. *J. Mol. Biol. 214*, 527−555.
(37) Xu, Y., Mayne, L., and Englander, W. (1998) Evidence for an unfolding and refolding pathway in cytochrome *c*. *Nature Struct. Biol. 5*, 774−778.
(38) Longo, M. A., and Combes, D. (1997) Influence of surface hydrophilic/hydrophobic balance on enzyme properties. *J. Biotechnol. 58*, 21−32.
(39) Vazquez-Duhalt, R., Fedorak, P. M., and Westlake, D. W. S. (1992) Role of enzyme hydrophobicity in biocatalysis in organic solvents. *Enzyme Microb. Technol. 14*, 837−841.
(40) Inada, Y., Takahashi, K., Yoshimoto, T., Ajima, A., Matsushima, A., and Saito, Y. (1986) Application of poly(ethylene glycol)-modified enzymes in biotechnological processes: organic solvents-soluble enzymes. *Trends Biotechnol. 4*, 190−194.
(41) Torres, E., Tinoco, R., and Vazquez-Duhalt, R. (1996) Solvent hydrophobicity predicts biocatalytic behaviour of lignin peroxidase and cytochrome *c* in aqueous solution of water-miscible organic solvents. *J. Biotechnol. 49*, 59−67.
(42) Liu, K. J., and Parsons, J. L. (1969) Solvents effects on the preferred conformation of poly(ethylene glycols). *Macromolecules 2*, 529−533.
(43) Varalakshmi, P., Lathika, K. M., Raghavan, K. G., and Singh, B. B. (1995) Altered physicochemical characteristics of polyethylene glycol linked beet stem oxalate oxidase. *Biotechnol. Bioeng. 46*, 254−257.
(44) Endo, S., Nagayama, K., and Wada, A. (1985) Probing stability and dynamics of proteins by protease digestion I: comparison of protease susceptibility and thermal stability of cytochromes *c*. *J. Biomol. Struct. Dyn. 3*, 409−421.
(45) Myer, Y. P. (1978) Circular dichroism spectroscopy of hemoproteins. *Methods Enzymol. 54*, 249−17.
(46) Woody, R. W. (1995) Circular Dichroism. *Methods Enzymol. 246*, 34−71.
(47) Greenfield, N. J. (1996) Methods to estimate the conformation of proteins and polypeptides from circular dichroism data. *Anal. Biochem. 235*, 1−10.
(48) Myer, Y. P., McDonald, L. H., Verma, B. C., and Pande, A. (1980) Urea denaturation of horse heart ferricytochrome *c*. Equilibrium studies and characterization of intermediate forms. *Biochemistry 19*, 199−207.
(49) Puett, D. (1973) The equilibrium unfolding parameters of horse and sperm whale myoglobin. Effects of guanidine hydrochloride, urea and acid. *J. Biol. Chem. 248*, 4623−4634.
(50) Knapp, J. A., and Pace, C. N. (1974) Guanidine hydrochloride and acid denaturation of horse, cow, and *Candida krussei* cytochromes *c*. *Biochemistry 13*, 1289−1294.
(51) Saito, Y., and Wada, A. (1983) Comparative study of GuHCl denaturation of globular proteins. I. Spectroscopic and chromatographic analysis of the denaturation curves of ribonuclease A, cytochrome *c*, and pepsinogen. *Biopolymers 22*, 2105−2122.
(52) Nall, B. T. (1996) Cytochrome *c* folding and stability. *Cytochrome c*. A multidisciplinary approach (Scott, R. A., and Mauk, G., Eds.) pp 167−200, University Science Books, Sausalito, CA.
(53) Busi, E., Howes, B. D., Pogni, R., Basosi, R., Tinoco, R., and Vazquez-Duhalt, R. (1999) Modified cytochrome *c*/H_2O_2 system: spectroscopic EPR investigation of the biocatalytic behaviour. *J. Mol. Catal. B: Enzymatic. 9*, 39−48.
(54) Donato, I. D., Magazú, S., Maisano, G., Majolino, D., Migliardo, P., and Pollicino, A. (1996) Hydration phenomena and hydrogen bond conectivity in polymeric aqueous solutions. *Mol. Phys. 87*, 1463−1469.
(55) Tasaki, K. (1996) Poly(oxyethylene)-water interactions: a molecular dynamics study. *J. Am. Chem. Soc. 118*, 8459−8469.

BC025561P